 © 1985 The Chemical Society of Japan Bull. Chem. Soc. Jpn., 58, 1—4 (1985)

Adsorption Properties of Pillar Interlayered Montmorillonite

Mutsuyoshi MATSUMOTO,*,† Minoru SUZUKI, (the late) Hiroshi TAKAHASHI, and Yasukazu SAITO
Institute of Industrial Sciene, The University of Tokyo,
22-1, Roppongi 7 Chome, Minato-ku, Tokyo 106
(Received March 31, 1984)

From analyses of Langmuir-type isotherms and α_s-plots for nitrogen adsorption, both the micropore volume and the external surface area have been determined for pillar interlayered montmorillonite (abbreviated as PILM) prepared by intercalating the polynuclear Al cation into the montmorillonite interlayer. The applicability of the Gurvitsch rule to microporous PILM samples was confirmed for adsorption of heptane, whereas the adsorbed amounts of polar adsorbates were dependent on dehydrated states of the alumina pillar. High density of benzene in the micropore independent of calcination temperature suggests some peculiar orientation of benzene in the adsorbed state due to its molecular shape. The interaction of a water molecule with the adsorption site is weak and dependent on the calcination temperature of PILM samples. On this basis, the inhibition of rehydration of the alumina pillar has been discussed.

The pore structure of a solid is essentially important for its adsorption properties. For example, the diffusion characteristics of benzene molecules adsorbed on pillar interlayered montmorillonite (abbreviated as PILM) are in contrast with those on faujasite-type zeolite, although both the adsorbents are similar in micropore size;[1] irreversible dehydration of the alumina pillar has been correlated with surface chemical properties of PILM.[2]

Since Langmuir-type isotherms for nitrogen adsorption on hydroxy-zirconium,[3] hydroxy-chromium,[4] and hydroxy-bismuth[5] montmorillonites were attributed to steric hindrance to the multilayer formation in micropores, elucidation has been expected of the adsorption behavior inside PILM micropores of various adsorbates including nitrogen. Moreover, some new clue to the characterization of surface chemical properties of PILM is necessary, since the generally adopted method of measuring heat of immersion[6] is inapplicable to microporous solids. In this study, we attempt to clarify surface chemical properties by measuring the adsorption enthalpy of water, because the small and polar molecule of water may penetrate with ease through pores of a solid during the adsorption process. An additional purpose is to examine whether or not surface hydroxyl groups can be regenerated, as it is important for the acidic nature of PILM catalysts.

Experimental

Montmorillonite. Otay montmorillonite, supplied from Ward's Natural Science Establishment, Inc., was separated by gravity sedimentation in water dispersion to obtain the fraction less than 2 μm in diameter, and was treated with NaCl (1.0 mol dm^{-3}) to obtain the mother material for PILMs in the Na ion exchanged form (hereafter the material is referred to as Na-Mont).

Preparation of Intercalation Compounds. Preparation of the polynuclear cation $[Al_{13}O_4(OH)_{24}(OH_2)_{12}]^{+7}$[7–9] and its intercalation into montmorillonite were done in the same manner as in previous studies.[1,2] The sample dried in an oven overnight at 393 K is referred to as PILM 120. This sample was calcined in air for 2 h at 473, 673, 873, or 1073 K (hereafter the calcined sample is referred to as PILM 200, PILM 400, PILM 600, or PILM 800, respectively). All these samples were kept in a vessel containing saturated aqueous solution of NH_4Cl to provide a constant humidity. A perspective view of PILM 120 is shown in Fig. 1.

Adsorption Analysis. Both volumetrical adsorption measurements with nitrogen at 77 K using an Orr surface-area

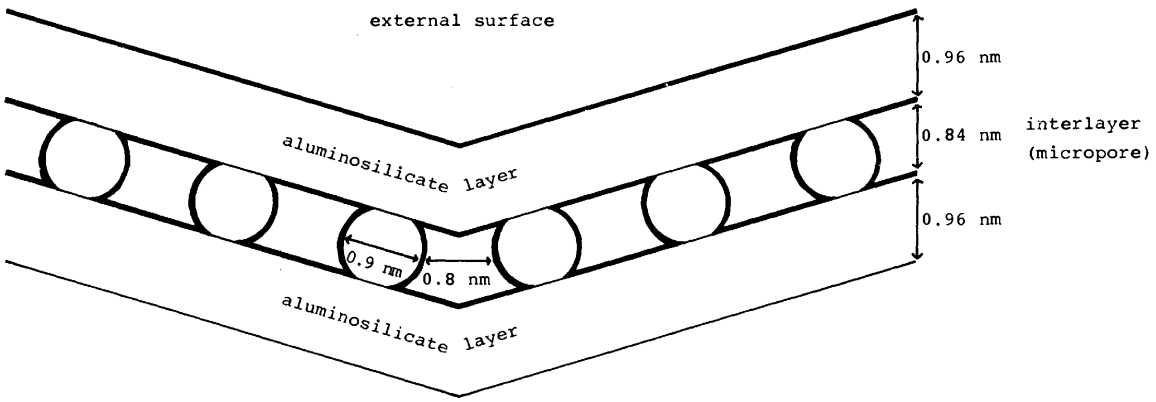

Fig. 1. Perspective view of the pillar interlayered montmorillonite, with the interdistance minimized for the homogeneous arrangement.

† Present address: National Chemical Laboratory for Industry, 1-1, Higashi, Yatabe-machi, Tsukuba-gun, Ibaraki 305.

pore-volume analyzer (2100 D, Micromeritics Instrument Corp.) and gravimetrical measurements at 298 K using a spring balance for heptane, benzene, 1-chlorobutane, and 1-nitropropane were conducted after a standard pretreatment of overnight evacuation ($<10^{-3}$ Pa) at 393 K.

Calorimetric Measurements of Water Adsorption. A twin conduction type calorimeter (Tokyo Riko Co., Ltd.) equipped with a vacuum system was used to detect the heat evolved during the adsorption process. Before measurement at 298 K, all samples were heat-treated at 393 K for 6 h under vacuum ($<10^{-3}$ Pa).

Results and Discussion

Estimation of the External Surface Area of Montmorillonite Samples with and without Interlayered Pillar. Figure 2 shows adsorption and desorption isotherms for nitrogen. The Langmuir-type adsorption, observed for all the samples except PILM 800, indicates the predominance of adsorption to fill up the micropore. The adsorption behavior in the middle pressure region will correspond to the adsorption on external surface, which may be ignored in the case of zeolite.[10] Abrupt change is noticed with the desorption isotherms at $p/p_0 \simeq 0.5$, resulting from the tensile strength effect.[11]

The α_s-method is useful for discriminating the monolayer capacity of external surface from the micropore capacity.[12,13] As for nonporous adsorbents, the external surface area, S_{ex}, is deduced from the slope of its α_s-plot, a straight line passing through the origin. In the case of microporous adsorbents, however, both the external surface and the micropore provide adsorption sites as far as the micropore is unfilled with adsorbate. Adsorption behavior different from that of nonporous solids would be expected; the α_s-plot provides a linear portion in the region of high coverage, whose slope gives the S_{ex} value for microporous solids.

Representative α_s-plots are shown in Fig. 3. Table 1 summarizes the S_{ex} values thus obtained from the slope of linear portion. The coincidence of the S_{ex} values among all the PILM samples except PILM 800 in Table 1 is remarkable. The α_s-plot for PILM 800 gives a straight line passing through the origin; thermal collapse of montmorillonite layer structure was previously observed in an X-ray diffraction pattern.[2]

Surface Areas of Montmorillonite Samples with and without Interlayered Pillar. The surface area, S, of adsorbent is generally evaluated by

$$S = v_a s N/M, \quad (1)$$

where v_a is the apparent monolayer capacity, s the cross-sectional area of adsorbate,[14] N Avogadro's number, and M the molar weight of adsorbate. Table 2 summarizes physical properties of adsorptives necessary for the adsorption analysis described later.

The v_a values of PILMs 120—600 were obtained from their Langmuir plots (for nitrogen $0.05<p/p_0<0.30$ and for the other adsorbates $0.10<p/p_0<0.35$). Since the adsorption isotherms of PILM 800 obeyed the BET equation, its S values were determined from BET

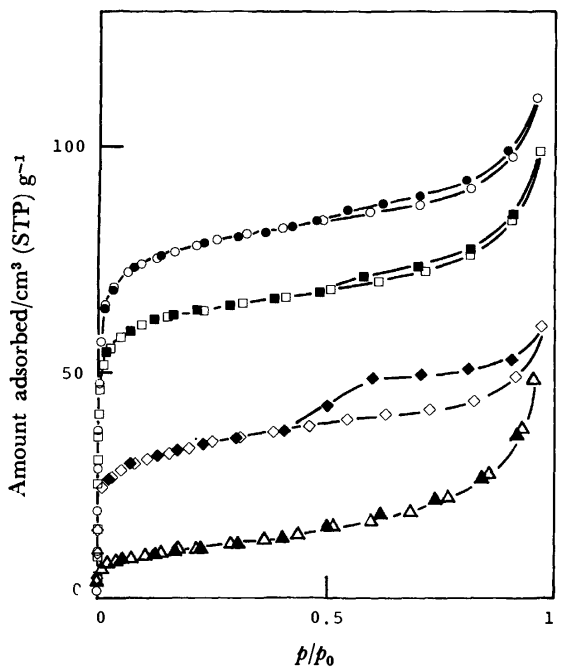

Fig. 2. Nitrogen adsorption and desorption isotherms of montmorillonite samples with and without the interlayered pillar at 77 K.
Open symbols: adsorption points, solid symbols: desorption polints. ○,●: PILM 120, □,■: PILM 400, △,▲: PILM 800, ◇,◆: Na-Mont.

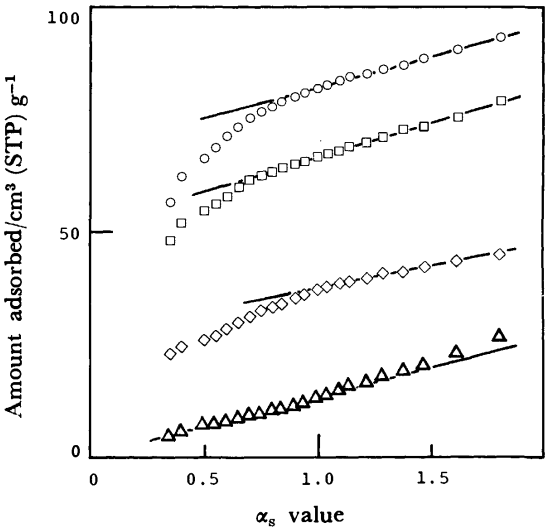

Fig. 3. The α_s-plot of montmorillonite sample with and without the interlayered pillar.
○: PILM 120, □: PILM 400, △: PILM 800, ◇: Na-Mont.

TABLE 1. EXTERNAL SURFACE AREAS OF MONTMORILLONITE SAMPLES WITH AND WITHOUT INTERLAYERED PILLAR AS CALCULATED FROM α_s-PLOTS

Adsorbent	PILM 120	PILM 200	PILM 400	PILM 600	PILM 800	Na-Mont
$S_{ex}/m^2\,g^{-1}$	38.7	42.8	40.7	46.8	38.7	28.6

TABLE 2. PHYSICAL PROPERTIES OF ADSORPTIVES NECESSARY FOR ADSORPTION ANALYSES

Adsorptive	Nitrogen	Heptane	Benzene	1-Chlorobutane	1-Nitropropane
Molar weight (M/g mol^{-1})	28.01	100.21	78.12	92.57	89.09
Density of liquid (ρ/g cm^{-3})	0.808[a)]	0.6796[b)]	0.8737[b)]	0.8866[c)]	1.0009[c)]
Cross-sectional area[d)] (s/nm^2)	0.162	0.631	0.436	0.446	0.305[e)]

a) At 77 K. b) At 298 K. c) At 293 K. d) Quoted from Ref. 14. e) Calculated with the equation: $s=1.091\times 10^{14}\ (M/\rho N)^{2/3}$.

TABLE 3. SURFACE AREA (S/m^2 g^{-1}) DETERMINED WITH VARIOUS ADSORBATES

Adsorbate[a)]	Nitrogen	Heptane	Benzene	1-Chlorobutane	1-Nitropropane
PILM 120	348.5	330.4	461.2	411.0	401.7
PILM 200	294.5	292.6	383.6	333.9	353.6
PILM 400	293.2	288.8	383.8	358.9	309.5
PILM 600	286.2	286.0	364.9	286.8	260.0
PILM 800[b)]	37.9	43.4	—[c)]	30.7	32.1

a) Nitrogen was adsorbed at 77 K and the other adsorbates at 298 K. Unless otherwise noted, adsorption obeyed the Langmuir equation. b) Adsorption obeyed the BET equation. c) Adsorption obeyed neither the BET nor the Langmuir equation.

plots (the p/p_0 range was the same as above) except the case of benzene. Table 3 shows surface area values of PILM samples thus derived from Eq. 1 with various adsorbates. The coincidence between the BET surface area, S (37.9 m^2 g^{-1}), and the α_s-plot external surface, S_{ex} (38.7 m^2 g^{-1}), for PILM 800 strongly supports the applicability of the α_s-method to the present system.

Applicability of the Gurvitsch Rule to Pillar Interlayered Montmorillonite. According to Breck and Grose,[15] the Gurvitsch rule on the amount of adsorbate taken up at saturation holds good for various types of zeolites, *i.e.*, a given adsorbent adsorbs different adsorbates up to the same amount as expressed in volume of liquid. This rule was applied to obtain the micropore volume of PILM samples as follows.

From the monolayer capacity, v_{ex}, of external surface obtainable from

$$S_{ex} = v_{ex}sN/M, \tag{2}$$

micropore capacity, v_{in}, is obtained as

$$v_{in} = v_a - v_{ex} \tag{3}$$

and is used to evaluate micropore volume, v, according to

$$v = v_{in}/\rho, \tag{4}$$

where ρ is the density of liquid.

Comparison of micropore volumes obtained with various adsorbates is useful for elucidating adsorption properties of PILM micropore. Figure 4 shows the relationship between the micropore volume for a polar or nonpolar adsorbate relative to that of nitrogen, v_{N_2}, and the calcination temperature. The dipole moment of each adsorbate is given in parentheses.

As far as the Gurvitsch rule is valid for the PILM micropore, all the values of v must be equal to v_{N_2}. Actually, the nonpolar adsorbate heptane gives a value of unity irrespective of calcination temperature, suggesting that the adsorption state in the micropore corresponds closely to liquid nitrogen.

The values for the polar adsorbates, 1-chlorobutane and 1-nitropropane, on the other hand, are larger than unity, especially with the samples for low calcination temperatures. Moreover, the deviation from unity is larger for 1-nitropropane (3.57 D) than for 1-chlorobutane (2.05 D). Since the irreversible dehydration of the alumina pillar proceeds in the calcination pretreatment on PILM samples,[2] water molecules and/or hydroxyl groups on the pillar surface should be responsible for the extraordinarily high density of these

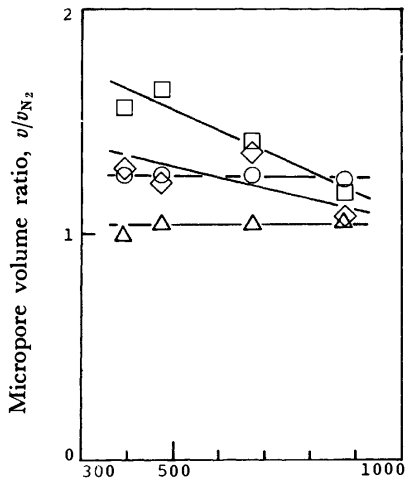

Fig. 4. Micropore volume ratio of PILM samples obtained with polar and nonpolar adsorbates as a function of calcination temperature.
△: heptane (0 D), ○: benzene (0 D), ◇: 1-chlorobutane (2.05 D), □: 1-nitropropane (3.57 D).

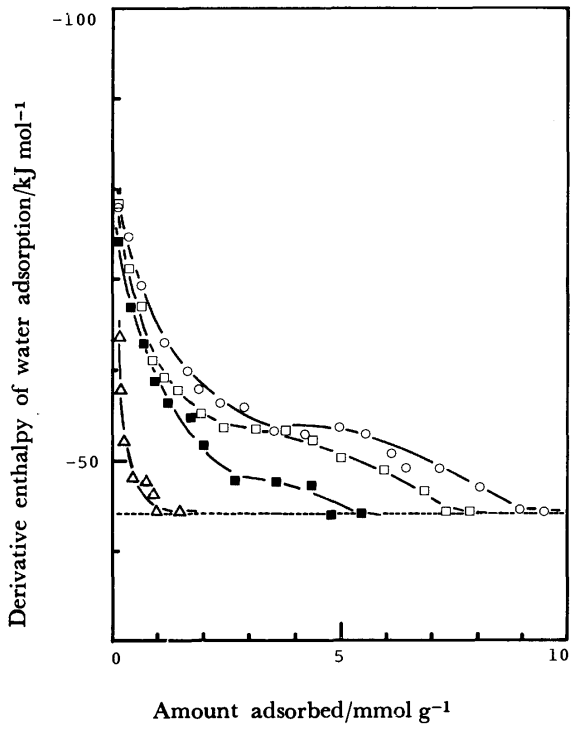

Fig. 5. Derivative enthalpy of water adsorption as a function of the amount adsorbed, with liquefaction enthalpy of water indicated by dashed line.
○: PILM 120, □: PILM 400, ■: PILM 600, △: PILM 800.

polar adsorbates. In addition, it is to be noted that the gradual decrease in the v/v_{N_2} values down to unity with elevating calcination temperature indicates the decisive influence of the alumina pillar on the adsorbate density. The assumption of homogeneous arrangement of the alumina pillars in the montmorillonite interlayer, therefore, is most likely.

The adsorbate density of benzene is high and independent of calcination temperature, which suggests a highly oriented adsorption of benzene due to its molecular shape under restriction of the slit width of PILM micropore.

Derivative Enthalpy of Water Adsorption on Pillar Interlayered Montmorillonite. Derivative enthalpies of water adsorption on PILM samples obtained by calorimetry are given in Fig. 5. In the range of sufficiently large amounts of water adsorbed, all the samples give almost the same values equal to the liquefaction enthalpy of water. The interaction of a water molecule with an adsorption site on a PILM sample is weaker than on zeolite[16] and decreases in degree with elevating calcination temperature.

The heat of immersion of α- and γ-alumina in water was reported to decrease with elevating pretreatment temperature in the relatively high temperature region; this phenomenon was ascribed to irreversible stabilization of dehydrated alumina surface.[17] Inhibition of the rehydration process would as well be responsible in the present PILM system.

References

1) M. Matsumoto, S. Shinoda, H. Takahashi, and Y. Saito, *Bull. Chem. Soc. Jpn.*, **57**, 1795 (1984).
2) M. Matsumoto, M. Suzuki, H. Takahashi, and Y. Saito, submitted to *Clays Clay Miner.*
3) S. Yamanaka and G. W. Brindley, *Clays Clay Miner.*, **27**, 119 (1979).
4) G. W. Brindley and S. Yamanaka, *Am. Mineral.*, **64**, 830 (1979).
5) S. Yamanaka, G. Yamashita, and M. Hattori, *Clays Clay Miner.*, **28**, 281 (1980).
6) A. C. Zettlemoyer, *Ind. Eng. Chem.*, **57**, 27 (1965).
7) G. Johansson, G. Lundgren, L. G. Sillén, and R. Söderquist, *Acta Chem. Scand.*, **14**, 769 (1960).
8) J. W. Akitt, N. N. Greenwood, B. L. Khandelwal, and G. D. Lester, *J. Chem. Soc., Dalton Trans.*, **1972**, 604.
9) D. E. W. Vaughan, "Proc. 5th Intern. Conf. Zeolite," ed by L. V. Rees, Heyden & Son, Ltd., London (1980), p. 94.
10) "Zeolite," ed by N. Hara and H. Takahashi, Kodansha, Ltd., Tokyo (1974).
11) O. Kadlec and M. M. Dubinin, *J. Colloid Interface Sci.*, **31**, 479 (1969).
12) M. R. Bhambhani, P. A. Cutting, K. S. W. Sing, and D. H. Turk, *J. Colloid Interface Sci.*, **38**, 109 (1972).
13) S. J. Gregg and K. S. W. Sing, "Adsorption, Surface Area and Porosity," 2nd ed, Academic Press, (1982), Chap. 4.
14) A. L. McClellan and H. F. Harnsberger, *J. Colloid Interface Sci.*, **23**, 577 (1967).
15) D. W. Breck and R. W. Grose, "Molecular Sieves," Advances in Chemistry Series 121, ed by W. M. Meier and J. B. Uytterhoeven, American Chemical Society, Washington, D. C. (1973), p. 319.
16) K. Tsutsumi and H. Takahashi, *Seisan Kenkyu*, **23**, 368 (1971).
17) T. Morimoto, K. Shiomi, and H. Tanaka, *Bull. Chem. Soc. Jpn.*, **37**, 392 (1964).

Sodium Sulfate Mixed with Rare Earth Sulfates(Ln=Y and Gd) and Silicon Dioxide as a Solid Electrolyte for a Sulfur Dioxide Detector

Nobuhito IMANAKA, Yasuo YAMAGUCHI, Gin-ya ADACHI,* and Jiro SHIOKAWA
Department of Applied Chemistry, Faculty of Engineering, Osaka University, Yamadaoka, Suita, Osaka 565
(Received May 14, 1984)

Sodium sulfate mixed with rare earth sulfates(Ln=Y and Gd) and silicon dioxide exhibits a Na_2SO_4-I-like phase as well as a small amount of silicon dioxide phase. The former phase is excellent in Na^+ ion conduction. The electrical conductivity of the Na_2SO_4–$Ln_2(SO_4)_3$–SiO_2(Ln=Y and Gd) systems is considerably higher than that of pure sodium sulfate. When the Na_2SO_4–$Ln_2(SO_4)_3$–SiO_2(Ln=Y and Gd) sample is applied as a solid electrolyte for a SO_2 gas concentration cell, the measured EMF is in good agreement with the calculated EMF for a SO_2 gas concentration range from 0.1% (1000 ppm) to 23%, and 0.32% (3200 ppm) to 10%, respectively.

Acid rain produced from the absorbtion of SO_2 and NO_2 in air is deteriorating the environment considerably in recent years. The control of the SO_2 and NO_2 in the exhausted gas and in the atmosphere is becoming a serious problem.

Alkali metal sulfates,[1-9] which are cation conductors at elevated temperature, have been applied as solid electrolytes for the SO_2 gas detector. Sodium sulfate holds the phase transformation from Na_2SO_4-III to Na_2SO_4-I.[10-26] The phase transformation, however, results in cracks in the electrolyte. The sulfate becomes soft at a temperature higher than approximately 1073 K. In addition, the electrical conductivity of Na_2SO_4 is appreciably lower than other Na^+ ion conductors such as NASICON.[27-32] Therefore, several attempts[33-37] to dope mono-, di-, or trivalent cations into sodium sulfate have been made to obtain higher electrical conductivity.

In our previous papers,[7-9,38] sodium vanadate and rare earth sulfates(Ln=Eu, Pr, and Y) have been doped in order to promote the oxidation from SO_2 to SO_3 and maintain the hig h conductive Na_2SO_4-I phase, and to increase the electrical conductivity.

In this investigation, silicon dioxide was added so as to obtain an effective network structure for Na^+ ion migration and in addition, to suppress the electrolyte becoming soft. Rare earth sulfates(Ln=Y and Gd) were also mixed to enhance the electrical conductivity. The suppression of the phase transformation from Na_2SO_4-I to Na_2SO_4-III was also attempted by mixing SiO_2 and $Ln_2(SO_4)_3$(Ln=Y and Gd) simultaneously with Na_2SO_4.

Experimental

Materials. Sodium sulfate(purity 99.99%) and silicon dioxide(purity 99.9%) were purchased from Wako Pure Chemical Industries Ltd. Yttrium(purity 99.9%) and gadlinium oxide(purity 99.99%) were bought from Shiga Rare Metal Industries Ltd. Yttrium and gadlinium sulfate were prepared by adding concd sulfuric acid into Y_2O_3 and Gd_2O_3, respectively. Sodium sulfate which is hygroscopic, and silicon dioxide were preheated before weighing. $Ln_2(SO_4)_3$ (Ln=Y and Gd) were also heated to eliminate the included water. Since $Ln_2(SO_4)_3$(Ln=Y and Gd) easily absorbs water, the real concentration of lanthanoid cation in the mixture was determined by the EDTA titration. Preheated materials were cooled in a desiccator, weighed, and mixed thoroughly in an agate mortar. Mixtures of Na_2SO_4–SiO_2 and Na_2SO_4–$Ln_2(SO_4)_3$–SiO_2(Ln=Y and Gd) were melted at 1473 K in air, then quenched in air. The resulting sample was pulverized in an agate ball, made into pellets under hydrostatic pressure (2.65×10^8 Pa) and then heated at 1073 K for 1 h in air.

Measurements. X-ray and thermal analyses were performed for the Na_2SO_4–SiO_2 and Na_2SO_4–$Ln_2(SO_4)_3$–SiO_2(Ln=Y and Gd) systems in order to investigate their phases and phase transformations using a Rigaku Rotaflex diffractometer equipped with a Cu target and a Rigaku Thermoflex, respectively. Electrical conductivities were measured by the complex impedance method[39] with a Hewlett Packard vector impedance meter 4800A. Electromotive force(EMF) measurements were carried out with a Takeda Riken Digital Multimeter TR-6841 by constructing the SO_2 gas concentration cell depicted in Fig. 1. Mixture gases of SO_2 ranging from 6% to 23% were prepared by controlling the SO_2 and the O_2

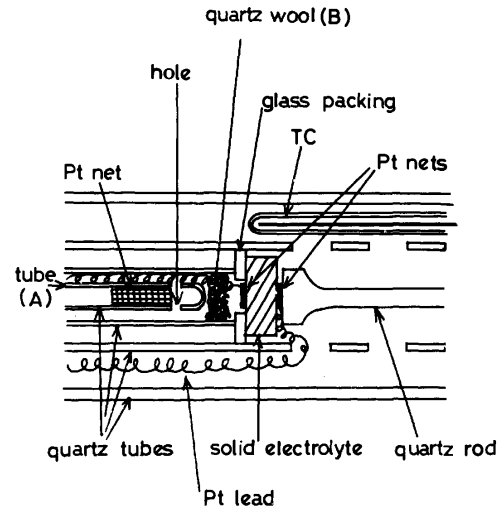

Fig. 1. The apparatus for the electromotive force (EMF) measurements.

gas flow volumes with self-made glass flow meters. The SO_2 gas concentration between 40 ppm and 11100 ppm was regulated by Standard Gas Generator(SGGU-711SD) from Standard Technology Co. The test SO_2 and O_2 gas mixture is introduced from the tube A depicted in Fig. 1. A Pt net is inserted so as to accelerate the oxidation of SO_2 to SO_3. The gas is led to the outer tube compartment through two small holes, and then reaches the electrolyte. The quartz wool is sacked in the place indicated by B shown in Fig. 1 in order to help to diffuse the gas uniformly and to avoid the occurrence of temperature gradient on the electrolyte surface. The ringed glass packing is fixed between the outer quartz tube of the test gas and the solid electrolyte by a spring loading a quartz rod so as to assure the separation of the test gas from the reference gas. The volume of the compartment for the reference SO_2 and O_2 gas mixture has been designed considerably larger compared with that for the test gas so that the SO_2–SO_3 equilibrium can be easily achieved.

Results and Discussion

Electrical Conductivity, Phases, and Thermal Properties. *Na_2SO_4–SiO_2 Systems*: Na_2SO_4–SiO_2 systems prepared are listed in Table 1 together with the results of X-ray and thermal analyses. All samples show the Na_2SO_4-III phase along with SiO_2. DTA curves also indicate a typical peak of the phase transformation from Na_2SO_4-III to Na_2SO_4-I at 513 K. Addition of silicon dioxide to sodium sulfate does not contribute to obtaining the Na_2SO_4-I-like phase which is excellent in the Na^+ ion conduction.

Electrical conductivity measurements for Na_2SO_4–SiO_2 systems are shown in Fig. 2. Mixing SiO_2 with Na_2SO_4 does not enhance the electrical conductivity. The discontinuity in the $\log(\sigma T)$-$1/T$ curve which is attributed to the III to I phase transformation, also exists for the Na_2SO_4–SiO_2 systems. The temperature at the break is about 513 K, which exactly coincides with the temperature obtained by the DTA measurements.

TABLE 1. THE PHASES AND THERMAL PROPERTIES OF Na_2SO_4–SiO_2

Sample No.	Na_2SO_4 (mol%)	SiO_2 (mol%)	Phases	DTA peak T/K
1	90	10	Na_2SO_4-III + SiO_2	513
2	70	30	Na_2SO_4-III + SiO_2	513
3	50	50	Na_2SO_4-III + SiO_2	513

The Na_2SO_4–SiO_2 systems, therefore, do not seem to be suitable for solid electrolytes because of their low electrical conductivities and because of the existence of the phase transformation from III to I.

Na_2SO_4–$Y_2(SO_4)_3$–SiO_2 Systems: The results of phase analyses and DTA measurements are presented in Table 2. X-Ray measurements indicate that a new phase, A, in which the peaks of Na_2SO_4-I-like phase are included, and a small amount of SiO_2 coexist. In sample No.1, some peaks of phase A split. Therefore, a symbol A′ is given to this phase instead of A. This sample(No.1) exhibits an endothermal peak with no gravimetric change at 593 K, showing that a phase transformation occurs. On the other hand, samples from No. 2 to 5 exhibit no phase transition.

Figure 3 illustrates the electrical conductivities results for Na_2SO_4–$Y_2(SO_4)_3$–SiO_2 systems. Sample No.1 exhibits relatively high conductivity. However, the discontinuity lies in the $\log(\sigma T)$ *vs.* $1/T$ curve approximately at 593 K. This temperature is identical with the result from DTA measurement. Similar $\log(\sigma T)$-$1/T$ curves were obtained for the samples of No, 2, 3, and 4. Their curves are nearly straight lines and their conductivities are about 20 times larger than that of Na_2SO_4 at 873 K. In the case of 14.8 mol% $Y_2(SO_4)_3$(No. 5), the electrical conductivity decreased. The cation vacancies are apt to form clusters which do not contribute to the cation conduction.

In the systems of Na_2SO_4–$Y_2(SO_4)_3$–SiO_2, the samples from No. 2 to 4 can be applied as solid electrolytes for a

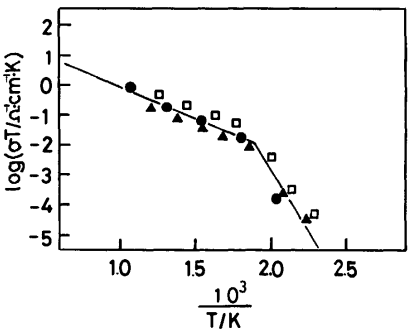

Fig. 2. Temperature dependences of electrical conductivities for the Na_2SO_4–SiO_2.
●: Na_2SO_4 : SiO_2 = 90 : 10,
□: Na_2SO_4 : SiO_2 = 70 : 30,
▲: Na_2SO_4 : SiO_2 = 50 : 50,
—: Na_2SO_4.

TABLE 2. THE PHASES AND THERMAL PROPERTIES OF Na_2SO_4–$Y_2(SO_4)_3$–SiO_2

Sample No.	Na_2SO_4 (mol%)	$Y_2(SO_4)_3$ (mol%)	SiO_2 (mol%)	Phases	DTA peak T/K
1	55.1	4.9	40.0	A′ + (small SiO_2)	593
2	52.2	7.7	40.1	A + (small SiO_2)	—
3	50.1	9.9	40.0	A + (small SiO_2)	—
4	48.1	11.8	40.1	A + (small SiO_2)	—
5	45.1	14.8	40.1	A + (small SiO_2)	—

A and A′: the phase which includes the peaks of Na_2SO_4-I-like phase.

SO_2 gas detector.

Na_2SO_4-$Gd_2(SO_4)_3$-SiO_2 Systems: The phases and thermal properties of Na_2SO_4-$Gd_2(SO_4)_3$-SiO_2 systems are tabulated in Table 3. The samples No. 1 to No. 4 exhibit a new phase α with a small amount of SiO_2. This phase is the phase where some peaks of phase A, are disappearing. The peaks of phase α' are slightly deviated from those of phase α toward low degree side except a peak at 31.6 degree. From thermal analyses, every sample exhibits no endo or exothermal peak on its DTA curve. The results of electrical conductivities for Na_2SO_4-$Gd_2(SO_4)_3$-SiO_2 systems are presented in Fig. 4. The electrical conductivities for the sample No. 1—3 show the highest values in the systems (at temperature higher than 781 K). In the case of 11.6mol% $Gd_2(SO_4)_3$, its conductivity decreased. This is because of the formation of cation vacancy clusters. When 17.2 mol% of $Gd_2(SO_4)_3$ is added(No. 5), the electrical conductivities becomes higher even at low temperatures. However, the bend in $\log(\sigma T)$ *vs.* $1/T$ curve appears at approximately 543 K.

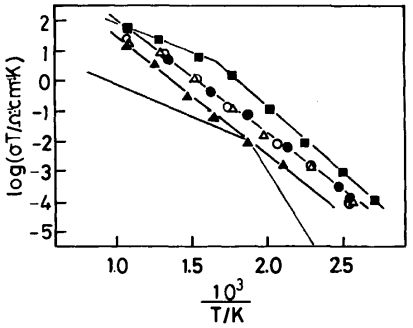

Fig. 3. Temperature dependences of electrical conductivities for the Na_2SO_4-$Y_2(SO_4)_3$-SiO_2.
-■-: $Na_2SO_4 : Y_2(SO_4)_3 : SiO_2 = 55.1 : 4.9 : 40.0$,
-○-: $Na_2SO_4 : Y_2(SO_4)_3 : SiO_2 = 52.2 : 7.7 : 40.1$,
-●-: $Na_2SO_4 : Y_2(SO_4)_3 : SiO_2 = 50.1 : 9.9 : 40.0$,
-△-: $Na_2SO_4 : Y_2(SO_4)_3 : SiO_2 = 48.1 : 11.8 : 40.1$,
-▲-: $Na_2SO_4 : Y_2(SO_4)_3 : SiO_2 = 45.1 : 14.8 : 40.1$,
——: Na_2SO_4.

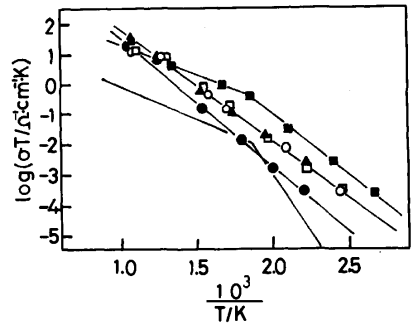

Fig. 4. Temperature dependences of electrical conductivities for the Na_2SO_4-$Gd_2(SO_4)_3$-SiO_2.
-□-: $Na_2SO_4 : Gd_2(SO_4)_3 : SiO_2 = 55.2 : 4.7 : 40.1$,
-○-: $Na_2SO_4 : Gd_2(SO_4)_3 : SiO_2 = 52.0 : 8.0 : 40.0$,
-▲-: $Na_2SO_4 : Gd_2(SO_4)_3 : SiO_2 = 51.0 : 8.2 : 40.8$,
-●-: $Na_2SO_4 : Gd_2(SO_4)_3 : SiO_2 = 48.2 : 11.6 : 40.2$,
-■-: $Na_2SO_4 : Gd_2(SO_4)_3 : SiO_2 = 43.8 : 17.2 : 39.0$,
——: Na_2SO_4.

In the Na_2SO_4-$Gd_2(SO_4)_3$-SiO_2 systems, the samples No. 1—3 are good candidates for solid electrolytes.

EMF Measurements: EMF measurements with the appropriate sample of Na_2SO_4-$Y_2(SO_4)_3$-SiO_2 (50.1 : 9.9 : 40.0) are shown in Fig. 5. The measured EMF was in good agreement with the calculated EMF, with the initial SO_2 gas concentration between 0.1% (1000 ppm) and 23%. When the initial SO_2 gas concentration was less than 0.1%, the measured EMF becomes lower than the calculated EMF. Figure 6 presents the variation of the EMF with the pertinent sample of Na_2SO_4-$Gd_2(SO_4)_3$-SiO_2 (51.0:8.2:40.8). The measured EMF coincided with calculated EMF, with the initial SO_2 gas range from 0.32% (3200 ppm) to 10%. When the initial SO_2 gas content was smaller than 0.32%, the difference between the measured and the calculated EMF became larger. The reason that the measured

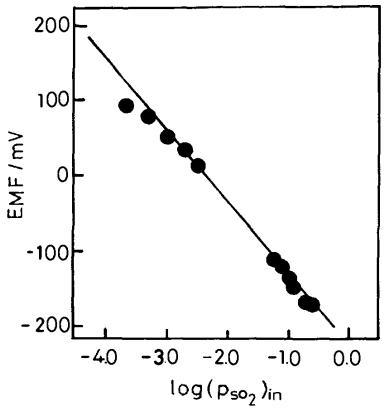

Fig. 5. Variation of the EMF for the concentration cell; $Pt|O_2(p_1'), SO_2(p_2')|Na_2SO_4$(9.9 mol% $Y_2(SO_4)_3$, 40.0 mol% SiO_2)$|O_2(p_1''), SO_2(p_2'')|Pt$, with $p_1''=0.996$ and $p_2''=0.004$ at 973 K.
—— is calculated EMF.[5]

Table 3. The phases and thermal properties of Na_2SO_4-$Gd_2(SO_4)_3$-SiO_2

Sample No.	Na_2SO_4 (mol%)	$Gd_2(SO_4)_3$ (mol%)	SiO_2 (mol%)	Phases	DTA peak T/K
1	55.2	4.7	40.1	α + (small SiO_2)	—
2	52.0	8.0	40.0	α + (small SiO_2)	—
3	51.0	8.2	40.8	α + (small SiO_2)	—
4	48.2	11.6	40.2	α + (small SiO_2)	—
5	43.8	17.2	39.0	α' + (small SiO_2)	—

α and α': the phase which includes the peaks of Na_2SO_4-I-like phase.

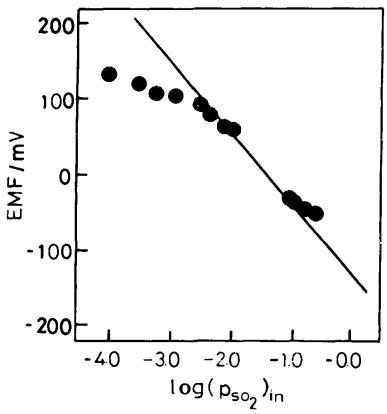

Fig. 6. Variation of the EMF for the concentration cell; Pt|$O_2(p_1')$, $SO_2(p_2')$|Na_2SO_4(8.2 mol% $Gd_2(SO_4)_3$, 40.8 mol% SiO_2)|$O_2(p_1'')$, $SO_2(p_2'')$|Pt, with $p_1''=0.966$ and $p_2''=0.034$ at 973 K.
—— is calculated EMF.[5)]

and the calculated EMF does not coincide at relatively lower SO_2 gas concentration, may be predominantly accounted to the inadequate oxidation of SO_2 to SO_3.

In conclusion, sodium sulfate mixed with $Ln_2(SO_4)_3$(Ln=Y and Gd) and SiO_2 maintains relatively high electrical conductivities. When Na_2SO_4-$Ln_2(SO_4)_3$-SiO_2 (Ln=Y and Gd) are applied as solid electrolytes for a sulfur dioxide gas sensor, they can detect the SO_2 gas in the initial SO_2 gas concentration range from 0.1% to 23%, and 0.32% to 10%, respectively.

The present work was partially supported by a Grant-in-Aid for Developmental Scientific Research No. 57850250 from the Ministry of Education, Science and Culture.

References

1) L. G. Boxall and K. E. Johnson, *J. Electrochem. Soc.*, **118**, 885 (1971).
2) M. Gauthier and A. Chamberland, *J. Electrochem. Soc.*, **124**, 1579 (1977).
3) M. Gauthier, A. Chamberland, A Bélanger, and M. Poirier, *J. Electrochem. Soc.*, **124**, 1584 (1977).
4) M. Gauthier, R. Bellemare, and A. Bélanger, *J. Electrochem. Soc.*, **128**, 371 (1981).
5) K. T. Jacob and D. B. Rao, *J. Electrochem. Soc.*, **126**, 1842 (1979).
6) W. L. Worrell, Pro. the International Meeting on Chemical Sensors, Fukuoka, 332 (1983).
7) N. Imanaka, G. Adachi, and J. Shiokawa, *Chem. Lett.*, **1983**, 287.
8) N. Imanaka, G. Adachi, and J. Shiokawa, *Denki Kagaku*, **51**, 93 (1983).
9) N. Imanaka, G. Adachi, and J. Shiokawa, *Bull. Chem. Soc. Jpn.*, **57**, 687 (1984).
10) J. P. Coughlin, *J. Am. Chem. Soc.*, **77**, 868 (1955).
11) Y. A. Badr, F. El-Kabbany, and M. Tosson, *Phys. Status Solidi A*, **53**, K51 (1979).
12) F. El-Kabbany, Y. Badr, and M. Tosson, *Phys. Status Solidi A*, **63**, 699 (1981).
13) Q. R. Goyal, V. V. Deshpande, and M. D. Karkhanavala, *Indian J. Chem.*, **9**, 1006 (1971).
14) J. E. D. Davies and W. F. Sandford, *J. Chem. Soc., Dalton Trans.*, **1975**, 1912.
15) B. N. Mehrotra, Th. Hahn, H. Arnold, and W. Eysel, *Acta Crystallogr., Sect. A*, **31**, S79 (1975).
16) V. Amirthalingam, M. D. Karkhanavala, and U. R. K. Rao, *Acta Crystallogr., Sect. A*, **33**, 522 (1977).
17) C. A. Cody, L. Dicarlo, and R. K. Darlington, *J. Inorg. Nucl. Chem.*, **43**, 398 (1981).
18) E. L. Kreidl and Ivan Simon, *Nature*, **181**, 1529 (1958).
19) Y. Saito, K. Kobayashi, and T. Maruyama, *Thermochim. Acta*, **53**, 289 (1982).
20) F. C. Kracek, *J. Phys. Chem.*, **33**, 1281 (1929).
21) F. C. Kracek and R. E. Gibson, *J. Phys. Chem.*, **33**, 1304 (1929).
22) F. C. Kracek and R. E. Gibson, *J. Phys. Chem.*, **34**, 188 (1930).
23) F. C. Kracek and C. J. Ksanda, *J. Phys. Chem.*, **34** 1741 (1930).
24) G. E. Brodale and W. F. Giauque, *J. Phys. Chem.*, **76**, 737 (1972).
25) K. Kobayashi and Y Saito, *Thermochim. Acta*, **53**, 299 (1982).
26) Y. Saito, K. Kobayashi, and T. Maruyama, *Solid State Ionics*, (**1981**) 393.
27) J. P. Boilot, J. P. Salanié, G. Desplanches, and D. Le Potier, *Mater. Res. Bull.*, **14**, 1469 (1979).
28) U. von Alpen, M. F. Bell, and W. Wichelhaus, *Mater. Res. Bull.*, **14**, 1317 (1979).
29) J. B. Goodenough, H. Y-P. Hong, and J. A. Kafalas, *Mater. Res. Bull.*, **11**, 203 (1976).
30) T. Takahashi, K. Kuwabara, and M. Shibata, *Solid State Ionics*, **1**, 163 (1980).
31) W. Bogusz, F. Krok, and W. Jakubowski, *Solid State Ionics*, **2**, 171 (1981).
32) U. von Alpen, M. F. Bell, and H. H. Höfer, *Solid State Ionics*, **3/4**, 215 (1981).
33) H. H. Höfer, W. Eysel, and U. v. Alpen, *J. Solid State Chem.*, **36**, 365 (1981).
34) H. H. Höfer, W. Eysel, and U. v. Alpen, *Mater. Res. Bull.*, **13**, 265 (1978).
35) R. M. Mupray and E. A. Secco, *Can. J. Chem.*, **56**, 2616 (1978).
36) K. L. Keester, W. Eysel, and Th. Hahn, *Acta Crystallogr., Sect. A*, **31**, S79 (1975).
37) H. H. Höfer, U. v. Alpen, and W. Eysel, *Acta Crystallogr., Sect. A*, **34**, S358 (1978).
38) N. Imanaka, G. Adachi, and J. Shiokawa, *Can. J. Chem.*, **61**, 1557 (1983).
39) J. E. Bauerle, *J. Phys. Chem. Solids*, **30**, 2657 (1969).

The Short Range Structure of Ion-polar Solvent Mixtures. Calculations by the RISM Integral Equations

Masaharu OHBA and Kiyoshi ARAKAWA*
Research Institute of Applied Electricity, Hokkaido University, Sapporo 060
(Received May 14, 1984)

The reference hypernetted chain like integral equation of the interaction site model is solved numerically for a solution of ions in a polar solvent. In our model, the ions and the solvent molecules are taken to be charged hard spheres and polar hard dumb-bells, respectively. Calculated pair correlation functions contain a great deal of interesting information on the short range structure of the ionic solutions: a solvated structure around ions and an effect of ionic charges upon the structure of the solvent. It is found that various types of associated structures of constituent species, such as simple ion pairs, ion triplets, and ion pairs separated by one solvent molecule exist in ionic solutions.

One of today's central problems of the physical chemistry of ionic solutions is to develop the theory based on the more realistic model for ionic solutions than the so called primitive model.[1] In the primitive model of ionic solutions, a solvent is considered as a continuum medium, in which ions are immersed, with the same dielectric constant as that of the pure solvent. For the last one decade, several authors proposed theories of ionic solutions in which microscopic structures of solvents were explicitly taken into account.[2-12] Many of these theories were concerned with a mixture of charged hard spheres and dipolar hard spheres.

Taking account of a structure of ions and solvent molecules, we proposed a theory[10] on the static dielectric function and site-site pair correlation functions of ionic solutions composed of polyatomic ions and polar polyatomic molecules based on the interaction site model. In the present paper, we obtain site-site radial distribution functions of ionic solutions composed of charged hard spheres and polar hard dumb-bells using the RISM integral equations.[13,14]

Recently, we proposed an RHNC-like integral equation of RISM-1[15] and solved the equation in the case of fluids composed of dipolar hard dumb-bells. Morriss and Cummings[16,17] presented Monte Carlo simulation results for site-site radial distribution functions and the dielectric constant of the polar hard dumb-bell fluids. A comparison of our results with their simulation results is also made in this paper. An agreement of these two results is fairly good, which encourages us to apply the RHNC-like integral equation of RISM-1 to ionic solutions.

In this paper, we extend the RHNC-like integral equation of RISM-1 to multi-component systems and solved it for ionic solutions composed of charged hard spheres and dipolar hard dumb-bells in order to investigate a short range structure of ionic solutions.

The RHNC-like Integral Equation for Fluid Mixtures

An extension of the RHNC-like integral equation of RISM-1[15] to the case of multi-component systems is made in this section.

We assume here that the molecule of type M has n_M interaction sites and a charge $q_{\alpha M}$ is sited on the α-th site of the molecule of type M. The total potential energy of the fluid mixture is assumed to be the sum over all pairs of the intermolecular potentials. The intermolecular potential between the i-th molecule of type M and the j-th molecule of type M', $U_{MM'}(i_M, j_{M'})$, is given as

$$U_{MM'}(i_M,j_{M'}) = \sum_{\alpha=1}^{n_M}\sum_{\gamma=1}^{n_{M'}} u_{\alpha M\gamma M'}(|\boldsymbol{r}_{iM}^{\alpha}-\boldsymbol{r}_{jM'}^{\gamma}|), \quad (1)$$

where $u_{\alpha M\gamma M'}(|\boldsymbol{r}_{iM}^{\alpha}-\boldsymbol{r}_{jM'}^{\gamma}|)$ is a site-site interaction between the pair of site αM and γM' and $\boldsymbol{r}_{iM}^{\alpha}$ the position of the α-th site of the i-th molecule of type M. The site-site interaction can be divided into two parts,

$$u_{\alpha M\gamma M'}(r) = u^{(0)}_{\alpha M\gamma M'}(r) + u^{(1)}_{\alpha M\gamma M'}(r). \quad (2)$$

Here, $u^{(0)}_{\alpha M\gamma M'}(r)$ is a short range part of the site-site interaction, which is treated as a reference potential, and the perturbation potential $u^{(1)}_{\alpha M\gamma M'}(r)$ is a long range Coulomb potential, that is,

$$u^{(1)}_{\alpha M\gamma M'}(r) = \frac{q_{\alpha M}q_{\gamma M'}}{4\pi\varepsilon_0 r}, \quad (3)$$

where ε_0 is the dielectric constant of vacuum.

The Ornstein-Zernike type equation for a multi-component system is

$$\tilde{\boldsymbol{h}}' = \tilde{\boldsymbol{\omega}}\tilde{\boldsymbol{c}}'\tilde{\boldsymbol{\omega}} + \tilde{\boldsymbol{\omega}}\tilde{\boldsymbol{c}}'\tilde{\boldsymbol{h}}', \quad (4)$$

where $\tilde{\boldsymbol{h}}'$, $\tilde{\boldsymbol{c}}'$, and $\tilde{\boldsymbol{w}}$ are matrices with elements $\sqrt{\rho_M\rho_{M'}}\tilde{h}_{\alpha M\gamma M'}(k)$, $\sqrt{\rho_M\rho_{M'}}\tilde{c}_{\alpha M\gamma M'}(k)$, and $\tilde{\omega}_{\alpha M\gamma M'}(k)$, respectively. ρ_M is the number density of molecules of type M. Hereafter, $\tilde{\boldsymbol{A}}'$ denotes a matrix with the element $\sqrt{\rho_M\rho_{M'}}\tilde{A}_{\alpha M\gamma M'}(k)$ and $\tilde{A}_{\alpha M\gamma M'}(k)$ is the Fourier transform of $A_{\alpha M\gamma M'}(r)$,

$$\tilde{A}_{\alpha M\gamma M'}(k) = \int d\boldsymbol{r} A_{\alpha M\gamma M'}(r)e^{-i\boldsymbol{k}\cdot\boldsymbol{r}}$$

$h_{\alpha M\gamma M'}(r)$ is the site-site total correlation function, and $c_{\alpha M\gamma M'}(r)$ is the site-site direct correlation function. $\omega_{\alpha M\gamma M'}(r)$ is the intramolecular pair correlation function

and the Fourier transform of $\omega_{\alpha M\gamma M'}(r)$ for rigid molecule is

$$\tilde{\omega}_{\alpha M\gamma M'}(k) = \delta_{MM'}\left\{\delta_{\alpha\gamma} + (1-\delta_{\alpha\gamma})\frac{\sin kl_{\alpha\gamma M}}{kl_{\alpha\gamma M}}\right\}, \quad (5)$$

where δ_{ab} is the Kronecker delta and $l_{\alpha\gamma M}=|r^{\alpha}_{iM}-r^{\gamma}_{iM}|$ the distance between the α-th site and the γ-th site of the same molecule of type M.

The Ornstein-Zernike type equation for a reference system is

$$\tilde{h}^{(0)\prime} = \tilde{\omega}\tilde{c}^{(0)\prime}\tilde{\omega} + \tilde{\omega}\tilde{c}^{(0)\prime}\tilde{h}^{(0)\prime}, \quad (6)$$

where a superscript (0) denotes the reference system quantity. From Eqs. 4 and 6, we obtain

$$\delta\tilde{h}' = \tilde{\chi}\{\boldsymbol{1}-\delta\tilde{c}'\tilde{\chi}\}^{-1}\delta\tilde{c}'\tilde{\chi}, \quad (7)$$

where $\tilde{\chi}=\tilde{\omega}+\tilde{h}^{(0)\prime}$, $\delta\tilde{h}'=\tilde{h}'-\tilde{h}^{(0)\prime}$, and $\delta\tilde{c}'=\tilde{c}'-\tilde{c}^{(0)\prime}$. $\boldsymbol{1}$ is the unit matrix and $\boldsymbol{A}^{-1}$ is the inverse matrix of $\boldsymbol{A}$.

An RHNC-like approximation of RISM-1 for the multi-component system is expressed as

$$\delta c_{\alpha M\gamma M'}(r) = \delta h_{\alpha M\gamma M'}(r) - \ln\frac{g_{\alpha M\gamma M'}(r)}{g^{(0)}_{\alpha M\gamma M'}(r)}e^{\beta u^{(1)}_{\alpha M\gamma M'}(r)}, \quad (8)$$

where $g_{\alpha M\gamma M'}(r)=h_{\alpha M\gamma M'}(r)+1$ is the site-site radial distribution functiion, $\beta=1/k_BT$, k_B the Boltzmann constant and T the absolute temperature. Combining Eq. 7 with Eq. 8, we can solve the integral equation when the reference system quantities are given.

As is shown in the appendix, $h_{\alpha M\gamma M'}(r)$ is a short range function in the case of ionic solutions as well as the case of polar fluids.[18] Then, the RHNC-like approximation, Eq. 8, implies the following asymptotic form of $c_{\alpha M\gamma M'}(r)$ at large r

$$c_{\alpha M\gamma M'}(r) \simeq -\beta q_{\alpha M}q_{\gamma M'}/4\pi\varepsilon_0 r. \quad (9)$$

However, Cummings and Stell[19] showed that Eq. 9 is not correct and the exact asymptotic forms of $c_{\alpha M\gamma M'}(r)$, for example, of a fluid composed of polar diatomic molecules is

$$c_{\alpha M\gamma M'}(r) \simeq -A\beta q_{\alpha M}q_{\gamma M'}/4\pi\varepsilon_0 r, \quad (10)$$

where A is the state dependent constant. All the closure relations of RISM-1 have the same asymptotic form Eq. 9. Thus, it seems that pair correlation functions calculated by the RISM-1 type integral equation have an incorrect long range nature. Nevertheless, the previous calculations showed that the RISM-1 equation gives good results for a short range structure of liquids.[14,20-22] Rossky *et al.*[23] showed that a modification of the asymptotic form of the closure relations produces only very small deviations in the site-site pair correlation functions at a short range region. Since we are interested in a short range structure of ionic solutions, we solve the Ornstein-Zernike type equation with the closure relation Eq. 8.

Applications to Ion-solvent Mixtures.

Model. A system considered is an 1:1 electrolyte solution. Cations(i+) and anions(i−) are charged hard spheres with the same diameter σ_{ii} and have charges $+q_i$ and $-q_i$, respectively. Solvent molecules(s) are fused hard spheres with the same diameter σ_{ss}, on whose center charges $+q_s$ and $-q_s$ are sited. The bond length of solvent molecules is l. An illustration of molecules is shown in Fig. 1. The reference potential is given as

$$u^{(0)}_{\alpha M\gamma M'}(r) = \begin{cases}\infty, & r<\sigma_{MM'}\\ 0, & r>\sigma_{MM'}\end{cases}, \quad (11)$$

where we assume that $\sigma_{is}=(\sigma_{ii}+\sigma_{ss})/2$. The system is electrically neutral, that is, $\rho_{i+}=\rho_{i-}\equiv\rho_i$. Because of the symmetry, we have $g_{i+i+}(r)=g_{i-i-}(r)$, $g_{i+i-}(r)=g_{i-i+}(r)$, $g_{s+s+}(r)=g_{s-s-}(r)$, $g_{s+s-}(r)=g_{s-s+}(r)$, $g_{i+s+}(r)=g_{s+i+}(r)=g_{i-s-}(r)=g_{s-i-}(r)$, $g_{i+s-}(r)=g_{s-i+}(r)=g_{i-s+}(r)=g_{s+i-}(r)$.

Computational Procedures. The function $\delta h_{\alpha M\gamma M'}(r)$ and $\delta c_{\alpha M\gamma M'}(r)$ have a discontinuity at $r=\sigma_{MM'}$, but $H_{\alpha M\gamma M'}(r)=\delta h_{\alpha M\gamma M'}(r)-\delta c_{\alpha M\gamma M'}(r)$ is a continuus function of r.[14,15,20] As is shown in the appendix, $h_{\alpha M\gamma M'}(r)$ for ionic solutions is a short range function. Thus, similar considerations in the previous paper[15] give us the following equations from Eqs. 7 and 8

$$\tilde{H}^{S\prime} = \tilde{\chi}\{\boldsymbol{1}-(\delta\tilde{c}^{S\prime}-\tilde{H}^{L\prime})\tilde{\chi}\}^{-1}(\delta\tilde{c}^{S\prime}-\tilde{H}^{L\prime})\tilde{\chi}-\delta\tilde{c}^{S\prime} \quad (12)$$

and

$$\delta c^{S}_{\alpha M\gamma M'}(r) = g^{(0)}_{\alpha M\gamma M'}(r)[\exp\{H^{S}_{\alpha M\gamma M'}(r)-\psi^{S}_{\alpha M\gamma M'}(r)\}-1] - H^{S}_{\alpha M\gamma M'}(r). \quad (13)$$

Here,

$$\delta c^{S}_{\alpha M\gamma M'}(r) = \delta c_{\alpha M\gamma M'}(r) + H^{L}_{\alpha M\gamma M'}(r),$$

$$H^{S}_{\alpha M\gamma M'}(r) = H_{\alpha M\gamma M'}(r) - H^{L}_{\alpha M\gamma M'}(r),$$

$$H^{L}_{\alpha M\gamma M'}(r) = \frac{\beta q_{\alpha M}q_{\gamma M'}}{4\pi\varepsilon_0 r}(1-e^{-\alpha r}),$$

$$\psi^{S}_{\alpha M\gamma M'}(r) = \frac{\beta q_{\alpha M}q_{\gamma M'}}{4\pi\varepsilon_0 r}e^{-\alpha r},$$

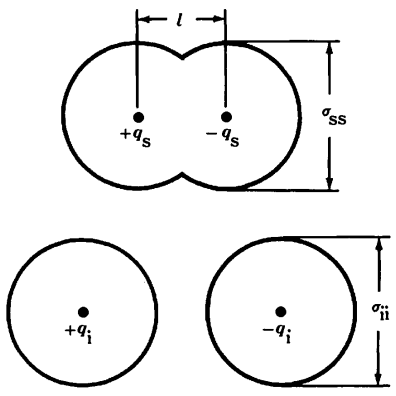

Fig. 1. The shapes of ions and a solvent molecule.

where a is a disposable parameter chosen so as to make the function $\psi^{S}_{\alpha M\gamma M'}(r)$ negligibly small at the termination of the finite range of r. Equations 12 and 13 involve only short range functions that can be numerically handled in the usual way. An iteration calculation is carried out by the use of Eqs. 12 and 13 with an initial guess $H^{S}_{\alpha M\gamma M'}(r)=0$, and is continued until the self consistency of

$$\left|\frac{\exp\{H^{S}_{\alpha M\gamma M'}(r)_{out}\}-\exp\{H^{S}_{\alpha M\gamma M'}(r)_{in}\}}{\exp\{H^{S}_{\alpha M\gamma M'}(r)_{in}\}}\right| < 10^{-6} \quad (14)$$

is satisfied. The site-site radial distribution function is finally obtained as

$$g_{\alpha M\gamma M'}(r) = g^{(0)}_{\alpha M\gamma M'}(r)\exp\{H^{S}_{\alpha M\gamma M'}(r) - \psi^{S}_{\alpha M\gamma M'}(r)\}. \quad (15)$$

Reference System Quantities. Reference system quantities are indispensable for solving the RHNC-like integral equation. It was shown that the PY-like approximation of RISM-1 gives good description of a structure of liquids with short range forces.[14,20] Therefore, a solution of the PY-like integral equation of RISM-1 is used as a reference system quantity. The PY-like approximation of RISM-1 is expressed as[14]

$$c^{(0)}_{\alpha M\gamma M'}(r) = g^{(0)}_{\alpha M\gamma M'}(r)\{1-e^{\beta u^{(0)}_{\alpha M\gamma M'}(r)}\}. \quad (16)$$

We transform Eqs. 6 and 16 into the following equations

$$\tilde{\boldsymbol{H}}^{(0)\prime} = \tilde{\boldsymbol{\omega}}(\boldsymbol{I}-\tilde{\boldsymbol{c}}^{(0)\prime}\tilde{\boldsymbol{\omega}})^{-1}\tilde{\boldsymbol{c}}^{(0)\prime}\tilde{\boldsymbol{\omega}}-\tilde{\boldsymbol{c}}^{(0)\prime}, \quad (17)$$

and

$$c^{(0)}_{\alpha M\gamma M'}(r) = y^{(0)}_{\alpha M\gamma M'}(r)\{e^{-\beta u^{(0)}_{\alpha M\gamma M'}(r)}-1\}, \quad (18)$$

where $y^{(0)}_{\alpha M\gamma M'}(r)=1+H^{(0)}_{\alpha M\gamma M'}(r)$ and $H^{(0)}_{\alpha M\gamma M'}(r)=h^{(0)}_{\alpha M\gamma M'}(r)-c^{(0)}_{\alpha M\gamma M'}(r)$. An interation calculation is carried out by the use of Eqs. 17 and 18 with an initial guess $H^{(0)}_{\alpha M\gamma M'}(r)=0$, and is continued until the self consistency of

$$\left|\frac{y^{(0)}_{\alpha M\gamma M'}(r)_{out}-y^{(0)}_{\alpha M\gamma M'}(r)_{in}}{y^{(0)}_{\alpha M\gamma M'}(r)_{in}}\right| < 10^{-6} \quad (19)$$

is satisfied. The reference system quantities are finally obtained as

$$g^{(0)}_{\alpha M\gamma M'}(r) = y^{(0)}_{\alpha M\gamma M'}(r)e^{-\beta u^{(0)}_{\alpha M\gamma M'}(r)} \quad (20)$$

and

$$\tilde{\boldsymbol{\chi}} = (\boldsymbol{I}-\tilde{\boldsymbol{\omega}}\tilde{\boldsymbol{c}}^{(0)\prime})^{-1}\tilde{\boldsymbol{\omega}}. \quad (21)$$

Results and Discussion

The system considered is characterized by six parameters as follows: the reduced number densities of ions and solvent molecules $\rho_i^*=\rho_i\sigma^3_{ii}$ and $\rho_s^*=\rho_s d^3$, the reduced charge of ions $q_i^*=(\beta q_i^2/4\pi\varepsilon_0\sigma_{ii})^{1/2}$, the reduced dipole moment of solvent molecules $\mu_s^*=(\beta\mu_s^2/4\pi\varepsilon_0 d^3)^{1/2}$, the reduced bond length of solvent molecules $L^*=l/\sigma_{ss}$, and the ratio of σ_{ii} to σ_{ss} $\sigma^*_{ii}=\sigma_{ii}/\sigma_{ss}$. Here, $\mu_s=q_s l$ is the magnitude of the dipole moment of solvent molecules and d, the diameter of the hard sphere whose volume is the same as the solvent molecule, is given by the following equation

$$d^3 = \sigma^3_{ss}(1+3L^*/2-L^{*3}/2). \quad (22)$$

The numerical calculations were carried out with a grid width $\Delta r=0.01\sigma_{ss}$ and the integrals were truncated at $r\approx 10\sigma_{ss}$. Calculations were checked by doubling the cutoff distance, and no meaningfull difference between the two calculations was found.

Comparisons with Monte Carlo Simulation Results for Polar Fluids. Recently, Monte Carlo calculations were carried out for dipolar hard dumb-bell fluids.[16,17] In this subsection, our results are compared with the

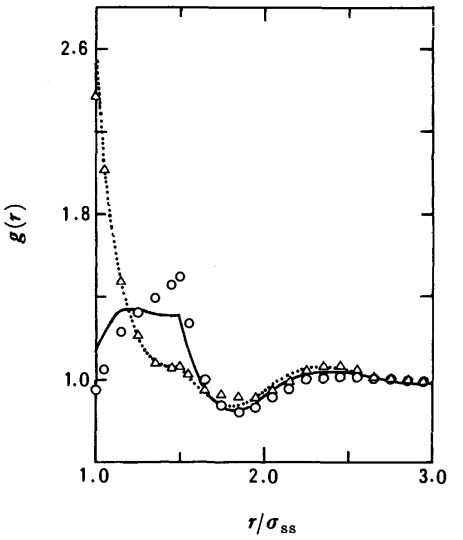

Fig. 2. The site-site radial distribution functions for the polar hard dumb-bell fluid at $\rho_s^*=0.78$, $\mu_s^*=1.17$ and $L^*=0.5$, ——: $g_{++}(r)$ by the RHNC-like equation, ·····: $g_{+-}(r)$ by the RHNC-like equation, ○: $g_{++}(r)$ by the Monte Carlo simulation, △: $g_{+-}(r)$ by the Monte Carlo simulation.

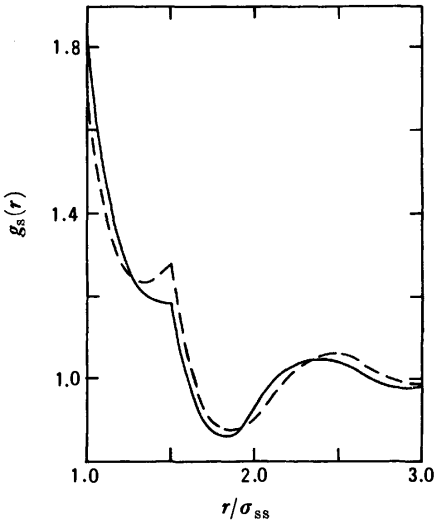

Fig. 3. The radial distribution functions of the centers of atoms. Parameters are the same as Fig. 2. ——: RHNC-like, ·····: Monte Carlo.

simulation results[16] of the polar hard dumb-bell fluid at $L^*=0.5$. $\rho_s^*=0.78$, and $\mu_s^*=1.17$.

Site-site radial distribution functions $g_{++}(r)$ and $g_{+-}(r)$ are shown in Fig. 2. An agreement between the simulation results and ours is good on the whole. Especially, the agreement of $g_{+-}(r)$ is very good except near a contact distance. The radial distribution function of the center of atoms $g_s(r)$ and the radial distribution function of charges $g_d(r)$ are shown in Figs. 3 and 4, respectively. Here, $g_s(r)$ and $g_d(r)$ are defined as

$$g_s(r) = \{g_{++}(r)+g_{+-}(r)\}/2$$

and

$$g_d(r) = \{g_{++}(r)-g_{+-}(r)\}/2.$$

$g_d(r)$ calculated using the interaction site approximation (ISA)[24] is also shown in Fig. 4. The ISA is defined as

$$h_{\alpha M\gamma M'}(r) = -1, \qquad r<\sigma_{\alpha M\gamma M'}$$

and

$$c_{\alpha M\gamma M'}(r) = -\beta u_{\alpha M\gamma M'}(r). \qquad r>\sigma_{\alpha M\gamma M'}$$

This is the molecular fluid analogue of the mean spherical approximation for simple fluids. Though our $g_s(r)$ is qualitatively correct, a small systematic difference between RHNC and Monte Calro results is found from Fig. 3. On the other hand, the agreement of $g_d(r)$ is good. It is said from Fig. 4 that the RHNC-like approximation is superior to the ISA. $\delta g(r)=g_s(r)-g^{(0)}(r)$ are plotted in Fig. 5, where $g^{(0)}(r)$ is the site-site radial distribution function of a nonpolar hard dumb-bell fluid with the same values of L^* and ρ_s^*. It is noted that $g_s(r)$ by ISA is equal to $g^{(0)}(r)$ calculated by the use of the PY-like approximation of RISM-1. Both the $\delta g(r)$ of RHNC and Monte Calro results are nearly equal to zero except at $r/\sigma_{ss}\approx 1-1.7$ where the RHNC result is qualitatively correct. This result shows that most of the disagreement of $g_s(r)$ of RHNC-like results with simulation ones comes from the use of approximate results as the reference system quantities. Thus, it is reasonable to expect that the use of the exact pair correlation functions obtained by computer simulations as reference system quantities gives an excellent result for short range structure of fluids.

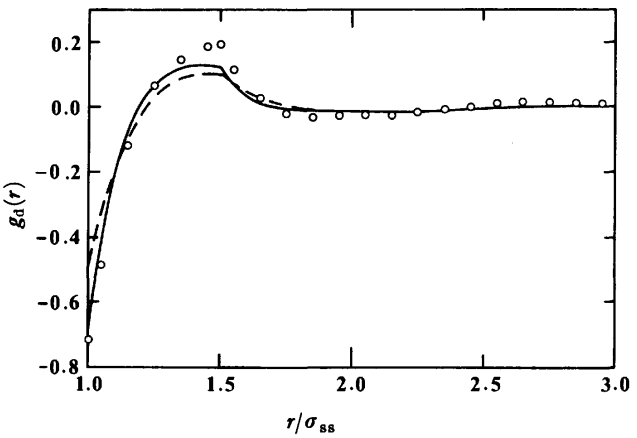

Fig. 4. The radial distribution functions of charges. Parameters are the same as Fig. 2. ——: RHNC-like, ----: ISA, O: Monte Carlo.

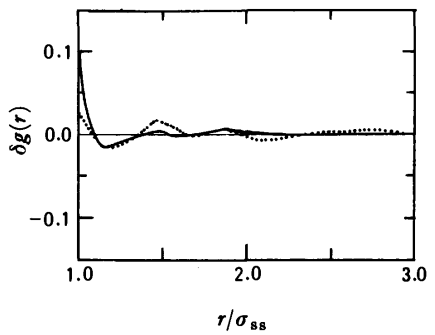

Fig. 5. δg (r). Parameters are the same as Fig. 2. ——: RHNC-like, ·····: Monte Carlo.

Distribution Functions of Ionic Solutions. The figures 6a—6c show the site-site radial distribution functions of an ionic solution. Broken curves in Fig. 6a are ion-ion radial distribution functions by the primitive model for the same state, which are calculated from the RHNC integral equation. The dielectric constant ε of a solvent used in calculations of the primitive model is given by $\varepsilon/\varepsilon_0=1+3y$, where $y=4\pi\beta\rho_s\mu_s^2/9$. This is consistent with the use of the RHNC-like approximation, because the asymptotic form Eq. 9 is obtained from Eq. 10 with $A=1$ and the approximation $A=1$ implies $\varepsilon/\varepsilon_0=1+3y$.[19] It is found from Fig. 6a that the primitive model gives an incorrect description on the short range nature of ion-ion radial distribution functions. The contact value of $g_{i+i-}(r)$ shown in Fig. 6a is large, which indicates that the degree of association of ionic specics is considerably large in this system. $g_{i+i+}(r)$

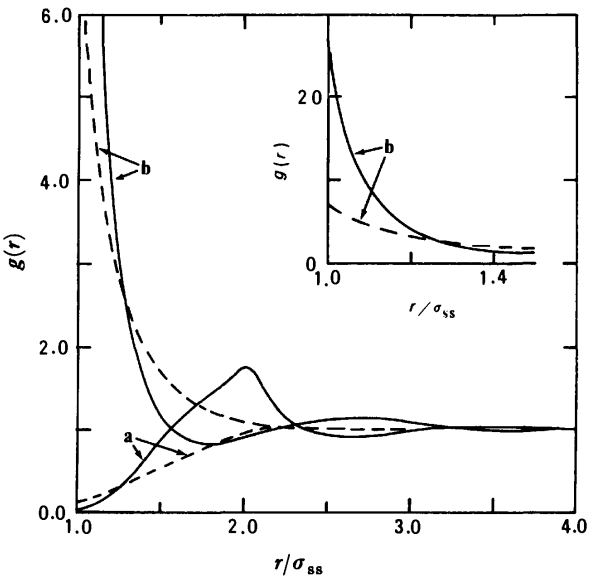

Fig. 6a. The ion-ion radial distribution functions for the ionic solution at $\rho_i^*=0.03$, $\rho_s^*=0.6$, $q_i^*=4.5$, $\mu_s^*=1.0$, $L^*=0.6$ and $\sigma_{ii}^*=1.0$. a: $g_{i+i+}(r)$, b: $g_{i+i-}(r)$. ——: the ion-solvent mixture, ----: the primitive model.

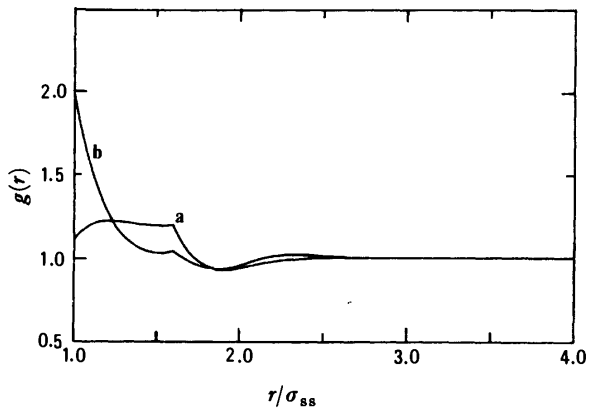

Fig. 6b. The solvent-solvent radial distribution functions for the ionic solution whose parameters are the same as Fig. 6a. a: $g_{s+s+}(r)$, b: $g_{s+s-}(r)$.

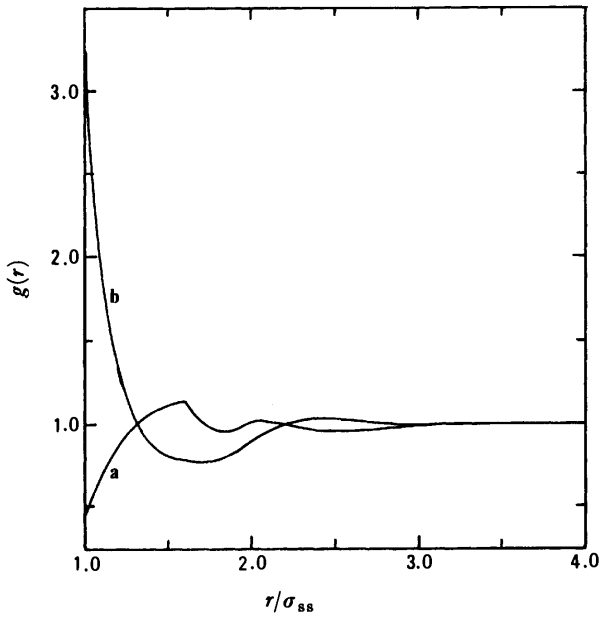

Fig. 6c. The ion-solvent radial distribution functions for the ionic solution whose parameters are the same as Fig. 6a. a: $g_{i+s+}(r)$, b: $g_{i+s-}(r)$.

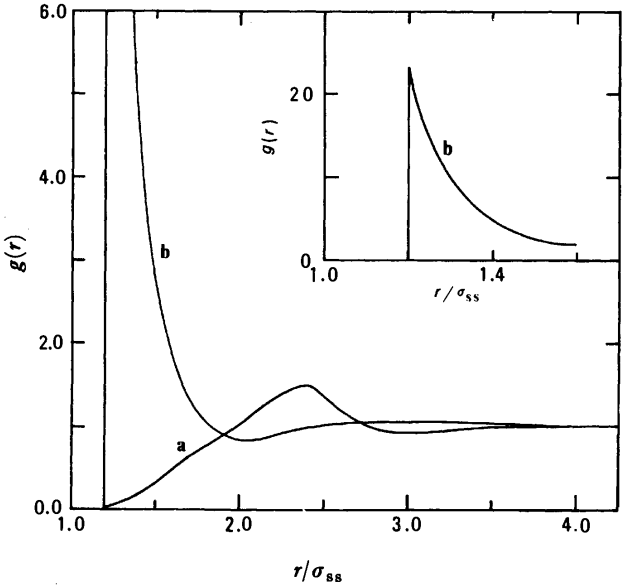

Fig. 7. The ion-ion radial distribution functions for the ionic solution whose parameters are the same as Fig. 6a except $\sigma_{ii}^*=1.2$. a: $g_{i+i+}(r)$, b: $g_{i+i-}(r)$.

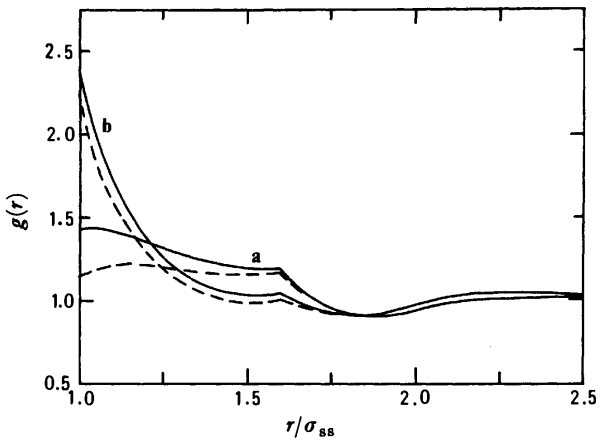

Fig. 8. The solvent-solvent radial distribution functions of the ionic solution at $\rho_i^*=0.05$, $\rho_s^*=0.6$, $\mu_s^*=1.0$, $L^*=0.6$ and $\sigma_{ii}^*=1.0$. a: $g_{s+s+}(r)$, b: $g_{s+s-}(r)$. ——: $q_i^*=4.5$, ----: $q_i^*=0.0$.

has a maximum at $r=2\sigma_{ss}=2\sigma_{ii}$. This maximum suggests the existence of ion triplets shown in Fig. 10a. In order to ascertain this consideration, an effect of the variation of the diameter of ions was investigated. Figure 7 shows the ion-ion radial distribution functions at the same parameters as that of Fig. 6 except $\sigma_{ii}^*=1.2$. The maximum of $g_{i+i+}(r)$ shifts to $r=2.4\sigma_{ss}=2\sigma_{ii}$, which supports the idea that the maximum at $r=2\sigma_{ii}$ comes from ion triplets.

Solvent-solvent radial distribution functions shown in Fig. 6b are similar to those of pure solvents whose details are described in Ref. 15. An effect of ionic charges on the solvent structure is found in Fig. 8. A system with $q_i^*=0$ is the mixture of polar hard dumbbells and neutral hard spheres. The values of solvent-solvent radial distribution functions at $q_i^*=4.5$ are larger than those at $q_i^*=0$ in a small r region. The behavior is explained as follows: ionic charges promote the association of ionic species, and resultantly, a probability that solvent molecules approach each other is enlarged. This effect is small in the case at $\rho_i^*=0.03$.

Ion-solvent radial distribution functions shown in Fig. 6c have cusps at $r/\sigma_{ss}=1+L^*$, which is the same as solvent-solvent radial distribution functions. These cusps come from the structure of solvent molecules and will be rounded off for the system with continuous potentials. The curves of $g_{i+s+}(r)$ and $g_{i+s-}(r)$ intersect each other, and $g_{i+s+}(r)<g_{i+s-}(r)$ at $r/\sigma_{ss}\approx 1$ and $g_{i+s+}(r)>g_{i+s-}(r)$ at $r/\sigma_{ss}\approx 1+L^*$, which is explained in a similar manner to the case of solvent-solvent radial distribution functions for pure solvent. These results imply that an atom of the solvent molecule with an opposite charge to an ion tends to orient toward the ion, that is, a solvated structure is formed around the ion.

It was found that a variation of the polarity of solvent molecules caused an interesting effect upon the short range structure of ionic solutions. $g_{i+i+}(r)$ and $g_{i+s+}(r)$ are shown in Fig. 9, and the contact values of $g_{i+i-}(r)$ and $g_{i+s-}(r)$ are shown in Table 1. With increasing μ_s^*, the maximum at $r/\sigma_{ss}=2$ of $g_{i+i+}(r)$ becomes small and a new maximum arises at $r/\sigma_{ss}\approx 1.5$. Further, a shoulder of $g_{i+s+}(r)$ near $r/\sigma_{ss}=1.4$ grows up to a maximum for $\mu_s^*=3$. Simultaneously, the contact value of $g_{i+i-}(r)$ decreases and the contact value of $g_{i+s-}(r)$ increases. These behaviors can be explained as follows. The ion-solvent interaction increases with increasing μ_s^*. As the result, the degree of association of ions themselves will decrease, and so the ion triplets will also decrease. Thus, the contact value of $g_{i+i-}(r)$ and the maximum at $r/\sigma_{ss}=2$ of $g_{i+i+}(r)$ will decrease with increasing μ_s^*. Further, because of the increment of ion-solvent interactions, a new type of ion pairs which, we suppose, has a structure shown in Fig. 10b will be formed, and thus the new maximum of $g_{i+i+}(r)$ and $g_{i+s+}(r)$ will arise near $r/\sigma_{ss}=1.5$. In order to ascertain the consideration, we calculated the Coulombic energy of an associated group of two cations and one solvent molecule which contact each other with an arrangement shown in Fig. 10b in vaccum, and determined the most stable structure of the group energitically. The results are shown in Table 2, where x is the distance between two cations, y the distance between the cation and the positive atom of the solvent molecule, u the electrostatic energy of the group. Parameters used in this calculation are the same as those in the case of Fig. 9, that is, $q_i^*=4.5$, $L^*=0.6$ and $\sigma^*_{ii}=1.0$. The distance x and y is roughly consistent with the position of the maximum of $g_{i+i+}(r)$ and $g_{i+s+}(r)$ at $\mu_s^*=3.0$, respectively. This result supports the consideration that the new maximums of $g_{i+i+}(r)$ and $g_{i+s+}(r)$ come from the ion pairs separated by one solvent molecule as shown in Fig. 10b. In a recent report, Levesque *et al.*[8] expected the existence of ion pairs separated by one solvent molecule as shown in Fig. 10c based on their LHNC and QHNC calculations of mixtures of

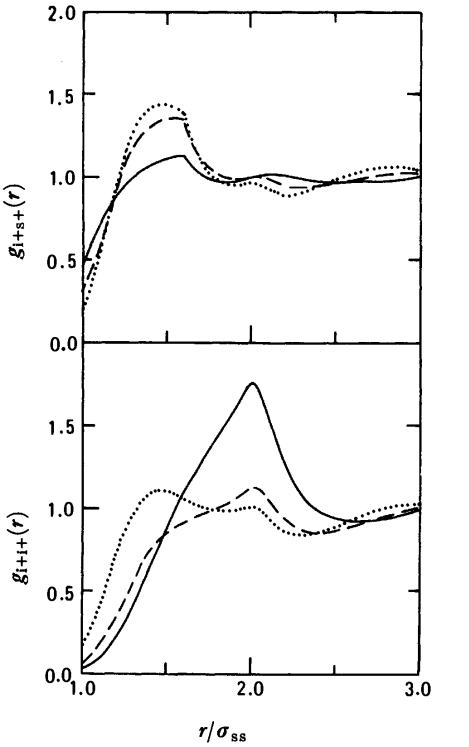

Fig. 9. $g_{i+i+}(r)$ and $g_{i+s+}(r)$ for the ionic solutions at $\rho_i^*=0.03$, $\rho_s^*=0.6$, $q_i^*=4.5$, $L^*=0.6$ and $\sigma^*_{ii}=1.0$. ——: $\mu_s^*=1.0$, ----: $\mu_s^*=2.0$, ·····: $\mu_s^*=3.0$.

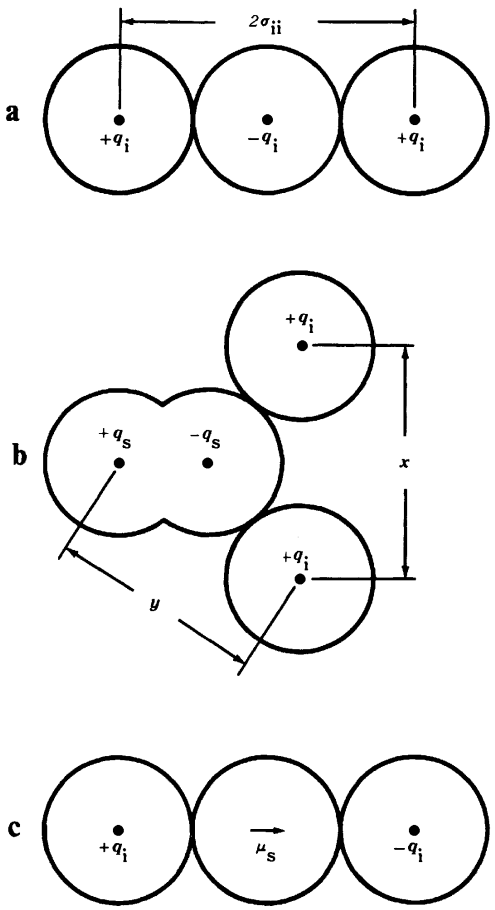

Fig. 10. Illustrations of the ion pairs and the ion triplets. → denotes the point dipole.

Table 1. Contact values of $g_{i+i-}(r)$ and $g_{i+s-}(r)$ at $\rho_s^*=0.6$, $\rho_i^*=0.03$, $q_i^*=4.5$, $L^*=0.6$, and $\sigma_{ii}^*=1.0$

μ_s^*	1	2	3
$g_{i+i-}(r)$	25.26	12.97	9.04
$g_{i+s-}(r)$	3.23	5.39	6.15

Table 2. The most stable structures and energies of the group of two cations and one solvent molecule at $q_i^*=4.5$, $L^*=0.6$, and $\sigma_{ii}^*=1.0$

μ_s^*	x/σ_{ss}	y/σ_{ss}	βu
1	1.85	1.35	5.8
2	1.70	1.41	0.2
3	1.59	1.44	−5.8

charged hard spheres and dipolar hard spheres. The ion pairs expected by Levesque *et al.* have a different structure from ours, which shows that the details of molecular structures must be considered when the short range structures of ionic solutions are investigated.

Concluding Remarks

Site-site radial distribution functions of pure polar fluids calculated with the RHNC-like integral equation of RISM-1 were compared with those of the Monte Carlo calculation. It was found from the comparison that the RHNC-like integral equation gives a fairly good result for the short range structure in polar fluids.

The short range structure in ionic solutions was also investigated by means of the RHNC-like integral equation. It was shown from the calculated site-site radial distribution functions that not only simple ion pairs but also ion triplets (Fig. 10a) and ion pairs separated by one solvent molecule (Fig. 10b) exist in ionic solutions and a solvated structure is formed around ions. The effect of a polarity of solvent molecules on the degree of association of ions and a change of the solvent structure caused by ionic charges have been investigated by the use of the RHNC-like integral equation.

Appendix

It is shown in this appendix that the total correlation functions of ionic solutions are short range functions. Here, we use the same notations as in Ref. 10, hereafter refered to as I.

From Eq. I. 2. 14, we obtain

$$\tilde{\boldsymbol{\chi}} = \tilde{\boldsymbol{\Omega}} + \tilde{\boldsymbol{\Omega}}\tilde{\boldsymbol{\phi}}^{(re)}\tilde{\boldsymbol{\Omega}}, \tag{A. 1}$$

where

$$\chi_{\alpha M \gamma M'}(r) = \rho_M \delta_{MM'}\omega_{\alpha\gamma M}(r) + \rho_M\rho_{M'}h_{\alpha M\gamma M'}(r) \tag{A. 2}$$

Eq. I. 4. 1 is expressed as

$$\tilde{\boldsymbol{\phi}}^{(re)} = -\frac{4\pi\beta}{\varepsilon(k)k^2}\boldsymbol{Z}. \tag{A. 3}$$

Combining Eq. A3 with Eq. A1, we have

$$\tilde{\boldsymbol{\chi}} = \tilde{\boldsymbol{\Omega}} - \frac{4\pi\beta}{\varepsilon(k)k^2}\tilde{\boldsymbol{\Omega}}\boldsymbol{Z}\tilde{\boldsymbol{\Omega}}. \tag{A. 4}$$

By inserting Eqs. I. 3. 11 and I. A. 1 into Eq. A. 4, and by expanding the right hand side of Eq. A4 in power series of k, we find the following equation for ionic solutions at small k

$$\tilde{\boldsymbol{\chi}} = \boldsymbol{\chi}^{(0)} + k^2\boldsymbol{\chi}^{(2)} + \cdots, \tag{A. 5}$$

where

$$\boldsymbol{\chi}^{(0)} = \boldsymbol{\Omega}^{(0)} - \frac{4\pi\beta}{K^2}\boldsymbol{\Omega}^{(0)}\boldsymbol{Z}\boldsymbol{\Omega}^{(0)}, \tag{A. 6}$$

and

$$\boldsymbol{\chi}^{(2)} = \boldsymbol{\Omega}^{(2)} - \frac{4\pi\beta}{K^2}(\boldsymbol{\Omega}^{(0)}\boldsymbol{Z}\boldsymbol{\Omega}^{(2)} + \boldsymbol{\Omega}^{(2)}\boldsymbol{Z}\boldsymbol{\Omega}^{(0)} - \frac{E}{K^2}\boldsymbol{\Omega}^{(0)}\boldsymbol{Z}\boldsymbol{\Omega}^{(0)}). \tag{A. 7}$$

Thus, the existence of $\boldsymbol{\chi}^{(2)}$ is verified, which means that $\chi(r)$ decays faster than r^{-5} at large r. $\omega_{\alpha\gamma M}(r)$ is intrinsically short range. Thus, we find from Eq. A2 that $h_{\alpha M\gamma M'}(r)$ of ionic solutions will decay faster than r^{-5} at large r.

References

1) J. C. Rasaiah and H. L. Friedman, *J. Chem. Phys.*, **48**, 2742 (1968); E. Waisman and J. L. Lebowitz, *ibid.*, **56**, 3086 (1972); G. Stell and B. Larsen, *ibid.*, **70**, 361 (1979).

2) L. Blum, *J. Chem. Phys.*, **61**, 2129 (1974); *J. Stat. Phys.*, **18** 451 (1978).

3) S. A. Adelman and J. M. Deutch, *J. Chem. Phys.*, **60**, 3935 (1974).

4) D. Y. C. Chan, D. J. Mitchell, and B. W. Ninham, *J. Chem. Phys.*, **70**, 2946 (1979).

5) S. A. Adelman, *J. Chem. Phys.*, **64**, 724 (1976).

6) J. S. Hφye and G. Stell, *J. Chem. Phys.*, **68**, 4145 (1978); **71**, 1985 (1979).

7) D. Y. C. Chan, D. J. Mitchell, B. W. Ninham, and B. A. Pailthorpe, *J. Chem. Phys.*, **69**, 691 (1978).

8) D. Levesque, J. J. Weis, and G. N. Patey, *J. Chem. Phys.*, **72**, 1887 (1980).

9) G. N. Patey and S. L. Carnie, *J. Chem. Phys.*, **78**, 5183 (1983).

10) M. Ohba and K. Arakawa, *J. Phys. Soc. Jpn.*, **50**, 743 (1981).

11) H. L. Friedman, *J. Chem. Phys.*, **76**, 1092 (1982).

12) F. Hirata, P. J. Rossky, and B. M. Pettitt, *J. Chem. Phys.*, **78**, 4133 (1983).

13) D. Chandler and H. C. Andersen, *J. Chem. Phys.*, **57**, 1930 (1972).

14) K. Kojima and K. Arakawa, *Bull. Chem. Soc. Jpn.*, **51**, 1977, (1978); **53**, 1795 (1980).

15) M. Ohba and K. Arakawa, *Bull. Chem. Soc. Jpn.*, **55**, 1387 (1982).

16) G. P. Morriss and P. T. Cummings, *Mol. Phys.*, **45**, 1099 (1982).

17) G. P. Morriss, *Mol. Phys.*, **47**, 833 (1982).

18) D. Chandler, *J. Chem. Phys.*, **67**, 1113 (1977).

19) P. T. Cummings and G. Stell, *Mol. Phys.*, **44**, 529 (1981); **46**, 383 (1982).

20) L. J. Lowden and D. Chandler, *J. Chem. Phys.*, **59**, 6587 (1973); **61**, 5228 (1974).

21) F. Hirata and P. J. Rossky, *Chem. Phys. Lett.*, **83**, 329 (1981).

22) F. Hirata, B. M. Pettitt, and P. J. Rossky, *J. Chem. Phys.*, **77**, 509 (1982).

23) P. J. Rossky, B. M. Pettitt, and G. Stell, *Mol. Phys.*, **50**, 1263 (1983).

24) G. P. Morriss and P. A. Monson, *Mol. Phys.*, **48**, 181 (1983).

Selective Hydrogenation of Conjugated Dienes Catalyzed by Thiocyanatotris(triphenylphosphine)cobalt(I)

Taisei NAKAYAMA and Hiroyoshi KANAI*
Division of Molecular Engineering, Graduate School of Engineering, Kyoto University, Sakyo-ku, Kyoto 606
(Received June 7, 1984)

Thiocyanatotris(triphenylphosphine)cobalt(I) prepared *in situ* from bis(thiocyanato)bis(triphenylphosphine)cobalt(II), triphenylphosphine, zinc bromide, selectively hydrogenated conjugated dienes to the corresponding cis-monomenes. The C_2-or/and C_3-methyl substituted 1,3-butadienes enhance the reactivity by a factor of 2.3 per one methyl group, while C_1- or/and C_4-methyl substituted 1,3-butadienes lower the reactivity by a factor of 1/23 per one methyl group. In the hydrogenation of cyclic conjugated dienes α-angle ($\angle$C–C=C) is closely related to the hydrogenation rate. The rates of hydrogenation in cyclic ethers are greater than those in acyclic ethers, but the cis-selectivity in acyclic ethers is much higher. Deuterium selectively adds to 1,3-butadiene and 2,5-norbornadiene (bicyclo[2.2.1]hepta-2,5-diene) to give 3,4-dideuterio-1-butene and *cis*-1,4-dideuterio-2-butene, and *endo,endo*-5,6-dideuterionorbornene and *endo,endo*-3,5-dideuterionortricyclene, respectively. A mechanism is proposed which derives from *anti*-π-allylcobalt hydride or delocalized nortricyclenylcobalt hydride as an intermediate.

Univalent cobalt complexes with halogen and pseudohalogen ligands were limited until recently.[1] The principal difficulties in the synthesis of Co(I) complexes are due to the capacity of Co(I) complexes for oxidation, reduction and disproportionation. The interest in Co(I) complex has been stimulated by studies in the field of stereochemistry[2] and catalysis.[3]

In the hydrogenation of 1,3-butadiene a cationic cobalt(I) complex, $[Co(PPh_3)_3]BF_3X$ (X=halogen),[3d] selectively gave 1-butene, while $CoX(bpy)_2$/zinc system (bpy=2,2′-bipyridyl) mainly gave *cis*-2-butene.[3h]

We reported here the selective hydrogenation of conjugated dienes with a cobalt(I) thiocyanate complex.

Experimental

Materials. 1,3-Butadiene was obtained from Takachiho Chemical Co. and distilled under vacuum. *trans*-1,3-Pentadiene, *trans*-2-methyl-1,3-pentadiene, *trans,trans*-2,4-hexadiene, 4-methyl-1,3-pentadiene and 2,3-dimethyl-1,3-butadiene were obtained from Aldrich Chemical Co. and distilled under vacuum. Isoprene and 1,3-cyclohexadiene were from Nakarai Chemical Co. and distilled under vacuum. Cyclopentadiene was prepared from the pyrolysis of dicyclopentadiene.[4] 1,3,5-Cycloheptatriene, 1,3-cyclooctadiene, 1,5-cyclooctadiene, β-myrcene and 2,5-norbornadiene were obtained from Nakarai Chemical Co. and used without further purification. 1,2-Butadiene was obtained from Tokyo Kasei Co. and distilled under vacuum.

Solvents were refluxed over lithium aluminium tetrahydride, distilled, and stored in a nitrogen atmosphere.

Preparation of Bis(thiocyanato)bis(triphenylphosphine)cobalt(II).[5] Cobalt(II) thiocyanate was prepared from cobalt(II) sulfate (Hayashi Junyaku Co.) and barium thiocyanate (Mitsuwa Kagaku Co.) by the literature method.[6] After $Co(SCN)_2$ (28 g, 98 mmol) was dissolved in acetone (300 ml) and the insoluble residue was filtered off, triphenylphosphine (48 g, 200 mmol) were added to the filtrate and the green solution was concentrated to *ca.* 100 ml by using an evaporator. Petroleum ether was added to the concentrated solution. The precipitate of $[Co(SCN)_2(PPh_3)_2]$ was collected, washed with petroleum ether for several times and dried: yield 32 g (67% based on $Co(SCN)_2$).

Hydrogenation Procedure. The catalyst was prepared *in situ* from the reduction of $[Co(SCN)_2(PPh_3)_2]$ 0.21 g (0.3 mmol) with Zn (3.0 mmol) and $ZnBr_2$ (1.0 mmol) in the presence of PPh_3 (0.3 mmol) in glyme (1,2-dimethoxyethane) (10 ml) under nitrogen. The solution, which was initially purple, turned brown after 2—3 h. Then substrates (2 mmol) were added and nitrogen was replaced by hydrogen. Hydrogenation was conducted at 17 °C with stirring under the constant pressure of hydrogen using the gas buret. The rate of hydrogenation was determined by hydrogen uptake and products were analyzed by gas chromatography (30% 2,4-dimethylsulfolane on C-22, 5.6 m, r.t.).

Isotopic exchange of H_2–D_2 and D_2–olefin were carried out by the analogous procedure. The deuterated products of 1,3-butadiene in H_2–D_2 mixed gas were analyzed by a gas chromatography–mass spectrometer (NEVA TE600, porapak Q, 110 °C, ionization voltage 10 V). Deuterated products of 1,3-butadiene and 2,5-norbornadiene were identified by ^{13}C and ^1H NMR spectra obtained on a JEOL FX-100 spectrometer.

Results and Discussion

Preparation of Co(I) Complex and Active Species. Sodium tetrahydroborate was ineffective to decompose the complex. Zinc can reduce $[Co(SCN)_2(PPh_3)_2]$ to the Co(I) complex, but it takes too much time. The activated zinc prepared from zinc halides and potassium,[7] or from zinc bromide, lithium and naphthalene[8] was not appropriate because they gave complexed compounds to lose reproducibility. We found that $[Co(SCN)_2(PPh_3)_2]$ was smoothly reduced by zinc in the presence of zinc bromide.[9] The effect of zinc bromide on the hydrogenation of 1,3-butadiene indicates that the highest activity was observed above the ratio of $ZnBr_2/Co=3.3$ (Fig. 1). Other Lewis acids, $AlCl_3$ and $FeCl_3$ were ineffective. Zinc bromide was the most effective among zinc halides.

The addition of triphenylphosphine increased the

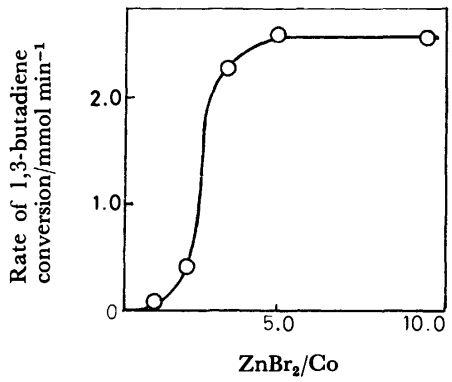

Fig. 1. Effect of zinc bromide on the hydrogenation of 1,3-butadiene.

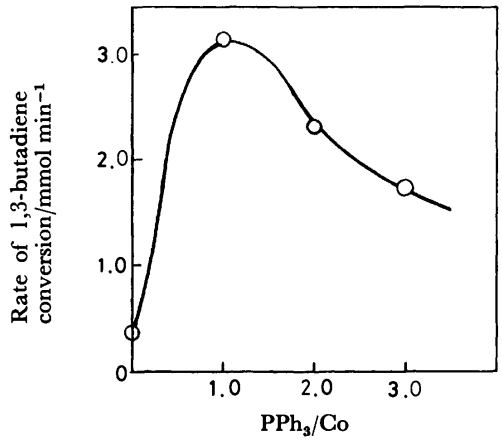

Fig. 2. Effect of triphenylphosphine on the hydrogenation of 1,3-butadiene.

yield of hydrogenation, but the excess inhibited (Fig. 2). The maximum yield at the 1:1 ratio of triphenylphosphine to the cobalt complex indicated that the precursor of the active species is [Co(SCN)(PPh3)3]. After the reduction of [Co(SCN)2(PPh3)2] in the presence of PPh3, ZnBr2, and Zn, the red-brown solution was separated from zinc by filtration. When 1,3-butadiene was introduced into the filtrate in an atmosphere of hydrogen, no reaction was observed. When butadiene was treated with another filtrate in contact with fresh zinc, hydrogenation began to occur. Zinc plays a role to keep the cobalt complex a univalent state. No anion exchange between [CoBr(PPh3)3] and NaSCN was observed in glyme at r.t. The red-brown solution where [CoBr(PPh3)3] was treated with Zn(SCN)2 caused hydrogenation of 1,3-butadiene, but hydrogen uptake stopped after 60 min by giving catalytically inactive green complex. Consequently, anion exchange method was not suitable to prepare the Co(I) complex.

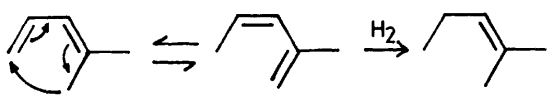

Scheme 1.

We have not isolated the Co(I)-thiocyanate complex. Putting all accounts together catalytic species must be [Co(SCN)(PPh3)3]. The presence of zinc is required as a reductant to keep the unstable complex active.

Hydrogenation of Unsaturated Hydrocarbons. Hydrogenation of unsaturated compounds were summarized in Table 1. Conjugated acyclic dienes were selectively hydrogenated to the corresponding cis-monoenes. No alkanes were observed. The rates of hydrogenation decreased in the following order; 2,3-dimethyl-1,3-butadiene>*trans*-2-methyl-1,3-butadiene-(Isoprene)>1,3-butadiene>*trans*-2-methyl-1,3-pentadiene>*trans*-1,3-pentadiene. *trans,trans*-2,4-Hexadiene was not hydrogenated. 4-Methyl-1,3-pentadiene was concluded to be hydroganated *via* 2-methyl-1,3-pentadiene, since hydrogenation products were the same as those of 2-methyl-1,3-pentadiene which had been formed in the course of hydrogenation. This reaction is similar to the 1,5-hydrogen shift explained by Frankel and Butterfield (Scheme 1).[10]

To investigate the coordination and reactivity sequences of conjugated dienes, the competitive hydrogenation of 1,3-butadiene and 2,3-dimethyl-1,3-butadiene was conducted. Since the hydrogenation of each dienes occurred at its own rate, the coordinating strength of dienes did not determine the reactivity sequence.

Among conjugated cyclic dienes, cyclopentadiene and 1,3-cyclohexadiene were selectively hydrogenated to the corresponding cyclomonoenes. 1,3,5-Cycloheptatriene was also hydrogenated to cycloheptene *via* 1,3- or 1,4-cycloheptadiene. No hydrogenation of 1,3- and 1,5-cyclooctadiene occurred. 1,5-Cyclooctadiene was isomerized to 1,3- and 1,4-cyclooctadienes. The composition of cyclooctadienes after 24 h were 1,3-cyclooctadiene: 1,4-cyclooctadiene: 1,5-cyclooctadiene= 4:29:67. 1,2-Butadiene was hydrogenated to butenes without selectivity but polymer was obtained as a by-product.

Although 2,5-norbornadiene is classified as a non-conjugated diene, Hoffmann *et al.* showed that its π-electron systems have direct through-space overlap interaction.[11] So it should be treated as one of conjugated dienes when it is coordinated to cobalt complex.

2,5-Norbornadiene was hydroganeted to bicyclo-[2.2.1]hept-2-ene (norbornene) and tricyclo[2.2.1.$0^{2,5}$]-heptane (nortricyclene). It is notable that nortricyclene is produced in the hydrogenation of norbornadiene by a cobalt catalyst, while it is barely produced by transition-metal complexes.[12] Parallel to the hydrogenation, dimerization occurred.[13] No dimerization of any other conjugated dienes in Table 1 was observed.

No hydrogenation occurred for following unsaturated compounds; 1-hexyne, styrene, *trans*-1-phenyl-1,3-butadiene, phenylacetylene, furan, and methyl acrylate.

Effect of Hydrogen Pressure, and the Concentrations of

TABLE 1. HYDROGENATION OF CONJUGATED DIENES CATALYZED BY $[Co(SCN)(PPh_3)_3]$ PREPARED *in situ* FROM $[Co(SCN)_2(PPh_3)_2]$, Zn AND $ZnBr_2$[a)]

Diene	Rate of H_2 uptake / 10^{-2} ml min^{-1}	Products / %
	10	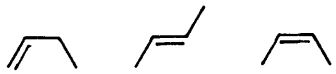 18 0 82
	23	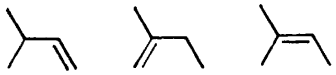 11 1 88
	50	3 97
	0.40	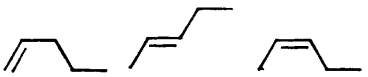 28 6 66
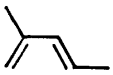	2.0	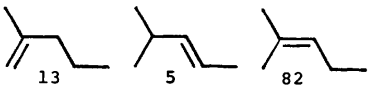 13 5 82
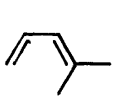	0.33	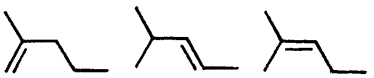 13 14 73
	0	
	21	100
	10	100
	0.06	100
	0	
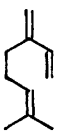	17[b)]	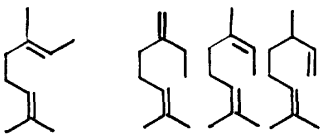 75 25
C=C=C-C	9.0	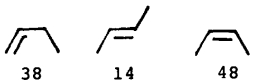 38 14 48 + Polymer
	3.0	55 48 68 32 + Dimers

a) Reactions were carried out as following conditions: diene 2 mmol, $[Co(SCN)_2(PPh_3)_2]$ 0.3 mmol, Zn 3.0 mmol, $ZnBr_2$ 1.0 mmol, glyme 10 ml, total pressure 1 atm at 17 °C.
b) β-Myrcene (1.2 mmol) was used.

Cobalt Complex and Dienes. Figure 3 illustrates the first order dependence upon hydrogen pressure. The first order dependence upon the concentration of the complex is observed up to a cobalt complex charge of 0.03 mol dm^{-3} which is the saturated concentration (Fig. 4). The hydrogenation is independent of the concentration of dienes except for β-myrcene. The lowering of the rate in the hydrogenation of β-myrcene with the elapse of time is attributed to the coordination of the diene products. Hydrogen uptake increases linearly with time, and products were not isomerized until dienes were almost consumed.

Solvent Effects. The nature of solvents has a significant effect on both the selectivity and the hydrogenation rate (Table 2). No reduction of [Co(SCN)$_2$-(PPh$_3$)$_2$] occurred in the following solvents; diethyl ether, dibutyl ether, and toluene. Methanol, ethanol, and acetonitrile were inadequate to make the complex dissociate into Co(SCN)$_2$ and PPh$_3$. The UV spectra of [Co(SCN)$_2$(PPh$_3$)$_2$]-Zn-ZnBr$_2$ in these solutions showed the same absorption bands as those of Co(SCN)$_2$ in the solutions except for the absorption bands attributed to triphenylphosphine.

Ethers can be typed into two groups, one is cyclic ethers and the other is acyclic polyethers. Acyclic ethers gave higher cis-selectivity than cyclic ones. The increase of n in $CH_3O(CH_2CH_2O)_nCH_3$ leads to the increase of cis-selectivity and the decrease of hydrogenation rate (Fig. 5). In a mixture of THF and glyme (ratio 1:1), THF controlled the hydrogenation rate and selectivity. The coordination strength of cyclic ethers toward the cobalt complex is larger than that of acyclic ethers. When crown ether (18-crown-6) was added to glyme (crown:Co=1:1 and 10:1) the hydrogenation rates were a little slower than that in glyme alone without change of selectivity. The high cis-selectivity in acyclic ethers seems to be attributed to the weak chelate coordination of free movable oxyetylene units.

Deuteration. Deuteration of 1,3-butadiene gave 3,4-dideuterio-1-butene **1** and *cis*-1,4-dideuterio-2-butene **2** which were identified by their ^{13}C NMR spectra. Hydrogen was selectively introduced into 1,3-butadiene *via* 1,2- and 1,4-addition. The isotopic effect is calculated as r_H/r_D=1.4. Hydrogenation products of 1,3-butadiene in H_2-D_2 mixed gas (ratio of H_2/

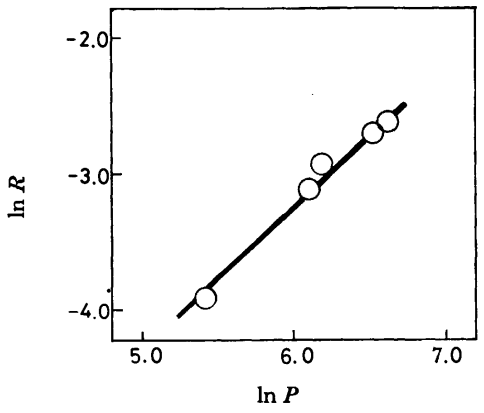

Fig. 3. Effect of hydrogen pressure; *P*: hydrogen pressure/mmHg, *R*: rate/ml(S.T.P.) min^{-1} (1 mmHg =133.2 Pa).

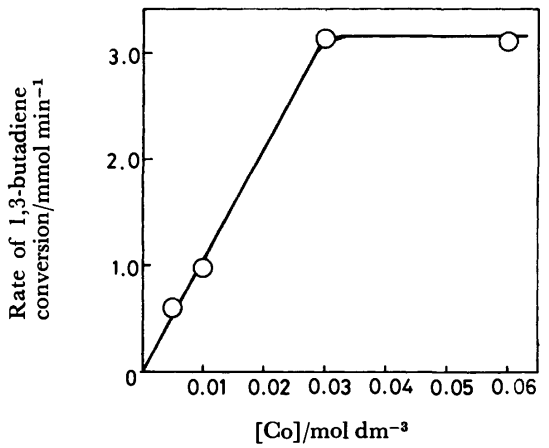

Fig. 4. Effect of the initial concentration of [Co(SCN)$_2$ (PPh$_3$)$_2$].

Table 2. Solvent effects on the hydrogenation of 1,3-butadiene[a)]

Solvent	Rate/ml min^{-1}	Butene composition/%	
		1-Butene	*cis*-2-Butene
Glyme	0.10	18	82
Diglyme	0.06	17	83
THF	0.08	53	47
Tetrahydropyran	0.04	45	55
1,3-Dioxolane	0.15	45	55
Dioxane	0.01	40	60
Glyme+THF (1 : 1)	0.11	51	49
Glyme+18-crown-6			
(Co : crown=1 : 1)	0.03	20	80
(Co : crown=1 : 10)	0.04	17	83

a) Solvent 10 ml, [Co] 0.03 mol dm^{-3}, 1,3-butadiene 2.0 mmol at 17 °C.

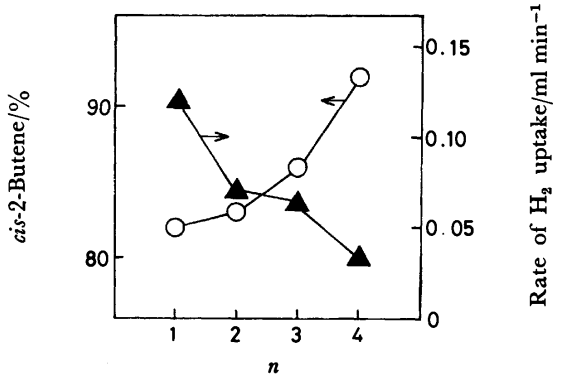

Fig. 5. Solvent effects on the hydrogenation of 1,3-butadiene ; solvents $CH_3O(CH_2CH_2O)_n$ CH_3.

D_2=1.08) were **1**, **2**, 1-butene and *cis*-2-butene. Mono- and polydeuterated products were not observed, so molecular identity was maintained.

Deuteration of norbornadiene was tried to investigate the stereochemistry of the addition of hydrogen. *endo, endo*-5,6-Dideuteriotricyclo[2.2.1]hept-2-one **3** and *endo,endo*-3,5-dideuteriotricyclo[2.2.1.$0^{2,5}$]heptane **4**, which were identified by their ^{1}H NMR spectra by comparison of those of authentic samples,[13] were obtained to ensure that hydrogen was added selectively via cis-endo-addition.

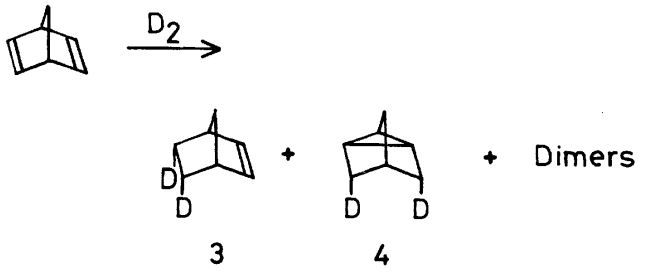

3 4

Methyl-substituted Effect on Acyclic Conjugated Dienes. We compared the rates of hydrogenation of methyl-substituted 1,3-butadienes (Table 3). The hydrogenation of C_1- or/and C_4-substituted 1,3-butadienes was faster than that of 1,3-butadiene, while the hydrogenation of C_1 or/and C_4-substitued 1,3-butadienes was slower. The substitution of methyl group at C_2 as seen in isoprene accelerates the hydrogenation rate 2.3 times as fast as that of 1,3-butadiene. 2,3-Dimethyl-1,3-butadiene can be estimated to be hydrogenated faster than 1,3-butadiene by a factor of 2.3^2=5.3 which is in fair agreement with the experimental value.

On the other hand, C_1- or C_4-subtituted methyl group lowers the hydrogenation rate by 1/23 time. The hydrogenation rate of *trans,trans*-2,4-hexadiene can be estimated to be $1/23^2$=0.002 time of that of 1,3-butadiene. The value is regarded as nearly zero. No hydrogenation of *trans,trans*-2,4-hexadiene occurred in practice. The hydrogenation rate of *trans*-2-methyl-1,3-pentadiene can be estimated to be 2.3×1/23=0.1 time of that of 1,3-butadiene. The value almost agrees with the experimental one on the basis of the order.

α-Angle Effect on the Hydrogenation of Cyclic Conjugated Dienes. The reason why cyclopentadiene, 1,3-cyclohexadiene and 1,3-cycloheptadiene were hydrogenated but 1,3-cyclooctadiene not, may be related to α-angles of cyclic dienes (Table 4). The hydrogenation rate is almost independent of β-angles. Strohmeier

Table 3. Hydrogenation of conjugated acyclic dienes

Diene	Substituent				Relative rate
	C_1	C_2	C_3	C_4	
	H	Me	Me	H	5.0
	H	Me	H	H	2.3
	H	H	H	H	1.0
	H	Me	H	Me	0.2
	H	H	H	Me	0.04
	H	H	H	Me,Me	0.03
	Me	H	H	Me	0

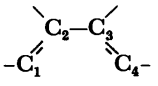

Table 4. Hydrogenation of conjugated cyclic compounds

Compound	Relative rate		α-Angle[a]	β-Angle[a]
	$[Co(SCN)(PPh_3)_3]$	$[Co(CN)_5]^{3-}$ [a]		
	1.0	1.0	109	110
	0.47	1.67	120.6	116.5
	0.003	0.71	121.8	127
	0	0	(126.46)[b]	(126.46)[b]

a) By Strohmeier and Iglauer.[15] b) Angle of cyclooctatetraene.

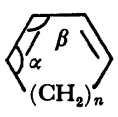

and Iglauer explained the ease of the hydrogenation of cyclic dienes by $[Co(CN)_5]^{3-}$ in terms of the strain energy of carbon-carbon bonding.[15]

Although no hydrogenation of 1,3- and 1,5- cyclooctadiene occurred, 1,5-cyclooctadiene was isomerized even in the absence of hydrogen. Hydrogen is not required for the isomerization of cyclooctadiene. The isomerization may occur *via* a 1,3-hydrogen shift with a π-allylcobalt hydride intermediate. The hydrogenation rates decrease in the order cyclopentadiene>1,3-cyclohexadiene>1,3-cycloheptadiene$\gg$1,3-cyclooctadiene. The smaller α-angle is, the more reactive the cyclic diene is. The ease of hydrogenation of cyclic dienes with small α-angle is related to the facile approach of hydrogen coordinated with cobalt toward coordinated dienes. Because α-angles are related to the distances between the C_1 and C_4 carbons of conjugated dienes and cobalt. On the crystallographic studies the distances between cobalt and C_1-carbon of π-cyclopentadienyl-1-phenylcyclopentadiene cobalt was 1.97 Å,[16] while that of *cis*-di-μ-carbonyl-bis[carbonyl-(π-cyclohexa-1,3-diene)cobalt] was 2.13 Å.[17]

Mechanism of Hydrogenation. A monomeric cobalt complex is an active species due to the first dependence of the cobalt concentration. The catalytic species must be $[Co(SCN)(PPh_3)_3]$. Zero-order dependence of butadiene indicates that the reaction between Co(I) complex and butadiene gives cobalt(I)-butadiene π-complex (Scheme 2). Hydrogen adds to the complex to form *anti*-1-methyl-π-allylcobalt hydride complex. Since *trans*-2-butene was not formed at all, no scrambling of the anti-complex to the syn-isomer occurred.[18] *anti*-π-Allylcobalt hydride complex produces *cis*-2-butene and 1-butene to regenerate the initial cobalt(I) complex.

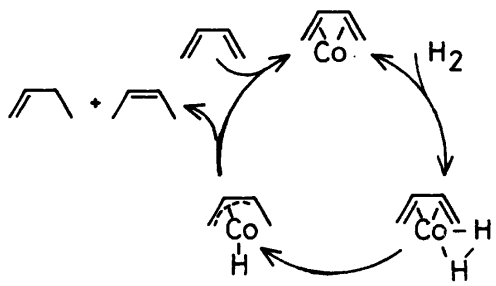

Co ≡ [Co(SCN)(PPh3)n]

Scheme 2.

In the case of norbornadiene, cobalt(I)-norbornadiene complex **5** is formed (Scheme 3). Then hydrogen reacts with the complex to form the delocalized nortricyclenylcobalt hydride complex **6**. When the hydride reacts *via* path I, norbornene is produced, and *via* path II, nortricyclene is produced.

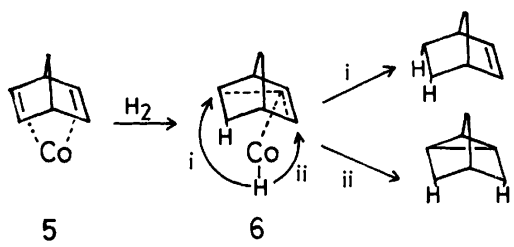

5 6

Scheme 3.

We are grateful to Dr. Sadayuki Mori of Chemical Research Institute, Kyoto University for performing mass spectrometric measurements.

References

1) F. A. Cotton and G. Wilkinson, "Advanced Inorganic Chemistry," 4th ed., John Wiley and Sons, New York (1980), pp. 779—783.

2) *e.g.*, Stereoelectronic effects of molecules-five coordinated complexes of transition metals. S. Otsuka, *Kagaku (Chemistry, Kyoto)* **34**, 202 (1979).

3) a) G. N. Schrauzer, J. H. Weber, and T. M. Beckham, *J. Am. Chem. Soc.*, **92**, 7078 (1979); b) L. Vaska, L. S. Chen, and W. V. Miller, *ibid*, **93**, 6671 (1971); c) K. Kawakami, T. Mizoroki, and A. Ozaki, *Bull. Chem. Soc. Jpn.*, **51**, 21 (1978); d) K. Kawakami, T. Mizoroki, and A. Ozaki, *J. Mol. Catal.*, **5**, 175 (1979); e) G. Fachinetti, C. Floriani, P. F. Zanazzi, and A. R. Zanzari, *Inorg. Chem.*, **18**, 3469 (1979); f) H. Kanai and K. Ishii, *Bull. Chem. Soc. Jpn.*, **54**, 1015 (1981); g) H. Kanai, *J. Mol. Catal.*, **12**, 231 (1983); h) H. Kanai, N. Yamamoto, K. Kishi, K. Mizuno, and K. Tarama, *J. Catal.*, **73**, 228 (1982).

4) R. B. Moffett, *Org. Synth.*, Coll. Vol. IV, 238 (1963).

5) F. A. Cotton, D. M. L. Goodgame, M. Goodgame, and A. Sacco, *J. Am. Chem. Soc.*, **83**, 4157 (1961).

6) A. Rosenheim and R. Cohn, *Z. Anorg. Chem.*, **27**, 289 (1901).

7) R. D. Rieke, S. J. Uhm, and P. M. Hudnall, *J. Chem. Soc., Chem. Commun.*, **1973**, 269.

8) R. D. Rieke, P. T. Li, T. P. Burns, and S. T. Uhm, *J. Org. Chem.*, **46**, 4323 (1981).

9) F. Toda and K. Iida, *Chem. Lett.*, **1976**, 695.

10) E. N. Frankel and R. O. Butterfield, *J. Org. Chem.*, **34**, 3930 (1969).

11) R. Hoffmann, E. Heilbronner, and R. Gleiter, *J. Am. Chem. Soc.*, **92**, 706 (1970).

12) a) M. J. Mirbach, T. Nyu Pyu, and A. Saus, *J. Organomet. Chem.*, **236**, 309 (1982); b) G. Platbrood and L. Wilputte-Steinert, *J. Organomet. Chem.*, **70**, 393 (1974); c) M. J. Mirbach, D. Steinmetz, and A. Saus, *J. Organomet. Chem.*, **168**, C13 (1979).

13) H. Kanai, Y. Watabe, and T. Nakayama, 49th National Meeting of the Chemical Society of Japan, Tokyo, Apr. 1984, Abstr., No. 3P05.

14) a) N. H. Werstiuk, *Can. J. Chem.*, **48**, 2310 (1970); b) G. Platbrood and L. Wilputte-Steinert, *Bull. Soc. Chim. Belg.*, **82**, 733 (1973).

15) W. Strohmeier and N. Iglauer, *Z. Phys. Chem.*, **61**, 29 (1968).

16) M. R. Churchill and R. Mason, *Proc. R. Soc. London,*

Ser. A, **279**, 191 (1964).
17) F. S. Stephens, *J. Chem. Soc., Dalton*, **1972**, 1752.
18) W. Rupilius and M. Orchin, *J. Org. Chem.*, **36**, 3604 (1971).

Carbon-13 NMR Chemical Shift and Electronic Structure of Solid Polypeptides as Studied by Tight-binding MO Theory. Polyglycine and Poly(L-alanine)

Takeshi YAMANOBE,* Isao ANDO,* Hazime SAITO,† Ryoko TABETA,†
Akira SHOJI,†† and Takuo OZAKI††
*Department of Polymer Chemistry, Tokyo Institute of Technology, Ookayama, Meguro-ku, Tokyo 152
†Biophysics Division, National Cancer Center Research Institute, Tsukiji, Chuo-ku, Tokyo 104
††Department of Industrial Chemistry, College of Technology, Gunma University, Kiryu-shi, Gunma 376
(Received June 13, 1984)

A tight-binding MO-sum-over-state theory has been used to calculate the ^{13}C NMR chemical shift of polyglycine having the forms I and II and that of poly(L-alanine) having the α-helix and β-sheet forms, in order to justify the origin of the conformation-dependent ^{13}C NMR chemical shift previously determined by the cross polarization-magic angle spinning technique. The calculated results on the carbonyl, C_α and C_β carbons were found to exhibit the conformation-dependent ^{13}C NMR chemical shifts comparable with the experimental data.

A recent development of the cross polarization-magic angle spinning (CP-MAS) NMR technique has provided useful information about the conformation of polypeptides in the solid state.[1-12] It has been demonstrated that the ^{13}C chemical shifts of the C_α, C_β, and carbonyl carbons are displaced up to 7 ppm, depending on the particular conformations such as the α-helix, β-sheet and ω-helix forms.

In a previous work,[7] we have justified by using a dipeptide fragment of poly(L-alanine), *N*-acetylalanine methylamide, and the finite perturbation theory(FPT) within the INDO MO framework[13-17] that the conformation-dependent ^{13}C chemical shift arises from changes of electronic structure varying with the dihedral angles (ϕ and ψ) of the skeletal bond. (On the other hand, Tonelli[33] has suggested that ^{13}C NMR chemical shifts of backbone carbonyl and side chain carbons in polypeptides provide information about their structure by means of the γ-gauche effect.) Such approaches are useful to obtain appropriate knowledge regarding the conformation of polypeptides. However, it may be necessary to clarify the following points: The specification of the long finite interaction length for the electronic structure, and the hydrogen bond's involved in the α-helix or β-sheet form are not always included sufficiently in the dipeptide.

Such a situation leads to the application of the tight-binding (TB) MO theory to the NMR chemical shift calculation for polypeptides without using the model compounds.[18] It is emphasized that the intrachain hydrogen bonds of the α-helix conformation are easily taken into account by this approximation. So far, the TB MO approximation has been used for describing the electronic structure of polymers with a periodic structure.[19-25] Thus, in this work we attempt to calculate the conformation-dependent ^{13}C chemical shift for polyglycine and poly(L-alanine) which was previously measured, on the basis of the TB MO approximation in order to gain an insight into the ^{13}C chemical shift in polypeptides.

Theory and Calculation

With the aid of the LCAO approximation and Bloch's theorem, the wave function for electrons in a polymer chain in which N-1 cells (or amino acid residues) interact with the original cell is expressed by[19-21]

$$\Psi_n(k,r) = \frac{1}{N}\sum_\nu \sum_j \exp(ikj) C_{\nu n}(k)\phi_\nu(r-ja), \quad (1)$$

where n is the band index; ν the atomic orbital in the j-th cell; N the total number of cells; l the number of atomic orbital in the cell; a the unit vector of translational symmetry and k the wave number. The parameters j and k vary from $-(N-1)/2$ to $(N-1)/2$ and from $-\pi/2$ to $\pi/2$, respectively, within the first Brillouin zone. The symbol i denotes the imaginary number. $\phi_p(r-ja)$ represents the p-th atomic orbital in the j-th cell and $C_{\nu n}(k)$ its expansion coefficient. Using Eq. 1, the Schrödinger equation for a polymer chain is given by

$$H(k) = \varepsilon(k)S(k), \quad (2)$$

where

$$H_{\mu\nu}(k) = \sum_j \exp(ikj)H^{0j}_{\mu\nu},$$
$$S_{\mu\nu}(k) = \sum_j \exp(ikj)S^{0j}_{\mu\nu}, \quad (3)$$

in which $H^{0j}_{\mu\nu}$ is the interaction between the μ-th atomic orbital in the original cell and the ν-th atomic orbital in the j-th cell. $S^{0j}_{\mu\nu}$ is the overlap integral between the μ-th atomic orbital in the original cell and the ν-th atomic orbital in the j-th cell. Thus, we can directly treat a polymer chain which has infinite length without model compounds such as a dimer,

trimer, *etc.* Previously, the electronic structure of polymers (including polyglycine and poly(L-alanine)) were calculated by means of the extended Hückel and CNDO MO theories and conformational energies were compared.[22-25]

Hence, we perform calculations within the framework of the extended Hückel approximation. It is said that the extended Hückel calculation should be compared among molecules with a similar structure, because, generally, such a calculation for polar molecules has a tendency to overestimate the electronic polarization. Therefore, it is considered that the extended Hückel method is significantly applicable to the conformation-dependent ^{13}C chemical shift calculation as done in this work. In the extended Hückel approximation, the diagonal and off-diagonal elements of the Hamiltonian are estimated as follows:

$$H^{00}_{\mu\mu} = -I_\mu$$
$$H^{0J}_{\mu\nu} = \frac{1}{2}KS^{0J}_{\mu\nu}(H^{00}_{\mu\mu}+H^{00}_{\nu\nu}), \quad (4)$$

where I_μ is the ionization potential energy of the μ-th orbital and K is taken to be 1.75. The valence-state ionization potential energy for the paticular atomic orbital used here is as follows:[26] I_{1s}=13.6 eV for hydrogen atom; I_{2s}=21.43 eV and I_{2p}=11.42 eV for carbon atom; I_{2s}=27.5 eV and I_{2p}=14.49 eV for nitrogen atom; I_{2s}=35.3 eV and I_{2p}=17.76 eV for oxygen atom. The Slater's effective nuclear charges used for hydrogen, carbon, nitrogen and oxygen atoms are 1.00, 3.25, 3.90, and 4.55, respectively.[26] Thus, we can directly obtain the expansion coefficients, $C_{\nu n}(k)$, and the electronic structure of an infinite regular polymer.

Using $C_{\nu n}(k)$, we estimate the ^{13}C NMR chemical shift of polyglycine and poly(L-alanine). In general, an NMR chemical shift can be written as

$$\sigma_A = \sigma^d_A + \sigma^p_A + \sigma', \quad (5)$$

where σ^d_A and σ^p_A are the diamagnetic and paramagnetic contributions, respectively. σ' is the contribution from neighbouring atoms. For the carbon atom, σ' is much smaller than 1 ppm and can be considered negligible. Thus, the ^{13}C NMR chemical shift can be estimated by the sum of σ^d and σ^p which are expressed by[18]

$$\sigma^d_A(k) = \frac{\mu_0}{4\pi}\frac{2e^2}{3m_e^2}\sum_\nu^A\sum_{\nu'}^A P_{\nu\nu'}(k)\langle\phi_\nu(r)|r^{-1}|\phi_{\nu'}(r)\rangle \quad (6)$$

$$\sigma^p_{A,\alpha\beta}(k) = -\frac{\mu_0}{4\pi}\frac{\hbar^2e^2}{m_e^2}\sum_m^{occ}\sum_n^{unocc}\sum_j^A\langle r^{-3}\rangle_{2p}({}^1E^n_m-{}^1E_0)^{-1} \quad (7)$$
$$\times\sum_B\sum_I^B (X(j,m,n,\beta,\gamma)X(l,n,m,\gamma,\alpha)$$
$$- Y(j,m,n,\beta,\gamma)Y(l,n,m,\gamma,\alpha)$$
$$+ X(j,m,n,\gamma,\alpha)X(l,n,m,\beta,\gamma)$$
$$- Y(j,m,n,\gamma,\alpha)Y(l,n,m,\beta,\gamma)),$$

where

$$P_{\nu\nu'}(k) = \sum_m^{occ} C^*_{\nu n}(k)C_{\nu' m}(k)$$
$$X(j,m,n,\beta,\gamma) = C^{R\beta}_{jm}C^{I\gamma}_{jn} + C^{R\beta}_{jn}C^{I\gamma}_{jm} - C^{R\gamma}_{jn}C^{I\beta}_{jm} - C^{R\gamma}_{jm}C^{I\beta}_{jn} \quad (8)$$
$$Y(j,m,n,\beta,\gamma) = C^{R\beta}_{jm}C^{R\gamma}_{jn} - C^{R\gamma}_{jm}C^{R\beta}_{jn} + C^{I\beta}_{jm}C^{I\gamma}_{jn} - C^{I\gamma}_{jm}C^{I\beta}_{jn}$$

in which j and l are orbitals on atoms A and B, respectively; $\sum_m^{occ}$ and $\sum_n^{unocc}$ are the summations over the occupied and unoccupied orbitals, respectively; α, β, γ=x, y, z in cyclic order; and R and I represent the real and imaginary parts of coefficient $C_{\nu n}(k)$, respectively.

The geometry data on polyglycine and poly(L-alanine) obtained from an X-ray diffraction analysis are used, and the dihedral angles (ϕ and ψ) are listed in Table 1. The structure of the hydrogen-bonded two polypeptide chains is shown in Fig. 1. The calculation for the two chains is carried out as a function of the hydrogen-bond length, R.

In the tight-binding MO calculation, it is important to determine the number of divisions for the wave vector, k. In a previous paper[18] on the ^{13}C chemical shift for polyethylene, we obtained the results that the ^{13}C chemical shift of polyethylene converges to a definite value as the number of the divisions increases. The magnitude of the variation of ^{13}C chemical shift is smaller than 0.1 ppm if the number of divisions exceeds 20. For this reason, we chose 60 and 30 points as the number of divisions for polyglycine and poly(L-alanine), respectively.

The calculations were performed on a HITAC M200H computer in the Computer Center of Tokyo Institute of Technology and a HITAC M200H computer in the Computer Center of Institute for Molecular Science, Okazaki.

Results and Discussion

Polyglycine. First, we are dealing with an isolated polymer chain. In Table 2 are shown the calculated and observed ^{13}C chemical shifts of a polyglycine chain with forms I and II. The calculated chemical

TABLE 1. THE DIHEDRAL ANGLE USED IN THE TB MO CALCULATION FOR POLYGLYCINE AND POLY(L-ALANINE)

	Dihedral angle (degree)	
	ϕ	ψ
Polyglycine[a]		
form I	−142.0	145.0
form II	−76.0	146.0
Poly(L-alanine)[b]		
α_R-helix	−66.8	−43.7
α_L-helix	66.8	43.7
β-sheet	−138.6	134.7

a) Refs. 27 and 28. b) α_R- and α_L-helix forms indicate the right-handed and left-handed β-helix forms, respectively. (Ref. 29).

Table 2. The observed and the calculated ^{13}C chemical shifts of an isolated polyglycine chain (in ppm)

	$\delta^{a)}_{obsd}$		$\sigma^{b)}_{calcd}$	
	form I	form II	form I	form II
CH_2	43.5	43.5	−127.2	−124.4
C=O	168.4	172.3	−236.7	−248.1

a) From TMS. The positive sign means deshielding. (Refs. 5 and 12). b) The negative sign means deshielding.

shift (σ) is a nuclear shielding constant and so the negative sign means deshielding. On the other hand, the negative sign of the observed chemical shift means shielding. Therefore, the relative difference in the calculated chemical shift (σ) should be compared with the observed chemical shifts (δ). The observed carbonyl ^{13}C chemical shift for form I appears at higher field by about 4 ppm than that for form II. The calculated ^{13}C chemical shift for form I appears at higher field by about 11 ppm than that in form II, which is in parallel with the experimental finding. There is no significant difference between the methylene ^{13}C chemical shifts for forms I and II within the experimental error. In this stage, we cannot determine whether the chemical shift for form I or II appears at higher field. On the other hand, the calculated ^{13}C chemical shift for form I appears at lower field by about 3 ppm than that for form II, so the calculation predicts the existence of a chemical shift difference (about 3 ppm) between forms I and II. It appears that the calculated shifts are somewhat exaggerated as compared with the observed values. Nevertheless, the observed trend that the ^{13}C chemical shift difference for the methylene carbon is considerably small compared with that for the carbonyl carbon, is reproduced qualitatively by the calculation. Accordingly, the overall trend in the observed conformation-dependent ^{13}C chemical shift of polyglycine can be qualitatively explained by the present calculation.[34]

Up to now we have dealt with an isolated polymer chain. However, real polymer chains in the solid state interact with each other. Especially, polyglycine has the hydrogen bond in both of forms I and II.[29-30] Form I has an antiparallel β-sheet structure and each chain has a hydrogen bond with both sides of the chains in the sheet. Form II has 3_1-helix structure and each chain is intermolecularly hydrogen-bonded to six surrounding chains. Therefore, it is important to investigate the effect of the hydrogen bond on the ^{13}C chemical shift. Then, we carried out a TB MO calculation on the ^{13}C chemical shift of polyglycine for forms I and II considering the effect of the hydrogen bond. In the TB MO

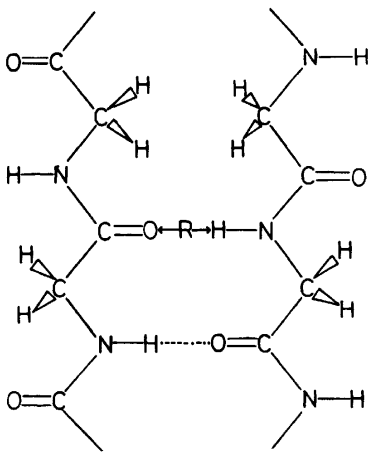

Fig. 1. The structure of two hydrogen-bonded β-sheet chains. R is the distance between oxygen and hydrogen atoms.

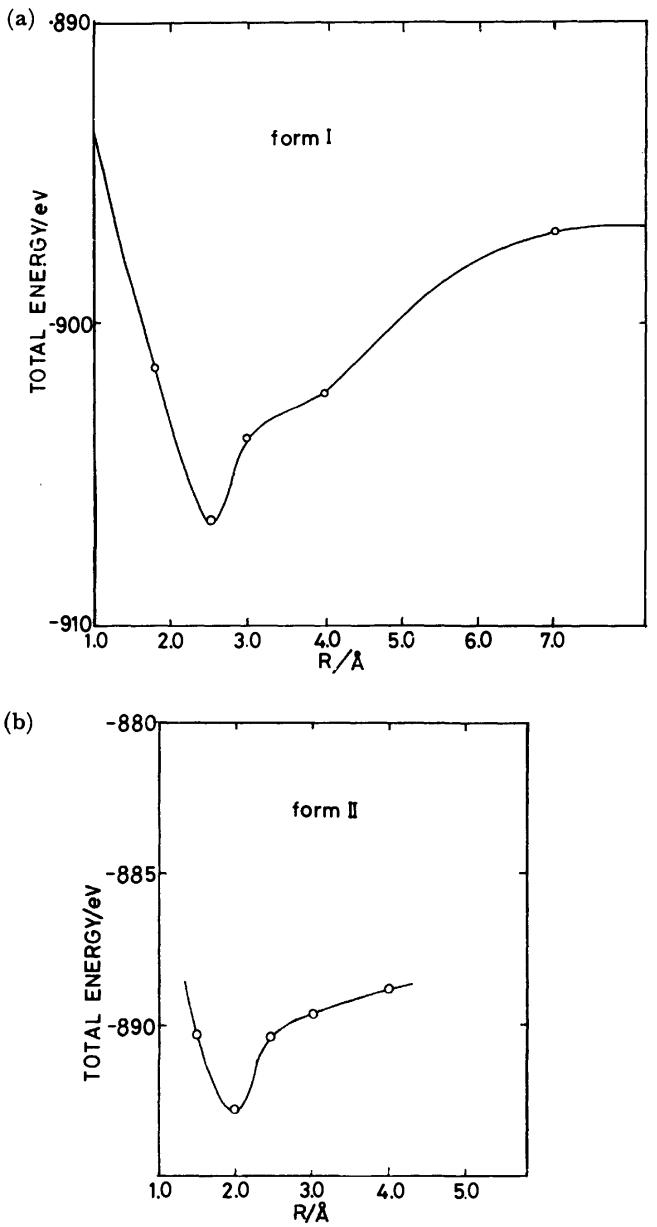

Fig. 2. The R dependence of the total electronic energy of polyglycine.
(a): form I, (b): form II.

calculation, it is not practical in this stage to treat the complete molecular structure of polyglycine in the solid state, which was determined from X-ray diffraction, because the TB MO calculation requires a very long calculation time and a large memory in the computer. Thus, instead of a real molecular structure, we will treat the two polyglycine chains which are hydrogen-bonded to each other (Fig. 1). In Fig. 1, R stands for the distance between the oxygen atom and the hydrogen atom bonded to the nitrogen atom. The TB MO calculation on the ^{13}C chemical shift was carried out as a function of R, in order to evaluate the influence of the hydrogen bond on the chemical shift. The calculation on form II was carried out in a similar manner. In Figs. 2 (a) and (b) is shown the R dependence of the total electronic energy of polyglycine in forms I and II, respectively. Obviously, form I has the energy minimum at about 2.5 A, and form II at 2.0 A. In the former the distance between the nitrogen and the oxygen atoms involved in the hydrogen bond for form I is longer than that for form II. It is known from an X-ray diffraction study that the distances between the nitrogen and oxygen atoms in forms I and II are 2.95 and 2.73 A, respectively.[30,31] Taking into account that the length of the N-H bond is 1.0 A, the above-calculated results are in parallel with the results found by X-ray diffraction: The length in form I is longer than that in form II.

Next, we will discuss the R dependence of the ^{13}C chemical shift for forms I and II. In Fig. 3(a) is shown the R dependence of the ^{13}C chemical shift of the carbonyl carbons for forms I and II. In the case of form I, for the carbonyl ^{13}C chemical shift moves downfield as R increases from 2 to 3.2 A, and upfield as R increases further from 3.2 A. In the case of form II, the carbonyl ^{13}C chemical shift moves downfield as R increases. Comparing this with the results for an isolated polymer chain, the carbonyl ^{13}C chemical shifts for both forms I and II appear largely downfield. This means that the carbonyl ^{13}C chemical shift moves largely downfield caused by the hydrogen bonding. At the minimum energy position (R=2.5 and 2.0 A for forms I and II, respectively), the carbonyl ^{13}C chemical shift for forms I and II are −274.9 and −286.2 ppm, respectively (Figs. 2 and 3). Thus, the carbonyl ^{13}C chemical shift for form I appears upperfield than that for form II, again consistent with the experimental finding. In Fig. 3(b) is shown the R dependence of the methylene ^{13}C chemical shift. The R dependence of the ^{13}C chemical shift of the methylene carbon is much smaller than that of the carbonyl carbon. Especially, the R dependence of the methylene ^{13}C chemical shift for form II is very small. This may be due to a fact that the carbonyl carbon is directly involved in the hydrogen bond, but the methylene carbon is not. In the case of form I, the methylene ^{13}C chemical shift moves to

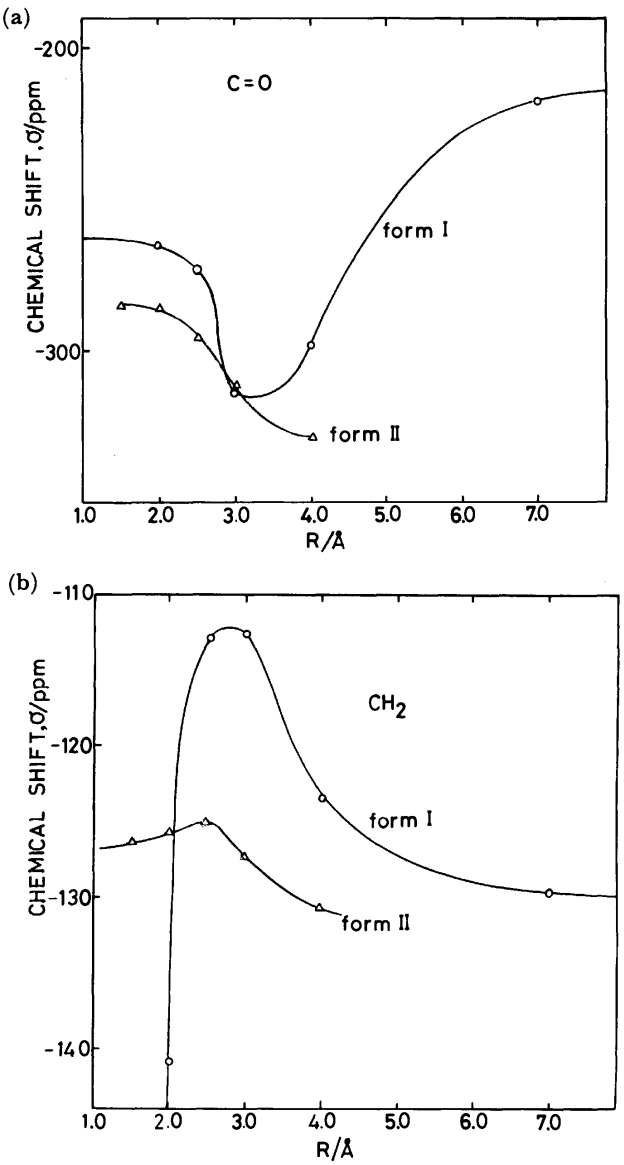

Fig. 3. The R dependence of the calculated ^{13}C NMR chemical shift of the carbonyl carbon (a) and methylene carbon (b) in polyglycine.
○: form I, △: form II.

upfield, as R increases from 2 to 2.8 A, and to downfield as R increases further from 2.8 A. In the case of form II, the ^{13}C chemical shift is similar to that of form I, but the magnitude of the change is much smaller compared with that for form I. At the minimum energy position the ^{13}C chemical shift of the methylene carbon for forms I and II are −112.9 and −126.0 ppm, respectively. Therefore it appears that the difference in ^{13}C chemical shift of the methylene carbon between forms I and II is much overemphasized. Experimentally, the ^{13}C chemical shift of the methylene carbon for form I is almost the same as that in form II. The ^{13}C chemical shift of the methylene carbon for form I changes largely in the vicinity of the energy minimum position, especially in the range of R between at 2.0

and 2.5 A. Therefore, this shows that the electronic structure of form I changes considerably in this region. As shown in Fig. 3(b), the ^{13}C chemical shift of the methylene carbon for form I moves to downfield as R decreases from the value at the energy minimum, and at the value of about 2.3 A it becomes almost equal to the ^{13}C chemical shift of the methylene carbon in form II. At this value of R, the ^{13}C chemical shift of the carbonyl carbon for form I appear at higher field than that for form II, and this result coincides with the observation. It is plausible that the R value obtained by the energy minimization of the two chains might be slightly modified by taking into account many chains in the solid state. Thus, by considering the hydrogen bond, we can reasonably explain the behavior of the ^{13}C chemical shift for forms I and II.

Poly(L-alanine) In Table 3 are shown the calculated and observed ^{13}C chemical shifts of poly(L-alanine). First, we consider the ^{13}C chemical shift of poly(L-alanine) taking the α-helix form. It is known that poly(L-alanine) has an right-handed α-helix(α_R-helix) form, but that the L-alanine residues are incorporated into the left-handed α-helix (α_L-helix) in D-alanine sequence in the random copolymers consisting of L- and D-alanines.[23] Therefore, we consider the ^{13}C chemical shifts of poly(L-alanine) in the α_R- and α_L-helix forms. We have already reported that the observed C_α and carbonyl ^{13}C chemical shifts of L-alanine residues incorporated into the α_L-helix form in the D-alanine sequence are between those in the β-sheet and α_R-forms and appears near that in the β-sheet form, while the C_β shift of the α_L-helix is close to that of the α_R-helix.[3-7] As seen from Table 3, the calculated ^{13}C chemical shifts of the C_α, C_β, and carbonyl carbons move to upfield (6.7 ppm), downfield (−1.3 ppm) and upfield(10.3 ppm), respectively, when the conformation changes from the α_R-helix to α_L-helix form. Experimentally, displacements of signals are 3.3, 0.0, 3.5, ppm for C_α, C_β, and carbonyl carbons, respectively. Therefore, the present calculation reproduces the experimental data.[34]

Next, we discuss the ^{13}C chemical shift for the β-sheet form. In the above calculation of α_R- and α_L-helix forms, we were able to include the O(=C) and H(-N)

Table 3. The observed and the calculated ^{13}C chemical shifts of an isolated poly(L-alanine) chain (in ppm)

	$\delta^{a)}_{obsd}$			$\sigma^{b)}_{calcd}$		
	α_R	α_L	β	α_R	α_L	β
$CH_3(C_\beta)$	14.9	14.9	19.9	−94.8	−96.1	−98.3
$CH(C_\alpha)$	52.4	49.1	48.2	−151.5	−144.8	−143.0
C=O	176.4	172.9	171.8	−278.1	−267.8	−245.8

a) From TMS. The positive sign means deshielding. (Refs. 3 and 7). b) The negative sign means deshielding.

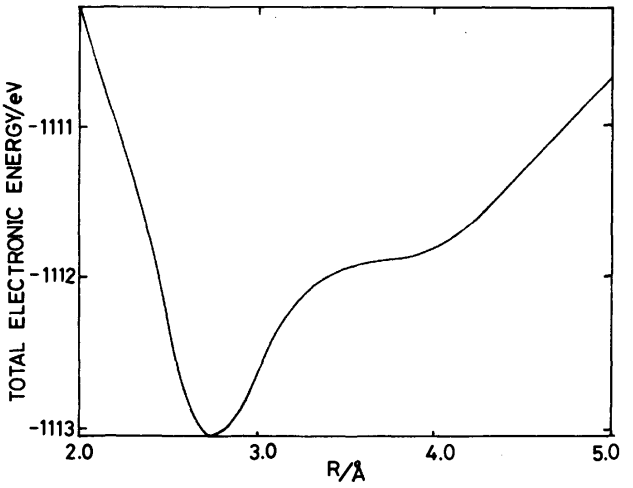

Fig. 4. The R dependence of the total electronic energy of poly(L-alanine) in the β-sheet form.

atoms making hydrogen bond without any difficulty. In the β-sheet form, where the hydrogen bonds are formed between chains, we calculated the ^{13}C chemical shift for the β-sheet form by taking into account the hydrogen bonds as a similar manner as that of polyglycine (Fig. 1). In Fig. 4 is shown the R dependence of the total electronic energy of poly(L-alanine). As seen from this figure, the energy minimum exists at R=2.75 A. From the results of an X-ray diffraction study, it is known that the distance between the nitrogen and oxygen atoms in the β-sheet form is 2.83 A.[29] If the distance between the nitrogen and hydrogen atoms is about 1.0 A, the distance between the oxygen and hydrogen atoms determined from the X-ray diffraction study is 1.83 A. The calculated results are longer than those from the X-ray diffraction, as also encountered in the calculation of forms I and II of polyglycine taking into account intermolecular hydrogen bonds. This may be due to the fact that the extended Hückel MO method is often apt to overestimate the polarity of a molecule. In Figs. 5 (a), (b), and (c) are shown the R dependences of the ^{13}C chemical shift of the C_α, C_β, and carbonyl carbons, respectively. It is shown that the ^{13}C chemical shifts of the C_α and C_β carbons moves to upfield from 2.0 to 3.6 A and downfield further from 3.6 A as R increases. On the other hand, in the case of the carbonyl carbon, the ^{13}C chemical shift moves to downfield from 2 to 3.7 A and then upfield above 3.7 A as R increases. The carbonyl carbon shows the largest R-dependence. This result agrees with the result for polyglycine. The carbonyl carbon is bonded directly to the oxygen atom by a double bond and a transfer of electrons from the carbon to the more electronegative oxygen occurs. At the energy minimum (R=2.75 A), the ^{13}C chemical shifts of the C_α, C_β, and carbonyl carbon are −144.5, −99.3, and −287.0 ppm, respectively, as seen from Fig. 5. These values of the C_α, C_β, and carbonyl carbon for the β-sheet form appear upperfield (7.0 ppm), lowerfield

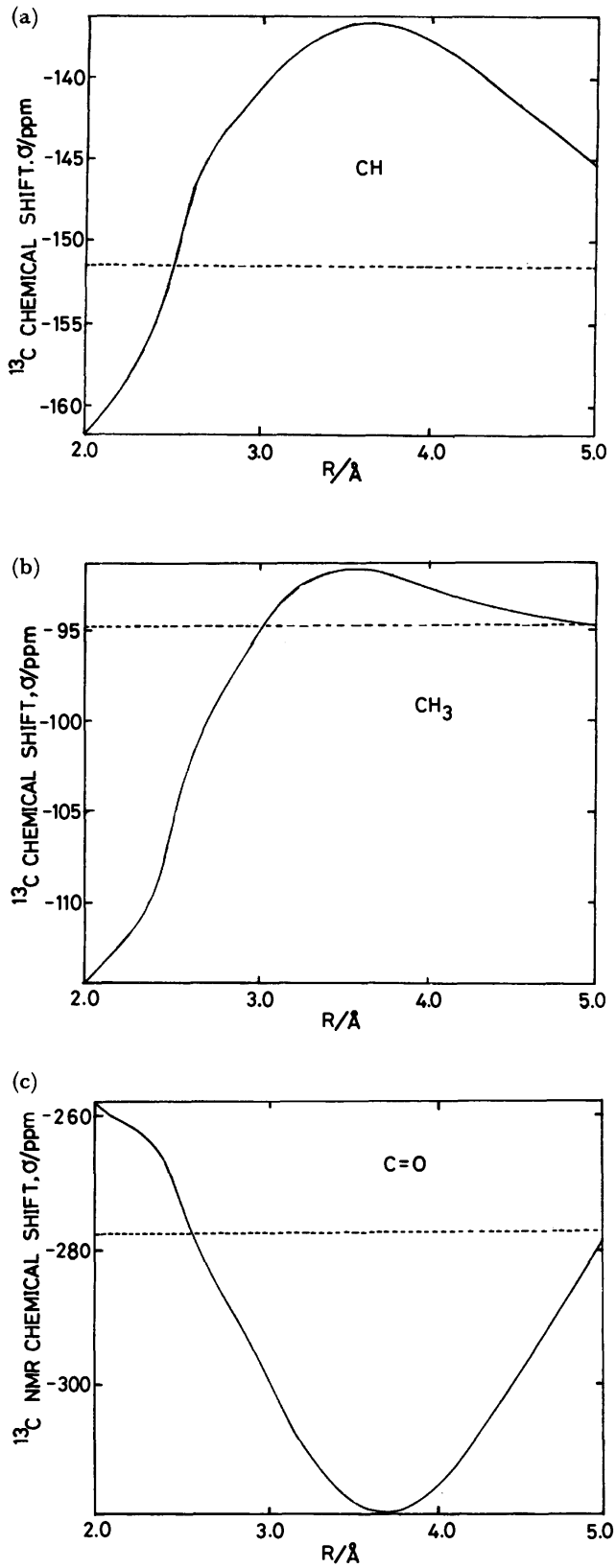

Fig. 5. The R dependence of the calculated ^{13}C NMR chemical shift of poly (L-alanine) in the β-sheet. The solid line is for two hydrogen-bonded β-sheet chains. The dashed line indicates the ^{13}C chemical shift value for an isolated α-helix chain.
(a): C_α, (b): C_β, (c): C=O.

(−4.5 ppm) and lowerfield (−8.9 ppm), respectively as compared with the shielding values of the α_R-helix form (Table 3). Experimentally, however, the ^{13}C NMR chemical shifts of the C_α, C_β, and carbonyl carbon for the β-sheet form appear upperfield (4.2 ppm), lowerfield (−5.0 ppm) and upperfield (4.6 ppm), respectively, compared with those for the α_R-helix. Therefore, it is shown that the calculated shielding constant for the carbonyl carbon at the minimum energy is not consistent with the experimental results, although the C_α and C_β chemical shifts are well reproduced. This is caused by that the carbonyl ^{13}C chemical shift is extremely sensitive to the hydrogen bond distance R. Another possibility is that the R value determined by the energy minimum should be slightly modified when many chains more than two chains are hydrogen-bonding in the real β-sheet form. Therefore, it is worthwhile to examine the "R" value which reproduces the experimental data instead of the R value at the energy minimum. For this, the ^{13}C chemical shift value for the α_R-form is indicated by the dashed line in Fig. 5. (The solid line indicates the ^{13}C chemical shift for the β-sheet form.) For the C_α, C_β, and carbonyl carbons both the lines intersect with each other at R=2.5 A, 3.0 A, and 2.56 A, respectively. Accordingly, the approximate value of R at which the calculated results are in parallel with the experimental result falls on the range of 2.5 to 2.56 A. This range is still longer than the length for the hydrogen bond determined from X-ray diffraction. Such an argument, however, arose from the use of an inadequate wavefunction such as the extended Hückel MO approximation. It is probable that this sort of problem might easily be resolved when more accurate wavefunctions such as CNDO, INDO or non-empirical theory are employed.

Nevertheless, the present calculation is very useful because the conformation-dependent ^{13}C chemical shifts in polypeptides are reproduced with some limitation. A more refined calculation using the tight-binding CNDO MO is in progress.

References

1) T. Taki, S. Yamashita, M. Satoh, A. Shibata, T. Yamashita, R. Tabeta, and H. Saitô, *Chem. Lett.*, **1981**, 1903.
2) D. Muller and H. R. Kircheldorf, *Polymer Bull.*, **6**, 101 (1981).
3) H. Saitô, R. Tabeta, A. Shoji, T. Ozaki, and I. Ando, *Macromolecules*, **16**, 1050 (1983).
4) H. Saitô, Y. Iwanaga, R. Tabeta, M. Narita, and T. Asakura, *Chem. Lett.*, **1983**, 427.
5) H. Saitô, R. Tabeta, T. Asakura, Y. Iwanaga, A. Shoji, T. Ozaki, and I. Ando, *Macromolecules*, **17**, 1405 (1984).
6) H. R. Kircheldorf and D. Muller, *Macromolecules*, **16**, 615 (1983).
7) I. Ando, H. Saitô, R. Tabeta, A. Shoji, and T. Ozaki, *Macromolecules*, **17**, 457 (1984).
8) H. R. Kircheldorf, M. Mutter, D. Muller, and H. Forster, *Biopolymers*, **22**, 1957 (1983).

9) A. Shoji, T. Ozaki, H. Saitô, R. Tabeta, and I. Ando, *Macromolecules*, **17**, 1472 (1984).
10) H. Saitô, R. Tabeta, I. Ando, T. Ozaki, and A. Shoji, *Chem. Lett.*, **1983**, 1437.
11) H. Saitô, M. Kameyama, M. Kodama, and C. Nagata, *J. Biochem.*, **92**, 233 (1982).
12) H. Saitô, R. Tabeta, A. Shoji, T. Ozaki, I. Ando, and T. Miyata, *Biopolymers*, **23**, 2279 (1984).
13) R. Ditchfield, D. P.Miller, and J. A. Pople, *J. Chem. Phys.*, **54**, 4186 (1971).
14) M. Kondo, I. Ando, R. Chûjô, and A. Nishioka, *J. Magn. Res.*, **24**, 315 (1976).
15) I. Ando and G. A. Webb, *Org. Mag. Reson.*, **15**, 111 (1981).
16) I. Ando and G. A. Webb, "Theory of NMR parameters," Academic Press, 1983.
17) K. A. K. Ebraheem and G. A. Webb, *Prog. NMR Spectroscopy*, **11**, 149 (1979).
18) T. Yamanobe, R. Chûjô, and I. Ando, *Mol. Phys.*, **50**, 1231 (1983).
19) "Electronic Structure of Polymers and Molecular Crystals," J. M. Andre and J. Ladik, Plenum Press, 1974.
20) J. M. Andre, J. Delhalle, and J. Ladik, "Quantum Theory of Polymers," ed by D. Reidel Publishing Co., 1978.
21) J. M. Andre, J. L. Bredas, J. Delhalle, J. Ladik, G. Leroy, and C. Moser, Lecture Notes in Physics 113: "Recent Advances in the Quantum Theory of polymers," Springer-Verlag, 1980.
22) A. Imamura, *J. Chem. Phys.*, **52**, 3168 (1970).
23) H. Fujita and A. Imamura, *J. Chem. Phys.*, **53**, 4555 (1970).
24) K. Morokuma, *Chem. Phys. Lett.*, **6**, 186 (1970); *J. Chem. Phys.*, **54**, 962 (1971).
25) A. Imamura and H. Fujita, *J. Chem. Phys.*, **61**, 115 (1974).
26) H. O. Pritchard and H. A. Skinner, *Trans. Faraday Soc.*, **49**, 1254 (1954).
27) L. Pauling, R. B. Corey, and H. R. Branson, *Proc. Natl. Acad. Sci. U. S. A.*, **37**, 729 (1951).
28) F. H. C. Crick and A. Rich, *Nature*, **176**, 780 (1955).
29) a) S. Arnott and A. L. Wonacott, *J. Mol. Biol.*, **21**, 371 (1966); b) S. Arnott, S. D. Dover, and A. Elliot, *J. Mol. Biol.*, **30**, 201 (1967).
30) B. Lotz, *J. Mol. Biol.*, **87**, 169 (1974).
31) G. N. Ramachandran, V. Sasisekharan, and C. Ramakrishnan, *Biochim. Biophys. Acta*, **112**, 168 (1966).
32) K. Ito, T. Nakahara, T. Shimanouchi, M. Oya, K. Uno, and Y. Iwakura, *Biopolymers*, **6**, 1759 (1968).
33) A. E. Tonelli, *J. Am. Chem. Soc.*, **102**, 7635 (1980).
34) In some conjugated aromatic compounds, it is known that there is the close relationship between the ^{13}C chemical shift and electron density on the carbon atom. However, it was found that the relationship between the conformation-dependent ^{13}C chemical shift and electron density on the C_α, C_β, and carbonyl carbon atoms does not exist.

 © 1985 The Chemical Society of Japan Bull. Chem. Soc. Jpn., 58, 30—35 (1985) [Vol. 58, No. 1

Interactions of Calcium Ions with Carbohydrates. The Crystal Structure of Calcium D-Glycero-D-gulo-heptonate Tetrahydrate

Tooru TAGA,* Taneno KAJI, and Kenji OSAKI
Faculty of Pharmaceutical Sciences, Kyoto University, Sakyo-ku, Kyoto 606
(Received June 30, 1984)

The crystal structure of the calcium salt of D-glycero-D-gulo-heptonic acid has been determined by the X-ray method. The crystal is monoclinic of space group $P2_1$ with unit-cell dimensions of a=10.064(1), b=10.540 (2), c=11.340(2) Å, and β=108.92(1)°. The intensity data for 1754 unique reflections were measured with an automatic diffractometer. A trial structure, obtained by the direct method, was refined by the full-matrix least-squares method to R=0.030. The two independent heptonate anions have different conformations, and they chelate a calcium ion in different ways. The calcium ion is surrounded by eight oxygen atoms in a deformed dodecahedral form, the Ca···O distances ranging from 2.40 Å to 2.48 Å. The distortion of the moleular strcuture of the heptonate anions due to the calcium chelation was discussed in relation to the calcium-binding sites on a linear carbohydrate chain.

The previous X-ray and NMR studies of interactions of calcium ions with carbohydrates in the solid and solution states have shown that the calcium ion is stereospecifically bound with a carbohydrate molecule and that the three-dimensional arrangement of the oxygen atoms of the carbohydrate chain is an important factor in forming a stable calcium-carbohydrate complex.[1] The geometry of the calcium-carbohydrate interactions in many crystalline complexes have been studied to date.[2] It has been reported that the C(6) carboxyl group of D-glucaric acid (II) is unlikely to interact with the calcium ion.[3-5] The carbohydrate chain of D-glycero-D-gulo-heptonic acid (I) has a relatively similar sequence to that of D-glucaric acid (II); the configurations around C(2), C(3), C(4), and C(5) in (I) correspond to the antipodal configurations around C(5), C(4), C(3), and C(2) respectively in (II). Thus the interactions of the calcium ions with the carboxylate (I) is of interest, and the X-ray analysis of the crystal structure of the title complex was undertaken. Since two crystallographically independent anions exist in the crystal structure, their molecular structures were compared in order to make clear the effect of the calcium chelation on the carbohydrate-chain structure.

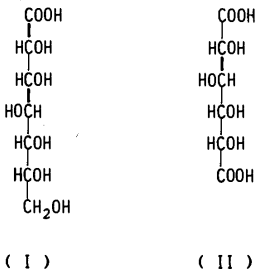

(I) (II)

Scheme 1.

Experimental

Transparent needle-like crystals were grown by evapolating an aqueous 2-propanol solution of the calcium salt of D-glycero-D-gulo-heptonic acid. The crystal data are: $Ca^{2+}[C_7H_{13}O_8^-]_2 \cdot 4H_2O$, MW=564.5, monoclinic, $P2_1$, Z=2, a=10.064(1), b=10.540(2), c=11.340(2) Å, β=108.92(1)°, and D_x=1.647 g/cm³. The space group $P2_1$ was indicated by the systematic absence of $0k0$ reflections with k odd. The unit-cell parameters were determined by a least-squares analysis of the angular settings of 22 high-angle reflections, measured on a Rigaku AFC-5 diffractometer using a graphite-monochromated Cu $K\alpha$ radiation (λ=1.54178 Å).

The intensity data were collected with the AFC-5 diffractometer operating with a RU-200 X-ray generator (40 KV, 150 mA), using a crystal with dimensions of 0.10×0.14×0.33 mm. A total of 1894 reflections were recorded in the range of $2\theta<120°$ in the $\omega-2\theta$ scanning mode with a scan speed of 4° min^{-1} in ω. The scan width was $\Delta(\omega)=0.8°+0.5\tan\theta$. The data were corrected for Lorentz and polarization factors, and then converted to the F_o structure factors. No absorption correction was applied.

The structure was solved with MULTAN78[6] using 445 reflections for phase-generation. The first E-map revealed one calcium ion and eight oxygen atoms surrounding the calcium ion. Subsequent E-map synthesized with the phases including the contributions of these atoms produced a complete non-hydrogen-atom structure. The trial structure was refined by the full-matrix least-squares method using a modified version of the ORFLS program.[7] The minimized quantity was $\sum w(|F_o|-k|F_c|)^2$, where k was the scale factor, and the weight w was equal to $1/[\sigma^2(F_o)+0.0023F_o)^2]$. All the hydrogen atoms were located from the difference Fourier maps synthesized after several cycles of the least-squares refinement optimizing the positional and anisotropic thermal parameters of the non-hydrogen atoms. The refinements including the positional and isotropic thermal parameters of the hydrogen atoms converged to R=0.030 and R_w=0.041 [$R_w=(\sum w|F_o-kF_c|^2/\sum|F_o|^2)^{1/2}$] for 1754 reflections [$F_o>3\sigma(F_o)$]. Scattering factors for Ca^{2+}, C, O, and H were obtained from the International Tables for X-ray Crystallography (1974).[8] All the computations were performed on a FACOM M-382 in the Data-processing Center of Kyoto University.

Results and Discussion

Table 1 lists the non-hydrogen-atom parameters and their estimated standard deviations. Table 2 lists the hydrogen-atom parameters and their estimated standard deviations. The bond distances and the bond

angles, and the torsion angles, for the non-hydrogen atoms are listed in Table 3 and Table 4 respectively. The anisotropic thermal parameters of the non-hydrogen atoms and the observed and calculated structure factors are preserved at the Chemical Society of Japan (Document No. 8503).

The crystal structure, stereographically illustrated in Fig. 1, is stabilized by the hydrogen bonds and the calcium-oxygen interactions. All the hydrogen atoms of the hydroxyl groups and of the water molecules participate in the hydrogen-bond network. The distances and angles for the hydrogen bonds are listed in Table 5. As is shown in Fig. 2, one calcium ion binds four heptonate anions and one water molecule. One heptonate anion chelates the calcium ion through the carboxyl oxygen O(1A) atom, together with the α-hydroxyl O(2) atom, a second anion through the O(4′) and O(5′) pair of hydroxyl groups, a third anion through the O(6) and O(7) pair of hydroxyl groups, and a fourth anion through the single carboxyl O(1B) atom. Consequently, the calcium ion is surrounded by eight oxygen atoms in a deformed dodecahedron arrangement, as is shown in Fig. 3. The Ca···O distances range from 2.40 Å to 2.48 Å. These distances are the usual distances observed in the other calcium-carbohydrate complex crystals.[9] As has been described in the Introduction, the carboxyl group of the heptonate anion was assumed to be unfavorable to the calcium binding. Actually, in the present crystal structure, the carboxyl oxygen atoms of the primed anion have no direct interactions with the calcium ion, although those of the unprimed anion are bound to the calcium ion.

Table 1. Atomic parameters for non-hydrogen atoms in Ca glucoheptonate $4H_2O$

Atom	x	y	z	B_{eq}/Å^2
CA2+	0.6039(1)	0.0 (0)	0.3985(1)	1.25(5)
C(1)	0.5431(3)	0.3072(3)	0.4248(3)	1.33(12)
C(2)	0.6755(3)	0.3151(3)	0.3860(3)	1.47(13)
C(3)	0.7990(3)	0.3696(3)	0.4920(3)	1.40(12)
C(4)	0.8023(3)	0.5132(4)	0.5134(3)	1.33(12)
C(5)	0.7982(3)	0.5895(3)	0.3980(3)	1.35(12)
C(6)	0.8011(3)	0.7316(3)	0.4222(3)	1.38(12)
C(7)	0.8293(3)	0.8070(4)	0.3183(3)	1.73(12)
O(1A)	0.4969(2)	0.1994(2)	0.4359(2)	1.83(8)
O(1B)	0.4940(2)	0.4109(2)	0.4448(2)	1.63(8)
O(2)	0.7127(2)	0.1911(2)	0.3589(2)	1.79(8)
O(3)	0.8038(2)	0.3113(2)	0.6084(2)	1.63(8)
O(4)	0.9310(2)	0.5430(2)	0.6093(2)	1.60(7)
O(5)	0.9177(2)	0.5523(3)	0.3631(2)	1.80(7)
O(6)	0.6663(2)	0.7743(2)	0.4223(2)	1.89(8)
O(7)	0.8106(2)	0.9390(2)	0.3376(2)	1.88(8)
C(1′)	0.0640(3)	1.0547(4)	0.0711(3)	2.11(12)
C(2′)	0.1561(3)	1.0968(4)	−0.0058(3)	1.90(12)
C(3′)	0.3131(3)	1.1078(4)	0.0688(3)	1.78(12)
C(4′)	0.3954(3)	0.9839(4)	0.0892(3)	1.54(13)
C(5′)	0.3376(3)	0.8809(3)	0.1528(3)	1.38(10)
C(6′)	0.4064(3)	0.7535(4)	0.1469(3)	1.54(12)
C(7′)	0.3588(4)	0.6515(4)	0.2175(3)	2.08(12)
O(1A′)	−0.0207(3)	0.9664(4)	0.0306(3)	3.60(13)
O(1B′)	0.0813(3)	1.1169(3)	0.1695(2)	2.82(10)
O(2′)	0.1353(3)	1.0216(3)	−0.1142(2)	2.95(10)
O(3′)	0.3780(3)	1.1879(3)	0.0008(3)	2.69(12)
O(4′)	0.5357(2)	1.0101(3)	0.1682(2)	1.86(7)
O(5′)	0.3689(2)	0.9215(2)	0.2801(2)	1.66(7)
O(6′)	0.3699(2)	0.7172(3)	0.0190(2)	2.03(8)
O(7′)	0.4266(3)	0.5362(3)	0.2067(2)	2.58(10)
O(W1)	0.7971(2)	1.0335(3)	0.5905(2)	2.25(9)
O(W2)	0.8261(4)	0.8726(3)	0.7854(3)	4.09(15)
O(W3)	0.7006(3)	0.9328(3)	0.0269(2)	2.38(10)
O(W4)	0.8461(3)	0.2466(4)	0.1943(3)	3.57(13)

Estimated standard deviations are given in parentheses. B_{eq} is isotropic equivalent of the anisotropic thermal parameter (Hamilton, 1959).

Table 2. Fractional coordinates and isotropic thermal parameters for hydrogen atoms in Ca glucoheptonate $4H_2O$

Atom	x	y	z	B_{iso}/Å^2
H2	0.649(4)	0.359(4)	0.317(3)	1.7(8)
HO2	0.770(5)	0.194(6)	0.314(4)	4.5(12)
H3	0.882(4)	0.345(5)	0.478(4)	2.4(8)
HO3	0.798(4)	0.229(5)	0.601(4)	3.3(10)
H4	0.721(4)	0.545(4)	0.543(4)	2.3(8)
HO4	0.913(4)	0.564(5)	0.680(4)	3.3(10)
H5	0.697(4)	0.578(4)	0.328(3)	1.4(7)
HO5	0.894(5)	0.540(6)	0.288(4)	5.0(13)
H6	0.878(4)	0.752(4)	0.501(4)	2.3(8)
HO6	0.627(5)	0.743(6)	0.468(4)	4.4(12)
H7A	0.768(4)	0.792(5)	0.249(4)	2.8(9)
H7B	0.920(4)	0.797(5)	0.308(4)	2.8(9)
HO7	0.891(4)	0.972(4)	0.357(4)	2.1(8)
H2′	0.115(4)	1.184(4)	−0.036(4)	2.3(8)
HO2′	0.132(6)	0.949(8)	−0.110(6)	6.8(16)
H3′	0.310(4)	1.148(5)	0.144(4)	2.4(8)
HO3′	0.339(4)	1.267(6)	−0.005(4)	3.5(10)
H4′	0.389(4)	0.952(5)	0.007(4)	2.3(9)
HO4′	0.585(4)	0.987(5)	0.129(4)	2.2(8)
H5′	0.234(4)	0.874(4)	0.112(3)	1.5(8)
HO5′	0.321(4)	0.891(5)	0.316(4)	2.6(9)
H6′	0.507(3)	0.761(4)	0.186(3)	0.8(7)
HO6′	0.438(4)	0.707(5)	0.004(4)	3.2(10)
H7A′	0.356(5)	0.677(6)	0.298(5)	4.6(12)
H7B′	0.250(4)	0.639(5)	0.185(4)	3.1(9)
HO7′	0.422(5)	0.484(6)	0.280(4)	4.4(12)
H(W1A)	0.874(4)	1.047(5)	0.590(4)	3.3(10)
H(W1B)	0.793(5)	0.967(6)	0.647(5)	4.7(11)
H(W2A)	0.831(5)	0.793(6)	0.786(4)	4.5(12)
H(W2B)	0.876(6)	0.901(7)	0.861(6)	6.4(15)
H(W3A)	0.795(5)	0.944(6)	0.052(4)	3.9(11)
H(W3B)	0.661(5)	0.964(6)	−0.041(4)	4.6(12)
H(W4A)	0.771(4)	0.220(5)	0.122(4)	2.6(9)
H(W4B)	0.915(5)	0.210(5)	0.179(4)	3.8(10)

A perspective drawing of the structures of the two independent heptonate anions with thermal ellipsoids of 50% probability is shown in Fig. 4. The backbone conformations of the two moieties differ from each other mainly in the torsion angles around the C(2)-C(3) bonds: the C(1)-C(2)-C(3)-C(4) torsion angle is −77.4(4)°, while the corresponding angle for the primed anion is 82.1(4)°. The conformational difference may be caused by the different intermolecular interactions around the carboxyl groups, since the calcium-oxygen interactions about the carboxyl groups differ remarkably, as has been described above. Apart from the large conformational difference about the C(2)-C(3) bonds, the bond distortions due to the calcium chelation became apparent upon comparing the corresponding bond distances and angles of the two anions (see Table 3). In particular, the C-C-O valence angles are greatly changed by the calcium chelation, and the internal C-C-O angles of the five-membered ring formed by the O-C-C-O linkage with the calcium ion are smaller than those in the absence of the calcium ion. The change in the torsion angles due to the calcium chelation is also remarkable (see Table 4). The calcium chelation tends to decrease the absolute values of the O-C-C-O torsion angles, and the O···O nonbonding distances between the adjacent hydroxyl groups are significantly shorter than the corresponding distances without calcium chelation: O(4′)···O(5′) 2.585(4) Å and O(6)···O(7) 2.636(3) Å for calcium chelation, while O(4)···O(5) 2.753(3) Å and O(6′)··· O(7′) 2.776(4) Å without calcium chelation. These O···O distances in the case of the calcium chelation are smaller than the sum of van der Waals radii (3.04 Å) and also of the ionic radii (2.80 Å) of oxygen atoms. Concerning a calcium chelation by the two hydroxyl oxygen atoms of a linear carbohydrate

TABL 3. BOND LENGTHS(l/Å) AND VALENCE ANGLES(ϕ/°) IN Ca GLUCOHEPTONATE $4H_2O$

Bond	Length	Bond	Length
C (1) - C (2)	1.535 (5)	C (1′) - C (2′)	1.530 (5)
C (1) - O (1 A)	1.249 (4)	C (1′) - O (1 A′)	1.245 (5)
C (1) - O (1 B)	1.250 (4)	C (1′) - O (1 B′)	1.257 (4)
C (2) - C (3)	1.533 (4)	C (2′) - C (3′)	1.536 (4)
C (2) - O (2)	1.420 (4)	C (2′) - O (2′)	1.420 (4)
C (3) - C (4)	1.532 (5)	C (3′) - C (4′)	1.523 (6)
C (3) - O (3)	1.443 (4)	C (3′) - O (3′)	1.435 (5)
C (4) - C (5)	1.525 (5)	C (4′) - C (5′)	1.520 (5)
C (4) - O (4)	1.430 (3)	C (4′) - O (4′)	1.433 (3)
C (5) - C (6)	1.521 (4)	C (5′) - C (6′)	1.522 (5)
C (5) - O (5)	1.437 (4)	C (5′) - O (5′)	1.439 (4)
C (6) - C (7)	1.522 (5)	C (6′) - C (7′)	1.508 (6)
C (6) - O (6)	1.430 (4)	C (6′) - O (6′)	1.428 (4)
C (7) - O (7)	1.430 (5)	C (7′) - O (7′)	1.418 (5)

Bond	Angle	Bond	Angle
C (2) - C (1) - O (1 A)	117.7 (3)	C (2′) - C (1′) - O (1 A′)	118.4 (3)
C (2) - C (1) - O (1 B)	115.8 (3)	C (2′) - C (1′) - O (1 B′)	114.8 (3)
O (1 A) - C (1) - O (1 B)	126.5 (3)	O (1 A) - C (1′) - O (1 B′)	126.8 (4)
C (1) - C (2) - C (3)	110.7 (3)	C (1′) - C (2′) - C (3′)	114.4 (3)
C (1) - C (2) - O (2)	109.0 (3)	C (1′) - C (2′) - O (2′)	112.6 (3)
C (3) - C (2) - O (2)	108.1 (2)	C (3′) - C (2′) - O (2′)	110.8 (3)
C (2) - C (3) - C (4)	117.7 (2)	C (2′) - C (3′) - C (4′)	115.5 (3)
C (2) - C (3) - O (3)	109.6 (3)	C (2′) - C (3′) - O (3′)	108.3 (3)
C (4) - C (3) - O (3)	106.5 (3)	C (4′) - C (3′) - O (3′)	105.4 (3)
C (3) - C (4) - C (5)	113.1 (3)	C (3′) - C (4′) - C (5′)	114.3 (3)
C (3) - C (4) - O (4)	107.8 (3)	C (3′) - C (4′) - O (4′)	107.9 (3)
C (5) - C (4) - O (4)	107.6 (3)	C (5′) - C (4′) - O (4′)	107.0 (3)
C (4) - C (5) - C (6)	111.8 (3)	C (4′) - C (5′) - C (6′)	111.1 (3)
C (4) - C (5) - O (5)	107.5 (2)	C (4′) - C (5′) - O (5′)	105.7 (2)
C (6) - C (5) - O (5)	110.5 (3)	C (6′) - C (5′) - O (5′)	110.6 (2)
C (5) - C (6) - C (7)	111.8 (3)	C (5′) - C (6′) - C (7′)	112.2 (3)
C (5) - C (6) - O (6)	110.3 (2)	C (5′) - C (6′) - O (6′)	108.1 (3)
C (7) - C (6) - O (6)	104.6 (2)	C (7′) - C (6′) - O (6′)	109.1 (3)
C (6) - C (7) - O (7)	108.8 (3)	C (6′) - C (7′) - O (7′)	108.7 (3)

TABLE 4. TORSION ANGLES (ϕ/°) IN Ca GLUCOHEPTONATE $4H_2O$

Bond	Angle	Bond	Angle
C(3)-C(2)-C(1)-O(1A)	−113.5(3)	C(3')-C(2')-C(1')-O(1A')	−130.7(3)
C(3)-C(2)-C(1)-O(1B)	65.0(3)	C(3')-C(2')-C(1')-O(1B')	50.7(4)
C(4)-C(3)-C(2)-C(1)	−77.4(4)	C(4')-C(3')-C(2')-C(1')	82.1(4)
C(4)-C(3)-C(2)-O(2)	163.2(3)	C(4')-C(3')-C(2')-O(2')	−46.6(4)
C(5)-C(4)-C(3)-C(2)	−56.7(3)	C(5')-C(4')-C(3')-C(2')	−56.5(4)
C(5)-C(4)-C(3)-O(3)	179.9(2)	C(5')-C(4')-C(3')-O(3')	−176.1(2)
C(6)-C(5)-C(4)-C(3)	179.8(2)	C(6')-C(5')-C(4')-C(3')	168.8(2)
C(6)-C(5)-C(4)-O(4)	−61.3(3)	C(6')-C(5')-C(4')-O(4')	−71.9(3)
C(7)-C(6)-C(5)-C(4)	167.5(2)	C(7')-C(6')-C(5')-C(4')	175.8(2)
C(7)-C(6)-C(5)-O(5)	47.9(3)	C(7')-C(6')-C(5')-O(5')	58.8(2)
O(2)-C(2)-C(1)-O(1A)	5.3(3)	O(2')-C(2')-C(1')-O(1A')	−2.9(4)
O(2)-C(2)-C(1)-O(1B)	−176.2(2)	O(2')-C(2')-C(1')-O(1B')	178.5(2)
O(3)-C(3)-C(2)-C(1)	44.4(3)	O(3')-C(3')-C(2')-C(1')	−160.0(3)
O(3)-C(3)-C(2)-O(2)	−75.0(3)	O(3')-C(3')-C(2')-O(2')	71.4(4)
O(4)-C(4)-C(3)-C(2)	−175.5(3)	O(4')-C(4')-C(3')-C(2')	−175.4(3)
O(4)-C(4)-C(3)-O(3)	61.0(3)	O(4')-C(4')-C(3')-O(3')	65.1(3)
O(5)-C(5)-C(4)-C(3)	−58.9(2)	O(5')-C(5')-C(4')-C(3')	−71.2(3)
O(5)-C(5)-C(4)-O(4)	60.1(3)	O(5')-C(5')-C(4')-O(4')	48.1(3)
O(6)-C(6)-C(5)-C(4)	−76.6(2)	O(6')-C(6')-C(5')-C(4')	−63.9(3)
O(6)-C(6)-C(5)-O(5)	163.8(2)	O(6')-C(6')-C(5')-O(5')	179.1(2)
O(7)-C(7)-C(6)-C(5)	171.8(1)	O(7')-C(7')-C(6')-C(5')	179.6(2)
O(7)-C(7)-C(6)-O(6)	52.4(2)	O(7')-C(7')-C(6')-O(6')	59.9(2)

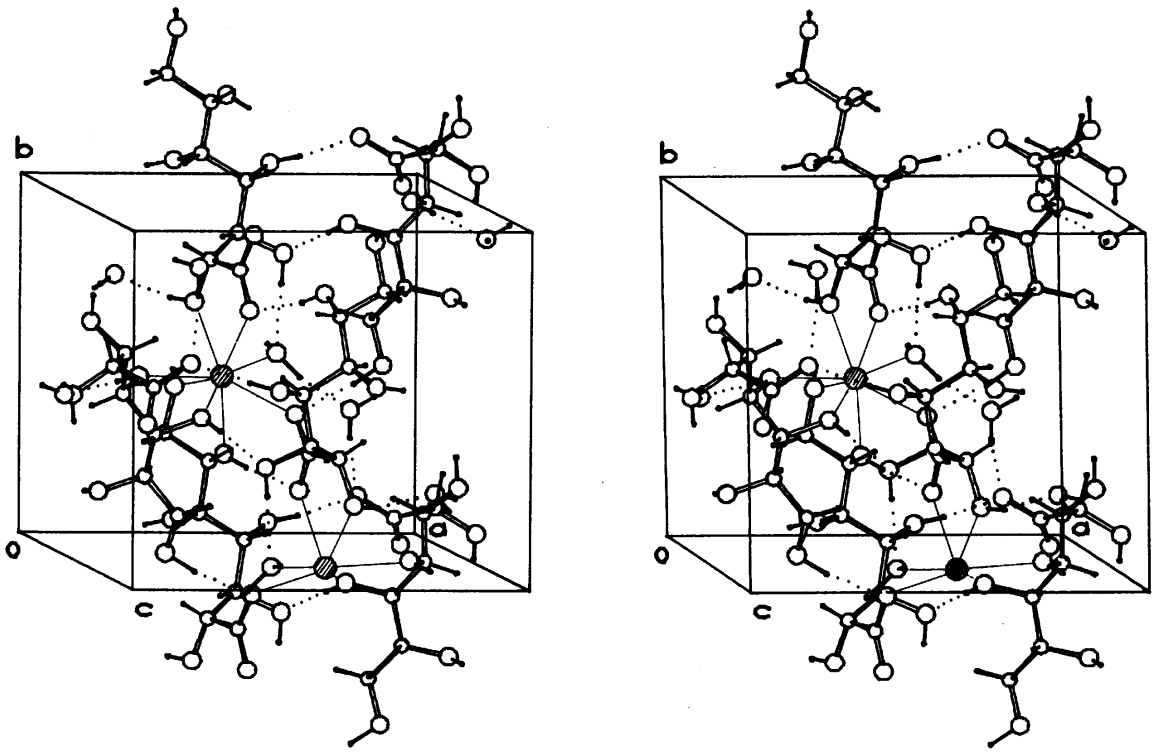

Fig. 1. Stereo view of the unit cell viewed approximately down the *c* axis. Thin and broken lines represent Ca···O interactions and hydrogen-bonds, respectively.

TABLE 5. HYDROGEN-BOND GEOMETRY

	Symmetry operation	O···O	H···O	H-O···O
O (2) -HO2···O (W4)		2.693 (5) Å	1.84 (6) Å	14 (3) °
O (3) -HO3···O (W1)	i	2.934 (4)	2.07 (5)	2 (2)
O (4) -HO4···O (1B')	ii	2.667 (4)	1.77 (5)	9 (2)
O (5) -HO5···O (2')	iii	2.717 (3)	1.91 (5)	6 (3)
O (6) -HO6···O (1A)	iv	2.760 (3)	1.96 (6)	9 (3)
O (7) -HO7···O (4)	v	2.704 (3)	1.87 (4)	2 (3)
O (2') -HO2'···O (W4)	vi	3.061 (5)	2.38 (8)	23 (5)
O (3') -HO3'···O (W3)	vi	2.688 (4)	1.79 (6)	9 (3)
O (4') -HO4'···O (W3)		2.777 (4)	1.97 (5)	2 (3)
O (5') -HO5'···O (3)	iv	2.719 (3)	1.93 (5)	3 (3)
O (6') -HO6'···O (3')	iii	2.637 (4)	1.89 (5)	8 (3)
O (7') -HO7'···O (1B)		2.882 (3)	1.94 (5)	16 (2)
O (W1) -H (W1A) ···O (5)	v	2.752 (3)	1.99 (4)	13 (3)
O (W1) -H (W1B) ···O (W2)		2.725 (4)	1.79 (6)	12 (3)
O (W2) -H (W2A) ···O (1B')	ii	2.843 (4)	2.05 (6)	16 (3)
O (W2) -H (W2B) ···O (1A')	vii	2.882 (4)	1.99 (6)	2 (4)
O (W3) -H (W3A) ···O (1A')	viii	2.814 (4)	1.96 (5)	17 (3)
O (W3) -H (W3B) ···O (7')	vi	2.765 (3)	1.96 (5)	2 (4)
O (W4) -H (W4A) ···O (6')	iii	2.695 (3)	1.76 (3)	10 (3)
O (W4) -H (W4B) ···O (1B')	ix	2.825 (5)	1.97 (5)	6 (4)

i	$+x, -1+y, +z$	iv	$1-x, 1/2+y, 1-z$	vii	$1+x, +y, 1+z$
ii	$1-x, 1/2+y, 1-z$	v	$2-x, 1/2+y, 1-z$	viii	$1+x, +y, +z$
iii	$1-x, -1/2+y, -z$	vi	$1-x, 1/2+y, -z$	ix	$1+x, -1+y, +z$

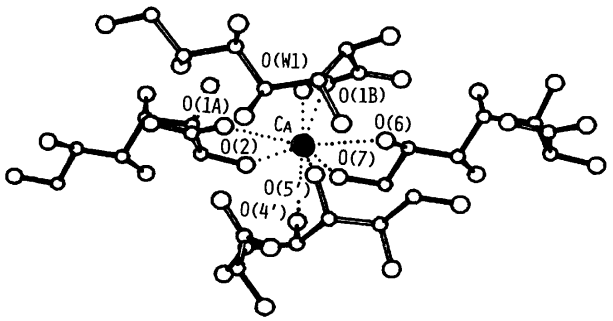

Fig. 2. Representation of the environment of the calcium ion.

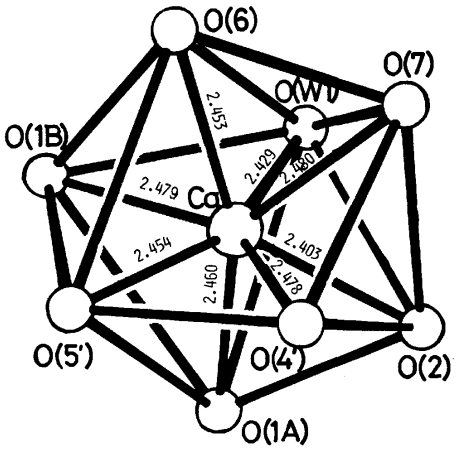

Fig. 3. Calcium-ion coordination shell.
Estimated standard deviations are 0.003 Å for the Ca···O distances.

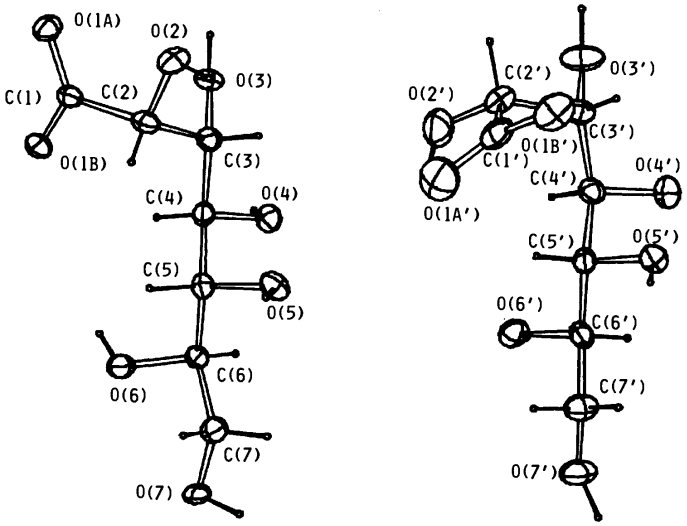

Fig. 4. Comparison of the molecular conformations of the two heptonate anions.

chain, it seems possible for four stable gauche conformations, represented as A1, A2, B1, and B2, to chelate a calcium ion. From a consideration of the bond distortions due to the calcium chelation described above, the B conformations are, however, unfavorable to the calcium chelation, because the calcium binding to B1 and B2 will decrease the absolute values of the O-C-C-O and C-C-C-C torsion angles and result in energetically unfavorable backbone conformations. On the other hand, the effects

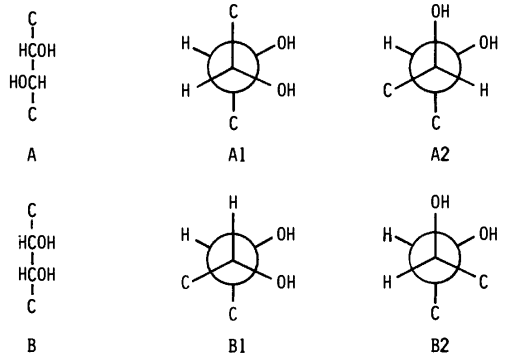

Scheme 2.

of such bond distortions on the A conformers are small. For A2, a decrease in the absolute O-C-C-O torsion angle accompanies the increase in the absolute C-C-C-C torsion angle. The calcium chelation through the O(4′) and O(5′) atoms in the present crystal corresponds to Al. To our knowlege, there are no calcium chelation by the B conformations in the reported crystal structures of the calcium linear-carbohydrate complexes.[10-12] In conclusion, the calcium chelation by the two hydroxyl oxygen atoms decreases the absolute value of the O-C-C-O torsion angle; this fact indicates that, in general, the calcium chelation by the linear carbohydrate chain occurs selectively at the site of the configuration A in which the two hydoxyl groups are located on opposite sides of the carbon chain in the Fischer notation.

References

1) S. L. Angyal, *Chem. Soc. Rev.*, **9**, 415 (1980).
2) H. Einspahr and C. E. Bugg, *Acta Crystallogr.*, **37**, 1044 (1981).
3) T. Taga and K. Osaki, *Bull. Chem. Soc. Jpn.*, **49**, 1517 (1976).
4) T. Taga, Y. Kuroda, and K. Osaki, *Bull. Chem. Soc. Jpn.*, **50**, 3079 (1977).
5) T. Taga, Y. Kuroda, and M. Ohashi, *Bull. Chem. Soc. Jpn.*, **51**, 2278 (1978).
6) P. Main, S. E. Hull, L. Lessinger, G. Germain, J.-P. Declercq, and M. M. Woolfson, "MULTAN 78. A System of Computer Programmes for the Automatic Solution of Crystal Structures from X-ray Diffraction Date," Universities of York and Louvain (1978).
7) W. R. Busing, K. O. Martin, and H. A. Levy, ORFLS. Report ORNL-TM-305, Oak Ridge National Laboratory, Tennessee (1962).
8) International Tables for X-ray Crystallography, Vol. IV, Birmingham, Kynoch Press (1974), pp. 71—151.
9) T. Taga, M. Ohashi, and K. Osaki, *Bull. Chem. Soc. Jpn.*, **51**, 1697 (1978).
10) S. Furberg and S. Helland, *Acta Chem. Scand.*, **16**, 2373 (1962).
11) R. Norrestam, P.-E. Werner, and M. Glehn, *Acta Chem. Scand.*, **22**, 1395 (1968).
12) W. J. Cook and C. E. Bugg, Acta Crystallogr., Sect. B., **29**, 215 (1973).

Excess Volume of Mixing of Quaternary Phosphonium Chlorides with Potassium Chloride in Water

Katsuko TAKAIZUMI* and Toshiki WAKABAYASHI
The College of General Education, Tohoku University, Kawauchi, Sendai 980
(Received July 2, 1984)

Volume changes upon mixing aqueous solutions of potassium chloride and the quaternary phosphonium chloride, n-$Bu_{4-n}Ph_nPCl$, (n=0—4), have been measured at various constant total ionic strengths (I=0.25, 0.5, 1.0) at 25 °C. Based on Friedman's theory for a mixed electrolyte solution, volume-interaction parameters, v_o, were determined at each ionic strength. The dependence of v_o on I shows that contributions to the excess volume due to structural effects of a pairwise interaction between the cations and triplet interactions including a single anion are most significant for the Bu_4P^+ ion and decrease with increasing n. A comparison of the v_o's with the excess-volume properties of the salts in each pure solution shows that the interaction between the phosphonium cations and the potassium ion results in negative contributions to the excess volume of mixing, which also decreases as n increases.

Measurements regarding the excess thermodynamic properties of aqueous mixed-electrolyte solutions have provided useful information on specific interactions between ions in solution.[1] Information on pairwise interactions between like-charged ions can be obtained by examining the mixing process of two kinds of electrolyte solutions containing a common counterion at constant ionic strength. Effects due to both the ionic atmosphere and oppositely charged ions are kept constant during the mixing process.

Wen and his associates[2,3] studied the excess volumes of mixing Δ_mV^E in the systems, tetraalkylammonium halides (R_4NX) and potassium halides, applying Friedman's theory[4] for mixed-electrolyte solutions. They found that the hydrophobic interactions between tetraalkylammonium ions are the major factors regarding the nonideal behavior of the mixtures in the case of R=propyl and butyl. They confirmed this conclusion by means of a more complete characterization of the hydrophobically induced cation-cation interaction.[5] They also suggested that cationic interactions between these R_4N^+ and K^+ ions gave positive contributions to Δ_mV^E.

In previous papers,[6,7] we determined the volume B-coefficients(B_v) for the quaternary phosphonium salts, n-$Bu_{4-n}Ph_nPX$, and concluded that the B_v's, which are all negative, reflect mainly the effects resulting from the cation-cation interactions. The time-averaged clathratelike hydration model seemed to be plausible for the butyl groups but not for the phenyl groups. Further, the B_v's were decomposed into contributions arising from the butyl-butyl, phenyl-phenyl, and butyl-phenyl interactions.

In this study, we carried out measurements to determine the excess volumes upon mixing quaternary phosphonium chloride with potassium chloride at constant ionic strength.

Experimental

Materials and Apparatus. The five quaternary phosphonium salts(n=0—4) were obtained and purified as previously reported.[8] The potassium chloride delivered from Merck(Suprapur) was used without further purification.

Volume changes upon mixing were measured using Hashitani's cells,[9] with some modification (Fig. 1). The cells(quartz) have a total capacity of *ca.* 60 cm^3. Each cell is divided into two rooms by a disk with a mirror surface. The room capacities were calibrated five times using conductivity water with a standard deviation of 0.004 cm^3. The capillary tubing attached at the top of the cap(Pyrex glass) had an inner diameter of *ca.* 0.6 mm with a minimum graduation of 0.0005 cm^3. This was calibrated using mercury. The inside of the capillary was coated with sillicon grease as previously reported.[10] Leakage of the solution through the disk separator was checked spectrophotometrically using a set of solutions, pure water(upper room) and a dye solution (lower room). No leakage was found.

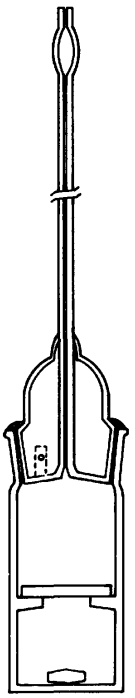

Fig. 1. The cell for measurering Δ_mV^E.

Measurements of $\Delta_m V^E$. Throughout the following procedures, the cells were kept in a water bath (25±0.003 °C). The two solutions, which had been degassed and equilibrated to the bath temperature, were introduced stepwise into each separated room. The cap was fixed with Decotinsky cement after adjusting the meniscus height in the capillary. The cell was thoroughly immersed in the bath and the equilibrium meniscus-height(initial volume) was read with a precision of 1×10^{-4} cm^3. Then, the disk separator was shifted by turning the cell upside down, the contents were thoroughly mixed by a magnetic stirrer, and the final meniscus-height(final volume) was measured.

Generally, for every mixing system, the measurements were carried out for more than ten of volume ratios and at ionic strengths of 0.25, 0.5, and 1.0 (mol kg^{-1}). The volume changes of mixing ranged from 0.002 to 0.03 cm^3.

Results and Discussion

The Friedman's theory for mixed electrolytes[4] leads to an expression for the excess volume of mixing two electrolyte solutions of identical ionic strength I as;

$$\Delta_m V^E/W = I^2 y(1-y)[v_o + (2y-1)v_1], \quad (1)$$

where W is the weight(kg) of the solvent water and y the mole ratio of one electrolyte to the total electrolytes and $v_0, v_1, ..$, are the volume-interaction parameters. The quantity of lhs. of Eq. 1 is the excess volume of mixing per kg of solvent and is related to the experimental data through the equation

$$\Delta_m V^E/W = mV_\phi(\text{mixture}) - ymV_\phi(\text{AX}) - (1-y)mV_\phi(\text{BX}) \quad (2)$$

where V_ϕ(MX) is apparent molar volume of MX in its pure solution, m the molality(equal to I in the present systems) and X, a common anion. The interaction parameters may be expressed as[11]

$$v_o = v_{\text{pairs}} + Iv_{\text{triplets}},\ v_1 = Iv^1_{\text{triplets}} \quad (3)$$

$$v_{\text{pairs}} = 2v^*_{AB} - v^*_{AA} - v^*_{BB}\cdots, \quad (4)$$

where v_{pairs} is the contribution to the excess volume of mixing from pairwise interactions between cations and v_{triplets} is the contribution from the triplet interactions of the cation-cation-anion type and; v^1_{triplets} is the contribution from the other types of triplet interactions. The v^*_{ij}'s are functions of ionic strength. In this paper, subscripts A and B stand for the phosphonium cation and the potassium ion, respectively. As employed by Wen and Nara,[3] the difference of excess volumes of two separate solutions, v^*, at an identical ionic strength I can be expressed by,

$$v^* = [V^E(\text{BX}) - V^E(\text{AX})]/I^2 = v^*_{BB} + 2v^*_{BX} - v^*_{AA} - 2v^*_{AX}\cdots \quad (5)$$

The excess volume can be written in the form,

$$V^E(\text{MX}) = m(V_\phi - \overline{V}^\circ) = m(A_v m^{1/2} + B_v m + C_v m^2 + \cdots) \quad (6)$$

where $\overline{V}^\circ$ is the standard partial molar volume of MX, and A_v is the Debye-Hückel limiting slope and; B_v, C_v,.. are empirical parameters. Combining Eq. 6 with Eq. 5, we obtain the relation,

$$v^* = B_v(\text{BX}) - B_v(\text{AX}) + I[C_v(\text{BX}) - C_v(\text{AX})]\cdots \quad (7)$$

In Fig. 2, the volume changes of mixing per kg of solvent water are plotted against the mole ratio of the phosphonium salt, y, at three ionic strengths and 25 °C. The height of a curve at y=0.5 gives v_o and the skewness is governed by v_1 (Eq. 1). As the ionic strength decreases, the skewness becomes less, and almost disappears at the lowest ionic strength, 0.25 mol kg^{-1}, for all systems examined. The values for the volume-interaction parameter v_o (Eq. 1) were determined from $\Delta_m V^E$ by a least-squares method based on Eq. 1 and are tabulated in Table 1, along with the B_v's.[6,7] Figure 3 is a plot of the v_o against the ionic strength, where the systems Me_4NBr/KBr and Bu_4NCl/KCl[2] are also shown, for comparison.

In general, two effects may be accompanied by the mixing process. One is the dilution effect for ions, which will result in a decrease in cosphere overlapping between the phosphonium cations as well as other ions. This effect for the salt AX at low concentrations is approximately expressed by the volume B-coefficient with a negative sign, $-B_v$(AX). Another is the effect due to the occurrence of a new type of cationic interaction pair, that is, the phosphonium cation and the K^+ ion, which is expressed by v^*_{AB} (Eq. 4).

As seen from Eqs. 3 and 4, the v_o value at I=0 reflects cationic pairwise interactions only. However, to experimentally determine $v_o(I=0)$ is very difficult because

Table 1. Volume interaction parameter v_o(Eq. 3) and v^*(Eq. 5)[a]

	Bu_4PCl		Bu_3PhPCl		Bu_2Ph_2PCl		$BuPh_3PCl$		Ph_4PCl	
I	v_o	v^*	v_o	v^*	v_o	v^*	v_o	v^*	v_o	v^*
0.25	6.7	13.3	4.4	8.5	3.4	6.6	3.1	5.3	2.8	5.3
0.5	5.0	10.7	2.7	7.0	2.1	5.6	2.0	4.8	1.8	4.8
1.0	2.3	7.2	1.2	4.9	1.1	4.2	1.0	3.9	1.0	4.0
B_v[b]	−16.71		−10.52		−7.87		−5.81		−5.77	

a) Units; v_o and v^*/cm^3 kg mol^{-2}, B_v/cm^3 dm^3 mol^{-2}. b) Ref. 6 and 7.

$\Delta_m V^E$ is proportional to the square of the ionic strength (Eq. 1). The curves in Fig. 3 suggest large positive values for $v_o(I=0)$, showing that the pairwise interactions are large for all the systems ($n=0$—4). If the assumption is made that the activity coefficients of the ions are constant independent of ionic strength, then we can expect a linear relation between v_o and I, as discussed by Wen[11] (*cf.* Eq. 3). Since the dependence of the activity coefficient of ions on ionic strength decreases with increasing I, we can conclude that the successive substitution of phenyl groups of the Ph_4P^+

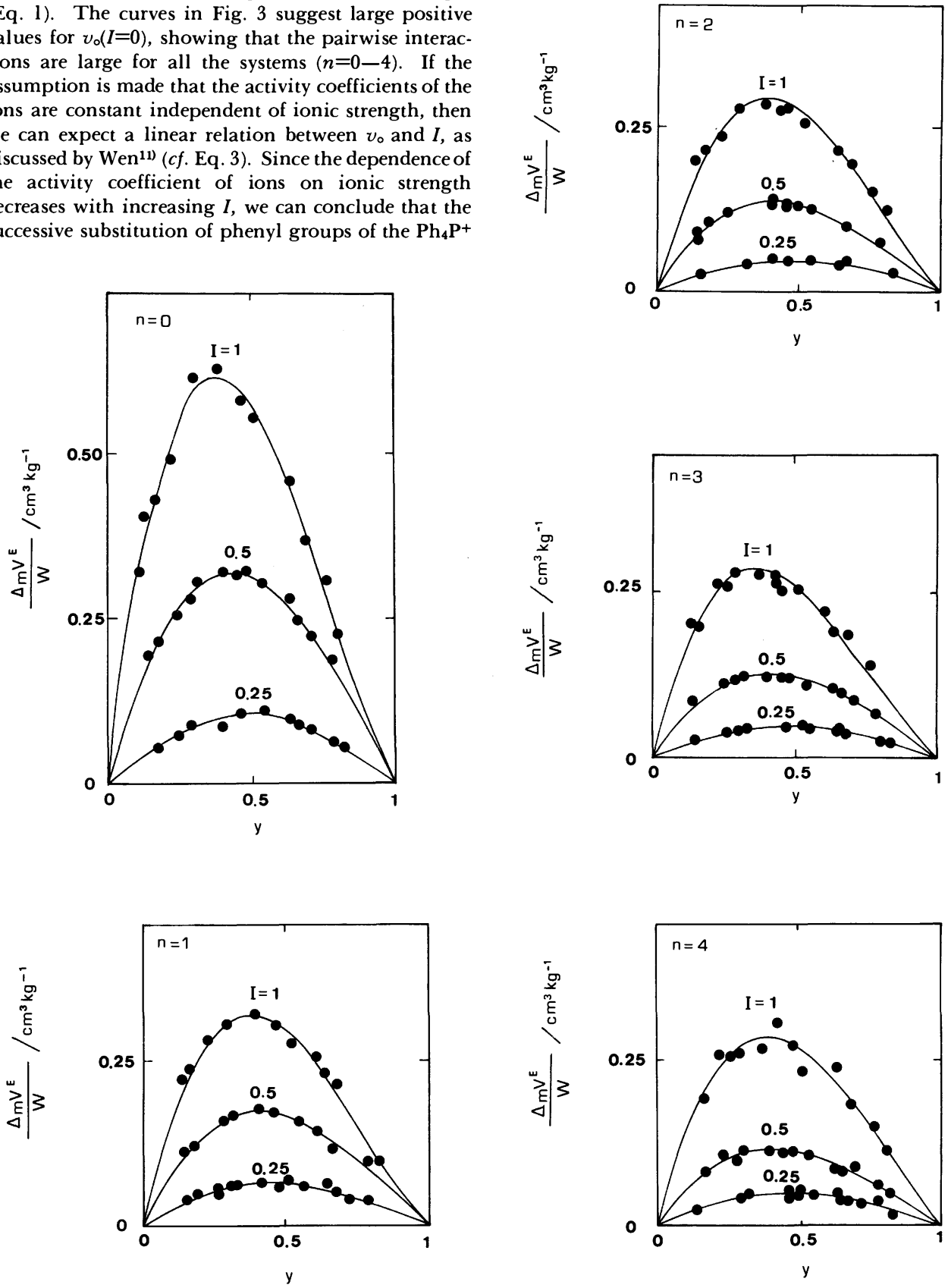

Fig. 2. The volume changes on mixing per kg of solvent water as functions of the mole ratio (y) of phosphonium chloride in the system, n-$Bu_{4-n}Ph_nPCl$/KCl ($n=0$—4), at 25 °C.

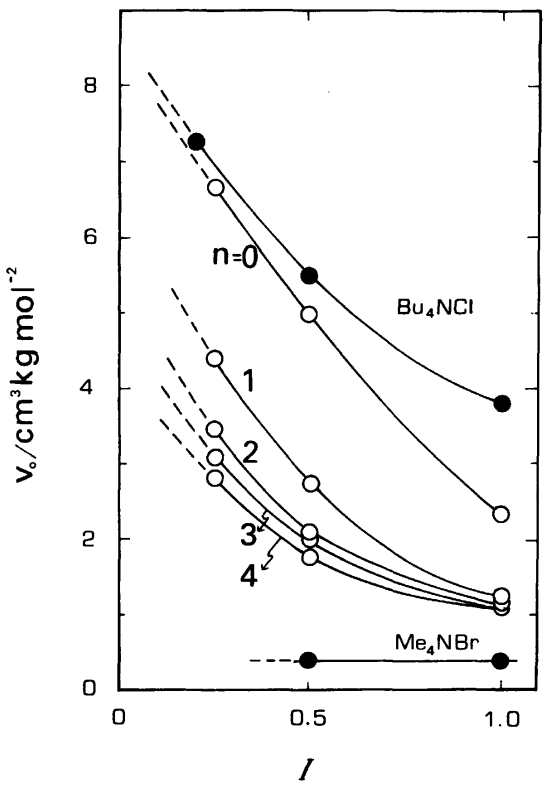

Fig. 3. The volume interaction paramenters v_o(-○-) in the systems, $Bu_{4-n}Ph_nPCl/KCl$ (n=0—4), as functions of ionic strength I, at 25 °C. The data for the systems Bu_4NCl/KCl and Me_4NBr/KBr, (-●-), were taken from Ref.2.

ion by butyl groups results in elevating the triplet and higher order interactions. This is illustrated in Fig. 3 and seems to be consistent with the clathrate-like hydration model for a butyl group assumed in previous studies.[6,7] The remarkable decrease in $V_o(Bu_4PX)$ with concentration was attributed to pairwise interaction between the cations in low concentrations and higher order interactions including the anions at high concentrations in which water-separated pairing of the cations was regarded as essential to reduce the solution volume.

It was shown in previous papers that the B_v's are negative for all the phosphonium halides (n=0—4) and mainly reflect contributions from the cation-cation interactions, that is, v_{AX}* in Eq. 5 would be relatively much smaller in magnitude than v_{AA}*. The small B_v value for KCl, 0.08 cm^3 mol^{-2} dm^3 [12], suggests that v_{BB}*+2v_{BX}* (Eq. 5) would be negligible in comparison with the large magnitudes of v_{AA}* for the phosphonium cations. A comparison of v_o's with v*'s (Table 1) reveals that all the v_o values are considerably smaller than the v* values, about halves of v*'s, even at the ionic strength of 0.25 where the v* values for all the systems are close to the magnitudes of B_v(AX)'s (*cf.* Eq. 7). Thus, it follows that the interactions between unlike cations (v_{AB}*) are mostly responsible for the differences between the magnitudes of v_{pairs} and v*. This difference is largest for a system with n=0 and decreases with n, indicating that the butyl cosphere-K^+ interaction results in decrease in solution volume.

This conclusion is contradictory to a suggestion made by Wen,[11] who attributed the difference found for the n-Bu_4NCl-KCl system to the Bu_4N^+-Cl^- interaction.

The second hydration layer, the B-zone in the Frank and Wen's hydration model, of the Bu_4P^+ ion would be more structured and, hence, more bulky than bulk water, as illustrated by a Monte Carlo simulation for a methane molecule in water.[13] Thus, the negative change in volume accompanied by the butyl-K^+ interaction is explicable if the assumption is made that the K^+ ion breaks the second layer structure of the butyl cosphere but not the first layer; if the K^+ ion breaks also the first layer a volume increase should be accompanied owing to disappearence of the caging effect,[11] which is assumed for clathrate-like hydration.

It is of interest to note that the interaction between the Ph_4P^+ and K^+ ions also contributes negatively to the solution volume, *i.e.*, v_{AB}*<0, even though the Ph_4P^+ ion behaves not always as a structure maker for solvent water[10] and its hydration dissimilar to clathrate-like one is assigned. In this regard, the Geiger's hydration model is of interest. Geiger[14] has simulated the effect of charges on the hydration of a nonpolar spherical solute with the size of a Xenon atom by the molecular dynamic technique. He obtained the result that the originally rigid hydrophobic hydration shell (zero charge) is "softened" from its inner sphere and its outer sphere remains more or less unchanged when electric charges below unit are given. If the delocalized charges on the phenyl groups[15,16] play a role in a way similar to this model, the water molecules in the B-zone of the groups would be more structured than bulk water and, hence, the interaction between the B-zone and the K^+ ion could result in a negative contribution to the solution volume due to a relaxing of the structured water in the B-zone to the bulk water.

For intermediate systems with n=1—3, the behavior found in v_{AB}* can be understood qualitatively as the sum of the effects found in the systems with n=0 and 4.

References

1) H. L. Anderson and R. H. Wood, "Thermodynamics of Aqueous Mixed Electrolytes," in "Water: A Comprehensive Treatise," ed by F. Franks, Plenum Press(1973), Vol. 3, Chap. 2, pp. 119—143.

2) W. Y. Wen and K. Nara, *J. Phys. Chem.*, **71**, 3907 (1967); W. Y. Wen, K. Nara, and R. H. Wood, *J. Phys. Chem.*, **72**, 3048 (1968).

3) W. Y. Wen and K. Nara, *J. Chem. Phys.*, **72**, 1137 (1968).

4) H. L. Friedman, *J. Chem. Phys.*, **32**, 1134 (1960); H. L. Friedman, "Ionic Solution Theory," Interscience, New York (1962).

5) W. Y. Wen, K. Miyajima, and A. Otsuka, *J. Phys. Chem.*, **75**, 2148 (1971).

6) T. Wakabayashi and K. Takaizumi, *J. Solution Chem.*, **11**, 565 (1982).
7) K. Takaizumi and T. Wakabayashi, *Bull. Chem. Soc. Jpn.*, **56**, 1896 (1983).
8) K. Takaizumi and T. Wakabayashi, *J. Solution Chem.*, **9**, 809 (1980).
9) T. Hashitani, *Bulletin of the Faculty of General Education, Tokyo University of Agriculture and Technology*, Vol. **14**, 84 (1978).
10) K. Takaizumi and T. Wakabayashi, *Bull. Chem. Soc. Jpn.*, **49**, 2194 (1976).
11) W. Y. Wen, "Aqueous Solutions of Symmetrical Tetraalkyl-ammonium Salts," in "Water and Aqueous Solutions," ed by R. A. Horne, Wiley-Interscience, (1971), Chap. 15, pp. 613—661.
12) F. H. Spedding, M. J. Pikal, and B. O. Ayers, *J. Phys. Chem.*, **70**, 2440 (1966).
13) M. Mezei and D. L. Beveridge, *J. Chem. Phys.*, **74**, 622 (1981).
14) A. Geiger, *Ber. Bunsenges. Phys. Chem.*, **85**, 52 (1981).
15) S. O. Gim and W. McFarlane, *Can. J. Chem.*, **46**, 2071 (1968).
16) E. Grunwald and G. Kohnstam, *J. Am. Chem. Soc.*, **82**, 5801 (1960).

 © 1985 The Chemical Society of Japan Bull. Chem. Soc. Jpn., 58, 41—46 (1985)

Delayed Fluorescence in Mixed Crystals Due to the Direct Resonance Interaction, as Revealed by Excitation Duration and Intensity Effects on the Decay Behavior

Shoji TAEN* and Yasuhiko GONDO

Department of Chemistry, Faculty of Science, Kyushu University 33, Hakozaki, Higashiku, Fukuoka 812

(Received July 6, 1984)

The decay of the temperature-independent delayed fluorescence observed in the mixed crystals of phenanthrene in the biphenyl host has been studied at 77 K. That triplet molecules are involved in the mechanism for the emission of temperature-independent delayed fluorescence has been shown by observing the intensities at the instances of the short-pulse excitations effected with different dark periods after the steady-state excitation. It has been found that both the excitation duration and the excitation light intensity affect the decay behavior of the temperature-independent delayed fluorescence. The decay after short-pulse excitation has been observed to be more rapid than the decay after prolonged excitation with the same intensity. When the excitation light intensity is increased with a fixed duration, the delayed fluorescence is observed to decay more rapidly. It is concluded that the decay behavior of the temperature-independent delayed fluorescence can be accounted for in terms of the direct-resonance-interaction mechanism.

The delayed fluorescence (DF) of organic compounds has attracted the attention of many investigators,[1] and different aspects of it, such as the temperature dependence,[2-6] the magnetic-field effect,[7-10] and the caging effect,[11] have been studied. Accordingly, the nature of DF is fairly well understood, and DF is now an important probe for studying excited states. For example, the singlet-triplet (S-T) absorption spectrum can be determined by measuring the DF excitation spectrum,[12] and the Davydov splitting in a certain CT molecular crystal was measured from the doublet DF-ODMR (optically detected magnetic resonance) signals.[13] However, some aspects of DF are still not understood. The existence of temperature-independent delayed fluorescence (TIDF) in organic mixed crystals, in addition to the usual temperature-dependent delayed fluorescence (TDDF), has been reported by several investigators.[3b,5,14,15] The mechanism for TDDF is ascribed to the triplet-triplet (T-T) annihilation between a thermally produced triplet exciton and a guest triplet state.[2-6] As for the mechanism for TIDF, though several possible mechanisms have been suggested thus far,[3,15] no definite one has been proposed. Because of the lack of sufficient experimental data on the TIDF, the discussion of the mechanism for TIDF has reached a dead end, and a breakthrough has been longed for.

Decay characteristics provide further knowledge about the mechanism for DF. In view of the nonexponential decay behavior of TIDF,[3,4] it was felt by the present authors that a careful study of the form of the decay curves would yield some information about the nature of TIDF. In a previous brief report on the benzo[*f*]quinoline-biphenyl mixed-crystal system, we have shown for the first time that the excitation duration markedly affects the decay behavior of TIDF at 77 K.[16] In this study, it has also been found that the excitation-light intensity affects the decay behavior of TIDF. We wish here to report these new effects and to discuss the mechanism for TIDF. Technically, the measurement of the excitation-light-intensity effect has been made possible as a result of the recent advent of data-processing instruments such as microcomputers and digital memories, which enable us to measure the decay curves of intrinsically weak TIDF easily and accurately.

Experimental

Chemicals and Samples. Phenanthrene (Tokyo Kasei, EP) was subjected to the chemical treatment described previously.[17] Biphenyl (Wako, EP) was twice recrystallized from ethanol and zone-refined over 200 passes. Then, a central portion of the ingot, the purest portion, was subjected to an additional 200 passes of zone refining. The polycrystalline samples were prepared between two fused-silica disks as has been described previously.[14] The guest concentration has been chosen to be fairly high, that is, 1.0×10^{-2} mol/mol, since the TIDF intensity is generally low.

Apparatus. Optical measurements were made on the apparatus illustrated in Fig. 1. The analyzing system consisted of a 220-mm grating monochromator (Spex, Doublemate 1672) equipped with a photomultiplier (HTV, R106), a DC preamplifier incorporating an operational amplifier (Teledyne Philbrick, 1009), a transient converter (Riken Denshi, TCB1000S-11), and a microcomputer (Fujitsu, MB25020). As a square-wave excitation source, mechanically-chopped radiation from a 250-W high-pressure mercury lamp (Ushio Electric, USH-250D) was used, in combination with a 5-cm optical-path aqueous filter. The mechanical chopping was effected by means of an electromagnetic shutter (shutter E in Fig. 1, Vincent Associates, 26LOAOX5), operated by means of a home-made control system incorporating multivibrators (Toshiba, TC4528BP) and Darlington configurations of transistors. When the excitation-light-intensity dependence was measured, calibrated neutral filters made of brass-wire gauze were used to modify the excitation-light intensity. Another shutter of the same model (shutter A in Fig. 1) was used in order to exclude the prompt fluorescence. Shutter A was opened with a delay time of about 5 ms after the cessation of excitation. The delay time is mainly determined by the operation of the control system. The intrinsic response time of the

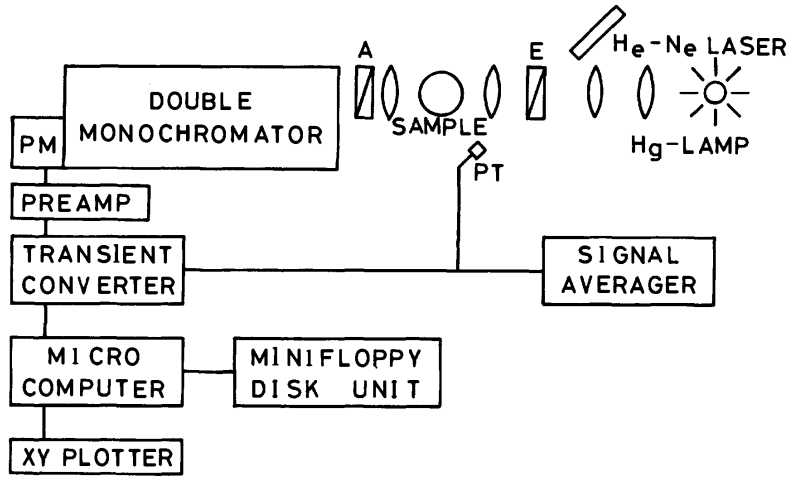

Fig. 1. A block diagram of the apparatus. A and E are electromagnetic shutters. PM and PT stand for photomultiplier and phototransistor, respectively.

shutters is claimed to be of the order of 1 ms. The delayed luminescence decay signals were memorized on the transient converter. After a measurement run, the data were transmitted from the transient converter to the microcomputer, utilizing an RS-232C interface with 9600 bauds. This interface circuit was a home-made one incorporating a UART (Intersil 6402). The transmitted data were stored on a minifloppy disk (Epson, F100A). The analyzed results were displayed on an XY plotter (Graphtec, MP1000). The operation of the shutter E was monitored on a digital memory device (Nicolet 1170 signal averager), displaying the output of a phototransistor illuminated by a He–Ne laser (NEC, GLG5000). The output signal in turn triggered the transient converter. The delayed luminescence spectra were measured in the square-wave excitation.

Results and Discussion

General Remarks on the Spectra and the Temperature Dependence of the Spectral Intensities. Figure 2 shows the delayed luminescence spectra obtained at 77 K with a train of square-wave excitations. For comparison, the prompt fluorescence spectrum is also shown in Fig. 2, comfirming that the observed DF is genuine. As the shortest wavelength fluorescence band tends to be affected by reabsorption, the excitation-duration effect and the excitation-light-intensity effect have been studied with the f band for DF. The phosphorescence decay curve has been observed on the p band, where the T–T absorption spectrum does not overlap the phosphorescence spectrum.[18] In this paper, t signifies the time elapsed after the cessation of excitation.

As has been reported by Misra,[15] the DF and phosphorescence intensities show characteristic temperature-dependences. As the temperature is raised from 6 K, the DF intensity is constant up to about 80 K. TIDF is observed throughout this temperature range. Then it increases to reach a maximum at about 160 K and decreases thereafter. The phosphorescence intensity decreases monotonically as the temperature is raised from 6 K to 180 K, and the DF observed at 77 K consists essentially of TIDF alone.

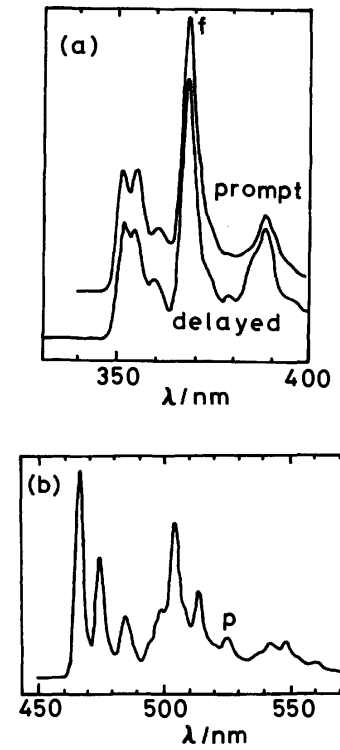

Fig. 2. Delayed luminescence and prompt fluorescence spectra. (a) Delayed and prompt fluorescence and (b) phosphorescence.

Energy Reservoir. As the spectrum of TIDF coincides with that of the prompt fluorescence, the final process of TIDF is a transition from the lowest excited singlet state to the ground state. However, TIDF emission continues for about 2.5 s after excitation is

removed. Therefore, the mechanism for TIDF must involve long-lived excited states. The most probable candidate for this energy reservoir is a triplet state. In this section, we will present experimental evidence that the guest triplet-state molecule is a constituent of the TIDF mechanism.

The phosphorescence decay is nearly exponential, with a lifetime of 3.8 s, and the TIDF intensity becomes negligible 2.5 s after the excitation light is extinguished. Consequently, that triplet molecules are involved can be shown by comparing the TIDF intensities at the instances of the short-pulse excitations effected with different dark periods after a steady-state excitation. The actual experimental procedure is as follows. The steady-state excitation is performed from −5 to 0 s, and then a 20-ms excitation is performed after a certain dark period in the course of the phosphorescence decay. The next set of 5-s and 20-ms excitations are performed after a period of darkness long enough for the triplet concentration, as estimated by monitoring the phosphorescence, to have fallen to a negligible value. The dark periods between the 5-s and 20-ms excitations have been chosen to be 0, 0.284, 0.549, 1.101, 1.616, 2.226, 2.750, 3.188, 3.750, 3.938, 4.490, 4.918, 9.740, and 60 s. The observed results are shown in Fig. 3, where, for comparison, the decay curve of phosphorescence is also shown. It may be noted that the intensities for the dark periods of 2.750 through 9.740 s are greater than that with the prolonged dark period of 60 s. Thus, it is proved that the guest triplet state is necessary for TIDF, since the excited state persisting for 10 s and disappearing at 60 s after excitation is the triplet state, as can be seen from the phosphorescence decay in Fig. 3.

The next problem to be solved is the number of triplet-state molecules which are required to produce one excited singlet state. Attempts were made to ascertain the dependence of the TIDF intensity, I_{TIDF}, on the phosphorescence intensity, I_P, when the excitation-light intensity, I_{exc}, was altered. The TIDF and phosphorescence intensities were measured as the integrated output obtained by the repetition of 20-ms excitations and 20-ms observations, with intervals of 10 ms between excitations and observations. The interdependence of $I_{TIDF} \propto I_P^{1.7}$ has thus been confirmed. The deviation from the square law may be brought about by the dead time of 10 ms in the operation of the two electromagnetic shutters, since the difference between the rates of disappearance of TIDF and of the phosphorescence is considerable. There are two alternative interpretations of this; *i.e.*, the above experimental facts indicate that two triplet-state molecules or one triplet-state molecule and one photon of excitation light produce one excited-singlet-state molecule, which is then responsible for TIDF. In phenanthrene, twice the energy of the lowest excited triplet state is larger than the value of the energy of the lowest excited singlet state. Consequently, both interpretations of the biphotonic nature are conceivable.

Possible Mechanisms. Here, in an effort to pick possible mechanisms for TIDF, we will list the mecha-

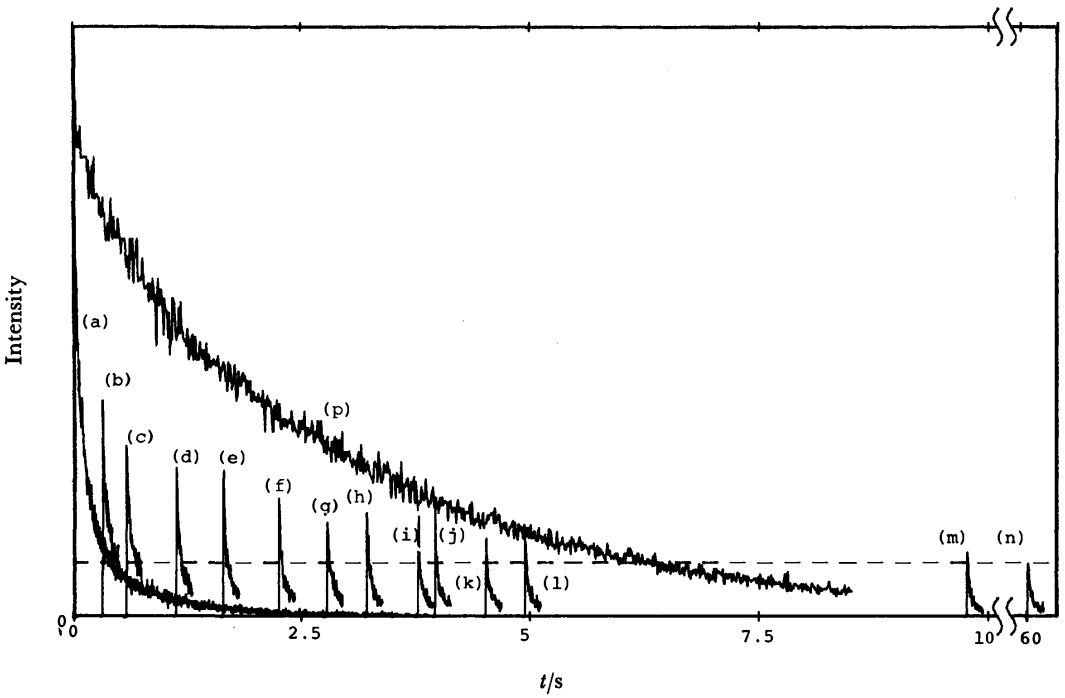

Fig. 3. Decay curves of delayed fluorescence and phosphorescence. (p) Phosphorescence decay after 5 s excitation. (a—n) TIDF decays by successive double pulse excitations. The excitation durations of the first and second pulses are chosen to be 5 s and 20 ms, respectively. The dark periods between the first and the second pulses are (a) 0, (b) 0.284, (c) 0.549, (d) 1.101, (e) 1.616, (f) 2.226, (g) 2.750, (h) 3.188, (i) 3.750, (j) 3.938, (k) 4.490, (l) 4.918, (m) 9.740, and (n) 60 s, respectively.

nisms proposed thus far for DF. The E-type,[1a] Williams-Stevens,[1a] exciton-splitting,[19] recombination,[20] trap,[4] P-type,[1a] exciton-migration,[2-6] direct-resonance-interaction,[3,4,19] double-excitation,[1a] and reabsorption mechanisms[1a-3,19] have all been proposed in the literature. According to the preceding discussion, the mechanism for TIDF must involve two triplet-state molecules or one triplet-state molecule and one photon of excitation. Then, the possible mechanisms for TIDF are the direct-resonance interaction, double-excitation, and reabsorption mechanisms.

In the case of the direct-resonance-interaction mechanism, two separately produced guest triplet molecules interact with each other and energy transfer occurs from one triplet-state molecule to the other. A highly excited state will eventually be produced, and once produced it will revert to the lowest excited singlet state or the triplet state with a significantly higher probability than excitation back to the initial state. The excited singlet state thus produced emits TIDF.

In the case of the double-excitation mechanism, a guest molecule is first excited to a triplet state, and then this triplet-state molecule is excited to a higher excited state X by a second quantum of light. The excited state X thereafter reverts partially to the lowest excited singlet state.

In the case of the reabsorption mechanism, one triplet molecule reaches a higher triplet/singlet state by reabsorbing the energy that another triplet radiates as phosphorescence.

Of these three mechanisms, the first, the direct-resonance interaction mechanism, is the most probable, because this is simply a special case of the mechanism for TDDF, as will be detailed below. The mechanism for TDDF may be summarized as follows:[4]

$$S_0 + h\nu \rightarrow S_1 \quad \text{(absorption)} \quad (1)$$
$$S_1 \rightarrow S_0 + h\nu \quad \text{(fluorescence)} \quad (2)$$
$$S_1 \rightarrow S_0 \quad \text{(relaxation)} \quad (3)$$
$$S_1 \rightarrow T_1 \quad \text{(intersystem crossing)} \quad (4)$$
$$T_1 \rightarrow S_0 + h\nu \quad \text{(phosphorescence)} \quad (5)$$
$$T_1 \rightarrow S_0 \quad \text{(relaxation)} \quad (6)$$
$$T_1 + T_1 \rightarrow S_1 + S_0 \quad \text{(annihilation)} \quad (7)$$
$$T_1 + T_1 \rightarrow T_1 + S_0. \quad \text{(annihilation)} \quad (8)$$

TDDF is ascribed to the fluorescence emitted by the S_1 state produced in the process of Eq. 7. Equation 7 is an abbreviated representation of thermal excitation, exciton migration, and annihilation and is realized as follows;

$$T_1 \rightleftarrows T_1^* \quad \text{(thermal excitation)} \quad (9)$$
$$T_1^* + S'_{0H} \rightleftarrows S_0 + T'_{1H} \quad \text{(energy transfer from guest to exciton)} \quad (10)$$
$$T'_{1H} + S_{0H} \rightleftarrows S'_{0H} + T_{1H} \quad \text{(exciton migration)} \quad (11)$$
$$T_{1H} + S_{0H} \rightleftarrows S_{0H} + T_{1H} \quad \text{(exciton migration)} \quad (12)$$
$$T_{1H} + S''_{0H} \rightleftarrows S_{0H} + T''_{1H} \quad \text{(exciton migration)} \quad (13)$$
$$T''_{1H} + T_1 \rightarrow S''_{0H} + S_1, \quad \text{(annihilation)} \quad (14)$$

where the subscript H identifies the host species; the primed symbols identify host molecules which are adjacent to guest molecules, and T_1^* is a vibrationally excited triplet state of the guest with an energy comparable to the host triplet-exciton band. (For more detailed information, Ref. 4 can be referred to.) Equation 9 represents a thermal excitation of the guest triplet state. As the mechanism for TDDF involves the thermal excitation of Eq. 9, TDDF can be said to depend on the temperature. Equation 12 stands for one-step migration or many-step migration, as the case may be. Equation 14 represents the process of energy transfer from a host triplet-state molecule to a guest triplet-state molecule. Kinoshita and McGlynn[4] assumed that the energy transfer of Eq. 14 was operative between adjacent molecules and explained the behavior of TDDF satisfactorily. However, we assume that energy transfer by long-range interaction can also be operative with a relatively small probability. This process may be rendered undetectable by competing fast exciton diffusion and process of Eq. 14 at high temperatures where TDDF is intense. At low temperatures where the process of Eq. 9 is ineffective, long-range direct-resonance interaction between guest molecules is predominant to give rise to DF, which is here called TIDF, because the fast, competing process favoring TDDF is absent. Therefore, Eqs. 9 through 13 do not apply at low temperatures; now, Eq. 7 represents not a sequence of processes, but really a one-step process. This mechanism does not need thermal excitation and is compatible with the experimental results described thus far. This mechanism for TIDF is the same as that proposed by Azumi and McGlynn in rigid glass.[19] The validity of their proposal has partly been proved by the experimental results of Nakashima *et al.*[21] According to Kellogg,[22] the necessary conditions for this type of energy transfer to occur are satisfied in phenanthrene.

Excitation-duration and Excitation-light-intensity Effects. In this section, we will show the experimental results of excitation-duration and excitation-light-intensity effects on TIDF decay. These two effects have been observed under exactly the same conditions except for the excitation duration and the excitation light intensity.

Figure 4 shows the observed TIDF decay curves. The excitation durations are chosen to be (a) 4.25, (b) 0.257, (c) 0.102, (d) 0.050, and (e) 0.021 s. It can easily be seen that shortening the excitation duration makes not only the TIDF intensity weak, but also the decay steep. The TIDF decay curves with excitations of more than 5 s are essentially the same as that with the excitation of 4.25 s.

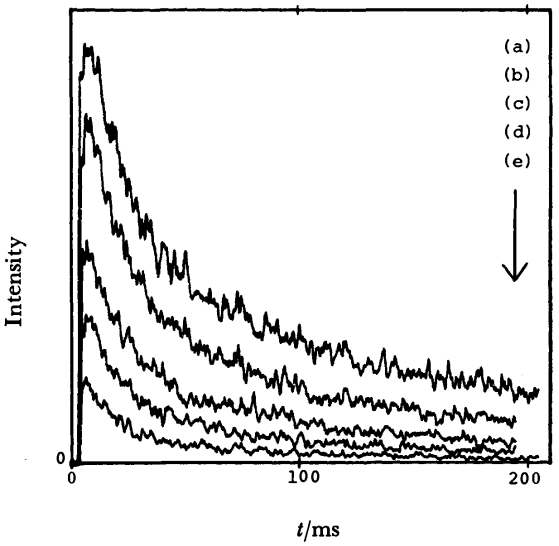

Fig. 4. Excitation duration effect on the delayed fluorescence decay at 77 K. Excitation durations are (a) 4.25 s, (b) 257 ms, (c) 102 ms, (d) 50 ms, and (e) 21 ms, respectively.

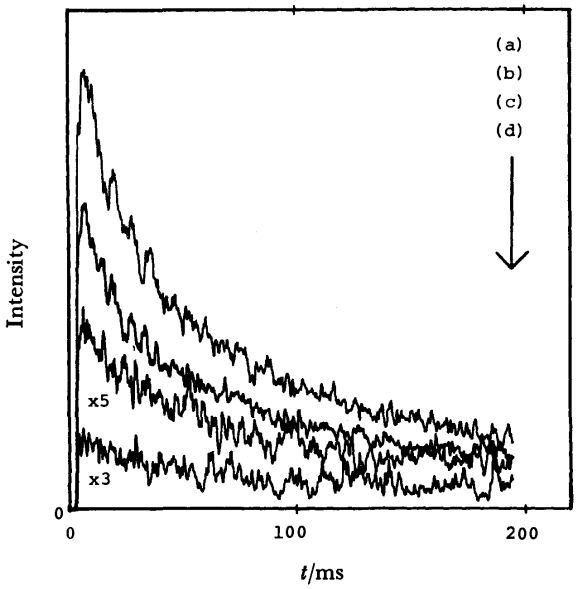

Fig. 5. Excitation light intensity effect on the delayed fluorescence decay observed at 77 K with a fixed excitation duration of 8.6 s. Relative excitation light intensities are (a) 1, (b) 0.6, (c) 0.1, and (d) 0.02, respectively.

Figure 5 shows the results of the observation of the excitation-light-intensity effect. The relative excitation light intensities are chosen to be 1, 0.6, 0.1, and 0.02.

When the excitation duration or excitation-light intensity are altered, the amount of light energy which is stored in the guests is changed. The TIDF intensities thus observed are greatly different from each other, as is shown in Figs. 4 and 5; in consequence, it is desirable to normalize the TIDF decay curves for the convenience of comparison. Figure 6 shows the normalized TIDF decay curves. The experimental conditions are as follows: (a) The excitation duration is 8.62 s; the relative excitation-light intensity is 1. (b) The excitation duration is 8.62 s; the relative excitation-light intensity is 0.02. (c) The excitation duration is 21 ms; the relative excitation-light intensity is 1. We can clearly see from this figure that (b) and (c) show opposite tendencies when we choose (a) as a reference.

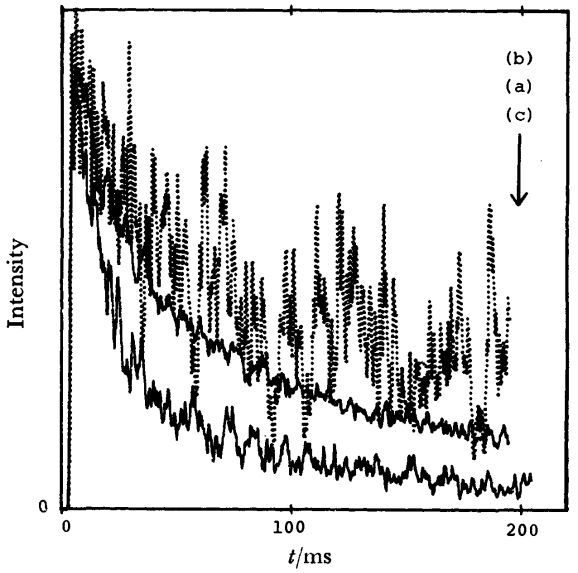

Fig. 6. Comparison between the excitation duration and excitation light intensity effects. Excitation durations are (a) 8.62 s, (b) 8.62 s, (c) 21 ms, respectively. Relative excitation light intensities are (a) 1, (b) 0.02, (c) 1, respectively.

The Mechanism for TIDF. In the foregoing sections, we have discussed the mechanism for TIDF and shown that the possible mechanisms for TIDF are the direct-resonance-interaction, double-excitation, and reabsorption mechanisms. In this section, we will consider the types of TIDF decay to be expected for the three possible mechanisms when the excitation duration and the excitation-light intensity are altered and will compare them with the experimental results shown in the preceding section.

If TIDF is caused by the direct-resonance-interaction mechanism, the energies from the two seperate guest triplet molecules are concentrated in a single guest molecule by the long-range direct interaction. Part of the resultant highly excited guest molecules are degraded into the lowest excited singlet state and then emit TIDF. We can now postulate that this interaction depends on the distance between the two interacting triplet molecules; the closer these two molecules, the higher the transfer probability. A triplet-state molecule far apart from other triplet-state molecules obeys the exponential decay law with the intrinsic transition probability. If another triplet-state molecule lies near the triplet-state molecule, this molecule obeys an exponential decay with an enhanced transition probability.

Therefore, the spatial distribution of the triplet-state molecules is important in this mechanism. In the case of the delta-pulse excitation, the distribution of the triplet-state molecules may be random at the moment of excitation. Consequently, the distances between triplet-state molecules are various and the decay laws to be obeyed are different for triplet-state molecules in different environments. As we observe the total TIDF intensity, the observed decay is a sum of the TIDF decays with different transition probabilities. In the case of the steady-state excitation, the situation is different from the case of the delta-pulse excitation. The distribution of the triplet-state molecules may be random at the initial stage of excitation, while interaction between triplet-state molecules is occurring. As pairs with shorter distances are annihilated with higher probabilities, pairs with longer distances survive with relatively higher probabilities. Therefore, the observed TIDF decay is a sum of the TIDF decays weighting slower components; *i.e.*, the TIDF decay after steady-state excitation contains more of the slowly decaying components than that after a delta-pulse excitation. In other words, a short excitation duration increases the relative number of pairs of triplet-state molecules with short distances. Contrary to this, decreasing the excitation-light intensity reduces the relative number of pairs of triplet-state molecules with short distances. Therefore, shortening the excitation duration quickens the TIDF decay, while decreasing the excitation light intensity makes it slower.

If the double-excitation mechanism is valid, the interaction between the excited states X is negligible. If X is confined within a molecule, the decay law is exponential. As a nonexponential decay is a necessary condition to observe the effect of excitation duration, the effect of excitation duration is not expected to appear in this case. If X is associated with more than one molecule, like an excimer and an exciplex, or with an electron-cation pair, TIDF will decay nonexponentially, and the effect of excitation duration may appear. When the excitation-light intensity is decreased, the total intensity of TIDF decreases, but the form of the decay curve does not change.

If the reabsorption mechanism is operative, a triplet-state molecule absorbs a photon of phosphorescence emitted by another triplet-state molecule and then undergoes the same processes as those in the direct-resonance-interaction mechanism. The effects of excitation duration and excitation-light intensity can be detected easily, judging from the fact that the triplet-state concentration is the major factor in the reabsorption and is affected both by the excitation duration and by the excitation-light intensity. Either shortening the excitation duration or decreasing the excitation-light intensity should have the same effect on TIDF decay.

Figure 6 shows the observed decay type, which is in accord with the prediction by the direct-resonance-interaction mechanism. Consequently, the observed effects of the excitation duration and excitation-light intensity can be reconciled only by adopting the direct-resonance-interaction mechanism for TIDF.

The present work was partially supported by Grant-in-Aid for Scientific Research Nos. 474221 and 347014 from the Ministry of Education, Science and Culture, and by the Ito Science Foundation.

References

1) a) C. A. Parker, "Advances in Photochemistry," Vol. 2, ed by W. A. Noyes, Jr., G. S. Hammond, and J. N. Pitts, Jr., Interscience Publishers, New York, N. Y. (1964), p. 305; b) C. A. Parker, "Photoluminescence of Solutions," Elsevier Publishing Company, Amsterdam (1968); c) J. B. Birks, "Photophysics of Aromatic Molecules," Wiley-Interscience, London (1970).

2) W. Güttler, J. U. von Schütz, and H. C. Wolf, *Chem. Phys.*, **24**, 159 (1977).

3) a) N. Hirota and C. A. Hutchison, Jr., *J. Chem. Phys.*, **42**, 2869 (1965); b) N. Hirota, *J. Chem. Phys.*, **43**, 3354 (1965).

4) M. Kinoshita and S. P. McGlynn, *Mol. Cryst.* **4**, 231 (1968).

5) G. F. Hatch and G. C. Nieman, *J. Chem. Phys.*, **48**, 4116 (1968).

6) T. N. Misra and S. P. McGlynn, *J. Chem. Phys.*, **44**, 3816 (1966).

7) R. C. Johnson, R. E. Merrifield, P. Avakian, and R. B. Flippen, *Phys. Rev. Lett.*, **19**, 285 (1967).

8) V. Ern and R. E. Merrifield, *Phys. Rev. Lett.*, **21**, 609 (1968).

9) M. Chabr and I. Zschokke-Gränacher, *J. Chem. Phys.*, **64**, 3903 (1976).

10) M. Chabr, U. P. Wild, J. Fünfshilling, and I. Zshokke-Gränacher, *Chem. Phys.*, **57**, 425 (1981).

11) S. Arnold, R. R. Alfano, M. Pope, W. Yu, P. Ho, R. Selsby, J. Tharrats, and C. E. Swenberg, *J. Chem. Phys.*, **64**, 5104 (1976).

12) P. Avakian, E. Abramson, R. G. Kepler, and J. C. Caris, *J. Chem. Phys.*, **39**, 1127 (1963).

13) J. U. von Schütz, W. Steudle, H. C. Wolf, P. Reineker, and U. Schmidt, *Chem. Phys. Lett.*, **79**, 1 (1981).

14) Y. Kusumoto, Y. Gondo, and Y. Kanda, *Chem. Lett.*, **1974**, 81; Y. Kusumoto, Y. Gondo, and Y. Kanda, *Bull. Chem. Soc. Jpn.*, **49**, 2706 (1976); Y. Kusumoto and Y. Gondo, *Mem. Fac. Sci., Kyushu Univ., Ser. C*, **14**, 51 (1983); S. Taen and Y. Gondo, *Mem. Fac. Sci., Kyushu Univ., Ser. C*, **13**, 237 (1982).

15) T. N. Misra, *J. Chem. Phys.*, **58**, 1235 (1973).

16) S. Taen and Y. Gondo, *Chem. Lett.*, **1982**, 911.

17) S. Yahiro, H. Sekiya, S. Taen, and Y. Gondo, *Mem. Fac. Sci., Kyushu Univ., Ser. C*, **13**, 227 (1982).

18) I. Taen, S. Taen, and Y. Gondo, *Mem. Fac. Sci., Kyushu Univ., Ser. C*, **13**, 221 (1982).

19) T. Azumi and S. P. McGlynn, *J. Chem. Phys.*, **38**, 2773 (1963); T. Azumi and S. P. McGlynn, *J. Chem. Phys.*, **39**, 1186 (1963).

20) G. Katagiri, K. Yakushi, H. Kuroda, K. Suga, N. Iwasaki, and M. Kinoshita, *Chem. Phys. Lett.*, **86**, 81 (1982).

21) N. Nakashima, Y. Kume, and N. Mataga, *J. Phys. Chem.*, **79**, 1788 (1975).

22) R. E. Kellogg, *J. Chem Phys.*, **41**, 3046 (1964).

 © 1985 The Chemical Society of Japan Bull. Chem. Soc. Jpn., 58, 47—51 (1985)

Solvent Effects on Chemical Reactivities of Conjugated Molecules

Takayuki OHMAE
Department of Chemistry, Faculty of Science, Tohoku University, Sendai 980
(Received July 11, 1984)

The propagator method is applied to the study of solvent effects on chemical reactivities of conjugated molecules. It is shoen that the number of π-electrons of a solute molecule (a conjugated molecule) controls the solvent effects on chemical reactivities. The obtained theory is applied to the study of solvent effects on selectivities of pericyclic reactions.

In recent years, a number of theoretical investigations of the solvent effects on electronic spectra and molecular structures have been made.[1-10] They can be classified in two different approaches: (1) The solvent effects are approximately described by explicitly considering one or numerous solvent molecules around the solute molecule;[1-3] (2) The virtual charge model in which the effects of solvent molecules are replaced by electrostatic continua and this allows the incorporation of the environmental effect into the Hamiltonian.[4-10]

On the other hand, there have been few theoretical studies of the solvent effects on chemical reactivities. Although reactions in the gas phase are simpler to deal with theoretically, the fact remains that most reactions occur actually in solutions. It is well known that the variation of solvent can change the rate and/or the reaction product.[11]

In this investigation it is shown that on the basis of the virtual charge model, the number of π-electrons of the solute molecule (the conjugated molecule) controls the solvent effects on the reactivities of pericyclic reactions.[12]

Hamiltonian

The reaction system in question is assumed to be well described by the following Hamiltonian[13,14] in the second quantized representation:

$$H_0 = \sum_s \alpha_s a_s^\dagger a_s + \sum_{s,t} \beta_{st} a_s^\dagger a_t + \sum_q h\omega b_q^\dagger b_q + \sum_q \sum_{s,t} (g_{st}^{q*} b_q^\dagger + g_{st}^q b_q) a_s^\dagger a_t, \quad (1)$$

where $a_s^\dagger$ and a_s are respectively the creation and annihilation operators for the π-electron at the s-th atom of the solute molecule, $b_g^\dagger$ and b_g are the creation and annihilation operators for the phonon with mode q, respectively, α_s is the coulomb integral, β_{st} the resonance integral, ω the phonon energy and g_{st}^q the electron-phonon interaction constant. In this model, the solvent is replaced by a phonon gas and the solvent-solute interaction by the electron-phonon interaction.[13]

The electron-photon interaction constant in Eq. 1 is defined by

$$g_{st}^q \equiv 4\pi i \frac{e^2 h}{2\gamma\omega} \frac{1}{q} \langle s | e^{iqx} | t \rangle, \quad (2)$$

where γ is given by the following formula;

$$\gamma \equiv \frac{4\pi}{\omega^2} \left(\frac{1}{\varepsilon_\infty} - \frac{1}{\varepsilon} \right)^{-1}, \quad (3)$$

where ε_∞ is the dielectric constant (ε) measured at the optical mode. The Hamiltonian is popular in the solid state phisics, and is successfully applied to a problem of electric resistance and so on.[14]

In this paper we neglect the mode dependence of the phonon energy. It is well known that the assumption is valid for polar media.

Propagator

In this chapter, we treat the propagator defined by

$$G_{rs}^0(t) \equiv -i\langle T[a_r(t) a_s^\dagger(0)] \rangle, \quad (4)$$

where $\langle \cdots \rangle$ denotes the ground state average, and T is the Wick time-ordering operator. Once the propagator is known, we can obtain the information about the eigenvalues and eigenvectors.[15,16]

We now introduce the Fourier transform of the propagator defined by

$$G_{rs}^0(z) \equiv \ll a_r;\ a_s^\dagger \gg = \int_{-\infty}^{+\infty} dt\, e^{izt} G_{rs}^0(t). \quad (5)$$

The Fourier transform satisfies the following equation of motion;

$$zG_{rs}^0(z) = \delta_{rs} + \ll [a_r,\ H_0];\ a_s^\dagger \gg, \quad (6)$$

where brackets [,] indicate a commutator. The commutation relation in Eq. 6 can be written as

$$[a_r,\ H_0] = \alpha_r a_r + \sum_u \beta_{ru} a_u + \sum_q \sum_u (g_{ru}^{q*} b_q + g_{ru}^q b_u) a_u. \quad (7)$$

The substitution Eq. 17 into Eq. 6 yields

$$zG_{rs}^0(z) = \delta_{rs} + \alpha_r G_{rs}^0(z) + \sum_u \beta_{ru} G_{us}^0(z) + \sum_q \sum_u g_{ru}^{q*} \ll b_q^\dagger a_u;\ a_s^\dagger \gg + \sum_q \sum_u g_{ru}^q \ll b_q a_u;\ a_s^\dagger \gg. \quad (8)$$

In evaluating $G^0_{rs}(z)$ by using this equation, we have to consider the higer order propagators:

$$M^{q\dagger}_{us}(z) \equiv \ll b^\dagger_q a_u;\ a_s \gg,$$
$$M^{q}_{us}(z) \equiv \ll b_q a_u;\ a_s \gg. \tag{9}$$

These propagators also satisfy the following equation of motion,

$$\begin{aligned} zM^{q\dagger}_{us}(z) &= (a_u-\omega)M^{q\dagger}_{us}(z) + \sum_v \beta_{uv}M^{q\dagger}_{vs}(z) \\ &+ \sum_l\sum_v g^{l*}_{uv}\ll b^\dagger_q b^\dagger_l a_v;\ a^\dagger_s\gg \\ &+ \sum_l\sum_v g^{l}_{uv}\ll b^\dagger_q b_l a_v;\ a^\dagger_s\gg \\ &- \sum_{v,t} g^{q}_{vt}\ll a^\dagger_v a_t a_u;\ a^\dagger_s\gg. \end{aligned} \tag{10}$$

To solve the above equation we assume as follows;[16]

$$\begin{aligned} \ll b^\dagger_q b_l a_v;\ a^\dagger_s\gg &= \langle b^\dagger_q b_l\rangle \ll a_v;\ a^\dagger_s\gg \\ &= \delta_{ql} n_q G^0_{vs}(z). \end{aligned} \tag{11}$$

Moreover we can assume that

$$\ll b^\dagger_q b^\dagger_l a_v;\ a^\dagger_s\gg = 0, \tag{12}$$

since the many phonon processes described by this propagator should be negligible. Further, we neglect higher order corrections to the electronic processes, that is,

$$\ll a^\dagger_v a_t a_u;\ a^\dagger_s\gg = 0. \tag{13}$$

Substituting the above approximations into Eq. 10, we obtain the following equation in the matrix notation,

$$z\mathbf{M}^{q\dagger}(z) = (\mathbf{h}-\omega)\mathbf{M}^{q\dagger}(z) + n_q\mathbf{g}^q\mathbf{G}^0(z), \tag{14}$$

or

$$\mathbf{M}^{q\dagger}(z) = n_q(z+\omega-\mathbf{h})^{-1}\mathbf{g}^q\mathbf{G}^0(z), \tag{15}$$

where

$$\mathbf{h} = \boldsymbol{\alpha} + \boldsymbol{\beta}. \tag{16}$$

Similarly $\mathbf{M}^q(z)$ is obtained as

$$\mathbf{M}^q(z) = (n_q+1)(z-\omega-\mathbf{h})^{-1}\mathbf{g}^{q*}\mathbf{G}^0(z). \tag{17}$$

Substituting Eqs. 15 and 17 into Eq. 8, we have the propagator, $\mathbf{G}^0(z)$, of the π-electron system in a solvent.

$$\begin{aligned} \mathbf{G}^0(z) = [&z-\mathbf{h}-\sum_q \mathbf{g}^{q*}n_q(z+\omega-\mathbf{h})^{-1}\mathbf{g}^q \\ &- \sum_q \mathbf{g}^q(n_q+1)(z-\omega-\mathbf{h})^{-1}\mathbf{g}^{q*}]^{-1}. \end{aligned} \tag{18}$$

Stabilization Energy

Let us consider a reagent, R, approaching atom r of a solvent molecule (see Fig. 1). The coulomb integral, α_s, and the resonance integral, β_{rs}, will undergo changes on approach of R. Assuming these changes or the perturbations, $\mathbf{v}$, to be small, the change of the total π-electron energy or the stabilization energy, ΔE, can be calculated by use of perturbation theory. ΔE is an energy change at the very beginning of the reaction and the reaction is expected to occur at the position where ΔE is smallest.[17]

The total π-electron energy is,

$$E_0 = \mathrm{Tr}\frac{1}{2\pi i}\int_c \mathrm{d}z\, z\mathbf{G}^0(z), \tag{19}$$

where $\mathbf{G}^0(z)$ is the matrix of the propagator, z the energy parameter and Tr the trace with respect to the arbitrary representation.[15,18] Integration contour, c, in Eq. 20 is the so-called Coulson contour shown in Fig. 2. Note that the integration includes the spin sum hereafter.

The stabilization energy[19-20] caused by the perturbation, $\mathbf{v}$, is

$$\begin{aligned} \Delta E &\equiv E - E_0 \\ &= \mathrm{Tr}\frac{1}{2\pi i}\int_c \mathrm{d}z\, z\mathbf{G}(z) - \mathrm{Tr}\frac{1}{2\pi i}\int_c \mathrm{d}z\, z\mathbf{G}^0(z) \\ &= \sum_n \frac{1}{n}\mathrm{Tr}\frac{1}{2\pi i}\int_c \mathrm{d}z\{\mathbf{G}^0(z)\mathbf{v}\}^n, \qquad (20) \\ &= -\frac{1}{2\pi i}\int_c \mathrm{d}z\, ln\ \mathrm{det}\{1-\mathbf{G}^0(z)\mathbf{v}\}, \qquad (21) \end{aligned}$$

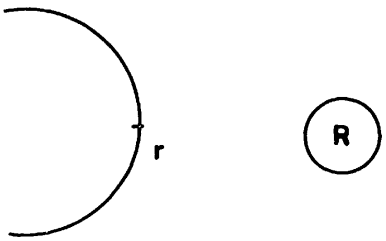

Fig. 1. R is reagent approaching a conjugated molecule.

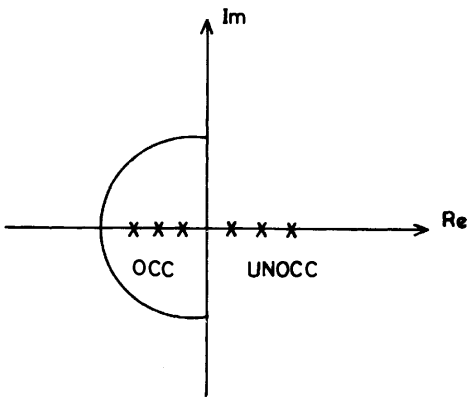

Fig. 2. Coulson contour.

where E and $\mathbf{G}(z)$ are the total π-electron energy and the propagator of the perturbed conjugated system, respectively.

It should be noted that Eqs. 20 and 21 are the straightforward generalization of the famous Coulson-Longuet-Higgins' perturbation formula.[19,21]

The substitution Eq. 18 into Eq. 20 yields

$$\Delta E = \sum_n \frac{1}{n} \mathrm{Tr} \frac{1}{2\pi i} \int_c dz [\{z-\mathbf{h}-\sum_q \mathbf{g}^{q*} n_q (z+\omega-\mathbf{h})^{-1} \mathbf{g}^q - \sum_q \mathbf{g}^q (n_q+1)(z-\omega-\mathbf{h})^{-1} \mathbf{g}^{q*}\}^{-1} \mathbf{v}]^n. \quad (22)$$

The reactivity of a chemical reaction is mainly determined by the first order term with respect to $\mathbf{v}$.[19] Accordingly, it is sufficient for us to study the first-order energy change

$$\Delta E^{(1)} \equiv \mathrm{Tr} \frac{1}{2\pi i} \int_c dz \{z-\mathbf{h}-\sum_q \mathbf{g}^{q*} n_q (z+\omega-\mathbf{h})^{-1} \mathbf{g}^q - \sum_q \mathbf{g}^q (n_q+1)(z-\omega-\mathbf{h})^{-1} \mathbf{g}^{q*}\}^{-1} \mathbf{v}. \quad (23)$$

Equation 23 is the general formula in our theory of the solvent effects on chemical reactivities.

Pericyclic Reaction

Let us consider ring closure reactions of conjugated chains. It is well known that selection rules of ring closure reactions can be generalized to those of pericyclic reactions.[12,19] Figure 3 shows the model of the ring closure reaction. The arrows stand for the basis functions, together with the phases.

For the sake of simplicity, let us now consider the case in which the chain is composed of n atoms and n π-electrons. If the ring closure reaction begins, the extra interaction, v, occurs between 0th and $(n-1)$th atoms:

$$v_{0,n-1} = v_{n-1,0} = v \begin{cases} >0, & \text{for the conrotatory mode} \\ <0, & \text{for the disrotatory mode.} \end{cases} \quad (24)$$

If a mode works to stabilize the solute molecule, *i.e*, $\Delta E^{(1)}<0$, we can choose this mode as the desired reaction path.

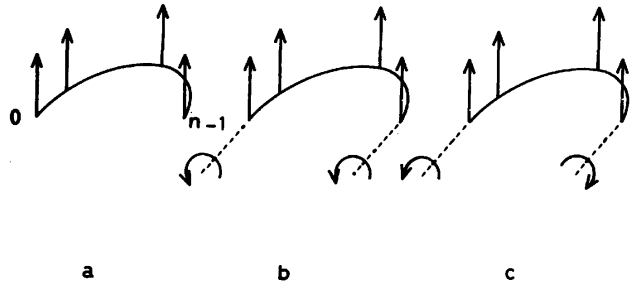

Fig. 3. Ring closure reaction, a: transition state, b: conrotatory mode, c: disrotatory mode.

The stabilization energy, $\Delta E^{(1)}$, in Eq. 23 can be expanded with respect to the electron-phonon interaction constant, $\mathbf{g}^q$,

$$\Delta E^{(1)} = \mathrm{Tr} \frac{1}{2\pi i} \int_c dz (z-\mathbf{h})^{-1} \mathbf{v} + \mathrm{Tr} \frac{1}{2\pi i} \times \int_c dz (z-\mathbf{h})^{-1} \sum_q \mathbf{g}^{q*} n_q (z+\omega-\mathbf{h})^{-1} \mathbf{g}^q (z-\mathbf{h})^{-1} \mathbf{v} + \mathrm{Tr} \frac{1}{2\pi i} \int_c dz (z-\mathbf{h})^{-1} \sum_q \mathbf{g}^q (n_q+1) \times (z-\omega-\mathbf{h})^{-1} \mathbf{g}^{q*} (z-\mathbf{h})^{-1} \mathbf{v} + \cdots. \quad (25)$$

The first term of Eq. 25 determines the selection rules of electrocyclic reactions.[12] This term has already been studied by Ohmae *et al.*[19] The second and third terms are responsible for the solvent effects on the selection rules of electrocyclic reactions in the lowest order. Equation 25 can be rewritten as

$$\Delta E^{(1)} \cong \Delta E_{\mathrm{rule}} + \Delta E_{\mathrm{solv}}, \quad (26)$$

where

$$\Delta E_{\mathrm{rule}} \equiv \mathrm{Tr} \frac{1}{2\pi i} \int_c dz (z-\mathbf{h})^{-1} \mathbf{v}, \quad (27a)$$

and

$$\Delta E_{\mathrm{solv}} \equiv \mathrm{Tr} \frac{1}{2\pi i} \int_c dz (z-\mathbf{h})^{-1} \sum_q \mathbf{g}^{q*} n_q (z+\omega-\mathbf{h})^{-1} \times \mathbf{g}^q (z-\mathbf{h})^{-1} \mathbf{v} + \mathrm{Tr} \frac{1}{2\pi i} \int_c dz (z-\mathbf{h})^{-1} \times \sum_q \mathbf{g}^q (n_q+1)(z-\omega-\mathbf{h})^{-1} \mathbf{g}^{q*} (z-\mathbf{h})^{-1} \mathbf{v}. \quad (27b)$$

First, we study the first term of Eq. 27b. We can treat this term by the representation in which the propagators are diagonal. Thus we have

$$\mathrm{Tr} \frac{1}{2\pi i} \int_c dz (z-\mathbf{h})^{-1} \sum_q \mathbf{g}^{q*} n_q (z+\omega-\mathbf{h})^{-1} (z-\mathbf{h})^{-1} \mathbf{v} = \sum_q n_q \sum_{i,j,k} \frac{1}{2\pi i} \int_c dz \frac{1}{z-\varepsilon_i} \mathbf{g}^{q*}_{ij} \frac{1}{z+\omega-\varepsilon_j} \mathbf{g}^q_{jk} \frac{1}{z-\varepsilon_k} \mathbf{v}_{kj}, \quad (28)$$

where ε_i is the orbital energy or the eigenvalue of $\mathbf{h}$. Now we suppose that the electron-phonon interaction constant, g^q_{ij}, has a dominant value between the highest occupied molecular orbital, HOMO, and the lowest unoccupied molecular orbital, LUMO. Equation 28 then reduces to

$$\sum_q n_q \sum_{i,j,k} \frac{1}{2\pi i} \int_c dz \frac{1}{z-\varepsilon_i} \mathbf{g}^{q*}_{ij} \frac{1}{z+\omega-\varepsilon_j} \mathbf{g}^q_{jk} \frac{1}{z-\varepsilon_k} \mathbf{v}_{kj} \cong \sum_q n_q v_{\mathrm{HH}} |g^q_{\mathrm{HL}}|^2 \frac{1}{2\pi i} \int_c dz \frac{1}{(z-\varepsilon_{\mathrm{H}})^2 (z+\varepsilon-\varepsilon_{\mathrm{L}})}$$

$$+\sum_q n_q v_{LL}|g^q_{HL}|^2\frac{1}{2\pi i}\int_c dz\frac{1}{(z-\varepsilon_L)^2(z+\omega-\varepsilon_H)}$$
$$=\sum_q n_q v_{HH}|g^q_{HL}|^2\frac{-1}{(\varepsilon_H-\varepsilon_L+\omega)^2}$$
$$+\sum_q n_q v_{LL}|g^q_{HL}|^2\frac{1}{(\varepsilon_H-\varepsilon_L-\omega)^2}$$
$$\cong -\sum_q n_q v_{HH}|g^q_{HL}|^2\frac{1}{(\varepsilon_H-\varepsilon_L+\omega)^2}, \quad (29)$$

where we have assumed that $(\varepsilon_H-\varepsilon_L-\omega)>(\varepsilon_H-\varepsilon_L+\omega)$, and HOMO and LUMO are given by the symbol H and L, respectively.

If we deal with the second term of Eq. 27b, the similar treatment gives

$$\sum_q(1+n_q)v_{LL}|g^q_{HL}|^2\frac{1}{(\varepsilon_H-\varepsilon_L+\omega)^2}. \quad (30)$$

Therefore, we have

$$\Delta E_{solv}=\sum_q|g^q_{HL}|^2\frac{-n_q v_{HH}+(1+n_q)v_{LL}}{(\varepsilon_H-\varepsilon_L+\omega)^2}. \quad (31)$$

In order to study the solvent effects on selection rules of electrocyclic reactions, it is necessary to examine v_{HH} and v_{LL}. As is shown in Eq. 24, the non-vanishing matrix elements of $\mathbf{v}$ are only $v_{0,n-1}$ and $v_{n-1,0}$ in the atomic orbital representation. We can decompose v_{AA} as follows:

$$v_{AA}=\sum_{s,t}\langle A|s\rangle\langle s|\mathbf{v}|t\rangle\langle t|A\rangle=2v_{0,n-1}p^A_{0,n-1}, \quad (32)$$

where $p^A_{0,n-1}$ is a partial bond order relating to the A th molecular orbital alone. The partial bond order is defined by using the propagator

$$p^A_{st}\equiv\frac{1}{2\pi i}\int_A dz g(s,t), \quad (33)$$
$$g(s,t)=\frac{\sin(n-t)\theta\sin(s+1)\theta}{\sin(n+1)\theta\sin\theta}, \quad (34)$$
$$z=2\cos\theta, \quad (35)$$

where $g(s,t)$ is the propagator between the s th and t th atoms of the conjugated chain molecule.[22] The contour A encloses only the pole at ε_A. From these equations we get

$$v_{AA}=(-1)^A\frac{4v}{n+1}\sin^2\frac{\pi A}{n+1}, \quad (36)$$

where

$$A=\frac{n+1}{\pi}\cos^{-1}\frac{\varepsilon_A}{2}. \quad (37)$$

The substitution Eq. 36 into Eq. 31 yields

$$\Delta E_{solv}\cong(-1)^H v\sum_q\frac{4}{n+1}\frac{|g^q_{HL}|^2}{(\varepsilon_H-\varepsilon_L+\omega)^2}$$
$$\times\left\{n_q\sin^2\frac{\pi H}{n+1}+(1+n_q)\sin^2\frac{\pi(H+1)}{n+1}\right\}$$
$$\propto(-1)^H v, \quad (38)$$

where H is a half of the number of the π-electrons. From this equation, we can calculate the solvent effects on the selection rules of electrocyclic reactions. The results obtained are summarized in Table 1.

Table 1. Solvent effects on the selectivity of the pericyclic reactions

Number of electron	sign of $(-1)^H$	sign of v[a]	sign of ΔE_{solv}	solvent effect[b]	selection rule
4m	+	+	+	unfavor	allowed
	+	−	−	favor	forbidden
4m+2	−	+	−	favor	forbidden
	−	−	+	unfavor	allowed

a) $v=\begin{cases}+ & \text{for conrotatory mode}\\ - & \text{for conrotatory mode}\end{cases}$

b) favor: The solvent effects accelerate the reaction
unfavor: The solvent effects disturb the reaction.

It has thus been shown that solvent effects depend on the number of π-electrons of the solute molecule only. The nature of the solvent reflects only on the magnitude of the solvent effects;

$$|g^q_{ij}|^2\propto\left(\frac{1}{\varepsilon_\infty}-\frac{1}{\varepsilon}\right). \quad (39)$$

It should be noted that allowed reactions are always disturbed by the solvent, but forbidden reactions are not. If we use the solvent which has the property of $|\varepsilon_\infty-\varepsilon|\gg 0$, we can expect to obtain the thermal reaction products which are the same as the photo chemical reaction ones.

We would like to thank Professor Takeshi Nakajima for helpful discussions.

References

1) P. Cremashi, A. Gamba, and M. Simonetta, *Theoret. Chim. Acta*, **31**, 155 (1973).
2) E. Clementi and G. Bolis, *J. Am. Chem. Soc.*, **99**, 5550 (1977).
3) A. Raudino, F. Zucarello, and G. Buemi, *J. Chem. Soc., Faraday Trans. 2*, **76**, 490 (1980).
4) G. Kloppman, *Chem. Phys. Lett.*, **1**, 200 (1967).
5) H. A. Germer Jr., *Theoret. Chim, Acta*, **34**, 145 (1974).
6) J. L. Rivail and D. Rinaldi, *Chem. Phys.*, **18**, 233 (1976).
7) S. Miertus and O. Kysel, *Chem. Phys.*, 21, 17, 33, 47 (1977).
8) O. Tapia and B. Silvi, *J. Phys. Chem.*, **84**, 2646 (1980).
9) S. Miertus, E. Scrocco, and J. Tomasi, *Chem. Phys.*, **55**, 177 (1981).
10) A. Botrel, F. Corre, and A. Le Beuze, *Chem. Phys.*, **74**, 383 (1983).

11) C. Reichart, *Pure Appl. Chem.*, **54**, 1867 (1982).
12) R. B. Woodward and R. Hoffman, "The Conservation of Orbital Symmetry," Verlag Chemie, Weinheim (1970).
13) R. D. Connon, "Electron Transfer Reactions," Butterworth (1980).
14) H. Haken, "Quantenfeldtheorie des Festkörpers," B. G. Teubner Stuttgart (1973).
15) D. N. Zubarev, *Soviet. Phys. Uspekhi.*, **3**, 320 (1960).
16) K. Nishikawa and S. Aono, *Prog. Theoret. Phys. (Kyoto)*, **50**, 830 (1973).
17) K. Higashi, H. Baba, and A. Rembaum, "Quantum Organic Chemistry," (Wiley & Sons, New York (1965)).
18) S. Aono and K. Nishikawa, *Bull. Chem. Soc. Jpn.*, **53**, 3418 (1980).
19) T. Ohmae, K. Nishikawa, K. Deguchi, and S. Aono, *Bull. Chem. Soc. Jpn.*, **54**, 2857 (1981).
20) K. Nishikawa, M. Yamamoto, and S. Aono, *J. Chem. Phys.*, **78**, 5031 (1983).
21) C. A. Coulson and H. C. Longuet-Higgins, *Proc. R. Soc. London, Ser. A*, **191**, 39 (1947); **192**, 16 (1947).
22) S. Aono, T. Ohmae, and K. Nishikawa, *Bull. Chem. Soc. Jpn.*, **54**, 1645 (1981).

High Resolution ^{29}Si Nuclear Magnetic Resonance Study on Gallosilicates with Zeolitic Structures

Shigenobu HAYASHI,* Kunio SUZUKI, Shigemitsu SHIN, Kikuko HAYAMIZU, and Osamu YAMAMOTO
National Chemical Laboratory for Industry, Tsukuba, Ibaraki 305
(Received July 14, 1984)

High resolution ^{29}Si nuclear magnetic resonance spectra have been measured using magic angle sample spinning technique for several gallosilicates and aluminosilicates with zeolitic structures. The number of gallium atoms coordinating to the SiO_4 tetrahedron was determined by the technique in the same manner as established for aluminium in aluminosilicates. The resonance lines were observed to shift to lower field by the substitution of silicon atoms with gallium as well as aluminium. The magnitudes of lower-field shifts were larger for the substitution by gallium than aluminium. The chemical shift ranges of ^{29}Si nuclei are discussed for gallosilicates with the values for aluminosilicates compared.

High resolution ^{29}Si nuclear magnetic resonance (NMR) spectroscopy in solids has recently become a powerful tool to study the structure of various silicates[1] and aluminosilicates.[2] In silicates the chemical shift of ^{29}Si nuclei depends on the degree of condensation of silicon-oxygen tetrahedra. On the other hand, aluminosilicates are composed of two kinds of tetrahedra, SiO_4 and AlO_4, and the ^{29}Si chemical shift correlates well with the degree of substitution of silicon by aluminium.

A zeolite is a crystalline aluminosilicate with many pores inside it. The pore size is an important factor in determining the selectivity of the catalytic reaction and of the molecular sieving. Various modifications have been carried out to change the pore size: for example, the substitution of silicon and aluminium by other elements, cation exchange, and modification of the surface. In some zeolites aluminium atoms can be replaced by gallium atoms, resulting in zeolitic gallosilicates.[3-6]

Vaughan *et al.*[7] have recently measured high resolution ^{29}Si NMR spectra of gallium faujasites and sodalite to study the effect of gallium substitution for aluminium on the ^{29}Si spectra, but no other works have been reported so far on gallosilicates. In the present work we have carried out an extensive study of high resolution ^{29}Si NMR spectra of various gallosilicates. The ^{29}Si chemical shift has been observed to change depending on the number of gallium atoms coordinating to the silicon-oxygen tetrahedron in the same manner as established for aluminosilicates. In addition to the one caused by the gallium atom, the ^{29}Si resonance line shifts by a crystallographical inequivalence. The range of the chemical shift in ^{29}Si spectra has been discussed, taking into consideration the effects of the substitution by gallium and of the crystallographical inequivalence, and the values for gallosilicates have been compared with those for aluminosilicates.

Experimental

Several gallosilicates were synthesized by the procedures described in Refs. 3—6. Aluminosilicates which have similar compositions and structures were synthesized for comparison. The structures of the synthesized zeolitic materials were checked by measuring powder X-ray diffraction patterns, and the compositions were determined by X-ray fluorescence (XRF) method.

High resolution ^{29}Si NMR spectra were measured by a Bruker CXP-100 pulsed spectrometer which was equipped with a probe for magic angle spinning of the sample and was operated at a resonance frequency of 17.9 MHz. An Andrew-type rotor[8] made of Delrin (polyoxymethylene) was spun at a rate of about 3.5 kHz. The angle of the rotation axis was determined by optimizing the ^{127}I spectrum of KI, using a procedure similar to that described in Ref. 9. Free induction decay signals observed after single pulse excitations were accumulated before Fourier transformation. The repetition times of the pulse excitations were between 2 and 10 s. Silicone rubber was used as an internal second reference, whose chemical shift is −22.0 ppm with respect to tetramethylsilane (TMS).[10] All the chemical shifts in this paper are referred to TMS.

The spectra were deconvoluted into several components with Lorentzian or Gaussian line shapes by a nonlinear least squares method using a FACOM M-380 computer.

Results and Discussion

NMR measurements have been performed for four kinds of zeolitic materials which were reported that aluminium can be substituted by gallium. Figures 1—4 show high resolution ^{29}Si spectra of gallosilicates as well as aluminosilicates in the increasing order of the Si/M ratio (M=Ga or Al). All the silicon atoms are equivalent crystallographically in the frameworks of hydroxysodalite and faujasite, while inequivalencies are present in offretite and ZSM-5.[11] The assignment of each peak observed in gallosilicates has been performed by analogy with aluminosilicates having similar composition and structure, as described below. Si(nM) used in this work means the silicon atom in an SiO_4 tetrahedron coordinated by n Al atoms.

Hydroxysodalite. The spectra for hydroxysodalites are shown in Fig. 1, and the results are summarized in Table 1. Spectra have been measured for three gallosilicates with different Si/Ga ratios,

Table 1. ^{29}Si Chemical shift, relative intensity of the resonance line, and Si/M ratio in hydroxysodalites[a)]

Sample	Chemical shift (ppm) and relative intensity (%)					Si/M (NMR)	Si/M (XRF)
	n[b)] = 4	3	2	1	0		
Gallium-containing (M=Ga)							
Hydroxysodalite (A)	−74.9(81)	−82.8(19)				1.05	1.15
(B)	−74.9(86)	−82.9(14)				1.04	1.14
(C)	−75.1(98)	−84(2)				1.005	0.2
Sodalite[c)]	−76.0	−82.4	−89.0	−94.9	−101.3	1.26	
Aluminium-containing (M=Al)							
Hydroxysodalite	−84(65)	−88(35)				1.10	

a) Lorentzian line shapes are assumed. b) n in Si(nM). c) From Ref. 7.

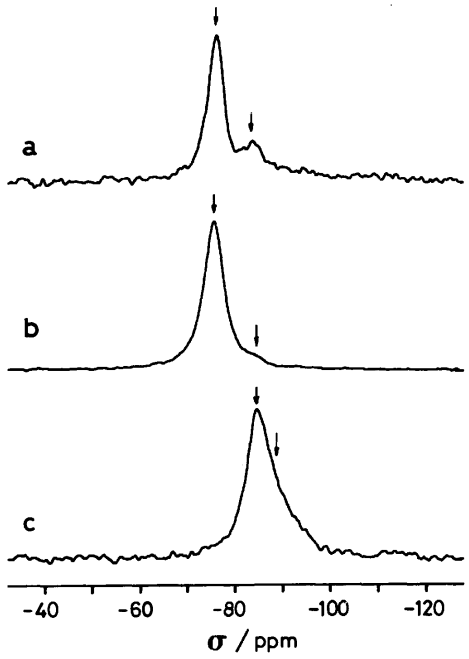

Fig. 1. High resolution ^{29}Si spectra of gallium-containing hydroxysodalite A (a) and C (b), and aluminium-containing hydroxysodalite (c). Arrows in the figure indicate the line positions.

and for one aluminosilicate. The observed peaks can be assigned to silicon atoms in Si(nM) configurations as shown in Table 1. The spectrum of the aluminosilicate has a line shape with a large asymmetry, which might be due to two overlapping lines attributed to Si(4Al) and Si(3Al). The chemical shifts of the two lines are determined to be −84 and −88 ppm. In gallosilicates the spectra are composed of two lines with chemical shifts, −75 and −83 ppm. By comparing the spectra with that of the aluminosilicate, the lines in the gallosilicates can be assigned to Si(4Ga) (−75 ppm) and Si(3Ga) (−83 ppm). The observed line shapes have been well fitted by using Lorentzian line shapes. The Si(nGa) line in gallosilicates shifts to lower field compared with the corresponding Si(nAl) line in aluminosilicate. The chemical shift values in Ref. 7 are also listed in Table 1, and the values obtained in the present work are in good agreement to the reported values.

The ratio of the number of silicon atoms to that of gallium or aluminium atoms (Si/M ratio) has been determined by the XRF method as well as the NMR method. The Si/M ratio from the NMR spectra was calculated assuming Loewenstein's rule,[12] that is, by using the following equation:

$$(\mathrm{Si/M}) = (\sum_{n=1}^{4} nI_n/4)^{-1}, \quad (1)$$

where I_n is a normalized intensity of the Si(nM) resonance line. Good agreements between the ratios obtained from the XRF and NMR methods are found in the cases of gallium-containing hydroxysodalite A and B within the experimental errors of the two methods. However, the discrepancy observed in gallium-containing hydroxysodalite C is too large to be explained by the experimental errors. Since the sample was found to be too rich in gallium atoms, it was considered to violate the Loewenstein's rule, as reported in Ref. 4, and hence Eq. 1 cannot be applied to this sample.

Faujasite. Figure 2 shows the spectra of faujasites containing Na ions. Four resonance lines are clearly observed in the aluminium-containing compound. Their chemical shifts are determined to be −83.6, −88.4, −93.8, and −99.2 ppm, which can be attributed to Si(4Al), Si(3Al), Si(2Al), and Si(1Al), respectively. A peak around −102 ppm is not clearly resolved but observed as a shoulder, which can be assigned to Si(0Al). The gallium-containing faujasite has also four clearly resolved lines. Their chemical shifts are −76.7, −83.3, −90.8, and −98.8 ppm, which can be assigned to Si(4Ga), Si(3Ga), Si(2Ga), and Si(1Ga), respectively, by analogy with the aluminium-containing compound. In both faujasites the spectra can be simulated well when a Lorentzian line shape is assumed for each line. The results are summarized in Table 2, together with the values in Ref. 7. The differences in the chemical shift between the neighboring

Table 2. ^{29}Si Chemical shift, relative intensity of the resonance line, and Si/M ratio in faujasites[a)]

Sample	Chemical shift (ppm) and relative intensity (%)					Si/M (NMR)	Si/M (XRF)
	n[b)]= 4	3	2	1	0		
Gallium-containing (M=Ga)							
NaX	−76.7(19)	−83.3(41)	−90.8(32)	−98.8(9)		1.47	1.58
NaX[c)]	−77.7	−84.2	−90.3	−96.4	−102.8	1.11	
NaX[c)]	−78.0	−84.2	−90.9	−97.4	−104.2	1.39	
NaY[c)]	−78.3	−84.6	−91.4	−98.2	−105.8	2.06	
Aluminium-containing (M=Al)							
NaX	−83.6(10)	−88.4(40)	−93.8(37)	−99.2(11)	−102(2)	1.63	1.75

a) Lorentzian line shapes are assumed. b) n in Si(nM). c) From Ref. 7.

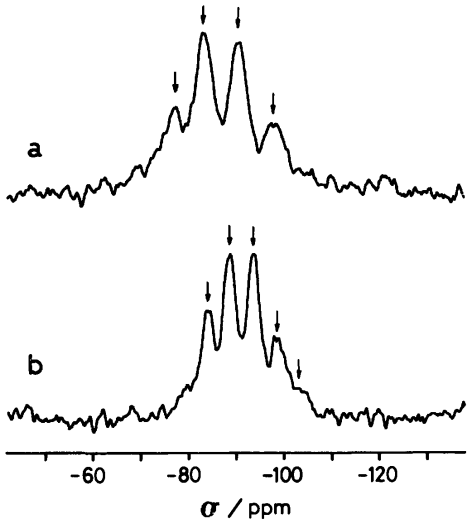

Fig. 2. High resolution ^{29}Si spectra of NaX-type faujasites containing gallium (a) and aluminium (b) atoms.

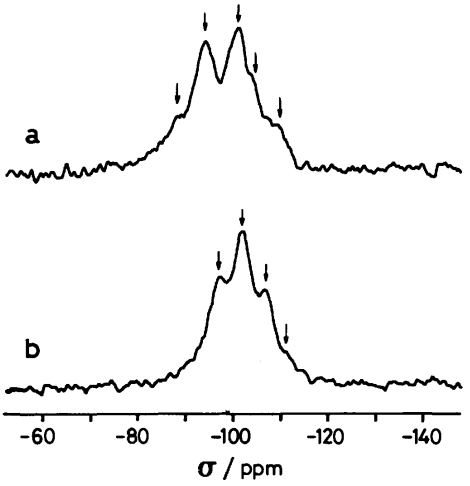

Fig. 3. High resolution ^{29}Si spectra of offretites containing gallium (a) and aluminium (b) atoms. Tetramethylammonium ion is included as the cation.

lines are 6—8 ppm for gallosilicates and 5—6 ppm for aluminosilicates. In gallosilicates the shift differences are a little larger in the present work than in Ref. 7. It can be concluded that a gallium atom deshields the silicon nucleus more than an aluminium atom.

Offretite. Figure 3 shows the spectra of offretites containing tetramethylammonium ion. Four lines are observed in the aluminum-containing compound, whose chemical shifts are −96.5, −101.7, −107.0, and −110.9 ppm. Nagy *et al.*[13] have measured the spectra of offretite with an Si/Al ratio of 3.8, and have made assignment as follows; −92 ppm to Si(3Al), −97 ppm to Si(2Al), −102 ppm to Si(1Al), and −107 and −112 ppm to Si(0Al). Two inequivalent sites however are present with the ratio of 2:1 in the framework of offretite, in contrast to hydroxysodalite and faujasite. Fyfe *et al.*[14] have reassigned the spectra of offretite by taking into consideration the effect of crystallographical inequivalence on the ^{29}Si chemical shift. The chemical shift dispersion for the two structurally inequivalent sites was reported to be about 5 ppm,[14] which is comparable in magnitude to the effect of the first nearest neighboring aluminium. According to the assignment of Fyfe *et al.*,[14] the lines observed in the present work are assigned as follows; −96.5 ppm to Si(2Al), −101.7 ppm to a mixture of Si(2Al) and Si(1Al), −107.0 ppm to a mixture of Si(1Al) and Si(0Al), and −110.9 ppm to Si(0Al). The fraction of each component is estimated as shown in Table 3, assuming that each Si(nAl) line consists of two lines with the intensity ratio of 2:1. Excellent agreement is obtained between the observed and estimated fractions, and the Si/M ratios obtained from the two methods are considered to agree within the experimental error.

In the spectra of gallium-containing offretite four resonance lines can be clearly observed, whose chemical shifts are −88.2, −94.6, −101.4, and −110.7 ppm. In addition to the four lines, there seems to exist at least one line between −101.4 and −110.7 ppm, whose chemical shift is calculated to be −104.5 ppm. They are tentatively assigned as shown in Table 3 by analogy with the aluminium-containing offretite, taking into

Table 3. ^{29}Si Chemical shift, relative intensity of the resonance line, and Si/M ratio in TMA-containing offretites[a)]

Chemical shift (ppm) and Obsd. intensity (%)	Estimated intensity (%) of Si(nM)					Si/M (NMR)	Si/M (XRF)
	n[b)]= 3	2	1	0	total		
Aluminosilicates (M=Al)							
−96.5 (40)		40			40		
−101.7 (36)		20	16		36		
−107.0 (18)			8	10	18		
−110.9 (6)				5	5		
total (100)		60	24	15	99	2.75	3.2
Gallosilicates (M=Ga)							
−88.2 (10)	10				10		
−94.6 (29)	5	24			29		
−101.4 (25)		12	13		25		
−104.5 (31)			7	20	27		
−110.7 (5)				10	10		
total (100)	15	36	20	30	101	2.92	2.8

a) Lorentzian line shapes are assumed. b) n in Si(nM).

Table 4. ^{29}Si Chemical shift, relative intensity of the resonance line, and Si/M ratio in H-type ZSM-5[a)]

Sample	Chemical shift (ppm) and relative intensity (%)				Si/M (NMR)	Si/M (XRF)
	n[b)]= 1	0				
Gallium-containing (M=Ga)						
(A)	−103.7 (13)	−112.3 (62)	−115.7 (25)		31	30
(B)		−110.6 (7)	−113.7 (82)	−116.9 (10)	—	194
Aluminium-containing (M=Al)						
(A)	−105.6 (9)	−112.3 (58)	−115.6 (33)		44	65
(B)	−104.5 (1)	−110.3 (13)	−113.2 (75)	−116.2 (11)	400	620

a) Gaussian line shapes are assumed. b) n in Si(nM).

consideration the effects of the first nearest neighboring gallium and the crystallographical inequivalence. The agreement between the observed and estimated fractions is not very good for the lines at −104.5 and −110.7 ppm. The discrepancy is considered to have its origin in the procedure of the deconvolution of the spectra. Since the three lines between −101 and −111 ppm overlap markedly, the observed fractions are considered to include appreciable errors. Furthermore, the line shape in the higher field appears to be different from a Lorentzian line shape, as shown in Fig. 3a, although Lorentzian line shapes are assumed for all lines. If the line shape can be assumed differently for each line based on a theoretical consideration, the observed spectra should be simulated very well, which is impossible at the present stage.

ZSM-5. ZSM-5 has a very high Si/M ratio compared with the materials described above, and has several sites which are inequivalent crystallographically. Figure 4 shows the spectra of H-type ZSM-5 with different Si/M ratios, and Table 4 summarizes the results. The observed spectra can be well simulated by assuming a Gaussian line shape for each component.

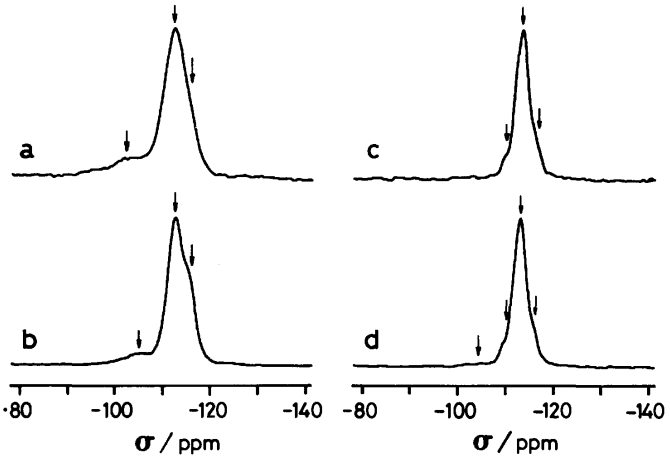

Fig. 4. High resolution ^{29}Si spectra of H-type ZSM-5. Gallium-containing A (a) and B (c), and aluminium-containing A (b) and B (d).

In aluminium-containing compounds with a lower Si/Al ratio, three lines are observed, whose chemical shifts are −105.6, −112.3, and −115.6 ppm. For the

ZSM-5 with a higher Si/Al ratio four lines are observed, whose chemical shifts are −104.5, −110.3, −113.2, and −116.2 ppm. The lines at about −105 ppm are attributed to Si(1Al), from the consideration of the Si/Al ratio obtained by the XRF method. The other lines are all assigned to Si(0Al), whose chemical shifts are dispersed because of the crystallographical inequivalence, as pointed out by Fyfe *et al.*[15]

The spectral shapes of the gallium-containing ZSM-5 are similar to those of the aluminium-containing ones with similar Si/M ratios. Three lines are observed in the sample with a lower Si/Ga ratio whose chemical shifts are −103.7, −112.3, and −115.7 ppm, while the sample with a higher Si/Ga ratio has three lines with chemical shifts of −110.6, −113.7, and −116.9 ppm. The line around −104 ppm is attributed to Si(1Ga), and the other lines are all attributed to Si(0Ga). It is reasonable that the Si(0Al) and Si(0Ga) lines have almost the same chemical shift.

Chemical Shift. The ranges of the chemical shift of Si(nM) lines in gallosilicates are summarized in Table 5, together with the values in aluminosilicates. The ranges of the chemical shifts of Si(nGa) lines cover lower field than the corresponding Si(nAl). In other words, gallium deshields ^{29}Si nucleus more than aluminium. The deshielding effects are 6—8 ppm per gallium atom and 5—6 ppm per aluminium atom when a nearest neighboring silicon atom is substituted by gallium or aluminium. In addition to the deshielding effect, the crystallographical inequivalence affects the chemical shift, which broadens the range of the chemical shift of each Si(nM) line.

Line Shape. In the procedure of the deconvolution a Lorentzian line shape was used for hydroxysodalite, faujasite, and offretite, while a Gaussian line shape was used for ZSM-5. In offretite, a Loretzian line shape is not suitable for the higher-field line. In other words, a Lorentzian line shape is suitable for the Si(nM) lines with n between 1 and 4, while a Gaussian line shape for Si(0M) line. There are two mechanisms of the line broadening: dipolar interaction between ^{29}Si and ^{27}Al or between ^{29}Si and ^{69,71}Ga, and distribution of aluminium and gallium in second and further nearest coordination spheres. The origin of the linewidth in aluminosilicates at high magnetic fields has been discussed by Fyfe *et al,*[17] and they concluded that the aluminium atoms in the second and further nearest coordination spheres produce the chemical shift dispersion of silicon nuclei. At the magnetic field used in the present work the dipolar interaction works in addition to the above mechanism, since the quadrupole interactions in ^{27}Al nuclei becomes larger at lower magnetic fields.[18] The mechanisms of the line broadening in gallosilicates are considered to be the same as those in aluminosilicates. The shape and width of each Si(nM) line reflect the contribution of the two mechanisms. In this work the linewidths of the ^{29}Si lines are found to be broader for gallosilicates than those for aluminosilicates. The gallium atoms in the second and further nearest coordination spheres may be one of the causes of the broader linewidth in gallosilicates, since the deshielding character is stronger in a gallium atom than in an aluminium atom.

In addition to the above mechanisms of the line broadening the site inequivalence makes the spectra very complex, sometimes producing the overlap of the resonance lines, as shown in offretite. The deconvolution of the ^{29}Si NMR spectrum is difficult when lines are heavily overlapped. The error in the fraction of each line produces a larger error in the calculated Si/Al ratio as the ratio becomes higher. The value obtained from the XRF method may have the experimental error of ±10%. Consequently, the Si/M ratios obtained from NMR and XRF methods are considered to agree well within the experimental errors in most cases.

Spin-lattice Relaxation Time. Spin-lattice relaxation times (T_1) of ^{29}Si nuclei in gallosilicates studied in this work range between 1 and 3 s at a resonance frequency of 17.9 MHz, which are the same order of magnitude as the T_1 values in aluminosilicates with similar structures. These results indicate that either a gallium atom as well as an aluminium atom have little contribution to the ^{29}Si spin-lattice relaxation, or the two atoms have the similar contribution to it if exists. Barron *et al.*[19] and Watanabe *et al.*[20] have measured the T_1 values of ^{29}Si nuclei in several layer aluminosilicates, and have correlated the T_1 value with paramagnetic impurities. In the case of the relaxation due to paramagnetic impurities all of the ^{29}Si nuclei should have the same T_1 value. independent of the number of coordinating aluminium atoms. In the present work however differences in the T_1 values are found among the peaks in the two NaX samples studied. There is a trend that the T_1 value of the Si(nM) line with higher n value becomes shorter. From the dependence of the T_1 value on the n value it can be concluded that aluminium and gallium nuclei contribute to the spin-lattice relaxation of ^{29}Si nuclei in gallosilicates and aluminosilicates.

TABLE 5. RANGES OF THE CHEMICAL SHIFTS (ppm) OF ^{29}Si NUCLEI IN GALLOSILICATES AS WELL AS ALUMINOSILICATES

n in Si(nM)	Gallosilicates (M=Ga)	Aluminosilicates (M=Al)	
		this work	Ref. 16
4	−74.9∼ −78.3	−84	−80∼ −87
3	−82.4∼ −94.6	−88	−88∼ −95
2	−89.0∼−101.4	−93.8∼−101.7	−93∼−100
1	−94.9∼−104.5	−99.0∼−107.0	−97∼−106
0	−101.3∼−116.9	−102∼−116.2	−102∼−113

The authors acknowledge Dr. K. Tanabe for constructing the computer program of Gaussian separation.

References

1) E. Lippmaa, M. Mägi, A. Samoson, G. Engelhardt, and A.-R. Grimmer, *J. Am. Chem. Soc.*, **102**, 4889 (1980).

2) E. Lippmaa, M. Mägi, A. Samoson, M. Tarmak, and G. Engelhardt, *J. Am. Chem. Soc.*, **103**, 4992 (1981).

3) K. Suzuki, Y. Kiyozumi, and S. Shin, Japan Patent 190818 (1983).

4) J. Selbin and R. B. Mason, *J. Inorg. Nucl. Chem.*, **20**, 222 (1961).

5) H. Bartes, E. I. Royport, H. Riterel, and F. Undel, Japan Patent 64213 (1983).

6) M. A. M. Bersma, M. F. M. Post, and L. Schappel, Japan Patent 16427 (1981).

7) D. E. W. Vaughan, M. T. Melchior, and A. J. Jacobson, "Intrazeolite Chemistry," American Chemical Society (1983), p. 231.

8) E. R. Andrew, *Prog. NMR Spectr.*, **8**, 1 (1972).

9) J. S. Frye and G. E. Maciel, *J. Magn. Reson.*, **48**, 125 (1982).

10) H. Marsmann, "NMR," Vol. 17, eds. P. Diehl, E. Fluck, and R. Kosfeld, Springer-Verlag, Berlin (1981), p. 152.

11) W. M. Meier and D. H. Olson, "Atlas of Zeolite Structure Types," Polycrystal Book Service (1978).

12) W. Loewenstein, *Am. Mineral.*, **39**, 92 (1954).

13) J. B. Nagy, Z. Gabelica, G. Debras, P. Bodart, and E. G. Derouane, *J. Mol. Catal.*, **20**, 327 (1983).

14) C. A. Fyfe, G. C. Gobbi, G. J. Kennedy, C. T. De Schutter, W. J. Murphy, R. S. Ozubko, and D. A. Slack, *Chem. Lett.*, **1984**, 163.

15) C. A. Fyfe, G. C. Gobbi, J, Klinowski, J. M. Thomas, and S. Ramdas, *Nature*, **296**, 530 (1982).

16) J. Klinowski, J. M. Thomas, C. A. Fyfe, and J. S. Hartman, *J. Phys Chem.*, **85**, 2590 (1981).

17) C. A. Fyfe, G. C. Gobbi, W. J. Murphy, R. S. Ozubko, and D. A. Slack, *Chem Lett.*, **1983**, 1547.

18) A. Abragam, "The Principles of Nuclear Magnetism," Oxford University Press, London (1961), p. 232.

19) P. F. Barron, R. L. Frost, and J. O. Skjemstad, *J. Chem. Soc., Chem. Commun.*, **1983**, 581.

20) T. Watanabe, H. Shimizu, A. Masuda, and H. Saito, *Chem. Lett.*, **1983**, 1293.

Fluorescence Emissions of Cycloalkanes and Mono-olefin by Controlled Electron Impact

Hirofumi KAWAZUMI, Tsuneaki UCHIDA, and Teiichiro OGAWA*
Department of Molecular Science and Technology, Kyushu University, Kasuga-shi, Fukuoka 816
(Received July 26, 1984)

Emission spectra of cyclohexane, methylcyclohexane, *trans*-decalin and tetramethylethylene were measured under the controlled electron-impact (5—100 eV) excitation. A broad band was observed in the ultraviolet region in addition to lines and bands from such fragments as H, CH, and C_2. This broad band was assigned to the fluorescence emission from the excited parent molecule, since its peak and lineshape resemble the fluorescence measured for liquid and since the threshold energy agrees with the absorption onset. The emission cross sections for these emissions were determined at an electron energy of 50 eV.

The intense absorption band of the saturated and mono-olefinic hydrocarbons lies in the far ultraviolet region.[1-2] A very weak broad fluorescence appears upon excitation by VUV photon,[3-8] UV two-photon,[9-10] X-ray[11] or β-ray.[12] Lipsky *et al.*[3-5] systematically investigated this fluorescence for a variety of normal and cyclic alkanes, and their alkyl derivatives; the fluorescence quantum yield increases almost linearly with number of carbon atoms for normal alkanes and depends on the molecular structure for cyclic and branched alkanes. The fluorescence lifetimes of these compounds are of the order of 10^{-9} s as measured by the excitation of the hydrogen flashlamp,[7] the synchrotron radiation,[8] the nitrogen laser[10] and the pulsed X-ray.[11]

The electron is a powerful excitation source, and it can induce not only an electric-dipole allowed but also an optically-forbidden transition.[13] Aromatic molecules show their characteristic emission which is apparently similar to optical fluorescence;[14-17] however, optically-forbidden levels are preferentially excited in the case of benzene.[18] Some of the amino compounds also show an excited molecular emission.[19] However, most organic molecules do not give their own fluorescence emission, mainly because nonradiative processes are fast.

We have recently obtained the fluorescence emission of such hydrocarbons as cyclohexane, methylcyclohexane, *trans*-decalin and tetramethylethylene upon the controlled electron-impact excitation, and discussed the dynamics of molecular excitation.

Experimental

The apparatus consists of a stainless steel collision chamber and a highly sensitive photodetection system. The collision chamber was evacuated with a 4″ oil-diffusion pump with a liquid nitrogen trap. The base pressure was of the order 10^{-5} Pa and the operating pressure was 2.7×10^{-2} Pa (uncorrected ionization gauge reading). Electrons from a tungsten filament were accelerated and collimated with electrostatic lenses, and were monitored with a Faraday cup. The sample was jetted into the collision region through a multichannel nozzle and was crossed to collide with the electron beam.

The optical emission produced in the collision region was observed through a quartz window and a quartz lens at an angle of 60° with respect to the electron beam. The spectrum in the entire region was recorded with a SPEX 1670 monochromator equipped with a 1200 grooves/mm grating blazed at 300 nm and with an HTV R585 photomultiplier. The spectrum in the 190—300 nm region was recorded with the same monochromator equipped with a 1200 grooves/mm grating blazed at 500 nm and used in the second order and with an HTV R166UH solar blind photomultiplier; this system offers a higher sensitivity in the above region. Photons were counted with an ORTEC 9315 photoncounter, and data were stored and analyzed with an NEC PC8800 microcomputer.

The instrumental response of the optical system was calibrated as a function of wavelength with a standard deuterium lamp. Corrected spectra were obtained in units of relative number of photons per wavenumber.

The excitation function and the threshold energy were measured with the latter optical system. The electron energy was calibrated with the threshold of N_2^+ (391.4 nm) at 18.75 eV and its energy resolution was ±0.8 eV.

Cyclohexane (Dojindo, luminasol grade), methylcyclohexane (Nakarai, spectroscopic grade), *trans*-decalin (Nakarai, guaranteed grade), tetramethylethylene (Tokyo Kasei, guaranteed grade), ethylene (Seitetsukagaku, research grade) and carbon monoxide (Takachiho, research grade) were used as supplied. The purity of cyclohexane was >99.98% from gas chromatographic analysis.

Results and Discussion

The emission spectrum of cyclohexane by controlled electron impact at an electron energy of 80 eV shows the Balmer lines of the excited hydrogen atom and bands of the CH (the A-X and B-X transitions) and C_2 (the d-a transition) radicals, as shown in Fig. 1. No molecular emission of cyclohexane was clear in this figure because of low sensitivity.

By using the more sensitive photodetection system for the 190—300 nm region as mentioned in the Experimental, a broad band could be observed for cyclohexane at an electron energy of 50 eV, as shown in Fig. 2. This spectrum was not corrected for the instrumental response. No vibrational structure was clear and the spectral feature did not vary with the bandpass width of 1—10 nm. In addition, atomic lines of C (247.9 nm), C^+

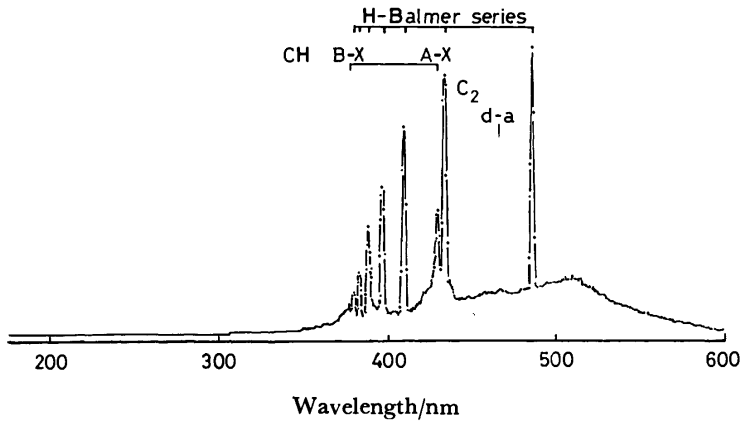

Fig. 1. A typical eminssion spectrum of cyclohexane by controlled electron impact. Electron energy 80 eV, Optical resolution 2 nm. Broad continuum (300—600 nm) is stray light from the hot filament.

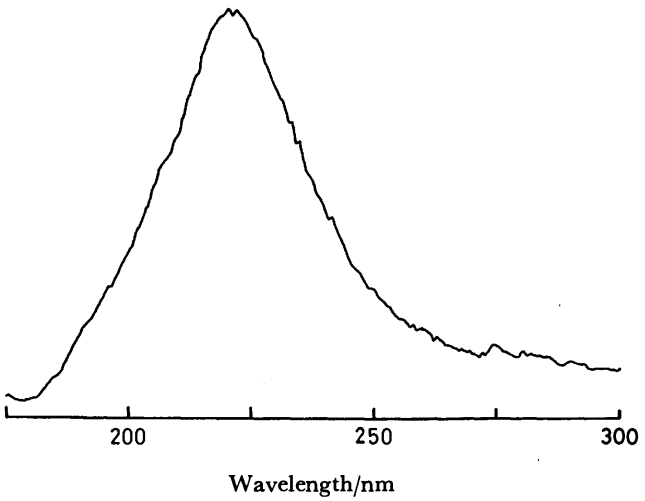

Fig. 2. Recorded fluorescence emission spectrum of cyclohexane by controlled electron impact taken at a higher sensitivity in the 190—300 nm region. Electron energy 50 eV, Optical resolution 2.5 nm.

(283.7 nm) and C^{++} (229.7, 269.8, and 272.5 nm) could be observed at 100 eV.

This broad band resembles the equilibrated fluorescence[3,5] excited optically for neat liquid. Thus, the observed band of cyclohexane is assigned to the fluorescence transition from the lowest excited singlet state (S_1) to the ground state (S_0). The intensity of the fluorescence emission was proportional to both the electron beam current (0—80 μA) and the gas pressure ((0.7—4.0)$\times 10^{-2}$ Pa); so the excited cyclohexane should be produced in a one-electron primary collision process.

The lifetime of the excited cyclohexane is 1.2—1.3 ns.[7] Therefore, no collisional relaxation of the S_1 state occurs in the pressure used. The peak and the band shape of the observed emission did not change for incident electron energies of 30—100 eV and agree with those of the equilibrated fluorescence. Thus, the major emitting state should be the S_1 state for all incident energies. The electron-impact excitation is a nonresonant process and is equivalent to the one by white light, whose maximum energy is that of the incident electron;[20] electrons can excite many vibronic levels simultaneously. Cyclohexane has a number of vibrational modes, and fluorescence from highly excited vibronic levels would lack any structural features. The fluorescence emission of aromatic hydrocarbons except benzene excited by electrons resembles the equilibrated fluorescence.[17] The trapped electron spectra for saturated hydrocarbons indicated excitation to the lowest triplet state as a result of electron exchange processes;[21] however, the transition from a triplet state should not give an intense emission as observed here.

The excitation function for the fluorescence emission of cyclohexane is shown in Fig. 3. The excitation function increased from threshold rapidly to 12 eV, and then decreased gradually to higher energies. The threshold energy was 6.9±1.0 eV, and agrees with the onset of the absorption spectrum (7.1 eV)[1] within experimental uncertainties. This finding supports that the observed emission is due to the S_1—S_0 transition. The highly excited states produced directly by electrons should decay nonradiatively or result in photodissociation.

Methylcyclohexane, *trans*-decalin and tetramethylethylene also show the broad fluorescence emission. Figure 4 shows their spectra taken at an electron energy of 50 eV; these spectra were smoothed and corrected for the wavelength response of the instrument. Each spectrum well resembles the fluorescence band measured for liquid,[3-6] as shown in Table 1; the vapor spectrum by photoexcitation was shown to be almost identical to the one for liquid. Therefore, they were assigned to the fluorescence emission from the excited parent molecules. No fluorescence, however, could be observed from ethylene with the present instrument. Its fluorescence quantum yield is extreme-

TABLE 1. WAVELENGTH OF THE MAXIMUM (λ_{max}) AND THE FULL WIDTH AT HALF MAXIMUM ($\Delta\lambda$) OF THE FLUORESCENCE EMISSIONS OF CYCLOALKANES AND MONO-OLEFIN

Compound	λ_{max}/nm		$\Delta\lambda$/nm	
	This work	Lipsky *et al.*	This work	Lipsky *et al.*
Cyclohexane	202	201[a]	32	34[a]
Methylcyclohexane	214	213[a]	41	39[a]
trans-Decalin	215	217[a]	43	44[a]
Tetramethylethylene	254	263[b]	36	40[b]

a) Ref. 5. b) Ref. 6.

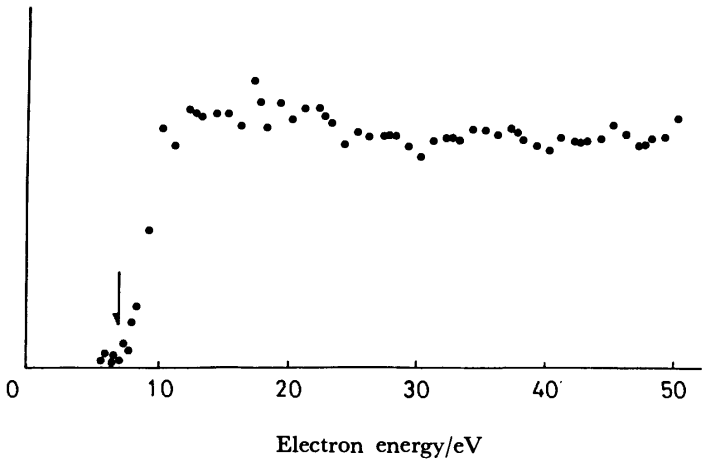

Fig. 3. Excitation function for the fluorescence emission of cyclohexane.

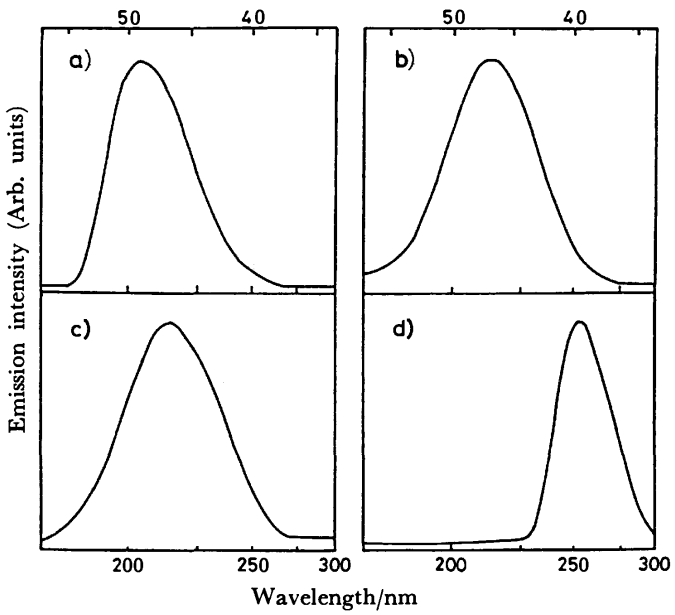

Fig. 4. Corrected emission spectra of (a) cyclohexane, (b) methylcyclohexane, (c) *trans*-decalin (d) tetramethylethlene. Electron energy 50 eV, Optical resolution 10 nm. All spectra are normalized at the intensity maxima.

ly small ($\phi_f < 4\times10^{-7}$) for neat liquid.[6]

The emission cross sections (σ_{em}) of these bands were measured with reference to the CO^+ emission (the B-($v'=0$)—X($v''=0$) transition, 219.0 nm,[22] by comparing the area of the corrected emission spectrum; the sensitivity of the ionization gauge (S)[23] was corrected. The results obtained at an electron energy of 50 eV are summarized in Table 2 together with the optical oscillator strength (f) of the corresponding absorption band[1,28] and the fluorescence quantum yield (ϕ_f).[5,6] The error would be about 50%; its major source is uncertainties in the pressure measurements. The emitting species do not escape from the viewing region during their lifetimes[6-8,24] of 10^{-8}—10^{-9} s.

When the energy of the incident electrons substantially exceeds the excitation energy of the molecule, the Born approximation is applicable; the excitation cross section into the level i ($\sigma_{exc}(i)$) is expressed by the optical oscillator strength ($f(i)$) and the transition energy ($E(i)$). The probability of optical emission from this level is proportional to the fluorescence quantum yield ($\phi_f(i)$). Thus, the emission cross section ($\sigma_{em}(i)$) is given as follows:[17,25]

$$\sigma_{em}(i) = \phi_f(i)\sigma_{exc}(i) = b\phi_f(i)f(i)/E(i)$$

where b is a proportionality constant. This equation can be used for an order of magnitude estimation of the excitation process by the controlled electron impact.

The emission cross sections of the hydrocarbons are

TABLE 2. EMISSION CROSS SECTIONS (σ_{em}) FOR THE S_1-S_0 TRANSITION OF HYDROCARBONS AT AN INCIDENT ELECTRON ENERGY OF 50 eV

Compound	$\sigma_{em}\times10^{17}$/cm^2	f	$\phi_f\times10^3$ [d]	S[e]
Cyclohexane	1.3	0.3[b]	8.8	6.4
Methylcyclohexane	1.7	—	11.2	6.7
trans-Decalin	13	—	23.0	9.6
Tetramethylethylene	2.6	0.01—0.02[c]	0.35	5.8
CO^+ ($B(v'=0)-X(v''=0)$)	0.98[a]	—	—	1.02

a) Ref. 22. b) Estimated value from the absorption spectrum in Ref. 1. c) Ref. 28. d) Refs. 5 and 6. e) Ref. 23.

much larger than that of benzene ($\sigma_{em}=4.8\times10^{-19}$ cm^2)[16] although the fluorescence quantum yields are contrary ($\phi_f=0.22$ for the zero point level of benzene),[26] because the excitation to the S_1 state of benzene is synmetry forbidden and less efficient ($f=0.0013$).[27]

The optical oscillator strength increases gradually with the number of C-C and C-H bonds for alkanes.[1] Therefore, the emission cross section shows a close correlation to the product of the optical oscillator strength and the fluorescence quantum yield for cycloalkanes. For tetramethylethylene, however, the fluorescence maximum is blue-shifted compared to that for neat liquid and for vapor (1.66×10^4 Pa with 8.47×10^4 Pa of N_2),[6] and the emission cross section is larger than expected from the optical oscillator strength and the fluorescence quantum yield. The observed emission originates from the S_1-S_0 transition for cycloalkanes. In contrast, the valence state (π^*) and the 3 s Rydberg state lie in the equivalent energy region for mono-olefins.[28] Hirayama *et al.* suggested that the emitting state is probably the Rydberg state and an internal conversion from the Rydberg state to the valence state is very efficient.[6] Since a collisional nonradiative decay may be suppressed under low-pressure conditions, the emission cross section of tetramethylethylene is large and its fluorescence band is shifted to blue.

The authors thank Professor Yukio Nishimura for his loan of the standard deuterium lamp.

References

1) J. W. Raymond and W. T. Simpson, *J. Chem. Phys.*, **47**, 430 (1967).
2) A. J. Merer and R. S. Mulliken, *Chem. Rev.*, **69**, 639 (1969).
3) F. Hirayama and S. Lipsky, *J. Chem. Phys.*, **51**, 3616 (1969).
4) F. Hirayama, W. Rothman, and S. Lipsky, *Chem. Phys. Lett.*, **5**, 296 (1970).
5) W. Rothman, F. Hirayama, and S. Lipsky, *J. Chem. Phys.*, **58**, 1300 (1973).
6) F. Hirayama and S. Lipsky, *J. Chem. Phys.*, **62**, 576 (1975).
7) W. R. Ware and D. V. O'connor, *Chem. Phys. Lett.*, **62**, 595 (1979).
8) H. Koizumi, T. Yoshimi, K. Shinsaka, S. Ashaoka, H. Nishimura, A. Yagishita, K. Ito, and Y. Hatano, Abstracts, 18th Fast Reaction Symposium, p. 24 (1983).
9) S. Dellonte, E. Gardini, F. Barigelletti, and G. Orlandi, *Chem. Phys. Lett.*, **49**, 596 (1977).
10) L. Flamigni, F. Barigelletti, S, Dellonte, and G. Orlandi, *Chem. Phys. Lett.*, **89**, 13 (1982).
11) M. S. Henry and W. P. Helman, *J. Chem. Phys.*, **56**, 5734 (1972).
12) L. Walter and S. Lipsky, *Int. J. Radiat. Phys. Chem.*, **7**, 175 (1975).
13) F. J. de Heer, *Int. J. Radiat. Phys. Chem.*, **7**, 137 (1975); K. Hirota, M. Hatada, and T. Ogawa, *ibid.*, **8**., 205 (1976); M. Robin, G. K. Schweitzer, and E. L. Wehry, *Appl. Spect. Rev.*, **17**, 165 (1981).
14) T. Ogawa, M. Tsuji, M. Toyoda, and N. Ishibashi, *Bull. Chem. Soc. Jpn.*, **46**, 2637 (1973).
15) K. C. Smyth, J. A. Shiavone, and R. S. Freund, *J. Chem. Phys.*, **61**, 4747 (1974).
16) C. I. M. Beenakker, F. J. de Heer, and L. J. Oosterhoff, *Chem. Phys. Lett.*, **28**, 324 (1974).
17) T. Ogawa, N. Yamami, M. Tsuji, and Y. Nishimura, *Bull. Chem. Soc. Jpn.*, **54**, 1203 (1981).
18) H. Kawazumi, T. Oomori, N. Yamami, and T. Ogawa, *Chem. Phys. Lett.*, **106**, 351 (1984).
19) C. A. F. Johnson, J. E. Parker, and H. P. Flitman, *J. Chem. Soc., Perkin Trans. II*, **1982**, 903.
20) R. L. Platzman, *Vortex*, **23**, 372 (1962).
21) H. H. Brongersma and L. J. Oosterhoff, *Chem. Phys. Lett.*, **3**, 437 (1969).
22) F. Arqueros and J. Campos, *J. Phys. B*, **14**, 2159 (1981).
23) F. Nakao, *Vacuum*, **25**, 431 (1975).
24) S. W. Jorgensen and G. Sorensen, *J. Chem. Phys.*, **62**, 2550 (1975).
25) M. Tsuji, T. Ogawa, and N. Ishibashi, *Chem. Phys. Lett.*, **26**, 586 (1974).
26) C. S. Parmenter and M. W. Schuyler, *Chem. Phys. Lett.*, **6**, 339 (1970).
27) E. Pantos, J. Philis, and A. Bolovinos, *J. Mol. Spectrosc.*, **72**, 36 (1978).
28) F. H. Watson, Jr., A. T. Armstrong, and S. P. McGlynn, *Theor. Chim. Acta*, **16**, 75 (1970).

Delayed Fluorescence of Zinc Porphyrin in Poly(vinyl alcohol) Film

Osamu OHNO, Youkoh KAIZU, and Hiroshi KOBAYASHI*
Department of Chemistry, Tokyo Institute of Technology, O-okayama, Meguro-ku, Tokyo 152
(Received July 27, 1984)

The delayed fluorescence was observed at room temperature with tetrakis(4-sulfophenyl)porphinatozinc ($ZnTPPS_4$) dyed on poly(vinyl alcohol) (PVA) film. In the film, the T-T annihilation is prohibited since any two molecules in the excited triplet can not encounter during their lifetime. Three types of luminescence emission were observed; fluorescence ($S_1 \rightarrow S_0$), phosphorescence ($T_1 \rightarrow S_0$) and delayed fluorescence ($T_1 \rightsquigarrow S_1 \rightarrow S_0$). The delayed fluorescence can be detected only at elevated temperatures where thermal activation from the lowest excited triplet can repopulate the lowest excited singlet.

The lifetimes of phosphorescence of (2,3,7,8,12,13, 17,18-octaethylporphinato)zinc (10 ms)[1] and (5,10,15, 20-tetraphenylporphinato)zinc (0.3 ms)[2] have been measured in toluene solution at ambient temperature. Upon low density excitation by a laser, encounters of the long-lived excited metalloporphyrin molecule in the lowest triplet state with another molecule in the ground state result in the formation of an ion-pair in solution ($^3P^* + P \rightarrow P^+ + P^-$). Upon high density excitation, however, the triplet-triplet annihilation is the path of the ion-pair formation.[1-4]

Since the initial population of the excited singlet state is dissipated in a short period after excitation, a delayed fluorescence is observed only when the lowest excited singlet state is repopulated. The triplet-triplet annihilation results in a population of the lowest singlet state. However, competitive to the bimolecular processes, the lowest excited singlet can be repopulated by a thermal activation of the long-lived excited molecule in the lowest triplet state at elevated temperatures. The delayed fluorescence by this mechanism has been reported on Pd porphyrins in liquid methyl methacrylate.[5] In the present work, the delayed fluorescence was studied with water-soluble zinc porphyrin dyed on the poly(vinyl alcohol) (PVA) film, in which any two excited porphyrin molecules can not encounter during their lifetime.

Experimental

Water-soluble tetrakis(4-sulfophenyl)porphin (H_2TPPS_4) was prepared by the method given elsewhere.[6] The sulfonation of all four phenyls of H_2TPP was confirmed by thin-layer chromatography using silica gel. Tetrasodium[tetrakis(4-sulfonatophenyl)porphinato]zinc ($ZnTPPS_4$) was prepared by refluxing H_2TPPS_4 and zinc perchlorate in an aqueous solution. $ZnTPPS_4$ thus obtained was purified by recrystallization from methanol and acetone. The counter ion of the sulfonates was converted to sodium by use of a cation-exchange resin column. Anal. Calcd for $ZnTPPS_4Na_4(H_2O)_3$: C, 46.35; H, 2.65; N, 4.91. Found: C, 46.24; H, 2.66; N, 4.78. $CuTPPS_4$ was also prepared by the similar method.

PVA films of 0.2 mm thickness were prepared by spontaneous evaporation of an aqueous solution of PVA (degree of polymerization: 1400) on a glass plate at ambient temperature during 10 days and then the films were heated at 80—90 °C for 1 h. The PVA film was sufficiently swelled in water before use and then dipped in an aqueous solution of the water-soluble porphyrin at 45 °C. After dried under dry nitrogen at ambient temperature, the film was used for measurements.

Luminescence emission and excitation spectra were recorded on a Hitachi fluorescence spectrophotometer model MPF-2A, equipped with a Hamamatsu Photonics photomultiplier R928. A component of the emission with a decay lifetime longer than 1 ms was detected through a rotating chopper which can cut the short-lived fluorescence. The decay lifetime of phosphorescence was measured on the Hitachi MPF-2A spectrophotometer equipped with its phosphorescence measuring attachment. The output from the instrument was AD converted and accumulated on a Kawasaki Electronica M-50E transient memory with its averager model TMC-400. The decay profile obtained from the data accumulated for 512 or 1024 times was analyzed on a Commodore CBM3032 microcomputer interfaced to the transient memory.

The sample film in a quartz tube was placed in a quartz Dewar vessel for emission measurements. Measurements were carried out at several temperatures obtained during elevation of the temperature in the vessel after the Dry Ice disappeared in Dry Ice-methanol mixture. The temperature of the film was measured by a thermocouple placed in the sample tube and regulated within an error less than 2 °C. Similar measurements were achieved also at temperatures obtained during cooling of hot water in the vessel.

Absorption spectra were measured on a Shimadzu recording spectrophotometer model MPS-50 and ESR spectra were taken on a JEOL-ME-3X spectrometer.

Results and Discussion

Absorption spectra of $ZnTPPS_4$ in PVA films conform to those observed with $ZnTPPS_4$ in methanol. A typical concentration of $ZnTPPS_4$ in the films used for the measurements was 10^{-4} M. ESR measurements were carried out on the PVA films dyed with $CuTPPS_4$ in the similar concentrations. The ESR spectra indicate that no appreciable interaction is present between copper porphyrin molecules in the film. In the medium, the molecules are isolated and in random orientation without forming dye aggregates such as dimer.

The ESR spectra of $CuTPPS_4$ in PVA film are in good agreement with those of magnetically diluted CuTPP in polycrystalline. Thus the effect of rotational and diffusional Brownian motions of the molecules in the

PVA film can be disregarded.[6]

$ZnTPPS_4$ in PVA film exhibits both phosphorescence (13000 cm^{-1}) and fluorescence (15000—16500 cm^{-1}) emission at ambient temperature, while only fluorescence is observed with $ZnTPPS_4$ in degassed water or methanol media. In the film, the rate of nonradiative process of the excited porphyrin in the lowest triplet state is decreased since the diffusional encounter processes are prohibited. In fact, paramagnetic metalloporphyrins $CuTPPS_4$ as well as $VOTPPS_4$ in the PVA film exhibit a strong phosphorescence even at room temperature.

The emission spectra were observed as shown in Fig. 1, where the component luminescence of decay lifetime shorter than 1 ms was cut by use of the phosphoroscope. Not only the phosphorescence at 13000 cm^{-1} but also the luminescence at 15000—16500 cm^{-1} were observed. The latter showed an identical spectral profile to that of the fluorescence but decayed with a lifetime which comformed to that of the phosphorescence.

Since the migration of molecules is prohibited in the film, the emission should be ascribed to the E(eosin)-type delayed fluorescence.[7] Repopulation of the lowest excited singlet is attributed to the thermal activation of the long-lived excited porphyrin in its lowest triplet. The thermal activation is possible only at elevated temperatures. In fact, the intensity of the delayed fluorescence decreases with lowering of temperature and is actually not detectable at temperatures below −20 °C.

The rate constants of intramolecular processes between three levels including the ground state (S_0), the lowest excited singlet and triplet (S_1, T_1) are defined as in Fig. 2. The ratio of the yields of delayed fluorescence and phosphorescence is given by

$$\phi_{df}/\phi_p = k_{-3} \times \frac{1}{k_p} \times \phi_f, \tag{1}$$

where ϕ_f stands for the yield of fluorescence. Since an equilibrium is established between S_1 and T_1 and thus

$$k_{-3}/k_3 = \frac{1}{3} \exp\{-\Delta E_{ST}/kT\}, \tag{2}$$

the Eq. 1 is rewritten as follows:

$$\phi_{df}/\phi_p = \frac{1}{3}\phi_f \frac{k_3}{k_p} \exp\{-\Delta E_{ST}/kT\} \tag{3}$$

where ΔE_{ST} is an energy gap between S_1 and T_1, 1/3, the ratio of the degeneracies of S_1 and T_1, k, Boltzmann constant and T, temperature. Provided that the ratio of the observed emission intensities is proportional to ϕ_{df}/ϕ_p,

$$\ln[I_{df}(660\text{ nm})/I_p(780\text{ nm})] = -\Delta E_{ST}/kT + \ln\left(\text{const} \times \frac{1}{3}\frac{k_3}{k_p}\right). \tag{4}$$

If k_p, k_3, and ϕ_f are temperature independent, a linear relation between $\ln[I_{df}(660\text{ nm})/I_p(780\text{ nm})]$ and $1/T$ is expected. The plots of $\ln[I_{df}(660\text{ nm})/I_p(780\text{ nm})]$ against $1/T$ result in a straight line as shown in Fig. 3. From the slope of the straight line, ΔE_{ST} was estimated as 3.5×10^3 cm^{-1} which was in good ageement with a gap between the observed fluorescence and phosphorescence maxima (3.9×10^3 cm^{-1}). If the minima of the excited singlet and triplet surfaces are shifted, the observed gap of phosphorescence and fluorescence peaks must be greater than the actual gap between S_1 and T_1. If k_{-3} is thermal in origin, rather than bimolecular, the excited states S_1 and T_1 will decay as

$$S_1 = c_1 \exp(-\alpha t) + c_2 \exp(-\beta t)$$
$$T_1 = c_3 \exp(-\alpha t) + c_4 \exp(-\beta t) \tag{5}$$

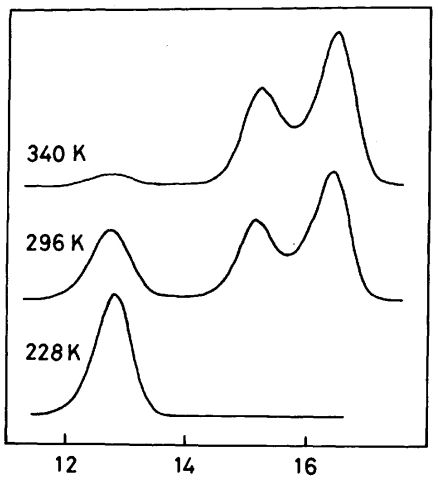

Fig. 1. Phosphorescence and delayed fluorescence of $ZnTPPS_4$ in PVA film at various temperatures.

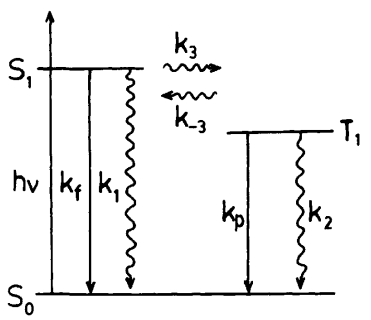

Fig. 2. Energy level diagram and the rate constants of intramolecular processes.
S_1 and T_1 stand for the lowest excited singlet and triplet states and S_0, the ground state.
⟶: radiative and ⇝: nonradiative processes.

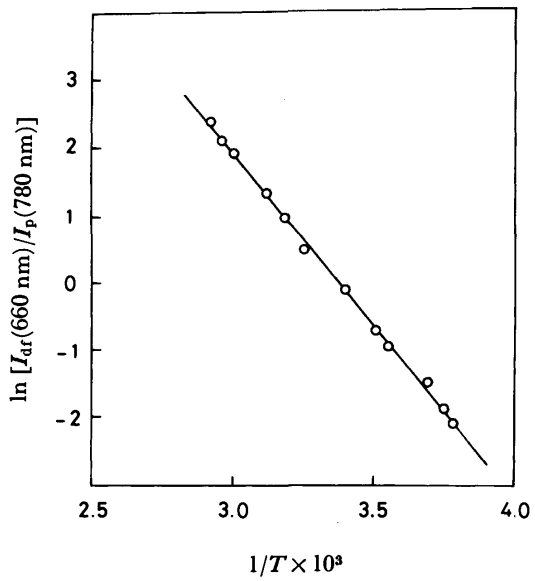

Fig. 3. Temperature dependence of ln [I_{df}(660 nm)/I_p(780 nm)].
I_{df}(660 nm) is the intensity of delayed fluorescence at 660 nm and I_p(780 nm), the intensity of phosphorescence at 780 nm.

where

$$\binom{\alpha}{\beta} = \frac{1}{2}\{(A+B) \pm \sqrt{(A-B)^2+4k_3k_{-3}}\} \quad (6)$$

and

$$A \equiv k_f + k_1 + k_3,$$
$$B \equiv k_2 + k_p + k_{-3}. \quad (7)$$

The faster component of decay ($\alpha > A = k_f + k_1 + k_3$) determines the lifetime of fluorescence. On the other hand, the slower component of decay determines the lifetimes of delayed fluorescence and phosphorescence which are approximated as

$$\beta = 1/\tau_p = 1/\tau_{df} = k_2 + k_p + k_{-3}(1-\phi_t) \quad (8)$$

where it is assumed that $k_{-3} \ll k_3$, $k_2 + k_f$, and ϕ_t stands for the yield of T_1 state. In fact, the observed decay curves in the ms time scale were of single exponential and yielded an identical lifetime regardless of the monitoring wavelengths, delayed fluorescence at 660 nm and phosphorescence at 780 nm, respectively. However the lifetime varies with temperature. Figure 4 shows the plots of the inverse lifetime of phosphorescence $1/\tau_p$ against temperature. It is noted that the lifetime is almost constant from liquid nitrogen temperature up to −20 °C but it decreases with elevation of temperature only above −10 °C. The delayed fluorescence can be detected above −10 °C where the lifetime of phosphorescence decreases. This indicates that $k_p + k_2$ of

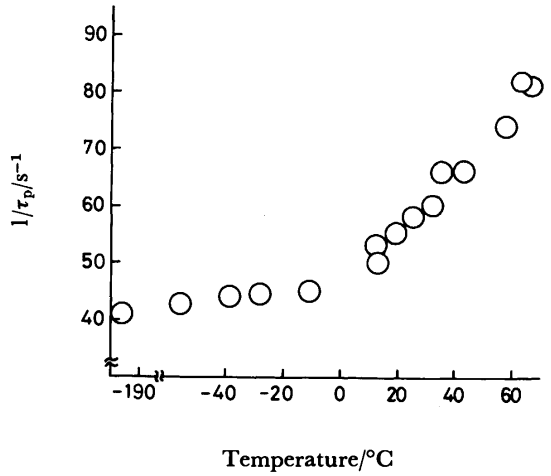

Fig. 4. Plots of the inverse phosphorescence lifetime versus temperature.

$ZnTPPS_4$ in PVA film increases only to a lesser extent with temperature but k_{-3}, the rate constant of activation in the thermal equilibrium between S_1 and T_1, is sufficiently increased with temperature only at elevated temperatures.

In fluid solution, the radiationless transition of the long-lived excited molecules is accelerated by a variety of diffusion-controlled bimolecular processes and thus the rate constant of nonradiative deactivation is sizable and heavily temperature dependent. Since the excited molecules cannot appreciably migrate during their lifetime in the polymer, the diffusion-controlled bimolecular mechanisms cannot play an important role in the relaxation of excited molecules.

In the present work, the metalloporphyrins fixed in the polymer film are isolated from the counterparts and this made it possible to study the intramolecular relaxation processes of excited metalloporphyrin in its lowest triplet by analysis of the temperature dependence of phosphorescence and delayed fluorescence.

References

1) J. Feltelson and D. Mauzerall, *J. Phys. Chem.*, **86**, 1623 (1982).
2) G. F. Stelmakh and M. P. Tsvirko, *Opt. Spektrosk.*, **49**, 511 (1980).
3) S. G. Ballard and D. C. Mauzerall, *J. Chem. Phys.*, **72**, 933 (1980).
4) J. F. Smalley, S. W. Feldberg, and B. S. Brunshwig, *J. Phys. Chem.*, **87**, 1757 (1983).
5) J. B. Callis, M. Gouterman, Y. M. Jones, and B. H. Henderson, *J. Mol. Spectrosc.*, **39**, 410 (1971).
6) H. Kobayashi, O. Ohno, Y. Kaizu, H. Hiratsuka, and Y. Tanizaki, *J. Phys. Chem.*, **86**, 114 (1982).
7) C. A. Parker, in "Advances in Photochemistry", Vol. 2, ed by W. A. Noyes, Jr.; G. S. Hammond and J. N. Pitts, Jr., Interscience Publishers, New York, (1964) p. 305.

 © 1985 The Chemical Society of Japan Bull. Chem. Soc. Jpn., 58, 65—72 (1985)

Infrared Intensities in Methyl Chloride. III. Improvement of the Anharmonic Force Field and the Analysis of the Overtone and Combination Band Intensities

Shigeo KONDO,* Yoshinori KOGA, and Taisuke NAKANAGA
National Chemical Laboratory for Industry, Tsukuba Research Center, Yatabe, Ibaraki 305
(Received August 3, 1984)

A recently obtained anharmonic *ab initio* force field of methyl chloride has been improved by the method of "predicate observations" using the observed values of the spectroscopic constants. The newly obtained force field was used to make re-analysis of the absorption intensities of the binary overtone and combination bands for CH_3Cl and CD_3Cl. Contribution from the electrical anharmonicity to the band intensities was estimated and compared with the *ab initio* result.

In Part II of the present series, we have analyzed the binary overtone and combination band intensities of CH_3Cl and CD_3Cl attempting to determine the values of the second derivatives of the dipole moment with respect to the normal coordinates ($\partial^2 P/\partial q_r \partial q_s$).[1] However, for some of the observed bands the predicted intensities were markedly different from the observed ones, where *ab initio* values were used for the second derivatives of the dipole moment. It seemed that some of the cubic force constants then available[2] contained relatively large errors. Therefore, we did not show the values of the second derivatives of the dipole moment derived therefrom.

Recently, the present authors have calculated the anharmonic potential function for methyl chloride as well as for methyl fluoride by *ab initio* MO method. Certainly, these theoretical force fields were obtained without any procedure of fitting to the observed values of the spectroscopic constants. Still, their values have been shown to remarkably well reproduce the observed values of the molecular constants such as the vibration-rotation constants, l-doubling constants, and the vibrational anharmonicity constants.[3] This means that if the calculations are made with well selected basis functions, the individual values of the theoretical (cubic) force constants are really close to the true values.

Furthermore, in a separate paper[4] we have shown for methyl fluoride that thus obtained anharmonic *ab initio* force field can be further refined by fitting the calculated values of the molecular constants still better to the observed values. In this manner, we have obtained a set of anharmonic force constants for methyl fluoride, which are able to estimate the mechanical contribution to the effective dipole moment in the excited vibrational states to an accuracy of at least a few thousandths of a Debye unit.[4]

Therefore, also in the case of methyl chloride since we have full cubic terms of the anharmonic force field derived from *ab initio* MO method, we expect that an improved set of anharmonic force constants be obtained through a similar analysis as adopted in methyl fluoride. And then, it will be possible to make a quantitative estimation of the values of the second derivatives of dipole moment from the analysis of the absorption band intensities of the two quantum transitions of this molecule.

Results

(1) Refinement of the Cubic Force Constants. In a previous paper,[3] the anharmonic force field of methyl chloride has been derived *ab initio* with Pople's 4-31G* basis set[5,6] and also Dunning's double zeta basis set augmented with the polarization functions for H, C, and Cl atoms (DZP).[7] The effect of the configuration interaction was also examined by using the Mφller-Plesset second-order perturbation theory (abbreviated as MP2).[8] The anharmonic force field was also calculated by adopting the MP2/DZP geometry as the reference geometry for the SCF calculations with 4-31G* and DZP basis sets. The five sets in total of the anharmonic force field thus obtained were found to be very similar to each other.

Furthermore, in order to moderate a systematic trend observed among these anharmonic force fields that the diagonal force constants for the bond stretching modes become smaller on going from lower levels of theoretical calculation to higher levels, and become closer to the observed values,[3] each set of the theoretical force constants was scaled by the observed quadratic force constants. For the scaling, the harmonic force field derived by Duncan *et al.*[9] was utilized. The scaled values of the force constants are summarized in Table 1.

In order to refine further the theoretical force constants thus obtained the method of "predicate observations" was utilized.[10] In this method, a parameter is tied to a "predicate" value by a spring whose strength can be adjusted arbitrarily. It was emphasized that the fitting procedure to the observed values of the molecular constants should not be too strict particularly when the concerned vibrational levels are involved in intramolecular resonances.[4]

In the actual calculation, the least-squares method was used, where in stead of the usual residual value the following quantity was minimized;

TABLE 1. SCALED VALUES OF THE *ab initio* CUBIC SYMMETRY FORCE CONSTANTS OF METHYL CHLORIDE[a,b]

F_{ijk}	I	II	III	IV	V	F_{ijk}	I	II	III	IV	V
111	−16.89	−17.49	−16.71	−17.33	−17.73	255	−0.37	−0.39	−0.35	−0.34	−0.33
112	−0.11	−0.18	−0.11	−0.10	−0.11	256	0.12	0.11	0.05	0.12	0.12
113	0.22	0.25	0.16	0.17	0.19	266	0.12	0.02	0.09	0.17	0.15
122	−0.09	−0.11	−0.09	−0.08	−0.07	344	0.33	0.38	0.34	0.35	0.31
123	0.04	−0.05	0.13	0.12	0.10	345	0.02	0.01	0.04	0.04	0.00
133	−0.48	−0.52	−0.52	−0.53	−0.52	346	−0.10	−0.11	−0.02	−0.03	−0.04
222	0.63	0.51	0.62	0.70	0.69	355	−0.01	0.00	−0.05	−0.05	−0.04
223	−0.57	−0.61	−0.67	−0.59	−0.60	356	0.01	0.01	0.02	0.05	0.06
233	0.67	0.64	0.44	0.54	0.75	366	−0.80	−0.82	−0.76	−0.75	−0.81
333	−16.88	−17.40	−16.51	−16.34	−16.88	444	−12.47	−13.00	−12.08	−12.62	−12.55
144	−17.34	−18.04	−17.02	−17.75	−17.67	445	−0.23	−0.27	−0.33	−0.36	−0.26
145	0.08	0.08	−0.01	0.00	0.06	446	0.10	0.11	−0.11	−0.11	−0.08
146	0.16	0.17	0.05	0.06	0.12	455	0.07	0.06	0.06	0.06	0.07
155	−0.25	−0.23	−0.19	−0.21	−0.24	456	0.02	0.02	0.18	0.20	0.08
156	0.05	0.02	−0.06	−0.01	−0.01	466	0.01	0.01	−0.04	−0.03	−0.03
166	−0.10	−0.11	−0.03	−0.04	−0.02	555	−0.07	−0.05	−0.04	−0.05	−0.04
244	0.10	0.12	0.07	0.10	0.07	556	−0.05	−0.08	−0.06	−0.05	−0.04
245	0.12	0.11	0.13	0.16	0.12	566	0.24	0.26	0.21	0.21	0.21
246	−0.03	−0.08	0.02	0.03	0.04	666	−0.45	−0.47	−0.43	−0.44	−0.41

a) Units are 10^{12} N m^{-2} for stretching, 10^{2} N m^{-1} rad^{-1} for stretch-stretch-bend, 10^{-8} N rad^{-2} for stretch-bend-bend, and 10^{-18}N m rad^{-3} for bending force constants. b) Set I is for 4-31G* at the consistent geometry, II for 4-31G* at MP2/DZP geometry, III for DZP at the consistent geometry, IV for DZP at MP2/DZP geometry, and V for MP2/DZP at the consistent geometry.

TABLE 2. OBSERVED AND CALCULATED VALUES OF x'S, g'S, α'S, AND q'S FOR $CH_3{}^{35}Cl$ UNITS ARE cm^{-1} FOR x AND g, AND 10^{-5} cm^{-1} FOR α AND q

	Obsd	Calcd[a]				
		I	II	III	IV	V
$x_{44}+3g_{44}$	15.3 (—) [b]	12.8	16.5	10.3	14.0	12.8
$x_{55}+3g_{55}$	−7.6 (10) [c]	−7.2	−7.3	−7.2	−7.2	−7.2
$x_{66}+3g_{66}$	5.7 (10) [c]	5.5	5.6	6.0	5.9	5.7
g_{45}	—	−11.3	−11.0	−11.1	−11.4	−11.0
g_{46}	—	1.5	2.1	0.6	0.5	1.0
g_{56}	−2.2 (10) [c]	−2.4	−2.5	−2.6	−2.6	−2.4
$\lvert\varphi_{122}\rvert$	57.0 (—) [d]	277.0	277.7	280.2	273.8	276.2
$\lvert\varphi_{155}\rvert$	99.8 (140) [d,e]	97.4	98.5	97.0	96.2	96.0
$\alpha_1{}^A$	5538 (500) [f]	5117	5405	5064	5285	5450
$\alpha_2{}^A$	−2297 (10) [g]	−2295	−2295	−2294	−2294	−2295
$\alpha_3{}^A$	850 (50) [h]	911	914	956	943	902
$\alpha_4{}^A$	2590 (100) [i]	2746	2780	2730	2760	2756
$\alpha_5{}^A$	4586 (10) [g]	4585	4585	4585	4584	4585
$\alpha_6{}^A$	−2536 (20) [j]	−2536	−2535	−2536	−2537	−2537
$\alpha_1{}^B$	−6 (500) [f]	1	−1	7	5	3
$\alpha_2{}^{B*}$	124 (500) [g]	124	114	133	127	135
$\alpha_3{}^B$	384 (5) [h,k]	384	385	385	384	384
$\alpha_4{}^B$	−18 (5) [i]	−22	−25	−22	−24	−23
$\alpha_5{}^{B*}$	−14 (500) [g]	−27	−30	−14	−18	−17
$\alpha_6{}^B$	163 (5) [j,k]	162	163	163	163	163
$q_4{}^{(+)}$	0 (10) [i]	5	5	9	8	6
$q_5{}^{(+)*}$	[0] (500) [g]	−3	−4	−5	−4	−5
$q_6{}^{(+)}$	−49 (10) [k]	−45	−45	−44	−44	−44

a) Calculated values for I, II, III, IV, and V are obtained from the force fields I, II, III, IV, and V in Table 4, respectively. b) Ref. 1. c) Ref. 12. d) Ref. 2. e) Ref. 13. f) Ref. 14. g) Ref. 15. h) Ref. 16. i) Ref. 17. j) Ref. 18. k) Ref. 19.

TABLE 3. OBSERVED AND CALCULATED VALUES OF x's, g's, α's, AND q's FOR $CD_3{}^{35}Cl$ UNITS ARE cm^{-1} FOR x AND g, AND $10^{-5}\,cm^{-1}$ FOR α AND q

	Obsd	Calcd[a]				
		I	II	III	IV	V
$x_{44}+3g_{44}$	9.8 (—) [b]	9.8	12.0	8.6	10.9	9.8
$x_{55}+3g_{55}$	—	−1.1	−0.8	−0.8	−1.1	−1.0
$x_{66}+3g_{66}$	—	2.3	2.4	2.5	2.4	2.4
g_{45}	−5.8 (—) [b]	−5.2	−4.9	−5.0	−5.2	−5.0
g_{46}	—	1.7	2.0	1.2	1.2	1.4
g_{56}	−6.0 (—) [b]	−1.0	−0.9	−1.0	−1.0	−0.9
$\lvert\varphi_{122}\rvert$	115.2 (—) [c]	199.1	196.9	204.8	199.4	200.3
$\lvert\varphi_{155}\rvert$	63.4 (—) [c]	65.5	66.8	68.1	67.1	65.9
$\alpha_1{}^A$	1950 (500) [d]	2084	2185	2070	2149	2210
$\alpha_2{}^A$	−915 (20) [e]	−937	−936	−940	−942	−934
$\alpha_3{}^A$	300 (500) [f]	405	407	427	423	397
$\alpha_4{}^A$	1253 (20) [g]	1248	1251	1247	1251	1251
$\alpha_5{}^A$	1537 (10) [e]	1541	1540	1539	1541	1541
$\alpha_6{}^A$	−900 (500) [d],[h]	−1007	−1003	−1008	−1007	−1008
$\alpha_1{}^B$	29 (500) [i]	21	19	25	25	24
$\alpha_2{}^{B*}$	122 (500) [e],[j]	90	84	98	94	95
$\alpha_3{}^B$	298 (5) [j]	296	298	293	294	297
$\alpha_4{}^B$	11 (5) [g]	12	13	12	13	13
$\alpha_5{}^{B*}$	−61 (500) [e],[j]	−52	−54	−44	−46	−46
$\alpha_6{}^B$	93 (5) [j]	93	93	91	92	92
$q_4{}^{(+)}$	—	12	12	16	16	13
$q_5{}^{(+)*}$	31 (500) [e],[j]	−1	−2	−3	−2	−3
$q_6{}^{(+)}$	3 (10) [j]	3	2	3	3	3

a) Calculated values for I, II, III, IV, and V are obtained from the force fields I, II, III. IV, and V in Table 4, respectively. b) Ref. 1. c) Ref. 2. d) Ref. 20. e) Ref. 21. f) Ref. 22. g) Ref. 23. h) Ref. 24. i) Ref. 25. j) Ref. 19.

$$\chi_0 = \chi_1 + \chi_2, \tag{1a}$$

where

$$\chi_1 = \sum_i W_i(E_i^{obsd} - E_i^{calcd})^2, \tag{1b}$$

and

$$\chi_2 = \sum_j w_j(p_j^{pred} - p_j)^2. \tag{1c}$$

Here, p_j^{pred} is the "predicate" value and p_j the current value of the jth force constant, and w_j is a weight factor.

As usual, the weight W_i for the ith observed constant E_i was determined as $1/(\Delta E_i)^2$, where ΔE_i is the estimated "error" in E_i.[2] It is to be noted, however, that the values ΔE_i employed here are in general much larger than the experimental uncertainties reported in the literature,[11-25] for they should also include uncertainties due to approximations used for the theoretical expressions of the constants.[26] The actual values for ΔE_i were rather arbitrarily chosen as listed in Tables 2 and 3.

On the other hand, in order to choose appropriate values for w_j, trial calculations were carried out a number of times, in each of which different values were adopted for w_j as in the case of methyl fluoride. Eventually, the value of 0.1 in the respective units, which are given in the footnote to Table 1, in general and the value of 0.3 for the diagonal stretching force constants were adopted for Δp_j, where $w_j=1/(\Delta p_j)^2$. These values are the same as those used in Ref. 4.

Once the values of ΔE_i and Δp_j are determined, the procedure for refining the force constants is straightforward. The calculation was carried out for the above mentioned five sets of anharmonic force field (Table 1). For example, in the case of 4-31G* with the consistent geometry, the original value of residual was χ_1=3270. Through the refinement, the value has been altered to be χ_1=11.0 (χ_2=25.7). Thus, the degree of agreement between the observed and calculated constants became better by more than two orders of magnitude in the residual value. Similarly, for the MP2/DZP case, through the refinement calculation, the residual value changed from χ_1=3860 to χ_1=10.2 (χ_2=28.2).

Table 4 shows the result of the refinement calculations. Comparison of the numbers listed in Tables 1 and 4 reveals that the changes in the individual cubic force constants are by no means large. Apart from the

TABLE 4. IMPROVED VALUES OF THE CUBIC SYMMETRY FORCE CONSTANTS OF METHYL CHLORIDE[a),b)]

F_{ijk}	I	II	III	IV	V
111	−17.03 (43)	−17.52 (38)	−16.87 (44)	−17.40 (39)	−17.73 (38)
112	−0.16 (15)	−0.20 (13)	−0.17 (15)	−0.13 (14)	−0.12 (13)
113	0.21 (14)	0.24 (14)	0.15 (14)	0.16 (14)	0.19 (14)
122	−0.08 (13)	−0.07 (16)	−0.08 (13)	−0.10 (13)	−0.09 (13)
123	0.01 (14)	−0.07 (13)	0.13 (13)	0.10 (14)	0.07 (14)
133	−0.44 (15)	−0.47 (15)	−0.43 (18)	−0.46 (17)	−0.49 (14)
222	0.69 (06)	0.69 (07)	0.69 (06)	0.70 (06)	0.71 (05)
223	−0.62 (10)	−0.59 (10)	−0.63 (12)	−0.62 (11)	−0.66 (10)
233	0.78 (14)	0.79 (16)	0.66 (21)	0.69 (17)	0.83 (12)
333	−16.93 (17)	−17.00 (20)	−16.77 (23)	−16.80 (22)	−16.97 (16)
144	−16.68 (53)	−17.02 (76)	−16.50 (45)	−16.86 (68)	−16.78 (68)
145	0.08 (14)	0.09 (14)	−0.01 (14)	0.00 (14)	0.07 (14)
146	0.15 (14)	0.14 (14)	0.04 (14)	0.04 (14)	0.10 (14)
155	−0.37 (10)	−0.35 (10)	−0.34 (10)	−0.35 (10)	−0.36 (10)
156	−0.10 (19)	−0.12 (19)	−0.17 (17)	−0.15 (19)	−0.13 (18)
166	−0.07 (12)	−0.05 (14)	−0.04 (12)	−0.08 (12)	−0.04 (12)
244	0.21 (19)	0.30 (26)	0.16 (16)	0.27 (24)	0.24 (24)
245	0.11 (14)	0.13 (16)	0.12 (14)	0.16 (15)	0.13 (15)
246	−0.05 (14)	−0.12 (15)	0.01 (14)	0.00 (15)	0.00 (15)
255	−0.30 (05)	−0.31 (05)	−0.31 (04)	−0.30 (05)	−0.30 (04)
256	0.00 (09)	0.01 (08)	0.02 (07)	0.01 (12)	0.01 (08)
266	0.18 (05)	0.17 (06)	0.16 (05)	0.18 (05)	0.16 (05)
344	0.13 (12)	0.13 (15)	0.15 (12)	0.13 (13)	0.13 (12)
345	−0.03 (15)	−0.04 (16)	0.00 (15)	0.00 (15)	−0.03 (15)
346	−0.06 (15)	−0.07 (16)	0.02 (15)	0.00 (15)	−0.01 (14)
355	−0.01 (14)	0.01 (14)	−0.05 (14)	−0.05 (14)	−0.04 (14)
356	0.05 (13)	0.05 (12)	0.07 (13)	0.09 (13)	0.07 (12)
366	−0.90 (06)	−0.90 (06)	−0.88 (06)	−0.88 (06)	−0.88 (06)
444	−12.48 (41)	−13.01 (41)	−12.10 (41)	−12.64 (41)	−12.56 (41)
445	−0.23 (14)	−0.26 (14)	−0.31 (14)	−0.35 (14)	−0.25 (14)
446	0.10 (14)	0.10 (14)	−0.11 (14)	−0.11 (14)	−0.08 (14)
455	−0.13 (09)	−0.12 (09)	−0.15 (10)	0.16 (10)	−0.13 (09)
456	−0.10 (16)	−0.11 (17)	0.00 (19)	0.02 (20)	−0.05 (17)
466	−0.03 (14)	−0.02 (14)	−0.07 (14)	−0.06 (14)	−0.06 (14)
555	−0.04 (15)	−0.02 (15)	−0.02 (15)	−0.03 (15)	−0.02 (15)
556	0.00 (12)	−0.02 (13)	0.00 (14)	0.02 (13)	0.00 (12)
566	0.27 (10)	0.27 (10)	0.25 (10)	0.25 (10)	0.25 (10)
666	−0.48 (12)	−0.49 (12)	−0.43 (13)	−0.44 (13)	−0.42 (13)

a) For the units, see footnote a) to Table 1. b) The results for I, II, III, IV, and V have been derived by adopting I, II, III, IV, and V in Table 1, respectively, as the "predicate" values. See text.

diagonal stretching force constants, most of them show changes less than 0.1 of the respective units. The numbers in the parentheses are one standard deviation resulting from the least-squares calculation under the present condition. It is to be noted that they can not simply be considered as the errors involved in their values.[4] The calculated values of the spectroscopic constants from these force constants are listed in Tables 2 and 3. Certainly, a very good agreement is obtained between the calculated and observed constants.

The obtained values of the force constants for the five cases are all very similar to each other; they actually agree with each other within the "standard errors" resulting from the present calculations.

(2) Binary Overtone and Combination Band Intensities. It is well known that the integrated intensity of a binary combination band is expressed by the following equation:[1,27]

$$A_{ss'} = 2.5066 \times (\omega_s + \omega_{s'}) d_f |Q_{ss'}|^2 Z_s Z_{s'} \{1 - e^{-\beta(\omega_s + \omega_{s'})}\}. \quad (2)$$

Similarly, for a binary overtone band,

$$A_{ss} = 2.5066 \times (2\omega_s) d_f |Q_{ss}|^2 Z_s^2 (1 - e^{-2\beta\omega_s}). \quad (3)$$

Here, ω_s is the sth normal frequency, d_f is the degeneracy of the upper vibrational state, β is $1/kT$, Z_s is the partition function for the sth normal vibration, $Z_s=1/\{1-\exp(-\beta\omega_s)\}$, and Q_{ss} and $Q_{ss'}$ are the transition moments calculated from the contact transformed dipole moment operator.[27] The numerical coefficient used in these equations is for the case where ω_s and φ_{rst} are given in cm^{-1}, P_r and P_{rs} in Debye units, and A_{ss} and $A_{ss'}$ in km mol^{-1}.

The actual expressions for the transition moments, Q_{ss} and $Q_{ss'}$, are given in Ref. 1 for different kinds of two quantum transitions of symmetric top molecules. They are given by the effective values of the second derivatives of the transformed dipole moment $\Omega_{ss'}^{\alpha}$ multiplied by different numerical factors as follows:[1] $Q_{ss}^{z}=\Omega_{ss}^{z}/2\sqrt{2}$, $Q_{ss'}^{z}=\Omega_{ss'}^{z}/2$, $Q_{st}^{x}=\Omega_{st}^{x}/2$, $Q_{tt}^{z}=\Omega_{tt}^{z}/2$, $Q_{tt}^{x}=\Omega_{tt}^{x}/2$, $Q_{tt'}^{z}=\Omega_{tt'}^{z}/\sqrt{2}$, and $Q_{tt'}^{x}=\Omega_{tt'}^{x}/\sqrt{2}$, where the index s denotes a nondegenerate mode and t denotes a degenerate mode.

The intensities of binary overtone and combination bands contain contributions both from electrical and mechanical anharmonicities. The mechanical contribution to the intensities may be obtainable if the normal coordinate cubic force constants and the values for $(\partial P/\partial q_r)$ are known. The former can be calculated from the anharmonic symmetry force field determined in the present study. They were calculated from the force field in Table 4 (case V) and are shown in Table 5. The phases of the normal coordinates used here is the same as in Part I of the present series.[11] On the other hand, the P_r values have also been determined in Part I and the actual values expressed in Debye units are summarized in Table 6.

Table 5. Normal coordinate cubic force constants φ_{rst} for methyl chloride.[a] Units are cm^{-1}

φ_{rst}	CH_3Cl	CD_3Cl	φ_{rst}	CH_3Cl	CD_3Cl
111	−1047.0	−627.6	255	−29.4	−7.8
112	−46.4	−64.7	256	−62.0	−42.8
113	6.2	−4.1	266	40.3	4.6
122	276.2	200.3	344	22.6	2.3
123	73.1	29.8	345	−17.9	−5.0
133	20.3	17.1	346	−65.0	−12.8
222	−119.4	−102.3	355	−15.2	−3.0
223	−71.1	−53.6	356	−34.4	−12.1
233	−30.0	−61.8	366	−67.0	−53.4
333	−259.5	−220.7	444	−815.5	−532.4
144	−1050.7	−659.9	445	−95.9	−65.5
145	0.5	25.6	446	7.6	−8.9
146	4.8	−10.4	455	−156.0	−112.6
155	96.0	65.9	456	152.0	75.1
156	−33.6	−34.3	466	169.3	105.9
166	398.9	220.0	555	−41.8	−24.2
244	47.3	29.0	556	31.2	19.1
245	−53.8	−17.8	566	−75.3	−37.6
246	−298.3	−192.1	666	−28.6	−22.5

a) Calculated from the cubic symmetry force constants V in Table 4.

Table 6. Summary of P_r^{α} values (Debye units)

P_r^{α}	CH_3Cl		CD_3Cl	
	Obsd[a]	Calcd[b]	Obsd[a]	Calcd[b]
P_1^z	−0.0778 (25)	−0.0920	−0.0756 (8)	−0.0936
P_2^z	0.0696 (28)	0.1107	0.0972 (15)	0.1420
P_3^z	0.1599 (32)	0.2177	0.1412 (28)	0.1923
P_4^x	−0.0368 (21)	−0.0605	−0.0303 (3)	−0.0534
P_5^x	0.0554 (19)	0.0504	0.0462 (18)	0.0406
P_6^x	−0.0384 (21)	−0.0400	−0.0171 (15)	−0.0189

a) Ref. 11. b) From 4-31G* calculation.

Table 7. Observed and calculated intensities for the overtones and combinations of CH_3Cl. Units are km/mol

Band	Obsd[a]	Calcd[b]		
		I[c]	II[d]	III[e]
$2\nu_4(//)$	0.290 (15)	0.750	0.694	0.735
$2\nu_4(\perp)$	0.429 (43)	1.751	1.773	1.772
$\nu_1+\nu_4$	0.92 (18)	1.679	1.617	1.665
$2\nu_1$		0.001	0.003	0.003
$\nu_4+\nu_5(//, \perp)$	3.02 (30)	2.106	1.888	1.966
$\nu_1+\nu_5$		1.047	1.028	1.058
$\nu_2+\nu_4$		1.568	1.642	1.603
$\nu_1+\nu_2$		0.013	0.005	0.005
$\nu_4+\nu_6(//)$	0.369 (37)	0.409	0.340	0.343
$\nu_4+\nu_6(\perp)$		0.097	0.102	0.097
$\nu_1+\nu_6$	0.134 (7)	0.215	0.217	0.214
$\nu_3+\nu_4$	0.164 (8)	0.396	0.375	0.382
$\nu_1+\nu_3$	0.205 (10)	0.113	0.147	0.147
$2\nu_5(//)$	4.16 (34)	2.642	5.688	2.726
$2\nu_5(\perp)$		0.771	0.010	0.264
$\nu_2+\nu_5$	0.316 (32)	0.550	0.473	0.445
$2\nu_2$	0.0	1.605	0.002	0.001
$\nu_5+\nu_6(//)$	0.004 (4)	0.801	0.237	0.387
$\nu_5+\nu_6(\perp)$	0.433 (43)	1.029	0.214	0.230
$\nu_2+\nu_6$	0.255 (13)	0.144	0.256	0.182
$\nu_3+\nu_5$	0.0	0.002	0.001	0.001
$\nu_2+\nu_3$	0.087 (5)	0.361	0.479	0.461
$2\nu_6(//, \perp)$	0.0	0.037	0.060	0.048
$\nu_3+\nu_6$	0.0	0.881	0.006	0.011
$2\nu_3$	?	0.014	0.049	0.045

a) Ref. 1. b) Second derivatives of the dipole moment by *ab initio* MO method (4-31G*) are taken into consideration. c) Mechanical contribution is from the force field in Ref. 2. d) Mechanical contribution is from the force field of V in Table 1. e) Mechanical contribution is from the force field of V in Table 4.

Tables 7 and 8 show the observed and calculated values of the absorption intensities of binary overtone and combination bands. In these tables, calculated intensities are shown for three cases; the first one is from

TABLE 8. OBSERVED AND CALCULATED INTENSITIES FOR THE OVERTONES AND COMBINATIONS OF CD_3Cl. UNITS ARE km/mol

Band	Obsd[a]	Calcd[b]		
		I[c]	II[d]	III[e]
$2\nu_4(//)$	0.202 (10)	0.364	0.339	0.357
$2\nu_4(\perp)$	0.284 (14)	0.911	0.916	0.917
$\nu_1+\nu_4$	0.224 (45)	0.844	0.812	0.834
$2\nu_1$		0.000	0.001	0.001
$\nu_4+\nu_5(//)$	0.91 (9)	0.022	0.028	0.027
$\nu_4+\nu_5(\perp)$		0.133	0.105	0.113
$\nu_2+\nu_4$		0.628	0.648	0.633
$\nu_1+\nu_5$		0.102	0.099	0.104
$\nu_1+\nu_2$	0.0	0.000	0.035	0.035
$\nu_4+\nu_6(//)$	?	0.165	0.127	0.126
$\nu_4+\nu_6(\perp)$	?	0.002	0.003	0.003
$\nu_3+\nu_4$	0.0	0.108	0.099	0.102
$\nu_1+\nu_6$	0.0	0.041	0.033	0.033
$\nu_1+\nu_3$	0.119 (6)	0.056	0.053	0.052
$2\nu_5(//)$	2.56 (13)	2.740	6.136	3.287
$2\nu_5(\perp)$		0.196	0.593	0.366
$\nu_2+\nu_5$	?	0.016	0.019	0.014
$2\nu_2$	1.29 (10)	0.759	1.543	1.460
$\nu_5+\nu_6(//)$	0.384 (38)	0.730	0.133	0.245
$\nu_5+\nu_6(\perp)$		0.035	0.038	0.031
$\nu_3+\nu_5$		0.232	0.169	0.167
$\nu_2+\nu_6$	?	0.060	0.126	0.094
$\nu_2+\nu_3$	0.125 (13)	0.393	0.468	0.456
$2\nu_6(//, \perp)$	0.0	0.033	0.012	0.010
$\nu_3+\nu_6$	0.0	0.113	0.003	0.003
$2\nu_3$	0.124 (12)	0.017	0.033	0.031

a) Ref. 1. b) Second derivatives of the dipole moment by *ab initio* MO method (4-31G*) are taken into consideration. c) Mechanical contribution is from the force field in Ref. 2. d) Mechanical contribution is from the force field of V in Table 1. e) Mechanical contribution is from the force field of V in Table 4.

TABLE 9. ANALYSIS OF THE TRANSITION DIPOLE MOMENT FOR CH_3Cl (IN $10^{-4}\times$D)

$rs(\alpha)$	I[a]	II[b]	III[c]	IV[d]
11 (z)		87		−99
12 (z)		30		−17
13 (z)	+94 (3)	4	90 (−98)	74
22 (z)	0 (109)	337	−337	−329
23 (z)	+82 (3)	0	82 (−82)	185
33 (z)		−289		193
14 (x)		42		−191
15 (x)		5		−143
16 (x)	+52 (2)	−13	65 (−39)	78
24 (x)		−1		172
25 (x)	−95 (5)	−35	−60 (130)	−77
26 (x)	+93 (3)	−101	194 (8)	179
34 (x)	+59 (2)	−4	63 (−55)	93
35 (x)	0 (61)	−5	5	−1
36 (x)	0 (68)	−27	27	5
44 (z)	−88 (3)	84	−172 (4)	−223
44 (x)	−75 (4)	29	−104 (46)	−182
45 (z)		−4		−30
45 (x)		0		−130
46 (z)		−24		106
46 (x)		3		28
55 (z)	+480 (20)	332	148 (−812)	55
55 (x)		−154		69
56 (z)	−11 (11)	−46	35 (57)	−65
56 (x)	−84 (5)	60	−144 (24)	−121
66 (z)	0 (89)	181	−181	−240
66 (x)	0 (63)	9	−9	2

a) Observed values of $\Omega_{rs}{}^{\alpha}$. Numbers in parentheses are the estimated errors. Their signs were so chosen that the resulting value of P_{rs} (see III) may agree better with the *ab initio* value (see IV). b) Mechanical anharmonicity obtained from set V of Table 4. c) Estimated values of P_{rs}; I—II. The numbers in parentheses are for the alternative signs of $\Omega_{rs}{}^{\alpha}$ in column I. d) *Ab initio* values of P_{rs} (Ref. 1).

the cubic force field in Ref. 2, the second from the scaled force field initially obtained with the MP2/DZP calculation (case V in Table 1), and the third one from the final force field (case V in Table 4). In all these calculations, the P_{rs} values obtained in Ref. 1 from *ab initio* MO calculation with 4-31G* basis set were utilized. Marked differences are observed between the first case and the other two cases, particularly in the values for $2\nu_2$, $\nu_5+\nu_6$, and $\nu_3+\nu_6$ of CH_3Cl, and $2\nu_2$ and $\nu_5+\nu_6$ of CD_3Cl. Certainly, this is due to the difference in the employed anharmonic force fields. If the values of the normal coordinate force constants listed in Table 5 are compared with those in Table 3 of Ref. 1, those concerned mainly with ν_2, ν_5, and ν_6 are markedly different between the two results. In fact, the values for the cubic force constants such as φ_{122}, φ_{222}, φ_{166}, φ_{256}, φ_{266}, φ_{356}, φ_{555}, φ_{556}, and φ_{666} have been improved very much.

On the other hand, the difference between the second and third cases is not so large. This is expected because the actual changes in the individual force constants were not large, although there was remarkable improvement on the agreement between the observed and calculated molecular constants. Also the latter improvement of the force field has yielded considerable changes in the calculated intensities of $2\nu_5$, $\nu_5+\nu_6$, and $\nu_2+\nu_6$ of both CH_3Cl and CD_3Cl molecules.

Tables 9 and 10 show the results of the analysis of the observed values of the transition dipole moment. In these tables, the column I shows the observed values of $\Omega_{rs}{}^{\alpha}$. These numbers are given with the signs. They were chosen as follows; at first, the contribution from the mechanical anharmonicity to $\Omega_{rs}{}^{\alpha}$ has been obtained by using the force constants for case V in Table 4 and is shown in column II. Then, the values of P_{rs} have been obtained by subtracting the numbers listed in column II from those in column I (and are shown in column III).

Table 10. Analysis of the transition dipole moment for CD_3Cl (in $10^{-4}\times$D)

$rs(\alpha)$	I[a]	II[b]	III[c]	IV[d]
11 (z)		68		−75
12 (z)	0 (100)	43	−43	−2
13 (z)	+82 (3)	8	74 (−90)	45
22 (z)	+450 (18)	615	−165 (−1065)	−142
23 (z)	+108 (6)	−24	132 (−84)	225
33 (z)	−168 (9)	−206	38 (374)	124
14 (x)		32		−154
15 (x)		0		−51
16 (x)	0 (52)	−4	4	33
24 (x)		−2		125
25 (x)		−12		−11
26 (x)		−72		136
34 (x)	0 (53)	−1	1	52
35 (x)		−2		87
36 (x)	0 (74)	−4	4	−8
44 (z)	−85 (3)	65	−150 (20)	−177
44 (x)	−71 (2)	21	−92 (50)	−148
45 (z)		−8		−17
45 (x)		1		−38
46 (z)		−20		77
46 (x)		4		2
55 (z)	+441 (12)	439	2 (−880)	56
55 (x)		−91		208
56 (z)		−63		−39
56 (x)		32		−6
66 (z)	0 (102)	128	−128	−160
66 (x)	0 (72)	12	−12	−8

a) Observed values of $\Omega_{rs}{}^{\alpha}$. Numbers in parentheses are the estimated errors. Their signs were so chosen that the resulting value of P_{rs} (see III) may agree better with the *ab initio* value (see IV). b) Mechanical anharmonicity obtained from set V of Table 4. c) Estimated values of P_{rs}; I—II. The numbers in parentheses are for the alternative signs of $\Omega_{rs}{}^{\alpha}$ in column I. d) *Ab initio* values of P_{rs} (Ref. 1).

The resulting values of P_{rs} for the two possible signs of $\Omega_{rs}{}^{\alpha}$ were compared with the theoretical values in column IV, the latter being obtained with Pople's 4-31G* basis set.[1] The signs given to the numbers in column I were so chosen that the resulting values of P_{rs} may agree better with the theoretical ones. In fact, if they are chosen in this manner, agreement between the observed and calculated values of P_{rs} is very good, *i.e.*, there is almost no doubt about the correctness of the present sign choice of $\Omega_{rs}{}^{\alpha}$. The numbers in parentheses in column III are those for the alternative signs of the transition moment.

Discussion

We did not show actual values of the errors involved in P_{rs} in Tables 9 and 10. This is because the errors involved in the force constants themselves are, as stated above, not well known. However, from comparison of the observed values of P_{rs} with the *ab initio* values listed in the same tables, the magnitudes of the errors may be on the average a few thousandths of a Debye unit.

On the other hand, it is well known that information on P_{rs} is also obtainable through observation of the dipole moment in the excited vibrational states.[28] By vibrationally averaging the transformed dipole moment operator[27] with a harmonic oscillator wave function, we obtain the expression for the dipole moment in each vibrational state;

$$\langle P\rangle_v = P_0 + \sum_a \delta P_a(v_a + d_a/2), \tag{4a}$$

where

$$\delta P_a = (1/2)\{P_{aa} - \sum_m P_m \varphi_{aam}/\omega_m\}. \tag{4b}$$

For CD_3Cl, Yamada and Hirota have measured the dipole moment in the ν_2 and ν_5 states; they obtained $\langle P\rangle_2$=1.90741(33), $\langle P\rangle_5$=1.90607(36), and $\langle P\rangle_0$= 1.90597(33) D.[21] Eq. (6) shows that from comparison of the dipole moment in the ν_2 and ν_5 states, respectively, with that of the ground state, we obtain the following quantities;

$$\delta P_2 = (1/2)\{P_{22} - P_1\varphi_{122}/\omega_1 - P_2\varphi_{222}/\omega_2 - P_3\phi_{223}/\omega_3\}, \tag{5}$$

and

$$\delta P_5{}^z = (1/2)\{P_{55}{}^z - P_1\varphi_{155}/\omega_1 - P_2\varphi_{255}/\omega_2 - P_3\varphi_{355}/\omega_3\}. \tag{6}$$

By substituting in these equations the above data for the dipole moment,[21] the observed values for the first derivatives (Table 6),[1] and the cubic force constants in Table 5, we obtain the values of P_{22}=−0.0243 D and $P_{55}{}^z$=−0.0034 D. If these values are compared with those resulting from the band intensities, *i.e.* P_{22}=−0.0165 D and $P_{55}{}^z$=0.0002 D (Table 10), the agreement between the two sets of data is about the magnitude we expected in the above for the errors in P_{rs}.

In this concern, it should be remembered that the expressions used for the intensity analysis has been derived through the contact transformation method.[1-27] The contribution of the mechanical anharmonicity calculated by using these equations may, therefore, contain large errors when there are close resonances. In the case of CD_3Cl, the values of P_{22} and $P_{55}{}^z$ derived from the intensity analysis may have suffered from the effect of this approximation. Considering this, the above discrepancy of the two sets of data could indicate the upper limit of the errors involved in the values of P_{rs} obtained in the present

analysis.

Now a study on the infrared intensities of binary overtone and combination bands of methyl fluoride is in progress in our laboratory. Also we are planning to extend similar studies on various molecules, *e.g.*, methyl bromide, formaldehyde, ethylene, and so forth.

References

1) S. Kondo, Y. Koga, T. Nakanaga, and S. Saëki, *Bull. Chem. Soc. Jpn.*, **57**, 16 (1984).

2) S. Kondo, Y. Koga, T. Nakanaga, and S. Saëki, *J. Mol. Spectrosc.*, **100**, 332 (1983).

3) S. Kondo, Y. Koga, and T. Nakanaga, *J. Chem. Phys.*, **81**, 1951 (1984).

4) S. Kondo, *J. Chem. Phys.*, in press.

5) a) R. Ditchfield, W. J. Hehre, and J. A. Pople, *J. Chem. Phys.* **54**, 724 (1971); b) W. J. Hehre and W. A. Lathan, *J. Chem. Phys.*, **56**, 5255 (1972).

6) P. C. Hariharan and J. A. Pople, *Theor. Chim. Acta*, **28**, 213 (1973).

7) a) S. Huzinaga, *J. Chem. Phys.*, **42**, 1293 (1965); b) T. H. Dunning, *J. Chem. Phys.*, **53**, 2823 (1970); c) T. H. Dunning, *Chem. Phys. Lett.*, **7**, 423 (1970); d) T. H. Dunning, *J. Chem. Phys.*, **55**, 3958 (1971).

8) C. Mφller and M. S. Plesset, *Phys. Rev.* **46**, 618 (1934); J. S. Binkley and J. A. Pople, *Int. J. Quant. Chem.* **9**, 229 (1975).

9) J. L. Duncan, D. C. McKean, and G. K. Speirs, *Mol Phys.* **24**, 553 (1972).

10) a) L. S. Bartell, D. J. Romenesko, and T. C. Wong, in "Chemical Society Specialist Periodical Report No. 20: Molecular Structure by Diffraction Methods," ed by L. E. Sutton and G. A. Sim, Vol. 3, The Chemical Society, London (1975); b) J. P. Champion, A. G. Robiette, I. M. Mills, and G. Graner, *J. Mol. Spectrosc.*, **96**, 422 (1982).

11) S. Kondo, Y. Koga, T. Nakanaga, and S. Saëki, *Bull. Chem. Soc. Jpn.*, **56**, 416 (1983).

12) N. Bensari-Zizi and C. Alamichel, *J. Mol. Spectrosc.*, **99**, 98 (1983) (x's and g's of CH_3Cl).

13) N. Bensari-Zizi and C. Alamichel, *Mol. Phys.* **43**, 1255 (1981) (φ_{155} of CH_3Cl).

14) M. Morillon-Chapey and G. Graner, *J. Mol. Spectrosc.*, **31**, 155 (1969).

15) M. Morillon-Chapey, G. Guelachvili, and P. Jensen, *Can. J. Phys.* **62**, 247 (1984) (CH_3Cl ν_2, ν_5, $2\nu_3$).

16) N. Bensari-Zizi and C. Alamichel, *J. Phys. (Paris)*, **42**, 209 (1981) ($\nu_1-\nu_3$ of CH_3Cl).

17) A. G. Maki and R. Thibault, *J. Chem. Phys.*, **48**, 2163 (1968); P. Jensen, S. Brodersen, and G. Guelachvili, *J. Mol. Spectrosc.*, **88**, 378 (1981).

18) J. C. Deroche, *J. Mol. Spectrosc.*, **69**, 19 (1978) (ν_6 of CH_3Cl).

19) M. Imachi, T. Tanaka, and E. Hirota, *J. Mol. Spectrosc.*, **63**, 265 (1976).

20) E. W. Jones, R. J. L. Popplewell, and H. W. Thompson, *Spectrochim. Acta*, **22**, 659 (1966); *ibid.*, **22**, 669 (1966).

21) C. Yamada and E. Hirota, *J. Mol. Spectrosc.*, **64**, 31 (1977).

22) J. L. Duncan, *J. Mol. Struct.*, **6**, 447 (1970).

23) R. W. Peterson and T. H. Edwards, *J. Mol. Spectrosc.*, **38**, 524 (1971).

24) Y. Morino and J. Nakamura, *Bull. Chem. Soc. Jpn.*, **38**, 443 (1965).

25) C. Betrencourt-Stirnemann and C. Alamichel, *J. Phys.*, **31**, 285 (1970) (ν_1 of $CD_3{}^{35}Cl$ and $CD_3{}^{37}Cl$).

26) I. M. Mills, "Molecular Spectroscopy: Modern Research," ed by K. N. Rao and C. W. Mathews, Acad. Press, New York (1972), p. 115.

27) J. Overend, "Vibrational Intensities in Infrared and Raman Spectroscopy," ed by W. B. Person and G. Zerbi, Elsevier Sci. Pub. Co., Amsterdam (1982), p. 203.

28) For example, see M. Toyama, T. Oka, and Y. Morino, *J. Mol. Spectrosc.*, **13**, 193 (1964).

 © 1985 The Chemical Society of Japan

The Phosphorescence Spectra of 9,10-Anthraquinone β- and β,β'-Sulfonates in an Aqueous Solution at 77 K

Akira KUBOYAMA* and Sanae Y. MATSUZAKI
National Chemical Laboratory for Industry, Tsukuba Research Center, Yatabe, Ibaraki 305
(Received March 8, 1984)

The nπ* phosphorescence spectra, and their excitation spectra and lifetimes of 9,10-anthraquinone-2-sulfonate, and -2,6- and -2,7-disulfonates in water–ethylene glycol 1:1 mixture at 77 K have been obtained. These phosphorescence spectra shift to the red with increases in the concentration of the solutions, and show an excitation-wavelength dependence. From the results obtained it is concluded that in the glassy solutions at 77 K an association of these quinones occurs, and that the phosphorescence state of the associates corresponds to the nπ* triplet excimer state, similar to that of the *p*-quinone aggregates in polycrystalline solutions at 77 K, previously studied.

Heretofore, we have studied the nπ* phosphorescence spectra of quinones in organic solvents at 77 K.[1] In this work, we examine the phosphorescence spectra of 9,10-anthraquinone β- and β,β'-sulfonates (9,10-anthraquinone is abbreviated as AQ in the following) in a glassy aqueous solution at 77 K. Investigations of the complex formation of these quinones with enzymes and cyclodextrins using these spectra are now in progress. These quinones have the following features favorable to the above studies. They are water-soluble and stable in the dark, have a large hydrophobic quinone moiety, and their phosphorescence spectra in a glassy aqueous solution at 77 K are relatively strong. Sodium AQ-2-sulfonate has been used in many photochemical[2] and biochemical[3] studies. However, few studies of the emission spectra of these quinones have been reported.

Experimental

Measurements. The phosphorescence spectra, and their excitation spectra and lifetimes in solutions were obtained at 77 K using an Aminco SPF-500 spectrofluorometer equipped with a photon counter (PM tube 1P28).[1] The energy distribution of the exciting radiation (a 250 W xenon arc lamp) and the spectral transmittance of the monochromator have not been taken into account. In the measurements, the sample solutions were rapidly cooled to 77 K. In some cases the results obtained using fast and slow cooling-speeds were compared. Water–ethylene glycol 1:1 mixture (H_2O–EG) which forms a glassy solution at 77 K was mainly used as a solvent. The pH value of this solvent was 6.8 at 26.0 °C. Methanol–ethanol 1:4 mixture which forms a glassy solution at 77 K was also used. The electronic absorption spectra in solution were obtained at room temperature using a Cary 17D self-recording spectrophotometer. In the measurements of high concentration solutions of the quinones, a 0.1 mm quartz cell of Gaskuro Kogyo Co. was used. Since the quinones are easily reduced in aqueous solutions by irradiation, especially at room temperature, care was taken to shield the sample solutions of the quinones from light.

Materials. Sodium AQ-2-sulfonate (AQ-2S) and disodium AQ-2,6-disulfonate (AQ-26S) of Tokyo Kasei Kogyo Co. were purified by recrystallization from water. Disodium AQ-2,7-disulfonate (AQ-27S) was purified by alumina column chromatography (eluent H_2O–EG). Their purity was checked by TLC (silica gel, developer water–propanol (3:7) mixture). Non-fluorescent water from Wako Junyaku Kogyo Co. was used. Ethylene glycol of Nakarai Kagaku Yakuhin Co. specially prepared for chromatography was used. No fluorescent impurity was detected in H_2O–EG. Spectrograde methanol and analytical-grade ethanol from Wako Junyaku Kogyo Co. were used without further purification.

Results and Discussion

In Fig. 1, the phosphorescence spectrum of AQ-2S in H_2O–EG shows a red-shift with increase in the concentration of the solutions, and an excitation-wavelength dependence, especially in the two medium concentrations (those in the spectra b and c). The spectra obtained with the 365 nm excitation are at longer wavelengths than those obtained with the 330 nm excitation. This excitation-wavelength dependence is very small in the low and high concentrations (those in the spectra a and d). These results suggest that the quinone molecules associate. The spectra in the low concentration (6.6×10^{-5} mol dm^{-3}) at the 330 nm excitation and in the high concentration (2.0×10^{-2} mol dm^{-3}) at the 365 nm excitation may be thought to be close to those of the quinone monomer and associate, respectively. The distance between these two spectra is *ca.* 600 cm^{-1}. Similar results were also observed in AQ-26S and -27S, as is seen in Figs. 2 and 3, but in these two quinones such a high concentration where the same spectra were obtained at the 330 and 365 nm excitations in the case of AQ-2S (the spectra d in Fig. 1) can not be realized because of the low solubility of these quinones in H_2O–EG.

The shapes of the spectra b and c of AQ-2S in the medium concentrations in Fig. 1 are similar to those of the spectra a and d in the low and high concentrations in Fig. 1. They are different from those of the simulation spectra in Fig. 4. The latter are composed of the two above-mentioned spectra which are thought to be close to those of the monomer and the associate. In Fig.

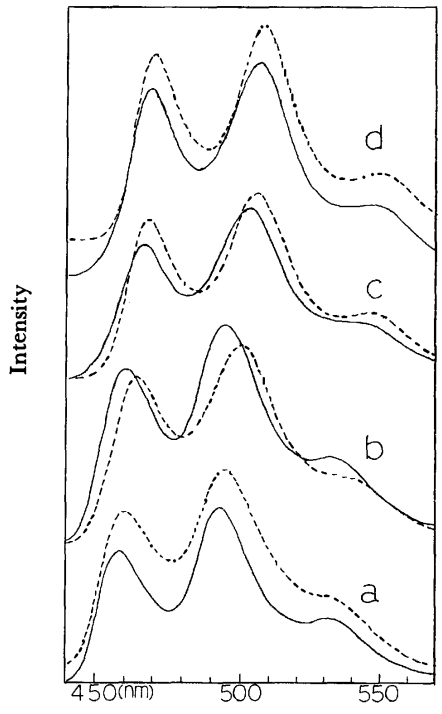

Fig. 1. Phosphorescence spectra of sodium 9,10-anthraquinone-2-sulfonate in the water–ethylene glycol mixture solution at 77 K, obtained without the rotating sector.
a: 6.6×10^{-5} M, b: 6.6×10^{-4} M, c: 6.6×10^{-3} M, d: 2.0×10^{-2} M, ——: 330 nm ex., ----: 365 nm ex. (In Figs. 1—8, M denotes the unit of mol dm^{-3}, and ex. does excitation.)

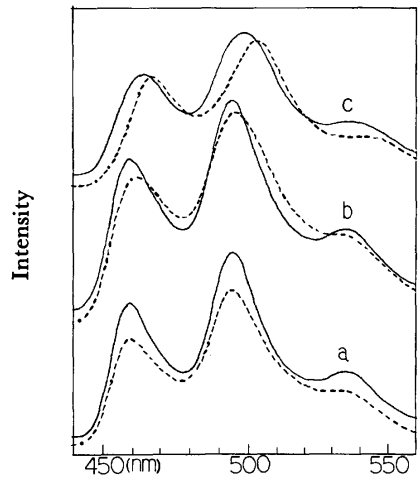

Fig. 2. Phosphorescence spectra of disodium 9,10-anthraquinone-2,6-disulfonate in the water–ethylene glycol mixture solution at 77 K, obtained without the rotating sector.
a: 6.0×10^{-5} M, b: 1.45×10^{-3} M, c: 1.2×10^{-2} M, ——: 330 nm ex., ----: 365 nm ex.

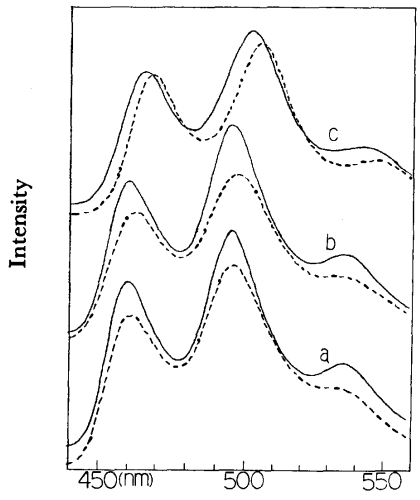

Fig. 3. Phosphorescence spectra of disodium 9,10-anthraquinone-2,7-disulfonate in the water–ethylene glycol mixture solution at 77 K, obtained without the rotating sector.
a: 6.5×10^{-5} M, b: 3.6×10^{-4} M, c: 7.9×10^{-3} M, ——: 330 nm ex., ----: 365 nm ex.

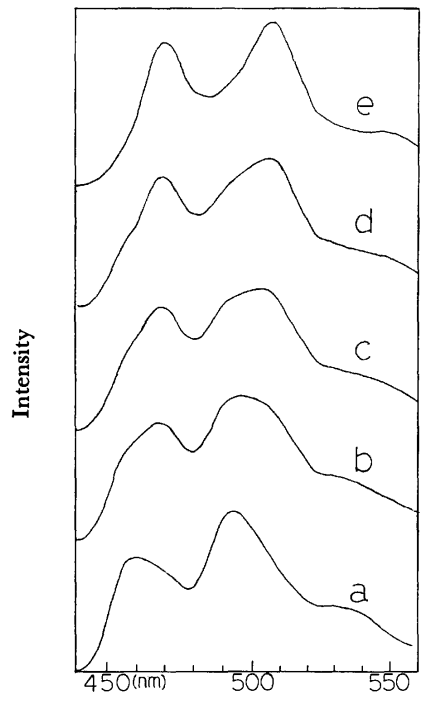

Fig. 4. Simulation spectra of sodium 9,10-anthraquinone-2-sulfonate composed of the spectra a (330 nm ex.) and d (365 nm ex.) in Fig. 1. The ratios of these two spectra in the spectra a—e are 4 : 1, 3 : 2, 1 : 1, 2 : 3, and 1 : 4, respectively.

l the peaks in the observed spectra are symmetrical, while in Fig. 4 most peaks in the simulation spectra are asymmetrical. Therefore, it is thought that there are more than one species in the number of the component molecules of the quinone associates, and consequently that in the high concentration solution the number of component molecules of the main part of the associates is greater than two, though its estimation is difficult at this stage. The spectra in the medium concentrations may be composed of the monomer and associates having various number of component molecules.

As is seen in AQ-2S (Fig. 5), the low-energy $\pi\pi^*$ absorption spectra[4] of these quinones in H_2O-EG at room temperature are broad and show only a small red-shift with increases in the concentration of the solutions. In Fig. 5, the peak wavelengths of the spectra 1 and 2 are 330 and 331 nm, respectively. The λ_{max} and molar absorption coefficients of the solutions of the concentrations lower than 1.8×10^{-3} mol dm^{-3} are almost constant.

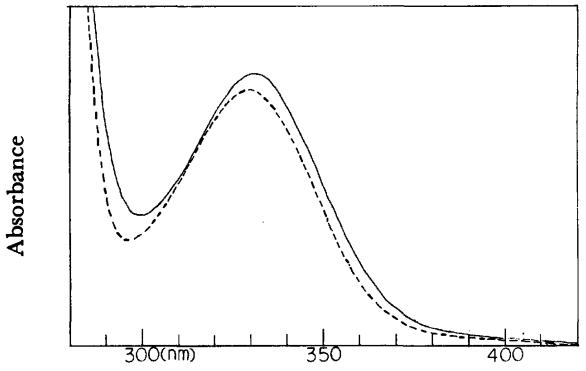

Fig. 5. Electronic absorption spectra of sodium 9,10-anthraquinone-2-sulfonate in the water–ethylene glycol solution at room temperature.
——: 2.0×10^{-2} M (spectrum 1), ----: 1.8×10^{-3} M (spectrum 2).
(The ordinate is arbitrary.)

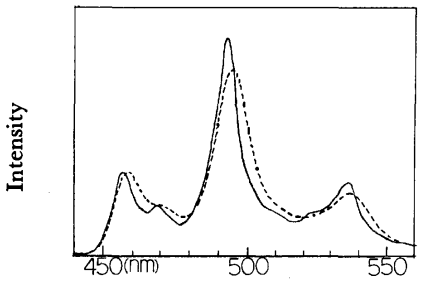

Fig. 6. Phosphorescence spectra of 9,10-anthraquinone (I) and sodium 9,10-anthraquinone-2-sulfonate (II) in the methanol–ethanol mixture solution at 77 K.
——: I 3.8×10^{-5} M, ----: II 6.1×10^{-5} M.

These phosphorescence spectra show a clear CO stretching vibrational structure and the phosphorescence lifetimes are around 2 ms, as is seen in Table 2. Since the phosphorescence spectra are similar to the $n\pi^*$ phosphorescence spectra of AQ[1b-1g] in organic solvents in position, vibrational structure, and lifetime, they also may be safely assigned to the $n\pi^*$ phosphorescence spectrum. As the electronic transition in the $n\pi^*$ phosphorescence spectra of AQ is orbitally forbidden,[5,6] the relative height of the shortest wavelength peak, 0-0 peak, in the phosphorescence spectrum of AQ-2S is also low in organic solvents, as is seen in Fig. 6,[7] while those in H_2O-EG in Fig. 1 are considerably larger. This may result from the symmetry-degradation of the quinone π-electronic system due to the strong, random hydrogen-bond formation between AQ-2S and water.

Table 1. Peak wavelengths, λ, of the phosphorescence spectra at 77 K

	Solvent	λ/nm			
AQ	M-E[b]	456.5	492	534.5	Fig. 6
AQ-2S[a]	M-E	458	493.5	535.5	Fig. 6
AQ-2S	H_2O-EG	456	491		Fig. 1[c]
AQ-2S	H_2O-EG	468.5	506		Fig. 1[d]
AQ-26S[a]	H_2O-EG	457	492.5		Fig. 2[c]
AQ-26S	H_2O-EG	465	501		Fig. 2[d]
AQ-27S[a]	H_2O-EG	459.5	495		Fig. 3[c]
AQ-27S	H_2O-EG	467.5	504.5		Fig. 3[d]

a) AQ-2S, -26S, and -27S denote sodium AQ-2-sulfonate and disodium AQ-26- and -27-disulfonates, respectively. b) M-E denotes the methanol-ethanol mixture solution. c) The values are for the low-concentration solutions (330 nm ex.). d) The values are for the high-concentration solutions (365 nm ex.).

Table 2. Observed phosphorescence lifetimes, τ, at 77 K

	Solvent	τ/ms	
AQ	M-E[b]	3.3	Fig. 6
AQ-2S[a]	M-E	2.3	Fig. 6
AQ-26S[a]	M-E	2.1	Ref. 10
AQ-2S	H_2O-EG	2.0	Fig. 1[c]
AQ-2S	H_2O-EG	2.3	Fig. 1[d]
AQ-26S	H_2O-EG	1.8	Fig. 2[e]
AQ-27S[a]	H_2O-EG	1.7	Fig. 3[e]

a) AQ-2S, -26S, and -27S denote sodium AQ-2-sulfonate and disodium AQ-26- and -27-disulfonates, respectively. b) M-E denotes the methanol-ethanol mixture solution. c) The value is for the low-concentration solution (330 nm ex.). d) The value is for the high-concentration solution (365 nm ex.). e) The values for the low-concentration solution (330 nm ex.) and the high-concentration solution (365 nm ex.) are almost the same.

As is seen in Fig. 7, the phosphorescence spectrum obtained with the slow rotating sector is far broader than that obtained with the fast rotating sector. In the spectra of the methanol-ethanol mixture solution of AQ-2S in Fig. 6, no such a sector-speed dependence of the phosphorescence spectra can be observed. In our previous work[1g] on methyl-substituted AQ's, results similar to the above sector-speed dependence of the phosphorescence spectra were obtained in non-saturated-hydrocarbon solutions. This may be due to there being a T_1 $n\pi^*$ level and a close-lying T_2 $\pi\pi^*$ level in AQ-2S in H_2O-EG, resulting from the strong hydrogen-bond formation between AQ-2S and water. There is a T_1 $\pi\pi^*$ level in the strongly solvated species. Consequently, in the spectra obtained with the slow rotating sector the sharp $n\pi^*$ and broad $\pi\pi^*$ spectra with different lifetimes overlap, as in the case of methyl-substituted AQ's.[1g] Since above-mentioned broad spectrum is observed only weakly, the phosphorescence spectrum obtained with the fast rotating sector contains the $\pi\pi^*$ spectrum as a very small contribution. The results similar to the above results are also observed in AQ-26S and -27S.

The phosphorescence excitation spectra of the low and high concentration solutions of AQ-2S are shown with that of a low-concentration solution of AQ-27S in Fig. 8. In these spectra, the weak long-wavelength part with a structure,[8] and the strong, broad short-wavelength part correspond to the S-S $n\pi^*$ and $\pi\pi^*$ absorption spectra, respectively.[9] In Fig. 8, the short-wavelength part of the excitation spectrum b of the high-concentration solution of AQ-2S is omitted, because the absorption in this wavelength region is very strong. The long-wavelength part of the excitation spectra in AQ-2S is almost the same in position and shape in the low- and high-concentration solutions. Similar results were obtained for AQ-26S and -27S. Therefore, the $n\pi^*$ absorption spectra of the monomer and associates of these quinones are at almost the same position. However, as mentioned before, the $n\pi^*$ phosphorescence spectra of these quinones shift considerably to the red with increases in the concentration. These circumstances are similar to those in the $n\pi^*$ phosphorescence spectra of the aggregates of the *p*-quinones, 1,4-naphthoquinone and 5,14:7,12-pentacenediquinone, in polycrystalline solutions at 77 K, previously studied.[1h] According to our previous work,[1h] the phosphorescence states of the quinone associates discussed here are also thought to correspond to the $n\pi^*$ excimer state. In these quinones, the $n\pi^*$ absorption spectra of the quinone monomer and associates are at almost the same position, as is mentioned above, while in the polycrystalline solutions the $n\pi^*$ absorption spectra of the aggregates are at shorter wavelengths than those of the corresponding quinone monomer, though the $n\pi^*$ phosphorescence spectra of these *p*-quinone aggregates appear at considerably longer wavelengths than those of the corresponding monomers.[10] This may indicate that the interaction between the quinone molecules in these associates is weaker than those in the *p*-quinone aggregates in the polycrystalline solutions.

With regards to the phosphorescence lifetimes shown in Table 2, the phosphorescence lifetimes of AQ-2S and -26S[11] in the methanol-ethanol mixture solution are considerably shorter than that of AQ

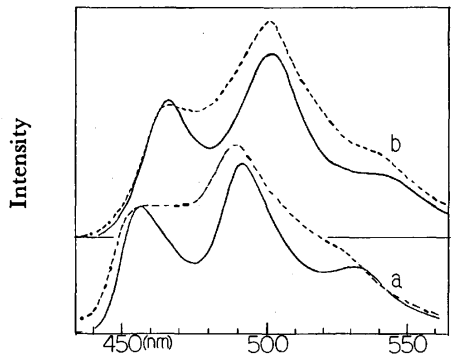

Fig. 7. Effect of the sector-speed on the phosphorescence spectra of sodium 9,10-anthraquinone-2-sulfonate in the water–ethylene glycol mixture solution at 77 K. a: 6.6×10^{-5} M, 330 nm ex., b: 6.6×10^{-3} M, 330 nm ex., —— with the fast-rotating sector (11500 min^{-1}), ---- with the slow-rotating sector (2070 min^{-1}).

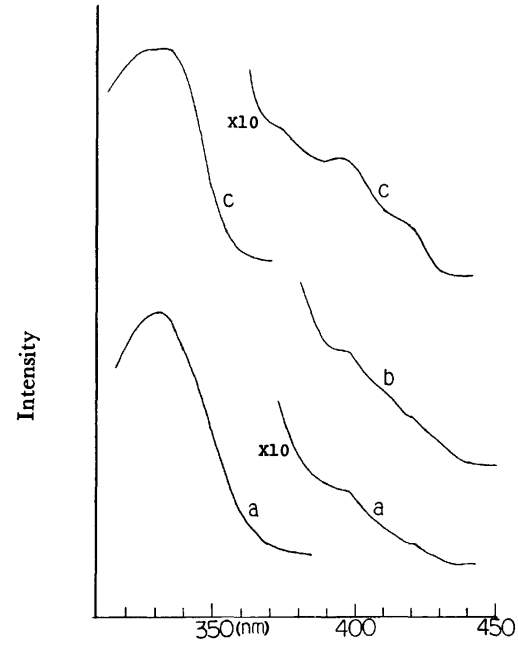

Fig. 8. Phosphorescence excitation spectra of sodium 9,10-anthraquinone-2-sulfonate (a,b) and disodium 9,10-anthraquinone-2,7-disulfonates (c) in the water–ethylene glycol mixture solution at 77 K.
a: 6.6×10^{-5} M, b: 6.6×10^{-3} M, c: 3.3×10^{-5} M.

and only slightly longer than the corresponding ones in H_2O-EG, in spite of the relative height of the 0-0 peak in the phosphorescence spectrum of AQ-2S in these two solutions being considerably different, as is seen in Figs. 1 and 6. In AQ also, the phosphorescence lifetimes of the methylcyclohexane and methanol-ethanol mixture solutions are both 3.3 ms, in spite of the relative height of the 0-0 peak in the latter solution being considerably larger than that in the former solution.[1g] In AQ-2S, the phosphorescence lifetime in the high-concentration solution is slightly longer than that in the low-concentration solution.

The association of these quinones is thought to be due to their having both a large hydrophobic quinone moiety and hydrophilic sulfonato anion groups. In the associates, the quinone molecules are thought to orient themselves, avoiding the strong steric hindrance of the sulfonato anion groups and overlapping their planar quinone moiety. The detailed structures of the associates can not be discussed at this stage.[1h]

References

1) a) A. Kuboyama and S. Yabe, *Bull. Chem. Soc. Jpn.*, **40**, 2475 (1967); b) A. Kuboyama, *ibid.*, **43**, 3373 (1970); c) A. Kuboyama and M. Anze, *Nippon Kagaku Kaishi*, **1972**, 229; d) A. Kuboyama and S. Matsuzaki, *ibid.*, **1973**, 2249; e) S. Y. Matsuzaki and A. Kuboyama, *Bull. Chem. Soc. Jpn.*, **51**, 2264 (1978); f) A. Kuboyama, *ibid.*, **51**, 2771 (1978); g) A. Kuboyama and S. Y. Matsuzaki, *ibid.*, **54**, 3635 (1981); *J. Nat. Chem. Lab. for Ind.*, **78**, 21 (1983); h) A. Kuboyama, Y. Kojima, and S. Y. Matsuzaki, *Bull. Chem Soc. Jpn.*, **56**, 2572 (1983); *J. Nat. Chem. Lab. for Ind.*, **79** 173 (1984).

2) For example, I. Loeff, A. Treinin, and H. Linschitz, *J. Phys. Chem.*, **87**, 2536 (1983); A. Roy and S. Aditya, *J. Photochem.*, **22**, 361 (1983).

3) For example, W. Oettmeier and W. Lockau, *Z. Naturforsch., C*, **28**, 717 (1973); A. A. Lamola, *Mol. Photochem.*, **4**, 107 (1972).

4) The $n\pi^*$ absorption spectra are observed as broad shoulders on the long-wavelength side.

5) The 0-0 peak in the $n\pi^*$ phosphorescence spectra of AQ in the normal paraffine Shpol'skii matrices is very weak.[1b]

6) K. E. Drabe, H. Veenvliet, and D. A. Wiersma, *Chem. Phys. Lett.*, **35**, 469 (1975); J. P. Galaup, J. Megel, and H. P. Trommsdorff, *ibid.*, **41**, 397 (1976); O. S. Khalil and L. Goodman, *J. Phys. Chem.*, **80**, 2170 (1976); N. S. Strokach and D. N. Shigorin, *Opt. Spectrosk.*, **43**, 34 (1977); E. Kanezaki, N. Nishi, and M. Kinoshita, *Bull. Chem. Soc. Jpn.*, **52**, 2836 (1979).

7) These spectra show no quinone-concentration and excitation-wavelength dependences.

8) In both the spectra a and b, two shoulders are observed at 420 and 397.5 nm.

9) The long-wavelength part of the excitation spectra in AQ-26S is close to that in AQ-27S in Fig. 8 in position and shape.

10) Similar long-wavelength $n\pi^*$ phosphorescence spectra have also been observed in polycrystalline solutions of *p*-benzoquinone and 2-methyl-AQ.[1h]

11) The phosphorescence spectrum of AQ-26S in the methanol-ethanol mixture solution is close to that of AQ-2S in position and shape.

Adsorption of Hydrophobic Anions onto Phospholipid Membranes. The Effect of Membrane Surface Charge

Hideo MATSUMURA,* Hiroyuki KAKOKI,† and Kunio FURUSAWA†
Electrotechnical Laboratory, Sakura-mura, Ibaraki 305
†*Department of Chemistry, The University of Tsukuba, Sakura-mura, Ibaraki 305*
(Received April 16, 1984)

Hydrophobic adsorption of tetraphenylborate ions (TPB) onto lipid membranes were studied at different pH's of aqueous phase by using lipid vesicles and monolayers. The amount of adsorbed TPB is much higher at pH 2 than at pH 7.4. This result indicates that the adsorption of hydrophobic ions is affected by the ionization state of surface polar groups of lipids, *i.e.*, that the membrane surface potential plays a role in the adsorption of hydrophobic ions.

Interactions of ions with phospholipid membranes have been intensively studied, especially, the binding of metal cations to negatively charged phospholipid membranes, which is now fairly well understood.[1-4] Interactions of organic ions with phospholipid membranes, however, have not yet been explored. Hydrophobic ions may be permeable through lipid bilayers *via* their hydrophobic interaction with lipid hydrocarbon chains. Therefore, hydrophobic anions and cations have been used as tracers to estimate the barrier height of membrane's electrical potential. The transport mechanism for hydrophobic ions passing through a lipid bilayer membrane has been studied by Ketterer *et al.*[5] They measured the conductance of tetraphenylborate ions through a black bilayer membrane of dioleoyllecithin, and proposed the "three-step model" that consists of adsorption, translocation, and desorption steps. In this model, the adsorption sites are considered to be located near the membrane-aqueous solution interface on the membrane side. Therefore, it is possible to determine the membrane potential by measuring the amount of these ions adsorbed from the aqueous phase. Further, it is significant to elucidate exactly the feature of adsorption of these ions from the aqueous phase.[6]

Andersen *et al.*[7] measured surface potential change of bacterial phosphatidylethanolamine monolayer on aqueous solution as a function of aqueous TPB concentration and proposed the discrete charge effect for the boundary potential model with a limiting number of adsorbed ions. In this sense, electrical charges near the membrane surface have a remarkable influence on the adsorption behavior of charged molecules toward the membrane. It is believed that charges on the membrane surface play a role in the binding of charged molecules such as metal ions and ionic detergents to the membrane.[8] In this work, the effect of the ionization state of surface polar groups on the adsorption of TPB onto a phospholipid membrane has been studied systematically by using phospholipid vesicles and monolayers as membrane samples.

Experimental

Bovin brain phosphatidylethanolamine (BPE), dipalmitoylphosphatidylethanolamine (DPPE), and dimyristoylphosphatidic acid (DMPA) were purchased from Sigma Chemical Co. (USA) to be used as phospholipids. Sodium tetraphenylborate was purchased from DOJINDO Laboratories (Japan). These were employed without further purification. The other reagents used were of analytical grade. All solutions of these substances were made with deionized and doubly distilled water.

BPE vesicles were prepared by sonication without using any buffer to eliminate the spurious effect of included buffer ions.[9] The amount of TPB adsorbed on these vesicles was measured as follows: 2 ml of a vesicle suspension was added to 2 ml of a TPB solution of known concentration in a glass-stoppered vial (5 ml). After the mixture had been left standing overnight at room temperature, the vesicle particles were separated from the medium liquid by ultrafiltration (MILLIPORE, PTGC). The concentration of TPB in the filtrate as well as in the original solution was measured by the inductively coupled Argon plasma method (Jarrell-Ash 975). From these measurements, the amount of adsorbed TPB per gram of vesicles was calculated by using a calibration curve.

Electrophoretic mobilities of large vesicles were determined at various pH values in an aqueous solution of 1×10^{-3} mol dm^{-3} KCl at 25 °C. The measurments were performed in a Rank Brother microelectrophoresis apparatus (MK-2) using a rectangular glass cell.

Monolayers of phospholipids were prepared by spreading a chloroform/ethanol (3:1) solution of DPPE or hexane/ethanol (9:1) solution of DMPA on the surface of a subphase solution containing 0.1 mol dm^{-3} NaCl and 0.01 mol dm^{-3} *Tris*-HCl buffer at pH 7.4 or HCl at pH 2 in an 80 ml Teflon trough. The subphase solution was continuously stirred with a glass-sealed 5 mm needle by a magnetic stirrer, except while the surface potential change being measured. A concentrated TPB solution was added to the solution, and this mixed solution was stirred for more than 30 min. Surface potentials of the monolayer were measured with a vibrating electrode against an Ag/AgCl reference electrode as a function of TPB concentration.

Results and Discussion

The degree of ionization of phospholipid polar groups depends on the pH of solution. It has been reported that a phosphatidylethanolamine (PE) membrane has net negative charges at neutral pH due to the deprotonating effect of the lower amino group on the vesicle surface[3] or due to hydrolytic degradation of PE molecules.[4] To confirm the state of ionization of our PE vesicles, electrophoretic mobility was measured in 0.001 mol dm^{-3} KCl aqueous solution. Figure 1 indicates that the PE vesicles have net negative surface charges at neutral pH and that the value decreases with decrease in pH value. This trend agrees qualitatively with the result of Papahadjopoulos[4] shown in Fig. 1, which was obtained with 0.145 mol dm^{-3} NaCl aqueous solution. Both data exhibit that electrophoretic mobilities converge to zero at pH 2. The membrane surface potential (or more exactly, the potential at the Stern layer) at pH 7.4 can be calculated, on the assumption of a Boltzmann distribution for the counter ions from our data and that of Papahadjopoulos, according to

$$\zeta = \phi_0 e^{-\kappa d}, \quad (1)$$

where ζ is the zeta potential, κ Debye's reciprocal length, d the distance from membrane surface to slipping plane, and ψ_0 the membrane surface potential. By this analysis using the ζ value at pH 7.4, the result of d=11 Å and ψ_0=−60 mV is obtained. Considering the value of d=10 Å for silica particles in 0.01 mol dm^{-3} NaCl solution, the value of d=11 Å is not so unrealistic as the distance in 0.1—0.001 mol dm^{-3} salt solution. Furthermore, as shown later, the estimated ψ_0 value (ψ_0=−60 mV) is in close agreement with the value derived from adsorption experiments.

In Fig. 2, adsorption isotherms for TPB on PE vesicles are shown in the form of semi-log plot, which were obtained at pH's 7.4 and 2 in 0.001 mol dm^{-3} KCl solution. From these data, it is possible to examine the surface potential effect on the adsorption by using the following relation:

$$[\mathrm{TPB}]_m = K[\mathrm{TPB}]_b e^{\psi_0 F/RT}, \quad (2)$$

where $[\mathrm{TPB}]_m$ is the concentration of TPB adsorbed on the membrane, $[\mathrm{TPB}]_b$ the residual concentration of TPB in the bulk solution, ψ_0 the membrane surface potential, K a constant independent of the surface potential term (K can be expressed by $K_{ad}e^{\Phi F/RT}$, where K_{ad} is the adsorption coefficient and Φ the electrostatic potential difference between membrane surface and adsorbing site), and the other symbols have the usual meanings. The solid lines in Fig. 2 are the curves obtained by calculation from Eq. 2 for two $Ke^{\psi_0 F/RT}$ values, which are different from each other by a factor of

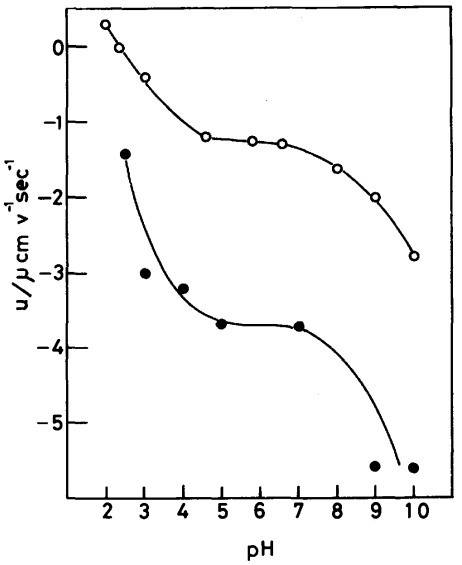

Fig. 1. Electrophoretic mobility-pH curves for PE vesicles.
(●): 0.001 mol dm^{-3} KCl, (○): Papahadjopoulos' data: 0.145 mol dm^{-3} NaCl.

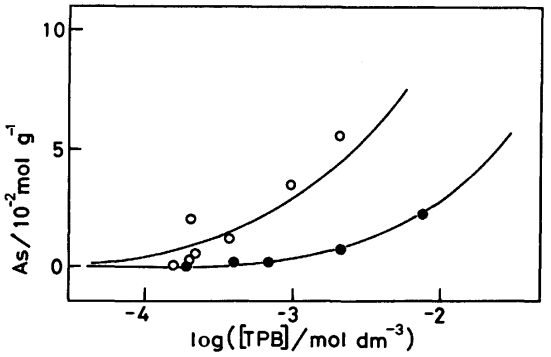

Fig. 2. Adsorption isotherms of TPB to PE vesicles.
(●): pH 7.4, (○): pH 2.

10, indicating that between the two cases there is a difference of about 60 mV in surface potential. As seen from Fig. 2, the two analytical curves fit the respective data very well, suggesting that the membrane surface potential at pH 7.4 is nearly −60 mV since the potential at pH 2 will become zero (see Fig. 1). An analogous discussion can be developed by using the data from the potential measurements on monolayer membranes. Potential change owing to TPB adsorption onto the monolayer can be given as follows on the simple capacitor model:

$$\Delta\Delta V = [\mathrm{TPB}]_m(F/C) = K_{ad}[\mathrm{TPB}]_b e^{\psi_0 F/RT} e^{\Phi F/RT}(F/C), \quad (3)$$

where Φ is the potential difference between membrane surface and adsorbing site, C the specific capacitance of the outer region of monolayer, K_{ad} the adsorption

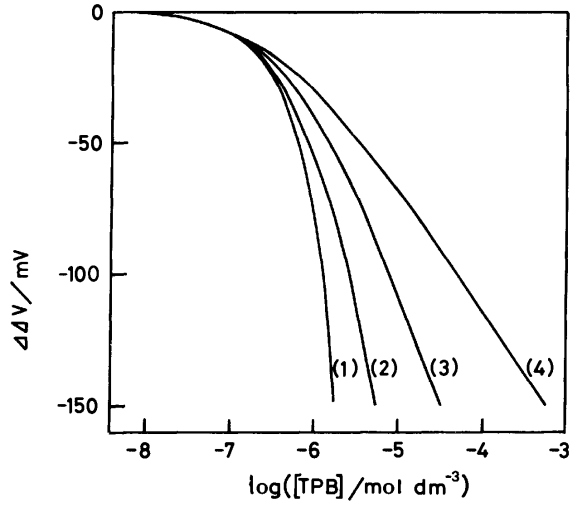

Fig. 3. Calculated curves from Eq. 3 for surface potential change of monolayer membrane. (1): $\Phi=0$, (2): $\Phi=0.2\Delta\Delta V$, (3): $\Phi=0.5\Delta\Delta V$, (4): $\Phi=\Delta\Delta V$.

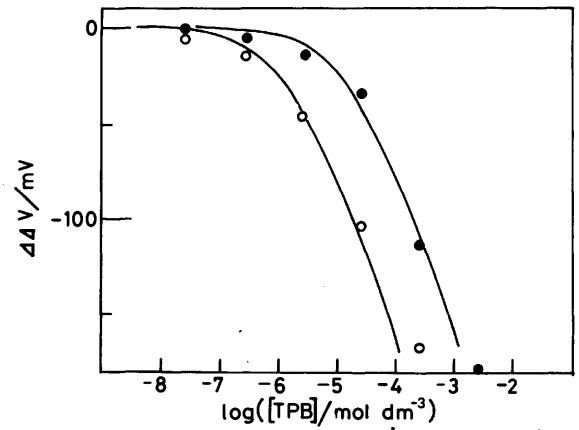

Fig. 5. Surface potential change of DMPA monolayer membrane *vs.* concentration of TPB (●): pH 7.4, (○) pH 2.

coefficient, ψ_0 the surface potential, and the other symbols have the usual meanings.

Figure 3 shows several calculated curves obtained from Eq. 3 by assuming ψ_0 is constant. In this case, Φ, is the electrostatic potential produced by adsorption of TPB on the membrane and expressed by the equation $\Phi=a\cdot\Delta\Delta V$. In the case if $a=1$, the full electrostatic potential produced by the adsorption of TPB molecules affects the adsorption of the next TPB molecule onto the membrane. In the case of $a=0$, the adsorption is affected by the chemical potential difference between solution and membrane and by the surface potential. In the experiments, intermediate cases with $0<a<1$ were observed. In Fig. 4, data of $\Delta\Delta V$ are plotted against the solution concentration of TPB (not against the residual concentration, though actually both are equal to each other) for the two values of pH. In these experiments, DPPE monolayers which have a packing density of

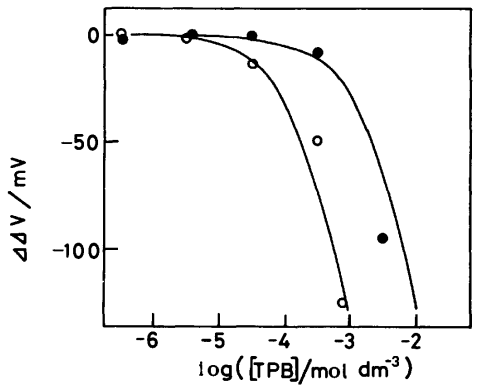

Fig. 4. Surface potential change of DPPE monolayer membrane *vs.* concentration of TPB. (●): pH 7.4, (○): pH 2.

1/80 molecule/Å^2 were used as the membrane sample. The solid lines in the figure are calculated curves from Eq. 3 in the case of $\Phi=0.2\Delta\Delta V$ for the two $K_{ad}(F/C)e^{\psi_0 F/RT}$ values differing from each other by a factor of 10. The agreement between the observed and calculated values is excellent if we take the experimental errors in consideration. If the capacitance value (C) in the boundary region is kept constant, there is expected to be about 60 mV difference in the surface potential of DPPE monolayer membrane between pH's 7.4 and 2. This value is in close agreement with the result estimated by the zeta potential analysis.

Similar behavior has been observed with DMPA monolayer membranes which have a packing density of 1/60 molecule/Å^2. In this case, calculated curves for $\Phi=0.5\Delta\Delta V$ were in close agreement with experimental data as shown in Fig. 5. These data suggest that there is a difference of about 60 mV in the surface potential of DMPA monolayer membrane between pH's 7.4 and 2.

The present analysis indicates that the adsorption equilibrium of TPB may be reasonably expressed by Eq. 3. This means that adsorption equilibrium exists between the concentration of TPB in the membrane, $[TPB]_m$, and the concentration of TPB at the membrane surface, $[TPB]_0$, which is represented by $[TPB]_b e^{\psi_0 F/RT}$. This is in good agreement with observations made on other charged molecules.

References

1) T. Seimiya, M. Ashida, Y. Heki, T. Muramatsu, I. Hara, and M. Hayashi, *J. Colloid Interface Sci.*, **55**, 388 (1976).

2) S. Ohki and R. Sauve, *Biochim. Biophys. Acta*, **511**, 377 (1978).

3) H. Hauser and M. C. Phillips, *Progress in Surface and Membrane Science*, **13**, 297 (1979).

4) D. Papahadjopoulos, *Biochim. Biophys. Acta*, **163**, 240 (1968).

5) B. Ketterer, B. Neumcke,and P. Läuger, *J. Membr. Biol.*, **5**, 225 (1971).

6) B. A. Levine, J. Sackett, and R. J. P. Williams, *Biochim. Biophys. Acta*, **550**, 201 (1979).
7) O. S. Andersen, S. Feldberg, H. Nakadomari, S. Levy, and S. Mclaughlin, *Biophys. J.*, **21**, 35 (1978).
8) S. Mclaughlin and H. Harary, *Biochemistry*, **15**, 1941 (1976).
9) S. Fujii, F. Kokufuta, and K. Furusawa, *Chem. Lett.*, **1978**, 555.

 © 1985 The Chemical Society of Japan Bull. Chem. Soc. Jpn., 58, 82—87 (1985) [Vol. 58, No. 1

Study of Chemisorption and Hydrogenation of 2-Butenes on Platinum by Temperature-programmed Desorption

Shinji TOKITAKA,† Hayao IMAMURA, and Susumu TSUCHIYA*
Department of Industrial Chemistry, Faculty of Engineering, Yamaguchi University, Tokiwadai, Ube 755
(Received May 10, 1984)

The temperature-programmed desorption (TPD) chromatograms of *cis*- and *trans*-2-butene from platinum black comprised three peaks (A, B, and C) with peak maxima at about 253, 373, and 573 K, respectively. Peak A was identified to be *cis*- or *trans*-2-butene and butane. Peaks B and C were from mixtures of *cis*- or *trans*-2-butene and butane with a trace amount of propylene. The propylene may have been formed from chemisorbed *cis*- or *trans*-2-butene by decomposition as the temperature was raised during the subsequent TPD. The reactivities of various types of chemisorbed hydrogen previously detected by TPD were also investigated with regard to the hydrogenation of 2-butenes. Two types of chemisorbed hydrogen, presumed to be present on the surface in the form of hydrogen atoms, chemisorbed on top of platinum atoms and in the bridge form of molecular hydrogen, were found to react with 2-butenes.

The existence of four different chemisorbed species of hydrogen (α, β, γ, and δ) on platinum surfaces has previously been detected by a temperature-programmed desorption (TPD) with peak maxima at about 170, 250, 360, and 570 K, respectively.[1] The TPD chromatogram with four peak maxima has been confirmed by Verbeeks and Sachtler.[2] These chemisorbed species were tentatively assumed to correspond to two types of molecularly chemisorbed hydrogen (one in a linear form (α) and the other in a bridge form (β)) and two types of hydrogen atoms (one adsorbed right on top of metal atoms (γ) and the other in the interstices between the metal atoms(δ)). The differences in their reactivities have been investigated for the H_2–D_2 exchange reaction[3] and for the hydrogenation of ethylene,[4] and of propylene.[5] The reactivity, however, was not necessary the same: β-hydrogen not involved in the H_2–D_2 exchange reaction did react with ethylene and propylene to form ethane and propane, respectively.[4,5] It is, therefore, important to investigate this matter more deeply.

In the present study, 2-butenes were employed as the reactants to investigate differences in the reactivity of various forms of chemisorbed hydrogen since it is the lowest olefin that can be hydrogenated and isomerized.

The isotope exchange involving reactant olefins during the hydrogenation in the presence of deuterium has been of interest to many investigators.[6] Information related to this matter can contribute to the understanding of the mechanism regarding the hydrogenation of olefins. If the reactant olefin molecules are more rapidly exchanged than hydrogenated, the deuterated olefin molecules may be stably chemisorbed on the surface. In previous cases (ethylene[4] and propylene[5]) deuterated olefin molecules which were chemisorbed could not be measured. Since the chemisorbed state is an intermediate state, related information on this species is of importance.

In the present study, the chemisorbed species were removed by the TPD technique and collected for further analysis in order to obtain information on the reaction mechanism.

Experimental

Apparatus and Materials. The apparatus used was the same as that used previously[4] and consisted, basically, of two parts. The first part consisted of an adsorption and a reaction system in which adsorption and reaction were measured in conventional manners. The second part consisted of a TPD system, in which adsorbed gas was later desorbed into a carrier-gas stream (N_2 or He) by means of the programmed heating of a catalyst. The concentration of the desorbed gas was measured and recorded by means of a thermal conductivity detector. The catalyst was platinum black from the same lot previously employed.[4] Its surface area was 3.2×10^3 cm^2/g and the amount used was 2.18 g. The initial reduction and the treatment of the catalyst between experiments have also been described previously.[4]

Cylinder hydrogen (99.975%) supplied by the Osaka hydrogen Co. was stored in a reservoir for use as a reactant after having been passed over platinized silica at 720 K and then through a liquid-nitrogen trap. The same cylinder hydrogen could also be fed through to the reactor for the reduction of the catalyst. Matheson's deuterium (99.5%) passed through a liquid-nitrogen trap was also used as a reactant. *cis*- and *trans*-2-butene obtained from Tokyo Kasei Kogyo Co., Ltd., were purified by repeated distillation *in vacuo*; the purity was confirmed by means of gas chromatography to be more than 99%. High-purity helium (99.995%) and high-purity nitrogen (99.999%), obtained from the Seitetsu Kagaku Co., Ltd., were used as carrier gases for TPD after being passed through a molecular sieve trap.

Procedure. In a typical experiment with *cis*-2-butene, for example, a known amount of *cis*-2-butene was adsorbed for 15 min at the experimental temperature. The reactor was then cooled to 238 K with the *cis*-2-butene present in the gas phase, and kept for 90 min. Following this, the carrier gas, helium, was diverted from the bypass into the reactor in order to remove the *cis*-2-butene in its gas phase. After 5 min the catalyst was heated in a programmed manner. The heating was stopped at about 800 K, after which the catalyst was

† Present address: Toyo Soda Co., ltd., Tokuyama, 746.

kept in a helium stream for 20 min at the same temperature as before cooling. A more detailed description of the TPD method has been given elsewhere.[7] Reproducible results were usually obtained by this procedure. When the results were not reproducible, however, the catalyst was treated with oxygen to oxidize any organic contamination, and was then reduced by hydrogen. This treatment improved the reproducibility considerably.

In the hydrogenation of *cis*- and *trans*-2-butene, various types of chemisorbed hydrogen were first prepared by the TPD technique described previously,[1,3,8] and then olefin was admitted to the reaction system to start the reaction. Helium was added to dilute the olefin when the circulating pump in the reaction system was operated. After the reaction, all the system except for the reactor was evacuated through a liquid-nitrogen trap to collect any condensable hydrocarbons, which were transferred to a sampler for analysis. The carrier gas was then diverted into the reactor, and any materials adsorbed on the catalyst were removed by TPD.

The reactants, the reaction mixtures, and the desorption products were identified by gas chromatography. The deuterated hydrocarbons obtained after the reaction were analyzed by means of a JEOL JMS D-100 mass spectrometer. Before subjecting the reaction mixtures to mass-spectrometric analysis, if possible, they were separated gas chromatographically to avoid any mutual interference of the mass spectra.

Results and Discussion

Temperature-programmed Desorption. Figure 1 shows some typical TPD chromatograms taken after the *cis*-2-butene had been adsorbed on platium black in the absence, or presence, of hydrogen with helium used as the carrier gas. The pressure of the *cis*-2-butene or hydrogen admitted was *ca.* 5×10^2 Pa, and the reaction temperature was 238 K. These four TPD chromatograms resemble each other, characteristically being composed of three peaks with peak maxima at about 253, 373, and 573 K. These peaks are referred to as A, B, and C in the order of appearance with an increase in the temperature. By gas-chromatographic analysis, peak A was indentified to be *cis*-2-butene and butane. Peaks B and C were identified to be mixtures of *cis*-2-butene and butane with a trace amount of propylene. It is suggested that the butane was formed by the self-hydrogenation of chemisorbed *cis*-2-butene when hydrogen was absent. The propylene may have been formed by decomposition from the chemisorbed *cis*-2-butene heated by TPD.

Similar results were obtained for *trans*-2-butene. The description mentioned above is applicable if the word "*cis*-2-butene" is replaced by "*trans*-2-butene".

Reactivity of Chemisorbed Hydrogen. Table 1 shows the results of the surface-hydrogenation experiments with hydrogen preadsorbed on platinum black in various forms (the surface reactant) and with gaseous *cis*- or *trans*-2-butene subsequently admitted into the reaction system (the gas-phase reactant). No gaseous hydrocarbon other than 2-butenes and *n*-butane was observed under the present experimental conditions. The double-bond migration and the *cis-trans* isomerization of butenes and the skeletal isomerization of butane could not be detected. The amounts of butane formed in Series C-2 and T-2 with δ-hydrogen agreed well with that in Series C-1 and T-1 in which *n*-butane was formed by a self-hydrogenation reaction. Apparently, δ-hydrogen hardly reacts with the gas-phase reactant under the present experimental conditions.

In Series C-3 and T-3 with δ- and γ-hydrogen preadsorbed on the surface, however, relatively larger amounts of butane were produced than for Series C-2 and T-2. In the TPD chromatogram obtained after one of 2-butenes was admitted to the preadsorbed hydrogen, where nitrogen was used as the carrier

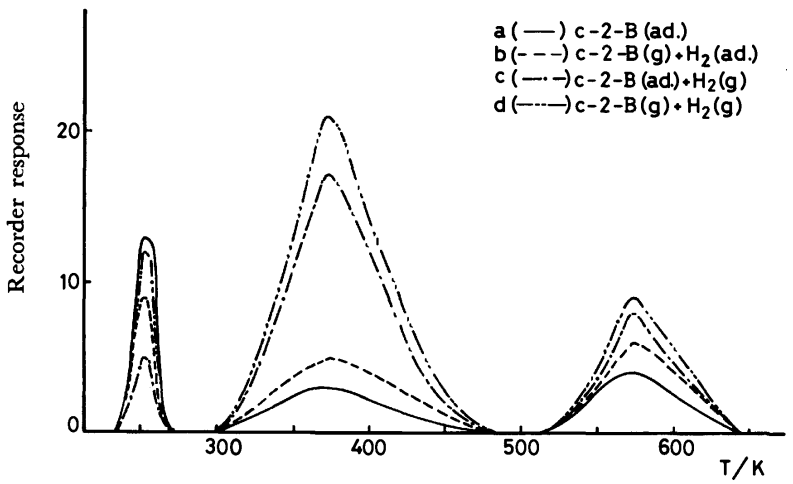

Fig. 1. TPD chromatograms of *cis*-2-butene on platinum.
(a): *cis*-2-Butene only was adsorbed, (b): H_2 was preadsorbed and *cis*-2-butene was subsequently admitted, (c): *cis*-2-Butene was preadsorbed and H_2 was subsequently admitted, (d): *cis*-2-Butene and H_2 were simultaneously admitted.

Table 1. Hydrogenation of *cis*-2-butene (series C1—C4) and of *trans*-2-butene (series T1—T4) on platinum black[a)]

Seriese	Surface reactant: Type of chemisorbed hydrogen and estimated amount[b)] (n/μmol)			Gas phase: Pressure of 2-butene (P/Pa)	Gas phase: Butane formed (n/μmol)
	β	γ	δ		
C-1	—	—	—	893	0.054
C-2	—	—	0.518	786	0.062
C-3	—	0.187	0.540	960	0.183
C-4	0.464	0.223	0.652	920	0.214
T-1	—	—	—	826	0.080
T-2	—	—	0.504	826	0.094
T-3	—	0.178	0.509	986	0.170
T-4	0.357	0.178	0.513	906	0.237

a) Catalyst weight, 2.18 g. Reaction temp 238 K, and reaction time, 90 min. b) Estimated from TPD chromatograms in comparable experiments.

gas, the γ-hydrogen disappeared, while δ-hydrogen was still present in almost the same amount. It is, therefore, clear that γ-hydrogen is involved in the hydrogenation.

In Series C-4 and T-4 in which β-, γ, and α-hydrogen were preadsorbed, the formation of butane was again observed. The contribution of β-hydrogen to the hydrogenation, however, was not clear at this stage, because the amounts of butane formed were not much different from those of γ-hydrogen. Since the amounts of butane formed in C-4 and T-4 were not very much different from those in C-3 and T-3, the results may suggest that β-hydrogen makes a minor contribution, if at all.

To elucidate the point, the preadsorbed hydrogen was partially displaced by deuterium before *cis*- or *trans*-2-butene was introduced, and the deuteriobutanes formed by hydrogenation were then analyzed. The participation of the different types of chemisorbed hydrogen was consequently elucidated. For the sake of simplicity, the word "hydrogen" in the present paper will hereafter stand for both isotopes, protium and deuterium, and, where necessary, the individual isotopes will be designated as H and D. The types of surfaces used were as follows: 1) δ-Hydrogen was displaced by deuterium, and γ- and β-hydrogen were displaced by protium (βH-γH-δD); 2) δ- and β-hydrogen were displaced by deuterium, and γ-hydrogen was displaced by protium (βD-γH-δD); 3) δ-Hydrogen was displaced by protium, and β- and γ-hydrogen were displaced by deuterium (βD-γD-δH). The method of preparation was described previously;[8)] the isolation of different types of chemisorbed hydrogen was confirmed by separate TPD experiments.

Table 2 shows the results of hydrogenation: The type of surface employed, the amounts of hydrogen preadsorbed and those of the individual deuteriobutanes formed by the hydrogenation are shown. The reactions were carried out at 238 K for 90 min. In the mass spectra of *cis*- or *trans*-2-butene, the reactant, the $m/e>56$ could not be observed, the ^{13}C contribution having been corrected; the H-D exchange between surface deuterium and gaseous *cis*- or *trans*-2-butene could not be detected.

Obviously, *cis*- and *trans*-2-butene were deuterated to deuteriobutanes over the βD-γH-δD, βD-γH-δH, and βH-γD-δH surfaces, but not over the βH-γH-δD surface. These results agree quite well with the above suggestions that δ-hydrogen does not, and γ-hydrogen does, participate in the hydrogenation. The results also suggest the participation of β-hydrogen, which was not clearly detected before.

It is natural that two possibilities for the participation of β-hydrogen be considered: 1) β-Hydrogen directly reacts with 2-butenes. 2) β-Hydrogen first converts to the γ-form and then reacts with 2-butenes. The very slow conversion of β-hydrogen to γ- and/or δ-hydrogen has previously been reported.[1)] In this case, olefin was absent and only hydrogen was present in the system. Therefore, if such conversion takes place during the hydrogenation, the conversion must proceed very fast and the 2-butenes also act as accelerators for the conversion. Since the conversion is actually the dissociation of a hydrogen molecule and the accelerator compound generally contacts with a reactant, 2-butenes must come into contact with β-hydrogen. The step is, namely, a direct reaction. Accordingly, these two types are essentially the same.

After the reaction, the reactant, *cis*- or *trans*-2-butene adsorbed and the product, butane, adsorbed on the surface were removed by TPD technique, and then analyzed by means of the mass spectrometer. The mass spectrometric analysis of reactant olefins chemisorbed and removed by TPD could not be succeeded in the previous cases with ethylene and propylene,[4,5)] because

Table 2. Hydrogenation of *cis*- and *trans*-2-butene with labeled hydrogen chemisorbed on platinum black[a)]

Type of surface employed	Surface reactant: Type of preadsorbed hydrogen and estimated amount[b)] (n/μmol)			Gas phase: Reactant type	Gas phase: Olefin pressure (P/Pa)	Deuteriobutanes formed (n/μmol)					
	β	γ	δ			d_0	d_1	d_2	d_3	d_4	Total
βH-γH-δD	0.357	0.178	0.509	*cis*-2	920	0.054	—	—	—	—	0.054
βD-γH-δD	0.464	0.223	0.638	*cis*-2	986	0.098	0.013	0.045	—	—	0.156
βD-γH-δH	0.366	0.183	0.527	*cis*-2	880	0.201	0.013	0.040	—	—	0.254
βH-γD-δH	0.460	0.219	0.629	*cis*-2	973	0.156	0.018	0.076	0.009	0.004	0.263
βH-γH-δD	0.339	0.174	0.495	*trans*-2	840	0.250	—	—	—	—	0.250
βD-γH-δD	0.357	0.178	0.513	*trans*-2	906	0.116	0.045	0.076	—	—	0.237
βD-γH-δH	0.375	0.187	0.536	*trans*-2	826	0.228	0.027	0.067	—	—	0.322
βH-γD-δH	0.335	0.170	0.491	*trans*-2	813	0.223	0.001	0.022	0.007	0.003	0.256

a) Catalyst weight, 2.18 g. Reaction temp 238 K, and reaction time 90 min. b) Estimated from TPD chromatograms in comparable experiments.

Table 3. TPD products after hydrogenation of *cis*- and *trans*-2-butenes

Type of surface employed	Reactant 2-butene	TPD peaks	Deuterio-2-butenes (n/μmol): Type	d_0	d_1	d_2	Total	Deuteriobutanes (n/μmol): d_0	d_1	d_2	Total
		A		0.06	—	—	0.06	0.03	—	—	0.03
βH-γH-δD	*cis*	B	*cis*	0.24	—	—	0.24	0.04	—	—	0.04
		C		0.10	0.01	—	0.11	0.02	—	0.01	0.03
		A		0.11	—	—	0.11	0.11	—	—	0.11
βH-γH-δD	*trans*	B	*trans*	0.13	—	—	0.13	0.15	—	—	0.15
		C		0.29	0.01	0.01	0.31	0.08	—	—	0.08
		A		0.06	0.01	—	0.07	0.04	0.01	0.01	0.06
βH-γD-δH	*cis*	B	*cis*	0.20	0.05	0.02	0.27	0.01	0.01	0.02	0.04
		C		0.11	0.01	—	0.12	0.03	0.01	0.02	0.06
		A		0.39	—	0.01	0.40	0.10	0.01	0.01	0.12
βH-γD-δH	*trans*	B	*trans*	0.27	0.01	0.02	0.30	0.09	—	0.01	0.10
		C		0.20	0.01	0.02	0.23	0.11	—	0.01	0.12
		A		0.14	0.01	—	0.15	0.06	0.01	0.03	0.10
βD-γH-δH	*cis*	B	*cis*	0.12	0.01	—	0.13	0.05	0.01	0.02	0.08
		C		0.16	0.02	0.01	0.19	0.06	0.02	—	0.08
		A		0.08	0.02	0.01	0.11	0.18	0.05	0.05	0.28
βD-γH-δH	*trans*	B	*trans*	0.03	0.01	0.01	0.05	0.17	—	0.01	0.18
		C		0.07	—	—	0.07	0.12	0.02	0.04	0.18

the amounts of olefins desorbed were too small to be transferred to the sampler for analysis. The results of *cis*- and *trans*-2-butene are shown in Table 3; deuterio-2-butenes and deuteriobutanes were observed. Since any deuteriobutene was not observed in the gase phase, the results suggest that the hydrogenation of chemisorbed *cis*- or *trans*-2-butene is easier than the desorption.

In peak A, any deuterio-2-butene was not observed in the case with βH-γH-δD surface. The result suggests that δ-deuterium does not react with *cis*- and *trans*-2-butene to form deuterio-2-butenes below 273 K. The formation of deuterio-2-butenes observed in the case of the βD-γH-δD and of the βD-γH-δH surfaces was therefore due to the participation of β-deuterium. In the case of the βH-γD-δH surface, the deuterio-2-butenes observed may have been formed by a reaction with γ-deuterium at 238 K.

In peak B, no deuterio-2-butenes was observed in the case of the βH-γH-δD surface. Since peak B appeared

between 290—490 K, and since δ-hydrogen, peak δ, appeared between 470—670 K, δ-deuterium does not suggestively participate in the H-D exchange reaction with 2-butenes. The result with βH-γD-δH surface is reasonably explained by the participation of γ-deuterium.

Small amounts of deuterio-2-butenes were observed in the case of the βD-γH-δD and of the βD-γH-δH surfaces, where the γ-hydrogen was protium. The results can be explained in such a way that the deuterio-2-butenes were formed from β-deuterium and 2-butenes at a lower temperature and, subsequently, desorbed by the rise of temperature.

Peak C appeared between 510—650 K, where δ-hydrogen mostly desorbed. In the case of the βH-γH-δD surface, therefore, the deuterium atoms in deuterio-2-butenes observed obviously came from δ-deuterium, which is only deuterium source.

In the case of the βD-γH-δH surface, some amounts of deuterio-2-butenes were observed. The result suggests that the deuterium atoms in the deuterio-2-butenes came from β-deuterium, and that deuterio-2-butenes formed at a lower temperature subsequently desorbed by the rise of temperature during TPD. In the case of the βH-γD-δH surface, deuterio-2-butenes observed may also be formed during TPD. The results with βD-γH-δD surface are qualitatively consistent with the explanation mentioned above.

The results of the mass spectrometric analysis of deuteriobutanes in peak A, B, and C shown in Table 3 agree quite well with the above suggestions that β- and γ-hydrogen do, and δ-hydrogen does not, participate in the hydrogenation.

In peak B, small amounts of deuteriobutanes were observed in the case of the βD-γH-δD and of the βD-γH-δH surface, where the γ-hydrogen was protium, but the β-hydrogen was deuterium. The results can be explained in such a way that the deuteriobutanes were formed from β-deuterium and 2-butene at a lower temperature and subsequently desorbed by the rise of temperature.

Peak C appeared between 510—650 K, where δ-hydrogen was mostly desorbed. In the case of the βH-γH-δD surface, therefore, the deuterium atoms in deuteriobutanes observed obviously came from δ-deuterium, which was the only deuterium source.

For the βD-γH-δH surface, some amounts of deuteriobutanes were observed. The result suggests that the deuterium atoms in the deuteriobutanes may have come from β-deuterium, and that deuteriobutanes formed at a lower temperature was subsequently desorbed by the rise of temperature during TPD. In the case of the βH-γD-δH surface, deuteriobutanes observed may also be formed during TPD. The results regarding the βD-γH-δD surface are qualitatively consistent with the explanation mentioned above.

A mass spectrometric analysis of propylene with regard to peaks B and C, was not carried out since the amount of propylene was too small to be separated from other components and from the carrier gas by condensation in the gas chromatograph stream. If any deuteriopropylene is observed, they are reasonably considered to have been formed from the chemisorbed deuteriobutenes by decomposition during TPD. The deuteriobutenes, however, do not necessary give the deuteriopropylenes which may depend on the degree of deuteration and the mechanism of decomposition of the chemisorbed deuteriobutanes.

Regarding the mechanism of the hydrogenation of olefins, extensive studies have been reported.[6,9,10] In the hydrogenation of ethylene over platinum catalyst, Bond-Wells mechanism may be accepted. According to the IR study by Soma (Soma-Noto),[10] π-adsorbed ethylene was easily hydrogenated at such low temperature as 195 K, and no hydrogenated species remained on the surface. The obsevation is consistent with the present result that the hydrogenation of *cis*- or *trans*-2-butene was more rapid than the desorption. Accordingly, the following scheme of the hydrogenation of *cis*- or *trans*-2-butene may be suggested. *cis*- or *trans*-2-butene is first chemisorbed on the surface and rapidly exchanged with the surface deuterium, without desorbing from the surface. The deuterio-2-butenes formed are stably chemisorbed on the surface with π-bond. Then, the deuterio-2-butenes are hydrogenated to deuteriobutanes and desorbed from the surface.

The four types of chemisorbed hydrogen were tentatively assigned on the basis of the previous results[1] and the postulates of other workers.[11-16] The γ- and δ-hydrogen were assigned to the weakly and strongly chemisorbed hydrogen atoms so far proposed. The α-hydrogen was assigned to the linearly chemisorbed hydrogen molecules. The β-hydrogen was the intermediate between α- and γ-hydrogen. Later, Primet *et al.*[17] and Dixon *et al.*[18,19] independently proposed their assignment on the basis of the IR studies. Dixon *et al.* deduced the existence of five kinds of hydrogen adsorption. Type I is physisorption, and the other four types, II—V, were corresponded to α—δ hydrogen.

It has previously been presumed that γ-hydrogen is present on the surface in the form of hydrogen atoms chemisorbed on top of platinum atoms, and that β-hydrogen is molecular hydrogen chemisorbed in a bridge form.[1] The difference in the reactivity may, accordingly, be due to the chemisorbed state, whether or not the H-H bond has been split. In the H_2-D_2 exchange reaction, β-hydrogen is not reactive, but it is reactive in the hydrogenation of olefins, and in the H-D exchange between the surface deuterium and 2-butenes. It is, accordingly, probable that a different tendency would be shown depending upon the sort of reaction; the explication of the other reactions awaits further investigations.

Conclusion

While some of the information could perhaps be obtained otherwise, the TPD technique in many cases can be used with unique advantage. Although the information that 2-butenes are more strongly chemisorbed than hydrogen on a catalyst had already been suggested on the basis of kinetic data,[9] it was more clearly shown by TPD, and in addition, the amounts of chemisorbed species could be estimated. Using isotopes, the individual chemisorbed species can be differently labeled, and the reactivity of each is separately measurable. The participation of various types of chemisorbed hydrogen in the 2-butenes hydrogenation were similar to that in the hydrogenation of ethylene and of propylene. γ-Hydrogen, presumed to be present on the surface in the form of hydrogen atoms chemisorbed on top of platinum atoms and β-hydrogen, presumed to be molecular hydrogen chemisorbed in a bridge form, were found to be involved in the 2-butenes hydrogenation. The information on the chemisorbed deuterio-2-butenes during the reaction revealed by the labeled TPD technique, suggests the following scheme of hydrogenation: *cis*- or *trans*-2-butene chemisorbed was first exchanged with deuterium to form deuterio-2-butenes, and before desorbing from the surface, the deuterio-2-butenes were hydrogenated to form deuteriobutanes.

The authors are grateful to Dr. Shizuo Fujisaki of this faculty for obtaining the mass spectra. This work was supported by a Grant-in-Aid for Scientific Research from the Ministry of Education, and by Watanabe foundation for which the authors' thanks are due.

References

1) S. Tsuchiya, Y. Amenomiya, and K. J. Cvetanović, *J. Catal.*, **19**, 245 (1970).
2) H. Verbeek and W. E. H. Sachtler, *J. Catal.*, **42**, 257 (1976).
3) S. Tsuchiya, Y. Amenomiya, and K. J. Cvetanović, *J. Catal.*, **20**, 1 (1971).
4) S. Tsuchiva and M. Nakamura, *J. Catal.*, **50**, 1 (1977).
5) S. Tsuchiya, M. Nakamura, and N. Yoshioka, *Bull. Chem. Soc. Jpn.*, **51**, 981 (1978).
6) G. C. Bond, "Catalysis by Metals," Academic Press, *New York, 1962, p. 229.*
7) K. J. Cvetanović and Y. Amenomiya, "Advances in Catalysis," ed by D. D. Eley, H. Pines, and P. B. Weisz, Vol. 17, p. 103, Academic Press, New York, 1967.
8) N. Yoshioka, M. Nakamura, and S. Tsuchiya, *Chem. Lett.*, **1977**, 445; S. Tsuchiya, *Hyomen*, 16 (2), 65 (1978).
9) G. C. Bond, and P. H. Wells, "Advances in Catalysis," ed by D. D. Eley, H. Pines, and P. B. Weisz, Vol. 15, p. 91, Academic Press, New York, 1964.
10) Y. Soma, *J. Catal.*, **59**, 239 (1979).
11) W. A. Pliskin and R. P. Eischens, *Z. Phys. Chem.*, **24**, 11 (1962).
12) T. Toya, *J. Res. Inst. Catal., Hokkaido Univ.*, **10**, 236 (1962).
13) R. Suhrmann, "Advances in Catalysis and Related Subject," ed by W. G. Frankenburg, V. I. Komarevsky, and E. K. Rideal, Vol. 7, (1955) p. 303.
14) J. C. P. Mignolet, *J. Chim. Phys.*, **54**, 19 (1957).
15) R. Suhrmann, G. Wedler, and H. Gentsch, *Z. Phys. Chem.*, **17**, 350 (1958).
16) W. H. Smith, H. C. Eckstrom, and F. Bär, *J. Phys. Chem.*, **72**, 369 (1968).
17) M. Primet, J. M. Basset., and M. V. Mathieu, *J. Catal.*, **28**, 368 (1973).
18) L. T. Dixon, R. Barth, and J. W. Gryder, *J. Catal.*, **37**, 368 (1975).
19) L. T. Dixon, R. Barth, R. J. Kokes, and J. W. Gryder, *J. Catal.*, **37**, 376, (1975).

Proton Transfer in the Excited State of 1- and 2-Methyl-4-amino-5*H*-[1]benzopyrano[3,4-*c*]pyridin-5-one Dimers and Complexes

Akira FUJIMOTO,* Junko NAKAMURA,† Iwao YAMAZAKI,††
Toshiro MURAO,††† and Kozo INUZUKA
Department of Applied Science, Faculty of Technology, Tokyo Denki University, Kanda, Chiyoda-ku, Tokyo 101
†*The Institute of Physical and Chemical Research, Wako, Saitama 351-01*
††*Institute for Molecular Science, Myodaiji, Okazaki 444*
(Received June 29, 1984)

The fluorescence rise and decay times and UV absorption spectra of 1-methyl-4-amino-5*H*-[1]benzopyrano-[3,4-*c*]pyridin-5-one (1-MBPP), 2-methyl-4-amino-5*H*-[1]benzopyrano[3,4-*c*]pyridin-5-one (2-MBPP), and the 1-MBPP/acetic acid and 2-MBPP/acetic acid systems have been measured in hydrocarbon and hydroxylic solvents at room temperature and 77 K. From these data, a rapid formation of proton-transferred species (tautomers) was found to occur in an excited state for 1-MBPP (or 2-MBPP) hydrogen-bonded dimers in hydrocarbon at 77 K, and for 1-MBPP (or 2-MBPP) hydrogen-bonded complexes with acetic acid in hydrocarbon at room temperature and 77 K. The rise times of the tautomer fluorescence for the dimers and complexes were less than 65 ps. The observed fluorescence lifetimes of the 1-MBPP and 2-MBPP monomers agreed well with the lifetimes calculated using the integrated absorption intensity and fluorescence quantum yield.

El-Bayoumi *et al.*[1] have presented the results of a time-resolved fluorescence study of an excited-state double proton transfer. The observed value of the rate constant for a deuterium transfer in a deuterated 7-azaindole dimer at 77 K was $1.9\times10^{8}\ s^{-1}$. Recently, Hetherington III *et al.*[2] have suggested that photo-excited dimers of 7-azaindole undergo a double proton transfer in less than 5 ps at room temperature and 77 K. The proton-transfer rate in an excited state is generally as fast as reported by them[1,2] and other workers.[3-5]

In a previous paper[6] we presented the emission spectra and polarization spectra of 1-methyl-4-amino-5*H*-[1]benzopyrano-[3,4-*c*]pyridin-5-one (1-MBPP), 2-methyl-4-amino-5*H*-[1]benzopyrano-[3,4-*c*]pyridin-5-one (2-MBPP), and the 2-MBPP acetic acid system (2-MBPP/AcOH) in glassy solvents at 77 K. In the course of this investigation, an anomalous fluorescence was observed with a maximum near 450 nm for 1-MBPP, near 436 nm for 2-MBPP, and near 460 nm for 2-MBPP/AcOH in hydrocarbon glassy solvents at 77 K. The anomalous fluorescence band was thought to have originated from the tautomer (imino-form) of the 1-MBPP and 2-MBPP formed by an intermolecular double proton transfer in the excited state of the doubly hydrogen-bonded dimer and complex of amino-form as shown in Schemes 1 and 2. In addition, the fluorescence spectra of the monomer, dimer (or complex) and tautomer, and the phosphorescence spectra of the monomer and dimer have been separately observed on the basis of concentration and tempera-

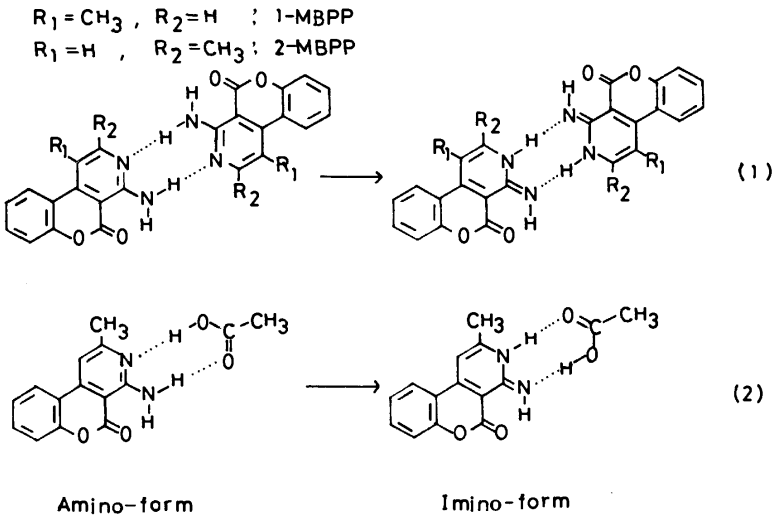

Schemes 1 and 2.

††† Present Adress: Hitachi Instrument Engineering Co., Ichige, Katsuta, Ibaraki 312.

ture effects on these emissions.[6] 7-Azaindole is known to show the double proton transfer in the excited state, where the phosphorescence spectrum greatly overlaps the tautomer fluorescence band.[7] 1-MBPP and 2-MBPP are, therefore, suitable for studying the dynamics of proton transfer in excited states.

In the present study, the fluorescence rise and decay times and the UV absorption spectra of 1-MBPP, 2-MBPP, 1-MBPP/AcOH, and 2-MBPP/AcOH in hydrocarbon and hydroxylic solvents at ambient temperature and 77 K were investigated in order to elucidate the proton-transfer mechanism in an excited state.

Experimental

Materials. 1-MBPP, 2-MBPP, acetic acid, and solvents were the same as in a previous paper.[6] Solvents used were as follows: (1) a mixed solvent of isopentane and methylcyclohexane (volume ratio 5:1) (IM), (2) a mixed solvent of ethanol and methanol (volume ratio 5:1) (EM), and (3) diethyl ether-isopentane-ethanol (volume ratio 5:5:2) (EPA). Concentrations of 1- and 2-MBPP were 1×10^{-4} mol dm^{-3} and that of the acetic acid was 5×10^{-4} mol dm^{-3}.

UV Absorption Measurements. The UV absorption spectra were obtained at room temperature and at 77 K with an Hitachi model 323 spectrophotometer. The UV absorption measurements at 77 K were carried out on rigid glass samples in a quartz cell of 5 mm path length placed in a glass Dewar vessel with quartz windows.

Fluorescence Time Profile Measurements. A nitrogen laser (Molectron UV24), a pumped dye laser (DL14), and a second-harmonic generator (a KDP crystal) were used for the nanosecond excitation.[8] The excitation wavelength was 305 nm (Rhodamine B/KDP, pulse duration 5 ns). A single-photon counting system (ORTEC) connected to a Spex 14 (0.75 m) monochromator and a HTV R1332 photomultiplier was used for the fluorescence lifetime measurements. More precise measurement with picosecond excitation was performed using a synchronously pumped, cavity-dumped dye laser (Spectra Physics 375 and 3445), operated with a mode-locked Ar^+ laser (Spectra Physics 171—18). The laser was operated with a repetition rate of 800 kHz and a pulse duration of 6 ps. The dye used was Na-fluorescein and its second harmonic (280 nm) was generated with a KDP crystal. Through a modification of the detecting systems, the apparent pulse width (fwhm) was found to be about 70 ps, and the rise and decay times were analyzed by a convolution-simulation method using the time profile of scattered laser light as a reference. Details of the experimental setup and single-photon counting systems for picosecond regions have been reported elsewhere.[9]

Results and Discussion

The UV absorption spectra of 1-MBPP in hydrocarbon[10] and hydroxylic[11] solvents at room temperature are shown elsewhere. The UV absorption spectra of 1-MBPP and 2-MBPP in IM and EM at 77 K are illustrated in Fig. 1 with those of 1-MBPP/AcOH and 2-MBPP/AcOH in IM at 77 K. The UV spectra of 1- and 2-MBPP in EPA at 77 K were similar to those in EM at 77 K. 1-MBPP and 2-MBPP in alcoholic solvents at room temperature as well as at 77 K exist as monomers, though they form hydrogen-bonded complexes with alcohols.[11] These molecules in IM at room temperature exist as monomers,[10] but at 77 K they are considered to form molecular complexes since the UV absorption spectra of 1- and 2-MBPP in IM are similar to those of hydrogen-bonded complexes of 1-MBPP/AcOH and 2-MBPP/AcOH in the same solvent at 77 K, respectively (Fig. 1). From the similarity of these UV absorption spectra, the model of the molecular complex for 1- and 2-MBPP is assumed to be the doubly hydrogen-bonded dimer of the amino-form as shown in Scheme 1.

The fluorescence lifetimes ($\tau_{f\,obsd}$) were measured at fluorescence band maxima ($\lambda_{f\,max}$) in various solvents at room temperature (Table 1) and 77 K (Table 2). An example of fluorescence decay curves observed by means of the single-photon counting method is presented in Fig. 2 for 1-MBPP at ambient temperature.

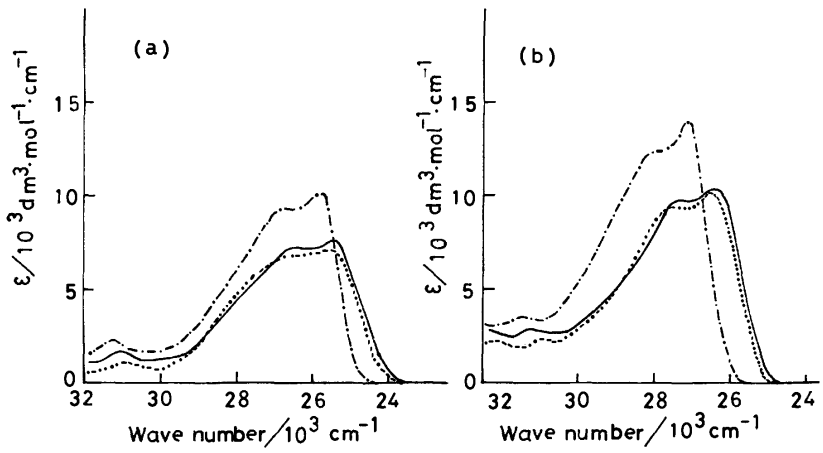

Fig. 1. UV absorption spectra of 1-MBPP (a) and 2-MBPP (b) in IM (——) and EM (—·—) at 77 K, with those of 1-MBPP/AcOH and 2-MBPP/AcOH (·····) in IM at 77 K.

TABLE 1. BAND MAXIMA ($\lambda_{f\,max}$), QUANTUM YIELDS (ϕ_f), OBSERVED LIFETIMES ($\tau_{f\,obsd}$), AND CALCULATED LIFETIMES ($\tau_{f\,calcd}$) OF 1-MBPP AND 2-MBPP FLUORESCENCE IN VARIOUS SOLVENTS AT ROOM TEMPERATURE WITH THOSE OF 1-MBPP/AcOH AND 2-MBPP/AcOH

System	Solvent	$\lambda_{f\,max}$ / nm	ϕ_f	$\tau_{f\,obsd}$ / ns	$\tau_{f\,calcd}$ / ns	$k_r \times 10^{-7}$ / s^{-1}	$k_{nr} \times 10^{-7}$ / s^{-1}
1-MBPP	IM	403	0.07	0.95	1.2	7.4	98
1-MBPP	EM	420[a)]	0.29[a)]	3.75	5.6	7.7	19
1-MBPP	EPA	420	0.29	3.77	5.4	7.7	19
1-MBPP/AcOH	IM	475	0.02	1.48	0.3	1.4	66
2-MBPP	IM	373	0.09	0.79	0.9	11	120
2-MBPP	EM	400[a)]	0.24[a)]	1.56	2.6	15	49
2-MBPP	EPA	398	0.23	1.50	2.7	15	51
2-MBPP/AcOH	IM	458	0.09	6.89	1.2	1.3	13

a) See Ref. 6.

TABLE 2. BAND MAXIMA ($\lambda_{f\,max}$), QUANTUM YIELDS (ϕ_f), OBSERVED LIFETIMES ($\tau_{f\,obsd}$), AND CALCULATED LIFETIMES ($\tau_{f\,calcd}$) FOR THE 1-MBPP AND 2-MBPP FLUORESCENCE IN VARIOUS GLASSES AT 77 K WITH THOSE OF 1-MBPP/AcOH AND 2-MBPP/AcOH

System	Solvent	$\lambda_{f\,max}$[a)] / nm	ϕ_f[a)]	$\tau_{f\,obsd}$ / ns	$\tau_{f\,calcd}$ / ns	$k_r \times 10^{-7}$ / s^{-1}	$k_{nr} \times 10^{-7}$ / s^{-1}
1-MBPP	IM	450	0.15	8.88	1.3	1.7	9.6
1-MBPP	EM	405	0.48	4.05	7.5	12	13
1-MBPP	EPA	401	0.43	2.43	6.7	18	23
1-MBPP/AcOH	IM	473	0.09	8.49	0.9	1.1	11
2-MBPP	IM	435	0.13	7.71	1.7	1.7	12
2-MBPP	EM	386	0.24	1.35	2.8	17	56
2-MBPP	EPA	384	0.24	1.42	2.6	17	54
2-MBPP/AcOH	IM	460	0.09	16.08	1.3	0.56	5.7

a) See Ref. 6.

The decay curve was found to be single exponential and the lifetime was 0.95 ns (Table 1). In Tables 1 and 2, the fluorescence quantum yields (ϕ_f) and the calculated fluorescence lifetimes ($\tau_{f\,calcd}$), deduced from the integrated UV absorption intensity and ϕ_f, are also shown together with the radiative (k_r) and nonradiative (k_{nr}) rate constants calculated from the fluorescence characteristics in several solvents at room temperature and 77 K, respectively.

The values of $\lambda_{f\,max}$ for 1- and 2-MBPP in IM glassy matrices and those for 1-MBPP/AcOH and 2-MBPP/AcOH are appreciably longer wavelengths than those in an alcoholic glass.[6] The values of $\tau_{f\,obsd}$ of 1-MBPP/AcOH and 2-MBPP/AcOH in nonpolar glass were greater than those of $\tau_{f\,calcd}$ estimated from the integrated absorption intensity of the hydrogen-bonded complex of amino-form and the fluorescence quantum yields observed at the band maxima (473 nm for 1-MBPP and 460 nm for 2-MBPP). This tendency was also seen for the cases of 1- and 2-MBPP in IM at 77 K. The results described above and the resemblance of the fluorescence characteristics of 1-MBPP and 2-MBPP in IM at 77 K indicate that the tautomer (imino-form) formation from the 1-MBPP and 2-MBPP hydrogen-bonded dimers (amino-form) occurs in the excited state, as given in Scheme 1, just as in the case of acid complexes in Scheme 2.[6] On the other hand, the values of $\tau_{f\,obsd}$ in alcoholic matrices at 77 K agreed with those of $\tau_{f\,calcd}$. This result is compatible with the assumption that 1-MBPP and 2-MBPP in an alcoholic solvent at 77 K (as well as at room temperature) behave like monomers, though they make hydrogen-bonded complexes with alcohol.

The tautomerization from benzopyranopyridine hydrogen-bonded dimers (amino-form) to imino-form was investigated with the picosecond laser induced fluorescence technique. The fluorescence rise times were observed at the tautomer fluorescence band at room temperature and 77 K. It is noted that there are fast and slow rise components in the tautomer fluorescence for 1-MBPP and 2-MBPP at 77 K, and for 1-MBPP/AcOH and 2-MBPP/AcOH at room temperature and 77 K, as summarized in Table 3. As described by Hetherington III *et al.* in the study on the proton

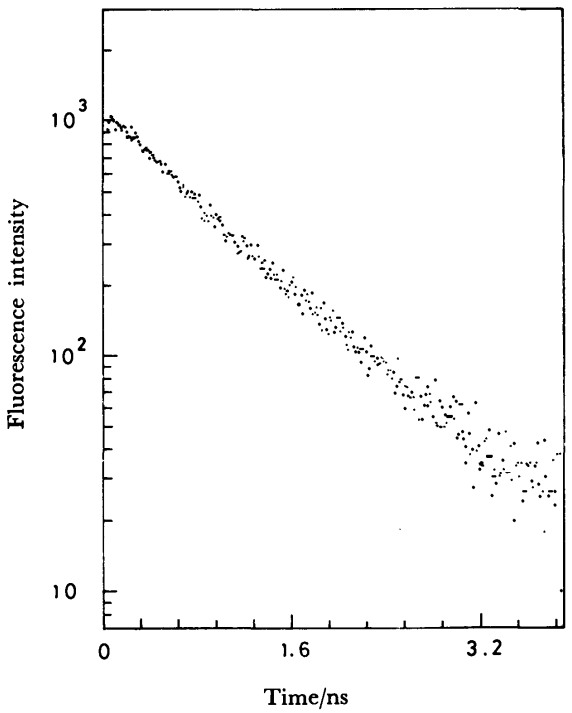

Fig. 2. Logarithmic plot of a fluorescence decay of 1-MBPP in IM at room temperature.
Excitation wavelength; 280 nm, Emission wavelength; 403 nm.

Table 3. Rise times of tautomer fluorescence for different systems in IM at room temperature and 77 K

System	Fast component	Slow component
	ps	ps
1-MBPP at 77 K	<20	~40
1-MBPP/AcOH at room temp	<20	~45
1-MBPP/AcOH at 77 K	<20	~65
2-MBPP at 77 K	<20	~35
2-MBPP/AcOH at room temp	<20	~45
2-MBPP/AcOH at 77 K	<20	~65

transfer of the 7-azaindole dimer,[2] the presence of fast and slow rise components in the tautomer fluorescence for 1- and 2-MBPP and their acetic acid complex systems suggests that there are two different pathways for the formation of the tautomer in an excited state: (a) the rapid proton transfer from the excited Franck-Condon state and (b) the relatively slow proton transfer from the excited state generated by energy relaxation from the excited Franck-Condon state.

The slow fluorescence rise times for 1-MBPP/AcOH and 2-MBPP/AcOH at room temperature were shorter than those for the same systems at 77 K. This result indicates that tautomer formation *via* pathway (b) at room temperature is more favored than at 77 K because proton transfer at room temperature occurs effectively across the barrier by thermal activation. In addition, the rise time of the dimer was shorter than that of heterogeneous systems such as 1-MBPP/AcOH. This result means that the barrier height in proton transfer in the excited state for homogeneous complexes is lower than that for heterogeneous complexes.

The intensity ratio of the fast and slow rise components in the tautomer fluorescence is thought to depend on the excitation wavelength. In the present case the excitation wavelength was 280 nm, about 9500—11700 cm^{-1} above the absorption edge of the complexes. A red edge excitation and time profile observation will give further information on the energy and proton transfer in an excited state.

References

1) M. A. El-Bayoumi, P. Avouris, and W. R. Ware, *J. Chem. Phys.*, **62**, 2499 (1975).
2) W. M. Hetherington III, R. H. Micheels, and K. B. Eisenthal, *Chem. Phys. Lett.*, **66**, 230 (1979).
3) W. Klopffer, *Advan. Photochem.*, **10**, 311 (1977).
4) K. K. Smith and K. J. Kaufmann, *J. Phys. Chem.*, **82**, 2286 (1978).
5) H. Shizuka, K. Matsui, Y. Hirata, and I. Tanaka, *J. Phys. Chem.*, **81**, 2243 (1977).
6) A. Fujimoto and K. Inuzuka, *Spectrochim. Acta, Part A*, **38**, 1035 (1982).
7) J. Waluk, H. Bulska, B. Pakula, and J. Sepiol, *J. Lumin.*, **24**, 519 (1981).
8) S. Ishikawa, J. Nakamura, and S. Nagakura, *Bull. Chem. Soc. Jpn.*, **53**, 2476 (1980).
9) I. Yamazaki, T. Murao, and K. Yoshihara, *Chem. Phys. Lett.*, **87**, 384 (1982).
10) A. Fujimoto and K. Inuzuka, *Bull. Chem. Soc. Jpn.*, **51**, 2781 (1978).
11) K. Inuzuka and A. Fujimoto, *Bull. Chem. Soc. Jpn.*, **52**, 939 (1979).

The Preparation and Spectral Properties of *trans(CN)*-$[Co(CN)_2(tmdda)]^-$ and -$[Co(CN)_2(L\text{-}ala)_2]^-$ Complexes

Kan KANAMORI,* Yoko NUNOMURA, Masumi TAKASHIMA, Kiyonori NAGATA, Kiyoyasu KAWAI, and Jinsai HIDAKA†

Department of Chemistry, Faculty of Science, Toyama University, Gofuku 3190, Toyama 930
†*Department of Chemistry, University of Tsukuba, Ibaraki 305*

(Received May 23, 1984)

All-*trans*- and *trans(CN),cis(N)*-$[Co(CN)_2(L\text{-}ala)_2]^-$ and *trans(CN)*-$[Co(CN)_2(tmdda)]^-$ were newly prepared; here, tmdda denotes trimethylenediamine-*N,N'*-diacetate. These complexes were characterized from their electronic absorption, NMR, and Raman spectra. The CD spectra of two *trans(CN)* isomers of the bis(L-alaninato)-complex are also presented.

There have been few reports on the preparation of *trans(CN)*-$[Co(CN)_2(N)_2(O)_2]$-type complexes, though many reports have appeared on *trans(CN)*-$[Co(CN)_2(N)_4]$-type complexes, where $(N)_2(O)_2$ denotes diamine-*N,N'*-diacetate or bis(amino carboxylate) and $(N)_4$ tetraammine[1] or bis(diamine).[2] For instance, three *cis(CN)*-$[Co(CN)_2(am)_2]^-$ isomers (am=amino carboxylate) have been reported for the glycinato complexes,[3,4] but the *trans(CN)* isomer has not yet appeared. Recently, work on synthesizing cobalt(III) complexes with a linear quadridentate O-N-N-O ligand, tmdda, have been reported, and it was suggested that tmdda prefers the *unsym-cis* to the *sym-cis* geometry, when the ligand coordinates to the Co^{III} ion.[5,6] This fact seems to reveal that the *trans(CN)* coordination is possibly formed in the preparation of the dicyano Co^{III} complex with tmdda.

The present work is concerned with the preparation of all-*trans*- and *trans(CN),cis(N)*-$[Co(CN)_2(L\text{-}ala)_2]^-$ and *trans(CN)*-$[Co(CN)_2(tmdda)]^-$, which are characterized by their electronic absorption, Raman, and NMR spectra. The CD spectra of the two isomers of $[Co(CN)_2(L\text{-}ala)_2]^-$ are also presented.

Experimental

Preparation. *1) Lithium* trans(CN)-*Dicyano(trimethylenediamine*-N,N'-*diacetato)cobaltate(III),* trans(CN)-*Li[Co(CN)$_2$(tmdda)].* To a solution of trimethylenediamine-*N,N'*-diacetic acid dihydrochloride[7] (5.2 g; 0.02 mol) in 200 cm^3 of water we added 4.5 g (0.02 mol) of $[CoCl(CN)(NH_3)_4]Cl$.[8] The mixture was adjusted to pH=8 with an aqueous NaOH solution, and then a small amount of activated charcoal was added. The mixture was stirred at 60 °C for 30 h. After removing the activated charcoal, the filtrate was adjusted to pH=7 with dilute acetic acid and diluted to 1 dm^3 with water. Then the charged compound was removed by passing it through a cation-exchange (Dowex 50W×8, Li^+ form) column and an anion-exchange (Dowex 1×8, Cl^- form) column. The eluate was concentrated to dryness with a rotary evaporator. The residue was washed with ethanol and dried. This dark-red intermediate product, which was presumed to be $[Co(CN)(tmdda)(NH_3)]$, was used in the next step without any purification. The intermediate product (4.5 g) and KCN (0.98 g; 0.015 mol) were kept at 60 °C in 200 cm^3 of dimethyl sulfoxide for 30 h. After the reaction solution has then been diluted to 2 dm^3 with water, a small amount of an insoluble material was filtered off. The filtrate was applied to an anion-exchange column (Dowex 1×8, 200-400 mesh, Cl^- form, 4×60 cm), and the adsorbed band was eluted with an aqueous LiCl solution (0.5 g/dm^3), separating into orange and orange-red bands. It was found from the spectral properties that the first, orange eluate contained the all-*cis*-$[Co(CN)_2(tmdda)]^-$ complex, with the second, orange red one contained the desired *trans(CN)*-$[Co(CN)_2(tmdda)]^-$ complex. The orange-red eluate was evaporated to dryness with a rotary evaporator, and the residue was washed with ethanol to remove the LiCl. The crude product was recrystallized from a small amount of water by adding methanol. Yield, 0.4 g. Found: C, 32.09; H, 4.52; N, 16.53%. Calcd for $Li[Co(CN)_2(tmdda)]\cdot 1.75H_2O = LiCoC_7H_{12}N_4O_4\cdot 1.75H_2O$: C, 32.05; H, 4.63; N, 16.61%.

2) Lithium trans(CN)-*Dicyanobis(L-alaninato)cobaltate(III),* trans(CN)-*Li[Co(CN)$_2$(L-ala)$_2$].* The two isomers of *trans(CN)*-$[Co(CN)_2(L\text{-}ala)_2]^-$ were obtained by a method similar to that in 1). That is, $[CoCl(CN)(NH_3)_4]Cl$ (9.0 g; 0.04 mol), L-alanine (7.2 g; 0.08 mol), and NaOH (3.2 g; 0.08 mol) were dissolved in a mixture of 100 cm^3 of dimethyl sulfoxide and 100 cm^3 of water; then the solution was stirred at 60 °C for 30 h. The intermediate product, which was supposed to be $[Co(CN)(L\text{-}ala)_2(NH_3)]$, was isolated by a manner similar to that used for $[Co(CN)(tmdda)(NH_3)]$. The intermediate product (5.6 g) and KCN (1.3 g; 0.02 mol) were kept at 60 °C in 200 cm^3 of dimethyl sulfoxide for 30 h. The reaction mixture was then diluted to 2 dm^3 with water and poured onto an anion-exchange column (Dowex 1×8, 200—400 mesh, Cl^- form; 4×60 cm). Four colored bands, yellow, pinkish red, orange-red, and orange, were obtained, in this order, by eluting with an aqueous NH_4Cl solution (1 g/dm^3). The first two bands (yellow and pinkish red) partially overlapped, so the eluates were combined and evaporated to dryness under reduced pressure. The yellow isomer and NH_4Cl were extracted from the residue with ethanol, leaving the pinkish red isomer, which was insoluble in ethanol. The yellow isomer was found to be the *cis(CN), trans(N)* isomer by comparing its electronic absorption spectrum with that of *cis(CN),trans(N)*-$[Co(CN)_2(gly)_2]^-$.[4] The pinkish red isomer was converted to lithium salt by rechromatography. The crude product was recrystallized by dissolving it in a small amount of water, and then adding methanol. It was found by

spectral measurements to be described later that this isomer has the all-*trans* configuration. After these two bands were removed, the eluent was changed from an aqueous NH_4Cl solution to an aqueous LiCl solution (1 g/dm^3). The orange isomer was found to be the all-*cis* isomer by comparing its electronic absorption spectrum with that of all-*cis*-[Co(CN)$_2$(gly)$_2$]$^-$.[4] The orange-red fraction was concentrated to dryness with a rotary evaporator, and the residue was washed with ethanol and recrystallized from a small amount of water by adding methanol. The orange-red isomer was assigned to have the *trans(CN)*, *cis(N)* configuration on the basis of the spectral properties to be described below. Yields, 0.5 g for the pinkish red isomer and 0.2 g for the orange-red isomer. Found for the pinkish red isomer: C, 28.62; H, 5.51; N, 15.56%. Calcd for Li[Co(CN)$_2$(L-ala)$_2$]·2.5H_2O·0.5CH_3OH=$LiCoC_8H_{12}N_4O_4$·2.5H_2O·0.5CH_3OH: C, 28.74; H, 5.39; N, 15.78%. The solvation of methanol was confirmed by the ^1H and ^{13}C NMR spectra. Found for the orange-red isomer: C, 27.82; H, 5.12; N, 16.10%. Calcd for Li[Co(CN)$_2$(L-ala)$_2$]·3H_2O=$LiCoC_8H_{12}N_4O_4$·3H_2O: C, 27.63; H, 5.22; N, 16.11%.

Measurements. The electronic absorption spectra were recorded with a Hitachi 220 spectrophotometer and the CD spectra, with JASCO J-20 and J-500 spectrophotometers. Raman spectra were recorded on a JASCO R-800 Laser Raman spectrophotometer with an excitation of the He–Ne laser (632.8 nm, 50 mW) in water and a disk. The IR spectra were recorded on a JASCO IRA-3 spectrophotometer, and the samples were provided as nujol mulls. The NMR spectra were recorded on JEOL FX-100 and FX-90Q spectrometers in D_2O. Sodium 2,2-dimethyl-2-silapentane-5-sulfonate (DSS) was used as the internal reference.

Results and Discussion

Structural Assignment. Figure 1 shows five geometrical isomers of [Co(CN)$_2$(N)$_2$(O)$_2$]-type complexes. All of them are possible for [Co(CN)$_2$(L-ala)$_2$]$^-$, while the possible isomers for [Co(CN)$_2$(tmdda)]$^-$ are reduced to three, *trans(CN)*, *cis(N)*, *cis(CN)*, *trans(O)*, and all-*cis*. Poznjac and Pawlowski[3] reported the preparations and spectroscopic properties of three *cis(CN)* isomers of [Co(CN)$_2$(gly)$_2$]$^-$ and two *cis(CN)* isomers of [Co(CN)$_2$(edda)]$^-$. Figure 2 shows the absorption spectra of the orange-red isomer of [Co(CN)$_2$(tmdda)]$^-$ and the pinkish red and orange-red isomers of [Co(CN)$_2$(L-ala)$_2$]$^-$; their data are summarized in Table 1. As the absorption spectrum of the orange isomer of [Co(CN)$_2$(tmdda)]$^-$ is quite similar to that of all-*cis*-[Co(CN)$_2$(edda)]$^-$,[5] it can be assigned to the all-*cis* one. On the other hand, the orange-red isomer of [Co(CN)$_2$(tmdda)]$^-$ can be assigned to the *trans(CN)* one, since the absorption spectrum differs distinctly from that of the *cis(CN)*,*trans(O)*-[Co(CN)$_2$(edda)]$^-$ (Table 1).

The orange-red isomer of [Co(CN)$_2$(L-ala)$_2$]$^-$ is also assignable to the *trans(CN)*,*cis(N)* one, since the d-d spectrum is quite similar to that of *trans(CN)*-[Co(CN)$_2$(tmdda)]$^-$, as may be seen in Fig. 2. The d-d spectrum of the pinkish red isomer differs remarkably from that of *trans(CN)*,*cis(N)*-[Co(CN)$_2$(L-ala)$_2$]$^-$ and those of the three *cis(CN)* isomers of [Co(CN)$_2$(gly)$_2$]$^-$[4] (Fig. 2 and Table 1). Consequently, the pinkish red isomer of [Co(CN)$_2$(L-ala)$_2$]$^-$ can be assigned to the all-*trans* one.

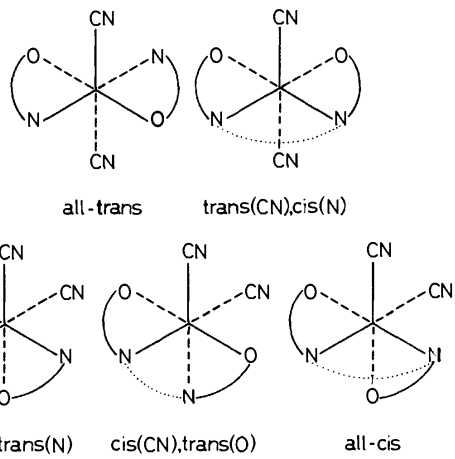

Fig. 1. Possible geometrical isomers of [Co(CN)$_2$(N)$_2$-(O)$_2$]-type complex; (N)$_2$(O)$_2$=(tmdda) or (L-ala)$_2$.

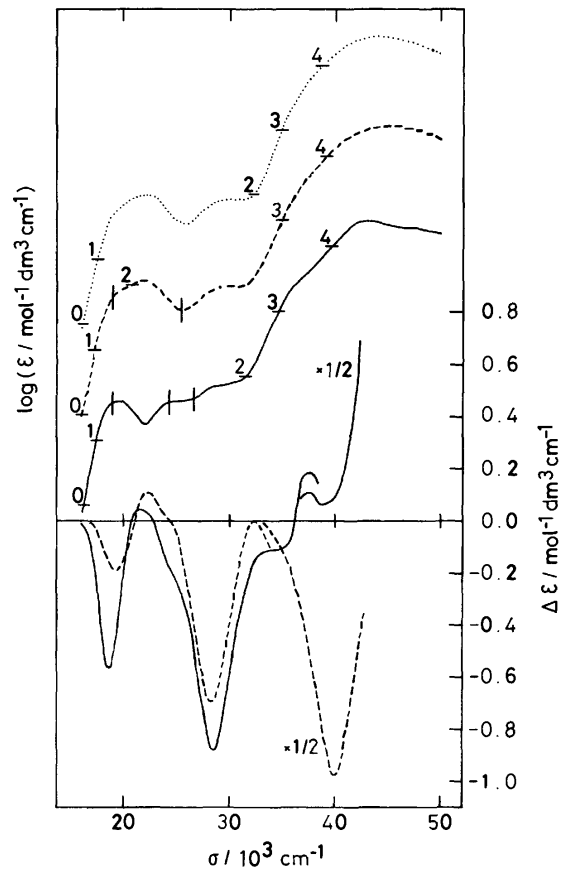

Fig. 2. Electronic absorption and CD spectra of *trans*-(*CN*)-[Co(CN)$_2$(tmdda)]$^-$, (·····), *trans(CN)*,*cis(N)*-[Co(CN)$_2$(L-ala)$_2$]$^-$, (----), and all-*trans*-[Co(CN)$_2$-(L-ala)$_2$]$^-$, (——). Short vertical lines show the predicted positions of the first d-d absorption band.

TABLE 1. ABSORPTION AND CD DATA OF $[Co(CN)_2(N)_2(O)_2]$-TYPE COMPLEXES (WAVE NUMBERS ARE GIVEN IN 10^3 cm^{-1} AND log ε AND $\Delta\varepsilon$ (IN PARENTHESES) mol^{-1} dm^3 cm^{-1})

Complex		First band	Second band	CT band
trans(CN)-[Co(CN]$_2$(tmdda)]$^-$		*ca.* 19 sh (1.7)	29.8 (1.91)	43.7 (4.39)
		21.5 (1.98)		
trans(CN),cis(N)-[Co(CN)$_2$(L-ala)$_2$]$^-$		*ca.* 19 sh (1.8)	*ca.* 30 sh (2.0)	*ca.* 37 (3.6)
		22.0 (2.05)		45.9 (4.41)
	CD	19.3 (−0.19)	28.2 (−0.69)	39.5 (−1.95)
	CD	22.2 (+0.11)		
		19.5 (1.60)	*ca.* 29 sh (1.8)	*ca.* 37 (3.5)
all-*trans*-[Co(CN)$_2$(L-ala)$_2$]$^-$		*ca.* 24 sh (1.5)		43.3 (4.35)
	CD	18.7 (−0.56)	28.2 (−0.88)	37.9 (+0.22)
	CD	21.5 (+0.04)		
	CD	*ca.* 24 sh (−0.2)		
cis(CN),trans(N)-[Co(CN)$_2$(gly)$_2$]$^-$ [a]		23.3 (2.34)	30.9 (2.13)	
cis(CN),trans(O)-[Co(CN)$_2$(gly)$_2$]$^-$ [a]		19.2 (1.84)	30.7 (2.14)	
		ca. 26 sh (1.9)		
all-*cis*-[Co(CN)$_2$(gly)$_2$]$^-$ [a]		21.1 (2.04)	30.5 (2.16)	
		24.4 (2.05)		
cis(CN),trans(O)-[Co(CN)$_2$(edda)]$^-$ [b]		19.4 (1.87)	30.5 (2.16)	
		ca. 26 sh (1.8)		
all-*cis*-[Co(CN)$_2$(edda)]$^-$ [b]		21.2 (2.08)	30.6 (2.06)	
		24.4 (1.95)		

a) Ref. 4. b) Values estimated from the figure in Ref. 3.

The ^{1}H and ^{13}C NMR spectra of the cobalt(III) complexes with tmdda have also been investigated.[5,6] The ^{13}C NMR spectrum of *trans(CN)*-[Co(CN)$_2$(tmdda)]$^-$ exhibits four resonance lines (at δ 28.88, 53.09, 60.08, and 183.60), corresponding to the four different carbon atoms; these lines are assignable to the resonances of -$CH_2\underline{C}H_2CH_2$-, -$NH\underline{C}H_2CH_2$-, -$NH\underline{C}H_2COO$-, and -$CH_2\underline{C}OO$- respectively, following the assignment of Gailey *et al.*[5] This observation indicates that the two glycinate moieties of the coordinated tmdda are equivalent, being consistent with the *trans(CN)* configuration. The six-membered backbone chelate ring of *trans(CN)*-[Co(CN)$_2$(tmdda)]$^-$ would take either the skew-boat or chair form. The middle methylene protons of the backbone trimethylenediamine ring would be in different magnetic environments to each other in the chair form, whereas they would be equivalent in the skew-boat form. In order to determine the conformation of the backbone chelate ring, the ^{1}H NMR spectra of *trans(CN)*-[Co(CN)$_2$(tmdda)]$^-$ were measured. Figure 3-A shows its ^{1}H NMR spectrum in D_2O acidified with D_2SO_4 (pD≈2), and Figure 3-B, that in D_2O. The proton-exchange rate of imino groups would be slow enough to give the observable signals in an acidified solution. In contrast, imino protons are expected to be quickly exchanged with deuterons in D_2O. From a comparison of Fig. 3-A with Fig. 3-B, the broad band at δ 5.8, which was observed only in the acidified D_2O, can be assigned to the imino protons. The doublet (at δ 3.35 and 3.27) and the multiplet (at *ca.* δ 2.5) in Fig. 3-A, which are transformed into a singlet and a simpler multiplet in D_2O (Fig. 3-B), can be assigned to the methylene protons adjacent to the imino groups. Two multiplets (at *ca.* δ 2.1 and

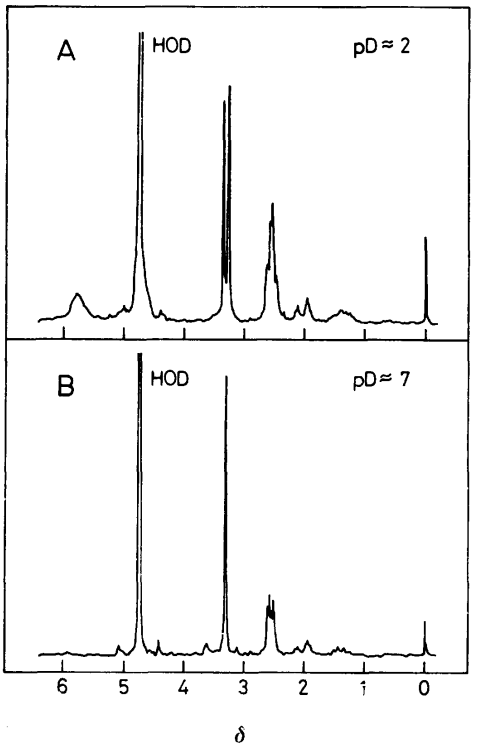

Fig. 3. ^{1}H NMR spectra of *trans(CN)*-[Co(CN)$_2$(tmdda)]$^-$ in D_2O acidified with D_2SO_4 (A) and D_2O (B). (Resonance lines around δ 1.4 are due to a contaminant in DSS.)

ca. 1.9), which remained unchanged by the deuteration of the imino groups, can be assigned to the middle methylene protons, though the integrated intensity was somewhat weaker than expected (the overall intensity of the two multiplets was about three-tenths of that of the multiplet at δ 2.5). This assignment is consistent with that of the middle methylene protons of a series of Co^{III}-tn complexes,[9] for which the middle methylene protons were assigned to the resonance lines near δ 2. The spacing of the two multiplets (δ 0.15) can not be explained on the basis of the spin-spin coupling between the middle methylene and the terminal methylene protons, since the spacing of the resonance lines due to the terminal methylene protons is much narrower than δ 0.15. Therefore, these two multiplets can be regarded as resonances of different protons in different magnetic environments. This fact suggests that the six-membered backbone chelate ring in the complex takes the chair form; in other words, the complex takes the *meso* form with respect to the coordinated nitrogen atoms.

The Raman spectrum gives useful information concerning the structural elucidation of Co^{III} complexes;[10,11] for instance, the Raman spectra in the skeletal stretching region were successfully applied to the differentiation of the isomers of [Co(gly)$_2$(AA)]-type complexes, where AA denotes en or ox.[11] The all-*trans* isomer can be regarded as having a C_{2h} symmetry, and then the Co-N and Co-O stretching vibrations are reduced to $2A_g+2B_u$, of which the A_g modes are Raman-active. On the other hand, the *trans(CN),cis(N)* isomer can be regarded as having a C_{2v} symmetry and the Co-N and Co-O stretching vibrations are reduced to $2A_1+2B_1$, of which all modes are Raman-active. The aqueous Raman spectra of the all-*trans*- and *trans(CN),cis(N)*-[Co(CN)$_2$(L-ala)$_2$]$^-$ complexes in the 650—450 cm^{-1} region are shown in Fig. 4 and correspond to those in the solid state well. The all-*trans* isomer exhibits two bands (581 and 537 cm^{-1}) in the Co-N and Co-O stretching vibration region, as expected from the symmetry. In contrast to the all-*trans* isomer, the *trans(CN),cis(N)* isomer exhibits three bands (595, 537, and 495 cm^{-1}) in the corresponding region. The fourth Raman-active band would be weak and concealed by the strong band at 595 cm^{-1}. The IR band at 577 cm^{-1} may be the counterpart of the concealed Raman band. These results confirm the assignment of the two isomers of [Co(CN)$_2$(L-ala)$_2$]$^-$ based on the absorption spectral behavior.

Absorption and CD Spectra. It has been suggested that, in the first absorption band of the *trans(CN)*-[Co(CN)$_2$(N)$_4$]-type complex ((N)$_4$=tetraammine or bis(diamine)), the position of the lower-energy component agrees with the one predicted from the semiempirical calculation,[12] whereas the position of the absorption component at a higher energy deviates from the one predicted.[1] This behavior in the first-absorption-band region is also realized in the present *trans(CN),cis(N)* isomer. The short vertical lines in Fig. 2 show the positions of the absorption components of the first absorption band, estimated in terms of the parameters, δ^1(CN)=32050 from [Co(CN)$_6$]$^{3-}$, δ^1(N)=21300 from [Co(en)$_3$]$^{3+}$, and δ^1(O)=16600 cm^{-1} from [Co(ox)$_3$]$^{3-}$. The splitting pattern of the first absorption band for the *trans(CN),cis(N)*-[Co(CN)$_2$(L-ala)$_2$]$^-$ isomer is similar to that of *trans(CN)*-[Co(CN)$_2$(NH$_3$)$_4$]$^+$;[1] namely, the higher energy component deviates remarkably from the one predicted. In the first absorption band of the all-*trans*-[Co(CN)$_2$(L-ala)$_2$]$^-$ isomer, however, the observed components agree fairly well with the predicted ones. This fact seems to deny that only *trans(CN)* arrangement is responsible for the deviation.

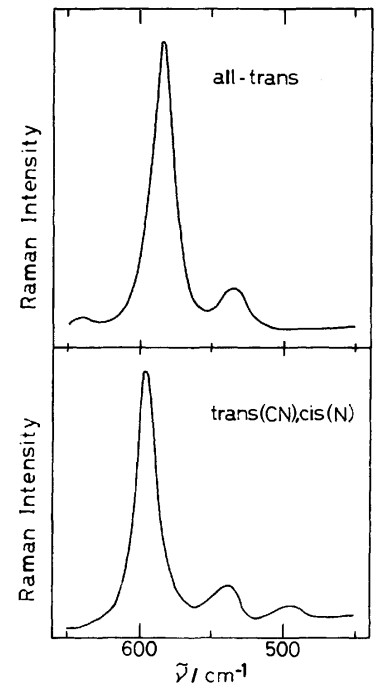

Fig. 4. Aqueous Raman spectra of the two isomers of *trans(CN)*-[Co(CN)$_2$(L-ala)$_2$]$^-$.

The CD spectra of *trans(CN),cis(N)*- and all-*trans*-[Co(CN)$_2$(L-ala)$_2$]$^-$ are mainly contributed by the *S*(C)-configuration of the L-alaninate ligand. In the d-d absorption-band region, the two isomers show similar CD patterns, though the CD spectrum of the all-*trans* isomer is somewhat stronger in intensity than that of the *trans(CN),cis(N)* isomer. Their CD bands in the second-absorption-band region are comparatively intense (Fig. 2 and Table 1). In contrast to the d-d absorption-band region, their CD spectra in the charge-transfer region (*ca.* 35—42×10^3 cm^{-1}) differ significantly from one another. It is apparent that the positive CD band (at 37.9×10^3 cm^{-1}) of the all-*trans* isomer corresponds to the absorption shoulder at *ca.* 37×10^3 cm^{-1}, and the negative CD band (at 39.5×10^3 cm^{-1}) of the *trans(CN),cis(N)* one, to the absorption

shoulder at *ca.* $37\times10^3\,cm^{-1}$. However, more data will be needed in order to discuss this CD spectral behavior in relation to the structural difference between the two geometrical isomers.

The authors wish to express their thanks to Professor Yoichi Shimura of Osaka University for his fruitful discussion.

References

1) K. Konya, H. Nishikawa, and M. Shibata, *Inorg. Chem.*, **7**, 1165 (1968).

2) M. Muto, T. Baba, and H. Yoneda, *Bull. Chem. Soc. Jpn.*, **41**, 2918 (1968); H. Kawaguchi and S. Kawaguchi, *Bull. Chem. Soc. Jpn.*, **46**, 3453 (1973); K. Kashiwabara, T. Yamanaka, K. Saito, N. Komatzu, N. Hamada, H. Nishikawa, and M. Shibata, *Bull. Chem. Soc. Jpn.*, **48**, 3631 (1975).

3) A. L. Poznjac and V. I. Pawlowski, *Z. Anorg. Allg. Chem.*, **465**, 159 (1980).

4) S. Fujunami and M. Shibata, *Bull. Chem. Soc. Jpn.*, **54**, 2959 (1981).

5) K. D. Gailey, K. Igi, and B. E. Douglas, *Inorg. Chem.*, **14**, 2965 (1975).

6) M. Okabayashi, K. Igi, and J. Hidaka, *Bull. Chem. Soc. Jpn.*, **52**, 753 (1979).

7) This ligand was prepared by modifying the method for ethylenediamine-*N*,*N*′-diacetic acid dihydrochloride; T. Kawato, H. Kanatomi, and I. Murase, *Bull. Chem. Soc. Jpn.*, **46**, 1723 (1973).

8) K. Ohkawa, J. Hidaka, and Y. Shimura, *Bull. Chem. Soc. Jpn.*, **39**, 1715 (1966).

9) I. R. Jonasson, S. F. Lincoln, and D. R. Stranks, *Aust. J. Chem.*, **23**, 2267 (1970).

10) K. Kanamori and K. Kawai, *Bull. Chem. Soc. Jpn.*, **53**, 2520 (1980); K. Kanamori and K. Kawai, *Bull. Chem. Soc. Jpn.*, **55**, 764 (1982); K. Kanamori, H. Ichinose, and K. Kawai, *Bull. Chem. Soc. Jpn.*, **55**, 1315 (1982).

11) T. F. Maruyama, K. Okamoto, J. Hidaka, and H. Einaga, *Bull. Chem. Soc. Jpn.*, **56**, 2610 (1983).

12) H. Yamatera, *Bull. Chem. Soc. Jpn.*, **31**, 2610 (1958).

Synthetic Inorganic Ion-exchange Materials. XXXVII. Ion-exchange Behaviors of Alkylammonium Ions on Hydrous Titanium Dioxide

Masamichi Tsuji,* Mitsuo Abe, and Minoru Orimo†
Department of Chemistry, Faculty of Science, Tokyo Institute of Technology, 2-12-1, Ookayama, Meguro-ku, Tokyo 152
(Received June 11, 1984)

Ion-exchange behavior of alkali hydroxide and alkylamines having different sizes and forms on hydrous titanium dioxide ion exchanger (HTDO) were studied. The uptakes of all the cations by HTDO indicated the ion-exchange stoichiometry at a pH range studied. The pH titration curves vary, depending on the cation species and the strength of the bases used: amorphous HTDO(Am-HTDO) behaves as a bifunctional acid towards strong bases and as a monofunctional acid towards weak bases. Am-HTDO shows an affinity series in the increasing order: large ions($(C_2H_5)_3NH^+$, $(CH_3)_4N^+$, and $(n\text{-}C_4H_9)_4N^+$)<ions in medium size ($CH_3NH_3^+$, $n\text{-}C_3H_7NH_3^+$, $n\text{-}C_4H_9NH_3^+$ *etc.*)<small ions(Na^+, K^+, and NH_4^+). The large ions suffer from a strong steric effect, because of the limited space of the ion-exchange site available. The results correlate with the pore size distribution: the pore radius ranged from 4 to 7 Å in Am-HTDO degassed at 40 °C by a rotary pump. The maximum volume occupied by the alkylammonium ions exchanged (0.2—0.3 cm^3/g), calculated by assuming cations to be unhydrated, is in good agreement with the value determined by N_2 gas adsorption (0.16 cm^3/g). An anatase-type HTDO showed a larger steric effect for uptake of the alkylammonium ions than that by the Am-HTDO, due to a decrease in the ion-exchange cavity.

Recently, ion-exchange selectivities on synthetic inorganic ion exchange materials have been studied.[1-4] Hydrous oxides and hydroxides of multivalent metals are reported to behave as selective ion exchangers towards a few metal ions. Hydrous titanium(IV) oxide showed selectivity for uranium(VI) in sea water.[5-7] Hydrous tin(IV) antimonate exhibited a unique selectivity sequence of $Na^+<K^+<Rb^+<Cs^+ \ll Li^+$ in an increasing order.[8] Hydrous manganese(IV) oxide in cryptomelane-type showed an unusual selectivity sequence towards alkali metal ions: $Li^+<Na^+<Cs^+ \ll K^+$, Rb^+. This exchanger shows a high selectilvity for the ions having the effective ionic radius[9] of 1.4 Å.[10,11] Crystalline antimonic(V) acid cation exchanger shows an excellent selectivity towards metal ions having an effective ionic radius of about 1 Å.[3] Cations larger than 6 Å in diameter cannot enter the cavity of crystalline antimonic acid.[12] Adsorption of Alkyl Orange dyes on silica gel indicated that a correlation exists with the molecular size of the dye.[13] It has been known that clinoptilolite cannot exchange alkylammonium ions larger than 6 Å.[14] These behaviors are well known as the ion-sieve action. No ion-sieve effect was observed on γ-zirconium phosphate ion exchanger, because of expansion along the c-axis by exchanging the large organic ions.[15] A steric effect can be expected for large spherical cations and long cations exchanged by HTDO, if it has a rigid framework and a small ion-exchange cavity.

The present paper describes the ion-exchange behaviors of univalent cations having different van der Waals dimensions on HTDO.

† Present address: 2-4-2, Nishigotanda, Shinagawa-ku, Tokyo Facility Management, KK.

Experimental

Ion-exchange Material. Am-HTDO was prepared by hydrolysis of $TiCl_4$ solution with NaOH solution.[16] Am-HTDO in H^+ form was obtained by removing Na^+ ions by percolation of 0.1 M HCl (1 M=1 mol dm^{-3}) solution into a column of Am-HTDO containing Na^+ ions (1 cmϕ×10 cm).

X-Ray and Thermal Analyses. X-Ray analysis with the powder method was carried out using Ni-filtered Cu-$K\alpha$ radiation with a JEOL diffractometer, Model JDX-7E. Thermogravimetry(TG) and differential thermal analysis (DTA) were undertaken with a Rigaku Denki thermoflex type thermal analyzer, Model 8001, at a heating rate of 10 °C min^{-1}.

Pore Size Distribution. The nitrogen gas adsorption isotherm of Am-HTDO was determined at 77 K by using N_2 gas adsorption equipment (Calro Erba, Co., Model Sorptomatic 1800). Prior to the measurement, degassing with a rotary pump was carried out until about 0.5 g of Am-HTDO in 50—100 mesh size became constant at 40 °C. A cross section of 16.2 $Å^2$ for N_2 molecule was employed.

pH Titration Curves. A 0.125 g portion of Am-HTDO in H^+ form was added into 12.5 cm^3 of (MCl+HCl) or (MCl+MOH) mixed solution of the ionic strength 0.1 at 30±0.5 °C in a thermostated bath, where M=Na, NH_4, and alkylammonium. It was shaken intermittently and allowed to stand until the concentration of M^+ ions became constant within the experimental error. Thereafter, pH values and the concentration of M^+ and Cl^- in the supernatant solution were determined. The pH measurement was carried out using a Toa Dempa pH meter, Model HM-5A. The concentrations of M^+ and Cl^- ions in the solution were determined by an "ion-exchange and titration" method: After neutralizing a 10 cm^3 aliquot with a standardized 0.1 M HNO_3 or 0.05 M NaOH solutions, the solution was percolated through Dowex 50W-X8 ion-exchanger column in H^+ form (1.0 cmϕ×10 cm) and then washed with water. The effluent was collected and titrated with standardized 0.05 M NaOH solution. The amount of M^+ ions in the solution was determined by sub-

tracting the amount of NaOH used for neutralization from the amount of the titrant. Cl^- ions in the equilibrated solution were determined by titrating with 0.03 M $AgNO_3$ solution using fluorescein as indicator after neutralization. Thus, the uptakes of M^+ and Cl^- ions by the Am-HTDO were calculated from the difference relative to the initial concentration.

Chemicals. $(n\text{-}C_4H_9)_4NOH$ was supplied as a 10% aqueous solution by Tokyo Kasei Ind. and other chemicals were supplied by Wako Pure Chemical Ind., Ltd. All chemicals were of analytical grade and used without further purification. Alkylammonium chloride solutions were prepared by neutralizing with dilute HCl solution.

Results and Discussion

Am-HTDO as an Ion-exchange Material. The Am-HTDO was characterized by X-ray diffraction and thermal studies. The X-ray powder pattern showed almost no distinct peak, indicating the product to be nearly amorphous. The crystallite sizes were estimated to be smaller than 20 Å in diameter. DTA curve showed an endothermic peak based on dehydration up to 200 °C and a sharp exothermic peak due to the transformation from nearly amorphous to the anatase modification at 400 °C. These features are in good agreement with those reported in our previous paper.[17] The composition of Am-HTDO obtained from the weight loss was $TiO_2 \cdot 1.84H_2O$ by assuming that the ignition product is TiO_2. The same composition was obtained in Am-HTDO kept in air at RT for 8 months, but it showed a weak anatase-type diffraction pattern, yielding a crystallite of about 30 Å.

Pore Size Distribution. The adsorption-desorption isotherm of N_2 gas on Am-HTDO was measured; this gives important informations about the pore structures of the solid. It shows the Langmuir-type[18] (Fig. 1). There was almost complete reversibility through the entire pressure range studied. A straight line was obtained on the BET plot,[19] giving S_{BET}= 345 m^2/g and C_{BET}=194. As long as the constant C_{BET} is lower than 200, a surface area, S_t, obtained by V_l-t plot based on the "MP method" by Brunauer, Mikhail and Bodor[20] shows good agreement with S_{BET}. In the present sample, S_t was 356 m^2/g, showing a discrepancy of 3.2%. This is a reasonable agreement, which permits use of V_l-t plot.

The pore volume distribution curve of Am-HTDO is shown in Fig. 2. The degassed Am-HTDO consists largely of micropores of 4—7 Å in hydraulic radius. The total pore volume was 0.16 cm^3/g. A sample degassed with a rotary pump until a constant weight was achieved showed a composition of $TiO_2 \cdot 1.2H_2O$. Hence, the skeleton of the Am-HTDO is still covered with hydrated and interstitial water. If the water could be removed more extensively without destruction of the ion-exchange sites or crystallization, a wider dis-

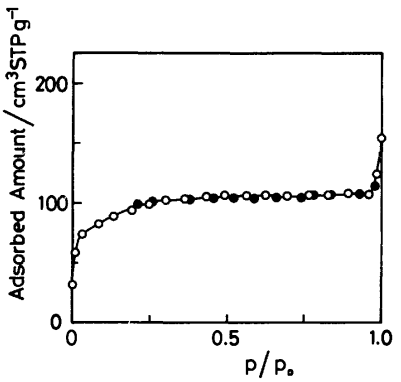

Fig. 1. Adsorption-desorption isotherm of N_2 on Am-HTDO at 77 K.
○: adsorption, ●: desorption.

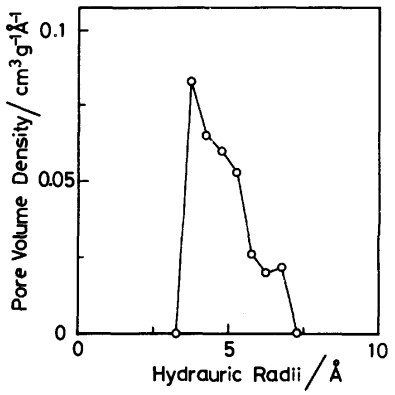

Fig. 2. Pore volume distribution curve of Am-HTDO.

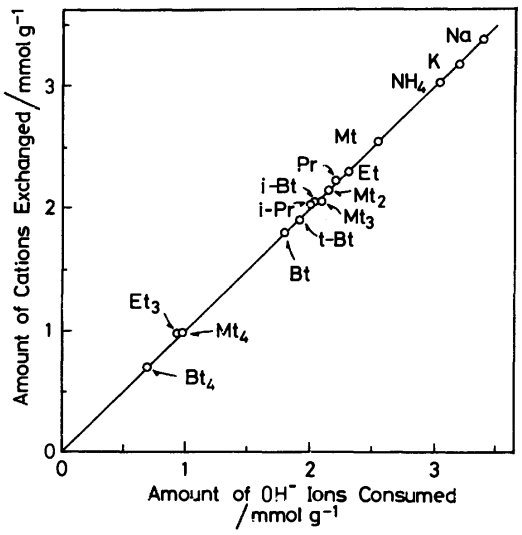

Fig. 3. Stoichiometry of ion-exchange reaction of alkylamines on Am-HTDO.
HTDO: 0.125 g, Soln: 0.1 M Amine or mixture of amine and the chloride, Total vol: 12.5 cm^3, Temp: 30 °C. Marks: Mt=$CH_3NH_3^+$, Et=$C_2H_5NH_3^+$, Pr=$C_3H_7NH_3^+$, Bt=$C_4H_9NH_3^+$, Mt_2=$(CH_3)_2NH_2^+$, Mt_3=$(CH_3)_3NH^+$, Mt_4=$(CH_3)_4N^+$, Et_2=$(C_2H_5)_2NH_2^+$, Et_3=$(C_2H_5)_3NH^+$, Bt_4=$(n\text{-}C_4H_9)_4N^+$.

tribution of pores accessible to nitrogen molecules would be obtained. However, degassing at elevated temperatures destroys the exchange sites.

Ion-exchange Stoichiometry for Various Alkylammonium Ions. The uptake of cations with different dimensions was studied in alkaline media(Fig. 3). The amount of hydroxide ions consumed was in good agreement with the amount of cation exchanged. This indicates the stoichiometry of the exchange reaction for all the cations used. Accordingly, almost all protons in Am-HTDO behave as a Brönsted acid. The uptake occurs through two possible schemes: One includes an exchange process with a replaceable proton,

$$-\overset{|}{\underset{|}{\text{Ti}}}\text{-OH} = -\overset{|}{\underset{|}{\text{Ti}}}\text{-O}^- + \text{H}^+ \qquad \text{(first step)}$$

$$-\overset{|}{\underset{|}{\text{Ti}}}\text{-O}^- + \text{R}_m\text{NH}^+_{n+1} = -\overset{|}{\underset{|}{\text{Ti}}}\text{-O-R}_m\text{NH}^+_{n+1} \qquad \text{(second step)}$$

and the other occurs through hydrogen bonding,

$$-\overset{|}{\underset{|}{\text{Ti}}}\text{-OH} + \text{R}_m\text{NH}_n = -\overset{|}{\underset{|}{\text{Ti}}}\text{-O-R}_m\text{NH}_{n+1}$$

where m and n are integer, and R denotes alkyl groups. However, the titration method cannot distinguish between the dissociation step and the adsorption step, because of the difficulty of the measurement of the H^+ ion concentration in the solid phase.

pH Titration Curve. It has been known that the Am-HTDO ion exchanger has an amphoteric character in aqueous solutions. The ion-exchange capacity towards Na^+ and Cl^- ions depends upon the pH of the solution used. The pH titration of the Am-HTDO ion exchanger was carried out in a pH range from 2 to 12, by using bases with different strengths, and geometrical forms and sizes in order to investigate the details of the change in the exchange capacity with pH values. A distinct break point can be found on each titration curve with strong bases at pH 7.5—8 irrespective of the geometrical dimensions of the cations (Fig. 4), while no break point is observed on the titration curves with weak bases over a wide range of pH studied (Fig. 5). Therefore the Am-HTDO acts as an apparent bifunctional acid towards strong bases and as an apparent monofunctional acid towards weak bases.

In the titration of a soluble weak acid with a strong base, generally the pH discontinuity at the end point is more obscure with decreasing strength of the base. Moreover, a steric effect also occurs in the case of the titration of inorganic ion-exchange materials having a rigid three-dimensional structure, as described below. The titration curves in Figs. 4 and 5 suggest these effects.

The uptakes for these cations were determined (Figs. 6 and 7). These results correspond well to each pH

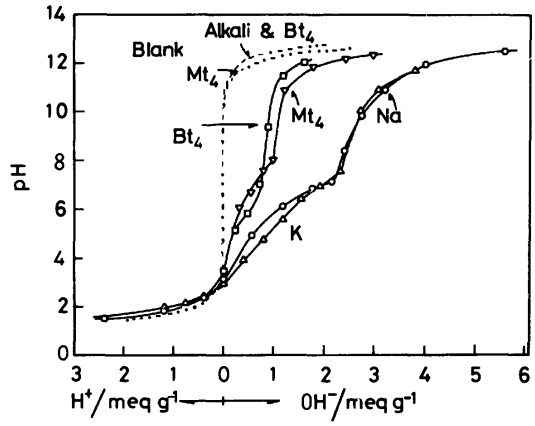

Fig. 4. pH Titration curves of Am-HTDO with strong bases having different size parameters.
Am-HTDO: 0.125 g, Soln: 0.1 M (MCl+HCl or MOH) mixed soln. (M=Bt_4, Mt_4, Na, and K). Notations are the same as in Fig. 3. Total vol.: 12.5 cm^3, Temp: 30±0.5 °C.

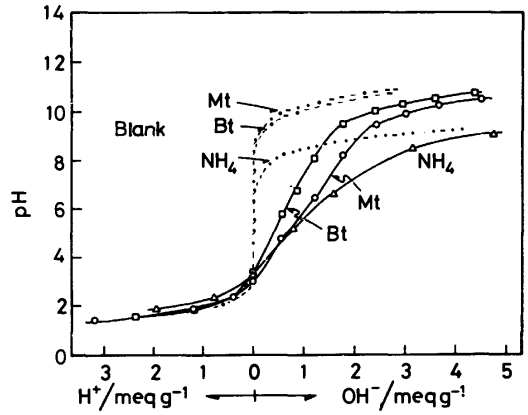

Fig. 5. pH Titration curves of Am-HTDO with weak bases having different size parameters.
The experimental conditions are the same as in Fig. 4.

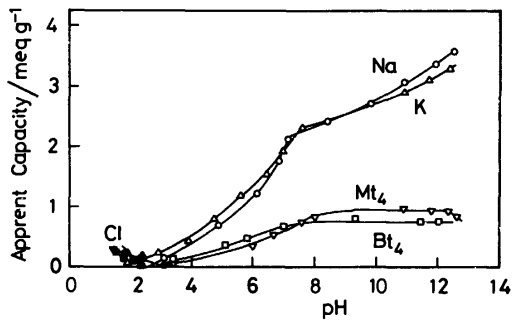

Fig. 6. Apparent capacities of spherical ions with different size parameters as a function of pH. Conditions are the same as in Fig. 4. Open marks are for cations and closed marks are for coexisting Cl^- ions.

Table 1. Amounts of alkylammonium ions having different dimensions exchanged by Am-HTDO

Cations	Dimension of Cations in Å[a]			Amounts exchanged	pH
	pK_a[d]	x-direction (length)	y-direction (width)	z-direction (height)	mmol/g	
NH_4^+	9.25	2.86	2.86	2.86	3.05	9.50
$CH_3NH_3^+$	10.65	4.9_1	4.0_0	4.0_0	2.55	11.0
$C_2H_5NH_3^+$	10.80	5.9_0	4.8_8	4.0_0	2.31	12.1
$(CH_3)_2NH_2^+$	10.73	6.4_2	4.2_8	4.0_0	2.25	12.3
n-$C_3H_7NH_3^+$	10.70	7.2_6	4.8_8	4.0_0	2.21	12.1
i-$C_3H_7NH_3^+$	—	6.5_2	5.5_6	4.7_7	2.03	12.1
$(CH_3)_3NH^+$	9.8[e]	6.4_2	6.1_0	4.1_7	2.06	11.6
n-$C_4H_9NH_3^+$	10.77	8.4_2	4.8_8	4.0_0	1.80	11.0
i-$C_4H_9NH_3^+$ [b]	—	7.5_1	5.5_6	4.7_7	2.05	12.0
$(C_2H_5)_2NH_2^+$ [b]	10.9[e]	7.5_9	6.0_5	4.0_0	2.25	12.3
t-$C_4H_9NH_3^+$	10.83	6.5_2	6.1_8	5.6_8	1.92	12.1
$(CH_3)_4N^+$	—	6.4_2	6.1_0	6.2_2	0.95	12.0
$(C_2H_5)_3NH^+$	10.8[e]	7.5_9	7.2_7	4.1_7	0.98	12.2
$(n$-$C_4H_9)_4N^+$ [b]	—	9.9_3	9.6_1	9.7_3	0.75	12.0
Na^+ [c]	—	2.04	2.04	2.04	3.40	12.0
K^+ [c]	—	2.76	2.76	2.76	3.20	12.0

a) Ref. 14. b) Estimated according to Ref. 14. c) Ref. 9. d) Ref. 27. e) Ref. 28.

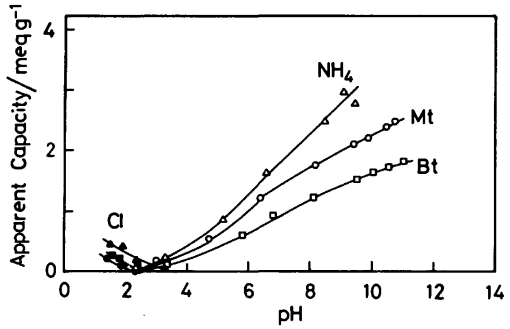

Fig. 7. Apparent capacities of NH_4^+ and nonspherical alkylammonium ions having different size parameters as a function of pH. Conditions are the same as in Fig. 5. Open marks are for cations and closed marks are for coexisting Cl^- ions.

titration curve in Figs. 4 and 5, indicating that the ion-exchange reaction is predominant over the whole range of pH studied. The apparent capacities for Na^+, K^+, $(CH_3)_4N^+$, and $(n$-$C_4H_9)_4N^+$ ions increase monotonically up to pH 7.5—8. At higher pH, the uptakes for Na^+ and K^+ ions having a small size show further increase, but those for large $(CH_3)_4N^+$ and $(n$-$C_4H_9)_4N^+$ ions constant up to pH 12. These suggest that smaller cations (Na^+, K^+) among strong bases can easily approach the ion-exchange sites present in micro-pores, while larger cations ($(n$-$C_4H_9)_4N^+$, $(CH_3)_4N^+$) are difficult of access to the micro-pores. At lower pH than 2, anion uptakes are predominant and a small uptake of Cl^- ions can be observed.

On the contrary, the apparent capacity for NH_4^+, $CH_3NH_3^+$, and n-$C_4H_9NH_3^+$ ions monotonically increases up to pH 10—11. With increasing dimensions, the apparent capacity decreased, when it was compared at pH>4.

A replaceable proton responsible for the ion-exchange reaction on various hydrous oxides and composite oxides has been determined by the butylamine titration method.[21,22] Johnson used butylamine as the titrating base for the reasons that it does not disturb the coloration at the end point using Hammet indicators and is not volatile. Many other authors have employed this base to determine the surface acid-sites.[23,24] The present results show that all the ion-exchange sites of Am-HTDO cannot be determined by the technique using this amine because of the steric hindrance. An alkali hydroxide or NH_3 aq. should be employed for the determination of the total protons responsible for the ion-exchange reaction of hydrous oxides of multivalent metals. However, an objection to the use of KOH can be found in the literature:[25] A silicate bond, $-\overset{|}{\underset{|}{Si}}-O-\overset{|}{\underset{|}{Si}}-$, is broken by the uptake of K^+ ions and the simultaneous consumption of OH^- ions on silica gel and the structure is rearranged. An uptake of Na^+ ions on hydrous tin(IV) oxide obeys a reversible ion-exchange reaction.[26] Hence, the breaking reaction of an $-\overset{|}{\underset{|}{Sn}}-O-\overset{|}{\underset{|}{Sn}}-$ bond will not be probable. Whether such a reaction including a break of $-\overset{|}{\underset{|}{Ti}}-O-\overset{|}{\underset{|}{Ti}}-$ occurs or not cannot be decided by the forward pH titration technique only.

Exchanged amounts of the alkylammonium ions having different van der Waals dimensions are compared in Table 1. Small spherical cations (NH_4^+, Na^+,

and K^+) of diameter<3 Å and ellipsoidally-shaped cations (n-$C_4H_9NH_3^+$ ions, *etc.*) can be exchanged to a greater extent. However, large ions>6 Å in dimension cannot fully replace a proton in the ion-exchange sites. Pore sizes of Am-HTDO vary over a range of 4—7 Å in radius (Fig. 2). These large organic ions are known to behave as a breaker of water structure in inorganic ion exchangers and exclude water molecules within the exchangers.[12] Water molecules in the Am-HTDO will be excluded more effectively than the degassing with a rotary pump when these large cations approach the ion-exchange sites. Thus, these alkylammonium ions can be exchanged.

The cross-section and volume of unhydrated cations were calculated, assuming the cations to be spheres (Na^+, NH_4^+) or prisms of elliptical cross-section (Table 2). The amounts of cations exchanged were plotted against the cross-section and the volume of the alkylammonium ion (Fig. 8 top and bottom, respectively). Uptakes of alkylammonium ions showed weak dependence on the cross-section, except n-$C_4H_9NH_3^+$, $(C_2H_5)_3NH^+$, and $(CH_3)_4N^+$ ions. These latter ions are very long or else very large spheres. The geometrical hindrance dose not permit these cations to be exchanged completely.

The uptakes decrease approximately linearly with increasing volumes of the unhydrated cations. The extent of the decrease is large for long (n-$C_4H_9NH_3^+$), wide ($(C_2H_5)_3NH^+$) or large spherical cations ($(CH_3)_4N^+$, $(n$-$C_4H_9)_4N^+$). It is due to the steric effect by these cations.

The maximum volume available for the ingoing ions can be estimated to be 0.2—0.3 cm^3/g. This value is comparable with that determined by N_2 adsorption (0.16 cm^3/g). It may be due to the effect of exclusion of water molecules by large cations exchanged that the former value is slightly large.

It has been known that an Am-HTDO in H^+ form is crystallized to an anatase-type while it is kept in the atmosphere at room temperature for a long period.[29]

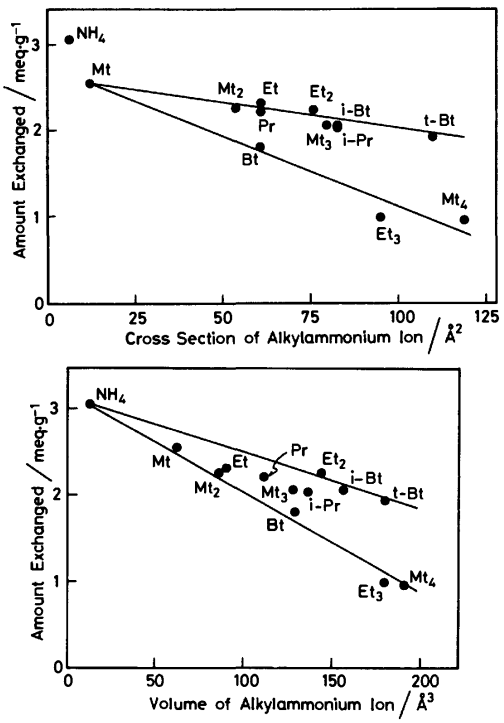

Fig. 8. Effect of the cross-section (top) and the volume (bottom) of unhydrated alkylammonium ions on the amount exchanged by Am-HTDO in H^+ form. Marks are the same as in Fig. 3.

Table 2. Total area and pore volume occupied by alkylammonium ions exchanged by Am-HTDO

Cations	Volume/Å³ of Unhydrated Cations	Cross-Section/Å² of Unhydrated Cations	Total Area m^2/g	Pore Volume cm^3/g
NH_4^+	12.5	6.3	38	0.023
$CH_3NH_3^+$	62	12	72	0.095
$C_2H_5NH_3^+$	90	61	367	0.125
$(CH_3)_2NH_2^+$	86	54	325	0.116
n-$C_3H_7NH_3^+$	111	61	367	0.147
i-$C_3H_7NH_3^+$	136	83	499	0.166
$(CH_3)_3NH^+$	128	80	481	0.158
n-$C_4H_9NH_3^+$	129	61	367	0.139
i-$C_4H_9NH_3^+$	156	83	499	0.192
$(C_2H_5)_2NH_2^+$	144	76	457	0.195
t-$C_4H_9NH_3^+$	180	110	662	0.208
$(CH_3)_4N^+$	191	119	716	0.109
$(C_2H_5)_3NH^+$	180	95	571	0.106
$(n$-$C_4H_9)_4N^+$	729	293	1763	0.329
Na^+	4.4	3.2	19	0.009
K^+	11.0	6.0	36	0.021

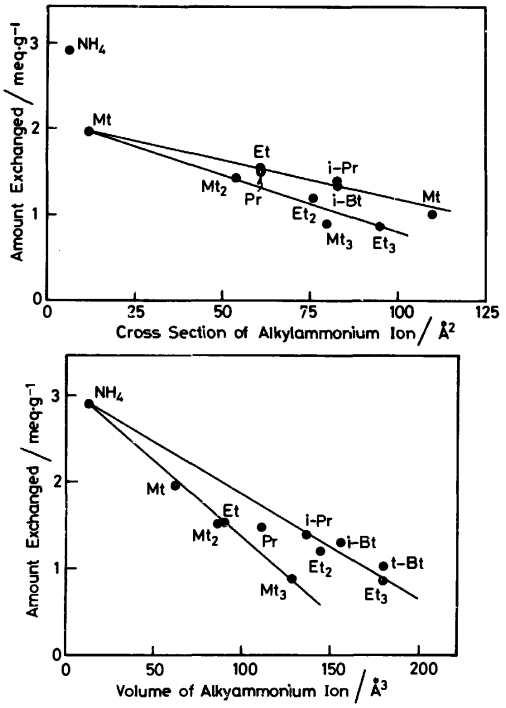

Fig. 9. Effect of the cross-section (top) and the volume (bottom) of unhydrated alkylammonium ions on the amount exchanged by An-HTDO in H^+ form. Marks are the same as in Fig. 3.

The Am-HTDO in H^+ form changed to An-HTDO having a crystallite size of about 30 Å after keeping it in the atmosphere for 8 months at room temperature. The An-HTDO showed about the same values as the Am-HTDO for the uptakes of NH_4^+ and $(C_2H_5)_3NH^+$ ions, while it showed a substantially decreased uptake for other alkylammonium ions (Fig. 9, top). This may be due to a decrease in the size of the cavity to accommodate the ingoing cations of medium size (5—7 Å). It suggests that the crystallization to the anatase-type causes shrinking of the Am-HTDO structure, followed by a decrease in the volume of the cavity necessary for the access to the ion-exchange sites. Consequently, the amounts exchanged more rapidly decreased with increasing volume of alkylammonium ions than Am-HTDO (Fig. 9, bottom). Thus, An-HTDO showed a larger steric effect than Am-HTDO.

The present authors are grateful to Mr. Kenta Ooi at the Government Industrial Research Institute, Shikoku, for the measurement of the pore size distribution.

References

1) V. Veselý and V. Pekárek, *Talanta*, **19**, 219 (1972).
2) V. Pekárek and V. Veselý, *Talanta*, **19**, 1245 (1972).
3) M. Abe, *Bunseki Kagaku*, **23**, 1254 (1974).
4) M. Abe, *Bunseki Kagaku*, **23**, 1561 (1974).
5) R. V. Davies, J. Kennedy, R. W. McIlroy, R. Spence, and K. M. Hill, *Nature (London)*, **203**, 1110 (1964).
6) N. J. Keen, *J. Brit. Nucl. Soc.*, **7**, 178 (1968).
7) N. Ogata, *Nippon Kaisui Gakkaishi*, **24**, 197 (1971).
8) M. Abe and K. Hayashi, *Solv. Extr. Ion Exchange*, **1**, 97 (1983).
9) R. D. Shannon and C. T. Prewitt, *Acta Crystallogr., Sect. B*, **25**, 925 (1969).
10) M. Tsuji and M. Abe, *Solv. Extr. Ion Exchange*, **2**, 253 (1984).
11) M. Tsuji and M. Abe, *Radioisotopes*, **33**, 218 (1984).
12) M. Abe, K. Yoshigasaki, and T. Sugiura, *J. Inorg. Nucl. Chem.*, **42**, 1753 (1980).
13) R. G. Haldeman and P. H. Emmett, *J. Phys. Chem.*, **59**, 1039 (1955).
14) R. M. Barrer, R. Pardopoulos, and L. V. C. Rees, *J. Inorg. Nucl. Chem.*, **29**, 2047 (1967).
15) A. Clearfield (Ed.), "Inorganic Ion Exchange Materials," CRC Press, Boca Raton, Fl. (1982), Chap. 1 by A. Clearfield.
16) Y. Inoue and M. Tsuji, *Bull. Chem. Soc. Jpn.*, **49**, 111 (1976).
17) M. Abe, M. Tsuji, S. P. Qureshi, and H. Uchikoshi, *Chromatogr.*, **13**, 626 (1980).
18) S. Brunauer, L. S. Deming, W. E. Deming, and E. Teller, *J. Am. Chem. Soc.*, **62**, 1723 (1940).
19) S. Brunauer, P. H. Emmett, and E. Teller, *J. Am. Chem. Soc.*, **60**, 309 (1938).
20) R. Sh. Mikhail, S. Brunauer, and E. E. Bodor, *J. Colloid Interface Sci.*, **26**, 45 (1968).
21) O. Johnson, *J. Phys. Chem.*, **59**, 827 (1955).
22) H. A. Benesi, *J. Phys. Chem.*, **61**, 970 (1957).
23) T. Takeda and S. Okazaki, *Nippon Kagaku Kaishi*, **1983** 608.
24) N. Yamagata, Y. Owada, S. Okazaki, and K. Tanabe, *J. Catal.*, **47**, 358 (1977).
25) R. M. Barrer, Discussion in "The Structure and Properties of Porous Materials," D. H. Everett and F. S. Stone (Ed.), Butterworths, London (1958), p. 290.
26) Y.Inoue and H. Yamazaki, *Bull. Chem. Soc. Jpn.*, **57**, 1534 (1984).
27) R. C. Weast (Ed.), Handbook of Chemistry and Physics, 54th, CRC Press, Cleveland, Ohio (1973—74), D-126.
28) Kagaku Binlan, The Chemical Society of Japan, Tokyo, 1975, p. 999.
29) M. Tsuji and M. Abe, 43th National Meeting of the Chemical Society of Japan, Tokyo, March 1981, Abstr. No. 1Z12.

 © 1985 The Chemical Society of Japan Bull. Chem. Soc. Jpn., 58, 103—108 (1985)

Electronic Spectra of the Aluminum(III) Complexes of 5,10,15,20-Tetraphenylporphin and 2,3,7,8,12,13,17,18-Octaethylporphin

Youkoh KAIZU, Naoaki MISU, Katsuhisa TSUJI,
Yoshiaki KANEKO, and Hiroshi KOBAYASHI*
Department of Chemistry, Tokyo Institute of Technology, O-okayama, Meguro-ku, Tokyo 152
(Received August 2, 1984)

Absorption, magnetic circular dichroism (MCD) and emission spectra as well as preparations of the aluminum(III) complexes of 5,10,15,20-tetraphenylporphin (TPP) and 2,3,7,8,12,13,17,18-octaethylporphin (OEP) are presented. On the basis of the spectral observations, the molecular parameters to describe the lowest (π,π^*) excited states of a typical metal porphyrin with only minor perturbation by the incorporated tervalent metal ion were determined. The orbital angular momenta in the excited states were evaluated from the MCD spectra as follows: TPPAlCl, $A_z=\pm3.0\,\hbar$ in Q_{00} band, $A_z=\pm0.61\,\hbar$ in B band and OEPAlCl, $A_z=\pm3.4\,\hbar$ in Q_{00} band, $A_z=\pm0.55\,\hbar$ in B band. A Davydov splitting of the Soret band observed for the μ-oxo dimer was interpreted in terms of the exciton coupling between two parallel porphyrin chromophores.

Aluminum(III) porphyrin is a typical porphyrin incorporated with a tervalent metal ion; characteristic Q and B bands in the visible and near-ultraviolet region, respectively, arise from the (π,π^*) excitations in the porphyrin ring with only minor perturbation from the outer-shell electrons of the central metal ion. On the other hand, the iron(III) porphyrins found in the heme proteins exhibit rather complicated spectral profiles attributable to the configuration-interaction admixtures of the porphyrin (π,π^*) excited states and the "porphyrin-to-iron" charge-transfer excited states.[1-4] Preparations of some aluminum(III) porphyrins have been reported,[5,6] however, the spectra of aluminum(III) porphyrins have received little attention until very recently.[7] A recent notable finding is that aluminum(III) porphyrin alkoxide behaves as the propagating end of the living polymerization of epoxide.[8]

In this paper, absorption and emission spectra as well as preparations of the aluminum(III) complexes of 5,10,15,20-tetraphenylporphin(TPP) and 2,3,7,8,12,13,17,18-octaethylporphin(OEP) are presented, since the spectra measured on the well-characterized samples of this particular reference porphyrin have never been reported. The spectra of the μ-oxo dimer, $(TPPAl)_2O$, which was prepared first in the present work, are also reported. The spectral character of the dimer is interpreted in terms of the exciton coupling model.

Experimental

Synthesis of Chloro(tetraphenylporphinato)aluminum(III) (TPPAlCl). The metal-free base ($TPPH_2$) was prepared from pyrrole and benzaldehyde by the method of Adler, *et al.*[9] A contamination of tetraphenylchlorin was oxidized by use of 2,3-dichloro-5,6-dicyano-*p*-benzoquinone.[10] $TPPH_2$(0.5 g) was vigorously refluxed for 1—2 h with anhydrous aluminum chloride(0.5 g) in dry benzonitrile (80 ml). The reflux was continued until no further change of the absorption spectrum was detected. If the metal insertion was incomplete, the mixture was refluxed again after addition of some anhydrous aluminum chloride. After cooled, the mixture was filtered and then excess hexane was added to the filtrate for completion of precipitation. (A trace of methanol facilitated precipitation of TPPAlCl from oily solutions which often appeared upon addition of hexane). The precipitates were collected by filtration, washed with hexane, and then dissolved in methanol (30—40 ml). After filtration of the methanol solution, 3 M HCl (1 M=1 mol dm^{-3}) was added for precipitation of the complex. The precipitates were collected on a filter, washed with 3 M HCl, dissolved in a smallest amount of acetone, and then recrystallized from the solution by addition of hexane. Reddish purple crystals thus obtained were $TPPAlCl\cdot4H_2O$. More reddish crystals of $TPPAlCl\cdot H_2O$ were obtained by drying $TPPAlCl\cdot4H_2O$ at 110—120 °C for 2 h.

Found: C, 76.12; H, 4.28; N, 7.98; Cl, 5.03%. Calcd for $C_{44}H_{30}N_4OAlCl$($TPPAlCl\cdot H_2O$): C, 76.24; H, 4.36; N, 8.08; Cl, 5.12%.

An effective metal insertion could not be achieved in pyridine, although the metal insertion in refluxing pyridine was reported in the case of meso- and etioporphin.[11]

Synthesis of Chloro(octaethylporphinato)aluminum(III) (OEPAlCl). The metal-free base ($OEPH_2$) was prepared by the method of Paine, *et al.*[12] from 3,4-diethyl-2-ethoxycarbonyl-5-methyl-pyrrole.[13]

Found: C, 80.87; H, 8.55; N, 10.38%. Calcd for $C_{36}H_{46}N_4$: C, 80.85; H, 8.67; N, 10.48%.

OEPAlCl was prepared in the similar way as described for preparation of TPPAlCl.

Found: C, 72.14; H, 7.52; N, 9.28; Cl, 5.42%. Calcd for $C_{36}H_{44}N_4AlCl$(OEPAlCl): C, 72.65; H, 7.45; N, 9.41; Cl, 5.96%.

The reaction of $OEPH_2$ and tris(acetylacetonato)aluminum(III) in phenol was reported.[5,6] However, $OEPH_2$ as well as $TPPH_2$ showed no significant reaction with tris(acetylacetonato)aluminum(III) in boiling benzonitrile.

Synthesis of Hydroxo(tetraphenylporphinato)aluminum(III) (TPPAlOH). By shaking of porphinatoaluminum(III)-chloride dissolved in a mixture of chloroform and methanol with an aqueous solution of $AgNO_3$, porphinatoaluminum(III) hydroxide was obtained in the chloroform layer. The reaction of conc H_2SO_4, which had been applied to the preparation of phthalocyaninatoaluminum-(III)hydroxide,[14,15] resulted in elimination of the central

metal ion.

TPPAlCl·H_2O (300 mg) was dissolved in a mixture of chloroform (300 ml) and methanol (30 ml). The solution was shaken with 100 ml of 0.1% aqueous solution of $AgNO_3$ and the chloroform layer was separated. To the chloroform layer, 20 ml methanol and 30 ml chloroform were added. The mixture was again shaken with 100 ml of 0.1% aqueous solution of $AgNO_3$. This procedure was repeated until no AgCl precipitated. The chloroform layer was thoroughly washed with water, being added an amount of chloroform and methanol to keep solubility of the complex. The chloroform solution thus obtained was concentrated up to a volume of 150 ml, and then 300 ml hexane was added for precipitation of the complex. The precipitate was dissolved in a smallest amount of methanol, concentrated by distillation of methanol and recrystallized by adding water. The crystals were thoroughly washed with 0.5 M aqueous ammonia and then water and recrystallized from a mixture of methanol and water. Purple crystals thus obtained were dried at 110—120 °C for 3 h.

Found: C, 78.29; H, 4.44; N, 8.37; Cl, 0.00%. Calcd for $C_{44}H_{31}N_4O_2Al$(TPPAlOH·H_2O): C, 78.33; H, 4.63; N, 8.30; Cl, 0.00%.

Synthesis of Hydroxo(octaethylporphinato)aluminum(III) (OEPAlOH). OEPAlOH was prepared by reaction of aqueous $AgNO_3$ with OEPAlCl in a similar way as described for preparation of TPPAlOH.

Found: C, 72.05; H, 7.83; N, 9.45%. Calcd for $C_{36}H_{47}N_4O_2Al$(OEPAlOH·H_2O): C, 72.70; H, 7.97; N, 9.42%.

Synthesis of μ-Oxo-bis[(tetraphenylporphinato)aluminum-(III)]. (TPPAl)$_2$O was obtained by heating TPPAlOH·H_2O at 300—340 °C for 10 h under reduced pressure (10^{-2}—10^{-3} mmHg).

Found: C, 81.65; H, 4.29; N, 7.98%. Calcd for $C_{88}H_{58}N_8OAl_2$ ((TPPAl)$_2$O): C, 81.59; H, 4.36; N, 8.65%.

A trace of TPPAlOH contamination in (TPPAl)$_2$O could not be eliminated by further purification because (TPPAl)$_2$O was not so stable in solution and not sublimable. The μ-oxo dimer exhibits a characteristic IR band of Al-O-Al at 1050 cm^{-1} (Fig. 1), which conforms to the band found in the μ-oxo dimer of aluminum phthalocyanine.[15]

The corresponding band of (OEPAl)$_2$O, however, could not be detected after heating OEPAlOH for several hours under reduced pressure in a variety of temperatures around the melting point of OEPAlOH. Preparation of (OEPAl)$_2$O by heating under reduced pressure has been reported, however, the reported IR spectrum lacks the characteristic Al-O-Al band.[16]

All other reagents and solvents used for preparations and measurements were commercially available. Benzonitrile was distilled under reduced pressure after dried over anhydrous sodium sulfate more than one night. Dichloromethane(CH_2Cl_2), chloroform($CHCl_3$) and carbon tetrachloride(CCl_4) were shaken with conc H_2SO_4 and then aqueous sodium hydrogencarbonate, washed with water, dried over anhydrous calcium chloride more than one night and then distilled. For further dehydration, CCl_4 was refluxed over phosphorus pentaoxide, distilled and then kept over sodium hydroxide. Methanol was purified by distillation after dried over $CaSO_4$.

Measurements. Electronic absorption spectra were taken on a Hitachi 220 A spectrophotometer. Since (TPPAl)$_2$O was stable only in concentrated solution, the intense absorption band was measured using a cell of 0.3 mm path length. On the other hand, the routine spectral measurements were carried out with solutions in quartz cuvetts of 1 cm path length. Emission and excitation spectra were recorded on a Hitachi MPF-2A fluorescence spectrophotometer equipped with a Hamamatsu Photonics photomultiplier R-928. Fluorescence intensity was corrected by the method of Lippert, *et al.*[17] Phosphorescence was detected on the fluorescence spectrophotometer attached with its phosphorescence device.

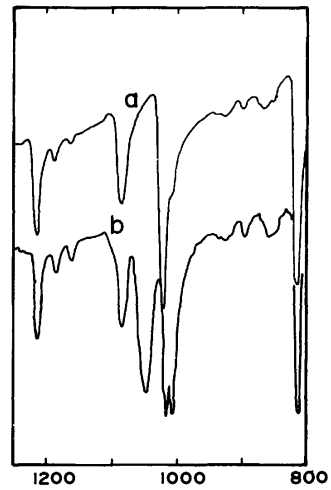

Fig. 1. IR spectra of TPPAlCl and (TPPAl)$_2$O in KBr disks.
a: TPPAlCl, b: (TPPAl)$_2$O.

Magnetic circular dichroism was measured on a JASCO J-500C spectropolarimeter with an electromagnet. The magnetic field was set at 1T.

Infrared spectra of TPPAlCl and (TPPAl)$_2$O in KBr disks were taken on a Hitachi 260-10 infrared spectrophotometer.

Results and Discussion

Absorption and fluorescence spectra of TPPAlCl and OEPAlCl in CCl_4 containing 2.5% methanol are shown in Fig. 2. The spectra of TPPAlOH and OEPAlOH were actually coincident with the spectra of the corresponding chloro complexes. In polar solvents such as methanol, ethanol, acetone, and acetonitrile, the complexes were stable. In non-polar solvents such as benzene and toluene, however, the complexes usually displayed a spectral drift for a period of time. A small amount of methanol added to the non-polar solvents stabilized the spectra and an increase in the concentration of methanol gives rise to a slight blue shift of each band. TPPAlOH and OEPAlOH in CH_2Cl_2 were rather stable and exhibited the spectral profiles given in Fig. 3. Absorption and fluorescence spectra of (TPPAl)$_2$O in CCl_4 are illustrated in Fig. 4. The spectra were rather stable only when the dimer was dissolved in CCl_4 which was treated with NaOH just before use.

The fluorescence spectra given in Figs. 2, 3, and 4 are

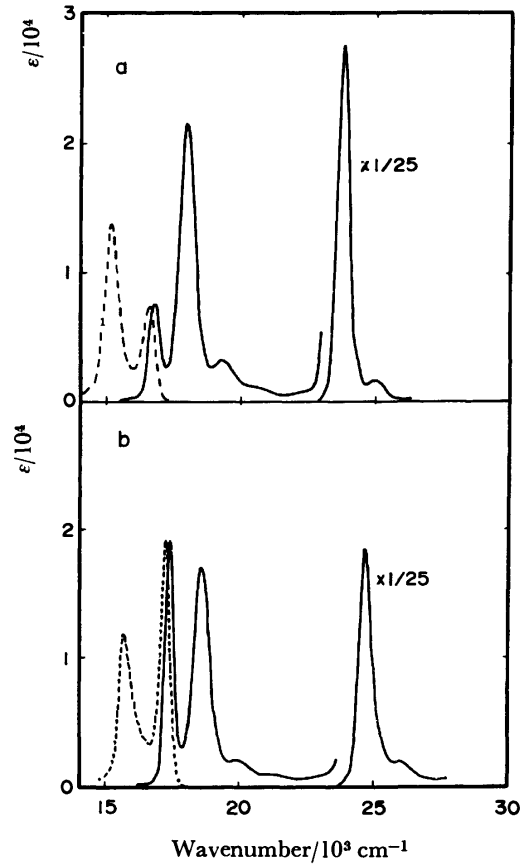

Fig. 2. Absorption and fluorescence spectra of TPPAlCl (a) and OEPAlCl (b) in methanol/CCl_4. (methanol: CCl_4=2.5: 97.5).
——: absorption, ----: emission.

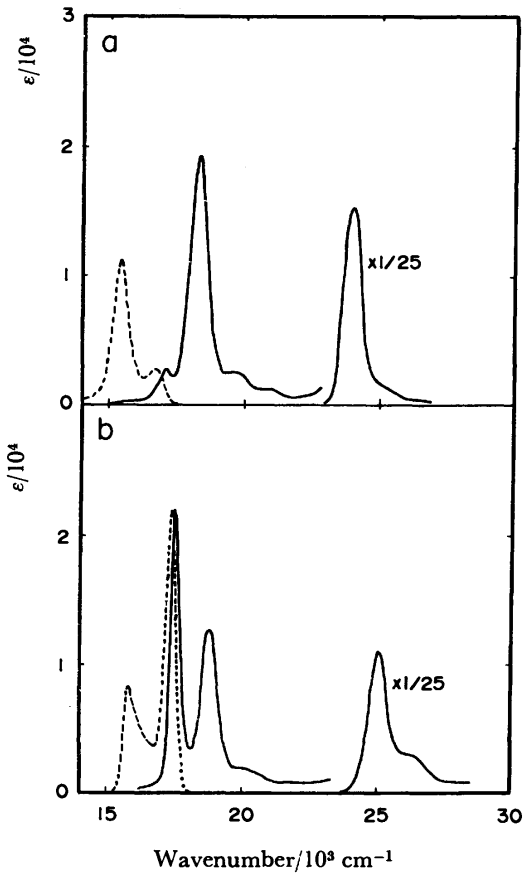

Fig. 3. Absorption and fluorescence spectra of TPPAlOH (a) and OEPAlOH (b) in CH_2Cl_2.
——: absorption, ----: emission.

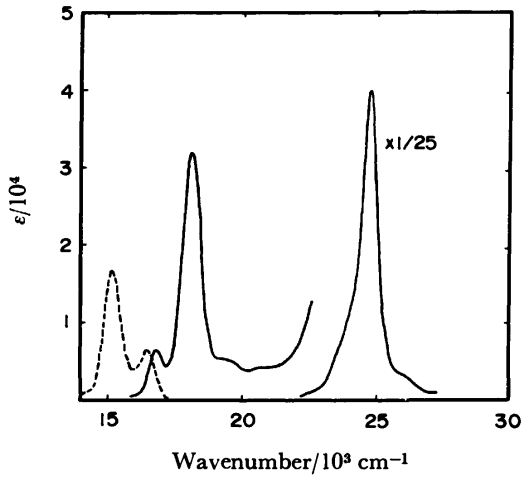

Fig. 4. Absorption and fluorescence spectra of $(TPPAl)_2O$ in CCl_4.

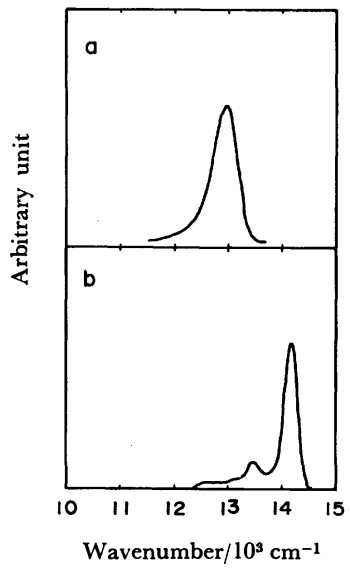

Fig. 5. Phosphorescence spectra of TPPAlCl (a) and OEPAlCl (b) in methanol glass at 77 K (uncorrected).

in a mirror image of the corresponding absorption spectra. The excitation spectra of fluorescence as well as phosphorescence were in good agreement with the absorption spectra. Figure 5 shows the phosphorescence spectra of the chloro complexes in ethanol at 77 K. Figure 6 shows the MCD spectra of TPPAlCl and OEPAlCl in methanol. The MCD spectra display a positive A term dispersion in each band. The ob-

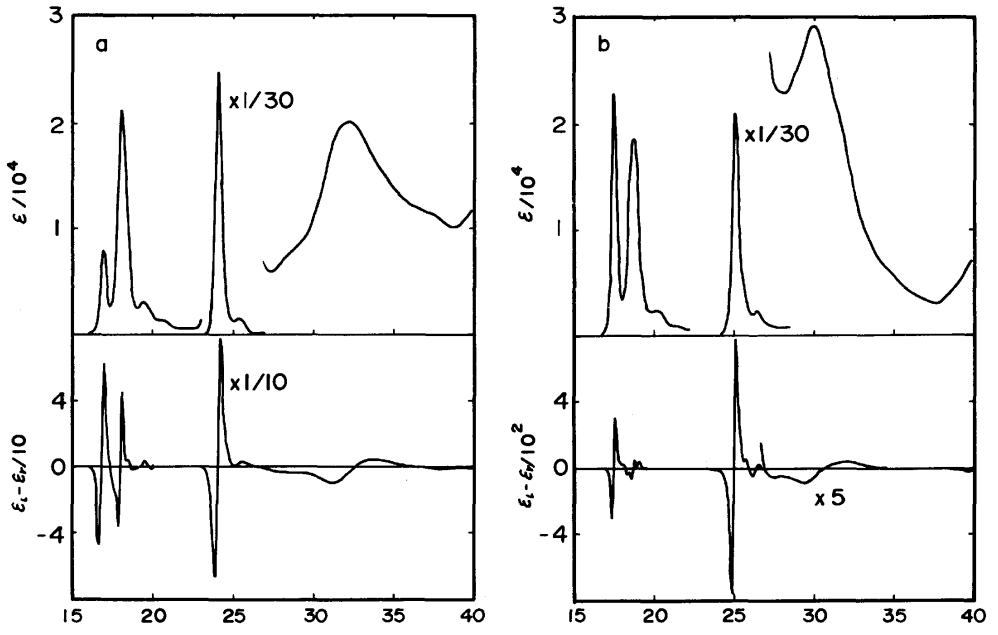

Fig. 6. MCD spectra of TPPAlCl (a) and OEPAlCl (b) in methanol.

served spectral characters are very similar to those of the typical (π,π^*) transition observed for the D_{4h} metalloporphins incorporated with a divalent metal ion such as Mg^{2+} and Zn^{2+}.

The lowest (π,π^*) excited states of metalloporphins are well described as a 50-50 admixture of the lowest excited configurations $(a_2)^2a_1e$ and $(a_1)^2a_2e$, where a_2 and a_1 are the highest filled orbital pair and e are the lowest vacant degenerate orbitals. Since the top filled orbitals are accidentally degenerate, their 50-50 admixtures $(a_2\pm ia_1)/\sqrt{2}$ are taken instead of individual a_2 and a_1 orbitals. The highest occupied orbital pair correspond to the degenerate orbital pair of the circular box model

$$|\pm 4) = f(\mathbf{r}) \exp[\pm 4i\theta], \tag{1}$$

where ± 4 denote the z components of orbital angular momentum $\lambda=4\hbar$, while the lowest vacant degenerate e orbitals are denoted as

$$|\pm 5) = f(\mathbf{r}) \exp[\pm 5i\theta]. \tag{2}$$

The one-electron excitations $|\pm 4)\rightarrow|\pm 5)$ and $|\mp 4)\rightarrow|\pm 5)$ give rise to two degenerate excited states with different total angular momenta $M_z=\pm 1\,\hbar$ and $M_z=\pm 9\,\hbar$, respectively. The ground state has zero angular momentum $M_z=0\,\hbar$. Thus the selection rule allows a pair of transitions of $\Delta M_z=\pm 1\,\hbar$, in which the angular momentum of the photons is conserved. The intense near-ultraviolet B(Soret) band is identified with the allowed transition pair $\Delta M_z=\pm 1\,\hbar$, whereas the weak Q band is characterized with the forbidden but vibronically allowed transition pair $\Delta M_z=\pm 9\,\hbar$. Table 1 shows the diagonal energies of the lowest excited states in terms of the exchange integrals

$$K_1 \equiv (4^*5|5^*4) = e^2\iint \frac{f^2(\mathbf{r}_1)f^2(\mathbf{r}_2)}{r_{12}} \exp[i(\theta_1-\theta_2)]d\tau_1 d\tau_2, \tag{3}$$

$$K_9 \equiv (-4^*5|5^*-4) = e^2\iint \frac{f^2(\mathbf{r}_1)f^2(\mathbf{r}_2)}{r_{12}} \exp[9i(\theta_1-\theta_2)]d\tau_1 d\tau_2, \tag{4}$$

and the off-diagonal one-electron term

$$\varepsilon \equiv -(4^*|\hat{\mathbf{h}}|-4) = \frac{1}{2}\{(a_1|\hat{\mathbf{h}}|a_1)-(a_2|\hat{\mathbf{h}}|a_2)\} \tag{5}$$

which arises from the fact that the a_2 and a_1 orbitals are not exactly degenerate in metalloporphins.

In the case of TPPAlCl in methanol, the Q band is observed at 16900 cm^{-1}($\varepsilon_{Q_{0,0}}$(max)=0.765×10⁴ M^{-1} cm^{-1}), and the B band at 24100 cm^{-1}(ε_B(max)=73.3×10⁴ M^{-1} cm^{-1}); the phosphorescence appears at 12900 cm^{-1}. The transitions to $^1(\pm 4\rightarrow\pm 5)$ are exclusively allowed. However, the off-diagonal element ε carries the spectral intensity from the allowed B transition to the forbidden Q counterpart. Assuming a Gaussian shape function with half-width $\tilde{\Gamma}$, the transition moment is evaluated from the observed absorption intensity,

$$|\mathbf{m}|^2 = 1.514\times 10^{-3}\{(\tilde{\Gamma}/\bar{\nu})\varepsilon(\max)/g\} \text{ (a.u.}^2\text{)}, \tag{6}$$

TABLE 1. THE LOWEST (π,π^*) EXCITED SINGLET AND TRIPLET STATES OF THE METALLOPORPHIN

$\|^{1,3}(-4\rightarrow+5)>$	$\|^{1,3}(+4\rightarrow-5)>$	$\|^{1,3}(+4\rightarrow+5)>$	$\|^{1,3}(-4\rightarrow-5)>$
$\Delta(4,5)+\binom{2}{0}K_9$	0	ε	0
	$\Delta(4,5)+\binom{2}{0}K_9$	0	ε
		$\Delta(4,5)+\binom{2}{0}K_1$	0
			$\Delta(4,5)+\binom{2}{0}K_1$

The top integer in ( ) stands for the excited singlet, while the bottom, for the excited triplet.
The excited states $|Q>$ and $|B>$ are described by

$$|Q> = -\sin\nu\,|^1(\pm4\rightarrow\pm5)> + \cos\nu\,|^1(\mp4\rightarrow\pm5)>$$
$$|B> = \cos\nu\,|^1(\pm4\rightarrow\pm5)> + \sin\nu\,|^1(\mp4\rightarrow\pm5)>,$$

where $\nu = \frac{1}{2}\tan^{-1}(\varepsilon/K_1 - K_9)$.

where g is the degeneracy of excited state, $g=2$ in this particular case, ε(max), and $\tilde{\nu}$ are molar absorption coefficient and wavenumber at the absorption maximum, respectively. The observed intensity ratio yields $|m(Q)|^2/|m(B)|^2=0.016$, where the values of $\tilde{f}(Q)$ and $\tilde{f}(B)$ are 520 cm^{-1} and 490 cm^{-1} respectively. Provided that $\Delta(4,5)=13800\ cm^{-1}$, $K_1=5100\ cm^{-1}$, $K_9=1600\ cm^{-1}$, and $\varepsilon=-900\ cm^{-1}$, not only the observed transition energies of the lowest triplet and singlet excited states but also the ratio $|m(Q)|^2/|m(B)|^2$ are well reproduced.

The corresponding values of OEPAlCl in methanol are as follows:

$$\Delta(4,5) = 15800\ cm^{-1},\ K_1 = 4400\ cm^{-1},\ K_9 = 1000\ cm^{-1}$$
$$\varepsilon = 1600\ cm^{-1}.$$

Here it is assumed that the a_1 orbital is higher than the a_2 orbital in OEPAlCl while it is reversed in TPPAlCl.[18]

The *ab initio* molecular orbital calculations even at the recent stage provide only poor predictions on the electronic excited states. However the screened potential molecular orbital approach yields a reasonable picture of the porphin excited states.[19,20] Theoretically evaluated values for metalloporphin are as follows;[20]

$$\Delta(4,5) = 13400\ cm^{-1},\ K_1 = 6600\ cm^{-1},\ K_9 = 1600\ cm^{-1}$$
$$\varepsilon = 1200\ cm^{-1}.$$

These results seem reasonable but still far from the observation.

The orbital angular momenta in the excited states were determined by computer simulations of the positive A term dispersions observed in the MCD spectra assuming Gaussian shape functions for the corresponding absorption bands.[21] The orbital angular momenta of TPPAlCl were obtained as $A_z=\pm3.0$ $\hbar$ and $A_z=\pm0.61\,\hbar$ in the excited states of Q_{00} and B band, respectively. This implies that the angular momenta of the highest occupied and the lowest vacant orbitals are $\lambda_4=1.2\,\hbar$ and $\lambda_5=1.8\,\hbar$, respectively. The corresponding values of OEPAlCl are as follows; $A_z=\pm3.4\,\hbar$ in Q_{00} band, $A_z=\pm0.55\,\hbar$ in B band, $\lambda_4=1.6\,\hbar$ and $\lambda_5=2.0\,\hbar$.

The absorption spectrum of the μ-oxo dimer as seen in Fig. 4 exhibits a remarkable blue shift of the B band with lower wavenumber tail extending to about 22000 cm^{-1} which is attributable to an exciton coupling in the B band. The dimer Q band is also blue-shifted but to a lesser extent. A similar spectral behavior has been found with the μ-oxo dimer $(TPPSc)_2O$, while the red shift of the dimer Q band was observed in the case of $(OEPSc)_2O$.[22]

The geometry of the μ-oxo dimer is assumed in D_{4d} symmetry. As revealed by X-ray analysis, the interplanar distance is greater than anticipated by the intermetal distance.[23,24] An extreme short intermetal distance has been found for the linear Al-O-Al bridge between two trigonal-bipyramidal pentacoordinated aluminum atoms.[25] In the case of $(TPPAl)_2O$, Al^{3+} ion can not displace much more than 0.5 Å out of the porphin plane, however, a doming distortion in two porphin skeletons results in an interplanar distance as high as 4.8 Å. Because of the small overlap between the π orbitals of two component porphins in such a distance, K_{AB}, an electrostatic interaction between the overlap charges (j_Aj_B) and (a_Aa_B), can be ignored. The exciton coupling arises only from the Coulomb interaction J_{AB} between two transition charges (j_Aa_A) and (j_Ba_B), which are often approximated by the interaction between two transition dipoles $\mathbf{m}_A$ and $\mathbf{m}_B$ on the counterparts A and B.

The basis sets of the exciton states are given by 50-50 admixtures of the local excited states; $|Q^+>=(|Q_A>+|Q_B>)/\sqrt{2}$, $|Q^->=(|Q_A>-|Q_B>)/\sqrt{2}$, $|B^+>=(|B_A>+|B_B>)/\sqrt{2}$, $|B^->=(|B_A>-|B_B>)/\sqrt{2}$. The interactions between these states are shown in Table 2, where

TABLE 2. THE INTERACTION BETWEEN THE LOWEST (π,π^*) EXCITED SINGLETS OF THE μ-OXO METALLOPORPHIIN DIMER

$\|Q^+>$	$\|Q^->$	$\|B^+>$	$\|B^->$
$E(Q)+\sin^2\nu J$	0	$-\sin\nu\cos\nu J$	
	$E(Q)-\sin^2\nu J$		$\sin\nu\cos\nu J$
		$E(B)+\cos^2\nu J$	
			$E(B)-\cos^2\nu J$

The exciton states are given by

$$|Q>=-\sin\phi\,|B^\pm>+\cos\phi\,|Q^\pm>$$
$$|B>=\cos\phi\,|B^\pm>+\sin\phi\,|Q^\pm>$$

where $\phi=\frac{1}{2}\tan^{-1}\{\mp\sin 2\nu/[E(B)-E(Q)\pm\cos 2\nu J]\}$.

$E(Q)$ and $E(B)$ are the energies of the component Q and B states in the μ-oxo dimer, which might be different from the monomer values and the interaction terms are given in units of $J=2(4_A{}^*5_A|5_B{}^*4_B)$.

Absorption spectrum of $(TPPAl)_2O$ exhibits the $Q_{0,0}$ band at 16900 cm^{-1} ($\varepsilon_{Q_{0,0}}(max)=0.650\times10^4$ M^{-1} cm^{-1}, $\tilde{\nu}=700$ cm^{-1}) and the B band at 24800 cm^{-1} ($\varepsilon_B(max)=100\times10^4$ M^{-1} cm^{-1}, $\tilde{\nu}=550$ cm^{-1}), respectively. Assuming the monomer values for $E(B)$ and $E(Q)$, the absorption spectrum of the μ-oxo dimer was reproduced for $J=1000$ cm^{-1}. The theory predicts that the allowed B state is in 25100 cm^{-1} and the forbidden one in 23100 cm^{-1} and thus the Davydov splitting is 2000 cm^{-1} in the B band while that of the Q band is less than 50 cm^{-1}. Conserving the monomer values only for two-electron terms K_1 and K_9, $E(Q)=16900$ cm^{-1}, $E(B)=24100$ cm^{-1} and $J=700$ cm^{-1} are evaluated from the transition energies and the intensity ratio observed for the μ-oxo dimer spectrum. On the other hand, the values, $E(Q)=16800$ cm^{-1}, $E(B)=23300$ cm^{-1} and $J=1500$ cm^{-1}, yield the forbidden and allowed B states in 21800 cm^{-1} and 24800 cm^{-1} respectively, and the corresponding Q states in 16800 cm^{-1} and 16900 cm^{-1}. The observed Davydov splitting in the B band is less than 3000 cm^{-1}.

The transition dipole $m\equiv\sqrt{2}(5|m|4)$ is estimated as 3.4 a.u. from the parameter values determined for TPPAlCl in methanol and thus J is evaluated as 3400 cm^{-1} for the parallel stacking by the approximation of dipole-dipole interaction $m^2/r_{AB}{}^3$ in a distance $r_{AB}=4.8$ Å. The diagonalization of the interactions using the parameters for TPPAlCl predicts a rather big splitting ($\approx$6800 cm^{-1}) in the B band. The value of J can be calculated by use of the wavefunctions obtained by molecular orbital calculations.[20] For $r_{AB}=4.8$ Å is obtained $J=4400$ cm^{-1}, which predicts a much greater splitting.

References

1) H. Kobayashi, Y. Yanagawa, H. Osada, S. Minami, and M. Shimizu, *Bull. Chem. Soc. Jpn.*, **46**, 1471 (1973).
2) H. Kobayashi, T. Higuchi, Y. Kaizu, H. Osada, and M. Aoki, *Bull. Chem. Soc. Jpn.*, **48**, 3137 (1975).
3) H. Kobayashi, T. Higuchi, and K. Eguchi, *Bull. Chem. Soc. Jpn.*, **49**, 457 (1976).
4) H. Kobayashi, *Adv. Biophys.* **8**, 191 (1975).
5) J. W. Buchler, G. Eikelmann, L. Puppe, K. Rohbock, H. H. Schneehage, and D. Weck, *Ann. Chem.*, **745**, 135 (1971).
6) J. W. Buchler, L. Puppe, K. Rohbock, and H. H. Schneehage, *Chem. Ber.*, **106**, 2710 (1973).
7) A. Harriman, *J. Chem. Soc., Faraday Trans. 1.*, **78**, 2727 (1982).
8) T. Aida and S. Inoue, *Macromolecules*, **14**, 1166 (1981).
9) A. D. Adler, F. R. Longo, J. D. Finarelli, J. Goldmacher, J. Assour, and L. Korsakoff, *J. Org. Chem.*, **32**, 476 (1967).
10) G. H. Barnett, M. F. Hudson, and K. M. Smith, *J. Chem. Soc., Perkin Trans. 1*, 1401 (1975).
11) A. Treibs, *Ann. Chem.*, **728**, 115 (1969).
12) J. B. Paine, III, W. B. Kirshner, D. W. Moskowitz, and D. Dolphin, *J. Org. Chem.*, **41**, 3857 (1976).
13) C. B. Wang and C. K. Chang, *Synthesis*, **1979**, 548.
14) P. A. Barrett, C. E. Dent, and R. P. Linstead, *J. Chem. Soc.*, **1936**, 1716.
15) J. E. Owen and M. E. Kenney, *Inorg. Chem.*, **1**, 334 (1962).
16) H. H. Inhoffen and J. W. Buchler, *Tetrahedron Lett.*, **1968**, 2057.
17) E. Lippert, W. Nagele, I. Seibold-Blandenstein, U. Staeger, and W. Voss, *Z. Anal. Chem.*, **170**, 1 (1959).
18) P. J. Spellane, M. Gouterman, A. Antipas, S. Kim, and Y. C. Liu, *Inorg. Chem.*, **19**, 386 (1980).
19) H. Sekino and H. Kobayashi, *J. Chem. Phys.*, **75**, 3477 (1981).
20) H. Sekino and H. Kobayashi, to be published.
21) P. N. Schatz, A. J. McCaffery, W. Suetaka, G. N. Henning, A. B. Ritchine, and P. J. Stephens, *J. Chem. Phys.*, **45**, 722 (1966).
22) M. Gouterman, D. Holten, and E. Lieberman, *Chem. Phys.*, **25**, 139 (1977).
23) A. B. Hoffman, D. M. Collins, V. W. Day, E. B. Fleischer, T. S. Srivastava, and J. L. Hoard, *J. Am. Chem. Soc.*, **94**, 3620 (1972).
24) J. F. Johnson and W. R. Scheidt, *Inorg. Chem.*, **17**, 1280 (1978).
25) Y. Kushi and Q. Fernando, *J. Am. Chem. Soc.*, **92**, 91 (1970).

The Determination of a Small Amount of Biological Constituent by the Use of Chemiluminescence. IV. A Highly Sensitive Detector for the HPLC of Protein

Tadashi HARA,* Motohiro TORIYAMA, and Takashi EBUCHI
Department of Chemical Engineering, Faculty of Engineering, Doshisha University, Karasuma Imadegawa, Kamigyo-ku, Kyoto 602
(Received August 23, 1984)

A highly sensitive detector for the HPLC of protein has been manufactured by making use of the phenomenon that the catalytic activity of copper(II) against the chemiluminescence between luminol and hydrogen peroxide is lowered in the presence of protein. According to the present detector, 2×10^{-4}—1×10^{-1} g/dm^3 protein could be determined, with the detection limit of 10 ng. By combining the present detector with a TSK-GEL G3000SW column, 2×10^{-3}—1×10^{-1} g/dm^3 ovalbumin could be determined, with the detection limit of 50 ng. The ovalbumin in 2×10^{-2} g/dm^3 could be determined by the internal-standard method with a coefficient of variation of 8.65% (n=5). Care had to be taken in the detection of the protein acting as a chemiluminescent catalyst.

As detectors for the high-performance liquid chromatography(HPLC) of protein, the following apparatus are now being used: a ultraviolet spectrophotometer(UV), a differential refractometer(RI), a light-scattering spectrophotometer, and so on. The detection limit of RI is inferior to that of UV.[1] A precise determination of protein by the use of a light-scattering spectrophotometer alone is difficult because the signal obtained with it is given by the product of the molecular weight of protein and its concentration.[2] UV is also unsuitable for application to an unknown sample because a measured value varies depending on the kind of protein, and the detection limit of 20 μg/cm^3 protein is still unsatisfactory for the determination of a small amount of protein in a clinical laboratory. To improve the detector sensitivity, a fluorometer has been applied to the determination of peptides after separation by means of HPLC.[3] On the other hand, a method for the flow-injection analysis of protein has been established by the present authors on the basis of the fact that the catalytic activity of copper(II) against the chemiluminescence (CL) between 5-amino-2,3-dihydro-1,4-phthalazinedione(luminol) and hydrogen peroxide(H_2O_2) is lowered in the presence of protein.[4] This method is applicable to the detection of 2×10^{-4}—1×10^{-1} g/dm^3 protein and is more sensitive than any others thus far reported. Moreover, this method shows a similar sensitivity for various kinds of proteins and makes a continuous determination of protein possible. Since this method was expected to be a promising post-column detector for the protein separated in an aqueous HPLC system without losing the inherent property of protein, the analytical conditions, detection limit, and so on were investigated.

Experimental

Reagents. All the reagents used were of a commercially available special grade. A 2.0×10^{-6} mol/dm^3 copper(II) solution was prepared by diluting a 2.0×10^{-2} mol/dm^3 copper(II) stock solution with a buffer solution(Buff-I)(pH 10.2) consisting of 0.1 mol/dm^3 boric acid and 0.1 mol/dm^3 potassium hydroxide. A 1.0×10^{-4} mol/dm^3 luminol solution was prepared by the use of the same buffer solution as above. A 5.0×10^{-4} mol/dm^3 H_2O_2 solution was prepared by diluting a 0.3 wt% H_2O_2 solution with distilled water. A 3.33×10^{-3} mol/dm^3 phosphate buffer solution(Buff-II; pH 6.19), consisting of a 2.67×10^{-3} mol/dm^3 potassium dihydrogenphosphate(KH_2PO_4) solution, a 6.67×10^{-4} mol/dm^3 disodium hydrogenphosphate(Na_2HPO_4) solution, and a 0.15 mol/dm^3 potassium chloride(KCl) solution, was prepared; it was also used as an eluent later on. The sample solutions of bovine serum albumin(BSA) (Sigma Chemical Co.), lysozyme (from chicken egg white) (Sigma Chemical Co.), ovalbumin (Sigma Chemical Co.), and the Gel Filtration Standard(Bio. Rad) were prepared by dissolving them in Buff-II and by diluting them with Buff-II.

Apparatus and Procedure. A HPLC system equipped with a CL detector was set up for the separation and determination of protein (Fig. 1). All the tubes (0.5 mm i.d.) and connectors(n) used were made of Teflon. Each solution of luminol(a) and H_2O_2(b), held at 25 °C by means of a thermostat(q) (Netsudenshi kogyo Co., Ltd.), and of copper(II)(c), held at room temperature, was fed by means of nitrogen gas of 3.3×10^5 Pa pressure gauge, the flow rate was adjusted to 1.0 cm^3/min by the use of a flow-meter equipped with a needle valve(h)(GILMONT). An eluent(buffer solution)(d) was fed at the flow rate of 1.0 cm^3/min by means of a pump(i) (Pharmacia High-precision Pump P-500). A 50-mm^3 portion of a mixed protein solution was injected into the eluent line through the sampling loop(k_1) and the seven-way cock(j_1) (Pharmacia Fine Chemicals, Valve-7), after which the protein was separated on the column(m) (TSK-GEL G3000SW column: 600×7.5 mm i.d.+TSK-GEL G3000SW guard column: 75×7.5 mm i.d.). The protein in an eluate was first mixed with a copper(II) solution, and then the resulting solution was further mixed with a H_2O_2 solution at the position W and with a luminol solution at the position X after having passed through a reaction tube(o) (0.64 m), held at 95 °C and a cooling tube(p) (0.40 m), held at 0 °C, in that order. Finally, the mixed solution was introduced into the same flow cell(r) as in the previous paper. The CL intensity

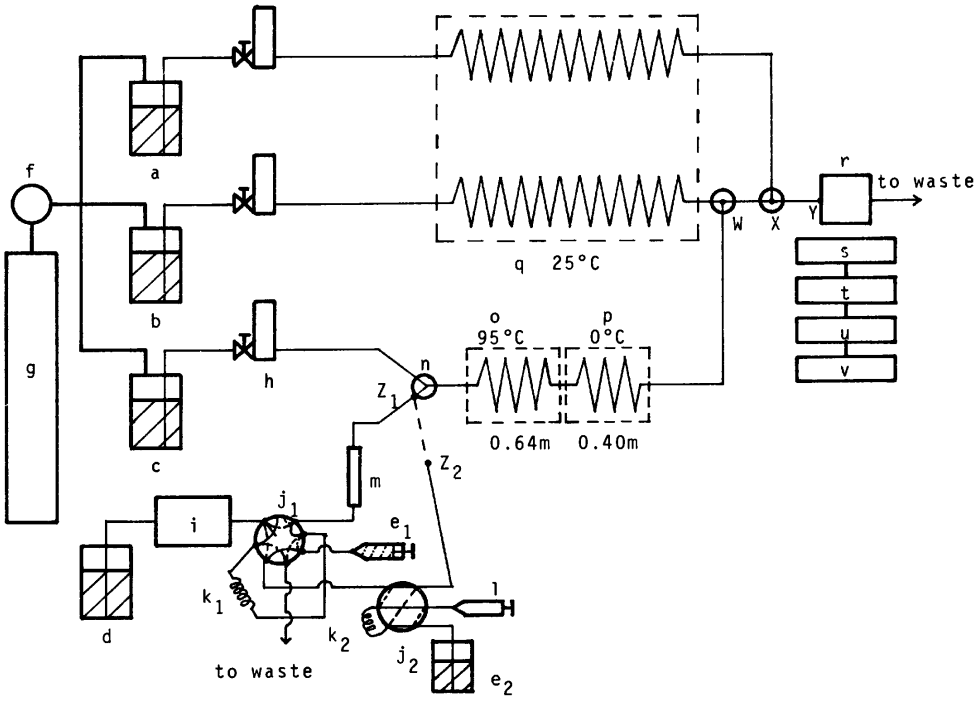

Fig. 1. Schematic diagram of the system equipped with CL detector.
a: Luminol solution, b: H_2O_2 solution, c: copper (II) catalyst solution, d: eluent (buffer solution), e_1 and e_2: sample solution, f: regulator, g: N_2 cylinder, h: flow-meter equipped with a needle valve, i: pump, j_1: seven-way cock, j_2: six-way cock, k_1 and k_2: sampling loop, l: syringe, m: cloumn, n: connector, o: reaction tube, p: cooling tube, q: thermostat, r: flow cell, s: photomultiplier, t: amplifier, u: recorder, and v: integrator.

was measured by means of a photomultiplier(s) (Hamamatsu TV Co., Ltd., R928), amplified with an amplifier(t) (Horiba Ltd., OPE-402), and recorded on a recorder(u) (Yokogawa Electric Works, Ltd., 3046), followed by the measurement of the peak area by the use of an integrator(v) (Shimadzu Chromatopac C-R2A). The distances between X and W or Y were 30 cm and 10 cm respectively.

The flow-injection analysis of protein by a direct-injection method was carried out by injecting a sample solution into the eluent line by operating a seven-way cock (j_1) and a six-way cock(j_2) equipped with a sampling loop(k_2) after connecting Z_1 with Z_2. Though a ghost peak appeared periodically owing to the exchange between the two cylinders in the pump(i), it did not interfere with the determination of the protein.

Results and Discussion

Characteristics of the Detector. The stability of a base line is generally indispensable for the exact determination of protein by means of HPLC. Though the CL intensity was significantly influenced by the temperature, no care was taken about the temperature except for a copper(II) solution in the previous paper. Therefore, no stable base line was obtained over a long period. In the present study, both the luminol solution and the H_2O_2 solution were held at 25 °C so as to give a stable base line. Since the flow rate of eluent in HPLC was generally less than 1.0 cm^3/min, a BSA sample solution was directly estimated by flow-injection analysis under the same conditions as were used in the previous paper except for the use of 1.0 cm^3/min instead of 10 cm^3/min for the flow rate of the buffer solution(Buff-I) (Fig. 1(d)). The detection limit of BSA was 40 ng in the previous paper, while it was 400 ng in this case. This was assumed to be due to the dilution of a sample solution, for the flow rate of each solution of copper(II), luminol, and H_2O_2 was 10 cm^3/min in the previous paper, while that of the buffer solution containing BSA in the present study was 1.0 cm^3/min. Therefore, the flow rate of each solution was selected as 1.0 cm^3/min. The diameter of the tubing was also changed from 1 mm to 0.5 mm so as to reduce the diffusion of a sample. Furthermore, the length of the reaction tube and the cooling tube were changed from 1.0 m to 0.64 m and from 1.6 m to 0.40 m respectively so as to provide the same residence time as in the previous paper. Under these conditions, the maximum diminution in the CL intensity based on the injection of protein was observed at a 1.0×10^{-4} mol/dm^3 luminol, a 5.0×10^{-4} mol/dm^3 H_2O_2, and a 2.0×10^{-6} mol/dm^3 copper(II) solution.

The calibration curve obtained by the flow-injection analysis of BSA, using the direct-injection technique at the above-mentioned flow rate and reagent concentra-

tion, is shown in Fig. 2, together with that obtained in the previous paper. According to the present detector, 2×10^{-4}—1×10^{-1} g/dm^3 BSA could be determined; its detection limit(S/N=2) was the same as in the previous paper. The coefficients of variation for ten measurements of 1×10^{-3} and 1×10^{-2} g/dm^3 BSA were 11.2% and 6.9% respectively. As can be seen from Fig. 2, the slope of the present calibration curve was about one, while that in the previous paper was about one-half. The difference between these two slopes may be supposed to be based on (1) the difference in the reaction conditions for the chelate formation between copper(II) and protein and/or (2) the difference between the residence times in the flow cell in the previous paper(about 0.3 s) and in the present paper(about 3.4 s).

Conditions for the Separation of Protein. A combination of the present detector and gel-permeation chromatography, in which proteins could be separated by the use of an aqueous eluent without changing the higher-order structure of protein, was devised for the separation of proteins. For this combination, care had to be taken in the use of an eluent with a pH value of around 7 against a TSK-GEL G3000SW column and of the alkaline solution for the chelate formation between copper(II) and protein and in the CL reaction.

The effects of the concentration of a phosphate buffer solution and a salt solution on the present detector in the gel-permeation chromatography of ovalbumin and lysozyme were also examined. The effect of the phosphate solution on the chelate formation between copper(II) and protein and the subsequent CL reaction is shown in Fig. 3. The results in Fig. 3 can be understood from the following experimental data.

The pH of the solution in a flow cell was inferred by measuring the pH value of the mixed solution consisting of distilled water, a Buff-I solution, and a phosphate buffer solution (3.33×10^{-2}, 3.33×10^{-3}, 3.33×10^{-4} mol/dm^3) containing a KH_2PO_4 solution and a Na_2HPO_4 solution in a volume ratio of 1:2:1; pH values of 9.8, 10.0, and 10.0 were found, in that order. This shows that the pH value of the solution in a flow cell is around the pH value desired for the measurements of the CL intensity.

On the other hand, the pH value of the mixed solution consisting of a Buff-I solution and a phosphate buffer solution (3.33×10^{-2}, 3.33×10^{-3}, 3.33×10^{-4} mol/dm^3), containing a KH_2PO_4 solution and a Na_2HPO_4 solution in a volume ratio of 1:1, was measured to ascertain the pH value in a reaction tube containing copper(II) and protein; the pH values 9.4, 9.9, and 9.9 were thus obtained.

In other words, the difference in the results of Fig. 3 may be concluded to be primarily due to the difference in the chelate formation by pH. Since the detection limits for A and B in Fig. 3 did not differ much from

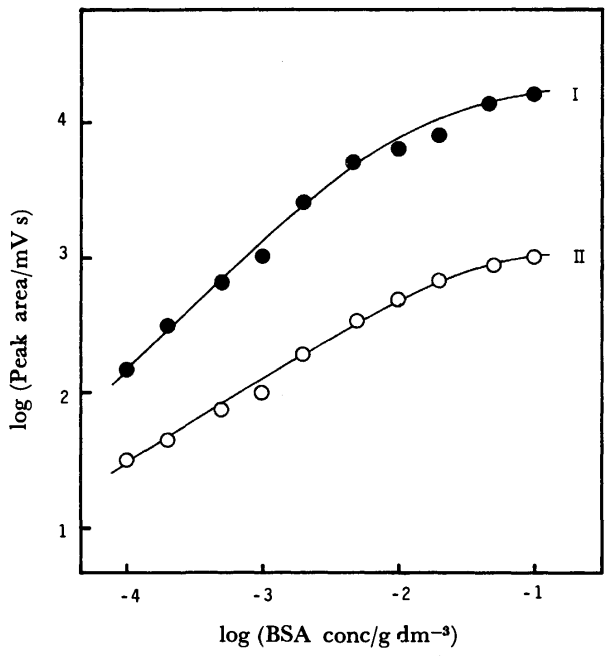

Fig. 2. Calibration curves of BSA by the present method and the previous method.
I: present paper and II: previous paper.
Conditions: previous paper; 5.0×10^{-4} mol/dm^3 luminol, 5.0×10^{-4} mol/dm^3 H_2O_2, 2.0×10^{-6} mol/dm^3 copper(II), and Buff-I(pH 10.15) as a buffer solution and present paper; 1.0×10^{-4} mol/dm^3 luminol, 5.0×10^{-4} mol/dm^3 H_2O_2, 2.0×10^{-6} mol/dm^3 copper(II), and Buff-II(pH 6.19) as a buffer solution.

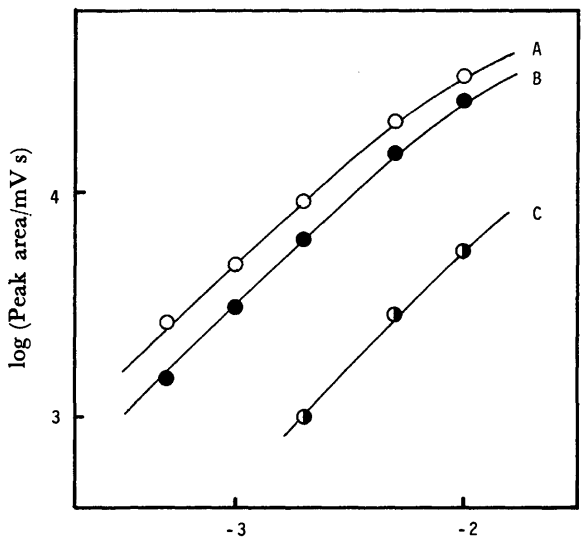

Fig. 3. Effect of concentration of phosphate buffer solution on the present detector.
A: 3.33×10^{-4} mol/dm^3-, B: 3.33×10^{-3} mol/dm^3-, and C: 3.33×10^{-2} mol/dm^3-phosphate buffer solution consisting of KH_2PO_4 solution and Na_2HPO_4 solution.
Conditions: 1.0×10^{-4} mol/dm^3 luminol, 5.0×10^{-4} mol/dm^3 H_2O_2, 2.0×10^{-6} mol/dm^3 copper (II), and ovalbumin as sample.

each other, and since a larger buffer capacity was desired for an eluent, a 3.33×10^{-3} mol/dm^3 phosphate buffer solution was chosen as the eluent for the HPLC.

The ionic strength of an eluent was enhanced by the addition of a salt to suppress the ionic adsorption of protein on the column. The effect of the added salt(KCl) on the present detector is shown in Fig. 4. The base line was lowered with an increase in the concentration of KCl, and then the CL intensity was influenced by the addition of KCl. The peak area in Fig. 4 is shown against the base line in a KCl-free ovalbumin solution. As can be seen from Fig. 4, the peak area was almost definite independent of the concentration of KCl, and the addition of KCl did not affect the reaction between copper(II) and ovalbumin. Since more than 0.2 mol/dm^3 of KCl reduced the CL intensity, and since the detection limits in the 0, 0.05, 0.10, and 0.15 mol/dm^3 KCl solutions were all approximately the same, a 0.15 mol/dm^3 KCl solution was selected as the optimum concentration.

Separation by Means of a Column. The number of theoretical plates was calculated from the peak width and the elution time recorded on recorder chart paper by injecting 1 μg of ovalbumin; the value of 1840 was thus obtained. According to the UV method, the number of theoretical plates 2488 was reported[5] to be obtained under the following conditions: a 0.1 mol/dm^3 phosphate buffer solution as an eluent, a flow rate of 0.875 cm^3/min, 100 μg of ovalbumin, and a 30.5-cm TSK-GEL G3000SW column. This value was calculated to be 5890 at the flow rate and the column length used in the present study.

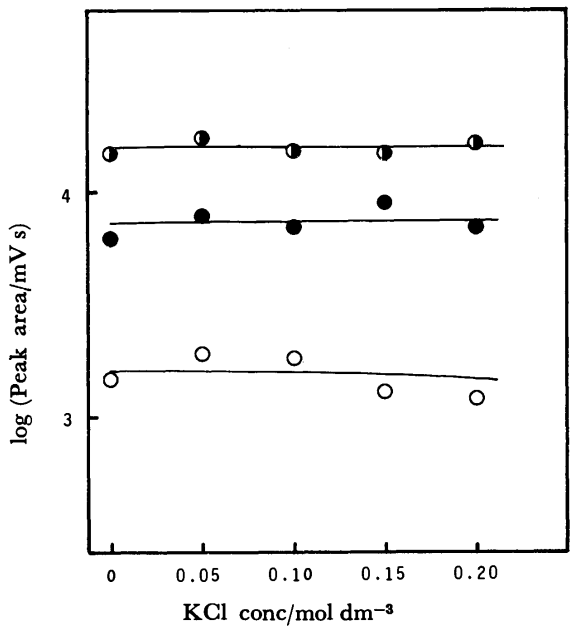

Fig. 4. Effect of added KCl on the present detector.
○: 5.0×10^{-4} g/dm^3-, ●: 2.0×10^{-3} g/dm^3-, and ◑: 5.0×10^{-3} g/dm^3-ovalbumin.
Conditions: 1.0×10^{-4} mol/dm^3 luminol, 5.0×10^{-4} mol/dm^3 H_2O_2, 2.0×10^{-6} mol/dm^3 copper (II), and 3.33×10^{-3} mol/dm^3 phosphate buffer solution consisting of 2.67×10^{-3} mol/dm^3 KH_2PO_4 solution and 6.67×10^{-4} mol/dm^3 Na_2HPO_4 solution.

It has usually been accepted in flow-injection analysis that the band broadening of a sample based on the diffusion in a tube can be neglected at a tube diameter of less than 0.5 mm. Since a tube 0.5 mm i.d. was used in the present study, the diffusion of a sample in the eluate seems not to lower the number of theoretical plates. Therefore, the lowering of the number of theoretical plates may be supposed to be attributed to the residence time in the flow cell, the amount of the sample, and so on.

A 18-mg sample(Gel Filtration Standard) of a mixture consisting of protein aggregates, thyroglobulin-(bovine), γ-globulin(bovine), ovalbumin(chicken), myoglobin(horse), and vitamin B-12 was dissolved in a 0.5-cm^3 Buff-II solution, and from the solution(Sample I) a 50-mm^3 fraction was taken, after which analysis was done by means of HPLC using a UV detector(Hitachi, Ltd., wavelength-tunable effluent monitor, 634). On the other hand, Sample I was diluted to 1:667 with Buff-II, and from the solution(Sample II) a 50-mm^3 fraction was taken, followed by analysis by means of HPLC using the present detector. The chromatograms thus obtained are shown in Fig. 5.

As can be seen from both chromatograms in Fig. 5, the D and E peaks in the chromatogram obtained by the present detector were relatively small in comparison with the A, B, and C. Furthermore, the D and E peaks appeared on the side opposite those in II of Fig. 5 when Sample I was diluted to 1 :200 and a 50-mm^3 fraction was similarly analysed.

Hemoglobin, catalase, and peroxidase, which are all hemoproteins containing an iron-porphine complex structure, have been well known to act as catalysts in the CL reaction. Since myoglobin is also a hemoprotein, it was expected to act more or less as a catalyst in the CL reaction.

The peak D of myoglobin in II of Fig. 5 was obtained by subtracting the inverse response based on the catalytic activity of myoglobin as a catalyst against the CL reaction from the response based on myoglobin as a protein. Vitamin B-12, containing a cobalt(II)-porphine complex structure in its central position, was experimentally confirmed by the authors to act as a weak catalyst against the CL reaction; then, the E peak was obtained by reasoning similar to that in case of the D peak.

To sum up, the present detector was shown to be a useful one for the sensitive detection of protein in an eluate from the HPLC column, though care had to be taken in the detection of protein acting as a catalyst against the CL reaction.

Determination by Means of a Column. Two calibration curves were obtained as follows: (I) each 50-

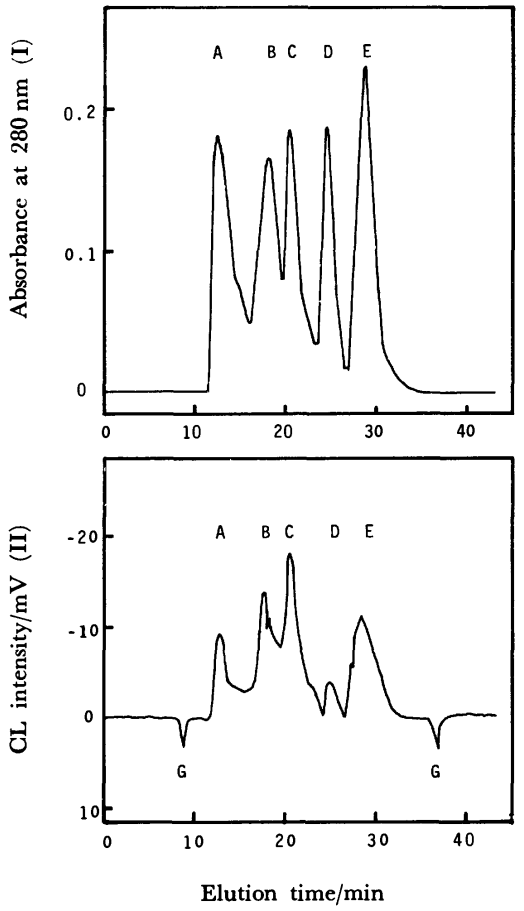

Fig. 5. Chromatograms of Gel Filtration Standard obtained by the present detector and the UV detector.
A: protein aggregates+thyroglobulin(bovine), B: γ-globulin(bovine), C: ovalbumin(chicken), D: myoglobin, E: vitamin B-12, and G: ghost peak.
Conditions: 3.33×10^{-3} mol/dm³ phosphate buffer solution(Buff-II)(pH 6.19) as eluent, load volume 50 mm³, I(UV detector); Range 1.28 and Sample-I: Gel Filtration Standard (18 mg mixture sample)/0.5 cm³ Buff-II, and II(present detector); Sample-II: Sample-I diluted to 1 : 667 with Buff-II.

mm³ portion in the concentration range of 2×10^{-3}—1×10^{-1} g/dm³ ovalbumin was injected into a separation column, and the ovalbumin in the eluate was monitored by means of the present CL detector, and (II) each 50-mm³ portion in the concentration range of 2×10^{-4}—1×10^{-1} g/dm³ ovalbumin was directly subjected to flow-injection analysis without using a separation column. The results obtained are shown in Fig. 6.

The coefficient of variation for five measurements of 2×10^{-2} g/dm³ ovalbumin in the former (I) was 12.7%. The deviation of the calibration curve II from a straight line can be understood in terms of the shortage of copper(II) in the reaction with ovalbumin; the shift of the calibration curve I to the higher side of ovalbumin concentration can also be understood by the dilution of the sample in a column. Here, the average recovery of 2×10^{-3}—2×10^{-2} g/dm³ ovalbumin

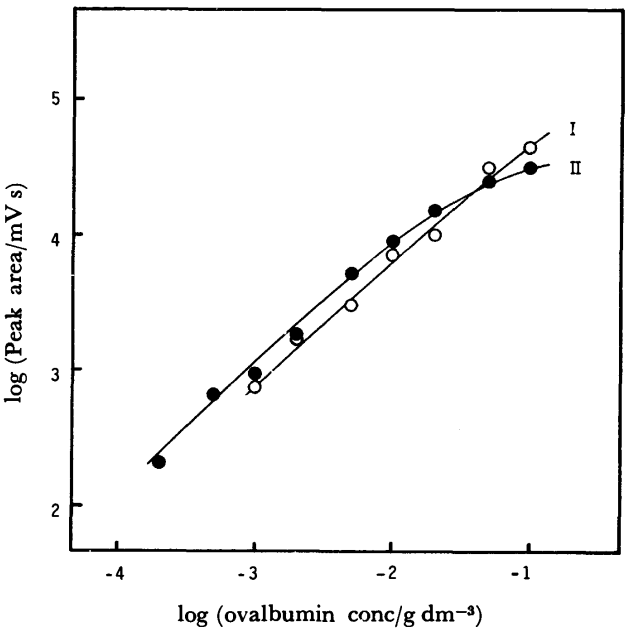

Fig. 6. Calibration curves of ovalbumin obtained by HPLC and flow-injection analysis.
I: through a column and II: column-free.
Conditions: injection volume 50 mm³, 1.0×10^{-4} mol/dm³ luminol, 5.0×10^{-4} mol/dm³ H_2O_2, 2.0×10^{-6} mol/dm³ copper(II), and Buff-II (pH 6.19) as buffer solution.

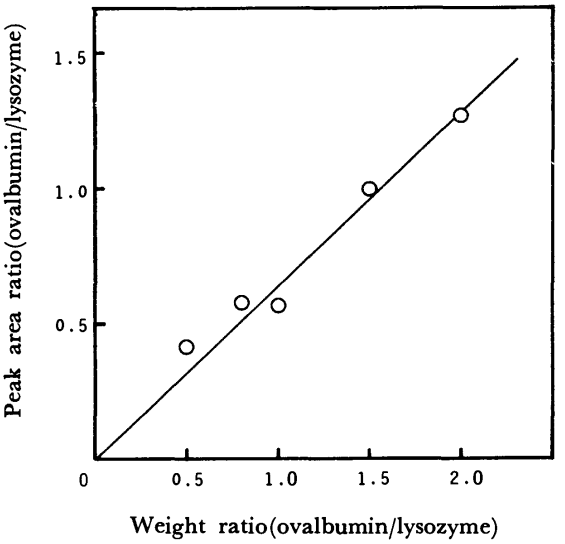

Fig. 7. Calibration curve of ovalbumin by use of lysozyme as internal standard.
Conditions: load volume 50 mm³, Buff-II (pH 6.19) as eluent, and 2.0×10^{-2} g/dm³ lysozyme as internal standard.

was 77.3%. Thus, the detection limit of the flow-injection analysis was 10 ng, while that of the column procedure was 50 ng.

Ovalbumin solutions of 1.0×10^{-2}, 1.6×10^{-2}, 2.0×10^{-2}, 3.0×10^{-2}, and 4.0×10^{-2} g/dm³ were determined by the use of a 2.0×10^{-2} g/dm³ lysozyme solution as the internal standard (Fig. 7). A linear relationship

was obtained between the weight ratio of ovalbumin to lysozyme and the ratio of the corresponding peak area. The coefficient of variation for five measurements of 2.0×10^{-2} g/dm^3 ovalbumin was 8.65%, and the internal standard method was shown to be superior to the absolute calibration method using the calibration curve I in Fig. 6.

To sum up, it has been found by the present authors that the catalytic activity of copper(II) against the CL between luminol and H_2O_2 is lowered in the presence of protein, and a sensitive and new detector for the HPLC of protein has been developed, 2×10^{-3}—1×10^{-1} g/dm^3 ovalbumin being determined within the detection limit of 50 ng. Since, however, the detection limit of the present detector was damaged by dilution and the low recovery which occurred when the present detector and HPLC were combined, some improvements overcoming these problems have to be done in future studies.

References

1) H. Kanaya and Y. Fujita, "Seikagakuteki Jikkenho," Maruzen, Tokyo (1983), p. 60.

2) T. Takagi, "Tanpakushitsu Peptide No Kosokuekitai Chromatography," ed by N. Utsui, S. Iwai, and F. Sakiyama, Kagaku Dojin, Kyoto (1984), p. 255.

3) S. Terabe, A. Tsuchitani, and T. Ando, *Bunseki Kagaku*, **33**, 361 (1984).

4) T. Hara, M. Toriyama, and K. Tsukagoshi, *Bull. Chem. Soc. Jpn.*, **57**, 1551 (1984).

5) E. Pfannkoch, K. C. Lu, and F. E. Regnier, *J. Chromatogr. Sci.*, **18**, 430 (1980).

 © 1985 The Chemical Society of Japan Bull. Chem. Soc. Jpn., 58, 115—119 (1985)

Benzylphenol Derivatives as Antioxidants for Autoxidation of Tetralin

Fukiko YAMADA,* Tomihiro NISHIYAMA, Yasuki SUZUURA, and Tatsuo YAMAMURA
Department of Applied Chemistry, Faculty of Engineering, Kansai University, Yamatecho, Suita, Osaka 564
(Received November 24, 1983)

A series of 4-benzylphenols, 2-methyl-4-benzylphenols, 4-methyl-2-benzylphenols and 4-methoxy-2-benzylphenols have been prepared and evaluated as antioxidants for tetralin at 60 °C by means of an oxygen-absorption method. Very good activities have been observed with a series of 4-methoxy-2-benzylphenols. The electrochemical oxidation potentials of these compounds were determined using linear-sweep voltammetry. The antioxidative activities were found to correlate with both the ^{13}C NMR chemical shifts (δ) of the *ipso*-carbon of the OH substituent and their peak potentials (E_p).

During the course of our studies of phenol derivatives as antioxidants,[1-5] compounds containing a diarylmethyl group with a phenolic hydroxyl group showed high activities as antioxidants for paraffin wax,[1,2] lard,[3] vitamin A,[4] mineral oils,[5] and greases.[5] In a recent study of benzylphenols,[6] we found that the introduction of a benzyl group to the *para*- and/or *ortho*-positions of the hydroxyl group on the benzene ring improved the antioxidative activities of phenols. Furthermore, the antioxidative activities of the benzylphenols increased with a decrease of the ^{13}C NMR chemical shifts (δ) of the *ipso*-carbon of the OH substituent.[6]

In this paper, the antioxidative activities of twenty compounds of four series of benzylphenols were evaluated by means of an oxygen-absorption method and are discussed in connection with their ^{13}C NMR chemical shifts and electrochemical oxidation data.

Experimental

Measurements. All the boiling and melting points were uncorrected. ^{13}C NMR spectra were recorded on a JNM-PS-100/EC-100 FT spectrometer operating at 25.15 MHz with complete proton decoupling. The pulse width and repetition time were 10.2 μs (for a 45° pulse) and 6 s, respectively. The spectra were observed as 2 mmol cm^{-3} solutions in $(CD_3)_2CO$ with a spectral width of 6250 Hz. Chemical shifts were referred to internal standard TMS. Mass spectra were obtained with a JEOL JMS-01SG Mattauch-Herzog double-focusing mass spectrometer at an ionizing voltage of 75 eV. GLC analyses were carried out on a Yanagimoto gas chromatograph(model GCG-550-T) using a 1.50-m column packed with Silicone SE-30 (10% wt).

Antioxidants. The benzylphenol derivatives studied in this work were as follows; 4-benzylphenol (**1**), 4-(α-methylbenzyl)phenol (**2**), 4-(α-ethylbenzyl)phenol (**3**), 4-(α-isopropylbenzyl)phenol (**4**), 4-benzhydrylphenol (**5**), 2-methyl-4-benzylphenol (**6**), 2-methyl-4-(α-methylbenzyl)-phenol (**7**), 2-methyl-4-(α-ethylbenzyl)phenol (**8**), 2-methyl-4-benzhydrylphenol (**9**), 2-methyl-4-(α, α-dimethylbenzyl)-phenol (**10**), 4-methyl-2-benzylphenol (**11**), 4-methyl-2-(α-methylbenzyl)phenol (**12**), 4-methyl-2-(α-ethylbenzyl)phenol (**13**), 4-methyl-2-(α-isopropylbenzyl)phenol (**14**), 4-methyl-2-benzhydrylphenol (**15**), 4-methoxy-2-benzylphenol (**16**), 4-methoxy-2-(α-methylbenzyl)phenol (**17**), 4-methoxy-2-(α-ethylbenzyl)phenol (**18**), 4-methoxy-2-(α-isopropylbenzyl)-phenol (**19**), and 4-methoxy-2-benzhydrylphenol (**20**).

Compounds **1**—**20** were prepared by Friedel-Crafts benzylations of the corresponding phenols in nitromethane using a catalyst for the desired time at a suitable temperature.[7,8] The reaction conditions for benzylations were as follows: (1) The reactions of the corresponding phenols with benzyl chloride or α-methylbenzyl chloride using $AlCl_3$ as the catalyst (1.0/1.0/0.1 molar ratio) at 60—70 °C gave the corresponding products, **1**, **7**, and **16**, respectively, (2) the reactions of the corresponding phenols with benzyl chloride using $ZnCl_2$ (1.0/1.0/0.1) at 25—45 °C gave products **6** and **11**, (3) the reactions of the phenols with α-ethylbenzyl alcohol, α-isopropylbenzyl alcohol, or benzhydrol using $ZnCl_2$ (1.0/1.0/1.0) at 25—45 °C gave products **3**, **4**, **5**, **8**, **9**, **13**, **14**, **15**, **18**, **19**, and **20**, respectively, and (4) the reactions of the phenols with styrene or α-methylstyrene using concd H_2SO_4 (1.0/1.0/1.0) at 30—60 °C gave products **2**, **10**, **12**, and **17**.

Each reaction was monitored using GLC analysis. The compound obtained was characterized by chemical shifts in the ^{13}C NMR spectrum. The physical properties and the results of elemental analyses of compounds **1**—**20** (prepared here) are summarized in Table 1.

Determination of Antioxidative Activity. Measurements of oxygen-absorption rates were performed with an isobaric gas-absorption apparatus under a closed-flow system (2.0±0.1 L oxygen/h) provided with an electrolyser using 50 cm^3 of tetralin containing an antioxidant (0.001 mol dm^{-3}) and azobis(isobutyronitrile) as the initiator (0.01 mol dm^{-3}). The oxidation temperature was kept at 60 ±0.1 °C and oxygen absorption was periodically measured in a constant-pressure closed system. Satisfactory and reproducible data were obtained.

The induction period (IP) and the oxidation rates both during and after the induction period were determined in the usual way.[9]

Tetralin used for the test was purified by shaking with concd sulfuric acid, dried with sodium, and distilled under an inert atmosphere.

Electrochemical Determination. Linear-sweep voltammograms were recorded for each compound (0.001 mol dm^{-3}) in acetonitrile with $LiClO_4$ (0.1 mol dm^{-3}) as a supporting electrolyte. The counter and working electrodes were made of platinum and the working electrode potential was referred to Ag/AgCl. Potential sweeps were generated by a Hokuto Denko HB-107A function generator in connection with a potentionstat Hokuto Denko HA-

TABLE 1. PHYSICAL PROPERTIES AND ANALYTICAL DATA OF **1—20** COMPOUNDS

Compound No.	Mp θ_m/°C or Bp θ_b/°C(Pa)	Yield/%	δ_c				Found (Calcd) (%)		M^+
			CH_3 or OCH_3	$CH_3(\alpha)$	$CH_3CH_2(\alpha)$	$(CH_3)_2CH(\alpha)$	C	H	
1	82.0—83.0	17.0					84.96 (84.75)	6.32 (6.57)	184
2	57.7—58.1	62.1		22.5			84.42 (84.81)	6.95 (7.12)	198
3	67.4—68.1	29.5			13.0; 29.2		84.72 (84.87)	7.84 (7.60)	212
4	62.0—62.9	26.5				21.9; 32.1	84.77 (84.91)	8.04 (8.02)	226
5	112.5—113.0	48.3					87.40 (87.66)	6.33 (6.20)	260
6	131 (133)	55.1	15.8				84.95 (84.81)	7.10 (7.12)	198
7	151 (133)	84.1	16.1	22.2			84.75 (84.87)	7.67 (7.60)	212
8	125 (133)	53.5	16.0		12.6; 28.8		84.73 (84.91)	8.10 (8.02)	226
9	99.8—100.3	67.5	16.2				87.88 (87.56)	6.40 (6.61)	274
10	121 (133)	20.3	16.4	29.0 29.7			85.02 (84.91)	8.13 (8.02)	226
11	133—134 (133)	61.5	20.5				84.76 (84.81)	7.25 (7.12)	198
12	142 (133)	40.4	20.7	20.7			84.58 (84.87)	7.69 (7.60)	212
13	128—129 (133)	36.6	20.9		13.1; 28.4		84.54 (84.91)	8.10 (8.02)	226
14	129—130 (133)	23.1	20.4			21.4; 21.8 31.2	84.81 (84.96)	8.56 (8.39)	240
15	133.2—134.1	79.2	20.7				87.35 (87.56)	6.53 (6.61)	274
16	96.6—98.1	42.0	55.2				78.65 (78.48)	6.63 (6.59)	214
17	63.9—64.8	52.8	55.4	20.9			78.88 (78.92)	7.08 (7.06)	228
18	84.4—85.0	45.6	55.5		12.9; 28.2		79.01 (79.31)	7.50 (7.49)	242
19	155.6—156.0	20.7	55.5			21.6; 22.0 31.5	79.88 (79.65)	7.85 (7.86)	256
20	110.8—111.2	40.4	55.5				82.84 (82.73)	6.26 (6.25)	290

104. All the measurements at the scan rate of 200 mV s^{-1} were carried out at 25 ±0.1 °C using a constant-temperature bath under a nitrogen atmosphere.

The acetonitrile was of optically pure grade and was free from water.

Results and Discussion

Activities of Antioxidants. Data regarding the activities of compounds **1—20** (denoted by the induction period, the stoichiometric factor, and the rates of the oxygen absorption) are listed in Table 2.

The autoxidation of tetralin at 60 °C was initiated by azobis(isobutyronitrile) (AIBN) and the inhibition by phenol derivatives can be described by the following chain-reaction schemes;[13,14]

Initiation: $\text{AIBN; RH} \xrightarrow{O_2} \text{RO}_2\cdot$ (1)

Propergation: $\text{RO}_2\cdot + \text{RH} \xrightarrow{k_p} \text{ROOH} + \text{R}\cdot$ (2)

$\text{R}\cdot + \text{O}_2 \longrightarrow \text{RO}_2\cdot$ (3)

Termination: $2\text{RO}_2\cdot \xrightarrow{k_t} \text{non-radical products}$ (4)

$\text{RO}_2\cdot + \text{ArOH} \xrightarrow{k_{inh}} \text{ROOH} + \text{ArO}\cdot$ (5)

Table 2. Activities of antioxidants along with ^{13}C chemical shifts of the *ipso*-carbon of the OH substituent and the oxidation potentials

Compound No.	IP/min	n[a]	$-d[O_2]/dt$[b] mol dm^{-3} min^{-1} (I) $\times 10^6$	$-d[O_2]/dt$[b] mol dm^{-3} min^{-1} (II) $\times 10^4$	δ_c/ppm	E_p/V	i_p/μA
1	62	0.45	17.3	5.7	156.0	1.512	92.2
2	56	0.40	15.9	5.2	156.2	1.530	93.7
3	69	0.50	15.5	5.7	156.0	1.519	89.5
4	69	0.50	12.9	5.9	155.4	1.490	89.3
5	50	0.36	14.3	6.4	156.2	1.526	72.3
6	186	1.34	12.0	2.6	153.7	1.388	76.3
7	177	1.27	13.1	1.9	153.8	1.403	79.0
8	182	1.31	12.3	1.5	153.7	1.371	45.9
9	168	1.21	10.6	4.1	154.2	1.386	51.8
10	157	1.13	11.4	8.4	153.5	1.359	62.5
11	213	1.53	9.2	2.0	153.0	1.351	52.8
12	252	1.81	8.1	1.7	152.1	1.323	51.2
13	221	1.59	8.1	1.7	153.2	1.349	52.5
14	217	1.56	10.3	1.7	152.6	1.341	51.3
15	215	1.55	9.6	3.1	153.0	1.339	51.8
16	434	3.12	3.1	7.3	149.0	1.040	55.8
17	452	3.25	3.0	7.3	148.7	1.023	52.9
18	460	3.31	3.1	7.1	149.1	1.049	55.4
19	454	3.27	3.3	7.9	148.8	1.043	51.5
20	406	2.92	3.3	7.2	149.3	1.055	49.9
Control	22			8.6			

a) The stoichiometries were determined at 60 °C by the induction-period method,[9,10] by using the values, the activity factor of the initiator, 0.6,[11] and the rate constant of decomposition of the initiator, 6.0×10^{-4} min^{-1} (the mean from the data in Ref. 12). b) The rates of oxygen absorption; (I) for an inhibited autoxidation during IP and (II) for an uninhibited oxidation after IP.

$$(n-1)RO_2\cdot + ArO\cdot \longrightarrow \text{non-radical products}, \quad (6)$$

where RH denotes the organic substrate (tetralin) and $RO_2\cdot$ is the peroxyl radical. In the presence of an antioxidant, ArOH, the oxidation chains become shortened, termination 4 is suppressed, and reactions 5 and 6 occur instead of 4. The induction period and the rates of inhibited and uninhibited oxidations can be represented by Eqs. I, II, and III, respectively;

$$IP = n[ArOH]/R_i \quad (I)$$

$$-d[O_2]/dt = k_p R_i[RH]/nk_{inh}[ArOH] \quad (II)$$

$$-d[O_2]/dt = k_p(R_i/2k_t)^{1/2}[RH] \quad (III)$$

where R_i is the rate of the chain initiation.

As can be seen from Table 2, the characterizations of the antioxidative activities can be expressed by three values: IP, n, and $-d[O_2]/dt$. These values are thought to be dependent on the structures of the phenol nuclei with various substituents at different positions. The length of IP increased in the order of **16—20** (4-methoxyphenols)> **11—15** (4-methylphenols)> **6—10** (2-methylphenols)> **1—5** (phenols). In each series, the compounds with an α-alkyl substituent possessed a longer IP than that of the α-phenyl substituent. Compounds **16—20** with a 4-methoxyl group exhibit much longer IP and, thus, higher stoichiometric factors (around n=3) in comparison with those of **1—15**.

For oxygen absorption during IP, much lower rates were found in compounds **16—20**, while higher rates were observed for **1—15**, (particularly **1—5**). According to Eq. II, the rate is proportional to the reciprocal of n. This relation is clearly illustrated in Fig. 1. On the other hand, the rates after IP are quite complicated. When all ArOH are consumed by reactions 5 and 6 (up to IP), the rate of autoxidation obeys Eq. III and is equal to that of the control test. In fact, the rates of **10** and **16—20** are close to 8.6. However, **1—15** (except for **10**) show much lower rates. This means that the retardation ability persists even after IP is over due to some products of the antioxidant. Figure 2 shows the tendency of IP values to increase with decreasing rates of **1—15** (except for **10**). Particularly, both groups **1**, **6** and **11** and **5**, **9** and **15** (with an α-phenyl substituent) show linear relations. This indicates the influence of a 2-methyl or 4-methyl substituent.

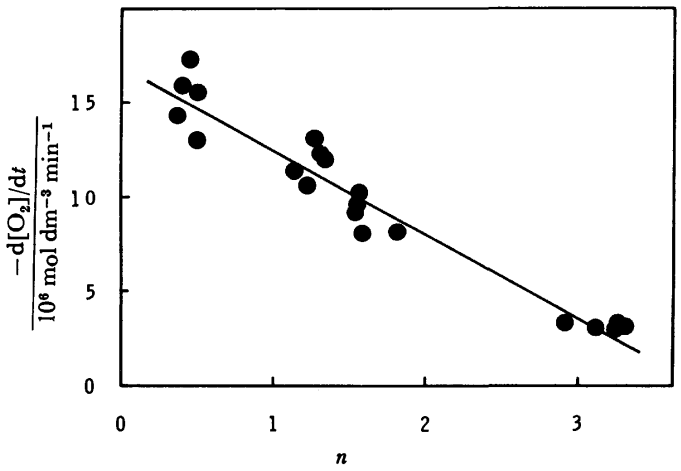

Fig. 1. plot of n *vs.* the rate of oxygen absorption; $r=0.969$.

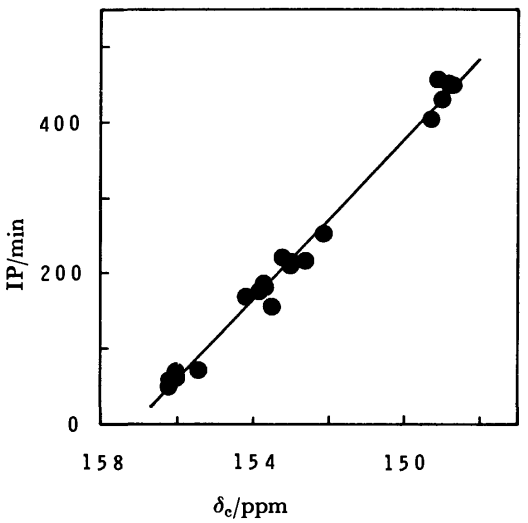

Fig. 3. Plot of IP *vs.* ^{13}C chemical shift of the *ipso*-carbon of OH; $r=0.994$.

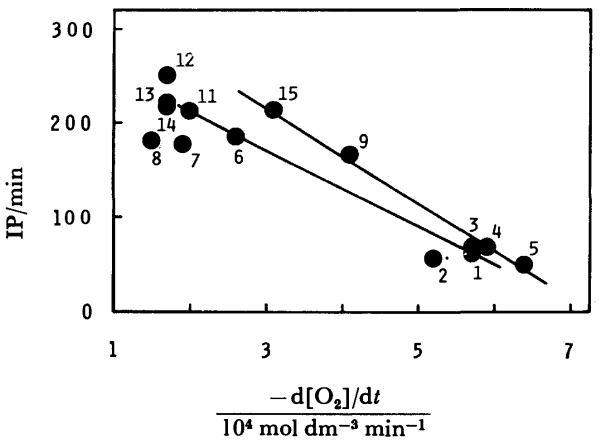

Fig. 2. Plot of IP *vs.* the rate of oxygen absorption.

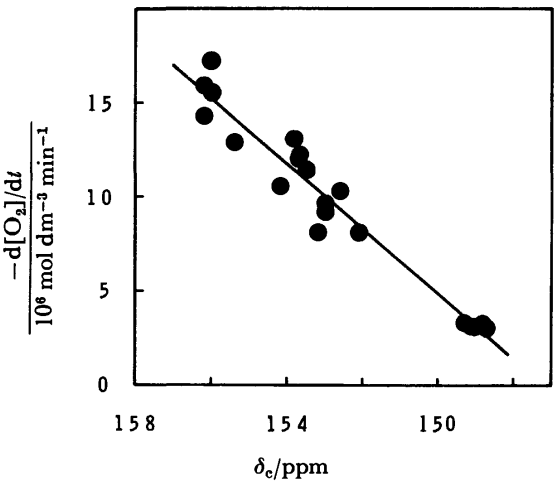

Fig. 4. Plot of the rate of oxygen absorption *vs.* ^{13}C chemical shift of the *ipso*-carbon of OH; $r=0.972$.

Correlations of Antioxidative Activities with ^{13}C Chemical Shifts and Oxidation Potentials. In order to understand the factors and mechanisms govering antioxidative activities of compounds **1—20**, several attempts were made to plot their IP values and the rates of oxygen absorption against the *ipso*-carbon chemical shifts of the OH substituents and the electrochemical oxidation potentials, respectively. The data used in this attempt are listed in Table 2.

Figure 3 shows the relation between the IP values and the *ipso*-carbon chemical shifts of the OH substituents. The plotted points fall on a straight line. This fact indicates that the IP values increase with the decreasing of the chemical shifts, and that the electron density on the *ipso*-carbon of the OH substituent governs antioxidative activity. In a previous paper,[15] we proved that the electron transmission through the *ipso*-carbon to the oxygen atom in phenols depends mostly upon the resonance contribution. Consequently, the total π-electron density of the oxygen atom may be increased by increasing the electron density of the *ipso*-carbon atom. According to a proposal by Morokuma *et al.*,[16] this will necessarily decrease the electronegativity of the oxygen atom and make the Coulomb integral of the σ orbital on the oxygen more positive. In the inhibition processes (reactions 5 and 6) the reactivities of phenolic hydrogen and the phenoxyl radical are the controlling factors. The reactivity of phenolic hydrogen for an attack on a peroxyl radical (electronegative radical) is greatly elevated by an increased π-electron density on the oxygen. Consequently, the reactivity of the phenoxyl radical produced can be elevated by an increased π-electron density.

Figure 4 also shows a linear relation between the rates of oxygen absorption during IP and the *ipso*-carbon chemical shifts of the OH substituents. The rates increase with increasing chemical shifts. From Eq. II, it is seen that the rate is proportional to

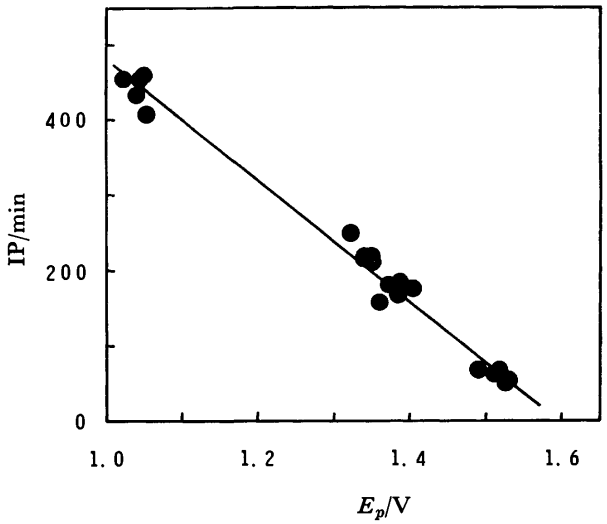

Fig. 5. Plot of IP *vs.* E_p; $r=0.993$.

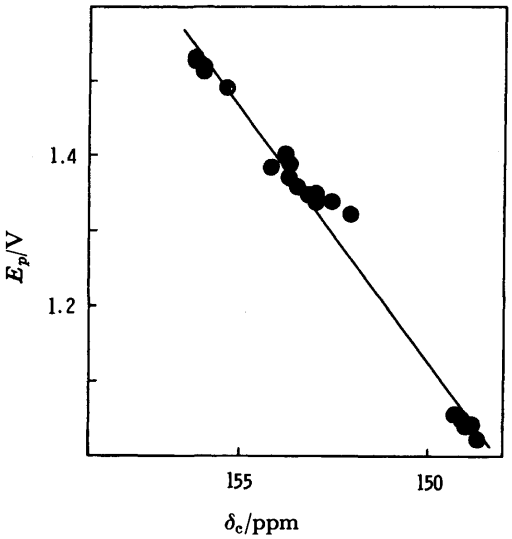

Fig. 6. Plot of E_p *vs.* ^{13}C chemical shift of the *ipso*-carbon of OH; $r=0.993$.

the reciprocal of n and k_{inh}. As was mentioned above, the activity of an antioxidant (which can be expressed by both n and k_{inh} values) is greatly elevated by an increased π-electron density on the phenolic oxygen.

The IP values show a linear relationship with the E_p values, as can be seen in Fig. 5. The IP values increase with a decreasing value of the oxidation potentials. In general, when the oxidation of a molecule is carried out at some potential, the reaction involves an initial electron loss, followed by proton migration. It is, therefore, thought that the simplicity of one-electron and one-proton transfers can be displayed by lower E_p values. In addition, there is the linear relationship between the *ipso*-carbon chemical shifts of the OH substituents and the E_p values, as can be seen in Fig. 6. This indicates that the easiness of one-electron and one-proton transfers is greatly increased by an increased electron density at the *ipso*-carbon of the OH substituent. The IP values were determined under an oxygen atmosphere while the electrochemical oxidations were performed in a solvent. The IP and E_p values were obtained for the different systems. Although the mechanism of the initial step of the inhibition is still unsettled, the above facts indicate that the oxidation of the phenol derivatives in these different systems proceed by a similar mechanism.

In conclusion, the ^{13}C chemical shift of the *ipso*-carbon of the OH substituent and the E_p value made it possible to estimate the antioxidative activity of a series of benzylphenol derivatives.

References

1) F. Yamada and S. Matsuda, *Kogyo Kagaku Zasshi*, **59**, 59 (1956).
2) S. Matsuda and F. Yamada, *Kogyo Kagaku Zasshi*, **60**, 566 (1957).
3) F. Yamada and S. Matsuda, *Kogyo Kagaku Zasshi*, **61**, 1257 (1958).
4) F. Yamada and S. Matsuda, *Kogyo Kagaku Zasshi*, **61**, 1478 (1958).
5) F. Yamada and S. Matsuda, *Kogyo Kagaku Zasshi*, **63**, 810 (1960).
6) F. Yamada, T. Nishiyama, and Y. Nakai, *J. Am. Oil Chem. Soc.*, **60**, 1651 (1983).
7) G. A. Olah, "Friedel-Crafts and Related Reaction," Wiley-Interscience, New York (1965), Vol. I-IV.
8) Y. Nakai and F. Yamada, *Org. Magn. Reson.*, **11**, 607 (1978).
9) C. E. Boozer, G. S. Hammond, C. E. Hamilton, and J. N. Sen, *J. Am. Chem. Soc.*, **77**, 3233 (1955).
10) E. C. Horswill, J. A. Howard, and K. U. Ingold, *Can. J. Chem.*, **44**, 985 (1966).
11) J. A. Howard and K. U. Ingold, *Can. J. Chem.*, **41**, 1744 (1963).
12) J. P. von Hook and A. V. Tobolsky, *J. Am. Chem. Soc.*, **80**, 779 (1958).
13) a) Y. Kamiya, "Yuki-sanka-hanno," Gihodo, Tokyo (1973), Chaps. 5 and 13; b) J. A. Howard, "Free Radicals," ed by J. K. Kochi, Wiley, New York (1973), Vol. II, Chap. 12.
14) G. W. Burton and K. U. Ingold, *J. Am. Chem. Soc.*, **103**, 6472 (1981).
15) Y. Nakai, T. Takabayashi, and F. Yamada, *Org. Magn. Reson.*, **13**, 94 (1980).
16) K. Morokuma, H. Kato, and K. Fukui, *Bull. Chem. Soc. Jpn.*, **36**, 541 (1963).

Synthesis of O-β-D-Glucopyranosyl-(1→2)-O-β-D-glucopyranosyl-(1→6)-D-glucopyranose; Dehydrative β-D-Glucosylation Using 2-O-Acetyl-3,4,6-tri-O-benzyl-D-glucopyranose

Shinkiti KOTO,* Naohiko MORISHIMA, Hiroko SATO, Yuko SATO, and Shonosuke ZEN
School of Pharmaceutical Sciences, Kitasato University, Shirokane, Minato-ku, Tokyo 108
(Received April 12, 1984)

A step-by-step synthesis of O-β-D-glucopyranosyl-(1→2)-O-β-D-glucopyranosyl-(1→6)-D-glucopyranose through the dehydrative β-D-glucosylation using 2-O-acetyl-3,4,6-tri-O-benzyl-D-glucopyranose and the ternary system of *p*-nitrobenzenesulfonyl chloride, silver trifluoromethanesulfonate, and triethylamine is described.

Our continuing study of glycosylation[1] has shown that the ternary system of *p*-nitrobenzenesulfonyl chloride (NsCl, Ns=$-SO_2C_6H_4NO_2(p-)$, silver trifluoromethanesulfonate (AgOTf, Tf=$-SO_2CF_3$), and triethylamine (Et_3N) induces selective β-D-glucosylation of glycosyl acceptors with the D-glucosyl donor having a free OH group at *C*-1 such as 2,3,4,6-tetra-*O*-benzyl-α-D-glucopyranose (**1**).[2] However, in any reaction with less reactive acceptors it almost always loses its selectivity.[3] To improve such an undesirable aspect, the benzyloxyl group at *C*-2 of **1** was replaced with an acetoxyl group, since an acyloxyl group at *C*-2 plays an important role in β-D-glycosylation using the 1-*O*-sulfonates.[4] Expectedly, the D-glucosylation with 2-*O*-acetyl-3,4,6-tri-*O*-benzyl-D-glucopyranose (**3**) yielded β-D-glucosides with excellent selectivity, while that with 6-*O*-acetyl-2,3,4-tri-*O*-benzyl-D-glucopyranose preferred to form α-D-glucosides.[5]

1,2,3,4,6-Penta-*O*-acetyl-β-D-glucopyranose (**2**) was readily converted into a D-glucosyl donor **3**[6] (α:β≈85:15) *via* a continuous four-stage through process.

D-Glucosylation of the primary OH group of methyl 2,3,4-tri-*O*-benzyl-α-D-glucopyranoside **4**[7] with **3** through the ternary system at 0 °C for 20 h gave the corresponding β-D-glucoside **5** in a 62% yield (Table 1). The β-selectivity was retained even in the D-glucosylation of the less reactive secondary OH group of methyl 2,3,6-tri-*O*-benzyl-β-D-glucopyranoside **6**[8] though the yield of the reaction was lowered. Thus, the β(1→4)-linked disaccharide **7** was selectively obtained at a 46% yield. The selectivity was also maintained in the D-glucosylation of the axial OH group of the galactose derivative **8**.[9] Therefore, it is, concluded that the acetoxyl group at *C*-2 controls the selectivity in dehydrative D-glucosylation irrespective of the type of OH group of D-glucosyl acceptor to produce β-D-glucoside in comparison with the previous experiments using **1**.[3]

Using the β-D-glucosylation described above, a linear trisaccharide **10** was synthesized as illustrated in Fig. 1. The first D-glucosylation of the acceptor **11**[10,11] with **3** was carried out using the ternary system; the gentiobiose derivative **12** was obtained selectively at a 61% yield. After deacetylation, the second glucosylation was performed by the ternary system to give the β-D-glucoside **14** at a 34% yield; an appreciable amount of the α-D-glucoside was isolated. In contrast to this, the use of **1** instead of **3** yielded the α-D-glucoside **15** as a significant by-product. A mixture of methanesulfonic acid ($MeSO_3H$) and $CoBr_2$[12] was useful for the first D-glucosylation to give **12** at a 41% yield. However, it was not at all useful for a second glucosylation of **13** with **3**. Deacetylation and successive hydrogenolysis of **14** afforded the trisaccharide **10**, whose ^{13}C NMR spectrum in D_2O was consistent with its proposed structure—6-*O*-β-sophorosyl-D-glucose.[13]

Experimental

Instrumentation for measuring the physical characteristics of the products was described in previous papers.[2,3,12] The D-glucosylation with the ternary system and the following processes were carried out in a manner which was detailed before.[2,3,5] The results of D-glucosylation are summarized in Table 1. The analytical and physical data of the products are listed in Table 2.

2-O-Acetyl-3,4,6-tri-O-benzyl-D-glucopyranose (3). 1,2,3,4,6-Penta-*O*-acetyl-β-D-glucopyranose (**2**, Kyowa, 1.0 g, 2.56 mmol) was treated in $CHCl_3$ (3.0 ml) containing AcBr (1.05 ml) and H_2O (0.23 ml) at room temperature for 2 h.[11] Evaporation and coevaporation with toluene gave a syrup which was dissolved in $MeNO_2$ (2.5 ml). 2,6-Dimethylpyridine (0.95 ml) and EtOH (1.15 ml) were added to the solution, which was then kept at room temperature overnight. The mixture was diluted with chloroform and washed with aq $NaHCO_3$ (5%). An organic layer was evaporated to dryness to give a syrup which was then heated in $PhCH_2Cl$ (14 ml) containing powdered KOH (7 g) for 2 h at 110 °C. Filtration and evaporation gave a syrup which was then stirred in aq AcOH (80%, 70 ml) for 2 h at room temperature. The mixture was diluted with toluene and an organic layer was washed with aq $NaHCO_3$ (5%) and water. After an evaporation, chromatography on a silica gel using a toluene–2-butanone system (gradient) gave a homogeneous syrup (R_f 0.18, toluene:2-butanone=6:1). This was crystallized from diisopropyl ether to afford **3** (0.37 g, 29%); ^1H NMR ($CDCl_3$, TMS): δ=2.00 (s, 3H, $C\underline{H}_3CO$), 3.44 (d, 1H, *J* 4.0 Hz, O<u>H</u>), 5.38 (dd, 1H, *J*=3.8 and 4.0 Hz, H-1).

Table 1. The results of glucosylation using the ternary reagent[a]

Run	**3**/mg	Acceptor	mg	NsCl mg	AgOTf mg	Et_3N μl	CH_2Cl_2 ml	Time[b] h	β-Glucoside obtained	Yield %	Solvent[c] for column chromatography[d]
1	64.0	**4**	46.4	37.7	43.7	24.0	0.50	20	**5**	62	TB[e]
2	64.0	**6**	46.4	37.7	43.7	24.0	0.50	24	**7**	46	TB[e]
3	101.4	**8**	67.0	54.4	63.1	34.0	0.78	45	**9**	65	TB[e]
4	320	**11**	270	189	219	119	2.7	24	**12**	61	TB[e]
5	93.2	**13**	142	54.8	63.8	34.2	0.75	48	**14**	34	DE[e]

a) The molar ratio of **3** to acceptor was 1.3 and that of each component of the ternary reagent to acceptor was 1.7. b) At 0 °C. c) TB=toluene-2-butanone, DE=$(CH_2Cl)_2$-AcOEt. d) On silica gel. e) A small amount of the α-glucoside was isolated (<5%).

Table 2. Physical and analytical data of compounds

Cpd	Mp θ_m/°C	$[\alpha]_D^{20}$ (*c*, solv)[a]	Mol. form	Calcd/% C	Calcd/% H	Found/% C	Found/% H	δ_C ($CDCl_3$, TMS)[b] C-1	C-1′	C-1″	CH_3CO
3[c]	129—130	+53° (1.0, C)	$C_{29}H_{32}O_7$	70.71	6.55	70.57	6.51	α 90.5, β 95.8	—	—	20.9
5	127—128	+15° (4.3, C)				73.04	6.69	98.2	101.2	—	21.0
7	—	+21° (1.8, C)	$C_{57}H_{62}O_{12}$	72.90	6.65	72.74	6.72	104.8	100.5	—	21.0
9	—	+28° (3.4, C)				72.68	6.73	98.6	102.1	—	21.0
10	—	−1° (0.8, W)	$C_{18}H_{32}O_{16}\cdot H_2O$	41.38	6.56	41.49	6.27	—	—	—	—
12	129—131	+15° (0.2, C)	$C_{63}H_{66}O_{12}$	75.29	6.63	74.73	6.69	95.5	101.2	—	21.0
13	100—103	+39° (1.3, C)	$C_{61}H_{64}O_{11}$	74.53	6.55	74.77	6.49	95.6	103.7	—	—
14	—	+28° (1.1, C)	$C_{90}H_{94}O_{17}$	74.67	6.54	73.96	6.46	95.2	102.1	100.4	20.9
15	—	+67° (0.6, C)	$C_{95}H_{98}O_{16}$	76.28	6.60	76.33	6.61	94.9	104.0	94.2	—
16	—	+34° (2.6, C)				76.08	6.60	95.5	102.0	102.4	—
17	—	+31° (1.0, C)	$C_{88}H_{92}O_{16}$	75.19	6.60	75.31	6.82	95.4	102.9	103.9	—

a) C=$CHCl_3$, W=H_2O. b) Measured at 25.1 MHz. c) Ref. 6, mp 128—129 °C, $[\alpha]_D^{22}$ +55° (*c* 1.1, $CHCl_3$).

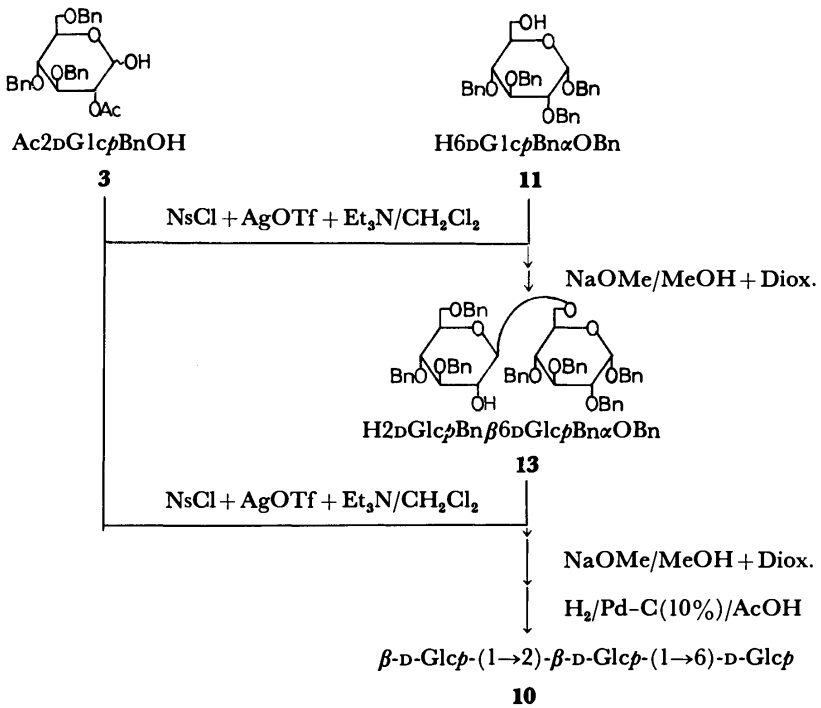

Fig. 1. Synthetic diagram[5] for the trisaccharide **10** (Bn=-CH_2Ph, Ns=-$SO_2C_6H_4NO_2$(*p*-), Tf=-SO_2CF_3).

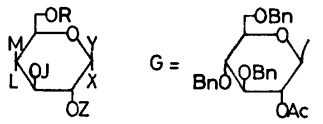

Cpd	X	Y	Z	J	L	M	R
1	OH,	H	Bn	Bn	OBn	H	Bn
2	H	OAc	Ac	Ac	OAc	H	Ac
4	OMe	H	Bn	Bn	OBn	H	H
5	OMe	H	Bn	Bn	OBn	H	G
6	H	OMe	Bn	Bn	OH	H	Bn
7	H	OMe	Bn	Bn	OG	H	Bn
8	OMe	H	Bn	Bn	H	OH	Bn
9	OMe	H	Bn	Bn	H	OG	Bn
12	OBn	H	Bn	Bn	OBn	H	G

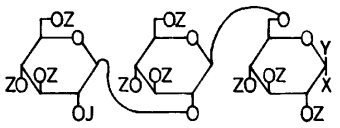

Cpd	X	Y	Z	J
10	OH,	H	H	H
14	OBn	H	Bn	Ac
16	OBn	H	Bn	Bn
17	OBn	H	Bn	H

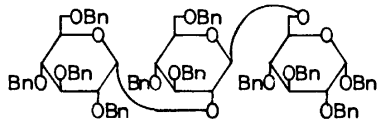

15

Alternative Synthesis of Benzyl 6-O-(2-O-Acetyl-3,4,6-tri-O-benzyl-β-D-glucopyranosyl)-2,3,4-tri-O-benzyl-α-D-glucopyranoside (12). To a stirring mixture of **11**[10,11] (82 mg, 0.17 mmol), **3** (90 mg, 0.17 mmol), and $CoBr_2$ (36.5 mg, 0.17 mmol) in CH_2Cl_2 (0.45 ml), $MeSO_3H$ (3.3 μl, 0.05 mmol) was added at 20 °C and stirring was continued for 2 h. After processing[12] and chromatography the product was shown to be **12** (69 mg, 41%).

Benzyl 2,3,4-Tri-O-benzyl-6-O-(3,4,6-tri-O-benzyl-β-D-glucopyranosyl)-α-D-glucopyranoside (13). Compound **12** (127.6 mg, 0.126 mmol) was treated with a mixture of methanolic NaOMe (0.3%, 4.3 ml) and 1,4-dioxane (4 ml) at 20 °C overnight. Chromatography on a silica gel with toluene–2-butanone system gave **13** (112.3 mg, 92%).

Benzyl O-(2,3,4,6-Tetra-O-benzyl-α- and -β-D-glucopyranosyl)-(1→2)-O-(3,4,6-tri-O-benzyl-β-D-glucopyranosyl)-(1→6)-2,3,4-tri-O-benzyl-α-D-glucopyranoside (15 and 16). Triethylamine (22 μl, 0.158 mmol) was added into a stirred mixture of **I**[14] (84 mg, 0.156 mmol, $\alpha:\beta \approx 95:5$), **13** (116.2 mg, 0.12 mmol), NsCl (35 mg, 0.158 mmol), and AgOTf (40 mg, 0.156 mmol) in CH_2Cl_2 (0.65 ml) at −40 °C. The bath temperature was gradually raised to 0 °C, at which temperature the reaction was continued overnight. After processing, chromatography on a silica gel with toluene–2-butanone (gradient) gave a syrup (46.6 mg, 39%) consisting of **15** and **16**. Rechromatography of this syrup on silica gel using $(CH_2Cl)_2$–AcOEt (gradient) gave pure **16** (25.1 mg, 21%) and then **15** (19.2 mg, 16%).

Benzyl O-(3,4,6-Tri-O-benzyl-β-D-glucopyranosyl)-(1→2)-O-(3,4,6-tri-O-benzyl-β-D-glucopyranosyl)-(1→6)-2,3,4-tri-O-benzyl-α-D-glucopyranoside (17). The trisaccharide derivative **14** (79.5 mg, 0.055 mmol) was treated in a mixture of methanolic NaOMe (0.4%, 2 ml) and 1,4-dioxane (4 ml) at 20 °C overnight. After chromatography on silica gel with toluene-2-butanone system gave **17** (73.8 mg, 96%).

Compound **17** (47 mg, 0.033 mmol) was heated in $PhCH_2Cl$ (0.8 ml) containing NaH (60%, 40 mg) at 135 °C for 16 h to give the aforementioned fully benzylated trisaccharide **16** (25 mg, 50%).

O-β-D-Glucopyranosyl-(1→2)-O-β-D-glucopyranosyl-(1→6)-D-glucopyranose (10). Two hydrogenolyses of **17** (47.4 mg, 0.034 mmol) in AcOH (6 ml) containing Pd–C (10%, 40 mg) under H_2 (340 kPa) and subsequent chromatography on silica gel with $CHCl_3$–MeOH (1:1) gave glassy **10** (10.0 mg, 59%); ^{13}C NMR (D_2O, ext. TMS): δ=62.0 (C-6′), 62.2 (C-6″), 69.9 (C-6α), 70.0 (C-6β), 70.8 (C-4′ and -4″), 70.9 (C-4α and -4β), 71.7 (C-5α), 72.8 (C-2α), 74.0 (C-3α), 75.0 (C-2″), 75.4 (C-2β), 76.2 (C-3β), 77.0 (C-5β, -3′, and -3″), 77.5 (C-5′ and -5″), 81.2 (C-2′), 93.5 (C-1α), 97.4 (C-1β), 102.6 (C-1′), and 103.8 (C-1″).

Similar hydrogenolysis of **16** (25 mg, 0.017 mmol) gave **10** (4 mg, 48%).

References

1) S. Koto, N. Morishima, and S. Zen, *J. Synth. Org. Chem.*, **41**, 701 (1983).

2) S. Koto, T. Sato, N. Morishima, and S. Zen, *Bull. Chem. Soc. Jpn.*, **53**, 1761 (1980).

3) S. Koto, S. Inada, T. Yoshida, M. Toyama, and S. Zen, *Can. J. Chem.*, **59**, 255 (1981); N. Morishima, S. Koto, M. Uchino, and S. Zen, *Chem. Lett.*, **1982**, 1183.

4) H. F. Vernay, E. S. Rachaman, R. Eby, and C. Schuerch, *Carbohydr. Res.*, **78**, 267 (1980); R. Eby and C. Schuerch, *ibid.*, **92**, 149 (1981).

5) S. Koto, N. Morishima, Y. Kihara, H. Suzuki, S. Kosugi, and S. Zen, *Bull. Chem. Soc. Jpn.*, **56**, 188 (1983).

6) M. A. E. Shaban and R. W. Jeanloz, *Carbohydr. Res.*, **52**, 103 (1976).

7) R. Eby and C. Scheurch, *Carbohydr. Res.*, **34**, 79 (1974).

8) S. Koto, N. Morishima, R. Kawahara, K. Ishikawa, and S. Zen, *Bull. Chem. Soc. Jpn.*, **55**, 1092 (1982).

9) N. Morishima, S. Koto, A. Sugimoto, M. Oshima, and S. Zen, *Bull. Chem. Soc. Jpn.*, **56**, 2849 (1983).

10) P. R. Adams, R. Harrison, T. D. Inch, and P. Rich, *Biochem. J.*, **155**, 1 (1976).

11) S. Koto, N. Morishima, T. Irisawa, Y. Hashimoto, M. Yamazaki, and S. Zen, *Nippon Kagaku Kaishi*, **1982**, 1651.

12) S. Koto, N. Morishima, and S. Zen, *Bull. Chem. Soc. Jpn.*, **55**, 1543 (1982).

13) T. Usui, N. Yamaoka, K. Matsuda, K. Tuzimura, I. Sugiyama, and S. Sato, *J. Chem. Soc., Perkin Trans. 1*, **1973**, 2425; K. Mizutani, H. Kajita, K. Tashima, and O. Tanaka, *Nippon Kagaku Kaishi*, **1982**, 1595.

14) S. Koto, N. Morishima, Y. Miyata, and S. Zen, *Bull. Chem. Soc. Jpn.*, **49**, 2639 (1976).

Synthesis of 3-Amino-5*H*-pyrido[4,3-*b*]indoles, Carcinogenic γ-Carbolines

Hiroshi AKIMOTO,* Akiyoshi KAWAI, and Hiroaki NOMURA
Central Research Division, Takeda Chemical Ind., Ltd., Juso, Yodogawa-ku, Osaka 532
(Received May 23, 1984)

The carcinogenic γ-carbolines 3-amino-1,4-dimethyl-5*H*-pyrido[4,3-*b*]indole (**1**) and 3-amino-1-methyl-5*H*-pyrido[4,3-*b*]indole (**2**) were synthesized efficiently by the following procedures. The key method involved the acid-catalyzed cyclization of 2-acetamido-3-(2-indolyl)alkanoic acids to 1,2-dihydro-γ-carbolines. This was followed by dehydrogenation to the γ-carbolinecarboxylates and conversion of the ester group to the carboxyl and finally to the amino one by Curtius rearrangement. Alternative methods involved the thermolysis of 4-(1-benzotriazolyl)-3,6-dimethyl-2-pyridinamine to synthesize **1** and the condensation of 3-acetylindole-2- acetonitrile with ammonia to synthesize **2**. The structures of γ-carbolines **1** and **2** were unambiguously established by comparing samples of each synthesized by the two different routes. A selective and one-step synthesis of ethyl 2-acetamido-3-(2-indolyl)alkanoates was newly exploited starting from diethyl acetamidomalonate and quaternary ammonium salts of 2-[1-(dimethylamino)alkyl]indoles.

In a preliminary communication,[1] we reported on the total synthesis of the carcinogenic γ-carboline derivatives, 3-amino-1,4-dimethyl-5*H*-pyrido[4,3-*b*]indole (named Trp-P-1, **1**) and 3-amino-1-methyl-5*H*-pyrido-[4,3-*b*]indole (named Trp-P-2, **2**).[2] This study was initiated in order to obtain sufficient amounts of samples to allow extensive biological studies, including carcinogenesis tests of **1** and **2**,[3] and has contributed to the development of new routes for the large-scale preparation of these γ-carbolines.

Massive research on environmental mutagenes and carcinogens over the last decade has led to the identification of many of these substances which occur in food, water and air.[3a] One series of such environmental agents, heterocyclic amines formed by pyrolysis of various amino acids and proteins, was identified as being mutagenic and has been intensively investigated by Sugimura and his co-workers.[3] The first isolated and highly potent mutagens among these compounds are the γ-carboline derivatives Trp-P-1 (**1**) and Trp-P-2 (**2**) isolated from protein pyrolysates[4] and more favorably tryptophan pyrolysates.[5] The structures of these carbolines have been determined from spectral data and, in the case of **1**, also from X-ray analysis.[5] These mutagens were suspected to be carcinogenic, based on their ability to induce morphological transformation of cultured mammalian embryo cells.[6,7] However, sufficient quantities of these compounds were needed for carcinogenicity tests in animals. Their preparation by tryptophan pyrolysis gave extremely low yields.[5] Thus, we developed new procedures for the large-scale synthesis of **1** and **2**.[1]

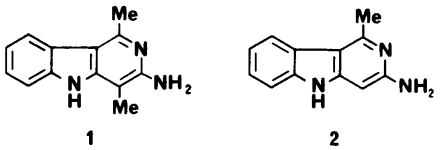

1 2

Fig. 1. Structures of Trp-P-1 (**1**) and Trp-P-2 (**2**).

Results and Discussion

Only a few reports have appeared regarding the synthesis of γ-carboline and its derivatives. They include 1) cyclization to the γ-carboline pyrrole ring by thermal decomposition of azidobenzenes or benzotriazoles containing a pyridine ring (Graebe-Ullmann type reaction),[8] 2) building the γ-carboline pyridine ring by cyclization of azomethines derived from 3-formylindole and amino acetal,[9] and 3) cyclization to 1,2,3,4-tetrahydro-γ-carbolines by thermal reaction of 4-piperidone phenylhydrazones (Fischer indole synthesis).[10] We tried three approaches to the synthesis of γ-carbolines **1** and **2**: A) Thermolysis of 4-(1-benzotriazolyl)-3,6-dimethyl-2-pyridinamine (**6**) in polyphosphoric acid, B) ring closure from 2-acetamido-3-(2-indolyl)alkanoic acids (**14a,b**) to 1,2-dihydro-γ-carbolines, followed by dehydrogenation, and C) building the γ-carboline pyridine ring by cyclization of the 2,3-disubstituted indole **19** with ammonia.

*Synthesis of 3-Amino-1,4-dimethyl-5*H*-pyrido[4,3-b]indole (1) by Route A.* A key intermediate for the synthesis of **1**, 3,6-dimethyl-4-nitro-2-pyridinecarboxylic acid (**3**), was prepared from 2,5-dimethylpyridine[11] and the nitro group was readily replaced by *o*-phenylenediamine to yield the *N*-phenyl-4-pyridinamine compound (**4**). Upon treatment with nitrous acid, this was converted to the 4-(benzotriazolyl)-pyridine derivative **5** in excellent yield. The carboxyl group of **5** was easily converted to the amino group by Curtius rearrangement using diphenylphosphoryl azide(DPPA)[12] to yield the 2-amino derivative **6**. Heating a sample of **6** in polyphosphoric acid gave the desired product **1**, which was isolated as colorless prisms of the acetic acid salt in moderate yield (46%) (Chart 1). Elemental analysis and mass spectroscopy supported the molecular formula of $C_{13}H_{13}N_3 \cdot CH_3COOH$. The UV spectrum of **1** showed several absorption maxima at 226,

244, 265, 267, 307, and 319 nm in an acidic solution, the pattern being comparable to that of γ-carboline.[13] The IR spectrum showed absorption bands at 1650 (CH_3COOH salt) and 1610 (γ-carboline) cm^{-1}. The ^1H NMR spectrum had signals for three methyl groups, acetic acid and those at the C-1 and C-4 positions at δ 2.08 (3H, s), 2.36 and 2.96 (each 3H, s), respectively, together with the four aromatic protons at δ 7.20—7.42 (3H, m) and 8.03 (1H, m).

Synthesis of 3-Amino-1,4-dimethyl-5H-pyrido[4,3-b]indole (1) by Route B. 2-Acetamido-3-(2-indolyl)-butyric acid (**14a**) was synthesized by subjecting the intermediary 2-[1-(dimethylamino)ethyl]indole (**11**), which was prepared from 2-indolecarboxylic acid (**7**) *via* 2-acetylindole (**8**), the dialkylamine **9** and *N,N*-dialkylformamide **10**, to malonic ester synthesis.[14] Quaternarization of **11** and subsequent reaction with diethyl acetamidomalonate gave 2-acetamido-3-(2-indolyl)butyrate (**13a**) in 81% yield from **11**. This ester was subjected to alkaline hydrolysis to yield 2-acetamido-3-(2-indolyl)butyric acid (**14a**) in quantitative yield. Treatment of **14a** with thionyl chloride in ethanol resulted in intramolecular cyclization and a simultaneous esterification to yield the dihydro-γ-carboline ester **15a**.[15] Dehydrogenation with sulfur quantitatively gave γ-carboline-3-carboxylate **16a**, and subsequent alkaline hydrolysis provided the γ-carbolinecarboxylic acid **17a** in high yield (68% yield from **13a**). The final step was Curtius rearrangement of **17a** using DPPA which gave **1** in 41% yield (Chart 2). Elemental analysis, UV, IR, and mass spectra gave results identical to those of the product obtained by route A.

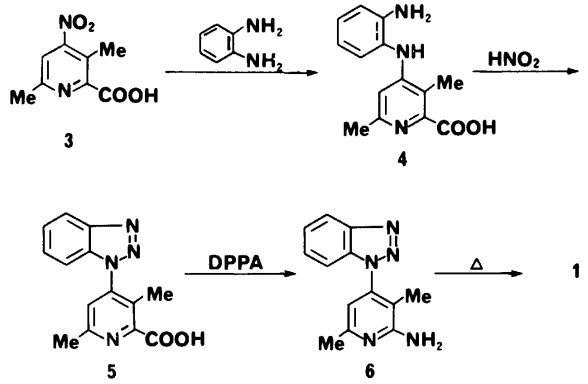

Chart 1. Synthesis of Trp-P-1 by Route A.

Synthesis of 3-Amino-1-methyl-5H-pyrido[4,3-b]indole (2) by Route B. Since route B was very efficient for the synthesis of **1**, we applied it to the synthesis of **2**. As described above, the trimethylammonium salt derived from 2-(dimethylaminomethyl)indole (**12**) was subjected to a malonic ester synthesis using diethyl acetamidomalonate, which yielded 2-acetamido-3-(2-indolyl)propionate (**13b**) in high yield (82%). This compound was cyclized to the dihydro-γ-carboline ester **15b** by treatment with thionyl chloride in ethanol. Dehydrogenation and alkaline hydrolysis, as in the synthesis of **17a** from **11**, gave γ-carbolinecarboxylic acid **17b** in good yield (77.8% from **13b**). Conversion of the carboxyl group to the amino function using DPPA yielded the desired γ-carboline **2** (Chart 2). The physical properties were determined with the crystalline acetic acid salt. The molecular for-

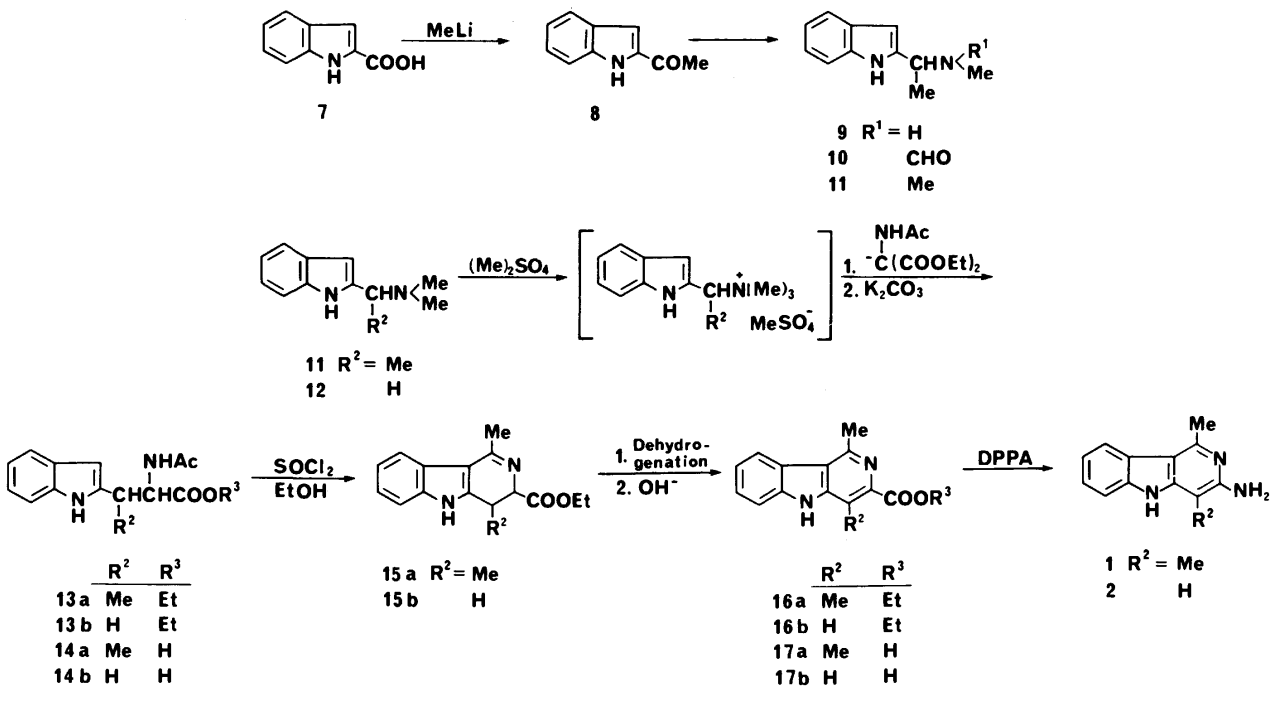

Chart 2. Synthesis of Trp-P-1 and Trp-P-2 by Route B.

mula agreed with $C_{12}H_{11}N_3 \cdot CH_3COOH$ on elemental analysis and mass spectroscopy. Its IR and UV spectra showed the absorption bands characteristic to γ-carboline and were very similar to those of **1** (the acetic acid salt). The structure was further supported by the ^1H NMR spectrum, which showed the signals at δ 1.93 (3H, s) due to acetic acid methyl protons, at δ 2.74 (3H, s) due to C-1 methyl protons, at δ 6.37 (1H, s) due to C-4 proton and at δ 7.07—7.53 (3H, m) and 7.97 (1H, d) due to four aromatic protons.

Synthesis of 3-Amino-1-methyl-5H-pyrido[4,3-b]indole (2) by Route C. In order to confirm the structure of **1**, the alternative, more short-cut method was exploited. Chart 3 shows the synthetic route of **2**, *via* indole-2-acetonitrile (**18**)[16] which was readily available from 2-(dimethylaminomethyl)indole (**12**). Compound **18** was converted to 2-acetylindole-2-acetonitrile (**19**) by the Vilsmeier-Haack reaction[17] with *N,N*-dimethylacetamide (DMA) and phosphoryl chloride. This key intermediate **19**, when treated with methanolic ammonia, underwent spontaneous condensation and aromatization to give the desired product **2** in 58% yield (Chart 3). The physical data regarding the product agreed with those of the sample obtained by route B.

Malonic Ester Synthesis Starting from 1-(2-Indolyl)alkylamines, 11 and 12. When quaternary ammonium salt derived from **11** and **12** were allowed to react with excess sodioacetamidomalonate in ethanol at room temperature, the corresponding monocarboxylates **13a,b** were obtained selectively and quantitatively without hydrolytic decarboxylation procedure (Table 1, runs 3 and 6). In each case, an equimolar quantity of diethyl carbonate was formed in the reaction mixture, offering some suggestion for the reaction mechanism.

In the present reaction, the composition and yields of the products were markedly influenced by changes in the reaction conditions, particularly, the molar ratio of 1-(2-indolyl)alkylamines **11** and **12** and sodioacetamidomalonate. In fact, an entirely different mode of reaction was encountered when the reaction was carried out using sodioacetamidomalonate in amounts less than equimolar to that of the quaternary salts derived from **11** and **12**. The reaction products were the indolylmethyl derivatives of 2-acetamidomalonates **20a,b** (Table 1, runs 1 and 4). When the sodiomalonate was used in slight excess of the equimolar quantity of **11**, the dihydropyrrolo[1,2-*a*]indole **21a** was produced selectively (Table 1, run 2).

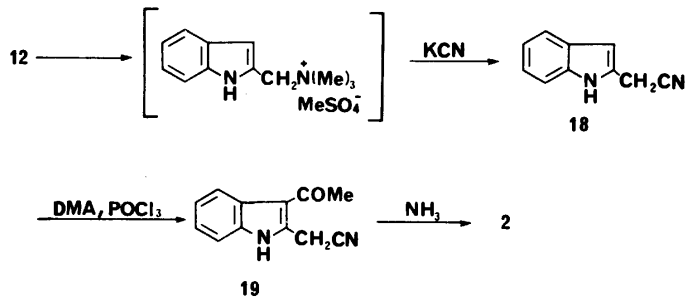

Chart 3. Synthesis of Trp-P-2 by Route C.

These substituted carboxylates, **20a,b**, **21a** and **13a,b**, when treated with alkali, gave the identical 2-acetamidoalkanoic acids **14a,b** in quantitative yields. Thus, this tricyclic hetero system **21** is assumed to be a precursor which can be readily converted to **13a,b**. Several attempts to isolate the tricyclic compound **21b** were unsuccessful under a range of reaction conditions, presumably due to the higher lability of **21b**, because the less hindered ring-carbonyl is considered to be more susceptible to nucleophile attack than that of the sterically more crowed pyrrolidone **21a** during the reaction. These results suggest that, under conditions using excess sodioacetamidomalonate, the reaction proceeds from 1-(2-indolyl)alkylamines **11** and **12** to the monocarboxylates **13a,b** *via* **20** and **21** (Chart 4). An intramolecular attack by the indole anionic nitrogen of **20** upon one of the malonic ester carbonyls results in the formation of the tricyclic pyrrolidone **21**, which, on attack by ethoxide, affords the corresponding monocarboxylates **13a,b**, through C–C bond cleavage of the pyrrolidone ring and another attack by ethoxide ion on the resulting ethoxycarbonyl group of the presumed intermediate (Chart 4). Thus, the present malonic ester-type reaction opens an efficient one-step synthesis of the 3-(2-indolyl)alkanoates, extending a two-carbon chain at the methyl position of the 2-indolylmethyl group

Table 1. Malonic ester synthesis starting from quaternary salts of **11** and **12**[a]

Run	Molar ratio: Sodiomalonate[b] / Quaternary salt of **11**[c]	Product ratio/%[d]: **20a**	**21a**	**13a**
1	0.98	82 (67)	16	2[e]
2	1.10	1	88 (71)	11
3	1.25	—	6	94 (81)[f]
	Sodiomalonate[b] / Quaternary salt of **12**[c]	**20b**	**21b**	**13b**
4	0.98	94 (76)	—	6[e]
5	1.10	42	—	58
6	1.25	3	—	97 (82)[f]

a) See text for reaction conditions. b) Calculated as sodium ethoxide which was employed in the reaction with the equimolar quantity of diethyl acetamidomalonate. c) Prepared from equimolar amounts of the corresponding amine **11** or **12** and dimethyl sulfate. d) For evaluation of the product ratios (%), each sample was analyzed by HPLC (Waters Associates; μ-Porasil, 3.9 mm × 30 cm, $CHCl_3$: AcOEt = 4 : 1; detection at 254 nm). Figures in parentheses express the isolated yields. e) Diethyl carbonate was not detected. f) A nearly quantitative yield of diethyl carbonate was detected by HPLC analysis.

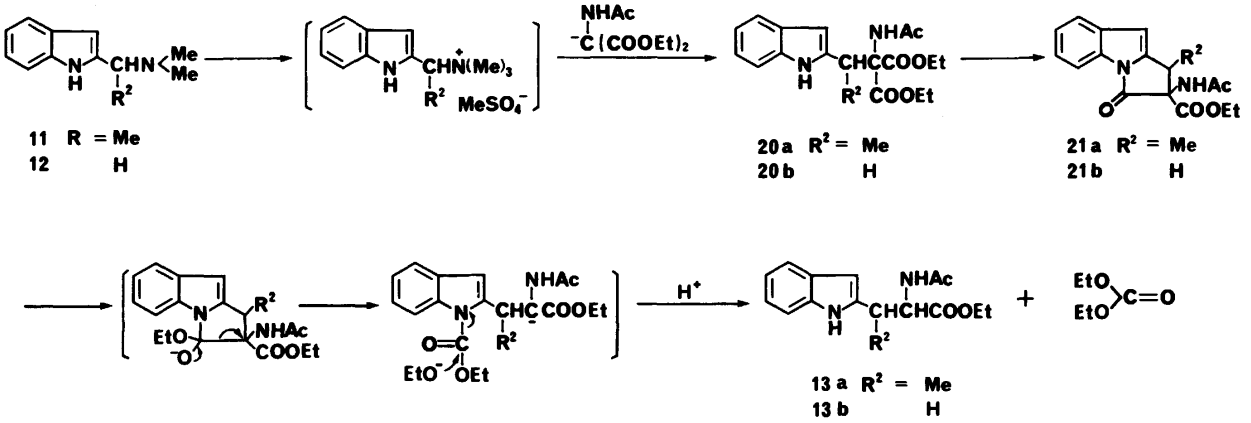

Chart 4. Reaction Mechanism of Monocarboxylic Ester Formation.

under mild reaction conditions.

Our new routes for synthesizing mutagenic γ-carbolines **1** and **2** are efficient and useful for preparing large quantities of these compounds. These methods enabled the synthesis of sufficient amounts of **1** and **2** for carginogenesis testing, including an almost one-year administration of **1** and **2** to mice, by Sugimura and his groups.[3,7] The results have proven that these γ-carbolines are carcinogenic.[3a,18]

Experimental

Melting points were measured on a Yanagimoto MP-S3 hot-plate apparatus and are uncorrected. Infrared spectra were recorded on a Hitachi 215 spectrometer. UV spectra were taken on a Hitachi EPS-3T spectrometer. Mass spectra were determined with a Hitachi RMU-6D spectrometer equipped with a direct-inlet system. ^{1}H NMR spectra were obtained using a Varian XL-100-12 instrument: Chemical shifts (δ) are expressed in ppm downfield from internal TMS. Preparative column chromatography was carried out on a Kieselgel 60 (E. Merck, Art. 7743).

3,6-Dimethyl-4-nitro-2-pyridinecarboxylic Acid (3). This compound was prepared from 2,5-dimethylpyridine according to a method[12] described in the synthesis of 6-ethyl-3-methyl-4-nitro-2-pyridinecarboxylic acid. Recrystallization from acetonitrile gave **3** as colorless needles: Mp 145—146 °C; IR (KBr) 3420, 3100, 1720, 1610, 1540, 1520, 1440, 1390, 1295, 1220, 1190, 1120, 960, 890, 800, and 780 cm^{-1}; ^{1}H NMR (CD_3OD) δ=2.46 (3H, s), 2.60 (3H, s), 7.67 (1H, s). Found: C, 48.99; H, 4.03; N, 14.38%. Calcd for $C_8H_8N_2O_4$: C, 48.98; H, 4.11; N, 14.28%.

3,6-Dimethyl-4-(2-aminophenylamino)-2-pyridinecarboxylic Acid (4). A solution of **3** (3.6 g) and *o*-phenylenediamine (5.4 g) in water (100 cm^3) was heated under reflux for 1 h, and evaporated *in vacuo*. The residue was charged on Amberlite XAD-II (500 cm^3) column which was then washed with water (1000 cm^3) and eluted with 20% aqueous MeOH. The combined fractions containing the desired product were evaporated *in vacuo* and gave a pale-yellow solid. Recrystallization from water provided colorless needles (4.4 g, 93%): Mp 241—242 °C; IR (KBr) 2700—2400, and 1600 cm^{-1}; ^{1}H NMR (CD_3OD) δ=2.03 (3H, s), 2.16 (3H, s), 5.80 (1H, s), 6.33—6.68 (3H, m). Found: C, 65.30; H, 5.79; N, 16.28%. Calcd for $C_{14}H_{15}N_3O_2$: C, 65.36; H, 5.88; N, 16.33%.

4-(1-Benzotriazolyl)-3,6-dimethyl-2-pyridinecarboxylic Acid (5). A 10% hydrochloric acid solution (30 cm^3) of **4** (2.0 g) was cooled in an ice bath and then sodium nitrite (1.1 g) in water (30 cm^3) was added. This mixture was left stainding at 0 °C for 2 h. The precipitated solid was collected, washed with 10% hydrochloric acid and dissolved in 2 mol dm^{-3} NaOH. The solution was filtered to remove any insoluble material and then hydrochloric acid was slowly added. Filtration and drying of the resulting crystalline precipitate gave the hydrochloride of **5** (2.25 g, 93%) as colorless needles: Mp 187—188 °C; IR (KBr) 2850—2300, and 1700 cm^{-1}; ^{1}H NMR (CD_3OD) δ=2.60 (3H, s), 2.93 (3H, s), 7.73 (3H, m), 8.13 (1H, m), 8.26 (1H, s). Found: C, 54.89; H, 4.36; N, 18.33; Cl, 11.69%. Calcd for $C_{14}H_{12}N_4O_2 \cdot HCl$: C, 55.18; H, 4.38; N, 18.39; Cl, 11.63%.

4-(1-Benzotriazolyl)-3,6-dimethyl-2-pyridinamine (6). A mixture of **5** (10 g), diphenylphosphoryl azide (DPPA; 10.8 g), and triethylamine (8.3 g) in *t*-BuOH (200 cm^3) was heated under reflux for 1.5 h and gave a residue when evaporated *in vacuo*. This was dissolved in ethyl acetate (200 cm^3), washed successively with saturated aqueous NaCl and saturated aqueous $NaHCO_3$, dried over $MgSO_4$ and evaporated. The resulting solid was dissolved in 25% HBr-acetic acid (140 cm^3) and the solution was kept standing at 0 °C for 30 min, then diethyl ether (140 cm^3) was added. When the mixed solution was left standing for another 1 h, a white precipitate separated. This was collected by filtration, washed with diethyl ether, and dried to give an amorphous powder (the hydrobromide of **6**). This material was suspended in 15% aqueous ammonia (140 cm^3) and extracted with ethyl acetate. The extract was washed with saturated aqueous NaCl, dried over $MgSO_4$, and evaporated *in vacuo*. Recrystallization of the residue from diethyl ether gave the free amino compound **6** (6.1 g, 78%) as pale yellow needles: Mp 139—140 °C; IR (KBr) 3320, 3200, 1620, and 1590 cm^{-1}; ^{1}H NMR ($CDCl_3$) δ=1.83 (3H, s), 2.34 (3H, s), 4.80 (2H, bs), 6.54 (1H, s), 7.40 (3H, m), 8.06 (1H, m). Found: C, 65.28; H, 5.34; N, 29.34%. Calcd for $C_{13}H_{13}N_5$: C, 65.26; H, 5.48; N, 29.27%.

2-Acetylindole (8). A solution of 2-indolecarboxylic acid (**7**; 14.2 g, Fluka AG, Switzerland) and methyl lithium, prepared from lithium (7.2 g) and methyl iodide (29 g), in

diethyl ether (300 cm^3) was refluxed for 1 h. The reaction mixture was poured into ice water and extracted with diethyl ether. The extract was washed with saturated aqueous NaCl, dried over $MgSO_4$ and evaporated to dryness *in vacuo*. Recrystallization of the residue from ethyl acetate gave 11.7 g (84%) of **8** as colorless needles: Mp 154—155 °C; IR (KBr) 3300, 1640, and 1610 cm^{-1}; ^1H NMR ($CDCl_3$) δ=2.57 (3H, s), 7.12 (2H, m), 7.40 (2H, m), 7.67 (1H, d). Found: C, 75.31; H, 5.62; N, 8.78%. Calcd for $C_{10}H_9NO$: C, 75.45; H, 5.70; N, 8.80%.

2-[1-(Methylamino)ethyl]indole (9). A solution of **8** (11.8 g) in 40% methanolic methylamine (350 cm^3) was heated under reflux for 5 h and left overnight at room temperature. After evaporation, the residue was dissolved in MeOH (200 cm^3) and treated with $NaBH_4$ (4.5 g) under stirring at room temperature for 1 h. Evaporation of the reaction mixture *in vacuo* gave a residue which was suspended in 4% aqueous NaOH (100 cm^3) and extracted with ethyl acetate. The extract was washed with saturated aqueous NaCl, dried over $MgSO_4$ and evaporated *in vacuo* to yield the desired product as colorless needles (11.0 g, 89%): Mp 95—95.5 °C; IR (KBr) 3170, 1450, 1430, and 1290 cm^{-1}; ^1H NMR ($CDCl_3$) δ=1.46 (3H, s), 2.33 (3H, s), 3.93 (1H, q), 6.30 (1H, s), 6.97-7.33 (3H, m), 7.50 (1H, m). Found: C, 75.88; H, 8.16; N, 16.01%. Calcd for $C_{11}H_{14}N_2$: C, 75.82; H, 8.10; N, 16.08%.

2-[1-(N-Formylmethylamino)ethyl]indole (10). A solution of **9** (25 g) and 4-nitrophenyl formate (28.8 g) in ethyl acetate (500 cm^3) was stirred at room temperature for 1 h. The reaction mixture was washed successively with 1 mol dm^{-3} NaOH and saturated aqueous NaCl, dried and evaporated *in vacuo*. Recrystallization of the residue from diethyl ether yielded the desired product as colorless needles (23.6 g, 91%): Mp 129—130 °C; IR (KBr) 3230, 3200, 1660, and 1300 cm^{-1}; ^1H NMR ($CDCl_3$) δ=1.67, 1.70 (3H, d, ratio 45:55), 2.67, 2.70 (3H, s, ratio 55:45), 4.96, 5.83 (1H, q, ratio 55:45), 6.46 (1H, s), 7.00—7.70 (4H, m), 8.13, 8.33 (1H, s, ratio 45:55). Found: C, 71.39; H, 6.98; N, 13.68%. Calcd for $C_{10}H_{14}N_2O$: C, 71.26; H, 6.98; N, 13.85%.

2-[1-(Dimethylamino)ethyl]indole (11). A mixture of **10** (45 g) and $LiAlH_4$ (10.6 g) in dry tetrahydrofuran (1000 cm^3) was placed in a flask equipped with a calcium chloride drying tube and stirred at room temperature for 1 h. After evaporation *in vacuo*, the residue was decomposed by the addition of water (100 cm^3) and extracted with diethyl ether. The extract was dried over $MgSO_4$ and evaporated *in vacuo*. The residual oil was distilled under reduced pressure to yield the desired product as a colorless oil (36 g, 86%): Bp 111—112 °C/1 mmHg (1 mmHg≈133.322 Pa), mp 48—49 °C (solidified on standing); IR (KBr) 3400, 2970, 1460, and 1300 cm^{-1}; ^1H NMR ($CDCl_3$) δ=1.35 (3H, d), 2.22 (6H, s), 3.75 (1H, q), 6.22 (1H, s), 6.95—7.30 (3H, m), 7.47 (1H, m), 8.53 (1H, bs). Found: C, 76.55; H, 8.69; N, 14.90%. Calcd for $C_{12}H_{16}N_2$: C, 76.56; H, 8.57; N, 14.88%.

Diethyl 2-Acetamido-2-[1-(2-indolyl)ethyl]malonate (20a). To a solution of **11** (500 mg, 2.65 mmol) in abs EtOH(5 cm^3), dimethyl sulfate (332 mg, 2.65 mmol) was added dropwise at a temperature below 35 °C. The solution was kept standing at room temperature for 1 h and was then added to an ice-cooled, stirred solution prepared from sodium (59.7 mg, 2.60 mmol) and diethyl acetamidomalonate (564 mg, 2.60 mmol) in abs EtOH (10 cm^3). The mixture was allowed to react at room temperature for 2 d and evaporated *in vacuo*. The resulting residue was dissolved in $CHCl_3$ and washed successively with water, aqueous Na_2CO_3, and dil HCl. Evaporation followed by recrystallization from benzene gave the desired product as an amorphous powder (641 mg, 67%): IR (KBr) 3380, 1735, 1720, 1690, 1670, and 1500 cm^{-1}; ^1H NMR ($CDCl_3$) δ=0.90 (3H, t), 1.26 (3H, t), 1.47 (3H, d), 1.96 (3H, s), 3.96 (1H, m), 4.30 (2H×2, q), 6.23 (1H, s), 7.00—7.67 (4H, m). Found: C, 63.17; H, 6.68; N, 7.81%. Calcd for $C_{19}H_{24}N_2O_5$: C, 63.32; H, 6.71; N, 7.77%.

Ethyl 2-Acetamido-1-methyl-3-oxo-1H-2,3-dihydropyrolo[1,2-a]indole-2-carboxylate (21a). This compound (2.35 g, 71%) was synthesized from the dimethylamino compound **11** (2.0 g) by a procedure similar to that described in the preceding section except that 1.1 equivalents of sodioacetamidomalonate were used. IR (KBr) 3360, 1750, 1740, 1680, and 1610 cm^{-1}; MS *m/z* 314 (M^+); ^1H NMR ($CDCl_3$) δ=1.07, 1.20 (3H, t, ratio 6:4) 1.30, 1.34 (3H, d, ratio 4:6), 2.06, 2.08 (3H, s, ratio 4:6), 3.87, 4.03 (1H, m, ratio 4:6), 4.14, 4.21 (2H, q, ratio 6:4), 6.25, 6.26 (1H, m, ratio 6:4), 7.20—7.50 (3H, m), 8.00 (1H, m). Found: C, 65.11; H, 5.80; N, 8.90%. Calcd for $C_{17}H_{18}N_2O_4$: C, 64.96; H, 5.77; N, 8.91%.

Ethyl 2-Acetamido-3-(2-indolyl)butyrate (13a). To a stirred solution of **11** (9.17 g, 48.8 mmol) in abs EtOH (50 cm^3), dimethyl sulfate (6.3 g, 48.8 mmol) was added dropwise at a temperature below 35 °C. The mixture, after being left standing at room temperature for 1 h, was added to an ice-cooled, stirred solution prepared from sodium (1.4 g, 61 mmol) and diethyl acetamidomalonate (10.6 g, 61 mmol) in abs EtOH (100 cm^3). The combined mixture was allowed to stand at room temperature for 3 d and then evaporated *in vacuo*. After work-up, the desired product was obtained as an amorphous powder (11.3 g, 81%): IR (KBr) 3370, 3360, 3300, 3260, 1730, 1650, 1550, and 1530 cm^{-1}; ^1H NMR (CD_3OD) δ=0.93, 1.16 (3H, t, ratio 1:9), 1.43 (3H, d), 1.90, 1.96 (3H, s, ratio 9:1), 3.56 (1H, q), 4.00, 4.16 (2H, q, ratio 1:9), 4.87, 4.89 (1H, d, ratio 1:9), 6.16, 6.26 (1H, s, ratio 1:9), 6.83—7.60 (4H, m). Found: C, 66.79; H, 6.98; N, 9.16%. Calcd for $C_{16}H_{20}N_2O_3$: C, 66.54; H, 6.99; N, 9.71%.

Ethyl 2-Acetamido-3-(2-indolyl)propionate (13b). From the dimethylamino compound[14] **12** (8.5 g), the desired product **13b** (11.0 g, 82%) was obtained as colorless needles by a procedure similar to that described in the preceding section: Mp 134—135 °C (from benzene); IR (KBr) 3420, 3300, 1740, 1620, 1220, 1200, 1175, and 1020 cm^{-1}; ^1H NMR ($CDCl_3$) δ=1.18 (3H, t), 1.93 (3H, s), 3.23 (2H, d), 4.17 (2H, q), 4.90 (1H, m), 6.23 (1H, s), 6.98—7.67 (4H, m). Found: C, 65.59; H, 6.73; N, 10.01%. Calcd for $C_{15}H_{18}N_2O_3$: C, 65.68; H, 6.61; N, 10.21%.

Malonic Ester Synthesis starting from 2-[1-(Dimethylamino)-alkyl]indoles (11 and 12). A solution of **11** or **12** (0.5 mmol) in abs EtOH (0.5 cm^3) was treated with dimethyl sulfate (0.5 mmol) at a temperature below 35 °C. After the mixture had stood at 20 °C for 1 h, it was added to an ethanolic solution (1.0 cm^3) prepared from equimolar quantities of 0.49, 0.55, or 0.63 mmol of sodium and diethyl acetamidomalonate (Table 1). The mixture was allowed to react at 20 °C for 3 d while being isolated from moisture. The product composition was analyzed by HPLC (μ-Porasil, 3.9 mm×30, $CHCl_3$:AcOEt=4:1). The results are summarized in Table 1.

2-Acetamido-3-(2-indolyl)butyric Acid (14a). *a)* A mixture of **20a** (185 mg) and Na_2CO_3 (180 mg) in water (2.0 cm^3) was refluxed for 15 h and then cooled. This was acidified with concd HCl (0.3 cm^3) and extracted with ethyl acetate. The extract was washed with saturated aqueous

NaCl, dried over $MgSO_4$ and evaporated to dryness *in vacuo*. Precipitation from aqueous EtOH gave the desired product as an amorphous powder (122 mg, 91%): IR (KBr) 3450, 3340, 1740, 1720, and 1600 cm^{-1}; ^1H NMR ($CDCl_3$) δ=1.41, 1.56 (3H, d, ratio 3:7), 2.03, 2.06 (3H, s, ratio 3:7), 3.56 (1H, m), 4.98 (1H, m), 6.36 (1H, m), 6.92—7.66 (4H, m). Found: C, 64.55; H, 6.36; N, 10.73%. Calcd for $C_{14}H_{16}N_2O_3$: C, 64.60; H, 6.20; N, 10.76%.

b) In a similar manner, the tricyclic carboxylate **21a** (288 mg) was subjected to alkaline hydrolysis and gave **14a** (239 mg, 92%).

c) The 2-acetamidobutyrate **13a** (2.15 g) similarly gave **14a** (1.71 g, 97%).

2-Acetamido-3-(2-indolyl)propionic Acid (14a). *a)* In a manner similar to that described in the preceding section, the 2-acetamidomalonate **20b** (3.46 g), on being refluxed in alkaline solution for 15 h, gave **14b** (2.41 g, 98%) as pale yellow needles: Mp 187—188 °C (lit,[14] 190—191 °C); IR (KBr) 3390, 3340, 1695, 1605, and 1535 cm^{-1}; ^1H NMR ($CDCl_3$) δ=1.92 (3H, s), 3.27 (2H, d), 4.80 (1H, m), 6.03 (1H, s), 6.77—7.57 (4H, m). Found: C, 63.57; H, 5.82; N, 11.46%. Calcd for $C_{13}H_{14}N_2O_3$: C, 63.40; H, 5.73; N, 11.38%.

b) The 2-acetamidopropionate **13b** (2.74 g) similarly gave **14b** (2.34 g, 95%).

Ethyl 1,4-Dimethyl-5H-3,4-dihydropyrido[4,3-b]indole-3-carboxylate (15a). To an ice-cooled, stirred suspension of **14a** (1.57 g) in EtOH (30 cm^3) was added dropwise thionyl chloride (1.5 cm^3). The mixture was refluxed for 30 min and evaporated *in vacuo*, giving a dark-red residue. This was dissolved in water (30 cm^3), washed with ethyl acetate and neutralized with 1 mol dm^{-3} NaOH to give the desired product (1.40 g, 86%) as an amorphous powder: IR (KBr) 1740, 1600, 1500, and 1470 cm^{-1}; ^1H NMR (CD_3OD) δ=0.77, (3H, t, ratio 3:7), 2.53, 2.58 (3H, s, ratio 3:7), 2.85, 2.92 (3H, s, ratio 3:7), 3.20, 3.55 (1H, d, ratio 3:7), 3.87, 3.93 (2H, q, ratio 3:7), 6.80—7.53 (4H, m). Found: C, 69.70; H, 6.65; N, 10.32%. Calcd for $C_{16}H_{18}N_2O_2 \cdot 1/4H_2O$: C, 69.92; H, 6.60; N, 10.19%.

Ethyl 1-Methyl-5H-3,4-dihydropyrido[4,3-b]indo-3-carboxylate (15b). In a manner similar to that described the 3-indolylpropionic acid **14b** (49.2 g) was treated with thionyl chloride and afforded **15b** (44.5 g, 87%) as pale yellow needles: Mp 181—183 °C (from EtOH); IR (KBr) 1735, 1605, 1545, and 1465 cm^{-1}; ^1H NMR (DMSO-d_6) δ=1.22 (3H, t), 2.43 (3H, s), 3.00 (2H, m), 4.15 (2H, q), 4.43 (1H, m), 7.00—7.47 (4H, m).

Ethyl 1,4-Dimethyl-5H-pyrido[4,3-b]indole-3-carboxylate (16a). A stirred suspension of **15a** (1.2 g) and sulfur (150 mg) in dry xylene (25 cm^3) was refluxed for 5 h. The reaction mixture was evaporated *in vacuo* to yield a yellow residue. Recrystallization from EtOH gave **16a** (1.11 g, 93%) as pale yellow needles: Mp 257—258 °C; IR (KBr) 1700, 1620, and 1200 cm^{-1}; ^1H NMR (DMSO-d_6) δ=1.30 (3H, t), 2.53 (3H, s), 2.80 (3H, s), 4.26 (2H, q), 7.00—7.66 (3H, m), 8.10 (1H, m). Found: C, 71.60; H, 5.92; N, 10.30%. Calcd for $C_{16}H_{16}N_2O_2$: C, 71.62; H, 6.01; N, 10.44%.

Ethyl 1-Methyl-5H-pyridoz[4,3-b]indole-3-carboxylate (16b).

a) By Dehydrogenation of 15b with Lead Tetraacetate: Lead tetraacetate (117 g) was added in small portions to an ice-cooled, stirred solution of **15b** (51.2 g) in dry pyridine (600 cm^3). The suspension was allowed to react at room temperature for 20 min and then poured into a mixture of ethyl acetate (2000 cm^3) and water (1000 cm^3) with stirring. The organic layer was separated and the aqueous layer was extracted with ethyl acetate. The combined extract was washed successively with saturated aqueous NaCl and saturated aqueous $NaHCO_3$, dried over $MgSO_4$ and evaporated to dryness *in vacuo*. Recrystallization of the resulting reddish solid from EtOH gave pale yellow needles (39.9 g, 78%): Mp 252—254 °C; IR (KBr) 1725, 1620, 1595, 1560, and 1345 cm^{-1}; ^1H NMR ($CDCl_3$) δ=1.45 (3H, t), 3.10 (3H, s), 4.47 (2H, q), 7.10—7.67 (4H, m), 8.13 (1H, s). Found: C, 70.65; H, 5.36; N, 10.84%. Calcd for $C_{15}H_{14}N_2O_5$: C, 70.85; H, 5.55; N, 11.02%.

b) By Dehydrogenation of 15b with Sulfur: In a manner similar to that described in the preceding section, the dihydro-γ-carbolinecarboxylate **15b** (25.6 g) was dehydrogenated with sulfur (3.3 g) to give the desired γ-carbolinecarboxylate **16b** (25.1 g, 98%) as pale yellow needles. All spectral and analytical data were identical with those of the sample described above.

1,4-Dimethyl-5H-pyrido[4,3-b]indole-3-carboxylic Acid (17a). A suspension of **16a** (268 mg) in EtOH-1 mol dm^{-3} NaOH (1:1, 5.0 cm^3) was refluxed for 5 h and then concentrated *in vacuo* to half of its original volume. The concentrate, after being neutralized with 1 mol dm^{-3} HCl (2.5 cm^3), gave a pale-yellow precipitate, which was collected by filtration, washed successively with water, ethanol and diethyl ether, and dried. Recrystallization from a large amount of boiling water gave **17a** (212 mg, 88%) as pale yellow prisms: Mp 283.5—284.5 °C; IR (KBr) 1640, 1620, and 1590 cm^{-1}; ^1H NMR (CD_3OD/NaOH) δ=2.67 (3H, s), 2.95 (3H, s), 7.13—7.73 (3H, m), 8.07 (1H, d). Found: C, 69.72; H, 4.87; N, 11.43%. Calcd for $C_{14}H_{12}N_2O_2$: C, 69.99; H, 5.03; N, 11.66%.

1-Methyl-5H-pyrido[4,3-b]indole-3-carboxylic Acid (17b). In a manner similar to that described in the preceding section, the γ-carboline-3-carboxylic acid ester **16b** (63.5 g) gave the desired 3-carboxylic acid **17b** (54.5 g, 96%) as pale yellow prisms: Mp 275—277 °C; IR (KBr) 1650, 1620, 1590, 1400, and 1220 cm^{-1}; ^1H NMR (CF_3COOH) δ=3.43 (3H, s), 7.73—7.93 (3H, m), 8.30 (1H, m), 8.62 (1H, s). Found: C, 63.68; H, 4.72; N, 11.46%. Calcd for $C_{13}H_{10}N_2O_2 \cdot H_2O$: C, 63.91; H, 4.90; N, 11.46%.

3-Acetylindole-2-acetonitrile (19). Indole-2-acetonitrile[16] (**18**; 1.56 g), prepared from indole-2-carboxylic acid (**7**; Fluka Chem. Corp., Swiss), was dissolved in a mixture of phosphoryl chloride (1.16 cm^3) and *N,N*-dimethylacetamide (3.0 cm^3), and this solution was heated at 85 °C for 2 h. The reaction mixture was poured onto crushed ice (20 g) and washed with ethyl acetate. Unreacted indole-2-acetonitrile (**18**; 840 mg) was recovered from the ethyl acetate layer. The aqueous layer was neutralized with 5 mol dm^{-3} NaOH and extracted with ethyl acetate–tetrahydrofuran (1:1). The extract was washed with saturated aqueous $NaHCO_3$ and dried over $MgSO_4$. After evaporation *in vacuo*, the residue was chromatographed on a column of silica gel using EtOH–$CHCl_3$ (3:7) as an eluent. Work-up, as usual, gave **19** (479 mg, 24%) as fine yellow needles: Mp 223—225 °C; IR (KBr) 3250, 2245, 1620, 1605, 1525, 1490, 1450, and 1180 cm^{-1}; ^1H NMR (DMSO-d_6) δ=2.63 (3H, s), 4.47 (2H, s), 7.07—7.67 (4H, m), 7.83—8.13 (1H, m). Found: C, 72.58; H, 4.98; N, 13.97%. Calcd for $C_{12}H_{10}N_2O$: C, 72.71; H, 5.08; N, 14.13%.

3-Amino-1,4-dimethyl-5H-pyrido[4,3-b]indole (Trp-P-1; 1). *a) Thermal Decomposition of 4-(1-Benzotriazolyl)-3,6-*

dimethyl-2-pyridinamine (6): A mixture of **6** (2.0 g) and polyphosphoric acid (16 g) was allowed to decompose by rapid heating over a free flame until evolution of nitrogen gas ceased. After the reaction mixture had cooled to room temperature, ice-water was added and the mixture was made strongly basic with 6 mol dm^{-3} NaOH and extracted with ethyl acetate. The extract was washed with saturated aqueous NaCl, dried over $MgSO_4$ and evaporated to dryness *in vacuo*. The residue was chromatographed on silica gel using 30% MeOH in ethyl acetate as an eluent. The fractions containing **1** were combined on the basis of TLC analysis and evaporated *in vacuo*, yielding a reddish yellow solid, which upon recrystallization from ethyl acetate (20 cm^3) containing a small amount of acetic acid (0.3 cm^3), gave the desired product, the acetic acid salt of **1** (1.04 g, 46%) as colorless prisms: Mp 248—256 °C; IR (KBr) 3350, 3050, 1650, 1550, and 1400 cm^{-1}; UV (0.1 mol dm^{-3} HCl/MeOH) 227 (ε 16000), 242 (sh, 24000), 265 (67000), 267 (sh, 66000), 307 (7900),and 318 (9800); MS *m/z* 211 (M^+); ^1H NMR (pyridine-d_5) δ=2.08 (3H, s), 2.36 (3H, s), 2.96 (3H, s), 7.20—7.42 (3H, m) 8.03 (1H, m). Found: C, 66.27; H, 6.42; N, 15.20%. Calcd for $C_{13}H_{13}N_3 \cdot CH_3COOH$: C, 66.40; H, 6.32; N, 15.49%.

b) By Curtius Rearrangement of 1,4-Dimethyl-5H-pyrido[4,3-b]indole-3-carboxylic Acid (17a): A mixture of **17a** (110 mg) and triethylamine (0.15 g) in DMA (5.0 cm^3) was kept at 60 °C for 1 h with stirring and cooled to 20 °C. DPPA (0.16 g) was added and the resulting mixture was allowed to react at room temperature for 2 h, during which time the suspension became almost clear. Aqueous acetic acid (50%, 2.0 cm^3) was added dropwise and the mixed solution was heated at 90 °C for 1 h, and then poured into ice-cooled aqueous NaOH (0.75 g in 20 cm^3). The combined mixture was extracted with ethyl acetate, and the extract, after being washed with saturated aqueous NaCl and dried over $MgSO_4$, was concentrated *in vacuo* to one-fifth of its original volume. The residual ethyl acetate solution, upon the treatment with acetic acid (0.3 cm^3), afforded the desired compound (51 mg, 41%) as colorless prisms. All spectral and analytical data were identical with those of the sample obtained by the method described above. The starting material (28 mg) was recovered from the aqueous layer of the ethyl acetate extraction when the pH of the solution was adjusted to 4.5 with concd HCl.

3-Amino-1-methyl-5H-pyrido[4,3-b]indole (Trp-P-2; 2).

a) By Curtius Rearrangement of 1-Methyl-5H-pyrido[4,3-b]-indole-3-carboxylic Acid (17b): Treatment of γ-carboline-3-carboxylic acid **17b** (1.13 g) by a procedure similar to that of section **1***b)* gave the desired product (594 mg, 46%) as colorless prisms: Mp 242—247 °C; IR (KBr) 1670, 1655, 1615, 1460, and 1400 cm^{-1}; UV (0.1 mol dm^{-3} HCl/MeOH) 224 (ε 13000), 243 (sh, 24000), 265 (64000), 269 (70000), 306 (5700), and 318 nm (6400); MS *m/z* 197 (M^+); ^1H NMR (DMSO-d_6) δ= 1.93 (3H, s), 2.74 (3H, s), 6.37 (1H, s), 7.07—7.53 (3H, m), 7.97 (1H, d). Found: C, 65.13; H, 5.71; N, 16.25%. Calcd for $C_{12}H_{11}N_3 \cdot CH_3COOH$: C, 65.36; H, 5.88; N, 16.33%.

b) By Cyclization Reaction of 3-Acetylindole-2-acetonitrile (19) with Ammonia: A solution of **19** (39.6 mg) in 20% methanolic ammonia was heated in a sealed tube at 100 °C for 5 h and evaporated *in vacuo*. The drak brown residue was purified through both silica-gel and alumina (Woelm B, Akt. I) columns, using MeOH in ethyl acetate as an eluent, to give **2** (23 mg, 58%). This product was dissolved in ethyl acetate. Then, a small amount of acetic acid was added and the acetic acid salt of **2** was obtained as colorless prisms. The physicochemical data were identical with those of the sample obtained by the method described above.

We are grateful to Dr. Katsura Morita, General Manager of this Division, and to Drs. Masahiko Fujino and Masao Nishikawa for their encouragement throughout this work. We also thank Dr. Morimasa Arakawa (Nard Institute, Ltd., Osaka) for his kind cooperation.

References

1) H. Akimoto, A. Kawai, H. Nomura, M. Nagao, T. Kawachi, and T. Sugimura, *Chem. Lett.*, **1977**, 1061.

2) At the almost same time, another synthetic method for Trp-P-2 has been reported by K. Takeda, T. Ohta, K. Shudo, T. Okamoto, K. Tsuji, and T. Kosuge, *Chem. Pharm. Bull.*, **25**, 2145 (1977).

3) a) "Environmental Mutagens and Carcinogens," ed by T. Sugimura, S. Kondo and H. Tanabe, University of Tokyo Press, Tokyo (1982); b) T. Sugimura, T. Kawachi, M. Nagao, M. Yamada, S. Takayama, N. Matsukura, and K. Wakabayashi, "Biochemical and Medical Aspects of Tryptophan Metabolism," ed by O. Hayaishi, Y. Ishimura and R. Kido, Elsevier/North-Holland and Biochemical Press, Amsterdam, (1980), p. 297.

4) T. Sugimura, M. Nagao, T. Kawachi, M. Honda, T. Yahagi, Y. Seino, S. Sato, N. Matsukura, T. Matsushima, A. Shirai, M. Sawamura, and H, Matsumoto, "Origins of Human Cancer," Cold Spring Habor Lab., Cold Spring Harbor, N.Y., (1977), p. 1561.

5) a) T. Sugimura, T. Kawachi, M. Nagao, T. Yahagi, Y. Seino, T. Okamoto, K. Shudo, T. Kosuge, K. Tsuji, K. Wakabayashi, Y. Iitaka, and A. Itai, *Proc. Jpn Acad.*, **53**, 58 (1977); b) T. Kosuge, K. Tsuji, K. Wakabayashi, T. Okamoto, K. Shudo, Y. Iitaka, A. Itai, T. Sugimura, T. Kawachi, M. Nagao, T. Yahagi, and Y. Seino, *Chem. Pharm. Bull.*, **26**, 611 (1978).

6) S. Takayama, Y. Katoh, M. Tanaka, M. Nagao, K. Wakabayashi, and T. Sugimura, *Proc. Jpn. Acad.*, **53**, 418 (1978).

7) S. Takayama, H. Hirakawa, and T. Sugimura, *Proc. Jpn. Acad.*, **54**, 418 (1978).

8) a) P. Nantka-Namirski and J. Zieleniak, *Acta Pol. Pharm.*, **34**, 449 (1977); b) P. A. S. Smith and J. H. Boyer, *J. Am. Chem. Soc.*, **73**, 2626 (1951).

9) L. K. Dalton, S. Demerac, and T. Teitei, *Aust. J. Chem.*, **22**, 185 (1969).

10) a) V. Boekelheide and C. Ainsworth, *J. Am. Chem. Soc.*, **72**, 2131 (1950); b) A. H. Cook and K. J. Reed, *J. Chem. Soc.*, **1945**, 399; c) U. Horlein, *Chem. Ber.*, **87**, 463 (1954).

11) E. Matsumura, M. Ariga, and T. Ohfugi, *Bull. Chem. Soc. Jpn.*, **43**, 3210 (1970).

12) K. Ninomiya, T. Shioiri, and S. Yamada, *Chem. Pharm. Bull.*, **22**, 1398 (1974).

13) H. Keberle, A. Rossi, and K. Hoffmenn, *Helv. Chim. Acta*, **42**, 907 (1959).

14) E. C. Kernfeld, *J. Org. Chem.*, **16**, 808 (1951).

15) Compounds **13a**, **14a**, and **15a** were each obtained as a diastereoisomeric mixture and used without separation for futher synthetic reaction.

16) W. Shindler, *Helv. Chim. Acta*, **40**, 2156 (1957).

17) a) A. Vilsmeier and Haack, *Chem. Ber.*, **60**, 119 (1927); b) W. C. Anthony, *J. Org. Chem.*, **25**, 2409 (1960).

18) Dr. T. Sugimura, National Cancer Center Research Institute, Tokyo, and his coworkers, before they used these synthetic products in their biological experiments, confirmed that these γ-carbolines were entirely identical with the corresponding samples obtained from tryptophan pyrolysates in all respects of their physicochemical properties and specific mutagenic activities toward *Salmonella typhimutium* TA98 and TA100.

 © 1985 The Chemical Society of Japan Bull. Chem. Soc. Jpn., 58, 131—135 (1985)

A Sudden-polarization Model to Predict Excited State Reactivity of β-*t*-Butylstyrene

Osamu KIKUCHI* and Hideki YOSHIDA
Department of Chemistry, The University of Tsukuba, Sakura-mura, Ibaraki 305
(Received June 2, 1984)

A model in which two zwitterions play a significant role was employed to account for solvent and substituent effects on photochemical reactions of β-*t*-butylstyrene. These zwitterions are formed by 90° rotation about the external C=C double bond. Semi-empirical MINDO/3 calculations showed that these zwitterions can be two channels which give the observed reacation products. The model also elucidated satisfactorily the photochemical reactions of para substituted β-*t*-butylstyrenes.

The photochemistry of β-*t*-butylstyrene has been established by Hixson.[1-6] Irradiation of β-*t*-butylstyrene in methanol solvent gave a methanol addition product, while irradiation in cyclohexane solvent gave a cyclopropane derivative which is considered to be derived by the 1,2-shift of a methyl group to the β carbon atom.[1] These reactions are singlet state processes.[1-3] The formation of the methanol addition product suggests that the excited singlet state of β-*t*-butylstyrene has a polar character. The formation of the cyclopropane derivative also suggests a polar character of the excited singlet state, since the carbon-to-carbon 1,2-shift of a methyl group occurs easily to the cationic center.[7]

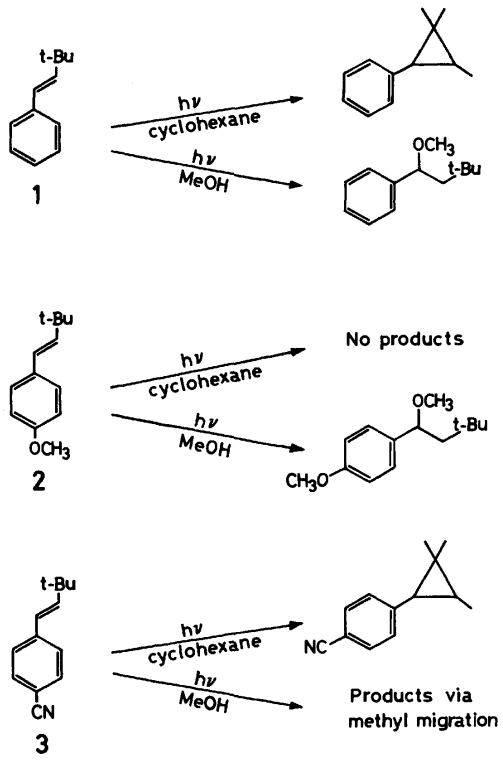

Scheme 1.

From the pairing theorem of the Hückel MO framework, the electron population of the HOMO→LUMO excited state of an even-alternant hydrocarbon is identical with that of the ground state, and the polarization of the excited singlet state of the hydrocarbon should not be large, even if a more sophisticated MO theory is applied to it. Thus the photochemical reaction of β-*t*-butylstyrene, which indicates the ionic character of the excited states, is very interesting from a mechanistic point of view.

The zwitterions, which have negative and positive charges separately, are formed by a rotation about the C-C double bond of an olefin.[8] This is "sudden-polarization" appeared in the 90°-twisted olefin. The sudden-polarization model is capable of elucidating the ionic character observed in the excited states of non-polar species. Some photochemical reactions have been well elucidated on the basis of this model.[9,10] In this paper we use the sudden-polarization model to explain the excited state reactivities of β-*t*-butylstyrene and its derivatives.

The closed-shell and open-shell SCF methods as well as two-configuration SCF method were employed for the calculation of the 90°-twisted structure within the semi-empirical MINDO/3 approximation.[11] The MINDO/3 CI method was used for the potential energy curves calculation along the rotation about the double bond of styrene.

Results and Discussion

Twisted Styrene. The $\pi \rightarrow \pi^*$ singlet state of an olefin is stabilized by a double-bond rotation which gives the 90°-twisted structure. The potential energy curves along this rotation of styrene were calculated by means of MINDO/3 CI which involves 50 and 48 configuration functions for the singlet and triplet states, respectively. Three lower singlet states and the lowest triplet state are shown in Fig. 1.

The 90°-twisted styrene has two non-bonding type MO's: one is the in-plane MO localized on the terminal carbon atom, ϕ_a, and the other is a π MO of the benzyl group, ϕ_b. The lowest singlet state of the 90°-twisted styrene is the ^{1}D diradical state in which each non-

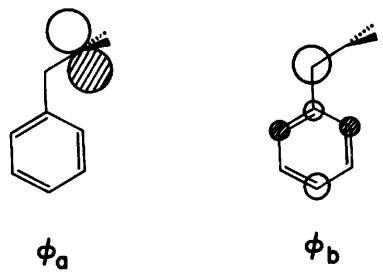

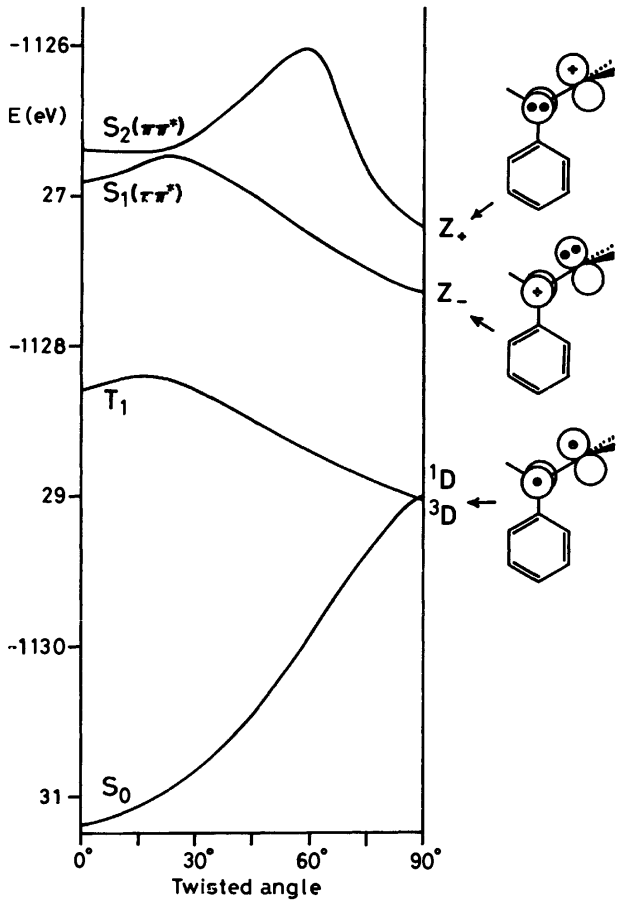

Fig. 1. Potential energy curves of styrene along the rotation about the double bond.
The structures employed were obtained by twisting the optimized ground state geometry. Three lower singlet and lowest triplet states are shown.

bonding MO is occupied by an unpaired electron. The lower excited singlet states involve the Z_- and Z_+ zwitterionic states, in which a pair of electrons occupy the ϕ_a orbital (Z_-) or ϕ_b orbital (Z_+). The electron occupations of these states are shown in Fig. 1.

As may be seen from Fig. 1, the Z_- state is lower in energy than the Z_+ state if the ground-state-twisted structure is considered. However, Bruckmann and Salem[12] pointed out that if the optimized structures corresponding to the Z_- and Z_+ zwitterions are sufficiently different from each other, both of the Z_- and Z_+ zwitterions should lie on the same lowest excited singlet energy surface at their optimized structures. This concept may rationalize the reaction processes of Scheme 1; the methanol addition product is derived from the Z_- zwitterion, while the cyclic isomerization product is from the Z_+ zwitterion *via* the 1,2-shift of a methyl group.

The electronic structure of the 90°-twisted styrene can be expressed in terms of three configurations:[13]

$$|a^2> = |\cdots\phi_a\bar{\phi}_a|$$
$$|b^2> = |\cdots\phi_b\bar{\phi}_b|$$
$$|ab> = \frac{1}{\sqrt{2}}\{|\cdots\phi_a\bar{\phi}_b| + |\cdots\phi_b\bar{\phi}_a|\}$$

The nearly degenerate orbitals of the 90°-twisted styrene, ϕ_a and ϕ_b, belong to different irreducible representations of the molecular symmetry group. The diradical ^1D state is thus expressed by the open-shell wavefunction, $|ab>$, while the zwitterionic states are expressed by two-configuration wavefunctions:

$$\Psi(Z_-) = \lambda|a^2> - \sqrt{1-\lambda^2}|b^2>$$
$$\Psi(Z_+) = \sqrt{1-\lambda^2}|a^2> + \lambda|b^2> \quad (\lambda \geqq 1/\sqrt{2})$$

For the 90°-twisted styrene, the mixing of $|a^2>$and $|b^2>$ is expected to be very small, since ϕ_a and ϕ_b have different symmetries and the value of $<a^2|H|b^2>$ is small.[14] Thus the zwitterionic states of the 90°-twisted styrene were calculated by the closed-shell SCF method, while the diradical state was calculated by the open-shell SCF method. The optimized structures of these states are shown in Fig. 2. The unpaired electron density of the ^1D state and the charge distributions of the Z_- and Z_+ states are shown in Fig. 3.

In order to understand the potential energy surface of the lowest excited singlet state of the 90°-twisted styrene, the energies of the diradical and zwitterionic states were calculated for three structures, II, III, and the ground-state twisted structure. The qualitative shapes of energy surfaces along the structural change among these three structures were obtained by simple interpolation (Fig. 4). The lowest excited singlet state has two energy minima corresponding to different polarizations, Z_- at the structure II and Z_+ at the structure III. The energy difference between these two minima was calculated to be small (22 kJ mol^{-1}).

Twisted β-t-Butylstyrene. Calculations on the 90°-twisted styrene showed two ionic channels on the energy surface of the lowest excited singlet state. This indicates two distinct photochemical pathways of styrene in which two zwitterions act as intermediates.[12]

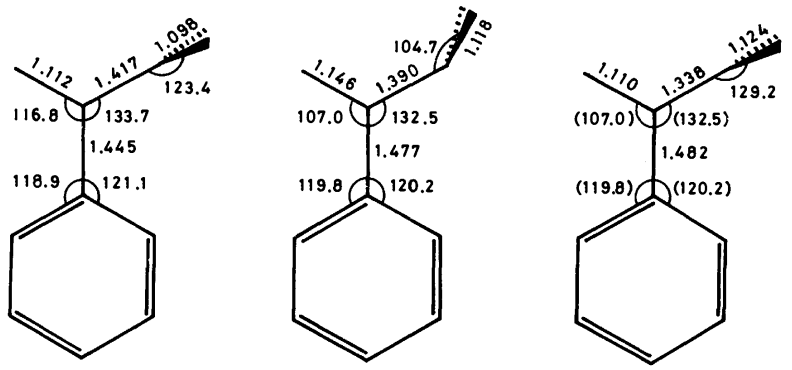

I II III

Fig. 2. Optimized structures of the 90°-twisted styrene.
I: Diradical structure, II: Z_- zwitterionic structure, III: Z_+ zwitterionic structure.
In the optimization of III the variables in parentheses were fixed.

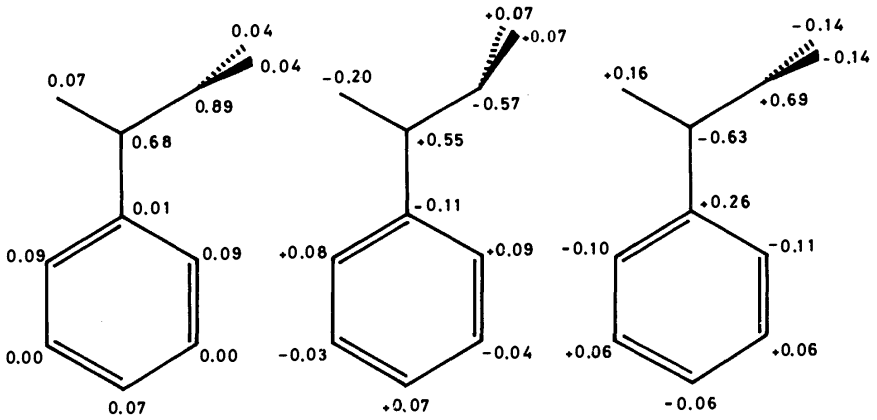

^1D Z_- Z_+

Fig. 3. Unpaired electron densities for the ^1D state and charge densities of the zwitterionic states.

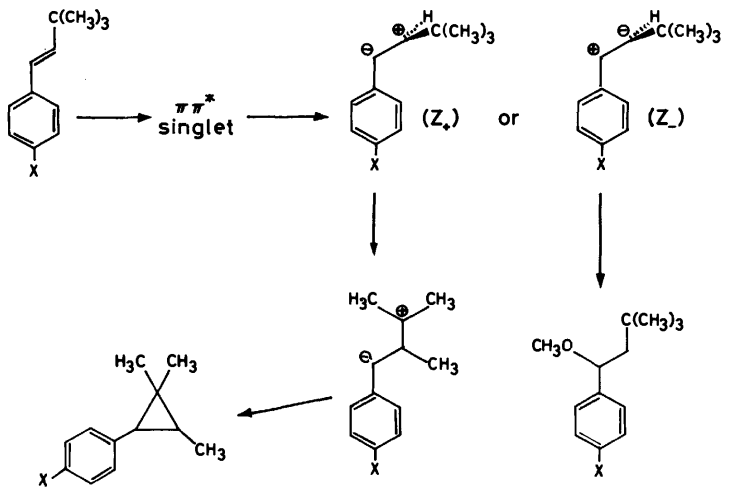

Scheme 2.

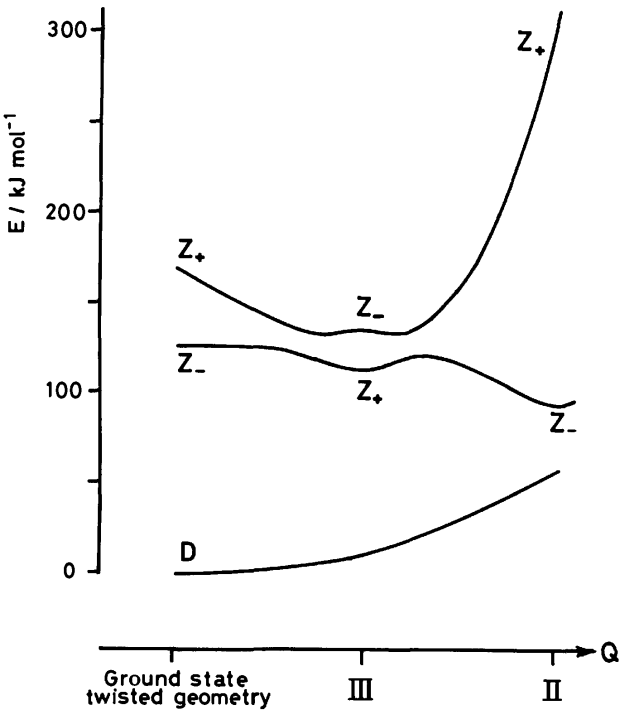

Fig. 4. Qualitative potential energy curves for the lowest singlet states of 90°-twisted styrene.
The coordinate Q indicates the structure of 90°-twisted styrene and is obtained by linear interpolation from the ground-state twisted structure to III, and from III to II; the structures II and III are shown in Fig. 2 and the ground-state twisted structure is obtained by 90° twisting of the ground state structure. The energies of the ^{1}D, Z$_-$, and Z$_+$ states were calculated for only these three structures and the energy curves were estimated by simple interpolation.

The photochemical reaction of β-*t*-butylstyrene can well be explained according to this concept (Scheme 2). The Z$_+$ zwitterion undergoes 1,2-methyl migration to the positive β carbon atom. This migration occurs very fast and is followed by cyclization to give the cyclopropane derivatives. In the Z$_-$ zwitterion, the methyl migration to the β carbon atom which has negative charge does not occur. The methanol addition product at the α carbon atom is obtained from the Z$_-$ zwitterionic state.

For the twisted styrene, the Z$_-$ state is more stable than the Z$_+$ one. In the case of β-*t*-butylstyrene, the Z$_+$ state may be stabilized by a *t*-butyl group. In order to estimate the relative stabilities of the Z$_-$ and Z$_+$ states of the 90°-twisted β-*t*-butylstyrene and its derivatives, the energies of ions **4**—**7** were calculated

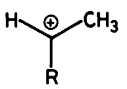

4a, R=H
b, R=C(CH$_3$)$_3$

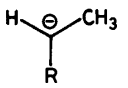

5a, R=H
b, R=C(CH$_3$)$_3$

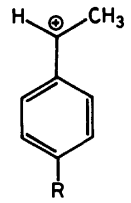

6a, R=H
b, R=CN
c, R=OCH$_3$

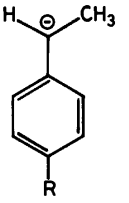

7a, R=H
b, R=CN
c, R=OCH$_3$

for their optimized geometries (Table 1). The change in the relative energy of the Z$_-$ and Z$_+$ states caused by the substitution of a *t*-butyl group at the β position was calculated by:

$$\{E(\mathbf{4a})-E(\mathbf{4b})\}-\{E(\mathbf{5a})-E(\mathbf{5b})\} = 37\ \text{kJ mol}^{-1}$$

This indicates that a *t*-butyl group at the β position stabilizes the Z$_+$ state by 37 kJ mol^{-1} in comparison with the Z$_-$ state. Since the Z$_+$ state of the unsubstituted styrene is 22 kJ mol^{-1} less stable than the Z$_-$ state, the Z$_+$ state of the 90°-twisted β-*t*-butylstyrene is expected to be 15 kJ mol^{-1} more stable than the Z$_-$ state. This energy difference is small and both of the Z$_+$ and Z$_-$ states of 90°-twisted β-*t*-butylstyrene can be the channels from which the methanol addition product and the cyclopropane derivative are formed. This agrees well with the dual pathways observed in the photochemical reaction of β-*t*-butylstyrene.[1)]

The energy differences between the Z$_+$ and Z$_-$ states of the *p*-OCH$_3$ and *p*-CN derivatives were estimated similarly. The results are shown in Table 2. The electron-withdrawing group (CN) at the para position stabilizes the Z$_+$ state, and the energy difference between the Z$_+$ and Z$_-$ states of 90°-twisted *p*-cyano-β-*t*-butylstyrene, 54 kJ mol^{-1}, is larger than that of β-*t*-butylstyrene. This indicates that in the photochemical reaction of *p*-cyano-β-*t*-butylstyrene, the Z$_+$ state may be the only channel from which the reaction product is

Table 1. MINDO/3 Energies of ions **4**—**7**

Ion	Energy/eV[a)]
4a	−318.272
4b	−944.548
5a	−326.057
5b	−951.952
6a	−1138.774
6b	−1442.322
6c	−1607.232
7a	−1146.283
7b	−1450.229
7c	−1614.233

a) All the geometries except the benzene ring were optimized.

Table 2. Relative energies (kJ mol^{-1}) of two zwitterions of twisted β-t-butylstyrenes

β-t-Butylstyrene	Z_-	Z_+
1	0	−15
2	0	+34
3	0	−54

formed. The Z_+ state will give the cyclopropane derivative, which agrees well with experiment.[1] In the case of *p*-methoxy-β-*t*-butylstyrene, the Z_- state was calculated to be 34 kJ/mol more stable than the Z_+ state, indicating that the photochemical reaction *via* the excited singlet state of *p*-methoxy-β-*t*-butylstyrene gives the methanol addition product from the Z_- zwitterion. This also agrees well with experiment.[1]

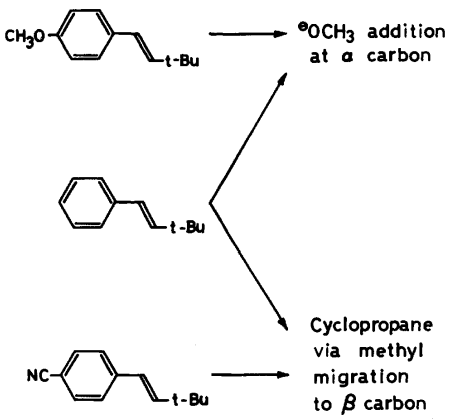

The photochemical reactions of β-*t*-butylstyrene and its derivatives were satisfactorily elucidated on the basis of the sudden-polarization model which involves the 90°-twisted structure. Existence of the twisted structure of β-*t*-butylstyrene was supported indirectly by experiment.[2] The trans and cis forms of *p*-cyano-β-*t*-butylstyrene gave the same primary reaction product, indicating a common intermediate of the 90°-twisted structure.[2] Another fact which may support the twisted structure of styrene is the formation of carbene intermediates[2,7] in the photochemical reactions of styrene derivatives, since carbenes would be expected to be derived easily from the 90°-twisted structure of olefins.[15] It has been shown here that the present modeling is useful to understand the photochemical reactions which appear to involve polar species.

The present results indicate that the excited-state reactivity of olefins can well be described by the MINDO/3 approximation if the correct configuration functions are employed. The energy diagram along the 1,2-hydrogen shift of the 90°-twisted ethylene has been obtained by *ab initio* 4-31G calculation.[15] For this reaction, the similar diagram was obtained when the MINDO/3 CI calculation was carried out. Also, the small CI calculation with the MINDO/3 approximation reproduced well the observed excitation energies of *s-trans*-butadiene and *s-trans*-acrylaldehyde.[16] Thus we feel the MINDO/3 method can be employed for the qualitative analysis of the excited state reactivity, although its parameters were determined so as to reproduce the ground state properties of organic molecules.

References

1) S. S. Hixson, *Tetrahedron Lett.*, **1973**, 277.
2) S. S. Hixson and T. P. Cutler, *J. Am. Chem. Soc.*, **95**, 3031 (1973).
3) S. S. Hixson, *J. Am. Chem. Soc.*, **98**, 1271 (1976).
4) S. S. Hixson, *J. Am. Chem. Soc.*, **97**, 1981 (1975).
5) S. S. Hixson, *Tetrahedron Lett.*, **1971**, 4211; *J. Am. Chem. Soc.*, **94**, 2505 (1972); S. S. Hixson and T. P. Cutler, *ibid.*, **95**, 3032 (1973).
6) H. Kristinsson and G. W. Griffin, *J. Am. Chem. Soc.*, **88**, 378 (1966); J. J. Brophy and G. W. Griffin, *Tetrahedron Lett.*, **1970**, 493.
7) One of the recent reviews on the rearrangement of carbocations is: M. Saunders, J. Chandradekhar, and P. V. R. Schleyer, "*Rearrangements in Ground and Excited States, 1*," ed by P. de Mayo, Academic Press, New York (1980)p. 1.
8) L. Salem, *Acc. Chem. Res.*, **12**, 87 (1979); V. Bonacic-Koutecky, P. Bruckmann, P. Hiberty, J. Koutecky, C. Leferestier, and L. Salem, *Angew. Chem., Int. Ed. Engl.*, **14**, 575 (1975).
9) T. Tezuka, O. Kikuchi, K. N. Houk, M. N. Paddon-Row, C. M. Santiago, N. C. Rondan, J. C. Williams, Jr., and R. W. Gandour, *J. Am. Chem. Soc.*, **103**, 1367 (1981).
10) G. J. M. Dormans, H. R. Fransen, and H. M. Buck, *J. Am. Chem. Soc.*, **106**, 1213 (1984).
11) R. C. Bingham, M. J. S. Dewar, and D. H. Lo, *J. Am. Chem. Soc.*, **97**, 1285 (1975).
12) P. Bruckmann and L. Salem, *J. Am. Chem. Soc.*, **98**, 5037 (1976).
13) L. Salem and C. Rowland, *Angew. Chem. Int. Ed. Engl.*, **11**, 92 (1972).
14) This was confirmed by the MC-SCF calculation with two configurations, $|a^2>$ and $|b^2>$; the value of λ was found to be very close to 1.0.
15) O. Kikuchi, *Bull. Chem. Soc. Jpn.*, **57**, 2007 (1984).
16) O. Kikuchi, H. Kubota, and K. Suzuki, *Bull. Chem. Soc. Jpn.*, **54**, 1126 (1981).

Synthesis of Licoisoflavone A and Related Compounds[1)]

Masao TSUKAYAMA,* Kunihiro FUJIMOTO,† Tokunaru HORIE,
Mitsuo MASUMURA, and Mitsuru NAKAYAMA††
Department of Applied Chemistry, Faculty of Engineering, Tokushima University, Minamijosanjima-cho, Tokushima 770
††*Department of Chemistry, Faculty of Science, Hiroshima University, Higashisenda-machi, Naka-ku, Hiroshima 730*
(Received June 19, 1984)

2′,4′,5,7-Tetrahydroxyisoflavone was partially benzoylated with benzoyl chloride to give 7-benzoyloxy-2′,4′,5-trihydroxyisoflavone. The condensation of the 7-(benzoyloxy)isoflavone with 2-methyl-3-buten-2-ol, followed by the hydrolysis of the resultant 3′-(3-methyl-2-butenyl)isoflavone gave licoisoflavone A. Its 5′-(3-methyl-2-butenyl) isomer was also synthesized from 5-benzoyloxy-2′,4′,7-trihydroxyisoflavone in a similar manner.

Licoisoflavone A was isolated from the roots of *Glycyrrhiza* spp. (Leguminosae) along with other flavonoids.[2)] The structure has been shown to be 2′,4′,5,7-tetrahydroxy-3′-(3-methyl-2-butenyl)isoflavone (**1**) on the basis of chemical and spectroscopic studies. In the continuation of our studies on the synthesis of isoflavones having 3-methyl-2-butenyl groups on the B ring,[3)] the present paper reports in detail the unambiguous synthesis of **1** to confirm the proposed structure of the natural isoflavone and its isomer [2′,4′,5,7-tetrahydroxy-5′-(3-methyl-2-butenyl)isoflavone] (**2**).

The condensation of 2,4-bis(benzyloxy)-6-hydroxyacetophenone (**3**) with 2,4-bis(benzyloxy)benzaldehyde gave 2,4,4′,6′-tetrakis(benzyloxy)-2′-hydroxychalcone (**4**) as a major product and 2′,4′,5,7-tetrakis(benzyloxy)-flavanone (**5**) as a minor product. A mixture of **4** and **5** was easily converted into the acetate (**6**) of **4**. The oxidative rearrangement of **6** with thallium(III) nitrate trihydrate[4)] in methanol, followed by the cyclization of the resultant compound with dilute hydrochloric acid gave the tetrakis(benzyloxy)isoflavone (**7**). The partial debenzylation of **7** with concd hydrochloric acid in acetic acid at 80 °C for 10 min gave the 5-hydroxyisoflavone (**8**). In the UV spectrum of **8**, the absorption maximum showed a bathochromic shift in the presence of aluminum chloride, and the ^{1}H NMR spectrum of **8** also showed three benzyl methylene proton signals and the 5-hydroxyl proton signal. The 5-(benzoyloxy)isoflavone (**9**), which was obtained by the benzoylation of **8** with benzoyl chloride in pyridine, was converted into 5-benzoyloxy-2′,4′,7-trihydroxyisoflavone (**10**) by the hydrogenolysis over 10% palladium on charcoal in methanol–ethyl acetate. The condensation of **10** with 2-methyl-3-buten-2-ol in the presence of boron trifluoride etherate in anhydrous dioxane gave a 3-methyl-2-butenyl compound (**11**) and a bis(3-methyl-2-butenyl) compound (**12**).

† Present address: Honny chemicals CO., Ltd., 3-1-33, Hiyoshi-cho, Nagata-ku, Kobe 653.

The ^{1}H NMR spectrum of **11** showed the presence of two methyl groups as a singlet at δ 1.61, one methylene group as a doublet (J=7 Hz) centering at δ 3.06, one methine proton as a triplet (J=7 Hz) centering at δ 5.18, and two aromatic protons as each singlet at δ 6.33 (3′-H) and 6.66 (6′-H), respectively. The ^{1}H NMR spectrum of **12** showed the presence of two 3-methyl-2-butenyl groups and one aromatic proton as a singlet at δ 6.57 (6′-H). Compound **12** was hydrolyzed with dilute alkali in a nitrogen atmosphere to give 2′,4′,5,7-tetrahydroxy-3′,

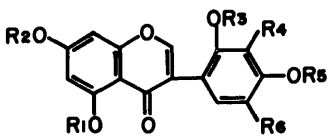

1 $R_1=R_2=R_3=R_5=R_6=H$, $R_4=(CH_3)_2C=CHCH_2$
2 $R_1=R_2=R_3=R_4=R_5=H$, $R_6=(CH_3)_2C=CHCH_2$
7 $R_1=R_2=R_3=R_5=PhCH_2$, $R_4=R_6=H$
8 $R_1=R_4=R_6=H$, $R_2=R_3=R_5=PhCH_2$
9 $R_1=PhCO$, $R_2=R_3=R_5=PhCH_2$, $R_4=R_6=H$
10 $R_1=PhCO$, $R_2=R_3=R_4=R_5=R_6=H$
11 $R_1=PhCO$, $R_2=R_3=R_4=R_5=H$, $R_6=(CH_3)_2C=CHCH_2$
12 $R_1=PhCO$, $R_2=R_3=R_5=H$, $R_4=R_6=(CH_3)_2C=CHCH_2$
13 $R_1=R_2=R_3=R_5=H$, $R_4=R_6=(CH_3)_2C=CHCH_2$
14 $R_1=R_2=R_3=R_5=CH_3CO$, $R_4=R_6=(CH_3)_2C=CHCH_2$
15 $R_1=R_2=R_3=R_5=CH_3CO$, $R_4=H$, $R_6=(CH_3)_2C=CHCH_2$
23 $R_1=R_2=R_3=R_4=R_5=R_6=H$
24 $R_1=R_3=R_4=R_5=R_6=H$, $R_2=PhCO$
25 $R_1=R_3=R_5=R_6=H$, $R_2=PhCO$, $R_4=(CH_3)_2C=CHCH_2$
26 $R_1=R_3=R_4=R_5=H$, $R_2=PhCO$, $R_6=(CH_3)_2C=CHCH_2$
27 $R_1=R_3=R_5=H$, $R_2=PhCO$, $R_4=R_6=(CH_3)_2C=CHCH_2$
28 $R_1=R_2=R_3=R_5=CH_3CO$, $R_4=(CH_3)_2C=CHCH_2$, $R_6=H$

Structure 1.

5′-bis(3-methyl-2-butenyl)isoflavone (**13**), which was converted into the tetraacetate (**14**). Compound **11** was hydrolyzed with dilute alkali in a nitrogen atmosphere to yield 2′,4′,5,7-tetrahydroxy-5′-(3-methyl-2-butenyl)isoflavone (**2**) (mp 232—234 °C). Compound **2** was converted into the tetraacetate (**15**) (mp 127—128 °C) and furthermore cyclized with concd hydrochloric acid in methanol to give the 3-(2,2-dimethyl-6-chromanyl)-4*H*-chromen-4-one (**16**) (mp 261—262 °C). The structure of **16** was further confirmed by the alternative unambiguous synthesis as described below.

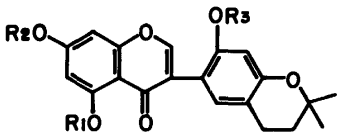

16 $R_1=R_2=R_3=H$
21 $R_1=R_2=R_3=PhCH_2$
22 $R_1=H$, $R_2=R_3=PhCH_2$

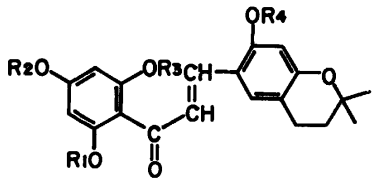

18 $R_1=R_2=R_4=PhCH_2$, $R_3=H$
20 $R_1=R_2=R_4=PhCH_2$, $R_3=CH_3CO$

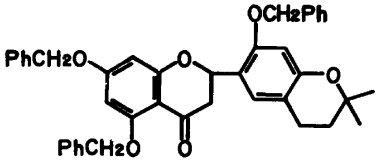

19

Structure 2.

The condensation of **3** and 7-benzyloxy-6-formyl-2,2-dimethylchroman (**17**) gave the 3-(2,2-dimethyl-6-chromanyl)-1-phenyl-2-propen-1-one (**18**) as a major product and the 2-(2,2-dimethyl-6-chromanyl)-4-chromanone (**19**) as a minor product. A mixture of **18** and **19** was converted into the acetate (**20**) of **18**. The oxidative rearrangement of **20** with thallium(III) nitrate trihydrate, followed by the cyclization of the resultant compound gave two 3-(2,2-dimethyl-6-chromanyl)-4*H*-chromen-4-ones (**21**) and (**22**). A mixture of **21** and **22** was hydrogenolyzed over 10% palladium on charcoal to give compound **16**.

From these results, the isoflavone **2** has been found to be a structural isomer of licoisoflavone A (**1**).

The hydrogenolysis of **7** over 10% palladium on charcoal, followed by the partial benzoylation of the resultant tetrahydroxyisoflavone (**23**) with benzoyl chloride in pyridine gave the 7-(benzoyloxy)isoflavone (**24**). In the UV spectrum of **24**, the absorption maximum did not show a bathochromic shift in the presence of sodium acetate. The condensation of **24** with 2-methyl-3-buten-2-ol gave two 3-methyl-2-butenyl compounds (**25**) and (**26**), and one 3′,5′-bis(3-methyl-2-butenyl)isoflavone (**27**). The ^1H NMR spectrum of **26** showed the presence of one 3-methyl-2-butenyl group and two aromatic protons as each singlet at δ 6.46 (3′-H) and 6.84 (6′-H), respectively. Both compounds **26** and **27** were also hydrolyzed to give **2** and **13**, respectively. The ^1H NMR spectrum of **25** showed the presence of one 3-methyl-2-butenyl group and two aromatic protons as each doublet (J=8 Hz) centering at δ 6.42 (5′-H) and 6.81 (6′-H), respectively. Therefore, compound **25** was shown to be 7-benzoyloxy-2′,4′,5-trihydroxy-3′-(3-methyl-2-butenyl)isoflavone, which was hydrolyzed with dilute alkali to give the desired isoflavone (licoisoflavone A) (**1**). Compound **1** was subsequently converted into the tetraacetate (**28**). In Tables 1 and 2, the UV and ^1H NMR spectral data for the synthetic isoflavone **1** and its tetraacetate **28** are shown to be identical with those for natural licoisoflavone A and its tetraacetate, respectively.[2]

On the basis of these results, the structure of licoisoflavone A was confirmed to be 2′,4′,5,7-tetrahydroxy-3′-(3-methyl-2-butenyl)isoflavone (**1**).

Table 1. Mp and UV spectra of isoflavones[a]

Compound	Mp θ_m/°C		λ_{max}/nm (log ε)
Licoisoflavone A (**1**)	120—122[b]	(EtOH)	266.5 (4.46), 339i (3.70)
(Natural)[1]	(111—113)	(EtOH + NaOAc)	277 (4.53), 330 (4.00)
		(EtOH + $AlCl_3$)	269 (4.48), 307i (3.90), 365 (3.43)
Tetraacetate (**28**)	149—150[b,c]	(EtOH)	247 (4.42), 296 (3.87), 335i (3.42)
(Natural)[1]	(136—138)		

a) i: Inflection point. b) The melting points were measured with a Yanagimoto micro-melting-point apparatus. c) The melting point of the tetraacetate (**28**) was not depressed by admixture with natural licoisoflavone A tetraacetate.

TABLE 2. ^{1}H NMR SPECTRA OF ISOFLAVONES[a)]

Compound (Solvent)	2-H	6-H 8-H	5'-H 6'-H	$(CH_3)_2C=CHCH_2$	OH or OAc
Licoisoflavone A (**1**) (DMSO)	8.11 (s)	6.22 (d_1) 6.39 (d_1)	6.36 (d_2) 6.76 (d_2)	1.62 (3H, s, CH_3) 1.72 (3H, s, CH_3) 3.26 (2H, d_3, CH_2) 5.21 (1H, t, CH=)	8.20, 9.24 10.75, 12.80 (each s or b)
Tetraacetate (**28**) ($CDCl_3$)	7.76 (s)	6.84 (d_1) 7.22 (d_1)	6.97 (d_2) 7.14 (d_2)	1.67 (6H, s, $CH_3\times2$) 3.22 (2H, d_3, CH_2) 5.03 (1H, t, CH=)	2.11, 2.28 2.34, 2.40 (each 3H, s)

a) s: Singlet. d_1, d_2, and d_3: Each doublet; J=2, 8, and 7 Hz, respectively. t: Triplet; J=7 Hz. b: Broad.

Experimental

All the melting points are uncorrected. The IR spectra were taken on a Hitachi 215 spectrophotometer, and the UV spectra on a Hitachi 124 spectrophotometer. The ^{1}H NMR spectra were measured with a Hitachi R-20 spectrometer (60 MHz), using tetramethylsilane as an internal standard (δ, ppm). Column chromatography and thin-layer chromatography were carried out on Kieselgel 60 (70—230 mesh) and with Kieselgel 60 F-254 (Merck).

2,4-Bis(benzyloxy)-6-hydroxyacetophenone (3). Potassium carbonate (41.4 g) was added to a solution of 2,4,6-trihydroxyacetophenone (16.8 g) and benzyl chloride (25 g) in *N,N*-dimethylformamide (DMF) (100 ml) in a nitrogen atmosphere at 150—153 °C with stirring, and the mixture was vigorously stirred at 150—153 °C for 40 min. Potassium carbonate was filtered off, and the solvent was removed under reduced pressure. The residue was crystallized from a small amount of methanol to give a mixture of two compounds, which showed R_f values of 0.39 and 0.49 on a silica-gel TLC plate [petroleum ether–1,2-dichloroethane (2:1)], respectively. The mixture was recrystallized from 1,2-dichloroethane to give the desired acetophenone **3** as colorless needles (9.1 g, 26%); mp 96—98 °C; R_f=0.39. Found: C, 75.59; H, 5.67%. Calcd for $C_{22}H_{20}O_4$: C, 75.86; H, 5.75%.

3-Benzyl-4,6-bis(benzyloxy)-2-hydroxyacetophenone was also obtained from the mother liquor by repeating recrystallization from ethyl acetate to give colorless needles (31.6 g, 31%); mp 111—112 °C; R_f=0.49. Found: C, 79.50; H, 5.88%. Calcd for $C_{29}H_{26}O_4$: C, 79.45; H, 5.94%.

2,4,4',6'-Tetrakis(benzyloxy)-2'-hydroxychalcone (4) and 2',4',5,7-Tetrakis(benzyloxy)flavanone (5). A mixture of **3** (10 g) and 2,4-bis(benzyloxy)benzaldehyde (10.2 g) was refluxed in the presence of piperidine (34 ml) in ethanol (200 ml) for 6 h to give yellow precipitates, which were collected by filtration. The precipitates were recrystallized from ethyl acetate to give **4** as yellow needles (11.5 g 68%); mp 146—147 °C. ^{1}H NMR ($CDCl_3$) δ=4.95 (2H, s, $C_6H_5C\underline{H}_2$), 5.01 (4H, s, $C_6H_5C\underline{H}_2\times2$), 5.03 (2H, s, $C_6H_5C\underline{H}_2$), 6.09 (1H, d, J=2 Hz, $C_{5'}$–H), 6.19 (2H, d, J=2 Hz, C_3–H and $C_{3'}$–H), 6.40 (1H, q, J=2 and 8 Hz, C_5–H), 6.81 (1H, d, J=8 Hz, C_6–H), 7.20—7.50 (20H, m, $C_6\underline{H}_5CH_2\times4$), 7.77 and 8.23 (each 1H, d, J=16 Hz, CH=), 12.78 (1H, s, OH). Found: C, 79.89; H, 5.63%. Calcd for $C_{43}H_{36}O_6$: C, 79.63; H, 5.56%.

The flavanone **5** was obtained from the mother liquor by repeating recrystallization from ethyl acetate as colorless needles (2.2 g, 11%); mp 159—161 °C. ^{1}H NMR ($CDCl_3$) δ=2.83—3.00 (2H, m, C_3–H), 5.04 (6H, bs, $C_6H_5C\underline{H}_2\times3$), 5.13 (2H, s, $C_6H_5C\underline{H}_2$), 5.68—5.94 (1H, m, C_2–H), 6.22 (2H, s, arom-H×2), 6.50—6.80 (2H, m, arom-H×2), 7.20—7.70 (21H, m, $C_6\underline{H}_5CH_2\times4$ and arom-H). Found: C, 79.90; H, 5.38%. Calcd for $C_{43}H_{36}O_6$: C, 79.63; H, 5.56%.

2'-Acetoxy-2,4,4',6'-tetrakis(benzyloxy)chalcone (6). Compounds **4** and **5** were converted into the acetate **6** by an acetic anhydride–sodium acetate method. Compound **6** was recrystallized from methanol–ethyl acetate to give pale yellow needles; mp 113—114 °C. ^{1}H NMR ($CDCl_3$) δ= 2.17 (3H, s, CH_3CO), 4.91 (2H, s, $C_6H_5C\underline{H}_2$), 5.00 (4H, s, $C_6H_5C\underline{H}_2\times2$), 5.02 (2H, s, $C_6H_5C\underline{H}_2$), 6.47—6.65 (4H, s, arom-H×4), 7.12—7.61 (21H, m, $C_6\underline{H}_5CH_2\times4$ and arom-H), 6.99 and 7.81 (each 1H, d, J=16 Hz, CH=). Found: C, 78.51; H, 5.54%. Calcd for $C_{45}H_{38}O_7$: C, 78.26; H, 5.51%.

2',4',5,7-Tetrakis(benzyloxy)isoflavone (7). After a mixture of **6** (10 g) and thallium(III) nitrate trihydrate (7 g) was stirred in methanol (1.6 l) at 32—35 °C for 8 h, 10% hydrochloric acid (80 ml) was added and the solution then refluxed for 3 h. After cooling, the precipitates (thallium compound) were filtered off and the solvent removed under reduced pressure. The residue was crystallized from a small amount of methanol and recrystallized from methanol to give **7** as colorless needles (7.4 g, 79%); mp 178—179 °C. ^{1}H NMR ($CDCl_3$) δ=5.00, 5.02, 5.04, and 5.17 (each 2H, s, $C_6H_5C\underline{H}_2$), 6.44—6.72 (5H, m, arom-H×5), 7.00—7.50 (20H, m, $C_6\underline{H}_5CH_2\times4$), 7.68 (1H, s, C_2–H). Found: C, 79.80: H, 5.34%. Calcd for $C_{43}H_{34}O_6$: C, 79.88; H, 5.26%.

2',4',7-Tris(benzyloxy)-5-hydroxyisoflavone (8). A mixture of concd hydrochloric acid (2 ml) and acetic acid (10 ml) was added to a solution of **7** (1 g) in acetic acid (6 ml), and the mixture heated with stirring at 80 °C for 10 min. Water was added to the reaction mixture to give pale yellow precipitates, which were recrystallized from methanol–ethyl acetate to give **8** as pale yellow needles (0.73 g, 85%); mp 117—119 °C. UV λ_{max} nm (log ε) (EtOH) 260 (4.57), 282.5 (4.20), 323i(3.65), (EtOH+NaOAc) 260.5 (4.58), 282.5 (4.22), 323i(3.68), (EtOH+$AlCl_3$) 273.5 (4.58), 309i(3.89), 375(3.65); ^{1}H NMR ($CDCl_3$) δ=5.04 (4H, s, $C_6H_5C\underline{H}_2\times2$), 5.09 (2H, s, $C_6H_5C\underline{H}_2$), 6.37—6.67 (5H, m, arom-H×5), 7.15—7.46 (15H, m, $C_6\underline{H}_5CH_2\times3$), 7.78 (1H, s, C_2–H), 12.00 (1H, s, OH). Found: C, 77.59; H, 4.94%. Calcd for $C_{36}H_{28}O_6$: C, 77.68; H, 5.07%.

5-Benzoyloxy-2',4',7-tris(benzyloxy)isoflavone (9). A mixture of **8** (2 g) and benzoyl chloride (1.67 ml) in pyridine (20 ml) was heated with stirring at 120 °C for 2 h. After cooling, the mixture was poured into ice-cold water and acidified with concd hydrochloric acid, extracted with ether, washed with aq sodium carbonate and water, and dried with sodium sulfate. The solvent was removed, and the residue recrystallized from 1,2-dichloroethane to give **9** as colorless needles (2.2 g, 90%); mp 155—157 °C. UV λ_{max} nm (log ε) (EtOH) 235.5 (4.64), 248i (4.53), 281sh (4.22), 301.5i (3.98), (EtOH+$AlCl_3$) 233.5 (4.67), 247.5i (4.53), 280sh (4.23), 301.5i (3.98); ^{1}H NMR (DMSO) δ=4.99, 5.02, and 5.27 (each 2H, s, $C_6H_5C\underline{H}_2$), 6.45—6.80 (3H, m, arom-H×3), 7.03 and 7.17 (each 1H, d, J=2 Hz, arom-H), 7.20—8.10 (20H, m, $C_6\underline{H}_5CH_2$×3 and $C_6\underline{H}_5CO$), 8.14 (1H, s, C_2–H). Found: C, 77.99; H, 4.84%. Calcd for $C_{43}H_{32}O_7$: C, 78.18; H, 4.85%.

5-Benzoylxoy-2',4',7-trihydroxyisoflavone (10). Compound **9** (2 g) was hydrogenolyzed over 10% palladium on charcoal (0.4 g) in a mixture of ethyl acetate (200 ml) and methanol (80 ml) at 30 °C until the uptake of hydrogen ceased. The catalyst was filtered off, and the solvent removed under reduced pressure. The residue was recrystallized from methanol-ethyl acetate to give **10** as colorless needles (1.1 g, 90%); mp 211—213 °C. UV λ_{max} nm (log ε) (EtOH) 237i (4.42), 250 (4.33), 260.5 (4.32), 301i (4.00), (EtOH+NaOAc) 260.5 (4.43), 297.5i (4.03), 327 (3.98), (EtOH+$AlCl_3$) 235 (4.50), 249.5i (4.33), 263 (4.22), 283 (4.14), 303i (3.88); ^{1}H NMR (DMSO) δ=6.05—6.45 (2H, m, arom-H×2), 6.60—7.40 (3H, m, arom-H×3), 7.45—8.20 (5H, m, C_6H_5CO), 8.05 (1H, s, C_2–H), 8.60—9.70 (2H, b, OH×2). Found: C, 67.69; H, 3.81%. Calcd for $C_{22}H_{14}O_7$: C, 67.69; H, 3.60%.

5-Benzoyloxy-2',4',7-trihydroxy-5'-(3-methyl-2-butenyl)isoflavone (11) and 5-Benzoyloxy-2',4',7-trihydroxy-3',5'-bis(3-methyl-2-butenyl)isoflavone (12). A solution of 2-methyl-3-buten-2-ol (0.32 ml) in anhydrous dioxane (10 ml) was gradually added to a solution of **10** (1 g) and boron trifluoride etherate (0.48 ml) in dioxane (42 ml) in a nitrogen atmosphere, and the mixture heated with stirring at 50 °C for 6 h. The reaction mixture was poured into ice-cold water and extracted with ether. The ethereal solution was washed with aq sodium hydrogencarbonate and dried with sodium sulfate. After the removal of the solvent, the residue was chromatographed over a silica-gel column with chloroform-ethyl acetate (3:1) to give two main products (R_f=0.75 and 0.24), respectively. The compound of R_f=0.24 was recrystallized from chloroform to give **11** as pale yellow prisms (261 mg, 22%); mp 180—182 °C. UV λ_{max} nm (log ε) (EtOH) 250.5i (4.33), 263 (4.34), 291sh (4.14), (EtOH+NaOAc) 261.5 (4.46), 301sh (4.07), 328 (4.02), (EtOH+$AlCl_3$) 248.5i (4.35), 266 (4.22), 285 (4.17); ^{1}H NMR (DMSO) δ=1.61 (6H, s, CH_3×2), 3.06 (2H, d, J=7 Hz, CH_2), 5.18 (1H, t, J=7 Hz, CH=), 6.33 (1H, s, $C_{3'}$–H), 6.66 (1H, s, $C_{6'}$–H), 6.74 (1H, d, J=2 Hz, C_6–H), 6.81 (1H, d, J=2 Hz, C_8–H), 7.45—8.15 (5H, m, C_6H_5CO), 8.01 (1H, s, C_2–H), 8.50—9.60 (2H, b, OH×2). Found: C, 70.57; H, 4.78%. Calcd for $C_{27}H_{22}O_7$: C, 70.73; H, 4.84%.

The compound of R_f=0.75 was a viscous pale yellow oil, compound **12** (325 mg, 26%), which did not crystallize. ^{1}H NMR (DMSO) δ=1.66 and 1.69 (each 6H, s, CH_3×2), 3.08—3.42 (4H, m, CH_2×2), 4.92—5.37 (2H, m, CH=×2), 6.57 (1H, s, $C_{6'}$–H), 6.75 (1H, d, J=2 Hz, C_6–H), 6.88 (1H, d, J=2 Hz, C_8–H), 7.50—8.20 (5H, m, C_6H_5CO), 8.10 (1H, s, C_2–H).

2',4',5,7-Tetrahydroxy-3',5'-bis(3-methyl-2-butenyl)isoflavone (13). Compound **12** (325 mg) was hydrolyzed with a 4% aq solution of sodium hydroxide (3 ml) in methanol (50 ml) in a nitrogen atmosphere at 50 °C for 1 h. The reaction mixture was acidified with dilute hydrochloric acid and extracted with ethyl acetate. The ethyl acetate solution was washed with aq sodium hydrogencarbonate, water, and dried with sodium sulfate. After the removal of the solvent, the residue was chromatographed over a silica-gel column with chloroform-acetone (10:1) to give **13** as a viscous pale yellow oil (95 mg, 36%), which did not crystallize. ^{1}H NMR ($CDCl_3$) δ=1.71 and 1.82 (each 6H, s, CH_3×2), 3.27 and 3.49 (each 2H, d, J=7 Hz, CH_2), 5.24 (2H, t, J=7 Hz, CH=×2), 5.60 (1H, bs, OH), 6.20 (1H, d, J=2 Hz, C_6–H), 6.29 (1H, d, J=2 Hz, C_8–H), 6.70 (1H, s, $C_{6'}$–H), 7.86 (1H, s, C_2–H), 12.17 (1H, s, OH).

2',4',5,7-Tetraacetoxy-3',5'-bis(3-methyl-2-butenyl)isoflavone (14). Compound **13** was converted into the tetraacetate **14** by an acetic anhydride-sodium acetate method. Compound **14** was chromatographed over a silica-gel column with chloroform-acetone (50:1) and recrystallized from ethyl acetate as colorless prisms; mp 170—171 °C. UV λ_{max} nm (log ε) (EtOH) 241 (4.46), 299 (3.89), 328 (3.37); ^{1}H NMR ($CDCl_3$) δ=1.68 (12H, s, CH_3×4), 2.09, 2.28, 2.33, and 2.40 (each 3H, s, CH_3CO), 3.18 (4H, d, J=7 Hz, CH_2×2), 4.85—5.42 (2H, m, CH=×2), 6.85 (1H, d, J=2 Hz, C_6–H), 7.00 (1H, s, $C_{6'}$–H), 7.24 (1H, d, J=2 Hz, C_8–H), 7.80 (1H, s, C_2–H). Found: C, 67.09; H, 5.74%. Calcd for $C_{33}H_{34}O_{10}$: C, 67.11; H, 5.80%.

2',4',5,7-Tetrahydroxy-5'-(3-methyl-2-butenyl)isoflavone (2). Compound **11** (83 mg) was hydrolyzed with a 4% aq solution of sodium hydroxide (3 ml) in methanol (40 ml) in a nitrogen atmosphere at 50 °C for 1 h. The reaction mixture was worked up in the same manner in the preparation of **13**. The resultant compound was chromatographed over a silica-gel column with chloroform-ethyl acetate (3:1), and recrystallized from dichloromethane-methanol to give **2** as pale yellow needles (32 mg, 50%); mp 232—234 °C. IR (KBr) 3430, 3200, 2960, 2915, 1650, 1615, 1505, 1440 cm^{-1}; UV λ_{max} nm (log ε) (EtOH) 266 (4.41), 301i (4.15), 341i (3.77), (EtOH+NaOAc) 277.5 (4.48), 301i (4.22), 334.5i (4.05), (EtOH+$AlCl_3$) 273 (4.44), 313i (3.93), 374 (3.43); ^{1}H NMR (DMSO) δ=1.67 (6H, s, CH_3×2), 3.14 (2H, d, J=7 Hz, CH_2), 5.26 (1H, t, J=7 Hz, CH=), 6.23 (1H, d, J=2 Hz, C_6–H), 6.38 (1H, d, J=2 Hz, C_8–H), 6.45 (1H, s, $C_{3'}$–H), 6.83 (1H, s, $C_{6'}$–H), 8.10 (1H, s, C_2–H), 8.70—9.64 (2H, b, OH×2), 12.96 (1H, s, OH); one OH proton was not observed. Found: C, 67.53; H, 5.05%. Calcd for $C_{20}H_{18}O_6$: C, 67.79; H, 5.12%.

2',4',5,7-Tetraacetoxy-5'-(3-methyl-2-butenyl)isoflavone (15). Compound **2** was converted into the tetraacetate **15** by an acetic anhydride-sodium acetate method. Compound **15** was recrystallized from ethyl acetate-petroleum ether to give colorless prisms; mp 127—128 °C. IR (KBr) 3070, 2970, 2940, 1785, 1650, 1630, 1500, 1435 cm^{-1}; UV λ_{max} nm (log ε) (EtOH) 244 (4.47), 300 (3.82); ^{1}H NMR ($CDCl_3$) δ=1.70 and 1.72 (each 3H, s, CH_3), 2.12, 2.28, 2.82, and 2.86 (each 3H, s, CH_3CO), 3.22 (2H, d, J=7 Hz, CH_2), 5.22 (1H, t, J=7 Hz, CH=), 6.84 (1H, d, J=2 Hz, C_6–H), 6.99 (1H, s, $C_{3'}$–H), 7.08 (1H, s, $C_{6'}$–H), 7.22 (1H, d, J=2 Hz, C_8–H), 7.78 (1H, s, C_2–H). Found: C, 64.19; H, 5.00%. Calcd for $C_{28}H_{26}O_{10}$: C, 64.38: H, 4.99%.

5,7-Dihydroxy-3-(7-hydroxy-2,2-dimethyl-6-chromanyl)-4H-chromen-4-one (16). A mixture of **2** (42 mg) and concd hydrochloric acid (1.9 ml) was refluxed in methanol (9 ml) for 4 h. The reaction mixture was poured into water to give precipitates, which were recrystallized from aq methanol to give **16** as colorless needles (37 mg, 88%); mp 261—262 °C. UV λ_{max} nm (log ε) (EtOH) 261 (4.44), 289sh (4.17), 337i (3.65), (EtOH+NaOAc) 271.5 (4.43), 302sh (4.15), 335sh (3.95), (EtOH+$AlCl_3$) 270.5 (4.47), 300i (4.10), 374 (3.64); ^{1}H NMR (DMSO) δ=1.28 (6H, s, CH_3×2), 1.72 and 2.62 (each 2H, t, J=7 Hz, CH_2), 6.18 (1H, d, J=2 Hz, C_6–H), 6.20 (1H, s, $C_{3'}$–H), 6.33 (1H, d, J=2 Hz, C_8–H), 6.82 (1H, s, $C_{6'}$–H), 8.08 (1H, s, C_2–H), 9.10 and 10.60 (each 1H, bs, OH), 12.88 (1H, s, OH). Found: C, 67.56; H, 4.98%. Calcd for $C_{20}H_{18}O_6$: C, 67.79; H , 5.12%.

7-Benzyloxy-6-formyl-2,2-dimethylchroman (17). A mixture of 6-formyl-7-hydroxy-2,2-dimethylchroman[5] (1.9 g), benzyl chloride (1.6 ml), and anhydrous potassium carbonate (4 g) in DMF (50 ml) was heated with vigorous stirring at 150 °C for 1.5 h. Potassium carbonate was filtered off, and the solvent removed under reduced pressure. The residue was extracted with ether, and the ethereal solution dried with sodium sulfate. The ethereal extract was chromatographed over a silica-gel column with chloroform–petroleum ether (1:1) to give **17** as a colorless liquid (2.1 g, 72%). ^{1}H NMR ($CDCl_3$) δ=1.33 (6H, s, CH_3×2), 1.78 and 2.71 (each 2H, t, J=7 Hz, CH_2), 5.05 (2H, s, $C_6H_5C\underline{H}_2$), 6.40 (1H, s, C_5–H), 7.36 (5H, s, $C_6\underline{H}_5CH_2$), 7.61 (1H, s, C_8–H), 10.36 (1H, s, CHO).

3-(7-Benzyloxy-2,2-dimethyl-6-chromanyl)-1-[2,4-bis(benzyloxy)-6-hydroxyphenyl]-2-propen-1-one (18) and 5,7-Bis(benzyloxy)-2-(7-benzyloxy-2,2-dimethyl-6-chromanyl)-4-chromanone (19). A mixture of **3** (4.1 g) and **17** (3.2 g) was refluxed in the presence of piperidine (15 ml) in ethanol (200 ml) for 6 h to give yellow precipitates. The precipitates were recrystallized from ethyl acetate to give **18** as yellow needles (3.5 g, 52%); mp 158—160 °C. ^{1}H NMR ($CDCl_3$) δ=1.34 (6H, s, CH_3×2), 1.72 and 2.46 (each 2H, t, J=7 Hz, CH_2), 4.97 (4H, s, $C_6H_5C\underline{H}_2$×2), 5.03 (2H, s, $C_6H_5C\underline{H}_2$), 6.07 (1H, d, J=2 Hz, $C_{5'}$–H), 6.16 (1H, d, J=7 Hz, $C_{3'}$–H), 6.30 (1H, s, C_3–H), 6.89 (1H, s, C_6–H), 7.21—7.45 (15H, m, $C_6\underline{H}_5CH_2$×3), 7.77 and 8.20 (each 1H, d, J=16 Hz, CH=). Found: C, 78.74; H, 6.16%. Calcd for $C_{41}H_{38}O_6$: C, 78.57; H, 6.11%.

The flavanone **19** was obtained from the mother liquor by silica-gel column chromatography with chloroform–hexane (5:1), and recrystallized from ethyl acetate to give colorless needles (0.15 g, 2%); mp 155—157 °C. ^{1}H NMR ($CDCl_3$) δ=1.34 (6H, s, CH_3×2), 1.79 (2H, t, J=7 Hz, CH_2), 2.60—3.10 (4H, m, C_3–H and CH_2), 5.01 (4H, s, $C_6H_5C\underline{H}_2$×2), 5.13 (2H, s, $C_6H_5C\underline{H}_2$), 5.64—5.98 (1H, m, C_2–H), 6.22 (2H, s, arom-H×2), 6.44 and 7.23 (each 1H, s, arom-H), 7.27—7.71 (15H, m, $C_6\underline{H}_5CH_2$×3). Found: C, 78.42; H, 6.04%. Calcd for $C_{41}H_{38}O_6$: C, 78.57; H, 6.11%.

3-(7-Benzyloxy-2,2-dimethyl-6-chromanyl)-1-[2-acetoxy-4,6-bis(benzyloxy)phenyl]-2-propen-1-one (20). Compound **18** and **19** were converted into the acetate **20** by an acetic anhydride–sodium acetate method. The compound **20** was recrystallized from methanol–ethyl acetate to give pale yellow needles; mp 143—144 °C. ^{1}H NMR ($CDCl_3$) δ=1.35 (6H, s, CH_3×2), 1.80 and 2.70 (each 2H, t, J=7 Hz, CH_2), 2.19 (3H, s, CH_3CO), 4.95 (2H, s, $C_6H_5C\underline{H}_2$), 5.02 (4H, s, $C_6H_5C\underline{H}_2$×2), 6.38—6.53 (3H, m, arom-H×3), 6.99 and 7.81 (each 1H, d, J=16 Hz, CH=), 7.12—7.49 (16H, m, $C_6\underline{H}_5CH_2$×3 and arom-H). Found: C, 77.16; H, 5.77%. Calcd for $C_{43}H_{40}O_7$: C, 77.22; H, 6.03%.

5,7-Bis(benzyloxy)-3-(7-benzyloxy-2,2-dimethyl-6-chromanyl)-4H-chromen-4-one (21) and 7-Benzyloxy-3-(7-benzyloxy-2,2-dimethyl-6-chromanyl)-5-hydroxy-4H-chromen-4-one (22). After a mixture of **20** (3 g) and thallium(III) nitrate trihydrate (7 g) was stirred in methanol (800 ml) at 35—37 °C for 4 h, 10% hydrochloric acid (40 ml) was added to the mixture, and the solution refluxed for 3 h. The reaction mixture was worked up in the same manner as in the preparation of **7**. The resulting compounds were chromatographed over a silica-gel column with chloroform to give two main compounds **21** (0.96 g, 33%) and **22** (1.1 g, 39%), respectively. Compound **21** was crystallized from ether–petroleum ether to give colorless prisms; mp 133—134.5 °C. ^{1}H NMR ($CDCl_3$) δ=1.31 (6H, s, CH_3×2), 1.75 and 2.70 (each 2H, t, J=7 Hz, CH_2), 4.94, 5.01, and 5.14 (each 2H, s $C_6H_5C\underline{H}_2$), 6.43 (3H, s, arom-H×3), 7.08 (1H, s, arom-H), 7.13—7.65 (15H, m, $C_6\underline{H}_5CH_2$×3), 7.68 (1H, s, C_2–H). Found: C, 78.79; H, 5.72%. Calcd for $C_{41}H_{36}O_6$: C, 78.82; H, 5.81%.

Compound **22** was crystallized from methanol to give pale yellow needles; mp 145—147 °C. ^{1}H NMR ($CDCl_3$) δ=1.34 (6H, s, CH_3×2), 1.79 and 2.75 (each 2H, t, J=7 Hz, CH_2), 5.00 and 5.10 (each 2H, s, $C_6H_5C\underline{H}_2$), 6.43 (2H, s, arom-H×2), 6.50 and 7.03 (each 1H, s, arom-H), 7.29 and 7.38 (each 5H, s, $C_6\underline{H}_5CH_2$), 7.18 (1H, s, C_2–H), 12.95 (1H, s, OH). Found: C, 76.33; H, 5.83%. Calcd for $C_{34}H_{30}O_6$: C, 76.39; H, 5.66%.

Another Synthesis of 5,7-Dihydroxy-3-(7-hydroxy-2,2-dimethyl-6-chromanyl)-4H-chromen-4-one (16). A mixture (1.66 g) of **21** and **22** was hydrogenolyzed over 10% palladium on charcoal (300 mg) in a mixture of ethyl acetate (150 ml) and methanol (150 ml) until the uptake of hydrogen ceased. After the catalyst was filtered off, the solvent was removed under reduced pressure. The residue was recrystallized from aq methanol to give **16** as colorless needles (650 mg); mp 261—262 °C [no depression in a mixed-melting-point determination with the 3-(2,2-dimethyl-6-chromanyl)-4*H*-chromen-4-one **16** synthesized above]. The ^{1}H NMR spectrum of the compound synthesized here was also identical with that of the 3-(2,2-dimethyl-6-chromanyl)-4*H*-chromen-4-one **16** synthesized above.

2',4',5,7-Tetrahydroxyisoflavone (23). Compound **7** (5 g) was hydrogenolyzed over 10% palladium on charcoal (1.7 g) in methanol (220 ml) until the uptake of hydrogen ceased. The catalyst was filtered off, and the solvent removed under reduced pressure. The residue was recrystallized from methanol to give **23** as pale yellow prisms (2.17 g, 97%); mp 255—256 °C. UV λ_{max} nm (log ε) (EtOH) 261.5 (4.38), 288i (4.15), (EtOH+NaOAc) 271.5 (4.36), 297i (4.09), 327 (3.97), (EtOH+$AlCl_3$) 271.5 (4.42), 301i (3.98), 375 (3.53); ^{1}H NMR (DMSO) δ=6.21 (1H, d, J=2 Hz, C_6–H), 6.29 (1H, q, J=2 and 8 Hz, $C_{5'}$–H), 6.37 (2H, d, J=2 Hz, $C_{3'}$–H and C_8–H), 6.96 (1H, d, J=8 Hz, $C_{6'}$–H), 8.12 (1H, s, C_2–H), 8.38—10.44 (3H, b, OH×3), 12.86 (1H, s, OH). Found: C, 62.72; H, 3.66%. Calcd for $C_{15}H_{10}O_6$: C, 62.94; H, 3.50%.

7-Benzoyloxy-2',4',5-trihydroxyisoflavone (24). Benzoyl chloride (0.88 ml) in anhydrous ether (15 ml) was gradually added to a solution of **23** (1.8 g) in pyridine (30 ml) in an ice bath, and the mixture stirred at 2—5 °C for 5.5 h. The reaction mixture was poured into ice-cold

water, acidified with concd hydrochloric acid, and allowed to stand overnight in a refrigerator to give precipitates. The precipitates were collected by filtration and recrystallized from methanol to give **24** as pale yellow prisms (914 mg, 37%); mp 212—213 °C. UV λ_{max} nm (log ε) (EtOH) 256 (4.50), 343i (3.54), (EtOH+NaOAc) 255 (4.50), 341i (3.60), (EtOH+$AlCl_3$) 264.5 (4.54), 383.5 (3.63); ^{1}H NMR (DMSO) δ=6.29 (1H, q, J=2 and 8 Hz, C$_{5'}$-H), 6.36 (1H, d, J=2 Hz, C$_{3'}$-H), 6.87 (1H, d, J=2 Hz, C$_6$-H), 7.04 (1H, d, J=8 Hz, C$_{6'}$-H), 7.19 (1H, d, J=2 Hz, C$_8$-H), 7.59—8.22 (5H, m, C_6H_5CO), 8.32 (1H, s, C$_2$-H), 8.87—10.17 (2H, b, OH×2), 12.88 (1H, bs, OH). Found: C, 67.68; H, 3.64%. Calcd for $C_{22}H_{14}O_7$: C, 67.69; H, 3.59%.

7-Benzoyloxy-2',4',5-trihydroxy-3'-(3-methyl-2-butenyl)isoflavone (25), 7-Benzoyloxy-2',4',5-trihydroxy-5'-(3-methyl-2-butenyl)isoflavone (26), and 7-Benzoyloxy-2',4',5-trihydroxy-3',5'-bis(3-methyl-2-butenyl)isoflavone (27). A solution of 2-methyl-3-buten-2-ol (0.39 ml) in anhydrous dioxane (10 ml) was gradually added to a mixture of **24** (1.2 g) and boron trifluoride etherate (0.57 ml) in dioxane (40 ml) in a nitrogen atmosphere, and the mixture heated with stirring at 51—53 °C for 6 h. The reaction mixture was worked up in the same manner as in the preparation of **11**. The resulting products were chromatographed over a silica-gel column with 1,2-dichloroethane–acetone (20:1) to give three main fractions, which showed R_f values of 0.88, 0.63, and 0.24 on a silica-gel TLC plate with 1,2-dichloroethane–acetone (20:1), respectively. The second fraction (R_f=0.63) was recrystallized from methanol to give the desired isoflavone **25** as pale yellow needles (250 mg, 18%); mp 165—167 °C. UV λ_{max} nm (log ε) (EtOH) 263.5 (4.54), (EtOH+NaOAc) 264.5 (4.51), 316sh (3.83), (EtOH+$AlCl_3$) 269 (4.55), 384 (3.41); ^{1}H NMR (DMSO) δ=1.64 and 1.73 (each 3H, s, CH_3), 3.33 (2H, d, J=7 Hz, CH_2), 5.24 (1H, t, J=7 Hz, CH=), 6.42 (1H, d, J=8 Hz, C$_{5'}$-H), 6.81 (1H, d, J=8 Hz, C$_{6'}$-H), 6.86 (1H, d, J=2 Hz, C$_6$-H, 7.13 (1H, d, J=2 Hz, C$_8$-H), 7.55—8.20 (5H, m, C_6H_5CO), 8.25 (1H, s, C$_2$-H), 8.28 and 9.38 (each 1H, s, OH), 12.86 (1H, s, OH). Found: C, 70.95; H, 4.73%. Calcd for $C_{27}H_{22}O_7$: C, 70.73; H, 4.84%.

The third fraction (R_f=0.24) was recrystallized from dichloromethane to give the 5'-(3-methyl-2-butenyl)isoflavone **26** as pale yellow needles (169 mg, 12%); mp 124—126 °C. UV λ_{max} nm (log ε) (EtOH) 255 (4.48), 317.5i (3.77), (EtOH+NaOAc) 253 (4.49), 318i (3.81), (EtOH+$AlCl_3$) 264 (4.52), 287i (4.23), 381 (3.68); ^{1}H NMR (DMSO) δ=1.68 (6H, s, CH_3×2), 3.17 (2H, d, J=7 Hz, CH_2), 5.27 (1H, t, J=7 Hz, CH=), 6.46 (1H, s, C$_{3'}$-H), 6.82 (1H, d, J=2 Hz, C$_6$-H), 6.84 (1H, s, C$_{6'}$-H), 7.12 (1H, d, J=2 Hz, C$_8$-H), 7.57—8.24 (5H, m, C_6H_5CO), 8.29 (1H, s, C$_2$-H), 9.04, 9.30, and 12.84 (each 1H, s, OH). Found: C, 70.95; H, 4.68%. Calcd for $C_{27}H_{22}O_7$: C, 70.73; H, 4.84%.

Compound **26** was hydrolyzed with dilute alkali to give the isoflavone **2**.

The first fraction (R_f=0.88) gave the 3',5'-bis(3-methyl-2-butenyl)isoflavone **27** as a viscous pale yellow oil (375 mg, 23%), which did not crystallize. ^{1}H NMR ($CDCl_3$) δ=1.77 and 1.85 (each 6H, s, CH_3×2), 3.30 and 3.54 (each 2H, d, J=7 Hz, CH_2), 5.28 (2H, d, J=7 Hz, CH=×2), 5.63 (1H, s, OH), 6.78 (1H, d, J=2 Hz, C$_6$-H), 6.97 (1H, d, J=2 Hz, C$_8$-H), 7.45—8.25 (6H, m, C_6H_5CO and C$_{6'}$-H), 8.00 (1H, s, C$_2$-H), 12.28 (1H, s, OH).

Compound **27** was hydrolyzed with dilute alkali to give the isoflavone **13**.

2',4',5,7-Tetrahydroxy-3'-(3-methyl-2-butenyl)isoflavone (Licoisoflavone A) (1). Compound **25** (180 mg) was hydrolyzed with a 4% aq solution of sodium hydroxide (3 ml) in methanol (55 ml) in a nitrogen atmosphere at 50 °C for 1.5 h. The reaction mixture was worked up in the same manner as in the preparation of **2**. The resulting compound was recrystallized from aq methanol to give the desired isoflavone **1** as pale yellow prisms (70 mg, 50%); mp 120—122 °C. IR (KBr) 3350, 2900, 1650, 1605, 1500, 1447 cm^{-1}. Found: C, 67.55; H, 5.03%. Calcd for $C_{20}H_{18}O_6$: C, 67.79; H, 5.12%.

2',4',5,7-Tetraacetoxy-3'-(3-methyl-2-butenyl)isoflavone (28). Compound **1** (licoisoflavone A) was converted into the tetraacetate **28** by an acetic anhydride–sodium acetate method. Compound **28** was recrystallized from ethanol to give colorless needles; mp 149—150 °C. IR (KBr) 2960, 2920, 1770, 1650, 1620, 1480, 1430 cm^{-1}. Found: C, 64.51; H, 4.73%. Calcd for $C_{28}H_{26}O_{10}$: C, 64.38; H, 4.99%.

The properties of this synthetic isoflavone (**1**) and its tetraacetate (**28**) were fully consistent with those of natural licoisoflavone A and its tetraacetate, respectively.

The authors are grateful to Professor Shoji Shibata, Meiji College of Pharmacy, and Dr. Takeshi Kinoshita, University of Tokyo, for supplying the sample of natural licoisoflavone A tetraacetate.

References

1) Part of this work was previously reported as a preliminary communication: M. Tsukayama, K. Fujimoto, T. Horie, Y. Yamashita, M. Masumura, and M. Nakayama, *Chem. Lett.*, **1982**, 675.

2) T. Kinoshita, T. Saitoh, and S. Shibata, *Chem. Pharm. Bull.*, **26**, 141 (1978).

3) M. Nakayama, S. Hayashi, M. Tsukayama, T. Horie, and M. Masumura, *Chem. Lett.*, **1978**, 879; M. Nakayama, S. Eguchi, S. Hayashi, M. Tsukayama, T. Horie, T. Yamada, and M. Masumura, *Bull. Chem. Soc. Jpn.*, **51**, 2398 (1978); M. Tsukayama, K. Fujimoto, T. Horie, M. Masumura, and M. Nakayama, *Heterocycles*, **22**, 261 (1984).

4) L. Farkas, A. Gottsegen, and M. Nógrádi, *J. Chem. Soc., Perkin Trans. 1*, **1974**, 305.

5) W. Stech, *Can. J. Chem.*, **49**, 1197 (1971).

The α-Chlorination of Aryl Ketones with Manganese(III) Acetate in the Presence of Chloride Ion

Takehiko TSURUTA, Tetsuya HARADA, Hiroshi NISHINO, and Kazu KUROSAWA*
Department of Chemistry, Faculty of Science, Kumamoto University, Kurokami 2-39-1, Kumamoto 860
(Received June 21, 1984)

The reaction of 2-(4-methoxyphenyl)-4-chromanone with $Mn(OAc)_3$ in the presence of LiCl gave 3,3-dichloro-2-(4-methoxyphenyl)-4-chromanone. The reactions of 2-phenyl-4-chromanone, 1-phenyl-1-propanone, 1,2-diphenylethanone, and 1-tetralone similarly yielded α,α-dichloro derivatives in good yields. 2,2,2-Trichloroacetophenones were obtained from 2,2-dichloroacetophenones, but in the absence of LiCl, 2,2-dichloroacetophenones gave 2,2,3,3-tetrachloro-1,4-butanediones. KCl, NaCl, NH_4Cl, $AlCl_3$, and $CaCl_2$ were also employed as the Cl^- ion source. Synthetic applicability and the reaction mechanisms are discussed briefly.

In a previous publication,[1] it was reported that the reaction of 4'-methoxyacetophenone with $Mn(OAc)_3$ in AcOH containing NH_4Cl yielded 2-chloro-4'-methoxyacetophenone and 2,2-dichloro-4'-methoxyacetophenone, and the reaction of the 2-chloro-4'-methoxyacetophenone with $Mn(OAc)_3$ in AcOH alone gave several dimeric compounds. This seemed to indicate that the reaction could provide a useful method for the total α-chlorination of some aryl ketones if an excess of $Mn(OAc)_3$–Cl^- is used. Therefore, the reactions of 2-phenyl-4-chromanones (**1a** and **1b**), 1-phenyl-1-propanone (**2**), 1,2-diphenylethanones (**3a** and **3b**), 1-tetralone (**4**), and 2,2-dichloroacetophenones (**5a—5d**) with $Mn(OAc)_3$ in the presence of various chloride ion sources such as LiCl, KCl, NH_4Cl, $CaCl_2$, and $AlCl_3$ in boiling AcOH were examined. These aryl ketones were chosen for the reason that they have at least one or two hydrogens at the α-position of the carbonyl function and are all enolizable ketones.

When 2-(4-methoxyphenyl)-4-chromanone (**1a**) was heated under reflux in AcOH containing $Mn(OAc)_3$ and LiCl, the products were found to be 3,3-dichloro-2-(4-methoxyphenyl)-4-chromanone (**6a**), 3-chloro-4'-methoxyflavone (**7**), and 4'-methoxyflavone (**8a**). A similar reaction of 2-phenyl-4-chromanone (**1b**) yielded 3,3-dichloro-2-phenyl-4-chromanone (**6b**) and flavone (**8b**).

The reactions of 1-phenyl-1-propanone (**2**) and 1-tetralone (**4**) gave the corresponding α,α-dichloro derivatives as the sole product.

When 1,2-bis(4-methoxyphenyl)ethanone (**3a**) was oxidized with $Mn(OAc)_3$–LiCl, the products were 2-acetoxy-1,2-bis(4-methoxyphenyl)ethanone (**13**), 1,2-bis(4-methoxyphenyl)ethanedione (**14a**), and *p*-anisic acid (**15a**). The formation of **13** can be accounted for by assuming a substitution of the chlorine atom by acetate ion in 2-chloro-1,2-bis(4-methoxyphenyl)ethanone (**16**) which may be formed as an intermediate. In fact, **16** gave **13** when heated in AcOH. 1,2-Diphenylethanone (**3b**), on the other hand, yielded the corresponding α,α-dichloro derivative (**11**) as the major product.

When 2,2-dichloro-4'-methoxyacetophenone (**5a**) was oxidized with $Mn(OAc)_3$–LiCl, it gave 2,2,2-trichloro-4'-methoxyacetophenone (**17a**) in almost quantitative yields (Table 1, Entry 7). 2,2-Dichloro-(**5b**), 2,2,4'-trichloro-(**5c**), and 2,2-dichloro-4'-methylacetophenones (**5d**) also yielded the corresponding 2,2,2-trichloroacetophenone (**17b—17d**) in excellent yields (Entries 9, 11, and 13). The reaction of **5a** with $Mn(OAc)_3$ in AcOH alone, on the contrary, resulted in the formation of a dimeric compound (**18a**) as in the reaction of 2-chloro-4'-methoxyacetophenone.[1] It was also found that **5c** gave another dimeric compound (**19**) together with **18c**.

The formation of 3,3-dichloro-2-phenyl-4-chromanones, **6a** and **6b**, has precedence. Weber and Birkner[2] have reported that the reaction of **1a** and **1b** with $CuCl_2$ for 8 h yielded **6a** (65.5%) and **6b** (27.2%), respectively. The reaction using $Mn(OAc)_3$–LiCl is certainly better than that reported because of a shorter reaction time (130 min) and a much higher yield (73% for **6a** and 74% for **6b**). It was also reported[3] that 2,2-dichloro-1-tetralone (**12**) was obtained by a two-step reaction of **4** with $FeCl_3$ (a 53% overall yield). Again this is poor when compared with ours.

In order to examine the reaction conditions in more detail, we chose 2-(4-methoxyphenyl)-4-chromanone (**1a**) as a substrate and carried out reactions under various conditions since **1a** gave several products in a previous experiment. Also, the products could be well separated on TLC. A previous study[1] revealed that the molar ratio of a substrate to $Mn(OAc)_3$ has considerable effect on the yield of products in the reaction of 4'-methoxyacetophenone with $Mn(OAc)_3$–NH_4Cl. An increase in the yield of **6a** was observed to be at the expence of **8a**, while increasing the amount of $Mn(OAc)_3$ (they stayed constant beyond the molar ratio of 1:7). In Table 2 a summary of the molar ratios and yields is presented.

Changing LiCl to other salts as a chloride ion source has some effect on the yields of the products (Table 3). It is demonstrated that KCl and NaCl are better salts and gave a much higher yield of **6a** than the other. $CaCl_2$ yielded a moderate amount of **8a**. NH_4Cl and

$AlCl_3$ were intermediary and gave *r*-3-acetoxy-*t*-2-(4-methoxyphenyl)-4-chromanone (**9**) together with **6a**, **7**, and **8a**. **9** was the major product in the reaction of **1a** with $Mn(OAc)_3$ alone (Entry 6). In the case of $AlCl_3$ it was necessary to acidify the reaction mixture with 2 M (1 M=1 mol/dm^3) hydrochloric acid to free the products from $AlCl_3$. All salts other than LiCl and $AlCl_3$ were only partially soluble in AcOH and some remained at the bottom of the flask. Although KCl gave the maximum yield of **6a**, it is better to use LiCl as the chloride ion source since KCl gives a rather poor yield in the case of 1,2-diphenylethanone (**11**, 50%).

The formation of the dimeric compound (**18a—d** and **19**) seems to suggest the radical nature of the reaction. The formation of **17a** in the reaction of **5a**, even in the absence of Cl^- ions (Table 1, Entry 8), indicates that **5a**, itself, could supply Cl^- ions. It can be postulated that the α-keto radical (A) produced from a 2,2-dichloroacetophenone by the action of a Mn(III) species is the common reaction intermediate both for the α-chlorination and for the formation of dimeric compounds. The intermediate A reacts with $Mn(OAc)_3/Cl^-$ to give **17a—d**, and in the absence of Cl^- ions dimerizes by a head-to-head coupling to give **18a—d** and by a head-to-tail coupling to give **19** (Scheme 1). When **19** was heated at 180 °C under reduced pressure, it isomerized to **18c**. This indicates that the dissociation of **19** to A (Ar=4-chlorophenyl) takes place and a recombination of A gives **18c**. Hydrolysis of **19** with aqueous AcOH yielded **5c** and 4-chlorobenzoic acid (**15c**). The formation of the α,α-dichloro derivatives in the reaction of other ketones can also be accounted for by the similar α-keto radical intermediates (-CO-CH- and -Co-CCl=).

It was thus shown that the reaction of $Mn(OAc)_3$-LiCl provides a facile and extremely simple procedure for α-chlorination of aryl ketones.

Experimental

All the ^{1}H-NMR spectra were recorded with a Hitachi-Perkin-Elmer R-24 spectrometer with tetramethylsilane as the internal reference. The proton decoupled ^{13}C-FT NMR spectra were measured for deuteriochloroform solutions at 100 MHz on a JEOL FX 100 spectrometer using tetramethylsilane as the internal reference. The IR spectra were taken for chloroform solutions on a JASCO IR A-1 grating spectrometer and the UV spectra were recorded for methanol solutions with a Hitachi EPS 3T spectrophotometer. The melting points were determined with a Yanagimoto micro-melting point apparatus and were not corrected.

Materials. 2-(4-Methoxyphenyl)-4-chromanone[4] (**1a**) 2-phenyl-4-chromanone[5] (**1b**), 1,2-bis(4-methoxyphenyl)-ethanone[6] (**3a**), 1,2-diphenylethanone[7] (**3b**), 2,2-dichloro-4′-methoxyacetophenone[8] (**5a**), 2,2-dichloroacetophenone[9] (**5b**) 2,2,4′-trichloroacetophenone[10] (**5c**), and 2,2-dichloro-4′-methylacetophenone[11] (**5d**) were prepared by the method described in the literature. 1-Phenyl-1-propanone (**2**) and 1-tetralone (**4**) were commercially available (Wako Pure Chemical Industries Ltd.).

Oxidations of Aryl Ketones with $Mn(OAc)_3$-Cl^-. The general procedure for the oxidation of aryl ketones with $Mn(OAc)_3$-Cl^- was as follows. To a heated solution of $Mn(OAc)_3 2H_2O$[12] (4—9 mmol) and Cl^- (10 mmol) in AcOH (20 ml), a ketone (1 mmol) was added. The mixture was then heated under reflux until the dark color of the solution

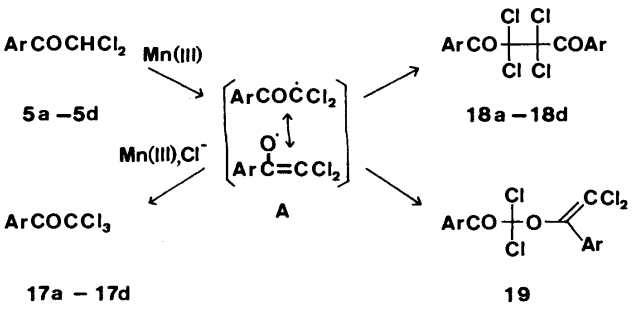

Scheme 1.

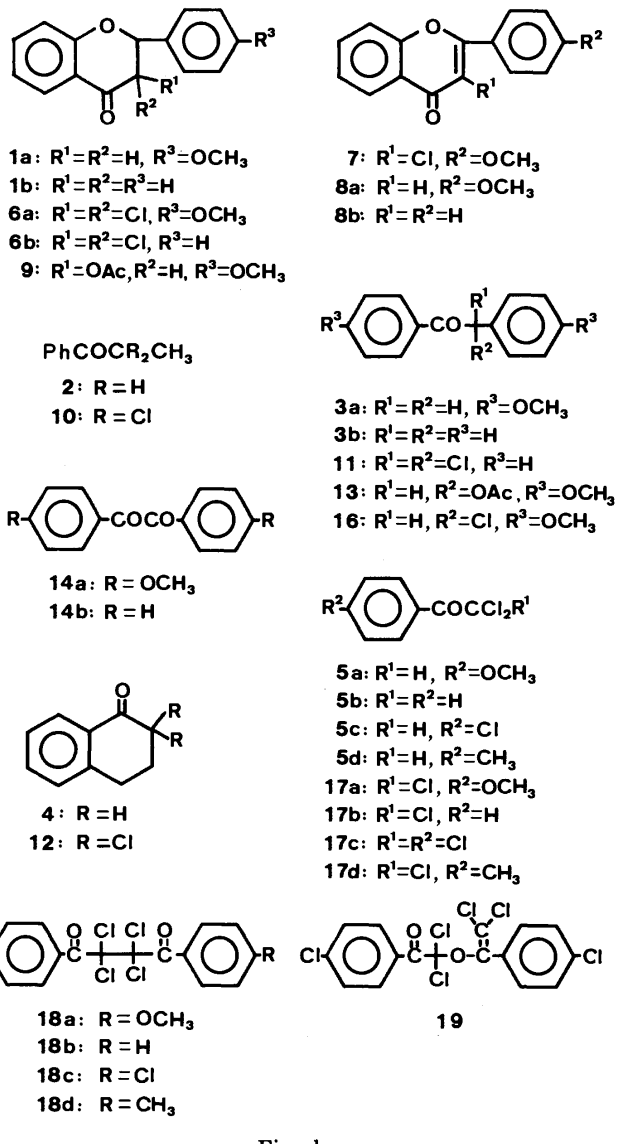

Fig. 1.

TABLE 1. REACTION OF ARYL KETONES WITH $Mn(OAc)_3$-LiCl

Entry	Substr.	Reaction conditions: Molar ratio of Substr : $Mn(OAc)_3$: LiCl	Time/min	Product (yield/%)[a]			
1	**1a**	1 : 7 : 10	130	**6a** (73)	**7** (6)	**8a** (12)	
2	**1b**	1 : 7 : 10	54	**6b** (74)		**8b** (9)	
3	**2**	1 : 9 : 10	180	**10** (93)			
4	**3a**	1 : 5 : 10	91		**13** (79)	**14a** (16)	**15a** (2)
5	**3b**	1 : 5 : 10	23	**11** (75)		**14b** (10)	**15b** (5)
6	**4**	1 : 5 : 10	11	**12** (78)[b]			
7	**5a**	1 : 4 : 10	180	**17a** (98)			
8	**5a**	1 : 2 : 0	95	**17a** (2)	**18a** (53)		**15a** (5)
9	**5b**	1 : 4 : 10	210	**17b** (95)			
10	**5b**	1 : 2 : 0	160		**18b** (42)		
11	**5c**	1 : 4 : 10	223	**17c** (94)			
12	**5c**	1 : 2 : 0	125		**18c** (38)	**19** (34)	
13	**5d**	1 : 4 : 10	94	**17d** (97)			
14	**5d**	1 : 2 : 0	280		**18d** (49)		

a) Yields based on the amount of substrate used. b) **4** was recovered (5%).

TABLE 2. REACTION CONDITIONS AND PRODUCT YIELDS FOR THE OXIDATION OF 2-(4-METHOXYPHENYL)-4-CHROMANONE (**1a**) WITH $Mn(OAc)_3$-LiCl

Entry	Reaction conditions: Molar ratio of **1a** : $Mn(OAc)_3$: LiCl	Time/min	Product (yield/%)[a] **6a**	**7**	**8a**
1	1 : 5 : 10	48	51	5	37
2	1 : 6 : 10	128	58	6	33
3	1 : 7 : 10	130	73	6	12
4	1 : 8 : 10	144	73	6	15
5	1 : 9 : 10	197	73	7	16

a) Yields based on the amount of the substrate used.

disappeared. The reaction mixture was diluted with water (60 ml) and then extracted with benzene (30 ml) twice. The combined benzene solution was washed with an aqueous sodium hydrogencarbonate solution and then evaporated *in vacuo*. Finally, the resulting products were purified on TLC with either benzene or chloroform as the eluting solvent, and then recrystallized or distilled. Yields are summarized in Tables 1, 2, and 3.

Oxidation Products of 2-(4-Methoxyphenyl)-4-chromanone (1a). *3,3-Dichloro-2-(4-methoxyphenyl)-4-chromanone (6a)*: Mp 133—134 °C (lit,[2] 129—131 °C). *3-Chloro-4'-methoxyflavone (7)*: Mp 141.5—142.5 °C (lit,[2] 143—144 °C). *4'-Methoxyflavone (8a)*: Mp 157—158 °C (lit,[13] 157—158 °C).

r-*3-Acetoxy-t-2-(4-methoxyphenyl)-4-chromanone (9)*: Colorless liquid (lit,[14] mp 96—97 °C).

Oxidation Products of 2-Phenyl-4-chromanone (1b). *3,3-Dichloro-2-phenyl-4-chromanone (6b)*: 141.8—142.3 °C (lit,[2] 144 °C). *Flavone (8b)*: Mp 99 °C (lit,[15] 97 °C).

2,2-Dichloro-1-phenyl-1-propanone (10): Colorless liquid (lit,[16] bp 83—87 °C/0.5 mmHg (1 mmHg=133.322 Pa)).

2,2-Dichloro-1-tetralone (12): Mp 79.5—79.9 °C (lit,[3] 79—80 °C).

Oxidation Products of 1,2-Bis (4-methoxyphenyl)ethanone (3a). *2-Acetoxy-1,2-bis(4-methoxyphenyl)ethanone (13)*: Mp 96.7—97 °C (lit,[17] 93.5 °C). *1,2-Bis(4-methoxyphenyl)ethanedione (14a)*: Mp 134—135.5 °C (lit,[18] 133 °C). p-*Anisic acid (15a)*: Mp 185 °C.

TABLE 3. INFLUENCE OF THE CHLORIDE ION SOURCE UPON THE OXIDATION OF 2-(4-METHOXYPHENYL)-4-CHROMANONE (**1a**) WITH $Mn(OAc)_3$-Cl^-

Entry	Reaction conditions: Salt	Molar ratio of **1a** : $Mn(OAc)_3$: Cl^-	Time/min	Produdt (yield/%)[a] **6a**	**7**	**8a**	**9**	**15a**
1	KCl	1 : 7 : 10	86	78	7	9		
2	NaCl	1 : 7 : 10	61	70		7	3	
3	NH_4Cl	1 : 7 : 10	46	46	2	13	6	3
4	$AlCl_3$	1 : 7 : 3.3	46	45	1	9	10	
5	$CaCl_2$	1 : 7 : 5	63	23	27	42		
6	None	1 : 6 : 0	17			22	41	12

a) Yields based on the amount of the substrate used.

2-Acetoxy-1,2-bis(4-methoxyphenyl)ethanone (13) from 2-Chloro-1,2-bis(4-methoxyphenyl)ethanone[19] (16). A solution of **16** (128 mg) in AcOH (20 ml) was heated under reflux for 90 min. Evaporation of the solvent *in vacuo* gave **13** (136 mg, 98%), identical with an authentic sample.

Dichloro-1,2-diphenylethanone (11): Mp 62.1—62.9 °C (lit,[20] 61—62 °C). *1,2-Diphenylethanedione (14b)*: Mp 94—95 °C. *Benzoic acid (15b)*: Mp 120 °C.

2,2,2-Trichloro-4'-methoxyacetophenone (17a): Bp 120—125 °C (bath temp)/0.02 mmHg (lit,[21] mp 33—35.3 °C).

2,2,2-Trichloroacetophenone (17b): Bp 105—110 °C (bath temp)/0.02 mmHg (lit,[10] 145 °C/25 mmHg).

2,2,2,4'-Tetrachloroacetophenone (17c): Bp 110—115 °C (bath temp)/0.02 mmHg (lit,[22] mp 28 °C).

2,2,2-Trichloro-4'-methylacetophenone (17d): Bp 115—120 °C (bath temp)/0.02 mmHg (lit,[23] 137 °C/10 mmHg).

Oxidation of Aryl Ketones with $Mn(OAc)_3$. The general procedure for the oxidation of aryl ketones with $Mn(OAc)_3$ was virtually identical with that for the reaction with $Mn(OAc)_3$–Cl^-.

2,2,3,3-Tetrachloro-1,4-bis(4-chlorophenyl)-1,4-butanedione (18a): Mp 145—146 °C (lit,[1] 145—146 °C).

2,2,3,3-Tetrachloro-1,4-diphenyl-1,4-butanedione (18b): Colorless Cubes; mp 94—95 °C (from light petroleum); IR 1700 cm^{-1} (–C=O): UV λ_{max} (ε) 265 nm (20900); ^{1}H-NMR ($CDCl_3$) δ=7.2—7.6 (6H, m, H-3', H-3", H-4', H-4", H-5', and H-5"), and 8.1—8.3 (4H, m, H-2', H-2", H-6', and H-6"). Found: C, 51.04; H, 2.67%. Calcd for $C_{16}H_{10}Cl_4O_2$: C, 51.07; H, 2.68%.

2,2,3,3-Tetrachloro-1,4-bis(4-chlorophenyl)-1,4-butanedione (18c): Colorless cubes; mp 167—168 °C (from light petroleum), IR 1712 cm^{-1} (>C=O); UV λ_{max} (ε) 219^{sh} (9000) and 276 nm (27700); ^{1}H-NMR ($CDCl_3$) δ=7.48 (4H, m, H-3', H-3", H-5', and H-5"), and 8.16 (4H, m, H-2', H-2", H-6', and H-6"); ^{13}C-NMR δ=183.958 (>C=O), 140.100 (=C–Cl), 132.118 (2×=C–H), 130.719 (=C–CO), 128.405 (2×=C–H), and 89.420 (–CCl_2–). Found: C, 43.09; H, 1.81%. Calcd for $C_{16}H_4Cl_6O_2$: C, 43.16; H, 1.81%.

4,β,β-Trichloro-α-[dichloro-(4-chlorobenzoyl)methoxy]styrene (19): Colorless cubes; mp 81.7—82.7 °C (from light petroleum); IR 1730 cm^{-1} (>C=O); UV λ_{max} (ε) 224^{sh} (17400) and 263 nm (15300); ^{1}H-NMR (DMSO-d_6) δ=7.64 (4H, m, H-2, H-3, H-5 and H-6), 7.69 (2H, m, H-3' and H-5'), and 8.18 (2H, m, H-2' and H-6'); ^{13}C-NMR δ=180.605 (>C=O), 144.788 (=C–O–), 140.709 (=C–Cl), 136.445 (=C–Cl), 132.547 (2×=C–H), 131.509 (2×=C–H), 129.438 (=C–CO), 128.707 (4×=C–H). 128.2 (=C–C(O)–), 120.486 (=CCl_2), and 109.765 (–CCl_2–). Found: C, 43.22; H, 1.81%. Calcd for $C_{16}H_8Cl_6O_2$: C, 43.16; H, 1.81%.

2,2,3,3-Tetrachloro-1,4-bis(4-methylphenyl)-1,4-butanedione (18d): Colorless cubes; mp 167.5—169.5 °C (from CCl_4–light petroleum); IR 1720 cm^{-1} (>C=O); UV λ_{max} (ε) 219^{sh} (7800) and 278 nm (23600); ^{1}H-NMR ($CDCl_3$) δ=2.40 (6H, s, 2×CH_3), 7.27 (4H, m, H-3', H-3", H-5', and H-5"), and 8.16 (4H, m, H-2', H-2", H-6', and H-6"). Found: C, 53.13; H, 3.44%. Calcd for $C_{18}H_{14}Cl_4O_2$: C, 53.47; H, 3.49%.

Isomerization of 4,β,β-Trichloro-α-[dichloro-(4-chlorobenzoyl)methoxy]styrene (19) to 2,2,3,3-Tetrachloro-1,4-bis(4-chlorophenyl)-1,4-butanedione (18a). **19** (33.9 mg) was heated in a glass tube at 180—190 °C under reduced pressure (15 mmHg) for 1 h. The product was recrystallized from light petroleum to give **18a** (28.9 mg, 85%), mp 167—168 °C.

Hydrolysis of 4,β,β-Trichloro-α-[dichloro-(4-chlorobenzoyl)-methoxy]styrene (19). A mixture of **19** (73.5 mg), AcOH (2 ml), water (1 ml), and concd hydrochloric acid (0.05 ml) was heated under reflux for 2 h. After the AcOH was removed *in vacuo*, the resulting substance was separated on TLC with carbon tetrachloride as the eluting solvent to give **5c** (27.5 mg, 74%), mp 61—62 °C (lit,[10] 51 °C) and 4-chlorobenzoic acid (**15c**) (6.9 mg, 26%), mp 244.5—245.5 °C (in a sealed tube) (lit,[24] 241.5 °C).

We wish to thank Professor Hitoshi Takeshita and Associate Professor Akira Mori of the Research Institute of Industrial Science, Kyushu University, for their measurements of the ^{13}C-NMR spectra.

References

1) K. Kurosawa and K. Yamaguchi, *Bull. Chem. Soc. Jpn.*, **54**, 1757 (1981).
2) F. G. Weber and E. Birkner, *Z. Chem.*, **19**, 292 (1979).
3) Y. Nakatani and M. Matsui, *Hgr. Biol. Chem.*, **32**, 734 (1968).
4) A. Edelstein and St. v. Kostanecki, *Ber.*, **38**, 1507 (1905).
5) A. Löwenbein, *Ber.*, **42**, 2348 (1909).
6) H. Apitsch, *Ber.*, **40**, 1803 (1907).
7) C. F. H. Allen and W. E. Barker, *Org. Synth.* Coll Vol. **II**, 156 (1943).
8) F. Kunckell and F. Johanssen, *Ber.*, **31**, 169 (1898).
9) H. Gautier, *Ann. Chim. Phys.*, **14**, 345 (1888).
10) H. Gaitier, *Ann. Chim. Phys.*, **14**, 402 (1888).
11) S. K. Morita, A. N. Ganguli, N. N. Chakravarti, and R. N. Adhya, *Tetrahedron Lett.*, **1971**, 199.
12) P. J. Andrulis, Jr., M. J. S. Dewar, R. Dietz, and R. L. Hunt, *J. Am. Chem. Soc.*, **88**, 5473 (1966).
13) K. v. Auwers and L. Anschütz, *Ber.*, **54**, 1558 (1921).
14) G. W. K. Cavill, F. M. Dean, A. McGookin, B. M. Marshall, and A. Robertson, *J. Chem. Soc.*, **1954**, 4573.
15) W. Feuerstein and St. v. Kostanecki, *Ber.*, **31**, 1760 (1898).
16) M. Ballester and J. Riera, *Anales Real. Soc. Espan.*, **56**, 897 (1960). *Chem. Abstr.*, **55**, 19876c (1961).
17) R. P. Barnes and W. M. Lucas, *J. Am. Chem. Soc.*, **64**, 2258 (1942).
18) M. Bösler, *Ber.*, **14**, 322 (1881).
19) G. Henne and A. Bruglants, *Bull. Soc. Chim. Belges*, **57**, 320 (1948).
20) B. Lachowicz, *Ber.*, **17**, 1161 (1884).
21) J. Houben and W. Fischer, *Ber.*, **60**, 1759 (1927).
22) H. Gaurier, *Ann. Chim. Phys.*, **14**, 403 (1888).
23) J. Houben and W. Fischer, *J. prakt. Chem.*, **123**, 313 (1929).
24) N. V. Sidgwick ad E. K. Ewbank, *J. Chem. Soc.*, **119**, 979 (1921).

Synthetic Studies on Germacranolides. Synthesis of Optically Active 3-Oxygenated 13-Norheliangolides[1)]

Chiaki KURODA,† Takayoshi NAKAMURA,†† Hiroshi HIROTA,* Katsumi ENOMOTO, and Takeyoshi TAKAHASHI*

Department of Chemistry, Faculty of Science, The University of Tokyo, Hongo, Bunkyo-ku, Tokyo 113

(Received June 25, 1984)

(3*R*,6*S*,7*S*,1(10)*E*,4*Z*)- and (3*R*,6*R*,7*S*,1(10)*E*,4*Z*)-3-Methoxymethoxy-13-nor-1(10),4-germacradieno-12,6-lactones were synthesized from (−)-carvone, utilizing anionic oxy-Cope rearrangement to construct a ten-membered ring compound.

A group of germacrane-type sesquiterpene lactones are known as "germacranolides," and a large number of germacranolides have been isolated from various species of plants in these years.[2)] Among them, (1(10)*E*,4*E*)- and (1(10)*E*,4*Z*)-1(10),4-germacradienolides constitute a group of "germacrolides" and that of "heliangolides," respectively.[3)] Most of germacranolides possess an α-exomethylene structure on γ-lactone ring, and some of them show significant anti-tumor activities.[4)] One of us and co-workers have isolated several kinds of germacranolides from plants of the genus *Eupatorium*.[5)] Hiyodorilactone A (**1**), a heliangolide isolated from *Eupatorium sachalinense* Makino, showed a strong inhibitory activity *in vivo* against the Ehrlich ascites carcinoma.[5a)] Synthetic studies on germacrolides have already been reported by many groups.[6)] But, those on heliangolides have been reported by only two groups, one is our preliminary report[1)] and the other is the total synthesis of **1** by Still's group,[7)] although a number of (1*E*,5*Z*)-1,5-cyclodecadiene derivatives without a lactone moiety were synthesized by the route involving oxy-Cope rearrangement,[8)] pyrolysis,[9)] or cyclization.[10)] We chose optically active C(3) oxygenated 13-norheliangolides as synthetic targets, because most of natural heliangolides have an oxygen function at C(3) position[11)] and the introduction of an α-methylene group to the γ-lactone ring in the final stage of the synthesis has been well-investigated.[12)] In this paper, we wish to report the preparation of (1*S*,4*R*,6*R*)-1-ethenyl-3-methyl-6-(1-methylethenyl)-2-cyclohexene-1,4-diol (**2**) from (−)-carvone (**3**) and the synthesis of (3*R*,6*S*,7*S*,

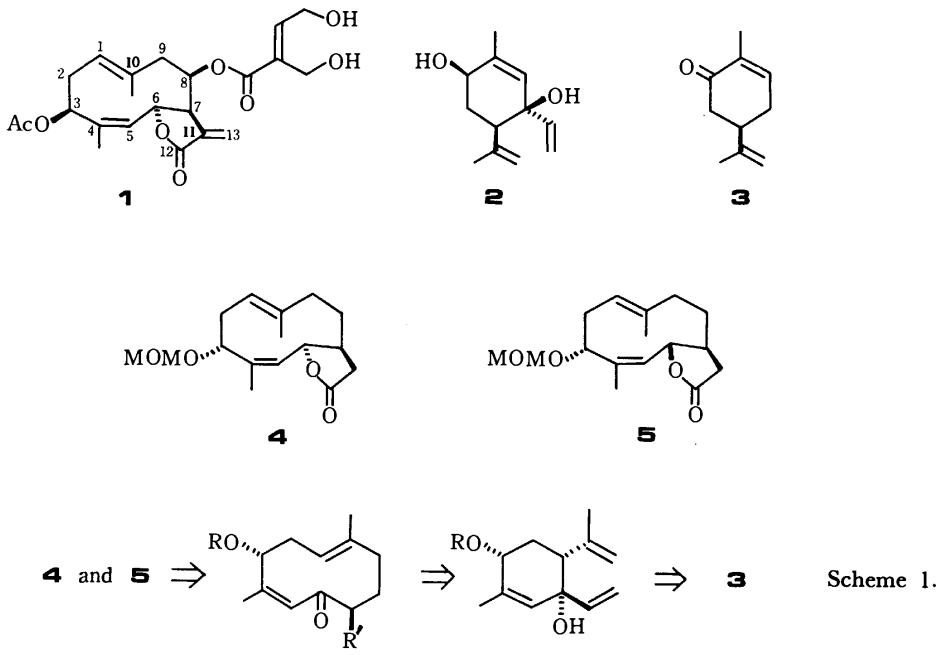

Scheme 1.

† Present address: Department of Chemistry, Faculty of Science, Rikkyo (St. Paul's) University, Nishi-Ikebukuro, Toshima-ku, Tokyo 171.

†† Present address: National Chemical Laboratory for Industry, Tsukuba Research Center, Yatabe, Ibaraki 305.

1(10)*E*,4*Z*)- and (3*R*,6*R*,7*S*,1(10)*E*,4*Z*)-3-methoxymethoxy-13-nor-1(10),4-germacradieno-12,6-lactones (**4** and **5**)[13] from **2** utilizing anionic oxy-Cope rearrangement as a key step, in detail.

Retro-synthetic pathway is shown in Scheme 1.

The first stage of the synthesis was a preparation of the diol (**2**) from an easily available optically active compound. We chose (−)-carvone (**3**) as a starting material. Several carvone derivatives oxygenated at allylic position have already been derived from carvone by three groups; Still's group had obtained **6** in 37% yield by 6 step reactions,[7] Miyashita and Yoshikoshi had prepared **7** in about 40% yield through eight synthetic intermediates,[14] and Noma and Nishimura had obtained **7** in 10% yield by microbial one step oxidation.[15] To obtain a large amount of **6**-type compound from carvone, we planned a direct allylic oxidation reaction of carveol derivative. The good hydroxyl-protecting group to carveol was turned out to be ester-type one (acetate or benzoate). When (−)-*cis*-carveol (**8**),[16] prepared by reduction of (−)-carvone (**3**) with lithium aluminum hydride, was acetylated and then treated with *t*-butyl chromate, a corresponding ketone (**9**) was obtained in 41% yield. When Collins reagent [chromium(VI) oxide-pyridine complex] was used instead of *t*-butyl chromate as an oxidizing agent, the reaction rate was very slow, and oxidation with selenium (IV) oxide gave no desired compound. Reaction of **9** with 1.4 equivalent moles of vinylmagnesium bromide gave trienes, **10** and **2**, in 28 and 6% yields, respectively. The acetate (**10**) was hydrolyzed by potassium carbonate in aqueous methanol to afford **2** in 85% yield. (Consequently, **2** was obtained from **9** in 30% yield.) No diastereomer of **2** was obtained. The stereochemistry at the vinyl- and hydroxyl-carrying carbon atom of **2** was deduced from the formation mechanism. When the benzoate of carveol was utilized instead of acetate in these consecutive reactions, allylic oxidation step gave a worse result and Grignard step gave a better one, and overall yield was almost the same as in the case of acetate. Anionic oxy-Cope rearrangement reaction of the diol (**2**) was examined. The secondary hydroxyl group of **2** was protected by methoxymethyl (MOM) group and then the resulting triene (**11**) was treated with potassium hydride and 18-crown-6 in tetrahydrofuran under reflux affording a cyclodecadienone (**12**) in 67% yield. When **2** was directly treated with the same conditions as above, only complex mixture was obtained. Any ten-membered ring compound could not be obtained when acetyl (compound **10**), trimethylsilyl, *t*-butyldimethylsilyl, or *t*-butyldiphenylsilyl protecting groups was used instead of MOM group. Although the geometry of olefinic double bonds of **12** could have already been expected from the reaction fashion of oxy-Cope

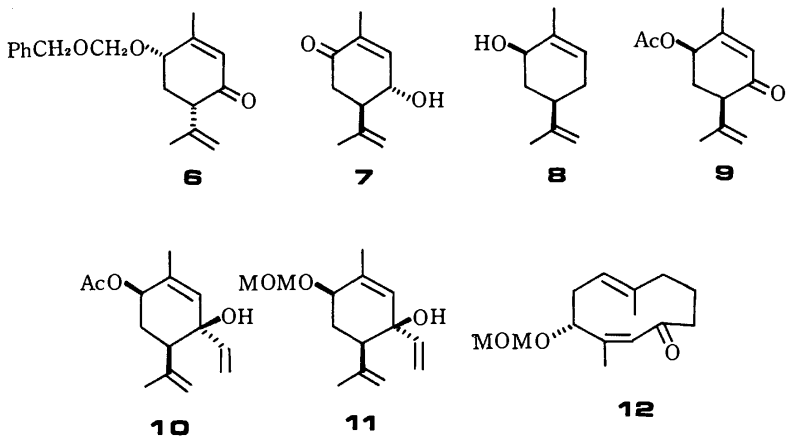

Table 1.[a] NOE data for **12**

Irradiated proton(s)	Observed proton	NOE[b]
C(10)-CH_3 (δ=1.56, 3H, s)	C(1)-H (δ=5.03, 1H, t, $J_{1,2\alpha}=J_{1,2\beta}=8$ Hz)	2%
	C(2β)-H (δ=2.51, 1H, ddd, $J_{1,2\beta}=8$ Hz, $J_{2\alpha,2\beta}=13$ Hz, $J_{2\beta,3\beta}=5.5$ Hz)	7%
	C(3β)-H (δ=4.88, 1H, dd, $J_{2\alpha,3\beta}=11$ Hz, $J_{2\beta,3\beta}=5.5$ Hz)	10%
C(4)-CH_3 (δ=1.79, 3H, s)	C(1)-H	15%
	C(5)-H (δ=6.07, 1H, s)	20%
C(2β)-H	C(3β)-H	12%

a) Assignment of signals was determined by decoupling experiments. b) Accuracies are about ±2%.

rearrangement, it was confirmed by NOE experiments. The result shown in Table 1 can only be interpreted based on the (1(10)*E*,4*Z*)-structure (**A**).[8] The ketone (**12**) was treated with lithium diisopropylamide followed by ethyl bromoacetate to give a keto ester (**13**) stereoselectively as a sole product in 74% yield. The stereochemistry at C(7) of **13** would be *S*(7α-H) from the reaction pathway as the following. That is, the enolate ion generated with lithium diisopropylamide would have a more stable 6*Z*-double bond, which can conjugate with 4*Z*-double bond, while the corresponding 6*E*-enolate can not do. On the enolate ion, methoxymethoxyl group at C(3) would take an equatorial form (**B**). Then, the electrophile would attack from the less hindered outer side of the ten-membered ring to give 7α-H configuration compound. This stereochemical assignment was supported by the following transformation into *cis*-lactone (**5**).

The keto ester (**13**) was reduced with sodium borohydride in ethanol to give a lactone (**5**) in 12% yield, together with more polar products which were suggested to be a keto alcohol (19%) and a diol (15%). The stereochemistry of **5** was decided to be 6*R*(6α-H) and 7*S*(7α-H) (**C**) from the NMR spectrum as follows. The methoxymethoxyl group at C(3α) is in axial conformation judging from the coupling constant of C(3β)-H (t, J=3 Hz). The chemical shift of C(6)-H (δ 6.01) is fairly low, which could be explained that C(6)-H is situated at the close position to the C(3α)-axial methoxymethoxyl oxygen, meaning that C(6)-H is α-oriented; large J values (7 and 11 Hz) observed for C(6)-H lead to a *cis*-lactone structure with C(6α)-H and C(7α)-H configuration for **5**. The *cis* lactone structure is also compatible with the formation mechanism that a hydride would attack C(6) carbonyl carbon preferentially from the less hindered outer side of the ten-membered ring. Consequently, the absolute stereostructure of **5** is established as (3*R*,6*R*,7*S*,1(10)*E*,4*Z*)-3-methoxymethoxy-13-nor-1(10),4-germacradieno-12,6-lactone.

No natural heliangolide possessing (6α-H,7α-H)-12,6-lactone has been known, even though several germacrolides of this type have been known (*e.g.* ursinolide A (**14**)).[17] In order to obtain *trans*-lactone, we planned to lactonize the hydroxy acid (**16**) with inversion at C(6) stereochemistry by activating the hydroxyl group. The keto ester (**13**) was hydrolyzed with potassium carbonate in aqueous methanol, and the resulting keto acid (**15**) was reduced with lithium borohydride to afford **16**. As the hydroxy acid (**16**) was easily lactonized into *cis*-lactone (**5**), **16** without purification was treated with *N*,*N*-dimethylformamide dineopentyl acetal in boiling toluene[18] to afford a lactone (**4**) in 15% yield from **13**.[19] The stereochemistry of the lactone (**4**), which has different physical data from those of *cis*-lactone (**5**), must have been *trans* (6*S*,7*S*), which was convincingly suggested from the formation mechanism.[18] The NMR spectral data were also compatible with the structure **4** when compared with those of natural heliangolide, eupasimplicin A (**17**).[20] Thus, the structure of **4** including the absolute stereochemistry was shown to be (3*R*,6*S*,7*S*,1(10)*E*,4*Z*)-3-methoxymethoxy-13-nor-1(10),4-germacradieno-12,6-lactone.

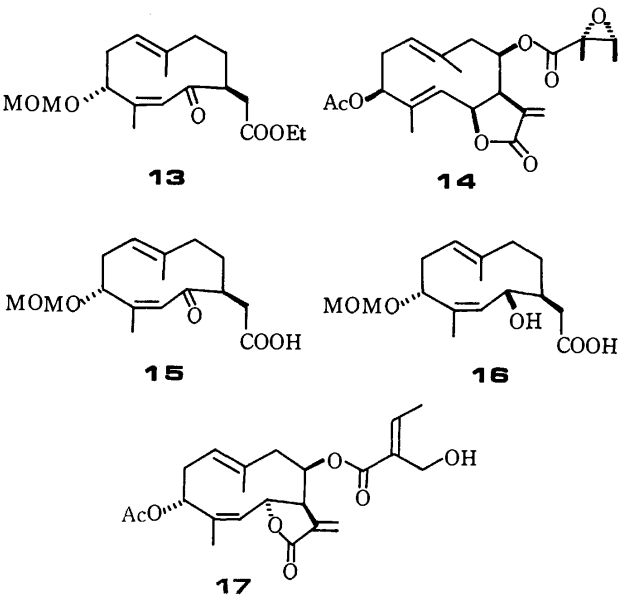

Experimental

General Procedures. All melting points were measured on a Mel-temp capillary melting point apparatus (Laboratory Devices) and uncorrected. Optical rotation was determined on a JASCO polarimeter DIP-SL. Ultraviolet absorption (UV) and infrared (IR) spectra were measured on a Hitachi 340 and a Hitachi 260-30 spectrometer, respectively. Mass (MS) spectra were run on a JEOL JMS-D300 mass spectrometer operating at 70 eV. Proton nuclear magnetic resonance (^{1}H NMR) spectra were taken using a Varian EM390 (90 MHz), a JEOL FX90Q (90 MHz), and a Brucker

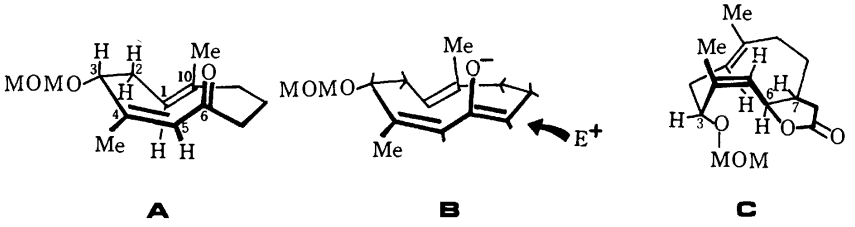

WH270 (270 MHz). Chemical shifts were expressed in δ (ppm) downfield from tetramethylsilane as an internal standard and coupling constants in Hz. Thin-layer chromatography (TLC) was carried out on Kieselgel 60 GF_{254} coated in 0.25 mm-thickness. Wakogel C-200 (Wako) and Florisil (100—200 mesh) were used for column chromatography. Liquid Chromatograph Model ALC/GPS 202/401 (Waters Assoc.) was used for high performance liquid chromatography (HPLC).

(−)-cis-Carvyl Acetate ((3R,5R)-3-Acetoxy-2-methyl-5-(1-methylethenyl)cyclohexene). To a solution of 6.7 g of (−)-*cis*-carveol (**8**) in 100 ml of pyridine was added 20 ml of acetic anhydride and the whole was stirred for about 12 h. After addition of 30 ml of methanol and removal of solvent *in vacuo*, the reaction mixture was extracted with ether as usual. After the removal of impurities at 40 °C under reduced pressure (10 mmHg; 1 mmHg=133.322 Pa), 8.11 g of acetate was obtained: bp 82—83 °C/2 mmHg; $[\alpha]_D^{11}$ −54.4° (*c* 6.99, EtOH); IR (neat) 1740, 1645, and 1240 cm^{-1}; NMR ($CDCl_3$) δ=1.62 (3H, br s), 1.72 (3H, s), 2.07 (3H, s, $-OCOCH_3$), 4.70 (2H, s, $-\underset{|}{C}=CH_2$), 5,42 (1H, br, C(1)-H), and 5.55 (1H, br, C(3)-H); MS *m/z* (%) 194 (M^+, 0.4), 152 (39), 134 (56), and 84 (100).

Allylic Oxidation of (−)-cis-Carvyl Acetate. To a solution of 5.0 g of (−)-*cis*-carvyl acetate in 70 ml of carbon tetrachloride was added 70 ml of a carbon tetrachloride solution of *t*-butyl chromate (prepared from 13 g of chromium(VI) oxide), 20 ml of acetic anhydride, and 7 ml of acetic acid, and the whole was refluxed for 1 d. A solution of oxalic acid (16 g) in 120 ml of water and then 50 g of oxalic acid were added. After removal of precipitate, ether was added for extraction. The ether layer was washed with aqueous sodium hydrogensulfite, saturated sodium hydrogencarbonate aqueous solution, and saturated brine, successively, and dried over sodium sulfate. After evaporation of solvent, the residue was chromatographed on a column of silica gel (80 g). Elution with hexane–ether (5:1) afforded 2.35 g of the unreacted starting material, and elution with hexane–ether (2:1) gave (4*R*,6*R*)-4-acetoxy-3-methyl-6-(1-methylethenyl)-2-cyclohexen-1-one (**9**, 1.22 g): an oil, $[\alpha]_D^{14}$ −52.2° (*c* 6.50, EtOH); IR (neat) 1740, 1680, 1635, and 1235 cm^{-1}; UV (EtOH) 228 nm (ε 9800); ^1H NMR ($CDCl_3$) δ=1.72 (3H, s, $CH_2=\underset{|}{C}-CH_3$), 1.91 (3H, s, C(3)-$CH_3$), 2.13 (3H, s, $-OCOCH_3$), 3.11 (1H, dd, *J*=4.5 and 13.5 Hz, C(6)-H), 4.79 and 4.95 (each 1H, br s, $-\underset{|}{C}=CH_2$), 5.7 (1H, br, C(4)-H), and 5.92 (1H, br s, C(2)-H); MS *m/z* (%) 208 (M^+, 0.5), 166 (17), and 98 (100); Found: *m/z* 208.1090. Calcd for $C_{12}H_{16}O_3$: 208.1097.

Grignard Reaction of the Keto Acetate (9). The Grignard reagent was prepared by heating the mixture of small pieces of magnesium ribbon (110 mg), 7 ml of dry tetrahydrofuran (dry THF; freshly distilled from lithium aluminum hydride), and vinyl bromide (0.35 ml) under nitrogen atmosphere. To the Grignard reagent cooled at 0 °C with ice-bath, a solution of **9** (675 mg) in THF (3.5 ml) was added, and the mixture was stirred for 20 min at room temperature. After addition of saturated ammonium chloride solution, the mixture was extracted with ether and then subjected to separation by silica gel (20 g) column chromatography. Elution with hexane–ether (5:1) gave **10** (157.0 mg), elution with hexane–ether (4:1) gave starting material (**9**; 189.1 mg), and then elution with hexane–ether (1:1) gave **2** (35.2 mg). (1*S*,4*R*,6*R*)-4-Acetoxy-1-ethenyl-3-methyl-6-(1-methylethenyl)-2-cyclohexen-1-ol (**10**): an oil, $[\alpha]_D^{14}$ −29.9° (*c* 5.58, EtOH); IR (neat) 3500, 1735, 1635, and 1235 cm^{-1}; ^1H NMR ($CDCl_3$) δ=1.68 (3H, t, *J*=0.5 Hz, $CH_2=\underset{|}{C}-CH_3$), 1.79 (3H, s, C(3)-Me), 2.09 (3H, s, $-OCOCH_3$), 4.8—5.5 (6H, m), and 5.87 (1H, dd, *J*=10 and 17 Hz, $-\underset{|}{C}-CH=CH_2$); MS *m/z* (%) 194 [$(M-42)^+$, 3], 176 (8), and 125 (100). Fragment ion peak due to $(M-CH_2CO)^+$ was observed at *m/z* 194.1308. Calcd for $C_{12}H_{18}O_2$: $M-C_2H_2O$, 194.1307. (1*S*,4*R*,6*R*)-1-Ethenyl-3-methyl-6-(1-methylethenyl)-2-cyclohexene-1,4-diol (**2**): crystals, mp 142.5—144.5 °C, $[\alpha]_D^{16}$ −23.9° (*c* 2.80, EtOH); IR (KBr disk) 3320, 3250, and 1635 cm^{-1}; ^1H NMR ($CDCl_3$) δ=1.80 (6H, s), 4.1 (1H, br, C(4)-H), 4.8—5.3 (5H, m), and 5.86 (1H, dd, *J*=10 and 17 Hz, $-\underset{|}{C}-CH=CH_2$); MS *m/z* (%) 194 (M^+, 0.2), 176 (1), 161 (5), and 126 (100). Found: C, 73.92%; H, 9.22%. Calcd for $C_{12}H_{18}O_2$: C, 74.19%; H, 9.34%.

Hydrolysis of the Acetate (10). A mixture of **10** (1.13 g) and potassium carbonate (1.8 g) in 80% aqueous methanol (120 ml) was stirred at room temperature for 1 h. After removal of methanol *in vacuo*, ether extraction was carried out as usual, and white crystals of **2** (786.7 mg) was afforded.

Methoxymethylation of the Diol (2). To a solution of **2** (174 mg) in dry acetonitrile (35 ml) were added triethylamine (3.5 ml) and methoxymethyl chloride (1.2 ml), and the mixture was refluxed for 8 h. After addition of saturated aqueous solution of sodium hydrogencarbonate and removal of acetonitrile *in vacuo*, ether extraction was done as usual. The mixture was separated by Florisil (20 g) column chromatography. Elution with hexane–ether (9:1) afforded 90.2 mg of methoxymethyl ether (**11**) and elution with ether gave unreacted diol (**2**; 55.2 mg). (1*S*,4*R*,6*R*)-1-Ethenyl-4-methoxymethoxy-3-methyl-6-(1-methylethenyl)-2-cyclohexen-1-ol (**11**): an oil, $[\alpha]_D^{16}$ −61.2° (*c* 4.25, EtOH); IR (neat) 3480 and 1640 cm^{-1}; ^1H NMR ($CDCl_3$) δ=1.79 (6H, s), 3.40 (3H, s, $-OCH_2OCH_3$), 4.05 (1H, br t, *J*=7.5 Hz, C(4)-H), 4.65 and 4.76 (each 1H, A and B parts of an ABq, *J*=6 Hz, $-OCH_2OCH_3$), 4.7—5.1 (5H, m), and 5.84 (1H, dd, *J*=10 and 17 Hz, $-\underset{|}{C}-CH=CH_2$); MS *m/z* (%) 193 [$(M-MOM)^+$, 4], 170 (36), and 108 (100). The fragment ion peak due to $(M-MOM)^+$ was observed at *m/z* 193.1236. Calcd for $C_{12}H_{17}O_2$: $M-C_2H_5O$, 193.1228.

Cyclodecadienone (12): (3R,1(10)E,4Z)-3-Methoxymethoxy-11,12,13-trinor-1(10),4-germacradien-6-one.[8] All the reactions were carried out under argon atmosphere. To a solution of potassium hydride (17 mg) in 10 ml of dry THF were added a THF (3 ml) solution of **11** (85.8 mg) and a solution of 18-crown-6 (107 mg) in THF (1.5 ml). After the mixture was refluxed for 1 h, the whole was cooled to room temperature, and subjected to ether extraction as usual. The products were separated by Florisil (7 g) column chromatography. Elution with hexane–ether (7:1) afforded the recovered starting material (**11**; 29.6 mg), and elution with hexane–ether (2:1) gave the cyclodecadienone (**12**; 37.5 mg): crystals, mp 52—53 °C (recrystallization from hexane), $[\alpha]_D^{11}$ −110.6° (*c* 3.02, EtOH); IR (film) 1680 and 1630 cm^{-1}; UV (EtOH) 235 nm (ε 5300); ^1H NMR ($CDCl_3$) δ=3.42 (3H, s, $-OCH_2OCH_3$), 4.65 and 4.67 (each 1H, A and B parts of an ABq, *J*=6 Hz, $-OCH_2OCH_3$), and signals listed in Table 1; MS *m/z* (%) 238 (M^+, 8), 193 (19), 169 (50), 81 (95), and 45 (100). Found: C, 70.47%; H, 9.57%. Calcd for $C_{14}H_{22}O_3$: C, 70.56%; H, 9.30%.

Keto Ester (13): *Ethyl (3R,7S,1(10)E,4Z)-3-Methoxymethoxy-6-oxo-13-nor-1(10),4-germecradien-12-oate.* A mixture of 1 ml of dry THF, 0.053 ml of diisopropylamine, and 0.24 ml of butyllithium (1.56 M hexane solution; 1 M=1 mol dm^{-3}) was stirred at −70 °C under nitrogen atmosphere, and a THF (1.5 ml) solution of **12** (74.7 mg) was added and the mixture was stirred at −70 °C for 45 min. Ethyl bromoacetate (0.15 ml) was added and the mixture was stirred at −23 °C (Dry Ice in carbon tetrachloride) for 5 h. Water was added and the mixture was extracted with ether as usual. Products were separated by Florisil (6 g) column chromatography. Elution with hexane–ethyl acetate (19:1) gave starting material (**12**; 26.2 mg). Elution with hexane–ethyl acetate (9:1) afforded the keto ester (**13**; 48.4 mg): an oil, $[\alpha]_D^{12}$ −39.5° (*c* 6.45, EtOH); IR (neat) 1735, 1680, and 1630 cm^{-1}; UV (EtOH) 238 nm (ε 5800); ^1H NMR ($CDCl_3$) δ=1.24 (3H, t, *J*=7 Hz, $-COOCH_2\underline{CH_3}$), 1.52 (3H, s, C(10)-Me), 1.80 (3H, s, C(4)-Me), 3.42 (3H, s, $-OCH_2OC\underline{H_3}$), 4.11 (2H, q, *J*=7 Hz, $-COOC\underline{H_2}CH_3$), 4.65 (2H, s, $-OC\underline{H_2}OCH_3$), 4.91 (1H, dd, *J*=6 and 11.5 Hz, C(3β)-H), 5.01 (1H, t, *J*=7 Hz, C(1)-H), and 6.23 (1H, br s, C(5)-H); MS *m/z* (%) 324 (M^+, 4), 255 (40), and 45 (100). Found: *m/z* 324.1948. Calcd for $C_{18}H_{28}O_5$: M, 324.1937.

Sodium Borohydride Reduction of the Keto Ester (13). Sodium borohydride (*ca.* 70 mg) was added to an ethanol solution (15 ml) of the keto ester (**13**; 76.3 mg), and the mixture was stirred at room temperature for 2 d. After addition of acetone to decompose the excess sodium borohydride and removal of solvent *in vacuo*, the products were extracted with ether as usual. The products were separated by Florisil (7 g) column chromatography. Elution with hexane–ethyl acetate (4:1) afforded the recovered starting material (**13**; 17.8 mg), the lactone (**5**; 5.2 mg), and a keto alcohol (9.8 mg). Elution with ethyl acetate gave a diol (7.5 mg). (3*R*, 6*R*,7*S*,1(10)*E*,4*Z*)-3-Methoxymethoxy-13-nor-1(10),4-germacradieno-12,6-lactone (**5**): an oil, $[\alpha]_D^{24}$ −110° (*c* 0.70, EtOH); IR (neat) 1765 cm^{-1}; ^1H NMR ($CDCl_3$) δ=1.46 (3H, s), 1.75 (3H, s), 3.36 (3H, s, $-OCH_2OC\underline{H_3}$), 4.36 (1H, t, *J*=3 Hz, C(3β)-H), 4.51 and 4.65 (each 1H, A and B parts of an ABq, *J*=6.5 Hz, $-OC\underline{H_2}OCH_3$), 5.37 (2H, m, C(1)-H and C(5)-H), and 6.01 (1H, dd, *J*=7 and 11 Hz, C(6)-H); MS *m/z* (%) 280 (M^+, 6), 248 (10), and 159 (100). Found: *m/z* 280.1656. Calcd for $C_{16}H_{24}O_4$: M, 280.1673.

Hydrolysis of the Keto Ester (13). As it was rather hard to separate **13** from **12** by Florisil column chromatography, the hydrolysis of a mixture of **12** and **13** was examined. To the mixture of **12** and **13** (35.6 mg) was added potassium carbonate (45 mg) in 80% aqueous methanol (3 ml), and the whole was stirred at room temperature for 8 h. After addition of water and evaporation of methanol, the mixture was extracted with ether. Aqueous layer was adjusted to approximately pH 3 by addition of dil. HCl, and was extracted with dichloromethane several times. From the ether layer 14.0 mg of **12** was recovered, and from the dichloromethane layer 18.3 mg of keto acid (**15**) was obtained. (3*R*,7*S*,1(10)*E*,4*Z*)-3-Methoxymethoxy-6-oxo-13-nor-1(10),4-germacradien-12-oic acid (**15**): an oil; IR (neat) 3400—2500 (br), 1710, and 1685 cm^{-1}; ^1H NMR ($CDCl_3$) δ= 1.52 (3H, s, C(10)-Me), 1.80 (3H, s, C(4)-Me), 3.07 (3H, s, $-OCH_2OC\underline{H_3}$), 4.63 (2H, s, $-OC\underline{H_2}OCH_3$), 4.96 (2H, m, C(1)-H and C(3β)-H), 6.20 (1H, m, C(5)-H), and 7.83 (1H, br, -COOH).

(3R,6S,7S,1(10)E,4Z)-3-Methoxymethoxy-13-nor-1(10),4-germacradieno-12,6-lactone (4). A mixture of the keto acid (**15**; 23.3 mg) in dry THF (2 ml) and about 10 mg of lithium borohydride was stirred at room temperature for 20 h. After addition of water and evaporation of THF, dil.HCl was gradually added to pH 4—5, and dichloromethane extraction was carried out several times. The extract was dried over sodium sulfate, and was concentrated into *ca.* 1 ml *in vacuo*. Toluene (6 ml) was added and the solvent (mainly dichloromethane) was removed under atmospheric pressure to give toluene solution (*ca.* 4 ml). To this toluene solution was added 0.03 ml of *N,N*-dimethylformamide dineopentyl acetal in toluene (0.4 ml), and the mixture was refluxed for 2 h. After removal of solvent, the reaction mixture was charged onto silica gel (*ca.* 3 g) column chromatography. Elution with benzene–ethyl acetate (5:1) gave 3.2 mg of *trans*-lactone (**4**), which was purified through HPLC (μ-Porasil; CH_2Cl_2). **4**: an oil, $[\alpha]_D^{19}$ +61° (*c* 0.04, EtOH); IR (neat) 1770 cm^{-1}; ^1H NMR ($CDCl_3$) δ=1.59 (3H, s, C(4)-Me), 1.75 (3H, br, C(10)-Me), 3.37 (3H, s, $-OCH_2OC\underline{H_3}$), 4.20 (1H, dd, *J*=6 and 9.5 Hz, C(3β)-H), 4.48 and 4.57 (each 1H, A and B parts of an ABq, *J*=7 Hz, $-OC\underline{H_2}OCH_3$), 4.55 (1H, br, C(1)-H), and 5.12 (2H, br, C(5)-H, and C(6β)-H) [Corresponding signals of eupasimplicin A (**17**)[20]: δ=5.60 (1H, dd, *J*=5 and 11 Hz, C(3β)-H) and 5.25 (2H, br, C(5)-H and C(6β)-H]; MS m/z (%) 280 (M^+, 1), 282 (12), and 81 (100). Found: *m/z* 280.1672. Calcd for $C_{16}H_{24}O_4$: M, 280.1672.

The authors with to thank Dr. Hajime Nagano, Ochanomizu University, for valuable discussions, Professor W. Clark Still, Columbia University, for the kind sending of the preprint on the total synthesis of hiyodorilactone A (**1**),[6] and Professor Tatsuo Miyazawa and Dr. Tatsushi Murae, Faculty of Science, the University of Tokyo, for the measurement of ^1H NMR spectra at 270 MHz.

References

1) Preliminary account of this report: C. Kuroda, H. Hirota, and T. Takahashi, *Chem. Lett.*, **1982**, 249.

2) *E.g.*: H. D. Fischer, N. H. Fischer, R. W. Franck, and E. J. Olivier, "Progress in the Chemistry of Organic Natural Products," Springer-Verlag, Wien (1979), pp. 50—133; T. K. Devon and A. I. Scott, "Handbook of Naturally Occurring Compounds," Academic Press, New York (1972), Vol. II, pp. 79—84.

3) D. Rogers, G. P. Moss, and S. Neidle, *J. Chem. Soc., Chem. Commun.*, **1972**, 142; *cf.* S. Neidle and D. Rogers, *ibid.*, **1972**, 140; S. M. Kupchan, J. E. Kelsey, and G. A. Sim, *Tetrahedron Lett.*, **1967**, 2863.

4) *E.g.*: E. Rodriguez, G. H. N. Towers, and J. C. Mitchell, *Phytochemistry*, **15**, 1573 (1976); S. M. Kupchan, *Pure Appl. Chem.*, **21**, 227 (1970), and references cited therein.

5) a) T. Takahashi, H. Eto, T. Ichimura, and T. Murae, *Chem. Lett.*, **1978**, 1345; b) T. Takahashi, T. Ichimura, and T. Murae, *Chem. Pharm. Bull.*, **27**, 2539 (1979).

6) E. J. Corey and A. G. Hortmann, *J. Am. Chem. Soc.*, **87**, 5736 (1965); M. Watanabe and A. Yoshikoshi, *J. Chem. Soc., Chem. Commun.*, **1972**, 698; Y. Fujimoto, T. Shimizu, and T. Tatsuno, *Tetrahedron Lett.*, **1976**, 2041; Y. Fujimoto, T. Shimizu, M. Ohmori, and T. Tatsuno, *Chem. Pharm. Bull.*, **27**, 923 (1979); P. A. Grieco and M. Nishizawa, *J. Org. Chem.*, **42**, 1717 (1977); P. A. Wender and J. C. Lechleiter, *J.*

Am. Chem. Soc., **102**, 6340 (1980); *cf.* A. Gopalan and P. Magnus, *ibid.*, **102**, 1756 (1980).

7) W. C. Still, S. Murata, G. Revial, and K. Yoshihara, *J. Am. Chem. Soc.*, **105**, 625 (1983). Hiyodorilactone A is identical with eucannabinolide (see the footnote (2) of this reference).

8) W. C. Still, *J. Am. Chem. Soc.*, **101**, 2493 (1979); **99**, 4186 (1977); *cf.* D. A. Evans and A. M. Golob, *ibid.*, **97**, 4765 (1975).

9) G. L. Lange, M. -A. Huggins, and E. Neidert, *Tetrahedron Lett.*, **1976**, 4409; J. R. Williams and J. F. Callahan, *J. Org. Chem.*, **45**, 4475 and 4479 (1980).

10) M. Kodama, Y. Matsuki, and S. Itô, *Tetrahedron Lett.*, **1976**, 1121.

11) The presence of C(3)-oxygenated functional group (chiral center) is necessary to keep an optical activity and fix conformation of the ten-membered ring compounds after oxy-Cope rearrangement.

12) *E.g.*: P. A. Grieco, *Synthesis*, **1975**, 67; R. B. Gammill, C. A. Wilson, and T. A. Bryson, *Synth. Commun.*, **5**, 245 (1975), and references cited therein.

13) Nomenclature numbering for germacranes is applied to that for cyclodecane derivatives in this paper for convenience sake.

14) M. Miyashita and A. Yoshikoshi, The 26th Symposium on the Chemistry of Natural Products, Kyoto, October, 1983 (Proceedings, p. 344).

15) Y. Noma and H. Nishimura, The 26th Symposium on the Chemistry of Perfumes, Terpenes, and Essential Oils, Yamagata, October, 1982 (Proceedings, p. 156).

16) R. Grandi, U. M. Pagnoni, R. Trave, and L. Garanti, *Tetrahedron*, **30**, 4037 (1974); L. Garver, P. van Eikeren, and J. E. Byrd, *J. Org. Chem.*, **41**, 2773 (1976), and references cited therein.

17) Z. Samek, M. Holub, U. Rychlewska, H. Grabarczyk, and B. Drożdż, *Tetrahedron Lett.*, **1979**, 2691.

18) H. Vorbrüggen and K. Krolikiewicz, *Angew. Chem., Int. Ed. Engl.*, **16**, 876 (1977); *cf.* H. Brechbühler, H. Büchi, E. Hatz, J. Schreiber, and A. Eschenmoser, *Angew. Chem.*, **75**, 296 (1963); H. Brechbühler, H. Büchi, E. Hatz, J. Schreiber, and A. Eschenmoser, *Angew. Chem., Int. Ed. Engl.*, **2**, 212, (1963); H. Brechbühler, H. Büchi, E. Hatz, J. Schreiber, and A. Eschenmoser, *Helv. Chim. Acta*, **48**, 1746 (1965).

19) Other products showing small R_f values on TLC were also formed. When **16** was treated with triphenylphosphine and diethyl azodicarboxylate, no desired product was obtained. *cf.* T. Kurihara, Y. Nakajima, and O. Mitsunobu, *Tetrahedron Lett.*, **1976**, 2455.

20) T. Takahashi, A. Utagawa, and T. Murae, The 23rd Symposium on the Chemistry of Perfumes, Terpenes, and Essential Oils, Tottori, October, 1979 (Proceedings, p. 276); *Chem. Abstr.*, **93**, 114734t (1980); eupasimplicin A (**17**), (3*R*,6*S*,7*S*,8*R*,1(10)*E*,4*Z*)-3-acetoxy-8-((2*E*)-2-hydroxymethyl-2-butenoyloxy)-1(10),4-germacradieno-12,6-lactone, was isolated from *Eupatorium chinense simpliciforium*.

 © 1985 The Chemical Society of Japan Bull. Chem. Soc. Jpn., 58, 152—157 (1985) [Vol. 58, No. 1

Hexacarbonylmolybdenum-induced Reaction of Isoxazoles. Cycloaddition of Isoxazoles with Acetylenic Esters and Related Reactions[1)]

Tomoshige KOBAYASHI and Makoto NITTA*
Department of Chemistry, School of Science and Engineering, Waseda University, Shinjuku-ku, Tokyo 160
(Received June 16, 1984)

In the presence of hexacarbonylmolybdenum, substituted isoxazoles undergo a cycloaddition reaction with dimethyl acetylenedicarboxylate across the C-4–C-5 bond to give 3,4-bis(methoxycarbonyl)pyridine derivatives. In a similar cycloadition of isoxazoles with methyl propiolate, 4-(methoxycarbonyl)pyridine derivatives were also obtained. The β-carbon atom of methyl propiolate could intervene in the bonding with the C-5 position of the isoxazoles regioselectively. A mechanism involving a complexed 2-oxa-3-azabicyclo[3.2.0]hepta-3,6-diene derivative and the subsequent N–O and C-1–C-5 bond cleavage leading to a complexed (β-keto vinyl)nitrene intermediate is proposed for the formation of pyridine derivatives. In order to clarify the mechanistic aspect, the reaction of 4-phenyl-2-oxa-3-azabicyclo[3.2.0]hepta-3,6-diene and its related compounds were also studied to give pyridine derivatives.

An isoxazole ring system has been the subject of an extensive investigation for its useful synthetic transformations. Its photochemical[2)] and thermal[3] reactions have been shown to isomerize to the corresponding ketoazirine derivatives. The catalytic hydrogenation of isoxazoles to β-amino enones is widely applicable in synthesis.[4)] Previously, we showed that [$Fe(CO)_5$], [$Fe_2(CO)_9$], and [$Mo(CO)_6$] effect the reductive cleavage of the N–O bond of substituted isoxazoles to give β-amino enones under mild conditions in the presence of water.[5)]

In contrast to these ring cleavage reactions, the cycloaddition of simple isoxazoles with olefins or acetylenic esters has not been accomplished,[6)] although the heterodiene system of 2,1-benzisoxazole derivatives has been shown to undergo a Diels-Alder reaction with *N*-phenylmaleimide,[7)] benzyne,[8)] and dimethyl acetylenedicarboxylate.[9)] The Diels-Alder reaction of 2,1-benzisoxazole with maleic anhydride has been shown to give only a starting material,[10)] although in a previous paper the reaction was reported to proceed.[11)]

This paper describes a [$Mo(CO)_6$]-induced cycloaddition of 3,5-disubstituted isoxazoles (**1a—f**) with acetylenic esters across the C-4–C-5 bond and the subsequent elimination of an oxygen atom to give pyridine derivatives, albeit, in low yields. Furthermore, [$Mo(CO)_6$]-induced reactions of 4-phenyl-2-oxa-3-azabicyclo[3.2.0]hepta-3,6-diene (**17**) and its related compound, **18** and **22**, were also studied to assess the mechanistic aspect of the above-mentioned cycloaddition reaction.

Results and Discussion

A benzene solution of isoxazoles **1a—f**, dimethyl acetylenedicarboxylate (DMAD), and [$Mo(CO)_6$] was refluxed for an adequate period to give the pyridine derivatives **2a—f**, as shown in Scheme 1. The reaction conditions and the yields of the products are summarized in Table 1 (Entries 1—6). The yields of the pyridines are rather poor and each of the reactions was accompanied by the formation of hexamethyl benzenehexacarboxylate (**4**) (10—20% yield based on DMAD used) and a mixture of more than three compounds. The latter mixture seemed to contain no methoxycarbonyl group and could not be separated. Thus, the structures have not been elucidated. Compound **4** could possibly be derived from [$Mo(CO)_6$]-induced trimerization of DMAD.[12)]

A similar reaction of isoxazoles **1a,d,e** with methyl propiolate (MP) afforded the pyridine derivatives **3a,d**. No pyridine bearing a methoxycarbonyl group at the 3-position could be detected. This fact clearly indicates that the β-carbon atom of MP connects regioselectively with the C-5-carbon atom of the isoxazole ring. In this case, the trimerization of MP was not observed. Since the thermal treatment of the isoxazole **1a** with DMAD in refluxing benzene afforded no adduct and **1a** was recovered quantitatively, [$Mo(CO)_6$] is indispensable for the present reaction.

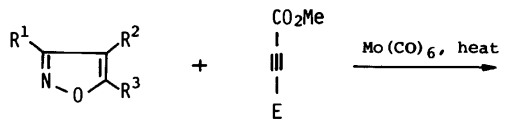

1

2: E = CO_2Me
3: E = H

4

1 and 2: a, $R^1=R^3=Ph$, $R^2=H$; b, $R^1=R^2=R^3=Ph$; c, $R^1=Ph$, $R^2=R^3=H$; d, $R^1=Ph$, $R^2=H$, $R^3=Me$, e, $R^1=Me$, $R^2=H$, $R^3=Ph$; f, $R^1=4\text{-}ClC_6H_4$, $R^2=R^3=H$.
3: a, $R^1=R^3=Ph$, $R^2=H$; d, $R^1=Ph$, $R^2=h$, $R^3=Me$.

Scheme 1.

Table 1. Reaction of isoxazoles **1a—f** with acetylenic esters[a] in the presence of $[Mo(CO)_6]$[b]

Entry	Isoxazole	Acetylenic Ester	Reaction Time/h	Pyridine (Yield/%)
1	**1a**	DMAD[c]	24	**2a** (28)
2	**1b**	DMAD	24	**2b** (22)
3	**1c**	DMAD	24	**2c** (16)
4	**1d**	DMAD	24	**2d** (26)
5	**1e**	DMAD	10	**2e** (12)
6	**1f**	DMAD	20	**2f** (11)
7	**1a**	MP[c]	24	**3a** (19)
8	**1d**	MP	20	**3d** (21)
9	**1e**	MP	10	**3d** (19)

a) 2.0 Molar equivalent of acetylenic ester to **1** was used. b) 1.0 Molar equivalent of $[Mo(CO)_6]$ to **1** was used. c) DMAD: dimethyl acetylenedicarboxylate; MP: methyl propiolate.

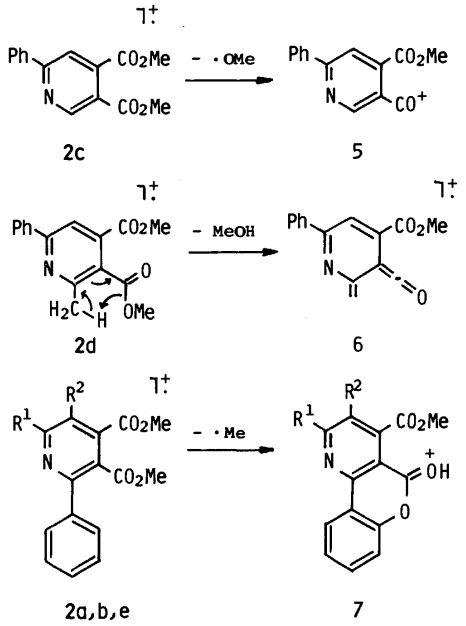

Scheme 2.

The structures of the pyridines were established by their spectral properties (NMR, IR, MS, and in part UV) and by a comparison of the physical data (mp and bp) with those of the authentic specimens. Only the pyridines, **2a** and **2f**, are new compounds. A comparison of their mass spectra revealed the position of the substituents. The main fragmentation pathways of the pyridines are illustrated in Scheme 2. The pyridine **2c** gives the ion **5** with *m/z* 240 (M^+-31), which is derived from the elimination of the MeO group. This fragmentation pattern is generally observed for compounds **2a—f** and **3a,d**. On the other hand, **2d** gives the ion **6** with *m/z* 253 (M^+-32), in addition to an ion with *m/z* 254 (M^+-31). The ion **6** indicates a loss of a methanol molecule through a general "ortho" effect. However, the spectrum of **3d**, which has a methoxycarbonyl group at the 4-position, did not exhibit the corresponding ion of M^+-32. Furthermore, **2a**, **2b**, and **2e**, all of which have a phenyl group adjacent to the methoxycarbonyl group at the 3-position, exhibit an ion of M^+-15 along with an ion of M^+-31. The former ion would be derived from a loss of a methyl group to give the ion **7**, which is stabilized by the phenyl group.[13] The mass spectrum of **3a** did not exhibit the corresponding ion of M^+-15. A comparison of the mass spectral data of the new pyridines with those typical fragmentations and the reaction sequences of the present reaction (*vide infra*) revealed the structure of **2a** and **2f** unequivacally.

Possible mechanistic pathways for the formation of the pyridines are outlined in Scheme 3. An initial complexation of the isoxazole to $[Mo(CO)_6]$ would give the n-donor complex **8**,[5] which has been shown to undergo an N-O bond cleavage to give the complexed nitrene intermediate **9**, collapsing to the corresponding β-amino enone **10** in the presence of water.[5] The factor allowing the facile N-O bond cleavage of **8** could be attributed to the delocalization of the p-d electron from molybdenum to the π* orbital of the isoxazole.[5] The addition reaction of several β-amino enones with DMAD has been shown to give no pyridines.[14] Furthermore, the β-amino enone, which is derived from the isoxazoles **1a**, did not undergo a reaction with DMAD under the present conditions. In the presence of DMAD or MP, **8** may undergo cycloaddition to give complex **13** *via* **11** (Path A). In the case of MP, the C-5-atom of the isoxazole in **8** seems to attack the more electron-deficient β-carbon atom of MP to afford **13** (E=H) (Path A). The regioselectivity affording **3a,d**, which have a methoxycarbonyl group at the 4-position, originate at this stage.

On the other hand, $[Mo(CO)_6]$-induced cyclobutane formation has been proposed for the reaction of 3-phenyl-2*H*-azirines with DMAD.[15] In some cases, $[Mo(CO)_6]$ has also been used for the metathetic reaction of acetylenes.[16] Therefore, an alternative mechanistic possibility may be a [2+2] cross-cycloaddition between **1** and an acetylenic ester to give **13** *via* a metallacycle such as **12** (Path B). Considering the facile n-donor complexation[5] of the isoxazole with $[Mo(CO)_6]$ species as well as the regioselectivity giving **3a,d**, Path A seems to be plausible over Path B.

It has been shown that the N-O and C-4-C-5 bond cleavage of 3,5-disubstituted isoxazolines afford the corresponding aldehydes and the complexed nitrene intermediate in the presence of $[Fe(CO)_5]$, $[Fe_2(CO)_9]$,[17] or $[Mo(CO)_6]$.[18] In a similar fashion, **13** would give the complexed nitrene intermediate **14**. The cyclization of **14** to produce **15** and the following ligand migration gives **16**, which collapses to afford the pyridines **2** or **3**.[19]

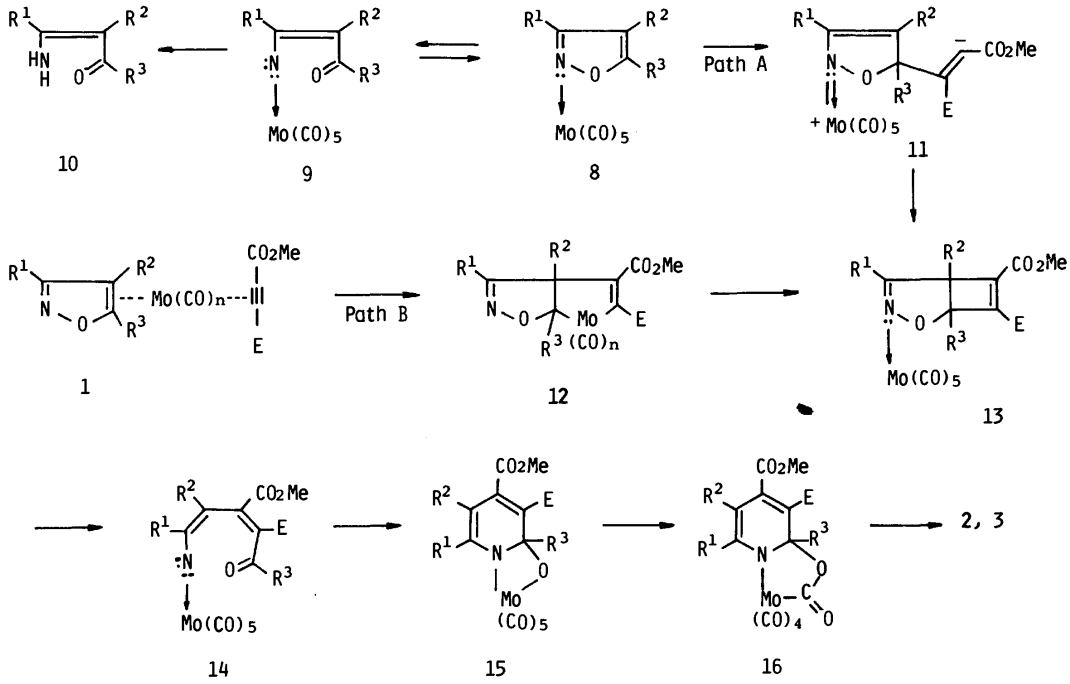

Scheme 3.

In order to study the possible intervention of complexes such as **13** and **14**, we investigated the reaction of 4-phenyl-2-oxa-3-azabicyclo[3.2.0]hepta-3,6-diene (**17**) and its benzoannelated compound **18** with $[Mo(CO)_6]$. As shown in Scheme 4, the reaction of **17** or **18** in refluxing benzene gave 2-phenylpyridine (**20**) or 3-phenylisoquinoline (**21**) in a 76 or 65% yield, respectively. A complexed nitrene intermediate, such as **19a,b** (cf. **14**), which could be derived from the cleavage of the N-O and C-1-C-5 bonds of an isoxazoline moiety, would also be a reasonable intermediate in the transformations. Thus, the intermediacy of **13** and **14** in Scheme 3 seems to be plausible. The $[Mo(CO)_6]$-induced cleavage of **17** is very similar to the photochemical N-O and C-1-C-5 bond-cleavage of **17** to give 3-(3-phenylazirin-2-yl)acrolein.[20] This fact also suggests the delocalization of the p-d electron from molybdenum to the π^* orbital of the C=N-O moiety of the complexed **17**.[17] The *in situ* preparation of $[Mo(CO)_3(MeCN)_3]$,[21] and the subsequent reaction with **17** at an ambient temperature gave **20** in a 76% yield. This fact may suggest that the ligand-exchange reaction of $[Mo(CO)_3(MeCN)_3]$ with **17** proceeds under mild conditions as compared to that of $[Mo(CO)_6]$ with **17**. The N-O bond cleavage of the complexed **17** and the subsequent ring-annelation occurs even at ambient temperature.

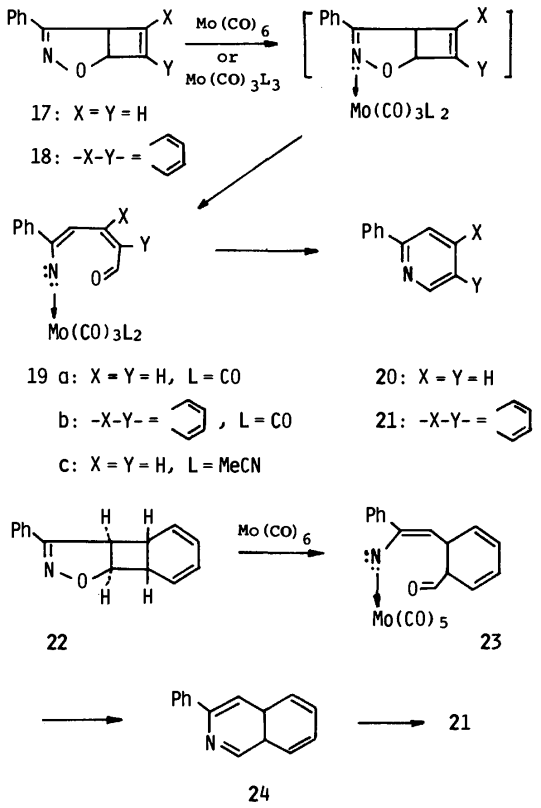

Scheme 4.

Furthermore, the reaction of **22**, which is a dihydrogenated analogue of **18**, with $[Mo(CO)_6]$ also afforded **21** in a 76% yield. The formation of **21** could be explained by an intervention of the complexed nitrene species **23**, ring-annelation giving **24**, and the subsequent dehydrogenation. Thus, the intramolecular ring-annelation of the complexed nitrene moiety with the carbonyl group, which is located in a preferable

stereochemical situation in compounds such as **14**, **19**, and **23**, seems to be general.

On the contrary, the complexed nitrene **31**, which is similar to **14** or **19a,b**, has been proposed as an intermediate of the $[Mo(CO)_6]$-induced transformation of (*Z*)-2-(3-oxo-1-phenyl)-2*H*-azirine derivative to pyrrole derivatives.[22] The yields of the products have not been mentioned, and no pyridine derivative has been obtained.[22] The steric and/or electronic effect of the benzoyl group in **31** seems to be reflected in the reaction pathway giving pyrrole derivatives. In contrast, the complex **14** or **19** bearing a benzoyl, acetyl, or formyl group could give only a pyridine ring. This fact may suggest that the electron-withdrawing property of the methoxycarbonyl group also affects the reaction pathway. A further confirmation of this point may be necessary.

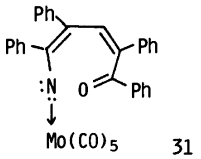

31

Scheme 5.

In conclusion, the $[Mo(CO)_6]$-induced cycloaddition of isoxazoles with acetylenic esters was suggested to give a 2-oxa-3-azabicyclo[3.2.0]hepta-3,6-diene skeleton. The N-O and C-1-C-5 bond-cleavage of the ring system was indicated to give the complexed (β-keto vinyl)nitrene intermediate, which collapses to the pyridine ring. The present reaction could also serve as a convenient method for the preparation of a series of [6](2,5)pyridinophane ring system.[23]

Experimental

The IR spectra were recorded on a Shimadzu IR-400 spectrometer. The NMR spectra were recorded on a Hitachi R-24 spectrometer and the chemical shifts are given in ppm (δ) relative to an internal $SiMe_4$ standard. Mass spectral studies were conducted using Hitachi RMU-60 spectrometer. All of the $[Mo(CO)_6]$-induced reactions were carried out under a dry nitrogen atmosphere. Solvents were purified and dried by the standard methods. The isoxazoles **1a**,[24] **1b**,[25] **1c**,[26] **1e**,[27] 2-oxa-3-azabicyclo[3.2.0]hepta-3,6-diene derivatives **17**,[28] and **18**[29] were prepared by methods described in the literature. The isoxazole **1f** was prepared by a procedure similar to that for 1c and was identified on the basis of physical data.[30] All of the melting points were uncorrected.

Preparation of Isoxazole **1d**. To a solution of benzhydroximoyl chloride (1.56 g, 10 mmol) and isopropenyl acetate (3.0 g, 30 mmol) in ether (100 cm^3), triethylamine (5 cm^3) was added over 1 h at 0 °C. After the mixture was stirred for 20 h, it was extracted with ether. The ether extract was dried over $MgSO_4$ and concentrated to give a crude product. This was purified by column chromatography on silica gel to give **1d** (794 mg, 50%); mp 41—42 °C (from hexane) (lit,[31] 42—43 °C); NMR ($CDCl_3$), δ=2.25 (3H, s), 6.10 (1H, s), 7.20—7.40 (3H, m), 7.60—7.80 (2H, m).

General Procedure for the Reaction of Isoxazoles **1a—f** *with DMAD in the Presence of* $[Mo(CO)_6]$. A solution of isoxazole **1** (2 mmol), DMAD (568 mg, 4 mmol), and $[Mo(CO)_6]$ (528 mg, 2 mmol) in benzene (10 cm^3) was refluxed for an adequate period. To this reaction mixture, hexane (10 cm^3) was added and filtered through Celite to remove insoluble materials. The filtrate was concentrated and the residue was separated by TLC on silica gel using chloroform as the eluent to give the pyridine derivative **2**, along with hexamethyl benzenehexacarboxylate (**4**)[12] (10—20% yield based on DMAD used) and an unidentified mixture (30—40 mg). The reaction times and the yields of the pyridines are summarized in Table 1. The structural proof for the pyridine derivatives **2a—f** were based on the following physical data. 3,4-Bis(methoxycarbonyl)-2,6-diphenylpyridine **2a**: mp 104—105 °C; IR (CCl_4), 1733 cm^{-1}; NMR (CCl_4), δ=3.72 (3H, s), 3.96 (3H, s), 7.20—7.80 (8H, m), 8.00—8.20 (2H, m), 8.17 (1H, s); MS, *m/z* (rel intensity), 347 (M^+, 41), 332 (100), 317 (5), 316 (22). Found: C, 72.91; H, 5.19; N, 4.11%. Calcd for $C_{21}H_{17}NO_4$: C, 72.61; H, 4.93; N, 4.03%. 3,4-Bis(methoxycarbonyl)-2,5,6-triphenylpyridine **2b**: mp 221—222 °C (from benzene)(lit,[32-34] 222—223 °C, 231 °C); IR ($CHCl_3$), 1742, 1739 cm^{-1}; NMR ($CDCl_3$), δ=3.57 (3H, s), 3.67 (3H, s), 7.10—7.80 (15H, m); MS, *m/z* (rel intensity), 423 (M^+, 100), 422 (89), 408 (48), 392 (13), 390 (13), 376 (17). 3,4-Bis(methoxycarbonyl)-6-phenylpyridine **2c**: mp 72.5—73 °C (from hexane) (lit,[35] 74 °C); IR ($CHCl_3$), 1731 cm^{-1}; UV (EtOH), λ_{max} (logε), 262 (4.28), 297 (4.33); NMR ($CDCl_3$), 3.96 (3H, s) 3.98 (3H, s), 7.35—7.60 (3H, m), 7.90 (1H, s), 7.95—8.20 (2H, m), 9.13 (1H, s); MS, *m/z* (rel intensity), 271 (M^+, 91), 240 (100), 236 (11), 212 (13). 3,4-Bis(methoxycarbonyl)-2-methyl-6-phenylpyridine **2d**: bp 140—150 °C (bath temp)/13.3 Pa [lit,[36] 175—185 °C (bath temp)/26.6 Pa]; IR ($CHCl_3$), 1743 cm^{-1}; UV (EtOH), λ_{max} (logε), 252 (4.33), 305 (4.24); NMR ($CDCl_3$), δ=2.70 (3H, s), 3.97 (3H, s), 3.98 (3H, s), 7.30—7.60 (3H, m), 7.85—8.20 (2H, m), 8.05 (1H, s); MS, *m/z* (rel intensity), 285 (M^+, 79), 254 (77), 253 (100), 226 (7), 195 (72), 167 (16). 3,4-Bis(methoxycarbonyl)-6-methyl-2-phenylpyridine **2e**: mp 116—117 °C (from CCl_4) (lit,[37] 215—217 °C); IR ($CHCl_3$), 1730 cm^{-1} NMR ($CDCl_3$), δ=2.65 (3H, s), 3.68 (3H, s), 3.88 (3H, s), 7.27—7.77 (5H, m), 7.55 (1H, s); MS, *m/z* (rel intensity), 285 (M^+, 34), 270 (100), 254 (39), 242 (9), 210 (2). 3,4-Bis(methoxycarbonyl)-6-(4-chlorophenyl)pyridine **2f**: mp 118—120 °C (from EtOH); IR ($CHCl_3$), 1724 cm^{-1}: NMR ($CDCl_3$), δ=3.92 (3H, s), 3.96 (3H, s), 7.45 (2H, d, *J*=8.8 Hz), 7.80 (1H, s), 7.95 (2H, d, *J*=8.8 Hz), 9.07 (1H, s); UV (EtOH), λ_{max} (logε), 266 (4.07), 276 (4.19); MS, *m/z* (rel intensity), 307 (M^+, 31), 305 (M^+, 100), 276 (27), 274 (72), 262 (1), 260 (3). Found: C, 58.97; H, 3.86; N, 4.79%. Calcd for $C_{15}H_{12}ClNO_4$: C, 58.93; H, 3.96; N, 4.58%.

General Procedure for the Reaction of Isoxazoles **1a, d, e** *with Methyl Propiolate (MP) in the Presence of* $[Mo(CO)_6]$. A solution of isoxazole **1** (1 mmol), MP (168 mg, 2 mmol), and $[Mo(CO)_6]$ (264 mg, 1 mmol) in benzene (10 cm^3) was refluxed for an adequate period. To this reaction mixture, hexane (10 cm^3) was added and filtered through Celite. The filtrate was concentrated, and the residue was purified by TLC on silica gel using benzene as the eluent to give the pyridine derivative **3**. The reaction times and the yields of the pyridines are summarized in Table 1 (Entries 7—9). The pyridine derivatives **3a,d** are known compounds and were

identified on the basis of the following physical data. 4-Methoxycarbonyl-2,6-diphenylpyridine **3a**: mp 104—105 °C (from hexane) (lit,[38] 104—105.5 °C); IR ($CHCl_3$), 1730 cm^{-1}; NMR ($CDCl_3$), δ=4.05 (3H, s), 7.45—7.68 (3H, m), 8.15—8.40 (2H, m), 8.27 (2H, s); MS, *m/z* (rel intensity), 289 (M^+, 100), 258 (2), 231 (93). 4-Methoxycarbonyl-2-methyl-6-phenylpyridine **3d**: mp 55—57 °C (from hexane) (lit,[39] 59—60 °C); IR (CCl_4), 1733 cm^{-1}; NMR (CCl_4), δ=2.64 (3H, s), 3.89 (3H, s), 7.25—7.45 (3H, m), 7.50 (1H, d, *J*=1.2 Hz), 7.90—8.10 (2H, s), 7.97 (1H, d, *J*=1.2 Hz); MS, *m/z* (rel intensity), 227 (M^+, 100), 196 (7), 169 (19) 127 (19).

Reaction of 3-Amino-1,3-diphenyl-2-propenone ***10a*** *with DMAD in the presence of [Mo(CO)$_6$].* A solution of **10a** (223 mg, 1 mmol), DMAD (284 mg, 2 mmol), and [$Mo(CO)_6$] (268 mg, 1 mmol) in 10 cm^3 of benzene was refluxed for 24 h. After the evaporation of the solvent, the residue was purified by TLC on silica gel using chloroform as the eluent to give unreacted **10a** (211 mg, 95%).

Reaction of 17 with [Mo(CO)$_6$]. A solution of **17** (171 mg, 1 mmol) and [$Mo(CO)_6$] (264 mg, 1 mmol) in 10 cm^3 of benzene was refluxed for 18 h. To this reaction mixture, hexane (10 cm^3) was added and filtered through Celite. The filtrate was concentrated and the residue was purified by TLC on silica gel using benzene as the eluent to give 2-phenylpyridine (**20**)[40] (118 mg, 76%).

Reaction of 17 with [Mo(CO)$_3$(MeCN)$_3$]. A solution of [$Mo(CO)_3(MeCN)_3$] was prepared from [$Mo(CO)_6$] (528 mg, 2 mmol) in 3 cm^3 of acetonitrile under reflux for 4 h.[20] After this solution was cooled to the ambient temperature, **17** (171 mg, 1 mmol) was added to the solution and it was stirred for 18 h. A workup similar to the one described above gave **20** (117 mg, 76%).

Reaction of 18 with [Mo(CO)$_6$]. A solution of **18** (140 mg, 0.63 mmol) and [$Mo(CO)_6$] (167 mg, 0.63 mmol) in 10 cm^{-3} of benzene was refluxed for 6 h. To this reaction mixture, hexane (10 cm^3) was added and filtered through Celite. The filtrate was concentrated and the residue was purified by TLC on silica gel using benzene as the eluent to give 3-phenylisoquinoline (21) (85 mg, 65%); mp 103—103.5 °C (from hexane); (picrate, mp 196.5—198 °C (from methanol) (lit,[41] mp 102—103.5 °C; picrate, mp 197—199 °C).

Reaction of 22 with [Mo(CO)$_6$]. A solution of **22** (223 mg, 1 mmol) and [$Mo(CO)_6$] (264 mg, 1 mmol) in 10 cm^3 of benzene was refluxed for 22 h. A similar workup followed by TLC on silica gel gave **21** (131 mg, 64%).

References

1) Preliminary report: see T. Kobayashi and M. Nitta, *Chem. Lett.*, **1983**, 1233.

2) E. F. Ullman and B. Singh, *J. Am. Chem. Soc.*, **88**, 1844 (1966); P. de Mayo, "Rearrangement of Ground and Excited States," Academic Press, New York, London, Toronto, Sydney, and San Francisco, 1980, Vol. 3.

3) T. Nishiwaki, T. Kitamura, and A. Nakano, *Tetrahedron*, **26**, 453 (1970); G. Aldous and J. H. Bowie, *J. Chem. Soc., Perkin Trans. 1*, **1975**, 16; K. L. Davis, R. C. Storr, and P. J. Whittle, *J. Chem. Soc., Chem. Commun.*, **1978**, 9.

4) A. R. Katritzky and A. J. Boulton, Adv. Heterocycl. Chem., Academic Press, New York, 1979, Vol. 25.

5) M. Nitta and T. Kobayashi, *Tetrahedron Lett.*, **23**, 3925 (1982); M. Nitta and T. Kobayashi, *J. Chem. Soc., Chem. Commun.*, **1982**, 877.

6) A. R. Katritzky and A. J. Boulton, Adv. Heterocycl. Chem., Academic Press, New York, 1978, Vol. 23, p 263.

7) E. C. Taylor, D. R. Eckroth, and J. Bartulin, *J. Org. Chem.*, **22**, 1899 (1967).

8) C. D. Campbell and C. W. Rees, *J. Chem. Soc. C*, **1969**, 748.

9) R. C. Boruah, J. S. Sandhu, and G. Thyagarajan, *J. Heterocycl. Chem.*, **18**, 1081 (1981).

10) R. M. Acheson and P. W. Poulter, *J. Chem. Soc. C*, **1960**, 2138.

11) A. Schönberg and A Mostafa, *J. Chem. Soc.*, **1943**, 654.

12) T. Sato, K. Shimizu, and H. Moriya, *J. Chem. Soc., Perkin Trans. 1*, **1974**, 1537.

13) R. A. Y. Jones and N. Sadighi, *J. Chem. Soc., Perkin Trans. 2*, **1977**, 412.

14) C. F. Huebner, L. Dorfman, M. N. Robison, E. Donoghue, W. G. Pierson, and P. Strachan, *J. Org. Chem.*, **28**, 3134 (1963).

15) A. Inada and H. Heimgartner, *Helv. Chim. Acta*, **65**, 1489 (1982).

16) A. M. F. Pettit and M. Blanchard, *J. Mol. Catl.*, **8**, 97 (1980).

17) M. Nitta and T. Kobayashi, *Chem. Lett.*, **1983**, 51; M. Nitta and T. Kobayashi, *J. Chem. Soc., Perkin Trans. 1*, **1984**, 2103.

18) M. Nitta, T. Kobayashi, and A. Yi, unpublished results.

19) F. Bellamy, *J. Chem. Soc., Chem. Commun.*, **1978**, 998.

20) T. Mukai, T. Kumagai, and O. Seshimoto, *Pure Appl. Chem.*, **49**, 287 (1977); T. Kumagai, M. Sawaura, C. Kabuto, and T. Mukai, *Nippon Kagaku Kaishi*, **1984**, 158.

21) D. P. Tate, W. R. Knipple, and J. M. Augle, *Inorg. Chem.*, **1**, 433 (1962).

22) F. Bellamy, *Tetrahedron Lett.*, **1978**, 4577.

23) M. Nitta and T. Kobayashi, *Tetrahedron Lett.*, **25**, 959 (1984).

24) G. A. Lee, *Synthesis*, **1982**, 508.

25) C. F. Beam, M. C. D. Dyer, R. A. Schwarz, and C. R. Houser, *J. Org. Chem.*, **35**, 1806 (1970).

26) K. Bast, M. Chust, R. Huisgen, W. Mack, and C. R. Sustmann, *Chem. Ber.*, **106**, 3258 (1973).

27) D. Nightingale and F. Wadsworth, *J. Am. Chem. Soc.*, **67**, 416 (1945).

28) G. Bianchi, R. Gandolfi, and P. Grunanger, *Tetrahedron*, **26**, 5133 (1970).

29) T. L. Gilchrist, E. E. Nun, and C. W. Rees, *J. Chem. Soc., Perkin Trans. 1*, **1974**, 1262.

30) T. A. Babushkina, G. K. Semin, S. D. Sokolov, and I. M. Yudintseva, *Izv. Akad. Nauk. SSSR, Ser. Khim.*, **1970**, 2376.

31) L. Claisen, *Ber. Deut. Chem. Ges.*, **40**, 3910 (1907).

32) T. Eicher, F. Abdesakan, G. Franke, and J. L. Weber, *Tetrahedron Lett.*, **1975**, 3915.

33) R. A. Y. Jones and N. Sadighi, *J. Chem. Soc., Perkin Trans. 1*, **1976**, 2259.

34) J. P. Freeman and M. J. Haddadin, *J. Org. Chem.*, **45**, 4898 (1980).

35) R. Boehm and K. Bournot, *Ber. Deut. Chem. Ges.*, **49**, 1570 (1916).

36) A. G. Bayer, *Chem. Abstr.*, **54**, 1873b (1964).

37) This mp is 100 °C higher than the reported datum: E.

Bushman and W. Stiglich, *Angew. Chem. Int. Ed. Engl.*, **13**, 484 (1974).
38) M. N. Tilichenko, *Chem. Abstr.*, **55**, 22308a (1965).
39) F. Bonadies, F. Savagnone, and M. L. Scarpatt, *Gazz. Chim. Ital.*, **108**, 87 (1978).
40) The Aldrich Library of NMR Spectra, Aldrich Chemical Co., Milwaukee, WI, Vol. IX, No. 49; The Aldrich Library of IR Spectra 1139G.
41) C. K. Bradsher and T. G. Wallis, *J. Org. Chem.*, **43**, 3817 (1978).

 © 1985 The Chemical Society of Japan Bull. Chem. Soc. Jpn., 58, 158—164 (1985) [Vol. 58, No. 1

Elucidation of the Origin of Substituent Effects. Theoretical Investigation of Field Effect in Aliphatic Systems by *ab initio* Molecular Orbital Calculation Using Simple Models

Naoki INAMOTO,* Shozo MASUDA, and Jun NIWA†

Department of Chemistry and Research Centre for Spectrochemistry, Faculty of Science, The University of Tokyo, Hongo, Tokyo 113

†*College of General Education, Nagoya University, Chikusa-ku, Nagoya 464*

(Received July 18, 1984)

The electronic substituent effect in the aliphatic systems was investigated using *ab initio* calculation at STO-3G and 4-31G levels. The relative energy changes, $\delta\Delta E$, in isodesmic reaction of the 4-substituted bicyclo[2.2.2]octane-1-carboxylic acids were compared with those for 1-substituted bicyclo[2.2.2]octanes(XC_8H_{13}), CH_3X, and H-X molecules perturbed with isolated pure point charges. The interaction energies between isolated dipole and point charge system, F-H···(±), were proportional to the reciprocal square of the distance between the center of dipole and the charge. Isodesmic reaction energies for the present systems at the distance longer than 5 Å can be practically explained by charge-dipole interaction. From the comparison of $\delta\Delta E$ in XCH_3···(±), XC_8H_{13}···(±), and XC_6H_5···(±) systems with those for X-H···(±), it was concluded that the pure field parameters for various substituents should be determined on the basis of the isodesmic reaction energy for X-H···(±) system. Correlations between $\delta\Delta E$ in X-H···(±) system and the field parameters recently proposed, σ_F and σ_I(gas), were generally better in the cases calculated at 4-31G level than those at STO-3G level.

The effect of a partial structural change on the chemical reactivities in organic compounds is one of long standing problems in physical organic chemistry.[1] Recently, some attempts to simplify complicated interactions in the systems have been made in order to make the physical meaning of substituent effect clear. Analyses of acidities and basicities in gas phase[2] free of solvent effect and *ab initio* molecular orbital (MO) calculations[3] of energy changes in isodesmic reactions[4] for isolated molecule systems[5] where only through-space effect is operative have deepened the understanding on the origin and mechanism of transmission of substituent effect.[1c-f]

Usually, the interactions between substituent and reaction (or probe) center have been explained in terms of four effects, namely, field effect (through-space effect),[1e,1f,6] σ-inductive effect (electronegativity or through-bonds effect),[7] resonance and hyperconjugation effects (charge transfer effect),[1,8] and polarization effect,[3a,8] although other effects have also been suggested.[1e]

We reported evidence for σ-inductive effect on spectral data at the adjacent position to substituent,[9] and established a reliable method to calculate inductive substituent parameters (ι; Gk., iota) as a measure of σ-inductive effect.[10] Reynolds, Taft, and Topsom[7] have reported that the charge densities at the hydrogen atom in the H-X molecules (at 6-31G* level) were well correlated with the group electronegativities of the substituents, because of the absence of the hyperconjugative interaction, and soon after, we also showed a similar relationship with our revised electronegativities.[11]

On the other hand, Streitwieser *et al.*[12] reported the results of *ab initio* MO calculations for the monosubstituted benzenes perturbed with positive and negative unit charges as a simple model of substituent effect, and suggested that the highly or weakly polarizable groups should not be included in the Hammett relationship on the basis same as normal substituents.

Recently, the scales of field effect (T_F,[13] σ_I(STO-3G),[10] F°,[8] and σ_F[7]) have been proposed on the basis of *ab initio* calculations of appropriate model systems at the STO-3G and 4-31G levels. However, usefulness of these scales is not so clear. Then we expected that a satisfactory interpretation for substituent effect might be obtained from a comparison of the energy changes in isodesmic reaction of 4-substituted bicyclo[2.2.2]octane-1-carboxylic acids (**1**) with those of 1-substituted bicyclo[2.2.2]octane perturbed with positive and negative point charges (**2**) as a simple model, though the acidities of **1** in gas phase have not been reported.

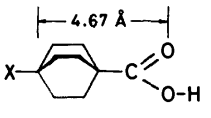

1

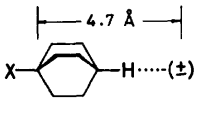

2

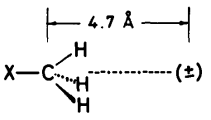

3

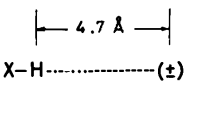

4

Systematic *ab initio* MO calculations for the through-space field effect in σ-bond systems **2**—**4** were

also carried out using perturbation with pure point charges to model nonbonded reaction center.

Calculation Methods

Calculations were performed on the *ab initio* STO-3G[14a] or/and 4-31G[14b] levels using the Gaussian-70[14c] and 80[14d] series of computer program, and the molecular geometries were taken from experimentally determined values.[15] The geometry of the carboxylate moiety in **1** was obtained to be $r_{C\text{-}O}$=1.27 Å and ∠OCO=130.4° from the optimized geometry of formate ion at the STO-3G level, and assumed to be constant for all substituted derivatives (**1**). The geometry of a pure dipole "substituent" having positive and negative point charges is the same as that used by Streitwieser *et al.*[12]

In other systems (**2**—**4**), perturbation of the systems was induced by both positive and negative point charges. The point charge was located at 1 Å from the 4-hydrogen atom in **2**, and at 4.7 Å from the methyl carbon and hydrogen atoms in **3** and **4**, respectively, along the X-C bond. Thus, the distances (4.7 Å) between *ipso*-carbon atom (hydrogen atom in **4**) and point charge in **2**—**4** are almost equal to that (4.67 Å) between C_4 atom and reaction center in **1**.

The following isodesmic reaction (Eq. 1) was used to evaluate the substituent effect on the above perturbed systems:

$$\underset{\mathbf{A}}{\text{X-R}} + \underset{\mathbf{B}}{\text{H-R}\cdots(\pm)} \rightleftharpoons \underset{\mathbf{C}}{\text{H-R}} + \underset{\mathbf{D}}{\text{X-R}\cdots(\pm)} \quad (1)$$

where X represents substituent and R-H is parent compound. The relative energy change ($\delta\Delta E$) in the above isodesmic reaction was obtained using Eq. 2.

$$\delta\Delta E = (E_C+E_D) - (E_A+E_B) = (E_D-E_A) - (E_B-E_C) = \Delta E_X - \Delta E_H \quad (2)$$

A negative value in $\delta\Delta E$ corresponds to a stabilizing effect compared with that of parent compound. All calculations were carried out on a FACOM M-382 computer at the Nagoya University Computation Center.

Results and Discussion

The total energies of the carboxylic acids (**1**) and the corresponding carboxylate ions, the relative energy changes ($\delta\Delta E$) in the isodesmic reaction (Eq. 3) of the series **1**,

$$XC_8H_{12}CO_2H + C_8H_{13}CO_2^- \rightleftharpoons C_8H_{13}CO_2H + XC_8H_{12}CO_2^- \quad (3)$$

and the relative charge densities (Δq_H) at the carboxyl hydrogen atom in **1** are given in Table 1.

The linear relationships between $\delta\Delta E$ and charge densities at a particular atom have been shown in the alkyl chlorides (STO-3G),[16] substituted phenols and benzoic acids (INDO[17] and STO-3G[18]), aliphatic aldehydes (STO-3G),[19] substituted anilines and toluenes (STO-3G),[20] and several isolated molecule systems.[6,13]

Correlation between the relative energy changes in the isodesmic reaction ($\delta\Delta E_{(1)}$) and Δq_H in the series **1** is as follows:

$$\delta\Delta E_{(1)} = 2135\Delta q_H - 0.056 \quad (r=0.9985,\ n=9,\ f=0.045)$$

Analogous correlation of $\delta\Delta E_{(1)}$ with $\Delta\sum q_O$(COOH) or $\Delta\sum q_O(COO^-)$, which is the sum of the relative charges on the both oxygen atoms in the carboxyl group of the series **1** or those in the corresponding carboxylate, respectively (see Table 1), shows that $\Delta\sum q_O(COO^-)$ can be used as a measure of $\delta\Delta E_{(1)}$ similarly to Δq_H, as shown in the following equations.

Table 1. Total energies of carboxylic acids **1** and their anions, relative energy for isodesmic reaction, and Δq_H and Δq_O of the carboxyl group

Substituent X	$XC_8H_{12}COO^-$ au	$XC_8H_{12}COOH$ au	$\delta\Delta E$ kcal mol^{-1} [a]	Δq(H) $\times 10^3$ (COOH)	$\Delta\sum q$(O)[b] $\times 10^3$ (COOH)	$\Delta\sum q$(O)[b] $\times 10^3$ (COO^-)
$-CH_3$	−530.37663	−531.12401	0.1	0.141	−0.156	0.170
-H	−491.80476	−492.55205	0.0	0.000	0.000	0.000
$-NH_2$	−546.11313	−546.85836	−1.3	−0.471	1.367	1.826
-OH	−565.63481	−566.37823	−2.4	−1.184	1.369	2.665
-CHO	−603.02569	−603.76839	−2.9	−1.317	1.815	3.226
-F	−589.26526	−590.00699	−3.5	−1.796	3.313	3.852
-CN	−582.36213	−583.09772	−7.3	−3.451	3.018	7.422
$-NO_2$	−692.51268	−693.24612	−8.7	−4.003	6.431	9.577
Dipole	−492.54771	−493.28027	−9.2	−4.229	6.788	9.262

a) 1 kcal mol^{-1}=4.184 kJ mol^{-1}. b) See the text.

$$\delta\Delta E_{(1)} = -1352\Delta\Sigma q_o(\mathrm{COOH}) - 0.327 \quad (r=0.943,\ n=9)$$

$$\delta\Delta E_{(1)} = -982\Delta\Sigma q_o(\mathrm{COO^-}) + 0.220 \quad (r=0.997,\ n=9)$$

In the case of the substituted phenols,[21] it has been found that the electron-donating groups deviate considerably from the correlation between the corresponding $\delta\Delta E$ values and the relative charges on the oxygen atom in the substituted phenoxides, because of conjugation of the oxide group with the π-electrons system.

The total energies of 1-substituted bicyclo[2.2.2]octanes, monosubstituted methanes, and H-X molecules at the STO-3G and 4-31G levels are given in Table 2. Table 3 shows $\delta\Delta E$ in the series **2**—**4** at both basis sets.

It was shown for the $CH_4\cdots(-)$ system as an example that the effect of slight change in bond length on $\delta\Delta E$ can be ignored in the case of the relative energy due to substituent effect as shown below. In Table 2, the C-H bond length of 1.10 Å was used. If the length is extend to 1.11 Å, the total energies of methane itself and methane perturbed with negative point charge were calculated to be −39.72450 and −39.72448 au, respectively. Thus the difference in $\delta\Delta E$ is 1×10^{-5} au (*ca.* 0.006 kcal mol^{-1} (1 cal=4.184 J)).

The electrostatic energy due to the interaction between dipole and point charge is calculated as the sum of the energies due to charge-permanent dipole interaction,[10] W_p (Eq. 4), and those due to charge-induced dipole interaction (polarizability effect),[10] W_α (Eq. 5):

$$W_p = -ep\cos\theta/(Dr^2) \quad (4)$$

$$W_\alpha = -e^2\alpha/(2Dr^4) \quad (5)$$

where e is the unit electric charge, p permanent dipole moment of substituent, θ the angle between the axis of dipole and the line joining the center of dipole and point charge, r the distance between the center of dipole and point charge, α group polarizability, and D dielectric constant of medium.

Recently, Yoder *et al.*[22] have evaluated the substituent effects on the energies of proton-transfer equilibria in gas phase using classical electrostatic model. Therefore, it is of interest to examine whether the electrostatic model can quantitatively account for the isodesmic reaction energies calculated by *ab initio* MO method in the cases of the systems **2**—**4**.

In order to test if Eq. 4 can be applied sufficiently to our models **2**—**4**, the perturbed energy changes at various distances between F-H, in which a contribution of polarizability effect is small because of a lower polarizability, and point charges were calculated at

Table 2. Total energies (au) of H-X, CH_3X, and 1-substituted bicyclo[2.2.2]octanes (XC_8H_{13})

Substituent X	H-X STO-3G	H-X 4-31G	CH_3-X STO-3G	CH_3-X 4-31G	XC_8H_{13} STO-3G
-CH_3	−39.72450	−40.13881	−78.30453	−74.11386	−346.05538
-H	−1.11676	−1.12676	−39.72591	−40.13881	−307.48345
-NH_2	−55.45339	−56.10364	−94.02601	−95.06490	−361.78996
-OH	−74.96454	−75.90681	−113.54451	−114.86937	−381.30980
-CHO	−112.35368	−113.69108	−150.94233	−152.68335	−418.70004
-F	−98.57077	−99.88726	−137.16877	−138.85696	−404.93877
-CN	−91.67519	−92.73132	−130.27080	−131.72657	−398.03009
-NO_2	−201.83118	−204.27805	−240.41178	−243.27215	−508.17817
Dipole	−1.83562	−1.84658	−40.44939	−40.86365	−308.21249

Table 3. Relative energies ($\delta\Delta E$) of isodesmic reactions (kcal mol^{-1})

Substituent X	X-H···(±) (**4**)				X-CH_3···(±) (**3**)				X-C_8H_{13}···(±) (**2**)	
	STO-3G		4-31G		STO-3G		4-31G		STO-3G	
	(+)	(−)	(+)	(−)	(+)	(−)	(+)	(−)	(+)	(−)
-CH_3	−0.2	0.0	−0.2	0.0	−0.3	0.1	−0.5	0.0	−0.5	0.0
-H	0.0	0.0	0.0	0.0	0.0	0.0	0.0	0.0	0.0	0.0
-NH_2	1.3	−1.4	1.8	−1.9	0.7	−0.9	1.2	−1.5	1.0	−1.4
-OH	2.4	−2.5	4.0	−3.9	1.7	−1.8	3.4	−3.6	2.3	−2.6
-CHO	1.4	−1.7	3.0	−3.3	1.9	−2.3	—	−4.4	2.5	−3.1
-F	3.2	−3.2	5.9	−5.7	2.6	−2.7	6.0	−5.9	3.5	−3.6
-CN	4.4	−4.7	6.2	−6.5	5.1	−5.5	7.1	−7.7	6.9	−7.6
-NO_2	5.5	−5.7	8.2	−8.3	6.0	−6.5	—	−9.8	8.4	−9.1
Dipole	7.0	−7.0	8.0	−8.0	7.0	−7.0	8.5	−8.6	9.7	−9.3

the 4-31G level. The results are shown in Table 4. A plot of $\log|\delta\Delta E|$ against $-\log r$ using the values (r=3.0—13.0 Å) listed in Table 4 showed a straight line having slope of nearly 2 (*i.e.*, 1.90 and 1.85 for negative and positive charges, respectively), as expected from Eq. 4.

It has been found that the polarization of the π-electron of ethylene[23] by $\overset{+}{N}H_4$ species approximately follows Eq. 4.

The effect of change of r on electrostatic field energies expressed by Eqs. 4 and 5 was also examined using the dipole moment of p=2.95 D[24] (1 D=3.333×10^{-30} C m) in gas phase and the longitudinal bond polarizability of α=31.3×10^{-25} cm^3 [25] for hydrogen cyanide perturbed with both positive and negative point charges as an example. As seen in Fig. 1, the W_p values in the cases of negative and positive charges are mutually reverse in the sign, but the W_α values always correspond to stabilization for both charges. The contribution of W_α at very close distance (within r=2 Å) amounts to above 40% of W_p, but that at longer distances than 5 Å decreases up to below a few percents of W_p. Therefore, the magnitude of electrostatic field effects at such a longer distance can be approximately evaluated using only Eq. 4.

Table 5 summarizes the values p, θ, α, W_p, and W_α in the series **2**, where (4.7+0.5$r_{C\text{-}X}$) Å is used as r, and p and θ are the values calculated at the STO-3G level. Group polarizabilities of substituents (α)[26] were calculated from the values of bond refractivity (R_D) for the D line. The correlation between $\delta\Delta E_{(2)\cdot\cdot(\pm)}$ (Table 3) and W_p or (W_p+W_α) for both point charges in the series **2** are as follows:

$$\delta\Delta E_{(2)\cdot\cdot(-)} \begin{cases} = 0.994W_p^{(-)} - 0.153 & (r=0.993,\ n=8) \\ = 0.968(W_p+W_\alpha)^{(-)} + 0.057 & (r=0.992,\ n=8) \end{cases}$$

$$\delta\Delta E_{(2)\cdot\cdot(+)} \begin{cases} = 0.946W_p^{(+)} - 0.093 & (r=0.989,\ n=8) \\ = 0.971(W_p+W_\alpha)^{(+)} + 0.121 & (r=0.991,\ n=8) \end{cases}$$

Thus, it is clear again that $\delta\Delta E$ in the series **2** (at r=5.5 Å as a mean) can be nearly interpreted using only Eq. 4.

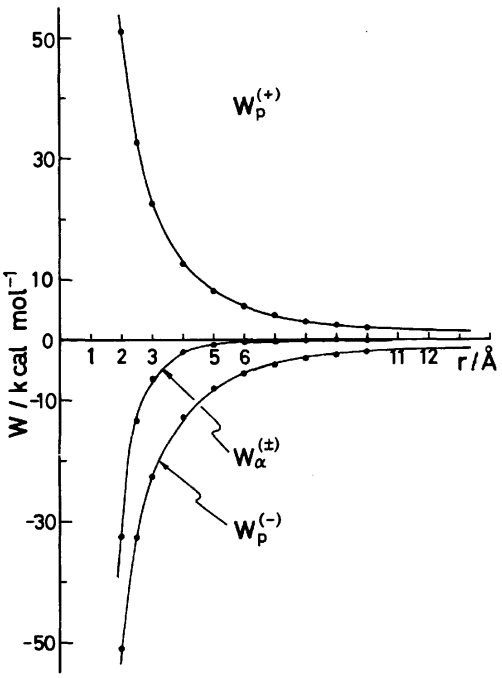

Fig. 1. Plots of electrostatic field energies (W_p and W_α) of hydrogen cyanide perturbed with both positive and negative point charges *vs.* the distances between the center of C-H bond and the point charges.

Table 4. $\delta\Delta E$ values[a] at various distances between F-H and point charges (4-31G level)

r/Å	1.0	3.0	4.7	7.0	10.0	13.0
$\delta\Delta E^{(-)}$/kcal mol^{-1}	−104.10	−14.29	−6.19	−2.91	−1.47	−0.89
$\delta\Delta E^{(+)}$/kcal mol^{-1}	61.17	12.98	5.92	2.84	1.44	0.87

a) The standard is the value in infinite distance.

Table 5. The values p, θ, α, W_p, and W_α in series **2**

Substituent X	p[a] / Debye[b]	θ[a] / degree	$\alpha\times10^{25}$ / cm^3	$\lvert W_p\rvert$ / kcal mol^{-1}	W_α / kcal mol^{-1}
-CH_3	0.00	0.00	22.408	0.000	−0.417
-H	0.00	0.00	4.075	0.000	−0.089
-NH_2	1.43	70.4	17.592	1.123	−0.335
-OH	1.56	51.6	10.092	2.290	−0.196
-CHO	1.76	43.3	22.313	2.980	−0.419
-F	1.37	0.00	3.2108	3.259	−0.063
-CN	3.49	0.00	21.639	8.195	−0.414
-NO_2	3.59	0.00	26.610	8.383	−0.504

a) Calculated at the STO-3G level. b) 1 D=3.333×10^{-30} C m.

In order to clarify whether the substituent effect on the acid dissociation energy in vacuum can be explained by the interaction with the carboxylate group, we examined the correlation between the dissociation energies of **1** ($\delta\Delta E_{(1)}$, Table 1) and the perturbation energies of **2** ($\delta\Delta E_{(2)\cdot\cdot(-)}$, Table 3) with negative charge. In the both cases, the distance (r) is almost same. The following linear relationship having a slope of nearly 1 was obtained, indicating that σ-inductive effect is unimportant in the systems **1**.

$$\delta\Delta E_{(1)} = 0.988\delta\Delta E_{(2)\cdot\cdot(-)} + 0.078$$
$$(r=0.9999,\ n=8,\ f=0.019)$$

We now discuss the polarizability effect on $\delta\Delta E$ from a slightly different point of view. Figure 2 (A) shows a substantially linear plot of $\delta\Delta E$ for the series **4** perturbed with positive charge *vs.* those perturbed with a negative one. Figures 2 (B) and (C) are also similar plots for the series **3** and **2**, respectively, two separate lines being obtained as expected from the result of monosubstituted benzenes perturbed with point charges.[12]

These plots indicate that the substituent effects are not independent of the nature of probe charge and molecular system. Most substituents having relatively large polarizability fall below the dotted line drawn through hydrogen, fluorine atoms, and dipole substituent having rather small polarizability. In comparison of these series, the series **4** showed the least deviation among them, while, the extent of the deviation in the series **3** and **2** becomes larger as the size of substrate increases. Hence, the deviation is probably attributed to the difference in the polarizability of the whole molecule. Thus the substituent parameters defined from data of relatively large molecules are considered to result in broadly scattered values for both negative and positive reaction probes, even in the absence of any specific solvent effects.

The charges at the hydrogen atom in the H-X molecules are free from hyperconjugative interaction,[7] while σ- and π-interactions between substituent and methyl group in monosubstituted methanes occur in the same fashion as in monosubstituted benzenes.[27] Then, it is interesting to compare the $\delta\Delta E$ values in some series having π-character with the $\delta\Delta E$ values in the series **1**.

Figure 3 shows the plots of the $\delta\Delta E$ values in the series **3**, **2**, and monosubstituted benzenes *vs.* those in the series **4** using a negative point charge perturbation, respectively. The lines shown in Fig. 3 are those drawn through dipole substituent and hydrogen atom.

As pointed out by Streitwieser *et al.*,[12] the dipole substituent is a substituent having only "field effect," and the substituents which deviate from the line may be accompanied by some additional effects such as polarization and resonance effects. Since the direct resonance interaction with perturbing negative charge is impossible in the systems **2**—**4**, the deviation from

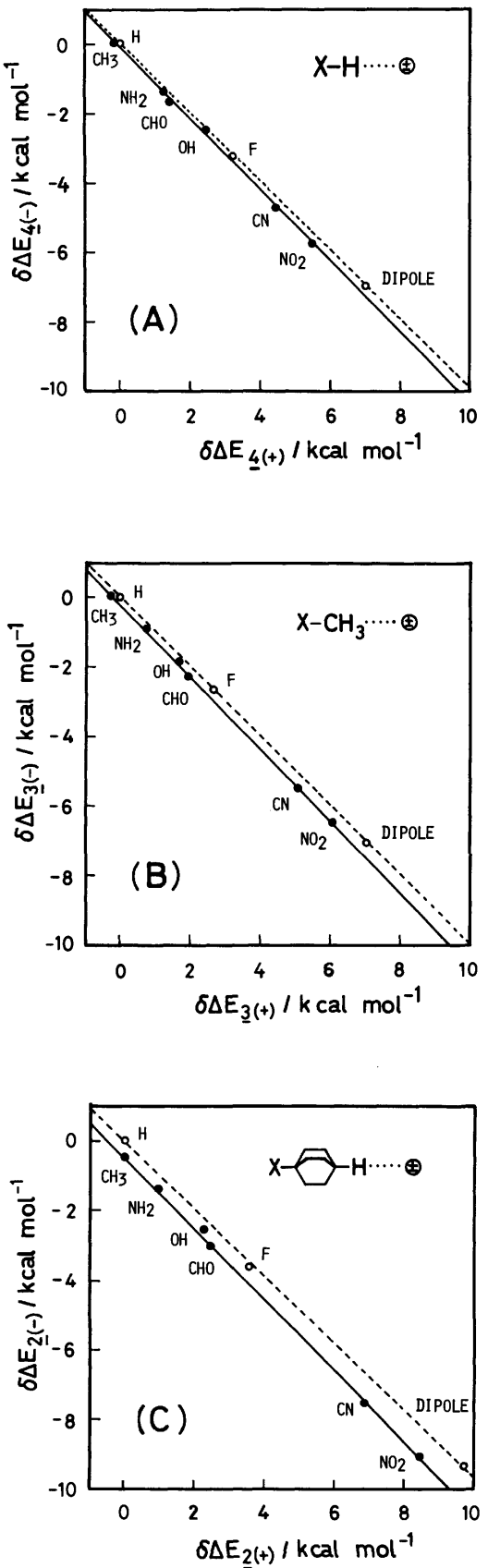

Fig. 2. Plots of isodesmic reaction energies ($\delta\Delta E$) for the aliphatic series perturbed with the point charges, (A) in the series **4**, (B) in the series **3**, and (C) in the series **2**.

Table 6. Comparison between $\delta\Delta E$ and W_p or σ_F and σ_I(gas)

Basis set	Model system	W_p[a]		σ_F[b]		σ_I(gas)[c]	
		Slope	r	Slope	r	Slope	r
STO-3G	**4**(−)	0.849	0.989	−8.61	0.976	−7.65	0.966
4-31G	**4**(−)	0.873	0.991	−12.68	0.994	−11.34	0.990
STO-3G	**4**(+)	0.822	0.984	8.41	0.980	7.44	0.966
4-31G	**4**(+)	0.845	0.983	12.77	0.997	11.35	0.988
STO-3G	**3**(−)	0.835	0.991	−9.42	0.926	−8.63	0.949
4-31G	**3**(−)	0.873	0.990	−14.72	0.973	−13.41	0.989
STO-3G	**3**(+)	0.790	0.986	9.08	0.939	8.28	0.958
4-31G	**3**(+)	0.807	0.976	14.54	0.981	12.12	0.999_9
STO-3G	**2**(−)	0.994	0.993	−13.01	0.926	−11.85	0.944
STO-3G	**2**(+)	0.946	0.989	12.62	0.940	11.45	0.953

a) $W_p = -ae(p\cos\theta/r^2)$, where a is slope. b) Refs. 1d and 6b. c) Ref. 1f.

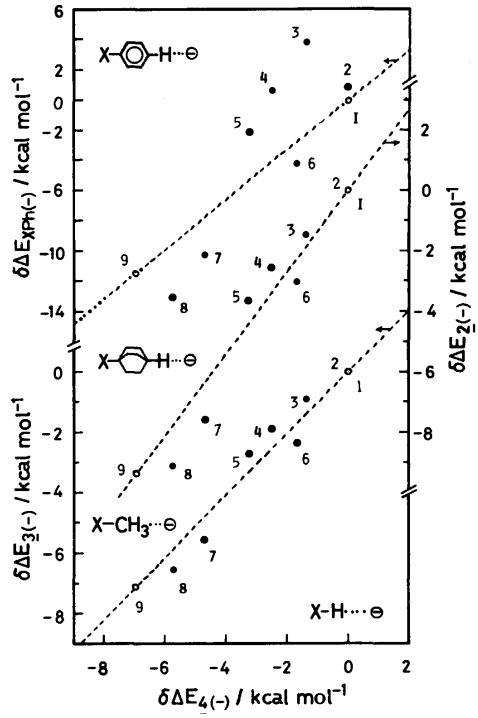

Fig. 3. Plots of the $\delta\Delta E$ in the series **3**, **2**, and monosubstituted benzenes *vs.* those in the series **4** using a negative point charge. 1: H, 2: CH_3, 3: NH_2, 4: OH, 5: F, 6: CHO, 7: CN, 8: NO_2, 9: Dipole.

the line shown in Fig. 3 must be attributed to the interaction of pseudo π-orbital of the methyl in the series **3** or alkyl group in the series **2** with appropriate orbital on the substituents.

Strong π-interaction is observed in the monosubstituted benzenes. For this negative point charge perturbation with substituted benzenes, the π-electron-donating groups such as fluoro, hydroxyl, amino, and methyl groups show a remarkable resonance destabilization, whereas the π-electron-withdrawing groups such as nitro, cyano, and formyl groups exhibit resonance stabilization.

However, deviation of electron-donating substituents from the line exhibits a different trend in aliphatic and aromatic series. From these analyses, it is concluded that pure field parameters for various substituents should reasonably be determined from the energy changes for the series of X-H··(±) system. Detailed analyses are in progress.

Finally, the correlation coefficients and slopes of the correlations between isodesmic energy changes ($\delta\Delta E$) and electrostatic energies (W_p) or various field parameters are summarized in Table 6. The σ_I(gas) values are those determined from acidities of phenols in gas phase.[2]

It is seen from Table 6 that the correlation coefficients using calculated electrostatic field energies (W_p) are generally quite good for all isodesmic energy changes. Correlations between $\delta\Delta E$ and σ_F or σ_I(gas) are generally better in the cases calculated at the 4-31G level than those calculated at the STO-3G level.

By the application of *ab initio* MO calculation, it was concluded that the field parameters, σ_I(gas), which were obtained from gas-phase acidities, can accurately be reproduced by $\delta\Delta E$ calculated at the 4-31G basis set. Thus, σ_I(gas) is a good measure of field effect in gas phase and *ab initio* calculation at the 4-31G basis set is the most suitable to examination of substituent effect, although the calculation is limited to rather small molecules for the present.

References

1) a) "Advances in Linear Free Energy Relationships," ed by N. B. Chapman and J. Shorter, Plenum, London (1972); "Correlation Analysis in Chemistry. Recent Advances," ed by N. B. Chapman and J. Shorter, Plenum, London (1978); b) S. Ehrenson, R. T. C. Brownlee, and R. W. Taft, *Progr. Phys. Org. Chem.*, **10**, 1 (1973); c) R. D. Topsom, *ibid.*, **12**, 1 (1976); d) R. D. Topsom, *Acc. Chem. Res.*, **16**, 292 (1983); e) W. F. Reynolds, *Progr. Phys. Org. Chem.*, **14**, 165 (1983), and references cited therein. f) R. W. Taft, *ibid.*, **14**, 247 (1983).

2) T. B. McMahon and P. K. Kebarle, *J. Am. Chem. Soc.*,

99, 2222 (1977); J. E. Bartmess, J. A. Scott, and R. T. McIver, Jr., *ibid.*, **101**, 6046, 6056 (1979); M. Fujio, R. T. McIver, Jr., and R. W. Taft, *ibid.*, **103**, 4017 (1981), and references cited therein.

3) a) W. J. Hehre, L. Radom, and J. A. Pople, *J. Am. Chem. Soc.*, **94**, 1496 (1972); b) W. J. Hehre and J. A. Pople, *ibid.*, **92**, 2191 (1970).

4) W. J. Hehre, R. Ditchifield, L. Radom, and J. A. Pople, *J. Am. Chem. Soc.*, **92**, 4796 (1970); *idem, Chem. Soc.* (A), **1971**, 2299.

5) P. G. Mezey and W. F. Reynolds, *Can. J. Chem.*, **55**, 1567 (1977).

6) a) R. D. Topsom, *J. Am. Chem. Soc.*, **103**, 39 (1981); b) S. Marriott and R. D. Topsom, *ibid.*, **106**, 7 (1984).

7) W. F. Reynolds, R. W. Taft, S. Marriott, and R. D. Topsom, *Tetrahedron Lett.*, **23**, 1055 (1982); S. Marriott, W. F. Reynolds, R. W. Taft, and R. D. Topsom, *J. Org. Chem.*, **49**, 959 (1984).

8) G. E. Fadhil and M. Godfrey, *J. Chem. Soc., Perkin Trans. 2*, **1982**, 933.

9) N. Inamoto and S. Masuda, *Tetrahedron Lett.*, **18**, 3287 (1977); idem, *Chem. Lett.*, **1978**, 177.

10) N. Inamoto and S. Masuda, *Chem. Lett.*, **1982**, 1007.

11) N. Inamoto and S. Masuda, *Chem. Lett.*, **1982**, 1003.

12) E. R. Vorpazel, A. Streitwieser, Jr., and S. D. Alexandros, *J. Am. Chem. Soc.*, **103**, 3777 (1981).

13) W. F. Reynolds, P. G. Mezey, and G. K. Hamer, *Can. J. Chem.*, **55**, 522 (1977); P. G. Mezey and W. F. Reynolds, *ibid.* **55**, 1567 (1977).

14) a) W. J. Hehre, R. F. Stewart, and J. A. Pople, *J. Chem. Phys.*, **51**, 2657 (1969); b) R. Ditchfield, W. J. Hehre, and J. A. Pople, *J. Chem. Phys.*, **54**, 724 (1971); W. J. Hehre and J. A. Pople, *ibid.*, **56**, 4233 (1972); c) W. J. Hehre, W. A. Lanthan, R. Ditchfield, M. D. Newton, and J. A. Pople, Program No. 236, Quantum Chemistry Program Exchange, Indiana University, Bloomington, Ind. d) J. S. Binkley, R. A. Whiteside, R. Khrishnan, R. Seegar, D. J. DeFrees, H. B. Schleyer, S. Topiol, L. R. Kahn, J. A. Pople, "Gaussian 80 An *Ab-Initio* Molecular Orbital program," Department of Chemistry, Carnegie-Mellon University, Pittsburg, 1980.

15) J. H. Callomon, H. Hirota, K. Kuchitsu, W. J. Lafferty, A. G. Maki, and C. S. Pote, "Structure Data on Free Polyatomic Molecules," ed by K. H. Hellweg, Springer-Verlag, West Berlin (1976), Vol. 7, Group 2 of Landort-Börnstein, New Series.

16) W. L. Jorgensen, *J. Am. Chem. Soc.*, **100**, 1049, 1057 (1978); *idem, Chem. Phys. Lett.*, **53**, 525 (1978).

17) S. Kang and D. L. Beveridge, *Theor. Chim. Acta*, **22**, 312 (1971); J. Calalem and A. Macias, *J. Chem. Soc., Perkin Trans. 2*, **1979**, 1632.

18) G. Kamistrer, A. Pross, L. Radom, and R. W. Taft, *J. Org. Chem.*, **45**, 1056 (1980).

19) J. E. Delben, *J. Am. Chem. Soc.*, **100**, 1673 (1978).

20) W. J. Hehre, M. Taagepera, R. W. Taft, and R. D. Topsom, *J. Am. Chem. Soc.*, **103**, 1344 (1981).

21) A. Pross, L. Radom, and R. W. Taft, *J. Org. Chem.*, **45**, 818 (1980).

22) C. S. Yoder and C. H. Yoder, *J. Am. Chem. Soc.*, **102**, 1245 (1980).

23) S. Marriott and R. D. Topsom, *J. Chem. Soc., Perkin Trans. 2*, **1984**, 113.

24) A. L. McClellan, "Tables of Experimental Dipole Moments," W. H. Freeman, San Francisco (1963).

25) K. G. Denbigh, *Trans. Faraday Soc.*, **36**, 936 (1940).

26) Values for CN, OH, and NO_2 groups calculated from R_D reported by A. L. Vogel, *J. Chem. Soc.*, **1948**, 1833.

27) K. B. Wiberg, *J. Am. Chem. Soc.*, **102**, 1229 (1980).

Cyclohepta[*b*][1,4]benzothiazines and Their Diazine Analogues. 1. Formation and Reactions of Cyclohepta-[*b*][1,4]benzothiazines[1]

Kimio SHINDO,* Sumio ISHIKAWA, and Tetsuo NOZOE*,†
Department of Chemistry, Faculty of Science, Josai University, 1-1 Keyakidai, Sakado-shi, Saitama 350-02
†*Tokyo Research Laboratories, Kao Corporation, 2-1-3 Bunka, Sumida-ku, Tokyo 131*
(Received July 18, 1984)

2-Chlorotropone reacted with *o*-aminobenzenethiol to give 2-(*o*-aminophenylthio)tropone, which readily cyclized in dilute methanolic HCl to afford the title benzothiazine (**9**). Although **9** was stable under basic conditions, its *N*-methyl cation reversibly afforded the ring-opened 2-[*o*-(methylamino)phenylthio]tropone in alkali. Oxidation of **9** with hydrogen peroxide in methanol underwent a rearrangement reaction to afford (exclusively) phenothiazine and its 1-formyl derivative. A similar H_2O_2 oxidation of 10-methoxycyclohepta[*b*][1,4]benzothiazine gave mainly methyl phenothiazine-1-carboxylate and 3-formyl-1-methoxy phenothiazine. Further oxidation of these products with hydrogen peroxide yielded thier *S*-oxides and *S,S*-dioxides. The reactivities of these cycloheptabenzothiazines are discussed in connection with those of the O- and N-analogues.

It was recently reported[2] by one of us (T.N.) that the condensation of 2-chloro- or 2-methoxytropone (**1a**, **b**) with *o*-aminophenol (**2**) gave 2-(*o*-hydroxyanilino)-tropone (**3**), which cyclized in acid to afford cyclohepta-[*b*][1,4]benzoxazine (**4**). Compound **4** and its derivatives were generally unstable in alkali (or, in some cases, even to the moisture in solvents) and readily reverted to **3** and further hydrolyzed to tropolone (**1**: X=OH) upon heating with an excess of alkali.[2,3]

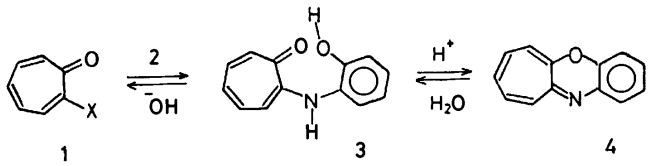

1 3 4

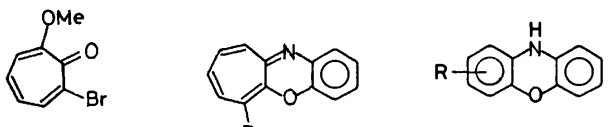

5 6 7

Moreover, reactive troponoids bearing two leaving groups, such as **5** and its isomers, were also found[4] to condense with **2**, to provide 6-bromocyclohepta[*b*]-[1,4]benzoxazine (**6**) and its isomers, which were then transformed into a wide variety of interesting derivatives of cycloheptabenzoxazine **4** and phenoxazine **7**.

This evidence led us to investigate the synthesis and properties of the S- and N-analogues of **4** in order to make a systematic study of these reactive troponoids fused with heterocycles.[5] Although the formation of cyclohepta[*b*][1,4]benzothiazine (**9**), corresponding 10(11*H*)-one **10**, and some of their derivatives from **1** (or **5**) and *o*-aminobenzenethiol (**8**), as well as the oxidative formation of *S*-oxide (**11**) and dioxide (**12**) with hydrogen peroxide, had been briefly reported earlier,[6,7] we now wish to describe their detailed preparation and

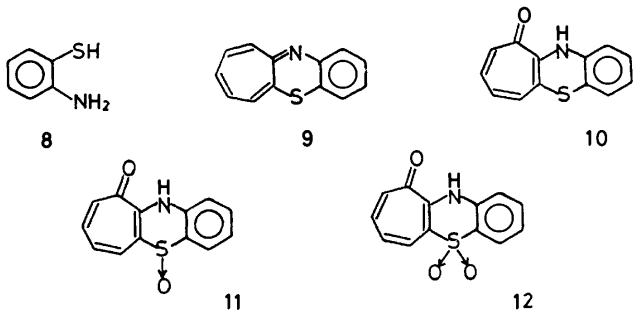

8 9 10

11 12

some new reactions of the title compound **9** and its derivatives.

Results and Discussion

We first studied the reaction of **1a** and **8** in methanol by means of reversed-phase, high-pressured liquid chromatography (HPLC). A stopped-flow apparatus was used to identify every product formed during the reaction[8] (see Fig. 1). It was found that an intermediate substance **14** that was formed at an early stage of the reaction was gradually transformed almost solely into the final product **9**. Besides these, the only remaining product detected was disulfide **13** from **8**. When the condensation of **1a** with **8** was conducted in the presence of an alkali in order to neutralize the liberated HCl, compound **14** (isolable as yellow needles, mp 120.5 °C) was produced exclusively. The 2-(*o*-aminophenylthio)tropone structure was unambiguously assigned to **14** on the basis of its IR, UV, NMR, and mass spectra as well as elemental analysis (for assignments of the spectral signals, see Experimental part). That the condensation of **1a** with **8** apparently took place by a nucleophilic attack of SH (rather than NH_2) group of **8** was in conformity with the generally known order of the nucleophilicity of these groups towards halotropones.[9]

The action of a trace amount of acid on **14** facilitated

cyclization to yield **9**, which remained stable and, in marked contrast to the afore-mentioned **4**, did not revert to **14** upon heating with methanolic potassium hydroxide. In a strong acid, compound **9** gave the red-colored monocation **9a** of a tropylium form as in the case of cation **4a** from **4**. It should be noted that these cationic species (**4a**,**9a**) are apparently different from the dark green-colored cation **15a** having a peripheral π-electron system which had been derived[5,10] from the N-analogue **15** in a strong acid.

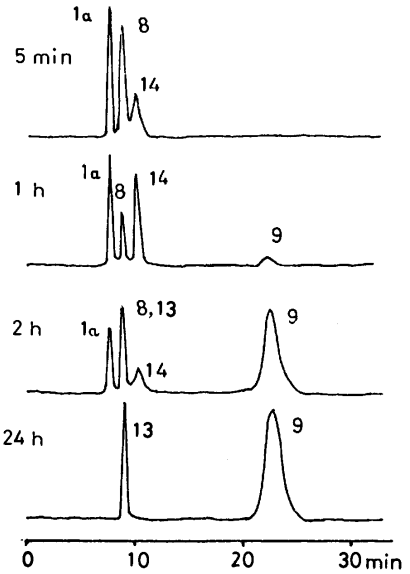

Fig. 1. Time dependent HPLC chromatogram of reaction of **1a** and **8** in MeOH at R.T.

The treatment of **9** with methyl fluorosulfate (magic methyl) yielded an inseparable mixture of the *N*-methyl cation **17** (see below) and **9a**, which, on basification, gave yellow needless **18**, along with recovered **9**. The structure of **18** was established on the basis of the spectral data (see Experimental) which closely resembled those of **14**, except for the presence of the *N*-methyl proton signal (NMR) at δ 2.09. Upon acidification, **18** gave the cyclized product **17**, isolable as the dark red BF_4^- salt. An appreciable down-field shift of the proton signals of the seven-membered ring in the NMR spectrum was strongly indicative of the cation **17**, predominantly in the tropylium form.

When **4** was likewise treated with magic methyl for comparison, a mixture of a similar cation **19** and **4a** was produced, which in turn led to aminotropone **20** and **4** upon basification. The structure of **20** was derived from the spectral data. On acidification, **20**

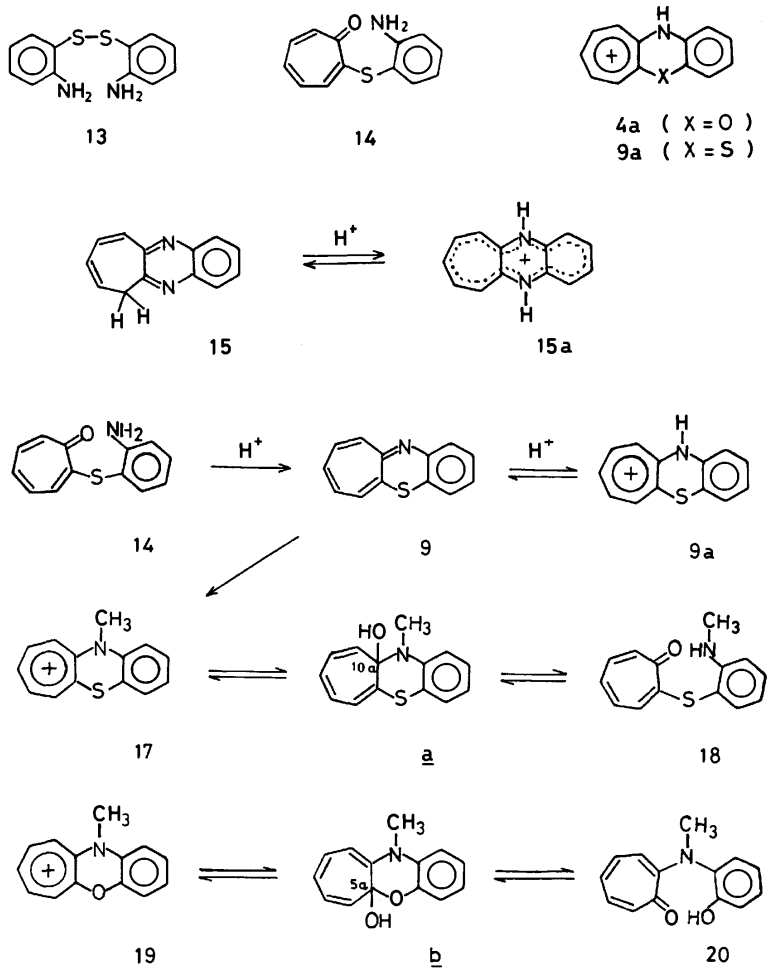

was found to cyclize to give **19** (isolable as BF_4^- salt) much faster than the case of **18** to **17**. The fact that the cation **17** was susceptible to a nucleophilic attack by OH^- at the 10*a*-position to give thiotropone **18** *via* an intermediate a, whereas its O-analogue **19** afforded aminotropone **20** *via* intermediate b by the OH^- attack at the 5*a*-position, is in accord with the results of theoretical calculations regarding the reactivities of these systems.[11]

We then studied the behaviors of **4** and the S-analogue **9** towards hydrogen peroxide. Treatment of compound **4** with H_2O_2 in methanol gave mainly cyclohepta[*b*][1,4]benzoxazin-10(11*H*)-one (**21**), along with small proportions of the hydrolyzed product **3** (*ca.* 3%) and the rearranged 1-formylphenoxazine[4] (**22**) (<1%). In contrast to oxazine **4**, compound **9** was

21 22

found exclusively to give a wide variety of rearrangement products. A close examination of this reaction using time-dependent HPLC (see Fig. 2) revealed that at the initial stage of the reaction, two main peaks (due to intermediates **23** and **24**) were observed. These gradually transformed into **23a** and **24a** and a small proportion of an additional product (**25**), and then finally gave products **23a** and **24a,b** as the main products. Presumable sequences of this oxidation reaction are summarized in Scheme 1. Although

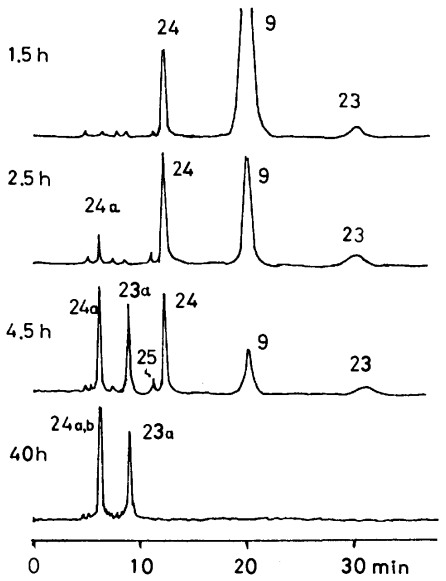

Fig. 2. Time dependent HPLC chromatogram of reaction of **9** and H_2O_2 in MeOH at R.T.

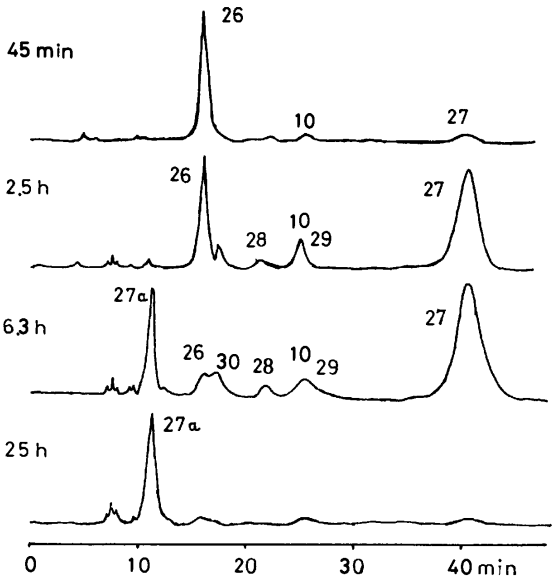

Fig. 3. Time dependent HPLC chromatogram of reaction of **26** and H_2O_2 in MeOH at R.T.

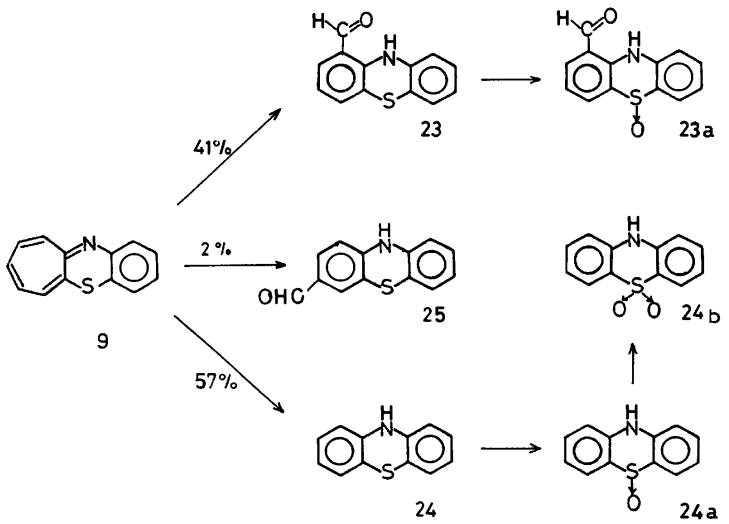

Scheme 1. H_2O_2 oxidation products from **9** in MeOH

compounds **23** and **25** both showed their molecular ion peaks at *m/z* 227 in the mass spectrum, the former (**23**) showed an IR absorption at 3300 cm^{-1} (NH) and characteristic ^{1}H-NMR signals at δ 10.00 (NH), 9.79 (CHO) and 7.17 (1H, dd, J=7.8 and 2.0 Hz), whereas the latter (**25**) showed the NH absorption at 3360 cm^{-1} and NMR signals at δ 8.90 (NH), 9.64 (CHO), and 7.30 (1H, d, J=1.8 Hz), thus permitting the assignments of 1-[12] and 3-formylphenothiazine structures to these products, respectively. Compound **24** was identified spectroscopically to be the known parent phenothiazine,[13] and **24a** and **24b** its *S*-monoxide and *S,S*-dioxides,[13] respectively. These *S*-oxides reverted to **23** and **24** upon redution with zinc duct.

In order to clarify the site of the H_2O_2 attack on the seven-membered ring of **9**, compound **26** (bearing a methoxyl group at the 10-position) was subjected to similar oxidation. The reaction was again monitored by periodical HPLC checking (see Fig. 3). Although the reaction appeared to be somewhat more complex compared with the oxidation of **9**, a transient product **27** and the final product **27a** were mainly formed. These compounds were identified by the spectral evidence to be methyl 1-phenothiazinecarboxylate[14] (**27**) and its *S*-oxide (**27a**). The probable sequences of this oxidation to yield these compounds and several minor products (**28**—**30**) are summarized in Scheme 2. The structure of 3-formyl-1-methoxyphenothiazine for **28** was derived from the NMR spectrum which showed two characteristic doublets at δ 7.12 and 7.04 (with J=1.5 Hz) due to isolated ring-protons, in addition to a singlet (δ 3.92) of a MeO group. Com ound **29** was identified to be 1-methoxyphenothia-

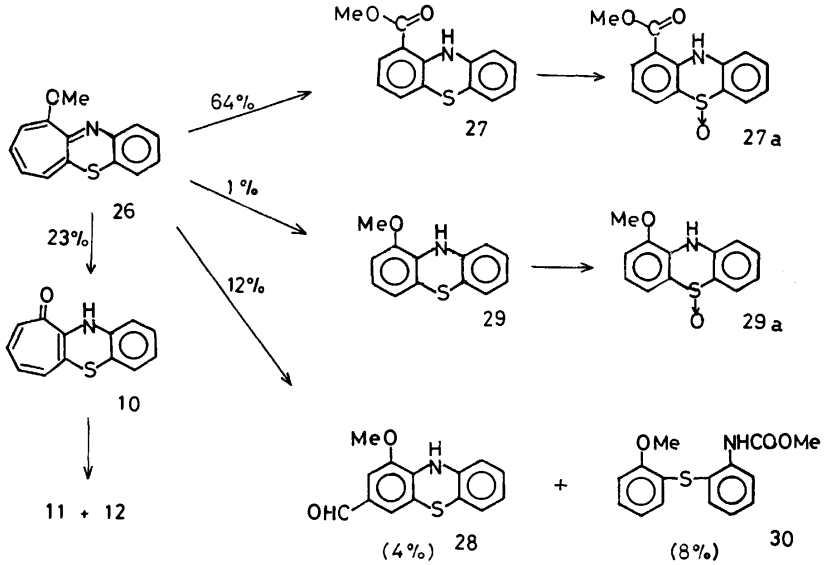

Scheme 2. H_2O_2 oxidation products from **26** in MeOH

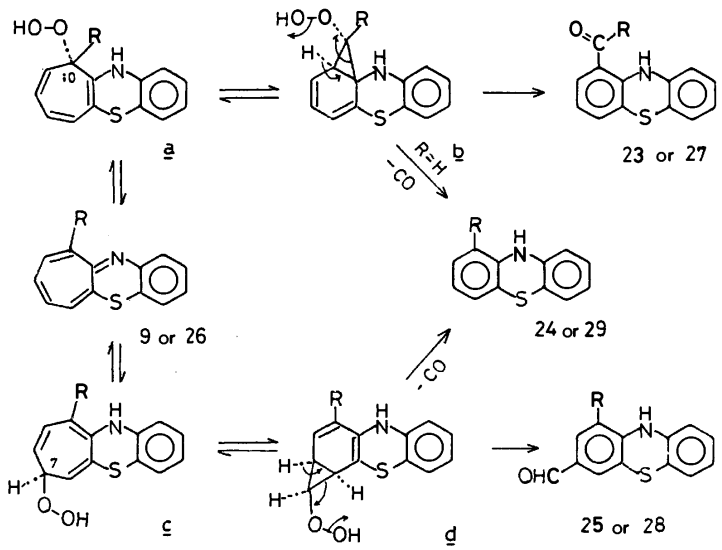

Scheme 3. R=H, OMe

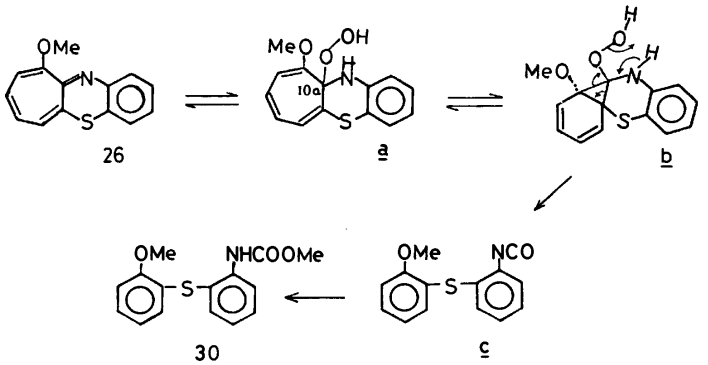

Scheme 4.

zine[15] on the evidence of IR, NMR, and mass spectra. Oxidation of **29** was found to afford *S*-oxide **29a**. Compound **30** was assigned to be methyl 2-(*o*-methoxyphenylthio)phenylcarbamate from the IR, NMR, and MS spectra. In addition to these oxidation products, the hydrolyzed product **10** was also isolated.

Possible Reaction Pathways for the Oxidation of Cyclohepta[b][1,4]benzothiazines. The ring-contraction of **9** and **26** to **23—28** are most likely to proceed by a nucleophilic attack of H_2O_2 preferentially at the 10- and then, to a considerably less extent, 7-positions to yield the intermediates a and c, followed by the sequential steps illustrated in Scheme 3. On the other hand, the oxidative degradation of **26** to **30** is considered to be initiated by an attack of hydrogen peroxide at the 10*a* position, followed by similar ring-contraction (illustrated in Scheme 4). This order of reactivities of cycloheptabenzothiazines towards nucleophiles is generally in agreement with predictions based on theoretical calculations.[11]

Although the exact mechanism of these oxidations accompanied by such a variety of facile rearrengements (as well as other reactivities of the title compounds and their N-analogues) are currently under detailed investigation. The present experimental results further demonstrate a part of the diversity of chemical reactions involving troponoid compounds, particularly when fused with certain heterocycles.

Experimental

Melting points were determined with a Yanagimoto MP-3S and are uncorrected. The IR spectra were taken on a Shimazu IR-400 or IR-450, and the UV spectra were recorded with a Shimazu UV-202 or a Hitachi 557 spectrometer. The NMR spectra were recorded with JEOL JNM-PS100 (100-MHz) and GX270 (270-MHz) spectrometers using TMS as the internal standard. The mass spectra were taken on Shimazu LKB9000 and JEOL JMS-01SG mass spectrometers. The HPLC was carried out with Hitachi gel #3011 with MeOH–hexane (9:1) as the solvent. The UV spectra in acid and alkali were taken after adding a drop of 3M HCl or 3M NaOH (1M=1 mol dm^{-3}) to the sample solution. TLC analyses were carried out with Merk Kieselgel 60F-254 and Alminium oxide F-254 plates.

2-(o-Aminophenylthio)tropone (14). A solution of **1a** (200 mg, 1.4 mmol) in methanol (1 ml) was slowly added, with stirring at 0 °C, to a solution of **2** (200 mg, 1.6 mmol) and sodium hydroxide (170 mg, 4.2 mmol) in methanol (2 ml), and the mixture was allowed to stand for one day at −5—0 °C. The precipitates were collected and recrystallized from acetone to give **14** (304 mg, 93%) as yellow needles; mp 120.5 °C; UV (MeOH) 243, 340, and 367 nm (log ε 4.34, 3.98, and 3.97); IR (KBr) 3430, 3340 (NH_2), and 1610 cm^{-1} (C=O); ^1H NMR (270 MHz in C_6D_6) δ=3.55 (2H, br, NH_2), 5.93—5.98 (2H, m, H-4,5), 6.28 (1H, dd, *J*=8 and 1.5 Hz, H-3′), 6.31 (1H, m, H-6), 6.54 (1H, d, *J*=10 Hz, H-3), 6.55 (1H, m, *J*=8.8 and 1.5 Hz, H-5′ or 4′), 6.96 (1H, d, *J*=12 Hz, H-7), 7.01 (1H, m, *J*=8.8 and 1.5 Hz, H-4′ or 5′), and 7.28 (1H, dd, *J*=8 and 1.5 Hz, H-6′), (270 MHz in $CDCl_3$) δ=4.33 (2H, br, NH_2), 6.68 (1H, m, H-5 or 4), 6.80 (1H, t, *J*=8 Hz, H-5′), 6.88—6.92 (2H, H-3 and H-4 or 5), 6.86 (1H, d, *J*=8 Hz, H-3′), 7.13 (1H, d, *J*=12 Hz. H-7), 7.22 (1H, m, H-6), 7.30 (1H, t, *J*=8 Hz, H-4′), and 7.38 (1H, d, *J*=8 Hz, H-6′); ^{13}CNMR (67.8 MHz in $CDCl_3$) δ=183.5, 157.4, 149.3, 137.5, 136.4, 135.5, 132.8, 132.0, 130.5, 128.5, 115.7, and 112.2; MS *m/z* 229 (M^+);

Anal. ($C_{13}H_{11}NSO$) C, H, N.

N-Acetyl Derivative; Yellow plates; mp 150.5 °C; UV (MeOH) 243, 342, and 367 nm (log ε 4.34, 3.95, and 3.96); IR (KBr) 3305 (NH), 1690 (C=O), and 1610 cm^{-1} (C=O); ^1H NMR (100 MHz in $CDCl_3$) δ=2.08 (3H, s, CH_3), 6.45—7.59 (8H, m, ar-H), 8.10 (1H, s, NH), and 8.55 (1H, d, *J*=9 Hz, H-3′); MS *m/z* 271 (M^+);

Anal. ($C_{15}H_{13}NSO$) C, H, N.

Cyclohepta[b][1,4]benzothiazine (9). A solution of **14** (30 mg, 0.13 mmol), in methanol (2 ml) containing a drop of conc hydrochloric acid was allowed to stand for 30 min at 20 °C. After removal of the solvent *in vacuo*, the residue was neutralized with aqueous $NaHCO_3$ and extracted with benzene. The extracts were combined, dried (Na_2SO_4), and evaporated *in vacuo*, thus giving **9** (27 mg, 97%) as red plates; mp 87 °C (from acetone), (lit,[6] 86—87 °C); ^1H NMR (250 MHz in $CDCl_3$) δ=6.04 (1H, dd, *J*=8.5 and 1.0 Hz, H-6), 6.12 (1H, ddt, *J*=11.0, 7.3 and 1.0 Hz, H-8), 6.14 (1H, d, *J*=12.0 Hz, H-10), 6.25 (1H, dddd, *J*=11.0, 8.5, 1.4, and 1.0 Hz, H-7), 6.31 (1H, ddd, *J*=12.0, 7.3, and 1.4 Hz, H-9), 6.79 (1H, ddd, *J*=7.5, 1.6 and 0.6 Hz, H-4), 6.92 (1H, td, *J*=7.5, 7.0, and 1.8 Hz, H-3), 7.01 (1H, td, *J*=7.5, 7.0, and 1.6 Hz, H-2), and 7.07 (1H, ddd, *J*=7.5, 1.8, and 0.6 Hz, H-1). (250 MHz in CF_3COOD) δ=6.74—6.82 (2H, m), 6.81 (1H, d, *J*=11 Hz, H-10 or 6), 7.03—7.14 (3H, m), 7.17 (1H, dd, *J*=10 and 1.5 Hz, H-6 or 10), 7.22 (1H, td, *J*=10 and 1 Hz, H-7 or 9), and 7.36 (1H, ddd, *J*=11, 10, and 1 Hz, H-9 or 7). ^{13}C-NMR (67.8 MHz in

$CDCl_3$) δ=125.5 (d), 126.5 (d), 127.5 (d), 127.6 (d), 128.7 (d), 131.4 (d), 133.5 (d), 133.6 (d), 134.2 (d), 134.4 (s), 143.4 (s), and 159.4 (s).

2-[o-(Methylamino)phenylthio]tropone (18). A solution of **9** (50 mg, 0.24 mmol) and methyl fluorosulfate (200 mg, 1.75 mmol) in dichloromethane (0.5 ml) was allowed to stand in a sealed flask for 48 h at room temperature. After removing the solvent and the excess sulfate *in vacuo*, the residue was diluted with aqueous $NaHCO_3$ and then extracted with $CHCl_3$. The extracts were combined and evaporated *in vacuo*. The residue was chromatographed on silica-gel thin-layer plates with 10:1 benzene–MeOH as the eluant, thus giving **18** (36 mg, 63%) and unreacted **9** (15 mg).

18: Yellow needles (from $CHCl_3$); mp 156—157 °C; UV (MeOH) 248, 277sh, 324, 340, 366, and 384 nm (log ε 4.33, 3.78, 3.92, 3.96, 3.92, and 3.83), (MeOH+HCl) 242, 282, 342, and 454 nm (log ε 4.27, 4.13, 3.93, and 3.61); IR (KBr) 3350 (NH) and 1620 cm^{-1} (C=O); ^1H NMR (270 MHz in C_6D_6) δ=2.09 (3H, s, CH_3), 4.53 (1H, s, NH), 5.92 (1H, ddd, *J*= 10.4, 8.0, and 1.5 Hz, H-4) 5.95 (1H, ddd, *J*=10.4, 7.0, and 1.5 Hz, H-5), 6.30 (1H, m, H-6), 6.35 (1H, d, *J*=8.0 Hz, H-3′ or 6′), 6.57 (1H, dd, *J*=8.0 and 1.5 Hz, H-3), 6.59 (1H, td, *J*=8.0 and 1.5 Hz, H-5′ or 4′), 6.98 (1H, d, *J*= 11.7 Hz, H-7), 7.17 (1H, td, *J*=8.0 and 1.5 Hz, H-4′ or 5′), and 7.36 (1H, dd, *J*=8.0 and 1.5 Hz, H-6′ or 3′).

Found: *m/z* 243.0688. Calcd for $C_{14}H_{13}NSO$: M, 243.0816.

2-(N-Methyl-o-hydroxyanilino)tropone (20). The reaction of **4** and methyl fluorosulfate was conducted in a manner similar to that for **9** described above, thus giving **20** in 50% yield: Yellow meedles (from $CHCl_3$); mp 132—133 °C; UV (MeOH) 246, 344, and 410 nm (log ε 4.24, 4.02, and 3.93), (MeOH+HCl) 228, 262, 272, 320, and 428 nm, (log ε 4.42 4.33, 4.39, 3.89, and 3.95); IR (KBr) 3420 (OH) and 1600 cm^{-1} (C=O); ^1H NMR (270 MHz in C_6D_6) δ=2.64 (3H, s, CH_3), 6.12 (1H, t, *J*=9 Hz, H-5), 6.28 (1H, d, *J*=10 Hz, H-3), 6.41 (1H, t, *J*=10 and 9 Hz, H-4), 6.44 (1H, ddd, *J*=12, 9, and 1.5 Hz, H-6), 6.58 (1H, dd, *J*=8 and 2 Hz, H-3′ or 6′), 6.61 (1H, td, *J*=8 and 1.5 Hz, H-4′ or 5′), 6.85 (1H, d, *J*=12 Hz, H-7), 6.96 (1H, td, *J*=8 and 2 Hz, H-5′ or 4′), and 7.18 (1H, dd, *J*=8 and 1.5 Hz, H-6′ or 3′).

Found: *m/z* 227.0928. Calcd for $C_{14}H_{13}NO_2$: M, 227.0942.

11-Methylcyclohepta[b][1,4]benzothiazinium Tetrafluoroborate (17). To a solution of **18** (10 mg) in methanol (1 ml) was added 42% HBF_4 (40 mg), and the mixture was set aside at room temperature, depositting crystals after several hours. The precipitates were filtered off, giving **17** (11 mg, 85%, combined with the second crop): Dark red needles; mp 162—164 °C; UV (MeOH) 240, 282, 340, and 452 nm (log ε 4.39, 4.26, 4.04, and 3.68); ^1H NMR (270 MHz in CD_3CN) δ=3.75 (3H, s, CH_3), 7.21 (1H, dd, *J*=7 and 1.5 Hz, H-4 or 1), 7.29 (1H, dd, *J*=7 and 1.5 Hz, H-1 or 4), 7.34 (1H, td, *J*=7 and 1.5 Hz, H-3 or 2), 7.39 (1H, td, *J*=7 and 1.5 Hz, H-2 or 3), 7.46 (1H, d, *J*=12 Hz, H-10 or 6), 7.57 (1H, td, *J*=8 and 3 Hz, H-8), 7.73 (1H, td, *J*=8 and 1.5 Hz, H-7 or 9), 7.76 (1H, dd, *J*=8 and 3 Hz, H-6 or 10), and 7.91 (1H, m, *J*=12, 8, and 1.5 Hz, H-9 or 7).

Anal. ($C_{14}H_{12}BF_4NO$) C, H, N.

11-Methylcyclohepta[b][1,4]benzoxazinium Tetrafluoroborate (19). The same treatment of **20** with HBF_4 as above gave **19** (89%) as dark red needles; mp 156—157 °C; UV (MeOH+HBF_4)[16] 228, 264, 272, 320, and 428 nm (log ε 4.31, 4.22, 4.31, 3.78, and 3.83); ^1H NMR (270 MHz in CD_3CN) δ=3.31 (3H, s, CH_3), 6.79 (1H, m, H-4 or 1), 6.99—7.08 (3H, m, H-2, 3, and 1 or 4), 7.10 (1H, d, *J*=12 Hz, H-6 or 10), 7.15 (1H, d, *J*=12 Hz, H-10 or 6), 7.26 (1H, t, *J*=9.5 Hz, H-8), 7.55 (1H, ddd, *J*=12, 9.5, and 1.5 Hz, H-7 or 9), and 7.75 (1H, ddd, *J*=12, 9.5, and 1.5 Hz, H-9 or 7).

Anal. ($C_{14}H_{12}BF_4NO$) C, H, N.

Oxidation of 9 with H_2O_2. Compound **9** was treated with various molar ratios (1:4—10) of 28% H_2O_2 in methanol at room temperature. Each product was identified by means of periodical checking using HPLC and TLC; most of the products were separated by preparative HPLC, and the yields were based on the peak areas.

1-Formylphenothiazine (23): Orange needles (from EtOH–$CHCl_3$); mp 80.5—81.0 °C (lit,[12] 80—81 °C); UV (MeOH) 240, 288, and 431 nm (log ε 4.46, 3.83, and 3.60); IR (KBr) 3300 (NH), 2860, 2760, and 1665 cm^{-1} (CHO); ^1H NMR ($CDCl_3$) δ=6.55—7.07 (6H, m), 7.17 (1H, dd, *J*=7.8 and 2.0 Hz, H-2), 9.79 (1H, s, CHO), and 10.10 (1H, br, NH); (Found: C, 68.70; H, 3.80; N, 6.63%; M^+ 227).

1-Formylphenothiazine 5-Oxide (23a): Yellow needles (from EtOH); mp 196—197 °C; UV (MeOH) 228, 305, and 375 nm (log ε 3.98, 3.70, and 3.57); IR (KBr) 3250 (NH), 2870, 2780, and 1665 cm^{-1} (CHO); ^1H NMR ($CDCl_3$) δ=7.24—7.41 (3H, m, H-3,7,9), 7.64 (1H, t, *J*=8 Hz, H-8), 7.97 (2H, d, *J*=8 Hz, H-4,6), 8.23 (1H, d, *J*=8 Hz, H-2), 10.09 (1H, s, CHO), and 11.67 (1H, br, NH); MS, *m/z* 243 (M^+).

Anal. ($C_{13}H_9NSO_2$) C, H, N.

3-Formylphenothiazine (25): Yellow needles (from MeOH); mp 194.5—196 °C; UV (MeOH) 242, 288, and 405 nm (log ε 4.39, 4.49, and 3.93); IR (KBr) 3320 (NH), 2850, 2760, and 1660 cm^{-1} (CHO); ^1H NMR ($CDCl_3$) δ=6.64—6.97 (5H, m, H-1,6,7,8,9), 7.30 (1H, d, *J*=1.8 Hz, H-4), 7.46 (1H, dd, *J*=8.2 and 1.8 Hz, H-2), 8.90 (1H, br, NH), and 9.64 (1H, s, CHO); MS, *m/z* 227 (M^+).

Anal. ($C_{13}H_9NSO$) C, H, N.

Phenothiazine 5-Oxide (24a): Pale yellow needles (from EtOH); mp 246—247 °C (lit,[13] 242—242.5 °C); ^1H NMR (DMSO-d_6) δ=7.17 (2H, ddd, *J*=7.8, 6.8, and 1.5 Hz, H-3,7), 7.38 (2H, dd, *J*=8.3 and 1.5 Hz, H-1,9), 7.56 (2H, ddd, *J*=8.3, 6.8, and 1.5 Hz, H-2,8), 7.86 (2H, dd, *J*=7.8 and 1.5 Hz, H-4,6), and 10.78 (1H, br, NH).

Reaction of 10-Methoxycyclohepta[b][1,4]Benzothiazine (26) with H_2O_2: Compound **26** was prepared from 7-methoxy-2-bromotropone and *o*-aminobenzenethiol according to the reported method.[6] The reaction of **26** with H_2O_2 was conducted in a manner similar to that described earlier for **9**, thus giving **10—12** and **27—30**.

26: Red oil; ^1H NMR ($CDCl_3$) δ=3.89 (3H, s, OCH_3), 6.08—6.38 (4H, m), and 7.01—7.36 (4H, m); MS, *m/z* 241 (M^+). Picrate, mp 183—184 °C (lit,[6] 184—185 °C).

Methyl 1-Phenothiazinecarboxylate (27): Yellow needles (from $CHCl_3$); mp 113.1—114.4 °C (lit,[14] 113—113.5 °C); UV (MeOH) 210, 240, 256, 316, and 388 nm (log ε 4.58, 4.56, 4.57, 3.62, and 3.87); IR (KBr), 3300 (NH) and 1680 cm^{-1} (C=O); ^1H NMR ($CDCl_3$) δ=3.89 (3H, s, CH_3), 6.51—7.11 (6H, m), 7.67 (1H, dd, *J*=7.8 and 1.5 Hz, H-2), and 9.91 (1H, br, NH); (Found: C, 65.62; H, 4.31; N, 5.62%; M^+, 257).

Methyl 10H-Phenothiazine-1-carboxylate 5-Oxide (27a): Yellow needles (from $CHCl_3$); mp 167.0—169.2 °C; UV (MeOH) 209, 229, 250, 296, and 361 nm (log ε 4.34, 4.33, 4.04, 4.09, and 3.87); IR (KBr) 3260 (NH) and 1690 cm^{-1} (C=O); ^1H NMR ($CDCl_3$) δ=4.01 (3H, s, OCH_3), 7.21 (1H, dd, *J*=7.8 and 6.8 Hz, H-7), 7.28 (1H, t, *J*=7.8 Hz, H-3), 7.33 (1H, d, *J*=8.3 Hz, H-9), 7.61 (1H, ddd, *J*=8.3, 6.8, and 1.5 Hz, H-8),

7.93 (1H, d, J=7.8 Hz, H-6), 8.17 (1H, dd, J=7.8 and 1.5 Hz, H-2 or 4), 8.34 (1H, dd, J=7.8 and 1.5 Hz, H-4 or 2), and 11.58 (1H, br, NH); MS, m/z 273 (M^+).

Anal. ($C_{10}H_{11}NSO_3$) C, H, N.

3-Formyl-1-methoxyphenothiazine (28): Yellow needles (from MeOH) mp 121 °C; UV (MeOH) 207, 246, 298, and 407 nm (log ε 4.38, 4.41, 4.35, and 3.82); IR (KBr) 3300 (NH) and 1660 cm^{-1} (C=O); ^1H NMR ($CDCl_3$) δ=3.92 (3H, s, OCH_3), 6.57 (1H, d, J=6.8 Hz, H-6 or 9), 6.61 (1H, br, NH), 6.88 (3H, m, H-7,8, and 9 or 6), 7.04 (1H, d, J=1.5 Hz, H-2 or 4), 7.12 (1H, d, J=1.5 Hz, H-4 or 2), and 9.68 (1H, s, CHO); MS, m/z 257 (M^+).

Anal. ($C_{14}H_{11}NSO_2$) C, H, N.

Methyl 2-(o-Methoxyphenylthio)phenylcarbamate (30): Pale yellow needles (from $CHCl_3$); mp 93.0 °C; UV (MeOH) 209, 239, and 289 nm (log ε 4.60, 4.26, and 3.79); IR (KBr) 3370 (NH) and 1740 cm^{-1} (C=O); ^1H NMR ($CDCl_3$) 3.73 (3H, s, OCH_3), 3.92 (3H, s, OCH_3), 6.79—7.63 (7H, m), 8.07 (1H, br, NH), and 8.21 (1H, dd, J=8.3 and 1.5 Hz, H-3 or 6); MS (70 eV), m/z (rel intensity) 290 (18), 289 (100; M^+), 258 (12), 257 (62), 214 (10), 200 (16), 199 (25), 198 (21), 186 (15), 167 (8), 150 (43), and 77 (8).

Anal. ($C_{15}H_{15}NSO_3$) C, H, N.

Cyclohepta[b][1,4]benzothiazin-10(11H)-one (10): Red needles (from MeOH); mp 168—169 °C (lit,[6] 168—169 °C); ^1H NMR (270 MHz in C_6D_6) δ=5.74 (1H, m, H-4), 5.84 (1H, dd, J=11.0 and 8.8 Hz, H-7) 6.22 (1H, d, J=11.0 Hz, H-6), 6.25 (1H, dd, J=11.7 and 8.8 Hz, H-8), 6.45—6.50 (3H, m, H-1,2,3), 6.99 (1H, d, J=11.7 Hz, H-9), and 8.74 (1H, s, NH).

Cyclohepta[b][1,4]benzothiazin-10(11H)-one 5-Oxide (11): Yellow needles (from EtOH); mp 196—197 °C (lit,[7] 207 °C); ^1H NMR (270 MHz in C_6D_6) δ=6.17 (1H, dd, J=11.0 and 8.8 Hz, H-7), 6.24 (1H, d, J=8.1 Hz, H-1), 6.56 (1H, dd, J=11.7 and 8.8 Hz, H-8), 6.74 (1H, dd, J=8.1 and 7.3 Hz, H-3), 6.84 (1H, dd, J=8.1 and 7.3 Hz, H-2), 7.04 (1H, d, J=11.7 Hz, H-9), 7.29 (1H, d, J=11.0 Hz, H-6), 7.55 (1H, d, J=8.1 Hz, H-4), and 10.12 (1H, s, NH).

Cyclohepta[b][1,4]benzothiazin-10(11H)-one 5,5-Dioxides (12): Yellow needles (from AcOH); mp 264—265 °C (lit,[7] 266 °C); ^1H NMR (270 MHz in C_6D_6) δ=6.17 (1H, dd, J=11.0 and 8.8 Hz, H-7), 7.27 (1H, d, J=11.7 Hz, H-9), 7.53 (1H, t, J=8.0 Hz, H-2 or 3), 7.64 (1H, dd, J=11.7 and 8.8 Hz, H-8), 7.81 (1H, t, J=8.0 Hz, H-3 or 2), 7.85 (1H, d, J=11.7 Hz, H-6), 8.03 (1H, d, J=8.0 Hz, H-1 or 4), 8.21 (1H, d, J=8.0 Hz, H-4 or 1), and 11.45 (1H, s, NH).

We wish to thank Professor Hiroshi Yamamoto for his helpful discussions and Professor Sumio Umezawa and Dr. T. Miyake (Inst. Bio-org. Chem., Kawasaki) for the NMR measurements with the Brucker WE-250 (250 MHz) spectrometer.

References

1) Presented at the 41th National Meeting of the Chemical Society of Japan, Higashi-Osaka, April 1980, Abstr., No. 2K34; at the 43rd Meeting, Tokyo, April 1981, Abstr., 1H42.

2) T. Nozoe, H. Okai, and T. Someya, *Bull. Chem. Soc. Jpn.*, **51**, 2185 (1978).

3) T. Nozoe and T. Someya, *Bull. Chem. Soc. Jpn.*, **51**, 3316 (1978).

4) T. Nozoe, T. Someya, and H. Okai, *Bull. Chem. Soc. Jpn.*, **52**, 1156 (1979); T. Someya, H. Okai, H. Wakabayashi, and T. Nozoe, *ibid.*, **56**, 2756 (1983).

5) T. Nozoe, *Pure Appl. Chem.*, **54**, 975 (1982).

6) T. Nozoe, T. Asao, and K. Takahashi, *Bull. Chem. Soc. Jpn.*, **34**, 146 (1961); T. Nozoe, T. Asao, and K. Takahashi, *ibid.*, **39**, 1980 (1966).

7) T. Nozoe, T. Asao, and K. Takahashi, *Bull. Chem. Soc. Jpn.*, **39**, 1988 (1966).

8) For the first examples of monitoring reactions by means of periodical checking using the reversed-phase HPLC, see T. Nozoe and J. Kawase, the 9th Japanese Symposium on the Chemistry of Nonbenzenoid Aromatic Compounds, Sendai, December, 1976, Abstr., p. 98.

9) T. Nozoe, K. Takase, and H. Matsumura, "Nonbenzenoid Aromatic Compounds" in "Dai Yuki Kagaku (Comprehensive Organic Chemistry)" ed by M. Kotake, Asakura Shoten, Tokyo (1960), Vol. 13, pp. 1—418.

10) a) T. Fukunaga, Presented at the 23rd IUPAC Congress, Boston, 1971, Abstr., p. 103; and private communication. b) K. Shindo, S. Ishikawa, and T. Nozoe, to be published.

11) T. Kurihara, S. Ishikawa, and T. Nozoe, to be published; reaction indexes (f_r^N) for nucleophilic reactions, **9**: C-5a (0.534), C-10 (0.499), C-7 (0.419); **26**: C-5a (0.510), C-10 (0.486), C-7 (0.375).

12) M. Harfenist, *J. Org. Chem.*, **27**, 4326 (1962); no spectral data were recorded in this paper.

13) S. P. Massie, *Chem. Rev.*, **54**, 797 (1954); H. Gilman and R. D. Nelson, *J. Am. Chem. Soc.*, **75**, 5422 (1953); N. L. Smith, *J. Org. Chem.*, **16**, 415 (1951); R. J. Warren, I. B. Eisdorfer, W. E. Thompson, and J. E. Zarembo, *J. Pharm. soc*, **55**, 144 (1966); C. Bodea and I. Silberg, "Advances in Heterocyclic Chemistry" ed by A. R. Katritzky and A. J. Boulton, Academic Press, Vol. 9, 321 (1968).

14) H. Gilman, D. A. Shirley and P. R. von Ess, *J. Am. Chem. Soc.*, **66**, 625 (1944); J. S. Driscoll and R. H. Nealey, *J. Heterocycl. Chem.*, **2**, 272 (1965); no spectral data were recorded.

15) A. M. Duffield, J. C. Craig, and L. R. Kray, *Tetrahedron*, **24**, 4267 (1968); J. C. Craig, D. E. Green, S. K. Roy, L. H. Piette, and K. O. Loeffler, *J. Med. Chem.*, **8**, 392 (1965).

16) Measured after adding a drop of aqueous HBF_4 to prevent the opening of the heterocyclic ring.

Aggregation Behavior of Amphiphiles Functionalized with Dipeptide Segments and Enantioselective Ester Hydrolysis in Their Bilayer Membranes†

Yukito MURAKAMI,* Akio NAKANO,†† Hidetsugu IKEDA, Toru IMORI, and Kazunari AKIYOSHI
Department of Organic Synthesis, Faculty of Engineering, Kyushu University, Hakozaki, Higashi-ku, Fukuoka 812
(Received July 19, 1984)

Four amphiphiles having dipeptide segments, which consist of one histidyl residue and another amino acid residue, and the dihexadecyl moiety for the double-chain segment (N^+C_5AlaHis2C_{16}, N^+C_5LeuHis2C_{16}, N^+C_5PheHis2C_{16}, and N^+C_5HisAla2C_{16}) were synthesized, and the aggregate morphology of them was characterized by electron microscopy and differential scanning calorimetry. The amphiphiles, which have the histidyl residue bound to the dihexadecylamine component (N^+C_5AlaHis2C_{16}, N^+C_5LeuHis2C_{16}, and N^+C_5PheHis2C_{16}) formed both multi- and single-walled aggregates in the aqueous dispersion state, while their sonicated solutions involved only single-walled vesicles. On the other hand, the amphiphile, which has the alanyl residue bound to the dihexadecylamine component (N^+C_5HisAla2C_{16}) afforded tubular aggregates in the aqueous dispersion. The hydrolysis of enantiomeric esters of various hydrophobic nature, which was carried out in the single-walled vesicles, showed relatively small enantioselectivity. The reasons for such catalytic performance of the vesicles were discussed from the kinetic and mechanistic viewpoints; the kinetic analysis being carried out on the basis of the organic pseudo-phase concept.

We have previously clarified that peptide amphiphiles having various amino acid residues form chemically and morphologically stable bilayer membranes in aqueous media.[1] Among them, amphiphiles bearing the histidyl residue behave not only as apoenzyme models of vitamin B_6-dependent enzymes effective in the transamination reaction of amino acids[2] but also as a functional model of hydrolytic enzymes acting on enantiomeric esters.[3]

In this work, we prepared amphiphiles having dipeptide segments, which consist of one histidyl residue and another amino acid residue, and the dihexadecyl moiety for the double-chain segment. The amphiphiles having such double-chain segment are expected to show the phase transition between the gel and liquid-crystalline states in the room temperature range,[1c] so that organic reactions in the vesicular phase can be readily carried out above and below their phase transition temperatures. The aggregate morphology of these amphiphiles in aqueous media and the enantioselective ester hydrolysis in their single-walled bilayer membranes were investigated. The molecular formulae and abbreviations of the present peptide amphiphiles and of the ester substrates are shown above.

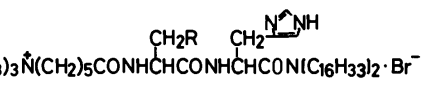

N^+C_5AlaHis2C_{16} : R =-H
N^+C_5PheHis2C_{16} : R =-C_6H_5
N^+C_5LeuHis2C_{16} : R =-$CH(CH_3)_2$

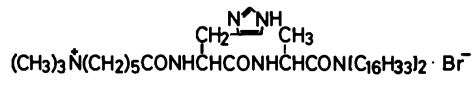

N^+C_5HisAla2C_{16}

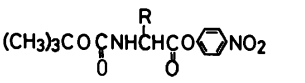

R = -CH_3 : BocAlaPNP
R = -$CH(CH_3)_2$: BocValPNP
R = -$CH_2CH(CH_3)_2$: BocLeuPNP

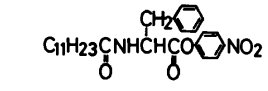

C_{12}PhePNP

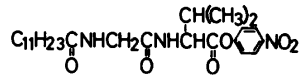

C_{12}GlyValPNP

Experimental

Spectroscopic data were taken on a JASCO DS-403G grating IR spectrophotometer and a Hitachi Perkin-Elmer R-20 NMR spectrometer. Melting points were measured with a Yanagimoto MP-S1 apparatus (hot-plate type). Experimental procedures for electron microscopy and differential scanning calorimetry (DSC) have been described elsewhere.[1-3] Optical rotations were measured with a Union Giken PM-71 high-sensitivity polarimeter.

N-(*t*-Butoxycarbonyl)-L-alanine, *N*-(*t*-butoxycarbonyl)-L-leucine, *N*-(*t*-butoxycarbonyl)-L-phenylalanine, *N*-(*t*-butoxycarbonyl)-N^{im}-benzyl-L-histidine, and the corresponding D-isomers were prepared from the corresponding amino acids and *O*-*t*-butyl *S*-(4,6-dimethyl-2-pyrimidinyl) thiocarbonate after the methods of Nagasawa *et al.*[4] *p*-Nitrophenyl esters of several *N*-(*t*-butoxycarbonyl)-L/D-amino acids (BocAlaPNP, BocValPNP, and BocLeuPNP) were obtained according to the procedures reported by Schnabel[5] and the products were identified by elemental analyses as well as by spectroscopic (NMR and IR) and polarimetric measurements. N^{α}-Hexadecanoyl-L-histidine (HisC$_{16}$) was prepared in a manner similar to that reported by Gitler *et al.*[6] for the preparation of N^{α}-tetradecanoylhistidine.[7] Octadecyltrimethylammonium

† Contribution No. 742 from this Department.

†† Present address: Department of Food Science, Toa University, Shimonoseki, Yamaguchi 751.

chloride (STAC) of Ishizu Pharmaceutical Co. was recrystallized from aqueous ethanol.

p-*Nitrophenyl* N^{α}_{val}-*(*N^{α}_{gly}-*Dodecanoylglycyl)*-L-*valinate (*L-C_{12}*GlyValPNP).* L-BocValPNP (1.1 g, 3.3 mmol) was dissolved in dry dichloromethane (30 ml). To the solution was added trifluoroacetic acid (25 g, 0.22 mol), and the mixture was stirred for 40 min at room temperature. The solvent was removed *in vacuo*, and the solid residue was washed with diethyl ether to give a white solid (0.8 g; mp 159—162 °C (decomp)). Elimination of the *t*-butoxycarbonyl group was confirmed by NMR spectroscopy. The amine component (0.8 g, 2.3 mmol) thus obtained, *N*-dodecanoylglycine (0.6 g, 2.3 mmol), and 1-hydroxybenzotriazole[8] (0.38 g, 2.8 mmol) were dispersed in dry dichloromethane (20 ml), and the mixture was cooled to 0 °C. Triethylamine (0.24 g, 2.3 mmol) and dicyclohexylcarbodiimide (0.58 g, 2.8 mmol) were added to the mixture in this sequence. The resulting mixture was stirred for 3 h at 0 °C, and then precipitates were removed by filtration. The solvent was removed *in vacuo*, and the residue was dissolved in ethyl acetate (100 ml). The solution was washed sequentially with 10% aqueous citric acid, 4% aqueous sodium hydrogencarbonate, and saturated aqueous sodium chloride. After being dried (Na_2SO_4), the solution was evaporated *in vacuo* to give a yellow oil which was subsequently purified by gel-filtration chromatography (Sephadex LH-20, methanol as an eluant): a white solid, yield 400 mg (10%); R_f on Silica Gel IB of J. T. Baker, 0.65 (ethyl acetate) and 0.14 (benzene); mp 76—78 °C, $[\alpha]_D^{25}$ −30.3° (*c* 1.0, dioxane). Found: C, 62.46; H, 8.20; N, 8.75%. Calcd for $C_{25}H_{39}N_3O_6$: C, 62.87; H, 8.23; N, 8.80%.

p-*Nitrophenyl* N^{α}_{val}-*(*N^{α}_{gly}-*Dodecanoylglycyl)*-D-*valinate (*D-C_{12}*GlyValPNP)*: mp 74—76 °C, $[\alpha]_D^{25}$ +30.5° (*c* 1.0, dioxane). Found: C, 62.63; H, 8.54; N, 8.32%.

p-Nitrophenyl N^{α}-dodecanoyl-D/L-phenylalaninates were synthesized according to the procedure by Ingles.[9]

p-*Nitrophenyl* N^{α}-*Dodecanoyl*-L-*phenylalaninate (*L-C_{12}-*PhePNP)*: mp 110.5—111.0 °C (lit,[10] 107.0—107.5 °C), $[\alpha]_D^{25}$ −11.9° (*c* 2.0, $CHCl_3$) [lit,[10] −11.4° (*c* 2.0, $CHCl_3$)]. Found: C, 68.90; H, 7.76; N, 6.01%. Calcd for $C_{27}H_{36}N_2O_5$: C, 69.20; H, 7.74; N, 5.97%.

p-*Nitrophenyl* N^{α}-*Dodecanoyl*-D-*phenylalaninate (*D-C_{12}-*PhePNP)*: mp 110.5—111.0 °C (lit,[10] 107.5—108.0 °C), $[\alpha]_D^{25}$ +11.0° (*c* 2.0, $CHCl_3$) [lit,[10] +11.9° (*c* 2.0, $CHCl_3$)]. Found: C, 68.98; H, 7.76; N, 6.00%.

The synthetic procedure for *N,N*-dihexadecyl-N^{α}_{his}-[N^{α}_{ala}-(6-trimethylammoniohexanoyl)-L-alanyl]-L-histidinamide bromide ($N^+C_5AlaHis2C_{16}$) is outlined in Scheme 1.

N,N-*Dihexadecyl*-N^{α}-*(t-butoxycarbonyl)*-N^{im}-*benzyl*-L-*histidinamide (1).* Dicyclohexylcarbodiimide (4.7 g, 23 mmol) was added with stirring to a dry dichloromethane solution (100 ml) of *N*-(*t*-butoxycarbonyl)-N^{im}-benzyl-L-histidine (6.6 g, 19 mmol), dihexadecylamine (8.9 g, 19 mmol) and 1-hydroxybenzotriazole[8] (3.9 g, 29 mmol) at 0 °C. The mixture was stirred for 3 h at 0 °C and for further 15 h at room temperature, and precipitates (*N,N'*-dicyclohexylurea) were removed by filtration. The solvent was removed *in vacuo*, and the residual oil was dissolved in ethyl acetate (200 ml). The solution was then washed sequentially with 10% aqueous citric acid, 5% aqueous sodium hydrogencarbonate, and saturated aqueous sodium chloride. After being dried (Na_2SO_4), the mixture was evaporated *in vacuo* to give an oil which was subsequently purified by centrifugal liquid chromatography with a combination of silica gel

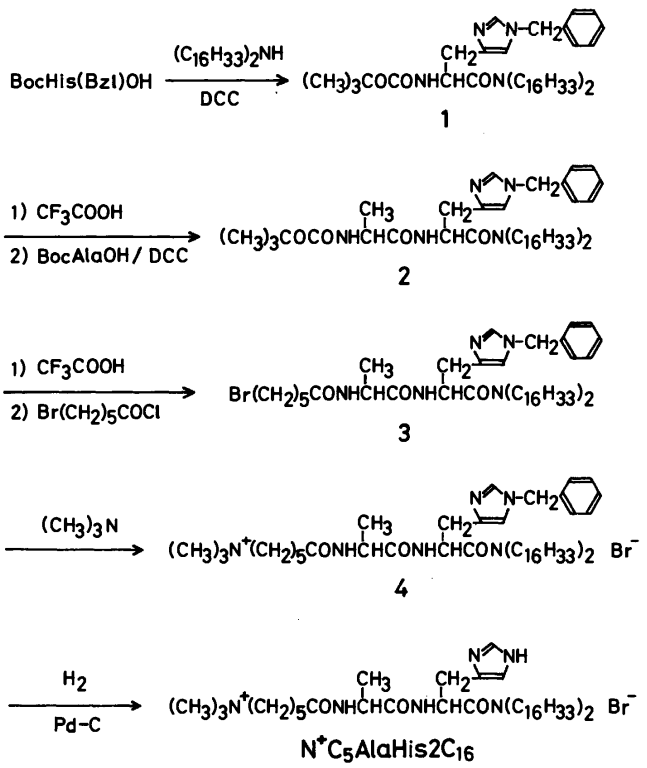

(Boc, t-butoxycarbonyl; Bzl, benzyl; DCC, dicyclohexylcarbodiimide)

Scheme 1.

(Wako Gel B5) and chloroform: a pale yellow solid, yield 8.1 g (54%); R_f (Silica Gel IB of J. T. Baker, ethyl acetate) 0.18, mp 63.0—65.5 °C; IR (Nujol) 3300 (NH), 1700 and 1640 cm^{-1} (C=O); ^{1}H-NMR ($CDCl_3$, TMS) δ=0.88 [6H, br t, $CH_3(CH_2)_{15}N$], 1.25 [56H, s, $CH_3(CH_2)_{14}CH_2N$], 1.40 [9H, s, $(CH_3)_3COCO$], 2.85 [2H, d, $CH(CH_2ImBzl)$], 2.9—3.4 [4H, m, $CH_3(CH_2)_{14}CH_2N$], 4.95 [2H, s, benzyl CH_2], 5.20 [1H, br t, $CH(CH_2ImBzl)$], 6.63 [1H, s, Im-5H], 7.0—7.3 [5H, m, phenyl H's], and 7.33 [1H, s, Im-2H].

N,N-*Dihexadecyl*-N^{α}_{his}-*[*N^{α}_{ala}-*(t-butoxycarbonyl)*-L-*alanyl]*-N^{im}-*benzyl*-L-*histidinamide (2).* Trifluoroacetic acid (25 g, 220 mmol) was added to a dry dichloromethane solution (20 ml) of **1** (4.7 g, 5.9 mmol), and the mixture was stirred for 2 h at room temperature. Evaporation of an excess amount of trifluoroacetic acid *in vacuo* below 40 °C gave a pale yellow oil (**1a**). Elimination of the *t*-butoxycarbonyl group was confirmed by NMR spectroscopy. The amine (**1a**) was dissolved in dry dichloromethane (30 ml) and the solution was cooled to 0 °C. Triethylamine (1.2 g, 11 mmol), *N*-(*t*-butoxycarbonyl)-L-alanine (1.1 g, 5.9 mmol), and 1-hydroxybenzotriazole[8] (1.2 g, 8.8 mmol), and subsequently dicyclohexylcarbodiimide (1.5 g, 7.1 mmol) were added to the solution at 0 °C with stirring. The resulting mixture was stirred for 3 h at 0 °C and for further 15 h at room temperature, and precipitates (*N,N'*-dicyclohexylurea) were removed by filtration. The solvent was removed *in vacuo*, and the residual oil was dissolved in ethyl acetate (200 ml). The solution was then washed sequentially with 10% aqueous citric acid, 4% aqueous sodium hydrogencarbonate, and saturated aqueous sodium chloride. After being dried (Na_2SO_4), the mixture was evaporated *in vacuo*

to give an oil which was subsequently purified by centrifugal liquid chromatography with a combination of silica gel (Wako Gel B5) and a dual solvent system (chloroform and then methanol): a pale yellow oil, yield 1.8 g (35%); R_f (Silica Gel IB of J. T. Baker, ethyl acetate) 0.56; IR (Nujol) 3200 (NH), 1720 and 1630 cm^{-1} (C=O); ^{1}H-NMR ($CDCl_3$, TMS) δ=0.85 [6H, br t, $CH_3(CH_2)_{15}N$], 1.25 [59H, s, $CH_3(CH_2)_{14}CH_2N$ and $CH(CH_3)$], 1.40 [9H, s, $(CH_3)_3$-COCO], 2.85 [2H, d, $CH(CH_2ImBzl)$], 2.7—3.8 [4H, m, $CH_3(CH_2)_{14}CH_2N$], 3.8—4.4 [2H, m, $CH(CH_2ImBzl)$ and $CH(CH_3)$], 4.95 [2H, s, benzyl CH_2], 6.60 [1H, s, Im-5H], 6.9—7.4 [5H, m, phenyl H's], and 7.33 [1H, s, Im-2H].

N,N-*Dihexadecyl*-N^{α}_{his}-[N^{α}_{ala}-(*6-bromohexanoyl*)-L-*alanyl*]-N^{im}-*benzyl*-L-*histidinamide* (**3**). Trifluoroacetic acid (25 g, 220 mmol) was added to a dry dichloromethane solution (10 ml) of **2** (1.8 g, 2.1 mmol), and the mixture was stirred for 2 h at room temperature. Evaporation of an excess amount of trifluoroacetic acid *in vacuo* below 40 °C gave a pale yellow oil (**2a**). Elimination of the *t*-butoxycarbonyl group was confirmed by NMR spectroscopy. The amine (**2a**) was dissolved in dry dichloromethane (30 ml), and the solution was cooled to 0 °C. After triethylamine (1.7 g, 16 mmol) being added dropwise, 6-bromohexanoyl chloride (0.9 g, 4.2 mmol) dissolved in dry dichloromethane (20 ml) was added dropwise to the mixture at 0 °C with stirring. The resulting mixture was stirred for 3 h at room temperature and then washed with 4% aqueous sodium hydrogencarbonate, 10% aqueous citric acid, and saturated aqueous sodium chloride in this sequence. After being dried (Na_2SO_4), the solution was evaporated *in vacuo* to give an oil which was subsequently purified by gel-filtration chromatography on a column of silica gel (Wako Gel C-100) with ethyl acetate as an eluant: a pale yellow oil, yield 0.88 g (45%); R_f (Silica Gel IB of J. T. Baker, ethyl acetate) 0.13; IR (Nujol) 3220 (NH) and 1650 cm^{-1} (C=O); ^{1}H-NMR ($CDCl_3$, TMS) δ=0.90 [6H, br t, $CH_3(CH_2)_{15}N$], 1.25 [59H, s, $CH_3(CH_2)_{14}CH_2N$ and $CH(CH_3)$], *ca.* 2.0 [6H, m, $BrCH_2(CH_2)_3CH_2CO$], 2.30 [2H, br t, $Br(CH_2)_4CH_2CO$], 2.9—3.5 [8H, m, $CH_3(CH_2)_{14}CH_2N$, $CH(CH_2ImBzl)$, and $BrCH_2(CH_2)_4CO$], 4.0—4.5 [2H, m, $CH(CH_2ImBzl)$ and $CH(CH_3)$], 5.40 [2H, s, benzyl CH_2], 6.95 [1H, s, Im-5H], 7.30 [5H, s, phenyl H's], and 8.95 [1H, s, Im-2H].

N,N-*Dihexadecyl*-N^{α}_{his}-[N^{α}_{ala}-(*6-trimethylammoniohexanoyl*)-L-*alanyl*]-N^{im}-*benzyl*-L-*histidinamide Bromide* (**4**). A benzene solution (60 ml) of **3** (880 mg, 0.94 mmol) was saturated with dry trimethylamine gas, and the solution was stirred overnight at room temperature. The solvent was removed *in vacuo* and the crude product was purified by gel-filtration chromatography on a column of Sephadex LH-20 with methanol as an eluant: a pale yellow solid, yield 610 mg (65%); R_f [Silica Gel IB of J. T. Baker, *t*-butyl alcohol-water-acetic acid (4:2:1 by volume; BWA)] 0.22; IR (Nujol) 3200 (NH) and 1630 cm^{-1} (C=O); ^{1}H-NMR ($CDCl_3$, TMS) δ=0.85 [6H, br t, $CH_3(CH_2)_{15}N$], 1.25 [59H, s, $CH_3(CH_2)_{14}CH_2N$ and $CH(CH_3)$], *ca.* 2.0 [6H, m, $N^+CH_2(CH_2)_3CH_2CO$], 2.30 [2H, br t, $N^+(CH_2)_4CH_2CO$], 2.8—3.7 [8H, m, $CH_3(CH_2)_{14}CH_2N$, $CH(CH_2ImBzl)$, and $N^+CH_2(CH_2)_4CO$], 3.40 [9H, s, $(CH_3)_3N^+$], 4.50 [2H, m, $CH(CH_2ImBzl)$ and $CH(CH_3)$], 5.30 [2H, s, benzyl CH_2], 7.00 [1H, s, Im-5H], 7.30 [5H, s, phenyl H's], and 8.10 [1H, s, Im-2H].

N,N-*Dihexadecyl*-N^{α}_{his}-[N^{α}_{ala}-(*6-trimethylammoniohexanoyl*)-L-*alanyl*]-L-*histidinamide Bromide* ($N^+C_5AlaHis2C_{16}$). A 700-mg sample of 10% PdC was added to **4** (610 mg, 0.61 mmol) dissolved in 80% aqueous acetic acid (40 ml), and hydrogen gas was introduced into the solution at 60 °C for 30 h with stirring. The catalyst was removed by filtration on Celite (Wako No. 545) with methanol. The filtrate was evaporated off *in vacuo*, and the residue was purified by gel-filtration chromatography on a column of Toyopearl HW-40 Fine with methanol as an eluant: a glassy solid, yield 360 mg (65%); R_f (Silica Gel IB of J. T. Baker, BWA) 0.20; mp 176 °C,[11] $[\alpha]_D^{26}$ −24.5° (*c* 1.0, ethanol); IR (Nujol) 1630 cm^{-1} (C=O); ^{1}H-NMR (CD_3OD, TMS) δ=0.90 [6H, br t, $CH_3(CH_2)_{15}N$], 1.25 [59H, s, $CH_3(CH_2)_{14}CH_2N$ and $CH(CH_3)$], *ca.* 2.0 [6H, m, $N^+CH_2(CH_2)_3CH_2CO$], 2.30 [2H, br t, $N^+(CH_2)_4CH_2CO$], 2.8—3.4 [8H, m, $CH_3(CH_2)_{14}CH_2N$, $CH(CH_2Im)$, and $N^+CH_2(CH_2)_4CO$], 3.10 [9H, s, $(CH_3)_3N^+$], 6.80 [1H, s, Im-5H], 7.60 [1H, s, Im-2H], the signals of $CHCH_3$ and $CH(CH_2Im)$ being obscured by the signal due to CD_3OH.

Similar experimental procedures were applied to the preparation of *N,N*-dihexadecyl-N^{α}_{his}-[N^{α}_{leu}-(6-trimethylammoniohexanoyl)-L-leucyl]-L-histidinamide bromide (N^+C_5-LeuHis2C_{16}), *N,N*-dihexadecyl-N^{α}_{his}-[N^{α}_{phe}-(6-trimethylammoniohexanoyl)-L-phenylalanyl]-L-histidinamide bromide (N^+C_5PheHis2C_{16}), and *N,N*-dihexadecyl-N^{α}_{ala}-[N^{α}_{his}-(6-trimethylammoniohexanoyl)-L-histidyl]-L-alaninamide bromide (N^+C_5HisAla2C_{16}).

$N^+C_5LeuHis2C_{16}$: mp 126 °C,[11] $[\alpha]_D^{26}$ −27.8° (*c* 1.0, ethanol), R_f (Silica Gel IB of J. T. Baker, BWA) 0.14; IR (Nujol) 1630 cm^{-1} (C=O); ^{1}H-NMR (CD_3OD, TMS) δ=0.70 [12H, m, $CH_3(CH_2)_{15}N$ and $CH_2CH(CH_3)_2$], 1.05 [59H, br s, $CH_3(CH_2)_{14}CH_2N$ and $CH_2CH(CH_3)_2$], *ca.* 2.0 [6H, m, $N^+CH_2(CH_2)_3CH_2CO$], 2.05 [2H, br t, $N^+(CH_2)_4CH_2CO$], 2.4—3.3 [8H, m, $CH_3(CH_2)_{14}CH_2N$, $CH(CH_2Im)$, and $N^+CH_2(CH_2)_3CH_2CO$], 2.90 [9H, s, $N^+(CH_3)_3$], 6.60 [1H, s, Im-5H], 7.30 [1H, s, Im-2H], the signals of $CHCH_2CH$-$(CH_3)_2$ and $CH(CH_2Im)$ being obscured by the signal due to CD_3OH.

$N^+C_5PheHis2C_{16}$: mp 130 °C,[11] $[\alpha]_D^{26}$ −11.4° (*c* 1.0, ethanol), R_f (Silica Gel IB of J. T. Baker, BWA) 0.09; IR (Nujol) 1640 cm^{-1} (C=O); ^{1}H-NMR (CD_3OD, TMS) δ= 0.90 [6H, br t, $CH_3(CH_2)_{15}N$], 1.20 [56H, s, $CH_3(CH_2)_{14}$-CH_2N], *ca.* 2.0 [6H, m, $N^+CH_2(CH_2)_3CH_2CO$], 2.30 [2H, br t, $N^+(CH_2)_4CH_2CO$], 2.7—3.5 [10H, m, $CH_3(CH_2)_{14}$-CH_2N, benzyl CH_2, and $N^+CH_2(CH_2)_4CO$], 3.20 [9H, s, $(CH_3)_3N^+$], 7.00 [1H, s, Im-5H], 7.20 [5H, s, phenyl H's], the signals of Im-2H, CHBzl, and $CH(CH_2Im)$ being obscured by the signal due to CD_3OH.

$N^+C_5HisAla2C_{16}$: mp 105 °C,[11] $[\alpha]_D^{26}$−11.9° (*c* 1.0, ethanol), R_f (Silica Gel IB of J. T. Baker, BWA) 0.20; IR (Nujol) 1625 cm^{-1} (C=O); ^{1}H-NMR (CD_3OD, TMS) δ=0.90 [6H, br t, $CH_3(CH_2)_{15}N$], 1.28 [59H, s, $CH_3(CH_2)_{14}CH_2N$ and $CH(CH_3)$], *ca.* 2.0 [6H, m, $N^+CH_2(CH_2)_3CH_2CO$], 2.30 [2H, br t, $N^+(CH_2)_4CH_2CO$], 2.9—3.5 [8H, m, $CH_3(CH_2)_{14}$-CH_2N, $CH(CH_2Im)$, and $N^+CH_2(CH_2)_4CO$], 3.10 [9H, s, $(CH_3)_3N^+$], 7.05 [1H, s, Im-5H], 8.10 [1H, s, Im-2H], the signals of $CH(CH_2Im)$ and $CHCH_3$ being obscured by the signal due to CD_3OH.

All the elemental analysis data for the present amphiphiles are summarized in Table 1.

Kinetic Measurements. Rates of *p*-nitrophenol liberation from *p*-nitrophenyl esters were measured at 400 nm with a Union Giken SM-401 high-sensitivity spectrophotometer.

Each run was initiated by adding a dioxane solution (20 μl) of a *p*-nitrophenyl ester (*ca.* 1.0×10^{-3} mol dm^{-3}) to a reaction medium (2.0 ml) which was pre-equilibrated at a desired temperature in a thermostated cell set in the spectrophotometer. The reaction medium was prepared as follows: an ethanol solution of a dipeptide amphiphile (90 μl, *ca.* 5.0×10^{-2} mol dm^{-3}) was taken into a sample tube and the solvent was removed completely. A 4.5-ml sample of an aqueous buffer was added to the residue, and the mixture was sonicated for 3 min with a probe-type sonicator at 30 W (W-220F, Heat Systems-Ultrasonics) and allowed to stand for 1 min at 5 °C. The ionic strength of sample solutions for the measurements was maintained at 0.05 with KCl.

Results and Discussion

Phase Transition and Aggregate Morphology. The phase transition parameters (enthalpy change, ΔH; temperature at peak maximum, T_m) of the molecular aggregates formed with the present amphiphiles in the aqueous dispersion were directly measured by differential scanning calorimetry (DSC) as summarized in Table 1. The T_m values of these amphiphiles are nearly identical with those of peptide amphiphiles having the same alkyl moieties (hexadecyl) in the double-chain portion. This indicates that the T_m value of the peptide amphiphile primarily depends on the alkyl-chain length of double-chain portion.[1c] On the other hand, the ΔH values are somewhat smaller than those of amphiphiles having the same double-chain segment prepared previously in our laboratory; *e.g.*, $N^+C_5Ala2C_{16}$, 32.6 kJ mol^{-1}.[1c] Since the ΔH value for the single-walled aggregate is generally much smaller than that for the corresponding multiwalled one,[1c] the present ΔH values seem to indicate that both single- and multi-walled aggregates are present in the aqueous dispersion state. This was clearly confirmed by electron microscopy. As shown in Fig. 1A, the aqueous dispersion of $N^+C_5LeuHis2C_{16}$ apparently involves single-walled vesicles in addition to multiwalled lamellae and vesicles. Similar electron micrographs were obtained with the aqueous dispersions of $N^+C_5AlaHis2C_{16}$ and $N^+C_5PheHis2C_{16}$. Such morphological behavior is reflected on the solubility properties of these amphiphiles; these three amphiphiles are more soluble and much less turbid in the

Table 1. Physical and analytical data of amphiphiles

Amphiphile	Formula	Elemental analysis[a]/%			DSC	
		C	H	N	T_m/°C	ΔH/kJ mol^{-1}
$N^+C_5AlaHis2C_{16}$	$C_{50}H_{97}BrN_6O_3+5/2H_2O$	62.78 (62.87)	10.57 (10.76)	8.60 (8.80)	24.8	27.6
$N^+C_5LeuHis2C_{16}$	$C_{53}H_{103}BrN_6O_3$	66.54 (66.84)	11.03 (10.90)	8.67 (8.83)	24.5	22.6
$N^+C_5PheHis2C_{16}$	$C_{56}H_{101}BrN_6O_3+3/2H_2O$	66.28 (66.37)	10.45 (10.34)	7.96 (8.29)	22.5	22.6
$N^+C_5HisAla2C_{16}$	$C_{50}H_{97}BrN_6O_3+3H_2O$	62.42 (62.28)	10.43 (10.76)	8.43 (8.71)	27.0	25.9

a) Calculated values are given in parentheses.

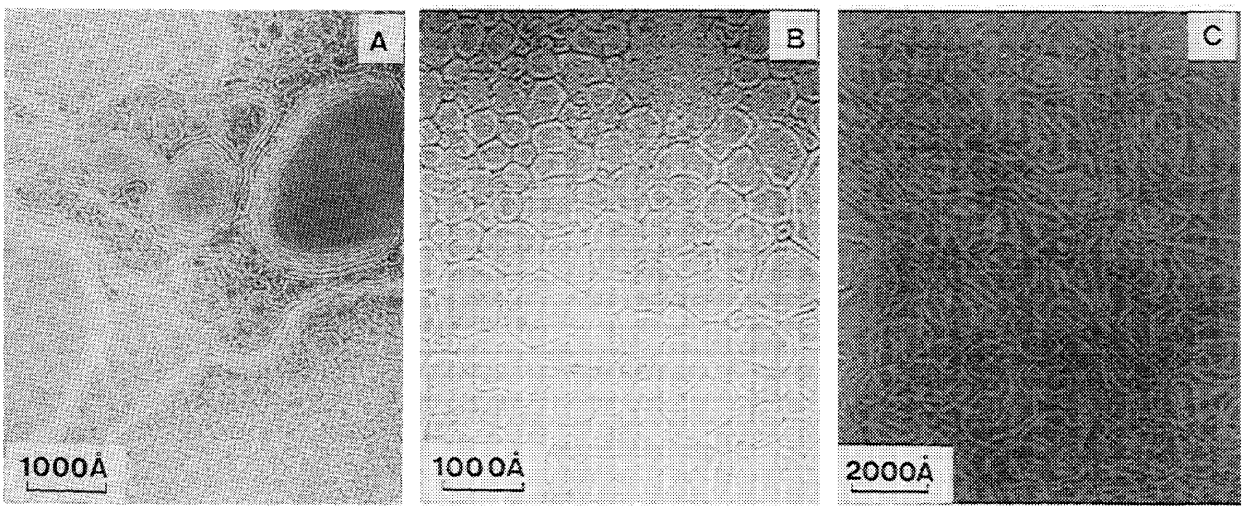

Fig. 1. Electron micrographs negatively stained with uranyl acetate: A, 5 mmol dm^{-3} aqueous dispersion of $N^+C_5LeuHis2C_{16}$; B, 5 mmol dm^{-3} aqueous solution of $N^+C_5LeuHis2C_{16}$ sonicated for 2 min at 30 W and subsequently allowed to stand for 5 min at 5 °C; C, 5 mmol dm^{-3} aqueous dispersion of $N^+C_5HisAla2C_{16}$.

dispersion state than other amphiphiles which have been synthesized previously in our laboratory.[1-3] The single-walled vesicles have never been observed with the latter amphiphiles in the dispersion state without sonication. The multiwalled aggregates were completely converted into the single-walled vesicles upon sonication of these aqueous dispersions for 2 min with a probe-type sonicator (Fig. 1B). Meanwhile, the aqueous dispersion of $N^+C_5HisAla2C_{16}$ involves exclusively tubular aggregates as clarified by electron microscopy (Fig. 1C). This indicates that the sequence of amino acid residues in the hydrogen-belt domain may largely control the aggregate morphology in the dispersion state.

Apparent Enantioselectivity in Ester Hydrolysis. The enantiomeric selectivity of the single-walled vesicles of the present amphiphiles exercised in the hydrolysis of various ester substrates was evaluated on the basis of apparent pseudo-first-order rate constants in an aqueous phosphate buffer (pH 7.47, μ 0.05 with KCl) at 15.0±0.1 °C. The first-order kinetics was found to hold at least up to 60% conversion of the substrate species under the conditions [S] ≪ [D]; S and D stand for substrate and amphiphile species, respectively (Table 2). In the micellar system of $HisC_{16}$ and STAC, the L-substrates are more favorably hydrolyzed than the corresponding D-isomers. On the other hand, the enantioselectivity demonstrated by the membrane systems depends on the hydrophobic nature of substrates employed; the L-isomers are more favorably hydrolyzed when less hydrophobic substrates are used (BocAlaPNP, BocValPNP, and BocLeuPNP), while the D-isomer is more reactive than the corresponding L-isomer in the case of C_{12}GlyValPNP that is largely hydrophobic. Above all, all the D-isomers are preferentially hydrolyzed in the single-walled vesicles of $N^+C_5LeuHis2C_{16}$ although the extent of selectivity is rather small.

Kinetic Analysis by Pseudo-Phase Concept. Various micellar reactions have been quantitatively analyzed on the basis of the Michaelis-Menten-type kinetics,[12] the ion-exchange model treatment,[13] and the pseudo-phase concept.[14] We employed in this work the pseudo-phase concept due to the following reasons. (i) The Michaelis-Menten treatment is based on the assumption that the interaction between substrate and aggregate species takes place at the 1 : 1 ratio; each aggregate incorporates only one substrate molecule. The aggregation number of the present single-walled vesicles is at least 4000—5000,[10] while that of ordinary micelles is *ca.* 100.[12] In the light of our previous study, a much larger number of substrate molecules are incorporated into each vesicle and the binding site concept needs to be introduced.[15] (ii) In the present reaction systems, the histidyl residue is covalently bound to amphiphile molecules, and consequently the catalyst species are exclusively placed in the vesicular domain and not in the bulk aqueous

Table 2. Apparent first-order rate constants for micelle- and vesicle-catalyzed hydrolysis of enantiomeric esters[a]

Catalyst[b]		Substrates				
		BocAlaPNP	BocValPNP	BocLeuPNP	C_{12}PhePNP	C_{12}GlyValPNP
$N^+C_5AlaHis2C_{16}$	k_L/s^{-1}	6.68×10^{-3}	1.81×10^{-3}	2.08×10^{-2}	3.90×10^{-2}	8.38×10^{-3}
(1.00×10^{-3})	k_D/s^{-1}	6.31×10^{-3}	1.34×10^{-3}	2.02×10^{-2}	4.09×10^{-2}	1.15×10^{-2}
	k_L/k_D	1.06	1.35	1.03	1.05[c]	1.37[c]
$N^+C_5PheHis2C_{16}$	k_L/s^{-1}	5.70×10^{-3}	2.19×10^{-3}	2.08×10^{-2}	5.05×10^{-2}	1.08×10^{-2}
(1.01×10^{-3})	k_D/s^{-1}	4.80×10^{-3}	1.56×10^{-3}	1.97×10^{-2}	5.11×10^{-2}	1.29×10^{-2}
	k_L/k_D	1.19	1.40	1.06	1.01[c]	1.20[c]
$N^+C_5LeuHis2C_{16}$	k_L/s^{-1}	7.05×10^{-3}	7.00×10^{-4}			1.06×10^{-2}
(1.05×10^{-5})	k_D/s^{-1}	7.77×10^{-3}	7.74×10^{-4}			1.26×10^{-2}
	k_D/k_L	1.10	1.11			1.19
$N^+C_5HisAla2C_{16}$	k_L/s^{-1}	2.46×10^{-3}	4.83×10^{-4}	5.55×10^{-3}	1.76×10^{-2}	3.95×10^{-3}
(1.01×10^{-3})	k_D/s^{-1}	2.35×10^{-3}	4.08×10^{-4}	4.76×10^{-3}	1.88×10^{-2}	7.60×10^{-3}
	k_L/k_D	1.05	1.18	1.17	1.07[c]	1.92[c]
$HisC_{16}$/STAC	k_L/s^{-1}	8.51×10^{-3}	2.56×10^{-3}	2.38×10^{-2}	1.10×10^{-1}	1.68×10^{-2}
(6.73×10^{-5}/	k_D/s^{-1}	7.14×10^{-3}	2.00×10^{-3}	8.55×10^{-3}	2.80×10^{-2}	8.37×10^{-3}
1.01×10^{-3})	k_L/k_D	1.19	1.28	2.78	3.93	2.01

a) In an aqueous phosphate buffer (5.0 mmol dm^{-3}) containing 1.0%(v/v) dioxane, 15.0±0.1 °C, pH 7.47, μ 0.05 (KCl). Initial concentrations in mol dm^{-3}: L-BocAlaPNP, 1.04×10^{-5}; D-BocAlaPNP, 1.01×10^{-5}; L-BocValPNP, 1.22×10^{-5}; D-BocValPNP, 1.29×10^{-5}; L-BocLeuPNP, 1.01×10^{-5}; D-BocLeuPNP, 1.07×10^{-5}; L-C_{12}PhePNP, 1.23×10^{-5}; D-C_{12}PhePNP, 1.10×10^{-5}; L-C_{12}GlyValPNP, 1.03×10^{-5} (vesicle), 5.15×10^{-6} (micelle); D-C_{12}GlyValPNP, 1.09×10^{-5} (vesicle), 5.45×10^{-6} (micelle). b) At the concentration (mol dm^{-3}) given in parentheses. c) Given as k_D/k_L.

phase. In addition, the ion-exchange treatment is not applicable to the present systems since all the substrates employed here are hydrophobic and nonionic. (iii) The bilayer domain may provide a steady and hydrophobic reaction site which is considered to be an organic pseudo-phase.

According to the Berezin's treatment based on the pseudo-phase concept, the pseudo-first-order rate constant, k_{obsd}, is given by Eq. 1 under the conditions employed for the present systems.[14,16]

$$k_{obsd} = \frac{k_m K_s D}{1 + K_s D} \quad (1)$$

This can be rearranged to give Eq. 2.

$$\frac{1}{k_{obsd}} = \frac{1}{k_m K_s D} + \frac{1}{k_m} \quad (2)$$

Here, k_m and K_s represent the intramembrane rate constant and the apparent binding constant for incorporation of a substrate into the single-walled vesicle, respectively; D designates the stoichiometric amphiphile concentration minus its critical aggregate concentration (CAC). A correlation of k_{obsd} with D is typically shown in Fig. 2a for the degradation of L-BocValPNP as catalyzed by $N^+C_5AlaHis2C_{16}$ and followed the saturation-type kinetics. The plot of $1/k_{obsd}$ *vs.* $1/D$ on the basis of Eq. 2 gave a straight line as illustrated in Fig. 2b. The k_m and K_s values for selected cases are summarized in Table 3. The K_s values for C_{12}GlyValPNP are larger than those for BocValPNP. This indicates that the substrate incorporation is largely controlled by the hydrophobic property of the substrates in addition to some orientational effect provided by the bilayer membranes.

As for the incorporation of BocValPNP, the binding constant increases in the following order with respect

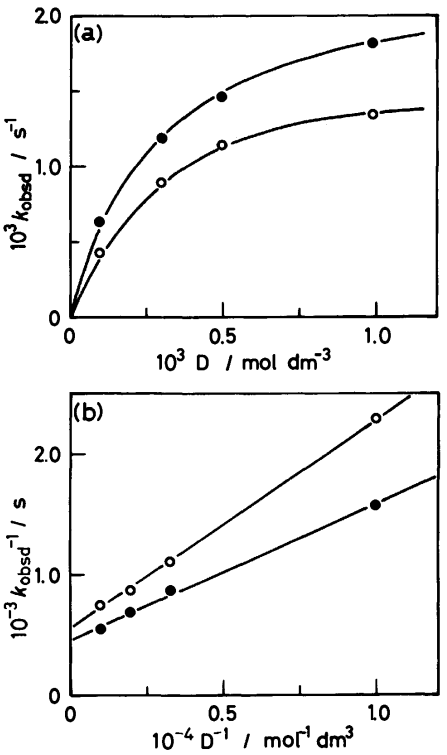

Fig. 2. Saturation-type kinetic behavior (a) and the corresponding double reciprocal plots (b) for the hydrolysis of L- (●) and D-BocValPNP (○) as catalyzed by $N^+C_5AlaHis2C_{16}$ in an aqueous phosphate buffer (5 mmol dm^{-3}) containing 1.0%(v/v) dioxane: pH 7.47, μ 0.05 (KCl), 15.5±0.1 °C. Initial concentrations: L-BocValPNP, 1.22×10^{-5}; D-BocValPNP, 1.29×10^{-5} mol dm^{-3}.

Table 3. Kinetic parameters for the hydrolysis of enantiomeric esters as catalyzed by vesicles[a]

Amphiphile[b]	Substrate		k_m/s^{-1}	$K_s/mol^{-1}\,dm^3$
$N^+C_5AlaHis2C_{16}$ (1.00×10^{-3}—1.00×10^{-4})	BocValPNP	L	2.15×10^{-3}	4.19×10^3
		D	1.65×10^{-3}	3.63×10^3
		L/D[c]	1.30	1.15
	C_{12}GlyValPNP	L	8.69×10^{-3}	2.16×10^4
		D	1.21×10^{-2}	1.13×10^4
		L/D[c]	1.39[d]	1.91
$N^+C_5LeuHis2C_{16}$ (1.05×10^{-3}—1.05×10^{-4})	BocValPNP	L	4.68×10^{-3}	1.76×10^2
		D	6.26×10^{-3}	1.41×10^2
		L/D[c]	1.34[d]	1.25
	C_{12}GlyValPNP	L	1.17×10^{-2}	9.95×10^3
		D	1.38×10^{-2}	1.06×10^4
		D/L[d]	1.18	1.07
$N^+C_5PheHis2C_{16}$ (1.01×10^{-3}—1.01×10^{-4})	BocValPNP	L	5.26×10^{-3}	6.90×10^2
		D	4.10×10^{-3}	6.00×10^2
		L/D[c]	1.28	1.15
$N^+C_5HisAla2C_{16}$ (1.01×10^{-3}—1.01×10^{-4})	C_{12}GlyValPNP	L	4.40×10^{-3}	1.93×10^4
		D	8.47×10^{-3}	7.20×10^3
		L/D[c]	1.93[d]	2.68

a) In an aqueous phosphate buffer (5.0 mmol dm^{-3}) containing 1.0%(v/v) dioxane, 15.0±0.1 °C, pH 7.47, μ 0.05 (KCl). As for initial concentrations of the substrates, see Table 2. b) At the concentration range (mol dm^{-3}) given in parantheses. c) Given as k_m^L/k_m^D and/or K_s^L/K_s^D. d) Given as k_m^D/k_m^L and/or K_s^D/K_s^L.

to the amphiphiles: N^+C_5LeuHis2C_{16}<N^+C_5PheHis2C_{16}<N^+C_5AlaHis2C_{16}. This means that the less the steric hindrance between the amino acid residue of the substrate and those of the amphiphiles is, the larger the substrate binding is. On the other hand, the k_m value does not change appreciably by the nature of the amphiphiles but increases largely by raising the hydrophobicity of the substrate: BocValPNP, $(1.6—6.3)\times10^{-3}$ s^{-1}; C_{12}GlyValPNP, $(0.4—1.4)\times10^{-2}$ s^{-1}. In addition, the apparent enantioselectivity (see the previous section) is primarily reflected on the k_m value.

pH Effect on Ester Hydrolysis. The pH-rate profiles for the hydrolysis of C_{12}GlyValPNP carried out in the micellar system composed of $HisC_{16}$ and STAC and in the vesicular phase of N^+C_5HisAla2C_{16} are shown in Fig. 3. The overall kinetic feature is in agreement with those of the previous studies which claim that the imidazolyl group is the catalytic species.[6,17] The acid dissociation from the cationic imidazolium group to the corresponding uncharged species gives the following pK_a values from the pH-rate profiles: $HisC_{16}$/STAC, 6.2; N^+C_5HisAla2C_{16}, 7.2. Thus, the present kinetic study mentioned above was carried out under the conditions that the uncharged imidazolyl group acts as the catalytic species. The imidazolyl group in the present micellar system must be placed in the cationic polar domain in the light of the previous investigations: *N*-tetradecanoylhistidine/CTAB, pK_a 6.20;[6] $HisC_{16}$/N^+C_5AlaC_{12}, pK_a 6.16.[7] On the other hand, the higher pK_a value observed in the vesicular system indicates that the imidazolyl group is placed in the significantly hydrophobic environment.

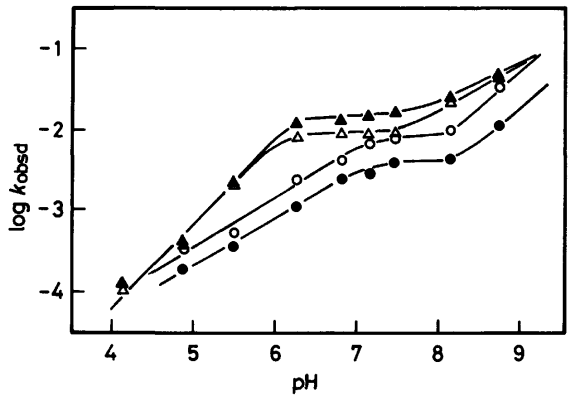

Fig. 3. Correlations of pH *vs.* rate for the hydrolysis of C_{12}GlyValPNP (L-Val, closed; D-Val, open) as catalyzed by the micellar system ($HisC_{16}$/STAC, triangle) and the vesicular system (N^+C_5HisAla2C_{16}, circle) in aqueous buffers containing 1.0% (v/v) dioxane at 15.0±0.1 °C and μ 0.05 (KCl): pH 4—6, citrate-borate buffer; pH 6—9, phosphate-borate buffer. Initial concentrations for the vesicular system: N^+C_5HisAla2C_{16}, 1.01×10^{-3}; L-C_{12}GlyValPNP, 1.03×10^{-5}; D-C_{12}GlyValPNP, 1.09×10^{-5} mol dm^{-3}. Initial concentrations for the micellar system: STAC, 1.01×10^{-3}; $HisC_{16}$, 6.73×10^{-5}; L-C_{12}GlyValPNP, 5.15×10^{-6}; D-C_{12}GlyValPNP, 5.45×10^{-6} mol dm^{-3}. Values of k_{obsd} are given in s^{-1}.

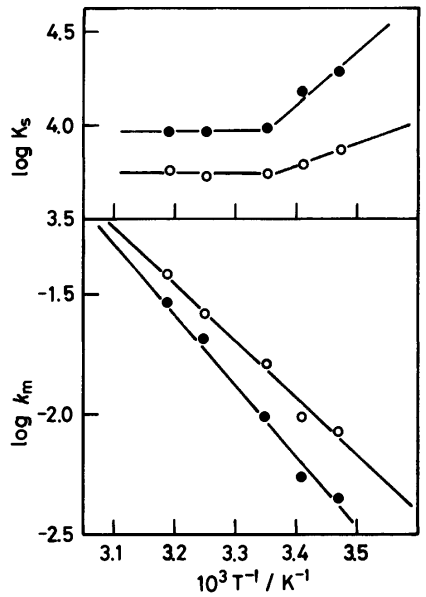

Fig. 4. Arrhenius plots for the hydrolysis of C_{12}-GlyValPNP (L-Val, ●; D-Val, ○) as catalyzed by N^+C_5HisAla2C_{16} in an aqueous phosphate buffer (5 mmol dm^{-3}) containing 1.0% (v/v) dioxane at pH 7.47 and μ 0.05 (KCl). Initial concentrations: N^+C_5HisAla2C_{16}, 1.01×10^{-3}; L-C_{12}GlyValPNP, 1.03×10^{-5}; D-C_{12}GlyValPNP, 1.09×10^{-5} mol dm^{-3}. Values of k_m and K_s are given in s^{-1} and mol^{-1} dm^3, respectively.

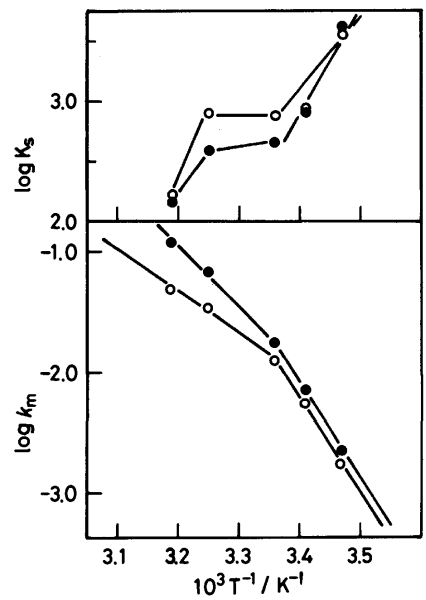

Fig. 5. Arrhenius plots for the hydrolysis of Boc-ValPNP (L-Val, ●; D-Val, ○) as catalyzed by N^+C_5AlaHis2C_{16} in an aqueous phosphate buffer (5 mmol dm^{-3}) containing 1% (v/v) dioxane at pH 7.47 and μ 0.05 (KCl). Initial concentrations: N^+C_5Ala-His2C_{16}, 1.00×10^{-3}; L-BocValPNP, 1.22×10^{-5}; D-BocValPNP, 1.29×10^{-5} mol dm^{-3}. Values of k_m and K_s are given in s^{-1} and mol^{-1} dm^3, respectively.

TABLE 4. ACTIVATION PARAMETERS FOR THE HYDROLYSIS OF ENANTIOMERIC ESTERS AS CATALYZED BY VESICLES[a)]

Amphiphile[b)]	Substrate	$\Delta G^{\ddagger}_{308}$ / kJ mol^{-1}	$\Delta H^{\ddagger}$ / kJ mol^{-1}	$\Delta S^{\ddagger}$ / J K^{-1} mol^{-1}
$N^+C_5HisAla2C_{16}$	L-C_{12}GlyValPNP	85.4	56.1	−95.8
(1.01×10^{-3})	D-C_{12}GlyValPNP	84.9	43.9	−133
	L-BocValPNP[c)]	82.4	77.4	−16.7
$N^+C_5AlaHis2C_{16}$	L-BocValPNP[d)]		144	−205
(1.00×10^{-3})	D-BocValPNP[c)]	84.1	67.8	−54.0
	D-BocValPNP[d)]		142	−197

a) In an aqueous phosphate buffer (5.0 mmol dm^{-3}) containing 1.0%(v/v) dioxane, pH 7.47, μ 0.05 (KCl). Initial concentrations in mol dm^{-3}: L-C_{12}GlyValPNP, 1.03×10^{-5}; D-C_{12}GlyValPNP, 1.09×10^{-5}; L-BocValPNP, 1.22×10^{-5}; D-BocValPNP, 1.29×10^{-5}. b) At the concentration (mol dm^{-3}) given in parentheses. c) For the range of 25—40 °C. d) For the range of 15—25 °C.

Phase-Transition Effect on Substrate-Binding and Intravesicular Rate Constants. The Arrhenius plots of the K_s and k_m values are shown in Figs. 4 and 5 for the combinations of $N^+C_5HisAla2C_{16}$–C_{12}GlyValPNP and $N^+C_5AlaHis2C_{16}$–BocValPNP, respectively. Apparently, the K_s values are much lower above the phase transition temperatures than the corresponding values below them. This seems to indicate that the fluidity of vesicular systems, which tends to be reduced as the hydrophobic and hydrogen-bonding interactions are enhanced, controls the substrate-binding process. As regards the Arrhenius plots of k_m values, there are break points in the phase transition range for the hydrolysis of both enantiomers of BocValPNP, while only a single straight line is drawn for the hydrolysis of each enantiomer of C_{12}GlyValPNP. This must reflect the fact that the BocValPNP molecules are placed in the vesicular surface domain between the charged head group and the hydrogen-belt region and consequently the molecular mobility of such substrates is much sensitive to their hydrogen-bonding interaction with the vesicular phase. On the other hand, the C_{12}GlyValPNP molecules are tightly fixed in the vesicular phase through the effective hydrophobic interaction, and the mobility of these molecules are hardly affected by the change in hydrogen-bonding mode. As for the hydrolysis of C_{12}GlyValPNP with $N^+C_5HisAla2C_{16}$ over the whole temperature range studied and that of BocValPNP with $N^+C_5AlaHis2C_{16}$ above the phase transition temperature, the unfavorable activation enthalpy is largely compensated by the favorable activation entropy. This is the reason why the enantioselectivity is not significantly large. Moreover, the absolute values of activation entropy are much smaller above T_m than those observed below it for the hydrolysis of BocValPNP. This must be due to the increased mobility of the substrate species above the phase transition temperature.

As regards the reaction mechanism, we have confirmed that the micelles formed with the peptide amphiphile having the histidyl residue enhances the ester hydrolysis partly by the general base catalysis.[7)] In the present vesicular systems, approximately half of the reaction proceeds through the general base mechanism; the hydrolysis of BocValPNP with $N^+C_5LeuHis2C_{16}$, 54% general base catalysis.[18)] This mechanism is operative in these molecular aggregate systems so as to reduce the direct steric hindrance between the substrate molecules and the active reaction sites within the vesicles. Thus, this mechanistic aspect provides the important reason why the enantioselectivity is not significantly large in the present systems.

In conclusion, the peptide amphiphiles having dipeptide segments yield characteristic molecular aggregates in the dispersion state, and the sequence of the amino acid residues may control the aggregate morphology. The hydrolysis reactions of enantiomeric esters of various hydrophobic nature, which were carried out in the single-walled vesicles, did not show large enantioselectivity primarily due to thermodynamic and mechanistic reasons. Since enzymes generally incorporate their specific substrates into their reaction sites most adequately for the transformation to the transition state from the stereochemical viewpoint,[19)] amphiphile molecules need to be designed so as to provide the efficient enantiomer-recognition sites through host-guest interactions.

References

1) a) Y. Murakami, A. Nakano, and K. Fukuya, *J. Am. Chem. Soc.*, **102**, 4253 (1980); b) Y. Murakami, A. Nakano, and H. Ikeda, *J. Org. Chem.*, **47**, 2137 (1982); c) Y. Murakami, A. Nakano, A. Yoshimatsu, K. Uchitomi, and Y. Matsuda, *J. Am. Chem. Soc.*, **106**, 3613 (1984).

2) Y. Murakami, A. Nakano, and K. Akiyoshi, *Bull. Chem. Soc. Jpn.*, **55**, 3004 (1982).

3) Y. Murakami, A. Nakano, A. Yoshimatsu, and K. Fukuya, *J. Am. Chem. Soc.*, **103**, 728 (1981).

4) T. Nagasawa, K. Kuroiwa, K. Narita, and Y. Isowa, *Bull. Chem. Soc. Jpn.*, **46**, 1269 (1973).

5) E. Schnabel, H. Klostermeyer, and H. Berndt, *Justus Liebigs Ann. Chem.*, **749**, 90 (1971).

6) C. Gitler and A. Ochoa-Solano, *J. Am. Chem. Soc.*, **90**, 5004 (1968).

7) Y. Murakami, A. Nakano, A. Yoshimatsu, and K. Matsumoto, *J. Am. Chem. Soc.*, **103**, 2750 (1981).
8) W. König and R. Geiger, *Chem. Ber.*, **103**, 788 (1970).
9) D. W. Ingles and J. R. Knowles, *Biochem. J.*, **104**, 369 (1967).
10) R. Ueoka, Doctral Dissertation, Kyushu University, 1982.
11) The value indicates the final melting point to the liquid state.
12) J. H. Fendler and E. J. Fendler, "Catalysis in Micellar and Macromolecular Systems," Academic Press, New York (1975).
13) F. H. Quina and H. Chaimovich, *J. Phys. Chem.*, **83**, 1844 (1979).
14) I. V. Berezin, K. Martinek, and A. K. Yatsimirskii, *Russ. Chem. Rev.*, **42**, 787 (1973).
15) Y. Murakami, A. Nakano, and A. Yoshimatsu, *Chem. Lett.*, **1984**, 13.
16) The observed reaction velocity, v, is given by the following equation.

$$v = v_o D\overline{V} + v_w(1-D\overline{V}) = k_o[A]_o[S]_o D\overline{V} + k_w[A]_w[S]_w(1-D\overline{V}) \quad (1\text{-}1)$$

Here, D, $\overline{V}$, and k stand for the amphiphile concentration minus its critical aggregate concentration (CAC), the partial molar volume of the amphiphile in the membrane, and the second-order rate constant, respectively; [A] and [S] are the concentrations of the amphiphile and the ester substrate, respectively; the subscripts, o and w, denote the quantities in the organic pseudo-phase and the bulk aqueous phase, respectively. The distribution coefficient, P_s, and the initial substrate concentration, $[S]_T$, are given as follows.

$$P_s = [S]_o/[S]_w \quad (1\text{-}2)$$
$$[S]_T = [S]_o D\overline{V} + [S]_w(1-D\overline{V}) \quad (1\text{-}3)$$

The binding constant for incorporation of the substrate into the organic pseudo-phase, K_s, is defined by Eq. 1-4, and $[S]_w$ and $[S]_o$ are given by Eqs. 1-5 and 1-6, respectively.

$$K_s = (P_s-1)\overline{V} \quad (1\text{-}4)$$
$$[S]_w = [S]_o/(1+K_sD) \quad (1\text{-}5)$$
$$[S]_o = P_s[S]_o/(1+K_sD) \quad (1\text{-}6)$$

By combining the relations, $[A]_o=1/\overline{V}$ and $[A]_w$=CAC, together with Eqs. 1-1, 1-5, and 1-6, we obtain Eq. 1-7.

$$v = k_o\frac{P_s[S]_o}{\overline{V}(1+K_sD)}D\overline{V} + k_w(\mathrm{CAC})\frac{[S]_o}{1+K_sD}(1-D\overline{V}) = \frac{k_oP_sD+k_w(\mathrm{CAC})(1-D\overline{V})}{1+K_sD}[S]_o = k_{obsd}[S]_o \quad (1\text{-}7)$$

Since the $(1-D\overline{V})$ term approximately equals 1 because of the low amphiphile concentration and k_w(CAC) can be neglected under the present conditions in addition to the fact that K_s nearly equals $P_s\overline{V}$, Eq. 1-7 is rearranged and simplified to give Eq. 1-8.

$$k_{obsd} = \frac{k_oK_sD}{\overline{V}(1+K_sD)} \quad (1\text{-}8)$$

By substitution of k_m for $k_o/\overline{V}$, Eq. 1-8 is converted into Eq. 1.

17) For example: Y. Ihara, R. Hosako, M. Nango, and N. Kuroki, *J. Chem. Soc., Chem. Commun.*, **1981**, 393.
18) A. Yoshimatsu, Doctral Dissertation, Kyushu University, 1983.
19) M. L. Bender, F. J. Kézdy, and C. R. Gunter, *J. Am. Chem. Soc.*, **86**, 3714 (1964).

Synthesis of 5-(Substituted Styryl)-2-aminotropones

Kimiaki IMAFUKU,* Toshio KOBAYASHI,† and Hisashi MATSUMURA††
Department of Chemistry, Faculty of Science, Kumamoto University, Kurokami, Kumamoto 860
(Received July 23, 1984)

The methylation of 4-styryltropolones with diazomethane afforded 2-methoxy-4-styryltropones (**2a**—g) and 2-methoxy-6-styryltropones. The reactions of **2a**—**g** with hydrazine gave 2-hydrazino derivatives, which were converted to 2-chloro derivatives **5a**—**g**. Ammonolysis of **5a**—**g** afforded 2-amino-5-styryltropones (**7a**—**g**) by *ciné* substitution reaction. The compounds **7a**—**g** were hydrolyzed to give the corresponding 5-styryltropolones. Some interesting by-products were also found in these synthetic processes.

Previously, we have studied long-range substituent effects on dissociation constants of some series of styryltropolone derivatives and transmission of the electronic effects between two aromatic rings which were connected by vinylene linkage.[1-4] In connection with these studies, the dissociation constants of some 5-(substituted styryl)-2-aminotropones were discussed.[5] This paper deals with their synthesis.

Results and Discussion

The condensations of 3-carboxy-4-carboxymethyltropolone with some substituted benzaldehydes gave 3-carboxy-4-styryltropolones, which were converted to 4-styryltropolones (**1a**—**g**) with carbon dioxide elimination.[6] Now, two new 4-styryltropolones (**1b**: R=*m*-CH_3 and **1d**: R=*m*-OCH_3) were obtained.

The methylations of **1a**—**g** with diazomethane afforded two isomeric 2-methoxy-4-styryl- (**2a**—**g**) and 2-methoxy-6-styryltropones (**3a**—**g**), which were previously reported[7] except for the new compounds **2b**, **d** and **3b**, **d**. Furthermore, treatments of **2a**—**g** with hydrazine gave 2-hydrazino-4-styryltropones (**4a**—**g**). The yields and characteristic data are summarized in Table 1.

Oxidative decompositions of **4a**—**g** in concentrated hydrochloric acid in the presence of copper(II) sulfate afforded 2-chloro-4-styryltropones (**5a**—**g**). The structures were confirmed by their analytical and spectral data, which are listed in Table 1. Further, in this reaction a trace amount of by-products were isolated. We could confirm structures of only two products from **4a** and **4b** to be 4-styryl- (**6a**)[8] and 4-(*m*-methylstyryl)tropone (**6b**). Other isolated ones were too small to analyze.

Reactions of 2-chloro-4-styryltropones (**5a**—**g**) with ammonia afforded 2-amino-5-styryltropones (**7a**—**g**) by *ciné* substitution reaction. These reactions also gave a new type of compounds, 2-amino-7-chloro-5-styryltropones (**8a**, **b**, **e**). These results were summarized in Table 1. Although some by-products were isolated in the cases of the ammonolysis of **5c**, **d**, **f**, **g**, their amounts were too small to establish their structures.

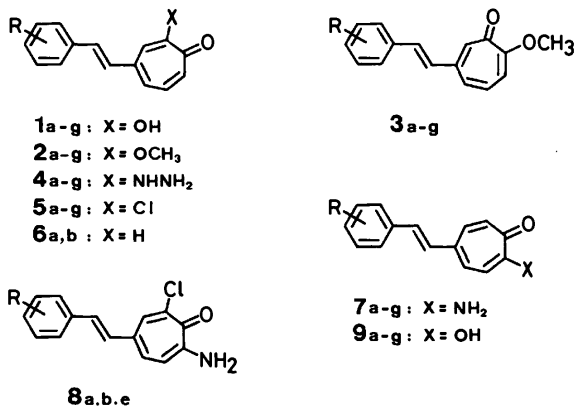

Scheme 1.

a R=H, **b** R=*m*-CH_3, **c** R=*p*-CH_3, **d** R=*m*-OCH_3, **e** R=*p*-OCH_3, **f** R=*m*-Cl, **g** R=*p*-Cl

The infrared spectra of the compounds **8a**, **b**, **e** are very similar to those of 2-amino-5-styryltropones **7** but show a little difference in the finger-print region. Their electronic spectra are also similar to those of **7** but show slightly bathochromic shift. These spectral data suggest that **8a**, **b**, **e** have a tropone ring and styryl group. The structure of **8a** was also confirmed by the fragmentation analysis in the mass spectrum.

In addition, 2-amino-5-styryltropones (**7a**—**g**) were hydrolyzed to afford 5-styryltropolones (**9a**—**g**).[9]

Experimental

The melting points were determined with a Yanagimoto MP-S2 apparatus and are uncorrected. The IR and UV spectra were taken on a JASCO IRA-1 and a Hitachi EPS-3T spectrophotometer, respectively. The NMR spectra were recorded with a Hitachi-Perkin-Elmer R-24 spectrometer (60 MHz). The mass spectrum was run on a JEOL JMS-01-SG2 apparatus.

4-Styryltropolones (1a—g). 4-Styryltropolones (**1a**—**g**) were prepared according to a previous work.[6]

2-Methoxy-4-styryltropones (2a—g) and 2-Methoxy-6-styryltropones (3a—g). An excess of diazomethane ethereal

† Present address: Minamata Senior High School, Nampukuji, Minamata 867.

†† Present address: Kumamoto Institute of Technology, Ikeda, Kumamoto 860.

TABLE 1. CHARACTERISTIC DATA

Compd	Yield %	Mp θ_m/°C	IR ($CHCl_3$) cm^{-1}	UV (CH_3OH) λ/nm (log ε)	NMR ($CDCl_3$) δ	Formula	Found (Calcd) (%) C	H	N
1b	48	93— 94	1600 (C=O)	315 (4.25) 402 (4.22)	2.33 (3H, s, CH_3) 6.9—7.3 (9H, m) 7.46 (1H, s, H-3)	$C_{16}H_{14}O_2$	80.49 (80.60	5.88 5.92)	
1d	22	106—107	1600 (C=O)	218 (4.30) 314 (sh, 4.33)	3.76 (3H, s, OCH_3) 6.8—7.4 (9H, m) 7.50 (1H, s, H-3) 8.73 (1H, br, OH)	$C_{16}H_{14}O_3$	75.40 (75.57	5.47 5.55)	
2b	40	Oil	1595 (C=O)	313 (4.41)	2.40 (3H, s, CH_3) 4.03 (3H, s, OCH_3) 6.9—7.4 (10H, m)	$C_{23}H_{19}N_3O_9$ [a]	57.35 (57.38	3.94 3.98	8.42 8.73)
2d	28	107	1590 (C=O)	282 (4.13) 396 (4.16)	3.86 (3H, s, OCH_3) 4.02 (3H, s, OCH_3) 6.8—7.4 (10H, m)	$C_{17}H_{16}O_3$	75.85 (76.10	6·03 6.01)	
3b	45	150—152	1590 (C=O)	314 (4.41)	2.34 (3H, s, CH_3) 3.88 (3H, s, OCH_3) 6.5—7.4 (10H, s)	$C_{17}H_{16}O_2$	80.62 (80.92	6.37 6.39)	
3d	35	140—141	1585 (C=O)	309 (4.47)	3.86 (3H, s, OCH_3) 3.94 (3H, s, OCH_3) 6.6—7.3 (9H, m) 7.40 (1H, s, H-3)	$C_{17}H_{16}O_3$	76.07 (76.10	6.21 6.01)	
4a	68	195 (189—190) [b]	3305 (NH) 3270 (NH) 1630 (C=O)	238 (4.09) 330 (4.56) 444 (3.92)	7.3—8.2 (m) [c]				
4b	89	163—164	3310 (NH) 3270 (NH) 1640 (C=O)	239 (4.08) 332 (4.56) 442 (3.73)	2.40 (3H, s, CH_3) 3.84 (2H, m, NH_2) 6.5—7.6 (10H, m) 8.0—8.1 (1H, m, H-3)	$C_{16}H_{16}N_2O$	76.08 (76.16	6.31 6.39	11.37 11.10)
4c	80	212	3310 (NH) 3265 (NH) 1630 (C=O)	240 (4.31) 334 (4.75) 442 (4.15)	2.40 (3H, s, CH_3) [c] 7.4—8.4 (10H, m)	$C_{16}H_{16}N_2O$	75.96 (76.16	6.44 6.39	11.23 11.10)
4d	99	173—174	3300 (NH) 3255 (NH) 1630 (C=O)	216 (4.39) 331 (4.50) 442 (3.98)	4.06 (3H, s, OCH_3) [c] 7.0—8.5 (10H, m)	$C_{16}H_{16}N_2O_2$	71.47 (71.62	5.94 6.01	10.35 10.44)
4e	64	198—200	3310 (NH) 3270 (NH) 1650 (C=O)	242 (4.10) 340 (4.50) 440 (4.04)	4.04 (3H, s, OCH_3) [c] 7.0—8.5 (10H, m)	$C_{16}H_{16}N_2O_2$	71.51 (71.62	5.94 6.01	10.24 10.44)
4f	86	191—192	3300 (NH) 3255 (NH) 1625 (C=O)	236 (4.15) 329 (4.58) 446 (3.96)	7.3—8.2 (9H, m) [c] 8.35 (1H, s, H-3)	$C_{15}H_{13}ClN_2O$	66.02 (66.06	4.74 4.80	10.14 10.27)
4g	95	223	3310 (NH) 3270 (NH) 1635 (C=O)	237 (4.13) 334 (4.55) 445 (3.94)	7.0—8.2 (9H, m) [c] 8.24 (1H, s, H-3)	$C_{15}H_{13}ClN_2O$	65.79 (66.06	4.80 4.80	10.08 10.27)
5a	32	110 (111—111.5) [b]	1615 (C=O)	242 (4.03) 282 (4.09) 276 (4.26)	6.9 (10H, m) 8.04 (1H, s, H-3)				

Table 1. (Continued)

Compd	Yield %	Mp θ_m/°C	IR ($CHCl_3$) cm^{-1}	UV (CH_3OH) λ/nm (log ε)	NMR ($CDCl_3$) δ	Formula	Found (Calcd) (%) C	H	N
5b	37	130—131	1610 (C=O)	243 (4.12) 284 (4.01) 380 (4.33)	2.28 (3H, s, CH_3) 6.9—7.5 (9H, m) 8.18 (1H, s, H-3)	$C_{16}H_{13}ClO$	74.54 (74.85	5.12 5.10)	
5c	52	140	1620 (C=O)	246 (4.14) 263 (4.12) 325 (4.02) 382 (4.17)	2.34 (3H, s, CH_3) 6.8—7.2 (5H, m) 7.23 (2H, d, J=8 Hz, H-3′,5′) 7.41 (2H, d, J=8 Hz, H-2′,6′) 8.09 (1H, s, H-3)	$C_{16}H_{13}ClO$	74.83 (74.85	5.19) 5.10)	
5d	37	118—119	1610 (C=O)	280 (4.28) 383 (4.39)	3.84 (3H, s, OCH_3) 6.6—7.4 (9H, m) 8.13 (1H, s, H-3)	$C_{16}H_{13}ClO_2$	70.20 (70.46	4.83 4.80)	
5e	45	111—112	1615 (C=O)	249 (4.23) 400 (4.38)	3.83 (3H, s, OCH_3) 6.6—7.3 (5H, m) 6.84 (2H, d, J=9 Hz, H-3′,5′) 7.48 (2H, d, J=9 Hz, H-2′,6′) 8.13 (1H, s, H-3)	$C_{16}H_{13}ClO_2$	70.28 (70.46	4.78 4.80)	
5f	36	182	1615 (C=O)	245 (4.14) 284 (4.17) 369 (4.26)	6.9—7.9 (9H, m) 8.12 (1H, s, H-3)	$C_{15}H_{10}Cl_2O$	64.78 (65.00	3.67 3.64)	
5g	28	146—147	1620 (C=O)	246 (4.12) 380 (4.43)	6.9 (9H, m) 8.11 (1H, s, H-3)	$C_{15}H_{10}Cl_2O$	64.79 (65.00	3.65 3.64)	
7a	43	207—208 (205—206) [b]	3510 (NH) 3360 (NH) 1595 (C=O)	236 (4.36) 242 (4.45) 285 (4.34) 389 (4.58)	5.8 (2H, br, NH_2) 7.0—7.6 (11H, m)				
7b	8	172	3510 (NH) 3350 (NH) 1595 (C=O)	237 (4.36) 244 (4.36) 285 (4.34) 391 (4.58)	2.37 (3H, s, CH_3) 5.88 (2H, br, NH_2) 6.5—7.8 (10H, m)	$C_{16}H_{15}NO$	80.79 (80.98	6.37 6.37	5.86 5.90)
7c	48	237	3510 (NH) 3360 (NH) 1585 (C=O)	244 (4.45) 288 (4.37) 394 (4.58)	2.35 (3H, s, OCH_3) 5.8 (2H, br, NH_2) 6.5—7.7 (10H, m)	$C_{16}H_{15}NO$	80.89 (80.98	6.36 6.37	5.63 5.90)
7d	24	162	3500 (NH) 3350 (NH) 1595 (C=O)	243 (4.48) 280 (4.34) 392 (4.58)	3.84 (3H, s, OCH_3) 5.9 (2H, br, NH_2) 6.7—7.5 (10H, m)	$C_{16}H_{15}NO_2$	75.62 (75.87	6.02 5.97	5.40 5.53)
7e	15	244—245	3510 (NH) 3360 (NH) 1595 (C=O)	245 (4.41) 295 (4.32) 398 (4.55)	3.83 (3H, s, OCH_3) 5.9 (2H, br, NH_2) 6.8—7.9 (10H, m)	$C_{16}H_{15}NO_2$	75.82 (75.87	6.02 5.97	5.25 5.53)
7f	20	244—246	3510 (NH) 3360 (NH) 1590 (C=O)	243 (4.45) 285 (4.35) 391 (4.58)	6.00 (2H, br, NH_2) 6.7—7.7 (10H, m)	$C_{15}H_{12}ClNO$	70.10 (69.91	4.57 4.69	5.35 5.43)
7g	22	231—232	3500 (NH) 3350 (NH) 1590 (C=O)	244 (4.54) 289 (4.50) 393 (4.69)	5.95 (2H, br, NH_2) 6.9—7.5 (10H, m)	$C_{15}H_{12}ClNO$	69.85 (69.91	4.76 4.69	5.26 5.43)

a) Picrate. b) H. Matsumura, *Nippon Kagaku Zasshi*, **81**, 1763 (1960). c) In CF_3COOH.

solution was added to a solution of 4-styryltropolone (**1a—g**) (1.0 g, 3.3—4.2 mmol) in chloroform (10 ml), and the mixture was allowed to stand for 2 d in a refrigerator. After removal of the solvents, the residue was chromatographed on three Wakogel B-10 plates (30×30 cm) with ethyl acetate. 2-Methoxy-4-styryltropones (**2a—g**) and 2-methoxy-6-styryltropones (**3a—g**) were obtained from the upper and lower band, respectively. Each methyl ether was recrystallized from benzene.

2-Hydrazino-4-styryltropones (4a—g). To a solution of 2-methoxy-4-styryltropone (**2a—g**) (1.0 g, 3.7—4.2 mmol) in ethanol (5 ml) was added 80% hydrazine hydrate (1.0 ml). The mixture was allowed to stand overnight at room temperature. The precipitate was collected and recrystallized from methanol to give 2-hydrazino-4-styryltropones (**4a—g**).

2-Chloro-4-styryltropones (5a—g). A hot solution of copper(II) sulfate pentahydrate (5 g) in water (6 ml) was added to a hot suspended solution of 2-hydrazino-4-styryltropones (**4a—g**) (500 mg) in concentrated hydrochloric acid (5 ml). The mixture was immediately cooled, diluted with water, and extracted with chloroform. The extract was dried over sodium sulfate, concentrated, and chromatogrpahed on a Wakogel C-100 column (50 g) with chloroform to afford 2-chloro-4-styryltropones (**5a—g**) (from methanol).

4-Styryltropones (6a, b). In the preparation of 2-chloro-4-styryltropones (**5a, b**), the second band in the chromatography gave 4-styryltropones (**6a, b**).

6a: Yellow crystals. Yeild, 9%. Mp 89—92 °C (lit,[8] 89—91 °C).

6b: Oil. Yield, 19%. IR ($CHCl_3$) 1625 (C=O), 1565 (C=C), 960 cm^{-1} (CH). Found: C, 86.23; H, 6.39%. Calcd for $C_{16}H_{14}O$ C, 86.45; H, 6.35%.

2-Amino-5-styryltropones (5a—g). A suspended solution of 2-chloro-4-styryltropone (**5a—g**) (100 mg) in ammonia-saturated absolute ethanol (6 ml) in a sealed tube was allowed to stand for 2 d at room temperature. After removal of the ammonia and ethanol, the residue was chromatographed on a Wakogel B-10 plate (20×20 cm) with ethyl acetate to give 2-amino-5-stytyltropones (**7a—g**) (from ethanol).

2-Amino-7-chloro-5-styryltropones (8a, b, e). In the preparation of 2-amino-5-styryltropones (**7a, b, e**), the upper fraction in the chromatography gave 2-amino-7-chloro-5-styryltropones (**8a, b, e**), respectively.

8a: Yellow needles (from benzene). Yield, 35%. Mp 186 °C. IR ($CHCl_3$) 3510 (NH), 3360 (NH), 1590 (C=O), 950 cm^{-1} (CH); UV (CH_3OH) 251 ($\log \varepsilon$ 4.24), 289 (5.32), 392 nm (4.46); MS *m/z* (%) 259 (M', 38), 257 (M, 100), 231 (M'—CO, 14), 229 (M—CO, 40), 194 ([231 and 229]–Cl, 25), 193 ([231 and 229]–HCl, 42). Found: C, 69.86; H 4.92; N, 5.31%. Calcd for $C_{15}H_{12}NOCl$: C, 69.90; H, 4.70; N, 5.44%.

8b: Yellow prisms (from benzene). Yield, 3%. Mp 177 °C. IR ($CHCl_3$) 3510 (NH), 3350 (NH), 1595 (C=O), 970 cm^{-1} (CH); NMR ($CDCl_3$) δ=2.36 (3H, s, CH_3), 6.12 (2H, br, NH_2), 6.8—7.5 (9H, m). Found: C, 70.75; H, 5.23; N, 5.10%. Calcd for $C_{16}H_{14}NOCl$: C, 70.72; H, 5.19; N, 5.15%.

8e: Yellowish brown needles (from benzene). Yield, 30%. Mp 208—210 °C. IR ($CHCl_3$) 3500 (NH), 3340 (NH), 1600 (C=O), 960 cm^{-1} (CH). Found: C, 66.73; H, 4.96; N, 4.63%. Calcd for $C_{16}H_{14}NO_2Cl$: C, 66.78; H, 4.96; N, 4.87%.

We wish to thank Professor Hitoshi Takeshita, Kyushu University, for his kind measurement of the mass spectrum.

References

1) K. Imafuku, *Yuki Gosei Kagaku Kyokaishi*, **38**, 79 (1980).
2) K. Imafuku, S. Nakama, and H. Matsumura, *Tetrahedron*, **26**, 1821 (1970).
3) K. Hamada, S. Nakama, K. Imafuku, K. Kurosawa, and H. Matsumura, *Tetrahedron*, **27**, 337 (1971).
4) K. Imafuku and H. Matsumura, *Bull. Chem. Soc. Jpn.*, **46**, 544 (1973).
5) T. Kobayashi, K. Imafuku, and H. Matsumura, *Bull. Chem. Soc. Jpn.*, **49**, 3606 (1976).
6) S. Nakama, K. Imafuku, and H. Matsumura, *Bull. Chem. Soc. Jpn.*, **43**, 3265 (1970).
7) K. Imafuku and H. Matsumura, *Bull. Chem. Soc. Jpn.*, **46**, 199 (1973).
8) K. Imafuku, *Yuki Gosei Kagaku Kyokaishi*, **38**, 809 (1980).
9) H. Higashi, K. Kurosawa, and H. Matsumura, *Bull. Chem. Soc. Jpn.*, **43**, 3236 (1970).

 © 1985 The Chemical Society of Japan Bull. Chem. Soc. Jpn., 58, 185—193 (1985)

Boron Trifluoride Etherate-catalyzed Backbone Rearrangement of 5α,10α-Epoxyalnusan-3β-yl Acetate and Partial Synthesis of Isomultiflorenol[1)]

Masaki Takai, Motoo Tori, Takahiko Tsuyuki, Takeyoshi Takahashi,* Akiko Itai,† and Yoichi Iitaka†

Department of Chemistry, Faculty of Science, The University of Tokyo,
†Faculty of Pharmaceutical Sciences, The University of Tokyo,
Hongo, Bunkyo-ku, Tokyo 113

(Received July 23, 1984)

Epoxidation of alnus-5(10)-en-3β-yl acetate with *m*-chloroperbenzoic acid gave a 5α,10α-epoxide, treatment of which with boron trifluoride etherate afforded multiflora-5,8-dien-3β-yl acetate. On hydrogenation and hydrolysis, the diene gave isomultiflorenol.

In the previous paper,[2)] the boron trifluoride etherate ($BF_3 \cdot OEt_2$)-catalyzed backbone rearrangement of 5,6-epoxyalnusan-3β-yl acetate was reported. Further investigation on a behavior of carbonium ions generated on B-ring was attempted. This paper describes the epoxidation of alnus-5(10)-ene derivatives, the $BF_3 \cdot OEt_2$-catalyzed backbone rearrangement of a 5α,10α-epoxy acetate, and also a preparation of isomultiflorenol (**1**)[3–7)] from one of the rearranged products.

Alnus-5(10)-en-3β-yl acetate (**4**),[8)] prepared from dendropanoxide (**5**),[9)] was subjected to the epoxidation with *m*-chloroperbenzoic acid (MCPBA) to afford a single epoxide (**6**) in a good yield. However, no information on the configuration of the epoxide ring could be obtained from any spectrum of **6** (See Experimental).

In order to determine the configuration of the epoxide (**6**), the following epoxidation reactions were examined. Alnus-5(10)-en-3β-ol (**7**) and its benzoate (**8**) were epoxidized with MCPBA under the same conditions as above to afford single epoxides (**9** and **10**), respectively. On acetylation, the epoxide (**9**) yielded an epoxy acetate, which was identical with **6**. Treatment of **10** with lithium aluminium hydride afforded an epoxy alcohol identical with **9**. Therefore, the epoxide rings of **6**, **9**, and **10** are in all the same configurations.

Since the signals due to 3α-protons of alnus-5(10)-en-3β-ol (**7**), -3β-yl acetate (**4**), and -3β-yl benzoate (**8**) were observed as double doublets at δ 3.44 (J=10 and 4 Hz), δ 4.69 (J=10 and 4 Hz), and δ 4.94 (J=10 and 4 Hz), respectively, in the ^1H NMR spectra, the substituents at C-3β exist in an equatorial orientation. From these facts, it could be understood why the 3β-oxygen functions did not participate in these epoxidation reactions, hence the reagent attacked exclusively from the less hindered α-side of the molecule (4β- and 9β-methyl groups are perpendicular to the 5,10-double bond plane, while the 4α-methyl group lies in the plane). Therefore, the epoxide rings of **6**, **9**, and **10** were considered to be in the α-configuration.

Then, epoxidation reactions of alnus-5(10)-en-3α-*O*-derivatives were examined. In the case of these 3α-*O*-derivatives, since the substituents at C-3α exist in an axial orientation, the bulky substituents block the α-side of the molecule and the attack of the epoxidizing reagent from the α-side was considered to be hindered. Epoxidation of alnus-5(10)-en-3α-ol (**11**) and its acetate (**12**) under the same conditions as above gave single epoxides (**13** and **14**), respectively, while 3α-benzoate (**15**), on epoxidation, gave two epoxides (**16** and **17**) in a ratio of 7:1. The relative configurations of the epoxide rings of **13**, **14**, and **16** were confirmed by the derivatization as in the case of the 3β-*O*-derivatives, and proved to be in all the same. These substituent effects are explained by the steric hindrance due to 4β- and 9β-methyl groups and partly by the hydrogen bond formation between the reagent and the 3α-axial hydroxyl group in the case of **11**, resulting in the exclusive formation of the α-epoxide (**13**). In the case of the benzoate (**15**), the attack from the α-side of the molecule was sterically slightly hinderded by the bulky benzoyloxyl group to afford the β-epoxide (**17**) as the minor product, while the acetoxyl group was not large enough to prevent the attack from the α-side. Thus the configurations of the epoxide rings of **13**, **14**, and **16** are concluded to be α.

These assignments of the epoxide rings were further confirmed by the Sharpless epoxidation.[10)] Epoxidation of alnus-5(10)-en-3α-ol (**11**) with vanadyl acetylacetonate ($VO(acac)_2$) and *t*-butyl hydroperoxide afforded a single epoxide which was identical with 5α,10α-epoxide (**13**) obtained by MCPBA. However epoxidation of alnus-5(10)-en-3β-ol (**7**) with the same conditions gave a single epoxide, but it was different from the 5α,10α-epoxide (**9**) obtained by MCPBA. From the spectral data and formation mechanism, it was concluded to be a 5β,10β-epoxide (**18**).

The epoxy-3β-ol (**9**), obtained by the reaction with MCPBA, was oxidized to give a keto epoxide (**19**) which was identical with that obtained by the oxidation of the epoxy-3α-ol (**13**); thus the epoxide rings of the 3β-*O*-derivatives (**6**, **9**, and **10**) and the 3α-*O*-derivatives (**13**, **14**, and **16**) are the same.

From these facts, the epoxidation reaction of these 5(10)-ene derivatives was shown to occur from the α-side of the molecule exclusively except for 5(10)-en-3α-yl benzoate (**15**). These results are opposite from those obtained for the epoxidation of alnus-5-en-3β-ol and its derivatives.[2]

The assignments of these epoxide rings were supported by the NMR spectral measurement (see Tables 1 and 2). The protons at C-3 of alnus-5(10)-en-3β-ol (**7**) and -3α-ol (**11**) resonated at nearly the same magnetic fields, while a remarkable difference in shift values due to the protons at C-3 was observed between 5α,10α-epoxy-3β-ol (**9**) and 5α,10α-epoxy-3α-ol (**13**); the 3α-H of **9** is deshielded by 0.34 ppm relative to that of **13**. This observation is ascribed to an anisotropic effect of an oxygen atom of the epoxide caused by a proximation of the 3α-axial proton of **9** to the oxygen atom.

This anisotropic effect is also observed in the ^{1}H NMR spectra of the corresponding acetates (**6** *vs.* **14**) and benzoates (**10** *vs.* **16**).

The same observations were given in the ^{1}H NMR spectral examination of 5β,10β-epoxides, although the differences are not so large, because the 3β-protons exist in an equatorial orientation. The 3β-protons of 5β,10β-epoxy-3α-ol (**20**), 5β,10β-epoxy-3α-yl acetate (**21**), and 5β,10β-epoxy-3α-yl benzoate (**17**) appeared at

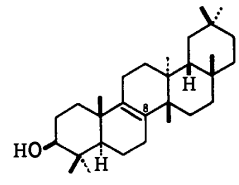

1

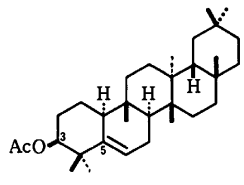

2

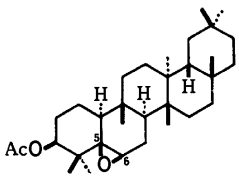

3

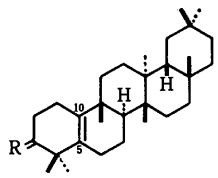

4 R=α-H, β-OAc
7 R=α-H, β-OH
8 R=α-H, β-OCOPh
11 R=α-OH, β-H
12 R=α-OAc, β-H
15 R=α-OCOPh, β-H

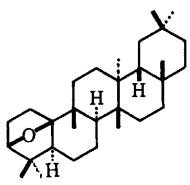

5

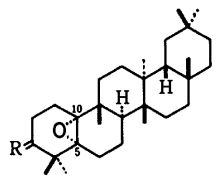

6 R=α-H, β-OAc
9 R=α-H, β-OH
10 R=α-H, β-OCOPh
13 R=α-OH, β-H
14 R=α-OAc, β-H
16 R=α-OCOPh, β-H
19 R=O

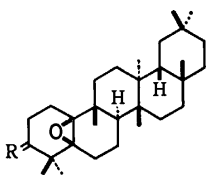

17 R=α-OCOPh, β-H
18 R=α-H, β-OH
20 R=α-OH, β-H
21 R=α-OAc, β-H
22 R=α-H, β-OAc
23 R=α-H, β-OCOPh

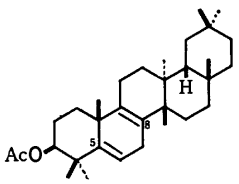

24

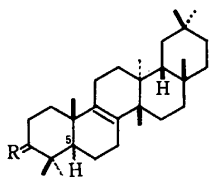

26 5α-H; R=α-H, β-OAc
27 5β-H; R=α-H, β-OAc
28 5β-H; R=α-H, β-OH
29 5α-H; R=O
30 5β-H; R=O

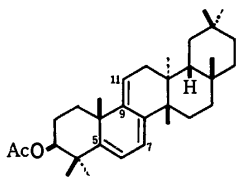

25

Table 1. The δ values of C-3 protons of alnus-5(10)-ene derivatives and 5,10-epoxyalnusane derivatives in the ^{1}H NMR spectra

	δ-values	
	C-3α protons of 3β-*O*- derivatives	C-3β protons of 3α-*O*- derivatives
5(10)-en-3-ol	**7** 3.44 dd J=10, 4	**11** 3.45 t-like J=4
5α,10α-epoxy-3-ol	**9** 3.58 dd J=10, 5	**13** 3.24 dt J=11, 3 3.52 d J=11 (-OH)
5β,10β-epoxy-3-ol	**18** 3.17 br s 2.71 br s (-OH)	**20** 3.41 dd J=7, 3
5(10)-en-3-yl acetate	**4** 4.69 dd J=10, 5	**12** 4.70 t J=4
5α,10α-epoxy-3-yl acetate	**6** 4.77 dd J=10, 4	**14** 4.47 dd J=7, 4
5β,10β-epoxy-3-yl acetate	**22** 4.36 dd J=11, 4	**21** 4.57 dd J=7, 3
5(10)-en-3-yl benzoate	**8** 4.94 dd J=10, 4	**15** 4.96 dd J=5, 3
5α,10α-epoxy-3-yl benzoate	**10** 5.02 dd J=11, 4	**16** 4.72 dd J=7, 3
5β,10β-epoxy-3-yl benzoate	**23** 4.62 dd J=10, 5	**17** 4.78 dd J=5.5, 3

TABLE 2. ^{13}C NMR SPECTRA OF ALNUS-5(10)-EN-3-OLS AND 5,10-EPOXYALNUSAN-3-OLS

7	11	9	13	18	20
18.6	18.6 t	16.7 t	16.7 t	15.6 t	15.9 t
18.8	18.8 q	17.2 q	18.4 q	18.1 q	18.0 q
20.5	19.0 t	18.3 q	18.6 q	18.9 q	18.9 q
20.7	20.5 q	18.7 q	19.5 t	19.9 q	19.7 t
21.0	21.2 q	19.9 q	19.8 q	20.6 t	21.1 q
23.2	23.1 q	20.6 q	21.4 q	21.0 q	21.1 q
24.7	25.9 t	23.5 t	24.1 t	24.7 t	22.6 q
27.0	27.0 t	24.4 t	24.2 t	25.4 q	24.5 t
27.7	28.0 q	26.1 t	25.5 q	28.1 s	28.1 s
28.2	28.2 s	28.1 s	28.2 s	29.0 t	29.5 t
30.1	30.1 t	29.0 t	28.8 t	29.9 s	30.0 s
31.0	31.0 s	30.0 s	30.1 s	31.6 q	31.7 q
31.6	31.8 t	30.2 t	30.2 t	31.8 t	31.8 s
31.8	31.8 q	31.9 q	32.0 q	32.2 t	32.2 t
32.2	32.2 q	32.1 q	32.1 q	32.2 q	32.2 q
32.3	32.4 t	32.4 t	32.4 t	32.7 t	32.6 t
32.9	32.9 t	32.9 t	32.9 t	32.9 t	32.8 t
35.1	35.1 q	34.9 q	34.9 q	35.1 q	35.2 q
35.5	35.5 t	35.3 t	35.3 t	35.5 t	35.5 t
36.1	36.1 t	36.0 t	36.0 t	35.9 t	36.0 t
37.5	37.6 s	36.9 s	36.9 s	37.6 s	37.7 s
38.3	38.3 s	37.9 s	37.1 s	37.8 s	37.8 s
39.4	38.8 s	38.6 s	37.9 s	38.8 s	38.8 s
39.4	39.4 t	* 38.8 d	* 38.7 d	39.4 t	39.4 t
39.5	39.5 s	39.2 t	39.2 t	39.4 s	39.5 s
42.8	42.8 d	39.3 s	39.3 s	42.6 d	42.7 d
* 47.9	* 47.8 d	42.9 d	42.9 d	* 49.6 d	* 49.7 d
** 76.2	** 75.5 d	71.0 s	71.4 s	71.8 s	69.7 s
131.7	130.0 s	71.9 s	73.3 s	73.6 s	** 72.7 d
137.3	137.4 s	** 72.2 d	** 76.5 d	** 76.5 d	72.8 s

* Assignable to C-8. ** Assignable to C-3.

lower fields than the 3α-protons of the corresponding 3β-alcohol (**18**), 3β-acetate (**22**), and 3β-benzoate (**23**), respectively.

In the ^1H NMR spectra of **13** and **18**, signals due to hydroxyl protons were observed at δ 3.52 and 2.71, respectively. Appearance of these signals is ascribed to the formation of hydrogen bond between the epoxide oxygen atom and the hydroxyl proton, resulting in the retardation of the exchange rate of the hydroxyl proton. This observation also supports the assignment of the epoxides, because the hydrogen bond could not be formed in 5α,10α-epoxy-3β-ol (**9**) nor 5β,10β-epoxy-3α-ol (**20**).

In the ^{13}C NMR spectrum of α-epoxy-3β-ol (**9**), a signal due to C-3 atom to which the proton resonating in a low field (δ 3.58) was attached, was observed in a higher field by 3.3 ppm than that of C-3 atom of α-epoxy-3α-ol (**13**). In the ^{13}C NMR spectra of β-epoxy alcohols, it was shown that C-3 atom of 3α-alcohol (**20**) resonated in a higher field relative to that of 3β-alcohol (**18**).

From the same reason, it is understood that C-8 atoms, bearing hydrogen atoms in α-orientation, of α-epoxides (**9** and **13**) resonate in a higher field by *ca.* 9 ppm than those of 5(10)-en-3-ols (**7** and **11**), while C-8 atoms of β-epoxides (**18** and **20**) resonates at nearly the same magnetic field as 5(10)-en-3-ols.

These observations described above are strongly indicative of the correct assignment of the epoxide rings.

The unequivocal proof for the structure of 5α,10α-epoxyalnusan-3β-yl acetate (**6**) was provided by X-ray single crystal analysis. The crystals of **6** belong to a monoclinic space group C_2, and the lattice parameters are a=13.446(4), b=6.739(2), c=32.257(7) Å, and β=103.71(3)°; z=4. Intensity data were measured on a Philips PW1100 automatic four-circle diffractometer using monochromated Cu $K\alpha$ radiation. A total of 2951 independent reflections with $F_o \geqq 2.5\sigma(F_o)$ were obtained by $2\theta-\theta$ scanning mode. The structure was solved by the direct method using the MULTAN 80 program and was refined by the block-diagonal least squares method. All hydrogen atoms were located on a difference electron density map. The final R-value was 0.056 assuming the anisotropic temperature factors for the non-hydrogen atoms and the isotropic ones

for the hydrogen atoms. The final atomic coordinates are listed in Table 3 and bond lengths and bond angles are listed in Tables 4 and 5.[11] Figure 1 is a computer-generated perspective drawing of the molecule of 5α,10α-epoxyalnusan-3β-yl acetate (**6**).

5α,10α-Epoxyalnusan-3β-yl acetate (**6**) was treated with $BF_3 \cdot OEt_2$ (1.2 equiv) in benzene to afford a reaction mixture, which was shown to consist of a main product (**24**; *ca.* 80% yield) and more than seven minor components by HPLC examination. The reaction mixture was subjected to separation by column chromatography to give the pure main product (**24**), $C_{32}H_{50}O_2$ (determined by the high-resolution mass spectrum), showed no chracteristic absorption maxi-

Table 3. Atomic positional parameters (×10⁴) and isotropic temperature factors (×10²) for non-hydrogen atoms of 5α, 10α-epoxyalnusan-3β-yl acetate (**6**) with estimated standard deviations in parentheses

Atom	x	y	z	B_{eq}[a]	Atom	x	y	z	B_{eq}[a]
C(1)	3874 (2)	2605 (0)	1572 (1)	422 (6)	C(19)	6057 (3)	69 (7)	3862 (1)	460 (6)
C(2)	3564 (3)	3303 (6)	1111 (1)	395 (5)	C(20)	6432 (3)	−918 (8)	4300 (1)	523 (7)
C(3)	4317 (3)	4817 (5)	1017 (1)	361 (5)	C(21)	7585 (3)	−421 (10)	4482 (1)	633 (9)
C(4)	5408 (3)	4000 (6)	1075 (1)	377 (5)	C(22)	8037 (3)	880 (9)	4179 (1)	571 (7)
C(5)	5765 (2)	3210 (5)	1529 (1)	328 (4)	C(23)	6112 (3)	5711 (7)	1010 (1)	530 (7)
C(6)	6882 (3)	2618 (8)	1662 (1)	496 (7)	C(24)	5444 (3)	2326 (7)	753 (1)	531 (7)
C(7)	7142 (2)	1077 (7)	2018 (1)	439 (6)	C(25)	5128 (3)	−1072 (5)	1939 (1)	440 (6)
C(8)	6508 (2)	1412 (5)	2351 (1)	303 (4)	C(26)	6268 (3)	3116 (6)	3203 (1)	431 (6)
C(9)	5361 (2)	1012 (4)	2138 (1)	278 (4)	C(27)	7037 (3)	−1899 (6)	2723 (1)	457 (6)
C(10)	5018 (2)	2486 (5)	1768 (1)	289 (4)	C(28)	8459 (3)	−2047 (9)	3776 (1)	630 (8)
C(11)	4734 (2)	1340 (6)	2475 (1)	350 (5)	C(29)	6277 (4)	−3205 (10)	4262 (1)	704 (9)
C(12)	5163 (2)	259 (6)	2896 (1)	353 (5)	C(30)	5799 (4)	−68 (13)	4598 (1)	875 (14)
C(13)	6273 (2)	861 (5)	3108 (1)	297 (4)	C(31)	3496 (3)	7192 (6)	496 (1)	451 (6)
C(14)	6954 (2)	367 (5)	2788 (1)	323 (4)	C(32)	3252 (5)	7673 (9)	22 (1)	766 (10)
C(15)	8049 (2)	1158 (8)	2972 (1)	487 (6)	O(1)	5461 (2)	4458 (3)	1846 (1)	373 (3)
C(16)	8386 (3)	1346 (8)	3461 (1)	559 (7)	O(2)	3962 (2)	5451 (4)	573 (1)	447 (4)
C(17)	7874 (2)	−46 (7)	3726 (1)	428 (6)	O(3)	3298 (3)	8235 (6)	764 (1)	728 (7)
C(18)	6687 (2)	−328 (5)	3530 (1)	342 (5)					

a) $B_{eq} = 8\pi(u_1^2 + u_2^2 + u_3^2)/3$.

Table 4. Bond lengths (*l*/Å) of 5α,10α-epoxyalnusan-3β-yl acetate (**6**) with estimated standard deviations in parentheses

Bond length		(*l*/Å)	Bond length		(*l*/Å)
Atom 1	Atom 2		Atom 1	Atom 2	
C(1)	-C(2)	1.523 (5)	C(12)	-C(13)	1.542 (4)
C(1)	-C(10)	1.520 (4)	C(13)	-C(14)	1.569 (5)
C(2)	-C(3)	1.517 (5)	C(13)	-C(18)	1.563 (4)
C(3)	-C(4)	1.537 (5)	C(13)	-C(26)	1.550 (5)
C(3)	-O(2)	1.461 (4)	C(14)	-C(15)	1.546 (4)
C(4)	-C(5)	1.525 (4)	C(14)	-C(27)	1.549 (5)
C(4)	-C(23)	1.537 (6)	C(15)	-C(16)	1.539 (5)
C(4)	-C(24)	1.542 (6)	C(16)	-C(17)	1.537 (6)
C(5)	-C(6)	1.514 (5)	C(17)	-C(18)	1.582 (4)
C(5)	-C(10)	1.486 (5)	C(17)	-C(22)	1.557 (6)
C(5)	-O(1)	1.456 (4)	C(17)	-C(28)	1.550 (7)
C(6)	-C(7)	1.526 (6)	C(18)	-C(19)	1.538 (5)
C(7)	-C(8)	1.539 (5)	C(19)	-C(20)	1.535 (5)
C(8)	-C(9)	1.556 (4)	C(20)	-C(21)	1.558 (6)
C(8)	-C(14)	1.562 (4)	C(20)	-C(29)	1.555 (9)
C(9)	-C(10)	1.538 (4)	C(20)	-C(30)	1.539 (7)
C(9)	-C(11)	1.540 (5)	C(21)	-C(22)	1.539 (7)
C(9)	-C(25)	1.546 (5)	C(31)	-C(32)	1.520 (6)
C(10)	-O(1)	1.454 (4)	C(31)	-O(2)	1.326 (5)
C(11)	-C(12)	1.529 (4)	C(31)	-O(3)	1.193 (5)

TABLE 5. BOND ANGLES (ϕ/°) OF 5α,10α-EPOXYALNUSAN-3β-YL ACETATE (**6**) WITH ESTIMATED STANDARD DEVIATIONS IN PARENTHESES

Bond angle			ϕ/°	Bond angle			ϕ/°
Atom 1	Atom 2	Atom 3		Atom 1	Atom 2	Atom 3	
C(2)	-C(1)	-C(10)	116.0 (2)	C(14)	-C(13)	-C(18)	108.7 (2)
C(3)	-C(2)	-C(1)	111.2 (3)	C(14)	-C(13)	-C(26)	111.6 (3)
C(4)	-C(3)	-C(2)	113.4 (3)	C(12)	-C(13)	-C(18)	111.0 (3)
C(4)	-C(3)	-O(2)	107.7 (3)	C(12)	-C(13)	-C(26)	107.2 (3)
C(2)	-C(3)	-O(2)	108.3 (3)	C(18)	-C(13)	-C(26)	110.4 (3)
C(5)	-C(4)	-C(3)	108.3 (3)	C(15)	-C(14)	-C(8)	108.5 (3)
C(5)	-C(4)	-C(23)	109.2 (3)	C(15)	-C(14)	-C(13)	109.0 (3)
C(5)	-C(4)	-C(24)	109.8 (3)	C(15)	-C(14)	-C(27)	107.4 (3)
C(3)	-C(4)	-C(23)	108.4 (3)	C(8)	-C(14)	-C(13)	109.8 (2)
C(3)	-C(4)	-C(24)	111.2 (3)	C(8)	-C(14)	-C(27)	110.3 (3)
C(23)	-C(4)	-C(24)	109.9 (3)	C(13)	-C(14)	-C(27)	111.7 (3)
C(6)	-C(5)	-C(4)	115.3 (3)	C(16)	-C(15)	-C(14)	116.4 (3)
C(6)	-C(5)	-C(10)	120.9 (3)	C(17)	-C(16)	-C(15)	117.2 (4)
C(6)	-C(5)	-O(1)	112.2 (3)	C(18)	-C(17)	-C(16)	113.1 (3)
C(4)	-C(5)	-C(10)	121.1 (3)	C(18)	-C(17)	-C(22)	109.1 (3)
C(4)	-C(5)	-O(1)	113.4 (3)	C(18)	-C(17)	-C(28)	112.1 (3)
C(10)	-C(5)	-O(1)	59.2 (2)	C(16)	-C(17)	-C(22)	107.2 (3)
C(7)	-C(6)	-C(5)	115.3 (3)	C(16)	-C(17)	-C(28)	107.8 (3)
C(8)	-C(7)	-C(6)	111.1 (3)	C(22)	-C(17)	-C(28)	107.2 (3)
C(9)	-C(8)	-C(7)	108.7 (3)	C(19)	-C(18)	-C(13)	112.0 (3)
C(9)	-C(8)	-C(14)	116.6 (2)	C(19)	-C(18)	-C(17)	111.8 (3)
C(7)	-C(8)	-C(14)	114.0 (3)	C(13)	-C(18)	-C(17)	113.8 (3)
C(10)	-C(9)	-C(8)	108.3 (2)	C(20)	-C(19)	-C(18)	116.8 (3)
C(10)	-C(9)	-C(11)	109.9 (2)	C(21)	-C(20)	-C(19)	109.5 (4)
C(10)	-C(9)	-C(25)	105.6 (2)	C(21)	-C(20)	-C(29)	110.2 (4)
C(8)	-C(9)	-C(11)	108.4 (2)	C(21)	-C(20)	-C(30)	109.4 (4)
C(8)	-C(9)	-C(25)	115.0 (3)	C(19)	-C(20)	-C(29)	110.4 (4)
C(11)	-C(9)	-C(25)	109.5 (3)	C(19)	-C(20)	-C(30)	107.8 (4)
O(1)	-C(10)	-C(1)	110.9 (2)	C(29)	-C(20)	-C(30)	109.5 (4)
O(1)	-C(10)	-C(5)	59.4 (2)	C(22)	-C(21)	-C(20)	113.1 (4)
O(1)	-C(10)	-C(9)	114.9 (2)	C(17)	-C(22)	-C(21)	112.2 (4)
C(1)	-C(10)	-C(5)	120.6 (3)	C(32)	-C(31)	-O(2)	110.9 (4)
C(1)	-C(10)	-C(9)	116.4 (2)	C(32)	-C(31)	-O(3)	124.9 (4)
C(5)	-C(10)	-C(9)	120.0 (3)	O(2)	-C(31)	-O(3)	124.2 (4)
C(12)	-C(11)	-C(9)	113.8 (3)	C(3)	-O(2)	-C(31)	118.2 (3)
C(13)	-C(12)	-C(11)	113.0 (3)	C(5)	-O(1)	-C(10)	61.4 (2)
C(14)	-C(13)	-C(12)	107.9 (2)				

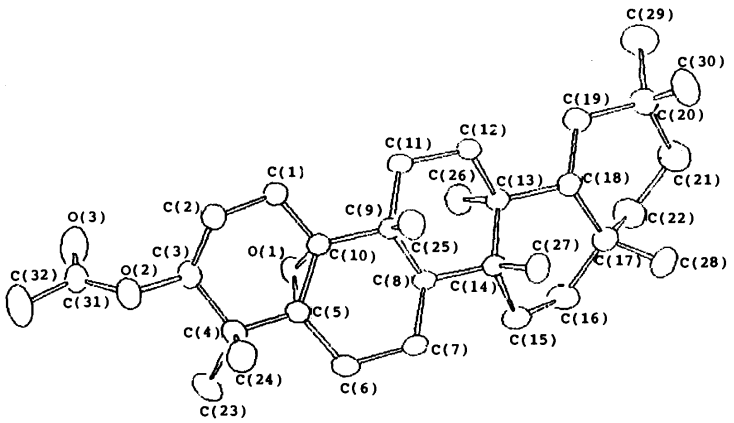

Fig. 1. Perspective view of 5α,10α-epoxyalnusan-3β-yl acetate (**6**).

mum above 210 nm, while the ^{1}H NMR spectrum revealed the presence of a doubly allylic methylene (δ 2.60, 2H; m) and an olefinic proton (δ 5.71, 1H; dd). The spectral data and mechanistic considerations lead to the structure, multiflora-5,8-dien-3β-yl acetate for the main product (**24**). The proposed structure was supported by the mass spectral measurement; the appearance of the fragment peaks at *m/z* 239 (**A**), *m/z* 227 (**B**), and *m/z* 171 (**C**) indicates the presence of the 5,8-diene structure.

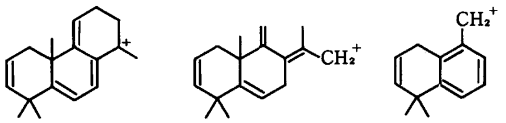

A $C_{18}H_{23}^+$ (*m/z* 239.1798) **B** $C_{17}H_{23}^+$ (*m/z* 227.1778) **C** $C_{13}H_{15}^+$ (*m/z* 171.1207)

The seven minor products obtained by the $BF_3 \cdot OEt_2$-catalyzed backbone rearrangement of **6** could not be identified, because of difficulty of the separation and a paucity of the material.

The diene (**24**) was treated with selenium dioxide[12] in boiling aqueous benzene to give a dehydrogenation product (**25**), the molecular formula, $C_{32}H_{48}O_2$, of which was given by the high-resolution mass spectrum. Since the ^{1}H NMR and UV spectra indicate the presence of a $\Delta^{5,7,9(11)}$-triene moiety, the stucture of the dehydrogenation product (**25**) is formulated as multiflora-5,7,9(11)-trien-3β-yl acetate.

The backbone rearrangement of 5α,10α-epoxyalnusan-3β-yl acetate (**6**) was shown to yield multiflora-5,8-dien-3β-yl acetate (**24**) as the main rearranged product, no further rearranged product being obtained much enough to be characterized. Although it is not clear the reason why further migration did not occur efficiently, the following account could be proposed. On attack of $BF_3 \cdot OEt_2$, the 5α,10α-epoxide ring would be cleaved to yield a carbonium ion on C-10 and a BF_3-coordinated oxygen-function at C-5α. A methyl group at C-9β would migrate to C-10 and then a migration of $C_{8\alpha}$–H to C-9α would follow immediately to afford a carbonium ion on C-8. If the BF_3-coordinated group is absent, it is expected to take place the further backbone rearrangement up to the C and D rings. However, since the BF_3-coordinated group at C-5α and the $C_{9\alpha}$–H are located in a 1,3-diaxial relationship, the neighboring group participation could assist the abstraction of the $C_{9\alpha}$–H, while the competitive migration of C_{14}–Me would be impeded, resulting in the interruption of the further backbone rearrangement.

The diene (**24**) in ethyl acetate was hydrogenated in the presence of 5% palladium on carbon for 3 d to give a hydrogenation product in 97% yield, which was shown to be a mixture of **26** and **27** in a ratio of 2:3 by GC examination. The mixture was subjected to separation by repeating column chromatography on silica gel to afford isomutiflorenyl acetate (**26**) and its 5β-*H* isomer (**27**). The spectral data of the former (**26**) were identical with those of literatures[4] and two compounds (**26** and **27**) exhibited nearly the same mass spectra characteristic of multiflor-8-ene skeleton.[13] Since the diene molecule (**24**) bends towards the α-side so much that the adsorption onto the surface of the catalyst was impeded, the hydrogenation from the α-side was hindered. On the other hand, the hydrogenation from the β-side was also hindered by the presence of 4β- and 10β-methyl groups. The fact that the hydrogenation had required a long reaction time could be explained by these two effects, which were estimated to be almost the same from the product ratio.

Isomultiflorenyl acetate (**26**) and its 5β-*H* isomer (**27**) were hydrolyzed with alkali to give isomultiflorenol (**1**)[6,14,15] and 5β-isomultiflorenol (**28**), respectively.

Thus the conversion of dendropanoxide (**5**) into isomultiflorenol (**1**) was achieved in 18% overall yield (6 steps) through thermodynamically favorable pathways,[16] which formally constitutes the total synthesis of isomultiflorenol (**1**).[17]

When the acetate mixture (**26** and **27**), obtained by the hydrogenation of the diene (**24**), was treated with 5% potassium hydroxide in methanol–tetrahydrofuran (5:1) at room temperature, the acetate (**26**) was easily hydrolyzed and afforded isomultiflorenol (**1**) within a half day, while most of the acetate (**27**) still remained intact; it required additional 4 d for completion of the hydrolysis of **27**.

Isomultiflorenol (**1**) and the 5β-*H* isomer (**28**) were subjected to Collins oxidation to give isomultiflorenone (**29**) and the 5β-*H* ketone (**30**), respectively. Isomultiflorenone (**29**)[15,18] exhibits IR absorption band at 1710 cm^{-1} and the positive Cotton effect. 5β-Isomultiflorenone (**30**) shows IR absorption band at 1715 cm^{-1}, intense fragment peaks at *m/z* 257 and *m/z* 245 chracteristic of the multiflor-8-ene skeleton,[13] and the negative Cotton effect.

Experimental[19]

Epoxidation of Alnus-5(10)-en-3β-yl Acetate (4). Alnus-5(10)-en-3β-ol (**7**), prepared from dendropanoxide (**5**), was acetylated with acetic anhydride in pyridine to give alnus-5(10)-en-3β-yl acetate (**4**), mp 289—293 °C. The acetate (**4**; 224 mg) was dissolved in chloroform (20 ml) and treated with MCPBA (208 mg) and disodium hydrogenphosphate dodecahydrate ($Na_2HPO_4 \cdot 12H_2O$; *ca.* 5 mg) at 0 °C for 7 h. The usual work-up gave a residue (224 mg; 97% yield), which was purified by silica-gel (30 g) column chromatography. Elution with benzene afforded 5α,10α-epoxyalnusan-3β-yl acetate (**6**), mp 272—273 °C (from $CHCl_3$–CH_3OH); IR (KBr) 1730, 1250, 1025, 990, and 980 cm^{-1}; ^{1}H NMR ($CDCl_3$) δ=0.97 (3H, s), 0.99 (6H, s), 1.02 (6H, s), 1.03 (6H, s), 1.15 (3H, s), 2.00 (3H, s), and 4.77 (1H, dd, J=10

and 4 Hz); MS *m/z* (%) 484 (M^+; 5), 466 (14), 406 (100), 391 (42), 227 (22), 205 (32), and 202 (46); Found: *m/z* 484.3867. Calcd for $C_{32}H_{52}O_3$: M, 484.3914.

Epoxidation of Alnus-5(10)-en-3β-ol (7). Alnus-5(10)-en-3β-ol (**7**; 118 mg) in chloroform (10 ml) was treated with MCPBA (122 mg) and $Na_2HPO_4 \cdot 12H_2O$ (*ca.* 5 mg) at 0 °C for 4 h. The usual work-up afforded 5α,10α-epoxyalnusan-3β-ol (**9**; quantitative yield), mp 247—248 °C (from acetone) (decomp); IR (KBr) 3450, 1690, 1050, 1020, 1000, and 970 cm^{-1}; ^1H NMR ($CDCl_3$) δ=0.94 (6H, s), 1.00 (6H, s), 1.01 (3H, s), 1.03 (3H, s), 1.07 (3H, s), 1.15 (3H, s), and 3.58 (1H, dd, *J*=10 and 5 Hz); MS *m/z* (%) 442 (M^+; 3), 427 (7), 424 (47), 409 (14), 406 (9), 391 (36), 245 (25), 206 (100), 201 (32), 109 (50), and 95 (54).

5α,10α-Epoxyalnusan-3β-ol (**9**; 37 mg) was treated with acetic anhydride (1 ml) and pyridine (4 ml) at room temperature for 14 h to give **6** in 95% yield.

Epoxidation of Alnus-5(10)-en-3β-yl Benzoate (8). Alnus-5(10)-en-3β-ol (**7**; 33 mg) was benzoylated with benzoyl chloride (1 ml) and pyridine (5 ml) at room temperature for 1 h to give the benzoate (**8**; 36 mg), mp 273—274 °C (from $CHCl_3$–acetone); IR (KBr) 1715, 1280, 1115, 705, and 685 cm^{-1}; ^1H NMR ($CDCl_3$) δ=0.96 (6H, s), 1.04 (12H, s), 1.14 and 1.18 (each 3H, s), 4.94 (1H, dd, *J*=10 and 4 Hz), and 7.35—8.14 (5H); MS *m/z* (%) 530 (M^+; 0.5), 515 (0.2), 408 (66), 393 (30), 365 (21), 205 (28), 203 (37), 190 (36), 189 (36), 187 (39), 175 (42), and 105 (100).

The benzoate (**8**; 33 mg) in chloroform (5 ml) was epoxidized with MCPBA (27 mg) and $Na_2HPO_4 \cdot 12H_2O$ (*ca.* 2 mg) at 0 °C for 3 h to afford 5α,10α-epoxyalnusan-3β-yl benzoate (**10**; 28 mg), mp 272—278 °C (from $CHCl_3$–CH_3OH) (decomp); IR (KBr) 1715, 1275, 1115, and 710 cm^{-1}; ^1H NMR ($CDCl_3$) δ=0.95, 0.99, 1.02, 1.04, 1.06, 1.08 (each 3H, s), 1.19 (6H, s), 5.02 (1H, dd, *J*=11 and 4 Hz), and 7.37—8.13 (5H); MS *m/z* (%) 546 (M^+; 0.6), 528 (3), 406 (43), 391 (41), 274 (18), 259 (20), 205 (30), 201 (19), 187 (24), 185 (25), 171 (41), and 105 (100).

On treatment with lithium aluminium hydride, the epoxy benzoate (**10**; 24 mg) afforded 5α,10α-epoxyalnusan-3β-ol (**9**; 15 mg) identical with an authentic sample.

Epoxidation of Alnus-5(10)-en-3α-ol (11). Alnus-5(10)-en-3α-ol (**11**, 21 mg), mp 255—258 °C, was dissolved in chloroform (5 ml) and treated with MCPBA (22 mg) and $Na_2HPO_4 \cdot 12H_2O$ (*ca.* 2 mg) at 0 °C for 1.5 h. The usual work-up gave 5α,10α-epoxyalnusan-3α-ol (**13**; 20 mg), mp 272—276 °C (from C_6H_6–CH_3OH) (decomp); IR (Nujol) 3480 cm^{-1}; ^1H NMR ($CDCl_3$) δ=0.95 (3H, s), 1.00 (9H, s), 1.02, 1.05 (each 3H, s), 1.17 (6H, s), 3.24 (1H, dt, *J*=11 and 3 Hz), and 3.52 (1H, d, *J*=11 Hz; disappeared on addition of D_2O); MS *m/z* (%) 442 (M^+; 0.8), 424 (79), 406 (17), 391 (46), 206 (100), 201 (48), 189 (38), 187 (35), 171 (35), 109 (65), and 95 (83).

5α,10α-Epoxyalnusan-3α-ol (**13**; 12 mg) was treated with acetic anhydride (3 ml) and pyridine (5 ml) at 120 °C for 4 h to give **14** in 53% yield.

Epoxidation of Alnus-5(10)-en-3α-yl Acetate (12). Alnus-5(10)-en-3α-yl acetate (**12**; 14 mg), mp 206—207 °C, in chloroform (3 ml) was epoxidized with MCPBA (21 mg) at 0 °C for 1.3 h to afford 5α,10α-epoxyalnusan-3α-yl acetate (**14**; 10 mg), mp 246—248 °C (from C_6H_6–CH_3OH); IR (KBr) 1740, 1255, 1030, 995, and 925 cm^{-1}; ^1H NMR ($CDCl_3$) δ=0.93 (3H, s), 1.03 (18H, s), 1.15 (3H, s), 2.03 (3H, s), and 4.47 (1H, dd, *J*= 7 and 4 Hz); MS *m/z* (%) 484 (M^+; 0.3), 409 (6), 406 (8), 391 (59), 248 (19), 227 (20), 205 (38), 201 (43), 189 (75), 187 (53), 137 (95), 109 (82), and 95 (100).

Epoxidation of Alnus-5(10)-en-3α-yl Benzoate (15). Alnus-5(10)-en-3α-ol (**11**) was treated with benzoyl chloride and pyridine to afford the benzoate (**15**), mp 175—177 °C (from $CHCl_3$–CH_3OH); IR (KBr) 1720, 1280, 1120, 755, and 710 cm^{-1}; ^1H NMR ($CDCl_3$) δ=0.96, 1.00, 1.01 (each 3H, s), 1.06, 1.09 (each 6H, s), 1.20 (3H, s), 4.96 (1H, dd, *J*=5 and 3 Hz), and 7.35—8.12 (5H); MS *m/z* (%) 530 (M^+; 4), 408 (93), 393 (36), 365 (33), 229 (21), 218 (24), 205 (39), 203 (37), 190 (39), 189 (45), 187 (40), 175 (39), and 105 (100).

Alnus-5(10)-en-3α-yl benzoate (**15**; 302 mg) in chloform (40 ml) was treated with MCPBA (246 mg) in the presence of $Na_2HPO_4 \cdot 12H_2O$ (*ca.* 10 mg) at 0 °C for 2 h. After the usual work-up, the reaction product was separated by column chromatography on silica gel (40 g) eluted with benzene to afford the major epoxide (**16**; 267 mg) and the minor epoxide (**17**; 35 mg). 5α,10α-Epoxyalnusan-3α-yl benzoate (**16**); mp 202—203 °C (from $CHCl_3$–CH_3OH); IR (KBr) 1720, 1275, 1115, and 715 cm^{-1}; ^1H NMR ($CDCl_3$) δ=0.96, 1.00, 1.03, 1.06 (each 3H, s), 1.10 (6H, s), 1.15, 1.17 (each 3H, s), 4.72 (1H, dd, *J*=7 and 3 Hz), and 7.38—8.18 (5H); MS *m/z* (%) 546 (M^+; 2), 528 (19), 406 (32), 391 (64), 310 (16), 205 (26), 201 (26), 189 (37), 187 (31), 137 (40), and 105 (100). 5β,10β-Epoxyalnusan-3α-yl benzoate (**17**); mp 154—155 °C (from $CHCl_3$–CH_3OH); IR (film) 1720, 1275, 1115, 1025, 940, and 710 cm^{-1}; ^1H NMR ($CDCl_3$) δ=0.97, 1.00, 1.02, 1.08 (each 3H, s), 1.09 (6H, s), 1.15, 1.20 (each 3H, s), 4.78 (1H, dd, *J*=5.5 and 3 Hz), and 7.33—8.18 (5H); MS *m/z* (%) 546 (M^+; 5), 424 (11), 406 (8), 391 (9), 288 (36), 274 (18), 273 (19), 219 (19), 218 (21), 205 (36), 189 (18), 185 (41), 137 (64), 109 (50), 105 (100), and 95 (61).

5α,10α-Epoxyalnusan-3α-yl benzoate (**16**; 22 mg) was treated with lithium aluminium hydride (5 mg) at room temperature for 30 min to give **13** in 68% yield.

5β,10β-Epoxyalnusan-3α-yl benzoate (**17**; 31 mg) was treated with a mixture of 5% potassium hydroxide (KOH) in methanol (6 ml) and tetrahydrofuran (THF) (2 ml) for 2 d to give 5β,10β-epoxyalnusan-3β-ol (**20**; 21 mg); mp 210—211 °C (from $CHCl_3$–CH_3OH); IR (KBr) 3580, 1070, and 965 cm^{-1}; ^1H NMR ($CDCl_3$) δ=0.95 (6H, s), 1.02 (12H, s), 1.03, 1.17 (each 3H, s), and 3.41 (1H, dd, *J*=7 and 3 Hz); MS *m/z* (%) 442 (M^+; 10), 427 (12), 424 (70), 406 (10), 391 (12), 218 (24), 206 (100), 205 (40), 201 (50), 187 (25), 179 (31), 137 (41), 109 (54), and 95 (60).

5β,10β-Epoxyalnusan-3α-ol (**20**; 14 mg) was treated with acetic anhydride (1 ml) and pyridine (3 ml) at 100 °C for 4 h to give 5β,10β-epoxyalnusan-3α-yl acetate (**21**; 15 mg); mp 173—174 °C (from $CHCl_3$–CH_3OH); IR (KBr) 1730, 1250, 1050, 1020, and 965 cm^{-1}; ^1H NMR ($CDCl_3$) δ=0.96 (6H, s), 0.98 (3H, s), 1.01 (9H, s), 1.05, 1.07, 2.03 (each 3H, s), and 4.57 (1H, dd, *J*=7 and 3 Hz); MS *m/z* (%) 484 (M^+; 41), 469 (16), 424 (19), 409 (18), 406 (17), 391 (12), 342 (11), 288 (98), 274 (62), 273 (60), 259 (21), 245 (28), 218 (79), 205 (91), 137 (100), 109 (59), and 95 (56).

Sharpless Epoxidation of Alnus-5(10)-en-3α-ol (11) and -3β-ol (7). Alnus-5(10)-en-3α-ol (**11**; 35 mg) was dissolved in benzene (7 ml) and treated with the benzene solution of *t*-butyl hydroperoxide (80 μl; 2.35 mmol/ml)[10a] and $VO(acac)_2$ (*ca.* 1 mg) at room temperature in nitrogen atmosphere for 4 h. The usual work-up afforded 5α,10α-epoxyalnusan-3α-ol (**13**; 32 mg), which was identical with that obtained by the MCPBA-epoxidation of **11**.

Alnus-5(10)-en-3β-ol (**7**; 47 mg) was treated with the ben-

zene solution of *t*-butyl hydroperoxide (100 μl) and VO (acac)$_2$ (*ca.* 1 mg) under the same conditions for 7 h to give 5β,10β-epoxyalnusan-3β-ol (**18**; 34 mg); mp 199—200 °C (from acetone); IR (film) 3380, 1055, 1030, 995, and 980 cm^{-1}; ^{1}H NMR ($CDCl_3$) δ=0.97 (6H, s), 1.03 (3H, s), 1.06 (9H, s), 1.10, 1.18 (each 3H, s), 2.71 (1H, br; disappeared on addition of D_2O), and 3.17 (1H, br; changed into a triplet (*J*=5 Hz) on addition of D_2O); MS *m/z* (%) 442 (M^+; 2), 424 (91), 409 (18), 406 (30), 391 (100), 227 (49), 206 (87), 205 (47), 201 (55), 189 (76), 187 (62), 137 (65), 109 (84), and 95 (95); high resolution MS *m/z* 442.3797. Calcd for $C_{30}H_{50}O_2$: M, 442.3809.

5β,10β-Epoxyalnusan-3β-ol (**18**; 30 mg) was treated with acetic anhydride (1 ml) and pyridine (2 ml) at room temperature for 40 h to give 5β,10β-epoxyalnusan-3β-yl acetate (**22**; 25 mg); mp 258.5—259.5 °C (from $CHCl_3$–CH_3OH); IR (KBr) 1735, 1250, and 1025 cm^{-1}; ^{1}H NMR ($CDCl_3$) δ=0.96 (6H, s), 1.01 (9H, s), 1.04 (6H, s), 1.17 (3H, s), 2.03 (3H, s), and 4.36 (1H, dd, *J*=11 and 4 Hz); MS *m/z* (%) 484 (M^+; 12), 469 (8), 466 (28), 451 (6), 424 (22), 409 (12), 406 (100), 391 (51), 342 (33), 288 (20), 274 (40), 259 (34), 218 (43), 205 (73), 137 (72), 109 (70), and 95 (83).

5β,10β-Epoxyalnusan-3β-ol (**18**; 31 mg) was benzoylated with benzoyl chloride (0.1 ml) and pyridine (2 ml) at room temperature for 1.5 h to give 5β,10β-epoxyalnusan-3β-yl benzoate (**23**; 23 mg); mp 245—246 °C (from $CHCl_3$–CH_3OH); IR (KBr) 1720, 1275, 1115, 1025, and 710 cm^{-1}; ^{1}H NMR ($CDCl_3$) δ=0.97, 1.03, 1.07, 1.20 (each 6H, s), 4.62 (1H, dd, *J*=10 and 5 Hz), and 7.38—8.12 (5H); MS *m/z* (%) 546 (M^+; 12), 424 (49), 409 (22), 406 (34), 391 (16), 342 (18), 288 (26), 274 (20), 273 (22), 249 (17), 218 (35), 205 (53), 137 (85), 105 (100), and 95 (52).

Oxidation of 5α,10α-Epoxyalnusan-3β-ol (9) and 5α,10α-Epoxyalnusan-3α-ol (13). 5α,10α-Epoxyalnusan-3β-ol (**9**; 56 mg) and -3α-ol (**13**; 22 mg) were oxidized with Collins reagent to give the same product, 5α,10α-epoxyalnusan-3-one (**19**; 43 mg and 11 mg, respectively), mp 261—263 °C (from $CHCl_3$–CH_3OH) (decomp); IR (KBr) 1710 and 980 cm^{-1}; ^{1}H NMR ($CDCl_3$) δ=0.94, 0.99 (each 3H, s), 1.04 (6H, s), 1.11, 1.13, 1.15, 1.17 (each 3H, s), and 2.24 (2H, t, *J*=6 Hz); MS *m/z* (%) 440 (M^+; 12), 425 (11), 422 (19), 407 (9), 205 (97), 204 (87), 177 (53), 137 (44), 123 (57), 109 (81), and 95 (100).

Backbone Rearrangement of 5α,10α-Epoxyalnusan-3β-yl Acetate (6). 5α,10α-Epoxyalnusan-3β-yl acetate (**6**; 121 mg) in benzene (30 ml) was treated with $BF_3 \cdot OEt_2$ (38 μl; 1.1 equiv) at room temperature in nitrogen atmosphere for 30 min. The reaction product, after addition of a saturated sodium hydrogencarbonate solution, was worked up as usual to give a residue (117 mg). The residue showed eight peaks at 12.8, 16.5, 18.9 (a main peak; a ratio of the product was estimated at *ca.* 80% from the peak hight), 21.1, 22.1, 23.9, 25.7, and 27.9 min on HPLC (column: μPORASIL, solvent system; 1% ether–hexane, 1 ml/min). The residue was chromatographed on alumina (Alumina Woelm N, Akt I. 35 g; impregnated with 15% silver nitrate). Elution with 5—10% ethyl acetate–hexane afforded a mixture (*ca.* 24 mg) of the minor products and the product, multiflora-5,8-dien-3β-yl acetate (**24**; 81.4 mg). The latter was purified by column chromatography on silica gel eluted with hexane–benzene to give pure **24**, mp 190—193 °C (from C_6H_6–CH_3OH); IR (KBr) 1735, 1250, 1035, 1020, and 990 cm^{-1}; ^{1}H NMR ($CDCl_3$) δ=0.98 (6H, s), 1.01 (3H, s), 1.10 (6H, s), 1.12, 1.14, 1.18, 2.04 (each 3H, s), 2.60 (2H, m), 4.50 (1H, dd, *J*=8 and 6 Hz), and 5.71 (1H, dd, *J*=5 and 3 Hz); ^{13}C NMR ($CDCl_3$) δ=19.2, 21.1, 21.3, 24.1, 25.1, 25.2, 25.2, 25.8, 27.1, 27.6, 28.3, 30.9, 31.1, 31.7, 33.1, 33.8, 34.2, 34.5, 34.5, 36.8, 36.8, 37.3, 38.4, 40.4, 40.7, 44.2, 79.1, 120.2, 131.1, 134.0, 146.4, and 170.7; MS *m/z* (%) 466 (M^+; 5), 406 (15), 391 (100), 239 (13), 227 (28), 187 (18), 185 (20), and 171 (43); high resolution MS *m/z* 466.3791 (Calcd for $C_{32}H_{50}O_2$: M, 466.3809), *m/z* 239.1798 (Calcd for $C_{18}H_{23}$: 239.1798), *m/z* 227.1778 (Calcd for $C_{17}H_{23}$: 227.1798), and *m/z* 171.1207 (Calcd for $C_{13}H_{15}$: 171.1174).

Dehydrogenation of Multiflora-5,8-dien-3β-yl Acetate (24). The diene (**24**; 39 mg) was heated with selenium dioxide in a mixture of benzene (5 ml) and water (5 drops) under reflux for 38 h to give multiflora-5,7,9(11)-trien-3β-yl acetate (**25**; 22 mg), mp 211—214 °C (from $CHCl_3$–CH_3OH); IR (KBr) 1740, 1250, 1035, 1005, 980, and 850 cm^{-1}; ^{1}H NMR ($CDCl_3$) δ=0.84, 0.96, 0.99, 1.02, 1.06, 1.09 (each 3H, s), 1.21 (6H, s), 2.07 (3H, s), 4.57 (1H, dd, *J*=6 and 5 Hz), 5.38 (1H, m), 5.57 (1H, d, *J*=6 Hz), and 5.89 (1H, d, *J*=6 Hz); UV λ(C_2H_5OH) 307 (ε 11600) and 317 nm (12200); MS *m/z* (%) 464 (M^+; 7), 404 (100), 389 (21), 251 (26), 237 (26), and 225 (80); high resolution MS *m/z* 464.3649 (Calcd for $C_{32}H_{48}O_2$: M, 464.3654), *m/z* 237.1645 (Calcd for $C_{18}H_{21}$: 237.1643), and *m/z* 225.1661 (Calcd for $C_{17}H_{21}$; 225.1644).

Hydrogenation of Multiflora-5,8-dien-3β-yl Acetate (24). A solution of multiflora-5,8-dien-3β-yl acetate (**24**; 103 mg) in ethyl acetate (70 ml) was hydrogenated in the presence of 5% palladium on carbon (470 mg) for 3 d to give hydrogenated products (101 mg), which showed two peaks at 16.3 and 21.4 min (peak hight ratio 3:2) on GC examination (column: Dexsil 300 GC, 2%, 1.5 m) and two peaks at 20.2 and 22.2 min (peak hight ratio 2:3) on HPLC examination. (column: μPORASIL, solvent system: 0.8% ether–hexane, 1 ml/min). The mixture was separated by repeating column chromatography on silica gel to give isomultiflorenyl acetate (**26**; 40 mg) and 5β-isomultiflorenyl acetate (**27**; 60 mg). Isomultiflorenyl acetate (**26**); mp 223—225 °C (from CH_2Cl_2–CH_3OH); IR (KBr) 1735, 1455, 1380, 1255, 1025, 1005, and 990 cm^{-1}; ^{1}H NMR ($CDCl_3$) δ=0.88, 0.96, 0.98 (each 6H, s), 1.06, 1.07, (each 3H, s), 2.03 (3H, s), and 4.48 (1H, dd, *J*=11 and 5 Hz); MS *m/z* (%) 468 (M^+; 58), 453 (15), 408 (21), 393 (23), 301 (28), 289 (17), 241 (26), 229 (27), 218 (64), 205 (100), 203 (47), and 189 (23). 5β-Isomultiflorenyl acetate (**27**); mp 151—152 °C (from CH_2Cl_2–CH_3OH); IR (film) 1730, 1245, and 1030 cm^{-1}; ^{1}H NMR ($CDCl_3$) δ=0.94 (3H, s), 0.97, 1.03 (each 6H, s), 1.06 (3H, s), 1.08 (6H, s), 2.04 (3H, s), and 4.54 (1H, t, *J*=3 Hz); MS *m/z* (%) 468 (M^+; 74), 453 (58), 408 (21), 393 (62), 301 (57), 289 (29), 241 (100), 229 (93), 205 (94), 203 (49), and 189 (58); high resolution MS *m/z* 468.3960. Calcd for $C_{32}H_{52}O_2$: M, 468.3965.

Hydrolysis of Isomultiflorenyl Acetate (26) and Its 5β-H Isomer (27). Isomultiflorenyl acetate (**26**; 15 mg) was treated with a mixture of 5% KOH in methanol (50 ml) and THF (10 ml) at room temperature in nitrogen atmosphere for 1 d. The usual work-up gave isomultiflorenol (**1**; 13 mg); mp 182—183 °C (from $CHCl_3$–CH_3OH); IR (Nujol) 3350 and 1025 cm^{-1}; ^{1}H NMR ($CDCl_3$) δ=0.80 (3H, s), 0.97 (9H, s), 0.99, 1.00, 1.06, 1.07 (each 3H, s), and 3.23 (1H, dd, *J*=11 and 5 Hz); MS *m/z* (%) 426 (M^+; 100), 411 (29), 408 (31), 393 (43), 259 (83), 247 (55), 241 (56), 229 (65), 218 (77), 205 (98), 204 (50), 191 (40), and 189 (44); high resolution MS *m/z* 426.3863. Calcd for $C_{30}H_{50}O$: M, 426.3862.

5β-Isomultiflorenyl acetate (**27**; 25 mg) was treated with

5% KOH in methanol–THF (5:1, 40 ml) under the same conditions as above for 4 d to afford 5β-isomultiflorenol (**28**; 20 mg); mp 159—159.5 °C (from ether-CH_3OH); IR (film) 3430, 1060, 950, and 935 cm^{-1}; ^1H NMR ($CDCl_3$) δ=0.98 (6H, s), 1.04 (12H, s), 1.09 (6H, s), and 3.33 (1H, t-like, J=3 Hz); MS m/z (%) 426 (M^+; 32), 411 (92), 408 (19), 393 (63), 259 (87), 247 (38), 241 (100), 229 (85), 205 (65), 203 (37), 189 (87), 109 (90), and 95 (88); high resolution MS m/z 426.3907 (Calcd for $C_{30}H_{50}O$: M, 426.3862), m/z 259.2060 (Calcd for $C_{18}H_{27}O$: 259.2060), m/z 247.2065 (Calcd for $C_{17}H_{27}O$: 247.2062), m/z 241.1944 (Calcd for $C_{18}H_{25}$; 241.1955), and m/z 229.1967 (Calcd for $C_{17}H_{25}$: 229.1956).

Oxidation of Isomultiflorenol (1) and 5β-Isomultiflorenol (28). Isomultiflorenol (**1**; 17 mg) in dichloromethane (5 ml) was oxidized with Collins reagent (4 ml; 17 eq) at room temperature for 16 min to give isomultiflorenone (**29**; 16 mg); mp 189—193 °C (from $CHCl_3$-CH_3OH); IR (KBr) 1710 cm^{-1}; ^1H NMR ($CDCl_3$) δ=0.97 (6H, s), 0.99 (3H, s), 1.06 (6H, s), 1.10 (9H, s), and 2.40—2.62 (2H, m); MS m/z (%) 424 (M^+; 16), 409 (7), 257 (48), 245 (39), 205 (100), 109 (38), and 95 (54). CD (c 0.016, $CHCl_3$, Amb. temp.) $[\theta]_{291}$ +1580 and $[\theta]_{323}$ −110.

5β-Isomutiflorenol (**28**; 18 mg) was oxidized with Collins reagent (4 ml; 16 eq) under the same conditions as above to give 5β-isomultiflorenone (**30**; 17 mg), mp 143—144 °C (from ether-CH_3OH); IR (KBr) 1715 cm^{-1}; ^1H NMR ($CDCl_3$) δ=0.97 (6H, s), 1.02 (3H, s), 1.10 (6H, s), 1.11, 1.14, 1.16 (each 3H, s) and 2.16—2.40 (2H, m); MS m/z (%) 424 (M^+; 16), 409 (11), 257 (73), 245 (60), 205 (100), 109 (39), and 95 (56); CD (c 0.016, $CHCl_3$, Amb. temp) $[\theta]_{314}$ −750, $[\theta]_{305}$ −880, and $[\theta]_{273}$ +120.

References

1) A preliminary account of this report: M. Takai, M. Tori, T. Tsuyuki, T. Takahashi, A. Itai, and Y. Iitaka, *Chem. Pharm. Bull.*, **32**, 2464 (1984).

2) M. Tori, M. Takai, Y. Matsumoto, Y. Moriyama, T. Tsuyuki, T. Takahashi, A. Itai, and Y. Iitaka, *Chem. Lett.*, **1983**, 527; M. Tori, M. Takai, Y. Matsumoto, Y. Moriyama, T. Tsuyuki, T. Takahashi, H. Ohnishi, A. Itai, and Y. Iitaka, *Bull. Chem. Soc. Jpn.*, **57**, 2490 (1984).

3) T. Itoh, T. Shigemoto, N. Shimizu, T. Tamura, and T. Matsumoto, *Phytochemistry*, **21**, 2414 (1982).

4) L. Cattel, G. Balliano, O. Caputo, and F. Viola, *Planta Med.*, **41**, 328 (1981).

5) J. Vaquette, J. L. Pousset, A. Cavé, P. Delaveau, and R. R. Paris, *Ann. Pharm. Fr.*, **31**, 49 (1973).

6) R. T. Aexel, R. B. Ramsey, and H. J. Nicholas, *Phytochemistry*, **11**, 2353 (1972).

7) H. N. Khastgir and P. Sengupta, *Chem. Ind. (London)*, **1961**, 1077.

8) H. R. Arthur and W. H. Hui, *J. Chem. Soc.*, **1961**, 551; J. H. Block and G. H. Constantine, Jr., *Phytochemistry*, **11**, 3279 (1972).

9) Dendropanoxide (**5**) was obtained from leaves of *Gilibertia triflidas* Makino, which were collected at the Botanical Gardens, Faculty of Science, the University of Tokyo. The authors would like to thank Mr. Eiichi Ishii for collection of leaves of the plant.

10) a) K. B. Sharpless and T. R. Verhoeven, *Aldrichimica Acta*, **12**, 63 (1979); b) K. B. Sharpless and R. C. Michaelson, *J. Am. Chem. Soc.*, **95**, 6136 (1973); c) S. Tanaka, H. Yamamoto, H. Nozaki, K. B. Sharpless, R. C. Michaelson, and J. D. Cutting, *J. Am. Chem. Soc.*, **96**, 5254 (1974).

11) The complete F_o–F_c data, anisotropic thermal parameters for non-hydrogen atoms, atomic posotional parameters and isotropic thermal parameters for hydrogen atoms are deposited as Document No. 8505 at the Office of the Editor of Bull. Chem. Soc. Jpn.

12) A. C. Paton, F. S. Spring, and R. Stevenson, *J. Chem. Soc.*, **1958**, 2640.

13) H. Budzikiewicz, J. M. Wilson, and C. Djerassi, *J. Am. Chem. Soc.*, **85**, 3688 (1963).

14) S. H. Rizvi, A. Shoeb, R. S. Kapil, and S. P. Popli, *Phytochemistry*, **19**, 2409 (1980).

15) P. Sengupta and H. N. Khastgir, *Tetrahedron*, **19**, 123 (1963).

16) Corey *et al.* reported a partial synthesis of multiflorenol from β-amyrin *via* energetically unfavorable pathways. I. Agata, E. J. Corey, A. G. Hortmann, J. Klein, S. Proskow, and J. J. Ursprung, *J. Org. Chem.*, **30**, 1698 (1965). On Hydrogenation in acetic acid in the presence of a platinum catalyst, multiflorenol is isomerized to isomultiflorenol (**1**).[7,15]

17) Conversion of friedelin into dendropanoxide (**5**): M. Tori, T. Torii, K. Tachibana, S. Yamada, T. Tsuyuki, and T. Takahashi, *Bull. Chem. Soc. Jpn.*, **50**, 469 (1977). Total synthesis of friedelin: R. E. Ireland and D. M. Walba, *Tetrahedron Lett.*, **1976**, 1071.

18) K. Seifert, H. Budzikiewicz, and K. Schreiber, *Pharmazie*, **31**, 816 (1976).

19) General procedures are the same as those described in lit.2.

Alkylation of Ketoxime with Dichloromethane Using Bases under Phase-transfer Conditions. Formation of Methylene Dioxime and Novel Heteromacrocyclic Compounds

Takahiro HOSOKAWA,* Toshiyuki OHTA, Yoshihiro OKAMOTO, and Shun-Ichi MURAHASHI*
Department of Chemistry, Faculty of Engineering Science, Osaka University, Machikaneyama, Toyonaka, Osaka 560
(Received July 26, 1984)

Ketoximes, when treated with KO_2 (1 equiv) in the presence of di-μ-chlorobis(2-methylallyl)dipalladium-(II) (0.1 equiv per Pd) in dichloromethane, give methylene dioximes in moderate yields. This alkylation of ketoximes with CH_2Cl_2 is also promoted by the use of potassium carbonate in the presence of phase-transfer catalysts such as 18-crown-6. Study on the reactivity of a series of ketoximes in these reactions shows that proton abstraction by base is a crucial step in the latter reaction. By contrast, in the former system the reactivity is supposed to be controlled by nucleophilicity of the oximate anion coordinated to palladium(II). Application of the present reaction to (*E,E*)-1,2-diketone dioxime such as dimethylglyoxime leads to the formation of novel 21-membered ring heteromacrocyclic compounds in which oxime units are sequentially linked by methylene bridge.

Previously we have reported palladium-induced deoximation[1] and Beckmann fragmentation of ketoximes[2] by the use of peroxobis(triphenylphosphine)palladium(II), $(PPh_3)_2Pd\langle^{O}_{O}$. During the course of the studies, we have found that the alkylation of ketoximes (**1**) with dichloromethane is promoted by KO_2 in the presence of palladium(II) catalyst to give methylene dioximes (**2**) of a novel class of compounds.[3] Since the reaction is one of the rare examples of the use of dichloromethane as both solvent and electrophile,[4] we have studied this type of reactions in detail.

Use of a simple base such as potassium carbonate in combination with a phase-transfer agent such as 18-crown-6 has promoted the reaction as well. However,

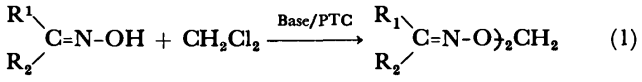

(1)

1 **2**

PTC: Phase-Transfer Catalyst

interestingly, these two systems have shown an inverse reactivity toward aryl and alkyl ketoximes.

Application of the reaction to 1,2-diketone dioximes, *e.g.*, dimethylglyoxime, has led to the synthesis of a novel heteromacrocyclic compound formed *via* a sequential oligomerization of the dioxime and dichloromethane. Although a variety of macrocyclic polyether and azacrown compounds have been reported in literatures,[5] there are few examples of heteromacrocycles containing oxime linkages. These are Vögtle's macrocyclic mono- and dioximes[6] prepared from 1,2-diketone dioximes and 1,ω-dichlorooligo-1-oxapropane $[Cl\{CH_2CH_2O\}_nCH_2CH_2Cl]$[7] and Sarlo's macrocyclic polyhydroximates formed *via* nucleophilic polymerization of acetonitrile oxide.[8] There has been, however, no precedent for the dioxime crowns such as **11** (*vide infra*) in which oxime units are sequentially linked by methylene bridges. This paper describes the alkylation of ketoximes with dichloromethane under phase-transfer conditions leading to the formation of methylene dioximes and dioxime crowns.

Results and Discussion

Reaction of Ketoximes with CH_2Cl_2 In the present study, ketoximes (**1**) have been generally allowed to react with an equimolar amount of KO_2 in dichloromethane in the presence of $[(2\text{-methylallyl})PdCl]_2$ (**3**) (0.1 equiv per Pd). Under the conditions, a relatively wide range of ketoximes, *e.g.*, 4-heptanone oxime, *d*-camphor oxime, and (*Z*)-2,2-dimethyl-5-phenyl-4-penten-3-one oxime, give the corresponding methylene dioximes (**2a**), (**4**), and (**5**) in moderate

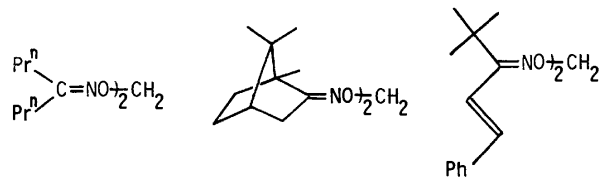

2a **4** **5**

yields (23—53%). If 2 equiv of KO_2 was used, the yields increased up to 60—96%. However, if KO_2 alone was used, entirely no reaction took place. Use of other palladium(II) complexes such as $PdCl_2(CH_3CN)_2$ and $Pd(OAc)_2$ as the catalyst also led to the alkylation of ketoximes. Since KO_2 is insoluble in dichloromethane, palladium(II) complexes are considered to act as a phase-transfer agent.

In this system, aryl ketoximes such as benzophenone oxime gave no appreciable amount of the alkylation product. By contrast, when the aryl ketoximes were treated with potassium carbonate (1.1 equiv) in dichloromethane containing 18-crown-6 (0.1 equiv), the corresponding methylene dioximes were formed in good yield (*e.g.*, 80% yield with benzophenone oxime).

Table 1. Formation of methylene dioximes **2** from a series of ketoximes **1**

Entry	Ketoxime **1**			Yield of methylene dioxime **2**/%			
	R_1	R_2		KO_2/Pd complex **3**[a]	K_2CO_3/18-c-6[b]	KO_2/18-c-6[b]	Bu^tOK/18-c-6[b]
1	C_3H_7	C_3H_7	(**1a**)	53 (96)[c]	0		
2	CH_3	CH_3	(**1b**)	45	0	27	74
3	$-(CH_2)_5-$		(**1c**)	39	0		
4	$PhCH_2CH_2$	$PhCH_2CH_2$	(**1d**)	36	19		
5	$PhCH_2$	$PhCH_2$	(**1e**)	24	65		(66)[a]
6	Ph	Ph	(**1f**)	7	83 (72)[a]	66	76
7	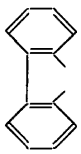		(**1g**)	2	90		
8	PhCO	Ph (*E*)	(**1h**)	0	92		

a) Isolated yield. b) In this system, yields were determined by ^1H NMR spectroscopy. c) Isolated yield when 2 equiv of KO_2 was used.

These results prompted us to examine the difference in reactivity between the two reaction systems using a series of ketoximes. From Table 1, it can be seen that in the former system aliphatic ketoximes afford higher yields of methylene dioxime than aryl ketoximes, whereas the opposite trend is observed in the latter (K_2CO_3/18-c-6). Further, the reactivities observed in both systems appear to change as a function of the p*K*a of ketoximes.[9]

Although potassium carbonate serves as an efficient, strong base in the presence of solid-liquid two phase catalysis,[10] it is not much basic as to promote the reaction with less acidic aliphatic ketoximes such as **1b** (Entries 1—3, Table 1). When K_2CO_3 was replaced with more basic Bu^tOK, the aliphatic ketoxime **1b** gives methylene dioxime **2b** in a good yield (74%). The use of KO_2 with 18-crown-6 gives **2b** only in 27% yield in accordance with the order of decrease in basicity ($Bu^tOK > KO_2 > K_2CO_3$).[11] Therefore, it is evident that proton abstraction from the oxime by base is a crucial step in this system. Note that there have been ample examples that KO_2 acts as a Brϕnsted base in the presence of phase-transfer agents.[12]

In the KO_2-Pd(II) system, more acidic ketoximes such as (**1d**)—(**1f**) led to the formation of palladium(II) complexes containing oximate ligands in 15—27% yield (based on Pd), along with the alkylation products. The complexes are formulated as $[(R_2C{=}NO)_2(R_2C{=}NOH)_2]Pd$ (**6**) by comparing the spectra data with those of the authentic complex **6a** (R= CH_2Ph) prepared from $Pd(acac)_2$ and dibenzyl ketone oxime.[13] Thus, when the oxime has lower pK_a, its anion is thought to successively coordinate to Pd(II) and has no nucleophilic ability enough to attack at the methylene carbon of dichloromethane.

The formation of methylene dioximes **2** is readily accounted for by succesive, nucleophilic displacement of an oximate anion to dichloromethane. In the former system (KO_2/Pd(II)), the oximate anion is probably formed *via* the following steps. At first, coordination of the nitrogen atom to Pd(II) complex takes place in dichloromethane solution. Superoxide anion ($O_2^{\cdot-}$) is then transfered into the organic phase *via* anion exchange (**7**→**8**) with the chloride ligand of Pd(II) complex. Electron transfer (**8**→**9**) followed by proton abstraction[14] results in the formation of oximate anion in the coordination sphere of palladium(II). Alternatively, the oximate anion may be

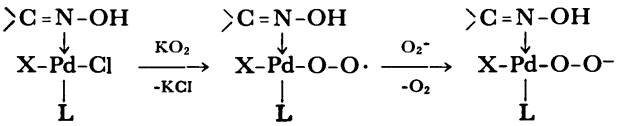

7 **8** **9**

directly formed from the coordinated oxime **7** by the action of KO_2 with releasing HOO·. In any case, depending on its nucleophilicity, the oximate anion thus produced attacks at the methylene carbon of CH_2Cl_2.[15] Since less acidic ketoximes readily undergo the reaction in this system, the acidity of oximes must be enhanced by its coordination to palladium(II).

Reaction of 1,2-Diketone Dioxime with CH_2Cl_2. Application of the present methods to 1,2-diketone dioximes (**10**) resulted in either formation of nitractable palladium complexes (KO_2/Pd(II)) or recovery of the starting materials (K_2CO_3/18-c-6). However, the use of Bu^tOK in the presence of 18-crown-6 led to a successful synthesis of novel dioxime crown compounds containing methylene linkages such as **11**.

The procedure for the synthesis of 21-membered ring compound **11a** is simple. To a suspended solution of (*E*,*E*)-2,3-butanedione dioxime (**10a**), Bu^t OK (2 equiv) and 18-crown-6 (0.1 equiv) in THF was slowly added an excess of dichloromethane, and the mixture

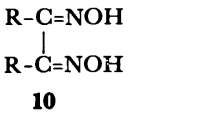

10

	Conf.	R
a;	(*E*,*E*)	Me
b;	(*E*,*E*)	Pr^i
c;	(*E*,*E*)	Pr^n
d;	(*E*,*E*)	Ph
e;	(*E*,*E*)	R,R=-$(CH_2)_4$-
f;	(*Z*,*Z*)	Cyclohexyl
g;	(*Z*,*Z*)	Pr^i
h;	(*Z*,*E*)	Pr^i

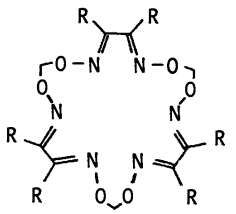

11

a; R=Me
b; R=Pr^i

was refluxed. After filtration of the reaction mixture and evaporation of the solvent and excess CH_2Cl_2, the residue was thoroughly washed with methanol to remove unreacted oxime **10a**. The remaining solid was recrystallized from MeOH-THF to give **11a** in 20% yield as colorless crystals. In the absence of 18-crown-6, no reaction takes place. However, the use of trioctylmethylammonium chloride (Capriquat) as a phase-transfer agent is comparatively effective in promoting the reaction. If THF is not used as the co-solvent, the yield of **11a** is reduced to ≈2%. A poor yield (4%) of **11a** is also resulted, when **10a** was treated with aqueous 20% NaOH solution in the presence of tetrabutylammonium hydrogensulfate (0.1 equiv) in CH_2Cl_2.

The same type of dioxime crown **11b** was obtained from (*E*,*E*)-2,5-dimethyl-3,4-hexanedione dioxime (**10b**) (R=Pr^i) in 21% yield by the same treatment (Bu^{t}OK/18-c-6). By contrast, (*E*,*E*)-dioxime **10c** of R=Pr^n gave **12**, in which four oxime units are linked by methylene bridges, in 40% yield.

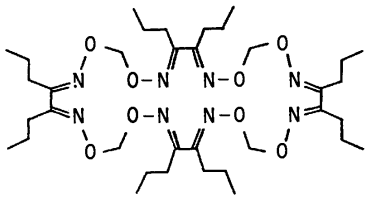

12

In the ^{1}H NMR spectra of **11a**, **11b**, and **12**, the -OCH_2O-protons appear as a singlet approximately at δ 5.50, and their $^{13}C\{^1H\}$ NMR spectra ($CDCl_3$) also exhibit only singlet due to the methylene carbon at δ 99.45 ppm for **11a** and δ 99.31 ppm for **12** relative to Me_4Si. These results indicate the equivalence of all the -OCH_2O- groups. In addition, the signal of alkyl substituent (R=Me, Pr^i, and Pr^n) in each compound has been shown to be magnetically equivalent (*vide infra*). These data also support the structures as illustrated above. The extent of oligomerization was determined by the mass spectra of the products.

Although (*E*,*E*)-dioximes appear to generally undergo the present sequential oligomerization, it is not the case for **10e** (R,R=-$(CH_2)_4$-) and **10d** (R=Ph). Thus, (*E*,*E*)-1,2-cyclohexanedione dioxime (**10e**) gave

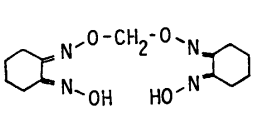

13

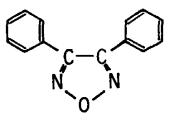

14

a 12% yield of **13**, a 2:1 adduct of the dioxime and CH_2Cl_2. (*E*,*E*)-benzil dioxime **10d** gave a 27% yield of 3,4-diphenylfurazan **14** formally *via* (*E*,*E*) ⇌ (*Z*,*E*) isomerization followed by dehydration.

As expected, the (*Z*,*Z*)-dioximes **10f** and **10g** do not undergo the present oligomerization, but intramolecular cyclization of a 1:1 adduct of the dioxime and CH_2Cl_2 takes place. Thus, **10f** (R=cyclohexyl) gave a 66% yield of 7*H*-3,4-dicyclohexyl-1,6,2,5-dioxadiazepine (**15a**), which is a previously unknown class of heterocyclic compounds. Similarly, (*Z*,*Z*)-dioxime **10g** afforded **15b** in 47% yield. In this case, a small amount (*ca.* ≈5%) of cyclic compound **16** containing

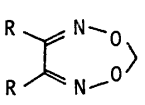

15

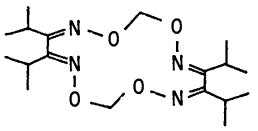

16

a; R=Cyclohexyl
b; R=Pr^i

two (*Z*,*E*)-oxime units was formed. The (*Z*,*E*)-configuration of this compound was assigned since the methyl signal of the two isopropyl group appears at different chemical shifts as two sets of doublets in its ^{1}H NMR spectrum.

The (*Z*,*E*)-dioxime **10h** (R=Pr^i) also gave the dioxadiazepine **15b** in 16% yield, but the expected product **16** was not formed. In any case, when the substituent is Pr^i, (*Z*,*E*) ⇌ (*Z*,*Z*) isomerization of the oxime group takes place during the reaction.

Experimental

General. NMR spectra were recorded on a 60-MHz Model JNM-MH-60 (Jeol) spectrometer; chemical shifts (δ) expressed in parts per million relative to Me_4Si. IR spectra were recorded on a Hitachi 215 spectrometer. Mass spectra were taken on a Hitachi RSM-4 mass spectrometer. Elemental analyses were determined on a Yanagimoto MT-2 CHN recorder. Potassium superoxide was obtained from Ventron, ground to a fine powder in a Ar-filled drybag, and stored in a desiccator prior to use. Di-μ-chlorobis(2-methylallyl)-dipalladium(II)[16] (**3**), palladium acetate(II),[17] bis(benzonitrile)dichloropalladium(II)[18] were prepared as the reported procedures. Dichloromethane was distilled from calcium hydride under argon or nitrogen. Ketoximes **1a-g** were prepared from the corresponding ketones according to the reported procedure. (*E*)-Benzil monoxime **1h** was prepared by the method of Taylor and Marks.[19] *d*-Camphor oxime, (*E*,*E*)-2,3-butanedione dioxime **10a** (dimethylglyoxime), (*E*,*E*)-benzil dioxime (**10d**), and (*E*,*E*)-1,2-cyclohexanedione dioxime (**10e**) are commercially available.

Three configurational isomers of (*E,E*)-**10b**, (*Z,Z*)-**10f**, and (*Z,E*)-**10h** were prepared from the oximation of 2,5-dimethyl-3,4-hexanedione. (*E,E*)-4,5-Octanedione dioxime (**10c**) and (*Z,Z*)-1,2-dicyclohexylethanedione dioxime (**10f**) were also prepared from the corresponding diketones. These details are described below.

*2,5-Dimethyl-3,4-hexanedione Dioxime (**10b**, **g**, and **h**).* To a solution of hydroxylamine hydrochloride (2.433 g, 0.035 mol) in 10 mL of water was added a soluton of 85% potassium hydroxide (2.307 g, 0.035 mol) in 6 mL of water in an ice bath. Into the cold solution was added 2,5-dimethyl-3,4-hexanedione[20] (1.990 g, 0.014 mol). The reaction mixture was stirred at 0 °C for 2 h and then at reflux for 2 h. After extraction with ether (10 mL×3), the extract was washed with water, shaken with brine, and dried over anhydrous magnesium sulfate. Concentration of the solvent followed by Kugelrohr distillation (55—60 °C/3 mmHg) (1 mmHg=133.322 Pa) gave 2,5-dimethyl-3,4-hexanedione monoxime (1.466 g, 67%). To a solution of the monooxime (1.415 g, 9.0 mmol) in 8 mL of 95% ethanol was added a solution of hydroxylamine hydrochloride (0.639 g, 9.2 mmol) and sodium acetate (1.292 g, 15.8 mmol) in 4 mL of water. The reaction mixture was refluxed for 4 h, and concentrated until the mixture became turbid, and then allowed to cool to room temperature. The white crystals were collected, washed thoroughly with water, and dried *in vacuo* at 50 °C. The crystals were found to contain three configurational isomers of the dioxime. Recrystallization from ether-petroleum ether afforded (*Z,Z*)-2,5-dimethyl-3,4-hexanedione dioxime **10g** (33%): mp 139—142 °C; IR (Nujol) 3260 (OH), 1100, 1048, 880, 715 cm^{-1}; ^1H NMR (DMSO-d_6) δ=0.73 (12H, d, J=7 Hz, $-CH_3$), 2.17 (2H, heptet, J=7 Hz, $\rangle CH$), 10.28 (2H, s, -OH). From the mother liquid, (*E,E*) and (*Z,E*)-isomers were separated by preparative TLC (SiO_2, ethyl acetate:hexane=3:7) in 2% and 6% yields, respectively. (*E,E*)-2,5-dimethyl-3,4-hexanedione dioxime (**10b**): R_f 0.45; IR (Nujol) 3250 (OH), 1155, 1102, 1060, 990, 970, 912, 845, 745 cm[1]; ^1H NMR (DMSO-d_6) δ=1.05 (12H, d, J=7 Hz, $-CH_3$), 2.30 (2H, heptet, J=7 Hz, $\rangle CH$), 10.78 (2H, s, -OH). (*Z,E*)-2,5-Dimethyl-3,4-hexanedione dioxime (**10h**): R_f 0.29; IR (Nujol) 3240 (OH), 1167, 1150, 1035, 1012, 932 895, 861, 742 cm^{-1}; ^1H NMR (DMSO-d_6) δ=0.99 (d, J=7 Hz, $-CH_3$, 6H), 1.03 (d, J=7 Hz, $-CH_3$, 6H), 2.30 (m, $\rangle CH$, 2H), 10.48 (s, -OH, 1H), 10.77 (s, -OH, 1H). The configuration assignment of these dioximes were made on the basis of their ^1H NMR signals of OH proton in DMSO-d_6, according to the method of Tanaka and Shinra.[21]

*(E,E)-4,5-Octanedione Dioxime (**10c**).* The oximation of 4,5-octanedione[20] by the similar manner as above gave (*E,E*)-4,5-octanedione dioxime (**10c**) as the sole product; mp 178—179.5 °C; IR (Nujol) 3220 (OH), 1150, 1042, 1020, 922, 893, 872, 761 cm^{-1}; ^1H NMR (DMSO-d_6) δ=0.70 (6H, m, $-CH_3$), 1.00—1.60 (4H, m, $-CH_2-$), 2.38 (4H, m, $-C(=N)-CH_2-$), 11.13 (2H, s, -OH). The (*E,E*)-configuration was assigned by the same method as above.

*(Z,Z)-1,2-Dicyclohexylethanedione Dioxime (**10f**).* The oximation of 1,2-dicyclohexylethanedione[20] by the similar manner as above gave the title compound as the sole product; mp 200 °C; IR (Nujol) 3250 (OH), 1115, 995, 960, 948, 893, 819, 810, 715 cm^{-1}; ^1H NMR (DMSO-d_6) δ=0.91—2.46 (20H, m, $-CH_2-$), 10.28 (2H, s, -OH). The configuration assignment of the dioxime was made similarly as above.

*Reaction of Ketoximes with Dichloromethane in the Presence of KO_2 and **3**. General Procedure.* In a drybag filled with argon, finely powdered potassium superoxide (4 mmol) was weighed and placed in a 100 mL flask containing a Teflon-coated magnetic stirrer bar, di-μ-chlorobis(2-methylallyl)dipalladium (**3**, 0.079 g, 0.2 mmol) and ketoxime (**1**, 4 mmol). Into the flask was added 40 mL of dichloromethane, and the reaction mixture was stirred for 72 h at room temperature under argon. After the resulting potassium chloride was removed by filtration, the filtrate was concentrated under reduced pressure. The products were separated by means of Al_2O_3 column chromatography. Generally, elution with a 7:3 mixture of hexane and ethyl acetate gave the methylene dioxime **2**. Unreacted ketoximes were recovered from further elution with ether or methanol. Analytically pure methylene dioximes were obtained by recrystallization or distillation. The results are summarized in Table 1. Spectral and analytical data of the methylene dioximes **2** obtained in this system are described below.

*Methylene Dioxime **2a**:* Bp 108—109 °C/3 mmHg; IR (neat) 1630 (C=N), 1146, 1005 (OCH_2O) cm^{-1}; ^1H NMR (CCl_4) δ=0.92 (12H, t, J=7 Hz, $-CH_3$), 1.48 (8H, m, $-CH_2-$), 2.13 (8H, q, J=7 Hz, $-CH_2C=N-$), 5.37 (2H, s, $-OCH_2O-$). Found: C, 66.58; H, 11.38; N, 10.36%. Calcd for $C_{15}H_{30}N_2O_2$: C, 66.62; H, 11.18; N, 10.10%.

*Methylene Dioxime **2b**:* Mp 39 °C; IR (Nujol) 1640 (C=N), 1150, 1020 (OCH_2O) cm^{-1}; ^1H NMR (CCl_4) δ=1.80 (12H, s, $-CH_3$,), 5.30 (2H, s, $-CH_2-$). Found: C, 53.04; H, 8.92; N, 17.85%. Calcd for $C_7H_{14}N_2O_2$: C, 53.14; H, 8.91; N, 17.71%.

*Methylene Dioxime **2c**:* Mp 47—48.5 °C; IR (Nujol) 1645 (C=N), 1135, 1020 (OCH_2O) cm^{-1}; ^1H NMR (CCl_4) δ=1.60 (12H, m, $-CH_2-$), 2.18 (4H, m, $-CH_2-$), 2.47 (4H, m, $-CH_2-$), 5.37 (2H, s, $-OCH_2O-$). Found: C, 65.75; H, 9.41; N, 11.49%. Calcd for $C_{13}H_{22}N_2O_2$: C, 65.51; H, 9.31; N, 11.76%.

*Methylene Dioxime **2d**:* Mp 73 °C; IR (Nujol) 1628 (C=N), 1150, 1028 (OCH_2O) cm^{-1}; ^1H NMR (CCl_4) δ=2.20—3.03 (16H, m, $-CH_2-$), 5.71 (2H, s, $-OCH_2O-$), 7.03—7.40 (20H, m, aromatic). Found: C, 81.27; H, 7.38; N, 5.42%. Calcd for $C_{35}H_{38}N_2O_2$: C, 81.04; H, 7.38; N, 5.40%.

*Methylene Dioxime **2e**:* Mp 102 °C; IR (Nujol) 1630 (C=N), 1148, 1024 (OCH_2O) cm^{-1}; ^1H NMR (CCl_4) δ=3.43 (4H, s, $-CH_2-$), 3.63 (4H, s, $-CH_2-$), 5.80 (2H, s, $-OCH_2O-$), 7.00—7.27 (20H, m, aromatic). Found: C, 80.71, H, 6.55; N, 6.10%. Calcd for $C_{31}H_{30}N_2O_2$: C, 80.49; H, 6.54; N, 6.06%.

*Methylene Dioxime **2f**:* Mp 90—91 °C IR (Nujol) 1150, 1020 (OCH_2O) cm^{-1}; ^1H NMR (CCl_4) δ=5.70 (2H, s, $-CH_2-$), 7.10—7.60 (20H, m, aromatic). Found: C, 79.99; H, 5.32; N, 6.79%. Calcd for $C_{27}H_{18}N_2O_2$: C, 79.78; H, 5.46; N, 6.89%.

*Methylene Dioxime **2g**:* Mp 211—211.5 °C; IR (Nujol) 1620 (C=N), 1021 (OCH_2O) cm^{-1}; ^1H NMR (CCl_4) δ=6.20 (2H, s, $-CH_2-$), 7.10—7.93 (14H, m, aromatic), 8.00—8.37 (2H, m, aromatic). Found: C, 80.86; H, 4.35; N, 7.30%. Calcd for $C_{27}H_{22}N_2O_2$: C, 80.58; H, 4.51; N, 6.96%.

*Methylene Dioxime **2h**:* Mp 99—100 °C; IR (Nujol) 1679 (C=O), 1668 (C=N), 1035 (OCH_2O) cm^{-1}; ^1H NMR (CCl_4) δ=5.76 (2H, s, $-CH_2-$), 7.03—8.03 (20H, m, aromatic). Found: C, 75.40; H, 4.72; N, 6.16%. Calcd for $C_{26}H_{22}N_2O_4$: C, 75.31, H, 4.79; N, 6.06%.

*Methylene Dioxime **4**:* Yield 32%; mp 68 °C; IR (Nujol) 1675 (=N), 1005 (OCH_2O) cm^{-1}; ^1H NMR ($CDCl_3$) δ=0.77 (6H, s, $-CH_3$), 0.90 (6H, s, $-CH_3$), 1.00 (6H, s, $-CH_3$),

1.07—2.73 (14H, m, $-CH_2-$, and >CH), 5.38 (2H, s, $-OCH_2O-$). Found: C, 72.50; H, 9.83; N, 7.82%. Calcd for $C_{21}H_{34}N_2O_2$: C, 72.79; H, 9.89; N, 8.09%.

Methylene Dioxime **5**: Yield 23%; bp 185 °C/0.15 mmHg; IR (neat) 1615 (C=N), 1245, 1075 cm^{-1}; ^1H NMR ($CDCl_3$) δ=1.36 (18H, s, $-Bu^t$), 6.30 (2H, s, $-CH_2-$), 7.15—7.48 (10H, m, =CH- and aromatic), 7.58—7.80 (4H, m, =CH- and aromatic).

The use of $Pd(OAc)_2$ or $PdCl_2(PhCN)_2$ in place of [(2-methylallyl)PdCl]$_2$ (**3**) in the reaction of **1b** (R=CH_3) under the conditions described above also gave the methylene dioxime **2b**. The isolable yield of **2b** were 42% with $Pd(OAc)_2$ and 34% with $PdCl_2(PhCN)_2$. In the reaction using 2 equiv of KO_2 under otherwise the same conditions as above, the methylene dioximes **2a** and **4** were isolated in 96% and 61% yield from **1a** and *d*-camphor oxime, respectively.

Formation of Oximate Palladium(II) Complexes **6**. The general procedure described above was followed by using 1,3-diphenyl-2-propanone oxime (**1e**, 0.901 g, 4 mmol), KO_2 (0.284 g, 4 mmol), di-μ-chlorobis(2-methylallyl)dipalladium(II) (0.079 g, 0.2 mmol) and 40 mL of CH_2Cl_2. Alumina column chromatography (Al_2O_3, 18 g) of the reaction mixture gave the methylene dioxime **2e** (0.219 g, 24%) from the elution of hexane and ethyl acetate (7:3, 20 mL). Further elution with ethyl acetate gave unreacted **1e** (0.429 g, 48%). The oximate complex **6a** (R=CH_2Ph), (0.060 g, 15% based on Pd) was obtained from CH_2Cl_2 elution. Recrystallization from CH_2Cl_2 and petroleum ether afforded analytically pure **6a**: mp 145—147 °C; IR (Nujol) 1600, 1590, 1095, 1074, 1055, 1030, 742, 695 cm^{-1}; ^1H NMR (CD_2Cl_2-$CDCl_3$) δ=2.83—4.13 (16H, m, $-CH_2-$), 6.77—7.03 (40H, m, aromatic) Found: C, 71.68; H, 5.72; N, 5.63%. Calcd for $C_{60}H_{58}N_4O_4Pd$: C, 71.68; H, 5.81; N, 5.57%.

The same reaction with **1d** (0.506 g, 2 mmol) gave the oximate complex **6b** (R=CH_2CH_2Ph), (0.061 g, 27% based on Pd), along with methylene dioxime **2d** (0.188 g, 36%). **6b**: mp 151 °C (decomp) IR (Nujol) 1602, 1580, 1157, 1090, 1030 cm^{-1}; ^1H NMR (CCl_4) δ=2.75 (32H, m, $-CH_2-$), 7.00—7.37 (40H, m, aromatic). Found: C, 73.07; H, 6.67 N, 5.06%. Calcd for $C_{68}H_{74}N_4O_4Pd$: C, 73.07; H, 6,67; N, 5.01%.

Benzophenone oxime (**1f**) also gave this type of complex. However, no attempt to isolate the complex in a pure state was made, owing to its difficulty in the separation from unreacted ketoxime **1f**.

Preparation of Complex **6a** *(R=CH_2Ph).* A solution of $Pd(acac)_2$ (0.219 g, 0.72 mmol) and ketoxime **1e** (0.885 g, 3.9 mmol) in dichloromethane (5 mL) was stirred at room temperature for 0.5 h. After removal of the solvent, recrystallization (CH_2Cl_2-hexane) of the resulting complex gave 0.825 g of the complex **6a** (86%), whose spectral data were identical with those of the aforementioned complex.

Reaction of Ketoximes with Dichloromethane in the Presence of K_2CO_3 and 18-Crown-6. General Procedure. In a 25 mL flask containing a Teflon-coated magnetic stirrer bar were placed the oxime (1.0 mmol), potassium carbonate (0.152 g, 1.1 mmol), and 18-crown-6 (0.026 g, 0.1 mmol). Into the flask was then added 10 mL of dichloromethane (distilled from CaH_2), and the reaction mixture was refluxed for 12 h under argon with stirring. After the resulting potassium chloride was removed by filtration, the filtrate was concentrated under reduced pressure. The residues which contain the methylene dioxime and/or unreacted oxime were analyzed by ^1H NMR spectroscopy to determine the product yield. Results are also shown in Table 1.

A typical experiment in this system is described as followed. A mixture of oxime **1f** (0.197 g, 1 mmol), K_2CO_3 (0.152 g, 1.1 mmol), and 18-crown-6 (0.026 g, 0.1 mmol) in CH_2Cl_2 (10 mL) was refluxed for 12 h with stirring. After work-up as decribed above, NMR analysis of the reaction mixture showed the presence of methylene dioxime **2f** in 83% yield with 17% of unreactive oxime. The reaction mixture was then chromatographed on alumina column (12 g) to give methylene dioxime **2f** (0.157 g, 72%) from the elution with 20 mL of petroleum ether and 25 mL of ether.

*3,4,10,11,17,18-Hexamethyl-1,6,8,13,15,20-hexaoxa-2,5,9,12,16,19-hexaazahenicosa-2,4,9,11,16,18-hexaene (**11a**).* In a 300 mL of flask containing a Teflon-coated magnetic stirrer bar were placed (*E,E*)-2,3-butanedione dioxime **10a** (3.832 g, 33 mmol), Bu^tOK (7.406 g, 66 mmol) and 18-crown-6 (0.872 g, 3.3 mmol), and into the flask was added THF (100 mL). To the resulting suspended solution was added dichloromethane (100 mL) such a rate to maintain a gentle reflux with stirring. After the addition was complete, the mixture was refluxed for 18 h, cooled, and filtered. The solvent and excess CH_2Cl_2 were removed under reduced pressure. The residue was thoroughly washed with methanol and recrystallized from THF-MeOH. Pure **11a** (0.846 g) was obtined in 20% yield. **11a**: Mp 270—271 °C; IR (Nujol) 1600 (C=N), 1120, 1005 (OCH_2O), 870, 795, 690 cm^{-1}; ^1H NMR ($CDCl_3$) δ=2.04 (18H, s, $-CH_3$), 5.74 (6H, s, $-CH_2-$); ^{13}C NMR ($CDCl_3$) δ=10.57 ($-CH_3$), 99.46 ($-CH_2-$), 155.64 (-C=N-), mass spectrum *m/z* 384 (M^+). Found: C, 47.07; H, 6.31; N, 22.15%. Calcd for $C_{15}H_{24}N_6O_6$: C, 46.87; H, 6.29; N, 21.87%.

*3,4,10,11,17,18-Hexaisopropyl-1,6,8,13,15,20-hexaoxa-2,5,9,12,16,19-hexaazahenicosa-2,4,9,11,16,18-hexaene (**11b**).* The reaction of (*E,E*)-2,5-dimethyl-3,4-hexanedione dioxime **10b** (0.152 g, 0.88 mmol) with Bu^tOK (0.199 g, 1.77 mmol) and 18-crown-6 (0.023 g, 0.088 mmol) in THF (6 mL) and CH_2Cl_2 (6 mL) gave **11b** (0.033 g, 21%) which was purified by preparative TLC (SiO_2, ethyl acetate:hexane=1:10). **11b**: Mp 140—148 °C; IR (Nujol) 1595 (C=N), 1060, 1030 cm^{-1}; ^1H NMR ($CDCl_3$) δ=1.14 (36H, d, *J*=7 Hz, $-CH_3$), 3.33 (6H, heptet, *J*=7 Hz, -CH), 5.63 (6H, s, $-CH_2-$); mass spectrum *m/z* 551 (M^+-1).

*3,4,10,11,17,18,24,25-Octapropyl-1,6,8,13,15,20,22,27-octaoxa-2,5,9,12,16,19,23,26-octaazaoctacosa-2,4,9,11,16,18,23,25-octaene (**12**).* This compound was prepared by the reaction of (*E,E*)-4,5-octanedione dioxime **10c** (1.033 g, 6 mmol) with Bu^tOK (1.346 g, 12 mmol) and 18-crown-6 (0.159 g, 0.6 mmol) in THF (20 mL) and CH_2Cl_2 (20 mL). The product (40% yield) was isolated by preparative TLC (SiO_2, ethyl acetate: hexane=1:15). Analytically pure sample was obtained by two additional preparative TLC. **12**: Mp 143—146 °C; IR (Nujol) 1595 (C=N), 1135, 1020 (OCH_2O) cm^{-1}; ^1H NMR ($CDCl_3$) δ=0.84 (24H, t, *J*=7 Hz, $-CH_3$), 1.14—1.73 (16H, m, $-CH_2-$), 2.63 (16H, t, *J*=7 Hz, $-CH_2C=N-$), 5.70 (8H, s, $-OCH_2O-$); ^{13}C NMR ($CDCl_3$) δ=14.13 ($-CH_3$), 19.93 ($-CH_2-$), 26.12 ($-CH_2-$), 99.32 ($-OCH_2O-$), 158.32 (-C=N-), mass spectrum *m/z* 736 (M^+). Found: C, 58.58; H, 8.70; N, 15.29%. Calcd for $C_{36}H_{64}N_8O_8$: C, 58.67; H, 8.75; N, 15.21%.

*7H-3,4-Dicyclohexyl-1,6,2,5-dioxadiazepine (**15a**).* This compound was prepared by the reaction of (*Z,Z*)-dicyclohexylethanedione dioxime **10f** (1.001 g, 4 mmol) with Bu^tOK (0.898 g, 8 mmol) and 18-crown-6 (0.106 g, 0.4 mmol) in

THF (20 mL) and CH_2Cl_2 (20 mL). The product (66% yield) was purified by preparative TLC (SiO_2, ethyl acetate:hexane=1:15). **15a**: Bp 135—136 °C/1 mmHg; IR (neat) 1600 (C=N), 1035 (OCH_2O), 990, 975 cm^{-1}; ^1H NMR ($CDCl_3$) δ= 0.98—2.58 (22H, m, $-CH_2-$), 5.28 (2H, s, $-OCH_2O-$); mass spectrum m/z 265 (M^++1). Found: C, 67.79; H, 9.13, N, 10.42%. Calcd for $C_{15}H_{24}N_2O_2$: C, 68.15; H, 9.15; N, 10.60%.

Reaction of (Z,Z)-2,5-Dimethyl-3,4-hexanedione Dioxime ***10g*** *with Dichloromethane.* In a 100 mL flask containing a Teflon-coated magnetic stirrer bar were placed (*Z,Z*)-2,5-dimethyl-3,4-hexanedione dioxime **10g** (1.033 g, 6 mmol), Bu^{t}OK (1.346 g, 12 mmol) and 18-crown-6 (0.159 g, 0.6 mmol). Into the flask was added CH_2Cl_2 (20 mL) with stirring, and then THF (20 mL) was slowly added to the resulting suspended solution in an ice bath. After the addition was complete, the mixture was refluxed for 20 h. cooled, and filtered. After removal of THF and CH_2Cl_2 under reduced pressure, the products were chromatographed on Al_2O_3. A mixture of **15b** and **16** obtained from the elution of ether was purified by preparative TLC (SiO_2, ethyl acetate:hexane=1:10). Pure **15b** (0.517 g) and **16** (0.044 g) were obtained in 47% and 4% yield, respectively. **15b**: Bp 60—61 °C/1 mmHg; IR (neat) 1605 (C=N), 1035 (OCH_2O), 975 cm^{-1}; ^1H NMR ($CDCl_3$) δ=1.25 (12H, d, J= 7 Hz, $-CH_3$), 2.68 (2H, heptet, J=7 Hz, >CH), 5.30 (2H, s, $-CH_2-$); mass spectrum m/z 184 (M^+). Found: C, 58.61; H, 8.57; N, 15.26%. Calcd for $C_9H_{16}N_2O_2$: C, 58.67; H, 8.75; N, 15.21%. **16**: Mp 82—83 °C; IR (Nujol) 1615 (C=N), 1260, 1020 (OCH_2O); ^1H NMR ($CDCl_3$) δ=1.14 (12H, d, J= 7 Hz, $-CH_3$), 1.19 (12H, d, J=7 Hz, $-CH_3$), 2.60 (4H, m, -CH), 5.55 (4H, s, $-CH_2-$); mass spectrum m/z 368 (M^+). Found: C, 58.99; H, 8.61; N, 14.87. Calcd for $C_{18}H_{32}N_4O_4$: C, 58.66; H, 8.75; N, 15.21.

Reaction of (Z,E)-2,5-Dimethyl-3,4-hexanedione Dioxime ***10h*** *with Dichloromethane.* In a 50 mL flask containing a Teflon-coated magnetic stirrer bar were placed (*Z,E*)-2,5-dimethyl-3,4-hexanedione dioxime **10h** (0.360 g, 2.1 mmol), Bu^{t}OK (0.471 g, 4.2 mmol) and 18-crown-6 (0.055 g, 0.21 mmol). Into the flask was added CH_2Cl_2 (10 mL) with stirring, and then THF (10 mL) was slowly added to the resulting suspended solution in an ice bath. After the addition was complete, the mixture was refluxed for 20 h, cooled, and filtered. After removal of THF and CH_2Cl_2 under reduced pressure, the residue was purified by preparative TLC (R_f 0.70, SiO_2, ethyl acetate:hexane=3:7) to give **15b** (0.043 g, 16%).

Reaction of (E,E)-1,2-Cyclohexanedione Dioxime ***10e*** *with Dichloromethane.* The reaction of (*E,E*)-1,2-cyclohexanedione dioxime **10e** (0.976 g, 6.8 mmol), Bu^{t}OK (1.526 g, 13.6 mmol) and 18-crown-6 (0.186 g, 0.68 mmol) in CH_2Cl_2 (80 mL) gave **13** (0.112 g, 12%) which was purified by silica-gel column chromatography (ether as eluting solvent). **13**: Mp 178—180 °C; IR (Nujol) 3200 (OH), 1620 (C=N), 1140, 1015 (OCH_2O), 820, 765 cm^{-1}; ^1H NMR ($CDCl_3$) δ=1.43—1.93 (8H, m, $-CH_2-$) 2.45—2.95 (8H, m, $-CH_2-$), 4.20—5.30 (2H, br, -OH), 5.85 (2H, s, $-OCH_2O-$). Found: C, 52.62; H, 6.66; N, 18.65%. Calcd for $C_{13}H_{20}N_4O_4$: C, 52.69; H, 6.80; N, 18.91%.

Reaction of (E,E)-Benzil Dioxime ***10d*** *with Dichloromethane.* The reaction of (*E,E*)-benzil dioxime **10d** (0.961 g, 4 mmol), Bu^{t}OK (0.896 g, 8 mmol) and 18-crown-6 (0.106 g, 0.4 mmol) in CH_2Cl_2 (40 mL) gave 3,4-diphenylfrazan **14** (0.236 g, 27%) which was purified by Al_2O_3 column chromatography (pentane:ether=9:1). **14**: Mp 91—92 °C; IR (Nujol) 1580 (C=N), 1075, 990, 890, 780, 760, 695 cm^{-1}; ^1H NMR (CCl_4) δ= 7.25—7.68 (10H, m, aromatic). Found: C, 75.75; H, 4.49; N, 12.76%. Calcd for $C_{14}H_{10}N_2O$: C, 75.66; H, 4.54; N, 12.61%.

References

1) K. Maeda, I. Moritani, T. Hosokawa, and S-I. Murahashi, *Tetrahedron Lett.*, **1974**, 797.

2) K. Maeda, I. Moritani, T. Hosokawa, and S-I. Murahashi, *J. Chem. Soc., Chem. Commun.*, **1975**, 689.

3) As a preliminary report, see; T. Hosokawa, T. Ohta, Y. Okamoto, S-I. Murahashi, *Tetrahedron Lett.*, **1980**, 1259. Synthesis of the same compound by similar methods has been independently reported by S. J. Kirsch and H. Schellig, *J. Org. Chem.*, **44**, 3970 (1979), and H. Shinozaki, N. Yoshida, and M. Tajima, *Chem. Lett.*, **1980**, 869.

4) K. Holmberg and B. Hansen, *Tetrahedron Lett.*, **1975**, 2303.

5) a) J. S. Bradshow and P. E. Stott, *Tetrahedron*, **36**, 461 (1980); b) G. W. Gokel, D. M. Dishong, R. A. Shultz, and V. J. Gatto, *Synthesis*, **1982**, 997.

6) W. Rasshofer, W. M. Müller, G. Oepen, and F. Vögtle, *J. Chem. Res.*, (S), 72; (M), 1001 (1978).

7) a) C. J. Pedersen, *J. Am. Chem. Soc.*, **89**, 7017 (1967); b) J. S. Bradshow, "Synthetic Multidentate Macrocyclic Compounds," ed by R. M. Izatt and J. J. Christensen, Academic Press, New York, 1978.

8) a) A. Brandi, F. D. Sarlo, and A. Guarna, *J. Chem. Soc., Perkin Trans, 1*, **1976**, 1827; b) F. D. Sarlo, A. Guarna, and G. P. Speroni, *J. Chem. Soc., Chem. Commun.*, **1977**, 549.

9) A similar trend of reactivity has been observed in the reaction of arylhydrazine and hydrazone with KO_2; see, C-I. Chern and J. S. Filippo, Jr., *J. Org. Chem.*, **42**, 178 (1977).

10) M. Fedorynski, K. Wojciechowski, Z. Matacz, and M. Makosza, *J. Org. Chem.*, **43**, 4682 (1978).

11) A. A. Frimer, G. Aljadeff, and J. Ziv, *J. Org. Chem.*, **48**, 1700 (1983).

12) a) E. Lee-Ruff, *Chem. Soc. Rev.*, **6**, 195 (1977); b) D. T. Sawyer, *Acc. Chem. Res.*, **13**, 105 (1979); c) D. T. Sawyer and M. J. Gibian, *Tetrahedron*, **35**, 1471 (1979); d) J. S. Valentine, "Biochemical and Clinical Aspects of Oxygen," ed by W. S. Caughey, Academic Press, New York (1979), pp. 659—677; e) D. T. Sawyer and J. S. Valentine, *Acc. Chem. Res.*, **14**, 393 (1981).

13) S. Imamura, T, Kajimoto, Y. Kitano and J. Tsuji, *Bull. Chem. Soc. Jpn.*, **42**, 805 (1969).

14) a) H. Suzuki, K. Mizutani, Y. Moro-oka, and T, Ikawa, *J. Am. Chem. Soc.*, **101**, 748 (1979); b) F. Sakurai, H. Suzuki, Y. Moro-oka, and T. Ikawa, *ibid.*, **102**, 1749 (1980); c) Y. Moro-oka and H. Suzuki, *J. Syn. Org. Chem. Jpn.*, **41**, 316 (1983).

15) It has been reported that the reaction of π-allyl palladium(II) complex **3** with KO_2 in CH_2Cl_2 gives μ-peroxobis(2-methylallyl)dipalladium(II) which behaves as a relatively stronger base.[14] However, this type of the complex is not involved in the present reaction, because when the complex was treated with dibenzyl ketone oxime in CH_2Cl_2, no methylene dioxime was formed. The only isolable product in this experiment was a trace or negligible amount of dibenzyl ketone. Although in one run the yield was 20%, its reproducibility was found to be poor in further runs.

16) W. T. Dent, R. Long, and A. J. Wilkinson, *J. Chem. Soc*, **1964**, 1585.
17) T. Hosokawa, S. Miyagi, S-I. Murahashi, and A. Sonoda, *J. Org. Chem.*, **43**, 2752 (1978).
18) J. R. Doyle, P. E. Slade, and H. B. Jonassen, *Inorg. Synth.*, **6**, 218 (1960).
19) T. W. J. Taylor and M. S. Marks, *J. Chem. Soc.*, **1930**, 2302.
20) The 1,2-diketone was prepared by a similar method reported by Y. Ogata and M. Yamashita, *Tetrahedron*, **27**, 3395 (1971).
21) M. Tanaka, T. Shono, and K. Shinra, *Anal. Chim. Acta.*, **46**, 125 (1969).

 © 1985 The Chemical Society of Japan Bull. Chem. Soc. Jpn., 58, 201—206 (1985)

Electrochemical Conversion of 2,3-Butanediol to Acetaldehyde by Oxidative Cleavage by a Periodate/Iodate Redox Mediatory System

Akiko YOSHIYAMA, Tsutomu NONAKA,* Manuel M. BAIZER,† and Tse-Chuan CHOU††

Department of Electronic Chemistry, Tokyo Institute of Technology, 4259 Nagatsuta, Midori-ku, Yokohama 227

†*Department of Chemistry, University of California, Santa Barbara, California 93106, U.S.A*

(Received July 30, 1984)

As electrochemical method was developed for converting 2,3-butanediol in dilute aqueous solutions to acetaldehyde by "in-cell" indirect anodic oxidation using a periodate/iodate redox mediatory system. Under optimum conditions, current efficiency for the desired acetaldehyde was close to 80% and the formation of by-products such as acetic acid, acetoin, and biacetyl was minimized or suppressed.

As part of a broad program pursued here and elsewhere whose main thrust is to explore the possibilites of converting electrochemically biomass-derived materials to (a) fuels or fuel components and/or (b) commercial organic chemicals, we have used 2,3-butanediol as a feedstock. Our results on the electrochemical conversion of this 1,2-diol to 2-butene (category *a* above)[1] and 2-butanone(category *b*)[2] had been reported; this paper concerns the conversion of the diol to acetaldehyde by electrooxidative cleavage.

It is well known that 1,2-diols,including 2,3-butanediol, can be cleaved with oxidizing reagents such as chromium(VI) oxide, peroxodisulfates, lead(IV) tetraacetate, diacetoxyiodobenzene and periodates to give two moles of the corresponding carbonyl compounds in a variety of yields and selectivities.[3,4] 1,2-Diols give also the carbonyl compounds by electrooxidation under a variety of electrolytic conditions.[5-14] The electrochemical method for the oxidative cleavage of the diols may be generally favorable from the point of view of avoiding the use of large amounts of expensive, poisonous and/or hazardous reagents. In this regard, we examined the electrochemical oxidation of 2,3-butanediol to acetaldehyde.

2,3-Butanediol is obtained as dilute aqueous solutions whose concentrations are lower than 10%, usually a few percent, by the fermentation of glucose and xylose.[15-18] Therefore, the electrolytic method suitable for such dilute solutions should be recommended, though the crude solutions from the fermentation can be concentrated by distillation; pure 2,3-butanediol is obtainable with considerable difficulty.[19,20]

In this work, either direct or indirect(using a redox mediator) electrooxidation of 2,3-butanediol to acetaldehyde in dilute (mainly *ca.* 1%) aqueous solutions was examined and it was found that the indirect oxidation using the periodate/iodate redox mediator resulted in high current efficiencies and selectivities for acetaldehyde.

Results and Discussion

Horányi *et al.*[21,22] reported that 2,3-butanediol was oxidized directly at a platinized platinum anode in a strongly acidic solution to give acetoin and biacetyl. In this oxidation, however, no cleaved products such as acetaldehyde and acetic acid were formed. In this work, the direct oxidation (Eq. 1) was first examined by using anodes other than platinized platinum in strongly acidic, neutral and strongly alkaline solutions. Electrolyses were carried out in a divided cell. Although acetaldehyde was formed in the direct oxidation, its current efficiency and selectivity were very low under a variety of conditions used. Even in the best case where a lead(IV) dioxide anode was used in a neutral solution, considerably large amounts of by-products such as acetic acid (15% current efficiency), acetoin(17%) and biacetyl(3%) were formed along with the desired acetaldehyde(24%).

$$CH_3\text{-}\underset{\displaystyle OH}{\underset{|}{CH}}\text{—}\underset{\displaystyle OH}{\underset{|}{CH}}\text{-}CH_3 \longrightarrow 2CH_3CHO + 2H^+ + 2e \qquad (1)$$

At the next stage of the investigation, the indirect oxidation using a suitable redox mediator was examined. Generally, either "in-cell" or "ex-cell" method may be available for indirect electrochemical oxidation and reduction. In this work, the "in-cell" method was favored, since it should be simpler in the whole system of electrolytic process.

As summarized by Torii,[23] a variety of organic and inorganic redox systems are available for indirect electro-oxidation of organic compounds. In this work, a periodate/iodate redox system was chosen as an electron-mediator, since 1,2-diols can generally cleaved by periodate oxidation to give the corresponding carbonyl compounds[3,4] and periodates are industrially produced by the electrochemical oxidation of iodates at lead(IV) dioxide anodes.[24-26] In addition, it has been confirmed by independent experiments that both periodates and iodates can not oxidize acetaldehyde. The indirect oxidation of 2,3-butanediol is pres-

†† Present address: Department of Chemical Engineering, Cheng-Kong University, Tainan, Taiwan, Republic of China.

ented by Eqs. 2 and 3.

At anode:

$$IO_3^- + 2OH^- \longrightarrow IO_4^- + H_2O + 2e \quad (2)$$

In solution:

$$CH_3\text{-}\underset{\underset{OH}{|}}{CH}\text{—}\underset{\underset{OH}{|}}{CH}\text{-}CH_3 + IO_4^- \longrightarrow 2CH_3CHO + IO_3^- + H_2O \quad (3)$$

The pH dependence of the chemical oxidation of 2,3-butanediol to acetaldehyde was first examined. As shown in Fig. 1, yields of acetaldehyde were high at pHs higher than 6, though no examination was carried out in alkaline solutions because in the latter case condensation reactions of aldehyde occur.

On the other hand, as shown in Fig. 2, current efficiencies for periodate formed in the electrooxidation of iodate at a lead(IV) dioxide anode were high at pHs lower than 6.

From these facts, it seemed to be difficult to obtain both the highest yield of acetaldehyde and the highest current efficiency for periodate at the same pH. It was expected that the best result in actual electrolysis of 2,3-butanediol in sodium iodate solutions would be obtained in a range of pH 5—7. As shown in Fig. 3, the current efficiency for acetaldehyde formed in the indirect electrochemical oxidation of 2,3-butanediol at the lead(IV) dioxide anode in phosphate buffer solutions containing sodium iodate was at a high level close to 80% at pH 5—9. The current efficiency was somewhat affected by anodic potentials and the highest value was obtained at 2.00 V *vs.* SCE.

Decrease of the current efficiency at lower pHs, shown in Fig. 3, might be due to unfavorable oxidation of 2,3-butanediol to by-products with anodically generated periodate(Eq. 2) since the oxidation proceeded more disadvantageously at such pHs, as shown in Fig. 1. However, no by-product was formed in the chemical oxidation with sodium periodate at such pHs. This fact suggests that the decrease of the current efficiency for acetaldehyde may be due to occurrence of electrochemical side reactions to form products other

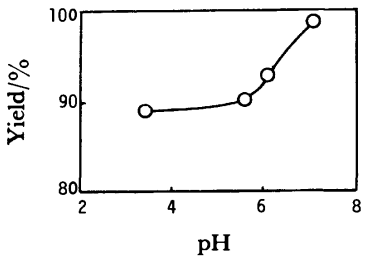

Fig. 1. pH-Dependence of Yield of Acetaldehyde Formed in the Chemical Oxidation of 2,3-Butanediol with Sodium Periodate.
2,3-Butanediol concentration, 0.1 M; Sodium periodate concentration, 0.2 M; Temperature, 40 °C; Reaction time, 20 s.

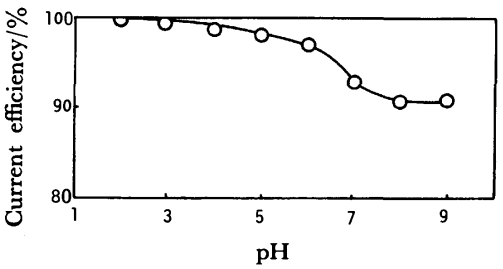

Fig. 2. pH-Dependence of Current Efficiency for Periodate Formed in the Electrochemical Oxidation of Sodium Iodate at a Lead Dioxide Anode.
Sodium iodate concentration, 0.2 M; Temperature, 38 °C; Anodic potential, 2.00 V *vs.* SCE

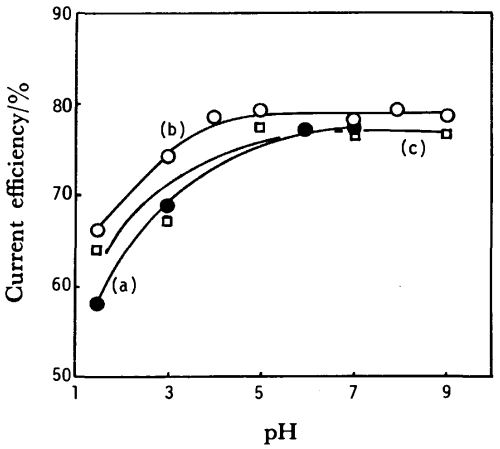

Fig. 3. pH-Dependence of Current Efficiency for Acetaldehyde Formed in the Indirect Electrochemical Oxidation of 2,3-Butanediol with a Periodate/Iodate Mediator at a Lead Dioxide Anode.
2,3-Butanediol concentration, 0.1 M; Sodium iodate concentration, 0.2 M; Temperature, 37 °C; Anodic potential, (a) 1.80 V *vs.* SCE, (b) 2.00 V, (c) 2.30 V; Charge passed, 0.67 F mol^{-1}.

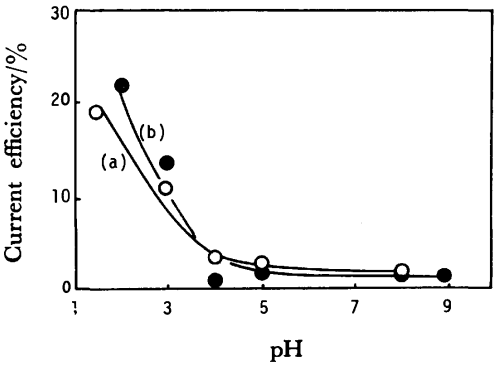

Fig. 4. pH-Dependence of Current Efficiencies for (a) Acetic Acid and (b) Acetoin Formed in the Indirect Electrochemical Oxidation of 2,3-Butanediol with a Periodate/Iodate Redox Mediator at a Lead Dioxide Anode.
2,3-Butanediol concentration, 0.1 M; Sodium iodate concentration, 0.2 M; Temperature, 37 °C; Charge passed, 0.67 F mol^{-1}; Anodic potential, 2.00 V *vs.* SCE.

than acetaldehyde. As shown in Fig. 4, the oxidation at the lower pHs provided larger amounts of by-products such as acetic acid and acetoin, while no biacetyl was formed at all pHs used. The oxidation potential of iodate seemed to be close to that of 2,3-butanediol (See Fig. 5) and the main products in the direct oxidation at the lead dioxide anode in the strongly acidic solution were acetic acid and acetoin. From these facts, the formation of the by-products at the lower pHs may be rationalized as due to the simultaneous direct oxidation with the indirect oxidation by electrogenerated periodate.

As shown in Fig.6 the highest current efficiency for acetaldehyde was obtained at 37 °C. Lower current efficiencies at higher temperatures might be partially due to loss of acetaldehyde by its evaporation.

The current efficiency for acetaldehyde was affected by the concentration of sodium iodate, as shown in Fig. 7. Lower efficiencies at lower concentrations may be due to simultaneous occurrence of the indirect and direct oxidation of 2,3-butanediol, the latter of which gave acetaldehyde in lower efficiencies. The direct oxidation should be relatively favorable at low concentration of sodium iodate, since the oxidation potential of 2,3-butanediol is not so far from that of sodium iodate even in a neutral solution (See Fig. 5). From the results in Fig. 7, concentrations higher than 0.2 M (1 M=1 mol dm^{-3}) should be desirable, but those higher than 0.3 M can not be actually used because of the limited solubility of sodium iodate in the electrolytic solution.

Curve(a) in Fig. 8 indicates that the current efficiency decreased with increase of concentration of 2,3-butanediol, when 0.67 F (1 F=96496 C) mol^{-1} of charge, which is proportional to the concentration, was passed. In such a manner of electrolysis, the ano-

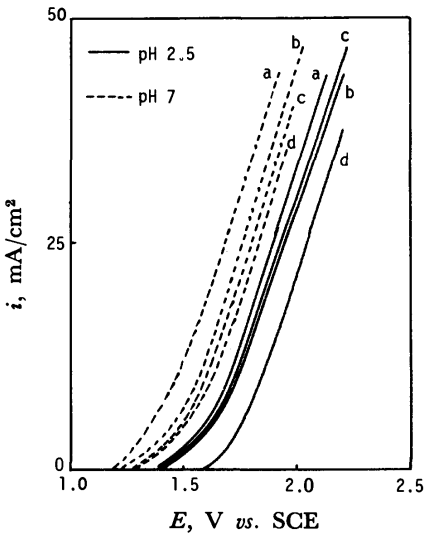

Fig. 5. *i-E* Curves at 37 °C and a Lead Dioxide Anode. (a): 0.2 M $NaIO_3$, (b): 0.1 M 2,3-Butanediol, (c): 0.08 M Acetaldehyde, (d): Background.

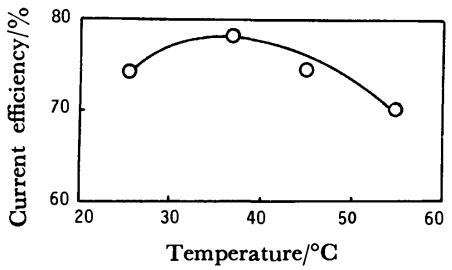

Fig. 6. Temperature-dependence of Current Efficiency for Acetaldehyde Formed in the Indirect Electrochemical Oxidation of 2,3-Butanediol with a Periodate/Iodate Redox Mediator at a Lead Dioxide Anode.
2,3-Butanediol concentration, 0.1 M; Sodium iodate concentration, 0.2 M; pH, 7; Anodic potential, 2.00 V *vs.* SCE; Charge passed, 0.67 F mol^{-1}.

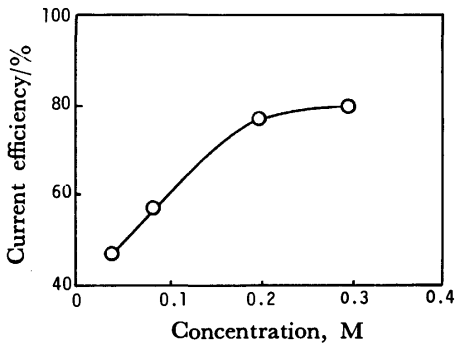

Fig. 7. Sodium Periodate Concentration-Dependence of Current Efficiency for Acetaldehyde Formed in the Indirect Electrochemical Oxidation of 2,3-Butanediol with a Periodate/Iodate Redox Mediator at a Lead Dioxide Anode.
2,3-Butanediol concentration, 0.1 M; pH, 7; Temperature, 37 °C; Anodic potential, 2.00 V *vs.* SCE; Charge passed, 0.67 F mol^{-1}.

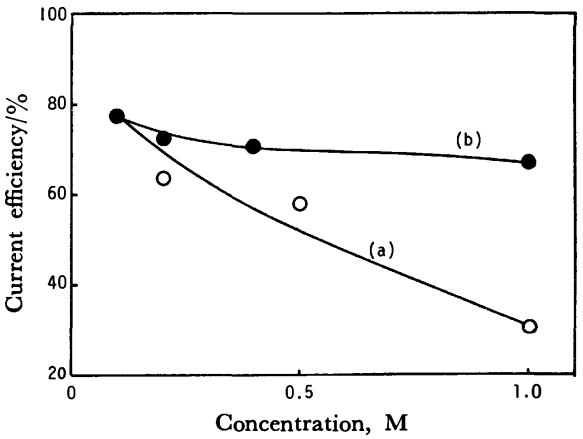

Fig. 8. 2,3-Butanediol Concentration-Dependence of Current Efficiency for Acetaldehyde Formed in the Indirect Electrochemical Oxidation of 2,3-Butanediol with a Periodate/Iodate Redox Mediator at a Lead Dioxide Anode.
Sodium iodate concentration, 0.2 M; pH, 7; Temperature, 37 °C; Anodic potential, 2.00 V *vs.* SCE; Charge passed, (a) 0.67 F mol^{-1} and (b) 0.0033 F for each concentration of 2,3-butanediol.

lyte should be acidified by the acid electrogenerated when large amounts of charge was passed at high concentration of 2,3-butanediol. In fact, after 0.67 F mol^{-1} (0.033 F for 50 mmol of 2,3-butanediol) was passed in 1.0 M 2,3-butanediol concentration, the pH decreased to 2.5 because of the insufficient buffering capacity of a phosphate solution used as the anolyte. Low current efficiency in this case also may be rationalized as due to simultaneous direct oxidation.

Curve(b) in Fig. 8 shows the results obtained by passing the same amount of charge(0.0033 F) at all the concentrations. In this case, a much smaller decrease of the current efficiency with increase of the concentration was observed, because the change of pH should be almost the same in each electrolysis.

From the above consideration, pH control is desired to obtain high current efficiencies, when such large amounts of charge are passed that high conversions of the starting 2,3-butanediol can be obtained when it is present in high concentrations. This point was further confirmed by Fig. 9. When large amounts of charge of 2.6 F mol^{-1} were passed without any pH control (to obtain almost 100% conversion), the current efficiencies for acetaldehyde and acetic acid were decreased and increased, respectively, as shown in Fig. 9.

Figure 9 also showes a result which was obtained by adjusting pH in the range of 7—6 by occasional addition of alkali during the electrolysis. Compared with the previous case, the result was improved.

When 2.5 F mol^{-1} of charge were passed in a high concentration (0.5 M, *ca.* 5%) of 2,3-butanediol under no pH control, the current efficiency for the desired acetaldehyde was lower than that for the by-product (acetic acid) as shown in Fig. 10. In this case, two more

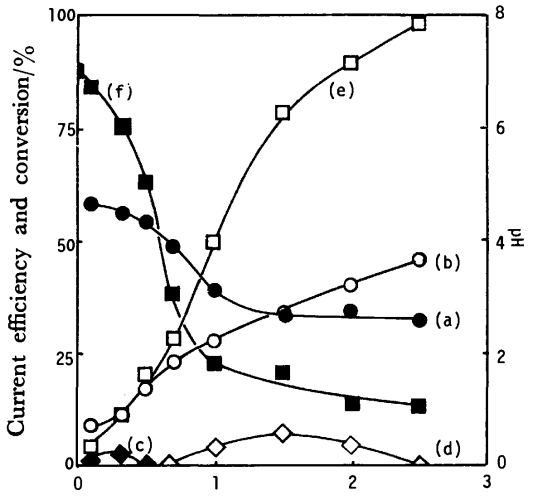

Fig. 10. Current Efficiencies for (a) Acetaldehyde, (b) Acetic Acid, (c) Acetoin and (d) Cyclic Acetal of 2,3-Butanediol, Conversion (e) of 2,3-Butanediol, and pH (f) in the Indirect Electrochemical Oxidation with a Periodate/Iodate Redox Mediator at a Lead Dioxide Anode.
2,3-Butanediol concentration 0.5 M (*ca.* 5%); Sodium iodate concentration, 0.2 M; Initial pH, 7 (not controlled); Anodic potential, 2.00 V *vs.* SCE; Temperature, 37 °C.

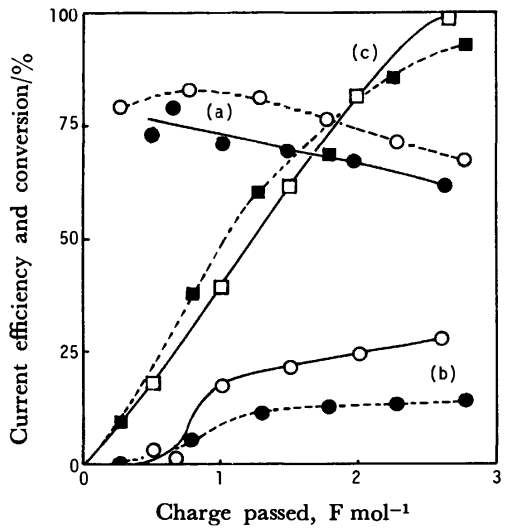

Fig. 9. Current Efficiencies for (a) Actealdehyde and (b) Acetic Acid, and Conversion (c) of 2,3-Butanediol in the Indirect Electrochemical Oxidation with a Periodate/Iodate Redox Mediator at a Lead Dioxide Anode: pH; ——, not controlled. ----, controlled at 7—6 by adding disodium hydrogenphosphate during the electrolysis.
2,3-Butanediol concentration, 0.1 M (*ca.* 1%); Sodium iodate concentration, 0.2 M; Initial pH, 7; Anodic potential, 2.00 V *vs.* SCE; Temperature, 37 °C.

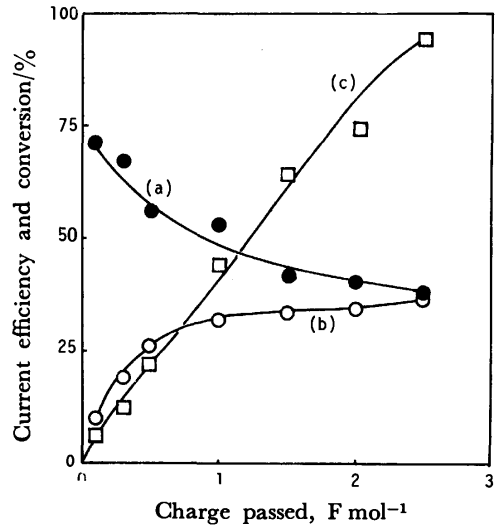

Fig. 11. Current Efficiency for (a) Acetaldehyde and (b) Acetic Acid, and Conversion (c) of 2,3-Butanediol in the Indirect Electrochemical Oxidation with a Periodate/Iodate Redox Mediator at a Lead Dioxide Anode.
2,3-Butanediol concenrtation, 0.5 M (*ca.* 5%); Sodium iodate concentration, 0.2 M; Initial pH, 7 (controlled at 7—6 by adding disodium hydrogenphosphate during the electrolysis); Anodic potential; 2.00 V. *vs.* SCE; Temperature, 37 °C.

by-products, acetoin and cyclic acetal of 2,3-butanediol(2,4,5-trimethyl-1,3-dioxolane), rose and fell in the course of the electrolysis. The pH control resulted in some improvements in the current efficiencies as shown in Fig. 11, but they were not satisfactory.

Acetaldehyde can not be oxidized with periodate, as described above, but it may be oxidized at an anode. In fact, acetaldehyde (0.48 M) was oxidized to acetic acid in 96% conversion and 78% current efficiency at 2.00 V *vs.* SCE (at lead(IV) dioxide anode) in a phosphate-buffered solution(pH 7) containing sodium iodate (0.2 M). Therefore, the decrease and increase of acetaldehyde and acetic acid, respectively, at high conversion of 2,3-butanediol is rationalized as due to the further oxidation of the former to the latter. To prevent the further oxidation, it should be effective to remove acetaldehyde from the anolyte by a suitable way during the electrolysis. This is a chemical engineering problem with which this paper is not concerned.

As described above, it was important to keep the pH in a suitable range and pH control was done by adding alkali to the anolyte during the electrolysis. There may be another way for the pH control, that is, the use of an undivided cell, which can be constructed more simply than divided ones. We attempted electrolyses in an undivided cell using a platinum cathode and lead(IV) dioxide anode, but good results could not be obtained because of the cathodic reduction of iodate to iodide (which was re-oxidized to iodine at the anode).

Conclusion

An optimization of the electrochemical conversion of 2,3-butanediol to acetaldehyde was established as follow: Electrolytic method, indirect oxidation; mediatory system, periodate/iodate redox; cell, divided; anode, lead(IV) dioxide; anodic potential, 2.00 V *vs.* SCE; pH, 7—6; temperature, 37 °C; concentration of sodium iodate, >0.2 M; concentration of 2,3-butanediol, several percent.

It is also recommended to remove acetaldehyde during the electrolysis so that it does not accumulate in the anolyte. For this purpose, continuous distillation and/or extraction may be available. If an efficient procedure for removing acetaldehyde is established, an "ex-cell" method for the indirect oxidation may become practicable, though it has not been established whether the "ex-cell" method is superior to the "in-cell" one.

Experimental

Materials. 2,3-Butanediol and lead(IV) dioxide anodes were supplied from Tokyo Kasei Kogyo Co. Ltd. and Sanwa Chemical Co. Ltd., respectively.

Electrolysis. An H-type divided cell with a sintered glass diaphragm and a potentiostat were used for controlled-potential electrolyses. Anodes were platinum (2.0×3.0 cm), lead(IV) dioxide (2.5×3.0 cm) and graphite (2.5×3.0 cm) plates. The direct oxidation of 2,3-butanediol was carried out in 0.5 M H_2SO_4, 1 M Na_2SO_4, and 1 M KOH, while anolytes for the indirect oxidation were phosphate-buffered solutions containing sodium iodate; 0.3 M Na_2HPO_4 (pH 9), Na_2HPO_4–NaH_2PO_4 (pH 8—4.5), 0.3 M Na_2HPO_4–0.5 M H_3PO_4 (pH 3), and NaH_2PO_4–H_2SO_4 (pH<3). Fifty mililiters of anolyte were used for each electrolysis.

Analysis. Starting 2,3-butanediol and all the products were analyzed by gas chromatography (1.5 m Chromosorb 101 column at 80—180 °C). Periodate was analyzed by the Fluery-Lange method.[22]

We are grateful to the Kajima Foundation for making possible Professor Chou's participation.

References

1) T. Nonaka and M. M. Baizer, *Electrochim. Acta*, **28**, 661 (1983).
2) M. M. Baizer, T. Nonaka, K. Park, Y. Saito, and K. Nobe, *J. Appl. Electrochem.*, **14**, 197 (1984).
3) Y. Ogata, "Yukikagobutsu no Sanka to Kangen (Oxidation and Reduction of Organic Compounds)," Nankodo, Tokyo, pp. 191, 248, 321, 343, 352 (1964).
4) H. O. House, "Modern Synthetic Chemistry," 2nd. Ed., W. A. Benjamin Inc., Monlo Park, p. 353 (1972).
5) A. Renard, *Ann. Chem.*, **17**, 313 (1879).
6) C. Neuberg, *Biochem. Z.*, **17**, 270 (1909).
7) W. Löb and G. Pulvermacher, *Biochem. Z.*, **17**, 343 (1909).
8) W. Löb and G. Pulvermacher, *Z. Elektrochem.*, **16**, 5 (1910).
9) E. Müller, *Z. Elektrochem.*, **27**. 565 (1921).
10) E. Tommila, *Ann. Acad. Sci. Fenn.*, **39**, 11 (1934).
11) T. Shono, Y. Matsumura, T. Hashimoto, K. Hibino, H. Hamaguchi, and T Aoki, *J. Am. Chem. Soc.*, **97**, 2546 (1975).
12) T. Shono, H. Hamaguchi, Y. Matsumura, and K. Yoshida, *Tetrahedron Lett.*, **1977**, 3625.
13) A. Yoshiyama, T. Goto, and T. Sekine, *J. Electrochem. Soc. Jpn.*, **49**, 532 (1981).
14) T. Fuchigami, T. Nonaka, C. Watanabe, A. Yoshiyama and T. Sekine, *J. Electrochem. Soc. Jpn.*, **51**, 812 (1983).
15) G. A. Adams and R. Y. Stanier, *Can. J. Res.*, **23B**, 1 (1945).
16) A. C. Blackwood, A. C. Neish, W. E. Brown, and G. A. Ledingham, *Can. J. Res.*, **25B**, 56 (1947).
17) A. C. Neish, A. C. Blackwood, F. M. Robertson, and G. A. Ledingham, *Can. J. Res.*, **25B**, 65 (1947).
18) A. C. Neish, A. C. Blackwood, F. M. Robertson, and G. A. Ledingham, *Can. J. Res.*, **26B**, 335 (1948).
19) A. C. Neish, *Can. J. Res.*, **23B**, 10 (1945).
20) D. Rose and W. S. King, *Can. J. Res.*, **23F**, 79 (1945).
21) G. Horányi, G. Inzelt and K. Torkos, *J. Electroanal. Chem. Interfacial Electrochem*, **106**, 305 (1980).
22) G. Horányi and G. Inzetl, *Ann. Univ. Sci. Budapestinensis de Rolando Eötvös Nominatase, Sec, Chim.*, **1980**, 47.
23) S. Torii, "Yukidenkaigosei (Organic Electrosyntheses)," Kodansha, Tokyo, p. 303 (1981).

24) H. H. Willard, and R. R. Ralston, *J. Electrochem. Soc.*, **62**, 239 (1932).
25) C. L. Mehltretter and C. S. Wise, *Ind. Eng. Chem.*, **51**, 511 (1959).
26) Y. Aiya, S. Fujii, K. Sugino and K. Shirai, *J. Electrochem. Soc.*, **109**, 419 (1962).
27) E. L. Fleury and J. Lange, *J. Pharm. Chem.*, **17**, 107, (1933).

Photoinduced Reduction of Methylviologen by Ascorbate Using Chlorophyllin in Liposome System

Seiji HIDAKA,† Eizo MATSUMOTO, and Fujio TODA*
†*Department of Synthetic Chemistry, Faculty of University of Tokyo, Hongo, Bunkyo-ku, Tokyo 113*
Department of Chemical Engineering, Faculty of Engineering, Tokyo Institute of Technology, Ookayama, Meguro-ku, Tokyo 152
(Received February 21, 1984)

Photoindeced electron transport across bilayer lipid membrane was studied, using chlorophyllin (Chln), a water-soluble derivative of chlorophyll. Photoreduction of methylviologen (MV^{2+}) by ascorbate was observed only in the liposome system containing ascorbate in the internal aqueous phase and MV^{2+} in the external aqueous phase. This suggests asymmetry of bilayer lipid membrane. This reaction rate was not affected by the addition of carbonyl cyanide *m*-chlorophenylhydrazone in the system buffered by tris(hydroxymethyl)aminomethane (Tris), but strongly affected by *N*-2-hydroxyethylpiperazine-*N'*-2-ethanesulfonic acid. In the system buffered by Tris, a proton carrier is not Chln having carboxyl groups but Tris possessing primary amine group. Replacement of the central Mg of Chln with Zn gives a higher rate of MV^{2+} photoreduction, but when Cu was used in place of Zn, photoreduction was not observed. The central metal may affect the redox potential and the life time of excited Chln.

Membrane-like structure plays an important role in bioenergetic systems. It is well-known that thylakoid membrane in chloroplast is indispensable to photosynthesis. There are three major functions in biological membrane. First, membrane is a barrier to separate the internal aqueous phase of cell from the external. Second, it can orient the functional units (enzyme, protein *etc.*) in the highly ordered forms. Third, it is a reaction medium of chemical and/or physical reactions. Consequently, thylakoid membrane enables active transport of electrons by interfering with back reaction and generates pH gradient to synthesize ATP.

There have been many reports on photoinduced electron transport across bilayer lipid membrane sensitized by chlorophyll,[1,2] amphiphilic Zn(II) porphyrins,[3,4] or Ru(II) complexes.[5,6] But these photosensitized redox reactions often occur effectively in homogeneous solutions.

We previously reported that photoinduced electron transport across bilayer lipid membrane can take place sensitized by chlorophyllin.[7] Chlorophyllin is a water-soluble derivative of chlorophyll, and a fairy green pigment which resembles chlorophyll in its photochemical reactivity.[8–10]

We report here that photoreduction of methylviologen by ascorbate using chlorophyllin as a sensitizer in liposome system. This reaction doesn't occur in homogeneous solution. Ascorbate is a reversible electron donor which is different from EDTA and triethanolamine as sacrificial electron donors.

Experimental

Materials. *Chlorophyllin* a: Chlorophyll a was extracted from fresh spinach leaves with cold acetone and purified according to the procedure of Omata and Murata.[11] Chlorophyllin a (Chln) was prepared from chlorophyll a by the method of Oster and his coworkers.[12]

Cu- and Zn-chlorophyllin a: Cu- and Zn-chlorophyll were prepared from their original chlorophyll using to the procedure of Onoue[13] and subsequently converted into Cu-chlorophyllin a (Cu-chln) and Zn-chlorophyllin a (Zn-chln).

Lecithin: Lecithin (phosphatidylcholine) was isolated from hen egg yolk and purified with the chromatographic procedure.[14]

Methylviologen (MV^{2+}) and carbonyl cyanide *m*-chlorophenylhydrazone (CCCP) were purchased from Sigma Chemical Co. and the other chemicals were reagent grade and used without further purification.

Liposome. Lecithin in chloroform was dissolved in benzene and colyophylized. Liposomes were prepared by sonicating lecithin in the solution buffered by 1 mol dm^{-3} Tris-Cl 0.1 mol dm^{-3} KCl (pH 7.5) under an N_2 atmosphere for 1 h at 4 °C. The dispersion was then centrifuged to remove metal fragments. External ions were separated from liposomes by gel-filtration on a 2×50 cm Sephadex G-50 column. The samples were purged of O_2 by bubbling a stream of Ar gas for 30 min at 4 °C.

Measurements. Photoreaction was carried out under an atmosphere of Ar gas sealed in the Pyrex tube with UV cell on the bottom. Light was irradiated with 500 W Xenon lamp (Ushio UXL-500D). Glass filters (Toshiba IRQ-25, OR-57) were used to isolate red light. Absorption spectra were measured on Hitachi spectrophotometer. Photoinduced electron transport was monitored by measuring the absorbance of reduced methylviologen ($MV^{+\cdot}$) at 605 nm.

Results and Discussions

Photoreduction of MV^{2+}. Transmembrane electron transport from ascorbate (Asc) to MV^{2+} sensitized by Chln was investigated in the various systems and the formation of $MV^{+\cdot}$ with time of irradiation as is shown in Fig. 1. In the homogeneous system, $MV^{+\cdot}$ was not observed. This is thought to be due to the rapid back reaction between oxidized ascorbate (DAH) and $MV^{+\cdot}$. In the liposome system containing MV^{2+} in the internal aqueous phase and Asc in the external, $MV^{+\cdot}$ didn't produce though the bilayer lipid membrane interfered with the back reaction. Photoreduc-

tion of MV^{2+} was observed only in the liposome system containing Asc in the internal aqueous phase and MV^{2+} in the external. The experimental results as described below were gained in this system.

The progressive spectral changes with time of irradiation are shown in Fig. 2. Chln in the liposome system showed a red absorption peak at 660 nm. However, on irradiation, a new absorption band appeared gradually at 690-nm as the 660 nm peak decreased. After the 690-nm peak was saturated, the absorption band due to $MV^{+\cdot}$ was observed to increase. From the previous experiment,[7,15] we confirmed the 690 nm absorbing species was an irreversible product of Chln (Chln'). In the present system, Chln didn't appear to sensitize MV^{2+} photoreduction but Chln' did and it was recycled because the spectrum after 20-min irradiation corresponded to that after 5-min irradiation when O_2 gas was added to the system to remove $MV^{+\cdot}$ absorption.

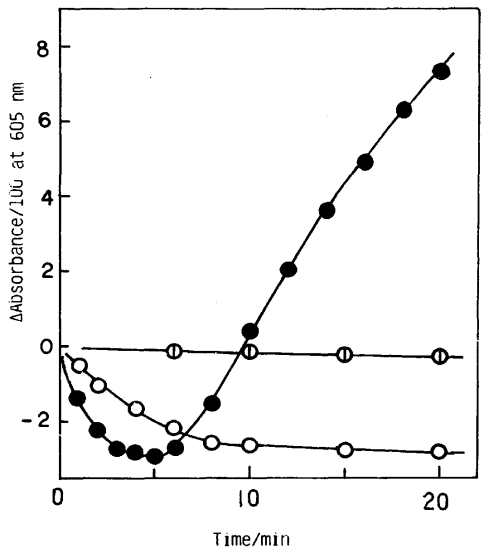

Fig. 1. Photoreduction of MV^{2+} in various systems. ①: [Chln] = 10 μmol dm^{-3}, [MV^{2+}] = 10 mmol dm^{-3}, [AscNa] = 10 mmol dm^{-3}, in Tris buffer, ○: [Chln] = 10 μmol dm^{-3}, [MV^{2+}] = 0.1 mol dm^{-3} (in), [AscNa] = 10 mmol dm^{-3} (out), in liposome system, ●: [Chln] = 10 μmol dm^{-3}, [AscNa] = 1 mol dm^{-3} (in), [MV^{2+}] = 10 mmol dm^{-3} (out) in liposome system.

The dependence of photoreduction rate of MV^{2+} on MV^{2+} concentration is shown in Fig. 3. The measurement of the concentration of $MV^{+\cdot}$ was based on the minimum absorbance at 605 nm as described above. The reduction rate increased rapidly with increasing the lower concentration region, and saturated at the higher concentration.

From these results, the reaction scheme is proposed and the difference of the reactivities of the two liposome systems is discussed. The reaction is thought to proceed as follows:

$$\text{Chln} \xrightarrow{h\nu} \text{Chln}' \quad (1)$$

$$\text{Chln}' \xrightarrow{h\nu} \text{Chln}'^{*} \quad (2)$$

$$\text{Chln}'^{*} + MV^{2+} \longrightarrow \text{Chln}'^{+\cdot} + MV^{+\cdot} \quad (3)$$

$$\text{Chln}'^{+\cdot} + \text{Asc}^{-} \longrightarrow \text{Chln}' + \text{DAH} \quad (4)$$

where Chln'* and Chln'$^{+\cdot}$ are excited Chln' and Chln' cation radical, respectively. The reaction (1) is the formation of the 690-nm absorbing species. The decrease of the absorbance at 605 nm at the initial step

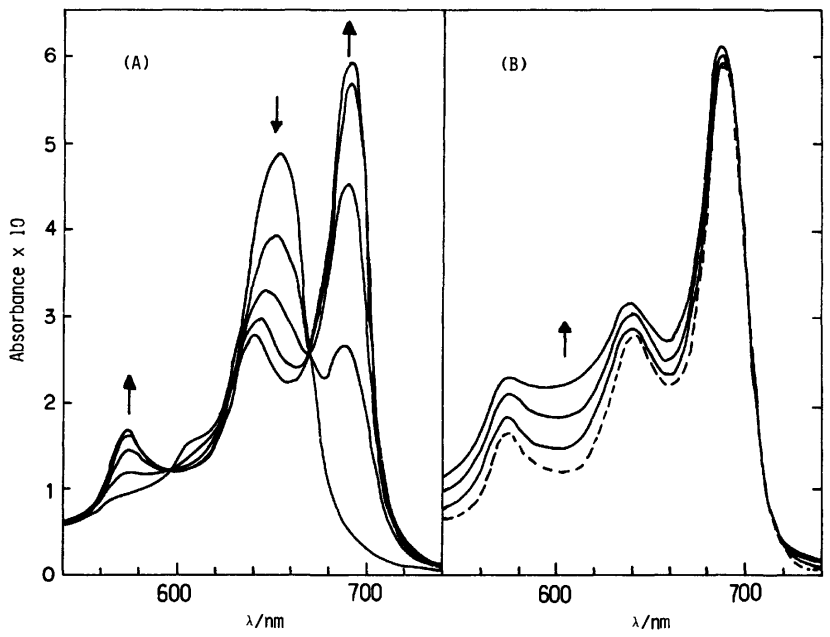

Fig. 2. Absorption spectra of liposome system.
(A) 0, 1, 2, 3, and 4 min after irradiation, (B) (——): 10, 15 and 20 min after irradiation and (----): bubbled O_2 after 20-min irradiation.

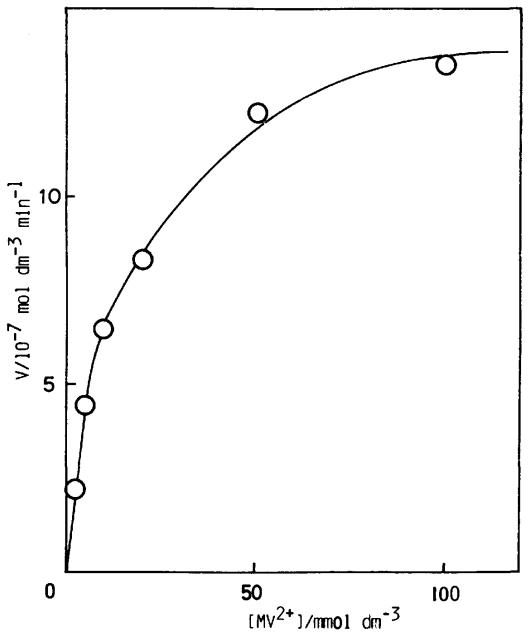

Fig. 3. Dependence of the reduction rate on MV^{2+} concentration.

was due to this reaction. The dependence of MV^{2+} photoreduction on MV^{2+} concentration is interpreted according to the scheme. In the lower MV^{2+} concentration, the reduction rate was determined by the reaction (3) and the observed rate was dependent on MV^{2+} concentration. On the other hand, as the reaction (3) was fast enough at the higher MV^{2+} concentration, the photoreduction rate was determined by the reaction (2). Therefore the observed rate was independent of MV^{2+} concentration.

The different results in the two liposome systems suggests asymmetry of bilayer lipid membrane. There have been several reports on asymmetry in sonicated liposomes.[16-20] The packing density of the inner-layer lipid molecules is more dense than that of the outer-layer lipid molecules owing to the difference of the curvature and causes the geometrical constraints to the head groups and the acyl chains of the inner-layer lipid molecules (Fig. 4[21]). This asymmetry facilitates the reaction (2) rather on the outer surface than on the inner surface. And another investigation indicates that the greater part of water-soluble Chln added to the liposome system exists on the outer surface.[15] Such a biased distribution of Chln is also more favorable to the reaction (2) on the outer surface than on the inner surface. Therefore, MV^{2+} photoreduction didn't occur in the liposome system containing MV^{2+}, in the internal and Asc in the external, but was observed in the liposome system containing Asc in the internal and MV^{2+} in the external.

Effect of CCCP. Chln was expected to play a role of a proton carrier as well as an electron carrier because Chln is tricarboxylic acid. The effect of CCCP was investigated in the liposome system buffered by

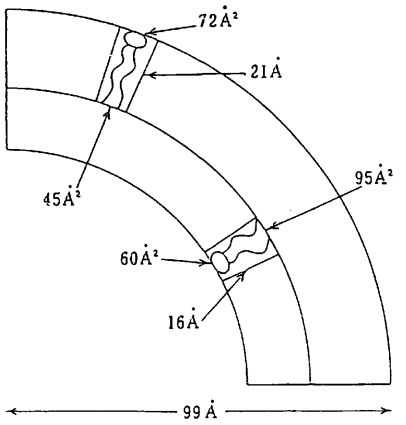

Fig. 4. Vesicle bilayer cross section showing the packing geometry of lipids within the inner and outer vesicle bilayer.

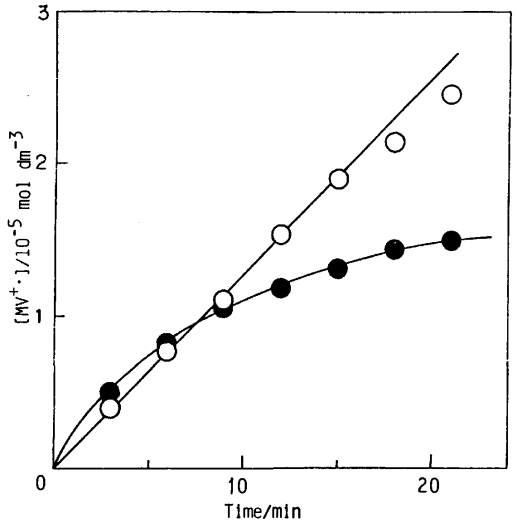

Fig. 5. Effect CCCP on MV^{2+} photoreduction in liposome system buffered by HEPES, pH 7.5.
●: without CCCP, ○: with 0.1 mmol dm^{-3} CCCP.

2-[4-(2-hydroxyethyl)-1-piperazinyl] ethanesulfonic acid (HEPES), pH 7.5 because HEPES is impermeable to membrane.[22,23] The addition of CCCP strongly affected MV^{2+} photoreduction as is shown in Fig. 5. Contrary to our expectation, Chln didn't transport protons with electrons in the absence of CCCP and the formation of membrane potential suppressed the photoreduction. But in the system buffered by Tris, pH 7.5 the effect of CCCP on the reaction rate was not observed. Without CCCP, $MV^{+\cdot}$ production was nearly linear, not saturated for our measurement time. It was reported that Tris could penetrate membrane and that 'Hill reaction' was hindered at the high concentration of Tris because Tris, having the primary amine group, acted as an uncoupler.[23,24] From a consideration of these reports, it is consistent to conclude that Tris played a part of a proton carrier in our system since the concentration of Tris was 1 mol dm^{-1}.

Effect of Central Metal. The effect of the central

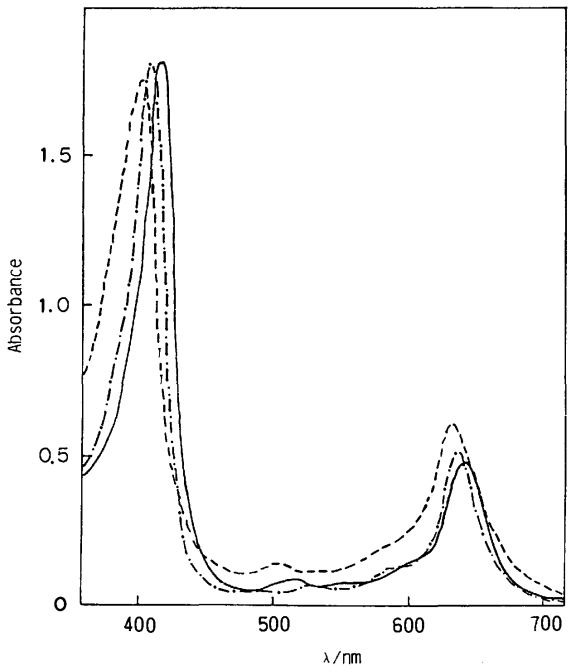

Fig. 6. Absorption spectra of chlorophyllin derivatives.
(——): Chln, (—·—): Zn-chln, (----): Cu-chln.

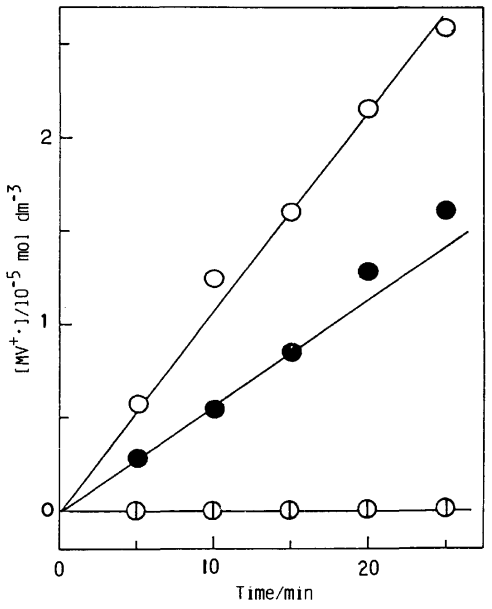

Fig. 7. Photoreduction of MV^{2+} sensitized by chlorophyllin derivatives.
●: Chln, ○: Zn-chln ⦶: Cu-chln.

metal of Chln on photoredox reaction was investigated by replacement of the central Mg with Cu or Zn. Though the spectra of these pigments bear much resemblance as is shown in Fig. 6, different photocatalytic reactivities were observed in MV^{2+} reduction as is shown in Fig. 7. The reactivity of pigment decreased in the order Zn-chln>Chln>Cu-chln=0. It is remarkable that Zn-chln reactivity was better than that of Chln which has the same Mg as chlorophyll, a natural photosynthetic pigment. The result indicates the redox potential and/or the life time of the excited state of Chln may depend on the central metal. The relative order of the redox potentials of these excited pigments may be Zn-chln>Chln>MV^{2+}>Cu-chln. Therefore Cu-chln couldn't sensitize the photoreduction of MV^{2+}.

The authors wish to express their thanks to Professor Kennichi Honda of University of Tokyo.

References

1) K. Kurihara, Y. Toyoshima, and M. Sukigara, *Nippon Kagaku Kaishi*, **1980**, 500.
2) W. E. Ford and G. Tollin, *Photochem. Photobiol.*, **38**, 441 (1983).
3) T. Katagi, T. Yamamura, T. Satio, and Y. Sasaki, *Chem. Lett.*, **1981**, 503.
4) T. Katagi, T. Yamamura, T. Saito, and Y. Sasaki, *Chem. Lett.*, **1982**, 417.
5) W. E. Ford, J. W. Otvos, and M. Calvin, *Nature*, **274**, 507 (1978).
6) C. Laane, I. Willner, J. W. Otvos, and M. Calvin, *Proc. Natl. Acad. Sci. U.S.A.*, **78**, 5928 (1981).
7) S. Hidaka and F. Toda, *Chem. Lett.*, **1983**, 1333.
8) G. Oster, S. B. Broyde, and J. S. Bellin, *J. Am. Chem. Soc.*, **86**, 1313 (1964).
9) L. P. Vernon, A. S. Pietro, and D. A. Limbach, *Arch. Biochem. Biophys.*, **109**, 371 (1965).
10) D. Brune and A. S. Pietro, *Arch. Biochem. Biophys.*, **141**, 371 (1970).
11) T. Omata and N. Murata, *Photochem. Photobiol.*, **31**, 183 (1980).
12) G. Oster, S. B. Broyde, and J. S. Bellin, *J. Am. Chem. Soc.*, **86**, 1309 (1964).
13) Y. Onoue, *Bull. Chem. Soc. Jpn.*, **54**, 1972 (1981).
14) C. H. Lea and D. H. Rhodes, *Biochemistry*, **60**, 355 (1975).
15) S. Hidaka, E. Matsumoto, and F. Toda, *Nippon Kagaku Kaishi*, in preparation.
16) R. J. Kostelnik and S. M. Castellano, *J. Magn, Reson.*, **9**, 291 91973).
17) J. A. Berden, R. W. Berker, and G. K. Radda, *Biochim. Biophys. Acta*, **375**, 186 (1975).
18) J. T. Mason and C. Huang, *Ann. N.Y. Acad. Sci. U.S.A.*, **308**, 29 (1978).
19) K. Machida and S. Ohnishi, *Biochim. Biophys. Acta*, **596**, 201 (1980).
20) B. A. Cornell, J. Middlehurst, and F. Separovic, *Biochim. Biophys. Acta*, **598**, 405 (1980).
21) C. Huang and J. T. Mason, *Proc. Natl. Acad. Sci. U.S.A.*, **75**, 308 (1978).
22) N. E. Good, *Arch. Biochem. Biophys.*, **96**, 653 (1962).
23) N. E. Good, G. D. Winget, W. Winter, T. N. Connolly, S. Izawa, and R. M. M. Singh, *Biochemistry*, **5**, 467 (1966).
24) T. Yamashita and W. L, Butler, *Plant Physiol.*, **44**, 435 (1969).

 © 1985 The Chemical Society of Japan Bull. Chem. Soc. Jpn., 58, 211—216 (1985)

Rearrangement Approaches to Cyclic Skeletons. I. Photochemical Rearrangement Approaches to (±)-Sesquicarene and (±)-Sirenin, [3—6] Fused-Ring Sesquiterpenes†

Tadao UYEHARA,* Jun-ichi YAMADA, Koichi OGATA, and Tadahiro KATO
Department of Chemistry, Faculty of Science, Tohoku University, Aramaki-Aoba, Sendai 980
(Received June 21, 1984)

The 4-alkyl, 4-alkenyl, and 4-aryl derivatives of bicyclo[3.2.2]nona-3,6-dien-2-one (**9**) were prepared from **9** itself by ultrasound-promoted Barbier reaction followed by PCC oxidation. Photochemical transformation of the 4-(4-methyl-3-pentenyl) derivative of **9**, namely **13**, in THF–water gave *endo*-7-[*exo*-7-(4-methyl-3-pentenyl)bicyclo[4.1.0]hept-2-ene]acetic acid (**14**). Acid **14** was converted into *endo*-7-methyl-*exo*-7-(4-methyl-3-pentenyl)bicylo[4.1.0]heptan-2-one (**4**), a key intermediate of (±)-sesquicarene and (±)sirenin total syntheses. Furthermore, a highly stereospecific total synthesis of (±)-sesquicarene was acomplished by the photochemical transformation of the 1-methyl derivative of **13** prepared from 2-methyltropone (**21**).

Sesquiterpene analogues of 2-carene, such as sesquicarene (**1**)[3] and sirenin (**2**),[2] have attracted a good deal of synthetic attention.[3,4] The prominent step of the synthesis of **1** and/or **2** is the stereospecific elabolation of a 7,7-disubstituted bicyclo[4.1.0]heptane skeleton. Well established methods to prepare the bicyclo[4.1.0]-heptane system are based on intramolecular carbene additions, such as from the carbenes (**3**[3a,c–e,g–k] and **5**, W=CH_3,[3b,f,k] CO_2CH_3,[3l] and CN[3o]) to the cyclo-

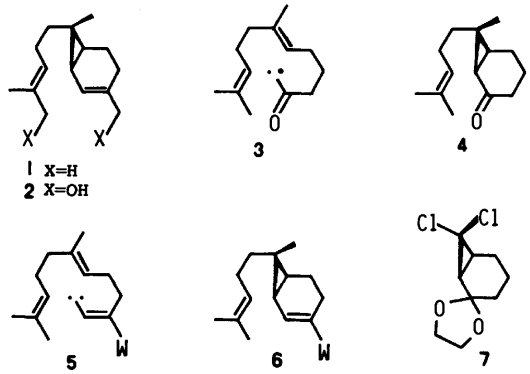

propanes (**4** and **6**), respectively. Another practical one is stereoselective displacement of the *exo*-chlorine of the acetal (**7**) by the cuprate derived from 5-bromo-2-methyl-2-propene followed by stereospecific transmetallation and then methylation to give the ethylene acetal of **4**.[3n]

Our interest in rearrangement approaches to terpene skeletons has prompted us to develop a new route to these [3—6] fused-ring compounds. In this paper, we wish to report the approaches to racemic sesquicarene (**1**) and sirenin (**2**) based on the photochemical transformation of the bridged compounds into the 2-carene derivatives (*vide infra*).

† A portion of this work has been published as a preliminary communication: T. Uyehara, K. Ogata, J. Yamada, and T. Kato, *J. Chem. Soc., Chem. Commun.*, **1983**, 17.

Results and Discussion

Bicyclo[3.2.2]nona-3,6-dien-2-one (**9**), derived from tropone (**8**) and ethylene as the 1,4-addition product,[5] is a photo-labile compound which was transformed into the methyl ester (**11**) by irradiation in methanol using a Hg-lamp through a Pyrex filter[6] (Scheme 1). This transformation is general not only for the bicyclo[3.2.2]nonadienones but also other bicyclo[3.2.x]dienones.[7,8] The process presumably involves the initial [3,3] sigmatropic rearrangement of **9** to the ketene intermediate (**10**) followed by addition of methanol.

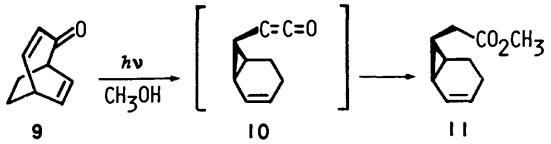

Scheme 1.

Since the conversion proceeds stereospecifically, we made a plan to prepare **4**, an established synthetic intermediate for both sesquicarene (**1**) and sirenin (**2**), starting from **8** and adopting the photochemical process. The synthetic route to **4** is outlined in Scheme 2.

Barbier reaction promoted by ultrasound irradiation[9] was taken to prepare the 1,2-addition product (**12**) selectively. Oxidation of the tertiary allylic alcohol (**12**) by pyridinium chlorochromate (PCC)[10] gave the α,β-unsaturated ketone (**13**) in a good yield.

Now, this two-step transformation is a general method for preparation of the C_4-substituted derivatives of **9** (**20**) from **9** itself *via* the allylic alcohol (**19**) as shown in Table 1. Run c shows that the oxidative transformation proceeded preferably on the C_3 bridge rather than on the side chain.

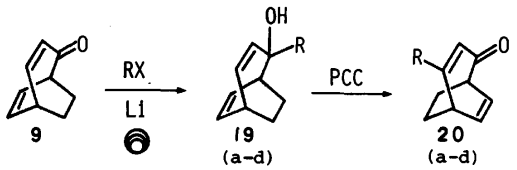

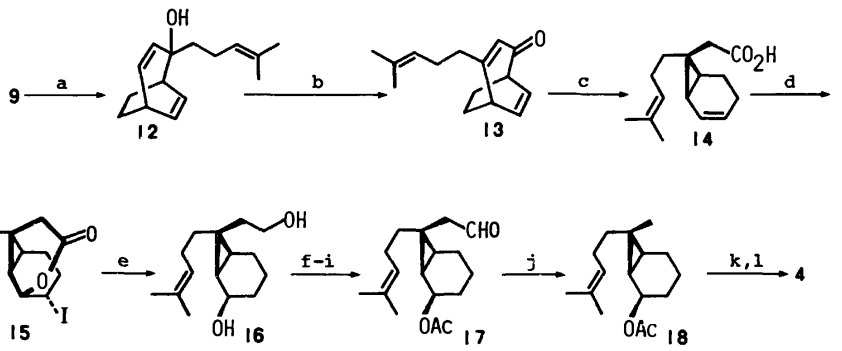

Scheme 2. Synthesis of *endo*-7-methyl-*exo*-7-(4-methyl-3-pentenyl)bicyclo[4.1.0]heptan-2-one (**4**)[a]. a) (a) $(CH_3)_2C{=}CHCH_2CH_2Br$, Li, THF, Ultrasounds, 45 min, 89%. (b) PCC, CH_2Cl_2, 87%. (c) *hv*, H_2O, THF, 88%. (d) I_2, $NaHCO_3$, H_2O–ether. (e) $LiAlH_4$, THF, reflux, 85% (from **14**). (f) TBDMS-Cl, DMAP, $N(CH_2CH_3)_3$, 76%. (g) Ac_2O, Py, 88%. (h) AcOH, THF, H_2O, 85%. (i) CrO_3–2Py, CH_2Cl_2, 83%. (j) $[Rh(PPh_3)_3]Cl$, PhCN, 145 °C, 5 min, 80%. (k) $LiAlH_4$, ether. (l) CrO_3–2Py, CH_2Cl_2, 84% (from **18**).

TABLE 1. ULTRASOUND-PROMOTED BARBIER REACTION FOLLOWED BY PCC OXIDATION OF BICYCLO[3.2.2]-NONA-3,6-DIEN-2-ONE (**9**), AN EFFICIENT TRANSFORMATION INTO THE C_4-SUBSTITUTED DERIVATIVES (**20a—d**)

Run	Halide (RX)	Solvent	Sonication (min)	**19** (Yield/%)	**20** (Yield/%)
a	CH_3I	Ether	30	—	78[a]
b	$(CH_3)_2CHBr$	THF	30	90	88
c	$CH_2{=}CCH_3Br$	THF	25	—	59[a]
d	PhBr	THF	40	—[b]	33[a]

a) Overall yield from **9**. b) A crude mixture, obtained quantitatively, gave a satisfactory ^{1}H-NMR spectrum.

The photochemical transformation of **13** to the acid (**14**), the prominent step of the synthesis, was carried out in aqueous THF using a 100 W-high pressure mercury lamp through a Pyrex filter.

When **14** was treated with iodine in the presence of sodium hydrogencarbonate, the unstable iodo lactone (**15**) was obtained as the sole product. Formation of **15** means not only that the expected stereochemistry of the 7-position is proven but also that the new carbon-oxygen bond is formed at the desired position. However, we could not reduce the C-I bond of **15** to the C-H bond without change of the other functional group. When **15** was treated with tributyltin hydride in cyclohexane, the desired lactone was isolated only in 34% yield. Reduction of **15** with lithium aluminium hydride is thus far a useful way to remove the iodine and to obtain the diol (**16**).

In order to remove one carbon from the *syn* side chain, we wanted to adopt decarbonylation by chlorotris(triphenylphosphine)rhodium.[11] Thus, **16** was converted into the acetoxy aldehyde (**17**). We examined several routes to the aldehyde, and found that the secondary hydroxyl group of **16** is oxidized easily and that the primary one is not oxidized selectively before protection of the other.

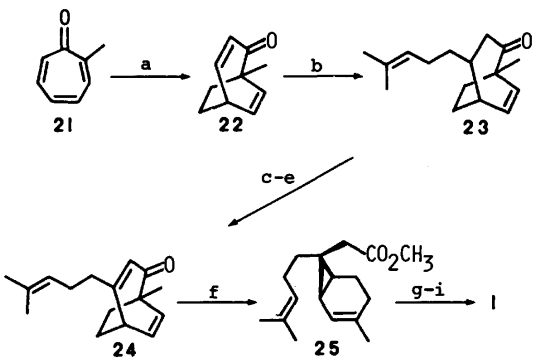

Scheme 3. Synthesis of (±)-sesquicarene (**1**)[a]. a) (a) Ref. 13. (b) $(CH_3)_2C{=}CHCH_2CH_2MgBr$, CuI, THF, 66%. (c) LDA, THF, then TMS-Cl. (d) NBS, THF. (e) LiBr, Li_2CO_3, DMF, 81% (from **23**). (f) *hv*, MeOH, 66%. (g) $LiAlH_4$, ether. (h) CrO_3–2Py, CH_2Cl_2, 80%, (from **25**). (i) $[Rh(PPh_3)_3]Cl$, CH_3CN, 145 °C, 5 min, 43%.

With just one equivalent of Wilkinson's complex, heating of a benzonitrile solution of **17** at 145 °C for 5 min is the most suitable conditions for the decarbonylation to give the acetate (**18**). The yield of **18** decreased when heating time was extended, because of instability of **18** under the reaction conditions.

Reduction of **18** with lithium aluminium hydride followed by oxidation with Collins reagent gave the desired ketone (**4**). Thus, a new sythetic route from tropone (**8**) to (±)-sesquicarene (**1**) and that of (±)-sirenin (**2**) have been established formally.

Next, an analogous sequence has been used to prepare (±)-sesquicarene (**1**) itself (outlined in Scheme 3).

1-Methylbicyclo[3.2.2]nona-3,6-dien-2-one (**22**) is one of the 1,4-addition products of 2-methyltropone (**21**) and ethylene.[12] Regioselective addition of 4-methyl-3-pentenylmagnesium bromide to **21** was carried out in the presence of copper(I) iodide in tetrahydrofuran. The major product of the reaction

was the enone (**23**). The stereochemistry of the homoprenyl side chain is uncertain.

In order to convert **23** into the dienone (**24**), the enol trimethylsilyl ether of **23** was treated with *N*-bromosuccinimide,[13] and the resulting mixture of α-bromo ketones was dehydrobrominated by heating with lithium bromide and lithium carbonate in *N,N*-dimethylformamide.

Photochemical transformation of **24** into the 2-carene derivative (**25**) was carried out by irradiation of a methanolic solution of **24**.

The ester (**25**) was changed into the aldehyde (**26**) by lithium aluminium hydride reduction followed by Collins oxidation. The hydrocarbon (**1**) derived from **26** by heating vigorously with Wilkinson's complex in acetonitrile was identical spectroscopically with natural sesquicarene.

Thus, the photochemical transformation of bicyclo[3.2.2]nona-3,6-dien-2-ones to the [3—6] fused-ring compounds is applicable to the synthesis of sesquiterpene analogues of 2-carene.

Experimental

General. Melting and boiling points are uncorrected. IR spectra (in CCl_4, unless otherwise mentioned) were recorded on a Hitachi Model 215 spectrometer. NMR spectra (in CCl_4, unless otherwise noted) were obtained on Jeol JNM-PMX60, Varian EM-390 90 MHz, and Varian XL-200 NMR spectrometers, using tetramethylsilane as an internal standared. The mass spectral studies were conducted using a Hitachi M-52 spectrometer.

Photochemical reactions were carried out in an immersion well through a Pyrex filter using a Riko 100 W high pressure mercury lamp, under an inert atmosphere. A Shimmyodai 150 W ultrasonic cleaner was used for the Barbier reactions. Tetrahydrofuran (THF) and ether were distilled from benzophenone ketyl under argon, immediately prior to use. Dichloromethane was distilled from P_2O_5 and stored on 4A molecular sieves. Pyridine (from BaO), triethylamine, *N,N*-dimethylformamide (DMF, from BaO), and acetonitrile (from P_2O_5) were purified by distillation. Diisopropylamine was distilled from CaH_2 under argon immidiately prior to use. 4-Methyl-3-pentenyl bromide,[14] pyridinium chlorochromate (PCC),[15] Collins reagent,[16] and Wilkinson's complex[17] were prepared by using literature procedures.

All reactions were monitored by analytical TLC using E. Merck precoated silica gel $60F_{254}$ plates. E. Merck silica gel 60 (70—230 mesh ASTM, twenty to fifty times (w/w)) was used for column chromatography.

*Ultrasound-Promoted Barbier Reactions of Bicyclo[3.2.2]nona-3,6-dien-2-one (**9**). Preparation of 2-(4-Methyl-3-pentenyl)-bicyclo[3.2.2]nona-3,6-dien-2-ol (**12**).* In a 200 ml round bottomed flask with a septum inlet, equipped with a three way stopcock, were placed 1.341 g (9.99 mmol) of **9** and 2.477 g (15.0 mmol) of homoprenyl bromide, and then the system was flushed with argon. After addition of 50 ml of dry THF and 0.41 g (59 mmol) of lithium, the flask was partly submerged in the ice-water filled bath of an ultrasonic cleaner and sonicated for 45 min. The excess lithium and organolithium compounds were destroyed by stirring with methanol and then with water. The bulk of THF was removed and then the remaining pot residue was extracted with three portions of ether. The combined extracts were washed with water and with saturated aqueous NaCl, and then dried over $MgSO_4$. Romoval of the solvent afforded 2.22 g of a pale yellow oil, and which was purified by column chromatography (15:1 hexane, ethyl acetate) to give 1.951 g (89%) of **12** as a colorless oil. **12**: IR 3620 (w), 3475 (m), 1640 (w) and 710 cm^{-1}; NMR δ=6.33 (1H, dd, J=8.3 and 7.5 Hz), 5.95 (1H, dd, J=8.3 and 7.5 Hz), 5.70 (1H, dd, J=10.5 and 7.8 Hz), 5.08 (1H, dd, J=10.5 and 2.4 Hz), 5.00 (1H, tm, J=6.9 Hz), 1.65 (3H, bs), and 1.61 (3H, bs).

*2-Methylbicyclo[3.2.2]nona-3,6-dien-2-ol (**19a**).* To a mixture 2.449 g (18.25 mmol) of **9**, 405 mg (58 mmol) of lithium and 73 ml of dry ether, prepared under argon, was added 3.88 g (27.3 mmol) of methyl iodide at 0 °C. After 30 min of sonication, the reaction mixture was allowed to stand at 0 °C for 15 min. The excess lithium and methyllithium were decomposed by methanol, and the ethereal solution was washed with water and then with saturated brine. After dried over $MgSO_4$, evaporation of the solvent left **19a** as a colorless oil, which was supplied without further purification to PCC oxidation. Distillation of a small portion (45—48 °C/0.2 Torr (1 Torr=133.322 Pa)) furnished an analytical sample. The major of **19a**: NMR δ=6.33 (1H, bt, J=7.5 Hz), 5.95 (1H, bt, J=7.5 Hz), 5.68 (1H, dd, J=10.8 and 8.0 Hz), 5.02 (1H, dd, J=10.8 and 2.4 Hz), and 1.18 (3H, s).

*2-Isopropylbicyclo[3.2.2]nona-3,6-dien-2-one (**19b**). (As General Procedure.)* A mixture of 490 mg (3.65 mmol) of **9**, 90 mg (3.9 eq) of lithium, 680 mg (0.52 ml, 1.5 eq) of isopropyl bromide, and 18 ml (5 ml/1 mmol of **9**) of THF was sonicated for 30 min at 0 °C. After stirring with methanol and then water, the solution was extracted with three portions of ether. The combined extracts were washed with water and saturated brine, and dried over $MgSO_4$. The solvent was removed *in vacuo* and the remaining oil (636 mg) was chromatographed on silica gel (10:1 hexane, ethyl acetate) to yield 583 mg (90%) of **19b**. The major of **19b**: NMR δ=6.32 (1H, bt, J=7.5 Hz), 5.89 (1H, bt, J=7.5 Hz), 5.70 (1H, dd, J=10.8 and 8.0 Hz), 5.17 (1H, dd, J=10.8 and 2.4 Hz), 0.92 (3H, d, J=6.9 Hz), and 0.9 (3H, d, J=6.9 Hz).

*PCC Oxidation of Bicyclo[3.2.2]nona-3,6-dien-2-ols (**12** and **19**). 4-(4-Methyl-3-pentenyl)bicyclo[3.2.2]nona-3,6-dien-2-one (**13**). (As General Procedure.)* To a solution of 3.214 g (14.91 mmol) of PCC in 22 ml of CH_2Cl_2 was added a solution of 1.627 g (7.45 mmol) of **12** in 75 ml of CH_2Cl_2 at room temperature, and the mixture was stirred for 2.5 h. After addition of 30 ml of ether, the solution was decanted from the black solids. The residue was washed in turn with several portions of ether. The combined etherial extracts were washed succesively with 5% aqueous NaOH, 1 M HCl (1 M=1 mol dm^{-3}), saturated aqueous $NaHCO_3$, and saturated aqueous NaCl, and dried over $MgSO_4$. The solvent was removed under reduced pressure, and the residue was chromatographed (15:1 hexane, ethyl acetate) to give 1.407 g (87%) of **13** as a pale yellow oil. **13**: IR 1665 (s) and 1635 (m) cm^{-1}; NMR δ=6.38 (1H, ddd, J=8.1, 7.4, and 1.4 Hz), 6.05 (1H, ddd, J=8.1, 7.4, and 1.4 Hz), 5.40 (1H,

bs), 5.05 (1H, bm), 3.37 (1H, dm, J=7.4 Hz), 3.08 (1H, dm, J=7.4 Hz), 1.68 (3H, s), and 1.62 (3H, s); MS, m/z (rel intensity), 216 (M^+, 14), 188 (80), 142 (52), and 69 (100). The 2,4-DNP derivative of **13**: C, 63.73; H, 6.10; N, 14.05%. Calcd for $C_{21}H_{24}N_4O_4$: C, 63.62; H, 6.10; N, 14.13%.

*4-Methylbicyclo[3.2.2]nona-3,6-dien-2-one (**20a**)*: Bp 82—84 °C/0.9 Torr; IR 1665 (s) and 1635 (m) cm^{-1}; NMR δ=6.37 (1H, ddd, J=8.4, 7.2, and 1.5 Hz), 6.02 (1H, ddd, J=9.0, 7.2, and 1.5 Hz), 5.42 (1H, m), 3.33 (1H, b, $W_{1/2}$=14.3 Hz), 3.07 (1H, b, $W_{1/2}$=14.3 Hz), and 2.01 (3H, d, J=1.5 Hz); MS, m/z (rel intensity) 148 (M^+, 100) and 133 (86). Found: C, 80.78; H, 8.34%. Calcd for $C_{10}H_{12}O$: C, 81.04; H, 8.16%.

*4-Isopropylbicyclo[3.2.2]nona-3,6-dien-2-one (**20b**)*: Bp 57—59 °C/0.3 Torr; IR 1660 (s), and 1630 (m) cm^{-1}; NMR δ=6.32 (1H, ddd, J=8.7, 7.1, and 1.4 Hz), 6.04 (1H, ddd, J=8.7, 7.1, and 1.4 Hz), 5.36 (1H, m), 3.33 (1H, dm, J=7.1 Hz), 3.16 (1H, dm, J=7.1 Hz), 2.42 (1H, septet, J=6.7 Hz), and 1.12 (6H, d, J=6.7 Hz); MS m/z (rel intensity) 176 (M^+, 51) and 133 (100). Found: C, 82.05; H, 9.32%. Calcd for $C_{12}H_{16}O$: C, 81.77; H, 9.15%. The 2,4-DNP derivative of **20b**: mp 146.7—148.9 °C. Found: C, 60.73; H, 5.77; N, 15.77%. Calcd for $C_{18}H_{20}N_4O_4$: C, 60.67; H, 5.66; N, 15.72%.

*4-(2-Methyl-2-propenyl)bicyclo[3.2.2]nona-3,6-dien-2-one (**20c**)*: Bp 58—60 °C/0.1 Torr; IR 1660 (s) and 1635 (m) cm^{-1}; NMR δ=6.38 (1H, ddd, J=8.9, 7.1, and 1.2 Hz), 6.10 (1H, ddd, J=8.9, 7.4, and 1.2 Hz), 5.63 (1H, m), 5.37 (1H, bs), 5.16 (1H, bs), 3.63 (1H, dm, J=7.4 Hz), 3.38 (1H, dm, J=7.4 Hz), and 2.1—1.7 (7H, m); MS, m/z (rel intensity) 174 (M^+, 100) and 130 (46). The 2,4-DNP derivative of **20c**: mp 159.2—160.8 °C. Found: C, 61.21; H, 5.33; N, 15.81%. Calcd for $C_{18}H_{18}N_4O_4$: C, 61.01; H, 5.12; N, 15.81%.

*4-Phenylbicyclo[3.2.2]nona-3,6-dien-2-one (**20d**)*: Mp 73.8—74.6 °C; IR 1660 (s) and 1630 (m) cm^{-1}; NMR δ=7.5—7.1 (5H, m), 6.50 (1H, ddd, J=8.9, 7.1, and 1.2 Hz), 5.81 (1H, dd, J=2.3 and 1.5 Hz), 3.73 (1H, dm, J=7.1 Hz), 3.46 (1H, dm, J=7.1 Hz), and 2.4—1.7 (4H, m); MS, m/z (rel intenaity), 210 (M^+, 100), 192 (51), 167 (61), and 105 (62). Found: C, 85.67; H, 6.71%. Calcd for $C_{15}H_{14}O$: C, 85.68; H, 6.71%.

*Photochemical Transformation of **13** into* endo-*7-[exo-7-(4-Methyl-3-pentenyl)bicyclo[4.1.0]hept-2-ene]acetic Acid (**14**).* To a solution of 1.002 g (4.63 mmol) of **13** in 350 ml of THF was added 35 ml of water, and the mixture was irradiated for 4 h. After removal of the bulk of the solvents, to the residue was added 10% aqueous NaOH. The basic solution was extracted once with ether, and acidified with 6 M HCl. After addition of saturated aqueous NaCl, the aqueous phase was extracted with two portions of ether. The extracts were combined, and dried over $MgSO_4$. Removal of the solvent gave 998 mg of a yellow oil, which was purified by column chromatography (3:1 hexane, ethyl acetate) to yield 955 mg (88%) of **14**: IR 1705 (s) cm^{-1}; NMR δ=9.0 (1H, b), 5.87 (1H, dm, J=10.5 Hz), 5.66 (1H, dm, J=10.5 Hz), 5.07 (1H, tm, J=6.9 Hz), 2.42 (1H, d, J=16.5 Hz), 2.43 (1H, d, J=16.5 Hz), 1.67 (3H, bs), and 1.62 (3H, bs). The methyl ester of **14**: bp 70 °C/0.15 Torr. Found: C, 77.10; H, 9.62%. Calcd for $C_{16}H_{24}O_2$: C, 77.38; H, 9.74%.

*Iodolactonization of **14**. Preparation of 7-Iodo-2-(4-methyl-3-pentenyl)-5-oxabicyclo[4.4.0.0^{2,10}]decan-4-one (**15**).* To a solution of 681.6 mg (2.91 mmol) of **14** in 19 ml of saturated aqueous $NaHCO_3$ was added a solution of 740 mg (2.92 mmol) of iodine in 25 ml of ether over a period of 20 min at room temperature in the dark. After 1 h of stirring, the mixture was diluted with water and ether, and extracted with several portions of ether. The ethereal extracts were combined, washed with 5% aqueous $Na_2S_2O_3$ and with saturated brine, and then dried over $MgSO_4$. Evaporation of the solvent without heating from outside gave 1.156 g of a pale yellow oil, which was supplied directly to the $LiAlH_4$ reduction. Flush column chromatography of a small portion furnished an analytical sample of **15**: NMR δ=5.22 (H_8, dd, J=8.7 and 3.5 Hz), 5.00 (1H, tm, J=6.9 Hz), 4.35 (H_7, q, J=3.5 Hz), 2.60 (H_3, d, J=19.1 Hz), 2.28 (H_3, d, J=19.1 Hz), 1.67 (3H, bs) and 1.61 (3H, bs).

*Reduction of Iodo lactone **15**. Preparation of* endo-*7-(2-Hydroxyethyl)*-exo-*7-(4-methyl-3-pentenyl)bicyclo[4.1.0]heptan-2-ol (**16**).* To a mixture of 280 mg (7.38 mmol) of $LiAlH_4$ and 5 ml of dry THF was added a solution of 1.156 g of **15**, obtained from 681.6 mg (2.91 mmol) of **14**, in 30 ml of dry THF at 0 °C. The reaction mixture was heated under reflux for 2 h. After cooling to 0 °C, the resulting suspension was treated by successive dropwise addition of a few ml of ethyl acetate, 0.3 ml of water, 0.3 ml of 15% aqueous NaOH, and 0.9 ml of water, and then allowed to warm to room temperature with stirring. The THF solution was filtered, and concentration of the filtrate *in vacuo* afforded 622.6 mg of a colorless oil. Purification of the product by column chromatography (1:1 hexane, ethyl acetate) gave 587.9 mg (85% from **14**) of **16**: IR 3250 (m), 1070 (m), and 1040 (m) cm^{-1}; NMR δ=5.49 (2H, bs), 5.01 (1H, tm, J=6.9 Hz), 4.06 (1H, b, $W_{1/2}$=21 Hz), 3.75 (2H, m), 1.65 (3H, s), and 1.58 (3H, s); MS, m/z (rel intensity) 230 (M^+, 2), 139 (100), and 138 (85). The diacetate of **16**: C, 70.75; H, 9.46%. Calcd for $C_{19}H_{30}O_4$: C, 70.77; H, 9.38%.

*Transformation of Diol **16** into* endo-*7-(2-Oxoethyl)*-exo-*7-(4-methyl-3-pentenyl)bicyclo[4.1.0]heptan*-trans-*2-yl Acetate (**17**).* In order to protect the primary hydroxyl group selectively, to a solution of 304.7 mg (1.28 mmol) of **16**, 145.1 mg (0.2 ml, 1.1 eq) of triethylamine, and a small amount of 4-dimethylaminopyridine in 10 ml of dry CH_2Cl_2 was added a solution of 242.5 mg (1.2 eqive) of *t*-butyldimethylsilyl chloride in 10 ml of dry CH_2Cl_2 under argon. After standing for 24 h at room temperature, the sulution was washed with saturated aqueous NH_4Cl, and dried over $MgSO_4$. Removal of the solvent gave 456.7 mg of the oily products, which were purified by chromatography (15:1 hexane, ethyl acetate) to give 341.4 mg (76%) of the monosilyl ether of **16**: NMR δ=4.98 (1H, tm, J=6.9 Hz), 4.22 (1H, m), 3.70 (2H, m), 3.19 (1H, m), 1.63 (3H, bs), 1.57 (3H, bs), 0.93 (9H, s), and 0.10 (6H, s).

To protect the secondary hydroxyl group, 1 ml of acetic anhydride was added to 314.4 mg (0.97 mmol) of the monosilyl ether in 3 ml of dry pyridine. After standing overnight at room temperature, evaporation of the solvent *in vacuo* gave 375.3 mg of the residue, which was chromatographed (15:1 hexane, ethyl acetate) to afford 333.1 mg (88%) of the acetate: IR 1735 (s) and 1020 (m) cm^{-1}. Found: C, 69.96; H, 10.77%. Calcd for $C_{23}H_{42}O_3Si$: C, 70.00; H, 10.73%.

In order to remove the silyl group, 332.2 mg (0.84 mmol) of the acetate was treated with a mixture of 1.7 ml of THF, 1.7 ml of water, and 5.1 ml of acetic acid[18] for 19 h at room temperature. The mixture was diluted with ether, and washed successively with water (four times), saturated aqueous $NaHCO_3$, and saturated brine, and then dried over $MgSO_4$. The solvent was removed *in vacuo*, and the remaining was purified by chromatography (2:1 hexane, ethyl acetate). Thus obtained was 198.5 mg (85%) of the hydroxy

hydride (50 mg, 1.32 mmol) in ether (20 ml) at 0 °C. The acetate: IR 1735 (s) and 1015 (s) cm^{-1}, NMR δ=5.25 (1H, qm, J=7.5 Hz), 5.01 (1H, tm, J=6.9 Hz), 3.67 (2H, m), 2.01 (3H, s), 1.66 (3H, bs), and 1.61 (3H, bs).

To a solution of 1.54 g 5.96 mmol) of Collins reagent in 24 ml of dry CH_2Cl_2 was added a solution of 278.5 mg (0.99 mmol) of the hydroxy acetate in 7 ml of CH_2Cl_2. After 7 min stirring at room temperature, the solution was decanted, and the black residue was washed with several portions of ether. The organic layers were combined, and washed successively with 5% aqueous NaOH, 5% HCl, saturated aqueous $NaHCO_3$, and saturated brine, and then dried over $MgSO_4$. Evaporation of the solvent gave 265.6 mg of an oil, which was purified by column chromatography (10:1 hexane, ethyl acetate) to give 229.7 mg (83%) of the unstable aldehyde, **17**: IR 2720 (w), 1740 (s), 1730 (s), and 1245 (s) cm^{-1}; NMR δ=9.72 (1H, t, J=2.3 Hz), 5.25 (H_2, m, $W_{1/2}$=18.8 Hz), 4.97 (1H, tm, J=6.9 Hz), 2.47 (2H, d, J=2.3 Hz), 1.95 (3H, s), 1.64 (3H, bs), and 1.57 (3H, s); MS, m/z (rel intensity) 278 (M^+, 1), 137 (79), 136 (100), 121 (52), and 82 (74).

Decarbonylation of **17**. *Preparation of* endo-*7-Methyl*-exo-*7-(4-methyl-3-pentenyl)bicyclo[4.1.0]heptan-2-yl Acetate* (**18**). A flask containing of a mixture of 153.8 mg (0.55 mmol) of **17**, 509.7 mg (0.55 mmol) of Wilkinson's complex and 2 ml of benzonitrile, prepared under argon, was immersed in a preheated oil bath at 145 °C for 5 min with stirring. The bulk of benzonitrile was removed by Kugelrohr distillation (100 °C/3 Torr) and the residure was stirred with ethanol, and then filtered. Concentration of the filtrate gave 362.4 mg of an oil, chromatography (15:1 hexane, ethyl acetate) of which gave 110.5 mg (80%) of **18**: bp 70 °C/1.5 Torr; IR 1740 (s) and 1245 (s) cm^{-1}; NMR δ=5.21 (H_2, m), 5.02 (1H, tm, J=6.9 Hz), 1.99 (3H, s), 1.68 (3H, s), 1.61 (3H, s), and 1.14 (3H, s); MS, m/z (rel intensity) 250 (M^+, 2), 190 (52), 147 (78), 121 (100), and 82 (75). Found: C, 76.55; H, 10.49%. Calcd for $H_{16}H_{26}O_2$: C, 76.75; H, 10.47%.

Preparation of endo-*7-Methyl*-exo-*7-(4-methyl-3-pentenyl)bicyclo[4.1.0]heptan-2-one* (**4**). To a suspension of 20 mg (0.527 mmol) of $LiAlH_4$ in 2 ml of dry ether was added a solution of 79.3 mg (0.317 mmol) of **18** in 10 ml of ether at 0 °C. After 20 min stirring, to the reaction mixture were added successively one drop of water, one drop of 15% aqueous NaOH, and three drops of water. After stirring untill a granular precipitate was formed, $MgSO_4$ was added to the mixture and filtered. Concentration of the filtrate gave 66.4 mg of the alcohol. An analytical sample was purified by chromatography (10:1 hexane, ethyl acetate). Treatment of the crude alcohol (66.4 mg) with 500 mg of Collins reagent in 10 ml of dry CH_2Cl_2 at room temperature for 5 min, followed by work-up as described above gave 61.3 mg of the crude product. Chromatography on silica gel (15:1 hexane, ethyl acetate) gave 55.1 mg (84%) of pure **4**: IR 1685 (s) cm^{-1}; NMR δ=5.00 (1H, tm, 6.9 Hz), 1.66 (3H, bs), 1.60 (3H, bs), and 1.10 (3H, s). Found: C, 81.31; H, 10.84%. Calcd for $C_{14}H_{22}O$: C, 81.50; H, 10.75%.

1,4-Addition of 4-Methyl-3-pentenylmagnesium Bromide to 1-Methylbicyclo[3.2.2]nona-3,6-dien-2-one (**22**). 4-Methyl-3-pentenylmagnesium bromide was prepared from 1.07 g (6.55 mmol) of homoprenyl bromide and 140 mg (6 mmol) of magnesium in 17 ml of dry THF. The solution of the Grignard reagent was added to a mixture of 507.8 mg (3.28 mmol) of **22** and 140 mg (0.66 mmol) of copper(I) iodide in 2 ml of dry THF at −24 °C *via* a double ended needle. The mixture was allowed to warm to room temperature with stirring, and cooled to 0 °C, and then treated with 6 ml of 10% H_2SO_4. After filtration through a Celite layer, the filtrate was extracted with several portions of ether. The combined extracts were washed successively with water, saturated aqueous $NaHCO_3$, and saturated brine, and the dried over $MgSO_4$. The solvent was removed *in vacuo*, and the residue (861 mg) was purified by chromatography (15:1 hexane, ethyl acetate) to give 505.3 mg (66%) of 1-methyl-4-(4-methyl-3-pentenyl)-bicyclo[3.2.2]non-6-en-2-one (**23**) as a colorless oil. **23**: IR 1700 (s) cm^{-1}; NMR δ=6.11 (1H, dd, J=9.3 and 7.2 Hz), 5.80 (1H, d, J=9.3 Hz), 5.00 (1H, tm, J=6.9 Hz), 1.67 (3H, bs), 1.60 (3H, bs), and 1.11 (3H, s); MS, m/z (rel intensity) 232 (M^+, 100) and 161 (55). The 2,4-DNP derivative of **23**: mp 108—109 °C (dec). Found: C, 63.89; H, 6.91; N, 13.71%. Calcd for $C_{22}H_{28}N_4O_4$: C, 64.06; H, 6.84; N, 13.51%.

Preparation of 1-Methyl-4-(4-methyl-3-pentenyl)-bicyclo[3.2.2]nona-3,6-dien-2-one (**24**). To a solution of 252.7 mg (0.35 ml, 2.5 mmol) of diisopropylamine in 8 ml of dry THF, prepared under argon, was added 1.7 ml (2.55 mmol) of 1.5 M hexane solution of *n*-BuLi at −72 °C. After 20 min of stirring, to the LDA solution was added a solution of 505.3 mg (2.18 mmol) of **23** *via* a double ended needle. The solution was kept at −72 °C for 15 min, and then at 0 °C for 30 min. To the solution was added 513.6 mg (0.6 ml, 4.73 mmol) of chlorotrimethylsilane *via* a syringe at 0 °C. After stirring at room temperature for 30 min, the solvent and the volatile components of the mixture was removed by a rotary evaporator, and the residue was diluted with 8 ml of dry THF. *N*-Bromosuccinimide (390 mg, 2.2 mmol) was added to a solution at 0 °C, and the mixture was stirred for 1 h, and then diluted with ether. The ethereal solution was washed with a 1:1 mixture of saturated aqueous $NaHCO_3$ and saturated brine, and with saturated brine.

After dried over $MgSO_4$, evaporation of the solvent gave 868.7 mg of a yellow oil, which was dissolved in 6 ml of dry DMF. To the solution were added 570 mg (6.6 mmol) of LiBr and 810 mg (11.0 mmol) of Li_2CO_3, and the mixture was heated at 100 °C for 4 h under an argon atmosphere. Dilution with water followed by extraction with three portions of ether and the usual work-up gave 668.9 mg of a brown oil. Purification by chromatography (15:1 hexane, ethyl acetate) gave 405.7 mg (81%) of **24**: IR 1660 (s) and 1630 (s) cm^{-1}; NMR δ=6.34 (1H, dd, J=9.3 and 7.5 Hz), 5.62 (1H, d, J=9.3 Hz), 5.42 (1H, bs), 5.03 (1H, bm), 3.07 (1H, bm), 1.69 (3H, bs), and 1.20 (3H, s); MS, m/z (rel intensity) 230 (M^+, 45), 202 (48), 147 (90), and 69 (100). The 2,4-DNP derivative of **24**: mp 117—118 °C. Found: C, 64.29; H, 6.48; N, 13.88%. Calcd for $C_{22}H_{26}N_6O_4$: C, 64.38; H, 6.38; N, 13.65%.

Photochemical Transformation of **24** *into the 2-Carene Derivative* **25**. After 3 h irradiation of a solution of 460.2 mg (2.0 mmol) of **24** in 300 ml of methanol, evaporation of the solvent gave 586.2 mg of an orange oil. Column chromatography of the crude oil (20:1 hexane, ethyl acetate) gave 346.7 mg (66%) of pure **25**: IR 1735 (s) cm^{-1}; NMR δ=5.49 (1H, bs), 5.01 (1H, J=6.9 Hz), 3.59 (3H, s), 2.26 (1H, d, J=15.9 Hz), 2.07 (1H, d, J=15.9 Hz), 1.65 (6H, bs), and 1.59 (3H, bs); MS, m/z (rel intensity) 262 (M^+, 53), 177 (100), 145 (73), and 119 (100). Found: C, 77.52; H, 10.23%. Calcd for $C_{17}H_{26}O_2$: C, 77.82; 9.99%.

Conversion of **25** *into (±)-Sesquicarene* (**1**). Ester **25**

(193.3 mg, 0.74 mmol) was reduced by lithium aluminium usual work-up as described previously gave the corresponging alcohol (172.8 mg). Oxidation of the alcohol by Collins reagent (1.15 g, 4.45 mmol) in CH_2Cl_2 (23 ml) at room temperature for 10 min, followed by the usual work-up and purification by chromatography (10: 1 hexane, ethyl acetate), gave the aldehyde (**26**) (136.7 mg, 80%). **26**: IR 2710(m) and 1725 (s) cm^{-1}; NMR δ=9.58 (1H, t, J=2.3 Hz), 5.53 (1H, bs), 5.00 (1H, tm, J=6.9 Hz), 2.21 (1H, dd, J=16.5 and 2.3 Hz), 2.17 (1H, dd, J=16.5 and 2.3 Hz), 1.65 (6H, bs), and 1.59 (3H, bs); MS, m/z (rel intensity) 232 (M^+, 66), 147 (100), 119 (52), and 93 (45). The 2,4-DNP derivative of **26**: mp 140—142 °C. Found: C, 64.13; H, 6.95; N, 13.31%. Calcd for $C_{22}H_{28}N_4O_4$: C, 64.06; H, 6.84; N, 13.58%.

A flask containing a mixture of 74.5 mg (0.32 mmol) of the aldehyde, 296.3 mg (0.32 mmol) of Wilkinson's complex, and 2 ml of acetonitrile was immersed in a preheated (145 °C) oil bath for 5 min. After removal of the solvent by a rotary evaporator, to the residue was added pentane and the mixture was filtered. Concentration of the filtrate followed by chromatography (pentane) gave 28.2 mg (43%) of pure *(±)-sesquicarene* (**1**): IR (neat) 2980 (s), 2925 (s), 2860 (s), 2730 (w), 1670 (w), 1650 (w), 1450 (m), and 1380 (m) cm^{-1}; NMR ($CDCl_3$) δ=5.56 (1H, b, $W_{1/2}$=9.0 Hz), 5.12 (1H, triplets of septet, J=7.0 and 1.4 Hz), 2.14—1.48 (6H, m), 1.68 (6H, bs), 1.62 (3H, bs), 1.39—1.05 (2H, m), 1.01—0.76 (2H, m), and 0.83 (3H, s); MS, m/z (rel intensity) 204 (M^+, 100), 161 (45), 135 (42), 134 (55), 133 (40), 122 (28) and 105 (38). Found: m/z 204.1855. Calcd for $C_{15}H_{24}$: 204.3546.

We are grateful to Dr. Yoko Naya, Suntory Institute for Bioorganic Research, for kindly providing the spectra of sesquicarene. This work was partially supported by Foundation for the Promotion of Research on Medicinal Resources.

References

1) Y. Ohta and Y. Hirose, *Tetrahedron Lett.*, **1968**, 1251.

2) L. Machlis, W. H. Nutting, and H. Rapoport, *J. Amer. Chem. Soc.*, **90**, 1674 (1968); **90**, 6434 (1968).

3) a) E. J. Corey and K. Achiwa, *Tetrahedron Lett.*, **1969**, 1837; b) *idem, ibid.*, **1969**, 3257; c) K. Mori and M. Matsui, *ibid.*, **1969**, 2729; d) *idem, ibid.*, **1969**, 4435; e) R. M. Coates and R. M. Freidinger, *Chem. Commun.*, **1969**, 871; f) T. Nakatani and A. Sato, *Agr. Biol. Chem.*, **33**, 1805 (1969); g) E. J. Corey, K. Achiwa, and K. A. Katzenellenbogen, *J. Am. Chem. Soc.*, **91**, 4318 (1969); h) J. J. Plattner, U. T. Bhalerao, and H. Rapoport, *ibid.*, **91**, 4933 (1969); i) P. A. Grieco, *ibid.*, **91**, 5660 (1969); j) K. Mori and M. Matsui, *Tetrahedron*, **26**, 2801 (1970); k) R. H. Coates and R. M. Freidinger, *ibid.*, **26**, 3487 (1970); l) E. J. Corey and K. Achiwa, *Tetrahedron Lett.*, **1970**, 2245; m) C. F. Garbers, J. A. Steenkamp, and H. E. Visagie, *ibid.*, **1975**, 3753; n) K. Kitatani, T. Hiyama, and H. Nozaki, *J. Am. Chem. Soc.*, **98**, 2362 (1976); o) T. Mandai, K. Hara, M. Kawada, and J. Nokami, *Tetrahedron Lett.*, **24**, 1517 (1983).

4) For reviews on synthesis of **1** and **2**: C. H. Heathcock, "The Total Synthesis of Natural Products," ed by J. ApSimon, John Wiley and Sons, New York (1973), Vol. 2, pp. 428—446; (1983) Vol. 5, pp. 313—318.

5) T. Uyehara and Y. Kitahara, *Chem. Ind. (London)*, **1971**, 354.

6) T. Uyehara and Y. Kitahara, *Synth. Commun.*, **2**, 405 (1972).

7) W. G. Dauben, K. Koch, S. L. Smith, and O. L. Chapmam, *J. Am. Chem. Soc.*, **85**, 2616 (1963); O. L. Chapman and J. D. Lassila, *ibid.*, **90**, 2449 (1968); O. L. Chapmam, M. Kane, J. D. Lassila, R. L. Loeschen, and H. E. Wright, *ibid.*, **91**, 6856 (1969); A. S. Kende, Z. Goldschmidt, and P. T. Izzo, *ibid.*, **91**, 6859 (1969).

8) For a review: D. I. Schuster, "Rearrangements in Ground and Excited States," ed by P. de Mayo, Academic Press, New York (1980), Vol. 3, Chap. 17, pp. 226—229.

9) J. L. Luche and J. C. Damiano, *J. Am. Chem. Soc.*, **102**, 7926 (1980).

10) W. G. Dauben and D. M. Michno, *J. Org. Chem.*, **42**, 682 (1977).

11) K. Ohno and J. Tsuji, *J. Am. Chem. Soc.*, **90**, 99 (1968).

12) T. Uyehara and Y. Kitahara, *Bull. Chem. Soc. Jpn.*, **52**, 3355 (1979).

13) L. Blanco., P. Amice, and J. M. Conia, *Synthesis*, **1976**, 194.

14) F. Medina and A. Manjarrez, *Tetrahedron*, **20**, 1807 (1964).

15) E. J. Corey and J. W. Suggs, *Tetrahedron Lett.*, **1975**, 2647.

16) J. C. Collins and W. W. Hess, *Org. Synth.*, **52**, 5 (1972).

17) J. A. Osborn and G. Wilkinson, *Inorganic Synth.*, **10**, 67 (1967).

18) E. J. Corey and A. Venkateswarlu, *J. Am. Chem. Soc.*, **84**, 6190 (1972).

 © 1985 The Chemical Society of Japan Bull. Chem. Soc. Jpn., 58, 217—222 (1985)

Reaction of Olefins with Malonamide in the Presence of Manganese(III) Acetate. Formation of α,β-Unsaturated γ-Lactones and γ-Lactams

Hiroshi NISHINO

Department of Chemistry, Faculty of Science, Kumamoto University, Kurokami, Kumamoto 860

(Received June 22, 1984)

The reaction of olefins with malonamide in the presence of manganese(III) acetate gave 2-buten-4-olides and/or 1*H*-pyrrol-2(5*H*)-ones in one-step, short reaction time, and moderate yields. The product distribution can be accounted for in terms of the stabilization of the intermediate carbocation in the oxidation process. The synthetic application and limitation, and the oxidation mechanism for the formations of α,β-unsaturated γ-lactones and γ-lactams are discussed.

It is known that ketones have been oxidized with manganese(III) acetate, $Mn(OAc)_3$, in acetic acid to form α-keto radicals, $\cdot CH_2COR$.[1,2] If the reaction is carried out in the presence of olefins, the α-keto radicals add to the olefins to give radical adducts which are converted to saturated or unsaturated ketones, or γ-keto esters either by gaining or losing hydrogen, or by further oxidation and taking up an acetate ion.[3] On the other hand, oxidation of readily enolizable ketones, such as β-diketones, with $Mn(OAc)_3$ gives the corresponding α,α'-diketo radicals, RCO-CH-COR.[4] Heiba and Dessau reported that acetylacetone was oxidized with $Mn(OAc)_3$ in the presence of olefins to form dihydrofurans in high yields.[5] In contrast, it was reported that the reaction of olefins and malonic acid in a 2:1 molar ratio (equivalent) in the presence of $Mn(OAc)_3$ yielded spirodi-γ-lactones in high yields.[6]

Recently, the author attempted the intramolecular oxidative cyclization of aromatic secondary amines with $Mn(OAc)_3$.[7] However, *N*-cyclized products were not obtained. These results led me to investigate the reaction of olefins with malonamide in the presence of $Mn(OAc)_3$. As the result, it was found that 2-buten-4-olides and/or 1*H*-pyrrol-2(5*H*)-ones were produced, but the desired spirodi-γ-lactams were not formed. In this paper, I will discuss the synthetic application and limitation, and the oxidation mechanism for the formations of α,β-unsatutrated γ-lactones and γ-lactams.

Results and Discussion

When malonamide was oxidized with $Mn(OAc)_3$ in the presence of 1,1-diphenylethene (**1a**), the reaction was finished within 1 min to give **2a**, **4a**, and benzophenone (**5a**). The major product **2a** showed a characteristic vinylic proton (δ=8.71) of 2-buten-4-olides in the lower field[8] and two broad singlets assigned to an amino group of which one was hydrogen-bonded according to the ^{1}H-NMR spectrum. Its IR spectrum revealed two carbonyl absorption bands and one olefinic absorption band. Therefore, the structure of **2a** was considered to be 2-carbamoyl-4,4-diphenyl-2-buten-4-olide, which was compatible with its mass spectrum. The minor product **4a** was determined to be 3,3,8,8-tetraphenyl-2,7-dioxaspiro[4.4]nonane-1,

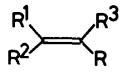

1a–j : R=H
8g.h.j : R=OAc
11 : $R^1=R^2=R^3$=4-MeOPh, R=CHO

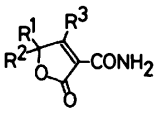

2a-h

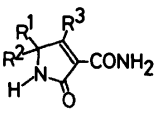

3f-j
3f': R^3=OH

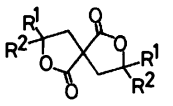

4a.b.k

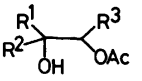

6a.c.g-i

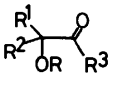

7g.h : R=H
7j : R=Ac

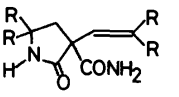

10 : R = 4-MeOPh

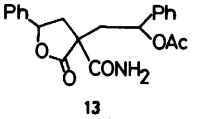

13

a: $R^1=R^2$=Ph, R^3=H
b: R^1=Me, R^2=Ph, R^3=H
c: $R^1=R^2=R^3$=Ph
d: R^1, R^2= , R^3=COOH
e: R^1, R^2= , R^3=H
f: $R^1=R^2$=4-MeOPh, R^3=H
g: $R^1=R^2$=4-MeOPh, R^3=Ph
h: $R^1=R^2=R^3$=4-MeOPh
i: R^1, R^2= , R^3=Ph
j: R^1, R^2= , R^3=Ph
k: R^1=Ph, $R^2=R^3$=H

6-dione of which ^{1}H-NMR, IR spectra, and the melting point were identical with those of an authentic sample.[6] The same reaction of 2-phenylpropene (**1b**), 1,1,2-triphenylethene (**1c**), fluorenylideneacetic acid (**1d**), and methylenecyclohexane (**1e**) gave the corresponding 2-buten-4-olides in moderate yields (Table 1).

On the other hand, when 1,1-bis(4-methoxyphenyl)-ethene (**1f**) was oxidized under the same reaction conditions, α,β-unsaturated γ-lactams (**3f** and **3f'**) were produced rather than the corresponding 2-buten-4-olide (**2f**). The structure of **3f** was determined to be 3-carbamoyl-5,5-bis(4-methoxyphenyl)-1*H*-pyrrol-2(5*H*)-one on the basis of the ^{1}H-NMR, ^{13}C-NMR, IR, and mass spectra. The ^{1}H-NMR spectrum of **3f'** was similar to that of **3f** except for the disappearance of a doublet assignable to a H-4 proton and the appearance of a broad singlet (δ=5.38) due to a hydroxyl group. Accordingly, the compound **3f'** was confirmed to be 3-carbamoyl-4-hydroxy-5,5-bis(4-methoxyphenyl)-1*H*-pyrrol-2(5*H*)-one. 3-Carbamoyl-3-[2,2-bis(4-methoxyphenyl)ethenyl]-5,5-bis(4-methoxyphenyl)-2-pyrrolidone (**10**) was also obtained.

The formation of the α,β-unsaturated γ-lactams deserves comment. It seems that the intermediate carbocation (**II**) tends to cyclize with a nitrogen atom of the carbamoyl group when it is stabilized by the resonance effect of the methoxyl group (Scheme 1). Then, the reaction of 1,1-bis(4-methoxyphenyl)-2-phenylethene (**1g**), 1,1,2-tris(4-methoxyphenyl)ethene (**1h**), 9-benzylidene-9*H*-xanthene (**1i**), and 9-benzylidene-9,10-dihydroanthracene (**1j**) with malonamide in the presence of $Mn(OAc)_3$ was tried. The reaction of **1g** or **1h** under the same reaction conditions certainly gave the corresponding α,β-unsaturated γ-lactam (**3g** or **3h**). However, the olefins (**1g** and **1h**) were also oxidized directly by $Mn(OAc)_3$ without the participation of malonamide to yield products (**5g**, **6g** and **6h**, **7g** and **7h**, **8g** and **8h**, and **9g** and **9h**). The same oxidation of **1i** and **1j** afforded the corresponding 1*H*-pyrrol-2-(5*H*)-ones (**3i** and **3j**) in good yields, as expected.

TABLE 1. REACTION OF OLEFINS WITH MALONAMIDE IN THE PRESENCE OF MANGANESE(III) ACETATE

	Molar ratio[a]	Time / min	Recovery / %	Product (yield/%)[b]								
1a	1 : 4 : 3	1	13	**2a** (56)		**4a** (5)	**5a** (4)					
1b	1 : 6 : 4	1		**2b** (38)		**4b** (3)	**5b** (4)					
1c	1 : 8 : 6	3	2	**2c** (69)				**6c** (8)				
1d	1 : 4 : 4	0.1		**2d** (48)			**5d** (5)					
1e	1 : 6 : 6	1		**2e** (26)								
1f	1 : 6 : 4	1	1	**2f** (9)	**3f** (18)	**3f'** (20)						**10** (11)
1g	1 : 10 : 4	2		**2g** (14)	**3g** (17)		**5g** (9)	**6g** (27)	**7g** (18)	**8g** (19)	**9g** (20)	
1h	1 : 10 : 4	2		**2h** (4)	**3h** (5)		**5g** (20)	**6h** (18)	**7h** (16)	**8h** (8)	**9h** (11)	**11** (3)
1i	1 : 10 : 4	1			**3i** (59)		**5i** (29)	**6i** (17)				**12** (20)
1j	1 : 10 : 4	0.2			**3j** (90)				**7j** (2)	**8j** (5)		

a) Substrate : malonamide : manganese(III) acetate. b) The yields were based on the amount of the substrate used.

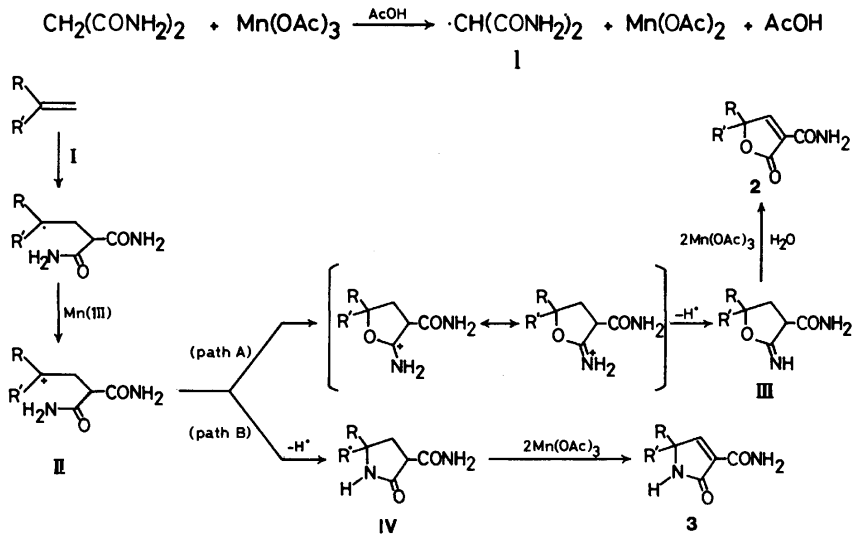

Scheme 1.

It is suggested that this reaction consists of two competing mechanisms. One is the direct oxidation of the substrate with $Mn(OAc)_3$ without the participation of malonamide (product **5**, **6**, **7**, **8**, and **9**). This mechanism has been explained as the electron-transfer mechanism represented by the aromatic acetoxylation[9] or the oxidation of α-glycols[10] with $Mn(OAc)_3$ alone. The other is a radical mechanism involving the malonamide radical (**I**) (product **2**, **3**, **4**, **10**, and **13**). The mechanism for the formation of the α,β-unsaturated γ-lactones and γ-lactams as depicted in Scheme 1 is deduced from the reaction of olefins with acetylacetone in the presence of $Mn(OAc)_3$.[5] At first, malonamide is readily oxidized with $Mn(OAc)_3$ to give the corresponding radical (**I**) which attacks olefins to form a benzyl radical. Then, the benzyl radical is subsequently oxidized to generate the intermediate carbocation (**II**). If cyclization occurs at the carbonyl oxygen of the carbamoyl group of the carbocation **II**, the imine **III** is formed (path A). The intermediate **III** is further oxidized and hydrolyzed upon work-up to give the α,β-unsaturated γ-lactone (**2**). When the carbocation **II** cyclizes on a nitrogen atom of the carbamoyl group, the pyrrolidone **IV** is elaborated and further oxidized to yield the 1*H*-pyrrol-2(5*H*)-one **3** (path B). It seems that it depends on the lifetime of **II** whether the carbocation **II** cyclizes on oxygen or nitrogen atom of the carbamoyl group. That is to say, when the carbocation **II** is stabilized by the delocalization of a positive charge, the carbocation **II** cyclizes on a nitrogen atom of the carbamoyl group. In fact, **1f—h** having two or three methoxyl groups or **1i**, **j** having a large molecular structure which can delocalize the positive charge produced the corresponding 1*H*-pyrrol-2(5*H*)-ones. 4-Butanolides derived from an attack on the olefins of the carboxymethyl radical (which was generated directly by the thermolysis of $Mn(OAc)_3$[11]) were not detected. This indicates that the malonamide radical (**I**) rather than the carboxymethyl radical was preferentially produced by the reaction. The malonamide radical (**I**) might be generated by the direct interaction of malonamide and $Mn(OAc)_3$, which is similar to the aromatic acetonylation mechanism reported by Kurz *et al.*[12] In view of the product yield, it seems that the radical mechanism prefers the electron-transfer mechanism under these reaction conditions (except for **1g** and **1h**).

This reaction of styrene (**1k**) gave not only α,β-unsaturated γ-lactone and γ-lactam, but also spirodi-γ-lactones (**4k**) and γ-lactone (**13**). Cyclohexene, cyclooctene, octene, and acenaphthylene under the same reaction conditions resulted in an intractable mixture. Therefore, it is thought that the formation of α,β-unsaturated γ-lactones and γ-lactams using this reaction is effective for the polar olefins, such as the 1,1-disubstituted olefins. Although it is well known that olefins are oxidized with $Mn(OAc)_3$ in acetic acid to afford γ-lactones in good yields,[11] this reaction is the first example that α,β-unsaturated γ-lactones and/or γ-lactams are produced in one-step, with a short reaction time, and in moderate yields.

Experimental

Measurements. All melting points are uncorrected. The ^{1}H-NMR spectra were recorded on a Hitachi Perkin-Elmer R-24 (60 MHz) or a JEOL JNM-GX-270 spectrometer (270 MHz) at room temperature. The ^{13}C-NMR spectra were obtained with a JEOL JNM-GX-270 spectrometer (68 MHz). All chemical shifts are recorded in the δ scale relative to TMS as an internal standard. The IR spectra were taken on a JASCO A-102 infrared spectrophotometer and all IR spectral data are expressed in cm^{-1}. The mass spectra were measured on a JEOL JMS-DX-300 mass spectrometer using a direct-insertion probe at 70 eV ionizing voltage.

Materials. The olefins (**1a—c**, **e—g**) and manganese(III) acetate dihydrate used were prepared according to a method described in the literature.[6,14] Fluorenylideneacetic acid (**1d**) was obtained by the standard procedure[15] from fluorenone and ethyl bromoacetate, mp 231.7—232.7 °C (lit,[16] mp 232 °C). 9-Benzylidene-9*H*-xanthene (**1i**) and 9-benzylidene-9,10-dihydroanthracene (**1j**) were synthesized from 9-xanthenone and anthrone, **1i**: mp 114—115 °C (EtOH) (lit,[17] mp 116 °C); Anal. ($C_{20}H_{14}O$) C, H, and **1j**: mp 133.0—133.5 °C (benzene); Anal. ($C_{21}H_6$) C, H. Styrene, cyclooctene, octene, acenaphthylene, and malonamide were obtained from a commercial sample of the Wako Pure Chemical Industries, Ltd.

Reaction of Olefins with Malonamide. The typical procedure for the reaction of olefins with malonamide in the presence of manganese(III) acetate was as follows. To a heated solution of olefin (1 or 2 mmol) and malonamide in acetic acid (25 ml), manganese(III) acetate was added (see Table 1). The solution was heated under reflux until the brown color of Mn(III) ion disappeared. The solvent was removed *in vacuo* and the residue was triturated with 2 M hydrochloric acid (1 M=1 mol dm^{-3}), followed by extraction with chloroform. The products were separated on TLC (Wakogel B-10) with chloroform or diethyl ether as the developing solvent. The yields are summarized in Table 1.

*Oxidation Products of 1,1-Diphenylethene (**1a**).* *2-Carbamoyl-4,4-diphenyl-2-buten-4-olide (**2a**)*: Colorless needles (from benzene/light petroleum), mp 167.5—168.0 °C; IR ($CHCl_3$) 3500—3200 (NH_2), 1757 and 1685 (C=O), and 1645 (C=C); ^{1}H-NMR ($CDCl_3$) δ=6.30 (1H, br. s, NH), 7.30 (10H, s, ArH), 7.67 (1H, br. s, NH), and 8.71 (1H, s, H-3); MS *m/z* 279 (M^+), 262, 236, 202, 189, 174, 165, 131, and 105. Found: *m/z* 279.08925. Calcd for $C_{17}H_{13}O_3N$: M, 279.08954.

*3,3,8,8-Tetraphenyl-2,7-dioxaspiro[4.4]nonane-1,6-dione (**4a**)*: Colorless needles (from benzene), mp 285 °C (lit,[6] mp 284.5—285.0 °C).

*Benzopenone (**5a**)*: Colorless plates (from methanol), mp 47—48 °C (lit,[18] mp 47—48 °C).

*Oxidation Products of 2-Phenylpropene (**1b**).* *2-Carbamoyl-4-methyl-4-phenyl-2-buten-4-olide (**2b**)*: Colorless plates (from benzene/light petroleum), mp 151—153 °C; IR ($CHCl_3$) 3500—3200 (NH_2), 1755 and 1684 (C=O), and

1643 (C=C); ^{1}H-NMR ($CDCl_3$) δ=1.87 (3H, s, CH_3), 6.41 (1H, br. s, NH), 7.37 (5H, s, ArH), 7.75 (1H, br. s, NH), and 8.46 (1H, s, H-3); MS *m/z* (rel intensity), 217 (M^+, 12), 202 (40), 175 (100), 158 (66), 131 (74), 105 (100), and 77 (70). Found: C, 66.20; H, 5.29; N, 6.33%. Calcd for $C_{12}H_{11}O_3N$: C, 66.35; H, 5.10; N, 6.45%.

*3,8-Dimethyl-3,8-diphenyl-2,7-dioxaspiro[4.4]nonane-1,6-dione (**4b**)*: It was confirmed by the ^{1}H-NMR spectrum that this compound consisted of three stereoisomers, (3*R**, 5*R**, 8*R**), (3*S**, 5*R**, 8*S**), and (3*R**, 5*R**, 8*S**).[6]

*Acetophenone (**5b**)*: The product **5b** was identical with an authentic sample.

*Oxidation Products of 1,1,2-Triphenylethene (**1c**). 2-Carbamoyl-3,4,4-triphenyl-2-buten-4-olide (**2c**)*: Colorless needles (from benzene), mp 230—231 °C; IR ($CHCl_3$) 3500—3100 (NH_2), 1744 and 1688 (C=O), and 1629 (C=C); ^{1}H-NMR ($CDCl_3$) δ=6.03 (1H, br. s, NH), 6.7—7.5 (15H, m, ArH), and 7.94 (1H, br. s, NH); MS *m/z* (rel intensity), 355 (M^+, 16), 338 (12), 309 (18), 292 (11), 266 (19), 182 (12), 165 (13), 145 (100), 129 (87), 105 (80), and 77 (57). Found: *m/z* 355.11970. Calcd for $C_{23}H_{17}O_3N$: M, 355.12084.

*1,1,2-Triphenyl-1,2-ethanediol 2-Acetate (**6c**)*: Colorless microcrystals (from benzene), mp 227 °C (lit,[6] mp 224.5—225.5 °C).

*Oxidation Products of Fluorenylideneacetic Acid (**1d**). 4'-Carbamoylspiro[fluorene-9,2'(5'H)-furan]-5'-one (**2d**)*: Pale yellow needles (from benzene/light petroleum), mp 241.5—242.5 °C; IR ($CHCl_3$) 3600—3100 (NH_2), 1758 and 1687 (C=O), and 1640 (C=C); ^{1}H-NMR (DMSO-d_6) δ=6.95—7.93 (10H, m, ArH and NH_2), 8.12 (1H, s, H-4); MS *m/z* (rel intensity), 277 (M^+, 100), 260 (95), 232 (81), 222 (88), 205 (66), 189 (62), 176 (63), and 165 (52). Found: *m/z* 277.07332. Calcd for $C_{17}H_{11}O_3N$: M, 277.07389.

*9-Fluorenone (**5d**)*: All spectral data of **5d** were compatible with an authentic sample.

*Oxidation Product of Methylenecyclohexane (**1e**). 3-Carbamoyl-1-oxaspiro[4.5]dec-3-en-2-one (**2e**)*: Colorless needles (from benzene/light petroleum), mp 154—155 °C; IR ($CHCl_3$) 3500—3200 (NH_2), 1741 and 1684 (C=O), and 1642 (C=C); ^{1}H-NMR ($CDCl_3$) δ=1.74 (10H, br. s, 5×-CH_2-), 6.90 (1H, br. s, NH), 7.78 (1H, br. s, NH), and 8.32 (1H, s, H-4); MS *m/z* (rel intensity), 195 (M^+, 4), 178 (100), and 152 (13). Found: C, 61.81; H, 6.79; N, 7.02%. Calcd for $C_{10}H_{13}O_3N$: C, 61.52; H, 6.71; N, 7.18%.

*Oxidation Products of 1,1-Bis(4-methoxyphenyl)ethene (**1f**). 2-Carbamoyl-4,4-bis(4-methoxyphenl)-2-buten-4-olide (**2f**)*: Colorless prisms (from benzene/light petroleum), mp 157 °C; IR ($CHCl_3$) 3500—3200 (NH_2), 1752 and 1683 (C=O), and 1643 (C=C); ^{1}H-NMR ($CDCl_3$) δ=3.75 (6H, s, 2×OCH_3), 6.35 (1H, br. s, NH), 6.74—7.26 (8H, m, ArH), 7.68 (1H, br. s, NH), and 8.64 (1H, s, H-3); MS *m/z* (rel intensity), 339 (M^+, 37), 322 (3), 295 (100), 251 (22), 237 (13), 204 (58), 161 (21), 135 (100), and 107 (20). Found: *m/z* 339.10658. Calcd for $C_{19}H_{17}O_5N$: M, 339.11067.

*3-Carbamoyl-5,5-bis(4-methoxyphenyl)-1H-pyrrol-2(5H)-one (**3f**)*: Colorless needles (from chloroform/light petroleum), mp 203 °C; IR ($CHCl_3$) 3500—3100 (NH_2), 1700 and 1671 (C=O), and 1631 (C=C); ^{1}H-NMR (DMSO-d_6) δ=3.74 (6H, s, 2×OCH_3), 6.83—7.36 (8H, m, ArH), 7.68 (1H, br. s, NH), 7.98 (1H, br. s, NH), 8.48 (1H, d, J=1.8 Hz, H-4), and 10.00 (1H, br. d, J=1.8 Hz, NH); ^{13}C-NMR (CD_3OD) δ=55.8, 70.6, 115.1, 128.5, 129.3, 133.2, 142.6, 160.9, 164.8, and 171.6; MS *m/z* (rel intensity), 338 (M^+, 2), 321 (7), 294 (100), 280 (46), 231 (9), 158 (10), 134 (49), and 119 (12). Found: *m/z* 338.12978. Calcd for $C_{19}H_{18}O_4N_2$: M, 338.12666.

*3-Carbamoyl-4-hydroxy-5,5-bis(4-methoxyphenyl)-1H-pyrrol-2(5H)-one (**3f'**)*: Colorless needles (from chloroform/light petroleum), mp 130—131 °C; IR ($CHCl_3$) 3500—3100 (NH and OH), 1653 (C=O), and 1618 (C=C); ^{1}H-NMR ($CDCl_3$) δ=3.79 (6H, s, 2×OCH_3), 5.38 (1H, br. s, OH), 6.45 (1H, br. s, NH), 6.84—7.32 (8H, m, ArH), 7.59 (1H, br. s, NH), and 8.32 (1H, br. s, NH); ^{13}C-NMR (CD_3OD) δ=55.8 (q), 88.0 (s), 95.4 (s), 114.8 (d), 129.4 (d), 131.4 (s), 161.4 (s), 168.2 (s), 179.2 (s), and 194.4 (s); MS *m/z* (rel intensity), 354 (M^+, 35), 311 (82), 294 (25), 226 (100), 211 (100), 195 (16), 183 (18), 168 (17), 152 (19), 135 (43), 113 (52), 92 (11), and 77 (19). Found: *m/z* 354.12294. Calcd for $C_{19}H_{18}O_5N_2$: M, 354.12157.

*3-Carbamoyl-3-[2,2-bis(4-methoxyphenyl)ethenyl]-5,5-bis(4-methoxyphenyl)-2-pyrrolidone (**10**)*: Colorless microcrystals (from carbon tetrachloride/light petroleum), mp 121—124 °C; IR ($CHCl_3$) 3550—3100 (NH), 1692 (C=O), and 1606 (C=C); ^{1}H-NMR ($CDCl_3$) δ=2.57 (1H, d, J=13.2 Hz, CH_2), 3.31 (1H, d, J=13.2 Hz, CH_2), 3.67 (3H, s, OCH_3), 3.72 (3H, s, OCH_3), 3.75 (3H, s, OCH_3), 3.78 (3H, s, OCH_3), 5.87 (1H, br. s, NH), 6.12 (1H, s, =CH-), 6.57—7.26 (17H, m, ArH and NH), and 8.25 (1H, s, NH); MS *m/z* (rel intensity), 578 (M^+, 3), 535 (100), 492 (15), 427 (11), 384 (8), 371 (30), 295 (39), 265 (20), 227 (74), 189 (19), 134 (19), and 121 (38). Found: *m/z* 578.24302. Calcd for $C_{35}H_{34}O_6N_2$: M, 578.24169.

*Oxidation Products of 1,1-Bis(4-methoxyphenyl)-2-phenylethene (**1g**). 2-Carbamoyl-4,4-bis(4-methoxyphenyl)-3-phenyl-2-buten-4-olide (**2g**)*: Colorless microcrystals (from benzene/light petroleum), mp 98—99 °C; IR ($CHCl_3$) 3600—3100 (NH_2), 1741 and 1684 (C=O); ^{1}H-NMR ($CDCl_3$) δ=3.71 (6H, s, 2×OCH_3), 6.15 (1H, br. s, NH), 6.57—7.40 (13H, m, ArH), and 7.80 (1H, br. s, NH); MS *m/z* (rel intensity), 415 (M^+, 40), 371 (60), 329 (25), 242 (30), 227 (20), and 135 (100). Found: *m/z* 415.14532. Calcd for $C_{25}H_{21}O_5N$: M, 415.14197.

*3-Carbamoyl-5,5-bis(4-methoxyphenyl)-4-phenyl-1H-pyrrol-2(5H)-one (**3g**)*: Colorless needles (from chloroform/light petroleum), mp 134—136, 225—226 °C; IR ($CHCl_3$) 3600—3100 (NH), and 1698 (C=O); ^{1}H-NMR (DMSO-d_6) δ=3.74 (6H, s, 2×OCH_3), 6.65—7.35 (13H, m, ArH), 7.38 (1H, br. s, NH), 8.01 (1H, br. s, NH), and 9.48 (1H, s, NH); MS *m/z* (rel intensity), 414 (M^+, 45), 371 (100), 307 (50), 240 (40), 210 (45), 134 (55), and 77 (12). Found: *m/z* 414.15650. Calcd for $C_{25}H_{22}O_4N_2$: M, 414.15796.

*4,4'-Dimethoxybenzophenone (**5g**)*: Colorless plates (from ethanol), mp 143—144 °C (lit,[19] mp 144 °C).

*1,1-Bis(4-methoxypheny)-2-phenyl-1,2-ethanediol 2-Acetate (**6g**)*: Colorless microcrystals (from benzene), mp 200—201 °C; IR ($CHCl_3$) 3600—3100 (OH) and 1735 (OAc); ^{1}H-NMR ($CDCl_3$) δ=1.96 (3H, s, OAc), 2.67 (1H, s, OH), 3.70 (3H, s, OCH_3), 3.80 (3H, s, OCH_3), 6.54 (1H, s, >CH-), and 6.67—7.51 (13H, m, ArH). Found: C, 73.55; H, 6.10%. Calcd for $C_{24}H_{24}O_5$: C, 73.45; H, 6.16%.

*2-Hydroxy-2,2-bis(4-methoxyphenyl)-1-phenylethanone (**7g**)*: Colorless needles (from benzene/light petroleum), mp 138—140 °C; IR ($CHCl_3$) 3600—3100 (OH) and 1666 (C=O); ^{1}H-NMR ($CDCl_3$) δ=3.63 (6H, s, 2×OCH_3), 4.93 (1H, br. s, OH), 6.60—7.80 (13H, m, ArH); MS *m/z* (rel intensity), 348 (M^+, 5), 242 (100), 227 (65), 211 (85), 135 (70), and 107 (70). Found: *m/z* 348.13133. Calcd for $C_{22}H_{20}O_4$: M, 348.13616.

*1-Acetoxy-2,2-bis(4-methoxyphenyl)-1-phenylethene (**8g**)*:

Colorless microcrystals (from ethanol), mp 101—102 °C; IR ($CHCl_3$) 1753 (OAc); ^{1}H-NMR ($CDCl_3$) δ=1.95 (3H, s, OAc), 3.67 (3H, s, OCH_3), 3.75 (3H, s, OCH_3), 6.55—7.45 (13H, m, ArH); MS *m/z* (rel intensity), 374 (M^+, 10), 332 (28), 278 (14), 242 (30), 223 (30), 212 (52), 205 (12), 196 (92), 180 (41), 168 (25), 149 (100), 135 (70), and 107 (10). Found: *m/z* 374.15023. Calcd for $C_{24}H_{22}O_4$: M, 374.15181.

*Benzoic Acid (**9g**)*: ^{1}H-NMR and IR spectral data were in agreement with an authentic sample.

*Oxidation Products of 1,1,2-Tris(4-methoxyphenyl)ethene (**1h**). 2-Carbamoyl-3,4,4-tris(4-methoxyphenyl)-2-buten-4-olide (**2h**)*: Colorless microcrystals (from benzene/light petroleum), mp 118—119 °C; IR ($CHCl_3$) 3600—3100 (NH_2), 1736 and 1680 (C=O); ^{1}H-NMR ($CDCl_3$) δ=3.76 (9H, s, 3×OCH_3), 5.8 (1H, br. s, NH), 6.60—7.22 (12H, m, ArH), and 8.0 (1H, br. s, NH). Found: *m/z* 445.15133. Calcd for $C_{26}H_{23}O_6N$: M, 445.15254.

*3-Carbamoyl-4,5,5-tris(4-methoxyphenyl)-1H-pyrrol-2(5H)-one (**3h**)*: Colorless needles (from chloroform/light petroleum), mp 188—189 °C; IR ($CHCl_3$) 3600—3100 (NH) and 1692 (C=O); ^{1}H-NMR (DMSO-d_6) δ=3.70 (3H, s, OCH_3), 3.72 (6H, s, 2×OCH_3), 6.65—7.30 (12H, m, ArH), 7.38 (1H, br. s, NH), 8.01 (1H, br. s, NH), and 9.46 (1H, s, NH). Found: *m/z* 444.17383. Calcd for $C_{26}H_{24}O_5N_2$: M, 444.16852.

*1,1,2-Tris(4-methoxyphenyl)-1,2-ethanediol 2-Acetate (**6h**)*: Colorless microcrystals (from benzene), mp 187.0—187.5 °C; IR ($CHCl_3$) 3600—3200 (OH) and 1734 (OAc); ^{1}H-NMR ($CDCl_3$) δ=1.95 (3H, s, OAc), 2.79 (1H, s, OH), 3.73 (3H, s, OCH_3), 3.75 (3H, s, OCH_3), 3.83 (3H, s, OCH_3), 6.61—7.61 (12H, m, ArH), and 6.83 (1H, s, >CH-). Found: C, 70.91; H, 6.32%. Calcd for $C_{25}H_{26}O_6$: C, 71.07; H, 6.20%.

*2-Hydroxy-1,2,2-tris(4-methoxyphenyl)-1-ethanone (**7h**)*: Colorless needles (from benzene/light petroleum), mp 118—119 °C; IR ($CHCl_3$) 3600—3200 (OH) and 1654 (C=O); ^{1}H-NMR ($CDCl_3$) δ=3.72 (9H, s, 3×OCH_3), 5.20 (1H, br. s, OH), and 6.68—7.82 (12H, m, ArH). Found: *m/z* 378.14591. Calcd for $C_{23}H_{22}O_5$: M, 378.14673.

*1-Acetoxy-1,2,2-tris(4-methoxyphenyl)ethene (**8h**)*: Liquid; IR ($CHCl_3$) 1751 (OAc); ^{1}H-NMR ($CDCl_3$) δ=1.98 (3H, s, OAc), 3.71 (6H, s, 2×OCH_3), 3.78 (3H, s, OCH_3), and 6.60—7.25 (12H, m, ArH); MS *m/z* (rel intensity), 404 (M^+, 25), 362 (50), 333 (23), 242 (48), 194 (40), and 152 (100). Found: *m/z* 404.16293. Calcd for $C_{25}H_{24}O_5$: M, 404.16238.

p-*Anisic Acid (**9h**)*: ^{1}H-NMR and IR spectral data were compatible with an authenitic sample.

*2,3,3-Tris(4-methoxyphenyl)-2-propenal (**11**)*: Colorless needles (from light petroleum), mp 126—127 °C; IR ($CHCl_3$) 1723 (CHO); ^{1}H-NMR ($CDCl_3$) δ=3.78 (9H, s, 3×OCH_3), 6.73—7.30 (12H, m, ArH), and 10.13 (1H, s, CHO); MS *m/z* (rel intensity), 374 (M^+, 3), 333 (100), 242 (78), 227 (80), 211 (70), 135 (70), and 107 (47). Found: *m/z* 374.15161. Calcd for $C_{24}H_{22}O_4$: M, 374.15181.

*Oxidation Products of 9-Benzylidene-9H-xanthene (**1i**). 4-Carbamoyl-3-phenyl-1,5-dihydrospiro[2H-pyrrole-2,9′-xanthen]-5-one (**3i**)*: Colorless prisms (from ethanol), mp 251 °C; IR (KBr) 3600—3000 (NH) and 1697 (C=O); ^{1}H-NMR (DMSO-d_6) δ=6.50—7.48 (13H, m, ArH), 7.52 (1H, br. s, NH), 8.20 (1H, br. s, NH), and 9.80 (1H, s, NH); MS *m/z* (rel intensity), 368 (M^+, 100), 351 (16), 325 (81), 295 (7), 281 (12), 222 (30), 204 (20), 195 (40), 168 (12), 146 (28), and 129 (60). Found: *m/z* 368.11536. Calcd for $C_{23}H_{16}O_3N_2$: M, 368.11609.

*9-Xanthenone (**5i**)*: Colorless needles (from ethanol), mp 175 °C (lit,[20] mp 173—174 °C). Found: C, 79.38; H, 4.16%. Calcd for $C_{13}H_8O_2$: C, 79.58; H, 4.11%.

*9-(α-Acetoxybenzyl)-9-xanthenol (**6i**)*: Colorless microcrystals (from benzene), mp 141—142 °C; IR ($CHCl_3$) 3600—3100 (OH) and 1740 (OAc); ^{1}H-NMR ($CDCl_3$) δ=1.93 (3H, s, OAc), 3.90 (1H, br. s, OH), 5.87 (1H, s, >CH-), and 6.38—7.70 (13H, m, ArH). Found: *m/z* 346.12230. Calcd for $C_{22}H_{18}O_4$: M, 346.12051.

*α,α-Diacetoxytoluene (**12**)*: Colorless microcrystals (from light petroleum), mp 45 °C (lit,[21] mp 45—46 °C); IR ($CHCl_3$) 1758 (OAc); ^{1}H-NMR ($CDCl_3$) δ=2.01 (6H, s, 2×OAc), 7.23—7.52 (5H, m, ArH), and 7.55 (1H, s, >CH-).

*Oxidation Products of 9-Benzylidene-9,10-dihydroanthracene (**1j**). 4′-Carbamoyl-3′-phenyl-1′,5′-dihydrospiro[anthracene-9(10H), 2′-[2H]pyrrol]-5′-one (**3j**)*: Colorless microcrystals (from ethanol), mp 248—249 °C; IR (KBr) 3600—3100 (NH) and 1670 (C=O); ^{1}H-NMR (DMSO-d_6) δ=2.94 (2H, br. s, CH_2), 5.71 (1H, br. s, NH), and 6.8—7.9 (15H, m, ArH and NH_2); MS *m/z* (rel intensity), 366 (M^+, 43), 293 (100), 233 (54), 208 (46), and 91 (29). Found: *m/z* 366.13415. Calcd for $C_{24}H_{18}O_2N_2$: M, 366.13683.

*9-Acetoxy-9-benzoyl-9,10-dihydroanthracene (**7j**)*: Colorless needles (from light petroleum), mp 151.5—152.0 °C; IR ($CHCl_3$) 1751 (OAc) and 1663 (C=O); ^{1}H-NMR ($CDCl_3$) δ=2.12 (3H, s, OAc), 3.31 (2H, s, CH_2), and 6.0—8.2 (13H, m, ArH). Found: *m/z* 342.12724. Calcd for $C_{23}H_{18}O_3$: M, 342.12560.

*9-(α-Acetoxybenzylidene)-9,10-dihydroanthracene (**8j**)*: Pale yellow needles (from ethanol), mp 214 °C; IR ($CHCl_3$) 1762 (OAc) and 1622 (C=C); ^{1}H-NMR ($CDCl_3$) δ=2.59 (3H, s, OAc), 4.94 (2H, s, CH_2), and 7.0—8.3 (13H, m, ArH). Found: *m/z* 326.12870. Calcd for $C_{23}H_{18}O_2$: M, 326.13068.

*Reaction of Styrene (**1k**) with Malonamide in the Presence of Manganese(III) Acetate.* The reaction was carried out by the same procedure described above (molar ratio, **1k**: malonamide:$Mn(OAc)_3$=1:4:4; reaction time, 1 min).

*3,8-Diphenyl-2,7-dioxaspiro[4.4]nonane-1,6-dione (**4k**)*: Three stereoisomers (yield; 4%) were isolated; (3*R**, 5*R**, 8*R**), mp 162—163 °C (lit,[6] mp 162—163 °C); (3*S**, 5*R**, 8*R**), mp 185—186 °C (lit, [6] mp 185—186 °C); (3*S**, 5*R**, 8*S**), mp 239—240 °C (lit,[6] mp 236—237 °C).

*2-(2-Acetoxy-2-phenylethyl)-2-carbamoyl-4-phenyl-4-butanolide (**13**)*: Yield, 5%; colorless needles (from benzene/light petroleum), mp 184—185 °C; IR ($CHCl_3$) 3600—3100 (NH_2), 1752 and 1687 (C=O); ^{1}H-NMR ($CDCl_3$) δ=2.07 (3H, s, OAc), 2.54 (2H, m, H-3), 2.93 (2H, d, J=8.4 Hz, CH_2), 5.42 (1H, t, J=8.4 Hz, >CH-), 5.81 (1H, br. s, NH), 5.93 (1H, dd, J=10.8 and 3.0 Hz, H-4), 7.15 (1H, br. s, NH), and 7.27 (5H, s, ArH); MS *m/z* (rel intensity), 367 (M^+, 1), 324 (2), 307 (2), 264 (6), 247 (25), 205 (100), 188 (65), 170 (67), 162 (58), 144 (11), 129 (37), 116 (25), 105 (68), and 77 (46). Found: *m/z* 367.13929. Calcd for $C_{21}H_{21}O_5N$: M, 367.14197.

The author wish to thank Mr. Hiromichi Matsuura of the Wakunaga Pharmaceutical Co. Ltd., Hiroshima, for his measurements of the ^{1}H-NMR (270 MHz), ^{13}C-NMR, and mass spectra. Thanks are also given to Mr. Kazuhiko Ichikawa of the Ichikawa Chemical Co. Ltd., Higashi Osaka, for his measurements of the mass spectra.

References

1) M. Okano and T. Aratani, *Bull. Chem. Soc. Jpn.*, **49**, 2811 (1976).
2) K. Kurosawa and K. Yamaguchi, *Bull. Chem. Soc. Jpn.*, **54**, 1757 (1981).
3) M. G. Vinogradov, S. P. Verenchikov, and G. I. Nikishin, *Izv. Akad. Nauk. SSSR, Ser. Khim.*, **1971**, 200; *Chem. Abstr.*, **75**, 5162 (1971). E. I. Heiba and R. M. Dessau, *J. Am. Chem. Soc.*, **93**, 524 (1971); *ibid.*, **94**, 2888 (1972).
4) G. I. Nikishin, M. G. Vinogradov, and T. M. Fedorova, *J. Chem. Soc., Chem. Commun.*, **1973**, 693.
5) E. I. Heiba and R. M. Dessau, *J. Org. Chem.*, **39**, 3456 (1974).
6) N. Ito, H. Nishino, and K. Kurosawa, *Bull. Chem. Soc. Jpn.*, **56**, 3527 (1983).
7) H. Nishino and K. Kurosawa, *Bull. Chem. Soc. Jpn.*, **56**, 1682 (1983).
8) A. Takeda, S. Tsuboi, and T. Sakai, *J. Org. Chem.*, **39**, 2601 (1974).
9) P. J. Andrulis, Jr., M. J. S. Dewar, R. Dietz, and R. L. Hunt, *J. Am. Chem. Soc.*, **88**, 5473 (1966); T. Aratani and M. J. S. Dewar, *ibid.*, **88**, 5479 (1966); P. J. Andrulis, Jr. and M. J. S. Dewar, *ibid.*, **88**, 5483 (1966).
10) S. A. Zonis and Yu. I. Kornilova, *Zhur. Obshchei Khim.*, **20**, 1252 (1950); *Chem. Abstr.*, **45**, 10196e (1951); S. A. Zonis and A. G. Pesina, *J. Gen. Chem., U. S. S. R.*, **20**, 1223 (1950); *Chem. Abstr.*, **46**, 3496i (1952).
11) J. B. Bush, Jr. and H. Finkbeiner, *J. Am. Chem. Soc.*, **90**, 5903 (1968); E. I. Heiba, R. M. Dessau, and W. J. Koehl, Jr., *ibid.*, **90**, 5905 (1968).
12) M. E. Kurz, V. Baru, and P-Nhi Nguyen, *J. Org. Chem.*, **49**, 1603 (1984).
13) E. I. Heiba, R. M. Dessau, and W. J. Koehl, Jr., *J. Am. Chem. Soc.*, **91**, 138 (1969).
14) K. Shishido, K. Okano, M. Shindo, and H. Nozaki, *J. Am. Chem. Soc.*, **79**, 3591 (1957).
15) H. Rupe and E. Busolt, *Ber.*, **40**, 4537 (1907).
16) E. D. Gergmann, H. Weiler-Feilchenfeld, and N. Mandel, *Vietnamica Chim. Acta*, **1966**, 129; *Chem. Abstr.*, **72**, 3276s (1970).
17) Ng. Ph. Buu-Hoï and Ng. D. Xuong, *J. Org. Chem.*, **16**, 1633 (1951).
18) C. S. Marvel and W. M. Sperry, *Org. Synth.*, Coll. Vol. **I**, 95 (1967).
19) M. Bösler, *Ber.*, **14**, 328 (1881).
20) A. F. Holleman, *Org. Synth.*, Coll. Vol. **I**, 552 (1967).
21) W. H. Perin, *J. Am. Chem. Soc.*, **20**, 590 (1867).

 © 1985 The Chemical Society of Japan Bull. Chem. Soc. Jpn., 58, 223—226 (1985)

Reactions of Dichloride Anion Radical with Nucleosides, Nucleotides, and Polynucleotides

Takeo TAKAHASHI, Kotaro YAMAUCHI, and Takahiro MASUDA*
Department of Chemistry, Faculty of Science, Tokyo Metropolitan University, Fukasawa, Setagaya-ku, Tokyo 158
(Received January 27, 1984)

Rate constants for reactions of dichloride anion radical with nucleosides, nucleotides, and polynucleotides were determined in neutral aqueous solutions of potassium chloride by the conventional flash photolysis. The reactivities of these compounds toward the anion radical are in the order: bases>nucleosides>nucleotides>polynucleotides. This trend is similar to that observed with the corresponding reactions with hydroxyl radical. A comparison of the reactivities of nucleosides, nucleotides, and polynucleotides toward dichloride anion radical with those toward hydroxyl radical has revealed that the reactivities of these compounds are governed mainly by their base moiety. This trend in the reactivities is discussed in terms of steric effect.

Reactions of nucleic acid and related compounds with dichloride anion radical produced in photolysis or radiolysis of aqueous chloride are of interest from biological point of view, considering their possible role in light or radiation induced damage on living cells. On the other hand, kinetic study on their reactions is expected to provide information on the relation between structure and reactivity of these biologically important molecules.

In previous studies,[1-3] rate constants for reactions of hydroxyl radical with nucleic acid bases, nucleosides, nucleotides, and polynucleotides were determined by the competition method using *N,N*-dimethyl-*p*-nitrosoaniline as a reference compound, and some trend observed in reactivities of bases, nucleosides, and nucleotides was explained in terms of steric hindrance, that is, mutual protection between base and sugar moieties. However, the applicability of this explanation is not examined for other radical reactions. Dichloride anion radical is known to resemble hydroxyl radical in oxidative nature but differ with respect to reactions with unsaturated compounds.[4-6] For the anion radical one-electron oxidation was found,[7,8] whereas addition to a double bond was observed for hydroxyl radical.

The present study was undertaken to ascertain whether or not the same explanation may apply to some trend in reactivities of a series of compounds toward dichloride anion radical. For this purpose, rate constants for reactions of dichloride anion radical with nucleosides, nucleotides, homopolynucleotides, and nucleic acids were determined in neutral aqueous solutions of KCl saturated with dinitrogen monoxide by the conventional flash photolysis. The rate constants obtained indicate that the trend in reactivities of these compounds is similar to that observed for reactions with hydroxyl radical. On the basis of these results, reactivities of these DNA related compounds are discussed from the view point of steric hindrance of substrates.

Experimental

Purine, 1-methylcytosine, D-ribose, 2-deoxyribose 5-phosphate, nucleosides, nucleotides, polynucleotides, ribonucleic acid (baker's yeast), and deoxyribonucleic acid (calf thymus) were obtained from Sigma Chemical Co. and used without further purification. The other chemicals were of reagent grade.

Solutions for irradiation were prepared by dissolving 1 mol dm^{-3} KCl and a desired amount of a substrate in triply distilled water and adjusting pH to 7. The solutions were subjected to bubbling of N_2O for 20 min immediately before flash photolysis. In UV-photolysis of the solutions, the following reactions are expected to take place:

$$Cl^- + h\nu \xrightarrow{197\ nm} Cl\cdot + e^-_{aq}, \quad (1)$$

$$Cl\cdot + Cl^- \rightleftharpoons Cl_2^-\cdot, \quad (2)$$

$$e^-_{aq} + N_2O \longrightarrow N_2 + \cdot OH + OH^-, \quad (3)$$

$$Cl_2^-\cdot + Cl_2^-\cdot \longrightarrow Cl_2 + 2Cl^-, \quad (4)$$

$$Cl_2^-\cdot + S \longrightarrow 2Cl^- + \text{product(s)}, \quad (5)$$

where S designates a substrate. By kinetic analysis of the rate of decay of dichloride anion radical due to Reactions 4 and 5, the rate constant of Reaction 5 was estimated. The procedure for the estimation was described in detail elsewhere.[6,9] Calculations in kinetic analysis and of solid angles were carried out with the aid of microcomputers PC-8001 and PC-8801 (Nippon Electric Co.).

Flash photolysis was carried out under the conditions of 10 μs duration and 200 J input energy with the same conventional apparatus, that had been described in a previous paper,[10] except additional use of a transient recorder TM-1410 (Kawasaki Electronica Co.). Decay rate of dichloride anion radical was measured by using the absorption at 350 nm with 7600 dm^3 mol^{-1} cm^{-1} taken as its absorption coefficient.[11]

Results and Discussion

Rate Constants for Reaction of Dichloride Anion Radical with Nucleic Acid Components in Aqueous

Solution. Rate constants for reactions of dichloride anion radical with nucleosides, nucleotides, and some related compounds are summarized in Table 1, together with the values previously reported for nucleic acid bases.[6] These values were obtained from more than fifteen experiments and their errors are expressed in standard deviation.

We failed in determination of the rate constant for the reaction with guanine because of its low solubility in neutral solution. The rate constant for the reaction with adenine could not be determined either, because a relatively long-lived absorption of a maximum at 335 nm appeared in the region of the absorption due to dichloride anion radical so that the decay process of the anion radical could not be followed in this case. Since the transient absorption was observed even in the absence of chloride ion, it may be attributable to a cation radical of adenine produced by the photoionization in aqueous solution

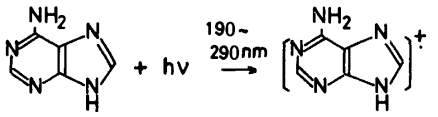

The species responsible for the transient absorption will be a neutral radical formed from the cation radical after deprotonation of N-9, because no absorption was observed for adenosine or adenosine 5′-phosphate in the time scale of flash photolysis:

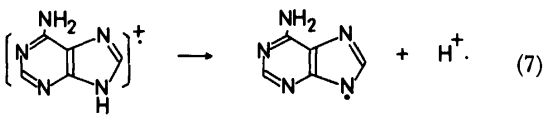

From the values given in Table 1, it is noticed that the reactivities of nucleic acid components may be arranged in the order: bases>nucleosides>nucleotides. The only exception was found for adenosine 5′-diphosphate. A duplicate determination resulted in fairly good reproducibility and this high value cannot be explained at the present stage of study. D-ribose or 2-deoxyribose 5-phosphate was chosen as a model compound of sugar or sugar phosphate moiety, respectively. Their low reactivities toward dichloride anion radical suggest that a hydrogen atom abstraction from these compounds occurs, as discussed by Hasegawa and Neta.[5]

In Table 2, rate constants for reactions with homopolynucleotides, ribonucleic acid, and deoxyribonucleic acid are summarized. They are presented as a value per nucleotide unit. Before flash photolysis, heat treatment was carried out on nucleic acids at 80 °C for 40 min in order to investigate the effect of conformational change on reactivity. An apparent increase in reactivity was observed after the treatment.

Mechanism of Reaction of Dichloride Anion Radical with Nucleoside. It has already been reported that dichloride anion radical reacts with a nucleic acid base to form 5 yl radical through one-electron oxidation and deprotonation[7,8]

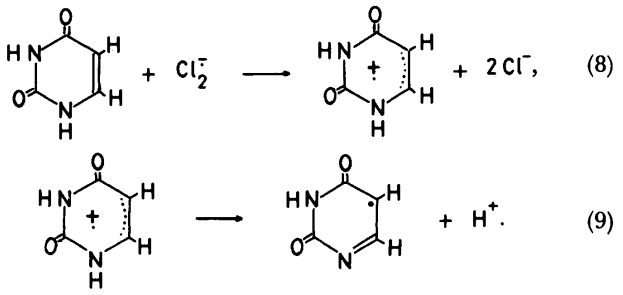

TABLE 1. RATE CONSTANTS FOR REACTIONS OF DICHLORIDE ANION RADICAL WITH NUCLEIC ACID BASES, NUCLEOSIDES, NUCLEOTIDES, AND RELATED COMPOUNDS

	Compound	Rate constant 10^8 dm^3 mol^{-1} s^{-1}
1.	Uracil[a]	2.8±0.1
2.	Uridine	1.6±0.3
3.	Uridine 5′-phosphate	1.5±0.2
4.	Cytosine[a]	3.5±0.1
5.	Cytidine	2.5±0.8
6.	Cytidine 5′-phosphate	2.2±0.6
7.	Thymine[a]	3.2±0.3
8.	Thymidine	2.4±0.2
9.	Thymidine 5′-phosphate	1.8±0.3
10.	Adenosine	3.2±0.5
11.	Adenosine 5′-phosphate	3.0±0.5
12.	Adenosine 5′-diphosphate	3.6±0.2
13.	Adenosine 5′-triphosphate	2.0±0.6
14.	Guanosine	14±7
15.	Guanosine 5′-phosphate	8.8±0.8
16.	D-Ribose	0.11±0.02
17.	2-Deoxyribose 5-phosphate	0.19±0.08
18.	Purine	0.52±0.08
19.	1-Methylcytosine	3.3±0.5

a) Ref. 6.

TABLE 2. RATE CONSTANTS FOR REACTIONS OF DICHLORIDE ANION RADICAL WITH HOMOPOLYNUCLEOTIDES AND NUCLEIC ACIDS

	Compound	Rate constant 10^8 dm^3 mol^{-1} s^{-1}
20.	Polyuridylic acid	0.98±0.22
21.	Polycytidylic acid	1.1±0.3
22.	Polyadenylic acid	1.5±0.1
23.	Ribonucleic acid	1.1±0.2
24.	Ribonucleic acid pretreated at 80 °C, 40 min	2.2±0.1
25.	Deoxyribonucleic acid	0.74±0.11
26.	Deoxyribonucleic acid pretreated at 80 °C, 40 min	1.4±0.3

On the other hand, it is well known that anion radical $Cl_2^{-}\cdot$ abstracts a hydrogen atom from an aliphatic compound as follows:[12,13]

$$RH + Cl_2^{-}\cdot \longrightarrow R\cdot + H^+ + 2Cl^-. \quad (10)$$

Therefore, two types of reactions are expected for nucleoside; one-electron oxidation of base ring (Reaction 8) and hydrogen abstraction from sugar moiety. Thus the apparent rate constant for the reaction of nucleoside, k, may be expressed by

$$k = f_1 k_b + f_2 k_s, \quad (11)$$

where k_b and k_s designate the rate constants independently determined for base and sugar, respectively, and f_1 and f_2 are correction factors for k_b and k_s, respectively, with respect to the bonding between base and sugar.

The correction factors will be evaluated by considering the following causes for the decrease in reactivity toward dichloride anion radical: 1) change in energy state due to formation of glycoside bond; 2) decrease in diffusion rate owing to increase in molecular size; 3) steric hindrance, that is, mutual protection of two moieties.

The effect of energy state on reactivity is evaluated from the rate constant determined for 1-methylcytosine. As shown in Table 1, the value for 1-methylcytosine, $(3.3\pm0.5)\times10^8$ dm^3 mol^{-1} s^{-1}, is closer to the value of cytosine than to that of cytidine or cytidine 5′-phosphate. This suggests that the change in energy state due to formation of glycoside bond does not significantly affect the reactivity toward dichloride anion radical at least in neutral aqueous solution.

Furthermore, the first ionization potentials determined by photoelectron spectroscopy for the nucleic acid components and related compounds are in the following orders for each series: uracil (9.6—9.45 eV) >uridine (9.0 eV)>1-methyluracil (8.74 eV); thymine (9.20—9.02 eV)>thymidine (8.7 eV); cytosine (9.1 eV)> 1-methylcytosine (8.655 eV)>cytidine (8.6 eV); adenine (8.48 eV)>adenosine (8.4 eV)>9-methyladenine (8.39 eV); guanine (8.28 eV)>9-methylguanine (8.02 eV)> guanosine (8.0 eV).[14-20] If the order of magnitude in gas phase does not change in the liquid phase, the order of magnitude suggests that a nucleoside or an *N*-methyl derivative is more reactive than a base in one-electron oxidation reaction.

In relation to diffusion rate, the reactivity would be affected by the encounter number of reactants in solution. The degree of this contribution will be evaluated by Smoluchowski's equation. Bowen and Martin[21] reported diffusion constants of some nucleosides, nucleotides, and purine bases in the presence and absence of salt such as KCl, $MgCl_2$, or $CaCl_2$. The values for adenine, adenosine, and adenosine 5′-phosphate are 7.7×10^{-6}, 5.2×10^{-6}, and 4.3×10^{-6} cm^2 s^{-1} in the presence of 5×10^{-3} mol dm^{-3} $MgCl_2$, respectively. From these values and the diffusion constant of the anion radical, 1.67×10^{-5} cm s^{-1}, which has been estimated from the rate constant of Reaction 4 by Debye's equation for diffusion-controlled reactions between charged species, 0.90 and 0.86 can be obtained as the relative reactivities of adenosine and adenosine 5′-phosphate, respectively, with unity taken for adenine. Since the observed values given in Table 1 are much less than the values estimated above from diffusion rate, the second cause will be eliminated.

The third possible cause is steric hindrance, namely mutual protection between base and sugar moieties. In Fig. 1, rate constants of nucleic acids and related compounds for hydroxyl radical are plotted against those for dichloride anion radical. In a previous paper,[6] we reported that a linear correlation with slope 11 was found between reactivities of pyrimidine bases toward hydroxyl radical and those toward dichloride anion radical.

For bases, nucleosides, nucleotides, polynucleotides, and nucleic acids, a similar correlation was observed, except for 2-amino derivatives of pyrimidine and purine. The slope 15 in the correlation is close to that found for pyrimidine bases. On the other hand, a slope of the correlation found for D-ribose and 2-deoxyribose 5-phosphate, 87.5, is close to that found for aliphatic dipeptides, 65.8.[6] These results suggest that the overall reactivity of a nucleoside, nucleotide,

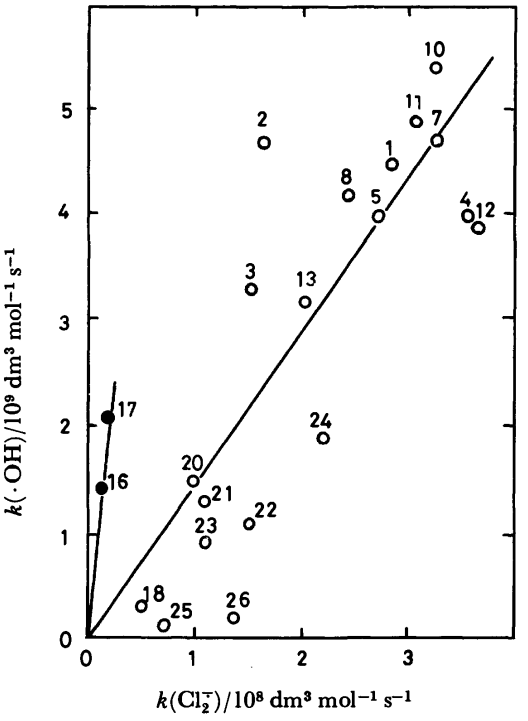

Fig. 1. $k(\cdot OH)$ *vs.* $k(Cl_2^-)$.
Figure associated with each plot corresponds to the number used in Tables 1 and 2.

polynucleotide, or nucleic acid is governed mainly by base moiety, the contribution of sugar or sugar phosphate moiety being negligible. Therefore, Eq. 11 is rewritten to $k=f_1k_b$.

The rate constant of a nucleoside will be predicted by the above equation, if f_1, the degree of protection of base moiety by sugar moiety, is estimated from the solid angle open to the attack of dichloride anion radical, as discussed in the case of hydroxyl radical.[2] Although for the addition reaction of hydroxyl radical C-5 has been proposed as the reaction site by ESR studies,[22,23] the reaction site on a pyrimidine base is not clear for one-electron oxidation. However, π-electron has been suggested to react with the anion radical (Reaction 8) by ESR studies.[7,8]

Therefore, by assuming that the reaction site on nucleoside for the anion radical is C-5 of pyrimidine ring, a calculation of f_1 was attempted for reactions of the anion radical with nucleosides. With each atom of sugar moiety projecting on the surface of unit sphere centered at C-5 of a base, the area of projection was determined as described in a previous paper.[2] Coordinates of nucleoside reported by Lakshiminarayanan and Sasisekharan[24] were used for the calculation of solid angles. Area was calculated for stepwise change of the torsional angle about the bond between N-1 and C-1′. Contact distances were taken as the sum of van der Waals radii. For the anion radical, the van der Waals radius was assumed as the average of the long and short axes, 0.25 nm. The estimated rate constants for uridine, cytidine and thymidine are given in Table 3.

They are presented as the values estimated for the upper and lower limits of protection. Compared with the case of hydroxyl radical, the agreement with the observed values is not good except uridine. This may be due to the assumption of the reaction site, because the effective size of π-orbital was neglected in the calculation. However, steric hindrance could provide values closer to observed ones.

The results obtained for homopolynucleotides and nucleic acids indicate that the reactivity toward dichloride anion radical depends on their conformation. The reactivity of a polynucleotide is 0.5—0.65 times as high as that of the corresponding nucleotide. This may be due to a protection by the sugar phosphate backbone. The reactivity of a nucleic acid is relatively high, in spite of its tight conformation. This will be explained in terms of the presence of guanosine 5′-phosphate, which is included in the molecules and very reactive to the anion radical. The increase in reactivity induced by heat treatment may also be understood in terms of conformational degradation.

Table 3. Estimated rate constants of reactions of nucleosides with dichloride anion radical

Compound	Rate constant 10^8 dm^3 mol^{-1} s^{-1}
Uridine	1.3—1.8
Cytidine	1.7—2.3
Thymidine	1.5—2.1

The results obtained for the reaction of dichloride anion radical can be understood in the same way with the reaction of hydroxyl radical. The explanation based on steric effect is probably applicable to reactions of these compounds with some other radicals in aqueous solutions.

References

1) T. Masuda, H. Shinohara, and M. Kondo, *J. Radiat. Res.*, **16**, 153 (1975).
2) H. Shinohara, T. Masuda, and M. Kondo, *J. Radiat. Res.*, **17**, 230 (1976).
3) T. Masuda, H. Shinohara, M. Eda, and M. Kondo, *J. Radiat. Res.*, **21**, 173 (1980).
4) G. E. Adams, J. E. Aldrich, R. H. Bisby, R. B. Cundall, J. L. Redpath, and R. L. Willson, *Radiat. Res.*, **49**, 278 (1972).
5) K. Hasegawa and P. Neta, *J. Phys. Chem.*, **82**, 854 (1978).
6) T. Masuda, T. Kimura, E. Kadoi, T. Takahashi, K. Yamauchi, and M. Kondo, *J. Radiat. Res.*, **24**, 165 (1983).
7) K. M. Bansal and R. W. Fessenden, *Radiat. Res.*, **75**, 497 (1978).
8) M. D. Sevilla, D. Suryanarayana, and K. M. Morehouse, *J. Phys. Chem.*, **85**, 1027 (1981).
9) T. Masuda, R. Gunji, T. Kimura, and K. Yamauchi, *Bull. Chem. Soc. Jpn.*, **56**, 3595 (1983).
10) T. Masuda, Y. Murata, K. Yamauchi, and M. Kondo, *J. Radiat. Res.*, **18**, 258 (1977).
11) M. Schöneshöfer, *Radiat. Phys. Chem.*, **1**, 505 (1969).
12) K. Bobrowski, *J. Phys. Chem.*, **84**, 3524 (1980).
13) T. Masuda, T. Hayashi, and M. Kondo, *J. Radiat. Res.*, **23**, 298 (1982).
14) D. Dougherty, K. Wittel, J. Meeks, and S. P. McGlynn, *J. Am. Chem. Soc.*, **98**, 3815 (1976).
15) S. Peng, A. Padva, and P. R. LeBreton, *Proc. Natl. Acad. Sci. U.S.A.*, **73**, 2966 (1976).
16) A. Padva, T. J. O'Donnell, and P. R. LeBreton, *Chem. Phys. Lett.*, **41**, 278 (1976).
17) C. Yu, S. Peng, I. Akiyama, J. Lin, and P. R. LeBreton, *J. Am. Chem. Soc.*, **100**, 2303 (1978).
18) J. Lin, C. Yu, S. Peng, I. Akiyama, K. li, Li Kao Lee, and P. R. LeBreton, *J. Am. Chem. Soc.*, **102**, 4627 (1980).
19) J. Lin, C. Yu, S. Peng, I. Akiyama, K. Li, Lee Kao Lee, and P. R. LeBreton, *J. Phys. Chem.*, **84**, 1006 (1980).
20) C. Yu, T. J. O'Donnell, and P. R. LeBreton, *J. Phys. Chem.*, **85**, 3851 (1981).
21) W. J. Bowen and H. L. Martin, *Arch. Biochem. Biophys.*, **107**, 30 (1964).
22) M. G. Ormerod and B. B. Singh, *Int. J. Radiat. Biol.*, **10**, 533 (1966).
23) C. Nicolau, M. McMillan, and R. O. C. Norman, *Biochim. Biophys. Acta*, **174**, 413 (1969).
24) A. V. Lakshminarayanan and V. Sasisekharan, *Biochim. Biophys. Acta*, **204**, 49 (1970).

Determination of Rate Constants for Reactions of Dichloride Anion Radical with Some Dipeptides in Aqueous Solution of KCl and $K_2S_2O_8$ by Flash Photolysis

Osamu NEDA, Kotaro YAMAUCHI, and Takahiro MASUDA*
Department of Chemistry, Faculty of Science, Tokyo Metropolitan University, Fukasawa, Setagaya-ku, Tokyo 158
(Received July 27, 1984)

Determination of rate constants for reactions of dichloride anion radical was conducted by conventional flash photolysis of aqueous solutions of KCl and $K_2S_2O_8$, where no participation of $HOCl^{-}\cdot$ is expected in decay kinetics of dichloride anion radical. The optimum conditions found for the determination are 0.1 mol dm^{-3} KCl and 10^{-4} mol dm^{-3} $K_2S_2O_8$. Under the present experimental conditions, $S_2O_8^{2-}$ serves to convert chloride ion to dichloride anion radical through reaction with hydrated electron produced by photolysis of chloride ion. For glycyltryptophan, the competition method was employed, because its transient absorption overlaps the absorption due to dichloride anion radical. The rate constants determined are almost the same as those obtained in N_2O-saturated aqueous solution of KCl (1 mol dm^{-3}). The reactivity of dipeptides toward dichloride anion radical is discussed.

Reaction of dichloride anion radical produced by radiolysis or photolysis of aqueous chloride with a protein molecule is an interesting subject, because physiological concentrations of the chloride ion in living cells are relatively high and because other dihalide anion radicals such as $Br_2^{-}\cdot$ were reported to react with proteins in a specific manner.[1-5] Rate constants for reactions of dichloride anion radicals with a variety of substrates have been determined in neutral aqueous solutions by radiation-chemical and photochemical method.[6-10] However, there remain some problems for the reported methods, because $HOCl^{-}\cdot$. is inevitably produced in radiolysis of neutral aqueous chloride and photolysis of N_2O-saturated aqueous chloride and because its absorption overlaps the absorption due to dichloride anion radical.[11] Furthermore, concentrations of chloride ion were inadequately high for protein, particularly in photolysis.

Peroxodisulfate ion reacts with hydrated electron to form $SO_4^{-}\cdot$, which oxidizes chloride ion to chlorine atom.[12,13] Chlorine atom is readily converted to dichloride anion radical in aqueous solution of potassium chloride:

$$e_{aq}^{-} + S_2O_8^{2-} \longrightarrow SO_4^{-}\cdot + SO_4^{2-}, \quad (1)$$

$$SO_4^{-}\cdot + Cl^{-} \longrightarrow SO_4^{2-} + Cl\cdot, \quad (2)$$

$$Cl\cdot + Cl^{-} \rightleftharpoons Cl_2^{-}\cdot. \quad (3)$$

In the present study, a determination of rate constants for reactions of dichloride anion radical with some biomolecules, especially dipeptides, was attempted in aqueous solutions of KCl including $K_2S_2O_8$, where no participation of $HOCl^{-}\cdot$ is expected. A comparison of the results obtained by the present method with those determined in N_2O-saturated solutions disclosed no essential difference between them.

Experimental

Peptides obtained from Nutritional Biochemicals Corp. were used without further purification. The other chemicals were all of reagent grade. Solutions for irradiation were prepared with triply distilled water by dissolving 0.1 mol dm^{-3} KCl, 10^{-4} mol dm^{-3} $K_2S_2O_8$, and a desired amount of substrate. The solutions were adjusted to pH 7 and subjected to bubbling of nitrogen for 20 min. Flash photolysis was carried out with a conventional apparatus under the conditions of 10 μs duration and 200 J input energy. Decay process of dichloride anion radical was monitored at 350 nm and analyzed on the basis of the following reactions:

$$Cl_2^{-}\cdot + Cl_2^{-}\cdot \longrightarrow Cl_2 + 2Cl^{-}, \quad (4)$$

$$Cl_2^{-}\cdot + S \longrightarrow 2Cl^{-} + \text{product(s)}. \quad (5)$$

The procedure of kinetic analysis was described in detail elsewhere.[9,10] Calculation was carried out with the aid of a microcomputer PC 8001 of Nippon Electric Co.

Results and Discussion

Optimum Conditions. In the presence of $S_2O_8^{2-}$, formation of dichloride anion radical was markedly enhanced even at low concentrations of chloride ion. Peroxodisulfate ions are photolyzed to give $SO_4^{-}\cdot$ as follows:[14,15]

$$S_2O_8^{2-} + h\nu \longrightarrow 2SO_4^{-}\cdot. \quad (6)$$

In addition to Reaction 1, therefore, Reaction 6 produces $SO_4^{-}\cdot$ and in turn increases the yield of dichloride anion radical through Reactions 2 and 3. However, formation of a large amount of the anion radical was found to be inadequate for analysis of the decay process, because it gave rise to a practical difficulty in monitoring absorption in the initial stage. Consequently, nitrogen-saturated solution of 0.1 mol dm^{-3} KCl and 10^{-4} mol dm^{-3} $K_2S_2O_8$ was chosen as an optimum condition for experimental reasons.

In this system, reaction of $SO_4^{-}\cdot$ with a substrate of dichloride anion radical was neglected because Reaction 2 takes place predominantly ($k_2=3.1\times10^8$ dm^3 mol^{-1} s^{-1}).[13] Similarly, bimolecular decay of $SO_4^{-}\cdot$ was neglected since the rate constant of Reaction 7 was reported to be 1.0×10^9 dm^3 mol^{-1} s^{-1} [16] and since $k_7[SO_4^{-}\cdot]$ was much less than $k_2[Cl_2^{-}\cdot]$:

$$SO_4^{-}\cdot + SO_4^{-}\cdot \longrightarrow S_2O_8^{2-}. \quad (7)$$

In fact, no absorption at 460 nm due to sulfate radical was observed in flash photolysis of the above solution. This implies that a decay of sulfate radical is almost complete within flash duration. The lifetime of sulfate radical was estimated to be 3.2×10^{-8} s from rate data for Reaction 2. In the present system, a complete consumption of hydrated electrons by Reaction 1 cannot be expected, because rate data of Reaction 1 suggest a possibility that at least several percent of hydrated electrons may react with dichloride anion radicals; this reaction causes a decrease in the yield of dichloride anion radicals. In any cases, the greater part of hydrated electrons will be consumed within flash duration, because the life time is estimated to be 1 μs. At 40 μs after start of flash, when analysis of the decay process starts, there may remain dichloride anion radicals as an overwhelming majority of reactive transients in the system.

Comparison of Rate Constants. Table 1 shows the rate constants determined by the present method, together with those obtained in N_2O-saturated solutions. Two kinds of substrates were taken for comparison, because dichloride anion radical abstracts a hydrogen atom from an aliphatic compound and oxidizes an unsaturated compound.[6,16,17] The values determined in the present study are in good agreement with those previously obtained in N_2O-saturated solutions. This implies that the contribution of $HOCl^{-}\cdot$ may be neglected in kinetic analysis based on the decay of the absorption at 350 nm. Since an OH-adduct of 5-aminouracil was observed in neutral N_2O-saturated solution,[10] the formation of hydroxyl radicals is confirmed. In neutral N_2O-saturated solutions, reactions

$$e_{aq}^{-} + N_2O \longrightarrow N_2 + \cdot OH + OH^{-}, \quad (8)$$

$$\cdot OH + Cl^{-} \rightleftharpoons HOCl^{-}\cdot \quad (9)$$

take place. The equilibrium constant of Reaction 9 was reported to be (0.70±0.13) dm^3 mol^{-1} by Jayson *et al.*[11] and hence the initial concentration of $HOCl^{-}\cdot$ is estimated as 70 percent of dichloride anion radicals on the assumption that Reaction 8 proceeds with 100 percent efficiency. Since the absorption coefficient at 350 nm is approximately half that of the dichloride anion radical,[11] the contribution of $HOCl^{-}\cdot$ amounts to about 26 percent of the absorbance at 350 nm. However, the decay constant of dichloride anion radical ($2k$ for Reaction 4) in N_2O-saturated solution was found to be essentially the same as that determined in the present system. Studying pulse radiolysis, Anbar and Thomas[8] pointed out that hydroxyl radicals formed in the bulk of a solution containing 10^{-3} mol dm^{-3} H_2O_2 do not produce any dichloride anion radicals (no change in absorbance at 365 nm). However, Jayson *et al.*[11] reported the transient spectrum of $HOCl^{-}\cdot$ and kinetic data for this species. The discrepancy cannot be interpreted at present, although the present results agree with the former.

Rate Constants of Dipeptides. In our previous paper,[8] rate constants for several aliphatic dipeptides reacting with dichloride anion radical were reported. The present method was applied to other dipeptides whose corresponding rate constants for the anion radical had not been determined. Values determined by the present method are listed in Table 2. The present method could not be applied to glycyltryptophan because of a transient absorption appearing in the region of the absorption due to dichloride anion radical. Tryptophan is known to yield an indolyl radical on one-electron oxidation and deprotonation.[19-22] The indolyl radical has another absorption with a maximum at 510 nm and is relatively long-lived. The decay constant in 0.1 mol dm^{-3} KCl was determined to be $(6.9\pm0.6)\times10^8$ dm^3 mol^{-1} s^{-1}. Since the dichloride anion radical has no absorption at 510 nm, a com-

Table 1. Comparison of rate constants determined in N_2O system with those in N_2-$K_2S_2O_8$ system

Compound	Rate constant/10^7 dm^3 mol^{-1} s^{-1}	
	N_2O	N_2-$K_2S_2O_8$
Thymine	32±3[a]	36±2
Cytosine	35±1[a]	35±2
Uracil	28±1[a]	28±3
Glycylvaline	4.1±0.5[b]	4.3±0.3
Glycylleucine	5.4±0.1[b]	5.1±0.1
Glycylisoleucine	5.8±0.7[b]	5.2±0.3

a) Ref. 9. b) Ref. 8.

Table 2. Rate constants of dichloride anion radical with several dipeptides

Peptide	Rate constant/10^7 dm^3 mol^{-1} s^{-1}
Glycylserine	4.0±0.2
Glycylthreonine	2.7±0.5
Glycylaspartic acid	3.9±0.2
Glycylasparagine	5.2±0.1
Glycylglutamic acid	2.7±0.4
Glycyllysine	3.4±0.7
Glycylproline	4.2±0.2
Glycylhistidine	21±3
Glycylphenylalanine	19±2
Glycyltyrosine	59±2
Glycyltryptophan	280±30[a]

a) Competition method.

petition kinetics was attempted to determine the rate constant for glycyltryptophan, in which use was made of the absorption at 510 nm due to the indolyl radical produced from glycyltryptophan through oxidation by dichloride anion radical:

$$Cl_2^{-\cdot} + TH \longrightarrow 2Cl^- + TH^{+\cdot}, \quad (10)$$

$$TH^{+\cdot} \longrightarrow T^{\cdot} + H^+, \quad (11)$$

where TH represents glycyltryptophan and TH^+ is the cation radical of glycyltryptophan produced by one-electron oxidation. $T^{\cdot}$ designates a neutral radical formed from the cation radical after deprotonation. Since glycyltryptophan yields also indolyl radical by photoionization according to

$$TH + h\nu \longrightarrow TH^+ + e_{aq}^-, \quad (12)$$

Reactions 5, 10, 11, and 12 should be considered in the competition kinetics. For the decrease in the absorbance at 510 nm caused by the presence of a substrate, the following equation is derived:

$$\frac{1}{A_0 - A} = \frac{1}{\varepsilon l[T^{\cdot}]}\left(1 + \frac{k_{10}[TH]}{k_5[S]}\right), \quad (13)$$

where A_0 and A designate the absorbances at 510 nm in the absence and presence of substrate, respectively at 150 μs after start of flash. A reciprocal plot of $(A_0 - A)$ *vs.* [TH]/[S] provides a straight line and k_{10}/k_5 is obtained from the slope and intercept as shown in Fig. 1. As reference substrates, were used glycylvaline, glycylleucine, glycylnorleucine, and glycyl-α-aminobutyric acid, because their reaction products have no absorption at 510 nm.

As shown in Table 2, dipeptides having C=C double bonds are more reactive than saturated ones toward the anion radical. For aliphatic dipeptides, the ratio of the rate constant with hydroxyl radical to that with the anion radical has been found to be about 66.[9] The reactivity of glycylproline can be explained in terms of this correlation. However, a large deviation from the correlation was observed for aliphatic dipeptides having such a functional group as hydroxyl, carboxyl, or carbamoyl group. Since the ratio of the rate constant with hydroxyl radical to that with dichloride anion radical is much less than 66 for the aliphatic dipeptide having some functional group, these groups may affect the reaction rate differently from hydroxyl radical working in hydrogen atom abstraction reaction.

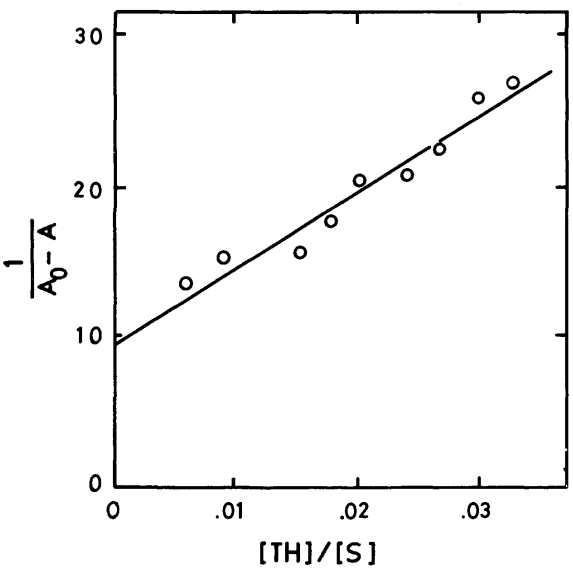

Fig. 1. Kinetic plots according to Equation 13. [TH] = 10^{-4} mol dm^{-3}. S: Clycylleucine.

Aromatic and heterocyclic dipeptides seem to undergo one-electron oxidation, because they are very reactive toward dichloride anion radicals. Glycyltryptophan is most reactive toward the anion radical in neutral solution as well as in acid solution.[1] Since tryptophan is often found in active sites of enzyme proteins and the physiological concentration of chloride ion is considerably high, the role of dichloride anion radical must be taken into consideration in radiation- or light-induced damage on biological systems.

References

1) G. E. Adams, J. E. Aldrich, R. H. Bisby, R. B. Cundall, J. L. Redpath, and R. L. Willson, *Radiat. Res.*, **49**, 278 (1972).
2) G. E. Adams, R. S. Bisby, R. B. Cundall, J. L. Redpath, and R. L. Willson, *Radiat. Res.*, **49**, 290 (1972).
3) J. L. Redpath, *Int. J. Radiat. Biol.*, **22**, 99 (1972).
4) P. B. Roberts, *Int. J. Radiat. Biol.*, **24**, 143 (1973).
5) G. E. Adams, J. L. Redpath, R. H. Bisby, and R. B. Cundall, *J. Chem. Soc., Faraday Trans. 1*, **69**, 1608 (1973).
6) K. Hasegawa and P. Neta, *J. Phys. Chem.*, **82**, 854 (1978).
7) T. Masuda, S. Shimada, and M. Kondo, *J. Radiat. Res.*, **20**, 209 (1979).
8) T. Masuda, T. Hayashi, and M. Kondo, *J. Radiat. Res.*, **23**, 298 (1982).
9) T. Masuda, T. Kimura, E. Kadoi, T. Takahashi, K. Yamauchi, and M. Kondo, *J. Radiat. Res.*, **24**, 165 (1983).
10) T. Masuda, R. Gunji, T. Kimura, and K. Yamauchi, *Bull. Chem. Soc. Jpn.*, **56**, 3595 (1983).
11) G. G. Jayson, B. J. Parsons, and A. J. Swallow, *J. Chem. Soc., Faraday Trans. 1*, **69**, 1597 (1973).
12) W. Roebke, M. Renz, and A. Henglein, *Int. J. Radiat. Phys. Chem.*, **1**, 39 (1969).
13) O. P. Chawla, and R. W. Fessenden, *J. Phys. Chem.*, **79**, 2693 (1975).
14) M.-S. Tsao and W. K. Wilmarth, *J. Phys. Chem.*, **63**, 346 (1959).
15) L. Dogliotti and E. Hayon, *J. Phys. Chem.*, **71**, 2511 (1967).
16) K. Bobrowski, *J. Phys. Chem.*, **84**, 3524 (1980).
17) M. D. Sevilla, D. Suryanarayana, and K. M. Morehouse, *J. Phys. Chem.*, **85**, 1027 (1981).
18) M. Anbar and J. K. Thomas, *J. Phys. Chem.*, **68**, 3829 (1964).
19) J. L. Redpath, R. Suntus, J. Ovadia, and L. I. Grossweiner, *Int. J. Radiat. Biol.*, **27**, 201 (1975).
20) D. V. Bent and E. Hayon, *J. Am. Chem. Soc.*, **97**, 2612 (1975).
21) E. J. Land and W. A. Prütz, *Int. J. Radiat. Biol.*, **32**, 203 (1977).
22) W. A. Prütz and E. J. Land, *Int. J. Radiat. Biol.*, **36**, 513 (1979).

The Crystal and Molecular Structures of Esculetin 6-Glucoside and 7-Glucoside

Katsuhiko UENO,* Masaru SHIRAKI, Mitsuhiko SATO,† and Norio SAITO††
Research Institute for Polymers and Textiles, Yatabe-Higashi 1-1-4, Tsukuba, Ibaraki 305
†*Department of Biology, Faculty of Science, Tokyo Metropolitan University, Setagaya-ku, Tokyo 158*
††*Chemical Laboratory, Meiji-gakuin University, Minato-ku, Tokyo 108*
(Received January 28, 1984)

The structures of two dihydroxycoumarin glucosides, esculetin 6-glucoside (**E6G**) and esculin 7-glucoside (**E7G**) have been determined by the X-ray analysis. The crystal data are: **E6G**, $C_{15}H_{16}O_9 \cdot 1.5H_2O$, orthorhombic $P2_12_12_1$ with a=11.358(2), b=36.850(9), c=7.663(1) Å and Z=8: and **E7G**, $C_{15}H_{16}O_9 \cdot 2H_2O$, orthorhombic $P2_12_12_1$ with a=4.507(1), b=13.077(3), c=27.748(5) Å and Z=4. Both structures were solved by the direct method and refined by the least-squares to the final R values of 0.073 (2036 reflections) for **E6G** and 0.069 (1037 reflections) for **E7G**. The geometries of the glucosyl linkages in **E6G** and **E7G** are different: the torsion angles around the glucosidic C-O bond are −58.2° and 14.3° for the two crystallographically independent **E6G** molecules and 9.9° for **E7G**. The glucosidation at the 6-hydroxyl group causes little effect on the conjugation of the coumarin moiety, whereas the conjugation is greatly decreased in the glucosidation at 7-hydroxyl group. This fact suggests that **E6G** is energetically more stable than **E7G**. The enzymatic transglucosidation from 7- to 6-hydroxyl group may proceed utilizing such an energy difference.

In the course of investigation on the biosyntheses of hydroxylated coumarin glucosides, characteristic transglucosidases were isolated from *Daphne odora* and *Cichorium intybus*. In *C.intybus*, it is considered that 7-*O*-(β-D-glucosyloxy)-6-hydroxycoumarin (or esculetin 7-glucoside: **E7G**) is formed from *p*-glucosyloxycinnamic acid, and that it is changed into 6-*O*-(β-D-glucosyloxy)-7-hydroxycoumarin (or esculetin 6-glucoside: **E6G**) by the action of transglucosidase.[1] A similar reaction has been observed for 7,8-dihydroxycoumarin (or daphnetin: **D**), where glucose is transferred from 7- to 8-hydroxyl group.[2] The transglucosidation to 7-hydroxyl group from 6- or 8-hydroxyl group was undetectable in either case. Figure 1 shows the above reactions schematically. In order to elucidate the mechanism, the structures of esculetin(**E**),[3] **D**,[4] daphnetin 8-glucoside(**D8G**)[5] and daphnetin 7-glucoside(**D7G**)[6] have been determined. The coumarin moiety of **D8G** has approximately the same structure as those of **D** and **E**, whereas that of **D7G** is significantly different from that of **D8G**. The glucosidation at 7-hydroxyl group has an important role in the resonance system of the coumarin moiety. Moreover, the geometries of the glucosyl linkages of **D8G** and **D7G** are different. It has been proposed that such structural difference is a factor for the transglucosidation from **D7G** to **D8G**. Present paper reports the structures of **E6G** and **E7G** and discusses the mechanism of another transglucosidation from **E7G** to **E6G** on the basis of the two structures.

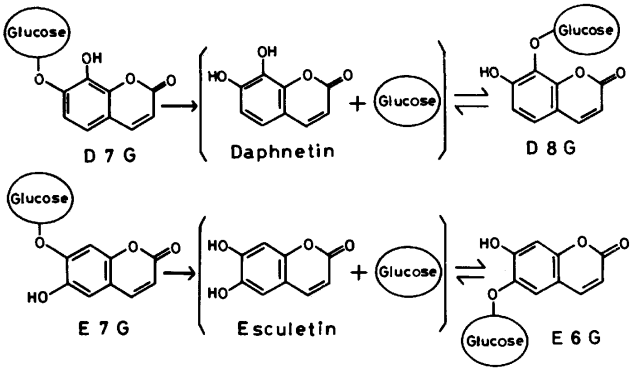

Fig. 1. Interconversions of dihydroxycoumarin 7-glucoside to 6- or 8-glucoside.

Experimental

Both crystals were prepared by slow evaporation from an aqueous ethanol solution. The lattice parameters and the intensity data up to 2θ=120° were obtained on a Nicolet P3/F four-circle diffractometer with graphite monochromated Cu $K\alpha$ radiation. An $\omega/2\theta$ scanning mode was applied with the scanning range and rate of 1.0° (ω) plus α_1—α_2 divergence and 1° (2θ)min^{-1}, respectively. Space groups were assigned from systematic absences. No correction was made for absorption. The densities were measured by flotation method in a mixture of dichloromethane and carbon tetrachloride. Crystal data of **E6G**; $C_{15}H_{16}O_9 \cdot 1.5H_2O$, F.W=367.3, orthorhombic $P2_12_12_1$, a=11.358(2), b=36.850(9), c=7.663(1) Å, U=3207.3 (11) Å^3, Z=8, needle, 0.08×0.04×0.18 mm^3 in size, D_x=1.524 g cm^{-3}, D_m=1.52 g cm^{-3}, μ(Cu $K\alpha$)=13.0 cm^{-1}, 2552 reflections measured of which 2036 had net intensities. Crystal data of **E7G**; $C_{15}H_{16}O_9 \cdot 2H_2O$, F.W=376.3, orthorhombic $P2_12_12_1$, a=4.507(1), b=13.077(3), c=27.748(5) Å, U=1635.4(6) Å^3, Z=4, thin plate, 0.08×0.04×0.02 mm^3 in size, D_x=1.528 g cm^{-3}, D_m=1.53 g cm^{-3}, μ(Cu $K\alpha$)=13.1 cm^{-1}, 1354 reflections measured of which 1037 had net intensities.

Structure Determination

Both structures were solved by the direct method[7] and the structural parameters were refined by the block-diagonal least-squares method. Anisotropic thermal parameters were applied for the non-hydrogen atoms. All the hydrogen atoms were located on difference electron density maps. The refinement including the

contribution of the hydrogen atoms with isotropic temperature factors converged to the R values of 0.073 and 0.069 for **E6G** and **E7G**, respectively. The weighting scheme used in the final stages were $w=((\sigma|F_o|)^2+(0.00012|F_o|)^2)^{-1}$ and $w=((\sigma|F_o|)^2+(0.00016|F_o|^2)^{-1}$ for **E6G** and **E7G**, respectively. Atomic scattering factors were taken from Ref. 8. The final atomic parameters are shown in Table 1.[9]

Results

The perspective drawings of the two crystallographically independent **E6G** molecules, **E6G(A)** and **E6G(B)**, and **E7G** with the numbering system of the atoms are shown in Fig. 2. Bond lengths and angles are listed in Table 2. The coumarin moieties are nearly planar.[9] The conformations of glucosyl linkages are different among the three molecules. In **E6G(B)** and **E7G**, the torsion angles around the glucosidic C-O bond, C(5)-C(6)-O(1')-C(1') for **E6G(B)** and C(8)-C(7)-O(1')-C(1') for **E7G**, are 14.3° and 9.9°, respectively, whereas the corresponding angle in **E6G(A)** is −58.2°. The former "in-plane" conformation appears to cause considerable intramolecular repulsion between the coumarin and glucose moieties, compared with the latter "out-of-plane" conforma-

Table 1. Positional and thermal parameters with standard deviations in parentheses

E6G

	x	y	z	B_{eq}/Å^2
O(1)A	0.2430(5)	0.2613(2)	0.0654(9)	3.01
C(2)A	0.1834(9)	0.2297(2)	0.0264(14)	3.12
C(3)A	0.0584(9)	0.2293(3)	0.0687(14)	3.37
C(4)A	0.0052(8)	0.2574(3)	0.1456(15)	3.34
C(5)A	0.0205(8)	0.3207(2)	0.2673(15)	2.99
C(6)A	0.0866(8)	0.3508(2)	0.2938(13)	2.36
C(7)A	0.2050(8)	0.3516(2)	0.2480(13)	2.54
C)8)A	0.2585(8)	0.3211(2)	0.1710(13)	2.40
C(9)A	0.1874(8)	0.2911(2)	0.1424(13)	2.49
C(10)A	0.0696(8)	0.2899(2)	0.1889(13)	2.32
O(2)A	0.2396(6)	0.2058(2)	−0.0385(11)	4.27
O(1')A	0.0404(6)	0.3815(2)	0.3792(9)	2.95
O(7)A	0.2660(5)	0.3829(2)	0.2794(10)	3.50
C(1')A	−0.0587(7)	0.3971(2)	0.2926(12)	2.00
C(2')A	−0.1254(8)	0.4180(2)	0.4305(13)	2.48
C(3')A	−0.2292(7)	0.4376(2)	0.3430(11)	1.68
C(4')A	−0.1824(7)	0.4609(2)	0.1941(13)	2.20
C(5')A	−0.1090(8)	0.4378(2)	0.0683(13)	2.16
C(6')A	−0.0539(9)	0.4588(2)	−0.0736(13)	2.77
O(2')A	−0.1716(6)	0.3950(2)	0.5595(9)	3.95
O(3')A	−0.2904(5)	0.4597(2)	0.4664(9)	2.85
O(4')A	−0.2840(5)	0.4755(2)	0.1009(9)	2.65
O(5')A	−0.0141(5)	0.4208(1)	0.1644(9)	2.36
O(6')A	0.0013(6)	0.4346(2)	−0.1943(8)	3.27
O(1)B	0.0308(5)	0.2453(2)	0.6352(10)	3.12
C(2)B	0.0946(10)	0.2183(3)	0.5556(14)	3.66
C(3)B	0.2136(10)	0.2259(3)	0.5053(16)	3.89
C(4)B	0.2626(9)	0.2594(2)	0.5348(14)	2.84
C(5)B	0.2429(7)	0.3212(2)	0.6654(14)	2.26
C(6)B	0.1727(8)	0.3458(2)	0.7479(13)	2.33
C(7)B	0.0544(8)	0.3382(2)	0.7848(13)	2.64
C(8)B	0.0064(8)	0.3041(2)	0.7510(14)	2.58
C(9)B	0.0806(8)	0.2795(2)	0.6696(14)	2.52
C(10)B	0.1941(8)	0.2864(2)	0.6231(13)	2.52
O(2)B	0.0406(7)	0.1900(2)	0.5301(11)	4.83
O(1')B	0.2058(5)	0.3798(2)	0.8065(9)	2.78
O(7)B	−0.0175(6)	0.3626(2)	0.8637(11)	4.25
C(1')B	0.3129(8)	0.3946(2)	0.7459(14)	2.82
C(2')B	0.3136(8)	0.4341(2)	0.8128(13)	2.53
C(3')B	0.4321(8)	0.4521(2)	0.7839(13)	2.34
C(4')B	0.5322(8)	0.4272(2)	0.8465(13)	2.24
C(5')B	0.5175(8)	0.3899(2)	0.7630(12)	1.94
C(6')B	0.6154(8)	0.3630(2)	0.8182(13)	2.50
O(2')B	0.2227(6)	0.4555(2)	0.7335(10)	3.30
O(3')B	0.4416(5)	0.4856(2)	0.8791(10)	3.26
O(4')B	0.6442(5)	0.4418(1)	0.7987(9)	2.45
O(5')B	0.4068(5)	0.3756(1)	0.8200(8)	2.08
O(6')B	0.6285(6)	0.3621(2)	1.0006(10)	3.57
O(1)W	0.4955(7)	0.3747(2)	0.2853(10)	4.23
O(2)W	0.2282(6)	0.4585(2)	0.3752(11)	4.26
O(3)W	0.4502(7)	0.4673(2)	0.2487(11)	5.61

E7G

	x	y	z	B_{eq}/Å^2
O(1)	0.6308(15)	0.1098(4)	0.3482(2)	3.57
C(2)	0.5803(21)	0.0217(7)	0.3209(3)	3.41
C(3)	0.3831(20)	0.0308(7)	0.2802(3)	3.83
C(4)	0.3393(20)	−0.0352(7)	0.2598(3)	3.32
C(5)	0.1584(20)	0.3024(7)	0.2885(3)	4.02
C(6)	0.2103(18)	0.3855(7)	0.3174(3)	2.70
C(7)	0.4106(19)	0.3749(5)	0.3556(3)	2.45
C(8)	0.5455(18)	0.2829(5)	0.3671(3)	2.58
C(9)	0.4870(16)	0.2011(5)	0.3367(3)	2.34
C(10)	0.3031(18)	0.2111(7)	0.2970(3)	3.23
O(2)	0.7150(15)	−0.0526(5)	0.3337(2)	4.74
O(6)	0.0790(15)	0.4759(5)	0.3073(2)	3.63
C(1')	0.6616(17)	0.4726(7)	0.4160(3)	2.35
C(2')	0.7473(17)	0.5864(5)	0.4215(3)	1.88
C(3')	0.9345(18)	0.6056(5)	0.4658(3)	2.16
C(4')	0.8036(17)	0.5541(6)	0.5096(3)	2.45
C(5')	0.7494(18)	0.4413(6)	0.4988(3)	2.33
C(6')	0.6015(20)	0.3835(6)	0.5402(3)	3.38
O(1')	0.4454(14)	0.4654(4)	0.3806(2)	2.95
O(2')	0.8838(13)	0.6233(4)	0.3796(2)	2.45
O(3')	0.9561(13)	0.7134(4)	0.4729(2)	2.75
O(4')	1.0524(13)	0.5638(4)	0.5478(2)	2.62
O(5')	0.5472(13)	0.4331(4)	0.4593(2)	2.25
O(6')	0.5567(14)	0.2777(4)	0.5293(2)	3.32
O(W1)	0.6246(16)	0.6556(5)	0.6108(2)	4.40
O(W2)	0.4833(17)	0.7322(5)	0.3268(3)	5.60

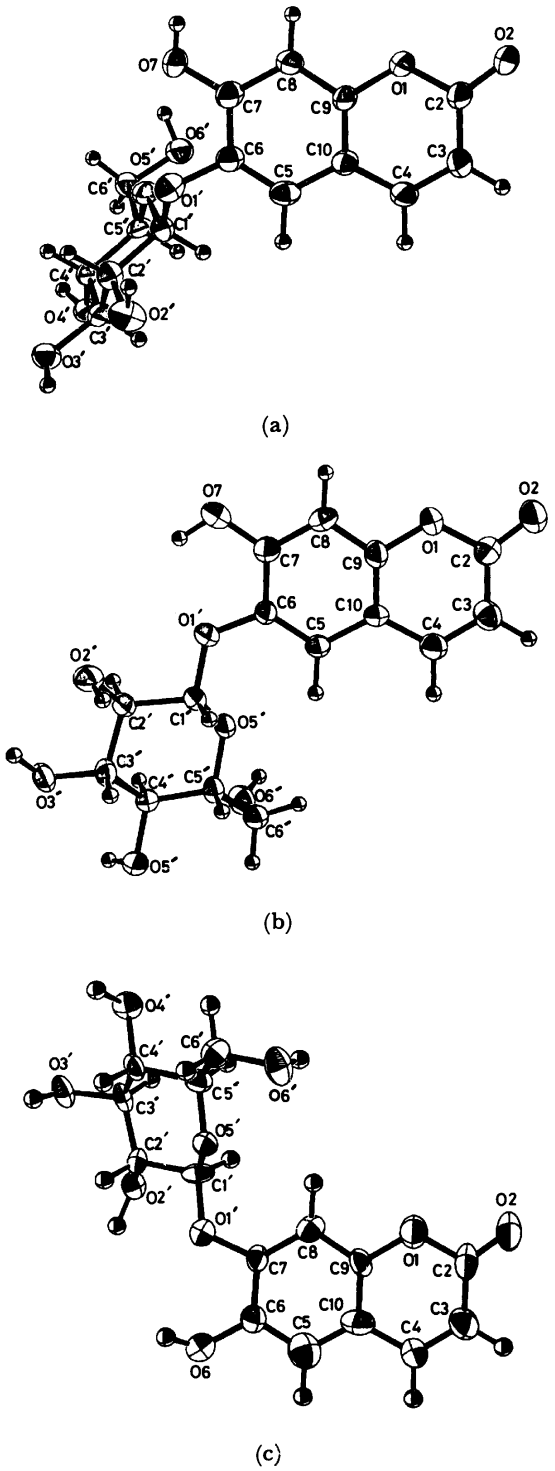

Fig. 2. Perspective drawing of the molecules with the numbering systems; (a): **E6G(A)**, (b): **E6G(B)**, (c): **E7G**.

tion. The angles of C(6)-O(1')-C(1') and C(5)-C(6)-O(1') in **E6G(B)** are 118.5(8)° and 126.2(8)°, which are significantly larger than those in **E6G(A)**, 113.7(7)° and 121.4(9)°, respectively. The corresponding angles in **E7G**, C(7)-O(1')-C(1') and C(8)-C(7)-O(1'), are 119.5(6)° and 125.4(7)°, respectively, and are similar to those of **E6G(B)**. They must be expanded to avoid the short contacts between the coumarin and glucose moieties.

In the benzene rings of **E6G(A)** and **E6G(B)**, the C(5)-C(6) bonds are significantly shorter than C(5)-C(10) and C(6)-C(7), and C(8)-C(9) is slightly shorter than C(7)-C(8). Such a quinonoid structure has been found in the structures of **D8G** and other 7-hydroxylated coumarins. In **E7G**, however, the six bonds in the benzene ring are approximately equivalent, as observed in **D7G**.

The glucose moieties in the three molecules are in C_1 chair conformations. The endo- and exocyclic torsion angles in the glucose portions are in good agreement with each other. The conformations around the C(5')-C(6') bond are trans-gauche in **E6G(A)** and **E7G** and gauche-gauche in **E6G(B)**. Each conformation corresponds to either of the two favored arrangement of the primary alcohol group in glucopyranoside.[10]

The bond lengths in the sequence of C(5')-O(5')-C(1')-O(1')-R have been discussed as an anomeric effect. Sundaralingam claimed that in α-pyranose C(5')-O(5')>O(5')-C(1')≃C(1')-O(1'), while in β-anomer C(5')-O(5')≃O(5')-C(1')>C(1')-O(1').[11] In **E6G** and **E7G**, however, C(5')-O(5') are longer by 0.019—0.041 Å than O(5')-C(1') and C(1')-O(1'). The same trend is observed in other aromatic β-glucosides so far determined such as in **D7G**, **D8G** and 1-naphthyl tetra-*O*-acetyl-β-D-glucoside,[12] and even in the α-anomer such as in *p*-nitrophenyl α-D-glucoside.[13] This indicates that in aromatic glucopyranosides, not only in α-anomer but also in β-anomer, C(5')-O(5') is longer than O(5')-C(1') and C(1')-O(1').

Figure 3 shows the crystal structure of **E6G** viewed along the c axis. The coumarin planes of **A** and **B** molecules are stacked alternately along the c axis. All the hydroxyl groups and water molecules make hydrogen bonds and form a three-dimensional network. The hydrogen bonding schemes around the glucose moieties are different between **A** and **B** as shown in Fig. 4. All the hydroxyl groups of **E6G(B)** participate in hydrogen bonds as a donor and an acceptor. In **E6G(A)**, on the other hand, O(2')H acts as a very weak donor and not an acceptor. The hydrogen bonding system of **E6G(B)** is apparently more favorable than that of **E6G(A)**.

The crystal structure of **E7G** viewed along the a axis is shown in Fig. 5. The molecules are connected by the hydrogen bonds to form sheets perpendicular to the c axis. The sheets are stacked along the c axis with the van der Waals contacts.

Discussion

The glucose moiety at the 7-position takes the "in-plane" conformation in **E7G** as in **D7G**. The torsion

Table 2. Bond lengths (l/Å) and angles (ϕ/°) with estimated standard deviations in parentheses

	E6G(A)	E6G(B)	E7G		E6G(A)	E6G(B)	E7G
O(1)-C(2)	1.379(13)	1.374(13)	1.395(11)	C(9)-C(10)	1.384(14)	1.361(14)	1.384(11)
O(1)-C(9)	1.396(12)	1.404(12)	1.393(10)	C(1')-C(2')	1.509(13)	1.543(15)	1.542(12)
C(2)-C(3)	1.455(15)	1.431(16)	1.441(13)	C(1')-O(1')	1.427(11)	1.410(13)	1.387(11)
C(2)-O(2)	1.196(14)	1.224(14)	1.198(11)	C(1')-O(5')	1.407(11)	1.396(12)	1.405(11)
C(3)-C(4)	1.337(16)	1.374(16)	1.320(13)	C(2')-C(3')	1.536(13)	1.513(14)	1.511(11)
C(4)-C(10)	1.442(15)	1.430(15)	1.464(13)	C(2')-O(2')	1.401(12)	1.435(12)	1.400(10)
C(5)-C(6)	1.353(15)	1.363(14)	1.369(13)	C(3')-C(4')	1.521(13)	1.536(14)	1.508(11)
C(5)-C(10)	1.399(15)	1.435(14)	1.379(13)	C(3')-O(3')	1.428(11)	1.438(12)	1.424(10)
C(6)-C(7)	1.389(14)	1.400(14)	1.398(13)	C(4')-C(5')	1.532(14)	1.525(13)	1.522(11)
C(6)-O(1')[a]	1.408(12)	1.384(12)	1.349(11)	C(4')-O(4')	1.458(12)	1.427(12)	1.422(10)
C(7)-C(8)	1.405(14)	1.391(14)	1.383(12)	C(5')-C(6')	1.532(14)	1.548(14)	1.527(12)
C(7)-O(7)[b]	1.366(13)	1.354(13)	1.379(11)	C(5')-O(5')	1.446(11)	1.430(11)	1.428(10)
C(8)-C(9)	1.384(14)	1.387(15)	1.386(11)	C(6')-O(6')	1.429(12)	1.405(12)	1.428(11)

a) C(6)-O(6) in **E7G**, b) C(7)-O(1') in **E7G**.

	E6G(A)	EG(B)	E7G		E6G(A)	EG(B)	E7G
C(2)-O(1)-C(9)	122.3(8)	121.3(8)	120.3(8)	C(5)-C(10)-C(9)	118.0(9)	118.3(9)	120.0(8)
O(1)-C(2)-C(3)	116.1(9)	118.4(10)	117.2(8)	C(6)-O(1')-C(1')[c]	113.7(7)	118.5(8)	119.5(6)
O(1)-C(2)-O(2)	116.8(10)	115.0(10)	115.1(8)	O(1')-C(1')-C(2')	106.0(7)	105.0(8)	108.1(7)
C(3)-C(2)-O(2)	127.1(10)	126.6(11)	127.6(8)	O(1')-C(1')-O(5')	106.8(7)	109.3(8)	108.9(6)
C(2)-C(3)-C(4)	121.9(10)	120.9(11)	122.2(8)	C(2')-C(1')-O(5')	110.7(7)	109.5(8)	111.1(7)
C(3)-C(4)-C(10)	121.1(10)	118.8(10)	121.3(8)	C(1')-C(2')-C(3')	108.6(8)	111.5(8)	112.4(6)
C(6)-C(5)-C(10)	120.4(10)	118.2(9)	120.3(9)	C(1')-C(2')-O(2')	111.9(8)	111.9(8)	111.0(6)
C(5)-C(6)-C(7)	121.0(10)	121.5(9)	118.4(8)	C(3')-C(2')-O(2')	107.9(8)	109.6(8)	111.9(6)
C(5)-C(6)-O(1')[a]	121.4(9)	126.4(9)	119.8(7)	C(2')-C(3')-C(4')	109.0(7)	110.6(8)	111.3(6)
C(7)-C(6)-O(1')[a]	117.4(9)	112.2(8)	121.8(7)	C(2')-C(3')-O(3')	110.7(7)	111.6(8)	108.3(6)
C(6)-C(7)-C(8)	120.5(9)	121.2(9)	122.9(7)	C(4')-C(3')-O(3')	110.1(7)	107.3(8)	110.9(6)
C(6)-C(7)-O(7)[b]	117.6(9)	122.3(9)	111.6(6)	C(3')-C(4')-C(5')	110.3(8)	108.9(8)	109.5(6)
C(8)-C(7)-O(7)[b]	121.9(9)	116.4(9)	125.4(7)	C(3')-C(4')-O(4')	107.4(7)	110.8(8)	107.6(6)
C(7)-C(8)-C(9)	116.9(9)	115.9(9)	116.4(7)	C(5')-C(4')-O(4')	109.1(8)	109.1(8)	109.9(6)
O(1)-C(9)-C(8)	115.5(9)	115.3(9)	115.5(6)	C(4')-C(5')-C(6')	113.7(8)	112.6(8)	113.5(7)
O(1)-C(9)-C(10)	121.3(9)	120.0(9)	122.7(7)	C(4')-C(5')-O(5')	109.0(8)	107.5(7)	109.1(6)
C(8)-C(9)-C(10)	123.2(9)	124.8(10)	121.7(7)	C(6')-C(5')-O(5')	106.6(8)	108.0(7)	105.2(6)
C(4)-C(10)-C(5)	124.7(10)	121.2(9)	123.5(7)	C(1')-O(5')-C(5')	110.8(7)	111.1(7)	113.2(7)
C(4)-C(10)-C(9)	117.2(9)	120.6(9)	116.0(8)	C(5')-C(6')-O(6')	109.6(8)	111.3(8)	112.3(7)

a) O(1') should be replaced by O(6) in **E7G**. b) O(7) should be replaced by O(1') in **E7G**. c) C(7)-O(1')-C(1') angle in **E7G**.

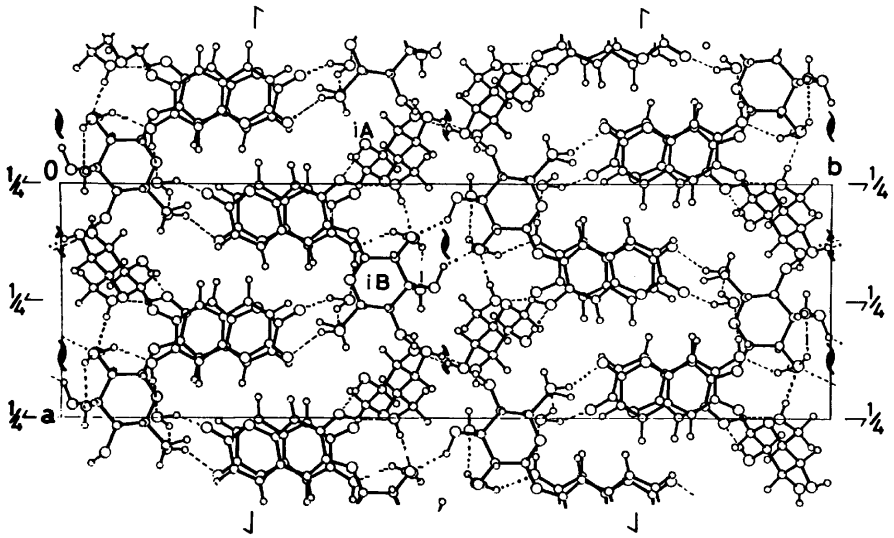

Fig. 3. The crystal structure of **E6G** viewed down the c axis. Hydrogen bonds are indicated by broken lines.

angles in the aromatic β-glucosides so far determined are summarized in Table 3. The glucose or alkyl moiety bonded to the hydroxyl group tend to take the "in-plane" conformation, in which π electrons of the oxygen atom of glucosyl linkage would take part in the resonance of the aromatic ring. Such an "in-plane" conformation would cause the intramolecular repulsion between the coumarin and glucose moieties as observed in the structures of **E7G** and **D7G**. The resonance energy brought about by the "in-plane" conformation may be compensated by the distorsion of the structure. **E6G** or **D8G**, however, is not required to take the "in-plane" conformation, since 6- and 8-hydroxyl group has little effect on the resonance of the coumarin moiety.

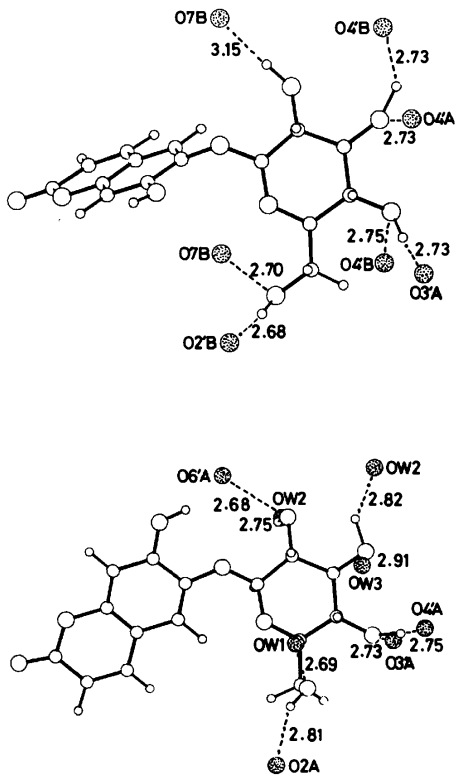

Fig. 4. Hydrogen bonding systems around the glucose moieties of **E6G**(upper; **A**, lower; **B** molecule).

Although **E6G(A)** has an "out-of-plane" conformation, **E6G(B)** is in an "in-plane" conformation. This may be explained by the difference of the hydrogen bond systems of the two molecules as shown in Fig. 4. The intramolecular repulsion in **E6G(B)** would be stabilized by the fairly strong intermolecular hydrogen bonds. In solution, therefore, **E6G** would have the structure close to that of **E6G(A)**.

The structures of the 7-hydroxylated coumarins are well explained by the resonance shown in Fig. 6. The benzene ring apparently takes a quinonoid structure in 7-hydroxycoumarin (umbelliferone: U),[16] 4-methylumlbelliferone,[17] **D**[4] and **E**.[3] Since **E6G** and **D8G** have essentially the same structure as those observed in the 7-hydroxylated coumarins, the glucosidation at the 8-hydroxyl group or at the 6-hydroxyl group causes little effect on the structure of the coumarin moiety. In **E7G** and **D7G**, however, the contributions of the limiting structure(II) is significantly smaller than those in **E6G** and **D8G**, respectively. In the structure of 7-ethoxycoumarin, recently determined, the contribution of (II) are apparently lowered compared with the structure of 7-hydroxycoumarin.[16] The glucosidation at the 7-hydroxyl group tends to decrease the cojugation effect. This seems to indicate that **E6G** and **D8G** are energetically more stable than **E7G** and **D7G**, respectively.

Although the structure of the active site of the enzyme is still unknown, the mechanism of the transglucosidation, as shown in Fig. 1, can be explained by the thermodynamic properties of the substrates and products. From the intermediate stationary state, both of forward and backward reactions could occur.

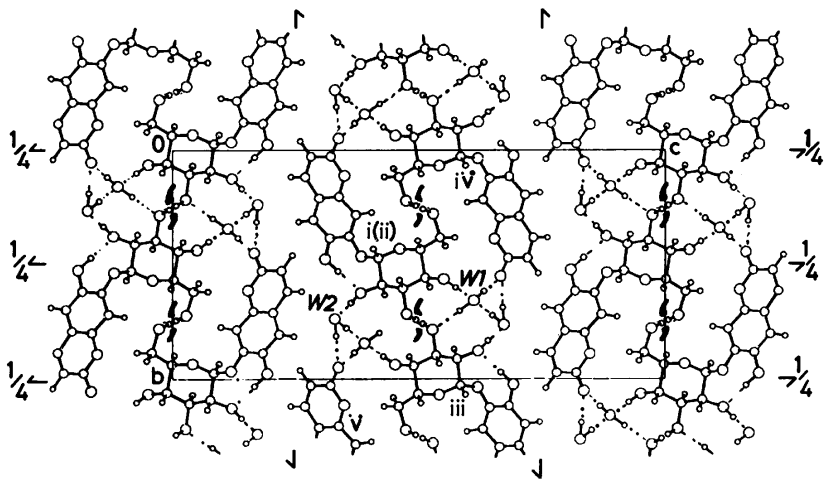

Fig. 5. The crystal structure of **E7G** viewed down the a axis. Hydrogen bonds are indicated by broken lines.

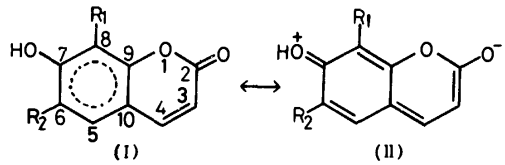

	E	D	U
R_1	H	OH	H
R_2	OH	H	H

Fig. 6. The conjugation system expected in 7-hydroxylated coumarins.

Table 3. Geometry of glycosyl linkages in aromatic glycosides

	ϕ/° a)	α/° b)	
E7G	9.9	119.6	This work
E6G(A)	−58.2	113.7	This work
E6G(B)	14.3	118.5	This work
D7G	13.8	118.5	6
D8G	−78.2	114.4	5
PNPNAG c)	16.4	120.0	14
PNPX d)	23.6	118.5	15
NTAG e)	11.2	119.7	12
U7E f)	2.6	117.7	16

a) Torsion angle around the bond between glycosidic O and aromatic C atoms (e.g., C(1')-O(1')-C(7)-C(8) in E7G). b) Valence angle of glycosidic oxygen atom. c) *p*-Nitrophenyl *β*-*N*-acetylglucosaminide. d) *p*-Nitrophenyl *β*-D-xylopyranoside. e) 1-Naphthyl tetraacetyl-*β*-D-glucoside. f) 7-Ethoxycoumarin.

However, the formation of **D8G** or **E6G** would be more favorable than that of **D7G** or **E7G**, since the former is energetically more stable than the latter. This should be a reason why glucose is transferred from 7-hydroxyl group to 8- or 6-hydroxyl group by the action of transglucosidase and the reverse is undetectable.

The authors are grateful to Professor Yoshio Sasada and Dr. Yuji Ohashi of Tokyo Institute of Tochnology for their valuable discussions and encouragement.

References

1) M. Sato and M. Hasegawa, *Phytochemistry*, **11**, 3149 (1972); M. Sato and M. Hasegawa, *ibid.*, **11**, 657 (1972).
2) M. Sato and M. Hasegawa, *Phytochemistry*, **10**, 2367 (1971).
3) K. Ueno and N. Saito, *Acta Crystallogr., Sect. B*, **33**, 283 (1977).
4) K. Ueno and N. Saito, *Acta Crystallogr., Sect.B*, **32**, 946 (1976).
5) K. Ueno, N. Saito, and M. Sato, *Bull. Chem. Soc. Jpn.*, **51**, 3170 (1978).
6) K. Ueno, M. Sato, and N. Saito, *Bull. Chem. Soc. Jpn.*, **56**, 1577 (1983).
7) J. Karle and H. Hauptman, *Acta Crystallogr.*, **9**, 635 (1956); J. Karle and I. L. Karle, *ibid.*,**21**, 849 (1966); G. Germain and M. M. Woolfson, *ibid., Sect. B*, **24**, 91 (1968).
8) "International Tables for X-Ray Crystallography," Kynoch Press, Birmingham (1974), Vol. **IV**, pp.72—73.
9) Lists of structure factors, anisotropic thermal parameters, atomic parameters for hydrogen atoms, torsional angles of glucose moieties, hydrogen bond parameters and equations of least-squares planes have been deposited as Document No. 8502. at the Office of the Chemical Society of Japan.
10) W. Klyne and V. Prelog, *Experimentia*, **16**, 521 (1960).
11) M. Sundaralingam, *Biopolymers*, **6**, 189 (1968); G. A. Jeffrey, J. A. Pople, J. S. Binkley, and S. Vishveshwara, *J. Am. Chem. Soc.*, **100**, 373 (1978).
12) M. W. Makinen and N. W. Isaacs, *Acta Crystallogr., Sect. B*, **34**, 1584 (1978).
13) P. Swaminathan, *Acta Crystallogr., Sect. B*, **38**, 184 (1982).
14) L. Brehm and J. Moult, *Proc. R. Soc. London, Sect. B*, **188**, 425 (1975).
15) K. Harata, *Acta Crystallogr., Sect. B*, **32**, 1932 (1975).
16) K. Ueno, *Acta Crystallogr., Sect. C*, to be published.
17) S. Shimizu, K. Kashino, and M. Haisa, *Acta Crystallogr., Sect.B*, **28**, 2485 (1972).

Fischer Tropsch Reaction over Reduced Molybdenum Catalysts Derived from Various Heteropoly Compounds

Hiroshi MIURA,* Hitoshi ISHIGURO, Masashi OSAWA, Kazunori SASAGAWA, Kazuo SUGIYAMA, and Tsuneo MATSUDA

Department of Applied Chemistry, Faculty of Engineering, Saitama University, Shimo-ohkubo, Urawa 338

(Received March 22, 1984)

The Fischer-Tropsch reaction was examined over reduced molybdenum catalysts using heteropoly compounds as catalyst precursors. Improvement in reducibility was realized by the use of heteropoly compounds. Metallic molybdenum powder with a very large surface area was obtained by the reduction of $H_3PMo_{12}O_{40}$. Its catalytaic activity was one order higher than conventional Mo catalysts. Using different salts of 12-molybdophosphoric acid, various additives were introduced under equivalent conditions and their addition effects were studied.

The catalytic hydrogenation of CO to form various hydrocarbons, the Fischer-Tropsch (FT) reaction, has been studied in detail for a long time. It is well known that group VIII elements such as Fe, Co, Ru, and Rh are active for this reaction, and most research regarding the FT reaction has been focused on these metal catalysts.[1-5] On the other hand, only a few studies have been reported for reactions over catalysts other than group VIII metals.[6-8]

The dissociation of CO is believed[9] to be an important process in the catalytic hydrogenation of CO. Fe and Ru have a great ability to dissociate CO, the reason for their high activity in the FT reaction. Among elements other than those from group VIII, molybdenum is reported[10] to have a high ability for CO dissociation and is worth noticing as a catalyst for the FT reaction. Saito and Anderson[7] examined CO hydrogenation over metallic molybdenum and several molybdenum compounds and found that reduced molybdenum is an active catalyst for the FT reaction. They reported the following order in activity: $Ni>Mo_2C>Mo(metal)>Mo_2N>MoO_2>MoO_3$. Murchison and Murdick[11] reported that molybdenum catalysts containing potassium are selective in the formation of C_2—C_5 hydrocarbons (LPG) and have a relatively high torelance for sulfur poisoning.

However, these studies have been carried out within a reaction temperature range of 623 to 673 K (more than 100 K higher than the group-VIII metals), indicating the mild activity of molybdenum. Because MoO_3 is not easily reduced, Saito and Anderson reduced their molybdenum catalysts at 873K. In order to obtain a more active catalyst, we tried to lower the reduction temperature using more reducible compounds as the catalyst precursors. Niiyama *et al.*[12] studied the initial stage of the reduction of heteropoly compounds and found that $H_3PMo_{12}O_{40}$ (HPMo) and its transition-metal salts are more easilly accessible to H_2 reduction than MoO_3. Therefore, we examined heteropolymolybdates as precursors of molybdenum catalysts. In addition, the use of heteropoly compounds makes it easy to estimate the effect of various additives which are introduced as the counter cation of heteropoly acid since each cation is placed in an equivalent position of the precursors.

Experimental

Catalyst Preparation. Although each catalyst was reduced with hydrogen before use (and its form changed), the chemical formula before reduction is used to express each catalyst.

MoO_3. Reagent grade ammonium heptamolybdate ($(NH_4)_6Mo_7O_{24}\cdot 4H_2O$, Wako Pure Chem.) was calcined in a flow of dry air at 773 K for 5 h. The resulting grey powder was submitted for catalytic studies. The grey MoO_3 was further purified following a method from the literature[13] and white powder was obtained. This MoO_3 was catalytically inactive and was used only as the raw material for heteropoly catalysts.

HPMo($H_3PMo_{12}O_{40}\cdot xH_2O$). According to the method of Tsigdinos[14] and Drechsel,[15] 12-molybdophosphoric acid was prepared as follows. 2.46 g of phosphoric acid (reagent grade, Wako Pure Chem.) was added to 150 ml of pure water and boiled with reflux for 30 min. 50 g of purified MoO_3 (white) was added stepwise and the mixture was allowed to boil for 6 h. After cooling, the insoluble contamination was removed by filtration. The objective compound was extracted with ether from the filtrate and dried. A yellow powder was obtained.

KPMo($KH_2PMo_{12}O_{40}\cdot xH_2O$).[14] A calculated amount of K_2CO_3 (reagent grade, Wako Pure Chem.) was added to an aqueous solution of HPMo so that the atomic ratio of K/Mo was 1/12. The solution was heated in a water bath until no more CO_2 was formed. After drying, a yellow powder was obtained.

MePMo($MeH_2PMo_{12}O_{40}\cdot xH_2O$; Me=Li, Na, Cs, Mg, Ca, Mn, Fe, Co, Ni, Cu, Zn). Alkali metal, alkaline earth and transition metal salts of HPMo were prepared in the same manner as the KPMo, following the method of Tsigdinos.[14] The atomic ratio Me/Mo was fixed at 1/12, except for CsPMo. In this case, the ratio was changed from 0.5/12 to 2/12.

Pretreatment. 1.0 g of catalyst was packed in a U-tube reactor attached with a 4-port valve, the weight of the reactor being measured in advance. After evacuating at room temperature for 10 min, the temperature was increased at a rate of 10 K/min. The temperature change

was controlled by a temperature programmer, Ohkura PG 3001, and the evacuation continued at 453 K for 1 h. After the evacuation treatment, the water content of the HPMo was found to be 0.2% from the weight loss after evacuation at 823 K. After cooling to room temperature, the 4-port valve was closed and the weight was measured. In a flow of hydrogen (high purity grade, Showa Denko Co., passed through activated copper and molecular sieve) the catalyst temperature was increased at a rate of 10 K/min and kept at 773 K for 4 h. After cooling slowly to room temperature in hydrogen, the weight of the catalyst was again measured. From the weight loss during the reduction treatment, the degree of reduction was determined.

Activity Measurement. The reactor was attached to a flow system in order to examine the CO hydrogenation. A premixed gas ($H_2/CO=2.98$, Takachiho Chem. Co.) was used as a reactant gas. After increasing the temperature in a hydrogen flow, the reactant gas was (30 ml/min, atmospheric pressure) passed through the catalyst at 503 K until the activity was stabilyzed (for 6 h). Then the activity was measured at 473—573 K. Products (CO, CO_2, and C_1—C_7 hydrocarbons) were analyzed by gas chromatography.

X-Ray Diffraction. In order to keep the sample from being exposed to air, the reduced (or spent) catalyst was removed from the reactor to a glass sample holder in a nitrogen atmosphare, covered with mylar film, and then submitted to an X-ray diffraction process.

Results and Discussion

MoO_3. The reduction of purified MoO_3 (white) was examined, but it was difficult to reduce it to metallic molybdenum. Even when the reduction temperature was raised to 873 K, the degree of reduction was less than 40% and it was catalytically inactive for the FT reaction. Unpurified MoO_3(grey) was also difficult to reduce and catalytically inactive when the reduction temperature was 773 K. However, when it was reduced at 873 K, the degree of reduction increased to 97.8%. An X-ray diffraction study of the reduced catalyst suggested that metallic molybdenum was formed by reduction. In this case, a mild activity in the FT reaction was found, consistent with Saito and Anderson.[7] In addition, the reduction of ammonium heptamolybdate (NH_4-Mo) was examined. NH_4-Mo was more easily reduced than MoO_3. Even at 773 K, the degree of reduction was 66%. Its catalytic activity was comparable to MoO_3 reduced at 873 K (Table 1).

HPMo. When HPMo was reduced in a hydrogen flow at 773 K, the degree of reduction was 98.1%. Apparently, the reduction of HPMo was easier than MoO_3. However, when HPMo was heated at 773 K *in vacuo* before reduction (so that the Keggin unit was destroyed), the reduction stopped at about 40%. Thus, not only the presence of phosphorus, but also the Keggin structure is required to improve the reducibility. The reduction temperature also affected the reducibility. The optimum temperature was 773 K and both higher and lower temperatures resulted in a lower degree of reduction (Fig. 1). The reduction of HPMo seems to proceed accompanied by the decomposition of the Keggin unit and at higher temperatures (when the rate of decomposition exceeds that of reduction), the reduction ceased before completion.

The reduced catalyst was submitted to X-ray diffraction analysis and only the diffraction lines of metallic molybdenum were found. By means of X-ray fluorescence, it was found that the P/Mo ratio does not change during the reduction process (Table 2). On the other hand, the IR band of the P-O bond disappeared

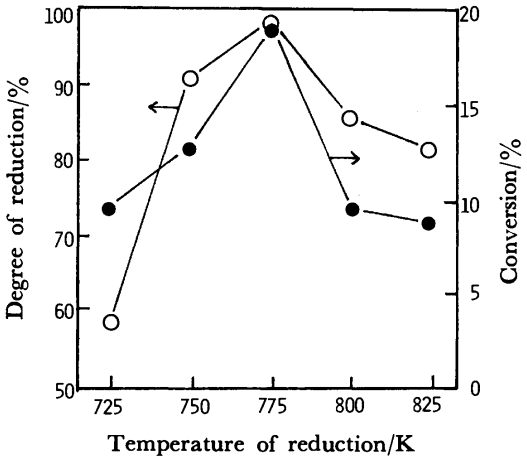

Fig. 1. Effect of reduction temperature on the degree of reduction and activity of HPMo.
-○-: degree of reduction, -●-: conversion (at 523K, amount of catalyst 1.0 g, flow rate 30 ml/min, $H_2/CO=2.98$).

Table 1. Reducibility and catalytic activity of various molybdenum compounds

Catal.	Reduction temp (K)	Degree of reduction (%)	Surface area (m^2/g)	X-ray Anal. (Diameter)*1 (Å)	Activity*2 523K	Activity*2 623K
MoO_3 (grey)	773	25.2	2.4	MoO_2	0.1	0.6
	873	97.8	11.8	Mo(440)	4.8	69.8
NH_4-Mo	773	66.0	5.9	Mo, MoO_2	5.6	—
HPMo	773	98.1	64.7	Mo(109)	74.1	—
MoO_3*3	873	(100)	7.5	Mo	—	61.5

*1: Particle size determined from the X-ray diffraction line broadening. *2: Rate of formation of hydrocarbons, μmol-C/min·g. *3: From Ref. 7 (Saito and Anderson).

TABLE 2. RESULTS OF THE ANALYSIS OF P/Mo RATIO BY MEANS OF X-RAY FLUORESCENCE

Specimen	P/Mo (atomic ratio)
HPMo (before reduction)	1.1/12
HPMo (after reduction)	0.9/12
NiPMo (after reaction)	1.1/12

after reduction. Nozaki *et al.*[16] reported that the formation of nickel phosphides such as Ni_3P or Ni_7P_3 was observed by the hydrogen reduction of $Ni_3(PO_4)_2$. Probably the phosphorus in HPMo is also reduced and is included in the metallic molybdenum phase.

The BET surface area after reduction was 64.7 m^2/g, which was in agreement with the particle size calculated from the X-ray line broadening (Table 1). This surface area was more than five times larger than MoO_3 (reduced at 873 K). The presence of phosphorus seems to inhibit the crystal grouth of molybdenum. As a metal powder obtained by the hydrogen reduction of an oxide at high temperatures, this metallic molybdenum has a very small particle size.

The catalytic activity of HPMo was much higher than MoO_3, owing to its large surface area. The reaction rate was even higher than for molybdenum carbide, which was reported[7] to be the most active among Mo compounds. However, the product distribution for HPMo was in agreement with that of MoO_3 (Fig. 4), suggesting that the presence of phosphorus had little effect on selectivity. The product distribution followed the Schulz-Flory distribution, with a propagation coefficient 0.44.

One of the features of the Mo catalysts (HPMo and MoO_3) compared with the group-VIII metals (such as Ru) is that the former produces CO_2 as an oxygen compound, whereas the latter forms H_2O. Another is that Ru changes the product distribution extensively with reaction temperature (Fig. 2), whereas Mo changes it only a little. As shown in Figs. 2 and 3, the selectivities of C_1—C_3 were almost constant for Mo at 483—533 K. Only the olefin/paraffin ratio changed with temperature. Such a stability in selectivity against reaction temperature is advantageous in practical operation because this reaction is exothermic and the heat of reaction tends to disturb the reaction.

We also tried to estimate the turnover frequency of this reaction over HPMo on the basis of the number of surface Mo atoms calculated from the BET surface area supposing that 1.73×10^{19} atoms are exposed per square meter.[17] The resulting turnover frequency was $2.6\times10^{-3}\ s^{-1}$ at 523 K, a value comparable to that of Ir ($2.6\times10^{-3}\ s^{-1}$ at 523 K)[18] which was the least-active metal among group-VIII elements.

Alkali Metal and Alkaline Earth Salts. HPMo has three protons per heteropolyanion which can be exchanged with various cations. We prepared three Cs salts, changing the content of Cs from 0.5 to 2 per

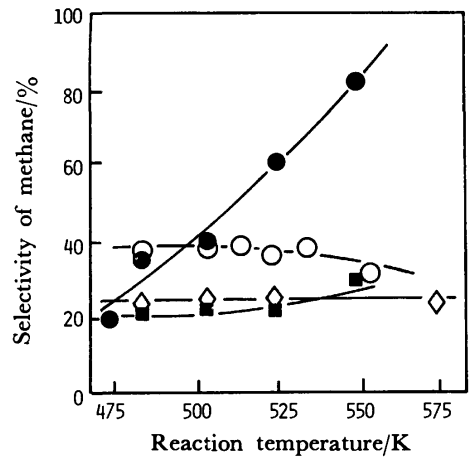

Fig. 2. Effect of reaction temperature on methane selectivity over Ru and various Mo catalysts.
-●-: Ru/alumina, -○-: HPMo, -◇-: CsPMo, -■-: CoPMo.

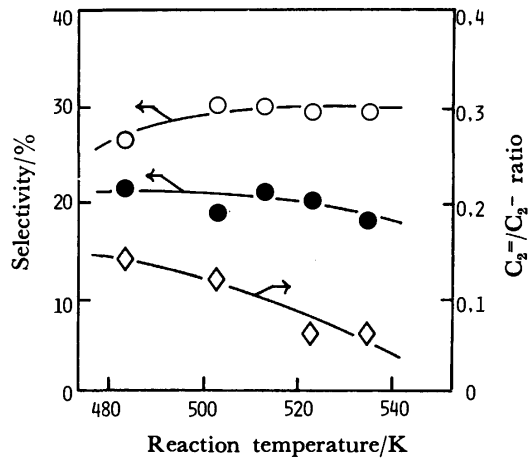

Fig. 3. Effect of reaction temperature on C_2 and C_3 selectivity and $C_2^=/C_2^-$ ratio over HPMo.
-○-: C_2 selectivity, -●-: C_3 selectivity, -◇-: $C_2^=/C_2^-$ ratio.

polyanion. The degree of reduction of $Cs_{0.5}$ and Cs_1 catalysts was 81—82%, in contrast to Cs_2 which was reduced only 52%. The activity of Cs_2 was also lower than $Cs_{0.5}$ and Cs_1, although no significant change in the product distribution was found for the Cs_1 and Cs_2 catalysts. Thus, the optimum content of an alkali metal seemed to be one cation per heteropolyanion.

The introduction of various alkali metals and alkaline earth cations into HPMo caused a decrease in the degree of reduction from 98.1% (HPMo) to 60(NaPMo)—82% (CsPMo). The catalytic activity also decreased, compared with HPMo. However, no correlation was found between the degree of reduction and activity. In order to increase the degree of reduction of KPMo, we prepared KNiPMo (which contain each one K^+ and Ni^+ per polyanion) and examined its catalytic activity. Although the degree of reduction of KNiPMo increased to 91% (compared with KPMo (74%)), the activity was lower than KPMo. Therefore, the change

Table 3. Results of the FT reaction over MoO_3, HPMo, and alkali metal or alkaline earth salts of HPMo

	MoO_3	HPMo	LiPMo	NaPMo	KPMo	CsPMO	MgPMo	CaPMo	KNiPMo
Temp/K	523	523	573	573	573	573	523	523	573
selectivity (%)									
C_1	36.9	36.1	31.6	18.1	21.0	24.5	26.8	28.3	29.6
C_2	25.0	27.0	25.2	30.8	35.0	33.5	28.0	30.0	32.5
C_3	16.1	16.7	17.7	26.5	24.8	23.0	27.5	24.4	19.0
C_4—C_7	22.0	20.1	25.4	24.6	19.2	19.0	17.8	17.4	18.9
$C_2^= + C_3^=$	3.1	2.0	4.4	29.9	29.6	32.7	6.5	13.9	28.3
Conv. (%)	2.4	31.3	29.4	14.4	21.5	10.3	11.8	1.3	15.0

Table 4. Results of the FT reaction over transition metal salts of HPMo at 523K

	MnPMo	FePMo	CoPMo	NiPMo	CuPMo	ZnPMo
C_1	30.1	21.5	20.9	25.3	25.5	24.8
C_2	30.5	22.6	26.1	27.9	32.6	25.8
C_3	23.5	33.5	21.1	28.0	27.6	30.6
C_4—C_7	15.8	22.5	32.0	18.8	14.6	18.8
$C_2^= + C_3^=$	4.6	8.3	12.2	7.9	8.3	11.2
Conv.	6.6	10.9	27.6	23.4	4.5	4.5

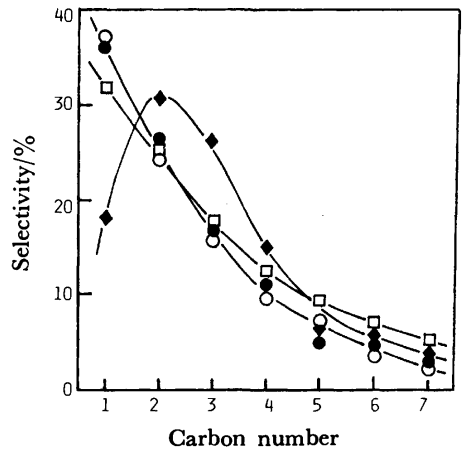

Fig. 4. Products distribution over MoO_3, HPMo, LiPMo and NaPMo.
-○-: MoO_3, -●-: HPMo, -□-: LiPMo, -◇-: NaPMo.

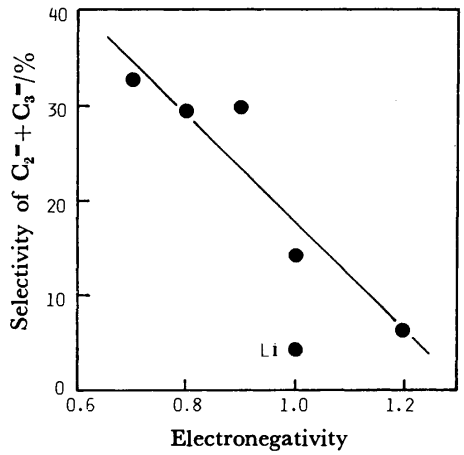

Fig. 5. Relation between electronegativity of alkali metals and alkaline earth metals and olefin selectivity over each salt of HPMo.

in the degree of reduction is not the main reason for activity loss by the introduction of K^+ and other alkali metal cations. Rather, the intrinsic interaction of cations and Mo seems to cause the effect.

The product distribution also changed with the introduction of these cations. Alkali metal salts produced less C_1 (methane) than HPMo or MoO_3 except LiPMo, which showed a product distribution similar to HPMo (Fig. 4). An increase in the C_2—C_3 selectivity was accompanied by a decrease in the C_1 selectivity. MgPMo and CaPMo showed an intermediate property between the two groups in selectivity. A sharp increase in olefin selectivity was observed for Na-, K-, and CsPMo. For CsPMo, the selectivity of the lower olefins (ethylene+propylene; $C_2^=+C_3^=$) was one order higher than that of HPMo. An increase in olefin selectivity was also observed for CaPMo, however it was only small for Li-and MgPMo. The formation of trace amounts of alcohols (mainly methanol) was found for na-, K-, and CsPMo.

Such a tendency of change in the product distribution caused by alkali metals (decrease in C_1 and increase in olefins) has also been observed for group-VIII metals such as Ru[19] and Fe.[20] As shown in Fig. 5, a correlation between the electronegativities of the cations and the olefin selectivity was found with the exception of LiPMo.

Transition Metal Salts. Various transition metal salts (Mn, Fe, Co, Ni, Cu, Zn) of HPMo were prepared and submitted to FT reactions. The amount of the bivalent cations introduced was fixed to one cation per

heteropolyanion. The activities of these catalysts were inferior to HPMo. A significant decrease in activity was observed after the introduction of Mn, Zn, and Cu. On the other hand, there was only a small decrease over Fe, Co, and Ni salts. The degree of reduction exceeded 90% (except Mn; 89%), and so the transition-metal salts appear to be easily reduced. (Especially, Fe-, Ni-, and CuPMo were almost completely reduced.) Perhaps these transition metals were reduced first and activated the hydrogen to accerelate the reduction of Mo.

A decrease in the C_1 selectivity was also observed as clearly as for the alkali metal salts. The C_1 selectivity of CoPMo (20.9%) was comparable to that of KPMo (21.0%). In the case of the alkali metal salts, the effect to suppress the C_1 selectivity was obtained at the expense of an activity loss, but Fe- and CoPMo realized the same effect with only a slight loss of activity. For Na-, K-, and CsPMo, a significant increase in the olefin selectivity was accompanied by a decrease of C_1. However, for the transition metal salt, olefin selectivity was less than half of that of the alkali metal salts even though the C_1 selectivity was in the same range. The relation between the C_1 selectivity and the olefin ($C_2^=+C_3^=$) selectivity is illustrated in Fig. 6. A clear correspondence between the two factors was observed except for Na-, K-, Cs-, and CaPMo.

If both a decrease in the C_1 selectivity and an increase in the olefin selectivity are brought about by a single driving fource (for example the electron donation from added elements to Mo), there must be a correspondence between the two selectivities. The behavior of the catalysts which fit on the curve of Fig. 3 seems to be such a case. On the other hand, Na-, K-, Cs-, and CaPMo also significantly promote olefin formation. The characteristic that distinguish these elements from others is that they have a strong common basicity. When basic sites are formed on a catalyst surface, they will abstract hydrogen from the surface alkyl group, which is formed by the surface polymerization of CH_2, and promote the formation of olefins.[19]

Mo Compounds Containing Co. In order to compare the additional effect of Co with CoPMo (which proved to be active and selective to C_2—C_3 among various heteropoly compounds) other Mo compounds containing Co were examined. Co-Mo-O (Co/Mo=1/12) was prepared by drying a mixture of aqueous solutions of cobalt nitrate and ammonium heptamolybdate. The product was calcined in air at 773 K for 5 h. X-Ray diffraction showed that it was a mixture of $CoMoO_4$ and MoO_3. $(NH_4)_3H_6[CoMo_6O_{24}]$ contains Co as a heteroatom, and is a different type of heteropoly compound from HPMo or CoPMo. We prepared it following a method described in the literature.[21]

The degree of reduction of Co-Mo-O was only 45.2%, and its activity for CO hydrogenation (conversion 1.8% at 523 K) was one order lower than CoPMo. The product distribution for Co-Mo-O was (as shown in Fig. 7) almost equal to that of HPMo or MoO_3, showing a poor addition effect of Co. Even though the ratio of Co and Mo is the same, CoPMo shows a more clear effect of Co than Co-Mo-O. This is because CoPMo (before reduction) contains Co and Mo in uniform concentrations in atomic level which results in a close interaction between the two elements after reduction. On the other hand, Co-Mo-O is a mixture of $CoMoO_4$ and MoO_3 and, thus, the ratio of Co/Mo is not uniform. Thus, the advantage of using heteropolymolybdates as the raw materials for a Mo catalysts is again suggested.

$(NH_4)_3H_6[CoMo_6O_{24}]$ is also a kind of heteropoly compound, but it was not as easily reduced as HPMo or CoPMo (the degree of reduction was 59.2%). The conversion of CO was only 5.2% at 523 K, perhaps due to the low degree of reduction. The product distribution (Fig. 7) showed the effect of Co, *i.e.* a decrease in

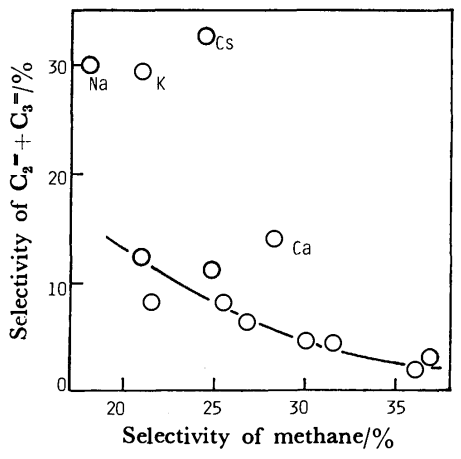

Fig. 6. Relation between methane selectivity and olefin selectivity over various salts of phosphomolybdate.

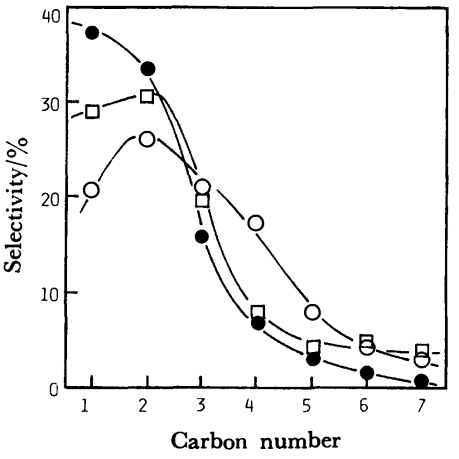

Fig. 7. Product distribution over Mo catalysts containing Co.
-○-: CoPMo, -●-: Co-Mo, -□-: $(NH_4)_3H_6[CoMo_6O_{24}]$.

the selectivity of C_1. It was not as clear as the case of CoPMo. Therefore, the effect of Co is more clearly observed when Co is the counter cation rather than the heteroatom.

Conclusions

1) 12-molybdophosphoric acid is an excellent precursor of metallic molybdenum owing to its reducibility. Thus, we could get a Mo catalyst with a very large surface area. Its activity for CO hydrogenation was one order higher than the conventional Mo catalyst. It was more active than Mo_2C, which was reported to be the most active among various molybdenum compounds.

2) It is possible to introduce various cations as additives using their salts of molybdophsphoric acid, and enables us to estimate their addition effect in equivalent conditions. Alkali metal and alkaline-earth cations suppressed the activity, but improved the selectivity for C_2—C_3 hydrocarbons, especially in the olefin formation.

3) Transition metal salts were reduced as easily as HPMo but the activity was lower than HPMo. By the addition of transition metals, the selectivity of methane decreased in the same manner as for the alkali metals. However, the addition effect was not so clear on the olefin formation as the alkali metals. Correlation was found between C_1 selectivity and olefin ($C_2^=+C_3^=$) selectivity except the salts of strong base cations (Na^+, K^+, Cs^+, and Ca^+).

4) The addition of cobalt was most effective on selectivity when cobalt was introduced as the counter cation of heteropoly acid.

References

1) M. A. Vannice, *Catal. Rev. Sci. Eng.*, **14**, 153 (1976).
2) P. J. Denny, D. A. Whan, *Catalysis* Vol. 2, The Chem. Soc., London (1978).
3) A. T. Bell, *Catal. Rev. Sci. Eng.*, **23**, 203 (1981).
4) H. Arakawa, *Hyomen*, **20**, 44 (1982).
5) M. Roper, "Catalysis in C_1 Chemistry," D. Reidel Co., Dordrecht, 1983.
6) T. Tsunoda, H. Ogasawara, M. Komiyama, S. Ozawa, and Y. Ogino, *Nippon Kagaku Kaishi*, **1982**, 305.
7) M. Saito and R. B. Anderson, *J. Catal.*, **63**, 438 (1980).
8) M. Kojima, E. Miyazaki, and I. Yasumori, *J. Chem. Soc., Chem. Commun.*, **1980**, 573
9) M. Araki and V. Ponec, *J. Catal.*, **44**, 439 (1976).
10) E. Miyazaki, *Hyomen*, **19**, 259 (1981).
11) C. B. Murchison and D. A. Murdick, *Hydrocarbon Processing*, **1981**, 159.
12) H. Niiyama, H. Tsuneki, and E. Echigoya, *Nippon Kagaku Kaishi* **1979**, 996.
13) "Shin Jikken Kagaku Koza," 8-III, p144, Maruzen Shuppan, Tokyo, 1976.
14) G. A. Tsigdinos, *Ind. Eng. Chem., Prod. Res. Devel.*, **13**, 267 (1974).
15) Ref. 13, p1413.
16) F. Nozaki and R. Adachi, *J. Catal.*, **40**, 166 (1975).
17) T. Keii "Shokubai Kagaku," P. 147, Tokyo Kagaku Dohjin, Tokyo, 1983.
18) M. A. Vannice, *J. Catal.*, **37**, 449 (1975).
19) R. D. Gonzalez and H. Miura, *J. Catal.*, **77**, 338 (1982).
20) H. Arakawa and A. T. Bell, *Shokubai*, **23**, 81 (1981).
21) L. C. Baker, B. Loev and T. P. McCutcheon, *J. Am. Chem. Soc.*, **72**, 2376 (1950).

Microwave Spectrum and Barrier to Internal Rotation of 4-Chlorophenol

Masao ONDA,* Takashi MOTODA, and Ichiro YAMAGUCHI
Department of Chemistry, Faculty of Science and Technology, Sophia University, Tokyo 102
(Received May 30, 1984)

Microwave spectra of 4-chlorophenol were observed in the frequency ranges 8—18 and 26.5—40 GHz. Rotational constants were obtained for the ground vibrational states of three isotopic species, $^{35}ClC_6H_4OH$, $^{37}ClC_6H_4OH$, and $^{35}ClC_6H_4OD$, and for the first excited state of C-Cl out-of-plane bending mode for $^{35}ClC_6H_4OH$. All the b-type Q-branch transition lines of the OH species split into doublets, but those of the OD species do not. The separation of doublets is 158.99±0.16 MHz for the ground state of $^{35}ClC_6H_4OH$. An analysis of the doublets on the basis of the pseudo-symmetric internal rotor model gives the barrier height to the internal rotation of hydroxyl group as V_2=13.98±0.37 kJ mol^{-1} for the ^{35}Cl species. The V_2 value obtained is compared with the theoretical V_2 value calculated for 4-X-phenols (X=H, F, Cl) by means of *ab initio* MO with the 4-31G basis set.

The microwave spectrum of phenol was reported for the first time by Kojima.[1] The barrier height V_2 was determined to be 13.16±1.20 kJ mol^{-1} from the observed splitting. In his method the hydroxyl group was assumed to be a pseudo-symmetric internal rotor. Following Kojima's paper, many theoretical and experimental articles on phenol have appeared.[2-6] One of them is the article on a strict Rotation-Internal Rotation (RIR) treatment by Mathier *et al.* and a more reliable V_2 value is given.[5]

The molecule of 4-fluorophenol has the same symmetry as that of phenol with respect to the overall and internal rotations. The far IR spectra of 4-fluorophenol were analyzed with the exact RIR treatment by Larsen and Nicolaisen.[7] In this paper, we report microwave spectra of three isotopic species of 4-chlorophenol and the value of V_2 as estimated according to Kojima's approximation.[1]

Experimental

The sample was obtained commercially and distilled *in vacuo*. The deuterated species (OD) was produced by mixing the normal species with D_2O in a wave-guide cell. The content of the *d*-species thus produced was estimated to be about 30% from the intensity ratio between the same rotational transitions of the deuterated and normal species. The microwave spectrum was measured with a conventional spectrometer using 100 kHz square-wave Stark modulation. The measured frequency regions were 8—18 and 26.5—40 GHz. The microwave sources for them were a synthesizer (HP-8672A) and a YIG tuned GaAs oscillator (Watkins-Johnson 5610-302FD), respectively. Measurements were made at room temperature with sample pressures of 3—7 Pa. The accuracy of the measured frequency was better than 0.1MHz for all lines except broadened ones with hyperfine components due to chlorine nucleus.

Results and Discussion

Analysis of Spectrum. Frequencies of spectral lines were predicted from a structural model which was constructed with structural parameters transferred from chlorobenzene[8] and phenol.[9] The components of the dipole moment were estimated as μ_a=1.65 D and μ_b=1.22 D from those of the two molecules mentioned above. From these predictions it was expected that the a-type transitions would be observed strongly for this molecule. This is in contrast to the case of phenol where μ_a=0.133 D and μ_b=1.217 D.[9] The spectrum consisted of many lines in the observed region. This complexity of the spectrum comes from the existence of two chlorine isotopic species in their ground and low frequency excited vibrational states. The initial step of assignment was made for the a-type R-branch transitions which were expected to appear as singlets with the assumed barrier to internal rotation of hydroxyl group. Some of the transitions with high K_{-1} were observed as doublets due to nuclear quadrupole coupling of chlorine. For $8_{3,6}$—$7_{3,5}$, $8_{3,5}$—$7_{3,4}$, $7_{2,6}$—$6_{2,5}$, and $7_{2,5}$—$6_{2,4}$, the separations of the doublets were about 1 MHz, which is consistent with those predicted by using χ-values obtained for chlorobenzene.[10] The assigned a-type R-branch transitions are given in Tables 1 and 2.

The b-type Q-branch transitions were expected to be doublets due to the internal rotation as seen in the b-type transitions of phenol.[1] The separation of the doublets depends on the barrier height of the internal rotor. It was predicted to be 27.6 to 467 MHz for V_2=18 to 12 kJ mol^{-1}. The upper and lower components of the doublets were searched for in the frequency region, which are located at the same distances from the predicted unperturbed frequencies as calculated from the results of analysis of the a-type R-branch transitions. The observed separations of the doublets were about 159 MHz. The observed b-type Q-branch transition frequencies and their splitting widths are given in Tables 1 and 2 and Table 3, respectively. Each component of b-type Q-branch transitions listed in the tables was observed as single line despite the perturbation of quadrupole coupling.

The rotational constants were obtained by least-

TABLE 1. OBSERVED FREQUENCIES IN MHz OF a-TYPE R-BRANCH AND b-TYPE Q-BRANCH[a] TRANSITIONS[b] FOR 4-$^{35}ClC_6H_4OH$

Transition	$v=0$	$v=1$	Transition	$v=0$	$v=1$
$7_{0,7}-6_{0,6}$	12472.11(8)		$19_{1,19}-18_{1,18}$	32404.05(−4)	32433.55(3)
$7_{1,7}-6_{1,6}$	12106.60(−3)		$19_{1,18}-18_{1,17}$	c)	34436.62(−13)
$7_{1,6}-6_{1,5}$	13108.16(−1)		$19_{2,18}-18_{2,17}$	c)	33788.00(−1)
$7_{2,6}-6_{2,5}$	12625.28(23)		$19_{2,17}-18_{2,16}$	35532.14(−7)	35555.93(7)
$7_{2,5}-6_{2,4}$	12803.44(−8)		$19_{3,17}-18_{3,16}$	34454.65(13)	34480.70(−19)
$8_{0,8}-7_{0,7}$	14195.25(4)		$19_{3,16}-18_{3,15}$	35171.11(−20)	35201.42(−27)[d]
$8_{1,8}-7_{1,7}$	13822.18(3)		$19_{4,16}-18_{4,15}$	34561.53(14)	
$8_{1,7}-7_{1,6}$	14961.63(−13)		$19_{4,15}-18_{4,14}$	34648.55(−15)	
$9_{0,9}-8_{0,8}$	15899.96(−5)		$20_{0,20}-19_{0,19}$	34133.82(1)	34163.79(−3)
$9_{1,9}-8_{1,8}$	15532.83(−7)		$20_{1,20}-19_{1,19}$	34074.65(−3)	34105.68(−7)
$9_{1,8}-8_{1,7}$	16806.49(−27)		$20_{1,19}-19_{1,18}$	36077.78(−6)	36098.75(−3)
$9_{2,8}-8_{2,7}$	16206.03(−2)		$20_{2,19}-19_{2,18}$	35480.72(8)	35507.82(19)
$9_{2,7}-8_{2,6}$	16570.57(−4)		$20_{2,18}-19_{2,17}$	37367.60(15)	37391.92(37)[d]
$10_{0,10}-9_{0,9}$	17587.85(−2)		$20_{3,18}-19_{3,17}$	36249.75(−16)	
$10_{1,10}-9_{1,9}$	17238.81(2)		$20_{3,17}-19_{3,16}$	37117.40(−2)	37149.35(12)
$10_{2,9}-9_{2,8}$	17989.60(3)		$20_{4,17}-19_{4,16}$	36396.21(12)	
$15_{1,14}-14_{1,13}$	27596.35(6)	27613.14(7)	$20_{4,16}-19_{4,15}$	36519.19(4)	
$15_{2,14}-14_{2,13}$	c)	26840.19(−5)	$21_{0,21}-20_{0,20}$	35789.31(−45)[d]	
$15_{2,13}-14_{2,12}$	28032.49(−9)	28053.45(−8)	$21_{1,21}-20_{1,20}$	35743.58(−13)	
$15_{3,13}-14_{3,12}$	27223.12(−1)	27244.45(−2)	$21_{1,20}-20_{1,19}$	37726.64(−18)	
$15_{3,12}-14_{3,11}$	27484.18(−9)	27507.61(2)	$21_{2,20}-20_{2,19}$	37192.45(2)	
$15_{4,12}-14_{4,11}$	27232.60(26)		$21_{3,19}-20_{3,18}$	38039.11(10)	
$15_{4,11}-14_{4,10}$	27249.24(−23)		$21_{3,18}-20_{3,17}$	39066.46(11)	
$16_{0,16}-15_{0,15}$	27526.57(4)	27549.21(3)	$21_{4,18}-20_{4,17}$	38230.80(10)	
$16_{1,16}-15_{1,15}$	27379.74(10)	27404.71(45)[d]	$21_{4,17}-20_{4,16}$	38400.41(1)	
$16_{1,15}-15_{1,14}$	29331.47(4)	29349.03(9)	$22_{0,22}-21_{0,21}$	37446.88(−21)	
$16_{2,15}-15_{2,14}$	28565.89(1)	28587.73(−0)	$22_{1,22}-21_{1,21}$	37411.26(−20)	
$16_{2,14}-15_{2,13}$	29927.67(−11)	29949.53(−1)	$22_{1,21}-21_{1,20}$	39367.42(3)	
$16_{3,14}-15_{3,13}$	29037.07(8)	29059.77(13)	$13_{2,11}-13_{1,12}$	12034.91(6)	
$16_{3,13}-15_{3,12}$	29386.55(−22)	29411.98(4)	$14_{2,12}-14_{1,13}$	12321.63(5)	
$16_{4,13}-15_{4,12}$	29062.50(18)	29085.93(28)[d]	$15_{2,13}-15_{1,14}$	12757.88(−0)	
$16_{4,12}-15_{4,11}$	c)	29112.79(−10)	$16_{2,14}-16_{1,15}$	13354.09(−14)	
$17_{0,17}-16_{0,16}$	29176.09(18)	29200.40(2)	$17_{2,15}-17_{1,16}$	14119.14(11)	
$17_{1,17}-16_{1,16}$	29057.13(19)	29083.15(1)	$18_{2,16}-18_{1,17}$	15058.12(10)	
$17_{1,16}-16_{1,15}$	31045.70(−20)	31064.12(−3)	$19_{2,17}-19_{1,18}$	16173.40(1)	
$17_{2,16}-16_{2,15}$	30305.17(11)	30328.23(3)	$20_{2,18}-20_{1,19}$	17462.97(−3)	
$17_{2,15}-16_{2,14}$	31810.81(10)	31833.17(−2)	$20_{3,17}-20_{2,18}$	18136.89(8)	
$17_{3,15}-16_{3,14}$	30847.26(−9)	30871.26(−1)	$23_{3,20}-23_{2,21}$	18256.52(−22)	
$17_{3,14}-16_{3,13}$	31302.87(−27)	31329.92(−21)	$35_{5,30}-35_{4,31}$		31521.43(−11)
$17_{4,14}-16_{4,13}$	30894.38(33)[d]	30918.98(13)	$36_{5,31}-36_{4,32}$	31041.11(−5)	30740.84(9)
$17_{4,13}-16_{4,12}$	30935.05(11)		$37_{5,32}-37_{4,33}$	30366.79(17)	30083.00(9)
$18_{0,18}-17_{0,17}$	30826.83(3)	30853.12(0)	$38_{5,33}-38_{4,34}$	29841.79(−7)	29577.32(−7)
$18_{1,18}-17_{1,17}$	c)	30759.50(6)	$39_{5,34}-39_{4,35}$	c)	c)
$18_{1,17}-17_{1,16}$	32740.52(8)	32759.46(−1)	$40_{5,35}-40_{4,36}$	29344.07(−2)	
$18_{2,17}-17_{2,16}$	32037.10(−7)	32061.58(−0)	$41_{5,36}-41_{4,37}$	29412.62(−4)	
$18_{2,16}-17_{2,15}$	33679.39(−4)	33702.64(11)	$42_{5,37}-42_{4,38}$	29713.73(−1)	29544.02(−5)
$18_{3,16}-17_{3,15}$	32653.54(10)	32678.51(−10)	$43_{5,38}-43_{4,39}$	30257.70(−1)	30114.03(5)
$18_{3,15}-17_{3,14}$	33232.36(26)	33260.84(−1)	$44_{5,39}-44_{4,40}$	31050.52(−1)	
$18_{4,15}-17_{4,14}$	32727.40(19)		$45_{5,40}-45_{4,41}$	32093.57(4)	
$18_{4,14}-17_{4,13}$	32787.65(−6)		$46_{5,41}-46_{4,42}$	c)	33314.26(−2)
$19_{0,19}-18_{0,18}$	32479.44(−0)	32507.58(−3)	$47_{5,42}-47_{4,43}$	c)	34862.94(1)

a) Center frequency of doublet. b) Figures in parentheses indicate the last digits of the difference: the observed minus calculated frequency. c) Overlapped by other lines. d) Not included in the least-squares fitting.

TABLE 2. OBSERVED FREQUENCIES IN MHz OF a-TYPE R-BRANCH AND b-TYPE Q-BRANCH TRANSITION[a)]

Transition	4-$^{35}ClC_6H_4OD$	4-$^{37}ClC_6H_4OH$	Transition	4-$^{35}ClC_6H_4OD$	4-$^{37}ClC_6H_4OH$
$15_{1,14}$-$14_{1,13}$		26956.47(5)	$18_{1,17}$-$17_{1,16}$		32008.16(−6)
$15_{2,13}$-$14_{2,12}$	27359.91(−22)	27325.11(20)	$18_{2,17}$-$17_{2,16}$	31317.75(29)	
$15_{3,13}$-$14_{3,12}$	26590.05(−3)		$18_{2,16}$-$17_{2,15}$		32846.58(−1)
$15_{3,12}$-$14_{3,11}$	26825.77(−11)	26792.29(−0)	$18_{3,16}$-$17_{3,15}$	31897.33(−16)	31870.10(−2)
$15_{4,12}$-$14_{4,11}$	26595.87(4)		$18_{3,15}$-$17_{3,14}$	32424.40(−19)	32378.40(16)
$15_{4,11}$-$14_{4,10}$	26610.76(8)		$18_{4,15}$-$17_{4,14}$	31960.94(9)	
$16_{0,16}$-$15_{0,15}$		26926.84(8)	$18_{4,14}$-$17_{4,13}$	32013.33(−11)	
$16_{1,16}$-$15_{1,15}$		26770.45(−2)	$19_{0,19}$-$18_{0,18}$		31769.65(6)
$16_{2,15}$-$15_{2,14}$	27920.45(4)		$19_{1,19}$-$18_{1,18}$		31686.79(6)
$16_{2,14}$-$15_{2,13}$	29213.07(24)		$19_{2,17}$-$18_{2,16}$		34661.16(−14)
$16_{3,14}$-$15_{3,13}$	28362.61(6)		$20_{1,20}$-$19_{1,19}$		33321.13(−9)
$16_{3,13}$-$15_{3,12}$	28679.19(2)	28641.34(−12)	$20_{1,19}$-$19_{1,18}$		35286.98(4)
$16_{4,13}$-$15_{4,12}$	28382.58(4)		$37_{4,33}$-$37_{3,34}$	26908.73(−12)	
$16_{4,12}$-$15_{4,11}$	28405.66(−19)		$38_{4,34}$-$38_{3,35}$	28191.52(−2)	
$17_{0,17}$-$16_{0,16}$	28542.77(−17)	28539.67(−4)	$39_{4,35}$-$39_{3,36}$	29679.95(−5)	
$17_{1,17}$-$16_{1,16}$	28418.78(−14)	28411.64(−6)	$40_{4,36}$-$40_{3,37}$	31360.71(7)	
$17_{1,16}$-$16_{1,15}$		30343.34(4)	$33_{5,28}$-$33_{4,29}$	34065.50(16)	
$17_{2,16}$-$16_{2,15}$	29622.31(4)	29606.15(1)	$34_{5,29}$-$34_{4,30}$	33129.36(−10)	
$17_{2,15}$-$16_{2,14}$	31054.75(24)	31017.82(−1)	$35_{5,30}$-$35_{4,31}$	32228.38(−35)	
$17_{3,15}$-$16_{3,14}$		30105.32(−15)	$36_{5,31}$-$36_{4,32}$	31393.66(−11)	
$17_{3,14}$-$16_{3,13}$	30545.65(−5)		$37_{5,32}$-$37_{4,33}$	30655.46(23)	
$17_{4,14}$-$16_{4,13}$	30171.14(17)	30141.47(11)	$39_{5,34}$-$39_{4,35}$	29582.68(0)	
$17_{4,13}$-$16_{4,12}$	30206.47(−1)	30174.63(−14)	$40_{5,35}$-$40_{4,36}$	29299.98(29)	
$18_{0,18}$-$17_{0,17}$		30153.92(5)			

a) Figures in parentheses indicate the last digits of the difference: the observed minus calculated frequency.

TABLE 3. OBSERVED SPLITTING IN MHz OF b-TYPE Q-BRANCH TRANSITIONS FOR $^{35}ClC_6H_4OH$

Transition $K_{-1}=2-1$	$v=0$	Transition $K_{-1}=5-4$	$v=0$	$v=1$
$13_{2,11}$-$13_{1,12}$	159.03	$36_{5,31}$-$36_{4,32}$	158.21	159.23
$14_{2,12}$-$14_{1,13}$	158.85	$37_{5,32}$-$37_{4,33}$	158.33	159.44
$15_{2,13}$-$15_{1,14}$	158.75	$38_{5,33}$-$38_{4,34}$	158.29	159.22
$16_{2,14}$-$16_{1,15}$	159.01	$39_{5,34}$-$39_{4,35}$	a)	a)
$17_{2,15}$-$17_{1,16}$	159.02	$40_{5,35}$-$40_{4,36}$	158.26	a)
$18_{2,16}$-$18_{1,17}$	158.89	$41_{5,36}$-$41_{4,37}$	158.31	a)
$19_{2,17}$-$19_{1,18}$	158.88	$42_{5,37}$-$42_{4,38}$	158.31	159.31
$20_{2,18}$-$20_{1,19}$	158.79	$43_{5,38}$-$43_{4,39}$	158.25	159.43
		$44_{5,39}$-$44_{4,40}$	158.25	a)
		$45_{5,40}$-$45_{4,41}$	158.25	a)
		$46_{5,41}$-$46_{4,42}$	a)	159.14
		$47_{5,42}$-$47_{4,43}$	a)	159.20
average	158.90(15)		158.27(6)	159.28(16)

a) Overlapped by other lines.

squares fitting of the transition frequencies listed in Tables 1 and 2. The values derived for the parameters are given in Table 4. Satellites which formed a series of lines with decreasing intensity were observed for low K_{-1} transitions near the ground vibrational lines. The most intense satellite lines were assigned to the transitions in the first excited state as specified in Table 1. On the basis of their intensity and inertia defect, this excited state is ascribed to the out-of-plane mode with the lowest vibrational frequency, namely, the C-Cl out-of-plane bending (165 cm^{-1}).[11] A search for the lines due to the OH torsional excited state was not successful.

Barrier to Internal Rotation. The splitting in the b-type Q-branch transitions was analyzed by using the same approximation as assumed for phenol molecule; a pseudo-symmetric internal rotor was assumed for O-H group.[1] The observed splittings of the doublets were almost independent of J for each K_{-1}–K'_{-1} series as seen in Table 3. However, the observed splittings for the two series of transitions, $J_{2,J-2}$–$J_{1,J-1}$ and $J_{5,J-5}$–$J_{4,J-4}$ of $^{35}ClC_6H_4OH$ (v=0), indicate that the splitting of the doublet varies depending on the K_{-1} values. Mathier *et al.*[5] pointed out the same K_{-1} dependency for phenol and gave an empirical formula for this dependency. Their empirical formula* was applied to the present analysis of 4-chlorophenol, and a virtual value of splitting independent of K_{-1} was obtained as 158.99±0.16 MHz (Table 5).

For the evaluation of barrier height the most uncertain parameter is I_1, the moment of inertia of the

* Split/MHz=158.99(16)−0.0175(25)×(K_{-1}^2+K'_{-1}^2) for $J_{K-1,K+1}$–$J_{K'-1,K'+1}$ of 4-$^{35}ClC_6H_4OH$. The virtual splitting was obtained by means of the least-squares method using the splitting widths in Table 3.[5]

TABLE 4. ROTATIONAL CONSTANTS, INERTIA DEFECT, AND INTERNAL ROTATION SPLITTING OF 4-CHLOROPHENOL[a)]

	4-$^{35}ClC_6H_4OH$		4-$^{35}ClC_6H_4OD$	4-$^{37}ClC_6H_4OH$
	$v=0$	$v=1$	$v=0$	$v=0$
A/MHz	5632.78(7)	5598.80(54)	5591.03(2)	5632.86(63)
B/MHz	975.573(4)	976.142(7)	951.854(3)	950.485(4)
C/MHz	831.655(4)	832.511(7)	813.505(3)	813.352(4)
τ_{aaaa}/MHz	−0.011(24)	−0.027(60)	−0.011[b)]	−0.011[b)]
τ_{bbbb}/MHz	−0.00011(2)	−0.00007(4)	−0.00011[b)]	−0.00011[b)]
τ_{aabb}/MHz	0.0004(5)	0.0009(11)	0.0004[b)]	0.0004[b)]
τ_{abab}/MHz	−0.00029(18)	−0.00047(35)	−0.00029[b)]	−0.00029[b)]
Δ/uÅ^2[c)]	−0.076(6)	−0.943(17)	−0.096(4)	−0.073(15)
σ/MHz[d)]	0.121	0.082	0.162	0.096
Split/MHz[e)]	158.99	159.28	<0.2	—

a) Figures in parentheses indicate the uncertainty involved in the last significant digits calculated as 2.5 times the standard deviation. b) Assumed. c) $\Delta=I_c-I_a-I_b$. d) Standard deviation for lines fitted. e) Average value of the splittings in the b-type Q-branch transitions.

TABLE 5. INTERNAL ROTATION PARAMETER

	4-$^{35}ClC_6H_4OH$	C_6H_5OH
Split/MHz	158.99(16)	111.998[a)]
I_a/uÅ^2	89.721(1)	89.439[a)]
I_1/uÅ^2	0.740(18)	0.743[a)]
F/GHz	688(16)	686
s	50.9(2)	53.7
V_2/kJ mol^{-1}	13.98(37)	14.71
		[14.44][a,b)]

a) Ref. 5. b) Obtained by RIR analysis.

hydroxyl group about the internal rotation axis. In the present analysis the following approximation is adopted: The a-axis coincides with the internal rotation axis and the center of mass of the hydroxyl group lies on the a-axis. The first moment equation was used to calculate the I_1 value, together with using the r_s b-coordinate of hydroxyl hydrogen (0.833±0.002 Å). The values of I_1 for the two molecules coincided well with each other as shown in Table 5.

The barrier height V_2 was calculated from the parameters in Table 5 by using the perturbation coefficients given by Lin and Swalen.[12] The error for I_1 arises from the ambiguity in the b-coordinate of the hydrogen atom, ±0.01 Å, which seems to be in the maximum allowable range. The b-type Q-branch transitions for $^{35}ClC_6H_4OD$ were not observed as doublet. The splittings, if any, were smaller than 0.2 MHz because no line broadening was recognized. They were predicted to be 0.41 MHz from the V_2 value obtained. The smaller splittings than 0.2 MHz of the transitions correspond to the higher V_2 than 15 kJ mol^{-1}. This result that the V_2 value for the OD species is higher than that of the OH species, is apparently the same as those in the case of phenol and 4-fluorophenol.[7]

To compare the V_2 value of 4-chlorophenol with that of phenol, the same approximation was applied to phenol; I_1 was calculated from the r_s coordinate of hydroxyl hydrogen because I_1 was roughly estimated in Kojima's paper. The V_2 value of phenol obtained on this approximation coincides with the value based on the RIR treatment within 2% as shown in Table 5.

Campagnero and Wood[13] assumed that the barrier height of 4-X-phenols is dependent mainly on the degree of double bond character in the C-O bond; if substituent X at 4-position is a strong π donor, the double bond character will decrease and thus the barrier height will decrease.[13] Larsen and Nicolaisen[7] explained the lower barrier height of 4-fluorophenol than that of phenol by the above theory. According to their theory, our result may be taken to indicate that the ability of chlorine as a π donor is lower than that of fluorine in 4-X-phenol.

Recently, the barrier in phenol has been calculated for a fully-optimized structure based on the STO-3G basis set[14] and also based on 4-31G for a rigidly rotating structure.[15] To compare the experimentally obtained barrier heights of 4-substituted phenols with MO theoretical ones, we calculated the total energies of the molecules with standard geometry and rigidly rotating hydroxyl group by using the 4-31G basis set without geometry optimization. The benzene ring was assumed as a regular hexagon in which the C-C bond length is equal to the mean value for the r_s length in phenol, 1.3912 Å. The other assumptions adopted were that the C-O bond lies on the C_{2v} axis of the ring and that the hydroxyl group rotates about the axis rigidly. The energy difference between the planar and orthogonal structures was taken as the theoretical barrier height. The results are given in Table 6. The MO theoretical barriers in Table 6 are lower than the experimental ones. However, it is interesting to have almost a constant ratio 1.5 of the experimental to theoretical value for the three molecules.

The *ab initio* calculation was carried out at the

TABLE 6. COMPARISON OF BARRIER HEIGHTS IN kJ mol^{-1} IN PARA-SUBSTITUTED PHENOLS

Molecule	Experimental	*ab initio*[a]	Ratio[b]
Phenol	14.44[c]	9.75	1.48
4-fluorophenol	12.05[d]	7.95	1.52
4-chlorophenol	13.98[e]	9.33	1.52

a) Calculation on the 4-31G basis set. b) Ratio= experimental/*ab initio*. c) Ref. 5. d) Ref. 7. e) This work.

Computer Center of the University of Tokyo by using the GSCF2 programmed by N. Kosugi.

References

1) T. Kojima, *J. Phys. Soc. Jpn.*, **15**, 284 (1960).
2) H. Forest and B. P. Dailey, *J. Chem. Phys.*, **45**, 1736 (1966).
3) C. R. Quade, *J. Chem. Phys.*, **47**, 1073 (1967); **48**, 5490 (1968).
4) T. Pedersen, N. W. Larsen, and L. Nygaard, *J. Mol. Struct.*, **4**, 59 (1969).
5) E. Mathier, D. Welti, A. Bauder, and Hs. H. Günthard, *J. Mol. Spectrosc.*, **37**, 63 (1971).
6) N. W. Larsen, E. Mathier, A. Bauder, and Hs. H. Günthard, *J. Mol. Spectrosc.*, **47**, 183 (1973).
7) N. W. Larsen and F. M. Nicolaisen, *J. Mol. Struct.*, **22**, 29 (1974).
8) G. Roussy and F. Michel, *J. Mol. Struct.*, **30**, 399 (1976).
9) N. W. Larsen, *J. Mol. Struct.*, **51**, 175 (1979).
10) W. Caminati and A. M. Mirri, *Chem. Phys. Lett.*, **12**, 127 (1971).
11) G. Varsanyi, "Assignments for vibrational spectra of 700 benzene derivatives," Adam Hilger, London (1974), p. 171.
12) C. C. Lin and J. D. Swalen, *Rev. Mod. Phys.*, **31**, 841 (1959).
13) G. E. Campagnero and J. L. Wood, *J. Mol. Struct.*, **6**, 117 (1970).
14) H. Konschin, *J. Mol. Struct*, **92**, 173 (1983).
15) L. S. Batchelder, J. Clymer, and J. L. Ragle, *J. Chem. Phys.*, **74**, 4791 (1981).

A Thermodynamic Study on Micellization of Nonionic Surfactant in Water and in Water-Ethanol Mixture by Gel Filtration

Ayako GOTO,* Masumi TAKEMOTO, and Fumio ENDO
Shizuoka College of Pharmacy, 2-2-1 Oshika, Shizuoka 422
(Received July 13, 1984)

Micellization of hexa(oxyethylene) dodecyl ether ($C_{12}E_6$) was studied in water and in ethanol-water mixtures at different temperatures by gel filtration on Sphacryl S-200. Standard enthalpies and entropies of micellization were determined from variation of critical micelle concentration(cmc) with temperature. Compensation plots were obtained, slopes for alcohol-water mixtures being indentical with that for pure water. Therefore, the micelle formation in water and ethanol-water mixtures has been explained in terms of its bulk structure. Gel fitration of $C_{12}E_6$ micelle with addition of a large amount of ethanol has led to a finding that the micelle size gradually becomes small with increasing ethanol content until micelles disappear above 35%v/v.

Thermodynamic studies on micellization are based on the assumption that monomer concentration is constant above cmc. However, any of the general methods, *e.g.*, the surface tension[1-3] and dye methods,[4,5] cannot verify the constancy of monomer concentration above cmc. We previously reported[6] that gel filtration of aqueous nonionic surfactant gave more reasonable cmcs than other methods, pointing out that monomer concentration became nearly constant at high concentrations of nonionic surfactant. Therefore, this method is effective for obtaining useful thermodynamic information regarding micellization.

In this research, we investigated the effect of temperature on the cmc of hexa(oxyethylene) dodecyl ether ($C_{12}E_6$) in water and in water-ethanol mixture by means of gel filtration for the purpose of elucidating thermodynamically the effect of ethanol on the micellization and the process of destruction of micelles by added ethanol.

Experimental

Materials. Hexa(oxyethylene) dodecyl ether,H-$(OCH_2CH_2)_6OC_{12}H_{25}$ ($C_{12}E_6$), was supplied from Nikko Chemical Co., Ltd. Sephacryl S-200 and Sephadex LH-60 used for gel filtration were purchased from Pharmacia Fine Chemicals. Distilled water was used after degassing *in vacuo*.

Gel Filtration. Sephacryl S-200 was mainly used because this gel hardly shrinks by added ethanol. The gel column was jacketed and maintained at a constant temperature within 0.1 °C. Tail analysis was carried out as previously reported.[6] Retention volumes of micelles (V_m) and monomer (V_f) and monomer concentration (C_f) were measured by the same method as described in our previous paper.[6]

Results and Discussion

Thermodynamic Studies on Micellization in Water. The effect of temperature (0—30 °C) on the behavior of $C_{12}E_6$ micelle in water was studied. Monomer concentrations measured on solutions in the range 4×10^{-5}—2×10^{-2} M (1 M=1 mol dm^{-3}) were plotted against total concentration (C_t) of $C_{12}E_6$ (Fig. 1). The monomer concentration increases toward a limiting concentration with increase in C_t at each temperature. The limiting concentration corresponding to cmc increases with lowering temperature. The plots, in Fig. 2, against temperature of ratio V_m/V_f obtained by gel filtration of 5×10^{-3} M $C_{12}E_6$ solution indicate that the hydrated micellar size increases with increase in temperature, in accord with Suzuki.[7] On the basis of the cmcs obtained by this tail analysis at various temperatures (Fig. 1), the standard free energy (ΔG°_m), standard enthalpy (ΔH°_m), and standard entropy (ΔS°_m) of micellization

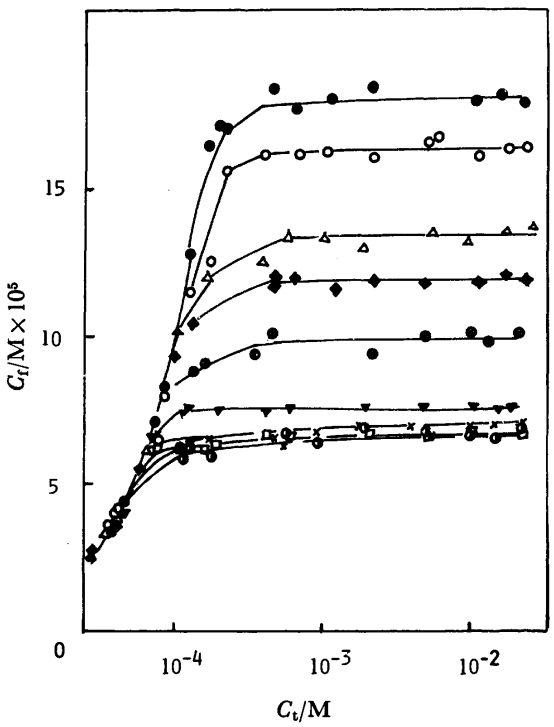

Fig. 1. Plots of Monomer Concentration, C_f, against Total Concentration, C_t.
●: 0 °C, ○: 2 °C, △: 5 °C, ◆: 10 °C, ⊗: 15 °C, ▼: 20 °C, ×: 25 °C, ◑: 27 °C, □: 30 °C.

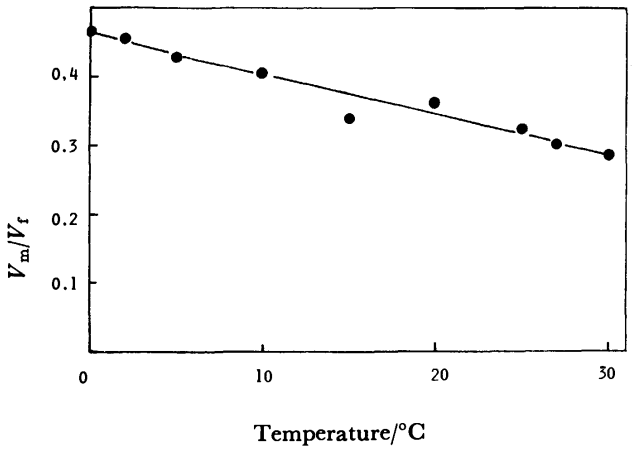

Fig. 2. Plots of V_m/V_f against Temperature.

were determined by use of the phase separation model. The standard free energy is obtained by

$$\Delta G_m^\circ \approx RT \ln \text{cmc}, \quad (1)$$

where cmc is expressed in mole fraction. The standard enthalpy of micellization can be obtained by

$$\Delta H_m^\circ = -RT^2[\mathrm{d}(\ln \text{cmc})/\mathrm{d}T]. \quad (2)$$

However, since ΔH_m° is dependent on temperature, values of ΔH_m° were obtained by fitting a quardratic function of the form[8]

$$\ln \text{cmc} = a/T^2 + b/T + c \quad (3)$$

to observed data and applying subsequently Eq. 2; values of ΔH_m° were calculated with a computer. Standard entropies of micellization were calculated from values of ΔH_m° and ΔG_m° by

$$\Delta S_m^\circ = (\Delta H_m^\circ - \Delta G_m^\circ)/T. \quad (4)$$

As shown in Table 1, the large positive entropy is responsible for the negative free energy of micellization since the enthalpy change is positive. This is caused by release of the ordered water from around the hydrocarbon chain on micellization.[14]

The Effect of Added Ethanol on Micellization. Figure 3 shows a tail analysis of aqueous $C_{12}E_6$ solution in the presence of ethanol using a column of Sephacryl S-200 at 25 °C. The retention volume of micelle and the monomer concentration increase with increase in ethanol content, indicating that the micelle becomes progressively unstable with decrease in its size. As the ethanol concentration rose to 20, 25, and 30%v/v, as shown in Fig. 4a, it became difficult to observe the presence of micelles from the tail part of $C_{12}E_6$ elution curve. Based on the finding from the elution curves of propyl *p*-hydroxybenzoate that the propyl ester is solubilized into $C_{12}E_6$ micelle in water,[9] a similar analysis was made on the system of $C_{12}E_6$-propyl *p*-hydroxybenzoate in ethanol-water mixtures (Fig. 5). The result suggested that micelles might be present even in 30%v/v ethanol. However, since Sephacryl S-200 can be used only for fractionation of substances with molecular weights 5000—250000, it seems difficult to distinguish clearly between micelles and monomer in higher concentrations than 30%v/v ethanol. When Sephadex LH gel was used (Fig. 4b) which can fractionate substances with molecular weights ranging from 500 to 10000 and is less influenced by organic additive, it could differentiate clearly the micelle and monomer even in 30%v/v ethanol. However, it seems likely that micelles are scarcely present above 35%v/v ethanol. The above results directly

Table 1. Values of thermodynamic parameters (cmc/M, ΔG_m° and ΔH_m°/kcal mol^{-1}, ΔS_m°/cal deg^{-1}) for $C_{12}E_6$ in water at various temperatures

T/°C	cmc	ΔG_m°	ΔH_m°	ΔS_m°
0	1.80×10^{-4}	−6.86	+9.68	+60.6
2	1.64×10^{-4}	−6.96	+9.18	+58.7
5	1.35×10^{-4}	−7.14	+8.45	+56.1
10	1.19×10^{-4}	−7.34	+7.26	+51.6
15	9.89×10^{-5}	−7.58	+6.11	+47.5
20	7.51×10^{-5}	−7.87	+5.00	+43.9
25	6.99×10^{-5}	−8.04	+3.93	+40.2
27	6.74×10^{-5}	−8.12	+3.51	+38.8
30	6.69×10^{-5}	−8.20	+2.89	+36.6

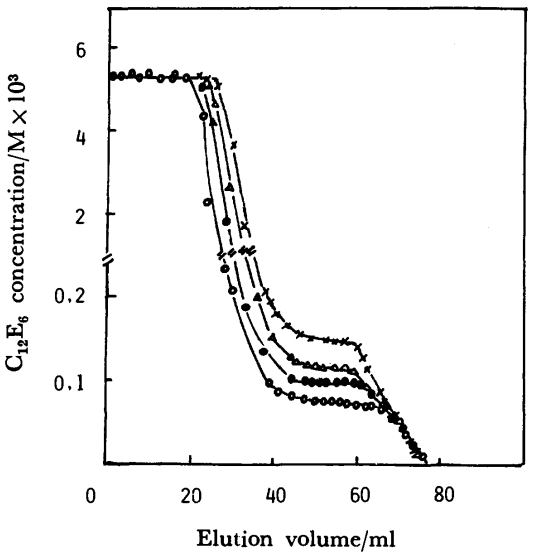

Fig. 3. Tail Analysis of Micellar $C_{12}E_6$ Solution on Sephacryl S-200.
○: without ethanol, ●: 5 % v/v ethanol, △: 10 % v/v ethnol, ×: 15 % v/v ethanol. $C_{12}E_6$ concentration, 5 mM.

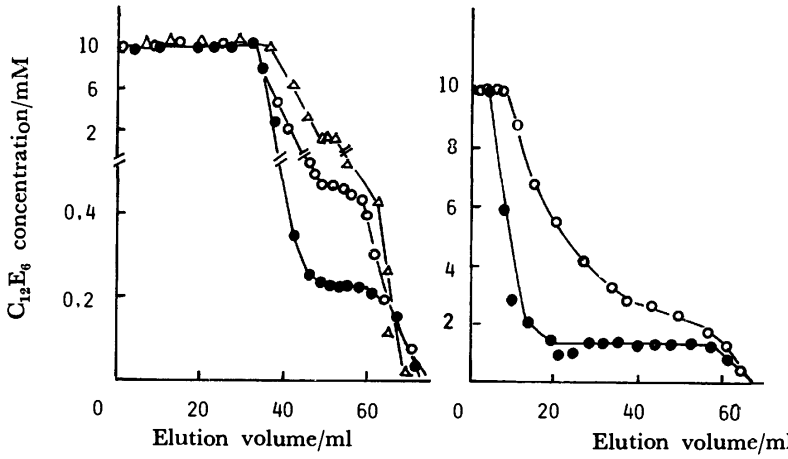

Fig. 4a. Tail Analysis for Elution Curves of 10 mM $C_{12}E_6$ in Ethanol-Water Mixtures on Sephacryl S-200 at 25 °C. ●: 20% v/v ethanol, ○: 25% v/v ethanol, △: 30% v/v ethanol.

Fig. 4b. Tail Analysis for Elution Curves of 10 mM $C_{12}E_6$ in Ethanol-Water Mixtures on Sephadex LH-60 at 25 °C. ●: 30% v/v ethanol, ○: 35% v/v ethanol.

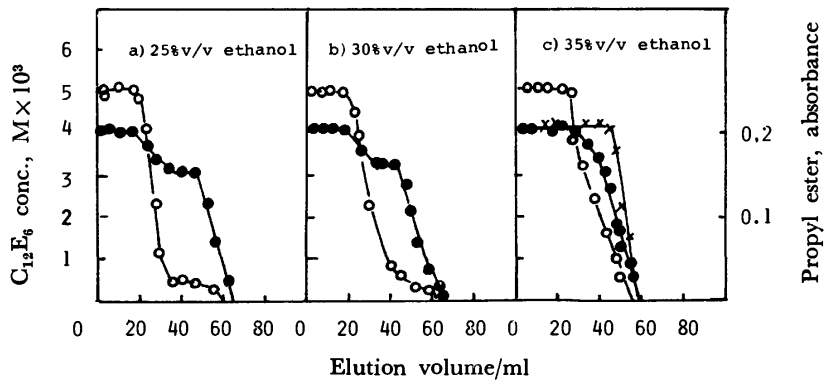

Fig. 5. Tail Analysis for Elution Curves of 0.278 mM Propyl *p*-hydroxybenzoate and 5 mM $C_{12}E_6$ in Ethanol-Water Mixtures on Sephacryl S-200 at 25 °C. ○: $C_{12}E_6$, ●: propyl *p*-hydroxybenzoate absorbance, ×: propyl *p*-hydroxybenzoate absorbance without $C_{12}E_6$

demonstrated that no micelles having a limiting size disappear suddenly with increasing ethanol content, whereas the micelle size becomes gradually small with micelles slowly disappearing. Deguchi *et al.*[10] assumed on the basis of charge-transfer interaction that the concentration of ethanol required for the destruction of $C_{12}E_7$ micelle is in the range 30—35%v/v, in consistency with the present result.

Figure 6 is a plot of C_f obtained by the gel filtration on Sephacryl S-200 against C_t at 2, 5, 10, and 15% v/v at 25 °C. Since the value of C_f increased toward a limiting concentration with increase in C_t at each ethanol content, it was also possible in the presence of ethanol to estimate cmc and to discuss the micellization thermodynamically. A general expression[11] for the solvent effect on nonionic surfactant micelle formation is

$$RT \ln [\mathrm{cmc}]/[\mathrm{cmc}]_0 = -(\mu_2^{s\circ} - \mu_2^{s\circ\prime}) + RT \ln X + RT \ln f, \quad (5)$$

where $[\mathrm{cmc}]_0$ is the cmc without organic additive, $\mu_2^{s\circ}$ and $\mu_2^{s\circ\prime}$ are the standard chemical potentials of the surfactant in bulk solutions of water and water-organic additive mixture, respectively, and X and f are the mole fraction and the activity coefficient of surfactant in the mixed micelle, respectively, both of which become unity when the solvent is pure water. The cmc-lowering effect of a solubilizate is explained in terms of mixed entropy and the reduction of activity on adding solubilizates.[11,12] If the organic additive is not solubilized into the micellar phase, the solvent effect on micellization may be due mainly to the contribution of $-(\mu_2^{s\circ} - \mu_2^{s\circ\prime})$. In this experiment, $\ln[\mathrm{cmc}]/[\mathrm{cmc}]_0$ increased with in-

Table 2. Values of thermodynamic parameters (cmc/M, ΔG_m° and ΔH_m°/kcal mol^{-1}, ΔS_m°/cal deg^{-1}) for $C_{12}E_6$ in water-ethanol mixture at various temperatures

T	5%v/v Ethanol				10%v/v Ethanol				15%v/v Ethanol			
°C	cmc	ΔG_m°	ΔH_m°	ΔS_m°	cmc	ΔG_m°	ΔH_m°	ΔS_m°	cmc	ΔG_m°	ΔH_m°	ΔS_m°
0	1.80×10^{-4}	−6.85	+5.55	+45.0	1.55×10^{-4}	−6.90	+5.41	+45.0	1.50×10^{-4}	−6.90	+7.90	+54.0
5	1.23×10^{-4}	−7.17	+3.94	+39.9	1.31×10^{-4}	−7.12	+3.88	+40.0	1.30×10^{-4}	−7.10	+5.22	+44.3
10	1.15×10^{-4}	−7.34	+2.27	+33.9	1.21×10^{-4}	−7.29	+2.34	+34.0	1.20×10^{-4}	−7.27	+2.53	+34.5
15	1.10×10^{-4}	−7.49	+0.68	+28.0	1.13×10^{-4}	−7.46	+0.85	+28.9	1.07×10^{-4}	−7.47	−0.07	+26.0
20	1.05×10^{-4}	−7.65	−0.86	+23.0	1.13×10^{-4}	−7.59	−0.58	+23.0	1.19×10^{-4}	−7.54	−2.58	+16.9
25	9.43×10^{-5}	−7.84	−2.34	+18.0	1.16×10^{-4}	−7.70	−1.97	+19.0	1.38×10^{-4}	−7.58	−5.01	+8.6

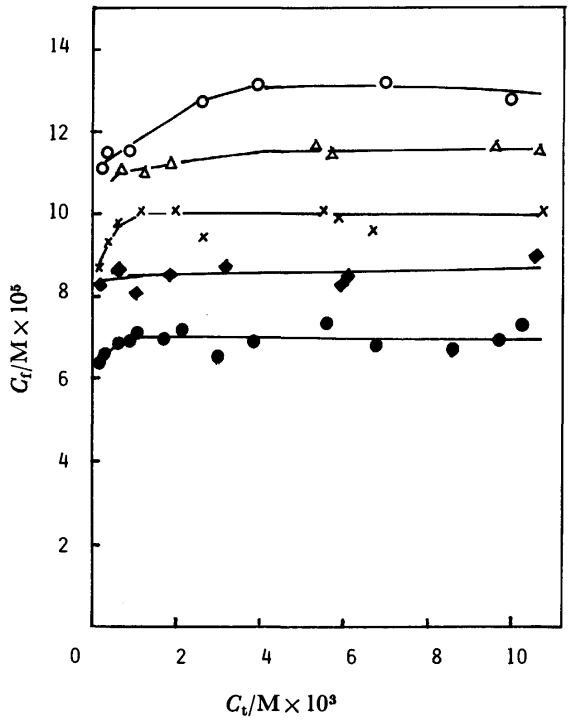

Fig. 6. Plots of Monomer Concentration, C_f, against Total Concentration, C_t in the presence of ethanol. ●: without ethnol, ◆: 2% v/v ethanol, ×: 5% v/v ethanol, △: 10% v/v ethanol, ○: 15% v/v ethanol.

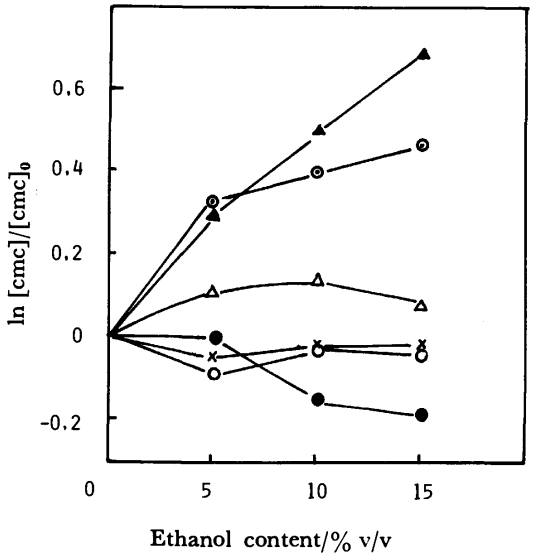

Fig. 7. Plots of ln[cmc]/[cmc]$_0$ against Ethanol Content. ●: 0 °C, ○: 5 °C, ×: 10 °C, △: 15 °C, ⊙: 20 °C, ▲: 25 °C.

creasing ethanol content at room temperature and hardly varied with ethanol content at low temperatures (Fig. 7). Therefore, the cmc-increasing effect of ethanol at room temperature is attributable to the increasing solvent power of these alcohol-water mixtures. It is of interest that the added ethanol hardly affects the micellization at low temperatures. This phenomenon may be explained as follows: the cmc-increasing effect attributable to the increasing solvent power of water-alcohol mixture would be compensated by the cmc-decreasing effect resulting from the solubilization of ethanol into $C_{12}E_6$ micelle. However, Nishikido *et al.*[13] reported that the solubilization of ethanol in nonionic micelle was negligible. We also investigated this system thermodynamically. Table 2 shows ΔG_m°, ΔH_m°, and ΔS_m° for the micellization in ethanol-water mixtures. The added ethanol caused a decrease in ΔH_m° and the micelle formation became exothermic in the neighborhood of room temperature as the content of ethanol increased (Table 2), while the micelle formation in water was endothermic as shown in Table 1. The entropy of micellization which has a large positive value in water, became small as the ethanol content increased (Table 2). Therefore, the cmc-increasing effect of ethanol at room temperature is ascribed to the weakness of the hydrophobic bond.[14] However, at low temperatures, the micellization in the presence of ethanol is responsible for the positive entropy. This indicates that the added ethanol might hardly destroy the structure of water at low temperatures.

Linear correlation between enthalpy and entropy changes has been observed for solution processes in aqueous media. This correlation is called the compensation phenomenon.[15-18] According to Lumry[15] the slope of compensation line has the dimension of temperature, T_c, in the range 220—290 K in

TABLE 3. T_c VALUES FOR MICELLIZATION IN DIFFERENT SYSTEMS

System	T_c/K	Reference
$C_{12}E_6$ in water	284 (r=1.000)	Present study
$C_{12}E_6$ in aqueous 5%v/v ethanol	289 (r=1.000)	Present study
$C_{12}E_6$ in aqueous 10%v/v ethanol	278 (r=0.999)	Present study
$C_{12}E_6$ in aqueous 15%v/v ethanol	280 (r=0.999)	Present study
Ionic surfactant in water (sodium dodecyl sulfate and cetyltrimethylammonium bromide)	283	8
Alkyltrimethylammonium bromide	313	19

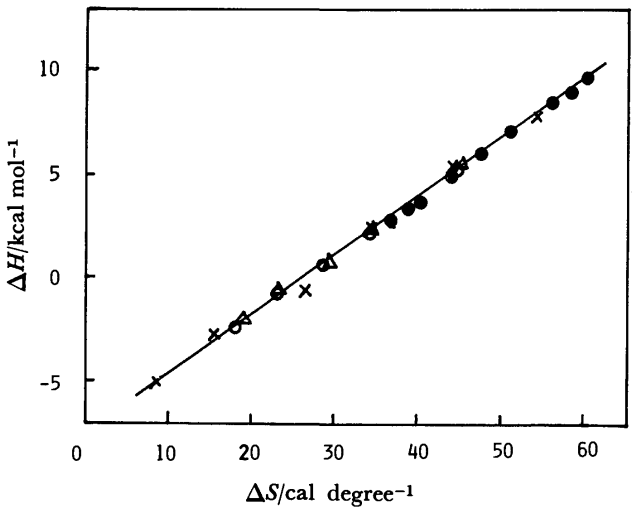

Fig. 8. Compensation plots of $C_{12}E_6$ Micellization.
●: without ethanol, ○: 5% v/v ethanol, △: 10% v/v ethanol, ×: 15% v/v ethanol.

aqueous media. Krishnan and Friedman[18] suggested that the entropy-enthalpy compensation was also observed in hydrophobic interactions. Sigh *et al.*[8] and Aoki *et al.*[19] found that their compensation plots obtained for the micellization of ionic surfactants in aqueous media were in accordance with Lumry's law.[15] Figure 8 shows compensation plots for nonionic surfactant micelle in water and in alcohol-water mixture. The compensation temperature of $C_{12}E_6$ micelle in water is 284 K, equal to that of ionic surfactant.[8] The compensation temperatures for alcohol-water mixtures are also in fair agreement with Lumry's law[15] (Table 3). Therefore, it is assumed that the micellization of $C_{12}E_6$ in water is related closely to the bulk structural property and proceeds even in the presence of ethanol essentially in a process similar to that in water.

References

1) E. H. Crook, G. F. Trebbi, and D. P. Ferdyce, *J. Phys. Chem.*, **68**, 3592 (1974).
2) B. W. Barry and D. I. D. Eleini, *J. Colloid Interface Sci.*, **54**, 339 (1976).
3) P. Becher and S. E. Trifillete, *J. Colloid Interface Sci.*, **43**, 485 (1973).
4) A. Ray and C. Nemethy, *J. Phys. Chem.*, **75**, 804 (1971).
5) K. Deguchi and K. Meguro, *J. Colloid Interface Sci.*, **38**, 596 (1972).
6) A. Goto, R. Sakura, and F. Endo, *J. Colloid Interface Sci.*, **67**, 491 (1978).
7) H. Suzuki, *Bull. Chem. Soc. Jpn.*, **49**, 1470 (1976).
8) H. N. Sigh, S. M. Saleem, and R. P. Sigh, *J. Phys. Chem.*, **84**, 2191 (1980).
9) A. Goto, F. Endo, and T. Higashino, *Bull. Chem. Soc. Jpn.*, in press.
10) K. Deguchi, T. Mizuno, and T. Meguro, *J. Colloid Interface Sci.*, **48**, 474 (1974).
11) K. Shirahama and R. Matuura, *Bull. Chem. Soc. Jpn.*, **38**, 373 (1965).
12) A. Goto, M. Nihei, and F. Endo, *J. Phys. Chem.*, **84**, 2268 (1980).
13) N. Nishikido, Y. Moroi, H. Uehara, and R. Matuura, *Bull. Chem. Soc. Jpn.*, **47**, 2634 (1974).
14) H. S. Frank and M. N. Evans, *J. Chem. Phys.*, **13**, 507 (1945).
15) R. Lumry and S. Rajender, *Biopolymers*, **9**, 1125 (1970).
16) C. Jolicoeur and P. R. Philip, *Can. J. Chem.*, **52**, 1834 (1974).
17) C. V. Krishnan and H. L. Friedman, *J. Solution Chem.*, **2**, 37 (1973).
18) C. V. Krishnan and H. L. Friedman, *J. Solution Chem.*, **2**, 119 (1973).
19) K. Aoki, T. Noda, K. Fuji, M. Murata, and K. Hiramatsu, *Yukagaku*, **33**, 20 (1984).

The Conformers of 2,2′-Bipyridine in the Phosphorescent Triplet State as Studied by Electron Spin Resonance and Phosphorescence

Mikio YAGI,* Kazuhiro MAKIGUCHI, Atsushi OHNUKI, Kazuhiro SUZUKI, Jiro HIGUCHI, and Shigeru NAGASE†

Department of Chemistry, Faculty of Engineering, Yokohama National University, Tokiwadai, Hodogaya-ku, Yokohama 240

†*Department of Chemistry, Faculty of Education, Yokohama National University, Tokiwadai, Hodogaya-ku, Yokohama 240*

(Received July 19, 1984)

Two sets of triplet-state ESR spectra corresponding to the *s-cis* and *s-trans* conformers of 2,2′-bipyridine have been observed in mixtures of water with various alcohols at 77K. The intensity ratio of the ESR signal for the *s-cis* conformer to that for the *s-trans* conformer depends on the composition of the mixture and on the sample-cooling rate. From the analysis of the phosphorescence spectra, the lowest triplet state of the *s-cis* conformer is estimated to be close to that of the *s-trans* conformer. An anomalous ESR signal which cannot be ascribed to either the *s-cis* conformer or the *s-trans* conformer has been observed in a 1-propanol-water mixture. The geometries of these conformers are discussed from their observed zero-field splitting parameters, together with their potential energy diagrams, as obtained by an *ab initio* calculation.

2,2′-Bipyridine (BPY) is a typical chelating agent for metal ions. The photophysics and photochemistry of complexes of BPY are under active investigation, with particular interest being taken in their application to solar-energy-conversion schemes. The *s-cis* and *s-trans* conformations are possible in BPY, as is shown in Fig. 1. The ground-state molecule has the *s-trans* conformation in solutions[1-3] or in the crystalline state.[4] The excited-state molecule also has the *s-trans* conformation in rigid solutions at low temperatures.[5] Although the *s-cis* conformer of free BPY was not observed until a few years ago, the chelated *s-cis* conformer undoubtedly exists in the metal-chelate compounds of BPY.[6-8]

Recently, we have succeeded, by using a poly(vinyl alcohol) (PVA) film as a host, in finding two sets of ESR spectra originating from the *s-cis* and *s-trans* conformers in the phosphorescent triplet states.[9,10] In rigid solutions, however, the triplet state BPY has for many years been considered to be in the *s-trans* conformation. In the present work, we have observed two sets of triplet-state ESR spectra of free BPY using mixtures of water with various alcohols (methanol, 1-propanol, 2-propanol, ethylene glycol, 1,2-propanediol, 1,3-propanediol, and glycerol) as rigid solvents.

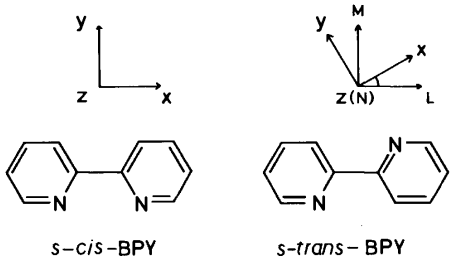

Fig. 1. Molecular structures and coordinate systems chosen for *s-cis*- and *s-trans*-2,2′-bipyridines.

The magnetic fine structure in an external magnetic field $\boldsymbol{B}$ can be described by the spin Hamiltonian:

$$\begin{aligned}\mathscr{H} &= g\mu_B \boldsymbol{B}\cdot\boldsymbol{S} + \boldsymbol{S}\cdot\boldsymbol{D}\cdot\boldsymbol{S} \\ &= g\mu_B \boldsymbol{B}\cdot\boldsymbol{S} - XS_x^2 - YS_y^2 - ZS_z^2 \\ &= g\mu_B \boldsymbol{B}\cdot\boldsymbol{S} + D[S_z^2 - (1/3)\boldsymbol{S}^2] + E(S_x^2 - S_y^2).\end{aligned}$$

Here, D is the zero-field splitting (ZFS) tensor with principal values of $-X$, $-Y$, and $-Z$, and D and E are the ZFS parameters. In the present work, the anisotropy of the g-tensor was neglected. Assuming a planar structure of the molecule in the phosphorescent triplet state, the coordinate axes were taken to be as shown in Fig. 1. For *s-cis*-BPY with the C_{2v} symmetry, the x axis is taken to be parallel to the central carbon-carbon bond which connects the two pyridine rings (hereafter, we will refer to such a direction as L), while for *s-trans*-BPY with the C_{2h} symmetry, the x axis should not be parallel to the direction L. Using such a difference in the direction of the principal axes of the ZFS tensor relative to the molecular axes, the two sets of X and Y peaks observed in the stretched PVA film were assigned as is shown in Fig. 2c.[10]

Experimental

The 2,2′-bipyridine (Aldrich) was purified by sublimation *in vacuo*. 1-Propanol (Tokyo Kasei G. R. Grade) was purified by distillation. The methanol (Dotite Spectrosol), 2-propanol (Dotite Spectrosol), ethylene glycol (Tokyo Kasei G. R. Grade), 1,2-propanediol (Tokyo Kasei G. R. Grade), 1,3-propanediol (Tokyo Kasei E. P. Grade), and glycerol (Wako Spectrosol) were used without further purification. The solvent mixtures were checked for the absence of an extraneous ESR signal prior to use. The solutions of BPY were prepared at the concentration of 3×10^{-3} mol dm^{-3}.

For the ESR measurements, the excitations were carried out using a Canrad-Hanovia 1 kW Xe-Hg lamp through a Toshiba UV-D33S glass filter, 5 cm of distilled water, and a Copal DC-495 electromechanical shutter. The decays of the ESR signals were measured by using a 1024-channel Kawasaki Electronica TM-1610S signal-averager system. The details of the ESR measurements were essentially the same as those reported previously.[10]

For the phosphorescence measurements, the excitations were done by the use of an Ushio USH-500D 500W mercury-arc lamp equipped with the glass filter mentioned above. The emissions from a sample were passed through a Jobin-Yvon HR-1000 monochromator and detected by means of a Hamamatsu Photonics R453 photomultiplier tube. All the measurements were carried out at 77K.

Results and Discussion

The ESR spectra of the phosphorescent triplet state of BPY were measured in ethanol and methanol-water (MeOH-H_2O) mixtures at 77K. The observed ESR spectra of the low-field $\Delta m_S=1$ transitions are shown in Fig. 2. For comparison, Fig. 2c shows the ESR spectrum observed in a stretched PVA film when the applied magnetic field $\boldsymbol{B}$ is parallel to the stretched direction s.

In the MeOH-H_2O mixtures, two sets of X and Y peaks and one set of Z peaks were observed, while in the ethanol solution only one set of X, Y, and Z peaks was observed. The X and Y peaks which can not be observed in the ethanol solution can reasonably be assigned to the *s-cis* conformer, for their resonance fields are almost the same as those for the *s-cis* conformer observed in the stretched PVA film. The ZFS parameters obtained are listed in Table 1.

The X and Y peaks assigned to the *s-cis* conformer of free BPY should not be attributed to signals from the complex with Zn^{2+}, which results from the contamination of polar solvents with traces of Zn^{2+}. The reasons for this assignment are as follows: (1) The ZFS parameters of the *s-cis* conformer are different from those of the Zn^{2+} complex, as is shown in Table 1; (2) the observed phosphorescence lifetime of the *s-cis* conformer in MeOH-H_2O (4:1 by volume) at 77K is 0.97s, while that of the Zn^{2+} complex is 1.16 s in the same solvent at the same temperature; (3) the intensity ratio of X peaks for the *s-cis* conformer to those for the *s-trans* conformer decreases as the MeOH content increases above 35wt% of MeOH, as is shown in Fig. 3. The last phenomenon suggests that the two sets of ESR

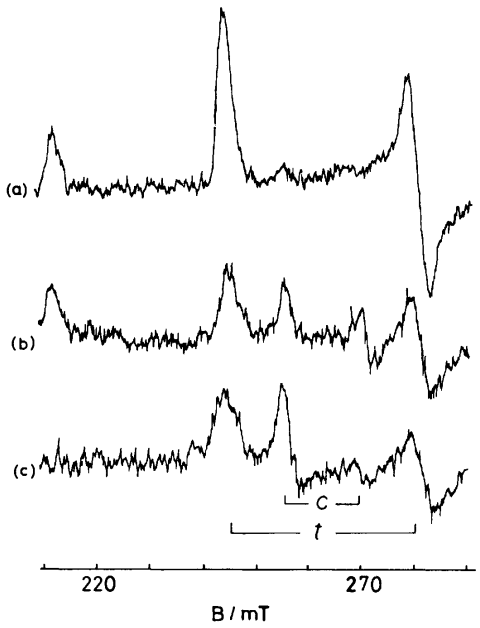

Fig. 2. ESR spectra of the low-field $\Delta m_S=1$ transitions for the phosphorescent triplet state of 2,2'-bipyridine at 77K. (a): In ethanol, (b): in MeOH-H_2O (3 : 1 by volume), (c): in a stretched PVA film with $\boldsymbol{B}$//s.

Table 1. ZFS parameters and lifetimes, τ, in the phosphorescent triplet states at 77 K

Molecule	Host	$\lvert X\rvert$ / cm^{-1}	$\lvert Y\rvert$ / cm^{-1}	$\lvert Z\rvert$ / cm^{-1}	$\lvert D\rvert$ / cm^{-1}	$\lvert E\rvert$ / cm^{-1}	D^{*} [a] / cm^{-1}	τ / s
s-trans-BPY	Ethanol	0.0487	0.0246	0.0737	0.1104	0.0121	0.1121	0.96
	PVA	0.0482	0.0237	0.0719[b]	0.1079	0.0123	0.1100	—
	MeOH-H_2O[c]	0.0479	0.0242	0.0722[b]	0.1081	0.0119	0.1102	0.97
	n-PrOH-H_2O[d]	0.0486	0.0242	0.0728[b]	0.1092	0.0122	0.1157	0.95
s-cis-BPY	PVA	0.0411	0.0317	0.0727[b]	0.1091	0.0047	0.1100	—
	MeOH-H_2O[c]	0.0411	0.0312	0.0723[b]	0.1084	0.0050	0.1102	0.97
	n-PrOH-H_2O[d]	0.0416	0.0316	0.0732[b]	0.1098	0.0050	0.1157	0.96
A-BPY	*n*-PrOH-H_2O[d]	0.0384	0.0317	0.0701[b]	0.1051	0.0033	—	0.94
B-BPY	*n*-PrOH-H_2O[d]	—	—	—	—	—	—	0.94
$[Zn(bpy)]^{2+}$	MeOH-H_2O[e]	0.0418	0.0306	0.0724	0.1087	0.0056	0.1090	1.16

a) Obtained from the observed resonance field of the $\Delta m_S=2$ transition with Kottis-Lefebvre's correction.[22] b) Obtained from X and Y by using the $X+Y+Z=0$ relation. c) MeOH-H_2O (4:1 by volume). d) *n*-PrOH-H_2O (35wt% of *n*-PrOH). e) Solutions of the complexes were prepared by the addition of $Zn(NO_3)_2$ (3×10^{-2} mol dm^{-3}) and free BPY (3×10^{-3} mol dm^{-3}) to the MeOH-H_2O (4:1 by volume) solution.

spectra should not be attributed to the formation of aggregates of BPY in MeOH-H_2O mixtures.

The intensities of the X peaks for the *s-cis* and *s-trans* conformers, $I_X(c)$ and $I_X(t)$ respectively, were measured as a function of the weight percentage of MeOH. The results are shown in Fig. 3. The $I_X(c)/\{I_X(c)+I_X(t)\}$ value increases with an increase in the amount of MeOH and gives a maximum at about 35wt% of MeOH.

In 1-propanol-water (*n*-PrOH-H_2O) mixtures, the situation is more complex. As is shown in Fig. 3, only one set of ESR signals corresponding to the *s-trans* conformer was observed in the *n*-PrOH-H_2O mixtures below 22wt% of *n*-PrOH. In the range from 23 to 29wt% of *n*-PrOH, the relative intensity of the X peaks for the *s-cis* conformer to those for the *s-trans* conformer increases with an increase in the amount of *n*-PrOH. In the range from 32 to 36wt% of *n*-PrOH, only one set of X peaks corresponding to the *s-cis* conformer was observed. As can clearly be seen in Fig. 3, there is a distinct discontinuity at 37wt% of *n*-PrOH. In the range from 38 to 100wt% of *n*-PrOH, only one set of the *s-trans* conformer signals was observed. At present we can not find the reason for the discontinuity observed at 37wt% of *n*-PrOH. However, it should be noted that, at 37wt% of *n*-PrOH, the mixed solvent forms a clear glass with a low cracking frequency and that the $\Delta m_S=1$ signals are too weak to be observed because of the very fast photochemical decomposition.

In *n*-PrOH-H_2O mixtures, the intensity ratio of the ESR signal for the *s-cis* conformer to that for the *s-trans* conformer depends on the sample-cooling rate. The results presented above were obtained with rapidly frozen samples. The sample-cooling rate was controlled by changing the penetration rate of a quartz sample tube (5 mm o.d.) into liquid nitrogen. In this experiment, the penetration rate could be changed between 2.5 and 300mm/min. In mixtures of 35wt% of *n*-PrOH, only one set of the *s-cis*-conformer signals was observed from rapidly frozen samples, while only one set of the *s-trans*-conformer signals was observed from slowly frozen samples. As is shown in Fig. 4c, two sets of the ESR signals which are not ascribed to the *s-cis* or *s-trans* conformer were observed for the samples precooled in the following manner: The bottom of the sample tube was placed in contact with the surface of liquid nitrogen for at least 10 min and then immersed in liquid nitrogen. The conformer which gives the relatively strong ESR signals at 260.1 and 270.8 mT will hereafter be denoted as the *A* conformer, while the conformer which gives the weak ESR signal at 265.7 mT will hereafter be denoted as the *B* conformer. On the other hand, the ESR signal at about 212 mT is broad and shows no structure. Although the conformation of the *A* conformer seems to be unclear, the ZFS pattern for this conformer may be assumed to be the same as those for the *s-cis* and *s-trans* conformers. The ZFS parameters thus obtained are listed in Table 1. The ZFS parameters of the *B* conformer was difficult to obtain because of its weak ESR signals. The phosphorescence lifetimes obtained from the decay of the ESR $\Delta m_S=1$ transition signal are also listed in Table 1. It is difficult to separate the observed ESR spectra into four component spectra by using a time-resolved technique because they have almost the same phosphorescence lifetime.

The *D* values of the *s-cis* and *s-trans* conformers are nearly the same, while that of the *A* conformer is smaller than those of these conformers. So long as the simple LCAO-MO's are used for the evaluation of spin distribution, however, one may roughly infer that the *D* values of the planar *s-cis* and *s-trans* conformers are nearly the same, this is in accord with the experimental results.[10] On the other hand, a preliminary π electron calculation made in our laboratory suggests that the *D* value of biphenyl becomes smaller by twisting

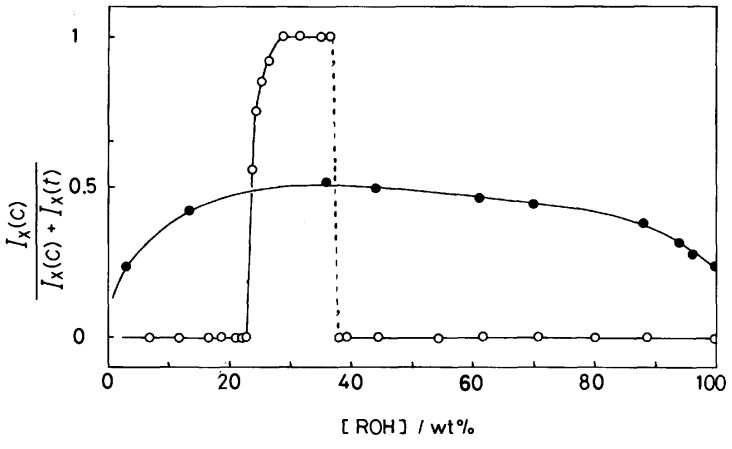

Fig. 3. Plots of $I_X(c)/\{I_X(c)+I_X(t)\}$ *versus* the weight percentage of MeOH and *n*-PrOH.
●: MeOH, ○: *n*-PrOH.

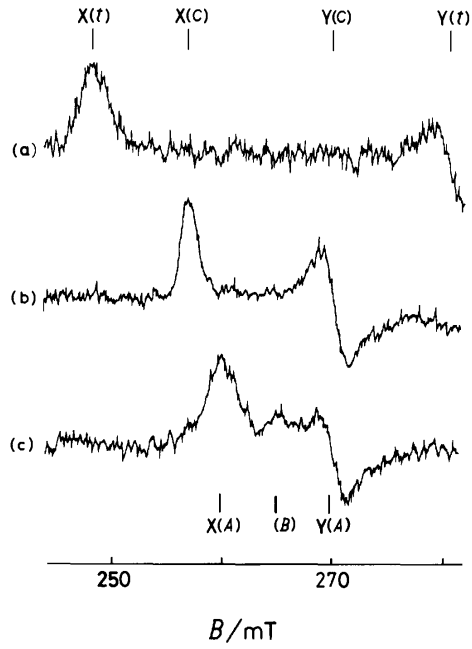

Fig. 4. ESR spectra of the low-field $\Delta m_S=1$ transitions for the phosphorescent triplet state of 2,2-bipyridine in *n*-PrOH–H_2O (35wt % of *n*-PrOH) at 77K. (a): For the slowly frozen sample, (b): for the rapidly frozen sample, (c): for the precooled sample.

around the inter-ring bond. As a result, it may be deduced that the *A* conformer has a nonplanar triplet state. In order to discuss the conformations of the lower electronic states more thoroughly, an *ab initio* calculation with a STO-3G basis set[11] was carried out for BPY, changing its inter-ring angle. At first, the optimized geometries of planar *s-cis*- and *s-trans*-BPY, with symmetries of C_{2v} and C_{2h} respectively, were determined by using the energy-gradient method.[12] The bond lengths and the bond angles thus obtained are shown in Fig. 5. When the geometry of each pyridine ring is maintained the same as in the *s-trans*-BPY, as given in Fig. 5, the SCF-MO's of the lowest-energy state were calculated by rotating the pyridine rings around the central single bond, C_2–$C_{2'}$. Using these SCF-MO's, the excitation energies of the lower electronic states were evaluated, including interactions among configurations which arise from one of the six highest occupied MO's to one of the four lowest unoccupied MO's in the ground state. The potential energy diagrams of BPY thus obtained are shown in Fig. 6.

The energy curve of the ground state (^{1}A) shown in Fig. 6 is nearly the same as that reported by Agresti *et al.*, in which the geometry of each pyridine ring was the same as the experimental one of *s-trans*-BPY.[13,14] In the present SCF-MO calculation, the geometry-optimized energy of the planar *s-cis* conformer obtained is 0.277 eV high in energy compared with that of the *s-trans* conformer. Therefore, the energy of the ground state near $\theta=180°$ can be expected to be lowered somewhat compared with that shown in Fig. 6. The lowest triplet state (^{3}B) is most stable at $\theta=0°$, and its energy curve is, in general, similar to that of biphenyl as obtained semiempirically by Imamura and Hoffmann.[15] On the other hand, the highest and the second highest occupied orbitals, and also the lowest and the second lowest unoccupied orbitals in the ground state, both degenerate at an angle of twist near $\theta=90°$. In this region, therefore, the second excited triplet state (^{3}A) is most stable and is located close to the lowest triplet state (^{3}B), as is shown in Fig. 6. As a result, the spin distributions and the ZFS parameters of these states may not differ much from each other

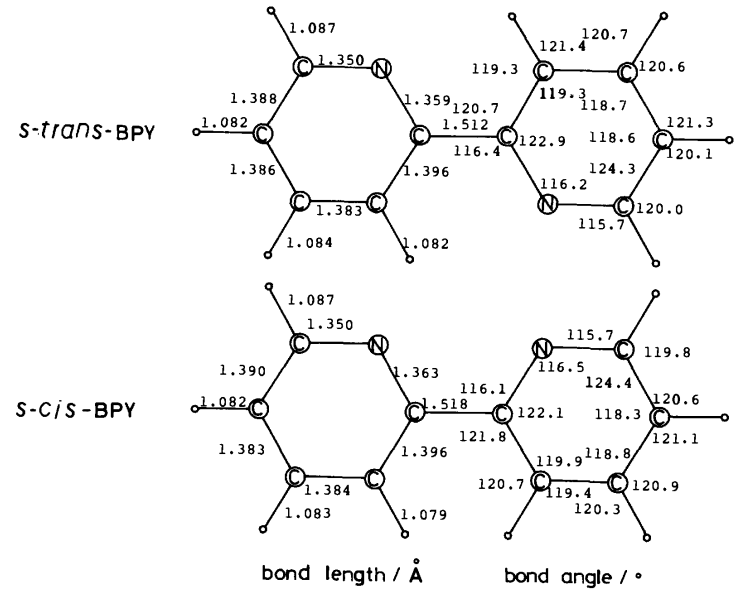

Fig. 5. Optimized geometries of *s-cis*- and *s-trans*-2,2'-bipyridines.

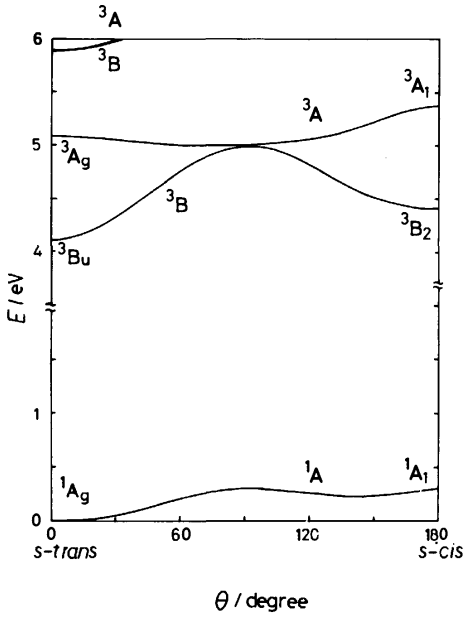

Fig. 6. Potential energy diagrams of 2,2'-bipyridine as a function of the angle of twist θ between the pyridine rings.

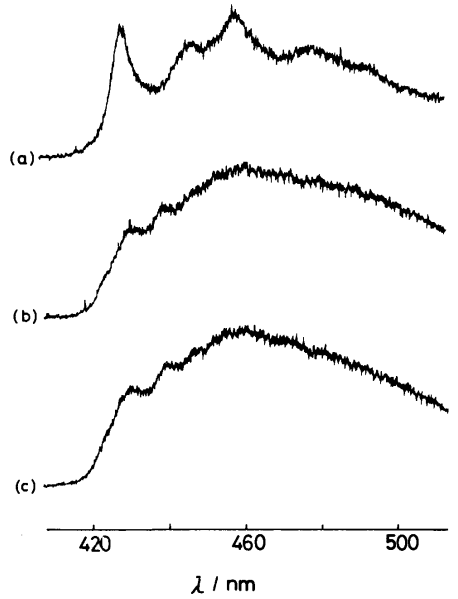

Fig. 7. Phosphorescence spectra of 2,2'-bipyridine in *n*-PrOH–H_2O (35wt % of *n*-PrOH) at 77K. (a): For the slowly frozen sample, (b): for the rapidly frozen sample, (c): for the precooled sample.

near θ=90°. Such a tendency may not be essentially changed if the approximations adopted are improved. Although the *A* conformer is most probably the nonplanar ^{3}B state, there remains another possibility that the *A* or *B* conformer is the ^{3}A state, if this state becomes the lowest excited triplet state near θ=90° under the influence of the medium. In the present work, however, a more detailed calculation of the triplet-state geometry with the intermolecular interaction was not carried out.

The phosphorescence spectra of BPY were measured in *n*-PrOH–H_2O (35wt% of *n*-PrOH) when the samples were cooled under the same conditions as in the ESR measurements. The results are shown in Fig. 7. When those results are compared with those of the ESR measurements, the phosphorescence spectra shown in Figs. 7a, 7b, and 7c may be interpreted as due to the *s-trans*, *s-cis*, and *A* and *B* conformers respectively. The phosphorescence spectrum shown in Fig. 7a is similar to that observed in ethanol at 90K.[16] The phosphorescence spectra of the *A* and *B* conformers (Fig. 7c) are almost the same as that of the *s-cis* conformer (Fig. 7b). The lineshape of the phosphorescence spectrum of the *s-trans* conformer is sharper than that of the *s-cis* conformer, while the lineshape of the ESR spectrum of the *s-trans* conformer is broader than that of the *s-cis* conformer. Although the phosphorescence spectra of the *s-cis*, *A*, and *B* conformers can not be exactly observed because of their broadness, the lowest triplet states of these conformers are estimated to be close to that of the *s-trans* conformer, 23400 cm^{-1}.

The ESR spectra of the *s-cis* and *s-trans* conformers were measured in MeOH–H_2O (4:1 by volume) with

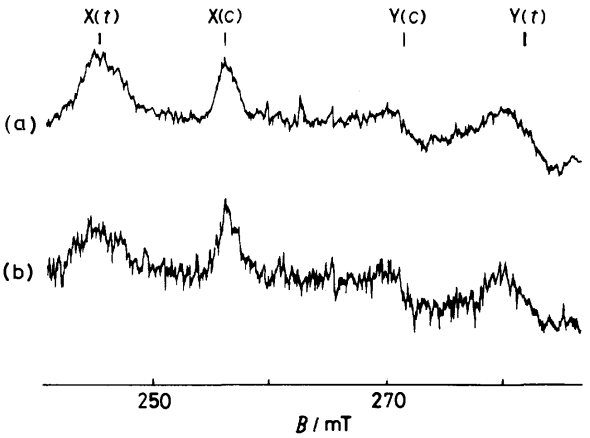

Fig. 8. ESR spectra of the low-field $\Delta m_S = 1$ transitions for the phosphorescent triplet state of 2,2'-bipyridine in MeOH–H_2O (4 : 1 by volume). (a): With A-type excitation, (b): with B-type excitation.

various filter combinations: A-type excitation, Toshiba UV-D33S glass filter; B-type excitation, Toshiba UV-D33S and UV-31 glass filters to cut off the short-wavelength region and obtain a transmission of 40% at 310 nm. The results are shown in Fig. 8. The intensity of the ESR signal of the *s-cis* conformer relative to that of the *s-trans* conformer increases under lower-energy excitation (B-type excitation). Therefore, the *s-cis* conformer has an absorption at a longer wavelength region than the *s-trans* conformer. This is in accord with the fact that the absorption of BPY coordinated to Zn^{2+} is shifted to a longer wavelength region than that of

free *s-trans*-BPY.[7]

Two sets of ESR spectra corresponding to *s-cis*- and *s-trans*-BPY's were observed in mixtures of water with 2-propanol, ethylene glycol, 1.2-propanediol, 1,3-propanediol, or glycerol, as well as with methanol or 1-propanol. The triplet-state BPY, which has for many years been considered to be in the *s-trans* conformation in rigid solutions, can easily be trapped in the *s-cis* conformation by the interactions between BPY and the solvent molecules in mixtures of water with various alcohols.

On the other hand, only one set of ESR spectra corresponding to *s-trans*-BPY has been observed in ethanol and in ethanol–water mixtures. Ethanol is generally used as a matrix for isolating free radicals or excited molecules. It is particularly interesting that ethanol acts as an exceptional solvent on the conformation of BPY. The reason for the unexpected behavior of ethanol could not be found in the present work. However, it should be noted that two sets of triplet-state ESR spectra have been observed with steric interactions for 2,2′- and 3,3′-dimethylbiphenyls in neat ethanol solutions at 77K.[17]

The heat-capacity measurements by Suga and Seki suggest that a rapid cooling of liquid ethanol yields the glassy liquid, but a slow cooling of the liquid yields a crystalline phase.[18,19] The dependence of the sample-cooling rate on the stable conformation of BPY observed in *n*-PrOH–H_2O may be related to the structures of the rigid solutions. We would expect that the use of a semirigid molecule like BPY as a probe would contribute to a deeper understanding of the molecular aspect of the rigid solution.

The calculation of geometry optimization was carried out at The Computer Center of The Institute for Molecular Science, using the IMSPAK,[20] while that of the configuration interaction was done at The Computer Centre of The University of Tokyo, using the GSCF2.[21] The authors wish to thank Dr. Nobuhiro Kosugi, Department of Chemistry, The University of Tokyo, for his kind advice in the use of the GSCF2. The present work was partially supported by Grand-in Aid for Scientific Research No. 57470004 and No. 58740213 from the Ministry of Education, Science and Culture.

References

1) K. Nakamoto, *J. Phys. Chem.*, **64**, 1420 (1960).
2) S. Castellano, H. Günther, and S. Ebersole, *J. Phys. Chem.*, **69**, 4166 (1965).
3) T. McL. Spotswood and C. I. Tanzer, *Aust. J. Chem.*, **20**, 1227 (1967).
4) L. L. Merritt, Jr. and E. D. Schroeder, *Acta Crystallogr.*, **9**, 801 (1956).
5) Y. Gondo and A. H. Maki, *J. Phys. Chem.*, **72**, 3215 (1968).
6) G. P. Rabold and L. H. Piette, *Spectrosc. Lett.*, **1**, 211 (1968).
7) T. Ohno and S. Kato, *Bull. Chem. Soc. Jpn.*, **47**, 2953 (1974).
8) J. Kotlicka and Z. R. Grabowski, *J. Photochem.*, **11**, 413 (1979).
9) T. Ito and J. Higuchi, *Chem. Lett.*, **1974**, 1519.
10) J. Higuchi, M. Yagi, T. Iwaki, M. Bunden, K. Tanigaki, and T. Ito, *Bull. Chem. Soc. Jpn.*, **53**, 890 (1980).
11) W. J. Hehre, R. F. Stewart, and J. A. Pople, *J. Chem. Phys.*, **51**, 2657 (1969).
12) A. Komornicki, K. Ishida, K. Morokuma, R. Ditchfield, and M. Conrad, *Chem. Phys. Lett.*, **45**, 595 (1977).
13) A. Agresti, M. Bacci, E. Castellucci, and P. R. Salvi, *Chem. Phys. Lett.*, **89**, 324 (1982).
14) V. Barone, F. Lelj, C. Cauletti, M. N. Piancastelli, and N. Russo, *Mol. Phys.*, **49**, 599 (1983).
15) A. Imamura and R. Hoffmann, *J. Am. Chem. Soc.*, **90**, 5379 (1968).
16) Y. Gondo and Y. Kanda, *Bull. Chem. Soc. Jpn.*, **38**, 1187 (1965).
17) B. J. Scheve and P. J. Wagner, *Chem. Phys. Lett.*, **25**, 324 (1974).
18) O. Haida, H. Suga, and S. Seki, *Proc. Jpn. Acad.*, **48**, 683 (1972).
19) H. Suga and S. Seki, *J. Non-Cryst. Solids*, **16**, 171 (1974).
20) K. Morokuma, S. Kato, K. Kitaura, I. Ohmine, S. Sakai, and S. Obara, "Program IMSPAK," IMS Library Program No. 372 (1980).
21) N. Kosugi, "Program GSCF2," Program Library, The Computer Centre, The University of Tokyo (1981).
22) P. Kottis and R. Lefebvre, *J. Chem. Phys.*, **39**, 393 (1963).

Optically Active (2-Aminoethyl)methylphenylarsine and (2-Aminoethyl)butylphenylarsine and Their Palladium(II) and Platinum(II) Complexes

Yoshiro SHIGETOMI, Masaaki KOJIMA, and Junnosuke FUJITA*
Department of Chemistry, Faculty of Science, Nagoya University, Nagoya 464
(Received August 28, 1984)

The chiral bidentate ligands, (2-aminoethyl)methylphenylarsine (mpan) and (2-aminoethyl)butylphenylarsine (bpan) were prepared and resolved by preparing their palladium(II) complexes containing, respectively, (*R*)-*N*,*N*-dimethyl-1-(2-naphthyl)ethylamine and (*S*)-*N*,*N*-dimethyl-α-methylbenzylamine. The optically actaive free arsine ligands can be readily liberated from the palladium(II) complexes, and complexes of the type, $[M^{II}X_2L]$ (M^{II}=Pd, Pt; X=Cl, Br, I; L= *R*-mpan, *S*-bpan) were prepared. The absorption and circular dichroism (CD) spectra of these and related complexes were recorded, and the absolute configurations of the arsenic atoms were assigned by comparing the CD spectra with those of analogous phosphine complexes. The optically active arsines in diethyl ether solution racemize by the addition of hydrochloric acid at room temperature, but their palladium(II) complexes in acetonitrile–ethanol solution containing hydrochloric acid are very optically stable and do not racemize by refluxing for a long time.

Otsuka *et al.* resolved chiral tertiary phosphines by fractional crystallization of their diastereomeric palladium(II) complexes containing optically active ortho-metallated *N*,*N*-dimethyl-α-methylbenzylamine or its analogs.[1,2] This method has been successfully applied to the resolution of bidentate chiral phosphines[3–6] and arsines.[5–8] The bidentate arsine ligands so far resolved, however, have a rigid framework such as *o*-phenylene[6–8] and quinolyl groups,[5] and no sterically flexible one such as (aminoalkyl)arsines has been reported, although several optically active metal complexes containing a flexible, linear quadridentate tetraarsine having two chiral arsenic donor atoms have been isolated.[9] We have succeeded in resolving (2-aminoethyl)methylphenylarsine (mpan) and (2-aminoethyl)butylphenylarsine (bpan) by use of $(-)_{589}$-di-μ-chloro-bis[(*R*)-*N*,*N*-dimethyl-1-(2-naphthyl)ethylamine-3*C*,*N*]dipalladium(II) and $(+)_{589}$-di-μ-chloro-bis[(*S*)-*N*,*N*-dimethyl-α-methylbenzylamine-2*C*,*N*]dipalladium(II), respectively. In this paper, we describe the preparation of these optically active arsines and their metal complexes of the type, $[M^{II}X_2L]$ (M^{II}=Pd, Pt; X=Cl, Br, I; L=mpan, bpan) as well as the analogous (2-aminoethyl)diphenylarsine (dpan) complexes, absorption and circular dichroism (CD) spectra of these complexes, and the absolute configurations and racemization of the chiral arsenic atoms.

Experimental

Free (aminoalkyl)arsines were handled under a nitrogen atmosphere until they formed air-stable palladium(II) and platinum(II) complexes. Tetrahydrofuran was dried with sodium and deoxygenated by distillation in a stream of nitrogen. Absorption, CD, and ^{1}H NMR spectra were recorded on a Hitachi 323 spectrophotometer, a JASCO J-40CS spectropolarimeter, and a JEOL JNM PMX 60 spectrometer, respectively. Optical rotations at 589 nm were measured with a JASCO DIP-4 polarimeter.

Diphenylarsine. Diphenylarsine was prepared by the method of Aquiar and Archibald,[10] and distilled under reduced pressure, bp 103—104 °C (133 Pa) (lit,[11] 87—90 °C (33 Pa)). ^{1}H NMR ($CDCl_3$) δ=4.97 (1H, s, AsH) and 7.13—7.76 (10H, m, C_6H_5).

(2-Aminoethyl)diphenylarsine, dpan. This compound was prepared by a method similar to that for (2-aminoethyl)diphenyl phosphine.[12,13] To a stirred solution of diphenylarsine (15.2 g, 66 mmol) in tetrahydrofuran (300 cm^3) was added a 15% (w/w) solution of butyllithium in hexane (45 cm^3, 73 mmol) over a period of 30 min at room temperature. After 1 h, aziridine (4.5 cm^3, 87 mmol) was added to the solution at 0 °C over a 15 min period. The mixture was heated at 50 °C for 1 h, then refluxed for 6 h, and allowed to stir at room temperature for 12 h. To the resulting brown solution was added deoxygenated water (2.5 cm^3), and after a while anhydrous sodium sulfate to remove excess water. After a few hours, the desiccant was filtered off, the solvent was removed by distillation, and the residual oil was distilled *in vacuo* to give (2-aminoethyl)diphenylarsine as a pale yellow viscous oil, bp 151—153 °C (133 Pa) (lit,[13] 140 °C (53 Pa)). Yield: 12.6 g (70%), ^{1}H NMR ($CDCl_3$) δ=1.25 (2H, s, NH_2), 2.15 (2H, t, $AsCH_2$), 2.91 (2H, t, NCH_2), and 7.17—7.77 (10H, m, C_6H_5).

(2-Aminoethyl)methylphenylarsine, mpan. Small pieces of sodium (2.4 g, 0.10 mol) were dissolved in liquid ammonia (150 cm^3). To this deep blue solution dpan (14.3 g, 5.2 mmol) was added with stirring. After 3 h, methyl iodide (18.2 g, 0.13 mol) was added to the resulting deep red solution, the color of which turning orange. Liquid ammonia was evaporated, and the residue was shaken with deoxygenated water–diethyl ether (60 cm^3–60 cm^3). The ethereal layer was separated and dried with anhydrous sodium sulfate. The desiccant was filtered off, the ether evaporated, and the residue was distilled at 95—98 °C and 133 Pa to give a colorless liquid. Yield: 7.0 g (63%). ^{1}H NMR ($CDCl_3$) δ=1.07 (2H, s, NH_2), 1.20 (3H, s, $AsCH_3$), 1.81 (2H, t, $AsCH_2$), 2.82 (2H, t, NCH_2), and 7.18—7.75 (5H, m, C_6H_5).

(2-Aminoethyl)butylphenylarsine, bpan. This compound was prepared by the same method as for mpan except that butyl bromide was used instead of methyl iodide. Bp 105—107 °C (133 Pa). Yield: 40%. ^{1}H NMR ($CDCl_3$)

δ=0.88 (3H, t, butylic CH_3), 1.1—1.8 (m, butylic $-CH_2-$), 1.23 (s, NH_2), 1.87 (t, $AsCH_2$), 2.87 (2H, t, NCH_2), and 7.23-7.77 (5H, m, C_6H_5).

The Diastereomers of [(R)-N,N-Dimethyl-1-(2-naphthyl)ethylamine-3C,N][(2-aminoethyl)methylphenylarsine]palladium(II) Complex, 1a and 1b. To a solution of $(-)_{589}$-di-μ-chloro-bis[(*R*)-*N*,*N*-dimethyl-1-(2-naphthyl)ethylamine-3*C*,*N*]dipalladium(II)[2] (2.04 g, 3.00 mmol) in benzene–methanol (10 cm^3–2 cm^3) was added a solution of mpan (1.28 g, 6.06 mmol) in benzene (3 cm^3). The mixture was stirred for 2 h at room temperature and then evaporated at 35 °C under reduced pressure until a small amount of white precipitate began to form. The precipitate was dissolved by heating at 45 °C, and the solution was allowed to stand overnight to yield colorless crystals. They were collected by filtration and recrystallized from methanol by adding benzene. No change in the $\Delta\varepsilon$ value was observed by repeated recrystallization. Yield (**1a**): 1.08 g. Found: C, 52.08; H, 5.82; N, 4.42%. Calcd for $PdC_{26.5}H_{35}N_2AsClO_{0.5}$=[Pd{(*R*)-$C_{10}H_6CH(CH_3)N(CH_3)_2$}(*R*-mpan)]Cl·1/2$CH_3OH$·1/2$C_6H_6$: C, 52.49; H, 5.82; N, 4.62%. $[\alpha]_{589}^{23}$ +135° (c 0.16, CH_3OH). Mp 175—179 °C. ^1H NMR ($CDCl_3$) δ=1.81 (3H, d, C-CH_3), 1.96 (3H, s, As-CH_3), 2.1—2.8 (4H, m, $-CH_2-$), 3.06 (6H, s, N-CH_3), 3.48 (1.5H, s, $C\underline{H}_3OH$), 3.93 (1H, q. -$\underline{C}H$-), 5.20 (2H, broad s, NH_2), and 7.2—8.1 (14H, m, $C_{10}H_6$, C_6H_5, and C_6H_6).

The mother liquor was evaporated to a volume of *ca.* 10 cm^3, and an aqueous solution (2 cm^3) of ammonium hexafluorophosphate (*ca.* 70 mg) was added to form a white precipitate. The mixture was heated at 50 °C and methanol was added dropwise until the precipitate dissolved completely. The solution was then allowed to stand at room temperature to yield a white powder. It was collected and recrystallized from methanol by adding benzene. Yield (**1b**): 0.69 g. Found: C, 42.74; H, 4.79; N, 3.67%. Calcd for $PdC_{23}H_{30}N_2AsPF_6$=[Pd{(*R*)-$C_{10}H_6CH(CH_3)N(CH_3)_2$}(*S*-mpan)]$PF_6$: C, 41.81; H, 4.58; N, 4.24%. $[\alpha]_{589}^{23}$ −229° (c 0.095, CH_3OH). Mp 208—211 °C (dec). ^1H NMR (CD_2Cl_2) δ=2.00 (3H, s, As-CH_3), 1.72 (3H, d, C-CH_3), 2.1—2.6 (4H, m, $-CH_2-$), 2.73 (3H, s, N-CH_3), 2.90 (3H, s, N-CH_3), 3.16 (2H, broad s, NH_2), 4.13 (1H, q, -$\underline{C}H$-), and 7.1—8.1 (11H, m, C_6H_5 and $C_{10}H_6$).

The Diastereomers of [(S)-N,N-Dimethyl-α-methylbenzylamine-2C,N][(2-aminoethyl)butylphenylarsine]palladium(II) Complex, 2a and 2b. To a solution of $(+)_{589}$-di-μ-chloro-bis[(*S*)-*N*,*N*-dimethyl-α-methylbenzylamine-2*C*,*N*]-dipalladium(II)[2,3] (1.13 g, 1.95 mmol) in benzene (10 cm^3) was added a solution of bpan (1.00 g, 3.95 mmol) in benzene (5 cm^3), and the mixture was stirred for 2 h at room temperature. Hexane (3 cm^3) was added with stirring. The mixture was allowed to stand for 1 h at room temperature to yield colorless crystals, and then cooled at 0 °C for 1 h to complete precipitation. The crystals were collected, washed with hexane, and recrystallized repeatedly from methanol by adding benzene until no change in the $\Delta\varepsilon$ values was observed. Yield (**2a**): 0.68 g. Found: C, 48.67; H, 6.39; N, 5.39%. Calcd for $PdC_{22}H_{34}N_2AsCl$=[Pd{(*S*)-$C_6H_4CH(CH_3)$-$N(CH_3)_2$}(*S*-bpan)]Cl: C, 48.64; H, 6.31; N, 5.16%. $[\alpha]_{589}^{23}$ +37° (c 0.042, CH_3OH). Mp 203—207 °C. ^1H NMR ($CDCl_3$) δ= 0.86 (3H, t, butylic CH_3) 1.1—2.8 (m, $-CH_2-$), 1.72 (d, -CHC$\underline{H}_3$-), 3.08 (6H, s, N-CH_3), 3.72 (1H, q, -$\underline{C}H$-), 5.20 (2H, broad s, NH_2) and 6.7—8.1 (9H, m, C_6H_4 and C_6H_5).

The mother liquor was evaporated to dryness. The residue was mixed with boiling water (200 cm^3), and the mixture was reduced in volume to about 40 cm^3. Ammonium hexafluorophosphate (*ca.* 60 mg) was added to yield a white precipitate. It was dissolved in a minimum amount of methanol, and the solution was allowed to evaporate slowly at room temperature to form colorless crystals, which were collected and recrystallized from methanol by adding benzene. Yield (**2b**): 0.89 g. Found: C, 40.56; H, 5.24; N, 4.29%. Calcd for $PdC_{22}H_{34}N_2AsPF_6$=[Pd{(*S*)-$C_6H_4CH(CH_3)N(CH_3)_2$}(*R*-bpan)]PF_6: C, 40.48; H, 5.25; N, 4.29%. $[\alpha]_{589}^{23}$ +75° (c 0.098, CH_3OH). Mp 169—173 °C. ^1H NMR ($CDCl_3$) δ=0.91 (3H, t, butylic CH_3), 1.2—2.6 (m, $-CH_2-$), 1.62 (d, -CHC$\underline{H}_3$-), 2.73 (3H, s, N-CH_3), 2.92 (3H, s, N-CH_3), 3.20 (2H, broad s, NH_2), 4.03 (1H, q, -$\underline{C}H$-), and 6.3—8.1 (9H, m, C_6H_5 and C_6H_4).

[(R)-N,N-Dimethyl-1-(2-naphthyl)ethylamine-3C,N][(2-aminoethyl)diphenylarsine]palladium(II) Chloride, 3. To a stirred solution of $(-)_{589}$-di-μ-chloro-bis[(*R*)-*N*,*N*-dimethyl-1-(2-naphthyl)ethylamine-3*C*,*N*]dipalladium(II)[2] (200 mg, 2.94×10^{-4} mol) in benzene (8 cm^3) was added a benzene solution (3 cm^3) of dpan (180 mg, 6.59×10^{-4} mol). After 2 h, hexane (2 cm^3) was added and the mixture was allowed to cool at 0 °C for 30 min to yield a white precipitate. It was collected by filtration, and recrystallized from methanol by adding benzene. Yield: 0.36 g. Found: C, 54.77; H, 5.83; N, 4.69%. Calcd for $PdC_{28}H_{32}N_2AsCl$=[Pd{(*R*)-$C_{10}H_6$-$CH(CH_3)N(CH_3)_2$}(dpan)]Cl: C, 54.83; H, 5.26; N, 4.57%. $[\alpha]_{589}^{23}$ −42° (c 0.103, CH_3OH). Mp 218—222 °C (dec). ^1H NMR ($CDCl_3$) δ=1.76 (3H, d, C-CH_3), 2.5—3.0 (4H, m, $-CH_2-$), 3.07 (3H, s, N-CH_3), 3.11 (3H, s, N-CH_3), 3.99 (1H, q, -$\underline{C}H$-), 5.31 (2H, broad s, NH_2), and 6.9—7.9 (16H, m, C_6H_5 and $C_{10}H_6$).

[(S)-N,N-Dimethyl-α-methylbenzylamine-2C,N][(2-aminoethyl)diphenylarsine]palladium(II) Chloride Monohydrate, 4. This complex was prepared from $(+)_{589}$-di-μ-chloro-bis-[(*S*)-*N*,*N*-dimethyl-α-methylbenzylamine-2*C*,*N*]dipalladium-(II)[2,3] and dpan by a method similar to that used for **3**. Yield: 90%. Found: C, 49.32; H, 5.52; N, 4.68%. Calcd for $PdC_{24}H_{32}N_2AsClO$=[Pd{(*S*)-$C_6H_4CH(CH_3)N(CH_3)_2$-}(dpan)]Cl·H_2O: C, 49.59; H, 5.55; N, 4.82%. $[\alpha]_{589}^{23}$ +41° (c 0.093, CH_3OH). Mp 208—211 °C (dec). ^1H NMR ($CDCl_3$) δ=1.66 (3H, d, C-CH_3), 2.4—2.9 (4H, m, $-CH_2-$), 3.04 (3H, s, N-CH_3), 3.12 (3H, s, N-CH_3), 3.86 (1H, q, -$\underline{C}H$-), 5.18 (2H, broad s, NH_2), 6.5—7.9 (14H, m, C_6H_5 and C_6H_4).

[PdCl2(R-mpan)]. A mixture of **1a** (56 mg, 9.20×10^{-5} mol) and sodium cyanide (45 mg, 9.18×10^{-4} mol) in water–diethyl ether (10 cm^3–10 cm^3) was stirred vigorously for 10 min and allowed to stand for a while. The ethereal phase was added to a stirred solution of palladium(II) chloride (17 mg, 9.59×10^{-5} mol) in acetonitrile (30 cm^3), the color of the mixture changing from orange to yellow. The mixture was stirred for 6 h at room temperature and then filtered. The filtrate was evaporated to a volume of *ca.* 5 cm^3, and the concentrate was applied on a column (ϕ12 mm×50 mm) of acid alumina. The product was eluted with 4:1 acetonitrile–ethanol. The eluate containing the main yellow band was collected and evaporated to a small volume to give yellow flocculent crystals of the palladium-(II) complex. Yield: 28 mg. Found: C, 28.20; H, 3.61; N, 4.06%. Calcd for $PdC_9H_{14}NAsCl_2$: C, 27.83; H, 3.63; N, 3.61%.

[$PdCl_2L$] (L=S-bpan and dpan). These complexes were prepared by a method similar to that for [$PdCl_2$(*R*-mpan)]. Yields: *ca.* 70%. Found: C, 33.55; H, 4.41; N, 3.17%. Calcd for $PdC_{12}H_{20}NAsCl_2$=[$PdCl_2$(*S*-bpan)]: C, 33.48; H, 4.68; N, 3.25%. Found: C, 37.46; H, 3.56; N, 3.33%. Calcd for $PdC_{14}H_{16}NAsCl_2$=[$PdCl_2$(dpan)]: C, 37.32; H, 3.58; N, 3.11%.

[$PdBr_2L$] (L=R-mpan, S-bpan, and dpan). These complexes were prepared by methods similar to those for the corresponding dichloro complexes using palladium(II) bromide instead of palladium(II) chloride. The complexes were isolated as orange crystals in 60—90% yields. Found: C, 22.64; H, 2.93; N, 2.94%. Calcd for $PdC_9H_{14}NAsBr_2$=[$PdBr_2$(*R*-mpan)]: C, 22.65; H, 2.94; N, 2.93%. Found: C, 27.10; H, 3.60; N, 2.55%. Calcd for $PdC_{12}H_{20}NAsBr_2$=[$PdBr_2$(*S*-bpan)]: C, 27.75; H, 3.88; N, 2.70%. Found: C, 31.79; H, 2.97; N, 2.94%. Calcd for $PdC_{14}H_{16}NAsBr_2$=[$PdBr_2$(dpan)]: C, 31.17; H, 2.99; N, 2.60%.

[PdI_2L] (L=R-mpan, S-bpan, and dpan). These complexes were prepared from [$PdCl_2L$] and NaI by metathesis. To a stirred solution of [$PdCl_2L$] (L=*R*-mpan, *S*-bpan, dpan; 9.0×10^{-5} mol) in 2:1 acetonitrile–ethanol (7 cm^3) was added an excess of sodium iodide (0.2 g, 1.33×10^{-3} mol), the color of the solution changing immediately from yellow to orange red. The solution was stirred for 1 h at 40 °C, and then evaporated to dryness. The residue was dissolved in a small amount of acetonitrile, and the solution was applied on a column (ϕ12 mm×60 mm) of acid alumina. On elution with 10:1 acetonitrile–ethanol, two red bands developed. The eluate containing the slower moving main band was collected and evaporated to a small volume to form red crystals in 50—65% yield. Found: C, 19.22; H, 2.33; N, 2.62%. Calcd for $PdC_9H_{14}NAsI_2$=[PdI_2(*R*-mpan)]: C, 18.92; H, 2.47; N, 2.45%. Found: C, 24.37; H, 3.15; N, 2.64%. Calcd for $PdC_{12.5}H_{20.75}N_{1.25}AsI_2$=[$PdI_2$(*S*-bpan)]·1/4$CH_3CN$: C, 24.07; H, 3.35; N, 2.81%. Found: C, 27.05; H, 2.64; N, 2.66%. Calcd for $PdC_{14}H_{16}NAsI_2$=[PdI_2(dpan)]: C, 26.55; H, 2.55; N, 2.21%.

[$PtCl_2$(R-mpan)]1/4CH_3CN. This complex was prepared by a method similar to that for the corresponding palladium(II) complex. A mixture of **1a** (250 mg, 4.12×10^{-4} mol) and sodium cyanide (200 mg, 4.08×10^{-3}mol) in water–diethyl ether (40 cm^3–40 cm^3) was stirred for 10 min, and then allowed to stand for a while. The ethereal layer was added to a stirred suspension of platinum(II) chloride (120 mg, 4.51×10^{-4} mol) in acetonitrile (300 cm^3). The resulting yellow solution was refluxed for 1 h, and then filtered. The filtrate was evaporated to a small volume to give a pale yellow precipitate. It was collected by filtration, dissolved in a small amount of acetonitrile, and the solution was applied on a column (ϕ12 mm×100 mm) of Toyopearl HW-40 (fine). The product was eluted with acetonitrile. The eluate containing the main yellow band was collected and evaporated to *ca.* 10 cm^3. The concentrate was applied again on a column (ϕ12 mm×100 mm) of acid alumina. By elution with acetonitrile–ethanol (5:1) the column showed a single pale yellow band. The yellow eluate was collected and evaporated slowly at room temperature to give pale yellow crystals. Yield: 50%. Found: C, 23.59; H, 3.00; N, 3.63%. Calcd for $PtC_{9.5}H_{14.75}N_{1.25}AsCl_2$: C, 23.41; H, 3.05; N, 3.59%.

[$PtCl_2$(dpan)]. This complex was prepared by a method similar to that for [$PtCl_2$(*R*-mpan)]1/4CH_3CN. When a solution of dpan in diethyl ether was mixed with a suspension of platinum(II) chloride in acetonitrile, a white precipitate formed. The mixture was refluxed for 2 h to give a clear pale yellow solution, from which the complex was obtained and purified in the same way as the above *R*-mpan complex. Yield: 50%. Found: C, 31.33; H, 2.90; N, 2.76%. Calcd for $PtC_{14}H_{16}NAsCl_2$: C, 31.19; H, 2.99; N, 2.60%.

[$PtBr_2$(R-mpan)]1/2CH_3CN. To a solution of [$PtCl_2$(*R*-mpan)]1/4CH_3CN (40 mg, 8.21×10^{-5} mol) in acetonitrile–ethanol (30 cm^3–30 cm^3) was added lithium bromide monohydrate (130 mg, 1.25×10^{-3} mol). The mixture was stirred at 60—65 °C for 3 h, cooled to room temperature, and then evaporated to dryness under vacuum. The residue was mixed with dichloromethane–H_2O (1:1) to extract the complex into the organic solvent. The dichloromethane was evaporated to 2 cm^3 and the concentrate was mixed with acetonitrile (1 cm^3) to give pale yellow crystals. They were purified by the same method as that for [$PtCl_2$(*R*-mpan)]·1/4CH_3CN. Yield: 50%. Found: C, 20.97; H, 2.68; N, 3.24%. Calcd for $PtC_{10}H_{15.5}N_{1.5}AsBr_2$: C, 20.48; H, 2.66; N, 3.58%.

[PtI_2(R-mpan)]. This complex was prepared by a method similar to that for [$PtBr_2$(*R*-mpan)]1/2CH_3CN using sodium iodide instead of lithium bromide. The complex was isolated as brownish orange plates in a 60% yield. Found: C, 16.47; H, 2.04; N, 2.03%. Calcd for $PtC_9H_{14}NAsI_2$: C, 16.38; H, 2.14; N, 2.12%.

[PtI_2(dpan)]. This complex was prepared from [$PtCl_2$(dpan)] by a method analogous to that for [PtI_2(*R*-mpan)]. Yield: 65%. Found: C, 23.34; H, 2.32; N, 1.61%. Calcd for $PtC_{14}H_{16}NAsI_2$: C, 23.29; H, 2.23; N, 1.94%.

Recemization of R-mpan**, *[$PdCl_2$(R-mpan)], and [$PdCl_2$(S)-bpan)].* A mixture of **1a** (50 mg, 8.25×10^{-5} mol) and sodium cyanide (40 mg, 8.16×10^{-4} mol) in water–diethyl ether (15 cm^3–15 cm^3) was stirred for 30 min. After a while, the ethereal phase was withdrawn and mixed with hydrochloric acid (*ca.* 0.08 cm^3, *ca.* 10^{-3} mol). The mixture was stirred for 1h at room temperature, and then mixed with a solution of palladium(II) chloride (15 mg, 8.46×10^{-5} mol) in acetonitrile (40 cm^3). The mixture was stirred for 2 h and then filtered. The filtrate was evaporated to *ca.* 20 cm^3, and neutralized with an ethanol solution of sodium hydroxide. The resulting yellow solution was applied on a column (ϕ12 mm×60 mm) of acid alumina, and the product was eluted with acetonitrile–ethanol (5:1). The eluate containing the main yellow band was confirmed to contain [$PdCl_2$(mpan)] by the absorption spectrum. However, the eluate showed no detectable CD in the region of 500—200 nm.

Solutions of [$PdCl_2$(*R*-mpan)] in acetonitrile–ethanol (4:1) and in the same solvent saturated with LiCl were refluxed for 4 h, and then the CD spectra were measured. Either spectrum was the same as that of the starting solution. To a solution of the complex in acetonitrile–ethanol (4:1) was added an excess of hydrochloric acid. The color of the solution changed immediately from yellow to red, indicating the formation of [$PdCl_3$(*R*-Hmpan)], where Hmpan represents $^+NH_3CH_2CH_2As(CH_3)(C_6H_5)$ coordi-

** The notation of the absolute configurations, *R* and *S*, for the tertiary arsine ligand is reversed upon liberation from a metal complex according to the rule.[14] However, the same notation as that for the coordinated arsine is used for the uncoordinated one throughout this paper.

nated to the Pd^{II} ion only through the arsenic atom. The solution was refluxed for 6 h, and then neutralized with an ethanol solution of sodium hydroxide. The resulting solution showed the same CD spectrum as that of the starting solution. The CD spectrum of [$PdCl_2$(*S*-bpan)] did not change by the same experiments, either.

Results and Discussion

Preparation and Characterization of the Arsine Ligands and the Complexes. The known compound, (2-aminoethyl)diphenylarsine (dpan) was prepared in fairly high yield (70%) by reaction of lithium diphenylarsenide with aziridine:

$$(C_6H_5)_2AsH \xrightarrow{n\text{-}C_4H_9Li} (C_6H_5)_2AsLi \xrightarrow{CH_2-CH_2 \diagdown\diagup NH} (C_6H_5)_2AsCH_2CH_2NHLi \xrightarrow{H_2O} \text{dpan}$$

This method is analogous to that for the corresponding phosphine.[12,13] To obtain dpan in good yield, it is essential to use pure $AsH(C_6H_5)_2$ isolated by distillation. New chiral (2-aminoethyl)methylphenylarsine (mpan) and (2-aminoethyl)butylphenylarsine (bpan) were prepared from dpan in liquid ammonia by a method similar to that for the corresponding phosphine analogs:[4]

$$\text{dpan} \xrightarrow{Na} NaC_6H_5AsCH_2CH_2NH_2 \xrightarrow[(RX=CH_3I,\ n\text{-}C_4H_9Br)]{RX} RC_6H_5AsCH_2CH_2NH_2$$

The chiral arsines, mpan and bpan were resolved into their enantiomers by fractional crystallization of the diastereomeric palladium(II) complexes, **1a** and **1b**, and **2a** and **2b**, containing, respectively, ortho-metallated (*R*)-*N*,*N*-dimethyl-1-(2-naphthyl)-ethylamine and (*S*)-*N*,*N*-dimethyl-α-methylbenzylamine. The less soluble **1a** and **2a** were isolated as the chlorides, whereas the more soluble **1b** and **2b** as the hexafluorophosphates. Except **2b** the diastereomers were separated in high purity as confirmed by the ^1H NMR and CD spectra. The separation of pure **2b** was difficult.

The optically active free (aminoalkyl)arsines were obtained from the diastereomers by treating with sodium cyanide in water, and by extracting with diethyl ether. The liberated ligands were used to prepare the [PdX_2L] (X=Cl, Br) and [$PtCl_2L$] complexes. The other halogeno complexes, [PdI_2L] and [PtX_2L] (X=Br, I), were prepared by metatheses from the dichloro complexes and sodium iodide or lithium bromide.

For complexes **1** and **2**, there are two possible geometrical isomers; the two nitrogen atoms can be either in the cis or trans positions to each other. For each complex only one of the geometrical isomers was formed as confirmed by ^1H NMR spectra. Kinoshita *et al.*[4] resolved (2-aminoethyl)butylphenylphosphine by forming a pair of diastereomeric palladium(II) complexes, **2a′** and **2b′**, with ortho-metallated (*S*)-*N*,*N*-dimethyl-α-methylbenzylamine. They assigned both diastereomers to the *cis*(*N*,*N*) isomer, since the ^1H NMR and ^{13}C NMR spectra exhibit large long-range couplings between the ^{31}P atom and the *N*-methyl protons ($^4J_{PPdNCH}$), and the *N*-methyl carbons ($^3J_{PPdNC}$), respectively. Such long-range couplings would be very small for the *trans*(*N*,*N*) configuration. Although such argument on couplings cannot be applied to the arsine complexes, the results that isomers **2a** and **2a′**, and **2b** and **2b′**, respectively show very similar ^1H NMR patterns strongly suggest that **2a** and **2b** also have the *cis*(*N*,*N*) configuration.

Since the σ-bonded carbon and the arsenic atoms induce the stronger trans effect than the amine nitrogen atom, the formation of the *cis*(*N*,*N*) isomer would be more favorable than the *trans*(*N*,*N*) one. Examination of molecular models indicates that the *trans*(*N*,*N*) isomer involves considerable steric interactions between the *N*-methyl groups and the substituent on the arsenic atom. Thus, all isomers **1a**—**4** can be assigned as the *cis*(*N*,*N*) configuration. Recently Allen *et al.*[5] resolved methylphenyl(8-quinolyl)phosphine and its arsenic analog with di-μ-chloro-bis[(*R*)-*N*,*N*-dimethyl-1-(1-naphthyl)ethylamine-C^2,*N*]dipalladium(II). In each case only one of geometrical isomers was formed, and X-ray crystal structure analysis of one of the diastereomers revealed the *cis*(*N*,*N*) configuration.

The optical activity of diastereomers **1a**—**2b** can be explained as a superposition of the two effects; one from the chiral arsine ligand and the other from the chiral ortho-metallated amine ligand. The observation that the CD spectra are nearly enantiomeric between diastereomers **1a** and **1b**, and between **2a** and **2b** suggests that the chiral arsine ligand has a dominating influence on the CD spectra (Figs. 1 and 2). In fact, the corresponding dpan complexes, **3** and **4** whose arsenic atoms are achiral show very weak CD. Thus the absolute configurations of the chiral arsenic atoms can be assigned from the CD spectra of the diastereomers. The CD pattern of **2a** is similar to that of the phosphine analog, **2a′** of the known absolute configuration (*S*(P)).[4] Thus the absolute configuration of the arsenic atom of **2a** is assigned as *S*. Diastereomer **1b** which shows a similar CD pattern to that of **2a** can be assigned to have the *S* configuration. Accordingly, the absolute configurations of the arsenic atoms of **2b** and **1a** can be assigned as *R*. Half the sum of the CD spectra of a pair of diastereomers should give the contribution due to the amine ligand. Actually, the calculated CD curves, $1/2[\Delta\varepsilon(\mathbf{1a})+\Delta\varepsilon(\mathbf{1b})]$ and $1/2[\Delta\varepsilon(\mathbf{2a})+\Delta\varepsilon(\mathbf{2b})]$ are similar to the observed spectra of **3** and **4**, respectively over the whole region (Figs. 1 and 2), indicating that the additivity in CD between the two effects holds for the diastereomers, and that

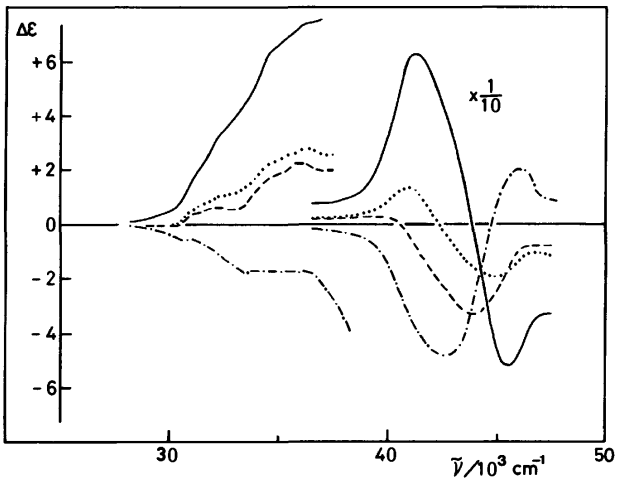

Fig. 1. CD spectra of [Pd{(*R*)-$C_{10}H_6CH(CH_3)N(CH_3)_2$}-(*R*-mpan)]Cl·1/2$CH_3OH$·1/2$C_6H_6$(**1a**, ——), [Pd{(*R*)-$C_{10}H_6CH(CH_3)N(CH_3)_2$}(*S*-mpan)]$PF_6$(**1b**, —·—), and [Pd{(*R*)-$C_{10}H_6CH(CH_3)N(CH_3)_2$}(dpan)]Cl(**3**, ----), and the mean CD curve of the two spectra for **1a** and **1b**.(·····).

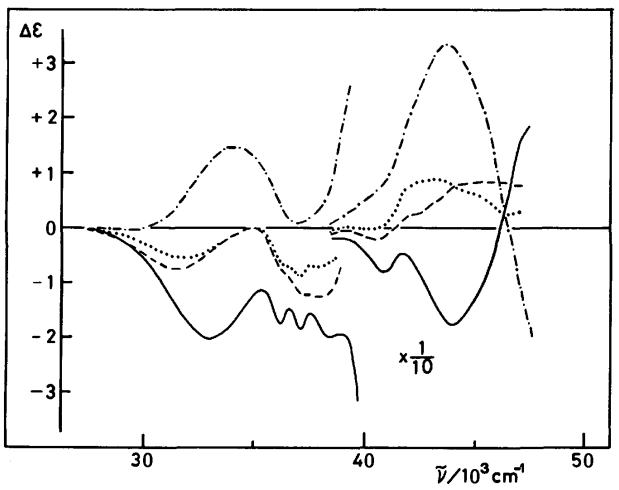

Fig. 2. CD spectra of [Pd{(*S*)-$C_6H_4CH(CH_3)N(CH_3)_2$}-(*S*-bpan)]Cl(**2a**, ——), [Pd{(*S*)-$C_6H_4CH(CH_3)N(CH_3)_2$}(*R*-bpan)]PF_6(**2b**, —·—), and [Pd{(*S*)-$C_6H_4CH(CH_3)N(CH_3)_2$}(dpan)]Cl(**4**, ----), and the mean CD curve of the two spectra for **2a** and **2b**(·····).

TABLE 1. ABSORPTION AND CD SPECTRA OF THE COMPLEXES IN ACETONITRILE

Complex	Absorption: $\tilde{\nu}_{max}/10^3$ cm^{-1} (log ε)	CD: $\tilde{\nu}_{ext}/10^3$ cm^{-1} ($\Delta\varepsilon$)
[$PdCl_2$(*R*-mpan)]	27.25(3.17) 36.1(3.84)[a] 40.52(4.05)	25.99(+0.76) 29.25(−0.63) 32.81(+0.066) 39.68(−12.75)
[$PdBr_2$(*R*-mpan)]	25.97(3.25) 32.0(3.38)[a] 37.50(4.12)	24.30(+0.28) 27.51(−0.45) 30.85(+0.43) 36.50(−9.93) 44.15(+19.25)
[PdI_2(*R*-mpan)]	22.96(3.53) 26.5(3.21)[a] 33.56(4.12) 41.2(4.29)[a]	24.27(−0.33) 28.05(+0.62) 32.73(−8.26) 36.5(+3.58)[a] 40.65(+16.69)
[$PdCl_2$(*S*-bpan)]	27.10(3.19) 35.7(3.80)[a] 40.50(4.06)	25.79(−0.64) 29.34(+0.78) 32.57(+0.14) 39.40(+12.28)
[$PdBr_2$(*S*-bpan)]	25.77(3.29) 31.01(3.43) 37.11(4.16)	24.27(−0.34) 27.74(+0.61) 30.77(+0.070) 36.36(+11.43) 43.48(−13.78)
[PdI_2(*S*-bpan)]-¼CH_3CN	22.99(3.47) 26.74(3.22) 33.64(4.07) 41.2(4.32)[a]	20.83(−0.035) 24.21(+0.30) 28.01(−0.26) 32.79(+7.07) 36.7(−0.39)[a] 41.24(+13.7)
[$PdCl_2$(dpan)]	26.67(3.23) 35.1(3.89)[a] 38.31(4.08)	
[$PdBr_2$(dpan)]	25.37(3.30) 30.40(3.40) 35.95(4.21)	
[PdI_2(dpan)]	22.17(3.55) 26.0(3.13)[a] 32.63(4.17) 41.0(4.33)[a]	
[$PtCl_2$(*R*-mpan)]-¼CH_3CN	29.0(2.35)[a] 33.22(3.00) 43.1(4.12)[a] 46.1(4.19)[a]	25.00(+0.044) 27.03(−0.031) 32.89(+0.57) 36.90(−0.45) 39.68(+0.30) 44.84(−13.1)
[$PtBr_2$(*R*-mpan)]-½CH_3CN	27.0(2.20)[a] 32.31(3.01) 41.7(4.02)[a] 45.5(4.29)[a]	24.21(+0.030) 26.67(−0.037) 31.55(+0.21) 34.06(+1.09) 43.86(−7.42)
[PtI_2(*R*-mpan)]	23.0(2.03)[a] 28.25(3.43) 33.19(3.13) 41.2(4.31)[a]	25.97(−0.26) 28.65(−0.013) 30.86(−0.20) 33.90(+1.03) 39.76(−12.09)
[$PtCl_2$(dpan)]	28.5(2.38)[a] 32.79(3.05) 42.0(4.16)[a] 45.10(4.37)	
[PtI_2(dpan)]	22.7(2.08)[a] 27.59(3.46) 32.89(3.13) 40.03(4.39)	

a) Shoulder.

the contribution from the chiral amine ligand is small.

Absorption and CD Spectra of [$M^{II}X_2L$] (M^{II}=Pd, Pt; X=Cl, Br, I; L=R-mpan, S-bpan). The elemental analyses and a comparison of the absorption spectral data (Table 1) with those of related complexes of dpan[15,16] support that these complexes are four-coordinate and square-planar. The low energy absorption bands with intensities log ε=3.0—3.5 may be assigned to predominantly a d-d transition, while those observed at energies higher than 30×10^3 cm^{-1} for the palladium(II) complexes and 35×10^3 cm^{-1} for the platinum(II) complexes will be assigned to charge-transfer transitions[15,17] (Figs. 3—6). The platinum(II) complexes show a shoulder (log $\varepsilon\approx$2.3) at the low energy side of the d-d absorption band, and the absorption may be assigned to the spin-forbidden transition. The patterns of the absorption spectra of [PtX_2(*R*-mpan)] (X=Cl, Br, I) are similar to those of the corresponding palladium(II) complexes, although all the bands of the former complexes are shifted by 5000—7000 cm^{-1} toward higher energy compared to the corresponding bands of the latter complexes. The spin-forbidden band at the lowest energy is pronounced for platinum(II) complexes (Figs. 4 and 6). In any series [$M^{II}X_2L$] (M^{II}=Pd, Pt), the energy of the d-d absorption band decreases in the order Cl>Br>I. When the phenyl group attached to the arsenic atom is replaced by an alkyl group, the d-d absorption band shifts to higher energy. Thus, the spectrochemical series of the arsine ligands is mpan≧bpan>dpan. For a series of bis(acetylacetonato)cobalt(III) complexes with analogous phosphine ligands a similar order has been reported; $NH_2CH_2CH_2P(CH_3)(C_6H_5)\geqq NH_2CH_2CH_2P(n\text{-}C_4H_9)(C_6H_5)>NH_2$-

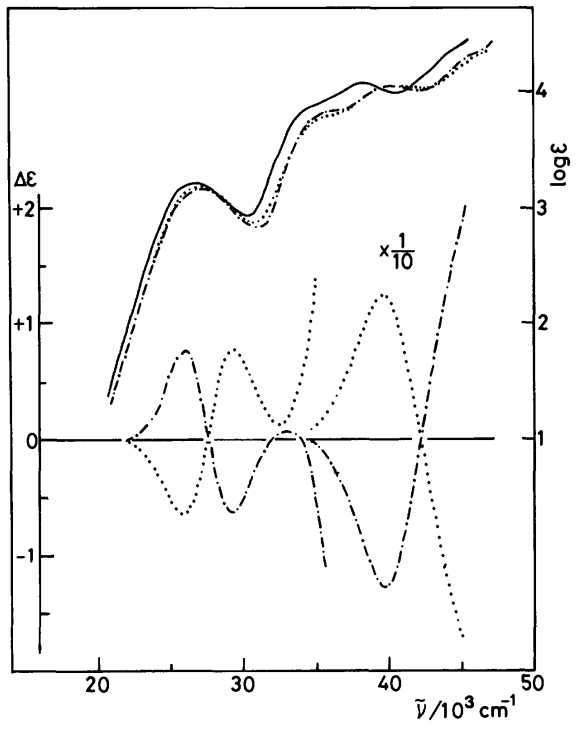

Fig. 3. Absorption and CD spectra of [$PdCl_2$(*R*-mpan)](—·—) derived from **1a**, and [$PdCl_2$(*S*-bpan)] (·····) derived from **2a**, and absorption spectrum of [$PdCl_2$(dpan)](——).

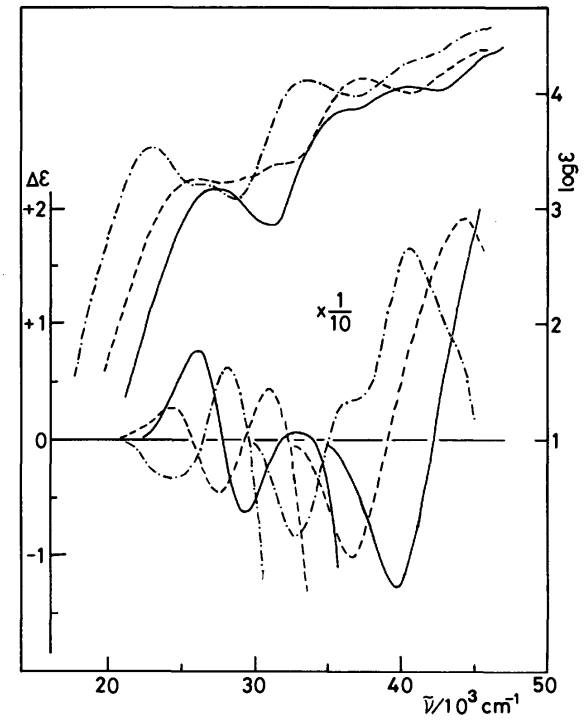

Fig. 4. Absorption and CD spectra of [PdX_2(*R*-mpan)], X=Cl(——), Br(----), and I(—·—).

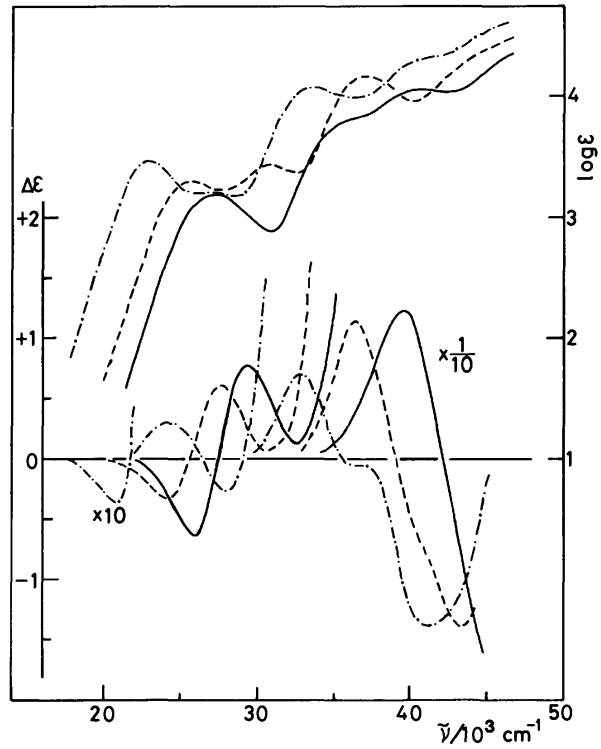

Fig. 5. Absorption and CD spectra of [PdX_2(*S*-bpan)], X=Cl(——), Br(----), and I(—·—).

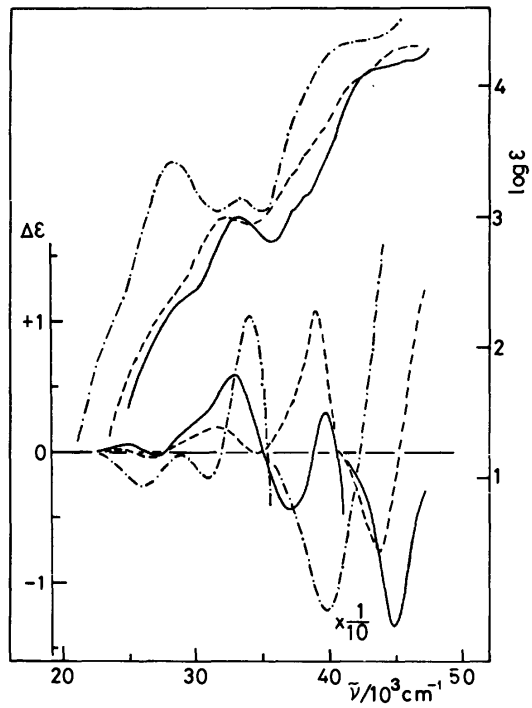

Fig. 6. Absorption and CD spectra of $[PtX_2(R\text{-mpan})]$, X=Cl(——), Br(----), aud I(—·—).

$CH_2CH_2P(C_6H_5)_2$.[18] The $[PdCl_2\{NH_2CH_2CH_2P(n\text{-}C_4H_9)(C_6H_5)\}]$ complex exhibits the d-d absorption band at a little higher energy than the corresponding bpan complex,[4] suggesting that an (aminoalkyl)phosphine ligand exerts a ligand field slightly greater than the corresponding arsine ligand.

Figure 3 shows the CD spectra of the dichloro-*R*-mpan and *S*-bpan palladium(II) complexes derived from **1a** and **2a**, respectively. The spectra are nearly enantiomeric over the whole region. The *S*-bpan complex shows the same CD pattern as that of $[PdCl_2\{(S)\text{-}NH_2CH_2CH_2P(n\text{-}C_4H_9)(C_6H_5)\}]$; a negative and a positive band from lower wave numbers in the region of the first absorption band.[4] These results support the previous assignments for the absolute configurations of the arsenic atoms of **1a—2b**. It should be noted that the CD strength of the bpan complex is about 2.5—3 times smaller than that of the phosphine analog. A similar decrease in CD strength accompanying the change of donor atom from the third to the fourth-row atom has been observed for the vicinal effect of $NH_2CH_2CH(CH_3)X^-$-*N*,*X* (X= S, Se) in the cobalt(III) complexes.[19]

In Figs. 4 and 5 the CD spectra of the complexes, $[PdX_2(R\text{-mpan})]$ (X=Cl, Br, I) and $[PdX_2(S\text{-bpan})]$ (X=Cl, Br, I), respectively, are shown. In either series of complexes all of the CD bands cause a systematic shift to smaller wave numbers as X proceeds from Cl through Br to I. The CD components in the region of the d-d absorption band decreases in magnitude in the order Cl>Br>I. For $[PdI_2(R\text{-mpan})]$ no positive CD band could be observed at *ca.* 21000 cm^{-1}, while the corresponding weak CD band for $[PdI_2(S\text{-bpan})]$ was observed at 20830 cm^{-1}.

The CD spectra of $[PtX_2(R\text{-mpan})]$ (X=Cl, Br, I) are similar to those of the corresponding palladium(II) complexes except that the former spectra shift to higher energy side by 5000—7500 cm^{-1} compared to the latter ones. The spectra of the Pt^{II} complexes show CD bands in the spin-forbidden band region, the corresponding CD bands being not observed in the spectra of the Pd^{II} complexes (Figs. 4 and 6).

Racemization of R-*mpan and Attempted Racemization of* $[PdCl_2$(R-*mpan*)*]* and $[PdCl_2$(S-*bpan*)*]*. It has been known that arsines and phosphines can be racemized catalytically, although in general they are thermally stable toward racemization.[21] For example, Horner and Hofer[21] reported that (+)-methylpropylphenylarsine in methanol solution racemizes in the presence of strong acid (HX). The rate is anion dependent and increases in the order $X=ClO_4^-<F^-<Cl^-<I^-$, the process presumably involving the rapid pseudorotation of a five-coordinate arsenic species.[22] Roberts and Wild[7] showed that *meso-o*-phenylenebis(methylphenylarsine) undergoes a halide-ion assisted epimerization in acidic methanol solution. The optically active arsine ligand, *R*-mpan, liberated from the diastereomeric palladium(II) complex (**1a**) was allowed to react with hydrochloric acid in diethyl ether at room temperature. The $[PdCl_2(mpan)]$ complex which was prepared from this mpan showed no detectable CD. The result shows that the arsine ligand undergoes racemization in the presence of hydrochloric acid.

Optically active quarternary phosphonium and arsonium salts also undego racemization in the presence of some anions such as Cl^- or Br^-, acid being not required.[24] Here again a similar account in terms of rapidly pseudorotating five-coordinate arsenic may be applicable. A metal complex with a chiral arsine ligand might undergo a halide-ion assisted racemization at the arsenic atom, if the metal ion assumes the role of a proton of a tertiary arsine or an alkyl group of a quarternary arsonium ion. Epimerization of a coordinated tertiary arsine within a chelate ring has been observed in $[CoX_2(tetars)]X$ (X=Cl, Br; tetars= $[(CH_3)_2As(CH_2)_3As(C_6H_5)CH_2\text{-}]_2$).[9,25] However, refluxing a solution of $[PdCl_2(R\text{-mpan})]$ (or $[PdCl_2(S\text{-bpan})]$) in acetonitrile-ethanol (4:1) for several hours in the presence of saturated lithium chloride or excess hydrochloric acid resulted in no racemization at a chiral arsenic center. These results indicate that the stability of chiral arsines toward racemization is greatly enhanced by coordination to a metal ion.

The authors wish to thank the Ministry of Education for Scientific Research Grant-in-Aid No. 58470032.

References

1) S. Otsuka, A. Nakamura, T. Kano, and K. Tani, *J. Am.*

Chem. Soc., **93**, 430 (1970).
2) K. Tani, L. D. Brown, J. Ahmed, J. A. Ibers, M. Yokota, A. Nakamura, and S. Otsuka, *J. Am. Chem. Soc.*, **99**, 7876 (1977).
3) N. K. Roberts and S. B. Wild, *J. Am. Chem. Soc.*, **101**, 6254 (1979).
4) I. Kinoshita, K. Kashiwabara, and J. Fujita, *Bull. Chem. Soc. Jpn.*, **53**, 3715 (1980).
5) D. G. Allen, G. M. McLaughlin, G. B. Robertson, W. L. Steffen, G. Salem, and S. B. Wild, *Inorg. Chem.*, **21**, 1007 (1982).
6) G. Salem and S. B. Wild, *Inorg. Chem.*, **22**, 4049 (1983).
7) N. K. Roberts and S. B. Wild, *J. Chem. Soc., Dalton Trans.*, **1979**, 2015.
8) N. K. Roberts and S. B. Wild, *Inorg. Chem.*, **20**, 1900 (1981).
9) B. Bosnich, W. G. Jackson, and S. B. Wild, *J. Am. Chem. Soc.*, **95**, 8269 (1973).
10) A. M. Aquiar and T. G. Archibald, *J. Org. Chem.*, **32**, 2628 (1967).
11) F. G. Mann and M. J. Pragnell, *J. Chem. Soc.*, **1965**, 4120.
12) K. Issleib and D. Haferburg, *Z. Naturforschg.*, **20b**, 916 (1965).
13) T. L. Morris and R. C. Taylor, *J. Chem. Soc., Dalton Trans.*, **1973**, 175.
14) R. S. Cahn, C. K. Ingold, and V. Prelog, *Angew. Chem., Int. Ed. Engl.*, **5**, 385 (1966).
15) T. L. Morris and R. C. Taylor, *J. Chem. Soc., Dalton Trans.*, **1973**, 175.
16) B. Chiswell, R. A. Plowman, and K. Verrall, *Inorg. Chim. Acta*, **6**, 275 (1972).
17) F. R. Hartley, *J. Organomet. Chem.*, **21**, 227 (1970).
18) I. Kinoshita, K. Kashiwabara, J. Fujita, T. Yamane, H. Ukai, and T. Ashida, *Bull. Chem. Soc. Jpn.*, **52**, 1413 (1979).
19) K. Nakabayashi, K. Doi, M. Kojima, and J. Fujita, *Bull. Chem. Soc. Jpn.*, **57**, 989 (1984).
20) J. B. Lambert, *Topics Stereochem.*, **6**, 19 (1971).
21) L. Horner and W. Hofer, *Tetrahedron Lett.*, **1965**, 4091.
22) F. H. Westheimer, "Rearrangements in Ground and Excited States," ed by P. de Mayo, Academic Press, New York (1980), Vol. 2, p. 229.
23) L. Horner and W. Hofer, *Tetrahedron Lett.*, **1965**, 3281.
24) W. G. Jackson and A. M. Sargeson, "Rearrangements in Ground and Excited States," ed by P. de Mayo, Academic Press, New York (1980), Vol. 2, p. 273.

Three-dimensional Aromaticity of Ferrocene

Jun-ichi AIHARA
Department of Chemistry, Faculty of Science, Shizuoka University, Oya, Shizuoka 422
(Received December 23, 1983)

The conjugated systems of ferrocene and related compounds were constructed using five equivalent 3d orbitals of iron and carbon $2p_z$ orbitals of the cyclopentadienyl or pentadienyl groups. Ferrocene with such a conjugated system was found to have positive resonance energy due to cyclic conjugation, and was characterized as a three-dimensional aromatic species.

Aromatic compounds have cyclic conjugated systems.[1,2] They are usually planar in geometry. In 1978, we showed that the concept of aromaticity can be extended to three-dimensional conjugated systems.[3,4] Graph-theoretical analysis identified tricarbonyliron complexes of olefins and *closo*-boranes as typical aromatics. Many compounds of this kind are in fact very stable, and undergo electrophilic substitution reactions.[5,6] Ferrocene is the most famous organometallic compound. However, its possible aromaticity has not been elucidated theoretically. In this paper, the author intends to resolve this problem by introducing a simplified bonding model of ferrocene[7,8] in combination with our graph theory of aromaticity.[1,2]

Theory

Ferrocene has strong covalent bonding between iron and cyclopentadienyl rings.[9,10] A large number of molecular orbital calculations have shown that the major bonding interactions between iron and rings involve a degenerate pair of iron 3d orbitals (d_{xz}, d_{yz}) and the π bonding orbitals of the rings.[9,10] Overlapping of these 3d orbitals with rings gives a three-dimensional conjugated system.

A convenient way of representing this situation is to use five equivalent hybridized 3d orbitals of iron as described by Powell[11] and by Pauling and McClure.[12] It was Herndon and Agranat who first constructed a Hückel-type molecular orbital model of ferrocene, using five equivalent 3d orbitals of iron.[7,8] We adopt their bonding model in what follows.

The directional character of five equivalent 3d orbitals is drawn in **1**, and overlap with $2p_z$ orbitals of two cyclopentadienyl rings generates a diagram which corresponds very closely to a staggered D_{5d} depiction of ferrocene with ten carbon-iron bonds given in **2**.[7,8] It is graphically shown in **3**, where five hybridized 3d orbitals of iron are represented by short horizontal lines. This indicates that the 3d orbitals can be treated formally as five hetero atoms. Eighteen valence electrons are then accommodated in this delocalized electron network.

The structure of ferrocene in the solid state deviates slightly from the staggered configuration.[13] However, in the gas phase it has an eclipsed configuration.[14] The rings are essentially free to rotate, and the configuration adopted in the crystal is susceptible to packing forces. No intrinsic barrier to internal rotation is predicted from the symmetry consideration of the occupied molecular orbitals.[9] The very low barrier observed may be attributable to van der Waals forces between the rings.[9] This allows us to take a staggered configuration of ferrocene for analyzing the degree of its aromaticity.

The resonance integral between each hybridized iron 3d and carbon $2p_z$ orbitals is set equal to that between two bonded carbon $2p_z$ orbitals. This is essentially the same approximation as adopted by Mingos to rationalize the stability of tricarbonyliron complexes of olefins.[15]

The Coulomb integral for iron 3d orbitals can be written as

$$\alpha = \alpha_c + h\beta_{c-c} \quad (1)$$

Here, α_c is the Coulomb integral for carbon $2p_z$ orbitals; β_{c-c} is the resonance integral between two bonded carbon $2p_z$ orbitals; and h is an appropriate constant. According to the widely accepted extended Hückel molecular orbital model, the Coulomb integral for iron 3d orbitals is -12.63 eV, which is slightly smaller than that for carbon 2p orbitals, -11.40 eV.[16] This implies that h might be positive in sign. However, the Coulomb integral for iron 3d orbitals is here set equal to that for carbon $2p_z$ orbitals. We dare adopt $h=0.0$ in order to have the iron 3d orbitals retain some electron-donating ability. This kind of treatment is required due to the neglect of iron 4s and 4p orbitals. Mingos adopted $h=1.0$ when he modeled conjugated systems of tricarbonyliron complexes of olefins using olefin π systems and only two of the iron 3d orbitals (d_{xz}, d_{yz}).[15] Our graph theory of aromaticity[1,2] was applied to the above bonding model of ferrocene pictured with $h=0.0$.

Results and Discussion

All atomic orbitals forming the ferrocene conjugated system are numbered as shown in **3**. The Hückel-type secular determinant for it can then be written as

$$D(X) = \begin{vmatrix} -X & 1 & 0 & 0 & 1 & 1 & 0 & 0 & 0 & 0 & 0 & 0 & 0 & 0 & 0 \\ 1 & -X & 1 & 0 & 0 & 0 & 1 & 0 & 0 & 0 & 0 & 0 & 0 & 0 & 0 \\ 0 & 1 & -X & 1 & 0 & 0 & 0 & 1 & 0 & 0 & 0 & 0 & 0 & 0 & 0 \\ 0 & 0 & 1 & -X & 1 & 0 & 0 & 0 & 1 & 0 & 0 & 0 & 0 & 0 & 0 \\ 1 & 0 & 0 & 1 & -X & 0 & 0 & 0 & 0 & 1 & 0 & 0 & 0 & 0 & 0 \\ 1 & 0 & 0 & 0 & 0 & -X & 0 & 0 & 0 & 0 & 1 & 0 & 0 & 0 & 0 \\ 0 & 1 & 0 & 0 & 0 & 0 & -X & 0 & 0 & 0 & 0 & 1 & 0 & 0 & 0 \\ 0 & 0 & 1 & 0 & 0 & 0 & 0 & -X & 0 & 0 & 0 & 0 & 1 & 0 & 0 \\ 0 & 0 & 0 & 1 & 0 & 0 & 0 & 0 & -X & 0 & 0 & 0 & 0 & 1 & 0 \\ 0 & 0 & 0 & 0 & 1 & 0 & 0 & 0 & 0 & -X & 0 & 0 & 0 & 0 & 1 \\ 0 & 0 & 0 & 0 & 0 & 1 & 0 & 0 & 0 & 0 & -X & 1 & 0 & 0 & 1 \\ 0 & 0 & 0 & 0 & 0 & 0 & 1 & 0 & 0 & 0 & 1 & -X & 1 & 0 & 0 \\ 0 & 0 & 0 & 0 & 0 & 0 & 0 & 1 & 0 & 0 & 0 & 1 & -X & 1 & 0 \\ 0 & 0 & 0 & 0 & 0 & 0 & 0 & 0 & 1 & 0 & 0 & 0 & 1 & -X & 1 \\ 0 & 0 & 0 & 0 & 0 & 0 & 0 & 0 & 0 & 1 & 1 & 0 & 0 & 1 & -X \end{vmatrix} \quad (2)$$

This determinant can be expanded into the characteristic polynomial $P(X)$ in this form:

$$\begin{aligned} P(X) &= (-1)^{15}D(X) \\ &= X^{15} - 20X^{13} + 155X^{11} - 4X^{10} - 600X^{9} \\ &\quad + 40X^{8} + 1245X^{7} - 160X^{6} - 1378X^{5} \\ &\quad + 300X^{4} + 760X^{3} - 240X^{2} - 160X + 64. \end{aligned} \quad (3)$$

The corresponding reference polynomial $R(X)$ can be constucted graph-theoretically.[1,2] It is expressed as

$$\begin{aligned} R(X) &= X^{15} - 20X^{13} + 155X^{11} - 590X^{9} + 1155X^{7} \\ &\quad - 1112X^{5} + 460X^{3} - 60X. \end{aligned} \quad (4)$$

$R(X)$ has been interpreted as a characteristic polynomial for the olefinic reference structure.

Roots of the equation $D(X)=0$ or $P(X)=0$ represent the orbital energies of the ferrocene conjugated system **3**. They are given relative to α_c and in units of $\beta_{c\text{-}c}$. Total electron energy is equal to twice the sum of the energies of all occupied orbitals. It is $18\,\alpha_c+20.780\beta_{c\text{-}c}$ for this eighteen-electron system. Roots of the equation $R(X)=0$ represent the orbital energies which the ferrocene conjugated system would possess if it were hypothetically olefinic in nature. They are also given relative to α_c and in units of $\beta_{c\text{-}c}$. Total electron energy calculated for this reference structure is $18\alpha_c+20.527\beta_{c\text{-}c}$.

The energy difference between the ferrocene conjugated system and its olefinic reference structure is 0.253β, where β is the absolute value of $\beta_{c\text{-}c}$. This is our way of evaluating the resonance energy arising from cyclic conjugation.[1-4] It follows that the resonance energy of **3** is 0.253β. This positive value indicates that the ferrocene conjugated system is more stable than its olefinic reference structure by this amount. Positive and negative resonance energies represent aromaticity and antiaromaticity, respectively.[1-4] Accordingly, ferrocene is classified as an aromatic compound.

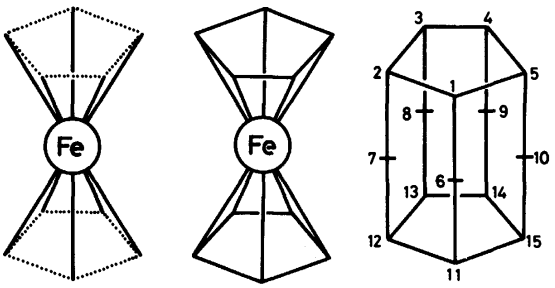

1 2 3

The resonance energy of ferrocene is comparable to that of benzene, 0.273β.[1-2] Considering that ferrocene is about twice as large as benzene, aromaticity of ferrocene, normalized with respect to the molecular dimension, is estimated to be about half that of benzene. In line with this ferrocene has been considered to be aromatic in its chemical behavior.[6,9,10] It is quite analogous in chemical reactivity to benzene. Furthermore, ferrocene is much more reactive toward electrophilic reagents than benzene. It rather resembles more reactive thiophene and phenol. In a previous paper,[17] we showed that more aromatic compounds are generally less reactive toward electrophiles. In this sense, ferrocene is chemically less aromatic than benzene. Theory and experiment thus agree qualitatively for the ferrocene conjugated system.

The resonance energy of a ferrocene-like conjugated system is a function of the h value defined in Eq. 1. It is maximized when h=0.3—0.4, and then takes the value of 0.296β. As far as h is larger than −0.5 but smaller than 1.5, the resonance enrgy stays positive in sign. This indicates that the system stays aromatic. Thus, not only tricarbonyliron complexes of olefins[3] but also ferrocene-like compounds

are highly delocalizable iron-organic systems with a considerable degree of aromatic stabilization.

Someone may depict ferrocene as a combination of two cyclopentadienide ions and one ferrous ion, attributing its aromaticity to the former ions. However, this model is not realistic at all. The resonance energy of the cyclopentadienide ion is 0.317β.[1,2] The resonance energy of ferrocene is much less than twice the resonance energy of this ion. Perturbation by the central iron atom is so great as to remove any simple prediction of aromaticity based on the cyclopentadienide ions only.

The resonance energy of open ferrocene,[18] *i.e.*, bis-(pentadienyl)iron, **4**, can be estimated according to the same procedure. Its conjugated system is similar in shape to that of ferrocene, but two C-C bonds are lacking. For simplicity, this open ferrocene is again assumed to take a staggered configuration. There still are three orientational isomers. They are pictured in **5**, **6**, and **7**. There of course is a possibility of facile rotation of the ligands in solution or in the gas phase.[18]

For isomer **5**, the two types of polynomials are

$$P(X) = X^{15} - 18X^{13} + 126X^{11} - 444X^{9} + 849X^{7} - 882X^{5} + 464X^{3} - 96X \quad (5)$$

and

$$R(X) = X^{15} - 18X^{13} + 126X^{11} - 436X^{9} + 783X^{7} - 698X^{5} + 266X^{3} - 32X. \quad (6)$$

For isomer **6**, the two types of polynomials are

$$P(X) = X^{15} - 18X^{13} + 126X^{11} - 442X^{9} + 832X^{7} - 8X^{6} - 832X^{5} + 36X^{4} + 408X^{3} - 44X^{2} - 76X + 16 \quad (7)$$

and

$$R(X) = X^{15} - 18X^{13} + 126X^{11} - 436X^{9} + 784X^{7} - 704X^{5} + 276X^{3} - 34X. \quad (8)$$

For isomer **7**, the two types of polynomials are

$$P(X) = X^{15} - 18X^{13} + 126X^{11} - 442X^{9} + 839X^{7} - 12X^{6} - 864X^{5} + 44X^{4} + 450X^{3} - 48X^{2} - 92X + 16 \quad (9)$$

and

$$R(X) = X^{15} - 18X^{13} + 126X^{11} - 436X^{9} + 785X^{7} - 708X^{5} + 280X^{3} - 36X. \quad (10)$$

The resonance energies are then calculated to be -0.189β for **5**, -0.160β for **6**, and -0.071β for **7**. This clearly shows that open ferrocene must be slightly antiaromatic and reactive in nature. In accord with this, open ferrocene is a relatively less tractable material, which readily decomposes to dipentadienyl and ferromagnetic iron byproducts.[18] It decomposed on attempted sublimation.

Wilson *et al.* determined the actual geometry of a tetramethyl derivative by X-ray crystallography,[18] and the structure was found to correspond closely to a geometry intermediate between **6** and **7**. It is not unlikely that this structure is chosen as a result of packing forces in the crystal. It is far from the most antiaromatic isomer **5**. By the way, **6**, represents the conjugated system of **4**.

Cyclopentadienyl(pentadienyl)iron, **8**, comes between ferrocene and open ferrocene. This semi-open

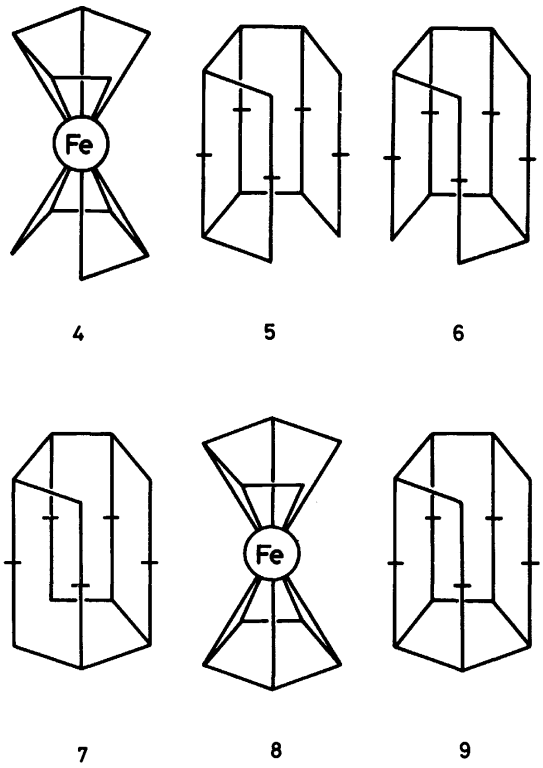

4 5 6

7 8 9

ferrocene has not been prepared yet. If this compound is assumed to have a staggered configuration, **9**, the following two polynomials are obtained:

$$P(X) = X^{15} - 19X^{13} + 140X^{11} - 2X^{10} - 516X^{9} + 18X^{8} + 1023X^{7} - 70X^{6} - 1089X^{5} + 134X^{4} + 580X^{3} - 112X^{2} - 120X + 32 \quad (11)$$

and

$$R(X) = X^{15} - 19X^{13} + 140X^{11} - 508X^{9} + 953X^{7} - 887X^{5} + 358X^{3} - 46X. \quad (12)$$

The resonance energy is then calculated to be 0.048β. Semi-open ferrocene is thus predicted to be essentially nonaromatic and olefinic in reactivity. Therefore, this compound may not be stable.

Comparing the resonance energies of ferrocene, semi-open ferrocene, and open ferrocene, we note that the resonance energy decreases in this order. This fact suggests that the cyclopentadienyl rings may play a key

role in stabilizing ferrocene-like conjugated systems. As we have seen, ferrocene is far from being an ionic species in the form of ferrous dicyclopentadienide. Its pentagonal substructures are firmly incorporated in the three-dimensional conjugated system. However, they still seem to be crucial to aromatic stabilization. It is quite possible that the electron-rich pentagonal rings are responsible for most part of the resonance energy.

Concluding Remarks

Our graph theory of aromaticity[1,2] is mathematically exact, in the sense that no parametrization is used in the framework of the theory. Its predictive capability depends solely on the validity of the bonding model employed. The bonding model adopted above for ferrocene and related compounds is fairly rough with omission of iron 4s and 4p valence orbitals. We believe that this bonding model is still practical enough to account for the aromatic origin of stabilization since it takes account of the predominant effect of iron 3d orbitals. At present, the resonance energy cannot be estimated for ferrocene of D_{5h} symmetry.

Our choice of Hückel parameters may not be based on physically sound grounds. However, the obtained resonance energies are consistent with chemical stabilities of the compounds. As has been referred to, the resonance energy of ferrocene is rather insensitive to the h value in Eq. 1. It is also fairly insensitive to the resonance integral between carbon $2p_z$ and hybridized iron 3d orbitals. Let this resonance integral be denoted by $k\beta_{c\text{-}c}$. The resonance energy of ferrocene is calculated to be 0.352β for $h=0$ and $k=0.8$ and 0.331β for $h=0$ and $k=0.5$. This further supports our view that ferrocene is basically aromatic in a thermodynamic sense. This compound can now be characterized as another example of three-dimensional aromaticity. This way of reasoning would become a new guiding principle in the field of organometallic chemistry, and would aid in developing simplified bonding models for a variety of complex organometallic compounds.

I gratefully acknowledge very helpful suggestions and comments from Prof. W. C. Herndon, without which this work would not have been finished.

References

1) J. Aihara, *J. Am. Chem. Soc.*, **98**, 2750 (1976).
2) M. Milun, I. Gutman, and N. Trinajstić, *J. Am. Chem. Soc.*, **99**, 1692 (1977).
3) J. Aihara, *Bull. Chem. Soc. Jpn.*, **51**, 1541 (1978).
4) J. Aihara, *J. Am. Chem. Soc.*, **100**, 3339 (1978).
5) E. L. Muetterties and W. H. Knoth, "Polyhedral Boranes," Marcel Dekker, New York (1968).
6) E. A. K. v. Gustorf, F.-W. Grevels, and I. Fischer, Eds., "The Organic Chemistry of Iron," Vol. I, Academic Press, New York (1978); Vol. II (1981).
7) W. C. Herndon and I. Agranat, *Isr. J. Chem.*, in press.
8) W. C. Herndon, private communication.
9) F. A. Cotton and G. Wilkinson, "Advanced Inorganic Chemistry: A Comprehensive Text," Fourth Ed., Wiley, New York (1980).
10) J. E. Huheey, "Inorganic Chemistry: Principles of Structure and Reactivity," Second Ed., Harper and Row, New York (1978).
11) R. E. Powell, *J. Chem. Educ.*, **45**, 45 (1968).
12) L. Pauling and V. McClure, *J. Chem. Educ.*, **47**, 15 (1970).
13) P. Seiler and J. D. Dunitz, *Acta Cryst., Ser. B*, **35**, 1068 (1979).
14) A. Haaland and J. E. Nilsson, *Acta Chem. Scand.*, **22**, 2653 (1968).
15) D. M. P. Mingos, *J. Chem. Soc., Dalton Trans.*, **1977**, 20, 26, 31.
16) J. W. Lauher and R. Hoffmann, *J. Am. Chem. Soc.*, **98**, 1729 (1976).
17) J. Aihara, *Bull. Chem. Soc. Jpn.*, **54**, 2268 (1981).
18) D. R. Wilson, A. A. DiLullo, and R. D. Ernst, *J. Am. Chem. Soc.*, **102**, 5928 (1980).

The Structure of Liquid Alcohols by Neutron and X-ray Diffraction. III. Liquid Structure of Methanol

Yukio TANAKA,† Norio OHTOMO,† and Kiyoshi ARAKAWA*
Research Institute of Applied Electricity, Hokkaido University, Sapporo 060
†*Faculty of Engineering, Hokkaido University, Sapporo 060*
(Received January 13, 1984)

A structure analysis of neutron and X-ray diffraction data of liquid methanol was performed by applying a general theoretical procedure for the fluid system composed of molecular clusters. The calculated structure factor curves are found to reproduce the essential features of observed ones. It was concluded that in liquid methanol chain clusters consisting of three or four hydrogen-bonded molecules are dominant on the average.

In the preceding neutron diffraction study of methanol[1] the structure of the molecule within liquid was determined. Its geometry was found to be different from that in gaseous phase,[2-4] which occurs from the strong influence of hydrogen-bond formation between molecules. Concerning the intermolecular structure of liquid methanol, however, there is still very few information.[5] Then, we aim here to elucidate the structure of the liquid, further, by applying a general theoretical procedure of analysis for the fluid system composed of molecular clusters, which was proposed recently.[6,7] Thus, we attempt to reproduce below the neutron and X-ray structure factors for comparing those with experimental data[1-5] comprehensively.

Theoretical Procedure of Analysis

Theory. The structure factor for molecular liquids obtained in diffraction experiments (neutron and X-ray) is generally expressed in the following form[8,9]

$$S_{m\eta}(Q) = N_m^{-1}\{\sum_n f_{n,\eta}\}^{-2}\langle \sum_{p,q} f_{p,\eta} f_{q,\eta} \exp(i\vec{Q}\cdot\vec{r}_{pq})\rangle, \quad \eta = N,X \qquad (1)$$

where p and q denote the p-th and q-th atoms in a sample, n the n-th atom in the molecule, $f_{p,\eta}$, $f_{q,\eta}$, and $f_{n,\eta}$ are the scattering amplitude of atoms p, q, and n, respectively, $\vec{r}_{pq}$ is the vector between the p-th and q-th atoms, N_m the number of molecules in the sample and $\hbar\vec{Q}$ the momentum transfer. The angular bracket $\langle\cdots\rangle$ means statistical average.

When a liquid is composed of molecular clusters of various sizes including monomers, the structure factor $S_{m\eta}(Q)$ is given in general by[7]

$$S_{m\eta}(Q) = \sum_\nu \frac{x_\nu}{\nu} f_1^\nu(Q) + \bar{f}_{2U}(Q)\{S_c(Q)-1\} + \sum_{\nu\geqq 2}\frac{x_\nu}{\nu} f_c^\nu(Q), \qquad (2)$$

where,

$$f_1^\nu(Q) = \{\sum_n f_{n,\eta}\}^{-2}\{\langle \sum_l^\nu |\sum_{n_l} f_{n_l,\eta}\exp(i\vec{Q}\cdot\vec{r}_{cn_l})|^2\rangle\}_\nu, \qquad (3)$$

$$f_c^\nu(Q) = \{\sum_n f_{n,\eta}\}^{-2}[\langle \sum_{l\neq l'}^\nu \exp(i\vec{Q}\cdot\vec{r}_{cll'}) \sum_{n_l,n_{l'}} f_{n_l,\eta} f_{n_{l'},\eta} \times \exp\{i\vec{Q}\cdot(-\vec{r}_{cn_l}+\vec{r}_{cn_{l'}})\}\rangle - \sum_{l\neq l'}^\nu \langle\exp(i\vec{Q}\cdot r_{cll'})\rangle \times \langle\sum_{n_l} f_{n_l,\eta}\exp(-i\vec{Q}\cdot\vec{r}_{cn_l})\rangle \times \langle\sum_{n_{l'}} f_{n_{l'},\eta}\exp(i\vec{Q}\cdot\vec{r}_{cn_{l'}})\rangle]_\nu, \qquad (4)$$

$$S_c(Q) = N_m^{-1}\langle\sum_{i,j}\exp(i\vec{Q}\cdot\vec{r}_{cij})\rangle \qquad (5)$$

and

$$\bar{f}_{2U}(Q) = \{\sum_n f_{n,\eta}\}^{-2}\sum_\nu \frac{x_\nu}{\nu}[\sum_l^\nu\{\sum_{n_l} f_{n_l,\eta} \times \langle\exp(i\vec{Q}\cdot\vec{r}_{cn_l})\rangle\}^2]_\nu. \qquad (6)$$

$x_\nu = \nu N_\nu/N_m$ (N_ν; the number of clusters consisting of ν molecules within the liquid). l and l' denote the molecules within a cluster and, i and j molecules in the sample. n_l labels the n-th atom in the l-th molecule within the cluster. $\vec{r}_{n_l n_{l'}}$ denotes the vector distance between atoms n_l and $n_{l'}$, $\vec{r}_{n_l}$ that from the center of molecule l to its n-th atom, $\vec{r}_{cll'}$ that between the centers of molecules l and l' and $\vec{r}_{cij}$ that between the centers of molecules i and j. $f_1^\nu(Q)$ and $f_c^\nu(Q)$ are the intramolecular and intermolecular contribution within the cluster, respectively, and $S_c(Q)$ the molecular center structure factor of liquids. $\sum_\nu (x_\nu/\nu) f_1^\nu$ ($=f_1(Q)$) is the overall averaged intramolecular contribution in the liquid.

Replacing $f_{n,N}$ in Eqs. 3, 4, and 6 with the coherent neutron scattering length b_n of atom n, we obtain the neutron structure factor $S_{mN}(Q)$. In the same way, we obtain the X-ray structure factor $S_{mX}(Q)$ by replacing the $f_{n,X}$ with the atomic form factor $f_n(Q)$ of atom n.[9]

Table 1. The structure of methanol molecule in liquid phase determined by neutron diffraction[1)]

r_{CO}/Å	r_{OD}/Å	r_{CD}/Å	DCD/degree	COD/degree	Methyl tilt/degree	τ/degree
1.435	0.990	1.085	109.5	109.5	0.0	15.0
1.440	0.985	1.090	109.5	115.0	0.0	free

τ is the dihedral angle concerning the internal rotation of the methyl group: $\tau=0°$ is the model with the staggered conformation.

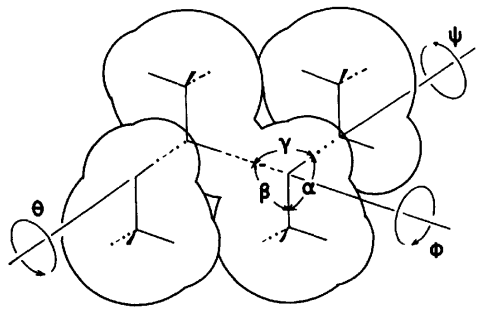

tetramer I

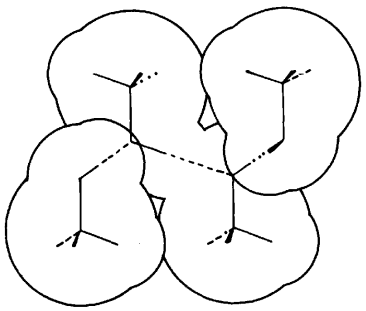

tetramer II

Fig. 1. The structure of the tetramer models I and II.

Structural Model of Liquid Methanol and Procedure of Calculation. According to the theory presented in the preceding item, we can calculate the two structure factors $S_{mX}(Q)$ and $S_{mN}(Q)$. The intramolecular structure of molecules in liquid methanol was determined uniquely in the preceding paper[1)] except the rotational angle of the methyl group: the two models with respect to the angle remain undiscriminated (the fixed angular position and the freely rotating one, Table 1). Then we calculate the $S_{mX}(Q)$ and $S_{mN}(Q)$ for the two intramolecular models in the present study.

The cluster model of liquid methanol is shown in Fig. 1, where two forms of linear tetramers are given.[10)] Concerning the model, we assumed the chain structure,[11)] *i.e.*, we neglect a branched conformation of clusters. Concerning the associated structure of the liquid, we performed calculation for five classes of liquids which are composed of identical clusters of ν molecules: The liquid consists of unbonded monomers ($\nu=1$), that of dimers ($\nu=2$), that of trimers ($\nu=3$) and that of tetramers ($\nu=4$, I and II in Fig. 1). The geometry of clusters are characterized by seven structural parameters: the hydrogen-bonded O–O distance r_{OO}, the angluar parameters α, β, γ, θ, ϕ, and ψ. The magnitudes of these parameters were varied in reference to the values tabulated in Table 2. In these cases, Eq. 2 is reduced to the following form,

Table 2. Range of parameters

Parameter	Range	Interval of variation
ν	1, 2, 3 and 4 (I and II)	
r_{HS}/Å	3.40—3.80	0.20
r_{OO}/Å	2.75—2.90	0.05
α,β,γ/degree	109.5—120.0	10.5
θ,ϕ,ψ/degree	0.0—360.0	45.0

r_{HS} is the effective hard-sphere diameter of molecules.

$$S_{m_\nu}(Q) = \frac{1}{\nu} f_i^\nu(Q) + \bar{f}_{2U}(Q)\{S_c(Q)-1\} + \frac{1}{\nu} f_c^\nu(Q). \tag{9}$$

Especially, for the liquid composed of monomer molecules,

$$S_{m_\nu}(Q) = f_i^1(Q) + \bar{f}_{2U}(Q)\{S_c(Q)-1\}, \tag{10}$$

which corresponds to the completely uncorrelated orientation model given by Page and Powles.[9)]

For calculating $S_{mX}(Q)$ and $S_{mN}(Q)$ with Eq. 9, the molecular center structure factor $S_c(Q)$ is required. The distribution of molecular centers in liquid methanol is assumed to be represented by the distribution for hard sphere fluids, and we substitute the structure factor $S_{HS}(Q)$ of hard sphere fluid[12)] (effective hard-sphere diameter, r_{HS}) for the $S_c(Q)$.

With respect to the magnitudes of Debye-Waller factors, we assume that the mean-square variation $2\gamma_{n|m|'}$ is in proportion to the interatomic distance $r_{n|m|'}$, *i.e.*, $\gamma_{n|m|'}=1/2D^2_{n|m|'}r_{n|m|'}$.[6,7,18)] The values of $D_{n|m|'}$ assigned are tabulated in Table 3.

Interpretation of X-ray and Neutron Diffraction Data

X-Ray and Neutron Data. Recently, X-ray structure factor data of liquid CH_3OH at 21.5 °C were reported by Magini *et al.*,[5)] which are shown in

Table 3. Root mean-square variation per unit length

Pair at atoms	$D_{n_in_i'}$/Å$^{1/2}$
Intramolecular pairs	0.06
Intermolecular pairs	
O···O	0.06
O···O—C	0.07
O···O···O	0.07
Other pairs	0.15
Intermolecular pairs including hydrogen atoms	
D···O	0.06
D···O—C	0.07
D···O—D	0.07
D—O···O	0.10
Other pairs	0.20
Between molecular centers	0.06
Between an atom and its molecular center	0.06

··· means a hydrogen bond.

Fig. 2 by full circles.** As seen in the figure, we can point out several distinctive features: the height and the position of its first peak, the hump at *ca.* Q=2.8 Å^{-1}, the broad peak at *ca.* 4—6 Å^{-1} and the shoulder at *ca.* Q=7.0 Å^{-1}. These features suggest the existence of interactions between molecules in the liquid. The neutron structure factor $S_{mN}(Q)$ of liquid CD_3OD at 10.0 °C obtained by authors[1] is given in Fig. 3 by open circles. In the figure, the behavior in the region of the hump ($Q\simeq$4 Å^{-1}) is distinctive as well as that of the first peak. The feature of the hump is due to the superposition of the contributions of intramolecular structure and intermolecular one.[1] Then, in our calculation, the structural model of liquid methanol is required to make a reproduction of these features on both experimental results.

Unbonded Monomer Model of Liquid Methanol. For the present purpose, we first calculated the X-ray and neutron structure factors for the liquid model consisting of unbonded monomers by using Eq. 10. The $S_{mX}(Q)$ and $S_{mN}(Q)$ curves obtained with r_{HS}=3.60 Å are compared with the X-ray and neutron diffraction results in Figs. 2 and 3, respectively. As clearly seen in these figures, the calculated curves can reproduce the fundamental behaviors of the experimental data, though discrepancies still remain in its detailed behavior. This means the dominance of the liquid structure as a randomly packed state of effective hard spheres, and shows the availability of the hard-sphere expression[12] for the molecular center distribution adopted in the present calculation.

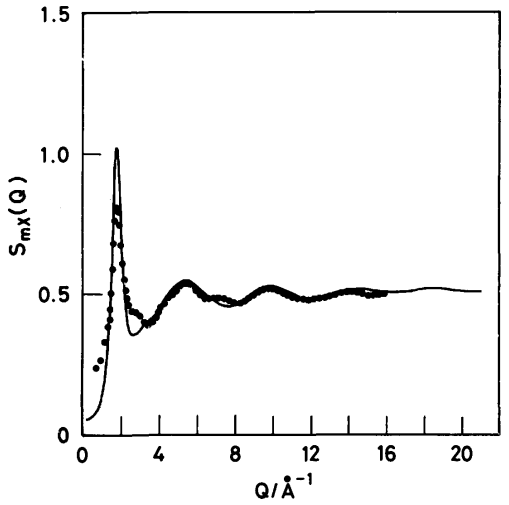

Fig. 2. Comparison between the calculated $S_{mX}(Q)$ for the unbonded monomer model and the observed X-ray structure factor $S_{mX}(Q)$.
——: Calculated $S_{mX}(Q)$ for the model with freely rotating methyl group,†† ●: observed $S_{mX}(Q)$. Observed data was transformed from the interference function $I(Q)$ by Magini et al.[5] by using the relation,[9]
$$S_{mX}(Q)=N_m^{-1}\{\sum_n f_n(Q)\}^{-2}I(Q).$$
††Concerning the rotation angle of the methyl group, there is no difference between the calculated $S_{mX}(Q)$ results for the two models (Table 1).

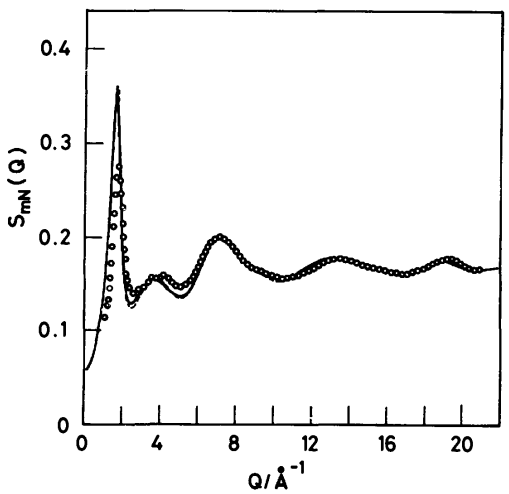

Fig. 3. Comparison between the calculated $S_{mN}(Q)$ curves for the unbonded monomer models and the observed neutron structure factor $S_{mN}(Q)$.
——: Calculated $S_{mN}(Q)$ for the model with freely rotating methyl group (Table 1), ----: calculated $S_{mN}(Q)$ for the model with fixed methyl group (Table 1), ○: observed $S_{mN}(Q)$.[1]

** Quite recently, Narten and Habenschuss have reported and X-ray diffraction study on liquid alcohols (*J. Chem. Phys.* **80**, 3387 (1984)). Their data is found substantially in agreement with that of Magini *et al.*, and concerning the intramolecular structure of methanol, they assignied a quite identical value of the C-O distance with that of Magini *et al.*

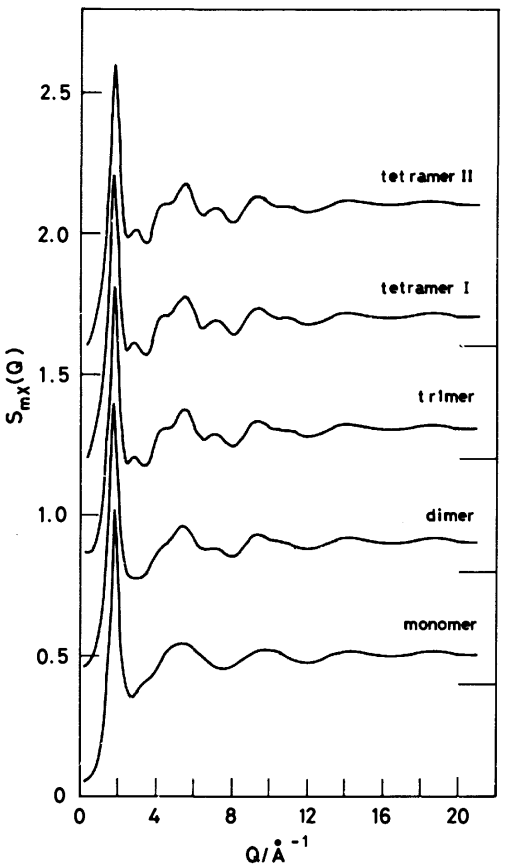

Fig. 4. The calculated $S_{mX}(Q)$ curves for five models.

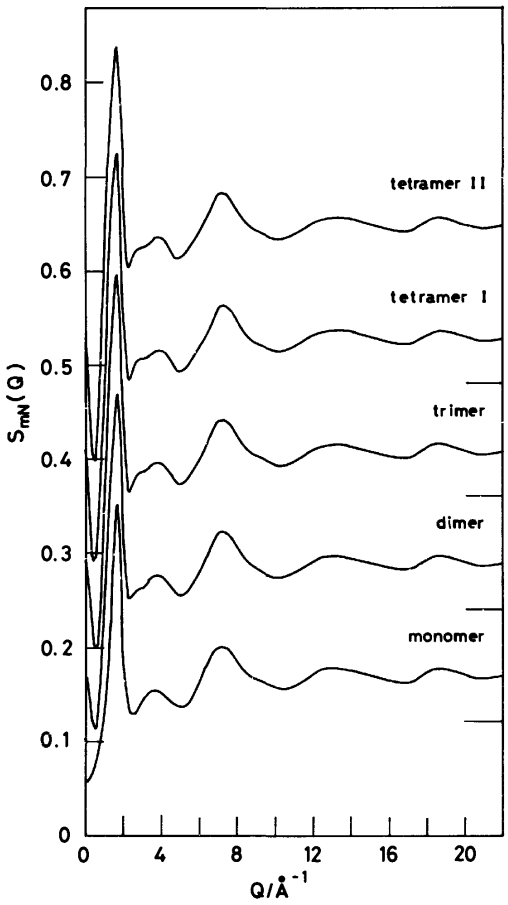

Fig. 5. The calculated $S_{mN}(Q)$ curves for five models with freely rotating methyl group.

The Best Fit Cluster Model. In Figs. 2 and 3 the discrepancies between the calculated curves and the observed data are seen in the intermediate Q region, 2.3—8.0 Å^{-1} for the X-ray result and 2.5—5.8 Å^{-1} for the neutron result. To explain these features, the calculations of $S_{mX}(Q)$ and $S_{mN}(Q)$ are required for the models of the liquid consisting of molecular culsters. The orientational configuration of the nearest neighbor molecules within liquid methanol is obtained from the combination of the X-ray and the neutron results.

We calculated the $S_{mX}(Q)$ and $S_{mN}(Q)$ for dimer fluid, trimer fluid and tetramer fluids (I and II) and the calculated curves are shown in Figs. 4 and 5. The geometrical parameters of the cluster model are determined as follows: r_{OO}=2.85 Å, $\alpha=\beta=\gamma=109.5°$, $\theta=\phi=\psi=0.0°$ and hard sphere diameter r_{HS}=3.6 Å (ξ= 0.363, ξ; packing fraction), which all are found to be identical for each oligomer fluid. As clearly seen in these figures, the characteristic features observed in the intermediate Q region (the hump at 2.8 Å^{-1}, the shoulder at *ca.* 4 Å^{-1} and that at 7.0 Å^{-1} in the X-ray curve and the hump at *ca.* 4 Å^{-1} in the neutron curve) are well-reproduced in the calculated curves for the trimer and tetramer models. Thus, we conclude that the liquid structure of methanol is regarded as the aggregates of the molecular clusters consisting of three or four linearly hydrogen-bonded molecules. The calculated curves of X-ray and neutron structure factors for trimer fluid are compared with the diffraction data in Figs. 6 and 7, respectively. Concerning the fitness of the calculated curves with the observed ones, we can not discriminate, which of the trimer and tetramer is better. In Fig. 7, the curves for the two models of the methyl-group rotation (freely rotating model and fixed one)[1] are shown.

Discussion

Molecular Center Distribution. In the present calculation, we assumed that the molecular center distribution in liquid methanol can be represented by the distribution in hard-sphere fluids and we substituted the $S_{HS}(Q)$ for the term $S_c(Q)$ in Eqs. 9 and 10. As mentioned in the preceding section, the features of the X-ray and neutron diffraction data were reproduced by the theoretical curves calculated under this assumption (Figs. 2—7). Especially, it is emphasized that the fundamental behaviors of diffraction data were explained by the use of the model of monomer fluid (Figs. 2 and 3). These facts mean the adequacy of

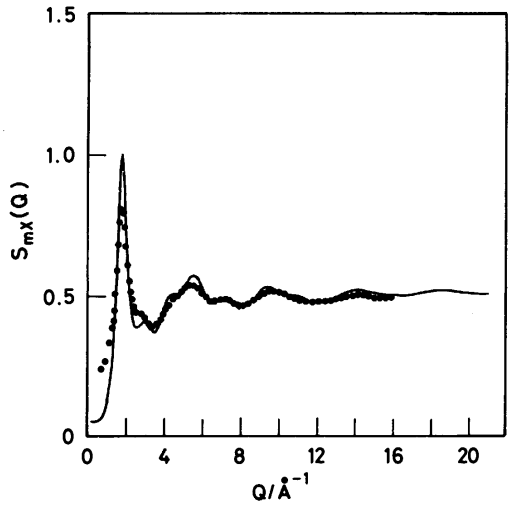

Fig. 6. Comparison between the calculated $S_{mX}(Q)$ for the trimer model and the observed X-ray structure factor $S_{mX}(Q)$.
——: Calculated $S_{mX}(Q)$, ●: observed $S_{mN}(Q)$.[5]

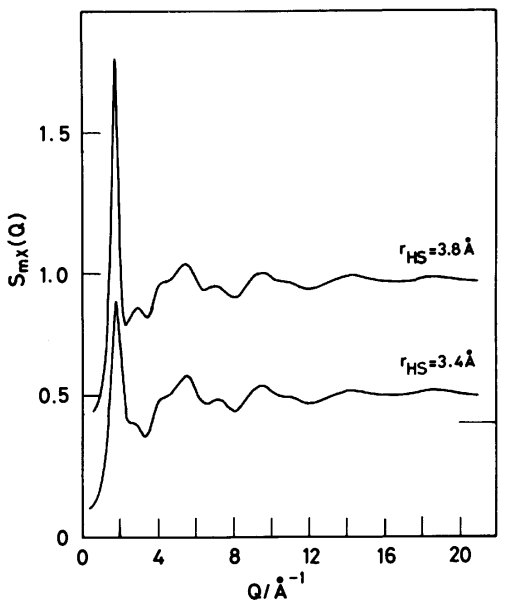

Fig. 8. The calculated $S_{mX}(Q)$ curves for the trimer models with r_{HS}=3.4Å and 3.8Å.

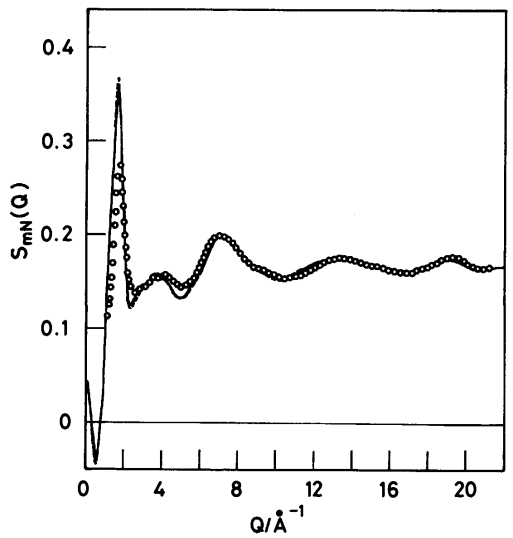

Fig. 7. Comparison between the calculated $S_{mN}(Q)$ for the trimer models and the observed neutron structure factor $S_{mN}(Q)$.
——: Calculated $S_{mN}(Q)$ for the model with freely rotating methyl group, ----: calculated $S_{mN}(Q)$ for the model with fixed methyl group, ○: observed $S_{mN}(Q)$.[1]

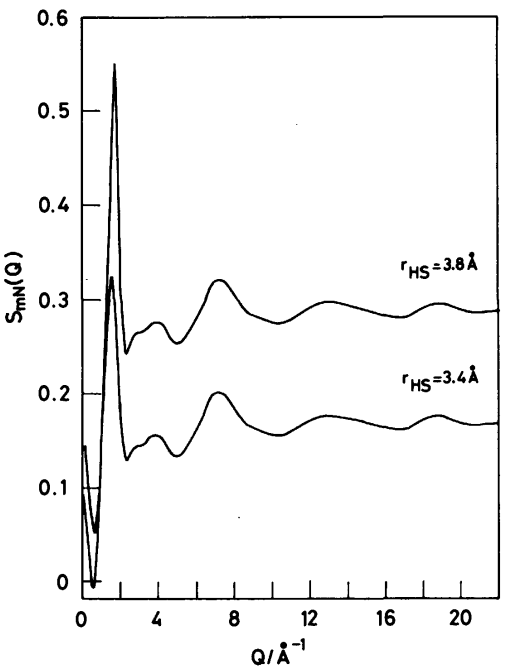

Fig. 9. The calculated $S_{mN}(Q)$ curves for the trimer models with r_{HS}=3.4Å and 3.8Å (freely rotating methyl group).

the assumption, and we can conclude that the liquid structure of methanol is expressed by the randomly-packed hard-sphere model as a rough approximation.

Concerning the hard sphere diameter as the effective size of molecules, we performed the calculation of X-ray and neutron structure factors, $S_{mX}(Q)$ and $S_{mN}(Q)$, for various magnitude of r_{HS}. When the r_{HS} increases, the height of the first peak increases rapidly as seen in Figs. 8 and 9. In the case of r_{HS}=3.4 Å (ξ= 0.306), the $S_{mX}(Q)$ curve in Fig. 8 shows improved agreement with the X-ray diffraction data, but, the first peak position of the $S_{mN}(Q)$ curve in Fig. 9 shifts to lower Q side and disagrees with the neutron diffraction data (Fig. 7). On the other hand, in the case of r_{HS}=3.8 Å (ξ=0.427), the heights of the first

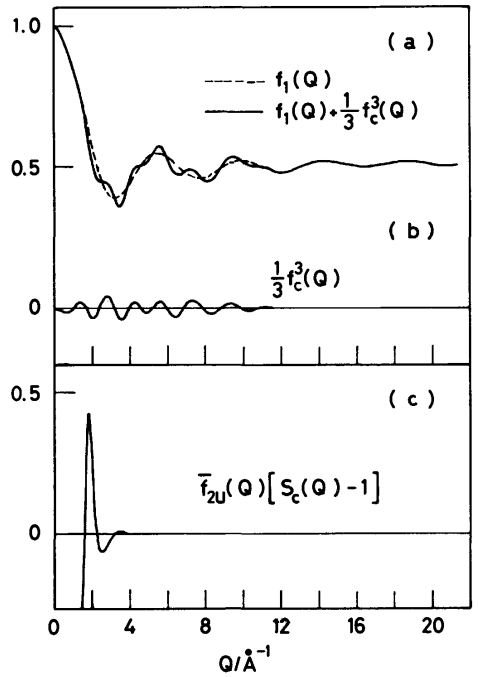

Fig. 10. Contribution of (a) $f_1(Q)$ $(=\frac{1}{3}f_1^3(Q))$ and $f_1(Q)+\frac{1}{3}f_c^3(Q)$, (b) $\frac{1}{3}f_c^3(Q)$ and (c) $\bar{f}_{2U}(Q)$ $\{S_c(Q)-1\}$ to the total $S_{mX}(Q)$ for the trimer model.

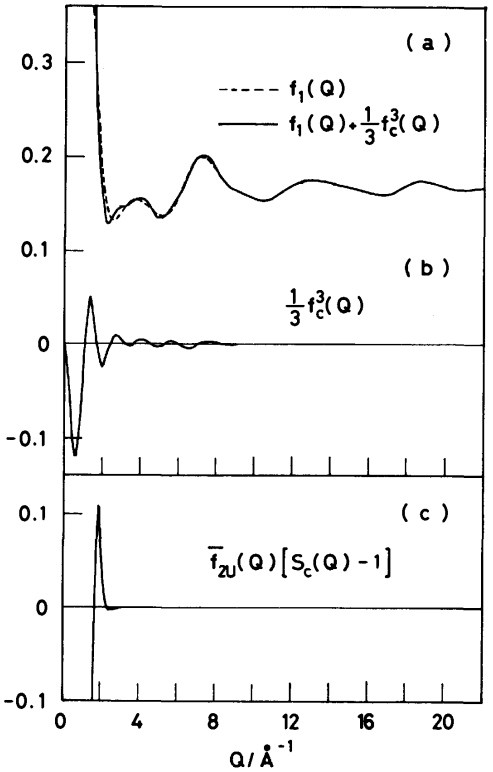

Fig. 11. Contribution of (a) $f_1(Q)$ $(=\frac{1}{3}f_1^3(Q))$ and $f_1(Q)+\frac{1}{3}f_c^3(Q)$, (b) $\frac{1}{3}f_c^3(Q)$ and (c) $\bar{f}_{2U}(Q)\{S_c(Q)-1\}$ to the total $S_{mN}(Q)$ for the trimer model with freely rotating methyl group.

peaks of the $S_{mX}(Q)$ and $S_{mN}(Q)$ curves are too high compared with experimental results. The hard sphere diameter is thus determined to be 3.6 Å (ξ= 0.363) at room temperature. Formerly, in crystals, Tauer and Lipscomb[11] gave the value of 3.88 Å for the methyl-methyl-interchain distances at −110 °C and 3.64 Å at −160 °C, and Wertz and Krue reported the value of 3.8 Å in the liquid state by X-ray diffraction.[13] Pettitt and Rossky showed the value of 3.9 Å for the distance as the result of the recent RISM calculation.[14] Concerning the packing fraction, there is no systematic studies for molecular fluids and only the cases of liquid alkali metals are available. According to the results, the packing fraction of liquid metals is about 0.45 near the melting point,[12,15] and decreases rapidly as the temperature increases.[16] Then, since the melting point of methanol is far below the room temperature, −94 °C for CH_3OH and −98 °C for CD_3OD, the present result that ξ=0.363 (r_{HS}=3.6 Å) at room temperature is acceptable. The value r_{HS}=3.6 Å is thus considered to be reasonable.

Hydrogen-bonded Structure in Liquid Methanol. In order to elucidate further the structure factors we examined the ingredients of the $S_{mX}(Q)$ and $S_{mN}(Q)$ for the trimer, by considering the terms in Eq. 9 and gave the terms in Figs. 10 and 11. In the higher Q region, the structure factor curve is practically composed of the $f_1(Q)$ term only.[17] On the other hand, the first peak is mainly composed of the sum of the curve $f_1(Q)$ and the curve $\bar{f}_{2U}(Q)\{S_c(Q)-1\}$. The sum of these curves corresponds to the $S_{mX}(Q)$ and $S_{mN}(Q)$ for monomer fluids. As seen in the figures, the shoulders and the hump for the $S_{mX}(Q)$ curve are originated from the term $1/3f_c^3(Q)$, which reflects the hydrogen-bonded structures within the cluster. The influence of the factor $1/3f_c^3(Q)$ appears mainly in the lower Q region. It is noticeable that the term $1/3f_c^3(Q)$ contributes to the total structure factor in a different way for $S_{mX}(Q)$ and $S_{mN}(Q)$. In the case of X-ray, its contribution remains up to 10—11 Å^{-1} (Fig. 10(b)). On the other hand in the case of neutron, it disappears virtually beyond the range of Q, 6—7 Å^{-1} (Fig. 11(b)).[1] The same trend is seen in the term $\bar{f}_{2U}(Q)\{S_c(Q)-1\}$ for each case (Figs. 10(c) and 11(c)).

Concering the hydrogen-bonded O-O distance r_{OO} which gives a criterion for the strength of hydrogen bonds as well as the O-D (or O-H) distance in liquid phase, no significant changes occur in calculated $S_{mX}(Q)$ and $S_{mN}(Q)$ curves when its magnitude is varied from 2.75 to 2.90 Å. Then, we assigned the value of r_{OO} to be 2.85 Å, which is identical with the value in the tetrahedral pentamer cluster in water.[6,7,18] Magini *et al.*[5] showed the value of 2.8 Å for the O-O distance by X-ray diffraction study. As the result of the Monte Carlo simulations for liquid methanol

at 25 °C, Jorgensen gave the value of 2.8 Å for the distance.[19] The present value is consistent with these values.

In the present study, we performed a structure analysis of X-ray and neutron diffraction data for methanol as an associated liquid by using a newly-proposed structure factor formula. The complete elucidation of the liquid structure of methanol is still left for future studies, of course, and we obtained here a chain-cluster model to represent its fundamental features approximately. The liquid methanol is thus considered as an aggregate of chain clusters consisting of three or four molecules linked with hydrogen bonds on the average.

References

1) Y. Tanaka, N. Ohtomo, and K. Arakawa, *Bull. Chem. Soc. Jpn.*, **57**, 644 (1984).
2) K. Kimura and M. Kubo, *J. Chem. Phys.*, **30**, 151 (1959).
3) R. M. Lees and J. G. Baker, *J. Chem. Phys.*, **48**, 5299 (1968).
4) M. C. L. Gerry, R. M. Lees, and G. Winnewisser, *J. Mol. Spectrosc.*, **61**, 231 (1976).
5) M. Magini, G. Paschina, and G. Piccaluga, *J. Chem. Phys.*, **77**, 2051 (1982).
6) N. Ohtomo, K. Tokiwano, and K. Arakawa, *Bull. Chem. Soc. Jpn.*, **54**, 1802 (1981).
7) N. Ohtomo, K. Tokiwano, and K. Arakawa, *Bull. Chem. Soc. Jpn.*, **55**, 2788 (1982).
8) E. Kálmán, G. Pálinkás, and P. Kovács, *Mol. Phys.*, **34**, 505 (1977).
9) D. I. Page and J. G. Powles, *Mol. Phys.*, **21**, 901 (1971).
10) The term "linear" means topologically linearly (one dimensionally) connected form of hydrogen-bonded structure.
11) K. J. Tauer and W. N. Lipscomb, *Acta Cryst.*, **5**, 606 (1952).
12) N. W. Ashcroft and J. Lekner, *Phys. Rev.*, **145**, 83 (1966).
13) D. L. Wertz and R. K. Kruh, *J. Chem. Phys.*, **47**, 388 (1967).
14) B. M. Pettitt and P. J. Rossky, *J. Chem. Phys.*, **78**, 7296 (1983).
15) N. Ohtomo and K. Arakawa, *J. Phys. Soc. Jpn.*, **51**, 1282 (1982).
16) Y. Tanaka, N. Ohtomo, and K. Arakawa, *J. Phys. Soc. Jpn.*, **52**, 2093 (1983).
17) Y. Tanaka, N. Ohtomo, and K. Arakawa, *Bull. Chem. Soc. Jpn.*, **57**, 2569 (1984).
18) N. Ohtomo, K. Tokiwano, and K. Arakawa, *Bull. Chem. Soc. Jpn.*, **57**, 329 (1984).
19) W. L. Jorgensen, *J. Am. Chem. Soc.*, **103**, 341 (1981).

Biionic Potential across Liquid Membranes with Some Anionic Surfactants

Kazuo NOMURA,* Akira MATSUBARA, and Hideo KIMIZUKA†
Laboratory of Chemistry, College of General Education, Kyushu University 01, Ropponmatsu, Fukuoka 810
†*Department of Chemistry, Faculty of Science, Kyushu University 33, Hakozaki, Fukuoka 812*
(Received August 13, 1984)

The biionic membrane potential was measured with the system in which a solution of calcium chloride was separated by a liquid membrane from a solution of another metal chloride. Four kinds of liquid membranes were prepared by dissolving calcium hexadecyl sulfate, stearate, cholate or deoxycholate in aqueous 1-octanol. All of the membranes studied were nearly permselective to cation. The membrane potential was analysed according to the Goldman-type equation based on the irreversible thermodynamics. The slope of a linear portion of the biionic potential *vs.* logarithmic activity curve showed fairly good agreement with the theoretical slope, *i.e.*, $2.303\times 2RT/(Z_{Ca}+Z_M)F$ per a ten-fold increase in activity, where Z_{Ca} and Z_M were the valencies of calcium ion and another metal ion M existing across a membrane, respectively. The selective permeation coefficients of various metal ions were estimated for each membrane. The surprisingly small differences in the selective permeation coefficient between uni- and bi-valent cations were observed for the liquid membranes with calcium stearate, cholate or deoxycholate, while the about ten-fold increase in the coefficient per valency was observed for the liquid membrane with calcium hexadecyl sulfate. These results were discussed according to the theory previously presented.

The ion transport across membrane has usually been explained by the Goldman-type equation. The equation of this type has been presented for a fixed-site membrane as a limiting form of the general equation on the basis of the irreversible thermodynamics by Kimizuka *et al.*[1-3] In the theory, the general expression of multiionic membrane potential has been derived without any assumptions concerning the distribution of concentration as well as that of potential within membrane. The theory has successfully been applied to the biionic system in which different multivalent ions exist across the membranes of some permselective ion-exchangers.[4,5]

The equation of the membrane potential for a liquid membrane with mobile sites has been derived on the basis of the Nernst-Planck equation by Sandblom *et al.*[6] The equation is expressed as a sum of the two logarithmic terms in the case of strong association between counter ion and membrane site, while being expressed as the single logarithmic term in the case of complete dissociation. Only when the unlikely assumption that the mobility of free site is much larger than that of counter ion is made, the equation for strong association can be reduced to the familiar form with the single logarithmic term. On the other hand, it is well known facts that the membrane potentials measured with liquid membranes can be expressed by the equation with the single logarithmic term, even when liquid membranes are prepared from solvents of low dielectric constant.[7,8]

The total flux of a permeable ion across a liquid membrane can be expressed by the equation of the same form as that for a fixed-site membrane, although the physical contents of the permeability coefficients are somewhat modified.[9-11] Thus, the Goldman-type equation with the single logarithmic term can also be derived from the flux equation in the same way as described elsewhere,[1-3] and is equally applicable to the liquid membrane systems.[10,11]

In the present study, the membrane potential was measured in the biionic systems with four kinds of thin liquid membranes. The results were analysed and discussed according to the Goldman-type equation.

Experimental

Materials. Calcium hexadecyl sulfate, $Ca(HS)_2$, was prepared from sodium hexadecyl sulfate according to the method of Lottermoser and Püschel.[12] Sodium hexadecyl sulfate was prepared from purified 1-hexadecanol obtained by fractional distillation of a commercial sample, as stated elsewhere.[13] Stearic, cholic and deoxycholic acids from Merck were neutralized with sodium hydroxide to sodium salts, from which calcium stearate, cholate and deoxycholate, abbreviated as $Ca(ST)_2$, $Ca(CH)_2$, and $Ca(DC)_2$, respectively, were prepared by metathesis in aqueous ethanol with the same procedure as described elsewhere.[14] All other reagents were of guaranteed grade and used without further purification.

Liquid membrane was prepared by dissolving a site species in water-saturated 1-octanol. The concentration of the site species in liquid membranes was *ca.* 10^{-3} M (1 M= 1 mol dm^{-3}).

Procedure. The following cell assembly, connected to the Orion digital pH meter, Model 701, was used for the measurement of membrane potential.

Ag|AgCl|Internal Solution (1.10×10^{-2} M $CaCl_2$)|
Liquid Membrane|External Solution|Calomel

For the liquid membranes with $Ca(ST)_2$, $Ca(CH)_2$, and $Ca(DC)_2$, the internal and external solutions were adjusted to pH=8.5 with 2×10^{-3} M Tris buffer. A body of the Orion calcium ion selective electrode and a Teflon millipore film (Fluoro Pore, No. FP080, 0.8 μm of pore size, 50 μm in thickness, Sumitomo Electric Co. Ltd.) as an inert porous matrix for liquid membranes were employed for construct-

ing the membrane electrode.

The external solution was stirred and all measurements were carried out at 25±0.02 °C.

Results and Discussion

For the liquid membranes with $Ca(ST)_2$, $Ca(CH)_2$, or $Ca(DC)_2$, the pH dependence of the membrane electrode potential, V, was studied at constant calcium ion concentration, as shown in Fig. 1. The potential for the liquid membrane with $Ca(ST)_2$ was independent of pH in the alkaline region of pH>8.5. A similar pH dependence was also observed with the calcium ion selective liquid membrane electrode using didecyl hydrogenphosphate site.[15] The potentials for the liquid membranes with $Ca(CH)_2$ or $Ca(DC)_2$ were unstable below pH 7, possibly being due to the dissolution of membrane site into aqueous phase.

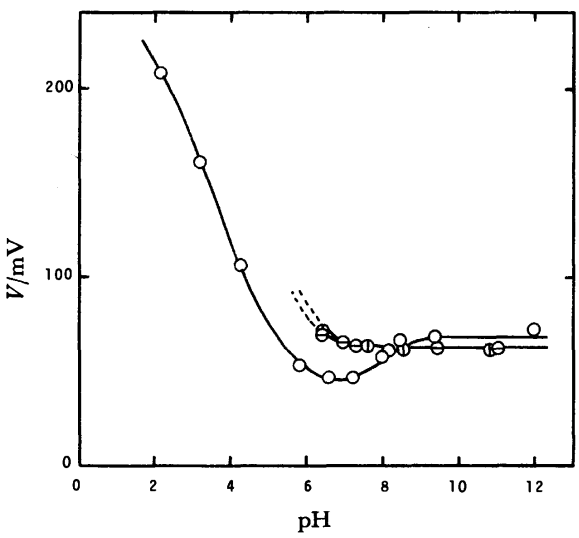

Fig. 1. Membrane electrode potential *vs.* pH curves. Liquid membranes with $Ca(ST)_2$, ○; $Ca(CH)_2$, ①; $Ca(DC)_2$, ⊖. $C_{Ca(I)}=C_{Ca(e)}=1.10\times10^{-2}$ M.

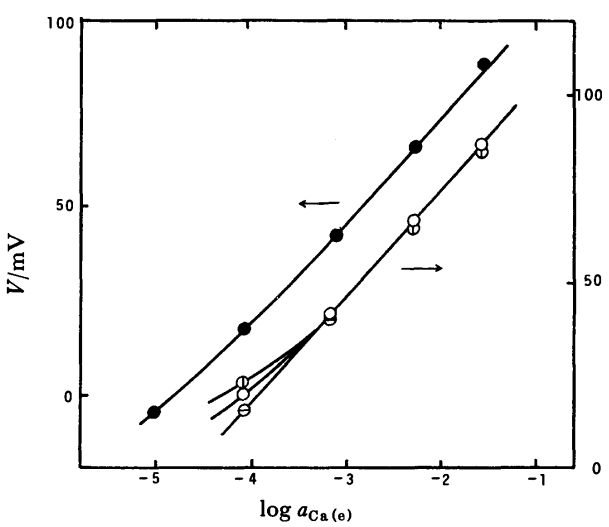

Fig. 2. Membrane electrode potential *vs.* logarithmic activity curves for the single electrolyte system of $CaCl_2$. Liquid membranes with $Ca(HS)_2$, ●; $Ca(ST)_2$, ○; $Ca(CH)_2$, ①; $Ca(DC)_2$, ⊖. $C_{Ca(I)}=1.10\times10^{-2}$ M. The pH's of aqueous phases were 5.6 for liquid membrane with sulfate site and 8.5 for those with carboxylate site.

The membrane electrode potential for the liquid membrane with $Ca(HS)_2$, measured at 10^{-1} M $CaCl_2$, was independent of pH in the range of pH>3.3.

The potentials of the membrane electrodes for all of liquid membranes studied were found to be linear against the logarithm of external calcium ion activity, as shown in Fig. 2. The values of ion activity were calculated according to the extended Debye-Hückel equation. Assuming that a membrane is ideally permselective to cation, the potential of the membrane electrode for the single electrolyte system of $CaCl_2$ is given as

$$V = V_{Ca} + V_o = -\frac{RT}{Z_{Ca}F}\ln\frac{a_{Ca(e)}}{a_{Ca(I)}} + V_o, \qquad (1)$$

where V_{Ca} is the membrane potential in the present system: $a_{Ca(e)}$ and $a_{Ca(i)}$, the activities of calcium ion in the external and internal solutions, respectively; R, gas constant: T, absolute temperature: F, Faraday constant: Z, valency; and V_o, the potential difference between the internal and external electrodes, including the liquid junction potential. Since the same internal solution was used throughout the experiment and the liquid junction potential is negligibly small, V_o can be regarded as constant. Therefore, the slope of the V *vs.* log $a_{Ca(e)}$ curve is approximately the same as that of the V_{Ca} *vs.* log $a_{Ca(e)}$ curve. The slopes of the linear portions shown in Fig. 2 are *ca.* 29 mV per decade for all of the liquid membranes studied, agreeing well with the theoretical slope predicted by Eq. 1. This indicates that these liquid membranes are ideally permselective to cation.

The measurements of the biionic potential were carried out on the systems in which the internal solution containing a constant concentration of $CaCl_2$ was separated by a liquid membrane from an external solution containing varying concentrations of another metal chloride. Typical results are shown in Figs. 3—5. When the membrane is ideally permselective to cation, the potential of the membrane electrode for the biionic system of Ca^{2+} and M^{Z_M+}, V', can be written as[4]

$$V' = V_{Ca,M} + V_o = \frac{2RT}{(Z_{Ca}+Z_M)F}\ln\frac{Z_M P_M a_{M(e)}}{Z_{Ca}P_{Ca}a_{Ca(I)}} + V_o, \qquad (2)$$

where $V_{Ca,M}$ is the membrane potential in the biionic system; and P, the membrane permeability. Assuming that the permeability ratio, P_M/P_{Ca}, and the concentration of $CaCl_2$ in the internal solution are constant, Eq. 2 becomes

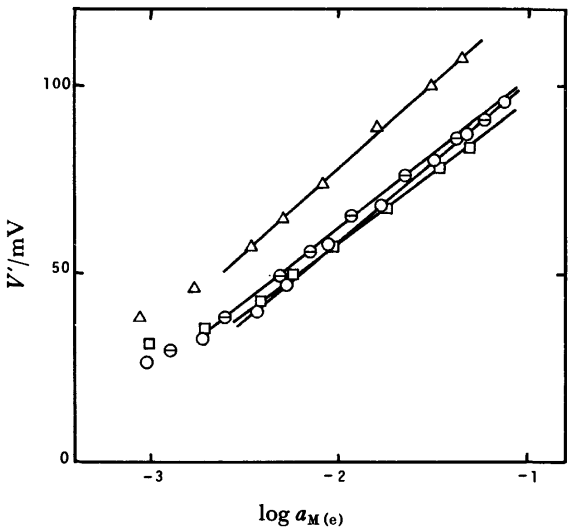

Fig. 3. Membrane electrode potential *vs.* logarithmic activity curves for the system Ca^{2+}(i)-M^{+}(e). Liquid membrane with $Ca(CH)_2$. M^+=Li^+, △; Na^+, ○; K^+, □; Cs^+, ⊖. $C_{Ca(I)}=1.10\times10^{-2}$ M. pH=8.5.

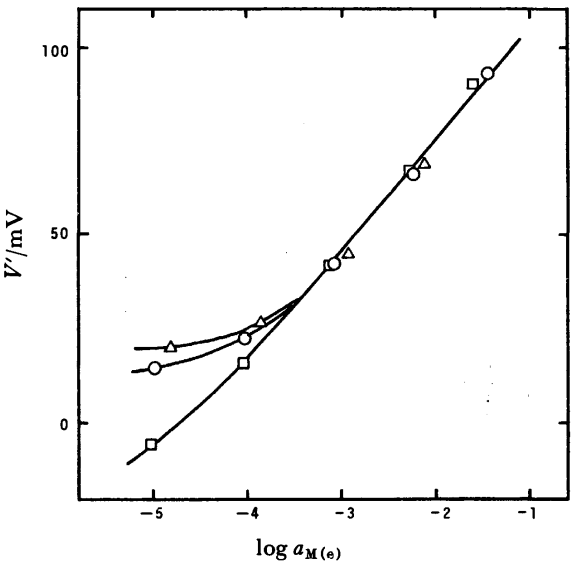

Fig. 4. Membrane electrode potential *vs.* logarithmic activity curves for the system Ca^{2+}(i)-M^{2+}(e). Liquid membrane with $Ca(HS)_2$. M^{2+}=Mg^{2+}, ○; Sr^{2+}, △; Ba^{2+}, □. $C_{Ca(I)}=1.10\times10^{-2}$ M. pH=5.6.

$$V' = \frac{2RT}{(Z_{Ca}+Z_M)F} \ln a_{M(e)} + \text{const.}, \quad (3)$$

where

$$\text{const.} = \frac{2RT}{(Z_{Ca}+Z_M)F} \ln \frac{Z_M P_M}{Z_{Ca} P_{Ca} a_{Ca(I)}} + V_o, \quad (4)$$

The slopes of linear portions in Figs. 3—5 were 37—41 (except 45 for the Ca^{2+}-Li^+ system), 30 and 21—22 mV per decade for the 2—1, 2—2, and 2—3 valent biionic systems, respectively, agreeing approximately with the theoretical slope predicted by Eq. 3, *i.e.*, 118/ (Z_{Ca}+Z_M) mV per decade.

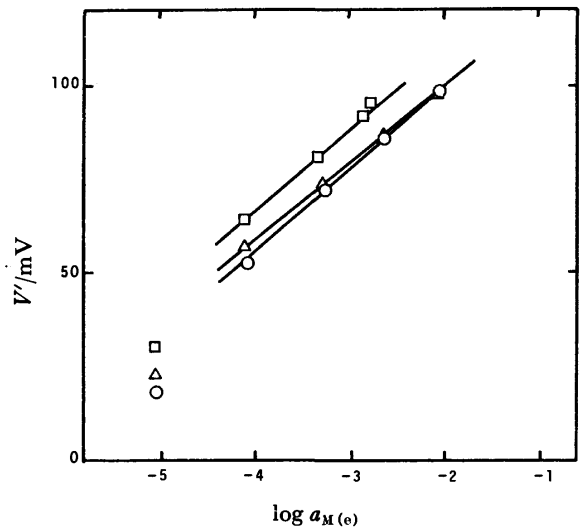

Fig. 5. Membrane electrode potential *vs.* logarithmic activity curves for the system Ca^{2+}(i)-M^{3+}(e). Liquid membrane with $Ca(HS)_2$. M^{3+}=Al^{3+}, ○; La^{3+}, △; $[Co(NH_3)_6]^{3+}$, □. $C_{Ca(I)}=1.10\times10^{-2}$ M. pH(i)= 5.6. The pH's of external solutions of Al^{3+}, La^{3+} and $[Co(NH_3)_6]^{3+}$ were 3.4—5.4, 5.2—5.5, and 5.5—5.4 depending upon the concentrations, respectively, where the electrode potential was independent of pH.

TABLE 1. SELECTIVE PERMEATION COEFFICIENTS, $K_{Ca,M}$

Ion, M	Liquid Membranes			
	$Ca(HS)_2$	$Ca(ST)_2$	$Ca(CH)_2$	$Ca(DC)_2$
Li^+	0.16	0.40	1.1	1.0
Na^+	0.06	0.18	0.37	0.41
K^+	0.07	0.19	0.37	0.38
Rb^+	0.07	—	—	—
Cs^+	0.09	0.20	0.44	0.39
Mg^{2+}	1.0	0.79	0.86	0.93
Sr^{2+}	1.0	0.46	0.50	0.55
Ba^{2+}	1.0	0.46	0.43	0.43
Cu^{2+}	1.3	—	—	—
Ni^{2+}	1.2	3.5	2.3	—
Co^{2+}	1.3	—	—	—
Al^{3+}	9.3	—	—	—
La^{3+}	10	—	—	—
$[Co(NH_3)_6]^{3+}$	17	—	—	—

The selective permeation coefficients of Z_M valent cation M, relative to Ca^{2+} ion, $K_{Ca,M}=Z_M P_M/Z_{Ca} P_{Ca}$, were estimated from the potential difference, $V'-V$, by using Eqs. 1 and 2. The results are shown in Table 1.

According to the previous theory,[11] the membrane permeability to cation M, P_M, can be expressed as

$$P_M = RT\bar{u}_M C_M^{to}/\{a_{M(e)} a_{M(I)}\}^{1/2} d, \quad (5)$$

where

$$\bar{u}_M = \alpha_M u_M + (1-\alpha_M) u_I, \quad (6)$$

and C_M^{to} denotes the mean total concentration of cation

M: d, the membrane thickness: u_M and u_I, the mean mobilities of cation M and ion pair I formed between cation M and site anion, respectively; and α_M, the dissociated fraction of cation M ($\alpha_M = C_M/C_M^{to} = 1-\nu_M C_I/C_M^{to}$, where ν_M is the stoichiometric coefficient of cation M in the ion-pair formation), all referred to the values within membrane. Inserting the following relation for the site species[11]

$$(\nu_M/\nu_S)\alpha_M u_S - (1-\alpha_M)u_I = 0 \tag{7}$$

into Eq. 6, we have

$$\bar{u}_M = \alpha_M\{u_M + (\nu_M/\nu_S)u_S\} \tag{8}$$

where ν_S is the stoichiometric coefficient of site anion S in the ion-pair formation; and u_S, the mean mobility of site anion. Assuming that the selective permeation coefficient, $K_{Ca,M}$, can be expressed as the ratio of $Z_M P_M$'s in the single electrolyte system, we have from Eqs. 5 and 8

$$\begin{aligned} K_{Ca,M} &= Z_M P_M / Z_{Ca} P_{Ca} \\ &= Z_M \bar{u}_M C_M^{to}\{a_{Ca(e)} a_{Ca(i)}\}^{1/2} / Z_{Ca}\bar{u}_{Ca} C_{Ca}^{to}\{a_{M(e)} a_{M(i)}\}^{1/2} \\ &= Z_M \alpha_M\{u_M + (\nu_M/\nu_S)u_S\}K_M / Z_{Ca}\alpha_{Ca} \\ &\quad \times \{u_{Ca} + (\nu_{Ca}/\nu_S)u_S\}K_{Ca} \end{aligned} \tag{9}$$

where K_{Ca} and K_M are the apparent partition coefficients of cations Ca^{2+} and M between the membrane and aqueous phases. This expression of the selective permeation coefficient has the same form as that for a fixed-site membrane,[3] except that u_M and C_M are replaced by $\bar{u}_M$ and C_M^{to}. Considering Eq. 7, Eq. 9 is reduced to the same limiting form as that derived by Sandblom *et al.* in the case of complete dissociation.

The noticeable feature seen among the estimated values of $K_{Ca,M}$ is the surprisingly small differences in the $K_{Ca,M}$ value between uni- and bivalent cations for the membranes with $Ca(ST)_2$, $Ca(CH)_2$, and $Ca(DC)_2$. Let us consider the case of $M=Na^+$ for the liquid membrane with $Ca(ST)_2$. Assuming that the mobility ratio, $\{u_{Na}+(\nu_{Na}/\nu_S)u_S\}/\{u_{Ca}+(\nu_{Ca}/\nu_S)u_S\}$, can be replaced by that in aqueous solution and using 50.15, 119.0[16], and 19.95 (extrapolated from the values for fatty acid anions of C_1—C_{14})[17] $ohm^{-1}\,cm^2\,mol^{-1}$ for the values of the limiting molar conductances of Na^+, Ca^{2+}, and stearate ions, respectively, Eq. 9 can be rewritten as

$$K_{Ca,Na} = 0.504(\alpha_{Na}/\alpha_{Ca})(K_{Na}/K_{Ca}) \tag{10}$$

According to Eq. 10, the $K_{Ca,Na}$ value is governed by the two ratios, *i.e.*, α_{Na}/α_{Ca} and K_{Na}/K_{Ca}. In the case of complete dissociation, the selective permeation coefficient is solely determined by the partition ratio. Experimental results with liquid membranes formed from solvents of high dielectric constant can be explained according to this reasoning.[8] However, in the case of partial dissociation, these two ratios usually exert the opposite effects on the selective permeation coefficient, *i.e.*, the strong affinity of an ion to the membrane site is favorable to the partition ratio, but not to the dissociation ratio.

The very small value of K_{Na}/K_{Ca} can be expected from the partition data of metal ions between the aqueous and the water-saturated 1-octanol phase with a partially neutralized polycarboxylic acid,[18] while the large value of α_{Na}/α_{Ca} can be expected from the conductance data for metal salts of the above polycarboxylic acid in water-saturated 1-octanol.[19] Thus, the partial cancellation of the K_{Na}/K_{Ca} value by the α_{Na}/α_{Ca} value seems to bring the $K_{Ca,Na}$ value close to those for bivalent cations, leading to the diminished valency effect on the selective permeation coefficient.

Contrary to the above membranes, the about tenfold increase in the $K_{Ca,M}$ value per valency were observed for the liquid membrane with $Ca(HS)_2$, as seen in Table 1. Because of the dissociable sulfate site, the α_{Ca} value of $Ca(HS)_2$ reachs 0.25 at the concentration of 2.5×10^{-3} M even in aqueous 1-octanol.[11] On the other hand, the association constant of sodium dodecyl sulfate in the dioxan–water mixture of the same dielectric constant as that of aqueous 1-octanol, *i.e.*, 8.92,[19] was obtained by the extrapolation, from which the α_{Na} value was estimated to be *ca.* 0.25 at the concentration of 2.5×10^{-3} M.[20] It is obvious from the estimated values of the dissociated fraction that the observed valency effect on the selective permeation coefficient can primarily be attributed to the partition ratio.

References

1) H. Kimizuka and K. Koketsu, *J. Theor. Biol.*, **6**, 290 (1964).
2) H. Kimizuka, *J. Theor. Biol.*, **13**, 145 (1966).
3) H. Kimizuka and K. Kaibara, *J. Colloid Interface Sci.*, **52**, 516 (1975).
4) A. Yamauchi and H. Kimizuka, *J. Theor. Biol.*, **30**, 285 (1971).
5) K. Kaibara, A. Yamauchi, and H. Kimizuka, *Mem. Fac. Sci., Kyushu Univ., Ser. C*, **8**, 247 (1973).
6) J. Sandblom, G. Eisenman, and J. L. Walker, Jr., *J. Phys. Chem.*, **71**, 3862 (1967).
7) M. A. Beg, M. Usman, and A. Nabi, *J. Electroanal. Chem.*, **112**, 347 (1980).
8) A. Jyo, M. Torikai, and N. Ishibashi, *Bull. Chem. Soc. Jpn.*, **47**, 2862 (1974).
9) A. Katchalsky and P. F. Curran, "Nonequilibrium Thermodynamics in Biophysics," Harvard Univ. Press, Cambridge, Mass. (1965), pp. 200—216.
10) A. Yamauchi, T. Minematsu, and H. Kimizuka, *Membrane* (in Japanese), **2**, 69 (1977).
11) K. Nomura, A. Matsubara, and H. Kimizuka, *Bull. Chem. Soc. Jpn.*, **54**, 1324 (1981).
12) A. Lottermoser and F. Püschel, *Kolloid-Z.*, **63**, 175 (1933).
13) R. Matuura, H. Kimizuka, S. Miyamoto, and R. Shimozawa, *Bull. Chem. Soc. Jpn.*, **31**, 532 (1958).

14) Y. Koga and R. Matuura, *Mem. Fac. Sci., Kyushu Univ., Ser. C*, **4**, 1 (1961).
15) J. W. Ross, "Ion Selective Electrodes," ed by R. A. Durst, National Bureau of Standards Special Publication 314, Washington, D.C. (1969), pp. 57—88.
16) R. Parsons, "Handbook of Electrochemical Constants," Butterworths Scientific Publications, London (1959), p. 85.
17) A. N. Campbell and G. R. Lakshminarayanan, *Can. J. Chem.*, **43**, 1729 (1965).
18) E. Pefferkorn and R. Varoqui, *J. Colloid Interface Sci.*, **52**, 89 (1975).
19) R. Varoqui and E. Pefferkorn, *J. Phys. Chem.*, **79**, 169 (1975).
20) G. D. Parfitt and A. L. Smith, *Trans. Faraday Soc.*, **61**, 2736 (1965).

Thermodynamic and Viscometric Studies on the Solution State of Surfynol 465 in Water

Shizuko SATO* and Hiroshi KISHIMOTO
Division of Physical Chemistry, Faculty of Pharmaceutical Sciences, Nagoya City University, Tanabe-dori, Mizuho-ku, Nagoya 467
(Received August 20, 1984)

The vapor-pressure depression, surface tension, density and viscosity of the aqueous solution of Surfynol 465, nonionic surfactant, α,α′-[2,4,7,9-tetramethyl-5-decyne-4,7-diyl]bis[ω-hydroxy-poly(oxyethylene)], were measured at various concentrations and 298.15 K, indicating cmc at 11—14×10^{-3} mol kg^{-1} and a second cmc at *ca.* 30×10^{-3} mol kg^{-1}. From vapor-pressure depression, the association numbers of first and second micelles were approximately estimated at 4 and 13—16, respectively. From the results of density and viscosity measurements, the molar volume and Einstein's parameter, *k*, were calculated, respectively. The cohesion between the two hydrophobic chains in monomer was suggested by the analysis of molar volume. It was estimated on the molar volume and *k* of Surfynol 465 that the hydration of two hydrophilic poly(oxyethylene) chains is significant in monomer as well as micelles, but scarcely changes through micelle formation. The effect of concentration on *k* was discussed with respect to the shape and interaction of micelles.

In comparison with the usual surfactant, whose molecule has a single group each for hydrophilic and hydrophobic moieties, such as sodium dodecyl sulfate or alkylphenol with poly(oxyethylene) side chain, surfactant with more than two hydrophilic or hydrophobic groups reveals very different characteristics in monomeric state as well as in micellar one with respect to various physicochemical properties. It is well known that such a polyfunctionality plays an important role in many biological systems, *e.g.* the role of phospholipid molecule with two hydrophobic groups in the membranes of cell and neuron. Concerning phosphatidylcholine,[1-3] a typical phospholipid known as forming a similar bilayer structure to red blood cell, and on sodium 1,2-bis(2-ethylhexyloxycarbonyl)ethane sulfonate, Aerosol OT, as well as its homologues,[4,5] which are typical anionic surfactants with two hydrophobic alkyl groups, we have investigated their physicochemical properties so far and found the characteristic features caused by their structures, *i.e.* amphiphiles with two hydrophobic chains. On nonionic surfactants, Kuwamura and Takahashi studied their surface-chemical properties, using acetal-type compounds which have one hydrocarbon chain and two poly(oxyethylene) hydrophilic groups.[6] Based upon the above informations, we are now studying various physicochemical properties of nonionic Surfynols which have two sets of one branched hydrocarbon chain and one poly(oxyethylene) chain at both sides of acetylene radical. In this work, we report the

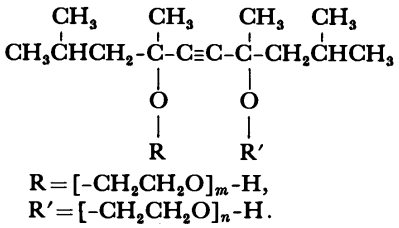

Fig. 1. Chemical structure of Surfynol 465. When m+n=10, the structure indicates Surfynol 465.

vapor-pressure depression, surface tension, density and viscosity of the aqueous solution of Surfynol 465, α,α′-[2,4,7,9-tetramethyl-5-decyne-4,7-diyl]bis[ω-hydroxyl-poly(oxyethylene)] with *ca.* ten oxyethylene segments in total (Fig.1).

Experimental

Materials. Surfynol 465 was obtained from Air Products and Chemicals, USA. NaCl was from Wako Pure Chemical Industries, Ltd., Japan. Deionized and twice-distilled water was used.

Procedures. The vapor-pressure depressions of Surfynol 465 and NaCl (reference) aq were measured with a Molecular Weight Apparatus model 115, Hitachi Ltd., Japan. Surface tension, σ, was measured by a drop-weight method, following Harkins, & Brown's correction.[7] Density, ρ, was determined with a digital precision densimeter (DMA 602/DMA 60, Anton Paar K.G., Austria) using air and water as calibration standards. Viscosity, η, was measured with a usual Ostwald viscometer. All measurements were carried out at 298.15 K±0.03 K for ρ and ±0.1 K for others.

Results and Discussion

Surfynol 465 is liquid and soluble in water at room temperature. The cloud point of 1—20 wt% aq solution exists in the range of 315—320 K, which was observed by the naked eye and plotted in Fig. 2. From the depression of vapor pressure in the very dilute aq solution, which is considered to be practically ideal, we estimated the number-average molar mass, *M*, of Surfynol 465 at 600 g mol^{-1}.

Using the molecular weight apparatus, we observed the difference in reading, Δ*R*, which indicates the vapor-pressure depression of water, against various molalities of Surfynol 465 in solution, *m*, and plotted the result in Fig. 3. The value of Δ*R* increased with *m*, approximately making a broken line, which had two breaks. The first sharp break is considered to indicate cmc (13.8×10^{-3} mol kg^{-1}) according to Brady *et al.*[8] The

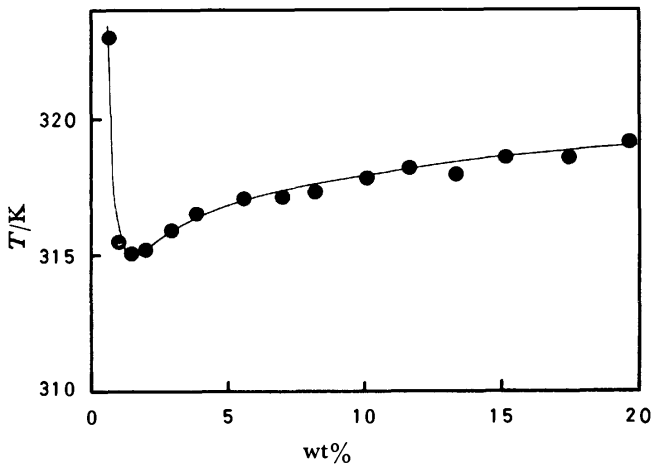

Fig. 2. Cloud point *vs.* wt% for Surfynol 465.

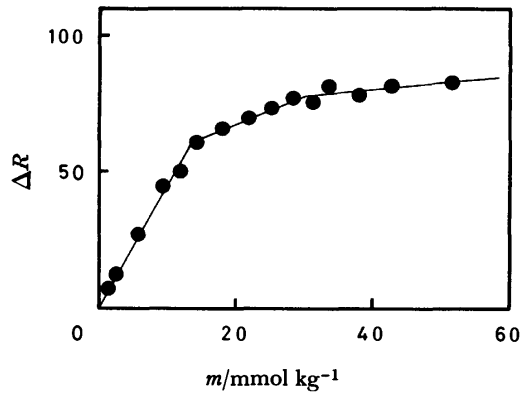

Fig. 3. Plots of ΔR *vs.* molality.

second slight break or bend suggests a second cmc.[4,5] Next, by the further analyses of the ΔR *vs.* m relation, we obtained the thermodynamic parameters for Surfynol 465, as follows. Since a real solution deviates from ideality with the increase of solute concentration, we must determine the activity coefficient of Surfynol 465, even if below cmc. Under the isopiestic condition between two solutions of reference and surfactant,

$$\nu_r m_r \phi_r = \nu m \phi, \tag{1}$$

where ν, m, and ϕ are the stoichiometric coefficient, molality and osmotic coefficient of water, respectively, for surfactant and those with suffix, r, are corresponding quantities for reference solute.[9,10] Adopting NaCl as reference, whose osmotic coefficient on $\nu_r=2$ is known over the necessary concentration range, and setting $\nu=1$, we obtained the ϕ *vs.* m relation shown in Fig. 4. The concentration, where ϕ dropped markedly, corresponds to cmc. The feature indicating the second cmc was scarcely recognized.

The activity coefficient, γ, and the activity, a, of surfactant can be calculated by Eq. 2 and 3.

$$-\ln \gamma = 1 - \phi + \int_0^m (1-\phi)/m \cdot dm \tag{2}$$

and

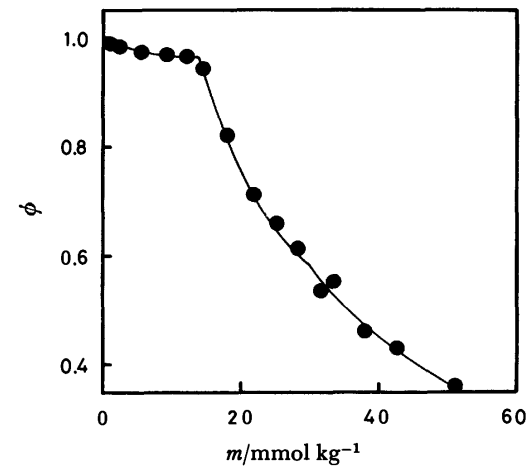

Fig. 4. Osmotic coefficient of water *vs.* molality.

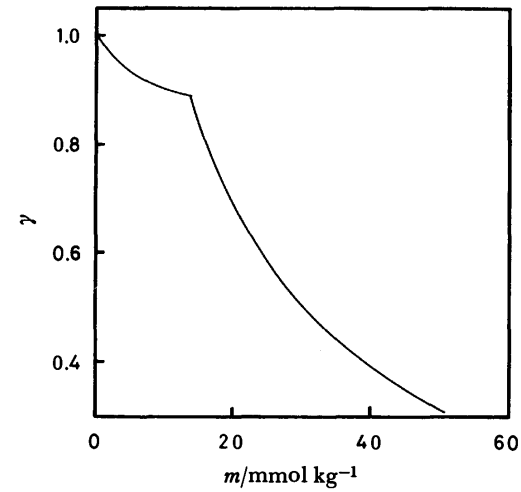

Fig. 5. Activity coefficient *vs.* molality.

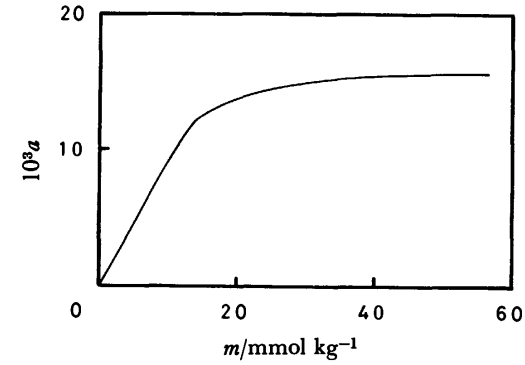

Fig. 6. Activity *vs.* molality.

$$a = \gamma m. \tag{3}$$

With the increase of m, γ decreased similarly to ϕ, also showing an abrupt fall at cmc (Fig. 5). As a result, above cmc the value of a became considerably restrained from increasing, hitherto almost proportionally to m (Fig. 6). The relation of a *vs.* m seems to be almost perfectly similar to the original relation of ΔR *vs.* m, in spite of the complex intermediates between them.

The similarity can be attributed to the nearly unit value of ϕ or the ideal nature of solute in low m.

Taking into consideration the general tendency that nonionic solutes behave more ideally than ionic solutes in water and in order to estimate the association number of Surfynol 465 in micelle, we approximately treated its aqueous solution as an ideal binary solution consisting of monomer and micelle, each of which has unit activity coefficient. As micellar species, we adopted a single kind of micelle with the association number, n, which is an average in the case of polydispersity. Then, we applied the Raoult's law to the ralation between ΔR and m (Fig. 3). The value of ΔR can be considered to be linear to the effective concentration of solute, C_{eff}, which is in an ideal solution the sum of molalities of surfactant in monomer and micelle, m_{mon} and m_{mic}, respectively, when C_{eff} is expressed in molality. Thus,

$$C_{\text{eff}} = m_{\text{mon}} + m_{\text{mic}}. \tag{4}$$

The molality of surfactant, which does not discriminate micelle from monomer, can be divided as

$$m = m_{\text{mon}} + nm_{\text{mic}}. \tag{5}$$

Then,

$$C_{\text{eff}} = m_{\text{mon}} + (m - m_{\text{mon}})/n. \tag{6}$$

The linearity of ΔR *vs.* m between cmc and second cmc can be simply explained, if both values of m_{mon} and n are assumed to be constant, m_{mon} being cmc. Calculating n as the ratio of two slopes of lines below and above cmc on ΔR *vs.* m, we obtained, *ca.* 4 for it.

For the analysis of ΔR *vs.* m relation above second cmc, the following two alternative approximations seems to be sufficient. First, approximating that the surfactant solution is an ideal ternary solution consisting of monomer, first micelle (hitherto simply called micelle) and second micelle, whose concentrations are cmc, second cmc minus cmc and m minus second cmc, respectively, we estimated the association number of second micelle at *ca.* 16 as the ratio of two slopes of lines below cmc and above second cmc on ΔR *vs.* m.[4,5] In this case, the linearity of ΔR *vs.* m holds at a constant association number of second micelle.

The second approximation assumes an ideal binary solution consisting of monomer and the second micelle, which forms from the transition of first micelle and grows in size, number or both with the increase of m above second cmc.[11] The association number of second micelle on the second approximation is not so easy to estimate directly from the slope of ΔR *vs.* m as the value on the first approximation, but is supposed to be somewhat smaller, owing to the consolidation of first micelles into second micelles at the second approximation.

Next in place of the above-mentioned phase-separation model, we considered an association equilibrium between monomer and micelle. For simplicity, we assumed also the monodispersity of micelle. Then,

$$(m_{\text{mic}}/\text{mol kg}^{-1})/(m_{\text{mon}}/\text{mol kg}^{-1})^n = K, \tag{7}$$

where K is the equilibrium constant. Combining Eq. 7 with Eqs. 4 and 5, which still hold, we have

$$\{(nC_{\text{eff}} - m)/\text{mol kg}^{-1}\}^n \cdot (n-1)^{1-n} = \{(m - C_{\text{eff}})/\text{mol kg}^{-1}\}/K, \tag{8}$$

or

$$n \ln \{(nC_{\text{eff}} - m)/\text{mol kg}^{-1}\} - (n-1) \ln (n-1) = \ln \{(m - C_{\text{eff}})/\text{mol kg}^{-1}\} - \ln K, \tag{9}$$

Converting ΔR into C_{eff} of Eq. 9 and calculating on a trial and error method, we obtained 15 for n, as seen in Fig. 7. To this value the association number of second micelle on the previously mentioned second approximation might be close.

From the inspection of σ *vs.* ln m curve, we assigned 11.1×10^{-3} mol kg^{-1} and 26.0 mN m^{-1} to cmc and the surface tension at cmc, σ_{cmc}, respectively (Fig. 8).

The surface excess, Γ, and the surface molecular area, A, of surfactant were calculated, by applying Gibbs' isotherm, Eq. 10, to the relation of σ with a, which had been calculated using Eq. 3.

$$\Gamma = -1/RT \cdot d\sigma/d\ln a, \tag{10}$$

and

$$A = 1/(L\Gamma), \tag{11}$$

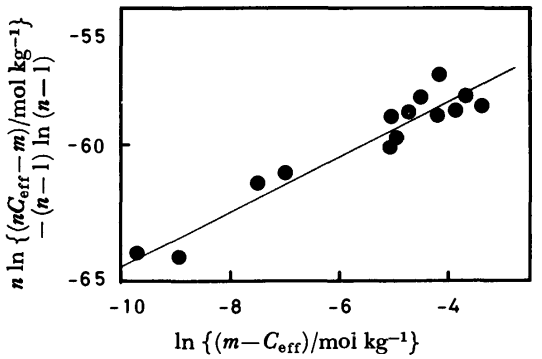

Fig. 7. Plot for the determination of association number.

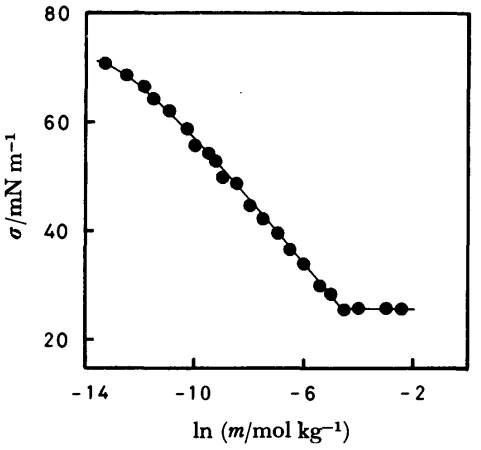

Fig. 8. Surface tension *vs.* logarithm of molality.

where L is Avogadro's number. We had 2.6×10^{-6} mol m^{-2} and 64.1 Å^2 molec^{-1} for Γ and A, respectively, near cmc.

In the course of study on acetal-type nonionic surfactant, Kuwamura and Takahashi[6] have reported that the cmc, σ_{cmc} and A of $CH_3(CH_2)_{12}CH(O(C_2H_5O)_5H)_2$, *i.e.* AG-14(10), at 293.15 K were 1.7×10^{-5} mol dm^{-3}, 36.2 mN m^{-1} and 54.5 Å^2 molec^{-1}, respectively. While the numbers of carbon, oxyethylene and poly (oxyethylene) chain of Surfynol 465 are same to those of AG-14(10), respectively, Surfynol 465 is about 650 times high in cmc, low by 10.2 mN m^{-1} in σ_{cmc} and large by 9.6 Å^2 molec^{-1} in A, each compared to AG-14(10). These discrepancies are considered to arise from the difference in the conformation of molecule in solution, wich is caused by the difference in the type of segment that connects two hydrophilic poly(oxyethylene) chains.

The relation between ρ and m makes two separate half lines, whose intersection gives cmc (12.4×10^{-3} mol kg^{-1}), as seen in Fig. 9. Owing to the lack of measurements beyond the second cmc, we could not describe the behavior of ρ or derived quantity *vs.* m at the formation of second micelle.

To obtain the apparent and partial molar volumes of surfactant, $^{\phi}V$ and V_s, respectively, we used the following relations.

$$^{\phi}V = \{(1+mM)/\rho - 1/\rho_o\}/m, \tag{12}$$

and

$$V_s = {}^{\phi}V + m(\mathrm{d}^{\phi}V/\mathrm{d}m), \tag{13}$$

where ρ_o is the density of water. The value of $^{\phi}V$ is plotted against m in Fig. 10.

Below cmc, surfactant exists only in monomeric form. There, the value of $^{\phi}V$ equals the apparent molar volume of monomer, $^{\phi}V_m$. According to Eq. 13, at infinite dilution the value of $^{\phi}V_m$ reduces to the standard partial volume of monomer, V_m°. From the inspection of Fig. 10, the following approximation can be expected at any concentration.

$$^{\phi}V_m \cong V_m^{\circ}. \tag{14}$$

Above cmc, assuming that $^{\phi}V$ is the average of monomeric and micellear contributions, we have

$$^{\phi}V = \mathrm{cmc}\cdot{}^{\phi}V_m/m + (m-\mathrm{cmc})^{\phi}V_M/m, \tag{15}$$

where $^{\phi}V_M$ is the apparent molar volume of surfactant in micelle. The $^{\phi}V$ of micelle formation, $\Delta_{mic}{}^{\phi}V$, is defined by Eq. 16.

$$\Delta_{mic}{}^{\phi}V \equiv {}^{\phi}V_M - {}^{\phi}V_m. \tag{16}$$

Then,

$$^{\phi}V = -\mathrm{cmc}\cdot\Delta_{mic}{}^{\phi}V/m + \Delta_{mic}{}^{\phi}V + {}^{\phi}V_m, \tag{17}$$

or

$$(m-\mathrm{cmc})/(^{\phi}V - {}^{\phi}V_m) = m/\Delta_{mic}{}^{\phi}V. \tag{18}$$

From plots of $^{\phi}V$ *vs.* $1/m$ (Fig. 11) and $(m-\mathrm{cmc})/(^{\phi}V-{}^{\phi}V_m)$ *vs.* m (Fig. 12), we can ascertain the validity of Eqs. 17 and 18 or retrospectively the assumption of Eq. 15, on the basis of the constancy of $^{\phi}V_M$ as well as $^{\phi}V_m$. From the above situation,

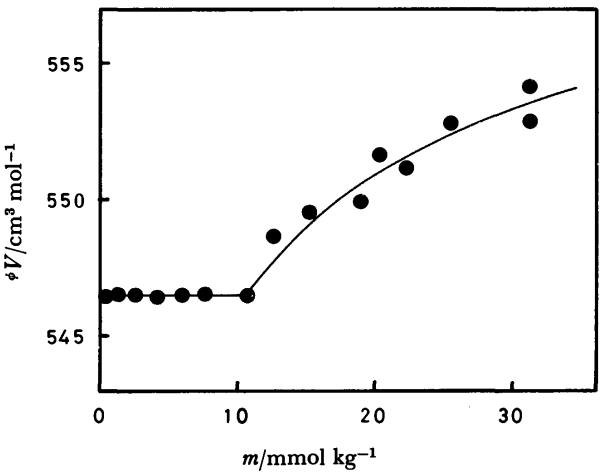

Fig. 10. Apparent molar volume *vs.* molality.

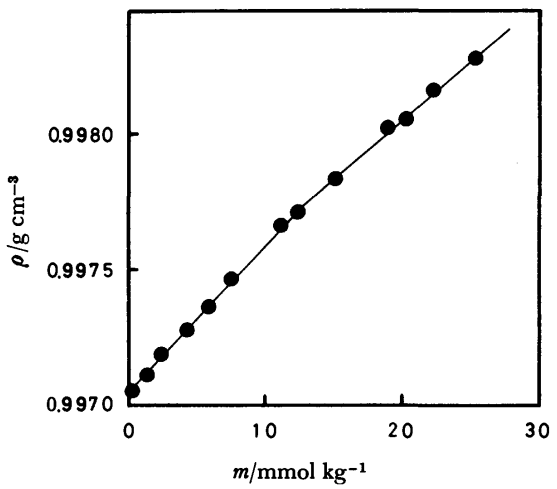

Fig. 9. Density *vs.* molality.

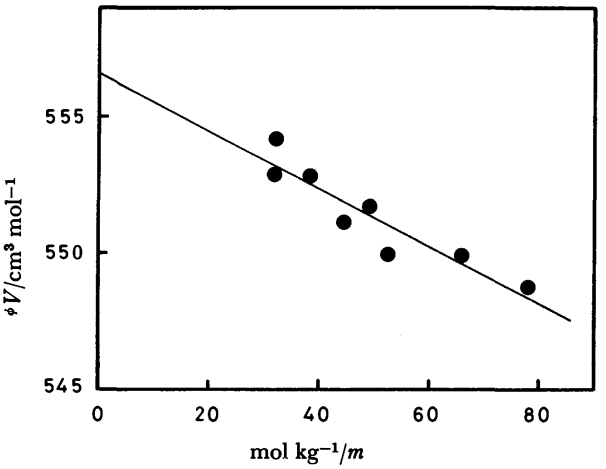

Fig. 11. Apparent molar volume *vs.* reciprocal of molality.

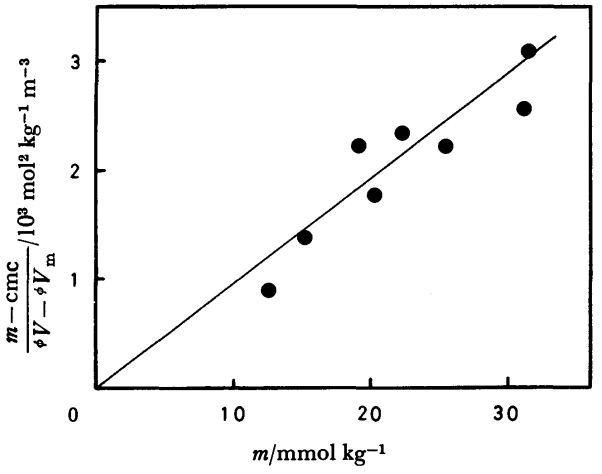

Fig. 12. $(m-\mathrm{cmc})/(^{\phi}V-^{\phi}V_{\mathrm{m}})$ *vs.* molality.

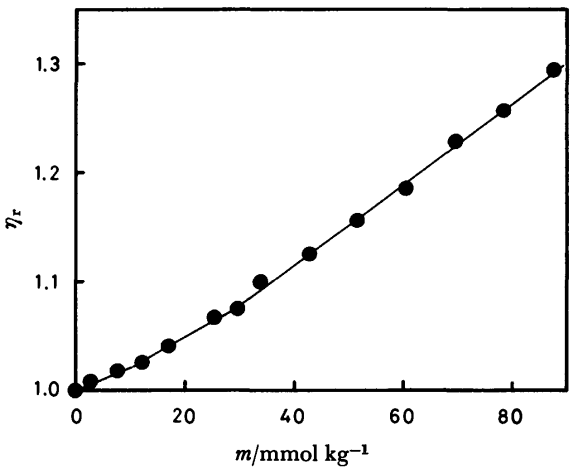

Fig. 13. Relative viscosity *vs.* concentration.

we can regard $^{\phi}V_{\mathrm{M}}$ and $\Delta_{\mathrm{mic}}{}^{\phi}V$ to be approximately equal to the standard partial volume of surfactant in micelle and of micelle formation, V°_{M} and $\Delta_{\mathrm{mic}}V^{\circ}$, respectively. From the analyses of Fig. 11 and 12, we estimated the V°_{m}, V°_{M}, and $\Delta_{\mathrm{mic}}V^{\circ}$ of Surfynol 465 at 546.5, 556.6, and 10.1 cm^3 mol^{-1}, respectively. As the optimal value of cmc for the above estimation, we used 10.6×10^{-3} mol kg^{-1} as cmc, which is slightly lower than the value estimated directly on the plot of ρ *vs.* m.

On the other hand, it is known with respect to $\Delta_{\mathrm{mic}}V^{\circ}$ that the contribution of methylene segment in one alkyl group is on the average *ca.* 1.5 cm^3 mol^{-1}, [12,13] which coincides with the molar volume change of methylene segment in paraffin at the transfer from solution state in water to liquid,[14] and the contribution of oxyethylene segment is considered to be negligible.[15] If the effect of acetylene group is ignored, the value of *ca.* 10 cm^3 mol^{-1} as $\Delta_{\mathrm{mic}}V^{\circ}$ of Surfynol 465, which has two hydrocarbon chains each with six carbons, suggests an entangling cohesion between the two chains in the surfactant molecule, dispersed in monomeric state, although the branching of hydrocarbon chains would also make the value of $\Delta_{\mathrm{mic}}V^{\circ}$ less in some degree. The above suggestion can be supported by the same case of Aerosol OT, which was studied by one of the authors and his co-worker using thermodynamic and spectrometric measurements.[4,5]

In order to study the micellar structure of Surfynol 465 from the rheological point of view, we measured the viscosity of its aqueous solution, η, against various m. The value of η increased rather monotonously with the increase of m, making only faint features near cmc and second cmc, as shown in Fig. 13 concerning the relative viscosity, η_r, *vs.* m. To make the effect of solute more conspicuous, we adopted the parameter of Einstein's formula, k, which is akin to reduced viscosity and defined by Eq. 19.[16]

$$k = (\eta_r - 1)/f, \tag{19}$$

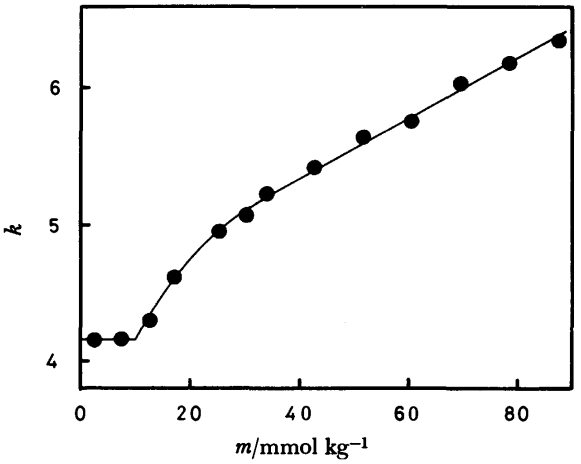

Fig. 14. Parameter of Einstein's viscosity formula *vs.* molality.

where f is the volume fraction of surfactant and can be approximately identified as the fraction of total apparent volume of surfactant, *i.e.* amount of surfactant, n_s, times $^{\phi}V$, in the volume of solution, V. Then,

$$f \cong n_s{}^{\phi}V/V = 1 - \rho/\{(1+mM)\rho_o\}, \tag{20}$$

The values of k were calculated from the results on η_r and ρ at various m and plotted in Fig. 14. Below *ca.* 10×10^{-3} mol kg^{-1}, which is approximately close to the previously described values of cmc, the value of k was constant at *ca.* 4, which is fairly higher than the theoretical value of 2.5 for spheres dispersed indepently of each other in medium. For its explanation, the deviation of molecular shape from sphere alone seems to be insufficient, since the monomer of Surfynol 465 dose not exist much differently from sphere, owing to the cohesion between its hydrophobic chains, which was previously mentioned. It is suggested that remarkable hydration occurs on the poly(oxyethylene) groups of Surfynol 465. As m increased above cmc, k increased and drew a parabola with a slight bend near second

cmc and a linear tail after it, showing the occurrence and multiplication of micelle having higher value of k than monomer. From the cause of higher k for micelle, the change in the hydration of poly (oxyethylene) group at micelle formation would be excluded, because the change is considered to be not significant, which was estimated on the analysis of $\Delta_{mic}V^{\circ}$, and might decrease k, even if it occurred, due to the dehydration and subsequent decrease of effective micellar size at micelle formation. Then, for the cause of higher k, there remain the following two factors: the shape and interaction concerning surfactant monomer and micelle.

In a dilute solution, the interaction between solutes can be excluded from discussion. Then, the shape of micelle is supposed to be significantly deviated from sphere in comparison with that of monomer, which is considered to be nearly spherical. With small n, the first micelle between cmc and second cmc is estimated to have the shape of either disk or short rod. The increase of k in this region with m is considered to result from the relative decrease of monomeric contribution to k, implying the convergence of k to the value of micelle itself. After passing through second cmc, the rate of increase in k on m recovered to show the linear increase of k, without any sign of convergence. Besides the long rod- or wide disk-like shape of second micelle with higher n, we might take into consideration the possible role played by the interaction between micelles, which facilitates a scaffold-structure, resulting in the so-called structural viscosity. Also, the possible increase of n with m might be the cause of increasing k. However, it seems to be necessary to study the micellar state above second cmc, or speaking with reserve, in a very higher concentration of Surfynol 465.

References

1) M. Ueno, R. Kitada, and H. Kishimoto, *Chem. Lett.*, **1978**, 1351.

2) C. Tanford, "The Hydrophobic Effect: Formation of Micelles and Biological Membranes," 2nd ed, John Wiley & Sons, New York (1980), Chap. 11.

3) S. Sato, and H. Kishimoto, *J. Colloid Interface Sci.*, **69**, 188 (1979); *ibid.*, **88**, 574 (1982).

4) M. Ueno and H. Kishimoto, *Nippon Kagaku Kaishi*, **1980**, 375.

5) M. Ueno, and H. Kishimoto, *J. Phys. Chem.*, **87**, 850 (1983).

6) T. Kuwamura and H. Takahashi, *Bull. Chem. Soc. Jpn.*, **45**, 617 (1972); H. Takahashi and T. Kuwamura, *ibid.*, **46**, 623 (1973); H. Takahashi, T. Fujiwara, and T. Kuwamura, *Yukagaku*, **24**, 36 (1975).

7) W. D. Harkins and F. E. Brown, *J. Am. Chem. Soc.*, **38**, 228 (1916); *ibid.*, **41**, 499 (1919).

8) A. P. Brady, H. Huff, and J. W. McBain, *J. Phys. & Colloid Chem.*, **55**, 304 (1951); H. Huff, J. W. McBain, and A. P. Brady, *ibid.*, **55**, 311 (1951).

9) R. A. Robinson and R. H. Stokes, "Electrolyte Solutions," 2nd ed, Butterworths, London (1970), Chap. 8.

10) H. Kishimoto and M. Ueno, *Yakugaku Zasshi*, **94**, 1408 (1974).

11) S. Ozeki and S. Ikeda, *J. Colloid Interface Sci.*, **87**, 424 (1982).

12) J. M. Corkill, J. F. Goodman, and T. Walker, *Trans. Faraday Soc.*, **63**, 768 (1967).

13) J. E. Desnoyers, R. De Lisi, C. Ostiguy, and G. Perron, "Solution Chemistry of Surfactants," Vol. I, ed by K. L. Mittal, Plenum Press, New York (1979), p. 221.

14) G. Nemethy and H. A. Scheraga, *J. Chem. Phys.*, **36**, 3401 (1962).

15) S. Kaneshina, M. Yoshimoto, H. Kobayashi, N. Nishikido, G. Sugihara, and M. Tanaka, *J. Colloid Interface Sci.*, **73**, 124 (1980); D. Guveli, S. S. Davis, and J. B. Kayes, *ibid.*, **86**, 213 (1982).

16) A. Einstein, "Investigations on the Theory of Brownian Movement," Dover Publications, New York (1956), p. 54.

Use of Propagators in the Hückel Model. V. Polarizabilities

Shigeyuki AONO and Kiyoshi NISHIKAWA
Department of Chemistry, Faculty of Science, Kanazawa University, Marunouchi Kanazawa 920
(Received September 6, 1984)

The ordinary perturbation theory is reformulated in terms of propagators. It is well known that, if the perturbing interaction has a single particle character, the additional energy up to the second order of the perturbation is expressed by bond orders and various polarizabilities. This is easily rewritten by use of propagators. In addition, under the tight-binding approximation, the propagators of linear and ring polyenes are expressed in simple analytical forms, which enable us to give also analytical expressions for bond orders and polarizabilities. A simple application is given to determine which is more stable, anthracene or phenanthrene.

The wave function plays a central role in the perturbation treatment of the quantum chemistry. The molecular orbital (MO) is usually constructed by the linear combination of atomic orbitals (LCAO). Since AO's are given as the basis set, the essential part of MO is LCAO coefficients. If any perturbing interaction is introduced, we begin with determining this effect on the wave function, and then obtain the first or second order correction to the physical quantity of interest in terms of LCAO coefficients.

It has been pointed out by Coulson and Longuet-Higgins[1] that the above mentioned procedure is not always necessary, but once the Hamiltonian matrix is given, any physical quantity is directly obtained by manipulating the corresponding determinant, not *via* wave functions. Let the Hückel determinant be

$$D(z) = \begin{vmatrix} \alpha_1 - z & \beta_{12} & \beta_{13} & \cdot & \cdot & \cdot \\ \beta_{21} & \alpha_2 - z & \beta_{23} & \cdot & \cdot & \cdot \\ \beta_{31} & \cdot & \cdot & \cdot & \cdot & \cdot \\ \cdot & \cdot & & & & \\ \cdot & \cdot & \cdot & \cdot & \cdot & \alpha_n - z \end{vmatrix}, \quad (1)$$

then we have the total enery of the system,

$$E = \frac{1}{2\pi i}\int_c dz \frac{\partial}{\partial z} \log D(z), \quad (2)$$

or the bond order q_{rs} between atomic sites r and s,

$$q_{rs} = (-)^{r+s+1}\frac{1}{2\pi i}\int_c dz \frac{D_{rs}(z)}{D(z)}, \quad (3)$$

where D_{rs} is the r,s cofactor of D, and the integration is done along the so-called Coulson contour in Fig. 1a, which encloses the poles corresponding to the occupied levels. For simplicity, here and hereafter we assume the occupied levels have two electrons with up and down spins, and the spin summation is included in the integration.

The above expressions are nothing but ones by using propagators, *e.g.*, the integrand of Eq. 3 is the r,s matrix element of the matrix propagator, as will be clarified in the followings. In this sence, the work of Coulson and Longuet-Higgins is not old in spirit. In the present work the elementary perturbation theory is reformulated in terms of propagators. Procedures look abstract, but are much simpler than usual ones. For the simplest systems as linear and ring polyenes, we have already obtained analytical expressions of propagators,[2] which enable us to express bond orders and various polarizabilities also in analytical form.

Perturbation Theory

The Hamiltonian of the system in question is given in matrix form, $\boldsymbol{H}$ which satisfies the eigenvalue equation,

$$\boldsymbol{H}|i\rangle = \varepsilon|i\rangle, \quad (4)$$

where we assume that $|i\rangle$ is a single-particle state, and forms a complete set;

$$\sum_i |i\rangle\langle i| = 1. \quad (5)$$

Let us introduce the Green's operator,

$$G = \frac{1}{z-\boldsymbol{H}} \quad (6a)$$

$$= \sum_i \frac{|i\rangle\langle i|}{z-\varepsilon_i}, \quad (6b)$$

of which matrix element with respect to atomic sites r,s is

$$G_{rs}(z) = \sum_i \frac{\langle r|i\rangle\langle i|s\rangle}{z-\varepsilon_i}. \quad (7)$$

If we integrate this along the Coulson contour, we obtain immediately

$$q_{rs} = \frac{1}{2\pi i}\int_c dz G_{rs}(z) = 2\sum_i^{occ} \langle r|i\rangle\langle i|s\rangle = 2\sum_i^{occ} C_{ri}C_{si}^*, \quad (8)$$

where the factor 2 is due to the spin sum, and in the final expression we have used LCAO coefficients. We can understand here q_{rs} is the so-called bond order. Next we consider the integral which gives the total energy,

$$E = \mathrm{Tr}\frac{1}{2\pi i}\int_c dz z\boldsymbol{G}(z) = \sum_s\sum_i \frac{1}{2\pi i}\int_c dz z\frac{\langle s|i\rangle\langle i|s\rangle}{z-\varepsilon_i} = 2\sum_i^{occ}\varepsilon_i, \quad (9)$$

where the factor 2 is due to the spin sum and we have also assumed that the set $\{|s\rangle\}$ is complete:

$$\sum_s |s\rangle\langle s| = 1. \quad (10)$$

Now we turn to the perturbation treatments. Almost all of them have already been done,[3] and then concentrate ourselves to connect with the conventional theory. The total Hamiltonian is devided into two parts:

$$\boldsymbol{H} = \boldsymbol{H}^0 + \boldsymbol{v}, \quad (11)$$

and $\boldsymbol{v}$ is assumed to be much smaller than $\boldsymbol{H}^0$ and further the propagator $\boldsymbol{G}^0$ for $\boldsymbol{H}^0$ is known. The perturbation expansion of G is as follows:

$$\boldsymbol{G} = \boldsymbol{G}^0 + \boldsymbol{G}^0\boldsymbol{v}\boldsymbol{G}^0 + \boldsymbol{G}^0\boldsymbol{v}\boldsymbol{G}^0\boldsymbol{v}\boldsymbol{G}^0 + \cdots. \quad (12)$$

If we take the effect of $\boldsymbol{v}$ into account up to the first order and integrate the r,s matrix elements of both sides along the Coulson contour, we obtain

$$\frac{1}{2\pi i}\int_c G_{rs}dz = \frac{1}{2\pi i}\int_c dz G^0_{rs} + \frac{1}{2\pi i}\int_c dz \sum_{tu} G^0_{rt}v_{tu}G^0_{us}. \quad (13)$$

Then we have a small change of the bond order q_{rs} caused by a specified v_{tu}

$$\delta q_{rs} = \frac{1}{2\pi i}\int_c dz(G_{rs}-G^0_{rs}) = \frac{1}{2\pi i}\int_c dz(G^0_{rt}v_{tu}G^0_{us} + G^0_{ru}v_{ut}G^0_{ts}). \quad (14)$$

If v_{tu} is real, namely, $v_{tu}=v_{ut}$, it follows that

$$\frac{\delta q_{rs}}{\delta v_{tu}} = \frac{1}{2\pi i}\int_c dz(G^0_{rt}G^0_{us} + G^0_{ru}G^0_{ts}) = \pi_{rs;tu}. \quad (15)$$

where we rewrite v_{tu} as δv_{tu}, stressing it be small. This is the bond-bond polarizability defined by Coulson. Other simpler polarizabilities are obtained as special ones of the above.

When v_{tu} is pure imaginary, say $v_{ut}=-v_{tu}$, we get

$$\bar{\pi}_{rs;tu} = \frac{1}{2\pi i}\int_c dz(G^0_{rt}G^0_{us} - G^0_{ru}G^0_{ts}). \quad (16)$$

This is employed by McWeeny in analysis of the ring current of aromatic compounds.[6] It is mentioned that using a explicit form of G^0_{rs} in Eq. 7, we can easily derive the common expression of $\pi_{rs;tu}$ in terms of LCAO coefficients.

Next placing Eq. 12 in the first line of Eq. 9 we have

$$E = \mathrm{Tr}\frac{1}{2\pi i}\int_c dz z(\boldsymbol{G}^0 + \boldsymbol{G}^0\boldsymbol{v}\boldsymbol{G}^0 + \boldsymbol{G}^0\boldsymbol{v}\boldsymbol{G}^0\boldsymbol{v}\boldsymbol{G}^0\boldsymbol{v}\boldsymbol{G}^0 + \cdots)$$

so that, up to the second order with respect to $\boldsymbol{v}$,

$$\delta E = E - E^0 = \mathrm{Tr}\frac{1}{2\pi i}\int_c (dz z(\boldsymbol{G}^0\boldsymbol{v}\boldsymbol{G}^0 + \boldsymbol{G}^0\boldsymbol{v}\boldsymbol{G}^0\boldsymbol{v}\boldsymbol{G}^0) = \mathrm{Tr}\frac{1}{2\pi i}\int_c dz\left(\boldsymbol{G}^0\boldsymbol{v} + \frac{1}{2}\boldsymbol{G}^0\boldsymbol{v}\boldsymbol{G}^0\boldsymbol{v}\right), \quad (17)$$

where the last result is obtained as follows: Remembering that $\boldsymbol{G}^0=(z-\boldsymbol{H}^0)^{-1}$, we integrate by parts and use the permutation invariability inside Tr.[4] In general $\boldsymbol{v}$ being complex:

$$v_{rs} = v^0_{rs} + iv'_{rs}, \quad v_{sr} = v^0_{rs} - iv'_{rs}, \quad (18)$$

and then using Eqs. 8 and 15, we obtain

$$\delta E = 2\sum_{(rs)} v^0_{rs}q_{rs} + \sum_{(rs)}\sum_{(tu)}(v^0_{rs}\pi_{rs;tu}v^0_{tu} + v'_{rs}\bar{\pi}_{rs;tu}v'_{tu}) \quad (19)$$

where (rs) means that the summation is carried out with respect to the bond (r,s), or under the restriction, $r<s$.

Analytical Expression for Bond Order and Polarizability

In the Hückel approximation, the propagators of linear and ring polyenes are obtained in analytical forms.[2] The r,s matrix element of the chain propagator is given as, in unit of β

$$G^0_{rs} = \frac{\sin(r+1)\theta \sin(n-s)\theta}{\sin(n+1)\theta \sin\theta}, \tag{20}$$

where the linear chain with n atomic sites is numbered as Fig. 2, and we omit the index indicating the chain length n without confusion, and further

$$z = 2\cos\theta. \tag{21}$$

This variable transformation maps the Coulson contour in Fig. 1a to that in Fig. 1b.

For the ring polyene shown in Fig. 3, we have (β=1)

$$R^0_{0k} = \frac{-1}{4\sin^2(n\theta/2)\sin\theta}(\sin(n-k)\theta + \sin k\theta). \quad (k \geqq 0) \tag{22}$$

This propagator consists of two parts: The first term in the bracket represents the effect arised from the ordinary propagation, $0\rightarrow 1\rightarrow 2\rightarrow\cdots\rightarrow k$, while the second term the reverse propagation.

The bond order of them are already given:[2] For the linear chain

$$q^L_{r+1,s+1} = \frac{1}{n+1}\left[\frac{\sin(s-r)\pi/2}{\sin(s-r)\pi/2(n+1)} - \frac{\sin(s+r)\pi/2}{\sin(s+r)\pi/2(n+1)}\right], \tag{23}$$

and for the ring

$$q^R_{0k} = \frac{2}{n^2}[(n-k)+k]\frac{\sin k\pi}{\sin k\pi/n}. \tag{24}$$

In the latter, the first term in the square bracket is due to the ordinary propagation, while the second due to the reverse propagation. Such interpretation is one of the remarkable results of propagator analysis and gives a profound understanding of chemical reactivity and stability.[4,5,7] We can observe that at the limit, $k\rightarrow 0$, either $q^L_{r,r+k}$ and q^R_{0k} tend to 1 (Coulson-Rushbrooke theorem), and other properties of the bond order are to be derived from these expressions.

Now we begin to evaluate polarizabilities. For the linear chain the most general one is

$$\pi^L_{rs;tu} = \frac{1}{2\pi i}\int_c dz(G^0_{rt}G^0_{us} + G^0_{ru}G^0_{ts}). \tag{25}$$

We know a symmetrical property, $G^0_{rs}=G^0_{sr}$, but we have to stress that the analytical expression (20) is avairable, for G^0_{rt} only if $t\geqq r$. Therefore the calculation carried out under the condition that $t\geqq r$, $s\geqq u$, $u\geqq r$, and $s\geqq t$, which corresponds to the case shown in Fig. 2a. Substituting Eq. 20 into Eq. 25, we have

$$\pi^{L(a)}_{rs;tu} = \frac{1}{2}\frac{1}{2\pi i}\int_c d\theta(-2\sin\theta)\frac{1}{\sin^2\theta\sin^2(n+1)\theta} \times[\sin(r+1)\theta\sin(n-t)\theta\sin(u+1)\theta\sin(n-s)\theta + \sin(r+1)\theta\sin(n-u)\theta\sin(t+1)\theta\sin(n-s)\theta]. \tag{26}$$

Some comments should be added. The factor, 1/2 is needed due to the fact the contour in θ plane goes round the origin twice while the contour in z plane does once. As to poles, θ=0 is not the pole (as mentioned in the second paper of Ref. 1), and real poles are

$$\theta_\mu = \frac{\pi\mu}{n+1}, \quad \mu = \pm 1, \pm 2, \cdots, \pm n. \tag{27}$$

If we assume for simplicity that n is even and every site offers an electron, the levels are doubly occupied from the bottom to the $\pm n/2$ and the result is as follows:

$$\pi^{L(a)}_{rs;tu} = \frac{-4}{(n+1)^2}\sum_{\mu=1}^{n/2}\frac{1}{\sin\theta_\mu} \{\sin(r+1)\theta_\mu\sin(n-t)\theta_\mu\sin(u+1)\theta_\mu\sin(n-s)\theta_\mu [(r+1)\cot(r+1)\theta_\mu + (n-t)\cot(n-t)\theta_\mu + (u+1)\cot(u+1)\theta_\mu + (n-s)\cot(n-s)\theta_\mu - \cot\theta_\mu] + \sin(r+1)\theta_\mu\sin(n-u)\theta_\mu\sin(t+1)\theta_\mu\sin(n-s)\theta_\mu [(r+1)\cot(r+1)\theta_\mu + (n-u)\cot(n-u)\theta_\mu + (t+1)\cot(t+1)\theta_\mu + (n-s)\cot(n-s)\theta_\mu - \cot\theta_\mu]\}, \tag{28}$$

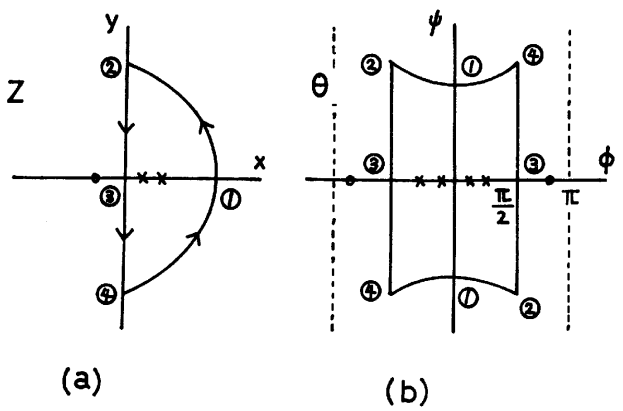

Fig. 1.

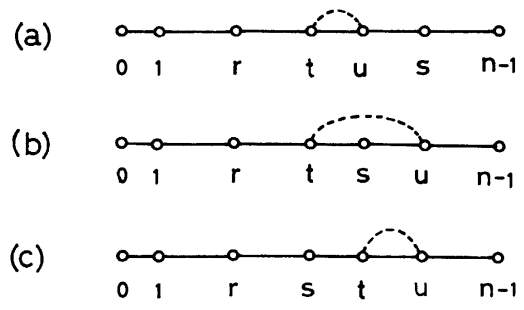

Fig. 2.

where the spin sum has been done. We can observe that the above result is valid for the exchange, $(r,s)\leftrightarrow(t,u)$.

There are other relations between pairs, (r,s) and (t,u) keeping $s>r$ and $u>t$, as shown in Figs. 2b and 2c. In the case of Fig. 2b, G^0_{us} in Eq. 25 should be read G^0_{su}, and then in order to obtain $\pi^{L(b)}_{rs;tu}$ we have to exchange u and s in the first square bracket of Eq. 28. In the case of Fig. 2c, $\pi^{L(c)}_{rs;tu}$ is obtained by exchanging not only u and s in the first term of the square bracket in Eq. 26 but also t and s in the second term. This makes two terms in Eq. 28 identical, and we denote the result for further investigations.

$$\pi^{L(c)}_{rs;tu} = \frac{-8}{(n+1)^2}\sum_{\mu=1}^{n/2}\frac{1}{\sin\theta_\mu}\{\sin(r+1)\theta_\mu \sin(n-t)\theta_\mu \sin(s+1)\theta_\mu \sin(n-u)\theta_\mu [(r+1)\cot(r+1)\theta_\mu + (n-t)\cot(n-t)\theta_\mu + (s+1)\cot(s+1)\theta_\mu + (n-u)\cot(n-u)\theta_\mu - \cot\theta_\mu]\}. \quad (29)$$

Other simpler polarizabilities will be obtained by the following procedures. One of self-polarizabilities, $\pi^L_{rs;tu}$ is obtained by putting $r=t$ and $s=u$, keeping $r,t<s,u$, therefore $\pi^{L(a)}_{rs;tu}$ or $\pi^{L(b)}_{rs;tu}$ should be used as a starting one, say,

$$\pi^L_{rs;rs} = (r=t,\ s=u \text{ in } \pi^{L(a)}_{rs;tu} \text{ or } \pi^{L(b)}_{rs;tu}). \quad (30)$$

Similar considerations lead to the followings:

$$\pi^{L(a)}_{r;tu} = (r=s \text{ in } \pi^{L(a)}_{rs;tu}) \text{ for } r \text{ inside } t-s,$$
$$\pi^{L(c)}_{r;tu} = (r=s \text{ in } \pi^{L(a)}_{rs;tu}) \text{ for } r \text{ outside } t-s,$$
$$\pi^{L(a)}_{rs;t} = \frac{1}{2}(t=u \text{ in } \pi^{L(a)}_{rs;tu}) \text{ for } t \text{ inside } r-s,$$
$$\pi^{L(a)}_{rs;t} = \frac{1}{2}(t=u \text{ in } \pi^{L(c)}_{rs;tu}) \text{ for } t \text{ outside } r-s,$$
$$\pi^L_{r;t} = \frac{1}{2}(r=s,\ t=s \text{ in } \pi^{L(c)}_{rs;tu}). \quad (31)$$

The last one is given explicitly as

$$\pi^L_{r;t} = \frac{-8}{(n+1)^2}\sum_{\mu=1}^{n/2}\frac{1}{\sin\theta_\mu}\sin^2(r+1)\theta_\mu \sin^2(n-t)\theta_\mu [(r+1)\cot(r+1)\theta_\mu + (n-t)\cot(n-t)\theta_\mu - \cot\theta_\mu] \quad (32)$$

which precisely coincides the result obtained by Coulson and Longuet-Higgins.[1] When $r=0$, the denominator cancels out one of the numerators, so that the summation can be carried out to get the result:

$$\pi^L_{0;t} = \frac{1}{2(n+1)^2}[(-)^t(2n-2t+1)\operatorname{cosec}(2t+3)\pi/2(n+1) + (-)^t(2n-2t+1)\operatorname{cosec}(2t+1)\pi/2(n+1) - 2\operatorname{cosec}\pi/2(n+1)], \quad (33)$$

which has been also obtained by the above-mentioned investigations.

Since $\bar{\pi}^L_{rs;tu}$ is expressed as

$$\bar{\pi}^L_{rs;tu} = \frac{1}{2\pi i}\int_c dz(G^0_{rt}G^0_{us} - G^0_{ru}G^0_{ts}), \quad (34)$$

the (a) and (b) types have non-vanishing values and the second half of Eq. 26 or 28 changes sign, but the (c) type not.

We turn to the case of ring polyenes with n sites which are numbered as shown in Fig. 3a. Using the ring propagators of Eq. 22 in Eq. 25, we have

$$\pi^{R(a)}_{rs;tu} = \frac{-1}{4}\frac{1}{2\pi i}\int_c d\theta(R^0_{rt}R^0_{us} + R^0_{ru}R^0_{ts}) = \frac{-1}{4}\frac{1}{2\pi i}\int_c d\theta\frac{1}{\sin^2(n\theta/2)\sin\theta}(\cos\bar{tr}\theta\cos\bar{su}\theta + \cos\bar{ur}\theta\cos\bar{st}\theta), \quad (35)$$

where, for example

$$\bar{tr} = n/2 - (t-r), \quad (36)$$

and the first and second terms of the second line are originated from the first and second terms of the first line, respectively. We present the result for each term separately, for convenience of the later investigation. Here we have poles:

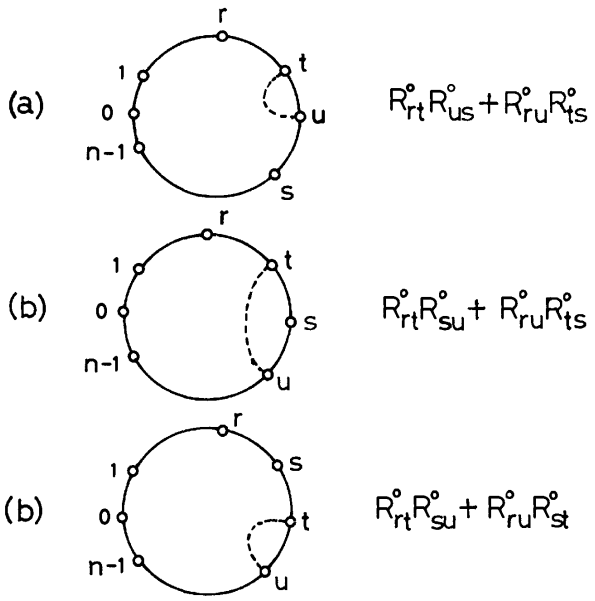

Fig. 3.

$$\theta_\mu = \frac{2\pi\mu}{n}, \quad \mu = 0, \pm 1, \pm 2, \cdots, n/2, \tag{37}$$

and the levels from 0 to $\pm n/4$ are doubly occupied. Unlike the case of the linear chain, $\theta=0$ is a real pole. The result are:

The first term of Eq. 35

$$= \frac{-1}{6} - \frac{1}{n^2}\left(\frac{1}{3} - \bar{tr}^2 - \bar{su}^2\right) + \frac{4}{n^2}\sum_{\mu=1}^{[n/4]} \frac{1}{\sin\theta_\mu} \cos\bar{tr}\theta_\mu \cos\bar{su}\theta_\mu \times (\cot\theta_\mu + \bar{tr}\tan\bar{tr}\theta_\mu + \bar{su}\tan\bar{su}\theta_\mu), \tag{38a}$$

and

The second term of Eq. 35

$$= \frac{-1}{6} - \frac{1}{n^2}\left(\frac{1}{3} - \bar{ur}^2 - \bar{st}^2\right) + \frac{4}{n^2}\sum_{\mu=1}^{[n/4]} \frac{1}{\sin\theta_\mu} \cos\bar{ur}\theta_\mu \cos\bar{st}\theta_\mu \times (\cot\theta_\mu + \bar{ur}\tan\bar{ur}\theta_\mu + \bar{st}\tan\bar{st}\theta_\mu). \tag{38b}$$

In the above the terms without summation arise from the pole, $\theta_u=0$, and others from poles, $\theta_u \neq 0$, and further $[n/4]$ is the Gauss notation, which means the maximum integer at most $n/4$. It is needless to say

$$\pi^{R(a)}_{rs;tu} = \text{Eq. 38a} + \text{Eq. 38b}. \tag{39}$$

For the cases shown in Fig. 3b and 3c, entirely the same treatments that have been done in the case of the linear chain hold. Namely

$$\pi^{R(b)}_{rs;tu} = [s\leftrightarrow u \text{ in the first term of Eq. 39}]$$
$$\pi^{R(c)}_{rs;tu} = [s\leftrightarrow u \text{ in the first term and } t\leftrightarrow s \text{ in the second term of Eq. 39}]. \tag{40}$$

but in $\pi^{R(c)}_{rs;tu}$ it does not happen that two terms are accidentally coincident as in $\pi^{L(c)}_{rs;tu}$. Further the relations as mentioned in Eqs. 30 and 31 also hold in this case.

It is rather striking that $\pi^{R}_{rs;tu}$ has a constant term, but it will be canceled out by a part of suceeding terms, as n tends to infinity.

The polarizability due to the imaginary perturbation, $\bar{\pi}^{R(a)}_{rs;tu}$ is simply obtained by changing the sign in Eq. 39:

$$\pi^{R(a)}_{rs;tu} = \text{Eq. 38a} - \text{Eq. 38b} \tag{41}$$

and for others the same relations hold.

Illustrative Example

As an example of previous treatments we consider which is more stable, anthracene (I) and phenanthrene (II). In each compound, the atomic sites are numbered as in Fig. 4. Namely, if we consider the ring polyene with fourteen sites as an unperturbed system, anthracene has additional bonds, (0,9) and (2,7), while phenanthrene has bonds, (0,9) and (1,6).

Considering that these bond formations are perturbation, we can estimate each stabilization energy. We begin with evaluating the first order energies:

$$\Delta E^{(1)}_{I} = 2v(q^R_{09} + q^R_{27}), \tag{42a}$$
$$\Delta E^{(1)}_{II} = 2v(q^R_{09} + q^R_{16}), \tag{42b}$$

where we put $v_{rs}=v_{sr}=v$. In the case of ring, the value of bond order depends only on the distance between sites along the ring perimeter, so that $q^R_{27}=q^R_{16}$ Therefore we can find no difference in the first order energies between I and II.

The second order energy is written in general as

$$\Delta E^{(2)} = \sum_{(rs)}\sum_{(tu)} v_{rs}\pi_{rs;tu}v_{tu}, \tag{43}$$

where the summations are carried out with repect to the bonds (r,s) and (t,u). Hence it follows that

$$\Delta E^{(2)}_{I} = v^2(\pi^R_{09;09} + \pi^R_{27;27} + 2\pi^R_{09;27}), \tag{44a}$$
$$\Delta E^{(2)}_{II} = v^2(\pi^R_{09;09} + \pi^R_{16;16} + 2\pi^R_{09;16}). \tag{44b}$$

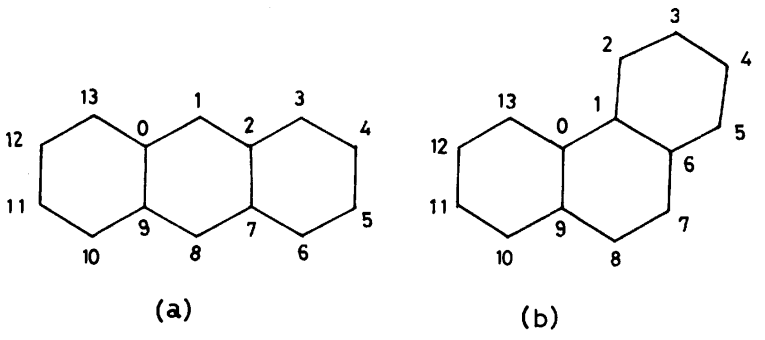

Fig. 4.

Thus we have a energy difference between I and II in the second order terms:

$$\begin{aligned}\Delta E &= \Delta E_{\mathrm{I}}^{(2)} - \Delta E_{\mathrm{II}}^{(2)} \\ &= 2v^2(\pi^R_{09;27} - \pi^R_{09;16}) \\ &= 2v^2(-0.00632/\beta - 0.08539/\beta) \\ &= -0.1834\beta, \end{aligned} \tag{45}$$

where in the final expression, β is recovered (note that polarizabilities are given in unit of β^{-1}), and we put $v=\beta$. Since β is negative, the result has a positive value. Therefore we can conclude that phenanthrene is more stable than anthracene.

Concluding Remarks

As long as the perturbing interaction is of a single particle character, the present treatment using propagator is quite general. Up to the second order of the perturbation, the additional energy and other physical quantities such as the diamagnetic susceptibility are expressed with bond orders and polarizabilities. The calculated results are solely depend upon, to what extent the zero-order propagators are already given.

As an advantage of our method, procedures are carried out without use of wave functions, so that we are able to analyze the problem under consideration in a compact and elegant way, and sometimes to insight the essential features of the subject. Some examples have been shown already in the analysis of chemical reactivities and stabilities.[4,7] For the simplest species such as linear or ring polyenes, the propagators are obtained in analytical forms. These are quite useful for qualitative and quantitative investigations of various chemical problems.

However we do not deny usefulness of the wave function. If we investigate too complicated species to take linear or ring polyene as an unperturbed system, the propagator of the starting substance is hardly obtained in an analytical way. Even in this case it is preferable that, at the stage of the general treatment, the problem is handled by the use of propagators, and then at the final calculating stage, the wave functions as accurate as possible should be used.

References

1) C. A. Coulson, and H. C. Longuet-Higgins, Proc. Roy. Soc. London, **A191**, 39 (1947), **A192**, 16 (1947), **A193**, 447, 456 (1948), **A195**, 188 (1948).

2) S. Aono, T. Ohmae, and K. Nishikawa, *Bull. Chem. Soc. Jpn.*, **54**, 1645 (1981).

3) S. Aono and K. Nishikawa, *Bull. Chem. Soc. Jpn.*, **53**, 3418 (1980).

4) T. Ohmae, K. Nishikawa, K. Deguchi, and S. Aono, *Bull. Chem. Soc. Jpn.*, **54**, 2857 (1981).

5) K. Nishikawa, M. Yamamoto, and S. Aono, *J. Chem. Phys.*, **78**, 5031 (1983).

6) R. McWeeny, *Mol. Phys.*, **1**, 311 (1958).

7) T. Ohmae, K. Nishikawa, K. Deguchi, and S. Aono, *Bull. Chem. Soc. Jpn.*, **54**, 3296 (1981).

Use of Propagators in the Hückel Model. VI. Magnetic Perturbation and Ring Current

Takayuki OHMAE, Kiyoshi NISHIKAWA, and Shigeyuki AONO
Department of Chemistry, Faculty of Science, Kanazawa University, Marunouchi, Kanazawa 920
(Received September 6, 1984)

The electron propagator in the magnetic field is investigated under the Hückel approximation, and the electronic energy and the aromatic ring current are evaluated. The perturbation treatment for the ring current developed by McWeeny is easily reformulated in terms of propagator and then the physical features involved in this problem have been made considerably clearer.

The diamagnetic anisotropy of an aromatic hydrocarbon may be attributed to induced currents flowing round the aromatic rings. This picture first proposed by Pauling,[1] has been quantum mechanically formulated by London,[2] and extensively studied, *e.g.*, by Pople[3] or by McWeeny.[4] Recently this problem is investigated in connection with aromaticity by Aihara,[5] who uses a graph-theoretical formalism. In this paper we reformulate the above mentioned treatments in terms of propagator. The physical contents beyond the previous works will not be expected, but the general and compact analysis might be helpful in a deeper understanding of this problem.

Hückel Hamiltonian with Magnetic Field

In treating species in the magnetic field, we use the basis set:

$$\chi_s(\mathbf{r}) = \chi_s^0(\mathbf{r})e^{-iA_s\cdot r/\Phi}, \quad \Phi = \hbar c/e, \tag{1}$$

where x_s^0 is the atomic orbital at s site in the absence of the magnetic field, A_s is the vector potential there and $\mathbf{r}$ is the position vector of electron. Meanwhile we manipulate in unit of $\Phi=1$ for simplicity, but if necessary we recover this constant. As usual the transfer integral β_{st} is approximately estimated as,

$$\begin{aligned}\beta_{st} &= \int d\mathbf{r}\chi_s^* H\chi_t \\ &= \int d\mathbf{r}e^{i(A_s-A_t)\cdot r}\chi_s^{0*}H\chi_t^0 \\ &\fallingdotseq e^{i(A_s-A_t)\cdot(R_s+R_t)/2}\int d\mathbf{r}\chi_s^{0*}H\chi_t^0 \\ &= \beta_{st}^0 e^{i\theta_{st}},\end{aligned} \tag{2}$$

where $\boldsymbol{R}_s$ is the position vector of the site s, and β_{st}^0 is the transfer integral in the absence of the magnetic field. In the Hückel approximation for the conjugated hydrocarbons, β_{st}^0's are constant, β only for the adjacent r and s. We proceed in unit of $\beta=1$ without confusion. In the above

$$\theta_{st} = \frac{1}{2}(\boldsymbol{A}_s-\boldsymbol{A}_t)\cdot(\boldsymbol{R}_s+\boldsymbol{R}_t) \tag{3}$$

from which it is apparent that

$$\theta_{st} = -\theta_{ts}. \tag{4}$$

A little more calculation of θ_{st} is useful for the later investigations. Remebering that

$$\boldsymbol{A}_s = -\frac{1}{2}H\boldsymbol{R}_s\times\boldsymbol{n}, \tag{5}$$

when the magnetic field, $\boldsymbol{H}=H\boldsymbol{n}$ is constant along the z axis (see Fig. 1), we obtain

$$\begin{aligned}\theta_{st} &= \frac{1}{2}(\boldsymbol{A}_s-\boldsymbol{A}_t)\cdot(\boldsymbol{R}_s+\boldsymbol{R}_t) \\ &= -\frac{1}{4}H[(\boldsymbol{R}_s-\boldsymbol{R}_t)\times\boldsymbol{n}]\cdot(\boldsymbol{R}_s+\boldsymbol{R}_t) \\ &= \frac{1}{2}H\boldsymbol{n}\cdot(\boldsymbol{R}_s+\boldsymbol{R}_t) \\ &= \boldsymbol{S}_{st}.\end{aligned} \tag{6}$$

Here $\boldsymbol{S}_{st}$ is the signed area of the triangle formed by the origin and the bond s—t, and counted positive if $s\rightarrow t$ is right handed about the normal $\boldsymbol{n}$.

Then we have the Hückel Hamiltonian with magnetic field as

$$H = \sum_s |s\rangle\alpha_s\langle s| + \sum_{st} e^{i\theta_{st}}\beta_{st}^0|s\rangle\langle t|, \tag{7}$$

and then with abbreviations:

$$\alpha_s = \alpha = 0, \quad \beta_{st}^0 = \beta = 1, \quad e^{i\theta_{st}} = \omega_{st}, \tag{8}$$

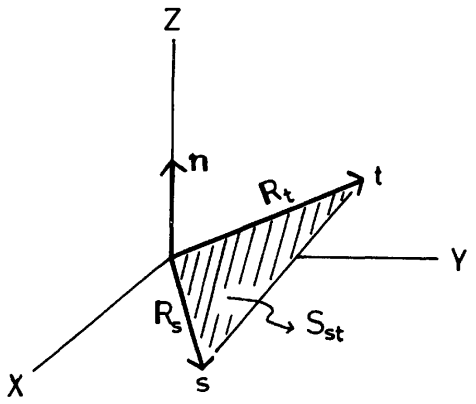

Fig. 1.

we can write, for example, for naphthalene, (see Fig. 4)

$$\begin{pmatrix} 0 & \omega_{12} & 0 & 0 & 0 & 0 & 0 & 0 & 0 & \omega_{1,10} \\ \omega_{21} & 0 & \omega_{23} & 0 & 0 & 0 & 0 & 0 & 0 & 0 \\ 0 & \omega_{32} & 0 & \omega_{34} & 0 & 0 & 0 & 0 & 0 & 0 \\ 0 & 0 & \omega_{43} & 0 & \omega_{45} & 0 & 0 & 0 & 0 & 0 \\ 0 & 0 & 0 & \omega_{54} & 0 & \omega_{56} & 0 & 0 & 0 & \omega_{5,10} \\ 0 & 0 & 0 & 0 & \omega_{65} & 0 & \omega_{67} & 0 & 0 & 0 \\ 0 & 0 & 0 & 0 & 0 & \omega_{76} & 0 & \omega_{78} & 0 & 0 \\ 0 & 0 & 0 & 0 & 0 & 0 & \omega_{87} & 0 & \omega_{89} & 0 \\ 0 & 0 & 0 & 0 & 0 & 0 & 0 & \omega_{98} & 0 & \omega_{9,10} \\ \omega_{10,1} & 0 & 0 & 0 & \omega_{10,5} & 0 & 0 & 0 & \omega_{10,9} & 0 \end{pmatrix} \tag{9}$$

Propagators

The propagators corresponding to the Hamiltonian in Eq. 7 are built similarly as the case without magnetic field.[6]

(i) The Edge of the Linear Chain Propagator. For the linear chain with n sites as numbered in Fig. 2a we have

$$\begin{aligned} {}^nG_0 &= {}^1G_0 + {}^1G_0 v_{01} {}^nG_{1\langle 0\rangle} v_{10} {}^nG_0 \\ &= {}^1G_0 + {}^1G_0 v_{01} {}^{n-1}G_0 v_{10} {}^nG_0, \end{aligned} \tag{10}$$

where ${}^nG_r$ is the $r-r$ matrix element of the matrix propagator for the n membered chain, and ${}^nG_{r\langle s\rangle}$ is one in the absence of the s site. Obviously

$${}^nG_0 = [({}^1G_0)^{-1} - v_{01} {}^{n-1}G_0 v_{10}]^{-1}. \tag{11}$$

Now we can understand that ${}^nG_0$ is independent of the magnetic field, because the phase factors of interaction terms arising from magnetic interactions cancel out with each other. Using abbreviations of Eq. 8 and changing variable as

$$z = 2\cos\theta, \tag{12}$$

we can obtain as before,[6]

$${}^nG_0 = \sin\theta / \sin(n+1)\theta, \tag{13}$$

(ii) The k-th Diagonal Element of the Linear Chain Propagator. In a similar way,

$${}^nG_k(\theta) = \frac{\sin(n-k)\theta \sin(k+1)\theta}{\sin(n+1)\theta \sin\theta}, \tag{14}$$

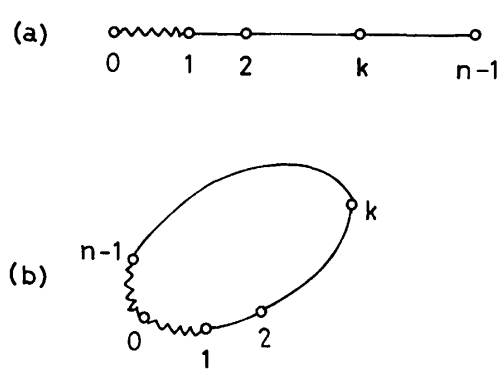

Fig. 2.

which also independent of the magnetic field.

(iii) The Off-diagonal Element of the Linear Chain Propagator. For simplicity, we deal with the three membered chain, a-b-c, and then obtain

$$\begin{aligned} {}^3G_{ac} &= {}^3G_a v_{ab} {}^3G_{b\langle a\rangle} v_{bc} {}^3G_{c\langle b\rangle} \\ &= \omega_{ab}\omega_{bc} {}^3G_{ac}^{(non)}, \end{aligned} \tag{15}$$

where ${}^3G_{ac}^{(non)}$ is the a—c matrix element of the 3-membered chain propagator in the absence of magnetic field. It is noted that in this case the propagator has a phase factor responsible to magnetic effect. In general,

$${}^nG_{k,k+l} = \omega_{k,k+1}\cdots\omega_{l-1,l} \frac{\sin(n-k-l)\theta \sin(k+1)\theta}{\sin(n+1)\theta \sin\theta}. \tag{16}$$

(iv) The Diagonal Element of the Ring Propagator. Observing Fig. 2b, we obtain

$$\begin{aligned} ({}^nR_0)^{-1} &= ({}^1G_0)^{-1} - v_{01} {}^nG_{1\langle 0\rangle} v_{10} - v_{0,n-1} {}^nG_{n-1\langle 0\rangle} v_{n-1,0} \\ &\quad - v_{01} {}^nG_{1,n-1\langle 0\rangle} v_{n-1,0} - v_{0,n-1} {}^nG_{n-1,1\langle 0\rangle} v_{n-1\text{-}0} \\ &= ({}^1G_0)^{-1} - 2^{n-1}G_0 - \omega_{01}\omega_{12}\cdots\omega_{n-1,0} {}^{n-1}G_{0,n-2}^{(non)} \\ &\quad - \omega_{0,n-1}\omega_{n-1,n-2}\cdots\omega_{10} {}^{n-1}G_{n-2,0}^{(non)}, \end{aligned} \tag{17}$$

where propagators appearing in the right-hand side are all non-magnetic. Noting that $\omega_{rs}=\omega_{sr}^*$, we get

$$\begin{aligned} ({}^nR_0)^{-1} &= ({}^1G_0)^{-1} - 2^{n-1}G_0 \\ &\quad - 2\cdot Re[\omega_{01}\omega_{12}\cdots\omega_{n-1,0}]^{n-1}G_{0,n-1}^{(non)} \\ &= 2\cos\theta - \frac{2\sin(n+1)\theta}{\sin\theta} - 2\cos HS \frac{\sin\theta}{\sin(n\theta)} \\ &= -\frac{4\sin\theta}{\sin n\theta} \sin(n\theta + HS/2)\cdot\sin(n\theta - HS/2). \end{aligned} \tag{18}$$

Here S is the area of ring counted positive, if the path goes round as $0\to1\to2\to\cdots\to n-1\to0$ in Fig. 2b.

(v) The Off-diagonal Element of the Ring Propagator. We devide ${}^nR_{ok}$ into two parts:

$${}^nR_{0k}^{(1)} + {}^nR_{0k}^{(2)}. \tag{19}$$

The former corresponds to the path with normal order, $0\to1\to2\cdots\to k$, while the latter to the reverse path $0\to n-1\to\cdots\to k$. Then we have

$$\begin{aligned} {}^nR_{0k}^{(1)} &= {}^nR_0 v_{01} {}^nG_{1k\langle 0\rangle} \\ &= {}^nR_0 {}^{n-1}G_{0,k-1}^{(non)} \omega_{01}\omega_{12}\cdots\omega_{k-1,k} \\ &= \frac{-\sin n\theta}{4\sin\theta\sin(n\theta+HS)/2\cdot\sin(n\theta-HS)/2} \\ &\quad \times \frac{\sin(n-k)\theta\sin\theta}{\sin n\theta\sin\theta} \omega_{01}\omega_{12}\cdots\omega_{k-1,k} \\ &= \frac{-\sin(n-k)\theta}{4\sin(n\theta+HS)/2\cdot\sin(n\theta-HS)/2} \cdot \omega_{01}\omega_{12}\cdots\omega_{k-1,k}, \end{aligned} \tag{20}$$

and similarly

$$\begin{aligned} {}^nR_{0k}^{(2)} &= \frac{-\sin k\theta}{4\sin\theta\sin(n\theta+HS)/2\cdot\sin(n\theta-HS)/2} \\ &\quad \times \omega_{k,k+1}^*\omega_{k+1,k+2}^*\cdots\omega_{n-2,n-1}^*\omega_{n-1,0}^*. \end{aligned} \tag{21}$$

Conclusively all the matrix elements of the ring propagator depend on magnetic field, while only the off-diagonal elements of the chain propagator does.

Energy

The total energies for various system will be calculated to estimate induced currents.

(i) Linear Chain with n *Sites and* n *Electrons.* The diagonal elements of this propagator in magnetic field are same as those of non magnetic case. Then the energy expression

$$E = \mathrm{Tr}\frac{1}{2\pi i}\int_c \mathrm{d}zzG(z) \tag{22}$$

leads to the same result as for the non-magnetic case. Namely

$$E = \sum_{k=0}^{n-1}\frac{-1}{\pi i}\int \mathrm{d}\theta \frac{\sin(n-k)\theta \sin(k+1)\theta \cos\theta}{\sin(n+1)\theta}$$
$$= 2\left[-1+\mathrm{cosec}\frac{\pi}{2(n+1)}\right]. \tag{23}$$

In the above, integration is carried out along the so-called Coulson contour mapped through the relation (12).[6,8] Poles of the first line of Eq. 23 are

$$\theta_r = \frac{\pi r}{n+1}, \quad r = \pm 1, \pm 2, \pm 3, \cdots, \pm n. \tag{24}$$

Among them poles up to $|n/2|$ are doubly occupied, which are enclosed by the contour. The integration above is assumed to include the spin sum.

(ii) Mono-ring with n *Sites and* N *Electrons.* Using Eq. 22, we obtain

$$E = \frac{n}{4\pi i}\int_c \mathrm{d}\theta \frac{\cos\theta \sin n\theta}{\sin(n\theta+HS/2)\cdot\sin(n\theta-HS/2)}. \tag{25}$$

Poles arising from the denominator are

$$\theta_r^+ = (2\pi r - HS)/n \text{ and } \theta_r^- = (2\pi r + HS)/n,$$
$$r = 0, \pm 1, \pm 2, \cdots, \pm(n/2-1), n/2 \tag{26}$$

in which ones up to $\pm n/4$ are occupied. Then calculations are straightforward:

$$E = \sum_\sigma \sum_r (-)^r\left[\frac{\cos(2\pi r-HS)/n\cdot\sin(2\pi r-HS)}{\sin(\pi r-HS)} + \frac{\cos(2\pi r+HS)/n\cdot\sin(2\pi r+HS)}{\sin(\pi r+HS)}\right]$$
$$= \sum_\sigma \sum_r \left(\cos\frac{2\pi r-HS}{n} + \cos\frac{2\pi r+HS}{n}\right)$$
$$= 2\sum_\sigma \sum_r \frac{\cos 2\pi r}{n}\frac{\cos HS}{n}, \tag{27}$$

where $\sum_\sigma$ indicates the spin sum which is carefully taken in the present case. In order to obtain Eq. 27 we have a useful relation

$$\sum_{r=1}^{k}\cos rx = \cos\frac{(k+1)x}{2}\sin\frac{kx}{2}/\sin\frac{x}{2} \tag{28}$$

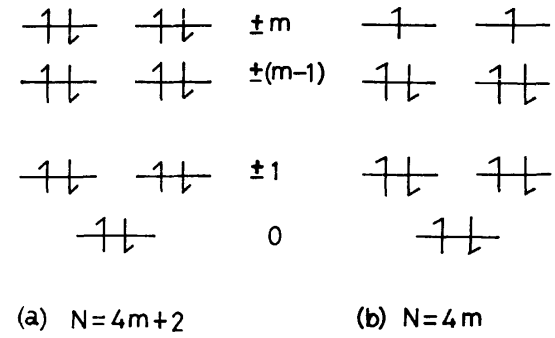

Fig. 3.

(a) The Closed System with N=4m+2 *Electrons:* In this case electrons occupy the levels as shown in Fig. 3a and then

$$\sum_\sigma \sum_{r=0}^{|m|}\cos\frac{2\pi r}{n} = 2\frac{\sin N\pi/2n}{\sin\pi/n}. \tag{29}$$

(b) The Open System with N=4m *Electrons:* Observing Fig. 3b, we get

$$\sum_\sigma \sum_{r=0}^{|m|}\cos\frac{2\pi r}{n} = 2\cos\frac{N\pi}{2n} + 2\frac{\sin(N-2)\pi/2}{\sin\pi/n} \tag{30}$$

Thus we have results; for the system with n sites and $4m+2$ electrons

$${}^nE_{4m+2} = 4\cos\frac{HS}{n}\cdot\frac{\sin N\pi/2n}{\sin\pi/n}, \tag{31}$$

and for the system with n sites ans $4m$ electrons

$${}^nE_{4m} = 4\cos\frac{HS}{n}\cdot\left(\cos\frac{N\pi}{2n} + \frac{\sin(N-2)\pi/2n}{\sin\pi/n}\right). \tag{32}$$

For special cases that number of sites is equal to that of electrons we have:

$${}^{4m+2}E_{4m+2} = 4\cos\frac{HS}{4m+2}\,\mathrm{cosec}\frac{\pi}{4m+2}, \tag{33}$$

$${}^{4m}E_{4m} = 4\cos\frac{HS}{4m}\cot\frac{\pi}{4m}. \tag{34}$$

Current

The ring current J is defined in terms of energy modified by magnetic field as follows.[7] The external field provokes an induced moment M opposing it and given by

$$M = -\frac{\delta E}{\delta H}, \tag{35}$$

or

$$M = \sum_k M_k = -\sum_k \frac{\delta E}{\delta f_k}\frac{\delta f_k}{\delta H}, \tag{36}$$

where

$$f_k = HS_k, \tag{37}$$

is the magnetic flux associated with the irreducible

circuit (ring). Our hypothesis is that the partial moment M_k of the k-th ring arises from an induced current J_k circulating around the ring and such that

$$M_k = \frac{1}{c} J_k S_k. \tag{38}$$

Therefore the current J_k is given by (recovering constant Φ_0)

$$J_k = -\frac{c}{\Phi_0}\frac{\delta E}{\delta f_k}. \tag{39}$$

It is needless to say that there is no current in the linear chain.

We want to apply Eq. 39 to various mono-ring compounds. For species corresponding to Eqs. 31 and 32

$${}^{n}J_{4m+2} = \frac{4\beta c}{n\Phi_0}\sin\frac{HS}{n\Phi_0}\frac{\sin N\pi/2n}{\sin \pi/n}, \tag{40}$$

$${}^{n}J_{4m} = \frac{4\beta c}{n\Phi_0}\sin\frac{HS}{n\Phi_0}\left(\cos\frac{N\pi}{2n} + \frac{\sin (N-2)\pi/2n}{\sin \pi/n}\right). \tag{41}$$

The area in the aboves is expressed by the use of the bond length d and the number of sites n as

$$S = \frac{nd^2}{4}\cot\frac{\pi}{n}. \tag{42}$$

At this stage it is instructive to make an order estimate of magnetic parameter such that for benzene $SH/\Phi_0 \sim 10^{-9}H$ which is very small even for $H \sim 10^4$ gauss. Accordingly it is good approximation that

$${}^{4m+2}J_{4m+2} = 4\beta\left(\frac{1}{4m+2}\right)^2\frac{cHS}{\Phi_0{}^2}\operatorname{cosec}\frac{\pi}{4m+2}, \tag{43}$$

$${}^{4m}J_{4m} = 4\beta\left(\frac{1}{4m}\right)^2\frac{cHS}{\Phi_0{}^2}\cot\frac{\pi}{4m}. \tag{44}$$

Next we calculate ${}^5J_6$, ${}^6J_6$, and ${}^7J_6$ which correspond to $C_5H_5^-$, C_6H_6, and $C_7H_7^+$, respectively. In the same approximation to obtain the previous results, we have

$$\begin{aligned} {}^5J_6 &= A\frac{\sin 6\pi/10}{\sin \pi/5} \fallingdotseq 1.6A, \\ {}^6J_6 &= A\frac{\sin 6\pi/12}{\sin \pi/5} = 2A, \\ {}^7J_6 &= A\frac{\sin 6\pi/14}{\sin \pi/5} \fallingdotseq 2.2A, \end{aligned} \tag{45}$$

with

$$A = \beta\frac{c}{\Phi_0{}^2}\frac{Hd^2}{4\pi}. \tag{46}$$

Hence ring currents increase significantly as number of sites increase although number of electrons remain constant.

Perturbation Treatment I

In the preceding section we have presented some examples in which propagators are obtained in a compact analytical form. Such a fortune can not be expected for more general or complicated systems. Hence a perturbation method will be preferable for the latter case. We are now going on as McWeeny has done.[4] In order to avoid the explicit use of the current density operator, we introduce a point dipole as a test body and evaluate the additional energy due to this effect and the effective magnetic field secondaly produced by the ring current. If a dipole moment $\boldsymbol{m}=m\boldsymbol{n}$ ($\boldsymbol{n}$ is the unit vector along z axis) is introduced at any point on the molecular plane, this point being chosen as origin, the vector potential at point r will be

$$A = -\frac{1}{2}H\boldsymbol{r}\times\boldsymbol{n} - m\frac{\boldsymbol{r}\times\boldsymbol{n}}{r^3}. \tag{47}$$

It is easily seen that Eq. 6 is replaced by

$$\begin{aligned} \theta_{st} &= S_{st}\left(H + \frac{m}{R_s^3} + \frac{m}{R_t^3}\right) \\ &= Ss_{st}\left(H + \frac{m}{\mathrm{d}^3}k_{st}\right), \end{aligned} \tag{48}$$

where areas are measured in unit of S, that of benzene ring, and distances are in unit of d, the C-C bond distance;

$$\begin{aligned} S_{st} &= Ss_{st}, \\ R_s &= r_s\mathrm{d}, \\ k_{st} &= \left(\frac{1}{r_s^3} + \frac{1}{r_t^3}\right). \end{aligned} \tag{49}$$

From the Hamiltonian in Eq. 7, we have a magnetic perturbation as

$$\begin{aligned} v &= \sum_{st}(e^{i\theta_{st}} - 1)|s\rangle\langle s| \\ &\fallingdotseq \sum_{st}\left(i\theta_{st} - \frac{1}{2}\theta_{st}^2\right)|s\rangle\langle s|. \end{aligned} \tag{50}$$

Here we have used the fact that $\theta_{st} \ll 1$, and note that v consists of the real and imaginary parts.

In general, if we wite the matrix element of v as

$$v_{rs} = v_{st}^0 + iv_{st}', \tag{51}$$

the energy change up to the second order of v is,[8]

$$\begin{aligned} \delta E = {} & 2\sum_{k<l} q_{kl}v_{kl}^0 \\ & + \sum_{k<l}\sum_{m<n}(v_{kl}^0\pi_{kl;mn}v_{mn}^0 + v_{kl}'\bar{\pi}_{kl;mn}v_{mn}'), \end{aligned} \tag{52}$$

where the bond order q_{rs} and the bond-bond polarizabilities $\pi_{kl;mn}$, $\bar{\pi}_{kl;mn}$ are given in terms of non-magnetic propagators as

$$q_{kl} = \frac{1}{2\pi\mathrm{i}}\int_c \mathrm{d}z\boldsymbol{G}_{kl}^0(z) \tag{53}$$

$$\pi_{kl;mn}(\bar{\pi}_{kl;mn}) = \frac{1}{2\pi\mathrm{i}}\int_c \mathrm{d}z(\boldsymbol{G}_{km}^0(z)\boldsymbol{G}_{nl}^0(z) \pm \boldsymbol{G}_{kn}^0(z)\boldsymbol{G}_{ml}^0(z)). \tag{54}$$

The above quantities are already been evaluated in analytic forms for simple species, linear chain and ring compounds.[8] However usual expressions in terms of LCAO coefficients are useful for more complicated molecules. It should be noted that if we use

$$G_{rs}(z) = \sum_i \frac{\langle r|i\rangle\langle i|s\rangle}{z-\varepsilon_i} \tag{55}$$

in Eqs. 53 and 54, we can easily obtain common expressions for them found in text-books.

$$q_{kl} = 2\sum_i^{\text{occ}} C_{ki}C_{li}^*, \tag{56}$$

$$\pi_{kl;mn}(\bar{\pi}_{kl;mn}) = 2\sum_i^{\text{occ}}\sum_j^{\text{un}} \frac{1}{\varepsilon_i-\varepsilon_j}(C_{ki}C_{mi}^*C_{lj}C_{mj}^* \pm C_{ki}C_{ni}^*C_{lj}C_{mj}^* + C_{kj}C_{mj}^*C_{li}C_{mi}^* \pm C_{kj}C_{nj}^*C_{li}C_{mi}^*). \tag{57}$$

Now the first order energy change $\delta E^{(1)}$ is

$$\begin{aligned}\delta E^{(1)} &= -\sum_{k<l} q_{kl}\theta_{kl}^2 \\ &= -\beta\left(\frac{S}{\Phi_0}\right)^2\sum_{k<l} q_{kl}s_{kl}^2\left[H^2+2H\left(\frac{m}{\mathrm{d}^3}\right)\times k_{kl}+\left(\frac{m}{\mathrm{d}^3}\right)^2 k_{kl}^2\right].\end{aligned} \tag{58}$$

The second order energy of which magnitude is same order to the first order one arises from the imaginary part of v, and then we obtain

$$\begin{aligned}\delta E^{(2)} &= \sum_{k<l}\sum_{m<n}\theta_{kl}\pi_{kl;mn}\theta_{mn} \\ &= \beta^2\left(\frac{S}{\Phi_0}\right)^2\sum_{k<l}\sum_{m<n}\bar{\pi}_{kl;mn}s_{kl}s_{mn}\left[H^2+\frac{mH}{\mathrm{d}^3}(k_{kl}+k_{mn})+\left(\frac{m}{\mathrm{d}^3}\right)^2 k_{kl}k_{mn}\right].\end{aligned} \tag{59}$$

The linear terms with respect to the test dipole m is needed to evaluate the effective field secondaly produced:

$$\begin{aligned}\delta E_{maq}(=-mH') &= \delta E_{maq}^{(1)} + \delta E_{maq}^{(2)} \\ &= -2\beta\left(\frac{S}{\Phi_0}\right)^2\frac{mH}{\mathrm{d}^3}(\sigma_1+\sigma_2),\end{aligned} \tag{60}$$

where σ_1 and σ_2 are dimensionless shielding constants:

$$\sigma_1 = \sum_{k<l} q_{kl}s_{kl}^2k_{kl}, \tag{61}$$

$$\sigma_2 = \sum_{k<l}\sum_{m<n}\beta\bar{\pi}_{kl;mn}s_{kl}s_{mn}\cdot\frac{1}{2}(k_{kl}+k_{mn}). \tag{62}$$

Thus we have completely reproduced the result obtained by McWeeny (see Eqs. (4,2) and (4,3) of Ref. 4).

Perturbation Treatment II

If we start with the transformed Hamiltonian given by McWeeny,[4] the procedure is much more simplified. McWeeny transformation is as follows: Introducing a new basis set,

$$\langle\bar{\chi}_a, \bar{\chi}_b, \bar{\chi}_c, \cdots| = \langle\chi_a, \chi_b, \chi_c, \cdots|U \tag{63}$$

where U is a diagonal matrix,

$$U = \mathrm{diag.}(1, \omega_{12}^*, \omega_{12}^*\omega_{23}^*, \cdots, \omega_{12}^*\omega_{23}^*\cdots\omega_{i-1,i}^*, \cdots). \tag{64}$$

Then we have a transformed Hamiltonian, $\tilde{H}=U^+HU$, or in details

$$\tilde{H}_{ij} = U_{ii}^*H_{ij}U_{jj}. \tag{65}$$

Remembering that $\omega_{ij}=\omega_{ji}^*$ and $|\omega_{ij}|=1$, we can see that H of naphthalene given in Eq. 9 is transformed to such that with all the near-diagonal ω's replaced by 1, say

$$\tilde{\omega}_{34} = \omega_{12}\omega_{23}\omega_{34}\omega_{12}^*\omega_{23}^*\omega_{34}^* = 1, \tag{66}$$

and

$$\tilde{\omega}_{10,1} = \omega_{12}\omega_{23}\cdots\omega_{9,10}\omega_{10,1} = e^{i\theta_{10\to1}}, \tag{67}$$

$$\tilde{\omega}_{10,5} = \omega_{12}\omega_{23}\cdots\omega_{9,10}\omega_{10,5}\omega_{12}^*\omega_{23}^*\cdots\omega_{45}^* = \omega_{56}\omega_{67}\cdots\omega_{9,10}\omega_{10,5} = e^{i\theta_{10\to5}}. \tag{68}$$

Thus we have

$$\tilde{H} = \begin{pmatrix} \cdot & 1 & \cdot & \cdot & \cdot & \cdot & \cdot & \cdot & \cdot & a \\ 1 & \cdot & 1 & \cdot & \cdot & \cdot & \cdot & \cdot & \cdot & \cdot \\ \cdot & 1 & \cdot & 1 & \cdot & \cdot & \cdot & \cdot & \cdot & \cdot \\ \cdot & \cdot & 1 & \cdot & 1 & \cdot & \cdot & \cdot & \cdot & \cdot \\ \cdot & \cdot & \cdot & 1 & \cdot & 1 & \cdot & \cdot & \cdot & b \\ \cdot & \cdot & \cdot & \cdot & 1 & \cdot & 1 & \cdot & \cdot & \cdot \\ \cdot & \cdot & \cdot & \cdot & \cdot & 1 & \cdot & 1 & \cdot & \cdot \\ \cdot & \cdot & \cdot & \cdot & \cdot & \cdot & 1 & \cdot & 1 & \cdot \\ \cdot & \cdot & \cdot & \cdot & \cdot & \cdot & \cdot & 1 & \cdot & 1 \\ a^* & \cdot & \cdot & \cdot & b^* & \cdot & \cdot & \cdot & 1 & \cdot \end{pmatrix}$$

$$= \begin{pmatrix} \cdot & 1 & \cdot & \cdot & \cdot & \cdot & \cdot & \cdot & \cdot & 1 \\ 1 & \cdot & 1 & \cdot & \cdot & \cdot & \cdot & \cdot & \cdot & \cdot \\ \cdot & 1 & \cdot & 1 & \cdot & \cdot & \cdot & \cdot & \cdot & \cdot \\ \cdot & \cdot & 1 & \cdot & 1 & \cdot & \cdot & \cdot & \cdot & \cdot \\ \cdot & \cdot & \cdot & 1 & \cdot & 1 & \cdot & \cdot & \cdot & 1 \\ \cdot & \cdot & \cdot & \cdot & 1 & \cdot & 1 & \cdot & \cdot & \cdot \\ \cdot & \cdot & \cdot & \cdot & \cdot & 1 & \cdot & 1 & \cdot & \cdot \\ \cdot & \cdot & \cdot & \cdot & \cdot & \cdot & 1 & \cdot & 1 & \cdot \\ \cdot & \cdot & \cdot & \cdot & \cdot & \cdot & \cdot & 1 & \cdot & 1 \\ 1 & \cdot & \cdot & \cdot & 1 & \cdot & \cdot & \cdot & 1 & \cdot \end{pmatrix}$$

$$+ \begin{pmatrix} \cdot & \cdot & \cdot & \cdot & \cdot & \cdot & \cdot & \cdot & \cdot & \bar{a} \\ \cdot & \cdot & \cdot & \cdot & \cdot & \cdot & \cdot & \cdot & \cdot & \cdot \\ \cdot & \cdot & \cdot & \cdot & \cdot & \cdot & \cdot & \cdot & \cdot & \cdot \\ \cdot & \cdot & \cdot & \cdot & \cdot & \cdot & \cdot & \cdot & \cdot & \cdot \\ \cdot & \cdot & \cdot & \cdot & \cdot & \cdot & \cdot & \cdot & \cdot & \cdot \\ \cdot & \cdot & \cdot & \cdot & \cdot & \cdot & \cdot & \cdot & \cdot & \bar{b} \\ \cdot & \cdot & \cdot & \cdot & \cdot & \cdot & \cdot & \cdot & \cdot & \cdot \\ \cdot & \cdot & \cdot & \cdot & \cdot & \cdot & \cdot & \cdot & \cdot & \cdot \\ \cdot & \cdot & \cdot & \cdot & \cdot & \cdot & \cdot & \cdot & \cdot & \cdot \\ \bar{a}^* & \cdot & \cdot & \cdot & \bar{b}^* & \cdot & \cdot & \cdot & \cdot & \cdot \end{pmatrix} \tag{69}$$

where

$$a = \omega_{1,10},\quad b=\omega_{5,10},\quad \bar{a}=1-a,\quad \bar{b}=1-b \tag{70}$$

The transformed Hamiltonian is thus written as

$$H = H_0 + v, \tag{71}$$

however, v has non-vanishing matrix elements only at bonds which complete circuits. In the case of naphthalene, if we draw the path seen in Fig. 4a, the bonds, 10→1 and 10→5 complete the naphthalene and benzene rings, respectively. The arrow showing enclosing direction suggests the sign of the ring area (see Eqs. 67 and 68).

The energy change due to magnetic interaction is

$$\begin{aligned}\delta E &= \mathrm{Tr}\frac{1}{2\pi \mathrm{i}}\int_c \mathrm{d}z z(\boldsymbol{G}(z)-\boldsymbol{G}^0(z)) \\ &= \mathrm{Tr}\frac{1}{2\pi \mathrm{i}}\int_c \mathrm{d}z z(\tilde{\boldsymbol{G}}(z)-\boldsymbol{G}^0(z)).\end{aligned} \tag{72}$$

In the above it is legitimate to replace $\boldsymbol{G}$ by $\tilde{\boldsymbol{G}}$ inside Tr.

The propagator $\tilde{\boldsymbol{G}}$ is given, by virtue of Eq. 71, as

$$\begin{aligned}\tilde{\boldsymbol{G}} &= \frac{1}{z-\boldsymbol{H}} = \frac{1}{z-\boldsymbol{H}_0-\boldsymbol{v}} \\ &= \frac{1}{z-\boldsymbol{H}_0} + \frac{1}{z-\boldsymbol{H}_0}\boldsymbol{v}\frac{1}{z-\boldsymbol{H}_0} \\ &\quad + \frac{1}{z-\boldsymbol{H}_0}\boldsymbol{v}\frac{1}{z-\boldsymbol{H}_0}\boldsymbol{v}\frac{1}{z-\boldsymbol{H}_0} + \cdots \\ &= \boldsymbol{G}^0 + \boldsymbol{G}^0\boldsymbol{v}\boldsymbol{G}^0 + \boldsymbol{G}^0\boldsymbol{v}\boldsymbol{G}^0\boldsymbol{v}\boldsymbol{G}^0 + \cdots\end{aligned} \tag{73}$$

Substituting this into Eq. 71 we can easily obtain, as has been done in the previous section, as

$$\begin{aligned}\delta E &= \mathrm{Tr}\frac{1}{2\pi \mathrm{i}}\int_c \mathrm{d}z\left(\boldsymbol{G}^0\boldsymbol{v} + \frac{1}{2}\boldsymbol{G}^0\boldsymbol{v}\boldsymbol{G}^0\boldsymbol{v}\right) \\ &= 2\sum_{m>n} q_{mn}v^0_{mn} + \sum_{m>n}\sum_{k>l} v'_{mn}\bar{\pi}_{mn;kl}v'_{kl},\end{aligned} \tag{74}$$

where v^0_{mn} and v'_{mn} are respectively the real and imaginary parts of v_{mn}, which is precisely

$$v_{mn} \doteqdot \beta\left(i\theta_{m\to n} - \frac{1}{2}\theta^2_{m\to n}\right), \tag{75}$$

with

$$\theta_{m\to n} = \frac{S}{\Phi_0}\left(s_{m\to n}H + \frac{m}{\mathrm{d}^3}\kappa_{m\to n}\right) \tag{76a}$$

and

$$\begin{aligned}s_{m\to n} &= s_{n,n+1} + s_{n+1,n+2} + \cdots s_{m-1,m} + s_{mn}, \\ \kappa_{m\to n} &= s_{n,n+1}k_{n,n+1} + s_{n+1,n+2}k_{n+1,n+2} + \cdots \\ &\quad + s_{mn}k_{mn}.\end{aligned} \tag{76b}$$

Namely, $s_{m\to n}$ is the area surrounded by the circle which goes round $n\to n+1\to\cdots\to m\to n$, and $\kappa_{m\to n}$ is understood similarly.

Using aboves in Eq. 74, we obtain

$$\delta E^{(1)} = -\beta\left(\frac{S}{\Phi_0}\right)^2\sum_{m>n} q_{mn}\left(Hs_{m\to n} + \frac{m}{\mathrm{d}^3}\kappa_{m\to n}\right)^2, \tag{77}$$

$$\delta E^{(2)} = \beta^2\left(\frac{S}{\Phi_0}\right)^2\sum_{m>n}\sum_{k>l}\bar{\pi}_{mn;kl}\left(HS_{m\to n} + \frac{m}{\mathrm{d}^3}\kappa_{m\to n}\right) \times\left(Hs_{k\to l} + \frac{m}{\mathrm{d}^3}\kappa_{k\to l}\right). \tag{78}$$

The linear terms with respect to m in Eqs. 77 and 78 yield

$$\begin{aligned}\delta E &= (-mH') = \delta E^{(1)}_{\mathrm{mag}} + \delta E^{(2)}_{\mathrm{mag}} \\ &= -2\beta\left(\frac{S}{\Phi_0}\right)^2\frac{m}{\mathrm{d}^3}(\sigma_1+\sigma_2),\end{aligned} \tag{79}$$

where

$$\begin{aligned}\sigma_1 &= \sum_{m,n} q_{mn}s_{m\to n}\kappa_{m\to n}, \\ \sigma_2 &= \sum_{m>n}\sum_{k>l}\beta\bar{\pi}_{mn;kl}\frac{1}{2}(s_{m\to n}\kappa_{k\to l} + s_{k\to l}\kappa_{m\to n}).\end{aligned} \tag{80}$$

In this treatment the summation is restricted to the bonds which complete circuits. Also note that $\bar{\pi}_{mn;kl}$ is given in unit of $1/\beta$. Eq. 79 gives the same result with that of the previous section, but with more transparent physical image.

Illustrative Examples

A few examples will be presented in order to faciliate understanding of the preceding treatment.

(1) Benzene. This is the case of one ring, and calculation becomes trivially simple. Go round the ring along the positive direction and the circuite is completed by the bond 6→1, then we have; $s_{6\to 1}=1$ and $\kappa_{61}=s_{12}k_{12}+s_{23}k_{23}+\cdots+s_{61}k_{61}$. Thus $\sigma_1=2/3\cdot\kappa_{1\to 6}$ and $\sigma_2=-5/9\cdot\kappa_{1\to 6}$. The secondary induced field at the test dipole is written as

$$H' = 2\beta\left(\frac{S}{\Phi_0}\right)^2\frac{H}{\mathrm{d}^3}\frac{1}{9}\kappa_{6\to 1}. \tag{81}$$

Further discussion is refered to Ref. 4.

(2) Naphthalene. It should be instructive to calculate in two alternative ways based on Fig. 4a and 4b. One of the purposes of the present example is that, as has been done intuitively, the whole effect of the (naphthalene) ring current is attributed to those of individual, constituent benzene rings.

(a) Bonds 10→5 and 10→1 together complete a positive circuite with $s_{10\to 5}=1$ and $s_{10\to 1}=2$. $\kappa_{10\to 5}$ is occuring

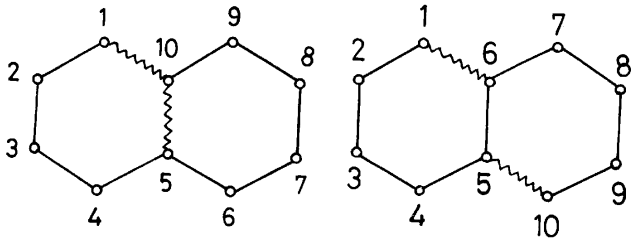

Fig. 4.

in the right hand side benzene ring, named R (while the left hand ring is called L). Then, if we write $\kappa_{10\to 1}=\kappa_R$, it should be that $\kappa_{10\to 1}=\kappa_R+\kappa_L$. Thus we obtain

$$\begin{aligned}\sigma_1 &= q_{1,10}(\kappa_R+\kappa_L) + q_{5,10}\kappa_L \\ &= 1.1094\kappa_R + 1.16277\kappa_L \end{aligned} \quad (82)$$

$$\begin{aligned}\sigma_2 &= -[\bar{\pi}_{5,10;5,10}\kappa_L + 2\bar{\pi}_{1,10;1,10}(\kappa_R+\kappa_L) \\ &\quad + \bar{\pi}_{5,10;1,10}(\kappa_R+3\kappa_L)] \\ &= -0.9880\kappa_R - 1.5063\kappa_L, \end{aligned} \quad (83)$$

where $\bar{\pi}$'s are in unit β. It should be stressed that as shown in Fig. 4, if we begin with drawing a path numbered there, circuits concerning with magnetic interaction are identically determined. In this respective, we call these circuits irreducible ones.

(b) The bonds 6→1 and 10→5 complete, respectively, the positive and negative circuits with $s_{6\to 1}=1$ and $s_{10\to 5}=-1$. Therefore noting that $\kappa_{6\to 1}=\kappa_R$ and $\kappa_{10\to 5}=-\kappa_L$, we obtain

$$\begin{aligned}\sigma_1 &= q_{16}(\kappa_R+\kappa_L) \\ &= 0.5547(\kappa_R+\kappa_L), \end{aligned} \quad (84)$$

and

$$\begin{aligned}\sigma_2 &= \bar{\pi}_{1,6;1,6}\kappa_R + \bar{\pi}_{5,10;5,10}\kappa_L + \kappa_{1,6;5,10}(\kappa_R+\kappa_L) \\ &= -0.4333(\kappa_R+\kappa_L), \end{aligned} \quad (85)$$

by the use of $\bar{\pi}_{1,6;1,6}=\bar{\pi}_{5,10;5,10}=-0.4660$ and $\pi_{1,6;5,10}=-0.0327$.

The both calculations (a) and (b) result in the same value,

$$\sigma_1 + \sigma_2 = 0.1214(\kappa_R+\kappa_L), \quad (86)$$

which tells us the invariant character, independent of choice of the original path. Finally we note that $-\kappa_p\to 1/r^3$ at large distance and each ring behaves like an induced dipole.

Conclusion

As has been seen in the previous sections, the propagator theory works well and easily reproduces the current results. One may say that it yields nothing new beyond traditional methods, but we insist that, by this way, the analysis is very much simplified, physical processes involved are made clearer, and the method itself is considerably general, even for the complicated phenomena.

References

1) L. Pauling, *J. Chem. Phys.*, **4**, 673 (1936).
2) F. London, *J. Phys. Radium*, **8**, 397 (1936).
3) J. A. Pople, *Mol. Phys.*, **1**, 175 (1958).
4) R. McWeeny, *Mol. Phys.*, **1**, 311 (1958).
5) J. Aihara, *J. Am. Chem. Soc.*, **101**, 5913 (1979); 103, 5704 (1981).
6) S. Aono and K. Nishikawa, *Bull. Chem. Soc. Jpn.*, **53**, 3418 (1980); S. Aono, T. Ohmae, and K. Nishikawa, *Bull. Chem. Soc. Jpn.*, **54**, 1645 (1981); K. Nishikawa, M. Yamamoto, and S. Aono, *J. Chem. Phys.*, **78**, 5031 (1983).
7) L. Salem, The Molecular Orbital Theory of Conjugated System, p 189 (Benjamin, 1966).
8) S. Aono and K. Nishikawa, previous paper.

A New Aspect on the Origin of an Anomalous Substituent Effect on the Azomethine Proton Chemical Shifts in 4-Substituted *N*-Benzylideneanilines

Ryoichi AKABA, Hirochika SAKURAGI, and Katsumi TOKUMARU*
Department of Chemistry, University of Tsukuba, Sakura-mura, Ibaraki 305
(Received July 14, 1984)

Carbon-13 chemical shifts, azomethine proton chemical shifts, and azomethine carbon–hydrogen coupling constants have been determined for *N*-benzylideneaniline and its several derivatives bearing *o*-methyl and/or *p*-nitro groups on the aromatic ring on the nitrogen atom (ring A). The anomalous upfield shift of the azomethine proton caused by introduction of a 4-nitro group on the ring A can be attributed to the increase in the twist angle θ_N of the ring A from the molecular plane containing the C=N bond.

Molecular conformations of *N*-benzylideneanilines have been studied by many workers,[1] and in previous papers, the present authors have shown that introduction of a 4-nitro group as well as 2,6-dimethyl groups increases the twist angle θ_N (formula shown below) in solution by UV spectroscopy,[1] and in gas phase by photoelectron spectroscopy.[2]

Concerning NMR of *N*-benzylideneanilines, one of the present authors reported with collabolators an anomalous substituent effect on the azomethine proton (H_7) chemical shifts for a series of 4-substituted *N*-benzylideneanilines, $C_6H_5CH{=}NC_6H_4$-X-4, in which with the increase in electron-withdrawing property of the 4-substituents H_7 exhibited an unexpected upfield shift (ρ=+0.04) whereas for a series of 4'-substituted *N*-benzylideneanilines, 4-Y-$C_6H_4CH{=}NC_6H_5$, H_7 exhibited a normal downfield shift (ρ=−0.16) with the increase in the electron-withdrawing property of the substituents.[3] The origin of this anomalous substituent effect has been argued,[4–9] for example, in terms of a through-space field effect,[3,5,6] but still remains puzzling.

We now wish to propose that this anomalous substituent effect originates primarily from the change of molecular conformation with the substituent as previously shown by UV[1] and photoelectron spectroscopy.[2] The present proposition is based on consideration that the introduction of an electron-withdrawing nitro group on the C-4 position of the anilino benzene ring (ring A) enhances delocalization of lone-pair electrons on the nitrogen atom into the ring A accompanied by an increase in the twist angle θ_N in solution, which leads to changes of the ring current effect by the ring A exerted on H_7, resulting in the anomalous upfield shift of its chemical shift.

Results and Discussion

The following six *N*-benzylideneanilines **1**—**6** have been examined for their carbon-13 chemical shifts, H_7 chemical shifts, and azomethine carbon (C_7)-hydrogen coupling constants. The results are summarized in Table 1, and schematically illustrated for the selected quantities in Fig. 1.

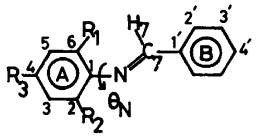

1; $R_1=R_2=R_3=H$
2; $R_1=H$, $R_2=CH_3$, $R_3=H$
3; $R_1=R_2=CH_3$, $R_3=H$
4: $R_1=R_2=H$, $R_3=NO_2$
5; $R_1=H$, $R_2=CH_3$, $R_3=NO_2$
6; $R_1=R_2=CH_3$, $R_3=NO_2$

Figure 1 indicates that on successive introduction of methyl groups on 2- and 2,6-positions of **1**, the chemical shift of C_7 shows an upfield shift from **1** to **2** by

TABLE 1. CHEMICAL SHIFTS FOR ^{13}C'S AND AZOMETHINE PROTONS ($CDCl_3$, ppm FROM TMS) AND AZOMETHINE CARBON-HYDROGEN COUPLING CONSTANTS ($CDCl_3$, Hz) FOR *N*-BENZYLIDENEANILINES **1**—**6**

Compound No.	C_1	C_2	C_3	C_4	C_5	C_6	$C_{1'}$	$C_{2'}$	$C_{3'}$	$C_{4'}$	C_7	H_7	$J(^{13}C\text{-}H)$
1	151.95	120.76	128.97	125.79	128.97	120.76	136.11	128.68	128.58	131.17	160.07	8.49	157.3[a]
2	150.92	131.71	130.97	125.50	126.58	117.44	136.36	128.53	128.53	130.97	159.00	8.40	158.5
3	151.12	126.87	127.95	123.60	127.95	126.87	136.01	128.63	128.34	131.27	162.37	8.25	159.6
4	157.82	121.15	124.87	145.50	124.87	121.15	135.53	129.97	128.88	132.25	162.46	8.46	158.6[a]
5	156.84	132.59	125.26	145.11	122.57	118.17	135.53	129.12	128.82	132.15	161.39	8.37	159.3
6	156.89	128.09	123.25	143.49	123.25	128.09	135.14	128.88	128.73	132.20	162.76	8.23	160.3

a) Ref. 3.

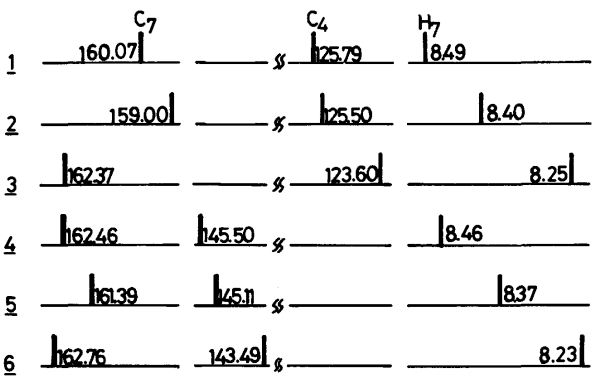

Fig. 1. Schematic illustration of the chemical shifts for C_4, C_7, and H_7 ($CDCl_3$, ppm downfield from TMS).

1.07 ppm, then a remarkable downfield shift from **2** to **3** by 3.37 ppm, C_7 of *3* resonating at much lower field than that of **1**. The chemical shift of C_4, as has already been reported by Kobayashi's group,[10] shows a slight upfield shift from **1** to **2** by 0.29 ppm, then a larger upfield shift from **2** to **3** by 1.90 ppm. The upfield shifts of C_4 and C_7 from **1** to **2** can be understood in terms of an inductive effect of the methyl group. However, the remarkable downfield shift of C_7 and the larger upfield shift of C_4 between **1** and **3** cannot be explained simply in terms of the inductive effect of the two methyl groups. These changes observed between **1** and **3** can be reasonably interpreted in terms that the introduction of the bulky 2,6-dimethyl groups forces the ring A to be highly twisted from the imino molecular plane. This distortion will cause the nitrogen lone pair to interact effectively with the aromatic π-system (n-π conjugation) to increase the electron density on C_4 leading to its upfield shift, as proposed previously.[11] The *N*-lone pair delocalization will succesively lead to the shift of electrons on C_7 to the nitrogen atom to decrease the electron density on C_7. The effect of the decrease in electron density on C_7 caused by the *N*-lone pair delocalization is predominant to the inductive effects of the two methyl groups finally giving the downfield shift of the C_7 chemical shift. The downfield shift of C_7 from **1** to **3** could also be explained in terms of a decrease of π-π conjugation throughout the π-system accompanied by the increase of the n-π conjugation. For example, β-vinyl carbon of 2,6-dimethylstyrene is reported to resonate at 6.2 ppm lower field than that of styrene, and this lower field shift was explained in terms of steric inhibition of resonance between the vinyl group and the phenyl group.[12] By analogy, the decrease of the π-π conjugation from **1** to **3** by the 2,6-dimethyl substitution may also cause a lowfield shift of C_7, which is in the same direction as predicted by the consideration on the increase of the n-π conjugation.

The above explanation that the twisting of the ring A from the molecular plane induces the significant lowfield shift of the C_7 carbon is supported by ^{13}C-H coupling constants. It is well known that the carbon-hydrogen coupling constant depends on the s character of the C-H bond,[13] and the larger s character is caused by the decrease of π electron density on the carbon atom. The ^{13}C-H coupling constant is increased from 157.3 (Hz) from **1** to 158.5 for **2**, then to 159.6 for **3**, which indicates that on successive introduction of the *o*-methyl groups on **1** the C_7-H bond increases in the s character possibly through the decrease in the π electron density on C_7.

On introduction of a 4-nitro group in **1**, C_7 exhibits a downfield shift by 2.39 ppm from **1** to **4**, which is of the same magnitude as observed between **1** and **3** with 2,6-dimethyl groups. However, 2,6-dimethyl substitution on **4**, in constrast with the effect on **1**, causes a very slight downfield shift of C_7 by only 0.30 ppm from **4** to **6**. These results suggest that the ring A of **4**, in spite of the absence of *o*-methyl groups, may be appreciably twisted like that of **3** in which the ring A is forced to be twisted by the effect of the *o*-methyl groups. The chemical shift of C_4 shows an upfield shift from **4** to **5** and to **6**, and the ^{13}C-H coupling constant for **4** is almost the same as for **2**, and then succssively increases on introduction of the *o*-methyl groups. These results suggest that, as in series of **1**, **2**, and **3**, the successive introduction of the *o*-methyl groups increases the twist angle θ_N accompanied by the decrease in the π electron density on C_7.

Concerning the H_7 chemical shifts, introduction of a nitro group on the C_4 position of each of **1**, **2**, and **3** anomalously shifts the H_7 chemical shifts to higher field by 0.02—0.03 ppm which is reproducible and beyond the experimental error. As to methyl substitution on **1** and **4**, monomethyl substitution of their 2-positions causes an upfield shift by 0.09 ppm, but further substitution by the second methyl group at their 6-positions results in a larger upfield shift by 0.14—0.15 ppm. Thus, the effect of the methyl group is not additive, which suggests that the larger upfield shift by the second methyl substitution might be due to the further distortion of the ring A by its introduction as well as its inductive effect. The increase in the twist angle θ_N by the successive methyl substitution will reduce the paramagnetic deshielding effect of the ring A exerted on H_7 resulting in its upfield shift. This view is further supported by a simple calculation of the chemical shift using McConnel's equation.[14] For example, when the unsusbtituted benzene ring (ring A) increases in the twist angle θ_N from 45° to 90°, H_7 can be estimated to resonate at a higher field of about 0.20 ppm.[15] These results coupled with the carbon-13 chemical shifts and the ^{13}C-H coupling constants suggest that the observed anomalous upfield shifts caused by the introduction of the 4-nitro group on **1**, **2**, and **3** could be attributed to the increase in the twist angle θ_N of the ring A from the molecular plane contaning C=N group.

Thus, introduction of the electron-withdrawing nitro group at the C_4 position of the ring A enhances the delocalization of the nitrogen lone pair electrons into the ring A, through so called n-π conjugation, accompanied by the increase in the twist angle θ_N which in turn reduces the paramagnetic deshielding effect of the ring A on H_7 finally resulting in its upfield shift. The observed values for the anomalous upfield shifts remain to be slight. This can be understood by partial cancelling of the upfield shift of H_7 by the twisting of the ring A, because the introduction of the 4-nitro group causes the decrease in electron density of C_7 which would lead to the downfield shift of H_7.

The above estimation that the 4-nitro group enhances the twist angle θ_N in solution is supported by our recent results by UV[1] and photoelectron spectroscopy[2] which indicates that the 4-nitro derivative **4** may be more twisted than **1** in solution and in gas phase, respectively. Also in view of the recent report by UV spectroscopy that the introduction of an electron-donating 4-dimethylamino group on **1** leads to reduction of the twist angle θ_N,[16] it is reasonable to consider that the introduction of an electron-withdrawing 4-nitro group tends to increase the twist angle θ_N.

Finally, it is worth noting that the present study shows that apparent substituent effects in NMR may arise from the changes of molecular conformations with substituents as well as from the electronic effects of the substituents.

Experimental

Materials. Preparations and characterizations of **1**—**6** are already reported.[1]

Spectral Measurements. *Carbon-13 NMR Spectra*: Carbon-13 NMR spectra were measured at room temperature (probe temperature 27 °C) on a JEOL FX-60 spectrometer operating in the Fourier transform mode with complete proton decoupling. The spectra were generally recorded at a pulse width of 4 μs, a pulse flip angle of 45°, and a repetition time of 5 s using $CDCl_3$ as a solvent. In some cases, single-frequency off-resonance decoupled spectra were also measured. Sample concentrations were usually 1 mol/dm³ in $CDCl_3$ solutions. Digital resolution was 0.74 Hz/point. Observed chemical shifts are reported in ppm downfield from internal tetramethylsilane.

Chemical shifts of the substituents (methyl group), which are not listed in the Table 1 are as follows; **2**: 17.79 (ppm), **3**: 18.23, **5**: 17.94, **6**: 18.33.

^1H-NMR Spectra: Azomethine proton chemical shifts were taken from a JEOL MH-100 spectrometer at room temperature in the external lock mode using $CDCl_3$ as a solvent and tetramethylsilane as an internal reference. We first examined the dilution shift for **4** as an example. The chemical shifts were as follows: 0.23 mol/dm³; 845.3 (Hz), 0.10 mol/dm³; 845.5, 0.08 mol/dm³; 845.6, 0.03 mol/dm³; 845.4. Thus, no dilution shifts were observed which allowed us to measure the chemical shifts for other componds in one concentration below *ca.* 0.1 mol/dm³. The chemical shifts listed in the Table 1 are those measured in the following concentrations: **1**: 0.10 (mol/dm³), **2**: 0.14, **3**: 0.11, **4**: 0.10, **5**: 0.09, **6**: 0.08.

Azomethine Carbon-Hydrogen Coupling Constants: The ^{13}C–H coupling constants were taken from a JEOL FX-60 or a Varian XL-100 spectrometer in $CDCl_3$ solutions by the gated decoupling technique combined with NOE mode.

References

1) R. Akaba, K. Tokumaru, and T. Kobayashi, *Bull. Chem. Soc. Jpn.*, **53**, 1993 (1980), and references cited therein.

2) R. Akaba, K. Tokumaru, T. Kobayashi, and C. Utsunomiya, *Bull. Chem. Soc. Jpn.*, **53**, 2002 (1980).

3) N. Inamoto, K. Kushida, S. Masuda, H. Ohta, S. Satoh, Y. Tamura, K. Tokumaru, K. Tori, and M. Yoshida, *Tetrahedron Lett.*, **1974**, 3617.

4) N. Inamoto, S. Masuda, K. Tokumaru, M. Yoshida, Y. Tamura, and K. Tori, *Tetrahedron Lett.*, **1975**, 3697.

5) N. Inamoto, S. Masuda, K. Tokumaru, K. Tori, and M. Yoshida, *Tetrahedron Lett.*, **1974**, 3701.

6) J. S. Sandhu, D. Mago, and B. J. Wakefield, *Tetrahedron Lett.*, **1975**, 1091.

7) A. S. Al-Tai, D. M. Hall,.and A. R. Mears, *J. Chem. Soc., Perkin Trans. 2*, **1976**, 133.

8) D. Mago, J. S. Sandhu, and B. J. Wakefield, *J. Chem. Soc., Perkin Trans. 2*, **1977**, 715.

9) M. Holík, J. Běluša, and B. Břicháček, *Collect. Czech. Chem. Commum.*, **43**, 610 (1978).

10) ^{13}C-NMR of **1**, **2**, and **3** have been reported by Yoshida, Minato, and Kobayashi, and the discussion has been made solely on the effect of ortho-methyl susbtitution on the C_4 chemical shifts.[11] These compounds have been reexamined for ^{13}C-NMR in an attepmt to get all data under the same conditions for the present purpose.

11) M. Yoshida, H. Minato, and M. Kobayashi, *Chem. Lett.*, **1976**, 1097.

12) K. S. Dahmi and J. B. Stothers, *Can. J. Chem.*, **43**, 510 (1965).

13) a) C. H. Yoder, R. H. Tuck, and R. E. Hess, *J. Am. Chem. Soc.*, **91**, 539 (1969); b) C. H. Yoder, C. D. Schaeffer, Jr., and R. E. Hess, *J. Chem. Eng. Data*, **17**, 385 (1972); c) N. Inamoto, S. Masuda, A. Terui, and K. Tori, *Chem. Lett.*, **1972**, 107.

14) H. McConnel, *J. Chem. Phys.*, **27**, 226 (1957).

15) The following bond distances were assumed for the calculation. C_7–H: 1.09 Å, C_7=N: 1.24, N–C_1: 1.46, C_1–C_2: 1.38, C_2–C_3: 1.40. All bond angles were assumed to be 120°.

16) J. Steiger and H. Zollinger, *Helv. Chim. Acta*, **58**, 800 (1975).

A Method for Determining Absolute Configuration of Cycloalkanamines and Related Compounds by CD Spectra of Their 2,4-Dinitrophenyl Derivatives

Masao KAWAI,* Teruhiko IWASE, Yasuo BUTSUGAN, and Ukon NAGAI†
Department of Synthetic Chemistry, Nagoya Institute of Technology, Showa-ku, Nagoya 466
†*Mitsubishi-Kasei Institute of Life Sciences, Minamiooya 11, Machida, Tokyo 194*
(Received July 16, 1984)

N-(2,4-Dinitrophenyl) derivatives of cycloalkanamines and related compounds having an amino and an aromatic groups in vicinal positions were prepared. Their CD spectra exhibited marked Cotton effect around 400 nm, the sign of which was shown to coincide with the chirality between the two chromophore-bearing bonds. This relation, as a special example of exciton chirality method, is useful for determining absolute configuration of cyclic compounds having a primary amino group.

Chiroptical properties of 2,4-dinitrophenyl (Dnp) derivatives of α-amino acids and related compounds have been investigated extensively.[1-10] Rules have been found which correlate the absolute configuration and the sign of the Cotton effect of the Dnp derivatives of chiral diamines,[1] arylalkylamines,[5] and cyclic secondary amines.[3] Dnp derivatives of L-α-amino acids with aromatic side chain (**1a**) exhibit characteristic CD spectra with negative Cotton effect around 400 nm.[2,5] Further study upon the related compounds led us to the proposal of Dnp-aromatic rule, which predicts negative and positive sign of $[\theta]_{\sim 400}$ value for the arylalkylamines of general formulas **2** and **2'**, respectively.[5] Based on ^{1}H NMR study and theoretical calculation of rotational strength it was concluded that staggered conformer **1b** is responsible for the negative Cotton effect around 400 nm of **1a**.[9] The conformer **1b**, designated as g^-, is characterized by the negative bond chirality between the C^α–NHDnp and C^β–Ar bonds. The present paper deals with CD spectra of carbocyclic analogs of **1a** in which the two chromophoric groups are conformationally fixed to have the same bond chirality as in **1b**. Theoretically, the chirality between electric dipole moments is the essential factor as discussed later. However, bond chirality is more familiar to organic chemists. So, "bond chirality" will be used throughout this paper as the reasonable and convenient approximation.

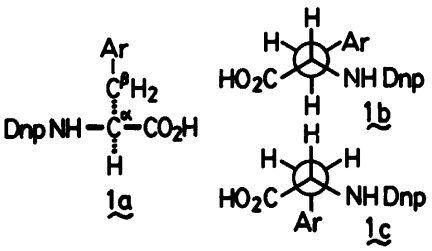

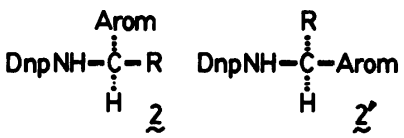

Arom : Achiral group which contains an aromatic chromophore

R : Nonaromatic group

Dnp derivatives of 2-substituted cyclohexanamines **3**—**6** were synthesized. Since the compounds **3**—**6** are considered to take stable chair conformation **7** with two bulky groups (DnpNH and Ar) in equatorial orientation, all of these Dnp derivatives **3**—**6** possess negative bond chirality between C–NHDnp and C–Ar bonds. CD spectra of **3**—**6** recorded in methanol solutions were reproduced in Fig. 1. As expected from theoretical consideration[9] all of these compounds exhibited marked negative Cotton effect around 400 nm. The conformationally fixed Dnp derivatives **3**, **4**, and **5** correspond to the staggered g^- conformers of Dnp derivatives of L-phenylalanine (**1a**, Ar=C_6H_5: $[\theta]_{410}$ −9100),[5] L-aspartic acid β-*p*-nitroanilide (**1a**, Ar=$CONHC_6H_4NO_2(p)$: $[\theta]_{400}$ −9200),[5] and *O*-benzoyl-L-serine (**1a**, Ar=$OCOC_6H_5$: $[\theta]_{408}$ −3400),[5] respectively. The magnitude of Cotton effect around 400 nm of **3**, **4**, and **5** were shown to be 2—3 times as large as the corresponding Dnp amino acids having conformational freedom, which supported the assumption that the staggered conformer g^- of Dnp derivatives of aromatic L-α-amino acids **1a** is responsible for their characteristic negative Cotton effect

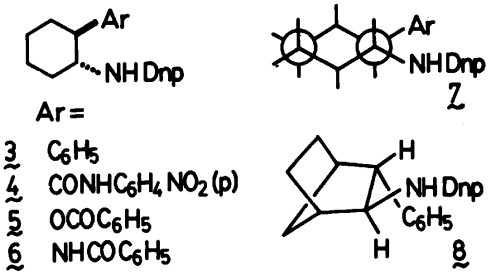

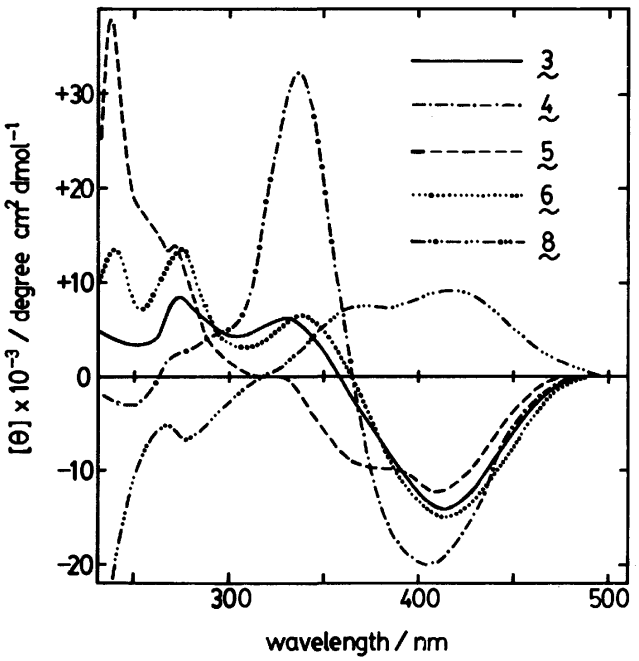

Fig. 1. CD spectra of **3**—**6** and **8** recorded in methanol.

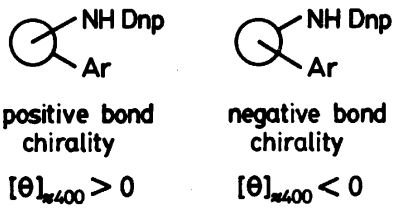

Fig. 2. Relation between bond chirality and sign of Cotton effect.
Ar implies a chromophore which contains an aromatic group.

around 400 nm. In order further to confirm the validity of the relation between bond chirality and the Cotton effect, the norbornane derivative **8** was synthesized. The CD spectrum of the Dnp derivative **8**, as also given in Fig. 1, exhibited positive Cotton effect at 416 nm in accordance with positive bond chirality of the C-NHDnp and C-C_6H_5 bonds. Thus it has been established that sign of the Cotton effect around 400 nm agrees with the bond chirality between C-NHDnp and C-Ar bonds for the conformationally fixed derivatives as described in this paper (Fig. 2).

Wakamiya *et al.*[11] already reported successful application of the relation between bond chirality and the sign of Cotton effect to structure elucidation of a natural product. In order to determine absolute configuration of galantinic acid (**9**), a constituent amino acid of a peptide antibiotic galantin

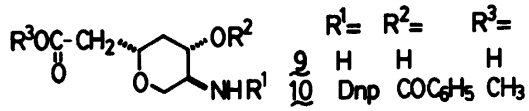

	R^1=	R^2=	R^3=
9	H	H	H
10	Dnp	COC_6H_5	CH_3

I,[12] micromolar amount of **9** was converted into *N*-Dnp-*O*-benzoyl derivative **10**. The CD spectrum of **10** exhibited prominent positive Cotton effect at 400 nm, which established the absolute configuration of **9** having positive chirality of the C-N and C-O bonds.[11]

Another example of application of the rule to oxacyclohexanamine derivative is the case of D-glucosamine derivative **11**, which was obtained apparently as a sole product by successive 2,4-dinitrophenylation and acetylation of D-glucosamine. Possible products of the reaction were anomers **11** and **11'**, which possess posi-

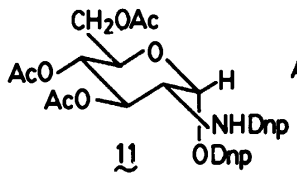

11

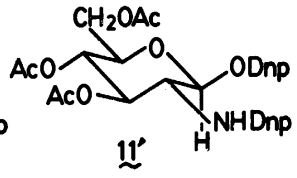

11'

tive and negative chirality between the C-NHDnp and C-ODnp bonds, respectively, corresponding to **1c** and **1b** in their chromophoric arrangement. Positive Cotton effect ($[\theta]^{25}_{400}$ +5100) and small coupling constant of the anomeric proton (δ_{DMSO-d_6} 6.48, d, J=3 Hz) in ^{1}H NMR spectrum established the structure **11**.

The agreement between bond chirality and the sign of Cotton effect is rationalized as follows: The Cotton effects in concern can be assumed to be due to exciton coupling of electric transition moments of the two chromophores as expressed by the equation[13]

$$R_a = \frac{\pi}{ch} \cdot \frac{\lambda_a \lambda_b}{\lambda_a^2 - \lambda_b^2} \cdot V \cdot [\boldsymbol{R} \cdot (\mu_a \times \mu_b)]$$

where R_a is rotational strength at wavelength λ_a generated by interaction of the electric transition moment μ_a at λ_a with μ_b at λ_b. V, $\boldsymbol{R}$, c, and h are interaction energy, directional vector from μ_a to μ_b, light velocity, and Planck's constant, respectively. Thus, the sign of term $V \cdot [\boldsymbol{R} \cdot (\mu_a \times \mu_b)]$ determines the sign of Cotton effect to be observed. The electronic spectra of DnpNH chromophore shows a shoulder band around 400 nm (ε 7000) along with strong main band at around 350 nm (ε 17000). SCF-MO[14] calculation showed that direction of the electric transition moment of the longest wavelength band of DnpNH chromophore is roughly parallel to the C-NHDnp bond.[1,15] Interaction of this transition moment with transition moments of the other chromophore is considered to generate the CD band observed around 400 nm. As for the other chromophore there usually exists a strong absorption band, the electric transition moment of which has a direction along the long axis of the chromophore;[16] *i.e.*, the direction of this transition moment is

exactly or approximately parallel to the C-Ar bond. Consequently the sign of the term $\boldsymbol{R}\cdot(\mu_a\times\mu_b)$ in the equation above is expected to coincide with the bond chirality between C-NHDnp and C-Ar bonds, when μ_a and μ_b are the transition moment of the longest wavelength band of DnpNH chromophore and the transition moment along the long axis of the other chromophore, respectively. Since the sign of V-term is positive in most cases usually encountered, the term $V\cdot[\boldsymbol{R}\cdot(\mu_a\times\mu_b)]$ also has the same sign as the bond chirality. Though the transition moments which are not parallel but rather perpendicular to the C-Ar bond are also present and interact with the moment of DnpNH chromophore, their contribution to the spectra are expected to be averaged out due to rotation around the C-Ar bond. Thus the sign of the Cotton effect around 400 nm is expected to agree with the bond chirality of C-NHDnp and C-Ar bonds of these compounds.

Cotton effect around 350 nm is assumed due to exciton coupling of the dipole moment of main band of DnpNH chromophore with dipole moments of the other chromophore. The extremum of CD spectrum at this region is shifted to longer wavelength when the Cotton effect has the same sign as that of 400 nm band as in **5** (shoulder) and **8** and at shorter wavelength when the sign of Cotton effects of 400 and 350 nm bands are different as in **3**, **4**, and **6** by overlapping of the two bands. In the case of **4** having *p*-nitroanilide group as the other chromophore whose absorption maximum is at about 315 nm,[8] another CD band which corresponds to this transition moment can be expected above 300 nm. No significant band is observed, however, around 315 nm in the CD spectrum of **4**, which is presumably due to the result of cancellation of opposite contributions from the two interactions with transition moments of 400 and 350 nm bands of DnpNH chromophore. Compounds **5** and **6** show different sign of Cotton effect around 350 nm in spite of the close similarity of the two compounds. Thus no simple relation seems to exist between the absolute configuration and the sign of Cotton effect around 350 nm, which is understandable from the dissimilarity between the direction of the correspoding transition moment and the C-NHDnp bond.[1]

In conclusion the relation between the absolute configuration of cycloalkanamines and the sign of Cotton effect around 400 nm of the Dnp derivatives was ascertained experimentally as given in Fig. 2 and was rationallized theoretically using exciton coupling mechanism. Thus it has been shown that absolute configuration can be determined chiroptically for a cyclic compound having a primary amino group, if suitable derivatization can afford a Dnp derivative in which C-NHDnp and C-Ar bonds possess unambiguous bond chirality.

The relation is valid when the chirality of interacting transition moments can be approximated by the bond chirality. In general, combination of conformational analysis and rotational strength calculation will afford useful information for predicting or explaining the CD spectra. The relation described here falls under the generalization "exciton chirality method" developed by Harada and Nakanishi.[17] Attempt to determine the absolute configuration of amino compounds with exciton chirality method using salicylideneamino chromophore was reported by Smith *et al.*[18,19]

Experimental

Melting points were uncorrected. UV and CD spectra were recorded in methanol solution at room temperature on a HITACHI 124 spectrometer and on a JASCO J-40 spectropolarimeter, respectively. Optical rotations were measured with a JASCO J-20 spectropolarimeter or a JASCO DIP-4 digital polarimeter. ^{13}C NMR spectra were determined with a Varian XL-200 spectrometer using sodium 2,2-dimethyl-2-silapentane-5-sulfonate as internal standard. ^{1}H NMR ($CDCl_3$, acetone-d_6, or DMSO-d_6 solution) and IR (KBr disk) spectra of all the derivatives, recorded on a HITACHI R-24 or R-24A spectrometer and on a JASCO IRA-1 or A-102 spectrophotometer, respectively, were consistent with the assigned structures.

(1R,2S)-N-(2,4-Dinitrophenyl)-2-phenylcyclohexanamine (3). (±)-*trans*-2-Phenylcyclohexanamine hydrochloride, mp 252—254 °C (lit,[20] mp 249—251 °C), was prepared from 2-phenylcyclohexanone oxime, mp 174—175 °C (lit,[20] mp 168—169 °C) as described by Masamune *et al.*[20] No significant amount of the *cis*-isomer was detected in the ^{13}C NMR of the dihydrochloride measured in D_2O solution (δ=24.8, 25.6, 31.4, 34.1, 49.0, 55.8, 128.5, 128.7, and 142.0). Optical resolution of (±)-*trans*-2-phenylcyclohexanamine using equimolar amount of (+)-tartaric acid was undertaken. Recrystallization from 3:1 (v/v) methanol–ether as described by Verbit and Price[21] afforded tartrate of (+)-amine as colorless needles, mp 150—151 °C, $[\alpha]_D$ +38° (c 0.85, methanol), while recrystallization from 1:5 (v/v) methanol–H_2O resulted in the crystallization of tartrate of (−)-amine as colorless prisms, mp 139—140 °C, $[\alpha]_D$ −16° (*c* 1.0, methanol). Usual workup of the tartrates gave (+)-(1*S*,2*R*)-2-phenylcyclohexanamine, mp 41.5—42 °C, $[\alpha]_D$ +51° (*c* 0.33, methanol) [lit,[21] mp 36—38 °C, $[\alpha]_D$ +45° (*c* 0.074, methanol)] and (−)-(1*R*,2*S*)-2-phenylcyclohexanamine, mp 43.5—44 °C, $[\alpha]_D$ −49° (*c* 0.28, methanol) [lit,[21] mp 37.5—39 °C, $[\alpha]_D$ −48° (*c* 0.2, methanol)]. A mixture of the levorotatory amine (70 mg, 0.43 mmol), 1-fluoro-2,4-dinitrobenzene (FDNB: 94 mg, 0.5 mmol), $NaHCO_3$ (53 mg, 0.63 mmol), acetone (5 mL), and H_2O (2 mL) was stirred at room temperature for 2 h. Usual workup followed by SiO_2 column chromatography (benzene–petroleum ether) gave **3** (125 mg, 85%), yellow needles from benzene–petroleum ether, mp 126.5—127 °C. UV 410 (sh, ε 6200), 353 (18500), and 257 nm (8800); CD $[\theta]_{415}$ −13600, $[\theta]_{358}$ 0, $[\theta]_{340}$ +6000, $[\theta]_{305}$ +4200, $[\theta]_{274}$ +8000, and $[\theta]_{250}$ +3400. Found: C, 63.50; H, 5.54; N, 12.30%. Calcd for $C_{12}H_{19}N_3O_4$: C, 63.33; H, 5.61; N, 12.31%.

(1R,2R)-2-(2,4-Dinitroanilino)cyclohexanecarboxylic Acid p-

Nitroanilide (4). (±)-*N*-Benzoyl-*trans*-2-aminocyclohexanecarboxylic acid was prepared from anthranilic acid as described by Hünig and Kahanek,[22] and was subjected to optical resolution according to Nohira *et al.*[23] to afford (−)-(1*R*,2*R*)-*N*-benzoyl-2-aminocyclohexanecarboxylic acid quinine salt, mp 134—136 °C, $[\alpha]_D$ −112° (*c* 2.3, ethanol) [lit,[23] mp 143—145 °C, $[\alpha]_D$ −111.6° (*c* 2.5, ethanol)]. Treatment of the quinine salt with 3M HCl (1M=1 mol dm^{-3}) gave (1*R*,2*R*)-*N*-benzoyl-2-aminocyclohexanecarboxylic acid, $[\alpha]_D$ −45° (*c* 0.66, ethanol) [lit,[23] $[\alpha]_D$ −44.5° (*c* 0.67, ethanol)]. The *N*-benzoyl derivative (96 mg, 0.39 mmol) was dissolved in a mixture of conc HCl (6 mL) and acetic acid (3 mL) and was refluxed for 24 h. Evaporation of the mixture afforded crude debenzoylated product, which was 2,4-dinitrophenylated with FDNB according to Sanger[24] to give (1*R*,2*R*)-2-(2,4-dinitroanilino)cyclohexanecarboxylic acid (101 mg, 83%). To the Dnp derivative (77 mg, 0.25 mmol) was added oxalyl dichloride (1.5 mL) and stirred overnight. Excess oxalyl dichloride was evaporated *in vacuo* and *p*-nitroaniline (250 mg, 1.8 mmol) in acetonitrile (2 mL) was added to the residue, which was stirred overnight. After the evaporation of the solvent the residue was washed with hot H_2O and recrystallized from acetone–ethyl acetate to give **4** (24 mg, 20%) as yellow needles, mp 259—261 °C. UV 400 (sh, ε 5800), 330 (24000), 266 (11000), and 219 nm (21800); CD $[\theta]_{406}$ −19800, $[\theta]_{368}$ 0, $[\theta]_{336}$ +32200, $[\theta]^{sh}_{275}$ +2400, $[\theta]_{263}$ 0, and $[\theta]_{250}$ −2500. Found: C, 52.67; H, 4.41; N, 16.00%. Calcd for $C_{19}H_{19}N_5O_7 \cdot 1/4H_2O$: C, 52.60; H, 4.53; N, 16.14%.

(1R,2R)-2-(2,4-Dinitroanilino)cyclohexyl Benzoate (5). (1*R*,2*R*)-2-Aminocyclohexanol (+)-tartrate[25] (44 mg, 0.17 mmol), supplied by Prof. T. Suami, was 2,4-dinitrophenylated with FDNB (62 mg, 0.33 mmol) and $NaHCO_3$ (76 mg, 0.90 mmol) in ethanol (1.7 mL) and H_2O (0.7 mL). The crude product was subjected to SiO_2 column chromatography (benzene–ethyl acetate) to afford (1*R*,2*R*)-2-(2,4-dinitroanilino)cyclohexanol (44 mg, 92%). To the ice-cooled solution of the Dnp derivative (44 mg, 0.16 mmol) in pyridine (0.4 mL) was added benzoyl chloride (0.06 mL, 0.5 mmol) and was stirred overnight at room temperature. After addition of 1 M H_2SO_4 (6 mL) the mixture was extracted with ethyl acetate. The extract was purified by SiO_2 column chromatography (benzene–hexane) and recrystallized from benzene–hexane to give **5** (43 mg, 71%) as yellow powder, mp 143—145 °C. UV 400 (sh, ε 6600), 349 (17700), 265 (9300), and 230 nm (22000); CD $[\theta]_{408}$ −12300, $[\theta]^{sh}_{370}$ −9600, $[\theta]_{320}$ 0, $[\theta]_{271}$ +13800, and $[\theta]_{238}$ +38100. Found: C, 59.39; H, 4.80; N, 10.73%. Calcd for $C_{19}H_{19}N_3O_6$: C, 59.21; H, 4.97; N, 10.90%.

(1R,2R)-N¹-Benzoyl-N²-(2,4-dinitrophenyl)-1,2-cyclohexanediamine (6). 1,2-Cyclohexanediamine (Tokyo Kasei Chemicals; 22.8 g, 0.2 mol) and adipic acid (29.2 g, 0.2 mol) were treated in 2-propanol as described in literature[26] to give *trans*-1,2-cyclohexanediamine adipate (50.0 g, 96%), which was converted into free diamine (13.0 g, 56%) with NaOH. The racemic diamine (8.0 g, 70 mmol) was resolved *via* (+)-tartrate according to Asperger *et al.*[27] to give (1*R*,2*R*)-1,2-cyclohexanediamine dihydrochloride (1.83 g, 27%): $[\alpha]_D$ −15.8° (*c* 2.53, H_2O) [lit,[27] $[\alpha]_D$ −15.8° (*c* 20, H_2O)]. A mixture of the hydrochloride (0.37 g, 2.0 mmol), FDNB (0.37 g, 2.0 mmol), and $NaHCO_3$ (0.60 g, 7.0 mmol) in ethanol (20 mL) and H_2O (10 mL) was stirred for 2 h at room temperature. After evaporation of ethanol benzoyl chloride (0.47 mL, 4 mmol) and 1 M NaOH (7.0 mL) were added and the mixture was stirred overnight. H_2O was added and the precipitate was collected by filtration and washed with H_2O. The precipitate was dissolved in ethanol and insoluble di-Dnp derivative was filtered off. The filtrate, which contained dibenzoyl derivative and *N*-benzoyl-*N'*-Dnp derivative, was concentrated *in vacuo* to induce crystallization of the latter compound. Recrystallization from ethanol gave **6** (63 mg, 8%) as yellow needles, mp 254—258 °C. UV 410 (sh, ε 7000), 352 (16000), 260 (sh, 10500), and 220 nm (17600); CD $[\theta]_{414}$ −15000, $[\theta]_{364}$ 0, $[\theta]_{338}$ +6400, $[\theta]_{310}$ +2900, $[\theta]_{274}$ +13500, $[\theta]_{253}$ +7000, and $[\theta]_{240}$ +13400. Found: C, 58.54; H, 5.25; N, 14.53%. Calcd for $C_{19}H_{20}N_4O_5 \cdot 1/4H_2O$: C, 58.68; H, 5.31; N, 14.41%.

(2S,3R)-2-(2,4-Dinitroanilino)-3-phenylnorbornane (8). Cyclopentadiene (60 g, 0.9 mol) and *trans*-β-nitrostyrene (60 g, 0.4 mol) in benzene (150 mL) were refluxed for 15 h to afford a mixture of stereoisomers of *trans*-5-nitro-6-phenyl-2-norbornenes (78.7 g, 91%), bp 126 °C/3 Torr (lit,[28] bp 110—115 °C/0.3 Torr; 1 Torr=133.322 Pa). This adduct (21.5 g, 0.1 mol) was treated with Sn (24 g, 0.2 mol) and acetic acid (90 mL) as described by Weinstock *et al.*[29] and the reaction mixture was purified by SiO_2 chromatography (ethyl acetate–acetone) to give *trans*-5-amino-6-phenyl-2-norbornenes (7.0 g, 38%), which was hydrogenated over 5% Pd–carbon in ethanol (120 mL) and 2M HCl (30 mL) at atmospheric pressure affording a mixture of 2-*endo*-amino-3-*exo*-phenyl- and 2-*exo*-amino-3-*endo*-phenylnorbornanes [TLC, SiO_2, benzene, R_f 0.7 (major) and 0.5 (minor), respectively]. The former (3.14 g, 15%) was separated from the latter by SiO_2 column chromatography (acetone–hexane) and resolved with (+)-tataric acid (2.35 g, 16 mmol) in ethanol according to Smith *et al.*[28] to give (2*S*,3*R*)-2-amino-3-phenylnorbornane (+)-tartrate (865 mg, 32%), mp 189—191 °C, $[\alpha]_D$ +42.7° (*c* 1.0, H_2O) [lit,[28] $[\alpha]_D$ +42° (*c* 1.0, H_2O)]. A mixture of the tartrate (169 mg, 0.5 mmol), FDNB (200 mg, 1.07 mmol), $NaHCO_3$ (200 mg, 2.38 mmol), ethanol (10 mL), and H_2O (5 mL) was stirred overnight at room temperature. Usual workup and preparative SiO_2 TLC (benzene) gave **8** (85 mg, 24%), yellow prisms from benzene–hexane, mp 168.5—169.5 °C. UV 410 (sh, ε 6000), 351 (16400), and 262 nm (8700); CD $[\theta]_{416}$ +9200, $[\theta]_{370}$ +7600, $[\theta]_{320}$ 0, $[\theta]_{280}$ −7100, and $[\theta]_{233}$ −44300. Found: C, 64.80; H, 5.47; N, 11.42%. Calcd for $C_{19}H_{19}N_3O_4$: C, 64.58; H, 5.42; N, 11.89%.

2,4-Dinitrophenyl 3,4,6-Tri-O-acetyl-2-deoxy-2-(2,4-dinitroanilino)-β-D-glucoside (11a). This compound was supplied by Dr. H. Kohno, who obtained **11a** during synthetic study of neamine[30] by 2,4-dinitrophenylation of 2-deoxy-2-amino-D-glucose followed by acetylation with acetic anhydride-pyridine. ^1H NMR (DMSO-d_6) δ=1.82 (3H, s, CH_3CO_2), 2.00 (3H, s, CH_3CO_2), 2.04 (3H, s, CH_3CO_2), 4.1—4.3 (3H, m, CH_2–O and CH–N), 5.1—5.6 (3H, m, 3×CH–O), 6.48 (1H, d, *J*=3 Hz, O–CH–O), 7.76 (2H, d, *J*=9 Hz, 2×*o'*–H of Dnp), 8.42 (1H, dd, *J*=9 and 3 Hz, *m'*–H of Dnp), 8.63 (1H, dd, *J*=9 and 3 Hz, *m'*–H of Dnp), 8.87 (1H, d, *J*=3 Hz, *m*–H of Dnp), and 8.90 (1H, d, *J*=3 Hz, *m*–H of Dnp); UV 400 (sh, ε 4400), 335 (18600) and 250 nm (19200); CD $[\theta]^{sh}_{400}$ +5100, $[\theta]_{334}$ +18000, $[\theta]_{315}$ 0, $[\theta]_{309}$ −6000, $[\theta]_{299}$ 0, $[\theta]_{278}$ +16000, $[\theta]_{258}$ 0, and $[\theta]_{248}$ −16000.

The authors are grateful to Professor Tetsuo Suami of Keio University and Dr. Hideki Kohno of Mitsubishi Chemical Industries Ltd. for their kind gifts of

optically active 2-aminocyclohexanol and D-glucosamine derivative, respectively. Thanks are also to Mrs. Motoko Arai for her technical assistances.

References

1) M. Kawai, U. Nagai, and T. Kobayashi, *Tetrahedron Lett.*, **1974**, 1881.
2) M. Kawai, U. Nagai, and M. Katsumi, *Tetrahedron Lett.*, **1975**, 2845.
3) U. Nagai and Y. Kani, *Tetrahedron Lett.*, **1977**, 2333.
4) M. Kawai and U. Nagai, *Tetrahedron Lett.*, **1977**, 3889.
5) M. Kawai, U. Nagai, M. Katsumi, and A. Tanaka, *Tetrahedron*, **34**, 3435 (1978).
6) U. Nagai, M. Kawai, T. Yamada, S. Kuwata, and H. Watanabe, *Tetrahedron Lett.*, **22**, 653 (1981).
7) U. Nagai, N. Taki, and M. Kawai, *Chem. Pharm. Bull.*, **29**, 1750 (1981).
8) K. Sato, M. Kawai, and U. Nagai, *Biopolymers*, **20**, 1921 (1981).
9) M. Kawai, U. Nagai, and A. Tanaka, *Bull. Chem. Soc. Jpn.*, **55**, 1213 (1982).
10) M. Kawai and U. Nagai, *Bull. Chem. Soc. Jpn.*, **55**, 1327 (1982).
11) T. Wakamiya, T. Ando, T. Teshima, and T. Shiba, *Bull. Chem. Soc. Jpn.*, **57**, 142 (1984).
12) J. Shoji, R. Sakazaki, Y. Wakisaka, K. Koizumi, M. Mayama, and S. Matsuura, *J. Antibiot.*, **28**, 122 (1975).
13) J. A. Schellman, *Acc. Chem. Res.*, **1**, 144 (1968).
14) Z. Yoshida and T. Kobayashi, *J. Chem. Phys.*, **54**, 4538 (1971).
15) DnpNH group is assumed to take planar conformation having a hydrogen bond between NH and *o*-NO_2 groups.
16) The electric transition moments of the longer wavelength π–π^* bands of *p*-nitroanilide, benzoate, and benzamide chromophores were shown to be aligned approximately along the long axis of the benzene ring by SCF-MO[14] calculation. Consequently, considering *s-trans* geometry of amide and ester moiety, the direction of those transition moments are roughly parallel to the chromophore attached bond C-Ar.
17) N. Harada and K. Nakanishi, *Acc. Chem. Res.*, **5**, 257 (1972).
18) H. E. Smith, J. R. Neergaard, E. P. Burrows, and F. Chen, *J. Am. Chem. Soc.*, **96**, 2908 (1974).
19) H. E. Smith, *Chem. Rev.*, **83**, 359 (1983).
20) T. Masamune, M. Ohno, M. Koshi, S. Ohuchi, and T. Iwadare, *J. Org. Chem.*, **29**, 1419 (1964).
21) L. Verbit and H. C. Price, *J. Am. Chem. Soc.*, **94**, 5143 (1972).
22) S. Hünig and H. Kahanek, *Chem. Ber.*, **86**, 518 (1953).
23) H. Nohira, K. Ehara, and A. Miyashita, *Bull. Chem. Soc. Jpn.*, **43**, 2230 (1970).
24) F. Sanger, *Biochem. J.*, **39**, 507 (1945).
25) S. Umezawa, T. Tsuchiya, and K. Tatsuta, *Bull. Chem. Soc. Jpn.*, **39**, 1235 (1966).
26) K. Yamamoto and S. Fujitake (Mitsui Toatsu Chemicals Co., Ltd.), Japan Kokai 70,29,655; *Chem. Abstr.*, **74**, 12700u (1971).
27) R. G. Asperger and C. F. Liv, *Inorg. Chem.*, **4**, 1492 (1965).
28) H. E. Smith and T. C. Willis, *Tetrahedron*, **26**, 107 (1970).
29) J. Weinstock, N. Schwartz; and M. F. Kormendy, *J. Org. Chem.*, **26**, 5427 (1961).
30) H. Kohno, H. Fukami, and M. Nakajima, *Agr. Biol. Chem.*, **39**, 1091 (1975).

 © 1985 The Chemical Society of Japan Bull. Chem. Soc. Jpn., 58, 309—315 (1985)

Enzymic Synthesis and Biochemical Activity of Various Indazole Adenine Dinucleotides[1)]

Shuichi TONO-OKA,* Yukiko TONE, Victor E. MARQUEZ,† David A. COONEY,† Isao SEKIKAWA, and Ichiro AZUMA

Section of Chemistry, Institute of Immunological Science, Hokkaido University, Kita-ku, Sapporo 060
†Laboratory of Medicinal Chemistry and Biology, National Cancer Institute, National Institutes of Health, Bethesda, Maryland 20205, U.S.A.

(Received July 23, 1984)

Each of 5- or 6-amino-, acetamido-, hydroxy-, methoxy-, and chloroindazoles (including an unsubstituted one) and β NAD were subjected to an NADase-catalyzed base-exchange reaction to produce a corresponding title compound with a 41—76% yield. A difficulty, due to the poor solubility in water of indazole bases, was overcome by the addition of DMSO (~20%) without a remarkable decrease in NADase activity. In most cases, the obtained dinucleotides were ascertained to be N^2-ribosylated compounds. From 5- and 6-aminoindazoles, however, N^1-ribosylated dinucleotide was also obtained as a minor product. In some of the N^2-ribosylated dinucleotides, an unusual tautomerism was suggested to occur on the benzene ring of an indazole moiety. Finally, the synthesized title compounds were examined for inhibition activity against NAD-linked inosine monophosphate dehydrogenase. Four compounds among them were markedly effective at a 10^{-3} M concentration.

Interestingly, porcine brain NADase catalyses an exchange reaction between the nicotinamide moiety of β NAD and the structurally related pyridine compound, besides the mere hydrolysis of the quaternary pyridinium linkage.[2-4)] Modifying this principle, we have previously prepared various new NAD analogs containing 3,4-disubstituted 1,4-dihydropyridine moiety.[5-7)] Moreover, the necessary conditions for the concerned replacing base for participating in the reaction have been discussed.[7)] Such NAD analogs can be useful intermediates leading to the naturally occurring pyridine nucleosides quantitatively.[6)] As for the biological aspect, some of the analogs have been observed to show significant immunological activities *in vitro*.[8)]

From the viewpoint of applying the enzymic synthesis to other nitrogen-containing heterocycle nucleotides, our interest has initially been focused on readily preparable indazole bases. Since no indazole adenine dinucleotide has been synthesized, chemically or enzymicly, this application of an exchange reaction to the indazole bases can be of great significance. On the other hand, in view of the NAD analogs, the dinucleotides are expected to show a possible inhibition activity against an NAD-linked dehydrogenase system, particularly inosine monophosphate (IMP) dehydrogenase which is a target enzyme for many antitumor agents.[9-10)] In this paper, we give a full account of the enzymic synthesis and characterization of new indazole adenine dinucleotides arising from 5- or 6-amino-, acetamido-, hydroxy-, methoxy-, and chloroindazoles (as well as an unsubstituted one), together with their biochemical activities against IMP dehydrogenase.

Results and Discussion

Preparation of Indazole Dinucleotides. When a replacing base shows a strong basicity ($pK_a \gtrsim 9$), no exchange reaction occurs because the concerned nitrogen atom is blocked by a protonation under the optimum conditions of NADase (pH 7.2).[7)] The indazole bases now used, however, are relatively weak in basicity ($pK_a \sim 5$)[11)] and have no substituent on the pyrazole ring which would cause a steric hindrance at the reaction site. Thus, the occurrence of a base exchange was expected. The only problem in carrying out the reaction was the poor solubility in water of the indazole compounds. The base concentration proved to be an important factor in promoting the formation of a new dinucleotide.[6)] Fortunately, the indazole bases were very soluble in DMSO, one of the typical aprotic solvents. Were it not for an extreme influence on the NADase activity, therefore, the addition of DMSO seemed favorable in view of enhancing base nucleophilicity as well as improving base concentration. In fact, no significant decrease in the activity was observed, even if DMSO (~20%) was added to get a suitable base concentration (20 mM††). The problem of base solubility in the reaction system was, thus, overcome.

Each indazole base and NAD were incubated with NADase at 37 °C in DMSO-containing Tris-HCl (pH 7.2) until the spot of NAD disappeared in TLC. After incubation, the rusulting mixture contained four major components: An unchanged indazole base, the NAD-derived nicotinamide, the desired product, and ADP-ribose. The mixture (after the removal of the enzyme, Tris-HCl, and DMSO) was subjected to column chromatography on DEAE-Sephadex to provide the desired dinucleotide in 41—76% yield (Table 1). Its purity was checked by TLC in two different develo-

†† 1 M=1 mol dm^{-3}.

ping systems and, if necessary, the chromatography was repeated.

Considering the two nitrogen atoms which form the indazole skeleton, though probably different in reactivity, the formation of two distinct dinucleotides can be anticipated in an enzymic reaction. In most cases, however, single dinucleotide was produced with no detectable amount of an alternative compound. As an exceptional case, a minor product was brought about from 5- and 6-aminoindazoles in *ca.* 10% yield besides the major one.

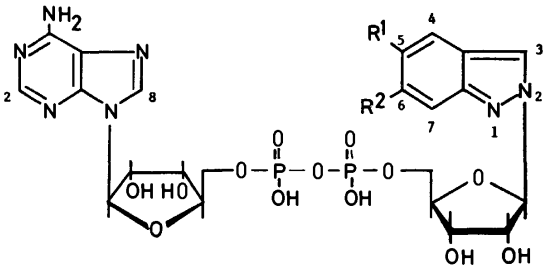

1: $R^1=R^2=H$
2: $R^1=NH_2$, $R^2=H$
3: $R^1=H$, $R^2=NH_2$
4: $R^1=NHAc$, $R^2=H$
5: $R^1=H$, $R^2=NHAc$
6: $R^1=OH$, $R^2=H$
7: $R^1=H$, $R^2=OH$
8: $R^1=OCH_3$, $R^2=H$
9: $R^1=H$, $R^2=OCH_3$
10: $R^1=Cl$, $R^2=H$
11: $R^1=H$, $R^2=Cl$

So far as we know, there has been no report concerning halogen-containing NAD analogs. Accordingly, an exchange reaction was also tried for the preparation of dinucleotides originating from 5-, 6-, and 4-chloroindazoles. As a result, we obtained the corresponding dinucleotides (**10—12**) in reasonable yield (Table 1), indicative of the availability of this method for halogen-containing bases as well.

Structural Characterization of Indazole Dinucleotides. In order to obtain structural information regarding the new compounds, we first compared their ^{1}H-NMR spectra with those of NAD and the corresponding indazole base. Relevant signals falling within δ 6.5—8.3 indicated the presence of indazole and adenine moieties (Table 1). In all cases, two anomeric protons appeared at δ 5.8—6.0 as clearly separate doublets, and ribose-linked ten protons at δ 4.2—4.8 overlapping one another. In addition, the phosphorus content was quantitatively analyzed to show 2 mol per molecule of the compound. These observations ascertained the indazole adenine dinucleotide of the products obtained.

By means of UV spectroscopy, we next examined the site of ribosylation in the indazole moiety of the dinucleotides. In the UV spectra, the absorption maxima of indazole chromophore was wrapped up with the adenine-derived strong absorption band at 260 nm, so that the dinucleotide (**1**) was led to the indazole mononucleotide (**15**) on cleavage of pyrophosphate linkage with phosphodiesterase (PDE), followed by chromatographic isolation. The UV spectrum of **15** was compared with those of 1- and 2-methylindazoles, because ribosylation or methylation was expected to produce similar inductive effects. Compound **15** closely resembles 2-methylindazole in its absorption curve, but differs markedly from 1-methylindazole (Fig. 1). Indazole mononucleotides formed from other dinucleotides also exhibited a similar

Table 1. Yields and ^{1}H-NMR spectral data of indazole adenine dinucleotides

Compd No.	Yield [b] %	Chemical shifts (δ, D_2O)[a] Indazole[c]					Adenine		Anomeric	
		H_3	H_4	H_5	H_6	H_7	H_2	H_8	ad-C_1' [d]	ind-C_1' [e]
1	54	8.29 s	7.53 d	7.19 dd	6.93 dd	7.40 d	7.97 s	8.24 s	5.99 d	5.87 d
2	41	8.17 s	n.o.[f]	—	6.89 d	7.32 d	7.95 s	8.10 s	5.94 d	5.86 d
3	43	8.21 s	7.42 d	6.62 d	—	n.o.[f]	7.97 s	8.16 s	5.91 d	5.87 d
4	72	8.21 s	7.53 d	—	7.00 d	7.31 d	7.90 s	8.12 s	5.98 d	5.79 d
5	47	8.24 s	7.41 d	6.70 d	—	7.51 s	7.90 s	8.06 s	5.98 d	5.79 d
6	73	8.13 s	6.75 d	—	6.80 dd	7.30 d	7.96 s	8.08 s	5.95 d	5.87 d
7	76	8.18 s	7.40 d	6.54 d	—	n.o.[f]	7.98 s	8.13 s	5.93 d	5.86 d
8	62	8.16 s	6.78 s	—	6.75 d	7.28 d	7.94 s	8.12 s	5.99 d	5.86 d
9	53	8.22 s	7.39 d	6.51 dd	—	6.66 d	7.99 s	8.13 s	5.95 d	5.86 d
10	62	8.23 s	7.42 d	—	7.01 dd	7.32 d	7.98 s	8.14 s	6.01 d	5.87 d
11	48	8.31 s	7.47 d	6.82 dd	—	7.30 d	7.99 s	8.09 s	6.01 d	5.83 d
12	48	8.27 s	—	7.09 dd	6.88 dd	7.28 dd	7.87 s	8.13 s	5.99 d	5.84 d
13	12	8.26 s	7.20 s	—	7.10 d	7.35 d	7.96 s	8.16 s	5.98 d	5.84 d
14	9	8.29 s	7.47 d	6.76 d	—	7.05 s	7.99 s	8.20 s	6.00 d	5.86 d

a) Chemical shifts of ribose-linked ten protons fell within δ 4.2—4.8 in all cases. b) Based on NAD used. c) Acetamido methyl protons of **4** and **5** appeared at δ 2.16 and 2.19, respectively, and methoxy methyl protons of **8** and **9** were observed at δ 3.76 and 3.81, respectively. d) J=4.2—4.4 Hz. e) J=4.0—5.4 Hz. f) Not observed.

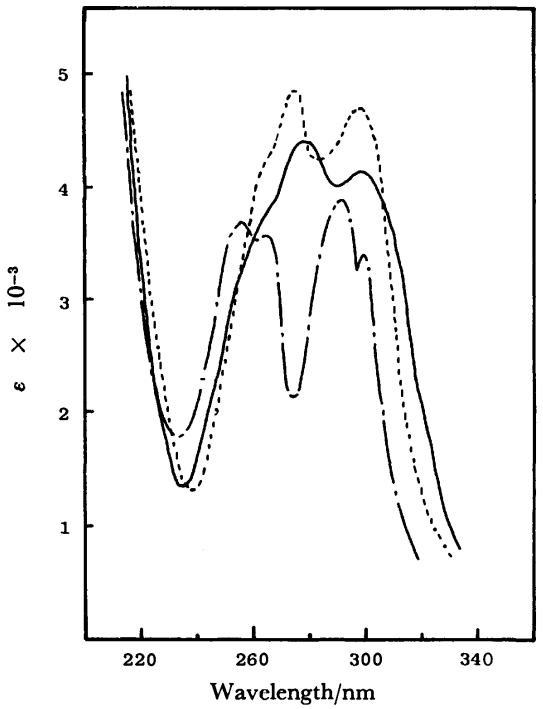

Fig. 1. UV spectral comparison of indazole mononucleotide (**15**) with 1- and 2-methylindazoles. (——): **15**; (— - —): 1-methylindazole; (-----): 2-methyl indazole.

bathochromic shift with somewhat hyperchromic effect. These observations indicate the quinonoid structure of mononucleotides, and consequently that the site of ribosylation is at the N^2-atom.

By ^{1}H-NMR spectroscopy, this reasoning could not be taken to a more definite conclusion. In order to gain further evidence, some appropriate N^1-acetylated indazoles (unsubstituted, 5-, and 6-acetamido ones) were submitted to the exchange reaction. Dinucleotides identical to **1**, **4**, and **5**, respectively, on ^{1}H-NMR spectral comparisons were produced in low yield. Upon incubation of the N^1-acetylated bases with NADase alone, however, no appreciable deacetylation occurred with N^1-acetyl group. These results strongly support the following conclusion: ADP-ribosylation occurred initially at the N^2-atom to form a 2-quaternary transient intermediate. Subsequently, the elimination of the N^1-acetyl group was accelerated by a strong electron-withdrawing effect of the quaternary nitrogen atom upon double-bond migrations, resulting in the quinonoid form of the indazole moiety.

Incidentally, the aforementioned minor products obtained with 5- and 6-aminoindazoles proved to be N^1-ribosylated dinucleotides (**13** and **14**) since their mononucleotides depicted a similar UV spectrum to that of the corresponding original base. Compounds **13** and **14** would arise from a certain proportion of the tautomeric 2*H*-indazole forms of the aminoindazoles although its existence has not been established.

The ^{1}H-NMR spectra in D_2O of compounds **2**, **3**, and **7** had no observable signal due to the aromatic proton (H_4 or H_7) adjacent to the amino or hydroxyl group. On the other hand, the corresponding signal was present as a singlet in compounds **4**, **5**, and **9** where the amino and hydroxyl substituents were blocked with acetyl and methyl groups, respectively (Table 1). Moreover, a signal was observed for the original amino- or hydroxyindazole, compound **13** and **14**. These facts suggest the occurrence of an unusual tautomerism on the benzene ring of the indazole moiety in **2**, **3**, and **7** which is probably dependent upon N^2-ribosylation. It is of interest to note that a signal due to H_4 appeared for compound **6**, whereas that due to H_7 disappeared for compound **7** under the same conditions (Fig. 2).

The assignment of the two doublets due to the anomeric protons remains unsettled. Thus, the respective coupling constants were estimated for the dinucleotides by a second-order approximation. As a consequence, the upfield signals were J=4.0—5.4 Hz, whereas the downfield ones were J=4.2—4.4 Hz. It can be expected that the dihedral angle between H-C_2'-C_1' and C_2'-C_1'-H in the ribose moiety of indazole side is somewhat changed by the difference in conformation of various kinds of the indazole bases. On the contrary, one can presume that the angle in the adenine side is little changed since the ribose moiety therein is under the influence of the same adenine base. Considering that the $J_{1',2'}$-value is reflected by the variation of the dihedral angle,[12] the upfield doublet can be assigned to the anomeric proton of indazole side, whereas the downfield one to that of adenine side (Table 1). In this connection, it is necessary to note that although respective chemical shifts and $J_{1',2'}$-values of a couple of mononucleotides were compared with each other, there was no unambiguous distinction between them in all cases.

Biochemical Activity of Indazole Dinucleotides against IMP Dehydrogenase. NAD-linked IMP dehydrogenase is known as one of the key rate-controlling enzymes of nucleic acid biosynthesis,[13] and many compounds which inhibit the enzyme have a more or less antitumor activity.[14,15] It is, therefore, of interest whether or not the indazole dinucleotides prepared here show an inhibitory effect on the dehydrogenase system. Some of those dinucleotides were examined for their ability to inhibit a partially purified IMP dehydrogenase from P388 leukemic cells. Among them, compounds **1**, **2**, **3**, and **6** showed an inhibition by 33 to 75% at a 10^{-3} M concentration (Table 2). At a 10^{-4} M concentration, however, none of them showed a significant level of inhibition, except for **2** which showed a 14% inhibition. Further investigations to correlate these results with actual features of cell proliferation are now in progress.

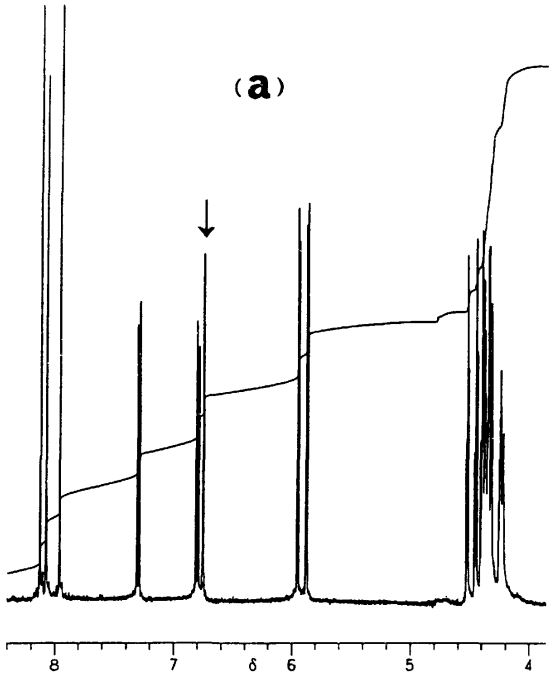

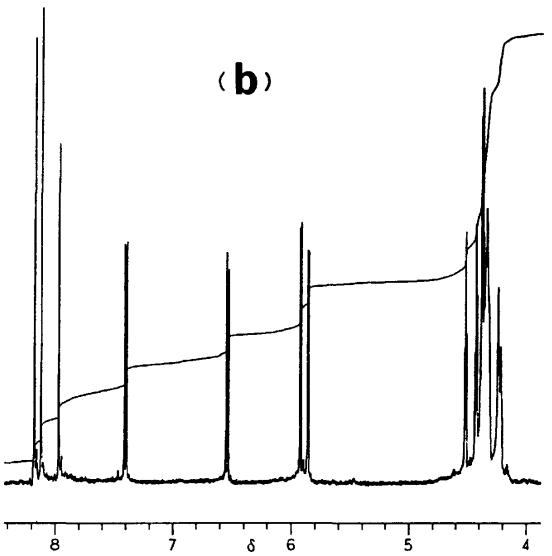

Fig. 2. 500 MHz ^1H NMR spectra of **6** (a) and **7** (b) in D_2O. (a) A signal assignable to H_4 is existent (an arrow). (b) A signal assignable to H_7 is nonexistent.

TABLE 2. INHIBITION ACTIVITY OF SOME OF INDAZOLE ADENINE DINUCLEOTIDES AGAINST IMP DEHYDROGENASE

Compd	Inhibition of IMP Dehydrogenase/%[a)]
1	33
2	75
3	55
4	0
5	0
6	75
7	5

a) At a 10^{-3} M concn of each compd.

Experimental

General. Melting points were measured with a Yamato MP-1 melting-point apparatus and are uncorrected. UV spectra were recorded on a Hitachi 200-20 spectrophotometer. ^1H-NMR spectra were determined on a JEOL GX-500 or a Varian XL-200 spectrometer in deuterium oxide with sodium 2,2-dimethyl-2-silapentane-5-sulfonate (DSS) as the internal standard. The abbreviations "s, d, and dd" denote "singlet, doublet, and double doublet," respectively. Optical rotations were measured on a Union PM-101 digital polarimeter. The ionic-strength and pH measurements were made with a Emuesu CD-35M II conductivity meter and a Radiometer PHM-26 pH meter equipped with a G-202 glass electrode, respectively. TLC was carried out on silica gel $60F_{254}$ HPTLC plates (Merck, 10 cm×10 cm) using 2-propanol–0.2% aq ammonia (7:3, v/v) and/or 1-propanol–0.3% aq acetic acid (3:2, v/v) as developing system. Column chromatographies were carried out on DEAE-Sephadex A-25 (HCO_3^--form) (column size: 2.5 cm×45 cm) monitored by LKB Uvicord II (254 nm). Phosphorus was determined colorimetrically by the method of Bartlett.[16] 1-Methyl- and 2-methylindazoles were obtained by the decarboxylation of respective 3-carboxylic acids.[17] β NAD (Grade III) and phosphodiesterase (PDE) (EC 3.1.4.1) were purchased from Sigma Chemical Co. Indazole, 5-, and 6-aminoindazoles were obtained from Aldrich Chemical Co.

Porcine Brain NADase (EC 3.2.2.5). The Crude particulate enzyme was prepared from a fresh porcine brain by the method of Zatman *et al.*[18] The colloidal supernatant fluid containing *ca.* 0.4 U[19]/ml of NADase activity was used without further purification.

N^1-*Acetylindazole.* Prepared by acetylation of indazole with acetic anhydride, and recrystallized from petroleum ether: Mp 44—46 °C (lit,[20] 42—43 °C).

N^1-*Acetyl-5-acetamidoindazole.* Prepared by acetylation of 5-aminoindazole with acetic anhydride, and recrystallized from benzene: Mp 167—169 °C. Found: C, 60.74; H, 5.12; N, 19.26%. Calcd for $C_{11}H_{11}N_3O_2$: C, 60.83; H, 5.07; N, 19.35%.

5-Acetamidoindazole. Prepared by the partial hydrolysis of the above compound with methanol–0.3% aq ammonia (60 °C, 3h), and recrystallized from methanol: Mp 203—205 °C. Found: C, 61.68; H, 5.16; N, 24.07%. Calcd for $C_9H_9N_3O$: C, 61.71; H, 5.14; N, 23.99%.

N^1-*Acetyl-6-acetamidoindazole.* Prepared by the acetylation of 6-aminoindazole with acetic anhydride, and recrystallized from benzene: Mp 187—189 °C. Found: C, 60.78; H, 5.06; N, 19.31%. Calcd for $C_{11}H_{11}N_3O_2$: C, 60.83; H, 5.07; N, 19.35%.

6-Acetamidoindazole. Prepared by the partial hydrolysis of the above compound, and recrystallized from methanol: Mp 253—255 °C. Found: C, 61.75; H, 5.18; N, 23.94%. Calcd for $C_9H_9N_3O$: C, 61.71; H, 5.14; N, 23.99%.

5-Hydroxyindazole. Prepared from 5-aminoindazole by the method of Davies,[21] and recrystallized from water: Mp 187—189 °C (lit,[21] 186 °C).

6-Hydroxyindazole. Prepared from 6-aminoindazole, and recrystallized from water: Mp 212—214 °C (lit,[21] 216 °C).

5-Methoxyindazole. Prepared from 4-methoxy-2-

methylaniline by diazotization followed by intramolecular cyclization, and recrystallized from ethanol–petroleum benzine: Mp 168—170 °C (lit,[22] 168—169 °C).

6-Methoxyindazole. Prepared from 6-hydroxyindazole by *O*-methylation with dimethyl sulfate, and recrystallized from petroleum benzine: Mp 125—127 °C (lit,[23] 124 °C).

5-Chloroindazole. Prepared from 2-amino-5-chlorotoluene, and recrystallized from benzene: Mp 122—124 °C (lit,[20] 118—120 °C).

6-Chloroindazole. Prepared from 2-amino-4-chlorotoluene, and recrystallized from benzene: Mp 175—177 °C (lit,[20] 175—177 °C).

4-Chloroindazole. Prepared from 2-amino-6-chlorotoluene, and recrystallized from benzene: Mp 158—160 °C (lit,[20] 155—157 °C).

Inhibition Activity against IMP Dehydrogenase. The assay was performed by the radiometric technique as reported previously:[24] NAD (1 mM), [2-^{3}H]IMP (0.075 mM), and each dinucleotide (1 mM or 0.1 mM) were incubated with P388 leukemic cell IMP dehydrogenase at 37 °C for 10 min, and then the reaction was terminated by 1 min of heating at 95 °C. The ^3H_2O arising from the oxidation of [2-^{3}H]IMP *via* [^{3}H] NAD was isolated by quantitative microdistillation and its tritium content was measured with a scintillation counter.

2H-Indazole Adenine Dinucleotide (1). Indazole (370 mg, 3.1 mmol) and NAD (780 mg, 1.1 mmol, neutralized to pH 7 with 0.2 M NaOH) were incubated with NADase (20 ml, 8 U) in DMSO (15 ml)-containing 0.1 M Tris-HCl (65 ml, pH 7.2) at 37 °C for 5 h. The incubation mixture was treated with 70% trichloroacetic acid (2 ml) and the denatured protein was removed by centrifugation. To the clear supernatant thus obtained, cold acetone (500 ml) was added, followed by standing overnight at 4 °C, to give white hygroscopic mass (708 mg). It was dissolved in water (30 ml) and then applied to a column (2.5 cm×25 cm) of DEAE-Sephadex (HCO_3^--form). The column was washed with 0.05 M NH_4HCO_3 (300 ml) to remove any free bases and then eluted with 0.4 M NH_4HCO_3 (pH 7.8). The first major component eluted, which showed a UV-absorption peak at 260 nm, was ADP-ribose. On further elution, the second major component was obtained and showed a UV-absorption peak at 264 nm. The eluate (200 ml) was immediately collected and lyophilized repeatedly to give **1** (375 mg) as ammonium salt. An analytical sample of **1** was obtained by drying over P_2O_5 *in vacuo* for 12 h at 40 °C: $[\alpha]_D^{23}$ −28.8° (*c* 0.59, H_2O); UV (H_2O) 264 (log ε 4.33) and *ca.* 293 nm (sh, log ε 3.78); ^{1}H-NMR (Table 1). Found: C, 34.17; H, 5.31; N, 16.76%. Calcd for $C_{22}H_{27}N_7O_{13}P_2 \cdot 2NH_3 \cdot 4H_2O$: C, 34.53; H, 5.36; N, 16.48%.

5-Amino-1H-indazole- and 5-Amino-2H-indazole Adenine Dinucleotides (13 and 2). 5-Aminoindazole (420 mg, 3.2 mmol) and NAD (620 mg, 0.9 mmol) were incubated with NADase (15 ml, 6 U) in DMSO (12 ml)-containing 0.1 M Tris-HCl (60 ml) for 5 h. The incubation mixture was treated in a similar manner as described above to give a pale-brown crude product (557 mg). It was dissolved in water (30 ml) and the water-insoluble part was removed by centrifugation. The clear supernatant was applied to a column (2.5 cm×40 cm) of DEAE-Sephadex. The column was then eluted with aq NH_4HCO_3, as described above. The eluate (60 ml) of the first major component posterior to the elution of ADP-ribose was immediately collected and lyophilized repeatedly to provide **13** (74 mg): $[\alpha]_D^{23}$ −33.0° (*c* 2.35, H_2O); UV (H_2O) 244 (log ε 4.31) and *ca.* 315 nm (log ε 3.55); ^{1}H-NMR (Table 1). Found: C, 35.39; H, 4.76; N, 16.81%. Calcd for $C_{22}H_{28}N_8O_{13}P_2 \cdot NH_3 \cdot 3H_2O$: C, 35.46; H, 4.97; N, 16.93%. After the elution of **13**, the second major component was eluted and showed a UV-absorption peak at 261 nm. The eluate (150 ml) was collected and lyophilized repeatedly to provide **2** (261 mg): $[\alpha]_D^{23}$ −38.7° (*c* 0.85, H_2O); UV (H_2O) 261 (log ε 4.27) and 330 nm (log ε 3.65); ^{1}H-NMR (Table 1). Found: C, 35.19; H, 4.90; N, 17.16%. Calcd for $C_{22}H_{28}N_8O_{13}P_2 \cdot NH_3 \cdot 3H_2O$: C, 35.46; H, 4.97; N, 16.93%.

6-Amino-1H-indazole- and 6-Amino-2H-indazole Adenine Dinucleotides (14 and 3). 6-Aminoindazole (390 mg, 2.8 mmol) and NAD (630 mg, 1.1 mmol) were incubated with NADase (15 ml, 6 U) in DMSO (15 ml)-containing Tris-HCl (70 ml) for 5 h. The pale brown crude mass (550 mg) obtained was separated by the chromatographic procedures as described for **13** to give **14** (55 mg) firstly: $[\alpha]_D^{23}$ −37.4° (*c* 0.19, H_2O); UV (H_2O) *ca.* 235 (sh, log ε 4.32), *ca.* 260 (log ε 4.21), and 296 nm (log ε 3.88); ^{1}H-NMR (Table 1). Found: C, 35.68; H, 5.09; N, 17.22%. Calcd for $C_{22}H_{28}N_8O_{13}P_2 \cdot NH_3 \cdot 3H_2O$: C, 35.46; H, 4.97; N, 16.93%. The chromatography was further continued as described for **2** to give **3** (276 mg) secondly: $[\alpha]_D^{23}$ −45.3° (*c* 0.19, H_2O); UV (H_2O) 263 (log ε 4.27) and 296 nm (log ε 3.92); ^{1}H-NMR (Table 1). Found: C, 35.39; H, 4.67; N, 16.67%. Calcd for $C_{22}H_{28}N_8O_{13}P_2 \cdot NH_3 \cdot 3H_2O$: C, 35.46; H, 4.97; N, 16.93%.

5-Acetamido-2H-indazole Adenine Dinucleotide (4). 5-Acetamidoindazole (540 mg, 3.0 mmol) and NAD (650 mg, 1.0 mmol) were incubated with NADase (15 ml, 6 U) in DMSO (5 ml)-containing Tris-HCl (60 ml) for 10 h. Chromatographic purification of the crude mass (600 mg) obtained, followed by repeated lyophilization, provided **4** (501 mg) as ammonium salt. An analytical sample of **4** was given by drying over P_2O_5 *in vacuo* for 12 h at 40 °C: $[\alpha]_D^{23}$ −31.2° (*c* 0.92, H_2O); UV (H_2O) 240 (log ε 4.38), *ca.* 260 (sh, log ε 4.22), and 310 nm (log ε 3.68); ^{1}H-NMR (Table 1). Found: C, 36.05; H, 5.70; N, 17.58%. Calcd for $C_{24}H_{30}N_8O_{14}P_2 \cdot 2NH_3 \cdot 3H_2O$: C, 35.85; H, 5.97; N, 17.43%.

6-Acetamido-2H-indazole Adenine Dinucleotide (5). 6-Acetamidoindazole (400 mg, 2.2 mmol) and NAD (600 mg, 0.9 mmol) were incubated with NADase (10 ml, 4 U) in DMSO (15 ml)-containing Tris-HCl (50 ml) for 12 h. The crude mass (545 mg) obtained was treated as described above to provide **5** (301 mg): $[\alpha]_D^{23}$ −20.6° (*c* 0.57, H_2O); UV (H_2O) 239 (log ε 4.32), *ca.* 265 (sh, log ε 4.13), and 297 nm (log ε 3.84); ^{1}H-NMR (Table 1). Found: C, 35.53; H, 5.78; N, 17.54%. Calcd for $C_{24}H_{30}N_8O_{14}P_2 \cdot 2NH_3 \cdot 3H_2O$: C, 35.85; H, 5.97; N, 17.43%.

Exchange Reaction with N^1-Acetyl Derivative of Indazole, 5-, and 6-Acetamidoindazoles. NAD (225 mg) and each of *N*^{1}-acetyl derivatives of indazole, 5-, and 6-acetamidoindazoles were incubated with NADase (5 ml, 2 U) in DMSO (5 ml)-containing 0.1 M Tris-HCl (30 ml) at 37 °C for 5—10 h. The, thus obtained, three dinucleotides (30—40 mg) were proved to be identical with **1**, **4**, and **5** from ^{1}H-NMR spectral comparisons, rcspectively. In all cases, no other detectable amount of dinucleotide was produced except for ADP-ribose.

5-Hydroxy-2H-indazole Adenine Dinucleotide (6).

NAD (958 mg, 1.4 mmol) and 5-hydroxyindazole (630 mg, 4.7 mmol) were incubated with NADase (10 ml, 4 U) in DMSO (5 ml)-containing Tris-HCl (50 ml) for 15 h. The reaction mixture was treated as previously described to provide a pale-brown mass of **6** (699 mg): $[\alpha]_D^{23}$ −38.3° (*c* 1.15, H_2O); UV (H_2O) 263 (log ε 4.33) and 319 nm (log ε 3.73); ^{1}H-NMR (Table 1). Found: C, 35.83; H, 5.01; N, 16.54%. Calcd for $C_{22}H_{27}N_7O_{14}P_2 \cdot 2NH_3 \cdot 2H_2O$: C, 35.42; H, 4.96; N, 16.90%.

6-Hydroxy-2H-indazole Adenine Dinucleotide (7). NAD (984 mg, 1.5 mmol) and 6-hydroxyindazole (625 mg, 4.7 mmol) were incubated with NADase (12 ml, 4.8 U) in DMSO (5 ml)-containing Tris-HCl (55 ml) for 12 h. The incubation mixture was treated as previously described to provide a pale-brown hygroscopic mass of **7** (764 mg): $[\alpha]_D^{23}$ −43.0° (*c*, 0.55, H_2O); UV (H_2O) 264 (log ε 4.30) and *ca.* 292 nm (sh, log ε 4.06); ^{1}H-NMR (Table 1). Found: C, 37.11; H, 4.82; N, 17.30%. Calcd for $C_{22}H_{27}N_7O_{14}P_2 \cdot 2NH_3 \cdot 1/2\,H_2O$: C, 36.75; H, 4.73; N, 17.54%.

5-Methoxy-2H-indazole Adenine Dinucleotide (8). A mixture of NAD (810 mg, 1.2 mmol), 5-methoxyindazole (420 mg, 2.9 mmol), and NADase (10 ml,4 U) was incubated in DMSO (8 ml)-containing Tris-HCl (70 ml) for 11 h. The incubation mixture was treated as previously described to give **8** (520 mg): $[\alpha]_D^{23}$ −25.5° (*c* 1.0, H_2O); UV (H_2O) 261 (log ε 4.27) and 310 nm (log ε 3.66); ^{1}H-NMR (Table 1). Found: C, 37.45; H, 4.92; N, 16.70%. Calcd for $C_{23}H_{29}N_7O_{14}P_2 \cdot 2NH_3 \cdot H_2O$: C, 37.27; H, 5.00; N, 17.01%.

6-Methoxy-2H-indazole Adenine Dinucleotide (9). A mixture of NAD (823 mg, 1.2 mmol), 6-methoxyindazole (325 mg, 2.2 mmol), and NADase (15 ml, 6 U) was incubated in DMSO (10 ml)-containing Tris-HCl (55 ml) for 15 h. The incubation mixture was treated as previously described to give a pale-yellow mass of **9** (452 mg): $[\alpha]_D^{23}$ −32.9° (*c* 0.78, H_2O); UV (H_2O) 266 (log ε 4.30) and *ca.* 290 nm (sh, log ε 4.04); ^{1}H-NMR (Table 1). Found: C, 37.22; H, 5.07; N, 16.68%. Calcd for $C_{23}H_{29}N_7O_{14}P_2 \cdot 2NH_3 \cdot H_2O$: 37.27; H, 5.00; N, 17.01%.

5-Chloro-2H-indazole Adenine Dinucleotide (10). A mixture of 5-chloroindazole (206 mg), NAD (750 mg), and NADase (10 ml) was incubated with DMSO (10 ml)-containing Tris-HCl (55 ml) for 10 h. The incubation mixture was treated as previously described to provide **10** (468 mg): $[\alpha]_D^{23}$ −22.1° (*c* 1.15, H_2O); UV (H_2O) 261 (log ε 4.18) and 305 nm (log ε 3.67); ^{1}H-NMR (Table 1). Found: C, 35.51; H, 4.57; N 16.64%. Calcd for $C_{22}H_{26}ClN_7O_{13}P_2 \cdot 2NH_3 \cdot H_2O$: C, 35.44; H, 4.56; N, 16.91%.

6-Chloro-2H-indaole Adenine Dinucleotide (11). A mixture of 6-Chloroindazole (310 mg), NAD (660 mg), and NADase (10 ml) was incubated in DMSO (8 ml)-containing Tris-HCl (50 ml) for 12 h. The reaction mixture was treated as previously described yielding a white hygroscopic mass of **11** (347 mg): $[\alpha]_D^{23}$ −33.1° (*c* 2.7, H_2O); UV (H_2O) 263 (log ε 4.17), *ca.* 300 (log ε 3.77), and *ca.* 310 nm (log ε 3.48); ^{1}H-NMR (Table 1). Found: C, 34.97; H, 4.62; N, 16.74%. Calcd for $C_{22}H_{26}ClN_7O_{13}P_2 \cdot 2NH_3 \cdot H_2O$: C, 35.44; H, 4.56; N, 16.91%.

4-Chloro-2H-indazole Adenine Dinucleotide (12). A mixture of NAD (660 mg), 4-chloroindazole (310 mg), and NADase (10 ml) was, similarly, incubated as described above. The incubated mixture was treated as previously described to give **12** (342 mg): $[\alpha]_D^{23}$ −35.6° (*c* 1.45, H_2O); UV (H_2O) 262 (log ε 4.19), 299 (log ε 3.74), and *ca.* 310 nm (sh, log ε 3.61); ^{1}H-NMR (Table 1). Found: C, 34.80; H, 4.66; N, 16.49%. Calcd for $C_{22}H_{26}ClN_7O_{13}P_2 \cdot 2NH_3 \cdot 2H_2O$: C, 34.60; H, 4.72; N, 16.51%.

Hydrolytic Cleavage of Dinucleotides to Mononucleotides. Compound **1** (120 mg) was incubated with PDE (0.4 U) in 0.2 M Tris-HCl (pH 8.8, 2 ml) containing 0.2 ml of 0.2 M $MgCl_2$ at 37 °C for 6 h. The reaction mixture, upon dilution with water (30 ml), was applied to a column (2.5 cm×15 cm) of DEAE-Sephadex. The column was eluted with 0.3 M NH_4HCO_3 to provide, in turn, AMP (54 mg) and 2*H*-indazole mononucleotide (**15**) (52 mg), separately. Spectral data regarding **15** were as follows: UV (H_2O) 276 (log ε 3.63) and 295 nm (log ε 3.56); ^{1}H-NMR (δ, D_2O) 8.64 (1H, s), 7.82 (1H, d, *J*=8.8 Hz), 7.68 (1H, d, *J*=8.8 Hz), 7.43 (1H, dd, *J*=8.8, 7.2 Hz), 7.18 (1H, dd, *J*=8.8, 7.2 Hz), 6.12 (1H, d, *J*=5.6 Hz), and 4.2—4.7 (5H, ribose). 5-Amino-2*H*-indazole mononucleotide (10 mg) was likewise obtained from compound **2** (20 mg), and its spectral data were as follows: UV (H_2O) 269 (log ε 3.72), 279 (log ε 3.70), and 330 nm (log ε 3.65); ^{1}H-NMR (δ, D_2O) 8.39 (1H, s), 7.57 (1H, d, *J*=9.0 Hz), 7.07 (1H, d, *J*=9.0 Hz), 6.04 (1H, d, *J*=5.4 Hz), and 4.1—4.7 (5H, ribose). The spectral data of 5-amino-1*H*-indazole mononucleotide (3.2 mg) obtained from compound **13** (8 mg) were as follows: UV (H_2O) 235 (log ε 4.17), *ca.* 270 (sh, log ε 3.65), and 311 nm (log ε 3.67); ^{1}H-NMR (δ, D_2O) 8.57 (1H, s), 7.54 (1H, s), 7.33 (1H, d, *J*=9.2 Hz), 7.22 (1H, d, *J*=9.2 Hz), 6.09 (1H, d, *J*=5.3 Hz), 4.1—4.7 (5H, ribose). Other mononucleotides also gave satisfactory spectral data compatible with the conclusion described in the text.

References

1) Partly reported in a preliminary communication: S. Tono-oka, I. Sekikawa, and I. Azuma, *Chem. Lett.*, **1983**, 805.

2) N. O. Kaplan and M. M. Ciotti, *J. Biol. Chem.*, **221**, 823 (1956).

3) L. S. Dietrich, I. M. Friedland, and L. A. Kaplan, *J. Biol. Chem.*, **233**, 964 (1958).

4) P. Walter and N. O. Kaplan, *J. Biol. Chem.*, **238**, 2823 (1963).

5) S. Tono-oka, A. Sasaki, H. Shirahama, T. Matsumoto, and S. Kakimoto, *Chem. Lett.*, **1977**, 1449.

6) S. Tono-oka, Y. Sasahara, A. Sasaki, H. Shirahama, T. Matsumoto, and S. Kakimoto, *Bull. Chem. Soc. Jpn.*, **54**, 212 (1981).

7) S. Tono-oka, *Bull. Chem. Soc. Jpn.*, **55**, 1531 (1982).

8) I. Saiki, S. Tono-oka, and I. Azuma, *Int Vitam. Nutr. Res.*, **51**, 239 (1981).

9) D. A. Cooney, H. N. Jayaram, G. Gebeyehu, C. R. Betts, J. A. Kelley, V. E. Marquez, and D. G. Johns, *Biochem. Pharmacol.*, **31**, 2133 (1982).

10) G. Gebeyehu, V. E. Marquez, J. A. Kelley, D. A. Cooney, H. N. Jayaram, and D. G. Johns, *J. Med. Chem.*, **26**, 922 (1983).

11) A. R. Katritzky, "Physical Methods in Heterocyclic Chemistry," Academic Press, New York (1963), Vol. I, p. 98.

12) R. M. Silverstein, G. C. Bassler, and T. C. Morrill, "Spectrometric Identification of Organic Compounds," 4th edition, John Wiley & Sons, New York (1981), p. 208.

13) R. C. Jackson, H. P. Morris, and G. Weber, *Biochem. J.*, **166**, 1 (1977).

14) J. H. Anderson and A. C. Sartorelli, *Biochem.*

Pharmacol., **18**, 2737 (1969).
15) M. J. Sweeney, D. H. Hoffman, and M. A. Estermann, *Cancer Res.*, **32**, 1803 (1972).
16) G. R. Bartlett, *J. Biol. Chem.*, **234**, 466 (1959).
17) V. Rousseau and H. G. Lindwall, *J. Am. Chem. Soc.*, **72**, 3047 (1950).
18) L. J. Zatman, N. O. Kaplan, S. P. Colowick, and M. M. Ciotti, *J. Biol. Chem.*, **209**, 467 (1954).
19) The 1 U is the amount of enzyme which will cleave 1 μ mol of the appropriate substrate per min.
20) C. Rüchardt and V. Hassmann, *Liebigs Ann. Chem.*, **1980**, 908.
21) R. R. Davies, *J. Chem. Soc.*, **1955**, 2412.
22) M. Tomita and T. Kitamura, *J. Pharm. Soc. Jpn.*, **80**, 21 (1960).
23) G. A. Jaffari and A. J. Nunn, *J. Chem. Soc.*, **1973**, 2371.
24) D. A. Cooney, Y. Wilson, and E. McGee, *Anal. Biochem.*, **130**, 339 (1983).

Preparation and Characterization of $[Fe_4S_4(SFc)_4]^{2-}$ and $[Mo_2Fe_6S_8X_3(SFc)_6]^{3-}$ (Fc=$C_5H_4FeC_5H_5$, X=EtS and MeO), and Their Catalytic Behaviors toward C_2H_2 Reduction

Koji TANAKA, Masami NAKAMOTO,† Yutaka TASHIRO, and Toshio TANAKA*
Department of Applied Chemistry, Faculty of Engineering, Osaka University, Yamada-oka, Suita, Osaka 565
†*Osaka Municipal Technical Research Instiute, Morinomiya, Joto-ku, Osaka 536*
(Received July 26, 1984)

Iron–sulfur and molybdenum–iron–sulfur clusters with ferrocenethiolate, $[Fe_4S_4(SFc)_4]^{2-}$ and $[Mo_2Fe_6S_8X_3(SFc)_6]^{3-}$ (Fc=$C_5H_4FeC_5H_5$, X=EtS and MeO), have been prepared as tetraalkylammonium salts. The reduction potentials of these clusters are more negative than those of the corresponding clusters with benzenethiolate suggesting that the ferrocencethiolate ligand has an electron donor ability stronger than the benzenethiolate ligand. Electronic absorption spectra reveal that the ferrocenethiolate ligand dissociates from the cluster anions in the electrochemically reduced states. The clusters can catalyze the reduction of C_2H_2 in water at pH 7.0 under the controlled potential electrolysis conditions. The rate of the reduction and the selectivity for the C_2H_4 formation are largely dependent on the clusters; the iron–sulfur cluster shows a higher activity than the molybdenum–iron clusters in the C_2H_2 reduction.

Studies of nitrogenase isolated from a variety of microorganisms have revealed that both iron and molybdenum–iron proteins are essential components in biological N_2 fixation.[1,2] The iron protein containing a Fe_4S_4 cluster is believed to function only as an electron-transfer catalyst.[3–5] The molybdenum–iron cofactor (MoFe-co) extracted from nitrogenase involves a novel molybdenum–iron–sulfur cluster,[6] which may be an active center for the reduction of N_2 to NH_3.[7–9] Although the structure of the MoFe-co is still ambiguous, the EXAFS studies suggest that both molybdenum and iron atoms in the MoFe-co are placed in sulfide-rich coordination sphere.[10–13] Most probable atomic ratios of Mo:Fe:S in the MoFe-co are 1:6:8—9, as determined by various chemical and physical techniques.[14] Holm *et al.* have developed a series of synthetic methods for molybdenum–iron single and double cuban clusters with chloride, alkanethiolate, and arenethiolate ligands.[9] The molybdenum–iron clusters prepared so far, however, seem to have still low iron contents relative to molybdenum in comparing with the MoFe-co. The present work was undertaken to incorporate extra iron atoms into the Fe_4S_4 as well as $MoFe_3S_4$ cores, using ferrocenethiolate in place of alkane- or arenethiolate as a ligand. The substitution of the ferrocenethiolate ligand at the cores may result in the increased stability of the cluster toward the oxidation owing to a strong electron-donating property of ferrocene. The stabilization of the cluster to the oxidation, particularly in the $[Fe_4S_4]^{2+}$ core, seem to be important in connection with high potential iron sulfur proteins which exhibit a stable $[Fe_4S_4]^{2+}/[Fe_4S_4]^{3+}$ redox couple.[15]

This paper reports the preparation and characterization of the title clusters I and II, and their catalytic abilities for the reduction of C_2H_2 in aqueous suspension under controlled potential electrolysis conditions.

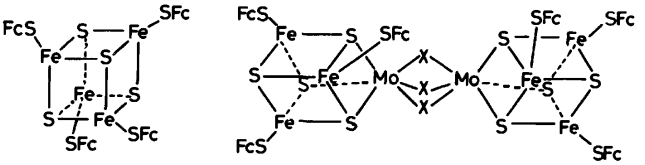

I II (X = SEt, OMe)

Fc = $C_5H_4FeC_5H_5$

Experimental

General Procedure and Materials. All manipulations were carried out under N_2 atmosphere. Solvents used for preparations and physical measurements were purified by distillation over dehydration chemicals; CaH_2 for MeCN, magnesium methoxide for MeOH, Na for THF, and CaO for DMF under reduced pressures of N_2. Ferrocenethiol,[16] $(Me_4N)_2[Fe_4S_4(SEt)_4]$,[17] and $(Et_4N)_3[Mo_2Fe_6S_8(SEt)_9]$,[18] were prepared according to the literature methods.

Preparation of $(Me_4N)_2[Fe_4S_4(SFc)_4]$ (Fc=$C_5H_4FeC_5H_5$). An MeCN (80 cm³) solution containing $(Me_4N)_2[Fe_4S_4(SEt)_4]$ (1.01 g, 1.17 mmol) and FcSH (2.04 g, 9.36 mmol) was stirred at 50 °C for 2 h during which time N_2 gas was bubbled into the solution about every 10 min. The resulting solution was evaporated to dryness under reduced pressure. The residual solid was dissolved in MeCN (40 cm³) and the solution was filtered on warming (35 °C). To the filtrate was added diethyl ether (15 cm³), and the solution was allowed to stand at 0 °C for 24 h to give black plates, which were collected by filtration, washed with diethyl ether, and dried *in vacuo*, 25% yield. Anal. Calcd for $C_{48}H_{60}Fe_8N_2S_8$: C, 42.12; H, 4.42; N, 2.04. Found: C, 41.77; H, 4.52; N, 2.07.

Preparation of $(Et_4N)_3[Mo_2Fe_6S_8(SEt)_3(SFc)_6]$. An MeCN (30 cm³) solution containing $(Et_4N)_3[Mo_2Fe_6S_8(SEt)_9]$ (0.36 g, 0.21 mmol) and FcSH (0.61 g, 2.78 mmol) was treated by the same procedure as the synthesis of $(Me_4N)_2[Fe_4S_4(SFc)_4]$ to afford black plates, in which only the terminal EtS group has been substituted by the FcS group, 62% yield. Anal. Calcd for $C_{90}H_{129}Fe_{12}Mo_2N_3S_{17}$: C, 40.36; H, 4.89; N, 1.59. Found: C, 40.20; H, 5.00; N, 1.72.

Preparation of $(Bu^n_4N)_3[Mo_2Fe_6S_8(OMe)_3(SFc)_6]$. As an attempt to incorporate the FcS group in the bridging position of Mo-Fe-S double cubane clusters, the following reaction was performed; to an MeOH (20 cm³) solution containing FcSH (4.31 g, 20 mmol) and MeONa (1.08 g, 20 mmol) was added a filtered MeOH solution (15 cm³) of $FeCl_3$ (0.81 g, 5.0 mmol), followed by the addition of $(NH_4)_2MoS_4$ (0.44 g, 1.60 mmol). After stirred for 17 h, the solution was diluted with MeOH (10 cm³) and filtered. To the filtrate was added slowly Bu^n_4NBr (1.61 g, 5.0 mmol) in MeOH (10 cm³) to give a black precipitate, which was collected by filtration and dissolved in MeCN (20 cm³) at 50 °C. After slow addition of MeOH (20 cm³), the solution was cooled to −10 °C to afford black plates of an Mo-Fe-S double cubane cluster with bridging MeO groups, which were collected by filtration, washed with MeOH, and dried *in vacuo*, 20% yield. Anal. Calcd for $C_{111}H_{171}Fe_{12}Mo_2N_3O_3S_{14}$: C, 45.87; H, 5.93; N, 1.45. Found: C, 45.62; H, 5.64; N, 1.44. The presence of three MeO groups in the cluster was confirmed as follows; HNO_3 (0.2 cm³) was added slowly to a small amount of the product (10 mg) in a test tube with a rubber stopper at 0 °C. The solution was heated at 50 °C to decompose the cluster completely, neutralized with concd aq NaOH at 0 °C, and then diluted with water to 2 cm³. The solution was analyzed on a gas chromatograph with a 2 m column filled with Gaschropack 54 (Gaschro Kogyo Co. Ltd) at 80 °C, then three moles of MeOH per one mole of the cluster decomposed were detected in the solution.

Reduction of C_2H_2 *in Water.* The reduction of C_2H_2 was carried out in a C_2H_2-saturated aqueous suspension of the tetraalkylammonium salt of $[Fe_4S_4(SFc)_4]^{2-}$ or $[Mo_2Fe_6S_8X_3(SFc)_6]^{3-}$ (7.0 μ mol, X=SEt, MeO) under the controlled potential electrolysis conditions using an Hg working electrode at −1.30—−1.40 V *vs.* SCF in a cell described in the previous papers.[19,20] pH Values of the suspension were maintained at 7.0±0.2 with an NaOH-H_3PO_4 buffer. Reaction products in the gaseous phase were determined quantitatively on a gas chromatograph with a 2 m column filled with unibeads 1S at 100 °C.

Physical Measurements. Electronic absorption and ^1H NMR spectra were measured with a Union SM 401 spectrophotometer and a JEOL PS-100 spectrometer, respectively. Cyclic voltammetry measurements were performed on a Hokuto Denko Model HA-301 potentiostat/galvanostat in DMF containing 0.1 mol dm⁻³ $Bu^n_4NClO_4$ as a supporting electrolyte, using a platinum disk-type electrode and a saturated calomel reference electrode (SCE).

Results and Discussion

It is well known that Bu^{t}S group of $[Fe_4S_4(SBu^t)_4]^{2-}$ is labile in solution.[21] Thus, $[Fe_4S_4(SFc)_4]^{2-}$ (Fc=$C_5H_4FeC_5H_5$) has easily been obtained as the tetramethylammonium salt by heating an MeCN solution containing $(Me_4N)_2[Fe_4S_4(SBu^t)_4]$ and excess FcSH at 50 °C with bubbling N_2 into the solution at a fixed time interval to remove Bu^{t}SH liberated. The ^1H NMR spectrum of the product in DMSO-d_6 shows three ring proton signals due to FcS at δ 4.60, 4.12, and 4.09 (Fig. 1a); the Bu^t proton signal originally observed in $[Fe_4S_4(SBu^t)_4]$ (δ 2.68)[22] completely disappeared, indicating that Bu^{t}S was substituted by FcS. Two different results have been reported in the substitution reaction of $[Mo_2Fe_6S_8(SEt)_9]^{3-}$ with alkanethiols; one is that both the terminal and bridging EtS groups are easily substituted,[23] and the other is that only the terminal EtS groups are active toward the substitution reaction.[24] The ^1H NMR spectrum for DMSO-d_6 solution of the product in the reaction of $[Mo_2Fe_6S_8(SEt)_9]^{3-}$ with FcSH shows the presence of three Fc-ring proton signals at δ 8.24, 4.16, and 3.85 as well as a S-CH_2 signal of the bridging EtS groups at δ 16.90, whereas the terminal EtS groups whose signals were observed in $[Mo_2Fe_6S_8(SEt)_9]^{3-}$ (S-CH_2-, δ 52.86 and S-CH_2-CH_3, δ 3.37) disappears (Fig. 1b). Similarly, the $[Mo_2Fe_6S_8(OMe)_3(SFc)_6]^{3-}$ cluster exhibits three signals due to Fc-ring protons at δ 8.20, 4.10, and 3.96 (Fig. 1c). No MeO proton signal has, however, been observed because of a large paramagnetic broadening, though the bridging MeO protons of $[Mo_2Fe_6S_8(OMe)_3(SPh)_6]^{3-}$ was reported to appear as a broad signal around δ −3.1 above 50 °C.[18]

Electrochemistry. The cyclic voltammogram of $[Fe_4S_4(SFc)_4]^{2-}$ in DMF gives a pair of cathode and anode peaks (E_c=−1.25 V, E_a=−1.10 V *vs.* SCE) which are a pseudo-reversible (2-/3-) couple (a in Fig. 2). The redox potential approximated by $E_{1/2}$ (Table 1) is about 40 mV negative compared with that of

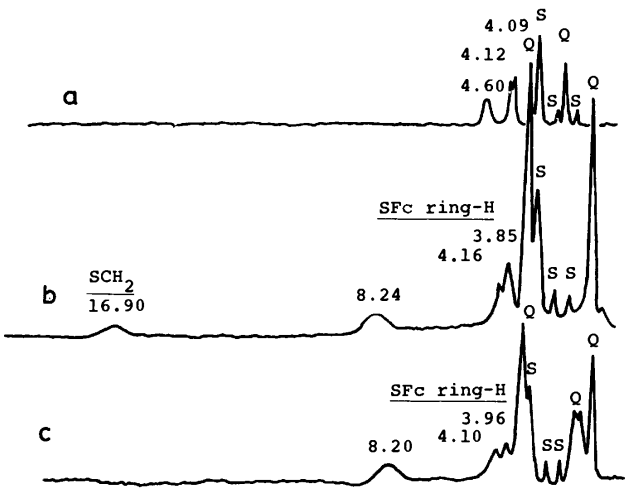

Fig. 1. Proton magnetic resonance spectra of $(Me_4N)_2[Fe_4S_4(SFc)_4]$ (a), $(Et_4N)_3[Mo_2Fe_6S_8(SEt)_3(SFc)_6]$ (b), and $(Bu^n_4N)_3[Mo_2Fe_6S_8(OMe)_3(SFc)_6]$ (c) in $(CD_3)_2SO$ at 298 K. Peaks due to the protons of the quaternary ammonium ion and the solvent are indicated by *Q* and *S*, respectively.

Table 1. Electrochemical and electronic spectral data for the clusters in DMF

Cluster	E/V *vs.* SCE			λ_{max}/nm (ε_M/mol^{-1} dm^2)		
	4-/5-	3-/4-	2-/1-			
$[Fe_4S_4(SFc)_4]^{2-}$		−1.18		310 (250000)	430 (140000)	600 (sh) [a]
$[Mo_2Fe_6S_8(SEt)_3(SFc)_6]^{3-}$	−1.34	−1.13	−0.08	308 (520000)	420 (290000)	580 (sh) [a]
$[Mo_2Fe_6S_8(OMe)_3(SFc)_6]^{3-}$	−1.37	−1.11	−0.12	308 (580000)	440 (220000)	

a) Shoulder.

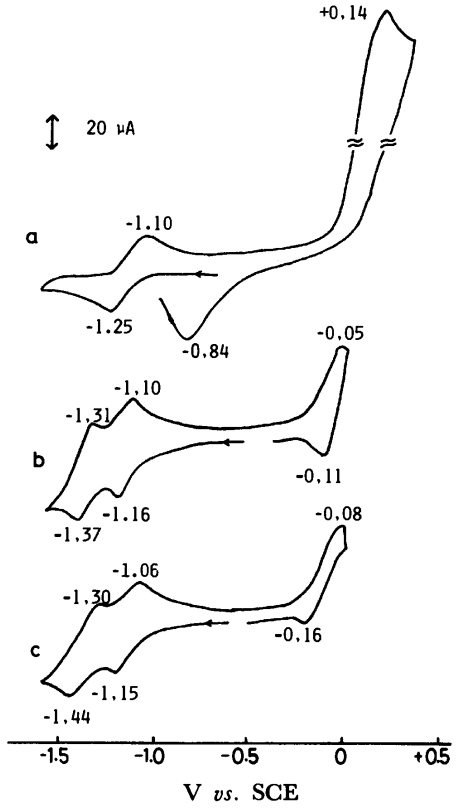

Fig. 2. Cyclic voltammograms of $[Fe_4S_4(SFc)_4]^{2-}$ (a), $[Mo_2Fe_6S_8(SEt)_3(SFc)_6]^{3-}$ (b), and $[Mo_2Fe_6S_8(OMe)_3(SFc)_6]^{3-}$ (c) in DMF containing 0.1 mol dm^{-3} $Bu^n_4NClO_4$; the scan rate 0.2 Vs^{-1}.

$[Fe_4S_4(SPh)_4]^{2-}$ in the same solvent.[25] This may be due to a donor ability of FcS stronger than PhS, as suggested for some cubane type clusters in which the more the electron-donating property of substituents is, the more negative shift the redox potential occurs.[26] On sweeping to positive potentials following to the occurrence of the pseudo-reversible couple, a strong anode peak appears at +0.14 V, followed by a cathode one at −0.84 V in the reverse scan (a in Fig. 2). The anode peak current is about 5—6 times larger than the cathode peak current and the potential difference between the these peaks is about 1 V. These results reveal that $[Fe_4S_4(SFc)_4]^{2-}$ is subject to the oxidation not only at the Fe_4S_4 core but also at the Fc moiety at +0.14 V, followed by irreversible chemical reactions. Thus, there has been observed no evidence for the presence of a stable (2-/1-) couple in $[Fe_4S_4(SFc)_4]^{2-}$, which is known to exist in high potential Fe-S proteins.[15]

In contrast to $[Fe_4S_4(SFc)_4]^{2-}$, $[Mo_2Fe_2S_8(SEt)_3(SFc)_6]^{3-}$ exhibits three reversible redox couples (3-/2-), (3-/4-), and (4-/5-) (b in Fig. 2), as confirmed by the observation that the potential difference between the anode and cathode peaks of each couple is 60 mV. The $[Mo_2Fe_6S_8(OMe)_3(SFc)_6]^{3-}$ cluster also displays three redox couples, the anode and cathode peak potentials being close to those of $[Mo_2Fe_6S_8(SEt)_3(SFc)_6]^{3-}$. The potential difference of each couple, however, is larger than 60 mV (c in Fig. 2), suggesting that the redox processes are pseudo-reversible. In addition, the cathode peak current at −0.16 V at sweep rate 0.2 Vs^{-1} is much smaller than that of the corresponding anode peak current at −0.08 V, and the cathode wave almost disappeared at sweep rate 0.02 Vs^{-1}. This result indicates that $[Mo_2Fe_6S_8(OMe)_3(SFc)_6]^{2-}$ generated by electrochemical oxidation is unstable even in the time scale of cyclic voltammetry. Thus, the Mo-Fe-S double cubane cluster bridged by EtS group may be more stable than that bridged by MeO.

Electronic Spectra. The electronic spectra of both $[Fe_4S_4(SFc)_4]^{2-}$ and $[Mo_2Fe_6S_8(SEt)_3(SFc)_6]^{3-}$ in DMF show two absorptions around 430 and 600 nm (solid line in Fig. 3), the latter of which has not been evident in the spectrum of $[Mo_2Fe_6S_8(OMe)_3(SFc)_6]^{3-}$ (Table 1). No distinct shoulder around 600 nm has been observed also in the corresponding clusters with PhS, $[Fe_4S_4(SPh)_4]^{2-}$ and $[Mo_2Fe_6S_8(SPh)_9]^{3-}$, however, the $[Fe_4S_4X_4]^{2-}$ cluster anions where X=Cl[27] and OPh[28] display a shoulder assignable to a transition within the Fe_4S_4 core in the 600—700 nm range. Thus, the shoulder around 600 nm of the present clusters may be ascribed to transitions within the Fe_4S_4 or $MoFe_3S_4$ cores. Another band around 430 nm of the present clusters is assigned to the charge-transfer transitions from terminal sulfur atoms to metal atoms of the cores on the basis of the close similarity of the spectral features to those of $[Fe_4S_4(SPh)_4]^{2-}$ [25] and $[Mo_2Fe_6S_8(SPh)_9]^{3-}$.[29]

The spectra in the course of the reduction of clusters were measured by the use of a OTTLE cell[30] under the controlled potential electrolysis conditions at 0.10—0.25 V more negative than the

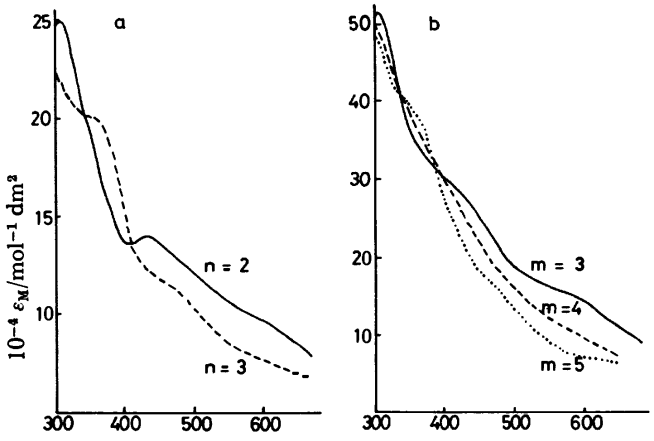

Fig. 3. Absorption spectra of (a) $[Fe_4S_4(SFc)_4]^{n-}$ (n= 2, 3) and (b) $[Mo_2Fe_6S_8(SEt)_3(SFc)_6]^{m-}$ (m=3, 4, 5) in DMF; the reduced forms with n=3 (a) and m= 4, 5 (b) were generated in an OTTLE cell by applying the potentials −1.50, −1.30, and −1.70 V (*vs.* SCE), respectively.

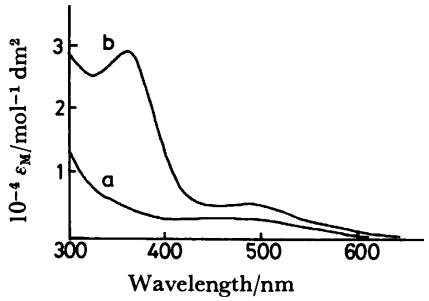

Fig. 4. Absorption spectra of FcSH (a) and FcS$^-$ (b) in DMF ; the latter was generated in an OTTLE cell by applying the potential −1.50 V (*vs.* SCE) to a solution of the Bu^n_4 N salt.

cathode peak potentials. The reduction of $[Fe_4S_4(SFc)_4]^{2-}$ at −1.50 V (*vs.* SCE) in DMF results in the decrease of absorbances around 430 and 600 nm, instead two new bands around 360 and 480 nm appear as shoulders (a broaken line in Fig. 3). The position of these shoulders are coincidence with those of absorptions appearing in the reduction of FcSH to FcS$^-$ by the controlled potential electrolysis at −1.50 V (*vs.* SCE) in DMF, as shown in Fig. 4. Thus, the reduction of $[Fe_4S_4(SFc)_4]^{2-}$ may result in a partial dissociation of FcS$^-$ as expressed in Eq. 1.

$$[Fe_4S_4(SFc)_4]^{2-} \underset{-e^-}{\overset{+e^-}{\rightleftharpoons}} [Fe_4S_4(SFc)_4]^{3-} \rightleftharpoons [Fe_4S_4(SFc)_3]^{2-} + FcS^- \quad (1)$$

The spectral change in the course of reduction was almost ceased in 30 min, except for the 360 nm band whose intensity continued to increase slowly for 1 h. The reoxidation of the resulting solution at −0.90 V (E_a=−1.10 V *vs.* SCE) recovered the 430 nm band up to more than 95%, and the 480 nm shoulder almost disappeared, although the 360 nm band still remained as a shoulder. Further oxidation at −0.50 V for 30 min resulted in complete disappearance of the 360 nm shoulder and the spectrum obtained finally was consistent with that of $[Fe_4S_4(SFc)_4]^{2-}$.

The spectral change during the electrochemical redox cycle of $[Mo_2Fe_6S_8(SEt)_3(SFc)_6]^{3-}$ in DMF is similar to that of $[Fe_4S_4(SFc)_4]^{2-}$; the reduction of $[Mo_2Fe_6S_8(SEt)_3(SFc)_6]^{3-}$ at −1.30 V (*vs.* SCE) results in weakening of the shoulder at 420 and 580 nm, and the appearance of a shoulder at 360 nm (a broken line in Fig. 3b). Further reduction at −1.70 V (*vs.* SCE) to produce $[Mo_2Fe_6S_8(SEt)_3(SFc)_6]^{5-}$ strengthens the absorbance at 480 nm as a shoulder as well as 360 nm (a broaken line in Fig. 3b). Further reduction at −1.70 V (*vs.* SCE) to produce $[Mo_2Fe_6S_8(SEt)_3(SFc)_6]^{5-}$ strengthens the absorbance at 480 nm as a shoulder as well as 360 nm (a dotted line in Fig. 3b). The absorbance at 360 nm attained to a constant value in about 30 min, which is much longer than the time required for the disappearance of the 420 nm band. The reoxidation at −0.50 V (*vs.* SCE) of the resulting solution also required more time for the disappearance of the 360 nm band than for the recovery of the intensity of the 420 nm band; the final spectrum of the solution was consistent with that of $[Mo_2Fe_6S_8(SEt)_3(SFc)_6]^{3-}$. Similar spectral changes were observed in the reduction (−1.30 and −1.70 V *vs.* SCE) and oxidation (−0.50 V *vs.* SCE) cycle of $[Mo_2Fe_6S_8(OMe)_3(SFc)_6]^{3-}$ in DMF, while no distinct shoulder appeared at 480 nm in the electrolysis at −1.70 V (*vs.* SCE). The reduction of $[Mo_2Fe_6S_8X_3(SFc)_6]^{3-}$ (X=SEt and OMe), therefore, also results in a partial dissociation of FcS$^-$ in DMF as expressed in Eq. 2.

$$[Mo_2Fe_6S_8X_3(SFc)_6]^{z-} \rightleftharpoons [Mo_2Fe_6S_8X_3(SFc)_5]^{(z-1)-} + FcS^- \quad (2)$$

z=4 and 5; X=SEt and OMe

Reduction of C_2H_2 by Clusters. It has been reported that $[Fe_4S_4(SPh)_4]^{3-}$ can reduce C_2H_2 in an aprotic solvent in the presence of CH_3COOH to give C_2H_4 selectively in a 60% yield,[31] and both $[Fe_4S_4(SPh)_4]^{2-}$ and $[Mo_2Fe_6S_8(SPh)_9]^{3-}$ catalyze the reduction of C_2H_2 to C_2H_4 in MeOH/THF under the controlled potential electrolysis conditions.[19] These results may be similar to the reduction of C_2H_2 by nitrogenase, where only C_2H_4 is produced with-

Table 2. Conditions for the reduction of C_2H_2 and the products distribution in H_2O (pH 7.0)

Catalyst[a]	Potential V *vs.* SCE	$\frac{C_2H_4}{H_2}$	$\frac{C_2H_4}{C_2H_6}$	TN[b]
$[Fe_4S_4(SFc)_4]^{2-}$	−1.30	0.79	11.1	1.65
$[Mo_2Fe_6S_8(SEt)_3(SFc)_6]^{3-}$	−1.40	0.29	11.1	1.38
$[Mo_2Fe_6S_8(OMe)_3(SFc)_6]^{3-}$	−1.40	0.22	10.0	0.63

a) 7 μmol. b) Turnover number; C_2H_4 mol/(cluster mol h).

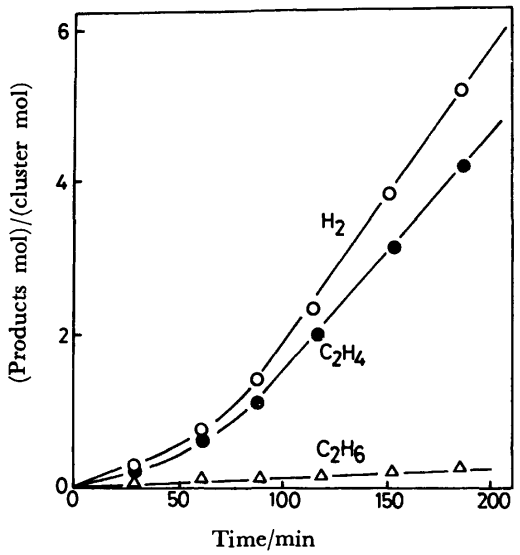

Fig. 5. Reduction of C_2H_2 catalyzed by $[Fe_4S_4(SFc)_4]^{2-}$ under the controlled potential electrolysis at −1.30 V (*vs.* SCE) in H_2O at pH 7.0.

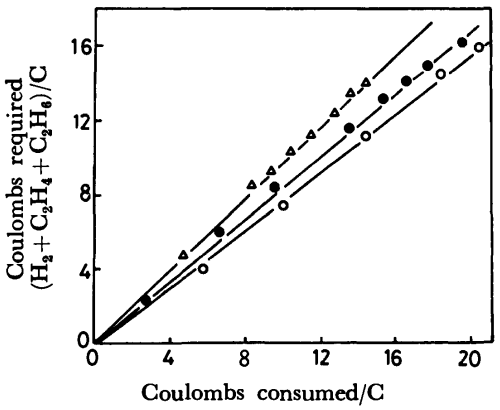

Fig. 6. Plots of the total number of coulombs required for the formation of all the products ($H_2+C_2H_4+C_2H_6$) *vs.* coulomb consumed in the reduction of C_2H_2 catalzed by $[Fe_4S_4(SFc)_4]^{2-}$ (○), $[Mo_2Fe_6S_8(SEt)_3(SFc)_6]^{3-}$ (●), and $[Mo_2Fe_6S_8(OMe)_3(SFc)_6]^{3-}$ (△) under the controlled potential electrolysis conditions in H_2O at pH 7.0.

out evolving C_2H_6 nor H_2.[32] Thus, the reduction of C_2H_2 by the reduced species of the present clusters may be of interest in comparing with that by nitrogenase. Since the present clusters are sparingly soluble in water, they were dispersed in water; a DMSO solution (1.0 cm³) of $[Fe_4S_4(SFc)_4]^{2-}$ (7 μ mol) was injected into C_2H_2-saturated water (20 cm³) containing Triton X-100 (0.01 cm³) as a surfactant and a supporting electrolyte. The controlled potential electrolysis of the solution at −1.30 V *vs.* SCE evolves C_2H_4 together with a small amount of C_2H_6 and a considerable amount of H_2, as shown in Fig. 5; the total mole of C_2H_4 and C_2H_6 produced in about 60 min exceeds the number of moles of the cluster used, confirming that the reduction of C_2H_2 proceeds catalytically. Similar catalytic reduction of C_2H_2 have occurred in water involving dispersed $[Mo_2Fe_6S_8X_3(SFc)_6]^{3-}$ (X=EtS, MeO) under the electrolysis at −1.40 V *vs.* SCE. The total numbers of coulombs required for the formation of all the products are related linearly with those consumed in the electrolysis conditions, as shown in Fig. 6, which indicates that the current efficiency for the C_2H_4, C_2H_6, and H_2 formation is essentially constant during the reaction. In addition, the electronic spectrum of the propylene carbonate extract of an aqueous suspension of either cluster in the working electrode cell after the electrolysis was identical in appearance with that in the same solvent, suggesting that most of the cluster used as a catalyst for the reduction of C_2H_2 has not been decomposed during the reaction.

The results of the reduction of C_2H_2 by the present clusters under the electrolysis conditions are collected in Table 2. Although the mole ratio C_2H_4/C_2H_6 evolved is nearly the same irrespective of the nature of the clusters used, the concomitant H_2 evolution in the reduction of C_2H_2 largely depends on the clusters; the mole ratio C_2H_4/H_2 increases in the order $[Mo_2Fe_6S_8(OMe)_3(SFc)_6]^{3-} < [Mo_2Fe_6S_8(SEt)_3(SFc)_6]^{3-} < [Fe_4S_4(SFc)_4]^{2-}$, and the rate of the C_2H_4 formation increased also in the same order. Thus, the Fe-S cluster may be concluded to exhibit not only a higher activity but also a better selectivity for the C_2H_2 reduction than the Mo-Fe-S clusters in the present reaction conditions, while the latter involves a skeltal more or less similar to MoFe-co as suggested by the EXAFS technique.[10,13]

References

1) W. E. Orme-Johnson and L. C. Davis, "Iron-Sulfur

Proteins," Vol. III, Ed. W. E. Lovenberg, Academic Press, New York (1977), p. 16.
2) L. E. Mortenson and R. N. F. Thorneley, *Ann. Rev. Biochem.*, **48**, 387 (1979).
3) B. E. Smith, D. J. Lowe, and R. C. Bray, *Biochem. J.*, **130**, 641 (1972).
4) B. E. Smith, D. J. Lowe, and R. C. Bray, *Biochem. J.*, **135**, 331 (1973).
5) B. E. Smith and G. Lang, *Biochem. J.*, **137**, 169 (1974).
6) V. K. Shah and W. J. Brill, *Proc. Natl. Acad. Sci., U. S. A.*, **78**, 348 (1981).
7) V. K. Shah, J. R. Chisnell, and W. J. Brill, *J. Biochem. Biophys. Res. Commun.*, **81**, 232 (1978).
8) H. Berndt, D. J. Lowe, and M. J. Yates, *Eur. J. Biochem.*, **86**, 133 (1978).
9) R. H. Holm, *Chem. Soc. Rev.*, **10**, 455 (1981).
10) S. P. Cramer, W. O. Gillum, K. O. Hodgeson, L. E. Mortenson, E. I. Stiefel, J. R. Chisnell, W. J. Brill, and V. K. Shah, *J. Am. Chem. Soc.*, **100**, 3814 (1978).
11) S. P. Cramer, K. O. Hodgeson, W. O. Gillum, and L. E. Mortenson, *J. Am. Chem. Soc.*, **100**, 3398 (1978).
12) B. Teo and B. A. Averill, *Biochem. Biophys. Res. Commun.*, **88**, 1454 (1979).
13) M. A. Antonio, B. Teo, W. H. Orme-Johnson, M. J. Nelson, S. E. Groh, P. A. Lindahl, S. M. Kanzlarich, and B. A. Averill, *J. Am. Chem. Soc.*, **104**, 4703 (1982).
14) M. J. Nelson, M. A. Lery, and W. H. Orme-Johnson, *Proc. Natl. Acad. Sci., U. S. A.*, **80**, 147 (1983).
15) C. D. Stout. "Iron-Sulfur Proteins," Vol. IV, Ed. T. G. Spiro, Academic Press, New York (1982), p. 99.
16) G. R. Knox and P. L. Pauson, *J. Chem. Soc.*, **1958**, 692.
17) B. A. Averill, T. Herskovitz, R. H. Holm, and J. A. Ibers, *J. Am. Chem. Soc.*, **95**, 3523 (1973).
18) G. Christou and C. D. Garner, *J. Chem. Soc., Dalton*, **1980**, 2354.
19) K. Tanaka, M. Tanaka, and T. Tanaka, *Chem. Lett.*, **1981**, 895.
20) K. Tanaka, Y. Imasaka, M. Tanaka, M. Honjo, and T. Tanaka, *J. Am. Chem. Soc.*, **104**, 4258 (1982).
21) L. Que, Jr, M. A. Bobrik, J. A. Iberse, and R. H. Holm, *J. Am. Chem. Soc.*, **96**, 4168 (1974).
22) M. A. Bobrik, L. Que, Jr, and R. H. Holm, *J. Am. Chem. Soc.*, **96**, 285 (1974).
23) G. Christou, C. D. Garner, F. E. Mabbs, and M. J. B. Drew, *J. Chem. Soc., Chem. Commun.*, **1979**, 91.
24) R. E. Palermo, P. P. Power, and R. H. Holm, *Inorg. Chem.*, **21**, 173 (1982).
25) B. V. Depamphilis, B. A. Averill, T. Herskovitz, L. Que, Jr, and R. H. Holm, *J. Am. Chem. Soc.*, **96**, 4159 (1974).
26) M. A. Bobrik, E. J. Laskowski, R. W. Johnson, W. O. Gillum, J. M. Berg, and R. H. Holm, *Inorg. Chem.*, **17**, 1402 (1978).
27) G. B. Wong, M. A. Bobrik, and R. H. Holm, *Inorg. Chem.*, **17**, 578 (1978).
28) W. E. Cleland, D. A. Holtman, M. Sabat, J. A. Ibers, G. C. DeFotis, and B. A. Averill, *J. Am. Chem. Soc.*, **105**, 6021 (1983).
29) G. Christou, P. K. Mascharak, W. E. Armstrong, G. C. Papaefthymiou, R. B. Frankel, and R. H. Holm, *J. Am. Chem. Soc.*, **104**, 2820 (1982).
30) D. Lexa, J. M. Saveant, and J. Zickler, *J. Am. Chem. Soc.*, **99**, 2786 (1977).
31) R. S. McMillan, J. Renaud, J. G. Reynold, and R. H. Holm, *J. Inorg. Biochem.*, **11**, 213 (1979).
32) R. W. F. Hardy, R. H. Holsten, J. K. Jackson, and R. C. Burns, *Plant Physiol*, **43**, 1185 (1968).

Spin Label Investigation of the Crown Ether. Complex Formation between the Veratrole Analogue of Phenoxyl-labeled Benzo-15-crown-5 and Alkali and Alkaline Earth Metal Salts in Frozen Solution

Kazuo MUKAI,* Michiyo TANII, Yohko YURUGI, Kunihiko TAJIMA, and Kazuhiko ISHIZU

Department of Chemistry, Faculty of Science, Ehime University, Matsuyama 790

(Received July 28, 1984)

A stable "phenoxyl-veratrole" (**2**), a veratrole analogue of "phenoxyl-benzo-15-crown-5" (**1**), was prepared and the complex formation between **2** and the alkali and alkaline earth metal salts has been studied by the ESR technique. Existence of the 2:1 complex of **2** with K^+, Rb^+, and Cs^+ salts was confirmed by the observation of the triplet ESR spectra in ethanol rigid matrix at 77 K. Essentially the same ***g***- and ***D***-tensor values were observed for all the 2:1 complexes, indicating similar conformation of the ligand molecule **2**. By comparing the observed *D* and *E* parameters with those of the 2:1 complexes reported for the alkali and alkaline earth metal complexes of **1** in a previous paper (Ref. 10), the structure of the 2:1 complex in ethanol rigid matrix was discussed. On the other hand, the results of the ESR measurements of the Li^+, Na^+, and alkaline earth metal complexes suggested a 1:1 complex formation between **2** and the metal salts.

Many investigations have been performed for the complex formation between crown ether and alkali and alkaline earth metal salts.[1-3] The stoichiometry of the crystalline complexes depends on the relative size of the "hole" in the crown ether and of the cation.[2-6] Such complex formations will be induced by the ion-dipole interaction between the positive ion and the cyclic polyether ring. On the other hand, Ungaro *et al.* have shown that a change in the 4-substituent for benzo-15-crown-5 (B15C5) can cause a significant change in the complex formation constant.[7] They reported that the effect may be as large as that caused by a change in the structure of the polyether ring.

The spin label investigation of the crown ether has given useful and important information about the formation and structure of the crown-metal complexes, as described in previous papers:[8,9] For instance, both the nitroxide- and galvinoxyl-labeled B15C5 compounds form 1:1 complexes with NaSCN and 2:1 complexes with KSCN, as reported for the native benzo-15-crown-5. However, the structure of the above 2:1 complexes in frozen solution is different from that of B15C5 obtained by X-ray analysis.[6]

Recently, we have prepared a stable phenoxyl derivative of benzo-15-crown-5 (hereafter called "phenoxyl-B15C5" (**1**)) (see Fig. 1) and studied the complex formation between the spin-labeled crown ether **1** and the alkali (Li^+, Na^+, K^+, and Rb^+) and alkaline earth (Mg^{2+}, Ca^{2+}, Sr^{2+}, and Ba^{2+}) metal salts by the ESR technique.[10] The result of ESR observation has established the new fact that two kinds of 2:1 complexes (hereafter called the dimer I_c and II_c complexes) having different structures (see Fig. 7 in Ref. 10) and a 1:1 complex coexist at equilibrium in all the ethanol solutions of **1** containing the above metal salts. The result is contrary to the well-known fact that the stoichiometry of the crystalline complexes depends on the relative size of the "hole" in the crown ether and of the cation, and suggests that van der Waals interaction between the aryloxyl groups substituted to the cyclic polyether ring may play an important role in the complex formation and in fixing the conformation of the complex, in addition to the above ion-dipole interaction.

In the present paper, in order to obtain further information on such complex formations, we have prepared a veratrole analogue of **1** (hereafter called "phenoxyl-veratrole" (**2**)) (see Fig. 1), in which the cyclic polyether ring is substituted by two methoxyl groups, and observed ESR spectra of its alkali and alkaline earth metal complexes in ethanol at 77 K.

Experimental

Quinol Derivative of Veratrole (3). **3** was synthesized by the reaction of lithium derivative of 4-bromoveratrole with 2,6-di-*t*-butyl-*p*-benzoquinone, according to the procedure used by us to prepare the quinol precursor of **1**.[10] **3** was recrystallized twice from ligroin (bp 90—105 °C) to give white crystals: Mp 122—123 °C; UV (EtOH) λ_{max} 282 nm (log ε=3.89); NMR (CCl_4) δ=1.18 (18H, s, *t*-Bu), 2.18 (1H, s, OH), 3.70 (6H, s, OCH_3), 6.38 (2H, s, *m*-ring), 6.68 (2H, s, aromatic H), 6.78 (1H, s, aromatic H) with Me_4Si as internal

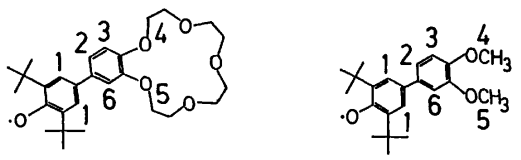

Phenoxyl-B15C5 (**1**) Phenoxyl-Veratrole (**2**)

Fig. 1. Molecular structures of phenoxyl-Bl5C5 (**1**) and phenoxyl-veratrole (**2**), and atomic numbering system.

standard.

Anal. Calcd for $C_{22}H_{30}O_4$: C, 73.71; H, 8.44%. Found: C, 73.42; H, 8.57%.

Phenol Derivative of Veratrole (4). **4** was synthesized by the reduction of **3** with Zn powder and concentrated HCl in methanol at 20 °C for 20 min.[11] **4** was recrystallized twice from ligroin (bp 95—105 °C) to give white crystals: Mp 135—136 °C; UV (EtOH) λ_{max} 268 nm (log ε=4.25); NMR (CCl_4) δ=1.45 (18H, s, *t*-Bu), 3.79 (3H, s, CH_3O), 3.81 (3H, s, CH_3O), 4.96 (1H, s, OH), 6.78 (1H, s, aromatic H), 6.83 (2H, s, aromatic H), 7.13 (2H, s, *m*-ring) with Me_4Si as an internal standard.

Anal. Calcd for $C_{22}H_{30}O_3$: C, 77.16; H, 8.83%. Found: C, 77.41; H, 9.00%.

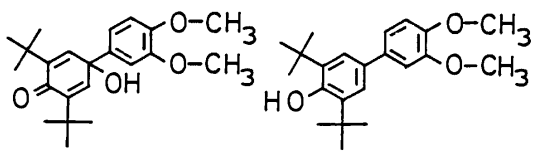

Quinol-Veratrole (**3**) Phenol-Veratrole (**4**)

Phenoxyl Derivative of Veratrole (Phenoxyl-veratrole) (2). Phenoxyl-veratrole (**2**) was prepared by the oxidation of corresponding phenol (**4**) with alkaline potassium hexacyanoferrate(III) in diethyl ether solvent under a nitrogen atmosphere, with the temperature kept between 0 and 5 °C.[12] **2** was isolated as stable dark brown crystals from the etherial solution: UV-vis (cyclohexane) λ_{max} 373 (log ε=3.71), 576 (log ε=2.93), 625 nm (log ε=3.05).

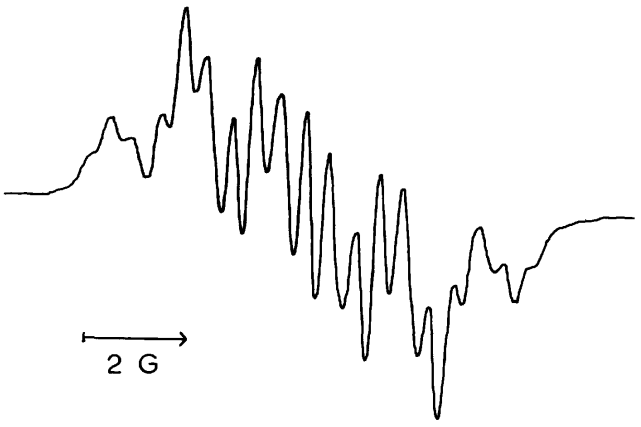

Fig. 2. ESR spectrum of **2** in ethanol at 20 °C.

The radical concentration was obtained from the results of the paramagnetic susceptibility measurements at 20 °C, after correcting for the diamagnetic contribution (χ_{dia}=−0.237×10^{-3} emu mol^{-1}) calculated by Pascal's method. The value of the radical concentration was 95%, assuming the Curie law. All the ESR spectra were measured in a sealed, degassed system.

Results and Discussion

Ethanol Solution ESR Spectrum of 2. The ethanol solution ESR spectrum of **2** has been measured at 20 °C (see Fig. 2). The observed hyperfine couplings are listed in Table 1. The value of each hyperfine splitting of phenoxyl-veratrole (**2**) is very close to the corresponding value of phenoxyl-B15C5 (**1**) radical,[10] except for the β-methyl and -methylene proton hyperfine splitting at O-4 (see Table 1). The g_{iso}-value (2.00416±0.00005) of **2** in an ethanol solution also show a good agreement with that (g_{iso}=2.00421± 0.00005) of **1** within the limits of experimental error. These results indicate that the effects of the substitution of the cyclic polyether ring by two methoxyl groups are very small to induce a change in the unpaired spin distribution of aryloxyl group.

Ethanol Rigid-matrix ESR Spectra of the Alkali and Alkaline Earth Metal Complexes of 2. An ethanol solution of **2** (3.0×10^{-3} mol dm^{-3}) containing equimolar KI salt gives an ESR spectrum consisting of (i) a central strong singlet and (ii) three pairs of absorption lines (X, X′; Y, Y′; and Z, Z′) on both sides of the central singlet at 77 K, as shown in Fig. 3 (a). A slightly asymmetric central line with a width of about 7.6 G at $g\cong2.0043$ shows a shape essentially the same as that of the metal-free **2** (ΔH_{msl}=6.9 G and $g\cong2.0042$), and the relative intensity of this central line changes depending on the ratio of the potassium salt to **2**. Therefore, this line is attributable to the 1 : 1 complex (hereafter called the monomer complex) between **2** and KI. The three pairs of absorption lines apparently represent zero-field splittings (zfs) arising from the intermolecular spin-spin dipolar interaction of two electrons in a triplet state. The result clearly indicates the formation of the 2 : 1 complex (hereafter called the dimer II_v complex) between **2** and KI. The zfs parameters (*D* and *E*) and *g*-tensor values observed for the dimer II_v complex are listed in Table 2.

First, the effects of positive ions on the complex for-

Table 1. Hyperfine couplings (a_i^H) and spin densities (ρ_i) of **1** and **2** in ethanol at 20 °C

		a_1^H	a_2^H	a_3^H	$a_4^{CH_3}$	a_6^H
2	ESR	1.41 G[a]	2.38	0.55	0.37	1.41
	ρ(exptl)	−0.0522	0.0881	−0.0204	0.0137[b]	0.0522
1	ESR	1.42 G	2.35	0.52	0.52[c]	1.42
	ρ(exptl)	−0.0526	0.0870	−0.0193	0.0128[b]	0.0526
	ρ(calcd)	−0.0296	0.0827	−0.0269	0.0105[b]	0.0341

a) Experimental errors, ±0.05 G. 1 G=10^{-4} T. b) Spin densities at O—4. c) Methylene proton hyperfine couplings.

TABLE 2. *D*- AND *g*-TENSOR VALUES OF THE COMPLEXES OF PHENOXYL-VERATROLE (**2**) WITH ALKALI METAL SALTS IN ETHANOL AT 77 K

Salts	$\frac{\lvert D\rvert^{a)}}{G}$	$\frac{\lvert E\rvert^{a)}}{G}$	$g_{xx}{}^{b)}$	g_{yy}	g_{zz}	g_{av}	Complex
LiI	a slightly asymmetric single line ($\Delta H_{msl}\cong 7.5$ G)						(1 : 1)
NaI	a slightly asymmetric single line ($\Delta H_{msl}\cong 7.8$ G)						(1 : 1)
KI	96.1	5.8	2.0062	2.0041	2.0031	2.0045	(2 : 1)
RbI	96.0	6.0	2.0057	2.0039	2.0032	2.0043	(2 : 1)
CsI	96.4	5.7	2.0063	2.0039	2.0028	2.0043	(2 : 1)
KBr	96.0	5.7	2.0062	2.0040	2.0032	2.0044	(2 : 1)
KSCN	96.0	5.8	2.0062	2.0040	2.0031	2.0042	(2 : 1)
KIO_4	a slightly asymmetric single line ($\Delta H_{msl}\cong 7.7$ G)						(1 : 1)
K_2SO_4	a slightly asymmetric single line ($\Delta H_{msl}\cong 7.3$ G)						(1 : 1)

a) The experimental errors in the values of $|D|$ and $|E|$ are ± 0.4 G. 1 G $=10^{-4}$ T. b) The experimental errors in the values of g_{xx}, g_{yy}, and g_{zz} are ± 0.0002.

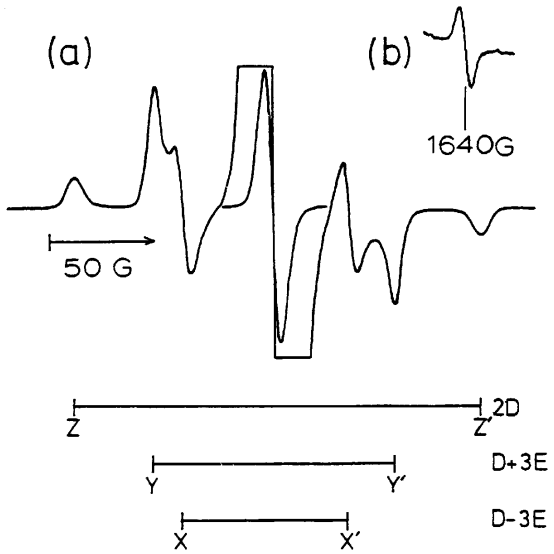

Fig. 3. ESR spectrum of the KI complex of **2** in ethanol at 77 K: (a) $\Delta m_s=\pm 1$ transition and (b) $\Delta m_s=\pm 2$ transition.

mation and on the molecular structure of the complex were studied. The ESR spectra of both the RbI and CsI complexes of **2** in ethanol at 77 K show shapes essentially the same as that of the KI complex, indicating the coexisting of a dimer and a monomer. As it is clear from the results shown in Table 2, the variation in zfs parameters with cations (K^+, Rb^+, and Cs^+) is almost negligible in the present dimer II_v complexes. On the other hand, ethanol solutions of **2** (3.0×10^{-3} mol dm^{-3}) containing equimolar alkali (LiI and NaI) and alkaline earth ($MgCl_2$, $SrCl_2$, and BaI_2) metal salts show a slightly asymmetric single line with a width of about 7 G located at $g\cong 2.004$ at 77 K, respectively, unequivocally suggesting 1 : 1 complex formation between **2** and the above salts.

Second, the effects of the negative ions (Br^-, I^-, SCN^-, IO_4^-, and SO_4^{2-}) on the complex formation and on the molecular structure of the complex have been studied. The anions were varied in the K^+ and Na^+ salts. ESR spectra of the KBr and KSCN complexes of **2** in ethanol rigid-matrix at 77 K are very similar to that of the KI complex, except for the difference in the central signal intensity, indicating the coexisting of a dimer II_v and a monomer. The observed ***D***- and ***g***-tensor values are summarized in Table 2. The result indicates that the effect of the change in anions is too small to induce the change in the molecular structure of the 2:1 complex. However, triplet ESR spectrum was not observed for the KIO_4 and K_2SO_4 complexes of **2**, suggesting the effect of anions on complex formation. On the other hand, similar single line ESR spectra were observed in all the Na complexes of **2** studied, indicating the 1:1 complex formation.

Here, an attempt to establish the molar ratio of the monomer and dimer II_v was achieved by observing the ethanol rigid-matrix ESR spectrum of **2** containing equimolar KI salt. The approximate ratio can be determined from the integrated spectral intensity of a first-derivative ESR absorption line.[13] The ratio obtained is monomer:dimer II_v=4:1.

The Structure of the 2:1 Complexes of **2** *with K^+, Rb^+, and Cs^+ Metal Salts.* As reported in a previous paper,[10] the results of the ESR observations have established the new fact that two kinds of 2:1 complexes (the dimer I_c and II_c complexes) having different structures and a 1:1 complex coexist at equilibrium in all the ethanol solutions of phenoxyl-B15C5 (**1**) containing the eight kinds of the alkali and alkaline earth metal salts. In addition, both in dimer I_c and II_c, the *D* and *E* values and *g*-tensor values observed for all the alkali and alkaline earth metal complexes remain constant, respectively, within the limit of experimental error, except for the small change in dimer II_c complexes of **1** with $SrCl_2$ and BaI_2. For instance, the *D* and *E* values and *g*-tensor values observed for the KI complex of **1** are $|D_I|$= 24.1 G, $|E_I|$=0.9 G, g^I_{xx}=2.0047, g^I_{yy}=2.0040 for dimer I_c, and $|D_{II}|$=97.6 G, $|E_{II}|$=6.5 G, g^{II}_{xx}=2.0061, g^{II}_{yy}=

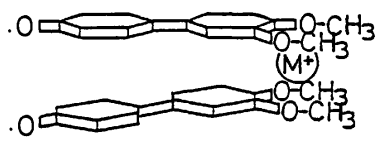

Fig. 4. Conformation of dimer II_v.

2.0036, g_{zz}^{II}=2.0026 for dimer II_c.

The result of the present ESR observations showed that a kind of 2:1 complex and a 1:1 complex coexist at equilibrium in the ethanol solutions of **2** containing the K^+, Rb^+, and Cs^+ metal salts. For instance, the *D*, *E*, and *g*-tensor values observed for the KI complex of **2** in ethanol rigid-matrix are $|D|$=96.1 G, $|E|$=5.8 G, g_{xx}=2.0062, g_{yy}=2.0041, and g_{zz}=2.0031, as listed in Table 2. It is very interesting that the phenoxyl-veratrole (**2**) having no crown ether ring forms 2:1 complex with alkali metal salts. And, further, these values are very similar to those observed for the dimer II_c complex of KI salt of **1**. As has been descrived in a previous section, **1** and the veratrole analogue (**2**) have similar spin distribution in a fluid solution. Therefore, the similarity of the *D*, *E*, and *g*-values observed for **1** and **2** suggests that the dimer II_v structure of the KI complex of **2** is similar to that of the dimer II_c structure of the KI complex of **1** (see Fig. 7 in Ref. 10). That is, the dimer II_v has a structure in which the aryloxyl radical parts of the complex overlap each other. From the results of the observed zfs parameters, a preferable conformation of the dimer II_v complex of **2** was assumed as illustrated in Fig. 4.

Many investigations have been performed for the complex formation between crown ether and alkali and alkaline earth metal salts, including B15C5, in solution and in the solid state.[1-7] The stoichiometry of the crystalline complexes depends on the relative size of the hole in the crown ether and of the cation. For instance, B15C5 with a hole 1.7—2.2 Å in diameter usually forms a 1:1 complex with Na^+ (diameter, 1.90 Å), because the Na^+ cation fits tightly in the crown cavity. But, it forms a 2:1 complex with K^+ (2.66 Å), the ion larger than the hole. Such complex formations will be induced by the ion-dipole interaction between the positive ion and the cyclic polyether ring. Therefore, by substituting the two methoxyl groups for the cyclic polyether ring, the above ion-dipole interaction will decrease considerably, and thus the complex formation will not be observed.

However, the result of the present investigation showed that the phenoxyl-veratrole (**2**), having no polyether ring, forms 2:1 complexes with alkali metal salts (K^+, Rb^+, and Cs^+). Further, the 2:1 complexes of **2** have a structure, in which the aryloxyl skeletons stack over one another, as shown in Fig. 4. It is probable that the van der Waals interaction between the two substituted aryloxyl groups induces such a complex formation and a conformation. On the other hand, the fact that the phenoxyl-veratrole (**2**) does not form 2:1 complex with LiI, NaI, and alkaline earth salts suggests that the ion-dipole interaction also play an important role in the above complex formation.

We are very grateful to Mr. Minoru Yamashita and Mr. Kyozo Ueda for their kind help in the synthesis of **2**. We also wish to thank Mr. Kazuyuki Fukuda for his kind help in the measurement of the ESR spectra.

References

1) C. J. Pedersen, *J. Am. Chem. Soc.*, **89**, 7017 (1967).
2) C. J. Pedersen, *J. Am. Chem. Soc.*, **92**, 386 (1970).
3) J. J. Christensen, D. J. Eatough, and R. M. Izatt, *Chem. Rev.*, **74**, 351 (1974), and references cited therein.
4) M. A. Bush and M. R. Truter, *J. Chem. Soc. Perkin Trans, 2*, **1972**, 341.
5) N. S. Poonia and M. R. Truter, *J. Chem. Soc. Dalton*, **1973**, 2062.
6) P. R. Mallinson and M. R. Truter, *J. Chem. Soc. Perkin Trans 2*, **1972**, 1818.
7) R. Ungaro, B. El Haj, and J. Smid, *J. Am. Chem. Soc.*, **98**, 5198 (1976).
8) K. Ishizu, H. Kohama, and K. Mukai, *Chem. Lett.*, **1978**, 227.
9) K. Mukai, N. Iida, and K. Ishizu, *Bull. Chem. Soc. Jpn.*, **55**, 1362 (1982).
10) K. Mukai, M. Yamashita, K. Ueda, K. Tajima, and K. Ishizu, *J. Phys. Chem.*, **87**, 1338 (1983).
11) A. Rieker and K. Scheffler, *Ann. Chem.*, **689**, 78 (1965).
12) E. Müller and K. Ley, *Chem. Ber.*, **87**, 22 (1954).
13) H. Yokoi and T. Isobe, *Bull. Chem. Soc. Jpn.*, **46**, 447 (1973).

Interaction of Galvinoxyl Radical with Ascorbic Acid, Cysteine, and Glutathione in Homogeneous Solution and in Aqueous Dispersions

Jyunichi TSUCHIYA, Teruaki YAMADA, Etsuo NIKI,* and Yoshio KAMIYA
Department of Reaction Chemistry, Faculty of Engineering, University of Tokyo, Hongo, Tokyo 113
(Received August 17, 1984)

The rates of interaction of galvinoxyl radical with ascorbic acid, cysteine, and glutathione have been studied in homogeneous solution and in water dispersions as a model reaction of vitamin E radical with these reducing agents in biological systems. The rate was measured by following the disappearance of galvinoxyl radical with absorption spectroscopy and electron spin resonance. In every system, galvinoxyl reacted with these reducing substrates and their relative reactivities decreased in the order of ascorbic acid>cysteine>glutathione. For any reducing substrate, the rate was fastest in homogeneous solution and slowest in micelle in Triton X-100 aqueous solution, and the rate in liposome system was in between.

The oxidation of polyunsaturated fatty acids in the lipids and its inhibition has received much attention recently in connection with its pathological effects in biological systems and preservation of foods.[1-8] Vitamin E has been known to act as an effective antioxidant.[9-12] A synergistic inhibition of oxidation by the combination of vitamin E with reducing agents has been suggested[13-19] and it has been observed experimentally that vitamin E radical reacts with ascorbic acid[13,20,21] and glutathione[21,22] to regenerate vitamin E.

In biological systems, most of vitamin E is present in lipophylic membranes, whereas ascorbic acid, glutathione, and cysteine are found in aqueous phase. Therefore, the interaction of vitamin E radical with these reducing agents must be more restricted than in homogeneous system and the effect of reaction medium must be quite important. In order to study the effect of reaction medium, the rates of interaction of galvinoxyl radical (**1**) with ascorbic acid, glutathione, and cysteine were measured both in homogeneous solution and in aqueous dispersions. Galvinoxyl was chosen as a model of vitamin E radical, since both are relatively stable phenoxyl radicals and galvinoxyl is much easier to locate in liposomal membranes and micelles than vitamin E radical (**2**).

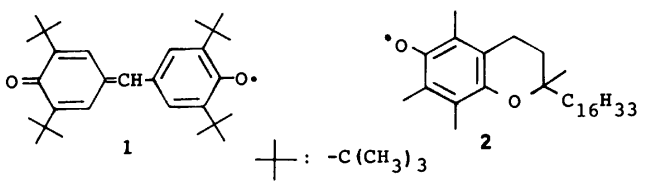

Experimental

Materials. Galvinoxyl, L-ascorbic acid, cysteine, and glutathione (reduced form) were of the highest grade available and used as received. *N,N'*-dioxide-2-methyl-*N*-(4-pyridinylmethylene)-2-propanamine (POBN) used as a spin trap was obtained from Aldrich. Dimyristoylphosphatidylcholine (PC) was obtained from Sigma and used without further purification. Ethyl palmitate, ascorbyl-6-stearate, and Triton X-100 were purchased from Tokyo Kasei Kogyo Co. and used as received.

Procedure. The micelle was prepared as follows using Triton X-100 as a nonionic surfactant. Appropriate amount of galvinoxyl was dissolved into ethyl palmitate and then 0.01 M (1 M=1 mol dm^{-3}) Triton X-100 aqueous solution was added. The mixture was shaken vigorously with a Vortex mixer for 1 min to obtain pale brownish micelle solution.

The liposome was prepared by the following method. PC and galvinoxyl (and other oil-soluble additives, when necessary) were dissolved in benzene or in benzene–ethanol (1:1 by volume) and the solution was taken into a small flask. The solvent was removed by evacuation on a water aspirator using a rotary evaporator to obtain a thin film on the flask wall. It was further evacuated under high vacuum. Appropriate amount of 0.1 M NaCl aqueous solution was then added and the film was slowly peeled off by shaking to obtain a milky liposome solution. In several experiments, the solution was sonicated using a Branson Sonifier Model 185.

The rate of disappearance of galvinoxyl was followed by absorption spectroscopy at 429 nm. The reaction was started by mixing the galvinoxyl solution with the reducing agent solution in a Pyrex glass ampoule immersed in a water bath maintained at the desired temperature. The solution was taken out periodically and analyzed.

The rate was also followed by electron spin resonance (ESR) spectroscopic analysis. ESR spectra were recorded on X-band JEOL FE1X spectrometer using a quartz flat cell.

Results

ESR Spectra of Galvinoxyl Radical. Figure 1 shows the ESR spectra of galvinoxyl radical in different media at different temperatures. In homogeneous solution, an isotropic ESR spectrum of galvinoxyl radical with good hyperfine splitting was observed. In micelle, the hyperfine structure showed good split at higher temperature. Similarly, the hyperfine splitting

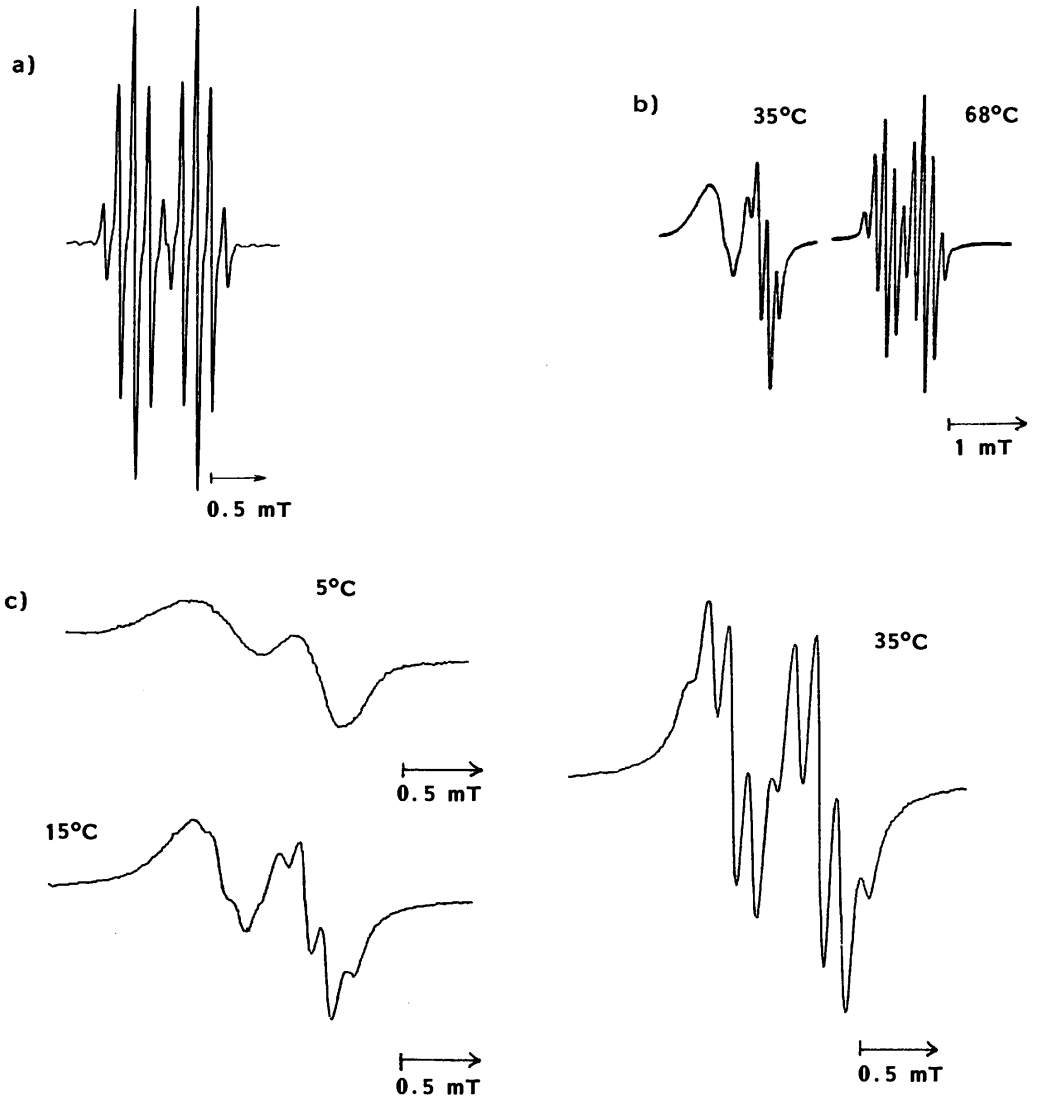

Fig. 1. ESR spectra of galvinoxyl radical in various media.
a) 0.50 mM galvinoxyl in benzene at room temperature under vacuum. b) In 10 mM Triton X-100 aqueous dispersion. c) In dimyristoyl PC liposome dispersed in 0.1 M NaCl aqueous solution.

was not satisfactory below 15 °C for the galvinoxyl incorporated into dimyristoyl PC liposome. The coupling constants for galvinoxyl are summarized in Table 1.

Interaction of Galvinoxyl Radical with Reducing Agents in Homogeneous Solution. When two methanol solutions containing 2.5 mM galvinoxyl and 25 mM ascorbic acid, respectively, were mixed at room temperature, galvinoxyl disappeared instantaneously. On the other hand, when galvinoxyl was mixed with cysteine or glutathione, galvinoxyl disappeared gradually with time and the first order plot gave a good straight line. The pseudo-first order rate constants obtained from this plot are summarized in Table 2.

Interaction in Micelle System. The galvinoxyl incorporated into micelle reacted with ascorbic acid, cysteine, and glutathione. Figure 2 shows an example

Table 1. Coupling constants of galvinoxyl radical in various media[a)]

Medium	Temp °C	a_p^{CH} mT	a_m^H mT
In homogeneous solution of benzene			
	25	0.583	0.140
		0.590[b)]	0.140[b)]
In ethyl palmitate micelle in Triton X-100			
aqueous dispersion	38	0.548	0.137
	48	0.552	0.140
	68	0.554	0.139
In dimyristoyl PC liposome in 0.1 M NaCl			
aqueous dispersion	25	0.594	0.142
	35	0.591	0.143
	46	0.588	0.142

a) Numbers in three decimal places may not be so accurate. b) Ref. 23.

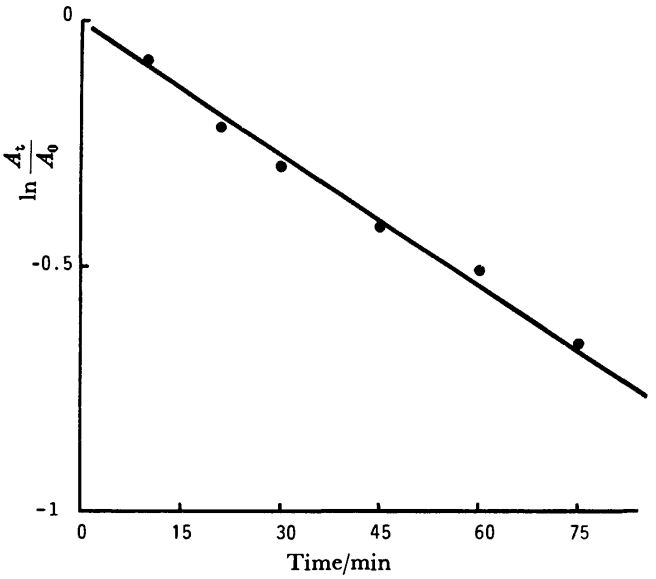

Fig. 2. Pseudo-first order plot of galvinoxyl radical for the reaction with ascorbic acid at 37 °C in Triton X-100 aqueous dispersion: 4 ml ethyl palmitate containing 10 mM galvinoxyl and 4 ml of 50 mM ascorbic acid in 10 mM Triton X-100 aqueous solution were mixed.

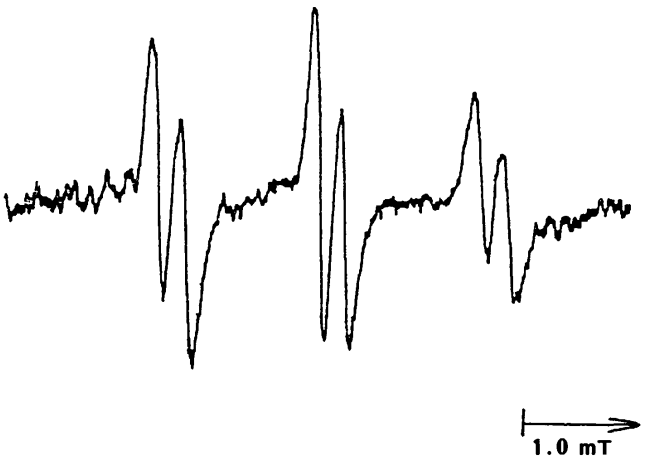

Fig. 3. ESR spectrum observed when POBN was dissolved in an aqueous solution during the interaction of galvinoxyl radical with glutathione in micelle system.

of the first order plot of the galvinoxyl radical in the reaction with ascorbic acid at 37 °C. The galvinoxyl is stable in the absence of ascorbic acid. The results with ascorbic acid are summarized in Table 3. The pseudo-first order rate constant was insensitive to the concentration of ascorbic acid and surfactant and also to the ratio of organic to aqueous fractions.

Interaction in Liposome System. Galvinoxyl incorporated into dimyristoyl PC liposome reacted with ascorbic acid, cysteine, and glutathione faster than in micelle system. Satisfactory first order plot was obtained. The results obtained in different systems are summarized in Table 4. In every case, the

Table 2. Rate of reaction of galvinoxyl radical (G) with ascorbic acid (AsA), Cysteine (CSH), and glutathione (GSH) at 37 °C in homogeneous solution[a] measured by absorption spectroscopy

[G] mM	Reactant	mM	$10^4 k$[d] s^{-1}
2.5[b]	AsA	25	e)
2.5[c]	AsA	25	e)
1.5	CSH	15	10
2.5	GSH	15	1.8
1.5	GSH	7.7	1.1
1.5	GSH	15	1.8
1.5	GSH	30	2.4
1.5	GSH	60	3.3
1.5	GSH	150	3.2
0.75	GSH	15	1.8
0.195[f]	GSH	0.81	2.8

a) Acetone/water=9/4 by v/v. b) In methanol. c) In acetone/methanol=15/8 by v/v. d) Pseudo-first order rate constant. e) The rate was too fast to be measured. f) In acetone/water=5/3 by v/v measured by ESR.

Table 3. Interaction of galvinoxyl radical (G) dissolved in ethyl palmitate (EP) micelle with ascorbic acid (AsA) in 10 mM Triton X-100 aqueous dispersion at 37 °C measured by absorption spectroscopy

G in EP [G] mM	ml	AsA in 10 mM Triton X-100 aq [AsA] mM	ml	$10^4 k$ s^{-1}
5	3	0	3	0
5	4	100	4	1.7
5	4	50	4	1.5
5	4	25	4	1.4
5	4	5	4	0.64
10	4	50	4	1.5
2.5	4	50	4	1.7
5	1	50	7	2.8
5	2	50	6	1.8
20	1	50	7	2.4
5	1	50	7[a]	1.7

a) In 100 mM Triton X-100 aqueous solution.

results obtained by absorption spectroscopy and ESR were in satisfactory agreement.

Discussion

Galvinoxy radical must interact with the reducing agents by a hydrogen atom abstraction. In fact, when a spin trap, POBN, was also dissolved in an aqueous phase in micelle system, new ESR spectra were observed as galvinoxyl disappeared in the presence of cysteine and glutathione. The example of the ESR spectrum is shown in Fig. 3 and the hyperfine

Table 4. Pseudo-first order rate constant (s^{-1}) for the interaction of galvinoxyl radical with ascorbic acid, cysteine, and glutathione in various reaction media at 37 °C

	Homogeneous solution[a]	Micelle[b]	Liposome[c]
Ascorbic acid	Too fast	1.7×10^{-4}	Too fast
Cysteine	1.0×10^{-3}	4.5×10^{-5}	6.5×10^{-4}
Glutathione	1.8×10^{-4}	1.7×10^{-5}	2.0×10^{-4}

a) In acetone/waser (9/4 by v/v). b) Galvinoxyl dissolved in ethyl palmitate in 10 mM Triton X-100 aqueous disperson. c) Galvinoxyl incorporated into dimyristoyl PC in 0.1 M NaCl aqueous dispersoin.

Table 5. Hyperfine splitting constants for the spin adducts of glutathione and cysteine radicals by POBN[a]

	a^N/mT	a^H_β/mT
Glutathione	1.495	0.230
Glutathione[b]	1.513	0.232
Cysteine	1.504	0.230

a) 1.18 mM galvinoxyl in Triton X-100 aqueous dispersion was reacted with 10 mM glutathione or cysteine. b) In ethanol/water (5/1 by v/v).[21]

splitting constants are given in Table 5. The same ESR spectra were observed when *t*-butoxyl radical was generated from di-*t*-butyl diperoxyoxalate containing POBN and glutathione or cysteine. Therefore, these spectra may well be ascribed to the spin adduct of glutathione radical or cysteine radical by POBN.[21]

Table 4 summarizes the rate constants for the interaction of galvinoxyl with the reducing agents in different systems. It shows that in every system the relative reactivities decrease in the order of ascorbic acid>cysteine>glutathione. It also shows that for any reducing agent the interaction proceeds most rapidly in homogeneous solution and most slowly in micelle system. The rate of interaction in liposome system was in between.

The lower reactivities in liposome and in micelle systems than in homogeneous solution must be ascribed to a lower mobility of galvinoxyl and to a lower accesibility of the reducing agent to galvinoxyl.

It must be important to compare the present results with the antioxidant activities of vitamin E and reducing agents. As reported previously,[13] vitamin E and vitamin C inhibited synergistically the oxidation of methyl linoleate in homogeneous solution. It was suggested that vitamin E scavenges the chain carrying peroxyl radical quickly and the resulting vitamin E radical reacts with vitamin C to regenerate vitamin E. As a consequence, only vitamin C was consumed at first and vitamin E decayed after vitamin C was depleted.

In the oxidation of soybean PC liposome initiated with an oil-soluble azo compound, vitamin C was not as good antioxidant as in the oxidation initiated with a water-soluble azo compound, but vitamin C was still suggested to react with vitamin E radical in the bilayer, regenerate vitamin E and reduce the rate of disappearance of vitamin E.[24]

Interestingly, in contrast to the oxidation in homogeneous solution and in liposome system mentioned above, vitamin C was not an effective antioxidant in the oxidation of methyl linoleate micelle in Triton X-100 aqueous dispersion initiated with an oil-soluble azo compound. However, even in this case, vitamin C could prolong the suppression period when 2,2,5,7,8-pentamethyl-6-chromanol, a vitamin E model, was located in micelle.

It may be also worth noting, that, although galvinoxyl incorporated into liposome reacted with vitamin C in an aqueous phase so rapidly, it reacted only slowly with ascorbyl-6-stearate incorporated into different liposome in the same water dispersion.

The results obtained in the present study and those of oxidations described above are in accordance with each other, although it must be considered that the location and behavior of galvinoxyl and vitamin E radicals in the membrane may not be identical. Furthermore, the location of phenoxyl radicals in micelle and liposome and the accesibility of reducing agents must also depend on the type of surfactant, composition of fatty acids in micelle and liposome, and other experimental variables.

In conclusion, the present results show that stable phenoxyl radicals react with reducing agents such as ascorbic acid, cysteine, and glutathione by a hydrogen atom abstraction not only in homogeneous solution but also in heterogeneous aqueous dispersions. This is another experimental support to the possible contribution of vitamin E and reducing agents in synergistic inhibition of peroxidation in biological systems.

References

1) "Oxygen Radicals in Chemistry and Biology," ed by Walter de Gruyter, Berlin, (1984).

2) "Oxygen Free Radicals and Tissue Damage" (Chiba Foundation Symp.), Excerpta Medica, Amsterdam, 1979.

3) "Biochemical and Medical Aspects of Active Oxygen," O. Hayaishi and K. Asada, ed by Japan Sci. Soc. Press, Tokyo, (1977).

4) "Oxygen and Oxygen Radicals in Chemistry and Biology," M. A. Rodgers and E. L. Powers, ed by Academic Press, New York, 1981.

5) W. S. Caughey, ed., "Biochemical and Medical Aspects of Oxygen," Academic Press, New York, (1979).

6) M. G. Simic and M. Karel, ed., "Autoxidation in Food and Biological Systems," Plenum, New ork, (1980).

7) K. Yagi, ed., "Lipid Peroxides in Biology and Medicine," Academic Press, New York, (1982).

8) "Free Radicals, Lipid Peroxidation and Cancer," D. C. H. McBrien and T. F. Slater, ed by Academic Press, London, (1982).
9) "Tocopherol, Oxygen, and Biomembranes," C. de Duve and O. Hayaishi, ed by Elsevier, Amsterdam, (1978).
10) "Vitamin E," M. J. Machlin, ed by Marcel Dekker, New York, (1980).
11) E. Niki, R. Tanimura, and Y. Kamiya, *Bull. Chem. Soc. Jpn.*, **55**, 1551 (1982).
12) G. W. Burton, A. Joyce, and K. U. Ingold, *Arch. Biochem. Biophys.*, **221**, 281 (1983).
13) E. Niki, T. Saito, A. Kawakami, and Y. Kamiya, *J. Biol. Chem.*, **259**, 4177 (1984).
14) A. L. Tappel, *Geriatrics*, **1968**, 97.
15) W. M. Cort, *J. Am. Oil Chem. Soc.*, **51**, 321 (1974).
16) H. W. Leung, M. J. Vang, and R. D. Mavis, *Biochim. Biophys. Acta*, **664**, 266 (1981).
17) E. Niki, T. Saito, and Y. Kamiya, *Chem. Lett.*, **1983**, 631.
18) L. R. C. Barclay, S. J. Locke, and J. M. MacNeil, *Can. J. Chem.*, **61**, 1288 (1983).
19) M. Nishikimi and L. J. Machlin, *Arch. Biochem. Biophys.*, **170**, 684 (1975).
20) J. E. Packer, T. F. Slater, and R. L. Willson, *Nature*, **278**, 737 (1979).
21) E. Niki, J. Tsuchiya, R. Tanimura, and Y. Kamiya, *Chem. Lett.*, **1982**, 789.
22) C. C. Reddy, R. W. Scholz, C. E. Thomas, and E. J. Massaro, *Life Sci.*, **31**, 571 (1982).
23) J. K. Becconsall, S. Clough, and G. Scott, *Trans. Faraday Soc.*, **56**, 459 (1960).
24) E. Niki, A. Kawakami, Y. Yamamoto, and Y. Kamiya, unpublished work.

 © 1985 The Chemical Society of Japan Bull. Chem. Soc. Jpn., 58, 331—335 (1985)

Natural Homologs of Gramicidin S. II.[1] Synthesis of Gramicidin S-2 and S-3

Sukekatsu NOZAKI* and Ichiro MURAMATSU†

Faculty of Pharmaceutical Sciences, Josai University, Sakado, Saitama 350-05

†*Department of Chemistry, College of Science, Rikkyo University, Nishi-Ikebukuro, Tokyo 171*

(Received August 21, 1984)

Two cyclic dodecapeptides corresponding to newly found members of gramicidin S family, gramicidin S-2: *cyclo*(-Val-Orn-Leu-D-Phe-Pro-Abu-Orn-Leu-D-Phe-Pro-), and gramicidin S-3: *cyclo*(-Abu-Orn-Leu-D-Phe-Pro-Abu-Orn-Leu-D-Phe-Pro-), were synthesized. In the synthesis, the linear decapeptide precursors of the antibiotics prepared by a combination of the "hold-in-solution" method and the usual liquid phase method were converted to cyclic ones in excellent yields by one-pot reaction using 1-ethyl-3-(3-dimethylaminopropyl)carbodiimide hydrochloride and 1-hydroxybenzotriazole. The synthesized antibiotics were identical with the natural products in HPLC analysis and assays of the antibiotic activities. The proposed structures for gramicidin S-2 and S-3 were confirmed. The CD spectra showed that the ring conformations of gramicidin S-2 and S-3 closely resemble each other and also that of gramicidin S-1, which has the already known structure.

In studies of gramicidin S, a peptide antibiotic produced by *Bacillus brevis* strain ATCC 9999 or the Nagano strain, it is known that replacement of the constituent amino acids in the antibiotic by other ones can occur because of the rather broad specificities of gramicidin S synthetases.[2] However, as the natural product only a single compound has been known, in which two identical pentapeptides join head to tail (Fig. 1. Gramicidin S-1).[3]

Recently we found that natural gramicidin S consists of at least 3 compounds; gramicidin S-1 as the major component with the known structure, and two minor ones, gramicidin S-2: *cyclo*(-Val-Orn-Leu-D-Phe-Pro-Abu-Orn-Leu-D-Phe-Pro-) and gramicidin S-3: *cyclo*(-Abu-Orn-Leu-D-Phe-Pro-Abu-Orn-Leu-D-Phe-Pro-) (Fig. 1).[1]

For investigation of the properties of the newly found minor components, chemical synthesis of them is required since isolation of the less abundant compounds from the mixture of the natural products exclusively depends on HPLC technique; providing of them in a sufficient amount is difficult in practice from the natural source.

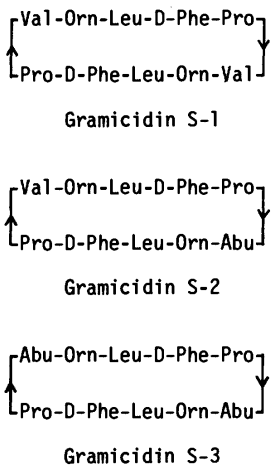

Fig. 1. Structures of gramicidin S-1, S-2, and S-3.

A convenient method was adopted for the preparation of gramicidin S-2 and S-3. The method (Fig. 2) includes rapid preparation of the tetrapeptide (**1**), effectual fragment condensation to give the C-terminal free decapeptides (**5a** and **5b**), and one-pot cyclization to afford the cyclic decapeptides (**7a** and **7b**).

The tetrapeptide (**1**) was synthesized by the "hold-in-solution" method[4] in an overall yield of 48% based on the C-terminal amino acid ester. The pentapeptides (**2a** and **2b**) derived from **1** were saponified to give the C-terminal free peptides (**3a** and **3b**), which were further converted to the N- and C-terminal free peptides (**4a** and **4b**). The coupling reaction of **3a**, which was preactivated by 1-ethyl-3-(3-dimethylaminopropyl) carbodiimide hydrochloride (WSCD·HCl)[5] and 1-hydroxybenzotriazole (HOBt)[6], and the amine components (**4a** and **4b**) afforded the C-terminal free decapeptides (**5a** and **5b**) in 96 and 93% yields, respectively. By acidolysis, the decapeptides (**5a** and **5b**) were converted to the N- and C-terminal free decapeptides (**6a** and **6b**), each of which was allowed to cyclize in anhydrous pyridine-DMF (1:1, 3×10^{-3} M peptide in the solvent (1 M=1 mol dm^{-3})) for 3 d at room temperature with the aid of 10 fold excess moles of WSCD·HCl and HOBt per mole of the peptide. After purification by gel filtration, the cyclic peptides, **7a** and **7b**, were obtained in 75 and 82% yields, respectively. Hydrogenolysis of the cyclic peptides (**7a** and **7b**) gave the desired peptides (**8a** and **8b**), whose homogeneities were confirmed by HPLC analysis, elemental analysis, and amino acid analysis of their acid-hydrolysates.

The present synthesis of gramicidins S demonstrates utility of the WSCD·HCl/HOBt procedure in preparation of the antibiotics. The procedure is quite effective not only for fragment condensation but also for cyclization. Recently successful one-pot cyclization using 5-nitro-2-pyridyl diphenylphosphinate was reported in a preparation of gramicidin S-1.[7] The

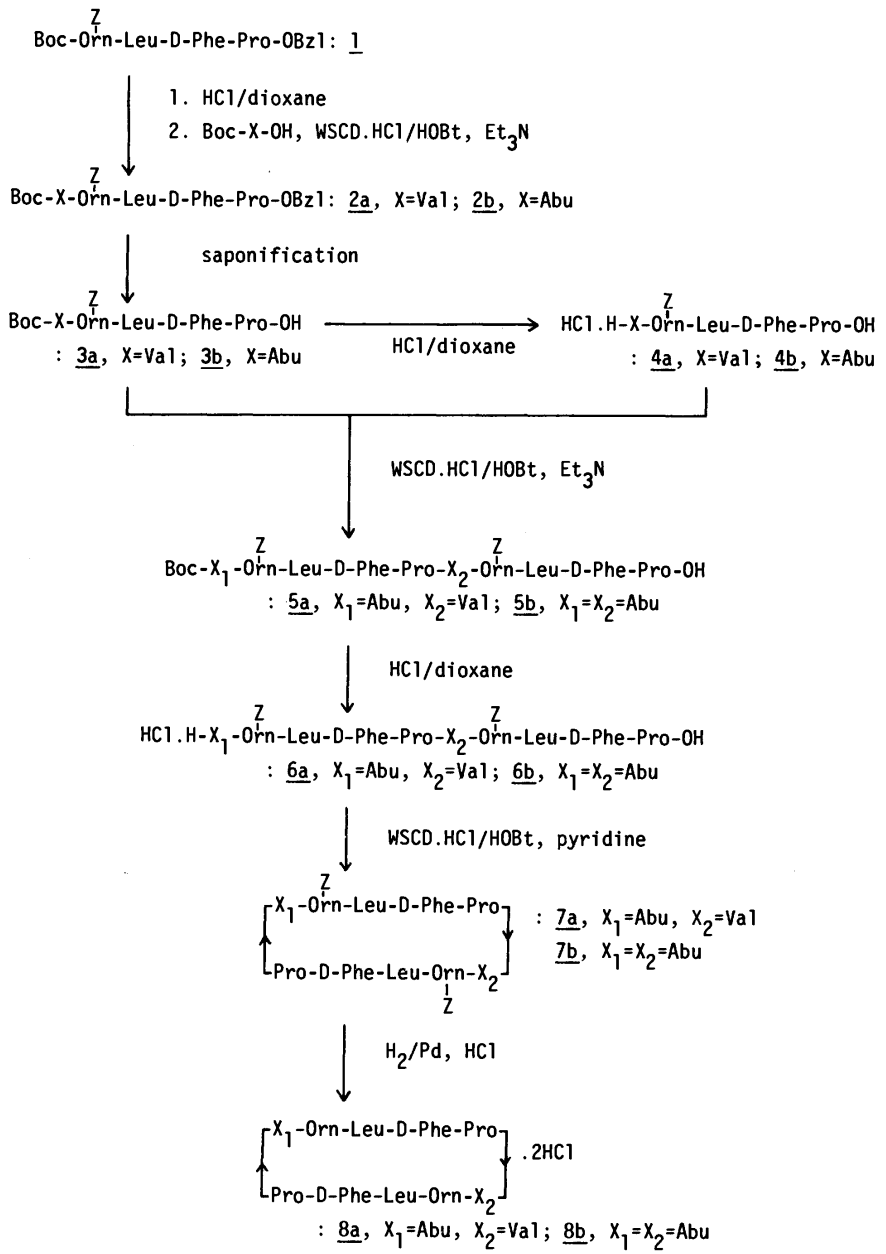

Fig. 2. Synthesis of gramicidin S-2 and S-3.

present convenient method employing the WSCD·HCl/HOBt procedure for one-pot cyclization may also be useful for synthesis of many cyclic peptides.

By HPLC analysis, **8a** and **8b** showed identical retention times with those of natural gramicidin S-2 and S-3 (hydrochlorides), respectively. The acetyl derivatives of **8a** and **8b** also gave identical HPLC profiles with those of the derivatives obtained from the natural antibiotics. The synthetic antibiotics showed the same degree of antibiotic activities as the natural ones (perchlorates) (Table 1). The CD spectra of **8a** and **8b** in ethanol were closely similar to those of the natural peptides (perchlorates). The data indicate that **8a** and **8b** are identical with natural gramicidin S-2 and S-3, respectively. The structures proposed for gramicidin S-2 and S-3 were confirmed.

The CD spectra of **8a** and **8b**, and of natural gramicidin S-1 (hydrochloride) in ethanol closely resembled each other with troughs near 207 nm and shoulders near 219 nm (Fig. 3-A). Addition of water to the peptides in ethanol produced slight decreases of the negative ellipticities near 207 nm, while the similarity found in the spectra of the three peptides was held unchanged (Fig. 3-B). The facts show that the ring conformations of the three gramicidins S are closely similar to each other.

The antibiotic activities of gramicidin S-1, S-2, and S-3 toward some test microorganisms resembled each other (Table 1).

Table 1. Antibiotic activities of synthetic and natural gramicidins S

Test organisms	Minimum inhibitory concentration (μg/ml)					
	Gramicidin S-1[a)]	**8a**	**8b**	Gramicidin S-1[b)]	Gramicidin S-2[b)]	Gramicidin S-3[b)]
Staphylococcus aureus JC-1	0.78	3.13	3.13	3.13	3.13	3.13
Staphylococcus epidermidis ATCC 14990	0.78	1.56	1.56			
Bacillus anthracis No. 119	3.13	3.13	3.13			
Bacillus subtilis ATCC 6633	1.56	3.13	3.13	3.13	3.13	1.56
Streptococcus pneumoniae IP-692	12.5	6.25	6.25			
Streptococcus pyogenes Cook Group A	3.13	3.13	3.13	6.25	6.25	6.25
Streptococcus faecalis O-0114	6.25	6.25	6.25			
Corynebacterium dyphtheriae Type Gravis	1.56	1.56	1.56	3.13	3.13	3.13
Listeria monocytogenes 4b F4	3.13	3.13	3.13			
Escherichia coli JC-2	>100	>100	100	>50	>50	>50
Salmonella typhi O-901-W	50	50	50			
Salmonella enteritidis No. 11	100	50	50			
Klebsiella pneumoniae PCI 602	>100	100	50			
Proteus vulgaris OX-19	>100	100	50			

a) The natural product. Hydrochloride. b) The natural product. Perchlorate. The data of the activity are cited from Lit. 1.

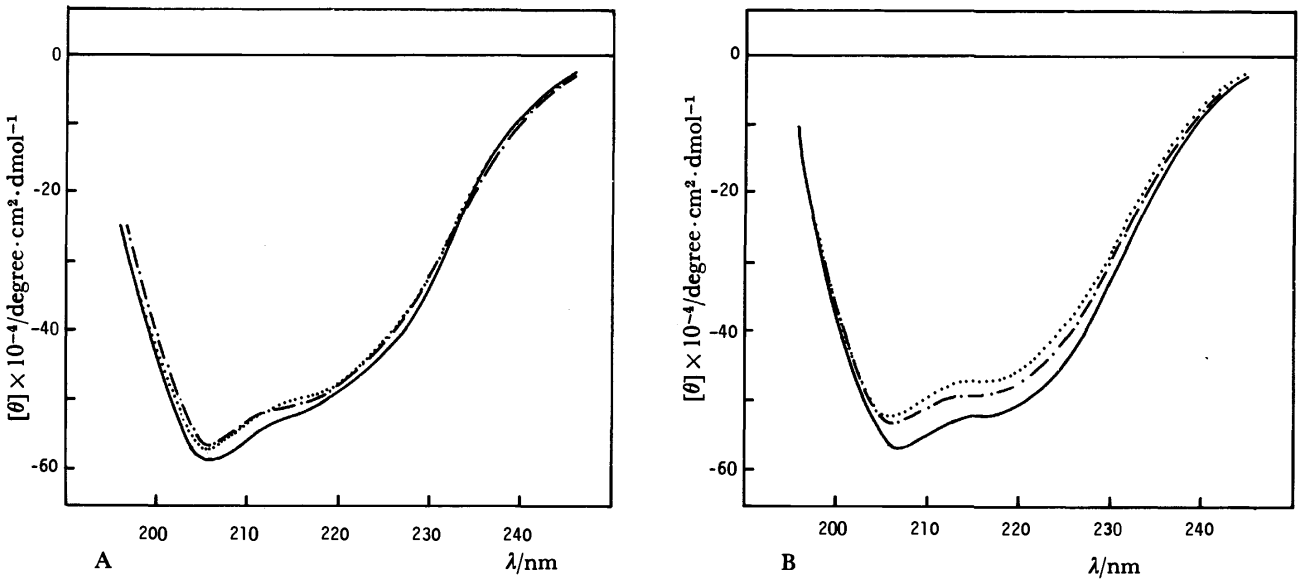

Fig. 3. CD spectra of gramicidins S. A: in ethanol, B: in ethanol-water, 1 : 1. Gramicidin S-1 hydrochloride: ——, **8a**: —·—·—, **8b**: ·····.

Experimental

Melting points were determined on a Mel-Temp apparutus and were uncorrected. CD spectra were obtained on a J-20A automatic recording spectropolarimeter (JASCO) using a calibrated 0.5 mm quartz cell. Amino acid analysis was carried out on a JLC-6AS automatic amino acid analyzer (JEOL). HPLC analysis was performed on a Partisil-10 ODS-3 column (4×250 mm, Whatman Ltd.) at a flow rate of 1.83 ml/min, which was maintained by a Milton Roy instrument minipump equipped with a JASCO PG-350D pulse dampener. The column effluent was monitored at 220 nm by a JASCO Uvidec 100-II spectrophotometer. The following solvent systems were used for the analysis; a: MeOH-water, 5/1; b: MeOH-water, 7/1; c: MeOH-5% $NaClO_4$, 4/1; d: MeOH-5% $NaClO_4$, 5/1; e: MeOH-4% ammonium acetate, 4/1; f: 2-propanol-5% $NaClO_4$, 2/3. For TLC, precoated silica-gel plates (Merck & Co., #5715) were used with the following solvent systems; a: 1-butanol-AcOH-water, 4/1/1; b: $CHCl_3$-MeOH-AcOH, 95/5/1. For elemental analysis, the samples were dried over P_2O_5 in high vaccum at 40 °C for 1 h unless otherwise noted. The natural peptides were isolated as the perchlorates by a similar method described in lit. 1. The hydrochlorides were obtained as follows: Gramicidin S-1 hydrochloride; The perchlorate was converted to the free peptide by reprecipitation from MeOH-0.5M $NaHCO_3$. The peptide was further converted to the hydrochloride by reprecipitation from MeOH-1 M HCl. Gramicidin S-2 and S-3 hydrochlorides;

Each perchlorate was dissolved in $CHCl_3$ and washed successively with 0.5 M $NaHCO_3$ and water. After removal of the solvent, the residue was dissolved in MeOH–1 M HCl and the solvent was evaporated to give a solid, which was reprecipitated from MeOH–ether.

Boc-Orn(Z)-Leu-D-Phe-Pro-OBzl (1). H-Pro-OBzl·HCl (1.209 g, 5 mM) in 1,2-dichloroethane (30 ml) was acylated successively by Boc-D-Phe-OH, Boc-Leu-OH, and Boc-Orn(Z)-OH (6 mM each) according to the procedures described in the literature.[4] The following reagents were used; Operation A: HOBt (6 mM), WSCD·HCl (7 mM). Operation B: 0.5 M $NaHCO_3$ (20 ml×2), water (20 ml), 0.1 M HCl (20 ml×2), water (20 ml×3). Operation C: 5.47 M HCl/dioxane (12 ml). Operation D: 2 M Na_2CO_3 (18 ml). Operation E: water (20 ml×3). After the final acylation, the reaction mixture was subjected to operation B and the organic layer was concentrated to give an oil. The desired peptide was obtained as a solid after chromatography on a silica-gel column (2.2×15 cm, $CHCl_3$–MeOH) followed by trituration in hexane: 1.960 g (48%), mp 76—85 °C (dec), $[\alpha]_D^{28}$ −59.9° (*c* 1, EtOH). Found: C, 66.22; H, 7.49; N, 8.26%. Calcd for $C_{45}H_{59}O_9N_5$: C, 66.40; H, 7.31; N, 8.60%.

Boc-Val-Orn(Z)-Leu-D-Phe-Pro-OBzl (2a). Boc-Val-OH (0.434 g, 2.0 mM), HOBt (0.270 g, 2.0 mM), HCl·H-Orn(Z)-Leu-D-Phe-Pro-OBzl (0.841 g, 1.12 mM, derived from **1**), Et_3N (0.16 ml, 1.12 mM) and WSCD·HCl (0.383 g, 2.0 mM) were allowed to react in DMF (3 ml) at room temperature overnight to give a mass, which was dissolved in AcOEt and washed successively with 0.1 M HCl, water, 0.5 M $NaHCO_3$, and water. The organic layer was concentrated and diluted with hexane to give precipitates, which were recrystallized from MeOH-AcOEt-hexane: mp 178—182 ° (dec), 0.667 g (65%), $[\alpha]_D^{29}$ −71.0° (*c* 1, EtOH). Found: C, 65.54; H, 7.78; N, 9.13%. Calcd for $C_{50}H_{68}O_{10}N_6$: C, 65.77; H, 7.51; N, 9.20%

Boc-Abu-Orn(Z)-Leu-D-Phe-Pro-OBzl (2b). Prepared in a similar way described above. Recrystallized from MeOH–AcOEt-hexane; mp 189—191 °C (dec), yield: 63%, $[\alpha]_D^{28}$ −68.8° (*c* 1, EtOH). Found: C, 65.22; H, 7.60; N, 9.24%. Calcd for $C_{49}H_{66}O_{10}N_6$: C, 65.46; H, 7.40; N, 9.35%.

Boc-Val-Orn(Z)-Leu-D-Phe-Pro-OH (3a). To a suspension of **2a** (0.612 g, 0.670 mM) in EtOH (30 ml) was added 2 M NaOH (3 ml) and the mixture was stirred for 2 h at room temperature. After addition of 1 M HCl (6 ml), the mixture was concentrated to a small volume, diluted with AcOEt and washed with 0.05 M HCl and water. The organic layer was concentrated and ether was added to give a solid: 0.468 g (85%), mp 122—125 °C (dec), $[\alpha]_D^{29}$ −41.2° (c 1, DMF). Lit:[8] mp 122—125 °C, $[\alpha]_D^{20}$ −39.0° (c 2.05, DMF).

Boc-Abu-Orn(Z)-Leu-D-Phe-Pro-OH (3b). Prepared from **2b** in a similar way described above. Reprecipitated from AcOEt–ether; mp 115—130 °C (dec), yield: 89%, $[\alpha]_D^{29}$ −41.6° (*c* 1, DMF). Found: C, 61.89; H, 7.79; N, 10.27%. Calcd for $C_{42}H_{60}O_{10}N_6$: C, 62.36; H, 7.48; N, 10.39%.

Boc-Abu-Orn(Z)-Leu-D-Phe-Pro-Val-Orn(Z)-Leu-D-Phe-Pro-OH (5a). Compound **3b** (0.400 g, 0.494 mM), HOBt (0.101 g, 0.75 mM), and WSCD·HCl (0.096 g, 0.5 mM) were allowed to react in DMF (3 ml) at room temperature for 40 min. To the solution was added **4a** (0.395 g, 0.521 mM, derived from **3a**, R_f^a 0.62), Et_3N (0.20 ml) and DMF (0.5 ml), and the mixture was stirred for 2 d. After removal of the solvent the desired peptide was solidified by addition of 0.1 M HCl. Reprecipitated from DMF–water: 0.727 g (96%), mp 174—180 °C (dec), R_f^b 0.36, $[\alpha]_D^{29}$ −67.3° (*c* 1, DMF). Found: C, 62.62; H, 7.67, N, 11.02%. Calcd for $C_{80}H_{112}O_{17}N_{12}\cdot H_2O$: C, 62.73; H, 7.50; N, 10.97%.

Boc-Abu-Orn(Z)-Leu-D-Phe-Pro-Abu-Orn(Z)-Leu-D-Phe-Pro-OH (5b). Prepared from **3b** (0.400 g, 0.494 mM) and **4b** (0.392 g, 0.529 mM, derived from **3b**, R_f^a 0.63) in a similar way described above. Reprecipitated from DMF-water: 0.701 g (93%), mp 111—116 °C (dec), R_f^b 0.32, $[\alpha]_D^{29}$ −53.5° (*c* 1, DMF). Found: C, 62.37; H, 7.41; N, 11.26%. Calcd for $C_{79}H_{110}O_{17}N_{12}\cdot H_2O$: C, 62.51; H, 7.44; N, 11.07%.

Cyclo*(-Abu-Orn(Z)-Leu-D-Phe-Pro-Val-Orn(Z)-Leu-D-Phe-Pro-) (7a).* A mixture of **6a** (0.207 g, 0.136 mM, derived from **5a**. Found in air-dried sample: C, 59.25; H, 7.48; N, 11.19%. Calcd for $C_{75}H_{104}O_{15}N_{12}\cdot HCl\cdot 4H_2O$: C, 59.14; H, 7.48; N, 11.03%), HOBt (0.193 g, 1.43 mM), and WSCD·HCl (0.274 g, 1.43 mM) were stirred in anhydrous DMF–pyridine (21 ml each, dried over Molecular Sieve 4 Å, Merck & Co., #5708) for 3 d at room temperature. After removal of the solvent, the residue was dissolved in $CHCl_3$ and was washed successively with 1 M HCl, water, 0.5 M $NaHCO_3$, and water. Removal of the solvent gave a crude product, which was purified by gel filtration on a Sephadex LH-20 column (1.2×96 cm, MeOH). Reprecipitated from MeOH–ether–hexane; mp 265—269 °C (dec), Retention time on the HPLC (RT)[b] 15.68 min, 0.146 g (75%), $[\alpha]_D^{28}$ −283° (*c* 0.3, EtOH). Found: C, 62.49; H, 7.40; N, 11.63%. Calcd for $C_{75}H_{102}O_{14}N_{12}\cdot 2H_2O$: C, 62.92; H, 7.46; N, 11.74%.

Cyclo*(-Abu-Orn(Z)-Leu-D-Phe-Pro-Abu-Orn(Z)-Leu-D-Phe-Pro-) (7b).* Prepared from **6b** (0.208 g, 0.138 mM, derived from **5b**. Found in air-dried sample: C, 59.23; H, 7.36; N, 11.15%. Calcd for $C_{74}H_{102}O_{15}N_{12}\cdot HCl\cdot 4H_2O$: C, 58.89; H, 7.41; N, 11.14%) in a similar way described above. Reprecipitated from MeOH–ether–hexane; mp 256—261 °C (dec), RT^b 12.30 min, 0.160 g (82%), $[\alpha]_D^{28}$ −289° (*c* 0.3, EtOH). Found: C, 62.84; H, 7.35; N, 11.91%. Calcd for $C_{74}H_{100}O_{14}N_{12}\cdot 2H_2O$: C, 62.69; H, 7.39; N, 11.86%.

Cyclo*(-Abu-Orn-Leu-D-Phe-Pro-Val-Orn-Leu-D-Phe-Pro-)·2HCl (8a).* Compound **7a** (0.109 g) was hydrogenated over Pd black (0.047 g) in EtOH (20 ml)-AcOH (10 ml). After removal of the catalyst by filtration, 1 M HCl (4 ml) was added to the filtrate, and the solvent was evaporated to give the desired peptide. Reprecipitation from EtOH–ether, 0.093 g (93%). Mp 270—273 °C (dec), $[\alpha]_D^{27}$ −267° (*c* 0.3 EtOH). RT^c 10.10 min, RT^e 17.97 min, RT^f 25.63 min. (Natural gramicidin S-2 hydrochloride: RT^c 10.12 min, RT^e 18.05 min, RT^f 25.62 min). Amino acid composition in acid-hydrolysate (6 M HCl, 110 °C, 20 h): Pro 2.09, Abu 1.07, Val 0.98, Leu 2.04, Phe 1.94, Orn 1.89. Found: C, 54.40; H, 7.92; N, 12.80%. Calcd for $C_{59}H_{90}O_{10}N_{12}\cdot 2HCl\cdot 6H_2O$: C, 54.16; H, 8.01; N, 12.85%. Acetyl derivative; mp 265—275 °C (dec). Found: C, 59.32; H, 7.88; N, 13.13%. Calcd for $C_{63}H_{94}O_{12}N_{12}\cdot 4H_2O$: C, 58.95; H, 8.01; N, 13.09%. RT^a 13.20 min, RT^d 12.60 min. SIMS *m/z*: 1211 $(M+H)^+$. (Acetyl derivative from the natural product: RT^a 13.20 min, RT^d 12.65 min. SIMS *m/z*: 1211 $(M+H)^+$).

Cyclo*(-Abu-Orn-Leu-D-Phe-Pro-Abu-Orn-Leu-D-Phe-Pro-)·2HCl (8b).* Prepared from **7b** (0.111 g) in a similar way as described above. Reprecipitated from

EtOH–ether, 0.090 g (89%), mp 272—274 °C (dec), $[\alpha]_D^{27}$ −263° (*c* 0.3, EtOH). RT^c 7.60 min, RT^e 13.12 min, RT^f 18.30 min. (Natural gramicidin S-3 hydrochloride: RT^c 7.62 min, RT^e 13.10 min, RT^f 18.37 min). Amino acid composition: Pro 2.05, Abu 2.07, Leu 2.04, Phe 1.93, Orn, 1.91. Found: C, 53.55; H, 7.75; N, 12.89%. Calcd for $C_{58}H_{88}O_{10}N_{12}\cdot 2HCl\cdot 6H_2O$: C, 53.82; H, 7.94; N, 12.99%. Acetyl derivative; mp 274—279 °C (dec). Found: C, 58.18; H, 7.69; N, 13.05%. Calcd for $C_{62}H_{92}O_{12}N_{12}\cdot 5H_2O$: C, 57.84; H, 7.99; N, 13.05%. RT^a 10.05 min, RT^d 9.57 min. SIMS *m/z*: 1197 $(M+H)^+$. (Acetyl derivative from the natural product: RT^a 10.08 min, RT^d 9.58 min. SIMS *m/z*: 1197 $(M+H)^+$).

We are indebted to the members of the Central Research Laboratory of Meiji Seika Kaisha Ltd. for measurement of mass spectra and for assays of the activity.

References

1) Part I: S. Nozaki and I. Muramatsu, *J. Antibiot.*, **37**, 689 (1984).

2) M. Altmann, H. Koischwitz, J. Salnikow, and H. Kleinkauf, *FEBS Lett.*, **93**, 247 (1978); Reviewed in E. Katz and A. L. Demain, *Bacteriol. Rev.*, **41**, 449 (1977).

3) Amino acids with no prefix are of L-configuration. The abbreviations for amino acids and peptides are in accordance with the rules of the IUPAC-IBU Commission of Biochemical Nomenclature. Other abbreviations are as follows: Boc=*t*-butoxycarbonyl, Z=benzyloxycarbonyl, OBzl=benzyl ester.

4) S. Nozaki and I. Muramatsu, *Bull. Chem. Soc. Jpn.*, **55**, 2165 (1982).

5) J. C. Sheehan, P. A. Cruickshank, and G. L. Boshart, *J. Org. Chem.*, **26**, 2525 (1961).

6) W. König and R. Geiger, *Chem. Ber.*, **103**, 788 (1970).

7) T. Mukaiyama, K. Kamekawa, and Y. Watanabe, *Chem. Lett.*, **1981**, 1367.

8) M. Ohno, T. Kato, S. Makisumi, and N. Izumiya, *Bull. Chem. Soc. Jpn.*, **39**, 1738 (1966).

4,4′,4″-Tris(levulinoyloxy)trityl as a New Type of Primary Hydroxyl Protecting Group

Mitsuo SEKINE* and Tsujiaki HATA
Department of Life Chemistry, Tokyo Institute of Technology, Nagatsuta, Midoriku, Yokohama 227
(Received August 27, 1984)

The 4,4′,4″-tris(levulinoyloxy)trityl (TLTr) group was introduced selectively on the 5′-oxygen of thymidine by use of *in situ* generated 4,4′,4″-tris(levulinoyloxy)trityl bromide. The TLTr group was found to be sufficiently stable to acids and readily removed by hydrazinolysis followed by warming to 50 °C in pyridine–acetic acid without damage of other protecting groups such as the *O*-acetyl and 4,4′-dimethoxytrityl groups. The utility of this new protecting group was demonstrated by the successful synthesis of thymidylyl(3′—5′)-thymidine where the TLTr group was employed as the 5′-hydroxyl-protecting group.

For synthetic work on polyfunctional natural products, a protecting group, which is removed under as mild conditions as possible, has often been required. Among a wide variety of unblocking agents reported, hydrazine has proved to be accessible in nucleotide chemistry.[1-4] Letsinger[1a] first reported β-benzoylpropionyl as a hydrazine-lable hydroxyl blocking group. Later, van Boom[2a] described levulinoyl as a more easily removable group. Very recently, Ogilvie[3] reported the use of the latter for protection of the exo amino groups of nucleosides. Matteucci[4] and we[5] also communicated dialkylamidines and phthaloyl, respectively, as hydrazine-labile blockers for the deoxyadenosine N^6-amino function.

We have found that the 4,4′,4″-tris(benzoyloxy)trityl (TBTr) group was rather stable to acids but yet susceptible to cleavage under alkaline conditions.[6] This hydrolytic cleavage was explained as the result of alkali-mediated elimination of rosolic acid from a 4,4′,4″-trihydroxytrityl ether initially formed. If the 4,4′,4″-trihydroxytrityl group could be removed under certain nonbasic conditions, we could choose various substituents capable of hydrolysis under mild conditions to design new "protected" protecting groups which satisfied the above mentioned stipulation.

Therefore, we have studied levulinoyloxy-substituted trityl as hydrazine-labile protecting groups. First, 4,4′,4″-tris(levulinoyloxy)tritanol (**1**) was prepared in 43% yield by levulination of rosolic acid. The tritanol was then converted to the trityl bromide (**2**) by treatment with acetyl bromide. This new reagent underwent facile 5′-*O*-tritylation with thymidine (**3**) in pyridine giving rise to the product (**4**) in 81% yield. Treatment of **4** with 80% acetic acid showed that the 4,4′,4″-tris(levulinoyloxy)trityl (TLTr) group had the same stability as the TBTr group ($T_{1/2}$=1 d, T_{com}=5 d).[6] On the other hand, hydrazinolysis of **4** with 1 M† H_2NNH_2 in hydrazine–acetic acid (3:2, v/v) at room temperature for 3 min gave quantitatively 5′-*O*-(4,4′,4″-trihydroxytrityl)thymidine (**5**). The latter was rapidly converted to **3** and rosolic acid by treatment with 80% acetic acid. Since our ultimate aim was to convert **5** to **3** under essentially neutral conditions, several experiments have been conducted. Some attempts to cleave the $(HO)_3Tr$–O ether bond of **5** oxidatively by using various metal salts[7] involving $FeCl_3$ and $CuCl_2$ have failed. Although **5** was expected to be decomposed to thymidine by passing it slowly through a silica-gel column, elution with CH_2Cl_2–MeOH gave a 80% recovery of **5** and a small amount (10%) of **3**. The final goal to conversion of **5** to **3** was achieved in pyridine–acetic acid (1:2, v/v) at 50 °C for 30 min. The hydrazine reaction of **4** followed by extraction and then warming in pyridine–acetic acid resulted in quantitative formation of **3**.

In order to see if the TLTr group can be used in the presence of other acid- or alkali-labile protecting groups, the syntheses of 3′-*O*-acetylthymidine (**6**) and 3′-*O*-(4,4′-dimethoxytrityl)thymidine (**7**) were conducted. Acetylation of **4** followed by unblocking of the TLTr group gave an 87% overall yield of **6**. Similarly, **7**, was obtained in 94% yield from **4**. The conditions for removal of the TLTr group described here proved to be very mild because the DMTr and acetyl groups were virtually stable.

Furthermore, to demonstrate the synthetic utility of the TLTr group, we tried to synthesize thymidylyl-(3′—5′)-thymidine 3′-phosphate (TpTp) by using this new hydroxyl-protecting group. Phosphorylation of **4** with cyclohexylammonium *S,S*-diphenyl phosphorodithioate (**8**)[8] in the presence of mesitylenedisulfonyl chloride (MDS)[9] gave the 3′-phosphorylated product

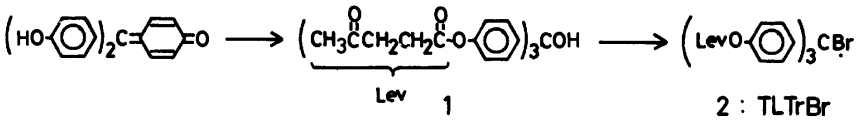

Scheme 1.

(**9**) in 86% yield. A similar hydrazinolysis of **9** and successive workup gave *S,S*-diphenyl thymidine 3'-phosphorodithioate (**10**) in 86% yield. The base-labile bis(phenylthio)phosphoryl group was found to be stable during these treatments. On the other hand, treatment of **9** with 3.3 M pyridinium phosphinate,[10,11] in pyridine resulted in quantitaive formation of Triethylammonium *S*-phenyl 5'-*O*-tris(levulinoyloxy)trityl]thymidine 3'-phosphorothioate (**11**). Upon this treatment, the TLTr group remained also intact. Condensation of **10** with **11** in the presence of MDS and 3-nitro-1,2,4-triazole (NT)[12] gave the dimer (**12**) in 82% yield. Treatment of **12** with AgOAc[5,13] in aqueous pyridine followed by ammonia gave TpTp in 91% yield.

Since the skeleton of the TLTr group is derived from a dye of rosolic acid, compounds containing the TLTr group can be readily detected as distinct orange spots upon heating TLC plates.

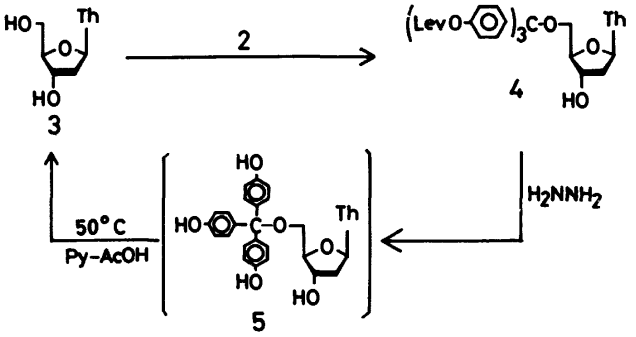

Scheme 2.

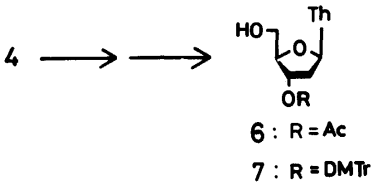

Scheme 3.

We have also examined the 9-[(4-levulinoyloxy)-phenyl]-9-xanthenyl and 4-dimethylamino-4',4''-bis(levulinoyloxy)trityl groups as the possible hydrazine-labile protecting groups. However, the former was found to be too unstable during silica-gel column chromatography, and the latter was stable on silica gel but the corresponding hydroxyl-substituted xanthenyl group resulted from the hydrazine treatment was resistant to the pyridine–acetic acid treatment even at 60 °C.

In conclusion, the TLTr group can be selectively introduced into a primary hydroxyl as an easily detectable group and used substantially as an equivalent of the levulinoyl group.

Experimental

^{1}H NMR spectra were recorded at 100 MHz on a JEOL JNM PS-100 spectrometer using tetramethylsilane as an internal standard. Column chromatography was performed with silica gel C-200 purchased from Wako Co. Ltd., and a mini pump for a goldfish basin was conveniently used to gain a medium pressure for rapid chromatographic separation. Rosolic acid and the other regents were purchased from Wako Co. Ltd.

4,4',4''-Tris(levlinoyloxy)tritanol (1). To a mixture of rosolic acid (29 g, 0.1 mol) and levulinic acid (23.2 g, 0.2 mol) in pyridine was added dicyclohexylcarbodiimide (41.2 g, 0.2 mol). After the solution was stirred for 2 h, water (1.8 ml) was added to hydrolyze the quinomethane initially formed to 4-hydroxy-4',4''-bis(levulinoyloxy)tritanol. After being stirred at 55 °C for 50 min, the solution was dried over powdered molecular sieves 3A (23 g) for 20 min and treated with levulinic acid (23.2 g, 0.2 mol) and dicyclohexylcarbodiimide (41.2 g, 0.2 mol) for 3 h. The mixture was quenched with water, filtered, extracted with CH_2Cl_2, dried over Na_2SO_4, and chromatographed on a silica-gel column with CH_2Cl_2 to yield **1** (26 g, 43%) as an oily material which gradually solidified upon standing: ^{1}H NMR ($CDCl_3$) δ=2.20 (s, 9H, $CH_3C(O)$), 2.81 (s, 12H, CH_2), 3.58 (br, 1H, OH), 6.93 (d, 6H, J=8.6 Hz, ArH), 7.22 (d, 6H, J=8.0 Hz, ArH). Calcd for $C_{34}H_{34}O_{10}$: C, 67.77; H, 5.69. Found: C, 67.82; H, 5.81.

5'-O-[4,4',4''-tris(levulinoyloxyl)trityl]thymidine (4). To a solution of **1** (5.0 g, 8.3 mmol) in benzene (28 ml) was added acetyl bromide (3.9 ml, 53 mmol). The mixture was

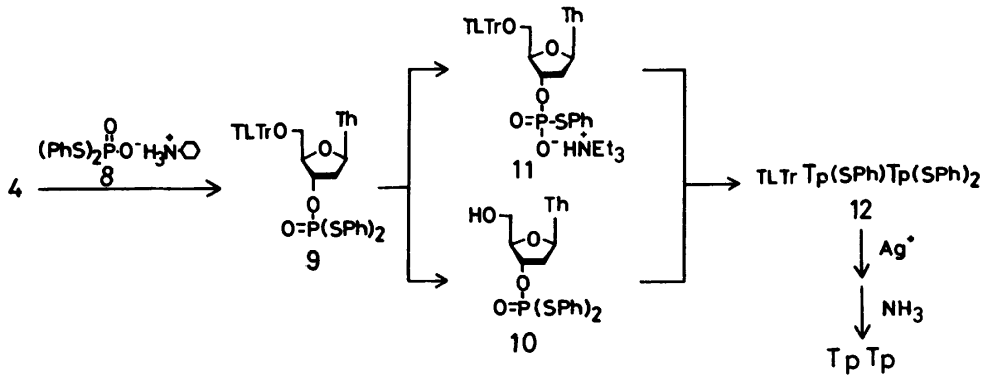

Scheme 4.

refluxed for 15 min, and then the benzene and excess reagent were removed by evaporation. The residue was coevaporated three times with dry benzene under reduced pressure and finally dissolved in pyridine (30 ml). This solution was added to **3** (1.34 g, 5.5 mmol) predried by repeated coevaporations with dry pyridine. The resulting solution was stirred for 10 h and then water was added. Extraction with CH_2Cl_2 followed by chromatography on silica gel gave **4** (3.7 g, 81%) as foam: ^1H NMR ($CDCl_3$) δ=1.61 (s, 3H, CH_3), 1.33 (m, 2H, 2'-H), 3.22 (m, 2H, 5'-H), 3.78 (s, 3H, CH-O), 4.01 (m, 1H, 4'-H), 4.40 (m, 1H, 3'-H), 5.03 (d, 1H, J=4 Hz, OH), 6.42 (t, 1H, J=7 Hz, 1'-H), 6.83 (d, 2H, J=5.2 Hz, ArH), 7.00—7.52 (m, 10H, ArH), 7.66 (s, 1H, 6-H), 10.71 (br, 1H, NH). Calcd for $C_{44}H_{46}O_{14}N_2$: C, 63.92; H, 5.61; N, 3.39. Found: C, 63.76; H, 5.48; N, 3.24.

3'-O-Acetylthymidine (6). To a solution of **4** (414 mg, 0.5 mmol) in dry pyridine (5 ml) was added acetic anhydride (1 ml). After being stirred for 3 h, the solution was quenched with water and extracted with CH_2Cl_2 (3×20 ml). The combined extracts were dried over Na_2SO_4, concentrated to dryness, and the residue was dissolved in 1 M H_2NNH_2 in pyridine–acetic acid (3:2, v/v, 7.5 ml). The same workup as described in the synthesis of **10** gave **6** (123 mg, 87%). This compound was identified with an authentic sample by comparison of their ^1H NMR spectra.

3'-O-(4,4'-Dimethoxytrityl)thymidine (7). To a solution of **4** (414 mg, 0.5 mmol) in dry pyridine (5 ml) was added 4,4'-dimethoxytrityl chloride (339 mg, 1 mmol). The mixture was kept at 70 °C for 4 h. Then, the same workup as described in the synthesis of **10** gave **7** (255 mg, 94%). This compound was identified with an authentic sample by comparison of their ^1H NMR spectra.

S,S-*Diphenyl 5'-O-[4,4',4''-tris(levulinoyloxy)trityl]thymidine 3'-Phosphorodithioate (9).* A mixture of **4** (3.26 g, 3.94 mmol) and **8** (1.81 g, 4.73 mmol) were rendered anhydrous by repeated evaporations with dry pyridine (2×5 ml) and finally dissolved in dry pyridine (20 ml). MDS (1.88 g, 5.92 mmol) was added to the solution and the mixture was stirred for 30 min. The solution was diluted with CH_2Cl_2 and washed with water and 5% $NaHCO_3$. The usual workup followed by chromatography gave **9** (4.06 g, 94%): ^1H NMR ($CDCl_3$) δ=2.22 (s, 9H, $CH_3C(O)$), 2.30 (m, 2H, 2'-H), 2.82 (s, 12H, CH_2), 3.28 (m, 2H, 5'-H), 4.01 (m, 1H, 4'-H), 5.25 (m, 1H, 3'-H), 6.23 (t, 1H, J=7.5 Hz, 1'-H), 6.95 (d, 6H, J=8.5 Hz, ArH), 7.28 (d, 6H, J=8.5 Hz, ArH), 7.15—7.62 (m, 11H, ArH and 5-H), 8.47 (br, 1H, NH). Calcd for $C_{56}H_{55}O_{15}N_2PS_2$: C, 61.64; H, 5.08; N, 2.57. Found: C, 61.53; H, 5.21; N, 2.44.

S,S-*Diphenyl Thymidine 3'-Phosphorodithioate (10).* Compound **9** (546 mg, 1 mmol) was dissolved with stirring in 1 M H_2NNH_2 in pyridine–acetic acid (3:2, v/v, 15 ml). After being kept for 3 min, the solution was diluted with CH_2Cl_2 and washed with water and 5% $NaHCO_3$. The CH_2Cl_2 extract was dried over Na_2SO_4, filtered, and evaporated to dryness under reduced pressure. The residue was dissolved in pyridine–acetic acid (1:2, v/v, 15 ml) and the solution was warmed at 50 °C for 30 min. At this time the TLTr group was completely removed. The solution was extracted with CH_2Cl_2 and washed with water and 5% $NaHCO_3$. After filtration the solvent was removed under reduced pressure, and the residue was chromatographed on a silica gel to yield **10** (218 mg, 86%). This compound was identified with an authentic sample by comparison of their ^1H NMR spectra.

Synthesis of Dimer 12. Compound **9** (262 mg, 0.24 mmol) was treated with a mixture of 5 M phosphinic acid in pyridine (2.4 ml) and triethylamine (1.2 ml) at room temperature for 30 min. At this time one of the two phenylthio group was removed completely. The mixture was diluted with CH_2Cl_2 and washed with water and 0.2 M triethylammonium hydrogencarbonate (10 ml). The CH_2Cl_2 extract was dried over Na_2SO_4, filtered, and evaporated to dryness under reduced presure. The residue was mixed with **10** (253 mg, 0.2 mmol) and 3-nitro-1,2,4-triazole (82 mg, 0.72 mmol), and rendered anhydrous by evaporation with dry pyridine (3×5 ml). The mixture was dissolved in dry pyridine (2 ml) and MDS (228 mg, 0.72 mmol) was added. After being stirred for 30 min, the solution was worked up as descrived in the case of **9**. Chromatography yielded **12** (244 mg, 82%).

Full Deprotection of 12. Compound **12** (58 mg, 0.04 mmol) was dissolved in a solution of silver acetate (668 mg, 4 mmol) in pyridine–water (2:1, v/v, 4 ml) and the solution was stirred at 50 °C for 9 h. The resulting solution was diluted with pyridine-water (2:1, v/v, 40 ml). Then, hydrogen sulfide gas was bubbled into the solution at 0 °C until a clear supernatant had been obtained. The excess gas was removed under reduced pressure with stirring and the solution was centrifuged to remove the precipitate. The supernatant was evaporated to dryness under reduced pressure and dissolved in pyridine (5 ml). Concentrated aqueous ammonia (45 ml) was added and the solution was kept with stirring at 50 °C for 4 h. Then, the excess ammonia was evaporated with stirring by an aspirator and rosolic acid was removed by extraction with CH_2Cl_2. The aqueous layer was concentrated under reduced pressure and the residue was chromatographed on Whatman 3 MM papers developed with 2-propanol-concentrated ammonia–water (6:1:3, v/v/v). A band at R_f 0.2 was cut and eluted with water to give TpTp (630 OD, 91%). This product (20 OD) was incubated with spleen phosphodiesterase (10 μg, Boehringer) in a mixture of 0.05 M ammonium acetate (pH 6.5, 0.4 ml) and 0.01 M pyrophosphate buffer (pH 6.5, 0.2 ml) for 10 h gave only Tp (21 OD).

This work was supported by a Grant-in-Aid form the Ministry of Education, Science and Culture of Japan.

References

1) a) R. L. Letsinger, M. H. Caruthers, P. S. Miller, and K. K. Ogilvie, *J. Am. Chem. Soc.*, **89**, 7146 (1967); b) G. Grams and R. L. Letsinger, *J. Org. Chem.* **33**, 2589 (1969); c) R. L. Letsinger and P. S. Miller, *J. Am. Chem. Soc.*, **91**, 3356 (1969); d) R. L. Letsinger, K. K. Ogilvie, and P. S. Miller, *ibid.*, **91**, 3360 (1969).

2) a) J. F. M. de Rooij, G. Wille-Hazeleger, P. H. Deursen, J. Serdijn, and J. H. van Boom, *Recl. Trav. Chim. Pays-Bas*, **98**, 537 (1979); b) J. A. J. den Hartog and J. H. van Boom, *ibid.*, **100**, 275 (1981); c) J. A. J. den Hartog, G. Wille, and J. H. van Boom, *ibid.*, **100**, 320 (1981).

3) K. K. Ogilvie, M. J. Nemer, G. H. Hakimelahi, Z. A. Proba, and M. Lucas, *Tetrahedron Lett.*, **23**, 2615 (1982).

4) B. C. Froehler and M. D. Matteucci, *Nucleic Acids Res.*, **11**, 8031 (1983).

5) A. Kume, M. Sekine, and T. Hata, *Nuclec Acids Res.*, **23**,

4365 (1982).

6) M. Sekine and T. Hata, *J. Org. Chem.*, **48**, 3011 (1983).

7) M. L. Mihailovic and Z. Cekovic, "The Chemistry of the Hydroxyl Group," ed by S. Patai, Interscience, New York (1971), Part 1, pp. 505—592; H. -U. Wagner and R. Gompper, "The Chemistry of Quinonoid Compounds," ed by S. Patai, Interscience, New York (1974), Part 2, pp. 1145—1178.

8) M. Sekine, K. Hamaoki, and T. Hata, *J. Org. Chem.*, **44**, 3772 (1979); M. Sekine, K. Hamaoki, and T. Hata, *Bull. Chem. Soc.Jpn.*, **54**, 3815 (1981); T. Hata, K. Yamaguchi, S. Honda, and I. Nakagawa, *Chem. Lett.*, **1978**, 507.

9) M. Sekine, J. Matsuzaki, and T. Hata, *Tetrahedron Lett.*, **22**, 3209 (1981).

10) M. Sekine and T. Hata, *J. Am. Chem. Soc.*, **105**, 2044 (1983).

11) S. Honda, K. Terada, Y. Satoh, M. Sekine, and T. Hata, *Chem. Lett.*, **1982**, 15; b) S. Honda, K. Urakami, K. Terada, K. Khono, M. Sekine, and T. Hata, *Tetrahedron*, **40**, 153 (1984).

12) C. B. Reese, R. C. Titmas, and L. Yau, *Tetrahedron Lett.*, **1978**, 2727.

13) M. Sekine, J. Matsuzaki, and T. Hata, *Tetrahedron Lete.*, **23**, 5287 (1982).

14) J. P. Horwitz, J. Chua, and J. A. Urabanski, *J. Org. Chem.*, **27**, 3300 (1962).

The Total Synthesis of (15*R*)- and (15*S*)-16-Hydroxyferruginol

Takashi MATSUMOTO,* Sachihiko IMAI, Shigekazu MIUCHI, and Hidenori SUGIBAYASHI
Department of Chemistry, Faculty of Science, Hiroshima University, Higashisenda-machi, Naka-ku, Hiroshima 730
(Received August 27, 1984)

In order to assign the absolute configuration of C-15 in natural 16-hydroxyferruginol, (5*S*,10*S*,15*R*)- (**1a**) and (5*S*,10*S*,15*S*)-8,11,13-abietatriene-12,16-diol (**1b**) have been synthesized. Optical resolution of 2-(2-methoxyphenyl)propanoic acid, prepared from methyl (2-methoxyphenyl)acetate, with cinchonidine afforded (*R*)- and (*S*)-enantiomers, which were converted into [(*R*)-4-methoxy-3-(2-methoxy-1-methylethyl)benzyl]triphenylphosphonium chloride (**3a**) and its (*S*)-isomer (**3b**) respectively. The Wittig reaction of (*R*)-(−)-α-cyclocitral with **3a**, followed by partial catalytic hydrogenation and intramolecular cyclization gave (5*S*,10*S*,15*R*)-12,16-dimethoxy-8,11,13-abietatriene (**16a**) together with its (5*S*,10*R*,15*R*)-isomer. Similarly, **3b** was also converted into (5*S*,10*S*,15*S*)-12,16-dimethoxy-8,11,13-abietatriene (**16b**) and its (5*S*,10*R*,15*S*)-isomer. Demethylation of **16a** gave **1a** which was identical with natural 16-hydroxyferruginol. The dimethoxy compound **16b** was also demethylated to give **1b**.

16-Hydroxyferruginol (**1**), a new tricyclic diterpene phenol possessing an abietane skeleton, has recently been isolated from the seed of *Thujopsis dolabrata* Sieb. et Zucc. var. *dolabrata* by Hasegawa and Hirose.[1] The structure **1** was elucidated by spectroscopic studies and by chemical transformation to the known (+)-ferruginol methyl ether. However, the absolute configuration at C-15 remained unsettled. In order to elucidate the unknown stereochemistry at C-15, we have attempted the total syntheses of (15*R*)-(**1a**) and (15*S*)-16-hydroxyferruginol (**1b**). The synthetic strategy was developed from the retrosynthetic analysis of the natural product (**1**), which involved the disconnection illustrated in Scheme 1.

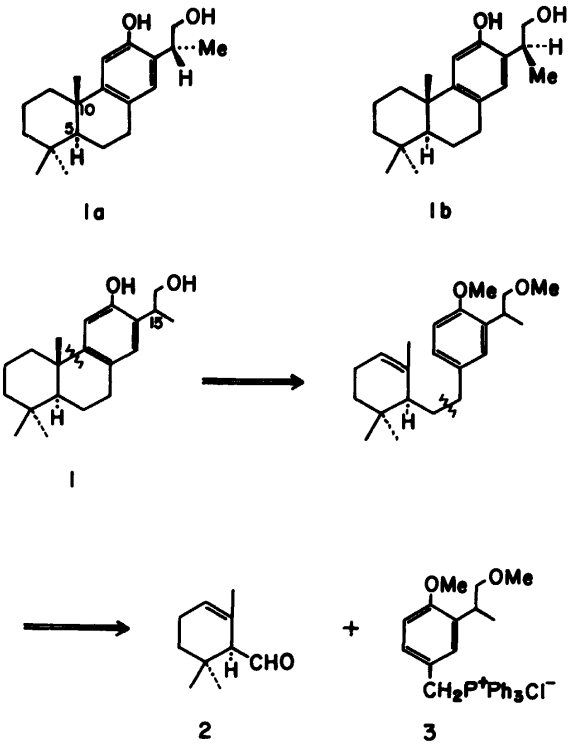

Scheme 1.

First, the optically active [4-methoxy-3-(2-methoxy-1-methylethyl)benzyl]triphenylphosphonium chloride (**3**) was prepared starting from methyl (2-methoxyphenyl)acetate (**4**) in the following manner. Methylation of **4** with methyl iodide in hexamethylphosphoric triamide and tetrahydrofuran in the presence of potassium *t*-butoxide afforded methyl 2-(2-methoxyphenyl)propanoate (**5**) which was hydrolyzed with aqueous sodium hydroxide in refluxing methanol to give the corresponding racemic acid (**6**). The racemic acid **6** was then resolved by means of cinchonidine to give (-)-acid (**6a**) and (+)-acid (**6b**), which were methylated with diazomethane to give the methyl esters, **5a** and **5b** respectively. Reduction of **5a** and **5b** with lithium aluminium hydride gave the corresponding alcohols, **7a** and **7b**. The absolute configurations of **7a** and **7b** were determined by the following correlation. Acetylation of **7a** with acetic anhydride in pyridine, followed by demethylation of the resulting acetate (**8a**) with anhydrous aluminium chloride and ethanethiol[2] in dichloromethane, afforded the phenolic compound (**9a**). This was then submitted to ozonization and the resulting acid was methylated with diazomethane to give the known methyl (*S*)-(+)-3-acetoxy-2-methylpropanoate[3] (**10a**). Similarly, the alcohol **7b** was correlated to methyl (*R*)-(−)-3-acetoxy-2-methylpropanoate (**10b**) *via* the corresponding acetate (**8b**) and phenol (**9b**). Thus, the absolute configurations of **7a** and **7b** were assigned to *R* and *S* respectively. The alcohols, **7a** and **7b**, were methylated respectively with methyl iodide and sodium hydride in 1,2-dimethoxyethane to give the dimethoxy compounds, **11a** and **11b**. Chloromethylation of **11a** with chloromethyl methyl ether in acetic acid, followed by treatment of the resulting benzyl chloride derivative (**12a**) with triphenylphosphine in refluxing benzene produced the desired [(*R*)-4-methoxy-3-(2-methoxy-1-methylethyl)benzyl]triphenylphosphonium chloride (**3a**). The

dimethoxy compound **11b** was also converted into the corresponding (*S*)-isomer (**3b**) *via* the benzyl chloride derivative (**12b**).

4 R=H, R'=Me
5 R=R'=Me
6 R=Me, R'=H

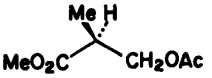

10a

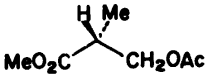

10b

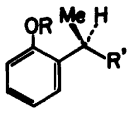

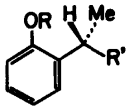

5a	R=Me, R'=CO_2Me	5b
6a	R=Me, R'=CO_2H	6b
7a	R=Me, R'=CH_2OH	7b
8a	R=Me, R'=CH_2OAc	8b
9a	R=H, R'=CH_2OAc	9b
11a	R=Me, R'=CH_2OMe	11b

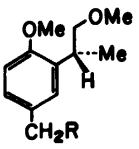

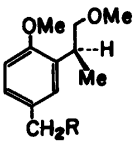

3a	R = $P^+Ph_3Cl^-$	3b
12a	R = Cl	12b

The Wittig reaction of (*R*)-(−)-α-cyclocitral (**2**)[4,5] with **3a** in benzene in the presence of butyllithium gave 6-[4-methoxy-3-(2-methoxy-1-methylethyl)styryl] -1,5,5-trimethylcyclohexene (**13a**) in 56.1% yield. The ^{1}H NMR spectrum of **13a** showed signals at δ 5.76 (double doublet, J=8.5 and 15 Hz) and 6.25 (doublet, J=15 Hz) due to the newly formed olefinic protons. These vicinal coupling constants (J=15 Hz) suggested the presence of a *trans*-disubstituted double bond in **13a**. The compound **13a** in ethanol was submitted to partial catalytic hydrogenation over Pd-C to afford the corresponding phenethyl derivative (**14a**: 94.1%). The intramolecular cyclization of **14a** with anhydrous aluminium chloride in benzene afforded (5*S*, 10*S*, 15*R*)-12,16-dimethoxy-8,11,13-abietatriene (**16a**: 49.0%) $[\alpha]_D$ +35.0° ($CHCl_3$) and its (5*S*,10*R*,15*R*)-isomer (**15a**: 35.3%). The *cis*-configuration of the A/B ring junction in **15a** was supported by its ^{1}H NMR spectrum which showed a signal due to the $C_{4\beta}$-methyl group at high field (δ 0.48) owing to the shielding effect of the aromatic C-ring. The Wittig reaction of **2** with **3b**, followed by partial catalytic hydrogenation of the resulting styryl derivative (**13b**: 54.9%) afforded the phenethyl derivative (**14b**: 89.4%). The intramolecular

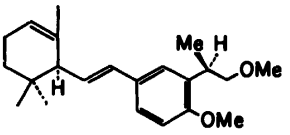

13a

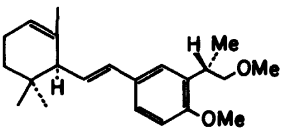

13b

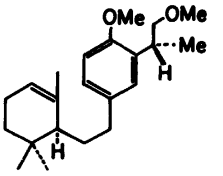

14a

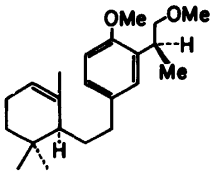

14b

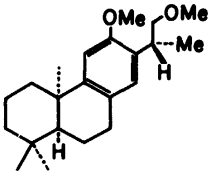

15a

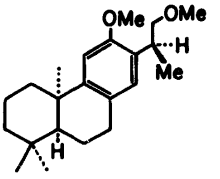

15b

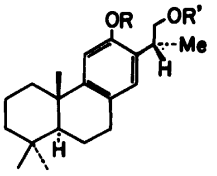

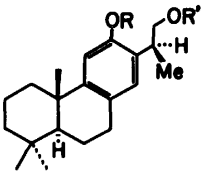

16a	R=R'=Me	16b
18a	R=R'=Ac	18b
19a	R=Me, R'=H	19b
20a	R=Me, R'=Ts	20b

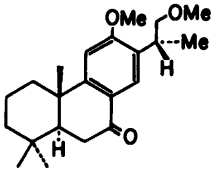

17a

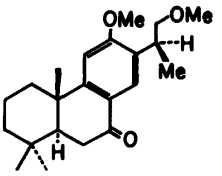

17b

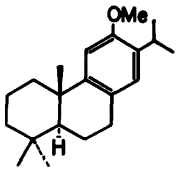

21

cyclization of **14b** with anhydrous aluminium chloride produced (5*S*,10*S*,15*S*)-12,16-dimethoxy-8,11,13-abietatriene (**16b**: 50.8%) $[\alpha]_D$ +60.4° ($CHCl_3$) together with its (5*S*,10*R*,15*S*)-isomer (**15b**: 40.5%). In order to increase the optical purity, the cyclization products (**16a** and **16b**) were oxidized with Jones reagent to give the crystalline 7-oxo derivatives, **17a** and **17b**. After recrystallization, **17a** and **17b** were converted into **16a** $[\alpha]_D$ +46.7° ($CHCl_3$) and **16b** $[\alpha]_D$ +68.7° ($CHCl_3$) by catalytic hydrogenation over Pd-C in the presence of perchloric acid. Demethylation of **16a** in dichloromethane with anhydrous aluminium chloride and sodium iodide in acetonitrile[6] at 35—40 °C under a stream of nitrogen afforded (5*S*,10*S*,15*R*)-8,11,13-abietatriene-12,16-diol (**1a**: 95.7%), mp 141—142.5 °C, $[\alpha]_D$ +65.7° ($CHCl_3$), which was identical with natural 16-hydroxyferruginol (lit,[1] mp 141—142 °C, $[\alpha]_D$ +36.6° ($CHCl_3$)). Similarly, the dimethoxy compound **16b** was also demethylated to give (5*S*,10*S*,15*S*)-8,11,13-abietatriene-12,16-diol (**1b**: 95.5%), mp 178—179 °C, $[\alpha]_D$ +44.6° ($CHCl_3$). Acetylation of **1a** and **1b** with acetic anhydride in pyridine gave the corresponding diacetates, **18a** and **18b**. Since the optical rotation value of the synthetic **1a** was somewhat larger than that reported for the natural product, the absolute configurations at C-5 and C-10 in **1a** and **1b** were subsequently confirmed by the following conversion. Methylation of **1a** with methyl iodide and anhydrous potassium carbonate in refluxing ethyl methyl ketone yielded 12-methoxy-8,11,13-abietatrien-16-ol (**19a**), which was converted into a tosylate[1] (**20a**). Reduction of **20a** with lithium aluminium hydride in ether afforded (+)-ferruginol methyl ether (**21**) $[\alpha]_D$ +63.3° ($CHCl_3$) (lit,[7] $[\alpha]_D$ +63.1° ($CHCl_3$)). The diol **1b** was also converted into **21** *via* the corresponding methyl ether (**19b**) and tosylate (**20b**).

From the above synthesis the absolute configuration of natural 16-hydroxyferruginol was conclusively assigned as 5*S*, 10*S*, 15*R*.

Experimental

All melting points are uncorrected. The IR spectra and optical rotations were measured in chloroform, and the ^1H NMR spectra in carbon tetrachloride at 60 MHz, with tetramethylsilane as an internal standard, unless otherwise stated; s: singlet, bs: broad singlet, d: doublet, dd: double doublet, m: multiplet. The column chromatography was performed using Merck silica gel (0.063 mm).

Methyl (±)-2-(2-Methoxyphenyl)propanoate (5). (2-Methoxyphenyl)acetic acid in ether was methylated with diazomethane to give a methyl ester (**4**).

To a solution of **4** (25.00 g) and hexamethylphosphoric triamide (25.0 ml) in dry tetrahydrofuran (300 ml) under a stream of nitrogen at −40—−30 °C was added potassium *t*-butoxide (15.57 g) over a 5 min period and then methyl iodide (8.70 ml) over a 20 min period. The mixture was stirred at −40—−30 °C for 30 min, poured into dilute hydrochloric acid, and extracted with ether. The ether extract was washed successively with aqueous sodium thiosulfate and brine, dried over sodium sulfate, and evaporated *in vacuo*. The residue was chromatographed on silica gel (300 g), using benzene as eluent, to give **5** (24.31 g: 93.7%). Found: C, 67.73; H, 7.36%. Calcd for $C_{11}H_{14}O_3$: C, 68.02; H, 7.27%.

(±)-2-(2-Methoxyphenyl)propanoic Acid (6). A mixture of **5** (2.58 g) and aqueous sodium hydroxide (20%: 4.8 ml) in methanol (20 ml) was refluxed for 1.5 h. After the methanol had been evaporated *in vacuo*, the residue was diluted with water, and then washed with ether. The alkaline solution was acidified with dilute hydrochloric acid and extracted with ether. The ether extract was washed with brine, dried over sodium sulfate, and evaporated *in vacuo* to give **6** (2.23 g: 93.1%) as a solid. This was recrystallized from acetone–petroleum benzine, mp 101—102 °C. Found: C, 66.39; H, 6.65%. Calcd for $C_{10}H_{12}O_3$: C, 66.65; H, 6.71%.

Resolution of (±)-6. A mixture of (±)-**6** (34.69 g) and cinchonidine (56.68 g) in ethyl acetate (1000 ml) was refluxed for 20 h. The solution was concentrated, allowed to stand at room temperature, and then filtered to give colorless crystals. This was recrystallized from ethyl acetate to give a cinchonidine salt (35.72 g), mp 106—111 °C, $[\alpha]_D$ −46.1°.

The above cinchonidine salt was suspended in dilute hydrochloric acid and extracted with ether. The ether extract was washed with brine, dried over sodium sulfate, and then evaporated to dryness. The residue was recrystallized from acetone–petroleum benzine to give (*S*)-(+)-2-(2-methoxyphenyl)propanoic acid (**6b**) (9.87 g), mp 94—96 °C, $[\alpha]_D$ +62.7° (*c* 2.32). Found: C, 66.65; H, 6.81%. Calcd for $C_{10}H_{12}O_3$: C, 66.65; H, 6.71%.

The mother liquor from the above recrystallization of the cinchonidine salt was evaporated *in vacuo*. The residue was suspended in dilute hydrochloric acid and extracted with ether. The ether extract was washed with brine, dried over sodium sulfate, and evaporated *in vacuo*. The residue was recrystallized from acetone–petroleum benzine to give (*R*)-(−)-2-(2-methoxyphenyl)propanoic acid (**6a**) (8.91 g), mp 94—96°C, $[\alpha]_D$ −67.8° (*c* 2.62). Found: C, 66.63; H, 6.84%. Calcd for $C_{10}H_{12}O_3$: C, 66.65; H, 6.71%.

(R)-(−)-2-(2-Methoxyphenyl)-1-propanol (7a) and Its (S)-(+)-Isomer (7b). *a)*: **6a** (8.914 g) was methylated with a solution of diazomethane in ether. After the usual work-up, the crude product was chromatographed on silica gel (200 g), using benzene as eluent, to give (*R*)-(−)-ester (**5a**) (8.791 g: 91.6%), $[\alpha]_D$ −69.4° (*c* 3.35).

A solution of **5a** (7.959 g) in dry ether (50 ml) was added dropwise to a stirred suspension of lithium aluminium hydride (1.436 g) in dry ether (80 ml) with cooling in an ice-water bath over a 15 min period. The mixture was stirred at room temperature for 1.5 h, poured into a mixture of ice and dilute hydrochloric acid, and extracted with ether. The ether extract was washed with brine, dried over sodium sulfate, and evaporated *in vacuo*. The residue was chromatographed on silica gel (50 g), using ether–benzene (1:9) as eluent, to give **7a** (6.530 g: 95.7%), $[\alpha]_D$ −6.1° (*c* 17.9).

b): **6b** (9.870 g) was methylated with diazomethane in ether to give (*S*)-(+)-ester (**5b**) (10.594 g: 99.6%), $[\alpha]_D$ +65.2° (*c* 4.68).

A solution of **5b** (11.915 g) in dry ether (50 ml) was reduced with lithium aluminium hydride (2.333 g) in dry ether (150 ml) to give **7b** (9.939 g: 97.5%), $[\alpha]_D$ +6.5° (*c* 18.8).

(R)-(−)-1-Acetoxy-2-(2-hydroxyphenyl)propane (9a) and Its

(S)-(+)-Isomer (9b). *a)*: A mixture of **7a** (659 mg) and acetic anhydride (2.0 ml) in pyridine (3.0 ml) was heated at 80—85 °C for 1.5 h. After the usual work-up, the crude product was chromatographed on silica gel (15 g), using benzene as eluent, to give (*R*)-(−)-acetate (**8a**) (695 mg: 84.2%), $[\alpha]_D$ −20.2° (*c* 3.92). Found: C, 69.01; H, 7.69%. Calcd for $C_{12}H_{16}O_3$: C, 69.21; H, 7.74%.

Anhydrous aluminium chloride (2.40 g) was added to a stirred solution of **8a** (620 mg) and ethanethiol (1.5 ml) in dichloromethane (7.0 ml) at 5—10 °C. The mixture was stirred at room temperature for 1 h, poured into a mixture of ice and dilute hydrochloric acid, and extracted with ether. The ether extract was washed with brine, dried over sodium sulfate, and evaporated *in vacuo*. The residue was chromatographed on silica gel (15 g), using ether–benzene (2:98) as eluent, to give **9a** (566 mg: 97.9%), $[\alpha]_D$ −11.6° (*c* 5.08).

b): **7b** (612 mg) was acetylated with acetic anhydride (1.5 ml) in pyridine (3.0 ml) to give (*S*)-(+)-acetate (**8b**) (652 mg: 85.0%), $[\alpha]_D$ +21.0° (*c* 9.72). Found: C, 68.91; H, 7.58%. Calcd for $C_{12}H_{16}O_3$: C, 69.21; H, 7.74%.

8b (647 mg) was demethylated with anhydrous aluminium chloride (2.481 g) and ethanethiol (2.3 ml) in dichloromethane (7.0 ml) to give **9b** (523 mg: 86.6%), $[\alpha]_D$ +12.4° (*c* 3.96).

Ozonization of 9a and 9b. *a)*: A solution of **9a** (523 mg) in methanol (20 ml) was ozonized at −20—−10 °C for 4 h. The solution was evaporated *in vacuo* and the residue was methylated with diazomethane in ether. The ether solution was washed successively with dilute hydrochloric acid and brine, dried over sodium sulfate, and evaporated. The residue was chromatographed on silica gel (15 g), using hexane–chloroform (3:7) as eluent, to give an ester (**10a**) (155 mg: 36.5%), $[\alpha]_D$ +14.9° (*c* 4.16), whose IR and ^{1}H NMR spectra were identical with those of methyl (*S*)-(+)-3-acetoxy-2-methylpropanoate.[3]

b): Ozonization of **9b** (523 mg) in methanol (20 ml), followed by esterification with diazomethane yielded methyl (*R*)-(−)-3-acetoxy-2-methylpropanoate (**10b**) (244 mg: 56.6%), $[\alpha]_D$ −15.2° (*c* 4.54).

(R)-(−)-1-Methoxy-2-(2-methoxyphenyl)propane (11a) and Its (S)-(+)-Isomer (11b). *a)*: A mixture of **7a** (6.530 g) and methyl iodide (3.3 ml) in 1,2-dimethoxyethane (20 ml) was added to a stirred suspension of sodium hydride (55%: 1.900 g) in 1,2-dimethoxyethane (20 ml) with cooling in an ice–water bath over a 35 min period. The mixture was stirred at room temperature for 2 h. After the addition of methanol, the mixture was poured into ice–dilute hydrochloric acid, and extracted with ether. The ether extract was washed successively with aqueous sodium thiosulfate and brine, dried over sodium sulfate, and evaporated *in vacuo*. The residue was chromatographed on silica gel (50 g: Merck 0.063—0.200 mm), using benzene as eluent, to give **11a** (6.726 g: 95.0%), $[\alpha]_D$ −29.8° (*c* 12.5).

b): The alcohol **7b** (9.939 g) was similarly methylated with methyl iodide (4.9 ml) and sodium hydride (55%: 2.890 g) in 1,2-dimethoxyethane (55 ml) to give **11b** (10.287 g: 95.5%), $[\alpha]_D$ +27.6° (*c* 10.6).

(R)-4-Methoxy-3-(2-methoxy-1-methylethyl)benzyl Chloride (12a) and Its (S)-Isomer (12b). *a)*: A round-bottomed flask containing a solution of **11a** (4.00 g) and chloromethyl methyl ether (2.8 ml) in acetic acid (4.0 ml) was fitted with a rubber stopper and then heated at 35—40 °C for 6 h. The mixture was cooled, poured into ice–aqueous sodium hydrogencarbonate, and extracted with ether. The ether extract was washed with brine, dried over sodium sulfate, and evaporated *in vacuo* to give the crude **12a** (5.00 g). This was used without purification in the next reaction. ^{1}H NMR: δ=1.21 (3H, d, J=7 Hz, $-\overset{|}{C}HCH_3$), 3.25 (3H, s, $-OCH_3$), 3.73 (3H, s, $-OCH_3$), 4.42 (2H, s, $-CH_2Cl$).

b): A solution of **11b** (5.00 g) and chloromethyl methyl ether (3.5 ml) in acetic acid (5.0 ml) was treated as described in *a)* to give the crude **12b** (5.90 g). This was used without purification in the next reaction.

[(R)-4-Methoxy-3-(2-methoxy-1-methylethyl)benzyl]triphenylphosphonium Chloride (3a) and Its (S)-Isomer (3b). *a)*: A mixture of **12a** (5.00 g) and triphenylphosphine (5.73 g) in dry benzene (5.0 ml) was refluxed for 1 h and then cooled. The precipitates were collected by filtration and washed with dry benzene to give the crude **3a** (10.29 g), mp 175—185 °C. This was used without purification in the next reaction.

b): A mixture of **12b** (5.90 g) and triphenylphosphine (6.77 g) in dry benzene (6.0 ml) was refluxed for 1.5 h and then treated as described in *a)* to give the crude **3b** (11.92 g), mp 176—186 °C. This was used without purification in the next reaction.

The Wittig Reaction of (R)-(−)-α-Cyclocitral with 3a and 3b. *a)*: A solution of butyllithium in hexane (15%: 4.0 ml) was added at 10—20 °C to a stirred suspension of **3a** (2.500 g) in dry benzene (15 ml) under a stream of nitrogen. The mixture was stirred at room temperature for 15 min and a solution of (*R*)-(−)-α-cyclocitral (**2**) (0.485 g) in dry benzene (2.5 ml) was added at 10—20 °C. After stirring at room temperature for 1.5 h, the reaction mixture was poured into dilute hydrochloric acid, and extracted with ether. The ether extract was washed with brine, dried over sodium sulfate, and evaporated *in vacuo*. The residue was triturated with hexane and the precipitated triphenylphosphine oxide was removed by filtration. The filtrate was evaporated and the residue was chromatographed on silica gel (30 g), using ether–hexane (2:98) as eluent, to give 6-[4-methoxy-3-(2-methoxy-1-methylethyl)styryl]-1,5,5-trimethylcyclohexene (**13a**) (0.583 g: 56.1%), $[\alpha]_D$ −316° (*c* 0.31); ^{1}H NMR: δ=0.89 (3H, s) and 0.95 (3H, s) ($-\overset{|}{C}(CH_3)_2$), 1.23 (3H, d, J=7 Hz, $-\overset{|}{C}HCH_3$), 1.63 (3H, bs, $=\overset{|}{C}CH_3$), 3.28 (3H, s) and 3.79 (3H, s) ($2-OCH_3$), 5.40 (1H, br, $-CH=\overset{|}{C}-$), 5.76 (1H, dd, J=8.5 and 15 Hz, $-\overset{|}{C}HCH=CH-$), 6.25 (1H, d, J=15 Hz, $-\overset{|}{C}HCH=CH-$).

b): A solution of butyllithium in hexane (15%: 88.0 ml) was added at 10—20 °C to a stirred suspension of **3b** (48.0 g) in dry benzene (250 ml) under a stream of nitrogen. The mixture was stirred for 5 min and a solution of **2** (9.31 g) in dry benzene (50 ml) was added at 10—20 °C. After stirring at room temperature for 1.5 h, the mixture was treated as described in *a)* to give the styryl derivative (**13b**) (11.0 g: 54.9%), $[\alpha]_D$ −287° (*c* 0.53). ^{1}H NMR: δ=0.89 (3H, s) and 0.95 (3H, s) ($-\overset{|}{C}(CH_3)_2$), 1.25 (3H, d, J=7 Hz, $-\overset{|}{C}HCH_3$), 1.64 (3H, bs, $=\overset{|}{C}CH_3$), 3.28 (3H, s) and 3.76 (3H, s) ($2-OCH_3$), 5.40 (1H, br, $-CH=\overset{|}{C}-$), 5.77 (1H, dd, J=8.5 and 15 Hz, $-\overset{|}{C}HCH=CH-$), 6.26 (1H, d, J=15 Hz, $-\overset{|}{C}HCH=CH-$).

Partial Catalytic Hydrogenation of 13a and 13b. *a)*: A suspension of **13a** (438 mg) and 5% Pd–C (253 mg) in ethanol (10 ml) was stirred at room temperature in an atmosphere of hydrogen. After one mol equivalent of hydrogen had been absorbed, the mixture was filtered. The filtrate was evaporated *in vacuo* and the residue was chromatographed on

silica gel (20 g), using ether–benzene (3:97) as eluent, to give the phenethyl derivative (**14a**) (414 mg: 94.1%), $[\alpha]_D$ −107° (*c* 5.22). Found: C, 79.65; H, 10.55%. Calcd for $C_{22}H_{34}O_2$: C, 79.95; H, 10.37%.

b): A suspension of **13b** (6.486 g) and 10% Pd-C (3.00 g) in methanol (50 ml) was stirred at room temperature in an atmosphere of hydrogen. After one mol equivalent of hydrogen had been absorbed, the mixture was treated as described in *a)* to give the phenethyl derivative (**14b**) (5.836 g: 89.4%), $[\alpha]_D$ −85.5° (*c* 6.12). Found: C, 79.85; H, 10.59%. Calcd for $C_{22}H_{34}O_2$: C, 79.95; H, 10.37%.

Intramolecular Cyclization of 14a and 14b. *a)*: Anhydrous aluminium chloride (2.246 g) was added at 5—15 °C to a solution of **14a** (5.565 g) in dry benzene (60 ml). The mixture was stirred at room temperature for 50 min, poured into ice-dilute hydrochloric acid, and extracted with ether. The ether extract was washed with brine, dried over sodium sulfate, and evaporated *in vacuo*. The residue was chromatographed on silica gel (300 g), using ether–hexane (2:98) as eluent, to give (5*S*,10*R*,15*R*)-12,16-dimethoxy-8,11,13-abietatriene (**15a**) (1.963 g: 35.3%). This was recrystallized from methanol: mp 79—80 °C, $[\alpha]_D$ −48.4° (*c* 2.03); ^{1}H NMR (C_6D_6): δ=0.48 (3H, s) and 0.93 (3H, s) (−C(CH$_3$)$_2$), 1.17 (3H, s, C_{10}–CH$_3$), 1.40 (3H, d, *J*=7 Hz, C_{15}–CH$_3$), 3.18 (3H, s, C_{16}–OCH$_3$), 3.50 (3H, s, C_{12}–OCH$_3$), 6.76 (1H, s) and 6.93 (1H, s) (C_{11}–H and C_{14}–H). Found: C, 79.83; H, 10.53%. Calcd for $C_{22}H_{34}O_2$: C, 79.95; H, 10.37%.

Further elution gave (5*S*,10*S*,15*R*)-12,16-dimethoxy-8,11,13-abietatriene (**16a**) (2.727 g: 49.0%) as an oil, $[\alpha]_D$ +35.0° (*c* 4.28); ^{1}H NMR (C_6D_6): δ=0.92 (6H, s, −C(CH$_3$)$_2$), 1.20 (3H, s, C_{10}–CH$_3$), 1.42 (3H, d, *J*=7 Hz, C_{15}–CH$_3$), 3.19 (3H, s, C_{16}–OCH$_3$), 3.53 (3H, s, C_{12}–OCH$_3$), 6.70 (1H, s) and 6.95 (1H, s) (C_{11}–H and C_{14}–H). Found: C, 79.77; H, 10.67%. Calcd for $C_{22}H_{34}O_2$: C, 79.95; H, 10.37%.

b): A solution of **14b** (5.836 g) in dry benzene (60 ml) was treated with anhydrous aluminium chloride (2.355 g) as described in *a)*. The crude product was chromatographed on silica gel (300 g), using ether–hexane (2:98) as eluent, to give (5*S*,10*R*,15*S*)-12,16-dimethoxy-8,11,13-abietatriene (**15b**) (2.166 g: 40.5%). This was recrystallized from methanol: mp 81—82 °C, $[\alpha]_D$ −16.9° (*c* 3.56); ^{1}H NMR (C_6D_6): δ=0.51 (3H, s) and 0.95 (3H, s) (−C(CH$_3$)$_2$), 1.20 (3H, s, C_{10}–CH$_3$), 1.44 (3H, d, *J*=7 Hz, C_{15}–CH$_3$), 3.18 (3H, s, C_{16}–OCH$_3$), 3.50 (3H, s, C_{12}–OCH$_3$), 6.80 (1H, s) and 6.96 (1H, s) (C_{11}–H and C_{14}–H). Found: C, 79.87; H, 10.59%. Calcd for $C_{22}H_{34}O_2$: C, 79.95; H, 10.37%.

Further elution gave (5*S*,10*S*,15*S*)-12,16-dimethoxy-8,11,13-abietatriene (**16b**) (2.769 g: 50.8%) as an oil, $[\alpha]_D$ +60.4° (*c* 4.56); ^{1}H NMR (C_6D_6): δ=0.92 (6H, s, −C(CH$_3$)$_2$), 1.19 (3H, s, C_{10}–CH$_3$), 1.45 (3H, d, *J*=7 Hz, C_{15}–CH$_3$), 3.21 (3H, s, C_{16}–OCH$_3$), 3.53 (3H, s, C_{12}–OCH$_3$), 6.65 (1H, s) and 6.90 (1H, s) (C_{11}–H and C_{14}–H). Found: C, 79.68; H, 10.63%. Calcd for $C_{22}H_{34}O_2$: C, 79.95; H, 10.37%.

(5S,10S,15R)-12,16-Dimethoxy-8,11,13-abietatrien-7-one (17a) and Its (5S,10S,15S)-Isomer (17b). *a)*: Jones reagent (2.5 mol dm^{-3}: 4.25 ml) was added to a stirred solution of **16a** (2.465 g) in acetone (35 ml) with cooling in an ice-water bath over a 5 min period. The mixture was stirred at this temperature for 10 min and then at room temperature for 2 h, diluted with water, and extracted with ether. The ether extract was washed with brine, dried over sodium sulfate, and evaporated *in vacuo*. The residue was chromatographed on silica gel (150 g), using ether–benzene (2:98) as eluent, to give the recovered **16a** (0.236 g: 9.6%). Further elution with ether–benzene (2:98 and then 5:95) gave **17a** (1.968 g: 76.6%). This was recrystallized from ethanol: mp 128—134 °C, $[\alpha]_D$ +27.8° (*c* 2.10); IR: 1664, 1601 cm^{-1}; ^{1}H NMR (C_6D_6): δ=0.74 (3H, s) and 0.80 (3H, s) (−C(CH$_3$)$_2$), 1.04 (3H, s, C_{10}–CH$_3$), 1.32 (3H, d, *J*=6 Hz, C_{15}–CH$_3$), 3.11 (3H, s, C_{16}–OCH$_3$), 3.42 (3H, s, C_{12}–OCH$_3$), 6.56 (1H, s, C_{11}–H), 8.33 (1H, s, C_{14}–H). Found: C, 76.78; H, 9.57%. Calcd for $C_{22}H_{32}O_3$: C, 76.70; H, 9.36%.

b): A solution of **16b** (2.610 g) in acetone (40 ml) was oxidized with Jones reagent (2.5 mol dm^{-3}: 4.50 ml) as described in *a)* to give the recovered **16b** (0.227 g: 8.7%) and (5*S*,10*S*,15*S*)-12,16-dimethoxy-8,11,13-abietatrien-7-one (**17b**) 2.405 g: 88.2%). This was recrystallized from ethanol: mp 140—141.5 °C, $[\alpha]_D$ +30.7° (*c* 4.53); IR: 1662, 1600 cm^{-1}; ^{1}H NMR (C_6D_6): δ=0.75 (3H, s) and 0.80 (3H, s) (−C(CH$_3$)$_2$), 1.05 (3H, s, C_{10}–CH$_3$), 1.33 (3H, d, *J*=6 Hz, C_{15}–CH$_3$), 3.13 (3H, s, C_{16}–OCH$_3$), 3.46 (3H, s, C_{12}–OCH$_3$), 6.58 (1H, s, C_{11}–H), 8.28 (1H, s, C_{14}–H). Found: C, 76.74; H, 9.46%. Calcd for $C_{22}H_{32}O_3$: C, 76.70; H, 9.36%.

Catalytic Hydrogenolysis of 17a and 17b. *a)*: A suspension of **17a** (254 mg), 10% Pd-C (125 mg), and 60% perchloric acid (0.15 ml) in ethyl acetate (5.0 ml) was stirred at room temperature in an atmosphere of hydrogen. After the hydrogen had been absorbed, the mixture was filtered. The filtrate was washed with brine, dried over sodium sulfate, and evaporated *in vacuo*. The crude product was chromatographed on silica gel (15 g), using ether–benzene (2:98) as eluent, to give **16a** (233 mg: 95.5%), $[\alpha]_D$ +46.7° (*c* 1.65). Found: C, 79.78; H, 10.53%. Calcd for $C_{22}H_{34}O_2$: C, 79.95; H, 10.37%.

b): A suspension of **17b** (500 mg), 10% Pd-C (250 mg), and 60% perchloric acid (0.30 ml) in ethyl acetate (10 ml) was hydrogenated to give **16b** (466 mg: 97.2%), $[\alpha]_D$ +68.7° (*c* 3.70). Found: C, 79.93; H, 10.55%. Calcd for $C_{22}H_{34}O_2$: C, 79.95; H, 10.37%.

(5S,10S,15R)-8,11,13-Abietatriene-12,16-diol (16-Hydroxyferruginol) (1a) and Its (5S,10S,15S)-Isomer (1b). *a)*: Anhydrous aluminium chloride (714 mg), sodium iodide (803 mg), and a solution of **16a** (177 mg) in dichloromethane (5.0 ml) were added in this order to acetonitrile (10.0 ml) with stirring at 0—5 °C under a stream of nitrogen over a 15 min period. The mixture was stirred at this temperature for 15 min and then at 35—40 °C for 5 h, poured into water, and extracted with ether. The ether extract was washed successively with aqueous sodium thiosulfate and brine, dried over sodium sulfate, and evaporated *in vacuo*. The residue was chromatographed on silica gel (20 g), using ether–hexane (1:1) as eluent, to give **1a** (155 mg: 95.7%). This was recrystallized from ether–hexane: mp 141—142.5 °C, $[\alpha]_D$ +65.7° (*c* 1.85) (lit,[1] mp 141—142 °C, $[\alpha]_D^{29}$ +36.6°); IR (KBr): 3505, 3275 cm^{-1}; ^{1}H NMR (90 MHz, $CDCl_3$): δ=0.94 (3H, s) and 0.96 (3H, s) (−C(CH$_3$)$_2$), 1.16 (3H, s, C_{10}–CH$_3$), 1.27 (3H, d, *J*=7 Hz, C_{15}–CH$_3$), 3.15 (1H, m, C_{15}–H), 3.64 (1H, dd, *J*=9 and 7 Hz) and 3.87 (1H, dd, *J*=9 and 4 Hz) (−CH$_2$OH), 6.76 (2H, s, C_{11}–H and C_{14}–H). Found: C, 79.51; H, 10.18%. Calcd for $C_{20}H_{30}O_2$: C, 79.42; H, 10.00%.

A mixture of **1a** (31.4 mg) and acetic anhydride (0.5 ml) in pyridine (0.5 ml) was heated at 75—80 °C for 1 h. After the usual work-up, the crude product was chromatographed on silica gel (5.0 g), using ether–hexane (15:85) as eluent, to give a diacetate (**18a**) (35.0 mg: 87.3%), $[\alpha]_D$ +59.4° (*c* 1.75);

^{1}H NMR ($CDCl_3$): δ=0.95 (6H, s, $-C(CH_3)_2$), 1.19 (3H, s, C_{10}–CH_3), 1.24 (3H, d, J=6 Hz, C_{15}–CH_3), 2.04 (3H, s, C_{16}–$OCOCH_3$), 2.31 (3H, s, C_{12}–$OCOCH_3$), 4.06 (2H, d, J=7 Hz, $-CH_2OAc$), 6.87 (1H, s) and 6.91 (1H, s) (C_{11}–H and C_{14}–H). Found: C, 74.92; H, 9.05%. Calcd for $C_{24}H_{34}O_4$: C, 74.57; H, 8.87%.

b): Anhydrous aluminium chloride (706 mg), sodium iodide (794 mg), and a solution of **16b** (175 mg) in dichloromethane (5.0 ml) were added in this order to acetonitrile (10.0 ml) with stirring at 0—5 °C under a stream of nitrogen over a 15 min period. The mixture was stirred at this temperature for 15 min and then at 35—40 °C for 5 h. After the work-up as described in *a)*, the crude product was recrystallized from acetone–hexane to give a diol (**1b**) (153 mg: 95.5%): mp 178—179 °C, $[\alpha]_D$ +44.6° (*c* 1.12); IR (KBr): 3545, 3260 cm^{-1}; ^{1}H NMR (90 MHz, $CDCl_3$): δ=0.92 (6H, s $-C(CH_3)_2$), 1.15 (3H, s, C_{10}–CH_3), 1.28 (3H, d, J=7 Hz, C_{15}–CH_3), 3.16 (1H, m, C_{15}–H), 3.68 (1H, dd, J=9 and 7 Hz) and 3.91 (1H, dd, J=9 and 4 Hz) ($-CH_2OH$), 6.77 (2H, s, C_{11}–H and C_{14}–H). Found: C, 79.28; H, 10.24%. Calcd for $C_{20}H_{30}O_2$: C, 79.42; H, 10.00%.

A mixture of **1b** (82.9 mg) and acetic anhydride (0.5 ml) in pyridine (0.5 ml) was heated at 75—80 °C for 1 h. After the usual work-up, the crude product was chromatographed on silica gel (10 g), using ether–hexane (7.5:92.5) as eluent, to give a diacetate (**18b**) (93.9 mg: 88.7%), $[\alpha]_D$ +37.1° (*c* 4.60), ^{1}H NMR ($CDCl_3$): δ=0.93 (6H, s, $-C(CH_3)_2$), 1.18 (3H, s, C_{10}–CH_3), 1.20 (3H, d, J=7 Hz, C_{15}–CH_3), 2.02 (3H, s, C_{16}–$OCOCH_3$), 2.31 (3H, s, C_{12}–$OCOCH_3$), 4.08 (2H, d, J=7 Hz, $-CH_2OAc$), 6.86 (1H, s) and 6.91 (1H, s) (C_{11}–H and C_{14}–H). Found: C, 74.52; H, 9.16%. Calcd for $C_{24}H_{34}O_4$: C, 74.57; H, 8.87%.

(5S,10S,15R)-12-Methoxy-8,11,13-abietatrien-16-ol (19a) and Its (5S,10S,15S)-Isomer (19b). *a)*: A mixture of **1a** (80.0 mg), methyl iodide (0.24 ml), and anhydrous potassium carbonate (320 mg) in ethyl methyl ketone (3.2 ml) was refluxed for 5 h. The mixture was cooled, diluted with water, and extracted with ether. The ether extract was washed successively with aqueous sodium thiosulfate and brine, dried over sodium sulfate, and evaporated *in vacuo*. The residue was chromatographed on silica gel (10 g), using ether–benzene (5:95) as eluent, to give **19a** (80.0 mg: 95.6%), $[\alpha]_D$ +62.3° (*c* 4.00); ^{1}H NMR: δ=0.95 (6H, s, $-C(CH_3)_2$), 1.17 (3H, d, J=6.5 Hz, C_{15}–CH_3), 1.18 (3H, s, C_{10}–CH_3), 3.74 (3H, s, C_{12}–OCH_3), 6.59 (1H, s) and 6.68 (1H, s) (C_{11}–H and C_{14}–H). Found: C, 79.72; H, 10.48%. Calcd for $C_{21}H_{32}O_2$: C, 79.70; H, 10.19%.

b): A mixture of **1b** (100 mg), methyl iodide (0.30 ml), and anhydrous potassium carbonate (400 mg) in ethyl methyl ketone (4.0 ml) was refluxed for 5 h. After the work-up as described in *a)*, the crude product was chromatographed on silica gel (10 g), using ether–hexane (5:95) as eluent, to give **19b** (96.5 mg: 92.3%), $[\alpha]_D$ +45.4° (*c* 4.83); ^{1}H NMR: δ=0.94 (6H, s, $-C(CH_3)_2$), 1.16 (3H, d, J=6.5 Hz, C_{15}–CH_3), 1.18 (3H, s, C_{10}–CH_3), 3.74 (3H, s, C_{12}–OCH_3), 6.60 (1H, s) and 6.68 (1H, s) (C_{11}–H and C_{14}–H). Found: C, 79.56; H, 10.46%. Calcd for $C_{21}H_{32}O_2$: C, 79.70; H, 10.19%.

(+)-Ferruginol Methyl Ether (21). *a)*: A mixture of **19a** (80.0 mg) and *p*-toluenesulfonyl chloride (80.0 mg) in pyridine (1.5 ml) was heated at 70—75 °C for 3.5 h. The mixture was cooled and diluted with ether. The ether solution was washed successively with dilute hydrochloric acid and brine, dried over sodium sulfate, and evaporated *in vacuo*. The residue was chromatographed on silica gel (10 g), using ether–benzene (3:97) as eluent, to give a tosylate (**20a**) (50.0 mg) and recovered **19a** (16.0 mg).

A mixture of **20a** (50.0 mg) and lithium aluminium hydride (45.0 mg) in dry ether (3.5 ml) was stirred at room temperature for 5 h. The mixture was poured into ice–dilute hydrochloric acid and extracted with ether. The ether extract was washed with brine, dried over sodium sulfate, and evaporated *in vacuo*. The crude product was chromatographed on silica gel (8.0 g), using hexane–benzene (9:1) as eluent, to give **21** (7.0 mg), $[\alpha]_D$ +63.3° (*c* 0.30) (lit,[7] $[\alpha]_D$ +63.1°). Further elution with ether–benzene (5:95) gave the alcohol **19a** (20.2 mg).

b): A mixture of **19b** (86.0 mg) and *p*-toluenesulfonyl chloride (78.0 mg) in pyridine (1.5 ml) was heated at 70—75 °C for 3.5 h. The mixture was treated as described in *a)* to give a tosylate (**20b**) (73.0 mg).

A mixture of **20b** (73.0 mg) and lithium aluminium hydride (65.0 mg) in dry ether (4.0 ml) was stirred at room temperature for 5 h. The mixture was treated as described in *a)* to give **21** (15.3 mg), $[\alpha]_D$ +61.4° (*c* 0.70) and **19b** (36.5 mg).

The authors are grateful to Professor Yoshiyuki Hirose, Science University of Tokyo, for kindly supplying the natural sample and the spectral data.

References

1) S. Hasegawa and Y. Hirose, *Phytochemistry*, **21**, 643 (1982).

2) M. Node, K. Nishide, M. Sai, K. Ichikawa, K. Fuji, and E. Fujita, *Chem. Lett.*, **1979**, 97.

3) T. Matsumoto, M. Takahashi, and Y. Kashihara, *Bull. Chem. Soc. Jpn.*, **52**, 3329 (1979).

4) C. H. Eugster, R. Buchecker, Ch. Tscharmer, G. Uhde, and G. Ohloff, *Helv. Chim. Acta*, **52**, 1729 (1969).

5) T. Matsumoto and S. Usui, *Bull. Chem. Soc. Jpn.*, **52**, 212 (1979).

6) M. Node, K. Ohta, T. Kajimoto, K. Nishide, E. Fujita, and K. Fuji, *Chem. Pharm. Bull.*, **31**, 4178 (1983).

7) T. Matsumoto and S. Takeda, *Chem. Lett.*, **1979**, 409.

The Total Synthesis of (±)-Megaphyllone Acetate, A Cytotoxic Neolignan

Takashi MATSUMOTO,* Sachihiko IMAI, Tadashi YAMAGUCHI, Masakazu MORIHIRA, and Masao MURAKAMI

Department of Chemistry, Faculty of Science, Hiroshima University, Higashisenda-machi, Naka-ku, Hiroshima 730

(Received September 3, 1984)

Conversion of 3-methoxy-4,5-methylenedioxybenzaldehyde into (2*RS*,3*SR*,4*RS*)-2-methoxycarbonyl-4-(3-methoxy-4,5-methylenedioxyphenyl)-3-methyl-4-butanolide (**11**) was carried out in seven steps *via* 1-acetoxy-1-(3-methoxy-4,5-methylenedioxyphenyl)propanone. The butanolide **11** was further converted into (2*RS*,3*SR*,3a*RS*,5*RS*)-3,3a,4,5-tetrahydro-5-methoxy-2-(3-methoxy-4,5-methylenedioxyphenyl)-3-methyl-3a-(2-propenyl)-6(2*H*)-benzofuranone (**22**) in eight steps. Reduction of **22** with lithium aluminium hydride followed by acetylation with acetic anhydride in pyridine afforded (±)-megaphyllone acetate.

Three cytotoxic neolignans, megaphone (**1**), megaphone acetate (**2**), and megaphyllone acetate (**3**), have been isolated from the root of *Aniba megaphylla* Mez. (Lauraceae) by Kupchan and his co-workers.[1] Each of these neolignans possesses four asymmetric centers and exhibits an *in vitro* inhibitory activity against cells derived from human carcinoma of the nasopharynx (KB). Recently, the total synthesis of racemic megaphone (**1**) and megaphone acetate (**2**) have been reported independently by four groups, Büchi,[2] Zoretic,[3] Hoye,[4] and ours.[5] As an extension of a previous work,[5] we describe here the stereoselective total synthesis of racemic megaphyllone acetate (**3**) starting from 3-methoxy-4,5-methylenedioxybenzaldehyde (myristicaldehyde)[6] (**5**) which was prepared from 3,4-dihydroxy-5-methoxybenzoic acid[7] (**4**). Our synthetic strategy was essentially the same as that reported in our previous work.

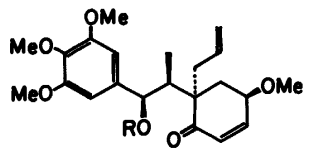

1 R=H
2 R=Ac

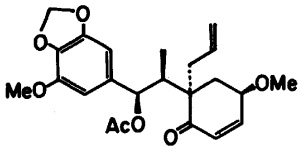

3

Condensation of **5** with methyl 2-chloropropanoate in tetrahydrofuran in the presence of potassium *t*-butoxide afforded a glycidic ester (**6**), which was hydrolyzed with aqueous sodium hydroxide in ethanol to give a sodium glycidate (**7**). This was decarboxylated with lead tetraacetate and pyridine in refluxing benzene[8] to afford 1-acetoxy-1-(3-methoxy-4,5-methylenedioxyphenyl)propanone (**8**) in 64% overall yield from **5**. Condensation of **8** in tetrahydrofuran with dimethyl malonate in the presence of titanium tetrachloride and pyridine yielded methyl 4-acetoxy-2-methoxycarbonyl-4-(3-methoxy-4,5-methylenedioxyphenyl)-3-methyl-2-butenoate (**9**) in 74% yield. The butenoate **9** was refluxed with concentrated hydrochloric acid in methanol to give a butenolide ester (**10**). Reduction of **10** with sodium borohydride in methanol followed by esterification with diazomethane gave a butanolide ester (**11**) in 33% yield along with its stereoisomer (**12**) and a keto diester (**13**) in 3% and 6% yields, respectively. A similar reduction of **13** with sodium borohydride provided **11** and **12** in 33% and 22% yields, respectively. The ^{1}H NMR spectrum of **11** showed a doublet signal due to the C-3 methyl at δ 0.81, while that of **12** showed a corresponding signal at δ 1.17. The appearance of the C-3 methyl signal in **11** in a very high field must be attributable to the shielding effect of the C-4 aromatic ring. Thus, the relative configurations of the methyl and aryl groups in **11** and **12** were assigned to be *cis* and *trans* dispositions, respectively. The *cis*-configurations of the methyl at C-3 and the hydrogen at C-2 in both **11** and **12** were also supported by the NOE measurements: irradiation of the methyl signals at δ 0.81 and 1.17 resulted in 16% and 14% enhancements of the C-2 proton signals at δ 3.35 and 3.39. Michael reaction of **11** in methanol with methyl vinyl ketone in the presence of triethylamine at 0—5 °C yielded a single keto lactone ester (**14**). This was hydrolyzed with aqueous sodium hydroxide in refluxing methanol and then decarboxylated with dilute hydrochloric acid to give a C-2 epimeric mixture of keto lactones (**15**) in 87% overall yield from **11**. Treatment of **15** with 1,2-ethanediol, trimethyl orthoformate, and boron trifluoride in dichloromethane afforded a mixture of the corresponding acetals (**16**) in 87% yield. To introduce an allyl group the acetal **16** was treated with allyl bromide and lithium diisopropylamide in 1,2-dimethoxyethane under a stream of nitrogen. The resulting single product (**17**) was hydrolyzed with dilute hydrochloric acid to give a keto lactone (**18**) in 68% overall yield from **16**. The relative configuration of the C-2 allyl and C-3 methyl groups in **17** was assigned to be *trans* by assuming the

introduction of the allyl group from the less hindered side of the molecule. Intramolecular aldol condensation of **18** with potassium *t*-butoxide in refluxing benzene was carried out and the crude product was immediately refluxed with *p*-toluenesulfonic acid in benzene to give an α,β-unsaturated ketone (**19**) in 66% yield. Subsequently, the introduction of a hydroxyl group at C-5 in **19** was carried out as follows.[9] The enone **19** in 1,2-dimethoxyethane was treated with chlorotrimethylsilane and lithium diisopropylamide under a stream of nitrogen to give a silyl enol ether. This was oxidized with *m*-chloroperbenzoic acid in dichloromethane in the presence of sodium hydrogencarbonate and then treated with triethylammonium fluoride to give the desired hydroxy enone (**20**) and its C-5 epimer (**21**) in 60% and 5% yields, respectively. In the ^{1}H NMR spectrum of the major alcohol **20**, a methine proton adjacent to the hydroxyl group exhibits both axial-axial (J=12 Hz) and axial-equatorial (J=5.5 Hz) vicinal coupling; while the corresponding proton in the minor alcohol **21** exhibits two equatorial-equatorial (J=5.5 and 3 Hz) vicinal coupling. Consequenly the hydroxyl groups in **20** and **21** are pseudoequatorial and pseudoaxial respectively. From these spectral data, the relative configurations of the hydroxyl and allyl groups in **20** and **21** were assigned respectively to be *trans* and *cis* dispositions. Methylation of **20** with diazomethane in ether in the presence of silica gel[10] afforded a methoxy enone (**22**) in 74% yield. This was reduced[11] with lithium aluminium hydride in refluxing tetrahydrofuran and the resulting alcohol was immediately acetylated with acetic anhydride in pyridine under a stream of nitrogen to give an acetate (**3**) in 71% yield. The ^{1}H NMR spectrum of the synthetic **3** was in good agreement with that published for natural megaphyllone acetate. A similar reduction of the enone **19** with lithium aluminium hydride followed by acetylation gave the corresponding acetate (**23**) in 82% yield.

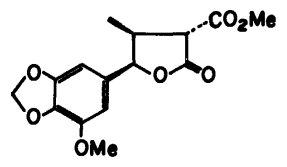

11

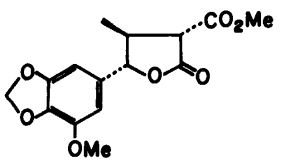

12

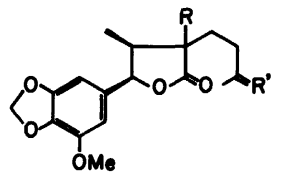

14 R=CO_2Me, R'=O
15 R=H, R'=O
16 R=H, R'=O(CH_2)$_2$O

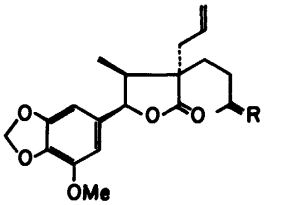

17 R=O(CH_2)$_2$O
18 R=O

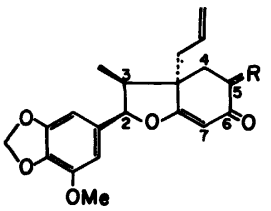

19 R=H_2
20 R= α-H, β-OH
21 R= α-OH, β-H
22 R= α-H, β-OMe

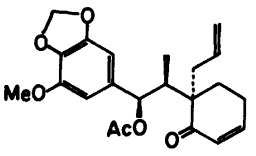

23

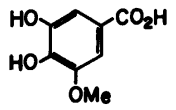

4

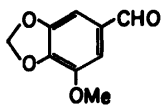

5

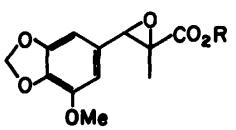

6 R=Me
7 R=Na

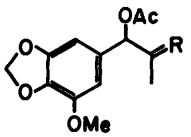

8 R=O
9 R=C(CO_2Me)$_2$

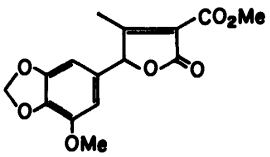

10

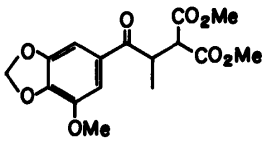

13

Experimental

All melting points are uncorrected. The IR spectra were measured in chloroform and the ^{1}H NMR spectra in deuteriochloroform at 90 MHz, with tetramethylsilane as an internal standard, unless otherwise stated; s: singlet, bs: broad singlet, d: doublet, bd: broad doublet, dd: double doublet, t: triplet, dt: double triplet, q: quartet, bq: broad quartet, m: multiplet. The column chromatography was performed using Merck silica gel (0.063 mm).

Methyl 3,4-Dihydroxy-5-methoxybenzoate. According to the method of Scheline,[7] 3,4-dihydroxy-5-methoxybenzoic acid (**4**) was prepared from gallic acid.

A mixture of the crude **4** (57 g) and concentrated sulfuric acid (6.0 ml) in methanol (250 ml) was refluxed for 6 h with a water separator containing 4-Å Molecular Sieves. The mixture was concentrated to a half volume, diluted with

brine, and extracted with ether. The ether extract was washed, successively, with aqueous sodium hydrogencarbonate and brine, dried over sodium sulfate, and evaporated *in vacuo*. The residue was recrystallized from benzene to give methyl 3,4-dihydroxy-5-methoxybenzoate (52 g: 76% from gallic acid), mp 115—118 °C, IR: 3550, 3350, 1713, 1622, 1521 cm^{-1}; ^1H NMR (60 MHz): δ=3.90 (6H, s, $-CO_2CH_3$ and $-OCH_3$), 5.4—6.4 (2H, br, 2-OH), 7.18 (1H, d, J=2 Hz) and 7.32 (1H, d, J=2 Hz) (aromatic protons).

3-Methoxy-4,5-methylenedioxybenzaldehyde (5). *a)*: Anhydrous potassium fluoride (88 g) was added to a stirred solution of methyl 3,4-dihydroxy-5-methoxybenzoate (50.0 g) in *N,N*-dimethylformamide (500 ml) and the mixture was stirred for 15 min. After the addition of dibromomethane (25.4 ml), the stirred mixture was refluxed for 2.5 h, cooled, diluted with ether, and then filtered. The filtrate was washed, successively, with brine, aqueous sodium hydroxide, and brine. The dried solution was evaporated *in vacuo* to give the crude methyl 3-methoxy-4,5-methylenedioxybenzoate (49.7 g). ^1H NMR (60 MHz): δ=3.89 (3H, s) and 3.95 (3H, s) ($-CO_2CH_3$ and $-OCH_3$), 6.04 (2H, s, $-OCH_2O-$), 7.17 (1H, d, J=2 Hz) and 7.28 (1H, d, J=2 Hz) (aromatic protons).

b): Lithium aluminium hydride (9.0 g) was added portionwise to a stirred solution of the above crude ester (49.7 g) in tetrahydrofuran (350 ml) with cooling in an ice-water bath. The mixture was refluxed for 2 h, cooled, poured into a mixture of ice and aqueous ammonium chloride, and then filtered. The filtrate was extracted with ethyl acetate. The ethyl acetate solution was washed with brine, dried over sodium sulfate, and evaporated *in vacuo* to give the crude 3-methoxy-4,5-methylenedioxybenzyl alcohol (41.0 g). ^1H NMR (60 MHz): δ=3.28 (1H, s, -OH), 3.85 (3H, s, $-OCH_3$), 4.46 (2H, s, $-C\underline{H}_2OH$), 5.90 (2H, s, $-OCH_2O-$), 6.46 (2H, s, aromatic protons).

c): Pyridinium dichlorochromate (186 g) was added to a stirred solution of the above crude alcohol (41.0 g) in dichloromethane (657 ml). The mixture was stirred at room temperature for 2 h and then filtered from a tarry residue, which was washed with ethyl acetate. The combined organic solution was washed with aqueous sodium hydrogencarbonate and brine, dried over sodium sulfate, and evaporated *in vacuo*. The residue was recrystallized from methanol to give **5** (26.0 g), mp 130—132 °C (lit,[6] mp 130—131 °C); IR: 1692, 1637, 1604 cm^{-1}; ^1H NMR (60 MHz): δ=3.98 (3H, s, $-OCH_3$), 6.10 (2H, s, $-OCH_2O-$), 7.04 (1H, d, J=2 Hz) and 7.12 (1H, d, J=2 Hz) (aromatic protons), 9.78 (1H, s, -CHO).

1-Acetoxy-1-(3-methoxy-4,5-methylenedioxyphenyl)propanone (8). *a)*: Potassium *t*-butoxide (50.50 g) was added to a stirred solution of 3-methoxy-4,5-methylenedioxybenzaldehyde (**5**) (54.05 g) and methyl 2-chloropropanoate (55.17 g) in tetrahydrofuran (810 ml) with cooling in an ice-water bath over a 10-min period. The mixture was stirred at 0—5 °C for 1.5 h and then at room temperature for 3 h, poured into ice-dilute hydrochloric acid, and extracted with ether. The ether extract was washed with brine, dried over sodium sulfate, and evaporated *in vacuo* to give a crude glycidic ester (**6**) (82.67 g) as an oil; IR: 1727, 1628 cm^{-1}; ^1H NMR (60 MHz): δ=1.36 (3H, s, $-\overset{|}{C}CH_3$), 3.80 (3H, s) and 3.90 (3H, s) ($-CO_2CH_3$ and $-OCH_3$), 4.22 (1H, s, $-\overset{|}{C}H-O-$), 5.97 (2H, s, $-OCH_2O-$), 6.47 (2H, s, aromatic protons).

b): Aqueous sodium hydroxide (13.2 g in 135 ml of water) was added, dropwise, to a stirred solution of the above crude **6** (82.67 g) in ethanol (1800 ml) with cooling in an ice-water bath. The mixture was stirred at room temperature for 3 h. The precipitates were collected by filtration and washed with ethanol to give a sodium glycidate (**7**) (68.00 g) as a colorless solid. Some additional **7** (8.00 g) was obtained from the filtrate.

Lead tetraacetate (112 g) was added to a stirred suspension of **7** (54.874 g) and pyridine (21.8 ml) in dry benzene (2000 ml) under a stream of nitrogen. The mixture was stirred at room temperature for 30 min, refluxed for 5 h, and then cooled. After the addition of 1,2-ethanediol (20 ml), the mixture was extracted with ether. The ether extract was washed with brine, dried over sodium sulfate, and evaporated *in vacuo*. The residue was chromatographed on silica gel (1200 g), using ether–benzene (1:99) as the eluent, to give **8** (34.254 g: 64.3% from **5**) as an oil. IR: 1743, 1731, 1639 cm^{-1}; ^1H NMR: δ=2.11 (3H, s) and 2.17 (3H, s) ($-COCH_3$ and $-OCOCH_3$), 3.91 (3H, s, $-OCH_3$), 5.87 (1H, s, $-C\underline{H}(OAc)-$), 6.00 (2H, s, $-OCH_2O-$), 6.59 (2H, s, aromatic protons). Found: C, 58.50; H, 5.34%. Calcd for $C_{13}H_{14}O_6$: C, 58.64; H, 5.30%.

Methyl 4-Acetoxy-2-methoxycarbonyl-4-(3-methoxy-4,5-methylenedioxyphenyl)-3-methyl-2-butenoate (9). A solution of **8** (26.638 g), dimethyl malonate (22.9 ml), and pyridine (145.3 ml) in dry tetrahydrofuran (270 ml) was added (over a 15-min period) to a stirred solution of titanium tetrachloride (65.9 ml) in dry tetrahydrofuran (850 ml) with cooling in an ice-water bath under a stream of nitrogen. The mixture was stirred at room temperature for 3.5 h, poured into ice–dilute hydrochloric acid, and extracted with ether. The ether extract was washed with brine, dried over sodium sulfate, and evaporated *in vacuo*. The residue was chromatographed on silica gel (600 g), using ether–benzene (2:98) as the eluent, to give **9** (28.046 g: 73.7%) as an oil. IR: 1730, 1640 cm^{-1}; ^1H NMR (60 MHz): δ=1.95 (3H, s), and 2.15 (3H, s) ($=\overset{|}{C}CH_3$ and $-OCOCH_3$), 3.78 (3H, s), 3.84 (3H, s), and 3.90 (3H, s) ($2-CO_2CH_3$ and $-OCH_3$), 5.95 (2H, s, $-OCH_2O-$), 6.65 (2H, s, aromatic protons), 6.87 (1H, s, $-C\underline{H}(OAc)-$). Found: C, 56.77; H, 5.18%. Calcd for $C_{18}H_{20}O_9$: C, 56.84; H, 5.30%.

2-Methoxycarbonyl-4-(3-methoxy-4,5-methylenedioxyphenyl)-3-methyl-2-buten-4-olide (10). A mixture of **9** (3.783 g) and concentrated hydrochloric acid (1.0 ml) in methanol (38 ml) was refluxed for 4 h. The mixture was concentrated and extracted with ethyl acetate. The ethyl acetate solution was washed with brine, dried over sodium sulfate, and evaporated *in vacuo* to give a crude **10** (2.953 g) as a solid, which was used without purification in the next reaction. IR: 1775, 1760 sh, 1720, 1633 cm^{-1}; ^1H NMR (60 MHz): δ=2.23 (3H, s, $=\overset{|}{C}CH_3$), 3.89 (6H, s, $-CO_2CH_3$ and $-OCH_3$), 5.60 (1H, s, C_4–H), 5.97 (2H, s, $-OCH_2O-$), 6.33 (1H, d, J=2 Hz) and 6.37 (1H, d, J=2 Hz) (aromatic protons).

Reduction of 10 with Sodium Borohydride. Sodium borohydride (0.376 g) was added to a stirred solution of the crude **10** (2.953 g) in methanol (38 ml) with cooling in an ice-water bath over a 5 min period. The mixture was stirred at room temperature for 30 min, poured into ice–dilute hydrochloric acid, and extracted with ethyl acetate. The ethyl acetate solution was washed with brine, dried over sodium sulfate, and evaporated *in vacuo*. The residue was

methylated with diazomethane in ether and the crude product was repeatedly chromatographed on silica gel, using ether–benzene (2:98) as the eluent, to give the following three compounds: **13**, **11**, and **12** in the order of elution.

a): Methyl 2-methoxycarbonyl-4-(3-methoxy-4,5-methylenedioxyphenyl)-3-methyl-4-oxobutanoate (**13**) (0.201 g: 6.0%), which was recrystallized from methanol, mp 83—85 °C. IR: 1747, 1728, 1672, 1628, 1602 cm^{-1}; ^1H NMR: δ= 1.18 (3H, d, J=7 Hz, $-CH(C\underline{H}_3)-$), 3.67 (3H, s) and 3.80 (3H, s) ($2-CO_2CH_3$), 3.94 (3H, s, $-OCH_3$), 3.5—4.3 (2H, m, $-C\underline{H}(CH_3)C\underline{H}(CO_2CH_3)_2$), 6.07 (2H, s, $-OCH_2O-$), 7.19 (1H, d, J=1.5 Hz) and 7.30 (1H, d, J=1.5 Hz) (aromatic protons). Found: C, 56.64; H, 5.57%. Calcd for $C_{16}H_{18}O_8$: C, 56.80; H, 5.36%.

b): (2*RS*,3*SR*,4*RS*)-2-Methoxycarbonyl-4-(3-methoxy-4,5-methylenedioxyphenyl)-3-methyl-4-butanolide (**11**) (0.999 g: 32.6%), which was recrystallized from methanol, mp 91.5—92.5 °C. IR: 1782, 1738, 1640 cm^{-1}; ^1H NMR: δ= 0.81 (3H, d, J=7 Hz, C_3-CH_3), 3.17 (1H, m, C_3-H), 3.35 (1H, d, J=6.5 Hz, C_2-H), 3.83 (3H, s) and 3.90 (3H, s) ($-CO_2CH_3$ and $-OCH_3$), 5.65 (1H, d, J=6.5 Hz, C_4-H), 5.98 (2H, s, $-OCH_2O-$), 6.38 (2H, s, aromatic protons). Found: C, 58.60; H, 5.41%. Calcd for $C_{15}H_{16}O_7$: C, 58.44; H, 5.23%.

c): (2*RS*,3*SR*,4*SR*)-2-Methoxycarbonyl-4-(3-methoxy-4,5-methylenedioxyphenyl)-3-methyl-4-butanolide (**12**) (0.084 g: 2.7%) as an oil. IR: 1782, 1738, 1640 cm^{-1}; ^1H NMR: δ=1.17 (3H, d, J=7 Hz, C_3-CH_3), 2.84 (1H, m, C_3-H), 3.39 (1H, d, J=12 Hz, C_2-H), 3.83 (3H, s) and 3.91 (3H, s) ($-CO_2CH_3$ and $-OCH_3$), 4.78 (1H, d, J=9.5 Hz, C_4-H), 5.99 (2H, s, $-OCH_2O-$), 6.55 (2H, s, aromatic protons). Found: C, 58.74; H, 5.22%. Calcd for $C_{15}H_{16}O_7$: C, 58.44; H, 5.23%.

Reduction of 13 with Sodium Borohydride. A solution of **13** (920 mg) in methanol (9.5 ml) was reduced with sodium borohydride (103 mg) as described above. The crude product was chromatographed on silica gel (50 g), using ether–benzene (2:98) as the eluent, to give the recovered **13** (85 mg: 9.2%), **11** (204 mg: 24.4%), and a 1:2.5 mixture of **11** and **12** (259 mg: 30.9%).

Michael Condensation of 11 with Methyl Vinyl Ketone. Triethylamine (1.40 ml) was added to a stirred solution of **11** (6.125 g) and methyl vinyl ketone (2.43 ml) in methanol (120 ml) with cooling in an ice–water bath. The mixture was allowed to stand in a refrigerator for 23 h, poured into ice–dilute hydrochloric acid, and extracted with ethyl acetate. The ethyl acetate solution was washed with brine, dried over sodium sulfate, and evaporated *in vacuo* to give a crude keto lactone ester (**14**) (7.592 g), which was used without purification in the next reaction. IR: 1773, 1715, 1633 cm^{-1}; ^1H NMR: δ=0.65 (3H, d, J=7.5 Hz, C_3-CH_3), 2.00—2.48 (2H, m, $-C\underline{H}_2CH_2CO-$), 2.14 (3H, s, $-COCH_3$), 2.48—3.08 (3H, m, $-C\underline{H}_2COCH_3$ and C_3-H), 3.74 (3H, s) and 3.89 (3H, s) ($-CO_2CH_3$ and $-OCH_3$), 5.66 (1H, d, J=6.5 Hz, C_4-H), 5.97 (2H, s, $-OCH_2O-$), 6.43 (1H, d, J=1.5 Hz) and 6.46 (1H, d, J=1.5 Hz) (aromatic protons).

Hydrolysis and Decarboxylation of 14. A mixture of the crude **14** (7.592 g) and 10% aqueous sodium hydroxide (5.0 ml) in methanol (86 ml) was refluxed for 3 h. The mixture was cooled, acidified with dilute hydrochloric acid, and then allowed to stand at room temperature for 30 min. After the methanol had been removed *in vacuo*, the residue was diluted with brine, and extracted with ethyl acetate. The ethyl acetate solution was washed with brine, dried over sodium sulfate, and evaporated *in vacuo*. The residue was chromatographed on silica gel (200 g), using ether–benzene (1:9) as the eluent, to give a mixture of (2*RS*,3*SR*,4*RS*)- and (2*SR*,3*SR*,4*RS*)-4-(3-methoxy-4,5-methylenedioxyphenyl)-3-methyl-2-(3-oxobutyl)-4-butanolide (**15**) (5.537 g: 87.0% from **11**); IR: 1771, 1716, 1637 cm^{-1}. The ^1H NMR spectrum of the mixture suggested the ratio of two C-2 epimers to be 57:43. ^1H NMR of the major compound: δ=0.78 (3H, d, J=6.5 Hz, C_3-CH_3), 2.16 (3H, s, $-COCH_3$), 3.88 (3H, s, $-OCH_3$), 5.45 (1H, d, J=7 Hz, C_4-H), 5.97 (2H, s, $-OCH_2O-$), 6.33 (2H, s, aromatic protons). ^1H NMR of the minor compound: δ=0.58 (3H, d, J=7 Hz, C_3-CH_3), 2.16 (3H, s, $-COCH_3$), 3.88 (3H, s, $-OCH_3$), 5.38 (1H, d, J=5.5 Hz, C_4-H), 5.97 (2H, s, $-OCH_2O-$), 6.42 (1H, d, J=2 Hz) and 6.46 (1H, d, J=2 Hz) (aromatic protons). Found: C, 63.49; H, 6.22%. Calcd for $C_{17}H_{20}O_6$: C, 63.74; H, 6.29%.

Acetalization of 15. A mixture of **15** (6.495 g), 1,2-ethanediol (11.3 ml), trimethyl orthoformate (22.0 ml), and boron trifluoride etherate (0.6 ml) in dichloromethane (130 ml) was stirred at room temperature for 12.5 h. The mixture was poured into water and extracted with ethyl acetate. The ethyl acetate extract was washed with brine, dried over sodium sulfate, and evaporated *in vacuo*. The residue was chromatographed on silica gel (200 g), using ether–benzene (1:9) as the eluent, to give a C-2 epimeric mixture of acetals (**16**) (6.395 g: 86.6%); IR: 1770, 1637 cm^{-1}. ^1H NMR of the major compound: δ=0.77 (3H, d, J=6.5 Hz, C_3-CH_3), 1.32 (3H, s, $-\underset{|}{C}CH_3$), 3.89 (3H, s, $-OCH_3$), 3.94 (4H, s, $-OCH_2CH_2O-$), 5.45 (1H, d, J=7 Hz, C_4-H), 5.97 (2H, s, $-OCH_2O-$), 6.36 (2H, s, aromatic protons). ^1H NMR of the minor compound: δ=0.58 (3H, d, J=7 Hz, C_3-CH_3), 1.32 (3H, s, $-\underset{|}{C}CH_3$), 3.89 (3H, s, $-OCH_3$), 3.94 (4H, s, $-OCH_2-CH_2O-$), 5.39 (1H, d, J=4 Hz, C_4-H), 5.97 (2H, s, $-OCH_2O-$), 6.43 (1H, d, J=2 Hz) and 6.47 (1H, d, J=2 Hz) (aromatic protons). Found: C, 62.69; H, 6.70%. Calcd for $C_{19}H_{24}O_7$: C, 62.62; H, 6.64%.

(2SR,3SR,4RS)-2-(3,3-Ethylenedioxybutyl)-4-(3-methoxy-4,5-methylenedioxyphenyl)-3-methyl-2-(2-propenyl)-4-butanolide (17). A solution of butyllithium in hexane (1.6 mol dm^{-3}, 9.38 ml) was added to a stirred solution of diisopropylamine (2.10 ml) in dry tetrahydrofuran (43 ml) at −70 °C under a stream of nitrogen. The mixture was stirred at −70 °C for 25 min and a solution of **16** (2.186 g) in dry tetrahydrofuran (6.0 ml) was added over a 5-min period. After 30 min, allyl bromide (3.57 ml) was added. The mixture was stirred at −70 °C for 25 min and then at −5—0 °C for 75 min, quenched with water, diluted with aqueous ammonium chloride, poured into dilute hydrochloric acid, and extracted with ethyl acetate. The extract was washed, successively, with dilute hydrochloric acid and brine, dried over sodium sulfate, and evaporated *in vacuo* to give the crude **17** (2.624 g), which was used without purification in the next reaction. IR: 1760, 1633 cm^{-1}; ^1H NMR (60 MHz): δ=0.67 (3H, d, J=7.5 Hz, C_3-CH_3), 1.29 (3H, s, $-\underset{|}{C}CH_3$), 2.47 (2H, bd, J=7 Hz, $-C\underline{H}_2CH=CH_2$), 3.88 (7H, bs, $-OCH_3$ and $-OCH_2CH_2O-$), 4.95—5.35 (2H, m, $-CH_2CH=C\underline{H}_2$), 5.54 (1H, d, J=6 Hz, C_4-H), 5.6—6.1 (1H, m, $-CH_2C\underline{H}=CH_2$), 5.94 (2H, s, $-OCH_2O-$), 6.37 (2H, bs, aromatic protons).

(2SR,3SR,4RS)-4-(3-Methoxy-4,5-methylenedioxyphenyl)-3-

methyl-2-(3-oxobutyl)-2-(2-propenyl)-4-butanolide (18). A mixture of the crude **17** (2.624 g) and 5% hydrochloric acid (1.3 ml) in methanol (26 ml) was stirred at room temperature for 3 h. The mixture was poured into brine and extracted with ethyl acetate. The extract was washed with brine, dried over sodium sulfate, and evaporated *in vacuo*. The residue was chromatographed on silica gel (100 g), using ether–benzene (5:95) as the eluent, to give **18** (1.463 g: 67.6% from **16**). This was recrystallized from chloroform–hexane, mp 114—114.5 °C IR: 1765, 1715, 1638 cm^{-1}; ^1H NMR: δ=0.68 (3H, d, J=7.5 Hz, C_3–CH_3), 1.42—2.13 (2H, m, $-C\underline{H}_2CH_2CO-$), 2.16 (3H, s, $-COCH_3$), 2.43 (2H, bd, J=7 Hz, $-C\underline{H}_2CH=CH_2$), 2.26—3.10 (3H, m, C_3–H and $-CH_2C\underline{H}_2CO-$), 3.90 (3H, s, $-OCH_3$), 5.04—5.33 (2H, m, $-CH_2CH=C\underline{H}_2$), 5.54 (1H, d, J=7 Hz, C_4–H), 5.56—6.03 (1H, m, $-CH_2C\underline{H}=CH_2$), 5.97 (2H, s, $-OCH_2O-$), 6.40 (1H, d, J=1.5 Hz) and 6.45 (1H, d, J=1.5 Hz) (aromatic protons). Found: C, 66.94; H, 6.72%. Calcd for $C_{20}H_{24}O_6$: C, 66.65; H, 6.71%. Further elution with ether–benzene (1:9) gave the recovered **15** (0.222 g).

(2RS,3SR,3aSR)-3,3a,4,5-Tetrahydro-2-(3-methoxy-4,5-methylenedioxyphenyl)-3-methyl-3a-(2-propenyl)-6(2H)-benzofuranone (19). Potassium *t*-butoxide (0.875 g) was added, portionwise, to a stirred solution of **18** (2.162 g) in dry benzene (22 ml) with cooling in an ice–water bath. The mixture was stirred at the same temperature for 5 min and then refluxed for 3 h. The mixture was cooled, poured into ice–dilute hydrochloric acid, and extracted with ethyl acetate. The extract was washed with brine, dried over sodium sulfate, and evaporated *in vacuo* to give an oily product.

A mixture of the above oily product and *p*-toluenesulfonic acid monohydrate (50 mg) in benzene (40 ml) was refluxed for 1 h, cooled, and diluted with ethyl acetate. The ethyl acetate solution was washed with aqueous sodium hydrogencarbonate and brine, dried over sodium sulfate, and evaporated *in vacuo*. The residue was chromatographed on silica gel (100 g), using ether–benzene (1:9) as the eluent, to give **19** (1.351 g: 65.8%). This was recrystallized from chloroform–hexane, mp 134—135 °C, IR: 1628 cm^{-1}; ^1H NMR: δ=0.53 (3H, d, J=7.5 Hz, C_3–CH_3), 2.56 (2H, d, J=7 Hz, $-C\underline{H}_2CH=CH_2$), 3.91 (3H, s, $-OCH_3$), 5.12—5.38 (2H, m, $-CH_2CH=C\underline{H}_2$), 5.54 (1H, s, C_7–H), 5.64—6.11 (1H, m, $-CH_2C\underline{H}=CH_2$), 5.78 (1H, d, J=5.5 Hz, C_2–H), 5.97 (2H, s, $-OCH_2O-$), 6.42 (2H, s, aromatic protons). Found: C, 69.90; H, 6.52%. Calcd for $C_{20}H_{22}O_5$: C, 70.16; H, 6.48%.

Hydroxylation of 19. A solution of butyllithium in hexane (1.6 mol dm^{-3}: 1.56 ml) was added dropwise to a stirred solution of diisopropylamine (0.42 ml) in dry 1,2-dimethoxyethane (6.8 ml) at −15 °C under a stream of nitrogen. The mixture was stirred at −15 °C for 15 min and a solution of **19** (342 mg) in dry 1,2-dimethoxyethane (3.0 ml) was added. After 15 min, chlorotrimethylsilane (0.64 ml) was added at −15 °C. The mixture was further stirred at room temperature for 2 h and the solvent was evaporated *in vacuo* under a stream of nitrogen. The residue was dissolved in dry hexane (30 ml) and then filtered. The filtrate was evaporated *in vacuo* under a stream of nitrogen to give a crude silyl enol ether.

A solution of the above crude product in dichloromethane (2.0 ml) was added to a stirred mixture of *m*-chloroperbenzoic acid (purity>90%: 326 mg) and sodium hydrogencarbonate (151 mg) in dichloromethane (20 ml) at −15 °C. The mixture was stirred at room temperature for 1 h, diluted with chloroform, and washed with aqueous sodium hydrogencarbonate. The dried solution was evaporated *in vacuo*. The residue was dissolved in dichloromethane (3.0 ml) and the resulting solution was added to a stirred solution of triethylammonium fluoride (484 mg) in dichloromethane (20 ml). The mixture was stirred at room temperature for 13.5 h, diluted with chloroform, and then washed successively with aqueous sodium hydrogencarbonate, dilute hydrochloric acid, and aqueous sodium hydrogencarbonate. The dried solution was evaporated *in vacuo*. The crude product was repeatedly chromatographed on silica gel (Merck 0.040—0.063 mm), using hexane–chloroform (4:6) as the eluent, to give the starting **19** (33.6 mg: 9.8%) and the following two alcohols.

(2*RS*,3*SR*,3a*RS*,5*RS*)-3,3a,4,5-Tetrahydro-5-hydroxy-2-(3-methoxy-4,5-methylenedioxyphenyl)-3-methyl-3a-(2-propenyl)-6(2*H*)-benzofuranone (**20**) (213.5 mg: 59.6%), which was recrystallized from chloroform–hexane, mp 160—161.5 °C. IR: 3480br, 1656sh, 1637sh, 1625 cm^{-1}; ^1H NMR: δ=0.54 (3H, d, J=7.5 Hz, C_3–CH_3), 1.81 (1H, t, J=12 Hz) and 2.37 (1H, dd, J=12 and 5.5 Hz) ($-C\underline{H}_2CH(OH)-$), 2.61 (2H, d, J=7 Hz, $-C\underline{H}_2CH=CH_2$), 3.52 (1H, bs, -OH), 3.90 (3H, s, $-OCH_3$), 4.34 (1H, dd, J=12 and 5.5 Hz, C_5–H), 5.15—5.43 (2H, m, $-CH_2CH=C\underline{H}_2$), 5.63 (1H, s, C_7–H), 5.70—6.18 (1H, m, $-CH_2C\underline{H}=CH_2$), 5.83 (1H, d, J=5.5 Hz, C_2–H), 5.98 (2H, s, $-OCH_2O-$), 6.40 (2H, s, aromatic protons). M^+, 358. Calcd for $C_{20}H_{22}O_6$: M^+, 358.

(2*RS*,3*SR*,3a*RS*,5*SR*)-3,3a,4,5-Tetrahydro-5-hydroxy-2-(3-methoxy-4,5-methylenedioxyphenyl)-3-methyl-3a-(2-propenyl)-6(2*H*)-benzofuranone (**21**) (17.6 mg: 4.9%), which was recrystallized from chloroform–hexane, mp 166—168 °C. IR: 3575, 3400br, 1637sh, 1624 cm^{-1}; ^1H NMR: δ=0.54 (3H, d, J=7.5 Hz, C_3–CH_3), 2.07 (1H, dd, J=15 and 5.5 Hz) and 2.22 (1H, dd, J=15 and 3 Hz) ($-C\underline{H}_2CH(OH)-$), 2.57 (1H, dd, J=13.5 and 8 Hz, $-C\underline{H}_AH_BCH=CH_2$), 2.86 (1H, dd, J=13.5 and 6 Hz, $-CH_A\underline{H}_BCH=CH_2$), *ca.* 2.6 (1H, m, C_3–H), 2.92 (1H, br, -OH), 3.91 (3H, s, $-OCH_3$), 4.10 (1H, dd, J=5.5 and 3 Hz, C_5–H), 5.11—5.40 (2H, m, $-CH_2CH=C\underline{H}_2$), 5.61 (1H, s, C_7–H), 5.89 (1H, d, J=5.5 Hz, C_2–H), 5.67—6.25 (1H, m, $-CH_2C\underline{H}=CH_2$), 5.79 (2H, s, $-OCH_2O-$), 6.40 (2H, bs, aromatic protons). M^+, 358. Calcd for $C_{20}H_{22}O_6$: M^+, 358.

(2RS,3SR,3aRS,5RS)-3,3a,4,5-Tetrahydro-5-methoxy-2-(3-methoxy-4,5-methylenedioxyphenyl)-3-methyl-3a-(2-propenyl)-6(2H)-benzofuranone (22). A cold solution of diazomethane (*ca.* 100 mmol) in ether (200 ml) was added to a stirred mixture of **20** (179.0 mg) and silica gel (9.0 g: Merck 0.040—0.063 mm) in dry tetrahydrofuran (15 ml) with cooling in an ice–water bath. Afer stirring at 0—5 °C for 30 min and then at room temperature for 1.5 h, the mixture was filtered to remove silica gel, which was washed well with chloroform. The filtrate was evaporated *in vacuo*. The residue was recrystallized from methanol to give **22** (101.0 mg: 54.1%), mp 154—155 °C. The mother liquor of recrystallization was evaporated *in vacuo* and the residue was chromatographed on silica gel (10 g: Merck 0.040—0.063 mm), using hexane–chloroform (6:4) as the eluent, to give an additional **22** (26.9 mg: 19.8%). IR: 1659sh, 1636, 1632 cm^{-1}; ^1H NMR: δ=0.54 (3H, d, J=7.5 Hz, C_3–CH_3), 1.88 (1H, t, J=12 Hz) and 2.28 (1H, dd, J=12 and 5.5 Hz) ($-C\underline{H}_2CH(OMe)-$), 2.33—

2.83 (3H, m, $-C\underline{H}_2CH=CH_2$ and C_3-H), 3.60 (3H, s, C_5-OCH_3), 3.91 (3H, s, $-OCH_3$), 3.98 (1H, dd, J=12 and 5 Hz, C_5-H), 5.17—5.43 (2H, m, $-CH_2CH=C\underline{H}_2$), 5.56 (1H, s, C_7-H), 5.70—6.18 (1H, m, $-CH_2C\underline{H}=CH_2$), 5.80 (1H, d, J= 5.5 Hz, C_2-H), 5.98 (2H, s, $-OCH_2O-$), 6.40 (2H, s, aromatic protons). Found: C, 67.47; H, 6.65%. Calcd for $C_{21}H_{24}O_6$: C, 67.73; H, 6.50%.

(±)-Megaphyllone Acetate (3). Lithium aluminium hydride (9.5 mg) was added to a stirred solution of **22** (93.1 mg) in dry tetrahydrofuran (5.0 ml) at room temperature. The mixture was refluxed for 2 h, cooled, poured into ice-water containing 15% hydrochloric acid (1.0 ml), and extracted with ether. The extract was washed with brine, dried over magnesium sulfate, and evaporated *in vacuo* under a stream of nitrogen. The residue was immediately acetylated with acetic anhydride (0.5 ml) in pyridine (5.0 ml) at 50 °C for 15 h in an atmosphere of nitrogen. After the usual work-up, the crude product was chromatographed on silica gel (20 g: Merck 0.040—0.063 mm), using hexane-chloroform (1:1) as the eluent, to give **3** (73.8 mg: 70.9%) as an oil, whose spectral data were identical with those reported for natural megaphyllone acetate. IR (CCl_4): 1745, 1676, 1636 cm^{-1}; ^1H NMR: δ=0.90 (3H, d, J=7 Hz, $-CH(C\underline{H}_3)-$), 1.87 (1H, dd, J=14 and 10 Hz) and 2.27 (1H, d of dd, J=14, 6, and 2 Hz) ($-C\underline{H}_2CH-(OCH_3)-$), 2.09 (3H, s, $-OCOCH_3$), 2.34 (2H, bd, J=7 Hz, $-C\underline{H}_2CH=CH_2$), 2.51 (1H, bq, J=7 Hz, $-C\underline{H}(CH_3)-$), 3.44 (3H, s, $-CH(OC\underline{H}_3)-$), 3.91 (3H, s, $-OCH_3$), 4.04—4.30 (1H, m, $-C\underline{H}(OCH_3)-$), 4.87—5.12 (2H, m, $-CH_2CH=C\underline{H}_2$), 5.35—5.82 (1H, m, $-CH_2C\underline{H}=CH_2$), 5.67 (1H, bs, $-C\underline{H}-(OCOCH_3)-$), 5.93 (2H, s, $-OCH_2O-$), 6.00 (1H, dd, J=10 and 2 Hz, $-COC\underline{H}=CH-$), 6.49 (1H, d, J=1.5 Hz) and 6.55 (1H, d, J=1.5 Hz) (aromatic protons), 6.89 (1H, dt, J=10 and 2 Hz, $-COCH=C\underline{H}-$). Found: C, 66.07; H, 6.88%; M^+, 416. Calcd for $C_{23}H_{28}O_7$: C, 66.33; H, 6.78%; M^+, 416.

(±)-Demethoxymegaphyllone Acetate (23). Reduction of a solution of **19** (250 mg) in dry tetrahydrofuran (20 ml) with lithium aluminium hydride (27.7 mg), followed by acetylation with acetic anhydride (2.5 ml) in pyridine (20 ml), was carried out as described regarding the preparation of **3**. The crude product was recrystallized from methanol to give **23** (179 mg: 63.2%), mp 115.5—116.5 °C. The mother liquor of recrystallization was evaporated *in vacuo* and the residue was chromatographed on silica gel (10 g), using ether-benzene (5:95) as the eluent, to give an additional **23** (51.3 mg: 18.2%). IR: 1737, 1666, 1640 cm^{-1}; ^1H NMR: δ=0.88 (3H, d, J=7.5 Hz, $-CH(C\underline{H}_3)-$), 2.09 (3H, s, $-OCOCH_3$), 2.33 (2H, bd, J=7 Hz, $-C\underline{H}_2CH=CH_2$), 2.47 (1H, bq, J=7.5 Hz, $-C\underline{H}(CH_3)-$), 3.91 (3H, s, $-OCH_3$), 4.83—5.11 (2H, m, $-CH_2CH=C\underline{H}_2$), 5.37—5.86 (1H, m, $-CH_2C\underline{H}=CH_2$), 5.71 (1H, bs, $-C\underline{H}(OCOCH_3)-$), 5.93 (2H, s, $-OCH_2O-$), 5.98 (1H, dt, J=10 and 2 Hz, $-COC\underline{H}=CH-$), 6.51 (1H, d, J=1.5 Hz) and 6.57 (1H, d, J= 1.5 Hz) (aromatic protons), 6.86 (1H, dt, J=10 and 4 Hz, $-COCH=C\underline{H}-$). Found: C, 68.44; H, 6.88%. Calcd for $C_{22}H_{26}O_6$: C, 68.38; H, 6.78%.

References

1) S. M. Kupchan, K. L. Stevens, E. A. Rohlfing, B. R. Sickles, A. T. Sneden, R. W. Miller, and R. F. Bryan, *J. Org. Chem.*, **43**, 586 (1978).

2) G. Büchi and P-S. Chu, *J. Am. Chem. Soc.*, **103**, 2718 (1981).

3) P. A. Zoretic, C. Bhakta, and R. H. Khan, *Tetrahedron Lett.*, **24**, 1125 (1983).

4) T. R. Hoye and M. J. Kurth, *Tetrahedron Lett.*, **24**, 4769 (1983).

5) T. Matsumoto, S. Imai, S. Usui, A. Suetsugu, S. Kawatsu, and T. Yamaguchi, *Chem. Lett.*, **1984**, 67.

6) K. N. Campbell, P. F. Hopper, and B. K. Campbell, *J. Org. Chem.*, **16**, 1736 (1951); M. Tomita and Y. Aoyagi, *Chem. Pharm. Bull.*, **16**, 523 (1968); Y. Asakawa, K. Tanikawa, and T. Aratani, *Phytochemistry*, **15**, 1057 (1976); G. E. Schneiders and R. Stevenson, *J. Org. Chem.*, **46**, 2969 (1981); M. Iinuma, T. Tanaka, and S. Matsuura, *Yakugaku Zasshi*, **103**, 994 (1983).

7) R. R. Scheline, *Acta Chem. Scand.*, **20**, 1182 (1966).

8) V. Reutrakul, Y. Srikirin, and S. Panichanun, *Chem. Lett.*, **1982**, 879.

9) G. M. Rubottom and J. M. Gruber, *J. Org. Chem.*, **43**, 1599 (1978).

10) K. Ohno, H. Nishiyama, and H. Nagase, *Tetrahedron Lett.*, **1979**, 4405.

11) W. F. Gannon and H. O. House, *Org. Synth.*, Coll. Vol. V, 294 (1973).

Total Synthesis of Antibiotic Althiomycin[1]

Kaoru INAMI and Tetsuo SHIBA*
Department of Chemistry, Faculty of Science, Osaka University, Toyonaka, Osaka 560
(Received September 3, 1984)

Total Synthesis of antibiotic althiomycin has been achieved starting from D-cysteine. The imide bond between thiazoline and the pyrrolinone part was constructed by coupling reaction of sodium salt of pyrrolinone with cysteine active ester or by photoreaction with diketene. The hydroxymethyl group attached on the carbon adjacent to C-2 of the thiazoline ring, was introduced by aldol condensation posterior to the thiazoline ring formation. The thiazole part was introduced in a final step in whole process of the total synthesis of the antibiotic. The synthetic althiomycin was identical with the natural antibiotic in all respects.

Althiomycin (**1**) was first isolated from *Streptomyces althioticus* by Umezawa and his collaborators in 1957[2] and then from other microorganisms by Sensi *et al.*[3] as well as Kunze *et al.*[4] This antibiotic inhibits the protein synthesis in both Gram-positive and negative bacteria.[5] The structural determination of althiomycin was carried out by Umezawa *et al.*,[6] Kirst *et al.*,[7] and us.[8] Althiomycin has two asymmetric centers, one of which, C-4 of the thiazoline ring, was deduced to be of *S* configuration, corresponding to D-cysteine residue, while the *exo* carbon atom adjacent to C-2 of the thiazoline ring, is still ambiguous, because this antibiotic is always isolated as the mixture of epimers concerning this asymmetric carbon. The geometric configuration of the aldoxime has been determined as *E* form from the result of X-ray analysis of the methanolysis product of althiomycin[7] as well as our synthetic study.[8] In order to investigate the structure-activity relationship of althiomycin, we first attempted the total synthesis of this antibiotic.

The synthetic pathway is based on the "stepwise elongation method" from C-terminal to N-terminal. Concerning the preparation of pyrrolinone part, 2,4-pyrrolidinedione (**2**) synthesized according to the method of Lowe *et al.*[9] was methylated with ethereal diazomethane to give 4-methoxy-3-pyrrolin-2-one (**3**) (yield 52.9%) as the major product and 2-methoxy-4-one isomer (**4**) (7.1%) as the minor one. The mixture was purified and separated by silica-gel column chromatography using the developing solvent of ethyl acetate–methanol 9:1. The predominant product (**3**) is completely identical with naturally derived pyrrolinone in all respects. As a preliminary experiment of acylation of the pyrrolinone, acid chloride method is solely successful among various kinds of acylation methods applied.

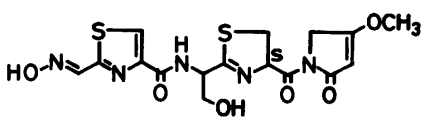

Althiomycin (1)

Fig. 1.

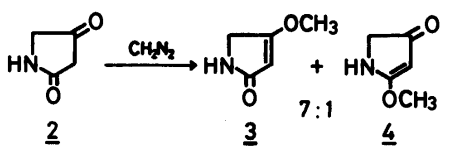

Fig. 2.

Secondly, the synthesis of the thiazoline part was performed by coupling method of the imino ether of *N*-protected glycine and D-cysteine ester. *N,S*-Ditrityl-D-cysteine diphenylmethyl ester (**6**) was prepared from D-cysteine *p*-toluenesulfonate *via* successive procedures of tritylation of mercapto and amino groups and esterification with diphenyldiazomethane. Both trityl (Trt) groups were removed with silver nitrate to give cysteine derivative with free amino and mercapto groups (**7**). The compound was coupled with ethyl benzyloxycarbonylaminoacetimidate[10] to obtain the thiazoline ester (**8**) (yield 73.9%). Removal of diphenylmethyl (DPM) group afforded the thiazolinecarboxylic acid (**9**).

With reference of results of the preliminary acylation of the pyrrolinone, the coupling of the thiazolinecarboxylic acid (**9**) with methoxypyrrolinone (**3**) was attempted using several carboxylic activation methods such as acid chloride, active ester, mixed anhydride, dicyclohexylcarbodiimide-4-dimethylaminopyridine, *N*-ethyl-5-phenylisoxazolium-3-sulfonate (Woodward's reagent "K"), azide, or triphenylphosphine-di-2-pyridyl disulfide (Mukaiyama's method). Amino activation methods like triethyloxonium tetrafluoroborate (Meerwein's reagent), 2-chloro-1-methylpyridinium iodide,[11] phosphazo, phosphite ester, and trimethylsilylation-acid chloride method[12] were also tried. However, the desired coupling product (**10**) could never be obtained by these methods because of a low reactivity of the imino group of the pyrrolinone and an instability of the thiazoline ring. Therefore, we next tried to apply a photoreaction of the thiazolinecarbonyl azide (**12**) with diketene according to the method exploited in the case of substituted benzoyl azides by Kato *et al.*[13] The corresponding azide (**12**) was synthesized from carboxylic acid **9** *via* successive procedures of conversion to the protected hydrazide with *t*-butyl carbazate, water-soluble carbodiimide (*N*-[3-(dimethylamino)propyl]-*N'*-ethylcarbodiimide), and

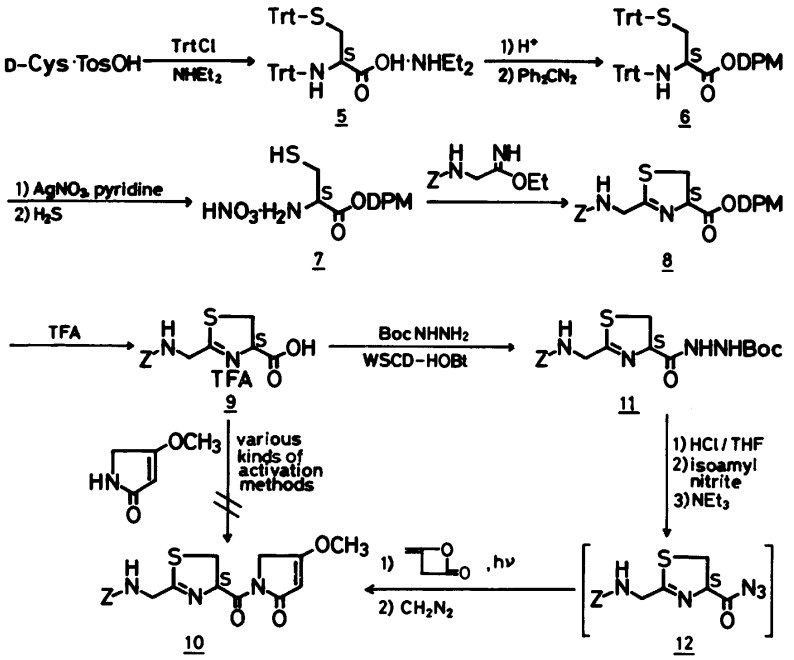

Fig. 3.

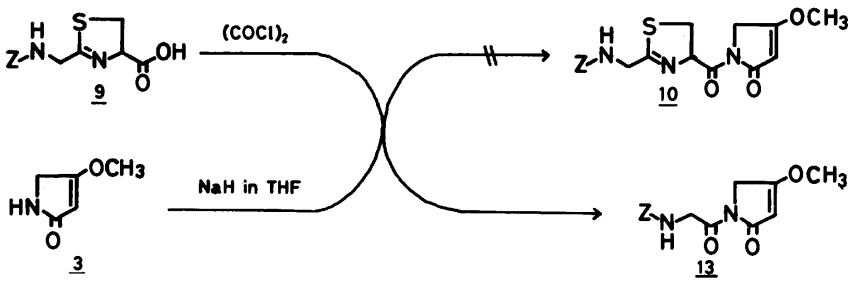

Fig. 4.

1-hydroxybenzotriazole, and then azidation with isopentyl nitrite followed by removal of *t*-butoxycarbonyl (Boc) group. A mixture of the azide (**12**) thus obtained without isolation and diketene distilled just before use was irradiated with a high-pressure mercury lamp through a quartz filter (HALOS PIH-100) in chloroform for 6 h at 0 °C under nitrogen atmosphere. The product was methylated with diazomethane to give the desired thiazoline-pyrrolinone compound (**10**). This route was, however, found to be disadvantageous concerning yield and reproducibility despite of searches of the good reaction condition.

Thus, we reinvestigated the coupling of the thiazoline part with the pyrrolinone to improve this synthesis. The defects in the above reaction seemed to be due to a low nucleophilicity of the imino group of the pyrrolinone ring. Therefore, we next tried a coupling of thiazolinecarbonyl chloride with sodium salt of the pyrrolinone prepared from **3** and sodium hydride. Actually the reaction afforded only glycylpyrrolinone (**13**), but not the desired thiazoline-pyrrolinone derivative (**10**), presumably because of the situation that C-2 of the thiazoline ring is more reactive than the carbonyl carbon of the acid chloride under these conditions. From results mentioned above, we then attempted the formation of the thiazoline ring after coupling of the cysteine active ester with sodium salt of the pyrrolinone. Each active ester (**14**—**16**) prepared from *N*-hydroxysuccinimide (HONSu), *N*-hydroxy-5-norbornene-*endo*-2,3-dicarboximide (HONb), or *p*-nitrophenol (HONp), was coupled with sodium salt of the pyrrolinone respectively. The products from both ONb and ONp esters were the cysteinylpyrrolinone (**18**), whereas that from ONSu ester was found to be *N*-[3-(cysteinyloxyaminocarbonyl)propionyl]-3-pyrrolin-2-one derivative (**17**) formed by ring opening of the succinimide. By comparison of two reactions using ONb and ONp esters, the former is superior to the latter both in respects of easiness in the treatment of the active esters and $[\alpha]_D$ of the product. The protected cysteinylpyrrolinone (**18**) thus obtained was deprotected with silver nitrate and hydrogen sulfide,

and then coupled with the imidic ether of benzyloxycarbonylglycine to afford the thiazoline-pyrrolinone derivative (**10**) in 39% yield. Formations of the thiazoline ring and the imide bond between the thiazoline and the pyrrolinone part were confirmed in long-range coupling (1 Hz) between the *exo* methylene of C-2 and the proton of C-4 in the thiazoline ring, and downfield shift (0.3 ppm) of methylene protons of the pyrrolinone ring in NMR respectively.

The aldol condensation for the thiazoline moiety with aqueous 35% formaldehyde solution in dimethyl sulfoxide at room temperature for 3 d afforded the hydroxymethyl compound (**19**) and its anhydro derivative in ratio of about 1 : 1 on TLC. However, when the aldol condensation was carried out by use of paraformaldehyde instead of formalin in degassed and anhydrous dimethyl sulfoxide, only the desired hydroxymethyl derivative was obtained as a sole product. The result of this reaction seems to be much dependent to the solvent used since this type of reaction for model compounds gave the β-hydroxy derivative in aprotic polar solvents such as dimethyl sulfoxide or *N*,*N*-dimethylformamide, while, in a protic solvent like methanol its anhydro derivative was obtained.[14]

The thiazole moiety, namely (*E*)-2-(hydroxyiminomethyl)-4-thiazolecarbonyl azide (**29**), was synthesized as shown in the scheme. For ethyl diethoxyacetate (**20**)[15] amidation, dehydration, and addition of hydrogen sulfide were successively carried out to result in the production of diethoxythioacetamide (**23**), which was then coupled with ethyl 3-bromopyruvate[16] to yield thiazole acetal (**24**). After removal of the acetal, the aldehyde was converted to oximes (**26**, **27**) with hydroxylamine hydrochloride. The (*E*)-aldoxime (**26**) was separated from (*Z*)-isomer (**27**) by silica-gel column chromatography and fractional recrystallization. The compound (**26**) thus obtained was then converted into thiazolecarbonyl azide (**29**) in the usual way.

Deprotection of the thiazoline-pyrrolinone compound **19** with anhydrous hydrogen fluoride followed by coupling with the thiazole part by the azide method was carried out under following conditions; the thiazoline-pyrrolinone derivative (**19**) was dissolved in anisole, and then anhydrous hydrogen fluoride was introduced to the solution at −78 °C. After deprotection procedure for 20 min at 0 °C, hydrogen fluoride

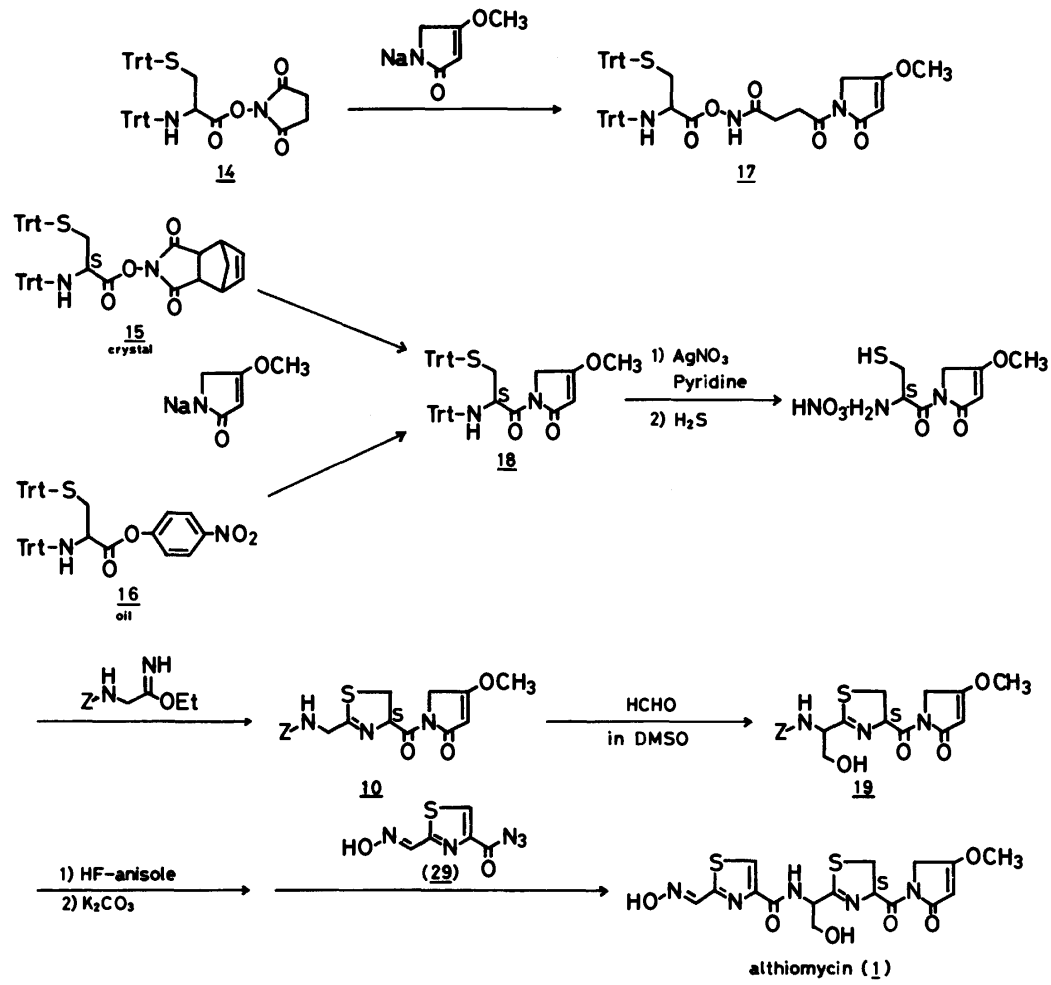

Fig. 5.

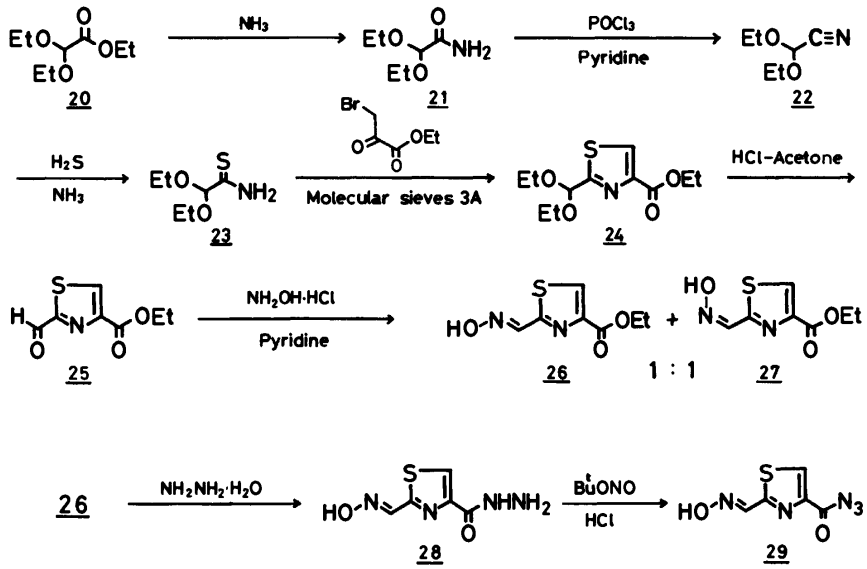
NH3
POCl3
Pyridine
20
21
22
H2S
NH3
Molecular sieves 3A
23
24
HCl-Acetone
NH2OH·HCl
Pyridine
25
26
1 : 1
27
NH2NH2·H2O
28
BuONO
HCl
29

Fig. 6.

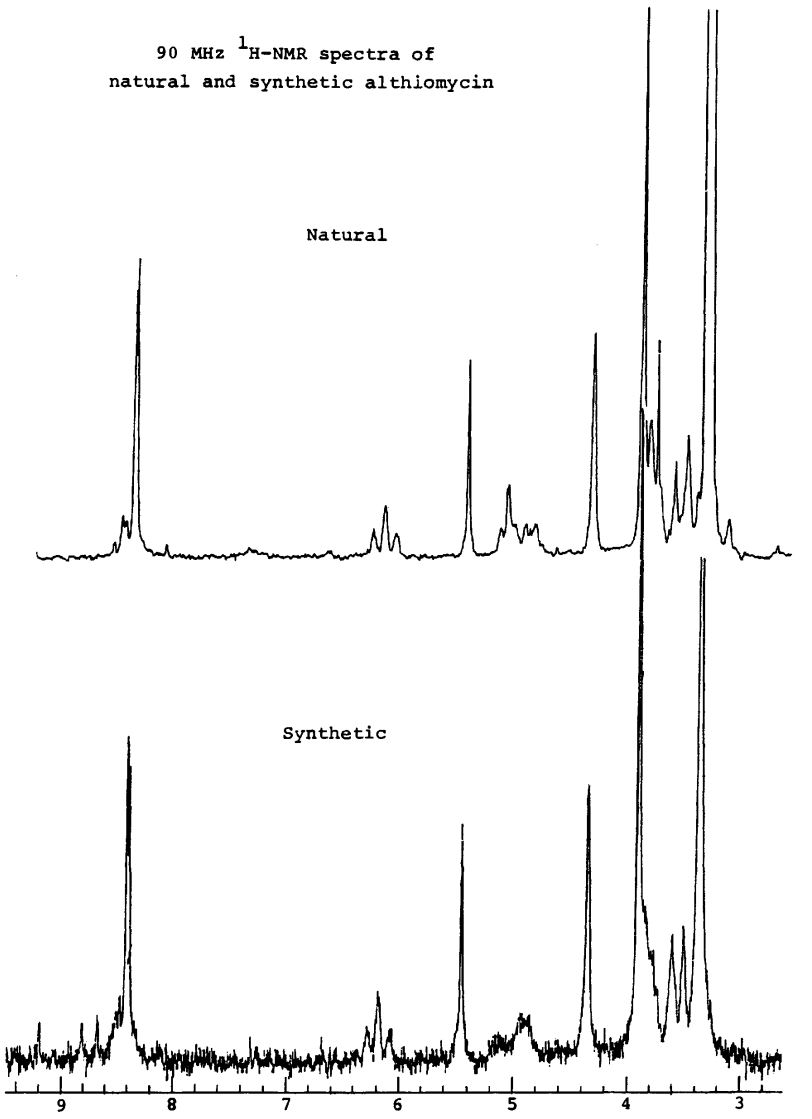
90 MHz 1H-NMR spectra of
natural and synthetic althiomycin
Natural
Synthetic
9
8
7
6
5
4
3

Fig. 7.

TABLE 1. COMPARISONS OF SYNTHETIC AND NATURAL ALTHIOMYCIN

		Synthetic	Natural
$[\alpha]_D^{20}$ (Methyl Cellosolve)		+22.3°	+20.8°
UV λ_{max}^{MeOH} (ε_{max})		223 nm (34100)	223 nm (38700)
		240 nm (26300)	240 nm (29900)
		286 nm (8200)	286 nm (8310)
TLC[a]	$CHCl_3$-MeOH 9:1	0.33	0.33
	Benzene-AcOEt 1:3	0.45	0.45
	Benzene-acetone 1:1	0.51	0.51
HPLC	31% CH_3CN[b]	7.4 min	7.4 min
	CH_3CN-MeOH-H_2O[c] (1:2:7)	25.4 min	25.4 min

a) Merck Kieselgel F_{254}. b) Nagel Nucleosil $7C_{18}$ (6 mm×250 mm), 1.5 ml/min. c) Waters Radialpak μ-Bondapak C_{18} (8 mm×100 mm), 1.0 ml/min

TABLE 2. MINIMUM INHIBITORY CONCENTRATION OF NATURAL AND SYNTHETIC ALTHIOMYCIN

Test organism	Synthetic	Natural
Staph. aureus ATCC 6538P	25	25
Staph. aureus MS353	25	25
Staph. aureus MS353 C36	25	25
Staph. aureus MS353 A0	25	25
Staph. aureus 0116	25	25
Staph. aureus 0119	25	25
Staph. aureus 0126	25	25
Staph. aureus 0127	25	25
Staph. epidermidis sp-al-1	25	25
Strept. pyogenes N.Y.5	3.1	3.1
Strept. pyogenes 1022	3.1	3.1
Strept. faecalis 1501	100	100
Strept. agalactiae 1020	6.3	6.3
Sarcina lutea ATCC 9341	1.6	1.6
Micrococcus flavus ATCC 10240	3.1	3.1
Corynebact. diphtheriae P.W.8	0.8	0.8
Bac. subtilis ATCC 6633	25	25
E. coli NIHJ-JC2	>100	>100
E. coli B	50	50
Klebs. pneumoniae ATCC 10031	6.3	6.3
Salm. typhosa H 901	>100	>100
Salm. enteritidis Gaertner	>100	>100
Shigella flexineri type 3a	50	25
Shigella sonnei E33	>100	>100
Proteus vulgaris OX19	50	50
Serratia carcescens	>100	>100
Ps. aeruginosa LAM1095	>100	>100

was evaporated off *in vacuo* as quickly as possible. The residual oil was neutralized with potassium carbonate, and coupled with thiazolecarbonyl azide in *N,N*-dimethylformamide for 3 h at room temperature. The product after purification by preparative silica-gel TLC (chloroform-methanol 9:1) was completely identical with natural althiomycin as shown in Table 1. Antibacterial activities of the synthetic althiomycin were also quite identical with those of the natural antibiotic (Table 2).

Experimental

All melting points are uncorrected. The IR spectra were determined on a JASCO A-100 grating infrared spectrophotometer; and the ^1H- and ^{13}C-NMR spectra, on a Varian XL-100-15 NMR spectrometer, a Jeol FX-90Q NMR spectrometer, a Jeol JNM-PMX 60 NMR spectrometer, and a Varian T-60 NMR spectrometer. The chemical shifts are given in δ, with TMS as the internal standard. The UV spectra were obtained with a Hitachi 124 spectrophotometer. The electron-impact and field-desorption mass spectra were obtained with a Jeol JMS-OlSG-2 mass spectrometer and Hitachi RM-50 spectrometer. The optical rotations were obtained with a Perkin-Elmer 141 polarimeter. The high performance liquid chromatography was performed on a Yanako liquid chromatograph model L-2000 and Shimadzu LC-5A liquid chromatograph. TLC was carried out by the ascending method on a Merck Kieselgel F_{254} and Woelm Kieselgel F_{254}.

4-Methoxy-3-pyrrolin-2-one (3). To a solution of 2,4-pyrrolidinedione (**2**)[9] (1.19 g, 12.0 mmol) in 100 ml of acetonitrile, was added excess diazomethane in ether and allowed to react for 10 h. After evaporation of excess diazomethane at 50 °C, the solution was concentrated *in vacuo* to give brown needles. Purification and separation by silica-gel column chromatography gave pale yellow solid (R_f 0.80 on TLC using a developing solvent chloroform–methanol 7:1). This solid was recrystallized from ethyl acetate and hexane; yield 0.72 g (53%). Mp 128—128.5 °C. Found: C, 53.05; H, 6.21; N, 12.36%. Calcd for $C_5H_7NO_2$: C, 53.09; H, 6.24; N, 12.38%. EI-MS: *m/z* (rel intensity) 113 (100), 98 (14), 86 (50), 83 (31), 70 (100), and 28 (52). 60 MHz ^1H-NMR ($CDCl_3$) δ=7.0 (1H, br.), 5.18 (1H, s), 3.98 (2H, s), 3.85 (3H, s).

1-Acetyl-4-methoxy-3-pyrrolin-2-one. To a solution of **3** (100 mg, 0.885 mmol) in 0.9 ml of chloroform, was added triethylamine (134 mg, 1.33 mmol) and acetyl chloride (208 mg, 2.65 mmol). A mixture was stirred for 2 h under ice-cooling and then diluted with chloroform. After washing with saturated aqueous sodium hydrogencarbonate and brine, the organic layer was dried over anhydrous magnesium sulfate and concentrated *in vacuo*. Purification by preparative silica-gel TLC (chloroform-methanol 9:1) gave

colorless needles; yield 121 mg (100%). Mp 92—92.5 °C. Found: C, 54.05; H, 5.86; N, 8.94%. Calcd for $C_7H_9NO_3$: C, 54.19; H, 5.85; N, 9.03%. EI-MS *m/z* (rel intensity), 155 (64), 113 (86), 99 (83), 70 (47), and 43 (100). 60 MHz ^{1}H-NMR ($CDCl_3$) δ=5.20 (1H, s), 4.30 (2H, s), 3.90 (3H, s), 2.50 (3H, s).

N,S-*Dityrityl-*D*-cysteine Diethylamine Salt (5).* To a solution of D-cysteine *p*-toluenesulfonate (13.1 g, 44.7 mmol) in 85 ml of degassed water, a solution of diethylamine (24.6 ml, 0.237 mol) in 85 ml of water was added dropwise with stirring for 5 min at 0 °C. To the reaction mixture, a solution of trityl chloride (37.4 g, 0.134 mol) in 290 ml of ether was added dropwise with a vigorous stirring for 10 min at −20 °C. After additional stirring for 1.5 h, the reaction mixture was extracted with chloroform and washed with water. The organic layer was concentrated *in vacuo* and residual oil was dissolved in 300 ml of 99% ethanol. To the solution, diethylamine (8 ml) was added and colorless prisms precipitated was collected; yield 27.2 g (89.8%). Mp 193—194 °C (dec). $[\alpha]_D^{20}$ −62.1° (*c* 1.50, chloroform). Found: C, 79.38; H, 6.72; N, 3.91; S, 4.50%. Calcd for $C_{45}H_{46}N_2O_2S$: C, 79.61; H, 6.83; N, 4.13; S, 4.72%.

Diphenylmethyl N,S-*Dityrityl-*D*-cysteinate (6).* To a suspension of *N,S*-ditrityl-D-cysteine diethylamine salt (19.9 g, 29.4 mmol) in 300 ml of ether, 10 ml of 3M aqueous (1 M= 1 mol dm^{-3}) citric acid was added with vigorous stirring for 40 min at 0 °C. The ethereal solution was washed with water and dried over anhydrous magnesium sulfate. The solution was concentrated *in vacuo* to 100 ml. To the solution, diphenyldiazomethane (5.70 g, 29.4 mmol) was added. After stirring for 1 d, the insoluble material was filtered off and the solution was concentrated *in vacuo*. The residue was recrystallized from ether and methanol; yield 19.3 g (84.8%). Mp 155—156 °C. $[\alpha]_D^{20}$ −44.4° (*c* 0.468, acetone). Found: C, 83.75; H, 5.87; N, 1.90; S, 4.09%. Calcd for $C_{54}H_{45}NO_2S$: C, 84.01; H, 5.88; N, 1.81; S, 4.15%. 60 MHz ^{1}H-NMR ($CDCl_3$) δ=7.30 (40H, m), 7.10 (1H, s), 6.30 (1H, s), 3.50 (1H, br.), 2.80 (1H, d), 2.40 (2H, d).

Diphenylmethyl D*-Cysteinate Nitrate (7).* To a solution of diphenylmethyl *N,S*-dityrityl-D-cysteinate (**6**) (19.2 g, 24.9 mmol) in 25 ml of benzene, a solution of silver nitrate (4.65 g, 27.4 mmol) and pyridine (2.20 ml, 27.4 mmol) in 40 ml of methanol was added and stirred for 1 d at room temperature. Through the reaction mixture, hydrogen sulfide was bubbled with stirring for 30 min at room temperature. Silver sulfide was filtered off and the filtrate was concentrated *in vacuo*. The residue was recrystallized from methanol and ether; yield 6.30 g (72.2%). Mp 123—125 °C. $[\alpha]_D^{20}$ +15.7° (*c* 2.84, *N,N*-dimethylformamide). Found: C, 54.95; H, 5.35; N, 7.78; S, 8.65%. Calcd for $C_{16}H_{18}N_2O_5S$: C, 54.84; H, 5.18; N, 8.00; S, 9.15%. 60 MHz ^{1}H-NMR ($CDCl_3$) δ=7.30 (10H, s), 6.93 (1H, s), 4.50 (1H, t, *J*=4Hz), 3.30 (2H, d, *J*=4Hz).

Diphenylmethyl (S)-2-(Benzyloxycarbonylaminomethyl)-2-thiazoline-4-carboxylate (8). To a solution of ethyl (benzyloxycarbonylamino)acetimidate[10] (4.25 g, 18.0 mmol) in 120 ml of absolute ethanol, diphenylmethyl D-cysteinate nitrate (6.30 g, 18.0 mmol) was added. The reaction mixture was stirred for 16 h at room temperature and concentrated *in vacuo*. The residual oil was dissolved in ethyl acetate and washed with water. The organic layer was dried over anhydrous magnesium sulfate and concentrated *in vacuo*. Recrystallization from acetone–hexane gave colorless crystals; yield 6.12 g (73.9%). Mp 94—96 °C. $[\alpha]_D^{14}$ −51.9° (*c* 1.15, benzene). Found: C, 67.76; H, 5.30; N, 6.06; S, 7.09%. Calcd for $C_{26}H_{24}N_2O_4S$: C, 67.81; H, 5.26; N, 6.08; S, 6.96%. 60 MHz ^{1}H-NMR ($CDCl_3$) δ=7.45 (15H, s), 6.88 (1H, s), 5.40 (1H, br.), 5.13 (1H, dt, *J*=2Hz, 10Hz), 5.08 (2H, s), 4.18 (2H, dd, *J*=2Hz, 7Hz), 3.52 (2H, d, *J*=10 Hz).

(S)-2-(Benzyloxycarbonylaminomethyl)-4-carboxy-2-thiazolinium Trifluoroacetate (9). A mixture of diphenylmethyl (*S*)-2-(benzyloxycarbonylaminomethyl)-2-thiazoline-4-carboxylate (6.12 g, 13.3 mmol) and trifluoroacetic acid (19.8 ml, 0.266 mol) was stirred for 30 min at 0 °C. To the reaction mixture, 200 ml of ether was added. The precipitate was collected and washed with ether, yield 4.43 g (81.6%). Mp>200 °C. 60 MHz ^{1}H-NMR (CF_3COOD) δ=7.34 (5H, s), 5.24 (2H, s), 4.70 (1H, br. t), 4.27 (2H, s), 3.74 (2H, br. d).

*(S)-N′-(*t*-Butoxycarbonyl)-2-(benzyloxycarbonylaminomethyl)-2-thiazoline-4-carbohydrazide (11).* To a solution of **9** (4.43 g, 10.9 mmol) in 20 ml of tetrahydrofuran, *t*-butyl carbazate (3.01 g, 22.8 mmol), 1-hydroxybenzotriazole (3.08 g, 22.8 mmol), and *N*-[3-(dimethylamino)propyl]-*N′*-ethylcarbodiimide hydrochloride (4.37 g, 22.8 mmol) were added successively and the mixture was stirred for 2 h at 0 °C. After additional stirring for 16 h at room temperature, the reaction mixture was concentrated *in vacuo* and dissolved in ethyl acetate. The solution was washed with saturated aqueous sodium hydrogencarbonate and brine. The organic layer was dried over anhydrous magnesium sulfate. The solution was concentrated *in vacuo*. Purification by silica-gel column chromatography (120 g, benzene–ethyl acetate 3:1) gave colorless oil; yield 2.60 g (58.7%). Found: *m/z* 408.1458. Calcd for $C_{18}H_{24}N_4O_5S$: *m/z* 408.1466. Found: C, 52.76; H, 6.31; N, 12.54; S, 6.61%. Calcd for $C_{18}H_{24}N_4O_5S \cdot 0.5C_4H_8O_2$: C, 53.08; H, 6.24; N, 12.38; C, 7.09%. 60 MHz ^{1}H-NMR ($CDCl_3$) δ=8.63 (1H, d, *J*=3Hz), 7.30 (5H, s), 6.85 (1H, d, *J*=3Hz), 6.00 (1H, br.t, *J*=6 Hz), 5.06 (2H, s), 5.03 (1H, tt, *J*=2Hz, 9Hz), 4.10 (2H, dd, *J*=2Hz, 6Hz), 3.53 (2H, d, *J*=9Hz), 1.45 (9H, s).

(S)-2-(Benzyloxycarbonylaminomethyl)-2-thiazoline-4-carbohydrazide Dihydrochloride. The protected hydrazide **11** (2.60 g, 6.37 mmol) was dissolved in 4.67 M hydrogen chloride in tetrahydrofuran (27.3 ml, 0.127 mol) and allowed to react for 2 h at 0 °C. To the reaction mixture, 300 ml of ether was added and the precipitate was collected; yield 2.05 g (84.4%). Mp 132—134 °C (dec). Found: C, 38.59; H, 5.18; N, 14.62; S, 8.03; Cl, 17.67%. Calcd for $C_{13}H_{18}N_4O_3SCl_2 \cdot H_2O$: C, 39.10; H, 5.05; N, 14.03; S, 8.41; Cl, 17.76%.

N,S-*Dityrityl-*D*-cysteine 5-Norbornene-*endo*-2,3-dicarboximidyl Ester (15).* To a suspension of *N,S*-ditrityl-D-cysteine diethylamine salt (**5**) (2.98 g, 3.86 mmol) in 200 ml of ether, 2 ml of 3 M aqueous citric acid was added. The reaction mixture was vigorously stirred for 30 min at 0 °C. An organic layer was washed with water and dried over anhydrous magnesium sulfate. The solution was concentrated *in vacuo* and the residual oil was dissolved in 15 ml of tetrahydrofuran. To the solution, *N*-hydroxy-5-norbornene-*endo*-2,3-dicarboximide (1.04 g, 5.79 mmol) and dicyclohexylcarbodiimide (0.950 g, 4.63 mmol) were added and stirred for 2 h at 0 °C. After additional stirring for 10 h at room temperature, the reaction mixture was concentrated *in vacuo*. The residual oil was dissolved in ethyl acetate, and the insoluble material was filtered off. The filtrate was washed with saturated aqueous sodium hydrogencarbonate and brine. The organic layer was dried over anhydrous magnesium sulfate and concentrated *in vacuo*. The residue

was recrystallized from ethyl acetate and hexane; yield 2.88 g (97.3%). Mp 194—195 °C (dec). $[\alpha]_D^{18}$ −63.4° (*c* 1.45, chloroform). Found: C, 78.10; H, 5.61; H, 3.67; S, 4.21%. Calcd for $C_{50}H_{42}N_2O_4S$: C, 78.31; H, 5.52; N, 3.65; S, 4.18%. 60 MHz ^{1}H-NMR ($CDCl_3$) δ=7.30 (30H, m), 7.00 (1H, br. s), 6.07 (2H, br. s), 3.78 (1H, m), 3.50 (2H, br. s), 3.25 (2H, br. s), 2.50 (2H, br. d), and 1.45—1.85 (2H, br. m).

1-(N,S-Dirityl-D-cysteinyl)-4-methoxy-3-pyrrolin-2-one (18). To a solution of 4-methoxy-3-pyrrolin-2-one (**3**) (5.60 g, 49.6 mmol) in 155 ml of anhydrous tetrahydrofuran, 60% sodium hydride (1.59 g, 39.7 mmol) was added. The mixture was heated under reflux for 10 min. To the solution, *N,S*-ditrityl-D-cysteine 5-norbornene-*endo*-2,3-dicarboximidyl ester (**15**) (24.0 g, 33.1 mmol) was added with vigorous stirring for 20 min at room temperature. Ethyl acetate was added to the reaction mixture, and the solution was washed with saturated aqueous sodium hydrogencarbonate and brine. An organic layer was dried over anhydrous magnesium sulfate and concentrated *in vacuo*. The residue was recrystallized from ethyl acetate and hexane; yield 20.3 g (87.9%). Mp 214—215 °C (dec). $[\alpha]_D^{21}$ −23.6° (*c* 2.02, chloroform). Found: C, 78.40; H, 5.94; N, 3.89; S, 4.50%. Calcd for $C_{46}H_{40}N_2O_3S$: C, 78.83; H, 5.75; N, 4.00; S, 4.57%. 100 MHz ^{1}H-NMR ($CDCl_3$) δ=7.0—7.6 (30H, m), 4.86 (1H, s), 4.84 (1H, br. s), 3.78 (3H, s), 3.77 (1H, d, *J*=18 Hz), 3.43 (1H, br. t), 3.34 (1H, d, *J*=18 Hz), 2.80 (1H, dd, *J*=6 Hz, 12 Hz), 2.58 (1H, dd, *J*=4 Hz, 12 Hz). 22.5 MHz ^{13}C-NMR ($CDCl_3$) δ=175.9, 172.2, 168.8, 146.1, 145.0, 129.8, 129.0, 127.8, 127.5, 126.5, 126.2, 94.3, 71.2, 66.5, 58.5, 54.4, 48.2, 36.8.

1-[(S)-2-(Benzyloxycarbonylaminomethyl)-2-thiazoline-4-carbonyl]-4-methoxy-3-pyrrolin-2-one (10). *i)* Via *Photoreaction*: To a suspension of (*S*)-2-(benzyloxycarbonylaminomethyl)-2-thiazoline-4-carbohydrazide dihydrochloride (1.33 g, 3.48 mmol) in 32 ml of degassed ethanol-free chloroform, isopentyl nitrite (0.673 ml, 3.44 mmol) and 4.20 M hydrogen chloride in tetrahydrofuran (0.815 ml, 3.44 mmol) were added at −18 °C and the stirring was continued for 25 min at −18 °C. The reaction mixture was neutralized with triethylamine (1.54 ml, 11.1 mmol). To the solution, diketene (2.65 ml, 3.48 mol) was added and irradiated with a 100 watt high-pressure mercury lamp (HALOS PIH-100) with a quartz filter under nitrogen atmosphere at 0 °C for 6 h. After concentration *in vacuo*, the residual oil was dissolved in 10 ml of chloroform and methylated with excess ethereal diazomethane with stirring for 2.5 h. After evaporation of diazomethane under reduced pressure, the solution was washed with saturated aqueous sodium hydrogencarbonate and brine. The organic layer was dried over anhydrous magnesium sulfate, and concentrated *in vacuo*. Purification by silica-gel preparative TLC (benzene–ethyl acetate 1:3) gave colorless oil; yield 67.7 mg (5.0%).

ii) Via *Sodium Salt of Pyrrolinone*: To a suspension of 1-(*N,S*-dirityl-D-cysteinyl)-4-methoxy-3-pyrrolin-2-one (**18**) (1.14 g, 1.63 mmol) in the mixture of 5.70 ml of methanol and 4.00 ml of benzene, pyridine (144 μl, 1.79 mmol) and silver nitrate (304 mg, 1.79 mmol) were added and stirring was continued for 4 h at room temperature. Hydrogen sulfide was bubbled through the reaction mixture for 20 min at room temperature. Silver sulfide was filtered off and the filtrate was concentrated *in vacuo*. To a solution of the residual oil in 22 ml of 99% ethanol, ethyl (benzyloxycarbonylamino)acetimidate[10] (385 mg, 1.63 mmol) was added and stirred for 20 h at room temperature. After concentration, the residual oil was dissolved in ethyl acetate and washed with saturated aqueous sodium hydrogencarbonate and brine. The organic layer was dried over anhydrous magnesium sulfate and concentrated *in vacuo*. The residue was recrystallized from ethyl acetate and hexane; yield 250 mg (39.4%). Mp 185—186 °C (dec). $[\alpha]_D^{20}$ +21.0° (*c* 0.879, chloroform). Found: C, 55.54; H, 4.94; N, 10.73; S, 8.02%. Calcd for $C_{18}H_{19}N_3O_5S$: C, 55.52; H, 4.92; N, 10.79; S, 8.23%. 100 MHz ^{1}H-NMR ($CDCl_3$) δ=7.36 (5H, s), 6.24 (1H, tt, *J*=1 Hz, 9 Hz), 5.54 (1H, br. s), 5.16 (1H, s), 5.15 (2H, s), 4.30 (2H, s), 4.26 (2H, dd, *J*=1 Hz, 5 Hz), 3.90 (3H, s), 3.61 (1H, dd, *J*=6 Hz, 9 Hz), and 3.50 (1H, dd, *J*=6 Hz, 9 Hz). 22.5 MHz ^{13}C-NMR ($CDCl_3$) δ=176.6, 171.9, 169.5, 169.0, 155.9, 136.4, 128.5, 128.0, 94.5, 78.1, 67.1, 58.8, 48.5, 43.7, and 35.7.

1-[(4S)-2-[1-(Benzyloxycarbonylamino)-2-hydroxyethyl]-2-thiazoline-4-carbonyl]-4-methoxy-3-pyrrolin-2-one (19). To a solution of 1-[(*S*)-2-(benzyloxycarbonylaminomethyl)-2-thiazoline-4-carbonyl]-4-methoxy-3-pyrrolin-2-one (**10**) (50.0 mg, 0.129 mmol) in 500 μl of degassed dimethyl sulfoxide, pulverized paraformaldehyde (77.0 mg, 2.57 mmol) was added. The mixture was stirred for 7 d at room temperature. The insoluble material was filtered off and the filtrate was dissolved in ethyl acetate. The solution was washed with water and dried over anhydrous magnesium sulfate. The solution was concentrated *in vacuo*. The residue was lyophilized; yield 52.7 mg (97.6%). Mp 71—73 °C. 100 MHz ^{1}H-NMR ($CDCl_3$) δ=7.34 (5H, s), 6.29 (1H, m), 5.88 (1H, m), 5.16 (1H, s), 5.13 (2H, s), 4.75 (1H, m), 4.28 (2H, s), 3.95—4.08 (3H, m), 3.90 (3H, s), 3.48 (1H, d, *J*=6 Hz), and 3.35 (1H, d, *J*=6 Hz). 22.5 MHz ^{13}C-NMR ($CDCl_3$) δ=177.0, 176.9, 169.7, 169.5, 156.6, 136.3, 128.5, 128.0, 94.4, 78.2, 67.1, 66.5, 58.9, 52.7, 48.4, and 34.1.

Diethoxyacetamide (21). A solution of ethyl diethoxyacetate[15] (42.7 g, 0.243 mol) in 2 l of 99% ethanol, was saturated with ammonia in a pressure bottle and kept at room temperature for 2 d. Concentration *in vacuo* gave colorless plates; yield 36.4 g (100%). Mp 80—81 °C. IR (Nujol) 1670 cm^{-1}. Found: C, 48.70; H, 8.91; N, 9.49%. Calcd for $C_6H_{13}NO_3$: C, 48.96; H, 8.90; N, 9.52%. 60 MHz ^{1}H-NMR ($CDCl_3$) δ=6.8 (2H, br.), 4.88 (1H, s), 3.73 (2H, q, *J*=7 Hz), 1.27 (6H, t, *J*=7 Hz).

Diethoxyacetonitrile (22). To a solution of diethoxyacetamide (**21**) (1.00 g, 6.80 mmol) in 16 ml of pyridine, phosphoryl chloride (1.15 g, 7.49 mmol) was added dropwise with stirring at −18 °C for 30 min. After additional stirring for 30 min, the reaction mixture was poured into about 100 g of cracked ice carefully. The mixture was extracted with ether and washed with 1M hydrochloric acid, brine, saturated aqueous sodium hydrogencarbonate, and brine successively. The organic layer was dried over anhydrous magnesium sulfate, and concentrated *in vacuo*. The residual oil was distilled under reduced pressure and collected a fraction boiling at 63—63.5 °C/ 22 mmHg: yield 0.78 g (89%). Found: C, 55.82; H, 8.69; N, 10.92%. Calcd for $C_6H_{11}NO_2$: C, 55.79; H, 8.59; N, 10.85%. 60 MHz ^{1}H-NMR ($CDCl_3$) δ=5.48 (1H, s), 3.73 (4H, q, *J*=7 Hz), and 1.25 (6H, t, *J*=7 Hz).

Diethoxythioacetamide (23). *i) From 21*: To a solution of diethoxyacetamide (**21**) (4.00 g, 27.2 mmol) in 50 ml of dry benzene, phosphorus pentasulfide (2.00 g, 9.00 mmol) was added portionwise with stirring during a period of 10 min at room temperature. After additional stirring for 10 min, an insoluble material was removed by decantation, and the

supernatant was washed with saturated aqueous sodium hydrogencarbonate and brine. The organic layer was dried over anhydrous magnesium sulfate, and concentrated *in vacuo*. The residue was recrystallized from benzene and hexane; yield 2.86 g (64.3%).

ii) From **22**: Through a solution of diethoxyacetonitrile (**22**) (580 mg, 4.50 mmol) in 300 ml of dry methanol containing 18 g of ammonia, hydrogen sulfide was bubbled with stirring for 16 h at room temperature. After hydrogen sulfide was removed by aeration, the solution was concentrated *in vacuo*. Recrystallization from benzene–hexane gave colorless needles; yield 0.73 g (100%). Mp 81—82 °C. IR (Nujol) 1600 cm^{-1} ($\nu_{C=S}$). Found: C, 44.18; H, 8.06; N, 8.54; S, 19.50%. Calcd for $C_6H_{13}NO_2S$: C, 44.15; H, 8.03; N, 8.58; S, 19.69%. 60 MHz ^{1}H-NMR ($CDCl_3$) δ=8.2 (2H, br.), 5.10 (1H, s), 3.75 (4H, q, J=7 Hz), and 1.20 (6H, t, J=7 Hz).

Ethyl 2-(diethoxymethyl)-4-thiazolecarboxylate (24). Ethyl 3-bromopyruvate[18] (0.37 g, 1.9 mmol) was added to a solution of diethoxythioacetamide (**23**) (0.37 g, 2.3 mmol) in 4 ml of dry ethanol, and the mixture was heated under reflux in the presence of Molecular Sieves 3A (about 1 g) for 30 min. The solution was concentrated *in vacuo*, extracted with ethyl acetate and washed with saturated aqueous sodium hydrogencarbonate and brine. The organic layer was dried over anhydrous magnesium sulfate and concentrated *in vacuo*. Purification by preparative TLC (chloroform–methanol 50:1) gave colorless oil; yield 0.49 g (100%). Found: C, 51.19; H, 6.68; N, 5.25; S, 11.79%. Calcd for $C_{11}H_{17}NO_4S$: C, 50.95; H, 6.61; N, 5.40; S, 12.36%. 60 MHz ^{1}H-NMR ($CDCl_3$) δ=8.30 (1H, s), 5.78 (1H, s), 4.48 (2H, q, J=7 Hz), 3.77 (4H, q, J=7 Hz), 1.40 (3H, t, J=7 Hz), and 1.25 (6H, t, J=7 Hz).

Ethyl 2-Formyl-4-thiazolecarboxylate (25). To a solution of ethyl 2-(diethoxymethyl)-4-thiazolecarboxylate (**24**) (1.59 g, 6.13 mmol) in 125 ml of acetone, 1 M hydrochloric acid (12.5 ml) was added and heated under reflux for 45 min. The reaction mixture was concentrated *in vacuo*, and the residual oil was extracted with ethyl acetate and washed with saturated aqueous sodium hydrogencarbonate and brine. The organic layer was dried over anhydrous magnesium sulfate, and concentrated *in vacuo*. The residue was recrystallized from ether and hexane; yield 1.13 g (100%). Mp 67—68 °C. IR (Nujol) 1720 and 1695 cm^{-1}. Found: C, 45.54; H, 3.75; N, 7.55; S, 17.25%. Calcd for $C_7H_7NO_3S$: C, 45.39; H, 3.81; N, 7.56; S, 17.31%. 60 MHz ^{1}H-NMR ($CDCl_3$) δ=10.13 (1H, d, J=1 Hz), 8.63 (1H, d, J=1 Hz), 4.53 (2H, q, J=7 Hz), and 1.43 (3H, t, J=7 Hz).

Ethyl (E)- and (Z)-2-(Hydroxyiminomethyl)-4-thiazolecarboxylate (26, 27). To a solution of ethyl 2-formyl-4-thiazolecarboxylate (**25**) (8.14 g, 44.0 mmol) in 70 ml of dry ethanol, pyridine (70.0 ml, 0.871 mol) and hydroxylamine hydrochloride (13.0 g, 0.187 mol) were added and heated under reflux for 1 h. The reaction mixture was concentrated *in vacuo*, and water (100 ml) was added to the residual oil. The precipitate was recrystallized from ethyl acetate and hexane; yield 8.04 g (91.4%). This solid is a mixture of (*E*)- and (*Z*)-aldoxime in ratio of about 1:1. Fractional recrystallization of the mixture from either ethyl acetate–hexane or methanol–ether gave colorless needles (**26**) and colorless powder (**27**). (*E*)-isomer **26**: Mp 183—184 °C. Found: C, 42.08; H, 4.01; N, 13.85; S, 15.91%. Calcd for $C_7H_8N_2O_3S$: C, 41.99; H, 4.03; H, 14.00; S, 16.01%. 100 MHz ^{1}H-NMR (DMSO-d_6): δ=12.24 (1H, s), 8.50 (1H, d, J=1 Hz), 8.40 (1H, d, J=1 Hz), 4.38 (2H, q, J=7 Hz), 1.36 (3H, t, J=7 Hz); (*Z*)-isomer **27**: mp 163—164 °C. Found: C, 42.09; H, 4.01; N, 13.87; S, 16.04%. Calcd for $C_7H_8N_2O_3S$: C, 41.99; H, 4.03; N, 14.00; S, 16.01%. 100 MHz ^{1}H-NMR (DMSO-d_6) δ=13.12 (1H, br. s), 8.67 (1H, d, J=1 Hz), 8.10 (1H, d, J=1 Hz), 4.39 (2H, q, J=7 Hz), 1.36 (3H, t, J=7 Hz).

(E)-2-(Hydroxyiminomethyl)-4-thiazolecarbohydrazide (28). To a solution of ethyl (*E*)-2-(hydroxyiminomethyl)-4-thiazolecarboxylate (**26**) (4.50 g, 22.5 mmol) in 40 ml of *N,N*-dimethylformamide, 100% hydrazine hydrate (24.0 ml, 0.494 mol) was added at 0 °C and allowed to react for 18 h at 5 °C. Colorless needles precipitated was collected and washed with a small amount of methanol; yield 3.50 g (89.7%). Mp>200 °C. Found: C, 32.30; H, 3.30; N, 29.70; S, 17.35%. Calcd for $C_5H_6N_4O_2S$: C, 32.25; H, 3.25; N, 30.09; S, 17.22%. 60 MHz ^{1}H-NMR (DMSO-d_6) δ=8.40 (1H, s), 8.32 (1H, s).

(E)-2-(Hydroxyiminomethyl)thiazole-4-carbonyl Azide (29). To a suspension of (*E*)-2-(hydroxyiminomethyl)-4-thiazolecarbohydrazide (**28**) (500 mg, 2.69 mmol) in 3 ml of *N,N*-dimethylformamide, *t*-butyl nitrite (350 μl, 2.96 mmol) and 4.67 M hydrogen chloride in tetrahydrofuran (1.27 ml, 5.92 mmol) were added at −50 °C. The reaction mixture was stirred for 3 h at −30 °C, extracted with ethyl acetate and washed with water. The organic layer was dried over anhydrous magnesium sulfate and concentrated *in vacuo*. The residue was recrystallized from acetone and hexane; yield 330 mg (62.3%). Mp 165—166 °C (dec). IR (Nujol) 2160 cm^{-1}. Found: C, 30.69; H, 1.64; N, 35.04; S, 16.58%. Calcd for $C_5H_3N_5O_2S$: C, 30.46; H, 1.53; N, 35.52; S, 16.26%. 60 MHz ^{1}H-NMR ($CDCl_3$–CD_3OD 1:1) δ=8.33 (1H, s), 8.32 (1H, s).

Althiomycin (1). To a solution of **19** (79.0 mg, 0.189 mmol) in 204 μl of anisole, anhydrous hydrogen fluoride (about 1 ml) was introduced at −78 °C within 10 min and stirred for a period of 20 min at 0 °C. Hydrogen fluoride was evaporated off *in vacuo* at 0 °C for 20 min. To a solution of the product in 1 ml of *N,N*-dimethylformamide, anhydrous potassium carbonate (781 mg, 5.66 mmol) was added at −78 °C. The reaction mixture was vigorously stirred for 5 min at room temperature under reduced pressure. Under cooling with Dry Ice–methanol bath, (*E*)-2-(hydroxyiminomethyl)-4-thiazolecarbonyl azide (**29**) (37.1 mg, 0.189 mmol) was added to the reaction mixture, which was stirred for 30 min at 0 °C and then for 2.5 h at room temperature. Ethyl acetate was added to this solution and washed with 0.1 M potassium phosphate buffer (pH 7.15) and water. The organic layer was dried over anhydrous magnesium sulfate and concentrated *in vacuo*. Purification by silica-gel preparative TLC using a developing solvent chloroform–methanol (9:1) gave colorless powder; yield 14.8 mg (17.9%). Mp 175—176 °C (dec). $[\alpha]_D^{27}$ +22.3° (*c* 0.065, Methyl Cellosolve). UV_{max} (CH_3OH) 223 nm (ε 34000), 240 nm (ε 25800), 286 nm (ε 8460). Found: C, 43.78; H, 4.38; N, 13.97; S, 12.95%. Calcd for $C_{16}H_{17}N_5O_6S_2 \cdot 0.5\ H_2O \cdot 0.5\ C_4H_8O_2$: C, 43.89; H, 4.50; N, 14.22; S, 13.02%. 90 MHz ^{1}H-NMR (DMSO-d_6) δ=8.40 (1H, br.s), 8.37 (1H, s), 8.35 (1H, s), 6.16 (1H, dt, J=3 Hz, 9 Hz), 5.43 (1H, s), 5.10 (1H, m), 4.90 (1H, m), 4.33 (2H, s), 3.89 (3H, s), 3.83 (2H, m), and 3.50 (2H, t).

The authors express our sincere thanks to Dr. Hamao Umezawa of Institute of Microbial Chemistry, and Dr. Hideo Sakakibara of the Research Laborato-

ries, Toyo Jozo Co. Ltd., for supplying natural althiomycin and giving kind suggestions. We also thank the Research Laboratories, Toyo Jozo Co. Ltd., for measurement of antibacterial activity. Authors deeply indebted to Mr. Kozo Sawada for his contribution in the initial stage of this work.

References

1) This work was presented at the 17th European Peptide Symposium, Prague (Czechoslovakia), August 1982 (T. Shiba and K. Inami, Peptides 1982, ed by K. Blaha, P. Malon. Walter de Gruyter & Co., Berlin, New York, p. 341 (1983)), and the 47th National Meeting of Chemical Society of Japan, Kyoto, April 1983, Abstr. No. 4H36; and reported in a preliminary form: K. Inami and T. Shiba, *Tetrahedron Lett.*, **25**, 2009 (1984).

2) H. Yamaguchi, Y. Nakayama, K. Takeda, K. Tawara, K. Maeda, T. Takeuchi, and H. Umezawa, *J. Antibiot., Ser.* **A10**, 195 (1957).

3) P. Sensi, R. Bollotta, and G. G. Gallo, *Antibiot. & Chemoth.*, **9**, 76 (1959).

4) B. Kunze, H. Reichenbach, H. Augustiniak, and G. Hofle, *J. Antibiot.*, **35**, 635 (1982).

5) H. Fujimoto, T. Kinoshita, H. Suzuki, and H. Umezawa, *J. Antibiot.*, **23**, 271 (1970).

6) H. Nakamura, Y. Iitaka, H. Sakakibara, and H. Umezawa, *J. Antibiot.*, **27**, 894 (1974); H. Sakakibara, H. Naganawa, M. Ohno, K. Maeda, and H. Umezawa, *ibid.*, **27**, 897 (1974); H. Sakakibara, H. Naganawa, M. Ohno, K. Maeda, and H. Umezawa, *J. Antibiot.*, **27**, 897 (1974).

7) H. A. Kirst, E. F. Szymanski, D. E. Dorman, J. L. Occolowitz, N. D. Jones, M. O. Chaney, R. L. Hamill, and M. M. Hoehin, *J. Antibiot.*, **28**, 286 (1975).

8) T. Shiba, K. Inami, K. Sawada, and Y. Hirotsu, *Heterocycles*, **13**, 175 (1979).

9) G. Lowe and H. W. Yeung, *J. Chem. Soc. Perkin I*, **1973**, 2907.

10) Y. Hirotsu, T. Shiba, and T. Kaneko, *Bull. Chem. Soc. Jpn.*, **40**, 2945 (1967).

11) A. Ishida and T. Mukaiyama, *Bull. Chem. Soc. Jpn.*, **51**, 2077 (1978).

12) M. Sakakibara and M. Matsui, *Agric. Biol. Chem.*, **37**, 1139 (1973).

13) T. Kato, Y. Suzuki, and M. Sato, *Chem. Pharm. Bull.*, **27**, 1181 (1979).

14) K. Yonetani, Y. Hirotsu, and T. Shiba, *Bull. Chem. Soc. Jpn.*, **48**, 3302 (1975); T. Shiba, K. Sawada, and Y. Hirotsu, *Heterocycles*, **10**, 133 (1978).

15) R. B. Moffet, *Org. Syn.* Coll. Vol. IV, 427 (1963).

16) P. F. Kruse, N. Geurkink, and K. L. Grist, *J. Am. Chem. Soc.*, **76**, 5796 (1954).

 © 1985 The Chemical Society of Japan Bull. Chem. Soc. Jpn., 58, 361—366 (1985)

Preparation and Properties of Oligocytidylates with 2′—5′ Internucleotide Linkage

Hiroaki SAWAI* and Masaji OHNO
Faculty of Pharmaceutical Sciences, University of Tokyo Hongo, Bunkyo-ku, Tokyo 113
(Received September 3, 1984)

Oligocytidylates upto a pentamer were prepared by lead(II) ion catalyzed polymerization of cytidine 5′-phosphorimidazolide in aqueous solution. 2′—5′ internucleotide linkage was preferentially formed. The yields of the 2′—5′ linked dimer, trimer, tetramer and pentamer were 17.0, 5.5, 1.9, and 0.7%, respectively. Some of their properties were studied by NMR, CD, UV, and chromatography and compared with the corresponding 3′—5′ linked oligomers which were prepared enzymatically.

Biological and physicochemical properties of 2′—5′ linked oligonucleotides have attracted widespread interest because unusual 2′—5′ linked oligoadenylates were isolated from interferon-treated cell and shown to be associated with the interferon's action.[1-3] Previously we have reported the preparation of 2′—5′ linked oligoadenylates by lead(II) ion catalyzed polymerization of adenosine 5′-phosphorimidazolide in aqueous solution.[4] The method provided a very simple preparative procedure for the 2′—5′ oligonucleotides. Preparation of other 2′—5′ linked oligonucleotides has been conducted by a similar procedure.[5,6] Oligoribonucleotides with 2′—5′ internucleotide linkage were preferentially formed by the reaction, though the yield and distribution of the resulting oligomers were different depending on the base moiety. In this paper, we report the synthesis of 2′—5′ linked oligocytidylates from cytidine 5′-phosphorimidazolide by lead(II) ion catalysis. Physicochemical properties of the 2′—5′ linked oligocytidylates are described and compared with the corresponding 3′—5′ linked oligocytidylates which were prepared by partial enzyme digestion of polycytidylate.

Results and Discussion

Cytidine 5′-phosphorimidazolide (ImpC) was prepared from cytidine 5′-phospate and imidazole using di-2-pyridyl disulfide and triphenylphosphine as a condensing agent.[5,7] Polymerization of ImpC was carried out in neutral aqueous solution in the presence of lead(II) nitrate as a catalysis. The starting ImpC disappeared almost completely in 3 d at room temperature. The reaction mixture was treated with Versenol solution to break the Pb^{2+}-nucleotide complex which was checked by HPLC. The solution was applied to a QAE-Sepahdex A-25 column and eluted with a linear gradient of triethylammonium hydrogencarbonate buffer. The elution profile is shown in Fig. 1. The separated products were further purified by paper chromatography when necessary. The peak identification and the yields of the products are given in Table 1. Oligocytidylates upto a pentamer were formed in the reaction. The lead(II) ion catalyzed internucleotide-bond formation is shown in Scheme 1. The oligocytidylates thus obtained were characterized by enzyme digestions, TLC and NMR. The 2′—5′ internucleotide linkage is not degraded with nuclease P_1 (N. P_1) and RNAse T_2 which degrades 3′—5′ internucleotide linkage. Both 2′—5′ and 3′—5′ internucleotide linkages are hydrolyzed with snake venom phosphodiesterase (VPDase) and by alkaline digestion. The internucleotide linkage and the chain length of the oligocytidylates were determined by sequential enzyme digestion using bacterial alkaline phosphatase (BAPF), N. P_1, VPDase and alkaline digestion. The yields of 2′—5′ linked dimer, trimer, tetramer and pentamer were 17.0, 5.5, 1.9, and 0.7%, respectively. The 3′—5′ linked dimer and trimer were isolated in 1.6 and 0.3%, respectively. Two linkage isomers, pC2′p5′pC3′p5′C and pC3′p5′pC2′p5′C, which appeared in peaks 10 and 11 were obtained in 2.8 and 1.4% yields, respectively. Three tetramers, containing one 3′—5′ and two 2′—5′ internucleotide linkage in a different position, were present in peak 12 along with 2′—5′ $(pC)_4$. The compound with a pyrophosphate bond, CppC, was obtained as a minor byproduct. Cytidine 3′,5′-cyclic phosphate which was formed by intramolecular phosphodiester bond formation was present in peak 4. Cyclic dicytidylates were obtained in 11.4% yield in peak 7. In contrast to the linear oligomers, 3′—5′ internucleotide linkage was predominant in the cyclic dicytidylates, as 3′—5′ linkage is conformationally preferable for the cyclic nucleotides. The cyclic dicytidylate with two 3′—5′ linkages was degraded with N. P_1 to cytidylic acid and insensitive to BAPF. The 3′—5′, 2′—5′ linked cyclic dicytidylate was hydrolyzed with N. P_1 to pC2′p5′C. The 2′—5′, 2′—5′ linked cyclic dimer was insensitive to N. P_1 but was digested with VPDase. The major feature of the reaction is preferential formation of 2′—5′ linked linear oligocytidylates. The yield and distribution of the products are comparable to those of the lead-ion catalyzed oligouridylates formation.[5] The yields and the selectivity of the 2′—5′ linked oligomers are lower than those of the oligoadenylates

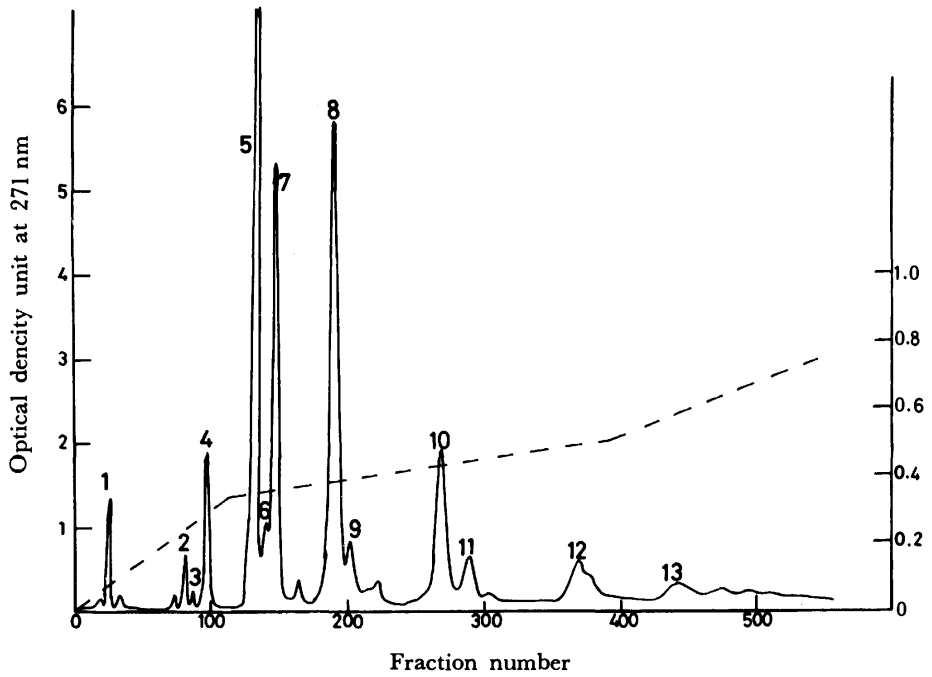

Fig. 1. Chromatography of the Products on QAE-Sephadex A-25 column. A linear gradient of triethylammonium hydrogencarbonate was used for elution (dotted line). The characterization of the peaks is listed in Table 1.

TABLE 1. OLIGOCYTIDYLATES OBTAINED FROM ImpC BY Pb^{2+} ION CATALYSIS

Peak No.	ODU_{271}	h(%)[a]	Identified Structure	Yield/%[b]
1	68.9		C	1.7
2	34	5.7	C2′p5′C	0.8
3	10	4.8	C3′p5′C	0.2
4	117		3′,5′-cyclic CMP	2.8
5	1243		pC	29.9
6	30		CppC	0.6
7	445	5.7[c]	-pCpC- (3′—5′, 3′—5′)	8.7
			(3′—5′, 2′—5′)	1.0
			(2′—5′, 2′—5′)	1.7
8	650	8.2	pC2′p5′C	17.0
9	64	5.7	pC3′p5′C	1.6
10	298	14.5[c]	pC2′p5′C2′p5′C	5.5
			pC2′p5′C3′p5′C	2.8
11	86	15.0	pC3′p5′C2′p5′C	1.4
			pC3′p5′C3′p5′C	0.3
12	212	15.2	pC2′p5′C2′p5′C2′p5′C	1.9
			pC2′p5′C3′p5′C2′p5′C	0.9
			pC2′p5′C2′p5′C3′p5′C	1.1
			pC3′p5′C2′p5′C2′p5′C	0.5
			Other oligomers	1.1
13	119	17.4	pC2′p5′C2′p5′C2′-p5′C2′p5′C	0.7
			Other oligomers	2.3

a) Hypochromicity estimated from alkaline hydrolysis. b) Yield obtained from UV_{271} after allowing the hypochromicity of each oligocytidylate. Total ODU_{271} of starting ImpC was 4160 (0.45 mmol). c) Mean hypochromicity of the compounds in the peak.

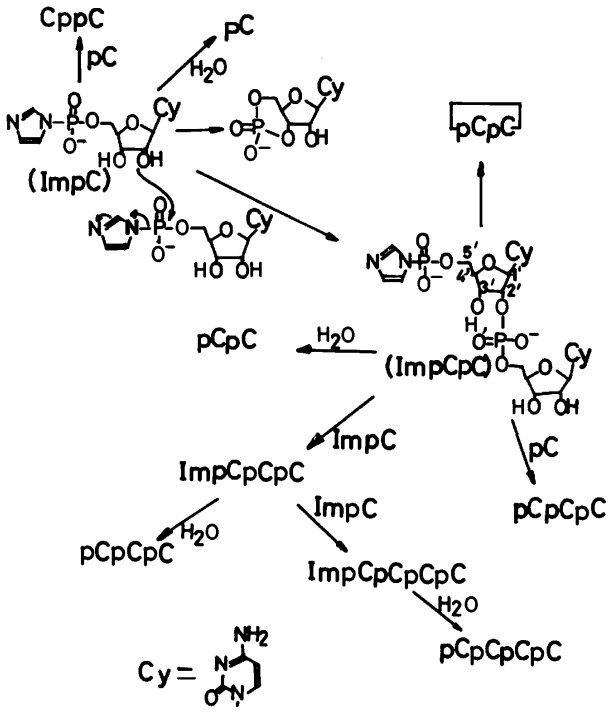

formation.[4] However, this procedure provides a simple synthetic method to the 2′—5′ linked oligocytidylates.

Table 2 lists R_f values of the 2′—5′ and 3′—5′ linked oligocytidylates. Paper chromatographic mobilities of 2′—5′ linked oligomers are large compared to those of the corresponding 3′—5′ linked

oligomers when buffer of high salt concentration was used as a developing solvent (solvent II). The result suggests that 2′—5′ linked oligomers have hydrophilic character and 3′—5′ linked oligomers have hydrophobic character. The same tendency was also observed in the 2′—5′ and 3′—5′ linked oligoadenylates, where the difference of the mobilities were larger.[4,8]

NMR data of the 2′—5′ and 3′—5′ linked oligocytidylates are listed in Table 3. Cytosine H-5 and H-6 protons of the 2′—5′ linked oligomers shows high-field shift compared to those of the 3′—5′ linked oligomers.

Figure 2 shows CD spectra of the 2′—5′ and 3′—5′ linked oligocytidylates at 27 °C. CD spectra of 2′—5′ and 3′—5′ linked tetracytidylates at 4, 27, and 55 °C are shown in Fig. 3. CD band of 3′—5′ linked oligomers is stronger than that of the 2′—5′ linked oligomers and increases with increasing the chain length. Temperature dependance and chain length dependance of the CD spectra of 3′—5′ linked oligomers are larger than those of 2′—5′ linked oligomers

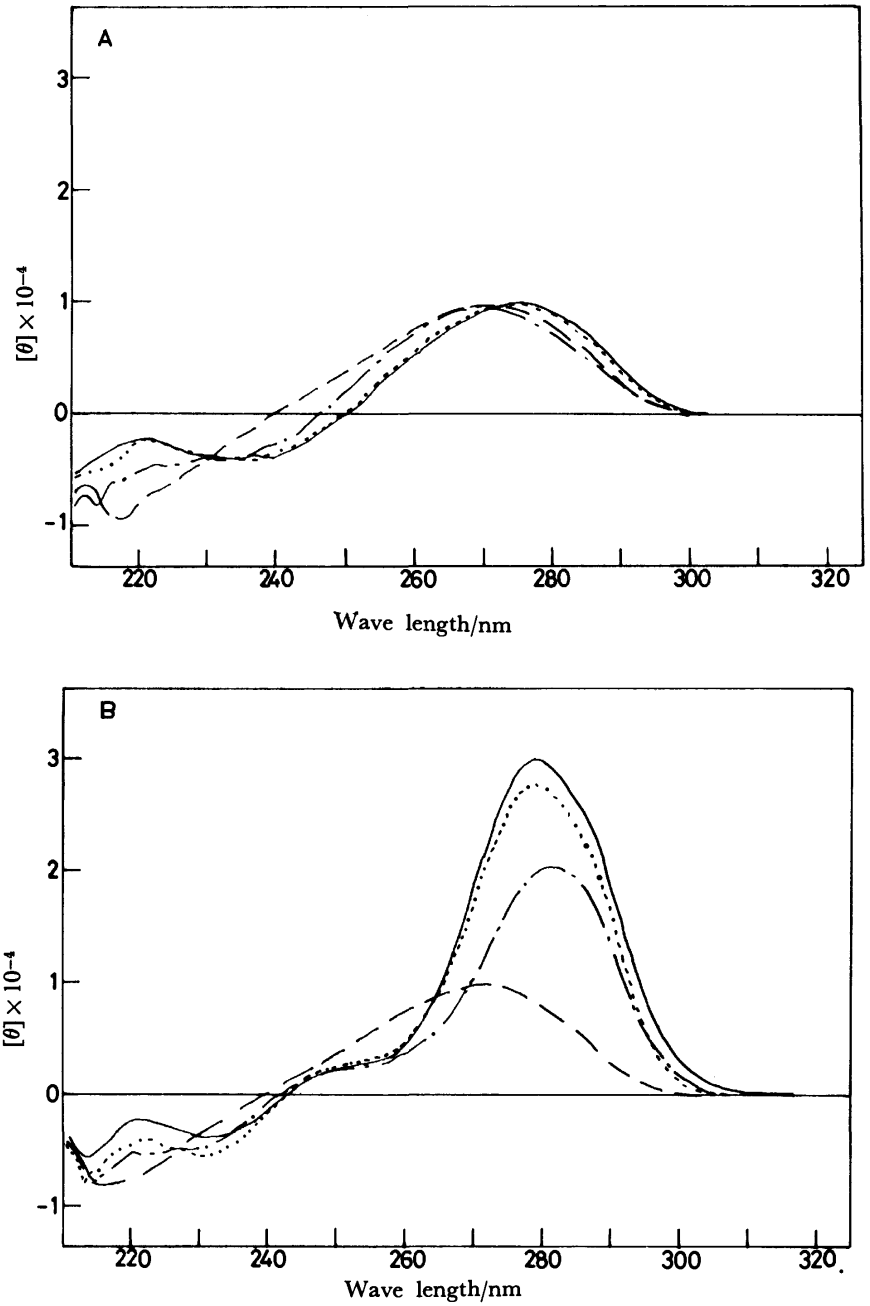

Fig. 2. CD Spectra of Oligocytidylates at 27 °C in 0.1 M Phosphate Buffer (pH 6.7).
A. 2′-5′ Linked Oligocytidylates. B. 3′-5′ Linked Oligocytidylates.
— — — pC, — — — $(pC)_2$, ---- $(pC)_3$, —— $(pC)_4$.

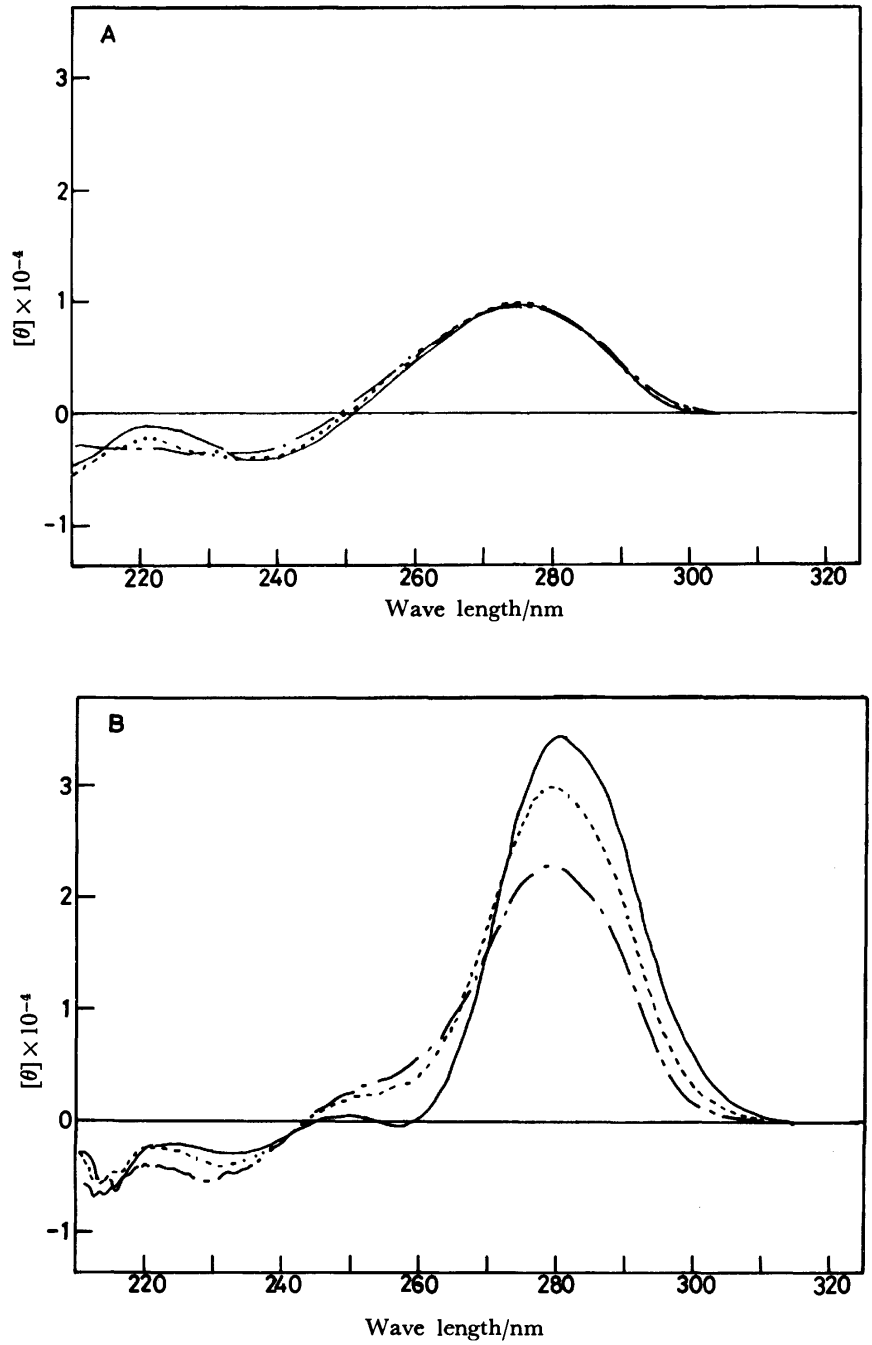

Fig. 3. CD Spectra of Tetracytidylates at 4, 27, and 55 °C in 0.1 M Phosphate Buffer (pH 6.7)
A. 2′—5′ Linked Tetracytidylate. B. 3′—5′ Linked Tetracytidylate.
—— 4 °C, ---- 27 °C, — — — — 55 °C.

which are similar to those of monomeric cytidylic acid. The CD data suggest that 3′—5′ linked oligomers possess higher ordered but more flexible structure than 2′—5′ linked oligomers. The character is also observed in the 2′—5′ and 3′—5′ linked oligoadenylates.[8] We tentatively believe that 3′—5′ linked oligomers can possess various conformations depending on the change of environment such as temperature and salt concentration, which is important for the function of RNA.

Experimental

Materials. Cytidine 5′-phosphoric acid was obtained from Yamasa. Cytidine 5′-phosphorimidazolide was prepared from pC and imidazole using di-2-pyridyl disulfide and triphenylphospine as a condensing agent by the similar method as published procedure.[5,7] Bacterial alkaline phosphatase (BAPF) and snake venom phosphodiestearase (VPDase) were from Worthington. Polycytidylic acid (sodium salt), nuclease p_1 (N. P_1) and nuclease SW were

Table 2. Chromatographic mobilities of the compounds

Compound	R_f value relative to pC	
	Solvent (I)	Solvent (II)
C	1.69	0.87
ImpC	1.67	
3′,5′-cyclic CMP	1.50	0.73
C2′p5′C	1.22	0.84
C3′p5′C	1.24	0.73
pC	1.00	1.00
CppC	1.00	0.88
-pCpC- (mixture)	1.20—1.25	0.61—0.77
pC2′p5′C	0.87	0.93
pC3′p5′C	0.85	0.91
pC2′p5′C2′p5′C	0.73	0.84
pC3′p5′C2′p5′C	0.72	0.81
pC3′p5′C3′p5′C	0.72	0.78
pC2′p5′C2′p5′C2′p5′C	0.58	0.75
2′-5′$(pC)_5$	0.38	0.70

Table 3. ^1H NMR of cytosine and H-1′ proton of oligocytidylates in D_2O at 25 °C (pD 6.7)

Compound	Chemical shift/δ (Coupling constant/Hz)		
	H-6($J_{5,6}$)	H-5($J_{5,6}$)	H-1′($J_{1',2'}$)
pC	8.07(7.6)	6.14(7.6)	6.00(3.7)
C3′p	7.85(7.6)	6.07(7.6)	6.00(5.2)
C2′p	7.79(7.6)	6.07(7.6)	5.94(4.0)
3′—5′$(pC)_2$	8.14(7.6)	6.07(7.6)	5.95(4.0)
	7.93(7.6)	6.07(7.6)	5.91(3.4)
2′—5′$(pC)_2$	7.87(7.6)	6.08(7.6)	6.18(6.4)
	7.81(7.6)	5.92(7.6)	5.87(3.4)
3′—5′$(pC)_3$	8.12(7.3)	6.03(7.6)	5.91(3.1)
	7.93(7.6)	6.00(7.3)	5.80(1.5)
	7.90(7.6)	6.00(7.3)	5.79(2.1)
2′—5′$(pC)_3$	7.80(7.3)	6.05(7.7)	6.12(5.5)
	7.79(7.6)	5.91(7.3)	6.10(5.8)
	7.61(7.3)	5.91(7.3)	5.88(3.7)

purchased from Seikagaku Kogyo.

Paper Chromatography and HPLC. Paper chromagtography was carried out by a descending technique on Whatman 3MM paper using solvent system (I), 1-propanol–aqueous ammonia (55:45), and (II), saturated ammonium sulfate–0.1 M sodium (1 M=1 mol dm^{-3}) acetate (pH 6.5)–2-propanol (79:19:2).

HPLC was performed with a Hitachi 638 using a RPC-5 column (4 mm×25 cm). RPC-5 was prepared from fine grannular poly(chlorotrifluoroethylene) and Adogen 464 by the modification of the method according to Pearson *et al.*[9] Elution was carried out with a linear gradient of $NaClO_4$ solution (0—0.01 M) buffered with 2.5 mM Tris acetate (pH 7.5).

Spectrometric Method. UV absorption spectra were recorded by a Shimazu MPS-5000 instrument in 0.1 M phosphate buffer (pH 6.7). NMR spectra were taken by a JEOL-GX-400 instrument using TSP-d_4 as an internal standard. The sample was passed through a short Dowex 50WX-8 (Na^+ form) column, evaporated under vacuum and repeated coevaporation with D_2O (1 ml×3). Concentration of the sample was about 5 mM per cytidine residue in D_2O (0.1 M phosphate buffer, pH 6.7). CD spectra were measured by a JASCO J-40 spectrometer using a 2 mm cell in 0.1 M phosphate buffer (pH 6.7).

Polymerization of ImpC. To an aqueous solution (6.8 ml) of ImpC (189 mg, 0.4 mmol, 4160 ODU_{270}), 0.8 ml of imidazole buffer (2 M, pH 6.5) and 0.4 ml of 0.25 M lead nitrate were added with stirring. The reaction mixture was kept at 20 °C for 5 d with stirring. Versenol buffer (0.6 ml×0.25 M, pH 7.0) was added to the reaction mixture to remove Pb(II) ion by Versenol-Pb^{2+} complex formation. HPLC of an aliquot showed the formation of oligocytidylates and the disapperance of ImpC. The solution was applied to a QAE-Sephadex A-25 column (30 mmϕ×45 cm). The column was eluted with a stepwise linear gradient of triethylammonium hydrogencarbonate buffer (1) H_2O-0.33 M (2×0.9 l), (2) 0.33 M—0.5 M (2×2 l), (3) 0.5 M—0.75 M (2×1 l). 15 ml of each fraction was collected every 12 min. UV absorption of each fraction was measured at 271 nm. The UV absorbing fractions were pooled and evaporated under vacuum below 30 °C. The excess triethylammonium hydrogencarbonate was removed by repeated evaporation after addition of water. The products were further purified by paper chromatography using solvent system (I) when necessary. The yield was calculated from ODU_{271} after allowing for the hypochromicity of each oligocytidylate. The hypochromicity was estimated by the ratio of UV absorption at 270 nm after and before alkaline hydrolysis of the oligocytidylate.

Enzymatic Synthesis of 3′—5′ Linked Oligocytidylates. Polycytidylic acid sodium salt (25 mg, 0.055 mmol) was digested with nuclease SW (400 units) in the solution (6 ml) containing sodium carbonate buffer (0.05 M, pH 10.3), NaCl (0.1 M), $MgCl_2$ (1 mM) and sodium acetate (2 mM) at 37 °C for 20 h. The reaction mixture was applied to a DEAE-Sephadex A-25 column (25 mmϕ×35 cm) and eluted with a linear gradient of triethylammonium hydrogencarbonate buffer (0.25 M—0.5 M, 2×1 l). 10 ml of each fraction was collected every 10 min. The UV absorbing fractions were pooled and evaporated under vacuum below 30 °C. The 3′—5′ linked di-, tri-, and tetra-cytidylates with 5′-terminal phosphate were obtained in 29% (1350 ODU_{270}, 0.016 mmol), 42% (1180 ODU_{270}, 0.023 mmol) and 18% (780 ODU_{270}, 0.01 mmol) yields, respectively.

Chracterization of the Oligocytidylates. Characterization of the products was carried out by means of sequential enzyme and alkaline hydrolysis. Each oligocytidylate was subjected to paper chromatography in solvent system (I) and (II). The UV absorbing spot on the paper developed with solvent system (I) was eluted with water and incubated with BAPF to remove 5′-terminal phosphate. The mixture was chromatographed on the paper with solvent system (I). The UV absorbing spot on the paper was eluted with water and incubated with N. P_I to degrade 3′—5′ internucleotide linkage. The mixture was analyzed by HPLC and paper chromatography in solvent system (I). The UV absorbing spot on the paper was eluted with water and incubated with VPDase and NaOH solution to degrade 2′—5′ internucleo-

tide linkage. The degraded products were analyzed by HPLC.

Digestion with BAPF was carried out by incubating a mixture of 0.5—1 μmol of nucleotide material in a 50 μl solution containing 0.1 M Tris-HCl (pH 8.05), 0.001 M $MgCl_2$ and 0.1 unit of the enzyme, at 37 °C for 2.5 h.

Digestion with N. P_1 was performed at 37 °C for 2.5 h in a mixture (50 μl) containing the nucleotide material (0.4—0.8 μmol), 0.006 M veronal acetate buffer (pH 5.75) and an enzyme (5 μg).

Degradation with VPDase was carried out at 37 °C for 2.5 h in a mixture (50 μl) containing the substrate (0.1—0.2 μmol), 0.01 M Tris-acetate (pH 8.0), 0.01 M $MgCl_2$ and enzyme solution (0.01 unit).

Alkaline hydrolysis was carried out at room temperature for 1 d in a mixture (50 μl) containing the substrate (0.1—0.2 μmol) in a 0.5 M NaOH solution.

The structure of the oligocytidylates was further confirmed by NMR, and by comparing the paper chromatography and HPLC with that of the authentic sample when available.

The authors are very grateful to professor H. Hirai, Mr. T. Kawamura, and Mrs. Y. Goto for their help in taking 400 MHz NMR, and to Dr. S. Higuchi for his aid in measuring CD spectra.

References

1) I. M. Kerr and R. E. Brown, *Proc. Natl. Acad. Sci. U. S. A.*, **75**, 256 (1978)
2) C. Baglioni, *Cell*, **17**, 255 (1979).
3) P. Lengyel, "Interferon 3," ed by I. Gresser, Academic Press, New York, (1980), p. 77.
4) H. Sawai, T. Shibata, and M. Ohno, *Tetrahedron*, **37**, 481 (1981).
5) H. Sawai and M. Ohno, *Chem. Pharm. Bull.*, **29**, 2337 (1981).
6) H. Sawai and M. Ohno, *Bull. Chem. Soc. Jpn*, **54**, 2759 (1981).
7) R. Lohrmann and L. E. Orgel, *Tetrahedron*, **34**, 853 (1978).
8) H. Sawai, *Nucleic Acid Res. Symp. Ser.*, No. 12, 189 (1983).
9) P. L. Pearson, J. F. Weiss, and A. D. Kelmers, *Biochim. Biophys. Acta*, **228**, 770 (1971).

 © 1985 The Chemical Society of Japan Bull. Chem. Soc. Jpn., 58, 367—373 (1985)

The Reaction of Azulene with Nitroethene. A New Route to 2-(1-Azulenyl)ethanamines

Shinji KUROKAWA* and Arthur G. ANDERSON, Jr.†

Department of Chemistry, Faculty of Education, Saga University, Honjo-machi, Saga 840

†*Department of Chemistry, University of Washington, Seattle, Washington 98195 U.S.A.*

(Received September 7, 1984)

Azulene and guaiazulene react with nitroethene to form substitution products having 2-nitroethyl, 2,4-dinitrobutyl, or 2-nitroethenyl groups at the 1(3)-position in low yields. The presence of formic acid prevented the formation of the dinitrobutyl compound, and increased the yield of the 2-nitroethyl derivative. A reaction course leading to these products is proposed. Reduction of 1-(2-nitroethyl)azulene and 1-(2-nitroethyl)-guaiazulene gave the corresponding amine compounds in good yields. This two-step process provides a new, improved route to 2-(1-azulenyl)ethanamines having a primary amino group. The amine products, like related biogenic amines, inhibited the contraction of smooth muscle.

2-Arylethanamine derivatives constitute an important class of physiologically active compounds related to biogenic amines.[1] In studying azulene analogs of biologically active amines, we have previously reported the synthesis of some *N*-alkyl and *N*-acyl derivatives of 2-(1-azulenyl)ethanamines[2] and 2-(4-azulenyl)ethanamine[3,4] compounds by ring aminoethylation and methyl side chain aminomethylation methods, respectively, and the effect of these compounds on specific enzyme activity.[2,4] These methods, however, were not successful for the preparation of azulenylethanamines having a primary amino group as in norepinephrine (noradrenaline), dopamine, serotonin, *etc.* The search for a synthetic route to this type of azulene compound led the investigation of the reaction of azulene and guaiazulene with nitroethene to form the corresponding 1-(2-nitroethyl) derivatives,[5] and the reduction of these to the primary amines.

Results and Discussion

Nitroethene (*ca.* 10% in benzene)[6] reacted with azulene (**1**) at room temperature to yield 1-(2-nitroethyl)azulene (**3**) (8%). Three by-products, **5** (6%), **6** (5%), and **8** (3%), were also formed. The structures of these compounds were determined by spectral analyses.

For example, the ^{1}H NMR spectrum of **6** showed a complicated splitting pattern for the 2,4-dinitrobutyl moiety. Analysis according to an ABX spin system[7] composed of nonequivalent (adjacent to an asymmetric center) α-methylene protons (3.61 and 3.82 ppm for AB) and a β-methine proton (4.94 ppm for X) afforded reasonable coupling constant of J_{AB}= 14.7, J_{AX}=6.3, J_{BX}=6.8 Hz. A coupling through 4σ-bonds (1.1 Hz)[8] was observed between the β-methine and δ-methylene protons (4.34 ppm) of the dinitro-

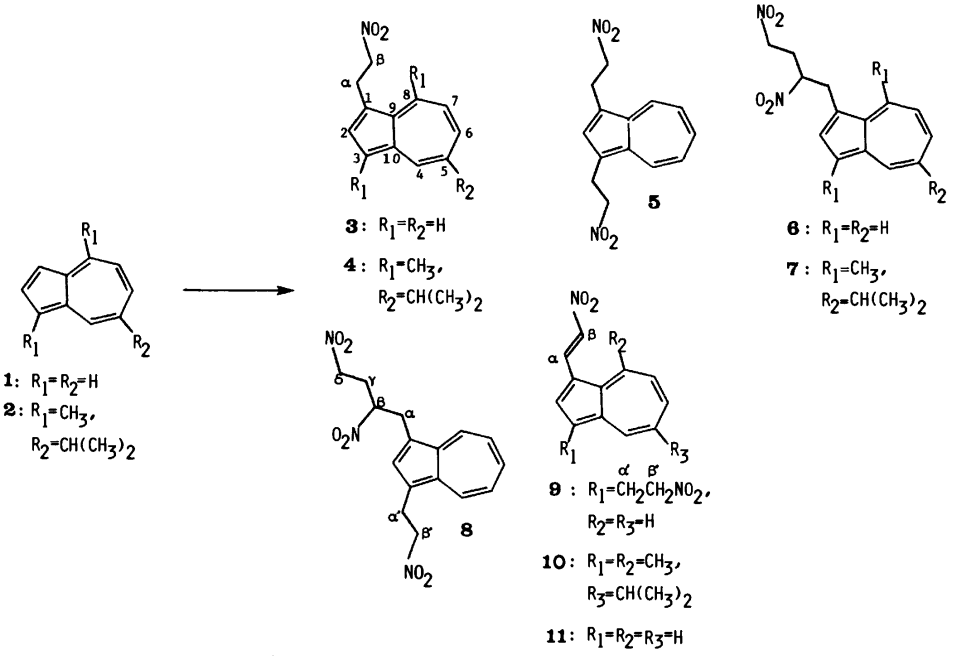

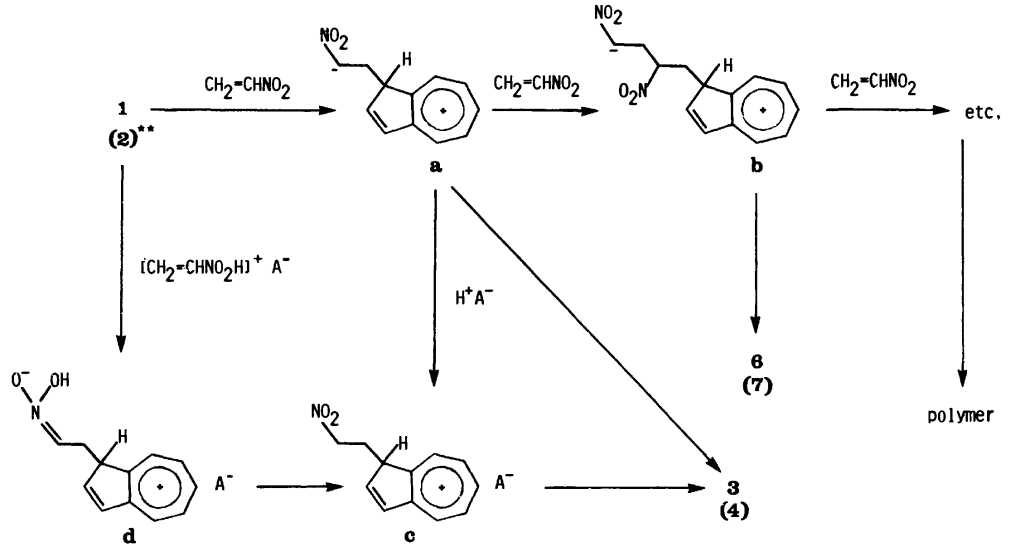

Scheme 1.

butyl group. The ^{1}H NMR spectrum of **8** showed the same splitting pattern for the dinitrobutyl group.

Analogously, guaiazulene (**2**) under the same conditions afforded **4** (9%), **7** (3%), and **10** (2%). The 2,4-dinitrobutyl group of **7** exhibited the same ^{1}H NMR splitting pattern as that of **6**. It was further characterized by its ^{13}C NMR spectrum which showed triplet signals for the α-, γ-, and δ-carbons and a doublet for the β-carbon of the assigned structure.

The 2-nitroethenyl product (**10**) had been previously prepared by the reaction of 1-formylguaiazulene with nitromethane,[9] but the configuration of the double bond was not determined. Our data indicate a trans configuration: i) The coupling constant ($J_{\alpha,\beta}$=13.0 Hz) for the olefinic protons in the ^{1}H NMR spectrum has the expected value when the electronegative nitro substituent is taken into account.[10] ii) The chemical shifts for the olefinic protons (7.56 and 8.93 ppm) show full conjugation of the double bond with the azulene ring. Molecular models indicate this to be possible only for the trans geometry. iii) The IR absorption at 956 cm^{-1} corresponds to a trans alkene.

A large amount of insoluble, polymeric material was also observed in these reactions. This was thought to be produced by polymerization of the nitroethene initiated by a nucleophile (*e.g.* **1** or **2**) (*cf.* Scheme 1. **1**→**a**→**b**→polymer). The formation of **6**, **7**, and **8** having a dinitrobutyl side chain provides support for this concept. This polymerization process would be suppresses if an acid was present to react with the intermediate to form **c** (Scheme 1). The effects of trifluoroacetic acid, formic acid, and ether-boron trifluoride (1/1) were examined (Table 1). As expected, the reaction yielding **7** was blocked, but also the yield of **4** was reduced except with formic acid.

Table 1. Reaction of guaiazulene (**2**) and nitroethene in the presence of acid (nitroethene: acid: **2**=1.5:1.5:1 in mole ratio. Benzene as the solvent)

Acid	Reaction conditions		Yield/%		
	Temp	Time/h	**4**	**7**	**10**
CF_3COOH	0 °C	1.5	5	—	0.2
HCOOH	Ambient	1.5	9	—	2
$BF_3 \cdot O(C_2H_5)_2$	Ambient	1.4	0.8	—	10
None	50 °C	3.5	47	9	2
HCOOH	50 °C	5	50	—	2

In another modification, nitroethene was added slowly to a solution of **2** preheated to 50 °C. This minimized the polymerization process and markedly increased the yield of **4** (47%) but also raised the yield of **7** to 9%. This procedure was then used in the presence of formic acid to give 50% of **4** with no detectable amount of **7**. In two runs, the one with the slower addition of nitroethene gave the higher yield of **4**.

Application of the improved method using 1.5 equivalents of nitroethene to **1**, however, gave only 21% of **3** along with 5% of the disubstitution product (**5**). With 3 equivalents of nitroethene at 60 °C the yields of **3** and **5** were 15 and 71%, respectively. A trace amount (≤0.4%) of 1-(2-nitroethenyl)-3-(2-nitroethyl)-azulene (**9**) was also obtained from these reactions. The structures of **9** was assigned by comparison of its spectral characteristics with those of **11**, which was prepared from 1-formylazulene by an established procedure.[11] As described earlier for **10**, the ^{1}H NMR and IR spectra were indicative of a trans double bond in **9** and **11**. Attempted nitroethylation of **11** to form **9** was unsuccessful. This suggests that the nitroethenyl group in **11** is deactivating the

** Corresponding guaiazulene derivatives are shown in parentheses.

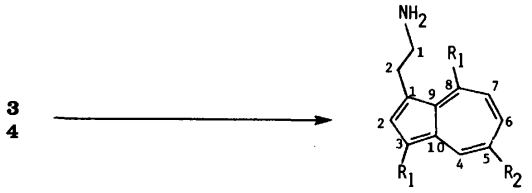

12 : $R_1=R_2=H$
13 : $R_1=CH_3$, $R_2=CH(CH_3)_2$

azulene ring and is formed after the nitroethyl group in the formation of **9** from **1**.

Scheme 1 summarizes the proposed reaction process of **1** with nitroethene. Intra- or intermolecular proton migration forms **3** from intermediate **a**. Alternatively, **a** can nucleophilically react with another molecule of nitroethene to form **b**, which can be converted to **6** or, by repetition of the process for **a**→**b** give polymeric material. The reaction of **3** with nitroethene would yield **5** or lead to **8**. The latter may also be formed by the reaction of **6** with nitroethene. Reaction of **a** with a protic acid would form **c** and prevent the process leading to **6** and polymer. The abstraction of a proton from **c** afford **3** if a sufficiently basic species is present. The action of formate ion to form **3** would account for the observation of the 1,3-disubstituted products, as **3** was shown to react further with nitroethene.

When a strong acid is present (*e.g.* trifluoroacetic acid), the conjugate acid of nitroethene could be formed and be the primary electrophilic reagent. If that event, **d** (formed directly from **1**) could tautomerize to give **c**, and **3** would be formed upon neutralization.

Hydride abstraction from the intermediate corresponding to **a** by one of the acidic species present would form the nitroethenyl side chains in **9** and **10**. This could have accounted for the increase in the yield of **10** when a Lewis acid was added (*cf.* $BF_3 \cdot O(C_2H_5)_2$ in Table 1). An indication of a possible oxidative dehydrogenation pathway (by air or nitro compounds[12]) to **9** and **10** from **5** and **4**, respectively, was provided by the observation that **4** yielded **10** readily when treated with palladized charcoal at room temperature, and even under reductive conditions.

The conversion of **3** and **4** into the corresponding primary amines (**12** and **13**) in good yields (79 and 77%) was effected by reduction with iron and acetic acid.[13] Other reduction trials with palladized charcoal and sodium borohydride[14] or lithium aluminum hydride were unsatisfactory. The chemical shifts and splittig patterns in the ^1H and ^{13}C NMR spectra of **12** and **13** compounds were in agreement with the assigned structures. Allyl fission of the aminoethyl side chain gave rise to the most abundant ion in the mass spectra, as previously observed for other azulenylethanamines.[2-4]

Compounds **12** and **13**, like related biogenic amines, strongly inhibited the contraction of smooth muscle.[15] Details of these studies will be reported elsewhere.

Experimental

All the melting points are uncorrected. Spectral data were recorded on the following instruments: UV, Hitachi 624 digital spectrometer with a Hitachi 056 recorder; IR, Hitachi 260-10 spectrometer; ^1H NMR, JEOL MH-100; ^{13}C NMR, JNM-FX 100; MS, JEOL-D 300 at 70 eV.

Nitroethene. This reagent was prepared from 2-nitroethanol and phthalic anhydride, and made into a *ca.* 10% benzene solution immediately after distillation:[6] ^1H NMR ($CDCl_3$) δ=4.78 (broad d, J=7.0 Hz, anti H), 5.94 (dd, J=15.0 and 2.0 Hz, syn H), and 6.41 (dd, J=7.0 and 15.0 Hz, $=C(NO_2)H$). The solutions of two preparative runs contained 9.7 and 11 wt% (by ^1H NMR) of nitroethene, respectively, and in the former case 3.4% of nitroethane was also noted: ^1H NMR ($CDCl_3$) δ=1.10 (t, J=7.0 Hz, CH_3) and 3.30 (q, J=7.0 Hz, CH_2).

Reaction of Azulene (1) and Nitroethene. A) Without Acid at Room Temperature. To an ice-cooled, stirred solution of 640 mg (4.99 mmol) of azulene in 35 cm^3 of dry dichloromethane was added dropwise, under dry nitrogen, 20 g of 9.7% benzene solution of nitroethene (containing 27 mmol of nitroethene) over a period of 30 min, and stirring was continued for 20 h more at room temperature. Removal of the solvent (reduced pressure) afforded a violet oil (7 spots on TLC over silica gel with benzene), which was chromatographed on a silica-gel column (elution with benzene) to give four products besides 80.2 mg (13%) of unchanged azulene eluted at first and recovered as violet crystals.

From the second eluate, 81.4 mg (8%) of 1-(2-nitroethyl)-azulene (**3**) was obtained as a blue oil: UV (C_2H_5OH) 237 (log ε 4.28), 263 (sh, 4.42), 268 (sh, 4.57), 272 (sh, 4.67), 276 (4.73), 280 (sh, 4.69), 286 (sh, 4.54), 295 (sh, 3.89), 328 (sh, 3.42), 332 (3.64), 342 (3.76), 524 (sh, 2.25), 550 (sh, 2.40), 571 (sh, 2.47), 588 (2.53), 608 (sh, 2.49), 638 (2.45), 668 (sh, 2.20), and 705 nm (2.02); IR (CCl_4) 3060, 3030 (aromatic CH), 2925 (CH_2), 1545, and 1378 cm^{-1} (NO_2); ^1H NMR ($CDCl_3$) δ=3.76 (2H, t, J=7.4 Hz, α-CH_2), 4.54 (2H, t, J=7.4 Hz, β-CH_2), 7.09 (1H, t, J=9.7 Hz, 5-H), 7.12 (1H, t, J=9.7 Hz, 7-H), 7.28 (1H, d, J=4.0 Hz, 3-H), 7.56 (1H, t, J=9.7 Hz, 6-H), 7.71 (1H, d, J=4.0 Hz, 2-H), and 8.22 (2H, dd, J=9.7 and 1.7 Hz, 4- and 8-H); ^{13}C NMR ($CDCl_3$) δ=25.5 (α-CH_2), 76.1 (β-CH_2), 117.3 (3-C), 122.4 (7-C), 123.0 (5-C), 122.9 (1-C), 132.9 (8-C), 136.1 (9-C), 136.7 (4-C), 136.9 (6-C), 137.9 (2-C), and 140.8 (10-C); MS

m/z (rel intensity) 201 (M^+; 80), 155 (M^+-NO_2; 100), and 141 ($M^+-CH_2NO_2$; 55).

Found: C, 71.97; H, 5.72; N, 6.37%. Calcd for $C_{12}H_{11}NO_2$: C, 71.63; H, 5.51; N, 6.96%.

From the third eluate, 67.5 mg (5%) of 1-(2,4-dinitrobutyl)-azulene (**6**) was obtained as blue crystals, mp 75—76 °C: UV (C_2H_5OH) 237 (log ε 4.47), 268 (sh, 4.69), 273 (sh, 4.79), 276 (4.84), 281 (4.80), 286 (sh, 4.68), 295 (sh, 4.17), 342 (4.01), 357 (3.86), 524 (sh, 2.44), 549 (2.56), 569 (sh, 2.62), 585 (2.66), 606 (sh, 2.62), 635 (2.58), 669 (sh, 2.30), and 701 nm (2.17); IR ($CHCl_3$) 1555 and 1370 cm^{-1} (NO_2); ^1H NMR ($CDCl_3$) δ=2.56 (2H, m, γ-CH_2), 3.61 and 3.82 (2H, symmetrical 8 lines, J=14.7, 6.8, and 6.3 Hz, α-CH_2), 4.34 (2H, dt, J=6.8 and 1.1 Hz. δ-CH_2), 4.94 (1H, m, β-CH), 7.14 (1H, t, J=9.7 Hz, 5-H), 7.16 (2H, t, J=9.7 Hz, 7-H), 7.30 (1H, d, J=4.0 Hz, 3-H), 7.60 (1H, t, J= 9.7 Hz, 6-H), 7.70 (1H, d, J=4.0 Hz, 2-H), 8.19 (1H, d, J=9.7 Hz, 4-H), and 8.27 (1H, d, J=9.7 Hz, 8-H); MS *m/z* (rel intensity) 274 (M^+; 24), 180 (M^+-2HNO_2; 11), 167 ($M^+-HNO_2-CH_2NO_2$; 18), and 141 ($M^+-C_3H_5N_2O_4$; 100).

Found: C, 61.11; H, 5.26; N, 9.96%. Calcd for $C_{14}H_{14}N_2O_4$: C, 61.31; H, 5.15; N, 10.21%.

From the fourth eluate, 76.7 mg (6%) of 1,3-bis(2-nitroethyl)azulene (**5**) was obtained as blue crystals, mp 95—96 °C: UV (C_2H_5OH) 238 (log ε 4.42), 271 (sh, 4.67), 275 (sh, 4.75), 279 (4.80), 283 (4.78), 289 (sh, 4.23), 346 (3.92), 362 (3.83), 560 (sh, 2.52), 600 (2.62), 647 (2.55), and 717 nm (sh, 2.14); IR ($CHCl_3$) 1550 and 1380 cm^{-1} (NO_2); ^1H NMR ($CDCl_3$) δ=3.72 (4H, t, J=7.4 Hz, α-CH_2), 4.64 (4H, t, J=7.4 Hz, β-CH_2), 7.12 (2H, t, J=9.7 Hz, 5- and 7-H), 7.59 (1H, t, J=9.7 Hz, 6-H), 7.59 (1H, s, 2-H), and 8.18 (2H, dd, J=9.7 and 1.7 Hz, 4- and 8-H); ^{13}C NMR ($CDCl_3$) δ=25.2 (α-CH_2), 76.1 (β-CH_2), 122.1 (1,3-C), 122.8 (5,7-C), 133.2 (4,8-C), 136.6 (9,10-C), 136.9 (6-C), and 138.5 (2-C); MS *m/z* (rel intensity) 274 (M^+; 63), 228 (M^+-NO_2; 47), 227 (M^+-HNO_2; 51), 214 ($M^+-CH_2NO_2$; 28), 182 (M^+-2NO_2; 23), 181 ($M^+-NO_2-HNO_2$; 83), and 167 ($M^+-HNO_2-CH_2NO_2$; 100).

Found: C, 61.83; H, 5.21; N, 10.13%. Calcd for $C_{14}H_{14}N_2O_4$: C, 61.31; H, 5.15; N, 10.21%.

From the last fraction, 53.1 mg (3%) of 1-(2,4-dinitrobutyl)-3-(2-nitroethyl)azulene (**8**) was obtained as a green oil: UV (C_2H_5OH) 238 (log ε 4.28), 266 (sh, 4.40), 270 (sh, 4.52), 275 (sh, 4.63), 279 (4.70), 284 (sh, 4.57), 298 (sh, 4.08), 345 (3.75), 363 (3.69), 446 (2.79), 562 (sh, 2.49), 585 (sh, 2.54), 596 (2.56), 640 (sh, 2.47), and 711 nm (2.02); IR ($CHCl_3$) 1560 and 1380 cm^{-1} (NO_2); ^1H NMR ($CDCl_3$) δ= 2.56 (2H, m, γ-CH_2), 3.70 (2H, symmetrical 8 lines, α-CH_2), 3.73 (2H, t, J=6.9 Hz, α'-CH_2), 4.37 (2H, dt, J= 6.9 and 1.7 Hz, δ-CH_2), 4.65 (2H, t, J=6.9 Hz, β'-CH_2), 4.90 (1H, m, β-CH), 7.61 (1H, t, J=10.3 Hz, 6-H), 8.16 (1H, d, J=10.3 Hz, 4-H), and 8.20 (1H, d, J= 10.3 Hz, 8-H); MS *m/z* (rel intensity) 347 (M^+; 54), 301 (M^+-NO_2; 52), 300 (M^+-HNO_2; 58), 287 ($M^+-CH_2NO_2$; 12), 254 ($M^+-NO_2-HNO_2$; 21), 253 (M^+-2HNO_2; 33), 227 ($M^+-2CH_2NO_2$; 12), 214 ($M^+-C_3H_5N_2O_4$; 75), 167 ($M^+-HNO_2-C_3H_5N_2O_4$; 100), and 153 ($M^+-CH_2NO_2-C_3H_5N_2O_4-H$; 80).

Found: C, 55.16; H, 4.87; N, 12.08%. Calcd for $C_{16}H_{17}N_3O_6$: C, 55.33; H, 4.93; N, 12.10%.

After the separation of these products, the solvent of the chromatography was changed to chloroform to afford an additional fraction, which was concentrated (reduced pressure) to leave 393 mg of brown solid. This material was insoluble in all organic solvents tested, but was soluble in mineral acid.

B) With Formic Acid at 50 °C. To a stirred solution of 130 mg (1.01 mmol) of azulene in 2 cm^3 of benzene, kept at 50 °C under dry nitrogen, was added dropwise a mixed reagent of 1.00 g (1.51 mmol) of 11% nitroethene solution and 69.4 mg (1.51 mmol) of formic acid during a period of 1 h, and stirring was continued for an additional 2 h at 50 °C. The reaction mixture was taken up in 100 cm^3 of benzene, washed with 10% potassium carbonate solution (50 cm^3×2), then with water (50 cm^3×3), dried on sodium sulfate, and concentrated (reduced pressure) to give a blue oil. Chromatography of the blue oil over silica gel (elution with benzene) gave 65.3 mg (50%) of unchanged **1**, 43.1 mg (21%) of **3**, 14.4 mg (5%) of **5**, and a small amount of brown crystalline material as the last fraction. The last fraction was rechromatographed over silica gel (benzene) to give 0.13 mg (0.5%) of 1-(2-nitroethenyl)-3-(2-nitroethyl)azulene (**9**) as dark brown crystals, mp 187—189 °C: UV (C_2H_5OH) 230 (log ε 4.20), 275 (sh, 4.22), 283 (4.26), 289 (sh, 4.24), 307 (sh, 3.95), 337 (3.88), 436 (sh, 4.11), and 448 nm (4.13); IR (KBr) 1550, 1318 (NO_2), and 950 cm^{-1} (trans CH); ^1H NMR ($CDCl_3$) δ=3.78 (2H, t, J=7.0 Hz, α'-CH_2), 4.73 (2H, t, J=7.0 Hz, β'-CH_2), 7.43 (1H, t, J=10.0 Hz, 5-H), 7.45 (1H, t, J=10.0 Hz, 7-H), 7.67 (1H, d, J=13.0 Hz, β-H), 7.81 (1H, t, J=10.0 Hz, 6-H), 7.96 (1H, s, 2-H), 8.31 (1H, d, J=10.0 Hz, 4-H), 8.58 (1H, d, J=13.0 Hz, α-H), and 8.55 (1H, d, J=10.0 Hz, 8-H); MS *m/z* (rel intensity) 272 (M^+; 72), 226 (M^+-NO_2; 42), 225 (M^+-HNO_2; 69); 178 (M^+-2HNO_2; 100), and 165 ($M^+-HNO_2-CH_2NO_2$; 98).

Found: N, 10.13%. Calcd for $C_{14}H_{12}N_2O_4$: N, 10.29%.

C) With Formic Acid at 60 °C. To a stirred solution of 64.0 mg (0.499 mmol) of azulene in 2 cm^3 of benzene, kept at 60 °C, was added dropwise a mixed reagent of nitroethene and formic acid (1.51 mmol in each) over a period of 1 h, and stirring was continued for an additional 2 h at 60 °C. The reaction mixture was worked up as described in *B* to give 1.50 mg (2%) of unchanged **1**, 14.8 mg (15%) of **3**, 97.1 mg (71%) of **5**, and 0.54 mg (0.4%) of **9**.

Synthesis of 1-(2-Nitroethenyl)azulene (11). To a stirred solution of 320 mg (1.47 mmol) of 1-formylazulene, which was prepared in a 76% yield according to Ref. 11, in 5 cm^3 of ethanol was added a mixed reagent of 100 mg (1.64 mmol) of nitromethane and 130 mg (1.55 mmol) of piperidine over a period of 10 min, and stirring was continued for 4 h more. Chromatography of the reaction mixture on a silica-gel column (dichloromethane) gave 31.4 mg (11%) of **11** as reddish-brown solid, besides 63 mg of reddish brown oil. After recrystallization from methanol containing a trace amount of acetone, **11** was obtained as dark brown crystals, mp 149—150 °C: UV (C_2H_5OH) 231 (log ε 4.22), 272 (sh, 4.28), 278 (4.32), 282 (4.32), 285 (4.31), 295 (sh, 4.19), 327 (sh, 3.82), 337 (3.85), 350 (sh, 3.81), 422 (sh, 4.05), 428 (sh, 4.08), and 443 nm (4.11); IR ($CHCl_3$), 1560, 1330 (NO_2), and 960 cm^{-1} (trans CH); ^1H NMR ($CDCl_3$) δ=7.20—7.68 (2H, m, 5- and 7-H), 7.56 (1H, d, J=4.0 Hz, 3-H), 7.85 (1H, d, J= 13.0 Hz, β-H), 7.94 (1H, t, J=10.0 Hz, 6-H), 8.24 (1H, d, J=4.0 Hz, 2-H), 8.52 (1H, d, J=10.0 Hz, 4-H), 8.74 (1H, d, J= 10.0 Hz, 8-H), and 8.78 (1H, d, J=13.0 Hz, α-H); MS *m/z* (rel intensity) 199 (M^+; 43) and 152 (M^+-HNO_2; 100).

Found: C, 72.31; H, 4.45; N, 6.97%. Calcd for $C_{12}H_9NO_2$: C, 72.35; H, 4.55; N, 7.03%.

In the attempted synthesis of **9** from **11**, **11** was treated at first with a 2 molar equivalent of the mixed reagent of nitroethene and formic acid at 50 °C, followed by treatment with an additional 2 molar equivalent of nitroethene at 80 °C. The recovery of **11** from each process was indicated by TLC (benzene–silica gel).

Reaction of Guaiazulene (2) and Nitroethene. A) Without Acid at Room Temperature. To an ice-cooled, stirred solution of 1.72 g (8.67 mmol) of guaiazulene in 35 cm^3 of dry dichloromethane was added dropwise 35 g (47 mmol) of 9.7% nitroethene solution during a period of 30 min, and stirring was continued for an additional 20 h at room temperature. Removal of the solvent (reduced pressure) and chromatography of the residue over silica gel (benzene) gave 2.38 g of blue oil, which was taken up in a mixed solvent of petroleum ether–benzene (220 cm^3) and extracted with 85% phosphoric acid (100 cm^3, then 50 cm^3×3). The acid layer was washed with petroleum ether (100 cm^3×3), diluted with ice-water (500 cm^3), and extracted with petroleum ether (100 cm^3, then 50 cm^3×3). The organic extract, after being washed with water (100 cm^3, then 50 cm^3×3), dried (sodium sulfate), and concentrated (reduced pressure), was chromatographed on a silica-gel column (benzene) to give three products.

From the first eluate, 203 mg (9%) of 1-(2-nitroethyl)-guaiazulene (**4**) was obtained as blue crystals, mp 85—89 °C: UV (C_2H_5OH) 246 (log ε 4.40), 287 (4.65), 291 (sh, 4.63), 305 (4.20), 336 (sh, 3.63), 346 (sh, 3.70), 352 (3.79), 369 (3.75), 544 (sh, 2.48), 614 (2.70), 668 (sh, 2.60), and 734 nm (sh, 2.23); IR (CCl_4) 1542 and 1378 cm^{-1} (NO_2); ^1H NMR ($CDCl_3$) δ=1.30 (6H, d, J=7.0 Hz, $CH(CH_3)_2$), 2.58 (3H, s, 3-CH_3), 2.82 (3H, s, 8-CH_3), 2.99 (1H, m, J=7.0 Hz, $CH(CH_3)_2$), 3.76 (2H, t, J=8.0 Hz, α-CH_2), 4.44 (2H, t, J=8.0 Hz, β-CH_2), 6.84 (1H, d, J=10.0 Hz, 7-H), 7.29 (1H, dd, J=10.0 and 2.0 Hz, 6-H), 7.37 (1H, s, 2-H), and 8.16 (1H, d, J=2.0 Hz, 4-H); ^{13}C NMR ($CDCl_3$) δ=12.8 (q, 3-CH_3), 24.6 (q, $CH(CH_3)_2$, 26.8 (q, 8-CH_3), 29.4 (t, α-CH_2), 37.7 (d, $CH(CH_3)_2$), 77.2 (t, β-CH_2), 120.1 (s, 1-C), 124.7 (s, 3-C), 127.1 (d, 7-C), 132.8 (s, 9-C), 133.8 (d, 4-C), 135.1 (d, 6-C), 138.1 (s, 10-C), 138.9 (d, 2-C), 139.9 (s, 5-C), and 144.6 (s, 8-C); MS m/z (rel intensity) 271 (M^+; 85), 225 (M^+-NO_2; 100), 224 (M^+-HNO_2; 44), and 211 ($M^+-CH_2NO_2$; 80).

Found: C, 75.52; H, 7.86; N, 5.12%. Calcd for $C_{17}H_{21}NO_2$: C, 75.25; H, 7.80; N, 5.16%.

From the second eluate, 89.2 mg (3%) of 1-(2,4-dinitrobutyl)guaiazulene (**7**) was obtained as a blue oil: UV (C_2H_5OH) 246 (log ε 4.29), 287 (4.50), 290 (sh, 4.49), 305 (4.08), 340 (sh, 3.54), 352 (3.64), 369 (3.62), 524 (sh, 2.31), 572 (sh, 2.50), 609 (2.57), 658 (sh, 2.48), and 731 nm (sh, 2.01); IR (CCl_4) 1540 and 1380 cm^{-1} (NO_2); ^1H NMR ($CDCl_3$) δ=1.31 (6H, d, J=7.0 Hz, $CH(CH_3)_2$), 2.54 (2H, m, γ-CH_2), 2.56 (3H, s, 3-CH_3), 2.90 (3H, s, 8-CH_3), 3.01 (1H, m, J=7.0 Hz, $CH(CH_3)_2$), 3.64 and 3.96 (2H, symmetrical 8 lines, J=14.9, 7.2, and 7.2 Hz, α-CH_2), 4.26 (2H, t, J=7.0 Hz, δ-CH_2), 4.88 (1H, m, β-CH), 6.91 (1H, d, J=11.0 Hz, 7-H), 7.32 (1H, dd, J=11.0 and 2.0 Hz, 6-H), 7.37 (1H, s, 2-H), and 8.13 (1H, d, J=2.0 Hz, 8-H); ^{13}C NMR ($CDCl_3$) δ=12.8 (q, 3-CH_3), 24.5 (q, $CH(CH_3)_2$), 26.9 (q, 8-CH_3), 29.7 (t, α-CH_2), 35.6 (t, γ-CH_2), 37.6 (d, $CH(CH_3)_2$), 71.0 (t, δ-CH_2), 87.1 (d, β-CH), 118.8 (s, 1-C), 124.8 (s, 3-C), 127.5 (d, 7-C), 133.0 (s, 9-C), 234.0 (d, 4-C), 135.2 (d, 6-C), 138.3 (s, 10-C), 139.8 (d, 2-C), 140.3 (d, 5-C), and 144.4 (s, 8-C); MS m/z (rel intensity) 344 (M^+; 48), 298 (M^+-NO_2; 15), 297 (M^+-HNO_2; 7), and 211 ($M^+-C_3H_5NO_2$; 100).

Found: C, 66.45; H, 6.96; N, 8.44%. Calcd for $C_{19}H_{24}N_2O_4$: C, 66.26; H, 7.02; N, 8.13%.

From the last fraction, 5.00 mg (2%) of 1-(2-nitroethenyl)-guaiazulene (**10**) was obtained as reddish-brown crystals, mp 154—155 °C. It was identical with that of Ref. 9 in its mp, IR, and ^1H NMR: UV (C_2H_5OH) 227 (log ε 4.02), 241 (4.06), 281 (sh, 4.01), 291 (4.07) 305 (sh, 3.91), 313 (sh, 3.77), 341 (3.77), 354 (3.76), 367 (sh, 3.44), 424 (sh, 3.88), 442 (4.06), and 466 nm (4.05); IR (CCl_4) 1540, 1310 (NO_2), and 956 cm^{-1} (trans CH); ^1H NMR ($CDCl_3$) δ=1.36 (6H, d, J=7.0 Hz, $CH(CH_3)_2$), 2.57 (3H, s, 3-CH_3), 3.11 (3H, s, 8-CH_3), 3.14 (3H, m, J=7.0 Hz, $CH(CH_3)_2$), 7.24 (1H, d J=10.5 Hz, 7-H), 7.48 (1H, dd, J=10.5 and 2.0 Hz, 6-H), 7.56 (1H, d, J=13.0 Hz, β-H), 7.75 (1H, s, 2-H), 8.12 (1H, d, J=2.0 Hz, 4-H), and 8.98 (1H, d, J=13.0 Hz, α-H); MS m/z (rel intensity) 269 (M^+; 59), 254 (M^+-CH_3; 11), 223 (M^+-NO_2; 27), 222 (M^+-HNO_2; 45), and 211 (M^+-CNO_2 100).

B) With Trifluoroacetic Acid at 0 °C. To an ice-cooled, stirred solution of 11% nitroethene in benzene (5.00 g; 7.53 mmol) was added dropwise 860 mg (7.54 mmol) of trifluoroacetic acid. This reagent was mixed dropwise with an ice-cooled, stirred solution of 1.00 g (5.04 mmol) of guaiazulene in 5 cm^3 of benzene over a period of 20 min; stirring was continued for a further 1 h under ice-cooling. The reaction mixture was poured into 100 cm^3 of ice-water, extracted with ether (500 cm^3×4), organic extract washed with 10% potassium carbonate solution (50 cm^3×2), then with water (50 cm^3×3), dried (sodium sulfate), and concentrated (reduced pressure) leaving a green oil. Chromatography of the oil on a silica-gel column (benzene) gave 226 mg (23%) of unchanged **2**, 64.0 mg (5%) of **4**, and 2.99 mg (0.2%) of **10**.

C) With Formic Acid at Room Temperature. A mixed reagent of nitroethene (7.53 mmol) and formic acid (7.54 mmol) was prepared in the same manner as described in *B*. This reagent was mixed dropwise with a stirred solution of 1.00 g (5.04 mmol) of guaiazulene in 6 cm^3 of benzene during a period of 20 min and stirring was continued for 1 h more at room temperature. After being extracted with ether (50 cm^3, then 25 cm^3×2), dried (sodium sulfate), and concentrated (reduced pressure), the reaction mixture was chromatographed over silica gel (benzene) to give a blue oil. This oil was taken up in 100 cm^3 of petroleum ether and extracted with 85% phosphoric acid (100 cm^3×3). The acid extract was diluted with 1 dm^3 of ice-water, and extracted with benzene (100 cm^3×3). Removal of the solvent and subsequent chromatography over silica gel (benzene) gave 157 mg (16%) of unchanged **2**, 129 mg (9%) of **4**, and 46.0 mg (2%) of **10**.

D) With Ether-Boron Trifluoride (1/1) at Room Temperature. To an ice-cooled, stirred solution of 1.00 g (5.04 mmol) of guaiazulene in 5 cm^3 of benzene was added dropwise 1.00 g (7.05 mmol) of ether-boron trifluoride (1/1) over a period of 5 min, and stirring was continued for an additional 20 min at room temperature. This solution was mixed dropwise with 5.00 g (7.53 mmol) of 11% nitroethene solution during a period of 30 min and stirring was continued for 3.5 h more. The reaction mixture was taken up into 100 cm^3 of petroleum

ether and extracted with 85% phosphoric acid (50 cm^3×3). Similar work up as described in *C* and subsequent chromatography over silica gel (benzene) gave 50.8 mg (5%) of unchanged **2**, 11.0 mg (0.8%) of **4**, and 134 mg (10%) of **10**.

E) Without Acid at 50 °C. To a stirred solution of 1.00 g (5.04 mmol) of guaiazulene in 5 cm^3 of benzene, kept at 50 °C, was added 5.00 g (7.53 mmol) of 11% nitroethene solution over a period of 1 h, and stirring was continued for additional 2 h at room temperature. The reaction mixture, after the usual work up as described in *D*, gave 162 mg (16%) of unchanged **2**, 637 mg (47%) of **4**, 163 mg (9%) of **7**, and 31.6 mg (2%) of **10**.

F) With Formic Acid at 50 °C. To a stirred solution of 2.00 g (10.1 mmol) of guaiazulene in 10 cm^3 of benzene was added a mixed reagent of 10.0 g (15.1 mmol) of 11% nitroethene solution and 700 mg (15.2 mmol) of formic acid during a period of 2 h, and stirring was continued for additional 3 h at 50 °C. The reaction mixture, after being worked up as in *D*, gave 44.0 mg (2%) of unchanged **2**, 1.36 g (50%) of **4**, and 61.2 mg (2%) of **10**.

A small scale experiment with the use of 200 mg (1.01 mmol) of **2**, accompanied with changes of the reaction time (1 h for addition of the mixed reagent, followed by 4 h for additional stirring), gave 10.0 mg (5%) of unchanged **2**, 133 mg (49%) of **4**, and 20.1 mg (7%) of **10**.

Reduction of 1-(2-Nitroethyl)azulene (3) with Iron and Acetic Acid. Ninety milligrams (1.61 mmol) of fine iron powder (200 meshes) was mixed with 1 cm^3 of 5% hydrochloric acid, rinsed with acetic acid (1 cm^3×2), and transferred to the reaction vessel with 2 cm^3 of acetic acid. To the stirred suspension of iron in acetic acid was added dropwise, under dry nitrogen, a solution of 38.6 mg (0.192 mmol) of **3** in 1 cm^3 of acetic acid over a period of 30 min (washed in with additional 1 cm^3 of acetic acid), and stirring was continued for 38 h more at room temperature. The progress of the reaction was checked by TLC (silica gel–benzene). The reaction mixture was poured into 30 cm^3 of ice-water. The precipitated iron powder was collected by decantation, washed throughly with 20 cm^3 of water and then with 50 cm^3 of chloroform, and the combined organic and aqueous solution was made alkaline by the addition of 50 cm^3 of 30% sodium hydroxide solution under ice-cooling. The chloroform layer was separated, and the aqueous solution was extracted with chloroform (50 cm^3, then 30 cm^3×2). The combined, dried (sodium sulfate), and concentrated (reduced pressure) organic extracts were chromatographed on a silica-gel column (7:3 chloroform–methanol) to give 0.75 mg (2%) of unchanged **3** and 25.8 mg (79%) of 2-(1-azulenyl)ethanamine (**12**) as blue prisms, mp 104—105 °C: UV (C_2H_5OH) 237 (log ε 4.22), 268 (sh, 4.52), 273 (sh, 4.64), 277 (4.71), 282 (4.66), 287 (sh, 4.52), 296 (sh, 3.79), 331 (sh, 3.55), 343 (3.68), 358 (3.38), 556 (sh, 2.41), 578 (sh, 2.47), 597 (2.52), 620 (sh, 2.46), 650 (2.43), 682 (sh, 2.15), and 720 nm (1.97); IR (CCl_4) 3390 and 1625 cm^{-1} (NH); ^1H NMR ($CDCl_3$) δ=1.36 (2H, s, NH_2), 3.21 (4H, 8 lines, CH_2-CH_2), 7.15 (1H, t, J=10.0 Hz, 5-H), 7.18 (1H, t, J=10.0 Hz, 7-H), 7.45 (1H, d, J=4.0 Hz, 3-H), 7.65 (1H, t, J=10.0 Hz, 6-H), 7.91 (1H, d, J=4.0 Hz, 2-H), 8.37 (1H, d, J=10.0 Hz, 4-H), and 8.42 (1H, d, J=10.0 Hz, 8-H); ^{13}C NMR ($CDCl_3$) δ=30.8 (2-CH_2), 53.3 (1-CH_2), 116.8 (3-C), 121.5 (7-C), 122.1 (5-C), 127.9 (1-C), 133.5 (8-C), 136.3 (4- and 9-C), 137.1 (6-C), 137.3 (2-C), and 140.6 (10-C); MS *m/z* (rel intensity) 171 (M^+; 14) and 141 ($M^+-CH_2NH_2$; 100).

Found: C, 84.06; H, 7.05; N, 8.20%. Calcd for $C_{12}H_{13}N$: C, 84.17; H, 7.65; N, 8.18%.

Reduction of 1-(2-Nitroethyl)guaiazulene (4). A) With Iron and Acetic Acid. To a suspension of 500 mg (8.95 mmol) of iron powder (200 meshes), treated as above with hydrochloric acid and acetic acid, in 12 cm^3 of acetic acid was added a solution of 270 mg (0.995 mmol) of **4** in 10 cm^3 of acetic acid over a period of 30 min (washed in with additional 5 cm^3 of acetic acid), and stirring was continued for 16 h more at room temperature. The reaction mixture, after being worked up as described in **3**, gave 60.2 mg (22%) of unchanged **4** and 184 mg (77%) of 5-isopropyl-3,8-dimethyl-2-(1-azulenyl)ethanamine (**13**) as a greenish blue oil: UV (log ε 4.02), 248 (4.19), 282 (sh, 4.40), 288 (4.47), 293 (4.46), 307 (4.02), 338 (sh, 3.45), 353 (3.62), 371 (3.58), 546 (sh, 2.33), 576 (sh, 2.52), 600 (sh, 2.57), 623 (2.59), and 673 nm (2.51); IR (CCl_4) 3390 and 1610 cm^{-1} (NH); ^1H NMR (CCl_4) δ=1.29 (6H, d, J=7.0 Hz, $CH(CH_3)_2$), 2.59 (3H, s, 3-CH_3), 2.87 (3H, s, 8-CH_3), 2.81—3.07 (1H, m, $CH(CH_3)_2$), 2.95 (2H, t, J=6.0 Hz, 1-CH_2), 3.32 (2H, t, J=6.0 Hz, 2-CH_2), 3.63 (2H, broad s, NH_2), 6.73 (1H, d, J=11.0 Hz, 7-H), 7.20 (1H, dd, J=11.0 and 2.0 Hz, 6-H), 7.49 (1H, s, 2-H), and 8.11 (1H, d, J=2.0 Hz, 4-H); ^{13}C NMR ($CDCl_3$) δ=12.8 (q, 3-CH_3), 24.5 (q, $CH(CH_3)_2$), 26.9 (q, 8-CH_3), 30.8 (t, 2-CH_2), 37.6 (d, $CH(CH_3)_2$), 52.9 (t, 1-CH_2), 124.2 (s, 3-C), 125.4 (s, 1-C), 126.2 (d, 7-C), 132.5 (s, 9-C), 133.2 (d, 4-C), 134.5 (d, 6-C), 137.7 (s, 10-C), 138.9 (d, 5-C), and 145.0 (s, 8-C); MS *m/z* (rel intensity) 241 (M^+; 14) and 211 ($M^+-CH_2NH_2$; 100).

Found: C, 84.21; H, 9.90; N, 5.32%. Calcd for $C_{17}H_{23}N$: C, 84.59; H, 9.60; N, 5.80%.

B) With Palladized Charcoal and Sodium Borohydride. To a stirred suspension of 5.0 mg (0.0047 mmol) of 10% palladized charcoal in 3 cm^3 of methanol, with bubbling of nitrogen below the surface, was added dropwise a solution of 10 mg (0.26 mmol) of sodium borohydride in 2 cm^3 of water, and then another solution of 27.0 mg (0.0995 mmol) of **4** in 5 cm^3 of 2 mol dm^{-3} methanolic sodium hydroxide. The mixture was refluxed for 1.5 h and cooled to room temperature. After the addition of 10 cm^3 of 1 mol dm^{-3} hydrochloric acid, the mixture was filtered to remove the catalyst, and the catalyst was washed with chloroform (30 cm^3×2). The combined organic and aqueous solution was worked up as described in *A* to give 7.06 mg (36%) of unchanged **4** and 5.10 mg (21%) of **13**.

Similar treatment of **4** with palladized charcoal in water and at low reaction temperature (30 min at room temperature) yielded 0.93 mg (5%) of **2**, 17.5 mg (65%) of unchanged **4**, and 1.23 mg (5%) of **10**.

C) With Lithium Aluminum Hydride. To a cooled (−50 °C), stirred solution of 10 mg (0.26 mmol) of lithium aluminum hydride in 0.5 cm^3 of THF was added dropwise another solution of 18.4 mg (0.0678 mmol) of **4** in 1 cm^3 of THF over a period of 5 min. This mixture was gradually brought to −4 °C, and kept for 20 min at −4 to −3 °C, during which period the color of the solution changed from blue to green. The reaction mixture was again cooled to −50 °C, mixed slowly with 2 cm^3 of 10% sodium hydroxide solution, and extracted with ether (5 cm^3×4). The usual work up of the organic extract gave 15.4 mg of dark resinous material and 1.34 mg (8%) of **13**.

We wish to thank Professor Hitoshi Takeshita

of Kyushu University for his kind measurements of the ^{13}C NMR spectra, and Dr. Koichi Sato of Hosei University, for generously giving us the specimen of 1-(2-nitroethenyl)guaiazulene.

References

1) See, for example, W. E. Coyne, "Medicinal Chemistry," 3rd ed, ed by A. Burger, Wiley Interscience, New York (1970), Part II, pp. 953—968; W. T. Comer and A. W. Gomoll, *ibid.*, pp. 1019—1056; D. J. Triggle, *ibid.*, pp. 1235—1282.

2) S. Kurokawa and A. G. Anderson, Jr., *Bull. Chem. Soc. Jpn.*, **56**, 2059 (1983).

3) S. Kurokawa, *Chem. Lett.*, **1981**, 1569.

4) S. Kurokawa, *Bull. Chem. Soc. Jpn.*, **56**, 2311 (1983).

5) Except the name of compounds, in which a side chain moiety being numbered as Az-$\overset{1}{C}$-$\overset{2}{C}$-$\overset{3}{C}$-$\overset{4}{C}$- (Az=azulene portion) according to IUPAC rules, the numbering of Az-$\overset{\alpha}{C}$-$\overset{\beta}{C}$-$\overset{\gamma}{C}$-$\overset{\delta}{C}$- is adopted for nitro compounds in this paper, in order to prevent a confusion in spectral assignments.

6) D. Ranganathan, C. B. Rao, S. Ranganathan, A. K. Mehrota, and R. Iyengar, *J. Org. Chem.*, **45**, 1185 (1980); R. Ranganathan, D. Ranganathan, and A. K. Mehrota, *J. Am. Chem. Soc.*, **96**, 5261 (1974).

7) B. Dishler, *Angew. Chem. Int. Ed. Engl.*, **5**, 623 (1960).

8) N. S. Bhacca and D. H. Williams, "Application of NMR Spectroscopy in Organic Chemistry, Illustrations from the Steroid Field," Holden-Day, San Francisco (1964), pp. 115—121.

9) K. Sato, M. Yamaguchi, and I. Ogura, *Kinki Daigaku Genshiryoku Kenkyusho Nenpo*, **18**, 51 (1981).

10) R. J. Abraham and P. Loftus, "Proton and Carbon-13 NMR Spectroscopy, An Integrated Approach," Heyden & Son (1978); translated into Japanese by Y. Takeuchi, "^{1}H NMR oyobi ^{13}C NMR Gaisetsu," Kagaku Dojin, Kyoto (1979), pp. 51—53

11) K. Hafner and C. Bernhard, *Justus Liebigs Ann. Chem.*, **625**, 108 (1959).

12) T. Sakan, "Zikken Kagaku Koza 17, Yuki Kagobutsu no Hanno I (Jyo)," ed by M. Kotake, Maruzen, Tokyo (1957), pp. 573—579.

13) N. Kornblum, W. D. Gurowitz, H. O, Lason, and D. E. Hardies, *J. Am. Chem. Soc.*, **82**, 3099 (1960); N. Kornblum and L. Fishbein, *ibid.*, **77**, 6266 (1955).

14) P. M. Babin, J. C. Sheeham, and R. E. Chandler, *Org. Synth.*, Coll. Vol. V, 30 (1973).

15) Biological activities of azulenylethanamines were investigated by Dr. Tsuyoshi Mizonishi at Department of Biology of Saga University, using established procedures.

Ternary Coordination Complexes Formed by Copper(II) with Thio- or Dithiodialkanoic Acids and Some Selected Ethyl-substituted Malonic Acids*

D. N. SHELKE
Chemistry Department, Marathwada University, Aurangabad 431004, India
(Received December 21, 1982)

Binary and ternary complexes formed by copper(II) with thio- or dithiodialkanoic acids and ethyl-substituted malonic acids have been investigated potentiometrically in an aqueous solution and the relevant stability constants have been evaluated using computer technique. Thio- and dithiodialkanoic acids were thiodiacetic, dithiodiacetic, 3,3′-thiodipropionic, and 3,3′-dithiodipropionic acids. The results are discussed in terms of substituent influences upon the chelation of the malonate dianions to the systems copper(II)–thiodialkanoic acids. It is suggested that in the mixed copper chelates containing thiodiacetic acid, the geometrical characteristics of the more basic ligand, governs the coordination of the other ligand.

The study of the coordination chemistry of transition metal complexes with thiodialkanoic (CT) acid ligands has received much attention in recent years and the applications of such complexes to a wide variety of problems of structure, bonding and mechanism are considerable. Initially the major attention was focussed to tridentate thiodialkanoic acids but now, with the advent of X-ray data, interest has been extended to ligands of greater or smaller denticity[1-3]. As part of our interest[4] in the bonding sites of thiodialkanoic aicds in mixed-ligand complexes, we have examined the coordinating tendencies of thiodialkanoic acids to the metal ions on the basis of thermodynamic parameters. We report here, in addition to a few data for binary complexes already reported[5-7], the equilibrium studies on mixed-ligand complex formation occurring, when copper(II) is mixed with thiodialkanoic acids and ethyl-substituted malonic acids. The mode of bonding in the ternary complex species involved is also examined.

Experimental

The ligands thiodiacetic acid (AT), dithiodiacetic acid (ADT), 3,3′-thiodipropionic acid (PT), 3,3′-dithiodipropionic acid (PDT), ethylmalonic and diethylmalonic (L) acids were obtained from Fluka (purum) or B.D.H. (AnalaR) and were used without purification. Metal ion was added as copper perchlorate and the concentration was estimated by EDTA titration.[8] All solutions were prepared in glass distilled water (pH=6.8 and conductivity=1.6×10^{-6} Mho). Details regarding other chemicals and the measurements have been described previously.[9,10]

Copper complex formation constants were evaluated from potentiometric titration curves of thiodialkanoic (CT) and ethyl-substituted malonic acids in the absence and presence of copper(II). Changes in pH were followed using glass and calomel electrodes and a ELICO Digital pH meter (L1-10 No. 1275). The accuracy of the pH meter was ±0.01 pH Unit. The glass electrode was calibrated in terms of hydrogen ion concentrations and titrations were carried out at 30 °C with an ionic background of 0.10 mol dm^{-3} ($NaClO_4$). Calculations were made with the aid of a computer programme[11] and carried out at the Tata Institute of Fundamental Research, Bombay.

* Presented at All India Symposium on "Mixed ligand chelates" Aurangabad, November 1982.

Results and Discussion

The protonation constants of the thiodialkanoic acids and ethyl-substituted malonic acids and the formation constants of copper(II) mono- and bis-complexes with these acids are presented in Table 1. The errors in the data obtained for the formation constants of binary and ternary systems were estimated to be 1±0.05 log units. Besides the direct experimental errors, the standard deviation of the equilibrium constants were between 0.01 and 0.05 for the systems studied. A representative data *i.e.*, copper(II)–ADT–ethylmalonic acid system, explains adequately the precision of the work (Table 2).

The overall stability constants $\beta^{Cu}_{Cu(CT)L}$ of the ternary complexes, together with the stability constants $K^{Cu(CT)}_{Cu(CT)L}$ and $K^{CuL}_{CuL(CT)}$, according to the following expression:

$$Cu + CT + L \rightleftharpoons Cu(CT)L ,$$

$$\beta^{Cu}_{Cu(CT)L} = \frac{[Cu(CT)L]}{[Cu][(CT)][L]} ,$$

$$Cu(CT) + L \rightleftharpoons Cu(CT)L ,$$

$$K^{Cu(CT)}_{Cu(CT)L} = \frac{[Cu(CT)L]}{[Cu(CT)][L]} ,$$

$$CuL + (CT) \rightleftharpoons CuL(CT) ,$$

$$K^{CuL}_{CuL(CT)} = \frac{[CuL(CT)]}{[CuL][(CT)]} ,$$

TABLE 1. LOGARITHMS OF ACIDITY CONSTANTS OF THIODIALKANOIC ACIDS (CT) AND SUBSTITUTED MALONIC ACIDS (L) AND LOGARITHMS OF STABILITY CONSTANTS OF THEIR BINARY COMPLEXES WITH COPPER(II) AT μ=0.1 mol dm^{-3} AND 30±0.1 °C

Ligand	Log $^{H}_{H(CT)}$	Log $^{H(CT)}_{H(CT)_2}$	Log $K^{Cu}_{Cu(CT)}$	Log $K^{Cu(CT)}_{Cu(CT)_2}$
AT[a]	4.28	3.08	4.58	3.20
PT[a]	4.93	3.87	2.55	—
ADT	3.81	2.88	3·46	—
PDT	4.60	3.90	1.61	—
Ethyl-malonic	5.48	2.85	4.95	2.82
Diethyl-malonic	6.96	2.02	4.94	2.74

a) From Refs. 4—7.

Table 2. Logarithms of equilibrium constants of copper(II)-ADT (CT)-ethylmalonic (L) acid system at $C_M = C_{CT} = C_L$, $\mu = 0.1$ mol dm^{-3}, and 30 ± 0.1 °C

pH	$[H^+] \times 10^4$	Log $K^{Cu}_{Cu(CT)L}$	Log $\beta^{Cu}_{Cu(CT)L}$	Log K_r	Log $K^{Cu(CT)}_{Cu(CT)L}$	Log $K^{CuL}_{CuL(CT)}$
3.90	1.151	−3.642	8.118	1.838	3.168	4.658
3.95	1.349	−3.643	8.117	1.837	3.167	4.657
4.00	1.203	−3.644	8.116	1.836	3.166	4.656
4.05	1.072	−3.645	8.114	1.835	3.165	4.655
4.10	0.955	−3.646	8.114	1.834	3.164	4.654
4.15	0.852	−3.647	8.112	1.833	3.162	4.652
4.20	0.759	−3.649	8.111	1.831	3.161	4.651
4.25	0.676	−3.645	8.113	1.834	3.165	4.654
Average		−3.646	8.117	1.835	3.165	4.654

Table 3. Logarithms of stability constants of the ternary complexes Cu(CT)L at $\mu = 0.1$ mol dm^{-3} and 30 ± 0.1 °C

System	Log $\beta^{Cu}_{Cu(CT)L}$[a]	Log $K^{Cu(CT)}_{Cu(CT)L}$	Log $K^{CuL}_{CuL(CT)}$
AT-ethylmalonic	8.93 (1)	3.98	4.35
AT-diethylmalonic	9.07 (3)	4.13	4.49
PT-ethylmalonic	7.13 (2)	2.18	4.58
PT-diethylmalonic	7.16 (4)	2.22	4.61
ADT-ethylmalonic	8.11 (1)	3.16	4.65
ADT-diethylmalonic	8.29 (2)	3.35	4.83
PDT-ethylmalonic	6.42 (3)	1.48	4.81
PDT-dimethylmalonic	6.54 (2)	1.60	4.93

a) The figures in parentheses are the standard deviations of the last decimal figure.

are presented in Table 3. The percentage distribution of the complexes formed in the copper(II)–dithiodiacetic–(ADT)–ethylmalonic (L) acid systems as a function of pH, is presented in Fig. 1.

In our earlier studies on mixed-ligand complexes, the tridentate nature of AT with copper(II) ion, has been reported.[5] These conclusions have been amply confirmed in subsequent studies involving tridentate thiodialkanoic acids particularly, copper(II) complex of AT.[12,13] The bonding nature of PT with copper (II) through the oxygen of the carboxylato group has been confirmed by Krebs *et al.*[14] by X-ray measurements. The structure consists of centrosymmetric complex unit in which the central Cu^{II} is in tetragonal planar arrangement, of two *trans*-coordinated water molecules and the carboxylato groups of two organic ligands. In view of the above, our potentiometric studies and observed stability constants (Table 1) suggest that PT and PDT bond through the oxygen atom of the carboxylato group whereas AT is coordinated through both oxygen atoms of the carboxylato groups and the sulfur atom. The stability constants obtained for ethylmalonic and diethylmalonic acids are also understandable.

Consequently, no simple relation exists between the stability of the ternary complexes and the basic properties of the dialkanoic acids. In these systems we note the sole formation of the 1 : 1 : 1 ternary species, with stability constant values higher than 0.6 would be expected from statistical considerations[15,16] as is apparent from Table 4, on examining the values of the stabilization parameters log K_r and Δ log K, defined by the following expressions:

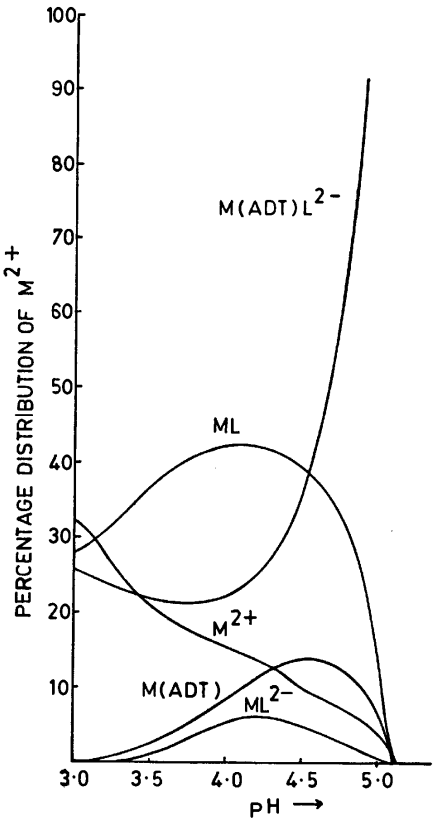

Fig. 1. Percentage distribution of various species present in ternary copper(II)–dithiodiacetic (ADT), ethylmalonic (L) acid system as a function of pH, M_2^+= copper ion_{free}, ML= copper ion-ethylamlonic, ML_2^{2-}= copper ion–(ethylmalonic)$_2$, M(ADT)=copper ion-dithiodiacetic and M (ADT)L^{2-}=copper ion-dithiodiacetic-ethylmalonic, $\mu = 0.1$ mol dm^{-3} ($NaClO_4$), Temp$= 30 \pm 0.1$ °C, $C_M = C_L = C_{ADT} = 2.0 \times 10^{-3}$ mol dm^{-3}.

$$Cu(CT)_2 + CuL_2 \rightleftharpoons 2Cu(CT)L\ ,$$

$$\log K_r = 2\log \beta^{Cu}_{Cu(CT)L} - (\log \beta^{Cu}_{Cu(CT)_2} + \log \beta^{Cu}_{CuL_2})$$

$$Cu(CT) + CuL \rightleftharpoons Cu(CT)L + Cu$$

$$\Delta \log K = \log \beta^{Cu}_{Cu(CT)L} - (\log K^{Cu}_{Cu(CT)} + \log K^{Cu}_{CuL}).$$

These results are of the same order of magnitude as

TABLE 4. STABILIZATION PARAMETERS $\Delta \log K$ AND $\log K_r$ FOR TERNARY COMPLEX FORMATION AT $\mu=0.1$ mol dm^{-3} AND 30 ± 0.1 °C

System	$-\Delta \log K$	$\log K_r$
AT-ethylmalonic	0.60	2.31
AT-diethylmalonic	0.46	2.55
PT-ethylmalonic	0.37	1.76
PT-diethylmalonic	0.33	1.87
ADT-ethylmalonic	0.30	1.83
ADT-diethylmalonic	0.11	2.09
PDT-ethylmalonic	0.14	1.99
PDT-diethylmalonic	0.01	2.19

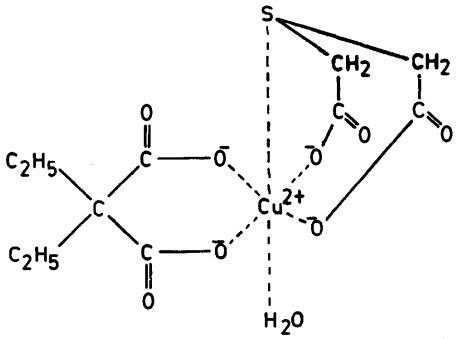

(Structure I)

those for previously studied complexes of copper(II) with thiodialkanoic acids and O–O donor ligands[17] and the following important conclusions may be drawn from the tabulated data.

(a) The $\Delta \log K$ values which are greater than −0.6 (Table 4) indicates the preferential formation of ternary complexes compared to the binary ones. This tendency to form mixed-ligand chelates is the same in the case of PT–ethylmalonic, PT–diethylmalonic and ADT–ethylmalonic acid system wherein $\Delta \log K$ are −0.37, −0.33, and −0.30 respectively.

(b) In the systems under investigation, the values of $\log K_r$ are significantly greater than 0.6 log units, demonstrating that the mixed-ligand complexes are more stable than the binary ones.[15]

(c) The introduction of two substituents increases the stability of ternary complexes in proportion to the size of the alkyl groups[18] (Table 3).

(d) The values of $\log K^{Cu(CT)}_{Cu(CT)L}$ and $\log K^{CuL}_{CuL_2}$ (Table 3) show the preferential formation of the ternary over the binary complexes. A comparison of $\log K^{CuL}_{CuL(CT)}$ with $\log K^{Cu(CT)}_{Cu(CT)_2}$ values, especially in the systems involving thiodiacetic acid as a secondary ligand, reveals the preferential formation of the ternary complexes over the corresponding binary bis ones.

(e) AT forms mixed complexes of exceptionally high stability with ethylmalonic and diethylmalonic acid because the ligand is coordinated through the thio group and two carboxyl groups. The highest value of $\log K_r$ for the AT–diethylmalonic acid system (2.55) accompanied by the highest stability for a $\log \beta^{Cu}_{Cu(CT)L}$ is due to the respective tridentate and bidentate nature of the two ligands. The bidentate diethylmalonic acid ligand occupies an equatorial position while the AT assumes an equatorial-axial coordination as shown in structure (I). The equatorial-axial coordination of AT with Cu^{II} has been recently reported on the studies of mixed-ligand complexes from X-ray data.[19]

(f) It can be seen from the experimental values of $\beta=^{Cu}_{Cu(CT)L}$ and the stabilization parameters $\Delta \log K$ and $\log K_r$ (Tables 3, 4) that the inductive effect of the alkyl group has no great influence on the stability of these systems. The presence of one or two substituents affects the reciprocal coplanarity of the two carboxylato group in different ways, giving rise to a different stability order in both binary and ternary complexes. In particular the presence of two bulky substituents as in the case of Cu(CT) DEt-mal. seems especially to favour the formation of the ternary species, probably by forcing the two carboxylato groups into the best position of chelation.

The computer was made available by the Tata Institute of Fundamental Research, Bombay. Thanks are due to Dr. D. V. Jahagirdar and Dr. L. G. Pardeshi for valuable suggestions. This research work is supported by the UGC, New Delhi.

References

1) H. Sigel, "Metal Ions in Biological Systems," Marcel Dekker Inc, New York, Vol. 2, p. 65 (1973), Vol. 5, p. 250 (1976), Vol. 9, p. 77 (1979).
2) F.J.C. Rossotti and R. J. Whewell, *J. Chem. Soc., Dalton Trans.*, **1979**, 257.
3) R. Cali, E. Rizzarelli, S. Samartano, and L. D. Pettit, *Thermochim. Acta*, **35**, 169 (1980).
4) D. N. Shelke and D. V. Jahagirdar, *J. Inorg. Nucl. Chem.*, **43**, 174 (1981).
5) D. N. Shelke, *Inorg. Chim. Acta*, **32**, L45 (1979).
6) D. N. Shelke and D. V. Jahagirdar, *J. Inorg. Nucl. Chem.*, **41**, 1635 (1979).
7) D. N. Shelke and D. V. Jahagirdar, *Indian. J. Chem.*, **16A**, 60 (1978).
8) A. I. Vogel "A Textbook of Quantitative Inorganic Analysis," Longman Press, London, p. 435 (1975).
9) D. N. Shelke, *J. Coord. Chem.*, **12**, 35 (1982).
10) D. N. Shelke and D. V. Jahagirdar, *J. Inorg. Nucl. Chem.*, **41**, 925, 929 (1979).
11) S. Ramamoorthy and P. G. Manning, *J. Inorg. Nucl. Chem.*, **32**, 1977 (1972).
12) R. M. Tichane and W. E. Bennett, *J. Am. Chem. Soc.*, **79**, 1293 (1957).
13) S. Ramamoorthy and M. Santappa, *Bull. Chem. Soc. Jpn.*, **42**, 411 (1969).
14) M. R. Udupa and B. Krebs, *Inorg. Chim. Acta*, **42**, 251 (1980).
15) J. I. Watters and R. De Witt, *J. Am. Chen. Soc.*, **82**, 1333 (1960).
16) D. N. Shelke and D. V. Jahagirdar, *Bull. Chem. Soc. Jpn.*, **49**, 2142 (1976).
17) D. N. Shelke and D. V. Jahagirdar, *J. Inorg. Nucl. Chem.*, **43**, 757 (1981).
18) D. N. Shelke, to be published.
19) R. P. Bonomo, E. Rizzarelli, N. Breseiani Pahor and G. Nardin, *J. Chem. Soc., Dalton Trans.*, **1982**, 681.

© 1985 The Chemical Society of Japan

NOTES

Bull. Chem. Soc. Jpn., 58, 377—378 (1985)

Promotion of Dehydrazination by Nitrobenzenesulfonyl Group from Phosphorus-hydrazone Adducts

Mitsuji YAMASHITA,* Jun TAKEUCHI, Kaname NAKATANI, Tatsuo OSHIKAWA, and Saburo INOKAWA†

Department of Chemistry, Faculty of Engineering, Shizuoka University, Hamamatsu 432

†*Department of Chemistry, Faculty of Science, Okayama University, Okayama 700*

(Received June 11, 1984)

Synopsis. Dehydrazination of adducts of phenylsulfonylhydrazones and phosphorus compounds was promoted by a nitro substituent on the ring to afford derivatives of a phosphine oxide and phosphonates.

Addition reaction of *p*-tolylsulfonylhydrazones with dimethyl phosphonate was reported to give the corresponding adducts, dimethyl 1-(*N'*-*p*-tolylsulfonylhydrazino)alkylphosphonates **3**, in 71—78% yields.[1] Adducts **3** was then dehydrazinated by a treatment with sodium tetrahydroborate to give **4** in 50—84% yields. The method provided a good tool to prepare phosphonates such as dimethyl isopropylphosphonate and *s*-butylphosphonate. However, in some cases where steric and ring strain factors operate, the dehydrazination reaction competed with the β-elimination reaction of dimethyl phosphonate from compound **3** giving the starting hydrazone.[2] The present paper deals with the preparation of *o*- and *p*-nitrophenylsulfonylhydrazones **5** and the reaction of **5** with some phosphorus compounds to improve the dehydrazination reaction by the nitro substituent by virtue of its electron withdrawing nature.

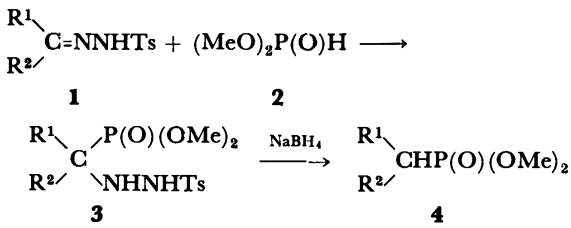

Results and Discussion

o- And *p*-nitrophenylsulfonylhydrazones **5** were prepared by the reaction of *o*- and *p*-nitrobenzenesulfonhydrazide with ketones in 1 M hydrochloric acid (1 M=1 mol dm^{-3}) at room temperature.

The reaction of **5a** (*o*-nitro derivative) with diphenylphosphine oxide (1:1.2, molar ratio) gave directly alkyldiphenylphosphine oxide **7** together with adduct **6**. The same reaction of **5b** (*p*-nitro derivative) gave solely **6b**. These results are summarized in Table 1. The table shows that the reaction at higher temperature gave higher yield of **7** than that at room temperature and that product **7** may be generated *via* intermediary **6**. Adduct **6b**, being produced from **5b** and diphenylphosphine oxide, was reduced by sodium tetrahydroborate to afford isopropyldiphenylphosphine oxide in overall yield of 66% from compound **5b**.

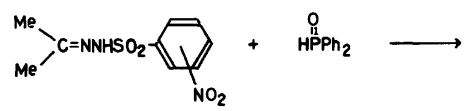

5a,b

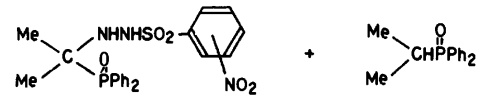

6a,b **7**

The reaction of **5** with dimethyl phosphonate was carried out in the presence of trifluoromethanesulfonic acid (condition A) or of excess dimethyl phosphonate (condition B) to give directly dimethyl alkylphosphonate **9** together with adduct **8** or to give solely compound **8** or **9** according to the substrate and reaction condition. The results are summarized in Table 2. The result that the ortho nitro substituent affords directly compound **7** or **9** in higher yield than the para one does may attribute more effective electron-withdrawal property of the ortho one and/or ortho effect. Enhancements of acidity constant of benzoic acids and anilinium salts in water and equiliblium constant of the reaction of benzoic acids with diphenylguanidine in benzene by ortho nitro substituent are known.[3]

The present results show that the dehydrazination of adducts **6** and **8** was promoted by the nitro substituent of benzenesulfonhydrazides giving phosphorus compounds **7** and **9**, and that the phosphorus compounds having a C-P bond such as tertiary phosphine oxides and phosphonates were prepared by one operation from hydrazone and phosphorus compounds having a P-H bond, *i.e.*, diphenylphosphine oxide and dimethyl phosphonate

TABLE 1. REACTION OF COMPOUND **5** (R=Me) WITH DIPHENYLPHOSPHINE OXIDE IN METHANOL FOR 24 h

Compound	*o*- or *p*	Temperature/°C	Yield of product/%	
			6	**7**
5a	*o*-	Room temperature	26	65
5a	*o*-	45	8	81
5b	*p*-	Room temperature	76	—

Table 2. Reaction of compound 5 with dimethyl phosphonate

Compound	R in 5	*o*- or *p*-	Reaction condition			Yield of product/%	
			A or B[a]	Time/h	Temp/°C	8	9
5a	Me	*o*-	A	20	30	—	93
5a	Me	*o*-	B	5	100	18	43
5b	Me	*p*-	A	20	30	35	53
5b	Me	*p*-	B	5	100	61	—
5c	Et	*o*-	A	20	30	—	61
5d	Et	*p*-	A	20	30	—	56
5e	Ph	*o*-[b]	A	20	30	13	38
5f	Ph	*p*-[c]	A	20	30	59	—

a) Reaction conditions A and B show the reaction in the presence of trifluoromethanesulfonic acid and large excess of dimethyl phosphonate, respectively. b), c) Recovered starting material was 31% and 8%, respectively.

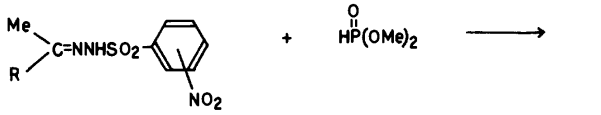

5

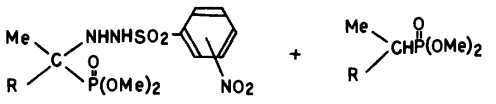

8 9

Experimental

Measurements. ^{1}H NMR spectra were measured on Hitachi R-24 (60 MHz) spectrometer with tetramethylsilane as an internal standard. IR spectra were recorded with Japan Spectroscopic Co., Ltd. A-3 infrared spectrophotometer. MS spectra were measured by Hitachi RMU DMG GC-MS spectrometer.

Materials. The following materials were synthesized according to reported methods: *o*-Nitrobenzenesulfonhydrazide, mp 101—102 °C (lit,[4] mp 101 °C), 92% yield from *o*-nitrobenzenesulfonyl chloride and 100% hydrazine hydrate; *p*-nitrobenzenesulfonhydrazide, mp 145 °C (lit,[5] mp 150—152 °C), 78% yield; diphenylphosphine oxide, mp 49 °C (lit,[6] mp 51—54 °C), 87% yield from phosphorus trichloride and benzene in the presence of aluminium chloride.

Synthesis of Acetone o-Nitrophenylsulfonylhydrazone (5a; R= Me, o-). Reaction of acetone (1.8 g, 30 mmol) with *o*-nitrobenzenesulfonhydrazide (6.0 g, 28 mmol) in 1 M hydrochloric acid overnight at room temperature gave precipitate. Recrystallization of the product from ethanol-water gave pure **5a** (4.2 g) in 59% yield, mp 144—147 °C (lit,[5] mp 147—148 °C), ^{1}H NMR ($CDCl_3$) δ, 1.77, 1.78 (2s, 6H, $2CH_3$), 7.2—7.3 (m, 1H, NH), and 7.6—8.4 (m, 4H, C_6H_4); IR ν_{max}^{KBr} cm^{-1}, 3250 (NH), 1650 (C=N), 1540, 1350 (NO_2), and 1180 (SO_2).

The following *o*- and *p*-nitrophenylsulfonylhydrazones (**5**) were prepared silimarly: Acetone *p*-nitrophenylsulfonylhydrazone (**5b**; R=Me, *p*-), 51% yield, mp 183—185 °C (lit,[7] 183—184 °C); 2-butanone *o*-nitrophenylsulfonylhydrazone (**5c**; R=Et, *o*-), 58% yield, mp 141—143 °C (lit,[7] mp 143—144 °C); 2-butanone *p*-nitrophenylsulfonylhydrazone (**5d**; R= Et, *p*-), 74% yield, mp 155—158 °C (lit,[7] mp 155—156 °C); acetophenone *p*-nitrophenylsulfonylhydrazone (**5f**; R= Ph, *p*-), 71% yield, mp 213—215 °C (lit,[7] mp 192 °C).

Reaction of 5a with Diphenylphosphine Oxide. Reaction of **5a** (0.50 g, 1.9 mmol) with diphenylphosphine oxide (0.46 g, 2.3 mmol) in methanol (5 ml) for 24 h at room temperature followed by evaporation of the solvent and separation of the reaction products by TLC gave isopropyldiphenylphosphine oxide **7a** (0.30 g) in 65% yield, mp 143—144 °C (lit,[8] mp 144—145 °C), together with **6a** (0.23 g) in 26% yield.

Spectral data for compound **7a** was as follows: ^{1}H NMR ($CDCl_3$) δ, 1.13 (dd, 6H, J_{HH}=7.0 Hz, J_{HP}=16.0 Hz, $2CH_3$), 2.1—2.8 (m, 1H, CH), and 7.0—8.2 (m, 10H, $2C_6H_5$); IR ν_{max}^{KBr} cm^{-1}, 1440 (P-Ph), 1180 (P=O), and 710 (C-P); MS, *m/z*, 244 (M^+).

^{1}H NMR for compound **6a** ($CDCl_3$) δ, 1.40 (d, 6H, J_{HP}=16.0 Hz, $2CH_3$) and 6.9—8.1 (m, 16H, $2C_6H_5$, C_6H_4, 2NH).

Reaction of 5a with Dimethyl Phosphonate. Reaction of compound **5a** (0.20 g, 0.78 mmol) with large excess of dimethyl phosphonate (6 ml) for 20 h at 30 °C followed by work-up gave dimethyl isopropylphosphonate[1] (0.11 g) in 93% yield.

Reaction of 5b with Diphenylphosphine Oxide. Reaction of **5b** (3.1 g, 12 mmol) with diphenylphosphine oxide (2.4 g, 12 mmol) in methanol (25 ml) for 24 h at room temperature followed by filtration of the product gave diphenyl-2-(*N'*-*p*-nitrophenylsulfonylhydrazino)propylphosphine oxide in 63% yield, mp 101—106 °C: ^{1}H NMR ($CDCl_3$) δ, 1.20 (d, J_{HP}=16.0 Hz, 6H, $2CH_3$), 3.40 (s, 2H, 2NH), and 7.4—8.4 (m, 14 H, $2C_6H_5$, C_6H_4).

References

1) S. Inokawa, Y. Nakatsukasa, M. Horisaki, M. Yamashita, H, Yoshida, and T. Ogata, *Synthesis*, **1977**, 179.

2) M. Yamashita, K. Nakatani, P. T. Long, and H. Yamashita, to be published.

3) L. P. Hammett, "Physical Organic Chemistry," 2nd ed, McGraw-Hill, New York (1970), Chap. 11.

4) A. H. Dann and W. Davies, *J. Chem. Soc.*, **1929**, 1050.

5) W. Davies, F. R. Storrie, and S. H. Tucker, *J. Chem. Soc.*, **1931**, 624.

6) United Kingdom Atomic Energy Authority, Fr. 1,314,704 (1963); *Chem. Abstr.*, **59**, 2860b (1963).

7) J. M. L. Cameron and F. R. Storrie, *J. Chem. Soc.*, **1934**, 1330.

8) M. I. Kabachnik, T. Ya. Medved, and Yu. M. Polikarpov, *Izv. Akad. Nauk SSSR, Ser. Khim.*, **1966**, 368; *Chem. Abstr.*, **64**, 15917 (1966).

Mechanochemical Changes of Neodymium Phosphates by Grinding

Hiroyuki NARIAI,* Itaru MOTOOKA, Mayumi DOI,† and Mitsutomo TSUHAKO†
Department of Chemistry, Faculty of General Education, Kobe University, Tsurukabuto, Nada-ku, Kobe 657
†*Kobe Women's College of Pharmacy, Kitamachi, Motoyama, Higashinada-ku, Kobe 658*
(Received March 7, 1984)

Synopsis. The effect of mechanochemical treatment on some neodymium phosphates was investigated. It is worth noting that on mechanochemical treatment $NdPO_4 \cdot 0.5H_2O$ (hexagonal) is gradually transformed into $NdPO_4$ (monoclinic) at room temperature, while thermal change of $NdPO_4 \cdot 0.5H_2O$ to $NdPO_4$ (monoclinic) happens at above 600 °C. Condensed phosphates, meta- and ultraphosphates, easily turned to X-ray amorphous structure by grinding.

Mechanochemical treatment influences structures, physical and chemical properties, and reactivity of solids. We have investigated the mechanochemical effect of various phosphates by grinding. In the present study, four neodymium phosphates ($NdPO_4$, $NdPO_4 \cdot 0.5H_2O$, $Nd(PO_3)_3$, and NdP_5O_{14}), were used. Rare earth phosphates were used for the laser materials, semiconductor, and ceramics, which have been studied for the last several years[1,2] The effecat of mechanochemical treatment on 1) X-ray diffraction patterns, 2) IR spectra, 3) DTA-TG diagrams, and 4 solubility of neodymium phosphates, was investigated.

Experimental

Neodymium phosphates used were prepared by the procedure described in a previous paper.[3] Grinding was performed with Ishikawa's grinding mill, AG-Z type, at a temperature range of 20—30 °C, humidity at 15—30%, in nitrogen atmosphere. The X-ray diffraction analysis was carried out with a Rigaku Denki Geigerflex diffractometer using nickel-filtered Cu $K\alpha$ radiation. Thermal analysis (DTA-TG) was carried out by a Rigaku 8002 SD thermal analyzer. The IR spectra were taken by means of a KBr tablet.

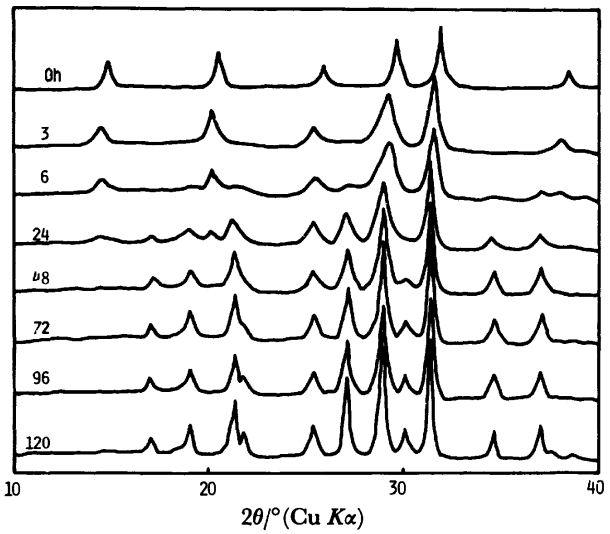

Fig. 1. X-Ray diffraction patterns of ground $NdPO_4 \cdot 0.5H_2O$.

Results and Discussion

Mechanochemical Changes of Orthophosphates. Figure 1 shows the X-ray diffraction patterns of $NdPO_4 \cdot 0.5H_2O$ at various stages of grinding. With grinding over 24 h, some new diffraction peaks, at 2θ= 17.5, 19.5, 22, 27.5, 30.5, 35, and 37.5°, appeared. These peaks coincided in position with those of $NdPO_4$ (monoclinic), and their intensities increased with further grinding. It is clear from this fact that $NdPO_4 \cdot 0.5H_2O$ turned to anhydrate ($NdPO_4$) by grinding. On the other hand, as for $NdPO_4$ (monoclinic), a remarkable change of X-ray diffraction patterns was not observed.

Figure 2 shows the IR spectra of $NdPO_4 \cdot 0.5H_2O$ by grinding. With grinding, the intensity of each absorption peak gradually decreased. Also, characteristic absorptions due to the O-H bond of water of crystallization in the region of 3400—3500 and 1600 cm^{-1} became weak, while those attributable to the P-O bond were gradually increased at about 960 and 560—580 cm^{-1}, and IR spectrum after 24 h's grinding coincided with that of anhydrate, that is, the water of crystallization was released and turned to the anhydrate ($NdPO_4$).

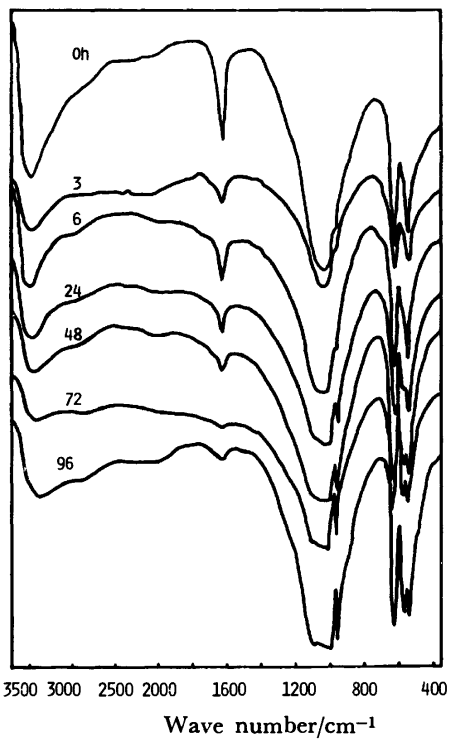

Fig. 2. IR spectra of ground $NdPO_4 \cdot 0.5H_2O$.

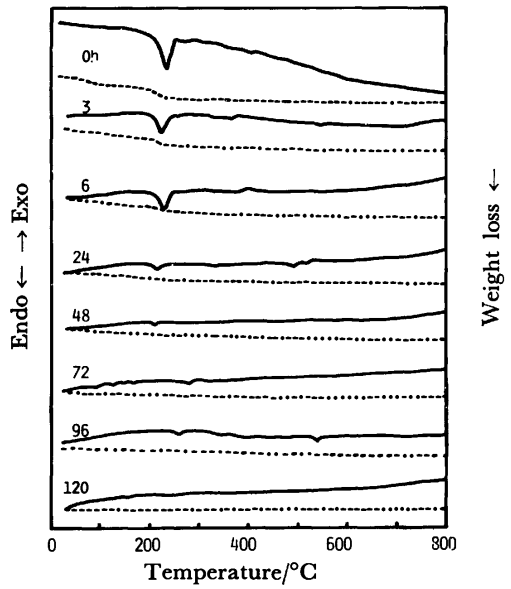

Fig. 3. DTA-TG curves of ground $NdPO_4 \cdot 0.5H_2O$. Solid line: DTA, dotted line: TG.

Figure 3 shows the DTA-TG curves of $NdPO_4 \cdot 0.5H_2O$ by grinding. An endothermic peak in the 210—220 °C region with a weight loss, being due to the dehydration of water of crystallization, decreased gradually with increasing the grinding time and almost disappeared in the samples ground for more than 24 h. When $NdPO_4$ (monoclinic) was ground, a remarkable change of DTA-TG curves was not observed. On heating, the thermal changes of $NdPO_4 \cdot 0.5H_2O$ were shown as follows:[3]

$$NdPO_4 \cdot 0.5H_2O(\text{hexagonal}) \underset{\text{standing in air}}{\overset{210-220\,^\circ C}{\rightleftarrows}}$$

$$NdPO_4(\text{hexagonal}) \begin{cases} \xrightarrow[\text{long time}]{600\,^\circ C} NdPO_4(\text{monoclinic}) \\ \xrightarrow[\text{short time}]{800\,^\circ C} NdPO_4(\text{monoclinic}) \end{cases}$$

On the other hand, in the case of mechanochemical treatment, the conversion of $NdPO_4 \cdot 0.5H_2O$ (hexagonal) to $NdPO_4$ (monoclinic) proceeds at room temperature for above 24 h. This finding is very interesting in view of the fact that the mechanochemical treatment had the same effect as heat energy on the transition of $NdPO_4 \cdot 0.5H_2O$ (hexagonal) to $NdPO_4$ (monoclinic), and this transition took place without X-ray amorphous structure.

Mechanochemical Changes of Condensed Phosphates. In order to compare the difference in mechanochemical changes of the structure of phosphates, two condensed phosphates, neodymium metaphosphate ($Nd(PO_3)_3$) and ultraphosphate (NdP_5O_{14}), were examined. Because an ultraphosphate is generally very unstable, crystalline substances are almost unknown.[4] Neodymium ultraphosphate is one of the stable, crystalline ones and their mechanochemical investigation have not been reported. The X-ray diffraction intensities of $Nd(PO_3)_3$ and NdP_5O_{14} decreased with increasing the grinding time, the line-width broadened, and their diffraction peaks disappeared at last. From their IR spectra, with grinding, the intensities of their absorption peaks decreased and the peak-width broadened because of X-ray amorphous structure. From the results of DTA-TG, the ground $Nd(PO_3)_3$ has an endothermic peak at about 100 °C with a weight loss by the dehydration of adsorbed water, and an exothermic one at about 650 °C, being due to the restoring of the lattice distortion produced by grinding. The exothermic peak increased gradually with grinding time. This shows that its crystal structure was distorted by grinding, and finally transformed to the X-ray amorphous structure; metaphosphate showed the structure change similar to alkaline metaphosphates,[5] that is, the increasing of amorphous substance with grinding time and the yielding of shorter-chain phosphate molecules as a result of random cleavage of the P-O-P linkage upon grinding. When NdP_5O_{14} was ground for more than 3 h, large weight loss at about 100 and 300—400 °C was observed. It is suggested from the results of X-ray diffraction patterns, IR spectra, and DTA that the crystal structure of neodymium ultraphosphate was very unstable for grinding.

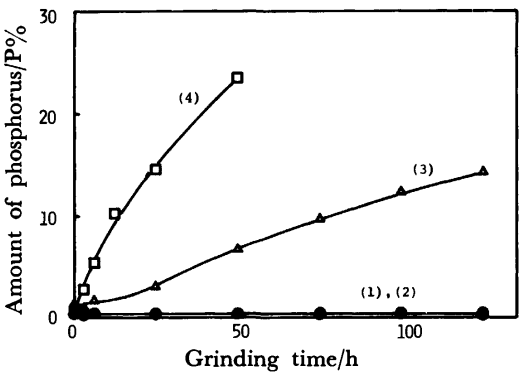

Fig. 4. Changes in the solubility of ground samples in water. (1): $NdPO_4$, (2): $NdPO_4 \cdot 0.5H_2O$, (3): $Nd(PO_3)_3$, (4): NdP_5O_{14}.

Solubility of Ground Samples in Water. Figure 4 shows the changes in the solubilities of various ground phosphates in water. Species dissolved was almost orthophosphate, seldom, pyrophosphate. The amounts of dissolved phosphates were 23.5% for ultraphosphate ground for 48h, and 14.3% for metaphosphate ground for 120h. But the ground samples of orthophosphates ($NdPO_4$ and $NdPO_4 \cdot 0.5H_2O$) were not entirely dissolved, showing that the crystal structure of condensed phosphates was rather unstable than those of orthophosphates on grinding.

References

1) B. C. Tofield, H. P. Weber, T. C. Damen, and G. A. Pasteur, *Appl. Phys.*, **9**, 435 (1974).
2) E. Snitzer, *Appl. Optics*, **51**, 1487 (1966).
3) M. Tsuhako, S. Ikeuchi, T. Matsuo, I. Motooka, and M. Kobayashi, *Nippon Kagaku Kaishi*, **1978**, 676.
4) C. Barthou, B. Blanzat, and J. M. Letoffe, *J. Appl. Phys.*, **52**, 6847 (1981).
5) I. Motooka, G. Hashizume, and M. Kobayashi, *Nippon Kagaku Kaishi*, **87**, 255, 953 (1966).

Phase Relations in the System $NH_4Ti_2P_3O_{12}$-$NH_4Zr_2P_3O_{12}$

Akira ONO
National Institute for Research in Inorganic Materials, 1-1 Namiki, Ibaraki, 305
(Received June 13, 1984)

Synopsis. Crystalline phases in the system $NH_4Ti_2P_3O_{12}$–$NH_4Zr_2P_3O_{12}$ were prepared in a high pressure vessel, and were investigated by X-ray method. New compounds, $(NH_4)_{1+x}Ti^{3+}{}_x(Ti^{4+},Zr)_{2-x}P_3O_{12}$ ($1 \geqq x$), with the langbeinite-type structure were produced under reducing conditions.

In recent years a number of compounds with the Nasicon-type structure have been studied in relation to the superionic conductor, Nasicon ($Na_3Zr_2Si_2PO_{12}$).[1-4] A characteristic framework of these compounds is that all the oxygen atoms are shared between MO_6 and TO_4 where M is Ti or Zr and T is Si,Al or P. Each octahedron is surrounded by six tetrahedra, and each tetrahedron by four octahedra. This framework with the formula $M_2(TO_4)_3$ can exist in three modifications: Nasicon-type, langbeinite-type and garnet-type structures.[5,6]

These structures may be conveniently described as a body-centered cubic rod packing or hexagonal packing of parallel cylinders.[7] For example, in the case of $KTi_2P_3O_{12}$ with cubic langbeinite-type structure,[8] the rods consist of a repeating sequence K, (K),O_3TiO_3,O_3TiO_3, where (K) is vacancy. The rods extend along four nonintersecting directions, parallel to the body diagonals of a cube. The P atoms in tetrahedral coordination hold the rods together. On the other hand, rods consist of a repeating sequence of K,O_3TiO_3,O_3TiO_3 in the rhombohedral $KTi_2P_3O_{12}$. The rods are oriented along the real axis $\bar{3}$.

Rhombohedral $NH_4Ti_2P_3O_{12}$ and $NH_4Zr_2P_3O_{12}$ were prepared,[9-11] but no cubic phase was obtained. However, solid solutions with cubic structure were produced during an investigation of the system $NH_4Ti_2P_3O_{12}$–$NH_4Zr_2P_3O_{12}$. The purpose of this work is to ellucidate phase relations in this and related systems.

Experimental

Reagents used for synthesis were $NH_4H_2PO_4$, TiO_2, and ZrO_2. All of them have a purity higher than 99%. These materials were weighed according to the prescribed proportion and mixed in an alcohol medium, and then dried at 323 K for 10 h. The ratio of P to (Ti+Zr) is 1.5 for all the starting materials except for two experimental runs where small amount of $NH_4H_2PO_4$ was added as a flux component to promote chemical reaction.

Three kinds of experiments were carried out. First, starting material was sealed in a gold capsule of 6 mm in diameter and 35 mm long with no water added. Second, double capsules were used. Starting material was sealed in an inner platinum capsule, and then hematite and water were put in between the inner and outer capsules in order to maintain low hydrogen fugacity. Third, a small amount of acetone was added to the starting material in a gold capsule in order to produce high hydrogen fugacity. The ratio $Ti^{4+}/(Ti^{4+}+Ti^{3+})$ in crystalline materials may be controlled by the hydrogen fugacity of fluid phase.

Synthesis was carried out in a cold seal high pressure vessel. Temperature was measured by an internal thermocouple, and pressure by a calibrated Heise Bourdon tube gauge.

X-ray powder patterns were recorded with a Toshiba diffractometer using Cu $K\alpha$ radiation. For unit cell determinations, the pattern was obtained at room temperature by the scanning speed of 0.25 degree 2θ per min. KCl or quartz powder was used as an internal standard.

Chemical analyses of the synthetic crystals were carried out with an electron probe microanalyzer (JXA 5A). $NH_4Ti_2P_3O_{12}$ prepared and analyzed before[10] was used as a standard. Apparent concentration was corrected by the procedure proposed by Bence and Albee.[12]

Results and Discussion

Experimental results are listed in Table 1 together with experimental conditions. X-ray studies on the products of the first kind of experiments (1—9 in Table 1) indicate that most of X-ray reflections could be indexed as a rhombohedral form. However, extra weak reflections were observed in four experimental products. These reflections could be indexed as a cubic form with the langbeinite-type structure. Cubic phases were not prepared by the second kind of experiments (10—13 in Table 1), suggesting that cubic phase is unstable under low hydrogen fugacity. On the other hand, cubic phases with blue colour were main products when acetone was added to the starting materials(14—19 in Table 1). These results suggest the presence of Ti^{3+} in the cubic phases. Further evidence for the existence of Ti^{3+} will be described afterward.

Formula unit volumes are presented on Fig. 1 as a function of the ratio Zr/(Zr+Ti) in the starting material. As is seen from Fig. 1, formula unit volumes slightly deviate from the Vegard's law. Two rhombohedral phases with different unit cell volume were present in the product obtained by the experiment 7 in Table 1. Chemical compositions of the coexisting phases were determined by using the relationship between composition and formula unit volume shown in Fig. 1, and plotted as circles A and B. The compositions of A and B are 0.56±0.03 and 0.09±0.01 in the Zr/(Zr+Ti) ratio, respectively.

The first and second kinds of experiments were unsuccessful in yielding a pure cubic phase. However, cubic phase with or without graphite was obtained by the third kind of experiments. Formula unit volume of the cubic phase is shown by the cross in Fig. 1. Two cubic phases with different unit cell volume were crystallized in two products (15 and 18), suggesting presence of an immiscibility field in the cubic solid solution system. One of the cubic phases in the product of experiment 15 showed weak X-ray peaks partially superimposed on nearby higher peaks.

Weight loss for the cubic phases(15 in Table 1) was 9.4 wt% at 1273 K, which was larger than the weight loss for $NH_4Ti_2P_3O_{12}$ (6.4%). Excess ammonium

Table 1. Experimental results

Run number	Starting material 100Zr/(Zr+Ti)	Temp K	Press GPa	Time h	Product[b]	Lattice constant/10^{-1} nm Rhombohedral a	Rhombohedral c	Cubic c
1	0	823	0.15	40	R	8.318	23.44	
2	8.6	823	0.15	40	R	8.328	23.51	
3	63	823	0.16	25	R, (C)	8.533	23.97	10.07
4	82	823	0.15	30	R, (C)	8.597	24.14	10.14
5	89	823	0.15	48	R, (C)	8.627	24.20	10.17
6	100	823	0.15	48	R	8.680	24.24	
7[a]	30	853	0.17	40	R	8.331 8.479	23.53 23.91	
8	20	878	0.19	48	R	8.33 8.450	23.53 23.87	
9	43	853	0.17	40	R, (C)	8.462	23.88	10.07
10	59	873	0.15	16	R	8.504	23.93	
11	63	828	0.15	40	R	8.511	23.90	
12	77	828	0.15	24	R	8.563	24.06	
13	89	828	0.15	40	R	8.621	24.17	
14	0	823	0.15	48	R, C, gr			9.922
15	22	823	0.15	40	C			9.970
16	42	828	0.15	6	C, gr			10.055
17	0	798	0.15	16	C, gr			9.925
18[a]	30	798	0.15	16	C, gr			10.09, 9.962
19	63	703	0.15	60	C			10.140

R: rhombohedral phase, C: cubic phase, gr: graphite, (—): minor product.
a) Small amount of $NH_4H_2PO_4$ was added. b) Fluid phase is present in all products.

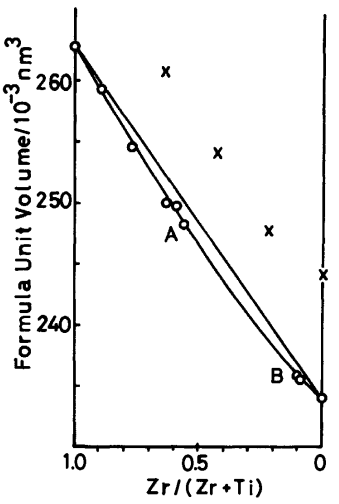

Fig. 1. Formula unit volume versus composition of starting materials. circle: rhombohedral phase not associated with cubic phase, cross: cubic phase prepared under reducing conditions, A—B; immiscibility field at 853 K, 0.17 GPa.

content may be explained by the presence of Ti^{3+} in the octahedral site. Chemical formula derived from the weight loss datum and the ratio of Zr to (Zr+Ti) in the cubic phase (0.22) is as follow: $(NH_4)_{1.55}Ti^{3+}_{0.55}Ti^{4+}_{1.01}Zr_{0.44}P_3O_{12}$.

Zirconium-free crystals were of sufficient sizes for analysis using an electron probe microanalyzer. Composition of the cubic phase is: TiO_2=37.68; P_2O_5=50.52 (wt%). Because discrimination of TiO_2 and Ti_2O_3 contents is impossible for our analytical method, value of TiO_2 is total titanium calculated as TiO_2. The analytical data is consistent with the theoretical value for $(NH_4)_2Ti^{3+}Ti^{4+}P_3O_{12}$: TiO_2=37.74; P_2O_5=50.29 (wt%). On the other hand, rhombohedral phase coexisiting with graphite and cubic phase gave the same composition as the standard $NH_4Ti_2P_3O_{12}$.

References

1) L. Hagman and P. Kierkegaard, *Acta Chem. Scand.*, **22**, 1822 (1968).
2) H. Y-P. Hong, *Mater. Res. Bull.*, **11**, 173 (1976).
3) F. d'Yvoire, M. Pintard-Screpel, E. Brety, and M. de la Rochere, *Solid State Ionics*, **10**, 851 (1983).
4) J. P. Boilot, G. Collin, and R. Comes, *J. Solid State Chem.*, **50**, 91 (1983).
5) R. G. Sizova, V. A. Blinov, A. A. Voronkov, V. V. Ilyukhin and N. V. Belov, *Sov. Phys. Crystallogr.*, **26**, 164 (1981).
6) V. B. Kalinin and S. Yu. Stefanovich, *Inorg. Mater.*, **18**, 1342 (1982).
7) M. O'Keefe and S. Andersson, *Acta Crystallogr Sect A.*, **33**, 914 (1977).
8) R. Masse, A. Durif, J-C. Guitel, and I. Tordjman, *Bull. Soc. Fr. Mineral. Cristallogr.*, **95**, 47 (1972).
9) A. Ono, *J. Mater. Sci.*, **19**, 2691 (1984).
10) A. Ono, *J. Solid State Chem.*, **56**, 3161 (1985).
11) A. Clearfield, B. D. Roberts and M. A. Subramanian, *Mater. Res. Bull.*, **19**, 219 (1984).
12) A. E. Bence and A. L. Albee, *J. Geol.*, **93**, 500 (1970).

Crystal Structure of Binuclear Copper(II) Complex with 3-Ethyl-2-pyridone and Magnetism of Its Homologues

Yuzo NISHIDA* and Sigeo KIDA
Department of Chemistry, Faculty of Science, Kyushu University 33, Fukuoka 812
(Received July 14, 1984)

Synopsis. The crystal structure of bis(*N*,*N*-dimethylformamide)tetrakis(3-ethyl-2-pyridonato)dicopper(II) was determined by X-ray diffraction method. Crystal data: Space group $P2_1/n$(monoclinic), a=9.906(1), b=13.494(3), c=14.029(2) Å, β=103.81(1)°. The crystal consists of centrosymmetric binuclear units in which two copper(II) ions are linked by four pyridonate anions similarly to copper(II) acetate monohydrate. The Cu–Cu distance is 2.55 Å. The cryomagnetic data revealed that $-2J$ values are in the range 360—405 cm^{-1} for the series of complexes.

It is well known that copper(II) acetate monohydrate consists of binuclear structure in which two copper(II) ions are bridged by four acetate anions with a short Cu–Cu distance(2.64 Å).[1] Similar structures were also observed for copper(II) complexes with 1,3-diphenyltriazene,[2] 1,7-diazaindene,[3] and adenine.[4] It is also known that 2-pyridone forms binuclear complexed with Ph(II), Mo(II), and Ru(II) ions similar to that of copper(II) acetate monohydrate.[5]

In 1972, Emori *et al.*[6] reported the preparation of Cu(2-pyridonato)$_2$·(2-pyridone), and they assumed that this complex has a structure similar to that of copper(II) acetate monohydrate based on the magnetic property. In this study a series of copper(II) complexes with 2-pyridone and its homologues have been prepared and characterized by the spectral and magnetic measurements. In order to confirm the binuclear structure, the crystal structure of one of them, bis(*N*,*N*-dimethylformamide)tetrakis(3-ethyl-2-pyridonato)dicopper(II) has been determined by X-ray diffraction method.

Experimental

Preparations. 2-Pyridone was obtained commercially. The substituted 2-pyridones were prepared by the published method.[7] The copper(II) complexes were prepared by the following way. A DMF (or DMSO) solution containing substituted 2-pyridone (0.01 mol) and copper(II) hydroxide (0.005 mol) was kept at 50 °C for five hours. From the filtrate, the complex was obtained as dark prisms.[8]

Magnetic Measurements. Magnetic susceptibilities were measured in the temperature range 90—300 K by the published method.[9] Magnetic moments were calculated by the equation, $\mu_{eff}=2.828\sqrt{(\chi-N\alpha)T}$, where χ and $N\alpha$ have usual meanings.[1]

Determination of the Cell Constant and Collection of the Intensity Data. A crystal with the approximate dimension of 0.3×0.2×0.3 mm^3 was used for the determination and the collection of intensity data at 294 K. The cell dimensions and the diffraction intensities were measured on a Rigaku AFC-5 Automatic Diffractometer by using graphite monochromated Mo $K\alpha$ radiation. Crystal data. Cu(3-ethyl-2-pyridonato)$_2$·DMF, FW=380.9, space group $P2_1/n$(monoclinic), a=9.906(1), b=13.494(3), c=14.029(2) Å, β=103.81(1)°, Z=4, D_c=1.39 g cm^{-3}, D_m=1.44 g cm^{-3} (by floatation method). All independent reflections within the range $3°<2\theta<55°$ were collected by the use of $2\theta-\theta$ scan mode with a scanning rate 6°(2θ) min^{-1}. A total 1973 independent reflections with $|F_o|>3\sigma(|F_o|)$ were used for the determination of crystal structure. The data were corrected for the Lorentz and polarization effects.

Structure Determination

The position of the copper atom was obtained from the three dimensional Patterson map. The positions of the other non-hydrogen atoms were located by the Fourier synthesis. There was a disorder in ethylcarbon atom (see Table 1). The structure was refined to R=0.065 for the observed reflections by a block-diagonal least-squares method using anisotropic temperature factors for non-hydrogen atoms. At the final stage of the refinement the difference Fourier map showed only featureless peaks. Anisotropic temperature factors of the non-hydrogen atoms and the complete F_o-F_c data are deposited as Documents No. 8506 at the Office of the Editor of the Bulletin of the Chemical Society of Japan. The final atomic coordinates, and the equivalent isotropic temperature factors are given in Table 1. All the calculations were carried out on a M-200 computer at the Computer Center of Kyushu University using the local version[10] of the UNICS system.[11] The atomic scattering factors were taken from the International Tables for X-Ray Crystallography.[12]

Results and Discussion

The perspective drawing of the structure of bis(*N*,*N*-dimethylformamide)tetrakis(3-ethyl-2-pyridonato)dicopper(II) is shown in Fig. 1 with selected bond lengths and bond angles. As has been expected, the crystal consists of centrosymmetric binuclear unit similar to that of copper(II) acetate monohydrate. The Cu–Cu distance is 2.55 Å, which is shorter than that of copper(II) acetate monohydrate (2.64 Å). The DMF molecule coordinates to the copper(II) atom at the apical position, forming a five-coordinated environment around the copper(II) ion.

The magnetic moments are summarized in Table 2. The magnetic moments of the complexes at room temperature are in the range 1.18—1.26 BM, implying that antiferromagnetic interaction is operating between two copper(II) ions. The temperature dependence of magnetic susceptibilities(90—300 K) of these complexes can be interpreted in terms of Bleaney-Bowers equation with the $-2J$, g and $N\alpha$ values listed in the Table 2.

All the electronic spectra of the compounds are similar to each other. In DMF the d-d band and the shoulder were observed at 17.4×10^3 cm^{-1} (log ε=2.41) and

Table 1. Atomic coordinates ($\times 10^4$), their estimated standard deviation (in parentheses) and equivalent isotropic temperature factors

Atom	x	y	z	B_{eq}/Å^2
Cu	96(1)	270(1)	9148(1)	4.3
O1	−652(6)	1522(4)	9496(4)	6.0
O2	−1817(5)	−223(5)	8720(3)	6.4
O3	−21(6)	832(5)	7593(4)	6.5
N1	−799(6)	1093(4)	11038(4)	4.7
N2	−2039(6)	−699(5)	10238(5)	4.8
C1	−978(8)	1763(6)	10287(5)	4.8
C2	−1550(8)	2715(6)	10408(7)	5.6
C3	−1858(9)	2947(7)	11282(7)	6.5
C4	−1661(9)	2240(7)	12051(7)	6.7
C5	−1120(9)	1322(7)	11902(6)	5.8
C6	−1751(10)	3451(6)	9558(7)	6.6
C7	−3119(10)	3243(8)	8808(7)	7.5
C8	−2574(8)	−593(6)	9262(6)	5.0
C9	−3987(9)	−879(8)	8840(7)	7.0
C10	−4771(10)	−1236(8)	9430(8)	7.3
C11	−4219(10)	−1336(7)	10457(7)	6.8
C12	−2862(10)	−1080(6)	10829(7)	5.8
C15	−1166(9)	1217(7)	7246(6)	6.0
N3	−1673(7)	1339(5)	6286(4)	5.6
C16	−882(10)	1011(8)	5577(6)	7.1
C17	−3077(10)	1753(8)	5909(8)	7.5
C13	−4462(17)	−853(17)	7730(11)	12.9
C14A[a)]	−4894(25)	−759(15)	7439(16)	7.0
C14B[a)]	−5835(20)	−796(20)	7158(15)	8.2

a) 50% probability.

25×10^3 cm^{-1} ($\log\varepsilon\approx2.7$) for bis(*N*,*N*-dimethylformamide)tetrakis(3-ethyl-2-pyridonato)dicopper(II). The shoulder at 25×10^3 cm^{-1} must correspond to 26.6×10^3 cm^{-1} band of copper(II) acetate monohydrate[1] which has been used for diagnosis of the binuclear structure, since the ligand itself has no absorption in this region.

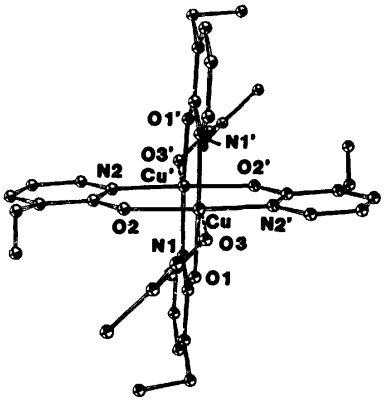

Fig. 1. Perspective drawing of binuclear structure of bis(*N*,*N*-dimethylformamide) tetrakis (3-ethyl-2-pyridonato) dicopper (II). Selected distances (Å): Cu'–Cu=2.550(1); Cu–O1=1.956(6); Cu–O2=1.961(6); Cu'–N1=2.003(6); Cu–N2'=1.997(6); Cu–O3=2.283(6). Selected bond angles (deg): O1–Cu–O2=88.3(3); O1–Cu–N2'=91.5(2); O1–Cu–N1'=171.9(2); O2–Cu–N2'=172.3(2); O2–Cu–O3=89.8(2); O2–Cu–N1'=89.5(2).

Table 2. Magnetic data of complexes

Complex	μ_{eff}/BM[a)]	$-2J$/cm^{-1}[b)]
$[Cu_2(pyr)_4(dmf)_2]$[c)]	1.24	365
$[Cu_2(pyr)_4(dmso)_2]$	1.26	360
$[Cu_2(3\text{-methyl-pyr})_4(dmf)_2]$	1.18	405
$[Cu_2(4\text{-methyl-pyr})_4(dmf)_2]$	1.20	400
$[Cu_2(3\text{-ethyl-pyr})_4(dmf)_2]$	1.22	395

a) 295 K. b) $-2J$ values were determined so that the experimental $\chi-T$ curves are simulated by Bleaney-Bowers equation ($g=2.15$, $N\alpha/10^{-6}$ cgs mol$^{-1}=60$, cgs mol$^{-1}\times4\pi\times10^{-6}\rightarrow$m^3 mol^{-1}). c) (pyr) represents 2-pyridonate anion.

References

1) M. Kato, H. B. Jonassen, and J. C. Fanning, *Chem. Rev.*, **64**, 99 (1964).
2) R. L. Martin and H. Waterman, *J. Chem. Soc.*, **1959**, 1359.
3) R. W. Brooks and R. L. Martin, *Inorg. Chem.*, **14**, 528 (1975).
4) A. Terziz, A. N. Beauchamp, and R. Rivest, *Inorg. Chem.*, **12**, 1166 (1973).
5) F. A. Cotton and R. A. Walton, "Multiple Bonds between Metal Atom," John Wiley & Sons, New York (1982).
6) S. Emori, I. Okano, and Y. Muto, *Bull. Chem. Soc. Jpn.*, **45**, 3717 (1972).
7) O. Seide, *Ber.*, **57**, 793, 1805 (1924).
8) The analytical data of the new compounds were deposited to the Editor of the Bulletin of the Chemical Society of Japan.
9) W. Kanda, H. Okawa, and S. Kida, *Bull. Chem. Soc. Jpn.*, **57**, 1159 (1984).
10) S. Kawano, *Rep. Comp. Cent. Kyushu Univ.*, **13**, 39 (1980).
11) "Universal Crystallographic Computer Program System(UNICS)," ed by T. Sakurai, The Crystallographic Society of Japan, Tokyo (1964).
12) "International Tables for X-Ray Crystallography", Vol. III, Kynoch Press, Birmingham (1962).

Synthesis of 2,6,8-Trinitro-4*H*-cyclopenta[*def*]phenanthren-4-one as an Electron Acceptor

Masahiro MINABE,* Masaaki YOSHIDA, and Okitoshi KIMURA

Department of Industrial Chemistry, Faculty of Engineering, Utsunomiya University, Ishiicho, Utsunomiya 321

(Received May 23, 1984)

Synopsis. 2,6,8-Trinitro-4*H*-cyclopenta[*def*]phenanthren-4-one (TNC) was synthesized by the nitration of the parent ketone. TNC formed charge-transfer complexes with polycyclic aromatic hydrocarbons (PAH). The property of TNC as an electron acceptor was compared with that of 2,4,7-trinitro-9*H*-fluoren-9-one (TNF). TNC was found to be a better complexing agent than TNF.

Many mono- and disubstituted derivatives of 4*H*-cyclopenta[*def*]phenanthrene (**1**) have been synthesized by electrophilic substitution.[1] However, there are few reports relating to polysubstituted derivatives of **1**.[2] Since polynitro ketones of **1** could be expected to be good electron acceptors as 2,4,7-trinitro-9*H*-fluoren-9-one (TNF),[3] we investigated the preparation of a polynitro derivative of 4*H*-cyclopenta[*def*]phenanthren-4-one (**2**).[4]

The present paper deals with the synthesis of 2,6,8-trinitro-4*H*-cyclopenta[*def*]phenanthren-4-one (TNC) and with a comparison of the properties of TNC with those of TNF.

Nitration of **2** with nitric acid in sulfuric acid at 0—55 °C afforded TNC in 70% yield as light-yellow needles. The positions of nitro groups were confirmed by a stepwise synthesis: nitration of the 2-nitro ketone (**3**)[4] gave TNC that was also obtained by reaction of the isomeric 8-nitro ketone (**4**).[4] Moreover, TNC was obtained by the nitration of the 2,6-dinitro ketone (**5**) that was isolated by the oxidation of 2,6-dinitro-8,9-dihydro compound (**6**).[4]

Carbonyl absorption in the IR spectrum of TNC is observed at higher wavenumber than that of TNF, while absorptions of parent **2** and 9*H*-fluoren-9-one appear at the same position. The red shift of the maximum of TNC in the UV spectra from that of **1** is greater than the case between TNF[3a] and 9*H*-fluoren-9-one.

The cyclic voltammogram of TNC is very similar to that of TNF.[5-8] TNC and TNF both exhibit the first reversible one-electron reductions at −0.38 V and −0.48 V *vs.* SCE, respectively, the latter of which agrees well with the reported value.[5,6] These findings suggest that charge transfer in the case of TNC may occur easier than for the case of TNF.

The π-π charge-transfer complexes of TNC with some PAH were isolated as stable solids of 1:1 molar ratio (Table 1). The shift of the nitro absorptions to a long-wavelength region of the IR spectra of these complexes may be associated with the charge-transfer energy of each complex as the relation between TNF complexes and their transition energies.[9]

The ability of TNC to act as an electron acceptor was compared with that of TNF using the binding constant (B*) which was the reverse of the *B*-value proposed by Harvey and Halonen.[10] The *B*-value is defined as $(R_{f_1}-R_{f_{11}})\times 100/R_{f_1}$, where R_{f_1} is the R_f-value of any PAH on the usual thin-layer chromatograph, and $R_{f_{11}}$ is the R_f-value of the same PAH on a plate doped with an acceptor. The constant *B** (which is defined as $R_{f_{11}}'/R_{f_1}$) is determined by a comparison of the R_f-value ($R_{f_{11}}'$) of a given acceptor on a plate doped by a donor with the R_{f_1} of the same acceptor on the usual plate. A large *B**-value indicates a large equilibrium constant in the donor-acceptor interaction. Table 2 illustrates the comparison of the *B**-constant of TNC with that of TNF using the plate doped with 9*H*-fluorene (**7**) as an electron donor. This finding apparently suggests that TNC is superior to TNF as an electron acceptor.

The CT absorption spectrum of TNC with diethylamine (DEA) is illustrated along with that of TNF-

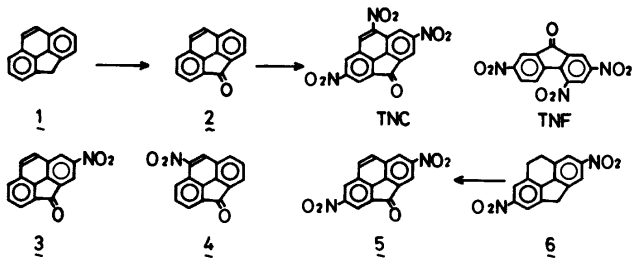

Table 2. Binding constants (*B**) of TNC and TNF

Compd	R_{f_1}	$R_{f_{11}}'$	*B**-value
TNC	0.37	0.46	1.24
TNF	0.42	0.47	1.12

Table 1. Properties of CT complexes of TNC with PAH

Donor	Yield %	Mp θ_m/°C (dec)	Color	IR (KBr) cm^{-1}	
				$\nu_{C=O}$	ν_{NO_2}
Phenanthrene	79	225—226	Yellow	1739	1537, 1530(s), 1335
7	88	211.0—211.5	Orange	1739	1537, 1335
1	89	240.0—240.5	Orange	1737	1544(s), 1530, 1337
Pyrene	87	291—292	Red	1740	1546, 1527, 1336

DEA in Fig. 1. A composit of the TNC-DEA system shows two maxima (450 and 560 nm). Also, the TNF-DEA curve has two maxima (520 and 630 nm) but the absorbance is less than that of the TNC complex. The formation constants (K) of these complexes were obtained at 25 °C by the Benesi-Hildebrand method:[11] K=1.88 lmol^{-1} for TNC at 560 nm and K=1.32 lmol^{-1} for TNF at 630 nm. The results suggest that TNC is a better complexing agent than TNF.

Experimental

All the melting points are uncorrected. The ^{1}H NMR, UV, and IR spectra were recorded on a Jeol JNM-C-60 HL, a Shimadzu UV-180, and a Jasco IRA-2 instrument, respectively. Satisfactory analytical data regarding the new compounds were obtained by elemental analyses (C, H, N, within ±0.3%) and a mass-spectra investigation.

Cyclic voltammograms were obtained with HMDE as the working electrode in aqueous dioxane (1:1 by volume) containing 50 mmol of $NaClO_4$. The solution was deoxygenated by bubbling for 30 min with dry nitrogen (99.999%).

Nitration of **2**. To a solution of **2** (4.1 g, 20 mmol) in H_2SO_4 (d=1.84 g cm^{-3}, 20 ml) was added a mixed acid of HNO_3 (d=1.49 g cm^{-3}, 5 ml) and concd H_2SO_4 (5 ml) below 0 °C for 15 min. The mixture was stirred at that temperature for a period of 1 h followed by stirring at 55 °C for an additional 15 min. A precipitate, formed after adding the mixture to ice water (300 ml), was filtered and washed with water. It was then dried overnight at 60 °C and chromatographed on a Kieselguhr column (45 mmϕ, 25 cm) with benzene. The yellow eluate was concentrated to a small volume to give 4.75 g (70%) of TNC, as light-yellow needles from ethyl acetate: mp 237—239 °C (dec). IR (KBr): $\nu_{C=O}$ 1740, ν_{NO_2} 1551, 1528, 1360, and 1342 cm^{-1}. NMR (DMSO-d_6): δ= 8.62—8.68 (2H, m) and 9.36—9.45 (3H, m). UV_{max} (EtOH): 207 (log ε 4.43), 266 (4.57), and 303 nm (4.23).

Oxime of TNC: mp 273.5—274.5 °C (dec). IR (KBr): ν_{OH} 3330, ν_{NO_2} 1544, 1536, and 1331 cm^{-1}. NMR (DMSO-d_6): δ=3.34 (1H, s, OH), 8.17 (1H, s), 8.42 (1H, s), 8.91 (1H, s), and 8.98—9.05 (2H, m). UV_{max} ($CHCl_3$): 250 (4.51), 313 (4.37), 380 (3.72), and 403 nm (3.61). B*-value: 1.15.

Hydrazone: mp 255.5—256.5 °C (dec). IR (KBr): ν_{NH_2} 3450, 3330, 3240, ν_{NO_2} 1552, 1524, and 1336 cm^{-1}. NMR (DMSO-d_6): δ=7.69—7.84 (1H, m), 8.43—8.57 (2H, m), 8.61—8.75 (2H, m), and 9.20 (2H, s, NH_2). UV_{max} ($CHCl_3$): 256 (4.41), 325 (4.34), and 416 nm (3.70). B*-value: 1.11.

Ethylene Dithioacetal: mp 310—311 °C (dec). IR (KBr): ν_{NO_2} 1543, 1529, and 1333 cm^{-1}. NMR (DMSO-d_6): δ=4.13 (4H, s), 8.95 (2H, s), 9.46 (1H, s), 9.59 (1H, s), and 9.68 (1H, s). UV_{max} ($CHCl_3$): 245 (4.27) and 292 nm (4.46).

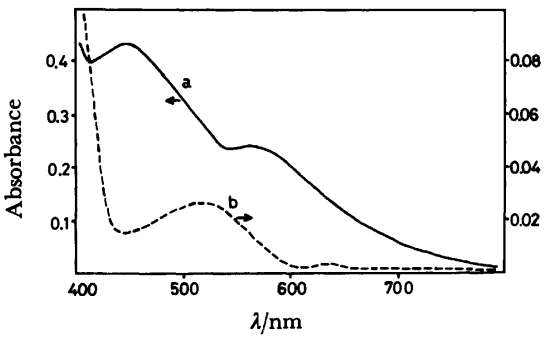

Fig. 1. CT absorption spectra of TNC and TNF with DEA in 1,2-dichloroethane at 25 °C.
(a): TNC(1.003×10^{-4} M, 1 M=1 mol dm^{-3})-DEA (4.71×10^{-1} M), (b): TNF(1.002×10^{-4} M)-DEA (4.71×10^{-1} M).

Nitration of **3**. Ketone **3** (75 mg, 0.3 mmol) was nitrated with HNO_3 (0.05 ml) in H_2SO_4 (10 ml) at 55 °C for 15 min to give 65 mg (64%) of TNC.

Nitration of **4**. A mixture of **4** (440 mg, 1.77 mmol), HNO_3 (0.5 ml), and H_2SO_4 (3.5 ml) was stirred at 70 °C for 1 h to afford TNC (175 mg, 28%).

Synthesis and Nitration of **5**. A nitro compound **6** (564 mg, 2 mmol) in benzene (120 ml) was refluxed with MnO_2 (10 g) for 12 h, followed by chromatography on a Kieselguhr column with benzene. The yellow eluate gave 361 mg (61%) of **5**: mp 351—352 °C (dec). IR (KBr): $\nu_{C=O}$ 1724, ν_{NO_2} 1524, and 1342 cm^{-1}. UV_{max} ($CHCl_3$): 262 (4.78), 312 (4.05), 322 (4.08), and 349 nm (3.74).

A mixture of **5** (60 mg, 0.2 mmol), HNO_3 (0.05 ml), and H_2SO_4 (10 ml) was maintained at 55 °C for 15 min to yield TNC (46 mg, 68%).

CT Complex of TNC with PAH. Typical Procedure. TNC (34 mg, 0.1 mmol) and **7** (17 mg, 0.1 mmol) were dissolved in a minimum quantity of HOAc with refluxing and allowed to cool to room temperature. A 45-mg (88%) of the complex was obtained as orange needles, mp 211.0—211.5 °C (dec).

Thin-layer Chromatography of Doped and Undoped Plates. TLC plates used in this experiment were purchased from E. Merck (TLC Silica gel 60; thickness 0.25 mm; 20×5 cm). The R_f-value was obtained using EtOAc/cyclohexane (1:2 by volume) as a developing solvent with the plate that was soaked in EtOAc/cyclohexane (1:2) for 5 min followed by drying at 60 °C for 20 min.

The R_f-value was determined on a plate that was soaked in a solution of EtOAc/cyclohexane (1:2) containing **7** (2%) for 5 min and dried at 60 °C for 20 min, using a developing solvent of EtOAc/cyclohexane (1:2) containing 2% of **7**. The value given in Table 2 is the average value for 10 runs.

The authors wish to thank Professor A. Yamada of the Technological University of Nagaoka for obtaining the cyclic voltammograms. Also, they thank Professor T. Toda for reading the manuscript.

References

1) For example: M. Yoshida, M. Kobayashi, M. Minabe, and K. Suzuki, *Bull. Chem. Soc. Jpn.*, **54**, 1159 (1981).
2) M. Yoshida, M. Minabe, W. Ookawa, and K. Suzuki, *Bull. Chem. Soc. Jpn.*, **56**, 1259 (1983).
3) a) M. Orchin and E. O. Woolfolk, *J. Am. Chem. Soc.*, **68**, 1727 (1946); b) M. Orchin, L. Reggel, and E. O. Woolfolk, *ibid.*, **69**, 1225 (1947).
4) M. Yoshida, S. Nagayama, M. Minabe, and K. Suzuki, *J. Org. Chem.*, **44**, 1915 (1979).
5) J. E. Kuder, J. M. Pochan, S. R. Turner, and D. F. Hinman, *J. Electrochem. Soc.*, **125**, 1750 (1978).
6) B. S. Ong, B. Keoshkerian, and T. I. Martin, *Chem. Ind. (London)*, **1984**, 110.
7) B. S. Ong, *J. Chem. Soc., Chem. Commun.*, **1984**, 266.
8) L. Ramaley and S. Gaul, *Can. J. Chem.*, **56**, 2381 (1978).
9) A. R. Lepley, *J. Am. Chem. Soc.*, **84**, 3577 (1962).
10) R. G. Harvey and M. Halonen, *J. Chromatogr.*, **25**, 294 (1966).
11) H. A. Benesi and J. H. Hildebrand, *J. Am. Chem. Soc.*, **71**, 2703 (1949).

^{119}Sn NMR Spectroscopic Determination of Diastereomeric Ratio of Some Optically Active Organotin Compounds

Junzo OTERA* and Toru YANO
Okayama University of Science, Ridai-cho, Okayama 700
(Received June 11, 1984)

Synopsis. Diastereomeric ratio of optically active organotin compounds, $R^*_2SnX_2$ and $R^1R^2R^3SnR^*$, was successfully determined by means of ^{119}Sn NMR spectra.

In the study of optically active organotin compounds, diastereomeric organotins play a versatile role[1] in the asymmetric induction at tin, the optical resolution, and the determination of optical purity. Accordingly, it is of great importance to determine the diastereomeric ratio conveniently. ^{1}H and ^{13}C NMR spectra may be applicable in some cases where spectra are simple and signals due to diastereomers are fully separated though these requirements being not always fulfilled. Development of an alternative method, therefore, is highly desirable. Pereyre *et al.* have reported that diastereomers of (*s*-Bu)$_4$Sn[2a] and $R_3SnCH(CH_3)CH_2CO_2(-)Men$[2b] (Men=menthyl) are distinguishable by means of ^{119}Sn NMR spectra. In the course of our studies on optically active allyltin compounds,[3] $R^*_2SnX_2$ and $R^1R^2R^3SnR^*$ proved to be versatile starting materials. Thus an effective method for quantitative determination of these diastereomers has been highly required for evaluating the degree of stereospecificity in the reaction of optically active allyltin compounds with aldehydes. Herein we wish to describe the usefulness of ^{119}Sn NMR spectra for this purpose.

On account of facile optical resolution of 2-phenylbutyric acid with various degree of optical purity,[4] 2-phenylbutyltin derivatives are suitable for attesting applicability of the ^{119}Sn NMR spectroscopy to quantitative diastereomeric determination. As shown in Fig. 1, optically active PB_2SnBr_2 (**1a**) (PB=2-phenylbutyl) that was prepared employing optically pure (*R*)-2-phenylbutylmagnesium chloride exhibits a singlet at δ 58.3 while racemic **1a** gives rise to two signals at 53.3 and 58.3. Thus it is reasonably concluded that the signal at lower field can be attributed to the (*R,R*)- and (*S,S*)-isomers and the other at higher field to the (*R,S*)- and (*S,R*)-isomers. The results of other compounds are summarized in Table 1. Since each signal of PB_2SnX_2 is unambiguously assigned analogously, one can deduce the diastereomeric ratio from the relative integral ratio. The results obtained by employing a PB group with various degree of optical purity are depicted in Fig. 2. Apparently the observed values are in good agreement with calculated ones based on ee of the used PB group.

Of particular interest is that this method can be applied to estimation of the degree of asymmetric induction at tin in the following type of reaction that is the most common method for introduction of a chirality at tin. Two optically active groups, (*R*)-PB and (*S*)-2-methylbutyl (MB) groups, were employed for this purpose. As shown in Table 1, ^{119}Sn NMR spectra of these compounds indeed gave rise to two signals, indicating diastereomeric selectivity to be 54 and 53%, respectively. It is also to be noted that the diastereomeric ratio itself is not affected by optical purity of R.

$$PhMeEtSnBr + RMgX \longrightarrow PhMeEtSnR$$
2a R=PB
b =MB

Experimental

^{119}Sn NMR spectra in proton gated decoupling mode were

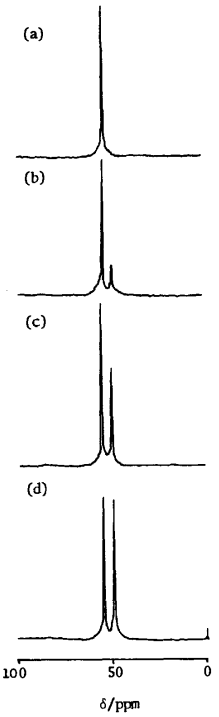

Fig. 1. ^{119}Sn NMR spectra of **1a** with a PB group of different optical purity. (a): Optically pure, (b): 78% ee, (c): 24% ee, (d): Racemic.

TABLE 1. ^{119}Sn NMR SPECTRA OF DIASTEREOMERIC ORGANOTIN COMPOUNDS

Compound		δ/ppm	
		Racemic	Optically active
1a	PB_2SnBr_2	53.5, 58.3[a]	58.3
1b	PB_2SnCl_2	90.5, 92.0[a]	92.0
1c	$PB_2Sn(CH_2CH=CH_2)_2$	−38.7, −39.1[a]	−39.1
2a	PhMeEtSnPB	−36.0, −36.9 (46 : 54)[b]	−36.0, −36.9 (46 : 54)[b]
2b	PhMeEtSnMB	−35.8, −36.0 (47 : 53)[b]	−35.8, −36.0 (47 : 53)[b]

a) Relative integral ratio is *ca.* 1 : 1. b) Relative integral ratio.

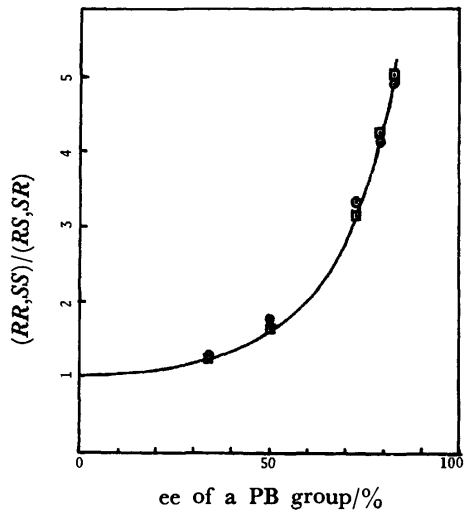

Fig. 2. Relation between ee of a PB group and (*RR*, *SS*)/(*RS*,*SR*) ratio. —— Calcualted; ⊙: Observed for **1a**, □: Observed for **1c**.

measured using a JEOL FX-100 spectrometer operating at 37.08 MHz at 22 °C. Field-frequency control was made with a deuterium-labelled solvent ($CDCl_3$) lock. The chemical shifts were determined relative to internal Me_4Sn, positive signs indicating low-field shifts from the reference, and were found to be accurate to ±0.1 ppm.

Optical resolution of 2-phenylbutyric acid was performed as the cinchonidine salt[4] into various degree of ee. Optically active 2-phenylbutyric acid thus obtained was converted into the corresponding chloride.[5] Optically active 2-methylbutyl bromide (ee>99%) was obtained by bromination of commercially available optically active 2-methyl-1-butanol (Aldrich Chemical Co.) with PBr_3.

Preparation of ***1a*** *and* ***1b***. To a dichloromethane solution (10 cm^3) of **1c**[3] (467 mg, 1 mmol) was added dropwise bromine (320 mg, 2 mmol) at 0 °C. The reaction mixture was evaporated to leave an oil that was chromatographed on silica gel (500:1 hexane-ether) to give **1a** (491 mg, 90%); ^1H NMR (CCl_4): δ=0.70 (6H, t, *J*=7.0 Hz), 0.96—2.21 (8H, m), 2.21—2.88 (2H, m), and 6.58—7.22 (10H, m). Found: C, 44.42; H, 4.54%. Calcd for $C_{20}H_{26}Br_2Sn$; C, 44.08; H, 4.81%. $[\alpha]_D^{22}$ for optically active **1a** −38.9 (*c* 2.14, benzene).

The chloride **1b** was prepared analogously employing sulfuryl chloride in place of bromine in 65% yield; ^1H NMR (CCl_4): δ=0.70 (6H, t, *J*=7.2 Hz), 0.90—2.17 (8H, m), 2.17—2.97 (2H, m), and 6.62—7.24 (10H, m). Found: C, 52.88, H, 6.03%. Calcd for $C_{20}H_{26}Cl_2Sn$; C, 52.68; H, 5.75%. $[\alpha]_D^{22}$ for optically active **1b** −51.9° (*c* 1.02, benzene).

Preparation of ***2a*** *and* ***2b***. To a THF solution (10 cm^3) of 2-phenylbutylmagnesium chloride prepared from 2-phenylbutyl chloride (471 mg, 2.79 mmol) and magnesium turnings (134 mg, 5.58 mmol), was added dropwise PhMeEtSnBr[6] (300 mg, 0.93 mmol) in THF (2 cm^3) at 0 °C. After being stirred for 2 h at room temperature, the reaction mixture was extracted with hexane-saturated ammonium chloride solution. The organic layer was washed with water and dried ($MgSO_4$). Evaporation and column chromatography (silica gel, hexane) of the resulting oil yielded **2a** (218 mg, 59%); ^1H NMR (CCl_4): δ=0.16, 0.18 (3H, s, diastereomeric), 0.66—2.10 (12H, m), 2.81 (1H, m), and 6.86—7.50 (10H, m). Found: C, 61.21; H, 7.60%. Calcd for $C_{19}H_{26}Sn$; C, 61.17; H, 7.22%.

The preparation of **2b** was carried out analogously employing 2-methylbutyl bromide in place of 2-phenylbutyl chloride in 63% yield; ^1H NMR (CCl_4); δ=0.48 (3H, s), 0.75—2.20 (16H, m), and 7.20—7.59 (5H, m). Found: C, 53.72; H, 8.30%. Calcd for $C_{14}H_{24}Sn$; C, 54.06; H, 7.78%.

References

1) M. Gielen, S. Simon, Y. Tondeur, and M. Van de Steen, *Isr. J. Chem.*, **15**, 74 (1976/77); U. Folli, D. Iarossi, and F. Taddei, *J. Chem. Soc. Perkin Trans. 2*, **1973**, 638; M. Lequan and R. M. Lequan, *J. Organomet. Chem.*, **226**, 35 (1982); A. Rahm and M. Pereyre, *ibid.*, **88**, 79 (1975).

2) a) A. Rahm, M. Pereyre, M. Petrand, and B. Barbe, *J. Organomet. Chem.*, **139**, 49 (1977); b) A. Rahm, M. Degueil-Castaing, and M. Pereyre, *Tetrahedron Lett.*, **21**, 4649 (1980).

3) J. Otera, Y. Kawasaki, H. Mizuno, and Y. Shimizu, *Chem. Lett.*, **1983**, 1529.

4) P. A. Levene, L. A. Mikeska, and K. Passoth, *J. Biol. Chem.*, **88**, 27 (1930).

5) J. S. Birtwistle, K. Lee, J. D. Morrison, W. A. Sanderson, and H. S. Mosher, *J. Org. Chem.*, **29**, 37 (1964).

6) PhMeEtSnBr was prepared by an analogous method for PhMe(i-Pr)SnBr. See, M. Gielen, J. Nasielski, and J. Topart, *Recl. Trav. Chim.Pays-Bas*, **87**, 1051 (1968); *Chen. Abstr*, **70**, 11779 (1980).

New Synthesis of *trans*-γ-Irone

Osamu TAKAZAWA,* Kunio KOGAMI, and Kazuo HAYASHI
Kawasaki Research Laboratories, T. Hasegawa Co., Ltd., 335 Kariyado, Nakahara-ku, Kawasaki 211
(Received June 20, 1984)

Synopsis. *trans*-γ-Irone was successfully synthesized starting from 3,4-dimethyl-2-cyclohexenone by seven-step reactions including $TiCl_4$-promoted reaction of enol silyl ether and cross-aldol reaction of vinyloxyborane.

Irones have been isolated from Iris oil as very important fragrant constituents.[1] Recently, Ohloff et al. have further identified *trans*-γ-irone (**1**) in Iris oil.[2] Concerning the synthesis of **1**, three methods have been reported.[3] Previously, we reported an efficient method for preparation of γ-ionone.[4] In this paper, we will describe an alternative method for synthesis of **1** starting from an easily accessible 3,4-dimethyl-2-cyclohexenone (**2**) in the similar manner as above. Our synthetic route is outlined in the following scheme.

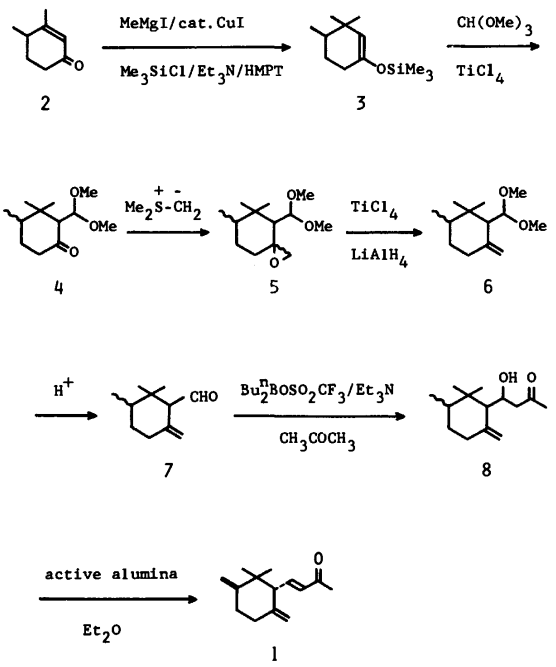

The reaction of 3,4-dimethyl-2-cyclohexenone (**2**) with methylmagnesium iodide in the presence of a catalytic amount of copper(I) iodide, followed by quenching with trimethylchlorosilane, triethylamine, and hexamethylphosphoric triamide, gave 3,3,4-trimethyl-1-trimethylsiloxy-1-cyclohexene (**3**) in a 70% yield.[5] 2-Dimethoxymethyl-3,3,4-trimethylcyclohexanone (**4**) was obtained in a 72% yield by the reaction of **3** with trimethyl orthoformate in the presence of $TiCl_4$.[6] The conversion of **4** to 4-dimethoxymethyl-5,5,6-trimethyl-1-oxaspiro[2.5]octane (**5**) was carried out in almost the same manner as reported,[7] that is, the reaction of **4** with dimethylsulfonium methylide gave **5** in a 61% yield. The deoxygenation of **5** with low valent titanium compound, prepared from $TiCl_4$ and $LiAlH_4$, afforded 6-methylene-2,2,3-trimethylcyclohexanecarbaldehyde dimethyl acetal (**6**) in an 83% yield, which was further converted to 6-methylene-2,2,3-trimethylcyclohexanecarbaldehyde (**7**)[3a] in a 79% yield by hydrolysis with 2 M HCl (1 M= 1 mol dm^{-3}).

Dibutyl(isopropenyloxy)borane, formed from acetone and dibutylboryl trifluoromethanesulfonate,[8] reacted with **7** to give a mixture of two stereoisomers (**8a** and **8b**) of 4-(6-methylene-2,2,3-trimethylcyclohexyl)-4-hydroxy-2-butanone (**8**) in a 79% yield, which was separated by silica-gel column chromatography. The aldols, **8a** and **8b**, were converted to *trans*-γ-irone (**1**) without accompanying *cis*-isomer on treatment with active alumina in 57% and 36% yields, respectively.

Experimental

Spectra. All bps are uncorrected. ^1H NMR spectra were recorded on a Hitachi R-24A spectrometer. Chemical shifts are reported on the δ scale relative to Me_4Si as an internal standard. IR spectra were taken using a JASCO IRA-2 spectrometer.

3,3,4-Trimethyl-1-trimethylsiloxy-1-cyclohexene (3). To a mixture of 2.8 M methylmagnesium iodide (50 ml, 140 mmol) in ether and copper(I) iodide (400 mg) was added dropwise a solution of 3,4-dimethyl-2-cyclohexenone (**2**) (12.40 g, 100 mmol) in dry ether (40 ml) at 0 °C, and the mixture was stirred for 1 h at 0 °C. Trimethylchlorosilane (30 ml), triethylamine (40 ml), and hexamethylphosphoric triamide (20 ml) were successively added at 0 °C and the mixture was stirred for 24 h at room temperature. The mixture was processed and the product was distilled to give **3** (14.80 g, 70%). Bp 90—93 °C/16 mmHg (1 mmHg=133.322 Pa); IR (neat) 1665 cm^{-1}; NMR (CCl_4) δ=0.15 (s, 9H), 0.82 (s, 3H), 0.88 (d, *J*=6.0 Hz, 3H), 0.98 (s, 3H), 1.2—2.1 (m, 5H), and 4.53 (m, 1H). Found: C, 67.83; H, 11.29%. Calcd for $C_{12}H_{24}SiO$: C, 67.86, H, 11.39%.

2-Dimethoxymethyl-3,3,4-trimethylcyclohexanone (4). To a cold solution (−78 °C) of trimethyl orthoformate (6.89 g, 65 mmol) in dry dichloromethane (100 ml) was added $TiCl_4$ (12.35 g, 65 mmol) under argon atmosphere. A solution of **3** (10.60 g, 50 mmol) in dry dichloromethane (10 ml) was added and the reaction mixture was stirred for 2 h at −78 °C. The mixture was quenched with methanol (20 ml) and poured into a 15% solution of K_2CO_3. After evaporation of the solvent, the residue was distilled to give **4** (7.70 g, 72%). Bp 88—90 °C/1.5 mmHg; IR (neat) 1715, 1125, and 1060 cm^{-1}; NMR (CCl_4) δ=0.75 (s, 3H), 0.90 (d, *J*=6.5 Hz, 3H), 0.97 (s, 3H), 1.2—2.5 (m, 5H), 2.28 (d, *J*=7.0 Hz, 1H), 3.20 (s, 3H), 3.27 (s, 3H), and 4.67 (d, *J*=7.0 Hz, 1H). Found: C, 67.14; H, 10.29%. Calcd for $C_{12}H_{22}O_3$: C, 67.26; H, 10.35%.

4-Dimethoxymethyl-5,5,6-trimethyl-1-oxaspiro[2.5]octane (5). A mixture of NaH (10 mmol) and dimethyl sulfoxide (5 ml) was stirred for 1 h at 65—70 °C and cooled to room temperature, and then tetrahydrofuran (30 ml) was added. A solution of trimethylsulfonium iodide (2.04 g, 10 mmol) in dimethyl sulfoxide (5 ml) was added dropwise at −20—−15

°C and stirred for 5 min. A solution of **4** (428 mg, 2 mmol) in tetrahydrofuran (5 ml) was added dropwise at the same temperature as above and the mixture was stirred overnight at 0 °C. The mixture was worked up and the product was subjected to silica-gel column chromatography to afford **5** (280 mg, 61%). IR (neat) 3030, 1130, 1075, and 1050 cm^{-1}; NMR (CCl_4) δ=0.80 (d, J=6.5 Hz, 3H), 0.86 (s, 3H), 1.05 (s, 3H), 1.3—2.2 (m, 6H), 2.46 (s, 2H), 3.30 (s, 3H), 3.37 (s, 3H), and 4.47 (d, J=3.0 Hz, 1H). Found: C, 68.23; H, 10.41%. Calcd for $C_{13}H_{24}O_3$: C, 68.38, H, 10.59%.

6-Methylene-2,2,3-trimethylcyclohexanecarbaldehyde Dimethyl Acetal (6). Tetrahydrofuran (16 ml) was added dropwise to $TiCl_4$ (1.29 g, 6.8 mmol) at −78 °C under argon atmosphere and the resulting complex was warmed to room temperature. $LiAlH_4$ (258 mg, 6.8 mmol) was added to the complex, and the mixture was stirred for 1 h, and then triethylamine (5.55 g, 55 mmol) was added. To this was added dropwise a solution of **5** (1.41 g, 6.2 mmol) in tetrahydrofuran (10 ml) on a water bath and the mixture was stirred for 1 h at room temperature. The mixture was worked up and the product was distilled to give **6** (1.09 g, 83%). IR (neat) 1120, 1060, and 890 cm^{-1}; NMR (CCl_4) δ=0.73 (s, 3H), 0.87 (d, J=6.0 Hz, 3H), 0.92 (s, 3H), 1.1—1.8 (m, 3H), 1.9—2.4 (m, 3H), 3.18 (s, 3H), 3.24 (s, 3H), 4.48 (d, J=6.5 Hz, 1H), 4.52 (m, 1H), and 4.70 (m, 1H).

6-Methylene-2,2,3-trimethylcyclohexanecarbaldehyde (7). To a solution of **6** (1.09 g, 5.1 mmol) in ether (30 ml) was added 2 M HCl (30 ml) and the mixture was stirred overnight at room temperature. After separation of the organic layer, it was washed with a saturated solution of $NaHCO_3$ and concentrated. The residue was distilled to give **7** (675 mg, 79%). Bp (bath temperature) 100—110 °C/10 mmHg; IR (neat) 1720, 1640, and 895 cm^{-1}; NMR (CCl_4) δ=0.78 (s, 3H), 0.84 (d, J=6.5 Hz, 3H), 1.05 (s, 3H), 1.2—2.1 (m, 3H), 2.25 (m, 2H), 2.71 (d, J=3.5 Hz, 1H), 4.74 (s, 1H), 4.90 (s, 1H), and 9.73 (d, J=3.5 Hz, 1H). Found: C, 79.36, H, 10.79%. Calcd for $C_{11}H_{18}O$: C, 79.47, H, 10.91%.

4-(6-Methylene-2,2,3-trimethylcyclohexyl)-4-hydroxy-2-butanone (8). To dibutylboryl trifluoromethanesulfonate (303 mg, 1.1 mmol) was added a solution of triethylamine (111 mg, 1.1 mmol) in ether (1.5 ml) at −78 °C under argon atmosphere and the mixture was warmed to room temperature. A solution of acetone (64 mg, 1.1 mmol) in ether (1 ml) was added at −78 °C and the mixture was stirred for 20 min. Then a solution of **7** (158 mg, 0.95 mmol) in ether (2 ml) was added dropwise and the mixture was stirred for 2.5 h at −78 °C. To the reaction mixture was added 1 M buffer solution (pH 7.0) of phosphoric acid (3 ml), methanol (10 ml), and a 30% solution of H_2O_2 (2 ml), successively, and the mixture was stirred for 20 min at room temperature. After addition of water (10 ml), methanol was removed under reduced pressure. The residue was extracted with dichloromethane and the solution was concentrated. Purification by silica-gel column chromatography afforded two stereoisomers (**8a** and **8b**) of **8** (169 mg, 79%). **8a** (117 mg, 55%): IR (neat) 3470, 3070, 1710, 1640, and 890 cm^{-1}: NMR (CCl_4) δ=0.75 (s, 3H), 0.79 (d, J=6.5 Hz, 3H), 1.08 (s, 3H), 1.2—2.3 (m, 6H), 2.15 (s, 3H), 2.52 (m, 2H), 3.22 (s, 1H), 4.50 (m, 2H), and 4.90 (m, 1H). Found: C, 74.86, H, 10.70%. Calcd for $C_{14}H_{24}O_2$: C, 74.95, H, 10.78%; **8b** (52 mg, 24%): IR (neat) 3500, 3070, 1705, 1635, and 885 cm^{-1}; NMR (CCl_4) δ=0.75 (s, 3H), 0.85 (d, J=6.5 Hz, 3H), 1.10 (s, 3H), 1.2—2.3 (m, 6H), 2.10 (s, 3H), 2.42 (d, J=6.0 Hz, 2H), 3.05 (s, 1H), 4.25 (m, 1H), 4.62 (m, 1H), and 4.75 (m, 1H). Found: C, 74.81, H, 10.84%. Calcd for $C_{14}H_{24}O_2$: C, 74.95, H, 10.78%.

trans-*γ-Irone (1).* To a solution of **8a** (55 mg, 0.25 mmol) in ether (5 ml) was added active alumina (0.5 g) and the mixture was stirred overnight at room temperature. Then the mixture was filtered and concentrated. The residue was subjected to silica-gel column chromatography to afford **1** (29 mg, 57%). IR (neat) 1675, 1620, and 890 cm^{-1}; NMR (CCl_4) δ=0.80 (s, 3H), 0.85 (d, J=6.0 Hz, 3H), 0.90 (s, 3H), 1.1—2.4 (m, 5H), 2.15 (s, 3H), 2.60 (d, J=9.0 Hz, 1H), 4.67 (s, 1H), 4.72 (s, 1H), 6.00 (d, J=16.0z4Hz, 1H), and 6.98 (dd, J=16.0 and 9.0 Hz, 1H). Spectral data of **1** were consistent with those of the authentic sample prepared by the method of Yoshikoshi *et al.*[3b]

In the same manner, **8b** was treated with active alumina to give **1** (36%).

The authors wish to express their thanks to Professor Teruaki Mukaiyama and Associate Professor Kazuhiko Saigo, the University of Tokyo for their helpful discussions.

References

1) a) F. Tiemann and P. Krüger, *Ber.*, **26**, 2675 (1893); b) V. Rautenstrauch and G. Ohloff, *Helv. Chim. Acta*, **54**, 1776 (1971); c) W. Krick, F.-J. Marner, and L. Jaenicke, *ibid.*, **67**, 318 (1984).

2) V. Rautenstrauch, B. Willhalm, W. Thommen, and G. Ohloff, *Helv. Chim. Acta*, **67**, 325 (1984).

3) a) J. Garnero and D. Joulain, *Bull. Soc. Chim. Fr.*, **1979**, 15; b) M. Miyashita, N. Makino, M. Singh, and A. Yoshikoshi, *J. Chem. Soc., Perkin Trans. 1*, **1982**, 1303; c) T. Kitahara, K. Tanida, and K. Mori, *Agric. Biol. Chem.*, **47**, 581 (1983).

4) T. Mukaiyama, K. Saigo, and O. Takazawa, *Chem. Lett.*, **1976**, 1033.

5) G. Stork and P. F. Hudrlik, *J. Am. Chem. Soc.*, **90**, 4462 (1968).

6) T. Mukaiyma and M. Hayashi, *Chem. Lett.*, **1974**, 15.

7) E. J. Corey and M. Chaykovsky, *J. Am. Chem. Soc.*, **87**, 1353 (1965).

8) T. Mukaiyama and T. Inoue, *Chem. Lett.*, **1976**, 559.

The Preparation of a Highly Active Raney Nickel Catalyst with Formation of a Recoverable Bayerite

Shigeo NISHIMURA,* Satoshi IKEDA, Makoto KINOSHITA, and Masaaki KAWASHIMA
Department of Applied Chemistry for Resources, Tokyo University of Agriculture and Technology, Koganei, Tokyo 184

(Received June 23, 1984)

Synopsis. In the presence of a properly prepared bayerite and a small amount of sodium hydroxide, Raney nickel–aluminium alloy is developed with water to give a highly active catalyst with formation of a recoverable bayerite. In hydrogenation of typical organic compounds the catalyst is even more active than the T-4 Raney nickel.

In 1959 one of the authors (S. N.) described a method for the preparation of a highly active Raney nickel catalyst in which the reaction of Raney alloy with water was initiated by partly leaching the alloy with a small amount of sodium hydroxide at 50 °C.[1] After an induction period of about 1 h, the alloy began to react with water violently and was developed extensively to give a product which had been covered with a large quantity of bayerite, a modification of crystalline aluminium trihydroxides. To obtain a highly active catalyst a concentrated sodium hydroxide solution was then added to remove the bayerite from the catalyst and complete the development. The Raney nickel thus prepared (denoted as T-4 when prepared from 40% nickel alloy) was more active than those prepared by usual procedures.[1] It seems that the extensive reaction of Raney alloy with water is promoted by the sodium hydroxide which has been regenerated by the hydrolysis of initially formed sodium aluminate, as suggested by Dirksen and Linden.[2] The violent reaction of Raney alloy with water that occurs after the induction period is probably caused by the transformation of the sodium aluminate into crystalline bayerite which in turn promotes the subsequent crystallization of amorphous aluminium hydroxide† and hence the hydrolysis of sodium aluminate, producing continuously sodium hydroxide for further development of the alloy (see Eq. 1). In fact, Taira and Kuroda

$$\mathrm{NaAlO_2} + 2\mathrm{H_2O} \rightleftharpoons \text{amorphous } \mathrm{Al(OH)_3} + \mathrm{NaOH} \xrightarrow{\text{bayerite}} \text{crystalline } \mathrm{Al(OH)_3} \text{ (bayerite)} \quad (1)$$

have shown that the addition of bayerite promotes the reaction of Raney alloy with water and prepared an active catalyst which was supported on bayerite and claimed to be resistant to deactivation, by developing the alloy with addition of bayerite.[3,4]

We have intended to improve the T-4 procedure with use of bayerite by which it may be possible to reduce the amount of sodium hydroxide required. In the course of this study it has been recognized that the action of bayerite to promote the reaction in Eq. 1 greatly depends on its preparation as well as reaction conditions, and, by using a properly prepared bayerite and suitable reaction conditions, the catalyst that is not combined with the bayerite formed can be prepared. Under these conditions the alloy can be developed extensively at a low temperature with use of only a small amount of sodium hydroxide to give a highly active catalyst, and at the same time the bayerite initially added as well as newly formed can easily be separated from the resulting catalyst merely by decantations. The bayerite thus recovered has been found to become reusable after treatment with a dilute hydrochloric acid. Whether the bayerite formed is deposited on the catalyst or not appears to depend on the nature of bayerite initially added as well as on the mode of the addition of sodium hydroxide. As described in the experimental part, the bayerite that promotes efficiently the reaction in Eq. 1 and gives the catalyst not combined with bayerite is prepared by the reaction of CO_2 gas with a rather concentrated solution of sodium aluminate at 40 °C. Such conditions suggest that the contamination of amorphous aluminium hydroxide or gelatinous boehmite should be avoided.[5] Further, to prepare a catalyst free from bayerite it is advisable to add the bayerite prior to the addition of sodium hydroxide. If we add the bayerite to the alloy after partly leached with sodium hydroxide, a catalyst which is firmly combined with bayerite tends to result, just as in the T-4 preparation where it is necessary to use a concentrated sodium hydroxide solution to remove the bayerite from the catalyst.[1]

As an example of the preparation, 0.5 g of Raney alloy powder (40% Ni) and 1 g of the bayerite prepared by the procedure given in Experimental are stirred in 10 ml of water at 40 °C. To this 0.03 ml of 20% sodium hydroxide is added and the mixture stirred for 30 min in which a violent reaction of the alloy with water almost subsides. At this stage the alloy is already developed to the extent of *ca.* 70% and the catalyst is sufficiently active for most hydrogenations (see the example in Table 1). To obtain the catalyst of the highest activity 0.3 ml of 20% sodium hydroxide is then added and the mixture stirred for 1 h at 40 °C. With one preparation the degree of oxidation of the aluminium in the alloy was estimated to be 81% at the final stage.[6] The catalyst thus prepared (denoted as N-4) has been more active than the T-4 catalyst in typical hydrogenations (Table 1). With benzonitrile, however, treatment with a larger amount of sodium hydroxide was

† The transformation of sodium aluminate to bayerite has been shown to occur according to the following scheme: sodium aluminate solution →amorphous hydroxide→gelatinous boehmite→bayerite [B. C. Lippens, "Structure and Texture of Aluminas," Uitgeverij Waltman, Delft (1961), p. 15].

Table 1. Hydrogenation of typical organic compounds with N-4 and T-4 Raney nickel catalysts[a]

Compound	Amount / mmol	Catalyst	Rate of H_2 uptake[b] / ml at STP min^{-1}	Time for hydrogenation / min
Cyclohexene	15	N-4	20.0	20
		T-4	18.0	26
Cyclohexanone	15	N-4	12.4	36
		N-4[c]	11.1	41
		N-4[d]	12.1	38
		T-4	9.4	45
Nitrobenzene	10	N-4	14.1	62
		T-4	11.1	90
Benzonitrile	5	N-4[e]	4.4	130
		T-4	4.4	130

a) The catalyst was prepared from 0.5 g of Raney alloy (40% Ni) each time before use. The compound was hydrogenated in 10 ml of methanol at 25 °C and atmospheric pressure. b) Average rate from 0 to 50% hydrogenation. c) The catalyst was prepared with use of 0.03 ml of 20% sodium hydroxide. d) The catalyst was prepared with the bayerite recovered two times. e) The catalyst was prepared with use of 0.5 ml of 20% sodium hydroxide.

favorable for the activity and both N-4 and T-4 catalysts showed the same activity.

The bayerite becomes grey in its color during the preparation. By treatment of the bayerite with a dilute hydrochloric acid, the bayerite turns almost white and becomes reusable for the N-4 preparation to give the catalyst of the same activity (see Table 1). Since the hydrochloric acid after the treatment was found to contain only a trace amount of nickel, the grey color of the bayerite after the preparation is presumed mostly due to the presence of fine particles of aluminium.

The procedure for the preparation of Raney nickel catalyst described here is advantageous not only for the use of only a small amount of sodium hydroxide but also for the easiness in controlling the highly exothermic reaction of aluminium oxidation which is often too violent to control in the reaction with a concentrated sodium hydroxide solution or in a sudden reaction with water after an induction period in the T-4 procedure. Further, it is also advantageous in that the degree of the development of the alloy can readily be controlled to a desired extent by the amount of sodium hydroxide employed and/or the reaction time. The present method is also recommended for obtaining a catalyst of reproducible activity.

Experimental

Preparation of the Bayerite Suitable to the Development of Raney Alloy. Twenty grams of aluminium grains are dissolved into a sodium hydroxide solution prepared from 44 g of sodium hydroxide and 100 ml of water. The solution is diluted to 200 ml and CO_2 gas is bubbled into the solution at 40 °C until small amounts of white precipitates are formed. The precipitates are filtered off and more CO_2 gas is bubbled into the filtrate. Then the solution is gradually cooled to room temperature under good stirring and left overnight with continued stirring. The precipitates thus formed (20—24 g) are collected, washed with warm water, and dried *in vacuo* over silica gel.[7]

Preparation of N-4 Raney Nickel and Recovery of Bayerite. In a 10 ml conical flask are placed 0.5 g of Raney alloy powder (40% Ni) and 1 g of the bayerite prepared by the procedure described above. To this 10 ml of distilled water is added and stirred well at 40 °C. Then 0.03 ml of 20% sodium hydroxide solution is added and the mixture stirred for 30 min at 40 °C in which a violent reaction almost subsides. Further 0.3 ml of 20% sodium hydroxide is added and the mixture stirred for 1 h at 40 °C. The upper layer is decanted with care not to let the catalyst flow away. The catalyst is washed three times with each 10 ml of distilled water and then three times with the same volume of methanol. The bayerite suspensions are combined and acidified with a dilute hydrochloric acid, and then warmed to 50—60 °C, when the grey color of the bayerite turns almost white. The bayerite is collected, washed well which water, and then dried *in vacuo* over silica gel. The bayerite thus recovered amounts to 1.4—1.6 g and can be reused repeatedly for the catalyst preparation. A specimen of the catalyst contained 0.192 g of nickel, 0.050 g of aluminium, and 0.036 g of acid insoluble materials.

Hydrogenation. All hydrogenations were performed in a small glass apparatus driven vibrationally at 25 °C and atmospheric pressure. After the catalyst had been shaken with hydrogen in methanol for 5 min, the compound to be hydrogenated was added with a syringe through a silicone rubber septum.

References

1) S. Nishimura, *Bull. Chem. Soc. Jpn.*, **32**, 61 (1959).
2) H. A. Dirksen and H. R. Linden, *Res. Bull. Inst. Gas Technol. Chicago*, **31**, 32 (1963).
3) S. Taira and A. Kuroda, Japan Patent 15059 (1968).
4) S. Taira and A. Kuroda, Japan Patent 9459 (1969).
5) G. Yamaguchi, K. Sakamoto, and K. Shirasuka, *Kogyo Kagaku Zasshi*, **61**, 307 (1968).
6) The degree of aluminium oxidation was determined from the amounts of evolved hydrogen (293 ml at STP) and adsorbed hydrogen (13.4 ml at STP, estimated from the hydrogenation of cyclohexanone in *t*-BuOH under an atmosphere of argon), on the basis that the alloy contained 39% of nickel.
7) The bayerite thus prepared usually contains a small amount of gibbsite as observed by an X-ray diffraction analysis. The bayerite recovered from the catalyst preparation has been found less contaminated with gibbsite.

Ring Transformation of 1,4 (or 1,6)-Disubstituted 3,5-Dinitro-2-pyridones with Sodio β-Keto Esters[1)]

Masahiro ARIGA,* Yasuo TOHDA, and Eizo MATSUMURA

Department of Chemistry, Osaka Kyoiku University, Minamikawahori-cho, Tennoji-ku, Osaka 543

(Received July 2, 1984)

Synopsis. The ring transformation of 1,6-dimethyl-, 1,4-dimethyl- and 4-methoxy-1-methyl-3,5-dinitro-2-pyridones with sodio β-keto esters to nitrosalicylic esters was investigated concerning the electronic effects of 4 and 6-substituents. The results were explained by the HSAB principle.

In the previous paper of this series,[2)] we reported the nucleophilic ring transformation of 1-substituted 3,5-dinitro-2-pyridones with some sodio β-keto esters to give nitrophenol derivatives together with *N*-substituted 2-nitroacetamides, and proposed a plausible reaction course including the stepwise formation of a bicyclic intermediate. Our interests have been directed to the investigation of the scope and limitation of these reactions. In this paper we describe the effects of the electron-donating substituents at the 4 or 6-position of 3,5-dinitro-2-pyridone on the nucleophilic attack of enolate ions of the β-keto esters.

Results and Discussion

As substrates 1,6-dimethyl- (**1a**), 1,4-dimethyl- (**1b**) and 4-methoxy-1-methyl- (**1c**) 3,5-dinitro-2-pyridones were employed, and diethyl sodio-3-oxopentanedioate (Na.DOPD) and ethyl sodioacetoacetate (Na. EAA) were used as the uncleophiles.

Treatment of **1a** with Na.DOPD at 50 °C in pyridine gave diethyl 2-hydroxy-4-methyl-5-nitro-1,3-benzenedicarboxylate (**2a**)[3)] and *N*-methyl-2-nitroacetamide (**3**) in 94.3 and 25.9%, respectively. Under somewhat milder conditions (25 °C) a colorless crystalline product (**4a**) was obtained in addition to **2a** and **3**. The product **4a** was easily converted to **2a** and **3** by the treatment with bases at 70 °C, and the ^{1}H-NMR spectrum of **4a** (see Experimental) behaved analogously to the bicyclic compounds reported in the previous paper.[2)] On the bases of these data **4a** was assigned to be diethyl 7-hydroxy-1,2-dimethyl-4,9-dinitro-3-oxo-2-azabicyclo[3.3.1]non-6-ene-6,8-dicarboxylate, an adduct of **1a** and DOPD.

From the reaction of **1b** with Na.DOPD, **2a**, **3**, and bicyclic compound, **4b**, were obtained. The similar reaction of **1c** with Na.DOPD gave diethyl 2-hydroxy-4-methoxy-5-nitro-1,3-benzenedicarboxylate (**2c**) together with **3** and bicyclic compound, **4c**.

From both the reactions of **1a** and **1b** with Na.EAA, ethyl 6-hydroxy-2-methyl-3-nitrobenzoate (**5a**)[4)] was solely yielded in addition to **3**; ethyl 2-hydroxy-4-methyl-5-nitrobenzoate which was anticipated as the alternative product was not obtained.

These facts suggest a probable course involving a preferential attack of the somewhat softer C-2 anion of EAA at the softer methyl-substituted 6 and 4-position of **1a** and **1b**, respectively. The subsequent intramolecular nucleophilic attack of the C-4 anion of EAA at the harder methyl-unsubstituted 4 or 6-position of the parent pyridone may lead to the same products, **4a** and **3** *via* the bicyclic intermediates.[5)] (Scheme 1, course a) The alternative course (b), however, is not to be discounted. Thus, the attack of the harder nucleophilic center of EAA, C-4 anion, at the harder methyl-unsubstituted position was followed by attack of the softer C-2 anion of EAA at the other position.[6)]

From the above results, it is difficult to decide which of the courses is more plausible.

On the other hand, from the reaction of **1c** with Na.EAA ethyl 2-hydroxy-4-methoxy-5-nitrobenzoate (**5c**) and **3** were obtained. The structure of **5c** was supported by the ^{1}H-NMR data and by the hydrolysis to 2-hydroxy-4-methoxy-5-nitrobenzoic acid.[7)]

This fact is interpreted as follows: The resonance effects of the nitro groups are decreased by the steric

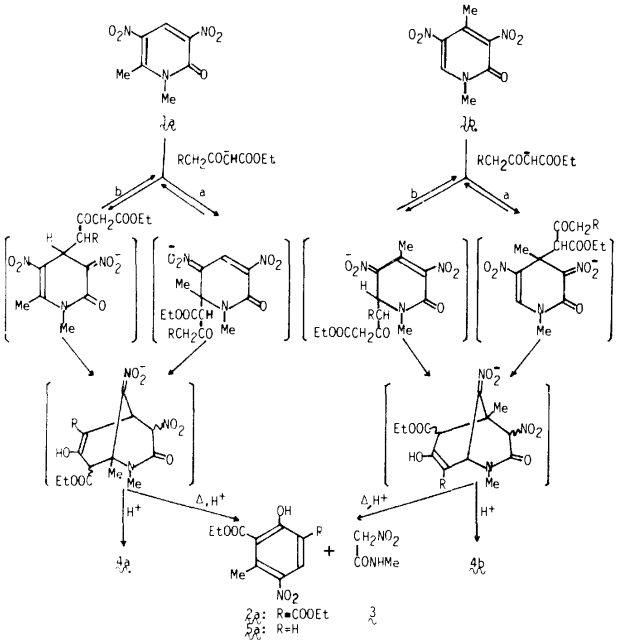

Scheme 1.

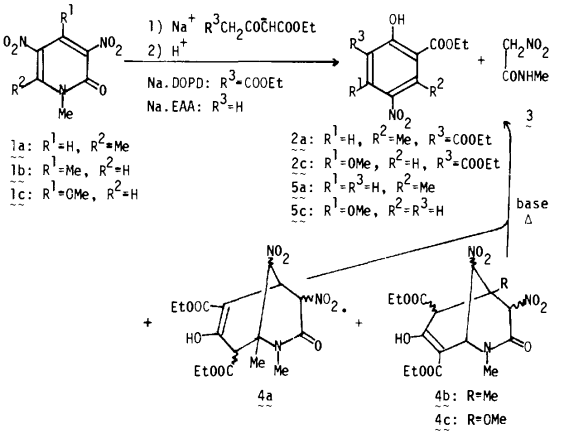

hydrance of the 4-methoxyl group, and the inductive effect of the 4-methoxyl group makes the C-4 position of the pyridone harder than the C-6 position, so the C-2 anion of Na.EAA attacks at the C-6 of the pyridone and C-2 of EAA at the C-4 of the pyridone.

Consequently, the sequence of the reaction steps could not be decided, neverthless the regiochemistry of the reaction could be explained by the HSAB principle, considering the electronic effects of the substituents.

Experimental

*Substrates, **1a**, **1b**, and **1c**.* These compounds were obtained from corresponding *N*-methyl-2-pyridones by the nitration with fuming nitric acid in acetic anhydride at room temperature.

*1,6-Dimethyl-3,5-dinitro-2-pyridone (**1a**).* Mp 135.5—136.0 °C. IR: 1695 cm^{-1} (C=O), 1570, 1340 (NO_2). NMR (acetone-d_6): δ=2.94 (3H, s), 3.78 (3H, s), 8.87 (1H, s).

*1,4-Dimethyl-3,5-dinitro-2-pyridone (**1b**).* Mp 155.0—156.0 °C. IR: 1695 cm^{-1} (C=O), 1570, 1340 (NO_2). NMR (acetone-d_6): δ=2.47 (3H, s), 3.74 (3H, s), 9.12 (1H, s).

*4-Methoxy-1-methyl-3,5-dinitro-2-pyridone (**1c**).* Mp 114.5—115.5 °C. IR: 1690 cm^{-1} (C=O), 1570, 1340 (NO_2). NMR (acetone-d_6): δ=3.72 (3H, s), 4.02 (3H, s), 9.12 (1H, s).

*The Reaction of **1** with Sodium Salts.* The method used here was the same as that described ealier.[2] Poor yield of **3** in all cases would be caused by acidity and lability of **3** to decompose under the reaction conditions.

*Diethyl 2-Hydroxy-4-methyl-5-nitro-1,3-benzenedicarboxylate (**2a**).* Colorless prisms (petroleum benzine), mp 69.0—70.0 °C. IR: 3100 cm^{-1} (O-H), 1745 (C=O), 1530, 1340 (NO_2). NMR ($CDCl_3$): δ=1.30 (3H, t, J=7 Hz), 1.44 (3H, t, J=7 Hz), 2.54 (3H, s), 4.44 (2H, q, J=7 Hz), 4.55 (2H, q, J=7 Hz), 8.49 (1H, s), 11.55 (1H, s).

*Diethyl 2-Hydroxy-4-methoxy-5-nitro-1,3-benzenedicarboxylate (**2c**).* Colorless needles (petroleum benzine), mp 100.0—100.5 °C. IR: 3200 cm^{-1} (O-H), 1740 (C=O), 1540, 1340 (NO_2). NMR ($CDCl_3$): δ=1.36 (3H, t, J=7 Hz), 1.39 (3H, t, J=7 Hz), 3.95 (3H, s), 4.39 (2H, q, J=7 Hz), 4.40 (2H, q, J=7 Hz), 8.57 (1H, s), 11.74 (1H, s).

*Diethyl 7-Hydroxy-1,2-dimethyl-4,9-dinitro-3-oxo-2-azabicyclo[3.3.1]non-6-ene-6,8-dicarboxylate (**4a**).* Colorless prisms (ethanol), mp 170.0—171.0 °C. IR: 1735 cm^{-1} (C=O), 1690 (C=O), 1550, 1320 (NO_2). NMR ($CDCl_3$): δ=1.28 (3H, t, J=7 Hz), 1.35 (3H, t, J=7 Hz), 1.53 (3H, s), 3.05 (3H, s), 3.72 (1H, s, H-8), 4.27 (4H, q, J=7 Hz), 4.37 (1H, dd, J=4 and 6 Hz, H-5), 5.59 (1H, *d*, J=6 Hz, H-9), 5.77 (1H, d, J=4 Hz, H-4), 12.64 (1H, s, 7-OH).

*Diethyl 3,7-Dihydroxy-2,5-dimethyl-4,9-dinitro-2-azabicyclo[3.3.1]nona-3,7-diene-6,8-dicarboxylate (**4b**).* Colorless prisms (ethanol), mp 151.0—152.0 °C. IR: 1750 cm^{-1} (C=O), 1670 (C=O), 1570, 1360 (NO_2). NMR ($CDCl_3$): δ=1.35 (3H, t, J=7 Hz), 1.41 (3H, t, J=7 Hz), 1.65 (3H, s), 3.16 (3H, s), 4.24 (1H, s, H-6), 4.27 (2H, q, J=7 Hz), 4.38 (2H, q, J=7 Hz), 4.85 (1H, d, J=3 Hz, H-1), 5.82 (1H, d, J=3 Hz, H-9), 12.41 (1H, s, 7-OH), 19.01 (1H, s, 3-OH, enol form).

*Diethyl 7-Hydroxy-5-methoxy-2-methyl-4,9-dinitro-3-oxo-2-azabicyclo[3.3.1]non-7-ene-6,8-dicarboxylate (**4c**).* Colorless prisms (ethanol), mp 198.0—199.0 °C. IR: 1750 cm^{-1} (C=O), 1690 (C=O), 1560, 1330 (NO_2). NMR ($CDCl_3$): δ=1.32 (3H, t, J=7 Hz), 1.45 (3H, t, J=7 Hz), 3.16 (3H, s), 3.60 (3H, s), 3.90 (1H, s, H-6), 4.30 (2H, q, J=7 Hz), 4.39 (2H, q, J=7 Hz), 4.93 (1H, d, J=4 Hz, H-1), 6.09 (1H, d, J=4H, H-9), 6.17 (1H, s, H-4), 12.38 (1H, s, 7-OH).

*Treatment of **4** with Sodium Ethoxide.* The raction was carried out according to the procedure described in Lit 2. From 208 mg of **5a** were obtained 112 mg (76.2%) of **2a** and 21 mg (41.3%) of **3**. Similarly, **2a** and **3** were yielded from **4b** in 58.7% and 28.8% yield, respectively, and **2c** in 27.9% and trace of **3**.

*Ethyl 6-Hydroxy-2-methyl-3-nitrobenzoate (**5a**).* Colorless needles (petroleum benzine), mp 58.0—58.5 °C. IR: 3200 cm^{-1} (O-H), 1670 (C=O), 1530, 1340 (NO_2). NMR ($CDCl_3$): δ=1.43 (3H, t, J=7 Hz), 2.60 (3H, s), 4.47 (2H, q, J=7 Hz), 6.85 (1H, d, J=9.5 Hz, H-5), 7.76 (1H, d. J=9.5 Hz, H-4), 11.33 (1H, s, 6-OH).

*Ethyl 2-Hydroxy-4-methoxy-5-nitrobenzoate (**5c**).* Colorless needles (petroleum benzine), mp 137.5—138.5 °C. IR: 3200 cm^{-1} (O-H), 1670 (C=O), 1540, 1340 (NO_2). NMR ($CDCl_3$): δ=1.41 (3H, t, J=7 Hz), 3.95 (3H, s), 4.31 (2H, q, J=7 Hz), 6.51 (1H, s, H-3), 8.48 (1H, s, H-6), 11.49 (1H, s, 2-OH).

Table 1. Reaction of 1,4- (or 1,6)-disubstituted 3,5-dinitro-2-pyridones with sodio β-keto esters*

Substrate	Reaction Conditions			Products (Yield/%)		
	Reagent	Mol. ratio	Temp			
1a	Na.DOPD	1.5	50 °C	**2a**(94.3)	**3**(25.9)	—
1a	Na.DOPD	1.5	25	**2a**(34.6)	**3**(7.8)	**4a**(46.9)
1b	Na.DOPD	1.5	50	**2a**(63.9)	**3**(17.2)	**4b**(23.6)
1b	Na.DOPD	3.0	70	**2a**(62.7)	**3**(16.9)	**4b**(23.6)
1b	Na.DOPD	1.5	25	**2a**(3.8)	—	**4b**(86.7)
1c	Na.DOPD	1.5	50	**2c**(62.2)	**3**(8.5)	**4c**(24.5)
1c	Na.DOPD	3.0	70	**2c**(64.2)	**3**(7.1)	**4c**(22.1)
1a	Na.EAA	3.0	70	**5a**(51.4)	**3**(11.3)	
1b	Na.EAA	3.0	70	**5a**(48.3)	**3**(8.3)	
1c	Na.EAA	3.0	70	**5c**(36.9)	**3**(8.5)	

* All the reactions were carried out in pyridine for 5 h.

Table 2. Analytical data of the substrates and products

Compound	Found(%)			Calcd(%)		
	C	H	N	C	H	N
1a	39.25	3.18	19.63	39.44	3.29	19.72
1b	39.16	3.09	19.82	39.44	3.29	19.72
1c	36.60	3.23	18.56	36.69	3.08	18.34
2a	52.47	4.95	4.95	52.52	5.09	4.71
2c	49.65	4.61	4.71	49.84	4.83	4.47
4a	46.05	4.81	10.11	46.26	5.10	10.12
4b	45.98	4.93	9.99	46.26	5.10	10.12
4c	44.56	5.14	9.61	44.55	4.90	9.74
5a	53.45	4.77	6.19	53.33	4.92	6.22
5c	49.70	4.68	5.51	49.80	4.95	5.80

References

1) The nucleophilic Reaction upon Electron-deficient Pyridone Derivatives. VII. for the preceding paper, see *Bull. Chem. Soc. Jpn.*, **57**, 1961 (1984).

2) E. Matsumura, M. Ariga, and Y. Tohda, *Bull. Chem. Soc. Jpn.*, **52**, 2413 (1979).

3) The authentic sample was obtained by usual nitration from diethyl 2-hydroxy-4-methyl-1,3-benzenedicarboxylate synthesized by the method of V. Prelog, O. Mezler and O. Jeger, *Helv. Chim. Acta*, **30**, 675 (1947).

4) The authentic sample was synthesized by nitration from ethyl 2-hydroxy-6-methylbenzoate. F. Bohlmann and K. Prezewowsky, *Chem. Ber.*, **97**, 1176 (1964).

5) E. Matsumura, Y. Tohda, and M. Ariga, *Bull. Chem. Soc. Jpn.*, **55**, 2174 (1982).

6) M. Strauss, T. Jensen, H, Schran, and K. O'Conner, *J. Org. Chem.*, **35**, 383 (1970).

7) N. Kaneniwa, *Yakugaku Zasshi*, **75**, 791 (1955).

Sulfur-Extrusive Rearrangement of α-Acylthio Ester by Lithium Amide

Kazuo Tsuzuki, Masaharu Akeyoshi, and Satoshi Ōmura*
School of Pharmaceutical Sciences, Kitasato University and The Kitasato Institute, Shirokane, Minato-ku, Tokyo 108
(Received August 11, 1984)

Synopsis. α-Acylthio esters readily undergo facile rearrangement to give β-keto esters on treatment with lithium amide at −78 °C. Thiolactone **3**, a key intermediate for thiolactonic antibiotics, was synthesized by utilizing the rearrangement.

In the course of synthetic studies[1] on the thiolactonic antibiotics, thiotetromycin[2] and thiolactomycin,[3] we treated ethyl 2-(benzoylthio)propanoate in dry tetrahydrofuran with 1.1 equiv lithium diisopropylamide at −78 °C (20 min) to obtain the corresponding β-keto ester [*m/z* 206(M^+), ν (neat) 1740 and 1690 cm^{-1}, δ ($CDCl_3$) 1.50 (3H, d, *J*=7 Hz) and 4.39 (1H, q, *J*=7 Hz)] in 93% yield. These spectral data suggest that it is ethyl 2-benzoylpropanoate. A similar reaction, using potassium *tert*-amylate and triphenylphosphine as a desulfurating agent which removes sulfur atom of the thiirane intermediate, was reported by Eschenmoser *et al.*[4] However, in our case the additive effect of desulfurating agent was not detected completely. In order to prove the generality and limitation of this rearrangement, several *S*-acyl derivatives obtained by *S*-acylation of 2-mercaptopropanoate and mercaptoacetate were treated with lithium amide and the results are summarized in Table 1. α-Acylthio esters except the *S*-acetyl (R^1=CH_3) derivative undergo facile rearrangement to yield the corresponding β-keto esters without a desulfurating agent in synthetically acceptable yield.

Attention was then turned to the application of this reaction to the synthesis of a key intermediate **3** containing the latent C-2 symmetry for thiolactonic antibiotics. Compound **1**[5] obtained by acylation of 2-mercaptopropanoate, on exposure at −78 °C with 1.1 equiv of lithium hexamethyldisilazanide for 20 min and then warming to room temperature in 1.5 h, provided β-keto ester **2**[5] as a mixture of diastereoisomers in 78% yield. Conversion of **2** to thiolactone **3**[5] was successfuly achieved in 49% yield by the following sequence: (1) deprotection of methoxymethyl group with $AgNO_3$; (2) hydrolysis of ester group; (3) thiolactonization by acidic work-up.

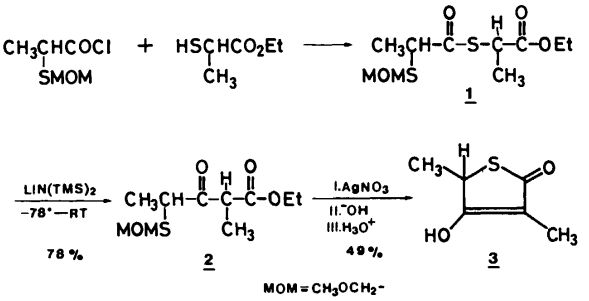

The ease of obtaining α-acylthio esters and the relatively mild conditions required for the rearrangement reaction might provide a useful tool for the construction of natural products.

References

1) K. Tsuzuki and S. Ōmura, *J. Antibiot.*, **36**, 1589 (1983).
2) S. Ōmura, Y. Iwai, A. Nakagawa, R. Iwata, Y. Takahashi, H. Shimizu, and H. Tanaka, *J. Antibiot.*, **36**, 109 (1983).
3) H. Oishi, T. Nato, H. Sasaki, K. Suzuki, T. Hayashi, H. Okazaki, K. Ando, and M. Sawada, *J. Antibiot.*, **35**, 391 (1982).

Table 1. Sulfur-extrusive rearrangement of α-acylthio esters by lithium amide

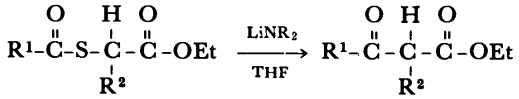

Entry[a]	R^1	R^2	R^3	Reaction conditions[b]	Yield/%[c]
1	Ph	Me	-Pr	−78 °C, 20 min	93
2	Ph	H	-Pr	−78 °C RT, 1 h	76
3	$Me(CH_2)_2$	Me	Me_3Si	−78 °C RT, 1.5 h	58
4	$Me(CH_2)_2$	H	Me_3Si	−78 °C RT, 2 h	54
5	Me_3C	Me	Me_3Si	−78 °C RT, 1.5 h	58
6	Me_3C	H	Me_3Si	−78 °C RT, 2 h	59

a) Satisfactory MS, ^1H NMR and IR spectroscopic data were obtained for all compounds. b) All reactions were carried out in THF under nitrogen at −78 °C for 20 min, and then warmed to room temperature. c) Isolated yield after silica-gel column chromatography.

4) M. Roth, P. Dubs, E. Gotschi, and A. Eschenmoser, *Helv. Chim. Acta*, **54**, 710 (1971).

5) **1**: MS *m/z* 266 (M^+); IR (neat) ν 1735, 1685 cm^{-1}; ^1H NMR ($CDCl_3$) δ=1.26 (3H, t, J=7 Hz), 1.50 (6H, d, J=7 Hz), 3.33 (3H, s), 3.70 (2H, q, J=7 Hz), 4.15 (2H, q, J=7 Hz), 4.67 (2H, AB, J=12 Hz). **2**: MS *m/z* 234 (M^+); IR (neat) ν 1740, 1715 cm^{-1}; ^1H NMR ($CDCl_3$) δ=1.25 (3H, t, J=7 Hz), 1.34 (3H, d, J=7 Hz), 1.44 (3H, d, J=7 Hz), 3.34 (3H, s), 3.78 (1H, q, J=7 Hz), 4.13 (2H, q, J=7 Hz), 4.15 (1H, q, J=7 Hz), 4.81 (2H, s). **3**: MS *m/z* 144 (M^+); IR (neat) ν 1605 cm^{-1}; ^1H NMR ($CDCl_3$) δ=1.63 (3H, d, J=7 Hz), 1.77 (3H, d, J=2 Hz), 4.20 (1H, qq, J=2 and 7 Hz).

Intramolecular [3+2] Cycloaddition of 2-Alkenyloxy-1-naphthaldehyde Oximes

Tomio SHIMIZU,* Yoshiyuki HAYASHI, and Kazuhiro TERAMURA
Department of Color Chemistry and Technology, Faculty of Industrial Arts, Kyoto Institute of Technology, Matsugasaki, Sakyo-ku, Kyoto 606
(Received August 11, 1984)

Synopsis. The thermal treatment of the mixture of 2-alkenyloxy-1-naphthaldehydes and hydroxylamine hydrochloride in ethanol gave intramolecular [3+2] cycloadducts, 1,3a,4,11c-tetrahydro-3*H*-naphtho[1′,2′:5,6]pyrano-[4,3-*c*]isoxazole hydrochlorides.

We have reported several intramolecular 1,3-dipolar cycloadditions of 2-(alkenyloxy)benzaldehyde (or 1-naphthaldehyde) arylhydrazones.[1] From the studies, it was found that the acid-catalyzed [3+2] cycloaddition was the most effective method for the preparation of cycloadducts.[1d] Several cycloadditions of analogous oximes have been reported; routes (a)[2] and (b)[3], respectively, consist of the intramolecular 1,3-dipolar cycloaddition of nitrile oxide or nitrone intermediates which were prepared from the oxidation or the thermal isomerization of aldehyde oximes. We report here the intramolecular [3+2] cycloaddition of 2-(alkenyloxy)-1-naphthaldehyde oximes.

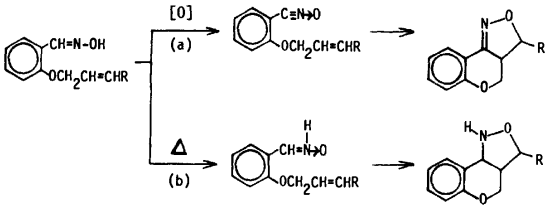

Results and Discussion

After the treatment of 2-(alkenyloxy)-1-naphthaldehyde (**1a—e**) with an excess amount of hydroxyamine hydrochloride in refluxing ethanol for 20 h, the intramolecular [3+2] cycloadducts, 1,3a,4,11c-tetrahydro-3*H*-naphtho[1′,2′:5,6]pyrano[4,3-*c*]isoxazole hydrochlorides (**2**), were obtained in the yields shown in Table 1. The treatment of **2** with triethylamine gave the free bases (**3**). The structures of **2** and **3** were established on the basis of elemental analyses and spectral data. The methine proton at 4-position of the isoxazolidine ring of **2** and **3** was observed as a multiplet at about δ 3 in ^{1}H NMR. An ambigous doublet at about δ 4.5 in the NMR spectra of **3** was assigned to be a proton at 3-position and it was converted into a simple doublet after adding D_2O. On the other hand, the proton of compounds **2** was observed as a doublet at about δ 5.6 because of the presence of the neighboring quaternary ammonium group. The observed coupling constants (6—7.5 Hz) of the bridgehead proton at 3-position suggest *cis* relationship with the bridgehead proton at 4-position and coupling constants (6—8 Hz) observed for the proton at 5-position suggest *trans* relationship with the proton at 4-position.[4]

Compounds **2** were also obtained after refluxing an ethanol solution containing 8% hydrogen chloride

Table 1. Yields of the reaction products (**2** and **3**)

Adduct	Yield/%	Adduct	Yield/%	Mp θ_m/°C
2a	10	**3a**	72	135—137
2b	33	**3b**	70	121—123
2c	14	**3c**[a]		
2d	8	**3d**	70	221—224
2e	60	**3e**	70	204—205

a) Not isolated.

Table 2. Spectral data of **2** and **3**

Compound	IR ν/cm^{-1}	NMR[a] (δ)
2a	2470 (N+H)	3.0—3.6 (m, 1H), 3.9 (t, 1H, J=11), 4.2—4.8 (m, 3H), 5.57 (d, 1H, J=6), 7.05—8.05 (m, 5H), 8.1—8.4 (m, 1H), 10.5 (br, 2H)[b]
2b	2500 (N+H)	1.5 (d, 3H, J=6), 2.7—3.2 (m, 1H), 4.0 (t, 1H, J=11), 4.3—4.8 (m, 2H), 5.5 (d, 1H, J=7), 7.0—8.1 (m, 5H), 8.3—8.6 (m, 1H), 10.8 (br, 2H)[b]
2c	2450 (N+H)	3.1—3.7 (m, 1H), 3.9—4.8 (m, 2H), 5.48 (d, 1H, J=6), 5.65 (d, 1H, J=7), 7.1—8.1 (m, 10H), 8.2—8.6 (m, 1H), 10.5 (br, 2H)[b]
2e	2450 (N+H)	1.27 (t, 3H, J=7), 3.1—3.7 (m, 1H), 3.9—4.9 (m, 5H), 5.1 (d, 1H, J=6) 7.05—8.3 (m, 6H), 10.5 (br, 2H)[b]
3a	3210 (NH)	2.5—3.2 (m, 1H), 3.4—4.4 (m, 5H), 4.48 (d, 1H, J=6), 4.9—5.4 (br, 1H)[b], 6.9—7.8 (m, 5H), 8.1—8.4 (m, 1H).
3b	3200 (NH)	1.4 (d, 3H, J=6), 2.2—2.7 (m, 1H), 3.75 (quintet, 1H, J=6), 3.8 (dd, 1H, J=2 and 11), 4.2 (dd, 1H, J=5 and 11), 4.68 (d, 1H, J=7.5), 5.0—5.4 (br, 1H)[b], 6.85—7.8 (m, 5H), 8.0—8.3 (m, 1H).
3d	3200 (NH) 2230 (CN)	3.0—3.6 (m, 1H), 4.0—4.5 (m, 2H), 4.65 (d, 1H, J=6), 4.5 (br, 1H)[b], 5.4 (d, 1H, J=8), 7.0—8.0 (m, 5H), 8.0—8.3 (m, 1H).

a) **2** were dissolved in DMSO-d_6 and **3** in $CDCl_3$. Coupling constants (J) are shown in hertz (Hz). b) This peak was disappeared by adding D_2O.

of 2-alkenyloxy-1-naphthaldehyde oximes (**5**). From the fact that **5** was stable for the thermal treatment in ethanol and recovered quantitatively, the formation of **2** can not be explained by the reaction *via* a nitrone intermediate (**6**), but a cationic intermediate (**4**).

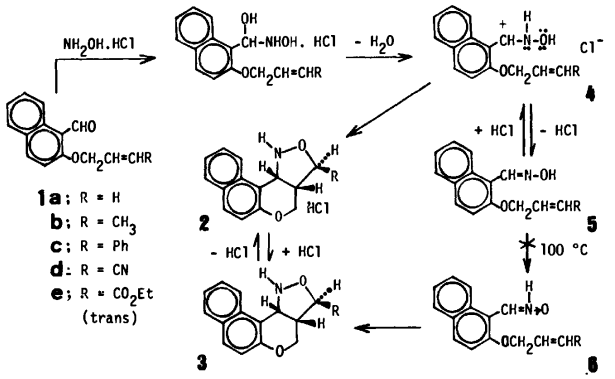

No cycloadducts could be obtained from the reaction mixture of 2-(alkenyloxy)benzaldehydes (**7a—7e**) and hydroxylamine hydrochloride, and only isolable compounds were salicylaldehyde oxime hydrochloride (**8**) (in 40—60% yields from **7a—c**) and 2-(alkenyloxy)benzaldehyde oximes (**9**) (in 90 and 10% yields from **7d** and **7e**, respectively). Phenol could not be detected after refluxing allyl phenyl ether in ethanol containing 8% HCl for 24 h, thus, the formation of **8** may be interpreted in terms of an acid-catalyzed intramolecular hydrolysis of **9**.

The results that **7** gave no cycloadduct (**10**) in the reaction may be explained by the comparison of the frontier molecular orbitals of the cationic intermediates (**4** and **11**). It is well-known[5] that the introduction of conjugated substituents (phenyl or naphthyl group) at the dipole increase in the HOMO energy and decrease in the LUMO energy and these effects of naphthyl group may be larger than those of phenyl group. While the intramolecular cycloaddition of **4** is only slightly more favorable than the other competitive reactions, the similar cycloaddition of **11** would be more unfavorable than the other competitive reactions, thus, **8** and **9** were formed.

Experimental

Measurements. All melting points are uncorrected. Satisfactory analytical data were obtained for the cycloadducts (**2a—c**, **3a**, **3b**, and **3d**)(±0.3% for C, H, and N).

Materials. The 2-(alkenyloxy)benzaldehydes (or -1-naphthaldehydes)(**7** or **1**)[1b] and those oximes (**9** and **5**)[2a] were prepared according to the method in the literature.

Reaction of 2-(Alkenyloxy)-1-naphthaldehydes (I) with Hydroxylamine Hydrochloride. A mixture of **1** (5 mmol) and hydroxylamine hydrochloride (1.0 g, 14 mmol) was refluxed in ethanol (50 ml) for 20 h with stirring. Evaporation of the solvent from the reaction mixture gave crystals, which were mixed well with benzene (30 ml) and filtered off, and the residue was washed with water and then dried *in vacuo* to give **2** in the yields shown in Table 1. The NMR spectra of **2** were shown in Table 2. The compounds **2** obtained above generally showed the broad melting points ranges (*ca.* 140—180 °C). In the case of **1a**, 2-allyloxy-1-naphthonitrile was also obtained in 80% yield from the filtrate by evaporation of the solvent (benzene); mp 64—65 °C (from ethanol), IR (Nujol): 2220 cm^{-1}, NMR ($CDCl_3$) δ: 4.73 (d, 2H, J=4 Hz), 5.1—5.6 (m, 2H), 5.7—6.4 (m, 1H), and 7.0—8.1 (m, 6H), Calcd for $C_{14}H_{11}NO$: C, 80.36; H, 5.30; N, 6.69%. Found: C, 80.25; H, 5.29; N, 6.71%. In the other cases, we could not isolate any by-products.

The Treatment of 2 with Triethylamine. Into a suspension of **2** in chloroform was added an excess mol of triethylamine, after which the mixture was stirred for 30 min at room temperature. The reaction mixture was then washed with water several times, and the organic layer was dried over anhydrous sodium sulfate. Evaporation of the solvent yielded crude naphthopyranoisoxazoles (**3**), which were recrystallized from ethanol to give pure materials in the yields shown in Table 1.

References

1) a) T. Shimizu, Y. Hayashi, Y. Nagano, and K Teramura, *Bull. Chem. Soc. Jpn.*, **53**, 429 (1980); b) T Shimizu, Y. Hayashi, Y. Kitora, and K. Teramura, *ibid.*, **55** 2450 (1982); c) T. Shimizu, Y. Hayashi, S. Ishikawa, and K Teramura, *ibid.*, **55**, 2456 (1982); d) T. Shimizu, Y. Hayashi M. Nakano, and K. Teramura, *ibid.*, **57**, 134 (1984).

2) a) R. Fusco, L. Garanti, and G. Zecchi, *Chim. Ind. (Milano)*, **57**, 16 (1975); L. Garanti, A. Sala, and G. Zecchi, *J. Org. Chem.*, **40**, 2403 (1975); b) G. A. Lee, *Synthesis*, **1982** 508.

3) W. Oppolzer and K. Keller, *Tetrahedron Lett.*, **1970** 1117.

4) R. Huisgen, R. Grashey, H. Hauck, and H. Seidel, *Chem. Ber.*, **101**, 2043 (1968), **102**, 736 (1969).

5) K. N. Houk, J. Sims, R. E. Duke, Jr., R. W. Strozier, and J. K. George, *J. Am. Chem. Soc.*, **95**, 7287 (1973).

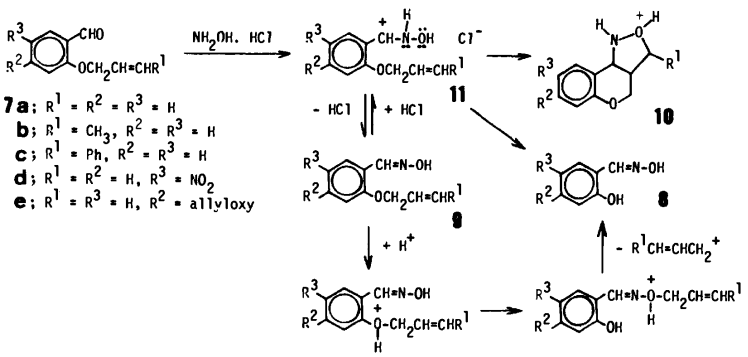

Alteration of Reaction Course in Thermolysis of *cis*-Diethylbis(tertiary phosphine)palladium(II) from Reductive Elimination to β-Elimination Process Induced by Addition of Tertiary Phosphine Ligand

Fumiyuki OZAWA, Kunihiko KURIHARA, Takakazu YAMAMOTO, and Akio YAMAMOTO*
Research Laboratory of Resources Utilization, Tokyo Institute of Technology, 4259 Nagatsuta, Midori-ku, Yokohama 227
(Received August 20, 1984)

Synopsis. Addition of tertiary phosphine to a solution containing *cis*-diethylbis(tertiary phosphine)palladium(II) alters thermolysis course of the complex from reductive elimination process liberating butane to β-hydrogen elimination process in which ethane and ethylene are released. Study with a deuterium-labeled ethyl complex indicates involvement of an internal metalation process.

Studies on thermolysis mechanisms of isolated dialkylpalladium complexes provide essential information for understanding basic properties of organopalladium complexes. Two most important concerted thermolysis pathways of dialkylpalladium complexes relevant to organic synthesis are reductive elimination and β-elimination.[1] Thus, information concerning controlling factors of these two pathways is of crucial importance for designing selective organic reactions promoted by palladium complexes.

In the previous reports[2,3] we showed that thermolysis courses of diethylbis(tertiary phosphine)palladium(II) complexes were dictated by their configurations, cis or trans.

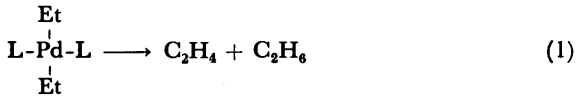

(L=PEt_3, PMe_2Ph, PEt_2Ph, $PMePh_2$, and $PEtPh_2$)

(L=PMe_2Ph and PEt_2Ph)

Trans isomers decompose through a clean β-elimination process to give ethylene and ethane in a 1:1 ratio, whereas cis isomers afford butane as the reductive elimination product. The β-elimination process of trans isomers is scarcely affected by addition of free tertiary phosphines to the systems and the reaction is assumed to proceed predominantly from four-coordinate species without predissociation of phosphine ligand.[3] In contrast, reductive elimination of the cis isomers is severely hindered by addition of phosphine ligands and a reaction mechanism proceeding through three-coordinate intermediates formed by partial dissociation of tertiary phosphine ligand has been proposed.[2,4] Further studies on the thermolysis reactions of *cis*-diethyl complexes revealed that addition of free phosphine ligands to the system not only retards the reductive elimination reaction but also forces to change the thermolysis course from the reductive elimination to the β-elimination process.

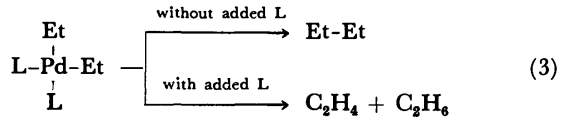

(L=PMe_2Ph, **1**; 1/2 $Ph_2P(CH_2)_2PPh_2$ (dppe), **2**; 1/2 $Ph_2P(CH_2)_3PPh_2$ (dppp), **3**; 1/2 $Ph_2P(CH_2)_4PPh_2$ (dppb), **4**)

TABLE 1. GASES EVOLVED ON THERMOLYSIS OF *cis*-$PdEt_2L_2$[a]

Run	L	Additive (mol dm^{-3})	Evolved gas ratio			Total amount[b]
			C_2H_4	C_2H_6	C_4H_{10}	
1	PMe_2Ph (**1**)	dmm (0.17)	0.00	0.00	*1.00*	0.94
2	PMe_2Ph (**1**)	PMe_2Ph (0.066) dmm (0.38)	0.03	0.04	*0.93*	0.76
3	PMe_2Ph (**1**)	PMe_2Ph (0.33)	*0.49*	*0.47*	0.04	0.95
4	PMe_2Ph (**1**)	PMe_2Ph (0.63)	*0.48*	*0.52*	0.00	0.86
5	1/2dppe (**2**)	dmm (0.38)	0.12	0.08	*0.81*	1.00
6	1/2dppe (**2**)	dppe (0.011) dmm (0.38)	*0.52*	*0.46*	0.02	0.72
7	1/2dppp (**3**)	dmm (0.38)	0.17	0.09	*0.75*	0.62
8	1/2dppp (**3**)	dppp (0.0087) dmm (0.38)	*0.47*	*0.50*	0.04	0.90
9	1/2dppp (**3**)	dppp (0.036)	*0.50*	*0.47*	0.04	0.89
10	1/2dppp (**3**)	dppp (0.26)	*0.50*	*0.48*	0.03	0.94
11	1/2dppb (**4**)	dmm (0.38)	0.17	0.09	*0.75*	0.62
12	1/2dppb (**4**)	dppb (0.12)	*0.48*	*0.50*	0.02	0.93

a) [Complex]=0.05—0.10 mol dm^{-3}. Solvent: toluene (run 1), Ph_2CH_2 (runs 2—12). Thermolysis temp (°C): r.t. (run 1), 70 (runs 2—12). b) Total amounts (mol/mol of complex)=$\{(1/2)(C_2H_4+C_2H_6)+C_4H_{10}\}$/(complex).

Table 1 summarizes distributions of hydrocarbons produced on thermolysis of four kinds of *cis*-diethyl complexes in solution in the presence and absence of free tertiary phosphines. Most of these reactions were carried out in the presence of dimethyl maleate (dmm). As previously mentioned,[2,3] dmm serves to trap $Pd(0)L_2$ species formed in thermolysis preventing decomposition of the $Pd(0)L_2$ species but does not affect the thermolysis of *cis*-$PdEt_2L_2$. The results in Table 1 clearly indicate that thermolysis course is effectively altered from the reductive elimination to the β-elimination pathway on addition of free phosphine ligands. Diphosphine coordinated compelexes **2—4** are more sensitive to addition of phosphines than complex **1** having monodentate ligand. Thermolysis rates in the systems with added phosphines were much slower than those without added phosphines. For example, complex **1** readily decomposes at room temperature to yield butane, while thermolysis of **1** (0.17 mol dm^{-3}) in Ph_2CH_2 containing 0.70 mol dm^{-3} of PMe_2Ph does not proceed at room temperature and takes place only at 60 °C. The reaction obeys the first order kinetics with respect to diethylpalladium concentration ($k_{obsd}=3.0\times10^{-5}\ s^{-1}$) and liberates ethylene and ethane in a 1 : 1 ratio.

Examination of the thermolysis products of *cis*-$Pd(CH_2CD_3)_2(PMe_2Ph)_2$ (**5**) provides further information on the thermolysis mechanisms of *cis*-diethyl complexes. Thermolysis of **5** in solution without added PMe_2Ph affords an almost quantitative yield of $CD_3CH_2CH_2CD_3$ as reported previously.[2] On the other hand, thermolysis of **5** in Ph_2CH_2 or C_6D_6 containing a ten fold excess amount of PMe_2Ph per palladium liberates a quantitative yield of CD_3CH_3, instead of CD_3CH_2D, together with a quantitative amount of $CD_2{=}CH_2$.

$$cis\text{-}Pd(CH_2CD_3)_2(PMe_2Ph)_2 \xrightarrow{\text{with } PMe_2Ph} CD_3CH_3 + CD_2{=}CH_2 \qquad (4)$$

Evidently no H-D scrambling in the ethyl groups is involved in these reductive elimination and β-hydrogen elimination processes. Furthermore, the ethane formation in thermolysis of the cis isomer arises by abstraction of hydrogen not from disproportionation of the two ethyl groups or from solvent but from the PMe_2Ph ligand. A similar hydrogen abstraction process from phosphine ligand has been suggested in thermolysis of *cis*-$Pt(CH_2CD_3)_2(Me_2P(CH_2)_2PMe_2)$ producing CD_3CH_3 and $CH_2{=}CD_2$.[5]

When the reductive elimination pathway is blocked in thermolysis of *cis*-$PdEt_2L_2$ by addition of tertiary phosphine ligand, the complex is forced to take another course. The most probable process suggested by the present study is internal ortho metalation of the starting *cis*-diethyl complex (**A**) involving C–H bond cleavage at the phenyl group in PMe_2Ph[6] to give **B**. The internally metalated diethyl(hydrido)palladium-(IV) species **B** then reductively eliminates ethane to give a monoethyl complex (**C**). Species **C** then undergoes β-elimination process liberating ethylene and forming a hydridopalladium complex (**D**), which is

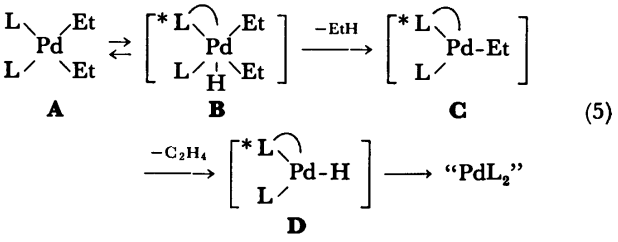

(5)

spontaneously converted into Pd(0) complex.

Experimental

All manipulations were carried out as reported previously.[2,3] Analysis of the gases evolved by thermolysis of *cis*-$Pd(CH_2CD_3)_2(PMe_2Ph)_2$ (**5**)[2] was carried out by GC-mass spectrometry (Hitachi M-80 spectrometer; column, Porapak Q; FD mass method). Structure of deuterated ethylene was confirmed by IR spectroscopy.[8] The rate constant for thermolysis of *cis*-$PdEt_2(PMe_2Ph)_2$ (0.17 mol dm^{-3}) in Ph_2CH_2 containing PMe_2Ph (0.70 mol dm^{-3}) at 60 °C was obtained by measuring the amounts of ethylene and ethane evolved with time using a Toepler pump.

Preparation of cis-*PdEt*$_2$*(dppp) (3) and* cis-*PdEt*$_2$*(dppb) (4).* *Cis*-diethyl complexes **3** and **4** were prepared by the reactions of $Pd(acac)_2$, $Al_2Et_3(OEt)_3$, and corresponding phosphine ligands in a manner similar to the preparation of *cis*-$PdEt_2$(dppe) (**2**)[9] and were identified by means of elemental analysis and IR and ^1H and $^{13}C\{^1H\}$ NMR spectroscopy.

References

1) J. K. Kochi, "Organometallic Mechanisms and Catalysts," Academic Press, New York (1978); J. Tsuji, "Organic Synthesis by Means of Transition Metal Complexes," Springer-Verlag, Berlin (1975); S. G. Davies, "Organotransition Metal Chemistry. Applications to Organic Synthesis," Pergamon Press, New York (1982); S. Murahashi, M. Yamamura, K. Yanagisawa, N. Mita, and K. Kudo, *J. Org. Chem.*, **44**, 2408 (1979); A. Sekiya and N. Ishikawa, *J. Organomet. Chem.*, **125**, 281 (1977) and **118**, 349 (1976); A. Minato, K. Tamao, T. Hayashi, K. Suzuki, and M. Kumada, *Tetrahedron Lett.*, **22**, 5319 (1981) and **21**, 845 (1980); T. Hayashi, M. Konishi, M. Fukushima, T. Mise, M. Kagotani, M. Tajika, and M. Kumada, *J. Am. Chem. Soc.*, **104**, 108 (1982); T. Hayashi, M. Konishi, Y. Kobori, M. Kumada, T. Higuchi, and K. Hirotsu, *ibid.*, **106**, 158 (1984).

2) F. Ozawa, T. Ito, Y. Nakamura, and A. Yamamoto, *Bull. Chem. Soc. Jpn.*, **54**, 1868 (1981).

3) F. Ozawa, T. Ito, and A. Yamamoto, *J. Am. Chem. Soc.*, **102**, 6457 (1980).

4) A. Gille and J. K. Stille, *J. Am. Chem. Soc.*, **102**, 4933 (1980); A. Moravsky and J. K. Stille, *ibid.*, **103**, 4182 (1981).

5) T. J. McCarthy, R. G. Nuzzo, and G. M. Whitesides, *J. Am. Chem. Soc.*, **103**, 3396 (1981).

6) G. W. Parshall, *Acc. Chem. Res.*, **3**, 139 (1970) and **8**, 113 (1975).

7) K. Tatsumi, R. Hoffmann, A. Yamamoto, and J. K. Stille, *Bull. Chem. Soc. Jpn.*, **54**, 1857 (1981).

8) T. Ikariya and A. Yamamoto, *J. Organomet. Chem.*, **120**, 257 (1976).

9) T. Ito, H. Tsuchiya, and A. Yamamoto, *Bull. Chem. Soc. Jpn.*, **50**, 1319 (1977).

Characterization of Catalyst for Coal Liquefaction. Exchange of Hydrogen Attached to Condensed Aromatics with Deuterium in Heavy Water over Catalyst

Tetsuro YOKONO,* Taro KOHNO, and Yuzo SANADA
Faculty of Engineering, Hokkaido University, North 13, West 8, Sapporo 060
(Received June 23, 1984)

Synopsis. The H-D exchange reaction of hydrogen atoms attached to condensed aromatics with deuterium atoms in D_2O over catalyst for coal liquefaction was studied by means of D-NMR. MoO_3/ZrO_2, MoO_3/SiO_2, Fe_2O_3-SO_4^{2-}, $SbCl_3$ and $ZnCl_2$ showed a significant catalytic activity for the exchange reaction. The H-D exchange ability was discussed in terms of the acidic properties and concentration of Mo^{5+} over supports for coal liquefaction catalysts.

There is a continuing interest in the surface properties of catalyst, particularly in their acid strength, the number and nature of the active sites, and the question of how the activity at these sites can be controled by chemical or physical treatment.

Little detailed information is available about catalytic activity of catalysts at high temperatures. The effect of the surface properties of catalysts on their role in coal liquefaction remains unclear. Our previous ESR study in the anthracene/$ZnCl_2$/H_2O system[1,2] suggested that an exchange reaction takes place between the hydrogen atoms in H_2O which is adsorbed on $ZnCl_2$ and the hydrogen atoms in anthracene (which is a model compound of coal). Furthermore, the hydrogen transfer reaction is known to play an important role in coal liquefaction and hydrogen exchange is one of these hydrogen transfer reactions. Thus the object of this study, as a model reaction for coal liquefaction, is to examine the H-D exchange reaction between the hydrogen atoms attached to condensed aromatics and the deuterium atoms in D_2O over metal oxide and metal chloride catalysts at high temperature by means of D-NMR.

Experimental

The metal oxide catalysts selected were as follows: MoO_3-SiO_2, MoO_3-ZrO_2, MoO_3-MgO, Fe_2O_3 and Fe_2O_3-SO_4^{2-}. These catalysts were prepared and supplied by Drs. K. Tanabe and H. Hattori, the Faculty of Science, Hokkaido University.[3] $ZnCl_2$ and $SbCl_3$ of guaranteed grade, as Lewis acid catalysts, were used for the experiments without further purification. Anthracene of G. R. grade was used as a model compound of coal.

Anthracene, catalyst and D_2O (molar ratio; 1:1:10) were mixed and sealed in a Pyrex tube reactor (10 mm diam× 500 mm) and heated in a vertical i.r. image furnace at a given temperature for a given time and then rapidly quenched. The heating rate was 10 K/min. The product was extracted with $CHCl_3$ in a ultrasonic vibrater. D-NMR spectra of the $CHCl_3$ soluble materials were obtained at room temperature using a Varian XL-200 spectrometer.

The ESR spectra of Mo^{5+} ions in the Mo-containing catalysts were obtained using a Varian E109 spectrometer employing 100 kHz modulation and a nominal operating frequency of 9 GHz.

Results and Discussion

Molybdenum Containing Catalyst Systems. Several metal oxide catalysts with different acidities were tested with respect to the H-D exchange reaction. The D-NMR spectrum of the product from the anthracene/MoO_3-ZrO_2/D_2O system which was allowed to react at 573 K for 15 min is shown in Fig. 1a. It is apparent that the H-D exchange reaction takes place over an acidic catalyst, MoO_3-ZrO_2. Assignment of deuterium atoms attached to anthracene is made by comparison with the proton chemical shifts of anthracene.[4] A similar spectrum was observed when MoO_3-SiO_2 was used. On the other hand, no significant exchange reaction was observed for the basic catalyst MoO_3-MgO, as shown in Fig. 1b.

The fact that MoO_3-ZrO_2 and MoO_3-SiO_2 are more active than MoO_3-MgO for the H-D exchange reaction might be explained by a great ability of ZrO_2 and SiO_2 to reduce MoO_3 to form lower bonding stages of Mo, such active species as Mo^{5+}, Mo^{4+} and so on.[5] Since Mo^{5+} is a paramagnetic

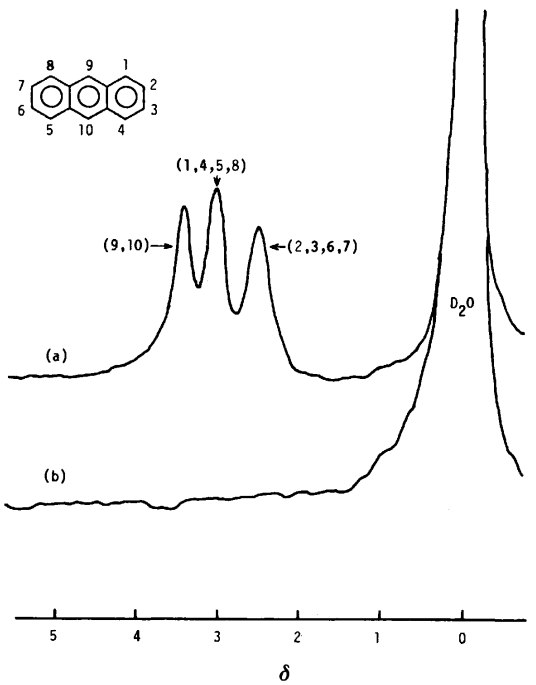

Fig. 1. D-NMR spectra of products from Anthracene/Catalyst/D_2O system.
(a): Anthracene/MoO_3-ZrO_2/D_2O 573 K, 15 min,
(b): Anthracene/MoO_3-MgO/D_2O 573 K, 15 min.

Table 1. Catalytic activity of MoO_3 over metal oxides for H-D exchange reaction on anthracene and their Mo^{5+} concentration

Catalyst	Exchanged product (%)	Mo^{5+} spin concentration (spins/g)
MoO_3/ZrO_2	8.3	2.52×10^{19}
MoO_3/SiO_2	8.2	1.42×10^{19}
MoO_3/MgO	0.0	0.77×10^{19}

species, it is detectable by ESR spectroscopy.[2] Table 1 shows the correlation between the propotion of the deuterium atoms incorporated in anthracene by the H-D exchange reaction and the Mo^{5+} spin concentrations in Mo-containing catalysts. The presence of reduced form of Mo species may be responsible for the H-D exchange reaction.

Iron Oxide Catalyst Systems. Fe_2O_3 is one of the most promising catalysts for the coal liquefaction process, because iron oxides and iron ore are disposable catalysts. One modification of Fe_2O_3 catalyst was attempted by including SO_4^{2-} ions.[3,6] The Fe_2O_3-SO_4^{2-} catalyst showed higher activity and selectivity for the liquefaction of both Akabira coal and Taiheiyo coal than those of pure Fe_2O_3 catalyst.[6]

The effect of SO_4^{2-} ion in Fe_2O_3 catalyst on coal liquefaction may be partly due to the increase in acid strength of catalyst. Therefore, it can be expected that SO_4^{2-} ion in Fe_2O_3 catalyst has an influence on the H-D exchange reaction of the anthracene/Fe_2O_3/D_2O system. In fact, evidence of such influence on the exchange reaction was obtained from the D-NMR spectrum of the product from the Fe_2O_3-SO_4^{2-}/anthracene/D_2O system which was allowed to react at 573 K for 15 min. On the other hand, any evidence of the H-D exchange reaction could not be obtained for pure Fe_2O_3 catalyst system.

Lewis Acid Catalyst Systems. Available evidence about metal chloride catalysts[7] suggests that Lewis acids first convert to Brönsted acids in the presence of water. Therefore, one can easily invoke a direct adduct of Lewis acid and anthracene as the intermediate allowing the H-D exchange. This consideration was confirmed directly by means of D-NMR for Lewis acid catalysts ($SbCl_3$, $ZnCl_2$) with anthracene.

The D-NMR spectrum of the product from the anthracene/$ZnCl_2$/D_2O system which was allowed to react at 483 K for 15 min is shown in Fig. 2a. It can be seen that the deuterium atoms are especially concentrated at the (9, 10) positions of anthracene. Fig. 2b indicates that a significant H-D exchange reaction also takes place over $SbCl_3$ catalyst, mainly at the (9, 10) and (1, 4, 5, 8) positions of the nuclei of anthracene.

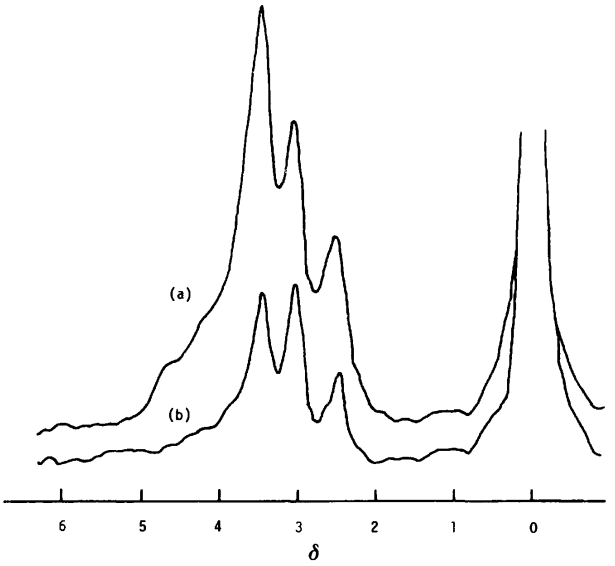

Fig. 2. D-NMR spectra of products from Anthracene/Lewis acid catalyst/D_2O system.
(a): Anthracene/$ZnCl_2$/D_2O 483 K, 15 min, (b): Anthracene/$SbCl_3$/D_2O 418 K, 15 min.

The deuterium distribution differs clearly from the case of the $ZnCl_2$ catalyst.

The D-NMR investigation of the H-D exchange reaction was extended to various polynuclear aromatics such as perylene, pyrene, phenathrene, benz[*a*]anthracene and naphthacene. Among the hydrocarbons so far tested, phenanthrene had the highest degree of H-D exchange reaction with respect to $ZnCl_2$ catalyst.

References

1) T. Kohno, T. Yokono, and Y. Sanada, The 45th National meeting of the Chemical Society of Japan, Tokyo, April, 1982, Abstr. No. 2X17.

2) T. Yokono, T. Kohno, Y. Sanada, E. Yamada, and S. Shimokawa, The 46th National Meeting of the Chemical Society of Japan, Niigata, October 1982, Abstr. No. 2E16.

3) K. Tanabe, A. Kayo, and T. Yamaguchi, *J. Chem. Soc., Chem. Commun.*, **1981**, 602.

4) P. Dirhl, "Nuclear Magnetic Resonance Spectroscopy of Nuclei Other than Protons," ed by T. Axenrod and G. A. Webb, John Wiley & Sone, Inc., New York (1974) pp. 275—285.

5) M. Niwa, M. Mizutani, M. Takahashi, and Y. Murakami, *J. Catal.*, **70**, 14 (1981).

6) K. Tanabe, H. Hattori, T. Yamaguchi, S. Yokoyama, J. Umematsu, and Y. Sanada, *Fuel*, **61**, 389 (1982); *Fuel Processing Tech.*, **8**, 117 (1984).

7) C. W. Zielke, R. T. Struck, J. M. Evans, C. P. Constanza, and E. Gorin, *Ind. Eng. Chem., Prod. Res. Dev.*, **5**, 155 (1966).

Optical and Magnetic Properties of Alkali-(18-Crown-6)-TCNQ Salts

Hideyuki NAKAYAMA and Kikujiro ISHII*
Department of Chemistry, Faculty of Science, Gakushuin University, Mejiro, Toshima-ku, Tokyo 171
(Received June 26, 1984)

Synopsis. Absorption spectra, ESR and static susceptibility were measured on TCNQ salts which incorporate Na^+- or K^+-(18-crown-6) as the cation unit. Results indicate that charge-transfer interaction between TCNQ anions is weak in the Na^+ salt, whereas it is very strong in the K^+ salt.

Physical processes in TCNQ (7,7,8,8-tetracyanoquinodimethan) salts are usually discussed laying stress only on the interaction between TCNQ molecules. We have recently shown,[1] however, that interaction of TCNQ with the cations is sometimes important in determining the electronic state in the TCNQ chain. Metal-(crown ether)-TCNQ ternary salts[2a-c] are good candidates for studying the effect of the cation-TCNQ interaction. We previously reported anomalous magnetic properties of some alkali-(crown ether)-TCNQ salts.[3] In the present note, we report an example in which a difference in the diameter of alkali cation causes a difference in the shape of the metal-(crown ether) unit, and the latter difference greatly affects the optical and magnetic properties of the TCNQ stacks. Substances studied were 1:1 TCNQ salts with N^+- or K^+-(18-crown-6) cation units, where 18-crown-6 stands for 1,4,7,10,13,16-hexaoxacyclooctadecane. The experimental procedures were almost the same as before.[3] Absorption spectra and ESR were measured on polycrystalline samples. On the K^+ salt, in addition, static magnetic susceptibility was measured. The absorption spectrum of the K^+ salt has been outlined.[2a]

Results and Discussion

Absorption Spectra. Absorption spectra of the two salts are shown in Fig. 1. In the spectrum of the Na^+ salt, the lowest energy band at 7.5×10^3 cm^{-1} is assigned to the charge-transfer(CT) excitation between TCNQ anions, since many alkali-TCNQ simple salts show CT band in this region.[4,5] Among the three small bands at 11.7, 13.0, and 15.0×10^3 cm^{-1}, the former two and the third are similar respectively to the absorptions of monomer $TCNQ^-$ and $TCNQ^-$ dimer in solution.[6] Therefore, these three bands could be explained by assuming the existence of $TCNQ^-$ monomers embedded at the impurity sites in a dimer-type crystal. However, these bands as a whole may reflect the electronic structure of the TCNQ molecules since the former two bands are too strong to be attributed to the impurity. A large peak at 27.2×10^3 cm^{-1} and a shoulder around 23×10^3 cm^{-1} are ascribed to local excitations in the TCNQ molecules. Energies of this peak and shoulder are almost the same as those respectively of other dimer and monor absorptions in solution.[6] Thus, the Na^+ salt is inferred to involve TCNQ columns with a weakly dimerized structure.

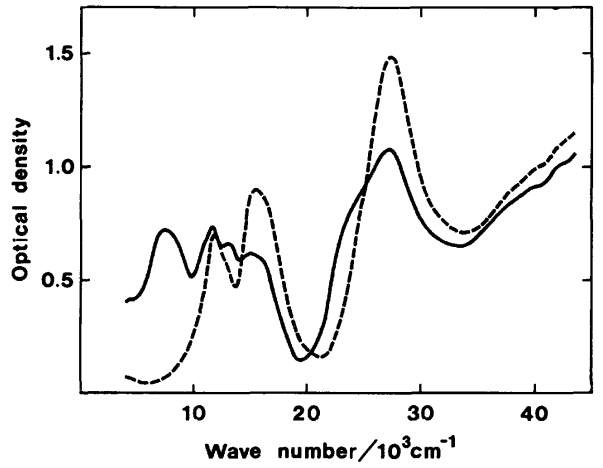

Fig. 1. Absorption spectra of powder samples; Na^+-(18-crown-6)- $TCNQ^-$ (——) and K^+-(18-crown-6)-$TCNQ^-$ (----).

The absorption spectrum of the K^+ salt (Fig. 1) is less complicated. There are three prominent bands at 11.8, 15.5, and 27.3×10^3 cm^{-1}. The first band is located in the energy region of one of the monomer $TCNQ^-$ excitations described before. However, it may be assumed that this band is a CT band associated with the excitation between two TCNQ anions since there is no absorption band in the lower-energy region beyond this band. The CT-band energy of a $TCNQ^-$ dimer is determined mainly by three terms,[4] *i.e.*, on-site Coulomb energy U, configuration-interaction(CI) energy t between ground and CT configurations, and CI-energy t' between CT- and locally-excited configurations. t increases the CT-band energy, whereas t' acts to decrease it. The above energy of the CT band implies that t is very large and, probably at the same time, t' is small in this salt. The crystal structure analyzed by Hirano *et al.*[7] indicates the existence of strong and isolated dimers of $TCNQ^-$ bound by the Coulomb interaction with K^+, the vector connecting two $TCNQ^-$ being almost perpendicular to their molecular plane. Thus the above assumptions for the molecular integrals are in harmony with the crystal structure, and the first assumption that the lowest-energy band is the CT band is reasonable. The local-excitation band at 27.3×10^3 cm^{-1} is sharp and has no shoulder on its lower-energy side. This fact is also in agreement with the crystal structure for which the thermal excitation of the monomer-like molecular arrangement seems to be difficult.

Magnetic Properties. The Na^+ salt showed a sharp and fairly strong ESR signal at room temperature at a g-value of 2.0029. The spin density was estimated to be 1.4×10^{23} mol^{-1} using purified DPPH as the standard. The temperature variation of the integrated intensity is shown in Fig. 2. While a thermally

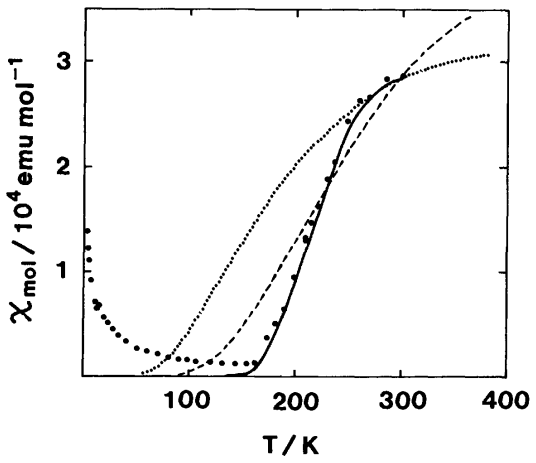

Fig. 2. Temperature dependence of the integrated ESR intensity of Na^+-(18-crown-6)-$TCNQ^-$. Solid line is the result obtained by subtracting the Curie-type contribution. Dashed and dotted lines are respectively the theoretical curves by the singlet-triplet model with J=0.069eV and the linear-Ising model with J= 0.038eV.

activated sharp signal is seen above 160 K, a weak and broad signal which obeys Curie's law is seen below this temperature. The latter signal is considered to come from isolated $TCNQ^-$ at the impurity sites in the crystal.[8] The variation of the thermally activated signal is revealed by subtracting the contribution from the impurity signal. Rise of the solid line thus obtained (Fig. 2) is steeper than the theoretical curves given by the singlet-triplet(ST) model[9] and the linear-Ising(LI) model.[10] The spin density at room temperature corresponds to those of a ST system with J=0.069 eV and a LI system with J=0.038 eV (Fig. 2). One possible cause of the steep rise of the present result is that the magnetic interaction between TCNQ anions is large in the low-temperature region and becomes weaker as the temperature is raised. This explanation is reasonable since the average distance between molecules increases because of the thermal expansion. The fact that the signal of the thermally activated spins is sharp over the whole temperature range where it is observed means that the magnetic excitons are mobile. These results imply that the dimerization of TCNQ anions is weak in this salt in agreement with the absorption spectrum.

We could not detect an ESR signal for the K^+ salt at room temperature at the maximum sensitivity of our instrument. To confirm that there are no spins, the static magnetic susceptibility was measured. The result $\chi=-2.9_8\times10^{-4}$ emu mol^{-1} agrees well with the diamagnetism estimated by Pascal's law. These observations indicate that the magnetic interaction between TCNQ anions is very strong in this salt, which agrees well with the absorption spectra and the crystal structure.

Shape of the Cation Unit and Property of the Crystal. The marked contrasts observed for the optical and magnetic properties of these two salts imply that their crystal structures are very different. It has been known that the size of the inner space of 18-crown-6 fits to the diameter of K^+ giving a cation unit with symmetric shape, but the diameter of Na^+ is smaller and consequently the shape of the cation unit is distorted.[11] This distortion seems not to favor good packing in the crystal. The structure and properties of TCNQ salts are determined by a critical balance between the Coulomb energy and the CT energy.[12] In the isolated dimer structure of the present K^+ salt,[7] the Coulomb attraction between K^+ and the cyano groups of the TCNQ molecules is inferred to compensate effectively for the repulsion between the TCNQ anions. Stabilization of the singlet ground state is, then, attained by the strong CT interaction.

References

1) A. D. Bandrauk, K. Ishii, K. D. Truong, M. Aubin, and A. W. Hanson, submitted to *J. Phys. Chem.*

2) a) M. Morinaga, T. Nogami, Y. Kanda, T. Matsumoto, K. Matsuoka, and H. Mikawa, *Bull. Chem. Soc. Jpn.*, **53**, 1221 (1980); b) T. Matsumoto, T. Nogami, H. Tanaka, and H. Mikawa *ibid.*, **55**, 369 (1982); c) K. Matsuoka, T. Nogami, T. Matsumoto, H. Tanaka, and H. Mikawa, *ibid.*, **55**, 2015 (1982).

3) K. Ishii, H. Nakayama, and F. Abe, *Chem. Phys. Lett.*, **91**, 73 (1982).

4) J. Tanaka, M. Tanaka, T. Kawai, T. Takabe, and O. Maki, *Bull. Chem. Soc. Jpn.*, **49**, 2358 (1976).

5) K. Yakushi, T. Kusaka, and H. Kuroda, *Chem. Phys. Lett.*, **68**, 139 (1979).

6) R. H. Boyd and W. D. Phillips, *J. Chem. Phys.*, **43**, 2927 (1965).

7) M. Hirano, T. Nogami, M. Morinaga, H. Horiuchi, M. Tokonami, Annual Meeting of Crystallogr. Soc Jpn. 1980, Abstr., P2—25.

8) C. F. Schwertdfeger, *Solid State Commun.*, **23**, 621 (1977).

9) D. Bijl, H. Kainer, and A. C. Rose-Innes, *J. Chem. Phys.*, **30**, 765 (1959).

10) J. C. Bonner and M. E. Fisher, *Phys. Rev.*, **135**, A640 (1964).

11) M. Dobler, J. D. Dunitz, and P. Seiler, *Acta Crystallogr., Sect B*, **30**, 2741 (1974); P. Seiler, M. Dobler, and J. D. Dunitz, *ibid., Sect B*, **30**, 2744 (1974).

12) R. M. Metzger and E. S. Arafat, *J. Chem. Phys.*, **78**, 2696 (1983); R. M. Metzger, E. S. Arafat, and C. S. Kuo, *ibid.*, **78**, 2706 (1983).

Formation Constants of Lanthanoid(III) Complexes with 4-(2-Thiazolylazo)resorcinol

Emiko OHYOSHI
Yatsushiro College of Technology, Hirayamashinmachi 2627, Yatsushiro, 866
(Received June 18, 1984)

Synopsis. The formation constants of the protonated (MHR) and normal (MR) complexes (1:1) of lanthanoids(III) with 4-(2-thiazolylazo)resorcinol (TAR, H_2R) have been determined spectrophotometrically by estimation of the free ligand. The MR complexes of TAR were less stable than the corresponding 4-(2-pyridylazo)resorcinol (PAR) complexes, but the relative stabilities were reversed for the MHR complexes.

4-(2-Thiazolylazo)resorcinol (TAR) gives intensely colored complexes with most metals and is widely used in analytical chemistry.[1] Shimizu and Momo reported that TAR is the most useful reagent for determination of Sc(III).[2] It is of interest to study complexation of lanthanoids(III) with TAR. As described previously, the method[3] developed for determination of complex formation constants by estimation of the free ligand was applicable to study the lanthanoid(III)-4-(2-pyridylazo)resorcinol (PAR) complexes.[4] In the present work, the method[3] was applied to the lanthanoid(III)-TAR system and the results were compared with those of the lanthanoid(III)-PAR system.[4]

Experimental

Materials. All chemicals used were of G.R. grade. TAR was obtained from Dojindo Chemical Co., and its purity was checked by using thin-layer chromatography.[5] A weighed quantity of TAR was dissolved in a small volume of 1.0 M (1 M=1 mol dm^{-3}) NaOH and the solution was diluted with distilled water to prepare the stock solution of 2.0×10^{-3} M. The lanthanoid(III) nitrate solutions except for Ce(III) were prepared by dissolving the calculated amounts of the respective oxides in nitric acid. The cerium(III) nitrate solution was prepared by dissolving $Ce(NO_3)_3\cdot2(NH_4NO_3)\cdot4H_2O$ in 10^{-2} M HNO_3 and the concentration was determined by EDTA titration. Hexamine and sodium nitrate were used to maintain the pH at 5—6.3 and the ionic strength at 0.1, respectively.

Procedure. The metal solution was added in small aliquots, 50 μl each, using a microliter pipet to a 10 ml of the buffered solution of TAR ($1.5—2.0\times10^{-5}$ M), to give the concentrations of $10^{-4}—5\times10^{-3}$ M. Before and after the addition of the metal for each 50 μl, the absorbance at the peak of TAR (420 or 440 nm) was measured by using a Shimadzu UV 200s spectrophotometer. No precipitation occurred under these experimental conditions.

Results and Discussion

As described previously,[3] metal complexes of TAR (H_2R), MHR, and MR, can indirectly be estimated by utilizing the ligand absorption peak. The absorbance at the free ligand peak measured in the absence (A_o) and the presence (A) of the metal under conditions where $C_M \gg C_R$ (C_M and C_R are the total concentrations of the metal and the ligand), *i.e.*, formation of the 1:1 complexes, MHR and MR, is assumed, can be related to their formation constants, K_{MHR} and K_{MR}, as follows (the charges are omitted for simplicity):

$$C_R = [MHR] + [MR] + [R'] \quad (1)$$

$$A = \varepsilon_{MHR}[MHR] + \varepsilon_{MR}[MR] + \varepsilon_{R'}[R'], \quad (2)$$

where R′ is the free ligand not combined with metal, and ε_{MHR}, ε_{MR}, and $\varepsilon_{R'}$ are the molar extinction coefficient of MHR, MR, and R′ at the free ligand peak, respectively. With the formation constants, $K_{MHR}=[MHR]/([M][HR])$ and $K_{MR}=[MR]/([M][R])$, the acid dissociation constants of H_2R, $K_1=[H][HR]/[H_2R]$ and $K_2=[H][R]/[HR]$, and α coefficient,[6] $\alpha_R=[R']/[R]$, Eqs. 1 and 2 can be brought into the following expressions:

$$[M](K_{MHR}K_1[H]+K_{MR}K_1K_2)/(\alpha_RK_1K_2) = C_R/[R'] - 1, \quad (3)$$

$$A/\varepsilon_{R'} = [R']\{1+(\varepsilon_{MHR}K_{MHR}K_1[H] + \varepsilon_{MR}K_{MR}K_1K_2)[M]/(\varepsilon_{R'}\alpha_RK_1K_2)\}. \quad (4)$$

Combining Eq. 3 with Eq. 4, and substituting C_M for [M] (since $C_M \gg C_R$) and A_o for $C_R\varepsilon_R$, we obtain

$$\frac{K_{MHR}K_1[H]+K_{MR}K_1K_2}{\alpha_RK_1K_2} - \frac{\varepsilon_{MHR}K_{MHR}K_1[H]+\varepsilon_{MR}K_{MR}K_1K_2}{\varepsilon_{R'}\alpha_RK_1K_2} \times\frac{A_o}{A} = (A_o/A-1)/C_M. \quad (5)$$

From Eq. 5, a linear relation between $(A_o/A-1)/C_M$ and A_o/A should be obtained at a constant pH where $\varepsilon_{R'}$ remains constant. The product of the intercept of the y axis ($y=(A_o/A-1)/C_M$), y_o, at a fixed pH and $\alpha_RK_1K_2$ is given as a function of [H]:

$$y_o \times \alpha_RK_1K_2 = K_{MHR}K_1[H] + K_{MR}K_1K_2 \quad (6)$$

According to Eq. 6, a linear plot of the left-hand side of Eq. 6 *vs.* [H] should be obtained in a pH range where no hydrolysis of metal ion occurs. From the slope and the intercept of the line, both K_{MHR} and K_{MR} can be determined.

By measuring the decrease of the absorbance at the peak of TAR (420 nm) with increasing metal concentrations at a constant pH, we plotted the relation expressed by Eq. 5. All the plots obtained at different pH values for different lanthanoids(III) yielded a straight line with a negative slope as expected. Since TAR shows a broad peak (410—440 nm), we tried to plot the data at another wavelength of 440 nm and ascertained the line having the same intercept (the slope is different). Figure 1 shows a typical set of plots at pH 5.50. The experimental data showed no detectable difference in the plots for Yb(III) and Lu(III) (line 1), for Dy(III) through Er(III) (line 3), and for Sm(III)

Table 1. Formation constants, K_{MHR} and K_{MR}, and proton dissociation constants of MHR, K^{H}_{MHR}, for TAR and PAR complexes of lanthanoids(III) $I=0.1$ ($NaNO_3$), 25 °C

Element	TAR			PAR[3,4]		
	$\log K_{MHR}$	$\log K_{MR}$	pK^{H}_{MHR}	$\log K_{MHR}$	$\log K_{MR}$	pK^{H}_{MHR}
La	3.61	6.93	6.12	3.18	8.91	6.57
Ce	4.08	7.44	6.08	3.78	9.61	6.47
Pr	4.27	7.65	6.06	3.95	9.78	6.47
Nd	4.40	7.79	6.05	4.07	10.02	6.35
Sm	4.71	8.10	6.05	4.28	10.25	6.33
Eu	4.71	8.10	6.05	4.28	10.25	6.33
Gd	4.71	8.10	6.05	4.28	10.25	6.33
Tb	4.71	8.10	6.05	4.28	10.25	6.33
Dy	4.71	8.10	6.05	4.29	10.36	6.23
Ho	4.71	8.10	6.05	4.29	10.47	6.12
Er	4.71	8.10	6.05	4.31	10.52	6.09
Tm	4.74	8.34	5.84	4.34	10.57	6.07
Yb	4.77	8.78	5.43	4.39	10.70	5.99
Lu	4.77	8.78	5.43	4.39	10.70	5.99

The relative errors of K_{MHR} and K_{MR} are 5—10% and 8—15% respectively.

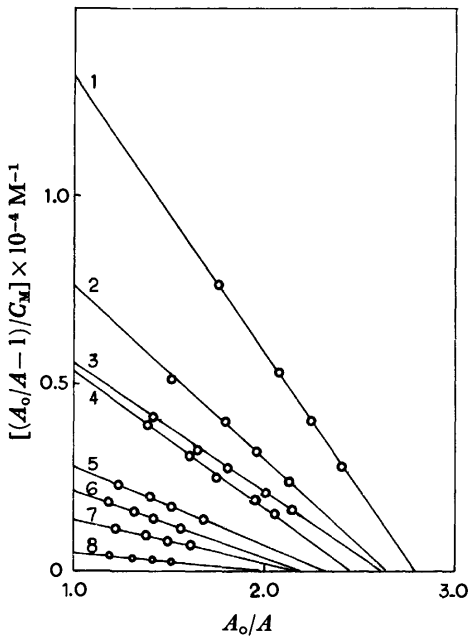

Fig. 1. Plots according to Eq. 5 at a constant pH of 5.50 for the system of TAR and lanthanoids (III). 1) Lu, Yb; 2) Tm; 3) Er, Ho, Dy; 4) Tb, Gd, Eu, Sm; 5) Nd; 6) Pr; 7) Ce; 8) La.

through Tb(III) (line 4), respectively. It is noted that lines 3 and 4 have a slightly different slope but almost the same intercept. This suggests that the degree of complex formation for Sm(III) through Er(III) is very similar to each other.

To determine the formation constants of MHR and MR complexes the relationship expressed by Eq. 6 was plotted for various lanthanoids(III). The values, $K_1=10^{-6.23}$ and $K_2=10^{-9.44}$[7] were used for calculation of $\alpha_R K_1 K_2$. All the plots exhibited straight lines, each of which had an intercept, indicating the presence of both MHR and MR, complexes. Table 1 shows the formation constants of MHR and MR, K_{MHR} and K_{MR}, obtained from the slope and the intercept of the plot of Eq. 6, and the proton dissociation constant of MHR, K^{H}_{MHR}, calculated by: $K^{H}_{MHR}=K_2K_{MR}/K_{MHR}$. The values were obtained by the least squares method. For comparison corresponding values for PAR are included.

In general, TAR forms less stable complexes with metal ions than PAR because of the lower basicity of the thiazole rings. From our results for the lanthanoids(III), this is valid only for the MR complexes. The MHR complexes are more stable than those of PAR. This parallels the protonation constants of the two ligands, HR^- and R^{2-} for TAR[7] ($pK_1=6.23$ and $pK_2=9.44$) and PAR[8] ($pK_1=5.50$ and $pK_2=12.30$). From the variation in the formation constants, K_{MHR} and K_{MR} (Table 1), with the atomic number, it is noticed that there are marked similarities between the coordinating tendencies of TAR and PAR to the lanthanoids(III): 1) The stabilities of MHR and MR complexes increase up to Sm(III); 2) After Sm(III) the K_{MHR} values are very close to each other; 3) The acidity of MHR which parallels the stability order of MR increases with the atomic number.

References

1) H. R. Hovind, *Analyst*, **100**, 769 (1975).
2) T. Shimizu and E. Momo, *Anal. Chim. Acta*, **52**, 146 (1970).
3) E. Ohyoshi, *Anal. Chem.*, **55**, 2404 (1983).
4) E. Ohyoshi, *Talanta*, **31**, 1129 (1984).
5) F. H. Pollard, G. Nickless, T. J. Samuelson, and R. G. Anderson, *J. Chromatogr.*, **16**, 231 (1964).
6) A. Ringbom, "Complexation in Analytical Chemistry," Interscience, New York (1963).
7) S. P. Mushran and L. Sommer, *Collect. Czech. Chem. Commun.*, **34**, 3693 (1969).
8) W. J. Geary, G. Nickless, and F. H. Pollard, *Anal. Chim. Acta*, **27**, 71 (1962).

The Facile Synthesis of Unsymmetrical Ketones Using Acetone Dimethylhydrazone

Masakazu YAMASHITA,* Kaoru MATSUMIYA, Minako TANABE, and Rikisaku SUEMITSU
Department of Applied Chemistry, Doshisha University, Kamikyo-ku, Kyoto 602
(Received June 27, 1984)

Synopsis. Unsymmetrical ketones were prepared by successive alkylation of acetone dimethylhydrazone. Application of this reaction to the synthesis of dihydrojasmone is described.

Ketones are one of the most important groups of compounds in the field of organic synthesis and many synthetic methods for their preparation have been reported. In this paper, we wish to report a facile and one stage synthetic method to synthesize unsymmetrical ketones using acetone dimethylhydrazone.[1] The outline of this method is shown in Scheme 1. After addition of butyllithium to a solution of acetone dimethylhydrazone[2] in THF at −5 °C under argon, 1-iodopentane was added and the mixture was stirred for 10 h at room temperature. After cooling the mixture to −5 °C again, butyllithium was again added followed by benzyl bromide. After stirring for 10 h, 2 mol dm^{-3} hydrochloric acid was added to hydrolyze the mixture and the organic material was extracted with ethyl acetate. Usual work up afforded pure 1-phenyl-3-nonanone in 94% yield. Other results are listed in Table 1.

The high yields of the products, the facility of the reaction procedure, and the mildness of the reaction conditions may make it possible to utilize this method for the syntheses of unsymmetrical ketones. The formation of the corresponding isomeric ketones (**1**) was negligible.[3]

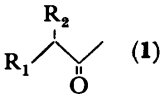

(**1**)

Using this method, synthesis of dihydrojasmone was carried out (Scheme 2). After successive alkylations and hydrolysis, 1-undecen-5-one (**2**) was obtained in 87% yield from acetone dimethylhydrazone. Oxidation of the terminal double bond to 2,5-undecanedione (95% yield) and the succeeding cyclization afforded the desired dihydrojasmone in 61% yield.

Experimental

The IR spectra were recorded on a Hitachi 260-10 Infrared Spectrophotometer, the NMR spectra were measured on a Hitachi R-600 FT-NMR Spectrometer, and the mass spectra were measured on a Hitachi RM-50 GC-MS. All the experiments were carried out under an atmosphere of argon. The tetrahydrofuran (THF) was dried by distillation from

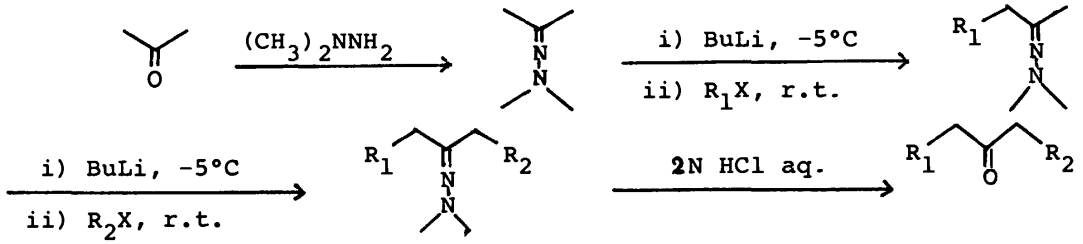

Scheme 1.

TABLE 1. SYNTHESIS OF UNSYMMETRICAL KETONES FROM ACETONE DIMETHYLHYDRAZONE

Run	R_1X	R_2X	Product	Yield/%[a]
1	CH_3I		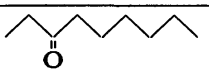	85
2		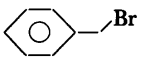	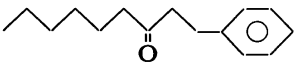	94
3	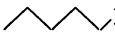		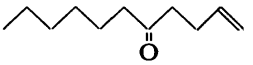	87
4	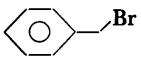	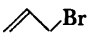	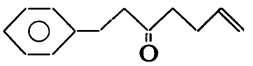	73
5		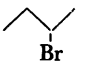	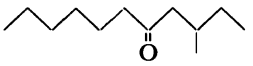	55
6		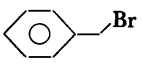	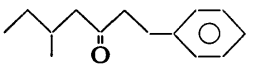	66

a) Isolated yield.

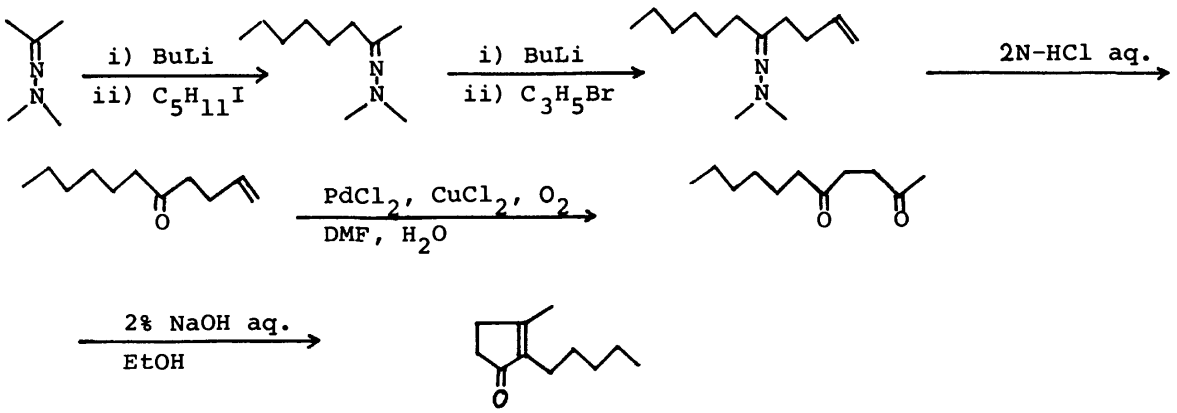

Scheme 2.

lithium aluminum hydride. The iodomethane, 1-iodopentane, benzyl bromide, allyl bromide, and 2-bromobutane were all commercial products and were distilled before use. Acetone dimethylhydrazone was prepared in 71% yield by refluxing acetone and dimethylhydrazine in benzene in the presence of catalytic amount of trifluoroacetic acid.

Representative Synthesis of 1-Phenyl-3-nonanone. Butyllithium (2.6 mmol) was added *via* a syringe at −5 °C to a solution of acetone dimethylhydrazone (2.4 mmol) in THF under argon. After 1 h, 1-iodopentane (2.4 mmol) was added and the mixture was stirred for 10 h at room temperature. After cooling the mixture to −5 °C again, butyllithium (2.6 mmol) and then benzyl bromide (2.6 mmol) were added, and the reaction mixture was stirred for 10 h at room temperature. Two mol dm^{-3} hydrochloric acid (10 ml) was added for hydrolysis and the organic material was extracted with ethyl acetate. The organic layer was washed with brine, dried over sodium sulfate, filtered, and concentrated *in vacuo*. The preparative TLC of the crude residue (silica gel, hexane–ethyl acetate 10:1) afforded pure 1-phenyl-3-nonanone (0.492g 94% yield).

Acetone Dimethylhydrazone. Bp 95 °C/760 Torr (1 Torr=133.322 Pa); NMR ($CDCl_3$) (δ): 1.93 (3H, s, C-CH_3), 1.97 (3H, s, C-CH_3), 2.04 (6H, s, N(CH_3)$_2$); IR (cm^{-1}): 1660, 1170, 1090; MS *m/z* (%): 100 (M^+, 8), 44 (90), 42 (83), 28 (100).

1-Undecen-5-one. NMR ($CDCl_3$) (δ): 0.88 (3H, t, -CH_3), 1.27—1.70 (10H, m, -CH_2-×5), 2.44 (4H, t, -CH_2COCH_2-), 4.86—6.18 (3H, m, -CH=CH_2); IR (cm^{-1}): 1710, 1640, 1130, 1080, 1000, 910; MS *m/z* (%): 168 (M^+, 18), 113 (56), 98 (68), 85 (100), 66 (79).

5-Methyl-1-phenyl-3-heptanone. NMR ($CDCl_3$) (δ): 0.83 (3H, d, -CHCH_3), 0.90 (3H, t, -CH_2CH_3), 1.15—1.38 (2H, m, -CH_2CH_3), 1.66—2.05 (1H, m), 2.20—2.38 (2H, m, -CHCH_2CO-), 2.78 (2H, t, -CH_2Ph), 2.83 (2H, t, -$COCH_2$-CH_2-), 7.24 (5H, s, -C_6H_5); IR (cm^{-1}): 1710, 1600, 1140, 1060, 1030; MS *m/z*: 204 (M^+).

The other compounds listed in Table 1 were identified by comparison of their IR, NMR, and mass spectra with those of authentic samples.

Synthesis of Dihydrojasmone from 1-Undecen-5-one. To a mixture of palladium chloride (60.5 mg, 0.34 mmol) and copper(II) chloride (173 mg, 1.0 mmol) in aqueous *N,N*-dimethylformamide (1.6 ml), 1-undecen-5-one (**2**) (0.191 g, 1.13 mmol) was gradually added under oxygen atmosphere. The mixture was stirred at room temperature for 40 h, poured into 5 mol dm^{-3} hydrochloric acid (15 ml), and extracted with ethyl acetate. The organic layer was washed with brine, dried over sodium sulfate, filtered, and concentrated *in vacuo*. Preparative TLC of the residual liquid gave 2,5-undecanedione 0.20 g (95% yield). The diketone (0.126 g, 0.68 mmol) was added to ethanol (3 ml) and 0.5 mol dm^{-3} aqueous sodium hydroxide (3 ml), and the mixture was refluxed for 7 h. The mixture was diluted with water and extracted with ethyl acetate. The organic layer was washed with brine, dried over sodium sulfate, filtered, and concentrated *in vacuo*. The preparative TLC of the residual liquid gave dihydrojasmone (0.070 g) in 61% yield. This compound was identified by comparison of IR, NMR, and mass spectra with those of a authentic sample.

References

1) Alkylation of acetone dimethylhydrazone with trideuteromethyl iodide and methyl iodide has been reported; M. E. Jung and T. J. Shaw, *Tetrahedron Lett.*, **1979**, 4149.

2) R. H. Wiley, S. C. Slaymaker, and H. Kraus, *J. Org. Chem.*, **22**, 204 (1957).

3) E. J. Corey and D. Enders, *Tetrahedron Lett.*, **1976**, 3, 11; *Chem. Ber.*, **111**, 1337, 1362 (1978); E. J. Corey, D. Enders, and M. G. Bock, *Tetrahedron Lett.*, **1976**, 7; D. Enders and P. Wenster, *ibid.*, **1978**, 2853; E. J. Corey and D. L. Boger, *ibid.*, **1978**, 4597.

 © 1985 The Chemical Society of Japan Bull. Chem. Soc. Jpn., 58, 409—413 (1985)

Structural Studies of Cyclo(L-histidyl-L-histidyl) and Its Metal Complexes

Yoshitane KOJIMA,* Tetsushi YAMASHITA, Shinya NISHIDE, Ken HIROTSU,* and Taiichi HIGUCHI
Department of Chemistry, Faculty of Science, Osaka City University, Sugimoto, Sumiyoshi-ku, Osaka 558
(Received June 25, 1984)

The crystal structure of cyclo(L-histidyl-L-histidyl) was determined by X-ray diffraction techniques, and was refined to a final R index of 0.066 for 680 reflections. This showed that one imidazolyl group of this compound faces the piperazine ring(folded) whereas the other is kept away from the ring(unfolded). A calculation using the α-β coupling-constant data of this peptide obtained by an ^1H NMR measurement shows that the ratio of a folded conformation to an unfolded one is 49:51 in D_2O. Also, NMR investigations of zinc(II) and silver(I) complexes with this peptide were carried out in D_2O.

Cyclic dipeptides(3,6-disubstituted 2,5-piperazinedione) are the simplest cyclic peptides of biological interest. The cyclic character of 2,5-piperazinedione simplifies the interpretation of NMR and other spectroscopic data and greatly limits the number of the preferred conformations. Numerous cyclic dipeptides have been studied in solution using NMR measurements.[1] Some of them have been studied the solid state by X-ray structural analyses.[2]

The most interesting result from the studies of cyclic dipeptides is that molecules containing an aromatic side chain (such as phenylalanyl, tyrosyl, and histidyl residues) tend to have a folded conformation with the aromatic ring facing the piperazine ring.[1a] An interaction between the aromatic ring and the piperazine ring (probably a dipole-induced dipole one) appears to have a great influence on the overall conformation of cyclic dipeptides.[2a]

We have mainly engaged in a study[3] of the metal complexes of cyclic dipeptides, including a histidyl residue in the solid state and in solution using X-ray diffraction methods and NMR techniques, respectively. These peptides are good model compounds for metalloproteins.

In a series of studies of the metal complexes of cyclic dipeptides, we suggested that the conformation of the cyclic dipeptide greatly affects the formation and conformation of the metal complex.[3]

This paper describes the X-ray crystallographic structure of cyclo(L-histidyl-L-histidyl)(abbreviated to CHH)·5/2H_2O with two imidazole rings on the same side of the piperazine ring. Also, the conformations of CHH and its metal complexes in an aqueous solution are discussed using NMR (^1H and ^{13}C) and the molecular-weight data.

Experimental

CHH and its silver(I) complexes were prepared according to methods reported earlier.[3a]

Preparations of Zinc(II) Complexes. A mixture of CHH (0.70 mmol) and zinc(II) nitrate (0.35 mmol) was completely dissolved in hot water (70 mdm^3). After standing at room temperature for a few days, a formed precipitate was filtered off. Mp 240—260° dec., Yield; 95%. Found: C, 36.87; H, 4.11, N; 24.65%. Calcd for Zn $(C_{12}H_{14}N_6O_2)_2(NO_3)_2\cdot 5/2H_2O$: C, 36.81; H, 4.25; N, 25.04%. Another complex was similarly obtained by the above procedure. Mp 209—222° dec., Yield; 85%. Found; C, 33.04; H, 3.65; N, 19.08%. Calcd for Zn-$(C_{12}H_{14}N_6O_2)_2(ClO_4)_2\cdot 7/2H_2O$: C, 32.91; H. 4.03; N, 19.19%.

X-Ray Crystallographic Procedure. A crystal (0.4×0.2×0.04 mm) grown from slow evaporation of an aqueous solution was used for data collection. Crystal data: $C_{12}H_{14}N_6O_2\cdot 5/2H_2O$ for CHH·5/2H_2O: M=319.3, orthorhombic, space group $P2_12_12$. On the basis of 20 reflections, the following unit-cell parameters were obtained: a=19.91(1), b=12.66(1), c=6.163(3) Å, V(for Z=4)=1553(2) Å^3, D_c=1.56 gcm^{-3}, and μ(Mo $K\alpha$)=1.31 cm^{-1}.

All unique diffraction maxima with $2°\leq 2\theta \leq 48°$ were recorded in the ω-scan mode using a computer-controlled four-circle diffractometer and graphite monochromated Mo $K\alpha$(0.7107 Å) X-rays. Of the 1448 reflections surveyed, 680 (47%) were judged observed ($I>3\sigma(I)$) after correction for Lorenz, polarization and background effects. No absorption correction was applied.

The structure was solved by MULTAN.[4a] All hydrogen atoms were located on difference electron density syntheses. Full matrix least-squares refinements of positional and anisotropic thermal parameters for non-hydrogen atoms and of positional parameters only for hydrogen atoms (to which isotropic temperature factors 1.0 Å^2 greater than those of the atoms bonded to them were assigned) led to a convergence at R=0.066 (R_w=0.054).[4b] Neutral atomic-scattering factors of Cromer and Waber[5] were used for all atoms.[6]

Other Measurements. The ^1H and ^{13}C NMR data were obtained in D_2O at 50°C using sodium 3-trimethylsilyl-1-propanesulfonate as an internal reference. The molecular weights of the zinc(II) complexes were measured in H_2O at 56°C using urea as a standard material. JEOL FX-100 (for ^1H and ^{13}C NMR spectra), PS-100 (for ^1H NMR spectra), and Knauer Vapor Pressure Osmometer (for molecular weight) apparatus were used for the measurements of the samples.

Results and Discussion

Crystal and Molecular Structures of CHH·5/2H_2O. The standard peptide notations and bond distances are shown for CHH in Fig. 1. All bond distances and angles agree well with the values for other related compounds.[2] A stereoscopic view of the molecular packing in a unit cell is shown in Fig. 2.[4c] There are nine protons (four from CHH and five from water molecules) available for hydrogen bonding, all of

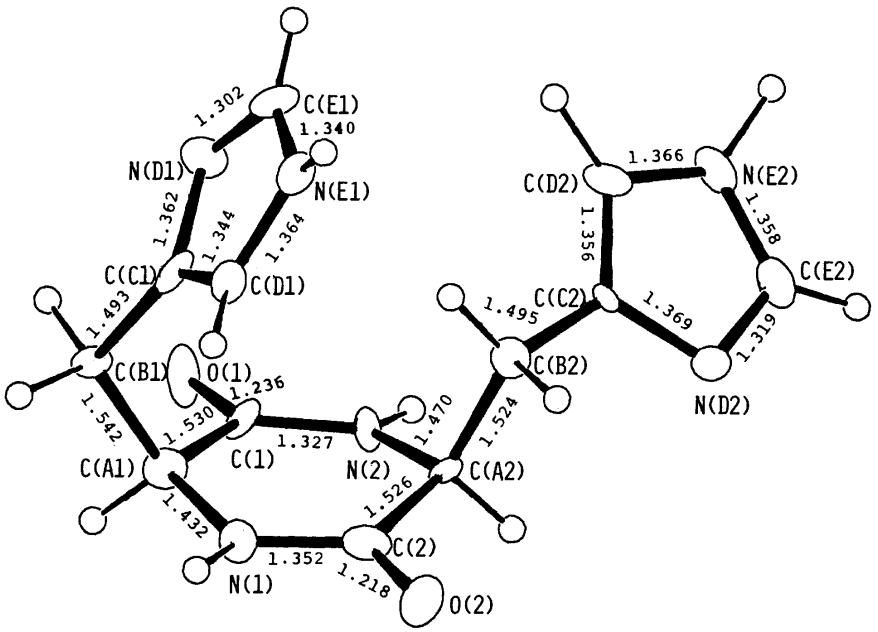

Fig. 1. Peptide notations and bond distances in cyclo(L-histidyl-L-histidyl). Standard deviations are 0.011—0.016 Å for all bond distances.

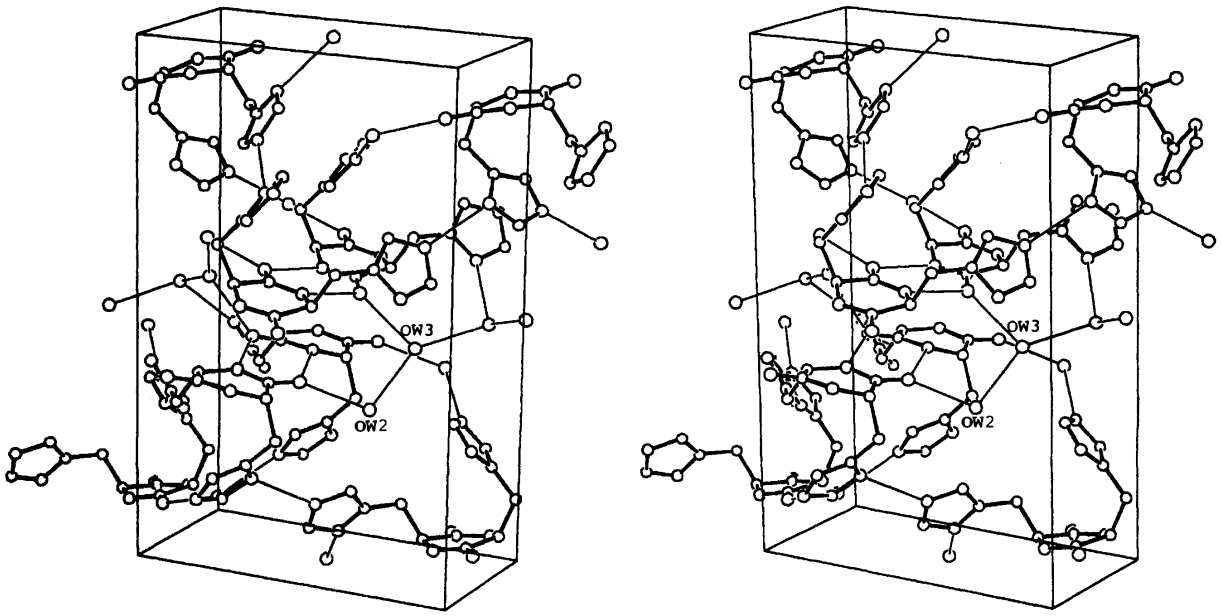

Fig. 2. Stereopicture of the molecular packing in cyclo(L-histidyl-L-histidyl). Thin lines indicate hydrogen bonding.

which are involved in intermolecular hydrogen bonds. Hydrogen bonds of the N-H···O type bind translationally equivalent piperazine rings in ribbons parallel to the c axis. Pairs of ribbons lie face-to-face across a two-fold axis such that one ribbon is connected to another ribbon through a O(1)···OW2···OW3···O(2) hydrogen-bonding scheme.

N(1), C(1), N(2), and C(2) atoms of the piperazine ring are coplanar within 0.03(1) Å with C(A1) and C(A2) deviate from this plane by 0.16(1) and 0.19(1) Å, respectively. The interplanar angles between the plane defined by N(1), C(1), N(2), and C(2) and the planes defined by C(1), C(A1), and N(1) and defined by C(2), C(A2), and N(2) are 12(1) and 13(1)°, respectively. Thus, the piperazine ring has a 'flagpole boat' conformation with cis α-carbon substituents quasi-axial. Both imidazole rings are planar within 0.02(1) Å, making angles of 56.8(5) and 46.6(5)° with the piperazine ring, respectively. Selected dihedral angles are given in Table 1. One imidazole ring is folded back over the piperazine ring with another imidazole ring kept away from the piperazine ring. This conformation is commonly found in 2,5-piperazinediones with aromatic residues.[2] The folded conformation of CHH with a 'flagpole boat' piperazine ring makes the intimate contacts between the imidazole ring and the piperazine ring possible and is compared with cyclo(glycyl-L-tyrosyl)[2a] and cyclo(L-leucyl-L-histidyl).[2e]

The short intramolecular contacts between the atom, five or more bonds apart are for N(1)···C(D1)= 3.26(1), C(1)···N(D1)=3.52(1), C(B2)···N(D1)= 3.87(1), C(B2)···N(E1)=3.74(1), C(B2)···C(D1)= 3.68(2), C(B2)···C(E1)=3.87(2), and C(2)···C(D1)=3.54(1) Å.

NMR of CHH and its Metal Complexes in D_2O. Table 2 shows β-proton chemical shifts, α-β coupling constants, and side-chain conformations for CHH and its metal complexes in D_2O. There are three possible conformations of CHH in solution. These conformations are described as follows: a folded-unfolded conformation (the same conformation in solid state), a folded-folded conformation (both imidazole rings hang over the piperazine ring) and an unfolded-unfolded (both imidazole rings are kept away from the piperazine ring). The results (folded/unfolded=49/51) for CHH shown in Table 2 appear to be consistent with a folded-unfolded conformation of CHH, but do not exclude the remaining two conformations when these two conformational isomers are present in an almost equal amount. According to the molecular structure of solid CHH, a folded-folded conformation is unlikely since the rotation of the unfolded imidazole ring around the C(A2)-C(B2) bond into a folded position produces unusual short contacts between the two imidazole rings. Cyclic dipeptides with aromatic rings usually prefer a folded conformation, but not an unfolded one in solution, as known from NMR studies.[1a] Thus, the major conformers of CHH in solution is a folded-unfolded one, which is similar to that of the solid state.

The ^1H NMR data in Table 2 indicates that the ratio of a folded form to an unfolded one is 8:92 for an $Ag(CHH)^+$ ion. Furthermore, the extremely low solubility of silver(I) complexes with CHH in protic and aprotic solvents suggests the preference of a polymeric form.

In addition, Table 2 shows that the chemical shift (2.7—3.1 ppm) of β-protons of a zinc(II) complex with CHH almost does not change from those (2.39 and 2.86 ppm) of CHH in spite of the broad and unresolved signals. Therefore, the side chain conformations of a zinc(II) complex are essentially identified with those of CHH. The broad and unresolved signal may be attributed to the rapid rotations about α-β carbon single bonds and the exchangeable coordination of nitrogen atoms [N(D1) or N(E1) and N(D2) or N(E2)] of imidazolyl groups to Zn^{2+} ions.

Table 3 shows the data of ^1H and ^{13}C NMR for CHH and its zinc(II) complex. It is suggested from Table 3

Table 1. Dihedral angles in cyclo(L-histidyl-L-histidyl)

Dihedral angle	Notation*	ϕ/°
C(2)-N(1)-C(A1)-C(1)	ϕ_1	17(1)
N(1)-C(A1)-C(1)-N(2)	ψ_1	−11(1)
C(A1)-C(1)-N(2)-C(A2)	ω_1	−8(1)
C(1)-N(2)-C(A2)-C(2)	ϕ_2	19(1)
N(2)-C(A2)-C(2)-N(1)	ψ_2	−12(1)
C(A2)-C(2)-N(1)-C(A1)	ω_2	−5(1)
N(1)-C(A1)-C(B1)-C(C1)	χ_1^1	58(1)
C(1)-C(A1)-C(B1)-C(C1)		−71(1)
C(A1)-C(B1)-C(C1)-N(D1)	χ_1^2	102(1)
C(A1)-C(B1)-C(C1)-C(D1)		−80(1)
N(2)-C(A2)-C(B2)-C(C2)	χ_2^1	−66(1)
C(2)-C(A2)-C(B2)-C(C2)		170(1)
C(A2)-C(B2)-C(C2)-N(D2)	χ_2^2	−63(1)
C(A2)-C(B2)-C(C2)-C(D2)		118(1)

*See Ref. 7.

Table 2. β-Proton chemical shifts, α-β coupling constants, and side chain conformation for cyclo(L-histidyl-L-histidyl) and its metal complexes in D_2O at 50 °C

Compound	β-proton chemical shifts $\delta(\Delta\delta^{a})$(ppm) high	low	α-β coupling constants Hz $J_{\alpha h\beta}$	$J_{\alpha l\beta}$	side chain conformations[b] F	U_I	U_{II}
CHH	2.39[c]	2.86[c]	6.6	4.2	49	15	36
$Zn(CHH)_2^{2+}$[d]	2.7—3.1[e]						
$Ag(CHH)^+$[f]	3.25[c] (0.86)	3.32[c] (0.46)	7.7	7.7	8	46	46

a) $\Delta\delta=\delta$[silver(I) complex ion]−δ(free ligand). b) Expressed in %; for notations and calculctions see Ref. 1. c) β-Methylene[C(B1) or C(B2)]and α-methine[C(A1) or C(A2)] protons of histidyl residues exhibit an ABX spin system, in which A and B are the β-protons and X is the α-proton. e) Broad and unresolved signals. f) $[Ag(CHH)(PF_6)]_n$ was used for the measurement.

Table 3. ^1H and ^{13}C chemical shifts(ppm) of CHH and $Zn(CHH)_2^{2+}$ in D_2O at 50 °C

Compound	Chemical shift, $\delta(\Delta\delta^{a})$ ^1H[b] HCAn	HCDn	HCEn	^{13}C[b] C(n)	C(An)	C(Bn)	C(Cn)	C(Dn)	C(En)
CHH	4.26	6.89	7.71	171.4	57.2	33.7	134.3	120.8	138.8
$Zn(CHH)_2^{2+}$[c]	4.35	6.90	7.97	171.5	57.0	32.1	131.6	122.9	139.1
	(0.09)	(0.01)	(0.26)	(0.1)	(−0.2)	(−1.6)	(−2.7)	(2.1)	(0.3)

a) $\Delta\delta=\delta$[zinc(II) complex ion]−δ(free ligand) b) n=1 and 2. c) $Zn(CHH)_2(NO_3)_2\cdot 5/2H_2O$ was used for the measurement.

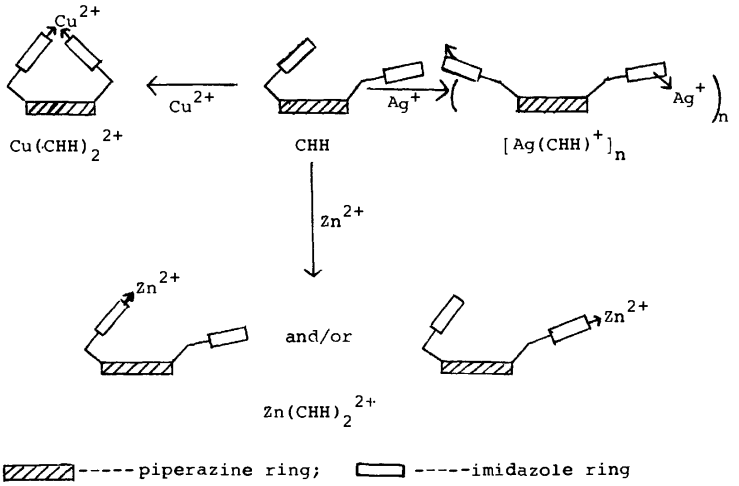

Fig. 3. The predominant conformations of cyclo(L-histidyl-L-histidyl) in complexations of Cu^{2+}, Ag^{+}, and Zn^{2+} ions.

that the imidazole nitrogen atom [N(Dn) or N(En); n=1 or 2] links to the Zn^{2+} ion on the basis of the up- or down-field shifts ($\Delta\delta$=0.26, −1.6, −2.7, and 2.1) of HCEn, C(Bn), C(Cn), and C(Dn) (n=1 and 2) of $Zn(CHH)_2^{2+}$ from CHH, respectively. This distinct shift may be due to the redistribution of electron densities owing to the binding of the imidazole nitrogen atom to the Zn^{2+} ion.[1c] On the other hand, it is indicated that the oxygen atoms of 2,5-piperazinedione do not coordinate to the Zn^{2+} ion on the basis of no distinct shifts ($\Delta\delta$=0.09, 0.1, and −0.2) of HCAn, C(n), and C(An)(n=1 and 2) of $Zn(CHH)_2^{2+}$ from CHH, respectively. Also, the earlier NMR measurements suggested that the imidazole nitrogen atom of CHH coordinates to the Ag^{+} ion, exclusively.[3a]

The molecular weights of zinc(II) complexes were obtained as follows. The perchlorate and nitrate of the $Zn(CHH)_2^{2+}$ ion are a monomeric form, and dissociate only into a complex ion and two anions: $Zn(CHH)_2^{2+}+2ClO_4^-$ (Calcd 813/3=271, Found 304) or $Zn(CHH)_2^{2+}+2NO_3^-$ (Calcd 738/3=246, Found 266). The molecular weight of a silver(I) complex could not be measured because of its extremely low solubility.

X-Ray, molecular weight, ^1H NMR, and CD studies of a copper(II) complex with CHH(reported earlier[3c]) reveal that both of the folded imidazole rings of CHH link to the Cu^{2+} ion, forming a 13-membered chelate rings by the N(E1) and N(E2) atoms. This observation is attributed to the coordination of CHH for the Cu^{2+} ion because of the too short distance(2.76 Å) between N(E1) and N(E2) makes the existence of a folded-folded conformer of free CHH impossible. In the case of the silver(I) complex ion (as described above) CHH prefers two unfolded imidazole rings whose nitrogen [N(Dn) or N(En); n=1 or 2] linearly coordinates to the Ag^{+} ion to give a polymeric material. In the zinc(II) complex ion, CHH has a folded imidazole ring and an unfolded one. However, at this stage, it is difficult to determine which (folded or unfolded) imidazole ring coordinates and, furthermore, which [N(Dn) or N(En); n=1 or 2] nitrogen atom of the imidazole ring links to the Zn^{2+} ion.

From a series of experimental results regarding CHH and its metal complexes, the predominant conformations of CHH in complexations of Cu^{2+}, Ag^{+}, and Zn^{2+} ions are assumed as shown in Fig. 3.

The authors wish to thank Prof. Toshio Miwa for his measurements of the NMR spectra and for helpful comments. They also wish to thank Mr. Junichi Gohda for the measurements regarding the elemental analyses. Also, the authors are indebted to the Crystallographic Research Center, Institute for Protein Research, Osaka University, for computer calculations.

References

1) a) K. D. Kopple and M. Ohnishi, *J. Am. Chem. Soc.*, **91**, 962 (1969); b) Y. Imanishi, *Adv. Polymer Sci.*, **20**, 1 (1976); c) C. M. Deber, V. Madison, and E. R. Blout, *Acc. Chem. Res.*, **9**, 106 (1976).

2) a) C.-F. Lin and L. E. Webb, *J. Am. Chem. Soc.*, **95**, 6803 (1973); b) M. Cotrait, M. Ptak, B. Busetta, and A. Heitz, *ibid.*, **98**, 1073 (1976); c) R. Ramani, K. Venkatesan, and R. E. Marsh, *ibid.*, **100**, 949 (1978); d) E. Benedetti, R. E. Marsh, and M. Goodman, *ibid.*, **98**, 6676 (1976); e) I. Tanaka, T. Iwata, N. Takahashi, and T. Ashida, *Acta Crystallogr., Sect. B*, **33**, 3902 (1977); f) M. Cotrait and M. Ptak, *ibid., Sect. B*, **34**, 528 (1978).

3) a) Y. Kojima, T. Yamashita, Y. Ishino, T. Hirashima, and T. Miwa, *Bull. Chem. Soc. Jpn.*, **56**, 3841 (1983); b) Y. Kojima, N. Ishio, T. Yamashita, and K. Hirotsu, *Chem. Lett.*, **1983**, 1365; c) Y. Kojima, *Transition Met. Chem.*, **4**, 269 (1979); d) M. Bressan, R. Ettore, F. Marchiori, and G. Valle, *Int. J. Peptide Protein Res.*, **19**, 402 (1982).

4) a) G. Germain, P. Main, and M. M. Woolfson, *Acta Crystallogr., Sect. B*, **26**, 274 (1970); M. M. Woolfson, *ibid., Sect. A*, **33**, 219 (1977); b) W. R. Busing, K. O. Martin, and H. S. Levy, "A Fortran Crystallographic Least Square Program," USAEC Report ORNL-TM-305, Oak Ridge Na-

tional Laboratory, Oak Ridge, TN, (1965); c) C. Johnson, "ORTEP, A Fortran Thermal-Ellipsoid Plot Program," USAEC Report ORNL-3794, Oak Ridge National Laboratory, Oak Ridge, TN, (1965).

5) D. T. Cromer, J. T. Waber, "International Tables for X-ray Crystallography;" J. A. Ibers, W. C. Hamilton, Eds.; Kynoch Press: Birmingham, England, (1974); Vol. IV, Table 2.2A, p. 72.

6) Fractional coordinates (Table 1), bond angles (Table 2), and observed and calculated structure factors (Table 3) are deposited as Document No. 8508 at the Office of the Editor of Bull. Chem. Soc. Jpn.

7) IUPAC-IUB Commision on Biological Nomenclature, *Biochemistry*, **9**, 3471 (1970).

Complete Magnetic Anisotropy Films for Perpendicular Recording Prepared by an Electroless Plating Method

Tetsuya OSAKA,* Ichiro KOIWA, Yutaka OKABE, Hiroshi MATSUBARA, Akihide WADA, Fumio GOTO,† and Norio SHIOTA†

Department of Applied Chemistry, School of Science and Engineering, Waseda University, Okubo, Shinjuku-ku, Tokyo 160

†*Microelectronics Research Labs, NEC Corporation, Miyazaki, Miyamae-ku, Kawasaki 213*

(Received July 7, 1984)

A complete magnetic anisotropy film was formed by an electroless plating method for a high-density perpendicular recording medium. The Co alloy plating bath, using ammoniacal malonate-tartrate-succinate mixed complexing agents was studied mainly by varying three main metal ion factors in the bath: *i.e.*, the concentrations of $NiSO_4$, NH_4ReO_4, and $MnSO_4$. The fine columnar structure of magnetic film in a cross section was confirmed by SEM observation. Three different kinds of eight-inch disks A, B, and C, were prepared under selected conditions with magnetic film thickness of 0.50, 0.25, and 0.20 μm respectively. The recording performance was evaluated with a Winchester ring head with a 0.33 μm gap length under various head-medium spacings. A perpendicular recording mode was confirmed, and the following recording densities were obtained: D_{50}=54 and 58 kFRPI for disk A, and 57 and 63 kFRPI for disk B when using 0.20 and 0.15 μm practical usable spacing respectively, and D_{50}=68 kFRPI for disk C when using the more advanced 0.12 μm spacing. It was suggested that the electroless cobalt alloy plating has a high potential as a process for producing perpendicular recording media.

Since the proposal of a perpendicular recording system by the Iwasaki school,[1,2] interest in it has exploded as a high potential technology to extend the limit of the present longitudinal recording system. Many workers have reported on perpendicular recording media, such as sputtered Co-Cr,[3] sputtered Ba ferrite,[4] evaporated Co-Cr[5] and coated Ba ferrite.[6] Recently, many extensive studies have been reported, not only of the medium but also of the perpendicular recording system, such as the spacing effect of the read/write conditions,[7] a comparison of the read/write characteristics between using a ring head and using a perpendicular head,[8] and the evaluation of the whole system for a perpendicular recording floppy disk drive.[9]

However, only a few attempts[10-13] have been made to use the electroless plating method to produce a medium which has higher productivity and cost performance. If the perpendicular medium could be obtained by means of an electroless plating method, as well as the longitudinal-recording-mode disk developed by NEC Corporation,[14] the realization of the system, with its merits of mass production and wear durability, would be accelerated.

With such considerations in view, the present authors attempted to prepare perpendicular recording media by means of an electroless plating. It was first reported by the present authors[10] that the perpendicular oriented c-axis of the cobalt hcp structure can be easily obtained by means of manganese codeposition into Co-Ni-P films; nevertheless, a very small amount of manganese is codeposited.[13] Moreover, the decrease in the saturation magnetization, which produces the completely magnetic anisotropy film, was performed by the rhenium codeposition into Co-Ni-Mn-P film.[15-18]

This communication reports the preparation of a new stable electroless bath for completely magnetic anisotropy films and their recording performance.

Experimental

Electroless cobalt alloy films were plated from an ammoniacal malonate-tartrate-succinate complexing-agent bath, whose composition and conditions were listed in Table 1. A polished electroless plated Ni-P film, composed of amorphous states, was usually used as a substrate, and an activated copper sheet was used only for the compositional analysis. The film composition of Co, Ni, Re, Mn, and P was determined 0.5 μm thick films by EPMA and X-ray fluorescence methods. The X-ray diffraction patterns and rocking curves for the plated films were measured by means of X-ray diffractometer with an Fe target. The magnetic properties were measured in 0.5μm thick films by the use of a vibrating sample magnetometer and a torgue magnetometer in a 10 kOe maximum applied field. Coercivities $Hc(\perp)$ and $Hc(//)$ were evaluated from the M-H hysteresis loops measured in perpendicular(⊥) and parallel(//) magnetic fields. The anisotropy field, Hk, was evaluated from the in-plane M-H hysteresis loop. SEM photographs for a cross section of the magnetic film were obtained by means of an Hitachi S-700 field emission SEM with a magnification of

TABLE 1. ELECTROLESS PLATING BATH COMPOSITION AND CONDITIONS

Chemicals	Concentration/mol dm^{-3}
$NaH_2PO_2 \cdot H_2O$	0.30
$(NH_4)_2SO_4$	0.50
$CH_2(COONa)_2 \cdot H_2O$	0.30
$C_2H_2(OH)_2(COONa)_2 \cdot 2H_2O$	0.20
$C_2H_4(COONa)_2$	0.30
$CoSO_4 \cdot 7H_2O$	0.06
$NiSO_4 \cdot 7H_2O$	0.06—0.16
NH_4ReO_4	0—0.009
$MnSO_4 \cdot 4$—$6H_2O$	0—0.09
Bath temperature	80°C
pH adjusted by NH_4OH	9.2

20000 and 50000. Eight inch disks were prepared with the bath conditions selected. The disk structure was the same as that reported in a previous paper.[12] The protective SiO_2 overcoat was formed by means of a spin-coat method.

Results and Discussion

Electroless Plating Bath for Perpendicular Recording Media. On the basis of various investigations for complexing agents, the ammoniacal malonate-tartrate-succinate mixed system was first selected, considering that sodium malonate and sodium tartrate tend to be favorable complexing agents for cobalt and perrhenate ions respectively, and further that sodium succinate tends to improve the $\Delta\theta_{50}$ value of the c-axis orientation. Moreover, the bath stability was improved by using a mixture of the three complexing agents.

Since the bath pH hardly affected the perpendicular orientation of the hcp structure and the magnetic anisotropy properties in the region between pH 8.8 and 9.4 in a manner dissimilar to that reported in the previous research,[13] the bath pH of 9.2, showing relatively favorable conditions, was chosen in this research.

The metal ion concentrations are a very important factor, like the complexing agents, in controlling magnetic properties. The cobalt sulfate was first fixed at 0.06 mol dm^{-3} in order to obtain optimum conditions for the other metal ion concentrations on the basis of the experimental results regarding the effect of the ratio of cobalt and phosphinate ions on the magnetic properties. Under the conditions at a fixed 0.06 mol dm^{-3} $CoSO_4$, the effects of the other metal ion concentrations of $NiSO_4$, NH_4ReO_4, and $MnSO_4$ on film properties were also investigated, as shown later.

The effects of the $NiSO_4$ concentration on the magnetic properties and the half width for the rocking curves of the (002) plane, $\Delta\theta_{50}$, have already been indicated in previous papers.[16,17] It was also reported there[16,17] that the optimum conditions for perpendicular magnetic anisotropy film were obtained in the $NiSO_4$ concentration region between 0.12 and 0.16 mol dm^{-3} at the fixed concentrations of 0.005 mol dm^{-3} NH_4ReO_4 and 0.05 mol dm^{-3} $MnSO_4$. In the above region, the magnetic anisotropy energy, *Ku*, became positive and reached its maximum value (1.6×10^5 erg cc^{-1}) at 0.12 mol dm^{-3} $NiSO_4$. The saturation magnetization, *Ms*, was also reported to gradually decrease with an increase in the $NiSO_4$ concentration.

From the effect of the $NiSO_4$ concentration on the compositional analysis for plated films, shown in a previous paper,[18] it was concluded that the increase in the $NiSO_4$ concentration caused the cobalt content to decrease and the nickel content to increase with constant values of 6 at% Re, 0.2 at% Mn, and 11 at% P.

The effect of the ammonium perrhenate concentration on the magnetic properties and the $\Delta\theta_{50}$ at the fixed concentrations of 0.12 mol dm^{-3} $NiSO_4$ and 0.05 mol dm^{-3} $MnSO_4$ is shown in Fig. 1. Since the Co-Ni-Mn-P films previously reported[12] did not become a complete magnetic anisotropy film, because of their higher *Ms* value, the rhenium codeposition into Co alloy film was intended to produce the *Ms* decrease in films. The demagnetized field, $Hd=4\pi Ms$, decreases with the decrease in Ms; therefore, a proper decrease in the *Ms* values could realize complete magnetic films with positive *Ku* values. Since it was very difficult to codeposit chromium into Co alloy film by means of an electroless plating method, whose codeposition could be easily deduced as a candidate from a sputtered Co-Cr film, the codeposition of rhenium, instead of chromium, was attempted in an effort to make the *Ms* decrease. The very small amount of NH_4ReO_4 into the bath made the Ms value decrease as shown in Fig. 1(b). Consequently, it produced a change in the *Ku* value from negative to positive, as may be seen in Fig. 1 (a). The other magnetic factors of *Hk* and ΔHc ($=Hc(\perp)-Hc(//)$) also showed optimum values in the concentration region between 0.003 and

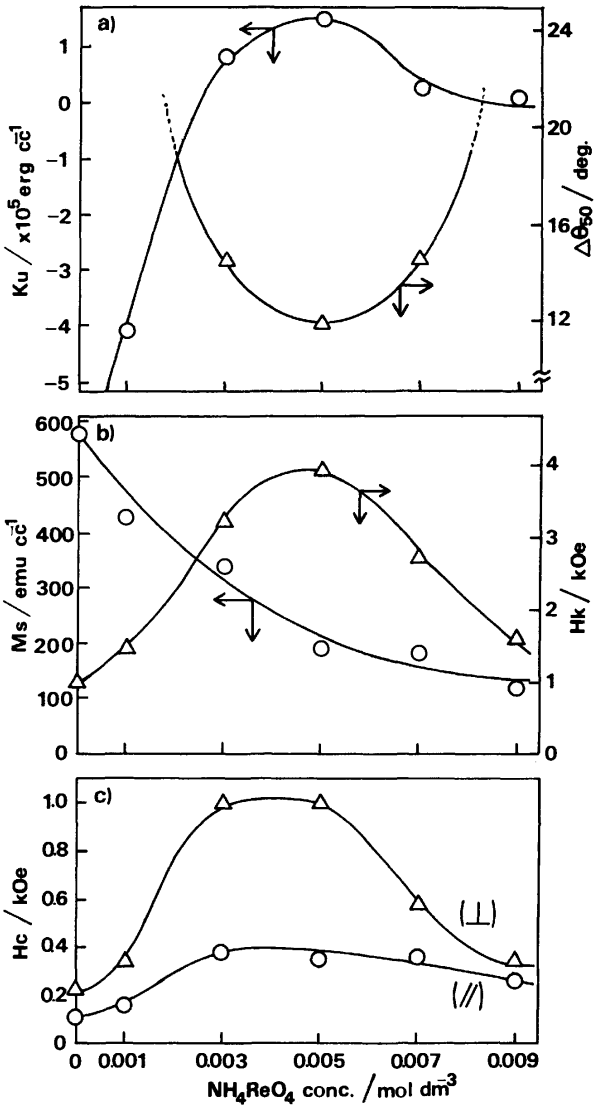

Fig. 1. Effects of NH_4ReO_4 concentration on magnetic properties and $\Delta\theta_{50}$ of (002) plane for plated films using 0.5 μm thickness.

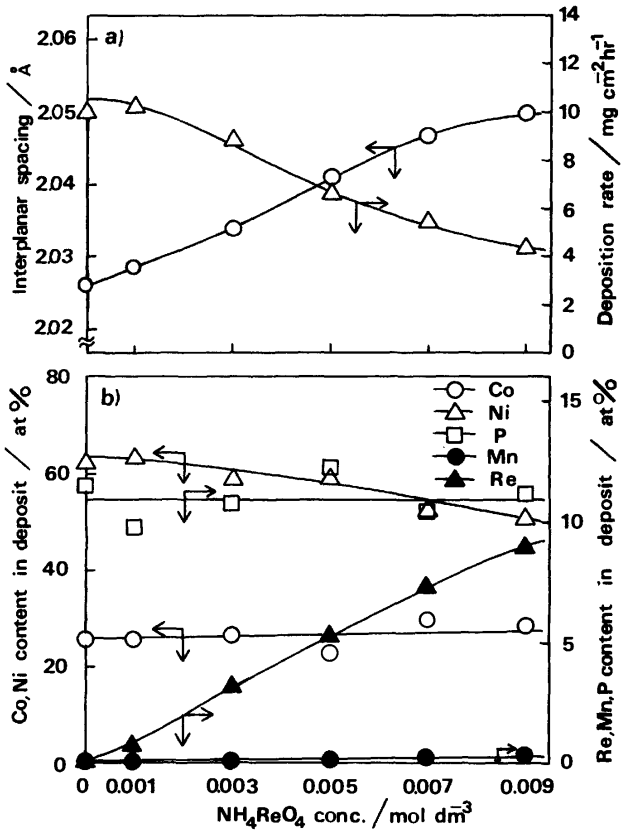

Fig. 2. Effect of NH_4ReO_4 concentration on film composition, interplanar spacing and deposition rate for plated films using 0.5 μm thickness.

0.006 mol dm^{-3} NH_4ReO_4. The $\Delta\theta_{50}$ value also reached its minimum in the same concentration region and reached the minimum value of 12 degrees at 0.005 mol dm^{-3} NH_4ReO_4.

The compositional analysis for the variation in the NH_4ReO_4 concentration is demonstrated in Fig. 2(b). The film composition for Co and P was independent of the NH_4ReO_4 concentration, while the increase in the NH_4ReO_4 concentration made the rhenium content increase linearly, accompanied by the decrease in the Ni content. The very small manganese codeposition (Mn=0.05—0.40 at%) slightly increased with the increase in the NH_4ReO_4 concentration. In Fig. 2(a), the interplanar spacing value, d, from the hcp structure, calculated from the X-ray diffraction patterns, increased with an increase in the NH_4ReO_4 concentration, *i.e.*, the increase in the Re content. This is unlike the case of the $NiSO_4$ variation, in which the d value was independent of the $NiSO_4$ concentration. It can be concluded by the above results that the replacement of Re atoms with Co atoms produces a widening of the d value in the hcp lattice, because the atomic radius of Re is larger than that of Co. For reference, the deposition rate of the films is also shown in Fig. 2(a). The deposition rate decreased with an increase in the NH_4ReO_4 concentration. It became 6—7 mg $cm^{-2}h^{-1}$ in the optimum condition region.

Figure 3 shows the effect of the $MnSO_4$ concentration on the magnetic properties and the $\Delta\theta_{50}$ value. As has already been stated, the $MnSO_4$ addition to the bath causes a perpendicular orientation of the hcp structure, in spite of the very small manganese codeposition into the film. The Ku and the $\Delta\theta_{50}$ values greatly increased and decreased, respectively, up to 0.04 mol dm^{-3} $MnSO_4$. The Ku value decreased with the increase in the $MnSO_4$ concentration from the above concentration. The X-ray diffraction peaks were not obtained in a $MnSO_4$ concentration region more than 0.05 mol dm^{-3}. The optimum conditions for magnetic properties lie in the region between 0.03 and 0.05 mol dm^{-3} $MnSO_4$. In Fig. 4(b), the dependence of the $MnSO_4$ concentration on the film composition indicates that each content is almost independent of the $MnSO_4$ concentration up to 0.03 mol dm^{-3}. Further, the phosphorus content increases

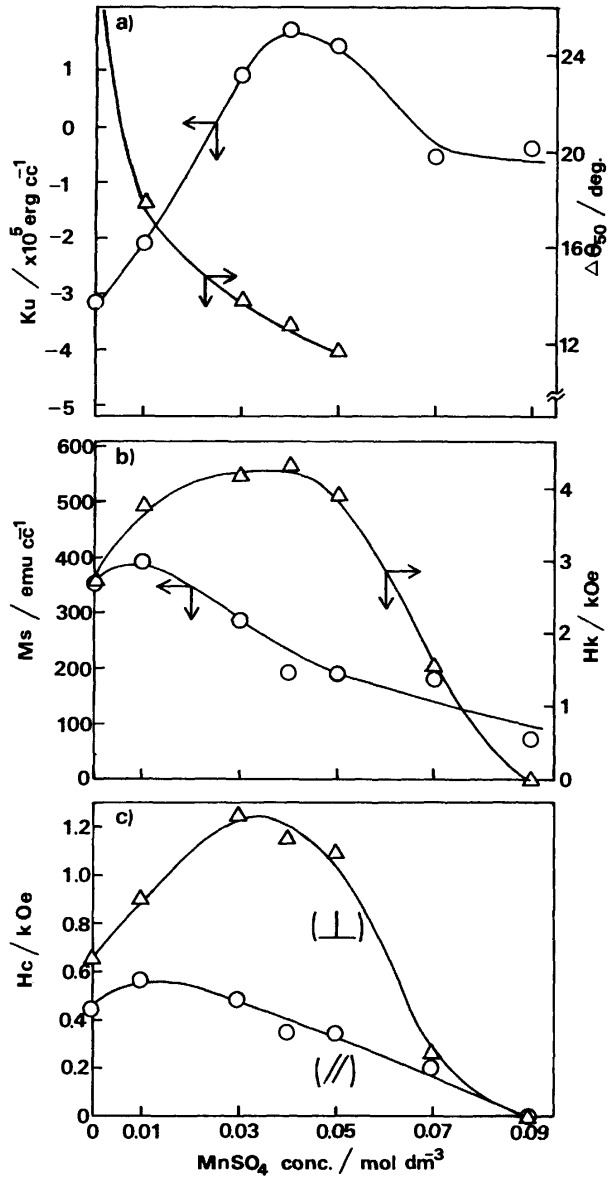

Fig. 3. Effect of $MnSO_4$ concentration on magnetic properties and $\Delta\theta_{50}$ of (002) plane for plated films using 0.5 μm thickness.

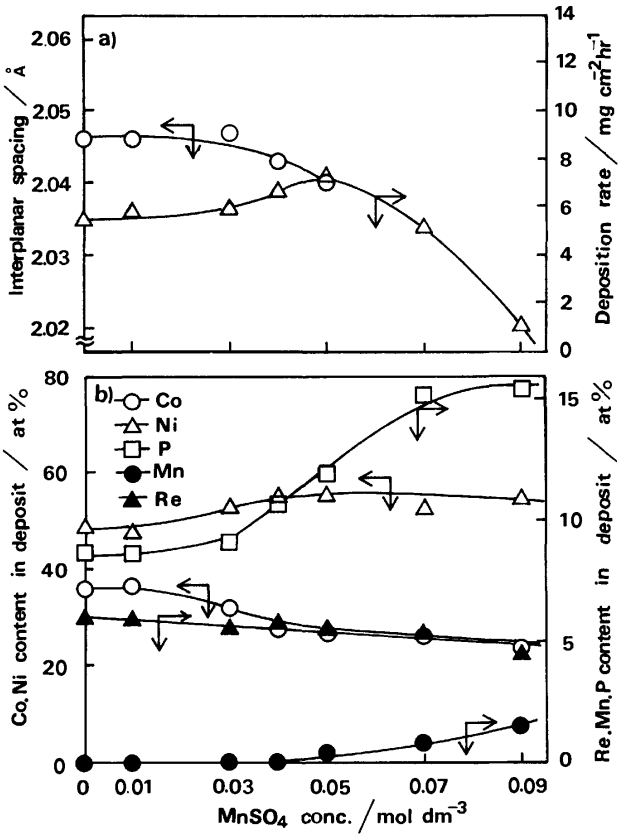

Fig. 4. Effect of $MnSO_4$ concentration on film composition, interplanar spacing and deposition rate for plated films using 0.5 μm thickness.

when the manganese starts to codeposit into the film. A small decrease in the *d* value also appeared from the initial point of Mn codeposition, as may be seen in Fig. 4(b). Thus, the variation in the *d* value and the increase in the P content simultaneously occurs upon the small amount of Mn codeposition. The effect of the manganese codeposition on the structure and its deposition mechanism are considered to be quite different from the rhenium codeposition, considering the reverse results regarding the *d* value variation in the Re and Mn codeposition. The amorphous states for non X-ray diffraction peaks in the concentration region of more than 0.05 mol dm^{-3} $MnSO_4$ is probably caused by the increase in the phosphorus content. The perpendicular orientation phenomenon produced by the addition of $MnSO_4$ can't be explained clearly in the present state. However, it might be assumed from the results of the small amount of manganese codeposition, in spite of the addition of a large amount of $MnSO_4$ to the bath, that the specifically adsorbed manganese intermediate at the interface causes the selective deposition at the initial deposition stage, and that, furthermore, thus the perpendicular orientation of the c-axis epitaxially grows on the initially selective deposited particles.

In Fig. 5, the most typical film thickness effect on the magnetic properties was obtained at one of the optimum conditions listed in Table 1, with the fixed

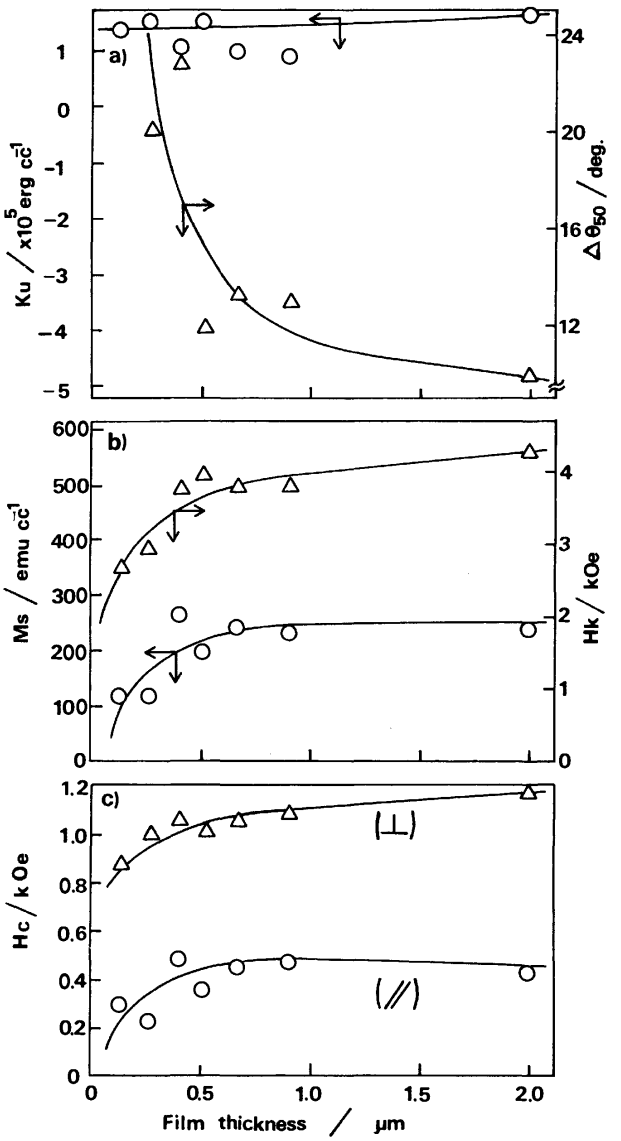

Fig. 5. Effect of film thickness on magnetic properties and $\Delta\theta_{50}$ of (002) plane for plated films.

concentrations of 0.12 mol dm^{-3} $NiSO_4$, 0.005 mol dm^{-3} NH_4ReO_4, and 0.05 mol dm^{-3} $MnSO_4$. The *Ku* value was interestingly independent of the film thickness. However, the other magnetic factors, *i.e.*, *Hk*, *Hc*(⊥), *Hc*(//), and *Ms*, depended on the film thickness in the initial thin region, up to 0.5 μm, and then reached constant values at a thickness of more than 0.5 μm. The structural factor, $\Delta\theta_{50}$, showed the largest dependence in the initial thin film region. It greatly improved with the increase in the film thickness, as may be seen in Fig. 5(a).

SEM Observation of Cross Section of Co Alloy Films. Figure 6 shows a typical cross section of Co alloy films plated to 0.5 μm under the same conditions as those in Fig. 5. Figures 6(a) and 6(b), which show the same cross section portion with different magnifications of 20000 and 50000 respectively, indicate the columnar growth structure of the hcp structure, although no clear columnar structure such as that shown

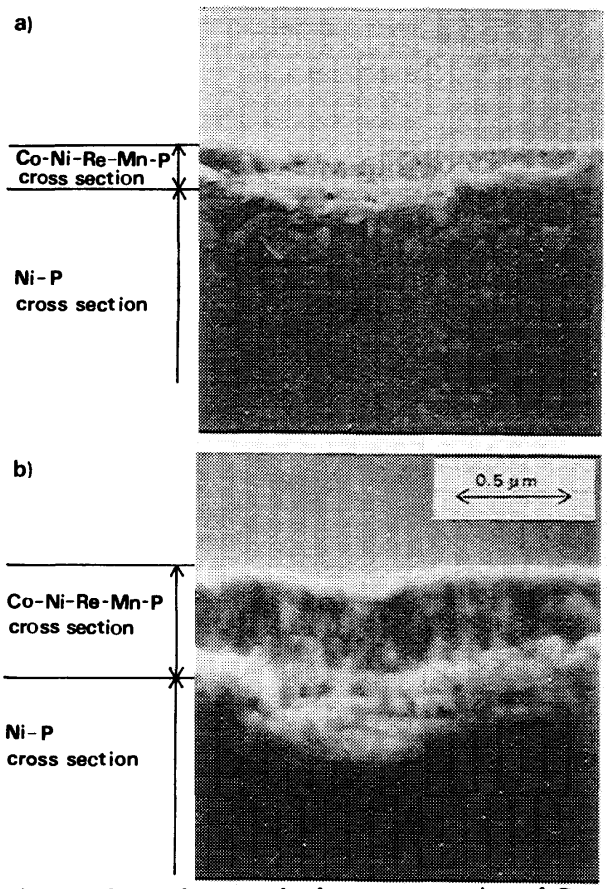

Fig. 6. SEM photographs for a cross section of Co alloy film plated 0.5 μm thick on Ni-P substrate. a) ×20000, b) ×50000.

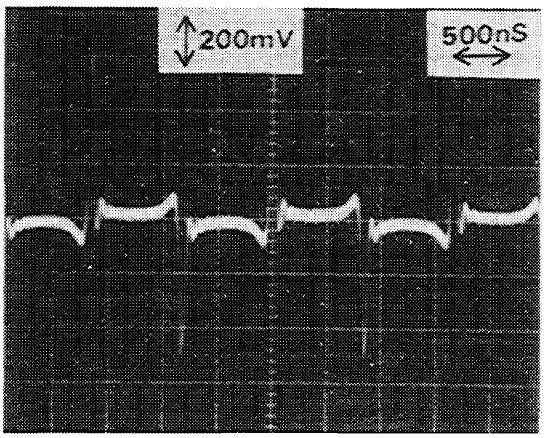

Fig. 7. Reproduced waveform at low recording density of 2540 FRPI for disk A using 0.20 μm spacing.

in previous results[12] is observed. Since the shape of the columnar structure at the cross section is reported to become unclear for the uniformly finer oriented film,[19] the film might be a finer oriented one, then the previously reported one.[12] By the SEM observation, the plated film is also concluded to be suitable for a perpendicular recording medium.

Read/Write Characteristics for Eight Inch Disks with a Combination of the Ring Head. Eight inch disks were prepared by using the optimum plating bath conditions listed in Table 1 at the fixed concentrations

TABLE 2. DISK AND HEAD CHARACTERISTICS

Items \ Disks	Disk A	Disk B	Disk C
Medium material		Co-Ni-Re-Mn-P	
Medium thickness/μm	0.50	0.25	0.20
Overcoat thickness/μm	0.05	0.05	0.02
Substrate material		Polished Ni-P on Al alloy	
Core material		Mn-Zn ferrite	
Gap length/μm		0.33	
Track width/μm		155	
Flying height/μm	0.10, 0.15 at 7.9 m/s at 12 m/s	0.10, 0.15 at 7.9 m/s at 12 m/s	0.10 at 7.9 m/s

of 0.12 mol dm^{-3} $NiSO_4$, 0.005 mol dm^{-3} NH_4ReO_4, and 0.05 mol dm^{-3} $MnSO_4$. The results for disks prepared at 0.10 mol dm^{-3} $NiSO_4$, under the same conditions as for the other factors, have already been reported in a previous paper.[16,17] The disk and head characteristics, as well as the read/write conditions, are shown in Table 2. The three medium thicknesses, *i.e.*, 0.20, 0.25, and 0.50 μm, and three head-medium spacings, 0.12, 0.20, and 0.25 μm, were used in these experiments. Here, the disks with magnetic film 0.50, 0.25, and 0.20 μm thick are designated as Disk A, Disk B, and Disk C respectively.

Figure 7 shows a typical reproduced waveform at a low bit density of 2540 FRPI for Disk A, with 0.20 μm head-medium spacing. The output voltage waveform at a low bit density in perpendicular magnetic recording in combination with the ring head is confirmed to display a dipulse shape.[20] As may be seen in Fig. 7, the dipulse shape at the low bit density recording is clearly observed. This finding supports the concept that the perpendicular recording mode is performed in a system using the plated disk combined with a ring head.

Figure 8 shows the recording density characteristics for Disks A, B, and C with the read/write conditions listed in Table 2. The recording density value at a half output voltage for a long wavelength, D_{50}, always became over 50 kFRPI under these conditions. The D_{50} values of the disks prepared at 0.12 mol dm^{-3} $NiSO_4$ were somewhat higher than the values for those prepared at 0.10 mol dm^{-3} $NiSO_4$, which were shown in the previous paper,[16,17] when the same read/write conditions are compared. This is due to the more advanced magnetic properties at the point of the 0.12 mol dm^{-3} $NiSO_4$ concentration. When considering the 0.33 μm head gap length, such recording density D_{50} values are fairly high. The recording density D_{50} values are scarcely restricted at all by the film properties, but are mainly restricted by the read/write conditions for such a magnetic anisotropy film, when using these read/write conditions. Figures 8(a) and 8(b) show the spacing effects on the recording characteristics for Disks A and B. The spacing decrease from 0.20 to 0.15 μm makes the D_{50} value higher. Furthermore, the medium thickness decrease also somewhat improves the D_{50}

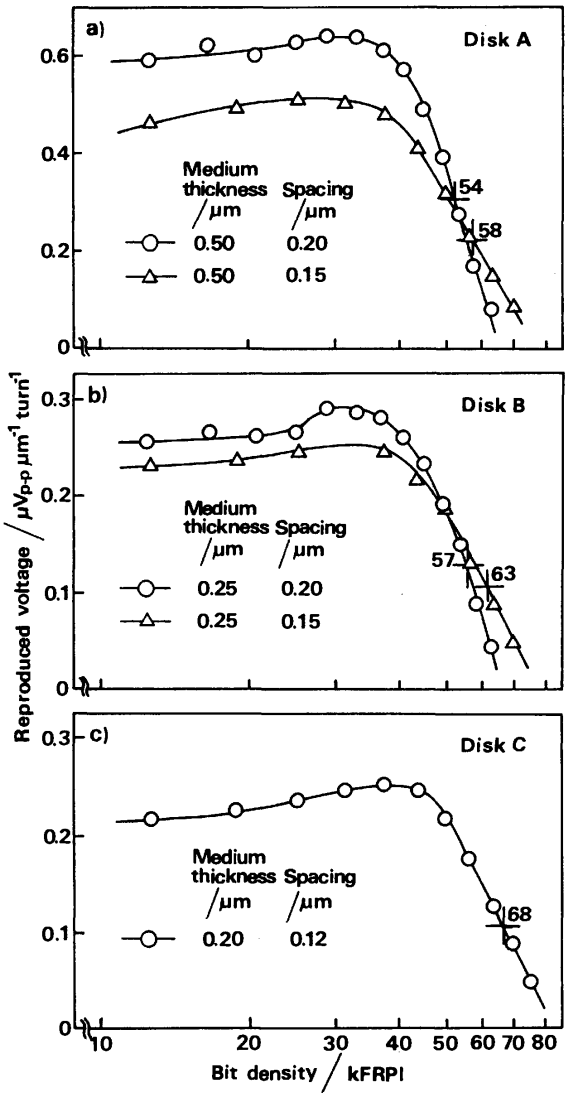

Fig. 8. Reproduced voltage dependence on recording density for Disks A, B, and C.

value. The spacing decrease from 0.25 to 0.20 μm more greatly developed the recording density D_{50} from 40 to 54 kFRPI, as was shown in previous papers.[17,18] Since a favorable *SNR* value and a flattened envelope were also obtained for these disks, with practically usable 0.20 μm spacing conditions, as in the previous data,[17] the electroless plated disks have been found to have a high potential for practical use. When the medium thickness and spacing values were reduced to 0.20 and 0.12 μm respectively, in obtaining a higher recording density, a high recording density, D_{50}= 68 kFRPI, was attained by using the 0.33 μm gap length head. The spacing used here means the total value of the 0.02 μm overcoat thickness and the 0.10 μm flying height. A very high potential for these plated disks as a perpendicular recording medium is also supported by such a high recording density with the more advanced read/write conditions.

The authors would like to thank Mr. Koichi Matsumi, Mr. Youji Suganuma, and Mr. Susumu Ito, in the Microelectronics Research Laboratories, NEC Corporation, for their encouragement during the research. The authors also wish to acknowledge the financial support of a grant from the Broadcasting Culture Foundation (Hoso Bunka Kikin).

References

1) S. Iwasaki and K. Takemura, *IEEE Trans. Magn.*, **MAG-11**, 1173 (1975).
2) S. Iwasaki and Y. Nakamura, *IEEE Trans. Magn.*, **MAG-13**, 1272 (1977).
3) S. Iwasaki and K. Ouchi, *IEEE Trans Magn.*, **MAG-14**, 849 (1978).
4) M. Naoe, S. Hasunuma, Y. Hoshi, and S. Yamanaka, *IEEE Trans Magn.*, **MAG-17**, 3184 (1981).
5) R. Sugita, T. Kunieda, and F. Kobayashi, *IEEE Trans. Magn.*, **MAG-17**, 3172 (1981).
6) O. Kubo, T. Ido, and H. Yokoyama, *IEEE Trans. Magn.*, **MAG-18**, 1122 (1982).
7) S. Iwasaki, D. E. Speliotis, and S. Yamamoto, *IEEE Trans. Magn.*, **MAG-19**, 1626 (1983).
8) C. S. Chi, K. A. Frey, R. A. Johnson, and W. T. Maloney, *IEEE Trans. Magn.*, **MAG-19**, 1608 (1983).
9) K. Yamamori, R. Nishikawa, T. Muraoka, and T. Suzuki, *IEEE Trans. Magn.*, **MAG-19**, 1701 (1983).
10) T. Osaka, F. Goto, N. Kasai, and Y. Suganuma, *Denki Kagaku*, **49**, 792 (1981).
11) F. Goto, T. Osaka, N. Kasai, I. Koiwa, H. Tanaka, M. Aoyama, and Y. Suganuma, Proc. of 1982 Sendai Symp. on Perpendicular Magn., Rec. (1982), p. 197.
12) T. Osaka, N. Kasai, I. Koiwa, F. Goto, and Y. Suganuma, *J. Electrochem. Soc.*, **130**, 568 (1983).
13) T. Osaka, N. Kasai, I. Koiwa, and F. Goto, *J. Electrochem. Soc.*, **130**, 790 (1983).
14) Y. Suganuma, H. Tanaka, M. Yanagisawa, F. Goto, and S. Hatano, *IEEE Trans. Magn.*, **MAG-18**, 1215 (1982).
15) K. Ito, O. Takano, and H. Matuda, Extended Abst. Conf. Metal Finish. Soc. Japan (1982), p. 8.
16) T. Osaka, I. Koiwa, Y. Okabe, H. Matsubara, A. Wada, and F. Goto, *Denki Kagadu*, **52**, 197 (1984).
17) F. Goto, T. Osaka, I. Koiwa, Y. Okabe, H. Matsubara, A. Wada, and N. Shiota, *IEEE Trans. Magn.*, **MAG-20**, 803 (1984).
18) T. Osaka, I. Koiwa, Y. Okabe, and F. Goto, Proc. of 11th Inter. Cong. of Metal Finishing, Israel (1984), p. 178.
19) M. Sagoi, R. Nishikawa, and T. Suzuki, IECE Tech. Group Meeting on Mag. Rec. Japan, **MR83-6** (1983).
20) S. Iwasaki, *IEEE Trans. Magn.*, **MAG-16**, 71 (1980).

Spectroscopic Behavior of the Alkali Salts of Noncyclic Polyethers: Evidence for Interaction between the End Groups[1)]

Kazuhisa HIRATANI
Industrial Products Research Institute, Higashi 1-chome, Yatabe-machi, Tsukuba-gun, Ibaraki 305
(Received July 7, 1984)

The electronic and fluorescence spectra of the alkali salts of noncyclic polyethers exhibiting selective transport for the lithium ion were investigated. In the electronic spectra hypochromicity in CH_2Cl_2 dependent on the kind of alkali metal ions was observed, and the magnitude of the hypochromic effect decreased in the following order: $Li^+>Na^+>K^+>Rb^+>Cs^+$. Using the polar solvents, EtOH and MeCN, instead of nonpolar CH_2Cl_2, the hypochromicity is small. Also, in the fluorescence spectra, the quenching phenomenon dependent on the kind of alkali metal ions appeared in the same sequence as the hypochromicity in the electronic spectra. It is suggested that these results, together with our previous results, support a stacking structure between the terminal aromatic rings of the lithium salt in a nonpolar solvent, which has been proposed from the inspection of the CPK model building.

We recently reported that a group of noncyclic polyethers, which have essentially the following framework (A), exhibit Li^+-selective transport through liquid membranes by functioning as a cation carrier.[2)]

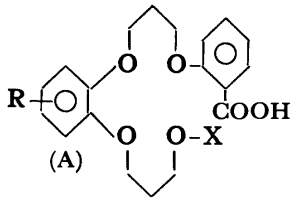

(A) X=aromatic group

When inspecting the CPK model building, it has been presumed that these compounds can form a pseudocyclic structure, the cavity of which has a diameter of 1.4—1.6Å. Furthermore the terminal groups (X= aromatic group) are presumed to overlap one another face-to-face to form a stacking structure, when hetero atoms are spatially directed to the inside. We concluded, therefore, that the lithium ion best fits the size of the cavity formed and can be transported by the (A)-type compound with high selectivity.

Here, the author attempts to verify this presumption by spectrophotometric methods. For this purpose, 1-[3-(*o*-carboxyphenoxy)propoxy]-2-[3-(8-quinolyloxy)propoxy]-4(or 5)-*t*-butylbenzene (**1**) (X=8-quinolyl, R=*t*-butyl in (A)) was used as a polyether carrier. This compound was chosen because the 8-quinolyl group has a strong absorbance maximum and strong fluorescence. The spectroscopic behavior of a 8-quinolyl terminal group may be able to give some information about the interaction between the polyether and the alkali metal ion as a counter cation of the carboxylate ion. For comparison, polyether **2** containing two oxyethylene chains was used as a **1**-analog.

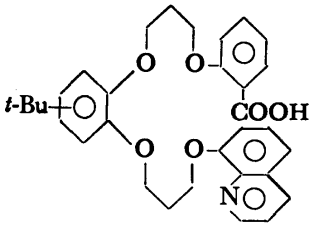

(1)

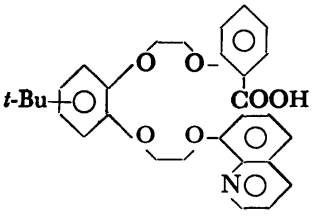

(2)

There are many reports that the stacking structure between inter- or intramolecular aromatic rings can be recognized by the electronic and NMR spectra. For example, it has been reported that the stacking between nucleic acid bases could be elucidated by the magnitude of their hypochromic effect on the absorbance of the aromatic rings, which increases with increasing stacking between them.[3)] In addition, the extent of the stacking between them can also be recognized by the chemical shifts of the protons on the aromatic rings in the NMR spectra.[3,4)] As previously-reported, we observed the upfield shift of the 2-position proton on the quinolyl group of **1** in the case of the lithium salt compared with other alkali salts of **1**.[2a)]

Results and Discussion

Electronic Spectra of the Salts of the Polyethers. The author first investigated the effect of the kind of alkali metal ions as a counter cation of the carboxylate ion of **1** and **2** on the absorptivity of their alkali salts. Figure 1 shows the results for the electronic spectra of the salts of **1** in CH_2Cl_2.[5)] The spectrum of each salt of **1** has one peak (*ca.* 280 nm) and one shoulder (303 nm). The shoulder at 303 nm was confirmed to be due to the absorbance of the quinolyl group because the position of the absorbance and the absorptivity of 8-(3-chloropropoxy)quinoline (λ_{max} 303 nm(CH_2Cl_2), ε 3.50×10^3) are almost in accord with those of the salts of **1**. The absorbance at *ca.* 280 nm for each salt of **1** is attributed to the other aromatic groups. The absorptivity appreciably changes in the electronic spectra with the kind of the alkali metal ion, whereas the positions of both absorbances change little in the range of 278 to 280 nm.

In Fig. 1, the absorptivity in CH_2Cl_2 increases with the increase of the size of the ionic diameter as follows: $Li^+<Na^+<K^+<Rb^+<Cs^+$. Apparently, the absorptivity of one terminal substituent (quinolyl group) is influenced by the kind of counter cation of the carboxylate ion of the other terminal substituent (*o*-carboxyphenyl group). Based on CPK model building, the linear distance between two terminal groups is at

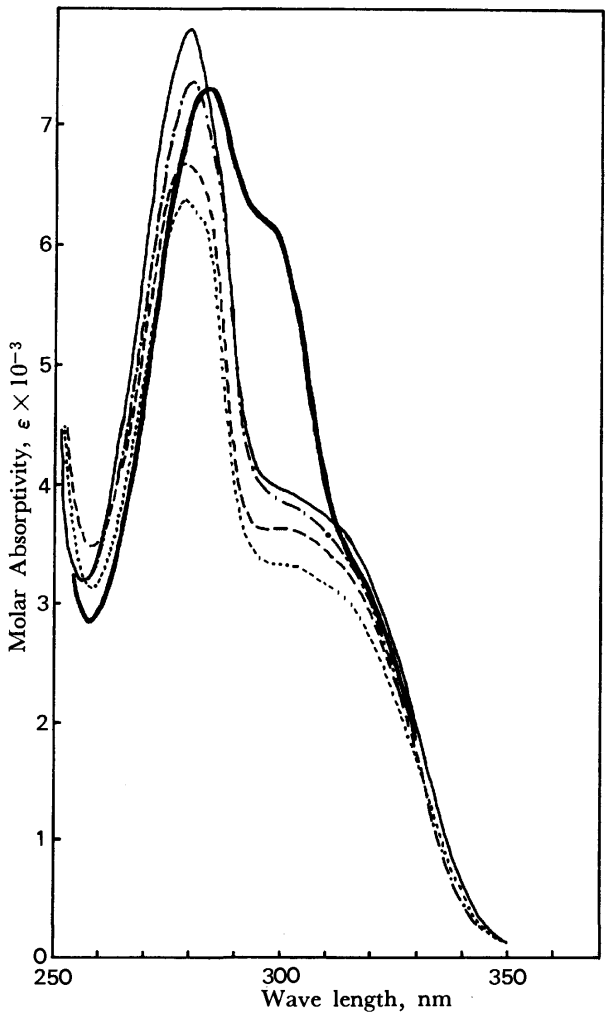

Fig. 1. Electronic absorption spectra of **1** and its alkali salts in methylene dichloride; concentration: 5.66 μmol/50 ml.[6] **1**: ——, Li^+ salt: ------, Na^+ salt: ----, K^+ salt: —·—·—, Cs^+ salt: ——

least 12 Å, when the molecule is linearly extended. The hypochromic effect (H, %) based on the absorptivity of the Cs^+-salt has been defined[3c] by the following equation:

$$H(\%) = \left(1 - \frac{\varepsilon_{M^+}}{\varepsilon_{Cs^+}}\right) \times 100 \qquad (1)$$

ε: molar absorptivity

M^+: alkali metal ions

Table 1 shows the hypochromic effect (H, %) at 303 nm calculated from this equation (1), which is based on the absorption maximum (shoulder) of the quinolyl group in the salts of **1**. The absorption spectra of the alkali salts of **2** were also measured under the same conditions, and the hypochromic effect at the absorption maximum (shoulder, 303 nm) are also shown in Table 1. In the case of the salts of **2**, it was observed that there is little difference in their hypochromic values. That is, their hypochromic effect is hardly dependent on the kind of alkali metal ion. The results in Table 1 may be closely associated with the following consideration

Table 1. Hypochromic effect (H, %)

Cation	Li	Na	K	Pb	Cs[a]
Ionic radius, Å	0.66	0.95	1.33	1.48	1.69
(1)	15.6	6.5	4.3	2.2	0
(2)	6.7	4.9	6.4	6.4	0

a) Molar absorptivity of the Cs^+-salt at 303 nm: (**1**) $\varepsilon_{Cs^+}=3.98\times10^3$, (2) $\varepsilon_{Cs^+}=3.89\times10^3$.

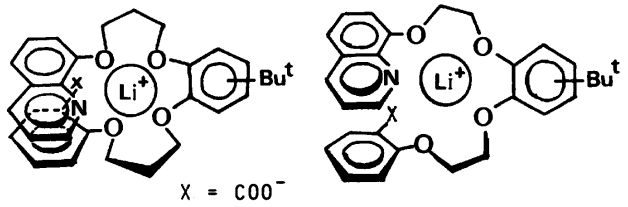

Fig. 2. Molecular structures of the lithium salt of the polyethers, **1** and **2**, on the basis of the CPK model building; a: Li^+ salt of **1**, b: Li^+ salt of **2**.

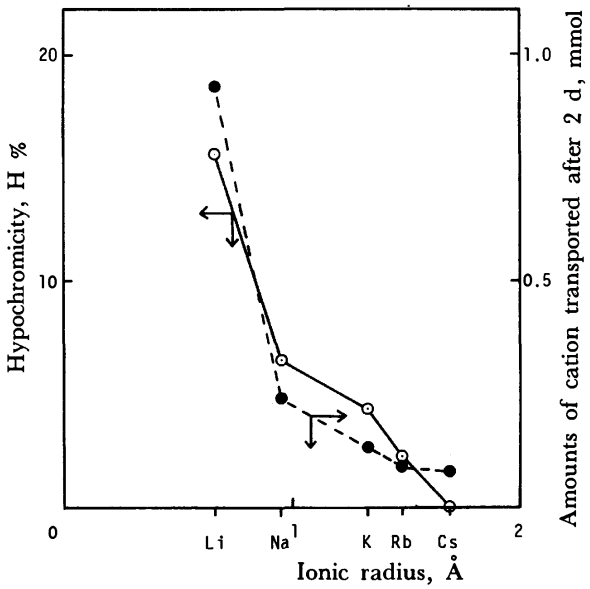

Fig. 3. Influence of the ionic radius of the alkali metal ions on the hypochromicity and the amounts of the cation transported.

based on CPK model building as previously-reported: i) when polyether **1** can form pseudocyclic structure, the lithium ion best fits the size of the cavity formed, which has a diameter of 1.4—1.6 Å, and then the terminal aromatic rings overlap one another face-to-face to form a stacking structure (Fig. 2-a), and ii) the terminal aromatic rings of **2**, on the contrary, can not overlap one another structurally, *i.e.*, on account of the bond angle, size of the terminal groups, *etc.*, as is shown in Fig. 2-b. Furthermore it is noted that the results of the selectivity for alkali metal ions in the transport experiment through a chloroform membrane by these polyethers are consistent with the spectroscopic behavior. The relationship between the hypochromicity and the amounts of cation transported[7] dependent on the kind of alkali metal ions is shown in Fig. 3.

Thus, the maximum hypochromic effect of the lithium salt of **1** in the electronic spectra is presumed to

TABLE 2. SOLVENT EFFECT IN THE ELECTRONIC SPECTRA OF THE SALTS OF (1) ON THE MOLAR ABSORPTIVITY

	CH_2Cl_2		MeCN		EtOH	
	λ_{max}	$\varepsilon\times10^{-3}$	λ_{max}	$\varepsilon\times10^{-3}$	λ_{max}	$\varepsilon\times10^{-3}$
free	284	7.43	284	7.07	282	6.80
	303	5.66	303	5.30	303	5.39
Li^+	279	6.53	278	6.49	280	6.85
	303	3.36	303	3.31	303	3.36
K^+	280	7.48	280	7.07	280	6.63
	303	3.81	303	3.45	303	3.18

reflect the stacking structure of the polyether carrier in the nonpolar solvents such as $CHCl_3$ and CH_2Cl_2. The solvent effects of the alkali salts of **1** on the hypochromic effect in the electronic spectra has been investigated: polar protic EtOH and polar aprotic MeCN used as solvents, and the results are shown in Table 2. Using EtOH, no change of absorptivity due to the kind of the alkali metal ions could be observed. For MeCN, the hypochromic effect by the kind of the alkali metal ions is not as large as in the case of a nonpolar aprotic solvent, CH_2Cl_2. From these results, it is considered that it is not necessary for the noncyclic polyether compound in such a polar solvent to form a pseudocyclic structure in order to wrap around the polar moiety (the alkali ion of the carboxylate), because the salts in a polar solvent could be solvated by the solvent and be solved in it.

The Fluorescence Spectra of the Alkali Salts of the Polyether 1. The fluorescence spectra of the alkali salts of **1** were measured in order to investigate further the interaction between the end groups of the salts of **1** in a nonpolar solvent.[8] The results are shown in Fig. 4. The fluorescence band, which appears on exposure to ultraviolet light by xenon lamp at 321 nm in CH_2Cl_2, is based on the quinolyl group. The relative intensity of the fluorescence maximum apparently decreases with the decrease of the ionic diameter of the alkali metal ion, although the maximum wave length of the fluorescence changes in the range of 386 to 391 nm is dependent on the kind of alkali metal ion.

The dependence of the quenching phenomenon on the kind of alkali metal ion is consistent with the hypochromicity in the electronic spectra, which suggests some interaction between the terminal aromatic groups. As reported recently,[2a] it has been presumed that in the NMR spectra the upfield shift of the proton at the 2-position of the quinolyl group in the case of the Li^+-salt of **1** is to be attributed to the shielding effect (ring-current effect) of the aromatic rings on account of the stacking structure between them. This phenomenon is in accord with the behavior both in the electronic and fluorescence spectra.

Thus, the results, which have been obtained here concerning the spectroscopic behavior of the alkali metal salts of the polyethers, reflect those of the cation selective transport by the polyether carriers through a chloroform liquid membrane. In conclusion, the mechanism of cation transport, which we have proposed,[2a] is supported spectrophotometrically: their cation selective transport might occur when the cation can become well incorporated into the pseudocavity of the polyethers formed and then they form the stacking structure between two terminal aromatic groups.

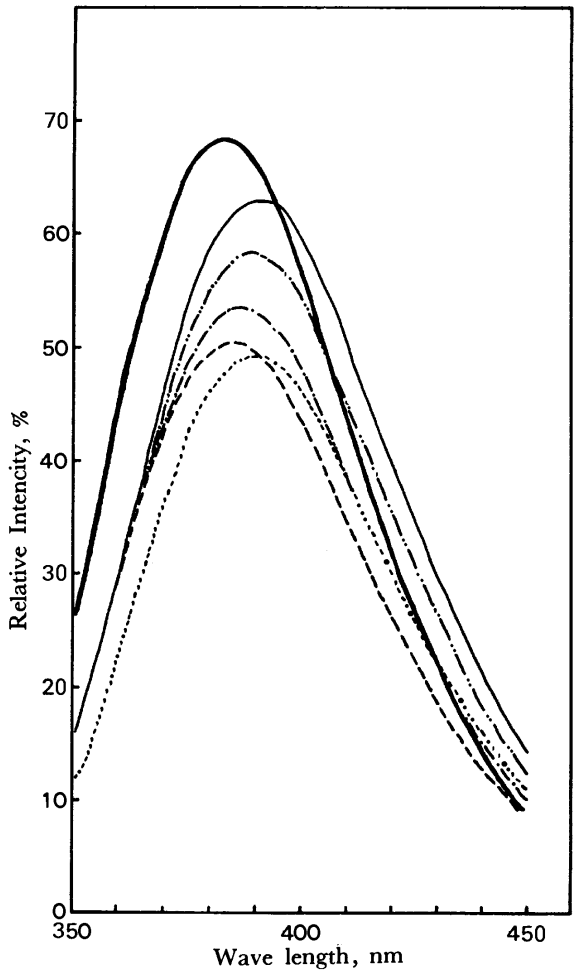

Fig. 4. Fluorescence spectra of the alkali metal salts of **1**; concentration: 5.66 μmol/50 ml of CH_2Cl_2, excitation at 321 nm. **1**: ——, Li^+ salt: ------, Na^+ salt: ----, K^+ salt: —·—·—, Rb^+ salt: —·····—, Cs^+ salt: ——

Experimental

Materials. 1-[3-(*o*-Carboxyphenoxy)propoxy]-2-[3-(8-quinolyloxy)propoxy]-4(or 5)-*t*-butylbenzene (**1**) and 1-[2-(*o*-carboxyphenoxy)ethoxy]-2-[2-(8-quinolyloxy)ethoxy]-4-(or 5)-*t*-butylbenzene (**2**) were obtained by the procedure reported previously.[2a] All solvents used were extra-pure grade reagents of Wako Pure Chemical Industries, LTD.,

which were tested for impurities spectrophotometrically before use. Sodium and potassium hydroxides were analytical grade reagents. Lithium, rubidium, and caesium hydroxides were reagent-grade.

General Spectrophotometric Measurement. Absorption spectra were measured on a Hitachi 330 spectrophotometer in the ultraviolet region. Fluorescence spectra were recorded on a Hitachi 204 fluorescence spectrophotometer.

Exactly, 3.0 mg of the polyether prepared was weighed into a 50 ml-measuring flask. About 5 ml of dichloromethane and 0.1 ml of aqueous solution containing 1.0 M (1 M=1 mol dm^{-3}) alkali metal ion were added. The flask was vigorously shaken for several hours and then the measuring flask filled with dichloromethane to the 50 ml mark. Both the electronic and fluorescence spectra of this solution were measured at room temperature. The alkali metal ions used were Li^+, Na^+, K^+, Rb^+, and Cs^+. In the case of the other solvents, the same procedure was followed. The molar absorptivity for each cation is shown in Fig. 1 and Table 2 for the electronic spectra. For the fluorescence spectra, the relative intensity for each cation is shown in Fig. 4.

References

1) Part X on "Synthesis and Properties of Noncyclic Polyether Compounds." Part IX: K. Taguchi, K. Hiratani, H. Sugihara, and K. Iio, *Chem. Lett.*, **1984**, 1457.

2) a) K. Hiratani, K. Taguchi, H. Sugihara, and K. Iio, *Bull. Chem. Soc. Jpn.*, **57**, 1976 (1984); b) K. Hiratani, *Chem. Lett.*, **1982**, 1021.

3) a) F. Hama, Y. Sakata, and S. Misumi, *Nucleic Acid Res., Spec. Publ.*, **8**, 131 (1980); b) *ibid.*, **10**, 73 (1981); c) *Tetrahedron Lett.*, **22**, 1123 (1981); d) K. Doyama, F. Hama, Y. Sakata, and S. Misumi, *ibid.*, **22**, 4101 (1981); e) F. Hama, Y. Sakata, S. Misumi, M. Aida, and C. Nagata, *ibid.*, **23**, 3061 (1982); f) K. Akahori, F. Hama, Y. Sakata, and S. Misumi, *Nucleic Acid Res., Spec. Publ.*, **11**, 265 (1982).

4) T. Otsubo, S. Mizogami, Y. Sakata, and S. Misumi, *Bull. Chem. Soc. Jpn.*, **46**, 3831 (1973).

5) Dichloromethane was used as a solvent for the spectroscopic measurement; its properties resemble those of chloroform used as a liquid membrane in the cation transport,[2] and it is more stable in the basic media than is chloroform.

6) The spectrum of the Rb^+ salt is not depicted because the curve is located in the narrow region between the curves of the Cs^+ and K^+ salts (*cf.* Table 1).

7) The results were obtained in the cation transport by **1** for five alkali metal ion species existing together in the source phase (see Ref. 2a).

8) It is difficult to conclude that the fluorescence quenching phenomenon necessarily reflects the formation of the stacking structure of **1**, because many other reasons for the phenomenon can also be considered. However, the results of the fluorescence is interestingly parallel with those of the electronic spectra.

The Effects of the pH and the Temperature on the Oxidation-reduction Properties of Adriamycin Adsorbed on a Mercury Electrode Surface

Kenji KANO, Tomonori KONSE, and Tanekazu KUBOTA*
Gifu Pharmaceutical University, 6-1 Mitahora-higashi 5-chome, Gifu 502
(Received July 18, 1984)

The effects of the pH and the temperature on the oxidation-reduction properties of the quinone moiety in adriamycin adsorbed on a mercury electrode surface have been investigated by means of cyclic d.c. voltammetry. The quinone waves have been fundamentally interpreted in terms of a two-step one-electron surface-redox reaction, even in a neutral or an alkaline solution, where the reduced product is liable to cause the following chemical reaction. The pH dependences of the standard surface-redox potential of the adsorbed adriamycin are −60 mV/pH (pH 2—6), −30 mV/pH (pH 7—8), and −60 mV/pH (pH 9—12). The semiquinone formation constant is 0.15 at pH 2—6 and 5 at pH 9—12. These results can be well explained by considering the protolytic equilibria of the phenolic hydroxyl groups among the oxidized, semiquinone, and reduced forms of adriamycin, the pK_a's of which are 8.53, 6.93, and 6.83 respectively. The thermodynamic constants of the semiquinone formation reaction at pH 4.5 have been determined to be $\Delta H=-24.6$ kJ mol^{-1} and $\Delta S=-99.7$ J K^{-1} mol^{-1}.

In a previous paper,[1] we have shown that adriamycin is strongly adsorbed on a mercury electrode surface and that the electrochemical redox reaction of the quinone moiety of the adsorbed adriamycin in an acidic solution can be well explained by the theory of a two-step one-electron redox reaction.[2] The apparent charge-transfer rate constants, redox potentials, and semiquinone formation constants of the surface-redox reaction have been determined at pH 2.69 and 4.54 using cyclic d.c. and a.c. voltammetry. These electrochemical and thermodynamic properties could be useful in an elucidation of the biological action mechanism of adriamycin.

In this paper, we have studied the pH dependence of the redox potential and the semiquinone formation constant in order to obtain information about the protolytic equilibria of the reduced and semiquinone forms as well as the oxidized (or parent) form of the adsorbed adriamycin. The protolytic equilibrium and the chemical stability of the oxidized form of adriamycin in the bulk solution have also been studied spectrophotometrically. Furthermore, we have investigated the thermodynamic property of the semiquinone formation reaction.

Experimental

Chemicals. Adriamycin hydrochloride and all the other chemicals used have been described elsewhere.[1]

Electrochemical Measurements. Cyclic d.c. voltammograms were recorded with a Yanagimoto P-1000 voltammetric analyzer, equipped with a Watanabe WX-4401 X-Y recorder. In the cyclic voltammetry at a sweep rate of more than 500 mV s^{-1}, an Iwatsu DM7100-DM711D digital memory (12 bit×1024 word, 5 μs/word) was used with the above system, while the voltage ramp was applied with an NF circuit FG-121B function generator.

All the voltammetric measurements were performed under potentiostatic conditions with a three-electrode system consisting of a hanging mercury drop working electrode (HMDE), a coiled platinum counter electrode, and a saturated calomel reference electrode (SCE). A fresh mercury drop from the HMDE was exposed to the electrolysis solution for a given period of time, t_{exp}, at a constant d.c. initial potential, E_i. Then the d.c. voltage scan was started from the E_i. Buffer solutions (0.2 mol dm^{-3} sodium acetate-nitric acid for pH 2.11—6.13; 0.1 mol dm^{-3} disodium hydrogenphosphate-nitric acid for pH 6.27—7.44; 0.2 mol dm^{-3} tris-(hydroxymethyl) methanamine-nitric acid for pH 7.89—9.00; 0.1 mol dm^{-3} sodium carbonate-nitric acid for pH 9.90—10.72; 0.05 mol dm^{-3} trisodium phosphate-nitric acid for pH 11.7) were used as the base solutions. The ionic strength of the base solutions was adjusted to 0.5 mol dm^{-3} with potassium nitrate. The other details of the electrochemical measurements have been described elsewhere.[1]

Spectral Measurements. The absorption spectra were recorded at room temperature in the usual manner with a Hitachi 323 spectrophotometer. To minimize decomposition errors, 20.0 μl of the adriamycin stock solution in methanol was injected into 2.00 ml of the buffer solution in a measuring cell just before recording the spectra. The concentration of adriamycin in the cell was chosen to be less than 1×10^{-5} mol dm^{-3} in order to eliminate the effect of the self-aggregation of adriamycin.[3,4]

Results and Discussion

A. pH Effect. Figure 1 shows the cyclic d.c. voltammogram of 1.46×10^{-6} mol dm^{-3} adriamycin at pH 4.54; it was recorded after $t_{exp}=4$ min at $E_i=-0.2$ V.

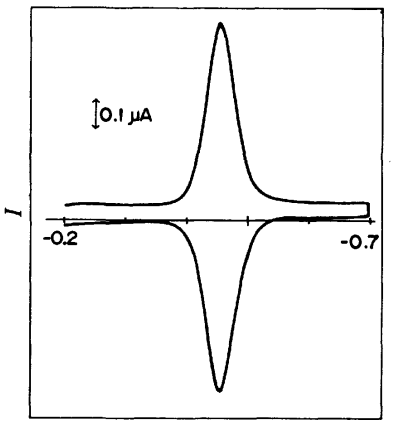

Fig. 1. Cyclic d.c. voltammogram of 1.46×10^{-6} mol dm^{-3} adriamycin at a pH 4.54 acetate buffer. $t_{exp}=4$ min at $E_i=-0.200$ V with $v=100$ mV s^{-1}.

A symmetrical pair of cathodic and anodic waves is observed. These waves are clearly to be ascribed to the surface-redox reaction of the quinone moiety in the adriamycin adsorbed on the mercury electrode.[1] When the voltammogram is recorded with an E_i value more positive than −0.3 V at pH 4.54, the peak potential, E_p^{dc}, and the half-peak width, $\Delta E_{p/2}^{dc}$, are −0.450 V and 52 mV respectively, regardless of the sweep rate, v, and the surface concentration of adriamycin, Γ.[5]

As has been described in a previous paper,[1] this wave can be interpreted in terms of a d.c. reversible two-step one-electron surface-redox reaction:[2,6]

$$\begin{aligned} O_{ad} + e &\rightleftharpoons S_{ad} \\ S_{ad} + e &\rightleftharpoons R_{ad} \end{aligned} \quad (1)$$

where O_{ad}, S_{ad}, and R_{ad} denote the oxidized (parent), semiquinone, and reduced forms of the adsorbed adriamycin respectively. In Scheme (1), the semiquinone formation constant, K, of the adsorbed adriamycin is defined by:

$$\begin{aligned} K &= [S_{ad}]^2/[O_{ad}][R_{ad}] \\ &= \exp[(F/RT)(E'_{o1} - E'_{o2})] \end{aligned} \quad (2)$$

where E'_{o1} and E'_{o2} are the standard surface-redox potentials of the O_{ad}/S_{ad} and S_{ad}/R_{ad} couples respectively. When $K<16$, the d.c. voltammogram has its maximum at the standard surface-redox potential of the O_{ad}/R_{ad} couple, E'_o, where E'_o is given by:

$$E'_0 = (E'_{o1} + E'_{o2})/2 \quad (3)$$

We can estimate the K value from $\Delta E_{p/2}^{dc}$ according to:

$$\zeta^4 - K\zeta^3 + (K - 4\sqrt{K} - 6)\zeta^2 - K\zeta + 1 = 0 \quad (4)$$

where $\zeta = \exp[(F/2RT)\Delta E_{p/2}^{dc}]$, or from the peak current, i_p, *vs.* the electricity, Q, plot according to:

$$i_p = (F/RT)Qv/(2+\sqrt{K}) \quad (5)$$

The K value at pH 4.54 has been determined to be 0.138±0.043 by the use of Eq. (4) and 0.126±0.034 by the use of Eq. (5). These values agree well with each other. The E'_{o1} and E'_{o2} values can be estimated by using the K value in Eq. (2) and the E'_o value in Eq. (3). The results are given in Table 1.

Table 1. Electrochemical and thermodynamic parameters of adriamycin adsorbed on a mercury electrode at various pHs

pH	K	E'_o	E'_{o1}	E'_{o2}
		V *vs.* SCE		
2.11	0.10	−0.299	−0.329	−0.270
2.60	0.15	−0.333	−0.357	−0.308
2.77	0.15	−0.340	−0.365	−0.315
3.05	0.14	−0.363	−0.389	−0.337
4.54	0.13	−0.450	−0.476	−0.424
5.02	0.19	−0.489	−0.510	−0.467
6.13	0.21	−0.538	−0.558	−0.518
6.27	0.15	−0.544	−0.569	−0.519
6.59	0.44	−0.570	−0.581	−0.560
7.14	0.52	−0.586	−0.594	−0.577
7.30	0.79	−0.600	−0.603	−0.597
7.44	0.77	−0.603	−0.607	−0.600
7.89	0.95	−0.625	−0.626	−0.625
8.45	1.78	−0.646	−0.638	−0.653
9.00	2.98	−0.680	−0.666	−0.694
9.90	3.42	−0.719	−0.703	−0.735
10.59	5.16	−0.755	−0.734	−0.776
10.68	5.37	−0.758	−0.736	−0.780
11.70	5.32	−0.829	−0.807	−0.850

Figure 2A shows the d.c. cyclic voltammogram of adriamycin at pH 7.44, which was recorded with v= 100 mV s^{-1} after t_{exp}=1 min at E_i=−0.4 V. Under these conditions, the cathodic and anodic waves are not symmetrical, and the peak potentials of the cathodic and anodic waves are −0.610 V and −0.642 V respectively. Where the voltammogram is recorded with v= 1000 mV s^{-1}, however, a symmetrical pair of cathodic and anodic waves is observed. These results indicate that the reversible electrochemical redox process of the parent compound is prevented at a relatively small v, *i.e.*, for a period of a few seconds, because of a subsequent irreversible chemical reaction of the semiquinone and/or reduced form adriamycin, and that the effect of the following chemical reaction can be disregarded at a large v. As was stated in the previous paper, this kind of chemical reaction can be observed even at pH 4.54 on electrolysis for a period of several minutes, but not in the voltammetry with v> 10 mV s^{-1}. This reaction may be considered as an irreversible elimination of the amino-sugar moiety, giving rise to 7-deoxyadriamycinone.[7] The chemical reaction rate of the reduced products increases with the pH. At any rate, we can estimate the E'_o and K values, and also the E'_{o1} and E'_{o2} values, from the cyclic voltammogram obtained with so large a v as to neglect the following chemical reaction.

With an increase in the pH to more than 8.5, the orange-red solution (pH<8) of the adriamycin turns blue-violet, indicating the acid dissociation of phenolic hydroxyl group in the parent molecule. Figure 3 shows the visible spectra of adriamycin at pH 6.00 and 10.72; they were recorded immediately after prep-

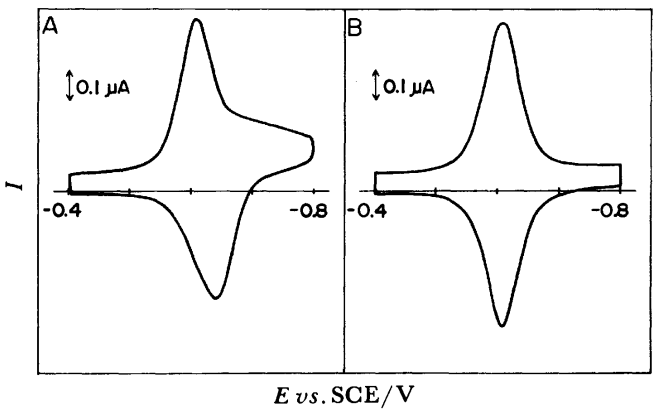

Fig. 2. Cyclic d.c. voltammograms of 4.77×10^{-6} mol dm^{-3} adriamycin at a pH 7.44 phosphate buffer with v=A) 100 mV s^{-1} and B) 1000 mV s^{-1}. t_{exp}=4 min at E_i=−0.400 V.

aration. In Fig. 4, the absorbance for 9.70×10^{-6} mol dm^{-3} adriamycin at 483.2 nm is plotted against the pH. Considering the protolytic equilibrium of the hydroxyl group of adriamycin, the total absorbance, A, at a constant analytical concentration is given by:

$$A = A_a + (A_b - A_a)\frac{K_a(\text{bulk})}{[H^+]+K_a(\text{bulk})} \quad (6)$$

where A_a and A_b represent the absorbance of the sufficiently acidic and alkaline solutions respectively, K_a (bulk) being the acid-dissociation constant of adriamycin in the solution. Regression analysis of A *vs.* pH plot was done using Eq. (6), where the absorbances at pH 6.00 and 10.72 were used for A_a and A_b respectively. The result is pK_a (bulk)=9.33±0.06. At pH 10.0, however, the absorbance decreases with the time, and the solution becomes almost colorless after about 2 h. This reaction can be interpreted as a base-catalyzed hydrolysis of the "deprotonated" adriamycin.[8]

To minimize the effect of the decomposition at pHs higher than 8.5, we recorded the voltammogram with v=1000 mV s^{-1} immediately after injecting the adriamycin stock solution into the deaerated base solution and exposing the electrode to the solution. The solid line in Fig. 5 represents the first scan of the multicyclic voltammogram recorded at pH 9.00 after t_{exp}=1 min at E_i=−0.400 V and with v=1000 mV s^{-1}. Two cathodic waves, I_c and I_c', are observed; their peak potentials are −0.680 V for the I_c wave and −0.772 V for the I_c' wave. In the anodic scan, only a symmetrical wave, I_a, is observed. The peak potential of the I_a wave is −0.680 V, coinciding with that of the I_c wave. The broken line in Fig. 5 represents the second scan, where we see that, although the I_c' wave disappears almost completely, the decrease in the wave height of I_c and I_a is small. In addition, the wave shape of the latter (I_c and I_a) is almost symmetrical, and the peak potentials coincide with those of the first scan. As a result, the pair of waves, I_c and I_a, may be considered to be practically d.c. reversible; then, the values of E_o', E_{o1}', E_{o2}' and K can be estimated. The origin of the I_c' wave is not clear at the present stage, but it may be due to the reorientation of the adsorbed molecules. In another interpretation, the appearance of the I_c' wave may be related to a following chemical reaction, such as the dimerization of the reduced form.[6]

Table 1 summarizes the electrochemical and thermodynamic parameters determined by means of the cyclic voltammetry. The K values are 0.1—0.2 at pH<6 and 3—5 at pH>9. In other words, the semiquinone formation reaction is thermodynamically favored at higher pHs. Figure 6 shows the pH dependence of E_o', E_{o1}', and E_{o2}'. The E_o' *vs.* pH plot is composed of three linear relations, the slopes being −60 mV/pH (pH 2—6), −30 mV/pH (pH 7—8), and −60 mV/pH (pH 9—12). The first and the second inflection points at pH 6.8 and 8.5 correspond to the acid-dissociation constants of the reduced and oxidized forms of the adsorbed adriamycin respectively. These findings lead us to consider the following protolytic and electrochemical equilibria:

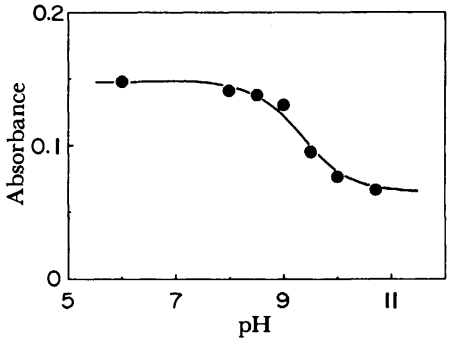

Fig. 4. pH dependence of absorbance for 9.70×10^{-6} mol dm^{-3} adriamycin at 483.2 nm. The solid line represents the regression curve calculated using the values of pK_a=9.33 for Eq. 6. (See text).

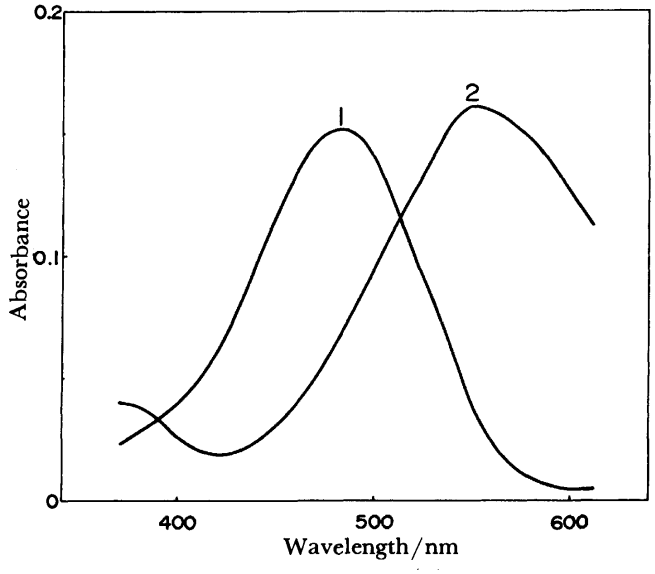

Fig. 3. Visible spectra of 9.70×10^{-6} mol dm^{-3} adriamycin at pH=1) 6.00 and 2) 10.72. The spectra were recorded immediately after preparation. (See text).

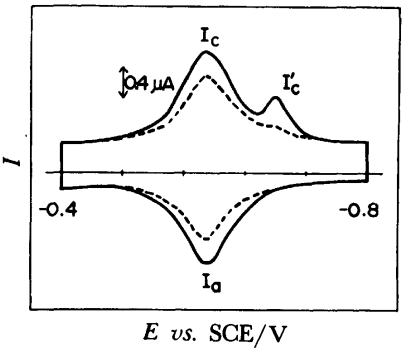

Fig. 5. Multi cyclic d.c. voltammogram of 1.38×10^{-6} mol dm^{-3} adriamycin at pH 9.00 tris buffer. t_{exp}= 1 min at E_i=−0.400 V. v=1000 mV s^{-1}. The solid and broken lines represent the first and second scans, respectively.

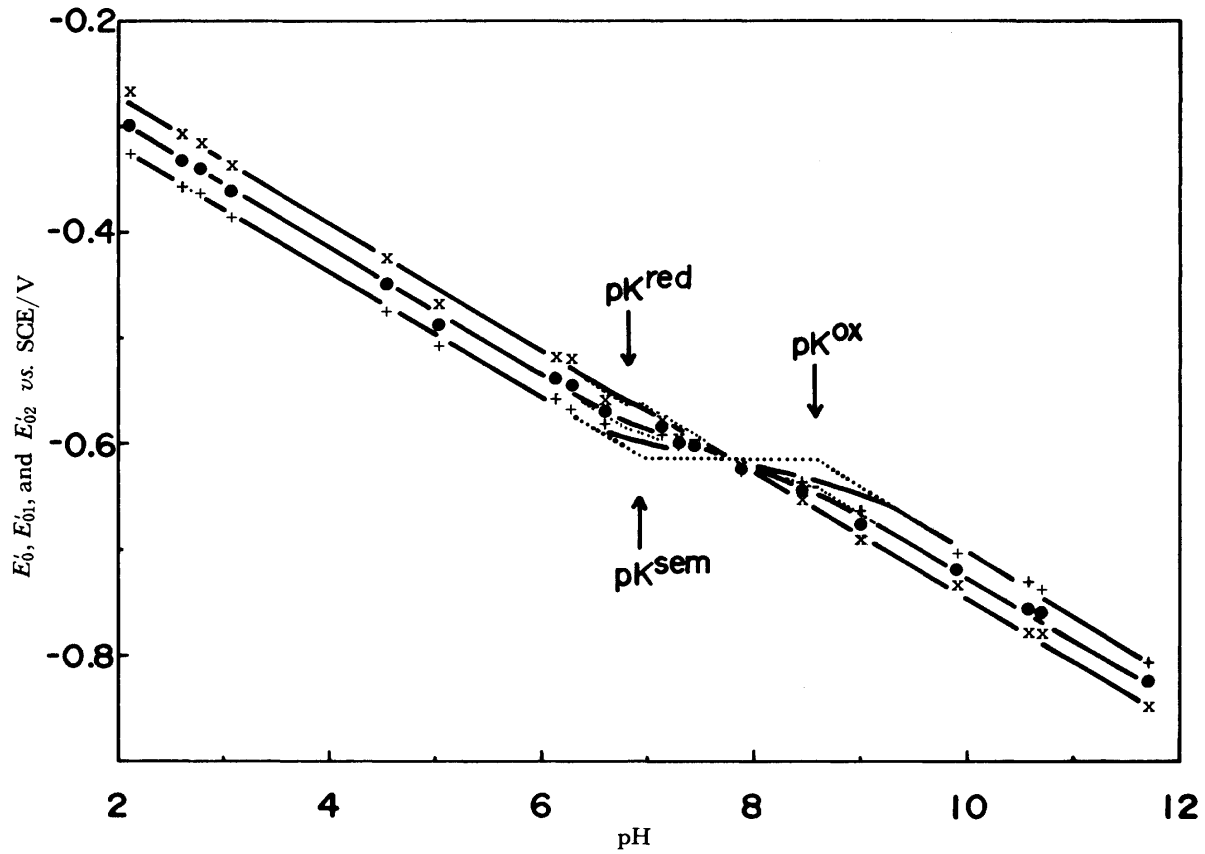

Fig. 6. Plots of E'_0 (●), E'_{01} (+), and E'_{02} (x) against pH. The solid lines represent the regression curves calculated using the values of $\bar{E}'_{01}$=−0.200 V, $\bar{E}'_{02}$= −0.153 V, pK_a^{ox}=8.53, pK_a^{sem}=6.93 and pK_a^{red}=6.83 for Eqs. 8—10.

$$\begin{array}{ccccc} (\text{Ox-H}_p)_{ad} & \overset{e,H^+}{\rightleftharpoons} & (\text{Sem-H}_{p+1})_{ad} & \overset{e,H^+}{\rightleftharpoons} & (\text{Red-H}_{p+2})_{ad} \\ H^+ \Big\| K_a^{ox} & & H^+ \Big\| K_a^{sem} & & H^+ \Big\| K_a^{red} \\ (\text{Ox-H}_{p-1})_{ad} & \overset{e,H^+}{\rightleftharpoons} & (\text{Sem-H}_p)_{ad} & \overset{e,H^+}{\rightleftharpoons} & (\text{Red-H}_{p+1})_{ad} \end{array} \quad (7)$$

where K_a^{ox}, K_a^{sem}, and K_a^{red} represent the acid-dissociation constants of the oxidized, semiquinone, and reduced forms respectively of the adriamycin adsorbed on a mercury electrode. The pH dependences of the E'_0, E'_{01}, and E'_{02} are now given by:

$$E'_0 = \frac{\bar{E}'_{01} + \bar{E}'_{02}}{2} + \frac{RT}{2F}\ln\left[\frac{[H^+]^3 + [H^+]^2 K_a^{red}}{[H^+] + K_a^{ox}}\right] \quad (8)$$

$$E'_{01} = \bar{E}'_{01} + \frac{RT}{F}\ln\left[\frac{[H^+]^2 + [H^+]K_a^{sem}}{[H^+] + K_a^{ox}}\right] \quad (9)$$

$$E'_{02} = \bar{E}'_{02} + \frac{RT}{F}\ln\left[\frac{[H^+]^2 + [H^+]K_a^{red}}{[H^+] + K_a^{sem}}\right] \quad (10)$$

where $\bar{E}'_{01}$ and $\bar{E}'_{02}$ correspond to E'_{01} and E'_{02} at pH=0 respectively. We have fitted Eqs.(8)—(10) to the three plots of E'_0, E'_{01}, and E'_{02} against the pH, using 5 parameters, $\bar{E}'_{01}$, $\bar{E}'_{02}$, pK_a^{ox}, pK_a^{sem}, and pK_a^{red}. Nonlinear least-squares analysis is performed by means of an NEC 8001 personal computer. The refined parameters are $\bar{E}'_{01}$=−0.200±0.002 V, $\bar{E}'_{02}$=−0.153±0.002 V, pK_a^{ox}= 8.53± 0.09, pK_a^{sem}=6.93±0.08 and pK_a^{red}=6.83± 0.09. In adriamycin, both the phenolic and amino groups should ionize in the pH region investigated. However, the amino group is located in the side-chain amino-sugar moiety separated from the aromatic ring by several saturated carbon atoms, so that the effect of the acid dissociation of the amino group on the redox potential should be negligible. Thus, we consider the phenolic hydroxyl group as an ionizable group in Scheme (7).[9] The present value of pK_a^{ox} (8.53) is smaller than the pK_a value of adriamycin (9.33) in the bulk solution. This disagreement is attributable to the difference between the adsorbed and dissolved states of adriamycin.

To our present knowledge, the determination of the acid-dissociation constant of the reduced and semiquinone forms of adriamycin is the first such case, though the values correspond not to the bulk state, but to the adsorbed state. The potentiometric titration may give information about the standard redox potential and the semiquinone formation constant of the bulk species.[10,11] This method, however, can not be applied to an unstable species such as adriamycin in a neutral or an alkaline solution.

On the other hand, the accelation of the chemical reaction rate following the electrochemical reduction in a neutral or an alkaline solution may be attributable to the instability of the deprotonated form of the reduced adriamycin and/or semiquinone intermediate. Here it is noteworthy to consider that, if the reduced (or

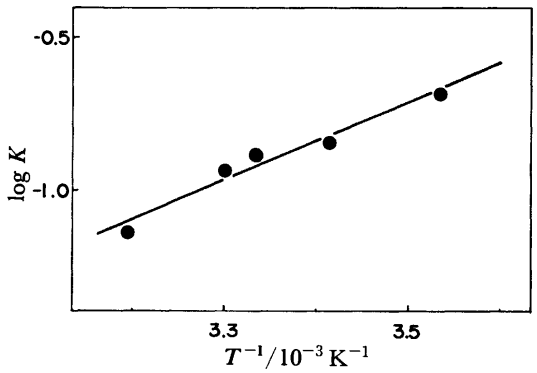

Fig. 7. Temperature dependence of the semiquinone formation constant of the adsorbed adriamycin in an acetate buffer (pH 4.54 at 25 °C).

semiquinone) form is generated in biological media (pH≈7.4), this species easily undergoes the elimination of the amino-sugar moiety to give 7-deoxyadriamycinone. This coincides with the fact that 7-deoxyaglycon is an important metabolite.[12,13]

B. Temperature Effect. We have further studied the temperature effect on the cyclic voltammogram of the adriamycin adsorbed on the HMDE in an acetate buffer (pH 4.54 at 25 °C). In the temperature range from 10 °C to 40 °C, the d.c. voltammogram is reversible and resembles that shown in Fig. 1. The peak potential shifts to the negative side with the increase in the temperature, the slope being $-0.9\,mV\,K^{-1}$. The half-peak width decreases with the increase in the temperature; in other words, the semiquinone formation constant, K, decreases with the temperature. Figure 7 shows the temperature dependence of the K value as determined by the use of Eq. 4.[14,15] The value of log K increases linearly with the reciprocal of the absolute temperature. The linear plot gives the enthalpy $\Delta H=-24.6\,kJ\,mol^{-1}$ and the entropy $\Delta S=-99.7\,J\,K^{-1}\,mol^{-1}$[16,17] for the semiquinone-radical-formation reaction ($O_{ad}+R_{ad}\rightarrow 2S_{ad}$). These values indicate that, because of the large negative entropy, the semiquinone formation reaction is not thermodynamically favored above 0 °C in an acidic solution.

References

1) K. Kano, T. Konse, N. Nishimura, and T. Kubota, *Bull. Chem. Soc. Jpn.*, **57**, 2383 (1984).

2) T. Kakutani and M. Senda, *Bull. Chem. Soc. Jpn.*, **53**, 1942 (1980).

3) R. J. Strurgeon and S. G. Schulman, *J. Pharm. Sci.*, **66**, 958 (1977).

4) F. Arcamone, "Topics in Antibiotic Chemistry," P. G. Sammes, ed., John Wiley & Sons, New York (1978), Vol. 2, pp. 185—211.

5) The adsorption process of adriamycin on an HMDE surface is diffusion-controlled, and Γ is given by a function of the t_{exp} and also the bulk concentration of adriamycin.[1]

6) V. Plichon and E. Laviron, *J. Electroanal. Chem.*, **71**, 143 (1976).

7) G. M. Rao, J. W. Lown, and J. A. Plambeck, *J. Electrochem. Soc.*, **125**, 534, 540 (1978).

8) The time-course analysis of the absorbance at 478 nm (pH 8.00—9.50) or 588 nm (pH 10.00—10.72) indicates that the decomposition is a (pseudo) first-order reaction. The evaluated apparent rate constants are ≈0 (pH 8, 9), 4.03×10^{-3} (pH 9.5), 1.14×10^{-2} (pH 10.0), and $1.59\times10^{-2}\,s^{-1}$ (pH 10.72).

9) The protolytic equilibrium involving the amino qroup affects the equilibrium involving the phenolic hydroxyl group, since overlapping protolytic equilibria are possible in adriamycin. Therefore, the pK_a's estimated in this work correspond to the apparent pK_a's.

10) W. H. Clark, "Oxidation-Reduction Potentials of Organic Systems," William & Wilkins, Batimore (1960), pp. 184—203.

11) R. D. Draper and L. L. Ingraham, *Arch Biochem. Biophys.*, **125**, 802 (1968).

12) V. P. Marshall, E. A. Reisender, L. M. Reineke, J. H. Johnson, and P. F. Wiley, *Biochemistry*, **15**, 4139 (1976).

13) S. Takahashi and N. R. Bachur, *J. Pharmacol. Exptl. Ther.*, **195**, 41 (1975).

14) Under the experimental conditions employed here, the adsorption of adriamycin on the HMDE surface is not in the equilibrium state, but is diffusion-controlled.[5] Therefore, Γ increases with an elevating temperature because of the increasing diffusion coefficient.[15] On the other hand, the K and E_0' values are independent of Γ,[1] so that, in this study, the effect(s) of the temperature (and also of the pH as well as the concentration and species of the supporting electrolytes) on the adsorption state is not taken explicitly into consideration.

15) K. Kano, I. Tokimitsu, T. Ikeda, and M. Senda, *Bull. Chem. Soc. Jpn.*, **57**, 648 (1984).

16) In this discussion, the change in the pH with the temperature is not taken into account; it is calculated to be 4.51 to 4.57 for the temperature change from 10 °C to 40 °C in the acetate buffer.[17] In this pH region, the K value is practically independent of the pH. Therefore, this correction for the pH change should not affect the estimated thermodynamic constants.

17) R. G. Bates, "Electrometric pH Determination," John Wiley & Sons, New York, London (1964), p. 108.

The Near Infrared Emission Band Observed in Electron Irradiated Xe and Xe in Other Rare Gases

Masako TANAKA,* Susumu SASAKI,† and Meiseki KATAYAMA
Department of Atomic Science and Nuclear Engineering Faculty of Engineering, Hokkaido University, Sapporo 060
(Received August 6, 1984)

The near-infrared emission spectra were studied for xenon diluted with krypton, argon, and neon, respectively, in order to estimate the origin of an emission band at 1260 nm which was previously observed at several hundred Torr (1 Torr=133.2 Pa) of pure Xe irradiated with pulses of high-energy electrons. A continuous band around 1260 nm was observed only in Xe-Ar mixtures. This band appeared at Xe pressures above 20 Torr (diluted in 600 Torr of Ar) while it was detected above 190 Torr in pure Xe. In Xe-Ar mixtures, three emission lines due to Xe $5d(3/2)_1$were also observed at 1700, 2020, and 2650 nm. On the basis of the reported kinetic data for the reactions of rare gas mixtures, the present results led to the conclusion that the band at 1260 nm was due to emission from highly excited excimer states, of which the dissociation limits were higher Rydberg states above the energy level of the Xe_2^+ ion.

The spectroscopy and kinetics of rare gas excimers have been studied mainly in the VUV region. Here, the continuous emissions (due to transitions from the lowest bound states to the repulsive ground state) were observed. According to theoretical studies of the excited states of Xe by Mulliken,[1] the emission or absorption due to the transitions between the energy levels of excited diatomic molecules is expected to occur in the NIR region. In this regard, Arai and coworkers reported the presence of absorption bands in the NIR region and the reactivity of the excimer with a number of simple molecules.[2] On the other hand, the deexcitation processes of higher Rydberg states have not been well studied, especially at high pressures such as are used for excimer lasers. As previously reported, we have found a new continuous band in the emission spectra of Xe in the NIR region, which occurs upon the irradiation of Xe and Xe (diluted with Ar) with pulses of high-energy electron. This band seemed to be due to molecular transitions related to higher Rydberg states. However, an assignment has not yet been made.[3] In this paper the NIR emission spectra of Xe and Xe, which were diluted in other rare gases, were studied in order to estimate the excited states of Xe leading to the new band. The emission spectra were qualitatively interpreted on the basis of the recently reported kinetic models.

Experimental

The experimental apparatus has been previously described.[3] The source of the electron pulses was the 45 Mev linac at Hokkaido University and the duration of the pulses was 3 μs. The emissions from the sample gases were detected in the reverse direction to the electron beam so that interference due to intense Cerénkov light in the Xe gas (upon irradiation) could be avoided in the infrared observation. A Hamamatsu TV p791 PbSe detector with a time constant of 2.5 μs was used. The spectra were obtained by plotting the peak intensities of the time-resolved signals against wavelength. The spectra region examined was 800—1600 nm for Xe-Ne and Xe-Kr mixtures, and 800—3200 nm for pure Xe and Xe-Ar mixtures. The observed band width of the spectra was about 15 nm at 825 nm with the 1.5-mm slit used during most of the experiment. When using a narrower slit, the signal accumulation and averaging were performed by using a Sord M223 Mark III computer.

Research-grade Xe (99.995%), Ar (99.999%), and Kr (99.995%) supplied by Nippon Sanso, Ne (99.999%) by Takachiho Kagaku Kogyo were used.

Results and Discussion

Emission Spectra in Pure Xe. Th emission spectrum which was obtained upon the irradiation of 635 Torr of Xe is shown in Fig. 1. The spectrum is essentially the same as that reported peviously,[3] but the present one was measured with a better optical resolution. The emission lines observed at 830, 890—910, 990, and 1080 nm were due to known atomic transitions: 6p—6s and 6p′—6s′. The continuous band at around 1260 nm was first reported by the authors in a previous paper.[3] It starts at about 1100 nm and continues to 1350 nm. The insert in Fig. 1 shown this

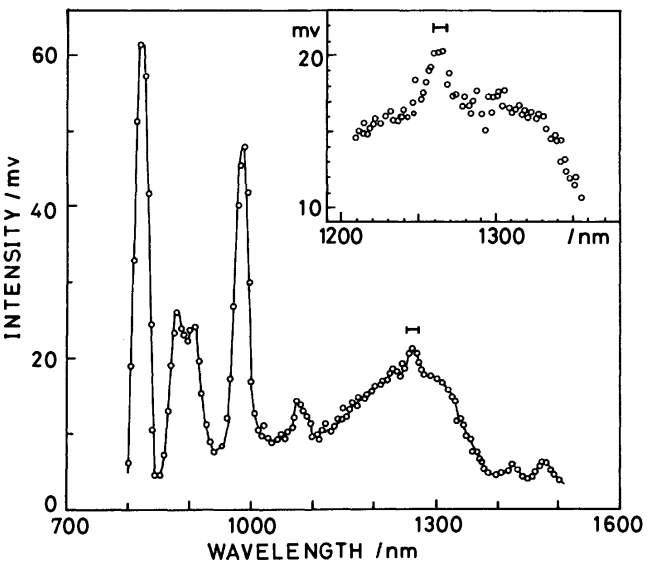

Fig. 1. The emission spectra of Xe in pure Xe at 630 Torr. The optical resolution is 20 nm. The spectrum in the insert was measured with 10 nm resolution.

†Present address: Central Research Laboratory, Mitsubishi Rayon Co. Ltd., Miyuki-cho, Otake 739-06.

band measured at a resolution of less than 10 nm. A narrow peak, which had not been detected at lower resolution, appeared and was assigned to the emission due to one of the 7s—6p atomic transitions. The possibility that this band was due to a 7p—5d transition ($3p_{10}$—$3d_5$ in Paschen notation, 1259.4 nm) was excluded since it has been reported that the branching ratio to $3d_5$ is very low.[4] No vibrational structures were observed at a 10-nm resolution, as shown in the insert. The band began to appear clearly at pressures above 190 Torr, and the pressure dependence of the peak intensity at 1260 nm was quadratic, which indicates that the band was due to a molecular transition.

One of the most important results reported in the previous paper was that the intensity of the band at 1260 nm was not affected by adding a small amount of SF_6, while the intensities of atomic lines decreased significantly. It is known that ion recombination and collisional state mixing are effectively inhibited by a small amount of SF_6.[5-7] Therefore, the ionic processes such as dissociative recombination of Xe_2^+ were ruled out as being the entity responsible for the 1260 nm band. Instead, the contribution of the direct excitation by the interaction of high-energy electron was considered.

Emission Spectra of Xe in Ne. Figure 2 shows the emission spectra of Xe in Ne. When 50 Torr of Xe was added to 510 Torr of Ne, the emission due to Ne completely disappeared, and the emission lines of Xe, which are due to the transitions 6p—6s and 7s—6p, were observed. However, no continuum emission was observed at 1260 nm except for a sharp 7s—6p line. Among the 6p—6s emission lines, the intensities of the lines due to the transition from $6p(1/2)_1$ ($2p_{10}$ in Paschen notation) at 980 and 1080 nm were very intense when the Xe pressure was low. The intensities of all emission lines decreased in the same manner as the Xe pressure increased, which indicates that these emissions were produced by energy transfer from excited Ne, and that the collisional state mixing occurred efficiently. Since all of the excited states of the Ne atoms lie at levels higher than the level of Xe^+ (12.127 ev), the excited Ne atoms can induce Penning ionization of Xe atoms, which leads to the production of an excited Xe atoms as follows; $Ne^*+Xe \rightarrow Ne+Xe^++e^-$, $Xe^++Ne+Xe \rightarrow Xe_2^++Ne$, $Xe_2^++e^- \rightarrow Xe^*+Xe$. It was estimated that the resultant energy levels of Xe* are the 6p states, if the electrons are thermalized and the dissociation energy of Xe_2^+ ion is about 1 ev.[6,8] Thus, it is considered that the 6p emissions which were observed in Fig. 2 were produced directly from the above-mentioned dissociative recombination. From the result that the 1260 nm band did not appear, it was concluded that the 6p states do not take part in the formation of the species responsible for the 1260 nm band.

Emission Spectra of Xe in Kr. The emission spectra in the irradiated Xe-Kr mixtures are shown in Fig. 3. Four emission lines due to 6p—6s transitions were observed at 830, 910, 980, and 1080 nm. The 7s—6p emission at 1260 nm, which was strong in the Xe-Ne mixtures, was very weak. The continuous band was not detected even at 100 Torr of Xe pressure.

It was considered that in this experiment the major part of the channel of energy transferred from the excited Kr to Xe was the excited Kr atoms in the 5s states. These were produced by deactivation in a cascade after the dissociative recombination of Kr_2^+. The role of the diatomic molecules, Kr_2^*, was less important, since the rate of the two-body collision of 5s Kr ($Kr^*+Xe \rightarrow Xe^*+Kr$) was much faster than that of the three-body collision ($Kr^*+2Kr \rightarrow Kr_2^*+Kr$) under the present experimental condition (P_{Xe}=higher than 5 Torr), where the former rate was 2.0×10^{-10} $cm^3 s^{-1}$[9] and the latter was 1.4×10^{-33} $cm^6 s^{-1}$.[9] An efficient dipole-dipole type energy transfer is possible between Kr $^3P_1$ and Xe $5d(7/2)_3$ and between Kr $^3P_2$ and Xe

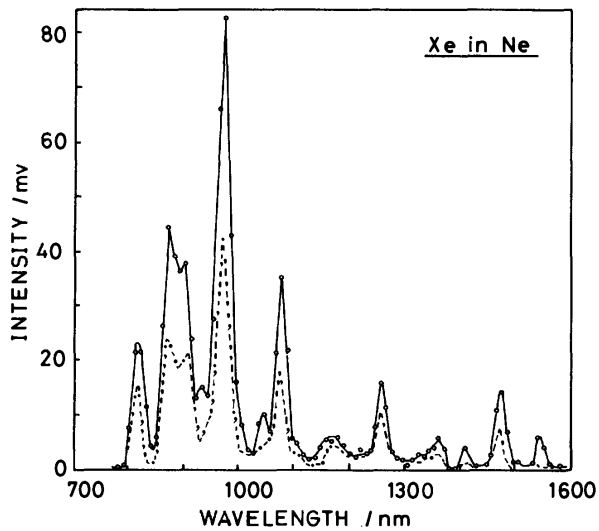

Fig. 2. The emission spectra of Xe in Xe-Ne mixtures at 50 Torr (——) and 80 Torr (----) of Xe in 510 Torr of Ne, respectively.

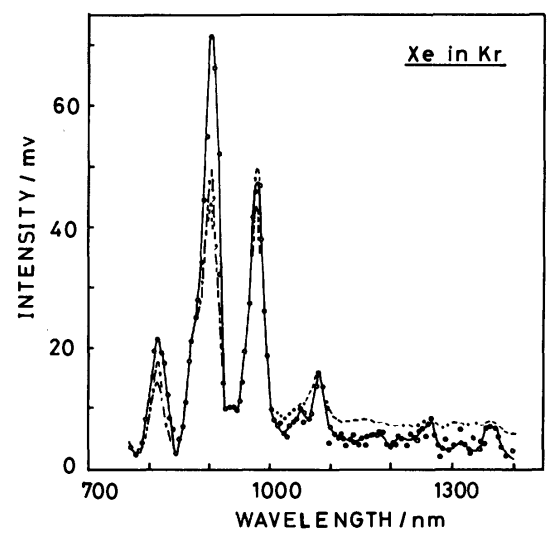

Fig. 3. The emission spectra of Xe in Xe-Kr mixtures at 20 Torr (——), 50 Torr (----), and 100 Torr (----) of Xe in 510 Torr of Kr, respectively.

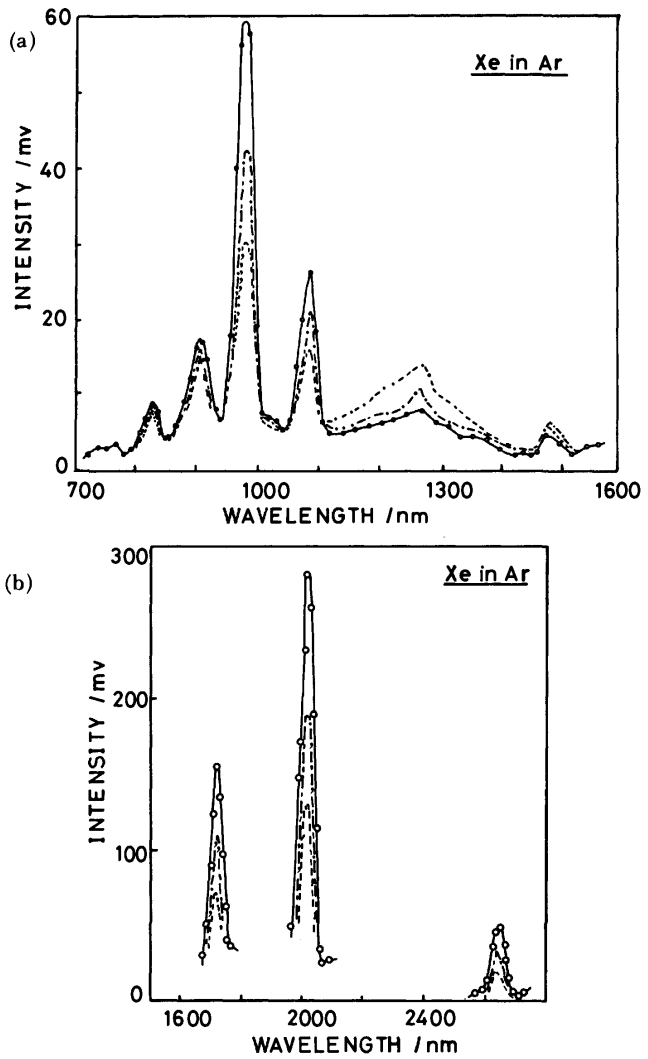

Fig. 4. (a) The emission spectra of Xe in Xe-Ar mixtures at 20 Torr (——), 50 Torr (----), and 80 Torr (----) of Xe in 640 Torr of total pressure, respectively.
(b) The emission bands of Xe 5d(3/2)$_1$ in Xe-Ar mixtures at 5 Torr (——), 10 Torr (----), and 20 Torr (----) of Xe in 640 Torr of total pressure, respectively.

5d(1/2)$_1$. Similarly, the second resonant state of Kr, $^1P_1$, can correlate with Xe 7s(3/2)$_1$. Accordingly, the observed emission lines due to 6p—6s transitions (Fig. 3) would be produced mainly by the de-excitation from lower 5d states and in a cascade from the 7s state. The absence of the continuous band at 1260 nm in the spectra implies that the lower 5d and 7s states of Xe are not involved in the formation of the species responsible for this band.

Emission Spectra in Xe-Ar Mixtures. In the Xe-Ar mixtures, the emissions due to the transition of 6p—6s of Xe and the 1260 nm band were observed, as shown in Fig. 4a. Figure 4b shows the emission lines due to Xe 5d(3/2)$_1$ at the wavelength from 1600 to 2800 nm, where the lines at 1700, 2020, and 2650 nm were observed. The lower states of these emissions are 6p(5/2)$_2$, 6p-(3/2)$_1$ and 6p(1/2)$_0$ (2p$_9$, 2p$_7$, and 2p$_5$ in Paschen notation), respectively. The intensities of the emission due to 6p(1/2)$_1$ (Paschen 2p$_{10}$) at 980 and 1080 nm were the most intense and decreased as the Xe pressure increased, whereas the emission lines at 825 and 900 nm were weak and insensitive to the Xe pressure. The Xe pressure dependence of the 5d emission was very similar to the 2p$_{10}$ emission. The band at 1260 nm began to appear at a Xe pressure greater than 20 Torr. The Xe pressure required to produce the appearance of this band was much lower in Ar compared with that observed in pure Xe, where the band began to appear above 190 Torr. Therefore, it is obvious that this band was induced by an energy transfer from Ar. The major part of the channel of the energy transfer from the excited Ar to Xe was considered to be the Ar atoms in 4s states rather than the lowest excimer state, Ar_2^*, as was considered for the reactions in Xe-Kr. Since all of the 4s states of Ar lie just below the ionization potential of Xe, the energy transfer from the excited Ar to Xe atoms will produce high Rydberg states in Xe. King, Piper and Setser studied the energy-transfer processes of metastable Ar atoms to Xe atoms and identified the emission lines extending from 7d to 10s[10] The production of similar highly excited states is possible in this type of experiment. In fact, the appearance of the emission due to Xe 5d(3/2)$_1$, shown in Fig. 4b, indicates the production of excited Xe atoms at higher Rydberg states, because it is known that in Xe-Ar mixture, the excitation of Ar $^3P_1$, or the selective excitation of higher Rydberg states of Xe above Xe_2^+ state leads to the 5d(3/2)$_1$ emission in VUV region.[11] The de-activation process of such higher Rydberg states has not been investigated except in studies of the collisional and radiative de-excitation of 7p states by Horiguchi and coworkers.[4] However, as the most probable reaction, the Hornbeck-Molner reaction, $Xe^*+Xe \rightarrow Xe_2^+ + e^-$, is known for the excited atoms above the energy state of Xe_2^+ ion (11.16 eV). According to the energetic model of the H-M reaction described by Hurst and Klots,[12] the formation of a highly excited diatomic molecule, Xe_2^{**}, would occur simultaneously with the H-M reaction, if the potential-energy curves for the collision of the highly excited atoms with a ground state atom are essentially parallel with those of the ion-atom system ($Xe^+ + Xe \rightarrow Xe_2^+$). Otherwise, the Xe_2^+ ions produced from the H-M reaction possibly undergo electron-ion recombination to form such highly excited excimers, as suggested by Mulliken[1] and Brodmann and coworkers.[13]

We attributed the band at 1260 nm to the emission from these highly excited excimer states. The Xe level closely resonant with Ar $^3P_1$ are the 9s states (11.58 eV). Then, if the potential minimum of the Xe_2^{**} formed from the 9s atom is as deep as that of the Xe_2^+ ion (0.97 eV), the lower state of this emission is estimated to be about 9.6 eV, which corresponds to the repulsive parts of the potential curves converging to the 6p levels. The band is so broad that it possibly involves several

deactivation processes.

In pure Xe, such highly excited excimer states can be formed by the direct excitation of the ground-state atoms or the vertical excitation of van der Waals molecules. The occurrence of direct excitation is supported by the fact that the addition of a small amount of SF_6 did not affect the emission intensity of the continuous band. On the other hand, the small effect of the addition of SF_6 was observed for the emission of Xe in Ar, in which a small decrease in the emission intensity at 1260 nm was clearly seen. This small decrease is considered to indicate that the ionic processes, such as the dissociative recombination of Ar_2^+, were involved in the formation of Xe_2^{**} in the Xe–Ar mixtures. However, the effect of the SF_6 observed was too small to give a reasonable interpretation so far.

It is less likely that the present band is related to the NIR absorption bands which were observed by Arai and coworkers,[2] because the emission bands could be detected only in the pure Xe and in Xe–Ar mixtures. The species, Xe_2^{**}, in this experiment may have a larger internuclear distance than the $^3\Sigma_u^+$ type excimers.

In conclusion, the continuous band which was observed at 1260 nm in irradiated pure Xe and in the Xe in Ar can be attributed to a transition from molecular states which were related to high Rydberg states just below the ionization potential of Xe and were formed by the Hornbeck-Molnar reaction, followed by ion recombination, or were formed simultaneously with the H–M reaction.

The authors would like to thank Dr. Takeaki Enoto, and Messrs. Hiroaki Tanida and Koichi Sato for their help in the operation of the linac.

References

1) R. S. Mulliken, *J. Chem. Phys.*, **52**, 5170 (1970)

2) S. Arai and R. F. Firestone, *J. Chem. Phys.*, **50**, 4575 (1969); T. Oka, K. V. S. Rao, J. L. Redpath, and R. F. Firestone, *ibid.*, **61**, 4740 (1974); S. Arai, Y. Oka, M. Koguma, and M. Imamura, *ibid.*, **68**, 4595 (1978).

3) M. Tanaka, S. Sasaki, and M. Katayama, *Bull. Chem. Soc., Jpn*, **56**, 1737 (1983).

4) H. Horiguchi, R. S. Chang, and D. W. Setser, *J. Chem. Phys.*, **75**, 1207 (1981).

5) J. LeCalvé, R. A. Gutchek, and O. Dutuit, *Chem. Phys. Lett.*, **47**, 470 (1977).

6) R. Cooper, F. Grieser, M. C. Sauer, Jr., and D. F. Sangster, *J. Phys. Chem.*, **81**, 2215 (1977).

7) A. Yokoyama, S. Takao, T. Ueno, and Y. Hatano, *Chem. Phys.*, **45**, 439 (1980).

8) Y-J. Shiu, M. A. Biondi, and D. P. Sipler, *Phys. Rev.*, **A15**, 494 (1977).

9) Y. Salamero, A. Birot, H. Brunet, H. Dijols, J. Galy, P. Millet, J. P. Montagne, *J. Chem. Phys.*, **74**, 288 (1981).

10) D. L. King, K. G. Piper, and D. W. Setser, *Trans. Faraday Soc.*, **72**, 177 (1976).

11) R. Brodmann and G. Zimmerer, *Chem. Phys. Lett.*, **56**, 434 (1976).

12) a) A. Hornbeck and J. P. Molnar, *Phys. Rev.*, **84**, 621 (1951); b) G. S. Hurst and C. E. Klots, in "Advances in Radiation Chemistry," Vol. 5, p. 23, ed by M. Burton and J. L. Magee. Wiley, New York, 1976.

13) R. Brodmann and G. Zimmerer, *Chem. Phys. Lett.*, **41**, 160 (1976).

 © 1985 The Chemical Society of Japan Bull. Chem. Soc. Jpn., 58, 433—436 (1985)

Asymmetric Transformation of DL-*p*-Hydroxyphenylglycine by a Combination of Preferential Crystallization and Simultaneous Racemization of the *o*-Toluenesulfonate

Chikara HONGO,* Masanori TOHYAMA, Ryuzo YOSHIOKA, Shigeki YAMADA,† and Ichiro CHIBATA††

Research Laboratory of Applied Biochemistry, Tanabe Seiyaku Co., Ltd., 16-89, Kashima-3-chome, Yodogawa-ku, Osaka 532

(Received October 8, 1984)

The asymmetric transformation of DL-*p*-hydroxyphenylglycine was achieved between two enantiomers by a combination of preferential crystallization of a desired enantiomer of *p*-hydroxyphenylglycine *o*-toluenesulfonate (HPG·*o*-TS) and the simultaneous racemization of the antipode. L-HPG·*o*-TS was easily racemized by heating at 100 °C in aqueous 95% (v/v) acetic acid in the presence of small amounts of salicylaldehyde and free DL-HPG. A supersaturated solution of DL-HPG·*o*-TS placed under such conditions for racemization was seeded with the crystals of D-HPG·*o*-TS, and added with DL-HPG and *o*-toluenesulfonic acid in order to provide continuously the supersaturated state of DL-HPG·*o*-TS as a driving force. As a result, 77.2% of DL-HPG added was transformed to D-isomer.

D-*p*-Hydroxyphenylglycine is useful as a side chain of semisynthetic penicillins or cephalosporins. Our previous paper[1] reported that DL-*p*-hydroxyphenylglycine was resolved by a preferential crystallization procedure in the form of salts with aromatic sulfonic acids such as benzenesulfonic acid, *o*-toluenesulfonic acid, and the like. The preferential crystallization procedure is considered to be a useful method for industrial purposes since it enables the desired optically active isomer to crystallize preferentially from a supersaturated solution of the racemic modification by the simple inoculation of the same isomer. In this procedure, however, there are several disadvantages[2-4] resulting from the fact that the crystallization of the desired isomer by inoculation leads to an excess of the undesired isomer in the solution and the resolution system is racemic as a whole.

The asymmetric transformation[3-5] by a combination of preferential crystallization of the desired isomer and the simultaneous racemization of the undesired isomer is very promising for industrial applications without the disadvantages described above. The asymmetric transformation of *N*-acyl amino acids has been successful[3,4] because *N*-acyl amino acids were easily racemized in the presence of a catalytic amount of acetic anhydride. Many DL-amino acids can be resolved in the form of salts with aromatic sulfonic acids or mineral acids.[1,6] In order to apply the asymmetric transformation to such amino acid salts, it is necessary to determine the conditions of racemization of amino acid salts.

We recently reported[7,8] that the salts of optically active amino acids with sulfonic acids or mineral acids could be racemized by heating moderately in a medium of acetic acid in the presence of small amounts of an aldehyde and free DL-amino acid, and the racemization method could be applied to asymmetric transformation of amino acids. Using the racemization method, we studied the asymmetric transformation by a combination of the optical resolution of DL-*p*-hydroxyphenylglycine *o*-toluenesulfonate (DL-HPG·*o*-TS) and the simultaneous racemization of the salt.

Since the solubility of DL-HPG·*o*-TS in acetic acid is very low (at 80 °C and 100 °C, 1.80 and 3.06 g/100 ml AcOH, respectively), it is preferable to use aqueous acetic acid to obtain a practical starting concentration for the asymmetric transformation. The effects of salicylaldehyde and DL-HPG on racemization of L-HPG·*o*-TS in aqueous acetic acid were examined. As shown in Table 1, the racemization of the salt was accelerated in the presence of salicylaldehyde, DL-HPG, or both. Although the rate of racemization, which is an important factor in this kind of asymmetric transformation, decreased with an increase in the water content of the acetic acid, a racemization rate sufficient for the asymmetric transformation was obtained by the presence of both salicylaldehyde and DL-HPG in aqueous 95% (v/v) acetic acid. Therefore, the asymmetric transformation was thereafter carried out in aqueous 95% (v/v) acetic acid. The rate of racemization was greatly influenced by temperature as shown in Fig. 1. A temperature higher than 90 °C was necessary for practical racemization.

When DL-HPG·*o*-TS was crystallized from a solution placed under the racemizing conditions as described above, the IR-spectrum and the melting point of the DL-HPG·*o*-TS obtained were identical with those of

TABLE 1. EFFECTS OF SALICYLALDEHYDE AND DL-HPG ON RACEMIZATION OF L-HPG·*o*-TS[a]

Additive[b]	Racemization degree/%		
	AcOH[c]	95% AcOH[d]	90% AcOH[d]
None	20	18	18
Salicylaldehyde	55	30	24
DL-HPG	76	66	49
Salicylaldehyde and DL-HPG	99	94	62

a) Reaction was carried out at 100 °C for 3 h. b) 0.2 Molar equivalent. c) Glacial acetic acid. d) Aqueous acetic acid.

†Present address: Research Planning & Investigation Division, Tanabe Seiyaku Co., Ltd., 16-89, Kashima-3-chome, Yodogawa-ku Osaka 532.

††Present address: Research & Development Headquarters, Tanabe Seiyaku Co., Ltd., 16-89, Kashima-3-chome, Yodogawa-ku, Osaka 532.

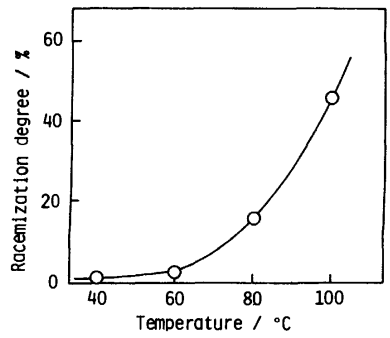

Fig. 1. Effect of temperature on racemization of L-HPG·*o*-TS.
The reactions were carried out for 1 h in aqueous 95% acetic acid in the presence of salicylaldehyde and DL-HPG.

racemic mixture of DL-HPG·*o*-TS obtained in our previous paper;[1] this indicates that DL-HPG·*o*-TS crystallizes as a racemic mixture suitable for the preferential crystallization procedure also under such racemizing conditions. The crystals of D-HPG·*o*-TS were confirmed to be not racemized under the above conditions for racemization in a liquid phase. Thus, the most essential requirement for this kind of asymmetric transformation was fulfilled.

Then, to find the possibility of the asymmetric transformation of DL-HPG, a batch-asymmetric transformation was carried out. The supersaturated solution of DL-HPG·*o*-TS placed under the racemizing conditions described above was seeded with the crystals of D-HPG·*o*-TS and stirred for 2 h. The crystallized crop and the second crop obtained from the mother liquor were analyzed. As a result, it was found that the preferential crystallization of seeded D-HPG·*o*-TS and the racemization of unseeded L-HPG·*o*-TS took place at the same time and 17% of DL-HPG·*o*-TS was transformed to D-HPG·*o*-TS.

Since the driving force for the preferential crystallization of a seeded isomer is provided only by the supersaturated state of the racemic modification, the yield of the enantiomer produced by this type of asymmetric transformation is dependent on the extent of the supersaturated state of the racemic modification. In a batch transformation, the yield is relatively low because the starting supersaturation degree is limited by the stability of the supersaturated state. To obtain a higher yield of the enantiomer, it is necessary to make up for the decrease of the supersaturation degree due to the preferential crystallization.

In the asymmetric transformation of DL-HPG·*o*-TS, the supersaturated state could not be continuously provided by cooling the solution because the racemization did not proceed at a low temperature (Fig. 1). In the present work, the supersaturated state was maintained continuously by suspending free DL-HPG in the reaction mixture and then by adding *o*-toluenesulfonic acid, thereto, to form the salt of DL-HPG·*o*-TS in the liquid phase. In this case, fortunately,

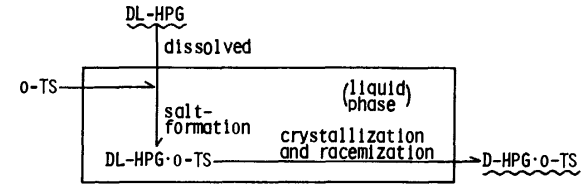

Fig. 2. Continuous asymmetric transformation of DL-HPG. ~~~, solid state.

the suspension of free DL-HPG is preferable since the presence of free DL-HPG in the liquid phase is essential for accelerating the racemization of L-HPG·*o*-TS. DL-HPG·*o*-TS resulting from free DL-HPG and the added *o*-toluenesulfonic acid can exist in a supersaturated state under an appropriate rate of the addition of *o*-toluenesulfonic acid, and can serve for the asymmetric transformation. The continuous asymmetric transformation presented here was carried out in such a suspension system in expectation of a repetition of the following process: dissolution of suspended DL-HPG, formation of DL-HPG·*o*-TS to result a supersaturated state, and preferential crystallization and simultaneous racemization toward the resulting DL-HPG·*o*-TS. The pathway is shown in Fig. 2.

o-Toluenesulfonic acid has two moles of water of crystallization which can not be easily removed. The addition of the dihydrate into the reaction mixture results in an increase of the water content in the reaction system and consequently in the lowering of the racemization rate. Therefore, *o*-toluenesulfonic acid dihydrate was dissolved in acetic anhydride, which reacted with the water of crystallization at 100°C to form acetic acid. This was added to the reaction system in the form of an acetic anhydride solution of *o*-toluenesulfonic acid dihydrate. The pouring speed of the *o*-toluenesulfonic acid solution, *i. e.*, the speed of producing a supersaturated state, was controlled to meet the rate of crystallization of D-HPG·*o*-TS and the rate of racemization of L-HPG·*o*-TS. Namely, into a heterogeneous mixture consisting of 19.0 g of DL-HPG·*o*-TS, 1.25 ml of salicylaldehyde, 51.0 g of free DL-HPG, and 100 ml of aqueous 95% (v/v) acetic acid, 2.0 g of crystals of D-HPG·*o*-TS was seeded at 100°C. Then, the solution consisting of 62.5 g of *o*-toluenesulfonic acid dihydrate and 62.5 ml of acetic anhydride was poured at the rate of 5.0 ml/h into the mixture maintained at 100°C under stirring. The precipitated crystals were separated to give 82.8 g of almost optically pure D-HPG·*o*-TS. The material remaining in the filtrate was nearly racemic. The change in the composition of both enantiomers by the reaction is shown in Fig. 3. The result suggests that 77.2% of suspended DL-HPG was transformed to D-HPG *via* the pathway as shown in Fig. 2. The D-HPG·*o*-TS obtained above was easily decomposed to D-HPG without racemization by neutralization.

The asymmetric transformation between two dia-

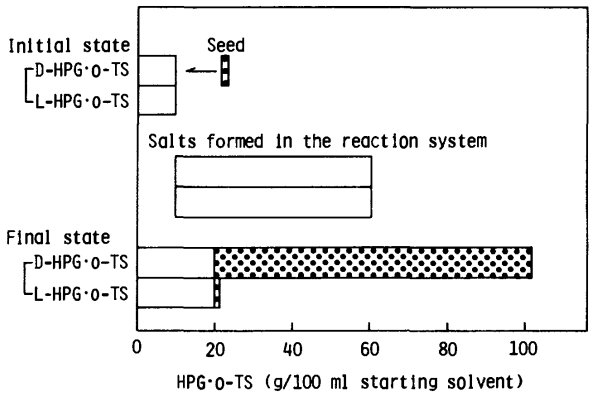

Fig. 3. The change in the composition of both enantiomers by continuous asymmetric transformation. ▩, crystals of HPG·*o*-TS; □, HPG·*o*-TS in solution.

stereoisomers by a combination of selective precipitation of the less soluble diastereoisomer and epimerization of the soluble diastereoisomer is well-known as an asymmetric transformation of the second order.[9] However, an asymmetric transformation between two enantiomers by a combination of preferential crystallization of a desired enantiomer and the simultaneous racemization of the antipode is unique and has not been reported except for a few examples.[3-5] It is necessary in this kind of asymmetric transformation to devise a way in which the supersaturated state is provided as a driving force. In the case of the asymmetric transformation of DL-HPG proposed here, the supersaturated state of DL-HPG·*o*-TS could be easily produced by adding DL-HPG and *o*-toluenesulfonic acid into the reaction system. If DL-HPG·*o*-TS in a supersaturated state is formed at a rate which meets the rates of preferential crystallization and racemization, the reaction proceeds in a high concentration of slurry state. The proposed method seems very promising for the industrial production of D-HPG because of its operational simplicity and high yield.

Experimental

Materials and Analyses. Optically active and racemic HPG manufactured by our company, Tanabe Seiyaku Co., Ltd., were used. *o*-Toluenesulfonic acid, salicylaldehyde, and other chemicals were obtained from Tokyo Kasei Kogyo Co., Ltd. Optically active and racemic HPG·*o*-TS were prepared in a manner described in a previous report.[1] All samples were dried overnight *in vacuo* at 40°C. Optical rotation was measured with a Perkin-Elmer 141 automatic polarimeter. The water content of samples was determined by the Karl-Fischer's method.

Racemization of L-*HPG·o-TS.* Unless otherwise noted, a mixture of L-HPG·*o*-TS (50 mg), DL-HPG (5 mg), salicylaldehyde (3 μl), and acetic acid containing 5% water (5 ml) was heated in a sealed tube at 100°C for 1 h or 3 h. After the reaction mixture was diluted with 1 M hydrochloric acid (5 ml (1 M=1 mol dm^{-3})), the optical rotation was measured. The racemization degree was calculated in the same way as described in a previous report.[7] The effect of DL-HPG or salicylaldehyde in acetic acid containing water and the effect of the reaction temperature are shown in Table 1 and Fig. 1, respectively.

Crystallization of DL-*HPG·o-TS from Racemizing Solution.* A mixture of DL-HPG·*o*-TS (3.8 g), DL-HPG (0.2 g), and salicylaldehyde (0.25 ml) was dissolved in acetic acid (20 ml) containing 5% water under reflux and maintained at 100°C. The solution was seeded with finely pulverized crystals of DL-HPG·*o*-TS (10 mg) and stirred for 5 h at the same temperature. The precipitated crystals were quickly separated by filtration, washed with a small amount of AcOH, and dried to give DL-HPG·*o*-TS (0.92 g) crystallized from racemizing solution. The melting point (213—215°C, dec) and IR-spectrum of the DL-HPG·*o*-TS were identical with those of racemic mixture of DL-HPG·*o*-TS shown in previous report.[1]

Stability of Crystalline D-*HPG·o-TS under Conditions for Racemization.* A mixture of DL-HPG·*o*-TS (1.0 g), DL-HPG (40 mg), and salicylaldehyde (50 mg) was dissolved in AcOH containing 2% water under reflux to prepare a solution saturated with DL-HPG·*o*-TS at 100°C. To the saturated solution maintained at 100°C, crystals of D-HPG·*o*-TS (2.0 g) were added. The heterogeneous reaction mixture was stirred for 5 h at the same temperature. The insoluble crystals were quickly separated by filtration, washed with a small amount of AcOH, and dried. The insoluble crystals proved to be optically pure D-HPG·*o*-TS (1.9 g), $[\alpha]_D^{25}$ −66.6° (c=1, water).

Asymmetric Transformation. Batch Transformation: A mixture of DL-HPG·*o*-TS (3.8 g), DL-HPG (0.2 g), salicylaldehyde (0.25 ml) and AcOH (20 ml) containing 5% water was heated under reflux until a complete solution occurred and was maintained at 100°C. The supersaturated solution was seeded with finely pulverized crystals of D-HPG·*o*-TS (0.2 g) and stirred for 2 h at the same temperature. The precipitated crystals were quickly separated by filtration, washed with a small amount of AcOH, and dried to give D-HPG·*o*-TS (0.85 g), $[\alpha]_D^{25}$ −66.6° (c=1, water), optical purity 100%. Subtracting 0.2 g of seeded D-HPG·*o*-TS, 0.65 g of pure D-HPG·*o*-TS was obtained. After the separation of D-HPG·*o*-TS, the filtrate was stirred at 20°C for 2 h and the precipitated crystals were collected by filtration to give DL-HPG·*o*-TS (2.66 g), $[\alpha]_D^{25}$ +0.6° (c=1, water). The mother liquor did not show any optical rotation. Therefore, the whole reaction mixture became 17.1% enantiomeric excess.

Continuous Transformation: A mixture of DL-HPG·*o*-TS (19.0 g) and aqueous 95% (v/v) acetic acid (100 ml) in a three-necked flask fitted with a mechanical stirrer and a condenser was heated under reflux until complete solution occurred. Then the flask was placed in an oil bath controlled at 100°C. Salicylaldehyde (1.24 ml) was added to the solution and DL-HPG (51.0 g) was suspended therein. After 20 min, into the heterogeneous reaction mixture were added under stirring finely pulverized crystals of D-HPG·*o*-TS (2.0 g) as seed crystals. To this was poured a solution consisting of *o*-toluenesulfonic acid dihydrate (62.5 g) and acetic anhydride (62.5 ml) at the rate of 5.0 ml/h by a Micro Feeder JP-W (Furue Science Co., Ltd.). At 5 h and 20 h after the addition of the seed crystals, 1.3 ml and 0.7 ml of salicylaldehyde were added to the mixture, respectively. The mixture was stirred at the same temperature for total 30 h. The precipitated crystals were quickly collected by filtration, washed with a small amount of acetic acid, and dried to give D-HPG·*o*-TS (82.8 g), $[\alpha]_D^{25}$ −64.9° (c=1, water), optical purity 97.4%.

After the separation of D-HPG·*o*-TS, the filtrate was stirred for 2 h at room temperature and the precipitated crystals were collected by filtration to recover DL-HPG·*o*-TS (18.2 g), $[\alpha]_D^{25}$ 0.0° (c=1, water). The filtrate did not show any optical rotation. The change in the composition of both enantiomers by the reaction is shown in Fig. 3.

Preparation of D-*HPG.* The D-HPG·*o*-TS (82.0 g) obtained above was dissolved in water (230 ml) at an elevated temperature and was treated with charcoal. The solution was adjusted to pH 6 with 5 M sodium hydroxide and allowed to stand in a refrigerator overnight. The resulting precipitates were collected, washed with water, and dried to give D-HPG (34.0 g), $[\alpha]_D^{25}$ −158.2° (c=1, M-HCl).

References

1) S. Yamada, C. Hongo, and I. Chibata, *Agric. Biol. Chem.*, **42**, 1521 (1978).

2) C. Hongo, S. Yamada, and I. Chibata, *Bull. Chem. Soc. Jpn.*, **54**, 1905 (1981).

3) C. Hongo, S. Yamada, and I. Chibata, *Bull. Chem. Soc. Jpn.*, **54**, 3286 (1981).

4) C. Hongo, S. Yamada, and I. Chibata, *Bull. Chem. Soc. Jpn.*, **54**, 3291 (1981).

5) W. J. Boyle, Jr., S. Sifniades, and J. F. Van Peppen, *J. Org. Chem.*, **44**, 4841 (1979).

6) A. Collet, M. J. Brienne, and J. Jacques, *Chem. Rev.*, **80**, 215 (1980).

7) S. Yamada, C. Hongo, R. Yoshioka, and I. Chibata, *J. Org. Chem.*, **48**, 843 (1983).

8) C. Hongo, R. Yoshioka, M. Tohyama, S. Yamada, and I. Chibata, *Bull. Chem. Soc. Jpn.*, **56**, 3744 (1983).

9) M. M. Harris, "Progress in Stereochemistry," ed by W. Klyne and P. B. D. Mare, Butterworths Scientific Publications, London (1958), Vol. 2, p. 157.

 © 1985 The Chemical Society of Japan Bull. Chem. Soc. Jpn., 58, 437—441 (1985)

Crystal and Molecular Structures of Fenethazine Hydrochloride and Its Cation Radical-Copper(II) Complex Salt

Atsuo OBATA, Masahiro YOSHIMORI, Koh-ichi YAMADA, and Hiroshi KAWAZURA*
Faculty of Pharmaceutical Sciences, Josai University, Keyakidai, Sakado, Saitama 350-02
(Received June 25, 1984)

The crystal structures of fenethazine hydrochloride hydrate (FTZ·HCl) and $[FTZ\,H]^{2+}\cdot[CuCl_4]^{2-}$ (FTZ-Cu) were determined. FTZ·HCl crystallized in the monoclinic space group $P2_1/a$ with $a=8.686(1)$, $b=31.660(2)$, $c=6.140(1)$ Å, $\beta=100.44(1)°$, $V=1660.5(3)$ Å^3, and $Z=4$. FTZ-Cu crystallized in the triclinic space group $P\bar{1}$ with $a=20.433(5)$, $b=12.721(4)$, $c=7.526(2)$ Å, $\alpha=91.31(3)$, $\beta=94.56(3)$, $\gamma=99.69(2)°$, $V=1920.9(1)$ Å^3, and $Z=4$. The structures were solved using the heavy-atom method and were refined by the block-diagonal least-squares method. The final R values were determined to be 0.052 for FTZ·HCl and 0.050 for FTZ-Cu. The formation of a cation radical causes the phenothiazine ring of the FTZ molecule to be flattened; the dihedral angle between benzene rings is increased from 140.3° for FTZ·HCl to 174.7 or 167.5° for FTZ-Cu. The 2-aminoethyl chain holds a trans conformation in FTZ-Cu and a near gauche form in FTZ·HCl. In FTZ·HCl crystals, the FTZ molecules form a layer along a in which the molecules array the phenothiazine ring as faced with the ring in the neighboring layer. In FTZ-Cu, two FTZ molecules form a pair with a close overlap of the phenothiazine rings, directed approximately perpendicular to a. The $CuCl_4^{2-}$ is located so as to counterbalance both the positive charge of the ring and the protonated amino group of the side chain.

It is well known that phenothiazine drugs have many therapeutical uses and that variations of substituents at the 2- and 10-positions in the tricyclic ring system are responsible for the diversity of pharmacological activities. Conformational studies on drugs with a 3-aminopropyl chain at the 10-position, which are mainly employed as tranquilizers, have been reported in connection with the structure-activity relationship.[1,2] However, no structural analysis has been described yet on drugs bearing a 2-aminoethyl substituent at the same position, showing the efficacy of antihistaminics. These types of drugs are easily converted into one-electron-oxidation products under relatively mild conditions owing to the low ionization potential of the phenothiazine ring.[3] Horse-radish peroxidase catalyzes 2-chloro-10-(3-dimethylaminopropyl)phenothiazine (chlorpromazine, CPZ) *in vitro* in the presence of hydrogen peroxide to the cation radical species.[4] Thus, it is expected that such cation radicals of the drugs may be generated *in vivo* and may play some kind of pharmacological role.[5]

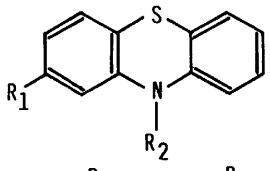

	R_1	R_2
CPZ :	Cl	$(CH_2)_3N(CH_3)_2$
PMZ:	H	$(CH_2)_3N(CH_3)_2$
FTZ :	H	$(CH_2)_2N(CH_3)_2$

In the course of our study regarding the interaction between neuroleptics and copper ions, we prepared stable complex salts of CPZ[6] and 10-(3-dimethylaminopropyl)phenothiazine (promazine, PMZ)[7] cation radicals with $[CuCl_4]^{2-}$ and determined their structures. So far, only the perchlorate salt of the CPZ cation radical has been obtained in crystal form among this type of drug,[8-10] though the structure has not been clarified. An application of a similar synthetic method[6] to 10-(2-dimethylaminoethyl)phenothiazine (fenethazine, FTZ) afforded stable crystals of the cation radical salt composed of $[FTZ\,H]^{2+}\cdot[CuCl_4]^{2-}$ (FTZ-Cu). In this paper we describe the crystal and molecular structures of FTZ·HCl and FTZ-Cu and discuss the structural differences between them.

Experimental

The FTZ·HCl was prepared by coupling *N,N*-dimethyl-2-chloroethylamine with phenothiazine[11] and crystallizing with water to yield white needles with the composition FTZ·HCl·H_2O. The FTZ-Cu was obtained as black plates according to a previously reported method.[7] Found: C, 40.06; H, 3.60; N, 5.57%. Calcd for $[FTZ\,H]^{2+}\cdot[CuCl_4]^{2-}$ ($C_{16}H_{19}N_2SCuCl_4$): C, 40.31; H, 4.02; N, 5.88%. The crystals were stable in air for several months when dried, although they decomposed slowly in aqueous solutions.

The X-ray diffraction data were measured on a Rigaku AFC-5 automatic four-circle diffractometer using graphite-monochromated Cu $K\alpha$ radiation ($\lambda=1.5418$ Å). The unit-cell parameters were refined from least-squares fits of 24 2θ values ($48<2\theta<52°$) for FTZ·HCl and 50 ($48<2\theta<53°$) for FTZ-Cu. The crystal data and a part of the experimental details are tabulated in Table 1. Intensities were measured by the θ–2θ scan technique and the counting time was 1 s. Each background was measured for 10 s at the begining and end of the scan range. During data collection, three standard reflections were monitored every 100 or 50 reflections and showed no significant variation in their intensities. For FTZ·HCl, 3226 reflections with $2\theta\leq130°$ were measured and 2297 independent reflections with $|F_o|>3\sigma(|F_o|)$ were used for the structure determination. For FTZ-Cu, 5557 reflections with $2\theta\leq120°$ were collected and 4478 reflections with $|F_o|>12\sigma(|F_o|)$ were used in the subsequent analysis. Each data set was corrected for Lorentz and polarization effects, but not for absorption.

The structures were solved using the heavy-atom and Fourier methods and were refined by the block-diagonal least-squares method. The minimized function was $\sum w(|F|-|F_c|)^2$,

where $w=1/[\sigma^2+(0.02F_o)^2]$. All the positional parameters and anisotropic thermal parameters for non-hydrogen atoms, and isotropic thermal parameters for hydrogen atoms were refined. All the parameter shifts in the final cycle of the refinement were less than 0.2σ for both compounds. The final R values were 0.052 for FTZ·HCl and 0.050 for FTZ-Cu.

The neutral atomic-scattering factors were taken from the International Tables for X-ray Crystallography.[12] All the calculations were carried out on a FACOM M-160F computer at Josai University using the UNICS III[13] and ORTEP[14] programs. The final positional and thermal parameters (with standard deviations) are given in Tables 2 and 3. Data regarding structure factors, anisotropic thermal parameters, and hydrogen-atom coordinates have been deposited in the office of the Chemical Society of Japan (Document No. 8507).

TABLE 1. CRYSTAL DATA AND EXPERIMENTAL DETAILS

	FTZ·HCl	FTZ-Cu
Formula	$C_{16}H_{18}N_2S$ HCl H_2O	$C_{16}H_{19}N_2S$ $CuCl_4$
F.W.	324.85	476.76
Crystal size/mm³	0.16×0.77×0.11	0.38×0.30×0.08
Crystal system	Monoclinic	Triclinic
Space group	$P2_1/a$	$P\bar{1}$
a/Å	8.686(1)	20.433(5)
b/Å	31.660(2)	12.721(4)
c/Å	6.140(1)	7.526(2)
α/°	—	91.31(3)
β/°	100.44(1)	94.56(3)
γ/°	—	99.69(2)
V/Å³	1660.5(3)	1920.9(1)
Z	4	4
F(000)	688	968
Dm/Mg m⁻³	1.307	1.636
Dc/Mg m⁻³	1.300	1.649
μ(Cu *Kα*)/mm⁻¹	3.21	7.87
Scan rate/° min⁻¹	3	4
Scan width/°	1.0	1.0
$2\theta_{max}$/°	130	120
R	0.052	0.050
Rw	0.053	0.057

TABLE 2. ATOMIC COORDINATES (×10⁴) AND EQUIVALENT ISOTROPIC THERMAL PARAMETERS FOR FTZ·HCl

	x	*y*	*z*	B_{eq}/Å²
Cl	−4094(1)	7923.3(3)	3938(1)	4.16(3)
O	2087(3)	7991(1)	5400(4)	5.9(1)
C(1)	2844(4)	8756(1)	10856(5)	3.8(1)
C(2)	4427(4)	8788(1)	9966(7)	5.1(1)
C(3)	4907(4)	8977(1)	7929(7)	5.7(1)
C(4)	3815(4)	9137(1)	6774(6)	4.7(1)
S(5)	813(1)	9284.5(3)	6145(1)	3.85(3)
C(6)	−1536(4)	9807(1)	8129(6)	4.3(1)
C(7)	−2717(4)	9930(1)	9827(7)	5.0(1)
C(8)	−2945(4)	9714(1)	11788(7)	4.9(1)
C(9)	−2014(4)	9371(1)	12081(6)	3.9(1)
N(10)	95(3)	8878(1)	10525(4)	3.0(1)
C(11)	1726(3)	8909(1)	9691(5)	2.9(1)
C(12)	2223(4)	9102(1)	7650(5)	3.3(1)
C(13)	−622(4)	9462(1)	8381(5)	3.2(1)
C(14)	−852(3)	9235(1)	10363(5)	2.9(1)
C(15)	−449(4)	8547(1)	12142(5)	3.2(1)
C(16)	−89(3)	8109(1)	11176(5)	2.8(1)
N(17)	−1366(3)	7942(1)	10056(4)	2.9(1)
C(18)	−1038(4)	7495(1)	9388(6)	4.2(1)
C(19)	−1627(4)	8204(1)	8132(5)	4.4(1)

TABLE 3. ATOMIC COORDINATES (×10⁴) AND EQUIVALENT ISOTROPIC THERMAL PARAMETERS FOR FTZ-Cu

	x	*y*	*z*	B_{eq}/Å²
Cu(A)	−3748.2(4)	−3257(1)	−2048(1)	2.91(3)
Cu(B)	1158.3(4)	−3093(1)	−3659(1)	2.61(3)
Cl(1)(A)	−2766(1)	−2629(1)	−597(2)	4.2(1)
Cl(2)(A)	−4388(1)	−2427(1)	−414(2)	3.8(1)
Cl(3)(A)	−4302(1)	−3120(2)	−4683(2)	5.1(1)
Cl(4)(A)	−3618(1)	−5015(1)	−2505(2)	4.1(1)
Cl(1)(B)	843(1)	−3012(1)	−858(2)	3.4(1)
Cl(2)(B)	1711(1)	−4487(1)	−3135(2)	3.21(4)
Cl(3)(B)	1883(1)	−2112(1)	−5287(2)	3.7(1)
Cl(4)(B)	198(1)	−2935(1)	−5170(2)	4.2(1)
C(1)(A)	5817(3)	1918(5)	6300(8)	3.7(2)
C(2)(A)	5494(3)	1351(6)	7601(9)	4.4(2)
C(3)(A)	5456(3)	250(6)	7667(9)	4.5(2)
C(4)(A)	5717(3)	−274(5)	6366(9)	4.1(2)
S(5)(A)	6305(1)	−507(1)	3441(2)	4.0(1)
C(6)(A)	6901(3)	−29(5)	515(9)	3.8(2)
C(7)(A)	7206(3)	612(6)	−702(9)	4.6(2)
C(8)(A)	7261(3)	1716(6)	−474(9)	4.6(2)
C(9)(A)	7020(3)	2156(5)	965(9)	4.0(2)
N(10)(A)	6463(2)	1978(3)	3699(6)	2.7(1)
C(11)(A)	6114(3)	1402(4)	4975(8)	2.8(2)
C(12)(A)	6038(3)	282(5)	5017(8)	3.1(2)
C(13)(A)	6650(3)	411(4)	1999(8)	2.9(2)
C(14)(A)	6706(3)	1523(4)	2246(7)	2.8(2)
C(15)(A)	6585(3)	3157(4)	3913(8)	2.9(2)
C(16)(A)	6021(3)	3575(4)	2855(8)	3.3(2)
N(17)(A)	6053(2)	4758(3)	3109(6)	2.5(1)
C(18)(A)	5475(3)	5058(5)	1978(9)	4.2(2)
C(19)(A)	6686(3)	5391(5)	2647(9)	3.9(2)
C(1)(B)	586(3)	1541(5)	1801(8)	3.0(2)
C(2)(B)	457(3)	798(5)	3078(8)	3.8(2)
C(3)(B)	598(3)	−219(5)	2884(9)	4.2(2)
C(4)(B)	864(3)	−509(5)	1392(8)	3.6(2)
S(5)(B)	1313(1)	−252(1)	−1793(2)	3.8(1)
C(6)(B)	1942(3)	760(5)	−4339(8)	3.7(2)
C(7)(B)	2180(3)	1609(5)	−5312(8)	4.0(2)
C(8)(B)	2014(3)	2599(5)	−4881(8)	3.9(2)
C(9)(B)	1630(3)	2741(5)	−3539(8)	3.3(2)
N(10)(B)	1023(2)	2046(3)	−1057(6)	2.6(1)
C(11)(B)	870(3)	1280(4)	252(7)	2.7(2)
C(12)(B)	1002(3)	229(4)	64(8)	3.1(2)
C(13)(B)	1563(3)	891(4)	−2908(7)	2.9(2)
C(14)(B)	1398(3)	1897(4)	−2475(7)	2.6(2)
C(15)(B)	835(3)	3110(5)	−745(8)	3.1(2)
C(16)(B)	1401(3)	3790(4)	440(8)	3.2(2)
N(17)(B)	1270(2)	4881(3)	911(6)	2.9(1)
C(18)(B)	702(4)	4860(5)	2061(9)	4.7(2)
C(19)(B)	1896(3)	5526(5)	1828(9)	4.6(2)

Results and Discussion

The FTZ-Cu displays a maximum (electronic spectrum) at 513 nm (ε 9500) in aqueous solution and at 560—580 nm (broad band) in the solid state. These appear also for the CPZ-Cu and PMZ-Cu complex salt and are ascribable to the cation radical species of the phenothiazine ring in agreement with the maximum wavelengths reported for the cation radicals of the same ring.[15]

The molecular structures and atom-numbering are given in Figs. 1 and 2, and the bond lengths and angles are listed in Table 4. As the difference Fourier maps revealed the hydrogen atom attached to the N(17) atom

Table 4. Bond lengths (l/Å) and angles (ϕ/°)

	FTZ-Cu		FTZ·HCl
	A	B	
C(1)-C(2)	1.375(9)	1.373(9)	1.388(4)
C(2)-C(3)	1.393(10)	1.380(10)	1.382(6)
C(3)-C(4)	1.365(10)	1.356(10)	1.379(6)
C(4)-C(12)	1.394(9)	1.400(8)	1.394(4)
C(11)-C(12)	1.409(8)	1.415(8)	1.391(4)
C(1)-C(11)	1.412(9)	1.399(8)	1.394(5)
C(6)-C(7)	1.360(9)	1.363(9)	1.380(5)
C(7)-C(8)	1.397(10)	1.397(10)	1.367(6)
C(8)-C(9)	1.372(10)	1.355(9)	1.385(5)
C(9)-C(14)	1.396(9)	1.396(8)	1.390(4)
C(13)-C(14)	1.408(8)	1.415(8)	1.397(4)
C(6)-C(13)	1.409(9)	1.399(9)	1.376(5)
S(5)-C(12)	1.718(6)	1.722(6)	1.760(3)
S(5)-C(13)	1.715(6)	1.719(6)	1.770(3)
N(10)-C(11)	1.391(7)	1.418(7)	1.420(4)
N(10)-C(14)	1.390(8)	1.391(7)	1.413(4)
N(10)-C(15)	1.483(7)	1.489(8)	1.461(4)
C(15)-C(16)	1.528(8)	1.533(8)	1.518(4)
C(16)-N(17)	1.504(7)	1.498(8)	1.503(4)
N(17)-C(18)	1.505(8)	1.500(9)	1.486(4)
N(17)-C(19)	1.476(7)	1.506(8)	1.494(4)
Cu-Cl(1)	2.221(2)	2.258(2)	
Cu-Cl(2)	2.235(2)	2.284(2)	
Cu-Cl(3)	2.230(2)	2.234(2)	
Cu-Cl(4)	2.319(2)	2.229(2)	
C(11)-C(1)-C(2)	121.2(6)	120.2(6)	120.3(3)
C(1)-C(2)-C(3)	121.0(7)	121.7(6)	120.2(4)
C(2)-C(3)-C(4)	119.1(6)	119.9(6)	120.1(3)
C(3)-C(4)-C(12)	120.8(6)	119.9(6)	120.0(3)
C(4)-C(12)-C(11)	121.2(6)	121.0(6)	120.4(3)
C(1)-C(11)-C(12)	116.6(5)	117.3(5)	119.0(3)
C(7)-C(6)-C(13)	120.6(6)	120.4(6)	120.3(3)
C(6)-C(7)-C(8)	119.2(7)	118.3(6)	119.6(3)
C(7)-C(8)-C(9)	120.9(6)	122.3(6)	120.8(3)
C(8)-C(9)-C(14)	121.6(6)	120.8(6)	120.3(3)
C(9)-C(14)-C(13)	117.1(6)	117.0(5)	118.1(3)
C(6)-C(13)-C(14)	120.7(5)	121.0(5)	120.9(3)
C(11)-N(10)-C(14)	124.5(5)	123.9(5)	118.3(2)
N(10)-C(11)-C(12)	122.1(5)	121.7(5)	118.9(3)
C(11)-C(12)-S(5)	124.2(5)	123.8(4)	119.0(2)
C(12)-S(5)-C(13)	102.4(3)	102.4(3)	99.0(2)
S(5)-C(13)-C(14)	124.6(5)	124.2(5)	118.8(2)
C(13)-C(14)-N(10)	121.8(5)	121.9(5)	118.7(2)
C(1)-C(11)-N(10)	121.3(5)	121.0(5)	122.2(3)
C(4)-C(12)-S(5)	114.7(5)	115.3(5)	120.5(3)
C(6)-C(13)-S(5)	114.6(4)	114.8(5)	120.3(3)
C(9)-C(14)-N(10)	121.1(5)	121.1(5)	123.2(3)
C(11)-N(10)-C(15)	117.6(5)	116.7(5)	118.3(2)
C(14)-N(10)-C(15)	117.9(4)	119.0(4)	120.0(2)
N(10)-C(15)-C(16)	108.1(4)	107.9(5)	111.7(2)
C(15)-C(16)-N(17)	113.1(4)	113.8(5)	112.6(2)
C(16)-N(17)-C(18)	107.5(4)	112.9(4)	110.0(2)
C(16)-N(17)-C(19)	113.6(5)	108.9(5)	113.3(2)
C(18)-N(17)-C(19)	110.5(5)	110.3(5)	111.1(2)
Cl(1)-Cu-Cl(2)	98.7(1)	94.2(1)	
Cl(1)-Cu-Cl(3)	139.4(1)	136.6(1)	
Cl(1)-Cu-Cl(4)	99.1(1)	99.1(1)	
Cl(2)-Cu-Cl(3)	96.8(1)	99.2(1)	
Cl(2)-Cu-Cl(4)	135.0(1)	133.9(1)	
Cl(3)-Cu-Cl(4)	95.9(1)	100.6(1)	

in both compounds, a positive charge in FTZ·HCl is located on the amino group of the side chain, and the same group together with the tricyclic ring in FTZ-Cu

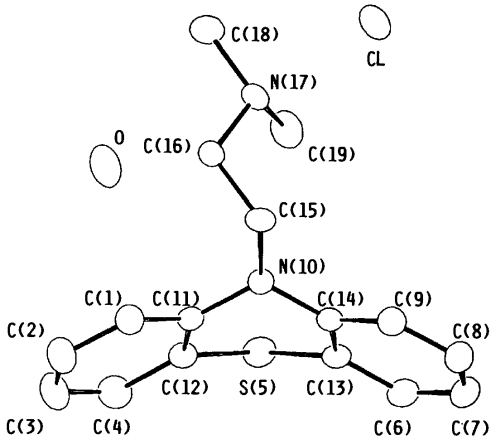

Fig. 1. Perspective view of FTZ·HCl·H_2O with 50% probability ellipsoids.

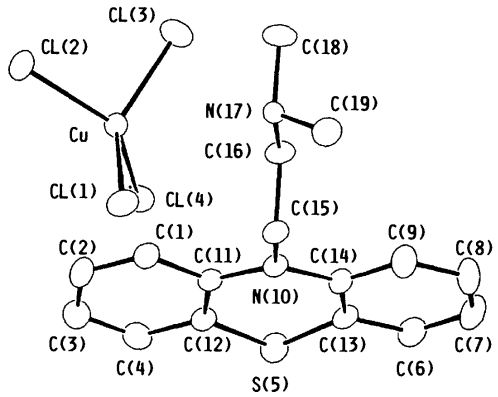

Fig. 2. Perspective view of $[FTZ\ H]^{2+}\cdot[CuCl_4]^{2-}$ (A) with 50% probability ellipsoids.

bears a positive charge. In the FTZ-Cu crystals there are two crystallographically independent FTZ molecules and two independent $[CuCl_4]^{2-}$ ions with different bond lengths and angles (hereafter discriminated by the notation A and B, respectively).

The conversion into the cation radical salt causes the almost planar geometry of the phenothiazine ring in the FTZ molecule as is obvious by a comparison of Figs. 1 and 2. The dihedral angle between the lateral benzene rings is 174.7° in FTZ-Cu (A) and 167.5° in FTZ-Cu (B). All the component atoms in the ring lie on a near plane, while the angle in FTZ·HCl is 140.3° owing to the folding of the ring around the S-N axis. This results in a bent boat-form. The C-N and C-S bond lengths in the thiazine ring of FTZ·HCl are approximately the same as those of *N*-methylphenothiazine (the C-N and C-S bond lengths are 1.402 and 1.764 Å, respectively).[16] The C-N-C and C-S-C angles in the ring are also in accordance with the 118° of the C-N-C angle and the 97° of the C-S-C in *N*-methylphenothiazine. These facts indicate that the positive charge on the protonated amino group of the side chain causes no significant perturbation in the structure of the phenothiazine moiety. On the other hand, the geometry of the thiazine ring in FTZ-Cu reveals a clear difference in comparison with that in

FTZ·HCl. The C-N and C-S bonds are shortened by the ranges of 0—0.03 and 0.04—0.05 Å, respectively. The C-N-C and C-S-C angles are spread by 5.4 (A) and 4.8 (B), and 3.3°, respectively, implying an increase of the double-bond characteristics of both bonds. In particular, the C-S bond lengths become shorter than the value of 1.740 Å reported regarding an aromatic molecule, dibenzothiophene.[17] The sums of the three bond angles around the N(10) atom amount to 359.6(9) (A) and 360.0(9)° (B). This indicates that the N(10) atom sustains a substantial sp^2 hybridization in contrast to the large sp^3 character of the corresponding N atom in the phenothiazine molecule.[18] These geometrical features signify that the π-electrons are delocalized over the tricyclic ring system by forming a cation radical salt. This situation is similar to the cases of the CPZ-Cu and PMZ-Cu complex salt.

The 2-aminoethyl chains of both compounds elongate into the direction approximately bisecting the external angle of C(11)-N(10)-C(14). The N(10)-C(15)-C(16)-N(17) torsion angles of 174.7° in FTZ-Cu (A) and of 181.7° in FTZ-Cu (B), holding trans conformations, are much greater than that of 89.0° in FTZ·HCl, being in a near gauche conformation. On the assumption that the cationic charge on the phenothiazine ring localizes in the center of the ring, tentative calculations demonstrate that the distances from the middle point between the S(5) and N(10) atoms in the ring to the N(17) atom in the side chain attain 4.002 Å in FTZ·HCl, and 4.650 (A) and 4.724 Å (B) in FTZ-Cu. This difference suggests that the two positive charges in the FTZ molecule of FTZ-Cu keep each other apart to make the electrostatic repulsion between them as small as possible.

Figures 3 and 4 show the crystal packing diagrams of both compounds. In the FTZ·HCl crystals, the FTZ molecules arrange themselves in layers along the a axis. Along the b axis, the phenothiazine moieties of the two FTZ molecules are coupled with the insertion of one of the lateral benzene rings into the void volume of the bent plane to one another. This packing fashion resembles that of 10H-phenothiazine-10-propionic acid as reported by S. M. C. Malmstrom *et al.*[19] It is interesting that the different substituents with an opposite polarity, such as a carboxyl and amino group, afford similar packing arrangements. The closest in-

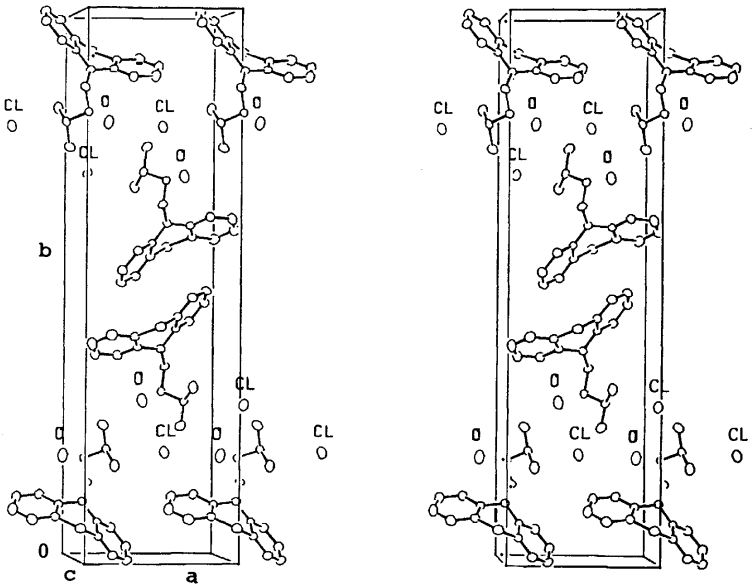

Fig. 3. Stereoscopic diagram of the crystal structure of FTZ·HCl·H_2O viewed down c.

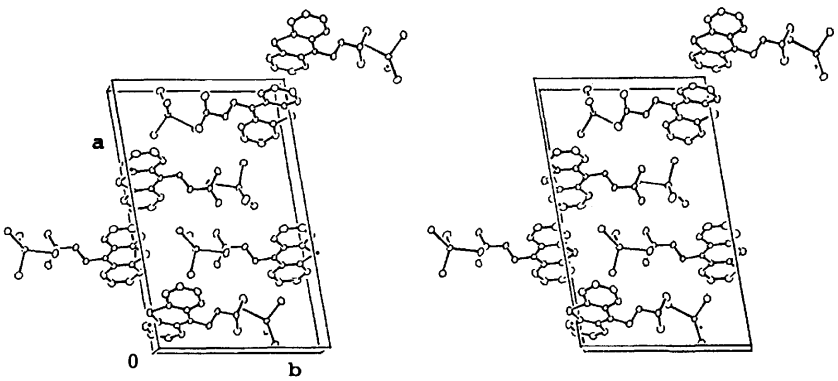

Fig. 4. Stereoscopic diagram of the crystal structure of $[FTZ\ H]^{2+\cdot}$-$[CuCl_4]^{2-}$ viewed down c.

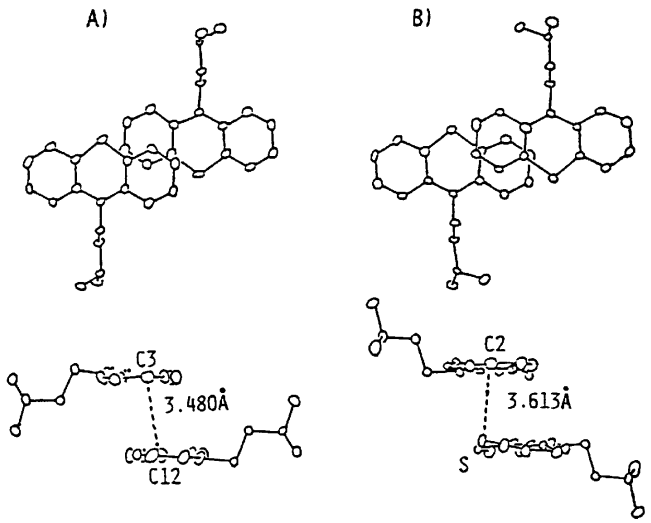

Fig. 5. Intermolecular overlap of the FTZ molecular pair in the $[FTZ\ H]^{2+\cdot}$ $[CuCl_4]^{2-}$ crystals.

termolecular contact is observed for C(7)-C(12^{ii}) [symmetry code: ii) $-x$, $-y$, $-z$] as 3.495(5) Å and all the other nonbonded contacts are greater than the sum of the van der Waals radii of the atoms. The chloride ions and the water molecules of crystallization are located in the vicinity of the ammonium groups of the side chains. The close contacts between these groups reveal the existence of a bridge structure linked with the hydrogen bonds (two hydrogen atoms of water are expressed as H(O1) and H(O2)): N(17)-Cl 3.042(2), H(17)-Cl 2.08(3), Cl-H(O2) 2.55(4), and H(O1)-Cl^{ii} 2.19(5) Å. In the case of the FTZ-Cu crystals, two crystallographically equivalent FTZ molecules form a pair with each other with the inversion centers to give a parallel overlap of the flattened phenothiazine rings. The side chains of the different pairs are stretched out in alternative directions as shown in Fig. 5; inside the faced planes (A) and outside the faced planes (B). The shortest intermolecular contact between the faced planes is seen for C(3)-C(12^{ii}) as 3.480(8) Å in an A pair, and for C(2)-S(5^{ii}) as 3.613(6) Å in a B pair. These values are within the van der Waals distances of the atoms, sufficiently indicating the intermolecular interaction between the faced rings. This type of dimer-like structure is widely seen in many organic radicals[20] and may contribute to the stabilization of the compounds in crystals. However, in the present case the degree of the ring overlap is relatively small.

The tetrachlorocuprate(2-) ions in which the copper atom has a pseudotetrahedral coordination sphere are positioned so as to neutralize the cationic charges of the phenothiazine ring and the protonated amino group in one pair and that of the ring in another pair. Among the coordinating chlorine atoms, the close nonbonded contacts occur around the Cl(4) (A) and Cl(1) (B) atom: Cl(4)(A)-N(17) 3.312(4), Cl(4)(A)-H(17) 2.56(5), Cl(1)(B)-N(17) 3.238(5), and Cl(1)(B)-H(17) 2.49(7) Å. These Cl-H distances are within the accepted hydrogen-bond range[21] and the Cl-N distances are considerably shorter than the van der Waals distances. This fact suggests that the electrostatic bonds that stand between N(17) and Cl(4)(A) or Cl(1)(B) are mediated through the hydrogen bonds.

In conclusion, FTZ-Cu differs largely from FTZ·HCl not only in its molecular structure but also in its crystal-packing mode. This differenece arises from the cation radical formation of the FTZ molecule. This fact might provide a clue to the explication of the pharmacological effect of the drug from a structural point of view, though it remains uncertain at the present stage.

The authors wish to express their thanks to Dr. Hiroshi Miyamae of the Faculty of Science at this University for sharing his expertize on X-ray analysis techniques.

References

1) A. S. Horn and S. H. Snyder, *Proc. Natl. Acad. Sci. U.S.A.*, **68**, 2325 (1971).
2) J. R. Rodgers, A. S. Horn, and O. Kennard, *J. Pharm. Pharmacol.*, **28**, 246 (1976); A. S. Horn, M. L. Post, and O. Kennard, *ibid.*, **27**, 553 (1975).
3) L. N. Domelsmith, L. L. Munchausen, and K. N. Houk, *J. Am. Chem. Soc.*, **99**, 6506 (1977).
4) J. E. Maruchin, *Pol. J. Pharmacol. Pharm.*, **28**, 277 (1976).
5) Cation Radicals of CPZ are thought to be responsible for the occasional side effects of long-term treatment by CPZ: M. S. Blois, *J. Invest. Dermatol.*, **45**, 475 (1965).
6) A. Obata, H. Kawazura, and H. Miyamae, *Acta Crystallogr., Sect. C*, **40**, 45 (1984).
7) The structure of PMZ cation radical salt has been reported just before our publication: R. B. Von Dreele and J. Harris, *Acta Crystallogr., Sect. C*, **39**, 170 (1983).
8) F. H. Merkle, C. A. Discher, and A. Felmeister, *J. Pharm. Sci.*, **53**, 965 (1964).
9) C. M. Gooley, H. Keyzer, and F. Setchell, *Nature (London)*, **223**, 80 (1969).
10) A. Ortiz, A. Gonzales, and J. I. Fernandez-alonso, *J. Solid State Chem.*, **40**, 210 (1981).
11) W. Schindler and F. Häfliger, *Helv. Chim. Acta*, **37**, 472 (1954).
12) "International Tables for X-ray Crystallography," Kynoch Press, Birmingham (1974), Vol. IV.
13) T. Sakurai and K. Kobayashi, *Rikagaku Kenkyusho Hokoku*, **55**, 69 (1978).
14) C. K. Johnson, ORTEP II, Report ORNL-5138, Oak Ridge National Laboratory, Oak Ridge, TN (1976).
15) Y. Iida, *Bull. Chem. Soc. Jpn.*, **44**, 663 (1971); S. Doi and Y. Matsunaga, *ibid.*, **48**, 3747 (1975); Y. Iida, *ibid.*, **51**, 3637 (1978).
16) S. S. C. Chu and D. Van der Helm, *Acta Crystallogr., Sect. B*, **30**, 2489 (1974).
17) R. M. Schaffrin and J. Trotter, *J. Chem. Soc.(A)*, **1970**, 1561.
18) J. Malrieu and B. Pullman, *Theor. Chim. Acta*, **2**, 293 (1964).
19) S. M. C. Malmstrom and A. W. Cordes, *Acta Crystallogr., Sect. B*, **28**, 325 (1972).
20) R. Foster, "Molecular Association," Academic Press, London (1975), p. 38.
21) G. C. Pimentel and A. L. McClellan, "The Hydrogen Bond," W. H. Freeman and Company, San Francisco (1960), p. 290.

Mössbauer Spectroscopic Studies of the Correlation between Molecular Structure and Sign of Quadrupole Splitting in Tris(β-diketonato)-iron(III) Complexes Utilizing Paramagnetic Relaxation Effects

Shigeru YAMAUCHI, Yoichi SAKAI, and Takeshi TOMINAGA*
Department of Chemistry, Faculty of Science, The University of Tokyo, Hongo, Bunkyo-ku, Tokyo 113
(Received July 16, 1984)

The change of the Mössbauer line shape with the paramagnetic relaxation time was studied in several tris(β-diketonato)iron(III) complexes to determine the sign of the quadrupole splitting. The correlation observed between the molecular structure and the sign of the quadrupole splitting demonstrates that the sign should depend on the bond angle (∠O-Fe-O) in iron(III) complexes.

The paramagnetic relaxation effects in Mössbauer spectroscopy have been ascribed to fluctuations of magnetic fields arising from flips of electronic spins.[1-3] Such magnetic fluctuations are either a spin-spin or spin-lattice relaxation process. The overall relaxation rate λ_t is expressed as $\lambda_t=\lambda_{SS}+\lambda_{SL}$, where λ_{SS} and λ_{SL} are relaxation rates *via* spin-spin and spin-lattice interactions, respectively. The relaxation time τ_t is the reciprocal of λ_t.

The line shape of the observed Mössbauer spectrum greatly depends on λ_t (or τ_t). The paramagnetic relaxation effects have been studied mainly for high-spin iron(III) species.[4-10] This is because there is a very small contribution from λ_{SL} to the relaxation rates which facilitates a discussion of the correlation between the Mössbauer line shape and the molecular structure.

It has been shown that the sign of the electric-field gradient can be determined by examining the asymmetry in a Mössbauer spectra *via* the paramagnetic relaxation processes.[11,12] Bancroft and co-workers[5] claimed that the asymmetric line shapes observed in Mössbauer spectra of a few tris(β-diketonato)iron(III) complexes indicate the presence of positive electric-field gradients. However, the experimental evidence seems to be too ambiguous to support their conclusion. Recently, we studied the paramagnetic relaxation effects in the Mössbauer spectra of eleven tris(β-diketonato)iron(III) complexes using the Mössbauer linewidth as a measure of the relaxation time. We found that the relaxation time increases with an increase in the iron-iron distance but decreases with an increasing temperature.[13] Although the Mössbauer spectra of most complexes were composed of a broad symmetric singlet, asymmetric peaks were observed in several complexes with relatively short relaxation times. Besides, there were complexes which seemed to have negative quadrupole splittings.

In general, it is difficult to definitely prove the presence of small quadrupole splittings. However, it should be possible to determine the sign as well as the presence of a small quadrupole splitting in high-spin iron(III) compounds by examining the change of the Mössbauer line shape associated with the paramagnetic relaxation time.

In the present work, we have measured the Mössbauer spectra of iron(III) complexes diluted in diamagnetic compounds in order to vary the paramagnetic relaxation time due to the spin-spin interaction. The temperature-dependence of the Mössbauer line shape in these systems was also examined because the relaxation time was varied with the temperature through the spin-lattice interaction.

Based on the sign of the quadrupole splitting determined utilizing paramagnetic relaxation effects, we discuss here the molecular structures, especially the coordinating bond angle of tris(β-diketonato)iron(III) complexes.

Experimental

Materials. The iron(III) compounds studied in this work are summarized in Table 1. Most compounds were synthesized and/or purified by modifying some procedures mentioned in the literature.[14-16] The purities of the ob-

TABLE 1. THE ELEMENTARY ANALYSES OF IRON(III) CHELATE COMPOUNDS

Complexes*	C (%)		H (%)		N or Cl (%)	
	Found	Calcd	Found	Calcd	Found	Calcd
$Fe(acac)_3$	50.80	51.02	6.27	5.95		
$Fe(tfa)_3$	34.91	34.92	2.64	2.34		
$Fe(3\text{-}Meacac)_3$	53.20	54.70	6.92	6.88		
$Fe(3\text{-}NO_2acac)_3$	37.33	36.91	3.99	3.72	8.38	8.61
$Fe(3\text{-}Clacac)_3$	38.63	39.47	4.00	3.97	23.85	23.30
$Fe(3\text{-}Phacac)_3$	66.52	68.17	5.70	5.72		
$Fe(trop)_3$	59.26	60.17	3.76	3.61		
$Fe(oxin)_3$	65.71	66.42	3.73	3.69	8.59	8.61

* acac: $CH_3COCHCOCH_3^-$, tfa: $CF_3COCHCOCH_3^-$, 3-Meacac: $CH_3COC(CH_3)COCH_3^-$, 3-NO_2acac: $CH_3COC(NO_2)COCH_3^-$, 3-Clacac: $CH_3COCClCOCH_3^-$, 3-Phacac: $CH_3COC(C_6H_5)COCH_3^-$, trop: $C_7H_5O_2^-$, oxin: $C_9H_6NO^-$.

tained compounds were checked by elementary analysis, and UV-visible and infrared spectroscopy. The results of the elementary analyses are summarized in Table 1.

Solid solutions of (Fe, Al)(oxin)$_3$ were prepared by coprecipitating oxinates of iron(III) and aluminum(III). After an 8-quinolinol (oxine) ethanol solution was added (slightly in excess) to an aqueous solution of $FeCl_3$ and $AlCl_3$ with known concentrations, the pH in the mixed solution was quickly adjusted to about 7 with a sodium acetate aqueous solution. The mole fraction of Fe(oxin)$_3$ in the precipitate was determined by means of colorimetry. Solvated compounds, Fe(acac)$_3$·2$CHCl_3$ and Fe(acac)$_3$·2CH_2Cl_2, were prepared by recrystallizing from each solvent[17] and their compositions were checked by measuring the weight-loss during storage in air after a Mössbauer measurement.

Measurements of Mössbauer Spectra. Mössbauer spectra were recorded at 78, 195, and 295 K using a Shimadzu MEG-2 or an Austin S-600 Mössbauer spectrometer. An iron foil was used for the calibration of Doppler velocity.

Results and Discussion

Determination of Sign of Quadrupole Splitting from Change in Mössbauer Line Shape. (a) Solid Solution: Figure 1 shows the Mössbauer spectra at 78 K of neat Fe(oxin)$_3$ and solid solutions of (Fe,Al)(oxin)$_3$. The line shape may be regarded as a symmetric doublet in the neat Fe(oxin)$_3$. The right (higher energy side) component of the doublet tends to collapse and broaden as the Fe(oxin)$_3$ content in solid solutions decreases, leading to larger distance between Fe(oxin)$_3$ molecules and thus to longer relaxaton time. The two peaks eventually merge into an asymetric single peak.[18] Since the electric-field gradient and the quadrupole splitting have the same sign in ^{57}Fe-Mössbauer spectroscopy, it is expected that the right side peak broadens first in the presence of positive quadrupole splitting whereas the left side peak collapses first in case of negative quadrupole splitting.[19] Accordingly, the change in the Mössbauer line shape shown in Fig. 1 reveals that the iron in Fe(oxin)$_3$ experiences a positive electric-field gradient and, hence, the sign of the quadrupole splitting is positive. Thus, it is shown that the sign of the quadrupole splitting in high-spin iron(III) compounds can be determined by examining the change in the Mössbauer line shape with a relatively small change in the relaxation time caused by the reduced spin-spin interaction due to the increased distance between Fe(oxin)$_3$ molecules in the (Fe, Al)(oxin)$_3$ system.

(b) Solvated Compound: Similar experiments were carried out to determine the sign of the quadrupole splitting in Fe(acac)$_3$. However, it proved quite difficult to determine the sign in the systems of (Fe,Al)-(acac)$_3$ and (Fe, Co)(acac)$_3$ with this method because of the very small quadrupole splitting expected in Fe-(acac)$_3$ and the difficulty in preparing solid solutions with slightly different Fe(acac)$_3$ contents. Accordingly, two solvated compounds, Fe(acac)$_3$·2$CHCl_3$ and Fe(acac)$_3$·2CH_2Cl_2, were prepared instead to increase the iron-iron distance slightly. The spectra of the solvated compounds at 78 K are shown in Fig. 2 together with neat Fe(acac)$_3$. In Fig. 2, a very small quadrupole splitting is seen in Fe(acac)$_3$ while a sharp singlet peak is observed in each solvated compound. The sharp peak-top position in the solvated compounds agrees exactly with that of the left-component peak in Fe-

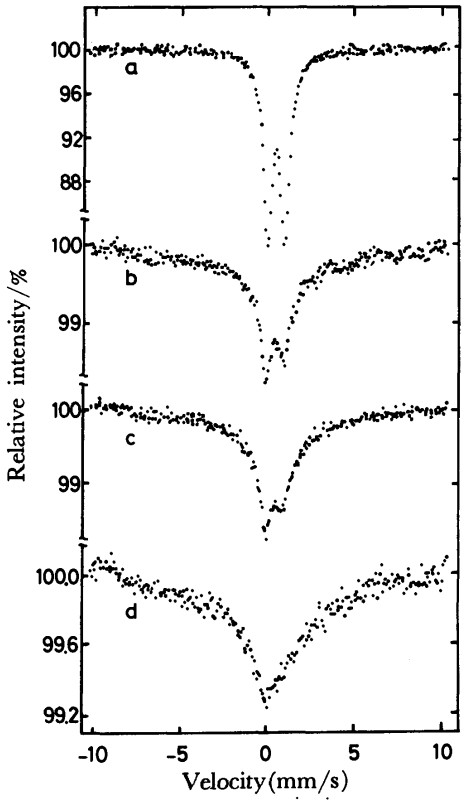

Fig. 1. Mössbauer spectra at 78 K of (Fe,Al) (oxin)$_3$ solid solutions with the Fe(oxin)$_3$ mole fraction of a) 1.0, b) 0.5, c) 0.4, and d) 0.3.

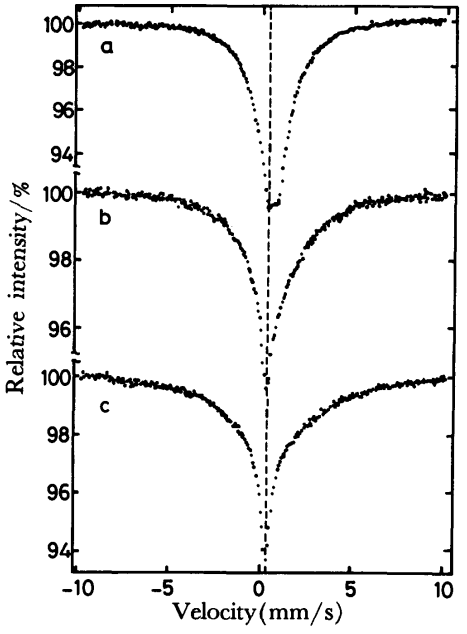

Fig. 2. Mössbauer spectra at 78 K of Fe(acac)$_3$ and its solvated compounds: a) Fe(acac)$_3$, b) Fe(acac)$_3$·2$CHCl_3$, and c) Fe(acac)$_3$·2CH_2Cl_2.

$(acac)_3$, indicated by the broken line. Furthermore, a slight asymmetry is observed in the line shape of the solvated compounds with a (probably) longer iron-iron distance than in $Fe(acac)_3$. Therefore, it is likely that the sign of the quadrupole splitting in $Fe(acac)_3$ is also positive.

(c) Temperature-dependence: The sign of the quadrupole splitting was determined for five kinds of tris(β-diketonato)iron(III) complexes and $Fe(trop)_3$[20] by examining the temperature-dependence of the Mössbauer line shape. For example, the Mössbauer spectra at 78, 195 and 295 K of $Fe(tfa)_3$ and $Fe(3\text{-}NO_2acac)_3$ are illustrated in Figs. 3 and 4, respectively.

It is seen in Fig. 3 that the absorption peak of $Fe(tfa)_3$ at 295 K splits in two: at 195 K the right side peak collapses. The spectrum at 78 K apparently has a single peak, although there remains a slight asymmetry. Such a change in the line shape of $Fe(tfa)_3$ with temperature (*i.e.*, relaxation time) may suggest the presence of a positive quadrupole splitting. Since the Mössbauer spectra of $Fe(3\text{-}Meacac)_3$ and $Fe(trop)_3$ showed a temperature-dependence similar to that of $Fe(tfa)_3$, their quadrupole splittings should be positive.

In contrast, the left component of the $Fe(3\text{-}NO_2acac)_3$ peak in Fig. 4 tends to collapse at lower temperatures, indicating the presence of a negative quadrupole splitting. Since the Mössbauer line shapes of $Fe(3\text{-}Phacac)_3$ and $Fe(3\text{-}Clacac)_3$ showed a temperature-dependence similar to that of $Fe(3\text{-}NO_2acac)_3$, the sign of their quadrupole splitting may be negative.

Correlation between Sign of Quadrupole Splitting and Molecular Structure. The sign of the quadrupole splitting may be correlated to the molecular structure in accordance with the point-charge model.[21] The

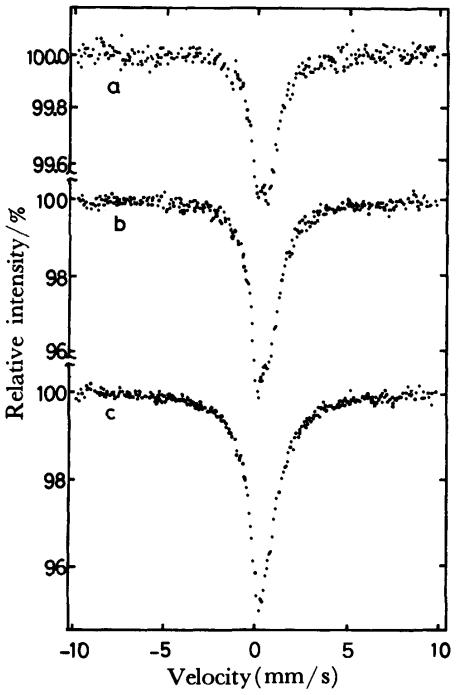

Fig. 3. Mössbauer spectra of $Fe(tfa)_3$ at a) 295 K, b) 195 K, and c) 78 K.

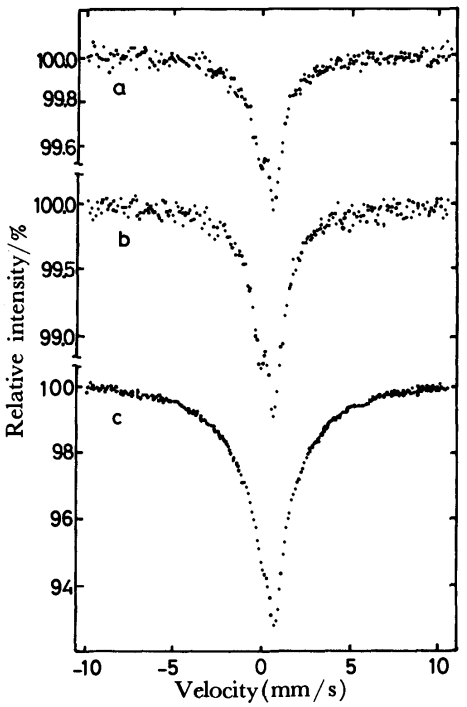

Fig. 4. Mössbauer spectra of $Fe(3\text{-}NO_2acac)_3$ at a) 295 K, b) 195 K, and c) 78 K.

quadrupole splitting in high-spin iron(III) compounds is determined by the electric-field gradient produced only by neighboring ions and atoms. The electric field gradient (eq) in tris(β-diketonato)iron(III) can be written as

$$eq = -12\rho \cos\alpha \cdot r^{-3}, \quad (1)$$

where ρ is the negative charge on an oxygen atom in β-diketonato ligand, r the iron-oxygen bond length, and α the bond angle $\angle$O-Fe-O (see Appendix). The quadrupole splitting (ΔEq) is given by

$$\Delta Eq = 1/2e^2qQ(1+\eta^2/3)^{1/2}, \quad (2)$$

where Q denotes the electric quadrupole moment of nucleus ($Q>0$ in ^{57}Fe) and η the asymmetric constant ($\eta=0$ in this case).

By putting equation(1) into equation(2), we obtain

$$\Delta Eq = -6e\rho Q \cos\alpha \cdot r^{-3}, \quad (3)$$

which implies that the sign of quadrupole splitting depends only on the angle α: the sign should be positive when $\alpha<90°$ and negative when $\alpha>90°$.

Meanwhile, average α values in $Fe(acac)_3$ and $Fe(trop)_3$ determined by X-ray diffractometry are 87.1°[22] and 77.8°[23] respectively. Based on the present model, the sign of a quadrupole splitting should be positive for both compounds, in agreement with the results deduced from the Mössbauer line shape in the present work. Thus, it may be assumed that the bond angle α is also smaller than 90° for $Fe(tfa)_3$ and $Fe(3\text{-}Meacac)_3$ whose quadrupole splittings proved to be positive based on the Mössbauer line shape.

It appears that α is larger than 90° in compounds complexed with ligand β-diketones containing more bulky 3-substituent groups such as $-NO_2$, $-C_6H_5$, and -Cl, while α is smaller than 90° in the compounds with ligands containing relatively smaller 3-substituent groups, *i.e.*, -H and $-CH_3$. Accordingly, it may be concluded that the bond angle α could be enlarged by the steric hindrance between complex molecules with a bulky 3-substituent group. A further study of these systems will be necessary to validate such a conclusion.

Appendix

If an ^{57}Fe nucleus is located at the origin of the coordinate system (Fig. 5), the electric-field gradient ($V_{zz}=eq$) due to point charges about the nucleus is given by

$$eq = \sum_i \rho_i r_i^{-3}(3\cos^2\theta_i - 1), \tag{4}$$

where ρ_i denotes the i-th point electric charge, θ_i the acute angle between the line segment from the i-th point to the origin and the Z axis (in accordance with the principal axis of electric-field gradient), r_i the distance between the i-th point charge and the origin, and e the protonic charge.

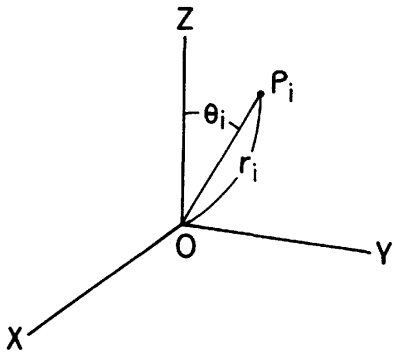

Fig. 5. Coordinates of point charges.

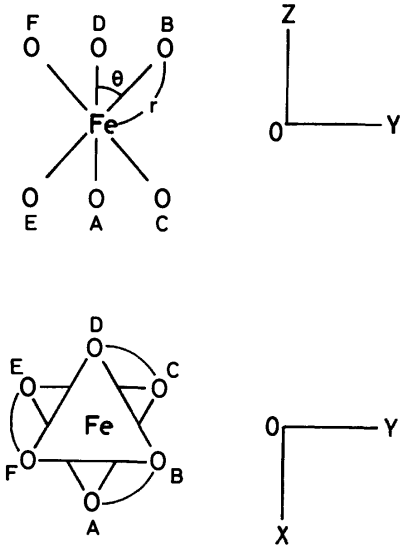

α = ∠AOB = ∠COD = ∠EOF

Fig. 6. Arrangement of coordinate atoms in tris(β-diketonato)iron(III) (Iron atom is situated on the origin(0,0,0)).

The Z axis can be determined in tris(β-diketonato)iron(III) complexes as illustrated in Fig. 6. If space coordinate of oxygen atom(A) in a ligand β-diketone is (rsin θ, 0, $-r\cos\theta$), that of oxygen atom(B) is ($1/2r\sin\theta$, $\sqrt{3}/2r\sin\theta$, $r\cos\theta$). The distance $\overline{AB}$ is given by

$$\overline{AB} = r(1+3\cos^2\theta)^{1/2}.$$

and ∠AOB (*i.e.* ∠O–Fe–O=α) is expressed as follows:

$$\cos\alpha = (1-3\cos^2\theta)/2. \tag{5}$$

Equation(5) also holds for the other two β-diketone ligands. Hence, putting equation(5) into equation(4), we obtain

$$eq = -2\cos\alpha \cdot \sum_i (\rho_i r_i^{-3}).$$

Assuming that each ρ_i or r_i is equivalent in three ligands, we can express the electric-field gradient as

$$eq = -12\rho\cos\alpha \cdot r^{-3}. \tag{6}$$

References and Notes

1) A. M. Afanas'ev and Y. Kagan, *Soviet Phys. JETP*, **18**, 1139 (1964).
2) H. H. Wickman, M. Klein, and D. A. Shirley, *Phys. Rev.*, **152**, 345 (1966).
3) M. Blume, *Phys. Rev. Lett.*, **14**, 96 (1965); *ibid.*, **18**, 305 (1967).
4) J. W. G. Wignall, *J. Chem. Phys.*, **44**, 2462 (1966).
5) G. M. Bancroft, A. G. Maddock, W. K. Ong, R. H. Prince and A. J. Stone, *J. Chem. Soc. (A)*, **1967**, 1966.
6) G. M. Bncroft and T. K. Sham, *J. Chem. Soc., Faraday Trans. 2*, **72**, 1706 (1976).
7) H. Sano, *J. Radioanal. Chem.*, **36**, 105 (1977).
8) Y. Sakai, K. Endo and H. Sano. *Int. J. Appl. Radiat. Isot.*, **32**, 435 (1981).
9) Y. Sakai, H. Nishioji, S. Yamauchi, and T. Tominaga, *Radiochem. Radioanal. Lett.*, **53**, 215 (1982).
10) J. Akashi and H. Sano, *Radiochem. Radioanal. Lett.*, **55**, 265 (1982).
11) M. Cox, B. W. Fitzsimmons, A. W. Smith, L. F. Larkworthy, and K. A. Rogers, *J. Chem. Soc., Chem. Commun.*, **1969**, 183.
12) N. Thrane and G. Trumpy, *Phys. Rev. B*, **1**, 153 (1970).
13) S. Yamauchi, Y. Sakai, H. Nishioji, and T. Tominaga, *Int. J. Appl. Radiat. Isot.*, **34**, 977 (1983).
14) R. G. Charles and M. A. Pawlikowski, *J. Phys. Chem.*, **62**, 440 (1958).
15) E. V. Dose, K. M. M. Murphy, and L. J. Wilson, *Inorg. Chem.*, **15**, 2622 (1976).
16) E. L. Muetterteis and C. M. Wright, *J. Am. Chem. Soc.*, **86**, 5132 (1964).
17) J. F. Steinbach and J. H. Burns, *J. Am. Chem. Soc.*, **80**, 1839(1958).
18) The Mössbauer spectrum at 78 K of (Fe,Al)(oxin)$_3$ was previously reported at a lower concentration Fe(oxin)$_3$ (3%) than in the present work, showing the line shape with the slower relaxation time reasonably.[24]
19) The magnetic hfs in the ^{57}Fe Mössbauer spectrum corresponds to six transitions ($\pm3/2\rightarrow\pm1/2$, $\pm1/2\rightarrow\pm1/2$ and $\pm1/2\rightarrow\mp1/2$), or combination of three doublets. In the presence of a quadrupole splitting, two lines corresponding

to $\pm 3/2 \rightarrow \pm 1/2$ and $\pm 1/2 \rightarrow \pm 1/2, \mp 1/2$ transitions respectively appear in the spectrum: the right hand (higher energy) component is attributed to the $\pm 3/2 \rightarrow \pm 1/2$ transitions if quadrupole splitting is positive, while the left hand component is attributed to the $\pm 3/2 \rightarrow \pm 1/2$ transitions for negative quadrupole splitting. Furthermore, the doublet due to the $\pm 3/2 \rightarrow \pm 1/2$ transitions has the largest splitting. Hence, there exists a range of magnetic relaxation time in which the $\pm 3/2 \rightarrow \pm 1/2$ line broadens whereas the $\pm 1/2 \rightarrow \pm 1/2, \mp 1/2$ lines are still sharp.[3]

20) Tropolone is not β-diketone, but $Fe(trop)_3$ is similar to tris(β-diketonato)iron(III) in magnetic properties and molecular structure.

21) G. M. Bancroft and R. H. Platt, "Advances in Inorganic Chemistry and Radiochemistry," ed by H. J. Emeléus and A. G. Sharpe, Academic Press, New York and London, Vol. 15, (1966) p. 59.

22) J. Iball and C. H. Morgan, *Acta Crystallogr.*, **23**, 239 (1967).

23) T. A. Hamoe and D. J. Watkin, *J. Chem. Soc., Chem. Commun.*, **1969**, 440.

24) K. Endo, M. Harada, Y. Sakai, and H. Sano, *J. Phys. (Paris), Colloq.*, **40**, C2-240 (1979).

A New Synthetic Model for Myoglobin: "Tulip Garden" Porphyrin

Shigeru TAKAGI, T. Ken MIYAMOTO,* and Yukiyoshi SASAKI
Department of Chemistry, Faculty of Science, The University of Tokyo, Hongo, Bunkyo-ku, Tokyo 113
(Received July 20, 1984)

A new model compound "tulip garden" porphyrin, has a long half-lifetime, thus satisfying the demand for the synthetic analogue of myoglobin. At the same time, "tulip garden" porphyrin has high O_2 affinities as compared to other protected porphyrins; especially, its Co(II) complex shows almost the same affinity ($P_{1/2}O_2$) as coboglobins. The difference in oxygen affinities between "tulip garden" and "picket fence-type" porphyrins can be ascribed to the bulkiness of pendant groups. The strong "side" influence of the adamantyl group can be expected to bring about a high O_2 affinity.

Considerable efforts have recently been made to develop synthetic model compounds which bind O_2 reversibly in a manner analogous to that of hemoglobin (Hb) and myoglobin (Mb).[1] These model compounds satisfy the demands for the formation of more stable oxygen adducts at room temperature and show high O_2 affinities equal to those of natural respiratory hemoprotein. In Hb and Mb, an important function of the heme pocket is to prevent dimeric interactions between hemes. In accordance with this requirement, sterically protected porphyrins ("superstructure porphyrins"[2]) have been synthesized in recent years. Such superstructures have a *hydrophobic pocket* on the single face of the porphyrin plane and help to *inhibit irreversible autoxidation*.[3] At room temperature, however, only a limited number of the protected porphyrins, most notably the "picket fence,"[4] "pocket,"[5] "capped,"[6] "doubly bridged,"[7] "hanging imidazole,"[8] and "cofacial"[9] porphyrins, bind O_2 reversibly.

The O_2 affinities and half-lifetimes of oxygen complexes differ from compound to compound. This variation is attributable to the electronic nature of porphyrins,[10] local polarity at the binding site,[2-11] the effect of solvation on the binding site,[12] and the steric effects on coordination to the metal center.[13] As far as the steric effects are concerned, we may consider two types of model compounds. In "capped" porphyrin[13] and "cyclophane heme,"[14] a series of compounds has been synthesized by changing the cavity size between the porphyrin plane and the capping aromatic ring, and the influence of the steric hindrance upon O_2 binding has been studied. On the other hand, the oxygen-binding properties of the "picket fence" porphyrins containing different pendant groups have hardly been investigated at all. In order to investigate of the steric effect caused by the bulkiness of the pendant groups, we need to design new model compounds.

We wish to report here the synthesis of a new model compound of Mb, "tulip garden" porphyrin **5a** (Fig. 1), which is "modified picket fence porphyrin." A reversible oxygenation based on its Fe(II) and Co(II) complexes is also described. We further synthesized "picket fence-type" porphyrin **5b** (Fig. 1), whose pendant moiety is the *t*-butyl group. The bulkiness of the adamantyl group may lead to very strong steric effect on the porphyrin **5a**. In order to compare the local polarity effects of binding sites, we also furthermore synthesized "camphanoyl fence" porphyrin **5c** (see Scheme 1).

Experimental

The synthetic procedure[15] to **5a**, **5b**, and **5c** is shown in Scheme 1, while the metallation procedure to the Co(II) and Fe(II) complexes is shown in Scheme 2.

5,10,15,20-Tetrakis(2-nitro-4-t-butylphenyl)-21H,23H-porphyrin **2**. The porphyrin **2** was prepared by the Rothemund condensation of pyrrole with a nitrobenzaldehyde derivative **1**.[16] A 259-g portion of **1** (1.25 mol) was dissolved in 2 dm^3 of glacial acetic acid. The solution was then heated to its boiling point with continuous stirring. A 95-g portion of pyrrole (1.42 mol) was added, drop by drop, to the boiling solution. The solution was then allowed to reflux for 3 h. After the solution has cooled to room temperature, the resulting black solution was left overnight. The purple crystals were filtered by suction and purified by silica gel chromatography, using

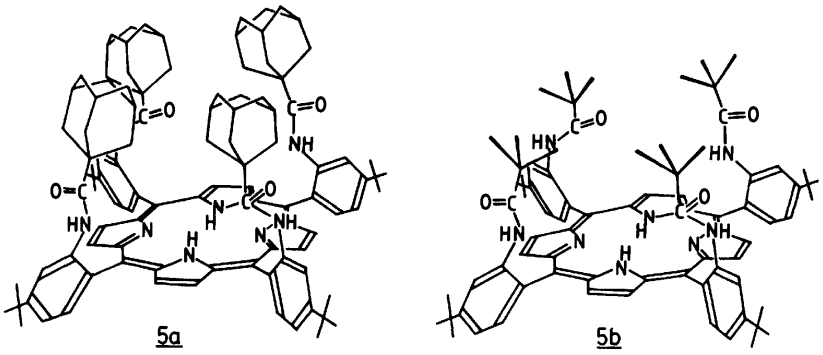

Fig. 1. "Tulip garden" porphyrin **5a** and "picket fence type" porphyrin **5b**.

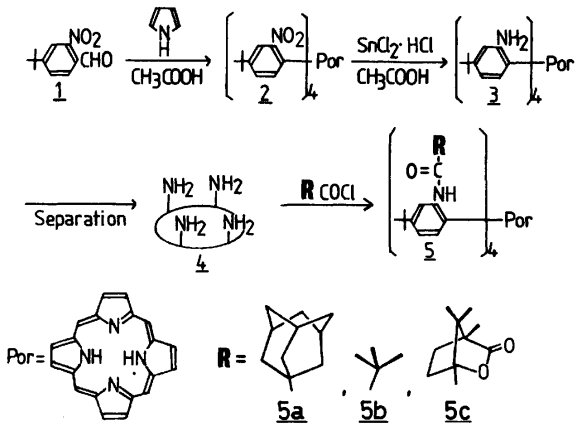

Scheme 1. Synthetic procedure to **5a**, **5b**, and **5c**.

$CHCl_3$ as the eluent. A 46.0-g portion of the porphyrin **2** (0.0451 mol) was thus obtained; the overall yield was 14.4% based on the **1** consumed: Anal. Calcd for $C_{60}H_{58}N_8O_8$: C, 70.71; H, 5.74; N, 10.99. Found: C, 70.76; H, 5.70; N, 11.14. ^1H NMR ($CDCl_3$) δ=−2.6 (2H, s, internal pyrrole H), 1.7 (36H, s, *t*-butyl H), 8.0—8.5 (12H, m, phenyl H), 8.6 (8H, s,β-pyrrole H). UV-*vis*. ($CHCl_3$) λ/nm (ε/$M^{-1}cm^{-1}$)[17] 423 (3.3×10^5), 517 (2.0×10^4), 553 (7.2×10^3), 594 (6.0×10^3), 651 (2.6×10^3).

5,10,15,20-Tetrakis(2-amino-4-t-butylphenyl)-21H,23H-porphyrin **3**. A 4.0-g portion of the porphyrin **2** (3.9 mmol) was dissolved in a mixture of concentrated hydrochloric acid (500 cm^3) and glacial acetic acid (1 dm^3) at room temperature. The resulting green solution was heated to 65 °C, and then a solution of 14 g (62 mmol) of $SnCl_2\cdot2H_2O$ dissolved in 100 cm^3 of the mixed solvent (HCl:CH_3COOH=1:2) was slowly added during a 30-min period. After heating for 1.5 h, crushed ice and water were poured into this solution. The porphyrin **3** was extracted with $CHCl_3$ from the resulting solution. The product was purified by alumina-column chromatography ($CHCl_3$). The average yield was 3.2 g (3.6 mmol, 92%): Anal. Calcd for $C_{60}H_{66}N_8$: C, 80.14; H, 7.40; N, 12.46. Found: C, 79.92; H, 7.67; N, 12.71. ^1H NMR ($CDCl_3$) δ=−2.6 (2H, s, internal pyrrol H), 1.5 (36H, s, *t*-butyl H), 3.4 (8H, s, NH_2), 7.0 (8H, d, phenyl H), 7.7 (4H, d, phenyl H), 8.8 (8H, s,β-pyrrole H). UV-*vis*. ($CHCl_3$) λ/nm (ε/$M^{-1}cm^{-1}$): 422 (2.3×10^5), 517 (1.7×10^4), 553 (6.1×10^3), 591 (5.3×10^3), 647 (2.8×10^3).

Separation of $\alpha,\alpha,\alpha,\alpha$-Isomer. The resulting porphyrin **3** was a mixture of four atropisomers in statistical abundance. The most polar one, the $\alpha,\alpha,\alpha,\alpha$-isomer, could be easily separated from the other three atropisomers by thin-layer[18] and column chromatography. Before isomer separation, the preferential isomerization to the $\alpha,\alpha,\alpha,\alpha$-isomer was carried out by the a modification of literature methods.[19] Eight grams of the porphyrin **3** were dissolved in 1.5 dm^3 of toluene. This solution was refluxed under Ar, and a 40-g portion of alumina (Merck alumina 90) was added six times every three hours. After refluxing for 20 h, the solution was cooled to the ambient temperature. The isomerized product was then extracted from the alumina with a $CHCl_3$/acetone mixed solvent. After the solvent had been removed, the residue was redissolved in a minimum amount of benzene. The benzene solution was poured into a column of silica gel (Wako gel C-200) prepared as a slurry in benzene. All the material was loaded, and 2:1 benzene/diethyl ether was passed through the column until the eluate became very pale. The desired $\alpha,\alpha,\alpha,\alpha$-isomer was left in the column and eluted with 2:1 benzene/acetone. The solvent was removed using a rotary evaporator at 30 °C. Yield: 6.5 g (81%).

"Tulip Garden" Porphyrin 5a. A 3.0-g portion (3.3 mmol) of the $\alpha,\alpha,\alpha,\alpha$-isomer **4** was dissolved in CH_2Cl_2 (200 cm^3) containing 10 cm^3 of pyridine. A 15-g portion (76 mmol) of 1-adamantanecarboxylic acid chloride was added, after which the solution was stirred for 3 h at the ambient temperature. A 200-cm^3 portion of 20% aqueous ammonia was then added, and the solution was stirred for an additional 30 min. The organic layer was separated and subsequently washed, first with dilute hydrochloric acid and then with aqueous ammonia. The solvent was evaporated using a rotary evaporator. The product was purified by chromatography on a silica-gel column (benzene), eluting with 3:1 benzene/ether. Yield 4.7 g (3.0 mmol, 91%): Anal. Calcd for $C_{104}H_{122}N_8O_4\cdot H_2O$: C, 79.95; H, 7.98; N, 7.15. Found: C, 79.52; H, 7.80; N, 7.24. ^1H NMR ($CDCl_3$) δ=−2.6 (2H, s, internal pyrrole H), 0.9—1.2 (60H, m, adamantyl H), 1.6 (36H, s, *t*-butyl H), 7.4—7.5 (12H, m, phenyl H), 8.9 (8H, s,β-pyrrole H), 8.9 (4H, d, NHCO). UV-*vis*. ($CHCl_3$) λ/nm (ε/$M^{-1}cm^{-1}$): 438 (3.5×10^4), 555 (8.3×10^3), 593 (6.5×10^3), 652 (2.5×10^3).

"Picket Fence-type" Porphyrin 5b and "Camphanoyl Fence" Porphyrin 5c. The synthetic procedure for **5b** and **5c** was similar to that used for **5a**. The porphyrin, **5b** or **5c**, was obtained by coupling the $\alpha,\alpha,\alpha,\alpha$-isomer **4** with pivaloyl chloride[20] or (−)-camphanoyl chloride respectively. The overall yield of **5b** was 95%, and that of **5c** was 60%: **5b** Anal. Calcd for $C_{80}H_{98}N_8O_4\cdot H_2O$: C, 76.65; H, 8.04; N, 8.94. Found: C, 76.55; H, 7.78; N, 8.77. ^1H NMR ($CDCl_3$) δ=−2.6 (2H, s, internal pyrrole H), 0.1 (36H, s, pivaloyl H), 1.6 (36H, s, *t*-butyl H), 7.2—7.8 (12H, m, phenyl H), 8.8 (8H, s,β-pyrrole H), 8.9 (4H, d, NHCO). UV-*vis*. ($CHCl_3$) λ/nm (ε/$M^{-1}cm^{-1}$): 423 (3.5×10^5), 515 (2.1×10^4), 549 (6.2×10^3), 589 (6.4×10^3), 646 (2.5×10^3). **5c** ^1H NMR ($CDCl_3$) δ=−2.6 (2H, s, internal pyrrole H), −0.1—1.3 (52H, m, camphanoyl H), 1.5 (36H, s, *t*-butyl H), 7.3—7.8 (12H, m, phenyl H), 8.4 (4H, d, NHCO), 8.8 (8H, s,β-pyrrole H). UV-*vis*.

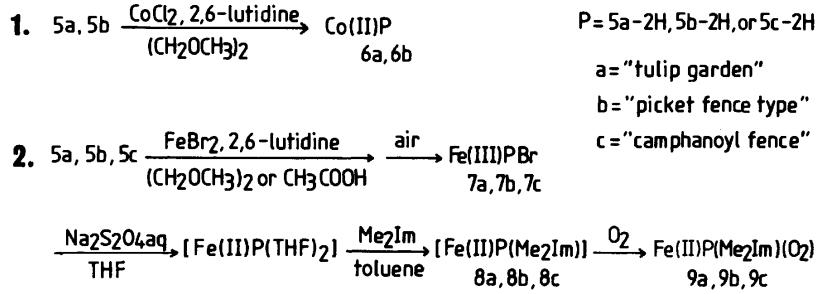

Scheme 2. Metallation procedure.

($CHCl_3$) λ/nm: 422, 517, 551, 582, 653.

Cobalt Insertion. A 1.0-g portion (0.65 mmol) of **5a**, 0.65 g (5.0 mmol) of anhydrous $CoCl_2$, and 0.20 cm^3 of 2.6-lutidine were dissolved in 100 cm^3 of 1,2-dimethoxyethane under Ar. The resulting solution was stirred for 3 h at room temperature. The solution was then brought to dryness, and the residue was redissolved in $CHCl_3$. The product was purified by alumina-column chromatography, using $CHCl_3$ as the eluent. Yield: 0.90 g (87%). The porphyrin **6b** was prepared by a similar procedure. Yield: (50%): **6a** Anal. Calcd for $CoC_{104}H_{120}N_8O_4 \cdot H_2O$: C, 76.96; H, 7.58; N, 6.90. Found: C, 77.03; H, 7.84; N, 6.65. UV-*vis.* ($CHCl_3$) λ/nm (ε/M^{-1} cm^{-1}): 419 (2.3×10^5), 532 (1.7×10^4). **6b** UV-*vis.* ($CHCl_3$) λ/nm: 414, 526.

Iron Insertion. **5a** (0.8 g), 2.6-lutidine (2 cm^3), and anhydrous $FeBr_2$[21] were dissolved in 200 cm^3 of 1,2-dimethoxyethane under oxygen-free conditions. The resulting solution was stirred for 3 h at the ambient temperature. The solution was then brought to dryness, and the product was purified using an alumina column ($CHCl_3$). The eluate was stirred with 10% hydrobromic acid. The solvent was then evaporated by means of a rotary evaporator. Yield: 0.82 g (95%). The porphyrin **7b** was prepared by a similar procedure. Yield: (60%). The porphyrin **7c** was obtained by the reaction in a mixed solvent of 1:1 $CHCl_3$/acetic acid. Yield: (70%). **7a** Anal. Calcd for $FeC_{104}H_{120}N_8O_4Br$: C, 74.24; H, 7.19; N, 6.66. Found: C, 73.90; H, 7.21; N, 6.77. UV-*vis.* ($CHCl_3$) λ/nm: 425, 514, 578, 660, 694. **7b** Anal. Calcd for $FeC_{80}H_{96}N_8O_4Br$: C, 69.94; H, 7.20; N, 7.96. Found: C, 70.17; H, 7.07; N, 8.18. UV-*vis.* ($CHCl_3$) λ/nm: 422, 512, 586, 656, 685. **7c** UV-*vis.* ($CHCl_3$) λ/nm: 421, 508, 578, 656.

Dioxygen Adducts of Fe(II) Complexes. A 2.0-g portion (1.2 mmol) of Fe(III) porphyrin **7a** was dissolved in a mixed solvent of 50% THF/benzene (v/v), after which the solution was purged with Ar to remove any O_2. Then a 100-cm^3 portion of the deoxygenated aqueous 0.2 M $Na_2S_2O_4$ solution was added to this solution of **7a**. When the mixture was vigorously stirred for 30 min, the dark brown solution turned red-orange. The aqueous layer was discarded, and the organic layer was dried using anhydrous Na_2SO_4. After removing the solution from Na_2SO_4 by filtration under Ar, the crude iron(II) complex was redissolved in 30 cm^3 of toluene containing 1,2-Me_2Im[22] and then 100 cm^3 of heptane was added, drop by drop, for crystallization. The precipitate **8a** was separated by filtration and dried *in vacuo*. All the operations were carried out under Ar or N_2 atmosphere. After the exposure of the **8a** to oxygen at atmospheric pressure for 1 d, a pure "dioxygen" complex **9a** was obtained as deep-violet crystals. The "dioxygen" complex **9b** was prepared by a similar procedure. **9c** was immediately oxidized to the iron(III) state, and so we could not obtain the pure "dioxgen" complex. For that reason, we used a THF/benzene solution of the crude iron(II) complex for the spectrophotometric measurement: **9a** Anal. Calcd for $FeC_{109}H_{128}N_{10}O_6$: C, 75.67; H, 7.46; N, 8.10. Found: C, 75.47; H, 7.57; N, 8.06.

Oxygen-affinity Measurement. The oxygen equilibria constants were determined by means of spectrophotometric O_2 titration. A Hitachi 340 recording spectrophotometer was used in all the experiments. The measurements were done at *ca.* 20 °C in a toluene[23] solution containing the corresponding imidazole.[24] In general, metalloporphyrin concentration of 50—80 μM were used, and the spectra were recorded in the 600—350 nm range. Any spectral changes were recorded, in the absence of O_2 and at various increasing partial pressures of O_2. The oxygen partial pressures were determined by the injection of known volumes O_2 into the tonometer. After the measurements, the reversibility was checked by bubbling a sample solution with Ar in order to obtain a spectrum identical with initial one.

Results

$$M(P)(B) + O_2 \rightleftharpoons M(P)(B)(O_2) \quad M = Co, Fe$$

In solution, five-coordinate porphyrin complexes are suitable for the measurement for the oxygen equilibrium, an appropriate N-base should, however, be chosen to ensure that the five-coordinate complex is the dominant species. Sterically hindered 2-substituted imidazoles exclusively form the five-coordinate adducts with Fe(II) porphyrins.[25,26] These hindered imidazole adducts are considered to mimic the T-state (low affinity) hemoglobin.[26] In the Fe(II) porphyrin/unhindered imidazole system, which can be expected to be a model system for the R-state (high affinity) hemoglobin,[26] six-coordinate bis-ligated adducts are the dominant species in solution.[25] Our porphyrin **5a** exerts a strong steric effect on the sixth coordinating position, but cannot restrain the coordination of 1-MeIm[27] in the pocket. In Co(II) porphyrins, both unhindered and hindered imidazoles form five-coordinate adducts.[28] For that reason, we choose the Fe(II) porphyrin/1,2-Me_2Im system the for T-state model and Co(II) porphyrin/1-MeIm system for the R-state model.

The spectrophotometric oxygen titrations of Fe(II) and of the Co(II) complexes were carried out in a toluene solution. Isosbestic points were found in all titrations. Figure 2 shows the spectral changes which took place when a toluene solution containing 1,2-Me_2Im

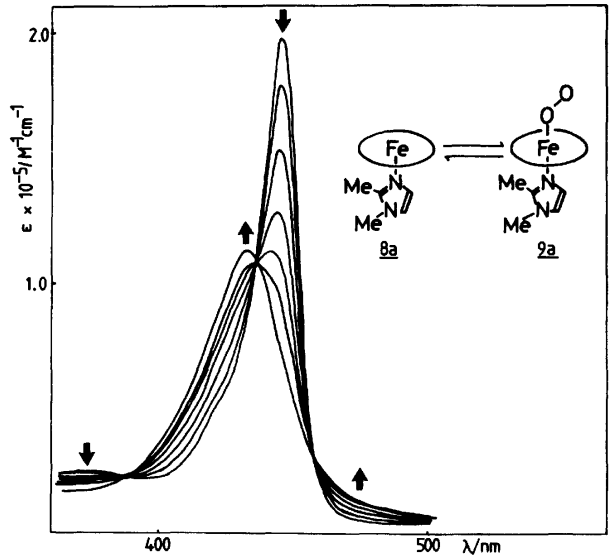

Fig. 2. Spectral changes of "tulip garden" iron(II) porphyrin under the various oxygen pressures. Arrows indicate the changes with increasing oxygen pressures.

TABLE 1. ELECTRON-ABSORPTION SPECTRA (TOLUENE)

Compound	λ/nm (ε/$M^{-1}cm^{-1}$)
6a(1-MeIm)	420(1.9×10^5), 537(1.1×10^4)
6a(1-MeIm)(O_2)	432(1.5×10^5), 554(1.3×10^4)
6b(1-MeIm)	416(*nd***), 536(*nd*)
6b(1-MeIm)(O_2)	423(*nd*), 549(*nd*)
8a	444(2.0×10^5), 540(7.3×10^3), 570(8.4×10^3), 613(4.3×10^3)
9a	432(1.1×10^5), 554(1.0×10^4), 592(5.3×10^3)
8b	432(*nd*), 535(*nd*), 565(*nd*)
9b	424(*nd*), 546(*nd*)

***nd*=not determined.

TABLE 2. HALF-SATURATION PRESSURES OF O_2 BINDING

Compound	$P_{1/2}O_2$ Torr
Co"tulip garden" (4.7×10^{-3} M 1-MeIm)	9.5
Co"picket fence type" (4.7×10^{-3} M 1-MeIm)	29
Fe"tulip garden" (9.9×10^{-2} M 1,2-Me_2Im)	26
Fe"picket fence type" (5.0×10^{-2} M 1,2-Me_2Im)	84

of Fe(II) porphyrin **8a** was exposed to various pressures of oxygen. However, the "camphanoyl fence" porphyrin Fe(II) complex was oxidized irreversibly, probably to the hydroxy iron(III) complex while the O_2 titration was being measured.[29] Both **9a** and **9b** showed full reversible oxygenation, and no spectrum of an oxidative species was observed within the period of the measurements. The electron-absorption data are listed in Table 1.

The Soret bands of the spectra were used for the spectrophotometric determination of oxygen-binding equilibria, because the most remarkable spectral changes throughout oxygenation took place at the Soret bands. The half-saturation pressures ($P_{1/2}O_2$) thus determined are listed in Table 2. The O_2 affinities of **8a** and **6a** (1-MeIm) were nearly three times those of **8b** and **6b** (1-MeIm). The half-lifetime for irreversible oxidation is >4d on **9a** and 36 h on **9b** at *ca.* 25 °C. In these ($P_{1/2}O_2$) and half-lifetime data, toluene was used as the solvent. The polarity effect of the solvent is negligible.

Discussion

(A) Half-lifetime. In synthetic analogues of Hb-Mb, it is desirable to form a stable oxygen adduct at room temperature. In this section, we will discuss the static stability of oxygen complexes. We consider that the half-lifetime of oxygen adducts at the ambient temperature indicates its static stability. The half-lifetimes of various oxygen complexes of Fe(II) porphyrins are given in Table 3. These data allow for comparison among a variety of synthetic Fe(II) porphyrins.

The protected porphyrins which have a nonprotic cavity on one side of the porphyrin plane, **9a**, **9b**, "FeTTTPP,"[2] "cofacial,"[9] "picket fence,"[4] "capped,"[48] "pocket,"[5] "doubly bridged,"[7] "hanging imidazole,"[8] and "cyclophane heme,"[31] showed long half-lifetimes (>5 h) at room temperature. In these models, the protected superstructures prevented bimolecular reactions between oxygen adducts and inhibited autoxidation. Other protected porphyrins, *e.g.*, "FeT(OMe)$_3$PP," "FeT(OEt)$_3$PP,"[32,33] and "strapped heme,"[34] whose superstructures could not prevent dimerization, binded O_2 partly reversibly at the ambient temperature. The subsequent autoxidation, however, took place immediately. Compared with these protected porphyrins, which oxygenated reversibly at room temperature, unprotected "chelated heme" had a short half-lifetime.[35] These data suggest that the protected superstructure is essential to stabi-

TABLE 3. HALF-LIFETIMES OF Fe(II) PORPHYRINS

Compound (base concentration)	$t_{1/2}$	Conditions	Ref.
FeTpivP (10^{-4} M 1,2-Me_2Im)	1 month	25 °C Toluene	3
Fepiv$_3$5CIm (tailed Im)	3 d		3
FePocpiv (0.1 M 1,2-Me_2Im)	1 d		5
(1.0 M 1-MeIm)	36 h		5
(0.1 M 1-MeIm)	7 h		5
FeMedPoc (0.1 M 1-MeIm)	2 d		5
Crown porphyrin (0.01 M 1-MeIm)	<3 min	24 °C DMA	44
(0.01 M 1-CPh$_3$Im)	>1 h	24 °C DMA	44
Fe-4-Cu	>12 h	25 °C Benzene	9
Fe-5-Cu	>12 h		9
FeTTTPP (1,2-Me_2Im)	>30 h	25 °C Toluene	2
(1,2-Me_2Im)	>2 h	60 °C Toluene	2
Chelated heme (tailed Im)	>10 s	25 °C CTAB	35
(tailed Im)	≈5 min	25 °C DMF	35
Fe(C_2-Cap) (0.64 M 1-MeIm)	5 h	25 °C Benzene	48
Basket handle (0.001 M 1-MeIm)	≈25 min	25 °C Toluene	45
(tailed Im)	≈30 min		45
(no axial base)	90 s		45
Hanging imidazole (tailed Im)	1 d	20 °C Toluene	8
Doubly bridged (tailed Im)	>2 d	20 °C DMF	7
9a (0.15 M 1,2-Me_2Im)	>4 d	20 °C Toluene	This work
9b (0.15 M 1,2-Me_2Im)	36 h		This work

lizing the oxygen complex at room temperature.

In the simple protoporphyrin/imidazole system, the oxygen adduct was less stable than "chelated heme." Although the protection was not enough to prevent dimerization, "hanging imidazole" porphyrin showed a long half-lifetime (1d).[8] In both "chelated heme" and "hanging imidazole" porphyrin, the imidazole arm was covalently linked to the porphyrin moiety, hence, the axial coordination was stabilized. Traylor[36] and Tsuchida[37] found that rigid and stable imidazole-heme coordination should result in a more stable oxygen adduct.

These protected porphyrins had various polarities at the ligand-binding site. "FeTTTPP" had a completely nonpolar pocket,[2] but other protected porphyrins were somewhat polar at the binding site. A series of "picket fence" and "pocket" porphyrins, whose polarities were quite similar, showed rather different values for their half-lifetimes (from 7 h to 1 month; see Table 3). Half-lifetime of "FeTTTPP" was over 30 h. Considering these variations of stability, it seems that the polarity is not strictly relevant to halflife time of oxygen adduct.

We will try to speculate tentatively on the relevance between the static stability and the polarity of a binding site. A related "picket fence" porphyrin complex, Fe(T*tos*PP)(N-Bu'Im) (where *tos*=*p*-toluenesulfonamide), underwent irreversible oxidation.[4] Our **9c** was also autoxidized immediately at room temperature. Both these models contained an electron-withdrawing moiety. We attribute the rapid oxidation of these two models, in spite of the inhibition of dimerization by the "picket fence," to the strong polarity of the amide protons, which permits the protonation of coordinated dioxygen and consequent oxidation. These results suggest that the local polarity effect on the stability of the oxygen complex may be small unless the polarity is too strong to promote the protonation and subsequent autoxidation.

The half-lifetime of **9a**, which was more protected than **9b**, was longer than that of **9b**. This suggests that complete protection brings about good stability of the oxygen adduct. The relationship between the stability and the steric hindrance is vague. At present, though, we consider that the steric hindrance is not very relevant to the half-lifetime.

(B) Half-saturation Pressure of Oxygen. The dynamic stability of oxygen binding is estimated by means of the half-saturation pressures of oxygen ($P_{1/2}O_2$). Table 4 contains the half-saturation pressures for the oxygenation of unhindered-imidazole complexes of various Co(II) porphyrins. Table 5 contains similar data for hindered-imidazole complexes of Fe(II) porphyrins. The variations in these $P_{1/2}O_2$values, particularly the difference in oxygen affinities between **9a** and **9b**, lead to several speculations about O_2-binding behavior. We consider that the oxygen affinities of these model compounds depend on four factors. We will discuss these four factors in the following paragraphs.

Table 4. O_2 affinities of Co(II) porphyrins (1-MeIm)

Compound	$P_{1/2}O_2$	Conditions	Ref.
CoMb (sperm whale)	30	20°C Water	46,47
CoTpivP	140	25°C Toluene	26
Co(T(*p*-OCH_3)PP)	10000	15°C Toluene	28
Co(C_2-Cap)	140000		42
6a	29	20°C Toluene	This work
6b	84	20°C Toluene	This work

Table 5. O_2 affinities of Fe(II) porphyrins (1,2-Me_2Im)

Compound	$P_{1/2}O_2$	Conditions	Ref.
FeTTTPP	508	25°C Toluene	2
FeTpivP	38		3
FePocpiv	12.6		12
FeMedPoc	12.4		12
FeTalPoc	4		12
Fe(C_2-Cap)	4000		42
Fe(Np C_2-Cap)	613	0°C Toluene	42
9a	9.5	20°C Toluene	This work
9b	26		This work

Local Polarity of Ligand-binding Site. The polarity of the ligand-binding site considerably influences the oxygen affinities. It has previously been suggested that an increased polarity should increase the oxygen affinities.[38] This suggestion has been based on the measurements on "flat," unprotected porphyrins. In protected porphyrins, also, however, we consider a similar tendency to be found.

Recently, structural studies of oxyMb[39] and oxyHb[40] have established that the N^{ε} of His E7 forms a hydrogen bond with the bound oxygen. The N^{ε} atom stabilizes the coordinated molecular oxygen with this hydrogen bond. Structural studies[41] have also shown that, in the solid state, there is no interaction between the amide proton and the bound dioxygen in the "picket fence" porphyrins. Consequently, we are unable to expect the stabilization of oxygen binding by means of the hydrogen bond in these model systems (not even in **9a**). However, these amide groups can be expected to increase the polarity at the ligand-binding site.

Momenteau and Lavallete[11] observed O_2 binding in two similar "hanging base" porphyrins. Changing the mode of attachment from amide to ether linkages resulted in a difference, by a factor of *ca.* 10, in $P_{1/2}O_2$ values. They concluded that the presence of the amide groups strongly increased the stability of the oxygenated complexes. "FeTTTPP," which had a completely nonpolar pocket, showed a rather low O_2 affinity in comparison to the "picket fence," "pocket," and **9a**. This large difference between the oxygen affinities was attributed primarily to the loss of polarity in the binding pocket of "FeTTTPP." A number of protected porphyrins, **9a**, **9b**, "picket fence," and "pocket" porphyrins, which included four amide groups around the binding site, showed high O_2 affinities.

These results suggest that the local polarity is a

significantly important factor in determining the O_2 affinity in encumbered model systems. As has been mentioned in Section (A), if the local polarity is too strong, as, *e.g.*, in **9c** and "FeT*tos*PP," the protonation and autoxidation happen rapidly even if the systems show high O_2 affinities. For that reason, these porphyrins are unsuitable as "biomimetic models" of natural oxygen carriers.

Polarity effects are expected to be similar within **9a**, **9b**, "picket fence," and "pocket" porphyrins. Therefore, the affinity differences among these model compounds, especially that between **9a** and **9b**, can not be explained by the local polarity effect. We must consider other factors in order to explain the differences.

Electronic Nature of the Porphyrin. Electronic effects have been extensively studied. Recently, Traylor *et al.*[10] found that the electronic nature of the heme had a striking effect on the O_2 affinity. The electronic nature of the series of protected porphyrins seems to be similar. Especially in **9a** and **9b**, we consider that the electronic natures of these two porphyrins quite resemble one another. As Collman *et al.*[12] mentioned in his report, other factors must be primarily responsible for the high O_2 affinities of the protected porphyrins.

Solvation Effect. Collman *et al.*[12] have discussed the solvation effects on "flat" and "protected" porphyrins. They suggested that, in "flat" iron porphyrins, the unligated five-coordinate form might be subject to a stronger solvation stabilization than the "protected" porphyrins. This stabilization of the five-coordinated species could account for the lower gaseous-ligand affinities of these "flat" porphyrins relative to "protected" porphyrins. They concluded that the solvation effect was the dominant factor responsible for the lower affinities of the "flat" hemes as compared to the "protected" hemes.

In "capped" porhyrins,[42] "[6.6]cyclophane,"[14] and "cofacial" porphyrins,[9] the O_2 affinities of these models were lower those of "flat" hemes ("chelated heme," or TPP), although a solution stabilization did not take place (see Table 6). The steric hindrance restrained the coordination of oxygen. This is reason why "capped," "[6.6]-cyclophane," and "cofacial" porphyrins indicated rather low O_2 affinities. In **9a** and **9b**, the solvation effects were considered to be almost the same. Even if the solvation effects of these two models were slightly different, the influence on the O_2 affinity should not be large. We consider that the solvation effect is the dominant factor in the difference between the O_2 affinities of "flat" hemes and those of "protected" hemes, however, among the "protected" hemes, a little difference in the solvation effect has no significant meaning on the O_2 affinities.

Steric Effect. The steric hindrance extensively influences the O_2 affinities of the protected porphyrins. Table 6 shows the $P_{1/2}O_2$ values of various porphyrin complexes.

TABLE 6. O_2 AFFINITIES OF SELECTED Fe(II) PORPHYRINS

Compound (base)	$P_{1/2}O_2$	Conditions	Ref.
[7.7]Cyclophane (1,5-DCI)	1.4	20°C Benzene	10
[6.6]Cyclophane (1,5-DCI)	696		10
Fe-4-Cu (1-MeIm)	31		9
Fe-5-Cu (THP Im)	5		9
Fe(Np C_2-Cap) (1-MeIm)	2.3		42
Fe(C_2-Cap) (1-MeIm)	4.5	0°C Toluene	42
Fe(C_3-Cap) (1-MeIm)	120-180		42
FePocpiv (1,2-Me_2Im)	12.6	25°C Toluene	12
FeMedPoc (1,2-Me_2Im)	12.4		12
FeTalPoc (1,2-Me_2Im)	4		12
9a (1,2-Me_2Im)	9.5	20°C Toluene	This work
9b (1,2-Me_2Im)	26		This work

The steric hindrance caused by the capping aromatic ring was termed "central" and "peripheral" effects by Basolo.[13] We call this "top" hindrance. The "top" hindrance was investigated in several kinds of protected porphyrins; "capped,"[13] "cyclophane,"[14] "cofacial,"[9] and "pocket"[12] hemes. Clayden *et al.*[43] studied the cavity size of "C_2-Cap," "C_3-Cap," and "Np C_2-Cap" using the paramagnetic shift and relaxation effects observed in these Co(II) complexes. The cavity size was varied in this order; "Np C_2-Cap">"C_2-Cap">"C_3-Cap." The O_2 affinities of these porphyrins decreased in exactly the same order.[42] Traylor *et al.*[14] measured the O_2 affinity of "[6.6]cyclophane" and "[7.7]cyclophane." "[7.7]cyclophane," whose cavity was larger than that of "[6.6] cyclophane," indicated a higher O_2 affinity. Chang *et al.*[9] obtained a similar result using "cofacial" porphyrins, "Fe-4-Cu," and "Fe-5-Cu." These three model systems, "capped," "cyclophane," and "cofacial" hemes, revealed a large steric effect on O_2 binding. The cavity size of "C_3-Cap," "[6.6]cyclophane," and "Fe-4-Cu" was too small for the coordination of dioxygen, and these three models had lower O_2 affinities than those of "flat" porphyrins.

A similar tendency of "top" hindrance is observed in "pocket" porphyrins.[12] The cavity size was changed in this order: "FeTalPoc">"FeMedPoc">"FePocpiv," the O_2 affinity varying in the same order. "FeMedPoc" and "FePocpiv" porphyrins had almost the same values for resulted in a difference, by a factor of *ca.* 10, in $P_{1/2}O_2$. In both porphyrins, the covalently attached benzene rings are rigidly constrained above the porphyrin ring. In contrast to these two porphyrins, the benzene ring of "FeTalPoc" was "floppy", and the O_2 affinity of this porphyrin was three times as high as those of "FeMedPoc" and "FePocpiv."

In the "top" hindrance, if the cavity size becomes too far small, the oxygen affinity is considerably decreased.

In the "pocket" porphyrins, the effects of cavity size and of rigidity are not yet clear.

The adamantyl moiety, which was the pendant group of **5a**, was bulkier than the *t*-butyl group of **5b**. The steric congestion attributable to the bulkiness of the pendant groups is termed "*side*" influence. This "*side*" influence has been scarcely studied in model systems, and it is not clear that "*side*" influence causes either the inhibition or the promotion of O_2 binding. At the beginning of this work, we set up a hypothesis that a strong "side" influence may produce a high O_2 affinity. As was expected, $P_{1/2}O_2$ values of these two models (**8a** and **8b**, **6a** and **6b**) were different, by a factor of *ca.* 3 (see Tables 4 and 6). "Tulip garden" porphyrins, **8a** and **6a**, demonstrated high O_2 affinities. The electronic nature, local polarity, solvation effect, and "top" hindrance are expected to be quite similar in these two types of model compounds, "tulip garden" and "picket fence-type" porphyrins. Only the steric "*side*" influence is dissimilar. These results suggest that the O_2 affinity is clearly dependent upon the bulkiness of the pendant groups.

Camphanoyl group of **8c** had the almost same bulkiness as the adamantyl moiety. Unfortunately, **8c** was rapidly autoxidized to the iron(III) state. For that reason, we could not estimate the "*side*" influence of **8c**.

References

1) R. D. Jones, D. A. Summerville, and F. Basolo, *Chem. Rev.*, **79**, 139 (1979).

2) K. S. Suslick and M. M. Fox, *J. Am. Chem. Soc.*, **105**, 3507 (1983).

3) J. P. Collman, *Acc. Chem. Res.*, **10**, 265 (1977).

4) J. P. Collman, R. R. Gagne, C. A. Reed, T. R. Halbert, G. Lang, and W. T. Robinson, *J. Am. Chem. Soc.*, **97**, 1427 (1975).

5) J. P. Collman, J. I. Brauman, T. J. Collins, B. L. Iverson, G. Lang, R. B. Pettman, J. L. Sessler, and M. A. Walters, *J. Am. Chem. Soc.*, **105**, 3038 (1983).

6) J. Almog, J. E. Baldwin, R. L. Dyer, and M. Peters, *J. Am. Chem. Soc.*, **97**, 226 (1975).

7) A. R. Battersby, S. A. J. Bartholomew, and T. Nitta, *J. Chem. Soc., Chem. Commun.*, **1983**, 1291.

8) M. Momenteau, B. Loock, D. Lavallette, C. Tetreau, and J. Mispelter, *J. Chem. Soc., Chem. Commun.*, **1983**, 962.

9) B. Ward, C.-B. Wang, and C. K. Chang, *J. Am. Chem. Soc.*, **103**, 5236 (1981).

10) T. G. Traylor, D. K. White, D. H. Campbell, and A. P. Berzinis, *J. Am. Chem. Soc.*, **103**, 4932 (1981).

11) M. Momenteau and D. Lavallete, *J. Chem. Soc., Chem. Commun.*, **1982**, 341.

12) J. P. Collman, J. I. Brauman, B. L. Iverson, J. L. Sessler, R. M. Morris, and Q. H. Gibson, *J. Am. Chem. Soc.*, **105**, 3052 (1983).

13) T. Hashimoto, R. L. Dyer, M. J. Crossley, J. E. Baldwin, and F. Basolo, *J. Am. Chem. Soc.*, **104**, 2101 (1982).

14) T. G. Traylor, M. J. Mitchell, S. Tsuchiya, D. H. Campbell, D. V. Stynes, and N. Koga, *J. Am. Chem. Soc.*, **103**, 5234 (1981).

15) T. N. Sorrell, *Inorg. Synth.*, **20**, 161 (1980).

16) ^{1}H NMR ($CDCl_3$) δ=1.4 (9H, s, *t*-butyl H), 7.8 (2H, s, phenyl H), 8.0 (1H, s, phenyl H), 10.9 (1H, s, CHO). MS (70 eV): *m/z* 207.23, $C_{11}H_{13}NO_3$ requires 207.23.

17) 1 M=1 mol dm^{-3}.

18) Atrop-isomers: R_f $\alpha, \beta, \alpha, \beta$, 0.97; $\alpha, \alpha, \beta, \beta$, 0.94; $\alpha, \alpha, \alpha, \beta$, 0.65; $\alpha, \alpha, \alpha, \alpha$, 0.05. (silicagel tlc, 2:1 benzene/ether).

19) a) J. Lindsey, *J. Org. Chem.*, **45**, 5215 (1980); b) C. M. Elliott, *Anal. Chem.*, **52**, 666 (1980).

20) Pivaloyl chloride was distilled under Ar immediately prior to use.

21) G. Winter, *Inor. Synth.*, **8**, 125 (1966).

22) 1,2-Me_2Im=1,2-dimethylimidazole.

23) We used spectro sol. (Dotite).

24) 1-Methylimidazole and 1,2-dimethylimidazole were distilled under reduced pressure from KOH, and stored under Ar.

25) J. P. Collman and C. A. Reed, *J. Am. Chem. Soc.*, **95**, 2048 (1973).

26) J. P. Collman, J. I. Brauman, K. M. Doxee, T. R. Halbert, S. E. Hayes, and K. S. Suslick, *J. Am. Chem. Soc.*, **100**, 2761 (1978).

27) 1-MeIm=1-methylimidazole.

28) a) F. A. Walker, *J. Am. Chem. Soc.*, **95**, 1150 (1973); b) F. A. Walker, *ibid.*, **95**, 1154 (1973).

29) In the spectrophotometric measurement, isosbestic points were maintained throughout the titration. The final spectrum obtained by exposing the solution to oxygen was, however, not exchanged by the vacuum removal of oxygen. λ/nm: 421, 578. a) T. K. Miyamoto, S. Tsuzuki, T. Hasegawa, and Y. Sasaki, *Chem. Lett.*, **1983**, 1587; b) M. J. Gunter, G. M. Mclaughlin, K. J. Berry, K. S. Murray, M. Irving, and P. E. Clark, *Inorg. Chem.*, **23**, 283 (1984).

30) 1 Torr=133.322 Pa.

31) T. G. Traylor, *Acc. Chem. Res.*, **14**, 102 (1981).

32) A. R. Amundsen and L. Vaska, *Inorg. Chim. Acta.*, **14**, L49 (1975).

33) L. L. Grazybski, R. J. Cheng, G. N. La Mar, and A. L. Balch, *J. Am. Chem. Soc.*, **104**, 5992 (1982).

34) a) A. R. Battersby, D. G. Buckley, S. G. Hartley, and M. Turnbull, *J. Chem. Soc., Chem. Commun.*, **1976**, 879; b) J. E. Baldwin, T. Klose, and M. Peters, *J. Chem. Soc., Chem. Commun.*, **1976**, 881; c) H. Ogoshi, H. Sugimoto, and Z. Yoshida, *Tetrahedron Lett.*, **49**, 4481 (1976).

35) W. S. Brinigar, C. K. Chang, J. Geibel, and T. G. Traylor, *J. Am. Chem. Soc.*, **96**, 5597 (1974).

36) C. K. Chang and T. G. Traylor, *Proc. Natl. Acad. Sci. USA*, **70**, 2647 (1973).

37) E. Tsuchida, H. Nishide, H. Yokoyama, R. Young, and C. K. Chang, *Chem. Lett.*, **1984**, 997.

38) a) H. C. Stynes and J. A. Ibers, *J. Am. Chem. Soc.*, **94**, 5125 (1972); b) C. J. Weschler, D. L. Anderson, and F. Basolo, *J. Am. Chem. Soc.*, **97**, 6707 (1975); c) T. G. Traylor and A. P. Berzinis, *Proc. Natl. Acad. Sci. USA*, **77**, 3171 (1980).

39) S. E. V. Phillips and B. P. Schoenborn, *Nature*, **292**, 81 (1981).

40) B. Shaanan, *Nature*, **296**, 683 (1982).

41) a) G. B. Jameson, G. A. Rodley, W. T. Robinson, R. R. Gagne, C. A. Reed, and J. P. Collman, *Inorg. Chem.*, **17**, 850 (1978); b) G. B. Jameson, E. S. Molinaro, J. A. Ibers, J. P. Collman, J. I. Brauman, E. Rose, and K. S. Suslick, *J. Am. Chem. Soc.*, **102**, 3224 (1980).

42) J. E. Linard, P. E. Ellis, Jr., J. R. Budge, R. D. Jones,

and F. Basolo, *J. Am. Chem. Soc.*, **102**, 1896 (1980).
43) N. J. Clayden, G. R. Moore, R. J. P. Williams, J. E. Baldwin, and M. J. Crossley, *J. Chem. Soc., Perkin Trans. 2*, **1983**, 1863.
44) C. K. Chang, *J. Am. Chem. Soc.*, **99**, 2819 (1977).
45) M. Momenteau and B. Loock, *J. Mol. Cat.*, **7**, 315 (1980).
46) B. M. Hoffman and D. H. Petering, *Proc. Natl, Acad. Sci. USA*, **67**, 634 (1970).
47) C. A. Spilburg, B. M. Hoffman, and D. H. Petering, *J. Biol. Chem.*, **247**, 4219 (1972).
48) J. Almog, J. E. Baldwin, and J. Huff, *J. Am. Chem. Soc.*, **97**, 227 (1975).

 © 1985 The Chemical Society of Japan Bull. Chem. Soc. Jpn., 58, 455—458 (1985)

Calorimetric Determination of Thermodynamic Parameters for the Dissociations of Acids in Dipolar Aprotic Solvents

Kosuke Izutsu,* Toshio Nakamura, Katsumi Takizawa, and Akihiko Takeda
Department of Chemistry, Faculty of Science, Shinshu University, Asahi, Matsumoto 390
(Received August 9, 1984)

A calorimetric method has been investigated for the determination of the thermodynamic parameters of acid dissociations in dipolar aprotic solvents. For the dissociations of monoprotonated bases BH^+ (B: aniline, pyridine, triethylamine, tributylamine, triethanolamine, 1,3-diphenylguanidine and 1,1,3,3-tetramethylguanidine) in *N,N*-dimethylformamide, dimethyl sulfoxide (DMSO), acetonitrile and propylene carbonate, the solutions of the bases were titrated with small volumes of a "strong acid," trifluoromethanesulfonic acid. In each solvent, there was an approximately linear relation of unit slope between ΔH°_{298} and ΔG°_{298}, showing that the difference in pK_a between different BH^+'s can mainly be attributed to the difference in the enthalpy term. As for the solvent effect on pK_a, however, the entropy term seems to play an important role. A preliminary study has shown that the calorimetric method is also applicable to the dissociations of HX-type weak acids (benzoic and salicylic acids in DMSO, for example), if the dissociation equilibria are not complicated by such reactions as homoconjugation.

Acid-base equilibria in dipolar aprotic solvents have been extensively studied, and fairly abundant data for acid-dissociation constants are available.[1] But the data concerning the thermodynamic parameters of acid dissociations are quite limited, and, in most cases, have been obtained from the effect of temperature on the dissociation constants. To our knowledge, no thermodynamic parameters of acid dissociation in dipolar aprotic solvents have been obtained calorimetrically.

In the present study, we used a calorimetric method to obtain thermodynamic parameters for acid dissociations in dipolar aprotic solvents. The main dissociations investigated were for monoprotonated bases BH^+ (Eq. (1)):

$$BH^+_{solv} \longrightarrow B_{solv} + H^+_{solv}. \quad (1)$$

The reactions which occur when a large amount (100 ml) of a base (B) solution is titrated with small amounts (10—60 μl to keep the heat of dilution negligibly small) of a strong acid (HA) can be considered to consist of the following three steps:

$$HA \longrightarrow (HA)_{solv}, \quad (2)$$

$$(HA)_{solv} \longrightarrow H^+_{solv} + A^-_{solv}, \quad (3)$$

$$H^+_{solv} + B_{solv} \longrightarrow BH^+_{solv}. \quad (4)$$

If we express the heat generated by reactions (2) and (3) by ΔH_1 (kJ mol^{-1}) and that by reactions (2), (3) and (4) by ΔH_T, the heat generated by reaction (4) is equal to $(\Delta H_T - \Delta H_1)$. Thus, the standard enthalpy ΔH°_{298} for the reaction (1) should also be equal to $(\Delta H_T - \Delta H_1)$. Here, ΔH_1 can be obtained by titrating the pure solvent with the "strong acid" HA. In the present study, we used trifluoromethanesulfonic acid as HA. It is one of the strongest acids and a pure, water-free product can be obtained easily. In *N,N*-dimethylformamide (DMF) and dimethyl sulfoxide(DMSO), it actually behaved as a strong acid and reliable values of ΔH_1 could be obtained. In acetonitrile(AN) and propylene carbonate (PC), however, the dissociation of the acid was not complete and only approximate ΔH_1-values could be obtained as will be described later. We also have studied preliminarily on the determination of thermodynamic parameters for the dissociations of HX-type weak acids.

Experimental

Apparatus and Reagents. A multi-purpose calorimeter, model MPC-11, of the Tokyo Riko Co. was used for calorimetric measurements. The cell assembly is shown in Fig. 1. Trifluoromethanesulfonic acid was added with a Gilmont ultra precision 250 μl-microburet S3100A (0.01 μl/div).

DMF, DMSO, and AN were the reagent grade products of Wako Chemicals Co., and PC was a synthetic grade Merck product. They were purified by the methods recommended in Ref. 2). Trifluoromethanesulfonic acid (Wako reagent grade) was purified by a distillation with a semimicro distilling apparatus. All the amines tested were Wako analytical grades. Tributylamine and triethanolamine were distilled under reduced pressures, and other amines were purified by the

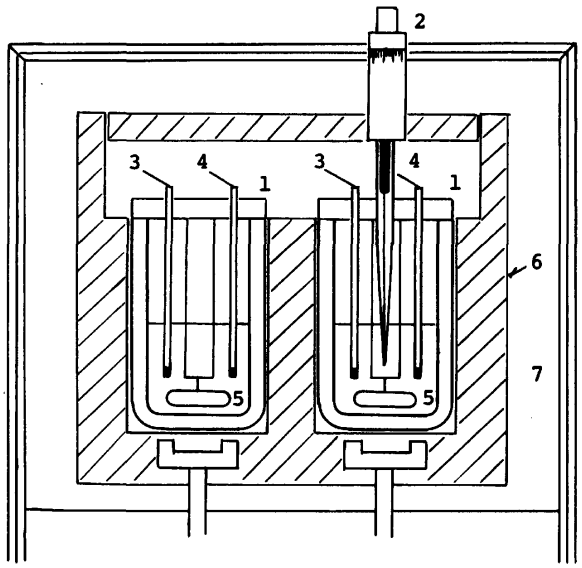

Fig. 1. Cell assembly for calorimetric measurements. 1: Dual cells, 2: microburet, 3: thermistor, 4: heater for calibration, 5: magnetic stirrer, 6: aluminum thermostat bath and 7, air thermostat bath.

methods described in a previous report.[3] Benzoic and salicylic acids (Wako reagent grades) were used as received.

Procedure for Monoprotonated Bases. To the cell was added 100 ml of the solution containing an appropriate amount of the base to be tested (in the case of ΔH_T measurement) or 100 ml of the pure solvent (in the case of ΔH_1 measurement). The cell and the microburet containing trifluoromethanesulfonic acid were set to the calorimeter as shown in Fig. 1 and kept for 2—3 h until they reached a uniform temperature of 25 °C (298 K). The amounts of the bases taken were 100 μl (0.0124 M, 1M=1 mol dm^{-3}) for pyridine, 100 μl (0.0109 M) for aniline, 200 μl (0.0143 M) for triethylamine, 250 μl (0.0105 M) for tributylamine, 200 μl (0.0150 M) for triethanolamine, 150 μl (0.0117 M) for 1,1,3,3-tetramethylguanidine and 211 mg (0.0100 M) for 1,3-diphenylguanidine. The solution in the cell was titrated with six aliquots of the acid, 10.0 μl (1.13×10^{-3} M) each, and, from the temperature changes, the heats corresponding to ΔH_1 and ΔH_T were obtained. The factor to convert temperature change to heat was determined for each solution with an accuracy of ±0.2% by using a built-in heater (accuracy: ±0.1%). During the titrations, the solutions were stirred with a magnetic stirrer at 280 rpm.

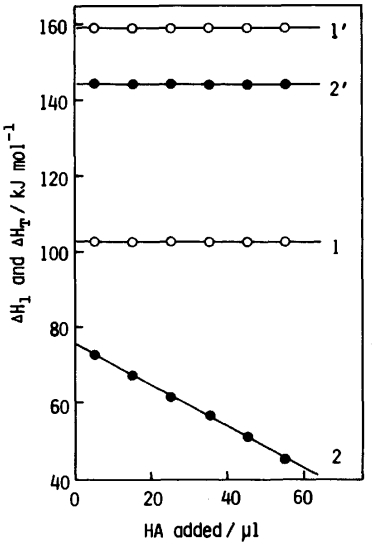

Fig. 2. ΔH_1 and ΔH_T (B=triethanolamine) *vs.* the volume of trifluoromethanesulfonic acid added. Lines 1 and 1′ in DMSO and 2 and 2′ in AN.

Results and Discussion

Thermodynamic Parameters for the Dissociations of Monoprotonated Bases. Measurements of ΔH_1: As described above, trifluoromethanesulfonic acid was added to 100 ml of the pure solvent six times in an aliquot of 10.0 μl (1.13×10^{-3} M) each. For DMF and DMSO, the heat generated each time was almost constant as line 1 in Fig. 2. ΔH_1, obtained from the average of these values, was 112.3±0.3$_2$ kJ mol^{-1} for DMF (n=4, where n is the number of similar measurements) and 102.9±0.3$_1$ kJ mol^{-1} for DMSO (n=6). In PC and AN, the determination of ΔH_1 encountered difficulties due to the incomplete dissociation of the acid. The heat generated by the addition of the acid decreased gradually with the increase of the acid concentration (line 2, Fig. 2). Because the decrease was approximately linear against the amounts of the acid added, we assumed that the value obtained by an extrapolation to zero concentration nearly corresponded to ΔH_1. It was 85.$_4$± 0.9 kJ mol^{-1} for PC (n=5) and 75.$_9$±0.6 kJ mol^{-1} for AN (n=6).

Measurements of ΔH_T: Trifluoromethanesulfonic acid was added to the solution of the base to be tested. The heat generated by each addition of the acid was almost constant (lines 1′ and 2′, Fig. 2) and ΔH_T was obtained as the average of the values. In Table 1 the results of ΔH_T are summarized. Most of the ΔH°_{298} values were obtained by the relation $\Delta H^\circ_{298}=(\Delta H_T-\Delta H_1)$. In DMF and DMSO, however, pK_a for aniline and pyridine were not large enough for the reaction (4) to be quantitative. In those cases, ΔH°_{298} were obtained from $(\Delta H_T-\Delta H_1)$ by correcting for the incompleteness of the reaction.

Thermodynamic Parameters: Thermodynamic parameters for the dissociations of monoprotonated bases are shown in Table 2. The values of ΔG°_{298} were calculated by the relation $\Delta G^\circ_{298}=-RT\ln K_a$. For most of the p$K_a$ we referred to the literature values[3-9], but we determined some of them in this work from the half-neutralization points of the potentiometric titra-

Table 1. Heats (ΔH_T) generated by reactions (2), (3), and (4) at 298 K

Bases	ΔH_T/kJ mol^{-1}			
	DMSO	DMF	PC	AN
Pyridine	129.0±0.9$_1$ (5)	134.6±0.2$_4$ (4)	118.3±0.4$_7$ (5)	120.0±0.2$_9$ (4)
Aniline	134.1±0.7$_5$ (5)	136.9±0.3$_6$ (4)	112.8±0.1$_8$ (4)	114.1±0.1$_8$ (4)
Triethanolamine	159.2±0.2$_9$ (4)	162.1±0.4$_0$ (4)	146.6±0.1$_8$ (4)	144.4±0.3$_8$ (4)
Tributylamine	165.5±0.1$_7$ (5)	167.0±0.4$_9$ (4)	154.4±0.6$_7$ (5)	154.8±0.4$_1$ (4)
1,3-Diphenylguanidine	161.3±0.6$_9$ (5)	166.9±0.1$_3$ (4)	142.5±0.3$_1$ (4)	146.5±0.2$_5$ (4)
Triethylamine	166.6±0.1$_9$ (6)	170.9±0.3$_4$ (4)	155.7±0.4$_6$ (6)	154.8±0.2$_3$ (5)
1,1,3,3-Tetramethylguanidine	190.7±0.3$_7$ (4)	—	—	—

The figures in parentheses show the number of measurements.

TABLE 2. THERMODYNAMIC PARAMETERS FOR THE DISSOCIATIONS OF MONOPROTONATED BASES IN DMSO, DMF, PC, AND AN (298 K)

Bases	$pK_a(BH^+)$	$\Delta G°_{298}$	$\Delta H°_{298}$	$-T\Delta S°_{298}$
		kJ mol^{-1}	kJ mol^{-1}	kJ mol^{-1}
		Dimethyl sulfoxide		
Pyridine	3.5[a](3.4[b])	20.0	26.9	−6.9
Aniline	3.7[a](3.6[b])	21.1	31.9	−10.8
Triethanolamine	7.4$_8$[c]	42.7	56.3	−13.6
Tributylamine	8.3[a]	47.4	62.6	−15.2
1,3-Diphenylguanidine	8.6[a]	49.1	58.4	−9.3
Triethylamine	9.0[b]	51.3	63.7	−12.4
1,1,3,3-Tetramethylguanidine	13.2[b]	75.3	87.8	−12.5
		N,*N*-Dimethylformamide		
Pyridine	3.3[d]	18.8	23.3	−4.5
Aniline	3.6$_6$[e] (4.3$_6$[f])	20.9	25.2	−4.3
Triethanolamine	7.5$_5$[d]	43.1	49.8	−6.7
Tributylamine	8.5$_7$[c]	48.9	54.7	−5.8
1,3-Diphenylguanidine	9.1[f](8.9[d])	51.9	54.6	−2.7
Triethylamine	9.2$_5$[d,f]	52.8	58.6	−5.8
		Propylene carbonate		
Aniline	10.0$_9$[g]	57.6	(27.4)	(30.2)
Pyridine	11.9$_2$[g]	68.0	(32.9)	(35.1)
Triethanolamine	15.8$_7$[c]	90.5	(61.2)	(29.3)
1,3-Diphenylguanidine	16.9$_8$[g]	96.9	(57.1)	(39.8)
Tributylamine	17.5$_2$[c]	99.9	(69.0)	(30.9)
Triethylamine	17.9$_4$[g]	102.3	(70.3)	(32.0)
		Acetonitrile		
Aniline	10.5$_6$[h]	60.2	(38.2)	(22.0)
Pyridine	12.3$_3$[h]	70.3	(44.1)	(26.2)
Triethanolamine	15.9$_3$[c]	90.9	(68.5)	(22.4)
1,3-Diphenylguanidine	17.9$_0$[h]	102.1	(70.6)	(31.5)
Tributylamine	18.0$_9$[h]	103.2	(78.9)	(24.3)
Triethylamine	18.4$_6$[h]	105.3	(78.9)	(26.4)

a) Ref. 4. b) Ref. 5. c) This work. d) Ref. 6. e) Ref. 7. f) Ref. 8. g) Ref. 3. h) Ref. 9. In the calculation of $\Delta G°_{298}$, the pK_a value without parentheses was used. The values of $\Delta H°_{298}$ and $-T\Delta S°_{298}$ in parentheses are somewhat approximate due to the reasons as described in text.

tions of the bases with trifluoromethanesulfonic acid (use of a glass pH-electrode). The pK_a of pyridine/pyridinium ion system was used as the reference.

In Figs. 3 and 4, the values of $\Delta H°_{298}$ and $-T\Delta S°_{298}$ were plotted against $\Delta G°_{298}$. For each solvent, there is an approximately linear relation of unit slope between $\Delta H°_{298}$ and $\Delta G°_{298}$ (though fairly big deviations are observed for 1,3-diphenylguanidine in PC and AN). Thus, for each solvent, the difference in pK_a values between different monoprotonated bases may mainly be attributed to the difference in the enthalpy term. As for the changes in pK_a with solvents (solvent effect on pK_a), however, the results in the figures show that the entropy term also takes a considerable part, though the reason for this has not been elucidated yet.

Thermodynamic Parameters for the Dissociation of Weak Acid HX. In dipolar aprotic solvents, the dissociation equilibria of weak acids of the type HX often become complicated due to such reactions as dimerization and homoconjugation. In the absence of such complicating reactions and when the acid HX is weak enough, the thermodynamic parameters for the dissociation (Eq. (5)) can be obtained by either of the following methods:

$$(HX)_{solv} \longrightarrow H^+_{solv} + X^-_{solv}. \quad (5)$$

i) The solution of R_4NX (tetraalkylammonium salt of X^-) is titrated by a strong acid HA. The thermodynamic parameters should be obtained by the same principle as in the above.

ii) The solution of the weak acid HX is titrated with an appropriate base B. Then, the reactions which occur can be expressed by:

$$B \longrightarrow B_{solv}, \quad (6)$$

$$(HX)_{solv} \longrightarrow H^+_{solv} + X^-_{solv}, \quad (7)$$

$$H^+_{solv} + B_{solv} \longrightarrow BH^+_{solv}. \quad (8)$$

The enthalpy for reaction (8) is known from the above work and that for reaction (6) can easily be determined. Thus, the enthalpy for reaction (7) should be obtained.

iii) The solution of a base B is titrated with the weak acid HX. The reactions which occur can be expressed by $HX \rightarrow (HX)_{solv}$ and Eqs. (7) and (8). Because

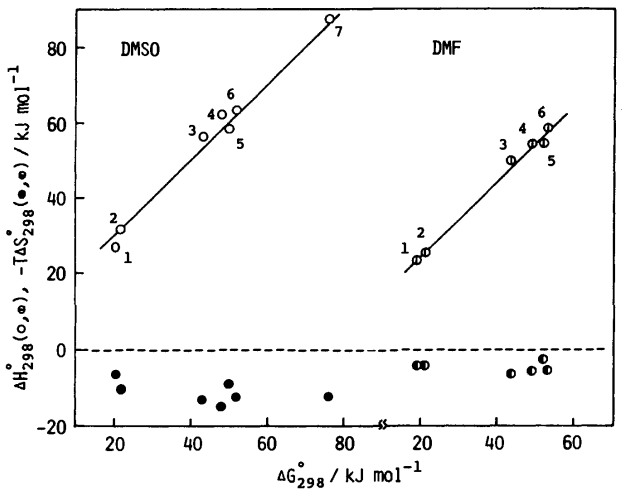

Fig. 3. Relations of ΔH°_{298} and $-T\Delta S^\circ_{298}$ *vs.* ΔG°_{298} in DMSO and DMF.
B: 1 pyridine, 2 aniline, 3 triethanolamine, 4 tributylamine, 5 1,3-diphenylguanidine, 6 triethylamine, and 7 1,1,3,3-tetramethylguanidine.

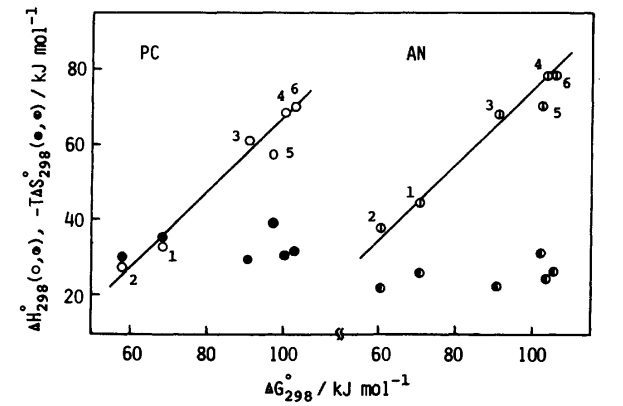

Fig. 4. Relations of ΔH°_{298} and $-T\Delta S^\circ_{298}$ *vs.* ΔG°_{298} in PC and AN (see the caption of Fig. 3).

the enthalpy for reaction (8) is known, that for reaction (7) can be obtained, if the enthalpy for HX→ $(HX)_{solv}$ is obtained separately.

In the present study, method ii) was employed for salicylic and benzoic acids in DMSO. For salicylic acid (pK_a=6.6, ΔG°_{298}=37.7 kJ mol^{-1} [10]), its solution in the cell was titrated with triethylamine ($pK_a(BH^+)$=9.0) and also with tetramethylguanidine (pK_a (BH^+)=13.2[5]). The titration with triethylamine gave ΔH°_{298} of 19.9 kJ mol^{-1} and that with tetramethylguanidine 20.3 kJ mol^{-1}.[11] The average of the two values, 20.1 kJ mol^{-1}, is somewhat larger (but probably more reliable) than 17.1 kJ mol^{-1} which we calculated using literature data of the changes of pK_a with temperature.[10] For benzoic acid (pK_a=10.6, ΔG°_{298}=60.5 kJ mol^{-1} [10]), the titration with tetramethylguanidine gave ΔH°_{298} of 35.6 kJ mol^{-1}[12] which is in good agreement with 35 kJ mol^{-1} obtained from the temperature effect on pK_a.[10]

In the above examples for HX-type weak acids, fair agreements were obtained between calorimetric results and the results from the temperature effect on pK_a. Usually, however, it is rather difficult in dipolar aprotic solvents to determine with enough precisions the temperature effect on pK_a. The calorimetric method as employed in the present work seems to be easier and give more reliable results for dissociations of both BH^+- and HX-type weak acids, if there is a "strong acid" which completely dissociates in the relevant solvents.

This work was partially supported by a Grant-in-Aid for Scientific Research from the Ministry of Education (No. 57470029).

References

1) I. M. Kolthoff and M. K. Chantooni, Jr., "Treatise on Analytical Chemistry" (I. M. Kolthoff and P. J. Elving, ed.), 2nd ed., Part I, Vol. 2, p. 239, Wiley (1979); K. Izutsu, Compilation of Acid Dissociation Constants in Dipolar Aprotic Solvents, Report for Commission on Electroanalytical Chemistry of IUPAC, to be published.

2) J. F. Coetzee, ed., "Recommended Methods for Purification of Solvents and Tests for Impurities", Pergamon (IUPAC) (1982).

3) K. Izutsu, T. Nakamura and I. Iijima, *Bull. Chem. Soc. Jpn.*, **52**, 2721 (1979).

4) J. Courtot-Coupez and M. LeDemezet, *Bull. Soc. Chim. Fr.*, **1969**, 1033.

5) I. M. Kolthoff, M. K. Chantooni, Jr., and S. Bhowmik, *J. Am. Chem. Soc.*, **90**, 23 (1968).

6) G. Demange-Guerin, *Talanta*, **17**, 1075 (1970).

7) E. Roletto and A. Vanni, *Talanta*, **24**, 73 (1977).

8) I. M. Kolthoff, M. K. Chantooni, Jr. and H. Smagowski, *Anal. Chem.*, **42**, 13 (1970).

9) J. F. Coetzee and G. R. Padmanabhan, *J. Am. Chem. Soc.*, **87**, 5005 (1965).

10) M. Perec, B. D. Struck and D. Trietenbach, *Electrochim. Acta*, **23**, 25 (1978).

11) ΔH° for reactions (6), (7), and (8) was $-34.1\pm0.2_5$ kJ mol^{-1} (n=3) with triethylamine and $-65.8\pm0.2_0$ kJ mol^{-1} (n=3) with tetramethylguanidine, while ΔH° for reaction (6) was 9.7 kJ mol^{-1} for triethylamine and 1.7 kJ mol^{-1} for tetramethylguanidine.

12) ΔH° of $-50.5\pm0.1_7$ kJ mol^{-1} (n=4) was obtained for reactions (6), (7), and (8) by extrapolation to the tetramethylguanidine concentration of zero.

^{59}Co Quadrupole Effects on the ^{1}H, ^{31}P, and ^{59}Co NMR Spectra of $HFeCo_3(CO)_9[P(OCH_3)_3]_3$ and the ^{1}H NMR Spectra of Other Derivatives

Taro SAITO* and Satoshi SAWADA
Department of Chemistry, Faculty of Engineering Science, Osaka University, Toyonaka, Osaka 560
(Received August 23, 1984)

The ^{1}H NMR spectra of $HMCo_3(CO)_{12}$ (M=Fe or Ru) and $HFeCo_3(CO)_{12-x}[P(OR)_3]_x$ (x=1—3, R=CH_3; x=3, R=C_2H_5 or C_6H_5) showed very broad signals centered near δ=−21 at 27 °C. The band widths were generally smaller for the compounds of larger molecular volume, at lower temperatures and with higher viscosity of the solvent. These data were interpreted in terms of the quadrupole effects of ^{59}Co nuclei to which the hydride proton was μ_3-bonded. Supporting evidence was obtained from the ^{31}P and ^{59}Co NMR spectra and the relaxation time T_1 of $HFeCo_3(CO)_9[P(OCH_3)_3]_3$.

In a previous paper[1] we reported the protonation of the coordinated dinitrogen by a highly acidic cluster hydride $HFeCo_3(CO)_{12}$ (**1**) (Fig. 1).[2] There was a long controversy over the position of the hydride ligand in this cluster[3-7] because ^{1}H NMR spectra did not show the signal for the proton[3,8] and no X-ray data were published. The problem seems to have been settled when the X-ray[8] and neutron[9] diffraction studies of a trimethyl phosphite-substituted derivative $HFeCo_3(CO)_9[P(OCH_3)_3]_3$ indicated unequivocally that the hydride existed on the Co_3 face. Although it seemed probable that the hydride ligand in the unsubstituted cluster **1** was also located on the Co_3 face from the X-ray crystallographic study of $Ph_3PAuFeCo_3(CO)_{12}$,[10] direct evidence was still not enough when the present study started.

During our study on the reaction of $Ni[P(OC_2H_5)_3]_4$ with **1**,[11] we found an unexpected high-field signal in the ^{1}H NMR spectra of a product which was later proved to be due to the hydride in $HFeCo_3(CO)_{11}[P(OC_2H_5)_3]$. The detection of the hydride signals is significant because (i) face-bridged μ_3-hydride cluster compounds[8,12-16] are interesting with respect to the dissociative adsorption of hydrogen molecules on metal surfaces.[9,17] and (ii) the information will be useful for the cobalt hydride cluster compounds showing very broad NMR signals difficult to detect. Thus, we have measured the NMR spectra of **1** and its derivatives and interpreted them.

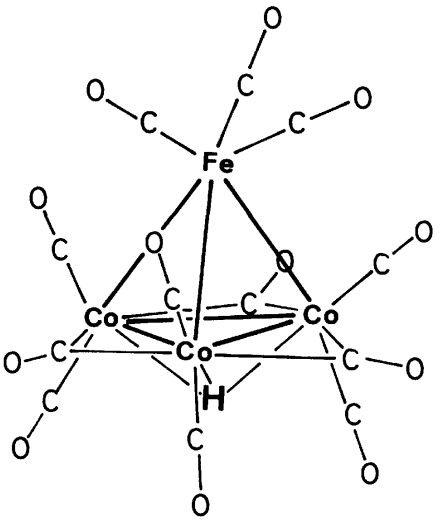

Fig. 1. Postulated structure of $HFeCo_3(CO)_{12}$.

Experimental

Hydridometalcarbonyl cluster compounds **1**—**7** (Table 1) were prepared by methods described in the literature with some modifications.[6,8,18] The compounds obtained after chromatography gave satisfactory elemental analyses and the absence of paramagnetic impurities was checked by the sharpness of the phosphite bands in the ^{1}H NMR spectra.

^{1}H NMR spectra were measured using a JEOL FX-100 FT NMR spectrometer at 100 MHz in the temperature range of +70—−60 °C. Chloroform-*d* solutions were used for the phosphite-substituted cluster compounds, but because of the low solubilities of the unsubstituted clusters $HMCo_3(CO)_{12}$

TABLE 1. HYDRIDE CHEMICAL SHIFTS AND HALF-HEIGHT WIDTHS OF ^{1}H NMR SPECTRA OF $HFeCo_3(CO)_{12-x}[P(OR)_3]_x$ AND $HRuCo_3(CO)_{12}$

Compound		δ[a]	$W_{h/2}$/Hz Temperature/°C				
			27	0	−20	−40	−60
$HFeCo_3(CO)_{12}$[b]	**1**	−21.1	487	472	201	93	56[c]
$HFeCo_3(CO)_{11}[P(OCH_3)_3]$	**2**	−21.4	366	217	133	85	62
$HFeCo_3(CO)_{10}[P(OCH_3)_3]_2$	**3**	−21.7	232	118	73	47	38
$HFeCo_3(CO)_9[P(OCH_3)_3]_3$	**4**	−22.1	137	78	49	29	28
$HFeCo_3(CO)_9[P(OC_2H_5)_3]_3$	**5**	−21.9	106	64	49	27	25
$HFeCo_3(CO)_9[P(OC_6H_5)_3]_3$	**6**	−21.0	91	61	45	39	51
$HRuCo_3(CO)_{12}$	**7**	−19.4	200	106	65	32	27[d]

a) Measured from a solvent peak and converted to δ values. b) Measured up to +70 °C and the line width was almost equal to that at 27 °C. c) −53 °C. d) −50 °C.

(M=Fe or Ru) in chloroform, they were dissolved in $Fe(CO)_5$ mixed with toluene-d_8 (5 vol%) for the measurements. $Fe(CO)_5$ did not affect the chemical shifts or line-widths of the spectra as compared with those recorded for saturated chloroform-*d* solutions which required many accumulations ($>10^4$ times) for the unsubstituted derivatives. Several hundred times accumulations were enough for the phosphite-substituted compounds. The relaxation times T_1 were obtained by the inversion recovery method. The effect of the sample viscosity on the line-width was tested for $HFeCo_3(CO)_9[P(OCH_3)_3]_3$ (**4**) in a chloroform-*d*/polyfluorinated hydrocarbon (Daifloil) (1:1) solvent which was about 3.5 times as viscous as pure chloroform-*d* indicated by a Ubbelohde viscosimeter at 27°C.

^{31}P NMR spectra were recorded at 40.7 MHz with JEOL FX-100 FT NMR spectrometer. Chloroform-*d* solutions with external standard (3% aq H_3PO_4) were used for the measurements.

^{59}Co NMR spectra were recorded at 63.8 MHz with JEOL GX-270 FT NMR spectrometer at the laboratory of JEOL. The compouds **2**—**4** were dissolved in chloroform-*d* and **1** was dissolved in $Fe(CO)_5$ mixed with toluene-d_8 (5 vol%) and external standard ($[Co(NH_3)_6]Cl_3$ or $[Co(en)_3]Cl_3$) was used for the measurements. The relaxation times T_1 were obtained by the inversion recovery method.

Results

Figures 2—4 illustrate variable temperature ^1H NMR spectra of **1**, **7**, and **4**, respectively. The spectra of **2**, **3**, **5**, or **6** are similar to those of **4** except chemical shifts and line-widths and the values are listed in Table 1. Variable temperature ^{31}P and ^{59}Co NMR spectra of **4** are shown in Figs. 5 and 6, respectively.

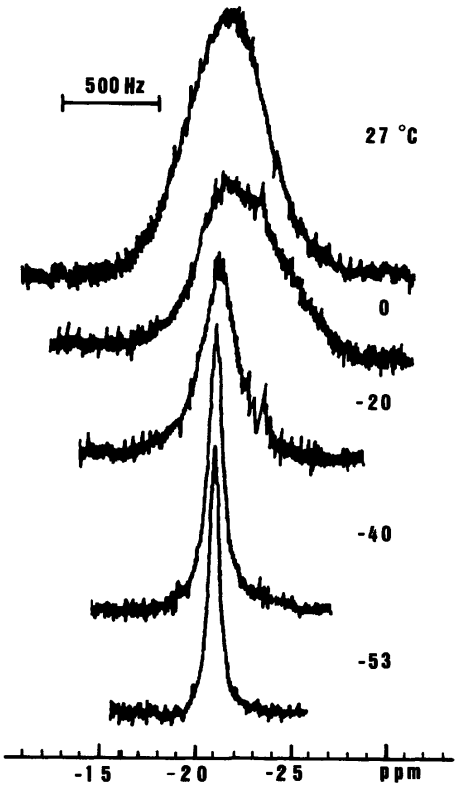

Fig. 2. Variable temperature ^1H NMR spectra of $HFeCO_3(CO)_{12}$ (**1**).

Fig. 3. Variable temperature ^1H NMR spectra of $HRuCo_3(CO)_{12}$ (**7**).

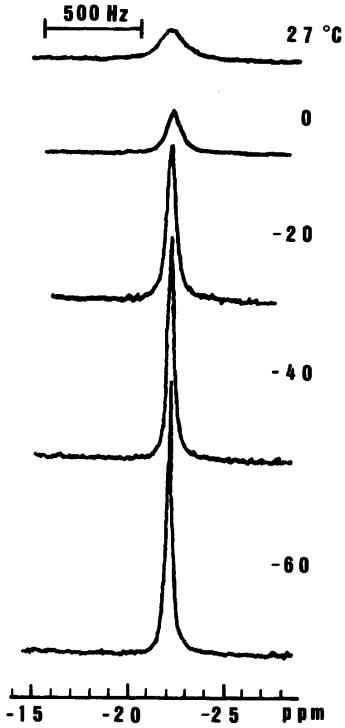

Fig. 4. Variable temperature ^1H NMR spectra of $HFeCo_3(CO)_9[P(OCH_3)_3]_3$ (**4**).

The ^1H NMR spectra indicated that the line-widths at half-signal height ($w_{h/2}$) were very broad and no couplings with ^{59}Co or ^{31}P nuclei were observed. The line-widths became narrower as the temperatures were lowered but the chemical shifts were invariable and no splittings of the major peaks resulted. A much sharper band of minor intensity (<1/20) appeared overlapped

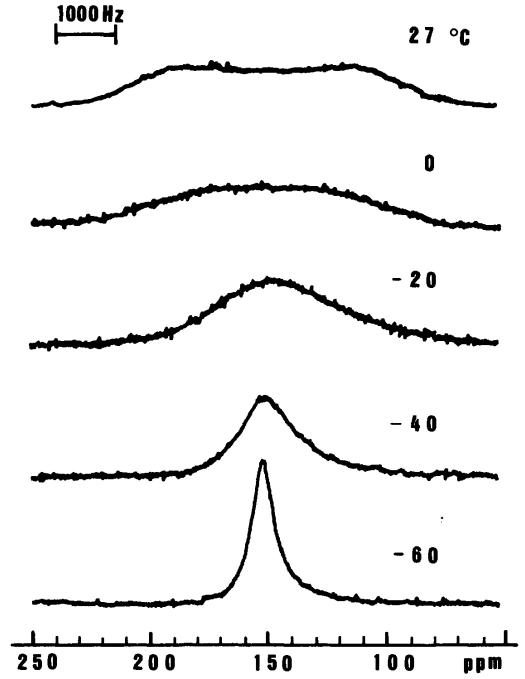

Fig. 5. Variable temperature ^{31}P NMR spectra of $HFeCo_3(CO)_9[P(OCH_3)_3]_3$ (**4**).

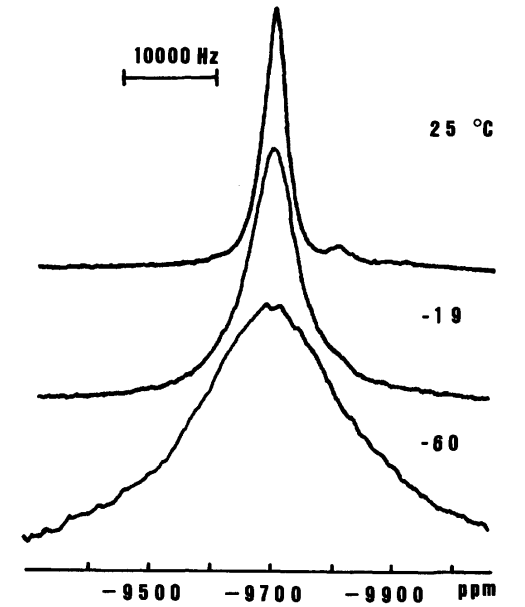

Fig. 6. Variable temperature ^{59}Co NMR spectra of $HFeCo_3(CO)_9[P(OCH_3)_3]_3$ (**4**). Chemical shifts were measured from $[Co(en)_3]Cl_3$ external standard.

on the major broad band and the signal intensities were temperature dependent.

The line-widths of a viscous solution of **4** in chloroform-*d*/Daifloil was 74 Hz as compared with 137 Hz of the pure chloroform-d_1 solution at 27 °C.

The ^{31}P NMR spectrum of **4** was a very broad saddle shaped doublet at 27 °C and became broad singlets at lower temperatures. The chemical shift (135.2 ppm) from the external H_3PO_4 standard did not change upon cooling the sample.

The chemical shifts and the line-widths of the ^{59}Co NMR spectra of **1**, **2**, **3**, and **4** at 27 °C are given in Table 2. The spectra of **1** and **4** are singlets and those of **2** and **3** are doublets, the higher field bands being assigned to the cobalt atoms coordinated with trimethyl phosphite.

Table 2. Chemical shifts and half-height widths of ^{59}Co NMR spectra of $HFeCo_3(CO)_{12-x}[P(OCH_3)_3]_x$

Compound		/ppm[a]	$W_{h/2}$/Hz
$HFeCo_3(CO)_{12}$	**1**	−3856	674
$HFeCo_3(CO)_{11}[P(OCH_3)_3]$	**2**	−3849 (1)[c]	1304
		−3913 (2)[c]	2065
$HFeCo_3(CO)_{10}[P(OCH_3)_3]_2$	**3**	−3836	b)
		−3863	
$HFeCo_3(CO)_9[P(OCH_3)_3]_3$	**4**	−3901	2609

a) Measured from $[Co(NH_3)_6]Cl_3$ external standard at 27 °C. b) Not resolved. c) Intensity ratio.

The relaxation times T_1 of the ^1H resonance of **4** were 207, 72, and 25 ms at 27, −20, and −60 °C, respectively. The T_1 for the ^{59}Co resonance of the same compound were 0.140, and 0.053 ms at 25, and −19 °C, respectively.

Discussion

The broad high-field signals in the ^1H NMR spectra of $HFeCo_3(CO)_{12-x}[P(OR)_3]_x$ show the calculated intensities relative to the phosphite protons and can be assigned to a single hydride proton. The signals for the unsubstituted $HMCo_3(CO)_{12}$(M=Fe or Ru) are also assignable to the hydride proton judging from the similarity of the chemical shifts and line shapes. The chemical shift values around $\delta=-21$ indicate that the hydrogens are bonded to transition metals and not to an oxygen atom of carbonyl groups.[19-21] Up-field shifts of about 0.3 ppm was observed by exchange of each carbonyl group on cobalt by a trimethyl phosphite, showing electron-donating influence of the latter ligand on the hydride proton. The proton chemical shift of the Co_3 face-bridged hydrides in $(\eta\text{-}C_5H_5)_4Co_4H_4$ was reported to be at $\delta=-23.06$[24] which is near the values of the present cluster hydrides. Thus it seems more likely that the hydride proton is bound to cobalt rather than to iron or ruthenium. The failure to detect the signals in the past[3,8] may be ascribable to the very broad nature of the resonance line due to the effect of the ^{59}Co quadrupole.[22,23]

The hydride spectra of cobalt hydride complexes generally do not show splittings due to scalar couplings of the proton with cobalt. For example, $HCo(CO)_2[P(OC_6H_5)_3]_2$[25] or $HCo[P(OC_2H_5)_3]_4$[26] show sharp resonance lines having splittings due to the coupling only with ^{31}P nuclei and $HCo(PF_3)_4$[22] shows a broad singlet with the width of about 180 Hz at room temperature. These spectral features are caused by the quadrupole of cobalt nuclei ($I=7/2$) which have the very short relaxation time T_1 except for the complexes with cubic symmetry around cobalt.[27]

The relaxation time T_1 of cobalt is expressed as follows:

$$\frac{1}{T_1}=\frac{3}{40}\frac{(2I+3)}{I^2(2I-1)}\left(\frac{e^2qQ}{\hbar}\right)^2\tau_c \quad (I=7/2), \qquad (1)$$

$$\tau_c = \frac{4\pi\eta' a^3}{3kT}, \quad (2)$$

where e^2qQ/h is electric quadrupole coupling constant, τ_c correlation time of molecular reorientation, η' viscosity, a molecular radius, k Boltzman's constant and T absolute temperature.[28,29] The spectral shapes of NMR spectra of the nuclei (I=1/2) coupled with quadrupolar nuclei have been analyzed by Pople[30] and Suzuki and Kubo.[31] Yamasaki[32] has extended it to ^{59}Co (I=7/2) and calculated the simulation spectra which are dependent on a parameter $\eta=2\pi JT_1$ where T_1 is relaxation time of cobalt and J is scalar coupling constant. Where η is small, the splittings due to the scalar couplings are not observed and the spectra broaden. However, when η is much smaller, the resonance of the nuclei (I=1/2) is out of the influence of cobalt and becomes sharper.

The T_1 of ^{59}Co is reciprocally proportional to τ_c and becomes smaller when the viscosity and molecular volume increase and the temperature decreases. As the viscosity of the solvent increases at lower temperatures, the effect of lowering the temperature on the T_1 is most pronounced. A typical example of the temperature effect was illustrated in the variable temperature ^{1}H, ^{31}P, and ^{59}Co NMR spectra of **4**. The T_1 of ^{59}Co decreased when the temperature was lowered and the spectra broadened (Fig. 6). On the other hand, ^{1}H and ^{31}P spectra became sharper at lower temperatures (Figs. 4 and 5). The line shapes of ^{31}P (I=1/2) spectra correspond to those of the simulation curves[32] at *ca.* η=0.5 for the spectrum at 27°C and *ca.* 0.2 for that at −20°C. The ^{1}H spectra are already singlets at 27°C and the line widths decrease at lower temperatures. Since the trimethyl phosphite ligands are bound to cobalt,[8,9] the line broadening mechanism for the ^{31}P nuclei is likely the same as that for the hydride. Namely, both the ^{1}H and ^{31}P spectra broaden because of the quadrupolar effect of ^{59}Co nuclei and sharpen at lower temperatures where the T_1 of ^{59}Co becomes much smaller.

The influence of viscosity upon the T_1 was evident from the comparison of the spectra in chloroform and in Daifloil. The increase of molecular volume by the phosphite exchange was also reflected in the decrease of line-widths (Table 1). For instance, by the approximation of regarding the cluster compounds as spheres, the molecular volume of **6** is calculated to be about twice that of **4**, and corresponding decrease of the line-widths was observed (Table 1).

The scrambling of carbonyl groups in $HFeCo_3(CO)_{12}$ and its derivatives was studied by ^{13}C and ^{17}O NMR spectroscopies.[33,34] It was shown that the scrambling was rather slow at lower temperatures, especially for the phosphite-substituted hydrides which have larger energy barrier for the fluxionality. As most of the ^{1}H NMR spectra of the present study were recorded below 27°C, the chemical shifts and line-widths are probably not influenced significantly by the carbonyl scrambling. The possibility that the sharpening of the spectra at lower temperatures may have been caused by hydride fluxionality can be ruled out because there were no chemical shifts and splittings of the signals which must have been shown in the temperature dependent spectra of the fluxional hydride. However a minor fraction of the hydride may be bound to iron or ruthenium,[7] since we observed a weak and sharp line overlapped on the broad main peak.

Conclusion

The present study has shown that the ^{1}H NMR spectra of the mixed carbonyl hydride complexes $HMCo_3(CO)_{12-x}[P(OR)_3]_x$ (M=Fe or Ru, x=0—3) have resonances in the normal region as transition metal hydrides but the line widths are murh broader than ordinary hydride complexes. We consider that the line broadening is caused by intermediate length of the relaxation time T_1 of cobalt, namely the T_1 is too short to show the ^{1}H-^{59}Co scalar couplings but too long to decouple the interaction completely. The T_1 could be remarkably reduced by lowering the temperature of the measurements, by raising the viscosity of the solvents or by increasing the molecular volume. When the T_1 became short enough in these ways, the hydride resonance was effectively "decoupled" and showed much narrower lines. As the spectral changes of the hydride resonance upon lowering temperature are similar to the behavior of ^{31}P NMR spectra of **4** in which trimethyl phosphites are coordinated to each cobalt,[8,9] the hydride proton must be bonded also to cobalt. It is reasonable to assume that the hydride is bonded to the Co_3 face in solution just as in the solid state.[8,9] The similarity of the ^{1}H NMR spectra of other derivatives including **1** or **7** suggests that the hydride ligands in these complexes are bonded also to the Co_3 face.

We wish to thank Mr. Yoshio Terawaki for the measurements of ^{1}H and ^{31}P NMR spectra and JEOL for the ^{59}Co NMR spectra. We thank also Professors Hiizu Iwamura, Yoji Arata and Akira Yamasaki for helpful suggestions and discussions.

References

1) H. Nishihara, T. Mori, Y. Tsurita, K. Nakano, T. Saito, and Y. Sasaki, *J. Am. Chem. Soc.*, **104**, 4367 (1982).

2) P. Chini, L. Colli, and M. Perald, *Gazz. Chim. Ital.* **90**, 1005 (1960).

3) M. J. Mays and R. N. F. Simpson, *J. Chem. Soc., (A)*, **1968**, 1444.

4) J. Knight and M. J. Mays, *J. Chem. Soc., (A)*, **1970**, 711.

5) J. W. White and C. J. Wright, *J. Chem. Soc., (A)*, **1971**, 2843.

6) C. G. Cooke and M. J. Mays, *J. Chem. Soc., Dalton Trans.*, **1975**, 456.

7) G. Bor, G. Sbrignadello, and K. Noack, *Helv. Chim. Acta*, **58**, 815 (1975).

8) B. T. Huie, C. B. Knobler, and H. D. Kaesz, *J. Am. Chem. Soc.*, **100**, 3059 (1978).
9) R. G. Teller, R. D. Wilson, R. K. McMullan, T. F. Koezle, and R. Bau, *J. Am. Chem. Soc.*, **100**, 3071 (1978).
10) J. W. Lauher and K. Wald, *J. Am. Chem. Soc.*, **103**, 7648 (1981).
11) T. Saito, unpublished.
12) M. R. Churchill, J. Wormald, J. Knight, and M. J. Mays. *J. Chem. Soc., Chem. Commun.*, **1970**, 458.
13) G. Huttner and G. Lorentz, *Chem. Ber.*, **107**, 996 (1974).
14) G. Huttner and H. Lorentz, *Chem. Ber.*, **108**, 973 (1975).
15) R. D. Wilson and R. Bau, *J. Am. Chem. Soc.*, **98**, 4687 (1976).
16) C. R. Eady, B. F. G. Johnson, and J. Lewis, *J. Chem. Soc., Chem. Commun.*, **1976**, 302.
17) E. L. Muetterties, *Science*, **196**, 839 (1977).
18) M. Hidai, M. Orisaku, M. Ue, Y. Koyasu, T. Kodama, and Y. Uchida, *Organometallics*, **2**, 292 (1983).
19) H. A. Hodalli, D. F. Shriver, and C. A. Ammlung, *J. Am. Chem. Soc.*, **100**, 5239 (1978).
20) G. Fachinetti, *J. Chem. Soc., Chem. Commun.*, **1979**, 396.
21) K. H. Whitmire and D. F. Shriver, *J. Am. Chem. Soc.*, **103**, 6754 (1981).
22) T. Kruck and W. Lang, *Angew. Chem.*, **77**, 860 (1965).
23) A. Davidson and D. L. Reger, *J. Organomet. Chem.*, **23**, 491 (1970).
24) J. Muller and H. Dorner, *Angew. Chem. Int. Ed.*, **12**, 843 (1973).
25) W. Hieber and H. Duchatsh, *Chem. Ber.*, **98**, 2933 (1965).
26) W. Kruse and R. H. Atalla, *J. Chem. Soc., Chem. Commun.*, **1968**, 921.
27) E. A. C. Lucken, K. Noack, and D. F. Williams, *J. Chem. Soc., (A)*, **1967**, 148.
28) S. Aime, G. Gervasio, L. Milone, and E. Rosenberg, *Transition Met. Chem.*, **1**, 177 (1976).
29) S. Aime, R. Gobetto, D. Osella, L. Milone, G. E. Hawkes, and E. W. Randall, *J. Chem. Soc., Chem. Commun.*, **1983**, 794.
30) J. A. Pople, *Mol. Phys.*, **1**, 168 (1958).
31) M. Suzuki and R. Kubo, *Mol. Phys.*, **7**, 201 (1964).
32) A. Yamasaki, M. Kojima, Y. Koike, M. Hirota, and S. Fujiwara, *Bull. Univ. Electrocommun. (Tokyo)*, **28**, 299 (1978).
33) S. Aime, L. Milone, D. Osella, and A. Poli, *Inorg. Chim. Acta*, **30**, 45 (1978).
34) S. Aime, D. Osella, L. Milone, G. E. Hawkes, and E. W. Randall, *J. Am. Chem. Soc.*, **103**, 5920 (1981).

Synthesis of Hg(II) Complexes of Cysteine-Containing Oligopeptides

Norikazu UEYAMA, Michio NAKATA, and Akira NAKAMURA*
Department of Macromolecular Science, Faculty of Science, Osaka University, Toyonaka, Osaka 560
(Received September 17, 1984)

Tetrapeptides, Z-Cys-Ala-Ala-Cys-OMe (Z=benzyloxycarbonyl), Z-Cys-Val-Val-Cys-OMe, and Z-Cys-Gly-Pro-Cys-OMe, having Cys-X-Y-Cys sequences were synthesized by using an acetamidomethyl (Acm) protecting group. The Hg(II) complexes of these peptides, Hg_2Cl_2(Z-Cys-Ala-Ala-Cys-OMe) **1**.[1] Hg(Z-Cys-Ala-Ala-Cys-OMe) **2**, Hg_2Cl_2(Z-Cys-Gly-Pro-Cys-OMe) **3**, Hg(Z-Cys-Val-Val-Cys-OMe) **4**, and Hg_2Cl_2(Z-Cys-Ala-Cys-OMe) **5** were synthesized by the reaction of the S(Acm) protecting peptides and $HgCl_2$ in *N,N*-dimethylformamide. Two Raman bands due to Cl-Hg-S of **1**, **3**, or **5** were observed at 314, 281, or 276 cm^{-1} in solid, whereas a single band due to S-Hg-S was found at 326 cm^{-1} for **2** or 327 cm^{-1} for **4**, in solid.

The tetrapeptide sequences of -Cys-X-Y-Cys- (X, Y=amino acid residues) serving as a macro-ring chelate with the cysteinyl thiolate coordinations are frequently found for metal binding sites of many of metal thiolate proteins: for example, Fe proteins; Cys(6)-Thr-Val-Cys(9) and Cys(39)-Pro-Leu-Cys(42) for *Clostridium pasteurianum* rubredoxin,[2] Cys(44)-Ser-Ser-Cys-(47) for *Spirulina plantesis* ferredoxin,[3] Cys(8)-Ile-Ala-Cys(11)- Gly-Ala-Cys(14) and Cys(35)-Ile-Asp-Cys(38)-Gly-Ala-Cys(41) for *Peptococcus aerogenes* ferredoxin:[4] Zn proteins; Cys(97)-Gly-Lys-Cys(100)-Arg-Val-Cys-(103) for horse liver alcohol dehydrogenase (E-chain),[5] Cys(137)-Lys-Tyr-Cys(140) for *Escherichia coli* aspartate carbamoyltransferase:[6] metallothioneins: Cys(21)-Lys-Gln-Cys(24), Cys(26)-Ala-Ser-Cys(29), and Cys(41)-Ala-Lys-Cys(44) for equine renal metallothionein 1B.[7] In such cases, conformational restriction due to the steric effects of the chelating tetrapeptides caused by side chains of the two amino acid residues, X and Y, interposed between the two cysteine residues definitively plays crucial roles on the stabilities of the chelate rings, the determination of geometries around a metal ion, and the revelation of enzymatic activities.

In order to elucidate the side chain conformational effects discussed above, we have been studying various metal complexes such as Pd(II)[8,9], Fe(III),[10] Co(II),[11] and Mo(IV, V)[12] of cysteine-containing tetrapeptide (Z-Cys-X-Y-Cys-OMe) in the relevance to the metal thiolate proteins. We were also interested in the formation of Hg(II) complexes of Z-Cys-Val-Val-Cys-OMe possessing more bulky side chains, Z-Cys-Gly-Pro-Cys-OMe having a restricted conformation with a Gly-Pro sequence,[13] and tripeptide, Z-Cys-Ala-Cys-OMe which contains only one amino acid residue between two cysteinyl residues. In biological systems with mercury, Hg(II) complexation with cysteine thiolate is involved in toxicity[14] and detoxicity. For example, mercuric reductase contains two active thiols which are proposed to bind Hg(II) ion to give RS-Hg-SR.[15] In this paper we describe detailed procedures for the syntheses of the cysteine-containing oligopeptides, Z-Cys-X-Y-Cys-OMe (X, Y=Ala; X, Y=Val; X=Gly and Y=Pro) and Z-Cys-Ala-Cys-OMe, and for the syntheses of Hg(II) complexes of the cysteine-containing peptides. We synthesized two types of Hg(II)/Cys-containing peptide complexes such as RS-Hg-SR and RS-Hg-Cl. The bulkiness and hydrophobicity around Cys residue may control the formation of either RS-Hg-SR or RS-Hg-Cl species.

Experimental

Materials. Glycine, L-alanine, L-valine, L-proline, L-cysteine hydrochloride, benzyloxycarbonyl chloride (Z-Cl), anhydrous hydrogen bromide in acetic acid (25%), DCC, and *N*-hydroxysuccinimide (HOSu) were purchased from Protein Research Foundation. Isobutyl chloroformate was purchased from Merck-Schuchardt and used without further purification. 2-(*t*-Butoxycarbonylthio)-4,6-dimethylpyrimidine (*t*-Boc-S) was obtained from Mitsubishi Chemical Industries Co., Ltd. Tetrahydrofuran (THF) and dioxane were distilled after refluxing over sodium. Acetonitrile was refluxed over calcium hydride and distilled. Purification of *N,N*-dimethylformamide (DMF) and triethylamine were purified by distillation. All other reagents used were of commercial grade.

Peptide Syntheses. Benzyloxycarbonyl derivatives of L-alanine, L-valine, and L-proline were prepared by the same procedures with Z-Cl cited in the literature.[16] *t*-Butoxycarbonyl derivative of L-alanine was prepared according to the literature method using *t*-Boc-S.[17] Glycine methyl ester hydrochloride was also prepared by the analogous method to a literature using thionyl chloride.[18] HCl·H-Cys(Acm)-OH was prepared by the modified method to a literature.[19]

1. Synthesis of Z-Cys(Acm)-Ala-Ala-Cys(Acm)-OMe Z-Cys(Acm)-OH. Benzyloxycarbonyl chloride (100 cm^3, 0.5 mol) and 4M NaOH solution (375 cm^3 (1 M=1 mol dm^{-3})) were added alternately to a solution of HCl·H-Cys(Acm)-OH (114.4 g, 0.5 mol) in 4 M NaOH solution (250 cm^3) over about 1.5 h period in an ice-cooled bath, and stirred for 3 h at room temperature. The product was obtained as an oil, which was crystallized on standing the chloroform solution, and recrystallized from ethyl acetate–ether: yield, 70 g (44%); mp 106—107 °C (dec); $[\alpha]_D$ −40.7° (*c* 0.905, methanol). Anal. Calcd for $C_{14}H_{18}N_2O_5S$: C, 51.52; H, 5.56; N, 8.58. Found: C, 51.50; H, 5.63; N, 8.40.

Z-Ala-Cys-(Acm)-OMe. A solution of Z-Ala-OH (45.0 g, 0.20 mol) and triethylamine (28.8 cm^3, 0.20 mol) in THF (200 cm^3) was cooled to −15 °C. To this solution was added iso-Boc-Cl (26.0 cm^3, 0.20 mol) with stirring at −15 °C. After 15 min, a solution of HCl·H-Cys(Acm)-OMe (60.0 g, 0.20 mol) and triethylamine (28.0 cm^3, 0.20 mol) in DMF (50 cm^3) was added with stirring at −15 °C. The reaction mixture was stirred for 1 h with cooling and then overnight at room temperature. The solution was concentrated under

reduced pressure. About 500 cm³ of water was added to the residue and the resulting white solid was collected on a glass filter, and washed sequentially with water, 4% $NaHCO_3$ aqueous solution, water, 2% HCl aqueous solution, and water. The product was dried over P_2O_5 *in vacuo*: yield, 50 g (61%); mp 143—145 °C (dec); $[\alpha]_D$ −21.7° (*c* 1.07, DMF). Anal. Calcd for $C_{18}H_{25}N_3O_6S$: C, 52.54; H, 6.12; N, 10.21. Found: C, 52.53; H, 6.12; N, 10.15.

Z-Ala-Ala-Cys(Acm)-OMe. To Z-Ala-Cys(Acm)-OMe (25 g, 0.06 mol) was added 25% HBr solution in acetic acid (50 cm³) at 0 °C. The solution was allowed to stand for 1.5 h with stirring at room temperature. Ether was added to this solution to precipitate HBr·H-Ala-Cys(Acm)-OMe. The supernatant was decanted off and the residue was washed with ether several times. The dipeptide hydrobromide salt obtained was dried over KOH *in vacuo*. To a solution of Z-Ala-OH (13.5 g, 0.06 mol) and triethylamine (8.3 cm³, 0.06 mol) in THF (200 cm³) was added iso-Boc-Cl (7.7 cm³, 0.06 mol) at −15 °C. After 15 min, a solution of HBr·H-Ala-Cys(Acm)-OMe and triethylamine (8.3 cm³, 0.06 mol) in DMF (30 cm³) was added with stirring at −15 °C. Following treatments were same as the syntheses of Z-Ala-Cys(Acm)-OMe: yield 10.5 g (36%); mp 183—186 °C (dec); $[\alpha]_D$ −32.9° (*c* 1.07, DMF). Anal. Calcd for $C_{21}H_{30}N_4O_7S$: C, 52.27; H, 6.27; N, 11.61. Found: C, 52.26; H, 6.32; N, 11.61.

Z-Cys(Acm)-Ala-Ala-Cys(Acm)-OMe. In order to remove the Z-group, Z-Ala-Ala-Cys(Acm)-OMe (2.3 g, 5 mmol) was treated with about 40 cm³ of 25% HBr/acetic acid. The resulting tripeptide hydrobromide salt, HBr·H-Ala-Ala-Cys(Acm)-OMe, was dried over KOH *in vacuo*. To a solution of Z-Cys(Acm)-OH (1.5 g, 5 mmol) and triethylamine (0.7 cm³, 5 mmol) in THF (100 cm³) was added iso-Boc-Cl (0.6 cm³, 5 mmol) at −15 °C. After 15 min, a solution of HBr·H-Ala-Ala-Cys(Acm)-OMe and triethylamine (0.7 cm³, 5 mmol) in DMF (20 cm³) was added with stirring at −15 °C. The reaction mixture was stirred for 1 h with cooling and stood overnight at room temperature. Subsequent work-up was done in the same manner as described for Z-Ala-Cys(Acm)-OMe: yield 1.2 g (36%); mp 210—213 °C (dec); $[\alpha]_D$ −33.6° (*c* 0.667, DMF). Anal. Calcd for $C_{27}H_{40}N_6O_9S_2$: C, 49.38; H, 6.14; N, 12.80. Found: C, 49.17; H, 6.15; N, 12.09.

t-Boc-Ala-Cys(Acm)-OMe. To a solution of *t*-Boc-Ala-OH (34.1 g, 0.18 mol) and triethylamine (24.8 cm³, 0.18 mol) in THF (200 cm³) was added iso-Boc-Cl (23.1 cm³, 0.18 mol) with stirring at −15 °C. After 15 min, an ice-cooled solution of HCl·H-Cys(Acm)-OMe (43.7 g, 0.18 mol) and triethylamine (24.8 cm³, 0.18 mol) in DMF (40 cm³) and chloroform (100 cm³) was added to the mixed anhydride solution with stirring at −15 °C. The reaction mixture was stirred for 1 h at 15 °C and overnight at room temperature. After evaporation of the solvent under reduced pressure, the addition of about 500 ml of saturated NaCl aqueous solution to the residue caused the separation of an oily material, which was extracted with ethyl acetate. The organic layer was washed sequentially with sat. NaCl aq, 4% $NaHCO_3$ aq solution saturated with NaCl, sat. NaCl aq, 10% citric acid aq solution saturated with NaCl, and sat. NaCl aq solution and dried over anhydrous Na_2SO_4. After the desiccant was filtered off, the solvent was removed under reduced pressure and ether was added to the residue to result in crystallization. The product was collected on a glass filter, washed with ether, and dried over silica gel *in vacuo*: yield, 32 g (47%); mp 85—86 °C (dec); $[\alpha]_D$ −48.7° (*c* 0.371, DMF). Anal. Calcd for $C_{15}H_{27}N_3O_6S$: C, 47.73; H, 7.21; N, 11.13. Found: C, 47.79; H, 7.20; N, 10.16.

t-Boc-Ala-Ala-Cys(Acm)-OMe. Hydrogen chloride gas was introduced into an ice-cooled solution of *t*-Boc-Ala-Cys(Acm)-OMe (20.4 g, 0.054 mol) in dioxane (150 cm³) for about 20 min to result in a white precipitate of HCl·H-Ala-Cys(Acm)-OMe. The reaction mixture was allowed to stand for about 30 min. After an addition of ether, the supernatant was decanted off. The dipeptide hydrochloride salt was washed with ether thoroughly and dried over KOH *in vacuo*. To a solution of *t*-Boc-Ala-OH (10.2 g, 0.054 mol) and triethylamine (7.5 cm³, 0.054 mol) with stirring at −15 °C for about 15 min. To this solution, an ice-cooled solution of the HCl·H-Ala-Cys(Acm)-OMe prepared previously and triethylamine (7.5 cm³, 0.054 mol) in DMF (10 cm³) and chloroform (100 cm³) was added with stirring under the continuous cooling. The reaction mixture was stirred at −15 °C for 1 h and at room temperature overnight. The solvent was removed under reduced pressure and about 500 cm³ of sat. NaCl aq solution was added to the residue. An oily material which was separated on the addition of the NaCl solution was extracted with ethyl acetate. Subsequent procedures were the same as described for *t*-Boc-Ala-Cys(Acm)-OMe: yield 4.2 g (17%); mp 144—145 °C (dec); $[\alpha]_D$ −34.1° (*c* 0.113, DMF). Anal. Calcd. for $C_{18}H_{32}N_4O_7S$: C, 48.20; H, 7.19; N, 12.49. Found: C, 47.23; H, 7.08; N, 12.07.

Z-Cys(Acm)-Ala-Ala-Cys(Acm)-OMe. Isobutyl chloroformate (0.9 cm³, 7 mmol) was added to a solution of Z-Cys(Acm)-OH (2.2 g, 7 mmol) and triethylamine (1.0 cm³, 7 mmol) in THF (10 cm³) with stirring at −15 °C. After 15 min, a solution of HCl·H-Ala-Ala-Cys(Acm)-OMe, which was prepared by a treatment of *t*-Boc-Ala-Ala-Cys(Acm)-OMe (3.1 g, 7 mmol) with HCl gas in dioxane (30 cm³), and triethylamine (1.0 cm³, 7 mmol) in a mixed solvent of DMF (5 cm³) and chloroform (10 cm³) was added to the above mixed anhydride solution at −15 °C with stirring. Subsequent treatments were the same as described for Z-Ala-Ala-Cys-(Acm)-OMe: yield 2.9 g (23%); mp 205—208 °C (dec); $[\alpha]_D$ −30.7° (*c* 0.200, DMF). Anal. Calcd for $C_{27}H_{40}N_6O_9S_2$: C, 49.38; H, 6.14; N, 12.80. Found: C, 48.88; H, 6.07; N, 12.41.

2. Synthesis of Z-Cys(Acm)-Ala-Cys(Acm)-OMe. Dipeptide, Z-Ala-Cys(Acm)-OMe (3.8 g, 9 mmol), was treated with 25% HBr/acetic acid (40 cm³) to result in formation of HBr·H-Ala-Cys(Acm)-OMe. A DMF solution (30 cm³) of the free-base dipeptide prepared from the hydrogen bromide salt and triethylamine (1.3 cm³, 9 mmol) was added to a THF solution (100 cm³) of a mixed anhydride prepared from Z-Cys(Acm)-OH (3.0 g, 9 mmol), triethylamine (1.3 cm³, 9 mmol), and iso-Boc-Cl (1.2 cm³, 9 mmol) at −15 °C. Usual work-up as described for the synthesis of Z-Cys(Acm)-Ala-Ala-Cys(Acm)-OMe gave a tripeptide, Z-Cys(Acm)-Ala-Cys(Acm)-OMe: yield 1.0 g (19%); mp 209—212 °C (dec); $[\alpha]_D$ −34.8° (*c* 1.07, DMF). Anal. Calcd for $C_{24}H_{35}N_5O_8S_2$: C, 49.22; H, 6.02; N, 11.96. Found: C, 48.43; H, 5.92; N, 11.43.

iso-Butyl chloroformate (1.0 cm³, 8 mmol) was added to a solution of Z-Cys(Acm)-OH (2.6 g, 8 mmol) and triethylamine (1.1 cm³, 8 mmol) in THF (80 cm³) with stirring at −15 °C. After 15 min, a solution of HCl·H-Ala-Cys(Acm)-OMe, which was prepared by a HCl treatment of *t*-Boc-Ala-Cys(Acm)-OMe (3.0 g, 8 mmol) in dioxane (50 cm³) and triethylamine (1.1 cm³, 8 mmol) in DMF (10 cm³) and chloroform (20 cm³), was added to the mixed anhydride solu-

tion at −15°C with stirring. After the same treatments as described above, Z-Cys(Acm)-Ala-Cys(Acm)-OMe was obtained: yield 4.0 g (85%); mp 211—212°C (dec); $[\alpha]_D$ −30.6° (*c* 0.197, DMF). Anal. Calcd for $C_{24}H_{35}N_5O_8S_2$: C, 49.22; H, 6.02; N, 11.96. Found: C, 48.12; H, 5.86; N, 11.44.

3. Synthesis of Z-Cys(Acm)-Val-Val-Cys(Acm)-OMe. *Z-Val-Cys(Acm)-OMe*: The peptide was prepared from Z-Val-OH and H-Cys(Acm)-OMe by the same procedure as mentioned for Z-Ala-Cys(Acm)-OMe. The crude materials were recrystallized from methanol. Yield 45%; mp 164—166°C; $[\alpha]_D$ −27.0° (*c* 0.97, DMF). Anal. Calcd for $C_{20}H_{29}N_3O_6S$: C, 54.65; H, 6.65; N, 9.56. Found: C, 54.58; H, 6.71; N, 9.53.

Z-Val-Val-Cys(Acm)-OMe: The peptide was prepared from Z-Val-OH and H-Val-Cys(Acm)-OMe by the same method mentioned above. The crude product was recrystallized from methanol. Yield 81%; mp 231—236°C (dec); $[\alpha]_D$ −25.2° (*c* 0.95, DMF). Anal. Calcd for $C_{25}H_{38}N_4O_7S$: C, 55.74; H, 7.11; N, 10.40. Found: C, 55.36; H, 7.09; N, 10.04.

Z-Cys(Acm)-Val-Val-Cys(Acm)-OMe: The peptide was synthesized from Z-Cys(Acm)-OH and H-Val-Val-Cys(Acm)-OMe by the same procedure for Z-Cys(Acm)-Ala-Ala-Cys(Acm)-OMe. The crude product was washed with ether and dried over P_2O_5 *in vacuo* and recrystallized from methanol. Yield 31%; mp 221—224°C (dec); $[\alpha]_D$ −29.3° (*c* 0.98, DMF). Anal. Calcd for $C_{31}H_{48}N_6O_9S_2$: C, 52.22; H, 6.80; N, 11.79. Found: C, 51.45; H, 6.73; N, 11.21.

4. Synthesis of Z-Cys(Acm)-Gly-Pro-Cys(Acm)-OMe. Z-Cys(Acm)-Gly-OMe was prepared from Z-Cys(Acm)-OH and H-Gly-OMe with the mixed anhydride method mentioned above. Z-Cys(Acm)-Gly-OH was obtained by hydrolysis with NaOH in methanol/dioxane. Z-Pro-Cys(Acm)-OMe was prepared from Z-Pro-OH and H-Cys(Acm)-OMe by the same procedure for Z-Ala-Cys(Acm)-OMe. Synthesis of HBr·H-Pro-Cys(Acm)-OMe was done by to the same method described for HBr·H-Ala-Cys(Acm)-OMe.

To the reaction mixture containing 2.5 g of Z-Cys(Acm)-Gly-OH, HBr·H-Pro-Cys(Acm)-OMe, and 1.1 cm³ of triethylamine in 20 cm³ of DMF was added 0.8 g of HOSu and, then, 1.5 g of DCC at 0°C. The reaction mixture was stirred for 1 h with cooling and overnight at room temperature. The solution was concentrated under reduced pressure. The residue was dissolved in chloroform and remaining *N,N'*-dicyclohexylurea was filtered off. The filtrate was washed sequentially with water, 2% HCl aq, water, 4% $NaHCO_3$ aq, and water, and dried over anhydrous Na_2SO_4. After removal of the solvent, Z-Cys(Acm)-Gly-Pro-Cys(Acm)-OMe was obtained as a white solid. Yield, 3.3 g (63%); mp 104°C; $[\alpha]_D$ −93.6° (*c* 0.50, methanol). Anal. Calcd for $C_{28}H_{40}O_9N_6S_2$: C, 50.25; H, 6.03; N, 9.58. Found: C, 50.10; H, 6.07; N, 9.46.

5. Syntheses of Hg(II)/Cys-containing Peptide Complexes. *HgCl(Z-Ala-cys-OMe).* A solution containing 100 mg of Z-Ala-Cys(Acm)-OMe and 65 mg of $HgCl_2$ in 3 cm³ of Me_2SO was stirred for several hours. A quick addition of 30 ml of water to the Me_2SO solution with cooling resulted in precipitation of a white powder, which was collected on a glass filter, washed with sat. NaCl aq and water, and dried over P_2O_5 *in vacuo*. Yield, 110 mg.

In order to secure a complete removal of Acm-group, it is preferable to use two equiv of $HgCl_2$ for an equiv of Acm-group. Mp 91—96°C. Anal. Calcd for $C_{15}H_{10}N_2SHgCl$: C, 31.31; H, 3.33; N, 4.87. Found: C, 31.23; H, 3.40; N, 4.97.

Hg_2Cl_2(Z-cys-Ala-Ala-cys-OMe) 1. To a solution of Z-Cys(Acm)-Ala-Ala-Cys(Acm)-OMe (200 mg, 0.3 mmol) in 10 cm³ of DMF was added 500 mg (1.0 mmol) of $HgCl_2$ during stirring at room temperature. After 5 h, 5 cm³ of NaCl-saturated water and 5 cm³ of methanol were added. Another addition of water (25 cm³) resulted in precipitation of white solids, which were collected with filtration, washed with 10% NaCl aq solution and with two portions of methanol, and dried over P_2O_5 *in vacuo*. Yield 190 mg. Anal. Calcd for $C_{21}H_{28}N_4O_7S_2Hg_2Cl_2$: C, 25.53; H, 2.87; N, 5.72. Found: C, 24.38; H, 2.92; N, 5.51.

Hg(Z-cys-Ala-Ala-cys-OMe) 2. The complex was synthesized from $Hg(OCOCH_3)_2$ (320 mg, 1.0 mmol) and Z-Cys(Acm)-Ala-Ala-Cys(Acm)-OMe (200 mg, 0.3 mmol) in DMF (10 cm³) by almost the same procedure employed for the synthesis of **1**. Anal. Calcd for $C_{21}H_{28}N_4O_7S_2Hg$: C, 35.23; H, 3.96; N, 7.90. Found: C, 37.11; H, 4.12; N, 7.95.

Hg_2Cl_2(Z-cys-Gly-Pro-cys-OMe) 3. The complex was synthesized by the same method described above. Yield 85%. Anal. Calcd for $C_{22}H_{28}N_4O_7S_2Hg_2Cl_2$: C, 26.50; H, 2.83; N, 5.65. Found: C, 24.13; H, 2.88; N, 5.26.

Hg(Z-Cys-Val-Val-Cys-OMe) 4. To a solution of Z-Cys(Acm)-Val-Val-Cys(Acm)-OMe (300 mg, 0.4 mmol) in 20 cm³ of DMF, 300 mg (1.1 mmol) of $HgCl_2$ was added at room temperature. White solids precipitated gradually. After 8 h, the precipitate was collected with filtration, washed with DMF, NaCl-saturated aq solution, and two portions of methanol. The product was dried over P_2O_5 *in vacuo*. Yield 76%. Anal. Calcd for $C_{25}H_{36}N_4O_7S_2Hg$: C, 39.02; H, 4.72; N, 7.32. Found: C, 42.00; H, 5.28; N, 8.03.

Hg_2Cl_2(Z-cys-Ala-cys-OMe) 5. The complex was synthesized by the same method as described for **4**. Anal. Calcd for $C_{18}H_{23}O_6N_3S_2Hg_2Cl_2$: C, 23.66; H, 2.54; N, 4.62. Found: C, 24.61; H, 2.72; N, 4.11.

Physical Measurements. Raman spectra of Hg(II)/Cys-containing peptide complexes in solid were taken on a Jasco R-800 spectrometer with exciting lines at 488.0 and 514.5 nm. Optical rotations were measured with an automatic polarimeter JASCO model DIP-4. Measurements of ^{1}H-NMR spectra were carried out on a Varian XL-100 spectrometer at 100 MHz at *ca.* 30°C. Purities of the synthetic peptides were checked by high-performance liquid chromatography on a WATERS model 6000 A and U6K equipped with WATERS μBondapak C18 column and detected at 254 nm with a Shimadzu spectrophotomeric detector SPD-1. An eluent system used was methanol/H_2O (2/1). The products were also characterized by ^{1}H-NMR spectra. Melting points were uncorrected.

Results and Discussion

Peptide Syntheses. The Acm-group has some distinctive advantages as the protecting group for cysteine thiolates especially in the construction of metallothiolate protein model complexes. It is cleaved in milder conditions than required for benzyl or *p*-methoxybenzyl derivative. Substitution of the Acm-group with Hg(II) ion and the subsequent removal of the Hg(II) ion with H_2S gas readily give SH-free peptides. Undesirable reducing reagents, such as 2-mercaptoethanol or dithiothreitol, are unnecessary

for the construction of metal complexes, *e.g.* iron-sulfur protein model complexes. An active site of metalloproteins has been known to be surrounded by hydrophobic environments particularly when they function as electron mediators.[20] Therefore, an investigation on the Hg(II)/Cys-containing peptide complexes should be carried out in various organic solvents because hydrophobic amino acid residues are involved.

In order to ensure the coordination of the cysteine thiolate to metal ion founds in metalloproteins, terminal amino and carboxyl groups must be protected by Z- or -OMe since Hg(II) readily coordinates to organic function groups such as COO^- and NH_2 groups as established by the X-ray analysis of $[MeHg]_2[SCMe_2CH(NH_2)CO_2]$.[21]

Reaction of Cys(Acm) Group with Hg^{2+}. Veber *et al.* reported that the Acm-group was deprotected in an aqueous solution at pH 4.0 by excess mercury(II) acetate.[22] A reaction between the (S-Acm)-peptide and $HgCl_2$ was performed in dimethyl sulfoxide (Me_2SO) because of insolubility of our fully protected peptides in water. An addition of water, which is crucial for the cleavage of the S-Acm bond with $HgCl_2$, resulted in precipitation of (S-Hg^{II}Cl)-peptide. Figure 1 shows the ^1H NMR of a mixture of Z-Ala-Cys(Acm)-OMe and $HgCl_2$ in Me_2SO. The spectrum (a) is ^1H-NMR spectrum of Z-Ala-Cys(Acm)-OMe in Me_2SO-d_6 showing cysteinyl C_β methylene protons and acetyl-(Acm) signals at 2.95 and 1.84 ppm, respectively. An

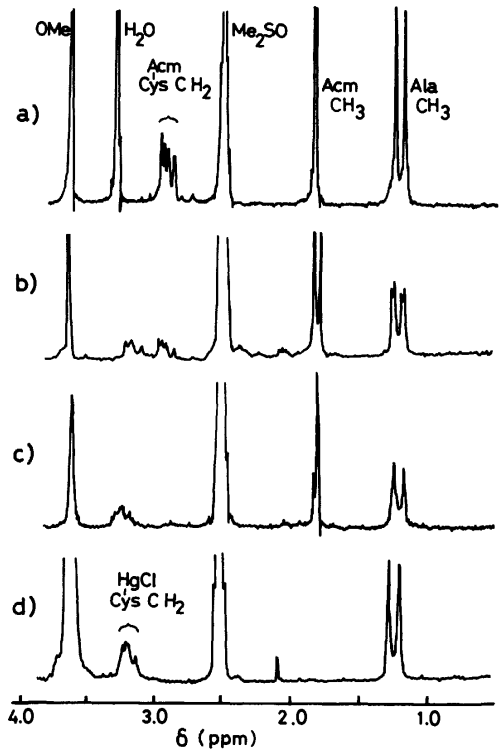

Fig. 1. a): H-NMR spectra of Z-Ala-Cys(Acm)-OMe (30 mg) in Me_2SO-d_6 (0.5 cm^3), b): (a) plus $HgCl_2$ (27 mg) in Me_2SO-d_6, c): (b) plus D_2O (0.2 cm^3), d): HgCl(Z-Ala-cys-OMe) (33 mg) in Me_2SO-d_6.

addition of $HgCl_2$ to the Z-Ala-Cys(Acm)-OMe solution resulted in an appearance of new signals at 3.17 and 1.80 ppm as shown in spectrum (b). The results suggests a direct interaction between the Hg(II) ion and the S atom. A subsequent addition of D_2O to the reaction mixture containing Z-Ala-Cys(Acm)-OMe and $HgCl_2$ gave spectrum (c) with disappearance of signals of the cysteine C_β methylene at 2.95 ppm and Acm acetyl at 1.84 ppm. The signal at 3.26 ppm coincided with cysteine C_β methylene signals of HgCl-(Z-Ala-cys-OMe) at 3.20 ppm represented by spectrum (d). These facts indicate that the addition of water forces the quantitative cleavage of the S-Acm bond by Hg(II) ion.

Two types of Hg(II) complexes were synthesized from the reaction between $HgCl_2$ and Cys-containing peptides. In the case of Z-Cys(Acm)-Val-Val-Cys(Acm)-OMe and Z-Cys(Acm)-Ala-Cys(Acm)-OMe in DMF, **4** and **5** having polymeric structures are obtainable without the addition of water. On the other hand, **1** and **3** were obtained with the addition of water to a DMF solution of $HgCl_2$ and the corresponding peptides. Such a mixed solvent system provides acidic conditions by the hydrolysis of $HgCl_2$ with the addition of water. The results indicate that under the acidic conditions the formation of HgCl(SR) (SR=Cys-containing peptide) predominates, whereas under neutral conditions, where competition of the formation between HgCl(SR) and $Hg(SR)_2$ occurs depending upon solubility. Actually, **2** was synthesized from the corresponding peptide and $Hg(OCOCH_3)_2$ in a weakly acidic aq DMF. The similar two types of the Hg(II)/cysteine complexes has been found to be formed in an aqueous solution by Hay and Porter.[23]

Raman Spectra of Hg(II)/Cys-containing Peptide Complexes. The two types of the complexes, *i.e.* Hg_2Cl_2(peptide)$_2$ and Hg(peptide)$_2$ was examined by their Raman spectra. Figure 2 shows the Raman spectra of Hg_2Cl_2(Z-cys-Ala-Ala-cys-OMe), Hg(Z-cys-Ala-Ala-cys-OMe), Hg_2Cl_2(Z-cys-Gly-Pro- cys-OMe), Hg(Z-cys-Val-Val-cys-OMe), and Hg_2Cl_2(Z-cys-Ala-cys-OMe) in solid state. The intensities of strong bands in the region of 280—320 cm^{-1} were proportional to that of a band at 1003 cm^{-1} due to phenyl of Z group.

The Hg_2Cl_2(peptide) complexes exhibited two strong bands at 281 and 314 cm^{-1}, whereas Hg(peptide) type provided only one strong band at 313—327 cm^{-1}. One strong Raman band is expected for linear S-Hg-S bonding ($D_{\infty h}$ symmetry). Two Raman bands should be observed for linear S-Hg-Cl structure ($C_{\infty v}$ symmetry). Therefore, a strong band at 327 cm^{-1} for Hg(Z-cys-Ala-Ala-cys-OMe) or Hg(Z-cys-Val-Val-cys-OMe) is assignable to ν(Hg-S). The ν(Hg-Cl) band of $HgCl_2$ was observed at 312 cm^{-1} in solid state, although ν(Hg-Cl) was reported to be observed at 348 cm^{-1} in inert gas matrices.[24] Tentatively two bands at 318 and 281 cm^{-1} for Hg_2Cl_2(Z-cys-Ala-Ala-cys-

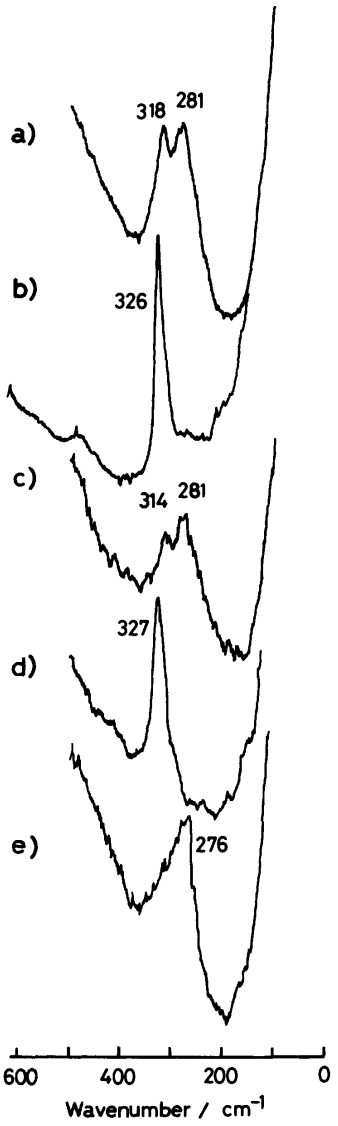

Fig. 2. Raman spectra of a): Hg_2Cl_2(Z-cys-Ala-Ala-cys-OMe), b): Hg(Z-cys-Ala-Ala-cys-OMe), c): Hg_2Cl_2(Z-cys-Gly-Pro-cys-OMe), d): Hg(Z-cys-Val-Val-cys-OMe), and e): Hg_2Cl_2(Z-cys-Ala-cys-OMe) in solid.

OMe) and at 314 and 281 cm^{-1} for Hg_2Cl_2(Z-cys-Gly-Pro-cys-OMe) are assigned to ν(Hg-S) and ν(Hg-Cl) by considering their masses. Two Raman bands have been observed at 349 and 325 cm^{-1} for PhHg(H_2-cys-OH)[25] and MeHg(H_2-cys-OH),[26] respectively.

It is interesting that one ν(Hg-S) band of Hg_2Cl_2-(Z-cys-Ala-cys-OMe) was observed at 276 cm^{-1}. The low frequency seemed unusual because the other S-Hg-Cl type complexes exhibit a band at 281 cm^{-1}. Similar low frequency bands were reported by Carty *et al.* for 3-coordinated Hg(II) in $[HgCl_2]_2[SCMe_2CH(NH_3)COOH]\cdot 2H_2O$.[27] The shift of ν(Hg-S) of Hg_2Cl_2(Z-cys-Ala-cys-OMe) may be attributed to the S-Hg-Cl bond weaken by the steric hindrance of two crowded Hg-S(cys) groups.

As described above, the Raman spectroscopy may be utilized as an important diagnostic tool for the characterization of cysteine-containing peptides. The present results will contribute to the investigation of Hg(II)-binding thiol sites surrounded by hydrophobic environments in proteins or burried in membrane. Reductive elimination of metallic mercury from Hg(Z-cys-X-Y-cys-OMe) complexes is important for a model reaction of mercuric reductase proposed to contain RS-Hg-SR in the active site. Further investigation on this point is in progress.

References

1) Small letter cys refers to a cysteinyl residue coordinating to a metal ion.
2) W. H. Orme-Johnson, *Annu. Rev. Biochem.*, **42**, 159 (1973).
3) K. K. Rao and H. Matsubara, *Biochem. Biophys. Res. Commun.*, **38**, 500 (1970).
4) H. Matsubara, R. M. Sasaki, D. K. Tsuchiya, and M. C. W. Evans, *J. Biol. Chem.*, **245**, 2121 (1970).
5) H. Ekulund, B. Nordstrom, E. Zeppezauer, G. Söderlung, I. Ohlsson, T. Boiwe, B.-O. Soderberg, O. Tapia, C.-I. Bränden, and Å. Åkeson, *J. Mol. Biol.*, **102**, 27 (1976).
6) H. L. Monaco, J. L. Crawford, and W. N. Lipscomb, *Proc. Natl. Acad. Sci. U.S.A*, **75**, 5276 (1978).
7) Y. Kojima, C. Berger, B. L. Vallee, and J. H. R. Kägi, *Proc. Natl. Acad. Sci., U.S.A*, **73**, 3413 (1976).
8) N. Ueyama, M. Nakata, and A. Nakamura, *Inorg. Chim. Acta*, **55**, L61 (1981).
9) N. Ueyama, K. Sasaki, M. Nakata, and A. Nakamura, *Bull. Chem. Soc. Jpn.*, **55**, 2364 (1982).
10) a) G. Christou, B. Ridge, and H. N. Rydon, *J. Chem. Soc. Chem. Commun.*, **1977**, 20; b) N. Ueyama, M. Nakata, and A. Nakamura, *Bull. Chem. Soc. Jpn.*, **54**, 1727 (1981).
11) M. Nakata, N. Ueyama, A. Nakamura, T. Nozawa, and M. Hatano, *Inorg. Chem.*, **22**, 3028 (1983).
12) a) A. Balasubramaniam and D. Coucouvanis, *Inorg. Chim. Acta*, **66**, L65 (1982); b) N. Ueyama, M. Nakata, A. Nakamura, M. Kamata, and S. Otsuka, *Inorg. Chim. Acta*, **80**, 207 (1983).
13) A Holmgren, B.-O. Soderberg, H. Ekulund, and C.-I. Branden, *Proc. Natl. Acad. Sci. U.S.A*, **72**, 2305 (1975).
14) a) L. Dunlap, *Chem. Eng. News*, **1971**, 22; b) J. M. Wood, *Adv. Environmental Sci. Technol.*, **2**, 39 (1971).
15) B. Fox and C. T. Walsh, *J. Biol. Chem.*, **257**, 2498 (1982).
16) M. Bergmann and L. Zervas, *Chem. Ber.*, **65**, 1192 (1932).
17) T. Nagasawa, K. Kuroiwa, K. Narita, and Y. Isowa, *Bull. Chem. Soc. Jpn.*, **46**, 1269 (1973).
18) M. Brenner and W. Huber, *Helv. Chim. Acta*, **36**, 1109 (1953).
19) D. F. Veber, J. D. Milkowski, R. G. Denkewalter, and R. Hirschmann, *Tetrhedron Lett.*, **1968**, 3057.
20) E. T. Adman, *Biochim. Biophys. Acta*, **549**, 107 (1979).
21) Y. S. Wong, N. J. Taylor, P. C. Chieh, and A. J. Carty, *J. Chem. Soc., Chem. Commun.*, **1974**, 625.
22) D. F. Veber, J. D. Milkowski, S. L. Varga, R. G. Denkewalter, and R. Hirshmann, *J. Am. Chem. Soc.*, **94**, 5456 (1972).
23) R. W. Hay and L. J. Poter, *Aust. J. Chem.*, **20**, 675 (1967).

24) A. Loewenschuss, A. Ron, and O. Schnepp, *J. Chem. Phys.*, **49**, 272 (1968); **50**, 2502 (1969).
25) A. J. Carty and R. Kishimoto, *Aust. J. Chem.*, **30**, 669 (1977).
26) N. J. Taylor, Y. S. Wong, P. C. Chieh, and A. J. Carty, *J. Chem. Soc., Dalton Trans.*, **1975**, 438.
27) A. J. Carty and N. J. Taylor, *J. Chem. Soc. Chem. Commun.*, **1976**, 214.

Synthesis of DMSO-$SbCl_5$ (1:1) Complex and Its Oxidizing Action toward Alcohols

Jiro YAMAMOTO,* Satoshi ITO, Takashi TSUBOI, Toshiaki TSUBOI, and Kumiko TSUKIHARA
Department of Industrial Chemistry, Faculty of Engineering, Tottori University, Koyama-cho, Tottori-shi 680
(Received May 21, 1984)

From an equimolar mixture of DMSO and $SbCl_5$ in carbon tetrachloride, a DMSO-$SbCl_5$(1:1) complex (**1**) was formed as a white precipitate in a quantitative yield. The structure of **1** was determined by X-ray crystallographic analysis. Butyraldehydes, para-substituted benzaldehydes and benzils were obtained by the oxidation of butylalcohols, para-substituted benzylalcohols and benzoins using **1** as an oxidizing agent.

In a series of investigations of synthetic reactions using $SbCl_5$ complexes with organic compounds having an oxygen atom, a new compound **1** was synthesized from DMSO and $SbCl_5$ and used as an oxidizing agent toward some alcohols. Benzils were formed in high yield on the oxidation of the corresponding benzoins by **1**. It was found that an oxygen and two chlorine atoms of **1** were used as the real reagents on the oxidation of benzoins.

Experimental

Synthesis of DMSO-$SbCl_5$ (1:1) Complex 1. A white precipitate was deposited immediately from the solution prepared by mixing 1.1 g (14 mmol) DMSO and 4.7 g (14 mmol) $SbCl_5$ in carbon tetrachloride (10 ml and 20 ml respectively) under cooling. The mixture was allowed to stand overnight. The products were collected by filtration, throughly washed with carbon tetrachloride followed by petroleum ether. The yield was 5.2 g (98.7%); mp 153 °C. IR (KBr) 1420, 1400, 1320, 1035, 980, 875, 500, and 300 cm^{-1}. UV ($CHCl_3$) 278 nm (ε 800). Found: C, 6.23%, H, 1.64%. Calcd for C_2H_5SO-$SbCl_5$: C, 6.37%; H, 1.60%.

Crystal Structure Analysis of the DMSO-$SbCl_5$ (1:1) Complex 1. The thin plate crystals grown from a benzene solution of **1** were orthorhobic, a=23.418(8) Å, b=13.517(5) Å, c=10.529 Å, $\alpha=\beta=\gamma=90°$, and space group Iba2. Intensity data were collected on a Rigaku four circle diffractometer with a Zr-filtered Mo-$K\alpha$ radiation, λ=0.7107 Å. A crystal was sealed in a glass capillary containing mother liquid to avoid deterioration of crystallinity during the intensity data collection. A total of 1588 non-zero unique intensity data up to 2θ=54° were measured by the θ—2θ scan technique.

The Patterson function followed by a minimum function, and successive Fourier and difference Fourier methods showed a disordered DMSO-$SbCl_5$ (1:1) complex together with a solvent molecule of benzene in an asymmetric unit. The initial structure was refined to an R-factor of 0.13, $R=\sum||F_o|-|F_c||/\sum|F_o|$, by the least squares method with an isotropic temperature factor for all the non-hydrogen atoms of the complex and the benzene molecule. Further refinement with an anisotropic temperature factor for the non-hydrogen atoms of **1** gave no appreciable improvement in the crystal structure. The reasons for the failure of the refinement may be because the intensity data have systematic errors from X-ray absorption by the crystal, the capillary and the mother liquid, and the benzene molecule loosely packed in the crystal. As a difference Fourier synthesis did not give any reasonable residual density, the structual analysis of the crystal was terminated at this stage. The atomic scattering factors were taken from the International Table for X-ray crystallography.[1] All the caluculations were carried out at the Computer Center of Tottori University. The final positional and thermal parameters with their estimated standard deviations are listed in Table 1.

Preparation of 2,2'-Dinitrobenzoin 5d. Crude **5d** was prepared by mixing both EtOH solution of *o*-nitrobenzaldehyde and KCN aqueous solution. Pure **5d** was obtained by crystallization with acetone-water (1:1) solution, mp 164—165 °C(lit,[2] 168—169 °C). *p*-Toluoin was also prepared in the same way, mp 86—87 °C (lit,[3] 88—89 °C). The commercially available benzoins, butyl alcohols and benzyl alcohols were used as received.

Oxidation of Benzoin 5a with DMSO-$SbCl_5$ (1:1) Complex 1. A mixture of **5a** (1.0 g, 4.7 mmol) and **1** (1.8 g, 4.7 mmol) was kept in nitromethane (5 ml) for 5 h at 40 °C. The reaction mixture was poured into ice-water and filtered. The filtrate was extracted with ether and the solution was dried with Na_2SO_4. After evaporation, the residue was separated by column chromatography (benzene-silicagel) to give benzil (**2**) (0.96 g, 96.8%). Dimethyl sulfide (**3**) was detected in the reaction mixture by gas chromatography (Injection: 170 °C, Column: 70 °C, N_2: 60 ml/min., Silicon SE 30). The reaction products were identified by comparison of their melting points and IR spectra with those of authentic samples.

Results and Discussion

The compound **1** immediately crystallized from an equimolar solution of DMSO and $SbCl_5$ in carbon

TABLE 1. POSITIONAL AND THERMAL PARAMETERS WITH THEIR ESTIMATED STANDARD DEVIATIONS IN PARENTHESES

Atoms	$x\times10^3$	$y\times10^3$	$z\times10^3$	B_{eq}/Å^2
Complex (**1**)				
Sb	128(3)	175(2)	0	3.71(0.03)
Cl(1)	59(10)	163(10)	160(10)	4.7 (0.2)
Cl(2)	202(11)	170(11)	153(11)	5.5 (0.2)
Cl(3)	61(12)	128(11)	−150(14)	6.3 (0.2)
Cl(4)	196(10)	199(10)	−160(12)	5.3 (0.2)
Cl(5)	117(13)	343(12)	18(23)	8.1 (0.3)
S(1)	143(17)	−56(17)	60(18)	3.6 (0.3)
S(2)	150(19)	−53(19)	−61(20)	4.3 (0.3)
O(1)	148(52)	32(52)	−48(53)	5.7 (1.3)
O(2)	140(37)	24(36)	41(36)	3.1 (0.8)
C(1)	92(35)	−135(36)	−5(94)	5.8 (0.8)
C(2)	208(37)	−116(38)	15(67)	5.9 (0.9)
Benzene				
C(3)	44(42)	390(42)	539(44)	6.0 (1.0)
C(4)	79(55)	389(55)	631(61)	7.9 (1.3)
C(5)	138(49)	397(47)	595(50)	6.5 (1.0)
C(6)	159(41)	395(41)	469(49)	6.2 (1.1)
C(7)	116(65)	396(61)	373(68)	9.2 (1.6)
C(8)	57(64)	396(63)	417(65)	9.4 (1.6)

tetrachloride in quantitative yield. The crystals **1** having a sharp mp were presumed to be DMSO-$SbCl_5$ (1:1), from the results of elemental analysis.

An X-ray crystallogrophic structure determination for **1** was undertaken. The structure **1** with bond lengths and their estimated standard deviations and the atomic numbering scheme are given in Fig. 1. The central metal atom exhibits a distorted octahedral coordination with five chlorine atoms and an oxygen atom of DMSO. The bond angles are listed in Table 2. The DMSO molecule is statistically disordered in the crystal. Two pairs of disordered positions were assigned for an oxygen and a sulfur atom. Each methyl carbon atom, however, was located at a single site. Consequently the methyl sites are shared with two disordered molecules. The bond distances of Sb-Cl for Cl(1), Cl(2), Cl(3), and Cl(5), 2.33 Å to 2.37 Å, are in good accord with those of $SbCl_5$-$PO(CH_3)_3$, 2.32 Å to 2.37 Å.[4] The Sb-Cl (5) bond is significantly shorter than the other Sb-Cl bonds. The bond angles for the two disordered oxygen, antimony and five chlorine atoms depart considerably from those of a regular octahedral structure. This distortion prevents the sulfur atom of DMSO from making abnormal short contacts with chlorine atoms.

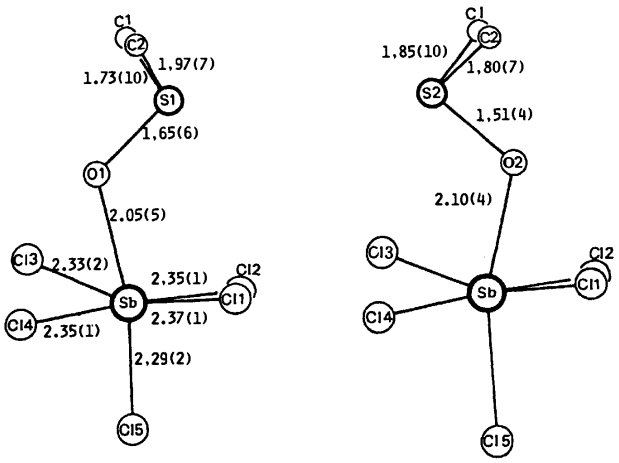

Fig. 1. Legand for Figure.
Molecular structure of DMSO-$SbCl_5$ (1:1) complex **1** together with bond length in Å and their estimated standard deviations in parentheses. Both $SbCl_5$ portions of two structures are common.

TABLE 2. BOND ANGLES FOR DMSO-$SbCl_5$ COMPLEX(**1**) WITH THEIR ESTIMATED STANDARD DEVIATIONS IN PARENTHESES

Bond angles	ϕ/°		ϕ/°
Cl(1)-Sb-Cl(2)	91.1(0.5)	Cl(1)-Sb-Cl(3)	162.6(0.6)
Cl(1)-Sb-Cl(4)	89.9(0.5)	Cl(1)-Sb-Cl(5)	93.0(0.7)
Cl(2)-Sb-Cl(3)	89.6(0.5)	Cl(2)-Sb-Cl(4)	175.0(0.5)
Cl(2)-Sb-Cl(5)	86.1(0.7)	Cl(3)-Sb-Cl(4)	90.7(0.5)
Cl(3)-Sb-Cl(5)	104.4(0.7)	Cl(4)-Sb-Cl(5)	89.8(0.7)
Cl(1)-Sb-O(1)	88.7(1.5)	Cl(1)-Sb-O(2)	74.9(1.0)
Cl(2)-Sb-O(1)	105.6(1.5)	Cl(2)-Sb-O(2)	83.0(1.1)
Cl(3)-Sb-O(1)	74.3(1.5)	Cl(3)-Sb-O(2)	87.9(1.1)
Cl(4)-Sb-O(1)	78.5(1.5)	Cl(4)-Sb-O(2)	101.2(1.1)
Cl(5)-Sb-O(1)	168.2(1.6)	Cl(5)-Sb-O(2)	163.5(1.2)
Sb-O(1)-S(1)	119.7(2.9)	Sb-O(2)-S(2)	122.6(2.3)
O(1)-S(1)-C(1)	103.2(3.7)	O(2)-S(2)-C(2)	97.2(2.8)
O(1)-S(1)-C(2)	94.8(3.0)	O(2)-S(2)-C(1)	94.2(3.4)
C(1)-S(1)-C(2)	100.4(3.8)	C(1)-S(2)-C(1)	96.4(3.7)

The oxidation of benzyl alcohol (**4a**) and its derivatives (methyl (**4b**), nitro (**4c**), and chloro (**4d**) in para-position) with equimolar **1** gave the corresponding benzaldehydes in moderate yields. The yield of benzaldehydes somewhat increased at reflux temperature in the cases of **4b**, **4c**, and **4d**. When air was conducted into the reaction mixture of **4a** and **1**, the yield of benzaldehyde (**5**) also increased (Table 3). The oxidation of butyl (**6a**), isobutyl (**6b**) and *s*-butyl alcohol (**6c**) with **1** also proceeded at room temperature to give butyraldehyde, isobutyraldehyde and ethyl methyl ketone respectively in moderate yields. When the reaction of the butyl alcohols (**6a**, **6b**, and **6c**) with **1** was carried out at 80 °C under air stream, the yield of carbonyl compounds increased. In the absence of **1**, the yield of **5** was only 2.5% even under aeration and refluxing conditions. Under similar conditions, butyl alcohols (**6a**, **6b**, and **6c**) were not oxidized at all.

In the oxidation of benzoin (**7a**), *p*-toluoin (**7b**), *p*-anisoin (**7c**), 2,2′-dinitrobenzoin (**7d**) and furoin (**8**) with **1**,the corresponding benzils or furil were formed in high yields at room temperature (Table 4). When the reactions of **7a** and **7b** with 1 were carried out at elevated temperature, the yields of the corresponding benzils were further improved. A 98.7% yield of **2** was also obtained at a low molar ratio (**7a**/1=0.5)

TABLE 3. THE OXIDATION OF BENZYL ALCOHOLS AND BUTYL ALCOHOLS WITH DMSO-$SbCl_5$ (1:1) COMPLEX **1**

X-C$_6$H$_4$-CH$_2$OH		Reaction conditions[a] Solvent	Temp °C	Time h	Yield of carbonyl compounds/%[b]
H	**2a**	CH_3NO_2	60	3	57.4[c,d]
CH_3	**2b**	benzene	Reflux	2	55.8
NO_2	**2c**	CH_3NO_2	Reflux	7	42.9
Cl	**2d**	CH_3NO_2	Reflux	1	10.5
Butyl alc.	**4a**	CH_3NO_2	80	2	47.3[c]
Isobutyl alc.	**4b**	CH_3NO_2	80	2	41.0[c]
s-Butyl alc.	**4c**	CH_3NO_2	80	2	50.9[c]

a) Molar ratio (Complex/Alcohols): 1 b) Carbonyl compounds were isolated as 2,4-dinitrophenylhydrazone c) Air was passed in the reaction mixture during reaction d) Yellow crystals (mp 58.0—59.0 °C, 5.5 wt.%) were obtained as a by-product.

Table 4. The oxidation of benzoins with DMSO-$SbCl_5$ (1:1) complex **1**

X-C$_6$H$_4$-CH(OH)-C(=O)-C$_6$H$_4$-X		Reaction conditions[a]			Products yield/%		Recovered starting materials/%
		Molar ratio (1/benzoins)	Temp °C	Time h	X-C$_6$H$_4$-C(=O)-C(=O)-C$_6$H$_4$-X	Tarrry products/Wt.%	
H	**7a**	1.0	Room temp.	24	94.2	2.0	Not detected
		1.0	80[b]	2	97.6	1.3	Not detected
		0.5	Reflux[c]	2	98.7(77.0)[d]	trace	Not detected
4,4'-CH_3	**7b**	1.0	Room temp.	24	79.4	8.0	10.1
4,4'-OCH_3	**7c**	1.0	Room temp.	24	77.1	7.0	10.0
		1.0	40	1	98.0(88.0)[d]	1.3	Not detected
2,2'-NO_2	**7d**	1.0	Room temp.	24	91.0	2.1	1.4
Furoin	**8**	1.0	5	1	75.3(31.0)[d]	10.0	4.0

a) Nitromethane was used as a solvent in most runs. b) DMSO was used as a solvent. c) A mixed solvent (30 ml benzene and 5 ml nitromethane) was used. d) In parenthesis, the yield of benzils studied by Dyke and Pritchard[5] are given.

(Table 4). In the oxidation of **7b** and **7c** with **1**, the yield of the corresponding benzils was low in comparison with **7a** and **7d** under the same conditions (Table 4). It seems to depend on the electron donating character of the methyl and methoxy groups.

The complexes of $SbCl_5$ with trimethylamine oxide, pyridine *N*-oxide[5] and *N,N*-dimethylbenzylamine oxide[6] were used in the oxidation of both **7a** and **8**. Dyke and Pritchard[7] also carried out the oxidation of **7a**, **7c**, and **8** using a DMSO-acetic acid medium. But **1** is a better reagent to give benzils from the corresponding benzoins in comparison with the reagents described above.[5-7] In the reaction of **4a**, **5a**, or **7a** with $SbCl_5$, the corresponding carbonyl compounds were not detected under the present mild conditions.

Increasing the ratio of **1** to **7a** resulted in increasing yields of both **2** and concomitant **3**, as shown in Fig. 2. It is evident that an oxygen atom in **1** is consumed in the oxidation of **7a**. In order to estimate the amount of chlorine which was consumed in the reaction of **7a** with **1** (10 h at 40 °C), the hydrogen chloride generated was transfered into aqueous silver nitrate solution by bubbling nitrogen gas through the reaction mixture. The oxidation of **7a** with **1** under these conditions should proceed essentially to completion (Table 4). The precipitated silver chloride corresponded to 88.6% of the expected value based on the assumption that two of the chlorine atoms in **1** are consumed as the oxidizing agent. Therefore, the present reaction may be shown by the following stoichiometry [Equation (a)].

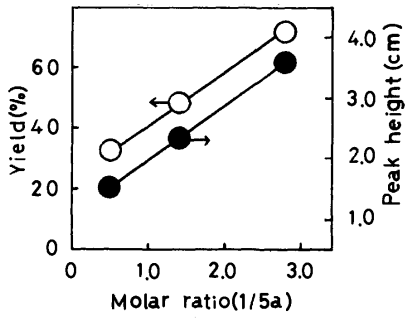

Fig. 2. The oxidation of benzoin **5a** with DMSO-$SbCl_5$ (1:1) complex **1**.
Reaction conditions: Benzoin 1.0 g (4.7 mmol) in nitromethane (10 ml) at 50 °C for 2 h.
○: Benzil, ●: $(CH_3)_2S$

$$2C_6H_5\text{-}\underset{\underset{O}{\|}}{C}\text{-}\underset{\underset{OH}{|}}{CH}\text{-}C_6H_5 + DMSO\text{-}SbCl_5 \longrightarrow$$

$$2C_6H_5\text{-}\underset{\underset{O}{\|}}{C}\text{-}\underset{\underset{O}{\|}}{C}\text{-}C_6H_5 + (CH_3)_2S + SbCl_3 + 2HCl + H_2O \quad (a)$$

When **7a** was allowed to stand with an equimolar combination of DMSO and $SbCl_3$ in nitromethane for 24 h at room temperature, the compound **2** was obtained in a 48% yield with **3**, but no hydrogen chloride was generated. Thus, the reaction of benzoins with **1** seems to proceed in the following two steps. When **1** was mixed with **7a** in nitromethane, hydrogen chloride generated immediately. Therefore, two chlorine atoms in **1** first react with **7a** to form **2** [Equation (b)] and subsequently another molecule of **7a** was also oxidized to **2** by the interaction of both DMSO and $SbCl_3$ [Equation (c)].

$$2C_6H_5\text{-}\underset{\underset{O}{\|}}{C}\text{-}\underset{\underset{OH}{|}}{CH}\text{-}C_6H_5 + DMSO\text{-}SbCl_5 \longrightarrow$$

$$2C_6H_5\text{-}\underset{\underset{O}{\|}}{C}\text{-}\underset{\underset{O}{\|}}{C}\text{-}C_6H_5 + DMSO + SbCl_3 + 2HCl \quad (b)$$

$$2C_6H_5\text{-}\underset{\underset{O}{\|}}{C}\text{-}\underset{\underset{OH}{|}}{CH}\text{-}C_6H_5 + DMSO + SbCl_3 \longrightarrow$$

$$2C_6H_5\text{-}\underset{\underset{O}{\|}}{C}\text{-}\underset{\underset{O}{\|}}{C}\text{-}C_6H_5 + (CH_3)_2S + SbCl_3 + H_2O \quad (c)$$

References

1) "International Tables for X-Ray Crystallography," Kynoch Press., Birmingham (1974), Vol. IV.
2) T. Ekecrantz and A. Ahlqvist, *Chem. Ber.*, **43**, 2602 (1910).
3) T. Ekecrantz and A. Ahlqvist, *Chem. Zentra.*, **1908, II**, 1689.
4) C. I. Branden and I. Lindqvist, *Acta Chem. Scand.*, **15**, 167 (1961).
5) J. Yamamoto, M. Murakami, N. Kameoka, M. Umezu, and T. Matuura, *Bull. Chem. Soc. Jpn.*, **55**, 345 (1982).
6) J. Yamamoto, Y. Tanioka, and M. Umezu, *Bull. Chem. Soc. Jpn.*, **55**, 3035 (1982).
7) M. V. Dyke and N. D. Pritchard, *J. Org. Chem.*, **32**, 3204 (1967).

 © 1985 The Chemical Society of Japan Bull. Chem. Soc. Jpn., 58, 473—476 (1985)

S_H2 Reactions of Triethylgermyl Radical with Thiosulfonic *S*-Esters and Selenosulfonic *Se*-Ester

Michio KOBAYASHI,* Masanori KOBAYASHI, and Masato YOSHIDA
Department of Chemistry, Faculty of Science, Tokyo Metropolitan University, Setagaya-ku, Tokyo 158
(Received June 25, 1984)

The triethylgermyl radical was found to react with thiosulfonic *S*-esters to generate sulfonyl radicals. The S_H2 character of this new reaction was confirmed by a C-13 CIDNP study and products analysis. Selenosulfonic *Se*-ester reacts with germyl radical in a similar way.

Aryl areneselenosulfonates (**1**) are known to suffer a Se–S cleavage by attack of carbon radicals.[1] On the contrary, arenethiosulfonates (**2**), sulfur analogs of selenosulfonic *Se*-ester, are thermally highly stable and are not cleaved by the attack of carbon radicals. For instance, when *S*-*p*-tolyl *p*-toluenethiosulfonate (**2a**) was refluxed in benzene in the presence of phenylazotriphenylmethane (PAT) or azobisisobutyronitrile (AIBN), almost no decomposition of **2a** was observed.

We have found that thiosulfonic *S*-esters are easily attacked by germyl radical more nucleophilic than carbon radical, at the S–S bond. Although many investigations of the reaction of germyl radicals with olefins and organic halides have been reported,[2] very little is known about the reactivity of the germyl radical with sulfur bonding. We have established the S_H2 character[3] of this new reaction and the results will be described in this paper.

Results and Discussion

When solutions of thiosulfonic *S*-esters $ArSO_2SAr'$ (**2**) are treated with 2 molar amounts of triethylgermane (**3**) in benzene in the presence of 0.2 molar equivalent of azobisisobutyronitrile for 17 h, thiosulfonic *S*-esters are decomposed completely and germyl esters of arenesulfonic acid (**4**) and thiogermane (**5**) are obtained in high yields.

$$2Et_3GeH + ArSO_2SAr' \xrightarrow{AIBN} ArSO_3GeEt_3 + Ar'SGeEt_3$$

(**3**) (**2**) (**4**) (**5**)

	Yield/%	Yield/%
a: Ar = Ar′ = *p*-Tol		
b: Ar = Ar′ = Ph	**4a** 96	**5a** 92
	4b 82	**5b** 82

Each product was identified by comparing its spectroscopic properties with those of the authentic samples prepared according to the literature.

Since thiosulfonic *S*-esters were found not to react with triethylgermane in the absence of AIBN, the above reaction was considered to be initiated by hydrogen abstraction from germane by a α-cyanoisopropyl radical and followed by radical chain reactions. The fact that germyl sulfonate (**4**), not germyl sulfinate (**6**), was isolated as the main product indicated the involvement of atmospheric oxygen. Therefore, the reaction of thiosulfonic *S*-esters with triethylgermane was carried out under deoxygenated conditions in the presence of AIBN. Under these conditions, the reactions proceeded only halfway and a part of **2** was recovered unchanged. No germyl sulfonate (**4**) but germyl sulfinate (**6**) and sulfone (**7**) were obtained as reaction products along with thiogermane (**5**).

$$ArSO_2SAr' + Et_3GeH \longrightarrow \underset{\underset{\text{(6a)}}{\overset{\|}{O}}}{ArSOGeEt_3} + Ar'SGeEt_3 \text{ (5a),(5b)} + \underset{\underset{\text{(7a)}}{CN}}{ArSO_2CMe_2}$$

Substrate	AIBN/2	Recovered (**2**)/%
2a	0.2	65
2c	1.0	24

Products (Yield/mol%)

6a (9), **5a** (24), **7a** (9)

6a (10), **5b** (68), **7a** (37)

These findings suggest that the sulfonyl radical can not abstract a hydrogen atom from triethylgermane and combine with germyl radical and α-cyanoisopropyl radical to form **6** and **7** respectively. Assuming this inactivity of sulfonyl radical as hydrogen abstractor, it was possible to explain why the reaction was stopped halfway in the absence of oxygen.

The above reaction may be expressed in the following reaction sequences.

$$AIBN \longrightarrow 2Me_2\dot{C}CN$$

$$Me_2\dot{C}CN + Et_3GeH \longrightarrow Et_3Ge\cdot + Me_2CHCN \quad (1)$$

$$Et_3Ge\cdot + ArSO_2SAr' \longrightarrow Et_3GeSAr' + ArSO_2\cdot \quad (2)$$

$$ArSO_2\cdot + Et_3Ge\cdot \longrightarrow \underset{\overset{\|}{O}}{ArSOGeEt_3} \quad (3)$$

$$ArSO_2\cdot + Me_2\dot{C}CN \longrightarrow \underset{\underset{CN}{|}}{ArSO_2CMe_2} \quad (4)$$

In the presence of atmospheric oxygen, the sulfonyl radical combines with oxygen to form a sulfonylperoxyl radical which can abstract a hydrogen atom from germane to regenerate germyl radical and thus start chain reaction.

$$ArSO_2\cdot + O_2 \longrightarrow ArSO_2OO\cdot \quad (5)$$

$$ArSO_2OO\cdot + Et_3GeH \longrightarrow ArSO_2OOH + Et_3Ge\cdot \quad (6)$$

$$ArSO_2OOH + Et_3GeH \longrightarrow ArSO_2OGeEt_3 + H_2O \quad (7)$$

Reaction (Eq. 2) is an S_H2 type reaction. To establish the S_H2 character for such a reaction shown below;

$$R\cdot + X\text{-}Y \longrightarrow RX + Y\cdot$$

it is essential to certify the formation of RX in high yield and also to verify that the expelled fragment Y is ejected from the solvent cage as a free radical unaccompanied by any radical partner.

We have confirmed the generation of free sulfonyl radicals in the reaction (Eq. 2) by C-13 CIDNP. When a sample tube containing a solution of **2a** and equimolecular PAT in nitrobenzene was inserted into the NMR probe previously heated at 90°C, the CIDNP signals shown in Fig. 1a were observed. These signals were attributed to the phenyl carbon atom C_1 in the starting material PAT and also to the phenyl carbon atom C_1 in *o*- and *p*-nitrobiphenyl which were formed by the attack of the phenyl radical generated from PAT on the solvent nitrobenzene; same signals could also be observed in the decomposition of PAT alone in nitrobenzene. All the thiosulfonic *S*-ester (**2a**) was recovered unchanged after the complete consumption of PAT. On the other hand, when the reaction of **2a** and PAT was carried out in the presence of an equimolecular amount of triethylgermane at 90°C, new CIDNP signals due to benzene (emission), *p*-tolyl triphenylmethyl sulfone (**8**), triphenylmethyl *p*-toluenesulfinate (**9**) were observed as shown in Fig. 1b. The latter reaction may be explained by the following reaction scheme.

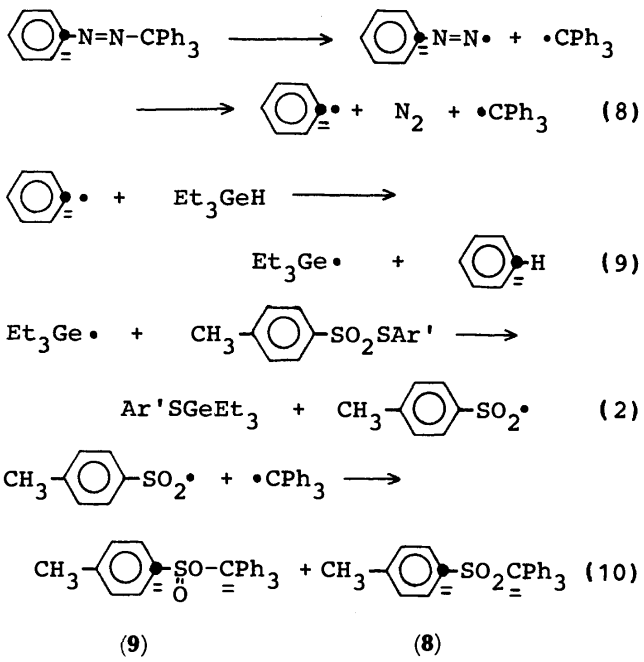

(= denotes the nuclear polarized carbon atoms)

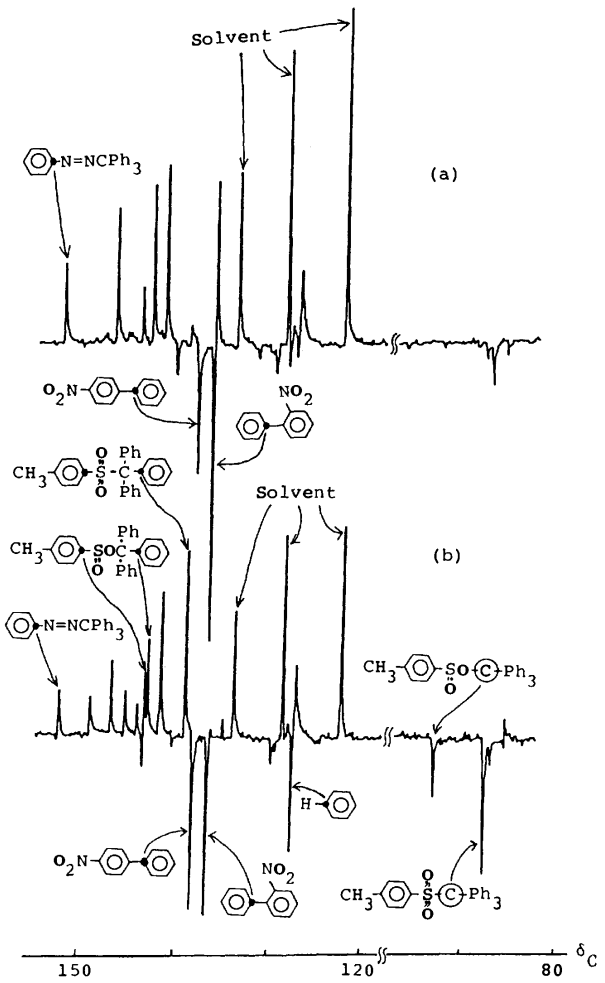

Fig. 1. ^{13}C-CIDNP spectra in the reaction of PAT and *p*-TolSO$_2$STol-*p* (a), and PAT, Et$_3$GeH, and *p*-TolSSO$_2$Tol-*p* (b) at 90°C in PhNO$_2$.

Since the nuclear spin of C_1 in the phenyl radical which diffused out of the solvent cage was polarized in β state, the benzene molecule formed by hydrogen abstraction from **3** should exhibit an emission signal. The germyl radical generated in this reaction (Eq. 9) attacked the sulfur atom of **2** to form thiogerman (**5**) and expelled a sulfonyl radical. The latter radical came diffused out of the solvent cage and reacted with a triphenylmethyl radical to form a new radical pair. Spin selection occurred during this encounter of the radical pair to result in nuclear β polarization at the tertiary carbon atom of the triphenylmethyl radical which had a smaller *g* value than the sulfonyl radical, thus causing an emission signal from the quarternary carbon atoms of **8** and **9**.

Se-Phenyl *p*-tolueneselenosulfonate (**1a**) is known to be decomposed easily by attack of carbon radicals on the selenium atom.[1] Reaction of **1a** with triethylgermane was also investigated.

Reaction between triethylgermane (**3**) and **1a** was found to proceed in the air without addition of any radical initiator, but in the presence of AIBN, the reaction was completed in a much shorter period. After the reaction, the triethylgermyl ester of *p*-toluenesulfonic acid (**4a**) and diphenyl diselenide (**10**) were obtained in almost quantitative yields.

$$Et_3GeH + p\text{-}TolSO_2SePh \xrightarrow[air]{AIBN} Et_3GeO\text{-}SO_2Tol\text{-}p + PhSeSePh$$
(**1a**) (**4a**) 93% (**10**) 98%

When the reaction was carried out under deoxygenated conditions, triethylgermyl sulfinate (**6a**), sulfone (**7**), and diselenide (**10**) were obtained.

$$Et_3GeH + (\mathbf{1a}) \xrightarrow[\text{In degassed tube}]{\text{AIBN (0.2 mol)}} Et_3Ge\text{-}O\text{-}S\text{-}Tol\text{-}p \quad (\mathbf{6a})\ 35\%$$
$$+ PhSeSePh + p\text{-}TolSO_2CMe_2 + (\mathbf{1a})\text{recovered}$$
$$\text{CN}$$
(**10**) 58% (**7**) 31% 23%

The reaction of the germyl radical with selenosulfonic *Se*-ester was considered to proceed similarly to the reaction of germyl radical and thiosulfonic *S*-ester:

$$Et_3Ge\cdot + (\mathbf{1a}) \longrightarrow Et_3GeSePh + p\text{-}TolSO_2\cdot \qquad (11)$$

The fate of the sulfonyl radical expelled was the same as in the case of thiosulfonic *S*-ester. Instead of phenylselenogermane (**11**), diphenyl diselenide (**10**) was isolated in high yield. In a separate experiment, it was confirmed that phenylselenogermane (**11**) reacted with selenosulfonic *Se*-ester (**1a**) to give **4a** and **10** in almost quantitative yields under atmospheric conditions (Eq. 12).

$$Et_3GeSePh + (\mathbf{1a}) \xrightarrow[O_2]{} p\text{-}TolSO_2OGeEt_3 + PhSeSePh \qquad (12)$$

Experimental

Materials. *Triethyl(p-tolylthio)germane (**5a**)*: To a solution of bromotriethylgermane (0.0209 mol) and *p*-toluenethiol (0.0209 mol) in 30 ml of benzene was added a solution of pyridine (0.0229 mol) in benzene (10 ml) at room temperature and stirred for 1.5 h. The precipitated pyridinium bromide was removed and the filtrate was washed with water, dried over anhydrous magnesium sulfate, and evaporated. The residue was purified by redistillation; yield 85%. Bp 121—122 °C/2 mmHg (1 mmHg=133.322 pa). Mass, *m/z* 284 (M^+); ^{1}H-NMR, 0.91—1.10 (m, 15H), 2.25 (s, 3H), 6.99, 7.26 (ABq, 4H, *J*=8.4 Hz); ^{13}C-NMR, 7.6, 8.6, 21.0, 129.3, 129.8, 134.9, 136.0.

*Triethyl(phenylthio)germane (**5b**)*: This was prepared from bromotriethylgermane and benzenethiol in a similar way to **5a**; yield 66%. Bp 105—107 °C/2 mmHg (lit,[4] 112—113 °C/1 mmHg). Mass, *m/z* 270 (M^+); ^{1}H-NMR, 0.90—1.07 (m, 15H), 7.05—7.47 (m, 5H); ^{13}C-NMR, 7.7, 8.6, 126.2, 128.4, 133.3, 134.9.

*Triethyl(phenylseleno)germane (**11**)*: To a solution of bromotriethylgermane (0.0299 mol) and equimolar benzeneselenol in 20 ml of benzene was added pyridine (0.0328 mol) in 10 ml of benzene under nitrogen stream at room temperature, and stirred for 1.5 h. After similar workup of the reaction mixture as for **5a**, **11** was obtained in 87% yield. Bp 130—132 °C/2 mmHg. Mass, *m/z* 316 (M^+); ^{1}H-NMR, 1.03 (s, 15H), 7.00—7.60 (m, 5H); ^{13}C-NMR, 8.1, 9.0, 125.7, 126.5, 128.5, 136.6.

Triethylgermyl p-*Toluenesulfonate (**4a**)*: A solution of triethylgermane (2.04 mmol) and *p*-toluenesulfonic acid (2.04 mmol) in toluene was refluxed for 24 h. After the evaporation of the solvent, the residue was purified by recrystallization from ethanol. Mp 69.5—70.0 °C. ^{1}H-NMR, 1.05—1.30 (m, 15H), 2.29 (s, 3H), 7.09, 7.56 (ABq, 4H, *J*=7.8 Hz); ^{13}C-NMR, 7.4, 9.1, 21.5, 126.5, 129.3, 137.9, 142.6; IR, (CCl_4), 1330, 1172 cm^{-1} (SO_2), 915 cm^{-1} (Ge-O).

*Triethylgermyl Benzenesulfonate (**4b**)*: This was prepared in a similar way to **4a**. Bp 185 °C/5 mmHg (lit,[5] 160 °C/1.3 mmHg. ^{1}H-NMR, 1.00—1.28 (m, 15H), 7.00—7.90 (m, 5H); ^{13}C-NMR, 7.3, 9.2, 126.4, 128.7, 132.2, 140.6; IR, (CCl_4), 1325, 1175 cm^{-1} (SO_2), 925 cm^{-1} (Ge-O).

Triethylgermyl p-*Toluenesulfinate (**6a**)*: This was prepared according to the literature.[6] ^{1}H-NMR, 1.08 (s, 15H), 2.31 (s, 3H), 7.22, 7.52 (ABq, 4H, *J*=7.8 Hz); ^{13}C-NMR, 7.5, 8.9, 21.4, 124.5, 129.4, 141.3, 148.1; IR, neat, 1120 cm^{-1} (S-O), 838 (Ge-O).

Cyanoisopropyl p-*Tolyl Sulfone (**7**)*: This was purified by recrystallization from methanol. Mp. 114—115 °C. ^{1}H-NMR, 1.67 (s, 6H), 2.43 (s, 3H), 7.36, 7.81 (ABq, 4H, *J*=8.4 Hz); ^{13}C-NMR, 21.1, 21.8, 57.5, 129.9, 130.4, 130.7, 146.5; IR, KBr, 1140, 1162, 1188, 1292, 1308, 1322 cm^{-1} (SO_2), 2240 cm^{-1} (CN); Anal. Found: C, 59.17; H, 5.95; N, 6.35%. Calcd for $C_{11}H_{13}NSO_2$: C, 59.17; H, 5.86; N, 6.27.

Thiosulfonic *S*-esters[7] and trietylgermane[8] were prepared according to the literature.

Reaction Between Triethylgermane and Thiosulfonic S-ester. Reaction in Air: A solution of triethylgermane (**3**) (1.0 mmol), thiosulfonic *S*-ester (**2a**) (0.5 mmol) and AIBN (0.2 mmol) in benzene (10 ml) was refluxed for 17 h. After the evaporation of the solvent under reduced pressure, the products were identified by ^{1}H- and ^{13}C-NMR.

Reaction Under Degassed Conditions: A solution of **2a** (0.622 mmol), **3** (0.622 mmol) and AIBN (0.124 mmol) in benzene (7 ml) was deoxygenated by a freeze-thaw cycle, sealed in an ampoule and heated at 80 °C for 38 h. The products were separated by column chromatography and identified by NMR.

CIDNP Measurement. Carbon 13 CIDNP was observed on JEOL FX-60 FT-NMR spectrometer at 90 °C; Ph-N=N-CPh_3 (C_1 of Ph: 152.1, A), Ph-$C_6H_4NO_2$-*p* (C_1 of Ph: 138.7, E), Ph-$C_6H_4NO_2$-*o* (C_1 of Ph: 137.3, E), *p*-$TolSO_2CPh_3$ (C_1' of Ph: 139.8, A, C_α: 87.3, E), and *p*-Tol(SO)$OCPh_3$ (C_1 of *p*-Tol: 141.0, A, C_α: 92.2, E, C_1' of Ph: 142.5, A).

References

1) T. Miura and M. Kobayashi, *J. Chem. Soc., Chem. Commun.*, **1982**, 438; T. G. Back, S. Collins, and R. G. Kerr, *J. Org. Chem.*, **48**, 3077 (1983); R. A. Gancarz and J. L. Kice, *J. Org. Chem.*, **46**, 4899 (1981).

2) M. Lesbre, P. Mazerolles, and J. Satgé, "The Organic Compounds of Germanium," Wiley-Interscience, New York (1971), Chap. 4.

3) K. U. Ingold and B. P. Roberts, "Free Radical Substitution Reactions," Wiley-Interscience, New York (1971), Chap. 7.

4) H. H. Anderson, *J. Org. Chem.*, **21**, 869 (1956).

5) J. Satgé, *Ann. Chim. (paris)*, **6**, 519 (1961); J. Dubac, G. Manuel, and P. Mazerolles, *C. R. Acad. Sci., Ser. C*, **271**,

465 (1970).
6) E. Lindner and K. Schardt, *J. Organomet. Chem.*, **44**, 111 (1972).
7) S. Oae, T. Takata, and Y. H. Kim, *Tetrahedron*, **37**, 37 (1981).
8) H. H. Anderson, *J. Am. Chem. Soc.*, **79**, 326 (1957).

 © 1985 The Chemical Society of Japan Bull. Chem. Soc. Jpn., 58, 477—480 (1985)

Liquid Crystal Materials with Sulfur Atoms Incorporated in the Principal Structure III. Trans and Cis Isomers of New Liquid Crystal Material: 2-(*p*-Substituted phenyl)-5-alkyl-1,3-dithianes

Yuichiro HARAMOTO * and Hiroyoshi KAMOGAWA
Department of Applied Chemistry, Yamanashi University, Takeda 4, Kofu 400
(Received August 11, 1984)

Trans and cis isomers of 2,5-disubstituted 1,3-dithianes were synthesized by the acid-catalyzed thioacetalization of *p*-substituted benzaldehydes and dithiols. The results of identifications of trans and cis isomers made by means of ^{13}C-NMR chemical shifts indicate that the isomerism occurred at the 5 position in the 1,3-dithiane ring. Benzaldehydes with electrondonating *p*-substituents produced less cis isomers than that with the cyano group, which seems to indicate the establishment of an equilibrium in the formation reaction between trans and cis isomers. Several electro-optic properties of *trans*- and *cis*-2-(*p*-cyanophenyl)-5-alkyl-1,3-dithianes were determined by using them as a dopant of mixture of liquid crystals. Mixture added with trans isomers was superior to that added with cis isomers in several points.

In recent years, we have synthesized 2,5-disubstituted 1,3-dithianes and 1,3-oxathianes[2,3,4] as novel analogs of the 1,3-dioxanes now in practical uses.[1] These compounds were produced in both trans and cis isomers. Then we analyzed these two isomers by means of ^{13}C-NMR to determine which isomer was trans and at what position the isomerism occurred in the 1,3-dithiane ring.

In addition to this, we compared several physical properties of trans and cis 2-(*p*-cyanophenyl)-5-alkyl-1,3-dithianes by using them as a dopant of liquid crystal mixtures.

Results and Discussion

2,5-Disubstituted 1,3-dithianes were synthesized *via* the following route.

In step **3**→**5**, the ^{1}H-NMR of the product indicated a splitting of the singlet due to the C-2 proton of the 1,3-dithiane ring, which was caused by the presence of two isomers, both trans and cis. In compound R′=CN, separation of trans and cis isomers was successfully carried out either by recrystallizations from hexane or by centrifugal liquid chromatography (CLC).

In compounds R′=OR, or CH_3, separation of trans and cis isomers was done by recrystallizations (5—7 times) from hexane to get pure one isomer. The mother liquors were collected and several recrystallizations were further effected to isolate some of the other isomer. In ^{1}H-NMR, these two isomers have different signal patterns of CH_2–S: isomer A with a broad rugged singlet proton signal at δ=2.5—2.9 and isomer B with a broad quintet signal at δ=2.4—3.5 (Table 1).

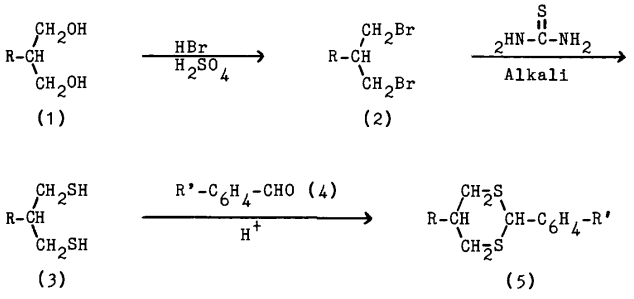

Fig. 1.

The ^{13}C-NMR characteristics of isomeric 2-(*p*-substituted phenyl)-5-alkyl-1,3-dithianes were investigated by means of the ^{1}H-complete decoupling (COM), ^{1}H-off resonance decoupling (OFR), and ^{1}H-selective decoupling (SEL) procedures. As C-2 and C-4, C-6 protons in the 1,3-dithiane ring show peculiar chemical shifts in ^{1}H-NMR, the ^{1}H-selective decoupling method was useful to determine the assignment in ^{13}C-NMR. In compounds R=C_2H_5, R′=CN, the difference in the ^{13}C-NMR chemical shift for the 1,3-dithiane ring carbons between isomers A and B (δ isomer A—δ isomer B) are 0.76 (C2), 1.79 (C4, C6), and 6.39 (C5) (Table 1).

These values indicate that the isomerism occurs at C5 with a large difference ($\Delta\delta$=6.39), and not at C2 ($\Delta\delta$=0.76).

In the ^{13}C-NMR data of 5-alkyl-1,3-dithiane, the C5 signal for 5-equatorial isomer lies at a lower magnetic field than that for 5-axial isomer.[5] Therefore, it is concluded that isomer A is 5-equatorial (trans) and B is 5-axial (cis).

With increasing purity, several trans isomers of this class began to exhibit the monotropic liquid crystal phase under a polarization microscope.[3] As two isomers (cis and trans) are white powder as produced, whereas two raw material compounds (**3**, **4**) are liquid, mixcd isomers are obtained in pure state after about two recrystallizations. At this point the mixture contains about 10% of cis isomer. This mixed isomer did not exhibit any liquid crystal phases. It is generally known that when two different liquid crystalline compounds with the same phase were mixed, the mixture exhibits the liquid crystal phase.[6] Therefore, cis isomer is considered to have no nematic liquid crystalline properties. In addition to this, some separable cis isomers (for example R=C_7H_{15}, R′=OC_2H_5; trans isomer of this compound exhibits the monotropic nematic liquid crystal phase: I 57 N 48 C) also did not exhibit any liquid crystal phases.

This fact supports that the cis isomers generally do not exhibit liquid crystal phases.

TABLE 1. ^1H AND ^{13}C-NMR CHEMICAL SHIFTS OF ISOMERIC 2-(*p*-SUBSTITUTED PHENYL)-5-ALKYL-1,3-DITHIANES, ^{13}C-NMR ($CDCl_3$)

Carbon No. (1,3-dithiane ring)	$R=C_2H_5$ Trans	$R'=CN$ Cis	δ trans—δ cis	$R=C_3H_7$ Trans	$R'=CN$ cis	δ trans—δ cis
2	50.77	50.01	0.76	50.77	50.06	0.71
4,6	37.06	35.27	1.79	37.38	35.60	1.78
5	37.22	30.83	6.39	35.22	28.88	6.34
Carbon No. (1,3-dithiane ring)	$R=C_4H_9$ Trans	$R'=CN$ Cis	δ trans—δ cis	$R=C_5H_{11}$ Trans	$R'=CN$ Cis	δ trans—δ cis
2	50.66	49.96	0.70	50.82	50.01	0.81
4,6	37.33	35.60	1.73	37.38	35.49	1.89
5	36.14	29.80	6.34	36.36	30.12	6.34

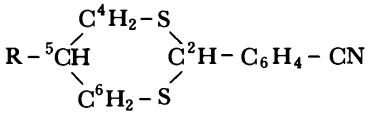

^1H-NMR ($CDCl_3$, δ)

R	R'	Trans	Cis
n-C_5H_{11}	OC_4H_9	0.7—2.1 (m, R-CH, OCH_2-C_nH_{2n+1}), 2.6—2.9 (m, 4H, CH_2-S), 3.9 (t, 2H, OCH_2), 5.06 (s, 1H, S>CH-), 6.65—7.5 (q, 4H, ArH)	0.7—2.1 (m, R-CH, OCH_2-C_nH_{2n+1}), 2.5—3.5 (m, 4H, CH_2-S), 3.9 (t, 2H, OCH_2), 5.03(s, 1H, S>CH-), 6.65—7.5 (m, 4H, ArH)
n-C_7H_{15}	OC_2H_5		
C_2H_5	CN	0.7—2.0 (m, R—CH), 2.6—2.9 (m, 4H, CH_2-S), 5.10 (s, 1H, S>CH-), 7.60 (s, 4H, ArH)	0.7—2.0 (m, R—CH), 2.4—3.5 (m, 4H, CH_2-S), 5.08 (s, 1H, S>CH-), 7.65 (s, 4H, ArH)
n-C_3H_7	CN		
n-C_4H_9	CN		
n-C_5H_{11}	CN		

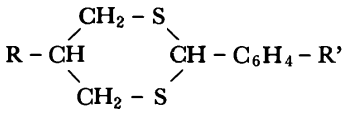

TABLE 2. CONTENTS OF TRANS AND CIS ISOMERS IN THE 2,5-DISUBSTITUTED 1,3-DITHIANES (5) SYNTHESIZED[a)]

R	R'	Trans (%)	Cis (%)
n-C_3H_7	CN	51	49
n-C_3H_7	CH_3	78	22
n-C_3H_7	OC_4H_9	80	20
n-C_5H_{11}	CN	64	36
n-C_5H_{11}	CH_3	78	22
n-C_5H_{11}	OC_4H_9	83	17

a) Determined gas-chromatographically Column: OV 17, 3m; Oven temp 250°C.

The production ratio of cis to trans isomers, as determined by means of gas chromatography (Table 2), seems to depend upon the kind of *p*-substituent (R') of compounds **5**. In step **3**→**5**, benzaldehyde **4** having the electron-donating substituent (R'), such as the alkyl and alkoxyl groups, produced much more C-5 equatorial isomer (trans) than C-5 axial isomer (cis). On the contrary, **4** with the electron-withdrawing substituent, such as the cyano group, produced both isomers in a nearly equal ratio.

This result is explainable as follows. In step **3**→**5**, possible configurations around C-5 and C-2 are as follows: C-5 Eq C-2 Ax, C-5 Eq C-2 Eq, C-5 Ax C-2 Ax, and C-5 Ax C-2 Eq. (Eq: equatorial, Ax: axial) As the C-2 substituent is the steric hindered *p*-substituted phenyl group, C-2 Ax should be converted to the more stable state C-2 Eq through the next equilibration

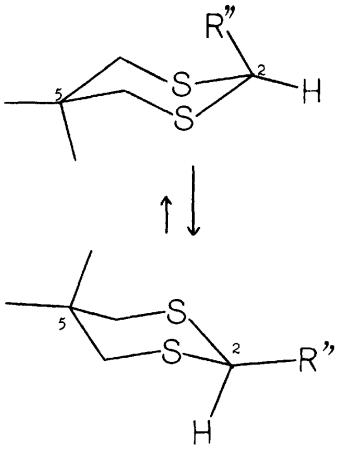

Fig. 2.

(Fig. 2).

Namely, C-5 Eq C-2 Ax and C-5 Ax C-2 Ax are converted to C-5 Ax C-2 Eq and C-5 Eq C-2 Eq, respectively. Therefore, C-2 configuration becomes all Eq. and the ratio of trans (C-5 Eq C-2 Eq) to cis (C-5 Ax C-2 Eq) should become nearly equal to unity. Nevertheless, in the 1,3-dithianes with the *p*-electron-donating phenyl group, trans isomers are produced more than cis isomers. In the 1,3-dithianes with the p-electron-donating phenyl group, the backward reaction of cis to trans may occur more readily owing to the reversible nature of the 1,3-dithiane ring formation and the stabilization of the carbocation at C-2 due to

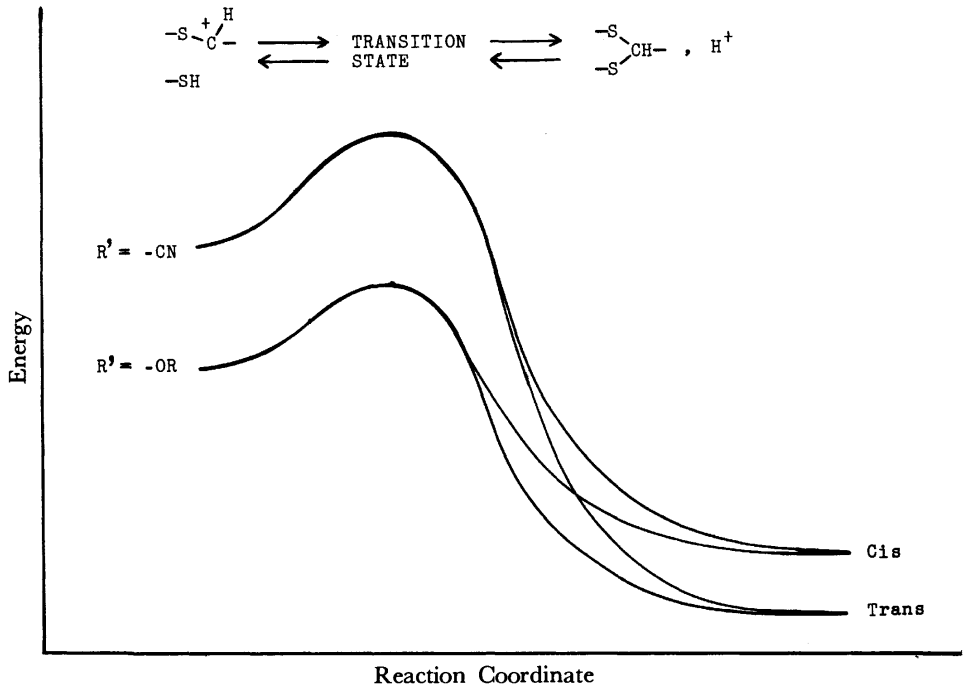

Fig. 3.

TABLE 3. COMPOSITION OF LIQUID CRYSTAL MIXTURE

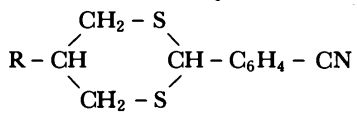

	Mixture T (trans) mol/%	Mixture C (cis) mol/%
[a]Base mixture	90	90
R=C_2H_5	5	5
R=n-C_4H_9	5	5

a) Composition of base liquid crystal mixture (Base mixture)

R	R'	mol/%
n-C_3H_7	OC_2H_5	8.8
n-C_3H_7	$OC_4H_9^n$	20.9
n-C_4H_9	OCH_3	17.9
n-C_4H_9	OC_2H_5	17.2
n-C_5H_{11}	OCH_3	18.7
C_2H_5-C_6H_4-COO-C_6H_4-CN		5.5
$C_4H_9^n$-C_6H_4-COO-C_6H_4-CN		5.5
$C_5H_{11}^n$-C_6H_4-C_6H_4-C_6H_4-CN		5.5

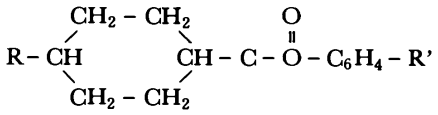

the electron -donation by R' (Fig. 3). Thus, this backward reaction (cis to trans) is equilibrium controlled,[7] energetically more favorable trans isomer will be produced in a higher ratio than cis isomer. In 1,3-dithiane with the *p*-cyanophenyl group, the electron-withdrawing substituent (CN) destabilizes the carbcation at C2, so that the activating energy of the backward reaction is too large to make the reaction thermodynamically-controlled.

Several electro-optic properties of *trans*-and *cis*-2-(*p*-cyanophenyl)-5-alkyl-1,3-dithianes by using them as a dopant of a mixture of liquid crystals were given in Table 4. And the compositions of mixture T (trans) and mixture C (cis) were given in Table 3. Threshold

TABLE 4. ELECTRO-OPTIC AND OTHER RELEVANT PROPERTIES

Threshold voltage (Vth)	Mixture T (trans) 1.82 V	Mixture C (cis) 1.69 V
Rising time (T_r)	100 m s	84 m s [c]
Decay time (T_d)	70 m s	89 m s
Birefringence (Δn)	0.103	0.090
Dielectric anisotropy ($\Delta\varepsilon$)	+5.37	+4.56
Steepness factor[a]	1.34	1.36
Temperature dependence[b]	0.35%/°C	0.53%/°C

a) Steepness factor=Vsat/Vth. b) Temperature dependence=$-1/V\text{th}(dV\text{th}/dT)$ Vth: threshold voltage, Vsat: saturated voltage c) Von=4 volt, Voff=0 volt.

voltage (Vth), rising time (T_r), decay time (T_d), birefringence (Δn), dielectric anisotropy ($\Delta\varepsilon$), steepness factor and temperature dependence of Vth were measured in mixture T and mixture C respectively.

Threshold voltage (Vth) of mixture C (cis) is smaller than that of mixture T (trans). Generally, Vth is proportional to the square root of $K/\Delta\varepsilon$.[8] (K: elastic constant). In mixture C, axial alkyl chain should weaken the interactions among liquid crystal molecules, so that K of mixture C seems to be smaller than that of mixture T. But $\Delta\varepsilon$ of mixture T is somewhat larger than that of mixture C. The result obtained for Vth must imply that K had larger influence than $\Delta\varepsilon$.

Rising time (T_r) of mixture T is longer than that of mixture C.

Generally, T_r is proportional to $\eta/(\Delta\varepsilon V^2 - K\pi^2)$.[9] Viscosity ($\eta$) of mixture containing 2 mol% of trans isomers (R=C_2H_5, C_4H_9) is 11 cp (25 °C), and that of cis isomers (R=C_2H_5, C_4H_9) is 13 cp. So η of mixture T is somewhat smaller than that of mixture C. Therefore values of viscosity (η) and $\Delta\varepsilon$ are support reverse result of T_r. But K of mixture C seems to be smaller than that of mixture T as written above. The result obtained for T_r must imply that difference of K had larger influence to T_r than differences of $\Delta\varepsilon$ and η. Since decay time (T_d) is proportional to η/K,[9] it is reasonable that the T_d of mixture T having larger K and smaller η is shorter than that of mixture C. In birefrigence (Δn), the value for mixture C is smaller than that for mixture T, so that mixture C must use a somewhat thick cell to gain a sufficient contrast. The facts that $\Delta\varepsilon$ of mixture T is somewhat larger, steepness factor is also superior, and temperature dependence is smaller, indicate that mixture T is superior to mixture C.

Experimental

IR, ^{1}H-NMR, ^{13}C-NMR, and mass spectra were obtained with a Hitachi 215 spectrophotometer, a JNM-PMX 60 spectrometer, a JNM-FX 90Q FT-NMR spectrometer, and a Hitachi RMU-6 MG spectrometer, respectively. Elemental analyses were carried out with a Perkin-Elmer 250 instrument. Centrifugal liquid chromatography was made with a Hitachi CLC-5 apparatus. Transition temperature and mesomorphic phases were determined by means of both a Mitamura Riken micro melting point apparatus equipped with polarizers and Rigaku Denki D.S.C. CN8059L1, CN8208A2. The viscosity (η) and dielectric anisotropy ($\Delta\varepsilon$), and birefringence (Δn) of liquid crystal mixtures were measured using a Tokyo Keiki E type rotating cone viscometer, a Yokokawa Hewlett Packard 4274A multi frequency LCR meter, and a Hitachi 340 spectrometer, respectively.

The measurement of liquid crystal properties are carried out by using 9.4 μm twisted nematic cells to ensure good guiding of the plane of polarization. Syntheses and detailed analytical data of compounds **1**, **2**, **3**, and **5** were written in a previous paper.[3] ^{1}H-NMR and ^{13}C-NMR data of separable cis and trans isomers are in Table 1.

The authors wish to express their gratitudes to Suwa Seikosha Co., Ltd. for extensive assistances in the measurement of liquid crystal properties.

References

1) D. Demus and H. Zaschke (to V. E. W. Kombinat Microelectronic) Japan Pat. Appl. No. 54-160916, Dec. (1980).

2) Y. Haramoto and H. Kamogawa, *J. Chem. Soc., Chem. Commun.*, **1983**, 75.

3) Y. Haramoto, A. Nobe, and H. Kamogawa, *Bull. Chem. Soc. Jpn.*, **57**, 1966, (1984).

4) Y. Haramoto, K. Akazawa, and H. Kamogawa, *Bull. Chem. Soc. Jpn.*, **57**, 3173, (1984).

5) E. L. Eliel, V. S. Rao, and F. G. Riddell, *J. Am. Chem. Soc.*, **98**, 3583, (1976).

6) G. W. Gray, and P. A. Winsor, "Liquid Crystal & Plastic Crystals"; Wiley: New York, **1974**; Vol. 1, p. 161.

7) E. L. Eliel and R. O. Hutchins, *J. Am. Chem. Soc.*, **91**, 2703, (1969).

8) H. Dewling, *Mol. Cryst. and Liq. Cryst.*, Vol. 19, 123, (1972).

9) E. Jackman and E.P. Raynes, *Phys. Lett.*, Vol. 39 A, p. 69 (1972).

Charge-transfer Complexes, Gas-liquid Chromatographic and Photochemical Characteristics, and Solvent Adducts of Polyphenylenes and Related Linear Polyphenyls[1)]

Yasuhiro FUJIOKA
Kyoto Pharmaceutical University, Misasagi-nakauchi-cho, Yamashina-ku, Kyoto 607
(Received May 12, 1984)

The absorption spectra of the charge-transfer (CT) complexes formed by two acceptors (tetracyanoethylene and 2,3-dichloro-5,6-dicyano-*p*-benzoquinone) with thirteen macrocyclic polyphenylenes and with thirty-eight linear polyphenyls were measured in dichloromethane. A linear relationship existing between the first transitions of the CT-complexes and those of the uncomplexed donor hydrocarbons made it possible to predict the CT-bands of new polyphenylenes and polyphenyls. By the gas-liquid chromatography using a glass capillary column, forty-nine polyphenyls and polyphenylenes, containing a large number of isomers, were successfully analyzed. The relationship between the retention times and the structure of linear polyphenyls was expressed by means of a simple empirical equation, and the equation was also applicable to the polyphenylenes by adding a correction factor. These equations are extremely useful for the estimation of the retention time and elution order and the structure of unknown polyphenyls and polyphenylenes. The reductive irradiation of *m,m,o,p,o*-pentaphenylene provided the bridged annulene compound. For six polyphenylenes and the related compounds, the criteria for the occurrence of the intramolecular photocoupling reaction were discussed. Among the examined polyphenylenes, *m,o,o,m,o,o*-hexaphenylene and *o,p,p,o,p,p,o,p,p*-nonaphenylene formed the adducts with several solvents.

In the preceding paper[2)] fourteen macrocyclic polyphenylenes have been synthesized to elucidate the relationship between the structures (the number and arrangement of the phenylene rings) and the physical properties such as infrared (IR), ultraviolet (UV), proton magnetic resonance (^{1}H NMR), and mass (MS) spectra on a series of linear and branched polyphenyls.[3)] The polyphenylenes have been characterized by the structure, in which both terminal rings of polyphenyls were linked to each other so that the rotation of pivot bonds was restricted significantly due to their rigid geometry. The results have indicated that the ^{1}H NMR and UV spectral studies provided useful conformational information, and the Hückel molecular orbital (HMO) calculations of the longest-wavelength absorption bands of polyphenylenes also gave additional grounds for their conformation deduced from their spectral data and Dreiding stereomodels.

The present study was undertaken to investigate several chemical behaviors of thirteen polyphenylenes {*m,m,o,p,o*-pentaphenylene (**1**); *m,m,o,m,m,o*- (**2**), *m,o,o,m,o,o*- (**3**), *o,o,p,o,o,p*- (**4**), *m,o,p,m,o,p*-(**5**), *o,p,o,p,o,p*-(**6**), *m,o,p,o,p,o*- (**7**), *m,o,m,o,m,o*- (**8**), *m,m,m,o,m,o*-(**9**), and *m*-hexaphenylene (**10**); *m,o,p,p,o,m,p*- (**11**) and *m,m,m,m,p,o,p*-heptaphenylene (**12**); and *o,p,p,o,p,p,o,p,p*-nonaphenylene (**13**)} as well as those of the closely related linear polyphenyls (**14**—**53**). So far, several studies have been reported on the charge-transfer (CT) complexes of biphenyl and three terphenyls,[4)] on the photodehydrocyclization of several *o*-terphenyl-type compounds,[5)] and further on the gas chromatographic analysis of linear and branched polyphenyls,[6)] but none on those of polyphenylenes. On the gas-liquid chromatography (GLC) of aliphatic or monocyclic compounds, it has been known that the "retention index" by Kováts serves to estimate their structure.[7)] Karger *et al.*[8)] and Ono[9)] have reported the applicability of the Hammet Equation for GLC using the series of isomers of phenols and anilines and of alkyl benzenes, respectively. In a programmed-temperature gas chromatography Solomon has suggested a relationship between elution temperatures and structures of polyphenyls, but their analytical conditions and the complex additive terms are to be improved.[6a)]

The CT-complexes have been formed by the donor hydrocarbons with two acceptors (tetracyanoethylene (TCNE) and 2,3-dichloro-5,6-dicyano-*p*-benzoquinone (DDQ)) in dichloromethane, and the relationship between the longest-wavelength absorption bands of the CT-complexes and those of the uncomplexed donors has been discussed. The gas-liquid chromatographic analysis of the polyphenylenes and polyphenyls has been performed and the relationship between the structures (the number and arrangement of the benzene rings) and the retention time has been formulated. In addition, the intramolecular photocoupling reactions and solvent adduct formations of polyphenylenes have also been discussed.

Results and Discussion

Charge-transfer Complexes. The CT-complexes between the donors (thirteen polyphenylenes (**1**—**13**) and thirty-eight related polyphenyls (**14**—**34**, **36**—**41**, and **43**—**53**)) and two acceptors (TCNE and DDQ) were prepared in dichloromethane[10)] and their absorption spectra were determined. The CT-complexes, which were characterized by the intensely colored solutions (orange to greenish blue), showed generally plural absorption bands for TCNE[12)] and only one band for DDQ. Tables 1 and 2 list the longest-wavelength absorption (first) CT-bands of the polyphenylenes and polyphenyls, respectively, and also the first bands of each uncomplexed hydrocarbon. Now the observed first transition energies (E_{ct}) for the CT-complexes are plotted against the observed first π-π^* transition ener-

Table 1. Longest-wavelength absorption bands of TCNE- and DDQ-polyphenylene CT-complexes[a] and of the donors[b] (λ_{max}/nm)

Compound No.	TCNE-complex	DDQ-complex	Donor
1	510	588	256 sh
2	485	565 sh	248 sh
3	540 sh	600 sh	242 sh
4	597	693	288 sh
5	547	630	264 sh
6	545 sh	630 sh	276 sh
7	525 sh	605 sh	237
8	505 sh	580 sh	254 sh
9	505 sh	590	252 sh
10	490 sh	—	247
11	590	687	312 sh
12	515 sh	610 sh	284 infl
13	625	703	320 sh

a) In dichloromethane. b) In cyclohexane (*cf.* Ref. 2).

Table 2. Longest-wavelength absorption bands of TCNE- and DDQ-polyphenyl CT-complexes[a] and of the donors[b] (λ_{max}/nm)

Compound[c] No.	TCNE-complex	DDQ-complex	Donor
$\phi\phi$ (**14**)	496	563	248
$\phi o\phi$ (**15**)	500 sh	560 sh	251 sh
$\phi m\phi$ (**16**)	496	563	247
$\phi p\phi$ (**17**)	555	637	276
$\phi oo\phi$ (**18**)	490 sh	560 sh	245 sh
$\phi om\phi$ (**19**)	502	570 sh	251 sh
$\phi op\phi$ (**20**)	552	639	278
$\phi mm\phi$ (**21**)	495	562	248
$\phi mp\phi$ (**22**)	537	613	268
$\phi pp\phi$ (**23**)	590	680	294
$\phi ooo\phi$ (**24**)	475 sh	545 sh	237
$\phi omo\phi$ (**25**)	500 sh	575 sh	250 sh
$\phi opo\phi$ (**26**)	535	625 sh	280
$\phi mom\phi$ (**27**)	498	573	249 sh
$\phi pop\phi$ (**28**)	563	648	284 sh
$\phi opm\phi$ (**29**)	493	575	275 sh
$\phi opp\phi$ (**30**)	585	680	295
$\phi mmm\phi$ (**31**)	494	560	249
ϕmpm (**32**)	505	590 sh	280 sh
$\phi pmp\phi$ (**33**)	558	640	280
$\phi mpp\phi$ (**34**)	572	672	296
$\phi oooo\phi$ (**36**)	465 sh	—	231
$\phi oomo\phi$ (**37**)	500 sh	570 sh	250 sh
$\phi oopo\phi$ (**38**)	495 sh	565	275 sh
$\phi moom\phi$ (**39**)	510	570	245
$\phi ommo\phi$ (**40**)	495 sh	580 sh	252 sh
$\phi poop\phi$ (**41**)	560	650	272
$\phi ompo\phi$ (**43**)	500 sh	625	272 sh
$\phi oppo\phi$ (**44**)	575	690	297
$\phi momm\phi$ (**45**)	493	562	250 sh
$\phi mopm\phi$ (**46**)	498	575 sh	249
$\phi pomp\phi$ (**47**)	560	643	275
$\phi opmm\phi$ (**48**)	493	575	277 sh
$\phi oppp\phi$ (**49**)	605	705	306
$\phi mmmm\phi$ (**50**)	492	565	249
$\phi mmpm\phi$ (**51**)	505	590	286 sh
$\phi pmmp\phi$ (**52**)	550	630	273
$\phi mppm\phi$ (**53**)	590	665 sh	296

a) In dichloromethane. b) In cyclohexane (*cf.* Ref. 3a-d and 3f). c) ϕ, o, m, and p refer to phenyl and to *o*-, *m*-, and *p*-phenylene rings.

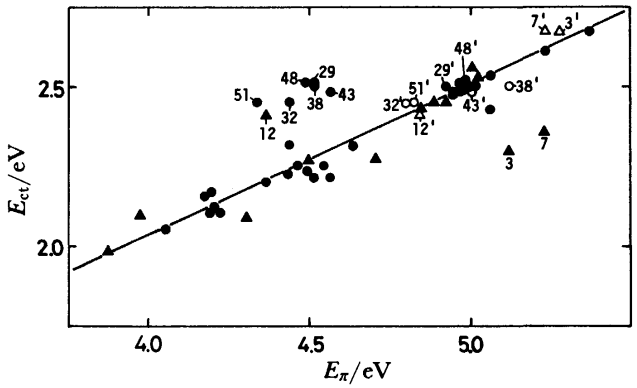

Fig. 1. Plot of the transition energy (E_{ct}) for the first CT-band of TCNE-donor complex *vs.* the energy (E_π) for the first π-π^* transition of the donor; the points are numbered according to the compound number in Tables 1 and 2; ●: Linear polyphenyls, ▲: polyphenylenes.

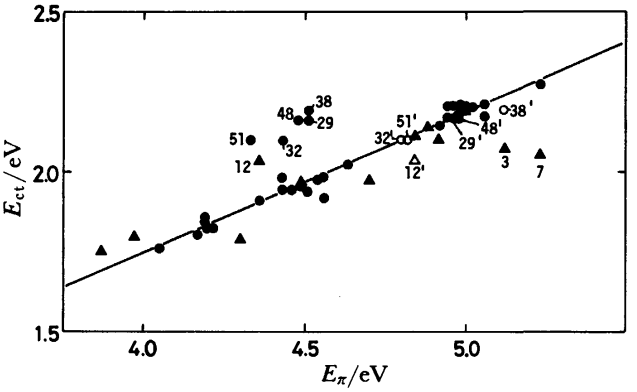

Fig. 2. Plot of the transition energy (E_{ct}) for the first CT-band of DDQ-donor complex *vs.* the energy (E_π) for the first π-π^* transition of the donor; the points are numbered according to the compound No. in Tables 1 and 2; ●: Linear polyphenyls, ▲: polyphenylenes.

gies (E_π) for the donor hydrocarbons (Figs. 1 and 2).

In Fig. 1, all but nine of the points lie approximately on a straight line (slope=0.47).[13] This linear relationship between E_{ct} and E_π is similar to that found previously for the CT-complexes between polycyclic aromatic hydrocarbons and trinitrofluorenone and defined by the following Eq. 1.[14]

$$E_{ct} = (1/2)E_\pi + C, \quad (1)$$

where C is a constant for the acceptor such as TCNE or DDQ.

The deviation of the values for compounds (**12**, **29**, **32**, **38**, **43**, **48**, and **51**) from the straight line is probably due to the obscurity of their real first CT-bands, because their first CT-bands were broad at the longer-wavelength side, and their E_{ct} were correlated to the energies of the second bands for the uncomplexed donors, in which all the first bands were observed as a shoulder or an inflection (the points with primed numbers in Fig. 1). For compounds, **3** and **7**, the deviation cannot be explained, even though the energies of the second CT-bands (465 and 460 nm, respectively) were

correlated to the energies of the second (235 nm) and first (237 nm) bands of the donors.[2]

An analogous correlation was observed between the CT-bands of DDQ-complexes and the first bands of the uncomplexed donors (Fig. 2; the slope of the fitted straight line=0.43).[15]

The foregoing results indicated that the polyphenylenes (containing 5—9 benzene rings) and polyphenyls (containing 2—6 benzene rings) formed the weak CT-complexes with TCNE or DDQ in solution, and an approximately linear relationship with a slope of one-half existed between the first transitions of the CT-complexes and those of the uncomplexed donors. Consequently, these results made it possible to predict the CT-bands of new polyphenylenes and polyphenyls.

Gas-liquid Chromatographic Characteristics. The retention times (t_R) of nine polyphenylenes (**1—9**) and a series of polyphenyls (**14—53**), having high boiling points and a large number of isomers, were determined at 5—15 different column temperatures (70—340 °C) using a glass capillary column (Dexsil 300GC as liquid phase).[16] For comparison the t_R at the same column temperature were calculated using Eq. 2

$$\log t_R = A \times 1/T + B \quad (2)$$

and the least squares method.[17] The log t_R at 250 °C thus determined are shown in Tables 3 and 4.

To investigate the structure-retention time correlation of the polyphenyls and polyphenylenes, the retention indexes (R_I) were firstly obtained as a simple difference between the log t_R of each polyphenyl and biphenyl (**14**) as a standard. Then, the comparison between the R_I-values of three terphenyls (**15—17**) and that of **14** gave the following estimated values for each phenylene unit: *o*- (0.74), *m*- (1.17), and *p*-phenylene (1.23). Further, by introduction of the correction factor

Table 3. Retention times and indexes of the linear polyphenyls

Compound[a] No.	log t_R=A×1/T+B		log t_R[b] (250 °C)	R_I	R'_I
	A	B			
φφ (**14**)	2968	−7.307	−1.632	0	
φoφ (**15**)	3515	−7.613	−0.892	0.74	0.74
φmφ (**16**)	3784	−7.694	−0.459	1.17	1.17
φpφ (**17**)	3822	−7.713	−0.405	1.23	1.23
φooφ (**18**)	3957	−7.767	−0.201	1.43	1.40
φmoφ (**19**)	4310	−8.158	0.083	1.72	1.72
φopφ (**20**)	4383	−8.220	0.161	1.79	1.79
φmmφ (**21**)	4746	−8.518	0.558	2.19	2.25
φmpφ (**22**)	4802	−8.541	0.644	2.28	2.31
φppφ (**23**)	4846	−8.574	0.694	2.33	2.38
φoooφ (**24**)	4536	−8.238	0.438	2.07	2.02
φomoφ (**25**)	4915	−8.767	0.633	2.27	2.33
φopoφ (**26**)	5027	−8.861	0.753	2.39	2.40
φmomφ (**27**)	5209	−9.043	0.916	2.55	2.62
φpopφ (**28**)	5424	−9.282	1.087	2.72	2.75
φmpoφ (**29**)	5528	−9.349	1.210	2.84	2.80
φoppφ (**30**)	5584	−9.427	1.248	2.88	2.87
φmmmφ (**31**)	5927	−9.795	1.537	3.17	3.23
φmpmφ (**32**)	6024	−9.797	1.721	3.35	3.31
φpmpφ (**33**)	6041	−9.824	1.726	3.36	3.35
φmppφ (**34**)	6062	−9.856	1.735	3.37	3.37
φpppφ (**35**)	6096	−9.874	1.782	3.41	3.43
φooooφ (**36**)	5178	−8.874	1.023	2.66	2.58
φomooφ (**37**)	5396	−9.188	1.127	2.76	2.88
φoopoφ (**38**)	5567	−9.414	1.244	2.88	2.94
φmoomφ (**39**)	5729	−9.511	1.445	3.08	3.15
φommoφ (**40**)	5779	−9.596	1.455	3.09	3.17
φpoopφ (**41**)	5896	−9.637	1.639	3.27	3.27
φopopφ (**42**)	5900	−9.640	1.643	3.28	3.29
φompoφ (**43**)	5905	−9.648	1.649	3.28	3.24
φoppoφ (**44**)	5927	−9.696	1.666	3.30	3.31
φmmomφ (**45**)	6237	−10.117	1.808	3.44	3.55
φmopmφ (**46**)	6379	−10.247	1.950	3.58	3.62
φpmopφ (**47**)	6410	−10.243	2.013	3.65	3.67
φmmpoφ (**48**)	6453	−10.234	2.104	3.74	3.72
φopppφ (**49**)	6496	−10.138	2.282	3.91	3.85
φmmmmφ (**50**)	6750	−10.455	2.451	4.08	4.14
φmmpmφ (**51**)	6758	−10.318	2.603	4.24	4.21
φpmmpφ (**52**)	6779	−10.309	2.652	4.28	4.26
φmppmφ (**53**)	6811	−10.345	2.678	4.31	4.28

a) Refer to the footnote c) to Table2. b) Observed values: $-0.30 < \log t_R < 1.70$; inserted values: $\log t_R < -0.30$ and $\log t_R > 1.70$.

TABLE 4. RETENTION TIMES AND INDEXES OF THE POLYPHENYLENES (**1**—**9**)

Compound[a] No.	log t_R=A×1/T+B		log t_R[b] (250°C)	R_I	R'_I
	A	B			
1	5232	−8.819	1.181	2.81	2.79
3	5629	−9.277	1.488	3.12	2.89
8	5705	−9.367	1.548	3.18	3.17
7	5762	−9.368	1.644	3.28	3.29
6	5789	−9.400	1.663	3.30	3.35
2	5878	−9.443	1.796	3.42	3.43
5	5953	−9.445	1.937	3.57	3.55
4	5957	−9.449	1.941	3.57	3.01
9	6276	−9.741	2.259	3.89	3.53

a) Refer to the footnote b) to Table 3.

for the number of the phenylene ring, $(0.96)^{n-1}$ (n: the total number of phenylene rings), following empirical Eq. 3 was obtained.

$$R'_I = (0.96)^{n-1} \times (0.74x+1.17y+1.23z+\alpha), \quad (3)$$

where x, y, and z are the number of *o*-, *m*-, and *p*-phenylene rings constituting each polyphenyl, respectively, and α is the correction factor for the substitution pattern of the phenylene rings. The values are estimated as follows: −0.01, −0.12, and −0.11 for an *o*-, *m*-, and *p*-phenylene rings adjacent to the *o*-phenylene ring, respectively, and +0.11 for a *m*- or *p*-phenylene ring adjacent to the *p*-phenylene ring.

The R'_I-values calculated by Eq. 3 are in good agreement with the experimental R_I-values (Table 3). The results are also confirmed by the approximate linear relation of the log t_R values to the R'_I-values (Fig. 3).[18] Care must be taken in appling indiscriminately a variety of analytical conditions. However, when unknown polyphenyls were bracketed with polyphenyls of known retention indexes, empirical Eq. 3 is useful for the estimation of the retention time, the elution order and the presumption of their structures.

Meanwhile the data of nine polyphenylenes (penta- and hexaphenylenes) are also listed in Table 4, which differ from the linear polyphenyls in not having both terminal rings. Empirical Eq. 4 for the polyphenylenes was derived from Eq. 3 by adding a new correction factor (β=−1.20).

$$R''_I = (0.96)^{n-1} \times (0.74x+1.17y+1.23z+\alpha) + \beta \quad (4)$$

The R''_I-values calculated by Eq. 4 are in fair agreement with R_I- or log t_R-values obtained from the experimental values except for compounds **3**, **4**, and **9** (Table 4 and Fig. 3). These results can be explained by the fact that compounds **1**, **2**, and **5**—**8**, showing a good agreement with experimental values, are nonplanar due to a spacial overcrowded conformation, while other compounds **3**, **4**, and **9** are more planar in the vapor phase.

Furthermore, when the R_I-values of the polyphenylenes were compared with those of the corresponding linear analogues (Table 5), the former gave approximately the same or somewhat larger R_I-values than the latter, except for **4** and **9** which showed clearly larger

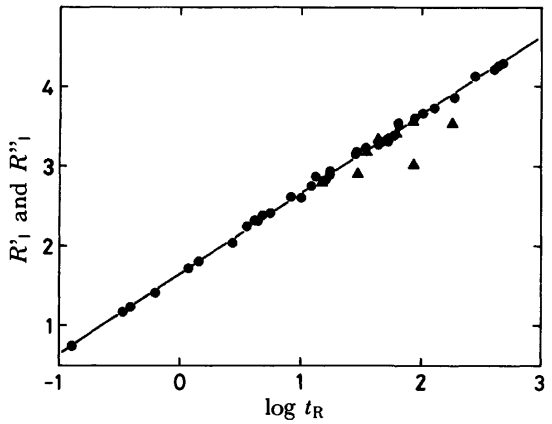

Fig. 3. Plot of the log of the retention time (log t_R) *vs.* the calculated retention index (R'_I and R''_I); ●: Linear polyphenyls, ▲: polyphenylenes.

values. That is to say, by the cyclization of the linear polyphenyls to the macrocyclic analogues the retention times were hardly affected or slightly delayed.

Foregoing results indicated that the relationship between the number and arrangement of benzene rings and the retention times of polyphenyls and polyphenylenes could be expressed by simple empirical equations, respectively. Both equations are very useful for the prediction of the retention time, elution order and the presumption of structures of unknown polyphenylenes and polyphenyls.

Photo-aryl Coupling Reaction. The bridged-annulene formation and photodehydrocyclization were examined by UV irradiation under degassed and oxidative conditions for compounds **1**, **5**, **6**, **9**, and **11**—**13** (except for **12** and **13** under the former conditions). Of these polyphenylenes, **1** and **6** correspond respectively to the di- and tribenzo analogues of the cyclophanes (**54** and **55**), for which the formation of the bridged annulenes (**54a** and **55a**) have been reported by Boekelheide *et al.*[19] (Scheme 1). In these attempts, the reductive coupling of **1** and the oxidative coupling of **1** and **6** gave the desired products, but other coupling reactions examined were unsuccessful.

When the degassed solution of **1** was irradiated, its color became immediately reddish orange (new absorption bands appeared at 372 (sh), 386, 468, and 498 nm) and then reddish orange needles (**1a**)

TABLE 5. COMPARISON OF R_I OF THE POLYPHENYLENES (**1**—**9**) WITH THOSE OF RELATED LINEAR POLYPHENYLS

Polyphenylene		Polyphenyl			
Compound[a)]	R_I	Compound[a)]	R_I[b)]	Compound[a)]	R_I
1 [m,m,o,p,o]	2.81	ϕopoϕ	2.39		
		ϕmopϕ	(2.68)	*cf.* ϕopmϕ	2.84
		ϕommϕ	(2.73)	*cf.* ϕmomϕ	2.55
3 [m,o,o,m,o,o]	3.12	ϕmoomϕ	3.08		
		ϕoomoϕ	2.76		
8 [m,o,m,o,m,o]	3.18	ϕmomoϕ	(3.17)	*cf.* ϕmoomϕ	3.08
				ϕommoϕ	3.09
7 [m,o,p,o,p,o]	3.28	ϕopopϕ	3.28		
		ϕomopϕ	(3.23)	*cf.* ϕompoϕ	3.28
		ϕopomϕ	(3.23)		
6 [o,p,o,p,o,p]	3.30	ϕopopϕ	3.28		
2 [m,m,o,m,m,o]	3.43	ϕommoϕ	3.09		
		ϕmommϕ	3.44		
5 [m,o,p,m,o,p]	3.57	ϕompoϕ	3.28		
		ϕmopmϕ	3.58		
		ϕpompϕ	3.65		
4 [o,o,p,o,o,p]	3.57	ϕpoopϕ	3.27		
		ϕoopoϕ	2.88		
9 [m,m,m,o,m,o]	3.89	ϕmommϕ	3.44		
		ϕommmϕ	(3.65)		
		ϕomomϕ	(3.17)	*cf.* ϕmoomϕ	3.08
				ϕommoϕ	3.09

a) Refer to the footnote c) to Table 2. b) The values in parentheses were calculated using Eq. 3.

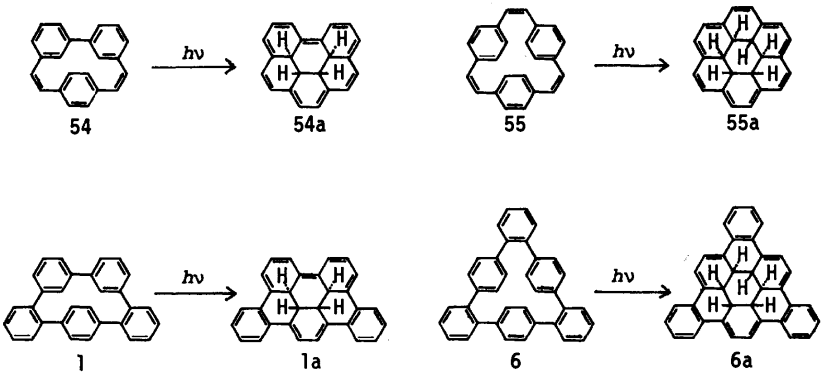

Scheme 1.

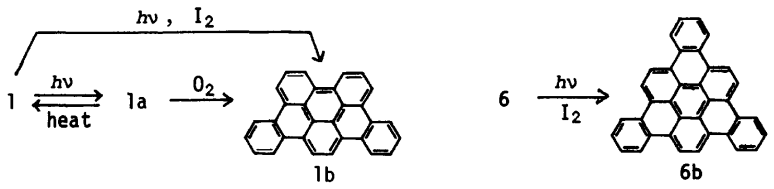

Scheme 2.

precipitated on prolonged irradiation.[20] On heating the colored solution or after standing it overnight at room temperature, it returned to the original colorless solution with the disappearance of the crystals. The reversible change was also confirmed by their absorption spectra.[21] On the other hand, in the presence of oxygen the irradiation yielded stable yellow needles (**1b**) *via* a reddish orange solution. The dehydrocyclized compound **1b** was also obtained by the photocoupling in the presence of iodine, and the absorption spectrum (λ_{max}: 228 (sh), 234, 256 (sh), 289, 300, 333, 349, 362, 368, 385, and 397 nm) was clearly distinguishable from those of **1** and **1a**.[22] The foregoing conversions can be reasonably summarized as shown in Scheme 2.

The irradiation of **6** gave dehydrocyclized compound **6b** in the presence of iodine, but not bridged annulene **6a** under the degassed conditions (Scheme 2).[24]

In connection with the photocoupling reactions of stilbene- and *o*-terphenyl-type compounds, the principal reasons for the occurrence of the coupling are summarized as follows: 1) the electron density on the carbon atoms undergoing coupling,[26] 2) the steric factors,[5a,c] 3) the nonexistence of the intermediate dihydro structures,[27] 4) the sum of the free valence numbers in the first excited state ($\sum Fr^*$) obtained for the atoms undergoing coupling and the localization energy (L^*).

The latter is the difference between the π-electron energy in the first excited state of the starting compound and that in the ground state of the intermediate dihydro derivative of the end product.[5c,27,28] Laarhoven *et al.*[5c], and Sato and Morita[28b] have independently carried out the calculation of the $\sum Fr^*$- and L^*-values by the HMO-method, and presented the critical values for the occurrence of the photocoupling: $\sum Fr^* > 1$ and $L^* < 3.45$, and $\sum Fr^* > 0.95$ and $L^* < 3.54$, respectively.

In order to consider the occurrence of the photocoupling reactions, the $\sum Fr^*$- and L^*-values of the polyphenylenes (**1**, **5**, **6**, **9**, **11**, and **12**), as well as those of the closely related compounds (**54**—**62**)[19,29] were calculated by the HMO-method (Table 6).

These values ($\sum Fr^*$ and L^*) indicate that the results of the photocoupling of the polyphenylenes and the related compounds may be explained on the basis of the criteria proposed by Sato and Morita, except for **6**, **9** and **55**. The photocoupling exceptions (**6** and **55**) may be correlated to the structures, in which three *p*-phenylene rings are fixed by three coplanar linkage. Meanwhile the uncoupled exception (**9**) is reasonably explained by the steric hindrance.

The foregoing results have indicated that the reaction indices ($\sum Fr^*$ and L^*) are useful as a measure for the occurrence of the photocoupling of macrocyclic polyphenylenes and cyclophanes with the coupling position on the macroring.

Formation of the Solvent Adducts. As described above, all the investigated aromatics formed the CT-complexes based on the weak affinity between the π-electrons of the donor and acceptor. Rapson *et al.* have previously reported the adduct-formation between *o*-tetraphenylene and a few solvents.[30] In the present study the formation of solvent adducts of the polyphenylenes was examined for several solvents, which is presumably due to the dipole-dipole interaction.

Among seven polyphenylenes (**1**—**6** and **13**) investigated, two compounds (**3** and **13**) formed successfully the adducts with several solvents, except for **3**-*m*-xylene and **13**-aniline. The thermogravimetric data are given in Table 7. The molar ratios of **3**-solvent adducts were 1:1 except for **3**-benzene (1:2), while those of **13**-solvent adducts were 1:2 except for **13**-*p*-xylene and **13**-pyridine (1:1). When some adducts (*e.g.*, **3**-benzene and **13**-*m*-xylene) were allowed to stand overnight in air at room temperature, the transparent

Table 6. Free valence numbers ($\sum Fr^*$) and localization energies ($L^*/-\beta$) for polyphenylenes and related cyclophanes

Compound No.		(1)	(6)	(5)	(9)	(11)
$\sum Fr^*$	●[a]	0.957	0.911	0.937	1.062	0.943
	○			0.896	0.867	0.900
L^*	●	2.627	3.523	3.411	3.231	3.469
	○			—[b]	—[b]	—[b]

Compound No.		(12)	(54)[c]	(55)[c]	(56)[d]	(57)[d]
$\sum Fr^*$	●[a]	0.946	0.979	0.932	0.957	0.953
	○				0.885	0.865
L^*	●	3.544	3.436	3.451	3.506	3.545
	○				3.626	3.920

Compound No.		(58)[e]	(59)[f]	(60)[f]	(61)[f]	(62)[g]
$\sum Fr^*$	●[a]	1.001	1.028	1.026	1.046	1.248
L^*	●	2.889	3.024	3.135	3.079	2.894

a) Coupling position. b) Nonexistence of intermediate dihydro structure. c), d), e), f), and g) refer to Refs. 19a, 19b, 29a, 29b, and 29c, respectively.

Table 7. Solvent adducts of polyphenylenes (**3** and **13**)

Solvent	**3**			**13**		
	Solvent release			Solvent release		
	Temp[a]/°C	%	mol	Temp[a]/°C	%	mol
benzene	110	25.2	2.0	151	18.3	2.0
toluene	101	14.9	0.9	107	19.3	1.8
o-xylene	87	17.1	0.9[b]	110	23.4	2.0
m-xylene		0		69	23.7	2.0
p-xylene	135	17.0	0.9	130	13.2	1.0
pyridine	110	13.9	0.9	159	10.2	1.0
aniline	109	16.9	1.0		0	

a) Temperature at which the maximum weight decrease in the DTG curve is observed. b) Adduct-formation temperature (%, mol): >60°C (0.22, 0.01); >50°C (0.41, 0.02); >40°C (2.54, 0.11); >30°C (15.76, 0.80); <30°C (17.10, 0.90).

crystals became opaque, and after a longer time disintegrated gradually to powder with the release of solvents. However, the adducts such as **3**-*p*-xylene and **13**-benzene were appreciably stable, especially in a tightly stoppered tube. The facts may be correlated to the solvent release temperatures of the adducts. Furthermore, for the **3**-*o*-xylene adduct the experimental results shown in Table 7 (footnote b) were obtained. Thus, **3** and *o*-xylene gave the approximately 1:1 adduct at temperatures under 30°C, but no adduct above 60°C. Consequently the formation of the adduct is obviously related with the solvent release.

The foregoing results suggested that the solvent adduct formation was limited to the particular polyphenylenes. Hence the adduct formation is different from the charge-transfer complex formation, and does not have an obvious correlation with the structures.

Experimental

Instruments. Melting points were determined with a Shimadzu DSC-30M differential scanning calorimeter. The absorption spectra were measured on a Shimadzu UV-240 spectrophotometer, and IR spectra on a Leitz III-G spectrophotometer. The molecular weights were determined with a Hitachi RMU-6MG mass spectrometer. The gas-chromatographic analyses were performed on a Shimadzu GC-7A gas chromatograph equipped with a flame ionization detector. The solvent releases of the adducts were measured by thermogravimetry using a Shimadzu TGA-30M thermogravimeter equipped with a Differentiator TD-30. The HMO calculations were carried out on Hewlett-Packard HP-85 or NEC PC-9801 personal computer.

Materials. The following polyphenylenes used were the authentic samples prepared previously[2]: *m,m,o,p,o*-pentaphenylene (**1**); *m,m,o,m,m,o*- (**2**), *m,o,o,m,o,o*- (**3**), *o,o,p,o,o,p*- (**4**), *m,o,p,m,o,p*- (**5**), *o,p,o,p,o,p*- (**6**), *m,o,p,o,p,o*- (**7**), *m,o,m,o,m,o*- (**8**), *m,m,m,o,m,o*- (**9**), and *m*-hexaphenylene (**10**); *m,o,p,p,o,m,p*- (**11**) and *m,m,m,m,p,o,p*-heptaphenylene (**12**); and *o,p,p,o,p,p,o,p,p*-nonaphenylene (**13**). Commercially available biphenyl (**14**) and terphenyls (**15**—**17**) were purified before use. Quater- to sexiphenyls (**18**—**53**) used were the authentic samples prepared previously.[3a-d,f] Commercially available tetracyanoethylene (TCNE) and 2,3-dichloro-5,6-dicyano-*p*-benzoquinone (DDQ) were purified before use, and dichloromethane (spectral-grade) was used without further purification.

Electronic Spectroscopic Measurements of Charge-transfer Complexes. Solutions of the complexes were prepared by dissolving the donors (0.005—0.05 mmol) in the acceptor-solution (10 ml) of known concentration (TCNE or DDQ; 0.01—0.1 mol/l) in dichloromethane, except for several sparingly soluble donors, for which they were prepared by saturating in the similar acceptor solution. The absorption spectra were measured in a 1- or 10-cm cell for the range 350—900 nm. The most reliable absorption maxima were obtained by the several determinations using the different concentrations of the two components or by the differential spectra with the acceptor absorption in known concentration.

Determination of Retention Times on the Gas-chromatographic Analyses. The retention times of polyphenyls and polyphenylenes were determined for 5 to 15 appropriate column temperatures in the range of 70—340°C and were corrected using methane gas. The samples were used as a benzene solution of approximately the same concentration except for a few less soluble compounds. The logarithm of retention time obtained (log t_R) was plotted against the reciprocal of the column temperature (T^{-1}, absolute temperature). All of the plots showed a linear relation[17] which was employed for the calculation of the t_R at 250°C. Other analytical conditions were as follows. Column: Dexsil 300GC glass-SCOT 10 m×0.3 mmϕ; acuracy of column temperature: ±0.1°C; carrier gas: He; flow rate: 0.70 ml/min; inlet pressure: 0.4 kg/cm^2; sprit ratio: 60:1; make-up gas: 40 ml.

Irradiation of the Degassed m,m,o,p,o-*Pentaphenylene (1) Solution.* A cyclohexane solution of **1** (8.97×10^{-5} mol/l) in a quartz cell (12 mmϕ) was carefully degassed, sealed, and irradiated using a low-pressure mercury lamp (2537 Å). After a short time the colorless solution turned into a reddish orange one, and the absorption spectrum showed an intensity decrease of the characteristic band (at 237 nm) of **1**, with an appearance of the additional bands of **1a** at 372 (sh), 386, 468, and 498 nm. After two minutes irradiation the solution showed no further change. When the irradiated colored solution was heated or allowed to stand overnight at room temperature, the solution turned into the original colorless one showing identical absorption spectrum.

The similar 5 minutes irradiation of **1** in a cyclohexane solution in the presence of air gave a pale yellow solution with the characteristic bands of **1b** at 228 (sh), 234, 256 (sh), 300, 333, 349, 362, 368, 385, and 397 nm, *via* a reddish orange

solution of **1a**.

Irradiation of m,m,o,p,o-*Pentaphenylene (1) in the Presence of Iodine.* A mixture of **1** (114 mg) and iodine (76 mg) in benzene (17 ml) was irradiated in a quartz cell under nitrogen atmosphere using a 500 W high-pressure mercury lamp for 20 h. The recrystallization of the product from xylene gave tribenzo[*b,n,pqr*]perylene (**1b**) as yellow needles; mp 390°C (lit,[31] 380°C); 107 mg (95%). IR: 697 w, 710 vw, 728 vw, 747 vs, 758 vs, 761 sh s, 799 s, 823 m, 833 vw, 838 vw, 857 w, 864 vw, 872 vw, 890 w, 899 cm^{-1} w. UV: $\lambda_{max}(\varepsilon)$ 228 (sh) (80700), 234 (103500), 256 (sh) (23100), 289 (74100), 300 (99500), 333 (15600), 349 (28400), 362 (27900), 368 (34200), 385 (2100), and 397 nm (600). (Found: C, 95.44; H, 4.50%; M^+, 376).

Irradiation of o,p,o,p,o,p-*Hexaphenylene (6) in the Presence of Iodine.* The irradiation of the solution of **6** (137 mg) and iodine (76 mg) in benzene (17 ml) was carried out in the same manner as **1**. The recrystallization of the product from dimethyl sulfoxide gave tribenzo[*a,g,m*]coronene (**6b**) as yellow needles; mp 550°C; 130 mg (96%). IR: 686 w, 747 vs, 753 sh s, 790 w, 811 s, 822 w, 827 m, 833 w, 858 w, 880 cm^{-1} w. UV: λ_{max} 221, 242, 254, 260, 300 (sh), 310, 323, 339, 348, 355, 363 nm. Found: C, 95.89; H, 4.00%; M^+, 450. Calcd for $C_{36}H_{18}$: C, 95.97; H, 4.03%; M^+, 450.

Solvent Adduct Formations of m,o,o,m,o,o-*Hexaphenylene (3) and* o,p,p,o,p,p,o,p,p-*Nonaphenylene (13).* The polyphenylenes, **3** and **13**, were crystallized from the following solvents: benzene, toluene, *o*-, *m*-, and *p*-xylene, pyridine, and aniline. They were crystallized out as solvated forms from each of the solvents, except for **3** from *m*-xylene and **13** from aniline.

3-Benzene: one-to-two adduct, colorless transparent plates. Found: C, 94.13; H, 5.94%. Calcd for $C_{36}H_{24}\cdot 2C_6H_6$: C, 94.07; H, 5.93%.

3-Toluene: one-to-one adduct, colorless transparent cubes. Found: C, 94.15; H, 5.90%. Calcd for $C_{36}H_{24}\cdot C_7H_8$: C, 94.12; H, 5.88%.

3-*o*-Xylene: one-to-one adduct, colorless transparent cubes. Found: C, 94.01; H, 6.08%. Calcd for $C_{36}H_{24}\cdot C_8H_{10}$: C, 93.91; H, 6.09%.

3-*p*-Xylene: one-to-one adduct, colorless transparent plates. Found: C, 93.95; H, 6.15%. Calcd for $C_{36}H_{24}\cdot C_8H_{10}$: C, 93.91; H, 6.09%.

3-Pyridine: one-to-one adduct, colorless transparent plates. Found: C, 92.00; H, 5.55; N, 2.60%. Calcd for $C_{36}H_{24}\cdot C_5H_5N$: C, 91.93; H, 5.46; N, 2.61%.

3-Aniline: one-to-one adduct, colorless plates. Found: C, 91.85; H, 5.61; N, 2.51%. Calcd for $C_{36}H_{24}\cdot C_6H_7N$: C, 91.77; H, 5.68; N, 2.55%.

13-Benzene: one-to-two adduct, colorless transparent cubes. Found: C, 94.33; H, 5.80%. Calcd for $C_{54}H_{36}\cdot 2C_6H_6$: C, 94.25; H, 5.75%.

13-Toluene: one-to-two adduct, colorless transparent cubes. Found: C, 94.00; H, 6.10%. Calcd for $C_{54}H_{36}\cdot 2C_7H_8$: C, 93.97; H, 6.03%.

13-*o*-Xylene: one-to-two adduct, colorless transparent cubes. Found: C, 93.81; H, 6.29%. Calcd for $C_{54}H_{36}\cdot 2C_8H_{10}$: C, 93.71; H, 6.29%.

13-*m*-Xylene: one-to-two adduct, colorless transparent cubes. Found: C, 93.75; H, 6.36%. Calcd for $C_{54}H_{36}\cdot 2C_8H_{10}$: C, 93.71; H, 6.29%.

13-*p*-Xylene: one-to-one adduct, colorless transparent cubes. Found: C, 94.15; H, 5.79%. Calcd for $C_{54}H_{36}\cdot C_8H_{10}$: C, 94.14; H, 5.86%.

13-Pyridine: one-to-one adduct, colorless needles. Found: C, 92.86; H, 5.35; N, 1.85%. Calcd for $C_{54}H_{36}\cdot C_5H_5N$: C, 92.76; H, 5.41; N, 1.83%.

The solvent releases of the adducts were determined under the following conditions: heating rate, 10°C/min; sample size, about 5 mg weighed accurately in a sealed cell with a pinhole; atmosphere, N_2 gas (40 ml/min).

The author wishes to thank Professor Aritsune Kaji of Kyoto University for his valuable discussions and suggestions.

References

1) Part XIV of "Studies of Polyphenyls and Polyphenylenes." For the preceding paper see Part XIII: Ref. 2.

2) Y. Fujioka, *Bull. Chem. Soc. Jpn.*, **57**, 3494 (1984).

3) a) S. Ozasa, N. Hatada, Y. Fujioka, and E. Ibuki, *Bull. Chem. Soc. Jpn.*, **53**, 2610 (1980); b) E. Ibuki, S. Ozasa, Y. Fujioka, and H. Kitamura, *Chem. Pharm. Bull.*, **28**, 1468 (1980); c) E. Ibuki, S. Ozasa, Y. Fujioka, M. Okada, and Y. Yanagihara, *ibid.*, **30**, 2369 (1982); d) S. Ozasa, Y. Fujioka, and E. Ibuki, *ibid.*, **30**, 2698 (1982); e) S. Ozasa, Y. Fujioka, H. Hashino, N. Kimura, and E. Ibuki, *ibid.*, **31**, 2313 (1983); f) *cf.* E. Ibuki, S. Ozasa, and K. Murai, *Bull. Chem. Soc. Jpn.*, **48**, 1868 (1975).

4) a) R. E. Merrifield and W. D. Phillips, *J. Am. Chem. Soc.*, **80**, 2778 (1958); G. Briegleb, J. Czekalla, and G. Reuss, *Z. Phys. Chem.* (Frankfurt am Main), **30**, 316 (1961); M. J. S. Dewar and H. Rogers, *J. Am. Chem. Soc.*, **84**, 395 (1962); M. J. S. Dewar and C. C. Thompson, Jr., *Tetrahedron Suppl.*, **7**, 97 (1966); b) A. R. Lepley and C. C. Thompson, Jr., *J. Am. Chem. Soc.*, **89**, 5523 (1967).

5) a) N. Kharasch, T. G. Alston, H. B. Lewis, and W. Wolf, *J. Chem. Soc., Chem. Commun.*, **1965**, 242; b) T. Sato, Y. Goto, and K. Hata, *Bull. Chem. Soc. Jpn.*, **40**, 1994 (1967); c) W. H. Laarhoven, Th. J. H. M. Cuppen, and R. J. F. Nivard, *Recl. Trav. Chim. Pays-Bas*, **87**, 687 (1968); d) T. Sato, *Yuki Gosei Kagaku Kyokai Shi*, **27**, 715 (1969); e) T. Sato, S. Shimada, and K. Hata, *Bull. Chem. Soc. Jpn.*, **42**, 766 (1969); *ibid.*, **44**, 2484 (1971).

6) a) P. W. Solomon, *U. S. At. Energy Comm.*, IDO-16912 (1964); b) F. Onuška and J. Janak, *Chem. Zvesti*, **22**, 929 (1968); S. Lukáč, *Collect. Czech. Chem. Commun.*, **33**, 2429 (1968).

7) E. Kováts, *Helv. Chim. Acta*, **41**, 1915 (1958); A. Wehrli and E. Kováts, *ibid.*, **42**, 2709 (1959).

8) B. L. Karger, Y. Elmehrik, and R. L. Stern, *Anal. Chem.*, **40**, 1227 (1968).

9) A. Ono, *Nippon Kagaku Zasshi*, **91**, 72 (1970); *ibid.*, **92**, 242, 429, 433, and 986 (1971).

10) All the CT-complexes in the present study could not be isolated as crystals (*cf.* crystalline complexes of the TCNE-paracyclophanes: Ref. 11).

11) D. J. Cram and R. H. Bauer, *J. Am. Chem. Soc.*, **81**, 5971 (1959); M. Sheehan and D. J. Cram, *ibid.*, **91**, 3553 (1969).

12) In a series of aromatic hydrocarbons including biphenyl and *p*-terphenyl, Lepley and Thompson have indicated a correlation between the energies of second CT-bands for their TCNE-complexes and the penultimate occupied HMO coefficients (in β-unit) for the hydrocarbons (Ref. 4b). However, the absorption spectra of a large majority of the TCNE-complexes examined in the present study

displayed commonly an absorption maximum or a shoulder near 400 nm as the second or the third CT-band. The energies of the CT-bands near 400 nm of polyphenyl- and polyphenylene-TCNE complexes are rather correlated with those of the E-bands near 200 nm of the respective donor hydrocarbons.

13) The line was fitted by the least squares method except the complexes of two groups (correlation coefficient: 0.95).

14) A. R. Lepley, *J. Am. Chem. Soc.*, **84**, 3577 (1962).

15) Correlation coefficient: 0.95.

16) For polyphenyls and polyphenylenes, as well as for the series of alkylbenzenes (Ref. 9), the saturation vapor pressures of substituted components were assumed to be proportional to those of unsubstituted components.

17) Correlation coefficients: lager than 0.999 for all compounds.

18) Correlation coefficient: 0.997.

19) a) R. B. DuVernet, T. Otsubo, J. A. Lawson, and V. Boekelheide, *J. Am. Chem. Soc.*, **97**, 1629 (1975); b) T. Otsubo, R. Gray, and V. Boekelheide, *ibid.*, **100**, 2449 (1978).

20) The crystals were not isolated due to the ready oxidative dehydrogenation.

21) The ^{1}H NMR spectra of **1a** could not be determined due to the poor solubility and the reversibility to **1**.

22) The radical anion (greenish blue) prepared from **1** with sodium in THF under nitrogen atmosphere showed the absorption maxima at 380 (sh), 415, 556, and 590 nm. In the presence of a trace of oxygen, however, the spectrum showed the bands at 363 (sh), 367, 384, 395 (sh), 421, 480, 534 (sh), 555, 676, 740, and 833 nm, and it was actually identical with that of the radical anion prepared from **1b**. This fact suggests that the radical anion undergoes an oxidative dehydrocyclization (*cf.* Ref. 23).

23) Ch. Elschenbroich, F. Gerson, and J. A. Reiss, *J. Am. Chem. Soc.*, **99**, 60 (1977).

24) The bridged-annulene formation from **55** to **55a** was unsuccessful at room temperature, but successful at −60 °C (Ref. 25 and 19). The examined compounds (**5**, **6**, **9**, and **11**) did not couple at −60 °C, though **6** was colored by irradiation in light blue.

25) D. J. Cram and K. C. Dewhirst, *J. Am. Chem. Soc.*, **81**, 5963 (1959).

26) F. B. Mallory, C. S. Wood, and J. T. Gordon, *J. Am. Chem. Soc.*, **86**, 3094 (1964).

27) M. Scholz, F. Dietz, and M. Mühlstädt, *Z. Chem.*, **7**, 329 (1967).

28) a) M. Scholz, M. Mühlstädt, and F. Dietz, *Tetrahedron Lett.*, **1967**, 665; b) T. Sato and T. Morita, *Bull. Chem. Soc. Jpn.*, **45**, 1548 (1972).

29) a) H. Blaschke and V. Boekelheide, *J. Am. Chem. Soc.*, **89**, 2747 (1967); b) R. H. Mitchell, R. J. Carruthers, and L. Mazuch, *ibid.*, **100**, 1007 (1978); c) J. R. Davy and J. A. Reiss, *Aust. J. Chem.*, **29**, 163 (1976).

30) W. S. Rapson, R. G. Shuttleworth, and J. N. van Niekerk, *J. Chem. Soc.*, **1943**, 326.

31) H. Reimlinger and A. van Overstraeten, *Chem. Ber.*, **91**, 2151 (1958).

A Comparative Study of Photoinduced Isomerizations between 1-*exo*- and 1-*endo*-Cyano-1a,7b-dihydro-1*H*-cyclopropa[*a*]naphthalenes

Hisako KOBAYASHI, Masahiko KATO,* and Toshio MIWA
Faculty of Science, Osaka City University, Sugimoto-3, Sumiyoshi-ku, Osaka 558
(Received June 30, 1984)

The titled compunds 1-*exo*-Cyano-1a,7b-dihydro-1*H*-cyclopropa[*a*]naphthalenes(**8a**), 1-*endo*-Cyano-1a, 7b-dihydro-1*H*-cyclopropa[*a*]naphthalenes(**8b**), were photolyzed in several solvents. The results were: (1) The isomerization proceeded faster in aprotic nonpolar solvents than in polar ones. (2) The 1-*endo* derivative (**8b**) rearranged faster than the 1-*exo*-isomer (**8a**). (3) **8b** was isomerized through Berson-Willcott rearrangement by the fission of bonds C_1-C_{7b} and C_1-C_{1a}, while **8a** gave 1-cyanomethylnaphthalene (**5b**) as a main product. (4) Examination with an optically active 1-*exo* derivative (**8a**) showed that the *exo-endo* interconversion occured by the simultaneous two centered (30%) and one centered (70%) epimerization.

The photochemical isomerization of 1-substituted 1a,7b-dihydro-1*H*-cyclopropa[*a*]naphthalenes (**1**) had been found to proceed in two directions (Scheme 1):[1-6] The rearrangements by the fission of the C_1-C_{7b} bond (Path a) to give 7-substituted 7*H*-benzocycloheptenes (**2**) and 2-substituted naphthalenes (**3**) and by the fission of the C_1-C_{1a} bond (Path b) to give 5-substituted 5*H*-benzocycloheptenes (**4**) and 1-substituted naphthalenes (**5**), in addition to the secondary photoproducts originating from **2** and **4**. The difference in photochemical reactivities between 1-*endo* and 1-*exo* substituted derivatives of **1** had been studied in methanol with 1-methoxycarbonylmethyl-3-isopropyl-1a,7b-dihydro-1*H*-cyclopropa[a]naphthalene (**6**), which gave the same products in different proportions.[4] The results were in line with the stereochemical course of the re-

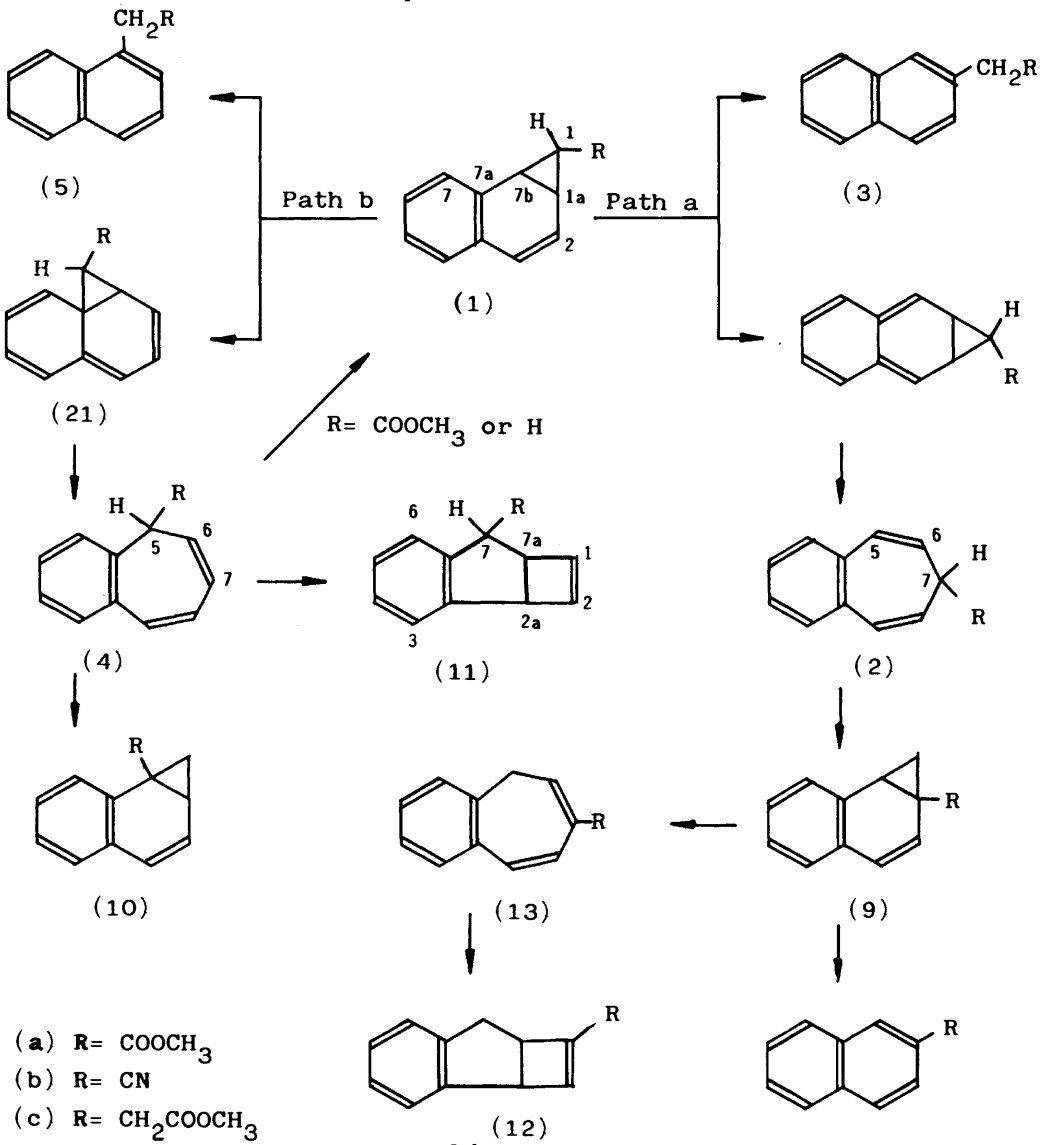

Scheme 1.

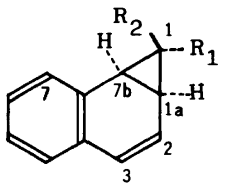

(7a) R_1= $COOCH_3$, R_2= H
(7b) R_1= H, R_2= $COOCH_3$
(8a) R_1= CN, R_2= H
(8b) R_1= H, R_2= CN

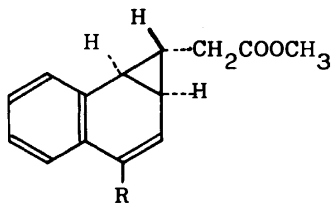

(6) R= i-Pr
(15) R= t-Bu
(16) R= H

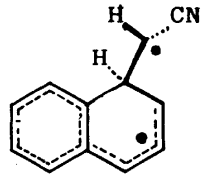

(14a)

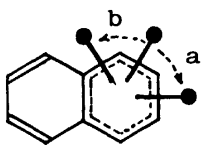

(18a)

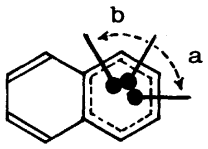

(18b)

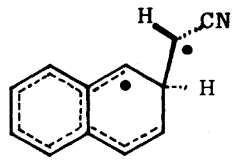

(17a)

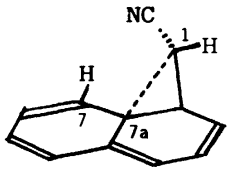

(19)

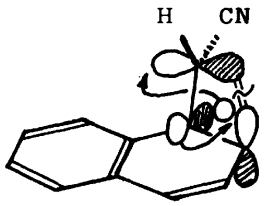

(20)

arangement established using optically active substrates.[3,5]

It is well known that the substitution with an electron-withdrawing group on the cyclopropane ring will have a strong affect on the bond strengths of the three membered ring under both ground and excited states.[7] Therefore, it was interesting to investigate the difference in photochemical reactivities between *exo* and *endo* isomers of 1-methoxycarbonyl- or 1-cyano-1a,7b-dihydro-1*H*-cyclopropa[*a*]naphthalene and to compare it with the photochemical behavior of *exo* and *endo* isomers of **6**. Swenton *et al.* found that when 1-deuterio-1-*exo*-methoxycarbonyl-1a,7b-dihydro-1*H*-cyclopropa[*a*]naphthalene (**7a**-1-d_1) was irradiated, though the typical products *via* path b were not detected, the deuterium atom on C_1 scrambled into the hydrogens on C_{1a} and C_{7b} of recovered **7a**,[2] which suggested that the rearrangement occurs in two directions. Later on, we reported that the direct irradiation at low temperature of 5-methoxycarbonyl-5*H*-benzocycloheptene (**4a**), which is assumed to be one of the primary photoproducts of the skeletal rearrangement of **7a**, gave exclusively 1-*endo*-methoxycarbonyl-1a,7b-dihydro-1*H*-cyclopropa[*a*]naphthalene(**7b**).[8] Beacause of the thermal instability of **7b** (facile Cope rearrangement),[8] comparison of the reactivities between exo and endo isomers of **7** was difficult.

Recently, the cyano derivatives (**8a** and **8b**) were obtained in stable crystalline forms,[6] therefore, we studied concurrently their photochemistry under direct irradiation in several solvents. The results were different from their isomerization under sensitized irradiation,[6] and also from the results obtained with **6**.[4]

Results

Irradiation of **8b** (*endo*) in benzene for 30 min resulted in a 94.3% recovery of the material. The mixture was composed of **8a** (yield, 2%), **8b** (35%), **9b** (11%),[10] **10b** (15%),[9] 7-cyano-[9] and 1-cyano-2a,7a-dihydro-7*H*-cyclobut[*a*]indene[9] (**11b**, 18%; **12b**, 8%). They were identified by direct comparison with the authentic samples obtained through direct irradiation of **4b**[9] and of 7-cyano-5*H*-benzocycloheptene (**13b**).[10]

The preparative photochemistry of **8a** has also been examined with an optically active isomer (see below) and **5b** was obtained as the main product, which was identical with an authentic sample prepared according

to the known procedure.[11]

In order to uncover the effect of the solvent polarity on the product composition,[9] the rearrangement of **8a** and **8b** was carried out in several solvents. The results are shown in Table 1. It is observed that the rates for disappearance of **8a** and **8b** are faster in aprotic nonpolar solvents than in polar ones. In every solvent, **8b** was consumed somewhat faster than **8a** and,

TABLE 1. PHOTOCHEMICAL REACTIONS OF **8a** AND **8b** IN VARIOUS SOLVENTS

a) in Methanol

Irradiation time/h	Compounds[a]									
From **8a**	**8**[b]	**11b**	**12b**	**4b**	**10b**	**9b**	**5b**	**A**[c,d]	**B**[c,d]	**C**[c,d]
1	92.6	0.0	0.0	0.0	0.0	0.6	6.0	0.34	—	—
2	80.0	1.05	0.95	1.4	1.3	3.4	8.9	0.35	0.70	0.86
3	70.7	1.05	1.35	1.1	1.3	4.6	13.4	0.35	0.80	0.58
4	67.4	1.8	1.8	1.6	2.6	6.0	16.5	0.35	0.73	0.77
5	59.0	2.25	2.55	2.1	3.3	8.6	19.4	0.41	0.72	0.68
							mean[d]	0.37	0.74	0.72
From **8b**										
1	82.5	1.8	0.4	6.2	4.4	3.1	0.0	0.28		
2	72.2	3.6	1.9	6.8	7.2	5.7	0.0	0.43		
3	61.9	6.9	2.1	5.6	11.2	9.0	0.0	0.47		
4	51.7	11.3	3.4	3.8	14.3	11.7	0.0	0.52		
5	41.7	18.9	3.7	3.0	18.2	13.2	0.0	0.42		
							mean	0.46		

b) in Acetonitrile

From **8a**	**8**	**11b**	**12b**	**4b**	**10b**	**9b**	**5b**	**A**[c,d]	**B**[c,d]	**C**[c,d]
1	86.9	1.2	0.3	0.5	1.0	2.3	7.0	0.27		
2	78.3	1.3	1.0	0.7	1.9	5.1	10.7	0.42	0.73	0.64
3	73.7	2.3	1.3	0.8	2.8	6.0	12.5	0.35	0.68	0.81
4	64.7	3.1	2.0	1.2	4.0	9.0	13.7	0.50	0.62	0.81
5	59.5	4.6	2.7	1.2	5.6	10.8	14.5	0.52	0.56	0.85
							mean	0.45	0.65	0.78
From **8b**										
1	78.7	3.9	1.2	1.7	6.9	5.3	0.0	0.52		
2	67.7	6.0	2.3	1.2	10.8	9.1	0.0	0.63		
3	59.4	7.3	2.3	0.8	13.7	12.4	0.0	0.67		
4	51.7	10.4	3.5	0.0	16.7	12.4	0.0	0.59		
5	41.9	12.4	4.7	0.0	17.7	16.2	0.0	0.69		
							mean	0.65		

c) in *t*-Butyl alcohol

From **8a**	**8**	**11b**	**12b**	**4b**	**10b**	**9b**	**5b**	**A**[c,d]	**B**[c,d]	**C**[c,d]
1	86.7	1.2	0.4	1.4	0.8	2.6	6.7	0.30	—	—
2	78.6	2.1	1.1	1.6	1.3	5.0	10.2	0.40	0.67	0.82
3	72.1	3.5	1.7	1.5	1.6	5.2	13.7	0.34	0.67	0.95
4	63.1	5.2	2.7	1.6	2.6	7.1	17.0	0.37	0.64	0.96
5	59.5	6.2	2.9	1.6	3.3	7.8	18.0	0.37	0.62	1.04
							mean	0.37	0.65	0.94
From **8b**										
1	80.4	5.0	1.3	5.1	3.0	4.4	0.0	0.44		
2	70.3	9.1	1.9	5.2	4.8	7.3	0.0	0.48		
3	62.5	15.3	3.7	4.9	10.5	10.5	0.0	0.46		
4	49.5	17.6	4.6	3.5	10.2	11.2	0.0	0.50		
5	44.9	21.6	5.3	2.6	10.3	10.8	0.0	0.47		
							mean	0.48		

d) in Benzene

From **8a**	**8**	**11b**	**12b**	**4b**	**10b**	**9b**	**5b**	**A**[c,d]	**B**[c,d]	**C**[c,d]
1	72.2	2.9	1.4	1.0	2.7	6.0	12.1	0.40	—	—
2	58.4	4.1	2.9	1.1	4.1	9.4	19.2	0.43	0.67	0.76
3	46.3	6.1	4.8	0.0	5.0	12.3	23.6	0.49	0.68	0.65
4	38.3	6.3	6.8	0.0	5.6	13.5	27.3	0.51	0.70	0.59
5	32.9	8.6	7.4	0.0	5.5	15.3	27.6	0.54	0.66	0.62
							mean	0.49	0.68	0.66

From **8b**										
1	72.1	9.7	2.4	1.2	9.9	2.2	0.0	0.22		
2	52.1	13.8	3.9	1.1	14.2	9.6	0.0	0.46		
3	39.8	17.9	6.4	0.0	18.5	11.6	0.0	0.49		
4	31.7	19.8	8.8	0.0	19.0	11.7	0.0	0.52		
5	22.2	23.3	10.7	0.0	19.2	13.3	0.0	0.56		
							mean	0.51		
e) in Cyclohexane										
From **8a**	**8**	**11b**	**12b**	**4b**	**10b**	**9b**	**5b**	**A**[c,d]	**B**[c,d]	**C**[c,d]
1	78.1	4.0	1.9	1.5	0.6	4.4	8.6	0.43	—	—
2	65.5	7.3	3.7	2.0	1.0	6.7	12.9	0.45	0.56	1.00
3	58.3	10.0	4.3	1.8	1.6	8.3	14.5	0.45	0.52	1.1
4	48.1	13.4	5.8	2.1	1.9	10.0	17.3	0.46	0.50	1.1
5	43.5	16.9	6.7	1.6	1.6	10.9	19.8	0.44	0.50	1.1
							mean	0.45	0.52	1.1
From **8b**										
1	77.5	10.0	2.5	3.3	2.0	4.1	0.0	0.43		
2	63.2	18.2	4.2	3.2	3.2	6.8	0.0	0.45		
3	51.0	25.9	5.4	2.7	3.9	7.5	0.0	0.40		
4	44.2	32.0	6.1	1.9	4.6	8.2	0.0	0.37		
5	32.9	34.4	9.4	1.9	5.2	11.5	0.0	0.50		
							mean	0.43		

a) The concentrations of **8a** and **8b** were kept constant throughout and their initial concentration was set equal to 100. All figures are normalized to those obtained in benzene. b) Compounds **8a** and **8b** were not distinguishable by GLC because of their thermal interconversion. c) Following product ratios are shown as **A**, **B**, and **C**: **A**=(**9b**+**12b**)/(**4b**+**10b**+**11b**+**5b**); **B**=**5b**/(**4b**+**10b**+**11b**+**5b**); **C**=(**4b**+**10b**+**11b**)/(**9b**+**12b**). d) To calculate the mean values of **A**, **B**, and **C**, the data of 1h-irradiation were omitted, where some of the products were formed in small amounts, hence, the margins of the error in **A**, **B**, and **C** seemed to be large.

although **5b** was not detected in the products from **8b**, it was the main product from **8a**.

Discussion

It was found that, in every solvent studied, **8a** produced **5b** in the largest quantity along with **9b** and **11b**, while **8b** gives mainly **11b** and **10b** (or **9b**). Dissimilar to the results of the direct irradiation of *exo*-**6** and *endo*-**6**,[4] the *exo-endo* interconversions of **8** were found to occur during irradiation, though the rates were very slow. To test the mechanism of the isomerization from **8a** to **8b** under direct irradiation, (+)-(1R)-**8a** ([α]$_D$ +103°) was photolyzed in benzene and the following compounds were isolated: **8b** (6%, [α]$_D$ +259° ±40°), **9b** (13%), and **3b** (19%), in addition to the recovered **8a** (48%, [α]$_D$ +94.2°±2°). This result indicates that the racemization of the starting material was 8.6±0.2% and the retention of optical activity for isomerization of **8a** was 45±7%. Thus, it is estimated that the one-centered epimerization (Scheme 2, Path i) in (1R)-**8a** was contaminated with the two-centered epimerization (Path ii) to an extent of 30%. This result was quite different from that under sensitized irradiation where the very fast one-centered epimerization was observed.[6] Under the sensitized conditions, a triplet biradical species (**14a**) could solely be the convincing intermediate, and hence no racemization of both carbon centers C_{1a} and C_{7b} was observed.

In order to discover if **5b** was formed through a biradical intermediate derived from **8a**, **8a** was irradiated in the presence of tributyltin hydride, a good

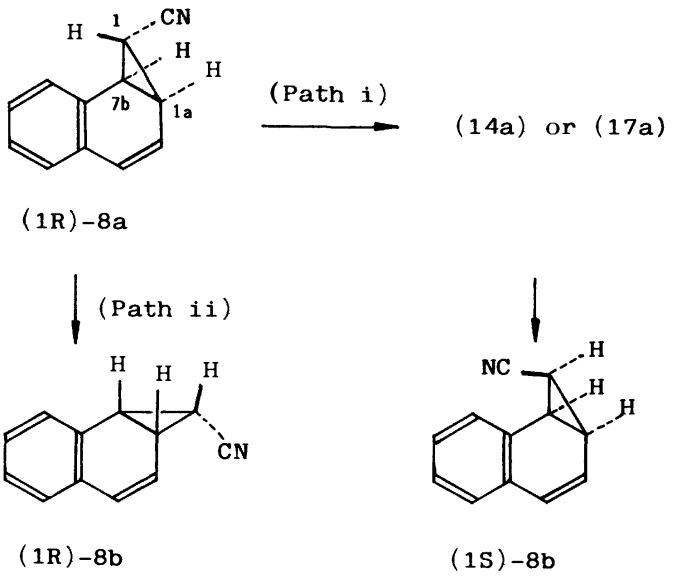

Scheme 2.

hydrogen donor,[12] or dideuterium selenide, a trapping agent.[13] In the presence of tributyltin hydride, however, no product other than those produced in the absence of these addenda was observed. In the presence of dideuterium selenide, neither was any deuterium incorporated into **5b**. These observations, in conjunction with the formation of **5b** even in benzene,[14] show that the isomerization of **8a** would occur either through a biradical in a solvent cage with a life-time too short to be trapped with such reagents or through an intramolecular concerted process which leads directly to **5b**. Such a process has been argued by

Lambert and Laarhoven in the photochemical di-π-methane rearrangement.[15]

As mentioned above, **6**, **15**, and **16** were found to rearrange in a concerted manner with inversion of the C-1 configuration in two directions, and a series of the rearrangement products following them has been established (Scheme 1).[3-5] Based on this knowledge, it is apparent that compounds **10b** and **11b** are formed *via* **4b** and compounds **9b** and **12b** *via* **2b**.[16] The process might proceed *via* an excited singlet state of **8a**, which will make bond reorganization follow either path a or path b to give **2b** and **4b**, respectively. It is possible that the rearrangement goes through a transient singlet biradical species such as **14a**.

Zimmerman introduced the K concept for predicting the multiplicity control of the di-π-methane rearrangement of 1,1,2,2-tetraphenyl-5,5-bis(methoxycarbonyl)-1,4-pentadiene and made a number of generalization to estimate the relative magnitude of K for different excited transition states or species.[17] A small K reaction is preferred by the singlet and the large K reaction is preferrd by the triplet species. In the generalization he proposed: "(1) Pericyclic reactions tend to have small *K*'s. (2) Biradical species with electron-withdrawing group on biradical centers have diminished *K*'s." According to his proposal, thus, transient biradical species such as **14** and **17** may possibly be in their singlet excited states if the transformation is not the concerted process. Sensitized irradiation *via* triplet states gave rise to different results.[6]

The schematic bird's eye-view of the movement of the exo-substituent on C-1 is shown in **18a** while that of the endo-substituent on C-1 in **18b**, where the ring carbons of **8** lie in a plane of the paper. The bonds to the substituents, H and CN, attached to C-1 are projected on the plane and are shown with a rod having a blackened circle at the end, which expresses a cyano group. The C-1 atom and the bonds from C-1 to the ring carbons are omitted. As the least-motion process should be energetically more favorable than the other,[18] the excited *endo*-isomer (**8b**) is expected to react toward both sides faster than the excited *exo*-isomer (**8a**). This trend is seen in all solvents, but especially in polar solvents. Thus, from Table 1, it is observed that the rates for the isomerization of **8a** and **8b** in several solvents stand in the decreasing order of: benzene, cyclohexane, acetonitrile, and *t*-butyl alcohol=methanol. This fact suggests that the transition state of this reaction would not be a polar one.

Similarities in the ratios (**A**) of the proportion of path a products (**9b**+**12b**) to that of path b products (**4b**+**10b**+**11b**+**5b**) in aprotic nonpolar solvents are observed on irradiation of **8a** and **8b** (in benzene, 0.50±0.01; in cyclohexane, 0.43±0.01). As compound **5b** is not formed from **8b**, **5b** must be formed from **8a** in compensation for the formations of **4b**, **10b**, and **11b**. The rates of the formation of **5b** are similar in every solvent, except in benzene. The values (**C**) of (**4b**+**10b**+ **11b**)/(**9b**+**12b**) for **8a** may be used as a criterium for how the path b is affected by solvents. The retardation (%) of the reaction through path b compared to that through path a in various solvents is obtained using cyclohexane as a standard: methanol (33%), acetonitrile (27%), *t*-butyl alcohol (12%), benzene (38%), and cyclohexane (0%). In accordance with these data, the molar fraction (**B**) of **5b** in path b products in methanol was found to be the highest (0.74±0.05), and in cyclohexane the lowest (0.52±0.04). The values for the other solvents were approximately the same (0.66± 0.05). These facts may be explained as follows. The solvation of the cyano group in **8a** will not be specifically hindered. In the movement of the *exo*-substituent (**18a**), the molecule seems not to alter any solvation energy along path a, but the movement in path b resulted in the loss of the solvation energy by the interference of the substituent with a hydrogen on C-7. Thus the pathway b (**4b**+**5b**+**10b**+**11b**) will be more or less unfavorable compared to path a (**9b**+ **12b**).[9] In **18b**, though one side facing the 6-membered ring is severly blocked to solvation, the degree of solvation is not much altered along both pathways a and b. The interaction of C_7-H with the solvated cyano group and the loss of solvation energy in **19** will raise the energy barrier for symmetry allowed excited Berson-Willcott rearrangement. The situation for solvation of **5b** would not differ from that of **8a**. Therefore, the molecular portion *via* the 1,2-hydrogen shift to **5b** will increase among the molecules following path b. The 1,2-hydrogen shift may also be the symmetry-allowed [$\sigma 2_a + \sigma 2_a$] in the excited state; the orbitals involved are shown in **20**.

A considerable rate acceleration and anomalies for the photoreaction of **8a** and **8b** were observed in benzene compared with the data in the other solvents studied. Similar phenomena had been observed for the photoreaction of **4b**.[9] The reason for the accleration in benzene is still unclear.

Orbital Symmetry Considerations. In order to obtain knowledge about the polarity signs of the lobes for the frontier orbitals during the Berson-Willcott rearrangement, we calculated some phases of the electronic states during the rearrangement of **1** (R=H) to 1,1a-dihydro-1*H*-cyclopropa[*a*]naphthalene (**21**; R=H) making use of the extended Hückel M. O. calculations.[19] The molecular geometry of norcaradiene was taken from the X-ray crystallographic analysis data of 2,5-dimethyl-7,7-dicyanobicyclo[4.1.0]hepta-2,4-diene[20] with some modifications of the double bond to that of a benzene ring (1.43 Å). In line with the Woodward-Hoffmann rule, the C-1 orbital-lobe of the HOMO at the half way of the rearrangement in 120° mechanism[4] comes near the C-7a orbital-lobe of the same mathematical sign (bonding; allowed), while that of the LUMO comes near the opposite sign of C-7a orbital-lobe (*anti*-bonding; forbidden). On the other hand, the C-1

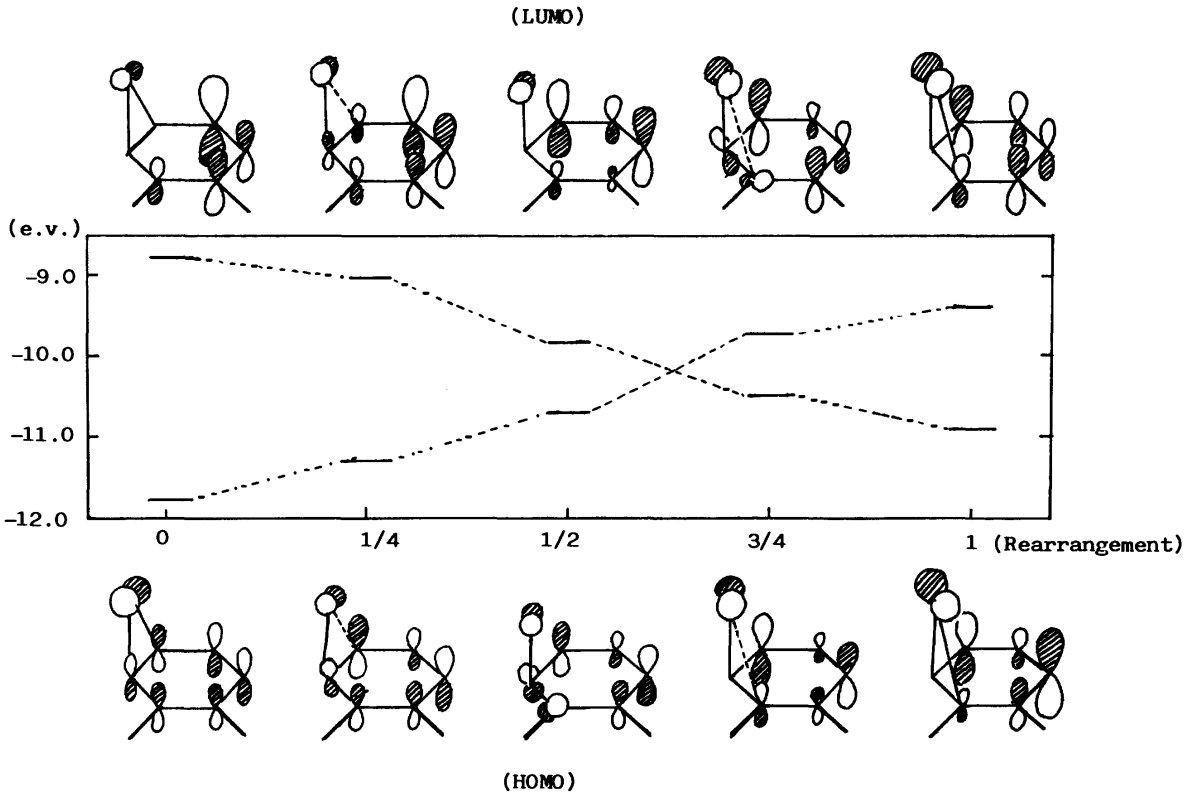

Fig. 1. The schematic orbital-lobes with their polarity signs and the corresponding orbital energy levels of the HOMO and the LUMO during rearrangement of 1 in the 60° mechanism.

orbital-lobe of the LUMO at the half way in 60° mechanism[4] comes near the C-7a orbital-lobe of the same sign (bonding; allowed). The schematic orbital-lobes with their polality signs and the corresponding orbital energy levels of the HOMO and the LUMO during rearrangement in 60° mechanism, calculated at the stages of the start, 1/4, 1/2, 3/4, and the complete rearrangements, are shown in Fig. 1. It is interesting to see that the LUMO (or HOMO) of the starting material is linked continuously with the HOMO (or LUMO) of **21** (R=H) in the polarity sings and their rough sizes of orbitals. The difference in the energy levels between the HOMO and the LUMO becomes smallest near the half way of the rerrangement. Though the calculations are classical, the rearrangement in the 60° mechanism would be photochemically allowed in the excited states, therefore, may proceed in a concerted manner.

Experimental

General Procedure. IR and ^{1}H-NMR were recorded according to the method given in the previous paper.[6,9] A Shimadzu Gas Chromatograph GC-4BM was used for the analytical purposes (Hydrogen ion flame detector). The column used was ϕ3.5 mm×1.0 m column charged with 3% Silicone OV-17 on Chromosorb WAW. For preparative column chromatography under medium pressure, a silica gel column (Merck Kiesegel 60, 230—400 mesh; ϕ8.2×500 mm) equipped with a F.M.I. pump (type RP-SY-1CSC) was used. For irradiation on a preparative scale, a solution charged in a vessel fitted with a Pyrex cooling jacket was purged with dry nitrogen for five min and internally irradiated with an Ushio High Pressure mercury lamp (HPL) (UM-452). The characterization of compounds, **4b**, **8a**, **8b**, **9b**, **10b**, **11b**, and **12b** had been reported previously.[1,2,8,9] In this experiment, the IR and NMR spectra, and the GLC retention times were compared with those of authentic specimens.

Irradiation of Racemic 8b. Racemic **8b** (54.8 mg; 0.33 mmol) dissolved in anhydrous benzene (40 mL) was irradiated internally with a HPL (UM-102) under ice-water cooling for 30 min. After evaporation of the solvent, the residue taken in benzene was filtered through a short column of silica gel (10 g) and the product chromatographed on 23 g of silica gel using 10% ether–hexane as solvent under medium pressure (1.2 atm). The products were **8a** (1.1 mg; 2%), **8b** (19.1 mg; 35%), **10b** (8.4 mg; 15%), **11b** (9.7 mg; 18%), **9b** (6.1 mg; 11%), and **12b** (4.3 mg; 8%). The ^{1}H NMR spectra of **10b** and **11b** were identical with those of the reported ones[9] and those of **9b** and **12b** were identical with the ones obtained by the photolysis of **13b**.[1,2] **9b**: NMR ($CDCl_3$) δ=0.43 (1H, d,d, J=4.4, 6.4 Hz), 2.12 (1H, d,d, J=9.7, 4.4 Hz), 3.9 (1H, bd, 6.4, 9.7 Hz), 6.19 and 6.39 (2H, AB type, J=9.8 Hz), 7.1—7.4 ppm (Ar-H). **12b**: NMR ($CDCl_3$) δ=3.02—3.28 (2H, m), 4.37 (1H, b), 7.02 (1H, bs), 7.1—7.3 ppm (Ar-H). **5b**: NMR ($CDCl_3$) δ=4.13 (2H, s), 7.4—7.65 (4H, m), 7.8—7.95 (3H, m). The GLC retention times (min) for them were also coincident with those of authentic specimens: Column temperature, 150 °C; hydrogen flow rate, 30 mL min^{-1}; retention times: **11b**, 4.3 min; **12b**, 4.6 min; **10b**, 5.8 min; **9b**, 6.2 min; **8**, 9.4 min.

Irradiation of Optically Active 8a. Optically active **8a** ([α]$_D$ +103°; 54.7 mg, 0.33 mmol) dissolved in anhydrous benzene (40 mL) was irradiated as described above. The products were **8a** (26.2 mg; 48%), **8b** (3.0 mg; 6%), **9b** (7.4 mg; 14%), and **5b**[11] (10.5 mg; 19%). The recovered **8a** and **8b** were

further purified by column chromatography under medium pressure (10% ether-hexane as an eluent): **8a** ($[\alpha]_D^{30}$ +94.2° (c=0.12 (CH_3OH)); **8b** ($[\alpha]_D^{31.5}$ +259° (c=0.15 (CH_3OH)).

Irradiation of 8a in the Presence of Tributyltin Hydride. **8a** (116 mg; 0.69 mmol) and hexadecane (24 mg; 0.11 mmol) were dissolved in anhydrous benzene and made up to 100 mL solution. This solution was divided into three portions; 40 mL, 30 mL, and 30 mL. To these solutions, tributyltin hydride (53% in tributyltin chloride) was added in the amounts of 1.51 g (10 mol-equivalent to **8a**), 619 mg (5.5 mol-equivalent), 227 mg (2 mol-equivalent), respectively. They were irradiated independently with a HPL (UM-102) for 30 min. The peak areas of the products analyzed by GLC were as follows: for 10 mol-equivalent of the hydride; **8**:**9b**:**5b**= 58:9:15.5; for 5.5 mol-equivalent; **8**:**9b**:**5b**=61:8.8: 13.0; for 2.0 mol-equivalent; **8**:**9b**:**5b**=59:9:15.3. (The data were obtained by taking the initial amount of **8a** as 100 and normalizing with the peak of hexadecane as constant).

Irradiation of 8a in the Presence of Dideuterium Selenide. To **8a** (56 mg; 0.33 mmol) dissolved in anhydrous benzene (15 mL) was added a solution of dideuterium selenide[21] in anhydrous benzene (1.75 mmol/25 mL) and the mixture was irradiated internally as above for 30 min. After irradiation (no precipitation of selenium was observed), the benzene solution was washed successively with 1 M aq sodium hydroxide (2 mL×2), water, saturated brine, and dried. Separation of the products by column chromatography gave **8b** (7 mg) and a mixture (41 mg) of **8a**, **9b**, and **5b**. Careful examination of ^1H NMR spectrum of the latter on the peak areas at 4.13 and 7.8—7.95 ppm for benzylic and α-protons of **5b**, respectively, shows that the resultant **5b** was not contaminated by more than 5% of the deuterated **5b**.

Comparison of the Photoreaction of 8a and 8b. The solvents used for photolysis were purified as reported earlier.[9] Methanol, t-butyl alcohol, acetonitrile, benzene, and cyclohexane were used as solvents. Each 1.0 mmol dm^{-3} solution of **8a** or **8b** was prepared in an appropriate solvent containing 0.10 mmol dm^{-3} of hexadecane as an internal standard. The photochemical reactions were carried out with the same technique (merry-go-round apparatus) described before.[9] Five tubes containing the same solution (5 mL) to be examined and two containing the benzene solution (5 mL) were photolyzed at the same time with a high pressure mercury lamp (UM-452) through a Pyrex filter under cooling (ice-water). During the irradiation, the test tube was taken out every one hour and each of 10 μL of the solution was examined by GLC with temperature programing (100 °C to 150 °C; 5 °C min^{-1}). The retention times of the products were as follows: Hexadecane, 9.1 min; **11b**, 12.3 min; **12b**, 13.1 min; **4b**, 13.9 min; **10b**, 14.3 min; **9b**, 14.7 min; **8**, 19.0 min; **5b**, 21 min. Each relative area of each peak was normalized to the area of the hexadecane and the data for each solvent were adjusted to the data obtained in benzene. The data in all solvents studied are listed in Table 1. No calibrations were made for each product because the use of a temperature programing technique might make the margin of error significant large. However, it may be said that the margin of error will be within 20% among different compounds and within 5% among the same compounds.

References

1) a) D. M. Madigan and J. S. Swenton, *J. Am. Chem. Soc.*, **93**, 6316 (1971); b) G. W. Gruber and M. Pomerantz, *ibid.*, **91**, 4004 (1969).

2) J. S. Swenton, K. A. Burdett, D. M. Madigan, T. Johnson, and P. D. Rosso, *J. Am. Chem. Soc.*, **97**, 3428 (1975).

3) M. Kato, M. Funakura, M. Tsuji, and T. Miwa, *J. Chem. Soc., Chem. Commun.*, **1976**, 63.

4) M. Kato, M. Tsuji, and T. Miwa, *Bull. Chem. Soc. Jpn.*, **51**, 1450 (1978).

5) M. Kato, K. Takatoku, S. Ito, M. Funakura, and T. Miwa, *Bull. Chem. Soc. Jpn.*, **53**, 3648 (1980).

6) M. Kato, H. Kobayashi, H. Yamamoto, K. Seto, S. Ito, and T. Miwa, *Bull. Chem. Soc. Jpn.*, **55**, 3523 (1982).

7) a) H. Günther, *Tetrahedron Lett.*, **1970**, 5173; b) S. W. Stayley, M. A. Fox, and A. Cairncross, *J. Am. Chem. Soc.*, **99**, 4524 (1977).

8) M. Kato, K. Takatoku, S. Ito, and T. Miwa, *Tetrahedron Lett.*, **1979**, 867.

9) H. Kobayashi, K. Takatoku, M. Kato, and T. Miwa, *Bull. Chem. Soc. Jpn.*, **56**, 3449 (1983).

10) J. S. Swenton, K. A. Burdett, D. M. Madigan, and P. D. Rosso, *J. Org. Chem.*, **40**, 1280 (1975).

11) N. G. Gaylord and E. I. Becker, *J. Org. Chem.*, **15**, 313 (1950).

12) G. S. Hammond and P. A. Leermakers, *J. Am. Chem. Soc.*, **84**, 207 (1962).

13) N. Kambe, K. Kondo, and N. Sonoda, *Chem. Lett.*, **1980**, 1629.

14) D. I. Schuster in "Rearrangements in Ground and Excited States" ed by P. de Mayo, Academic Press, New York (1980) Vol. 3, p. 199.

15) J. J. Lambert and W. H. Laarhoven, *J. Am. Chem. Soc.*, **106**, 1736 (1984).

16) We could not study the photochemistry of **2b**, because it was very sensitive to base and was contaminated with **13b** when prepared from benzotropylium fluoroborate and sodium cyanide in acetonitrile.[9]

17) H. E. Zimmerman, *Acc. Chem. Res.*, **15**, 312 (1982). The value of K can be obtained approximately by use of Hückel or SCF LCAO MO coefficients:

$$K_{kl}=\sum_{r,t} C_{rk}C_{rl}C_{tk}C_{tl}\gamma_{rt}.$$

18) a) J. Hine, "Advances in Physical Organic Chemistry" ed by V. Gold and D. Bethell, Academic Press, New York (1977), Vol. 15, p. 1; b) J. A. Altmann, O. S. Tee, and K. Yates, *J. Am. Chem. Soc.*, **98**, 7132 (1976).

19) O. Kikuchi, "A Series of Monographs on Modern Trends in Chemistry (No. 6); Bunshikidoho. Denshikeisanki ni yoru sono Katsuyou," Kodansha, Tokyo (1971), p. 153.

20) C. J. Fritchie, Jr., *Acta Cryst.*, **20**, 27 (1966).

21) G. R. Waitkins and R. Shutt, *Inorg. Synth.*, **2**, 183 (1946): The procedure was followed by D_2O instead of H_2O.

 © 1985 The Chemical Society of Japan Bull. Chem. Soc. Jpn., 58, 497—504 (1985)

Hydrolysis of Active Esters of Aliphatic Carboxylic Acids with Cyclic Dipeptide Catalysts Consisting of L-Histidine and Different Aliphatic α-Amino Acids

Yoshihiko MASUDA, Masao TANIHARA, Yukio IMANISHI,* and Toshinobu HIGASHIMURA
Department of Polymer Chemistry, Faculty of Engineering, Kyoto University, Yoshida Honmachi, Sakyo-ku, Kyoto 606
(Received July 2, 1984)

The hydrolyses of a series of *p*-nitrophenyl carboxylates with different acyl chains were investigated at 25 °C, pH 7.8 using cyclic dipeptides[*cyclo*(-L- or D-Xyz-His-) consisting of L-histidine (L-His) and an α-amino acid (Xyz) with different aliphatic side chains] as catalysts. Consequently, *cyclo*(-D-Leu-L-His-) and *cyclo*(-D-Val-L-His-) were found to be specifically effective catalysts for the hydrolysis of *p*-nitrophenyl laurate. These trans (D-L-type) cyclic dipeptides were much more efficient catalysts than their diastereomers, and were more reactive than imidazole, despite the fact that the former are less basic than the latter. The conformation of the cyclic peptides in solution was investigated using proton magnetic resonance spectroscopy and the relationship between conformation and catalytic activity was investigated. Consequently, it was found that the hydrophobic interaction between a catalyst and a substrate and the stereochemical fit for the cooperation of functional groups in the intramolecular nucleophilic catalysis are very important in order to attain a highly efficient catalysis. It was also found that the functional groups should have a certain size and flexibility in order to realize an effective stereochemical fit between functional groups of catalysts and substrates.

The specific catalysis of hydrolytic enzymes has been shown to depend upon the intramolecular cooperation of side-chain functional groups which are confined to a specific spatial conformation by the influence of the secondary structure of a polypeptide chain. In order to develop a catalyst with an enzyme-like character, the use of cyclic peptides seemed to be promising.[1] On the basis of this view, we synthesized cyclic dipeptides consisting of leucine and histidine and investigated the catalysis in the hydrolysis of *p*-nitrophenyl carboxylates. A very high catalytic activity of *cyclo*(D-leucyl-L-histidine)[*cyclo*(-D-Leu-L-His-)] in the hydrolysis of *p*-nitrophenyl laurate [$CH_3(CH_2)_{10}COOC_6H_4NO_2$] at 25 °C, pH 7.9 in 20% dioxane/water at the substrate concentration of 3.0×10^{-5} mol dm^{-3} has been reported by us.[2] *Cyclo*(-D-Leu-L-His-) (pK_a=6.00) is less basic than imidazole (pK_a=7.05) and the former was less efficient than the latter as a catalyst for the hydrolysis of *p*-nitrophenyl esters of short-chain carboxylic acids. However, it was specifically reactive for the hydrolysis of $CH_3(CH_2)_{10}COOC_6H_4NO_2$, that is, in the above conditions the second-order rate constant k_{cat} was 34—68 dm^3 mol^{-1} min^{-1} which was several tens of times as large as k_{cat}=1.9 dm^3 mol^{-1} min^{-1} by imidazole. It was considered that the hydrophobic interaction between the catlyst and the substrate should have played an important role in the above reactions.

It should be interesting to confirm if the above explanation is commonly applicable to other combinations of catalysts and substrates. This sort of investigation will be effective to explore a substrate-selective catalysis, that is, an efficient catalysis for a specific substrate, by controlling the structure of the cyclic peptide.

Experimental

Cyclic Dipeptides. *N*-Benzyloxycarbonyl α-amino acid or *N*-*t*-butoxycarbonyl α-amino acid and L-histidine methyl ester were condensed by an active ester method or with dicyclohexylcarbodiimide to obtain a linear dipeptide blocked at both terminals. A benzyloxycarbonyl group and *t*-butoxycarbonyl group were removed by catalytic hydrogenation and HCl/dioxane, respectively. The cyclization was carried out by refluxing in methanol. Cyclic dipeptides were recrystallized from water or a water/acetone mixture. It should be emphasized that ion-exchanging resins were not used to purify the intermediates and the products. Syntheses of *cyclo*(-Gly-L-His-), *cyclo*(-L-Leu-L-His-) and *cyclo*(-D-Leu-L-His-) have been reported previously.[2] *Cyclo*(-L-Ala-L-His-), mp 252—254 °C. Calcd for $C_9H_{12}N_4O_2$: C, 51.92; H, 5.81; N, 26.91%. Found: C, 51.70; H, 5.54; N, 26.96%. *Cyclo*(-D-Ala-L-His-), mp 235—236 °C. Calcd for $C_9H_{12}N_4O_2\cdot H_2O$: C, 47.78; H, 6.24; N, 24.76%. Found: C, 47.71; H, 6.10; N, 24.40%. *Cyclo*(-L-Phe-L-His-), mp 263 °C. Calcd for $C_{15}H_{16}N_4O_2$: C, 63.37; H, 5.67; N, 19.17%. Found: C, 63.07; H, 5.60; N, 20.00%. *Cyclo*(-D-Phe-L-His-), mp 255—257 °C. Found: C, 63.17; H, 5.53; N, 19.76%. *Cyclo*(-L-Val-L-His-), mp 220—224 °C. Calcd for $C_{11}H_{16}N_4O_2$: C, 55.92; H, 6.83; N, 23.71%. Found: C, 55.72; H, 6.89; N, 23.02%. *Cyclo*(-D-Val-L-His-), mp 228—230 °C. Found: C, 55.88; H, 6.68; N, 23.46%. *Cyclo*(-DL-Nle-L-His-), mp 207—213 °C. Calcd for $C_{12}H_{18}N_4O_2\cdot H_2O$: C, 53.72; H, 7.51; N, 20.88%. Found: C, 54.41; H, 7.32; N, 20.77%.

To synthesize *cyclo*(-D-Pip-L-His-) a racemic pipecolic acid-(2-piperidinecarboxylic acid) was optically resolved to obtain (*R*)-pipecolic acid(D-Pip). (+)-Tartaric acid was added to the racemic pipecolic acid to form a (*R*)-pipecolic acid — (+)-tartaric acid complex. To the complex, lead (IV) acetate was added to remove (+)-tartaric acid and to obtain (*R*)-pipecolic acid.[3] (*R*)-Pipecolic acid — (+)-tartaric acid complex, mp 182—185 °C (lit,[3] 182 °C), $[\alpha]_D$ 19.9 (H_2O) (lit,[3] 20.0). (*R*)-pipecolic acid, $[\alpha]_D$ 26.6 (H_2O)(lit,[4] 26±1). (*R*)-*N*-(Benzyloxycarbonyl)pipecolic acid was condensed with methyl L-histidinate using *N*-ethoxycarbonyl-2-ethoxy-1,2-dihydroquinoline to obtain a linear dipeptide blocked at both terminals. The subsequent procedure leading to *cyclo*-(-D-Pip-L-His-) was the same as the above. (*R*)-*N*-(Benzyloxycarbonyl)pipecolic acid, mp 110—113 °C (lit,[4] 112—113 °C); $[\alpha]_D$ 60.0 (AcOH) (lit,[5] 57.2±1). *Cyclo*(-D-Pip-L-His-), mp 185—195 °C. Calcd for $C_{12}H_{16}N_4O_2$: C, 58.05; H, 6.50; N, 22.57%. Found: C, 58.21; H, 6.57; N, 22.34%.

Methyl *N*-methoxycarbonyl-L- or D-leucyl-L-histidinate

(MeOCO-L or D-Leu-L-His-OMe) was used as a reference catalyst for the hydrolysis. They were synthesized in the same way as reported previously.[2]

Substrate. Vaious carboxylic acids were condensed with *p*-nitrophenol using dicyclohexylcarbodiimide, and the active esters were purified by recrystallization from ethanol. All esters were proven to be pure by an elemental analysis. Syntheses and purifications of *p*-nitrophenyl acetate [$CH_3COOC_6H_4NO_2$], 3-phenylpropionate [$Ph(CH_2)_2COOC_6H_4NO_2$] and laurate [$CH_3(CH_2)_{10}COOC_6H_4NO_2$] have been reported previously.[2] *p*-Nitrophenyl 5-phenylvalerate[$Ph(CH_2)_4COOC_6H_4NO_2$], mp 64.5—65.0°C. Calcd for $C_{17}H_{17}NO_4$: C, 68.22; H, 5.72; N, 4.68%. Found: C, 68.07; H, 5.80; N, 4.90%. *p*-Nitrophenyl decanoate [$CH_3(CH_2)_8COOC_6H_4NO_2$], mp 32.5—33°C. Calcd for $C_{16}H_{23}NO_4$: C, 65.51; H, 7.90; N, 4.77%. Found C, 65.75; H, 7.91; N, 4.74%. *p*-Nitrophenyl cyclohexanecarboxylate [$c\text{-}C_6H_{11}COOC_6H_4NO_2$], mp 50°C. Calcd for $C_{13}H_{15}NO_4$: C, 62.64; H, 6.07, N, 5.62%. Found: C, 62.91; H, 6.11; N, 5.56%. *p*-Nitrophenyl pivalate-[$Me_3CCOOC_6H_4NO_2$], mp 98—99°C (lit,[5] 94—95°C).

Hydrolytic Reaction. Hydrolyses were carried out at 25°C, pH 7.8 (KH_2PO_4–NaOH buffer) in 20% dioxane/water mixture. The catalyst concentration with respect to the imidazolyl group was in the range 1.65—11.2×10^{-4} mol dm^{-3}. It was lowered to 5.49×10^{-5} mol dm^{-3} when the effect of the dilution of the catalyst was examined. The substrate concentration was 3.0×10^{-5} mol dm^{-3}. However, the concentration of $CH_3(CH_2)_{10}COOC_6H_4NO_2$ and $CH_3(CH_2)_8COOC_6H_4NO_2$ was 6.0×10^{-6} mol dm^{-3} or 2.0×10^{-6} mol dm^{-3} to avoid association. A mixture of the buffer solution and the aqueous catalyst solution was kept at a constant temperature in an ultraviolet cell and a dioxane solution of substrate, which was kept at the same temperature, was added to start the hydrolytic reaction. By this procedure, an excellent reproducibility of the reaction was obtained even when a slight turbidity was observed in the hydrolysis of $CH_3(CH_2)_{10}COOC_6H_4NO_2$. To determine the reaction rate, a JASCO UVIDEC-1-type spectrophotomer was employed. The concentration of the *p*-nitrophenolate ion liberated in the reaction was determined by the absorbance at 400 nm, and the rate of hydrolysis was calculated. Optical cells having optical path lengths of 1 cm and 5 cm were used when the substrate concentration was 3.0×10^{-5} mol dm^{-3} and 6.0×10^{-6} mol dm^{-3} or 2.0×10^{-6} mol dm^{-3}, respectively. A second-order rate constant k_{cat} was calcutated from the pseudo-first-order rate constant k_1, the rate constant for the spontaneous hydrolysis k_w, and the effective imidazolyl concentration under reaction conditions. With all cyclic dipeptide catalysts the side-chain imidazolyl group of L-histidyl residue is in its neutral form at pH 7.8, so that the effective concentration is the same as the total concentration. On the other hand, with imidazole as a catalyst the fraction of catalytically active imidazole was 0.85 at pH 7.8. The second-order kinetics has been described previously.[2] The catalytic activities were compared in terms of k_{cat}.

Conformational Analysis. The side-chain conformation of cyclic peptides in solution was investigated by 220 MHz and 100 MHz ^1H nuclear magnetic resonance (NMR) spectroscopy. Varian HR-220 and HA-100 spectrometers were used. Dimethyl-d_6-sulfoxide(Me_2SO-d_6) and D_2O (NaOD–KD_2PO_4 buffer, pH 7.8) were used as solvent. Tetramethylsilane (Me_4Si) was used as an internal standard for the Me_2SO-d_6 solution. Sodium 2,2-dimethyl-2-silapentane-5-sulfonate[$Me_3Si(CH_2)_3SO_3Na$] and Me_4Si were used as an internal standard and an external standard for the D_2O solution, respectively.

Results and Discussion

The Hydrolysis of p-*Nitrophenyl Laurate with* Cyclo-*(-*L-*or* D-*Leucyl-*L-*Histidyl).* In a series of experiments to confirm the previous experimental results, we could not reproduce the rapid hydrolysis of $CH_3(CH_2)_{10}COOC_6H_4NO_2$ by *cyclo*(-D-Leu-L-His-) under the same conditions. A trace amount of some long-chain alkylamine, which was contaminated into the *cyclo*-(-D-Leu-L-His-) synthesized in the previous way, might have catalyzed the apparently fast hydrolysis. It has been reported that the hydrolyses of *p*-nitrophenyl esters of long-chain carboxylic acids are greatly accelerated by long-chain alkylamine.[6,7] Since a trace amount of long-chain alkylamine may be concentrated in a cyclic peptide during the purification with anion-exhange resin Amberlite IRA-400 which was used in the previous experiments, cyclic peptide catalysts were resynthesized without using ion-exchangers in the present investigation. The hydrolytic experiments of $CH_3(CH_2)_{10}COOC_6H_4NO_2$ with a pure *cyclo*(-D-Leu-L-His-) and related peptide catalysts were carried out nearly the same conditions as before, and k_{cat} values are shown in Table 1 together with other data. It is remarkable that the k_{cat} value, by pure *cyclo*(-D-Leu-L-His-), is much smaller than that reported previously. We must conclude that k_{cat}=34—68 $dm^3 mol^{-1} min^{-1}$ reported in a previous paper is much larger than the real value. The origin of the error is perhaps some hydrophobic amine contaminated from an ion-exchanger during the synthesis of *cyclo*(-D-Leu-L-His-).

Table 1. Second-order rate constants(k_{cat}, $dm^3 mol^{-1} min^{-1}$) for the hydrolysis of *p*-nitrophenyl laurate[a]

Catalyst	pK_a	$[S]_0^{b)}$=6.0×10^{-6} mol dm^{-3}	$[S]_0^{b)}$=3.0×10^{-5} mol dm^{-3}	
			Present experiment	Previous experiment
None (k_w, min^{-1})	—	0.24×10^{-3}	0.07×10^{-3}	0.20×10^{-3}
Imidazole	7.05	1.6	3.8	1.9
MeOCO-L-Leu-L-His-OMe	6.60	1.3	0.73	≈0
MeOCO-D-Leu-L-His-OMe	6.60	2.7	0.77	0.18
Cyclo(-L-Leu-L-His-)	6.25	0.05	0.08	0.25
Cyclo(-D-Leu-L-His-)	6.00	2.6	1.1	34—68

a) 25°C, pH 7.8, 20% dioxane/water. b) Initial substrate concentration.

However, it was not possible to isolate and identify the hydrophobic amine.

In previous experiments in which the substrate concentration was 3.0×10^{-5} mol dm^{-3}, sometimes the solution was trubid and precipitation occurred during the reaction. In these cases, the first-order plot with respect to the concentration of the reaction product was not linear. In view of several papers,[8,9] $CH_3(CH_2)_{10}COOC_6H_4NO_2$ tends to associate in a 20% dioxane/water solution at a concentration of 3.0×10^{-5} mol dm^{-3} and the association affects the k_{cat} value. A similar situation will be met with $CH_3(CH_2)_8COOC_6H_4NO_2$, too. Therefore, the hydrolyses of $CH_3(CH_2)_{10}COOC_6H_4NO_2$ with pure cyclic dipeptides containing L-histidine were carried out at substrate concentrations of 6.0×10^{-6} mol dm^{-3} and 2.0×10^{-6} mol dm^{-3}, which seemed to be low enough to avoid association. Under these conditions the reaction solution was nearly transparent. In particular, at the substrate concentration of 2×10^{-6} mol dm^{-3}, the reaction solution was perfectly transparent, and a first-order plot on the basis of the absorption due to dissociated *p*-nitrophenolate ion was linear except for the very early stage of the hydrolysis of $CH_3(CH_2)_{10}COOC_6H_4NO_2$. The k_{cat} values were determined from the linear part of first-order plot and are summarized in Table 2. In Table 2 the effect of dilution of catalyst on k_{cat} is also shown.

In Table 2, the catalyst dilution does not induce a definite change in k_{cat}. Therefore, the catalysts should be completely soluble under the conditions employed in the present investigation. An inspection of the experimental data shown in Tables 1 and 2 shows that a substrate dilution from 3.0×10^{-5} mol dm^{-3} to 6.0×10^{-6} mol dm^{-3} increased k_{cat} for $CH_3(CH_2)_{10}COOC_6H_4NO_2$ with peptide catalysts, that the reproducibility of the hydrolyses of $CH_3(CH_2)_{10}COOC_6H_4NO_2$ and $CH_3(CH_2)_8COOC_6H_4NO_2$ at a concentration 6.0×10^{-6} mol dm^{-3} is excellent, and that the further dilution of both substrates from 6.0×10^{-6} mol dm^{-3} to 2.0×10^{-6} mol dm^{-3} increased the k_{cat} values again. Since the aggregation of these hydrophobic substrates in 20% dioxane/water at a concentration of 2.0×10^{-6} mol dm^{-3} is suppressed to the minimum extent as described above, the k_{cat} values obtained at 2.0×10^{-6} mol dm^{-3} are regarded as the true values. It is remarkable that the cyclic peptides, consisting of D-leucyl or D-valyl and L-histidyl residues, have a high catalytic activity toward $CH_3(CH_2)_{10}COOC_6H_4NO_2$ under diluted conditions as compared to imidazole. It should be a marked result because these cyclic peptide catalysts are less basic than imidazole. The binding of hydrophobic substrates by a hydrophobic side chain of leucyl or valyl residue must have increased the reaction rate. In fact, in a mixed solvent containing more dioxane, the k_{cat} of *cyclo*(-D-Leu-L-His-) and *cyclo*(-D-Val-L-His-) was much smaller than that of imidazole as shown in Table 3.

Most interestingly, the catalysis by *cyclo*(-D-Leu-L-His-) or *cyclo*(-D-Val-L-His-) was much stronger than that by *cyclo*(-L-Leu-L-His-) or *cyclo*(-L-Val-L-His-), although both enantiomorphic pairs of catalysts are considered to be equally hydrophobic. The different activities of enantiomorphic catalysts may have been caused by different orientations of side chains in these cyclic dipeptides. In *cyclo*(-L-Leu-L-His-) or *cyclo*(-L-Val-L-His-), the side chains exist at the opposite side of the cyclic dipeptide plane.[10] To realize the hydrophobic binding of a substrate in an aqueous solution and subsequent intramolecular nucleophilic catalysis, *cyclo*(-D-Leu-L-His-) and *cyclo*(-D-Val-L-His-)

TABLE 2. EFFECTS OF DILUTION OF CATALYST AND SUBSTRATE ON THE SECOND-ORDER RATE CONSTANT (k_{cat}, dm^3 mol^{-1} min^{-1}) FOR THE HYDROLYSIS OF HYDROPHOBIC ESTERS WITH HYDROPHOBIC CYCLIC DIPEPTIDE CATALYSTS

Effect of Catalyst Dilution[a]

Catalyst	Low[b]	Intermediate[c]	High[d]
None (k_w, min^{-1})	2.6×10^{-4}	3.4×10^{-4}	3.3×10^{-4}
Imidazole	1.8	1.4	0.31
Cyclo(-D-Val-L-His-)	2.6	2.7	1.8
Cyclo(-D-Leu-L-His-)	2.5	3.2	2.4

a) 25°C, pH 7.8, 20% dioxane/water, $[CH_3(CH_2)_{10}COOC_6H_4NO_2]_0=6.0\times10^{-6}$ mol dm^{-3}. b) [Catalyst]=$(5.49—5.87)\times10^{-5}$ mol dm^{-3}. c) [Catalyst]=$(1.64—1.76)\times10^{-4}$ mol dm^{-3}. d) [Catalyst]=$(4.94—5.28)\times10^{-4}$ mol dm^{-3}.

Effect of Substrate Dilution[e]

Catalyst	$CH_3(CH_2)_8COOC_6H_4NO_2$		$CH_3(CH_2)_{10}COOC_6H_4NO_2$		
	6.0×10^{-6} mol dm^{-3}	2.0×10^{-6} mol dm^{-3}	6.0×10^{-6} mol dm^{-3}		2.0×10^{-6} mol dm^{-3}
None (k_w, min^{-1})	0.86×10^{-3}, 0.38×10^{-3}	0.47×10^{-3}, 0.59×10^{-3}	0.21×10^{-3}, 0.34×10^{-3}		0.22×10^{-3}
Imidazole	7.4, 7.1	9.7	1.6	1.4	4.9
Cyclo(-L-Val-L-His-)	1.1	1.2		0.15	0.11
Cyclo(-D-Val-L-His-)	9.9	3.5		2.7	16
Cyclo(-L-Leu-L-His-)	1.4	1.2	0.50	0.68	0.15
Cyclo(-D-Leu-L-His-)	1.6	6.3	2.6	3.2	16

e) 25°C, pH 7.8, 20% dioxane/water, [Catalyst]=$(1.65—1.80)\times10^{-4}$ mol dm^{-3}.

Table 3. Second-order rate constants (k_{cat}, $dm^3 mol^{-1} min^{-1}$) for the hydrolysis of p-nitrophenyl laurate[a]

Catalyat	20% dioxane/water		50% dioxane/water	
None (k_w, min^{-1})	0.21×10^{-3}	0.22×10^{-3}[b]	2.6×10^{-3}	0.21×10^{-3}[b]
Imidazole	1.6	4.9[b]	2.3	1.9[b]
Cyclo(-D-Val-L-His-)	—	16[b]	—	0.67[b]
Cyclo(-D-Leu-L-His-)	2.6	—	0.5	—

a) 25°C, pH 7.8, $[CH_3(CH_2)_{10}COOC_6H_4NO_2]_0=6.0\times10^{-6}$ mol dm^{-3}. b) $[CH_3(CH_2)_{10}COOC_6H_4NO_2]_0=2.0\times10^{-6}$ mol dm^{-3}.

Table 4. Second-order rate constants(k_{cat}, $dm^3 mol^{-1} min^{-1}$) for the hydrolysis of *p*-nitrophenyl acetate and *p*-nitrophenyl decanoate by various cyclic dipeptide catalysts *Cyclo*(-Xyz-L-His-)[a]

Xyz residue	Gly	L-Als	D-Ala	L-Phe	D-Phe	L-Val	D-Val	L-Leu	D-Leu	Imidazole
pK_a	6.20	6.25	6.20	6.35	6.35	6.35	6.40	6.25	6.00	7.05
$CH_3COOC_6H_4NO_2$	1.5	1.9	2.2	1.9	3.2	1.9	3.5	1.6	3.2	17.5
$CH_3(CH_2)_8COOC_6H_4NO_2$	—	—	—	0.4[b]	1.9[b]	1.2	3.5	1.2	6.3	9.7

a) 25°C, pH 7.8, 20% dioxane/water, $[S]_0=3.0\times10^{-5}$ mol dm^{-3} for $CH_3COOC_6H_4NO_2$, 2.0×10^{-6} mol dm^{-3} for $CH_3(CH_2)_8COOC_6H_4NO_2$. b) $[S]_0=3.0\times10^{-5}$ mol dm^{-3}. c) $[S]_0=6.0\times10^{-6}$ mol dm^{-3}.

Table 5. Second-order rate constants(k_{cat}, $dm^3 mol^{-1} min^{-1}$) for hydrolysis of *p*-nitrophenyl esters of aliphatic carboxylic acids with different acyl chain lenghts by hydroophobic cyclic dipeptide catalysts[a]

Catalyst	$CH_3COOC_6H_4NO_2$	$Ph(CH_2)_2COOC_6H_4NO_2$	$Ph(CH_2)_4COOC_6H_4NO_2$	$CH_3(CH_2)_8COOC_6H_4NO_2$	$CH_3(CH_2)_{10}COOC_6H_4NO_2$
Cyclo(-Gly-L-His-)	1.5	1.7	3.5	—	1.1
Cyclo(-L-Phe-L-His-)	1.9	1.9	1.2	0.4	—
Cyclo(-D-Phe-L-His-)	3.2	3.4	2.5	1.9[b]	0.8[b]
Cyclo(-L-Val-L-His-)	1.9	1.6	—	1.2[c]	0.11[c]
Cyclo(-D-Val-L-His-)	3.5	3.7	2.4	3.5[c]	16[c]
Cyclo(-L-Leu-L-His-)	1.6	1.5	—	1.2[c]	0.15[c]
Cyclo(-D-Leu-L-His-)	3.2	4.1	2.1	6.3[c]	16[c]
Cyclo(-DL-Nle-L-His-)	3.7	4.2	3.4	—	—
Imidazole	17.5	14.0	8.9	9.7[c]	4.9[c]

a) 25°C, pH 7.8, 20% dioxane/water, $[S]_0=3.0\times10^{-5}$ mol·dm^{-3}. b) $[S]_0=6.0\times10^{-6}$ mol dm^{-3}. c) $[S]_0=2.0\times10^{-6}$ mol dm^{-3}.

must have a suitable orientation of the functional groups and a stereochemical fit with a substrate.

Hydrolysis Catalyzed by Cyclic Dipeptides Carring an Alkyl Side Chain of Different Chain Lengths. The hydrophobicity of cyclic dipeptide catalysts can be controlled by the kind of α-amino acid (Xyz) which is coupled with L-histidine in the cyclic dipeptide. Thus, we can investigate the effect of the nature of cyclic dipeptide catalysts on the hydrolyses of a highly hydrophobic $CH_3(CH_2)_8COOC_6H_4NO_2$ and a less hydrophobic $CH_3COOC_6H_4NO_2$. The experimental results are summarized in Table 4.

The basicities of the side-chain imidazolyl groups of cyclic dipeptides are lower by *ca.* 0.7 pK unit than that of imidazole. The basicities are not seriously affected by the different natures and configurations of the α-amino acid residues which are coupled with L-histidine in the cyclic dipeptides.

For the hydrolysis of $CH_3COOC_6H_4NO_2$, which has the shortest acyl chain among the substrates investigated, imidazole was the most efficient catalyst and none of the cyclic dipeptide catalysts used were found to be more efficient than imidazole. No particular interaction, such as a hydrophobic interaction, seems to operate between $CH_3COOC_6H_4NO_2$ and the cyclic dipeptides. As a consequence, the cyclic dipeptide catalysts, which are less basic and are accompanied by a higher steric hindrance in the nucleophilic reaction, are less efficient than imidazole. It should be pointed out that with all diastereomeric catalysts a D-L-type dipeptide is somewhat more(up to twice) reactive than an L-L-type cyclic dipeptide. As will be described subsequently, this difference must be due to a less steric hindrance in the reaction of an imidazolyl group of the D-L-type cyclic dipeptide.

On the other hand, in the hydrolysis of $CH_3(CH_2)_8COOC_6H_4NO_2$, which has a long acyl chain, cyclic dipeptide catalysts carrying a bulky side chain were found to be relatively reactive. More interestingly, under these conditions *cyclo*(-D-Xyz-L-His-) s were 3—5 times more reactive than their diastereomers. This reactivity difference should be ascribed to a favorable orientation of the side chains of *cyclo*(-D-Xyz-L-His-) in the intramolecular catalysis toward a bound substrate.

Next, the hydrolytic reactions of *p*-nitrophenyl carboxylates having different lengths of an acyl chain with some hydrophobic cyclic dipeptide catalysts were investigated. The experimental results are summarized in Table 5.

The second-order rate constants k_{cat} for the hydrol-

yses with imidazole as a catalyst decreased on going from $CH_3COOC_6H_4NO_2$ to $CH_3(CH_2)_{10}COOC_6H_4NO_2$. The same trend was also observed in a hydrolyses catalyzed by L-L-type cyclic dipeptide catalysts. These experimental findings indicate an increasing steric hindrance against a nucleophilic attack by imidazole or an imidazolyl group as the length of the acyl chain of the substrates increases.

On the other hand, the k_{cat} values for the hydrolyses catalyzed by D-L-type cyclic dipeptides did not decrease markedly as the acyl chain length of the substrates increased. Interestingly, in the hydrolysis of $CH_3(CH_2)_{10}COOC_6H_4NO_2$, *cyclo*(-D-Val-L-His-) and *cyclo*(-D-Leu-L-His-) were more reactive than imidazole. In these experimental results, the important contribution of the hydrophobic binding of $CH_3(CH_2)_{10}COOC_6H_4NO_2$ by the hydrophobic cyclic dipeptides is again indicated.

The reactivity difference between the *cyclo*(-D-Xyz-L-His-)s, where Xyz is Leu, Val, and Phe, and their diastereomers is much larger in the hydrolysis of $CH_3(CH_2)_{10}COOC_6H_4NO_2$ than in the hydrolysis of $CH_3(CH_2)_8COOC_6H_4NO_2$, which is in turn larger than those in the hydrolyses of $CH_3COOC_6H_4NO_2$, $Ph(CH_2)_2COOC_6H_4NO_2$, and $Ph(CH_2)_4COOC_6H_4NO_2$. In other words, the more important the hydrophobic interaction between substrate and cyclic dipeptide, the larger the reactivity difference between the diastereomers of the cyclic dipeptides. *Cyclo*(-D-Xyz-L-His-) is intrinsically more reactive in a nucleophilic reaction toward $CH_3COOC_6H_4NO_2$, $Ph(CH_2)_2COOC_6$-H_4NO_2, and $Ph(CH_2)_4COOC_6H_4NO_2$ because of less steric hindrance than *cyclo*(-L-Xyz-L-His-). In addition to this, the conformation of *cyclo*(-D-Xyz-L-His-) is far more favorable in the intramolecular reaction toward a bound substrate than that of *cyclo*(-L-Xyz-L-His-).

Conformational Analysis of Side-Chain Group of Cyclic Peptide by Nuclear Magnetic Resonance Spectroscopy. An attempt was made to elucidate the hydrolytic activity — conformation relationship of the cyclic peptide catalysts through an analysis of the side-chain conformation of the cyclic peptides by NMR spectroscopy.

^1H NMR spectra of *cyclo*(-Xyz-L-His-) in Me_2SO-d_6 or D_2O solution were obtained, and the chemical shifts (δ^α, δ^β) of H^α and H^β of the two α-amino acid residues and the coupling constants($J^{\alpha\beta}$) between them were determined. These values are summarized in Table 6.

The $J^{\alpha\beta}$ values were substituted into a Karplus-type equation, by which the proportions of conformers existing in three conformational energy minima were calculated with reference to the internal rotation around the C^α-C^β bond. On that basis, the proportion F, which represents the folded conformation with the side chain stacking over the plane of cyclic dipeptide, and the proportion U, which represents the unfolded conformation with the side chain protruding outside the plane of cyclic peptide, were calculated and are shown in Table 7. In the same table, those values that have been determined by NMR spectroscopy with *cyclo*(-L- or D-Leu-L-His-) and *cyclo*(-Gly-L-His-) are also shown.[10]

The backbone conformation of these cyclic dipeptides was not investigated in detail. However, it may be considered, on the basis of the previous conclusion obtained with *cyclo*(-L- or D-Leu-L-His-),[10] that L-L-type cyclic dipeptides take a flagpole-boat conformation and that D-L-type cyclic dipeptides assume a nearly planar conformation. In all the cyclic dipeptides investigated, the fraction with a folded conformation of the side chain of L-histidyl residue was more than 1/3, the statistical value. This tendency is particularly marked for D_2O. The folded conformation is stabilized by an aromatic — amide interaction between an imidazolyl group and the backbone of the cyclic di-

TABLE 6. CHEMICAL SHIFT (δ, ppm) AND COUPLING CONSTANT (J, Hz) OF H^α AND H^β OF *Cyclo*(-Xyz-L-His-) IN ^1H NMR SPECTRUM[a]

Xyz residue	Solvent	L-His residue			Xyz residue		
		δ^α	δ^β	$J^{\alpha\beta}$	δ^α	δ^β	$J^{\alpha\beta}$
L-Ala	Me_2SO-d_6	4.09	2.87	5.0	3.84	0.99	7.0
			3.04	6.0			
D-Ala	Me_2SO-d_6	4.02	2.93	5.0	3.44	1.19	6.3
L-Phe	Me_2SO-d_6	4.16	2.86	5.0	3.89	1.68	4.0
						2.61	9.0
D-Phe	Me_2SO-d_6	3.24	≈2.84	—[b]	3.87	2.87	4.2
						3.10	5.3
L-Val	Me_2SO-d_6	4.08	2.79	4.1	3.67	2.04	3.5
			3.08	7.6			
D-Val	Me_2SO-d_6	4.05	2.83	4.8	3.39	2.11	4.0
			3.06	6.8			
L-Val	D_2O	4.88	3.52	5.2	4.35	2.33	4.2
			3.72	4.5			
D-Val	D_2O	4.87	3.52	4.1	3.92	2.67	3.0
			3.71	4.4			

a) The standard substance is Me_4Si in Me_2SO-d_6 and capillary Me_4Si in D_2O. b) Overlapping with H^β signal obstacled the determination of the coupling constant.

TABLE 7. SIDE-CHAIN ORIENTATION OF *Cyclo*(-Xyz-L-His-) IN SOLUTION AS DETERMINED BY ^1H NMR SPECTROSCOPY[a]

Xyz residue	Solvent	L-His residue		Xyz residue	
		F(%)	*U*(%)	*F*(%)	*U*(%)
Gly	Me_2SO-d_6	56	44	—[d]	—[d]
L-Ala	Me_2SO-d_6	47	53	—[d]	—[d]
D-Ala	Me_2SO-d_6	56	44	—[d]	—[d]
L-Phe	Me_2SO-d_6	56	44	29	71
D-Phe	Me_2SO-d_6	—[c]	—[c]	61	39
L-Val	Me_2SO-d_6	41	59	—[e]	—[e]
D-Val	Me_2SO-d_6	42	58	—[e]	—[e]
L-Leu	Me_2SO-d_6	48	52	29	71
D-Leu	Me_2SO-d_6	38	62	38	62
Gly[b]	D_2O	57	42	—[d]	—[d]
L-Val	D_2O	59	41	—[c]	—[c]
D-Val	D_2O	68	32	—[c]	—[c]
L-Leu	D_2O	70	30	22	78
D-Leu	D_2O	60	40	50	50

a) The standard substance is Me_4Si in Me_2SO-d_6 and capillary Me_4Si in D_2O. b) The standard substance is $Me_3Si(CH_2)_3SO_3Na$. c) Coupling constant was not determined (see Table 3). d) No C^γ atom is present. e) Two methyl groups are present at the γ position.

peptide. This interaction seemed to be more important in D_2O than in Me_2SO.[11,12] The high-field shift of the H^α signal of a D-Xyz residue of *cyclo*(-D-Xyz-L-His-), as compared with that of L-Xyz residue of *cyclo*-(-L-Xyz-L-His-) (see Table 6), might be due to a magnetic-shielding effect of the imidazolyl group. This indicates a molecular conformation in which H^α of D-Xyz residue protrudes over the plane of the imidazolyl group in the folded conformation of the side chain of the L-histidyl residue. Similarly, in Table 6, the H^β signal of the L-Xyz residue in *cyclo*(-L-Xyz-L-His-) is shifted to a higher magnetic field than the H^β signal of the D-Xyz residue in *cyclo*(-D-Xyz-L-His-). When two H^β atoms are concerned, they are nonequivalent and one of them is more strongly shifted to a high field than the other. These phenomena might have been caused by a magnetic-shielding effect of the imidazolyl group, and again indicate a folded conformation of the side chain of L-histidyl residue in which the H^β of L-Xyz residue protrudes over the plane of imidazolyl group.

These experimental NMR spectroscopy results indicate that in *cyclo*(-D-Xyz-L-His-) two side chains exist on different sides of the almost planar backbone plane of the cyclic dipeptide, and that in *cyclo*(-L-Xyz-L-His-) two side chains exist on the same side of the boat-type plane of the cyclic dipeptide. This conclusion means that the molecular conformation[10] proposed previously for *cyclo*(-L- or D-Leu-L-His-) is commonly available in other cyclic dipeptides. It is, therefore, conceivable to say that a conformation in which an isobutyl side chain of the D-Leu residue exists on the other side of an imidazolylmethyl side chain of the L-His residue with respect to the cyclic dipeptide backbone enables a stereochemical fit in binding a long-chain $CH_3(CH_2)_{10}COOC_6H_4NO_2$ by hydrophobic interaction with the isobutyl group and in the intramolecular nucleophilic attack by the imidazolylmethyl group.

There are two γ-methyl groups in *cyclo*(-L- or D-Val-L-His-), so that a Karplus-type equation is not applicable to this cyclic dipeptide. Therefore, the internal rotation around the C^α-C^β bond cannot be investigated on the basis of the coupling constant. In this cyclic peptide, however, one or two methyl groups are present in an unfolded position in any rotational state. Therefore, with *cyclo*(-D-Val-L-His-) a conformation becomes available in which one or two methyl groups situate fairly close to the backbone of the cyclic dipeptide and on the other side of the imidazolylmethyl group. This sort of arrangement of the functional groups may provide a favorable stereochemical fit with $CH_3(CH_2)_{10}COOC_6H_4NO_2$ for a concerted hydrophobic binding — intramolecular nucleophilic catalysis.

Cyclo(-D-Phe-L-His-) was found not to be so effective for the hydrolysis of *p*-nitrophenyl esters of long-chain carboxylic acids, although the side chain benzyl group of the Phe residue may well be hydrophobic comparable to the isobutyl side chain of the Leu residue and the isopropyl side chain of the Val residue. The reason for the low catalytic activity may exist in the peculiar orientation of the two side chains of *cyclo*(-D-Phe-L-His-). It is desirable to know the conformation of *cyclo*(-D-Phe-L-His-) in an aqueous solution, because the hydrolysis was carried out in a 20% dioxane/water mixture. Unfortunately, for the limited solubility of *cyclo*(-D-Phe-L-His-) in water, only the conformation in Me_2SO was investigated. As shown in Table 6, the NMR chemical shift of the H^α of the Phe residue in *cyclo*(-D-Phe-L-His-) is nearly the same as that in *cyclo*(-L-Phe-L-His-). In other words, the H^α of the Phe residue in *cyclo*(-D-Phe-L-His-) is free from the magnetic-shielding effect of the imidazolyl group of the His residue, which is a significant exception in the *cyclo*(-D-Xyz-L-His-) series. This indicates that the extent of the folded orientation of the imidazolylmethyl side chain of His residue in *cyclo*(-D-Phe-L-

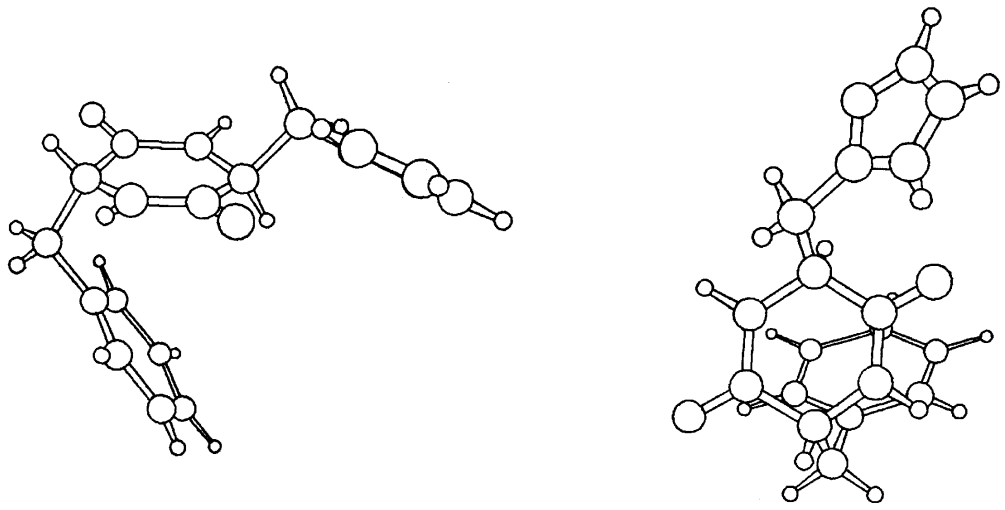

(a) (b)

Fig. 1. Molecular conformation of *cyclo*(-D-Phe-L-His-) in Me_2SO-d_6 simulated by computer. Internal rotation angles: amide bond, planar cis; ϕ, −9.3°; ψ, 9.3°: His-χ^1, gauche: Phe-χ^2, 90°. Bond lengths and bond angles were usual values.
a, side view, b, top view.

His-) is less than that of others. As shown in Table 7, the folded conformation of the side-chain benzyl group of *cyclo*(-D-Phe-L-His-) amounts to nearly 60% in Me_2SO. The contribution of the folded conformation will be more important in an aqueous solution than in Me_2SO. Since the amide — aromatic interaction of the cyclic peptide backbone is stronger with a phenyl group than with an imidazolyl group,[11,12] *cyclo*(-D-Phe-L-His-) should have been forced to take the conformation depicted in Fig. 1 in an aqueous solution. Evidence supporting the conformation of Fig. 1 is collected in Table 6. For example, the NMR signal of the H^{α} of His residue in *cyclo*(-D-Phe-L-His-) shifts extensively to the upfield. This means that the benzyl group of the Phe residue situates very near to the H^{α} of the His residue. This type of arrangement of functional groups should lead to a poor stereochemical fit for the hydrophobic binding of *p*-nitrophenyl esters of long-chain carboxylic acids and the intramolecular nucleophilic attack.

Effect of the Nature of Hydrophobic Group on the Intramolecular Cooperation of a Hydrophobic Binding Group and a Nucleophilic Catalytic Group. It has been shown that the orientation of functional groups in the side chains of a cyclic dipeptide consisting of a hydrophobic D-amino acid and L-histidine is suitable to their intramolecular cooperation toward the hydrolysis of hydrophobic nitrophenyl carboxylates.[2] It was also shown above that subtle change in the structure of a hydrophobic side chain delicately influences the intramolecular cooperation, as in *cyclo*(-D-Phe-L-His-). To elucidate this point and to gain more information regarding the design of an efficient catalyst, the effect of the structure of the hydrophobic group in both catalyst and substrate on the reactivity was investigated.

First of all, $Me_3CCOOC_6H_4NO_2$ and *c*-$C_6H_{11}COOC_6H_4NO_2$ were chosen as the *p*-nitrophenyl carboxylates to be tested. They have a hydrophobic acyl chain which is different in structure from those investigated so far. These esters were hydrolyaed with a series of *cyclo*(-L- or D-Xyz-L-His-) and the experimental results are shown in Table 8.

Either $Me_3CCOOC_6H_4NO_2$ or *c*-$C_6H_{11}COOC_6H_4NO_2$ carries a highly hydrophobic acyl chain. However, both were not hydrolyzed efficiently with *cyclo*(-D-Xyz-L-His-) bearing a hydrophobic side chain. According to the examination regarding the molecular model, the acry group of $Me_3CCOOC_6H_4NO_2$ is spheric. Therefore, the arrangement of the acyl group and the ester group of a substrate does not fit with the arrangement of the functional groups of *cyclo*(-D-Xyz-L-His-). Similary, the cyclohexane ring of *c*-$C_6H_{11}COOC_6H_4NO_2$ assumes a rigid conformation, which makes a stereochemical fit between functional groups of the substrate and the catalyst difficult. This situation must have led to the sluggish reaction.

Next, *cyclo*(-D-Pip-L-His-) was synthesized as a cata-

Table 8. Second-order rate constants(k_{cat}, $dm^3 mol^{-1} min^{-1}$) for the hydrolysis of *p*-nitrophenyl pivalate and *p*-nitrophenyl cyclohexanecarboxylate by hydrophobic cyclic dipeptide catalysts *Cyclo*(-Xyz-L-His-)[a]

Xyz residue	Gly	L-Phe	D-Phe	L-Val	D-Val	L-Leu	D-Leu	DL-Nle	Imidazole
$Me_3CCOOC_6H_4NO_2$	0.2	0.02	0.04	—	0.03	0.04	0.10	0.06	0.2
c-$C_6H_{11}COOC_6H_4NO_2$	1.0	0.8	2.0	1.1	2.1	0.7	1.9	—	8.3

a) 25 °C, pH 7.8, 20% dioxane/water, $[S]_0 = 3.0 \times 10^{-5}$ mol dm^{-3}.

Table 9. Second-order rate constants(k_{cat}, $dm^3 mol^{-1} min^{-1}$) for the hydrolysis of *p*-nitrophenyl esters of several aliphatic carboxylic acids by *Cyclo*(-D-Pip-L-His-)[a]

Substrate	$CH_3COOC_6H_4NO_2$	$Ph(CH_2)_2COOC_6H_4NO_2$	$CH_3(CH_2)_8COOC_6H_4NO_2$	$c\text{-}C_6H_{11}COOC_6H_4NO_2$
Cyclo(-D-Pip-L-His-)	0.9	1.3	0.5	1.8
Imidazole	17.5	14.0	7.4[b]	8.3

a) 25°C, pH 7.8, 20% dioxane/water, $[S]_0=3.0\times10^{-5}$ mol dm^{-3}. b) $[S]_0=6.0\times10^{-6}$ mol dm^{-3}.

lyst having a rigid hydrophobic functional group, and was used in the hydrolyses of *p*-nitrophenyl carboxylates. The experimental results are shown in Table 9.

In the hydrolysis catalyzed by *cyclo*(-D-Pip-L-His-), an efficient catalysis, as has been observed with other hydrophobic cyclic dipeptides [*cyclo*(-D-Xyz-L-His-)], was never observed. According to Bláha *et al.*,[13,14] the backbone of the cyclic dipeptide containing pipecolic acid, *cyclo*(-D-Pip-Gly-), *cyclo*(-D-Pip-L-Leu-), and *cyclo*(-D-Pip-L-Phe), is nearly planar. The piperidine ring of the Pip residue is not so strained as to seriously alter the backbone conformation of the cyclic dipeptide. As estimated from $J^{\alpha\beta}$ of the NMR spectrum of *cyclo*(-D-Pip-L-His-) in Me_2SO-d_6, 70% of the imidazolylmethyl groups take the folded form (*F*) and the rest (30%) the unfolded form (*U*). Therefore, *cyclo*(-D-Pip-L-His-) takes nearly the same conformation of functional groups as other hydrophobic *cyclo*(-D-Xyz-L-His-). The unexpectedly low catalytic activity of *cyclo*(-D-Pip-L-His-) should therefore be due to the insufficient flexibility of the peperidine ring of the Pip residue to inhibit a satisfactory stereochemical fit of functional groups between catalyst and substate.

The above experimental results indicate that cylic dipeptides consisting of a hydrophobic D-amino acid and an L-histidine could be an efficient catalyst for the hydrolysis of hydrophobic *p*-nitrophenyl carboxylates, that the efficient catalysis is based upon a satisfactory stereochemical fit of functional groups between catalyst and substrate, and that the functional group should bear a certain size and a moderate flexibility in order to attain the sterochemical fit.

References

1) Y. Imanishi, *Adv. Polym. Sci.*, **20**, 1 (1976).
2) Y. Imanishi, M. Tanihara, T. Sugihara, and T. Higashimura, *Chem. Lett.*, 261 (1975); *Biopolymers*, **16**, 2203 (1977).
3) J. P. Greenstein and M. Winitz, Chemistry of Amino Acids, Vol. 3, John Wiley & Sons, N. Y., (1961) p. 2538.
4) L. Balaspiri, B. Penke, J. Petres, and K. Kovacs, *Monatsh. Chem.*, **101**, 1177 (1970).
5) C. Huggins and J. Lapides, *J. Biol. Chem.*, **170**, 467 (1947).
6) C. A. Blyth and J. R. Knowles, *J. Am. Chem. Soc.*, **93**, 3017 (1971).
7) D. Oakenfull, *J. Chem. Soc., Perkin Trans.* **2**, 1006 (1973).
8) F. M. Menger and C. E. Portnoy, *J. Am. Chem. Soc.*, **90**, 1875 (1968).
9) Y. Murakami, Y. Aoyama, and M. Kida, *J. Chem. Soc., Perkin Trans. 2*, **1977**, 1947.
10) M. Tanihara, Y. Imanishi, and T. Higashimura, *Biopolymers*, **16**, 2217 (1977).
11) K. D. Kopple and D. H. Marr, *J. Am. Chem. Soc.*, **89**, 6193 (1967).
12) K. D. Kopple and M. Ohnishi, *J, Am. Chem. Soc.*, **91**, 962 (1969).
13) J. Vicăr, M. Budišinský, and K. Bláha, *Collect. Czecho. Chem. Commun.*, **38**, 1940 (1973).
14) J. Vicăr, J. Smolíková K. Bláha, *Collect. Czecho. Chem. Commun.*, **38**, 1957 (1973).

 © 1985 The Chemical Society of Japan Bull. Chem. Soc. Jpn., 58, 505—507 (1985)

Disproportionation of Cyclohexadienes Catalyzed by Metallic Nickel

Mutsuji SAKAI,* Toshiya KIMURA, Toshiaki NAKAOKA, Yasumasa SAKAKIBARA, and Norito UCHINO
Department of Polymer Science and Engineering, Kyoto Institute of Technology, Matsugasaki, Sakyo-ku, Kyoto 606
(Received August 10, 1984)

Cyclohexadienes, 1,3-cyclohexadiene (**1**) and 1,4-cyclohexadiene (**2**), disproportionated to benzene (**3**) and cyclohexene (**4**) in the presence of catalytic amounts of metallic nickel prepared from nickel halides and zinc powder in *N,N*-dimethyformamide (DMF) under nitrogen.

In the preceding paper, the authors pointed out that a small amount of benzene was formed in the hydrogenation of 1,4-cyclohexadiene by a $Ni(acac)_2$–$Al_2Et_3Cl_3$–PPh_3 catalyst.[1] Recently, it has been reported that Ziegler catalysts prepared from Co(II) or Ni(II) alkanoates and alkylaluminiums are active for the disproportionation of cyclohexadienes to benzene and cyclohexene.[2] Homogeneous catalysts (Cr,[3] Zr,[4] Ru,[5] Rh,[6] and Ir[7] compounds) are known for the disproportionation of cyclic dienes. In many cases, isomerization took place simultaneously. Catalytic reactions involving disproportionation and dehydrogenation are also noted with heterogeneous metal calalysts (Ni,[8] Rh,[9] and Pd[10] catalysts). We have found that metallic nickel (colloidal state) prepared from anhydrous nickel halides and zinc powder was active for the disproportionation of cyclohexadienes. Compared with other metal catalysts, advantages of the metallic nickel catalyst are negligible isomerization and dehydrogenation, and easy access to the reagents. The utility of metallic nickel for catalytic reactions will be further extended.

$$\text{Cyclohexadiene} \xrightarrow[\text{under } N_2]{NiBr_2\text{–Zn, in DMF}} \underset{(3)}{\text{Benzene}} + \underset{(4)}{\text{Cyclohexene}}$$

(1,3-Cyclohexadiene, **1**; 1,4-Cyclohexadiene, **2**)

Experimental

Materials. Metal halides, metal powders, and alkylaluminium compounds were commercially available and used without further purification. Solvents and dienes were dried and distilled under nitrogen before use. $[NiBr_2(PPh_3)_2]$ was prepared according to the literature.[11]

Procedure. A typical reaction of **1** is as follows. To a 50 cm^3 flask fitted with a septum inlet and a magnetic stirrer were added anhydrous nickel bromide (44 mg, 0.2 mmol) and zinc powder (65 mg, 1.0 mmol) in *N,N*-dimethylformamide (DMF) (15 cm^3). After the atmosphere was replaced with nitrogen the catalyst was allowed to stand overnight at room temperature. The mixture became a black solution containing fine metallic nickel. To the mixture was added **1** (400 mg, 5 mmol) in DMF (5 cm^3), and the mixture was stirred with a magnetic stirrer and kept in a thermostated bath. The reaction was stopped by adding a dilute hydrochloric acid solution and the aqueous mixture was shaken with toluene. The toluene extract was washed with water, dried over anhydrous calcium chloride, and subjected to GLC analysis.

Analysis. The gas chromatographic analyses were performed on a Shimadzu GC-8A instrument with a TC detector and helium carrier gas using a 3 m column of 20% bis(2-cyanoethyl) ether on Celite 545. The amounts of products were determined by the peak areas of chromatogram using *p*-xylene as an internal standard.

Results and Discussion

Cyclohexadienes (**1** and **2**) disproportionated to **3** and **4** by metallic nickel. The results are shown in Table 1. The catalyst prepared from anhydrous nickel chloride or bromide and zinc powder was most effective for the disproportionation reaction. Bis(acetylacetonato)nickel, nickel acetate, nickel sulfate, nickel hydroxide, and cobalt bromide have little activity for the reaction. Zinc powder was more effective as a reductant than magnesium and manganese powders. Three times amounts of zinc powder to nickel bromide were sufficient to reduce nickel(II). When sodium borohydride was used as a reductant, the hydrogenation of **1** took place predominantly to give **4**. Table 2 shows the effect of solvent. DMF, hexamethylphosphoric triamide (HMPA), and methanol were good solvents for the disproportionation. However, little disproportionation reaction occurred in dimethyl sul-

TABLE 1. NICKEL CATALYSTS FOR THE DISPROPORTIONATION OF **1**[a]

Catalyst	Solvent	Temp	Time	Composition/mol%				Total
		°C	h	**1**	**2**	**3**	**4**	yield/%
$NiBr_2$–Zn(powder)	DMF	60	2	Trace	0	46	54	95
$NiCl_2$–Zn(powder)	DMF	60	2	2	0	46	52	98
$NiBr_2$–Mn(powder)	DMF	60	2	66	0	15	20	94
$NiBr_2$–Mg(powder)	DMF	60	2	79	0	9	12	98
$Ni(acac)_2$–Zn(powder)	DMF	60	2	99	0	1	Trace	96
$NiBr_2$–$NaBH_4$	DMF	60	2	81	0	1	17	98
$Ni(acac)_2$–$AlEt_3$	Toluene	20	10 min	1	1	41	57	98
$Ni(acac)_2$–$Al_2Et_3Cl_3$	Toluene	20	2	100	0	0	Trace	95

a) **1**, 5 mmol; Ni compound, 0.2 mmol; reductant, 1.0 mmol; solvent, 20 cm^3.

foxide (DMSO), acetonitrile, tetrahydrofuran (THF), and toluene. Under a nitrogen atmosphere, the mixture consisting of nickel bromide and zinc powder in DMF turned black after stirring for 5 h at room temperature. Resulting nickel did not precipitate and could not be separated by filtration. The catalyst mixture containing colloidal nickel was used as it was. It was not deteriorated over a long period and stable to water; however, it was air sensitive. An active species for the disproportionation may be metallic nickel since the reaction was retarded significantly by the addition of triphenylphosphine, as shown in Table 3. The disproportionation of **1** was studied in the temperature range from 0 to 100 °C, as shown in Fig. 1. At 100 °C the catalyst was satisfactorily active.[12] Table 4 shows that the 1,3-diene disproportionated faster than the 1,4-diene did. Little isomerization of cyclohexadienes was observed. 1-Methyl-1,4-cyclohexadiene (**5**), 1,3-cyclooctadiene (**6**), and 1,5-cyclooctadiene (**7**) did not react and remained unchanged under similar reaction conditions.

Table 2. Effect of solvent[a)]

Solvent	Time	Composition/mol%				Total
	h	1	2	3	4	yield/%
DMF	2	Trace	0	46	54	95
HMPA	2	1	0	46	53	98
Methanol	2	0	0	47	53	87
DMSO	30	96	0	2	2	97
Acetonitrile	30	99	0	1	0	86
THF	30	99	0	0	1	95
Toluene	30	99	0	1	0	91

a) **1**, 5 mmol; $NiBr_2$, 0.2 mmol; Zn, 1.0 mmol; solvent, 20 cm^3; temp, 60 °C.

In Scheme 1 the most probable mechanism of the disproportionation of **1** is illustrated and metallic nickel is represented as Ni(0) (one atom). Nickel(II) is reduced to nickel(0) by zinc. Nickel(0) is colloidal and so fine that it has large surface area and many reaction sites. The diene **1** is activated by coordination (adsorption) on the active site of nickel(0). The cleavage of allylic C–H bond of **1** by nickel(0) (oxidative addition) gives a nickel hydride intermediate, followed by insertion reaction, β-hydrogen elimination, and reductive elimination to give **3** and **4**. No disproportionation of **4** occurs, probably because of its weak coordination. The diene **2** also disproportionated with nickel(0) under the conditions, but much more

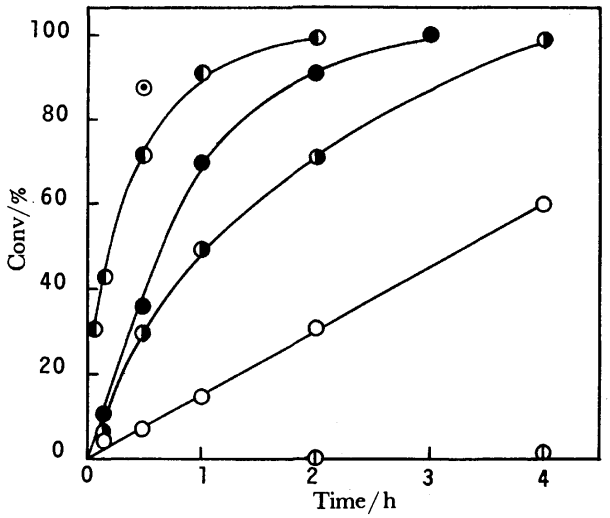

Fig. 1. Effect of temperature.
1, 5 mmol; $NiBr_2$, 0.2 mmol; Zn, 0.6 mmol; DMF, 20 cm^3; temperature (°C) — ◑: −30, ○: 0, ◑: 20, ●: 40, ◐: 60, ⊙: 100.

Table 3. Effect of additive[a)]

Catalyst	Additive	Conv	Composition/mol%				Total
	(mmol)	%	1	2	3	4	yield/%
$NiBr_2$–Zn	—	100	Trace	0	46	54	95
$NiBr_2$–Zn	PPh_3(0.4)	5	95	0	2	3	97
$NiBr_2(PPh_3)_2$–Zn	— (0.4)	11	89	0	5	6	98
$NiBr_2$–Zn	H_2O(100)	95	5	0	41	54	89

a) **1**, 5 mmol; Ni compound, 0.2 mmol; Zn, 1.0 mmol; DMF, 20 cm^3; temp, 60 °C; time, 2 h.

Table 4. Effect of substrate[a)]

Substrate	Time	Composition/mol%				Total
(mmol)	h	1	2	3	4	yield/%
1(5)	2	Trace	0	46	54	95
1(18)	2	47	Trace	26	27	98
	6	1	Trace	48	51	92
2(5)	2	0	30	31	38	93
	6	0	19	37	44	90
1(2)+**2**(3)	2	0	30	33	38	93
4(5)	30	0	0	1	99	95[b)]
5(5)	50	No Reaction				
6(5)	50	No Reaction				
7(5)	50	No Reaction				

a) $NiBr_2$, 0.2 mmol; Zn, 1.0 mmol; DMF, 20 cm^3; temp, 60 °C. b) Trace amounts of cyclohexane were detected.

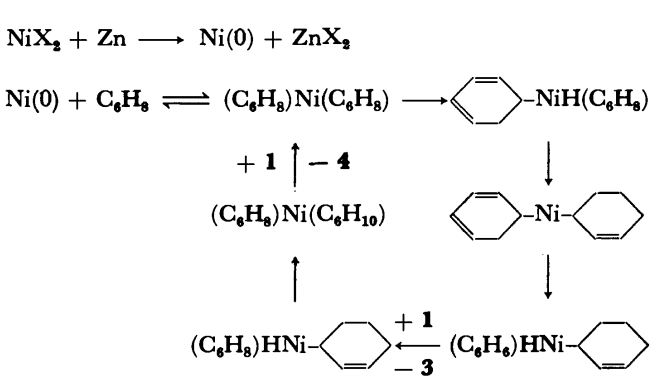

Scheme 1.

slowly. Triphenylphosphine occupies the active site of nickel(0) and blocks the coordination of diene.

References

1) M. Sakai, F. Harada, Y. Sakakibara, and N. Uchino, *Bull. Chem. Soc. Jpn.*, **55**, 343 (1982).

2) C. B. Hanson, *Tetrahedron Lett.*, **21**, 1581 (1980).

3) E. N. Frankel, *J. Catal.*, **24**, 358 (1972).

4) a) S. Datta, S. S. Wreford, R. P. Beatty, and T. J. McNeese, *J. Am. Chem. Soc.*, **101**, 1053 (1979); b) M. B. Fischer, E. J. James, T. J. McNeese, S. C. Nyburg, B. Posin, W. Wong-Ng, and S. S. Wreford, *J. Am. Chem. Soc.*, **102**, 4941 (1980).

5) a) J. E. Lyons, *J. Catal.*, **28**, 500 (1973); b) P. Pertici, G. Vitulli , M. Paci, and L. Porri, *J. Chem. Soc., Dalton Trans.*, **1980**, 1961.

6) a) K. Moseley and P. M. Maitlis, *J. Chem. Soc., (A)*, **1970**, 2884; b) M. Green and T. A. Kuc, *J. Chem. Soc., Dalton Trans.*, **1972**, 832.

7) J. E. Lyons, *J. Chem. Soc., Chem. Commun.*, **1969**, 564.

8) L. K. Freidlin, I. L. Popova, and T. P. Dadze, *Izv. Akad. Nauk SSSR, Ser. Khim.*, **1972**, 2204: *Chem. Abstr.*, **78**, 71065 (1973).

9) L. K. Freidlin and I. L. Popova, *Izv. Akad. Nauk SSSR, Ser. Khim.*, **1968**, 1514: *Chem. Abstr.*, **69**, 105590 (1968).

10) a) V. M. Gryaznov and V. D. Yagodovskii, *Kinet. Katal.*, **4**, 404 (1963): *Chem. Abstr.*, **59**, 9368 (1963); b) S. Carra, P. Beltrame, and V. Ragaini, *J. Catal.*, **3**, 353 (1964).

11) K. Yamamoto, *Bull. Chem. Soc. Jpn.*, **27**, 501 (1954).

12) A homogeneous nickel catalyst prepared from $Ni(acac)_2$–$Al_2Et_3Cl_3$–PPh_3, being effective for the selective hydrogenation of **2**, was deactivated at 90 °C.

Oxidative Cyclization of 3-(3-Heterocycle-substituted 2-Propenoyl)tropolones

Masaaki HONDA and Kimiaki IMAFUKU*
Department of Chemistry, Faculty of Science, Kumamoto University, Kurokami, Kumamoto 860
(Received August 11, 1984)

3-[3-(2-Furyl)-2-propenoyl]- (**2a**), 3-[3-(2-thienyl)-2-propenoyl]- (**2b**), 3-[3-(3-thienyl)-2-propenoyl]- (**2c**), and 3-[3-(3-pyridyl)-2-propenoyl]tropolone (**2d**) were prepared by the condensation of 3-acetyltropolone with the corresponding heterocyclic aldehydes. The compounds **2a—d** were oxidized with selenium dioxide to afford 2-heterocycle-substituted cyclohepta[*b*]pyran-4,9-diones, while oxidation with both alkaline hydrogen peroxide and 2,3-dichloro-5,6-dicyano-*p*-benzoquinone gave 2-(heterocycle-substituted methylene)-2*H*-cyclohepta-[*b*]furan-3,8-diones.

Previously, we reported that 3-cinnamoyltropolones were oxidized with selenium dioxide,[1] alkaline hydrogen peroxide,[2] and 2,3-dichloro-5,6-dicyano-*p*-benzoquinone (DDQ)[3] to afford flavonoid-like compounds. The present paper deals with the synthesis and oxidative cyclization of 3-(2-propenoyl)tropolones having a five- or six-membered heterocyclic ring at 3-position on the 2-propenoyl group and the effects of the heterocyclic ring on the cyclization.

Results and Discussion

Synthesis. 3-Acetyltropolone (**1**) reacted with heterocyclic aldehydes at room temperature in the presence of potassium hydroxide solution to afford each of 3-(3-heterocycle-substituted 2-propenoyl)tropolones (**2a—d**). Their structures were established by the spectral data and elemental analysis, which are summarized in Table 1.

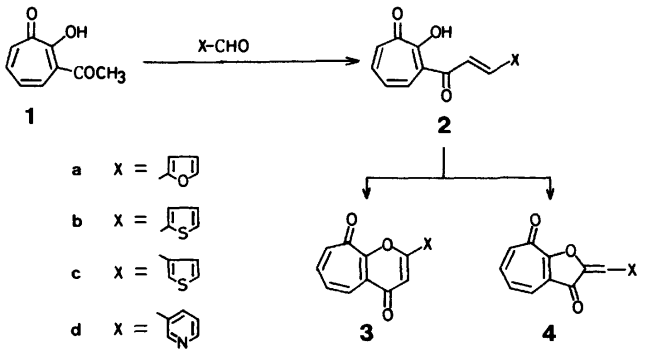

Scheme 1.

Oxidation with Selenium Dioxide. In flavonoid chemistry, Mahal *et al.* found that 2′-hydroxychalcones were oxidized with selenium dioxide to give flavones.[4] When a solution of 3-(3-heterocycle-substituted 2-propenoyl)tropolones (**2a—c**) in dioxane were refluxed in the presence of selenium dioxide, 2-heterocycle-substituted cyclohepta[*b*]pyran-4,9-diones (**3a—c**) were isolated. Their structures were determined by the spectral data and elemental analysis, which are summarized in Table 2.

The reaction of **2d**, which has a pyridine ring, did not give a desired product but a tarry material. The variation of the reaction conditions, such as molar ratio, solvent, reaction time, *etc.*, did not improve the reaction.

Oxidation with Alkaline Hydrogen Peroxide. It is well known that 2′-hydroxychalcones are oxidized with alkaline hydrogen peroxide to give the corresponding flavonols (Algar-Flynn-Oyamada reaction)[5,6] and that, if a methoxyl group is present at the 6′-position of the chalcones, aurones rather than flavonols are obtained.[7] In troponoid, we found that 3-cinnamoyltropolones were oxidized with alkaline hydrogen peroxide to give 2-arylmethylene-2*H*-cyclohepta[*b*]furan-3,8-diones.[2]

TABLE 1. CHARACTERISTICS FOR 3-(2-PROPENOYL)TROPOLONES (**2a—d**)

Compd	Yield	Mp	IR ($CHCl_3$)	UV (CH_3OH)	NMR ($CDCl_3$)	Analysis (%)
	%	θ_m/°C	cm^{-1}	λ/nm(log ε)	δ	Found (Calcd)
2a	46	139—140	1710 1630	243 (4.51) 331 (4.47)	6.4—6.6 (1H, m) 6.7—7.9 (9H, m)	$C_{14}H_{10}O_4$ C 69.53 (69.42) H 4.25 (4.16)
2b	61	187—189	1675 1600	242 (4.34) 330 (4.28)	6.9—7.9 (10H, m)	$C_{14}H_{10}O_3S$ C 65.10 (65.10) H 3.61 (3.90)
2c	83	173—174	1670 1600	240 (4.40) 315 (4.24)	6.8—7.8 (10H, m)	$C_{14}H_{10}O_3S$ C 65.40 (65.10) H 3.86 (3.90)
2d	56	184—185	1690[a] 1605	245 (4.50) 305 (4.37) 360 (3.83)	4.8—6.0 (1H, br)[b] 6.6—7.6 (6H, m) 7.6—7.8 (1H, m) 8.0—8.3 (1H, m) 8.5—8.7 (1H, m) 8.8—9.0 (1H, m)	$C_{15}H_{11}NO_3$ C 71.37 (71.14) H 4.42 (4.38) N 5.60 (5.53)

a) KBr. b) DMSO-d_6.

Table 2. Characteristics for the products (**3a—c**)

Compd	Yield	Mp	IR ($CHCl_3$)	UV (CH_3OH)	NMR ($CDCl_3$)	Analysis (%)
	%	θ_m/°C	cm^{-1}	λ/nm(log ε)	δ	Found (Calcd)
3a	31	210—211	1638 1602	255 (4.25) 327 (4.42)	6.6—6.9 (1H, m) 6.92 (1H, s) 7.0—8.3 (6H, m)	*m/z* M^+ for $C_{14}H_8O_4$ 240.0422 (240.0422)
3b	54	211—212	1640 1600	257 (4.30) 332 (4.42)	6.81 (1H, s) 6.9—8.2 (7H, m)	$C_{14}H_8O_3S$ C 65.71 (65.61) H 3.22 (3.15)
3c	56	212—214	1632 1598	223 (4.43) 253 (4.36) 317 (4.30)	6.91 (1H, s) 7.0—8.4 (7H, m)	*m/z* M^+ for $C_{14}H_8O_3S$ 256.0226 (256.0194)

Table 3. Characteristics for the products (**4a—d**)

Compd	Yield/%		Mp	IR ($CHCl_3$)	UV (CH_3OH)	NMR ($CDCl_3$)	Analysis (%)
	H_2O_2 Oxidn	DDQ Oxidn	θ_m/°C	cm^{-1}	λ/nm(log ε)	δ	Found (Calcd)
4a	37	45	211(dec)	1715 1645	235 (4.36) 282 (4.08) 395 (4.22) 440 (4.28)	6.5—6.8 (1H, m) 7.0—7.8 (7H, m)	$C_{14}H_8O_4$ C 69.68 (70.00) H 3.35 (3.36)
4b	12	33	191—192	1710 1640	230 (4.32) 285 (4.05) 391 (4.16) 446 (4.28)	6.8—8.0 (8H, m)	$C_{14}H_8O_3S$ C 65.77 (65.61) H 3.19 (3.15)
4c	42	15	214—215	1710 1650	228 (4.34) 290 (4.01) 375 (3.96) 423 (3.83)	6.7—8.3 (8H, m)	$C_{14}H_8O_3S$ C 65.67 (65.61) H 3.32 (3.15)
4d	7	8	230(dec)	1710 1645	228 (4.51) 274 (4.24) 368 (4.25) 412 (4.08)	7.0—8.0 (6H, m) 8.3—9.1 (3H, m)	*m/z* M^+ for $C_{15}H_9NO_3$ 251.0585 (251.0583)

When 3-(3-heterocycle-substituted 2-propenoyl)tropolones (**2a—d**) were oxidized with hydrogen peroxide in the presence of sodium hydroxide, 2-(heterocycle-substituted methylene)-2*H*-cyclohepta[*b*]furan-3,8-diones (**4a—d**) were obtained. Their structures were deterimed by the spectral data and elemental analysis, which are summarized in Table 3.

In the reaction, large excess of hydrogen peroxide or alkali decreased the yields of the products. In addition, the heterocyclic aldehydes were detected in the reaction mixture by the NMR measurements.

Oxidation with DDQ. In dehydrocyclization of 3-cinnamoyltropolones with DDQ, we found that unsubstituted and 3-methoxy-substituted 3-cinnamoyltropolones gave the flavone-like compounds, while the other 2- and/or 4-methoxy-substituted ones gave aurone-like compound.[3] Thus, it was expected that π-rich five-membered heterocycle-substituted 3-(2-propenoyl)tropolones might give the aurone-like products, while π-defficient six-membered heterocycle-substituted 3-(2-propenoyl)tropolones might give the flavone-like products. However, a mixture of the compounds **2a—d** and DDQ in dry benzene was refluxed to afford **4a—d** in all the cases. The difference between the five- and six-membered heterocyclic ring was not observed.

Experimental

The melting points were determined with a Yanagimoto MP-S2 apparatus and are uncorrected. The IR and UV spectra were taken on a JASCO IRA-1 and a Hitachi EPS-3T spectrophotometer, respectively. The NMR spectra were recorded with a Hitachi-Perkin-Elmer R-24 spectrometer (60 MHz). The high-resolution mass spectra were obtained with a JEOL DX-300 apparatus.

*3-(3-Heterocycle-substituted 2-Propenoyl)tropolones (**2a—d**).* Potassium hydroxide solution (5%, 40 ml) was added to a mixture of 3-acetyltropolone (**1**) (1.6 g, 10 mmol) and heterocyclic aldehyde (20 mmol) in 50% aqueous methanol (60 ml). After stirring for 24 h at room temperature, the mixture was diluted with water (100 ml) and acidified with 3 M (1 M=1 mol dm^{-3}) hydrochloric acid to give a precipitate, which was recrystallized from ethanol to afford 3-(3-heterocycle-substituted 2-propenoyl)tropolone (**2a—d**).

Selenium Dioxide Oxidation. A mixture of **2** (**a**, **b**, or **c**) (1.0 mmol) and selenium dioxide (584 mg, 5.0 mmol) in dioxane (10 ml) was refluxed for 36 h. The solvent was evaporated off, and the residue was diluted with ethanol (100 ml) and stirred for 2 h in the presence of Raney nickel (580 mg, 10 mmol). After filtration and removal of the ethanol, the residue was dissolved in chloroform, washed with a saturated sodium hydrogencarbonate solution and water, and dried over sodium sulfate. Evaporation residue was chromatographed on a Wakogel B-10 plate (30×30 cm) with diethyl ether and recrystallized from ethanol–dichloro-

methane to give 2-heterocycle-substituted cyclohepta[*b*]-pyran-4,9-dione (**3a—c**).

Alkaline Hydrogen Peroxide Oxidation. To a suspended solution of **2** (**a**, **b**, **c**, or **d**) (2.0 mmol) in ethanol (40 ml) was added 30% hydrogen peroxide (2 ml) under stirring at 0 °C. After addition of 12% potassium hydroxide solution (10 ml), the stirring was continued for 5 h. The mixture was acidified with 3 M hydrochloric acid and extracted with chloroform. The extract was concentrated and chromatographed on a Wakogel B-10 plate (30×30 cm) with chloroform and recrystallized from benzene to to give 2-(heterocycle-substituted methylene)-2*H*-cyclohepta[*b*]furan-3,8-dione (**4a—d**).

DDQ Oxidation. A mixture of **2** (**a**, **b**, **c**, or **d**) (1.0 mmol) and DDQ (450 mg, 2.0 mmol) in dry benzene (20 ml) was refluxed for 20 h. The reaction mixture was poured into a saturated sodium carbonate solution (100 ml) and extracted with chloroform. The extract was washed with water, dried over sodium sulfate, and brought to dryness by evaporation of the solvent. The residue was recrystallized from benzene to give **4a—d**.

We wish to thank Professor John F. W. McOmie, University of Bristol, England, for his valuable suggestion. We are also grateful to Mr. Hiromichi Matsuura, Wakunaga Pharmaceutical Co., Ltd., Hiroshima, for his kind measurements of the high-resolution mass spectra.

References

1) K. Imafuku, A. Yamane, and H. Matsumura, *Yuki Gosei Kagaku Kyokai Shi*, **38**, 308 (1980).
2) K. Yamaguchi, K. Imafuku, and H. Matsumura, *Yuki Gosei Kagaku Kyokai Shi*, **38**, 998 (1980).
3) K. Imafuku and K. Yamaguchi, *Bull. Chem. Soc. Jpn.*, **54**, 2855 (1981).
4) H. S. Mahal, H. S. Rai, and K. Venkataraman, *J. Chem. Soc.*, **1935**, 966.
5) J. Algar and J. P. Flynn, *Proc. Roy. Irish Acad., (B)*, **42**, 1 (1934); *Chem. Abstr.*, **29**, 161 (1935).
6) T. Oyamada, *Nippon Kagaku Kaishi*, **55**, 1256 (1934).
7) T. A. Geissman and D. K. Fukushima, *J. Am. Chem. Soc.*, **70**, 1686 (1948).

Reaction of Substituted Benzaldehydes with Sodium Hydrogensulfide or Sodium Sulfide in Liquid Ammonia

Yuji TAKIKAWA,* Kazuaki SHIMADA, Tetsuo MINAMI, Ryu SATO,† and Saburo TAKIZAWA
Department of Applied Chemistry, Faculty of Engineering, Iwate University, Morioka, Iwate 020
†*Department of Resource Chemistry, Faculty of Engineering, Iwate University, Morioka, Iwate 020*
(Received August 23, 1984)

Reactions of substituted benzaldehydes with sodium hydrogensulfide in the presence of nitrobenzene, nitrosobenzene, or azobenzene in liquid ammonia produce the corresponding benzyl alcohols and benzamides. On the other hand, reaction of benzaldehyde with sodium sulfide produces benzyl alcohol and benzamide. A reaction mechanism has been proposed which involves benzaldehyde anion radical.

The Cannizzaro reaction has been considered as one of the most fundamental reactions in organic chemistry.[1] A variety of mechanisms for this reaction have been proposed,[2] and the mechanism presently accepted involves a hydride transfer. Radical chain mechanisms have been suggested[3] but discounted mainly because radical initiators or inhibitors have no significant effect on reaction rate.[4] Recently, however, Chung[5] has evidenced a possible involvement of radical intermediates in a Cannizzaro reaction consuming benzaldehyde-α-d in alkaline aqueous dioxane or dioxane alone; a formation of monodeuterated benzyl alcohol-α-d_1 suggests formation of benzaldehyde anion radical, followed by hydrogen atom abstraction from solvent. Ashby *et al.*[6] have studied reaction of benzaldehydes having electron-withdrawing substituents with NaOH in THF/HMPA (9:1) by EPR spectroscopy and obtained evidence for existence of paramagnetic species in solution. In our previous paper,[7] we have reported that reaction of 9-nitroanthracene with NaSH in liquid ammonia gave 10,10′-di-aci-nitro-9,9′,10,10′-tetrahydro-9,9′-bianthryl, di-9-anthryl disulfide, anthracene, and anthraquinone. These products suggest formation of 9-nitroanthracene anion radical by transfer of electron generated from NaSH-liq NH_3 to 9-nitroanthracene. This result urged us to attempt oxidation-reduction reactions *via* single electron-transfer by using NaSH- or Na_2S-liq. NH_3. In this paper, we report results on reaction of substituted benzaldehydes with NaSH or Na_2S in liquid ammonia.

Results and Discussion

Benzaldehyde (**1**) reacts with liquid ammonia in the presence and absence of NaSH to give *N*,*N*′-dibenzylidene-α,α-toluenediamine quantitatively, and no such oxidation-reduction as the well-known Cannizzaro reaction occurs (Runs 1 and 2 in Table 1). However, addition of a small amount of nitrobenzene in this reaction system gave benzyl alcohol and benzamide in 27 and 25% yields, respectively, besides a small amount of *N*-benzylideneaniline (Run 3 in Table 1). On the other hand, reaction of **1** with $Na_2S \cdot 5H_2O$ in liquid ammonia gave benzyl alcohol and benzamide in good yields without formation of *N*,*N*′-dibenzylidene-α,α-toluenediamine (Run 5 in Table 1). Reaction of substituted benzaldehydes with NaSH in the presence of nitrobenzene gave the corresponding benzyl alcohols and benzamides (Runs 6—9 in Table 1). This reaction was also catalyzed by nitrobenzene derivatives such as *m*-dinitrobenzene and 1,3,5-trinitrobenzene (Runs 2—4 in Table 2). On the other hand, no formation of benzyl alcohol or benzamide was effected by addition of either aromatic nitro compounds, such as *p*-dinitrobenzene, 1-nitronaphthalene,[8] and 9-nitroanthracene,[7] which give substitution products in reaction with NaSH in liquid ammonia, or nitro compounds, such as *p*-nitroaniline, *p*-nitrotoluene, and nitromethane, which have high polarographic half-wave potentials (Runs 5—10

Table 1. Reactions of substituted benzaldehydes with NaSH or $Na_2S \cdot 5H_2O$ in liq. NH_3[a]

$$R\text{—}C_6H_4CHO \xrightarrow[\text{liq}\cdot NH_3,\ 40\,^\circ C,\ 5\,h]{\text{NaSH or } Na_2S\cdot 5H_2O} R\text{—}C_6H_4CH_2OH + R\text{—}C_6H_4CONH_2$$

Run	Substituent R	Additive (mmol)	NaSH/mmol	$Na_2S \cdot 5H_2O$/mmol	Yield/%	
					R—$C_6H_4CH_2OH$	R—$C_6H_4CONH_2$
1[b]	H	—	—	—	0	0
2[b]	H	—	2	—	0	0
3	H	Nitrobenzene (0.25)	2	—	27	25
4	H	Azobenzene (1)	2	—	35	32
5	H	—	—	2	37	37
6	2-OCH_3	Nitrobenzene (2)	2	—	43	34
7	4-OCH_3	Nitrobenzene (2)	2	—	32	—[c]
8	4-CH_3	Nitrobenzene (2)	2	—	27	—[c]
9	4-Cl	Nitrobenzene (2)	2	—	26	—[c]

a) Substituted benzaldehyde: 2 mmol. Substituted *N*-benzylideneaniline were produced when nitrobenzene was added. b) *N*,*N*′-Dibenzylidene-α,α-toluenediamine was quantitatively obtained. c) Not determined.

Table 2. Reactions of benzaldehyde with NaSH in the presence of a nitro compound in liq. NH_3[a]

Run	Nitro compound (mmol)		Yield/% Benzyl alcohol
1	Nitrobenzene	(0.25)	27
2	*m*-Dinitrobenzene	(0.25)	24
3	*m*-Dinitrobenzene	(0.1)	34
4	1,3,5-Trinitrobenzene	(0.1)	28
5	1-Nitronaphthalene	(0.25)	4
6	*p*-Nitroaniline	(2.0)	Trace
7	*p*-Nitrotoluene	(2.0)	Trace
8	*p*-Dinitrobenzene	(2.0)	0
9	9-Nitroanthracene	(2.0)	0
10	Nitromethane	(2.0)	0

a) Benzaldehyde and NaSH: 2 mmol; liq. NH_3: 10 ml; temp: 40 °C; time: 5 h.

Table 3. Reactions of benzaldehyde with NaSH in the presence of a reductant of nitrobenzene in liq. NH_3[a]

Run	Reductant	NaSH/mmol	Yield/% Benzyl alcohol
1	PhNO	2	10
2	PhNHOH	2	0
3	PhN(O)=NPh	2	0
4	PhN=NPh	2	31
5	PhNHNHPh	2	0
6	$PhNH_2$	2	0
7	PhN=NPh	0	0
8	PhNHNHPh	0	0

a) Benzaldehyde and reductant: 2 mmol; liq. NH_3: 10 ml; temp: 40 °C; time: 5 h.

in Table 2). Because nitrobenzene was easily reduced by NaSH in liquid ammonia to give aniline, azobenzene, and other reductants,[8] we investigated whether the catalytic behavior for the formation of benzyl alcohol and benzamide was due to the addition of nitrobenzene or its reductant. Nitrobenzene, nitrosobenzene, and azobenzene were found to exhibit the catalytic behavior for the formation of benzyl alcohol as shown in Table 3. Azoxybenzene, phenylhydroxylamine, hydrazobenzene, and aniline did not exhibit the catalytic behavior. Moreover, reactions of nitrobenzene or its reductants with NaSH at 40 °C for 5 h in liquid ammonia were investigated, results obtained being shown in Table 4. Both nitrobenzene and nitrosobenzene, showing the catalytic behavior, reacted with NaSH in liquid ammonia to give azobenzene, whereas azobenzene, after allowed to react with NaSH, resulted in almost complete recovery of itself only with formation of a small amount of hydrazobenzene. Accordingly, azobenzene is one of catalyzers for the formation of benzyl alcohol and benzamide in the reaction of **1** with NaSH in liquid ammonia. However, we can't deny that nitrobenzene and nitrosobenzene themselves act also as catalyzers.

On the other hand, the reaction of **1** with $Na_2S \cdot 5H_2O$ produced benzyl alcohol and benzamide in good yields (Run 5 in Table 1).

This reaction was investigated in such solvents as Et_2NH, Et_3N, MeOH, DMF, and HMPA, results obtained being shown in Table 5. The reaction with NaSH occurred only in such solvents[9,10] as liquid ammonia and HMPA which are favorable for single electron-transfer reaction,[11,12] but the reaction with $Na_2S \cdot 5H_2O$ occurred in various organic solvents.

Attempted reaction of benzophenone with NaSH in the presence of azobenzene in liquid ammonia at 40 °C for 5 h resulted only in recovery of the substrate. An addition of formalin (37%) to this reaction system, however, led to formation of benzhydrol in 27% yield;

Table 4. Reactions of nitrobenzene or its reductants with NaSH in liq. NH_3[a]

Run	Substrate	Yield/%						
		$PhNO_2$	PhNO	PhNHOH	PhN(O)=NPh	PhN=NPh	PhNHNHPh	$PhNH_2$
1	$PhNO_2$	62	0	0	0	Trace	0	26
2	PhNO	0	0	b)	0	37	b)	11
3	PhNHOH	0	0	b)	b)	0	b)	0
4	PhN(O)=NPh	0	0	0	0	0	99	0
5	PhN=NPh	0	0	0	0	92	8	0
6	PhNHNHPh	0	0	0	0	0	100	0
7	$PhNH_2$	0	0	0	0	0	0	100

a) Substrate and NaSH: 2 mmol; liq. NH_3: 10 ml; temp: 40 °C; time: 5 h. b) Not determined.

Table 5. Reactions of substituted benzaldehydes with NaSH or $Na_2S \cdot 5H_2O$ in various solvents[a]

Run	Substituent R	Solvent	Additive (mmol)	NaSH/mmol	$Na_2S \cdot 5H_2O$/mmol	Temp/°C	Yield/% Benzyl alcohol
1	H	Et_2NH	$PhNO_2$ (2)	2	—	Reflux	Trace
2	H	Et_3N	$PhNO_2$ (2)	2	—	Reflux	Trace
3	H	DMF	PhN=NPh (1)	2	—	80	Trace
4	H	HMPA	PhN=NPh (1)	2	—	80	20
5	4-Cl	Et_2NH	—	—	2	Reflux	7
6	4-Cl	Et_3N	—	—	2	Reflux	32
7	4-Cl	MeOH	—	—	2	Reflux	25
8	4-Cl	HMPA	—	—	2	80	35

a) Substituted benzaldehyde: 2 mmol; solvent: 4 ml; time: 5 h.

reaction with $Na_2S \cdot 5H_2O$ in the presence of formalin (37%) in liquid ammonia under the same conditions yielded benzhydrol in 58% yield. These results suggest that the methylenic hydrogen generated newly in the alcohol is not the hydrogen in H_2O, NH_3, or NaSH but the one in formaldehyde. Consequently, the formation of benzyl alcohol and benzamide in the reaction of substituted benzaldehydes with NaSH or $Na_2S \cdot 5H_2O$ in liquid ammonia is taken to be a result of an intermolecular reaction.

The following facts have been disclosed on the reaction of substituted benzaldehydes with NaSH in liquid ammonia.

1. The reaction with liquid ammonia in the absence and presence of NaSH produces *N,N'*-dibenzylidene-α,α-toluenediamine quantitatively.
2. The reaction proceeds only in the presence of an additive such as nitrobenzene, nitrosobenzene, or azobenzene which are good electron acceptors.
3. No sulfur-containing products are produced.
4. *N,N'*-dibenzylidene-α,α-toluenediamine formed by the reaction of benzaldehyde with ammonia does not react with NaSH in the presence of azobenzene in liquid ammonia.
5. The methylenic hydrogen generated newly comes from the formyl group in benzaldehydes.
6. The reaction proceeds only in liquid ammonia or HMPA.

Since **1** reacts with ammonia in the absence and presence of NaSH to give *N,N'*-dibenzylidene-α,α-toluenediamine quantitatively, the formation of benzyl alcohol and benzamide is not a simple Cannizzaro-like reaction *via* intermolecular reaction of **1** with hemiaminal, which has been formed from **1** and ammonia.

Another Cannizzaro-like reaction

$$\underset{\mathbf{1}}{PhCHO} + NaSH \xrightarrow[liq.\,NH_3]{} Ph\text{-}\underset{\displaystyle SH}{\overset{\displaystyle O^-}{\overset{|}{C}}}\text{-}H \xrightarrow{1}$$

$$PhCH_2OH + PhCOSH \xrightarrow{NH_3} PhCONH_2 + H_2S$$

is also conceivable. This mechanism, however, is also denied because in this reaction no sulfur-containing products are obtained and because the reaction of thiobenzoic acid with liquid ammonia at 40°C for 5 h gives ammonium thiobenzoate quantitatively.

The other Cannizzaro-like reaction

$$PhN{=}NPh + NH_3 \rightleftharpoons Ph\overset{+}{N}H{=}NPh + NH_2^- \xrightarrow{1}$$

$$Ph\text{-}\underset{\displaystyle NH_2}{\overset{\displaystyle O^-}{\overset{|}{C}}}\text{-}H \xrightarrow{1} PhCH_2OH + PhCONH_2$$

is also conceivable, but, in conflict with this sequence, the reaction of **1** with ammonia in the presence of azobenzene gives *N,N'*-dibenzylidene-α,α-toluenediamine, no benzyl alcohol or benzamide being formed (Run 8 in Table 3). Accordingly, this mechanism is also unlikely.

Meanwhile, as described above, the reduction of **1** by hydrazobenzene is also unlikely (Runs 5 and 8 in Table 3).

Since the reactions in question proceed only in the presence of an additive such as nitrobenzene, nitrosobenzene, or azobenzene which are good electron acceptors,[10,11] a reaction mechanism involving single electron-transfer, as shown in Scheme 1, may be considered as one of plausible mechanisms.

The polarographic half-wave potentials (−0.45—0.04 V in H_2O) of nitrobenzene, nitrosobenzene, and azobenzene are lower than those (−1.15—−0.77 V in H_2O) of substituted benzaldehydes and benzophenone. Accordingly, the initiation step is an electron-transfer to azobenzene from NaSH as an electron-donor species in liquid ammonia,[7] and the subsequent electron-transfer to benzaldehyde from azobenzene anion radical generates benzaldehyde anion radical. It then abstracts hydrogen atom from benzaldehyde to form benzyl alcoholate and benzoyl radical. The benzyl alcoholate in turn abstracts proton from solvent to afford benzyl alcohol. Meanwhile, the benzoyl radical reacts with NH_3 to afford benzamide. A solution of NaSH in HMPA at room temperature assumes an intense blue color. This solution liberate gradually H_2S and elemental sulfur according to

$$2\,NaSH \xrightarrow{HMPA} (2\,Na^+ e^-) + (2\,HS\cdot),$$

$$(2\,HS\cdot) \longrightarrow (HSSH) \longrightarrow H_2S + \frac{1}{8} S_8.$$

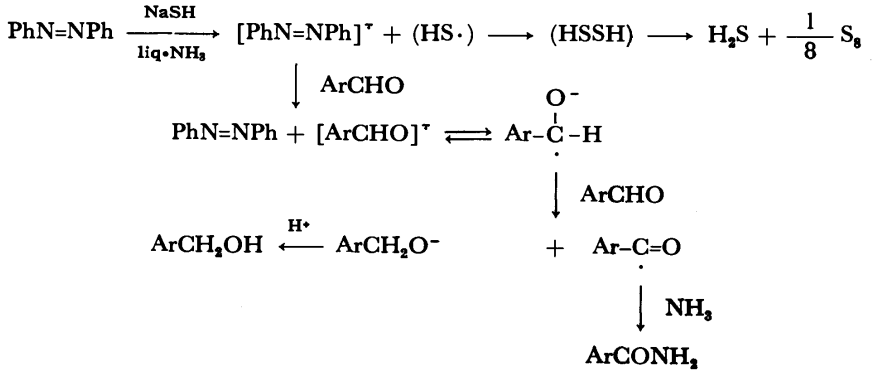

Scheme 1.

These results also support the single electron-transfer mechanism. We investigated these reactions by EPR spectroscopy in HMPA, but the signals obtained were too broad to allow us to make their assignment.

Experimental

General. The reagents used were commercial reagent-grade materials except 9-Nitroanthracene and were purified by recrystallization or distillation prior to use. 9-Nitroanthracene was prepared and purified according to the literature.[13] IR spectra were recorded on a Hitachi 295 infrared spectrophotometer. ^1H NMR spectra were recorded on a Hitachi R-22 (90 MHz) spectrometer in carbon tetrachloride or deuteriochloroform solution containing tetramethylsilane as an internal standard. Mass spectra were recorded on a Hitachi RMU-6M spectrometer with a direct inlet system operating at 20 eV. GLC analysis was carried out with a Hitachi 063 gas chromatograph. For column chromatography Wakogel C-300 was used. Products obtained were identified by comparing IR, NMR, MS, GLC, and MP data with those of authentic samples.

Reaction of Benzaldehyde (1) with NaSH in the Presence of Nitrobenzene in Liq. NH_3. A solution of **1** 212 mg (2 mmol), NaSH (98%) 114 mg (2 mmol), and nitrobenzene 31 mg (0.25 mmol) in liq. NH_3 (10 ml) in a titanium autoclave under nitrogen atmosphere was stirred at 40 °C for 5 h. After removal of NH_3, CCl_4 was added to the reaction mixture. The yields of benzyl alcohol (27%), and *N*-benzylideneaniline (9%) and *N,N'*-dibenzylidene-*α,α*-toluenediamine (5%) were determined by measuring NMR intensities of methylene and methine groups, respectively, using *p*-nitrotoluene as an internal standard in CCl_4 solution. The aqueous solution of residue was extracted with $CHCl_3$. After removal of $CHCl_3$, the residue was separated by silica-gel column chromatography using $CHCl_3$ as an eluent to give benzamide in 25% yield.

Reaction of Substituted Benzaldehydes with NaSH in the Presence of Various Nitro Compounds in Liq. NH_3. A solution of a substituted benzaldehyde (2 mmol), NaSH (98%) 114 mg (2 mmol), and a nitro compound (0.1—2.0 mmol) in liq. NH_3 (10 ml) in a titanium autoclave under nitrogen atmosphere was stirred at 40 °C for 5 h. The reaction mixture was treated as in the case of the reation with nitrobenzene added. Results obtained are summarized in Tables 1 and 2.

Reaction of Benzaldehyde (1) with NaSH in the Presence of a Reductant of Nitrobenzene in Liq. NH_3. A solution of 212 mg (2 mmol), NaSH (98%) 114 mg (2 mmol), and a reductant (2 mmol) in liq. NH_3 (10 ml) in a titanium autoclave under nitrogen atmosphere was stirred at 40 °C for 5 h. After removal of NH_3, CCl_4 was added to the reaction mixture. The yield of benzyl alcohol was determined by measuring the NMR intensity of the methylene group using *p*-nitrotoluene as an internal standard in CCl_4 solution.

Reaction of Nitrobenzene or its Reductants with NaSH in Liq. NH_3. A solution of nitrobenzene or its reductants (nitrosobenzene, phenylhydroxylamine, azoxybenzene, azobenzene, hydazobenzene, or anilne,) (2 mmol), and NaSH (98%) 114 mg (2 mmol) in liq. NH_3 (10 ml) in a titanium autoclave under nitrogen atmosphere was stirred at 40 °C for 5 h. After removal of NH_3, CCl_4 was added to the reaction mixture, and filtered. After removal of CCl_4, the residue was separated by silica-gel column chromatography using $CHCl_3$ as an eluent to give reductants of nitrobenzene. Results obtained are summarized in Table 4.

Reaction of Benzaldehyde (1) with $Na_2S \cdot 5H_2O$ in Liq. NH_3. A solution of **1** 212 mg (2 mmol) and $Na_2S \cdot 5H_2O$ 336 mg (2 mmol) in liq. NH_3 (10 ml) in a titanium autoclave under nitrogen atmosphere was stirred at 40 °C for 5 h. The reaction mixture was treated similarly to give benzyl alcohol and benzamide in 35 and 37% yield, respectively.

Reaction of Benzophenone with NaSH in the Presence of Azobenzene and Formalin in Liq. NH_3. A solution of benzophenone 364 mg (2 mmol), NaSH (98%) 114 mg (2 mmol), azobenzene 182 mg (1 mmol), and formalin (37%) 162 mg (2 mmol) in liq. NH_3 (10 ml) in a titanium autoclave under nitrogen atmosphere was stirred at 40 °C for 5 h. After removal of NH_3, the reaction mixture was extracted with $CHCl_3$. After removal of $CHCl_3$, the residue was separated by silica-gel column chromatography using $CHCl_3$ as an eluent to give benzhydrol in 27% yield.

Reaction of Benzophenone with $Na_2S \cdot 5H_2O$ in the Presence of Formalin in Liq. NH_3. A solutin of benzophenone 364 mg (2 mmol), $Na_2S \cdot 5H_2O$ 336 mg (2 mmol), and formalin (37%) 405 mg (5 mmol) in liq. NH_3 (10 ml) in a titanium autoclave under nitrogen atmosphere was stirred at 40 °C for 5 h. Similar treatment of the reaction mixture gave benzhydrol in 58% yield.

References

1) T. A. Geissman, *Org. React.*, **II**, 94 (1944).
2) C. G. Swain, A. L. Powell, W. A. Sheppard, and C. R. Morgan, *J. Am. Chem. Soc.*, **101**, 3576 (1979), and references cited therein.
3) F. Haber and R. Willstater, *Ber.*, **64**, 2851 (1931).
4) E. R. Alexander, *J. Am. Chem. Soc.*, **69**, 289 (1947).
5) Sung-Kee Chung, *J. Chem. Soc., Chem. Commun.*, **1982**, 480.
6) E. C. Ashby, D. T. Coleman III, and M. P. Gamasa, *Tetrahedron Lett.*, **24**, 851 (1983).
7) Y. Takikawa, T. Abe, R. Sato, and S. Takizawa, *Chem. Lett.*, **1980**, 25.
8) Y. Takikawa and S. Takizawa, *Nippon Kagaku Kaishi*, **1972**, 761.
9) G. Lepoustre and M. J. Sinko, "*Metal-Ammonia Solution*," W. A. Benjamin (1964).
10) N. Kornblum, S. C. Carlson, and R. G. Smith, *J. Am. Chem. Soc.*, **101**, 647 (1979).
11) A. Ishitani and S. Nagakura, *Bull. Chem. Soc. Jpn.*, **38**, 367 (1965).
12) N. Kornblum and S. Singaram, *J. Org. Chem.*, **44**, 4727 (1979).
13) E. B. Charles, D. C. Clinton, M. Charles, Jr., and E. R. Joseph, *Org. Synth., Coll. Vol.* **IV**, 711 (1963).

The Synthesis of the Chloro and Dichloro Derivatives of 2,10-Dihydroxydicyclohepta[*b,d*]furan-3,9-diones

Tomoyuki KUSABA, Akira MORI,† and Hitoshi TAKESHITA*,†

Graduate School of Engineering Sciences, 39, Kyushu University, Kasuga-koen, Kasuga, Fukuoka 816

†*Research Institute of Industrial Science, 86, Kyushu University, Kasuga-koen, Kasuga, Fukuoka 816*

(Received September 3, 1984)

4,8-Dichloro- and 5,7-dichloro-2,10-dihydroxydicyclohepta[*b,d*]furan-3,9-diones were synthesized. Although the latter could be obtained by condensation of 4-chloro-*p*-tropoquinone and its hydroquinone, the former required the hydrolysis of condensate of 3-chloro-*p*-tropoquinone and 7-chloro-5-hydroxy-2-methoxytropone. This mixed condensation led to several unsymmetrically substituted derivatives in improved yields.

In 1968, Norin and Baggaley[1] reported a structural study on a dimeric troponoid constituent from a conifer, *Juniperus utahensis Lemm.*, utahin (**1a**).[2] They suggested its identity with the oxidative condensation product obtained *via* several routes from hinokitiol (4-isopropyltropolone)[3,4] but was reluctant to draw a final conclusion as to its structure. A similar condensate (**1b**) has been obtained from 4-methyltropolone by Haworth *et al.*[5] Recently, we have reported the synthesis of the parent compound, 2,10-dihydroxydicyclohepta[*b,d*]furan-3,9-dione[6] (**2**), from 5-hydroxytropolone (**3**) and *p*-tropoquinone (**4**),[7] as well as the unambiguous synthesis of **1a**.[8]

In this paper, we wish to describe the synthesis of 4,8-, 5,7-, and 1,8-dichloro derivatives as well as the controlled mixed condensation of the tropoquinones with 5-hydroxy-2-methoxytropones.

First two chloro-*p*-tropoquinones have been prepared as follows: 4-Chloro-*p*-tropoquinone (**5**) was easily prepared by means of DDQ (2,3-dichloro-5,6-dicycano-*p*-benzoquinone)-oxidation of 4-chloro-5-hydroxytropolone (**6**) which was derived from *p*-tropoquinone (**4**)[9] with hydrochloric acid.[10] On the other hand, 3-chloro-*p*-tropoquinone (**7**) was prepared from 5-acetoxytrpolone (**8**) *via* 5-acetoxy-2-methoxytropone (**9**), 4-acetoxy-2-chloro-7-methoxytropone (**10**), and 3-chloro-5-hydroxytropolone (**11**) by sequential reactions with diazomethane, *N*-chlorosuccinimide (NCS),[11] hydrochloric acid in acetic acid, and the DDQ-dehydrogenation.

Following our previous methods, preparation of the 5,7-dichloro derivative (**12**) was carried out in two ways; the first was the partial reduction of **5** with acetic acid to yield **12** in 32% yield. The major reaction path in this case was, however, the reduction of **5** to its hydroquinone, **6**. The second was the coupling of **5** and **6** in tetrahydrofuran (THF) to give **12** in 22% yield. Again the reduction of **5** to **6** was the preferred process; this has led us to conclude that THF is also suitable for the reduction of tropoquinones to 5-hydroxytropolones.

Moreover, attempts to prepare 4,8-dichloro derivative (**13**) or 1,8-dichloro derivative (**14**) by the two methods failed; again, the reduction of **7** to **11** was exclusive. Therefore, we have modified the substrate to the 2-methoxytropone derivative based on the following grounds.

Since 3-bromotropolone (**A**) has been known to exist mainly as the tautomeric form of 3-bromo-2-hydroxytropone (**Aa**),[12] the predominant tautomer of 3-chloro-5-hydroxytropolone (**11**) must be a similar 3-chloro-2,5-dihydroxytropone (**11a**). From the view on this bond fixation, the condensation of **11** must be facilitated at C-4 over C-6. On the other hand, a steric hindrance from the adjacent chlorine atom must disfavor the condensation at C-4. Consequently, the attempted

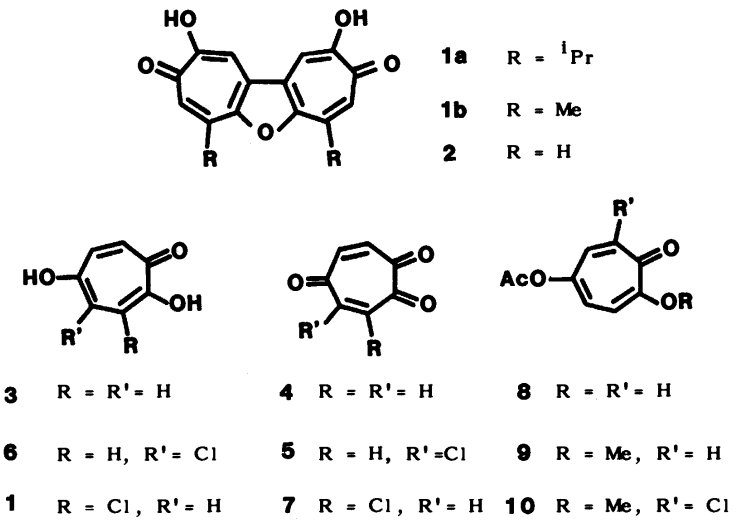

Scheme 1.

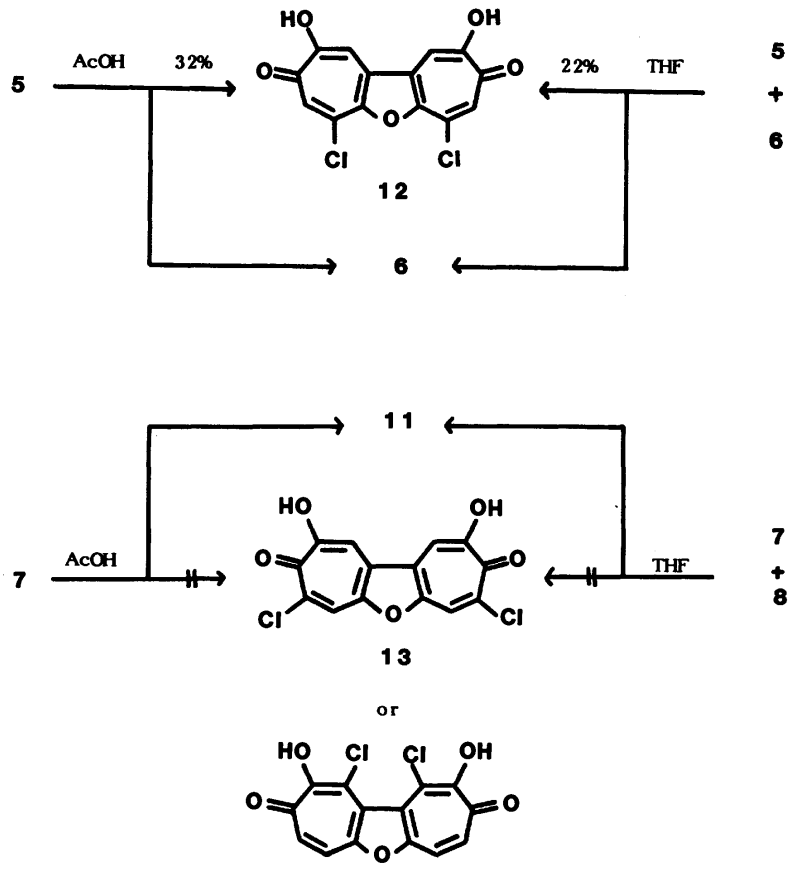

Scheme 2.

condensation of **11** with the quinone, **7**, which also possesses an adjacent chlorine atom at the reactive site, C-4, should merely have resulted in the reduction of **7** to **11**.

Thus, in view of the bond alternation, the fixed C=C bond system of **11** in the 2-chloro-7-hydroxy form would facilitate the condensation. This can be simply done by making a monomethyl ether. A mild condensation of 2-chloro-4-hydroxy-7-methoxytropone (**15**), which could be prepared from **10** by a 33%-aqueous acetic acid-hydrolysis, with **7** at 15—25 °C furnished two condensates in 24% yield with a 4:1 ratio; they are 4,8-dichloro-2-methoxy derivative (**16**) and 1,8-dichloro-10-methoxy derivative (**17**). From the mixture, the major product, **16**, was isolated after methylation to 4,8-dichloro-2,10-dimethoxy derivative (**18**) by sublimation. The hydrochloric acid-hydrolysis of **18** or **16** in acetic acid afforded **13**. Thus, the use of the 5-hydroxy-2-methoxytropones has not only provided an entry for mixed types of condensates, but also improved the yields for the single species condensates; *e.g.*, when 5-hydroxy-2-methoxytropone (**19**), which could be prepared easily from **9**, was mixed with **4** in THF at 15—25 °C for 15 min, the condensate isolated in 45% yield was the 2-methoxy derivative (**20**). This compound **20** was characterized as 2-acetoxy-10-methoxy derivative (**21**), and 2,10-dimethoxy derivative (**22**).

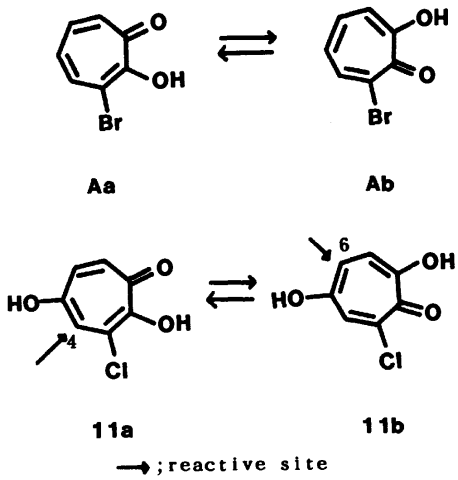

Scheme 3.

Similarly, the condensation products of **7** and **19**, isolated by consecutive treatments with hydrochloric acid in acetic acid and with acetic anhydride, were 2,10-diacetoxy-1-chloro derivative (**23**) and 2,10-diacetoxy-4-chloro derivative (**24**). Further, the condensations of **4** with **15** and **5** with **19** gave 4-chloro-2-methoxy derivative (**25**) and 7-chloro-2-methoxy derivative (**26**) in regiospecific fashion, respectively. The hydrolysis of **25** and **26** yielded 4-chloro (**27**) and 5-chloro (**28**) derivatives.

In conclusion, appropriate combinations of the

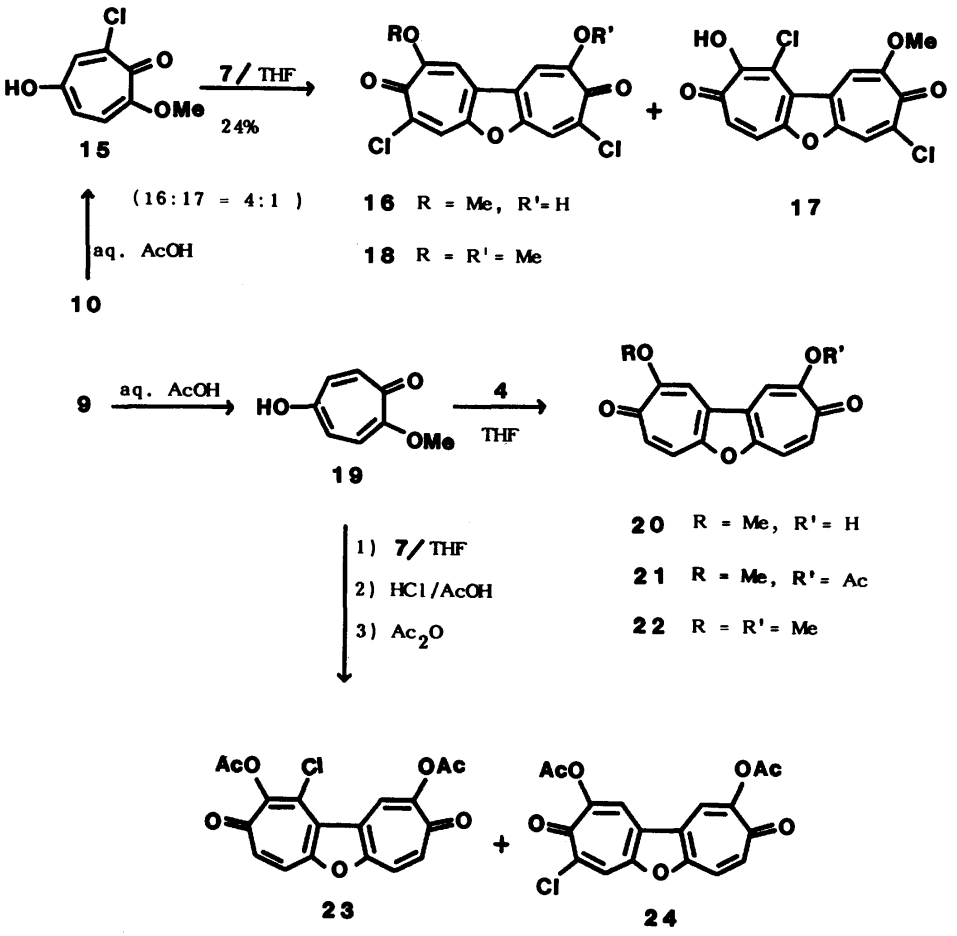

Scheme 4.

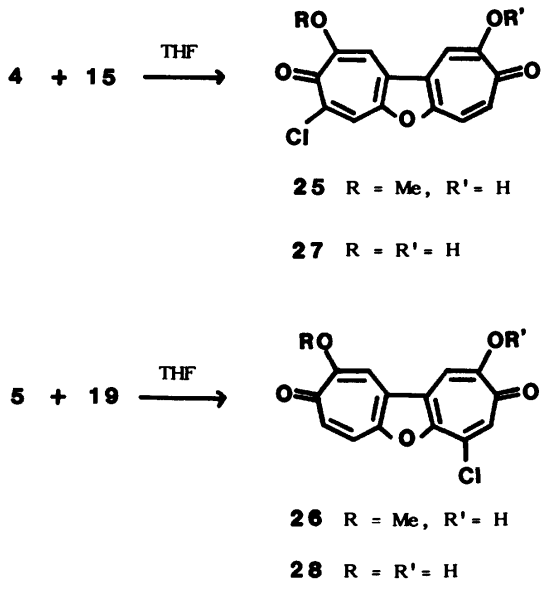

Scheme 5.

two components, *p*-tropoquinones and 5-hydroxy-2-methoxytropones, are capable of leading to various kinds of the dicyclohepta[*b*,*d*]furandione derivatives in improved yields, some of which are indeed quantitative after subtracting the amounts of recovered troponoids. Various aspects of the chemistry of these condensed furan derivatives are under investigation.

Experimental

Elemental analyses were performed with a Hitachi 026 Model CHN Analyzer by Miss M. Yamaguchi and S. Hirashima, at this Institute. The mps were measured by a Yanagimoto Micro-mp Apparatus, and were uncorrected. The IR spectra were taken either in CCl_4 solutions or as KBr disks with a Jasco Model A 102 spectrometer. The NMR spectra were measured, in $CDCl_3$ solution unless otherwise stated, by a JEOL FX100 Model Spectrometer, and the chemical shifts were expressed in the δ unit from the internal TMS. The mass spectra were measured on a JEOL OlSG Model Apparatus.

Preparation of 4-Chloro-p-tropoquinone (5). To an acetone solution (10 cm^3) of **6**[9] (260 mg), was added an acetone solution (5 cm^3)of DDQ (375 mg) at 15—25 °C. After 10 min, the acetone was removed *in vacuo*, and the residue was washed with benzene. The benzene washings were combined, concentrated, and chromatographed on a silica-gel column with benzene to yield pale yellow needles, mp 91—93 °C (decomp), **5**, 198 mg (77%) [Found: C, 49.32; H, 1.84%. Calcd for $C_7H_3O_3Cl$: C, 49.29; H, 1.78%. MS *m/z*, 170 and 172 (M^+). ^1H NMR δ=6.83 (1H, d, J=13 Hz), 6.97 (1H, d, J=13 Hz), and 7.30 (1H, s). ^{13}C-NMR δ=133.3, 133.7, 137.6, 147.2, 179.6, 182.5, and 183.4. IR ν 3050, 1655, 1630, 1600, 1235, 920, and 855 cm^{-1}].

Preparation of 5-Acetoxytropolone (8). To an AcOH solution (20 cm^3) of **3** (2.50 g), Ac_2O (2 cm^3) was added at 100 °C for 1 h, and the mixture was refluxed for 1.5 h. The reaction mixture was distilled *in vacuo*, and the residue

washed with $CHCl_3$ to recover the insoluble **3**, 1.28 g (51%). From the filtrate, colorless crystals, **8**, 1.60 g (100%), mp 107—108 °C (lit,[13] 110—111 °C) [^{1}H NMR δ=2.29 (3H, s), 7.08 (2H, dd, J=11, 1.5 Hz), 7.16 (2H, dd, J=11, 1.5 Hz), and 8.37 (1H, br. s). ^{13}C NMR δ=20.9, 122.6 (2C), 131.6 (2C), 149.3, 169.4 (2C), and 170.7], were isolated after recrystallizations from EtOAc–hexane (1:2).

Preparation of 5-Acetoxy-2-methoxytropone (9). A $CHCl_3$ solution (10 cm^3) of **8** (1.6 g) was treated with an Et_2O solution of CH_2N_2 at 0 °C to give **9**, 1.6 g (94%), colorless crystals, mp 85—86 °C [Found: C, 61.97;, H, 5.25%. Calcd for $C_{10}H_{10}O_4$: C, 61.85; H, 5.19%. ^{1}H NMR δ=2.29 (3H, s), 3.93 (3H, s), 6.65 (1H, d, J=11 Hz), 6.80 (1H, ddd, J=11, 2, 1 Hz), 7.01 (1H, dd, J=13, 2 Hz), and 7.16 (1H, dd, J=13, 1 Hz). ^{13}C NMR δ=20.8, 56.4, 110.5, 123.6, 133.8, 135.9, 148.9, 164.0, 169.3, and 179.3. MS m/z, 194 (M^+). IR ν 3000, 1760, 1570, 1200, 1145, and 910 cm^{-1}].

Preparation of 4-Acetoxy-2-chloro-7-methoxytropone (10) from 9 and NCS. A benzene solution (30 cm^3) of **9** (1.00 g) and NCS (830 mg) was refluxed for 24 h with stirring. The mixture was heated *in vacuo* to remove the solvent. Pale yellow crystalline residue was washed with benzene, and the washings chromatographed on a silica-gel column; the eluent obtained from EtOAc–hexane (2:1) was **10**, 560 mg (77%), pale yellow needles, mp 112—113 °C [Found: C, 52.53; H, 3.87%. Calcd for $C_{10}H_9O_4Cl$: C, 52.53; H, 3.98%. ^{1}H NMR δ=2.29 (3H, s), 3.94 (3H, s), 6.72 (1H, d, J=11 Hz), 6.86 (1H, dd, J=11, 2 Hz), and 7.67 (1H, d, J=2 Hz). ^{1}H NMR δ=20.8, 56.8, 111.1, 124.3, 133.5, 143.0, 145.9, 162.2 169.2 and 172.5. MS m/z, 228 and 230 (M^+). IR ν 3030, 2950, 1760, 1625, 1610, 1595, 1220, 1160, 1125, and 990 cm^{-1}], and subsequently, the recovered **9**, 380 mg (38%), was obtained.

Preparation of 3-Chloro-5-hydroxytropolone (11). A glacial AcOH solution (5 cm^3) of **10** (210 mg) and conc HCl (1 cm^3) was refluxed for 4 h. The mixture was heated *in vacuo* to remove the solvent, and the residue washed with EtOAc and recrystallized from MeOH–EtOAc to give **11**, colorless needles, mp 221—222 °C (decomp), 149 mg (94%) [Found: C, 48.62; H, 2.92%. Calcd for $C_7H_5O_3Cl$: C, 48.72; H, 2.93%. ^{1}H NMR (CD_3OD) δ=7.00 (1H, dd, J=12, 3 Hz), 7.30 (1H, d, J=12 Hz), and 7.65(1H, d, J=3 Hz). ^{13}C NMR (CD_3OD) δ=123.5, 123.9, 129.7, 140.2, 157.9, 163.6, and 167.8. MS m/z, 172 and 174 (M^+). IR ν 3200—2400, 1585, 970, 960, 930, 850, and 760 cm^{-1}].

Preparation of 3-Chloro-p-tropoquinone (7). Under the similar conditions to those in the preparation of **5** from **6**, **11** (48 mg) was converted to **7**, 38 mg (80%). Recrystallizations from benzene gave pale yellow crystals, mp 73—74 °C (decomp) [Found: C, 49.51; H, 1.75%. ^{1}H NMR δ=6.84 (2H, d, J=1 Hz) and 7.30 (1H, t, J=1 Hz). ^{13}C NMR δ=133.8, 137.2, 138.5, 143.4, 180.2, 184.5, and 184.8. MS m/z, 170 and 172 (M^+). IR ν 3030, 1695, 1660, 1320, 1170, 925, 880, 860, and 850 cm^{-1}].

Formation of 5,7-Dichloro Derivative (12) by Partial Reduction of 5. An AcOH (3 cm^3) solution of **5** (104 mg) was refluxed for 1.5 h with stirring. The solvent was removed *in vacuo*, and the residue washed with MeOH. The residue thus obtained was sublimed on a cold finger to give **12**, yellow needles, mp>300 °C, 8 mg (32%) [Found: C, 51.79; H, 2.08%. Cacld for $C_{14}H_6O_5Cl_2$: C, 51.72; H, 1.86%. ^{1}H NMR (CF_3COOD) δ=8.24 (2H, s) and 8.32 (2H, s). MS m/z, 324 and 326 (M^+). IR ν 3250, 3050, 1620, 1590, 1540, 1510, and 1400 cm^{-1}]. From the MeOH soluble fractions, 79 mg (75%) of **6** was obtained.

Condensation of 5 with 6. To a THF solution (10 cm^3) of **6** (252 mg), a THF solution (5 cm^3) of **5** (249 mg) was added at once. The mixture was kept at 15—25 °C under N_2 atmosphere for 16 h with stirring. After the removal of the solvent *in vacuo*, the residue was washed with a small amount of MeOH. Insoluble solid material was collected by filtration to give **12**, 33 mg (22%). From the MeOH washings, 348 mg (69%) of **6** was obtained.

Attempted Formation of 4,8-Dichloro Derivative (13) or 1,8-Dichloro Derivative (14). *a)*: A THF solution (4 cm^3) of **7** (43 mg) and **11** (43 mg) was kept at room temperature for 2 d. The solvent was removed *in vacuo*, and the residue crystallized from MeOH to give 76 mg (100%) of **11**. No other compound was identified.

b): An AcOH solution (2 cm^3) of **7** (38 mg) was refluxed for 2 h, and the solvent removed *in vacuo*; the pale yellow crystals obtained by recrystallizations from MeOH were **11**, 39 mg (100%).

Preparation of 2-Chloro-4-hydroxy-7-methoxytropone (15). An aqueous AcOH solution (33%, 3 cm^3) of **10** (200 mg) was heated at 100 °C for 10 h with stirring. The mixture was then evaporated *in vacuo* and the residue washed with EtOAc, and recrystallized from MeOH to give **15**, 155 mg (95%), mp 170—173 °C (decomp) [Found: C, 51.37; H, 3.82%. Calcd for $C_8H_7O_3Cl$: C, 51.49; H, 3.79%. ^{1}H NMR (CD_3OD) δ=3.88 (3H, s), 6.77 (1H, dd, J=11, 2.5 Hz), 7.15 (1H, d, J=11 Hz), and 7.85 (1H, d, J=2.5 Hz). ^{13}C NMR (CD_3OD) δ=57.2, 116.3, 118.7, 133.2, 146.2, 157.8, 159.9, and 172.9. MS m/z, 186 and 188 (M^+). IR ν 3050—2500, 1615, 1590, 1540, 1480, 1475, 1450, 1440, 1355, 1250, 1220, 1000, 835, and 755 cm^{-1}].

The Condensation of 7 with 15 to 4,8-Dichloro-10-methoxy Derivative (16) and 1,8-Dichloro-10-methoxy Derivative (17). To a THF suspension (30 cm^3) of **15** (830 mg), a THF solution (20 cm^3) of **7** (1.00 g) was added at once under N_2 atmosphere. The mixture was kept at 15—25 °C for 16 h. The solvent was removed *in vacuo*, and the residue washed with MeOH. The insoluble mass was passed through a Celite column with $CHCl_3$ to yield a 4:1-mixture of **16** and **17**, 380 mg (24%). Droplet-counter-current distribution fractionation of the mixture with $CHCl_3$–AcOH–H_2O (2:2:1) led to a separation of **16**, yellow crystals, mp 274—277 °C (decomp) [Found: C, 53.07; H, 2.33%. Calcd for $C_{15}H_8O_5Cl_2$: C, 53.12; H, 2.38%. MS m/z, 338, 340, and 342 (M^+). ^{1}H NMR δ=4.08 (3H, s), 7.16 (1H, s), 7.75 (1H, s), 8.27 (1H, s), and 8.40 (1H, s). IR ν 3500—3300, 3250, 3040, 1615, 1570, 1510, 900, and 860 cm^{-1}], and **17**, yellow crystals, mp 225—227 °C (decomp) [Found: M. W., 337.9750. Calcd for $C_{15}H_8O_5{}^{35}Cl_2$: M. W., 337.9749. ^{1}H NMR δ=4.04 (3H, s), 7.39 (1H, d, J=12 Hz), 7.85 (1H, d, J=12 Hz), 8.24 (1H, s), and 8.69 (1H, s). IR ν 3150, 1615, 890, and 850 cm^{-1}]. From the MeOH washings, the troponoids, **11** and **15**, 1.4 g (1:1), were recovered.

Methylation of 16 to 18. To a $CHCl_3$ solution (50 cm^3) of **16** (345 mg) was treated with ethereal CH_2N_2 to form precipitates, 223 mg, which were collected and sublimed at 300 °C to obtain 219 mg (55%) of colorless crystals, mp> 300 °C, **18** [Found: C, 54.30; H, 2.90%. Calcd for $C_{16}H_{10}O_5Cl_2$: C, 54.41; H, 2.86%. ^{1}H NMR δ=4.08 (6H, s), 7.12 (2H, s), and 8.25 (2H, s). MS m/z, 352, 354, 356 (M^+). IR ν 3025, 2940, 1615, 1580, and 990 cm^{-1}].

Hydrolysis of 16 to 13. An AcOH solution (4 cm^3) containing conc HCl (1 cm^3) of **16** (41 mg) was heated at 90 °C for 24 h. After evaporation of the mixture, the residue was washed with MeOH and sublimed on a cold finger to yield

yellow needles, **13**, mp>300 °C, 33 mg (85%) [Found: C, 51.90; H, 2.16%. Calcd for $C_{14}H_6O_5Cl_2$: C, 51.72; H, 1.86%. ^{1}H NMR (CF_3COOD) δ=8.38 (2H, s) and 8.75 (2H, s). MS *m/z*, 324, 326, 328 (M^+). IR ν 3250, 3040, 1620, 1590, 1570, 1500, and 1450 cm^{-1}].

Preparation of 5-Hydroxy-2-methoxytropone (19). A 50%-aqueous AcOH solution (10 cm^3) of **9** (600 mg) was heated at 90 °C for 16 h. The mixture was evaporated to dryness, and the residue washed by AcOEt. The crystalline residue was sublimed on a cold finger to yield **19**, pale yellow needles, mp 154—155 °C, 423 mg (91%) [Found: C, 62.99; H, 5.25%. Calcd for $C_8H_8O_3$: C, 63.15; H, 5.30%. ^{1}H NMR (CD_3OD) δ=3.86 (3H, s), 6.74 (1H, dd, J=11, 2 Hz), 7.11 (1H, d, J=11 Hz), and 7.24 (2H, d, J=2 Hz). ^{13}C NMR (CD_3OD) δ=56.6, 116.4, 119.1, 134.1, 138.1, 160.6, 161.9, and 178.5. IR ν 3100—2400, 1595, 1535, 980, 858, 840, and 780 cm^{-1}].

Condensation and Acetylation of 19 with 4 to 2-Acetoxy-10-methoxy Derivative (21). To a THF suspension (10 cm^3) of **19** (210 mg), a THF solution (10 cm^3) of **4** (190 mg) was added at 15—25 °C. After 16 h with stirring, the mixture was heated *in vacuo* to remove the solvent, and, without further purifications, was acetylated by Ac_2O (5 cm^3), and kept at 100 °C until the mixture became homogeneous. After cooling the mixture, the solvent was removed *in vacuo*, and the residual mass washed with EtOAc, and crystallized from $CHCl_3$ to give 275 mg (100%) of **21**, mp 237—239 °C [Found: C, 65.11; H, 3.80%. Calcd for $C_{17}H_{12}O_6$: C, 65.38; H, 3.87%. ^{1}H NMR δ=2.40 (3H, s), 4.01 (3H, s), 6.94 (1H, s), 7.16 (1H, d, J=12 Hz), 7.22 (1H, d, J=12 Hz), 7.54 (1H, d, J=12 Hz), 7.61 (1H, d, J=12 Hz), and 7.68 (1H, s). ^{13}C NMR δ=20.7, 56.6, 102.0, 119.3, 122.5, 123.8, 124.5, 125.4, 134.2, 136.4, 151.5, 153.6, 154.1, 161.3, 168.7, 178.1, and 179.8]. EtOAc-soluble fractions gave a mixture of 2,5-diacetoxytropone and **9**, 209 mg.

Hydrolysis of 21 to 10-Methoxy Derivative (20). A 50%-aqueous AcOH solution (10 cm^3) of **21** (275 mg) was heated at 100 °C with stirring for 16 h. After the solvent was evaporated, the residue was sublimed on a cold finger to give **20**, 220 mg (93%), mp>300 °C [Found: C, 66.54; H, 3.87%. Calcd for $C_{15}H_{10}O_5$: C, 66.67; H, 3.73%. ^{1}H NMR (CF_3COOD) δ=4.63 (3H, s), 8.09 (1H, d, J=12.5 Hz), 8.44 (1H, d, J=12.5 Hz), 8.53 (1H, d, J=11.7 Hz), 8.58 (1H, s), 8.97 (1H, d, J=11.7 Hz), and 9.03 (1H, s). MS *m/z*, 270 (M^+). UV ($CHCl_3$) λ_{max}: 263 nm (ε=29600), 272 (36200), 299 (18000), 321 (15200), 380 (20500), 396 (30800), and 411 (28500). IR ν 3250, 3050, 1610, 1565, 1520, 1460, 1410, 1250, 1200, 1155, 1110, and 980 cm^{-1}].

Methylation of 20 to 2,10-Dimethoxy Derivative (22). A $CHCl_3$ solution (3 cm^3) of **20** (50 mg) was treated with CH_2N_2 in Et_2O at 0—5 °C. Sublimation on a cold finger of the mixture yielded **20**, yellow crystals, mp 227—230 °C, 22 mg (57%) [Found: M. W., 284.0685. Calcd for $C_{16}H_{12}O_5$: M. W., 284.0684. ^{1}H NMR δ=4.08 (6H, s), 7.05 (2H, s), 7.21 (2H, d, J=13 Hz), and 7.62 (2H, d, J=13 Hz). ^{13}C NMR δ=56.5 (2C,) 103.0 (2C), 123.8 (2C), 124.9 (2C), 134.1 (2C), 151.7 (2C), 161.0 (2C), and 179.9 (2C). IR ν 1610, 1560, and 1520 cm^{-1}].

Condensation of 19 with 7 and Subsequent Transformation to 2,10-Diacetoxy-1-chloro Derivative (23) and 2,10-Diacetoxy-4-chloro Derivative (24). To a THF suspension (2 cm^3) of **19** (95 mg), a THF solution (4 cm^3) of **7** (106 mg) was added at 15—25 °C under N_2 atmosphere. The solvent was removed *in vacuo*, the resultant residue washed with MeOH, and the reddish yellow crystalline solid directly hydrolyzed in AcOH (7 cm^3) with conc HCl (1.5 cm^3) at 100 °C for 16 h. After evaporation of the solvent *in vacuo*, the residue, 74 mg, was acetylated with Ac_2O (7 cm^3) at 100 °C for 16 h. After removal of Ac_2O *in vacuo*, the residue was chromatographed on a silica-gel column to give at first, yellow crystals, **24**, mp 225—226 °C, 43 mg (50%) [Found: C, 57.47; H, 3.33%. Calcd for $C_{18}H_{11}O_7Cl$: C, 57.69; H, 2.96%. ^{1}H NMR δ=2.38 (3H, s), 2.40 (3H, s), 7.27 (1H, d, J=13 Hz), 7.60 (1H, s), 7.68 (1H, d, J=13 Hz), 7.69 (1H, s), and 8.30 (1H, s). ^{13}C NMR δ=20.5 (2C), 118.4, 118.8, 122.3, 122.7, 125.2, 137.3, 144.2, 151.6, 152.1, 154.3, 154.7, 168.3 (2C), 171.9, and 178.1. IR ν 3050, 2940, 1765, 1615, 1580, 1540, 1375, 1350, 1190, 1115, 1050, 930, and 855 cm^{-1}], and subsequently, other yellow needles, mp 158—159 °C, **23**, 2 mg (2%) [Found: C, 57.75; H, 3.13%. Calcd for $C_{18}H_{11}O_7Cl$: C, 57.69; H, 2.96%. ^{1}H NMR δ=2.38 (3H, s), 2.43 (3H, s), 7.17 (1H, d, J=12.5 Hz), 7.25 (1H, d, J=12.7 Hz), 7.64 (1H, d, J=12.5 Hz), 7.66 (1H, d, J=12.7 Hz), and 8.76 (1H, s). ^{13}C NMR δ=20.4, 20.6, 121.2, 121.4, 123.6, 125.2, 125.4, 133.1, 135.8, 136.9, 151.6, 152.9, 153.0, 154.7, 167.1, 168.4, 176.1, and 178.1. MS *m/z*, 374 and 376 (M^+). IR ν 3050, 2950, 1770, 1620, 1585, and 1179 cm^{-1}].

From the MeOH soluble fractions of the condensation reaction mixture, **11** and **9**, 98 mg (44%) were obtained.

Condensation of 15 with 4. Formation of 4-Chloro-2-methoxy Derivative (25): To a THF solution (2 cm^3) of **15** (164 mg), a THF solution (4 cm^3) of **4** (120 mg) was added at once under N_2 atmosphere. After stirring for 48 h the solvent was removed, and the residue washed with MeOH. The residue was collected by filtration and washed again with MeOH to give yellow crystals, mp>300 °C, **25**, 113 mg (35%) [Found: C, 59.00: H, 3.13%. Calcd for $C_{15}H_9O_5Cl$: C, 59.13; H, 2.98%. ^{1}H NMR (CF_3COOD) δ=4.44 (3H, s), 8.18 (1H, d, J=12 Hz), 8.38 (1H, s), 8.51 (1H, d, J=12 Hz), 8.87 (1H, s), and 8.95 (1H, s). MS *m/z*, 304 and 306 (M^+). UV ($CHCl_3$) λ_{max}:268 nm (ε=31600), 276 (37600), 299 (20000), 405 (32900), and 422 (32900). IR ν 3300, 3050, 1610, 1570, 1520, 1470, 1405, 1240, 1170, and 980 cm^{-1}].

Hydrolysis of 25 to 27. An AcOH solution (3 cm^3) of **25** (50 mg) and conc HCl (1 cm^3) was heated at 100 °C for 24 h. After removal of solvent *in vacuo*, the residue was sublimed on a cold finger to give yellow crystals, mp>300 °C, **27**, 44 mg (95%) [Found: C, 57.82; H, 2.70%. Calcd for $C_{14}H_7O_5Cl$: C, 57.85; H, 2.43%. ^{1}H NMR (CF_3COOD) δ=8.30 (1H, d, J=11.7 Hz), 8.40 (1H, s), 8.61 (1H, d, J=11.7 Hz), 8.81 (1H, s), and 8.83 (1H, s). UV ($CHCl_3$) λ_{max}:271 nm (ε=33100), 278 (39200), 302 (18100), 330 (13500), 394 (20700), 412 (31600), and 427 (27600). IR ν 3250, 3050, 1630, 1600, 1565, 1550, 1460, 1250, 1170, 1120, 880, 850, and 840 cm^{-1}].

Acetylation of 27 to 24. An Ac_2O solution (3 cm^3) of **27** (26 mg) was heated at 100 °C for 20 h to form yellow crystals, mp 225—226 °C, 28 mg (78%), which was identical with **24**.

Condensation of 19 with 5. To a THF suspension (10 cm^3) of **19** (69 mg), a THF solution (4 cm^3) of **5** (77 mg) was added at 15—25 °C. After 16 h, the mixture was heated *in vacuo* to remove the solvent, the residue was washed with MeOH to recover **19**, 40 mg (57%), and **6**, 42 mg (55%), and the residue sublimed *in vacuo* to give yellow crystals, mp 292—294 °C (decomp), 58 mg (100%), **26** [Found: C, 58.84; H, 2.97%. Calcd for $C_{15}H_9O_5Cl$: C, 59.13; H, 2.98%. ^{1}H NMR (CF_3COOD) δ=4.61 (3H, s), 8.28 (1H, s), 8.52 (1H, d, J=12 Hz), 8.65 (1H, s), 8.96 (1H, s), and 8.99 (1H, d, J=12 Hz). MS *m/z*, 304 and 306 (M^+). IR ν 3250, 3030, 1605, 1570, 1545, and 1510 cm^{-1}].

Hydrolysis of 26 to 5-Chloro Derivative (28). An AcOH

solution (3 cm^3) of **26** (17 mg) and conc HCl(1.5 cm^3) was heated at 100°C for 4 h. Then, the mixture was evaporated *in vacuo*, and the residue trituated with MeOH, and sublimed on a cold finger to give **28**, 15 mg (83%) [Found: C, 57.82; H, 2.70%. Calcd for $C_{14}H_7O_5Cl$: C, 57.85; H, 2.43%. ^1H NMR (CF_3COOD) δ=8.16 (1H, d, J=12 Hz), 8.30 (1H, s), 8.44 (1H, s), 8.54 (1H, d, J=12 Hz), and 8.60 (1H, s). IR ν 3250, 3050, 1620, 1560, 1540, and 1519 cm^{-1}].

References

1) K. H. Baggaley and T. Norin, *J. Chem. Soc., Chem. Commun.*, **1968**, 233.

2) J. Runeberg, *Acta Chem. Scand.*, **14**, 797 (1960).

3) T. Nozoe, S. Ebine, S. Itô, and A. Konishi, *Proc. Jpn. Acad.*, **27**, 10 (1951).

4) T. Nozoe, S. Seto, S. Itô, M. Sato, and T. Katono, *Proc. Jpn. Acad.*, **28**, 488 (1952).

5) P. Akroyd, R. D. Haworth, and P. R. Jefferies, *J. Chem. Soc.*, **1954**, 286.

6) To avoid repetitions of lengthy names for these tricyclic compounds, they are expressed with the term, "derivative," unless otherwise specified for substituents on the C-2 and C-10, this is equivalent to 2,10-dihydroxydicyclohepta[*b*,*d*]-furan-3,9-dione.

7) H. Takeshita, T. Kusaba, and A. Mori, *Chem. Lett.*, **1982**, 701.

8) H. Takeshita, T. Kusaba, and A. Mori, *Chem. Lett.*, **1983**, 1371.

9) S. Itô, Y. Shoji, H. Takeshita, M. Hirama, and K. Takahashi, *Tetrahedron Lett.*, **1975**, 1075.

10) S. Itô and M. Hirama, *Tetrahedron Lett.*, **1976**, 2339.

11) This is an extended version of the Takase-Yasunami's NBS-bromination of 2-methoxytropone to 2,4-dibromo-7-methoxytropone. See K. Takase, M. Yasunami, and Y. Sasagawa, *Chem. Lett.*, **1980**, 205.

12) H. Sugiyama, S. Itô, and T. Nozoe, *Tetrahedron Lett.*, **1965**, 179.

13) T. Nozoe, S. Seto, S. Itô, M. Sato, and T. Katono, *Sci. Repts. Tohoku Univ. Ser. I*, **37**, 191 (1953).

 © 1985 The Chemical Society of Japan Bull. Chem. Soc. Jpn., 58, 521—524 (1985)

Photochemical Electron-transfer Reaction between Aromatic Olefins and Metal Ions. Dependence of the Reaction Course on the Structure of the Olefins

Masanobu KOJIMA,*†,†† Hirochika SAKURAGI,† and Katsumi TOKUMARU†

†*Department of Chemistry, University of Tsukuba, Sakura-mura, Ibaraki 305*

††*Faculty of Liberal Arts, Shinshu University, 3-1-1 Asahi, Matsumoto 390*

(Received September 11, 1984)

To investigate the photochemical electron transfer from aromatic olefins to copper(II) or iron(III) ions, a series of substituted styrenes (**1**) was irradiated in the presence of copper(II) or iron(III) salts in methanol, which gave dimethoxylated monomers (**2**) and one or more of three types of dimethoxylated dimers [α,α- (**3**), α,β- (**4**), and β,β-dimers (**5**)]. The formation of these products are reasonably attributed to the participation of the cation radicals of the olefins generated by electron transfer from the excited olefins to the metal ions. Substituents on the substrates are found to govern the reaction products.

Recently, much attention has been paid to the photochemical electron-transfer processes from the viewpoint of mechanistic photochemistry, energy storage, photoimaging, preparative chemistry, *etc.*[1] On photochemical electron transfer involving styrenes, investigations were reported for the excitation of organic electron acceptors like 1,4-dicyanobenzene or methyl 4-cyanobenzoate followed by electron transfer to their excited state from ground-state styrenes to give the cation radicals of the olefins.[2—4] On the other hand, few investigation was done for the electron transfer from the excited styrene to an acceptor except a short report by Tsutsumi and Murai that the irradiation of styrene (**1a**) in the presence of copper(II) perchlorate in methanol gave a dimethoxylated monomer **2a** and a dimethoxylated dimer (α,α-dimer **3a**) as isolatable products.[5]

$$\underset{\textbf{1a}}{PhCH{=}CH_2} \xrightarrow[Cu^{2+}/MeOH]{254\ nm} \underset{\textbf{2a}}{PhCH(OMe)CH_2OMe} + \underset{\textbf{3a}\ (\alpha,\alpha\text{-dimer})}{[PhCH(CH_2OMe)\text{-}]_2}$$

To get deeper insight into the electron transfer from the excited organic compounds, particularly aromatic olefins, to metal ions, a series of styrene derivatives **1** were irradiated in the presence of copperr(II) and iron(III) salts. This paper discribes the results of the reaction; 1) the irradiation gives in addition to **2** and **3**, other isomeric dimethoxylated dimers **4** (α,β-dimer) and **5** (β,β-dimer), 2) the reaction products are similar to those of the electrolysis of the styrene **1** with a platinum anode in the same solvent,[6a] 3) the reaction course of the cation radicals of **1** is controlled by the substituents on the α-, β-, and p-carbons of the olefins **1**.

Results

Photochemical Reaction of Substituted Styrenes in the Presence of Metal Ions in Methanol. In a typical run, styrene (**1a**, 28 mmol) was irradiated in the presence of copper(II) perchlorate (56 mmol) in methanol (300 cm^3) under nitrogen stream at room temperature with a 160-W low pressure mercury lamp for 40 h. After the irradiation, 70% of **1a** was consumed and a dimethoxylated monomer **2a** (yield 41% based on **1a** consumed) was obtained in addition to three types of dimethoxylated dimers [α,α- (**3a**, yield 4%), α,β- (**4a**, 0.7%), β,β- (**5a**, 1.5%)] (see Scheme 1). During the irradiation, a small amount of metallic copper was precipitated. The structure of the products was identified from spectral data in comparison with authentic samples obtained from the anodic oxidation of **1a** in methanol with a platinum or a graphite anode.[6] The yields of the reaction products were determined by GLPC analysis.

In control experiments, when **1a** was left standing in methanol with $Cu(ClO_4)_2$ for 25 d under nitrogen atmosphere at room temperature without irradiation, **1a** was completely recovered, and also irradiation of **1a** in the presence of $Cu(ClO_4)_2$ in methanol with bromine lamp (effective longer than 400 nm) through a Pyrex filter under nitrogen atmosphere at room temperature gave only a trace amount of **2a**. Moreover, UV spectra of the mixture of **1** and $Cu(ClO_4)_2$ in methanol did not show any new absorption band.

Other styrene derivatives **1** were likewise irradiated in the presence of $Cu(ClO_4)_2$ in methanol. The results are summarized in Table 1 together with the oxidation potentials of the olefins. The use of iron(III) perchlorate instead of copper(II) perchlorate in the photochemical reaction of **1a—d** in methanol gave **2a** (12%),

$$\underset{\textbf{1a-g}}{ArCR{=}CHR'} \xrightarrow[Cu^{2+}/MeOH]{h\nu} \underset{\textbf{2a-g}}{ArCR(OMe)CHR'OMe} + \underset{\textbf{3a-c,e}\ (\alpha,\alpha\text{-dimer})}{[ArCR(CHR'OMe)\text{-}]_2} + \underset{\textbf{4a}\ (\alpha,\beta\text{-dimer})}{PhCH(OMe)CH_2CH(Ph)CH_2OMe} + \underset{\textbf{5a-d,f,g}\ (\beta,\beta\text{-dimer})}{[ArCR(OMe)CHR'\text{-}]_2}$$

a: Ar=Ph, R=R'=H; **b**: Ar=4-ClC_6H_4, R=R'=H;
c: Ar=Ph, R=Me, R'=H; **d**: Ar=R=Ph, R'=H;
e: Ar=Ph, R=H, R'=Me; **f**: Ar=4-MeC_6H_4, R=R'=H;
g: Ar=4-$MeOC_6H_4$, R=R'=H

Scheme 1.

TABLE 1. PHOTOCHEMICAL REACTION OF STYRENE DERIVATIVES IN THE PRESENCE OF COPPER(II) ION

	ArCR=CHR′ 1	Eox[a] (V)	Conv. (%)	Dimethoxylated Monomer (2,%)[b]	Dimethoxylated Dimers (%)[c] α,α (3)	α,β (4)	β,β (5)
1a	$PhCH=CH_2$	1.95	70	41	4	0.7	1.5
1b	$4\text{-}ClC_6H_4CH=CH_2$	1.76	58	13	35	—	6
1c	$PhCMe=CH_2$[d]	1.60	54	45	5	—	2
1d	$Ph_2C=CH_2$[e]	1.48	53	39	—	—	2
1e	PhCH=CHMe	1.38	67	12	37	—	—
1f	$4\text{-}MeC_6H_4CH=CH_2$	1.38	63	42	—	—	5
1g	$4\text{-}MeOC_6H_4CH=CH_2$[f]	1.15	79	trace	—	—	34

a) Oxidation potential *vs.* Ag/0.1 mol/dm³ $AgNO_3$ in MeCN. b) Yield for **2**: [(moles of 2)/(moles of **1** consumed)]×100. c) Yield for **3**, **4**, or **5**: [(moles of **3**, **4**, or **5**)/(moles of **1** consumed)]×200. d) Another product: $PhCMe_2OMe$ (20%). e) Other products: Ph_2CO (10%) and $Ph_2C(OMe)Me$ (28%). f) Other products: $4\text{-}MeOC_6H_4CH(OMe)Me$ (12%) and *trans*-1,2-bis(4-methoxyphenyl)cyclobutane (10%).

2b (13%), **2c** (24%), and **2d** (24%), respectively, but did not afford any other isolatable products.

Discussion

Substituent Effect on the Selectivity for Products. As Table 1 shows, **1a**, **1b**, and **1c** with the higher oxidation potentials among **1**'s afforded **2**, α,α-dimer **3**, and β,β-dimer **5**, accompanied by α,β-dimer **4** from **1a**. On the other hand, **1d**, **1f**, and **1g** with the lower oxidation potentials gave no α,α-dimer **3** but exclusively β,β-dimer **5** together with **2**. On the basis of the above selectivity for the production of the dimethoxylated dimers, **1a**, **1b**, and **1c** are now classified as group I olefins, while **1d**, **1f**, and **1g** as group II olefins. **1e** is classified as group I in view that irradiation of **1e** with $Cu(ClO_4)_2$ in methanol gave exclusively α,α-dimer **3e** together with **2e** but no β,β-dimer **5e**, although **1e** has the same oxidation potential as **1f** of group II. As the above results indicate, the selectivity for production of dimethoxylated dimers is governed by the substituent on the α-, β-, or *p*-carbon of **1**; group II olefins with electron-donating groups such as *p*-methyl or *p*-methoxyl group tend to produce β,β-dimer **5** selectively, while group I olefins without electron-donating groups on the aromatic nucleus tend to give α,α-dimer **3** rather than β,β-dimer **5**.

Mechanism. Formation of the various products is satisfactorily understood in terms of a mechanism depicted in Scheme 2.

The initial step after the excitation of **1** is certainly the electron transfer from the excited state of **1** to the metal ions to generate the cation radical **6**.

In group I olefins, the production of α,α-dimer **3** seems to be plausible only through dimerization of radical **7**, which results from the addition of methanol to β-carbon of the cation radical **6**. Also, radical **7** will collapse into α,β-dimer **4** through addition to the olefins, or be further oxidized by copper(II) ion into carbocation **8** finally giving rise to **2**. However, in the photochemical reactions of group II olefins, production of neither α,α-dimer **3** nor α,β-dimer **4** suggests that radical **7** does not participate as a reaction intermediate. In cation radicals **6** arising from group II olefins as compared with those arising from group I olefins, the positive charge tends to be more highly distributed on the aromatic ring and concurrently the unpaired electron must have higher density on the terminal carbon. This situation can be schematically expressed by a resonance canonical form (**6a**) and was actually observed in ESR spectrum of the cation radicals of *N*,*N*-dimethylalkenamines generated by electrolysis.[7] Therefore, **6** from group II olefins, owing to their higher spin density on their terminal carbon atoms, will more facilely add to olefins than those from group I olefins finally leading to β,β-dimer **5**, and consequently, due to the less positive charge population on their terminal carbon atoms, will react with methanol on their α-carbon atoms to give radical **9**, which will be further oxidized by copper(II) ion to give carbocations **10** finally affording **2**.[8]

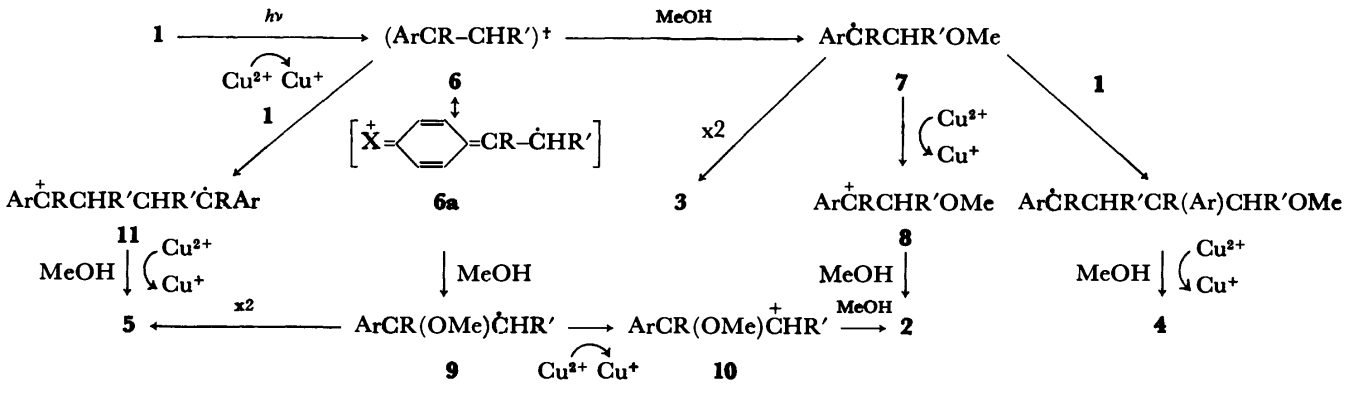

Scheme 2.

For the methanolysis of the cation radical **6**, electron transfer between **1d** and excited electron acceptors like 1,4-dicyanobenzene and 1-cyanonaphthalene in methanol was reported to give anti-Markownikoff adduct of methanol to the olefin through the formation of radical **7d** as an intermediate.[2d] It is noticeable that, in the present reaction of group I olefins, methanolysis of the intermediate cation radical **6** occurs by the same orientation as the above reaction, however, for group II olefins, methanolysis of the cation radical **6** proceeds by a different orientation giving **9**.

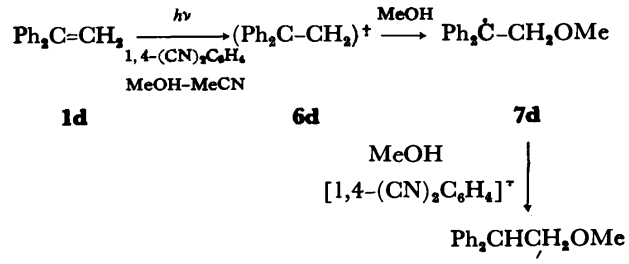

The free-energy change (ΔG) for the electron-transfer processes from the excited olefin to metal ions is given by Eq. 1,[9] where $E(D/D^+)$ and $E(A^-/A)$ are the oxidation potential of the donor (D) and the reduction potential of the acceptor (A), respectively, and $e_0^2/\varepsilon\alpha$ is the energy gained by bringing the two ion radicals to the encounter distance (α) in a solvent of dielectric constant ε (methanol, $\varepsilon_{25°}$=32.7) and estimated to be 0.065 eV (1.5 kcal/mol) in methanol. The singlet energies, E_s, of 4-methoxystyrene and styrene are obtained from the fluorescence spectrum or literature,[10] respectively. In Table 2 are listed the calculated values of ΔG for the olefins. The electron-transfer process from the excited olefins to copper(II) ion is shown to be exothermic.

$$\Delta G(\text{kcal/mol}) = 23.06[E(D/D^+) - E(A^-/A) - e_0^2/\varepsilon\alpha] - E_s \quad \text{(kcal/mol)} \quad \text{(Eq. 1)}$$

The proposed mechanism in Scheme 2 requires the second electron transfer from radical **7** or radical **9** to metal ions. The free-energy change of this process cannot be easily estimated because the oxidation potentials of radical **7** and **9** cannot be measured.[11] However, their oxidation potentials seem to lie at more cathodic levels than the reduction potentials of the metal ions. Therefore, the second electron-transfer process seems also exothermic as reported by Kochi *et al.*[12-14]

Table 2. Singlet energies of the olefins and calculated ΔG values, using Eq. 1, for the electron-transfer process involving the singlets of the olefins and copper(II) ion

	Eox/V[a]	Ered/V[b]	*Es* (kcal/mol)	*ΔG* (kcal/mol)
$PhCH=CH_2$	1.95	—	98[c]	−33
$4\text{-}MeOC_6H_4CH=CH_2$	1.15	—	94[d]	−48
$Cu(ClO_4)_2$	—	−0.88		

a) Oxidation potential. b) Reduction potential. c) Taken from S. L. Murov, "Handbook of Photochemistry," Marcel Dekker, New York (1973), p. 20. d) Obtained from the fluorescence spectrum.

Experimental

The IR spectra were obtained from a Hitachi 260-50 infrared spectrophotometer and a Hitachi 260-10 infrared spectrophotometer. The NMR spectra were recorded on a JEOL JNM-MH-100 spectrometer, a JEOL-FX-100 spectrometer, and a JEOL-FX-90Q spectrometer. The mass spectra were determined with a Hitachi RMU-6MC mass spectrometer. Gas-liquid phase chromatographic analysis was performed on a Hitachi 163 gas chromatograph equipped with a flame ionization detector.

Materials. Styrene, 4-chlorostyrene, α-methylstyrene, 1,1-diphenylethylene, and *trans*-β-methylstyrene were commercial samples from Wako Pure Chemical Industries. 4-Methylstyrene and 4-methoxystyrene were prepared by decarboxylation of the corresponding cinnamic acids as described in the literature.[15] Copper(II) perchlorate and iron(II) perchlorate were purchased from Kanto Chemical.

Preparation of Authentic Samples. Authentic samples of dimethoxylated monomers **2** (except for **2c**) and dimethoxylated dimers (except for **3b**, **3c**, and **3e**) were prepared by anodic oxidation of olefins **1** in methanol.[6]

Preparation of 1,2-Dimethoxy-1-phenylpropane (2e). Metallic sodium (1 g, 43 matom) was dissolved in 100 cm^3 of methanol and then freshly distilled β-methylstyrene (4.5 g, 38 mmol) was added to the mixture. The mixture was subjected to constant-current (1 A) elctrolysis at a platinum plate anode (approximate area 60 cm^2) with a platinum wire as a cathode and SCE as a reference electrode under argon atmosphere at room temperature for 2 h. Because a current was not able to be maintained at 1 A after 2 h, constant-current electrolysis was continued at 0.1 A for 3 h. The electrolysis mixture was diluted with water (300 cm^3) and extracted with dichloromethane (80 cm^3×2). The organic layer was washed with water, dried (Na_2SO_4), and analyzed by GLPC. The products obtained by evaporation of the dichloromethane solution were separated with flash-column chromatography.[16] The structures of the products were determined on the basis of their spectral data and elemental analysis.

PhCH(OMe)CH(Me)OMe (2e), erythro-*form*: Bp 59 °C/4 mm; MS: *m/z* 180 (M^+), 149, 121 (100%), 117, 105, 91; IR (neat): 1100 cm^{-1}, ν_{C-O}; ^{1}H-NMR ($CDCl_3$): δ=1.12 (d, *J*= 8 Hz, 3H, Me), 3.16 (s, 6H, 2MeO), 3.18 (m, 1H, CH), 4.14 (d, *J*=4 Hz, 1H, CH), 7.30 (s, 5H, Ph); ^{13}C-NMR ($CDCl_3$): δ= 139.2 (s), 128.0 (d), 127.4 (d), 86.0 (d), 80.6 (d), 57.1 (q), 57.0 (q), 14.3 (q); Found: C, 73.30; H, 8.92%. Calcd for $C_{11}H_{16}O_2$: C, 73.29; H, 8.94%. *threo*-form: Bp 62 °C/4 mm: MS: *m/z* 180 (M^+). 149, 121 (100%), 117, 105, 91; IR (neat): 1100 cm^{-1}, ν_{C-O}; ^{1}H-NMR ($CDCl_3$): δ=0.92 (d, *J*=7 Hz, 3H, Me), 3.24 (s, 3H, OMe), 3.40 (s, 3H, OMe), 3.50 (m, 1H, CH), 4.08 (d, *J*=7 Hz, 1H, CH), 7.28 (s, 5H, Ph); ^{13}C-NMR ($CDCl_3$): δ=139.1 (s), 128.2 (d), 127.8 (d), 127.6 (d), 87.4 (d), 80.0 (d), 57.3 (q), 57.0 (q), 15.6 (q); Found: C, 73.19; H, 8.86%. Calcd for $C_{11}H_{16}O_2$: C, 73.29; H, 8.94%.

Measurements of the Oxidation Potentials of Styrenes. Cyclic voltammetric data were obtained using a three-electrode cell with a Hokuto HA-201 potentiostat and a Hokuto HB-104 function generator. The working electrode was a platinum wire (1 mm diameter) sealed into glass and a counter electrode was a platinum gauze. A $Ag/AgNO_3$ (0.1 mol/dm^3)

electrode was used as a reference electrode and 0.1 mol/dm^3 tetraethylammonium perchlorate as supporting electrolyte. The current-potential curves were recorded directly from the output of the potentiostat on a Rika Denki RW-11 X-Y recorder. The measured value for **1d** agreed well with the reported value.[17]

Irradiation of Styrenes with Copper(II) Salt in Methanol. A solution of styrenes **1** (5 g, 28—48 mmol) in methanol (300 cm^3) containing copper(II) perchlorate (21—36 g, 56—96 mmol) was irradiated under a nitrogen stream at room temperature with a 160-W low pressure mercury lamp (Riko UVL-160LA) for 49 h. The reaction mixture was diluted with water (500 cm^3) and extracted with dichloromethane (100 cm^3×2). The organic layer was washed with water and dried (Na_2SO_4). After evaporation of the solvent, the residue was subjected to flash-column chromatography[16] on silica gel to give **2**, **3**, **4**, and **5**. The structures of the products (**2**, **3**, **4**, and **5**) were confirmed from their spectral data and elemental analysis, or by comparison of their spectral data with those of authentic samples. The organic layer was analyzed by GLPC to determine the yields of the products (Table 1).

1,2-Dimethoxy-2-phenylpropane (2c): Oil; bp 64°C/3 mm; MS: *m/z* 165, 149, 134 (100%); IR (neat): 1070—1140 cm^{-1}, $\nu_{C\text{-}O}$; ^{1}H-NMR ($CDCl_3$): δ=1.52 (s, 3H, Me), 3.10 (s, 3H, OMe), 3.30 (s, 3H, OMe), 3.40—3.50 (ss, 2H, OCH_2), 7.15—7.50 (m, 5H, aromatic H); ^{13}C-NMR ($CDCl_3$): δ= 142.5 (s), 128.1 (d), 127.2 (d), 126.5 (d), 80.8 (t), 78.9 (s), 59.5 (q), 50.6 (q), 20.1 (q); Found: C, 72.97; H, 9.02%. Calcd for $C_{11}H_{16}O_2$: C, 73.30; H, 8.95%.

1,4-Dimethoxy-2,3-bis(4-chlorophenyl)butane (3b): Mp 127—128°C; MS: *m/z* 342 (M^{++}2), 340 (M^+), 310, 308, 172, 170 (M^+/2), 169, 156, 139; IR (KBr): 1100 cm^{-1}, $\nu_{C\text{-}O}$; ^{1}H-NMR ($CDCl_3$): δ=3.08 (s, 6H, 2MeO), 3.16—3.34 (broad, 6H, 2CH and $2CH_2$), 7.20 (s, 8H, aromatic H); ^{13}C-NMR ($CDCl_3$): δ= 140.4 (s), 132.4 (s), 129.8 (d), 128.5 (d), 74.5 (t), 58.9 (q), 47.7 (d); Found: C, 63.81; H, 5.93; Cl, 20.80%. Calcd for $C_{18}H_{20}Cl_2O_2$: C, 63.72; H, 5.94; Cl, 20.90%.

1,4-Dimethoxy-2,3-dimethyl-2,3-diphenylbutane (3c): Oil; a 1:1 mixture of *meso*- and *dl*-form; MS: *m/z* 221, 149 (M^+/2, 100%), 134; IR(neat): 1100 cm^{-1}, $\nu_{C\text{-}O}$; ^{1}H-NMR ($CDCl_3$): δ= 1.30 and 1.40 (s, 6H, 2Me), 3.15 and 3.18 (s, 6H, 2MeO), 3.34 and 3.60 (m, 4H, $2OCH_2$), 6.80—7.40 (m, 10H, 2Ph); ^{13}C-NMR ($CDCl_3$): δ=142.9 (s), 128.7 (d), 126.8 (d), 125.9 (d), 78.1 (t), 58.8 (q), 47.8 (s), 47.6 (s), 20.6 (q), 20.3 (q); Found: C, 80.44; H, 8.58%. Calcd for $C_{20}H_{26}O_2$: C, 80.49; H, 8.78%.

2,5-Dimethoxy-3,4-diphenylhexane (3e): Mp 175—176°C; MS: *m/z* 267, 209 (100%), 150; IR(KBr): 1130—1070 cm^{-1}, $\nu_{C\text{-}O}$; ^{1}H-NMR ($CDCl_3$): δ=0.74 (d, 6H, 2Me), 3.20 (m, 2H, 2CH), 3.20 (s, 6H, 2MeO), 3.22 (broad, 2H, 2CH), 7.24—7.60 (m, 10H, 2Ph); ^{13}C-NMR ($CDCl_3$): δ=140.9 (s), 130.4 (d), 127.7 (d), 126.1 (d), 76.1 (d), 56.3 (q), 54.3 (d), 17.0 (q); Found: C, 80.69; H, 8.82%. Calcd for $C_{20}H_{26}O_2$: C, 80.54; H, 8.72%.

References

1) a) M. R. Gordon and W. R. Ware, ed., "The Exciplexes," Academic Press, New York, N. Y. (1975); b) *Chem. Soc. Jpn. Ed.*, "Kagaku Sosetsu," **1982**, 33.

2) a) T. Asanuma, M. Yamamoto, and Y. Nishijima, *J. Chem. Soc., Chem. Commun.*, **1975**, 608; b) M. Yamamoto, T. Asanuma, and Y. Nishijima, *J. Chem. Soc., Chem. Commun.*, **1975**, 53; c) T. Asanuma, M. Yamamoto, and Y. Nishijima, *J. Chem. Soc., Chem. Commun.*, **1975**, 56; d) R. A. Neuteufel and D. R. Arnold, *J. Am. Chem. Soc.*, **95**, 4080 (1973).

3) Y. Shigemitsu and D. R. Arnold, *J. Chem. Soc. Chem. Commun.*, **1975**, 407.

4) T. Asanuma, T. Gotoh, A. Tsuchida, M. Yamamoto, and Y. Nishijima, *J. Chem. Soc., Chem. Commun.*, **1977**, 485.

5) S. Murai and S. Tsutsumi, *Bull. Chem. Soc. Jpn.*, **39**, 198 (1966).

6) a) M. Kojima, H. Sakuragi, and K. Tokumaru, *Chem. Lett.* **1981**, 1707; b) T. Inoue and S. Tsutsumi, *Bull. Chem. Soc. Jpn.*, **38**, 661 (1965); c) E. Engels, H. J. Schäfer, and E. Steckhan, *Justus Liebigs Ann. Chem.* 204 (1977).

7) J. M. Fritsch, H. Weingarten, and J. D. Wilson, *J. Am. Chem. Soc.*, **92**, 4038 (1970).

8) In the case of **1e** with the same oxidation potential as **1f**, which gave β,β-dimer **5f** selectively in the photochemical reaction with the metal ions, the result that α,α-dimer **3e** was selectively obtained but no β,β-dimer **5e** was obtained suggests that cation radical **6e** scarcely interacts with copper(II) ion or the difficulty of addition to β-carbon of another molecule because of the steric hindrance by a methyl group on the β-carbon.

9) D. Rehm and A. Weller, *Isr. J. Chem.*, **8**, 259 (1970).

10) S. L. Murov, "Handbook of Photochemistry," Marcel Dekker, New York, (1973), p. 20.

11) Miller *et al.* have reported the correlation between the ionization energy and the oxidation potentials of aromatic compounds. If the oxidation potentials of free radicals correlate with their ionization energy similarly to above neutral molecules, the oxidation potentials of radicals **7** and **9** might be estimated; a) L. L. Miller, G. D. Nordblom, and E. A. Mayeda, *J. Org. Chem.*, **37**, 916 (1972); b) M. Kobayasi, "Physicochemical Properties of Free Radicals" in "Chemistry of Free Radicals," ed by H. Sakurai and K. Tokumaru, Nankodo (1967).

12) J. K. Kochi, "Organometallic Mechanism and Catalysis," Academic Press (1978), p. 11.

13) J. K. Kochi and A. Bemis, *J. Am. Chem. Soc.*, **90**, 4038 (1968).

14) J. K. Kochi, A. Bemis, and C. L. Jenkins, *J. Am. Chem. Soc.*, **90**, 4616 (1968).

15) R. H. Wiley and N. R. Smith, *Org. Synth.*, Coll. Vol. **IV**, 731 (1963).

16) W. C. Still, M. Kahn, and A. Mitra, *J. Org. Chem.*, **43**, 2923 (1978).

17) D. R. Arnold and A. J. Maroulis, *J. Am. Chem. Soc.*, **98**, 5931 (1976).

Molecular Design of Crown Ethers. 3.[1] Extraction of Alkaline Earth and Heavy Metal Picrates with 14- to 17-Crown-5 and 17- to 22-Crown-6

Yoshihisa INOUE,* Mikio OUCHI, and Tadao HAKUSHI
Department of Applied Chemistry, Himeji Institute of Technology, 2167 Shosha, Himeji, Hyogo 671-22
(Received September 13, 1984)

The solvent extraction of alkaline earth and heavy metal picrates with a series of ring-contracted and ring-enlarged crown ethers has been carried out in order to reveal the effects of methylene-chain length upon cation-binding ability. Compared with the parent 3*m*-crown-*m*, the ring-contracted crown ethers and their sila analogues possess limited extractabilities, often as low as those for the corresponding glymes. On the other hand, the ring-enlarged crown ethers, in general, show gradual, but not drastic, decreases in extractability for most cations with increasing methylene-chain length. Interestingly, the extractabilities for Ag^+, Tl^+, and Ba^{2+} do not decrease monotonously with ring expansion; in particular 16-crown-5 is a better extractant for Ag^+ than 15-crown-5 and even than 18-crown-6. These results are accounted for in terms of cavity size, conformation, and molecular symmetry of crown ethers. Effects of cation hydration upon extractability and the limitations of solvent extraction technique are also discussed.

Despite the extensive work on crown ether chemistry, the effect of methylene-chain length between two adjacent oxygen atoms of a crown ether upon its complexation ability has not been explored systematically until very recently. Recent investigations from this laboratory[2-4] have shown that, compared with common, symmetrical 3*m*-crown-*m* ethers (*m*=5,6), the ring-contracted and ring-enlarged (3*m*+*n*)-crown-*m* ethers (*n*=−1 to 4) exhibit drastic changes in cation-binding ability with alkali metal ions, endowing (3*m*+*n*)-crown-*m* characteristic cation-selectivities which are distinctly different from those for 3*m*-crown-*m*. It is interesting and significant that the introduction of extra methylene(s), which lower the crown ether's molecular symmetry, does not simply lead to monotonous decreases in complexation ability for all alkali cations but results in unequal decreases or even in an enhancement of cation-binding ability. 16-Crown-5, for example, possesses higher cation-binding ability and selectivity for Na^+ than 15-crown-5. More recently, Kimura *et al.*[5] have shown that, among 13- to 16-crown-4 derivatives, 14-crown-4 is most selective for Li^+ over any other alkali or alkaline earth metal ions. These selectivity shifts or enhancements caused by changing methylene-chain length between two adjacent oxygen atoms have been attributed to the changes in cavity size and/or conformation of the crown ether ring.[2-4]

In this paper, we report our results on the effects of ring contraction and ring enlargement upon cation-binding abilities for alkaline earth and heavy metal ions assessed by solvent extration studies. The extractabilities for alkali,[3,4] alkaline earth, and heavy metal ions are compared and discussed in terms of cavity size, conformation, and molecular symmetry of the crown ethers and also in terms of cation hydration energy. The limitations of solvent extraction as a method for evaluating complexation ability of crown ethers are also considered.

Results

Solvent extractions from aqueous solutions (3.0×10^{-3} M† in salt) of alkaline earth and heavy metal picrates were performed at 25.0±0.1 °C with dichloromethane solutions (3.0×10^{-3} M in ligand) of a variety of symmetrical and less-symmetrical crown ethers and their acyclic analogues under the same conditions employed earlier for alkali metal picrates.[2-4] The % extractabilities (% *Ex*), defined as % picrate extracted into the organic phase, were measured twice and the average values are shown in Table 1; two independent measurements gave very close % *Ex* values with error of <0.5%. This equimolar condition has been employed,††

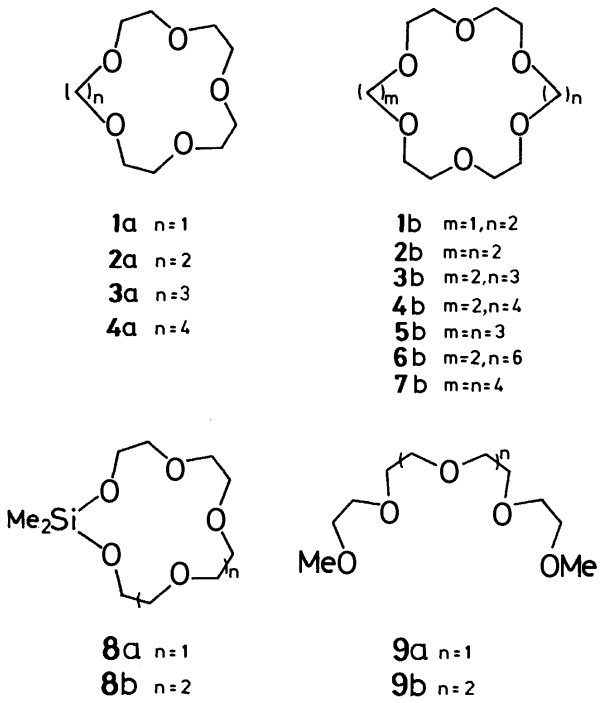

Chart 1.

†1M=1 mol dm^{-3}.

††Added in proof. E. Weber has indicated in a private communication that his group is going to employ the same equimolar condition to assess cation-binding ability of crown ethers. We propose that this condition is adopted widely for the facile assessment and that the results are accumulated for comparison.

Table 1. Solvent extraction of aqueous metal picrates[a]

Ligand	% Ex[b]					
	Ag^+	Tl^+	Mg^{2+}	Ca^{2+}	Sr^{2+}	Ba^{2+}
14-Crown-5 (**1a**)	0.8	1.1	0.5	0.5	0.5	1.5
Sila-14-crown-5 (**8a**)	0.3	1.6	<0.1	<0.1	<0.1	1.5
15-Crown-5 (**2a**)	26.7	29.2	0.7	1.5	8.0	25.3
16-Crown-5 (**3a**)	35.7	18.1	0.3	0.8	4.5	15.4
17-Crown-5 (**4a**)	13.8	7.8	0.7	0.7	0.9	2.1
Tetraglyme (**9a**)	0.2	1.0	<0.1	<0.1	0.2	1.3
17-Crown-6 (**1b**)	6.1	5.4	0.5	0.6	1.4	7.4
Sila-17-crown-6 (**8b**)	0.6	3.5	<0.1	<0.1	1.9	8.8
18-Crown-6 (**2b**)	31.3	73.2	2.5	26.2	69.0	75.8
19-Crown-6 (**3b**)	8.5	35.8	0.6	1.6	52.4	68.1
asym-20-Crown-6 (**4b**)	8.1	43.8	0.1	0.4	34.4	71.6
sym-20-Crown-6 (**5b**)	3.6	9.8	0.4	0.3	13.0	54.3
asym-22-Crown-6 (**6b**)	2.9	14.3	0.1	0.3	2.8	48.6
sym-22-Crown-6 (**7b**)	8.1	5.3	0.6	0.4	0.3	14.2
Pentaglyme (**9b**)	0.5	3.3	0.1	0.1	3.1	36.4

a) Temperature 25.0±0.1 °C; aqueous phase (10 mL): [picrate]=3.0×10^{-3} M; organic phase (CH_2Cl_2, 10 mL): [ligand]=3.0×10^{-3} M. b) Extractability defined as % picrate extracted into the organic phase.

Table 2. Extraction equilibrium constants (K_{ex})[a] for 1:1 complexation of alkaline earth and heavy metal ions with some crown ethers[b]

Ligand	log K_{ex}				
	Ag^+	Tl^+	Ca^{2+}	Sr^{2+}	Ba^{2+}
15-Crown-5 (**2a**)	5.00	5.08	6.49	7.26	<9.20[c]
16-Crown-5 (**3a**)	5.25	4.63	6.16	7.02	7.74
17-Crown-5 (**4a**)	4.40	4.13	5.98	6.14	6.55
18-Crown-6 (**2b**)	5.09	6.71			
19-Crown-6 (**3b**)	4.24	5.28			
asym-20-Crown-6 (**4b**)	4.08	5.45	5.79	8.47	

a) Unit of K_{ex}: M^{-2} for monovalent and M^{-3} for divalent cations. b) Dichloromethane-water system at 25.0 °C. c) Least-square-means calculation gives a slope of 1.34 in this particular case, indicating the participation of 1:2 sandwitch type complex to some extent; the actual value K_{ex} value must be lower.

since the cation-selectivity sequence judged from the % Ex values coincides with that from the extraction equilibrium constants (K_{ex}).[2,3]

With selected combinations of crown ethers and mono- and divalent cations, the extraction equilibium constants (K_{ex}) and the complex stoichiometeries (n) for n:1 crown ether-cation complexes were also determined. The solvent extraction of a metal picrate MA_m (m=1 or 2) with n molecules of a crown ether (CE) is expressed by the following overall extraction equilibrium,

$$M_{aq}^{m+} + m A_{aq}^{-} + n CE_{org} \overset{K_{ex}}{\rightleftharpoons} [M(CE)_nA_m]_{org}$$

and the equilibrium constant (K_{ex}) is given by Eq. 1.

$$K_{ex} = \frac{D_M}{[A^-]_{aq}^m [CE]_{org}^n} \quad (1)$$

where

$$D_M = \frac{[M(CE)_nA_m]_{org}}{[M^{m+}]_{aq}} \quad (2)$$

Modification of Eq. 1 leads to the following equation.

$$\log(D_M/[A^-]_{aq}^m) = n \log[CE]_{org} + \log K_{ex} \quad (3)$$

Extraction studies were carried out under a variety of conditions to determine extraction equilibrium constant K_{ex} and complex stoichiometry n; [ligand]=0.5—5.0×10^{-3} M and [picrate]=3.0×10^{-3} M. As exemplified in Figure 1, in the most cases the plots of log (D_M/$[A^-]_{aq}^m$) *versus* log $[CE]_{org}$ gave straight lines with a slope (n) of unity, indicating that 15- to 17-crown-5 and 18- to 20-crown-6 form 1:1 crown ether-cation complexes under the conditions employed. The logK_{ex} values are given as intercepts of the straight lines; the results are listed in Table 2.

Discussion

Ring-contracted Crown Ethers 1 and 8. As can be seen from Table 1, all the ring-contracted crown ethers **1** and their sila analogues **8** possess extremely low extractabilities for the alkaline earth and heavy metal ions as compared with the symmetrical ligands 15-crown-5 (**2a**) and 18-crown-6 (**2b**), respectively. The extractabilities may more appropriately be compared with the corresponding glymes **9**. Similarly poor extraction ability has been previously reported in solvent extractions of alkali metal picrates with the same ring-contracted crown ethers **1** and **8**.[4,6] It was shown there that removal of a methylene group from a symmetrical crown ether results in nearly complete loss

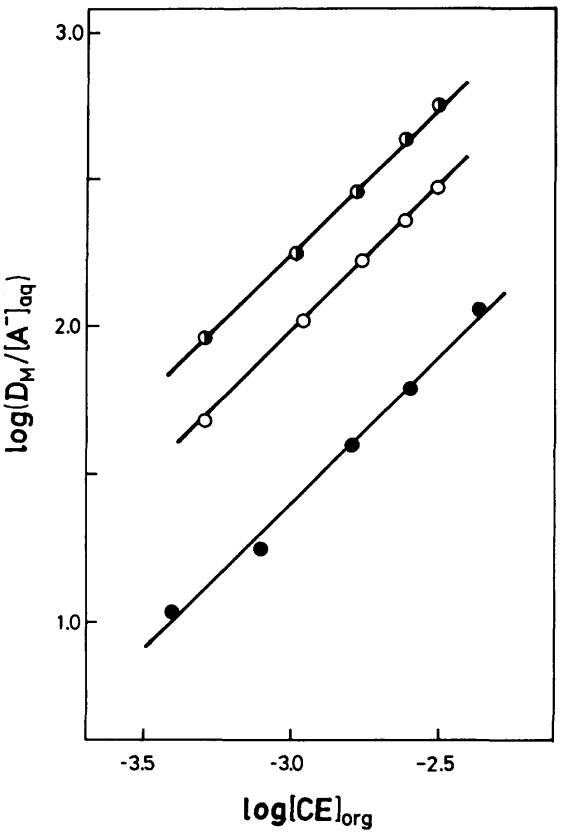

Fig. 1. Plots of $\log(D_M/[A^-]_{aq})$ versus $\log[CE]_{org}$ obtained in extraction experiments on 15- to 17-crown-5 **2a**(○), **3a**(◑), and **4a**(●) with silver picrate.

of complexing ability for most cations examined.

As has already been proposed in the extraction of alkali metal ions, the origin of the drastic reduction in cation-binding ability for alkaline earth and heavy metal ions is probably due not to diminished cavity size but to the conformational disorder induced by the ring contraction, since the removal of a methylene group does not reduce significantly the cavity size of crown ether and the replacement of the O–C–O linkage of **1** by a longer O–Si–O linkage to give **8** does not contribute to raise the extractability. Examinations of CPK space-filling molecular models also support the irregular spatial arrangement of the donor oxygen atoms; one of the five or six donor atoms cannot be accommodated in the plane of the remaining donor atoms, while the cavity sizes are *ca.* 1.7 Å for **1a**, **2a**, or **8a** and 2.5—2.6 Å for **1b**, **2b**, or **8b**. It is clear that, in this situation, one of the formal donor oxygen atoms no longer acts as an effective donor atom; this may be the major reason for the drastic decrease in the extractability of the ring contracted crown ethers **1** and **8**.

Ring-enlarged Crown Ethers **3**—**7**. The introduction of extra methylene (s) at one or two transannular position (s) of the symmetrical 3*m*-crown-*m* gives ring-enlarged crown ethers. In general, these crown ethers of low symmetry, *i.e.* 16- and 17-crown-5 and 19- to 22-crown-6 possess lower % *Ex* or K_{ex} values for the cations examined in this study. This is also the case with the solvent extraction of alkali metal picrates with the same crown ethers.[3] For most cations, the % *Ex* or K_{ex} value decreases gradually or, in some cases, drastically with increasing methylene-chain length, although even the extremely enlarged 17-crown-5 **4a** and 22-crown-6 **6b**, **7b** are still the better ligands than the corresponding glymes **9**. Interestingly, the % *Ex* for Ba^{2+} is relatively insensitive to the ring expansion and therefore the less symmetrical crown ethers **3b**—**7b** exhibit higher Ba^{2+} selectivity than the parent 18-crown-6 **2b**. It is also noted that the highest selectivity for Ba^{2+} is given not by the crown ethers but by acyclic pentaglyme **9b**.

The major reason for the gradual decrease in % *Ex* or K_{ex} is certainly the lower symmetry, or in other words the less-favorable spatial arrangement of donor oxygen atoms, resulting from the ring expansion. In this context, the comparison of % *Ex* for the *asym*- and *sym*-isomers of 20- and 22-crown-6 is interesting. The % *Ex* values for *sym*-isomers **5b** and **7b** are considerably lower than those for *asym*-isomers **4b** and **6b** except for the complexation of Ag^+ with 22-crown-6. It may be concluded that, when the same number of methylene group is introduced into a crown ether, the double extension of methylene-chain length at the transannular positions giving a *sym*-crown ether is much more effective in diminishing cation-binding ability than the single extension giving an *asym*-crown ether. This is probably due to the greater deformation of spatial arrangement of donor atoms induced by the double, rather than single, extension of methylene-chain length.

Some exceptions to the gradation of % *Ex* or K_{ex} are seen at the same time in the extraction of Ag^+, Tl^+, and Ba^{2+}. In spite of the increased methylene-chain length, *asym*-20-crown-6 (cavity size 3.3 Å) exhibits somewhat higher % *Ex* values for Tl^+ (cation diameter 3.00 Å) and Ba^{2+} (2.72 Å) than 19-crown-6 (2.7 Å), although the % *Ex* values are considerably lower than those for the parent 18-crown-6. These irregular increases in % *Ex* may roughly be accounted for in terms of the size-fit concept[7]—relationship between relative sizes of cation and crown cavity; see Table 3 for these quantities.[8] A more remarkable result was obtained in the extraction of Ag^+ with 16-crown-5. In contrast to the monotonous decreases in % *Ex* or K_{ex} for the other cations, 16-crown-5 exhibits fairly higher % *Ex* and K_{ex} values for Ag^+ than the parent 15-crown-5 or even than 18-crown-6, preserving the 1:1 stoichiometry. This may be an exceptional case in which 18-crown-6 does not show the highest cation-binding ability, although Gokel *et al.*[9] have reported that 18-crown-6 shows the highest stability constants (K_s) for Na^+, K^+, NH_4^+, and Ca^{2+} in the homogeneous solution. This preferential extraction of Ag^+ by 16-crown-5 may originate from the "nesting" interaction in the 1:1 complex with Ag^+ as is the case with Na^+. It has been shown previously[2,3] that 16-

TABLE 3. CAVITY SIZE OF THE CROWN ETHERS AND CATION DIAMETER AND HYDRATION ENERGY ($-\Delta G^{s}_{H_2O}$) OF CATIONS

Ligand	Cavity diameter, Å[a]	Cation	Diameter, Å[b]	$-\Delta G^{s}_{H_2O}$, kcal/mol[c]
14-Crown-5 (**1a**)	1.7	Na^+	2.04	98
15-Crown-5 (**2a**)	1.7	K^+	2.76	81
16-Crown-5 (**3a**)	1.8	Rb^+	2.98	76
17-Crown-5 (**4a**)	2.0	Cs^+	3.40	68
17-Crown-6 (**1b**)	2.5	Ag^+	2.30	114
18-Crown-6 (**2b**)	2.6	Tl^+	3.00	82
19-Crown-6 (**3b**)	2.7	Mg^{2+}	1.44	454
asym-20-Crown-6 (**4b**)	3.3	Ca^{2+}	2.00	379
sym-20-Crown-6 (**5b**)	3.0	Sr^{2+}	2.32	340
asym-22-Crown-6 (**6b**)	3.4	Ba^{2+}	2.72	314
sym-22-Crown-6 (**7b**)	3.9			

a) Estimated by CPK molecular models. b) Reference 8b. c) Reference 13.

TABLE 4. EXTRACTABILITY (% *Ex*), EXTRACTION EQUILIBRIUM CONSTANT (K_{ex}), AND STABILITY CONSTANT (K_s) AT 25 °C FOR 15-crown-5 AND 18-crown-6

Ligand	Binding constant	Cation									Ref
		Na^+	K^+	Rb^+	Cs^+	Ag^+	Tl^+	Mg^{2+}	Ca^{2+}	Sr^{2+}	Ba^{2+}	
15-Crown-5	% *Ex*	13.2	14.3	9.6	3.3	26.7	29.2	0.7	1.5	8.0	25.3	a)
	log K_{ex}	4.52	4.40	4.29	3.74	5.00	5.08		6.49	7.26	<9.20	a)
		(≡1.0)	(0.97)	(0.95)	(0.83)	(1.11)	(1.12)					
	log K_s	3.48	3.77		2.18	3.62			2.18	2.63		b)
	(MeOH)	(≡1.0)	(1.08)		(0.63)	(1.04)						
	log K_s	0.70	0.74	0.62	0.8	0.94	1.23			1.95	1.71	c)
	(H_2O)	(≡1.0)	(1.06)	(0.89)	(1.14)	(1.34)	(1.76)					
18-Crown-6	% *Ex*	6.3	69.0	57.6	36.7	31.3	73.2	2.5	26.2	69.0	75.8	a)
	log K_{ex}	3.89	6.20	5.96	5.17	5.09	6.71					a)
		(0.63)	(≡1.0)	(0.96)	(0.83)	(0.82)	(1.08)					
	log K_s	4.36	6.06	5.32	4.79	4.58			3.86	5.5	7.04	b)
	(MeOH)	(0.72)	(≡1.0)	(0.88)	(0.79)	(0.76)						
	log K_s	0.80	2.03	1.56	0.99	1.50	2.27			2.72	3.87	c)
	(H_2O)	(0.39)	(≡1.0)	(0.77)	(0.49)	(0.74)	(1.11)					

a) This work and reference 3. b) Reference 12. c) Reference 11.

crown-5 possesses the highest extractability and selectivity for Na^+ among alkali metal ions, which is explained by the most favorable cavity size and orientation of the donor atoms for 1:1 complexation with Na^+, *i.e.* "nesting" interaction, and by the less-favorable "perching" interaction with the larger cations, K^+, Rb^+, Cs^+. The same situation may be attained in the 1:1 complex of 16-crown-5 with heavy metal ions. Taking into account of the axial development of hybrid orbital of silver ion originating from the d_{z^2}-s mixing,[10] Ag^+ (formal cation diameter 2.30 Å) is considered to be better accommodated in the cavity (1.8 Å) of 16-crown-5 than in the smaller cavity (1.7 Å) of 15-crown-5.

It is concluded that the cation-binding ability of the ring-enlarged crown ethers for monovalent cations is determined by a critical balance between the enlarged cavity size and the reduced molecular symmetry, although the cation selectivity is well accounted for in terms of the size-fit concept. It is also shown that the unfavorable effect of the conformational change induced by ring enlargement may be minimized or cancelled, in particular, with the size-fitted cations like Na^+ and Ag^+, but leads to the drastic decrease of extractability with the mismatched cations. This discriminating effect can be utilized as a tool to enhance the cation selectivity as demonstrated in the complexations of Na^+ and Ag^+ with 16-crown-5 and of Ba^{2+} with 19- to 22-crown-6.

Limitations of Solvent Extraction Technique. The solvent extraction of aqueous metal picrates has been employed as a facile method to assess cation-binding ability of crown ethers. However there may be some ambiguities with the binding ability assessed by this technique, since the extractability (% *Ex*) or extraction equilibrium constant (K_{ex}) would not necessarily be determined only by the cation-binding ability of ligand and the other factor might have a dominant effect.[9] In Table 4, the % *Ex* and K_{ex} values for 15-crown-5 and 18-crown-6 are compared with the corresponding stability constants (K_s) in homogeneous solution determined by the other investigators.[11,12] With monovalent cations, the K_{ex}, or % *Ex*, values parallel exactly the K_s values in methanol, indicating that the cation-binding ability and cation selectivity can be assessed quantitatively by the solvent extraction technique at least for monovalent cations.

Serious discrepancy is however found between the K_{ex} and K_s values for divalent cations. Thus the size-fit concept fails to explain the extractability trend for alkaline earth metal ions. This is most evident with

15- to 17-crown-5. As can be seen from Tables 1, 2, and 4, the K_{ex} or % *Ex* values for Mg^{2+} and Ca^{2+} are quite low for these ligands, although the cation diameters of these divalent cations (Mg^{2+} 1.44Å, Ca^{2+} 2.00Å)[8b] would fit in the cavity of 15-crown-5 (1.7Å), 16-crown-5 (1.8Å), or 17-crown-5 (2.0Å). By contrast, the formally mismatched larger cations, *i.e.* Sr^{2+} and Ba^{2+}, are extracted more efficiently. These results strongly suggest that, in the solvent extraction of divalent cations, the extractability and cation-selectivity cannot be discussed by the size-fit concept alone and the other factor plays a primary role to determine the above quantities.

The major difference between the series of mono- and divalent cations is not the cation diameter but the energy of hydration. As listed in Table 3, the divalent cations possess much higher free energy of hydration ($\Delta G^{\circ}_{H_2O}$) than the monovalent ones; $-\Delta G^{\circ}_{H_2O}$ values are 68—114 kcal/mol* for the monovalent cations, while 314—454 kcal/mol for the divalent ones.[13] This does not immediately mean that the cation of higher hydration energy encounters greater difficulty upon complexation with a ligand, since the higher hydration energy also promises stronger interaction with the donor oxygen atoms of the ligand as well as water molecules. Indeed, judged from the K_s values obtained in homogeneous solutions (Table 4), the cation selectivities among the divalent cations appear to be accounted for in terms of the size-fit concept. The major difficulty for the divalent cations to be extracted into the organic phase may originate from the incomplete dehydration of the cation upon extraction. Iwachido *et al.*[14] have reported that the cation extracted into the organic phase in the form of 1:1 complex with a crown ether is not entirely dehydrated and the number of water molecule coextracted with a cation is much greater for the divalent than monovalent cations; for example, the hydration numbers for M^{n+}-dibenzo-18-crown-6 complex in nitrobenzene are: Na^+ 1.2; K^+–Cs^+ 0.1; Ca^{2+} 5.1; Sr^{2+} 4.9; Ba^{2+} 4.4. Therefore, although the organic phase and the crown ether reported are different from those used in this study, the discrepancy between the K_{ex} and K_s values for divalent cations probably ascribable to the higher barrier for the heavily hydrated complex to be extracted into the organic phase.

In conclusion, it is evident that the solvent extraction technique works well with monovalent cations to give appropriate K_{ex} or % *Ex* trends in accord with the K_s trends, but is inadequate as a metod to assess cation-binding ability and cation selectivity of crown ethers for di- and probably tri-valent cations.

Experimental

Material. *Crown ethers.* The ring-contracted crown ethers **1** were prepared by the method described by Kawakami *et al.*[6] Commercially available 3*m*-crown-*m* **2** (Nisso Co.) and sila crown ethers **8** (Petrarch Systems Inc.) were used without further purification. The ring-enlarged crown ethers **3**—**7** and glymes **9** were synthesized as reported previously.[3]

Metal Picrates. *Alkali metal picrates* were prepared from picric acid and the corresponding metal hydroxide as reported.[2-4]

Silver Picrate. Picric acid (4.1 g, 18 mmol) was dissolved in hot water (100 mL), to which silver oxide (2.0 g, 8.6 mmol) was added slowly and the mixture was stirred for additional 10 min at that temperature.[15] The precipitate formed upon cooling was recrystallized twice from ethanol and then once from water to give 0.6 g (20% yield) of silver picrate.

Thallium picrate was prepared from picric acid (3.4 g, 15 mmol) and thallium oxide (3.0 g, 7.1 mmol) in hot water according to the procedure described above. Recrystallization twice from water gave 2.5 g (81%) of thallium picrate.

Alkaline earth metal picrates were prepared from picric acid (4.6 g, 20 mmol) and the corresponding metal carbonate (10 mmol) in hot water according to the procedure described above.[16] Recrystallization twice from water gave 0.6 g (11%) of magnesium picrate, 0.9 g (15%) of calcium picrate, 0.9 g (14%) of strontium picrate, or 3.0 g (50%) of barium picrate. Magnesium, calcium, and strontium picrates were pentahydrates, and barium picrate was anhydrous salt.

Extraction Studies. The general procedures employed were similar to those described in previous papers.[2-4] The concentration of heavy metal picrate in the organic phase was determined from its absorption at 375 nm in a 1:1 mixture of dichloromethane and acetonitrile. The molar extinction coefficients at 375 nm of silver and thallium picrates are 18800 and 18900 $M^{-1}cm^{-1}$, respectively. The concentration of alkaline earth metal picrate in the organic phase was determined according to the procedure in the literature.[16] After the phase separation, 5 mL of the dichloromethane phase was withdrawn and evaporated to dryness, to which was added 5 mL of acetonitrile. After further dilution, if necessary, with acetonitrile, the picrate concentration in acetonitrile was determined from its absorption at 374 nm. The molar extinction coefficients at 374 nm for magnesium, calcium, strontium, and barium picrates are 29400, 29700, 29500, and 29000 $M^{-1}cm^{-1}$, respectively.

This work was partially supported by a Grant-in-Aid (No. 59550583) from the Ministry of Education, Japan, which is gratefully acknowledged. Stimulative discussion with Prof. G. W. Gokel, University of Maryland, is also acknowledged.

*1 cal=4.184 J.

References

1) For part 2 of this series, see: M. Ouchi, Y. Inoue, K. Wada, and T. Hakushi, *Chem. Lett.*, **1984**, 1137. Taken in part from the Ph. D. Dissertation of M. O. (1984), Himeji Institute of Technology.

2) M. Ouchi, Y. Inoue, H. Sakamoto, A. Yamahira, M. Yoshinaga, and T. Hakushi, *J. Org. Chem.*, **48**, 3168 (1983).

3) M. Ouchi, Y. Inoue, T. Kanzaki, and T. Hakushi, *J. Org. Chem.*, **49**, 1408 (1984).

4) M. Ouchi, Y. Inoue, T. Kanzaki, and T. Hakushi, *Bull. Chem. Soc. Jpn.*, **57**, 887 (1984).

5) K. Kimura, S. Kitazawa, and T. Shono, *Chem. Lett.*, **1984**, 639.

6) Y. Kawakami, J. Suzuki, and Y. Yamashita, *Polymer J.*, **9**, 519 (1977).

7) C. J. Pedersen and H. K. Frensdorf, *Angew. Chem., Int. Ed. Engl.*, **11**, 16 (1972).

8) a) The cavity sizes were determined by CPK space-filling molecular models. b) The cation diameters are quoted from: R. D. Shannon and C. T. Prewitt, *Acta Crystallogr Sect. B.*, **25**, 925 (1969).

9) See, for example: G. W. Gokel, D. M. Goli, C. Minganti, and L. Echegoyen, *J. Am. Chem. Soc.*, **105**, 6786 (1983).

10) a) L. E. Orgel, *J. Chem. Soc.*, **1958**, 4186; b) R. A. Cotton and G. Wilkinson, "Advanced Inorganic Chemistry," 2nd Ed., Wiley, New York, NY, 1972, Chapter 30.

11) R. M. Izatt, R. E. Terry, B. L. Haymore, L. D. Hansen, N. K. Dalley, A. G. Avondet, and J. J. Christensen, *J. Am. Chem. Soc.*, **98**, 7620 (1976).

12) J. D. Lamb, R. M. Izatt, C. S. Swain, and J. J. Christensen, *J. Am. Chem. Soc.*, **102**, 475 (1980).

13) R. M. Noyes, *J. Am. Chem. Soc.*, **84**, 513 (1962).

14) a) T. Iwachido, M. Kimura, and K. Toei, *Chem. Lett.*, **1976**, 1101; b) T. Iwachido, M. Minami, A. Sadakane, and K. Toei, *ibid.*, **1977**, 1511.

15) T. Maeda, K. Kimura, and T. Shono, *Fresenius Z. Anal. Chem.*, **298**, 363 (1979).

16) T. Maeda, K. Kimura, and T. Shono, *Fresenius Z. Anal. Chem.*, **313**, 407 (1982).

Synthesis and Properties of Gramicidin S Analogs Containing D-Phe-L-Pro-D-Val or L-Phe-L-Pro-D-Val Sequences in Place of D-Phe-L-Pro-L-Val Sequence in the β-Turn Part of the Antibiotic

Makoto TAMAKI,* Tadashige OKITSU, Mie ARAKI, Honami SAKAMOTO, Michiaki TAKIMOTO, and Ichiro MURAMATSU†

Department of Chemistry, Faculty of Science, Toho University, Miyama, Funabashi-shi, Chiba 274
†*Department of Chemistry, College of Science, Rikkyo University, Nishi-ikebukuro, Tokyo 171*

(Received September 18, 1984)

In order to investigate the contribution of configurations of amino acid residues around Pro residues in gramicidin S to its activity and conformation, [D-Val$^{1,1'}$]- and [D-Val$^{1,1'}$ L-Phe$^{4,4'}$]-gramicidin S were synthesized by a liquid-phase method. The CD spectra of these analogs and gramicidin S in aqueous solutions differ from each other, indicating that these peptides have different conformations. These analogs have practically no activity against the Gram-positive microorganisms tested, indicating the importance of the presence of the D-Phe-Pro-Val sequence in gramicidin S regarding activity.

Gramicidin S (GS)[1] is an antibiotic cyclodecapeptide isolated from *Bacillus brevis*. Its secondary structure has been established as an antiparallel β-sheet conformation (Fig. 1).[2] This conformation is characteristically featured (with the orientation of side chains) in such a way that the charged Orn side chains are situated on one side of the molecule and the hydrophobic Val and Leu side chains are situated on the other side. The side-chain arrangement is apparently held together by a rigid conformation containing two D-Phe-Pro type II′ β-turns.[2,3] In studies regarding the structure-activity relationship of GS, it has been proposed that this specific conformation is necessary in order to exhibit an antibiotic activity.[4]

Recently, we reported in studies of an antibiotic cyclododecapeptide, gratisin, that the configurations of amino acid residues around Pro residues in synthetic isomers greatly affect their conformation, and that the activity of *cyclo*(-Val-Orn-Leu-D-Phe-Pro-D-Tyr-)$_2$ was similar to that of GS against *Bacillus subtilis* and stronger than that of *cyclo*(-Val-Orn-Leu-D-Phe-Pro-Tyr-)$_2$.[5] In connection with these results, it is of interest to study the relationship between configurations of amino acid residues around Pro residues in GS and its secondary structure or antibiotic activity.

Kawai *et al.*[6] synthesized [L-Ala$^{4,4'}$]-GS, in which D-Phe-Pro-Val sequences in GS were replaced with Ala-Pro-Val sequences, and elucidated the structure-activity relationship.

In the present paper, we wish to describe the synthesis and antibiotic activity of [D-Val$^{1,1'}$]- and [D-Val$^{1,1'}$, L-Phe$^{4,4'}$]-GS (Fig. 2), in which the D-Phe-Pro-Val sequence in GS is replaced, respectively, with D-Phe-Pro-D-Val and Phe-Pro-D-Val. We also wish to discuss the relationship between partial sequences around Pro residues and CD patterns in GS and the analogs.

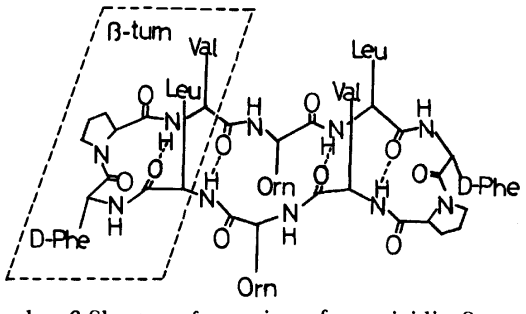

Fig. 1. β-Sheet conformation of gramicidin S.

The synthetic routes of [D-Val$^{1,1'}$]-GS (**7**) and [D-Val$^{1,1'}$, L-Phe$^{4,4'}$]-GS (**13**) are shown in Schemes 1 and 2. In the synthesis of protected [D-Val$^{1,1'}$]-GS (**6**), the Boc-dipeptide ester (**1**) was synthesized with DCC and HOBt, and then converted into the hydrazide (**2**). The Z-tripeptide benzyl ester (**3**) was obtained with DCC and HOBt by stepwise elongation as an oil. The hydrogenolysis of **3** gave the tripeptide (**3′**). The coupling of **2** and **3′** was carried out using an azide method and afforded the Boc-pentapeptide (**4**), which in part was converted into the Boc-pentapeptide succinimido ester (**4′**) with 1-ethyl-3-(3-dimethylaminopropyl)carbodiimide (WSCD) and HOSu. The coupling of **4′** and the pentapeptide derived from **4** afforded the Boc-decapeptide (**5**) which was converted into the decapeptide succinimido ester (**5′**). The cyclodecapeptide (**6**) was derived by the cyclization of **5′** in pyridine at 60°C for 2 h in a 25% yield. In the synthesis of

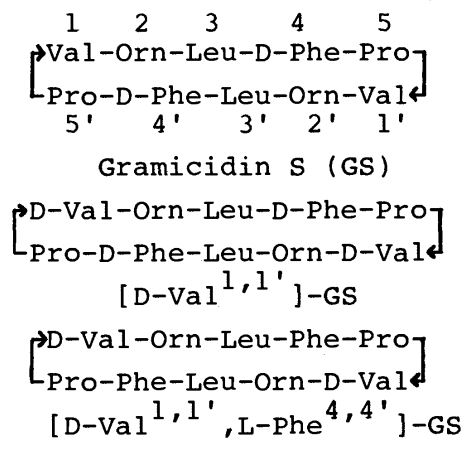

Fig. 2. Primary structures of gramicidin S and its analogs.

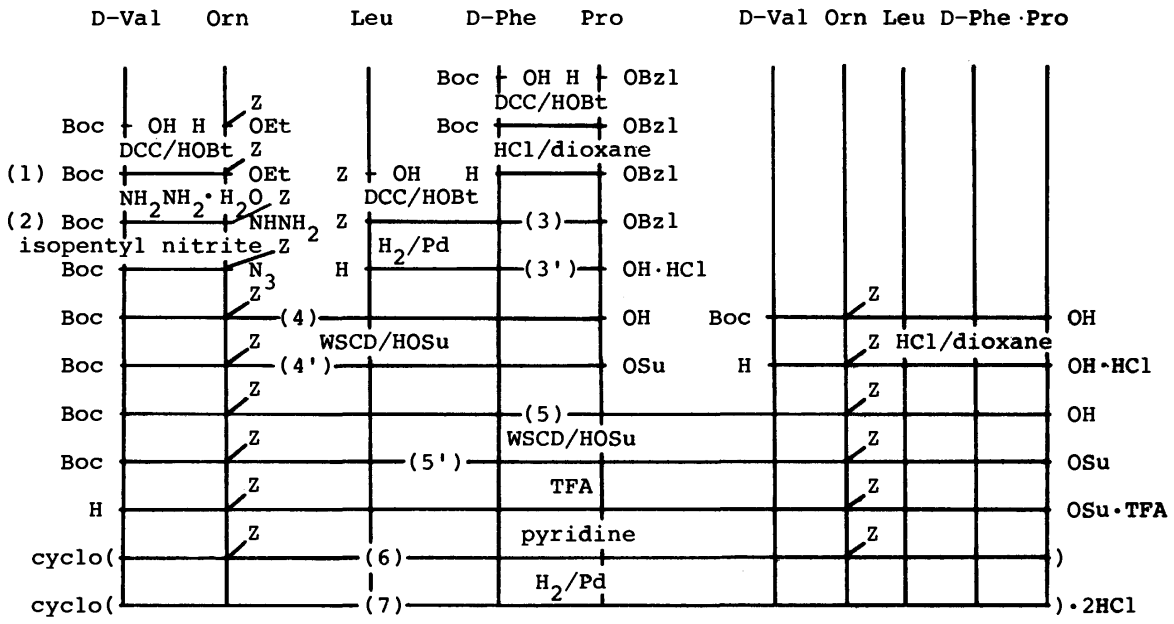

Scheme 1. Synthesis of [D-Val$^{1,1'}$]-GS.

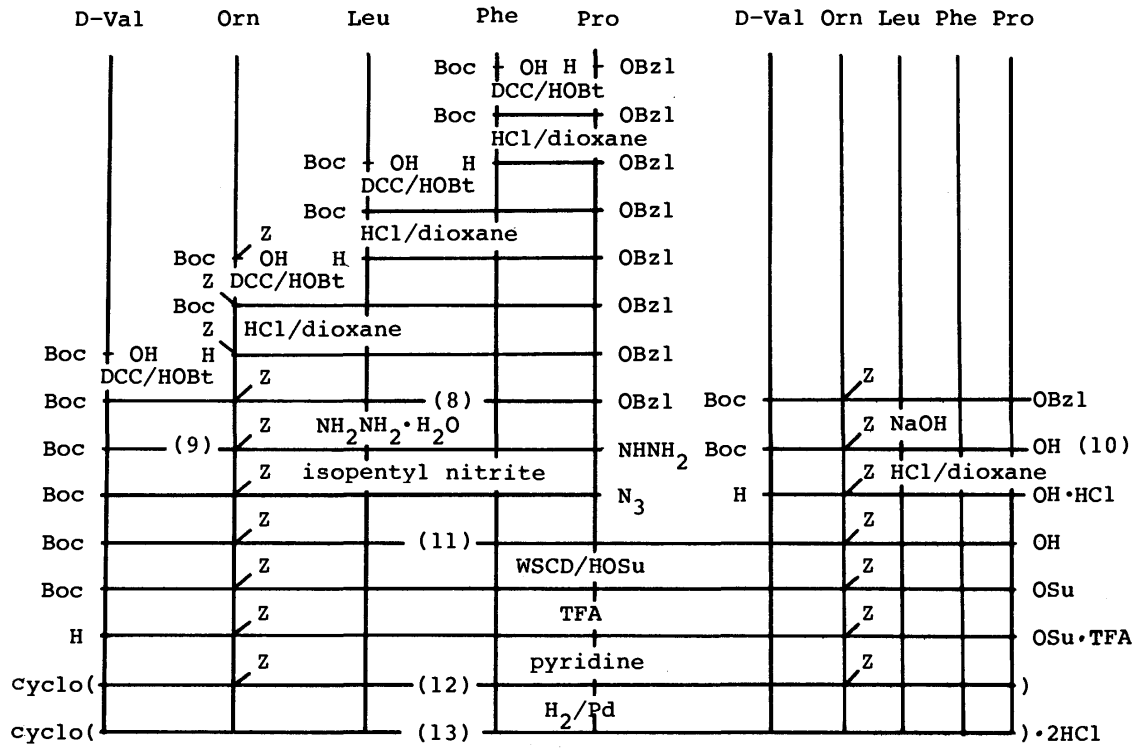

Scheme 2. Synthesis of [D-Val$^{1,1'}$, L-Phe$^{4,4'}$]-GS.

protected [D-Val$^{1,1'}$, L-Phe$^{4,4'}$]-GS (**12**), the Boc-pentapeptide benzyl ester (**8**) was synthesized by stepwise elongation using DCC and HOBt from the Pro benzyl ester. A part of **8** was converted into the hydrazide (**9**), and another part was saponified to obtain the Boc-pentapeptide (**10**). The coupling of **9** and the pentapeptide derived from **10** was carried out using an azide method and afforded the Boc-decapeptide (**11**). The cyclization of **11** was performed using an active ester method in a similar manner as described regarding the synthesis of [D-Val$^{1,1'}$]-GS. The desired peptide was obtained in a 47% yield. The masking groups of **6** and **12** were removed by hydrogenolysis. Their homogeneity was confirmed by thin-layer chromatography, cellulose plate electrophoresis, elemental analysis, amino acid analysis, high-performance liquid chromatography (HPLC) and secondary ion mass spectrometry (SIMS).

The CD spectra of [D-Val$^{1,1'}$]-GS, [D-Val$^{1,1'}$, L-Phe$^{4,4'}$]-GS, and GS in aqueous solutions are shown in Fig. 3. The spectral shapes of these peptides differ from each other, indicating that they have different conforma-

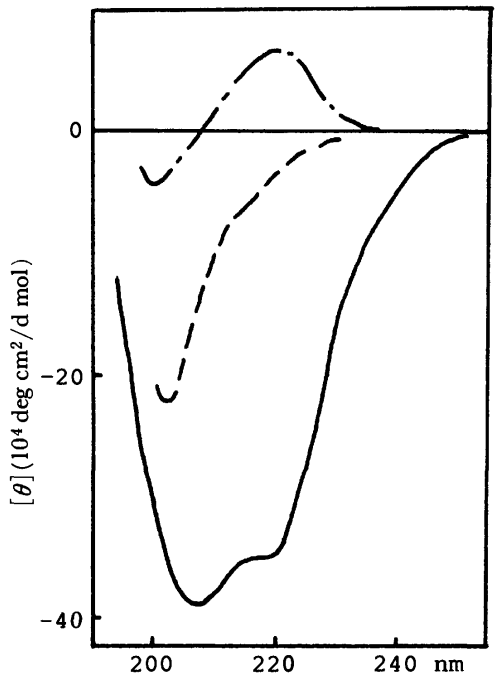

Fig. 3. CD spectra of GS and its analogs in aqueous solution.
——, GS: ---, [D-Val$^{1,1'}$]-GS: –·–, [D-Val$^{1,1'}$, L-Phe$^{4,4'}$]-GS.

tions in aqueous solutions. Recently, in CD spectroscopic studies of cyclododecapeptide gratisin, we reported that the CD spectra of synthetic isomers could be classified into four groups, and that the isomers belonging to each group possess analogous partial sequences around the Pro residues. That is, L-X-Pro-L-Y, D-X-Pro-L-Y, L-X-Pro-D-Y, and D-X-Pro-D-Y.[5] Each CD spectrum of [D-Val$^{1,1'}$]-GS, [D-Val$^{1,1'}$, L-Phe$^{4,4'}$]-GS and GS showed a similar pattern to that of the gratisin isomer having the corresponding partial sequences around the Pro residues (D-X-Pro-D-Y, L-X-Pro-D-Y and D-X-Pro-L-Y, respectively). The CD pattern of [L-Ala$^{4,4'}$]-GS[6] also resembles that of the gratisin isomer having a L-X-Pro-L-Y partial sequence. It is interesting that the CD spectra of these peptides related with both GS and gratisin are dependent on the particular sequence around the Pro residue, although these peptides have a different number of ring members. The CD spectra of [Pro$^{4,4'}$, Asn$^{5,5'}$]-GS and [Pro$^{4,4'}$, D-Ala$^{5,5'}$]-GS reported by Sato *et al.*[7] also showed a similar sequence dependence, although the Pro residues occupy positons different from 5 and 5′ in GS. Moreover, the CD spectrum of *cyclo*(-Leu-Orn-Leu-Orn- Leu-D-Phe-Pro-)$_2$ synthesized by Ando *et al.*[8] was also similar to that of GS. This may result from the presence of a D-X-Pro-L-Y partial sequence in the peptide. These results indicate that the CD spectra of these peptides in aqueous solutions reflect the partial sequences around the Pro residues, which affect (largely) the conformation of these peptides.

[D-Val$^{1,1'}$]-GS showed antibiotic activity only against *Corynebacterium diphtheriae* at a concentration of 25 μg/ml, and no activity toward the other Gram-positive microorganisms tested. [D-Val$^{1,1'}$, L-Phe$^{4,4'}$]-GS showed no antibiotic activity against all the Gram-positve microorganisms tested. That is, the D-Phe-Pro-Val sequences in GS can not be substituted by Phe-Pro-D-Val or D-Phe-Pro-D-Val sequence without affecting the activity. In gratisin analogs, several isomers containing different sequences in the corresponding part were more or less active.[5] The significant difference between GS and gratisin in this regard may result from the distinction of their rings, in other words, the flexibility of the β-turn parts.

Experimental

All the melting points are uncorrected. The CD spectra were obtained using a JASCO spectropolarimeter (model J-500). The CD spectroscopy of GS and its analogs was carried out with an aqueous solution of their dihydrochlorides. The molecular weights of GS analogs and several intermediary products were determined by secondary ion mass spectrometry (SIMS) using a Hitachi M-80B mass spectrometer and fast atom bomberdment (FAB) mass spectrometry using a JMS D-300 mass spectrometer. Amino acid analyses were carried out using a Hitachi 835 amino acid analyzer, after hydrolysis of the peptides in 6 M HCl (1 M=1 mol dm^{-3}) at 110°C for 24 h. HPLC was performed by an ODS column (φ 4.6×250 mm) using MeOH–5% $NaClO_4$ aq (5:1)[1] as eluting solvent. Thin-layer chromatography was performed on Merck silica-gel F_{254} plates with the following solvent systems (v/v): R_f^1, $CHCl_3$–MeOH (9:1); R_f^2, $CHCl_3$–MeOH–AcOH (95:5:3); R_f^3, *n*-BuOH–AcOH–H_2O (4:1:1); R_f^4, *n*-BuOH–pyridine–AcOH–H_2O (4:1:1:2).

Boc-D-Val-Orn(Z)-OEt (1). DCC (2.9 g, 14 mmol) was added to a solution of Boc-D-Val (3.0 g, 14 mmol), HOBt (2.1 g, 15.5 mmol), Orn(Z)-OEt·TsOH (6.5 g, 14 mmol) and TEA (2 ml, 14 mmol) in $CHCl_3$ (70 ml) at 0°C. This solution was stirred for 3 h at 0°C and overnight at room temperature. After the reaction mixture was concentrated *in vacuo*, AcOEt (20 ml) was added to the residue, and insoluble substance was removed by filtration. The filtrate was then diluted with AcOEt (150 ml). The solution was washed (successively) with 5% citric acid, water, 5% Na_2CO_3 and water, and then dried over sodium sulfate. After removal of the drying agent, the solvent was evaporated *in vacuo*. The product was recrystallized from hot AcOEt; yield, 4.56 g (65%); mp 130—132 °C; $[\alpha]_D^{29}$ −4.0° (*c* 1, DMF); R_f^1 0.88, R_f^2 0.68. Found: C, 61.25; H, 7.98; N, 8.53%. Calcd for $C_{25}H_{39}O_7N_3$: C, 60.83; H, 7.96; N, 8.51%.

Boc-D-Val-Orn(Z)-NHNH$_2$ (2). A solution of **1** (4.0 g, 8.1 mmol) and hydrazine hydrate (5 ml) in DMF (15 ml) was allowed to stand for 24 h at room temperature. The solution was concentrated, and then water was added to the residue. The resulting solid was collected by filtration; yield, 3.5 g (90%); mp 179—180°C; $[\alpha]_D^{29}$ −9.7° (*c* 1, DMF); R_f^1 0.41; R_f^2 0.44. MS (FAB), *m/z* 480 (MH^+). Found: C, 57.65; H, 7.82; N, 14.32%. Calcd for $C_{23}H_{37}O_6N_5$: C, 57.60; H, 7.78; N, 14.60%.

Z-Leu-D-Phe-Pro-OBzl (3). The coupling of Boc-D-Phe (5.4 g, 20 mmol) and Pro-OBzl·HCl (5.15 g, 20 mmol) were performed by the method described in the preparation of **1**. The product was dissolved in 4 M HCl/dioxane

(30 ml) containing anisole (0.5 ml) at 0°C. After stirring for 30 min at room temperature, the solution was concentrated *in vacuo*. The residue was dissolved in $CHCl_3$ (30 ml). The solution was washed by 5% Na_2CO_3 and water under cooling with an ice bath. To this solution were added Z-Leu (5.3 g, 20 mmol), HOBt (2.96 g, 22 mmol) and DCC (5.15 g, 20 mmol). The mixture was treated in a similar way to that described in the preparation of **1**. The crude tripeptide was purified by chromatography on a silica-gel column (2×40 cm) using a solvent system of $CHCl_3$–MeOH (50:1). The fractions containing the desired product were combined and concentrated. The product was obtained as an oil in a yield of 3.18 g (27% calculated from Pro-OBzl as the starting material). R_f^1 0.80, R_f^2 0.65.

Boc-D-Val-Orn(Z)-Leu-D-Phe-Pro-OH (4). Compound **3** (2.64 g, 4.4 mmol) was dissolved in 90% MeOH (30 ml), and then 1 M HCl (4.4 ml) was added to the solution. The mixture was hydrogenated in the presence of Pd black for 10 h. After removal of the catalyst, the filtrate was concentrated *in vacuo*. To a solution of **2** (2.1 g, 4.4 mmol) in DMF (20 ml) were added 9 M HCl/dioxane (1.4 ml, 12.6 mmol) and isopentyl nitrite (0.7 ml, 5.0 mmol) at −40°C. After stirring at −20°C for 15 min, TEA (1.8 ml, 12.6 mmol) was added at −40°C. This mixture was combined with a solution of the total amount of the H-Leu-D-Phe-Pro-OH prepared above and TEA (1.25 ml, 8.8 mmol) in DMF (12 ml). The mixture was stirred at 0°C for 3 d, and concentrated. The residue was dissolved in AcOEt (100 ml). The solution was washed with 5% citric acid, water, 5% Na_2CO_3 and water, and dried. After the removal of the drying agent, the solution was evaporated. The product was recrystallized from MeOH–ether; yield, 3.05 g (84%); mp 191—192°C; $[\alpha]_D^{29}$ −36.7° (*c* 1, DMF); R_f^1 0.37, R_f^2 0.39. MS (FAB), *m/z* 823 (MH^+). Found: C, 62.57; H, 7.81; N, 10.14%. Calcd for $C_{43}H_{62}O_{10}N_6$: C, 62.76; H, 7.59; N, 10.21%.

Boc-[D-Val-Orn(Z)-Leu-D-Phe-Pro-]$_2$-OH (5). To a solution of **4** (1.17 g, 1.4 mmol) in DMF (7 ml) was added HOSu (0.35 g, 3 mmol) and WSCD·HCl (0.52 g, 2.7 mmol) at 0°C, and then the mixture was stirred for 48 h at room temperature. The solution was evaporated, and then water was added to the residue. The resulting solid, Boc-D-Val-Orn(Z)-Leu-D-Phe-Pro-OSu (**4'**), was collected by filtration, and washed with water and dried. Another crop of **4** (1.17 g, 1.4 mmol) was dissolved in 4 M HCl/dioxane (10 ml) containing anisole (0.5 ml) at 0°C. After stirring at room temperature for 30 min, the solution was concentrated *in vacuo*. To a solution of H-D-Val-Orn(Z)-Leu-D-Phe-Pro-OH prepared above and TEA (0.4 ml, 2.8 mmol) in DMF (8 ml) at 0°C was added **4'** derived from **4**. The mixture was left to stand for 2 h at 0°C and overnight at room temperature. The solution was evaporated, and the residue was dissolved into AcOEt (200 ml). The solution was washed with 5% citric acid and water, and was evaporated. The product was recrystallized from MeOH–ether; yield, 1.37 g (64%); mp 146—148°C; $[\alpha]_D^{29}$ −38.3° (*c* 1, DMF); R_f^1 0.32, R_f^2 0.42. Found: C, 62.91; H, 7.67; N, 10.75%. Calcd for $C_{81}H_{114}O_{17}N_{12}\cdot H_2O$: C, 62.93; H, 7.56; N, 10.87%.

cyclo[-D-Val-Orn(Z)-Leu-D-Phe-Pro-]$_2$ (6). Boc-[D-Val-Orn(Z)-Leu-D-Phe-Pro-]$_2$-OH (0.94 g, 0.6 mmol) was converted into the succinimido ester (**5'**) by the method described for **5**. It was dissolved in TFA (10 ml) containing a few drops of anisole at 0°C. The mixture were stirred for 30 min at room temperature and then concentrated. The residue, the trifluoroacetate of the decapeptide active ester, was triturated with ether, collected by filtration and dissolved in DMF (8 ml). The solution was added dropwise into pyridine (400 ml) at 60°C. After stirring for 3 h at 60°C, the solvent was evaporated, and then water was added to the residue. The resulting solid was collected by filtration, washed with water and dried. The product was purified by reprecipitaion from MeOH–ether; yield, 0.21 g (25%); mp 146—148°C; $[\alpha]_D^{29}$ −58.0° (*c* 0.5, DMF); R_f^1 0.73, R_f^2 0.70. Found: C, 63.89; H, 7.56; N, 11.81%. Calcd for $C_{76}H_{104}O_{14}N_{12}\cdot H_2O$: C, 63.93; H, 7.48; N, 11.77%.

cyclo(-D-Val-Orn-Leu-D-Phe-Pro-)$_2$·2HCl (7). **6** (100 mg, 0.07 mmol) was hydrogenated in 90% MeOH (35 ml) containing 1 M HCl (0.14 ml) in the presence of Pd black for 8 h. After removal of the catalyst, the filtrate was concentrated *in vacuo*. The product was purified by gel filtration on a Sephadex LH-20 column (1×150 cm) using MeOH as solvent, and by reprecipitation from MeOH–ether; yield, 40 mg (47%); mp 241—243°C (dec.); $[\alpha]_D^{29}$ −55.1° (*c* 0.2, EtOH); R_f^3 0.55, R_f^4 0.71. Amino acid ratios: Val, 0.93; Orn, 0.90; Leu, 1.05; Phe, 1.07; Pro, 1.07. MS (SIMS), *m/z* 1141 ($C_{60}H_{93}O_{10}N_{12}$; MH^+) Found: C, 55.93; H, 7.68; N, 12.83%. Calcd for $C_{60}H_{92}O_{10}N_{12}\cdot 2HCl\cdot 4H_2O$; C, 56.01; H, 7.99; N, 13.06%.

Boc-D-Val-Orn(Z)-Leu-Phe-Pro-OBzl (8). This product was synthesized with DCC and HOBt by stepwise elongation from Pro-OBzl·HCl (2.57 g, 10 mmol) as described for the preparation of **3**. The product was purified by a silica-gel column (2.2×40 cm) using $CHCl_3$–MeOH (50:1) as a solvent, and the fractions containing the desired product were combined and concentrated. The product was recrystallized from MeOH–ether; yield, 4.6 g (50%); mp 92—96°C; $[\alpha]_D^{29}$ −37.9° (*c* 1, DMF); R_f^1 0.80, R_f^2 0.59. Found: C, 66.08; H, 7.55; N, 9.09%. Calcd for $C_{50}H_{68}O_{10}N_6$: C, 65.77: H, 7.51, N, 9.20%.

Boc-D-Val-Orn(Z)-Leu-Phe-Pro-NHNH$_2$ (9). Compound **8** (1.49 g, 1.63 mmol) was treated with hydrazine hydrate (1.5 ml) as described for the preparation of **2**; yield, 0.95 g (70%); mp 132—135°C; $[\alpha]_D^{29}$ −32.0° (*c* 0.5, DMF); R_f^1 0.55, R_f^2 0.44. Found: C, 60.54; H, 7.75; N, 13.03%. Calcd for $C_{43}H_{64}O_9N_8\cdot H_2O$: C, 60.40; H, 7.77; N, 13.10%.

Boc-D-Val-Orn(Z)-Leu-Phe-Pro-OH (10). In a solution of **8** (1.01 g, 1.1 mmol) in MeOH (24 ml) and dioxane (12 ml), 1 M NaOH (2.3 ml) was added. The solution was stirred for 5 h at room temperature. After the addition of water (10 ml), the solution was evaporated, and then 10% citric acid was added to the residue. The resulting solid was collected by filtration, washed with water and dried. The product recrystallized from MeOH–ether; yield, 0.68 g (75%); mp 134—136°C; $[\alpha]_D^{29}$ −28.6° (*c* 0.5, DMF); R_f^1 0.50, R_f^2 0.44. Found: C, 62.42; H, 7.71: N, 10.48%. Calcd for $C_{43}H_{62}O_{10}N_6$: C, 62.76; H, 7.59; N, 10.21%.

Boc-[D-Val-Orn(Z)-Leu-Phe-Pro-]$_2$-OH (11). This compound was prepared from **9** (0.62 g, 0.73 mmol) and **10** (0.6 g, 0.73 mmol) as described for the preparation of **4**. The product was purified by gel filtration on a Sephadex LH-20 column (2.5×120 cm) using MeOH as solvent, and recrystallization from MeOH–ether; yield, 0.74 g (66%); mp 150—151°C; $[\alpha]_D^{29}$ −37.1° (*c* 0.5, DMF); R_f^1 0.40, R_f^2 0.40. Found: C, 62.86; H, 7.35; N, 10.84%. Calcd for $C_{81}H_{114}O_{17}N_{12}\cdot H_2O$: C, 62.93; H, 7.56; N, 10.87%.

cyclo[-D-Val-Orn(Z)-Leu-Phe-Pro-]$_2$ (12). This compound was prepared from **11** (0.41 g, 0.27 mmol) as described for the preparation of **6**. The product was purified

by silica-gel column chromatography, and recrystallization from MeOH–ether; yield, 179 mg (47%); mp 218—219 °C; $[\alpha]_D^{29}$ −22.0° (*c* 0.5, DMF); R_f^1 0.66, R_f^2 0.41. Found: C, 64.31; H, 7.59; N, 12.23%. Calcd for $C_{76}H_{104}O_{14}N_{12}$: C, 64.75; H, 7.43; N, 11.92%.

cyclo(-D-*Val-Orn-Leu-Phe-Pro-*)$_2$·2HCl (**13**). This compound was prepared from **12** (105 mg, 0.074 mmol) as described for the preparation of **7**; yield, 66 mg (74%); mp 239—241 °C; $[\alpha]_D^{29}$ −31.8° (*c* 0.2, EtOH); R_f^3 0.68, R_f^4 0.65. Amino acid ratios: Val, 0.95; Orn, 1.03; Leu, 1.03; Phe, 1.00; Pro, 1.00. MS(SIMS), *m/z* 1141 ($C_{60}H_{93}O_{10}N_{12}$, MH^+). Found: C, 56.03; H, 7.78; N, 13.08%. Calcd for $C_{60}H_{92}O_{10}N_{12}\cdot 2HCl\cdot 4H_2O$: C, 56.01; H, 7.99; N, 13.06%.

Cellulose Plate Electrophoresis. It was carried out with cellulose (Avicel) plate and with a solvent system of HCOOH–AcOH–MeOH–H_2O (1:3:6:10 v/v, PH 1.4) for 2 h at 500 V/20 cm. Each of analogs revealed a single spot, the mobility being the same as that of GS.

Microbiological Assays. The microorganisms employed were *Stapylococcus aureus* ATCC 6538, *Streptomyces pyogenes* N.Y.5, *Corynebacterium diphtheriae* P.W.8, *Micrococcus pyogenes* ATCC 10240, *Bacillus subtilis* ATCC 6633, *Escherichia coli* NIHJ-JC2 and *Proteus vulgaris* OX 19. The minimum concentration of the compounds necessary for the complete inhibition of growth of these microorganisms was determined by an agar dilution method with 10^6 organisms per milliter.

We are grateful to the staff of the Research Laboratories of Toyo Jozo Co. for elemental analyses, microbiological assays and the measurements of FAB Mass, and also to Professor Makoto Suzuki, Meijo University, for the measurement of SIMS.

References

1) Recently, it was reported that natural GS is a mixture of several homologs. The GS used in the present paper corresponds to GS-1 in the report: S. Nozaki and I. Muramatsu, *J. Antibiotics.*, **37**, 689 (1984).

2) D. C. Hodgkin and B. M. Oughton, *Biochem. J.*, **65**, 752 (1957).

3) Amino acid residues with no plefix are of L-configuration. The abbreviations for amino acids and peptides are in accordance with the rules of IUPAC-IBU Commission of Biological Nomencalture. Abbreviations used are as follows: Boc, *t*-butoxycarbonyl; Z, benzyloxycarbonyl; OBzl, benzyloxy; OEt, ethoxy; DCC, dicyclohexylcarbodiimide; WSCD, 1-ethyl-3-(3-dimethylaminopropyl)carbodiimide; HOBt, 1-hydroxybenzotriazole; HOSu, *N*-hydroxysuccinimide; TFA, trifluoroacetic acid; TEA, triethylamine; NMM, *N*-methylmorpholine; DMF, *N*,*N*-dimethylformamide; AcOEt, ethyl acetate.

4) N. Izumiya, T. Kato, H. Aoyagi, M. Waki, and M. Kondo, "Synthetic Aspects of Biologically Active Cyclic Peptide-Gramicidin S and Tyrocidines," Kodansha, Tokyo, and Halsted Press, New York (1979), pp. 49—97.

5) a) M. Tamaki, M. Takimoto, S. Sofuku, and I. Muramatsu, "Peptide Chemistry 1982," ed by S. Sakakibara, Protein Research Foundation, Osaka (1983) pp. 111; b) M. Tamaki, *Bull. Chem. Soc. Jpn.*, **57**, 3210 (1984).

6) M. Kawai and U. Nagai, *Biopolymers.*, **17**, 1549 (1978).

7) K. Sato and U. Nagai, *Bull. Chem. Soc. Jpn.*, **56**, 3329 (1983).

8) S. Ando, H. Takiguchi and N. Izumiya, *Bull. Chem. Soc. Jpn.*, **56**, 3781 (1983).

Syntheses of Four Stereoisomers of β-Methyllanthionine.

Tateaki WAKAMIYA, Yoshiaki ODA, Koichi FUKASE, and Tetsuo SHIBA*
Department of Chemistry, Faculty of Science, Osaka University, Toyonaka, Osaka 560
(Received September 27, 1984)

Four stereoisomers of β-methyllanthionine were synthesized by coupling of *N*-benzyloxycarbonyl-3-methyl-D-cysteine with β-chloroalanine. ^{1}H NMR analysis and retention time in amino acid analysis were studied on these compounds.

β-Methyllanthionine is a unique sulfide amino acid which was first found as a constituent of peptide antibiotics subtilin[1] and nisin[2] and also occurred in yeast.[3] Recently, the same amino acid was observed in a new angiotensin converting enzyme inhibitor, ancovenin.[4] The configuration of this amino acid in

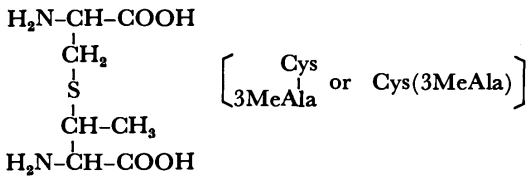

β-Methyllanthionine = (3-Methylalanin-3-yl)cysteine

all these biologically active peptides was determined to be of (2*R*)-*S*-[(2*S*,3*S*)-3-methylalanin-3-yl]cysteine.[5] To confirm this result synthetically, we prepared four stereoisomers in which the configuration of α-carbon atom of 3-methylalanine part was fixed in *S* configuration corresponding to D-amino acid. Another four possible compounds of *R* configuration on α-carbon atom of 3-methylalanine moiety were not prepared in this work, since all the physicochemical properties except the opposite sign of specific rotation are obtainable from the corresponding enantiomer with (2*S*)-3-methylalanyl configuration. Although Okawa *et al.* reported the syntheses of two enantiomers of protected *threo*-β-methyllanthionine by addition of *N*-benzyloxycarbonyl-L-cysteine benzyl ester to benzyl *N*-benzyloxycarbonyl-(2*S*,3*S*)- or (2*R*,3*R*)-3-methyl-2-aziridinecarboxylate, other enantiomers and free forms of all diastereoisomers have not yet been known in their physical properties.[6]

The synthesis of β-methyllanthionine in this investigation was attempted by coupling of *N*-benzyloxycarbonyl-3-methylcysteine with β-chloroalanine. For this purpose both *threo*- and *erythro*-3-methyl-D-cysteine were required. The *threo* compound was prepared by our previous method *via* an addition of thiocarboxylic acid to aziridinecarboxylic acid derivative obtained from threonine.[7] On the other hand, the *erythro* compound was obtained by S_N2 substitution of *p*-toluenesulfonyloxy group on β-carbon atom of threonine derivative with thiobenzoic acid[8] as shown in Fig. 1. From the amino acid analysis of the product, we could assure that the reaction proceeded without racemization to form *erythro*-3-methyl-D-cysteine, *i.e.*, (2*S*,3*R*)-3-methylcysteine.

Coupling of each *N*-benzyloxycarbonyl-3-methyl-

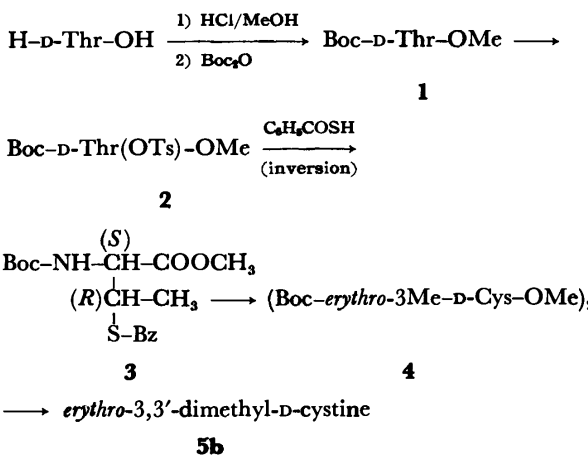

Fig. 1. Preparative scheme of *erythro*-3,3′-dimethyl-D-cystine. Boc=*t*-butoxycarbonyl.

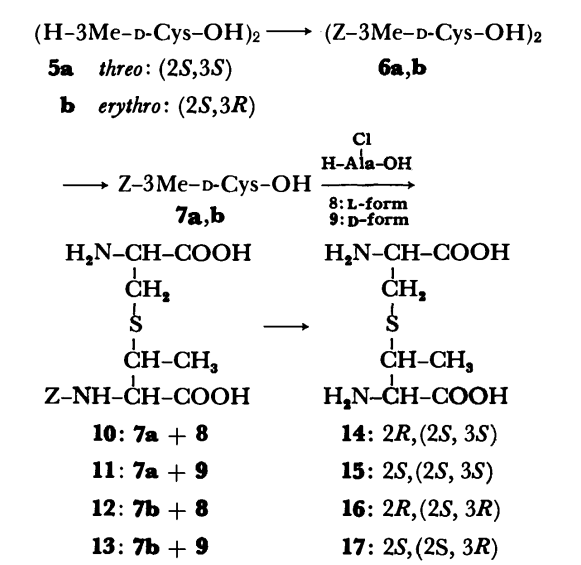

Fig. 2. Preparation of four stereoisomers of β-methyllanthionine.

cysteine (**7a** and **7b**) with L- or D-β-chloroalanine (**8** or **9**) was carried out according to the procedure for the preparation of *meso*-lanthionine by Photaki *et al.*[9] (Fig. 2). Each coupling product, **10**—**13**, was then treated with hydrogen bromide in glacial acetic acid to give corresponding β-methyllanthionine, **14**—**17**, respectively. Physicochemical properties of the compounds **6**—**17** were listed in Table 1. Retention times of final products in amino acid analysis were also given in Table 1. ^{1}H NMR analysis of the compounds **10**—**17** was summarized in Table 2.

TABLE 1. ANALYTICAL DATA OF STEREOISOMERS OF β-METHYLLANTHIONINE AND THE COMPOUNDS RELATED TO THEIR SYNTHESES

Compound	Yield/%	Mp (θ_m/°C, dec)	$[\alpha]_D$/°	Formula	Found (Calcd) (%) C	H	N	S	Retention time in amino acid analysis (min)
6a	96	oil	−28.5(t=32°C)[b]	$C_{24}H_{28}N_2O_8S_2$	53.44 (53.72	5.42 5.26	5.30 5.22	11.93 11.95)	
6b	89	oil	+135(t=19°C)[b]	$C_{24}H_{28}N_2O_8S_2$	53.52	5.14	5.25	11.99	
7a[a]	quant	oil		$C_{12}H_{15}NO_4S$					
7b[a]	quant	oil		$C_{12}H_{15}NO_4S$					
10	53	191—193	−15(t=24°C)[c]	$C_{15}H_{20}N_2O_6S$	50.71 (50.55	5.64 5.66	7.78 7.86	8.98 9.00)	
11	35	204—208	−31(t=24°C)[c]	$C_{15}H_{20}N_2O_6S$	50.41	5.64	7.80	8.81	
12	48	192—195	+46(t=27°C)[c]	$C_{15}H_{20}N_2O_6S$	50.52	5.68	7.84	9.00	
13	53	189—190	−20(t=27°C)[c]	$C_{15}H_{20}N_2O_6S$	50.18	5.65	7.64	8.81	
14	87	228—231	−36(t=23°C)[d]	$C_7H_{14}N_2O_4S$ with $0.6H_2O$ (36.07	36.03 6.57	6.33 12.02	11.91 13.76)	13.71	54.0
15	89	205—206	−48(t=23°C)[d]	$C_7H_{14}N_2O_4S$ with $1.1H_2O$ (34.73	34.53 6.74	6.73 11.57	11.42 13.24)	13.73	54.0
16	quant	258—261	+53(t=23°C)[d]	$C_7H_{14}N_2O_4S$ with $0.6H_2O$ (36.07	36.16 6.57	6.38 12.02	12.16 13.76)	13.33	62.3
17	90	203—226	+5.0(t=27°C)[d]	$C_7H_{14}N_2O_4S$ with $0.9H_2O$ (35.26	35.42 6.68	6.53 11.75	11.68 13.44)	13.41	51.4

a) These compounds were used for the next coupling without purification to avoid reoxidation. b) c 1.18 in ethanol. c) c 0.25 in 1M HCl. d) c 0.22 in 1M HCl. e) Column: Hitachi #2618 resin (one column method, 0.9× 25 cm, 55°C), buffer: 0.20 M sodium citrate (pH 3.0).

TABLE 2. CHEMICAL SHIFTS OF THE COMPOUNDS **10—17** IN ^{1}H NMR

Compound	Cys part 2-CH	Cys part 3-CH_2	3MeAla part 2-CH	3MeAla part 3-CH	3MeAla part 3-CH_3	Z group —CH_2—	Z group C_6H_5—
10[a]	4.38(dd)	3.26(—)[c]	4.54(d)	3.52(m)	1.37(d)	5.17(s)	7.46(s)
11[a]	4.40(t)	3.30(d)	4.56(d)	3.58(m)	1.41(d)	5.18(s)	7.44(s)
12[a]	4.45(t)	3.29(d)	4.65(d)	3.54(m)	1.30(d)	5.22(s)	7.50(s)
13[a]	4.00(t)	3.53(d)	4.64(d)	3.71(m)	1.40(d)	5.18(s)	7.42(s)
14[b]	3.90(dd)	3.13(—)[c]	3.81(d)	3.49(m)	1.40(d)	—	—
15[b]	3.97(t)	3.17(d)	3.89(d)	3.55(m)	1.46(d)	—	—
16[a]	4.52(t)	3.39(d)	4.45(d)	3.72(m)	1.41(d)	—	—
17[b]	4.05(t)	3.19(d)	3.98(d)	3.57(m)	1.34(d)	—	—

Abbreviations; s: singlet, d: doublet, dd: double doublet, t: triplet, m; multiplet.
a) Measured in 2 M DCl. b) Measured in D_2O. c) Three peaks due to A_2B system were observed.

Of four stereoisomers of β-methyllanthionine obtained, (2*R*)-*S*-[(2*S*,3*S*)-3-methylalanin-3-yl]cysteine (**14**) was identical with the natural one from nisin or ancovenin confirming the assumed structure unequivocally. Now, these synthetic compounds will be useful as authentic samples for structural determination of β-methyllanthionine of unknown configuration when found newly in nature.

Experimental

All melting points are uncorrected. The NMR spectra were obtained with Varian XL-100-15 spectrometer and sodium 2,2-dimethyl-2-silapentane-5-sulfonate (DSS) was used as the external standard. Chemical shifts were given by δ value (ppm) from DSS. Specific rotations were measured with a Perkin-Elmer 141 polarimeter. Amino acid analysis was carried out with a Hitachi KLA-5 analyzer.

N-t-Butoxycarbonyl-D-threonine Methyl Ester (1). To a solution of D-threonine methyl ester hydrochloride[7a] (12.8 g, 75.6 mmol) in anhydrous methanol (160 ml) were added dropwise triethylamine (11.5 g, 113 mmol) and di-*t*-butyl dicarbonate (18.1 g, 83.2 mmol) under ice cooling. The reaction mixture was stirred overnight at room temperature and then concentrated *in vacuo*.

Ethyl acetate extract from an oily residue obtained was washed successively with water, saturated sodium chloride solution, 10% citric acid solution, saturated sodium hydrogencarbonate solution, and saturated sodium chloride solution. The extract was dried over magnesium sulfate and concentrated *in vacuo* to give **1** as an oily product: yield 15.0 g (85.2%); $[\alpha]_D^{32}$ +7.7° (c 1.0, $CHCl_3$). Found: C, 50.10; H, 8.17; N, 5.79%. Calcd for $C_{10}H_{19}NO_5 \cdot 0.3H_2O$[10]: C, 50.33; H, 8.28; N, 5.87%.

N-t-Butoxycarbonyl-O-p-toluenesulfonyl-D-threonine Methyl Ester (2). To a solution of **1** (9.70 g, 41.6 mmol) in pyridine (120 ml) was added *p*-toluenesulfonyl chloride (79.4 g, 416 mmol) under cooling in an ice–salt bath. The reaction mixture was stirred for 3 h in the chilled bath and then in an ice bath until the starting material disappeared. The reaction mixture was poured onto crushed ice and extracted with ethyl acetate (1 l×2). The extract was subjected to the general aqueous washing procedure as mentioned above.

Ethyl acetate layer was then dried over magnesium sulfate and concentrated *in vacuo*. An oily residue thus obtained was purified by silica-gel column chromatography. Elution with benzene removed unreacted *p*-toluenesulfonyl chloride. The desired *p*-toluenesulfonate **2** was eluted with ethyl acetate as an oily product: yield 14.9 g (92.5%); $[\alpha]_D^{32}$ −15.5° (*c* 1.39, CH_3OH). Found: C, 52.28; H, 6.62; N, 3.59; S, 8.26%. Calcd for $C_{17}H_{25}NO_7S \cdot 0.2H_2O$[10]: C, 52.22; H, 6.55; N, 3.58; S, 8.20%.

S-Benzoyl-N-t-butoxycarbonyl-erythro-3-methyl-D-cysteine Methyl Ester (3). To a solution of potassium hydroxide (10.5 g, 187 mmol) in methanol (100 ml) was added thiobenzoic acid (25.7 ml, 219 mmol). The mixture was stirred for 5 min at room temperature and then concentrated *in vacuo* to give potassium thiobenzoate which was dried in a vacuum desiccator. To potassium thiobenzoate transferred in a reaction vessel was added the compound **2** (18.4 g, 47.5 mmol) in DMF (61 ml) under nitrogen atmosphere with cooling in an ice bath. The solution was stirred for 64 h at room temperature and the reaction mixture was extracted with ethyl acetate. The extract was washed with saturated sodium chloride, sodium hydrogencarbonate and then sodium chloride solutions. Ethyl acetate layer was dried over magnesium sulfate and concentrated *in vacuo*. An oily residue was column-chromatographed on silica gel (Merck #7734, 7×19 cm). Elution with benzene–ethyl acetate (19:1) gave pure **3** as an oily product: yield 7.59 g (45.2%); $[\alpha]_D^{17}$ −23.7° (*c* 1.65, $CHCl_3$). Found: C, 57.23; H, 6.53; N, 3.94; S, 9.06%. Calcd for $C_{17}H_{23}NO_5S \cdot 0.1H_2O$[10]: C, 57.48; H, 6.58; N, 3.94; S, 9.03%.

N,N'-Bis(t-butoxycarbonyl)-erythro-3,3'-dimethyl-D-cystine Dimethyl Ester (4). Debenzoylation and oxidation of the compound **3** (100 mg, 0.28 mmol) were carried out in a similar manner as described in the previous paper.[7] After usual treatment of the reaction mixture as described in preparation of **3**, crude product was purified by column chromatography on silica gel (Merck #7734, 0.8×17 cm). Pure oily material was obtained by an elution with benzene-ethyl acetate (9:1): yield 60 mg (85%); $[\alpha]_D^{17}$ +52.9° (*c* 1.14, $CHCl_3$). Found: C, 48.56; H, 7.35; N, 5.65; S, 12.60%. Calcd for $C_{20}H_{36}N_2O_8S_2$: C, 48.37; H, 7.31; N, 5.64; S, 12.91%.

erythro-3,3'-Dimethyl-D-cystine (5b). A suspension of **4** (1.57 g, 3.16 mmol) in 6M† HCl (40 ml) was heated for 2 h at 110°C. The hydrolyzate was concentrated *in vacuo* and the residue was dissolved in 50% ethanol (30 ml). The solution was neutralized by an addition of pyridine to give crystalline product which was recrystallized from water and ethanol: yield 722 mg (85.1%); mp 177—183°C (dec); $[\alpha]_D^{19}$ +515° (*c* 1.02, 1 M HCl). Found: C, 35.13; H, 6.15; N, 10.07; S, 23.46%. Calcd for $C_8H_{16}N_2O_4S_2 \cdot 0.3H_2O$[10]: C, 35.10; H, 6.11; N, 10.23; S, 23.42%.

N,N'-Bis(benzyloxycarbonyl)-threo- and erythro-3,3'-dimethyl-D-cystine (6a and 6b). To a solution of the compound **5a**[7] or **5b** (900 mg, 3.36 mmol) in 1 M sodium hydroxide (13 ml) was added benzyloxycarbonyl chloride (1.1 ml, 7.1 mmol) under ice cooling. The solution was stirred for 2 h at 0°C and then extracted with ether. The aqueous layer acidified with 2 M HCl was extracted with ethyl acetate. The ethyl acetate extract was washed with saturated sodium chloride solution, dried over magnesium sulfate, and concentrated *in vacuo*. Each benzyloxycarbonyl derivative **6a** and **6b** was obtained respectively as an oily substance.

N-Benzyloxycarbonyl-threo- and erythro-3-Methyl-D-cysteine (7a and 7b). Disulfide derivative **6a** or **6b** (688 mg, 1.28 mmol) was dissolved in methanol (2.7 ml) and concentrated hydrochloric acid (0.83 ml) was added to the solution under ice cooling. To the solution was added zinc powder by portions and the suspension was stirred in an ice bath until the disulfide disappeared. The reaction mixture was filtered to remove zinc powder and the filtrate was concentrated *in vacuo*. The residue was dissolved in ethyl acetate and the solution was washed with saturated sodium chloride solution. Ethyl acetate layer was dried over magnesium sulfate and concentrated *in vacuo* to obtain mercapto derivative **7a** or **7b** respectively as an oily product.

Coupling of Mercapto Derivative with β-Chloroalanine. Mercapto derivative **7a** or **7b** (679 mg, 2.52 mmol) was dissolved in 4.4 M potassium hydroxide (1.5 ml). To the solution warmed at 50°C were added β-chloroalanine hydrochloride (403 mg, 2.52 mmol)[11] and 2.6 M potassium hydroxide (1.9 ml). The solution was warmed at 50°C for 30 min and at room temperature for 44 h under argon atmosphere. The reaction mixture was acidified and extracted with ether. Aqueous layer was concentrated *in vacuo* and the residue dissolved in a small amount of 2 M ammonium hydroxide was applied to HP-20 column (3×16 cm). Elution with water and 50% methanol gave desired product which was crystallized by trituration with methanol and ether.

Analytical sample was obtained by further column chromatography on Amberlite IRCG-50 (H^+ form) using water as an eluent. Pure material was recrystallized from water.

β-Methyllanthionine (14—17). Each *N*-benzyloxycarbonyl-β-methyllanthionine derivative (**10—13**) (340 mg, 0.96 mmol) obtained above was dissolved in 25% HBr in glacial acetic acid (12 ml). To the solution kept at room temperature for 2 h was added ether to precipitate respective β-methyllanthionine as hydrobromide. A solution of the hydrobromide in a small amount of water was neutralized with pyridine. Addition of methanol and ether to the solution gave a free amino acid (**14—17**) respectively which was recrystallized from water and methanol. The data of physical properties of these products (**14—17**) were shown in Table 1 and 2.

The authors are deeply indebted to Ajinomoto Co. Ltd., for the supply of D-threonine.

†1M=1 mol dm^{-3}.

References

1) a) G. Alderton, *J. Am. Chem. Soc.*, **75**, 2391 (1953); b) E. Gross, H. H. Kiltz, and E. Nebelin, *Hoppe-Seyler's Z. Physiol. Chem.*, **354**, 810 (1973).

2) E. Gross and J. L. Morell, *J. Am. Chem. Soc.*, **93**, 4634 (1971).

3) P. F. Downey and S. Black, *J. Biol. Chem.*, **228**, 171 (1957).

4) Y. Kido, T. Hamakado, T. Yoshida, M. Anno, Y. Motoki, T. Wakamiya, and T. Shiba, *J. Antibiot.*, **36**, 1295 (1983).

5) J. R. Knox and P. C. Keck, *Biochem. Biophys. Res. Commun.*, **53**, 567 (1973).

6) K. Nakajima, H. Oda, and K. Okawa, *Bull. Chem. Soc. Jpn.*, **56**, 520 (1983).

7) a) T. Wakamiya, K. Shimbo, T. Shiba, K. Nakajima, M. Neya, and K. Okawa, *Bull. Chem. Soc. Jpn.*, **55**, 3878

(1982); b) T. Wakamiya, K. Fukase, K. Shimbo, and T. Shiba, *Bull. Chem. Soc. Jpn.*, **56**, 1559 (1983).

8) The use of thioacetic acid did not give a desirable result.

9) I. Photaki, I. Samouilidis, S. Caranikas, and L. Zervas, *J. Chem. Soc. Perkin I*, **1979**, 2599.

10) Complete removal of water from the oily product was extremely difficult because of very hygroscopic property.

11) a) E. Fischer and K. Raske, *Ber.*, **40**, 3717 (1907); b) G. B. Brown and V. du Vigneaud, *J. Biol. Chem.*, **137**, 611 (1940).

Magnetic Properties of Conjugated Systems. Bond Orders and Imaginary Bond-Bond Polarizabilities of "Acyclic" Bonds†

Noriyuki MIZOGUCHI
Department of Physics, Meiji College of Pharmacy, Nozawa, Setagaya-ku, Tokyo 154
(Received June 28, 1984)

Within the London-McWeeny formalism of the π-electron magnetic properties, the contribution of each bond in a conjugated system to the London susceptibility is studied. By using the relations between the bond orders P_{rs} and the imaginary bond-bond polarizabilities $\bar{\pi}_{(rs)(tu)}$ proved in a previous paper, it is shown that two equations, $P_{rs}+\beta\bar{\pi}_{(rs)(rs)}=0$ and $\bar{\pi}_{(rs)(vw)}=0$, hold for the "acyclic" bond r-s in a conjugated system. The equations show that no bonds in acyclic conjugated systems or in acyclic fragments of cyclic systems make any contributions to the London susceptibilities (or to the ring currents) of the systems. On the basis of these equations, the expression for the London susceptibility is simplified. Moreover, we will discuss the relationships between the above equations and some consequences of McWeeny's unitary transformation.

In 1937 London first laid the foundations of the quantum mechanical theory of π-electron magnetic properties using the Hückel molecular orbital method.[1-4] The π-electron contribution to the magnetic susceptibility of a conjugated system is called the London susceptibility.[5] Pople[6] and McWeeny[7] modified London's method to estimate the proton NMR shielding constants.

It is well-known that, within the London formalism, an external, uniform, magnetic field perpendicular to the molecular plane has no effect on noncyclic conjugated systems.[1-4,8] By using graph theory,[9] Aihara[10] reexamined Pople's approach and showed that the London susceptibility of a polycyclic conjugated molecule can be expressed as a sum of the circuit susceptibilities over all the circuits found in the system.[11] Recently, using Coulson's integral formula,[12] we have proved the circuit rule for the magnetic susceptibility, which states that the circuit susceptibility for the $(4n+2)$-membered circuit is diamagnetic, while that for the $(4n)$-membered circuit is paramagnetic.[11]

In McWeeny's perturbation approach,[3,7] the London susceptibility is expressed in terms of the bond order[12] and the imaginary bond-bond polarizability.[7] Recently we[13] ourselves have proved several general relations between bond orders and imaginary bond-bond polarizabilities, which reflect the local topological nature of the bonds considered, *i.e.*, the mode of branching.

As has been mentioned above, the relationship between the magnetic properties and the structure has been extensively studied. However, it has not been known how each bond in acyclic conjugated systems and in acyclic fragments of cyclic systems contributes to the London susceptibilities. In the present paper, by the use of the relations between the bond orders and the imaginary bond-bond polarizabilities we will reexamine the properties of the bond orders and imaginary bond-bond polarizabilities for the bonds in those systems. The physical meanings of the equations obtained will also be discussed. Moreover, we will study the relationships between the equations thus obtained and some consequences of McWeeny's unitary transformation.

London Susceptibility and Relations between Bond Orders and Imaginary Bond-Bond Polarizabilities

Following London,[1-4] the Hückel matrix elements of a planar conjugated hydrocarbon, in the presence of an external, uniform, magnetic field, $\boldsymbol{H}$, perpendicular to the molecular plane, are given by:

$$h_{rr} = \alpha, \tag{1a}$$

$$h_{rs}\begin{cases} = \beta\exp(iw_{rs}) & \text{if atoms } r \text{ and } s \text{ are adjacent,} \\ = 0 & \text{otherwise,} \end{cases} \tag{1b}$$

where α is the Hükel Coulomb integral, where β is the Hückel resonance integral in the absence of the field, which is assumed to be equal for all the bonds in the molecule, and where w_{rs} is given by:

$$w_{rs} = (e/\hbar c)\, S_{rs} H = -\, w_{sr}. \tag{2}$$

In Eq. 2, e, $\hbar$, and c are the usual fundamental constants with these symbols, S_{rs} is the signed area of the triangle formed by an arbitrary origin and the bond r-s, and H is the field strength. With respect to the zero-field atomic orbital, the matrix elements of the perturbation due to the magnetic field are:

$$\Delta_{rs} = h_{rs} - \beta = \beta(iw_{rs} - \frac{1}{2} w_{rs}^2 + \cdots\cdots). \tag{3}$$

In McWeeny's notation[7] the partial London susceptibility for the J-th MO, χ_J, is given by:

$$\chi_J = 2\beta\left(\frac{e}{\hbar c}\right)^2 \left\{\sum_{(rs)} p_{J,rs} S_{rs}^2 + \sum_{(rs)}\sum_{(tu)} \beta\bar{\pi}_{J,(rs)(tu)} S_{rs} S_{tu}\right\}, \tag{4}$$

where the sum runs over all the bonds in the molecule and where $P_{J,rs}$ and $\bar{\pi}_{J,(rs)(tu)}$ are, respectively, the partial Coulson bond order of the bond r-s[14] and the partial imaginary bond-bond polarizability between the bonds r-s and t-u for the J-th MO:[15]

$$P_{J,rs} = C_{rJ}\, C_{sJ}, \tag{5}$$

and:

†This is Part II in a series in which Ref. 13 is Part I.

$$\pi_{J,(rs)(tu)} = \sum_{K(\neq J)} \frac{(C_{rJ}C_{sK} - C_{sJ}C_{rK})(C_{tK}C_{uJ} - C_{uK}C_{tJ})}{(X_J - X_K)\beta} \quad (6)$$

where X_J and C_{rJ} are, respectively, the orbital energy (in units of β) and the coefficient of the r-th AO of the J-th MO in the absence of the magnetic field and where the sum runs over all the unperturbed molecular orbitals except the J-th MO.

We have proved several relations between partial bond orders and partial imaginary bond-bond polarizabilities for each nondegenerate MO for the bonds in the two subgraphs, G1 and G2, shown in Fig. 1:[13]

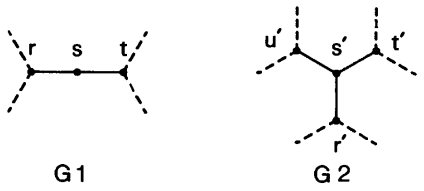

Fig. 1. Subgraphs G1 and G2.

for the bonds in the subgraph G1:

A' $\pi_{J,(vw)(rs)} = \pi_{J,(vw)(st)}$,

B' $P_{J,rs} + \beta\pi_{J,(rs)(rs)} = P_{J,st} + \beta\pi_{J,(st)(st)}$,

C' $P_{J,rs} + \beta\pi_{J,(rs)(rs)} = \beta\pi_{J,(rs)(st)}$,

for the bonds in the subgraph G2:

D' $\pi_{J,(vw)(r's')} = \pi_{J,(vw)(s't')} + \pi_{J,(vw)(s'u')}$,

E' $P_{J,r's'} + \beta\pi_{J,(r's')(r's')} = \beta\pi_{J,(r's')(s't')} + \beta\pi_{J,(r's')(s'u')}$,

where v-w is an arbitrary bond. The partial imaginary bond-bond polarizabilities in the relations A' and D' must be mutual.

Bond Orders and Imaginary Bond-Bond Polarizabilities of "Acyclic" Bonds

A bond (edge) in a molecular graph may be classified into one of two types, an "acyclic" bond or a "cyclic" bond. They are defined as follows: The deletion of a "cyclic" bond from a molecular graph reduces the number of rings in the molecular graph, but the deletion of an "acyclic" bond does not. For example, the bonds 1-7, 2-8, 3-9, 4-10, 5-11, and 6-12 in the [6]-radialene molecular graph G3 shown in Fig. 2 are "acyclic" because the deletion of any one of these bonds does not reduce the number of rings in G3. All the other bonds in G3 are "cyclic." Edge 1-7 in the biphenyl molecular graph G4 in Fig. 2 is "acyclic." Of course, all the bonds in an acyclic system are "acyclic."

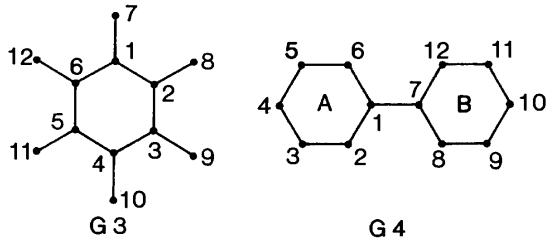

Fig. 2. Molecular graphs G3 and G4.

"Acyclic" and "cyclic" bonds play drastically different roles in the calculations of the magnetic properties of conjugated molecules. For the "acyclic" bond r-s we have the following equations:

$$\pi_{J,(rs)(vw)} = 0, \quad (7)$$

$$\pi_{(rs)(vw)} = 0, \quad (8)$$

$$P_{J,rs} + \beta\pi_{J,(rs)(rs)} = 0, \quad (9)$$

and:

$$P_{rs} + \beta\pi_{(rs)(rs)} = 0, \quad (10)$$

where v-w is an arbitrary bond except in the case of the bond r-s. Here, it should be noted that two quantities, $P_{J,rs}$ and $\pi_{J,(rs)(rs)}$, are not zero for any bonds, and that the (total) self imaginary bond-bond polarizabilities of bonds in an arbitrary closed-shell system are positive:[13]

$$\pi_{(rs)(rs)} > 0. \quad (11)$$

By virtue of the relations A'—E', Eqs. 7—10 will be illustrated for several typical systems. For the sake of simplicity, only Eqs. 7 and 9 will be discussed in detail because Eqs. 8 and 10 can be easily derived from Eqs. 7 and 9 respectively.

A) It will be convenient for the later discussions to prove initially Eqs. 7 and 9 for a terminal "acyclic" bond, a-b, shown in Fig. 3. By substituting the vari-

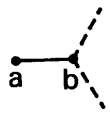

Fig. 3. Terminal "acyclic" bond a—b.

ational constraint for the carbon atom (vertex) a:

$$-X_J C_{aJ} + C_{bJ} = 0, \quad (12)$$

into Eq. 7, and with some manipulations, the partial mutual imaginary bond-bond polarizability between the bond a-b and an arbitrary bond, v-w, is rewritten as follows:

$$\beta\pi_{J,(ab)(vw)} = \sum_{K\neq J} \{C_{aJ}C_{aK}(-C_{vK}C_{wJ} + C_{wK}C_{vJ})\}$$

$$= \sum_{K} \{C_{aJ}C_{aK}(-C_{vK}C_{wJ} + C_{wK}C_{vJ})\}, \quad (13)$$

where the sum $\sum_{K(\neq J)}$ has been replaced by the sum $\sum_{K}$. Since from the orthonomalities of AO's and MO's, we have[16]

$$\sum_{J} C_{rJ}C_{sJ} = \delta_{rs}, \quad (14)$$

the right-hand side of Eq. 13 vanishes. Hence, it follows that

$$\pi_{J,(ab)(vw)} = 0. \quad (15)$$

In a similar way, we can show that

$$\beta\pi_{J,(ab)(ab)} = \sum_{K} \{C_{aJ}C_{aK}(-C_{aK}C_{bJ} + C_{bK}C_{aJ})\}$$

$$= -C_{aJ}C_{bJ}. \quad (16)$$

Thus, we have proved that

$$P_{J,ab} + \beta\pi_{J,(ab)(ab)} = 0. \tag{17}$$

Therefore, it has been shown that Eqs. 7 and 9 are valid for the bond, *a-b*, shown in Fig. 3.

B) Next, two acyclic systems will be discussed. First, let us take linear polyene with N carbon atoms G5 in Fig. 4. We have already shown in the preceding section

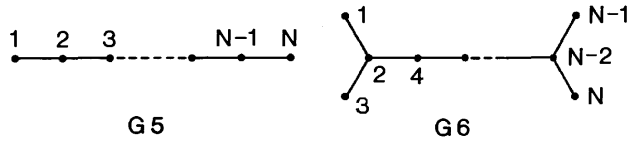

Fig. 4. Molecular graphs G5 and G6.

that Eqs. 7 and 9 hold for the bond, 1-2, in G5 because the bond corresponds to the bond, *a-b*, in Fig. 3. By only applying the relations A′ and B′ and Eqs. 15 and 17 to all the other bonds in G5, we easily obtain:

$$\pi_{J,(j\,j+1)(k\,k+1)} = 0, \tag{18}$$

and:

$$P_{J,j\,j+1} + \beta\pi_{J,(j\,j+1)(j\,j+1)} = 0, \tag{19}$$

where j, k=1, 2,···, N-1 and $j \neq k$.

Second, consider the molecular graph G6 shown in Fig. 4. We have already proved for the terminal bonds, 1-2, 2-3, (N-2)—(N-1), and (N-2)—N, in G6 in the previous section:

$$\pi_{J,(rs)(vw)} = 0, \tag{20}$$

and:

$$P_{J,rs} + \beta\pi_{J,(rs)(rs)} = 0, \tag{21}$$

where r-s stands for one of the bonds 1-2, 2-3, (N-2)—(N-1), and (N-2)—N and where v-w is an arbitrary bond. The application of the relation D′ to the bond 2-4 gives:

$$\pi_{J,(12)(vw)} = \pi_{J,(23)(vw)} + \pi_{J,(24)(vw)}. \tag{22}$$

From Eqs. 20 and 22, it follows that

$$\pi_{J,(24)(vw)} = 0. \tag{23}$$

From the relation E′ we obtain:

$$P_{J,24} + \beta\pi_{J,(24)(24)} = \beta\pi_{J,(24)(12)} + \beta\pi_{J,(24)(32)}. \tag{24}$$

Because of Eq. 20, the two terms on the right-hand side of Eq. 24 vanish, and so:

$$P_{J,24} + \beta\pi_{J,(24)(24)} = 0. \tag{25}$$

Further, by applying the relation A′ and Eq. 23 (and the relation B′ and Eq. 25) to the other bonds in G6, we can easily show that Eq. 7 (and Eq. 9) holds for all the bonds in G6.

C) Acyclic fragments in cyclic systems will be discussed in this section. The molecular graph of the biphenyl G4 in Fig. 2 shows one "acyclic" bond, 1-7. The relation E′ gives:

$$P_{J,12} + \beta\pi_{J,(12)(12)} = \beta\pi_{J,(12)(71)} + \beta\pi_{J,(12)(61)}. \tag{26}$$

From the relation C′ we obtain:

$$P_{J,12} + \beta\pi_{J,(12)(12)} = \beta\pi_{J,(12)(61)}. \tag{27}$$

A comparison of Eq. 26 with Eq. 27 gives:

$$\pi_{J,(12)(71)} = 0. \tag{28}$$

By applying the relation A′ to other bonds in the ring A and by using Eq. 28, we obtain:

$$\pi_{J,(17)(vw)} = 0, \tag{29}$$

where v-w is an arbitrary bond in the ring A of G4. In the same way, one can show that Eq. 29 holds for any bonds in the ring B.

From the relation E′, the following equation is obtained:

$$P_{J,17} + \beta\pi_{J,(17)(17)} = \beta\pi_{J,(17)(21)} + \beta\pi_{J,(17)(61)}. \tag{30}$$

The relation A′ gives:

$$\pi_{J,(17)(12)} = \pi_{J,(17)(61)} = -\pi_{J,(17)(21)}, \tag{31}$$

where we have used the following equation:[13]

$$\pi_{J,(rs)(tu)} = -\pi_{J,(sr)(tu)} = -\pi_{J,(rs)(ut)}. \tag{32}$$

From Eqs. 30 and 31, we obtain:

$$P_{J,17} + \beta\pi_{J,(17)(17)} = 0. \tag{33}$$

Accordingly, it has been shown that Eqs. 7 and 9 hold for the "acyclic" bond, 1-7, in G4.

The last example is the molecular graph with an acyclic fragment, G7, shown in Fig. 5. It seems evident

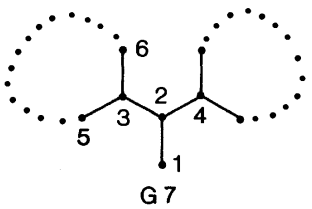

Fig. 5. Molecular graph with acyclic fragment G7.

that Eqs. 7 and 9 are valid for the bond 1-2 in G7. For the bond 2-3, the relation D′ gives:

$$\pi_{J,(23)(vw)} = \pi_{J,(35)(vw)} + \pi_{J,(36)(vw)}, \tag{34}$$

where v-w is an arbitrary bond. From Eq. 32, we obtain:

$$\pi_{J,(36)(vw)} = -\pi_{J,(63)(vw)}, \tag{35}$$

and from the relation A′:

$$\pi_{J,(35)(vw)} = \pi_{J,(63)(vw)}. \tag{36}$$

Equations 35 and 36 show that the right-hand side of Eq. 34 vanishes:

$$\pi_{J,(23)(vw)} = 0. \tag{37}$$

Similarly, it is shown that

$$\pi_{J,(24)(vw)} = 0. \tag{38}$$

From the relation E′, the following equation is obtained:

$$P_{J,23} + \beta\pi_{J,(23)(23)} = \beta\pi_{J,(32)(53)} + \beta\pi_{J,(32)(63)}. \tag{39}$$

Because of Eq. 37, the right-hand side of Eq. 39 vanishes, hence,

$$P_{J,23} + \beta\pi_{J,(23)(23)} = 0. \quad (40)$$

In the same manner, one can show that Eq. 9 is valid for the bond 2-4. Thus, we have shown that Eqs. 7 and 9 are valid for all the "acyclic" bonds in G7.

The above examples make it obvious that Eqs. 7 and 9 hold for any "acyclic" bonds in an arbitrary system. It should be noted that Eqs. 7 and 9 are not valid for degenerate MO's. However, it can easily be shown that Eqs. 8 and 10 hold also for bonds in closed-shell molecules, even with degenerate energy levels, provided that the (total) imaginary bond-bond polarizabilities, not in the form of Eq. 41, but in that of Eq. 42, are used:[13]

$$\bar{\pi}_{(rs)(tu)} = \sum_J \sum_{(K\neq J)} g_J \frac{(C_{rJ}C_{sK} - C_{sJ}C_{rK})(C_{tK}C_{uJ} - C_{uK}C_{tJ})}{(X_J - X_K)\beta}, \quad (41)$$

$$\bar{\pi}_{(rs)(tu)} = 2\sum_J^{\text{occ}} \sum_K^{\text{unocc}} \frac{(C_{rJ}C_{sK} - C_{sJ}C_{rK})(C_{tK}C_{uJ} - C_{uK}C_{tJ})}{(X_J - X_K)\beta}, \quad (42)$$

where g_J is the occupation number of the J-th MO and where $\sum^{\text{occ}}$ and $\sum^{\text{unocc}}$, respectively, run over occupied and unoccupied MO's.

Simplified Expression for London Susceptibility

The London susceptibility has usually been expressed in the form of Eq. 4.[3,7] The first term on the right-hand side of Eq. 4 is a first-order correction of the second term in Δ_{rs} (see Eq. 3), namely, of $-(\beta/2)\,w_{rs}^2$ (second-order with respect to the field strength, H), while the second term is a second-order correction of the first term in Δ_{rs}, namely, of i βw_{rs} (first- order with respect to H). However, a partial bond order and a partial self imaginary bond-bond polarizability always appear in the form of the sum of the two quantities, *i.e.*, in the form of $P_{J,rs}+\beta\bar{\pi}_{J,(rs)(rs)}$ in the relations B′, C′, and E′ and in Eqs. 9 and 10. When we consider the contributions of individual bonds in a molecule to its London susceptibility, it may, therefore, be appropriate to rewrite χ_J in the following form:

$$\chi_J = 2\beta\left(\frac{e}{\hbar c}\right)^2\left[\left\{\sum_{(rs)}(P_{J,rs}+\beta\pi_{J,(rs)(rs)})\right)S_{rs}^2\right\} + \sum_{(rs)\neq(tu)}\sum \beta\pi_{J,(rs)(tu)}S_{rs}S_{tu}\Big]. \quad (43)$$

Then, each term in Eq. 43 may be interpreted as follows: each term in the first sum on the right-hand side of Eq. 43, namely, $P_{J,rs}+\beta\bar{\pi}_{J,(rs)(rs)}$, is associated with the π- electron energy change due to an alternation in the resonance integral of the bond r-s itself, while each term in the second sum, namely, the mutual imaginary bond-bond polarizability $\bar{\pi}_{J,(rs)(tu)}$, is associated with that due to the changes in the resonance integrals of the bonds r-s and t-u.

Now we can clarify the physical meaning of Eqs. 7—10. The equations mean that no "acyclic" bonds make any contributions to the London susceptibility. Therefore, it may be more appropriate to rewrite the expression for χ_J in this simplified form:

$$\chi_J = 2\beta\left(\frac{e}{\hbar c}\right)^2\left[\sum_{(rs)}^{\text{"cyclic"}}\left\{(P_{J,rs}+\beta\pi_{J,(rs)(rs)})S_{rs}^2\right\} + \sum_{(rs)\neq(tu)}^{\text{"cyclic"}}\sum_{(tu)}^{\text{"cyclic"}} \beta\pi_{J,(rs)(tu)}S_{rs}S_{tu}\right], \quad (44)$$

where the sum runs over only all the "cyclic" bonds in the molecule. The above expression reduces the number of bonds which must be calculated. In the case of [6]-radialene, for example, the number is reduced to half. The set of Eqs. 7—10 provides an alternative way of explaining the well-known fact that the London susceptibilities of any acyclic conjugated systems are zero.

It has been pointed out that the magnitude of the London susceptibility is partially quenched if bond alternation occurs.[15,17] We can prove that the equations corresponding to the relations A′—E′ and to Eqs. 7—10 hold for bonds of molecules with bond alternation.[18]

Ring Current and Equations 7—10

The expression for the ring current[2,19,20] can be derived more easily from the expression for the partial London susceptibility in the form of Eq. 44 than from that in the form of Eq. 4 without the use of the "current-density" formalism.[21-23]

Assume, as in the usual way,[2] that the London susceptibility arises from an induced circulation of π-electrons along the framework of carbon atoms in a conjugated molecule (ring current). Further, the induced ring current may formally be considered as a sum of individual "bond currents" associated with each bond in the molecule.[20,23,24] Then, the "bond current" intensity of the bond r-s, J_{rs}, is given by:[20]

$$J_{rs} = (P_{rs} + \beta\pi_{(rs)(rs)})S_{rs} + \sum_{(tu)}\beta\pi_{(rs)(tu)}S_{tu}, \quad (45)$$

where the sum runs over all the bonds except the bond r-s. The above equation shows that the "bond current" of the bond r-s arises from the contributions of two types; one is that due to the first term on the right-hand side of Eq. 45, *i.e.*, $P_{rs}+\beta\bar{\pi}_{(rs)(rs)}$, which is associated with an alternation in the resonance integral of the bond r-s itself, while the other is that due to the mutual imaginary bond-bond polarizability in the second term, $\bar{\pi}_{(rs)(tu)}$, which is associated with a change in the resonance integral of the other bond, t-u.

Equations 7—10 indicate that, if the bond r-s is "acyclic," then the change in the resonance integral, due to the applied field, of the bond r-s (see Eq. 3) has no effect on the induction of the "bond current" of the bond r-s itself or on the induction of the "bond current" of any of the other bonds in the system. As a result, we may reasonably conclude that, when there are no rings

in a system, the (ring) current does not arise. As in the case of Eq. 44, it is sufficient also for Eq. 45 to sum over only the "cyclic" bonds in the molecule.

The "bond current" is entirely equivalent to the concept of the "ring current" as long as the "bond current" is conserved. The set of the relations A'—E' ensures that the "bond current" intensity given by Eq. 45 is conserved.[25] In this connection, it is interesting to notice that the relations A'—E' show that the two quantities, $P_{J,rs}+\beta\bar{\pi}_{J,(rs)(rs)}$ and $\bar{\pi}_{J,(rs)(tu)}$, obey Kirchhoff's law.[13]

The Relationship between Eqs. 7—10 and Some Consequences of McWeeny's Unitary Transformation

McWeeny has shown that, by virtue of a suitable unitary transformation, the sums in Eq. 44 may be reduced to the sums of one bond in each ring.[7] Gayoso and Boucekkine[26] have proposed a further unitary transformation which generalizes that devised by McWeeny. In the present paper, the transformation devised by Gayoso and Boucekkine will be used and called simply "McWeeny's unitary transformation." It seems that it will be significant and interesting to discuss the relationship between Eqs. 7—10 and some consequences of McWeeny's unitary transformation for "acyclic" bonds.

The matrix of the unitary transformation, $\boldsymbol{U}$, is a diagonal matrix, whose elements are given by:

$$U_{11} = 1,\ U_{rr} = (a_{1j}a_{jk}\cdots\cdots a_{tr})^*, \tag{46}$$

where the asterisk stands for the complex conjugate and where

$$a_{rs} = h_{rs}/\beta = \exp(iw_{rs}), \tag{47}$$

and where $(1j)(jk)\cdots(tr)$ is a sequence of edges (bonds) representing the shortest chain between the vertex (atom) labelled 1 and that labelled r in a chosen spanning tree of the original molecular graph. A tree which connects all the vertices of a graph, G, is called a spanning tree of G.[19,27] The bond which must be added to the particular spanning tree in order to reform the original graph, G, is called the "circuit-completing" bond.[7] Let $\bar{\boldsymbol{h}}$ be the transformed matrix of $\boldsymbol{h}$ due to $\boldsymbol{U}$:

$$\bar{\boldsymbol{h}} = \boldsymbol{U}^\dagger \boldsymbol{h}\, \boldsymbol{U}. \tag{48}$$

The non-zero elements, h_{rs}, corresponding to the "circuit-completing" bonds are transformed to the non-zero elements, $\bar{h}_{rs}$, while all the other non-zero elements, h_{rs}, are transformed to β.

Consider biphenyl again. Figure 6 shows a spanning tree, T, whose "circuit-completing" bonds are the bonds 1-6 and 7-8. The matrix elements of biphenyl are transformed as follows:

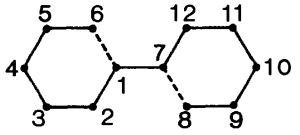

Fig. 6. Spanning tree of the biphenyl molecular graph T.

for the elements corresponding to all bonds except 1-6 and 7-8, for instance:

$$\begin{aligned}\bar{h}_{56} &= U_{55}^* h_{56} U_{66} \\ &= (a_{12}a_{23}a_{34}a_{45})h_{56}(a_{12}a_{23}a_{34}a_{45}a_{56})^* \\ &= \beta, \end{aligned} \tag{49-a}$$

$$\bar{h}_{17} = U_{11}^* h_{17} U_{77} = h_{17}(a_{17})^* = \beta, \tag{49-b}$$

for elements corresponding to the "circuit-completing" bonds 1-6 and 7-8:

$$\begin{aligned}\bar{h}_{16} &= U_{11}^* h_{16} U_{66} = h_{16}(a_{12}a_{23}a_{34}a_{45}a_{56})^* \\ &= \beta\exp\{-i(w_{12}+w_{23}+w_{34}+w_{45}+w_{56}+w_{61})\} \\ &= \beta\exp(-iw_{\mathrm{A}}), \end{aligned} \tag{49-c}$$

$$\bar{h}_{78} = \beta\exp(iw_{\mathrm{B}}). \tag{49-d}$$

In the above equations, we have defined for each ring:

$$w_{\mathrm{R}} = (e/\hbar c)S_{\mathrm{R}}H, \tag{50}$$

where S_{R} is the signed area of a ring, R, of G4. Accordingly, we have certainly found that all the non-zero elements of h_{rs} corresponding to all bonds except the "circuit-completing" bonds are transformed to β. The set of Eqs. 49 shows that all the perturbation due to the applied magnetic field can be thought of as being concentrated in only one bond (edge) of each ring (in this case, the bonds 1-6 and 7-8).[7,19] By virtue of the relations A'—E' we can also perform the "concentration of perturbation."[19]

The elements of $\boldsymbol{U}$ are dependent on the graph of a chosen spanning tree (see Eq. 46), but one can draw many spanning trees for one molecular graph.[19,27] However, the above example shows that, by the unitary transformation, the matrix elements corresponding to any "acyclic" bonds in an arbitrary system are transformed to β, irrespective of the choice of spanning tree. This means that an "acyclic" bond behaves as if the magnetic field was not applied. Therefore, it follows that all the non-zero Hückel Hamiltonian matrix elements of an acyclic system are changed to β. In other words, the Hückel Hamiltonian matrix of an acyclic conjugated system in the presence of the magnetic field is transformed to the field-free Hückel Hamiltonian matrix of the system by the unitary matrix.

Now it may be apparent that the consequences of the unitary transformation correspond to the fact that Eqs. 7—10 hold for "acyclic" bonds. However, it should be noted that there is a difference between Eqs. 7—10 and the consequences of the unitary transformation. Equations 7—10 show that, in the case of acyclic systems, the coefficient of each element of the perturbation matrix, Δ_{rs}, in Eq. 43 is zero, hence, the second-order energy change with respect to the field strength H is zero. On the other hand, the consequences due to the unitary transformation for acyclic systems mean that all the elements of the perturbation matrix, Δ_{rs}, for

the transformed Hamiltonian matrix, $\bar{h}$, are zero, and so the energy change due to the applied field is exactly zero. Of course, in our perturbation approach, the first-order energy change with respect to the field strength, H, vanishes for all arbitrary systems, even with rings.[3)]

References

1) F. London, *J. Phys. Radium*, **8**, 397 (1937).
2) L. Salem, "The Molecular Orbital Theory of Conjugated Systems," W. A. Benjamin, New York (1966), Chap. 4.
3) J. D. Memory, "Quantum Theory of Magnetic Resonance Parameters," McGraw-Hill, New York (1968), Chap. 6.
4) C. W. Haigh and R. B. Mallion, "Progress in Nuclear Magnetic Resonance Spectroscopy," Vol. 13, ed by J. W. Emsley, J. Feeney, and L. H. Sutctliffe, Pergamon, Oxford (1980), p. 303.
5) H. J. Dauben, Jr., J. D. Wilson, and J. L. Laity, *J. Am. Chem. Soc.*, **91**, 1991 (1969); "Nonbenzenoid Aromatics," Vol. 2, ed by J. P. Snyder, Academic Press, New York (1971), Chap. 3.
6) J. A. Pople, *Mol. Phys.*, **1**, 175 (1958).
7) R. McWeeny, *Mol. Phys.*, **1**, 311 (1958).
8) J. A. Pople, *J. Chem. Phys.*, **37**, 53 (1962).
9) A. Graovac, I. Gutman, and N. Trinajstić, "Topological Approach to the Chemistry of Conjugated Molecules," Springer-Verlag, Berlin (1977), Chap. 2.
10) J. Aihara, *J. Am. Chem. Soc.*, **101**, 5913 (1979); **103**, 5704 (1981). Aihara used the term "ring susceptibility" in these papers. However, as has been mentioned in Ref. 11, the term "circuit susceptibility" is more appropriate than "ring susceptibility" in the discussion of the London susceptibility.
11) N. Mizoguchi, *Chem. Phys. Lett.*, **106**, 451 (1984).
12) C. A. Coulson and H. C. Longuet-Higgins, *Proc. R. Soc. London, Ser. A*, **191**, 39 (1947); **192**, 16 (1947).
13) N. Mizoguchi, *Bull. Chem. Soc. Jpn.*, **56**, 1588 (1983).
14) Y. Ooshika, *J. Phys. Soc. Jpn.*, **12**, 1296 (1957).
15) T. Nakajima and S. Kohda, *Bull. Chem. Soc. Jpn.*, **39**, 804 (1966).
16) M. Hida, "Yuki Ryosi Kagaku Nyumon, Kisohen," Gakkai Shuppan Senta, Tokyo (1981), Chap. 4.
17) H. C. Longuet-Higgins and L. Salem, *Proc. R. Soc. London Ser. A*, **257**, 445 (1960); J. A. Pople and K. G. Untch, *J. Am. Chem. Soc.*, **88**, 4811 (1966).
18) N. Mizoguchi, to be discussed elsewhere.
19) R. B. Mallion, *Proc. R. Soc. London, Ser. A*, **341**, 429 (1975).
20) R. B. Mallion, *Mol. Phys.*, **25**, 1415 (1973).
21) J. A. Pople, *Proc. R. Soc. A*, **239**, 5416 (1958).
22) C. P. Slichter, "Principles of Magnetic Resonance," Harper and Row, New York (1963), Chap. 4.
23) A. T. Amos and H. G. Ff. Roberts, *Mol. Phys.*, **20**, 1073 (1971).
24) Y. B. Vysotsky, *Theoret. Chim. Acta.*, **159**, 467 (1981).
25) N. Mizoguchi, to be discussed elsewhere.
26) J. Gayoso and A. Boucekkine, *C. R. Acad. Sc.* Paris, C, **272**, 184 (1971).
27) R. B. Mallion, *Chem. Phys. Lett.*, **36**, 170 (1975).

 © 1985 The Chemical Society of Japan Bull. Chem. Soc. Jpn., 58, 546—549 (1985) [Vol. 58, No. 2

Calorimetric Studies of the Interaction between the Lecithin and Copolymers of L-Lysine and L-Leucine

Masayuki NAKAGAKI* and Emiko OKAMURA
Faculty of Pharmaceutical Sciences, Kyoto University, Yoshida-Shimoadachicho, Sakyo-ku, Kyoto 606
(Received June 29, 1984)

The interaction between the dimyristoyl phosphatidylcholine (DMPC) bilayers and aqueous copolymers of L-lysine and L-leucine was investigated by means of differential scanning calorimetry. None of the copolymers had any effects on the transition temperature of DMPC, irrespective of the lysine/leucine ratio, although the pretransition peak disappeared. The transition enthalpy did not appreciably change upon the addition of copolymers if the leucine fraction was small (<0.25), but it remarkably decreased upon the addition of a copolymer with a large leucine content (>0.3). The latter case suggests the penetration of copolymers into the hydrophobic region (hydrocarbon-chain region) of DMPC as a result of the hydrophobic effect of leucine residues. On the contrary, copolymers of a small leucine content can penetrate at most into the polar region of DMPC because of the electric charge derived from lysine residues, indicating the effect of the copolymer composition on the penetrability of a copolymer into lipid layers.

The interaction between proteins or polypeptides and lipid membranes has been studied by means of various kinds of physicochemical techniques. It is considered that calorimetric studies are useful in investigating the effect of these proteins or polypeptides on the state of lipid membranes, particularly on the fluidity of hydrocarbon chains or on the phase transition of these membranes. Many calorimetric studies have thus been carried out of the systems of various lipids and proteins or polypeptides,[1-6] and different effects of proteins on the lipid phase transition have been proposed.[7]

The surface pressures of lecithin monolayers spread on lysine-leucine copolymer solutions were measured, and the penetration of these copolymers into lecithin monolayers was investigated in our previous study.[8] It was found, in that study, that the extent of penetration was dependent on the copolymer composition: The penetration was less when the leucine fraction in the copolymer, X_{Leu}, was smaller than 0.25, while it was remarkable at a X_{Leu} value larger than 0.3. Under our experimental conditions, however, all the copolymers are randomly coiled, and the conformational changes are not induced in the bulk solution.[8] Therefore, some kinds of substantial changes in lipid membranes should be regarded as possible reasons for the above penetration.

In the present study, differential scanning calorimetry (DSC) has been carried out in order to investigate the interaction between these copolymers and lecithin bilayers, and to discuss the characteristic properties of lecithin-copolymer interaction in some detail.

Experimental

Materials. As lecithin, L-α-dimyristoyl phosphatidylcholine (DMPC) from the Sigma Chemical Company was used without further purification. The random copolymers of lysine and leucine were the same as those previously used.[8] These copolymers were dissolved in redistilled water.

Differential Scanning Calorimetry. The differential scanning calorimetry was carried out on a Shimadzu DSC-30 calorimeter. The samples were prepared as follows: A 2—5 mg portion of the lipid was weighed in an aluminium sample pan. A copolymer solution of known concentration (0—20.3 mg/0.1 ml) was then added by capillary. After the lipid and the solution had been mixed with a pin at 30—40 °C and dispersed uniformly, the pan was hermetically sealed. The samples were heated and cooled at a constant rate of 5 °C/min. All scans were repeated for at least three cycles in order to confirm that the observed transition profile was reproducible. The water/lipid ratio was high enough to form multibilayers or lamellar phases of DMPC. Palmitic acid (mp 62.65 °C; enthalpy of melting, 10.0 kcal mol^{-1}) was used to standardize the apparatus for a quantitative heat determination. The peak areas were measured by weighing paper cutouts of the peaks.

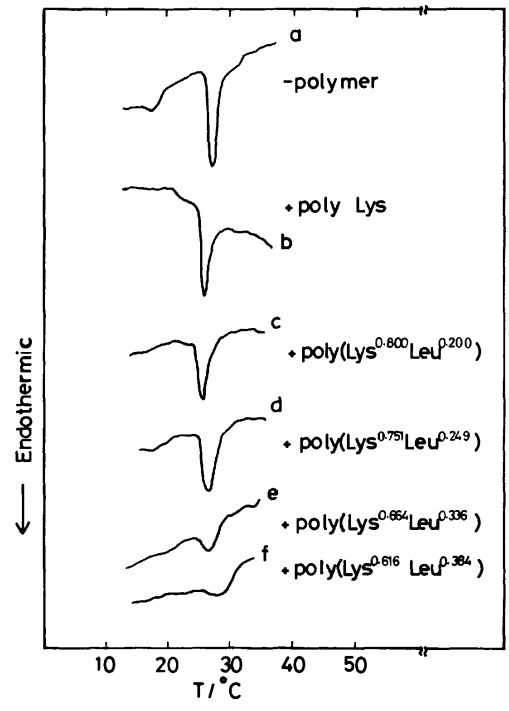

Fig. 1. DSC thermograms of DMPC dispersed in aqueous polymer solution.
(a): Without polymer, (b): with poly Lys, (c): with poly($Lys^{0.800}Leu^{0.200}$) (d): with poly($Lys^{0.751}Leu^{0.249}$) (e): with poly($Lys^{0.664}Leu^{0.336}$) and (f): with poly-($Lys^{0.616}Leu^{0.384}$). Heating rate: 5 °C/min.

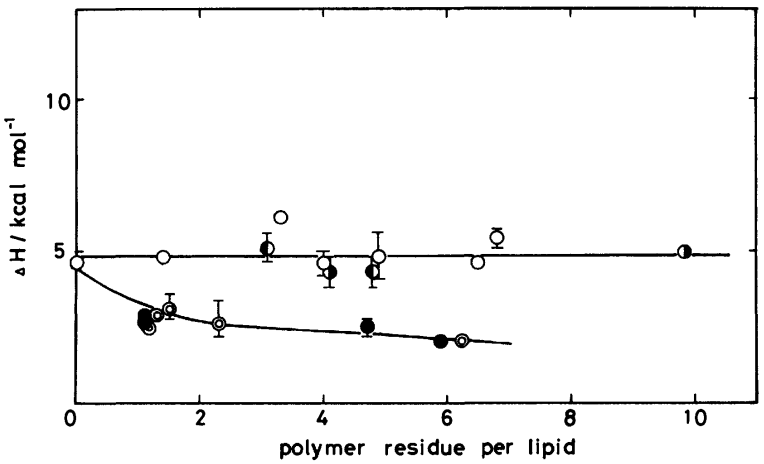

Fig. 2. The dependence of the calorimetric enthalpy of transition (ΔH) of DMPC on the polymer content in DMPC-polymer system: poly Lys (○), poly($Lys^{0.800}Leu^{0.200}$) (◑), poly($Lys^{0.751}Leu^{0.249}$) (◐) poly($Lys^{0.664}Leu^{0.336}$) (●), and poly-($Lys^{0.616}Leu^{0.384}$) (◎).

Results and Discussion

DSC Curves of DMPC Multilayers in Copolymer Solutions. Figure 1 shows the DSC curves upon the heating of DMPC dispersed in water containing various copolymers. It is known that phospholipids dispersed in excess water form lamellar phases.[9] The heating curve accompanied by the gel-to-liquid crystalline transition of pure DMPC is shown in Fig. 1-(a); it indicates that the main transition is at 24°C, and the pretransition, at 15°C. The calculated value of the calorimetric enthalpy change, ΔH, was 4.6 kcal mol^{-1}. Figures 1-(b)—(f) give the DSC heating curves of DMPC dispersed in aqueous copolymer solutions of various lysine-leucine ratios. The copolymer concentration was 10 mg/0.1 ml. In each case, the pretransition peak disappeared upon the addition of a copolymer. However, the transition temperature (the onset of main transition), T_c, did not change.

Calorimetric Enthalpy Change Accompanied by Phase Transition. The calorimetric enthalpy change, ΔH, accompanied by the gel-to-liquid crystalline transition of DMPC, is calculated from the peak area, and the values are plotted against the polymer residue/lipid ratio in Fig. 2. In the case of polylysine or the copolymers containing a small leucine fraction (<0.25), the ΔH values did not appreciably change compared with the case without copolymers (pure DMPC alone), irrespective of the value of the polymer/lipid ratio. On the other hand, the ΔH values are decreased by the addition of copolymers with large leucine fraction (>0.3). The values of ΔH are decreased with an increase in the polymer/lipid ratio and asymptotically converge, similarly in the case of the lecithin-gramicidin A system previously reported.[10]

The Effect of the Copolymer Composition. The dependencies of the transition temperature (T_c) and the enthalpy change (ΔH) of DMPC on the copolymer composition were established. The results when the polymer residue/lipid ratio is 5 are shown in Fig. 3. A similar tendency was found in the case of other polymer residue/lipid ratios (not shown). As is shown in Fig. 3-(a), the transition temperature was almost constant and was not appreciably different from that of pure DMPC (24°C), irrespective of the copolymer composition. The values of ΔH were, however, dependent on the copolymer composition: (1) if the leucine fraction (X_{Leu}) was smaller than 0.25, the ΔH values were almost constant (4.3—4.8 kcal mol^{-1}) and not appreciably different from that of pure DMPC (4.6 kcal mol^{-1}), irrespective of the composition of the added copolymers, and (2) in the cases of X_{Leu} values larger than 0.34, the ΔH's were decreased remarkably to 2.3—2.5 kcal mol^{-1}.

According to the differential scanning calorimetry studied by Susi *et al.*,[11] T_c is increased and ΔH is

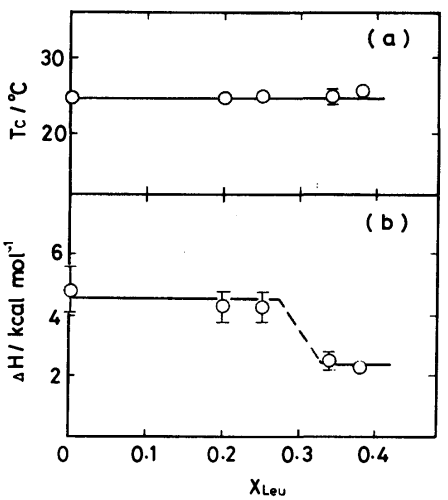

Fig. 3. The dependence of (a) the transition temperature (T_c) and (b) the enthalpy of transition (ΔH) of DMPC, on the leucine fraction of copolymers (X_{Leu}), at the polymer residue/lipid ratio of 5.

decreased in the case of polylysine-DMPC liposomal systems. This seems to contradict our present results. However, this apparent contradiction may be ascribed to the difference in experimental conditions, such as the method of preparation or the polymer/lipid ratio. Under the present conditions, no appreciable effects on T_c and ΔH were observed upon the addition of polylysine except for the disappearance of the pretransition, while the ΔH values were decreased by the addition of copolymers with a large leucine fraction, suggesting the effect of the leucine fraction of the copolymer on the membrane behavior.

The Mechanism of the Interaction between Lecithin and Lysine-Leucine Copolymers. The enthalpy change in the lecithin bilayer membrane accompanied by a phase transition, ΔH, was dependent on the leucine fraction of the copolymer, X_{Leu}, as has been described above. Further, the ΔH values are remarkably decreased around a X_{Leu} value of 0.3, which corresponds to the region with a sharp increase in the surface pressure of a lecithin monolayer upon the addition of copolymers.[8] On the other hand, copolymers had no effects on the transition temperature of the lecithin. It is, therefore, ascertained that the remarkable surface pressure increase of a lecithin monolayer in the presence of copolymers[8] was not due to the conformational change of copolymers.

Papahadjopoulos *et al.* have suggested three categories of protein-lipid interactions according to the correlation in calorimetric studies between the membrane permeability and the monolayer-area expansion.[7] Our results for the lysine-leucine copolymers will be discussed in comparison with their suggestion, and a plausible mechanism for the interaction between lecithin and lysine-leucine copolymers will be considered.

First, the interaction between lecithin and copolymers with a leucine fraction smaller than 0.25 may correspond to the Group 1 interaction in Ref. 7. According to the Papahadjopoulos postulate, no effects on monolayer expansion have been observed at a high value of the initial surface pressure (25 mN m^{-1}). In our results, a small increase in the area per molecule was observed in the low-surface-pressure region, while the extent of the increase becomes smaller at a higher surface pressure. Further, as has been described in Ref. 7, the enthalpy change of the transition, ΔH, of neutral phospholipids such as lecithin did not appreciably change; this also coincides with our present result. According to the results of Papahadjopoulos *et al.*,[7] this interaction is ascribable to the binding of the protein to the surface of lipid bilayers, without any penetration into the hydrocarbon region.

On the other hand, the interaction between lecithin and copolymers of a leucine fraction larger than 0.34 may correspond to the Group 3 interaction in Ref. 7. In this case, the surface pressure of a lipid monolayer increases as has previously been reported in Ref. 8, while the enthalpy change in the transition(ΔH) decreases. The transition temperature (T_c), however, does not change appreciably, These phenomena are attributable to the fact that proteins or polypeptides penetrate deeply into the hydrophobic domain. The deep penetration of proteins or polypeptides enhances the monolayer expansion.[8] By this hydrophobic interaction between lipids and proteins, the number of free lipid molecules decreases, and finally the ΔH value decreases. Since only a few lipid molecules participate in this interaction, and the bilayer is almost unperturbed,[7] no appreciable effects are observed on the transition temperature of a lipid, T_c.

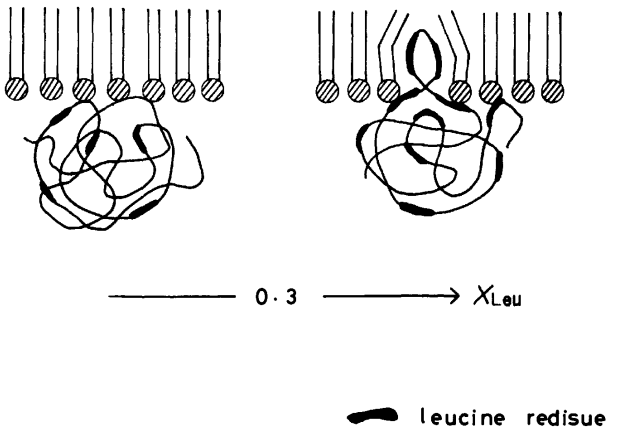

Fig. 4. A schematic model of the possible interaction between lecithin and lysine-leucine copolymers.

In the interaction between lecithin and lysine-leucine copolymers, the copolymers with a leucine fraction,X_{Leu}, smaller than 0.3, at most, interact only with the polar region of the lipid membrane because of the large electric charge derived from the lysine residues of the copolymer. On the other hand, the copolymers with X_{Leu} values larger than 0.3 penetrate into the hydrocarbon region of bilayers because of the hydrophobicity of the leucine residues. Figure 4 shows a schematic model of the possible interaction between lecithin and copolymers.

It has been accepted that the penetration ability of proteins into lipid membranes depends mainly on both the hydrophobicity and the electrostatic character of such proteins and polypeptides. Furthermore, it is of great interest that a change in the amino-acid composition of a copolymer also induces a remarkable increase in the penetration ability into lipid layers.

We are grateful to Professor Dr. J. T. Yang and Dr. Shigeo Kubota for the gift of the lysine-leucine copolymers.

References

1) D. Papahadjopoulos, *J. Colloid Interface Sci.*, **58**, 459 (1977).

2) R. M. Epand and R. Epand, *Biochim. Biophys. Acta*, **602**, 600 (1980).

3) J. M. Boggs, J. G. Stollery, and M. A. Moscarello,

Biochemistry, **19**, 1226 (1980).

4) M. Nakagaki, T. Handa, and C. Sehara, Yakugaku Zasshi, **101**, 774 (1981).

5) E. Bernard, J. -F. Faucon, and J. Dufourcq, *Biochim. Biophys. Acta*, **688**, 152 (1982).

6) J. R. Silvius, "Lipid-Protein Interactions," ed by P. C. Jost and O. H. Griffith, A Wiley-Interscience Publication, John Wiley & Sons, New York (1982), Vol. 2, Chap. 7, p. 265, and also the refs. cited therein.

7) D. Papahadjopoulos, M. Moscarello, E. H. Eylar, and T. Isac, *Biochim. Biophys. Acta*, **401**, 317 (1975).

8) M. Nakagaki, E. Okamura, and S. Kubota, *Bull. Chem. Soc. Jpn.*, **56**, 3730 (1983).

9) M. Nakagaki, T. Handa, and K. Ohashi, *Yakugaku Zasshi*, **99**, 1 (1979).

10) D. Chapman, B. A. Cornell, A. W. Elisaz, and A. Perry, *J. Biol.*, **113**, 517 (1977).

11) H. Susi, J. Sampugna, J. W. Hampson, and J. S. Ard, *Biochemistry*, **18**, 297 (1979).

 © 1985 The Chemical Society of Japan Bull. Chem. Soc. Jpn., 58, 550—552 (1985) [Vol. 58, No. 2

The Electrical Properties of Calcium Sulfide Doped with Lanthanum Sulfide and Zirconium Sulfide

Gin-ya ADACHI,* Nobuhito IMANAKA, Mineo SATO, and Jiro SHIOKAWA
Department of Applied Chemistry, Faculty of Engineering, Osaka University, Yamadaoka, Suita, Osaka 565
(Received July 5, 1984)

Calcium sulfides doped with tri- and tetravalent metal sulfides were prepared. Their electromotive forces (EMF) were measured on a galvanic cell(Fe+FeS| Solid Electrolyte| Cu+Cu_2S) where the solid electrolyte was a material in a CaS-Ln_2S_3-MS_2 system. The cell, using calcium sulfide doped with La_2S_3 and ZrS_2, exhibited an EMF value as high as the one calculated for thermodynamical equilibrium. The CaS-La_2S_3-ZrS_2 solid electrolyte showed, predominantly, an ionic conduction in the sulfur pressure range from 10^{-4} to 10^2 Pa with an activation energy of approximately 56.7 kJ·mol^{-1}, which was lower than for CaS and CaS-La_2S_3.

Galvanic cell techniques, applying CaO-stabilized zirconia[1,2] and calcium fluoride,[3-7], had been investigated to determine the chemical potentials of sulfur at elevated temperatures. When ZrO_2(CaO) was used as the electrolyte, a metal oxide was formed at the interface of the metal sulfide electrode and the electrolyte, according to the following equilibrium equation:

$$MS(s) + 3/2O_2(g) = MO(s) + SO_2(g)$$

It is necessary that the resulting metal oxide is insoluble in the metal sulfide electrode. When CaF_2 was used as the electrolyte, on the other hand, the sulfur chemical potential was first converted to a calcium chemical potential and then to a fluorine chemical potential, where F^- anions were mobile species in the CaF_2 solid electrolyte. Therefore, the electromotive force(EMF) became less accurate because of the double chemical potential conversion.

Recently, calcium sulfide[8-10] has been found to be a Ca^{2+} ionic conductor at elevated temperatures. Otowa *et al.*[9] measured the isotope tracer diffusion coefficients of sulfur and proved that the electric charge carrier in the ionic-conductive calcium sulfide is predominantly the Ca^{2+} ions. Attempts[11-16] have been concentrated on applying calcium sulfide to a solid electrolyte in order to determine the sulfur chemical potentials. However, calcium sulfide holds several disadvantages. One is its lower electrical conductivity. The other is the presence of a region where electronic conduction cannot be ignored. The doping of a tri-, or tetravalent ion into calcium sulfide[12-16] has been carried out in order to improve its electrical properties.

In this study, tri- and tetravalent metal sulfides were doped into calcium sulfide so as to increase the Ca^{2+} ion vacancies and to obtain a larger sulfur pressure independent region. EMF measurements were conducted by constructing a galvanic cell (Fe+FeS and Cu+Cu_2S as electrodes) for the purpose of examing the possibilities of the calcium sulfide doped with metal sulfides as an electrolyte. The sulfur pressure dependency on the electrical conductivity were also investigated on a sample with the most promising properties.

Experimental

Materials. Calcium sulfate dihydrate ($CaSO_4·2H_2O$; impurity, Chloride: max. 0.003%, Nitrate: max. 0.005%, Heavy metals: 0.001%, Copper: 0.0005%, Lead: 0.0005%, Arsenic: 0.0001%, Iron: 0.001%) was purchased from Wako Pure Chemical Indusries Ltd.. Lanthanum (purity: 99.9%) and yttrium (purity: 99.9%) oxides were secured from Shinetsu Chemical Co. Ltd.. Zirconium (purity: 97%), titanium (purity: 99.5%) and neobium (purity: 99.9%), and wolfram (purity 99.9%) metals were bought from Mitsuwa's Pure Chemicals, and Wako Pure Chemical Industries Ltd., respectively. FeS (Practical Grade) and Cu_2S (purity: 99.99%) were purchased from Wako Pure Chemical Industries Ltd. and Mitsuwa's Pure Chemicals, respectively. Pure calcium sulfide was prepared by heating $CaSO_4·2H_2O$ in a carbon boat at 973 K for 2 h and then at 1273 K for 5 h under a flowing gas atmosphere of hydrogen sulfide (purity: 99%). Lanthanum and yttrium chloride were prepared by adding a diluted hydrochloric acid aqueous solution to La_2O_3 and Y_2O_3, respectively. Ln_2S_3 (Ln=La and Y) were obtained by heating $LnCl_3$ (Ln=La and Y) in a carbon boat at 673 K for 2 h in an argon gas flowing atmosphere and then at 1273 K for 5 h in an H_2S gas flow. Metal sulfides (M=Zr, Ti, W, and Nb) were prepared by heating a mixture of the metal and sulfur in an evacuated quartz capsule at 773 K for 2 h and at 1273 K for 5 h. The CaS, Ln_2S_3 (Ln=La and Y), and MS_2 (M=Zr, Ti, W, and Nb) was thoroughly mixed in an agate mortar. The cation ratio in the CaS–Ln_2S_3–MS_2 system was 96:2:2 for Ca^{2+}, Ln^{3+}, and M^{4+}, respectively. The mixture was made into pellets with a pressure of 6.7×10^8 Pa. Sintering of the pellets was performed for 4 h at 1273 K in a flow of hydrogen sulfide gas. The samples were analysed using an X-ray diffraction apparatus (Rigaku's Rotaflex diffractometer with Cu $K\alpha$ radiation). The preparation of the electrodes (Fe+FeS and Cu+Cu_2S) was also conducted by sintering the pellets of the metal and metal sulfide (50:50 by molecular weight) for 3 h at 773 K in an argon gas-flow atmosphere.

Measurements. The apparatus for the EMF measurements (galvanic cell technique) is illustrated in Fig. 1. A good contact between the electrolyte and the electrodes was assured by pushing the quartz rod B to the quartz tube A with springs. The electrical conductivity was also measured with the apparatus shown in Fig. 1. In the conductivity measurements, a gold film was deposited on both surfaces of the sample with Shinku Kiko's vacuum-deposition apparatus (ULVAC, VP-C2A) so as to reduce the resistance between the sample and the platinum plate electrodes. The electrical conductivity was measured with a Hewlett Packard vector impedance meter 4800A (from 5 Hz to 500 kHz). The sulfur pressure was controlled by the regulation of the hy-

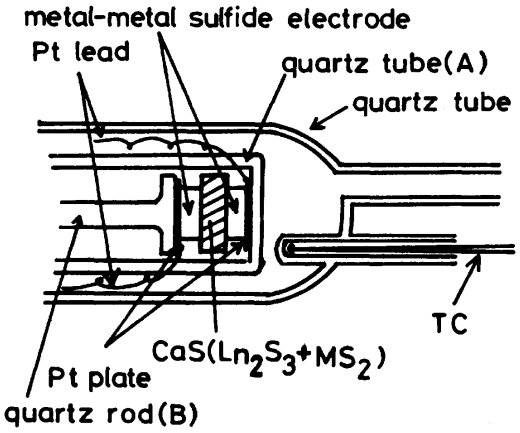

Fig. 1. The apparatus for the EMF and the electrical conductivity measurements.

TABLE 1. THE PROPERTIES OF $CaS-Ln_2S_3-MS_2$ SOLID ELECTROLYTES

composition (Ca^{2+}:Ln^{3+}: M^{4+} =96:2:2)	EMF/mV[1]	invasion of Cu^+	Average ionic radius of dopants[2]/nm
$CaS-La_2S_3-ZrS_2$	40	No	0.102
$CaS-La_2S_3-TiS_2$	40	Yes	0.096
$CaS-La_2S_3-WS_2$	0	Yes	0.099
$CaS-La_2S_3-NbS_2$	0	Yes	0.100
$CaS-Y_2S_3-ZrS_2$	40	Yes	0.095
$CaS-Y_2S_3-TiS_2$	11	No	0.089

1) Measured at 973 K. 2) Ca^{2+}(0.114 nm), La^{3+} (0.117 nm), Y^{3+}(0.104 nm), Zr^{4+}(0.086 nm), Ti^{4+} (0.0745 nm), W^{4+}(0.080 nm), Nb^{4+}(0.082 nm). These ionic radii are cited from the reference.[17]

drogen and hydrogen sulfide gas-flow volumes by flow meters. A noninductive resistance furnace was used in order to avoid any noise in both the EMF and conductivity measurements.

Results and Discussion

By X-ray diffraction analysis, samples of $CaS-Ln_2S_3$ (Ln=La and Y)-MS_2 (M=Zr, Ti, W, and Nb) were found to form solid solution. The properties of these solutions are summarized in Table 1. The invasion of the Cu^+ ion from the $Cu-Cu_2S$ electrode into the solid electrolyte occurred in samples of $CaS-La_2S_3-MS_2$ (M =Ti, W, and Nb) and $CaS-Y_2S_3-ZrS_2$. When the $CaS-Y_2S_3-TiS_2$ sample was employed as a solid electrolyte, the measured EMF was considerably lower than the calculated EMF at 973 K, which is derived from the Gibbs free energy data of Oishi *et al.*[4] and Brooks.[18] On the other hand, the cell with calcium sulfide doped with La_2S_3 and ZrS_2 exhibited an EMF as high as the calculated value. In addition, the Cu^+ ion invasion from the electrode disappeared. For the $CaS-La_2S_3-ZrS_2$ electrolyte, the average ionic radius of the dopants was 0.102 nm,[17] which is the closest to the ionic radius of Ca^{2+} (0.114 nm)[17] for the three component systems.

A good candidate for a solid electrolyte in the three component systems is considered to be the $CaS-La_2S_3-ZrS_2$ system.

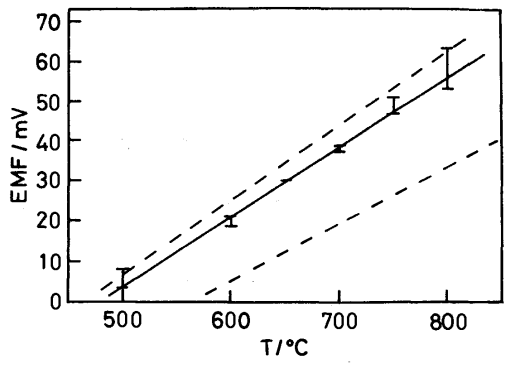

Fig. 2. The temperature dependences of the EMF for $Fe+FeS|CaS$(2 atom% La_2S_3 and 2 atom% ZrS_2)$|Cu+Cu_2S$ cell.
The maximum and minimum EMF (---) are calculated from the Gibbs free energy data of Oishi *et al.*[4] and Brooks,[18] and Alcock and Richardson[19] and Nagamori,[20] respectively.

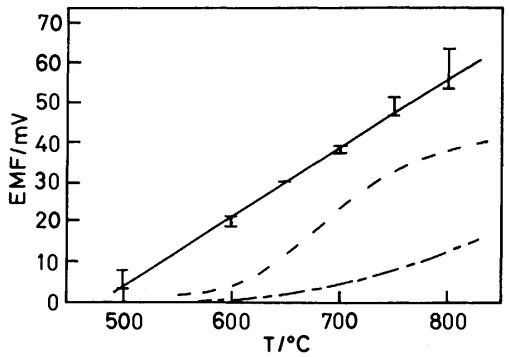

Fig. 3. The temperature dependences of the EMF for Fe+FeS|Solid electrolyte|$Cu+Cu_2S$ cell.
——: CaS(2 atom% La_2S_3 and 2 atom% ZrS_2), ———: CaS(5 atom% La_2S_3), ——: CaS.

The EMF results for the $CaS-La_2S_3-ZrS_2$ electrolyte are presented in Fig. 2. The maximum and minimum EMF were calculated from the Gibbs free energy data of Oishi *et al.*[4] and Brooks,[18] and Alcock and Richardson[19], and Nagamori,[20] respectively. The measured EMF shows itself in well within the calculated EMF range.

A comparison of the EMF results for cells using CaS, $CaS-La_2S_3$,[15] and $CaS-La_2S_3-ZrS_2$ systems is shown in Fig. 3. The calcium sulfide in which La_2S_3 was held in a solid solution, exhibited a higher EMF compared with the calcium sulfide alone. This was attributed to the formation of cation vacancies during doping. In the $CaS-La_2S_3-ZrS_2$ system, the EMF properties were appreciably improved in comparison with both CaS and $CaS-La_2S_3$.

The sulfur pressure dependency of the electrical conductivity is illustrated in Fig. 4. The conductivities are independent of the sulfur pressure variation for all samples measured at 700, 800, and 900 °C. This result indicates that electrical conduction is predominantly ionic in an $CaS-La_2S_3-ZrS_2$ system. In a previous work,[11] it was reported that calcium sulfide exhibits a

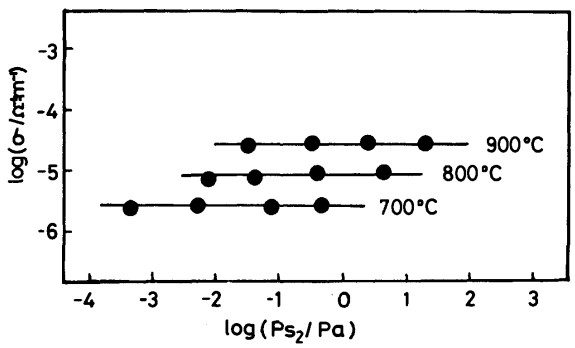

Fig. 4. The variation of the electrical conductivity of CaS(2 atom% La_2S_3 and 2 atom% ZrS_2) with sulfur pressure at 700, 800, and 900°C.

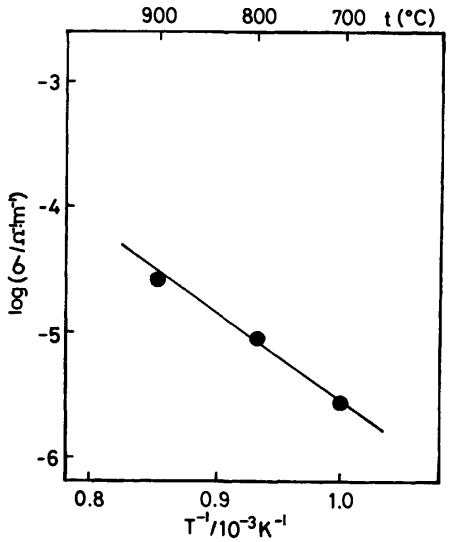

Fig 5. The temperature dependences of the electrical conductivity for CaS(2 atom% La_2S_3 and 2 atom% ZrS_2) under an atmosphere of H_2/H_2S=1.5/1.

P-type conduction at log P_{S_2} higher than approximately −6. In our earier paper,[15] electronic conduction was found to appear in the CaS-La_2S_3 system, at log P_{S_2} lower than about −5.5. By doping La_2S_3 and ZrS_2 simultaneously into CaS, the ionic conduction becomes dominant. The electronic conduction seems to be negligibly small compared with the ionic conduction due to the Ca^{2+} migration.

The temperature dependences of the log σ are shown in Fig. 5. From the slope of the line, the activation energy for the CaS-La_2S_3-ZrS_2 system was calculated to be 56.7 kJ·mol^{-1}. This value is smaller than both 99.6 kJ·mol^{-1} [11] for CaS, and 79.9 kJ·mol^{-1} [15] for CaS-La_2S_3.

The migration of a Ca^{2+} ion from a cation site to a cation vacancy becomes easier after increasing the number of cation vacancies.

In conclusion, the EMF characteristics of CaS with Cu+Cu_2S and Fe+FeS electrodes are remarkably improved by the doping of La_2S_3 and ZrS_2 simultaneously into the host CaS. The conduction mechanism of the CaS-La_2S_3-ZrS_2 solid solution is predominantly ionic. The CaS-La_2S_3-ZrS_2 system has the potential of being utilized as a solid electrolyte for a galvanic cell over a large range of sulfur pressures (10^{-4} to 10^2 Pa).

References

1) H. R. Larson and J. F. Elliott, *Trans. Metall. Soc. AIME*, **239**, 1713 (1967).
2) K. Sadakane, M. Kawakami, and K. Goto, *Tetsu to Hagane*, **63**, 432 (1977).
3) S. Aronson, *J. Inorg. Nucl. Chem.*, **29**, 1611 (1967).
4) T. Oishi, T. Fujimura, K. Ogura, and J. Moriyama, *Nippon Kinzoku Gakkai Shi*, **40**, 969 (1976).
5) K. T. Jacob, D. B. Rao, and H. G. Nelson, *J. Electrochem. Soc.*, **125**, 758 (1978).
6) T. A. Ramanarayanan and W. L. Worrell, *J. Electrochem. Soc.*, **127**, 1717 (1980).
7) W. L. Worrell, *Solid State Ionics*, **3/4**, 559 (1981).
8) H. Nakamura and K. Gunji, *Nippon Kinzoku Gakkai Shi*, **42**, 635 (1978); *Trans. Jpn. Inst. Met.*, **21**, 375 (1980).
9) T. Otowa, M. Kobayashi, K. S. Goto, and M. Someno, *Nippon Kinzoku Gakkai Shi*, **43**, 1181 (1979).
10) Von T. L. Wen, W. Weppner, and A. Rabenau, *Z. Anorg. Allg. Chem.*, **497**, 93 (1983).
11) K. Nagata and K. S. Goto, *Metall. Trans.*, **5**, 899 (1974).
12) W. L. Worrell, V. B. Tare, and F. J. Bruni, 3rd International Symposium of the High Temperature Technology, Asilomar, California, 1967 Abstr., No. 503.
13) K. Ono, K. Ishihara, and J. Moriyama, *Nippon Kinzoku Gakkai Shi*, **44**, 185 (1980).
14) K. Ono, T. Oishi, and J. Moriyama, *Solid State Ionics*, **3/4**, 555 (1981).
15) M. Sato, N. Imanaka, G. Adachi, and J. Shiokawa, *Mater. Res. Bull.*, **16**, 215 (1981).
16) A. Egami, T. Onoye, and K. Narita, *Solid State Ionics*, **3/4**, 617 (1981).
17) R. D. Shannon, *Acta Crystallogr., Sect. A*, **32**, 751 (1976).
18) A. A. Brooks, *J. Am. Chem. Soc.*, **75**, 2464 (1953).
19) C. B. Alcock and F. D. Richardson, *Nature*, **168**, 661 (1951).
20) M. Nagamori, *Metall. Trans., Sect. B*, **7B**, 67 (1976).

Solvent Effects on the Monomer-Dimer Equilibrium and Dimerization of the 1-Methyl-2-methoxycarbonylpyridinyl Radical

Hirami SHIMOISHI, Shozo TERO-KUBOTA,† and Yusaku IKEGAMI*
Chemical Research Institute of Non-Aqueous Solutions, Tohoku University, Katahira 2-1-1, Sendai 980
(Received August 2, 1984)

Solvent effects on the hyperfine splitting constants, monomer-dimer equilibrium, and kinetic parameters of the dimerization of the 1-methyl-2-methoxycarbonylpyridinyl radical have been examined in detail, using methylcyclohexane, toluene, 2-methyltetrahydrofuran, acetone, and acetonitrile as the solvents. A comparatively large activation energy for the fast step in the two-step dimerization mechanism suggests strongly that the dimeric intermediate is the 2,2′-dimer of the radical, which subsequently rearranges to the stable 4,4′-dimer.

Equilibrium between the 1-methyl-2-methoxycarbonylpyridinyl radical (R) and the covalently bonded dimer (D) was discussed in our previous papers.[1,2] Since the equilibrium lies largely in favor of D at room temperature, and since D decomposes reversibly to generate R upon irradiation with light in the near-UV region, the dimerization mechanism showing a two-step decay of R in 2-methyltetrahydrofuran (MTHF) was successfully elucidated by kinetic ESR spectroscopy.[3] In this study, however, the structure of the dimeric intermediate (DI) in the two-step decay process of R was left for further investigation, though the π-complex dimer was suggested for it. Concerning the structure of DI, a kinetic study of the dimerization of the 1-alkyl-4-phenylpyridinyl radicals suggests the 4,4′-dimer as DI; it subsequently rearranges to the stable 2,2′-dimer through the [3,3]sigmatropic mechanism.[4] The activation energy for the DI formation was too large (>27 kJ mol^{-1}) for us to suggest the π-complex dimer as DI. Because of the short lifetime of DI, the attempted spectroscopic analysis of DI has been unsuccessful.[3]

We then examined the thermodynamic parameters of the equilibrium and kinetic parameters for the dimerization in various solvents with a view to establishing the magnitude of solvent dependence for these parameters and also whether or not the two-step mechanism can be used in solvents with different polarities. We are also interested in solvent effects on neutral radicals, as have been reported previously for the stable 1-methyl-4-methoxycarbonyl- and 1-methyl-4-acetyl-pyridinyl radicals.[5] The present examination provides valuable information about solvent effects on the equilibrium system formed by a pyridinyl radical with an intermediate stability.

Methylcyclohexane, toluene, MTHF, acetone, and acetonitrile were used as solvents. The Block-Walker reaction field parameters were adopted in discussing the experimental data. This paper will end by proposing the 2,2′-dimer of R as a favorable structure for DI.

Experimental

Materials. The pyridinyl radical R was prepared by the reduction of 1-methyl-2-methoxycarbonylpyridinium iodide with 3% sodium amalgam in degassed acetonitrile, purified by distillation as previously reported,[1] and then dissolved in the desired solvent. Commercial methylcyclohexane (spectral grade) was dried over sodium metal, degassed, and then distilled under a vacuum. The purification of the other solvents has been described in a previous paper.[6]

Concentration of the Species. The addition of 1,1-dimethyl-4,4′-bipyridinium dichloride (methylviologen) to a solution of R and D caused a quantitative electron-transfer reaction, thus generating the methylviologen cation radical. The total concentration of the species was determined from the absorption measurement of the cation radical (ε 13000 at λ_{max} 605 nm). An electronic double-integrator of ESR signals was used to determine the concentration of R. A benzene solution of 2,2-diphenyl-1-picrylhydrazyl was used as the standard sample, and the concentration was determined from its optical absorbance (ε 14150 at 519 nm). The ESR sensitivity-variation in different solvents was calibrated with an internal standard of strong pitch in a capillary tube.

ESR Spectroscopy. A Varian E-109E EPR spectrometer was used for the ESR measurements. The system of kinetic ESR spectroscopy has been described previously.[3]

Results and Discussion

Solvent Effects on the Hyperfine Splitting Constants of R. In a previous paper,[5] an expression for the solvent effects on the hyperfine splitting (hfs) constants of a free radical was derived by obtaining the π-electron spin densities of the radical in solution by means of the perturbation theory; it was demonstrated that, for some neutral radicals, the hfs constants are correlated with the Block and Walker reaction-field parameter of $\theta(\varepsilon_r)=3\varepsilon_r(\ln\varepsilon_r)/(\varepsilon_r\ln\varepsilon_r-\varepsilon_r+1)-6/(\ln\varepsilon_r)-2$, where ε_r is the relative permittivity of the solvent.[7] We then used this parameter to express the solvent dependence of the hfs constants for the present radical. The equilibrium ($2R \rightleftharpoons D$) system showed well-resolved hfs of the ESR spectrum in all solvents, and each spectrum was analyzed with six splitting constants, to which the assignments were given by comparing them with the spin densities calculated by the McLachlan procedure. Plots of the hydrogen and nitrogen hfs constants (a_{obsd}) *vs.* $\theta(\varepsilon_r)$ are shown in Fig. 1. In this figure, the sign of each a_{obsd} value was chosen according to these relations; $a^H_{obsd}=Q^H_{CH}\,\rho_{calcd}$, with $Q^H_{CH}<0$,[8] and $a^N_{obsd}=Q^N\rho^\pi_N+Q^N_{CN}\times\sum\rho^\pi_{CN}$, with $|Q^N|>|Q^N_{CN}|$ and positive Q^N,[9,10] nega-

†Present address: Institute for Molecular Science, Myodaiji, Okazaki 444.

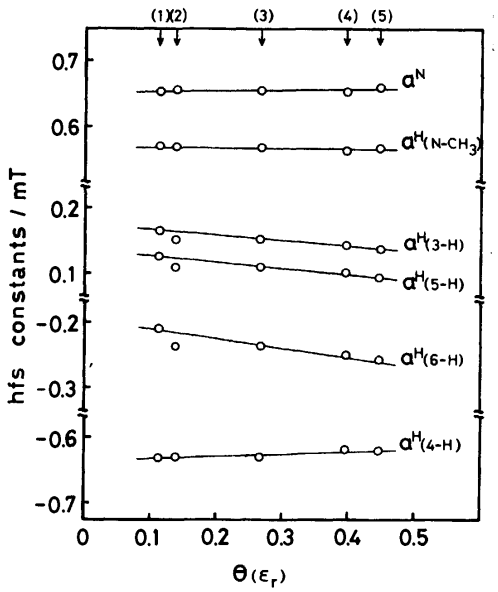

Fig. 1. Relationship between the hfs constants of R and the Block-Walker's parameters, $\theta(\varepsilon_r)$. The numbers in parentheses correspond to solvents. (1) Methylcyclohexane, (2): toluene, (3): MTHF, (4): acetone, and (5): acetonitrile.

tive spin densities appearing at the 3 and 5 positions.

The correlation between the values of a_{obsd} and $\theta(\varepsilon_r)$ is good, though the plots for the toluene solvent deviate significantly from the lines obtained by the least-squares method. The deviation is probably due to a specific interaction, such as a charge-transfer mechanism between the radical and the solvent toluene. The variations in the a_{obsd} values with the change in the solvent are small, the largest change being observed at the 6 position from 0.208 mT in methylcyclohexane to 0.256 mT in acetonitrile. Accordingly, the solvent effects on the spin distribution are not very large, not even for the density at the 2 position with the largest spin density in the pyridine ring; therefore, the dimerization mechanism is not influenced by the perturbation in the shape of the singly occupied molecular orbital due to the change in solvent. Therefore, the solvent effects described hereinafter will mainly be ascribed to the stabilization of the energy level by solvation.

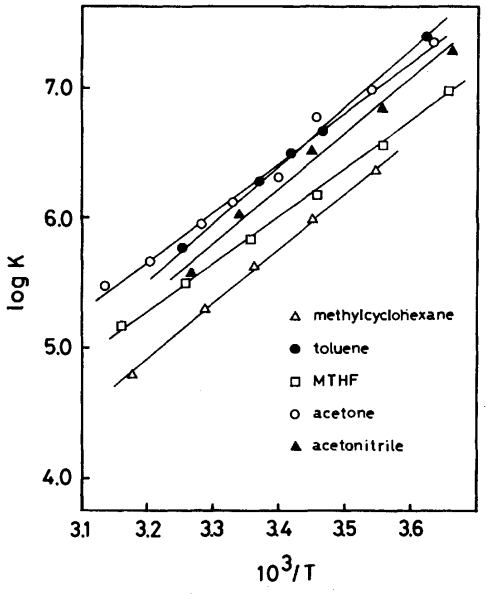

Fig. 2. Monomer-dimer equilibrium constants (K) *vs.* $1/T$.

Solvent Effects on the Monomer-Dimer Equilibrium. The monomer-dimer equilibrium constant is expressed as $K=[D]/[R]^2=([Total]-[R])/2[R]^2$, where [Total] is the total concentration of D and R, which can be determined by titration with 1,1′-dimethyl-4,4′-bipyridinium dichloride. [R] is determined by the use of an electronic double-integrator of ESR signals. The measurements were carried out at temperatures between 3 °C and 45 °C. Plots of log K *vs.* $1/T$ afforded a good straight line for each solvent, as is shown in Fig. 2. The thermodynamic parameters obtained from these linear relationships are listed in Table 1. The equilibrium tends to shift towards the D side with an increase in the solvent polarity. Plots of the free energy change (ΔG) against $\theta(\varepsilon_r)$ gave a linear relationship, with the exception of the value in toluene, as is shown in Fig. 3. The enthalpy change (ΔH) also shows a solvent dependence, the absolute value ($|\Delta H|$) becoming smaller with an increase in the solvent polarity.

Because R has a dipole moment, while that of D is equal to zero or very small, the stabilization of R by solvation with polar solvents would be larger than that of D. The solvation enthalpy, $\Delta\Delta H$, is assumed to be the difference between the dimer-formation enthalpy in a solution (ΔH_{solv}) and that *in vacuo* (ΔH_{vac});[11] therefore, $\Delta\Delta H_{solv}=\Delta H_{solv}-\Delta H_{vac}=\Delta H_{D,solv}-\Delta H_{2R,solv}$, where

Table 1. Thermodynamic parameters for the monomer-dimer equilibrium of R in various solvents

Solvent	ΔH	ΔS	$\Delta G^{a)}$	$K^{a)}$
	kJ mol^{-1}	J K^{-1} mol^{-1}	kJ mol^{-1}	mol^{-1} dm^3
Methyl-cyclohexane	−82.5	−170	−31.8	3.86×10^5
Toluene	−86.7	−172	−35.5	1.66×10^6
MTHF	−69.0	−121±4	−32.9	7.44×10^5
Acetone	−74.1	−129	−35.6	1.89×10^6
Acetonitrile	−76.5	−141	−34.5	1.10×10^6

a) At 25 °C.

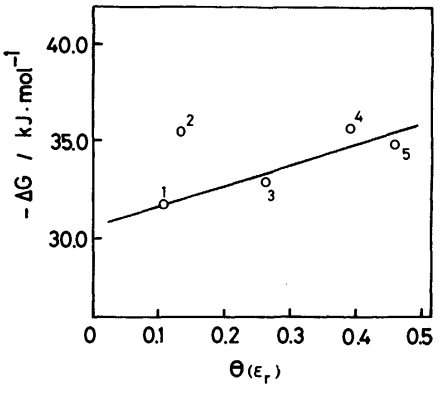

Fig. 3. Free energy change (ΔG) at 25°C *vs.* the Block-Walker's parameters ($\theta(\varepsilon_r)$).

$\Delta H_{D,solv}$ and $\Delta H_{2R,solv}$ are the solvation enthalpies of D and R respectively. As the dipole moment of methylcyclohexane is approximately zero, the enthalpy change in this solvent is assumed to be that under a vacuum. Then, $\Delta H_{vac}=\Delta H_{methylcyclohexane}=-82.5$ kJ mol^{-1}. For the case of the acetone solvent, $\Delta\Delta H_{acetone}$ becomes 8.4 kJ mol^{-1}; this positive value indicates the large stabilization of the R side. In a similar way, the solvation free energy is obtained: $\Delta\Delta G_{acetone}=-3.8$ kJ mol^{-1}; this indicates that D is stabilized by the solvation at this temperature. The difference in signs of $\Delta\Delta G$ and $\Delta\Delta H$ is caused by the entropy term: $\Delta\Delta S_{acetone}=\Delta S_{acetone}-\Delta S_{vac}=41$ JK^{-1} mol$^{-1}=\Delta S_{D,acetone}-\Delta S_{2R,acetone}$. Since $\Delta S_{methylcyclohexane}$ ($\simeq\Delta S_{vac}$) is largely negative (Table 1), the positive $\Delta\Delta S_{acetone}$ value can be explained if there is a stronger orientation of acetone molecules to R than to D. It is thus assumed that the ΔS value of -170 JK^{-1} mol^{-1} in methylcyclohexane is mostly the entropy change for D formation and that, in acetone, the $\Delta\Delta S_{acetone}$ value contributes positively to ΔS, suppressing it to the observed value (-129 JK^{-1} mol^{-1}). Consequently, the importance of the entropy term in polar solvents is established for the present equilibrium system.

Kinetic Parameters of Dimerization. In our previous paper,[3] a kinetic ESR study aimed at the dimerization of R generated by the flash photolysis of D in MTHF was described. Similar examinations for R in methylcyclohexane exhibited the growth-and-decay curves shown in Fig. 4. The following features were recognized in the same manner as in MTHF: (1) a two-step decay of R is observed around -65 °C, as shown in Fig. 4b; (2) the decay of the fast step observed at tempratures below -40 °C is represented as a reversible second- and first-order for the range of -95—-70 °C; (3) the slow step is a first-order decay in the -40—40 °C range, and (4) no change in the hfs pattern is exhibited. The same features were observed in toluene and acetone. In acetonitrile, the measurements were carried out at temperatures above -40 °C, and a first-order decay was observed.

Although the fast step could be treated as a second-order reaction, some deviations were observed because of the influence of the reverse reaction. Therfore, the step was treated as a reversible second- and first-order reaction, k_1 one which can be represented by the following equation:

$$2k_1t=-\frac{1}{2[\bar{R}]}\ln\left|\frac{[R]-[\bar{R}]}{[R]+[\bar{R}]}\Big/\frac{[R]_0-[\bar{R}]}{[R]_0+[\bar{R}]}\right|$$

where [R], [$\bar{R}$], and [R]$_0$ are the concentration, the pre-equilibrium concentration, and the initial concentration of the radical respectively. The plots based on this equation gave good linear relationships, as is shown in Fig. 5a. The Arrhenius plots yielded an activation energy (E_{a1}) of 28.9 kJ mol^{-1} and a frequency factor (A) of 1.5×10^{14} mol^{-1} dm^3 s^{-1}. These values and the rate constant obtained by extrapolation to 25 °C are

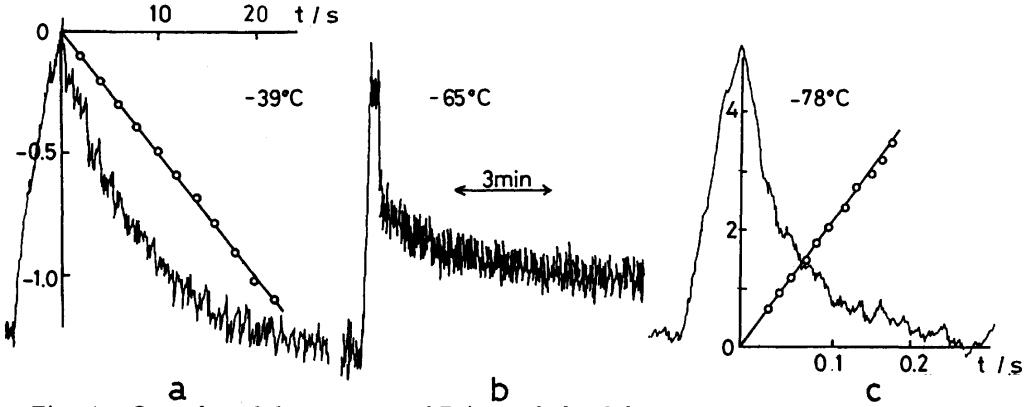

Fig. 4. Growth-and-decay curves of R in methylcyclohexane.
a: The first-order decay at -39 °C; the unit of the vertical axis is $\ln([R]-[\bar{R}])/([R]_0-[\bar{R}])$.
b: Two-step decay at -65 °C. c: The reversible second- and first-order decay at -78 °C; the unit of the vertical axis is

$$-\frac{1}{2[\bar{R}]}\ln\left|\frac{[R]-[\bar{R}]}{[R]+[\bar{R}]}\Big/\frac{[R]_0-[\bar{R}]}{[R]_0+[\bar{R}]}\right|.$$

TABLE 2. ACTIVATION PARAMETERS FOR THE DIMERIZATION OF R IN VARIOUS SOLVENTS

Solvent	Fast step				Slow step			
	log A	E_{a1}	$\Delta G_1^{a)}$	$2k_1^{a)}$	log A	E_{a2}	$\Delta G_2^{a)}$	$k_2^{a)}$
	mol^{-1} dm^3 s^{-1}	kJ mol^{-1}	kJ mol^{-1}	mol^{-1} dm^3 s^{-1}	s^{-1}	kJ mol^{-1}	kJ mol^{-1}	s^{-1}
Methyl-cyclohexane	14.2	28.9	20.9	1.4×10^9	11.8	56.9	62.8	63.8
Toluene	9.5	15.9	34.7	5.1×10^6	10.9	54.8	65.3	21.3
MTHF[b)]	10.88	20.9	31.8	1.6×10^7	10.98	54.4	64.4	28.0
Acetone	10.7	19.2	31.4	2.0×10^7	8.32	42.7	68.6	6.15
Acetonitrile					12.9	65.3	64.4	31.8

a) At 25 °C, b) From Ref. 3.

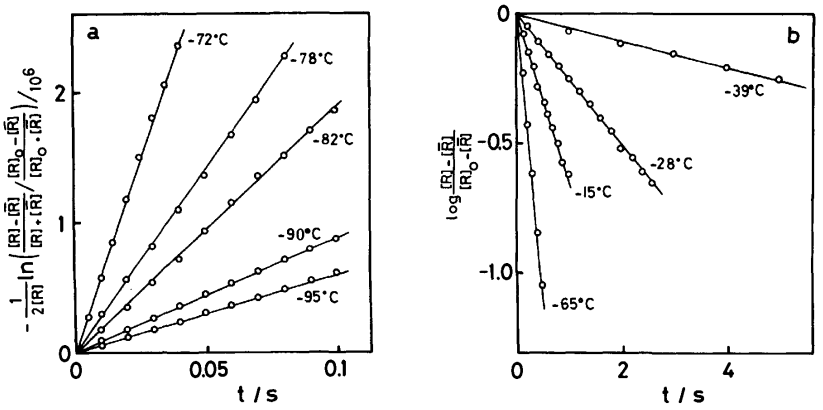

Fig. 5. (a) Reversible second- and first-order plots for the fast step and (b) first-order plots for the slow step in the decay of R in methylcyclohexane.

shown in Table 2, together with those obtained using toluene, MTHF, and acetone as solvents. The rate constant in methylcyclohexane is comparable to that in a diffusion-controlled reaction.[12]

The E_{a1} value of 28.9 kJ mol^{-1} in methylcyclohexane tends to decrease with an increase in the solvent polarity, showing 19.2 kJ mol^{-1} in acetone, while the ΔG value at 25 °C increases and k_1 decreases with an increase in the solvent polarity. The relationship between the ΔG values and the solvent parameters $\theta(\varepsilon_r)$ was poor, though a tendency could be recognized. The activation parameters for the fast step are also indicative of a great influence of the frequency factor upon k_1. The ΔS values, as estimated from the A values, are 4.5, −17.1, −10.7, and −11.5 JK^{-1} mol^{-1} for R in methylcyclohexane, toluene, MTHF, and acetone respectively. It is noteworthy that a positive value is obtained for methylcyclohexane. Since the fast step passes through a transition state in which two radicals are oppositely oriented to each other by the dipole-dipole interaction, the positive ΔS value presumably originates from the strong interaction between two radicals, regardless of the nonpolar solvent molecules. This orientation would be reduced in its strength by solvation to R in polar solvents, resulting in the negative ΔS values, because the solvation corresponds to the reduction of the dipole moment of the radical.

The rate constant, k_2, of the slow step is represented by this equation:

$$k_{obsd} = \frac{k_2}{2}t = -\ln\frac{[R] - [\bar{R}]}{[R]_0 - [\bar{R}]}$$

The good relationships shown in Fig. 5b were obtained for the measurements in methylcyclohexane. The activation parameters obtained from the Arrhenius plots are summarized in Table 2 for the results in five solvents.

The E_{a2} value has a tendency to decrease with an increase in the solvent polarity. The large value for acetonitrile is abnormal. As a long irradiation of the acetonitrile solution caused significant damage to the sample, there may be a specific interaction between the sample and the solvent. The values of ΔG_2 and k_2 show that the reaction becomes slow with an increase in the ΔG_2. Concerning the solvent dependence of ΔG_2, the plots *vs.* $\theta(\varepsilon_r)$ showed a good relationship among the solvents except for a slight deviation for toluene.

Preequilibrium between R and DI. The above results clearly prove that the radicals generated by the photolysis of D rapidly establish a preliminary equilibrium. In the irradiation with a strong, short light pulse, the initial concentrations of R and DI immediately after the irradiation are represented as $[R]_0$ and $[DI]_0$ respectively. At the preequilibrium, these concentrations become $[\bar{R}]$ and $[\overline{DI}]$ respectively. The constant (K_1) can be determined from the following equation:

$$K_1 = \frac{[\overline{DI}]}{[\bar{R}]^2} = \frac{[R]_0 - [\bar{R}]}{2[\bar{R}]^2}$$

since $[DI]_0/([R]_0 - [\bar{R}]) \ll 1$.

The measurements were performed at the shutter speed of 1/15 s, using a UV-29 glass filter at temperatures between −70 °C and −95 °C. Under these conditions, however, accurate values for K_1 could not be obtained. For instance, the measurement in methylcyclohexane gave no fine signal because the formation of DI was very rapid. The reliable results obtained in toluene, MTHF, and acetone were in these ranges: $K_1 = (1.0—2.0) \times 10^7$ mol dm^{-3} (at −75 °C) and $\Delta H_1 = -23—-33$ kJ mol^{-1}.

On the Structure of DI. The above results can enable us to draw a free energy *vs.* reaction coordinate

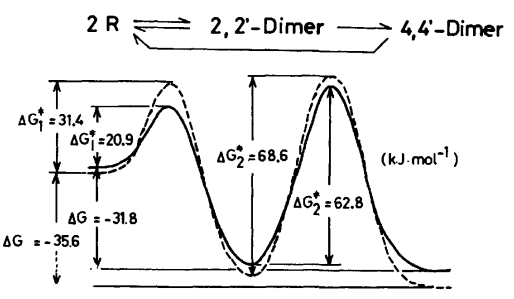

Fig. 6. A free energy at 25 °C *vs.* reaction coordinate diagram for the dimerization of R proceeding *via* DI. ——: in methylcyclohexane. -----: in acetone.

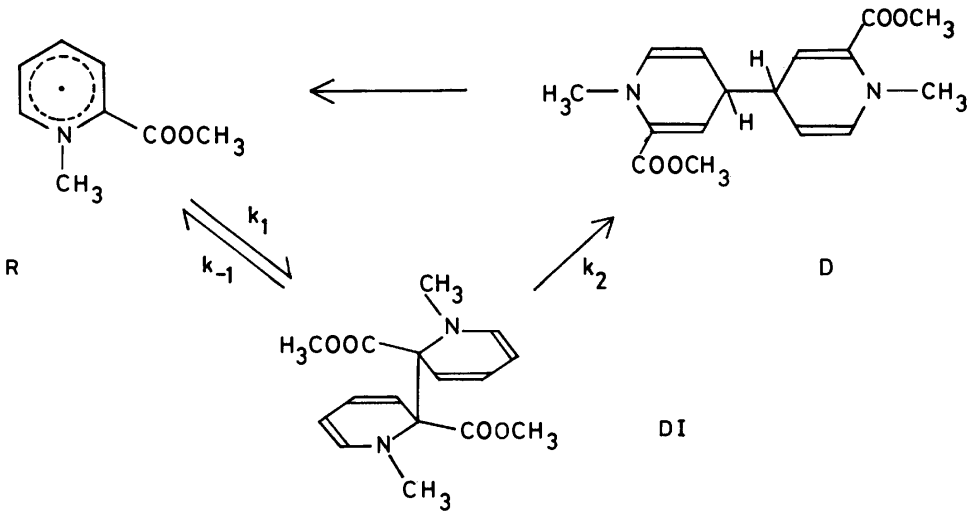

diagram for the present dimerization, as depicted for the methycyclohexane and acetone solvents in Fig. 6.[13] The structure of D reported previously[1] was recently confirmed by NMR measurements at a temperature below 0 °C, the spectrum disclosing that the dimer consists of two diastereoisomers.[14]

Concerning the structure of DI, the previous paper[3] suggested that DI was a singlet π-complex with a sandwich-like structure and expected that a charge-transfer absorption due to the complex would be observed. Further examinations, however, provided no evidence supporting the π-complex structure.

The observation of the two-step decay of R in all five solvents means that the dimerization mechanism does not differ with the solvent, and the relatively large E_{a1} values strongly imply that DI is a σ-bonding dimer rather than a π-complex. The value of 28.9 kJ mol^{-1} in methylcyclohexane is not conceivable for the E_{a1} of π-complex formation. Since free radicals are apt to react at positions with a high spin density, it is simply assumed that the coupling point is the 2 position, where the highest spin density is indicated by the McLachlan calculation.[2] The transformation of the intermediate 2,2′-dimer into the stable 4,4′-dimer can be interpreted as a [3,3]sigmatropic rearrangement, by analogy with the dimerization of the 1-alkyl-4-phenylpyridinyl radicals.[4]

References

1) J. Hermolin, M. Levin, Y. Ikegami, M. Sawayanagi, and E. M. Kosower, *J. Am. Chem. Soc.*, **103**, 4695 (1981).

2) Y. Ikegami, M. Sawayanagi, and S. Kubota, *Heterocycles*, **15**, 1027 (1981).

3) S. Tero-Kubota, Y. Sano, and Y. Ikegami, *J. Am. Chem. Soc.*, **104**, 3711 (1982).

4) K. Akiyama, S. Tero-Kubota, and Y. Ikegami, *J. Am. Chem. Soc.*, **105**, 3601 (1983).

5) T. Abe, S. Tero-Kubota, and Y. Ikegami, *J. Phys. Chem.*, **86**, 1358 (1982).

6) S. Kubota and Y. Ikegami, *J. Phys. Chem.*, **82**, 2739 (1978).

7) H. Block and S. M. Walker, *Chem. Phys. Lett.*, **19**, 363 (1973).

8) K. Akiyama, S. Kubota, and Y. Ikegami, *J. Phys. Chem.*, **85**, 120 (1981).

9) H. Zeldes and R. Livingston, *J. Phys. Chem.*, **77**, 2076 (1973).

10) T. Rakowsky and J. K. Dohrmann, *Ber. Bunsenges. Phys. Chem.*, **83**, 495 (1979).

11) C. Reichardt, "Solvent Effects in Organic Chemistry," Verlag Chemie Weinheim, New York (1979), p. 53.

12) G. B. Watts and K. U. Ingold, *J. Am. Chem. Soc.*, **94**, 491 (1972).

13) In this figure, the ΔG value for the 2R⇌2,2′-dimer equilibrium is assumed to be about 30 kJ mol^{-1}, which was estimated from the K_1 value at 25 °C obtained by the extrapolation of the values measured in the range of −70—−95 °C.

14) Y. Ikegami and others, unpublished results.

The Spin Exchange of Nitroxide Radicals with Ni^{2+} Ions in SDS Micellar Solutions

Masayuki AIZAWA
Electrotechnical Laboratory, 1-1-4, Umezono, Sakuramura, Niiharigun, Ibaraki 305
(Received August 7, 1984)

The spin-exchange rate of three kinds of hydrophobic nitroxide radicals with paramagnetic ions, Ni^{2+} ions, was measured in an aqueous sodium dodecyl sulfate (SDS) micellar solution at 30 °C. In the presence of SDS micelles, two of the three radicals had their spin-exchange rates accelerated, whereas the rate of the other radical was deaccelerated. These strange results were interpreted on the basis of a different solubilized location of the radicals in SDS micelles. The translational mobility of the Ni^{2+} ions on a micellar surface was estimated from the spin-exchange rate in the accelerated systems.

In preceding studies,[1-3] my coworkers and I investigated the molecular motion of hydrophobic nitroxide radicals solubilized in surfactant micelles by means of the ESR method. The translational mobility of the radicals in micelles[3] was estimated from the magnitude of the spin-exchange rate between the radicals.

The spin-exchange interaction[4] is one of the intermolecular magnetic interaction, occurring upon an intermolecular collision between paramagnetic particles. Due to this fact, the spin-exchange rate is proportional to the rate of intermolecular collisions. One can, therefore, calculate the translational diffusion coefficient from the spin-exchange rate constant if an appropriate model is applied for the diffusion process.

In the present study, the spin-exchange rate of nitroxide radicals with Ni^{2+} ions in micellar solutions was measured in order to investigate how the presence of surfactant micelles affects the collisions between ions and organic molecules in water. If the information on the collisional process in micelles can be obtained, it will be utilized for understanding the mode of ion-binding to the micellar surface and the reaction mechanism of a micellar catalysis.

Experimental

Three kind of nitroxide radicals (Fig. 1) were used as solubilizates. The synthesis of the two of them, 2,2,6,6-tetramethyl-4-benzoyloxy-1-piperidinyloxyl (BzONO, Fig. 1(a)) and 2,2,6,6-tetramethyl-4-myristoyloxy-1-piperidinyloxyl (MyONO, Fig. 1(b)), has been reported elsewhere.[1,3] The other nitroxide radical, 2,2,6,6-tetramethyl-4-(1-naphtoyloxy)-1-piperidinyloxyl (NpONO, Fig. 1(c)), was synthesized by the reaction of the corresponding acid chloride with a nitroxide alcohol, and was purified in a way similar to that described in the literature.[5] The results of an elemental analysis of NpONO was as follows: Found: C, 73.52; H, 7.38; N, 4.26%. Clcd for $C_{20}H_{24}O_3$: C,73.59; H, 7.41; N, 4.29%; mol wt 326.4.

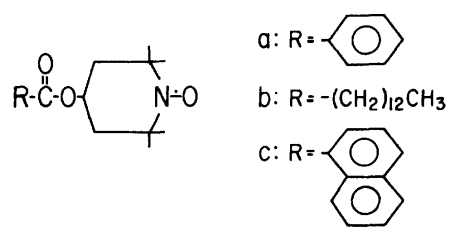

Fig. 1. (a) BzONO, (b) MyONO, and (c) NpONO.

Sodium dodecyl sulfate (SDS) of a specially prepared reagent and nickel nitrate of a guaranteed grade were purchased from Nakarai Chemicals Ltd. The SDS was recrystallized several times from ethanol-water solutions and was further purified by the method of Harrold.[6] The paramagnetic salt was used without further purification.

ESR spectra of the nitroxide radicals solubilized in SDS solutions with various amounts of Ni^{2+} ions were recorded on a JEOL model FE1X spectrometer at 30±0.5 °C.

The concentration of Ni^{2+} ions in sample solutions was determined by chelatometric titration.

Results and Discussion

As is well known, the usual ESR spectrum of nitroxide radicals in solutions consists of three lines owing to the contact interaction between an electron spin (S=1/2) and a ^{14}N nuclear spin (I=1). The three lines correspond to the ^{14}N nuclear spin quantum numbers, M_I=+1, 0, and −1, toward the high-field direction.

In the present study, the three lines broaden their linewidths (in the same manner) with an increase in the concentration of Ni^{2+} ions. I, therefore, will discuss the behavior of the lowest field line (M_I=+1) as a representative line.

In Fig. 2, the peak-to-peak linewidth, $W(+1)$, of the three nitroxide radicals in 5.2wt% SDS solutions are

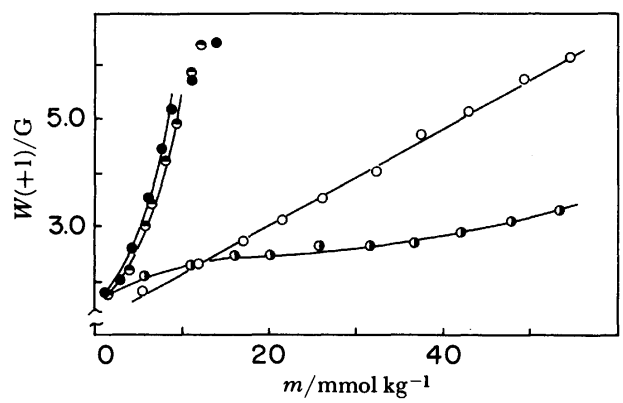

Fig. 2. Plots of the linewidth, $W(+1)$, *vs.* the concentration of Ni^{2+} ion, m, in various systems. ○: (BzONO+Ni^{2+})/water, ◑: (BzONO+Ni^{2+})/SDS, ◓: (NpONO+Ni^{2+})/SDS, and ●: (MyONO+Ni^{2+})/SDS. [SDS]=5.2 wt%.

plotted as a function of the concentration, m, of Ni^{2+} ions. A similar plot of BzONO in water is also shown in the same figure; because of low solubility in water, the spectrum of the other two radicals, NpONO and MyONO, could not be measured.

In the presence of the spin-exchange interaction, $W(+1)$ (that is, the spin-spin relaxation rate, $T_2^{-1}(+1)$) is theoretically described by the spin-exchange rate constant, k_e, and the concentration of the paramagnetic ion, m, in the following expression;

$$W(+1) = (2/\sqrt{3})T_2^{-1}(+1) = (2/\sqrt{3})\{T_{20}^{-1}(+1)+k_e m\} \quad (1)$$

where $T_{20}^{-1}(+1)$ is the spin-spin relaxation rate when no spin-exchange interaction occurs. Thus, it can be predicted that the $W(+1)$ increases linearly with the m.

As can be seen from Fig. 2, the prediction is valid only in the case of BzONO in water. The $W(+1)$-m plots of NpONO and MyONO in the SDS solutions curve upwards steeply, and that of BzONO exhibits little dependence on m.

Most of the SDS molecules in the 5.2wt% SDS solutions dissolve as micelles and the nitroxide radicals are solubilized into micelles. The nonlinear plots in the cases of SDS solutions may be related to this fact.

Comparing these plots with each other, it can be seen that the spin-exchange rates of NpONO and MyONO with paramagnetic ions are accelerated, whereas that of BzONO is deaccelerated in the presence of SDS micelles. The spin-exchange interaction occurs upon collisions between paramagnetic particles. This finding indicates that the SDS micelle affects the collision process between the nitroxide radical and the Ni^{2+} ion.

I will consider why such inverse effects are brought about in the same SDS solutions. There are three possible ways to explain this.

The first possibility is that the retarding effect in the (BzONO+Ni^{2+})/SDS system is an apparent phenomenon caused by the superposition of the signal of BzONO in the bulk solution onto that in the micellar phase. From the solubility value of BzONO into the SDS solution,[7] however, it can be estimated that the more than 99% of the BzONO molecules exist in the micellar phase in the case of the 5.2wt% SDS solution. Thus, the above possibility is implausible.

The second possibility is that the mobility of BzONO in SDS micelles is very low in comparison with the other two radicals. The BzONO molecule, however, has the smallest value of the rotational correlation time, τ_c, in the SDS micelle among the three radicals used (*cf.* Table 1). The values of τ_c were calculated according to a well-known formula.[8] This implies that the BzONO molecule is most mobile in its rotational mode; a similar phenomenon holds also in the translational mode.

The third possibility is that the solubilized location of BzONO in the SDS micelle is not available for an effective collision with paramagnetic ions. It is well known that the isotropic hyperfine splitting constant, a_N is a parameter which reflects the polarity of the microscopic environment where the nitroxide group exists: The value of a_N increases with the polarity.[9] From the a_N values given in Table 1, it can be seen that the BzONO molecule is located in the more polar region of the SDS micelle than is the NpONO or MyONO molecule.

Table 1. The isotropic hyperfine splitting constant, a_N, and the rotational correlation time, τ_c

	[SDS](wt%)	a_N/G	$\tau_c/10^{-10}$ s rad^{-1}
(BzONO+Ni^{2+})/SDS	0	17.0	0.35
	5.2	16.8	0.96
	7.6	16.7	
(NpONO+Ni^{2+})/SDS	0	16.9	
	5.2	16.4	2.4
(MyONO+Ni^{2+})/SDS	1.3	16.6	
	2.6	16.6	
	3.9	16.6	
	5.2	16.6	3.4

Assuming that the SDS micelle is an ordinary spherical micelle with the Stern layer and the diffuse layer being used as the binding regions of the counterions, I think that the nitroxide group of BzONO is in the diffuse layer, whereas that of NpONO or MyONO is near the Stern layer: The nitroxide group of BzONO protrudes from the micellar surface. When Ni^{2+} ions are added to SDS solutions, they will initially become bound to the Stern layer and then, to the diffuse layer with a further increase in their concentration. Consequently, a nitroxide group of BzONO in the diffuse layer cannot collide with the Ni^{2+} ions bound to the Stern layer.

On the basis of the above idea, I can predict that the spin-exchange rate of BzONO increases at higher concentrations of Ni^{2+} ions where the Ni^{2+} ions become bound to the diffuse layer. Figure 3 shows the $W(+1)$-m plots of BzONO for two solutions with different amounts of SDS over a wider range of m. It is

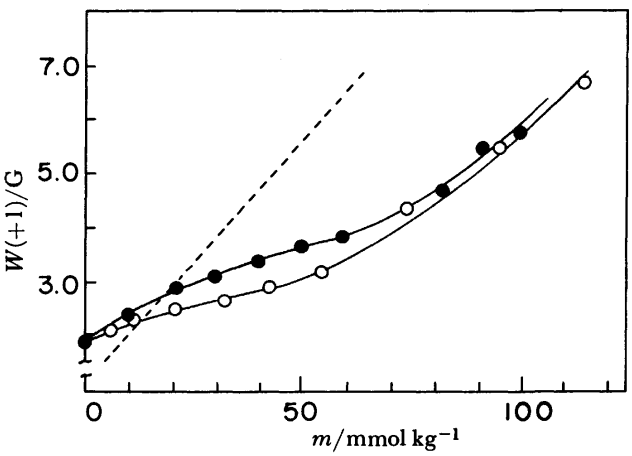

Fig. 3. Plots of $W(+1)$ *vs.* m in (BzONO+Ni^{2+})/SDS systems with the SDS concentrations of 5.2 wt%: (○) and 7.6 wt%: (●). Dashed line is a similar plot of (BzONO+Ni^{2+})/water.

noticeable that $W(+1)$ varies consistently with prediction. The concentration where a sharp increase in $W(+1)$ begins, corresponds to a sufficient content to neutralize about 50% of the negative charges of the micellar dodecyl sulfate ions. This finding coincides with Zayev's results[10] regarding proton NMR relaxation studies on a system similar to the present one. Zayev has discovered two binding areas of the Cu^{2+} ion onto SDS micelles. One is an area of complete binding up to a Cu^{2+} ion content of 50—60% with respect to that equivalent to dodecyl sulfate ions. This area corresponds to the Stern layer. The other is the area of weak binding above the Cu^{2+} ion content; this area corresponds to the diffuse layer.

It is additionally noticeable (in Fig. 3) that until the sharp increase in $W(+1)$ begins, the $W(+1)$ in 7.6wt% SDS solutions is greater than that in 5.2wt% SDS solutions. This fact may imply that the BzONO in a micelle interacts with Ni^{2+} ions bound onto the other micelles.

From the above discussion, it is concluded that the deaccelerating effect of SDS micelles on the spin-exchange rate of BzONO with paramagnetic ions results from the solubilized location of BzONO emerging outside from the micellar surface.

In order to investigate the acceleration in the ($NpONO+Ni^{2+}$)/SDS or ($MyONO+Ni^{2+}$)/SDS system, the $W(+1)$ of MyONO in the solutions with various amounts of SDS was measured as a function of the Ni^{2+} ion concentration. The data obtained are plotted in Fig. 4. In all the solutions, the accelerating effect can be observed (*cf.* the straight dashed line in the figure). A similar plot of MyONO in water will be depicted by a straight line with a smaller slope than of the dashed line.

In this case, the accelerating effect results from the condensation of Ni^{2+} ions on the micellar surface and, moreover, from an appropriate solubilized location of the nitroxide group of MyONO for colliding with the Ni^{2+} ions: Its nitroxide group exists in the Stern layer.

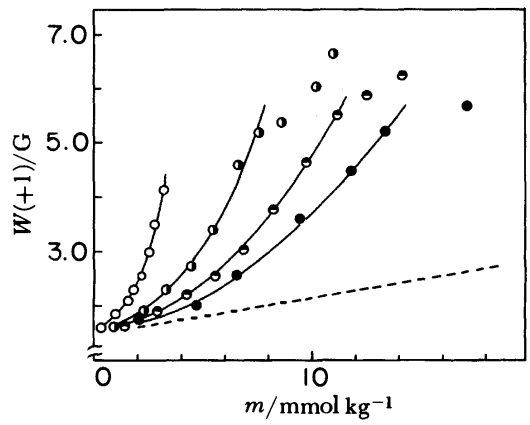

Fig. 4. Plots of $W(+1)$ *vs.* m in ($MyONO+Ni^{2+}$)/SDS systems with the SDS concentrations of 1.3 wt%: (○); 2.6 wt%: (◑); 3.9 wt%: (◓); 5.2 wt%: (●). Dashed line is a similar plot of ($BzONO+Ni^{2+}$)/water.

If the above idea holds, plots of $W(+1)$ against the mole ratio, X_r, of Ni^{2+} ions on the micellar surface in these solutions will be on the same line. The X_r was defined by the following equation;

$$X_r = n(Ni^{2+})/\{n(DS^-) + n(MyONO)\} \quad (2)$$

where $n(Ni^{2+})$ is the number of Ni^{2+} ions bound onto one micelle on the assumption that all Ni^{2+} ions are bound onto micelles, $n(DS^-)$ the number of dodecyl sulfate ion in one micelle, being equal to the aggregation number=62,[11] and n(MyONO) is the number of MyONO solubilized in one micelle, being equal to unity in the present case. I assumed that $n(DS^-)$ and n(MyONO) are approximately constant. Strictly speaking, they will change with an increase in the concentration of Ni^{2+} ions.

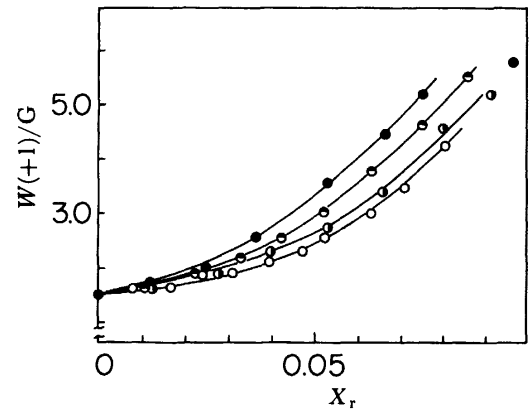

Fig. 5. Plots of the linewidth, $W(+1)$ *vs.* the mole ratio, X_r, of Ni^{2+} ion on the micellar surface in ($MyONO+Ni^{2+}$)/SDS systems with the SDS concentrations of 1.3 wt%: (○); 2.6 wt%: (◑); 3.9 wt%: (◓); 5.2 wt%: (●).

Figure 5 shows the obtained $W(+1)$-X_r plots. They are not on a common line, but on upwardly curved lines (their curvatures become greater with the SDS concentration). This fact indicates that the above assumption regarding $n(DS^-)$ and n(MyONO) is inadequate, and/or that there is an intermicellar interaction which induces the spin-exchange with the Ni^{2+} ions bound to other micellar surfaces.

In the plots, the departure from linearity might be a result of the distribution of the number of bound Ni^{2+} ions per micelle. In previous studies,[2,3] my coworkers and I investigated the spin-exchange between BzONO or MyONO molecules solubilized in SDS micelles. We obtained similar curved lines in plots of $W(+1)$ against the mole fraction of radicals in the SDS micelles. The curved lines could be successfully simulated by considering the distribution of the number of radical molecules per micelle. The non-linear behavior of some observed parameters in several other studies regarding micellar solution[12,13] was interpreted using a similar model.

Consequently, in an estimation of the translational diffusion coefficients of Ni^{2+} ions bound to a SDS micellar surface, I will analyze the $W(+1)$-X_r plots in

consideration of the distribution of Ni^{2+} ions. The analysis is in progress; the results will be described in my next paper. Qualitatively, in comparison with the previous results of the lateral diffusion of MyONO in the SDS micelle,[3] I can presume that the translational mobility of Ni^{2+} ions on the micellar surface are not extremely different from that of MyONO solubilized in the micelle.

I wish to thank Professor H. Uedaira of Hokkaido University for his helpfull discussions.

References

1) M. Aizawa, T. Komatsu, and T. Nakagawa, *Bull. Chem. Soc. Jpn.*, **50**, 3107 (1977).
2) M. Aizawa, T. Komatsu, and T. Nakagawa, *Bull. Chem. Soc. Jpn.*, **52**, 980 (1979).
3) M. Aizawa, T. Komatsu, and T. Nakagawa, *Bull. Chem. Soc. Jpn.*, **53**, 975 (1980).
4) Yu. N. Molin, K. M. Salikhov. and K. I. Zamaraev, "Spin Exchange," Springer-Verlag, Berlin, Heidelberg, New York (1980).
5) E. G. Rozantsev, V. A. Golubev, and M. B. Neiman, *Bull. Acad. Sci. USSR*, **1965**, 379.
6) S. P. Harrold, *J. Colloid Sci.*, **15**, 280 (1960).
7) V. A. Gaevoj, N. N. Kalibabchuk, and V. S. Kuts, *Kolloidn. Zh.*, **45**, 756 (1983).
8) J. Martinie, J. Michon, and A. Rassat, *J. Am. Chem. Soc.*, **97**, 1818 (1975).
9) O. W. Kolling, *Anal. Chem.*, **49**, 591 (1979).
10) Ye. Ye. Zayev, *Kolloidn. Zh.*, **41**, 1179 (1979).
11) J. H. Fendler and E. J. Fendler, "Catalysis in Micellar and Macromolecular Systems," Academic Press, New York, N. Y. (1975), p. 20.
12) Y. Wada, K. Hamamoto, and N. Mataga, *Chem. Phys. Lett.*, **53**, 242 (1978).
13) U Khuanga, B. K. Selinger, and R. McDonald, *Aust. J. Chem.*, **29**, 1 (1976).

Fluorescence of RbH and RbD Formed by Irradiating the Mixed Gases Rb+H_2 and Rb+D_2 with Laser Light

Hajime KATÔ,* Yukiko TOYOSAKA, and Tomonari SUZUKI
Department of Chemistry, Faculty of Science, Kobe University, Nada-ku, Kobe 657
(Received August 22, 1984)

When a mixture of ^{85}Rb, $^{85}Rb_2$, and D_2 was irradiated by laser light at 5145 or 4880 Å, small visible particles appeared and the fluorescence spectra were observed. By analyzing these spectra, we determined the rotational constants B_v and the centrifugal distortion constants D_v and H_v for the $X\ ^1\Sigma^+$ and $A\ ^1\Sigma^+$ states of ^{85}RbD. By considering the isotopic dependence of the Dunham coefficients, we determined various molecular constants of ^{85}RbH whose values were in good agreement with the observed fluorescence spectra of ^{85}RbH excited by laser lines at 4762, 4765, and 4880 Å. The process of RbH formation is discussed.

In 1975, Tam, Moe, and Happer reported that micron-size visible particles were produced in a cell filled with cesium and hydrogen upon Ar^+-laser irradiation at 4545 or 4579 Å.[1] The pressure broadening of the 7p→6s doublets at 4555 and 4593 Å allowed a substantial pumping of the Cs atoms from the ground state $6s\ ^2S_{1/2}$ to the $7p\ ^2P_{3/2}$ or $7p\ ^2P_{1/2}$ state

$$Cs(6s) + h\nu \longrightarrow Cs(7p). \quad (1)$$

They suggested that the particles (often called "laser snow") were crystals of cesium hydride salt produced by the following reactions:

a) $$Cs(7p) + H_2 \longrightarrow CsH + H, \quad (2)$$

or

$$Cs(7p) + H_2 \longrightarrow Cs(6s) + H_2(v), \quad (3)$$

$$Cs(6s) + H_2(v) \longrightarrow CsH + H, \quad (4)$$

where $H_2(v)$ represents a vibrationally excited hydrogen molecule.

b) Collisions with other CsH molecules lead to a $(CsH)_2$ molecule, which would further polymerize to form crystals of CsH. Particle formation was also observed when rubidium, mixed with H_2, was irradiated at 4880 or 4765 Å. In this case, the first step in the process was the production of excited Rb_2 ($C\ ^1\Pi_u$) molecules. The process regarding RbH formation is interesting.

There are few previous spectroscopic analyses of RbH. In 1939 Gaydon and Pearse[2] observed the $A\ ^1\Sigma^+ \rightarrow X\ ^1\Sigma^+$ transition of RbH in the 4680 to 6540 Å region in emission. Bartky[3] observed the absorption spectrum of RbD. He showed that the previous vibrational assignment of the $A\ ^1\Sigma^+$ state of RbH had to be changed, and gave revised molecular constants for RbH. Hsieh *et al.*[4] observed the laser-induced fluorescence spectra of RbH excited by an Ar^+ laser line at 4765 Å.

Here, we report the laser-induced fluorescence spectra of RbD excited at 5145 and 4880 Å, and of RbH excited at 4762, 4765, and 4880 Å. Since the vibrational constant ω_e of RbD is about $(\mu^{RbH}/\mu^{RbD})^{1/2}$ times that of RbH (where μ^{RbD} and μ^{RbH} are the reduced masses of RbD and RbH, respectively), we observed the fluorescence lines of RbD by about $(\mu^{RbD}/\mu^{RbH})^{1/2}$ times that of RbH in a given energy region. Hence, we could determine more accurate potential curves for RbD than for RbH. We report on the rotational constants B_v and the centrifugal constants D_v and H_v, which are independent of the method of least squares, for the $X\ ^1\Sigma^+$ and $A\ ^1\Sigma^+$ states of RbD. The potential curves of the $X\ ^1\Sigma^+$ and $A\ ^1\Sigma^+$ states and the Franck-Condon factors of the $A\ ^1\Sigma^+ - X\ ^1\Sigma^+$ transition are calculated. The fluorescence spectra of RbD excited by laser lines at 4880 and 5145 Å are compared with the calculated results. By using the isotopic dependence of diatomic Dunham coefficients, we determined the molecular constants of RbH. By referring to the potential energy curves of H_2, Rb_2, and RbH, we estimated the processes of RbH formation.

Experimental

^{85}Rb metal was obtained by the reduction of $^{85}RbCl$ (Oak Ridge National Laboratory, 99.78% of $^{85}RbCl$ and 0.22% of $^{87}RbCl$). A mixture of 120 mg of $^{85}RbCl$ and 120 mg of Ca metal granules was enclosed in a breakable glass tube of 6 mm o.d. with a slender neck. It was enclosed in an exhaused Pylex glass tube of 10 mm o.d. We broke the neck of the glass tube and heated the contents to 450 °C for 20 min. The heating caused the ^{85}Rb metal to become volatilized. This ^{85}Rb metal was driven into a cooler part of the tube and was sealed off.

The optical cells were constructed from Corning 1720 aluminosilicate glass tube of 13 mm o.d., and were baked for 8 h (1 h=60 min) at 600 °C in a vacuum of 10^{-6} Torr (1 Torr= 133.322 Pa). A mixture of the ^{85}Rb metal and the H_2 or D_2 (500 Torr) in the cell (at temperatures ranging from 300 to 500 °C) was irradiated at various frequencies of an Ar^+ laser. The vapor pressures of Rb and Rb_2 at 400 °C were estimated to be about 14 and 0.24 Torr, respectively. The experimental arrangement to measure the fluorescence spectra was the same as that reported in our previous paper.[5] The monochromator was calibrated using atomic Hg and Kr lines (Oriel, spectral lamps C-13-61 and C-13-12), and the accuracy of the line position measurements was within $\pm 0.3\ cm^{-1}$.

Results and Discussion

When a mixture of ^{85}Rb, $^{85}Rb_2$, and D_2 was irradiated by a multimode 4880 Å Ar^+ laser line, we observed the appearance of small visible particles. The laser power was 1.0 W and the beam diameter was 2 mm. The flu-

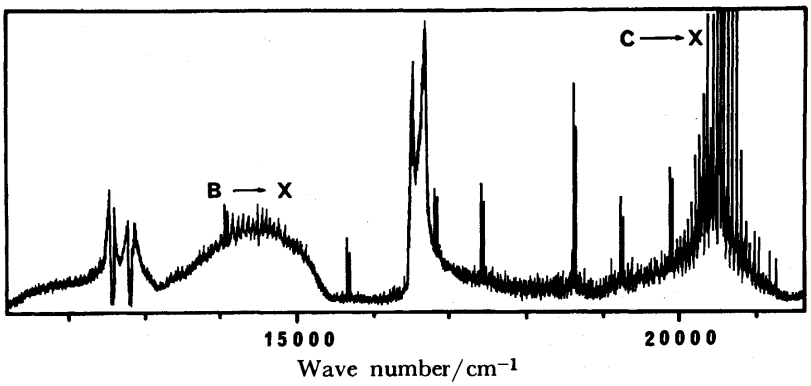

Fig. 1. Fluorescence spectrum of a mixture of ^{85}Rb metal and D_2 irradiated by the 4880 Å Ar^+ laser line. The cell temperature was 400°C. A spectral slit width of 1 cm^{-1} was used. A series of P, R doublet are the resonance fluorescence $A\ ^1\Sigma^+(v'=14,\ J'=4)\rightarrow X\ ^1\Sigma^+(v'',\ J''=3$ and 5) of ^{85}RbD. Rb atomic fluorescence at 12816 cm^{-1} ($5p^2P_{3/2}\rightarrow 5s^2S_{1/2}$) and 12578 cm^{-1} ($5p^2P_{1/2}\rightarrow 5s^2S_{1/2}$) appeared self-reversed due to the large optical density of atomic Rb. All the other bands are the fluorescence of Rb_2 (See Ref. 20).

orescence spectrum (Fig. 1) was observed. The fluorescence of Rb_2, the atomic lines of Rb ($5p\ ^2P_{3\,2}\rightarrow 5s\ ^2S_{1\,2}$) and Rb ($5p\ ^2P_{1\,2}\rightarrow 5s\ ^2S_{1\,2}$), and a series of P and R doublets with a vibrational spacing which can be identified as the fluorescence of RbD were observed. The molecular constants of the $X\ ^1\Sigma^+$ and $A\ ^1\Sigma^+$ states were reported by Bartky.[3] We identified the rotational quantum number J of the P, R doublet to be P ($J''=5$) and R ($J''=3$) from the observed spacing of the doublet. Since the R-branch was observed at the higher frequency side of the laser line, the series of P and R doublets were identified as the resonance fluorescence of ^{85}RbD originating from the excitation $A\ ^1\Sigma^+$ ($v'=14,\ J'=4$)$\leftarrow X\ ^1\Sigma^+$ ($v''=0,\ J''=5$). The vibrational quantum number $v''=0$ was assigned since any anti-Stokes P, R doublet of RbD was not observed, and $v'=14$ was assigned by referring the energy of the laser line and the calculated transition energies.

In the region near each resonance P and R doublet, we observed fluorescence lines from rotational levels of the excited state populated by a collision-induced rotational-energy transfer. A spectrum of the rotationally resolved $v'=14\rightarrow v''=3$ band is shown in Fig. 2. Similar spectra were observed when the cell was irradiated by a 5145 Å Ar^+ laser line, and the assignment of the transition could be achieved in the same way. The observed line positions and the relative intensities of the resonance lines of ^{85}RbD excited at 4880

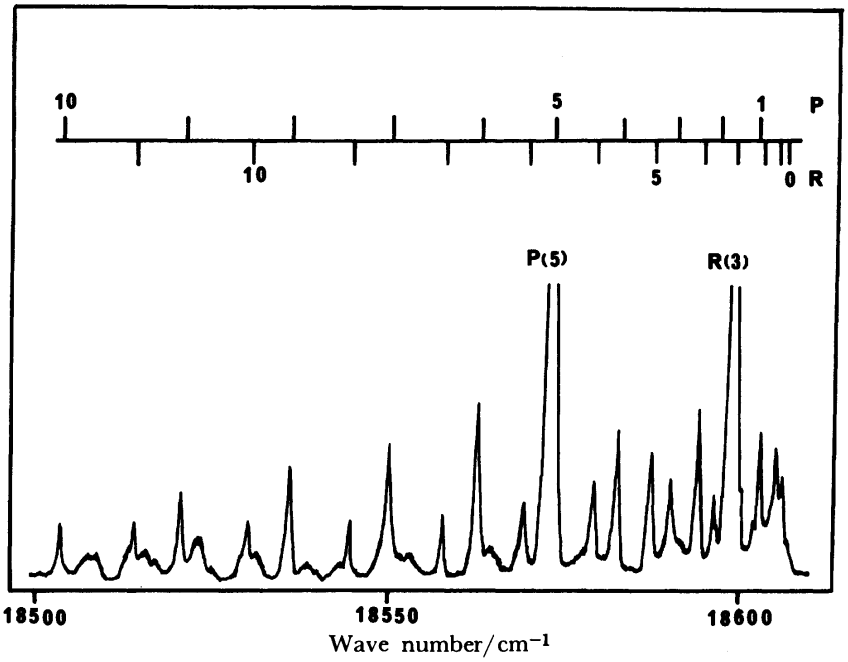

Fig. 2. Fluorescence lines from rotational levels of the excited state in the near region of the resonance fluorescence lines $A\ ^1\Sigma^+(v'=14,\ J'=4)\rightarrow X\ ^1\Sigma^+(v''=3,\ J''=3$ and 5) of ^{85}RbD. Assignments are shown above each line.

and 5145 Å are listed in Table 1.

The line positions $\sigma(v'J'-v''J'')$ of a fluorescence series can be represented by the energy difference between the $(v'J')$ and $(v''J'')$ vibrational-rotational levels of the excited and ground states:

$$\sigma(v'J' - v''J'') = T_{e'} + E_{v'J'} - E_{v''J''}, \quad (5)$$

where

$$E_{vJ} = \sum_{ij} Y_{ij}\left(v+\frac{1}{2}\right)^i J^j(J+1)^j, \quad (6)$$

T_e is the electronic term energy separation, and the Dunham coefficients Y_{ij}[6] are determined to reproduce the observed line positions. The transition energies calculated from the molecular constants reported by Bartky are in good coincidence with the observed

TABLE 1. WAVE NUMBERS AND RELATIVE INTENSITIES OF THE RESONANCE FLUORESCENCE LINES OF ^{85}RbD EXCITED BY THE λ=4880 Å AND λ=5145 Å LASER LINES

The (14,4)→(v'', J'') series excited by λ=4880 Å line			The (13,30)→(v'', J'') series excited by λ=5145 Å line		
(v'', J'')	σ_{vac}/cm^{-1}	Intensity[a]	(v'', J'')	σ_{vac}/cm^{-1}	Intensity[a]
(0, 3)	20513.8	10.0	(0, 29)	19607.0	10.0
(0, 5)	20485.3	—	(0, 31)	19428.5	—
(1, 3)	19861.5	2.1	(1, 29)	18976.8	15.7
(1, 5)	19834.7	2.3	(1, 31)	18802.0	14.3
(2, 3)	19223.4	1.5	(2, 29)	18360.6	3.5
(2, 5)	19196.9	2.0	(2, 31)	18188.8	2.9
(3, 3)	18599.0	3.7	(3, 29)	17757.9	1.2
(3, 5)	18573.1	4.8	(3, 31)	17588.5	2.3
(5, 3)	17391.6	2.1	(4, 29)	17169.0	6.2
(5, 5)	17366.6	2.6	(4, 31)	17003.4	6.0
(6, 3)	16807.7	1.5	(5, 29)	16593.5	1.3
(6, 5)	16783.4	1.8	(5, 31)	16430.9	1.0
(8, 3)	15680.3	1.7	(6, 29)	16031.3	0.8
(8, 5)	15656.9	2.2	(6, 31)	15871.6	1.3
(11, 3)	14085.7	1.0	(7, 29)	15481.9	3.6
(11, 5)	14064.5	1.4	(7, 31)	15325.5	3.3
			(10, 29)	13911.7	1.9
			(10, 31)	13763.9	1.7

a) Relative intensity as the intensity of a transition to v''=0 is 10.

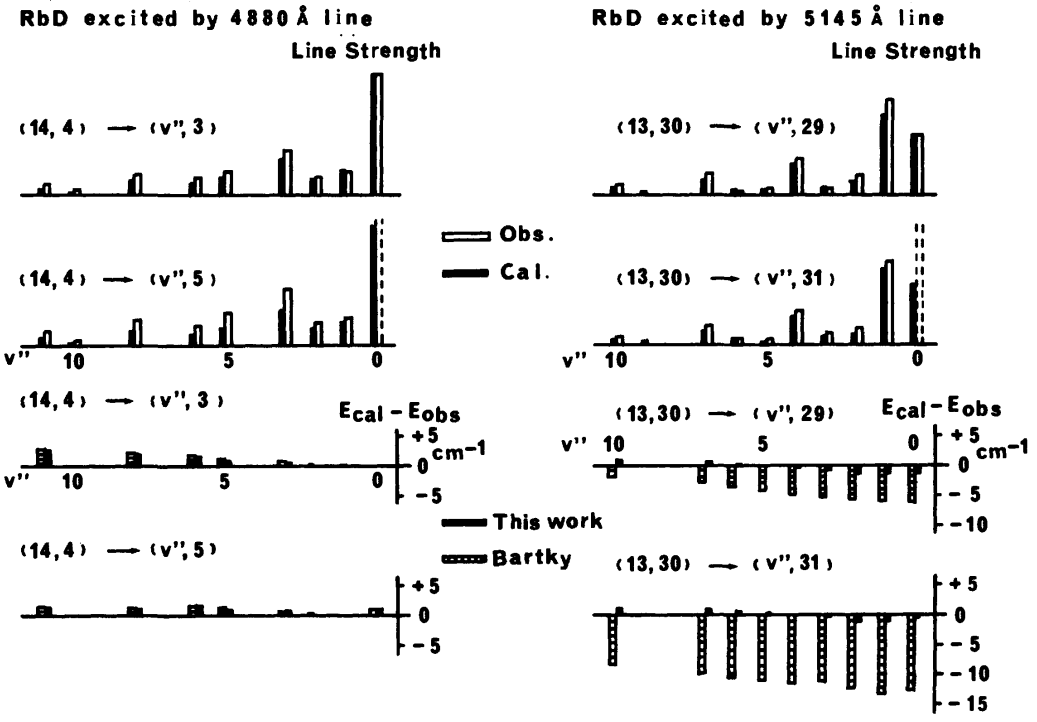

Fig. 3. Comparison between the calculated and observed relative line strengths for fluorescence series $A\ ^1\Sigma^+(v'=14,\ J'=4)\rightarrow X\ ^1\Sigma^+(v'',\ J''=3$ and 5) and $A\ ^1\Sigma^+(v'=13,\ J'=30)\rightarrow X\ ^1\Sigma^+(v'',\ J''=29$ and 31) of ^{85}RbD excited by the 4880 and 5145 Å Ar$^+$ laser lines, respectively (upper 4 figures). Lower 4 figures show the transition energy difference, $E_{cald}-E_{obsd}$ (in units of cm^{-1}), which is the difference of the transition energies between the observed ones and the ones calculated by using molecular constants determined by this work and by Bartky.[3]

energies for the transitions between states of small rotational quantum numbers J, but the coincidence of the transition energies for large J is poor (See Fig. 3). We adopted the vibrational constants reported by Bartky as Y_{io}, and the rest of the Dunham coefficients Y_{ij} ($j \neq 0$) for the $X\ ^1\Sigma^+$ state were determined by a least squares fitting of all the observed transition energies.

The rotation-vibration energy of a diatomic molecule is conventionally expanded in the form[7]

$$E_{vJ} = G(v) + B_vJ(J+1) - D_vJ^2(J+1)^2 + H_vJ^3(J+1)^3 + \cdots, \quad (7)$$

where $G(v)$ is the energy of the rotationless molecule in the vibrational state v, B_v is the corresponding

Table 2. Potential curves of the $X\ ^1\Sigma^+$ ($J=0$) and $A\ ^1\Sigma^+$ ($J=0$) states of the ^{85}RbD molecule

v''	$X\ ^1\Sigma^+$ state Energy	r_-[a]	r_+[a]	v'	$A\ ^1\Sigma^+$ state Energy	r_-[a]	r_+[a]
	cm^{-1}	Å	Å		cm^{-1}	Å	Å
		r_e=2.37 Å				r_e=3.87 Å	
0	331.6	2.22	2.54	0	77.0	3.53	4.20
1	983.9	2.12	2.69	1	233.9	3.29	4.43
2	1622.2	2.06	2.80	2	396.6	3.13	4.58
3	2246.5	2.02	2.89	3	564.5	3.01	4.70
4	2857.0	1.98	2.98	4	737.3	2.91	4.81
5	3453.9	1.95	3.07	5	914.3	2.83	4.90
6	4037.5	1.92	3.15	6	1095.1	2.76	4.99
7	4607.8	1.90	3.23	7	1279.3	2.69	5.08
8	5165.0	1.87	3.30	8	1466.6	2.64	5.16
9	5709.3	1.85	3.38	9	1656.4	2.59	5.24
10	6241.0	1.84	3.46	10	1848.4	2.55	5.31
11	6760.1	1.82	3.53	11	2042.3	2.51	5.39
12	7266.9	1.80	3.61	12	2237.7	2.47	5.46
13	7761.4	1.79	3.68	13	2434.3	2.44	5.53
14	8244.0	1.78	3.76	14	2631.7	2.40	5.61
15	8714.8	1.76	3.84	15	2829.8	2.38	5.68
				16	3028.2	2.35	5.75
				17	3226.7	2.32	5.82
				18	3425.1	2.30	5.90
				19	3623.1	2.28	5.97
				20	3820.5	2.26	6.04
					D_o=9614.6 cm^{-1}		
					T_o=17964.4 cm^{-1}		

a) r_- and r_+ are the classical minimum and maximum internuclear separation, respectively, for a vibrational level v''.

Table 3. Rotational constants $B_{v'}$ and centrifugal distortion constants $D_{v'}$ and $H_{v'}$ for the $X\ ^1\Sigma^+$ and $A\ ^1\Sigma^+$ states of ^{85}RbD

v''	$X\ ^1\Sigma^+$ state $10^{-1}B_{v'}$	$10^4D_{v'}$	$10^9H_{v'}$	v'	$A\ ^1\Sigma^+$ state $B_{v'}$	$10^4D_{v'}$	$10^9H_{v'}$
0	0.15160[a]	0.321[a]	0.52[a]	0	0.57172[a]	0.311[a]	5.59[a]
1	0.14902	0.320	0.52	1	0.58850	0.306	4.46
2	0.14645	0.318	0.53	2	0.60261	0.302	3.66
3	0.14390	0.317	0.53	3	0.61465	0.291	2.36
4	0.14136	0.315	0.53	4	0.62372	0.285	2.66
5	0.13884	0.313	0.53	5	0.63185	0.280	1.25
6	0.13633	0.312	0.53	6	0.63758	0.266	1.04
7	0.13385	0.310	0.52	7	0.64168	0.261	1.08
8	0.13137	0.308	0.52	8	0.64464	0.252	0.33
9	0.12892	0.305	0.51	9	0.64611	0.242	0.38
10	0.12648	0.303	0.50	10	0.64651	0.236	0.43
11	0.12405	0.301	0.49	11	0.64609	0.230	0.26
12	0.12164	0.298	0.47	12	0.64486	0.223	0.34
13	0.11925	0.296	0.40	13	0.64302	0.220	0.49
14	0.11683	0.299	0.11	14	0.64074	0.216	0.40
15	0.11427	0.312	−0.48	15	0.63806	0.211	0.26
				16	0.63501	0.206	−0.04
				17	0.63161	0.197	−0.69
				18	0.62781	0.184	−1.50
				19	0.62358	0.165	−2.41
				20	0.61894	0.141	−3.17

a) In units of cm^{-1}.

rotational constant, and D_v and H_v are the centrifugal distortion constants. The Dunham coefficients Y_{ij}, which were determined in order to reproduce or extrapolate the measured line positions, depend on the statistical nature of the fitting, and the values are often highly correlated with the number of expanded terms. An accurate vibrational constant $G(v)$ can be obtained by fitting it to the line positions of $J=0$ or small J.

We used a direct approach to separate the effects due to B_v from those due to D_v, H_v, *etc.* as the constants independent of the fitting. In the Rydberg-Klein-Rees (RKR) method[8] the potential curve is derived from the vibrational constant $G(v)$ and the rotational constant B_v. Primitive RKR potential curves of the $X\,^1\Sigma^+$ and $A\,^1\Sigma^+$ states were calculated for the vibrational constant $G(v)$ and the approximate rotational constant

$$B_v = \sum_i Y_{i1}\left(v+\frac{1}{2}\right)^i. \tag{8}$$

Once an approximate potential curve was obtained, the centrifugal distortion constants could be theoretically evaluated as constants independent of the fitting.[9,10] By using a computer program of Hutson,[11] we calculated the centrifugal distortion constants. These theoretical values were used to obtain more reliable rotational constants and an improved RKR curve. This procedure was iterated until it converged. The RKR potential energy curves obtained in this way are listed in Table 2, and the rotational constant B_v and centrifugal distortion constants D_v and H_v for the $X\,^1\Sigma^+$ and $A\,^1\Sigma^+$ states are listed in Table 3.

Once a potential curve was constructed, the vibrational wave functions and the eigenvalues were obtained by solving the radial Schrödinger equation.[12] The line strengths of the emission are proportional to $\nu^4|\langle v'|v''\rangle|^2$, where the electric transition moment is assumed to be constant over the range of vibrations v' and v''. ν is the frequency of a transition and $|\langle v'|v''\rangle|^2$, is the Franck-Condon factor. A comparison of the observed and calculated intensity distributions as well as the transition energy difference, $E_{cald}-E_{obsd}$, are shown in Fig. 3 for the $A\,^1\Sigma^+$ ($v'=14$, $J'=4$)$\rightarrow$ $X\,^1\Sigma^+$ (v'', $J''=3$ and 5) and $A\,^1\Sigma^+$ ($v'=13$, $J'=30$)$\rightarrow$ $X\,^1\Sigma^+$ (v'', $J''=29$ and 31) transitions. This confirms that the present vibrational assignments are correct regarding intensity distribution.

The isotopic dependence of the Dunham coefficients Y_{ij} of a diatomic molecule has been studied.[6,13] Except for very precise data, the Dunham coefficients Y_{ij}^A and Y_{ij}^B of two isotopic molecules (A and B, respectively) are expressed to a very good approximation by[7]

$$Y_{ij}^A/Y_{ij}^B = (\mu^B/\mu^A)^{j+1/2}, \tag{9}$$

where μ^α (α=A, B) is the reduced mass of an isotopic molecule. We expanded the centrifugal constants D_v and H_v in the form of Eq. (8) for the rotational constant B_v as

$$D_v = -\sum_i Y_{i2}(v+1/2)^i, \text{ and } H_v = \sum_i Y_{i3}(v+1/2)^i, \tag{10}$$

TABLE 4. DUNHAM TYPE COEFFICIENTS FOR THE $X\,^1\Sigma^+$ AND $A\,^1\Sigma^+$ STATES OF THE ^{85}RbH MOLECULE. ALL VALUES ARE GIVEN IN cm^{-1}

$X\,^1\Sigma^+$ state	$A\,^1\Sigma^+$ state
Y_{10}=936.94	Y_{10}=211.74
Y_{20}=−14.205	Y_{20}=6.47
Y_{30}=0.815×10^{-1}	Y_{30}=−0.253
Y_{01}=3.0195	Y_{40}=0.304×10^{-2}
Y_{11}=−0.7071×10^{-1}	Y_{01}=1.12898
Y_{21}=−0.392×10^{-3}	Y_{11}=0.5133×10^{-1}
Y_{31}=0.1147×10^{-3}	Y_{21}=−0.5923×10^{-2}
Y_{41}=−0.596×10^{-5}	Y_{31}=0.2638×10^{-3}
Y_{02}=−0.127×10^{-3}	Y_{41}=−0.481×10^{-5}
Y_{12}=0.31×10^{-5}	Y_{02}=−0.121×10^{-3}
Y_{22}=−0.114×10^{-5}	Y_{12}=0.0
Y_{32}=0.194×10^{-6}	Y_{22}=0.1677×10^{-5}
Y_{42}=−0.102×10^{-7}	Y_{32}=−0.2176×10^{-6}
Y_{03}=0.3×10^{-8}	Y_{42}=0.859×10^{-8}
Y_{13}=0.18×10^{-8}	Y_{03}=0.43×10^{-7}
Y_{23}=−0.85×10^{-9}	Y_{13}=−0.126×10^{-7}
Y_{33}=0.140×10^{-9}	Y_{23}=0.105×10^{-8}
Y_{43}=−0.75×10^{-11}	Y_{33}=0.176×10^{-10}
	Y_{43}=−0.373×10^{-11}

The Dunham-type coefficients Y_{ij} of ^{85}RbD were determined by a least-squares fitting of the values in Table 3. Then, by using Eq. (9), we obtained the Dunham-type coefficients of ^{85}RbH. The results are listed in Table 4.

The transition energies calculated from the constants in Table 4 agreed satisfactorily with the observed series of fluorescence lines of ^{85}RbH excited at 4762, 4765, and 4880 Å. A comparison of the observed and calculated intensity distributions as well as the transition energy difference, $E_{cald}-E_{obsd}$, are shown in Fig. 4 for the observed series of resonance fluorescence of ^{85}RbH excited at 4762 Å. From the figure we see that the molecular constants determined by Hsieh *et al.* are less accurate than the ones determined by Bartky for the transitions with a small rotational quantum number J. The constants reported by Bartky are in good coincidence with the observed values for transitions with a small J. However, for large J agreement was poor, as it was for RbD.

The RKR potential energy curves for the $X\,^1\Sigma^+$ and $A\,^1\Sigma^+$ states of ^{85}RbH were calculated for the molecular constants in Table 4, and the results are listed in Table 5. The molecular constants $\omega_e x_e$ ($=-Y_{20}$) and α_e ($=-Y_{11}$) of the $A\,^1\Sigma^+$ state are abnormally negative, and the potential energy curve approaches its asymptote unusually slowly with increasing internuclear distance. The exceptional potential form of the $A\,^1\Sigma^+$ state of alkali metal hydrides has been explained to be the result of strong mixing between two zero-approximation states of the ionic and covalent character.[14] The dissociation energy D_e of the $X\,^1\Sigma^+$state of RbH was estimated to be 14580±600 cm^{-1}.[15]

Let us now discuss the process of RbH formation. The potential curves of H_2 ($X\,^1\Sigma_g^+$), Rb_2 ($X\,^1\Sigma_g^+$ and $C\,^1\Pi_u$), and RbH ($X\,^1\Sigma^+$ and $A\,^1\Sigma^+$) are schematically shown in Fig. 5. Accurate spectroscopic data of H_2

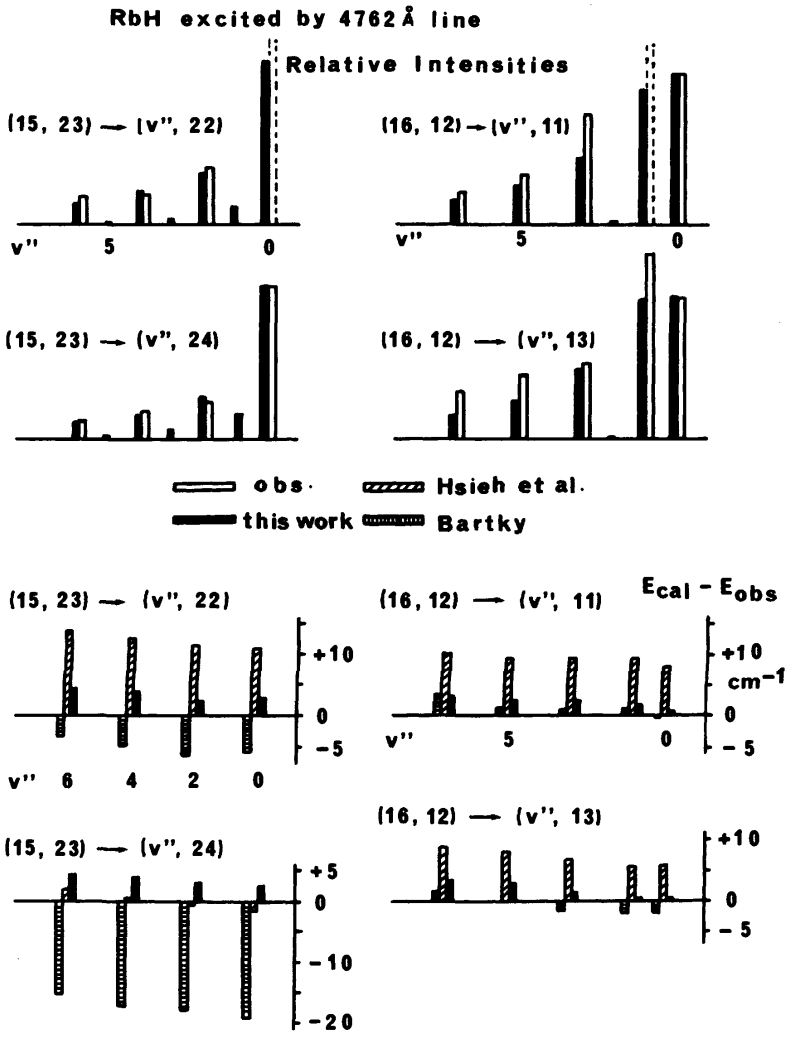

Fig. 4. Comparison between the calculated and observed relative line strengths for the fluorescence series $A\ ^1\Sigma^+(v'=15, J'=23) \rightarrow X\ ^1\Sigma^+(v'', J''=22$ and 24) and $A\ ^1\Sigma^+(v'=16, J'=12) \rightarrow X\ ^1\Sigma^+(v'', J''=11$ and 13) of ^{85}RbH excited by the 4762 Å Ar^+ laser line (upper 4 figures). Lower 4 figures show the transition energy difference, $E_{cald}-E_{obsd}$ (in units of cm^{-1}), which is the difference of transition energies between the observed ones and the ones calculated by using the molecular constants determined by this work, by Bartky,[3] and by Hsieh *et al.*[4]

have been reported for the Lyman bands ($B\ ^1\Sigma_u^+ - X\ ^1\Sigma_g^+$) and the RKR potential curve of the $X\ ^1\Sigma_g^+$ state has been fairly well established.[16-18] The dissociation energy D_e of the $X\ ^1\Sigma_g^+$ state of H_2 has been determined to be $38284\pm15\,cm^{-1}$.[18] The dissociation energy D_e of the $X\ ^1\Sigma_g^+$ state of Rb_2 has been determined to be $3950\pm160\,cm^{-1}$, and energy of the bands of the $C\ ^1\Pi_u - X\ ^1\Sigma_g^+$ transition have been represented by

$$\begin{aligned} E(v',v'') = 20835.1 &+ [36.46(v'+1/2) \\ &- 0.124(v'+1/2)^2] - [56.78(v''+1/2) \\ &- 0.0785(v''+1/2)^2 - 0.00083(v''+1/2)^3] \end{aligned} \quad (11)$$

in units of cm^{-1}.[19] Brom and Broida[20] assigned the excitation of Rb_2 irradiated at 4880 Å as the $X\ ^1\Sigma_g^+$ ($v''=8$) $\rightarrow C\ ^1\Pi_u$ ($v'=3$) transition. Hence, the excited Rb_2 molecule has about $17000\,cm^{-1}$ of excess energy when it is dissociated into two Rb ($5s\ ^2S_{1/2}$) atoms.

The dissociation energies D_0 of H_2 and RbH molecules are 36000 and $14000\,cm^{-1}$, respectively. The excited Rb_2 molecule does not have a potential energy which exceeds the difference between the dissociation energies of H_2 and RbH. Hence, the formation of RbH in the ground state $X\ ^1\Sigma^+$ through the primary reaction

$$Rb_2(C^1\Pi_u) + H_2 \longrightarrow RbH + H + Rb(5^2S) \quad (12)$$

or through two step reaction: vibrational activation

$$Rb_2(C\ ^1\Pi_u) + H_2 \longrightarrow Rb_2(X\ ^1\Sigma_g^+) + H_2(v) \quad (13)$$

followed by

$$H_2(v) + Rb(5^2S) \longrightarrow RbH + H, \quad (14)$$

which is analogous to the one suggested for CsH formation, is impossible from the energy requirements of the reaction.

The spectra for a mixture of ^{85}Rb and H_2 were sim-

TABLE 5. POTENTIAL CURVES OF THE $X\ ^1\Sigma^+$ ($J=0$) AND $A\ ^1\Sigma^+$ ($J=0$) STATES OF THE ^{85}RbH MOLECULE

v''	$X\ ^1\Sigma^+$ state Energy	r_- [a]	r_+ [a]	v'	$A\ ^1\Sigma^+$ state Energy	r_- [a]	r_+ [a]
	cm^{-1}	Å	Å		cm^{-1}	Å	Å
		r_e=2.37 Å				r_e=3.87 Å	
0	465.1	2.19	2.58	0	109.1	3.47	4.26
1	1373.9	2.08	2.75	1	333.0	3.19	4.53
2	2255.0	2.02	2.89	2	567.6	3.01	4.71
3	3108.9	1.97	3.02	3	811.6	2.87	4.85
4	3936.1	1.92	3.13	4	1063.7	2.77	4.98
5	4737.2	1.89	3.25	5	1322.6	2.68	5.10
6	5512.5	1.86	3.35	6	1587.3	2.61	5.21
7	6262.5	1.83	3.46	7	1856.5	2.54	5.32
8	6987.9	1.81	3.57	8	2129.4	2.49	5.42
9	7688.9	1.79	3.67	9	2405.0	2.44	5.52
10	8366.3	1.77	3.78	10	2682.3	2.40	5.63
11	9020.3	1.76	3.89	11	2960.7	2.36	5.73
12	9651.5	1.74	3.99	12	3239.4	2.32	5.83
13	10260.5	1.73	4.11	13	3517.8	2.29	5.93
14	10847.6	1.72	4.22	14	3795.3	2.26	6.03
15	11413.5	1.71	4.34	15	4071.4	2.23	6.14
				16	4345.7	2.20	6.24
				17	4617.8	2.18	6.35
				18	4887.4	2.16	6.45
				19	5154.4	2.14	6.56
				20	5418.6	2.12	6.67
					T_0=17863.9 cm^{-1}		

a) r_- and r_+ are the classical minimum and maximum internuclear separation, respectively, for a vibrational level v''.

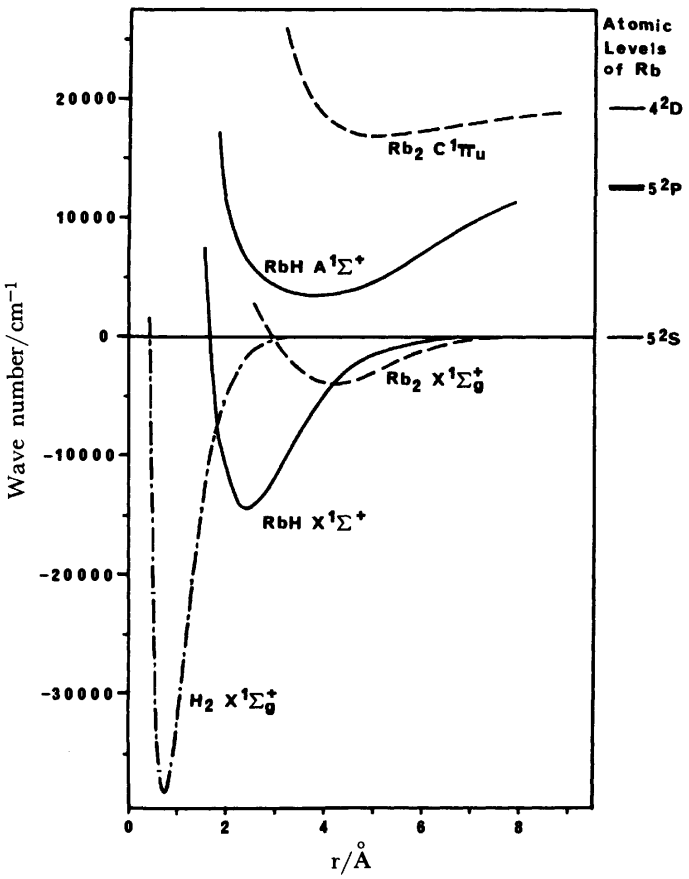

Fig. 5. Potential energy curves of $H_2(X\ ^1\Sigma_g^+$: RKR in Ref. 17), Rb_2 ($X\ ^1\Sigma_g^+$: RKR calculated from molecular constants in Ref. 21, and $C\ ^1\Pi_u$: Morse), and RbH($X\ ^1\Sigma^+$ and $A\ ^1\Sigma^+$: RKR in Table 5).

ilar to those shown in Figs. 1 and 2. We observed the resonance fluorescence of Rb_2, fluorescence of Rb_2 from the energy transferred states, and the atomic lines of Rb(5p $^2P_{1/2}\rightarrow$5s $^2S_{1/2}$) and Rb(5p $^2P_{3/2}\rightarrow$5s $^2S_{1/2}$) in addition to the resonance fluorescence of RbH. The density of H_2, Rb, and Rb_2 in the cell at 400°C are about 10^{19}, 5×10^{17}, and 10^{16} cm^{-3}, respectively. The excited Rb_2 molecule collides mostly with a H_2 molecule, and about once in ten with a Rb atom. The $H_2(v)$ molecule which was vibrationally excited through the reaction (13) collides mostly with a H_2 molecule in the ground state and will lose some of its vibrational energy. The reaction (14) would require vibrational excitation of the H_2 molecule to $v>6$, which will not be possible under our experimental conditions. A reaction with a Rb atom in the excited state 5p $^2P_{3/2}$ or 5p $^2P_{1/2}$ (it requirs $H_2(v>2)$) would be possible. However, this would not be the main process of the RbH formation, since the density of the Rb(5p $^2P_{1/2}$ and 5p $^2P_{3/2}$) atoms are low. Under our experimental conditions we have not observed fluorescence from highly excited Rb atoms, such as Rb(6p) and Rb(4d). This was the same for a cell containing only rubidium. Hence, there is no possibility of the reaction through a multi-photon process. By estimating from the energy requirments of the reaction, the most probable process of RbH formation would be a bimolecular reaction *via* an exciplex [Pb_2*H_2]

$$Rb_2(C\ ^1\Pi_u) + H_2(X\ ^1\Sigma_g^+) \longrightarrow [Rb_2{}^*H_2] \longrightarrow 2RbH(X\ ^1\Sigma^+). \quad (15)$$

However, nothing is known about the possible existence of the transient complex [Rb_2*H_2], and more

work is necessary to clearify this situation.

H. K. thanks the Ministry of Education, Science and Culture for Grant-in-Aid for Scientific Research No. 58490020. A part of the calculations were carried out at the computer center of IMS.

References

1) A. Tam, G. Moe, and W. Happer, *Phys. Rev. Lett.*, **35**, 1630 (1975).
2) A. G. Gaydon and R. W. B. Pearse, *Proc. R. Soc. London*, **173**, 28 (1939); *ibid.*, **173**, 37 (1939).
3) I. R. Bartky, *J. Mol. Spectrosc.*, **21**, 1 (1966).
4) Y. K. Hsieh, S. C. Yang, A. C. Tam, K. K. Verma, and W. C. Stwalley, *J. Mol. Spectrosc.*, **83**, 311 (1980).
5) H. Katô and C. Noda, *J. Chem. Phys.*, **73**, 4940 (1980).
6) J. L. Dunham, *Phys. Rev.*, **41**, 721 (1932).
7) G. Herzberg, "Spectra of Diatomic Molecules," Van Nostrand Reinhold, New York (1950), pp. 107, 109, and 141.
8) R. Rydberg, *Z. Phys.*, **73**, 376 (1931); O. Klein, *ibid.*, **76**, 226 (1932); A. L. G. Rees, *Proc. Phys. Soc., Ser. A*, **59**, 998 (1947).
9) J. M. Hutson, *J. Phys. B*, **14**, 851 (1981).
10) R. N. Zare, A. L. Schmeltekopf, W, J. Harrop, and D. L. Albritton, *J. Mol. Spectrosc.*, **46**, 37 (1973).
11) J. M. Hutson, QCPE Program No. 435 (1982).
12) R. N. Zare, *J. Chem. Phys.*, **40**, 1934 (1964); University of California Radiation Laboratory Report, UCRL-10925, 1963.
13) J. K. G. Watson, *J. Mol. Spectrosc.*, **80**, 411 (1980).
14) R. S. Mulliken, *Phys. Rev.*, **50**, 1028 (1936).
15) S. C. Yang, D. D. Nelson, Jr., and W. C. Stwalley, *J. Chem. Phys.*, **78**, 4541 (1983).
16) G. Herzberg and L. L. Howe, *Can. J. Phys.*, **37**, 636 (1959).
17) S. Weissman, J. T. Vanderslice, and R. Battino, *J. Chem. Phys.*, **39**, 2226 (1963).
18) M. L. Ginter and R. Battino, *J. Chem. Phys.*, **42**, 3222 (1965).
19) N. Tsi-Ze and T. San-Tsiang, *Phys. Rev.*, **52**, 91 (1937).
20) J. M. Brom Jr. and H. P. Broida, *J. Chem. Phys.*, **61**, 982 (1974).
21) C. D. Caldwell, F. Engelke, and H. Hage, *Chem. Phys.*, **54**, 21 (1980).

Reaction in the System $N(CH_3)_4$-ZrO_2-P_2O_5-H_2O. Preparation and Characterization of Framework Zirconium Phosphates $(NH_4)_xH_{1-x}Zr_2(PO_4)_3$ and $HZr_2(PO_4)_3$

Tsuyoshi KIJIMA* and Yoshiyuki YAJIMA
National Institute for Research in Inorganic Materials, Sakura-mura, Niihari-gun, Ibaraki 305
(Received July 3, 1984)

The hydrothermal reaction in the system ZrO_2-P_2O_5-H_2O in the presence of tetramethylammonium ions was examined within the temperature range 160—350 °C. This reaction resulted in the formation of framework zirconium phosphates $(NH_4)_xH_{1-x}Zr_2(PO_4)_3 \cdot yH_2O$ ($0.6 \leq x \leq 1$, $y \leq 0.3$) as well as some other phases, including two tetramethylammonium intercalates. The framework phases were rhombohedral with lattice constants of, *e.g.*, $a=8.669$ and $c=24.23$ Å for $x=1.0$. These phases were deammonated at 400—640 °C and converted to the proton-exchanged form $HZr_2(PO_4)_3$. The protons of this phase are easily exchanged by unhydrated Li^+ and Na^+ ions, but not by K^+ and Cs^+, owing to the sieving effect of the bottleneck in the $(Zr_2P_3O_{12})^{-1}$ framework. The acid strength of the proton form is a little weaker than that of α-zirconium phosphate.

Inclusion phenomena have attracted increasing attention in inorganic chemistry. In previous papers concerned with molecular inclusion, we reported the adsorption of amino acids by layered zirconium phosphates[1] and the complexation of copper(II)-montmorillonite with a modified cyclodextrin.[2] Recently, another type of application has been made in preparing several useful micro-porous compounds, such as zeolite ZSM-5[3] and framework aluminophosphates,[4] by a method in which their organic base-including precursors were hydrothermally crystallized prior to the decomposition of the complexing moieties.

Zirconium phosphate, other than with a layered structure, can be obtained with a framework structure. This phase is the end member of the zirconium phosphate silicate $M_{1+x}Zr_2Si_xP_{3-x}O_{12}$ ($0 \leq x \leq 3$, M=univalent cation). It is represented by a composition of $x=2$ and M=Na (NASICON) with a fast Na^+ ion conductivity and has an open three-dimensional skeleton framework with four cavities per formula weight.[5] It is, therefore, of interest to apply the inclusion crystallization method to the NASICON system.

An attempt was, thus, made to examine a hydrothermal reaction in the system ZrO_2-P_2O_5-H_2O in the presence of tetramethylammonium (TMA) ions.

In the present study, we obtained framework zirconium phosphates $(NH_4)_xH_{1-x}Zr_2(PO_4)_3$ and $HZr_2(PO_4)_3$ in addition to two tetramethylammonium intercalates. Alberti has already reported that the proton exchanged form of $MZr_2(PO_4)_3$ is obtained by washing $LiZr_2(PO_4)_3$ with dilute HCl.[6] After the present work was underway, we learned that Ono[7] prepared the ammonium- and the proton-exthanged forms of $MZr_2(PO_4)_3$ by a hydrothermal reaction using the system NH_3-ZrO_2-P_2O_5-H_2O. Clearfield, Roberts and Subramanian[8] also reported the hydrothermal synthesis of these two phases using the amine or ammonium exchanged forms of α-zirconium phosphate as a starting material or the reaction of NH_4Cl with $Zr(NaPO_4)_2$.

Experimental

Hydrothermal experiments were carried out as follows. To a 1:1 mixed aqueous solution of 1 mol dm^{-3} $ZrOCl_2$ and 1 mol dm^{-3} tetramethylammonium bromide, a 1 mol dm^{-3} phosphoric acid solution was added to keep the P/Zr ratio constant at 1.5 or 4. After the pH value of the reaction mixture had been adjusted to 0.8—9 with a 10% tetramethylammonium hydroxide solution, the mixture was sealed in a gold capsule or stainless steel bomb (fitted with a Teflon liner) and kept for 2—10 d at 160, 220, 280, 310, or 350 °C. The resulting solids were centrifuged, washed with distilled water and dried at 40 °C in air. Measurements of X-ray diffraction, TG traces, and infrared (IR) transmission were made using the same instruments and procedures as described elsewhere.[1] A wet analysis of zirconium and phosphorus was conducted by modifying the method of Clearfield, Blessing and Stynes.[9] An analysis of C, H, N loss on ignition was made using a conventional method. Ion exchange experiments were performed by the following procedure: 0.01—0.02 g of solid was contacted with 3 cm^3 of distilled water, followed by the addition of 0.5 cm^3 of a 1.0 mol dm^{-3} MCl solution. After each equilibration at 25 °C, the pH of the supernatant was measured, which enabled us to evaluate the number of protons released to the solution. A qualitative measurement of the acid strength was made in the same manner as previously described.[10]

Results and Discussion

The products resulting from the hydrothermal reactions were characterized primarily by their X-ray diffraction patterns and the results are summarized in Fig. 1. The two phases which give X-ray diffraction profiles similar to those of $NaZr_2(PO_4)_3$ and $KZr_2(PO_4)_3$[5] are denoted as NASICON(I) and NASICON(II), respectively. The numbers for the other phases designate the first interplanar spacing in their respective powder patterns. In the temperature range below 300 °C, the three phases labelled 12.6, 10.5, and 9.9 were obtainable as a single phase and the phases labelled 9.2 and 8.6 coexisted with the NASICON(I) phase. At higher temperature the NASICON(II) phase was obtained as a single phase at pH 1—9 and a mixture of some less crystalline phases, including the NASICON(I) phase, appeared at pH 0.8.

Among the three single phases labelled by numbers,

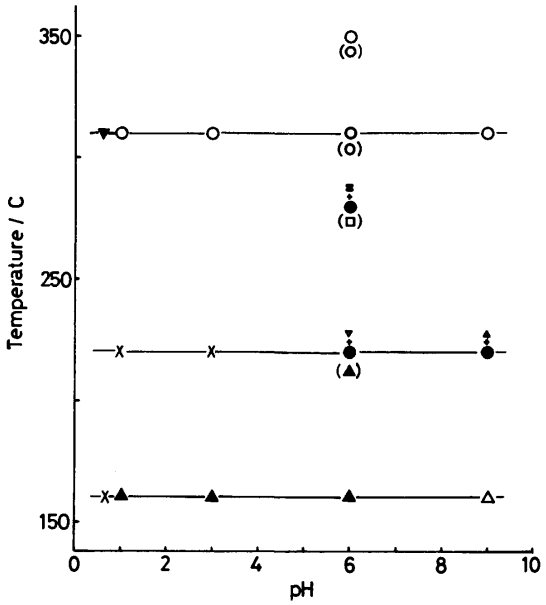

Fig. 1. Reaction diagram for the system TMA-ZrO_2-P_2O_5-H_2O.
●: NASICON(I), ○: NASICON(II), △: 12.6, ▲: 10.5, □: 9.9, ■: 9.2, ▽: 8.6, ×: amorphous, ▼: a mixture of some low crystalline phases, including phase NASICON(I). The phases obtained using reaction mixtures with a P/Zr ratio of 4 are shown in parentheses.

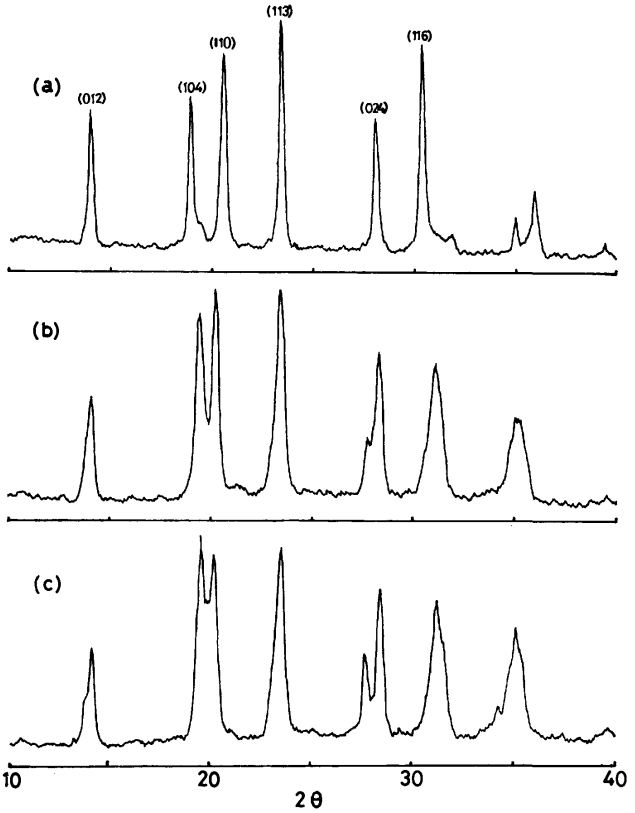

Fig. 2. X-Ray diffraction patterns of (a) sample A, (b) sample A-1, and sample A-2 for Cu$K\alpha$ rays. Main reflections are indexed for sample A.

composition analysis was made on phases 10.5 and 9.9 with high crystallinity. N, C, H analyses of these two phases yielded: N, 1.89; C, 6.23; H, 2.49 and N, 1.83; C, 6.12, H, 2.39 wt% or 1:3.85:18.4 and 1:3.90:18.3 in molar ratio, respectively. Both phases were also found to convert to α-ZrP_2O_7 upon heating to 1000°C. On the basis of the above results, in connection with the TG data, phases 10.5 and 9.9 can be identified as the TMA intercalates of α-zirconium phosphate, with compositions of $ZrH_{1.52}(TMA)_{0.48}(PO_4)_2 \cdot 0.6\ H_2O$ and $ZrH_{1.54}(TMA)_{0.46}(PO_4)_2 \cdot 0.4H_2O$, respectively. These two intercalates expanded their layers by as little as 3.1 or 2.5Å over that of the anhydrous form of α-zirconium phosphate. These values are much less than 6.9Å for the van der Waals diameter of the TMA ion. This is probably because the methyl groups of intercalated TMA ions would dip under the surface of the phosphate layer, due to an ionic attraction with the surface oxygens.

A similar but more detailed characterization was made on the NASICON(II) -type samples obtained. Table 1 lists data concerning the composition and structure of two typical samples prepared under different conditions. Both samples exhibited similar X-ray diffraction patterns, one of which is shown in Fig. 2(a). An organic analysis of sample A (obtained from a phosphorus-rich reaction mixture) yielded: N, 2.23; C, 0.32; H, 0.62 wt% or 1:0.17:3.89 in molar ratio, indicating that the NASICON(II) phase includes NH_4^+ ions, probably produced by the thermal decomposition of the TMA ions. An analysis of the deammonated form of sample A gave: ZrO_2, 51.2; P_2O_5, 44.5 wt% or 1:1.51 in P/Zr ratio. From the above data and the TG traces (described later), the composition of sample A was determined (Table 1). Sample B, obtained from a reaction mixture with a P/Zr ratio of 1.5, yielded solids containing fewer ammonium ions. The observed X-ray diffraction peaks for both samples were indexed on the basis of hexagonal cells with the lattice constants listed in Table 1. It has been noticed that the ammonium-exchanged form of $MZr_2(PO_4)_3$ contracted along the a axis and expanded along the c axis, compared to the Li, Na, or K forms.[5]

Figure 3 shows the TG curves for samples A and B. Upon heating, the ammonium form releases its water at 280—350°C and undergoes deammonation at 400—

Table 1. Preparation conditions of $(NH_4)_xH_{1-x}(PO_4)_3$ and their characterization

Sample	Hydrothermal cond. p/Zr	pH	T/°C	t/h	Composition	Lattice const.[a] a/Å	c/Å
A	4	6	310	60	$(NH_4)_{1.0}Zr_2(PO_4)_3 \cdot 0.07H_2O$	8.669	24.23
B	1.5	6	350	120	$(NH_4)_{0.62}H_{0.38}Zr_2(PO_4)_3 \cdot 0.13H_2O$	8.694	24.19

a) Rhombohedral.

TABLE 2. STRUCTURAL AND ION EXCHANGE PROPERTIES OF THE CALCINED FORMS OF $(NH_4)_xH_{1-x}(PO_4)_3$

Sample	Calcination cond. Precursor	T/°C	t/h	X-ray pattern	Ion exchange capacity/meq g^{-1} for Li^+	Na^+	K^+	Cs^+
A						0.015		
A-1	A	600	1	NASICON-like	1.95	1.99	0.088	0.039
A-2	A	600	2	NASICON-like	1.78	1.83		
A-3	A	600	12	NASICON-like	1.25	1.47	0.087	0.042
B						0.008		
B-1	B	520	12	NASICON-like	1.54	1.43	0.027	0.009

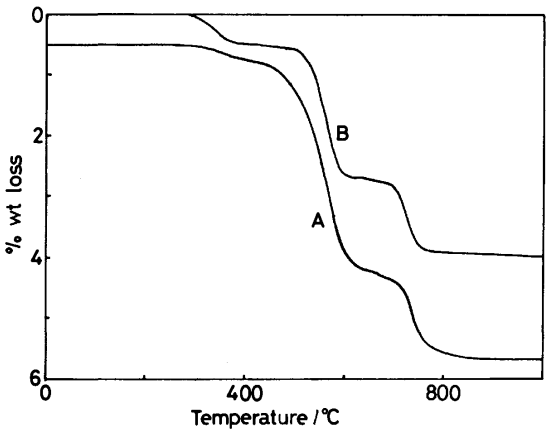

Fig. 3. TG curves for (A) sample-A and (B) sample-B with a heating rate of 10°C min^{-1}. The vertical scale for (A) is shifted by 0.5%.

640°C to convert to the proton analogue $HZr_2(PO_4)_3$. This conversion was confirmed by an IR observation. During the second weight loss, the NH_4^+ deformation band at 1440 cm^{-1} disappears and the band due to OH stretching appears at 3645 cm^{-1}. The third weight loss at higher temperatures is due to the condensation of the phosphate groups.

Ion-exchange-capacity measurements on samples A and B and their calcined products were made using the procedure described before. In each run, the pH of an equilibrated solution decreased from an initial value of *ca.* 4.5 to 2—3.5 in 24—30 h and remained constant for longer times. The data obtained are summarized in Table 2. The X-ray diffraction profiles of the calcined products were characterized by the shift of the two diffraction peaks corresponding to the (104) and (110) reflections of the ammonium form as well as by the broadening or splitting of the peaks corresponding to its (012) and (124) reflections, as shown in Fig. 2 (b) and (c). For sample A-1, calcined at 600 °C for 1 h, the ion exchange capacities for Li^+ and Na^+ ions are close to 2.14 mmol g^{-1} for the theoretical capacity of $HZr_2(PO_4)_3$, while those for K^+ and Cs^+ are 25—55 times smaller than the theoretical value. The X-ray diffraction and IR patterns of sample A-1 were changed to those for $LiZr_2(PO_4)_3$ or $NaZr_2(PO_4)_3$ after treatment with their corresponding chloride solution, but little affected by using KCl and CsCl solutions. These findings indicate that the protons in $HZr_2(PO_4)_3$ are exchanged by unhydrated Li^+ and Na^+ ions which are 0.74 and 1.02 Å in ionic radius, respectively. Also, protons other than surface protons are unreplaceable by K^+ and Cs^+ ions which are 1.38 and 1.70 Å in ionic radius, respectively. Because of their isomorphous structures, the diameter of a bottleneck formed by three ZrO_6 octahedral edges and three PO_4 tetrahedral edges for $HZr_2(PO_4)_3$ would be close to that for $NaZr_2(PO_4)_3$, *i.e.*, twice the difference of the Na-O distance[11] and O^{2-}-ion radius (or 2.3 Å). This diameter is large enough to allow Li^+ and Na^+ ions to diffuse into the cavity in the $(Zr_2P_3O_{12})^-$ framework, but too small for K^+ and Cs^+ ions. Thus, that the selectivity of $HZr_2(PO_4)_3$ for Li^+ and Na^+ uptakes is much higher than that for the others can be attributed to an ion-sieving effect of the intracrystalline bottleneck. It has also been noticed that the number of protons replaceable by Li^+ and Na^+ ions decreases with an increase in calcination time. However, the number of protons replaceable by K^+ and Cs^+ remains unaltered. One possible explanation for this behavior may be that the condensation of inner HPO_4^{2-} group in $HZr_2(PO_4)_3$ proceeds in preference to that of the surface ones.

TABLE 3. ACID STRENGTH OF $HZr_2(PO_4)_3$ AND α-ZIRCONIUM PHOSPHATE IN WATER[a]

	Ho +4.8	+3.3	+1.5	−3.0	−5.6	
$HZr_2(PO_4)_3$	+	+*	−	−	−	This work
α-zirconium phosphate	+	+	−	−	−	Ref. 10

a) +, Acidic color; −, basic color; +*, see text.

The acid strength of $HZr_2(PO_4)_3$ in water as well as in benzene was qualitatively determined using sample A-1. This compound was found to have, qualitatively, the same acid strength of Ho≥3.3 in both liquids. The data obtained are shown in Table 3, along with those for α-zirconium phosphate.[10] For Ho=+3.3, however, the triphosphate solid rapidly became pale red on contact with the indicator, but turned pale gray in 1 h or more. Such fading was not observed for the α-zirconium phosphate. These results indicate that the acid strength of $HZr_2(PO_4)_3$ in a little weaker than that of α-zirconium phosphate.

The authors wish to thank Mr. Y. Ogura and Y. Masuda for the preparation of high pressure bombs, Dr. M. Onoda for helpful advice regarding X-ray analysis, and Dr. F. Okamura and M. Goto for their fruitful

advice and encouragement during this work.

The essence of this article was presented in Abst. No. 4Q32 of the 49th National Meeting of the Chemical Society of Japan, 1984 (received December 10, 1983).

References

1) T. Kijima, S. Ueno, and M. Goto, *J. Chem. Soc., Dalton Trans.*, **1982**, 2499.

2) T. Kijima, J. Tanaka, M. Goto, and Y. Matsui, *Nature*, **310**, 45 (1984).

3) U. S. Patent 3702886.

4) S. T. Wilson, B. M. Lok, C. A. Messina, T. R. Cannan, and E. M. Flanigen, *J. Am. Chem. Soc.*, **104**, 1146 (1982).

5) H. Y-P. Hong, *Mat.Res. Bull.*, **11**, 173 (1976); J. B. Goodenough, H. Y-P. Hong, and J. A. Kafalas, *ibid.*, **11**, 203 (1976).

6) G. Alberti, "Inorganic Ion Exchange Materials," ed by A. Clearfield, CRC Press, Boca Raton, Fla. (1982), p. 98.

7) A. Ono, *J. Mater. Sci.*, **19**, 2691 (1984).

8) A. Clearfield, B. D. Roberts, and M. A. Subramanian, *Mat. Res. Bull.*, **19**, 219 (1984).

9) A. Clearfield, R. H. Blessing, and J. A. Stynes, *J. Inorg. Nucl. Chem.*, **30**, 2249 (1968).

10) T. Kijima and M. Goto, *Thermochim. Acta*, **63**, 33 (1983).

11) L. Hagman and P. Kierkegaard, *Acta Chem. Scand.*, **22**, 1822 (1968).

Mössbauer Study of ^{60}Co γ-Ray Irradiated $Fe_xMg_{1-x}(NH_4)_2(SO_4)_2 \cdot 6H_2O$

Nobuhiko SAKAI,* Fumiko SAKAI,† and Hisashi SEKIZAWA
The Institute of Physical and Chemical Research, Wako, Saitama 351-01
†*The Institute for Solid State Physics, The University of Tokyo, Roppongi, Minato-ku, Tokyo 106*
(Received July 19, 1984)

The γ-ray radiolytic oxidation of Fe^{2+} ions in $Fe_xMg_{1-x}(NH_4)_2(SO_4)_2 \cdot 6H_2O$ ($x=1.0$, 0.75, 0.56, 0.35, and 0.075) is studied by Mössbauer spectroscopy. For $x \leqq 0.75$, a part of Fe^{2+} ions remain unoxidized even after heavy irradiation of ^{60}Co γ-rays in contrast to the complete disappearance of Fe^{2+} ions for $x=1.0$. At least three kinds of Fe^{3+} ions are produced, and two of them order magnetically at liquid He temperature. Their saturated relative amount after heavy irradiation depends on the concentration of Fe, and is well explained by the random distribution probability of Fe and Mg ions among the six neighboring metallic sites around the Fe^{2+} ion.

Irradiation of ^{60}Co γ-rays induces oxidation of Fe^{2+} ions in hydrated salts. This phenomenon has been explained by the OH radical mechanism, *i.e.* energetic electrons created by the γ-ray Compton scattering or the photo-electron effect induce OH radicals along their paths from coordination H_2O molecules around Fe^{2+} ions, and these OH radicals oxidize the Fe^{2+} to Fe^{3+} ions.[1-3] A Mössbauer spectroscopic study of the oxidation of Fe^{2+} ions in $FeSO_4 \cdot nH_2O$[1] supported the OH radical mechanism. The oxidation occurs when n is not zero, and the chemical formula of the final radiolytic product was proposed to be $Fe_x(OH)_y(SO_4)_z \cdot nH_2O$,[1] and an accurate formula was later established in the case of $FeSO_4 \cdot 7H_2O$ to be $Fe(OH)(SO_4) \cdot 2H_2O$.[2] Electron and γ-ray irradiation experiments on $Fe(NH_4)_2(SO_4)_2 \cdot 6H_2O$ also indicate radiolysis of the water of crystallization.[4,5] The OH radical mechanism due to the electron capture process of ^{57}Co to ^{57}Fe was also suggested by a Mössbauer experiment on ^{57}Co-doped hydrated salts. However, except for the coordination water, little is known about the effect of the environment around a Fe atom on the oxidation of Fe^{2+} by γ-ray irradiation in a hydrated salt. Even though the water molecules around a Fe^{2+} are necessary to oxidize Fe^{2+} to Fe^{3+} at the primary step of the oxidation process, it is not clear whether their presence itself is sufficient or not for the final stabilization of Fe^{3+} ions in solids.

Besides the studies of the OH radical oxidation, after-effects of Auger ionization following electron capture were studied[6] using several ^{57}Co-labelled Co(III) complexes having no H_2O molecules. In some cases, depending on the structure of neighboring molecules, Fe(II) states were observed in emission spectra, which led to the conclusion that fragmentation of the parent molecules occurred as a consequence of the Auger ionization. Furthermore, emission spectra of ^{57}Co-labelled Co(III) complexes, containing various anions in the second coordination sphere, revealed that the yield of Fe(II) state was strongly affected by the presence of oxalate anions in the second coordination sphere.[7]

In the present study, a mixed crystal system $Fe_xMg_{1-x}(NH_4)_2(SO_4)_2 \cdot 6H_2O$ was prepared to examine the effect of the environment around a Fe^{2+} ion on its oxidation induced by the γ-ray irradiation. Here, the environment around a Fe^{2+} ion is characterized by a local distribution of Mg^{2+} ions which is expected to be stable under γ-ray irradiation.

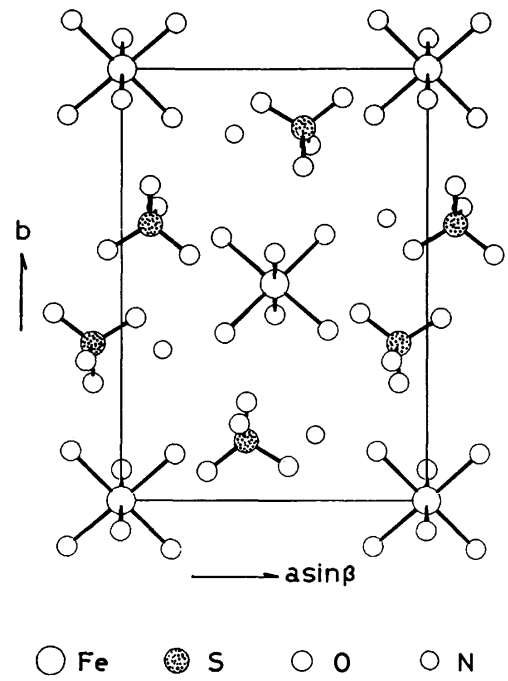

Fig. 1. Crystal structure of $Fe(NH_4)_2(SO_4)_2 \cdot 6H_2O$. The dimensions of the unit cell are $a=9.324$ Å, $b=12.65$ Å, $c=6.24$ Å, and $\beta=106.8°$.[8]

The crystal structure of ammonium magnesium sulfate hexahydrate, $Mg(NH_4)_2(SO_4)_2 \cdot 6H_2O$, is isomorphous to that of $Fe(NH_4)_2(SO_4)_2 \cdot 6H_2O$, and a desired amount of Mg ions can be mixed without changing the monoclinic crystal structure of $Fe(NH_4)_2(SO_4)_2 \cdot 6H_2O$. A unit cell of this crystal is shown in Fig. 1. Each Fe ion in this crystal structure is surrounded by six H_2O, two NH_4, and two SO_4 molecules as first neighbors. Further apart, there are six Fe ions as second neighbors. If only the first neighbors around a Fe^{2+} ion contribute to the stabilization of a Fe^{3+} ion produced by irradiation, the ratio of Fe^{2+} to the induced Fe^{3+} ions should remain constant after the same irradiation dose, independent of a different Mg concentration. Therefore, if the ratio of Fe^{2+} to Fe^{3+} ions is found to change with the concentration of Mg ions, we can say that the stablization of the induced Fe^{3+}

ions are affected by the second neighboring Mg, Fe ions, or other molecules.

Experimental

Mixed crystals of $Fe_xMg_{1-x}(NH_4)_2(SO_4)_2\cdot 6H_2O$ were prepared by dissolving commercially available reagents of x amount of $Fe(NH_4)_2(SO_4)_2\cdot 6H_2O$ and $1-x$ amount of $Mg(NH_4)_2(SO_4)_2\cdot 6H_2O$ into water for x=1.0, 0.8, 0.6, 0.4, and 0.1. Concentrations of Fe in the precipitated mixed crystals from saturated solution at room temperature were determined by chemical analysis to be 0.75, 0.56, 0.35, and 0.075 for x=0.8, 0.6, 0.4, and 0.1, respectively. The observed X-ray diffraction patterns of the mixed crystals were equivalent to that of $Fe(NH_4)_2(SO_4)_2\cdot 6H_2O$. The mixed polycrystals were irradiated by ^{60}Co γ-rays at temperatures below 42°C in loosely sealed glass tubes. The ^{60}Co γ-ray irradiation was accomplished up to 5.23×10^9 rad(H_2O). The dose rate was between 2.80 and 2.93×10^6 rad(H_2O)/h.

After being irradiated with the desired amount of dose, a part of each specimen was separated from the glass tube and mixed with vacuum grease for the Mössbauer spectroscopic analysis. After the heavy irradiation, the specimens were broken to fragile blocks, and the specimen with x=1.0 slightly moistened. Their colors were white or yellow-brown depending on the concentration of Fe ions. After an irradiation of 5.23×10^9 rad(H_2O), $Fe(NH_4)_2(SO_4)_2\cdot 6H_2O$ crystals turned almost totally to blocks of transparent acicular crystals. The dimensions of each crystal were about 0.01 mm in diameter and 0.2 mm in length.

Results

Measurements of the Mössbauer spectra of the irradiated samples were made mainly at room temperature, and partly at liquid N_2 and liquid He temperatures. The Mössbauer spectra were analyzed by a computer processing which includes least squares fitting of Lorentzian curves to the experimental absorption peaks, with a correction for the base-line sag. The same recoilless fraction was assumed for all the Fe ions. The assignments for Fe^{3+} in the following are based on the values of the isomer shifts of the corresponding absorption peaks.

$Fe(NH_4)_2(SO_4)_2\cdot 6H_2O$: The Mössbauer spectra of the irradiated $Fe(NH_4)_2(SO_4)_2\cdot 6H_2O$ specimens measured at room temperature are shown in Fig. 2. The fitted absorption peaks are shown in the figure by the solid curves. Before irradiation, only the quadrupole-split peaks of Fe^{2+} were observed. The Fe^{3+} peaks are successfully analyzed under an assumption of two kinds of quadrupole-split peaks(Fe^{3+} (1) and Fe^{3+} (2)). The Fe^{2+} peaks disappeared completely on heavy irradiation above 3.66×10^9 rad(H_2O), and no changes were observed in the Mössbauer spectra by further irradiation up to 5.23×10^9 rad(H_2O). The Mössbauer spectrum of a sample irradiated to 5.23×10^9 rad(H_2O) was also measured at 4.2 K and shown in Fig. 3a. The peaks of Fe^{3+} radiolytic products in this specimen can be resolved at least into three components, and two of

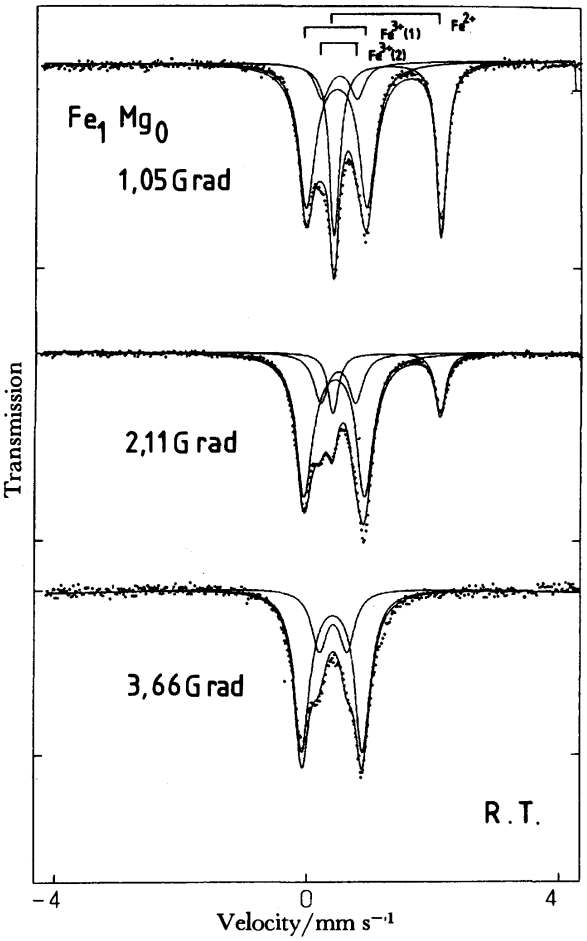

Fig. 2. Mössbauer spectra of $Fe(NH_4)_2(SO_4)_2\cdot 6H_2O$ irradiated by ^{60}Co γ-rays. The solid lines are the calculated absorption peaks.

them are in magnetically ordered states. The major component denoted by Fe^{3+} (1a) evidently corresponds to the recognized acicular small crystals. The minor component denoted by Fe^{3+} (1b) in the figure was not resolved in the room-temperature spectrum, and is considered to be included in the Fe^{3+} (1) component. The values of the hyperfine magnetic fields and other Mössbauer parameters are tabulated in Table 1, together with those at room temperature.

The total amount of Fe^{3+} approaches nearly exponentially to a constant value in relation to the γ-ray dose. From the Fe^{3+}/Fe ratio determined by the computer fitting, the G value (the number of Fe^{3+} ions produced for each 100 eV of energy absorbed) is evaluated to be 2.65±0.35 for the ^{60}Co γ-ray dose below 2.7×10^9 rad(H_2O); the ratio of the atomic number Z to the mass number A for the specimen and that for water were used to estimate the absorbed dose in the specimen.

The effect of humidity on the oxidation was examined in some cases. A specimen in a sealed tube with CaO as desiccant was irradiated. After an irradiation of 1.1×10^9 rad, the remaining Fe^{2+} peak became broad and the amount of Fe^{3+} was markedly higher, *i.e.* Fe^{2+}/Fe was lower in comparison with the irradiation

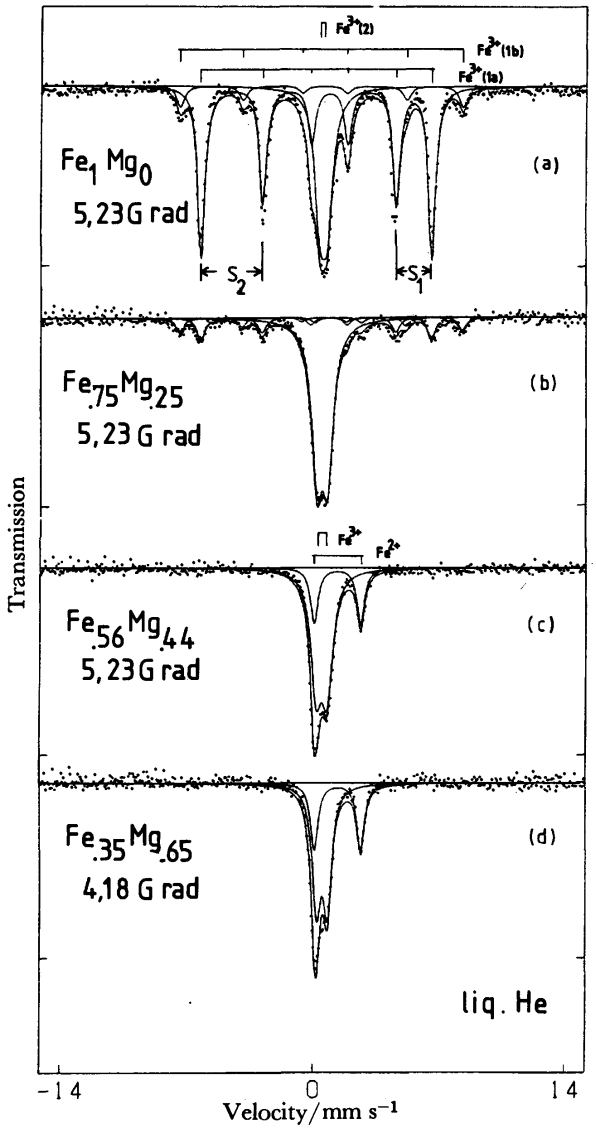

Fig. 3. Mössbauer spectra of γ-ray irradiated $Fe_xMg_{1-x}(NH_4)_2(SO_4)\cdot 6H_2O$ measured at 4.2 K.

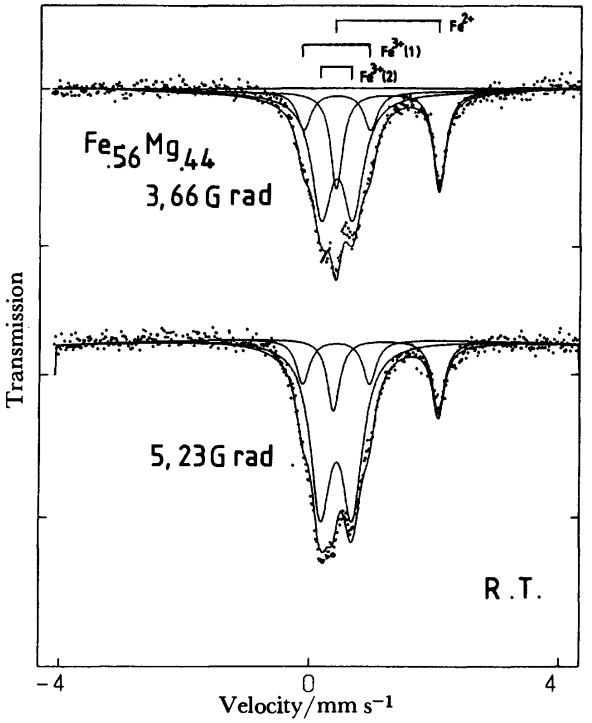

Fig. 4. Mössbauer spectra of γ-ray irradiated $Fe_{0.56}Mg_{0.44}(NH_4)_2(SO_4)_2\cdot 6H_2O$ measured at room temperature.

in air (see Fig. 6). On the contrary, the Fe^{2+}/Fe ratio was higher when a specimen was irradiated together with a small amount of water.

$Fe_xMg_{1-x}(NH_4)_2(SO_4)_2\cdot 6H_2O$: The Mössbauer spectra of the irradiated mixed crystals with $x=0.56$ and $x=0.075$ measured at room temperature are shown in Figs. 4 and 5, respectively. The Fe^{2+} quadrupole splitting of $x=0.075$ is 2% smaller than that of $x=1.0$. All spectra were analyzed by assuming two Fe^{3+} components ($Fe^{3+}(1)$ and $Fe^{3+}(2)$). The best fitted values of the quadrupole splitting and the isomer shift of $Fe^{3+}(2)$ were not the same for all the spectra and distributed to some extent as tabulated in Table 1. In the case of the specimen with $x=0.56$, some of the Fe ions retain the Fe^{2+} state even after the irradiation of 5.32×10^9 rad(H_2O) which was sufficient in the case of $Fe(NH_4)_2(SO_4)_2\cdot 6H_2O$ to change all Fe^{2+} ions to Fe^{3+}. The suppression of the radiolytic oxidation of Fe^{2+} ions is more significant for $x=0.075$ as can be seen in Fig. 5. Almost 85% of Fe ions still remain in the Fe^{2+} state after an irradiation of 2.8×10^9 rad(H_2O). The ratio of the remaining Fe^{2+} to the total Fe *versus* the γ-ray dose is plotted in Fig. 6. It should be noted that the Fe^{2+}/Fe ratios measured at liquid N_2 temperature agreed with those at room temperature within 5%. Then, the assumption that Fe^{2+} and Fe^{3+} ions have the same recoilless fraction is fairly good. It is characteristic that all the curves for the Fe^{2+}/Fe ratios are saturated. The

TABLE 1. MÖSSBAUER PARAMATERS OF γ-IRRADIATED $Fe_xMg_{1-x}(NH_4)_2(SO_4)_2\cdot 6H_2O$

Component	T	ΔE_Q	δ(Fe)[a]	H_{hf}	4ε[b]
	K	mm s^{-1}	mm s^{-1}	kOe	mm s^{-1}
Fe^{2+}	300	1.71±0.03(x=1.0)	+1.25±0.02		
		1.67±0.03(x=0.1)			
$Fe^{3+}(1)$	300	0.96±0.03	+0.42±0.03		
(1a)	4.2		+0.24±0.02	396.3	−1.41
(1b)	4.2		+0.24±0.02	485.8	−0.36
$Fe^{3+}(2)$	300	0.35—0.45	+0.40—+0.45		
$Fe^{3+}(3)$	300	0.19±0.03	+0.36±0.03		

a) Relative to metallic iron. b) $4\varepsilon=S_1-S_2$; for the definitions of S_1 and S_2, see Fig. 3a.

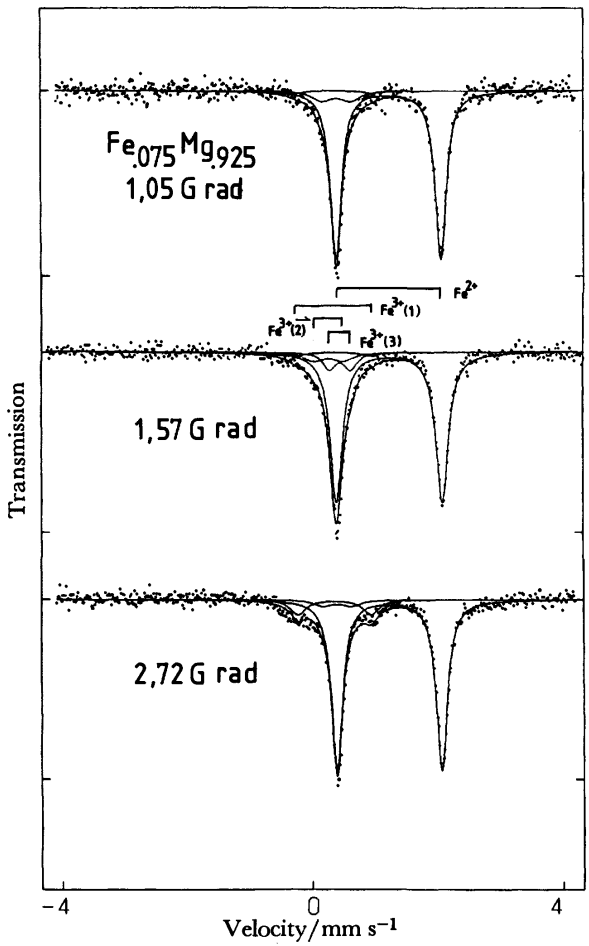

Fig. 5. Mössbauer spectra of γ-ray irradiated mixed crystal $Fe_{0.075}Mg_{0.925}(NH_4)_2(SO_4)_2 \cdot 6H_2O$ measured at room temperature.

saturated final value of the Fe^{2+}/Fe ratio is lower for higher concentration of Fe ions.

Figure 3b shows a spectrum of the specimen with $x=0.75$ measured at 4.2 K after an irradiation of 5.23×10^9 rad(H_2O). The $Fe^{3+}(1)$ component having a large quadrupole splitting at room temperature orders magnetically, but the rest of the $Fe^{3+}(2)$ having a smaller splitting does not. The room-temperature Mössbauer spectrum of $x=0.56$ contains a small amount of the $Fe^{3+}(1)$ component. However, no magnetically split peaks were observed at 4.2 K for this specimen (see Fig. 3c). This can be ascribed to the weak intensities of these absorption peaks.

Discussion

The Mössbauer spectra of the mixed crystals $Fe_xMg_{1-x}(NH_4)_2(SO_4)_2 \cdot 6H_2O$ show that the relative amount of the Fe^{3+} radiolytic products to the total Fe varies remarkably with the concentration of Mg ions. The evaluated absorbed dose in each mixed crystal from the Z/A ratio different slightly from one another, but their mutual deviations are only within 2%. Thus the large differences in the saturated ratios of the remaining Fe^{2+} to the total Fe (Fig. 6) can not be explained by these slight differences between the absorbed doses in the mixed crystals.

We notice that there are two kinds of Fe^{3+} ($Fe^{3+}(1)$ and $Fe^{3+}(2)$) in the spectra shown in Figs. 2—4; one of them orders magnetically at 4.2 K and another does not. There is a possibility of another Fe^{3+} component ($Fe^{3+}(3)$) to exist, which has a much smaller quadrupole splitting, in the spectra of $x=0.075$ and 0.35, because its addition is effective in obtaining a better fitted spectrum as shown in Fig. 5; this component does not order magnetically at 4.2 K.

In Fig. 7, the summed saturated ratio of the magnetically ordered components ($Fe^{3+}(1)=Fe^{3+}(1a)+Fe^{3+}(1b)$) to the total Fe, and that of the rest Fe^{3+} ($Fe^{3+}(2,3)$) are plotted separately. We can analyze the behavior of these ratios as follows. Since the ratios depend on the Fe concentration, the spacial statistical average for the distribution of Fe in the mixed crystal seems to be related to these ratios. Assuming a random distribution of Fe and Mg atoms among the simple cubic lattice, we can estimate the probability that we find N or more than N Fe atoms within a sphere with radius

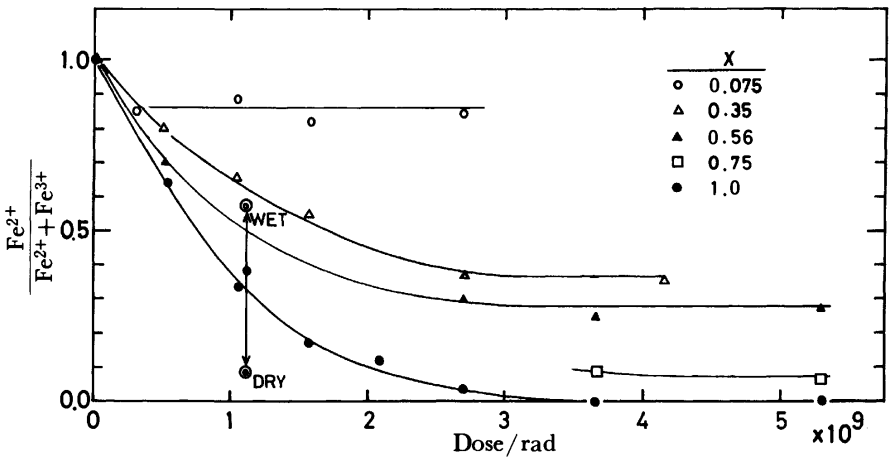

Fig. 6. Fe^{2+}/Fe ratios determined by the calculated Mössbauer absorption intensities. The notations WET and DRY for $x=1.0$ denote the specimens irradiated with water and CaO, respectively.

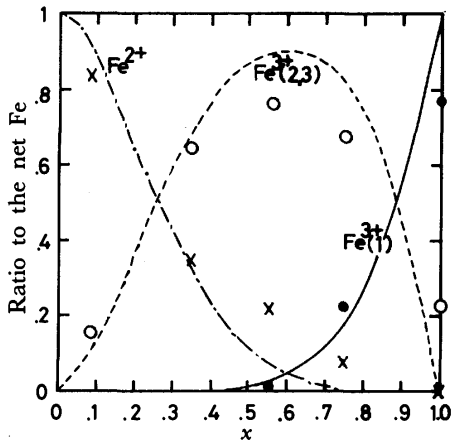

Fig. 7. The ratios of the saturated amount of Fe^{3+} ions induced by γ-ray irradiation and the remaining Fe^{2+} ions. The notations $Fe^{3+}(1)$ and $Fe^{3+}(2,3)$ denote the magnetically ordered component and the rest one, respectively.

R around an Fe atom. Figure 8 shows the concentration dependence of this probability. The unit of the radius is the lattice constant of the simple cubic lattice. The change of the probability becomes steep as the radius increases, that is, as the number of the sites in the sphere increases. The observed ratios shown in Fig. 7 change rather gradually against the Fe concentration. Then the effective local environment, which is considered to be related to the formation of stable Fe^{3+} ions, is best characterized by the probability for R= 1.0. This means that only the neighboring six metallic-ion sites are strongly related to the radiolysis of a Fe atom.

Using the probability for R=1.0, we can interpret the saturated ratios of the remaining Fe^{2+}, $Fe^{3+}(1)$, and $Fe^{3+}(2,3)$. When a Fe^{2+} is initially surrounded by six or five Mg ions ($N<2$), this Fe^{2+} ion cannot be oxidized into a stable Fe^{3+} ion by the ^{60}Co γ-ray irradiation (dot-dashed curve: N=2 curve of Fig. 8(a) being inverted), even though water molecules exist as the nearest neighbors. The ratio of the $Fe^{3+}(2,3)$ components can be explained by the total probability that any number of Fe ions from 2 to 5 initially occupies the neighboring six metallic-ion sites (dashed curve: the vertical distance from the curve 2 to 6 of Fig. 8a). The distributed values of the quadrupole splitting of $Fe^{3+}(2,3)$ component as mentioned in Table 1 reflect the occurrence of the different sites of this component. Furthermore, if the neighboring six metallic ion sites around a Fe^{2+} ion are initially all occupied by Fe ions, this Fe^{2+} ion is oxidized and has a possibility to recrystallize into the new compounds denoted by $Fe^{3+}(1)$. The calculated probability is shown in the figure by a solid curve.

The above proposed interpretation implies that the Fe^{3+} ions are stabilized only when more than one Fe^{3+} states are produced among the neighboring six sites at the same time or within the relaxation time of Fe^{3+} states, and these Fe^{3+} states are probably stabilized by constituting a Fe^{3+} ion cluster. In a low Fe concentration region, these clusters are considered to be created isolatedly, and Fe^{3+} ions ($Fe^{3+}(2,3)$) in the clusters cannot be in a magnetically ordered state, at least above 4.2 K. In a high Fe concentration region, $x>0.5$, a part of the created clusters can segregate new Fe^{3+} compounds (Fe^{3+}(1a,1b)), because the original mixed crystal possesses many paths which connect Fe ions without interruption by Mg ions. According to the percolation theory, the percolation probability of the simple cubic lattice is 0.254 for the site property.[9]

This simple model, however, does not completely explain the observed ratios; fairly large Fe^{2+} ratios above x=0.5, and the existence of the nonmagnetic component at x=1.0. It should be emphasized that the proposed model describes only the initial circumstance around a Fe^{2+} ion, and does not specify the process of recrystallization of the material, which will occur

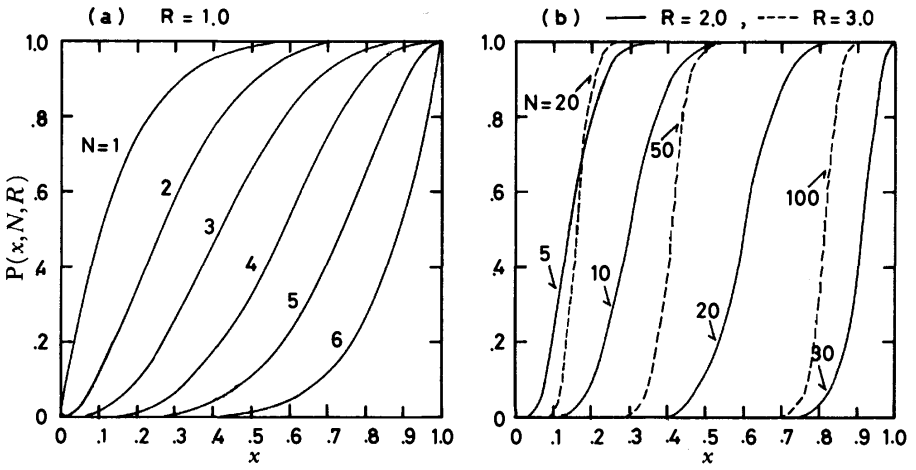

Fig. 8. The probabilities that N or more than N Fe atoms are found in a sphere of radius R. Fe atoms with a concentration of x are assumed to be dispersed at random on the simple cubic lattice sites. (a) R=1.0, and the number of the lattice sites in the sphere, N_s, is 6. (b) solid curves; R=2.0 and N_s=32, dashed curves; R=3.0 and N_s=122.

during irradiation for several months. Therefore, during recrystallization, the model-calculated ratios of Fe^{3+} ions will be modified. As mentioned above, humidity evidently affected the formation of the Fe^{3+} compound. Particularly, when the initial amount of water of crystallization is not the same as the final one, as it probably is in the present case, excess water molecules will play an important role in the recrystallization process, which act to suppress the formation of Fe^{3+} ions. The amount of the remaining Fe^{2+} ions above $x=0.5$, which is larger than the model-calculated value, seems to be due to this excess water. Thus, the final amount of Fe^{3+} ions is the result of at least two competitive processes; the OH radical process which is considered to be an important mechanism at the primary step of the radiolysis, and the following recrystallization process.

The radiolytic chemical reaction which produces Fe^{3+}(1a) component from $Fe(NH_4)_2(SO_4)_2\cdot 6H_2O$ is considered to be

$$Fe(NH_4)_2(SO_4)_2\cdot 6H_2O \rightsquigarrow Fe(NH_4)_2(OH)(SO_4)_2\cdot nH_2O + 1/2H_2 + (5-n)H_2O, \quad (n<5),$$

because i) the radiolytic product did not have an odour of ammonia, and ii) SO_4 molecules are not separated by the γ-ray irradiation in the case of $FeSO_4\cdot 7H_2O$. The measured X-ray diffraction pattern of the radiolytic product from $Fe(NH_4)_2(SO_4)_2\cdot 6H_2O$ could not be found in the X-ray powder diffraction file.[10] To the authors' knowledge, a material having the chemical formula $Fe(NH_4)_2(OH)(SO_4)_2\cdot nH_2O$ is not known.

Conclusion

The ^{60}Co γ-ray irradiation induced the oxidation of Fe^{2+} ions in a mixed salt $Fe_xMg_{1-x}(NH_4)_2(SO_4)_2\cdot 6H_2O$ (x=1.0, 0.75, 0.56, 0.35, and 0.075). At least three kinds of Fe^{3+} states were clearly observed, and the relative saturated amount of the induced Fe^{3+} ions to the total Fe ions in each mixed salt varied remarkably with the concentration of Mg ions. This phenomenon can not be explained only by the presence of the coordination water. The simple six-neighbor metallic site model, which represents the effective initial environment around a Fe^{2+} ion, well explains the characteristic concentration dependence of the saturated amounts of these Fe^{3+} radiolytic products. This result suggests that the initial environment, which includes only the neighboring six metallic ion sites around a Fe^{2+} ion, strongly affects the formation of the final Fe^{3+} products from this mixed hydrated salt. It is interpreted that the induced Fe^{3+} states are only stabilized when more than one Fe^{3+} ions are produced among the neighboring six sites at the same time or within the relaxation time of Fe^{3+} states, and these Fe^{3+} states are probably stabilized by constituting a Fe^{3+} cluster. In a high Fe concentration region, these clusters can segregate new Fe^{3+} compounds. However, to clarify the discrepancy between the model-calculated ratios and the experimental ones, more detailed consideration on the recrystallization process is required.

We are grateful to Dr. T. Okada for his helpful advice on the Mössbauer measurements, and Mr. K. Nakano for his assistance in the operation of the γ-irradiation equipment.

References

1) J. Meyers, J. Ladrière, M. Chavee, and D. Apers, *J. Phys. (Paris)*, **37**, C6-905 (1976).
2) N. Sakai, H. Sekizawa, and K. Ôno, *J. Inorg. Nucl. Chem.*, **43**, 1731 (1981).
3) Ph. Gütlich, S. Odar, B. W. Fitzsimmons, and N. E. Erickson, *Radiochim. Acta*, **10**, 147 (1968).
4) G. K. Wertheim and D. N. E. Buchanan, *Chem. Phys. Lett.*, **3**, 87 (1969).
5) W. Triftshäuser and P. P. Craig, *Phys. Rev.*, **162**, 274 (1967).
6) A. Nath, M. D. Klein, W. Kündig, and D. Lichtenstein, "Mössbauer Effect Methodology," ed by I. J. Gruverman, Plenum Press, New York, (1970), Vol. 5, p. 163.
7) H. Sano and T. Ohnuma, *Bull. Chem. Soc. Jpn.* **48**, 266 (1975).
8) H. Montgomery, R. V. Chastain, J. J. Natt, A. M. Witkowska, and E. C. Lingafelter, *Acta Cryst.*, **22**, 775 (1967).
9) V. K. S. Shante and S. Kirkpatrick, *Adv. Phys.*, **20**, 325 (1971).
10) "Powder Diffraction File (1983)," JCPDS International Centre for Diffraction Data, U.S.A.

The Distribution of Mercury, Arsenic, and Antimony in Sediments of Kagoshima Bay

Hayao SAKAMOTO
Department of Chemistry, Faculty of Science, Kagoshima University, Koorimoto, Kagoshima 890
(Received September 8, 1984)

Mercury, arsenic, and antimony were determined in marine sediments collected from Kagoshima Bay, and their distribution was investigated. The contents of mercury, arsenic, and antimony in surface sediments were higher than those in the marine sediments of the open ocean. The average contents of mercury, arsenic, and antimony in surface sediments in the northern part of the bay were higher than in the southern part. The high-temperature sediments (about 200 °C) in the vicinity of a sea bottom fumarole, located at a depth of about 200 m in the northern part of the bay, showed abnormal concentrations of mercury, arsenic, and antimony derived from the fumarole gas; the contents of these components decreased sharply with an increase in the distance from the fumarole. A high degree of positive correlation was found among the contents of the three components (mercury, arsenic, and antimony) over the northern part of the bay. In contrast, no such correlation was observed in the southern part of the bay. This is in accord with the fact that volcanic activity is more vigorous in the northern than in the southern part of the bay.

In November, 1973, high pollution with mercury exceeding the "provisional permissible level for mercury contained in fishes and shellfishes (0.4 mg kg^{-1})" was found[1] in some of the *Trichiurus lepturus* caught in the northern part of Kagoshima Bay.

Investigations of other types of fish then followed, and autonomous regulation was extended to include ten other types of fish (*Trachurus japonicus, Nemipterus bathybius, Conger myriaster, etc.*) by August, 1975. Concurrently, extensive studies[2-4] of the mercury pollution of fishes living in Kagoshima Bay, investigation of possible pollution sources,[5-7] and medical checks[8-10] of the local inhabitants have been carried out by the aid of the central and local governments. In spite of these efforts, however, the mechanism of the pollution of fish with mercury is not yet absolutely clear.

Mercury, arsenic, and antimony are elements of special interest in connection with volcanic activity[11,12] because of the volatility they exhibit as elements and in the form of compounds.

This study will concentrate on the volatile components (mercury, arsenic, and antimony) derived from volcanic activity based on the notion that volcanic activity must be related to the marine environment of Kagoshima Bay. The horizontal and vertical distributions of the mercury concentration in sea water of Kagoshima Bay have previously been reported.[13] This paper describes the results of concentrations on mercury, arsenic, antimony in marine sediments collected from Kagoshima Bay.

Experimental

General Circumstances of Kagoshima Bay. Kagoshima Bay is a narrow inner bay (about 75 km long and about 25 km wide)—an arm of the sea penetrating far into the land from south to north.

Its bottom has unique topographic features, as may be seen from the vertical section shown in Fig. 1. Sakurajima Volcano, standing between the central and northern parts of the bay, separates the two sea areas, which communicate

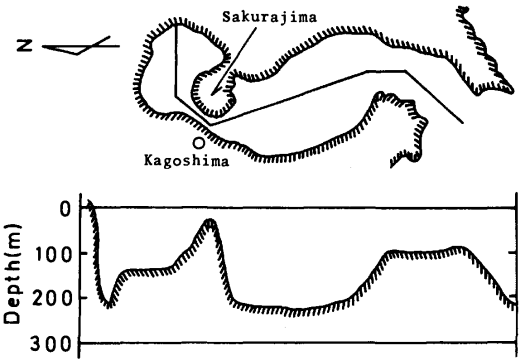

Fig. 1. Vertical section of Kagoshima Bay.

with each other only through Nishi Sakurajima Suidō, a shallow area about 40 m deep. Thus, sea-water exchange between the northern part (140 to 200 m deep) and the open ocean is not easy. The progress of pollution in the whole bay caused by human activities, both connected with daily living and industrial, is also dictated by the sea-water exchange because of the intricate topography of the bay's bottom. Considerable fumarolic activity is observed around Points **A** and **B** in the northern part of Kagoshima Bay (Fig. 2); this activity influence the marine environment in a number of ways. On the other hand, the speed of sediment accumulation in Kagoshima Bay is high due to the emissions from Minamidake of Sakurajima Volcano, which has continued to be active since October, 1955. The effects of the volcano emissions upon the sediments will be reported in a separate paper.

Methods of Collecting and Preserving Sedimentary Samples. A Smith-McIntyre spring-loading grab was used to collect surface sediments, and a Fhleger bottom sampler, equipped with a plastic inner tube 3.3 cm in inside diameter, was employed for the investigation of the vertical distribution. The sediment sample collected was immediately cut at 10 cm intervals; each fragment was enclosed in a polystyrene bottle, refrigerated at the site, and then brought back to our laboratory. Each sample was then suction-filtered with a 0.45 μm Millipore filter, air-dried (taking care to avoid any extraneous contamination), and ground in an agate mortar. The uniform sediment samples thus obtained were preserved for the subsequent determination of mercury, arsenic, and antimony.

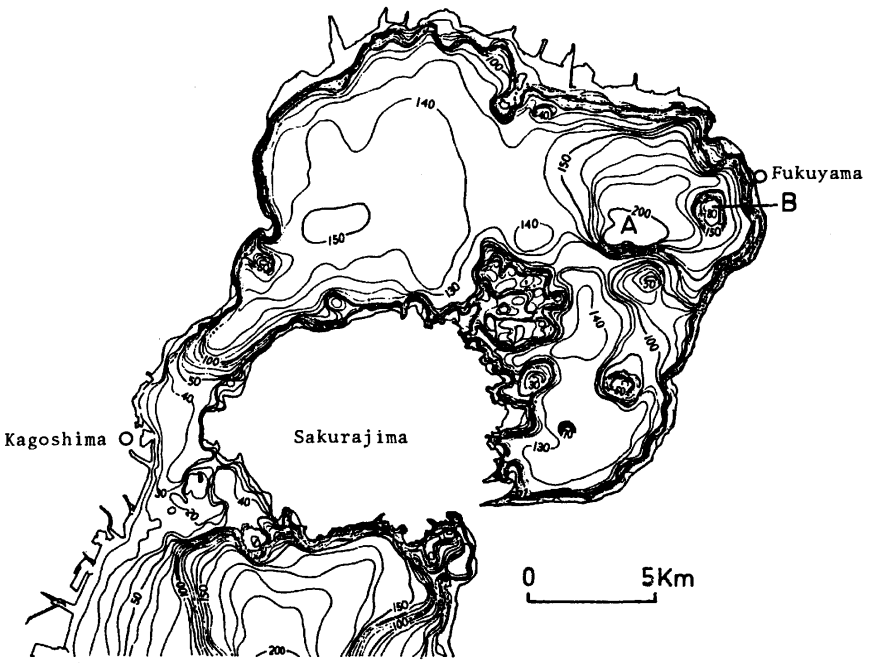

Fig. 2. Topographical map of northern Kagoshima Bay and the locations (A and B) where the submarine fumarolic activities were found.

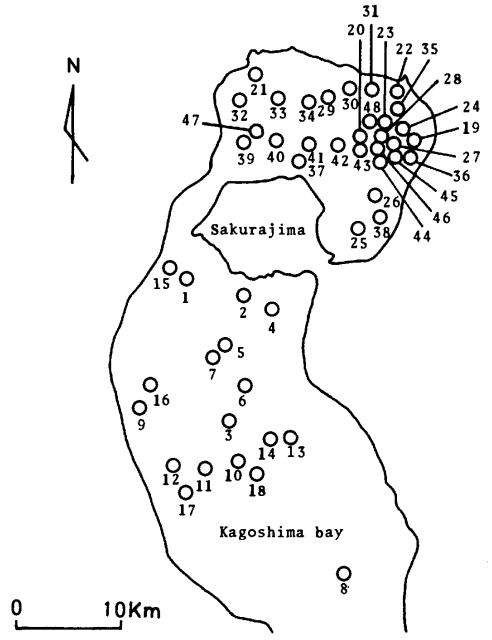

Fig. 3. Sampling stations of marine sediments in Kagoshima Bay.

Sampling Stations in Kagoshima Bay. The sediment sampling stations in Kagoshima Bay are shown in Fig. 2 and Fig. 3; the station numbers are tabulated in Table 1.

Apparatus. The apparatus used included a Rigaku Mercury SP (this apparatus was connected to an Ohkura recorder); a Hitachi spectrophotometer Model 101; an Iwaki-KM (Model V-D) shaker, and a Shimadzu-MAF atomic-absorption spectrophotometer.

Reagents. *Standard Solution of Mercury(II), 1 mg cm^{-3}*: Dissolve 1.354 g of mercuric chloride in 10 cm^3 of 5 mol dm^{-3} sulfuric acid, and dilute to 1000 cm^3 with water.

Standard Solution of Arsenic(III), 1 mg cm^{-3}: Dissolve 1.320 g of diarsenic trioxide in 10 cm^3 of 10 mol dm^{-3} sodium hydroxide, and dilute to 1000 cm^3 with water.

Standard Solution of Antimony(III), 1 mg cm^{-3}: Dissolve 1.874 g of antimony trichloride in water, and dilute to 1000 cm^3 with water.

The acids used (sulfuric acid, nitric acid, hydrochloric acid, hydrofluoric acid, perchloric acid) and potassium permanganate were all analytical-special-reagent-grade for the measurements of the toxic metals.

Procedure for the Determination of Mercury. A sediment sample (0.02 to 0.20 g), homogenized as much as possible under wet or air-dried conditions, was weighed out into a porcelain boat previously ignited to exclude any trace of mercury that might be left adhered, and covered with an addition agent (calcium hydroxide and sodium carbonate, both ignited at 700°C and then mixed in a 1:1 volume ratio). The analytical sample thus prepared was heated in the furnace of a mercury analyzer at about 300°C for three minutes, and then at about 700°C for four minutes to complete the decomposition; the mercury vapor thus evolved was caught in a potassium permanganate solution acidified with sulfuric acid[14] or with a porous gold collector.[15] In the method using a porous gold collector, once the collector heating time is properly set on the timer, the evolution of mercury vapor and its measurement by cold vapor atomic-absorption spectrometry are performed automatically, giving results of a high reproducibility in a short time.

Procedure for the Determination of Arsenic. A sediment sample (0.05 to 0.20 g) was weighed out into a Teflon beaker; 4 cm^3 of perchloric acid (60%), 3 cm^3 of sulfuric acid (96 to 98%), 8 cm^3 of hydrofluoric acid (46%), and 2 cm^3 of potassium permanganate solution (2%) were then added, and the mixture was heated on a hot plate (100°C) to effect decomposition and subsequently evaporated to dryness. After cooling, 3 cm^3 of 12 mol dm^{-3} hydrochloric acid and 6 cm^3 of

redistilled water were added to dissolve the residue, and the solution was transferred into an arsine generator, where the arsenic was separated as arsine (AsH_3) by the addition of arsenic-free zinc and determined by the Ag-DDTC method.[16] The results of this method showed good agreement with those obtained by atomic-absorption spectrometry.[17]

Procedure for the Determination of Antimony. A sediment sample (0.05 to 0.50 g), weighed out into a porcelain crucible, was fused with 2.5 g of potassium pyrosulfate. After cooling to room temperature, 10 cm^3 of 6 mol dm^{-3} hydrochloric acid, 10 cm^3 of 6 mol dm^{-3} sulfuric acid, and 5 cm^3 of redistilled water were added to dissolve the fusion product, the solution was transferred into a separating funnel, and the antimony was determined by the Rhodamine B method.[18]

The contents of mercury, arsenic, and antimony in the marine-sediment samples were measured according to the methods described above. Actual analysis was made on air-dried samples. Separately, part of each sample was heated at 110 °C for 6 h to determine the weight loss; the measurements were then converted to the values on a bone-dry basis.

Results and Discussion

Contents of Mercury, Arsenic, and Antimony in Surface Sediments (0 to 10 cm deep). The analytical results for the contents of mercury, arsenic, and antimony in surface sediments (0 to 10 cm deep) of Kagoshima Bay are shown in Table 1. In the following discussion,

Table 1. Mercury, arsenic, and antimony contents in surface sediments of Kagoshima Bay

Station No.	Depth/m	Sampling Date	Content/mg kg^{-1} [a]			Remarks
			Hg	As	Sb	
1	144	Sept. 21, '76	0.034	8.12	0.62	Southern Kagoshima Bay
2	170	Sept. 22, '76	0.042	7.23	0.59	Southern Kagoshima Bay
3	226	Sept. 21, '76	0.108	7.48	1.45	Southern Kagoshima Bay
4	160	Sept. 21, '76	0.017	4.57	1.25	Southern Kagoshima Bay
5	217	Oct. 12, '76	0.063	6.74	1.37	Southern Kagoshima Bay
6	226	Oct. 30, '76	0.034	7.64	2.05	Southern Kagoshima Bay
7	218	Dec. 5, '76	0.055	7.34	1.27	Southern Kagoshima Bay
8	185	Dec. 5, '76	0.040	7.39	1.16	Southern Kagoshima Bay
9	13	Mar. 10, '77	0.0084	8.06	0.66	Southern Kagoshima Bay
10	210	Mar. 10, '77	0.060	6.97	1.08	Southern Kagoshima Bay
11	110	Mar. 10, '77	0.040	6.32	1.20	Southern Kagoshima Bay
12	36	Mar. 10, '77	0.016	7.61	1.49	Southern Kagoshima Bay
13	100	Mar. 10, '77	0.014	5.48	0.54	Southern Kagoshima Bay
14	200	Mar. 10, '77	0.030	7.73	0.56	Southern Kagoshima Bay
15	80	Nov. 6, '77	0.014	7.22	1.74	Southern Kagoshima Bay
16	40	Nov. 6, '77	0.050	8.35	1.84	Southern Kagoshima Bay
17	150	Nov. 6, '77	0.047	6.27	0.81	Southern Kagoshima Bay
18	215	Nov. 6, '77	0.095	4.75	1.20	Southern Kagoshima Bay
19	78	Aug. 12, '76	0.0024	6.53	1.35	Northern Kagoshima Bay
20	140	Oct. 12, '76	0.107	10.6	1.74	Northern Kagoshima Bay
21	25	Oct. 29, '76	0.143	12.0	4.39	Northern Kagoshima Bay
22	38	Oct. 30, '76	0.030	15.8	2.75	Northern Kagoshima Bay
23	190	Oct. 30, '76	0.092	19.1	4.97	Northern Kagoshima Bay
24	180	Oct. 30, '76	0.026	8.64	4.16	Northern Kagoshima Bay
25	140	Oct. 30, '76	0.016	8.43	3.23	Northern Kagoshima Bay
26	118	Dec. 6, '76	0.017	9.34	1.22	Northern Kagoshima Bay
27	202	Jan. 21, '77	0.370	16.2	3.14	Northern Kagoshima Bay
28	210	Apr. 17, '77	0.240	17.3	2.80	Northern Kagoshima Bay
29	115	Oct. 29, '77	0.060	9.65	2.92	Northern Kagoshima Bay
30	104	Oct. 29, '77	0.069	22.0	3.36	Northern Kagoshima Bay
31	40	Oct. 29, '77	0.174	20.0	4.16	Northern Kagoshima Bay
32	135	Oct. 29, '77	0.099	10.6	1.31	Northern Kagoshima Bay
33	145	Nov. 6, '77	0.078	9.50	1.51	Northern Kagoshima Bay
34	140	Nov. 6, '77	0.200	9.54	1.21	Northern Kagoshima Bay
35	140	Nov. 6, '77	0.247	13.3	2.27	Northern Kagoshima Bay
36	195	Nov. 6, '77	0.240	9.68	2.37	Northern Kagoshima Bay
37	30	Nov. 6, '77	0.032	5.80	1.00	Northern Kagoshima Bay
38	100	Nov. 6, '77	0.034	6.19	1.45	Northern Kagoshima Bay
39	150	Sept. 20, '79	0.058	7.7	1.66	Northern Kagoshima Bay
40	155	Sept. 20, '79	0.096	5.8	1.17	Northern Kagoshima Bay
41	140	Sept. 20, '79	0.103	5.5	3.76	Northern Kagoshima Bay
42	140	Sept. 20, '79	0.115	8.1	3.94	Northern Kagoshima Bay
43	190	Sept. 20, '79	0.219	8.8	3.40	Northern Kagoshima Bay
44	195	Sept. 20, '79	0.198	6.8	2.87	Northern Kagoshima Bay
45	200	Sept. 20, '79	0.731	14.1	4.41	Northern Kagoshima Bay
46	192	Oct. 5, '79	0.529	18.0	4.82	Northern Kagoshima Bay
47	150	Sept. 21, '76	0.030	7.33	2.83	Northern Kagoshima Bay

48	205	Nov. 6, '77	0.34_0	8.2_5	1.3_0	Northern Kagoshima Bay
A-1	200	Sept. 9. '77	0.66_8	$18._8$	$10._7$	Vicinity of a sea bottom fumarole
A-2	200	Sept. 11. '77	0.32_4	$12._5$	9.2_2	Vicinity of a sea bottom fumarole
A-3	200	Sept. 11. '77	267	297	1080	Vicinity of a sea bottom fumarole
A-4	200	Sept. 11. '77	1.4_3	$20._2$	$11._2$	Vicinity of a sea bottom fumarole
A-5	200	Sept. 11. '77	256	113	276	Vicinity of a sea bottom fumarole
A-6	200	Sept. 13. '77	116	464	11200	Vicinity of a sea bottom fumarole
A-7	200	Sept. 15. '77	0.45_9	$15._5$	8.7_3	Vicinity of a sea bottom fumarole
A-8	200	Sept. 15. '77	0.63_5	7.9_0	6.6_1	Vicinity of a sea bottom fumarole
A-9	200	Sept. 15. '77	0.34_4	$12._9$	7.4_8	Vicinity of a sea bottom fumarole
A-10	200	Aug. 25. '78	0.61_0	$12._6$	7.6_1	Vicinity of a sea bottom fumarole
A-11	200	Aug. 25. '78	1.3_9	$38._2$	$33._2$	Vicinity of a sea bottom fumarole
A-12	200	Aug. 25. '78	2.1_5	$48._5$	$48._8$	Vicinity of a sea bottom fumarole
A-13	200	Aug. 26, '78	0.96_1	$16._1$	$12._8$	Vicinity of a sea bottom fumarole
A-14	200	Aug. 27. '78	$76._7$	200	121	Vicinity of a sea bottom fumarole
A-15	200	Aug. 27. '78	$37._0$	105	131	Vicinity of a sea bottom fumarole
B-1	100	Sept. 12. '77	0.10_5	$15._5$	2.5_0	Vicinity of a sea bottom fumarole
B-2	100	Sept. 12. '77	0.015	$13._0$	1.5_2	Vicinity of a sea bottom fumarole
B-3	100	Sept. 14. '77	0.042	7.6	1.5_5	Vicinity of a sea bottom fumarole
B-4	100	Aug. 24. '78	0.012	8.5	1.4_1	Vicinity of a sea bottom fumarole

a) The contents of mercury, arsenic, and antimony are coverted to these values when samples are heated at 110 °C for 6h.

TABLE 2. MERCURY, ARSENIC, AND ANTIMONY CONTENTS IN SURFACE SEDIMENTS OF KAGOSHIMA BAY

		Content/mg kg^{-1}(110 °C, 6 h dry basis)						
		Hg		As		Sb		
Sampling station		$\overline{X_A}$[d]	$\overline{X_G}$[e]	$\overline{X_A}$[d]	$\overline{X_G}$[e]	$\overline{X_A}$[d]	$\overline{X_G}$[e]	n[f]
Northern Kagoshima Bay	A[a]	$50._8$	4.0_3	$92._1$	$39._6$	864	$43._7$	15
	B[b]	0.04_4	0.03_0	$11._2$	$10._7$	1.7_5	1.7_0	4
	C[c]	1.5_7	0.09_1	$11._0$	$10._2$	2.7_2	2.4_2	30
Southern Kagoshima Bay		0.04_3	0.03_5	6.9_6	6.8_7	1.1_6	1.0_7	18

a) A is the area 200 m-deep within *ca.* 100 m from the center of the fumarole group. b) B is the area 78 m-deep within *ca.* 50 m from the center of the fumarole group. c) C is the area excluding A and B. d) $\overline{X_A}$ is the arithmetic mean. e) $\overline{X_G}$ is the geometric mean. f) n is the number of determined samples.

Kagoshima Bay is divided into two sections by the line connecting Kagoshima City and Sakurajima: The southern part (Stn. 1 to 18) and the northern part (Stn. 19 to 48, A and B). The results for the northern part are summarized in Table 2, in which data are separately shown for the 200 m station (A), the 78 m station (B), and the other stations (C). $\overline{X_A}$ represents the arithmetic mean; $\overline{X_G}$ the geometric mean, and n; the number of samples collected. It is apparent from the table that the contents of mercury, arsenic, and antimony at the 200 m station (A) are abnormally high. The data for the 200 m and 78 m stations are those of sediment samples collected in a past survey; (an investigation by the government and Kagoshima prefecture, in which the author paticipated as a member, which was carried out to determine if the mercury derived from volcanic activity is responsible for the mercury pollution of fishes and shellfishes).

These samples were collected by means of a submarine boat (HAKUYO; displacement, 6.6 tons) while visually observing the sea-bottom fumarole. No abnormal values, such as those seen at the 200 m station, were found at the 78 m station. This difference may probably be correlated to the fact that the fumarole gas at the 78 m station is relatively low in temperature and has a composition similar to that of natural gas, while the fumarole gas at the 200 m station is considerably high in temperature (the max. was 215 °C) and contains much hydrogen *etc.*[6] The average values of mercury, arsenic, and antimony in the surface sediments collected from the southern part, in which volcanic activity is milder, are lower than those in the northern part.

Horizontal Distribution of Mercury, Arsenic, and Antimony in Surface Sediments of Kagoshima Bay. Figures 4—6 show the horizontal distribution on mercury, arsenic, and antimony in surface sediments collected at 48 stations over the entire area of Kagoshima Bay.

Higher contents of these compositions are observed in the northern part, particularly in the vicinity of the 200 m-deep fumarole and in the area near the estuary of the river Amori, flowing down from the Kirishima Volcano region. This suggests a close correlation of the mercury, arsenic, and antimony components to volcanic activity.

Sedimentary samples with abnormally high concentrations of mercury, arsenic, and antimony, as collected near the 200 m deep fumarole, have never been found in any ship survey from sea level.

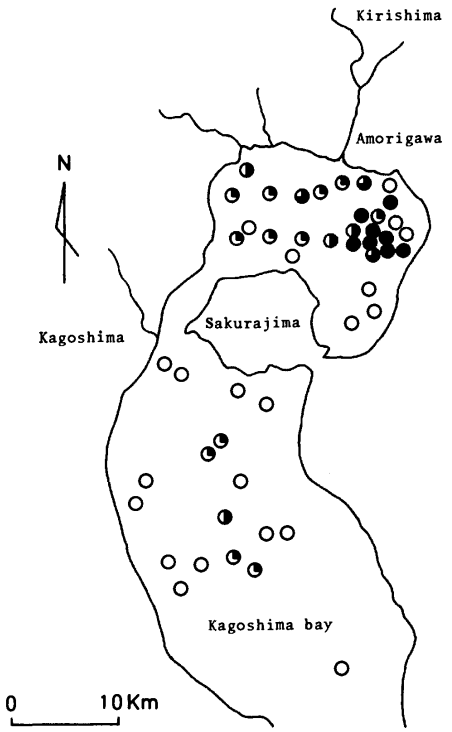

Fig. 4. Horizontal distribution of mercury in surface sediments of Kagoshima Bay.

Hg mg kg^{-1} [a]	No. of samples
○ ≦0.05	21
◔ 0.06—0.10	12
◑ 0.11—0.15	4
◕ 0.16—0.20	3
● 0.21≦	8

a) 110°C, 6h dry basis.

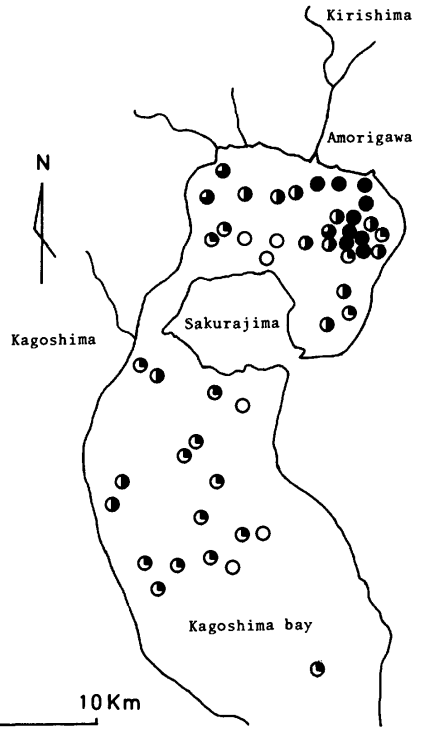

Fig. 5. Horizontal distribution of arsenic in surface sediments of Kagoshima Bay.

As mg kg^{-1} [a]	No. of samples
○ ≦ 6.0	6
◔ 6.1— 8.0	17
◑ 8.1—10.0	13
◕ 10.1—12.0	3
● 12.1≦	9

a) 110°C, 6h dry basis.

Let us now compare the mercury content in surface sediments collected in Kagoshima Bay with those in other inner bays.

Already reported are 0.12—0.33 mg kg^{-1} for Funka Bay,[19] 0.115—0.794 mg kg^{-1} for Tokyo Bay,[20] 0.190—0.550 mg kg^{-1} for Osaka Bay,[19] and 0.1—0.2 mg kg^{-1} for Tokuyama Bay[21] (20 cm deep). Compared with these values, the range of mercury concentrations observed in the southern and northern parts of Kagoshima Bay are lower (except for the vicinity of the 200 m-deep fumarole); 0.008—0.10$_8$ mg kg^{-1} (geometric mean: 0.033 mg kg^{-1}) and 0.002—0.73$_1$ mg kg^{-1} (geometric mean: 0.087 mg kg^{-1}) respectively.

However, an unusually high concentration range of 0.45$_9$—267 mg kg^{-1} (geometric mean: 4.0$_3$ mg kg^{-1}) is found in the limited area in the vicinity of the 200 m-deep fumarole.

Vertical Distribution of Mercury, Arsenic, and Antimony in Sediments of Kagoshima Bay. Figure 7 shows the vertical distribution of mercury, arsenic, and antimony contained in sediments of the northern (Stn. 48) and southern (Stn. 18) parts of Kagoshima Bay. In this figure, the contents of mercury, arsenic, and antimony (abscissa) are plotted against the depth (ordinate) (10 cm-interval vertical sections from the surface of the sediment to a depth of 100 cm).

In the southern part (Stn. 18), little change is observed in the contents of mercury, arsenic, and antimony with the depth. In the northern part (Stn. 48), on the other hand, the vertical distribution is uneven for mercury and arsenic. This figure also shows higher contents for all of the components in the northern than in the southern part. This tendency is also the case with the other sampling stations.

Relationship between Mercury and Arsenic Contents in Surface Sediments Around the Fumarole in the Northern Part. Figure 8 shows the relationship between the mercury and arsenic contents in the surface sediments collected at the 200 m-deep station around the fumarole in the northern part of Kagoshima Bay. As can be seen from the figure, a fairly high degree of positive correlation exists between the two (correlation coefficient: 0.65).

Relationship between Arsenic and Antimony Contents in Surface Sediments Around the Fumarole in the Northern Part. Figure 9 shows the relationship between the contents of arsenic and antimony in the same samples as have been used to describe the relationship between mercury and arsenic. Here, also, there is a high degree of positive correlation (correlation coefficient: 0.83).

Relationships of Mercury, Arsenic, and Antimony Contents to the Distance from the Fumarole (200 m-Deep

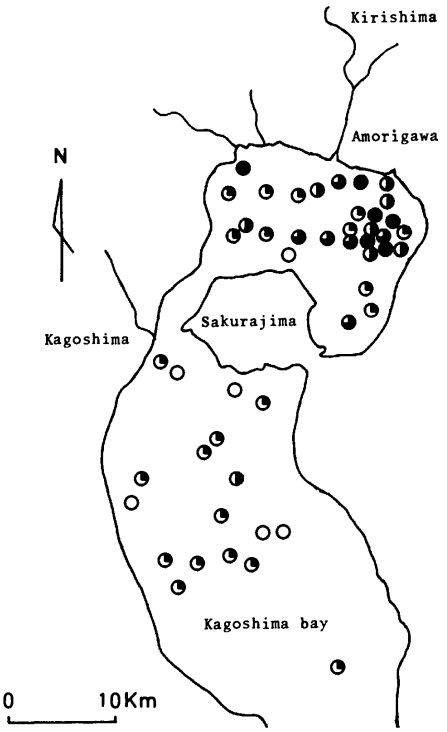

Fig. 6. Horizontal distribution of antimony in surface sediments of Kagoshima Bay.

Sb mg kg^{-1} a)	No. of samples
○ ≦1.0	6
◔ 1.1—2.0	22
◑ 2.1—3.0	8
◕ 3.1—4.0	6
● 4.1≦	6

a) 110°C, 6h dry basis.

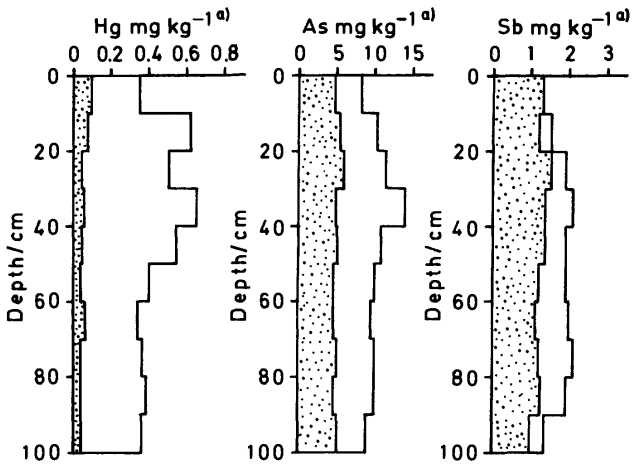

Fig. 7. Vertical profiles of mercury, arsenic, and antimony in sediments of Kagoshima Bay.
□: Stn. 48 (Northern Kagoshima Bay)
▨: Stn. 18 (Southern Kagoshima Bay)
a) 110°C, 6h dry basis.

Locations in the Northern Part). Figure 10 shows the relationships between the contents of mercury, arsenic, and antimony in surface sediments and the distance from the fumarole. It is apparent from these figures that abnormal concentrations of mercury, arsenic, and antimony are observed only at hot positions near the fumarole. The contents of these components sharply decrease with the distance between the sampling position and the fumarole, gradually approaching the background level of the open ocean.

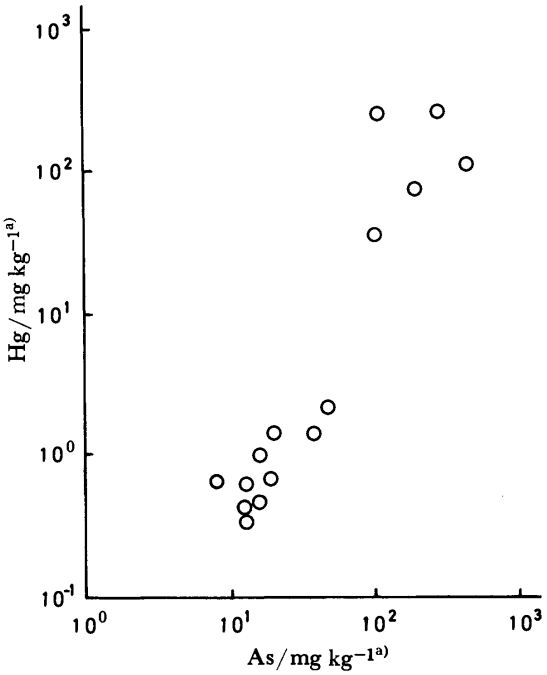

Fig. 8. Relationship between the mercury and arsenic contents in surface sediments around the fumarole at the 200m-deep locations.
a) 110°C, 6h dry basis.

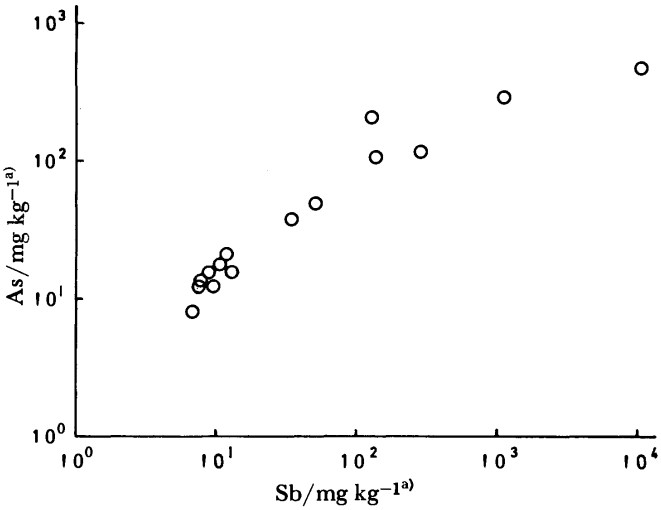

Fig. 9. Relationship between the arsenic and antimony contents in surface sediments around the fumarole at the 200m-deep locations.
a) 110°C, 6h dry basis.

Correlations among Mercury, Arsenic, and Antimony Contents in Surface Sediments in Kagoshima Bay. Table 3 shows the correlation coefficients among the contents of mercury, arsenic, and antimony in surface sediments in the northern and southern parts of Kagoshima Bay. As may be apparent from this table, a higher degree of positive correlation is found among

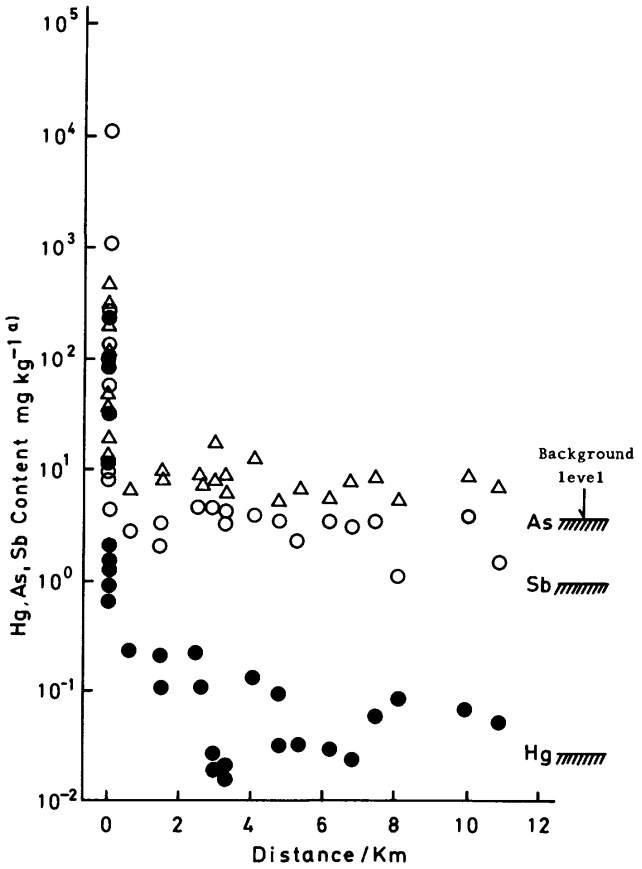

Fig. 10. Relationships between the mercury, arsenic, antimony, and the distance from the fumarole at the 200m-deep locations.
a) 110°C, 6h dry basis.
●: Mercury, △: Arsenic, ○: Antimony.

TABLE 3. MUTUAL CORRELATION COEFFICIENTS OF MERCURY, ARSENIC, AND ANTIMONY IN MARINE SURFACE SEDIMENTS OF KAGOSHIMA BAY

(I)[a]

	As	Sb	Hg
As			
Sb	0.13		
Hg	−0.12	0.19	

(n^{c})=18)

(II)[b]

	As	Sb	Hg
As			
Sb	0.88		
Hg	0.81	0.89	

(n^{c})=39)

a) (I) is southern Kagoshima Bay. b) (II) is northern Kagoshima Bay. c) (n) is the number of determined samples.

the contents of mercury, arsenic, and antimony in the northern than in the southern part. This is in accord with the more vigorous volcanic activity in the former than in the latter part.

It may be considered that factors such as geological circumstances (Kirishima and Sakurajima) and the intricate submarine topography of the northern part.

Conclusion

The horizontal and vertical distributions of the contents of mercury, arsenic, and antimony in the sediments collected from Kagoshima Bay have been studied. The results may be summarized as follows: (1) The distribution of mercury, arsenic, and antimony contents in the surface sediments of Kagoshima Bay revealed high concentrations of these components in a limited area in the northern part. (2) The vertical distribution of these components in sediments of Kagoshima Bay clearly showed higher concentrations in the northern than in the southern part. Little change was observed in the contents with the depth in the sediments of the southern part, but apparent changes with depth were noticed in the sediments of the northern part. (3) A high degree of correlation was found among the three components (mercury, arsenic, and antimony) in surface sediments of the northern part, but no such close correlation existed among those in the southern part. (4) Abnormal concentrations of mercury, arsenic, and antimony were found at a hot position, 200 m deep, near the center of volcanic activity in the northern part, and a sharp decrease in the contents of these components was observed with the increasing distance from the fumarole. This suggests that these components have been deposited as a result of volcanic activity which both took place in the past and are under way at present. (5) It has already been demonstrated[6] that all sediments containing mercury, arsenic, and antimony in markedly high concentrations are also rich in montmorillonite, stibnite, and dolomite.

It may thus be concluded that the abnormally high concentrations of mercury, arsenic, and antimony found in surface sediments at the hot position 200 m deep near the fumarole in the northern part of Kagoshima Bay is derived from natural volcanic activity at the sea bottom and is not caused by human activities.

Studies of the mechanism of mercury concentration in fishes are under way in various fields of research, but a satisfactory explanation has not yet been reached. For a complete elucidation, it would be essential to continue monitoring of water quality, sediments, living things, volcanic activity, and other phenomena in the bay.

The author wishes to express his thanks to Professor Masaakira Kamada of Kagoshima University, Professor Joyo Ossaka of the Tokyo Institute of Technology, Professor Takejiro Ozawa of Saitama University, and Dr. Junichi Hirabayashi of the Tokyo Institute of Technology for their helpful discussions. The author is also indebted to the Environmental Government and Environmental Pollution Control Section of Kagoshima Prefecture and the Institute of Environmental Pollution and Public Health of Kagoshima Prefecture for their practical assistance,

such as in the collection of samples, as well as for their endlessly helpful discussions during this investigation.

References

1) Environmental government and Environmental Pollution Control Section of Kagoshima Prefecture, "Report of Environmental Survey of Mercury Pollution in Kagoshima Bay," 2 (1975).

2) M. Kamada, T. Onishi, and H. Sakamoto, "Study of the Submarine Volcanic Activity of Northern Kagoshima Bay and Influences in the Environment," 55 (1976).

3) J. Ossaka, J. Hirabayashi, T. Ozawa, T. Onishi, and H. Sakamoto, "Study of the Submarine Volcanic Activity, in the Northern Area of Sakurajima," 48 (1977).

4) M. Kamada, H. Sakamoto, and N. Yonehara, "Study of the Submarine Volcanic Activity in the Northern Area of Sakurajima," 64 (1977).

5) Kagoshima Prefecture, "Report of Environmental Survey on Mercury Pollution in Kagoshima Bay" (1977).

6) Kagoshima Prefecture, "Report of Environmental Survey on Mercury in Kagoshima Bay" (1978).

7) Fisheries Laboratory of Seikaiku, "Report of Mercury Pollution Surveys in Kagoshima Bay" (1978).

8) Kagoshima Prefecture, "Environmental White Paper," 240 (1976).

9) Kagoshima Prefecture, "Environmental White Paper," 162 (1977).

10) Kagoshima Prefecture, "Environmental White Paper," 158 (1978).

11) S. M. Siegel and B. Z. Siegel, *Nature*, **233**, 471 (1971).

12) B. Z. Siegel and S. M. Siegel, *Environ, Sci. Technol.*, **12**, 1036 (1978).

13) H. Sakamoto, *Nippon Kagaku Kaishi*, **1985**, 35.

14) H. Sakamoto and M. Kamada, *Rep. Fac., Kagoshima Univ., (Math., Phys. & Chem.)*, **13**, 63 (1980).

15) H. Sakamoto and M. Kamada, *Nippon Kagaku Kaishi*, **1981**, 32.

16) Testing Methods for Industrial Wastewater, TIS K 0102, 176 (1981).

17) M. Yamamoto, K. Urata, K. Murashige, and Y. Yamamoto, *Spectrochimica Acta*, **36B**, 671 (1981).

18) Testing Methods for Industrial Wastewater, JIS K 182 (1981).

19) K. Matsunaga, S. Montani, R. Kobayashi, Y. Maita, S. Fukase, and J. Ishii, *Geochim. J.*, **12**, 287 (1978).

20) E. Mastumoto, K. Kato, and K. Matsunaga, *Chikyukagaku*, **17**, 48 (1983).

21) H. Tsubota, M. Ambe, Y. Dokiya, N. Higo, T. Saisho, M. Kamada, S. Horibe, and T. Yoshida, "Environmental Science of the Sea," Kouseishiya Kouseikaku, 259 (1983).

 © 1985 The Chemical Society of Japan Bull. Chem. Soc. Jpn., 58, 588—591 (1985) [Vol. 58, No. 2

Studies of the Complexes of Np(V) with Inorganic Ligands by Solvent Extraction with Thenoyltrifluoroacetone and 1,10-Phenanthroline. I. Carbonato Complexes

Yasushi INOUE* and Osamu TOCHIYAMA

Department of Nuclear Engineering, Faculty of Engineering, Tohoku University, Aramaki-aza-Aoba, Sendai 980

(Received September 11, 1984)

The complex formation of Np(V) in a carbonate medium has been studied in 1 mol dm^{-3} $NaClO_4$ at pH 6.5—8.3 and 25 °C using the solvent-extraction method with thenoyltrifluoroacetone (TTA) and 1,10-phenanthroline. The formation constants of the complexes of Np(V) with CO_3^{2-} were $\log(\beta_1/\text{mol}^{-1}\,\text{dm}^3)=4.14\pm0.01$ and $\log(\beta_2/\text{mol}^{-2}\text{dm}^6)=6.78\pm0.01$, with no indication of the formation of HCO_3^- complexes. Based on these constants, the distribution of chemical species of neptunium are discussed under various conditions encountered in natural water.

The solution chemistry of neptunium has received much attention in recent years since the ^{237}Np in radioactive wastes will have a long-term radiological toxicity in the human environment. Since this element most probably exists as a quinquevalent state in neutral solutions, the study of the complex formations of Np(V) in aqueous solutions is very important for the understanding of the behavior of this element in natural water.

In spite of this importance, quinquevalent neptunium has not been extensively studied due to its reduced reactivity with various ligands as a result of its low ionic potential. However, recent studies[1,2] by means of solvent extraction with thenoyltrifluoroacetone (TTA) and 1,10-phenanthroline (phen) revealed that Np(V) still forms considerably stable complexes with many organic ligands such as hydroxy carboxylic acids, dicarboxylic acids, amino carboxylic acids and some other widely used chelating reagents.

This induced us to study the complex formation of Np(V) with some inorganic anions using the same solvent extraction technique. Among inorganic anions, the carbonate ion deserves special attention because of its pronounced tendency to interact with cations and because of its wide distribution in the environment. Since the formation of carbonato complexes is expected to affect the movement of neptunium in natural water, reliable stability constants are required for estimating the behavior of the element in the environment.

The present paper deals with the determination of the formation constants of Np(V)-carbonato complexes by means of solvent extraction with TTA and phen, and the distribution of chemical species of neptunium in solutions under various conditions are discussed based on the obtained results.

Experimental

Reagents. The ^{239}Np tracer was prepared by milking from ^{243}Am (obtained from the Commissariat a l'Energie Atomique) by the method of Sill,[4] and adjusted to the quinquevalent state by evaporation to dryness and dissolution in water.[5] Thenoyltrifluoroacetone and 2-morpholinoethanesulfonic acid monohydrate (MES) were obtained from Dojindo Laboratories (Kumamoto, Japan) and used without further purification. The solutions of these chemicals were freshly prepared just prior to use.

Procedures. To avoid the possible contamination by any complex-forming substances or by neptunium with a valence state other than quinquevalent (which might be introduced during milking), the following back-extraction procedure was adopted. The ^{239}Np tracer was first extracted into an organic (3-methyl-1-butanol or dichloromethane) solution containing the desired concentrations of TTA and phen. A 4-cm^3 portion of this organic solution containing ^{239}Np was then mechanically shaken for 15 min (140 times/min) at 25±1 °C in a glass tube with the same volume of aqueous solution containig 1 mol dm^{-3} sodium perchlorate, buffer reagents (a proper mixture of 0.1 mol dm^{-3} of MES and 0.1 mol dm^{-3} of tris(hydroxymethyl)aminomethane (THAM)) and a variable concentration of sodium hydrogencarbonate. After phase separation, a 1-cm^3 portion of each phase was pipetted into a counting tube and the γ-activity of each phase was measured with a well-type NaI(Tl) scintillation counter. The remaining part of the aqueous phase was used for the pH measurement.

Calculation of Stability Constants. The distribution ratio D of Np(V) in the presence of the complexing agent (X) can be expressed by:

$$D = D_0/(1+\sum\beta_n[X]^n), \quad (1)$$

where D_0 is the distribution ratio of Np(V) in the absence of the complexing agent, and β_n is the overall formation constant of the Np(V) complex with the ligand X (charges of ions are omitted for simplicity). Equation 1 is equivalent to linear function:

$$y = f(x), \quad (2)$$

where

$$y = 1/D,$$
$$f(x) = 1/D_0 + \sum(\beta_n/D_0)x^n,$$

and

$$x = [X].$$

A set of data (x_i, y_i) was analyzed by the least-squares method to determine the β_n values. Since the counting-time of the γ-activity was set to make the relative statistical errors of the total counts approximately constant, residuals of observed ratios, y, were expected to be proportional to the value of $1/D$ from error propagation rules. Although the observed value of $1/D$ is not error free, this value gives a good basis for an estimate of the weight of the observation. Therefore, the least-squares fitting was carried out to minimize the follow-

ing sum of the weighted squares of the residuals:

$$S = \sum\{y_i - f(x_i)\}^2/y_i^2. \quad (3)$$

This procedure is nearly equivalent to obtain a best fit of the plots of log D against log [X] to Eq. 1.

Results

The distribution ratio of Np(V) in the presence of a complexing agent can be expressed by Eq. 1. In the presence of a polybasic acid as a complexing agent, however, there is a possibility of the formation of different types of complexes; that is, the ligands in different stages of dissociation can react with Np(V). When ligands HL and L (charges omitted) can react with Np(V) in solution, the ratio D_0/D, the reciprocal of which is equivalent to the fraction of neptunium in the form of free ion (NpO_2^+), is given by:

$$D_0/D = 1 + \sum\beta'_n[HL]^n + \sum\beta_n[L]^n, \quad (4)$$

where β'_n and β_n are the overall formation constants of the respective complexes:

$$\beta'_n = [M(HL)_n]/[M][HL]^n, \quad (5)$$

$$\beta_n = [ML_n]/[M][L]^n, \quad (6)$$

where M=NpO_2^+. The concentration of HL and L can be related in terms of the acid dissociation constant:

$$K_a = [H][L]/[HL]. \quad (7)$$

Thus, Eq. 4 becomes:

$$D_0/D = 1 + \sum B'_n[HL]^n = 1 + \sum B_n[L]^n, \quad (8)$$

where

$$B'_n = \beta'_n + \beta_n K_a^n/[H]^n, \quad (9)$$

and

$$B_n = \beta'_n[H]^n/K_a^n + \beta_n. \quad (10)$$

Measurement of D as a function of [HL] or [L] leads to the apparently constant values of B'_n or B_n, provided that the extraction is carried out in a medium buffered at constant pH. Since B'_n or B_n is the function of pH, as expressed by Eq. 9 or 10, a set of B'_n or B_n obtained at various pH discloses the contribution of each series of complex formation to give the constant values, β'_n and β_n.

Six series of experiments were carried out on solutions ranging from pH 6.5 to 8.3 to obtain a distribution ratio at various added concentrations of sodium hydrogencarbonate. In each series of experiments, the distribution ratio was obtained in a medium buffered at constant pH. The pH of the aqueous phase drifted during extraction; the pH after shaking differed from the initial pH by less than 0.4 unit in each series of experiments and the experimental values of D were corrected to those at a constant pH by using experimental extraction curves which were obtained previously.[3] The concentration of a particular species of carbonate, [HCO_3^-] or [CO_3^{2-}], at an equilibrium pH was calculated according to the following relationship:

$$C_L = [H_2CO_3] + [HCO_3^-] + [CO_3^{2-}] = [H_2CO_3](1 + K_1/[H^+] + K_1K_2/[H^+]^2), \quad (11)$$

where

$$K_1 = [H^+][HCO_3^-]/[H_2CO_3] = 10^{-6.02}\ \text{mol dm}^{-3}, \quad (12)$$

$$K_2 = [H^+][CO_3^{2-}]/[HCO_3^-] = 10^{-9.57}\ \text{mol dm}^{-3}, \quad (13)$$

at 25 °C, μ=1.0.[6] In the calculation, the concentration of the undissociated acid in the organic phase was assumed to be negligibly small. To ascertain the validity of this assumption, two kinds of solvents, 3-methyl-1-butanol and dichloromethane, were used as an organic diluent. Plots of log(D/D_0) *vs.* log([HCO_3^-]/mol dm^{-3}) and log([CO_3^{2-}]/mol dm^{-3}) are given in Figs. 1 and 2, respectively. The plots in Figs. 1 and 2 give the values of B'_n and B_n in Eq. 8, respectively, if HL and L denote HCO_3^- and CO_3^{2-}, respectively. Since the plots in Fig. 2 indicate that the B_n values in Eq. 10 are independent of pH, it can be safely concluded that the complex formation of Np(V)

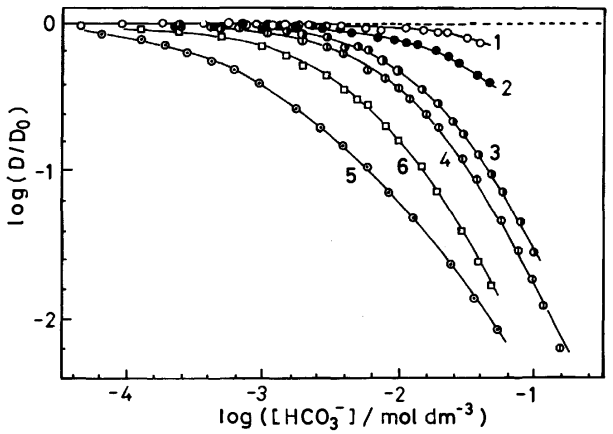

Fig. 1. Plots of log(D/D_0) *vs.* log([HCO_3^-]/mol dm^{-3}). pH: (1) 6.50, (2) 7.00, (3) 7.50, (4) 7.80, (5) 8.30, (6) 8.11. (1)—(5): C_{TTA}=10^{-4} mol dm^{-3}, C_{phen}=10^{-2} mol dm^{-3} in 3-methyl-1-butanol. (6): C_{TTA}=10^{-3} mol dm^{-3}, C_{phen}=10^{-2} mol dm^{-3}, in dichloromethane.

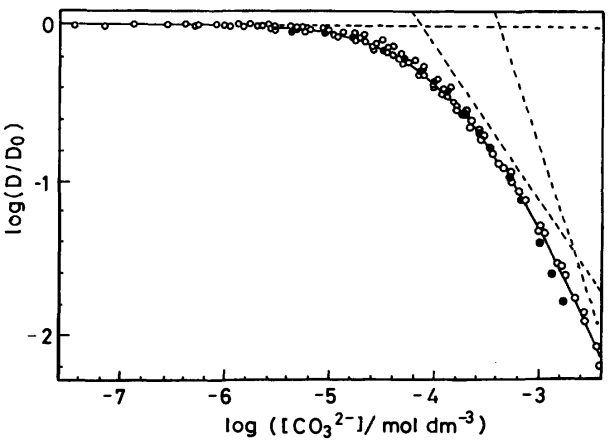

Fig. 2. Plots of log(D/D_0) *vs.* log([CO_3^{2-}]/mol dm^{-3}). ○: pH 6.50—8.30, C_{TTA}=10^{-4} mol dm^{-3}, C_{phen}=10^{-2} mol dm^{-3}, in 3-methyl-1-butanol. ●: pH 8.11, C_{TTA}=10^{-3} mol dm^{-3}, C_{phen}=10^{-2} mol dm^{-3} in dichloromethane.

with HCO_3^- is negligibly small in the pH region investigated, that is, only the carbonate ion CO_3^{2-} participates in the complex formation. We cannot distinguish between MCO_3^- and $M(OH)(HCO_3)^-$; the behavior of these species in the solvent extraction system is identical since the latter merely differs from the former in having an additional H_2O. However, it is quite unreasonable to imagine the formation of $M(OH)(HCO_3)^-$ since even a positively charged NpO_2^+ ion does not form any complexes with an HCO_3^- ion. The formation of mixed hydroxo-carbonato complexes such as $M(OH)(CO_3)^{2-}$, $M(OH)_2(CO_3)^{3-}$, $M(OH)(CO_3)_2^{4-}$, *etc.* can also be eliminated since the formation of these kinds of complexes would give a pH dependence to a family of plots of $\log(D/D_0)$ *vs.* $\log([CO_3^{2-}]/\text{mol dm}^{-3})$. This can be easily understood when we regard $CO_3\cdot nH_2O^{2-}$ as HL and $OH\cdot CO_3\cdot(n-1)H_2O^{3-}$ as L in Eqs. 8—10. Therefore, we can conclude that only carbonate complexes are present in the solution within the pH range studied. A least-squares study of these six series of experiments (113 points) resulted in:

$$\log(\beta_1/\text{mol}^{-1}\text{dm}^3) = 4.14 \pm 0.01,$$
$$\log(\beta_2/\text{mol}^{-2}\text{dm}^6) = 6.78 \pm 0.01.$$

Although higher complexes such as $M(CO_3)_3^{5-}$ cannot be excluded, it was difficult to detect them because the concentration of CO_3^{2-} and pHs greater than those adopted in the present experiment would result in the oxidation of Np(V) to Np(VI), as discussed below.

Discussion

Figure 3 shows the fraction of Np(V) in the form of a particular carbonato complex as a function of carbonate ion concentration at equilibrium, evaluated using the stability constants obtained in the present experiment. NpO_2^+ predominates when the equilibrium carbonate concentration is lower than $10^{-4.5}$ mol dm^{-3}. The equilibrium concentration of various species in distilled water exposed to air can be estimated with the use of Eq. 11 and Henry's law:

$$K_H = [H_2CO_3]/P_{CO_2}, \quad (14)$$

where P_{CO_2} is a partial pressure of carbon dioxide. By substituting $K_H=10^{-1.48}$ mol dm^{-3} atm^{-1},[7] $P_{CO_2}=10^{-3.5}$ atm, $pK_1=6.02$, $pK_2=9.57$, and

$$[H^+] \simeq [HCO_3^-], \quad (15)$$

we obtain:

$$[H_2CO_3] = 10^{-5.0}\ \text{mol dm}^{-3},$$
$$[H^+] = [HCO_3^-] = 10^{-5.5}\ \text{mol dm}^{-3},$$
$$[CO_3^{2-}] = 10^{-9.6}\ \text{mol dm}^{-3},$$

and

$$C_L = 10^{-4.8}\ \text{mol dm}^{-3}.$$

When experiments are carried out which exclude the dissolution of more carbon dioxide than the equilibrium concentration in distilled water exposed to air, Np(V) does not form substantial amount of carbonato complexes since the concentration of the carbonate ion never exceeds $C_L=10^{-4.8}$ mol dm^{-3}. In some natural systems like sea water and inland water, however, the pH is controlled by other coexisting components than dissolved carbon dioxide. Hence, the concentration of carbon dioxide depends on the equilibrium pH controlled by the solutes. At equilibrium, the concentration of the carbonate ion can be expressed as:

$$[CO_3^{2-}] = P_{CO_2}K_HK_1K_2/[H^+]^2. \quad (16)$$

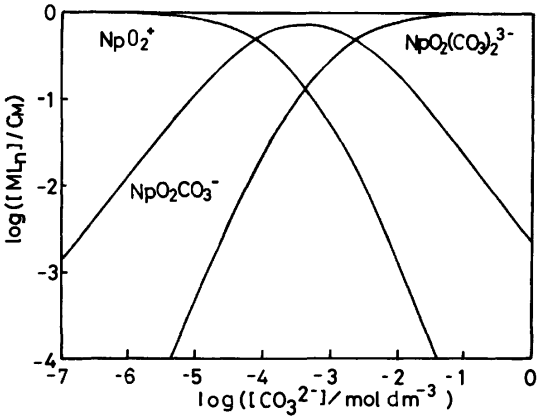

Fig. 3. Logarithmic diagram of the Np(V)–carbonate system.

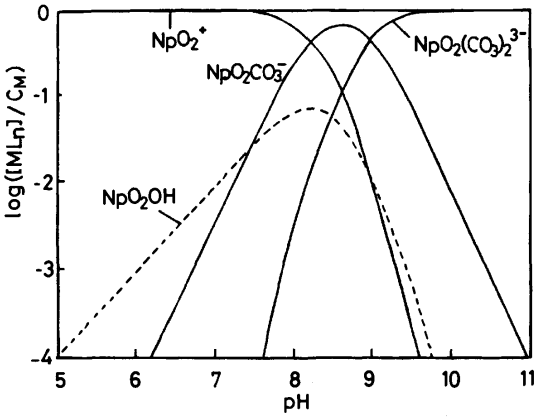

Fig. 4. Logarithmic diagram of the Np(V)–carbonate–hydroxide system at $P_{CO_2}=10^{-3.5}$ atm.

Figure 4 shows the fractional distribution of the chemical species of Np(V) in a solution in equilibrium with an atmosphere of $P_{CO_2}=10^{-3.5}$ atm as a function of pH. In the calculation, hydrolysis constants of Np(V) are taken from the table compiled by Allard *et al.*[8]

$$[MOH]/[M^+][OH^-] = 10^{5.0}\ \text{mol}^{-1}\ \text{dm}^3,$$
$$[M(OH)_2^-]/[M^+][OH^-]^2 = 10^{10}\ \text{mol}^{-2}\ \text{dm}^6.$$

As compared with the diagram in the absence of carbon dioxide,[9] chemical species of Np(V) predominating in a slightly alkaline solution drastically change from hydroxo to carbonato complexes. The precipitation of hydroxides should be markedly suppressed in the presence of an equilibrium amount of carbonate ions.

Diagrams for a tracer neptunium-carbonate-hydroxide system at $P_{CO_2}=10^{-3.5}$ atm were constructed in the

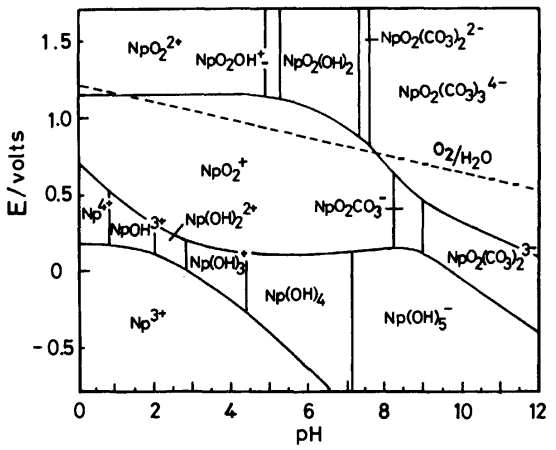

Fig. 5. Potential-pH diagram of tracer neptunium–carbonate–hydroxide system at $P_{CO_2}=10^{-3.5}$ atm.

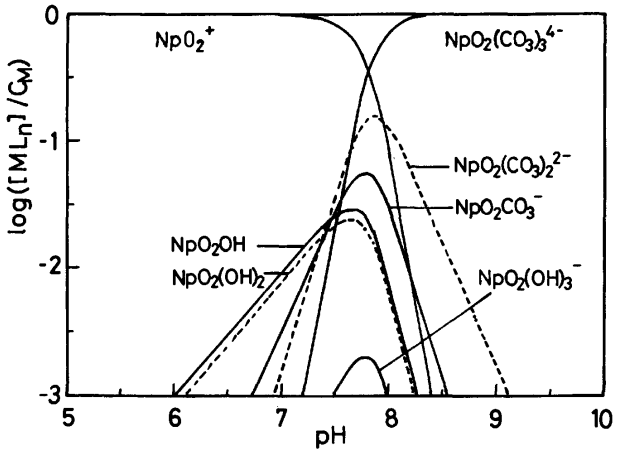

Fig. 6. Logarithmic diagram of tracer neptunium–carbonate–hydroxide system at $P_{CO_2}=10^{-3.5}$ atm and $P_{O_2}=1/5$ atm.

same manner as previously described.[9] They are shown in Figs. 5 and 6 in the form of potential-pH and fraction-pH diagrams. Hydrolysis constants and standard potentials for redox reactions were taken from a table compiled by Allard *et al.*[8] Since reliable data for carbonato complexing of Np(VI) are unavailable,[10] the data for U(VI):[6]

$$\log(\beta_1/\mathrm{mol^{-1}\,dm^3}) = 9.02,$$

$$\log(\beta_2/\mathrm{mol^{-2}\,dm^6}) = 16.22,$$

and

$$\log(\beta_3/\mathrm{mol^{-3}\,dm^9}) = 21.54$$

for

$$\beta_m = [UO_2(CO_3)_m^{2-2m}]/[UO_2^{2+}][CO_3^{2-}]^m,$$

were used as a substitute. Since uranium and neptunium in the same valence state generally have similar formation constants, a small disparity in the constants of U(VI) and Np(VI) will only slightly influence the predictions. The formation of carbonato complexes of Np(III) and Np(IV) are considered negligible as compared with the formation of hydroxo complexes by the analogy of other ter- and quadrivalent actinoids. The fraction-pH diagram was constructed at the potential of the solution in equilibrium with 1/5 atm O_2:

$$E = 1.219 + (RT/F)\ln([H^+]/\mathrm{mol\,dm^{-3}}). \quad (16)$$

This potential is shown by a dashed line in Fig. 5. Figures 5 and 6 clearly indicate that the sexivalent state is stabilized by carbonato complexing in slightly alkaline solutions at $P_{CO_2}=1/5$ atm. Even under reducing conditions, neptunium is not expected to form hydroxides which lead to precipitation but to form soluble carbonato complexes of Np(VI) or Np(V). Since it is not unusual for natural water to experience this kind of condition, the concentration of a carbonate ion must be carefully estimated or analyzed in order to predict the geochemical behavior of neptunium.

References

1) Y. Inoue and O. Tochiyama, *Polyhedron*, **2**, 627 (1983).
2) Y. Inoue, O. Tochiyama, and T. Takahashi, *Radiochim. Acta*, **31**, 197 (1982).
3) Y. Inoue and O. Tochiyama, *Radiochim. Acta*, **31**, 193 (1982).
4) C. W. Sill, *Anal. Chem.*, **38**, 802 (1966).
5) Y. Inoue and O. Tochiyama, *J. Inorg. Nucl. Chem.*, **39**, 1443 (1977).
6) A. E. Martell and R. M. Smith, "Critical Stability Constants," Plenum Press, New York (1977).
7) A. L. Horvath, "Physical Properties of Inorganic Compounds SI Units," Edward Arnold Limited, London (1975), p. 168.
8) B. Allard, H. Kipatsi, and J. O. Liljenzin, *J. Inorg Nucl. Chem.*, **42**, 1015 (1980).
9) Y. Inoue and O. Tochiyama, *Tech. Repts., Tohoku Univ.*, **47**, 263 (1982).
10) B. S. Jensen, "Migration Phenomena of Radionuclides into the Geosphere," Harwood Academic Publishers for the Commission of the European Communities, New York (1982), Part A.

Über den Effekt der Schwingungsmühle auf Thermische Zersetzung von Ammoniumhydrogenamidophosphat

Choichiro SHIMASAKI,* Shigenobu OOKAWA, und Ryuichi ISHIZAKA
Fakultät für Ingenieurwissenschaften, Universität Toyama, Nakagawasonomachi, Takaoka-shi, Toyama 933
(Eingangsdatum: 19. März 1984)

Das von einer Schwingungsmühle gemahlte Ammoniumhydrogenamidophosphat ($NH_4HPO_3NH_2$) hat es herausgestellt, daß nach einer Stunde Laufzeit die erste endotherme Spitze in DSC Kurven in zwei Teile geteilt wird. Die Absorption infolge NH und Zwitterions in IR Spektren wird vom Einfuß der Schwingungsmühle verändert. Das Ergebnis unterstützt eine Transformation von $NH_4HPO_3NH_2$ nach einer Zwischenphase, die durch die starke Wasserstoffbindung zwischen NH und POH gebildet worden hat.

Bei thermischer Zersetzungsreaktion vom Ammoniumsalz der Phosphorsäure bilden sich hohe Anteile von Ammoniak und Phosphorsäure. Demzufolge wurde das Ammoniumsalz der Phosphorsäure als flammensicherer und feuerbeständiger Agent für Zellulosematerialien gebraucht. Einige Forschungen[1] wurden über die thermischen Zersetzung der obigen Verbindung ausgeführt, aber der Mechanismus der Zersetzungsreaktion ist noch nicht vollständig erforscht.

In der früheren Abhandlung[2] wurde die thermische Zersetzungsreaktion mit DTA, DSC, und TG erforscht. In der jetzigen Abhandlung wird der Effekt der Mechanochemie auf die thermische Zersetzungsreaktion untersucht und die Veränderung der physikochemischen Eigenschaften von $NH_4HPO_3NH_2$ diskutiert.

Durchführung der Experimente

Materialien. $NH_4HPO_3NH_2$ wurde nach der Methode zusammengesetzt,[3] die in der früheren Abhandlung beschrieben ist. Das Produkt wurde unter 3333 Pa bei Raumtemperatur für zwei Tage getrocknet und mit Daten von IR Spektren[4] und Röntgenbeugungsbildern identifiziert.[5]

Gef.: P, 29,96; N(gesamt), 24,25; N-NH_4, 12,16%. Ber. für $H_7N_2O_3P$: P, 29,16; N(gesamt), 24,56; N-NH_4, 12,28%.

Apparate und Verfahren. Der Ammoniakgehalt wurde mit Lösung der Schwefelsäure nach der Kjeldahl Methode bestimmt. Der Phosphorgehalt wurde mittels Ionenaustauschchromatographie[6] analysiert und mittels Papierchromatographie[7] mit saure und basische Lösungsmitteln getrennt. Die DTA, DSC, und TG Kurven wurden in der Luft mit einer Aufheizgeschwindigkeit von 5 °C/min mit einem Rigaku TG-DTA, TG-DSC Thermoflex aufgenommen. Für DTA und DSC wurde α-Al_2O_3 als Bezugsmittel gebraucht. Die Röntgenbeugungsbilder wurden mit einem Shimadzu-Beugungsmesser (Cu $K\alpha$-Strahlung, Ni-gefiltert) erhalten. Die IR Spektren wurden mittels Präparation von KBr-Preßlingen mit einem Beugungsgitter IR Spektrometer der JASCO aufgenommen. Die Schwingungsmühle wurde nur in der Luft gebraucht. $NH_4HPO_3NH_2$ (3,0 g) und eine Stahlstange (Diameter 0,025 m, Länge 0,045 m) wurden in einen 100-ccm-Stahltoph hineingetan und dann mit der Schwingungsmühle von Laboratoriumgröße (Heiko Seisakusho AG) gemahlen. Der spezifische Oberflächenraum wurde nach der BET Methode geschätzt, die Stickstoff bei 77 K adsorbieren läßt.

Ergebnisse und Diskussion

Thermische Analyse. Abbildungen 1 und 2 zeigen den Effekt der Schwingungsmühle auf DSC und TG von $NH_4HPO_3NH_2$. Die DSC Kurven ergeben drei endotherme Spitzen in der frühen Stufe der Laufzeit der Schwingungsmühle. Die erste Spitze (E_{D_1}), die in zwei Teile geteilt ist, verschiebt sich auf die Seite der Tiefentemperatur mit Laufzeit der Schwingungsmühle. Die zweite Spitze (E_{D_2}), die bei 470—480 K für die untersuchten Verbindungen beobachtet wird, kann von Bildung des Ammoniummetaphosphates abhängig sein. Das wurde mittels Ionenaustauschchromatographie, Papierchromatographie, und Röntgenbeugungsbilder von allen Proben beobachtet, die vor und hinter E_{D_2} in den DSC Kurve herausgenommen wurden. Die Stelle von E_{D_2} verschiebt sich ein wenig auf die Seite der Tiefentemperatur mit zunehmender Laufzeit der Schwingungsmühle und die Spitzenintensität wächst. Die letzte, große, breite Spitze (E_{D_3}) wird im Temperaturgebiet 530—650 K beobachtet, in welchem $NH_4HPO_3NH_2$ zu Metaphosphorsäure zersezt wird. Die TG Kurven in

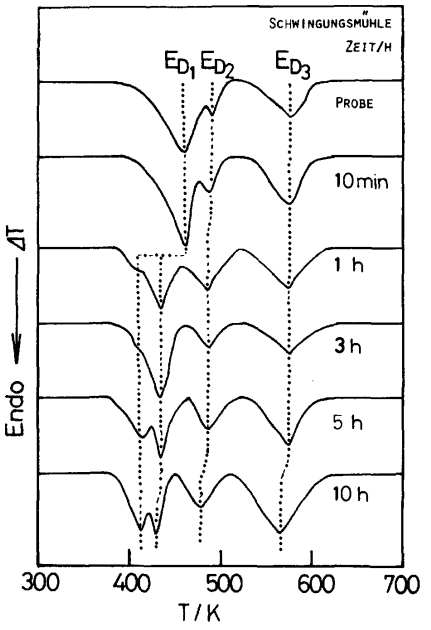

Abb. 1. Variationen von DSC Kurven für $NH_4HPO_3NH_2$ mit Laufzeit der Schwingungsmühr.

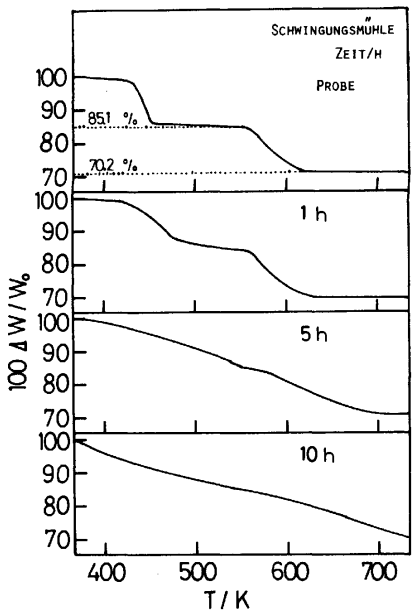

Abb. 2. Variationen von TG Kurven für $NH_4HPO_3NH_2$ mit Laufzeit der Schwingungsmühle.

Abb. 2 zeigen, daβ der Prozeβ der Zersetzung von $NH_4HPO_3NH_2$ in zwei Stufen ausgeführt wird. Die Zahlenwerte, die auf der punktierten Linie von TG Kurven (Abb. 2) liegen, zeigen die berechneten Werte der Gewichtverluste, die dem aus der Probe austretendem Ammoniak entsprechen. Es gibt keine deutliche Hochebene in den TG Kurven bei der Verlängerung der Laufzeit der Schwingungsmühle. Aus dieser undeutlichen Hochebene ergibt sich, daβ beides die Transition der Amidogruppe zu Ammoniak und die Auslassung des Ammoniaks vom Zwischenprodukt gleichzeitig im gemahlten Material verlaufen. Diese Arbeit hat es ins klare gebracht, daβ die Stelle der Spitzen von DTA und DSC und die Anfangstemperatur der Zersetzung von $NH_4HPO_3NH_2$ sich auf die Seite der hohen Temperaturen mit zunehmender Aufheizgeschwindigkeit verschieben.

Veränderung in Größe und Form. Die Veränderungen in Größe und Form der Partikel von $NH_4HPO_3NH_2$ mit Laufzeit der Schwingungsmühle werden in Abb.

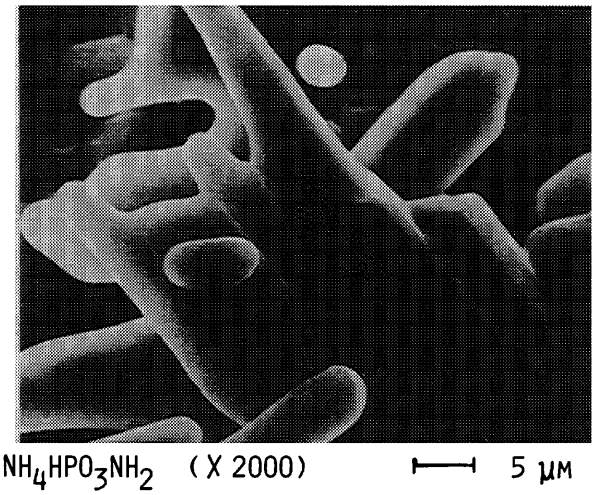

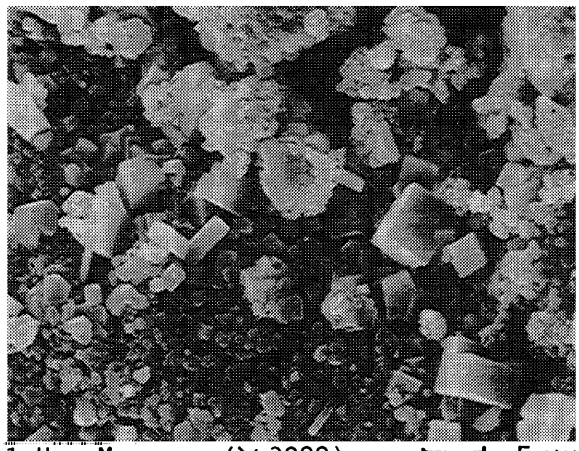

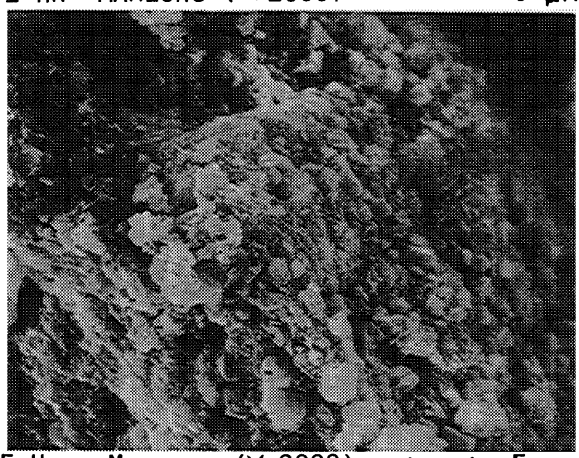

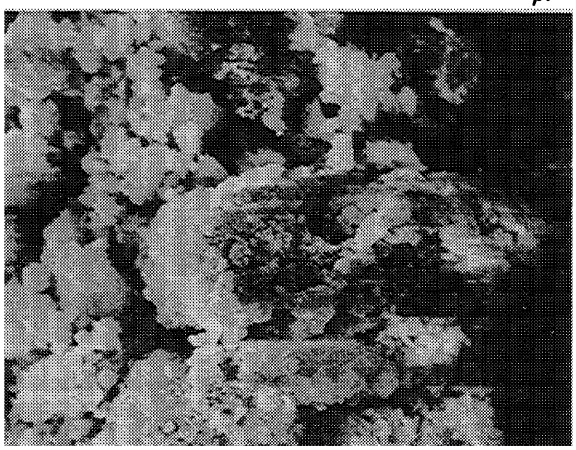

Abb. 3. Elektronenmikrophotographie vom gemahlten $NH_4HPO_3NH_2$ in verschiedenen Abstanden.

3 bei verschiedenen Abständen dargestellt. Die erste brettförmige Partikel wird im gemahlten $NH_4PO_3NH_2$ nach einer Stunde bemerkt. Der Durchmesser der Partikel, die über fünf Stunden gemahlt wurde, nahm um 0,5—2,0 μm ab.

Röntgenbeugungsbild und Spezifischer Oberflächeraum. In den drei größten Intensitätslinien des Röntgenbeugungsbildes von $NH_4HPO_3NH_2$ sind die entsprechenden Abstände (*d*-Werten in Å) 5,72, 4,23, und 4,28. Diese Spitzenintensitäten nehmen mit zunehmender Laufzeit

der Schwingungsmühle bedeutend ab. Die Röntgenbeugungsbilder auf dem Gebiete zwischen 2,98 und 8,85 Å überlappen gegenseitig. Für Bestimmung der Kristallitengröβe nach der Scherrer Methode,[8] wurde die Beugungslinie von 2,23 Å des unentschiedenen Millerschen Indexes ausgewählt, um Überlappung zuvermeiden. Die Halbwertsbreite der Beugungslinie zu 2,23 Å wird mit zunehmender Laufzeit der Schwingungsmühle verbreitert. Das Phänomen wurde bereits nach zehn Minuten Laufzeit der Schwingungsmühle beobachtet. Die Kristallitengröβe nahm von 500 zu 160 Å mit zunehmender Laufzeit der Schwingungsmühle ab. Der nach der BET Methode bestimmte spezifische Oberflächenraum von $NH_4HPO_3NH_2$ ist 2,0 M^2/g und der der über zwei Stunden gemahlten Partikel ist 2,5—3,5 M^2/g; Die Laufzeit der Schwingungsmühle hat nur kleinen Einfluβ. Es ist nach diesem Ergebnis verständlich, daβ die Agglomeration von primären Partikeln mit zunehmender Laufzeit der Schwingungsmühle vergröβert wird.

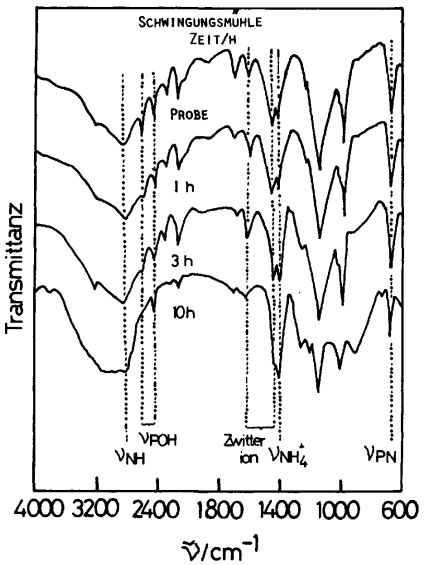

Abb. 4. IR-Spektren vom gemahlten $NH_4HPO_3NH_2$ in verschiedenen Abständen.

IR Spectra. Abbildung 4 zeigt den Effekt der Schwingungsmühle auf IR Spektren von $NH_4HPO_3NH_2$. Auf den Kurven erscheint auch ein freies NH zwischen 3000 und 3600 cm^{-1}. Eine zwischenmolekulare Brücke NH wird zwischen 2810 und 2840 cm^{-1} unter einer Verschiebung durch Wasserstoffbindung auf tiefere Frequenz gesehen. Die Bänder bei 1615 und 1470 cm^{-1}, die aus Bildung des Zwitterions entstehen, erfahren einen Einfluβ im Verhältnis zu der Zeitspanne, in welcher die Mühle in Betrieb gewesen ist. Aus den Veränderungen der IR Spektren von $NH_4HPO_3NH_2$ mit zunehmender Laufzeit der Schwinungsmühle scheint es somit erlaubt zu schlieβen, daβ gemäβ der Betriebszeit der Mühle die Fraktion der starken Wasserstoffbindung zwischen NH und POH zunimmt. Wahrscheinlich hängt diese starke Wasserstoffbindung mit der Transformation von $NH_4HPO_3NH_2$ ins

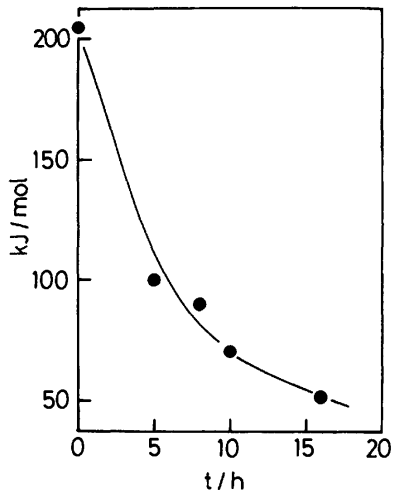

Abb. 5. Variationen von Aktivierungsenergie mit Laufzeit der Schwingungsmühle.

Zwitterion $NH_4PO_3^-NH_3^+$ zusammen.

Kinetik der Thermischen Zersetzung im Festen Zustand. Die Kinetik der thermischen Zersetzung wurde im Temperaturgebiet von 420 bis 470 K untersucht. In Analyse der isothermischen DSC-Kurve, nach Mcghie *et al.*,[9] konnte man annehmen, daβ die Fläche unter der Spitze die Gesamtzersetzungswärme darstellt. Die vollständige Geschwindigkeitsgleichung für die thermische Zersetzung ergibt sich aus der Gleichung

$$k/\mathrm{min}^{-1} = 3.6 \times 10^{22} \exp[(-208.6 \pm 0.2)/RT].$$

Dieser Wert der Aktivierungsenergie stimmte am besten mit E_A=203,5±0,5 kJ/mol überein, die aus DTA Kurven nach der Kissinger Gleichung[10] berechnet wurde. Diese Resultate wurden so bestimmte, daβ beide DTA und DSC die gleiche Aktivierungsenergie haben konnte. Abbildung 5 zeigt den Effekt der Schwingungsmühle auf die Aktivierungsenergie des Desamidierenes von $NH_4HPO_3NH_2$. Die Aktivierungsenergie nimmt mit zunehmender Laufzeit der Schwingungsmühle ab. Aus den obigen Resultaten läβt sich annehmen, daβ die Zunahme des amorphen Zustandes und die Leichtigkeit der Transformation der Amidogruppe zu Ammoniumion von einander abhängig sind.

Literaturen

1) P. Klement und O. Koch, *Chem. Ber.*, **87**, 333 (1954); M. Goehring und J. Sambeth, *ibid.*, **90**, 232 (1957).
2) C. Shimasaki, Y. Oono, F. Takai, M. Shoji, und M. Yoshizawa, *Nippon Kagaku Kaishi*, **1982**, 376.
3) F. A. Cotton, "Inorganic Syntheses," Vol. XIII, p. 23 (1972).
4) D. E. C. Corbridge und E. J. Lowe, *J. Chem. Soc.*, **1954**, 493.
5) A. H. Herzog und M.L. Nielsen, *Anal. Chem.*, **30**, 1490 (1958).
6) E. Kobayashi, *Nippon Kagaku Zasshi*, **85**, 317 (1964).
7) E. Karl-Kroupa, *Anal. Chem.*, **28**, 1091 (1956).
8) P. Schherrer, *Göttinger Nachrichten*, **2**, 98 (1918).
9) A. R. Mcghie, P. S. Kalyanaraman, und A. F. Garito, *J. Polym. Sci., Polym. Lett. Ed.*, **16**, 335 (1978).
10) H. E. Kissinger, *Anal. Chem.*, **29**, 1702 (1957).

Theory of Time-resolved Resonance Raman Scattering from Vibrationally Hot Molecules

Yuichi FUJIMURA,* Yukiyoshi OHTSUKI, and Takeshi NAKAJIMA
Department of Chemistry, Faculty of Science, Tohoku University, Sendai 980
(Received April 7, 1984)

A theory of time-resolved resonance Raman scattering (RRS) from molecules is developed. The time-resolved RRS cross section is defined as a product of the time-dependent vibronic energy distribution and the scattering cross section from the single vibronic level. The theory is applied to the time-resolved RRS from vibrationally hot molecules whose vibronic distribution characterized by a canonical distribution with temperature higher than that of the heat bath relaxes to the equilibrium one in the presence of a collisional vibrational relaxation. Analytical expressions for the time-resolved RRS cross section are derived within a displaced harmonic oscillator model. It is shown that in the strong coupling case the intensities of the Stokes and anti-Stokes Raman bands in the rigorous resonance case vary inversely as the time-dependent average vibrational occupation number. Some model calculations are performed to illustrate the time-dependent intensity changes of the Raman bands.

Time-resolved Raman spectroscopy is one of the attractive methods for studying relaxation dynamics taking place in highly non-equilibrium ground or electronically excited states of molecules. There have been a considerable number of experimental results on the application of the time-resolved Raman spectroscopy to vibronically excited molecules, photochemical and biological intermediates and so on.[1,2]

Let us consider vibrationally hot molecules characterized by a canonical distribution with temperature T^0 higher than that of the heat bath T. This distribution relaxes to the equilibrium distribution with T after collisional vibrational relaxations. The vibrational energy distribution in the v vibrational state at time t is given as[3]

$$\rho_v(t) = \{1 - \exp[-u(t)]\}\exp[-vu(t)], \tag{1}$$

where

$$u(t) = \log\left[\frac{\exp[-z(t)]\{1-\exp(\theta-\theta^0)\}-\exp(\theta)\{1-\exp(-\theta^0)\}}{\exp[-z(t)]\{1-\exp(\theta-\theta^0)\}-\{1-\exp(-\theta^0)\}}\right], \tag{2}$$

with $z(t)=\kappa t\{1-\exp(-\theta)\}$, $\theta=\hbar\omega/kT$ and $\theta^0=\hbar\omega/kT^0$ in which κ is the collisional vibrational relaxation constant, and ω is the frequency of the vibrational mode of the molecule. The canonically hot molecules are produced by a shock wave method[4] or by a radiationless transition following an optical excitation[5] *etc.* The collisional vibrational relaxation of the hot molecules in the presence of heat bath molecules has mainly been investigated by using the time-resolved one-photon absorption technique so far.[5] The typical relaxation times are in micro to nanoseconds region, depending on the pressure of the perturber molecules. Application of the time-resolved Raman spectroscopy to the investigation of the relaxation mechanism has not been reported. It is interesting to mention the difference in the band structure between the time-resolved one-photon absorption spectra and the time-resolved Raman spectra to be observed. The former consists of a structureless, broad bands,[5] and on the other hand, the latter should consist of vibrational Stokes and anti-Stokes band structures in a highly non-equilibrium condition. The broad band structure in the absorption spectra originates mainly from electronic relaxations taking place in the optically excited electronic state. Compared with the time-resolved absorption method, the time-resolved Raman scattering method may make a significant contribution to analyzing the relaxation mechanism from the view point of the band structure mentioned above.

In this paper we present an applicability of the time-resolved Raman spectroscopy to analyzing the relaxation mechanism of the canonically hot molecules and show how the collisional vibrational relaxation reflects the time-resolved Raman spectra. For this purpose we derive an expression for the cross section of the time-resolved resonance Raman scattering. To our knowledge, there are few theoretical papers on the time-resolved Raman spectroscopy applied to highly non-equilibrium system so far. Luzzi and Vasconcellos,[6] and Vasconcellos and Luzzi[7] have developed a theoretical study of the time-resolved Raman scattering from a highly photoexcited semiconductor plasma by using the Zubarev non-equilibrium ensemble method. In the next section we use the generating function method to derive the time-resolved resonance Raman scattering cross section. This method has been proved to be a powerful method for deriving the Raman scattering cross section of molecules.[8,9]

Theory

We consider a resonance Raman scattering (RRS) from initial state $a\{v\}$ to final state $a\{v'\}$ *via* resonant state $b\{m\}$ where a and b denote the initial (final) and resonant electronic states, respectively, and { } denote the relevant vibrational states. The time-resolved RRS differential cross section in a solid angle $d\Omega$ per unit scattered photon frequency ω_2, $d^2\sigma(\omega_1,\omega_2,t)/d\Omega d\omega_2$ is defined as

$$\frac{d^2\sigma(\omega_1,\omega_2,t)}{d\Omega d\omega_2} = \sum_v \rho_v(t)\frac{d^2\sigma_v(\omega_1,\omega_2)}{d\Omega d\omega_2}, \tag{3}$$

where ω_1 is the incident photon frequency, $d^2\sigma_v(\omega_1,\omega_2)/d\Omega d\omega_2$ is the RRS differential cross section from single vibronic level (SVL) v, and $\rho_v(t)$ is the population of the initial vibrational state v at time t. In this treatment, it is assumed that the time-dependence of the population can be observed after transient effects have terminated. The single vibronic level RRS cross section is expressed as

$$\frac{d^2\sigma_v(\omega_1,\omega_2)}{d\Omega d\omega_2} = C\omega_1\omega_2^3 \sum_{v'} \frac{\Gamma_{av',av}}{(\omega_{v',v}-\omega_1+\omega_2)^2+\Gamma_{av',av}^2} \times \left| \sum_m \frac{M_{av',bm}(2)M_{bm,av}(1)}{i(\omega_{bm,av}-\omega_1)+\Gamma_{bm,av}} \right|^2, \quad (4)$$

where $C=(2\pi\hbar^2\varepsilon_0c^4)^{-1}$, and $M_{bm,av}$ (1)represents the component of the transition moment along the polarization direction $\hat{e}_1$ between two vibronic states bm and av. $\Gamma_{av',av}$ and $\Gamma_{bm,av}$ are the dephasing constant associated with the initial and final states, and that with the resonant and initial states, respectively.

In order to derive an expression for the time-resolved RRS differential cross section, it is convenient to express Eq. 4 in terms of the generating function,

$$\frac{d^2\sigma_v(\omega_1,\omega_2)}{d\Omega d\omega_2} = \frac{1}{2}C\omega_1\omega_2^3|M_{ab}^0(2)M_{ba}^0(1)|^2\int_0^\infty d\tau\int_0^\infty d\tau'\int_{-\infty}^\infty d\xi \times \exp[i\xi(\omega_1-\omega_2)+i\omega_1(\tau'-\tau) - \Gamma_{ba}(\tau+\tau') - \Gamma_{v'v}|\xi|]G_v(\tau,\tau',\xi), \quad (5)$$

where the generating function for the single vibronic level RRS, $G_v(\tau,\tau',\xi)$ takes the form,

$$G_v(\tau,\tau',\xi) = \langle v|\exp[i\hat{H}_b\tau/\hbar]\exp[-i\hat{H}_a\xi/\hbar]\exp[-i\hat{H}_b\tau'/\hbar] \times \exp[i\hat{H}_a(\xi-\tau+\tau')/\hbar]|v\rangle. \quad (6)$$

In deriving Eq. 5, the vibrational quantum number dependence of the dephasing constants has been omitted, that is, Γ_{ba} and $\Gamma_{v'v}$ should be interpreted as the average electronic and vibrational dephasing constants, respectively, and the Condon approximation has been used, that is, electronic transition moments $M_{ab}^0(2),M_{ba}^0(1)$ are independent of the nuclear coordinates.

In the displaced harmonic oscillator model, in which the Hamiltonians of the initial (final) electronic and the resonant electronic states are given by

$$\hat{H}_a = \frac{\hbar\omega}{2}(\hat{p}^2+q^2) = \hbar\omega(\hat{b}^\dagger\hat{b}+\frac{1}{2}), \quad (7a)$$

and

$$\hat{H}_b = \frac{\hbar\omega}{2}[\hat{p}^2+(q-\Delta)^2]+\varepsilon^0 = \hat{H}_a - \frac{\hbar\omega\Delta}{\sqrt{2}}(\hat{b}+\hat{b}^\dagger) + \frac{\hbar\omega\Delta^2}{2} + \varepsilon^0, \quad (7b)$$

we can derive the generating function, Eq. 6 as

$$G_v(\tau,\tau',\xi) = \exp\left[\frac{i\varepsilon^0(\tau-\tau')}{\hbar} + \frac{\Delta^2}{2}\{\exp(i\omega\tau)-1\} + \frac{\Delta^2}{2}\{\exp(-i\omega\tau')-1\} + \lambda^*(\tau)\lambda(\tau')\exp(-i\omega\xi)\right]L_v(|\alpha(\tau,\tau',\xi)|^2), \quad (8)$$

where ω is the frequency of the harmonic oscillator, Δ is the dimensionless displacement between the equilibrium positions in the initial and resonant states and ε^0 represents the electronic energy gap between the bottoms of the two electronic states. A detailed derivation is given in Appendix A. In Eq. 8, L_v, the Laguerre polynomials, is defined as

$$L_v(|\alpha(\tau,\tau',\xi)|^2) = \sum_{k=0}^{v} \frac{v!(-|\alpha(\tau,\tau',\xi)|^2)^k}{(k!)^2(v-k)!}, \quad (9)$$

with

$$\alpha(\tau,\tau',\xi) = \lambda(\tau) - \lambda(\tau')\exp(-i\omega\xi), \quad (10)$$

and

$$\lambda(\tau) = \frac{\Delta}{\sqrt{2}}\{1-\exp(-i\omega\tau)\}.$$

Substituting Eqs. 1 and 5 with Eq. 8 into Eq. 3, and carrying out summation over v, we obtain

$$\frac{d^2\sigma(\omega_1,\omega_2,t)}{d\Omega d\omega_2} = \frac{1}{2}C\omega_1\omega_2^3|M_{ab}^0(2)M_{ba}^0(1)|^2\int_0^\infty d\tau\int_0^\infty d\tau'\int_{-\infty}^\infty d\xi \times \exp[i\xi(\omega_1-\omega_2)+i\omega_1(\tau'-\tau) - \Gamma_{ba}(\tau+\tau')-\Gamma_{v'v}|\xi|]G(\tau,\tau',\xi), \quad (11)$$

where

$$G(\tau,\tau',\xi) = \exp\left[i\varepsilon^0(\tau-\tau')/\hbar - \{v(t)+1\}\left\{\frac{\Delta}{\sqrt{2}}\lambda^*(\tau) + \frac{\Delta}{\sqrt{2}}\lambda(\tau')-\lambda^*(\tau)\lambda(\tau')\exp(-i\omega\xi)\right\} - v(t)\left\{\frac{\Delta}{\sqrt{2}}\lambda(\tau)+\frac{\Delta}{\sqrt{2}}\lambda^*(\tau') - \lambda(\tau)\lambda^*(\tau')\exp(i\omega\xi)\right\}\right], \quad (12)$$

and $v(t)=\{\exp[u(t)]-1\}^{-1}$, which is the average vibrational occupation number at time t. In deriving Eq. 11 the following formula has been used,

$$\sum_{v=0}^{\infty}\exp[-vu(t)]L_v(|\alpha(\tau,\tau',\xi)|^2) = \frac{\exp[-|\alpha(\tau,\tau',\xi)|^2v(t)]}{1-\exp[-u(t)]}. \quad (13)$$

Equation 12 has the same structure as that of the generating function for the RRS cross section of molecules in the thermal equilibrium.[8] An analytical expression for the time-resolved RRS cross section can easily be derived from Eq. 11 with Eq. 12:

$$\frac{d^2\sigma(\omega_1,\omega_2,t)}{d\Omega d\omega_2} = C\omega_1\omega_2^3|M_{ab}^0(2)M_{ba}^0(1)|^2\exp[-\{2v(t)+1\}\Delta^2] \times \left(\sum_{k=0}^{\infty}\sum_{l=0}^{\infty}\frac{\left[\{v(t)+1\}\frac{\Delta^2}{2}\right]^k\left\{v(t)\frac{\Delta^2}{2}\right\}^l}{k!l!}\right.$$

$$\times \frac{\Gamma_{v'v}}{[\{\omega_1-\omega_2-(k-l)\omega\}^2+\Gamma_{v'v}^2]}\Bigg)$$

$$\times\left|\sum_{p=0}^{k}\sum_{q=0}^{l}\sum_{r=0}^{\infty}\sum_{u=0}^{\infty}\binom{k}{p}\binom{l}{q}(-1)^{r+u}\frac{\left[\{v(t)+1\}\frac{\Delta^2}{2}\right]^r}{r!}\frac{\left\{v(t)\frac{\Delta^2}{2}\right\}^u}{u!}\right.$$

$$\left.\times\frac{1}{[\mathrm{i}\{\omega_1-\varepsilon^0/\hbar-(p-q+r-u)\omega\}+\Gamma_{ba}]}\right|^2. \quad (14)$$

In the case in which the molecular system is characterized by a high temperature, that is, $\{2v(t)+1\}\Delta^2/2 \gg 1$ is satisfied, an approximate expression for the time-resolved RRS can be used. In this case expanding $\exp(\pm i\omega\tau)$ and $\exp(\pm i\omega\tau')$ in Eq. 12 to the second order,[10] substituting the resulting expression into Eq. 11 and carrying out the integration over ξ, we obtain

$$\frac{d^2\sigma(\omega_1,\omega_2,t)}{d\Omega d\omega_2} \simeq C\omega_1\omega_2^3|M_{ab}^0(2)M_{ba}^0(1)|^2$$

$$\times\sum_{k=0}^{\infty}\sum_{l=0}^{\infty}\frac{\{S_{v1}(t)\}^k\{S_v(t)\}^l}{k!l!}\frac{\Gamma_{v'v}|F^{(k+l)}(\omega_1)|^2}{[\{\omega_1-\omega_2-(k-l)\omega\}^2+\Gamma_{v'v}^2]}, \quad (15)$$

where

$$F^{(k+l)}(\omega_1)=\int_0^\infty d\tau(\omega\tau)^{k+l}$$

$$\times\exp\left[i\left(\frac{\varepsilon^0}{\hbar}+\frac{\Delta^2\omega}{2}-\omega_1\right)\tau-\Gamma_{ba}\tau-\frac{S(t)\omega^2\tau^2}{2}\right], \quad (16)$$

$S_{v1}(t)=\{v(t)+1\}\Delta^2/2$, $S_v(t)=v(t)\Delta^2/2$, and $S(t)=S_{v1}(t)+S_v(t)$. Equation 16 can be expressed in terms of the repeated integrals of the error function defined by[11]

$$i^{(n)}\mathrm{erfc}(z)=\frac{2}{\sqrt{\pi}}\int_z^\infty\frac{(x-z)^n}{n!}\exp(-x^2)dx, \quad (17)$$

as

$$F^{(k+l)}(\omega_1)=$$

$$\frac{\sqrt{\pi}}{2}\frac{(k+l)!}{\omega}\left\{\frac{2}{S(t)}\right\}^{(k+l+1)/2}\exp(z^2)i^{(k+l)}\mathrm{erfc}(z), \quad (18)$$

with

$$z=\left\{\Gamma_{ba}-i(\varepsilon^0/\hbar+\frac{\Delta^2}{2}\omega-\omega_1)\right\}^2/[\{2S(t)\}^{1/2}\omega]. \quad (19)$$

In the high temperature case, anti-Stokes bands as well as Stokes bands make a significant contribution to the Raman spectra. Expressions for the time-resolved RRS, Eqs. 14 and 15 consist of the Rayleigh, Stokes, and anti-Stokes components:

$$\frac{d^2\sigma(\omega_1,\omega_2,t)}{d\Omega d\omega_2}=\frac{d^2\sigma^{(R)}(\omega_1,\omega_2,t)}{d\Omega d\omega_2}$$

$$+\sum_{n=1}^{\infty}\left\{\frac{d^2\sigma^{(ST-n)}(\omega_1,\omega_2,t)}{d\Omega d\omega_2}+\frac{d^2\sigma^{(AST-n)}(\omega_1,\omega_2,t)}{d\Omega d\omega_2}\right\}, \quad (20)$$

where the first, second and the last terms represent the Rayleigh scattering, n-th order Stokes and n-th order anti-Stokes cross sections, respectively. For example, the cross sections for the n-th order Stokes and anti-Stokes bands in Eq. 15 can be expressed by putting $n=k-l$ and $n=l-k$ as

$$\frac{d^2\sigma^{(ST-n)}(\omega_1,\omega_2,t)}{d\Omega d\omega}$$

$$=\sum_{l=0}^{\infty}\frac{S_{v1}^{n+l}S_v^l}{(n+l)!l!}|F^{(n+2l)}(\omega_1)|^2\frac{\Gamma_{v'v}}{\{(\omega_1-\omega_2-n\omega)^2+\Gamma_{v'v}^2\}}, \quad (21)$$

and

$$\frac{d^2\sigma^{(AST-n)}(\omega_1,\omega_2,t)}{d\Omega d\omega_2}=\sum_{l=0}^{\infty}\frac{S_{v1}^lS_v^{n+l}}{l!(n+l)!}|F^{(n+2l)}(\omega_1)|^2$$

$$\times\frac{\Gamma_{v'v}}{\{(\omega_1-\omega_2+n\omega)^2+\Gamma_{v'v}^2\}}, \quad (22)$$

respectively where $S_{v1}=S_{v1}(t)$, $S_v=S_v(t)$ and the expression for the Rayleigh scattering band is equivalent to Eqs. 21 or 22 with $n=0$. The cross sections for the n-th order Stokes and anti-Stokes bands in Eq. 14 can be evaluated in the similar way.

Discussion

In the previous section we have derived an expression for the time-resolved RRS from molecules in which the initial distribution is characterized by a canonical distribution with higher temperature than that of the heat bath. One of the merits of carrying out the summation over v in Eq. 3 to derive the expression for the time-resolved RRS differential cross section is spontaneously to bring about concept of time-dependent average occupation numbers $v(t)$. The average occupation number decreases as the molecular system becomes cool because of the collisional vibrational relaxation. Intensities of anti-Stokes bands originate from the nonzero average occupation numbers. In order to demonstrate the time-dependence of the RRS spectra we perform a model calculation of the Raman band intensity. Figure 1 shows the time-resolved RRS spectra of molecules whose initial distribution is characterized by a canonical distribution with temperature $T^0=800$ K at the initial time and relaxes to the equilibrium one with 300 K after collisional vibrational relaxations. The broken and solid lines represent the RRS spectra at $\kappa t=0$ and 2 in a unit of κ, respectively. These Raman bands are calculated by using Eq. 14 under the rigorous resonance condition $\omega_1=\varepsilon^0/\hbar$. The average vibrational occupation numbers $v(t)$ at $\kappa t=0$, and 2 are 3.52 and 1.99, respectively. The parameters used in the calculation are vibrational frequency $\omega=200\,\mathrm{cm}^{-1}$, dimensionless displacement $\Delta=0.5$, the damping constants $\Gamma_{ba}=100\,\mathrm{cm}^{-1}$, and $\Gamma_{v'v}=20\,\mathrm{cm}^{-1}$. We can see the increase in the intensities of the Rayleigh and first-order Stokes Raman bands with the development of time. Higher order Stokes and anti-Stokes Raman bands, on the other hand, decrease in their intensities.

Figure 2 shows time-resolved RRS spectra in the

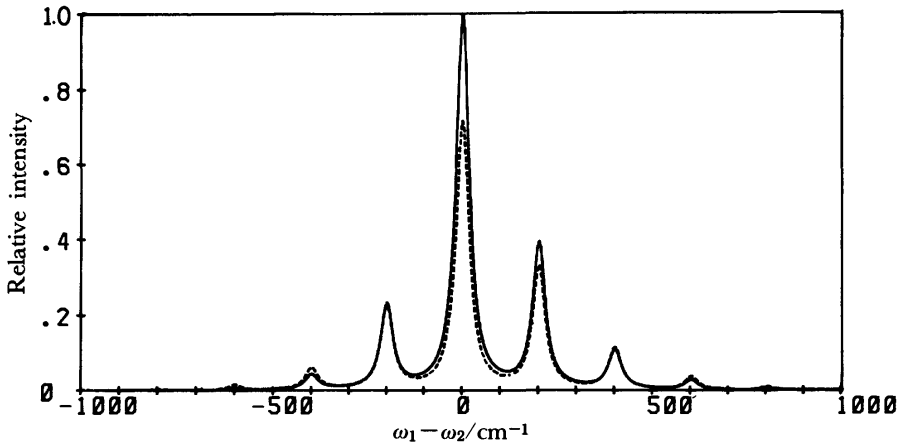

Fig. 1. The calculated time-resolved resonance Raman spectra. The broken and solid lines represent the Raman spectra for $\kappa t=0$ and 1.0 in a unit of κ, respectively. The resonant condition $\omega_1=\varepsilon^0/\hbar$ is assumed. The constants used are $T^0=800\,\mathrm{K}$ and $T=300\,\mathrm{K}$ for the initial and thermal equilibrium temperatures, $\omega=200\,\mathrm{cm}^{-1}$ for the frequency of the displaced harmonic oscillator with dimensionless displacement $\Delta=0.5$, and $\Gamma_{ba}=100\,\mathrm{cm}^{-1}$, and $\Gamma_{v'v}=20\,\mathrm{cm}^{-1}$ for the dephasing constants. The calculation is carried out by using Eq. 14.

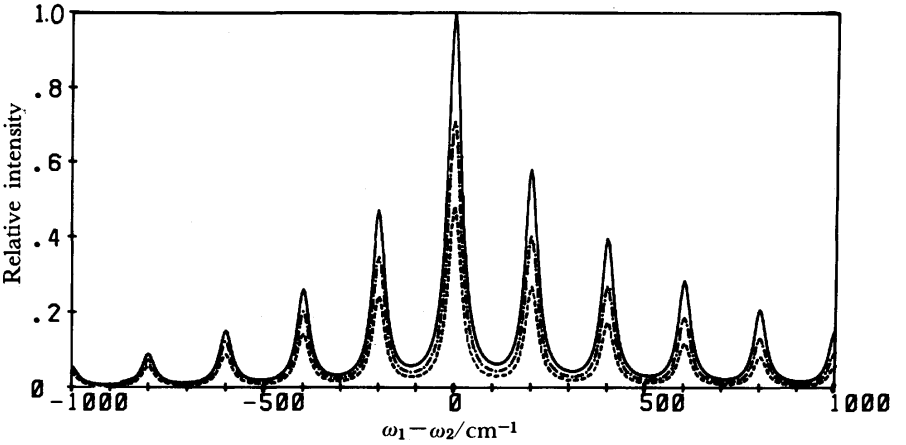

Fig. 2. The calculated time-resolved resonance Raman spectra in a strong coupling case. The broken, dotted broken, and solid lines represent the Raman spectra at $\kappa t=0$, 1.0 and 2.0, respectively. The constants used are $T^0=2000\,\mathrm{K}$ and $T=300\,\mathrm{K}$, $\Delta=2.0$ and the other constants are the same as those in Fig. 1. The resonant condition $\omega_1=\varepsilon^0/\hbar+\Delta^2\omega/2$ is assumed. The calculation is carried out by using Eq. 15. The average occupation numbers $v(t)$ at $\kappa t=0$, 1.0 and 2.0 are 9.51, 6.25 and 4.25, respectively.

strong coupling case. Here $\Delta=2.0$ and $T^0=2000\,\mathrm{K}$ are taken, and the other parameters are the same as those in Fig. 1. The calculation has been carried out by using Eq. 15. It was assumed that $\omega_1=\varepsilon^0/\hbar+\omega\Delta^2/2$ which corresponds to the classical resonance condition. From Fig. 2, we can see that in the strong coupling case n-th order anti-Stokes bands as well as the Stokes bands increase in their intensities with the time development. The average occupation numbers at $\kappa t=0$, 1, and 2 are $v(t)=9.51$, 6.25, and 4.25, respectively. In order to understand this time-dependent behavior we derive an analytical expression for the time-dependent Raman scattering cross section, Eq. 16 in the resonance condition. In the strong coupling case and further in the case in which $\{v(t)+1/2\}^{1/2}\Delta\omega>\Gamma_{ba}$ is satisfied and the damping effects (Γ_{ba}) can be neglected, noting that

$$F^{(p)}(\omega_1=\varepsilon^0/\hbar+\omega\Delta^2/2)=\frac{1}{\omega}\left(\frac{\pi}{2}\right)^{1/2}S^{-1/2}(p-1)!!S^{-p/2}, \tag{23a}$$

for even p, and

$$F^{(p)}(\omega^1=\varepsilon^0/\hbar+\omega\Delta^2/2)=\frac{1}{\omega}S^{-1/2}(p-1)!S^{-p/2}, \tag{23b}$$

for odd p, we can obtain an analytical expression for Stokes band intensity, Eq. 21 as

$$\frac{\mathrm{d}^2\sigma^{(ST-n)}(\omega_1,\omega_2,t)}{\mathrm{d}\Omega\mathrm{d}\omega_2}=S^{-1}\Xi^{(ST-n)}, \tag{24}$$

with

$$\Xi^{(ST-n)} = \frac{1}{\omega^2}\sum_{l=0}^{\infty}\left(\frac{S_{v1}}{S}\right)^{n+l}\left(\frac{S_v}{S}\right)^{l} \times \frac{\{(n+2l-1)!!\}^2}{(n+l)!l!}\frac{\Gamma_{v'v}}{\{(\omega_1-\omega_2-n\omega)^2+\Gamma_{v'v}^2\}}, \quad (25a)$$

for odd n, and with

$$\Xi^{(ST-n)} = \frac{\pi}{2\omega^2}\left[\sum_{l=0}^{\infty}\left(\frac{S_{v1}}{S}\right)^{n+l}\left(\frac{S_v}{S}\right)^{l} \times \frac{\{(n/2+l-1)!!\}^2}{(n+l)!l!}\frac{\Gamma_{v'v}}{\{(\omega_1-\omega_2-n\omega)^2+\Gamma_{v'v}^2\}}\right], \quad (25b)$$

for even n, where $S=S(t)$. Equation 24 indicates that the time-dependence of the Stokes band intensities originates mainly from S^{-1} for high temperatures because $S_{v1}/S_v \sim 1$ and therefore $\Xi^{(ST-n)}$ is independent of time. Similarly, the time-dependence of the anti-Stokes bands originates from S^{-1}:

$$\frac{d^2\sigma^{(ST-n)}(\omega_1,\omega_2,t)}{d\Omega d\omega_2} \propto S^{-1}(t) \propto v(t), \quad (26a)$$

and

$$\frac{d^2\sigma^{(AST-n)}(\omega_1,\omega_2,t)}{d\Omega d\omega_2} \propto S^{-1}(t) \propto v(t). \quad (26b)$$

These expressions explain why the Raman bands in the strong coupling case increase in their intensities with the time development as shown in Fig. 2. It should be noted that Eqs. 26 are valid for the short time domain in which the strong coupling can be defined.

In summary in this paper we have developed a theory of the time-resolved RRS from molecules. The time-resolved RRS cross section is defined as a product of the SVL RRS cross section and its time-dependent population which is derived from the master equation. As an example we have applied the theory to the RRS from molecules whose population distribution is given by a canonical distribution characterized by temperature T^0 higher than that of the heat bath. It is shown that the time-resolved resonance Raman scattering method can be used to clarify the relaxation mechanism of canonically hot molecules. In a subsequent paper other types of the populations relaxation will be taken into account.

Appendix A

Derivation of the generating function for the SVL resonance Raman scattering cross section. In this Appendix we derive the generating function of the cross section for the resonance Raman scattering from single vibronic level v in the displaced harmonic oscillator model. In theory section it is shown that the generating function $G_v(\tau,\tau',\xi)$ takes the form,

$$G_v(\tau,\tau',\xi) = \langle v|\exp[i\hat{H}_b\tau/\hbar]\exp[-i\hat{H}_a\xi/\hbar]\exp[-i\hat{H}_b\tau'/\hbar] \times \exp[i\hat{H}_a(\xi-\tau+\tau')/\hbar]|v\rangle \quad (A.1)$$

Substituting the following expression into Eq. (A. 1)

$$\exp[i\hat{H}_b\tau/\hbar] = \exp[i\varepsilon_a^0\tau/\hbar + \frac{\Delta^2}{2}\{\exp(i\omega\tau)-1\}]\exp[i\hat{H}_a\tau/\hbar] \times \exp[-\lambda(\tau)\hat{b}^\dagger]\exp[\lambda^*(\tau)\hat{b}], \quad (A.2)$$

we obtain

$$G_v(\tau,\tau',\xi) = \exp[i\varepsilon_a^0(\tau-\tau')/\hbar + \frac{\Delta^2}{2}\{\exp(i\omega\tau)-1\} + \frac{\Delta^2}{2}\{\exp(-i\omega\tau')-1\}]\,A_v(\tau,\tau',\xi), \quad (A.3)$$

where

$$A_v(\tau,\tau',\xi) = \langle v|\exp[i\hat{H}_a\tau/\hbar]\exp[-\lambda(\tau)\hat{b}^\dagger]\exp[\lambda^*(\tau)\hat{b}] \times \exp[-i\hat{H}_a\xi/\hbar]\exp[-i\hat{H}_a\tau'/\hbar] \times \exp[-\lambda(-\tau')\hat{b}^\dagger]\exp[\lambda^*(-\tau')\hat{b}] \times \exp[i\hat{H}_a(\xi-\tau+\tau')/\hbar]|v\rangle, \quad (A.4)$$

with $\lambda(\tau)=\Delta/\sqrt{2}\{1-\exp(-i\varepsilon\tau)\}$. Equation A. 2 has been derived by using the Feynman disentangle technique.[9] Applying the Boson operator technique[9] to Eq. A. 4, we can obtain

$$A_v(\tau,\tau',\xi) = \exp[\lambda^*(\tau)\lambda(\tau')\exp(-i\omega\xi)]\langle v| \times \exp[-\alpha(\tau,\tau',\xi)\exp(i\omega\tau)\hat{b}^\dagger] \times \exp[\alpha^*(\tau,\tau',\xi)\exp(-i\omega\tau)\hat{b}]|v\rangle, \quad (A.5)$$

where

$$\alpha(\tau,\tau',\xi) = \lambda(\tau)-\lambda(\tau')\exp(-i\omega\xi). \quad (A.6)$$

Noting that

$$|v\rangle = \frac{1}{\sqrt{v!}}(\hat{b}^\dagger)^v|0\rangle, \quad (A.7)$$

we can rewrite Eq. A. 5 as

$$A_v(\tau,\tau',\xi) = \exp[\lambda^*(\tau)\lambda(\tau')\exp(i\omega\xi)]\frac{1}{v!} \times \langle 0|\hat{b}^v\exp[-\alpha(\tau,\tau',\xi)\exp(-i\omega\tau)\hat{b}^\dagger] \times \exp[\alpha^*(\tau,\tau',\xi)\exp(i\omega\tau)\hat{b}](\hat{b}^\dagger)^v|0\rangle, \quad (A.8)$$

which is expressed as

$$A_v(\tau,\tau',\xi) = \exp[\lambda^*(\tau)\lambda(\tau')\exp(i\omega\xi)]\frac{1}{v!} \times \langle 0|\{b-\alpha(\tau,\tau',\xi)\exp(-i\omega\tau)\}^v \times \{\hat{b}^\dagger+\alpha(\tau,\tau^\dagger,\xi)\exp(i\omega\tau)\}^v|0\rangle = \exp[\lambda^*(\tau)\lambda(\tau')\exp(i\omega\xi)]\frac{1}{v!} \times \sum_{k=0}^{\infty}\frac{(v!)^2\{-|\alpha(\tau,\tau',\xi)|^2\}^{(v-k)}}{(k!)^2(v-k)!}, \quad (A.9)$$

where we have used the relation

$$(\hat{b}^\dagger+\alpha^*)^v|0\rangle = \sum_{k=0}^{v}\frac{v!(\alpha^*)^{v-k}}{(v-k)!\sqrt{k!}}|k\rangle. \quad (A.10)$$

Equation A. 9 can be expressed in terms of the Laguerre polynomials which is defined by

$$L_v(|\alpha|^2) = \sum_{k=0}^{v}\frac{v!(-|\alpha|^2)^k}{(k!)^2(v-k)!}, \quad (A.11)$$

as

$$\Lambda_v(\tau,\tau',\xi) = \exp[\lambda^*(\tau')\lambda(\tau)\exp(i\omega\xi)]L_v(|\alpha(\tau,\tau',\xi)|^2). \tag{A.12}$$

Substituting Eq. A. 12 into Eq. A. 3 we obtain the expression for the generating function:

$$\begin{aligned} G_v(\tau,\tau',\xi) = \exp[&i\varepsilon^0(\tau-\tau')/\hbar \\ &+ \frac{\Delta^2}{2}\{\exp(i\omega\tau)-1\} + \frac{\Delta^2}{2}\{\exp(-i\omega\tau')-1\} \\ &+ \lambda^*(\tau)\lambda(\tau')\exp(-i\omega\xi)]L_v(|\alpha(\tau,\tau',\xi)|^2). \end{aligned} \tag{A.13}$$

References

1) G. H. Atkinson, "Advances" in Infrared and Raman Spectroscopy ed by R. J. H. Clark and R. E. Hester, (Heyden, London, 1982) Vol. 9, p. 1, and references therein.

2) T. Kobayashi and K. Yokoyama, *Kagaku No Ryoiki*, **36**, 509 (1982).

3) E. W. Montroll and K. E. Shuler, *J. Chem. Phys.*, **26**, 454 (1957).

4) D. C. Astholz, L. Brouwer, and J. Troe, *Ber. Bunsenges. Phys. Chem.*, **85**, 559 (1981).

5) N. Nakashima and K. Yoshihara, *J. Chem. Phys.*, **79**, 2727 (1983).

6) R. Luzzi and A. R. Vasconcellos, *J. Raman Spectry.*, **10**, 28 (1981).

7) A. R. Vasconcellos and R. Luzzi, *J. Raman Spectry.*, **14**, 39 (1983).

8) Y. Fujimura and S. H. Lin, *J. Chem. Phys.*, **71**, 3733 (1979).

9) Y. Fujimura and S. H. Lin, *J. Chem. Phys.*, **70**, 247 (1979).

10) R. Englman and J. Jortner, *Mol. Phys.*, **18**, 145 (1970).

11) "Handbook of Mathematical Functions," ed by M. A. Abramowitz and I. A. Stegun, of Dover, New York (1965).

 © 1985 The Chemical Society of Japan Bull. Chem. Soc. Jpn., 58, 601—610 (1985)

Orbital Phase Design of Acyclic Electron Localizing and Delocalizing π-Conjugated Polyions and Related Systems

Satoshi INAGAKI,* Koji IWASE, and Hirofumi KAWATA
Department of Chemistry, Faculty of Engineering, Gifu University, Yanagido, Gifu 501-11
(Received May 1, 1984)

Acyclic localization-delocalization of electrons in π-conjugated hydrocarbon polyions was predicted in terms of the continuity-discontinuity of the phase of the component orbitals. Many pairs of electron-localizing and -delocalizing conjugated polyions were designed as the model systems of which the relative stabilities have not been explored so far.

The concept of localization and delocalization of electrons is fundamental in organic chemistry. Among the prominent examples are the $4n+2$ π electron rule for aromaticity[1] and the stereoselection rule for pericyclic reactions.[2] The frontier orbital theory for chemical reactivity[3] emphasizes the delocalization between the molecules or bonds. The charge transfer force for intermolecular complexation of electron donor and acceptor[4] belongs to this category. An introduction of orbital symmetry or phase arguments[2,3] makes substantial progress in the theory of cyclic localization and delocalization. Chemical reactions *via* cyclic transition state are under control of the frontier orbital phase of the reacting molecules or parts of molecules or under the conservation of orbital symmetry.

Recently, mechanism of cyclic delocalization among more than two molecules, molecular fragments, or bonds was examined to derive the orbital phase continuity conditions for cyclic delocalization:[5] (a) The most electron-donating orbitals out of phase; (b) the most electron-accepting orbitals in phase; (c) the most electron-donating and -accepting orbitals in phase. The most electron-donating orbital is the HOMO of molecular systems, a bonding orbital of a bond, or a non-bonding orbital of lone-pair electrons. The most electron-accepting orbital is the LUMO of molecular systems, an anti-bonding orbital of a bond, or a vacant orbital on cationic centers. Electron-delocalizing systems are here defined as those which meet the three orbital phase requirements simultaneously. Otherwise, conjugate systems are classified into electron-localizing ones. The orbital phase conditions were already shown[5,6] to cover the aromaticity rule and the stereoselection rule.

More recently, cyclic orbital interaction was shown to be contained in acyclic conjugation.[7] The orbital phase conditions for cyclic delocalization are also applicable to estimating the degree of acyclic delocalization. Unfortunately, the related chemical phenomena observed so far are limited. In this paper we attempt to explore some new aspects of acyclic conjugation in view of continuity and discontinuity of orbital phase. π-Conjugated hydrocarbon polyions are employed as the model species.

Orbital Phase Design

Suppose that four orbitals, a, b, c, and d, interact in a cyclic manner in which the orbital sequence is illustrated in **1**. The interaction is hereafter denoted by the cyclic (a, b, c, d) interaction. The orbitals treated here are limited to occupied (p) and vacant (p*) p-orbitals of ionic centers and bonding (π) and anti-bonding (π*) orbitals of a π-bond. The π and π* orbitals can interact with the others at the same or different atomic orbitals. The former one-centered interaction is denoted by the subscript, 1, the latter two-centered interaction by 2. The other subscripts, s (suprafacial) and a (antarafacial), are introduced to specify whether an orbital takes part in cyclic interaction at the same or opposite side of orbital lobes. For a given set of orbitals, there are many possible modes of cyclic interactions which differ from one another in the orbital sequence, the interacting lobe (s or a) or center (1 or 2). Some interactions are those contained in real molecular systems, the others being not. The orbital interactions are subjected to the orbital phase analysis to predict that the associated molecular systems are electron-localizing or -delocalizing.

We start with cyclic (π_s, p_s, π^*_s, p_s) interactions. The orbital sequence and the interacting lobes are given there. Whether the π and π* orbitals interact at one or two centers makes a difference. There are four modes of interactions: (π_{1s}, p_s, π^*_{1s}, p_s) (**2**), (π_{2s}, p_s, π^*_{2s}, p_s) (**3**), (π_{2s}, p_s, π^*_{1s}, p_s) (**4**), (π_{1s}, p_s, π^*_{2s}, p_s) (**5**) interactions. When we apply the orbital phase condition, we can classify the cyclic orbital interactions into electron-localizing and -delocalizing ones. The p and π orbitals are electron-donating orbitals, and the π* orbital is an electron-accepting orbital.

In **2** all relations between the neighboring orbitals meet the phase requirements: The electron-donating π and p orbitals out of phase, the donating p and accepting π* orbitals in phase. The interaction is electron-delocalizing. The conditions cannot simultaneously be satisfied in **3**, where the dotted line between the p_s and π_{2s} orbitals in phase indicates that the phase relation is opposite to the requirement. The interaction is electron-localizing. Similarly, the remaining interactions, **4** and **5**, are predicted to be delocalizing and localizing, respectively. The cyclic orbital in-

teractions, **2** and **3**, are associated with real acyclic conjugated species, as previously shown[7] and will be briefly described in the following paragraph: The electron-delocalizing interaction **2** with trimethylenemethane (TMM) dianion (**6**) and the localizing interaction **3** with butadiene (BD) dianion (**7**). There are no actual acyclic systems related to the remaining interactions (**4**, **5**).

Dianions of TMM and BD are considered to be composed of two anionic centers and a double bond. The electron delocalization among the three systems is described in terms of the configuration interactions or the orbital interactions as is schematically represented in Fig. 1a.[7] An electron shifts from an anionic center to the double bond through the interaction of the ground-state configuration, G, with the electron-transferred configuration, T_1. The configuration interaction is approximated to be the interaction of the p-orbital of the anionic center with the π^* orbital of the double bond. An electron hole results from the transfer. The hole can be supplied with an electron from the double bond through the interaction of the transferred configuration with the locally-excited configuration, E. The T_1-E configuration interaction corresponds to the p-π orbital interaction. As a result the G-T_1-E configuration interaction or the π-p-π^* orbital interaction is involved in the above process. There is an analogous process starting with an electron shift from the other anionic lone-pair orbital. The process involves the G-T_2-E configuration interaction or the π-p-π^* orbital interaction, where the p orbital is different from that in the aforementioned process. All interactions are suprafacial. Now we realize that the delocalization involves the cyclic (π_s, p_s, π^*_s, p_s) interaction. In the TMM dianion both anionic centers interact with the same carbon of the double bond. The π and π^* orbitals take part in cyclic interaction at one center (π_{1s},π^*_{1s}) as is shown in **2**. In the BD dianion the anionic centers interact with the different carbons of the double bond. The two-centered interactions at the π and π^* orbitals (π_{2s} and π^*_{2s}) are involved in cyclic interaction (**3**).

We have examined cyclic (π_s,p_s,π^*_s,p_s) interactions which have been found to include the orbital interactions for the dianions of TMM and BD. We replace p_s by p^*_s to examine the corresponding dications. Similar arguments lead to a (π_{1s}, p^*_s, π^*_{1s}, p^*_s) interaction (**8**) and a (π_{2s}, p^*_s, π^*_{2s}, p^*_s) interaction (**9**) in place of **2** and **3**. The interactions are similarly associated with real systems; those corresponding to **4** and **5** being not. The interaction, **8**, is electron-delocalizing, while **9** is electron-localizing. The delocalizing interaction is contained in the TMM dication (**10**), the localizing one in the BD dication (**11**) as is shown in Fig. 1b. An electron shifts from a double bond to a cationic center through the G-T_1 interaction. The configuration interaction is approximated to the π_s-p^*_s interaction. The transferred electron goes back to the π^* orbital through the T_1-E interaction or through the p^*_s-π^*_s orbital interaction. There is another way of electron delocalization *via* the other cationic center

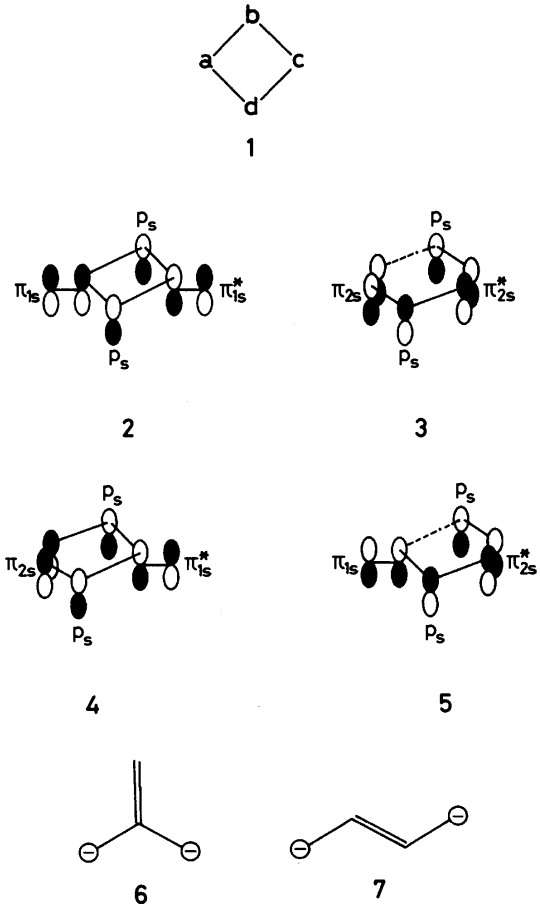

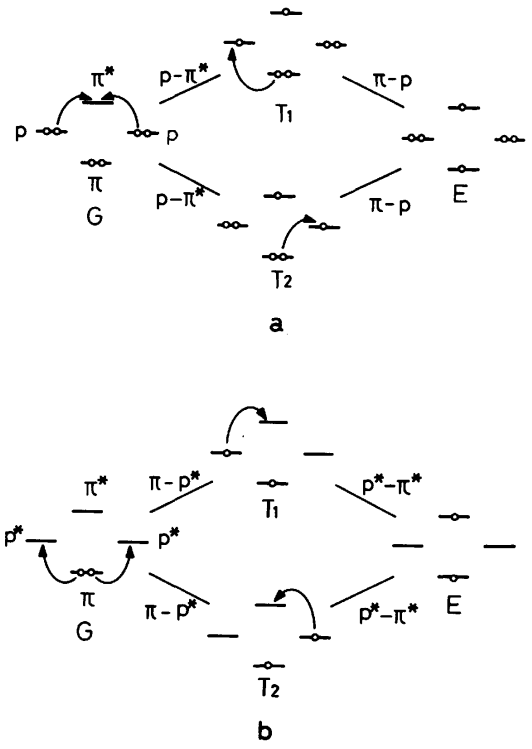

Fig. 1.

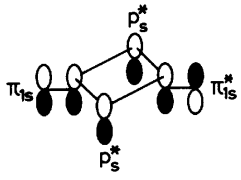
8

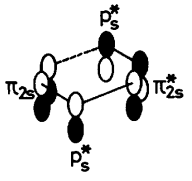
9

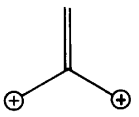
10

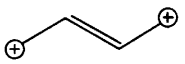
11

through the G-T_2-E interaction or through the π_s-p*$_s$-π^*_s interaction. As a result, the delocalization among two cationic centers and a double bond contains the cyclic (π_s, p*$_s$, π^*_s, p*$_s$) interaction. The delocalizing **8** with one-centered interactions of π and π^* orbitals is associated with the TMM dication, the localizing **9** with the BD dication.

We have described the suprafacial (π_s, p$^{(*)}_s$, π^*_s, p$^{(*)}_s$) interactions and treat here their antarafacial analogues, the (π_a, p$^{(*)}_s$, π^*_a, p$^{(*)}_s$) interactions. The antarafacial counterparts of the suprafacial interactions for the divalent ions of TMM and BD, and these only, are associated with real systems. The electron-delocalizing interaction (**2**) contained in TMM dianion corresponds to the (π_{1a}, p_s, π^*_{1a}, p_s) interaction (**12**). That (**8**) contained in TMM dication corresponds to the (π_{1a}, p*$_s$, π^*_{1a}, p*$_s$) interaction (**13**). These are related to the antarafacial analogues of the TMM divalent ions, where a double bond interacts with two ionic centers at the same carbon (**14** and **15**). Electron-localizing counterparts are the (π_{2a}, p_s, π^*_{2a}, p_s) and (π_{2a}, p*$_s$, π^*_{2a}, p*$_s$) interactions (**16** and **17**). The related systemes are the antarafacial analogues of BD divalent ions (**18** and **19**).

We have described cyclic (π, p$^{(*)}$, π^*, p$^{(*)}$) interactions and found that the orbital interactions (**2**, **3**, **8**, **9**, **12**, **13**, **16**, **17**) are associated with the real molecular systems (**6**, **7**, **10**, **11**, **14**, **15**, **18**, **19**), respectively. Although there are many other possible interactions of four orbitals, none of them are contained in real polyvalent ions. We will here design electron-localizing and -delocalizing species with more electric charges by fusing the cyclic orbital interaction units for the divalent ions singled out above. Charge (positive or negative) does not alter the conclusion with respect to localization and delocalization,[8] as can be seen in the preceding arguments. The following will be confined to polyanions.

We first fuse the suprafacial interaction units, *i.e.*, the delocalizing interaction, **2**, and the localizing interaction, **3**. The fusion of **2** at one of p_s's gives rise to a delocalizing chain of cyclic orbital interaction (**20**). The related system is polyanion where

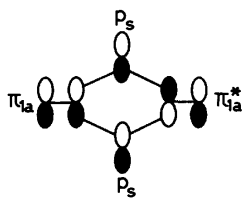
12

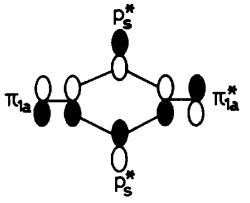
13

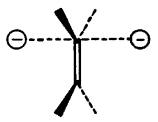
14

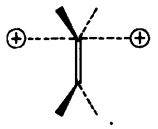
15

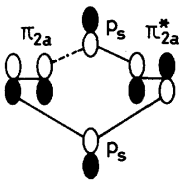
16

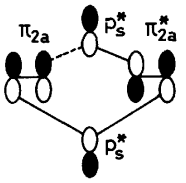
17

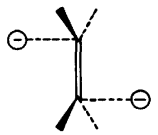
18

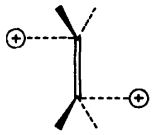
19

each neighboring pair of TMM dianions share one of anionic centers (**21**). The localizing counterpart (**22**) similarly derives from **3**. The cyclic orbital interaction corresponds to the polyanion (**23**) where anionic centers are shared by BD dianions. The two-site fused interactions (**24** and **25**) are those contained in the delocalizing dianion (**26**) and the localizing dianion (**27**).

Secondly, we fuse the antarafacial interaction units, *i.e.*, the delocalizing interaction (**12**) and the localizing interaction (**16**). Similar arguments lead to the delocalizing (**28**) and localizing (**29**) chains of cyclic orbital interactions in case of one-site fusion. These are associated to ions and double bonds stacked alternately (delocalizing **30** and localizing **31**). The two-site fusion gives rise to the delocalizing (**32**) and localizing (**33**) arrays of orbitals, which are those contained in **34** and **35**, respectively.

We have described the cyclic interactions of two p$^{(*)}$'s, π and π^* orbitals, which have been shown to be contained in the divalent ions of TMM and BD (**6**, **7**, **10**, **11**) and their corresponding antarafacial analogues (**14**, **15**, **18**, **19**) and designed electron-localizing and -delocalizing polyions (**21**, **23**, **26**, **27**, **30**, **31**, **34**, **35**) by fusing them at one and two sites. We will next describe cyclic orbital interactions of one p orbital and three of π or π^* orbitals. The real acyclic systems

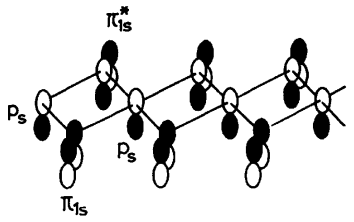

20

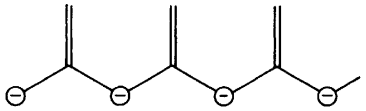

21

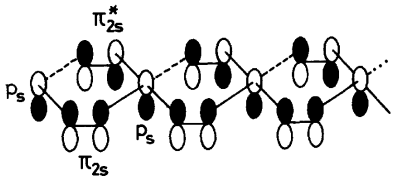

22

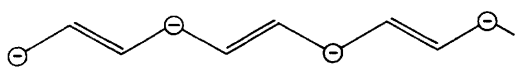

23

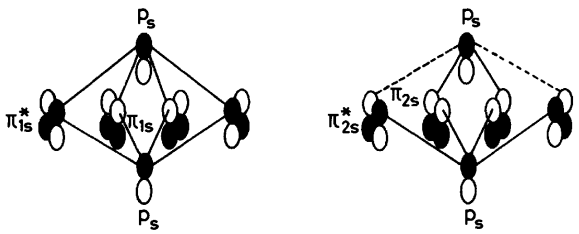

24 25

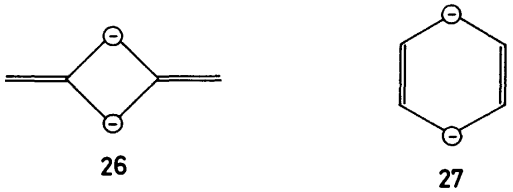

26

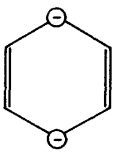

27

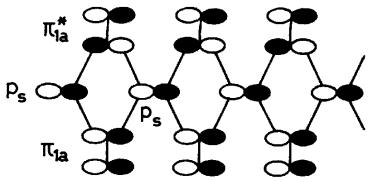

28

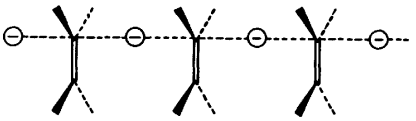

30

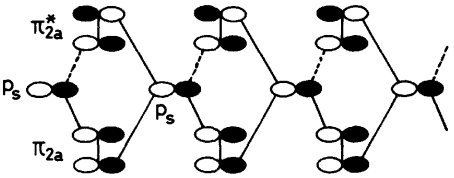

29

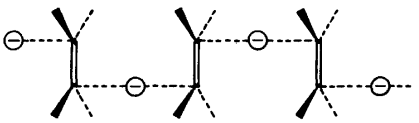

31

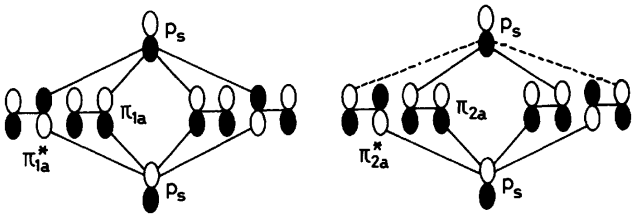

32 33

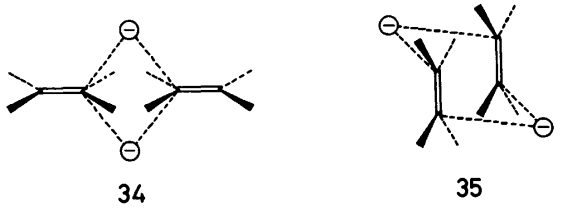

34 35

represented by some interactions, *i.e.*, the (p, π^*, π^*, π) interactions (**36**, **38**) and (p, π^*, π, π) interactions (**37** and **39**), are monovalent ion units, *i.e.*, the conjugated anions, **40** and **41**, as will be shown in the following paragraph. We will then design some dianions by fusing the cyclic orbital interaction units in a different manner.

The mechanism of electron delocalization from the anionic center to the distant double bond through the middle bond in **40** and **41** is shown in Fig. 2a. An electron shifts from the anionic center to the middle bond through the G-T_1 or p-π^* interaction. The transferred electron shifts farther to the terminal bond through the T_1-T_3 or π^*-π^* interaction. The process involves the p-π^*-π^* interaction. There is another path for the distant delocalization. An electron shifts from the middle to terminal bond through the G-T_2 or π-π^*

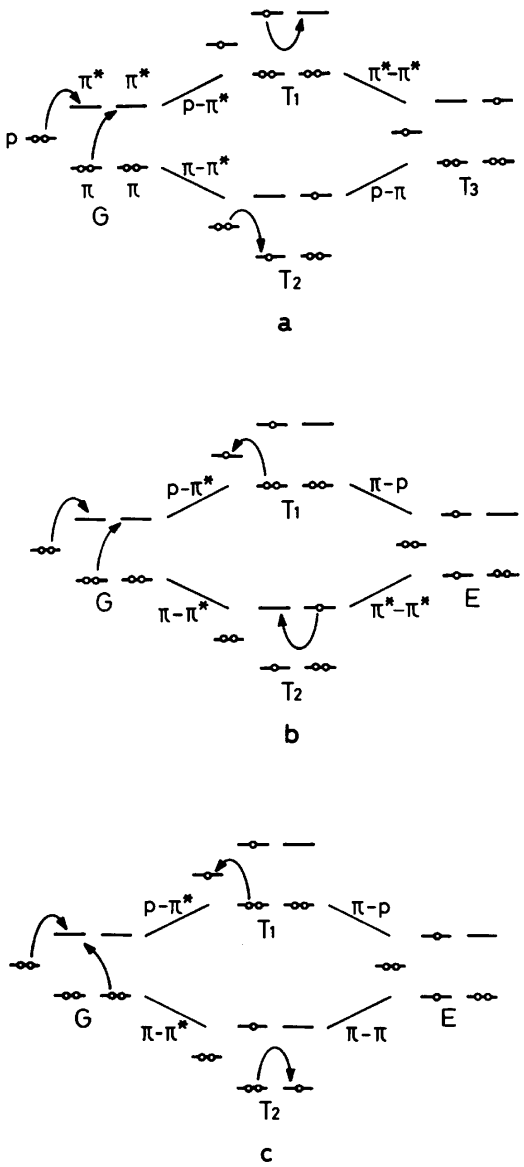

Fig. 2.

interaction, leaving an electron hole in the middle π bond. The hole then shifts to the anionic center through the T_2-T_3 or p-π interaction. The process involves p-π-π^* interaction. As a result, the distant delocalization *via* the two paths contains the (p_s, π^*_s, π^*_s, π_s) interactions (**36—39**).

The cyclic interactions are identical with that involved in a way of polarization of the middle bond (Fig. 2b). The electron shift from the anionic center to the middle bond leaves an electron hole which moves to the latter. The process involves the G-T_1-E or π_s-p_s-π^*_s interaction. In the other path, an electron first shifts from the middle to terminal bond and then back to the former through the G-T_2-E or π_s-π^*_s-π^*_s interaction. As a result, the polarization involves the same (p_s, π^*_s, π^*_s, π_s) interaction as the distant delocalization. The dual property of the cyclic orbital interaction should be noted for forthcoming arguments.

Another polarization path is shown in the bottom half of Fig. 2 c. The electron shift from the terminal to middle bond leaves an electron hole, which moves to the latter through the G-T_2-E or π_s-π_s-π^*_s interaction. This forms a different cyclic (p_s, π_s, π_s, π^*_s) interaction with the π_s-p_s-π^*_s interaction, which has been shown in the preceding paragraph to be involved in the polarization of the middle bond (The top halves of Fig. 2b and 2c represent the identical process).

We have shown that cyclic orbital interactions of one p orbital and three π and π^* orbitals are contained in the conjugated monoanions. The cyclic orbital interaction with the dual nature—the distant delocalization of the lone-pair electrons and the polarization of middle bond—is favored by phase continuity (**36**) in the anion **40**, and disfavored by phase discontinuity (**38**) in the anion **41**. The cyclic orbital interaction for the polarization only is favored by phase continuity (**39**) in **41**, and disfavored by phase discontinuity (**37**) in **40**.

Now we design cyclic orbital interactions for dianions by fusing the delocalizing interaction units derived

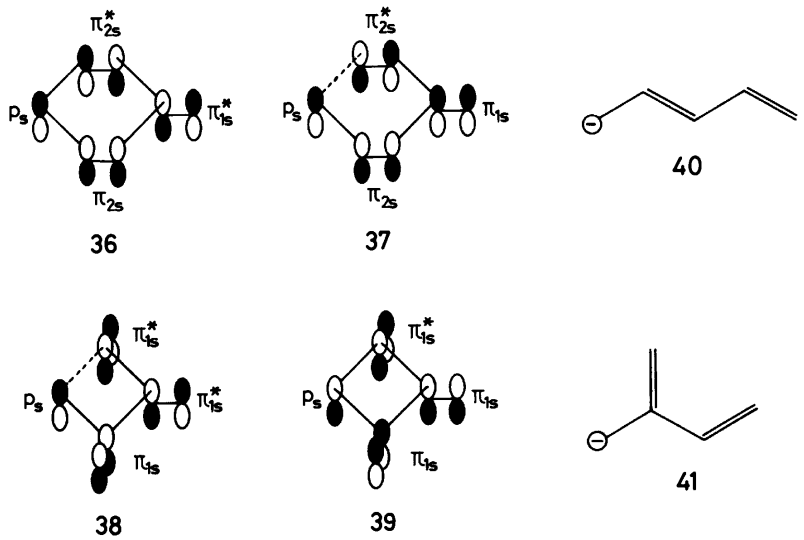

from the monoanions. The interaction (**36**) for the delocalization-polarization in **40** and that (**39**) for the polarization in **41** are combined to share the neighboring pair of π_{2s} and π^*_{1s} in **36** and that of π_{1s} and π^*_{1s} in **39**. The resulting orbital interaction (**42**) is associated with the dianion (**43**) where the diene moieties in the monoanions are superimposed. When the orbital interactions (**36**) for the delocalization-polarization are combined with each other to share the π^*_{1s}-π^*_{2s} pairs, a cyclic interaction (**44**) for the dianion **45** is generated. A combination of the interactions (**39**) for the polarization to share the π_{1s}-π_{1s} pairs leads to a cyclic interaction (**46**) for the dianion (**47**).

Now we predict the relative stabilities of the designed dianions. The cyclic orbital interaction unit (**36**) with the dual nature of delocalization and polarization should contribute to more stabilization than the polarization interaction (**39**). The stability is then expected to increase with the number of the delocalization-polarization interactions involved if there is no extra-stabilization on fusion. In the dianion **45** the cyclic orbital interaction units are both the delocalization-polarization interactions. The dianion **43** contains one, the remaining (**47**) none. The stability then decreases in the order of **45**>**43**>**47**. However, the fusion of orbital interaction units can enhance the effects of each other as significantly as to invert the ordering. A pair of orbitals shared on fusion in **42** is a primary[9] interaction between electron-donating and accepting orbitals. In addition, the cyclic six-orbital (p, π^*, π^*, p, π, π) interaction in **42** satisfies the phase continuity requirements. In contrast, the orbital interactions shared in **44** and **46** are secondary[9] between electron-donating orbitals or between electron-accepting orbitals. The extra-stabilization due to the fusion should be smaller, if any. In addition, the cyclic six-orbital (p, π^*, π^*, p, π, π) interactions do not satisfy the phase continuity requirements.[10] The extra-stabilization on fusion is then expected to be greater in **43**. The stability ordering of **43** and **45** might be inverted.

The conjugate dianions designed in the preceding sections are considered to be vinylogues of TMM and BD dianions. There is a pair of corresponding vinyl-

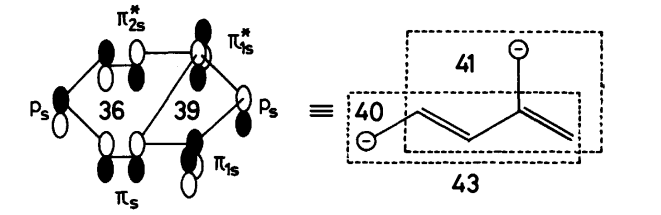

42

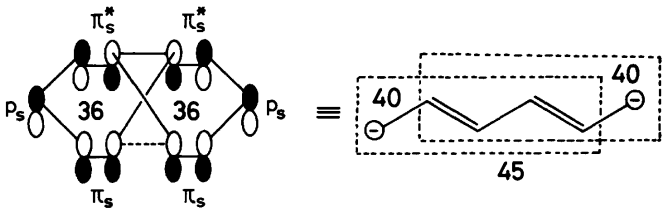

44

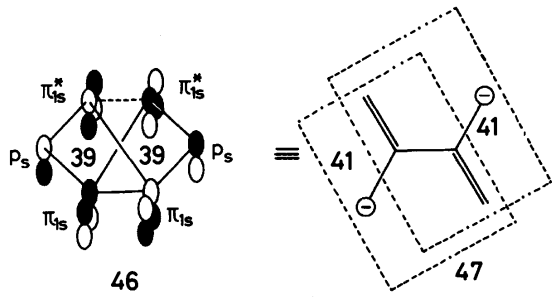

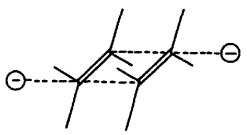

48

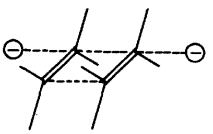

49

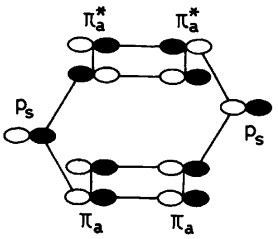

50

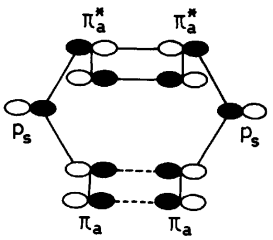

51

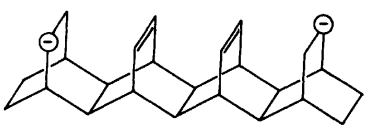

52

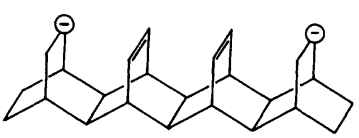

53

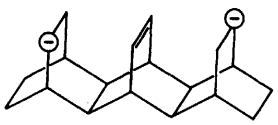

54

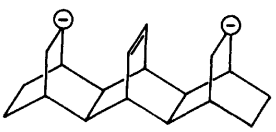

55

ogues of the antarafacial analogues (**14** and **18**) of the TMM and BD dianions, where two juxtaposed π-bonds interact with two anionic centers in a different manner as shown in **48** and **49**. The interactions involved are cyclic six-orbital (p_s, π^*_a, π^*_a, p_s, π_a, π_a) interactions, **50** and **51**. The cyclic six-orbital interaction is favored by the phase continuity (**50**) for **48** and disfavored by the phase discontinuity (**51**) for **49**. It follows that **48** is more stable than **49**. The relative stability makes a contrast with the aforementioned stability of the antarafacial analogues (**14**, **18**) of the TMM and BD dianions. We could experimentally examine the prediction by preparing such polycyclic species as **52**—**55**.

Geometry Optimization

The preceding orbital phase arguments have been limited to the localization-delocalization of π electrons, and have not taken into account the effects of σ electrons and inner-shell electrons. It is necessary to examine whether these effects may modify or alter the orbital phase predictions, and to supplement the qualitative arguments by means of numerical values. Molecular geometries of some ions are optimized by *ab initio* molecular orbital calculations with STO-3G basis set. The geometries fully optimized under given symmetry constraints are shown in Fig. 3. The relative energies of the isomers to be compared are listed in Table 1.

The TMM dianion is estimated to be more stable by 22.5 kcal mol^{-1}† than the BD dianion. The relative stability is consistent with the orbital phase prediction[7] and with the experimental observation.[11] The bond lengths also support the preceding arguments. The bond alternation is remarkable in the electron-localizing BD dianion. The small distance (1.35 Å) between the inner carbons suggests a double bond character while the distance between the inner and outer carbons is long (1.47 Å). The carbon–carbon bond length (1.42 Å) in the electron-delocalizing TMM dianion is intermediate between those in the BD dianion.[12] Similar results are obtained for the TMM and BD dications. The energy difference is 18.1 kcal mol^{-1}. The bond lengths are 1.43 Å in the TMM dication, and 1.36 Å and 1.50 Å in the BD dication.

The one-site fusion is found to still retain the delocalization and localization characters of the unit dianions. The fully cross-conjugated C_7H_9 trianion[13] (**21**) is more stable by 7.6 kcal mol^{-1} than the fully linearly conjugated C_7H_9 trianion[14] (**23**). The bond alternation in the linear trianion is similar to that in the BD dianion. The short bond length is 1.35 Å, the long bond lengths being 1.47 Å and 1.48 Å. All the carbon–carbon bond lengths (1.41, 1.43, and 1.47 Å) in the cross trianion range between those in the linear trianion. Noteworthy is that the distance between the fused and central carbons in the TMM dianion unit is close to the larger distance in the linear trianion. The cross trianion tends to shift from the one-site fused pair of TMM dianions to two allyl anions connected with each other at their central carbons by an anionic carbon.

The two-site fusion of the TMM and BD dianion units gives rise to the four and six-membered ring dianions (**26**, **27**). The direct comparison of the thermodynamic stabilities due to π-electron delocalization is hampered by ring strain. The instability of benzene dianion is also a direct result of the Hückel rule. It is more interesting to compare the delocalizing dianion (**26**) with its four-membered ring isomer (**56**). The delocalizing **26** was estimated to be more stable by 29.2 kcal mol^{-1}. The bond lengths range less widely (1.36—1.46 Å). The structure of the 1,3-isomer deviates from formally fused TMM dianions toward a combined system of anionic centers and exocyclic double bonds. The 1,2-isomer tends to obtain a property of linearly-conjugated dianion by lengthning a bond in the ring.

Geometry optimization of C_6H_8 dications shows that the relative stability decreases in the order of **57**>**58**>**59**. The stability of **57** relative to **58** suggests the importance of the extra-stabilization by sharing the primary orbital interaction corresponding to **42** for the dianions. A conspicuous feature in the optimized geometry is a strong tendency toward two allyl cations. The linear dication appreciably alternates

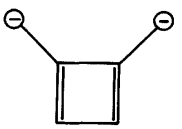

56

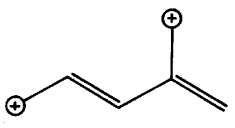

57

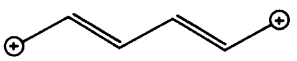

58

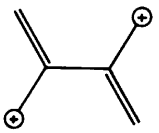

59

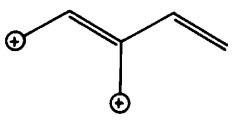

60

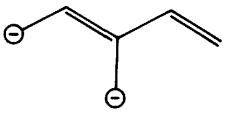

61

†1 cal=4.184 J.

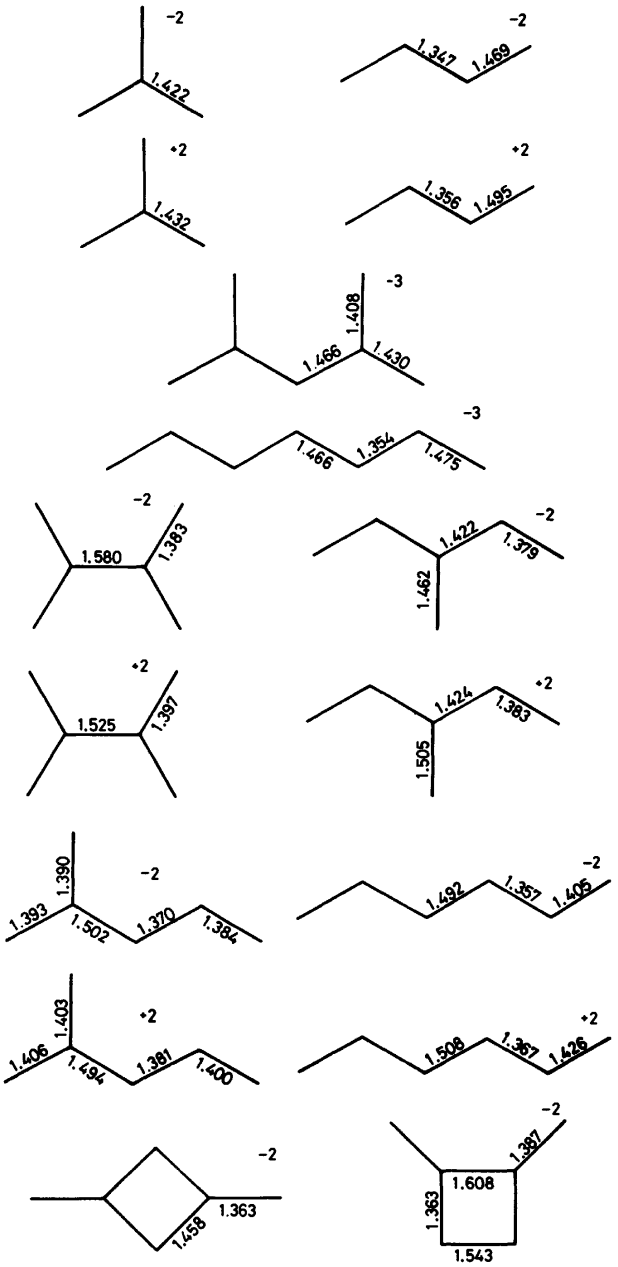

Fig. 3.

TABLE 1. RELATIVE ENERGIES (kcal/mol) AND RESULTS OF CONFIGURATION ANALYSIS[a]

Molecule	Geometry optimization		Configuration analysis[c]			
	Point group	Relative energy[b]	GT	TE	TT	Total
6	D_{3h}	0	0.430	0.139	—	0.569
7	C_{2h}	+22.46	0.286	0	—	0.286
10	D_{3h}	0	0.452	0.144	—	0.596
11	C_{2h}	+18.10	0.257	0	—	0.257
21[d]	C_{2v}	0	0.725	0.208	0.014	0.947
23[d]	C_{2v}	+7.62	0.561	0.001	0.017	0.579
26	D_{2h}	0	0.606	0.136	—	0.742
56	C_{2v}	+29.21	0.490	0.070	0.034	0.594
43	C_s	0	0.586	0.108	0.037	0.731
45	C_{2h}	+1.24	0.534	0.042	0.036	0.612
47	D_{2h}	+17.27	0.586	0.111	0.010	0.707
61	C_{2v}	+53.40	0.590	0.039	0.145	0.774
57	C_s	0	0.626	0.113	0.037	0.776
58	C_{2h}	+1.31	0.524	0.043	0.032	0.598
59	D_{2h}	+12.64	0.658	0.011	0.014	0.683
60	C_{2v}	+53.31	0.601	0.046	0.153	0.800

a) With STO-3G basis set. b) The reference is the total energy of the most stable isomer. c) Each term is defined in the text (Eq. 3). d) Trianion.

the single and double bonds. The remaining isomer of C_6H_8 dications, **60**, which has an electron-localizing BD dication unit, is the least stable. The geometry suggests that the dication is a combination of a pentadienyl cation and a cationic center. These results are almost the same as those of the dianionic analogues[15] (**43**, **45**, **47**, **61**).

Electron Configuration Analysis for Many System Interaction

The *ab initio* calculations almost completely support the orbital phase predictions on the relative stabilities of the polyions, and give more detailed information of molecular geometries. Here we attempt to look into the relation of these calculated properties with the mechanism of electron delocalization among many bonds, cationic and anionic centers. We are concerned with the delocalization of π-electrons in conjugate polyions, composite systems of double bonds and anionic or cationic centers. The ground-state configuration (G) has two electrons in each bonding orbital of double bonds and in each non-bonding orbital on the anionic centers, and no electron in p-orbitals on the cationic centers. The delocalization is expressed by mixing the electron transferred configurations (T) and locally-excited configurations (E) into G. The ground-state wavefunction is then formulated as

$$W = C_G G + \sum_T C_T T + \sum_E C_E E + \quad (1)$$

In the transferred configuration an electron is shifted from an occupied orbital of a bond or an anionic center to a vacant orbital of another bond or a cationic center. In the locally-excited configuration an electron is promoted from the bonding orbital to the antibonding orbital in a bond.

In general there are many Kekulé structures for a given molecule. A Kekulé structure corresponds to a ground-state configuration. It is meaningful to analyze how electrons delocalize starting from the main Kekulé structure. The electron configuration analysis for many system interaction (ECAMSI)[16] is employed to single out the main Kekulé structure. The wavefunction is subjected to ECAMSI for different ground-state configurations or Kekulé structures. The calculations yield the coefficients of G, T, and E configurations. The main Kekulé structure is one with the biggest C_G.

Some quantities are defined to examine the delocalization in a quantitative manner. The integration of the normalized wavefunction (Eq. 1) all over the space leads to the following equation:

$$1 = C_G^2 + \sum_T C_T^2 + \sum_E C_E^2 + \sum_T 2C_G C_T S(G,T) + \sum_{T_1>T_2} 2C_{T_1} C_{T_2} S(T_1,T_2) + \sum_{T,E} 2C_T C_E S(T,E) + \quad (2)$$

The square terms are the weights of electron configurations. The first cross terms represent the contribution from the G-T configuration interactions. This can be used as a measure of adjacent delocalization through the neighboring occupied and unoccupied orbital interactions. The second cross terms represent the contribution from the T-T configuration interactions. This can be used as a measure of distant delocalization beyond more than one systems through the interactions between the neighboring occupied orbitals and between the neighboring vacant orbitals. The third cross terms represent the contribution from the T-E configuration interactions. This can be used as a measure of polarization of bonds. The coefficients of configurations show the extent of contribution of each configuration to the electronic structure of a molecule. It has been shown that the ratios of coefficients of various configurations to that of the ground state configuration (C/C_G) are more preferable for comparing electronic structures of different molecules.[7b] We discuss the results of configuration analysis on the basis of the coefficient ratios. The GT, TT, and TE terms of interest are defined as follows:

$$GT = \sum_T 2C_G C_T S(G,T)/C_G^2$$
$$TT = \sum_{T_1>T_2} 2C_{T_1} C_{T_2} S(T_1,T_2)/C_G^2$$
$$TE = \sum_{T,E} 2C_T C_E S(T,E)/C_G^2 \quad (3)$$

The main Kekulé structures are confirmed to be such forms as drawn. The results of configuration analysis on the optimized geometries are listed in Table 1. The relative stabilities are completely paralleled with the sums of three terms for the dianions of TMM and BD and for the one-site fused trianions. A difference in the electronic structures comes from the double bond polarization. There is no double bond polarization (C_E=0.0 therefore TE=0.0) in the electron-localizing isomers (**7**, **11**, **23**), as has been predicted by the phase discontinuity of the cyclic orbital interaction. In the delocalizing ones the polarization contributes as significantly as the adjacent delocalization. According to perturbation theory the adjacent delocalization should be similar for the localizing and delocalizing pairs. The increment of the GT term in the delocalizing isomers is considered to be induced by the allowed polarization

The GT and TE terms of the delocalizing two-site fused dianion (**26**) are greater than those of the reference species (**56**), as was predicted. The relative stability can be similarly understood to be also due to the allowed bond polarization and the induced increment of the adjacent delocalization.

The most stable C_6H_8 dianion (**43**) has a greater sum of the three terms than the second (**45**). The magnitude of the GT term in **43** is due to the enhanced mixing of the transferred configuration or primary interaction between the π-π* interaction shared by the fused cyclic orbital interactions as has been described (**42**). The configuration coefficient ratio (0.24) of the transferred

configuration is larger than that (0.17) of the corresponding transferred configuration in **45**. A similarly expected difference in polarization is found in the coefficient ratios. The locally-excited configuration ratio (0.32) for the cross-conjugated double bond in **43** is more than twice greater than that (0.13) in **45**.

There is a limit to the parallelism between the simply predicted or calculated stabilities and the results of configuration analysis. The sum of the three terms for the dianions (**47** and **61**) of lower stabilities are greater than that of more stable **43** or **45**. A possible explanation for the lost parallelism might be related with the "multiplicity" of the main Kekulé structure. The main Kekulé structure is uniquely determined "singlet" for **43** and **45** for which the sum of the three terms of configuration analysis is well correlated to the total energy. There is one more equivalent Kekulé structure for **47** and **61**, which are then expressed by the "doublet" Kekulé structures. The multiplicity arises from the discrepancy in symmetry between Kekulé structures and molecular geometries. Lower symmetry of Kekulé structures might enforce "undesirable" electronic rearrangements to recover the symmetry of electronic structures imposed by molecular geometries. The artificial failure inevitably results in overestimation of GT, TT, and TE terms.

The authors thank Prof. Paul von Ragué Schleyer of Universität Erlangen-Nürnberg for private communication of their results in prior to publication and stimulating criticisms on our manuscript. The *ab initio* molecular orbital calculations were carried out on a HITAC-M200H computer, Institute for Molecular Science, with IMSPACK programs. The other calculations were carried out on a FACOM-M382 computer, Nagoya University Computer Center. This work was supported by Grant-in-Aid for Scientific Research from the Ministry of Education, Science, and Culture.

References

1) E. Hückel, *Z. Phys.*, **70**, 204 (1931); **76**, 628 (1932).

2) R. B. Woodward and R. Hoffmann, "The Conservation of Orbital Symmetry," Academic Press, New York, (1970).

3) K. Fukui, "Theory of Orientation and Stereoselection," Springer-Verlag, Heidelberg, (1975).

4) R. S. Mulliken and W. B. Person "Molecular Complexes," Wiley, New York, (1969).

5) K. Fukui and S. Inagaki, *J. Am. Chem. Soc.*, **97**, 4445 (1975); S. Inagaki, H. Fujimoto, and K. Fukui, *ibid.*, **98**, 4693 (1976).

6) S. Inagaki and Y. Hirabayashi, *J. Am. Chem. Soc.*, **99**, 7418 (1977).

7) a) S. Inagaki and Y. Hirabayashi, *Chem, Lett.*, **1982**, 709; b) S. Inagaki, H. Kawata, and Y. Hirabayashi, *Bull. Chem. Soc. Jpn.*, **55**, 3724 (1982).

8) a) The pioneering works by Clark, Schleyer and their collaborators have been encountered with greater difficulties in preparing dications[b] than dianions[c] of TMM, and they have been tempted to throw doubt on the thermodynamic stability of the dications. The TMM dianion with a phenyl group on each methylene was readily prepared at 20°C, whereas a reasonable synthetic route to the corresponding triphenyl TMM dication leads only to ring closure or intramolecular Friedel-Crafts reaction involving the aromatic moiety. This contrast may be attributable to the kinetic cause: Electrophilic aromatic substitutions are familiar while the substrates of nucleophilic ones are limited. The difficulties have been demonstrated by other attempts, but the origins seem unclear. There may be no well-established grounds for claiming that polycations and polyanions have similar stabilities. The similarities, which allow us to exclude a group of counterparts (polycations) from the arguments in the text, are the relative stabilities of the isomeric ions. Meaningful is the comparison of the TMM dication with the BD dication, but not that of the dication with the dianion; b) K. Schötz, T. Clark, H. Schaller, and P. v. R. Schleyer, *J. Org. Chem.*, **49**, 733 (1984); c) D. Wilhelm, T. Clark, P. v. R. Schleyer, K. Buckl, and G. Boche, *Chem. Ber.*, **116**, 1669 (1983).

9) According to the perturbation theory the interaction between electron-donating and accepting orbitals is contained in the second-order energy terms, whereas those between donating orbitals and between accepting orbitals are contained in higher-order terms.[5]

10) On fusion there appears another cyclic six-orbital interaction, *i.e.*, (p, π^*, π, p, π^*, π) interaction. The orbital phase is continuous. However, the continuity does not promote electron delocalization because the donating and accepting orbitals are excessively alternated along the chain in the orbital cycle. For more details see the continuity and discontinuity of cyclic conjugation.[6]

11) N. S. Mills, J. Shapiro, and M. Hollingsworth, *J. Am. Chem. Soc.*, **103**, 1263 (1981).

12) a) Some molecular orbital calculations of more realistic models with coordinated Li atoms have been reported. In the BD "dianion" lithium cations were indicated to bridge the terminal carbons symmetrically and doubly.[b] The most stable structure of TMM "dianion" has a 1,3- and 1,3'-bridged structure (C_2)[c], which was, however, found to be different from the X-ray structure of tribenzylidenemethane di(lithium tetramethylethylene diamine (TMEDA))[c]: one lithium bridges the 1,3 positions of a allyl system while the other bridges the remaining carbons in 1,2-manner. The models for this structure (C_s) and with the highest symmetry (D_{3h}) were calculated to be higher in energy by about 4 kcal mol^{-1}. Anyway, we think that our dianion model is sufficient to compare the relative stabilities of polymetallated hydrocarbon isomers of the same number of carbons and charges but topologically different carbon skeletons; b) P. v. R. Schleyer, *Pure & Appl. Chem.*, **55**, 355 (1983); c) D. Wilhelm, H. Dietrich, T. Clark, W. Mahdi, A. J. Kos, and P. v. R. Schleyer, *J. Am. Chem. Soc.*, **106**, 7279 (1984).

13) R. B. Bates, W. A. Beavers, M. G. Greene and J. H. Klein, *J. Am. Chem. Soc.*, **96**, 5640 (1974).

14) J. J. Bahl, R. B. Bates, W. A. Beavers, and C. R. Launer, *J. Am. Chem. Soc.*, **99**, 6126 (1977).

15) S. Inagaki, H. Kawata, and Y. Hirabayashi, *J. Org. Chem.*, **48**, 2928 (1983) and references cited therein.

16) S. Inagaki and Y. Hirabayashi, *Bull. Chem. Soc. Jpn.*, **51**, 2283 (1978) and references cited therein.

 © 1985 The Chemical Society of Japan Bull. Chem. Soc. Jpn., 58, 611—617 (1985)

Catalysis by Transition Metal Carbides. VI. Hydrogenation of Carbon Monoxide over WC, W_2C, and W Powder Catalysts

Isao KOJIMA,* Eizo MIYAZAKI, Yasunobu INOUE,† and Iwao YASUMORI††

Department of Chemistry, Tokyo Institute of Technology, Ookayama, Meguro-ku, Tokyo 152

†*Analytical Center, Nagaoka Technological University, Nagaoka 949-54*

††*Department of Applied Chemistry, Kanagawa University, Rokkakubashi, Yokohama 221*

(Received May 24, 1984)

WC, W_2C, and W were comparatively studied for CO hydrogenation to reveal the catalytic role of carbon alloyed with metals. The main products of the reaction were CH_4, CO_2, and H_2O on these catalysts, but the kinetic data obtained for WC catalyst were different from those for W_2C and W catalysts: *i.e.*, the apparent activation energies for CO consumption and for CH_4 formation on WC were found to be about three times larger than those on W_2C or W. Furthermore, the catalytic activity of WC was about 20 times larger than that of W_2C and W. It was suggested that the hydrogenation of CO on WC proceeds *via* direct hydrogenation of adsorbed CO forming a CHO adsorbed species as an intermediate, whereas on W_2C and W catalysts, dissociation of CO occurs in the initial step, followed by further hydrogenation of adsorbed carbon to form CH_4. X-ray photoelectron spectroscopic (XPS) studies on WC and W_2C showed that the WC surface catalytically activated was almost free from graphite carbon and oxygen as poison, but W_2C surface was largely covered with graphite carbon. These distinctive catalytic behavior differences between the carbide catalysts are discussed on the basis of the structure of the active surfaces.

The hydrogenation of carbon monoxide is a current problem in research on heterogeneous catalysis, and has been studied by many investigators on supported and unsupported metal catalysts.[1,2,3] Recently, it has been shown that the transition metal carbides form a new group of catalysts for the hydrogenation of benzene,[4] ethylene,[5,6] and carbon monoxide.[7,8] For the hydrogenation of carbon monoxide, the metal carbides were found to produce higher molecular weight hydrocarbons involving olefins other than methane.[7] A subsequent kinetic study suggested that the adsorbed CO and H atoms form an intermediate of CH_xO type prior to the C-O bond rupture.[8]

From the point of view of catalyst modification by alloying metals with carbon, the states of the carbon species are of importance in understanding the difference in the catalytic properties between metal carbides and the original pure metals. For example, McCarty and Madix found that the carbide-carbon on the Ni(110) plane changes its catalytic properties like those of copper metal for the decomposition of formic acid.[9] Boudart and coworkers reported that W and Mo catalysts modified by C and O atoms exhibit activity and selectivity resembling those of Group VIII transition metals.[10,11] Ross and Stonheart reported that the electrocatalytic activity of tungsten carbide was sensitive to surface composition.[12,13] The unique physical properties such as extremely high melting point, metal-like thermal and electronic conductivities, superconductivity *etc.* of transition metal carbides can be closely related to their electronic structure derived from the coexistence of covalent, metallic and ionic bonds. They have been extensively studied both experimentally and theoretically.[14] However, little effort has been devoted to understanding their chemical reactivity and catalysis. In particular, the question as to how the carbon incorporated in metals affects the catalytic activity still remains open.

In the present study, the hydrogenation of CO was investigated on WC, W_2C, and W in order to reveal the catalytic behavior of the transition metal carbides. Attention was focused on the reaction mechanisms over these catalysts and on the structure of active sites which are responsible for the catalysis. By the use of computer aided analysis of pressure dependencies, a surface intermediate of CHO species was concluded to be formed during the reaction on WC, whereas, it was expected on W_2C and W that CO first dissociates into C and O atoms on the surface, followed by hydrogenation to produce methane. XPS technique was used to examine the surface states of the catalysts.

Experimental

The kinetic measurements of the reaction were carried out using a recirculation reactor, 520 ml in volume, with a liquid nitrogen cold trap for removing the condensable products from the reaction system during the course of the reaction. The reaction products were analyzed using gas chromatography and mass spectrometry. The powdered materials, WC, W_2C, and W (≈300 mesh) of high purity (>99%) were purchased from Fru-uchi Chemicals Co. X-ray diffraction measurement of WC exhibited only the peaks due to monocarbide, but the diffraction peaks of W_2C catalyst showed a slight trace of metallic tungsten. Before the kinetic measurements, WC was catalytically activated by heating *in vacuo* at 700 °C as described elsewhere.[5] W_2C and W were reduced at 600 °C in an atmosphere of hydrogen at 100 Torr (1 Torr=133.322 Pa) until there was no further formation of H_2O, and subsequently evacuated at 700 °C. The material balance of carbon in the reaction system was maintained within ±5%. The BET surface area of WC measured by Kr adsorption was 1.5 $m^2 g^{-1}$, which was almost identical to the area of the other powdered carbide catalysts. XPS spectra were recorded on a Hewlett-Packard 5950A ESCA spectrometer using monochromatic Al $K\alpha$ exciting radiation. The samples pressed into discs were transferred into the preparation chamber of the spectrometer and subjected to *in situ* heat-treatment *in vacuo* or in hydrogen at 700 °C.

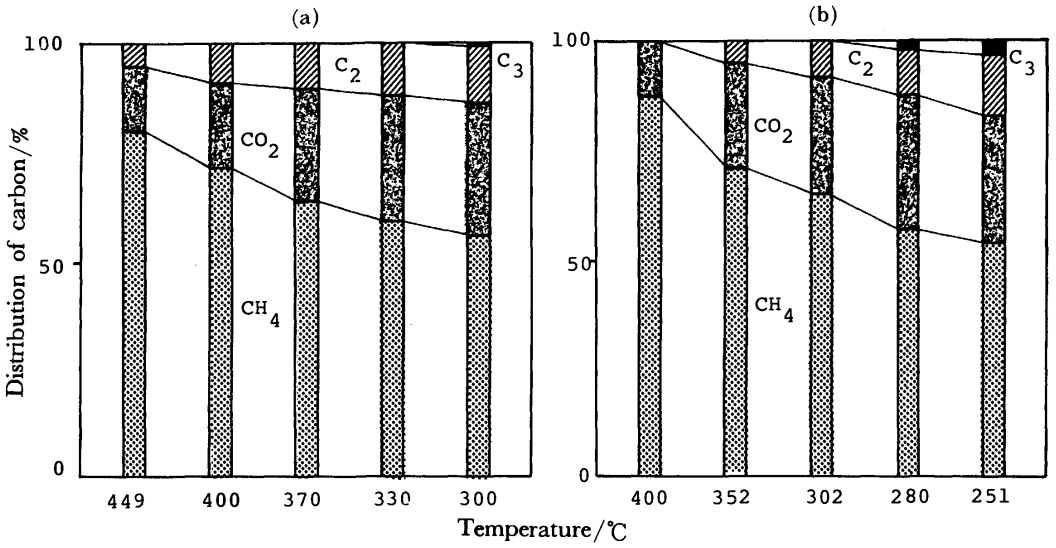

Fig. 1. %-Distribution of carbon containing products for the CO hydrogenation by (a) W_2C and (b) WC.

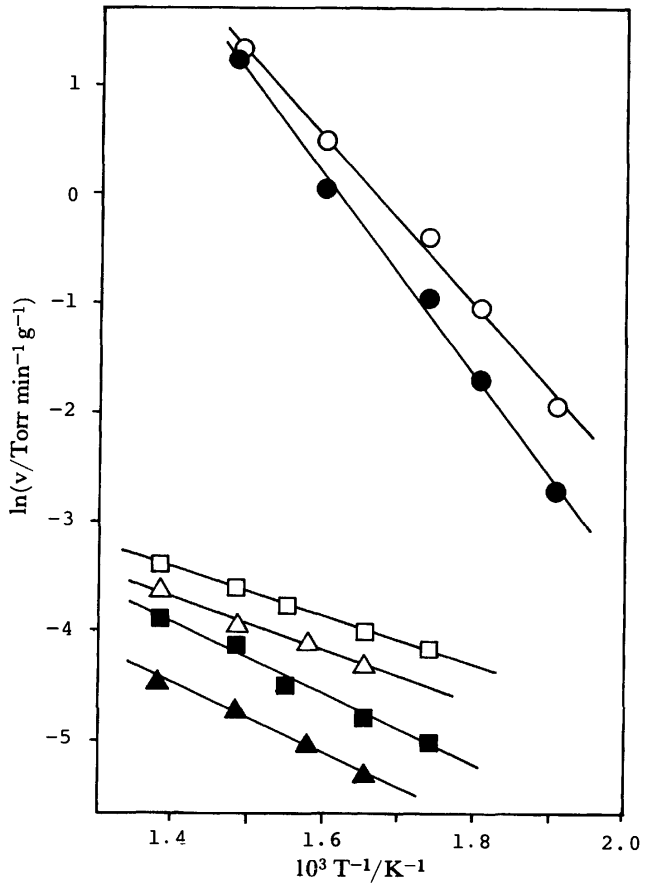

Fig. 2. Dependence of catalytic activities on reaction temperatures for the CO hydrogenation by WC, W_2C, and W.
○, ●: WC, □, ■: W_2C, and △, ▲: W.
Open and close symbols are for the rates of CO consumption and CH_4 formation, respectively.

Result

Figure 1 shows the variation of product distributions with reaction temperature on WC and W_2C. The main products were CH_4, CO_2, and H_2O on WC catalyst at temperatures above 400 °C, and the formation of hydrocarbons of higher molecular weight became appreciable at lower temperatures even at high values of the H_2/CO ratio. Among the metal carbide catalysts investigated here and elsewhere,[7,8] WC is most liable to produce methane. The distribution of products on W catalyst was almost identical to that on W_2C.

Figure 2 shows the dependence of the initial rates of CO consumption and of CH_4 formation on the reaction temperature during the CO hydrogenation under the initial pressures of H_2 at 100 Torr and CO at 10 Torr. The apparent activation energies for CO consumption and CH_4 formation were respectively 64.4 and 76.1 kJ mol^{-1} on WC, 18.4 and 26.8 kJ mol^{-1} on W_2C, and 20.1 and 25.9 kJ mol^{-1} on W catalysts. It is noted that the two values for W_2C and W catalysts are very close in both processes and the values for WC are about three times larger than for W or W_2C catalyst. The catalytic activity ratio of WC, W_2C, and W per unit weight were 200:1.4:1 at 400 °C. The amounts of CO chemisorbed at 0 °C were determined to be 4×10^{14} and 5×10^{13} mol cm^{-2} on the activated WC and W_2C, respectively. This finding indicates that the WC catalyst is roughly 20 times more active per CO-site than W_2C catalyst.

The pressure dependence of the reaction rates was investigated on WC and W_2C at the reaction temperature of 400 °C, where the main products were CH_4, H_2O, and CO_2. The results are shown in Figs. 3 to 5, and they are summarized in Table 1. The reaction orders of the rates of CO consumption and CH_4 formation are similar to those on the transition metals such as Ni, Pd, Rh, Ru *etc.*[15] However, characteristic features on the carbide catalysts can be seen in the reaction orders for the formation of H_2O and CO_2 on WC; *i.e.*, the order for H_2O formation exceeds unity with respect to H_2 pressure, but is negative with respect to CO pressure. Furthermore, the order for CO_2

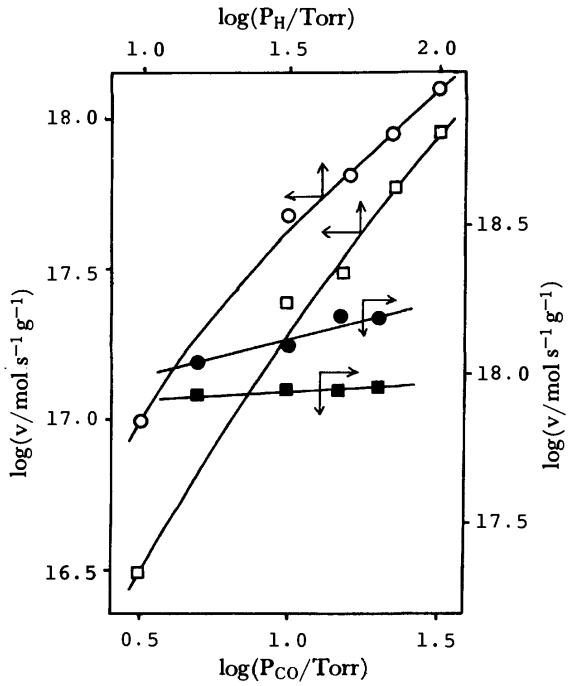

Fig. 3. Dependence of reaction rates of CO consumption (○, ●) and of CH_4 formation (□, ■) on the pressure of CO (open) and H_2 (close) for the CO hydrogenation by WC.

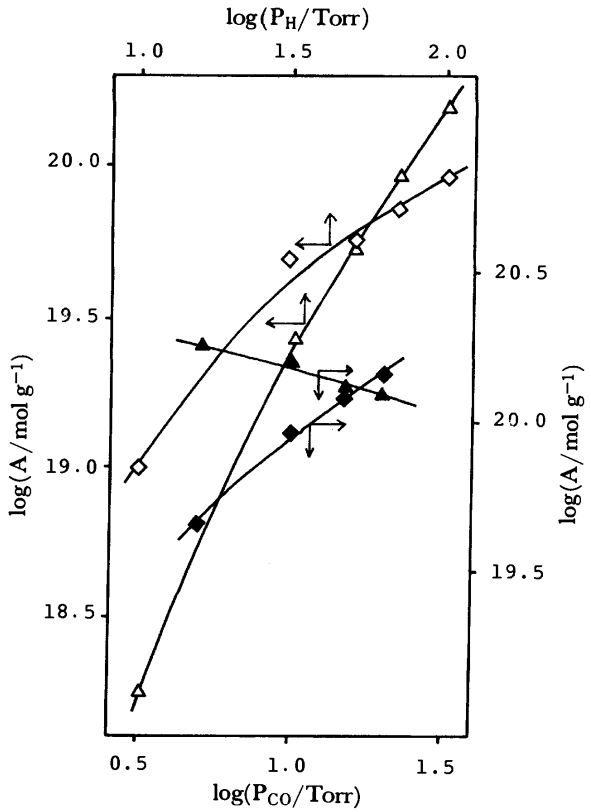

Fig. 4. Dependence of reaction rates of CO_2 formation (◇, ◆) and of H_2O formation (△, ▲) on the pressure of CO (open) and H_2 (close) for the CO hydrogenation by WC.

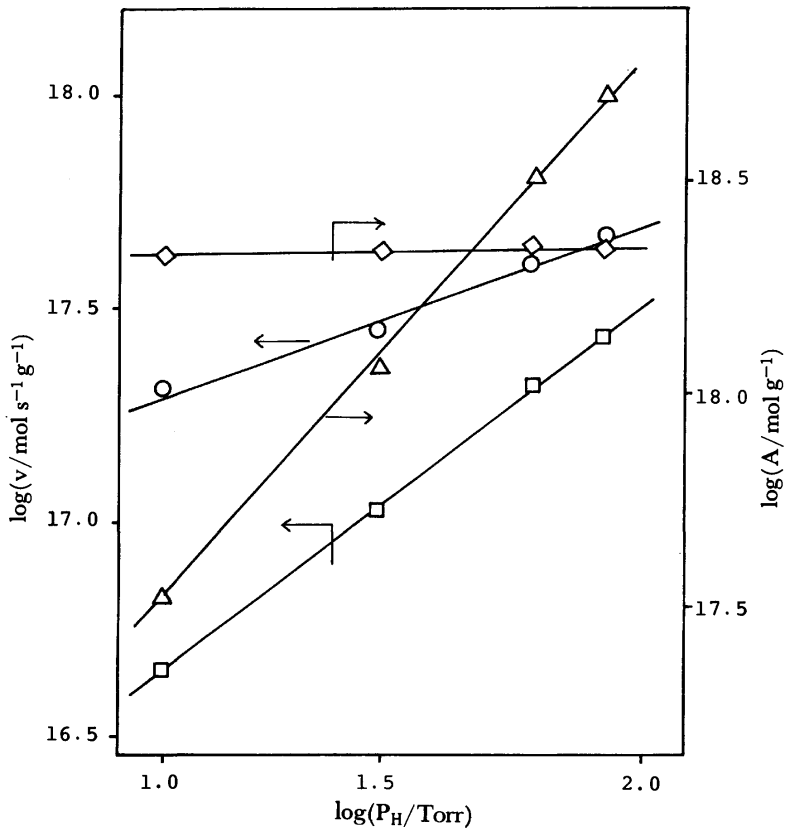

Fig. 5. Dependence of reaction rates on the pressure of H_2 for the CO hydrogenation by W_2C. ○: CO consumption, □: CH_4 formation, ◇: CO_2 formation, and △: H_2O formation.

TABLE 1. PRESSURE DEPENDENCE OF REACTION RATES ON WC AND W_2C

	r_{CO}		r_{CH_4}		$\bar{r}_{H_2O}$		$\bar{r}_{CO_2}$	
	x	y	x	y	x	y	x	y
WC	0.9	0.3	1.2	0.1	1.5	−0.3	0.6	0.7
W_2C	0.4	—	0.8	—	1.0	—	0.0	—

r (or $\bar{r}$)$=k P_H^x P_{CO}^y$, where r represents the initial rate, and $\bar{r}$ is the average rate estimated from the amount produced in a constant initial period of reaction, 10 min.

formation is positive with respect to H_2 pressure. These characteristics of pressure dependence are in common with those on other metal carbides such as TiC, TaC, and Mo_2C. While, on W_2C, the orders of H_2O and CO_2 with respect to H_2 pressure are 1.0 and nearly zero, respectively.

In a previous XPS study on TaC and WC,[5] the peaks assigned only to the pure state of the respective metal monocarbide were observed when the samples were heated *in vacuo* at temperatures higher than the temperatures required for activation, while the oxidized states of the metals were observed in the lower temperatures. In the present case of WC and W_2C, the characteristic peaks due to the oxides disappeared after the activation treatments were made (Figs. 6 and 7). As shown in Fig. 7(a), the catalytically activated WC exhibited a typical peak only at 283.2 eV which can be attributed to carbide carbon, indicating that the surface was almost free from graphite-like contaminant. However, the superimposed peaks were observed with almost equal intensity at 284.8 and 283.5 eV for the

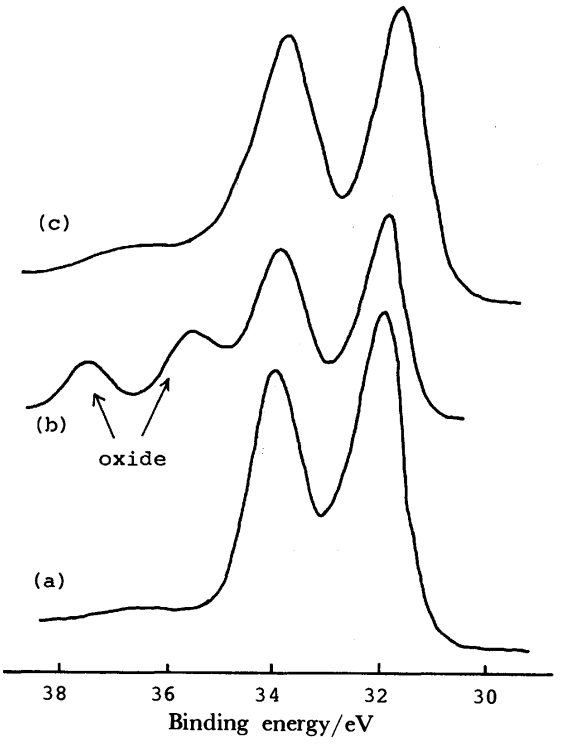

Fig. 6. XPS spectra of W 4f region for WC and W_2C. (a) activated WC, (b) untreated WC, and (c) activated W_2C.

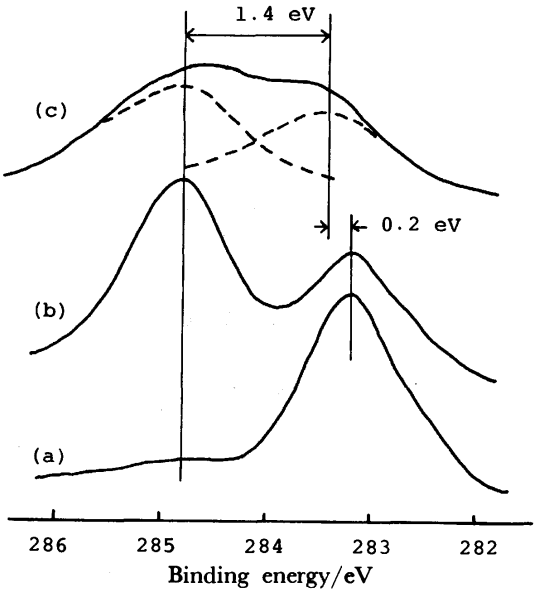

Fig. 7. XPS spectra of C 1s region for WC and W_2C. (a) activated WC, (b) untreated WC, and (c) activated W_2C.

activated W_2C (Fig. 7(c)). The existence of the former peak indicates that the surface of W_2C is largely covered with graphite-like carbon. The C 1s peak of WC was found to shift toward lower binding energy relative to that of graphite carbon by 1.6 eV, suggesting that the electrons are transferred from the W to C atoms. It is of note that the observed shift of W_2C, 1.4 eV was smaller than that of WC.

Discussion

Structure of Active Sites. The present kinetic measurements of CO hydrogenation showed a remarkable difference among the WC, W_2C, and W catalysts. The latter two catalysts exhibited very similar activation energies, specific activities and product distributions. WC, on the contrary, exhibited a marked catalytic activity; the activation energies for CH_4 formation and CO consumption were about three times larger than those on W_2C and W, and the specific activities were larger by about 20 times. This different catalytic behavior among the catalysts may arise from the different states of the active sites distributed on the surfaces. Figure 8 shows the crystal structures of WC and W_2C and the periodic arrangement of constituent atoms for $(10\bar{1}0)$ and (0001) planes. These carbides have similar hexagonal structures: The monocarbide consists of an alternate stacking of W- and C-layers along the c-axis direction, whereas W_2C has a series of a unit consisting of two W-layers and a C-layer.[14] As for the $(10\bar{1}0)$ plane of these carbides, both W and C atoms compose the uppermost layer in contact with each other, whereas either of W- or C-atoms compose the uppermost layer for the (0001) plane. Although there is little knowledge concerning the surface structure of WC, an ISS study on the single crystal faces of TiC by

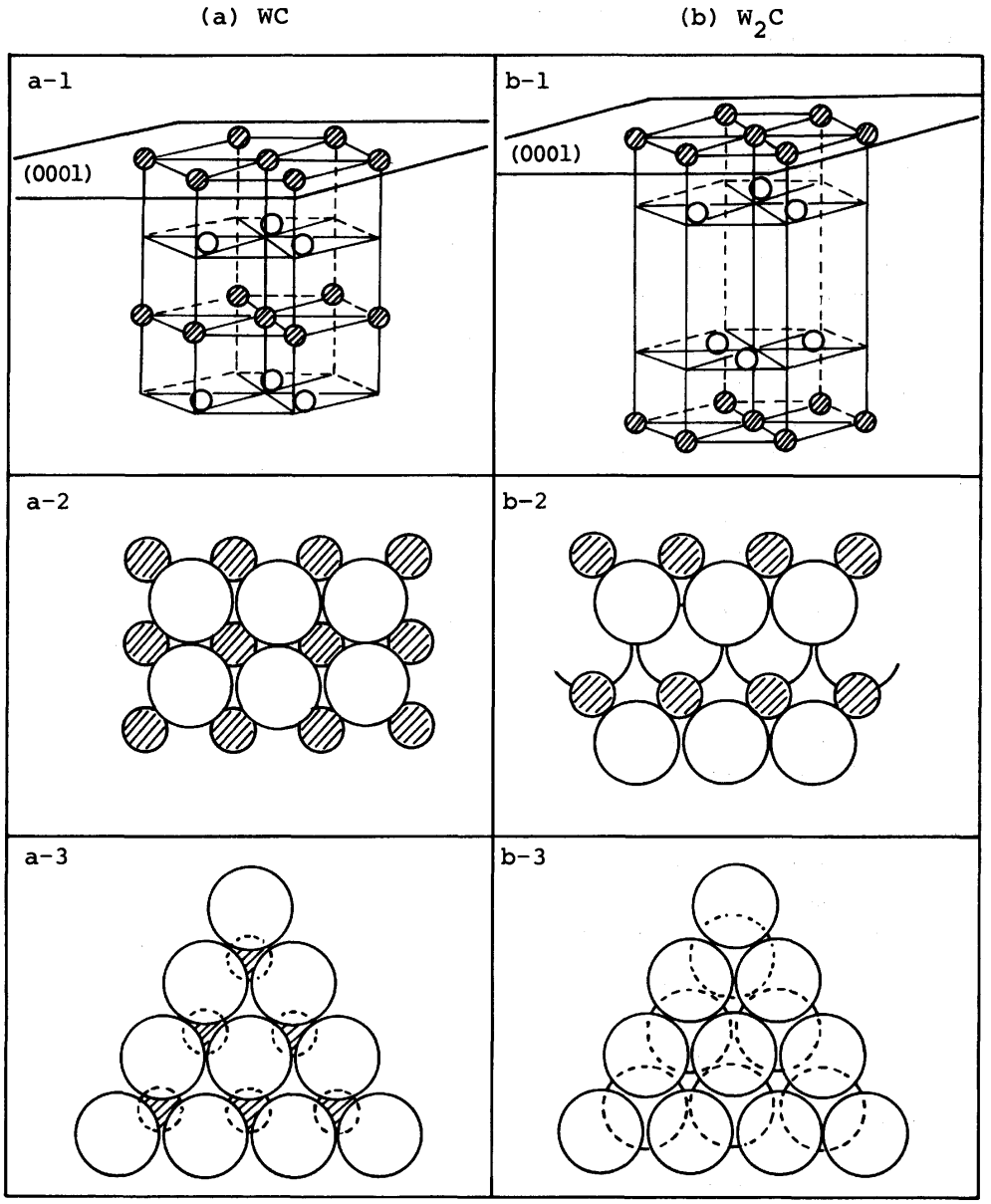

Fig. 8. Structures of (a) WC and (b) W_2C.
1: crystal structure, 2: $(10\bar{1}0)$ face, and 3: (0001) face.
○: W atom, and ◐: C atom.

Oshima *et al.*[16] gives some assistance for describing the behavior of the WC surface. It revealed that with the TiC (111) face Ti atoms compose the uppermost layer and the adsorption rate of oxygen on the (111) face is 100 times larger than that on the (100) face.[16] It is of note that the structures of the (0001) and $(10\bar{1}0)$ faces of WC resemble those of the (111) and (001) faces of TiC, respectively. More recently, Aono *et al.* reported that the carbon vacancies on the TiC (100) plane were very active for the adsorption of oxygen.[17] If carbon vacancies are formed on the WC surface during the activation treatments and are responsible for the catalytic reaction, the catalytic behavior of WC is expected to become closer to that of W_2C, which is opposed to the experimental facts obtained here. Furthermore, considering the uptake of CO adsorption, 30—40 percent of the total surface atoms of WC are estimated to be catalytically effective. This suggests that the surface vacancies are less likely to contribute to the hydrogenation of CO.

It is found that the surface of activated WC is free from contaminants such as oxygen and graphite-like carbon. However, a large amount of graphite residues remains on W_2C even after the high temperature treatment *in vacuo*, and the adsorption amount of CO on W_2C is very small in comparison with that on WC. From the previous study on TaC, the surface graphite acts as a strong poison for the catalytic reaction of ethylene hydrogenation. Assuming that the metal atoms are exposed as the uppermost surface layer of WC (0001) and W_2C (0001) faces as in TiC, the (0001) faces are expected to be catalytically more active than the $(10\bar{1}0)$ faces. With WC (0001) surface, the electronic state of the uppermost W atoms should be strongly

modified by the underlying C atoms. This effect is thought to be responsible for the suitable modification of the catalytic properties of surface-exposed W atoms. On the other hand, the nature of the W_2C (0001) surface might be similar to the pure W metal because the second layer also consists of W atoms. Therefore, metallic atoms of the W_2C (0001) surface with high chemical reactivity may strongly bind with contaminants such as graphite carbon or oxygen atoms, resulting in a reduction of the catalytically effective area to only a few per cent of the total surface.

Bradshaw *et al.*[18] performed angle-resolved photoemission measurements of TiC (111) and TiC (100) surfaces. They found that TiC (111) yielded a Ti-terminated (1×1) structure after annealing at 1000°C *in vacuo* and thus the prepared surface readily adsorbed hydrogen molecules, whereas TiC (100) showed no evidence of H_2 adsorption. These findings also suggest that metal-terminated polar surfaces are mainly responsible for the catalytic activities of refractory metal carbides.

Reaction Mechanisms. There is no general agreement of the nature of the reaction intermediates or of the reaction mechanism for CO hydrogenation on metallic catalyst surfaces: Some authors proposed that CO molecules first dissociate into carbon and oxygen atoms. This is followed by hydrogenation of the former adsorbate to produce methane or other higher hydrocarbons and by hydrogenation of the adsorbed oxygen atoms to produce water or by their reaction with CO to produce CO_2 molecules.[2,3,19,20] However, other investigators advocate that the adsorbed CO and H_2 form an oxygen containing surface species, CH_xO (x=1—3), prior to the C-O bond breaking.[1,21,22] In a previous paper,[8] we proposed the latter mechanism for the CO hydrogenation on TaC, TiC, and Mo_2C catalyst mainly for the following reasons:

(i) The adsorbed oxygen atoms on these carbide catalysts are tightly bound to the surfaces and can not be eliminated near the reaction temperatures, regardless of the presence or absence of hydrogen in the gas phase.

(ii) The facts that the reaction order of H_2O formation with respect to the hydrogen pressure exceeds unity and that the formation of CO_2 is enhanced by an increase in H_2 pressure; this suggests the existence of some attractive interaction between chemisorbed CO and H atoms. Thus on WC catalyst, similar reaction mechanism to those proposed previously are likely to contribute to the hydrogenation of CO on WC as follows:

$$CO \overset{K_1}{\rightleftharpoons} CO(a) \tag{1}$$

$$H_2 \overset{K_2}{\rightleftharpoons} 2H(a) \tag{2}$$

$$CO(a) + xH(a) \overset{K_3}{\rightleftharpoons} CH_xO(a) \tag{3}$$

$$CH_xO(a) + 2H(a) \overset{k_4}{\longrightarrow} CH_x(a) + H_2O \tag{4}$$

$$CH_xO(a) + CO(a) \overset{k_5}{\longrightarrow} CH_x(a) + CO_2 \tag{5}$$

$$CH_x(a) + (4-x)H(a) \overset{k_6}{\longrightarrow} CH_4 \tag{6}$$

where (a) denotes an adsorbed state, and K_i or k_i is the equilibrium or rate constant, respectively, of step i.

Assuming that the rate determining step exists in the elimination step of the oxygen atom in the CH_xO species to cause the C-O bond rupture and that all preceding steps are in quasi-equilibrium, the rates of the formation of H_2O and CO_2 are given respectively as

$$R_{H_2O} = \frac{k_4 K_1 (K_2)^{1+x/2} K_3 P_H^{1+x/2} P_{CO}}{(1+\sqrt{K_2 P_H}+K_1 P_{CO})^3} \tag{I}$$

$$R_{CO_2} = \frac{k_5 K_1^2 (K_2)^{x/2} K_3 P_H^{x/2} P_{CO}^2}{(1+\sqrt{K_2 P_H}+K_1 P_{CO})^2}. \tag{II}$$

From these rate expressions, one can estimate possible reaction orders with respect to H_2 and/or CO pressures. Comparing them with the experimental data,

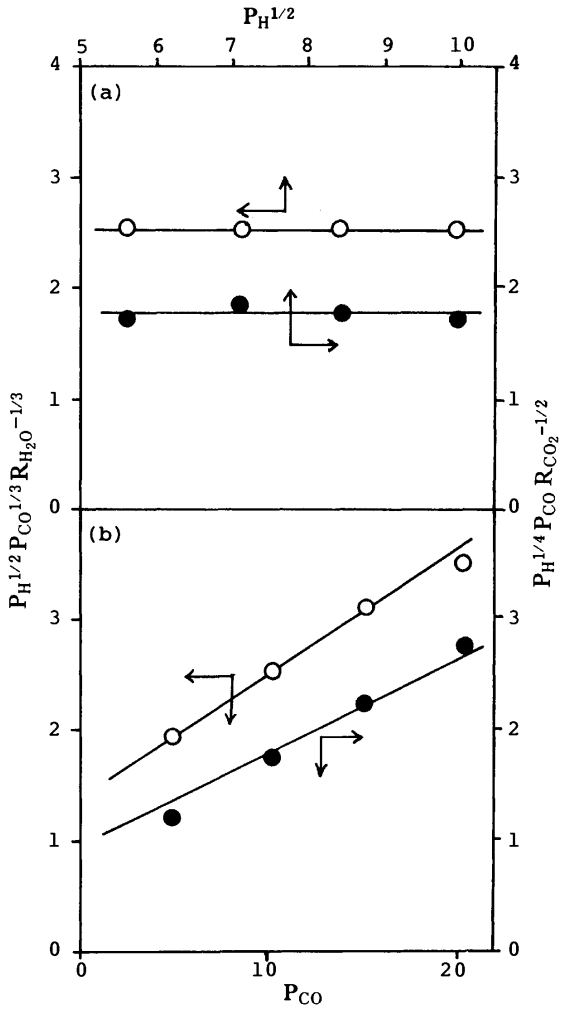

Fig. 9. Least square fitting of pressure dependency by applying the equations (I) and (II) with x=1.
(a) Dependency on H_2 pressure and (b) on CO.
Open and closed circles are the experimental data for the formation of H_2O and CO_2 taken from Fig. 4, respectively.

as described in the previous paper, the value of x can be estimated to be 1 or 2. In order to choose a more restricted value, a least square fitting was achieved between the pressure dependencies given in Fig. 4 and the rate equations of (I) and (II). The best fit was attained when x was unity. Figures. 9(a) and (b) show the results and the optimized values of K_1 and K_2 are known to be 0.082 and 0.0, respectively. By using the value of 2 for the x, an unreasonable negative value for $\sqrt{K_2}$ was obtained.

On the other hand, as described above, the active surface of W_2C behaves like a metallic W surface. Since the dissociation of the C-O bond on a metallic W surface is known to be a non-activated process,[23] it is more likely on W_2C that CO molecules initially dissociate into adsorbed C and O atoms on the surface. Thus, the apparent activation energy of the CO hydrogenation is lower on W_2C and W than on WC. These considerations lead us to a dissociative reaction scheme on W_2C and W catalysts as follows:

$$CO \overset{K_7}{\rightleftharpoons} C(a) + O(a) \quad (7)$$

$$H_2 \overset{K_8}{\rightleftharpoons} 2H(a) \quad (8)$$

$$O(a) + 2H(a) \xrightarrow{k_9} H_2O \quad (9)$$

$$O(a) + CO(a) \xrightarrow{k_{10}} CO_2 \quad (10)$$

$$C(a) + 4H(a) \xrightarrow{k_{11}} CH_4 \quad (11)$$

Provided that the rate-determining step is the elimination of an adsorbed oxygen atom from the surface and that the preceding steps, (7) and (8) are in quasi-equilibrium, the rate equations for the formation of CO_2 and H_2O can be obtained as (III) and (IV).

$$R'_{H_2O} = \frac{k_9 K_7^{1/2} K_8 P_H P_{CO}^{1/2}}{(1+\sqrt{K_7 P_{CO}})^3} \quad (III)$$

$$R'_{CO_2} = \frac{k_{10} k_7^{1/2} P_{CO}^{3/2}}{(1+\sqrt{K_7 P_{CO}})} \quad (IV)$$

Considering the material balance of carbon in the reaction system leads to the rate equation of (V) for the formation of CH_4.

$$R'_{CH_4} = R'_{H_2O} + R'_{CO_2} \quad (V)$$

These rate equations are consistent with the experimental reaction orders shown in Table 1. A marked difference of the rate equations is seen between WC and W_2C; *i.e.*, formation of CO_2 depends on the hydrogen pressure on WC but does not depend on W_2C.

Bell *et al.*[3,19] investigated the reaction pathway involving CO dissociation on Ru catalyst in which they assumed the rate to be controlled in the step of the hydrogenation of the CH_x surface species. The present rate equations are not in accord with their mechanism, because the rate-determining step is different. Since the bonding energy of an oxygen atom to metals is stronger on a W surface (651 kJ mol^{-1}) than on a Ru surface (396 kJ mol^{-1}),[23] thereby the elimination of adsorbed oxygen atom from the surface may control the overall rate of CO hydrogenation on W_2C and W catalysts.

References

1) M. A. Vannice, *Catal. Rev.*, **14**,153 (1976).
2) V. Ponec, *Catal. Rev.*, **18**, 151 (1978).
3) A. T. Bell, *Catal. Rev.*, **23**, 203 (1981).
4) E. Miyazaki, *Nippon Kagaku Kaishi*, **1973**, 1388.
5) I. Kojima, E. Miyazaki, Y. Inoue, and I. Yasumori, *J. Catal.*, **59**, 472 (1979).
6) I. Kojima, E. Miyazaki, Y. Inoue, and I. Yasumori, *J. Catal.*, **73**, 128 (1982).
7) I. Kojima, E. Miyazaki, and I. Yasumori, *J. Chem. Soc., Chem. Commun.*, **1980**, 573.
8) I. Kojima and E. Miyazaki, *J. Catal.*, **89**, 168 (1984).
9) J. G. McCarty and R. J. Madix, *J. Catal.*, **38**, 402 (1975).
10) R. B. Levy and M. Boudart, *Science*, **181**, 547 (1973).
11) M. Boudart, S. T. Oyama, and L. Leclercq, "Proceding of 7th Intern. Congr. Catalysis, Tokyo, 1980," Kodanshya, Tokyo (1981), p. 578.
12) P. N. Ross, Jr. and P. Stonheart, *J. Catal.*, **39**, 298 (1975).
13) P. N. Ross, Jr. and P. Stonheart, *J. Catal.*, **48**, 42 (1977).
14) L. E. Toth, "Transition Metal Carbides and Nitrides," Academic Press, New York/London (1971).
15) H. Arai, *Yukagaku*, **27**, 15 (1978).
16) C. Oshima, T. Tanaka, M. Aono, R. Nishitani, S. Kawai, and F. Yajima, *Appl. Phys. Lett.*, **35**, 822 (1979).
17) M. Aono, Y. Hou, R. Souda, C. Oshima, S. Otani, and Y. Ishizawa, *Phys. Rev. Lett.*, **50**, 1293 (1980).
18) A. M. Bradshaw, J. F. van der Veen, F. J. Himpsel, and D. E. Eastmann, *Solid State Commun.*, **37**, 37 (1980).
19) S. C. Kellner and A. T. Bell, *J. Catal.*, **67**, 175 (1981).
20) Y. Kobori, H. Yamasaki, S. Naito, T. Onishi, and K. Tamaru, *J. Chem. Soc., Faraday Trans. 1*, **78**, 1473 (1982).
21) D. W. Mckee, *J. Catal.*, **8**, 240 (1967).
22) T. Mori, H. Masuda, H. Imai, A. Miyamoto, S. Baba, and Y. Murakami, *J. Phys. Chem.*, **86**, 2753 (1982).
23) E. Miyazaki, *J. Catal.*, **65**, 84 (1980).

Thermodynamic Analysis of the Potentiometric Titrations of Polypeptides Accompanying the Coil-Beta Conversion

Hiroshi MAEDA
Department of Chemistry, Faculty of Science, Nagoya University Chikusa-ku Nagoya 464
(Received August 14, 1984)

The stability of uncharged β-structure of polypeptides from potentiometric titrations is examined based on thermodynamic considerations with special references to the aggregation and/or precipitation of polypeptides and the irreversible nature of the titration. It is concluded that most of the reported data on various kinds of polypeptides approximately represent the stability of the β-structure. Diverse stabilities exhibited by reported data can be partly ascribed to different extents of the stacking of the pleated sheets.

The stability of the β-structure, an important secondary structure found in proteins, in aqueous media has been studied.[1-15] For an intermolecularly associated β-structure, the free energy of association is derived from the concentration dependence of the conversion.[1] However, all other studies have evaluated the free energy change based on the potentiometric titrations.[2-15]

The interpretations of the potentiometric titrations accompanied by the coil-β conversion are often ambiguous because of slow attainment of equilibrium and/or irreversible behavior. These complex situations originate mainly, not always, from the aggregation and/or precipitation of the polypeptides. Under this situation, the reported values of the free energy change of the conversion are only nominal and apparent. These values are called here tentatively the apparent free energy change, ΔG_{app}, which is defined as follows in the case of poly (weak acid).[16-18]

$$-\Delta G_{app} = 2.303RT\int_{-\infty}^{pH_1}(\alpha_c - \alpha^*)\mathrm{d\,pH}$$
$$= 2.303RT\left[\int_0^1 pH^*d\alpha^* - \int_0^1 pH_c d\alpha_c\right]$$
$$= 2.303RT\int_0^1 (pH^* - pH_c)d\alpha \qquad (1)$$

Here, α_c and α^* (pH_c and pH*) represent, respectively, the degrees of ionization (the values of pH) of the reference solution and the actual solution (including the case with phase separation). The upper limit of the integral, pH_1, corresponds to the pH where α_c coincides with α^*. In the reference solution, random coils are titrated without being converted to the β-structure when protonated. In other words, in the reference solution, only random coils are present at any pH. In the actual solution, the β-structure is formed at low values of pH or at low charge densities. The fraction of random coils at zero ionization is assumed to be negligible in the present study.

Potentiometric titrations accompanying the β-coil conversion have been performed on four different groups of polypeptides; poly(L-tyrosine),[2-7] poly(L-lysine) (PLL)[8,9] poly[*S*-(carboxymethyl)-L-cysteine][10-12] (poly[Cys(CH_2COOH)]) and poly[*S*-(2-carboxyethyl)-L-cysteine] (poly[Cys(CH_2CH_2COOH)]),[12,13] and copolypeptides of L-lysine with L-valine[14] and L-isoleucine.[15] The reported values of ($-\Delta G_{app}$) differ markedly; about 1.25 kJ mol^{-1} for poly(L-tyrosine),[3-7] 590 J mol^{-1} for poly(L-lysine),[8] 3.51 kJ mol^{-1} and 4.60 kJ mol^{-1} for poly[Cys(CH_2COOH)] and poly[Cys(CH_2CH_2-COOH)], respectively[12] and 3.76 kJ mol^{-1} and 2.15 kJ mol^{-1} for poly(L-valine)[14] and poly(L-isoleucine), respectively.[15]

It is pertinent, therefore, to examine whether or not these reported diverse values of ($-\Delta G_{app}$) can be accepted as representing different stabilities of the β-structures formed by different kinds of side chains.

In the present study, the relation between the apparent free energy change (ΔG_{app}) and the stability of the β-structure is analyzed at first when the aggregation or the precipitation of polypeptides occurs. Then, a conventional procedure to evaluate ΔG_{app} from titration data as well as the effect of polypeptide concentration on the stability of the β-structure is examined. Finally, as an example of the usefulness of the present approach, a new interpretation is proposed on the stability of the β-structure of poly(L-lysine) from the titration data.

Theoretical

Relation between the Stability of the β-Structure and ΔG_{app}. In the potentiometric titrations with aggregation of polymers, the thermodynamic analysis has shown that ($-\Delta G_{app}$) consists of essentially two contributions.[19]

$$-\Delta G_{app} = \Delta\mu_p(0)/x + (n_w/n_p)\Delta\mu_w(0)/x \qquad (2)$$

and

$$\Delta\mu_p(0) = \mu_p^c(0) - \mu_p^\beta(0) \qquad (3)$$

Here μ_p and μ_w are the chemical potentials of the polymer component (taken as protonated species) and solvent (water), respectively. Numbers of moles of these components are denoted by n_p and n_w. $\Delta\mu_p(0)$ represents the difference between the chemical potentials of the protonated species of random coil (superscript c) and β-structure (superscript β). The second term of rhs of Eq. 2 represents the solvent contribution.[19,20] When the number of dissociable sites per polymer x is not too small, the solvent contribution is shown to be negligible.[19] In the present study, the second term of Eq. 2 is always neglected. This approximation is valid

for synthetic polypeptides considered in the present study. In the case of proteins, however, the solvent contribution of Eq. 2 can be significant in a certain case.[19] In the case of unimolecular conversion, such as the helix-coil conversion, the concentration dependent terms (cratic terms) of the chemical potential are identical for both conformations. Hence, $\Delta\mu_p(0)$ reduces to the corresponding standard part $\Delta\mu_p^*(0)$. When aggregation occurs, on the other hand, $\Delta\mu_p^*(0)$ can be evaluated from $\Delta\mu_p(0)$ after the correction for the cratic part is made. Further, $\mu_p{}^{\beta*}(0)$ itself can vary with concentration if the "crystallinity" of the β-structure depends on the concentration, as is likely in the case of crystalline polymers. In this sense, the effect of aggregation on ΔG_{app} can be said to be dual, even when the solvent contribution is ignored (which represents also the effect of aggregation).

The effect of phase separation on ΔG_{app} has been developed recently for a simple case where neither conformational change nor aggregation occurs in the solution phase and where the potentiometric equation for the polymers in the precipitated phase is given by Eq. 4.[20]

$$d\mu_p = -2.303\,RT\alpha_b x\,d\,pH \tag{4}$$

The result is given as follows:

$$-\Delta G_{app} = \Delta\mu_p(0)/x - 2.303(RT/C_p{}^t)\int_{-\infty}^{pH_c} C_p(\alpha-\alpha_b)d\,pH. \tag{5}$$

Here, the integration extends over the entire region of precipitation. In this region, the solution (degree of ionization α) and the precipitates (degree of ionization α_b) are in equilibrium with each other. The solubility C_p increases with pH and eventually coincides with the total concentration $C_p{}^t$ in the single solution region ($pH \geq pH_c$). The second term is suggested to be negligible in ordinary cases.[20] Although the effect of aggregation in the solution phase is not taken into account in the derivation of Eq. 5, the effect can be included in the term $\Delta\mu_p(0)/x$ according to the result of the preceding paragraph. Therefore, for the most of the data encountered in the present study, $-\Delta G_{app}$ can be approximated to $\Delta\mu_p(0)/x$, *i.e.*, Eq. 6 holds.

$$-\Delta G_{app} = \Delta\mu_p(0)/x. \tag{6}$$

However, as discussed later, the effect of phase separation could be significant in the case of poly(L-lysine).

It is important to examine the applicability of Eq. 4 to the β-precipitates. As shown experimentaly in a particular example,[21] β-precipitates contain a considerable amount of water, *i.e.*, the β-precipitates most likely consist of a gel which is uniform like a solution. Consequently, Eq. 4 holds for the β-precipitates to a good approximation. Stacked aggregates are also present in a gel constituting crosslinkages. However, as shown later, titration of β-precipitates occurs approximately for those dissociable sites on the surface of the aggregates and those sites inside the stacked aggregates are not titrated. In the course of titration, pleated sheets are peeled off from stacked aggregates. However, this disintegration process does not affect $\mu_p{}^{\beta}$ but the solubility C_p.

Examination of the Procedure of Evaluating ΔG_{app} from Experimental Data. In the present section, the procedure to evaluate ΔG_{app} from titration curves will be examined.

In all the data published up to now, identical values of pK_o were assumed for both random coil and the β-structure. In the case of poly (L-lysine),[8] both β-sheet and random coil limbs are discriminated clearly and they can be reasonably extrapolated to the same point pK_o. In the case of poly[Cys(CH_2COOH)] and its side chain homolog, however, the extrapolation of the β-sheet limb cannot be made unambiguously. In the case of poly(L-tyrosine), the situation is reversed. Extrapolation can be made only from the β-sheet limb and hence pK_o is assumed to be identical with $pK_o{}^{\beta}$. When the stacking of the pleated sheets occurs appreciably, the dissociable sites belonging to adjacent pleated sheets in the interior of the stacked aggregates will have a different value of pK_o, $pK_o{}^{\beta}$, from normal one found in the state of random coils. If $pK_o{}^{\beta}$ is greater than pK_o, $-\Delta G_{app}$ will be greater than reported values in each case discussed above.

In the titration of the stacked aggregates, what is likely to occur is such that titration proceeds with the sites located on the surface of the aggregates and that the sites buried in the interior of the aggregates are not titrated. When the surface charge density of the aggregates increases, the aggregates split into small aggregates or pleated sheets are peeled off one by one from the aggregates, or both. Consequently, there are a number of dissociable sites on the pleated sheets which have normal pK_o at any stage of titration. Under this situation, pK_o remains unchanged, on one hand, irrespective of the degree of ionization α. On the other hand, the distribution of charged and uncharged sites becomes highly deviated from a uniform distribution. The degree of ionization of the surface, α', is much higher than the nominal value α. In Fig. 1, titration curves of hypothetical system are schematically drawn, where a well-defined aggregate species is in equilibrium with unstacked pleated sheet. The titration curve of the aggregate (curve d) differs from that of unstacked pleated sheet (curve c), simply because α and α' are not identical. In other words, an important consequence of the difference between α and α' is included in the titration data themselves when integrated. Also, the question about the term $\log[\alpha/(1-\alpha)]$ does not cause any trouble, as seen below. It is obvious that the quantity pK^* ($=pH^*-\log[\alpha/(1-\alpha)]$) along curve (d) and in the transition region no longer represents the same physical meaning as attached to it in ordinary potentiometric titrations. However, the integral $\int_0^1 (pK^*-pK_c)\,d\alpha$ correctly reduces to the integral

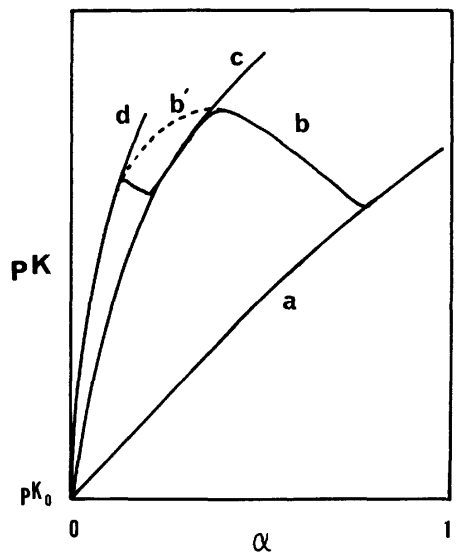

Fig. 1. Schematic titration curves for a hypothetical system where a well-defined stacked aggregate is in equilibrium with unstacked pleated sheet. Titration curves: (a) random coil, (b) actual system (pK^* *vs.* α), (c) single (unstacked) pleated sheet, and (d) stacked aggregate. Dashed curve (b′) represents the titration curve found on poly[Cys(CH_2CH_2COOH)], corresponding to a mixture of various kinds of aggregates.

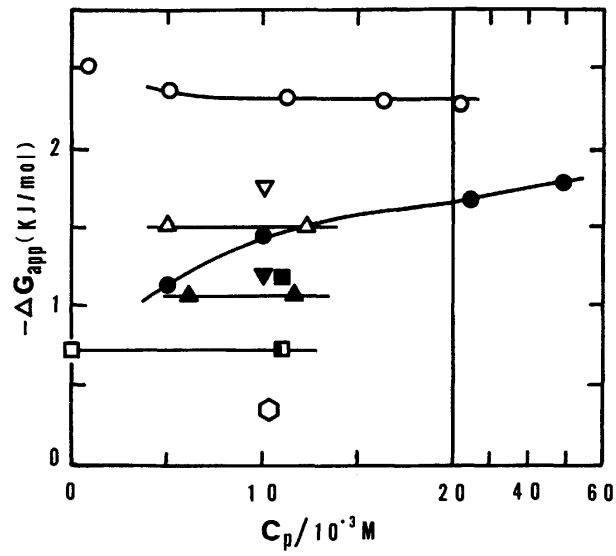

Fig. 2. Dependence of apparent free energy change (ΔG_{app}) on the polypeptide concentration (C_p) at 25°C in the media of ionic strengths 0.1—0.2 M (with a few exceptions). Poly(L-lysine): (○) (DP=670—837).[8] Poly(L-tyrosine): (□) (DP=445),[6] (◧),[5] and (■) (DP=1370).[3,6] Poly[Cys(CH_2COOH)]: (△) (DP=304) and (▲) (DP=50),[11] (▽) (DP=360) and (▼) (DP=62).[12] Poly[Cys(CH_2CH_2COOH)]: (○) (DP=206),[12] and (●) (DP=97).[13]

$\int_0^1$(pH*−pH_c) dα, which is the required quantity in Eq. 1. In this way, the difference between α and α' does not affect the evaluation of ΔG_{app}.

In the titration of poly(L-tyrosine) at high concentrations, titration curves similar to curve (b) in Fig. 1 are reported.[2,4] In the case of poly[Cys(CH_2COOH)], however, a titration curve like curve (b) has never been observed. A distribution about the number of pleated sheets in aggregates is expected and the side-by-side aggregation of pleated sheets is also likely. Under this situation, disintegration of aggregates occurs in diverse ways. As a result of their superposition, the titration curve (b) will be modified as shown by dotted line (b′) in Fig. 1. This kind of titration curve (b′) is observed in poly[Cys(CH_2COOH)] and poly[Cys(CH_2CH_2COOH)]. On the other hand, the titration curves of poly(L-lysine)(PLL) do not show any trace of the stacking as far as this diagnostic tool is concerned. However, fluorescence studies have suggested the stacking of the pleated sheets of PLL.[22-25] Thus, the titration behavior of PLL is different from those of other groups of polypeptide also in this respect.

Effects of Polymer Concentration. Experimentally obtained concentration dependence is summarized in Fig. 2 for the data at 25°C in 0.1—0.2 M (1 M=1 mol dm^{-3}) ionic strength (with a few exceptions). In the case of poly(L-tyrosine) represented by squares, very close values of ($-\Delta G_{app}$) were obtained at 1.1×10^{-2} M[5] and 2×10^{-4} M.[5] In the case of poly[Cys(CH_2COOH)], negligible concentration dependence was found on two samples (DP=304 and 50).[11] For comparison, results on other samples are also shown (DP=360 and 62).[12] In the case of poly[Cys(CH_2CH_2COOH)], the effect of the concentration was extensively examined. Negligible dependence resulted for a high molecular weight sample (DP=206),[12] while a considerable dependence was found on another sample (DP=62).[13] In summary, concentration dependence of the titration curves is negligible except for one example (poly[Cys[CH_2CH_2COOH). DP=62) even when aggregation and/or precipitation occur with increasing concentration. Although extensive study on poly[Cys(CH_2COOH)] and poly(L-tyrosine) in this respect is desirable, we accept the conclusion for the moment and consider its implication.

The chemical potential of the polymer in a random coil can be generally written as follows:

$$\mu_p^c(0) = \mu_p^{c*}(0) + RT\ln a_c = \mu_p^{c*}(0) + RT\ln C_p^t y_p(0). \quad (7)$$

Here a_c and y_p (0) represent the activity and activity coefficient of uncharged random coils, respectively. Generally, explicit expression for $\mu_p^{\beta}(0)$ is not easily obtained, since detailed knowledge on the β-structure is scarcely available. At first, the simplest case is considered where the β-structure can be characterized as forming a pseudophase like detergent micells, as proved to be in the case of poly[Cys(CH_2COOH)] at a concentration range higher than about 1×10^{-3} M.[26] This situation, although simple, is valid for other polypeptides in the same concentration range. In this case, $\mu_p^{\beta}=\mu_p^{\beta*}$ and $\mu_p^{\beta*}(0)$ depends on the concentration only when "crystal structure" varies with the concentration. The chemical potential difference $\Delta\mu_p(0)/x$ is given by Eq. 8 in this case.

$$-\Delta G_{app} = \Delta\mu_p(0)/x = \Delta\mu_p^*(0)/x + (RT/x)\ln C_p^t y_p(0), \quad (8)$$

In this way, $(-\Delta G_{app})$ or $\Delta\mu_p(0)/x$ has to vary with C_p^t through the second term of rhs of Eq. 8, aside from the possible concentration dependence of $\Delta\mu_p^*(0)/x$. However, the second term changes only by $(RT/x)\times 2.303\times 2\simeq 5RT/x$, which amounts to 125 J mol^{-1} for $x=100$ when C_p^t is changed by 100 times. It is now clear that for the high molecular weight samples shown in Fig. 2, the variation of the second term is practically negligible either because x is sufficiently large or because the examined concentration range is not wide enough. Therefore, the apparent inconsistency is solved, which is found between the formal dependence on C_p^t predicted by Eq. 8 and the actually observed independence on C_p^t. Moreover, it is inferred that the "crystal structure" remains constant irrespective of the concentration in these examples. The constant values of thus $(-\Delta G_{app})$ correspond to $\Delta\mu_p^*(0)/x$ under this situation.

$$-\Delta G_{app} = \Delta\mu_p^*(0)/x. \quad (9)$$

However, the values of $(-\Delta G_{app})$ differ considerably for polypeptides of different side chains as well as for different chain lengths, as exhibited in Fig. 2. Different values of the standard chemical potential difference can be partly ascribed to different "crystal structures." For example, the stacking of the pleated sheets is suggested to occur in the case of poly[Cys(CH_2COOH)] under the conditions shown in Fig. 2.[26,27] The extent of the stacking becomes negligible at the concentration range around 1×10^{-4} M[26] or lower.[27] Since the tendency of the stacking of the pleated sheets is stronger in the case of poly[Cys(CH_2CH_2COOH)],[28,29] the observed values of $(-\Delta G_{app})$, which is equivalent to $\Delta\mu_p^*(0)/x$, for these two polypeptides represent the stabilities of the stacked pleated sheets.

In the case of poly(L-tyrosine), the β-structures at the two concentrations differ considerably. At 1.1×10^{-2} M, the approximation of pseudophase is probably good, based on the results on the molecular weight measurements.[3] Hence, Eq. 9 is expected to hold at this concentration. On the other hand, unimolecular β- structure without aggregation is suggested at 2×10^{-4} M.[6,30] The observed values of $(-\Delta G_{app})$ at this concentration can be also regarded as $\Delta\mu_p^*(0)/x$ because the concentration terms in the chemical potentials cancel out each other just as in the case of the helix-coil transition, when activity coefficients of uncharged polypeptide in the two conformations are approximated to be identical. Similar values of $\Delta\mu_p^*(0)/x$ for both aggregated and unaggregated pleated sheets indicate either that the aggregation at 1.1×10^{-2} M does not involve the stacking of pleated sheets or that the single pleated sheet at 2×10^{-4} M is folded over on itself (self-stacking) as proposed by Auer *et al.*[6,7,30,31] The idea of self-stacking is interesting and it is hoped that the idea will be developed both experimentally and theoretically.

In Eq 9, $(-\Delta G_{app})$ is experimentally obtained and hence independent of the concentration scale employed, while μ_p^{c*} and hence $\Delta\mu_p^*(0)$ depend on it. If the concentration scale is changed from C_p^t to $C_p^{t\prime}=C_p^t\,\xi$, ξ being the conversion factor, $\Delta\mu_p^*(0)/x$ also changes to $[\Delta\mu_p^*(0)/x]'=\Delta\mu_p^*(0)/x+(RT/x)\ln\xi$. The difference $[(RT/x)\ln\xi]$ can be again very small owing to the factor x, unless an extraordinary conversion factor is used such as $\xi=10^x$. Consequently, it can be that $\Delta\mu_p^*(0)/x$ depends, in principle, on the concentration scale but the difference arising from the change of the concentration scale is practically negligible.

Contrary to many examples discussed above, on the other hand, the titration curves are dependent on the polymer concentration for a low molecular weight sample of poly[Cys(CH_2CH_2COOH)],[13] as shown in Fig. 2. Judging from the molecular weight of the used sample, the β-structure is formed by intermolecular association of extended chains to a considerable extent.[26] However, judging from the CD spectra, the fraction of the β-structure is large, very close to the completion, and hence the concentration dependence cannot be ascribed to the effect on the association equilibrium. Therefore, the observed concentration dependence can be understood as representing the situation that the extent of the stacking of the pleated sheets increases with C_p^t.

A New Interpretation of the Titration Data of Poly(L-lysine). As shown in Fig. 2, the stability of the β-structure of PLL is considerably smaller than that of other polypeptide consisting of tyrosine or cysteine derivatives, in spite of a contribution from the hydrophobic interaction which has been suggested for the β-structure of PLL.[8,9,14,15,32] Instead of discussing possible sources for this low stability of β-PLL, a completely different point of view is presented in this section, according to which the stability at 25 °C can be greater than what is given by $(-\Delta G_{app})$.

At 25 °C, an irreversible β-to-coil conversion of PLL takes place when titrated from uncharged to charged states, while a reversible coil-to-helix conversion occurs when titrated from charged to uncharged states. Marked time dependence of pH was reported during the titration from β to coil,[8] showing a slow dissociation of β-aggregates in comparison to helix-coil interconversion. The titration curve does not represent a simple β-to-coil conversion, but it represents a complex conversion from the β-structure to the mixture of the α-helix and random coils: The relative populations of these two states varying with pH. This should be the case, otherwise the titration could be reversible. For the potentiometric titration with separation of phases, Eq. 5 can be rewritten in the case of poly (weak bases) as follows.

$$-\Delta G_{app} = \Delta\mu_p(0)/x - 2.303(RT/C_p^t)\int_{pH_c}^{\infty}(\alpha-\alpha_b)C_p\,d\,pH \quad (10)$$

Here α and α_b represent the degree of ionization or protonation of the solution and the precipitates, respectively. The reason why the second term is negligible in ordinary cases resides in the respect that the solubility varies sharply with pH and hence the integrand remains finite only for a very narrow pH range. The effect of the equilibrium between the helix and random coil is dual. First, it will increase the solubility more than what is expected for the case that only random coils are present. Secondly, the increased solubility will vary gradually with pH, simply because the addition of HCl not only dissociates the β-aggregates but also it converts the α-helices to random coils. The latter process keeps the solubility unchanged. As a result of these two effects, the integrand is expected to remain finite over a wide range of pH. These considerations lead to the interpretation that the second term of Eq. 10 can contribute significantly in the irreversible titration of PLL and hence the term $(-\Delta G_{app})$ underestimates $\Delta\mu_p(0)/x$ considerably. Therefore, it is not unreasonable to expect a value of $\Delta\mu_p(0)/x$ larger than 590 J mol^{-1} $(-\Delta G_{app})$ at 25°C from the titration data of PLL.[8] This consideration predicts that $(-\Delta G_{app})$ increases with temperature (positive ΔH_{app}) even in the case that $\Delta H=0$, simply because both irreversible conversion and phase separation become significant as temperature decreases. A value of 3.64 kJ mol^{-1} was obtained for ΔH_{app} from the temperature dependence of ΔG_{app} including the data corresponding to irreversible titrations.[8] On the other hand, a small temperature dependence (ΔH_{app}=540 J mol^{-1}) was obtained from the titrations accompanying the coil-to-β conversion and limited within soluble range.[9] The present analysis can explain reasonably a large difference between these two values of ΔH_{app}. Conversely, the present point of view based on Eq. 10 is experimentally supported.

Summary

1. Most of the reported values of ΔG_{app} evaluated from the potentiometric titrations accompanying the β-coil conversion, can be approximately accepted as representing $\Delta\mu_p^*(0)/x$, the standard chemical potential difference (per residue) of uncharged polypeptides between the β-structure and random coil state.

2. The values of $\Delta\mu_p^*(0)/x$ vary markedly depending on the kind of side chains.

3. Different values of $\Delta\mu_p^*(0)/x$ are best understood as arising from different extents of "crystallinity" rather than from different extents of the conversion from disordered to the β-conformation. In the case of the β-structure, "crystallinity" corresponds to the extent of the stacking of the pleated sheets.

4. In the case of poly(L-lysine), present analysis suggests that the apparent free energy change $(-\Delta G_{app})$ from irreversible titration with precipitation underestimates the stability of the β-structure.

References

1) H. Maeda, K. Saito, and S. Ikeda, *Bull. Chem. Soc. Jpn.*, **56**, 602 (1983).
2) E. Patrone, G. Conio, and S. Brighetti, *Biopolymers*, **9**, 897 (1970).
3) M. B. Senior, S. L. H. Gorrell, and E. Hamori, *Biopolymers*, **10**, 2387 (1971).
4) G. Conio, E. Patrone, and F. Salaris, *Macromolecules*, **4**, 283 (1971).
5) A. Cosani, M. Palumbo, M. Terbojevich, and E. Peggion, *Int. J. Peptide Protein Res.*, **6**, 457 (1974).
6) R. P. McKnight and H. E. Auer, *Macromolecules*, **9**, 939 (1976).
7) H. E. Auer and R. P. McKnight, *Biochemistry*, **17**, 2798 (1978).
8) D. Pederson, D. Gabriel, and J. Hermans, Jr., *Biopolymers*, **10**, 2133 (1971).
9) A. Cosani. M. Terbojevich, L. Romanin-Jacur, and E. Peggion, "Peptides, Polypeptides and Proteins," ed by E. R. Blout *et al.* John Wiley, New York, (1974), p. 166.
10) S. Ikeda, *Bull. Chem. Soc. Jpn.*, **43**, 1686 (1970).
11) S. Makino and S. Sugai, *Biopolymers*, **9**, 1049 (1970).
12) H. Maeda and S. Ikeda, *Biopolymers*, **14**, 1623 (1975).
13) H. Maeda and S. Ikeda, *Biopolymers*, **10**, 2525 (1971).
14) R. Mandel and G. D. Fasman, *Biopolymers*, **14**, 1633 (1975).
15) B. Walter and G. D. Fasman, *Biopolymers*, **16**, 17 (1977).
16) B. H. Zimm and S. A. Rice, *Mol. Phys.*, **3**, 391 (1960).
17) M. Nagasawa and A. Holtzer, *J. Am. Chem. Soc.*, **86**, 538 (1964).
18) J. C. Leyte and M. Mandel, *J. Polym. Sci.*, **A2**, 1879 (1964).
19) H. Maeda, *J. Phys. Chem.*, **79**, 1680 (1975).
20) H. Maeda, *J. Phys. Chem.*, **88**, 5129 (1984).
21) H. Maeda and S. Ikeda, *Biopolymers*, **12**, 2121 (1973).
22) J. Lynn and G. D. Fasman, *Biochem. Biophys. Res. Commun.* **33**, 327 (1968).
23) G. Witz and B. L. van Duuren, *J. Phys. Chem.*, **77**, 648 (1973).
24) S. Ichimura and M. Zama, *Biopolymers*, **16**, 1449 (1977).
25) Y. Sato and R. W. Woody, *Biopolymers*, **19**, 2021 (1980).
26) H. Maeda, Y. Gatto, and S. Ikeda, *Macromolecules*, **17**, 2031 (1984).
27) H. Maeda, K. Kadono, and S. Ikeda, *Macromolecules*, **15**, 822 (1982).
28) K. Ooi, H. Maeda and S. Ikeda, *Biopolymers*, **19**, 1743 (1980).
29) H. Maeda and K. Ooi, *Biopolymers*, **20**, 1549 (1981).
30) E. Patton and H. E. Auer, *Biopolymers*, **14**, 849 (1975).
31) H. E. Auer and H. Miller-Auer, *Biopolymers*, **21**, 1245 (1982).
32) C. R. Snell and G. D. Fasman, *Biochemistry*,. **12**, 1017 (1973).

 © 1985 The Chemical Society of Japan Bull. Chem. Soc. Jpn., 58, 623—630 (1985)

ESR Spectra of Six-coordinate Cobalt(III) Tetraphenylporphyrin Cation Radicals Generated by Electrochemical Oxidation II.[1] Axial Ligand and Solvent Effects

Kohji ICHIMORI, Hiroaki OHYA-NISHIGUCHI,* Noboru HIROTA, and Kiyoko YAMAMOTO†

Department of Chemistry, Faculty of Science, KyotoUniversity, Sakyo-ku, Kyoto 606

†*The Institute of Physical and Chemical Research, Wako, Saitama 351-01*

(Received August 15, 1984)

The ESR spectra of the π-cation radical generated electrochemically from 5,10,15,20-tetraphenylporphyrinatocobalt(II), [Co^{II}(tpp)], have been observed in the presence of various anions and in solvents such as halogenated hydrocarbons, nitriles, ethers, ethanol, and organic acids. From the analyses of these spectra, the π-cation radical has been found to coordinate axially the anion or the solvent according to the order of its coordinating ability; BF_4^-, ClO_4^-, PF_6^-, NO_3^-<nitriles<halogen anions<ethanol<CF_3COO^-, AcO^-, SCN^-, CN^-. The singly-occupied molecular orbital has been assigned to be always $a_{2u}\pi$ orbital regardless of the axial ligands. The spin densities on N and Co much increase due to the axial ligation. It has been further confirmed that the spin polarization mechanism mainly contributes to the appearance of the spin density on Co. These axial-ligand effects are quantitatively explained by a model calculation of the CNDO/2 MO method.

The redox behavior of metalloporphyrins has been widely investigated from biological and biochemical interests and it has been known that most of metalloporphyrins are converted into their π-cation radicals by the oxidation of their porphyrin rings as well as of their central metal ions.[2] Some of natural porphyrins can be oxidized into their π-cation radicals under mild conditions,[3] but such readily oxidizable porphyrins have been rarely found in synthetic ones so far. It has been found that by thermal and light activations 5,10,15,20-tetraphenylporphyrinatocobalt(III) chloride, [Co^{III}(tpp)]Cl, in chlorinated hydrocarbons is converted partially and reversibly into a paramagnetic species, which was identified by ESR as the [Co^{III}(tpp)]$^{2+\cdot}$ π-cation radical coordinating axially two chlorides.[4] From the studies using electrochemical techniques,[1,4b] it has been shown that this radical is also generated by the one-electron oxidation of [Co^{III}(tpp)]Cl or the subsequent two-electron oxidation of [Co^{II}(tpp)] in the same solvents with tetrabutylammonium chloride (TBACl) as a supporting electrolyte. On the other hand, when $TBABF_4$ or $TBAClO_4$ was used, a different paramagnetic species was produced. It was concluded from the ESR observation that the π-cation radical coordinates different anions which perturb its electronic state. These results motivate us to examine in detail the effects of the coexisting anions and solvents on the ESR spectra of the π-cation radical. The ESR spectroscopy is a powerful means for investigating the microscopic structures of the complexes in solutions. Therefore, we have examined the ESR spectra of the π-cation radical using various combinations of anions and solvents.

In this paper, we first describe which anions or solvents are coordinated by the π-cation radical under different conditions and then discuss their effects on the electronic state of the π-cation radical. Secondly, we have made a model calculation of closed-shell CNDO/2 MO method including the cobalt AO in order to fully understand the effect of axial ligation. The results of the calculation will be compared with the experimental results.

It has been known that the electronic states of natural porphyrins are perturbed by their axial ligands, which is related to the bioactivities of the enzymes containing metalloporphyrins.[5] It is hoped that this results will be helpful for understanding their activities.

Experimental

Materials. [Co^{II}(tpp)] and [Co^{III}(tpp)]Cl were prepared by method previously reported.[6] [Co^{III}(tpp)]Br and [Co^{III}(tpp)]$_2(SO_4)$ were prepared in a similar way using HBr and H_2SO_4, respectively, instead of HCl for [Co^{III}(tpp)]Cl preparation.[7] They were identified by elemental analyses and absorption spectra. Dichloromethane (DCM), acetonitrile (ACN), propionitrile (PCN), butyronitrile (BCN), and nitromethane were of spectroscopic grade and dried over Woelm 200 neutral alumina. Tetrahydrofuran (THF), 1,2-dimethoxyethane (DME), and dibromomethane (DBM) were distilled over CaH_2 before use. Ethanol of spectroscopic grade was distilled over magnesium ethoxide immediately prior to use. Trifluoroacetic acid (TFA) and trifluoroacetic anhydride (TFAA) of special grade were used without further purification. $TBABF_4$, $TBAClO_4$, TBACl, and TBABr were commercially obtained. $TBABF_4$ and $TBAClO_4$ of polarographic grade were used without further purification. TBABr was recrystallized once from ethyl acetate–ether (3:1). $TBAPF_6$,[8a] $TBANO_3$,[8b] and TBAF[8c] were prepared according to the methods reported elsewhere. $TBAPF_6$ and $TBANO_3$ recrystallized twice from ethanol–water and benzene, respectively, were confirmed by elemental analyses. TBAF was stored in ether under nitrogen atmosphere. The salts were dried *in vacuo* at room temperature before use except for TBACl which was dried at 90 °C. The preparations of dibenzo-18-crown-6 (DB18C6) complexes with potassium salts were carried out according to the methods given by Pedersen.[9]

Apparatus and Procedures. The ESR spectra were taken with JEOL PE-3X or FE-3X spectrometer equipped with a temperature controller. The Co^{III}(tpp) π-cation radical was generated by electrochemical two-electron oxidation of [Co^{II}(tpp)] otherwise noted, using various electrolytes and

solvents. The best temperature for the ESR measurement depended on the solvent. In most cases, the ESR spectra were measured at temperatures 10 to 20 °C above the melting point of the solvent. The procedure for the ESR measurement combined with electrochemical technique and the method of *g*-value calibration were described previously.[1] Here we only mention the usage of tetrabutylammonium salts and DB18C6·KX complexes (X=CN^-, SCN^-, and AcO^-). Some of the salts used here have been found to function both as the axial ligand source for the cation radical and as the supporting electrolytes. But those salts comprising such an anion as CN^-, SCN^-, or AcO^- could not be used as the supporting electrolyte, since they are very hygroscopic and/or difficult to be purified. Thus on the occasion of introducing such anions into sample solution, DB18C6·KX was added to the solution together with $TBAPF_6$ which acts only as the supporting electrolyte.[10] This method of preparing the sample solution may be generally useful for studying anion effects in nonaqueous solvents in electrolysis. DB18C6 was confirmed to have no effect on the ESR spectra by itself.

Results

The π-cation radical exists in solution as a free ion or a complex with the coexisting anion or the solvent whose effect is reflected sensitively on the ESR spectrum. Table 1 shows the parameters of the π-cation radical. In the following the results are classified into several groups by the electrolyte and solvent, denoted as electrolyte/solvent. The electrolytes should also be recognized as the source of anions coordinated by the π-cation radical.

$TBAPF_6$, $TBABF_4$, $TBAClO_4$, $TBANO_3$/DCM, DBM. It was suggested in the previous paper[1] that the π-cation radical in the system of $TBAClO_4$/DCM or $TBABF_4$/DCM might be complexed with ClO_4 or BF_4. This was deduced from the marked difference between the ESR spectra of these systems and that of TBACl/DCM system in which the π-cation radical was shown to coordinate the chloride. However, there was no direct evidence of BF_4^- or ClO_4^- ligation in the ESR spectra. We have tried to clarify whether or not the π-cation radical coordinates these anions by observing its ESR spectra in the *inert* solvent such as DCM or DBM in the presence of BF_4^-, ClO_4^-, PF_6^-, and NO_3^- (weak-ligand anions).

Table 1. ESR parameters of Co^{III} (tpp) π-cation radical

Solvent	Anion	Axial Ligand	*T* °C	*g* (±0.0002)	ΔH[a] mT	hfcc/mT Co	N	X[b]
DCM	BF_4^-	c)	−70	2.0031	4.53	0.57	(0.18)	—
	ClO_4^-	c)	−70	2.0031	4.41	0.57	(0.18)	—
	PF_6^-	c)	−70	2.0031	4.52	0.57	(0.18)	—
	NO_3^-	c)	−70	2.0031	4.59	0.6	—	—
	SO_4^{2-}	c)	−60	2.0031	4.41	0.57	—	—
	F^-	F^-	−70	2.003	7.98	—	—	2.68
	Cl^-	Cl^-[d]	−70	2.0029	8.0	1.03	0.28	0.22
	CN^-	CN^-	−55	2.0033	8.1	1.02	0.26	—
	SCN^-	SCN^-	−65	2.0028	9.1	1.20	(0.25)	—
	AcO^-	AcO^-	−74	2.0072	7.1	0.92	0.20	—
DBM	BF_4^-	c)	−48	2.0028	4.0	—	—	—
	ClO_4^-	c)	−45	2.0028	3.92	—	—	—
	PF_6^-	c)	−45	2.0029	3.9	—	—	—
	Cl^-	Cl^-	−48	2.0035	7.97	1.02	—	—
	Br^-	Br^-	−48	2.008	10.0	—	—	—
PCN	BF_4^-	PCN[d]	−70	2.0034	4.46	0.60	0.19	—
	ClO_4^-	PCN[d]	−70	2.0034	4.47	0.60	0.19	—
	PF_6^-	PCN	−65	2.0034	4.46	0.60	0.19	—
	Cl^-	Cl^-	−70	2.0035	8.55	1.10	0.26	0.22
	CN^-	CN^-	−60	2.0035	8.1	1.07	0.27	—
ACN	PF_6^-	ACN	−34	2.0038	4.76	—	—	—
BCN	PF_6^-	BCN	−70	2.0034	4.51	—	—	—
CH_3NO_2	BF_4^-	CH_3NO_2	−24	2.0037	4.83	—	—	—
	PF_6^-	CH_3NO_2	−30	2.0037	4.81	—	—	—
	ClO_4^-	CH_3NO_2	−26	2.0037	4.80	—	—	—
EtOH	BF_4^-	EtOH	−70	2.0042	4.36	—	—	—
	PF_6^-	EtOH	−70	2.0042	4.35	—	—	—
	Cl^-	EtOH	−68	2.0041	4.33	—	—	—
	CN^-	CN^-	−65	2.0033	8.0	1.02	0.24	—
	SCN^-	SCN^-	−65	2.0030	9.0	1.2	—	—
DME+THF	BF_4^-	c)	−80	2.003	(3.55)	—	—	—
TFA+TFAA	—	CF_3COO^-	−30	2.0051	4.78	(0.65)	—	—
	BF_4^-	CF_3COO^-	−30	2.0052	4.81	(0.65)	—	—
	F^-	CF_3COO^-	−30	2.0050	4.73	(0.65)	—	—
	Cl^-	CF_3COO^-	−30	2.0051	4.70	(0.65)	—	—

a) Total peak-to-peak width including hfcc. b) Axial ligand. c) The π-cation radical was not ligated. d) Previous work.

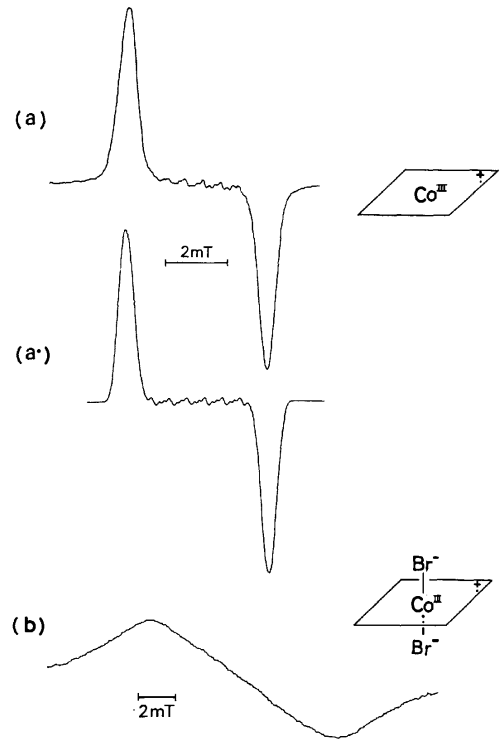

Fig. 1. The ESR spectra of [Co^{III}(tpp)] π-cation radical in the presence of weak-ligand anion and halogen anion: a) $TBABF_4$/DCM at −70°C, a') The computer simulation of a), b) TBABr/DBM at −48°C. The parallelograms in Figs. 1—3 indicate the porphyrin π-system.

The ESR spectra obtained in DCM did not depend on these anions, indicating that the π-cation radical did not coordinate these anions. A typical spectrum is shown in Fig. 1a. Partially resolved hyperfine structures (hfs) due to cobalt and nitrogen nuclei are seen in the spectrum. It is simulated with g=2.0031, a_{Co}= 0.57 mT, a_N=0.18 mT, and linewidth of 0.30 mT.

In DBM the anion dependence of the ESR spectra was not also observed. The hyperfine coupling constants (hfcc) could not be obtained from the ESR spectra because of line-broadening (Fig. 1b). The g-value and the total peak-to-peak width (ΔH_{pp}) were independent of the anions used (see Table 1). The possibility of the ligation of these anions was excluded, but there still remained the possibility of solvent ligation in these systems. The ligation of DBM is expected to cause a large g-value shift owing to the large spin-orbit interaction of bromine. Since the g-value was near that of free spin, it is concluded that the π-cation radical does not coordinate DBM. The g-value in DCM was almost equal to that in DBM and thus the same conclusion is derived for DCM, which is consistent with the inertness of DCM in ligation. The one-electron oxidation of [Co^{III}(tpp)] (1/2)SO_4 in $TBAPF_6$/DCM gave the same ESR spectrum as described above. Therefore, it is also concluded that the π-cation radical does not coordinate SO_4^{2-}.

TBAF, TBACl, TBABr/DCM, DBM. Halogen anions are considered to have moderate coordinating ability and the π-cation radical is expected to coordinate these anions in the inert solvents. TBACl/DCM system has already been examined and Cl hfs was observed.[1] In TBAF/DCM system the ESR spectrum consisted of two components: a central sharp line (ΔH_{pp}=1.5 mT) and a broad line having two peaks on the both sides of the central line. The former was attributed to the H_2tpp radical generated by the loss of the cobalt ion, since there was no splitting due to the cobalt nuclei (I=7/2). The latter showed an additional large splitting due to the fluorine nucleus (2.68 mT), indicating that the π-cation radical coordinates the fluoride.

In TBACl/DBM, the π-cation radical coordinates the chloride as in TBACl/DCM. The ESR spectrum had a similar a_{Co} but was broader than that of in TBACl/DCM. In TBABr/DBM the presence of bromide gave a very broad ESR spectrum of the π-cation radical. The large g-value (2.008) and ΔH_{pp} (10 mT) indicate the ligation of the bromide, but because of the broadness a_{Co} or a_{Br} could not be estimated (Fig. 1b). The one-electron oxidation of [Co^{III}(tpp)] Br in TBABr/DBM gave the same spectrum. TBAF/DBM and TBABr/DCM systems gave no ESR spectra probably because the π-cation radical was unstable in these systems. TBAI was examined in both solvents, but no ESR spectra were observed.

DB18C6·KCN, ·KSCN, ·KOAc+TBAPF$_6$/DCM. Strong ligands such as CN^-, SCN^-, and AcO^- were introduced in the form of DB18C6 potassium complexes mentioned in the previous section. These anions gave considerable changes to the ESR spectra and therefore the π-cation radical is considered to coordinate these anions. The cobalt hfcc's were comparable with that found for the radical complexed with chloride but varied somewhat depending on the anions.

Figure 2a gives the ESR spectrum of the π-cation radical in DB18C6·KCN+$TBAPF_6$/DCM system, which shows well resolved hfs. The spectrum was simulated with one Co (a_{Co}=1.02 mT), four N (a_N=0.26 mT) and eight H (a_H=0.03 mT) nuclei. The nitrogen hfs of the cyanide was not observed. This indicates that the cyanide is bound to the π-cation radical with the carbon, not the nitrogen. On the other hand, the spectrum in DB18C6·KSCN+$TBAPF_6$/DCM system (Fig. 2b) could not be simulated with 1Co, 4N, and 8H. By taking the hfs due to the nitrogen nuclei of the thiocyanate into consideration, the spectrum was well simulated with 1Co (a_{Co}=1.20 mT), 6N (a_N=0.25 mT) and 8H (a_H=0.03 mT), though there was an ambiguity of the a_N value. This result leads to the conclusion that the π-cation radical has N-bound thiocyanate in this system.

The acetate had a peculiar effect on the π-cation radical (Fig. 2c). Though the acetate does not contain a heavy atom, the g-value (2.0072) was much larger than

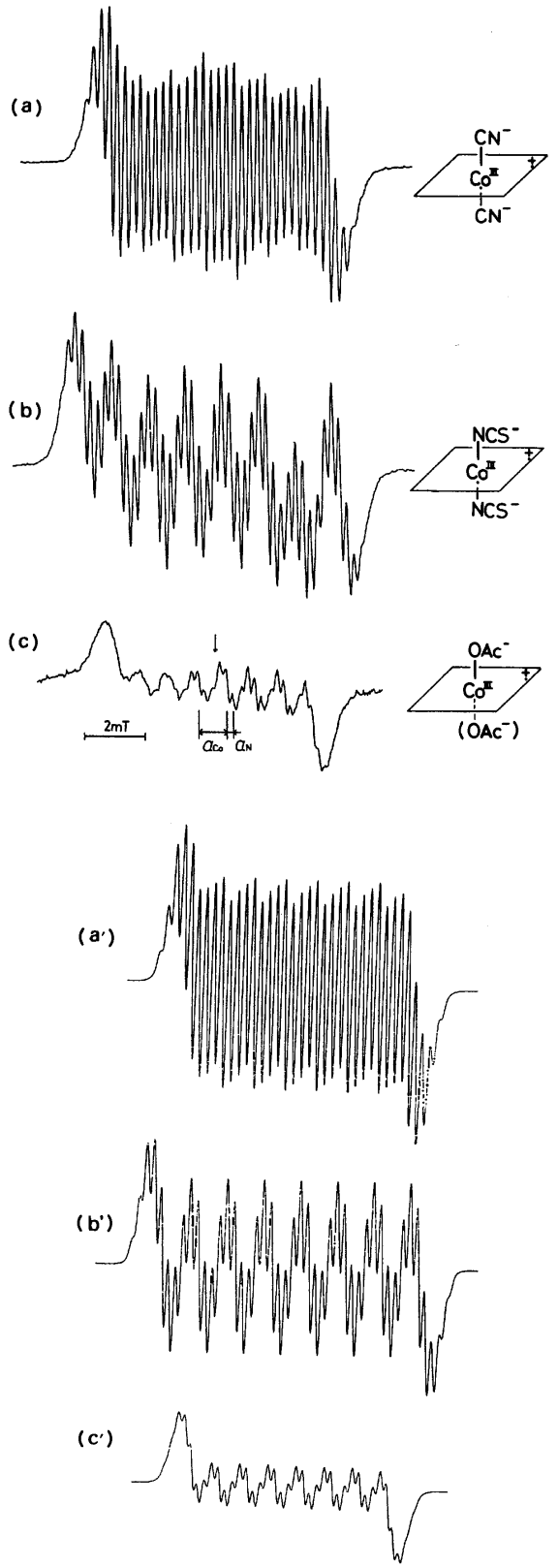

Fig. 2. The ESR spectra of [Co^{III}(tpp)] π-cation radical in the presence of strong ligands: a) DB18C6·KCN+$TBAPF_6$/DCM at −55 °C, b) DB18C6·KSCN+$TBAPF_6$/DCM at −65 °C, c) DB18C6·KOAc+$TBAPF_6$/DCM at −74 °C, a'), b'), c') The computer simulations of a), b), and c), respectively. The linewidths of these spectra depend on Co m_I, but this effect was not considered in these simulations.

that of free spin. It has been said that the assymmetric axial ligation causes a large g-value of the π-cation radical (2.0056) in the case of [Co^{III}(tpp)](py)Cl.[1] It is suggested that five-coordination or the up-and-down axial ligation by different ligands results in the displacement of the cobalt ion and the cobalt d orbital interacts with the singly-occupied a_{2u} π orbital. In the case of the acetate, the π-cation radical is likely to be five coordinate or coordinate two oxygen atoms of the acetate, causing the large g-value shift mentioned above.

The ESR spectrum of DB18C6·KCl+$TBAPF_6$/DCM system was identical with that of TBACl/DCM system. This result shows that the use of DB18C6 does not affect the ESR spectra.

The Effect of Various Solvents in the Presence of Weak-ligand Anions. We also examined in detail the effects of other solvents, using the electrolytes comprised by BF_4^-, ClO_4^-, PF_6^-, and NO_3^-. As in the case of DCM or DBM, the ESR spectra did not depend on the coexisting anions. No hfs in the ESR spectra were observed except for the case of PCN. But the g-value and ΔH_{pp} proved to be a good measure of the ligation state of the π-cation radical. As shown in Table 1, the g-values are different depending on the solvent, and are larger than 2.003, that is, the value in DCM or DBM. Thus it is concluded that the π-cation radical coordinates these solvents in the presence of weak-ligand anions.

Solvent Effects in the Presence of Halogen Anions and Strong-ligating Anions. Since the halogen anions are nucleophiles and so the π-cation radical is subject to undergo reaction with them, the ESR spectra were observed only in a few cases. In TBACl/PCN reported previously,[1] the ESR spectrum was almost the same as in TBACl/DCM, indicating that the chloride also is bound to the π-cation radical and the solvent had only a slight effect. On the other hand, the ESR spectra in EtOH did not change between the halogen anions and weak-ligand anions. This indicates that in EtOH the π-cation radical does not coordinate the halogen anions but EtOH. In both nitriles and EtOH, such anions as CN^-, SCN^-, AcO^- gave almost the same ESR spectra as in DCM, showing that the π-cation radical coordinates these anions.

In the mixed solvent of TFA and TFAA, Co^{II}(tpp) was autoxidized into its π-cation radical. The ESR spectrum was easily observed with a large g-value (2.0050), which might be due to the effect of CF_3COO^- ligation as in the case of AcO^-. The ESR spectrum was not changed by the addition of the weak-ligand anions or the halogen anions. But the addition of SCN^- or CN^- gave the superimposed spectra of three species, the ΔH_{pp} of which were 8 mT, 4 mT, and 1.5 mT. The corresponding species could be assigned as the π-cation radical binding SCN^- or CN^-, that binding CF_3COO^-, and that without the cobalt ion, respectively. Therefore, the coordinating ability of this solvent

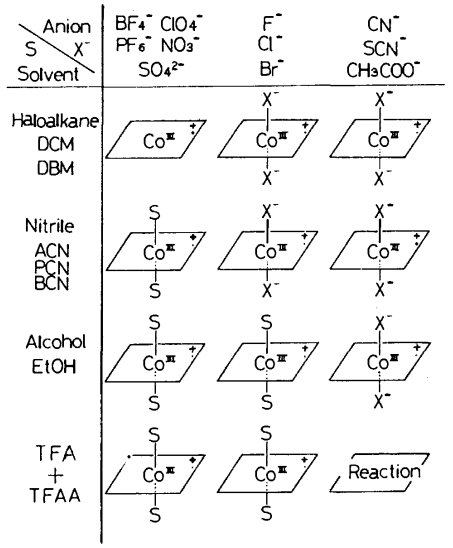

Fig. 3. A diagram for the structure of [Co^{III}(tpp)] π-cation radical in various solvents and in the presence of various anions. X^- and S denote coexisting anion and solvent, respectively.

competes with that of SCN^- or CN^-. Consequently, the order of coordinating ability to the π-cation radical is; BF_4^-, ClO_4^-, PF_6^-, NO_3^-, SO_4^{2-}<nitriles<halogen anions<EtOH<CF_3COO^-, AcO^-, SCN^-, CN^-.

As described in the above sections, the states of axial ligation of the π-cation radical in various solvents and in the presence of various anions are clarified by the change of the ESR spectra. The results are summarized in Fig. 3. The π-cation radical coordinates the anion and solvent according to the order of coordinating ability,well-known as the spectrochemical series.

Discussion

The Axial-ligand Effect on the Electronic State of the π-Cation Radical. As assigned first by the PPP-SCF MO calculation,[12] the singly-occupied molecular orbitals (SOMO) of the two-electron oxidation products of cobalt porphyrins are a_{1u} or a_{2u} π orbital in D_{4h} symmetry, not the 3d orbital of the cobalt ion. This has been confirmed by the fact that their g-values are quite isotropic and near the free-spin value. It has been considered that the a_{1u} and a_{2u} orbitals of metalloporphyrins are nearly degenerate.[13] Indeed, in the case of Co(oep) and Co(etioporphyrin) π-cation radicals, the order of the a_{1u} and a_{2u} π orbitals changes depending on the counter ion: In the presence of weak-ligand anions or F^-, the a_{2u} orbital is the SOMO, while a_{1u} for Br^-.[14] The nature of SOMO can be directly determined by the observation of nitrogen hfs, since the a_{2u} orbital has large spin densities on the nitrogen nuclei, but the a_{1u} has nodes on them. As shown in Table 1, the nitrogen hfs of the order of 0.2 mT was observed regardless of the nature of the ligands. Thus it is concluded that the SOMO is always the a_{2u} orbital different from the oep or etioporphyrin cases. It is noteworthy that the nitrogen hfs is increased by axial ligation.

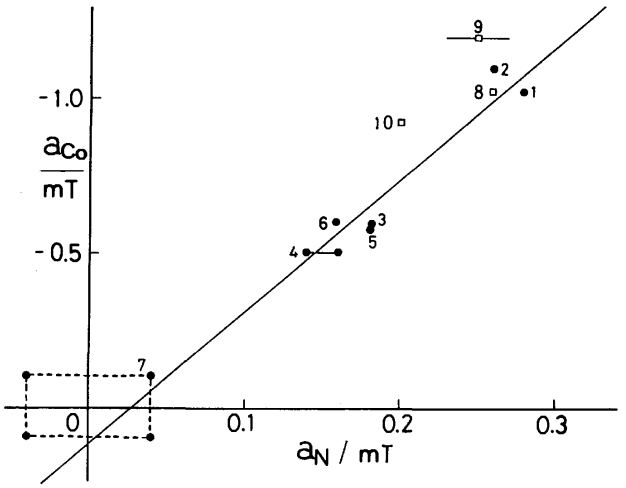

Fig. 4. A correlation between a_{Co} and a_N of some Co(III) porphyrin π-cation radicals; 1: [Co^{III}(tpp)]-Cl_2 (in DCM), 2: [Co^{III}(tpp)]Cl_2 (in PCN), 3: [Co^{III}-(tpp)]$(BF_4)_2$ (in DCM), 4: [Co^{III}(tpp)]$(ClO_4)_2$ (in DCM), 5: [Co^{III}(tpp)]$(ClO_4)_2$ (in BCN), 6: [Co^{III}(pr)$_4$p]-$(ClO_4)_2$ (in BCN), 7: [Co^{III}(oep)]$(ClO_4)_2$ (in DCM), 8: [Co^{III}(tpp)]$(CN)_2$ (in DCM), 9: [Co^{III}(tpp)]$(SCN)_2$ (in DCM), 10: [Co^{III}(tpp)]$(OAc)_2$ (in DCM). This figure is composed by the addition of strong ligand cases (□: 8—10) to Fig. 4. in Ref. 1.

The ESR spectra of the π-cation radical exhibit the ^{59}Co hfs (a_{Co}=0.5—1.2 mT), which indicates that there is a small spin density on the central cobalt ion (at most 0.9%). In D_{4h} symmetry a_{2u} orbital and cobalt s and d orbital cannot overlap with each other. Thus it is necessary to consider a mechanism to interpret the ^{59}Co hfs.

It has been proposed that there is a linear relationship between a_N and ρ_N^π, represented by

$$a_N = Q_{N\text{-}Co}^{Co} \times \rho_N^\pi + \alpha \quad (1)$$

where $Q_{N\text{-}Co}^{Co}$ is a proportionality constant and ρ_N^π is the π-electron spin density on the nitrogen nuclei. The first term represents the contribution from the spin polarization of the σ-electrons in the Co-N bonds by the π-electron spin density on the nitrogen nuclei. The second term means the contribution from the direct overlap between the a_{2u} orbital and the cobalt orbitals. Figure 4 shows a correlation between a_{Co} and a_N listed in Table 1, in addition to those reported previously.[1] The validity of Eq. 1 is further confirmed by the present study. It is seen that α in Eq. 1 is small. Therefore, a_{Co} is mainly produced by the spin polarization mechanism. But when the π-cation coordinates SCN^- or AcO^-, there seems to be a slight deviation from the liner relationship, which is probably caused by the overlap between the p orbital of axial ligands and the a_{2u}.

The CNDO/2 Calculations. In order to explain the observed results, we have made CNDO/2 MO calculations[19] extended to treat metal ions. The parameters used in these calculations are listed in Table 2.

Table 2. The CNDO/2 parameters

Atom		H	C	N	F	Cl	Co
$\zeta^{a)}$	s	1.2	1.6083	1.9237	2.5638	2.033	1.423
	p		1.5679	1.9170	2.5500	2.033	1.423
	d						2.830
	Ref.	14	15	15	15	15	16
$(I_p+A_p)/2$(eV)$^{b)}$	s	7.176	14.051	19.316	32.272	21.591	4.176
	p		5.572	7.275	11.180	8.708	1.160
	d						5.839
$-\beta_A^\circ$ (eV)$^{c)}$	s	9	21	25	39	22.33	17.1
	p		21	25	39	22.33	4.76
	d						28.0

a) Basis set exponentials. b) The average potentials between ionization potential (I_p) and electron affinity(A_p) from Ref. 17. c)Bonding parameters from Refs. 15 and 18, Case III.

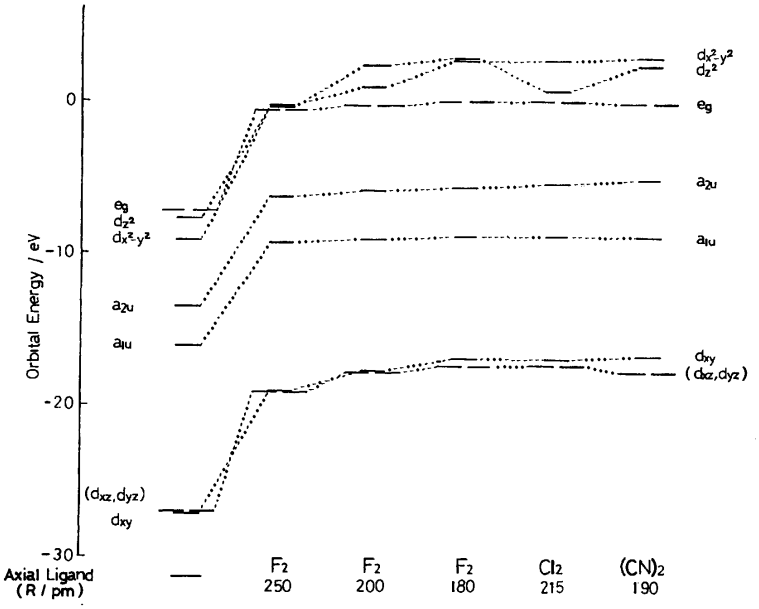

Fig. 5. Molecular orbital energy levels for $[Co^{III}(tmp)]X_2$ (X=F, Cl, CN). R denotes Co–X distance. The d orbitals in this figure denote those orbitals whose electron densities are distributed mainly on the Co 3d orbital (at least 60%). The other orbitals can be characterized as the tmp π orbital.

The geometry of the porphyrin skeleton was obtained from a crystallographic study of $[Co^{II}(tpp)]$ S_4 symmetry.[20] The phenyl groups were replaced with methyl groups for simplifying the calculations. The geometries of the methyl groups were estimated from covalent radii and angles as well as those of hydrogen atoms attached to the pyrrole rings. From the ESR investigations of the π-cation radical of 5,10,15,20-tetraphenylporphyrinatozinc(II), Zn^{II}(tmp), the property of its SOMO has been known to be almost the same as that of Zn^{II}(tpp) π-cation radical.[13,21] Then the tmp skeleton was used instead of the tpp skeleton in our calculations. The axial ligands (F^-, Cl^-, and CN^-) were also placed on both sides of the tmp plane keeping the axial symmetry. The fluoride was placed at the distances of 250, 200, and 180 pm from the cobalt ion. From this one can estimate the effects of axial ligand field on the π-cation radical as a function of distance. The effects of the chloride and cyanide were also examined by taking their distances from the cobalt ion as 215 and 190 pm, respectively, which were obtained from the crystal structure studies (116 pm for C–N distance).[22,23] The order of the ligand field strength is $F^- < Cl^- \ll CN^-$. The π-cation radical free from axial ligation ($[Co^{III}(tpp)]^{2+}\cdot$) was also calculated for comparison.

The calculation was carried out under S_4 symmetry. Figure 5 shows the calculated energy levels. Other results are listed in Table 3. Strictly speaking, the notations of a_{1u}, a_{2u}, and e_g orbitals are only appropriate in D_{4h} symmetry, but they are also used here conventionally. The SOMO is always the a_{2u} π orbital in agreement with the ESR observations mentioned above. The energy difference between the a_N and a_{Co} orbitals is quite large in each case compared with the energy shift due to the axial ligand, which makes the a_{2u} always SOMO. Both orbitals grow slightly more unstable with the strength of the axial ligand field, the extent of which is slightly larger for a_{2u} than for a_{1u}. In Co(oep) and Co(etioporphyrin), both π orbitals are energetically

TABLE 3. THE RESULTS OF CNDO/2 CALCULATIONS

X[a]			—	F	F	F	Cl	CN
R[b]/pm			—	250	200	180	215	190
ρ[c]	Co	$3d_{x^2-y^2}$	0.83	0.28	0.25	0.12	0.12	0.08
		$3d_{z^2}$	0.01	0.01	0.02	0.03	0.03	0.03
		$4p_z$	5.43	0.01	0.16	0.41	0.00	0.44
	N	$2p_z$	4.97	7.24	8.41	8.88	9.61	9.92
	C_{meso}	$2p_z$	10.18	8.58	9.92	10.30	10.05	8.88
	C_α	$2p_z$	0.84	0.31	0.33	0.30	0.22	0.21
	X[a]	2s	—	0.03	0.07	0.12	0.10	1.08,[e] 0.01[f]
		$2p_z$	—	9.80	3.72	1.99	2.34	2.69,[e] 0.88[f]
a_N[d]/mT			0.138	0.201	0.233	0.247	0.267	0.276
Net Charge	Co		+0.915	+0.905	+0.909	+0.947	+0.529	+0.589
	X[a]		—	−0.613	−0.584	−0.531	−0.341	−0.354

a) Axial ligand. b) The distance between the Co and axial ligand. c) Electron spin density. d) See Text. e) For C. f) For N.

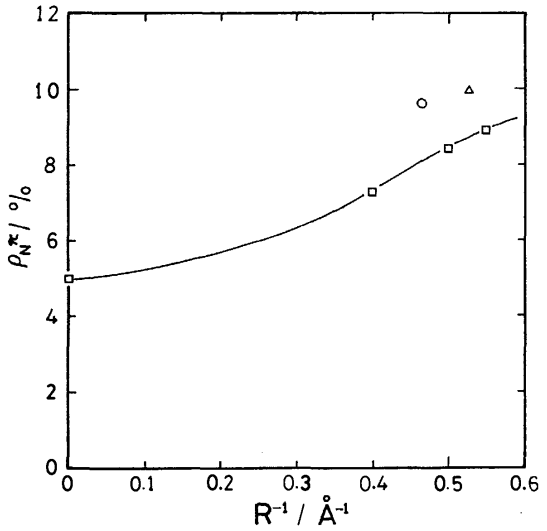

Fig. 6. A correlation between the spin density on the nitrogen nuclei (ρ_N^π) and Co–X distance (R) of $[Co^{III}(tmp)]X_2$ π-cation radical (X: axial ligand); □: $[Co^{III}(tmp)]F_2$, ○: $[Co^{III}(tmp)]Cl_2$, △: $[Co^{III}(tmp)](CN)_2$. The point at $R^{-1}=0$ denotes $[Co^{III}(tmp)]^{2+\cdot}$ π-cation radical free from axial ligation.

very close to each other and so small energy difference shift due to the change of axial ligand field causes the alternation of their SOMO. It is also noted that the energy of Co; $3d_{z^2}$ orbital is strongly affected by the axial ligation, which is consistent with the prediction by the conventional crystal field theory for D_{4h} symmetry.

The spin density on the a_{2u} SOMO is mainly distributed on the nitrogen $2p_z$ orbitals and the carbon $2p_z$ orbitals at the meso positions as expected. Figure 6 shows the relation between the spin density on the nitrogen π orbitals (ρ_N^π) and the distance between the cobalt ion and the axial ligands (R). From the points for $[Co^{III}(tmp)]^{2+\cdot}$ and $[Co^{III}(tmp)]F_2$, one can recognize that ρ_N^π becomes larger as the fluoride approaches the cobalt ion and reaches the value about twice as large as that of $[Co^{III}(tmp)]^{2+\cdot}$. This is in good agreement with the experimentally observed trend that by the axial ligation a_N increased from 0.18 mT for the weak-ligand anions to 0.28 mT for Cl^-. The change from F^- to Cl^- and CN^- gives further small increment for ρ_N^π. Thus it is concluded that the ligand field strength plays the principal role in increasing ρ_N^π.

The a_N's listed in Table 3 are calculated using the McConnell-type equation: $a_N=Q^N_{N(C2H)}\rho_N^\pi$, where $Q^N_{N(C2H)}$ has the value of 2.78 mT, applicable to a nitrogen bonded to two carbon atoms and a proton.[24] The calculated a_N for Cl^- or CN^- is in good agreement with the observed value. The a_N for a weak-ligand anion has the intermediate value between $[Co^{III}(tmp)]^{2+\cdot}$ and $[Co^{III}(tmp)]F_2$ (R=180 pm) and so it is suggested that the weak-ligand anion exists in the vicinity of the cobalt ion, having an electrostatic effect on the a_{2u} SOMO.

The orbitals of the axial ligands directly overlap with a_{2u} SOMO, producing the hfs of the axial ligands. The calculated spin densities on the axial ligands have the value compatible with the observed hfs but the large ambiguity of the Q-value for F or Cl prevents us from making a quantitative discussion.

The cobalt $4p_z$ orbital can mix with the SOMO. The lowering symmetry enables the cobalt $3d_{x^2-y^2}$ and $3d_{xy}$ to mix with the SOMO. In $[Co^{III}(tmp)]^{2+\cdot}$, the spin density on the cobalt $4p_z$ orbital is calculated to be large because of this mixing. However, even in the presence of weak-ligand anions, their electrostatic effects reduce this direct overlap between the cobalt orbitals and the SOMO. In fact, when the π-cation radical coordinates anions, these cobalt orbitals carry only at most 0.4% of spin density and cannot contribute so much to the ^{59}Co hfs. Therefore, as mentioned in the previous part, the ^{59}Co hfs is produced mainly by ρ_N^π through the spin polarization mechanism.

The authors are grateful to Dr. Hisayoshi Kobayashi of Kyoto Prefectural University for supplying them the program of CNDO MO calculation. They also express their thanks to the Data Processing Center of Kyoto University for the use of FACOM M-200 computer.

References

1) Part 1: H. Ohya-Nishiguchi, M. Kohno, and K. Yamamoto, *Bull. Chem. Soc. Jpn.*, **54**, 1923 (1981).

2) D. G. Davis, "Electrochemistry of Porphyrins," in "The Porphyrins," ed by Dolphin, Academic Press Inc.,

New York (1978),Vol. 5, p. 127.

3) An interesting note with regard to horseradish peroxidase was reported: G. H. Loew and Z. S. Harman, *J. Am. Chem. Soc.*, **102**, 6173 (1980).

4) a) K. Yamamoto, J. Uzawa, and T. Chijimatsu, *Chem. Lett.*, **1979**, 89; b) K. Yamamoto, M. Kohno, and H. Ohya-Nishiguchi, *ibid.*, **1981**, 255.

5) W. D. Hewson and L. P. Hager, "Peroxidases, Catalases, and Chloroperoxidase," in "The Porphyrins," ed by Dolphin, Academic Press Inc., New York (1978), Vol. 7, p. 295.

6) K. Yamamoto and S. Tonomura. *Sci. Papers Inst. Phys. Chem. Res.*, **58**, 122 (1964).

7) K. Yamamoto. *Sci. Papers Inst. Phys. Chem. Res.*, **70**, 71 (1976).

8) a) E. C. Johnson. T. Niem. and D. Dolphin, *Can. J. Chem.*, **56**, 1381 (1978); b) N. L. Cox, C. A. Kraus, and R. M. Fuoss, *Trans. Faraday Soc.*, **31**, 749 (1935); c) E. J. Corey and A. Venkateswarlu, *J. Am. Chem. Soc.*, **94**, 6190 (1972).

9) C. J. Pedersen, *J. Am. Chem. Soc.*, **89**, 7017 (1967).

10) The DB18C6·KX complexes did not act well as supporting electrolyte.

11) The ΔH_{pp} is given by $\Delta H_{pp}=7a_{Co}+\Delta H$, where ΔH is the linewidth, ΔH_{pp} is used as a measure of a_{Co}, when a_{Co} is unresolved.

12) C. Weiss, H. Kobayashi, and M. Gouterman, *J. Mol. Spectrosc.*, **19**, 415 (1965).

13) J. Fajer and M. S. Davis, "Electron Spin Resonance of Porphyrin Cations and Anions," in "The Porphyrins," ed by Dolphin, Academic Press Inc., New York (1978), Vol. 4, p. 197.

14) D. Dolphin. A. Forman, D. C. Borg, J. Fajer. and R. H. Felton, *Proc. Nat. Acad. Sci. U. S. A.*, **68**, 614 (1971).

15) E. Clementi and D. L. Raimondi, *J. Chem. Phys.*, **38**, 2686 (1963).

16) M. Zerner and M. Gouterman, *Theor. Chim. Acta*, **4**, 44 (1966).

17) D. W. Clark, N. S. Hush, and J. R. Yandle, *J. Chem. Phys.*, **57**, 3503 (1972).

18) E. Kai and K. Nishimoto, *Int. J. Quantum. Chem.*, **18**, 403 (1980).

19) J. A. Pople and D. L. Beveridge, "Approximate Molecular Orbital Theory," McGraw-Hill, New York (1970), p. 57.

20) P. Madura and W. R. Scheidt, *Inorg. Chem.*, **15**, 3182 (1976).

21) J. Fajer, D. C. Borg, A. Forman, A. D. Adler, and V. Valedi. *J. Am. Chem. Soc.*, **96**, 1238 (1974).

22) T. Sakurai, K. Yamamoto, H. Naito, and N. Nakamoto, *Bull. Chem. Soc. Jpn.*, **49**, 3042 (1976).

23) A. Wolberg, *Acta Crystallogr., Sect. B*, **25**, 161 (1969).

24) J. R. Bolton, "Electron Spin Density," in "Radical Ions," ed by E. T. Kaiser and L. Kevan, John Wiley & Sons, New York. London. Sydney, (1968), p. 1.

 © 1985 The Chemical Society of Japan Bull. Chem. Soc. Jpn., 58, 631—633 (1985)

DNA Sequence and Intramolecular Evolutionary Tree of Calmodulin Gene. Application of Maximum Likelihood Method

Yôichi IIDA

Department of Chemistry, Faculty of Science, Hokkaido University, Sapporo 060

(Received September 19, 1984)

DNA sequences of calmodulin genes taken from chicken and electric eel were examined to investigate the molecular evolution of its protein. One notable feature of the amino acid coding region of the gene is that it can be subdivided into four domains having a similar amino acid sequence. In the present paper, an intramolecular evolutionary tree was constructed with the DNA sequences of the four domains.

Origin and evolution of protein is one of the most important problems in biology and biochemistry. In previous papers,[1-4] we studied the molecular evolution of calmodulin (CaM), one of the calcium-binding proteins. It has four calcium-binding sites, and interacts reversibly with Ca^{2+} to form a calmodulin-Ca^{2+} complex.[5] CaM plays an important role in regulating various enzymatic reactions or cellular processes. It contains 148 amino acids and has a trimethylated lysine at position 115. One notable feature of CaM is that it is widely distributed throughout eukaryotes and that the primary amino acid sequence is highly conservative against evolution. Another interesting feature is that the primary structure of CaM has internal homology, that is, it can be subdivided into four domains having a similar amino acid sequence. It is also found that the amino acid sequence homology is greatest when the first domain (residues 8 to 40) is aligned with the third (residues 81 to 113), and the second domain (residues 44 to 76) is aligned with the fourth (residues 117 to 148). In order to explain this fact, a two-step intragenic duplication model was proposed to the primary amino acid sequence of CaM.[2] In this model, it is assumed that an ancestral one-domain quarter-calmodulin (AQ) underwent an elongation by the first intragenic duplication, which resulted in an ancestral two-domain half-calmodulin (AH). In the period from the birth of AH to the next intragenic duplication (stage 1 in Fig. 4 of Ref. 2), AH underwent evolutionary changes and some replacements of amino acids occurred in it. At the end of stage 1, the second intragenic duplication took place, resulting in an ancestral four-domain calmodulin (AC). In the period from the birth of AC to the present time (stage 2 in Fig. 4 of Ref. 2), AC underwent further evolution and some replacements of amino acids took place.

DNA Sequence of Calmodulin Gene

Previously, using the data on the primary amino acid sequences, we attempted to confirm the above two-step intragenic duplication model.[3] Using the common ancestor method together with the maximum parsimony technique, we constructed an intramolecular evolutionary tree of the four domains of CaM. At that time, however, only the primary amino acid sequences were available for such purposes, and the observed difference of amino acid residues of CaM between the domains was attributed to the difference of nucleotides between the corresponding codons. Referring to "the genetic code," we assumed that the difference of amino acids was given by the least number of nucleotide substitutions of the codons.

Recently, Lagáce *et al.* isolated m RNA of CaM from the electroplax of electric eel (*Electrophorus electricus*), and its cDNA (DNA complementary to m RNA) has been cloned and sequenced.[6] Moreover, Putkey *et al.* isolated the m RNA from chicken brain and determined the primary nucleotide sequence of its cDNA.[7] For the two biological species, the nucleotide sequences of the amino acid coding regions were aligned and compared in Fig. 1 of Ref. 4. Comparison of the corresponding codons revealed that the situation is more complex than has been expected, that is, the difference of the corresponding codons was not always given by the least number of nucleotide substitutions of codons. Corrections for multiple and revertant changes at homologous sites appear to be important to estimate the evolutionary distances between homologous sequences. It is also found that nucleotide substitutions have occurred most frequently at the third positions of codons and that those substitutions are synonymous with respect to the kinds of the amino acid residues. The synonymous nucleotide substitutions have also occurred at the first positions of codons; such mutations are only allowed in the leucine and arginine residues.

In view of these results, we should examine whether the actual DNA sequences of CaM gene may lead to the same intramolecular evolutionary tree as was given previously by the primary amino acid sequences or not. This was done with the cDNA sequences of the chicken and eel CaM genes. In Fig. 1, we show the nucleotide sequences of the four domains of the genes. For each of the biological species, we construct an intramolecular evolutionary tree of the four domains by using "maximum likelihood method."

Intramolecular Evolutionary Tree and Maximum Likelihood Approach

In order to construct an evolutionary tree in terms of DNA sequence data, several approaches are known, such as maximum parsimony method to estimate the

c DNA Sequence of Chicken Calmodulin

Domain 1	CAG ATT GCA GAA TTC AAA GAA GCT TTT TCA CTA TTT GAC AAG GAT GGT
	GAT GGT ACT ATA ACT ACA AAG GAG TTG GGG ACT GTG ATG AGA TCA CTT
Domain 2	ACA GAA GCA GAA TTA CAG GAC ATG ATC AAT GAA GTA GAC GCT GAT GGC
	AAT GGC ACA ATT GAC TTC CCA GAG TTT CTG ACA ATG ATG GCA AGA AAA
Domain 3	AGC GAA GAA GAA ATT AGA GAA GCG TTC CGT GTG TTT GAC AAG GAT GGT
	AAT GGT TAC ATT AGT GCT GCA GAA CTT CGT CAT GTG ATG ACA AAT CTT
Domain 4	ACA GAT GAA GAA GTT GAT GAA ATG ATT AGG GAA GCA GAC ATT GAT GGT
	GAT GGT CAA GTA AAC TAT GAA GAG TTT GTA CAG ATG ATG ACA GCG AAG

c DNA Sequence of Electric-Eel Calmodulin

Domain 1	CAG ATT GCT GAG TTC AAG GAG GCG TTT TCC CTC TTT GAC AAA GAT GGT
	GAC GGC ACC ATC ACC ACC AAA GAG CTG GGT ACT GTG ATG CGC TCT CTG
Domain 2	ACC GAG GCA GAG CTG CAG GAC ATG ATC AAT GAA GTG GAT GCT GAC GGC
	AAT GGA ACA ATA GAC TTC CCG GAG TTC CTG ACC ATG ATG GCC AAG AAA
Domain 3	AGT GAA GAA GAG ATC CGA GAA GCC TTC CGA GTT TTT GAC AAG GAC GGT
	AAT GGC TAC ATC AGT GCA GCC GAG TTG CGA CAT GTC ATG ACT AAC TTG
Domain 4	ACG GAC GAG GAG GTG GAT GAG ATG ATC CGA GAG GCC GAC ATC GAT GGC
	GAC GGC CAG GTG AAC TAT GAA GAG TTC GTG CAA ATG ATG ACT GCA AAG

Fig. 1. The nucleotide sequences of the four domains of the calmodulin (CaM) genes of chicken and eel. For each domain, 96 nucleotides were taken from the c DNA sequence data. See the text and Refs. 6 and 7.

common ancestor sequence and matrix method to estimate pairwise similarity of the sequences.[8] However, most data on DNA sequences involve moderate to large amount of change, such as multiple and revertant changes. In such cases, the maximum parsimony method may fail to construct a correct evolutionary tree, because this method does not take into consideration such probabilistic process of multiple and revertant changes. On the other hand, the matrix method has a difficulty in that it does not make full use of the information available in the original sequences. It has been also pointed out that simple clustering technique based on pairwise similarities can give inconsistent estimates of an evolutionary tree if rates of evolution are sufficiently unequal in different lineages.[9] A third approach invloves method which tries to avoid the above difficulties and to make explicit and efficient use of all of the sequence data by formulating a probabilistic or statistical model of evolution. As such an attempt, Felsenstein proposed an algorithm to evaluate the likelihood of an evolutionary tree.[8] The likelihood of the tree is defined by the product of the probabilities of change in each tree segment, times the prior probability of the ancestral state. The most probable evolutionary tree can be obtained by maximizing such a likelihood value. A computer program was written for the maximum likelihood method.

This method was then applied to our case of CaM genes. We took nucleotide sequence data of the four domains, as shown in Fig. 1. Each domain is composed of 96 nucleotides, which correspond to 32 amino acid residues. For each of the chicken and eel CaM genes, the result computed by the maximum likelihood method shows that the evolutionary tree given by Fig. 2 is the most probable. The maximum likelihood value,

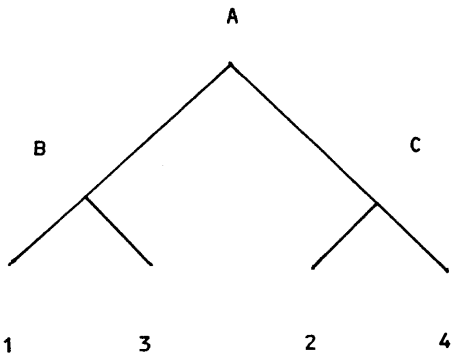

Fig. 2. The intramolecular evolutionary tree of the four domains of the chicken or eel calmodulin (CaM) gene estimated by the maximum likelihood method. This tree shows that the domains 1 and 3 diverged from the common ancestor B, while the domains 2 and 4, from the common ancestor C. B and C had diverged from the common ancestor A.

log likelihood, is calculated as -450.00 in the case of chicken, while it is -477.53 in the case of eel. Figure 2 shows that the domains 1 and 3 came from the common ancestor of B, and the domains 2 and 4, from the common ancestor of C. The common ancestors, B and C, had diverged from the common ancestor A. The evolutionary tree estimated by the cDNA sequence data coincides well with that described previously by the maximum parsimony method together with the amino acid sequence data.[3] Our previous two-step intragenic duplication model is reconfirmed by the present evolutionary tree (for the reason, refer to Ref. 3).

In Table 1, we show data on the optimal branch length, $\hat{p}$, in each tree segment of the evolutionary tree (Fig. 2), together with its 95% confidence limit value. In each of the biological species, the nucleotide sequence of the domain 1 has longer branch length from the

TABLE 1. DATA ON THE OPTIMAL BRANCH LENGTH, $\hat{p}$, IN EACH TREE SEGMENT OF THE EVOLUTIONARY TREE OF THE FOUR DOMAINS, TOGETHER WITH ITS 95% CONFIDENCE LIMIT VALUE

From	To	Chicken			Electric Eel		
		$\hat{p}$	95% Confidence Limits		$\hat{p}$	95% Confidence Limits	
Domain 1	B	0.4080	(0.2518,	0.5642)	0.4824	(0.3086,	0.6561)
B	Domain 3	0.2247	(0.0591,	0.3904)	0.3047	(0.1103,	0.4991)
B	C	0.3736	(0.2069,	0.5403)	0.3884	(0.1936,	0.5831)
Domain 2	C	0.3539	(0.2034,	0.5044)	0.4627	(0.2958,	0.6296)
C	Domain 4	0.2065	(0.0492,	0.3638)	0.2585	(0.0654,	0.4515)

For the nucleotide sequences of the four domains of chicken or eel calmodulin (CaM) gene, the evolutionary tree is given by Fig. 2.

common ancestor of B than does that of the domain 3. Similarly, the sequence of the domain 2 has longer branch from the common ancestor of C than does that of the domain 4. The distance between any two domains can be calculated by adding the $\hat{p}$ value of each tree path. It is found that distances between domains have appreciably large values of $\hat{p}$, that is, the sum of $\hat{p}$'s is always greater than 1/2. A reason for this is that nucleotides at the third positions of codons have changed considerably.[4] In spite of this, the distance between the domains 1 and 3 or between the domains 2 and 4 is nearest in both of the chicken and eel genes. The $\hat{p}$ data of Table 1 will be valuable for further discussion on the molecular evolution of CaM gene.

We wish to thank Dr. J. Felsenstein for showing us his computer programs.

References

1) Y. Iida, *Bull. Chem. Soc. Jpn.*, **55**, 2683 (1982).
2) Y. Iida, *J. Mol. Biology*, **159**, 167 (1982).
3) Y. Iida, *Bull. Chem. Soc. Jpn.*, **57**, 2665 (1984).
4) Y. Iida, *Bull. Chem. Soc. Jpn.*, **57**, 2667 (1984).
5) See, for example, "Calcium Binding Proteins and Calcium Function," ed by R. H. Wasserman *et al.*, North Holland, New York (1977).
6) L. Lagáce, T. Chandra, S. L. C. Woo and A. R. Means, *J. Biol. Chem.*, **258**, 1684 (1983).
7) J. A. Putkey, K. F. Ts'ui, T. Tanaka, L. Lagáce, J. P. Stein, E. C. Lai and A. R. Means, *J. Biol. Chem.*, **258**, 11864 (1983).
8) J. Felsenstein, *J. Mol. Evol.*, **17**, 368 (1981).
9) D. H. Colless, *Syst. Zool.*, **16**, 289 (1970).

Solvent Effects on Chemical Reactivities II. Aromatic Substitution Reactions

Takayuki OHMAE
Department of Chemistry, Faculty of Science, Tohoku University, Sendai 980
(Received September 21, 1984)

The propagator method is applied to the study of solvent effects on reactivities of aromatic substitution reactions. We obtain the following set of results: (1) The influence of nonpolar solvent on electrophilic reactions is opposite to that on nucleophilic reactions; (2) the solvent which has the large dielectric constant weakens the directive power of a substituent group; (3) frontier orbitals control solvent effects on the chemical reactivities of aromatic substitution reactions.

Several theories have been proposed to explain experimental results of aromatic substitution reactions.[1-3] Fukui *et al.* have proposed the frontier electron theory.[4,5] Their theory was first introduced in discussing the orientation in electrophilic substitution reactions. Afterward, the theory has been applied not only to electrophilic, but also to radical and nucleophilic substitution reactions as well as addition reactions in conjugated molecules, showing its utility, through a satisfactory agreement of theory with experiment.[6,7]

In a previous work, we have successfully studied solvent effects on selectivities of pericyclic reactions using the propagator method.[8] In this paper, we investigate influences of nonpolar solvent on reactivities of aromatic substitution reactions.

Propagator

The reaction system in question is assumed to be well described by the following hamiltonian in the second quantized representation:[8]

$$\mathbf{H}_0 = \sum_s \alpha_s \mathrm{a}_s^\dagger \mathrm{a}_s + \sum_{s,t} \beta_{st} \mathrm{a}_s \mathrm{a}_t + \sum_q \mathrm{h}\omega \mathrm{b}_q^\dagger \mathrm{b}_q + \sum_q \sum_{s,t} (g_{st}^{q*} \mathrm{b}_q^\dagger + g_{st}^q \mathrm{b}_q) \mathrm{a}_s^\dagger \mathrm{a}_t, \quad (1)$$

where $\mathrm{a}_s^\dagger$ and a_s are respectively the creation and annihilation operators for the π-electron at the s th atom of a solute molecule, $\mathrm{b}_q^\dagger$ and b_q are the creation and annihilation operators for the phonon with mode q, respectively, α_s is the coulomb integral, β_{st} the resonance integral, ω the phonon energy and g_{st}^q the electron-phonon interaction constant. In this model, the solvent is replaced by a phonon gas and solvent-solute interaction by the electron-phonon interaction.[8,9] This model is realistic for nonpolar solvents.

The electron-phonon interaction constant is related with the dielectric constant, ε, of a solvent:

$$g_{st}^q \propto \left(\frac{1}{\varepsilon_\infty} - \frac{1}{\varepsilon}\right)^{1/2}, \quad (2)$$

where ε_∞ is the dielectric constant of the solvent measured at the optical mode.

The propagator, $\mathbf{G}^0(z) \equiv (z-\mathbf{H}_0)^{-1}$, which describes the electronic structure of the solute molecule interacting with solvents, is easily obtained with some approximations:[8,10]

$$\mathbf{G}^0(z) = [(z-\mathbf{h}) - \sum_q \boldsymbol{g}^{q*} n_q (z-\mathbf{h}+\omega)^{-1} \boldsymbol{g}^q - \sum_q \boldsymbol{g}^q (n_q+1)(z-\mathbf{h}-\omega)^{-1} \boldsymbol{g}^{q*}]^{-1}, \quad (3)$$

where

$$\mathbf{h} = \sum_s \alpha_s \mathrm{a}_s^\dagger \mathrm{a}_s + \sum_{s,t} \beta_{st} \mathrm{a}_s^\dagger \mathrm{a}_t. \quad (4)$$

Once the propagator is known we can obtain the eigenvalues and eigenvectors of $\mathbf{H}_0$.

Frontier Electron Density

Let us consider the frontier electron density:

$$f_r^{\mathrm{E}} \equiv \frac{1}{2\pi \mathbf{i}} \int_{\mathrm{H}} \mathrm{d}z \mathbf{G}_{rr}^0(z), \quad (5a)$$

$$f_r^{\mathrm{N}} \equiv \frac{1}{2\pi \mathbf{i}} \int_{\mathrm{L}} \mathrm{d}z \mathbf{G}_{rr}^0(z), \quad (5b)$$

where f_r^{E} and f_r^{N} are respectively the electron density of the highest occupied molecular orbital, HOMO, and the that of the lowest unoccupied molecular orbital, LUMO, and the contours H and L respectively enclose the poles ε_{H} and ε_{L} (see Fig. 1).

It is well known that the chemical reactivity is well correlated with the frontier electron density:[5] 1) in case of reactions with electrophilic reagents, that position having the higher density of HOMO is more susceptible to attack; 2) in case of reactions with nucleophilic reagents, that position having the higer density of LUMO is reactive.

Now, it is well known that the variation of solvent can change the rate and/or the reaction products. In case of aromatic substitution reactions, the variation of solvent changes the isomer ratio of products. In order to study this problem, it is sufficient for us to examine the solvent effects on the frontier electron density.

It is said that the interaction between the solute and the solvent is small, *i.e.*, $|g_{ij}^q| \ll 1$, in the aromatic substitution reaction.[12] Therefore, the propagator in Eq. 3 is well approximated as follows;

$$\mathbf{G}^0(z) \cong (z-\mathbf{h})^{-1} + (z-\mathbf{h})^{-1} \sum_q \boldsymbol{g}^{q*} n_q (z+\omega-\mathbf{h})^{-1} \boldsymbol{g}^q (z-\mathbf{h})^{-1} + (z-\mathbf{h})^{-1} \sum_q \boldsymbol{g}^q (n_q+1)(z-\omega-\mathbf{h})^{-1} \boldsymbol{g}^{q*} (z-\mathbf{h})^{-1}. \quad (6)$$

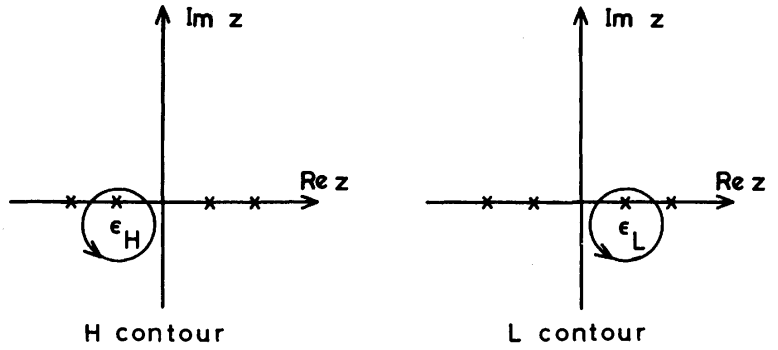

Fig. 1. Contours H and L.
ε_H is the energy of HOMO.
ε_L is the energy of LUMO.

Substituting Eq. 6 into Eqs. 5a and 5b, we obtain the frontier electron density including the solvent effect. For f_r^E,

$$
\begin{aligned}
f_r^E &\equiv \frac{1}{2\pi\mathbf{i}}\int_H dz G^0_{rr}(z) \\
&= \frac{1}{2\pi\mathbf{i}}\int_H dz \langle r|\{(z-\mathbf{h})^{-1} \\
&\quad + (z-\mathbf{h})^{-1}\sum_q \boldsymbol{g}^{q*} n_q (z-\mathbf{h}+\omega)^{-1}\boldsymbol{g}^q (z-\mathbf{h})^{-1} \\
&\quad + (z-\mathbf{h})^{-1}\sum_q \boldsymbol{g}^q (n_q+1)(z-\mathbf{h}-\omega)^{-1}\boldsymbol{g}^{q*}(z-\mathbf{h})^{-1}\}|r\rangle \\
&= f_r^{0E} + \sum_q\sum_{i,j} n_q |\langle r|i\rangle|^2 |g^q_{ij}|^2 \frac{1}{2\pi\mathbf{i}}\int_H dz \frac{1}{(z-\varepsilon_i)^2(z-\varepsilon_j+\omega)} \\
&\quad + \sum_q\sum_{i,j} (n_q+1)|\langle r|i\rangle|^2 |g^q_{ij}|^2 \frac{1}{2\pi\mathbf{i}}\int_H dz \frac{1}{(z-\varepsilon_i)^2(z-\varepsilon_j-\omega)} \\
&\cong f_r^{0E} + \sum_q n_q |\langle r|H\rangle|^2 |g^q_{HL}|^2 \frac{1}{2\pi\mathbf{i}}\int_H dz \frac{1}{(z-\varepsilon_H)^2(z-\varepsilon_L+\omega)} \\
&\quad + \sum_q n_q |\langle r|L\rangle|^2 |g^q_{HL}|^2 \frac{1}{2\pi\mathbf{i}}\int_H dz \frac{1}{(z-\varepsilon_L)^2(z-\varepsilon_H+\omega)} \\
&\quad + \sum_q (n_q+1)|\langle r|H\rangle|^2 |g^q_{HL}|^2 \frac{1}{2\pi\mathbf{i}}\int_H dz \frac{1}{(z-\varepsilon_H)^2(z-\varepsilon_L-\omega)} \\
&\quad + \sum_q (n_q+1)|\langle r|L\rangle|^2 |g^q_{HL}|^2 \frac{1}{2\pi\mathbf{i}}\int_H dz \frac{1}{(z-\varepsilon_L)^2(z-\varepsilon_H-\omega)} \\
&\cong f_r^{0E} + \sum_q (2n_q+)1 |g^q_{HL}|^2 \frac{f_r^{0N}-f_r^{0E}}{(\varepsilon_H-\varepsilon_L)^2}, \qquad (7)
\end{aligned}
$$

where we assume that the electron-phonon interaction constant has a dominant value between HOMO and LUMO. Moreover, we can approximate

$$\frac{1}{2\pi\mathbf{i}}\int_H dz \frac{1}{(z-\varepsilon_L)^2(z-\varepsilon_H+\omega)} \cong \frac{1}{(\varepsilon_H-\varepsilon_L)^2}, \qquad (8)$$

since $|\omega/\varepsilon| \ll 1$. Similarly f_r^N is obtained as

$$f_r^H \cong f_r^{0N} - \sum_q (2n_q+1)|g^q_{HL}|^2 \frac{f_r^{0N}-f_r^{0E}}{(\varepsilon_H-\varepsilon_L)^2} \qquad (9)$$

In Eqs. 7 and 9, f_r^{0E} f_r^{0N} are respectively the usual density of HOMO and LUMO.

It should be noted here that the sign of the second term of Eq. 7 is opposete to that of Eq. 9. This shows that the solvent effect on electrophilic reactions is opposite to that on nucleophilic reactions.

Solvent Effect Index

We define a solvent effect index, τ_r,

$$\tau_r \equiv \frac{f_r^{0N}-f_r^{0E}}{(\varepsilon_H-\varepsilon_L)^2}. \qquad (10)$$

In kindred reactions, the factors in Eqs. 7 and 9 which depend on the phonon mode q can be assumed to be of the same order. So the solvent effects on chemical reactivities are classified by the above index: in case of reactions with electrophilic reagent, that position having the large value of τ_r becomes susceptible to attack; in case of reactions with nucleophilic reagent, that position having the negative value of τ_r becomes more reactive.

The solvent effect indexes of several monosubstituted benzenoids (see Fig. 2) are listed in Table 1. Calcula-

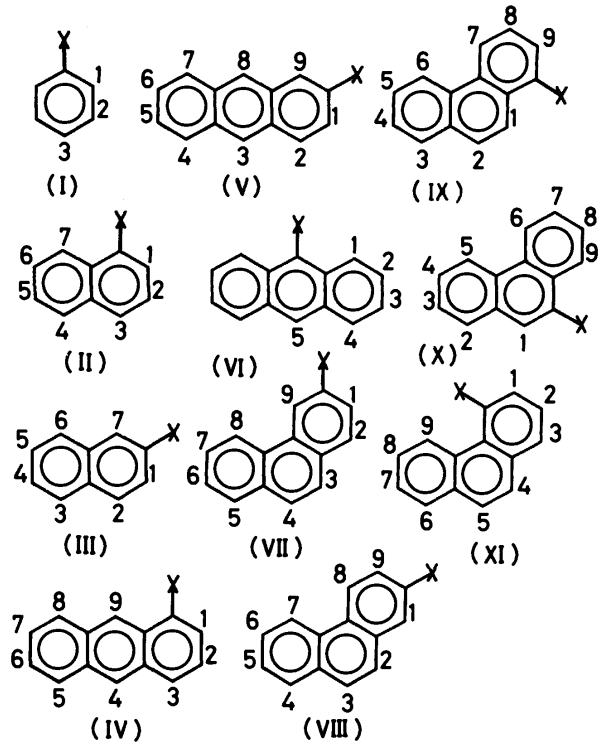

Fig. 2. Monosubstituted benzenoids.

tions are performed within the simple Hückel approximation. The parameters are taken from reference 2.

Table 1 shows the characteristic of the solvent effects on aromatic substitution reactions: 1) Substituent groups have a material effects; for example, at the sites 1 and 2 of molecule I with *ortho-*, *para*-directors, *e.g.*, OH, CH_3, Cl, and OCH_3, electrophilic reactions become favorable: on the contrary at the site 3 of molecule I with a *metha*-director, *e.g.*, NO_2, electrophilic reactions becomes favorable; this fact conclusively shows that solvent effects depend on the nature of the solute molecule only; 2) the stronger the directive power of *ortho-*, *para*-directors, the larger absolute value τ_r.

In conclusion, it should be noted that the solvent which has the large dielectric constant weakens the directive power of a substituent group. If we use the solvent which have the large dielectric constant, we can obtain the reaction products which are minor in the usual reaction conditions. For example, we can obtain the resolcinol using the substitution reaction of the

TABLE 1. SOLVENT EFFECT INDEXES OF MONOSUBSTITUTED BENZENOIDS

Molecule	Site X	OH	CH_3	Cl	OCH_3	NO_2
I	1	0.147	0.072	0.083	0.177	−0.037
	2	0.243	0.120	0.120	0.259	−0.145
	3	−0.121	−0.182	−0.157	−0.099	0.122
II	1	−0.215	−0.141	−0.054	−0.171	0.234
	2	0.113	0.035	0.019	0.123	−0.145
	3	−0.075	−0.133	−0.042	−0.010	0.035
	4	0.262	0.095	0.048	0.288	−0.318
	5	0.141	0.063	0.029	0.146	−0.164
	6	0.026	−0.013	−0.001	0.047	−0.047
	7	0.348	0.144	0.068	0.366	−0.416
III	1	0.171	0.115	0.059	0.164	−0.158
	2	0.296	0.038	0.026	0.326	−0.398
	3	0.325	0.063	0.038	0.350	−0.421
	4	−0.021	−0.051	−0.024	0.011	−0.014
	5	0.156	0.055	0.030	0.160	−0.185
	6	0.189	−0.005	0.003	0.234	−0.280
	7	−0.111	−0.122	−0.055	−0.026	0.056
IV	1	−0.443	−0.196	−0.088	−0.394	0.569
	2	0.099	0.016	0.009	0.112	−0.160
	3	−0.415	−0.229	−0.101	−0.343	0.478
	4	0.218	0.015	0.018	0.280	−0.376
	5	0.235	0.079	0.041	0.255	−0.333
	6	0.160	0.059	0.029	0.166	−0.218
	7	0.060	0.009	0.006	0.075	−0.099
	8	0.323	0.120	0.059	0.334	−0.438
	9	0.516	0.150	0.079	0.556	−0.755
V	1	0.237	0.062	0.054	0.237	−0.276
	2	0.205	0.009	0.010	0.205	−0.323
	3	0.500	0.046	0.046	0.500	−0.740
	4	0.272	0.031	0.031	0.272	−0.392
	5	0.026	−0.012	−0.009	0.026	−0.051
	6	0.150	0.021	0.019	0.150	−0.212
	7	0.164	0.004	0.007	0.164	−0.252
	8	0.126	−0.039	−0.027	0.126	−0.229
	9	−0.396	−0.101	−0.088	−0.396	0.568
VI	1	0.322	0.138	0.070	0.327	−0.399
	2	−0.104	−0.071	−0.030	−0.077	0.112
	3	0.177	0.083	0.041	0.179	−0.216
	4	0.075	0.010	0.011	0.101	−0.103
	5	−0.412	−0.289	−0.116	−0.307	0.450
VII	1	−0.053	0.012	0.004	−0.055	0.094
	2	0.187	0.034	0.022	0.217	−0.260
	3	0.327	0.090	0.052	0.363	−0.426
	4	0.116	−0.028	−0.006	0.174	−0.205
	5	0.169	0.032	0.022	0.198	−0.232
	6	0.002	−0.001	−0.001	0.002	−0.004
	7	0.144	0.030	0.019	0.168	−0.196
	8	0.101	0.026	0.016	0.114	−0.132
	9	−0.197	−0.090	−0.043	−0.164	0.225

Table 1. Continued

	1	−0.091	−0.057	−0.026	−0.030	0.069
	2	0.287	−0.019	−0.009	0.317	−0.384
	3	0.342	0.018	0.008	0.362	−0.439
	4	0.232	0.025	0.012	0.246	−0.298
VIII	5	−0.048	0.003	0.002	−0.037	0.042
	6	0.191	0.001	0.000	0.205	−0.249
	7	0.069	0.028	0.014	0.083	−0.100
	8	0.064	−0.025	−0.012	0.082	−0.111
	9	0.112	0.029	0.014	0.130	−0.129
	1	0.265	0.042	0.038	0.286	−0.083
	2	0.178	0.023	0.024	0.209	−0.265
	3	0.242	0.105	0.058	0.242	−0.303
	4	0.021	0.015	0.004	0.016	−0.018
IX	5	0.145	0.033	0.026	0.157	0.203
	6	0.185	0.109	0.053	0.170	−0.209
	7	−0.250	−0.165	−0.084	−0.196	0.271
	8	0.163	0.035	0.026	0.173	−0.231
	9	−0.198	−0.054	−0.035	−0.177	0.274
	1	−0.199	−0.146	−0.062	−0.124	0.199
	2	0.104	0.021	0.014	0.126	−0.138
	3	0.018	0.013	0.003	0.014	−0.014
	4	0.021	−0.030	−0.007	0.053	−0.059
X	5	0.150	0.072	0.032	0.144	−0.167
	6	0.033	−0.012	0.002	0.051	−0.064
	7	0.210	0.081	0.045	0.218	−0.258
	8	−0.024	−0.011	−0.007	−0.023	0.032
	9	0.162	0.025	0.027	0.190	−0.237
	1	−0.117	−0.089	−0.042	−0.067	0.111
	2	−0.023	−0.024	−0.013	−0.017	0.013
	3	−0.184	−0.177	−0.089	−0.114	0.146
	4	0.267	0.018	0.015	0.301	−0.367
XI	5	0.358	0.096	0.056	0.378	−0.455
	6	0.296	0.129	0.072	0.299	−0.353
	7	−0.017	0.006	0.003	−0.014	0.019
	8	0.195	0.042	0.026	0.208	−0.252
	9	0.159	0.113	0.061	0.157	−0.176

hydroxyl group.

References

1) A. Streitwieser, Jr., "Molecular Orbital Theory for Organic Chemistry," John Wiley (1961).

2) T. Yonezawa, C. Nagata, H. Kato, A. Imamura, and K. Morokuma, "Introduction to Quantum Chemistry," (in Japanese), Kagaku dohjin (1983).

3) K. Higashi, H. Baba, and A. Rembaum, "Quantum Organic Chemistry," John Wiley (1965).

4) K. Fukui, T. Yonezawa, and H. Shingu, *J. Chem. Phys.*, **20**, 722 (1952).

5) K. Fukui, T. Yonezawa, C. Nagata and H. Shingu, *J. Chem. Phys.*, **22**, 1433 (1954).

6) I. Fleming, "Frontier Orbitals and Organic Chemical Reactions," John Wiley (1976).

7) K. Fukui, "Chemical Reactions and Electron Orbital," (in Japanese), Maruzen (1976).

8) T. Ohmae, to be published.

9) R. D. Connon, "Electron Transfer Reactions," Butterworth (1980).

10) T. Ohmae, K. Nishikawa, K. Deguchi, and S. Aono, *Bull. Chem. Soc. Jpn.*, **54**, 3296 (1981).

11) C. Reichart, *Pure & Apple. Chem.*, **54**, 1867 (1982).

In-Plane Vibrational Modes of Guanine from an *ab Initio* MO Calculation

Yoshifumi NISHIMURA, Masamichi TSUBOI,* Shigeki KATO,†,†† and Keiji MOROKUMA†
Faculty of Pharmaceutical Sciences, University of Tokyo, Hongo, Bunkyo-ku, Tokyo 113
†*Institute for Molecular Science, Myodaiji, Okazaki 444*
(Received October 12, 1984)

Harmonic force constants, in-plane vibrational frequencies, and in-plane vibrational modes of guanine have been calculated by an *ab initio* MO method. The force constants were calculated by the use of an energy gradient method with STO-3G basis set, and then they were corrected into "4-31G force constants" by the scaling factors given by us previously for the case of uracil. The corrected set of force constants could reproduce the observed frequencies of guanine, guanine-7, 9-$^{15}N_2$, guanine-1,3,*amino*-$^{15}N_3$ (at positions 1, 3 and amino), guanine-8-*d* (at position 8), guanine-1,9, *amino*-d_4 (at amino and iminos), and guanine-d_5. The calculated vibrational modes could also account for the results of earlier experiments on infrared and Raman spectra of guanine residues in 5'-GMP and other nucleotides.

This is our second paper in a series of *ab initio* MO studies of the internal force field of nucleic acid. The previous one[1] dealt with uracil, and the present paper deals with guanine.

The vibrational spectroscopic studies of the guanine residue have now begun to provide a good insight into the conformation of nucleic acids. This residue has been found to cause many of the Raman lines of DNA and RNA,[2-12] and some of them are found to be useful to diagnose the polynucleotide conformation.[2-3-8,12] The location of a strong guanine Raman line around 650 cm^{-1}, for example, is sensitive to the internal rotation angle around the glycosidic bond and to the pseudo-rotation phase angle of the five-membered ribose ring directly linked to the guanine residue.[2,3] To establish such a spectrum-conformation correlation, it is necessary to clarify the normal mode of vibration for each Raman line of the guanine residue.

For a normal coordinate treatment, it is essential to obtain a reliable set of force constants of the molecule. In the previous paper,[1] we showed that it is practical to calculate the force constants of a big molecule, namely uracil, by the use of an *ab initio* MO method with STO-3G basis set, and it was possible to predict to a significant extent the vibrational modes by the use of "4-31G" force constants which were reached by a correction from the STO-3G force constants. Thus, the calculation could reproduce the observed frequencies, not only of uracil itself, but also of *C*, *C*-dideuterouracil, *N*, *N*-dideuterouracil, perdeuterouracil, and a uracil-$^{15}N_2$ residue.

In this paper, we report a similar study on guanine. Delabar and Majoube[13] reported the experimental frequencies, not only for guanine itself, but also for its three deuterated derivatives and two ^{15}N-substituted derivatives. All the normal frequencies and the corresponding vibrational modes of these guanine derivatives have been calculated in the present study and we can predict satisfactorily the observed frequencies.

Computational Details

The geometry and the harmonic force constants were calculated by the use of IMSPACK program.[14] We optimized the geometry of guanine without any constraint starting from a geometry which had been optimized under the constraint that the molecule is planar. This initial geometry was kindly provided by Mrs. Aida.[15] Our new optimization did not cause any significant change. The internal coordinates adopted here are shown in Fig. 1. Here, the redundancy of the angular coordinates caused by the ring system has been removed by the method of Pulay *et al.*[16]

The vibrational frequencies and the normal modes of vibration were calculated by a program written by us, which is a modified version of NCTB program written by Shimanouchi *et al.*[17] The force constants calculated from the STO-3G basis set were corrected into "4-31G" force constants by the use of the scaling factors, which are given in the previous paper (Table 1 and Eq. (4)) on uracil.[1] These were obtained by a direct comparison of the actually calculated force constants both with the STO-3G and 4-31G basis sets for urea, acrylaldehyde, and formamide. It will be shown below that they are useful for guanine as well as for uracil. Let us also mention here of our trial calculations on imidazole. We have calculated the force constants of imidazole with the STO-3G and the 3-21G basis sets. The STO-3G force constants were then corrected by the use of our scaling factors, and the results were found to be in a good agreement with the 3-21G force constants. The off-diagonal elements of the STO-3G force constant matrix of guanine, smaller than 0.1 mdyn/Å for the stretching-stretching, 0.03 mdyn for the stretching-bending, and 0.01 mdyn·Å for the bending-bending are taken to be zero, so that the number of non-zero force constants turned out to be 171.

Results and Discussion

Equilibrium Geometry. The optimized geometry calculated using the STO-3G basis set is given in Table 1. This should correspond to the geometry of the free guanine molecule, but it showed a good coincidence

†† Present address: Department of Chemistry, College of General Education, Nagoya University, Chikusa-ku, Nagoya 464.

$S_1 = \Delta r_1$	νN_1C_2 str.
$S_2 = \Delta r_2$	νC_2N_3 str.
$S_3 = \Delta r_3$	νN_3C_4 str.
$S_4 = \Delta r_4$	νC_4C_5 str.
$S_5 = \Delta r_5$	νC_5C_6 str.
$S_6 = \Delta r_6$	νC_6N_1 str.
$S_7 = \Delta r_7$	νC_6O str.
$S_8 = \Delta r_8$	νN_1H str.
$S_9 = \Delta r_9$	νC_2NH_2 str.
$S_{10} = \Delta r_{10}$	νNH str.
$S_{11} = \Delta r_{11}$	νNH str.
$S_{12} = \Delta r_{12}$	νC_5N_7 str.
$S_{13} = \Delta r_{13}$	νN_7C_8 str.
$S_{14} = \Delta r_{14}$	νC_8N_9 str.
$S_{15} = \Delta r_{15}$	νN_9C_4 str.
$S_{16} = \Delta r_{16}$	νC_8H str.
$S_{17} = \Delta r_{17}$	νN_9H str.
$S_{18} = \beta_3-\beta_4+\beta_5-\beta_6+\beta_1-\beta_2$	δR_6 I
$S_{19} = 2\beta_3-\beta_4-\beta_5+2\beta_6-\beta_1-\beta_2$	δR_6 II
$S_{20} = \beta_4-\beta_5+\beta_1-\beta_2$	δR_6 III
$S_{21} = \beta_{18}-0.8090169\beta_{19}+0.309017\beta_{20}+0.309017\beta_{16}-0.8090169\beta_{17}$	δR_5 I
$S_{22} = -1.1180339\beta_{19}+1.8090169\beta_{20}-1.8090169\beta_{16}+1.1180339\beta_{17}$	δR_5 II
$S_{23} = \beta_7-\beta_8$	δCO bend.
$S_{24} = \beta_9-\beta_{10}$	δN_1H bend.
$S_{25} = \beta_{11}-\beta_{12}$	δC_2N bend.
$S_{26} = 2\beta_{15}-\beta_{13}-\beta_{14}$	δNH_2 scis.
$S_{27} = \beta_{13}-\beta_{14}$	δNH_2 rock.
$S_{28} = \beta_{23}-\beta_{24}$	δN_9H bend.
$S_{29} = \beta_{21}-\beta_{22}$	δC_8H bend.

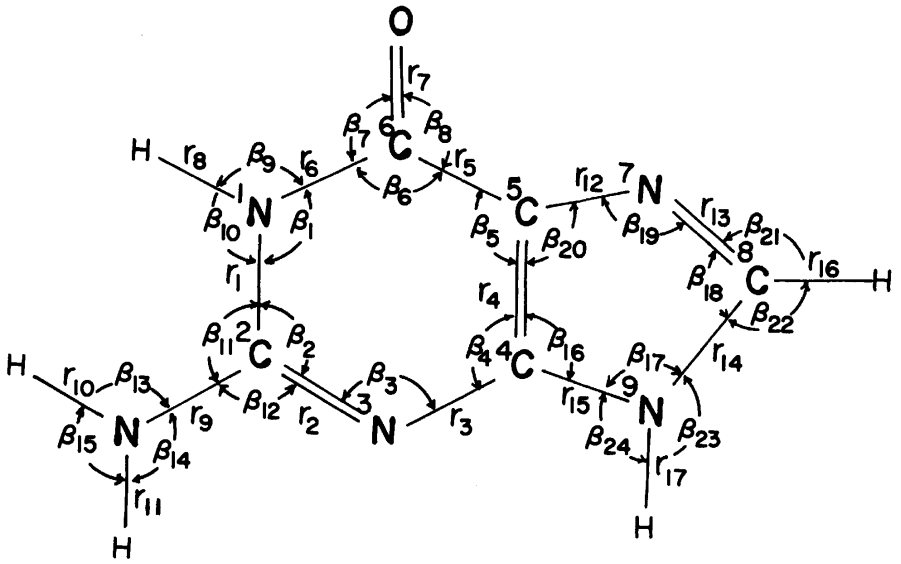

Fig. 1. Internal coordinates of the guanine molecule.

with the averaged values of the bond lengths and bond angles found in the X-ray crystallographical analyses of many guanine derivatives.[18] The averaging may cause a cancelling one another of various effects of intermolecular forces in the crystals to result in an experimental geometry of a guanine molecule, somewhat free from intermolecular force field. It is an interesting finding that the skeletal geometry (involving C, N, and O) of the guanine molecule calculated with the STO-3G basis set reproduced such an experimental geometry.

Force Constants (corrected). The "4-31G" force constants after the correction from the STO-3G force constants, are shown in Tables 2-A—E. In Table 2-A, the diagonal elements of the force constants matrix are shown. The stretching force constants of the ring system varies from 6.427 mdyn/Å for the C_6N_1 to 9.636 mdyn/Å for the N_7C_8 bond, and it is found that the greater force constant corresponds to the shorter bond length. The off-diagonal elements among the

stretching coordinates of the six-membered ring system are nearly equal to the corresponding elements of the uracil molecule[1] as shown in Table 2-B. The off-diagonal elements for the "ortho" positions are

TABLE 1. BOND LENGTHS IN THE GUANINE MOLECULE (unit: Å, 1Å=0.1 nm)

	Calcd on STO-3G	Obsd[a]
N1C2[b]	1.400	1.375
C2N3	1.318	1.327
N3C4	1.403	1.355
C4C5	1.376	1.377
C5C6	1.477	1.415
C6N1	1.455	1.393
C6O	1.218	1.239
N1H	1.021	
$C2NH_2$	1.390	1.341
NH	1.013	
C5N7	1.414	1.389
N7C8	1.312	1.304
C8N9	1.397	1.374
N7C4	1.390	1.377
C8H	1.083	
N9H	1.020	

a) Reference 18. b) see Fig. 1.

TABLE 2. FORCE CONSTANTS OF THE GUANINE MOLECULE, CALCULATED ON THE STO-3G BASIS SET, AND THEN CORRECTED AS DESCRIBED IN THE TEXT

A. Diagonal Elements

Numbering of internal coord.[a]	Force const.[b]	Classification
1.	7.980	
2.	8.967	
3.	7.174	S_{6r}
4.	8.524	
5.	6.458	
6.	6.427	
7.	13.482	
8.	8.098	
9.	8.518	S_{6p}
10.	8.428	
11.	8.445	
12.	7.129	
13.	9.636	S_{5r}
14.	8.249	
15.	8.817	
16.	6.296	S_{5p}
17.	8.213	
18.	2.005	
19.	2.012	
20.	1.782	Δ_r
21.	2.581	
22.	2.721	
23.	1.203	
24.	0.616	
25.	1.392	
26.	0.572	Δ_p
27.	0.698	
28.	0.512	
29.	0.586	

a) See Fig. 1. b) Units: mdyn/Å for S's and mdyn.Å for Δ's where 1Å=0.1 nm.

B. Off-Diagonal Elements between One of the Ring Stretching Coordinates (S_{6r} and S_{5r}) and Another

Internal coord.[a]	Force const.[c]	Classification
1- 2.	0.852	
1- 3.	−0.455	
1- 5.	−0.376	
1- 6.	0.535	
2- 3.	0.328	
2- 4.	−0.352	
2- 5.	0.337	
2- 6.	−0.199	S_{6r}–S_{6r}
3- 4.	0.650	
3- 5.	−0.236	
3- 6.	0.204	
4- 5.	0.524	
4- 6.	−0.236	
5- 6.	0.415	
1-14.	0.202	
1-15.	−0.112	
2-12.	−0.145	
2-13.	0.144	
2-14.	−0.169	
3-13.	−0.231	S_{6r}–S_{5r}
3-15.	0.470	
5-12.	0.367	
5-13.	−0.176	
5-15.	−0.137	
6-13.	0.117	
4-12.	0.804	
4-13.	−0.230	
4-14.	−0.292	
4-15.	0.826	
12-13.	0.476	
12-14.	−0.305	S_{5r}–S_{5r}
12-15.	−0.317	
13-14.	0.976	
13-15.	0.182	
14-15.	0.378	

a) See Fig. 1. c) Unit: mdyn/Å, where Å=0.1 nm.

C. Off-Diagonal Elements between Ring-Stretching and Ring-Deformation Coordinates

Internal coord.[a]	Force const.[d]	Classification
1-19.	−0.298	
1-21.	0.116	
2-18.	0.441	
2-19.	0.704	
2-20.	−0.138	
3-18.	0.411	
3-19.	0.610	
3-20.	0.204	
3-21.	−0.136	
3-22.	0.314	Δ_r–S_{6r}
4-20.	−0.186	
4-21.	0.403	
5-20.	−0.229	
5-21.	−0.091	
5-22.	−0.196	
6-19.	0.142	
6-20.	0.230	
6-22.	−0.193	

12-18.	−0.223	
12-19.	0.175	
12-20.	0.190	
12-21.	−0.821	
12-22.	0.164	
13-19.	−0.173	
13-22.	−0.812	
14-19.	−0.162	Δ_r–S_{5r}
14-21.	0.267	
14-22.	0.525	
15-18.	0.248	
15-19.	0.155	
15-20.	−0.284	
15-21.	−0.567	
15-22.	−0.306	

a) See Fig. 1. d) Unit: mdyn.

D. Off-Diagonal Elements between the Ring-Stretching and Peripheral-Stretching (or Deformation) Coordinates

Internal coord.[a)]	Force const.[e)]	Classification
1- 9.	0.472	
1-23.	0.119	
1-24.	−0.205	
1-25.	0.477	
2- 8.	−0.098	
2- 9.	0.937	
2-23.	−0.048	
2-25.	−0.441	
2-27.	0.054	
3- 9.	−0.169	
3-23.	0.054	
3-24.	0.055	S_{6r}–S_{6p}, or Δ_p
3-28.	0.032	
4- 7.	−0.161	
4-23.	−0.085	
4-25.	−0.032	
4-28.	0.061	
5- 7.	0.632	
5- 9.	−0.168	
5-23.	0.225	
6- 7.	1.074	
6-23.	−0.489	
6-25.	−0.087	
14- 9.	0.090	
12-23.	−0.056	
13-23.	0.046	
13-29.	0.157	
14-28.	0.041	S_{5r}–S_{5p}, or Δ_p
14-29.	−0.190	
15-23.	0.037	
15-28.	−0.051	
15-29.	0.060	

a) See Fig. 1. e) Units: mdyn/Å for S-S's and mdyn for S-Δ's (Å=0.1 nm).

E. Some Other Off-Diagonal Elements

Internal coord.[a)]	Force const.[f)]	Classification
7-18.	0.258	
7-19.	−0.362	
7-23.	−0.111	
7-25.	0.033	
8-18.	−0.093	
8-25.	−0.057	
9-18.	0.187	
9-19.	0.133	
9-20.	0.271	S_{6r}–Δ_r, or Δ_p
9-26.	−0.188	
9-27.	0.048	
10-11.	−0.184	
10-25.	−0.076	
10-26.	0.050	
10-27.	0.059	
11-25.	0.044	
11-27.	−0.072	
16-21.	−0.108	S_{5r}–Δ_r
18-22.	0.481	
18-23.	−0.081	
18-29.	−0.031	
19-21.	−0.242	
19-23.	0.124	
19-24.	0.118	
19-25.	−0.082	
19-27.	0.032	
20-22.	−0.441	
20-23.	−0.165	
20-24.	0.080	
20-25.	0.078	
21-22.	−0.106	Δ_r–Δ_r, or Δ_p
21-28.	0.048	
22-25.	−0.045	
22-28.	0.101	
22-29.	−0.088	
23-24.	0.070	
23-25.	−0.046	
23-27.	0.011	
24-25.	−0.012	
24-27.	−0.012	
25-26.	−0.044	
25-27.	−0.180	
26-27.	−0.012	

a) See Fig. 1. f) Units: mdyn for S-Δ's, and mdyn.Å for Δ-Δ's(Å=0.1 nm).

positive, those for the "meta" positions are negative, and those for the "para" positions are positive. Their absolute values are all greater than 0.2 mdyn/Å except for the off-diagonal element between the N_1C_2 stretching and the C_4C_5 stretching coordinates, which is nearly zero. The anomalously small value of this element is considered to be caused by a perturbation by the five-membered ring system, which shares the C_4C_5 bond with the six-membered ring. The off-diagonal elements on the five-membered ring system are nearly equal to those of imidazole molecule (the data are not shown here)[19] except for those involving the C_4C_5 stretching coordinate. It is rather surprising that some of the off-diagonal elements of the stretching coordinates of two bonds located far apart from each other, such as r_1 & r_{14} and r_3 & r_{13}, are as great as 0.2 mdyne/Å as shown in Table 2-B. We could never predict such effectual values of them without the present *ab initio* MO calculation. Also in the calculation, many non-zero off-diagonal elements between the ring stretching and the ring deformation coordinates are found as shown in Table 2-C. The off-diagonal elements among the ring vibrations and the peripheral vibrations are given in Table 2-D and Table 2-E.

Vibrational Frequencies. For the uracil molecule, we showed that the calculated vibrational frequencies using the corrected force constants ("4-31G" force constants) are almost uniformly greater by 8% than the observed fundamental frequencies. Therefore, in our present study on guanine we scaled down the vibrational frequencies by the factor of 0.92. The calculated vibrational frequencies, thus scaled, and the calculated modes are given in Table 3. The calculated frequencies of deuterated guanines are shown in Table 4. In parentheses in these tables, calculated ^{15}N isotope shifts are also given: The first numerical value here indicates the shift (cm^{-1}) for the product in which N_1, N_3, and amino-*N* are substituted by ^{15}N's, namely for pyrimidinic substitution, and the second one the shift for the product, in which N_7 and N_9 are substituted by ^{15}N's, namely for imidazolic substitution.

The largest isotope shift for the pyrimidinic substitution is calculated to be $-24\,cm^{-1}$ for ν_{21} (at 1026 cm^{-1}), and this corresponds to the observed isotope shift ($-26\,cm^{-1}$) for the $1052\,cm^{-1}$ Raman line. For imidazolic substitution, the largest shift is calculated to be $-21\,cm^{-1}$ for ν_{22} ($985\,cm^{-1}$), and this is actually observed ($-20\,cm^{-1}$) for the $950\,cm^{-1}$ line.

In this way, it was attempted to correlate every calculated frequency with an observed frequency by taking an agreement in the isotope effect into account. This attempt was mostly successful except for those in the frequency range higher than $2000\,cm^{-1}$. The difficulty in the higher frequency region is probably caused by the hydrogen bonds. In our calculation, no hydrogen bonding effect was taken into account, whereas the observed frequencies are taken from the solid state guanine whose N_1H and N_9H groups are involved in intermolecular NH···N hydrogen bonds.

The difficulty due to the hydrogen bonds seems to extend into the NH in-plane bending range (1350—1420 cm^{-1}) in a less prominent manner. The amount of couplings of the N_1–H bending modes with some skeletal stretching modes may be sensitive to the diagonal and off-diagonal force constants involving these NH bending coordinates. Therefore only a slightly improper prediction of the force constants may fail in explaining observed ^{15}N-shifts (for $1420\,cm^{-1}$ band, for example). In this frequency region, therefore the calculated vibrational modes should be taken with some reservation, even if the vibrational frequencies predicted for ν_{13}, ν_{14}, and ν_{15} are in good agreement with the observed ones (Table 3).

For the whole other spectral range, however, our present calculation has provided a very good set of vibrational frequencies, which fits the experimental results in a nealy perfect manner.

Vibrational Modes. *I. 4000—2000 cm^{-1}*: In this frequency region, special care must be taken in correlating the calculated and observed vibrations, because many of the infrared and Raman bands here are under severe perturbation by hydrogen bonds. Our present calculation shows that the vibration at 3686 cm^{-1} is the amino antisymmetric stretching and that at $3496\,cm^{-1}$ is the amino symmetric stretching.

In the infrared spectrum on the other hand, 2′,3′-benzylidene-5′-tritylguanosine dissolved in deuteriochloroform shows two bands due to the molecule free from any hydrogen bond at 3515 and $3407\,cm^{-1}$.[20] These two may correspond to the above two. In that solution, however, other bands due to some guanine-guanine association complexes are also found at 3480, 3355, 3305, and $3230\,cm^{-1}$. The vibrational modes of the hydrogen-bonded NH_2 and those of NH are not the subject of our present study.

In the case of C_8–H stretching vibration, the situation is simpler. The calculation shows that the vibration at $3132\,cm^{-1}$ is the C_8–H stretching and that at $2338\,cm^{-1}$ is the C_8–D stretching. On the other hand, a strong Raman line is observed of 5′GMP (guanosine 5′-monophosphate) in D_2O solution at $3125\,cm^{-1}$, and of the C_8-deuterated derivative in H_2O solution at $2325\,cm^{-1}$.[21] The hydrogen bondings at the N–H groups do not seem to affect the C_8–H vibration in the same molecule.

II. 2000—1100 cm^{-1}: A strong infrared band and a medium intensity Raman line around $1700\,cm^{-1}$ of guanine and guanine derivatives have been assigned to the C=O stretching vibration by a number of researchers, and this mode is reproduced in our calculation (ν_6 in Table 3).

In the Raman spectra of guanine, deuterated guanines, and 5′GMP in H_2O and D_2O solutions in the 1620—$1500\,cm^{-1}$ region, there are always three Raman lines, at 1610, 1580, and $1530\,cm^{-1}$.[22-24] These Raman lines are considered to correspond to the ring stretching vibrations, ν_8, ν_9, and ν_{10}, whose vibrational modes are shown in Table 3 as well as in Fig. 2. The calculated vibration ν_7 is the NH_2 scissoring, but this has never been identified in the Raman spectra of guanine and guanine derivatives. The calculated vibrations, ν_9 and ν_{11}, must correspond to the observed Raman lines at $1580\,cm^{-1}$ and $1480\,cm^{-1}$ of 5′GMP in H_2O solution, respectively. Those two Raman scatterings show marked resonance effect with the absorption bands at 278 and/or 253 nm.[25] In these excited states, the geometry of the guanine molecule is supposed to be deformed along these two normal coordinates which are shown in Fig. 2 (ν_9 and ν_{11}).

The Raman line at $1480\,cm^{-1}$ shows a large frequency shift as great as $-23\,cm^{-1}$ upon the C_8–H deuteration,[21] and this was used as a monitor line of the C_8–H deuterium exchange kinetics.[21] In our calculation, this large shifts is well reproduced ($-27\,cm^{-1}$) as shown in Table 5 (k=11). This $1480\,cm^{-1}$ Raman line also shows a marked frequency shift and/or intensity change on the coordination at N_7 of heavy metal ions and on N_7 protonation.[22,24,25] This is also understandable because the calculated normal modes (as shown in Fig. 2) involves a big movement of the N_7 atom, and the

TABLE 3. VIBRATIONAL FREQUENCIES (cm^{-1}) OF THE GUANINE MOLECULE (CALCULATED NORMAL FREQUENCIES ω AND OBSERVED FUNDAMENTAL FREQUENCIES ν)

Numbering of nomal coord (k)	Calcd ω (isotope shifts)[a]	Vibrational modes[b]	Obsd ν[c] (isotope shifts) IR	Raman
1	3686(−12, 0)	NH_2 anti sym. str(97)	3515[d]	
2	3554(0, −9)	N_9H str(99)		
3	3522(−8, 0)	N_1H str(100)		
4	3496(−5, 0)	NH_2 sym. str(100)	3407[d]	
5	3132(0, 0)	C_8H str(98)		3125[e]
6	1802(−2, 0)	C_6O str(71), C_5C_6 str(17)	1702(−6, 0)	1678(−2,)
7	1661(−10, −1)	NH_2 sci(37), C_2NH_2 str(28)	1675(−9, 0)	
8	1630(−6, −8)	ring str(75)	1638(−7, 0)	1604(−4,)
9	1601(−7, 0)	NH_2 sci(44), ring str(34)	1565(−5,)	1552(−3, −5)
10	1581(−6, −1)	ring str(56)	1550(0,)	1535(,)
11	1526(−4, −10)	ring str(81), C_8H bend(22)	1477(−3, −2)	1480(2,)
12	1464(−4, −6)	ring str(85)	1464(−2, −9)	1468(−4, −8)
13	1415(−2, −15)	ring str(67), N_9H bend(22)	1420(−5, −2)	1422(−5, −2)
14	1350(−1, −3)	ring str(55), N_1H bend(13)	1375(−4, −3)	1392(−4, −4)
15	1343(−8, −2)	N_1H bend(37), ring str(27)	1362(−6, −4)	1361(−6, −4)
16	1273(−5, −14)	ring str(76), C_8H bend(13)	1261(−1, −10)	1266(0, −14)
17	1174(−3, −4)	ring str(38), C_8H bend(32)	1174(−4, −7)	1188(−4, −8)
18	1146(−12, −3)	ring str(78), CO bend(13)	1216(−8, 0)	1232(−12, −5)
19	1102(−6, −3)	ring str(36), NH_2 rock(28)	1150(−12, −1)	1161(−11,)
20	1079(−7, −5)	ring str(30), NH_2 rock(25)	1118(−7, −3)	
21	1026(−24, −1)	ring str(51), ring def(13)	1042(−23, 0)	1052(−26,)
22	985(0, −21)	ring def(81)	950(−1, −20)	940(−2, −19)
23	833(−17, −7)	ring def(62), ring str(33)	850(−15, −4)	850(−17,)
24	661(−8, 0)	CO bend(27), ring def(28)	703(−6, 1)	712(−4,)
25	619(−6, −2)	ring breathing (50)	645(−5, −3)	651(−5, −3)
26	533(−5, −4)	ring def(55)	557(−6, −2)	568(−10,)
27	481(−6, −3)	ring def(69)	501(1, 1)	496(−3, −4)
28	332(−4, 0)	C_2NH_2 bend(49), CO bend(23)	404(−5, 1)	400(−6, −1)
29	311(−2, −2)	CO bend(20), ring def(31)	348(−1, −2)	343(0,)

a) The first numerical value (cm^{-1}) in each pair of parentheses indicates the shift for the $^{15}N_3$ substitution at positions 1, 3 and amino, and the second one for the $^{15}N_2$ substitution at positions 7 and 9. b) Potential energy distribution (%) calculated is given in parentheses. c) Ref. 13. d) Ref. 20. e) Ref. 21.

TABLE 4. CALCULATED NORMAL FRQUENCIES AND ISOTOPE SHIFTS OF GUANINE DEUTERATED DERIVATIVES

	Guanine	Guanine-d_1	Guanine-d_4	Guanine-d_5
1	3686(−12, 0)[a]	3686(−12, 0)	3132(0, 0)[b]	2736(−17, 0)
2	3554(0, −9)	3554(0, −9)	2736(−17, 0)	2622(0, −15)
3	3522(−8, 0)	3522(−9, 0)	2622(0, −15)	2588(−13, 0)
4	3496(−5, 0)	3496(−5, 0)	2588(−13, 0)	2530(−8, 0)
5	3132(0, 0)[b]	2338(0, 0)[b]	2530(−8, 0)	2337(0, 0)[b]
6	1802(−2, 0)	1802(−2, 0)	1794(−1, 0)	1794(−1, 0)
7	1661(−10, −1)[c]	1660(−11, −1)[c]	1619(−3, −6)	1617(−3, −6)
8	1630(−6, −8)	1627(−6, −8)	1594(−13, −1)	1594(−14, −1)
9	1601(−7, 0)	1601(−7, 0)	1569(−6, −1)	1566(−7, −1)
10	1581(−6, −1)	1578(−7, −1)	1515(−3, −10)	1486(−3, −11)
11	1526(−4, −10)	1499(−4, −9)	1449(−6, −5)	1448(−6, −7)
12	1464(−4, −6)	1461(−3, −10)	1385(−2, −15)	1371(−2, −14)
13	1415(−2, −15)	1394(−1, −15)	1327(−1, −9)	1286(−2, −11)
14	1350(−1, −3)	1345(−6, 0)	1279(−14, −6)	1274(−17, −5)
15	1343(−8, −2)	1327(−5, −5)	1233(−12, −8)	1220(−10, −9)
16	1273(−5, −14)	1248(−7, −14)	1166(−8, −2)[c]	1159(−9, −1)[c]
17	1174(−3, −4)[d]	1145(−11, −2)	1146(−4, −4)[d]	1066(−9, −2)
18	1146(−12, −3)	1120(−1, −7)	1063(−8, −2)	980(−6, −1)
19	1102(−6, −3)	1088(−12, −1)	980(−1, −8)	974(−4, −23)
20	1079(−7, −5)	1026(−24, −1)	971(−14, −16)	930(−7, −4)[d]
21	1026(−24, −1)	983(−1, −22)	873(−13, −2)	872(−13, −1)
22	985(0, −21)	885(−5, −4)[d]	852(−2, −1)	813(−4, 0)
23	833(−17, −7)	814(−13, −5)	788(−11, −5)	772(−8, −4)
24	661(−8, 0)	660(−9, −1)	613(−6, −1)	613(−6, −1)
25	619(−6, −2)	616(−6, −2)	603(−6, −1)	603(−6, −1)
26	533(−5, −4)	529(−5, −4)	508(−3, −3)	506(−3, −3)
27	481(−6, −3)	479(−6, −3)	469(−5, −3)	468(−6, −3)
28	332(−4, 0)	332(−4, 0)	317(−1, −1)	314(−1, −1)
29	311(−2, −2)	305(−2, −2)	289(−3, −1)	286(−3, −1)

a) In each pair of parentheses, the first numerical value indicates the shift for the $^{15}N_3$ sunstitution at positions 1, 3, and amino, and the second one for the $^{15}N_2$ substitution at positions 7 and 9. b) C_8H or C_8D stretching vibration. c) NH_2 or ND_2 scissoring vibration. d) C_8H or C_8D bending vibration.

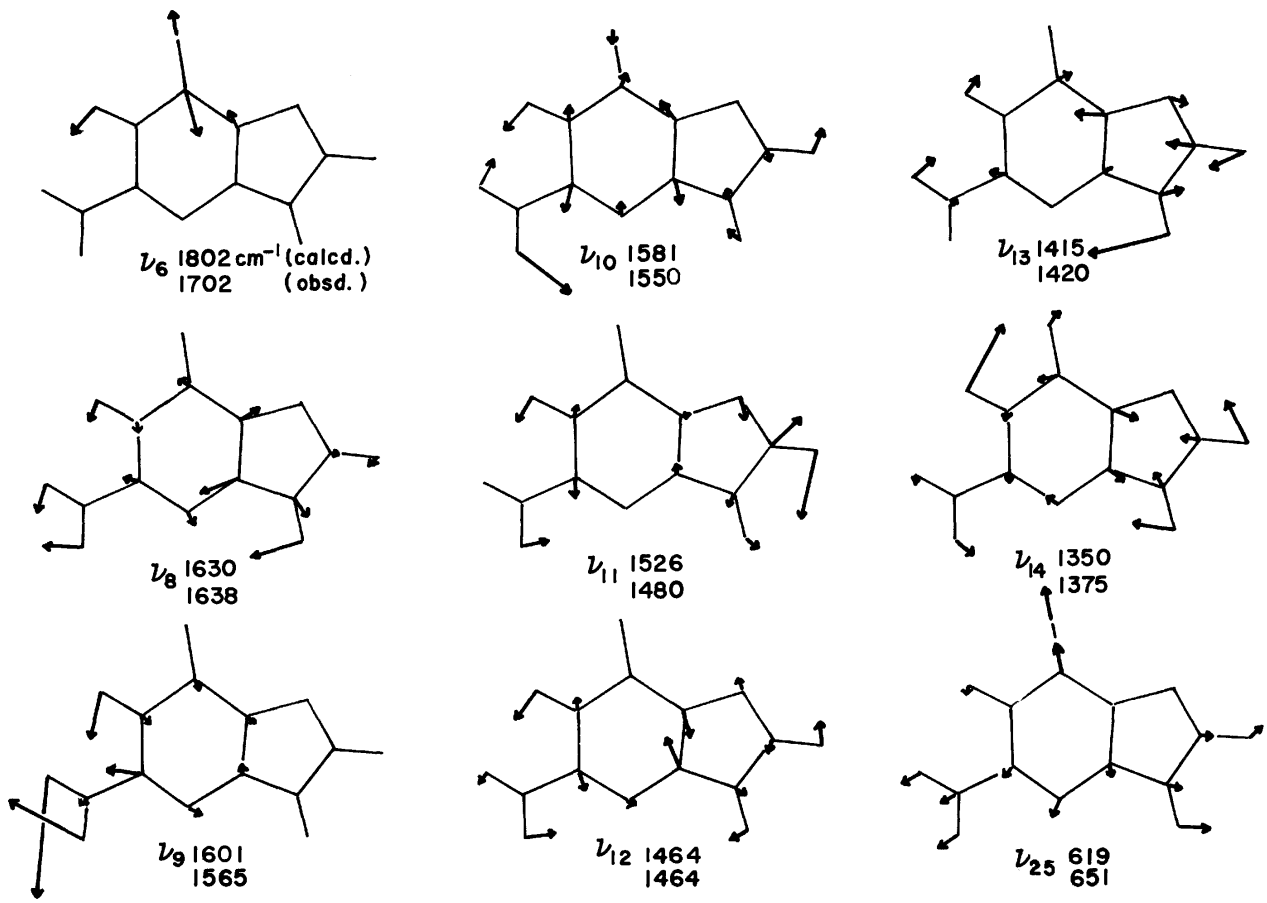

Fig. 2. Normal modes of vibration, calculated with the "4-31G force constants" which were reached by a correction from the STO-3G force constants of guanine. Calculated normal frequency (upper numerical value) and observed fundamental frequency (lower) are also given in cm^{-1} for each mode.

TABLE 5. CALCULATED AND OBSERVED FREQUENCIES (IN cm^{-1}) OF SOME OF THE GUANINE VIBRATIONS WITH THE ISOTOPE SHIFTS DUE TO THE C_8-DEUTERATION

Numbering of normal coord. (k)	Calcd	Obsd (5'GMP)[a]
6	1802 (0)[b]	1680 (−5)
7	1661 (−1)	—
8	1630 (−3)	1605 (+3)
9	1601 (0)	1576 (0)
10	1581 (−3)	1538 (−11)
11	1526 (−27)	1487 (−23)
12	1464 (−3)	—
13	1415 (−21)	1415 (−7)
14	1350 (−5)	1365 (−8)
15	1343 (−16)	1324 (−19)
25	619 (−3)	671 (−10)
26	533 (−4)	586 (−2)
27	481 (−2)	501 (−1)

a) From Ref. 21. b) The amount of shift (in cm^{-1}) by the C_8-deuteration is given in each pair of parentheses.

calculated potential energy distribution of C_8N_7 stretching in this vibration is as high as 42%. Therefore, this Raman scattering is naturally sensitive to a perturbation at N_7.

As has already been mentioned, the contribution of the N_1H, N_9H, and NH_2 bending modes in the vibrations in the 1450—1100 cm^{-1} region are not clearly predicted by the present calculation. However, the contribution of the C_8–H deformation mode has been satisfactorily predicted. The calculated vibrations at 1174 cm^{-1} for guanine, at 885 cm^{-1} for guanine-d_1, at 1146 cm^{-1} for guanine-d_4, and at 930 cm^{-1} for guanine-d_5 should involve a great amount of C_8–H or C_8–D in-plane bending mode (see Table 4). These vibrations are correlated with observed IR bands at 1174 cm^{-1}, 926 cm^{-1}, 1168 cm^{-1}, and 897 cm^{-1}, respectively.[13] Thus, the C_8-deuteration effect in *N*-deuterated guanine as well as undeuterated guanine spectra have been clearly reproduced and explained by our calculation.

III. Vibrations with Frequencies below 1100 cm^{-1}: In this frequency region, no complexity coming from the NH bending modes is involved any more. The calculated frequencies and their ^{15}N isotope effects of the ν_{20}, ν_{21}, ν_{22}, ν_{23}, ν_{24}, ν_{25}, and ν_{26} vibrations can be clearly correlated with what were actually observed. The calculated vibrational modes given in Table 3 are considered to be quite useful.

In particular, the ring breathing vibration should be mentioned. Raman spectroscopic studies of nucleic acids have so far showed that a strong and sharp Raman lines at 780, 790, and 725 cm^{-1} of uracil, cytosine, and

adenine, respectively, are assignable to the ring breathing vibrations.[1,22-24] For guanine residues, in 5'GMP for example, no strong Raman line has been found in the frequency region higher than 700 cm^{-1}; instead a much broader and weaker line was observed around 680 cm^{-1}.[22,25] This line has been considered to correspond to some kind of ring breathing vibration perturbed by some ring deformations.[23] However, this Raman line at 650 cm^{-1} is strong enough in the spectrum of solid state guanine.[13] Our present calculation has now predicted that this line is nearly pure ring breathing vibration. Our recent study on guanosine residues indicates that this ring breathing frequency is appreciably affected by the sugar conformation and by the torsion angle around the glycosidic bond connecting the guanine and ribose moieties.[2,3] The broadness and weakness of the 670 cm^{-1} line of 5'GMP in H_2O, therefore, would mean that various conformations are involved in the solution whose frequencies are slightly different from one another.[27] Such a flexibility of the 5'GMP conformation in solution would be removed in the solid state or in a regular-form polynucleotide. On the basis of this argument, a strong, sharp Raman line should be observed if the conformation of 5'GMP is fixed. This is what is actually found as has been detailed elsewhere.[2,3,27]

As shown in Fig. 2, the calculated vibrational mode (ν_{25}) involves a big movement of the N_9 atom and the position-9 hydrogen atom. In the guanosine molecule, this hydrogen is replaced by the sugar, so that the ring breathing vibration should cause a coupling with a vibration in the sugar part. This is a qualitative explanation of the observed dependence of the ring breathing frequency upon the ribose conformation. More detailed description as for how it depends is given in a previous article.[3]

This work was supported by a grant (No. 57060004) from the Ministry of Education, Science, and Culture of Japan. The numerical calculations were carried out at the Computer Center of IMS.

References

1) Y. Nishimura, M. Tsuboi, S. Kato, and K. Morokuma *J. Am. Chem. Soc.*, **103**, 1354 (1981).

2) Y. Nishimura, M. Tsuboi, T. Nakano, S. Higuchi, T. Sato, T. Shida, S. Uesugi, E. Ohtsuka, and M. Ikehara, *Nucleic Acids Res.*, **11**, 1579 (1983).

3) Y. Nishimura, M. Tsuboi, and T. Sato, *Nucleic Acids Res.*, **12**, 6901 (1984).

4) E. W. Small and W. L. Peticolas, *Biopolymers*, **10**, 1377 (1971).

5) S. Mansy and W. L. Peticolas, *Biochemistry*, **12**, 2650 (1976).

6) L. Lafleur, J. Rice, and G. J. Thomas, Jr., *Biopolymers*, **11**, 2423 (1972).

7) B. Prescoff, R. Gamache, J. LIvermento, and G. J. Thomas, Jr., *Biopolymers*, **13**, 1821 (1974).

8) F. M. Pohl, A. Ranade, and M. Stockburger, *Biochim. Biophys. Acta*, **335**, 85 (1973).

9) J. Rice, L. Lafleur, G. C. Medeiros, and G. J. Thomas, Jr., *J. Raman Spectrosc.*, **1**, 207 (1973).

10) R. Savoie, H. Klump, and W. L. Peticolas, *Biopolymers*, **17**, 1335 (1978).

11) S. Brahms, J. Vergne, J. G. Brahms, E. D. Gupta, Ph. Bucher, and Th. Koller, *J. Mol. Biol.* **162**, 473 (1982).

12) T. J. Thaman, R. Lord, H. J. Wang, and A. Rich, *Nucleic Acids Res.*, **9**, 5443 (1981).

13) J.-M. Delabar and M. Majoube, *Spectrochim. Acta*, **34A**, 129 (1978).

14) K. Morokuma, S. Kato, K. Kitaura, I. Ohmine, S. Sakai, and S. Obara, IMS Computer Center Library Program, No. 0372 (1980).

15) M. Aida and C. Nagata, to be published.

16) P. Pulay, G. Fogarasi, F. Pang, and J. E. Boggs, *J. Am. Chem. Soc.*, **101**, 2550 (1979).

17) T. Shimanouchi, Computer Programs for Normal Coordinate Treatment of Polyatomic Molecules, Department of Chemistry, University of Tokyo.

18) R. Taylor and O. Kennard, J. Mol. Struct., **78**, 1 (1982).

19) Y. Nishimura, M. Tsuboi, S. Kato, and K. Morokuma, to be published.

20) Y. Kyogoku, R. C. Lord, and A. Rich, *Science* **154**, 518 (1966).

21) M. J. Lane and G. J. Thomas,Jr., *Biochemistry*, **18**, 3839 (1979).

22) R. C. Lord and G. J. Thomas,Jr., *Spectrochim. Acta*, **23A**, 2551 (1967).

23) M. Tsuboi, S. Takahashi, and I. Harada, "Physico-Chemical Properties of Nucleic Acids," ed by J. Duchesne, Academic Press, London, New York, 1973, Vol. 2, p. 91.

24) K. A. Hartman, R. C. Lord, and G. J. Thomas,Jr., "Physico-Chemical Properties of Nucleic Acids," ed by J. Duchesne, Academic Press, Lomdon, New York, 1973, Vol. 2, p. 1.

25) Y. Nishimura, A. Y. Hirakawa, and M. Tsuboi, "Advances in Infrared and Raman Spectroscopy," Vol. 5, R. J. H. Clark and R. E. Hester, Eds., Heyden, London, 1978, Chap. 4.

26) G. Y. H. Chu, S. Mansy, R. E. Duncan, and T. S. Tobias, *J. Am. Chem. Soc.*, **100**, 593 (1978).

27) Y. Nishimura, I. Sakuma, and M. Tsuboi, *Nucleic Acids Ras.*, Symp. Ser. **12**, 177 (1983).

Catalytic Function of Cobalt(III) Complexes with *N,N'*-Disalicylideneethylenediamine on Oxygenation of *t*-Butylphenols

Yūko Aimoto, Wakako Kanda, Sadatoshi Meguro,† Yūji Miyahara, Hisashi Ōkawa,* and Sigeo Kida

Department of Chemistry, Faculty of Science, Kyushu University 33, Hakozaki, Higashiku, Fukuoka 812
†*Department of Forest Products, Faculty of Agriculture, Kyushu University 46-08, Hakozaki, Higashiku, Fukuoka 812*
(Received May 24, 1984)

Catalytic oxygenation of *t*-butylphenols has been examined with the cobalt(III) complexes with *N,N'*-disalicylideneethylenediamine (H_2salen), K[Co(salen)CO_3], Na[Co(salen)$(N_3)_2$], K[Co(salen)$(CN)_2$], [Co(salen)$(py)_2$]PF_6, and [Co(salen)$(NH_3)_2$]PF_6. The CO_3-complex showed a high catalytic activity while the other complexes a low or no catalytic activity. Based on electronic and ESR spectral investigations, it has been shown that the reaction is initiated by the direct oxidation of *t*-butylphenols by the CO_3-complex through a phenolatocobalt(III) intermediate.

Reversible oxygen-carrying functions of cobalt(II) complexes with Schiff base ligands are well known.[1,2] Recently, catalytic oxidations of *t*-butylphenols[3-11] and indoles[12,13] by the use of such cobalt(II) complexes have become of interest as models for biological oxidations, since the catalysis in biological systems is considered to involve the activation of molecular oxygen by metalloenzymes. In the oxygenation of *t*-butylphenols with [Co(salpr)] (salpr^{2-}=bis(3-salicylideneaminopropyl)amine anion), it has been shown that the reaction is initiated by the hydrogen abstraction from the phenol by the superoxocobalt(III) complex [Co(salpr)O_2] initially formed.[9-11] On the other hand, the catalytic function of [Co(salen)](salen^{2-}=*N,N'*-disalicylideneethylenediamine anion) in oxygenations of *t*-butylphenols is less known, though it is generally thought that its oxygen complex takes part in the initiation of the reactions.[3]

It is also shown that [Co(salen)] acts as a good catalyst for oxygen delignification.[14] In the oxidative degradation of guaiacol as a model for the oxygen delignification, the catalytic activity of [Co(salen)] decreases in the order of additives in aqueous solution: $NaHCO_3$>Na_2CO_3>NaOH.[15] Under these conditions [Co(salen)] must be oxidized to a cobalt(III) complex. However, the species formed in alkaline aqueous media have not been characterized as yet.

The objects of this study are (1) to isolate and characterize the cobalt(III) complex derived from [Co(salen)] in aqueous solution containing hydrogencarbonate ion and (2) to examine catalytic activities of this cobalt(III) complex and its related complexes on the oxygenations of *t*-butylphenols, in the hope of obtaining an insight into the catalytic function of [Co(salen)] in the oxygenation reaction.

Experimental

Isolation of the Cobalt(III) Complex Formed in Aqueous Potassium Hydrogencarbonate Solution. [Co(salen)] (5 g) was suspended in a solution of $KHCO_3$ (10 g) in water (300 cm^3). Then chloroform (30 cm^3) was added, and the mixture was stirred for a week at room temperature. The deep green aqueous layer was separated and evaporated to dryness at a temperature lower than 40 °C. The crude product thus obtained was recrystallized from cold water containing potassium hydrogencarbonate (5%) to form green prisms.

Found: C, 43.45; H, 3.81; N, 6.06%. Calcd for $C_{17}H_{14}N_2O_5CoK\cdot 5/2H_2O$: C, 43.50; H, 4.08; N, 5.97%.

Syntheses of Other Cobalt(III) Complexes. Na[Co(salen)$(N_3)_2$]: An aqueous solution of NaN_3 (1 g) was added to a solution of K[Co(salen)CO_3]$\cdot 5/2H_2O$ (hereafter denoted as CO_3-complex, 450 mg) in water (10 cm^3). Soon the $(N_3)_2$-complex separated as brown crystals.

Found: C, 43.34; H, 3.29; N, 25.51%. Calcd for $C_{16}H_{14}N_8O_2CoNa\cdot 1/2H_2O$: C, 43.55; H, 3.43; N, 25.39%.

[Co(salen)N_3]: The $(N_3)_2$-complex (30 mg) was dissolved in water (40 cm^3) to form a reddish brown solution, from which brown crystals separated. They were collected, washed with water, and dried *in vacuo*.

Found: C, 49.75; H, 4.31; N, 17.76%. Calcd for $C_{16}H_{14}N_5O_2Co\cdot H_2O$: C, 49.88; H, 4.19; N, 18.18%.

K[Co(salen)$(CN)_2$]: This complex ($(CN)_2$-complex) was obtained as yellowish orange crystals by the reaction of the CO_3-complex and an excess amount of KCN in water.

Found: C, 51.20; H, 3.49; N, 13.23%. Calcd for $C_{18}H_{14}N_4O_2CoK\cdot 1/2H_2O$: C, 50.82; H, 3.55; N, 13.17%.

[Co(salen)$(py)_2$]PF_6: The CO_3-complex (460 mg) was dissolved in water (15 cm^3) containing pyridine (10 cm^3). To the resulted red solution was added an aqueous solution of KPF_6 to give the $(py)_2$-complex as orange prisms.

Found: C, 49.69; H, 3.85; N, 8.92%. Calcd for $C_{26}H_{24}N_4O_2CoF_6P\cdot 1/2H_2O$: C, 49.70; H, 3.85; N, 8.92%.

[Co(salen)py]PF_6: The $(py)_2$-complex was left standing in a vacuum desiccator over P_2O_5 for a week to give the monopyridine adduct.

Found: C, 45.24; H, 3.58; N, 7.84%. Calcd for $C_{21}H_{19}N_3O_2CoF_6P\cdot 1/2H_2O$: C, 45.18; H, 3.61; N, 7.53%.

[Co(salen)$(NH_3)_2$]PF_6: This complex ($(NH_3)_2$-complex) was obtained in a way similar to that for the $(py)_2$-complex.

Found: C, 37.40; H, 4.07; N, 10.98%. Cacd for $C_{16}H_{20}N_4O_2CoF_6P\cdot 1/2H_2O$: C, 37.44; H, 4.12; N, 10.92%.

Oxygenation Reactions of t-*Butylphenols.* Oxygenation reactions of 2,4,6-tri-*t*-butylphenol and 2,6-di-*t*-butyl-4-methylphenol were examined by the use of the CO_3-, $(N_3)_2$-, $(CN)_2$-, $(py)_2$-, and $(NH_3)_2$-complexes as catalysts. The reactions were carried out by stirring an ethanolic solution containing a substrate and a catalyst for 12 h at room temperature, where the concentration of the substrate was 1×10^{-1} M (1 M=1 mol dm^{-3}) and the [substrate]/[catalyst] ratio was 50. Oxygenation products were separated by preparative thin-

layer chromatography with alumina as an adsorbent or by high-speed liquid chromatography (column; Zorbax-ODS, 15 cm: eluent; acetonitrile–water (4:1)). Identifications of the products were performed by comparing the NMR and IR spectra and melting points of the products with those of authentic samples.

Physical Measurements. Infrared spectra were measured on a Hitachi Infrared Spectrometer Model 215 on KBr disks. Electronic spectra were recorded on a Shimadzu Multipurpose Spectrophotometer Model MPS-5000. ESR spectra (X-band) were recorded on a JES-FE3X Spectrometer. Conductivity measurements were carried out with a Yanagimoto Conductivity Output Model MY-8 in ethanol, the cell constant being determined by the use of tetraethylammonium chloride.

Results and Discussion

The CO_3-complex exhibits the IR bands at 1590 and 1290 cm^{-1}, which are assigned to the vibration of bidentate carbonate group.[16] Absorption spectrum of this complex in water containing excess potassium hydrogencarbonate shows a d-d band at 16.3×10^3 cm^{-1} and an intraligand transition band at 26.6×10^3 cm^{-1} (Fig. 1). The spectrum resembles the spectra of *cis*-β-[Co(salen)(acac)][17] and its homologs.[18–21] All these facts indicate that the CO_3-complex adopts a *cis*-β octahedral configuration with nonplanar $salen^{2-}$ and bidentate carbonate ion (Fig. 2a).

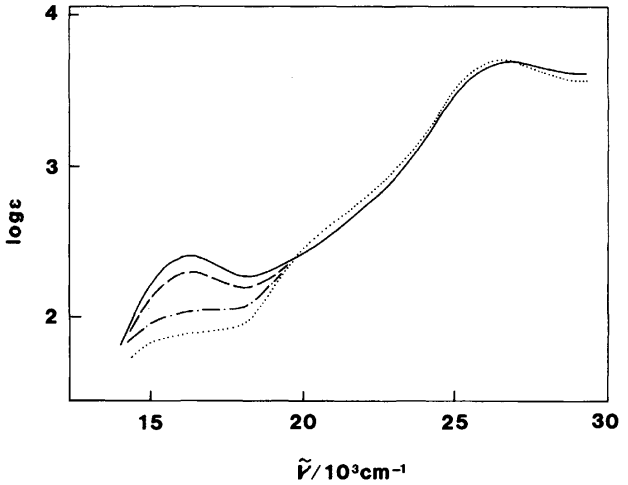

Fig. 1. Absorption spectra of the CO_3-complex: (——) in 10% $KHCO_3$ (1×10^{-3} M), (— —) in 1% $KHCO_3$ (1×10^{-3} M), (— · —) in water (1×10^{-2} M), and (·····) in water (1×10^{-3} M).

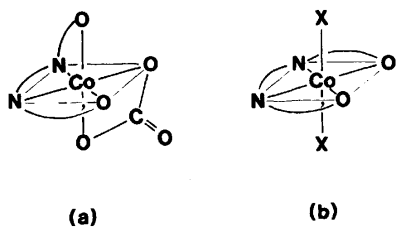

Fig. 2. Schematical representations of (a) *cis*-β-[Co(salen)CO_3]$^-$ and (b) *trans*-[Co(salen)X_2]$^-$ ($^-O\cap N\cap N\cap O^- = N,N'$-disalicylideneethylenediaminate ion).

As is seen in Fig. 1, the 16.3×10^3 cm^{-1} band diminishes its extinction coefficient with lowering of the hydrogencarbonate concentration or diluting the solution with water. This spectral behavior suggests the ligand substitution and/or the configurational change of the complex in aqueous solution. Since the electronic spectrum of a dilute aqueous solution is very similar to that of *trans*-[Co(salen)$(H_2O)_2]^+$,[22] the following equilibrium is supposed for the complex: *cis*-β-[Co(salen)$CO_3]^- + 2H_2O \rightleftharpoons$ *trans*-[Co(salen)$(H_2O)_2]^+ + CO_3^{2-}$. Therefore, we presume that either *cis*-β-[Co(salen)$CO_3]^-$ or *trans*-[Co(salen)$(H_2O)_2]^+$ functions as a catalyst in the oxidative degradation of guaiacol.[15] In oxygen delignification in a dilute sodium hydroxide solution, *trans*-[Co(salen)$(H_2O)_2]^+$ must be the active species. However, this does not rule out the possibility of the catalytic function of *cis*-β-[Co(salen)$CO_3]^-$ in oxygen delignification in the presence of bicarbonate or carbonate ion.

It is also noted in this study that the CO_3-complex can be used as a starting material for the preparation of *trans*-[Co(salen)$X_2]^-$ (X=N_3, CN) and [Co(salen)$B_2]^+$ (B=py, NH_3) (Fig. 2b).

The oxygenation reactions of 2,4,6-tri-*t*-butylphenol and 2,6-di-*t*-butyl-4-methylphenol have been examined by the use of the CO_3-, $(N_3)_2$-, $(CN)_2$-, $(py)_2$-, and $(NH_3)_2$-complexes as catalysts, and the results are given in Table 1. The characterized major products are quinol (**1**), quinone (**2**), and peroxide (**3**) (Fig. 3). In the case with 2,4,6-tri-*t*-butylphenol as the substrate, the CO_3-

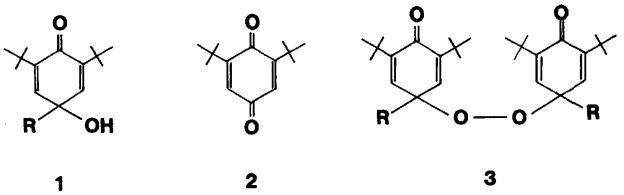

1 2 3

Fig. 3. Oxygenation products from *t*-butylphenols: (1) quinol, (2) quinone, and (3) peroxide.

Table 1. Oxygenation of *t*-butylphenols[a]

Catalyst	Substrate[b]	Conv/%	Products[c]/%		
			1	2	3
K[Co(salen)CO_3]	TBP	100	11	38	42
Na[Co(salen)$(N_3)_2$]	TBP	29	2	13	11
K[Co(salen)$(CN)_2$]	TBP	0			
[Co(salen)$(py)_2$]PF_6	TBP	0			
[Co(salen)$(NH_3)_2$]PF_6	TBP	0			
K[Co(salen)CO_3]	DBMP	45	30	15	0
Na[Co(salen)$(N_3)_2$]	DBMP	0			
K[Co(salen)$(CN)_2$]	DBMP	0			
[Co(salen)$(py)_2$]PF_6	DBMP	0			
[Co(salen)$(NH_3)_2$]PF_6	DBMP	0			

a) Reaction condition: [catalyst]=2×10^{-3}M, [substrate]/[catalyst]=50, 12 h in ethanol at room temperature. b) TBP=2, 4, 6-tri-*t*-butylphenol and DBMP=2, 6-di-*t*-butyl-4-methylphenol. c) **1**: quinol, **2**: quinone, and **3**: peroxide (*cf.* Fig. 3).

complex exhibited a high catalytic activity while the $(N_3)_2$-complex a low activity. Other complexes showed practically no catalytic activity. In the case with 2,6-di-*t*-butyl-4-methylphenol, only the CO_3-complex showed a catalytic activity. The main oxygenation product in the former was the peroxide, while the product in the latter was the quinol. It should be noted that the same oxygenation products have been obtained by the use of Co(salen) as the catalyst.[6]

The catalytic activities of the cobalt(III) complexes evidently depend upon the fifth and sixth ligands. For obtaining an insight into the differences in catalytic activities of the complexes, the absorption spectra in ethanol were investigated. The CO_3-complex in ethanol shows bands at 14.2×10^3 and $\approx21\times10^3$ cm^{-1}, attributable to d-d and intraligand transitions respectively (Fig. 4). This spectrum markedly differs from those of *cis*-β-$[Co(salen)CO_3]^-$ and *trans*-$[Co(salen)(H_2O)_2]^+$. Its molar conductivity has been determined to be 34 Ω^{-1} mol^{-1} cm in ethanol, which falls in the range for 1:1 electrolytes.[23] This indicates that carbonate ion is still bonded to the metal in this solvent. It is likely that the complex takes a configuration either of tetragonal pyramid with a unidentate carbonate ion at the apex or of an elongated octahedron with a carbonate ion and a solvent molecule at the apical positions.

The electronic spectra of the $(N_3)_2$-complex are shown in Fig. 4. The spectrum in ethanol differs from that in water containing excess of sodium azide. Further, $[Co(salen)N_3]$ shows the same spectrum as that of the $(N_3)_2$-complex in ethanol. These facts imply that the possible species of the $(N_3)_2$-complex in ethanol is $[Co(salen)N_3]$ or $[Co(salen)N_3(EtOH)]$.

A marked spectral change was also observed for the $(CN)_2$-complex when measured in water containing excess potassium cyanide and in ethanol (Fig. 5). Thus, the complex must have undergone some change in

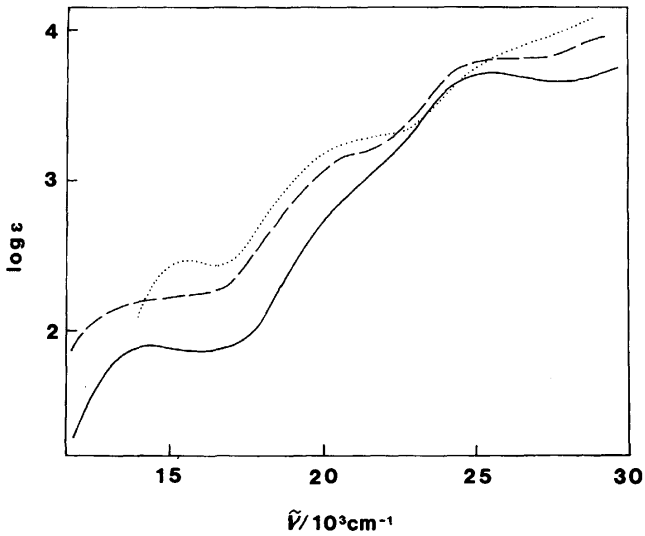

Fig. 4. Absorption spectra of the CO_3-complex in ethanol (——) and the $(N_3)_2$-complex in 2% NaN_3 solution (·····) and in ethanol (— —).

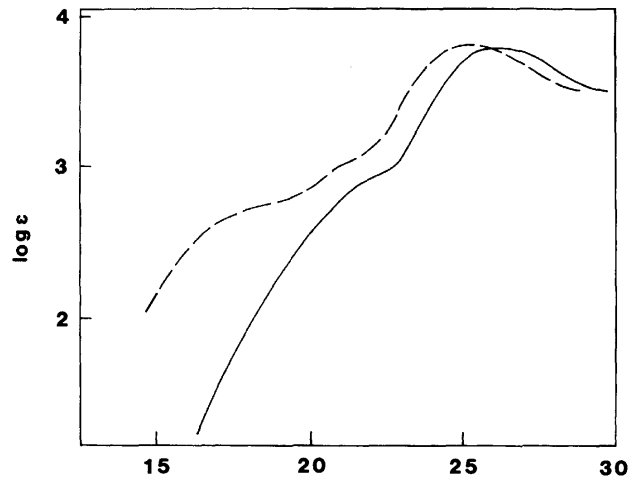

Fig. 5. Absorption spectra of the $(CN)_2$-complex in 2% KCN solution (——) and in ethanol (— —).

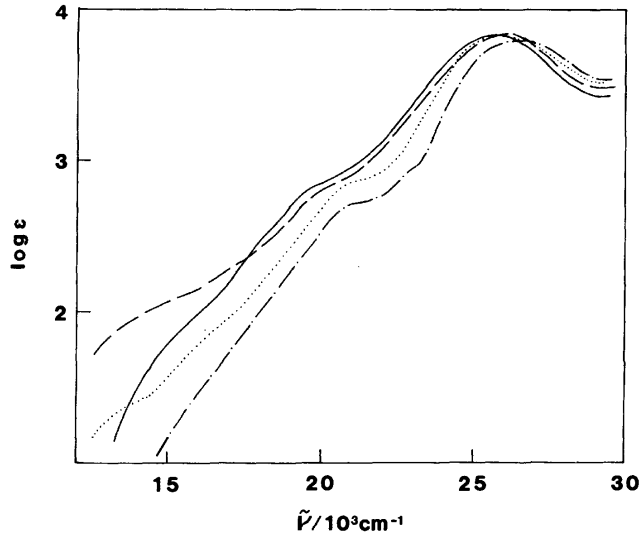

Fig. 6. Absorption spectra of the $(py)_2$-complex in pyridine (——) and in ethanol (— —) and the $(NH_3)_2$-complex in 18% ammonia (— · —) and in ethanol (·····).

ethanol in more or less degree. The spectrum in ethanol is characterized by an absorption at $\approx18\times10^3$ cm^{-1}. A similar absorption band was observed for the five-coordinate [RCo(salen)] (R=alkyl anion) and its homologs.[24-27] We have examined the electronic spectra of the ethanol solutions of the CO_3-complex containing potassium cyanide in various amounts, and found that the extinction coefficient at $\approx18\times10^3$ cm^{-1} becomes maximal when [Co]/[CN]=1. This suggests that [Co(salen)(CN)] or [Co(salen)(CN)(EtOH)] is formed in the solution.

Each spectrum of the $(py)_2$- and $(NH_3)_2$-complexes in ethanol differs from the spectrum in water containing the corresponding base (Fig. 6). Hence, the complex species in ethanol differs from $[Co(salen)B_2]^+$. Since the spectra of the $(py)_2$-complex and $[Co(salen)(py)]PF_6$ are practically the same in ethanol, the species in both solutions are likely to be $[Co(salen)(py)]^+$ or [Co(salen)-

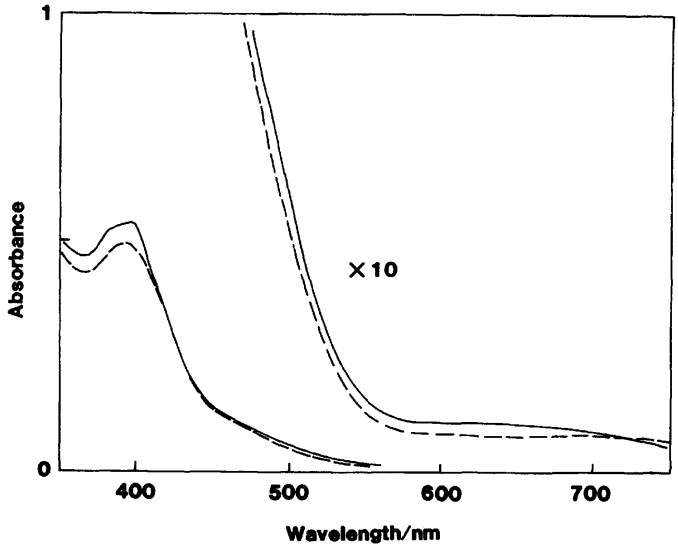

Fig. 7. Electronic spectral change on adding 2,4,6-tri-*t*-butylphenol to an ethanolic solution of the CO_3-complex: (——) CO_3-complex (1×10^{-3} M) and (——) CO_3-complex (1×10^{-3} M)+2,4,6-tri-*t*-butylphenol (1×10^{-2} M).

$(py)(EtOH)]^+$. A similar feature is supposed for the $(NH_3)_2$-complex in ethanol.

Above spectral investigations suggest that all the complexes take an essentially identical configuration; a tetragonal pyramid or an elongated octahedron. Therefore, it is difficult to explain the catalytic activity of the CO_3-complex solely in terms of configurational aspect.

It seems that the high catalytic activity of the CO_3-complex relative to the other complexes is attributable to the high lability of the carbonate ion. In order to verify this, the absorption spectrum of the CO_3-complex in the presence of ten times of 2,4,6-tri-*t*-butylphenol was examined under a nitrogen atmosphere. As seen in Fig. 7, the intensity around 390 nm increased and a new absorption appeared around 630 nm when the substrate was added, suggesting the generation of 2,4,6-tri-*t*-butylphenoxyl radical.[28] Further, this complex/substrate solution exhibited a three-lined ESR signal with a coupling constant of 1.7 gauss near $g\approx2.0$. This signal is very similar to that of 2,4,6-tri-*t*-butylphenoxyl radical,[29] though the hyperfine structures due to the tertiary butyl groups are absent probably because of the presence of the paramagnetic species ([Co(salen)]) in the solution. All these facts indicate that the CO_3-complex oxidizes the phenol to the phenoxyl radical. The preliminary electrochemical investigations have revealed that the Co^{III}/Co^{II} redox potential of the CO_3-complex (−1.2 V *vs.* SCE in ethanol, glassy carbon electrode) is much lower than that of the $(py)_2$-complex.[30,31] This fact suggests that the electron transfer between the CO_3-complex and a *t*-butylphenol is of inner-sphere rather than outer-sphere, through a five-coordinate intermediate with the phenolate group at the apical position. Thus, the mechanism of the catalytic oxygenation with the CO_3-complex may be represented as follows: (1) The substitution of the apical carbonate ion for the phenolate ion to form a phenolatocobalt(III) intermediate, (2) the intramolecular electron transfer to generate Co^{II} (salen) and the phenoxyl radical, and (3) the progression of radical reactions with molecular oxygen (Fig. 8).

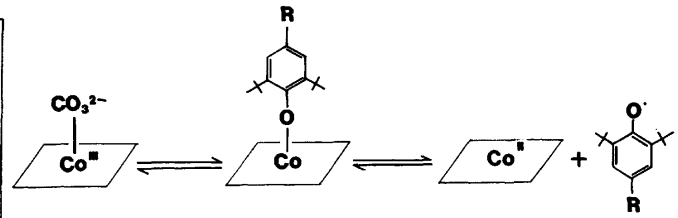

Fig. 8. Catalytic scheme for the oxygenation with the CO_3-complex.

Table 2. Oxygenation of 2,4,6-tri-*t*-butylphenol with [Co(salen)] in the presence of additives[a]

Additive	Conv/%	Products[b]/%		
		1	2	3
none[c]	85	—	24	53
KCN	0			
py	0			

a) Reaction condition: [catalyst]=2×10^{-3} M, [substrate]/[catalyst]=50, [additive]/[catalyst]=10, 12 hrs in ethanol at room temperature. b) *Cf.* Fig. 3. c) Results from Ref. 6, the solvent being methanol.

It is shown that the phenol/phenoxyl redox potential depends upon the substituent on the ring and becomes lower when a more electron donative substituent is introduced into the ring.[32] The ready oxidation of 2,4,6-tri-*t*-butylphenol relative to 2,6-di-*t*-butyl-4-methylphenol is probably due to the generation of the phenoxyl radical in a higher concentration in the former, since the *t*-butyl group is slightly more electron donative than the methyl group. Indeed, the electronic spectrum of the CO_3-complex (in ethanol under nitrogen atmosphere) showed a very little increase around 400 and 630 nm when 2,6-di-*t*-butyl-4-methylphenol (ten times) was added.

The low catalytic activities of the $(N_3)_2$-, $(CN)_2$-, $(py)_2$-, and $(NH_3)_2$-complexes may be due to the difficulties in forming the phenolatocobalt(III) intermediate with these complexes, because of the strong donating abilities of the apical ligands compared with the phenolate ion.

We have further examined the catalytic activity of [Co(salen)] on the oxygenation reactions of *t*-butylphenols in the presence of a donating additive. The results are given in Table 2. Contrary to a high catalytic activity in the absence of an additive,[6] the activity of [Co(salen)] for the oxygenation reaction was almost suppressed on adding cyanide ion or pyridine to the reaction system. This fact again demonstrates that the additives coordinate at the apical position of the air-oxidized Co^{III} (salen) and thence deactivate the catalytic function of [Co(salen)].

References

1) T. D. Smith and J. R. Pilbrow, *Coord. Chem. Rev.*, **39**, 295 (1981).
2) R. T. Jones, D. A. Summerville, and F. Basolo, *Chem. Rev.*, **79**, 139 (1979).
3) L. H. Vogt, Jr., J. G. Wirth, and H. L. Finkbeiner, *J. Org. Chem.*, **34**, 273 (1969).
4) A. Nishinaga, T. Itahara, and T. Matsuura, *Chem. Lett.*, **1974**, 667.
5) T. J. Fullerton and S. P. Ahern, *Tetrahedron Lett.*, **1976**, 139.
6) A. Nishinaga, K. Watanabe, and T. Matsuura, *Tetrahedron Lett.*, **1974**, 1291.
7) A. Nishinaga, T. Shimizu, and T. Matsuura, *Tetrahedron Lett.*, **21**, 1261 (1980).
8) A. Nishinaga, H. Tomita, and T. Matsuura, *Tetrahedron Lett.*, **21**, 1265 (1980).
9) A. Nishinaga, K. Nishizawa, H. Tomita, and T. Matsuura, *J. Am. Chem. Soc.*, **99**, 1289 (1977).
10) A. Nishinaga, H. Tomita, K. Nishizawa, T. Matsuura, S. Ooi, and K. Hirotsu, *J. Chem. Soc., Dalton*, **1981**, 1504.
11) A. Zombeck, R. S. Drago, B. B. Corden, and J. H. Gaul, *J. Am. Chem. Soc.*, **103**, 7580 (1981).
12) A. Nishinaga, *Chem. Lett.*, **1975**, 273.
13) M. N. Dufour-Ricroch and A. Gaudemer, *Tetrahedron Lett.*, **1976**, 4079.
14) T. J. Fullerton and S. P. Ahern, *Tappi*, **61**, 37 (1978).
15) S. Meguro, K. Sakai, and H. Imamura, *Mokuzai Gakkaishi*, in press.
16) K. Nakamoto, "Infrared Spectra of Inorganic and Coordination Compounds," 2nd ed., Wiley-Intersci., New York (1970), p. 169.
17) K. Day and R. L. De, *Z. Anorg. Allg. Chem.*, **402**, 120 (1973).
18) S. N. Podder and D. K. Biswas, *J. Inorg. Nucl. Chem.*, **31**, 565 (1969).
19) M. Nakamura, H. Ōkawa, T. Inazu, and S. Kida, *Bull. Chem. Soc. Jpn.*, **55**, 2400 (1982).
20) R. A. D. Wentworth and T. S. Piper, *Inorg. Chem.*, **4**, 202 (1965).
21) L. J. Boucher, *Inorg. Chim. Acta*, **6**, 29 (1972).
22) S. Yamada, H. Nishikawa, and E. Yoshida, *Proc. Japan Acad.*, **40**, 211 (1964).
23) W. J. Geary, *Coord. Chem. Rev.*, **7**, 81 (1971).
24) G. Costa, G. Mestroni, and L. Stefani, *J. Organomet. Chem.*, **7**, 493 (1967).
25) R. H. Bailes and M. Calvin, *J. Am. Chem. Soc.*, **69**, 1886 (1947).
26) M. Calvin, R. H. Bailes, and W. K. Wilmarth, *J. Am. Chem. Soc.*, **68**, 2254 (1946).
27) M. Calvin and C. H. Barkelew, *J. Am. Chem. Soc.*, **68**, 2267 (1946).
28) E. J. Land, G. Porter, and E. Strachan, *Trans. Faraday Soc.*, **57**, 1885 (1961).
29) K. Mukai, H. Nishiguchi, K. Ishizu, Y. Deguchi, and H. Takaki, *Bull. Chem. Soc. Jpn.*, **40**, 2731 (1967).
30) G. Costa, G. Mestroni, A. Puxeddu, and E. Reisenhofer, *J. Chem. Soc. (A)*, **1970**, 2870.
31) D. F. Averill and R. F. Broman, *Inorg. Chem.*, **17**, 3389 (1978).
32) H. Mauser and B. Nickel, *Angew. Chem.*, **77**, 378 (1965).

Crystal Structure of Nonstoichiometric Tetranuclear Platinum Compound, *cis*-Diammineplatinum α-Pyrrolidone Violet, $[Pt_4(NH_3)_8(C_4H_6NO)_4](PF_6)_2(NO_3)_{2.56}\cdot 5H_2O$

Kazuko MATSUMOTO

Department of Chemistry, School of Science and Technology, Waseda University, Okubo, Shinjuku-ku, Tokyo 160

(Received July 19, 1984)

Nonstoichiometric platinum tetranuclear compound, *cis*-Diammineplatinum α-Pyrrolidone Violet, $[Pt_4(NH_3)_8(C_4H_6NO)_4](PF_6)_2(NO_3)_{2.56}\cdot 5H_2O$, has been synthesized and the crystal structure has been solved with X-ray diffraction analysis. The crystal is triclinic with the space group of $P\bar{1}$ and cell dimensions of a=13.530(8), b=19.242(9), c=10.222(3) Å, α=96.56(9), β=93.82(9), γ=74.64(8)°, V=2547.4 Å^3, and Z=2. The structure have been solved by heavy atom method and the final discrepancy index R_1 was 0.094 and R_2 was 0.090. The cation is structurally identical with those of *cis*-Diammineplatinum α-Pyridone Yellow(PPY), $[Pt_4(NH_3)_8(C_5H_4NO)_4]^{4+}$, *cis*-Diammineplatinum α-Pyridone Blue(PPB), $[Pt_4(NH_3)_8((C_5H_4NO)_4]^{5+}$, and *cis*-Diammineplatinum α-Pyrrolidone Tan(PPT), $[Pt_4(NH_3)_8(C_4H_6NO)_4]^{6+}$, and consists of four platinum atoms linked in a chain with bridging pyrrolidone ligands. Each platinum atom is cis coordinated by two ammine ligands and either two exocyclic oxygen atoms or two deprotonated ring nitrogen atoms of α-pyrrolidone ligands. The Pt-Pt bond distances are 2.848(2), 2.875(2), 2.839(2), and 2.875(2) Å, which are intermediate between those of PPY and PPB, indicating that the average platinum oxidation state is between 2.0 and 2.25. According to the potentiometric oxidative titration of the compound using Ce(IV), the average platinum oxidation state is 2.14 and therefore the compound is considered to consist of 44% of $[Pt_4(NH_3)_8(C_4H_6NO)_4]^{4+}$ and 56% of $[Pt_4(NH_3)_8(C_4H_6NO)_4]^{5+}$.

Although a class of dark blue platinum compounds, so called "Platinum Blues," was first reported as early as 1908[1] and have attracted interest of chemists because of their abnormally deep blue color and paramagnetic nature,[2-4] their structure and formulas have long been unknown, because they are unstable in solution, difficult to synthesize reproducibly and to obtain crystals.

Recently, Barton *et al.* first reported the synthesis of crystalline *cis*-Diammineplatinum α-Pyridone Blue (PPB), $[Pt_4(NH_3)_8(C_5H_4NO)_4](NO_3)_5\cdot H_2O$, and solved the structure by X-ray analysis.[5,6] The compound is a tetranuclear chain cation, whose neighboring platinum atoms are bridged by amide oxygen and deprotonated amide nitrogen atoms. Three of the platinum atoms are formally in the oxidation state of +2, and the remaining one is +3; that is, the average platinum oxidation state is +2.25, although the four platinum atoms are actually rather equivalent and the one unpaired electron is delocalized over the four platinum atoms.[6]

Following the synthesis and structure determination of PPB, several platinum-blue related compounds have been isolated and structurally elucidated. These include *cis*-Diammineplatinum α-Pyridone Yellow (PPY), $[Pt_4(NH_3)_8(C_5H_4NO)_4](NO_3)_4$,[7] *cis*-Diammineplatinum 1-Methylhydantoin Yellow (PHY), $[Pt_4(NH_3)_8(C_4H_5N_2O_2)_4](NO_3)_4\cdot H_2O$,[8] *cis*-Diammineplatinum α-Pyrrolidone Tan (PPT), $[Pt_4(NH_3)_8(C_4H_6NO)_4](NO_3)_6\cdot 2H_2O$,[9,10] and *cis*-Diammineplatinum α-Pyrrolidone Green (PPG), $[Pt_4(NH_3)_8(C_4H_6NO)_4](NO_3)_{5.48}\cdot 3H_2O$.[11] The last compound is nonstoichiometric, being a mixture of diamagnetic hexavalent PPT cation and paramagnetic PPB-corresponding quinquevalent cation. This nonstoichiometry has been confirmed both with single crystal X-ray diffraction analysis and magnetic susceptibility measurement.[11] PPT consists of two Pt(II) and two Pt(III) atoms, whose two unpaired electrons are strongly diamagnetically coupled.[10] PPY and PHY have all their four platinum atoms in the oxidation state of 2+ and are therefore diamagnetic. These compounds reveal that "Platinum Blues" are a class of compounds whose platinum oxidation state can be varied without basic structural change and the color varies according to the platinum oxidation state.

In this paper, another platinum blue related compound, *cis*-Diammineplatinum α-pyrrolidone Violet (PPV), is reported. This compound is nonstoichiometric, being a mixture of PPB-corresponding quinquevalent cation and PPY-corresponding quadrivalent cation. A preliminary report on the structural analysis of the compound has been publlshed previously,[12] Therefore the details of the crystal structure is reported here, together with the result of the potentiometric oxidative titration using Ce(IV), which confirms the average platinum oxidation state of 2.14.

Experimental

Preparation. The preparation procedure of the compound has been already reported in Ref. 12. The results of the elemental analyses are: Found: C, 10.79; H, 3.32; N, 11.70; Pt, 43.4%. Calcd for $[Pt_4(NH_3)_8(C_4H_6NO)_4](PF_6)_2(NO_3)_{2.56}\cdot 5H_2O$: C, 10.72; H, 3.27; N, 11.38; Pt, 43.55%.

Crystal Data. The single crystal of the compound used for intensity measurement was 0.25×0.2×0.1 mm. Preliminary Weissenberg photographs of the crystal showed it is monoclinic. Unit cell parameters were obtained from least-squares fit of 20 reflections in the range of $20°<2\theta<35°$ measured on a Philips PW1100 diffractometer using graphite-monochromated Mo $K\alpha$ radiation. The crystal data are as follows:

$[Pt_4(NH_3)_8(C_4H_6NO)_4](PF_6)_2(NO_3)_{2.56}\cdot 5H_2O$
triclinic $P\bar{1}$
a = 13.530(8)

$b = 19.242(9)$
$c = 10.222(3)$ Å
$\alpha = 96.56(9)$
$\beta = 93.82(9)$
$\gamma = 74.64(8)°$
$v = 2547.4$ Å^3
MW = 1791.9
$Z = 2$
$D_m = 2.40$
$D_x = 2.34$ g cm^{-3}
$\mu = 117.4$ cm^{-1} (for Mo $K\alpha$ radiation)

Data Collection. All the intensities within $3°<2\theta<55°$ were measured on a Philips PW1100 four-cirle diffractometer. The scan mode was ω—2θ, with a scan rate of 2° min^{-1} in 2θ. The scan range was calculated for each reflection according to the formula, $\omega=1.2+0.3\tan\theta$, and stationary-crystal, stationary-counter background measurement was employed. The background measurement time, T_{bck}, was determined according to the formula, T_{bck}=(scan time)/$2(I_{bck}/I_{int})^{1/2}$, where I_{bck} (counts/s) is average value preliminarily measured at both ends and I_{int} (counts/s) is the value of the peak. The measurement was carried out on a crystal sealed in a glass capillary in order to avoid crystal deterioration after long irradiation. Three standard reflections were monitored every two hours, however only random statistical fluctuations were observed throughout the measurement. The data were corrected for the Lorentz-polarization effects and absorption. A total of 8377 reflections with $|F_o|\geq 3\sigma(|F_o|)$ were used for calculation.

Solution and Refinement of the Structure. The coordinates of the four platinum atoms were found from a Patterson map, and a series of block-diagonal least-squares refinements followed by Fourier synthesis revealed all the oxygen, nitrogen, and carbon atoms in the α-pyrrolidonate and ammine ligands. After further refinement of the coordinates with anisotropic temperature factors for all the atoms, a difference synthesis was calculated and all the nitrate and hexafluorophosphate anions and water molecules of crystallization were located. Hydrogen atoms could not be located even with a difference synthesis using the refined coordinates of all the atoms. The structure was finally refined with anisotropic temperature factors for all the atoms to the final discrepancy index of R_1=0.094 and R_2=0.090, where $R_1=\sum||F_o|-|F_c||/\sum|F_o|$ and $R_2=[\sum w_i||F_o|-|F_c||^2/\sum w_i|F_o|^2]^{1/2}$. The weight of each reflection was determined as $w_i=1/\sigma^2(F_o)$. Atomic scattering factors were taken from Ref. 13, and the anomalous dispersion corrections were based on Ref. 14. All the calculations were performed with the local version of

TABLE 1. POSITIONAL AND ISOTROPIC PARAMETERS WITH THEIR STANDARD DEVIATIONS IN PARENTHESES. POSITIONAL PARAMETERS ARE MULTIPLIED BY 10^5 FOR PLATINUM AND BY 10^3 FOR THE OTHER

	X	Y	Z	B_{eq}/Å^2
PT 1	2758 (10)	6696 (7)	3671 (14)	3.0(1)
PT 2	12852 (12)	18015 (7)	9033 (16)	3.5(1)
PT 3	48319 (11)	55246 (6)	40591 (13)	2.9(1)
PT 4	46160 (13)	67446 (7)	26392 (14)	3.6(1)
NH1	−76 (3)	110 (2)	−99 (3)	4.3(4)
NH2	−80 (2)	100 (2)	183 (3)	4.0(3)
NH3	51 (3)	255 (2)	−40 (4)	5.7(4)
NH4	45 (3)	246 (2)	250 (3)	5.1(4)
NH5	533 (3)	473 (2)	249 (3)	4.9(4)
NH6	336 (4)	545 (2)	371 (3)	5.6(4)
NH7	490 (3)	631 (2)	70 (3)	4.9(4)
NH8	319 (3)	704 (2)	221 (3)	5.0(4)
O11	131 (2)	30 (1)	−106 (2)	3.7(3)
N11	216 (2)	121 (2)	−61 (3)	3.7(3)
C11	200 (3)	60 (2)	−121 (3)	3.3(3)
C21	282 (3)	30 (2)	−226 (4)	5.0(4)
C31	353 (6)	82 (4)	−206 (7)	10.2(7)
C41	308 (5)	141 (3)	−97 (6)	7.6(6)
O12	124 (2)	21 (1)	176 (3)	4.4(4)
N12	206 (2)	114 (2)	214 (3)	3.9(4)
C12	189 (3)	50 (2)	236 (4)	4.4(4)
C22	263 (4)	16 (2)	343 (5)	5.2(5)
C32	339 (5)	61 (4)	371 (7)	9.4(7)
C42	291 (4)	131 (3)	292 (6)	6.9(5)
O13	614 (3)	557 (1)	446 (2)	5.5(4)
N13	610 (4)	660 (2)	303 (3)	6.7(5)
C13	664 (3)	603 (2)	376 (4)	4.3(4)
C23	774 (4)	602 (3)	393 (5)	6.0(5)
C33	774 (6)	668 (4)	327 (10)	11.5(7)
C43	670 (5)	694 (3)	262 (7)	7.5(6)
O14	438 (2)	628 (1)	564 (2)	4.1(3)
N14	434 (3)	723 (1)	448 (3)	4.0(3)
C14	432 (3)	697 (2)	561 (4)	4.0(3)
C24	408 (4)	750 (2)	675 (4)	4.8(4)
C34	411 (7)	819 (3)	622 (6)	9.9(7)
C44	423 (6)	804 (2)	472 (4)	8.4(7)
P 1	617 (1)	138 (1)	−40 (1)	4.3(4)
P 2	289 (1)	349 (1)	191 (1)	5.8(4)
F 1	698 (2)	144 (1)	−145 (3)	6.7(6)
F 2	707 (3)	129 (2)	67 (4)	9.8(8)
F 3	542 (3)	134 (2)	65 (3)	7.8(6)
F 4	529 (2)	152 (2)	−147 (4)	9.4(8)
F 5	639 (3)	55 (1)	−76 (4)	10.0(7)
F 6	604 (3)	223 (1)	−1 (3)	8.9(6)
F 7	333 (6)	277 (3)	109 (7)	20.9(11)
F 8	393 (4)	373 (3)	191 (7)	16.1(10)
F 9	337 (5)	318 (3)	328 (4)	15.0(11)
F10	241 (4)	425 (2)	271 (6)	14.8(10)
F11	190 (5)	321 (5)	218 (8)	22.1(13)
F12	251 (6)	378 (3)	67 (5)	19.1(13)
N 1	291 (3)	530 (2)	5 (3)	4.8(4)
N 2	790 (3)	290 (2)	113 (4)	5.6(4)
N 3	12 (5)	826 (3)	425 (5)	4.7(4)
N 4	38 (17)	462 (20)	409 (27)	31.2(14)
O 1	265 (4)	504 (2)	−97 (4)	9.0(8)
O 2	386 (3)	520 (2)	34 (4)	7.3(5)
O 3	233 (4)	563 (2)	84 (4)	9.4(7)
O 4	832 (3)	260 (2)	13 (3)	6.5(6)
O 5	824 (3)	263 (2)	223 (4)	7.5(6)
O 6	704 (3)	337 (2)	110 (3)	7.0(6)
O 7	−56 (8)	840 (6)	344 (10)	11.9(9)
O 8	96 (6)	833 (4)	437 (7)	9.6(8)
O 9	−47 (12)	855 (8)	503 (15)	15.9(13)
O10	115 (12)	497 (7)	410 (10)	13.9(11)
O11	−43 (15)	465 (10)	480 (21)	22.7(12)
O12	23 (17)	459 (17)	286 (26)	39.3(13)
OW 1	−36 (21)	593 (9)	27 (25)	24.4(14)
OW 2	−52 (8)	397 (5)	159 (13)	7.8(7)
OW 3	418 (48)	87 (28)	347 (46)	21.3(9)
OW 4	30 (25)	836 (15)	553 (10)	24.2(11)
OW 5	76 (11)	789 (6)	311 (11)	10.0(8)
OW 6	−4 (13)	−102 (6)	385 (14)	14.3(10)
OW 7	−24 (16)	−206 (15)	444 (16)	18.0(12)
OW 8	−200 (16)	366 (9)	437 (17)	16.1(14)
OW 9	−200 (12)	402 (7)	393 (14)	10.9(9)
OW10	−205 (10)	328 (7)	492 (15)	11.0(10)
OW11	651 (30)	159 (12)	396 (32)	29.9(12)

the program UNICS (Sakurai, 1967) and ORTEP (Johnson, 1965).

The final positional and thermal parameters of non-hydrogen atoms are listed in Table 1. The observed and calculated structure factors and anisotropic temperature factors are avilable at the office of this Bulletin (Document No. 8516).

Oxidative Titration. In order to confirm the average platinum oxidation state, oxidative titration using Ce(IV) was carried out. The titration was monitored potentiometrically by using platinum *vs.* AgCl electrodes. The titrant Ce(IV) was prepared by dissolving ammonium cerium(IV) sulfate in 0.36 mol dm^{-3} sulfuric acid to the concentration of 6.1×10^{-3} mol dm^{-3}. About 0.01 g of *cis*-Diammineplatinum α-Pyrrolidone Violet was weighed and dissolved in 40 ml of 0.1 mol dm^{-3} nitric acid. Both the titrand and the titrant were degassed with argon before titration and were also protected from the air by argon flow during the titration.

Description of the Structure and Discussion

Unit cell has two independent platinum tetranuclear cations. The structure of one of them and the atomic-numbering schemes are depicted in Ref. 12. The interatomic distances and bond angles within the cations are listed in Tables 2 and 3, respectively. The cation consists of four platinum atoms linked in a chain with bridging pyrrolidone ligands. Each platinum atom is cis coordinated by two ammine ligands and either two exocyclic oxygen atoms or two deprotonated ring nitrogen atoms of α-pyrrolidone ligands. Each cation has crystallographic center of symmetry at the midpoint of Pt1-Pt1′ and Pt3-Pt3′ bonds, respectively. These central Pt-Pt bondings are achieved by partial metal-metal bonding and probably also by hydrogen bonding between ammine hydrogen atoms and exocyclic oxygen atoms of α-pyrrolidone ligands coordinated to adjacent platinum atoms. The structure of the cation is basically identical with those of PPB, PPY, PHY, PPT, and PPG. The Pt-Pt bond distances are closely related to the average platinum oxidation state in the tetranuclear platinum chain compounds[10] as well as in one-dimensional platium complexes.[15] The Pt-Pt bond length of PPV suggests that the compound consists of platinum atoms with intermediate oxidation state between 2.0 and 2.25.[12] The compound contains 2.56 nitrate anions per cation as concluded later in the discussion of the oxidative titration using Ce(IV). From the X-ray diffraction analysis, two nitrate anions (N1 and N2) have been located with statistical weight of unity, and another two (N3 and N4), with statistical weight of less than unity. The latter two are considered to be distributed in the crystal lattice with a weight of 0.56/2. However, no definite conclusion can be drawn concerning the platinum oxidation state, simply from the number of nitrate anions found in the crystal lattice. The average platinum oxidation state has been confirmed by oxidative titration and the detail is described later in this paper.

Table 2. Interatomic distances (l/Å) within the cations with their estimated standard deviations in parentheses

Coordination Spheres			
Pt1–Pt2	2.848(2)	Pt3–Pt4	2.839(2)
Pt1–Pt1′	2.875(2)	Pt3–Pt3′	2.875(2)
Pt1–NH1	1.99(3)	Pt3–NH5	2.10(2)
Pt1–NH2	2.09(3)	Pt3–NH6	2.04(4)
Pt1–O11	2.02(2)	Pt3–O13	1.82(5)
Pt1–O12	1.98(2)	Pt3–O14	2.06(2)
Pt2–NH3	2.10(3)	Pt4–NH7	2.08(2)
Pt2–NH4	2.13(3)	Pt4–NH8	1.90(4)
Pt2–N11	2.05(2)	Pt4–N13	1.98(5)
Pt2–N12	1.96(3)	Pt4–N14	2.01(2)
Pt2–F11	3.15(8)		
Pyrrolidone Rings			
O11–C11	1.26(4)	O13–C13	1.51(5)
C11–C21	1.54(5)	C13–C23	1.49(6)
C21–C31	1.56(10)	C23–C33	1.52(10)
C31–C41	1.53(8)	C33–C43	1.50(9)
N11–C41	1.49(7)	N13–C43	1.28(8)
O12–C12	1.26(5)	O14–C14	1.30(4)
C12–C22	1.52(5)	C14–C24	1.46(4)
C22–C32	1.51(9)	C24–C34	1.51(7)
C32–C42	1.62(9)	C34–C44	1.53(7)
N12–C42	1.44(6)	N14–C44	1.52(4)

Table 3. Interatomic bond angles (ϕ/°) in the cations with their estimated standard deviations in parentheses

Coordination Spheres			
Pt2–Pt1–Pt1′	166.53(6)	Pt4–Pt3–Pt3′	168.31(6)
NH1–Pt1–NH2	91.3(13)	NH5–Pt3–NH6	90.6(16)
NH1–Pt1–N11	96.7(11)	NH5–Pt3–O13	90.8(15)
NH1–Pt1–N12	136.6(11)	NH5–Pt3–O14	178.0(9)
NH2–Pt1–N11	137.3(11)	NH6–Pt3–O13	176.5(19)
NH2–Pt1–N12	94.6(11)	NH6–Pt3–O14	90.3(15)
N11–Pt1–N12	52.5(9)	O13–Pt3–O14	88.2(14)
NH3–Pt2–NH4	90.0(14)	NH7–Pt4–NH8	90.3(15)
NH3–Pt2–O11	89.1(11)	NH7–Pt4–N13	90.5(17)
NH3–Pt2–O12	139.2(11)	NH7–Pt4–N14	176.4(11)
NH4–Pt2–O11	139.7(10)	NH8–Pt4–N13	170.6(20)
NH4–Pt2–O12	97.8(10)	NH8–Pt4–N14	89.1(15)
O11–Pt2–O12	52.1(6)	N13–Pt4–N14	89.5(17)
Pyrrolidone Rings			
Pt2–N11–C11	123 (2)	Pt4–N13–C13	120 (3)
Pt2–N11–C41	120 (3)	Pt4–N13–C43	128 (3)
Pt1–O11–C11	122 (2)	Pt3–O13–C13	122 (2)
N11–C11–O11	129 (3)	N13–C13–O13	124 (3)
N11–C11–C21	109 (3)	N13–C13–C23	111 (4)
O11–C11–C21	122 (3)	O13–C13–C23	124 (3)
C11–C21–C31	104 (4)	C13–C23–C33	100 (4)
C21–C31–C41	107 (5)	C23–C33–C43	108 (6)
C31–C41–N11	103 (4)	C33–C43–N13	108 (5)
Pt2–N12–C12	126 (2)	Pt4–N14–C14	132 (2)
Pt2–N12–C42	119 (3)	Pt4–N14–C44	118 (2)
Pt1–O12–C12	123 (2)	Pt3–O14–C14	122 (2)
N12–C12–O12	127 (3)	N14–C14–O14	121 (3)
N12–C12–C22	111 (3)	N14–C14–C24	116 (3)
O12–C12–C22	123 (3)	O14–C14–C24	123 (3)
C12–C22–C32	106 (4)	C14–C24–C34	103 (3)
C22–C32–C42	104 (4)	C24–C34–C44	108 (3)
C32–C42–N12	104 (4)	C34–C44–N14	103 (3)

TABLE 4. CHARACTERISTIC BOND LENGTHS IN COORDINAITON SPHERES OF PLATINUM TETRANUCLEAR COMPOUNDS

Compound	Av Pt oxdn state	Distance (l/Å) Pt–Pt	Pt–L_{axial}	Ref
$[Pt_4(NH_3)_8(C_5H_4NO)_4](NO_3)_4$ α-pyridone (PPY)	2.0	2.88[a] 3.13[b]		7
$[Pt_4(NH_3)_8(C_4H_5N_2O_2)_4](NO_3)_4 \cdot H_2O$ 1-methylhydantoin (PHY)	2.0	3.131[a] 3.204[b]		8
$[Pt_4(NH_3)_8(C_4H_6NO)_4](PF_6)_2(NO_3)_{2.56} \cdot 5H_2O$ α-Pyrrolidone (PPV)	2.14	2.848[a] 2.839[a] 2.875[b] 2.875[b]	3.15 (PF_6^-)	this work
$[Pt_4(NH_3)_8(C_5H_4NO)_4](NO_3)_5 \cdot H_2O$ α-Pyridone (PPB)	2.25	2.7745[a] 2.8770[b]	3.32 (NO_3^-)	6
$[Pt_4(NH_3)_8(C_4H_6NO)_4](NO_3)_{5.48} \cdot 3H_2O$ α-Pyrrolidone (PPG)	2.37	2.764[a] 2.761[a] 2.739[b] 2.724[b] 2.740[a] 2.753[a]	3.21 (NO_3^-) 2.95 (NO_3^-)	11
$[Pt_4(NH_3)_8(C_4H_6NO)_4](NO_3)_6 \cdot 2H_2O$ α-Pyrrolidone (PPT)	2.5	2.70[a] 2.71[b] 2.70[a]	2.60 (NO_3^-) 2.72 (NO_3^-)	10

a) Bond length related to terminal Pt–Pt bond. b) Bond length related to central Pt–Pt bond.

TABLE 5. CHARACTERISTIC BOND ANGLES IN PLATINUM TETRANUCLEAR COMPOUNDS

Compound	Dihedral angle,[c] deg τ	Dihedral angle,[c] deg ω	Pt–Pt–Pt Angle, deg	Ref
PPY	30.0[a]	21	158.40	7
PHY			160.5	8
PPV	26.2[a] 23.2[a]	0.9 3.2 1.1 4.5	166.53 168.31	This work
PPB	27.4[a]	21.7 23.9	164.60	6
PPG	24.5[a] 26.9[a] 17.4[b] 15.9[b]	0.8 0.8 16.8 1.2 12.8 0.2 3.8 7.0	166.6 168.5 167.2 170.9	11
PPT	18.7[a] 21.2[b]	4.1 4.5 5.0 5.1	170.4 168.8	10

a) Bond angle related to terminal Pt–Pt bond. b) Bond angle related to central Pt–Pt bond. c) τ is the tilt angle betewen adjacent platinum coordination planes and ω is the torsion (or twist) angle about the Pt–Pt vector.

Tables 4 and 5 summarizes the geometric features of PPY, PPV, PPB, PPG, and PPT. In PPY, PPV, and PPB the interior Pt–Pt bonds are longer than the terminal ones, while in PPT they are almost equal, and in PPG the relation is reversed. Comparing the difference of the terminal and central Pt–Pt bond lengths in these tetranuclear cations, it seems that the difference of the bond lengths between terminal and central Pt–Pt bonds is specific to the bridging amide ligand and the difference is larger in α-pyridone compounds than α-pyrrolidone ones. The difference is also dependent on the platinum oxidation state and, as the average oxidation state is increased, the difference seems to be decreased. Comparing PPV, PPG, and PPT, the tilt sngle τ shows a slightly decreasing tendency as the platinum oxidation state is increased. This is a result of the shortening of the Pt–Pt bond as the platinum oxidation state is increased. Since the N(ring)···O(exocyclic) bite distance (about 2.3Å) is shorter than the Pt–Pt distance, the tilt angle τ is decreased as the platinum oxidation state is increased and the Pt–Pt bond distance is decreased. Concerning the torsion angles ω about the Pt–Pt vector, there seems to be a distinct difference between α-pyridone compounds and α-pyrrolidone ones. While in PPY and PPB, where the amide ligand is α-pyridone, the angles are about 22°, most of them are decreased to less than 6° in PPG, PPT, and PPV containing α-pyrrolidone. The reason for the remarkably different two ω angles larger than 10° in PPG still remains unexplained even with the present structural analysis of PPV. The small ω values less than 6° signify that the bridging N(ring) and O(exocyclic) in the α-pyrrolidone are almost overlapped when viewed along the Pt–Pt vector for α-pyrrolidone compounds, PPV, PPG, and PPT, while in α-pyridone compounds, PPY and PPB, ω values are about 22°, which suggest that N(ring) and O(exocyclic) are twisted about the Pt–Pt vector. Apart from these tetranuclear compounds, there are several amidate-bridged Pt(II) dimers whose structures have been studied by X-ray diffraction analyses. These include $[Pt_2(NH_3)_4(C_5H_4NO)_2](NO_3)_2 \cdot 2H_2O$ (α-pyridone dimer),[16] $[Pt_2(NH_3)_4(C_6H_7N_2O_2)_2]$ $(NO_3)_2 \cdot H_2O$ (1-methylthymine dimer),[17] $[Pt_2(NH_3)_4(C_5H_5N_2O_2)_2]$-

$(NO_3)_2 \cdot 3H_2O$ (1-methyluracil dimer,[18] $[Pt_2(NH_3)_4(C_5H_6N_3O)_2]$-$(NO_3)_2 \cdot 2H_2O$ (1-methylcytosine dimer).[20] The torsion angles ω in these dimers are all within the range of 13° to 20°, except in 1-methylthymine dimer, where ω is 1.0°. It seems, therefore, the torsion angle is specific to each amide ligand and the effect of platinum oxidation state on ω value is less, compared with that of an amide ligand.

No significant difference was observed in Pt-O, Pt-N, and Pt-NH_3 bond lengths among the six tetranuclear platinum compounds and these values are within the range normally observed in related platinu-(II) ammine complexes.[16-28] The coordination sphere of each platinum atom is almost planar. The shifts of each platinum atom from the least-squares planes are Pt1 0.05Å, Pt2 0.06Å, Pt3 0.04Å, and Pt4 0.02Å. The average P-F distance in PF_6^- anions is 1.57Å with the standard deviation of 0.04Å. All the N-O distances and bond angles within the nitrate anions are within the usual values (average N-O distance, 1.24Å).

Table 6. Possible hydrogen bonding (Å) in the crystal lattice[a)]

NH1···OW6 (i)	3.15(16)	O4···NH8(v)	3.09(4)
NH5···O10(ii)	3.03(13)	NH2···OW4(vi)	2.94(17)
O13···NH6(ii)	2.87(4)	OW8···O14(vi)	3.18(21)
O5···NH2(iii)	3.05(4)	NH4···OW4(vi)	3.08(27)
O5···OW9(iii)	2.97(13)	NH6···OW10(vi)	3.01(12)
O4···NH1(iii)	2.96(3)	O14···OW10(vi)	3.07(12)
NH4···O5(iv)	2.92(5)	NH6···OW8(vi)	3.02(17)
NH1···O4(iv)	2.96(3)	O14···OW8(vi)	3.18(21)
NH3···O4(iv)	3.01(5)	NH1···OW5(vii)	3.07(13)
NH7···O6(v)	3.07(5)	OW1···NH3(vii)	2.86(18)
NH8···O4(v)	3.09(4)	O1···OW2(vii)	3.08(10)
NH7···O2(v)	3.05(4)		

a) Roman numerals refer to the symmetry translations as follows: i(−x, −y, −z), ii(1−x, 1−y, 1−z), iii(1+x, y, z), iv(−1+x, y, z), v(1−x, 1−y, −z), vi(−x, 1−y, 1−z), vii(−x, 1−y, −z).

Table 6 summarizes the possible hydrogen bondings in the crystal lattice. The crystal packing is shown in Fig. 1. The axial coordination to platinum atoms at both ends of the chain is important in regard to the relation between the Pt-L_{axial} bond length and platinum oxidation state. Hollis *et al.* reported that axial coordination is favored and the Pt-L_{axial} bond distance is decreased with increasing platinum oxidation state, from a review of amidatebridged dinuclear and tetranuclear compounds of platinum(II) and platinum-(III).[29] In the present compound, only one loose coordination, Pt2-F11 3.15(8)Å, is found as shown in Table 2, and no other significant coordination to platinum atoms at chain ends are observed within 3.5-Å range. This is probably due to the low average platinum oxidationstate of the compound. The bond length 3.15Å of Pt2-F11 is slightly shorter than the axial bond length of 3.32Å for Pt-O(NO_3^-) found in PPB, even if we take into consideration the difference of the ionic radii of O^{2-} (1.40Å) and F^- (1.33Å). It is rather comparable to 3.21Å of Pt-O(NO_3^-) found in PPG. The axial bond length would therefore be determined firstly by average platinum oxidation state, however it is also affected by other forces probably imposed by the crystal packing.

The results of the potentiometric oxidative titration with Ce(IV) in 0.29 mol dm^{-3} and 0.93 mol dm^{-3} HNO_3 are shown in Fig. 2. Both results show that the average platinum oxidation state is 2.14, however, the titration curve is different. While in 0.29 mol dm^{-3} HNO_3 the compound is directly oxidized to Pt(III) state, in 0.93 mol dm^{-3} HNO_3, it is first oxidized to $Pt^{2.5+}$ and secondly to Pt(III), as shown in Fig. 2. From the relation curve

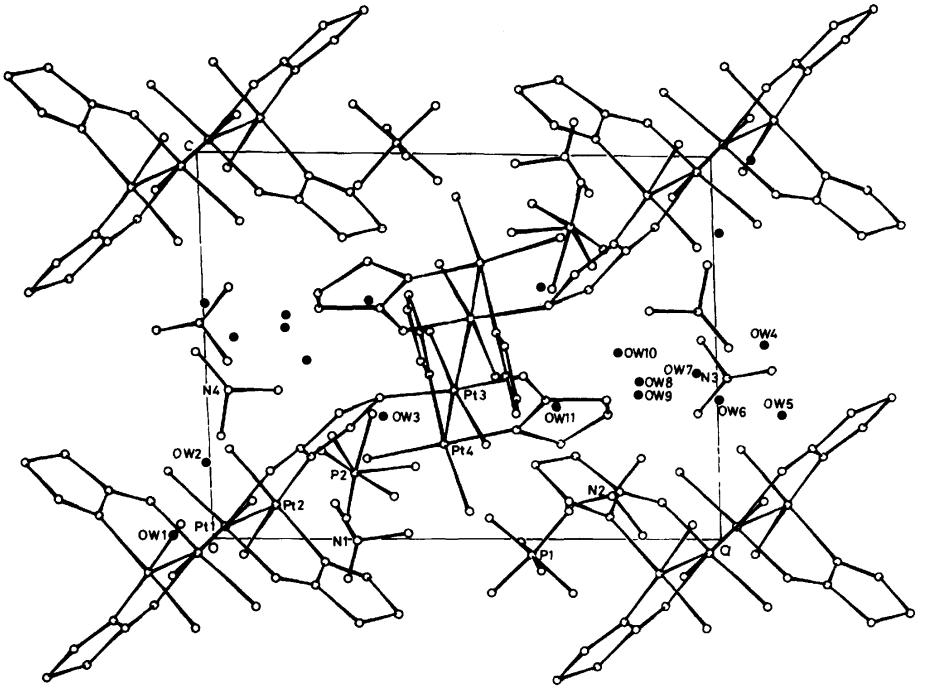

Fig. 1. Crystal structure of $[Pt_4(NH_3)_8(C_4H_6NO)_4](PF_6)_2(NO_3)_{2.56} \cdot 5H_2O$.

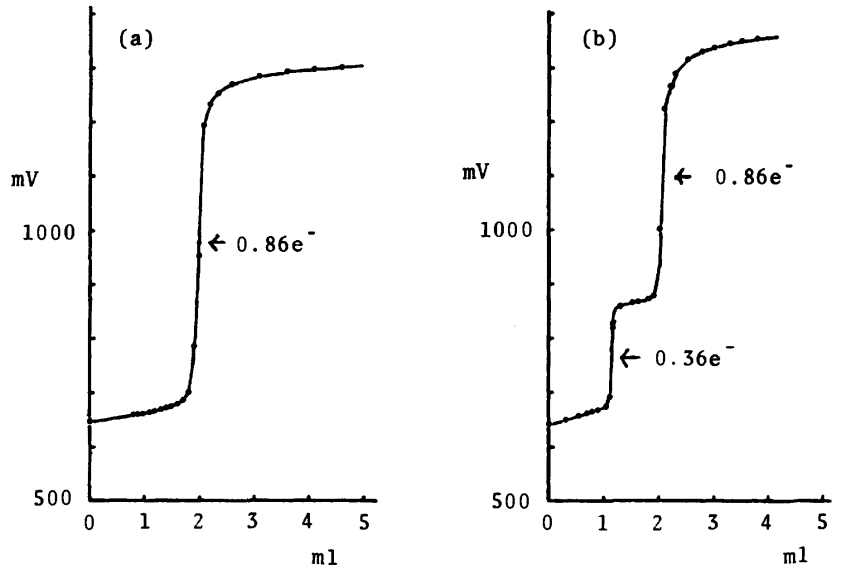

Fig. 2. Potentiometric oxidative titration of PPV with Ce(IV); (a) 0.29 mol dm^{-3} HNO_3 solution, (b) 0.93 mol dm^{-3} HNO_3 solution.
The titrations were monitored by using platinum *vs.* AgCl electrodes.

of Pt–Pt bond distance and average platinum oxidation state,[11] the average platinum oxidation state in the present compound is 2.10 (from the terminal Pt–Pt bond lengths) or 2.25 (from the central Pt–Pt bond lengths). Since the relation still seems to require more data to be recognized as established, we currently adopt the result of oxidative titration and determine the average platinum oxidation state as 2.14. This means that the compound is $[Pt_4(NH_3)_8(C_4H_6NO)_4](PF_6)_2(NO_3)_{2.56}\cdot 5H_2O$, being a mixture of 44% of $[Pt_4(NH_3)_8(C_4H_6NO)_4]^{4+}$ and 56% of $[Pt_4(NH_3)_8(C_4H_6NO)_4]^{5+}$. The fact that the existence ratio of the two cations is nearly 1:1 does not seem to mean any particular inter-cationic or inter-cation and -anion interactions, since there seems no significant interacions between them in the crystal psck-ing. Therefore it seems probable that other crystals with different existence ratio exist. Such possibility is now under investigation.

References

1) K. A. Hofmann and G. Bugge, *Ber. Dtsch. Chem. Ges.*, **41**, 312 (1908).
2) B. Lippert, *J. Clin. Haematol.*, **7**, 26 (1977).
3) J. H. Burness, M. J. Bandurski, L. J. Passman, and B. Rosenberg, *J. Clin. Haematol.*, **7**, 508 (1977).
4) C. M. Flynn, Jr., T. S. Viswanathan, and R. B. Martin, *J. Inorg. Nucl. Chem.*, **39**, 437 (1977).
5) J. K. Barton, H. N. Rabinowitz, D. J. Szalda, and S. J. Lippard, *J. Am. Chem. Soc.*, **99**, 2827 (1977).
6) J. K. Barton, D. J. Szalda, H. N. Rabinowitz, J. V. Waszezak, and S. J. Lippard, *J. Am. Chem. Soc.*, **101**, 1434 (1979).
7) L. S. Hollis and S. J. Lippard, *J. Am. Chem. Soc.*, **103**, 1230 (1981).
8) J.-P. Laurent, P. Legape, and F. Dahan, *J. Am. Chem. Soc.*, **104**, 7335 (1982).
9) K. Matsumoto and K. Fuwa, *J. Am. Chem. Soc.*, **104**, 897 (1982).
10) K. Matsumoto, H. Takahashi, and K. Fuwa, *Inorg. Chem.*, **22**, 4086 (1983).
11) K. Matsumoto, H. Takahashi, and K. Fuwa, *J. Am. Chem. Soc.*, **106**, 2049 (1984).
12) K. Matsumoto and K. Fuwa, *Chem. Lett.*, **1984**, 569.
13) "International Tables for X-Ray Crystallography," Kynoch Press, Vol. IV, Birmingham (1974).
14) D. T. Cromer, *Acta Crystallogr.*, **18**, 17 (1965).
15) A. H. Reis, Jr. and S. W. Peterson, *Inorg. Chem.*, **15**, 3186 (1976).
16) L. S. Hollis and S. J. Lippard, *J. Am. Chem. Soc.*, **105**, 3494 (1983).
17) C. J. L. Lock, H. J. Peresie, B. Rosenberg, and G. Turner, *J. Am. Chem. Soc.*, **100**, 3371 (1978).
18) R. Faggiani, C. J. L. Lock, R. J. Pollock, B. Rosenberg, and G. Turner, *Inorg. Chem.*, **20**, 804 (1981).
19) R. Faggiani, B. Lippert, C. J. L. Lock, and R. A. Speranzini, *J. Am. Chem. Soc.*, **103**. 1111 (1981).
20) B. Lippert, D. Neugebauer, and U. Schubert, *Inorg. Chim. Acta*, **46**, L11 (1980).
21) S.-M. Wu and R. Bau, *Biochem. Biophys. Res. Commun.*, **88**, 1435 (1979).
22) B. Lippert, C. J. L. Lock, and R. A. Speranzini, *Inorg. Chem.*, **20**, 808 (1981).
23) R. Faggiani, B. Lippert, and C. J. L. Lock, *Inorg. Chem.*, **21**, 3210 (1982).
24) R. Faggiani, B. lippert, C. J. L. Lock, and R. Pfab, *Inorg. Chem.*, **20**, 2381 (1981).
25) B. Lippert, C. J. L. Lock, and R. A. Speranzini, *Inorg. Chem.*, **20**, 335 (1981).
26) R. Faggiani, B. Lippert, and C. J. L. Lock, *Inorg. Chem.*, **19**, 295 (1980).
27) B. Lippert, *Inorg. Chem.*, **20**, 4326 (1981).
28) L. S. Hollis and S. J. Lippard, *Inorg. Chem.*, **22**, 2600 (1983).
29) L. S. Hollis and S. J. Lippard, *J. Am. Chem. Soc.*, **103**, 6761 (1981).

Reactions of the $[PtCl_2L_2]$ Complexes (L=Sulfide or Tertiary Phosphine) with β-Diketonate Anions

Fumiyo SASAKURA, Kiyoshi ISOBE,* and Shinichi KAWAGUCHI*,†

Department of Chemistry, Faculty of Science, Osaka City University, Sumiyoshiku, Osaka 558

†*Kinki University, Sayamacho, Minamikawachigun, Osaka 589*

(Received August 18, 1984)

cis- and *trans*-$[PtCl_2(Et_2S)_2]$ as well as $[PtCl_2(EtSCH_2CH_2SEt)]$ reacted with thallium(I) β-diketonates, Tl(β-dik), to give complexes containing a central-carbon-bonded β-dik ligand. The reaction of *cis*-$[PtCl_2(PEt_3)_2]$ with Tl(acac) (acac=acetylacetonato) did not give an acetylacetonato complex, but resulted in $[Pt(CO_3)(PEt_3)_2]$, while *trans*-$[PtCl_2(PEt_3)_2]$ yielded [PtCl(acac)(PEt_3)]. $[Pt(PPh_3)_2(H_2O)_2](ClO_4)_2$ derived from *cis*-$[PtCl_2(PPh_3)_2]$ reacted with K(acac) and K(tfac) (tfac=trifluoroacetylacetonato) to afford $[Pt(acac)(PPh_3)_2]ClO_4$ and $[Pt(tfac)(PPh_3)_2]$-ClO_4, respectively. Bases such as Et_3N, K(acac), and K(tfac) removed a proton from the latter complex to give $[Pt(tfac(2-)\text{-}C,O)(PPh_3)_2]$ containing a *C,O*-chelated tfac dianion.

Bis(acetylacetonato)platinum(II) was first prepared by Werner by the reaction of the tetrachloroplatinate(II) with acetylacetone in basic aqueous solution,[1] and the yield reported by Grinberg and Chapurskii[2] was only 35%.[3] The low yield was caused partly by formation of $[Pt(acac)(acac\text{-}C^3)Cl]^-$ as a by-product which contains the central-carbon-bonded acetylacetonate anion (acac-C^3) as a ligand.[4] This complex seems to be produced by the ligand substitution reaction of $[Pt(acac)Cl_2]^-$ with an acac anion and it is worth noting that the [Pt(acac)Cl] moiety prefers the central carbon bonding to the oxygen bonding when it accepts the acac anion as a unidentate ligand.

Recently the reaction between $[Pd(acac)_2]$ and diethylamine to afford $[Pd(acac)(acac\text{-}C^3)(Et_2NH)]$[5] was found by kinetic and equilibrium studies to proceed not directly but *via* $[Pd(acac)(Et_2NH)_2](acac)$.[6] When the diethylamine ligand is replaced by an acac anion, the $[Pd(acac)(Et_2NH)]^+$ moiety also favors the central carbon bonding over the oxygen bonding. On the other hand, *trans*-$[PdCl(C_5H_3(6\text{-}Cl)N\text{-}C^2)(PEt_3)_2]$, which contains the 6-chloro-2-pyridyl group as a carbon-bonded ligand, reacts with thallium(I) β-diketonate such as acetylacetonate, trifluoroacetylacetonate, and hexafluoroacetylacetonate to afford *trans*-$[Pd(\beta\text{-dik-}O)(C_5H_3(6\text{-}Cl)N\text{-}C^2)(PEt_3)_2]$.[7] In this case the $[Pd(C_5H_3(6\text{-}Cl)N\text{-}C^2)(PEt_3)_2]^+$ group prefers oxygen bonding to central carbon bonding of the unidentate β-diketonate ligand.

In recent years very extensive studies have been performed on the reactions of bis(β-diketonato) palladium-(II) and -platinum(II) complexes with various nitrogen bases,[8] tertiary phosphines,[9] and arsines[9b] to convert the *O,O'*-chelated β-diketonate anion to other several types of coordination modes. Factors which favor each of these coordination modes were also investigated. As an extention of these studies, reactions of the $[PtCl_2L_2]$-type complexes containing dialkyl sulfides and tertiary phosphines as L with thallium(I) β-diketonates have been examined, and the results are reported in this paper.[10]

Experimental

Preparation of Complexes. Thallium(I) β-diketonates were prepared by the method analogous to that reported for thallium(I) benzoylacetonate.[11] Potassium acetylacetonate and trifluoroacetylacetonate were obtained by adding acetylacetone or trifluoroacetylacetone to a methanol solution of potassium hydroxide and concentrating the reaction product. Starting complexes, *cis*- and *trans*-$[PtCl_2(SEt_2)_2]$,[12] *cis*- and *trans*-$[PtCl_2(PEt_3)_2]$,[13] *cis*-$[PtCl_2(PPh_3)_2]$,[14] and *trans*-$[PtHCl(PEt_3)_2]$[15] were also prepared according to literatures. 1,2-Bis(ethylthio)ethane, $C_2H_5SCH_2CH_2SC_2H_5$ (S-S), was prepared in the following way similar to that used for 1,2-bis-(methylthio)ethane.[16] Sodium (0.5 g) was dissolved in ethanol and the solution was concentrated to get nearly saturated solution of sodium ethoxide. Ethanethiol (1.5 cm^3) was added to the solution and the mixture was stirred at room temperature for 15 h, when the colorless solution turned to light yellow. 1,2-Dibromoethane (0.83 cm^3) was then added to the solution in small portions. The mixture was heated under reflux for 10 h. After separation of sodium bromide by filtration the solution was refluxed for an additional hour. Water was added to the reaction mixture and the heavy oil layer was separated. The water layer was extracted with diethyl ether. The organic solutions were combined, passed through a column of anhydrous sodium sulfate, and distilled under reduced pressure (bp 37 °C/3 Torr, 1 Torr=133.322 Pa) to obtain colorless liquid (0.7 g).

The following procedures including evaporation of solvents in a rotary evaporator were carried out at room temperature unless otherwise stated.

*(Acetylacetonato)(acetylacetonato-C³)(diethyl sulfide)platinum-(II), [Pt(acac)(acac-C³)(Et₂S)] (**1a**)*: A methanol solution (15 cm^3) of Tl(acac) (0.681 g, 2.25 mmol) was added drop by drop to a methanol solution (15 cm^3) of *cis*-$[PtCl_2(Et_2S)_2]$ (0.500 g, 1.12 mmol) with stirring. Color of the solution changed from yellow to colorless and thallium(I) chloride precipitated. After being stirred for 3 h, the precipitate was filtered off and the filtrate was evaporated to dryness. The residue was treated with dichloromethane and remaining Tl(acac) was separated by filtration. After concentration of the solution, diethyl ether was added to the concentrate to obtain a white precipitate of **1a**. The yield was 0.201 g (37%).

*[Pt(tfac)(tfac-C³)(Et₂S)] (**1b**)*: A mixture of *cis*-$[PtCl_2(Et_2S)_2]$ (0.400 g, 0.90 mmol) and Tl(tfac) (0.640 g, 1.84 mmol) in methanol (30 cm^3) was stirred for 3 h. After separation of TlCl and evaporation of the solvent, the residue was dissolved in dichloromethane and Tl(acac) was filtered off. The yield was 0.186 g (35%).

*[Pt(hfac)(hfac-C³)(Et₂S)] (**1c**)*: The reaction of *cis*-$[PtCl_2(Et_2S)_2]$ with Tl(hfac) in a similar way as above gave **1c** in a 30%

yield. Complexes **1b** and **1c** are readily soluble in diethyl ether, while **1a** is sparingly soluble in the same solvent.

Dichloro[1,2-bis(ethylthio)ethane]platinum(II), [$PtCl_2$(S-S)], was prepared by a method analogous to that exemplified by Cross *et al.*[17] Aqueous solution of an equimolar mixture of $K_2[PtCl_4]$ and the disulfide was stirred for 4 h and then heated under reflux for 1 h. A yellow precipitate was filtered, dried, and recrystallized from hot dichloromethane. The yield was 79%.

[PtCl(acac-C³)(S-S)] (2): A methanol solution (15 cm^3) of Tl(acac) (0.240 g, 0.79 mmol) was added to a suspension of [$PtCl_2$(S-S)] (0.330 g, 0.79 mmol) in methanol (15 cm^3) and the mixture was stirred for 5 h. After separation of TlCl, the solvent was evaporated to dryness. The residue was treated with dichloromethane (10 cm^3) and Tl(acac) was filtered off. The filtrate was again concentrated to dryness and the residue was treated with diethyl ether. A light yellow solid of **2** was purified by reprecipitation from dichloromethane–diethyl ether. The yield was 0.216 g (48%).

[Pt(CO_3)(PEt_3)$_2$] (3): A methanol solution (15 cm^3) of Tl(acac) (0.600 g, 2.00 mmol) was added dropwise to a solution of *cis*-[$PtCl_2(PEt_3)_2$] (0.500 g, 1.00 mmol) in methanol (15 cm^3) through which carbon dioxide was being passed. The mixture was stirred for 5 h under CO_2 bubbling. After separation of TlCl the solvent was evaporated to dryness. The residue was dissolved in a small amount of dichloromethane containing a very small portion of pyridine. Diethyl ether was carefully added until the solution became turbid and the mixture was allowed to stand overnight. White crystals (0.087 g) were obtained in an 18% yield.

[Pt(PPh_3)$_2$(H_2O)$_2$](ClO_4)$_2$ (4): A methanol solution (10 cm^3) of silver perchlorate (0.250 g, 1.19 mmol) was added to a suspension of *cis*-[$PtCl_2(PPh_3)_2$] (0.470 g, 0.60 mmol) in chloroform (10 cm^3). Both solutions were cooled with ice in advance and the mixture was stirred at 0 °C for 5 min. After separation of silver chloride, the filtrate was evaporated to dryness under cooling. A white solid of **4** (0.280 g) was obtained in a 49% yield after purification by reprecipitation from dichloromethane–diethyl ether at room temperature.

[Pt(acac)(PPh_3)$_2$]ClO_4 (5a): A methanol solution (15 cm^3) of K(acac) (0.020 g, 0.13 mmol) was added drop by drop to a suspension of complex **4** (0.100 g, 0.11 mmol) in the same solvent (15 cm^3). After stirring for 24 h, a precipitate of potassium perchlorate was filtered off and the filtrate was evaporated to dryness. The residue was purified by reprecipitation from dichloromethane–diethyl ether and the yield was 0.049 g (49% yield).

[Pt(tfac)(PPh_3)$_2$]ClO_4 (5b): A methanol solution (5 cm^3) of K(tfac) (0.080 g, 0.43 mmol) was added to a dichloromethane solution (30 cm^3) of **4** (0.400 g, 0.43 mmol) and the mixture was stirred for 16 h. After separation of potassium perchlorate, the yellow filtrate was concentrated to dryness. The residue was dissolved in dichloromethane and precipitated K(tfac) was separated by filtration. The filtrate was concentrated to 2—3 cm^3. On addition of diethyl ether to the concentrate a light yellow precipitate appeared, which was purified by reprecipitation from chloroform–hexane. The yield was 0:208 g (50%).

[Pt(acac)(PEt_3)$_2$]PF_6 (6): Acetylacetone (1 cm^3) was added to a methanol solution (15 cm^3) of *trans*-[PtHCl(PEt_3)$_2$] (0.500 g, 1.10 mmol) and to this solution was added dropwise a methanol solution (15 cm^3) of silver hexafluorophosphate (0.270 g, 1.10 mmol). After stirring of the mixture for 24 h, silver chloride was filtered off and the filtrate was concentrated to about one-half volume. Scratching of the flask stimulated crystallization. A white precipitate was recrystallized from dichloromethane–diethyl ether. The yield was 0.236 g (32%).

[Pt(tfac(2—)-C,O)(PPh_3)$_2$] (7): A methanol solution (30 cm^3) containing complex **4** (0.340 g, 0.35 mmol) and K(tfac) (0.140 g, 0.73 mmol) was stirred for 24 h. After separation of potassium perchlorate, the yellow filtrate was evaporated to dryness. The residue was dissolved in a small amount of dichloromethane. Diethyl ether was added carefully to the solution until the upper portion of the solution became turbid and the mixture was allowed to stand overnight. A white crystalline product (0.077 g) was obtained in a 25% yield.

Complex **7** was also derived from **5b** by treating with bases.

(i) Triethylamine (0.036 g, 0.36 mmol) was added drop by drop to a methanol solution (20 cm^3) of complex **5b** (0.222 g, 0.23 mmol) and the mixture was stirred for 19 h. The solution was then evaporated under reduced pressure to leave an oily substance, which was dissolved in a tiny amount of dichloromethane. Diethyl ether was added dropwise to the solution to deposite a white precipitate, which was recrystallized from dichloromethane–diethyl ether. The yield was 0.040 g (20%). When a ten times molar amount of triethylamine was employed the yield of **7** was improved to 36%.

(ii) A methanol solution (15 cm^3) of K(acac) (0.043 g, 0.31 mmol) was added to a solution of **5b** (0.301 g, 0.31 mmol) in the same solvent (15 cm^3) and the mixture was stirred for 24 h. Work-up similar to that starting with **4** gave **7** (0.103 g) in a 38% yield. Employment of an equimolar amount of K(tfac) instead of K(acac) gave a similar yield of **7**.

[PtCl(acac)(PEt_3)] (8): A methanol solution (30 cm^3) containing *trans*-[$PtCl_2(PEt_3)_2$][13] (0.300 g, 0.60 mmol) and Tl(acac) (0.630 g, 2.1 mmol) was stirred for one week. After separation of thallium(I) chloride by filtration, the filtrate was evaporated under reduced pressure to leave an oily substance, which was dissolved in a mixture (15 cm^3) of diethyl ether and petroleum ether (1:2 by volume). Scratching of the flask stimmulated crystallization of the product, which was dissolved in the smallest amount of dichloromethane and passed through a column (40 cm×ϕ1.3 cm) of silica gel. A mixture (60 cm^3) of benzene and petroleum ether (1:2 by volume) was used as the eluant. A light yellow solid (0.18 g) was obtained by evaporation of the eluate. Purity of the product was not good, giving unsatisfactory analysis. The IR and ^1H NMR data in comparison with those for [PtCl(acac)(PMe_2Ph)][18] showed that the product is **8** contaminated with the starting complex.

Measurements. Infrared spectra were measured in Nujol mulls with JASCO IR-E (4000—650 cm^{-1}), Hitachi EPI-L (700—200 cm^{-1}), and JASCO DS 701 G (4000—200 cm^{-1}) spectrophotometers. Electronic spectra were taken on a Hitachi EPS-3T recording spectrophotometer and ^1H NMR spectra on a JNM MH-100 instrument with tetramethylsilane as an internal reference. Molecular weight was determined with a vapor pressure osmometer manufactured by Knauer in West Berlin, West Germany.

Results and Discussion

Characterization of Complexes. Results of elemental analysis and molecular weight determination for

TABLE 1. ANALYTICAL DATA FOR THE NEWLY PREPARED COMPLEXES

Complex		Found (Calcd)		
		C(%)	H(%)	Mol wt[a]
[Pt(acac)(acac-C^3)(Et_2S)]	(**1a**)	34.43(34.78)	4.97(5.00)	482(484)
[Pt(tfac)(tfac-C^3)(Et_2S)]	(**1b**)	28.46(28.43)	3.02(3.07)	574(591)
[Pt(hfac)(hfac-C^3)(Et_2S)]	(**1c**)	24.04(24.04)	1.76(1.73)	
[PtCl(acac-C^3)(S-S)]·CH_2Cl_2	(**2**)	25.16(25.52)	4.17(4.10)	532(565)
[Pt(CO_3)(PEt_3)$_2$]	(**3**)	31.89(31.77)	6.21(6.15)	486(491)
[Pt(PPh_3)$_2$(H_2O)$_2$](ClO_4)$_2$	(**4**)	45.05(45.30)	3.64(3.59)	
[Pt(acac)(PPh_3)$_2$]ClO_4	(**5a**)	54.36(54.05)	4.15(4.09)	830(911)
[Pt(tfac)(PPh_3)$_2$]ClO_4	(**5b**)	50.03(50.65)	3.50(3.53)	929(972)
[Pt(acac)(PEt_3)$_2$]PF_6	(**6**)	30.03(30.23)	5.37(5.52)	604(676)
[Pt(tfac(2−)-*C,O*)(PPh_3)$_2$]	(**7**)	55.64(56.49)	3.93(3.82)	

a) Determined in dichloromethane (0.01—0.03 mol dm^{-3}) at 27°C.

TABLE 2. CHARACTERISTIC IR BANDS (cm^{-1})[a]

Complex	ν(C⋯⋯O)+ν(C⋯⋯C) of chelated β-dik	ν(C=O) of C^3-bonded β-dik	Others
1a	1560 vs, 1525 vs	1690 vs	
1b	1660 s, 1590 vs	1720 vs	
1c	1608 vs	1750 vs	
2		1650 vs	ν(Pt–Cl) 310 m
3			ν(C=O) 1660 vs, 1630 s, 1610 s
			ν(C–O) 1195 vs, 990 s
5a	1560 vs, 1530 vs		ν(ClO_4) 1100 vs
5b	1600 vs, 1530 m		ν(ClO_4) 1100 vs
6	1570 vs, 1535 vs		ν(PF_6) 840 vs
7	1620 vs, 1597 s		
8[b]	1560 vs, 1540 s		ν(Pt–Cl) 305 m

a) vs=very strong, s=strong, m=medium. b) [PtCl(acac)(PEt_3)].

TABLE 3. ^1H NMR SIGNALS IN $CDCl_3$[a]

Complex	Chelated β-dik		*C*-Bonded β-dik		Neutral ligand		
	CH_3	CH	CH_3	CH	CH_3	CH_2	Ph
1a	1.85	5.35(4)	2.18	4.78(128)	1.32	2.57	
	1.92						
1b	2.08	6.00(6)	2.32	5.30(124)	1.35	2.63	
	2.10		2.36		1.28		
1c		6.38(4)		5.80(b)	1.30	2.60	
2			2.11	4.98(112)	1.42	2.78, 3.02	
3					1.20	1.89	
5a	1.50	5.58(4)					7.32
5b	1.66	5.97(5)					7.29
6	1.87	5.19(4)			1.07	1.71	
7	2.80[c]	5.10					7.29
	(58)						
8	2.00	5.58(5)			1.20	2.00	

a) Chemical shifts in ppm from internal Me_4Si. Figures in parentheses give the J(Pt-H) values. b) Indiscernible. c) CH_2 bound to platinum in the tfac(2−)-*C,O* ligand, appearing as a doublet of doublets with ^3J(*cis*-P-H)=6.0 Hz and ^3J(*trans*-P-H)=12 Hz flanked by the ^{195}Pt satellites.

the newly prepared complexes are collected in Table 1, and their characteristic IR bands are shown in Table 2. These data are consistent with the proposed structures of these complexes, the IR data for complexes **1a**, **1b**, and **1c** supporting coexistence of chelated and central-carbon-bonded β-diketonate ligands.

The ^1H NMR signals listed in Table 3 are readily assigned based on the proposed structures. For example, complex **1a** exhibits four methyl signals at 1.32, 1.85, 1.92, and 2.18 ppm. The triplet signal at 1.32 ppm is assigned to the methyl protons of diethyl sulfide. The relative intensity of the δ 2.18 signal corresponds to six protons and it is ascribed to methyl protons of the carbon-bonded acac ligand. The remaining two signals of equal intensity come from two methyl groups of the chelated acac anion. By reference to the case of [Pd(acac)(acac-C^3)L] (L=PPh_3, py, and Et_2NH),[5] the higher-field signal (δ 1.85) is assigined to the methyl group positioned trans to the carbon-bonded acac ligand and the δ 1.92 signal to that cis to the acac-C^3 ligand. Both of two methine signals are flanked by ^{195}Pt satellites and the δ 4.78 signal show-

ing a very strong coupling to Pt is unequivocally assigned to the methine group bound to the metal.

Since the tfac anion forms an unsymmetric chelate ring, the following two geometrical isomers are conceivable for complex **1b**. Three signals at 1.35, 2.08,

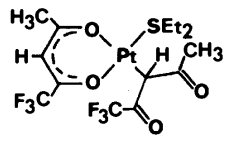

cis-(Me, L)-1b

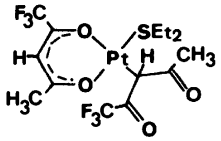

trans-(Me, L)-1b

and 2.32 ppm are assigned similarly to the case of **1a** to methyl protons of Et_2S, chelated tfac, and carbon-bonded tfac, respectively. Each of these signals is accompanied by a minor signal at 1.28, 2.10 or 2.36 ppm indicating contamination with a geometrical isomer as expected. Unfortunately, the corresponding pair of signals are so close to each other as to preclude measurement of the area ratio. Unequivocal assignment of the two sets of signals to these isomers is difficult, but minor signals are tentatively assigned to the *trans*-(Me, L) isomer, since of the two methyl signals at 2.08 and 2.10 ppm from the chelated tfac anion, the minor lower-field one is assigned to the methyl protons positioned cis to the carbon-bonded tfac ligand by reference to the case of **1a**.

It is worth noting that the product from the reaction between *trans*-[$PtCl_2(Et_2S)_2$] and Tl(tfac) gives the same ^1H NMR spectrum as above. During the preparative reactions the platinum(II) complexes seem to undergo geometrical isomerization to yield a thermodynamically favored mixture of isomers. Recently Cattalini and his collaborators studied kinetically the reactions of *cis*- and *trans*-[$PtCl_2(Me_2S)_2$] with pyridine and other nitrogen bases (L) to afford *cis*- and *trans*-[$PtCl_2(Me_2S)L$] and found that the reactions of the cis complex were complicated by its tendency to isomerize to the more stable trans isomer.[19]

Complex **4** was prepared by the reaction of *cis*-[$PtCl_2(PPh_3)_2$] with silver perchlorate in a mixture of chloroform and methanol at 0 °C. Two molecules of water retained per one platinum atom seem to have come from the organic solvents and be coordinated with the metal, perchlorate anions lying in the outer sphere. Hartley and his coworkers[20] prepared the [$Pt(PPh_3)_2L_2$]-(ClO_4)$_2$-type complexes containing various solvent molecule as L and found that anhydrous perchlorate complexes are explosive (**Caution!**). Fortunately complexes **4**, **5a**, and **5b** containing perchlorate in the outer sphere could be handled safely.

The ^1H NMR spectra of complexes **5a**, **5b**, and **6** are simple. Methyl protons of the acac and tfac ligands in **5a** and **5b**, respectively, resonate at much higher field than those in **1a** and **1b** owing to the anisotropic shielding effect of the phenyl rings in the ancillary triphenylphosphine ligands.[5] Thus the chemical shift of methyl protons of acac in **6**, which contains PEt_3 in place of PPh_3 in **5a**, coincides with that for **1a**. The PEt_3 ligands in **3** and **6** exhibit the 2:2:3:2:1 quintet signal in the methyl proton region and another symmetric quintet signal of methylene protons in accordance with the cis arrangement.[21] The IR and ^1H NMR data for complex **7** nearly coincide with those reported by Okeya *et al*,[9b] certifying that the same tfac (2—)-*C*,*O* chelate was obtained from the present reactions.

Synthetic Reactions. The reactions of *cis*-[$PtCl_2(Et_2S)_2$] with twice molar amounts of Tl (β-dik) gave [Pt(β-dik)(β-dik-C^3)(Et_2S)].

The reaction was almost complete by one hour and a half in either case as evidenced by the quantitative yield of TlCl and absence of the starting complex on the thin layer chromatogram(TLC) of the reaction mixture on silica gel. Although stirring was continued for three hours (Experimental), yields of complexes **1** were not high (30—37%), but products other than **1** could not be detected.

The reactions of *trans*-[$PtCl_2(Et_2S)_2$] with Tl(β-dik) (β-dik=acac, tfac, and hfac) were solwer than those of the cis complex, giving the same products **1a**—**1c**. Thus, the TLC assay showed that the starting complex remained in the reaction mixture even after being stirred for four hours and was exhausted after seven hours. The yield of TlCl also increased slowly with time for several hours.

The difference in reactivities of *cis*- and *trans*-[$PtCl_2(Et_2S)_2$] with Tl(β-dik) to give complexes **1** seems to accord with the stronger trans effect of the sulfide than that of chloride, and to suggest that the rate controlling step is displacement of the chloride ligand. (The above-mentioned substitution of Me_2S in [$PtCl_2(Me_2S)_2$] with a neutral ligand proceeds more slowly for the cis isomer than for the trans complex due to the stronger trans effect of the sulfide.[18])

Bis(β-diketonato)platinum(II) complexes react with a number of nitrogen bases[8d] and tertiary phosphines[9b-d] to give various types of complexes, but [Pt(acac)$_2$] does not react with excess Et_2S under various conditions. Converesely the reaction between [$PtCl_2(Et_2S)_2$] and Tl(acac) did not yield [Pt(acac)$_2$] beyond **1a**. Even when [$PtCl_2(Et_2S)_2$] was first treated with silver perchlorate to remove chloride ligands and then forced to react with K(acac), only complex **1a** was produced.

On the other hand, lowering of reaction temperature

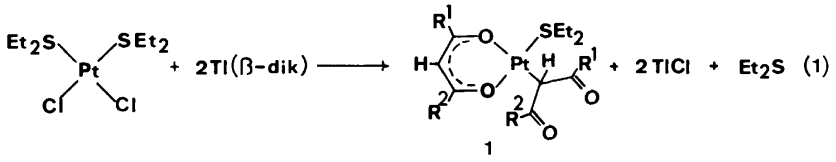

1

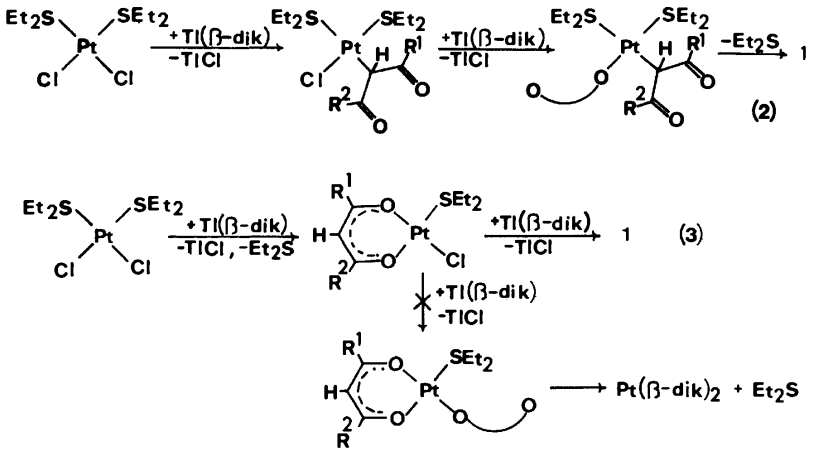

or decreasing of the amount of Tl(acac) depressed the rate and yield of **1a** but gave no intermediary product. Thus no clue was obtained to find either of the chelated and carbon-bonded β-diketonate ligands of **1** entered first into the coordination sphere.

In the case of $[PtCl_2(S\text{-}S)]$, complex **2** was formed exclusively. No other product was obtained even when excess Tl(acac) up to ten times moles was employed. These results indicate that the $[PtCl(S\text{-}S)]^+$ moiety prefers the central carbon bonding to the oxygen bonding of acac, and that $[PtCl(acac\text{-}C^3)(S\text{-}S)]$ (**2**) is thermodynamically more stable than other conceivable complexes such as $[Pt(acac)(S\text{-}S)]X$ (X=Cl or acac), $[Pt(acac\text{-}C^3)_2(S\text{-}S)]$, and $[Pt(acac\text{-}C^3)(acac\text{-}O)(S\text{-}S)]$.

Production of **2** might suggest that in reaction 1 the β-diketonate carbanion first substitutes a chloride ligand and the second β-diketonate anion replaces the other chloride anion to form an *O*-unidentate linkage and then a sulfide ligand is expelled to close the chelate ring (Eq. 2).

Another alternative mechanism also looks reasonable: A β-dik chelate is first formed and the $[Pt(\beta\text{-dik})(SEt_2)]^+$ moiety favors the carbon bonding of the second β-dik anion over the oxygen bonding which should be stabilized by intramolecular substitution to close the chelate ring (Eq. 3).

It is rather surprizing that complexes **1** and **2** containing a carbon-bonded β-dik ligand were obtained in methanol, since in the following palladium(II) case the carbon bonding of acac is completely disfavored in methanol.[6]

$$[Pd(acac)_2] + 2\,Et_2NH \overset{K_1}{\rightleftharpoons} [Pd(acac)(Et_2NH)_2](acac)$$

$$[Pd(acac)(acac\text{-}C^3)(Et_2NH)] + Et_2NH \overset{K_2}{\rightleftharpoons} [Pd(acac)(Et_2NH)_2](acac)$$

Thus $K_1=32.9\pm1.1\ dm^6\ mol^{-2}$ and $K_2=0.224\pm0.007\ dm^3\ mol^{-1}$ in dichloromethane at 25 °C, but in methanol at 25 °C $K_1=(3.93\pm0.04)\times10^6\ dm^6\ mol^{-2}$ and K_2 was immeasurablly large, no trace of the carbon-bonded acac complex being detected in the equilibrium mixture.[6]

If the latter mechanism (Eq. 3) is the case for the present sulfide complex, the tendency of the $[Pt(acac)(Et_2S)]^+$ moiety to favor the carbon bonding of acac may be very much greater than that of $[Pd(acac)(Et_2NH)]^+$. At the present stage of investigation, it is difficult to conclude which of the two mechanisms is operative.

In contrast with the case of *cis*-$[PtCl_2(Et_2S)_2]$ (Eq. 1), the reaction of *cis*-$[PtCl_2(PEt_3)_2]$ with Tl(acac) did not give any acetylacetonato complex, but resulted in $[Pt(CO_3)(PEt_3)_2]$ (**3**). The observed IR bands included in Table 2 accord with the bidentate coordination of the carbonate ion.[22] When the reaction was carried out under the atmospheric condition, the yield of **3** was as low as a few percent. Addition of water and bubbling of carbon dioxide through the methanol solution improved the yield of **3** to 18%. Conversely the same reaction under nitrogen gave no trace of **3**.

In either case the reaction of Tl(acac) with *cis*-$[PtCl_2(PEt_2)_2]$ to remove the chloride ligands was complete, since the yield of TlCl was almost quantitative and the UV spectrophotometric assay of the filtrate confirmed acetylacetone molecules in a satisfactory yield. Concentration of the solution by evaporation under reduced pressure resulted in a viscous substance, which showed broad IR bands in the 3600—3200 cm^{-1} region and at 1600 cm^{-1} indicative of the aqua or hydroxo ligand.

Thus the reaction sequence to form **3** might be shown by Eq. 4, although the aqua and hydroxo complexes presumed as intermediates have not been isolated.

$$cis\text{-}[PtCl_2(PEt_3)_2] \xrightarrow[-2TlCl]{+2Tl(acac)+2H_2O} cis\text{-}[Pt(H_2O)_2(PEt_3)_2](acac)_2 \xrightarrow[-2acacH]{} cis\text{-}[Pt(OH)_2(PEt_3)_2] \xrightarrow[-H_2O]{+CO_2} [Pt(CO_3)(PEt_3)_2] \quad (4)$$

3

On the other hand, the reaction of *trans*-$[PtCl_2(PEt_3)_2]$ with Tl(acac) was much slower than that of the cis isomer and gave $[PtCl(acac)(PEt_3)]$ instead of the carbonato complex **3**. Such a difference between the two isomers in reactivities and products may be

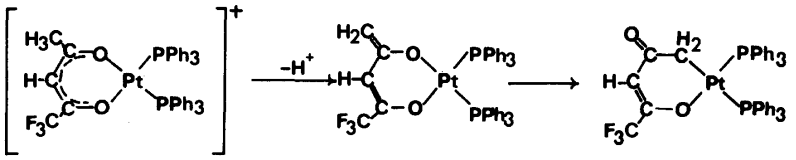

rationalized based on the strong trans effect of triethylphosphine.

The chloride ligand in *cis*-$[PtCl_2(PEt_3)_2]$ is readily substituted by a carbonyl end of acac anion, which may fail in displacing a PEt_3 ligand to close the chelate ring and be in turn replaced by a water molecule. On the contrary, the chloride ligand in *trans*-$[PtCl_2(PEt_3)_2]$ is less readily substituted by an acac anion, but the dangling carbonyl group of the *O*-unidentate acac ligand may release more easily a PEt_3 ligand which is labilized by the other PEt_3 molecule positioned trans to each other. The bond between the metal and the remaining chloride is strengthened in [PtCl(acac)(PEt_3)] and is not readily cleaved by attack of another acac anion.

When the chloride ligand in *trans*-$[PtHCl(PEt_3)_2]$ was removed by silver hexafluorophosphate in methanol containing acetylacetone, $[Pt(acac)(PEt_3)_2]PF_6$ (**6**) was resulted. Geometrical isomerization probably followed by dihydrogen evolution rather than displacement of a PEt_3 ligand seems to have been induced by acetylacetone.

cis-Dichlorobis(triphenylphosphine)platinum(II) is less reactive than the corresponding triethylphosphine complex and hardly reacts with Tl(β-dik). When the chloride ligands were removed by silver perchlorate, $[Pt(PPh_3)_2(H_2O)_2](ClO_4)_2$ (**4**) was obtained, which is slightly soluble only in haloalkanes such as chloroform and dichloromethane and was characterized by elemental analysis and IR spectra. A very broad and strong band at 1100 cm^{-1} and a band of medium intensity at 625 cm^{-1} suggest that the perchlorate ions lie in the outer sphere.[23] The aqua ligands in **4** can be readily substituted by other ligands. Thus **4** reacted with K(acac) in methanol at room temperature to give $[Pt(acac)(PPh_3)_2]ClO_4$ (**5a**). Similarly the reaction of **4** with an equimolar amount of K(tfac) in a mixture (1:6 by volume) of methanol and dichloromethane gave $[Pt(tfac)(PPh_3)_2]ClO_4$ (**5b**). On the other hand, the reaction of **4** with a twice molar amount of K(tfac) in methanol gave rise to [Pt(tfac(2−)-*C,O*)(PPh_3)$_2$] (**7**).

Complex **7** was previously obtained by Okeya *et al* by the reaction of $[Pt(tfac)_2]$ with PPh_3 and shown to contain a *C,O*-chelated trifluoroacetylacetonate dianion.[9b] More recently similar palladium(II) complexes [Pd(tfac(2−)-*C,O*)LL′] containing triphenylphospine, pyridine and their derivatives as L and L′ were prepared, and the molecular structure of the complex containing triphenylphosphine and 2,6-dimethylpyridine as neutral ligands was confirmed by X-ray analysis.[9e] Complex **7** was inferred to be produced through deprotonation of the chelated tfac ligand by the outer-sphere tfac anion in the presumed intermediate $[Pt(tfac)(PPh_3)_2](tfac)$.[9c] Now the cationic complex was isolated as **5b**, of which reactions with various bases were examined.

Potassium acetylacetonate and trifluoroacetylacetonate as well as triethylamine were successful in abstracting a proton from **5b** to give **7**. On the other hand, pyridine derivatives such as 4-amino-, 4-dimethylamino- and 2,6-dimethylpyridines were proved to be unsuccessful in giving **7**, although they were effective in deprotonating $[Pd(tfac)(PPh_3)_2]^+$ to afford [Pd(tfac-(2−)-*C,O*)(PPh_3)L].[9e] The tfac ligand in **5b** was displaced by pyridines and complexes $[Pt(PPh_3)_2L_2](ClO_4)_2$ containig 4-amino- and 4-dimethylaminopyridines as L were isolated and characterized, the yields being 10 and 29%, respectively. These results suggest that the Pt(II) tfac chelate is more labile than the corresponding Pd(II) chelate against the nucleophilic attack of nitrogen bases. Deprotonation of the chelating tfac monoanion by a base may produce a dienediolate intermediate as was postulated in the case of the Pd(II) complexes.[9e]

We wish to thank Mr. Junichi Gohda for elemental analyses.

References

1) A. Werner, *Chem. Ber.*, **34**, 2584 (1901).

2) A. A. Grinberg and I. N. Chapurskii, Russ. *J. Inorg. Chem.*, **4**, 137 (1959).

3) Recently a revised procedure of preparation was proposed to attain a higher yield (75%). S. Okeya and S. Kawaguchi, *Inorg. Synth.*, **20**, 65 (1980).

4) X-Ray molecular structure: R. Mason, G. B. Robertson, and P. J. Pauling, *J. Chem. Soc. (A)*, **1969**, 485.

5) S. Baba, T. Ogura, and S. Kawaguchi, *Bull. Chem. Soc. Jpn.*, **47**, 665 (1974).

6) S. Matsumoto and S. Kawaguchi, *Bull. Chem. Soc. Jpn.*, **53**, 1577 (1980).

7) H. Tanaka, K. Isobe, S. Kawaguchi, and S. Okeya, *Bull. Chem. Soc. Jpn.*, **57**, 1850 (1984).

8) a) S. Okeya and S. Kawaguchi, *Inorg. Chem.*, **16**, 1730 (1977); b) S. Okeya, H. Sazaki, M. Ogita, T. Takemoto, Y. Onuki, Y. Nakamura, B. K. Mohapatra, and S. Kawaguchi, *Bull. Chem. Soc. Jpn.*, **54**, 1978 (1981); c) S. Okeya, H. Yoshimatsu, Y. Nakamura, and S. Kawaguchi, *ibid.*, **55**, 483 (1982); d) S. Okeya, Y. Nakamura, and S. Kawaguchi, *ibid.*, **55**, 1460 (1982).

9) a) S. Okeya, T. Miyamoto, S. Ooi, Y. Nakamura, and S. Kawaguchi, *Inorg. Chim. Acta*, **45**, L135 (1980); b) S. Okeya, Y. Nakamura, S. Kawaguchi, and T. Hinomoto, *Inorg. Chem.*, **20**, 1576 (1981); c) S. Okeya, Y. Nakamura, and S. Kawaguchi, *Bull. Chem. Soc. Jpn*,. **54**, 3396 (1981); d) S. Okeya, Y. Nakamura, S. Kawaguchi, and T. Hinomoto, *ibid.*,

55, 477 (1982); e) S. Okeya, Y. Kawakita, S. Matsumoto, Y. Nakamura, S. Kawaguchi, N. Kanehisa, K. Miki, and N. Kasai, *ibid.*, **55**, 2134 (1982); f) S. Ooi, T. Matsushita, K. Nishimoto, Y. Nakamura, S. Kawaguchi, and S. Okeya, *Inorg. Chim. Acta*, **76**, L55 (1983).

10) In this paper the *O,O'*-chelated monoanions of β-diketones such as acetylacetone, trifluoroacetylacetone, and hexafluoroacetylacetone are abbreviated by β-dik, acac, tfac, and hfac, respectively, and β-dik-C^3 and β-dik-*O* represent the central-carbon-bonded and *O*-unidentate β-diketonate monoanions, respectively. The *C,O*-chelated dianion of trifluoroacetylacetone is shown by tfac(2−)-*C,O*.

11) W. H. Nelson, W. J. Randall, and D. F. Martin, *Inorg. Synth.*, **9**, 52 (1967).

12) G. B. Kauffman and D. O. Cowan, *Inorg. Synth.*, **6**, 211 (1953).

13) J. Chatt and R. G. wilkins, *J. Chem. Soc.*, **1952**, 273.

14) R. D. Gillard and M. F. Pilbrow, *J. Chem. Soc., Dalton Trans.*, **1974**, 2320.

15) J. Chatt and B. L. Shaw, *J. Chem. Soc.*, **1962**, 5075.

16) G. T. Morgan and W. Ledburg, *J. Chem. Soc.*, **1922**, 2882.

17) R. J. Cross, I. G. Dalgleish, G. J. Smith, and R. Wardle, *J. Chem. Soc., Dalton Trans.*, **1972**, 992.

18) J. M. Jenkins and B. L. Shaw, *J. Chem. Soc. (A)*, **1966**, 770.

19) L. Canovese, L. Cattalini, G. Marangoni, G. Michelon, and M. L. Tobe, *Inorg. Chem.*, **20**, 4166 (1981).

20) J. A. Davies, F. R. Hartley, and S. G. Murray, *J. Chem. Soc., Dalton Trans.*, **1980**, 2246.

21) W. J. Louw, *Inorg. Chem.*, **16**, 2147 (1977).

22) K. Nakamoto, "Infrared and Raman Spectra of Inorganic and Coordination Compounds," 3rd ed., Wiley-Interscience, New York (1978), p. 243.

23) B. J. Hathaway and A. E. Underhill, *J. Chem. Soc.*, **1961**, 3091.

Synthesis of 6-Alkylpurine Derivatives by Nickel-complex-catalyzed Coupling Reaction of 6-(Methylthio)purine Derivatives with Grignard Reagents[1)]

Hideyuki SUGIMURA and Hisashi TAKEI*
Department of Life Chemistry, Tokyo Institute of Technology, Nagatsuta, Midoriku, Yokohama 227
(Received July 11, 1984)

6-(Methylthio)purine reacted with RMgX (R=C_6H_5, $CH_3(CH_2)_nCH_2$ (n=2 to 6), $C_6H_5CH_2CH_2$, $(CH_3)_2C{=}CHCH_2CH_2$) in the presence of 5 mol% [$NiCl_2(Ph_2PCH_2CH_2CH_2PPh_2)$] in refluxing THF for 8 h to afford 6-aryl or 6-alkylpurines in 62—74% yields. By applying this reaction to 6-(methylthio)purine nucleoside, 6-(4-methyl-3-pentenyl)-9-β-D-ribofuranosylpurine was synthesized.

In the previous paper,[2)] we reported that heterocyclic thiols or sulfides reacted with Grignard reagents in the presence of a nickel-phosphine complex to give coupling products. This reaction serves as a new and convenient method for the introduction of alkyl and aryl groups to heterocyclic nuclei.

In this report, we describe an application of the method to the synthesis of 6-alkyl and 6-arylpurine derivatives, which correspond to N^6 carbon analogs of cytokinin,[3)] by the coupling reaction of 6-(methylthio)purine (**1**) and 6-(methylthio)purine nucleosides (**3**) with Grignard reagents catalyzed by nickel-phosphine complex.

Henderson and his coworkers[4)] reported the synthesis of 6-(4-methyl-3-pentenyl)purine (**2h**) by the reaction of dianion of 6-methylpurine with 3-methyl-2-butenyl bromide, though the yield was not satisfactory (25%). We tried the coupling reaction of readily available 6-(methylthio)purine (**1**) with 4-methyl-3-pentenylmagnesium bromide in the presence of [$NiCl_2$(dppp)] (dppp=$Ph_2PCH_2CH_2CH_2PPh_2$), and **2h** was obtained in 71% yield.

Then, we also examined the coupling reaction with other alkyl and aryl Grignard reagents and the desired 6-substituted purines were obtained in good yields. The results were summarized in Scheme 1.

Next, we applied this coupling reaction to the synthesis of 6-alkyl-9-β-D-ribofuranosylpurine. Recently, Pichat *et al.*[5)] reported the palladium-catalyzed coupling reaction of Grignard reagents with silylated derivatives of 8-bromopurine nucleosides. The reaction utilizes direct C-alkylation method of purine nucleosides, though the yields of the products were low (10—33%). We examined the coupling reaction of 4-methyl-3-pentenylmagnesium bromide with 9-(2′,3′-*O*-isopropylidene-5′-*O*-monomethoxytrityl or 5′-*O*-*t*-butyldimethylsilyl-β-D-ribofuranosyl)-6-(methylthio)purine (**3a** or **3b**) in the presence of [$NiCl_2$(dppp)] or [$NiCl_2(PPh_3)_2$]. The results were shown in Table 1.

When [$NiCl_2$(dppp)] was used as a catalyst, the yields were unsatisfactory probably because of bulkiness of the sulfides (run 1—3). According to our observation during the study of the nickel catalyzed coupling reac-

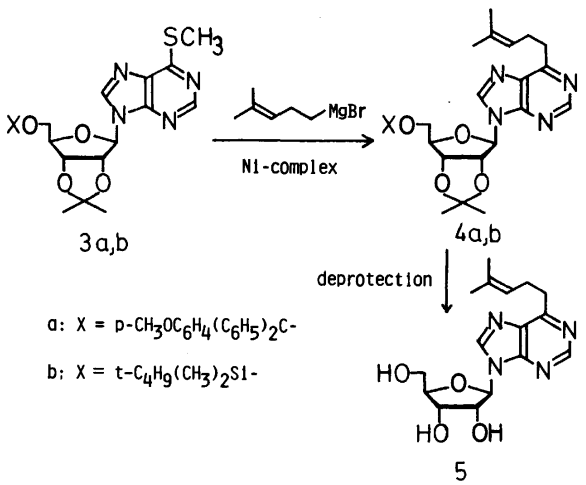

Scheme 2.

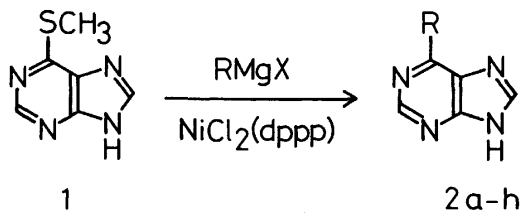

R	Isolated Yield (%)	R	Isolated Yield (%)
2a: C_6H_5	68	2e: n-C_7H_{15}	67
2b: n-C_4H_9	74	2f: n-C_8H_{17}	68
2c: n-C_5H_{11}	62	2g: $C_6H_5CH_2CH_2$	72
2d: n-C_6H_{13}	62	2h: $(CH_3)_2C{=}CHCH_2CH_2$	71

Scheme 1.

TABLE 1. COUPLING REACTION OF **3** WITH 4-METHYL-3-PENTENYLMAGNESIUM BROMIDE.[a)]

Run	Sulfide	Ni-complex[b)]	Isolated Yield (%)	
			4	**3** (Recovered)
1	**3a**	A	21	34
2[c)]	**3a**	A	29	13
3	**3b**	A	35	56
4	**3a**	B	43	17
5	**3b**	B	53	2

a) All reactions were carried out in refluxing ether for 6 h. Molar ratio of Ni-complex/sulfide/Grignard reagent is 0.05/1.00/1.1, unless otherwise noted. b) Ni-complex A: [$NiCl_2$(dppp)]. B: [$NiCl_2(PPh_3)_2$]. c) Three Eqs. of Grignard reagent was used.

TABLE 2. MP AND NMR SPECTRA OF THE COUPLING PRODUCTS **2a**—**h**.

Compound	Mp (θ_m/°C)[a]	NMR (δ) (in $CDCl_3$)
2a	243 sublime (283)[8]	7.30—7.80 (5H, m), 8.47 (1H, s), 8.84 (1H, s)
2b	134.5—135	0.63—2.20 (7H, m), 3.07—3.44 (2H, t, J=8Hz), 8.28 (1H, s), 8.91 (1H, s)
2c	128.5—129.5	0.57—2.27 (9H, m), 3.24 (2H, t, J=8Hz), 8.38 (1H, s), 8.92 (1H, s)
2d	95—96	0.69—2.16 (11H, m), 3.24 (2H, t, J=7Hz), 8.22 (1H, s), 8.90 (1H, s)
2e	94—95	0.63—2.13 (13H, m), 3.38 (2H, t, J=8Hz), 8.37 (1H, s), 8.96 (1H, s)
2f	89—90	0.59—2.20 (15H, m), 3.25 (2H, t, J=8Hz), 8.36 (1H, s), 8.94 (1H, s)
2g	131—132 (134.5—136)[4]	2.95—3.87 (4H, m), 7.03 (5H, s), 8.20 (1H, s), 8.85 (1H, s), 10.17—10.93 (1H, b)
2h	116.5—117 (115.5—116.5)[4]	1.51 (3H, s), 1.58 (3H, s), 2.30—2.95 (2H, m), 2.95—3.56 (2H, m), 5.12 (1H, m), 8.45 (1H, s), 8.93 (1H, s)

a) Mp in parentheses are those of literatures.

TABLE 3. MP, NMR, AND UV SPECTRA OF **3a**—**b**, **4a**—**b**, AND **5**

Compound	Mp (θ_m/°C)	NMR (δ) (in $CDCl_3$)	UV λ_{max}/nm	UV λ_{min}/nm
3a	—[a]	1.34 (3H, s), 1.57 (3H, s), 2.64 (3H, s), 3.24 (2H, d, J= 6Hz), 3.75 (3H, s), 4.33—4.57 (1H, m), 4.80—5.03 (1H, m), 5.30—5.50 (1H, m), 6.05 (1H, d, J=2Hz), 6.62 (2H, d, J= 8Hz), 6.89—7.33 (12H, m), 7.92 (1H, s), 8.44 (1H, s)	282, 289(sh) (in 95% C_2H_5OH)	247
3b	71—73	0.06 (6H, s), 0.82 (9H, s), 1.36 (3H, s), 1.58 (3H, s), 2.64 (3H, s), 3.63—3.80 (2H, m), 4.20—4.43 (1H, m), 4.74—4.93 (1H, m), 5.06—5.25 (1H, m), 6.02 (1H, d, J=3Hz), 7.93 (1H, s), 8.48 (1H, s)	283, 290 (in CH_3OH)	241, 287
4a	—[b]	1.38 (3H, s), 1.61 (9H, s), 2.35—2.77 (2H, m), 3.02—3.40 (4H, m), 3.72 (3H, s), 4.33—4.70 (1H, m), 4.81—5.57 (3H, m), 6.07 (1H, d, J=2HZ), 6.67 (2H, d, J=9Hz), 6.98—7.29 (12H, m), 8.02 (1H, s), 8.64 (1H, s)	262 (in 95% C_2H_5OH)	255
4b	—[b]	0.00 (6H, s), 0.82 (9H, s), 1.43 (3H, s), 1.59 (3H, s), 1.62 (6H, s), 2.46—2.82 (2H, m), 3.09—3.42 (2H, m), 3.78—3.93 (2H, m), 4.32—4.57 (1H, m), 4.87—5.43 (3H, m), 6.23 (1H, d, J= 2Hz), 8.25 (1H, s), 8.91 (1H, s)	250(sh), 263 289(sh) (in CH_3OH)	232
5	80—83.5[c]	(in $CDCl_3$-D_2O) 1.54 (3H, s), 1.62 (3H, s), 2.28—2.68 (2H, m), 2.85—3.18 (2H, m), 3.63—3.94 (2H, m), 4.37—4.54 (1H, m), 4.68—5.27 (3H, m), 5.77—6.00 (1H, m), 8.15 (1H, s), 8.56 (1H, s)	262 (in CH_3OH)	239
			250(sh), 263 (pH 1)	226
			269 (pH 10)	242

a) Foam. b) Syrup. c) Freezed dry; lit. Mp 48—49°C.[5b]

tion, $[NiCl_2(PPh_3)_2]$ is more favorable catalyst with bulky sulfides than $[NiCl_2(dppp)]$. Indeed, by using $[NiCl_2(PPh_3)_2]$ in place of $[NiCl_2(dppp)]$, the yields of **4a** and **4b** were improved (run 4 and 5). In these cases, however, 6-unsubstituted purine nucleosides were also obtained as by-products. These by-products, produced by the replacement of methylthio group by hydrogen atom, may be formed by the β-elimination of intermediate nickel complexes.[6]

Deprotection of both **4a** and **4b** was easily performed by a standared manner[7] and 6-(4-methyl-3-pentenyl)-9-β-D-ribofuranosylpurine (**5**) was obtained.

Experimental

Typical Procedure for the Coupling Reaction of 6-(Methylthio)purine (1) with Grignard Reagents. To 166 mg (1 mmol) of **1** and 26 mg (0.05 mmol) of $[NiCl_2(dppp)]$ in 10 ml of anhydrous THF under an argon atmosphere at room temperature was added an ethereal solution of Grignard reagent (2.5 mmol). The solution was stirred for 8 h at refluxing temperature. After cooling, the reaction mixture was quenched with saturated aqueous solution of NH_4Cl, and neutralized with saturated aqueous $NaHCO_3$ solution. The insoluble solid was filtered off through Celite and the Celite was washed with ethanol. The filtrate and the washings were combined and evaporated under reduced pressure. The residue was extracted five times with dichloromethane, the combined extracts were washed and dried over anhydrous $MgSO_4$. The solvent was evaporated and the product was isolated by TLC. All products gave satisfactory elemental analyses. The melting points and NMR spectra of them were summarized in Table 2.

Coupling Reaction of 3a or 3b with 4-Methyl-3-pentenylmagnesium Bromide. To 0.3 mmol of **3a** or **3b**, and 0.05 equiv of a nickel-phosphine complex in 10 ml of anhydrous ether under an argon atmosphere was added an ethereal solution of 4-methyl-3-pentenylmagnesium bromide (1.1 equiv). The mixture was refluxed for 6 h. The reaction mixture was quenched with saturated aqueous solution of NH_4Cl, neutralized with saturated aqueous $NaHCO_3$ solution and

filtered through Celite *in vacuo*. The resulting mixture was separated and the aqueous phase was extracted twice with ether. The combined extracts were washed and dried over anhydrous $MgSO_4$. The solvent was evaporated and the product was isolated by TLC. Resulted **4a** and **4b** were deprotected by a standard manner to yield 6-substituted purine nucleoside **5** in 32—53%. The melting points and spectral data of **3a—b**, **4a—b**, and **5** were summarized in Table 3. The compounds except **3a** and **4a—b** gave satisfactory elemental analyses. **3a** and **4a—b** couldn't be purified completely because they were obtained as foam or syrup. But NMR spectra of them well agreed with the assigned structures.

References

1) Presented at the 43rd Annual Meeting of the Chemical Society of Japan, Tokyo, Abstr. II, p. 933 (1981).

2) H. Takei, M. Miura, H. Sugimura, and H. Okamura, *Chem. Lett.*, **1979**, 1447.

3) S. Matsubara, *Phytochemistry*, **19**, 2339 (1980) and references cited therein.

4) T. R. Henderson, C. R. Frihart, N. J. Leonard, R. Y. Schmitz, and F. Skoog, *Phytochemistry*, **14**, 1687 (1975).

5) a) N. Cnog-Dahn, J. P. Beaucourt, and L. Pichat, *Tetrahedron Lett.*, **1979**, 3159; b) After this work had been completed, the coupling reaction of 9-(2′,3′,5′-tris-*O*-*t*-butyldimethylsilyl-β-D-ribofuranosyl)-6-chloropurine with aryl and alkyl Grignard reagents catalyzed by [$NiCl_2$(dppp)] was reported: D. E. Bergstrom and P. A. Reday, *Tetrahedron Lett.*, **23**, 4191 (1982).

6) H. Okamura, M. Miura, and H. Takei, *Tetrahedron Lett.*, **1979**, 43; B. M. Trost and P. Lornstein, *Tetrahedron Lett.*, **22**, 3463 (1981).

7) E. g., T. W. Greene, "Protective Groups in Organic Synthesis," John Wiley & Sons, New York (1981), Chap. 2.

8) *Chem. Abst.*, **65**, 5472c (1966).

 © 1985 The Chemical Society of Japan Bull. Chem. Soc. Jpn., 58, 667—674 (1985)

Chemistry of 1,2-Thiaphosphole 2-Sulfides I. Cycloaddition Reactions of 1,2-Thiaphosphole 2-Sulfides with Some Dienophiles

Hideyuki TANAKA, Shunichi KAMETANI, Takao SAITO, and Shinichi MOTOKI*

Department of Chemistry, Faculty of Science, Science University of Tokyo, Kagurazaka, Shinjuku-ku, Tokyo 162

(Received August 7, 1984)

2,9-Dithia-1-phosphabicyclo[4.3.0]nona-3,7-diene 1-sulfides have been prepared by the reaction of α,β-unsaturated ketones with P_4S_{10} in the presence of NEt_3. 1,2-Thiaphosphole 2-sulfides generated by the thermolysis of the phosphabicyclo compounds underwent cycloaddition reactions with acrylonitrile, styrene, butyl vinyl ether and norbornene to give the [4+2]cycloadducts, respectively.

During the course of the work on the preparation of α,β-unsaturated thione dimers and the cycloaddition reactions of their monomers with various dienophiles,[1] it has been found that attempts to isolate monomeric 1-arylmethylene thiopinacolones **2** resulted in the formation of the unexpected phosphorus(V)-containing compounds **3**.[2] In boiling benzene **3** generated α,β-unsaturated thione monomers **2** and 1,2-thiaphosphole 2-sulfides **4**, both of which could be trapped by acrylonitrile as [4+2]cycloadducts **5** and **6**.[3] To our knowledge, the proposed intermediates **4** are the first representatives of five-membered heterocyclic dienes, S-P(=S)=C-C=C, though analogous π-bonded phosphorus compounds, -(S=)P=C<, have been prepared recently.[4]

In the present paper, we wish to report the detailed study on the cycloaddition reactions of this interesting cyclic heterodienes **4** with a variety of dienophiles leading to P-S-C bridging [4+2]cycloadducts.

Results and Discussion

At first, some additional phosphabicyclo compounds were prepared as starting materials. The results are summarized in Table 1. The yields increased with an increasing electron donating property of the para-substituents of the aromatic rings as in the case of the preparation of the thione dimers.[5] X-Ray difraction analysis was performed for **3a**[6] and the structures of **3b**, **3c**, **9**, and **10** were confirmed by comparison of

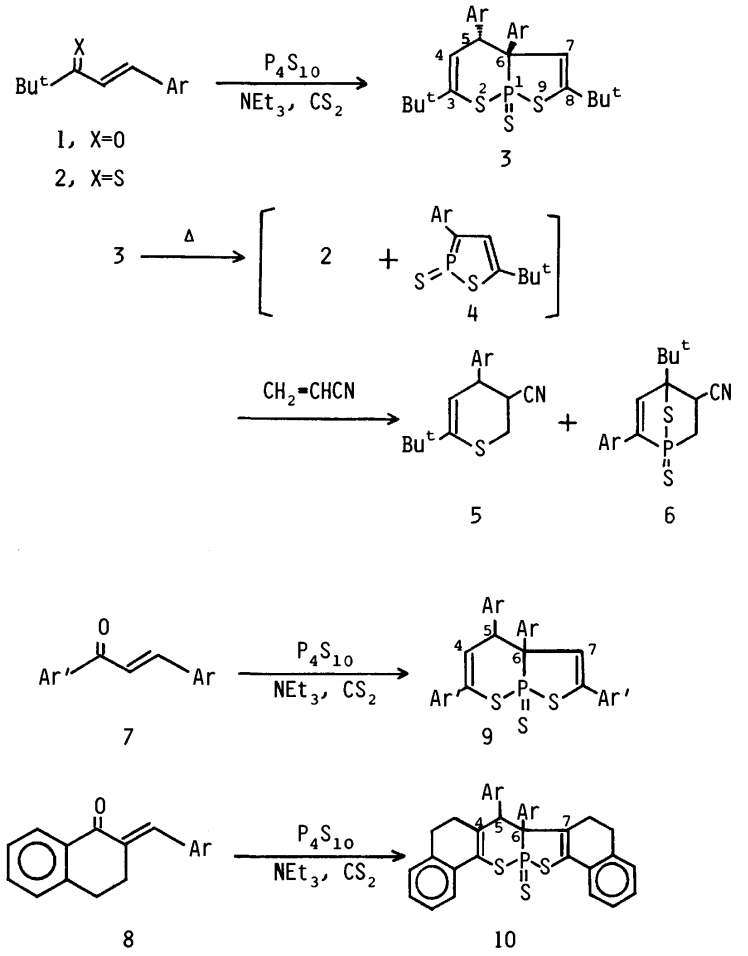

Scheme 1.

TABLE 1. PREPARATIONS OF PHOSPHABICYCLO COMPOUNDS **3**, **9**, AND **10**

Compound[a)]	Ar	Ar'	Reaction time/h	Mp(dec) θ_m/°C	Yield/%
3a	Ph	(*t*-Bu)	20	206—209	20
3b	*p*-$CH_3C_6H_4$	(*t*-Bu)	20	210—212	30
3c	*p*-ClC_6H_4	(*t*-Bu)	10	220—223	10
9a	Ph	Ph	2	155—159	43
9b	*p*-$CH_3OC_6H_4$	Ph	2	144—146	57
9c	*p*-$CH_3C_6H_4$	Ph	2	165—167	45
9d	*p*-ClC_6H_4	Ph	2	178—180	39
9e	Ph	*p*-$CH_3OC_6H_4$	2	157—158	70
9f	Ph	*p*-$CH_3C_6H_4$	2	161—162	41
9g	Ph	*p*-ClC_6H_4	2	178—179	14
10a	Ph	—	2	172—174	6
10b	*p*-$CH_3OC_6H_4$	—	2	189—191	22
10c	*p*-ClC_6H_4	—	2	144—146	8

a) All the compounds are colorless crystals.

TABLE 2. ^1H AND ^{13}C NMR SPECTRAL DATA OF **3**, **9**, AND **10** (δ(J Hz))

Compound	H(4)	H(5)	H(7)	J_{HH}	$^4J_{H(4)P}$	$^3J_{H(5)P}$	$^3J_{H(7)P}$	C(5)	C(6)	$^2J_{C(5)P}$	$J_{C(6)P}$
3a	6.26	4.76	5.76	5.5	5.5	19.5	41.0	55.5	75.5	2.4	42.7
3b	6.24	4.72	5.76	5.5	5.5	20.0	42.0	54.7	75.4	2.4	42.7
3c	6.17	4.67	5.66	5.5	5.5	20.0	42.0	54.9	74.8	2.4	43.9
9a	6.82	5.06	6.35	5.0	5.5	18.0	42.0	56.7	77.2	2.9	42.7
9b	a)	4.96	6.30	5.0	a)	18.0	42.0	55.9	77.0	2.4	41.5
9c	6.82	5.00	6.33	6.0	5.5	20.0	42.0	56.2	77.1	4.0	41.5
9d	6.74	4.96	6.23	6.0	5.5	20.0	42.0	56.2	76.6	2.4	41.5
9e	a)	5.02	6.22	5.0	a)	18.0	42.0	56.7	77.4	2.4	43.9
9f	6.78	5.04	6.29	5.0	5.5	18.0	42.0	56.7	77.2	2.4	41.5
9g	6.82	5.04	6.32	5.0	5.5	18.0	42.0	56.8	77.4	2.4	41.5
10a	—	4.28	—	—	—	28.0	—	56.4	71.9	3.7	41.5
10b	—	4.89	—	—	—	38.0	—	56.5	75.5	≃0	41.5
10c	—	4.30	—	—	—	28.0	—	55.5	71.2	2.4	53.7

a) Superimposed on Ar–H. b) Chemical shifts of the signals of C-3, C-4, C-7, and C-8 were not assigned.

their NMR spectral data with those of **3a** (Table 2). The signals of the hydrogen atoms attached to the bicyclic skeleton (H-4, H-5, and H-7) and those of the skeletal saturated carbon atoms (C-5 and C-6) showed characteristic H-P and C-P couplings.[7]

Treatment of the thione dimers with P_4S_{10} and NEt_3 in refluxing carbon disulfide also produced the phosphabicyclo compounds. P_4S_{10} is cleaved by liquid NH_3 or NEt_3 to produce diverse complex species containing P, S, and N, *e.g.*, $(NH_4)[PS_2(NH_2)_2]$, $(NH_4)_2[PS_3(NH_2)]$.[8] Therefore it is assumed that the attack of NEt_3 upon P_4S_{10} generates the reactive species, X-(S=)P=S (*e.g.*, X=$Et_3NH^+S^-$), which reacts with α,β-unsaturated thiones to form an intermediate **I** in a similar manner to Lawesson's Reagent (L.R.)[9] (Scheme 2). In the case of L. R. (X=*p*-$CH_3OC_6H_4$), I is actually obtained as a stable compound. But when X is P_4S_{10} fragment as in the present study, it would be an effective leaving group and can be removed readily under suitable reaction conditions. Accordingly it is rationally considered that by action of a base, NEt_3, H-3 proton is eliminated with X to form 1,2-thiaphosphole 2-sulfide **II** which subsequently undergoes cycloaddition reaction as 2π system with the thione monomer (4π) to afford the phosphabicyclo compound **III**.

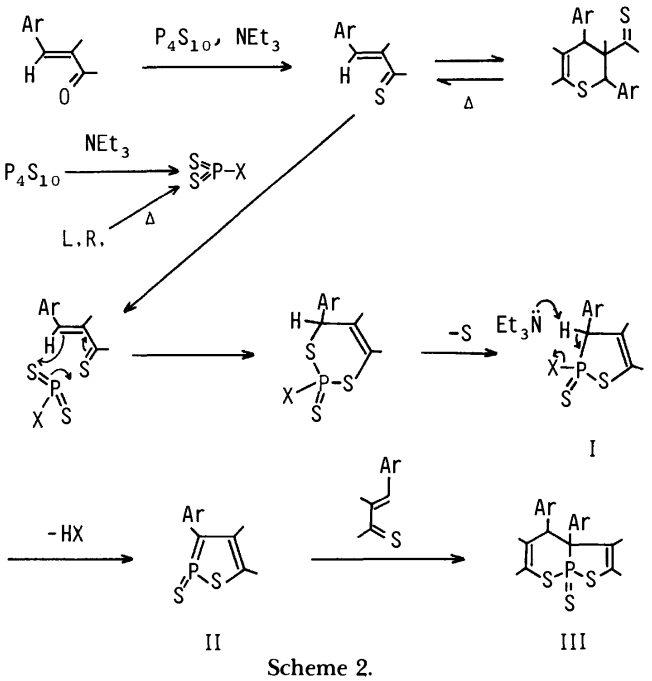

Scheme 2.

The reaction of **3a** with acrylonitrile in refluxing benzene gave 1,4-cycloadducts **5a**, ***endo*-6a** and a small amount of ***exo*-6a** without the formation of any regioisomers (Table 3). The cycloadduct **5a** was easily identified by comparison with the authentic compounds reported previously[1] and the structure of ***endo***-

Table 3. Reactions with acrylonitrile, styrene, butyl vinyl ether and norbornene

Material	Dienophile	Reaction time/h	Product					
				Mp θ_m/°C	Yield/%		Mp (dec) θ_m/°C	Yield/%
3a		26	**5a**	137—138	96	***endo*-6a**	142—143	54
						***exo*-6a**	135—136	3
3b	"	18	**5b**	156—157	37	***endo*-6b**	174—176	15
3c	"	27	**5c**	149—151	86	***endo*-6c**	145—147	45
9a	"	2	**15a**	131—132	94	***exo*-16a**	155—156	13
9c	"	2	**15b**	154—155	86	***exo*-16b**	155—156	14
						***endo*-16b**	164—167	29
10a	"	4	**17a**	223—225	90	***exo*-18a**	175—177	23
10b	"	1.5	**17b**	126—128	68	***exo*-18b**	171—172	25
9a		2	**19**	129—131	69	***endo*-20**	a)	86
10a	"	3	**21a**	176—178	77	**22a**	134—135	44
10b	"	1	**21b**	143—144	72	**22b**	177—179	56
9a		4.5	**23**	a)	15	**24**	a)	7
10a	"	7.5	**25**	a)	19	**26**	148—149	36
9a		2	**27a**	140—142	75	***exo-exo*-28a**	160—161	72
9c	"	4.5	**27b**	126—127	84	***exo-exo*-28b**	179—181	34
						***endo-exo*-28b**	150—151	39
10a	"	8	**29a**	99—100	53	***exo*-30a**	229—230	48
10b	"	1.5	**29b**	124—125	27	***exo*-30b**	211—213	23

a) Oils.

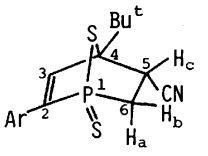

endo-6

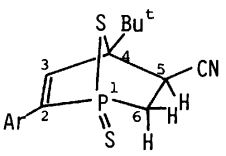

exo-6

a, Ar=C_6H_5 b, Ar=p-$CH_3C_6H_4$ c, Ar=p-ClC_6H_4

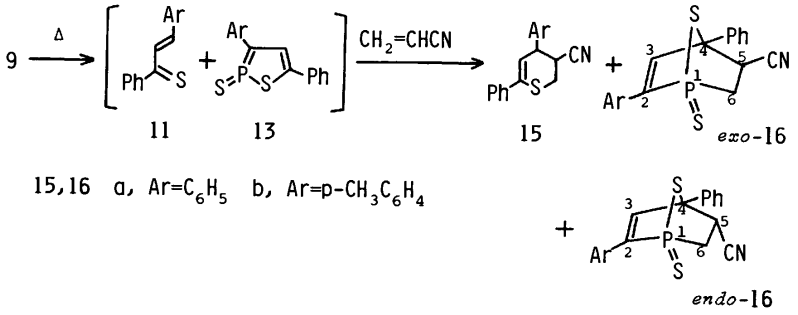

11 13 15 *exo*-16

15,16 a, Ar=C_6H_5 b, Ar=p-$CH_3C_6H_4$

endo-16

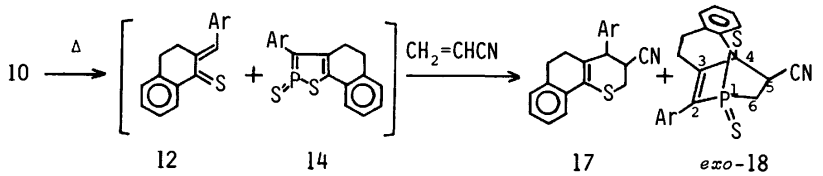

12 14 17 *exo*-18

17,18 a, Ar=C_6H_5 b, Ar=p-$CH_3OC_6H_4$

Scheme 3.

6a was confirmed by X-ray analysis.[6] The cycloadducts ***endo*- and *exo*-6a** showed sharp IR absorptions of ν_{CN} at 2250 cm^{-1}, and their mass spectra showed molecular ion peaks and the fragments due to retro cycloaddition reaction. In the ^{13}C NMR spectra of ***endo*- and *exo*-6a**, the signals of the methylene carbon

TABLE 4. ^{13}C NMR SPECTRAL DATA OF CYCLOADDUCTS (δ (J/Hz))

Adduct	C(2)	C(3)	C(4)	C(5)	C(6)	CN	$J_{C(2)P}$	$^2J_{C(3)P}$	$^2J_{C(4)P}$	$^2J_{C(5)P}$	$J_{C(6)P}$	$^3J_{PCN}$
***endo*-6a**	146.1	141.1	74.9	33.4	42.4	119.6	59.8	9.8	19.5	3.7	42.7	7.4
***exo*-6a**	146.4	141.4	a)	34.4	42.4	119.8	61.0	12.2	a)	6.1	44.0	3.7
***endo*-6b**	145.9	140.1	75.4	33.6	42.4	119.7	59.8	11.0	19.5	3.7	44.0	8.5
***endo*-6c**	144.9	141.6	75.4	33.4	42.4	119.5	59.8	9.8	19.5	3.7	44.0	7.3
***exo*-16a**	147.0	144.6	68.8	41.0	40.6	118.3	58.6	11.0	24.4	4.9	42.7	3.7
***exo*-16b**	146.6	143.5	68.8	41.0	40.5	118.4	58.6	11.0	24.4	4.9	42.7	3.7
***endo*-16b**	148.2	141.3	66.6	38.7	40.3	118.0	≃0	9.8	≃0	2.4	42.7	9.8
***endo*-18a**	139.8	155.5	66.2	40.1	41.3	118.2	64.6	11.0	24.4	4.9	41.5	3.7
***exo*-18b**	139.4	154.2	66.2	40.3	41.2	118.3	64.7	12.2	24.4	4.9	42.7	3.7
***endo*-20**	145.3	142.0	69.7	56.3	44.2	—	58.6	9.8	24.4	4.9	42.7	—
22a	137.6	155.7	67.5	56.4	41.8	—	63.5	9.8	25.6	4.9	42.7	—
22b	143.4	154.3	75.1	56.4	41.7	—	60.0	11.0	25.6	4.9	42.7	—
24	138.2	144.0	67.0	84.4	42.1	—	52.5	8.6	22.0	2.4	42.7	—
26	140.3	155.5	70.2	80.8	44.0	—	64.7	13.4	24.4	3.7	41.5	—
***exo-exo*-28a**	147.0	149.7	69.9	58.1	55.4	—	57.4	9.8	29.3	6.1	40.3	—
***exo-exo*-28b**	146.7	148.7	69.9	58.2	55.3	—	58.6	9.8	30.5	6.1	40.3	—
***endo-exo*-28b**	145.1	145.4	68.2	58.7	59.2	—	52.5	9.8	29.3	6.1	40.3	—
***exo*-30a**	139.0	155.7	66.0	62.3	57.4	—	58.6	9.8	29.3	6.1	40.3	—
***exo*-30b**	138.3	154.6	66.0	62.3	57.5	—	52.5	11.0	29.3	6.1	39.0	—

a) Superimposed on $CDCl_3$.

(***endo*-6a**; δ=42.42, ***exo*-6a**; δ=42.40) showed large C-P coupling constants (***endo*-6a**; J_{CP}=42.7 Hz, ***exo*-6a**; J_{CP}=44.0 Hz). This suggests that the methylene carbon is directly bonded to the phosphorus atom.[7] The ^1H NMR spectrum of ***endo*-6a** showed double double doublets of three sets of protons at δ=2.51 (J_{HH}=3.5, 14.0 Hz, J_{HP}=7.5 Hz), 3.07 (J_{HH}=9.5, 14.0 Hz, J_{HP}=14.0 Hz) and 3.64 (J_{HH}=3.5, 9.5 Hz, J_{HP}=4.5 Hz), which are assigned to the H_a, H_b, and H_c by spin decoupling experiments, respectively. The coupling constant value of H_c agreed with those of *exo* proton in 2-substituted norbornene ring system.[10] The ^1H NMR of ***exo*-6a** showed signals of H-5 proton at δ=3.08—3.32 and of H-6 (*gem*-AB) protons at δ=2.70—2.86. The coupling pattern was unambiguously different from that of ***endo*-6a**. *Endo* configuration of cyano group in **6b** and **6c** was determined by comparing their coupling pattern of H_a~H_c with that of ***endo*-6a**. Neither ***exo*-6b** nor ***exo*-6c** was obtained.

Similarly, the thermolysis of **9** or **10** in the presence of acrylonitrile yielded **15** and **16**, or **17** and **18** (Table 3). The reactions proceeded more rapidly than that of **3**. The products **15** and **17** were identfied as [4+2]-cycloadducts of **11** and **12** with acrylonitrile, respectively.[1] The structure and configuration of the adduct **16** were determined by comparing their spectral data with those of **6a** (*endo*, *exo*) as described above. The ^{13}C NMR spectral data of **18** indicated that the cyano group was linked to the carbon atom at 5-position. It is difficult to determine exactly the configuration of cyano group in **18** by ^1H NMR spectra, however, it was presumed to be *exo* because C-P coupling constants of *endo* cyano carbon were 7.3—9.8 Hz in the adducts **6** and **16**, whereas those of the *exo* were 3.7 Hz (Table 4).

With styrene **9** or **10** produced **19**[1] and **20** or **21**[1] and **22**, respectively. Table 3 shows that the orientation of the 1,4-cycloadducts (**20**, **22**) agrees with that of the

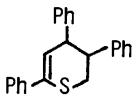

19

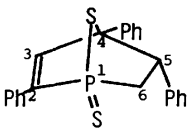

endo-20

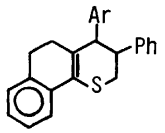

21

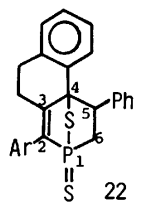

22

21,22 a, Ar=C_6H_5 b, Ar=p-$CH_3OC_6H_4$

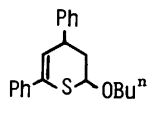

23

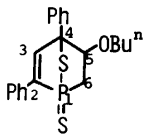

24

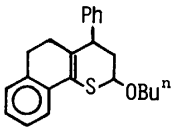

25

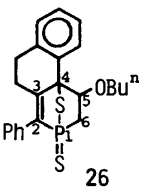

26

acrylonitrile-adducts (**16**, **18**). The ^1H NMR coupling pattern of **20** agreed with that of the *endo*-adduct **6** or **16**.

The thermolysis of **9** with butyl vinyl ether gave **23**[1] and **24**. In the adduct **24**, the ^{13}C NMR spectral data proved that butoxyl group was linked to the C-5 carbon. The signal of the C-5 carbon showed small coupling constant $^2J_{C(5)P}$(2.4 Hz) as compared with

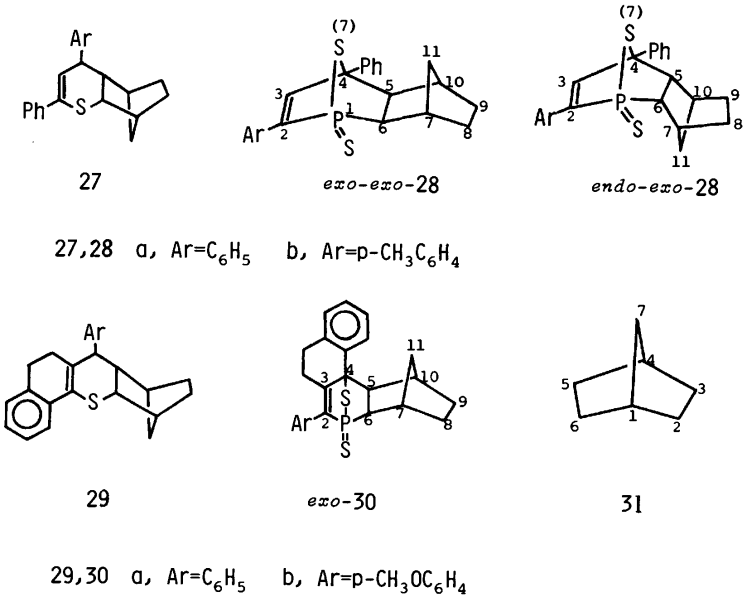

Fig. 1. The configurations of cycloadducts with norbornene. In 2-substituted norbornane, the *exo*-2 group usually shifts the resonance of the C-7 carbon upfield by 1.3—4.4 ppm from the one in norbornane **31** while the *endo*-2 group usually shifts the resonamce of C-6 carbon upfield by 4.9—9.7 ppm from one in **31**[11] (Table 5).

$J_{C(6)P}$ and shifted downfield owing to the butoxyl group (Table 4). Similarly, the reaction of **10** with butyl vinyl ether afforded **25**[1] and **26**. The configurations of **24** and **26** could not be determined.

The reaction of **9** with norbornene gave **27**[1] and **28**. In the case of **9c**, two stereo isomers of **28b** were obtained. In general, the chemical shift of the bridged carbon of *exo* substituted norbornane should shift upfield from that of norbornane **31** due to steric repulsion.[11] One isomer showed the resonance of the C-11 carbon at δ=34.8 shifted upfield by 4.1 ppm from that of **31**. The other isomer had the resonance at δ=30.4 shifted upfield by 8.0 ppm. The chemical shifts of the C-8 and C-9 carbons of both isomers did not change from those of **31** (Table 5). Therefore, both of the isomers would be *exo* with respect to the norbornyl skeleton. On the other hand, the C-2 and C-3 olefinic carbons[11] of the latter isomer resonated upfield by 1.6—3.3 ppm as compared with those of the former, hence the configuration of the latter with respect to 1-phospha-7-thiabicyclo[2.2.1]heptene 1-sulfide ring system would be *endo*; namely the former isomer is ***exo-exo*-28b** and the latter is ***endo-exo*-28b**. The reaction of **10** with norbornene gave **29** and **30**. In the ^{13}C NMR of **30**, the chemical shifts of the C-8 and C-9 carbons did not change, while the C-11 carbon resonated upfield by 6.3 ppm from that of **31**. Therefore, the configuration should be *exo* with respect to norbornyl ring.

As described above, it has been found that 1,2-thiaphosphole 2-sulfides react as cyclic heterodienes readily and regioselectively with acrylonitrile, styrene or butyl vinyl ether.[12] Besides the cycloaddition, other varied reactions can be expected for the 1,2-thiaphosphole 2-sulfides. The reaction with some nucleophiles are now under investigation.

Table 5. ^{13}C NMR Chemical shifts of norbornane **31** and cycloadducts **28b** (J_{CP}/Hz)

Carbons	**31**	*exo-exo*-**28b**		*endo-exo*-**28b**	
	δ	δ	J_{CP}	δ	J_{CP}
C-2	—	146.7	58.6	145.1	52.5
C-3	—	148.7	9.8	145.4	9.8
C-7(C-1)	36.8	39.1		38.5	
C-8(C-2)	30.1	30.7	17.1	32.1	15.9
C-9(C-3)	30.1	30.7		32.9	
C-10(C-4)	36.8	36.6	3.7	36.2	2.4
C-11(C-7)	38.7	34.8		30.7	

Experimental

All the melting points are uncorrected. IR spectra were measured on a Hitachi Model 260-10 spectrometer. ^1H and ^{13}C NMR spectra were recorded on a JEOL JNM-FX 100 spectrometer in $CDCl_3$ solution using Me_4Si as internal standard (^1H; at 100 MHz, ^{13}C; at 25 MHz). ^{13}C NMR spectral data are shown in Tables 2, 4, and 5. ^{31}P NMR spectra were recorded at 40 MHz on a JEOL JNM-FX 100 spectrometer using 85% H_3PO_4 as external standard. Mass spectra were recorded on a Hitachi double focusing mass spectrometer (RMU-7M) operating at an ionizing potential of 70 eV. Elemental analyses of sulfur and phosphorus were performed for some representative compounds. All α,β-unsaturated ketones were prepared by the Aldol condensation of the corresponding ketone with aldehyde.[13] Acrylonitrile, styrene, butyl vinyl ether and norbornene were obtained commercially.

General Procedure for the Preparation of 2,9-Dithia-1-phosphabicyclo[4.3.0]nona-3,7-diene 1-Sulfides. A suspension of α,β-unsaturated ketone (0.04 mol), P_4S_{10} powder (12 g) and NEt_3 (24 cm^3) in dry carbon disulfide (320 cm^3) was gent-

ly refluxed (50—55 °C) under a nitrogen atmosphere (Reaction times are shown in Table 1). The reaction mixture was filtered and the filtrate was evaporated. The residue was chromatographed on silica gel (Wakogel C-200). The solvent was evaporated and the residue was recrystallized from chloroform–ethanol giving the product as colorless crystals.

*3,8-Di-t-butyl-5,6-diphenyl-2,9-dithia-1-phosphabicyclo[4.3.0]-nona-3,7-diene 1-Sulfide (**3a**).* Chromatographed by eluting with benzene–hexane (2:3); ^{1}H NMR ($CDCl_3$) δ=1.22 (s, 9H), 1.27 (s, 9H), 4.76 (dd, 1H, J_{HH}=5.5 Hz, J_{HP}=19.5 Hz), 5.76 (d, 1H, J_{HP}=41.0 Hz), 6.26 (dd, 1H, J_{HH}=5.5 Hz, J_{HP}=5.5 Hz), and 7.00—7.30 (m, 10H); ^{31}P NMR ($CDCl_3$) δ=117.1 (dd, J_{PH}=41.0, 19.5 Hz); MS *m/z* (rel intensity) 470 (M^+; 3), 266 (19), 234 (47), 204 (34), 203 (32), and 147 (100). Found: C, 66.33; H, 6.48; S, 20.46; P, 6.43%. Calcd for $C_{26}H_{31}S_3P$: C, 66.35; H, 6.64; S, 20.43; P, 6.58%.

*3,8-Di-t-butyl-5,6-bis(p-methylphenyl)-2,9-dithia-1-phosphabicyclo[4.3.0]nona-3,7-diene 1-Sulfide (**3b**).* Chromatographed by eluting with benzene–hexane (2:3); ^{1}H NMR ($CDCl_3$) δ=1.21 (s, 9H), 1.27 (s, 9H), 2.23 (s, 3H), 2.29 (s, 3H), 4.72 (dd, 1H, J_{HH}=5.5 Hz, J_{HP}=20.0 Hz), 5.76 (d, 1H, J_{HP}=42.0 Hz), 6.24 (dd, 1H, J_{HH}=5.5 Hz, J_{HP}=5.5 Hz), and 6.90—7.30 (m, 8H); MS *m/z* (rel intensity) 498 (M^+), 280 (8), 248 (65), 218 (22), 203 (41), and 161 (75). Found: C, 67.50; H, 7.12; S, 19.39; P, 6.31%. Calcd for $C_{28}H_{35}S_3P$: C, 67.43; H, 7.07; S, 19.28; P, 6.21%.

*3,8-Di-t-butyl-5,6-bis(p-chlorophenyl)-2,9-dithia-1-phosphabicyclo[4.3.0]nona-3,7-diene 1-Sulfide (**3c**).* Chromatographed by eluting with benzene–hexane (2:3); ^{1}H NMR ($CDCl_3$) δ=1.22 (s, 9H), 1.27 (s, 9H), 4.67 (dd, 1H, J_{HH}=5.5 Hz, J_{HP}=20.0 Hz), 5.66 (d, 1H, J_{HP}=42.0 Hz), 6.17 (dd, 1H, J_{HH}=5.5 Hz, J_{HP}=5.5 Hz), and 6.90—7.30 (m, 8H); MS *m/z* (rel intensity) 538 (M^+), 300 (20), 268 (54), 238 (27), 233 (94), and 181 (100). Found: C, 57.90; H, 5.43; S, 18.16; P, 5.80%. Calcd for $C_{26}H_{29}Cl_2S_3P$: C, 57.88; H, 5.42; S, 17.83; P, 5.74%.

*3,5,6,8-Tetraphenyl-2,9-dithia-1-phosphabicyclo[4.3.0]nona-3,7-diene 1-Sulfide (**9a**).* Chromatographed by eluting with benzene–hexane (1:1); ^{1}H NMR ($CDCl_3$) δ=5.06 (dd, 1H, J_{HH}=5.0 Hz, J_{HP}=18.0 Hz), 6.35 (d, 1H, J_{HP}=42.0 Hz), 6.82 (dd, 1H, J_{HH}=5.0 Hz, J_{HP}=5.5 Hz), and 7.18—7.58 (m, 20H); ^{31}P NMR ($CDCl_3$) δ=116.8; MS *m/z* (rel intensity) 254 (100), 224 (15), 223 (30), and 191 (60). Found: C, 70.61; H, 4.78; S, 19.12; P, 5.56%. Calcd for $C_{30}H_{23}S_3P$: C, 70.56; H, 4.54; S, 18.83; P, 6.07%.

*5,6-Bis(p-methoxyphenyl)-3,8-diphenyl-2,9-dithia-1-phosphabicyclo[4.3.0]nona-3,7-diene 1-Sulfide (**9b**).* Chromatographed by eluting with benzene–hexane (1:1); ^{1}H NMR ($CDCl_3$) δ=3.70 (s, 3H), 3.74 (s, 3H), 4.96 (dd, 1H, J_{HH}=5.0 Hz, J_{HP}=18.0 Hz), 6.30 (d, 1H, J_{HP}=42.0 Hz), and 6.66—7.54 (m, 19H); ^{31}P NMR ($CDCl_3$) δ=116.6; MS *m/z* (rel intensity) 284 (100), 269 (25), 254 (18), and 253 (19). Found: C, 67.18; H, 4.83%. Calcd for $C_{32}H_{27}O_2S_3P$: C, 67.35; H, 4.83%.

*5,6-Bis(p-methylphenyl)-3,8-diphenyl-2,9-dithia-1-phosphabicyclo[4.3.0]nona-3,7-diene 1-Sulfide (**9c**).* Chromatographed by eluting with benzene–hexane (1:1); ^{1}H NMR ($CDCl_3$) δ=2.26 (s, 3H), 2.30 (s, 3H), 5.00 (d, 1H, J_{HH}=6.0 Hz, J_{HP}=20.0 Hz), 6.33 (d, 1H, J_{HP}=42.0 Hz), 6.82 (dd, 1H, J_{HH}=6.0 Hz, J_{HP}=5.5 Hz), and 6.92—7.56 (m, 18H); MS *m/z* (rel intensity) 300, 268 (100), 238 (13), 237 (18), and 205 (29). Found: C, 71.27; H, 5.20%. Calcd for $C_{32}H_{27}S_3P$: C, 71.34; H, 5.05%.

*5,6-Bis(p-chlorophenyl)-3,8-diphenyl-2,9-dithia-1-phosphabicyclo[4.3.0]nona-3,7-diene 1-Sulfide (**9d**).* Chromatographed by eluting with benzene–hexane (1:1); ^{1}H NMR ($CDCl_3$) δ=4.96 (dd, 1H, J_{HH}=6.0 Hz, J_{HP}=20.0 Hz), 6.23 (d, 1H, J_{HP}=42.0 Hz), 6.74 (dd, 1H, J_{HH}=6.0 Hz, J_{HP}=5.5 Hz), and 6.96—7.54 (m, 18H); MS *m/z* (rel intensity) 288 (100), 258 (24), 257 (28), and 225 (36). Found: C, 62.32; H, 3.81%. Calcd for $C_{30}H_{21}Cl_2S_3P$: C, 62.71; H, 3.65%.

*3,8-Bis(p-methoxyphenyl)-5,6-diphenyl-2,9-dithia-1-phosphabicyclo[4.3.0]nona-3,7-diene 1-Sulfide (**9e**).* Chromatographed by eluting with benzene–hexane (1:1); ^{1}H NMR ($CDCl_3$) δ=3.77 (s, 3H), 3.78 (s, 3H), 5.02 (dd, 1H, J_{HH}=5.0 Hz, J_{HP}=18.0 Hz), 6.22 (d, 1H, J_{HP}=42.0 Hz), and 6.66—7.50 (m, 19H); ^{31}P NMR ($CDCl_3$) δ=117.0; MS *m/z* (rel intensity) 284 (100), 253 (25), and 221 (9). Found: C, 67.58, H, 4.97%. Calcd for $C_{32}H_{27}O_2S_3P$: C, 67.35; H, 4.77%.

*3,8-Bis(p-methylphenyl)-5,6-diphenyl-2,9-dithia-1-phosphabicyclo[4.3.0]nona-3,7-diene 1-Sulfide (**9f**).* Chromatographed by eluting with benzene–hexane (1:1); ^{1}H NMR ($CDCl_3$) δ=2.33 (s, 6H), 5.04 (dd, 1H, J_{HH}=5.0 Hz, J_{HP}=18.0 Hz), 6.29 (d, 1H, J_{HP}=42.0 Hz), 6.78 (dd, 1H, J_{HH}=5.0 Hz, J_{HP}=5.5 Hz), and 7.06—7.44 (m, 18H); MS *m/z* (rel intensity) 268 (100), 238 (27), 237 (49), and 205 (29). Found: C, 71.35; H, 5.34%. Calcd for $C_{32}H_{27}S_3P$: C, 71.34; H, 5.05%.

*3,8-Bis(p-chlorophenyl)-5,6-diphenyl-2,9-dithia-1-phosphabicyclo[4.3.0]nona-3,7-diene 1-Sulfide (**9g**).* Chromatographed by eluting with benzene–hexane (1:1); ^{1}H NMR ($CDCl_3$) δ=5.04 (dd, 1H, J_{HH}=5.0 Hz, J_{HP}=18.0 Hz), 6.32 (d, 1H, J_{HP}=42.0 Hz), 6.82 (dd, 1H, J_{HH}=5.0 Hz, J_{HP}=5.5 Hz), and 7.16—7.56 (m, 18H); MS *m/z* (rel intensity) 288 (100), 258 (1), 257 (2), and 225 (29). Found: C, 62.38; H, 3.74%. Calcd for $C_{30}H_{21}Cl_2S_3$ P: C, 62.17; H, 3.65%.

*6b,7-Diphenyl-5,6,6b,7,8,9-hexahydro-14,15-dithia-14a-phosphabenz[4,5]indeno[1,2-b]phenanthrene 14a-Sulfide (**10a**).* Chromatographed by eluting with benzene–hexane (2:3); ^{1}H NMR ($CDCl_3$) δ=1.24—2.98 (m, 8H), 4.28 (d, 1H, J_{HP}=28.0 Hz), and 6.86—7.60 (m, 18H); ^{31}P NMR ($CDCl_3$) δ=123.7; MS *m/z* (rel intensity) 530, 312 (30), 280 (100), 250 (9), and 249 (17). Found: C, 72.70; H, 4.70; S, 17.62; P, 5.12%. Calcd for $C_{34}H_{27}S_3P$: C, 72.44; H, 5.01; S, 17.06; P, 5.49%.

*6b,7-Bis(p-methoxyphenyl)-5,6,6b,7,8,9-hexahydro-14,15-dithia-14a-phosphabenz[4,5]indeno[1,2-b]phenanthrene 14a-Sulfide (**10b**).* Chromatographed by eluting with benzene–hexane (2:3); ^{1}H NMR ($CDCl_3$) δ=1.54—2.74 (m, 8H), 3.75 (s, 6H), 4.89 (d, 1H, J_{HP}=38.0 Hz), and 6.66—7.52 (m, 16H); ^{31}P NMR ($CDCl_3$) δ=109.4; MS *m/z* (rel intensity) 310 (100), 279 (25). Found: C, 69.43; H, 5.32%. Calcd for $C_{36}H_{31}O_2S_3P$: C, 69.32; H, 5.17%.

*6b,7-Bis(p-chlorophenyl)-5,6,6b,7,8,9-hexahydro-14,15-dithia-14a-phosphabenz[4,5]indeno[1,2-b]phenanthrene 14a-Sulfide (**10c**).* Chromatographed by eluting with benzene–hexane (2:3); ^{1}H NMR ($CDCl_3$) δ=1.57—1.84 (m, 8H), 4.30 (d, 1H, J_{HP}=28.0 Hz), and 7.00—7.58 (m, 16H); MS *m/z* (rel intensity) 314 (100), 285 (22), and 283 (22). Found: C, 64.63; H, 3.97%. Calcd for $C_{34}H_{27}Cl_2S_3P$: C, 64.65; H, 3.99%.

General Procedure for the Cycloaddition Reactions of the 2,9-Dithia-1-phosphabicyclo[4.3.0]nona-3,7-diene 1-Sulfides with Dienophiles. A solution of the 2,9-dithia-1-phosphabicyclo[4.3.0]nona-3,7-diene 1-sulfide (2 mmol) and dienophile (6 mmol) in dry benzene (5 cm^3) was refluxed under a nitrogen atmosphere until all the phosphabicyclo compound had been consumed as indicated by TLC. The solvent was evaporated and the residue was chromatographed on silica gel (Wakogel C-200). The solvent was evaporated and the residue was recrystallized from ethanol to give the cycloadduct.

*6-t-Butyl-3-cyano-4-phenyl-3,4-dihydro-2H-thiopyran (**5a**).* Chromatographed by eluting with benzene–ligroin (1:1); IR

(KBr) 2250 cm^{-1} (CN); ^1H NMR ($CDCl_3$) δ= 1.22 (s, 9H), 3.00—3.40 (m, 3H), 3.78 (dd, 1H, J_{HH}=4.8 Hz), 5.66 (d, 1H, J_{HH}=4.8 Hz), and 7.20—7.30 (m, 5H); MS *m/z* (rel intensity) 257 (M^+; 30), 203 (63), and 147 (100). Found: C, 74.68; H, 7.47; N, 5.37; S, 12.74%. Calcd for $C_{16}H_{19}NS$: C, 74.66; H, 7.44; N, 5.44; S, 12.46%.

6-t-Butyl-3-cyano-4-(p-methylphenyl)-3,4-dihydro-2H-thiopyran (**5b**). Chromatographed by eluting with benzene–hexane (2:1); IR (KBr) 2250 cm^{-1} (CN); ^1H NMR ($CDCl_3$) δ=1.21 (s, 9H), 2.34 (s, 3H), 2.90—3.40 (m, 3H), 3.60—3.80 (m, 1H), 5.63 (d, 1H, J_{HH}=5.0 Hz), and 7.00—7.20 (m, 4H); MS *m/z* (rel intensity) 271 (M^+; 29), 218 (22), 203 (100), and 161 (70). Found: C, 75.39; H, 7.85; N, 5.17%. Calcd for $C_{17}H_{21}NS$: C, 75.23; H, 7.80; N, 5.16%.

6-t-Butyl-3-cyano-4-(p-chlorophenyl)-3,4-dihydro-2H-thiopyran (**5c**). Chromatographed by eluting with benzene–hexane (1:1); IR (KBr) 2250 cm^{-1} (CN); ^1H NMR($CDCl_3$) δ=1.22 (s, 9H), 2.98—3.36 (m, 3H), 3.78 (dd, 1H, J_{HH}=4.6 Hz), 5.60 (d, 1H, J_{HH}=4.6 Hz), and 7.06—7.36 (m, 4H); MS *m/z* (rel intensity) 291 (M^+; 25), 238 (41), 203 (40), and 181 (100). Found: C, 65.79; H, 6.02; N, 4.77%. Calcd for $C_{16}H_{18}NClS$: C, 65.85; H, 6.22; N, 4.80%.

*4-t-Butyl-*endo*-5-cyano-2-phenyl-7-thia-1-phosphabicyclo[2.2.1]hept-2-ene 1-Sulfide* (**endo-6a**). IR (KBr) 2250 cm^{-1} (CN); ^1H NMR ($CDCl_3$) δ=1.34 (s, 9H), 2.51 (ddd, 1H, J_{HH}=3.5, 14.0 Hz, J_{HP}=7.5 Hz), 3.07 (ddd, 1H, J_{HH}=9.5, 14.0 Hz, J_{HP}= 14.0 Hz), 3.64 (ddd, 1H, J_{HH}=3.5, 9.5 Hz, J_{HP}=4.5 Hz), and 7.05—7.72 (m, 6H); ^{31}P NMR ($CDCl_3$) δ=−28.9; MS *m/z* (rel intensity) 319 (M^+; 2), 266 (100), 251 (22), 234 (52), 219 (85), and 203 (18). Found: C, 60.18; H, 5.77; N, 4.41; S, 20.02; P, 9.78%. Calcd for $C_{16}H_{18}NS_2P$: C, 60.16; H, 5.68; N, 4.39; S, 20.07; P, 9.70%.

exo-6a: IR (KBr) 2250 cm^{-1} (CN); ^1H NMR ($CDCl_3$) δ=1.39 (s, 9H), 2.70—2.86 (m, 2H), 3.08—3.32 (m, 1H), and 6.72—7.70 (m, 6H); MS *m/z* (rel intensity) 319 (M^+; 2) 266 (100), 251 (22), 234 (29), 219 (22), and 203 (17). Found: C, 60.32; H, 5.60; N, 4.35%. Calcd for $C_{16}H_{18}NS_2P$: C, 60.16; H, 5.68; N, 4.39%.

*4-t-Butyl-*endo*-5-cyano-2-(p-methylphenyl)-7-thia-1-phosphabicyclo[2.2.1]hept-2-ene 1-Sulfide* (**endo-6b**). IR (KBr) 2250 cm^{-1} (CN); ^1H NMR ($CDCl_3$) δ=1.32 (s, 9H), 2.36 (s, 3H), 2.48 (ddd, 1H, J_{HH}=3.0, 13.0 Hz, J_{HP}=7.5 Hz), 3.04 (ddd, 1H, J_{HH}=10.0, 13.0 Hz, J_{HP}=13.0 Hz), 3.60 (ddd, 1H, J_{HH}=3.0, 10.0 Hz, J_{HP}= 4.0 Hz), and 6.92—7.64 (m, 5H); MS *m/z* (rel intensity) 333 (M^+; 2), 280 (100), 265 (21), and 248 (39). Found: C, 61.56; H, 5.97; N, 4.18%. Calcd for $C_{17}H_{20}NS_2P$: C, 61.24; H, 6.05; N, 4.20%.

*4-t-Butyl-*endo*-5-cyano-2-(p-chlorophenyl)-7-thia-1-phosphabicyclo[2.2.1]hept-2-ene 1-Sulfide* (**endo-6c**). IR (KBr) 2250 cm^{-1} (CN); ^1H NMR ($CDCl_3$) δ=1.34 (s, 9H), 2.50 (ddd, 1H, J_{HH}=3.0, 14.0 Hz, J_{HP}=7.5 Hz), 3.08 (ddd, 1H, J_{HH}=10.0, 14.0 Hz, J_{HP}=14.0 Hz), 3.64 (ddd, 1H, J_{HH}=3.0, 10.0 Hz, J_{HP}=4.5 Hz), and 7.04—7.68 (m, 5H); MS *m/z* (rel intensity) 355 (M^+; 1), 302 (44), 287 (11), 270 (23), and 255 (37). Found: C, 54.25; H, 5.00; N, 3.94%. Calcd for $C_{16}H_{17}NClS_2P$: C, 54.31; H, 4.84; N, 3.96%.

exo-5-Cyano-2,4-diphenyl-7-thia-1-phosphabicyclo[2.2.1]hept-2-ene 1-Sulfide (**exo-16a**). Chromatographed by eluting with benzene–ligroin (1:1); IR (KBr) 2250 cm^{-1} (CN); ^1H NMR ($CDCl_3$) δ=2.82—3.04 (m, 2H), 3.54—3.80 (m, 1H), and 6.82—7.68 (m, 11H); ^{31}P NMR ($CDCl_3$) δ=−52.6; MS *m/z* (rel intensity) 286 (15), 254 (100). Found: C, 63.90; H, 4.35; S, 19.35; P, 8.88%. Calcd for $C_{18}H_{14}NS_2P$: C, 63.70; H, 4.16; S, 18.89; P, 9.13%.

exo-5-Cyano-2-(p-methylphenyl)-4-phenyl-7-thia-1-phosphabicyclo[2.2.1]hept-2-ene 1-Sulfide (**exo-16b**). Chromatographed by eluting with benzene–ligroin (1:1); IR (KBr) 2250 cm^{-1} (CN); ^1H NMR ($CDCl_3$) δ=2.36(s, 3H), 2.64—3.12 (m, 2H), 3.50—3.80 (m, 1H), and 7.04—7.60 (m, 10H); MS *m/z* (rel intensity) 353 (M^+; 1), 300 (30), and 268 (100). Found: C, 64.44; H, 4.32%. Calcd for $C_{19}H_{16}NS_2P$: C, 64.57; H, 4.56%.

endo-16b: IR (KBr) 2250 cm^{-1} (CN); ^1H NMR ($CDCl_3$) δ= 2.38 (s, 3H), 2.58 (ddd, 1H, J_{HH}=4.0, 13.0 Hz, J_{HP}=8.0 Hz), 3.12 (ddd, 1H, J_{HH}=9.0, 13.0 Hz, J_{HP}=13.0 Hz), 4.06 (ddd, 1H, J_{HH}=4.0, 10.0 Hz, J_{HP}=3.0 Hz), and 7.12—7.70 (m, 10H); MS *m/z* (rel intensity) 353 (M^+), 300 (24), and 268 (100). Found: C, 64.38; H, 4.28%. Calcd for $C_{19}H_{16}NS_2P$: C, 64.57; H, 4.56%.

exo-10-Cyano-7-phenyl-2,3-benzo-11-thia-8-phosphatricyclo-[6.2.1.$0^{1,6}$]undec-6-ene 8-Sulfide (**exo-18a**). Chromatographed by eluting with benzene–hexane (3:2); IR (KBr) 2250 cm^{-1}(CN); ^1H NMR ($CDCl_3$) δ=2.58—3.52 (m, 7H) and 7.14—7.67 (m, 9H); ^{31}P NMR ($CDCl_3$) δ=−52.1; MS *m/z* (rel intensity) 365 (M^+), 312 (34), and 280 (100). Found: C, 65.75; H, 4.71; S, 17.96; P, 8.28%. Calcd for $C_{20}H_{16}NS_2P$: C, 65.73; H, 4.41; S, 17.55; P, 8.48%.

exo-10-Cyano-7-(p-methoxyphenyl)-2,3-benzo-11-thia-8-phosphatricyclo[6.2.1.$0^{1,6}$]undec-6-ene 8-Sulfide (**exo-18b**). Chromatographed by eluting with benzene–hexane (1:2); IR (KBr) 2250 cm^{-1} (CN); ^1H NMR($CDCl_3$) δ=2.40—3.56 (m, 7H), 3.82 (s, 3H), and 6.80—7.72 (m, 8H); MS *m/z* (rel intensity) 395 (M^+), 342 (3), and 310 (100). Found: C, 63.87; H, 4.89%. Calcd for $C_{21}H_{18}ONS_2P$: C, 63.87; H, 4.58%.

endo-5-Phenyl-2,4-diphenyl-7-thia-1-phosphabicyclo[2.2.1]hept-2-ene 1-Sulfide (**endo-20**). Chromatographed by eluting with benzene–hexane (1:2); ^1H NMR ($CDCl_3$) δ=2.48—4.20 (m, 3H), 6.60—6.76 (m, 1H), and 6.80—7.92 (m, 15H); MS *m/z* (rel intensity) 390 (M^+; 1), 287(2), and 254 (100).

7,10-Diphenyl-2,3-benzo-11-thia-8-phosphatricyclo[6.2.1.$0^{1,6}$]undec-6-ene 8-Sulfide (**22a**). Chromatographed by eluting with benzene; ^1H NMR ($CDCl_3$) δ=1.42—3.80 (m, 6H), 4.42—4.60 (m, 1H), and 6.34—7.79 (m, 14H); ^{31}P NMR ($CDCl_3$) δ= −49.6; MS *m/z* (rel intensity) 416 (M^+), 312 (6), 280 (100), and 249 (10). Found: C, 71.83; H, 5.34; S, 15.47; P, 7.26%. Calcd for $C_{25}H_{21}S_2P$: C, 72.09; H, 5.08; S, 15.39; P, 7.44%.

7-(p-Methoxyphenyl)-10-phenyl-2,3-benzo-11-thia-8-phosphatricyclo[6.2.1.$0^{1,6}$]undec-6-ene 8-Sulfide (**22b**). Chromatographed by eluting with benzene–hexane (1:1); ^1H NMR ($CDCl_3$) δ= 1.40—3.60 (m, 5H), 3.86 (s, 3H), 4.40—4.64 (m, 1H), and 6.75—7.82 (m, 13H); MS *m/z* (rel intensity) 446 (M^+), 342 (6), and 310 (100). Found: C, 69.82; H, 5.41%. Calcd for $C_{26}H_{23}OS_2P$: C, 69.93; H, 5.19%.

5-Butoxy-2,4-diphenyl-7-thia-1-phosphabicyclo[2.2.1]hept-2-ene 1-Sulfide (**24**). Chromatographed by eluting with benzene–hexane (1:1); ^1H NMR ($CDCl_3$) δ=0.60—1.48 (m, 9H), 2.00—2.32 (m, 1H), 2.76—3.00 (m, 1H), 3.12—3.40 (m, 1H), and 7.00—7.76 (m, 11H).

10-Butoxy-7-phenyl-2,3-benzo-11-thia-8-phosphatricyclo[6.2.1.$0^{1,6}$]undec-6-ene 8-Sulfide (**26**). Chromatographed by eluting with benzene–hexane (3:4); ^1H NMR ($CDCl_3$) δ=0.39—1.56 (m, 7H), 2.34—3.00 (m, 7H), 3.12—3.36 (m, 1H), 3.80—4.16 (m, 1H), and 7.00—7.60 (m, 9H); MS *m/z* (rel intensity) 412 (M^+), 378 (1), 346 (1), 312 (13), 280 (100), and 215 (31). Found: C, 66.84; H, 6.20%. Calcd for $C_{23}H_{25}OS_2P$: C, 66.96; H, 6.11%.

8,10-Diphenyl-11-thia-1-phosphatetracyclo[6.2.$1^{3,6}$.$0^{2,7}$]dec-9-ene 1-Sulfide (**exo-exo-28a**). Chromatographed by eluting

with benzene–hexane (3:2); ^{1}H NMR ($CDCl_3$) δ=0.94—3.10 (m, 10H), 7.03—7.67 (m, 11H); ^{31}P NMR ($CDCl_3$) δ=−44.4; MS *m/z*' (rel intensity) 380 (M^+; 2), 286 (100), 254 (8), 223 (10), and 121 (14). Found: C, 69.71; H, 5.82; S, 17.18; P, 7.88%. Calcd for $C_{22}H_{21}S_2P$: C, 69.45; H, 5.56; S, 16.85; P, 8.14%.

10-(p-Methylphenyl)-8-phenyl-11-thia-1-phosphatetracyclo-[6.2.1^{3,6}.0^{2,7}]dec-9-ene 1-Sulfide (**exo-exo-*28b***). Chromatographed by eluting with benzene–hexane (1:2); ^{1}H NMR ($CDCl_3$) δ=0.92—3.07 (m, 10H), 2.36 (s, 3H), and 6.97—7.66 (m, 10H); MS *m/z* (rel intensity) 394 (M^+; 3), 300 (100), and 268 (19). Found: C, 70.33; H, 5.92%. Calcd for $C_{23}H_{23}S_2P$: C, 70.02; H, 5.88%.

endo-exo-*28b*: ^{1}H NMR ($CDCl_3$) δ=0.68—3.40 (m, 10H), 2.36 (s, 3H), and 6.90—7.68 (m, 10H); MS *m/z* (rel intensity) 394 (M^+; 5), 300 (100), and 268 (15). Found: C, 70.30; H, 5.82%. Calcd for $C_{23}H_{23}S_2P$: C, 70.02; H, 5.88%.

9-Phenyl-13,14-benzo-15-thia-8-phosphapentacyclo[6.6.1.1^{3,6}.-0^{1,10}.0^{2,7}]hexadeca-9,13-diene 8-Sulfide (**exo-*30a***). Chromatographed by eluting with benzene; ^{1}H NMR ($CDCl_3$) δ=0.82—3.32 (m, 14H) and 7.16—7.58 (m, 9H); ^{31}P NMR ($CDCl_3$) δ=−41.3; MS *m/z* (rel intensity) 406 (M^+; 3), 312 (100), 280 (9), and 249 (10). Found: C, 70.94; H, 5.75; S, 15.55; P, 7.80%. Calcd for $C_{24}H_{23}S_2P$: C, 70.91; H, 5.70; S, 15.77; P, 7.62%.

9-(p-Methoxyphenyl)-13,14-benzo-15-thia-8-phosphapentacyclo-[6.6.1.1^{3,6}.0^{1,10}.0^{2,7}]hexadeca-9,13-diene 8-Sulfide (**exo-*30b***). Chromatographed by eluting with benzene–hexane (1:1); ^{1}H NMR ($CDCl_3$) δ=1.78—3.32 (m, 14H), 3.80 (s, 3H), and 6.80—7.64 (m, 8H); MS *m/z* (rel intensity) 436 (M^+; 1), 342 (100), and 310 (10). Found: C, 69.01; H, 6.01%. Calcd for $C_{25}H_{25}OS_2P$: C, 68.78; H, 5.77%.

The authors wish to thank Professor Tokiko Uchida for performing the X-ray analysis. The authors also would like to thank Mr. Ryoichi Yamabe for his technical assistance.

References

1) T. Karakasa and S. Motoki, *J. Org. Chem.*, **43**, 4147 (1978); **44**, 4151 (1979).

2) Treatment of chalcones **7** or 2-arylmethylene-1-tetralones **8** (0.1 mol) with P_4S_{10} (10 g) and NEt_3 (10 cm^3) in carbon disulfide at room temperature afforded the corresponding thione dimers. However, when the thionation of 1-arylmethylenepinacolones **1** was carried out under the same reaction conditions, no reaction took place. Treatment of these ketones (0.1 mol) with large amount of P_4S_{10} (30 g) and NEt_3 (60 cm^3) in refluxing carbon disulfide is suitable for the preparation of phosphabicyclo compounds **3**, **9**, and **10**.

3) H. Yamaguchi, S. Kametani, T. Karakasa, T. Saito, and S. Motoki, *Tetrahedron Lett.*, **1982**, 1263.

4) M. Caira, R. H. Neilson, W. H. Watson, P. Wisian-Neilson, and Z. -M. Xie, *J. Chem. Soc., Chem. Commun.*, **1984**, 698; J. -M. Alcaraz and F. Mathey, *Tetrahedron Lett.*, **1984**, 207; T. Kawashima, T. Tomita, and N. Inamoto, *Phosphorus and Sulfur*, **16**, 9 (1983); R. H. Neilson, *ibid.*, **18**, 43 (1983); F. Mathey, *ibid.*, **18**, 101 (1983).

5) T. Karakasa and S. Motoki, unpublished work.

6) T. Uchida, K. Kozawa, T. Saito, and S. Motoki, *Bull. Chem. Soc. Jpn*, **57**, 1985; 1990 (1984).

7) E. F. Moony, "Annual Reports on NMR Spectroscopy," Academic Press, New York (1973), Vol. 5B, p. 12; J. Emsley and D. Hall, "The Chemistry of Phosphorus," Harper & Row, Publishers, London (1976).

8) G. Nickless, "Inorganic Sulphur Chemistry," Elsevier Publishing Company, Amsterdam (1968), p. 309.

9) S. Kametani, H. Ohmura, H. Tanaka, and S. Motoki, *Chem. Lett.*, **1982**, 793; A. Ecker, I. Boie, and U. Schmidt, *Angew. Chem., Int. Ed. Engl.*, **10**, 191 (1971).

10) E. I. Snyder and B. Franzus, *J. Am. Chem. Soc.*, **86**, 1166 (1964); P. Laszlo and P.von R. Schleyer, *ibid.*, **86**, 1171 (1964); H. Günther and G. Jikeii, *Chem. Revs.*, **77**, 599 (1977).

11) J. B. Stothers, "Carbon-13 NMR Spectroscopy," Academic Press, New York (1972), p. 68, p. 414; G. C. Levy, R. L. Lichter, and G. L. Nelson, "Carbon-13 Nuclear Magnetic Resonance for Organic Chemists," Wiley, New York (1972), p. 61.

12) Tentative CNDO/2 calculations of the FMO's show that the reaction is LUMO (1,2-thiaphosphole 2-sulfide)-controlled with styrene and butyl vinyl ether, while with acrylonitrile HOMO (1,2-thiaphosphole 2-sulfide)-controlled. This prediction of the regioselectivity with styrene and butyl vinyl ether is in agreement with the experimental results, but is opposite with acrylonitrile.

13) E. P. Kohler and H. M. Chadwell, *Org. Synth.*, **1**, 78 (1932); A. Hassner, N. H. Cromwell, and S. J. Davis, *J. Am. Chem. Soc.*, **79**, 230 (1957).

A Potent Pyridoxal Model Capable of Promoting Transamination and β-Elimination of Amino Acids

Hiroki KONDO,* Jun-ichi KIKUCHI, Shinji UCHIDA, Tatsuya KITAMIKADO, Eiji KOYANAGI, and Junzo SUNAMOTO

Department of Industrial Chemistry, Faculty of Engineering Nagasaki University, Nagasaki 852

(Received September 3, 1984)

N-Dodecylpyridoxal chloride (**1a**) has been synthesized as a potent pyridoxal 5′-phosphate model. The equilibrium constant for Schiff base formation of **1a** with phenylalanine (21000 M^{-1}) in 3 mM hexadecyltrimethylammonium chloride (CTACl) micelle is over a thousand times larger than that for the *N*-methyl counterpart (**1b**). The Schiff base of **1a** and phenylalanine exists over a broad pH range of 5—11 in two ionic forms, HSB and SB^-, that differ in the protonation state at the azomethine group. These Schiff bases undergo transamination at 30 °C in the absence of a metal ion at considerably different rates; 1.33×10^{-3} and 1.5×10^{-5} s^{-1} for HSB and SB^-, respectively. Likewise, the former species exhibited 11 times higher reactivity in the β-elimination of *O*-phosphonoserine catalyzed by **1a** in 3 mM CTACl at 40 °C. These results indicate unambiguously the importance of a positive charge on the azomethine nitrogen as well as the one residing on the pyridine nitrogen in vitamin B_6 catalysis. The kinetic α-deuterium isotope effect of 5.1 in the transamiantion of phenylalanine with **1a** at pH 7.7 and 30 °C revealed that α-hydrogen abstraction takes place in the transition state.

Pyridoxal 5′-phosphate (PLP)-dependent enzymes play a pivotal role in the metabolism of amino acids.[1,2] Such metabolic reactions comprise transamination, decarboxylation *etc.* It is well known that these reactions can be duplicated in nonenzymatic systems, but rather unphysiological conditions such as high temperature, presence of metal ions[3] and/or high buffer salts[4] are usually needed to promote the reaction. It is, hence, clear that factors responsible for a more efficient catalysis of the coenzyme in enzymatic systems remain to be elucidated. In light of the fact that the PLP catalysis appears to be subject to general acid-base catalysis in the enzyme active site[5,6] as well as in model systems,[4,7] we have envisioned that duplication of this aspect of catalysis would generate a potent pyridoxal model capable of mediating reactions of amino acids under ambient conditions. The present model system consists of a pyridoxal bearing a dodecyl group on the pyridine nitrogen (**1a**) and a hexadecyltrimethylammonium chloride (CTACl) micelle.[8] The positive charge residing on the pyridine ring exerts a strong electron-withdrawing effect on the Schiff base of amino acid, and hydroxide ions concentrated at the cationic micellar surface are expected to serve as a base catalyst.[9] It was found that this system is an excellent catalyst of transamination and β-elimination reactions of ordinary amino acids in the absence of metal ions.

Experimental

Materials. Pyridoxal hydrochloride was obtained from Wako Pure Chemical Ind., Osaka. Pyridoxal methochloride (**1b**) was prepared according to the literature.[10] DL-Phenylalanine and DL-[α-^{2}H]phenylalanine were prepared by the literature method.[11] The deuterium content in the latter was determined as 95.4% by mass spectroscopy.[12] *O*-Phosphonoserine was either prepared[13] or purchased from Sigma. Other L-amino acids, ammonium molybdate and other common chemicals were obtained from Wako. Sodium tetraphenylborate and EDTA were the products of Dojindo, Kumamoto. CTACl was the same as that used previously.[14] Rabbit muscle lactate dehydrogenase and NADH were obtained from Boehringer Mannheim and Kyowa Hakko, Tokyo, respectively.

1-Dodecylpyridoxal Chloride (1-dodecyl-4-formyl-3-hydroxy-5-hydroxymethyl-2-methylpyridinium Chloride, 1a). "Pyridoxal inner monomethyl acetal"[10] (1,3-dihydro-1-methoxy-6-methylfuro [3,4-c]pyridin-7-ol, 0.50 g, 3 mmol) was allowed to react with dodecyl iodide (3.0 g, 10 mmol) in 12 ml of refluxing dry MeOH–benzene (5:1 by vol) for 200 h. The solvents were removed *in vacuo* and 100 ml of ether was added to the residue. The precipitate formed was collected by filtration. It was purified by column chromatography twice on a Sephadex LH-20 (Pharmacia) column (1.2×30 cm) with MeOH as eluant. The product was obtained as a light yellow oil in 20% yield.

An aqueous solution (50 ml) of "1-dodecylpyridoxal iodide inner monomethyl acetal" prepared above was mixed with an aqueous suspension of silver chloride, prepared fresh from silver nitrate and potassium chloride. The mixture was stirred at room temperature for 2 h. After removing the solid by filtration, the pH of the filtrate was brought to 2 with hydrochloric acid. Evaporation of the solvent left a very hygroscopic yellow oil. TLC (silica gel) R_f 0.08 (CH_3CN). NMR (DMSO-d_6) δ 0.86 (t, J=5 Hz, 3H), 1.0—2.0 (m, 20H), 2.71 (s, 3H), 4.61 (t, J=7 Hz, 2H), 5.04 (d, J=14 Hz, 1H), 5.18 (d, J=14 Hz, 1H), 6.81 (s, 1H), 8.72 (br s, 1H).

Apparatus. Electronic absorption spectra were taken on a Hitachi 124 or 200 spectrophotometer. Rapid-scanning spectra were determined with a Union Giken RA-401 spectrophotometer furnished with a rapid scanning device RA-415. Fluorescence spectra were recorded on a Hitachi 650-10 fluorescence spectrophotometer. ^{1}H NMR spectra were obtained on a Jeol JNM-MH-100 spectrometer. Mass spectra were determined with a Jeol JMS-DX 300 mass spectrometer in the chemical ionization mode. The pH values of aqueous solutions were read on a Toa pH meter HM-5A fitted with a combination electrode GS-195C.

Equilibria. For determining equilibrium constants for the formation of a Schiff base of **1a** or **1b** with amino acids, a number of aqueous solutions containing $1-3\times10^{-4}$ M† **1a** or **1b** and 0—1 M amino acid at various pH values were prepared

† 1 M=1 mol dm^{-3}.

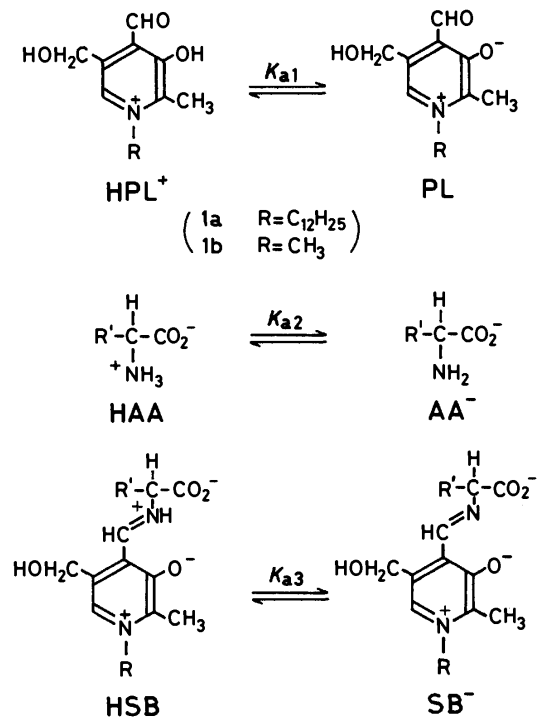

Scheme 1.

in the absence or presence of 3 mM CTACl.[15] Equilibria of Schiff base formation were attained within 10 min and absorption spectra were determined at 30.0 °C. The pertinent equilibria are depicted in Scheme 1. With **1b**, the two ionic species of Schiff base, HSB and SB^-, were detected spectroscopically over the pH range 7—11. On the other hand, HSB species was hardly visible with **1a** in 3 mM CTACl in the same pH region, though the equilibrium constant for the Schiff base formation is much greater with this system. A pH jump-rapid scanning spectroscopy, however, allowed one to observe HSB species (see below).

The data were analyzed in a way similar to those described previously,[16-18] but with some simplifications where possible. The pH-dependent (K_{pH}, Eq. 1) and independent equilibrium constants (K, Eq. 2) for the Schiff base formation are those defined by Metzler.[15] In a micellar **1a** and phenylalanine system, the Schiff base formation is complete at 10 mM amino acid at pH 9—11 and only a single ionic species each is present for **1a**, phenylalanine and Schiff base in that pH region. Hence, the spectrum determined at pH 11 at the highest amino acid concentration represents the intrinsic spectrum of SB^- whose absorption maximum is located at 393 nm. Furthermore, the K_{pH} values obtained in this pH region are set equal to the pH-independent equilibrium constant K. The intrinsic spectrum of HSB was obtained by a pH jump-rapid scanning technique. To determine the pK_a values of Schiff base and phenylalanine in the micelle, steady state spectral data at pH 4.7, 5.6, 6.0, and 11.0 (16 points) were analyzed by iterative computations until a minimum value of the sum of residual squares U is reached (Eq. 3).[16]

$$K_{pH} = \frac{[SB]_T}{[PL]_T \cdot [AA]_T} \quad (1)$$

$$K = \frac{[SB^-]}{[PL] \cdot [AA^-]} \quad (2)$$

$$U = \sum_{i,j,k} (A^{obs}_{ijk} - A^{cal}_{ijk})^2 \quad (3)$$

$$A^{cal}_{ijk} = \sum_{k,l} \varepsilon_{kl} \cdot C_{ijl} \quad (4)$$

Caluculated absorbance A^{cal}_{ijk} at a given pH i, amino acid concentration j and wavelength k is the sum of contributions of HPL^+, PL, HSB, and SB^- (Scheme 1 and Eq. 4).

Rapid Scanning Spectroscopy. Following two stock solutions were prepared: Solution (A) contained 0.40 mM **1a**, 30 mM phenylalanine and 3 mM CTACl in 10 mM borate buffer, pH 12 and Solution (B) contained 3 mM CTACl and dilute hydrochloric acid. Equal volumes of both solutions were mixed to bring the pH of the resulting solution to ≈4 and an electronic absorption spectrum was recorded at 1 ms intervals (Fig. 1). The absorption band centered at 430 nm disappeared gradually with a half life ≈14 s, finally to make the solution colorless. This phenomenon is explained in terms of rapid protonation to SB^- and subsequent slow dissociation of HSB into its constituents.

Kinetics of Transamination. An aqueous solution (3 ml) of 10 mM phenylalanine, 3 mM CTACl and 0.10 mM EDTA in 10 mM phosphate buffer at a specified pH value was placed in a cuvette and thermally equilibrated at 30.0 °C. A solution of **1a** (30 μl) was injected and the whole mixture was agitated quickly. The concentration of **1a** in the mixture was 0.10 mM. A decrease of the Schiff base absorption was followed continuously at its absorption maximum wavelength. The rate of transamination was determined by Eq. 5.

$$-\frac{d[SB]_T}{dt} = k_{obsd}[SB]_T \quad (5)$$

As the Schiff base formation is not always complete, the rate constant k_{obsd} obtained by Eq. 5, was converted to the specific rate constant of the Schiff base (k) with the aid of Eq. 6, which is derived by a combination of Eqs. 1 and 7 as well as an assumption that the amino acid concentration does not change throughout the reaction, *i.e.*, $[AA]_T \simeq [AA]_0$.

$$k_{obsd} = \frac{k \cdot K_{pH} \cdot [AA]_0}{1 + K_{pH} \cdot [AA]_0} \quad (6)$$

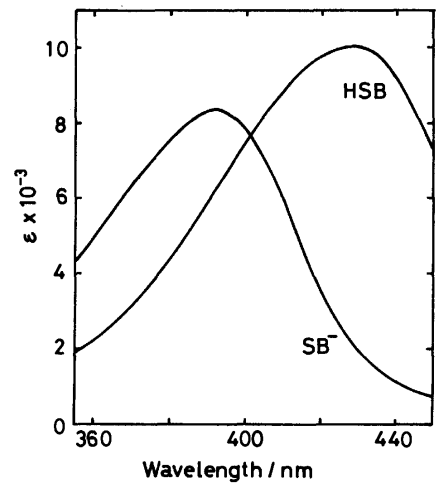

Fig. 1. Electronic absorption spectra of the HSB and SB^- Schiff base of **1a** and phenylalanine in 3 mM CTACl. The trace for HSB was obtained by pH-jump rapid scanning spectroscopy. Details are given under Experimental.

$$\frac{d[PL]_T}{dt} + \frac{d[SB]_T}{dt} + \frac{d[Product]_T}{dt} = 0 \quad (7)$$

β-Elimination of O-Phosphonoserine. Reaction rates were determined by quantitating colorimetrically the inorganic phosphate liberated.[19] A reaction mixture (6 ml) containing 20 mM substrate, 5 mM EDTA and 3 mM CTACl and adjusted to a specified pH value with sodium hydroxide was placed in a constant temperature bath of 40.0 °C. The reaction was started by the addition of 300 μl of **1a** or **1b** solution, the final concentration of the catalyst being 0.50 mM. A 1 ml-aliquot was withdrawn at appropriate time intervals and transferred to a flask containing 1 ml of 3.1 mM sodium tetraphenylborate to precipitate most of the surfactant. A 4 ml-aliquot of molybdate solution, prepared according to Taussky and Shorr,[19] was added and the whole mixture swirled for 1 min. The precipitate was removed by ultrafiltration through a 0.05 μm pore size filter paper (Millipore). The absorbance of the filtrate was read at 720 nm.

Reaction rates (v) were linear with time in the initial stage of the reaction. Combination of a rate equation (Eq. 8) and K_{pH} (Eq. 1) yields Eq. 6′, from which the specific rate constant of the Schiff base (k) is obtained.

$$v = k[SB]_T \quad (8)$$

$$v = \frac{k \cdot K_{pH}[AA]_0 \cdot [PL]_0}{1 + K_{pH} \cdot [AA]_0} \quad (6')$$

Product Analysis. Keto acids produced by transamination of phenylalanine and β-elimination of *O*-phosphonoserine were identified spectroscopically after conversion to their 2,4-dinitrophenylhydrazones. Pyruvic acid was also quantitated by the "coupled assay," in which pyruvic acid is reduced with NADH and lactate dehydrogenase and the remaining NADH is determined by fluorescence spectroscopy.[8] Formation of the pyridoxamine form of **1a** upon transamination with phenylalanine was revealed by an increase in fluorescence intensity at ~438 nm of a reaction mixture.[8] This compound was also confirmed by TLC on silica gel, in which a new ninhydrin-positive fluorescent spot became visible with the progress of reaction.

Results

Schiff Base Formation. The acid dissociation constant (pK_{a1}) of the 3-hydroxyl group of **1a** and **1b** was determined by spectroscopic titrations in water at 30.0 °C as 3.7 or 4.0, respectively. The acid form of either compound possesses an absorption maximum at 296 nm, while the ionized form at 323.5 nm. Whereas the absorption spectrum of **1b** was not affected by SDS or CTACl micelles, the spectrum of **1a** is red-shifted considerably in either micelles. Thus the λ_{max} value of 323.5 nm is shifted to 330.5 and 326 nm in 3 mM CTACl and SDS micelles, respectively. In addition, the pK_{a1} value of **1a** is altered to 2.6 and 4.9 in the CTACl and SDS micelles, respectively. These data indicate that **1a** forms a mixed micelle with the two surfactants.

The equilibrium constant for the Schiff base formation between **1a** or **1b** and amino acid was determined by spectral measurements of solutions that contain varying amounts of amino acid at different pH values.[15] The Schiff base exists over a pH range of 7—11 in two ionic forms, *i.e.*, protonated or ionized with respect to the azomethine group (Scheme 1). The former Schiff base species of **1b** and phenylalanine has a λ_{max} at 416 nm and the latter at 380 nm. The equilibrium constant K defined by Eq. 2 was also determined as 17 M^{-1}. The formation of Schiff base of phenylalanine was enhanced greatly with **1a** in the presence of 3 mM CTACl, but only a single ionic species that has a λ_{max} at 393 nm was discernible in the neutral to alkaline media. This species is likely to be SB^- and the red-shift by 13 nm from that of the corresponding **1b** species is explicable in terms of its location in the micellar phase. The polarity of the micellar environment of the Schiff base was assessed by determining the Schiff base absorption as a function of dioxane concentration in water. As shown in Fig. 2, the λ_{max} shifts to the blue as the dioxane content in the medium is increased. The value of 393 nm in the CTACl micelle corresponds to the polarity of 46% dioxane in water.

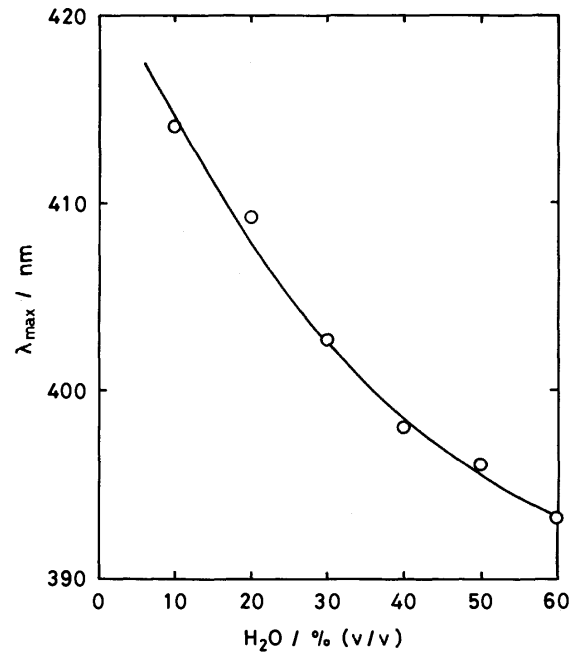

Fig. 2. Relationship of the absorption maximum of SB^- of **1a** and phenylalanine with the water content in dioxane.

The HSB species of the Schiff base of **1a** and phenylalanine in 3 mM CTACl was observed at lower pH values of ≈5. This species possesses an absorption maximum at 430 nm, again shifted to the red by 14 nm from the corresponding Schiff base species of **1b**. Analysis of the spectroscopic data in this pH region yielded the results summarized in Table 1. The equilibrium constant of 21000 M^{-1} is over 1000 times greater than the corresponding value for the **1b** system (17 M^{-1}). Based on the former value, molar distribution of the two Schiff base species of 0.10 mM **1a** and 10 mM phenylalanine is depicted over a broad pH

TABLE 1. EQUILIBRIUM CONSTANTS AND SPECTROSCOPIC DATA FOR THE SCHIFF BASES OF PHENYLALANINE WITH **1a** OR **1b**

Aldehyde	K[a)]/M^{-1}	pK_{a3}[b)]	λ_{max}/nm (ε_{max}/$M^{-1}\cdot cm^{-1}$)	
			HSB	SB^-
1a	21,000	5.0	430(10,000)	393(8,300)
1b	17	8.0	416(8,400)	380(7,900)

a) Defined by Eq. 2. b) For definition see Scheme 1.

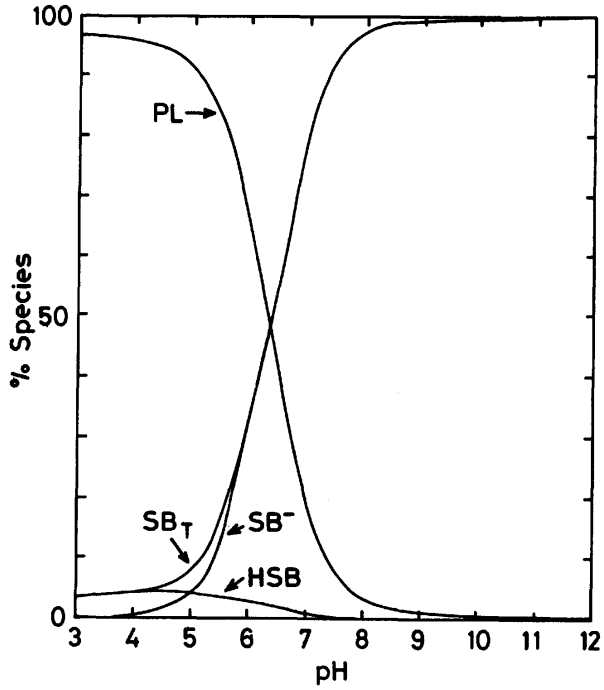

Fig. 3. pH-Distribution profile for HSB and SB^- species of the Schiff base of 0.10 mM **1a** and 10 mM phenylalanine in 3 mM CTACl. The following numerical values are employed: K 21000 M^{-1}; pK_{a1} 2.6; pK_{a2} 8.7; pK_{a3} 5.0.

range in the micelle (Fig. 3). The origin of favorable Schiff base formation in this system stems from the hydrophobic interaction of the apolar side chain of amino acid with the micelle. Owing to this interaction a large portion of phenylalanine is partitioned in the micellar phase to form a Schiff base with **1a** residing there. As stated previously,[8] the equilibrium constant is highly dependent on the hydrophobicity of amino acids; the more hydrophobic, the greater is the equilibrium constant. This view is further supported by the fact that equilibrium constants for hydrophilic amino acids such as glutamic acid and *O*-phosphonoserine are comparable with the corresponding values for **1b** or pyridoxal (see below).

One peculiarity encountered in the Schiff base of *O*-phosphonoserine with **1a** in 3 mM CTACl at pH 9 should be worth mentioning. At low amino acid concentrations, the Schiff base formation is observed with a λ_{max} at 387 nm, but further addition of amino acid was not accompanied by a steady build-up of that absorption. Analysis of these spectroscopic data led to a molar extinction coefficient of ≈2000 for SB^- species. The value is quite untenable, as all Schiff bases of pyridoxal and related compounds share a common chromophore which is responsible for the absorption in the visible region with a molar extinction coefficient of 6000—10000.[15-18,20] It is speculated that highly anionic *O*-phosphonoserine may change the micellar structure of CTACl significantly and/or the amino acid may not be partitioned in the micelle to a large extent for some reasons which we are not aware at present. Hence, an extinction coefficient of 7000 was assumed for the SB^- species of *O*-phosphonoserine and this value was used for the evaluation of K_{pH} in the micellar system. The K value for this amino acid is estimated as 7 M^{-1}.

Another point to note is the low pK_a value (5.0) of the Schiff base of **1a** and phenylalanine in the micelle. It is well known that acid dissociation is enhanced at a cationic micellar surface typically by one pH unit (see above), but the change as large as ≈3 pH units cannot be explained by the micellar effect of concentrating hydroxide ions at its surface alone. Since the micellar environment of the Schiff base is less polar (see above), ionization of the iminium proton may be facilitated to generate SB^- species which is electrically neutral with respect to the azomethine group.

Transamination of Phenylalanine. The Schiff base of **1a** formed in 3 mM CTACl micelle undergoes a slow spectral change from 393 to 335 nm.[21] This phenomenon is compatible with transamination of an aldimine into a ketimine, and eventually into its components (Eq. 9). The product analysis supported

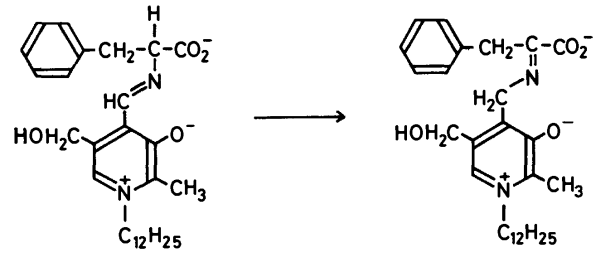

(9)

this interpretation. The rate of transamination was determined from the decay of Schiff base absorption at 30.0°C. It should be noted here that as this reaction, like most other nonenzymatic PLP-dependent reactions of amino acids,[3] is accelerated drastically by traces of a metal ion, an appropriate amount of EDTA was supplemented to all reaction solutions to suppress this metal ion effect. The amount of EDTA was decided by the following criteria. The rate obtained in the absence of EDTA was considerably greater than that in its presence because of a metal ion(s) contaminating the reagents used in these experiments, but it was decreased by an incremental addition of the chelator. There is a certain concentration of EDTA beyond which further addition of the reagent brought about no more rate-suppressing effect. At this concentration, addition of 1×10^{-5} M copper(II) or iron(III) ion did not give out any rate acceleration. Hence, the rates

Table 2. Rate constants for the transamination of **1a** with phenylalanine in 3 mM CTACl at 30.0 °C in the presence of 0.10 mM EDTA[a)]

pH	$k_{obsd}\times10^5/s^{-1}$	$k\times10^4/s^{-1}$
4.8	4.07	6.22
5.3	6.63	5.77
5.9	7.10	2.63
8.0	1.39	0.15

a) Rates were determined as described under Experimental and were analyzed with the aid of Eqs. 5 and 6.

determined in the presence of EDTA represent true rates of the Schiff base, free from metal contamination.

As the Schiff base formation is virtually complete under the present conditions over the pH range 9—11 (Fig. 3), kinetic data were analyzed in terms of a first-order equation with respect to the Schiff base. In cases where the Schiff base formation is incomplete, the determined rate was corrected for with the aid of Eq. 6. The rate constants thus obtained are listed in Table 2. The data were analyzed in terms of different reactivities of the two ionic species of Schiff base involved in the reaction (Eq. 10), where X_{HSB} and X_{SB^-} stand for the

$$k = k_1 \cdot X_{HSB} + k_2 \cdot X_{SB^-} \quad (10)$$

molar fraction of each species. The more acidic species (HSB) has a rate constant $1.33\times10^{-3}\,s^{-1}$ and the other (SB^-) $1.5\times10^{-5}\,s^{-1}$, thus the former is 89 times more reactive. To gain a further insight into the reaction mechanism of this nonenzymatic transamination, kinetic α-deuterium isotope effects of Schiff base have been investigated. The k_H/k_D of 5.1 was obtained for DL-phenylalanine and its α-deuterated counterpart at 30.0 °C and pH 7.7. This value compares with the isotope effect of 9.2 for the transamination of alanine with 4-formyl-3-hydroxy-1-methylpyridinium chloride under similar conditions,[21)] suggesting that α-hydrogen abstraction takes place in the transition state in both reactions.

β-Elimination of O-Phosphonoserine. *O*-Phosphonoserine undergoes β-elimination in the presence of **1b** or **1a**-CTACl (Eq. 11).[11)] The spontaneous reac-

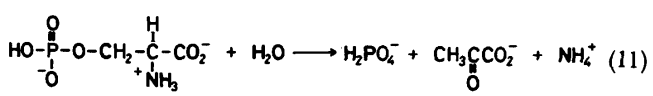

(11)

tion and its CTACl catalysis were negligible under the present reaction conditions, indicating that the β-elimination proceeds via a Schiff base. First, the apparent catalytic efficiency of **1a** and **1b** was compared. The initial rate with **1a** and 3 mM CTACl in the presence of 5 mM EDTA was $6.3\times10^{-8}\,M\cdot s^{-1}$ at pH 9.0 and 40.0 °C, whereas the corresponding value with **1b** was $4.3\times10^{-9}\,M\cdot s^{-1}$, thus the former catalyst being 15 times more effective. The K_{pH} values for **1a** and **1b** at pH 9.0 were 3.8 and 0.5, respectively. Based on these figures, the above rate constants were converted to the specific rate constants of the Schiff base (mainly SB^- species). The numerical values were $1.0\times10^{-3}\,s^{-1}$ for **1a** and $0.9\times10^{-3}\,s^{-1}$ for **1b**, demonstrating that both Schiff bases possess a roughly identical reactivity.

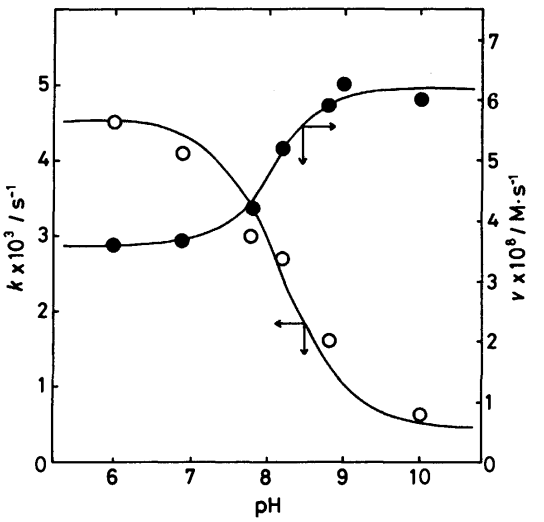

Fig. 4. pH-Rate profiles for the β-elimination of *O*-phosphonoserine in the presence of 0.50 mM **1a** and 5 mM EDTA in 3 mM CTACl at 40.0 °C. Closed circles represent the observed rates and they were converted to the rate constants of the Schiff base with the aid of Eq. 6′ (open circles). The theoretical curve is drawn based on the rate constants 4.6×10^{-3} and $4.2\times10^{-4}\,s^{-1}$ and the acid dissociation constant (pK_{a3}) 8.0.

The pH-dependence of the reaction rates in the presence of **1a** and CTACl is shown with closed circles in Fig. 4. By using the known K_{pH} values, a new pH-rate profile is constructed for the specific rate constant of the Schiff base (open circles and the sigmoid curve connecting them). The sigmoidal curve is interpreted in terms of different reactivities of the two Schiff base species (Eq. 10). The rate constants k_1 and k_2 obtained by this analysis were 4.6×10^{-3} and $4.2\times10^{-4}\,s^{-1}$, respectively. This result of the higher reactivity of HSB is compatible with the following metal ion effect on the elimination. Addition of 0.50 mM copper(II) ion, equimolar to **1a**, brought about a rate increase to $3.0\times10^{-6}\,M\cdot s^{-1}$ at pH 9.0 and 40.0 °C. Supposing that the copper(II) ion forms only a 1:1 Schiff base complex, the specific rate constant of the Cu^{2+}-SB^- species is $7.9\times10^{-2}\,s^{-1}$, 190 times as large as that of SB^-. Since the metal is divalent, it should exert a stronger electron-withdrawing effect, among other effects, than does a proton, thus rendering the α-proton of the Schiff base more labile.

It is also noted that the pK_a of the Schiff base of *O*-phosphonoserine with **1a** (8.0) is much higher than that of phenylalanine, but rather is close to that of phenylalanine and **1b**. This fact and the band location of 387 nm suggest that the Schiff base of *O*-phosphonoserine resides in a micellar domain more polar than that for the Schiff base of phenylalanine.

Discussion

As described above, the present pyridoxal model is

capable of promoting transamination and β-elimination of ordinary amino acids in the absence of metal ions. The reactions are presumed to take place in a mixed micelle of CTACl and **1a**. This view is substantiated by the following observations. The critical micelle concentration of CTACl was estimated as 1.2 mM under the present reaction conditions from an increase in the fluorescence intensity of 8-anilino-1-naphthalenesulfonic acid (ANS). A similar transition in the fluorescence intensity of ANS was found to occur at 0.16 mM CTACl in the presence of 0.10 mM **1a**, suggesting that the latter enhances the micellar aggregation of the former. The notion that **1a** and its Schiff base reside in the apolar micellar phase is supported by the large red-shift of their absorption bands and by the change in their pK_a (see Results). A large proportion of hydrophobic amino acids such as phenylalanine is partitioned in the micelle, thereby enhancing the Schiff base formation with **1a** residing there. This in turn is responsible for the facile transformation of the resulting Schiff base.

In addition to the enhanced Schiff base formation, this system has one more advantage in exploring pyridoxal-dependent reactions. Owing to the *N*-substitution in **1a**, the number of Schiff base species derived therefrom is limited (usually two, if we ignore acid dissociation of an amino acid side chain) over the wide pH range. These two are present in fair amounts under the condition of kinetic experiments, provide distinctly different absorption spectra and their reactivities can be assessed precisely. Based on the kinetic analysis of the transamination of phenylalanine and β-elimination of *O*-phosphonoserine, it is concluded that HSB, protonated at the azomethine group, is more reactive than SB^-.[22] This result is understandable in view of the fact that the primary role of PLP is to play as an electron sink[1-3] and that an electron-withdrawing ability of the Schiff base is greater when it bears more net positive charges. Others, however, dealing with similar data provided an opposite interpretation.[23] The reason for this discrepancy is not known.

This finding may be relevant to the enzymatic PLP catalysis. Absorption bands similar to that for the HSB species of **1a** and amino acid (430 nm) are obtained for some of the PLP-dependent enzymes.[24-26] This band location is characteristic for a Schiff base carrying a proton on the azomethine nitrogen. Whether or not the Schiff base bears a proton on the pyridine nitrogen cannot be decided, as the two forms of the Schiff base provide quite similar spectra.[16] Nonetheless, the fact that the *N*-substituted form is more reactive than the unsubstituted Schiff base[21,22] suggests that enzyme-bound PLP might carry a proton on the nitrogen, which is donated by an acidic group of the active site. This idea is supported by the recent crystallographic data on aspartate aminotransferase, in which the nitrogen of enzyme-bound PLP is hydrogen-bonded by an aspartate residue from the active site.[27,28] It is, hence, tempting to conclude that both the ring and azomethine nitrogen of the Schiff base need be protonated for PLP to perform its function of facilitating an electronic shift from the amino acid portion.

A general base catalysis as well as the general acid catalysis discussed above may be responsible for the high efficiency of the coenzyme in the enzymatic systems. The group involved in this function is the lysine amino moiety that binds PLP in the absence of a substrate.[5,6] A similar mode of base catalysis was observed in nonenzymatic systems also.[4,7] By analogy, hydroxide ions concentrated on the cationic micellar surface are a potential candidate to serve as a base catalyst.[8,9] Whether such a mechanism is working or not in the present system remains to be proven in the future. The fact that the α-deuterium isotope effect obtained in the micellar system is smaller than that for the nonmicellar reaction may provide a clue to solve this problem. At any rate, incorporation of a "powerful" base in our system should enhance the reactivity of the catalyst and further work is being continued along this line in this laboratory.

The authors are grateful to Professor Y. Murakami of Kyushu University for the use of his rapid scanning spectrophotometer. They also thank Dr. K. Sakata of Kyushu Institute of Technology for measuring mass spectra. This work was supported by a Grant-in-Aid for Special Project Research 57102007 from the Ministry of Education, Science and Culture, and by a grant from the Saneyoshi Scholarship Foundation.

References

1) E. E. Snell and S. J. Dimari, "The Enzymes," 3rd ed., ed by P. D. Boyer, Academic Press, New York, Vol. II, Chap. 7 (1970).
2) A. E. Braunstein, "The Enzymes," 3rd ed., ed by P. D. Boyer, Academic Press, New York, Vol. IX, Chap. 10 (1973).
3) D. E. Metzler, Y. Ikawa, and E. E. Snell, *J. Am. Chem. Soc.*, **76**, 648 (1954).
4) T. C. Bruice and R. M. Topping, *J. Am. Chem. Soc.*, **85**, 1480 (1963).
5) Y. Morino, A. M. Osman, and M. Okamoto, *J. Biol. Chem.*, **249**, 6684 (1974).
6) C. W. Fearon, J. A. Rodkey, and R. H. Abeles, *Biochemistry*, **21**, 3790 (1982).
7) Y. Murakami and H. Kondo, *Bull. Chem. Soc. Jpn.*, **48**, 125 (1975).
8) H. Kondo, J. Kikuchi, and J. Sunamoto, *Tetrahedron Lett.*, **24**, 2403 (1983).
9) Y. Murakami and H. Kondo, *Bull. Chem. Soc. Jpn.*, **48**, 541 (1975).
10) D. Heyl, E. Luz, S. A. Harris, and K. Folkers, *J. Am. Chem. Soc.*, **73**, 3430 (1951).
11) D. M. Yamamoto, D. A. Upson, D. K. Linn, and V. J. Hruby, *J. Am. Chem. Soc.*, **99**, 1564 (1977).
12) L. C. Kurz and C. Frieden, *J. Am. Chem. Soc.*, **102**, 4198 (1980).
13) D. Samuel and B. L. Silver, *J. Chem. Soc.*, 289 (1963).
14) J. Sunamoto, H. Kondo, T. Hamada, S. Yamamoto, Y.

Matsuda, and Y. Murakami, *Inorg. Chem.*, **19**, 3668 (1980).
15) D. E. Metzler, *J. Am. Chem. Soc.*, **79**, 485 (1957).
16) K. Nagano and D. E. Metzler, *J. Am. Chem. Soc.*, **89**, 2891, (1967).
17) Y. Murakami, H. Kondo, and A. E. Martell, *J. Am. Chem. Soc.*, **95**, 7138 (1973).
18) C. M. Metzler, A. Cahill, and D. E. Metzler, *J. Am. Chem. Soc.*, **102**, 6075 (1980).
19) H. H. Taussky and E. Shorr, *J. Biol. Chem.*, **202**, 675 (1953).
20) D. Heinert and A. E. Martell, *J. Am. Chem. Soc.*, **85**, 183 (1963).
21) J. R. Maley and T. C. Bruice, *Arch. Biochem. Biophys.*, **136**, 187 (1970).
22) H. Kondo, K. Morita, T. Kitamikado, and J. Sunamoto, *Bull. Chem. Soc. Jpn.*, **57**, 1031 (1984).
23) K. Tatsumoto, A. E. Martell, and R. J. Motekaitis, *J. Am. Chem. Soc.*, **103**, 6197 (1981).
24) W. J. Jenkins, D. A. Yphantis, and I. W. Sizer, *J. Biol. Chem.*, **234**, 51 (1959).
25) H. Kumagai and H. Yamada, *J. Biol. Chem.*, **245**, 1767 (1970).
26) M. Moriguchi, T. Yamamoto, and K. Soda, *Biochemistry*, **12**, 2969 (1973).
27) G. C. Foru, G. Eichele, and J. N. Jansonius, *Proc. Natl. Acad. Sci.*, **77**, 2559 (1980).
28) E. G. Harutyunyan, V. N. Malashkevich, S. S. Tersyan, V. M. Kochkina, Yu. M. Torchinsky, and A. E. Braunstein, *FEBS Lett.*, **138**, 113 (1982).

Selective Hydrogenation of Cyclooctadienes Using Colloidal Palladium in Poly(*N*-vinyl-2-pyrrolidone)

Hidefumi HIRAI,* Hitoshi CHAWANYA, and Naoki TOSHIMA
Department of Industrial Chemistry, Faculty of Engineering, The University of Tokyo, Hongo, Bunkyo-ku, Tokyo 113
(Received September 10, 1984)

Selective hydrogenation of 1,3-, 1,4-, and 1,5-cyclooctadiene to cyclooctene was carried out at 30 °C under atmospheric hydrogen pressure using colloidal palladium which was prepared by reducing palladium(II) chloride with refluxing methanol in the presence of poly(*N*-vinyl-2-pyrrolidone). The yields of cyclooctene were 99.9% and 97.8% for hydrogenation of 1,3- and 1,5-cyclooctadiene, respectively at the point that an equimolar hydrogen was uptaken by cyclooctadienes. The hydrogenation rate of 1,3- and 1,4-cyclooctadiene (R_1) is expressed as $R_1=k_1[H_2][Pd]$, and that of 1,5-cyclooctadiene (R_2) is expressed as $R_2=k_2[H_2]^{0.7}[Pd]$, where k_1 and k_2 are the rate constants. Alcohols were found to be good solvents for hydrogenation. In particular the fastest rate and the highest selectivity for monoene were observed in methanol among the solvents examined. Effect of bases on the monoene selectivity has also been investigated.

There have been numerous attempts to prepare highly dispersed metal catalysts supported on inorganic materials such as silica, alumina, and active carbon. Dispersion of the metal plays an important role in exhibiting high activity and selectivity of the catalyst.

On the other hand there are relatively little studies on colloidal metals homogeneously dispersed in a liquid phase. Rampino and Nord[1,2] reported that a colloidal dispersion of palladium with an average diameter of 700 Å was prepared by reducing aqueous palladium(II) hydroxide with molecular hydrogen in the presence of poly(vinyl alcohol).

Recently the present authors reported that colloidal noble metals were formed in good reproducibility by reducing the corresponding metal salts with primary or secondary alcohols or ethers in the presence of water-soluble vinyl polymers.[3,4] These colloidal metals were found to have smaller particle sizes (average particle diameters of 10—53 Å), and narrower particle size distributions than those prepared by reduction with molecular hydrogen. During the investigation of catalytic activity of the colloidal dispersions of noble metals, we have found that colloidal palladium prepared by reduction of palladium(II) chloride with methanol in the presence of poly(*N*-vinyl-2-pyrrolidone) catalyzes partial hydrogenation of cyclopentadiene,[5] and methyl esters of unsaturated fatty acid[6] to the corresponding monoenes. In the present paper we describe the selective hydrogenation of three isomers of cyclooctadiene to cyclooctene with the colloidal plladium.[7]

Experimental

Materials. Poly(*N*-vinyl-2-pyrrolidone) K-90 (Tokyo Chemical Industry Co. Ltd.; degree of polymerization, 3200) and palladium(II) chloride ($PdCl_2$) were used without further purification. 1,5-Cyclooctadiene, 1,3-cyclooctadiene, and cyclooctene were distilled under nitrogen before use. 1,4-Cyclooctadiene was prepared from 1,3-cyclooctadiene by bromination followed by reduction according to the literature.[8] All solvents were distilled and stored under nitrogen. Extra pure grade hydrogen (Nippon Oxygen Co. Ltd.; 99.99999% of purity) was passed through a Deoxo column (Nippon Engelhard, Ltd.) before use to remove trace amounts of oxygen. A commercial palladium catalyst used for comparison was 5% palladium on active carbon (Pd-C, Nippon Engelhard, Ltd.; surface area of Pd, 200 m^2/g-Pd).

Preparation of Colloidal Dispersion of Palladium. All manipulations were carried out under nitrogen atmosphere, using the solvents which were deaerated by purging with nitrogen.

Pd-PVP-MeOH/NaOH: Palladium(II) chloride (5.9 mg, 0.033 mmol) was dissolved in methanol (25 cm^3) by stirring the mixture overnight. Poly(*N*-vinyl-2-pyrrolidone) (151 mg, 1.36 mmol of monomeric units) was dissolved in methanol (20 cm^3). The combined mixture of these two solutions was gently heated with a water bath and brought to reflux. After the solution was refluxed for 30 min, a solution of sodium hydroxide (6.6 mg, 0.17 mmol) in methanol (5 cm^3) was added dropwise to the refluxing solution. The solution was refluxed for further 10 min to give a homogeneous dark brown dispersion of colloidal palladium protected by poly(*N*-vinyl-2-pyrrolidone).

Pd-PVP-MeOH/H_2O: A solution of palladium(II) chloride (5.9 mg) in methanol (25 cm^3) was combined with a solution of poly(*N*-vinyl-2-pyrrolidone) (151 mg) in water (25 cm^3). The mixed solution was refluxed over a water bath for 4 h, resulting in dark brown colloidal dispersion of palladium protected by poly(*N*-vinyl-2-pyrrolidone).

Electron Microscopy and Particle Size Determination. The sample film was prepared by evaporating a small amount of the colloidal dispersion of palladium to dryness on a collodion film which was coated with a carbon layer. The electron micrographs were taken at 100 kV at a magnification of 100000. The diameters of 200—900 particles of palladium in an arbitrarily chosen area were measured in an enlarged (4.4×) photograph. The particle size distribution and the number average particle diameter were determined on the basis of these results.

Hydrogenation of Cyclooctadienes. The reaction flask immersed in a thermostated water bath (30 °C) was evacuated and then flushed with hydrogen for 3—4 times. A solvent [(19−x) ml] and a colloidal dispersion of palladium (x ml) was then introduced into the flask and the mixed solution was stirred for 1 h to be saturated with hydrogen. A substrate diluted with a solvent for hydrogenation (1 cm^3) was injected into the reaction flask to start the reaction. Hydrogen uptake under a constant atmospheric pressure was monitored with a gas burette. Initial rates of hydrogenation (in H_2 mol/

Pd mol s) were calculated from the initial rates of hydrogen uptake.

The product was analyzed by GLPC with a flame ionization detector using helium as a carrier gas and a 30 m× 0.28 mmϕ glass capillary column coated with Silicone OV-101 at 55 °C

Kinetic Measurements. Initial rates of hydrogenation of cyclooctadienes with the colloidal palladium (Pd-PVP-MeOH/NaOH) were measured as a function of catalyst concentration, substrate concentration, and hydrogen pressure. Standard conditions are as follows: catalyst concentration=0.01 mmol dm^{-3} (0.1 mmol dm^{-3} for 1,5-cyclooctadiene), substrate concentration=25 mmol dm^{-3}, and hydrogen pressure=728 Torr (1 Torr≈133.322 Pa). Each variable was changed over the following range: catalyst, 0.002—0.01 mmol dm^{-3} (0.02—0.1 mmol dm^{-3} for 1,5-cyclooctadiene); substrate, 5—50 mmol dm^{-3}; hydrogen pressure, 180—728 Torr. The dependence of the rate on hydrogen pressure was measured in mixed gases of hydrogen and nitrogen at 1 atm. The concentration of hydrogen in the solution was determined from the partial pressure of hydrogen using Henry's law.

Under these reaction conditions, the hydrogenation rates were independent of the stirring rates of magnetic stirrers. Thus the reactions were not mass transfer limited.

Results

Preparation of the Colloidal Dispersion of Palladium. Palladium(II) chloride and poly(*N*-vinyl-2-pyrrolidone) were dissolved in methanol to form a yellow solution. After the solution was refluxed for 30 min, a methanol solution of sodium hydroxide was added to the refluxing solution, which caused a color change of the solution to dark brown. Further refluxing for 10 min gave a dark brown homogeneous dispersin of colloidal palladium, abbreviated as Pd-PVP-MeOH/NaOH.

When methanol/water (1/1, v/v) was used as a solvent instead of methanol in the case mentioned above, reduction of palladium ions took place even without addition of sodium hydroxide, resulting in a colloidal dispersion, Pd-PVP-MeOH/H_2O.

Electron micrographs of these colloidal dispersions (Figs. 1 and 2) show formation of well-dispersed palladium particles ranging from 10 to 120 Å in diameter. More than 98% of the particles in the colloidal dispersion, Pd-PVP-MeOH/NaOH, had a diameter below 30 Å, and the average diameter was determined to be 18 Å from the micrograph. In the colloidal dispersion of Pd-PVP-MeOH/H_2O 92% of the particles had a diameter below 30 Å, and the average diameter was determined to be 23 Å.

These colloidal dispersions were so stable that no precipitates of palladium metal appeared and the catalytic activities were unchanged after storing the dispersions under air for a year.

Hydrogenation of Cyclooctadienes. The colloidal palladium, Pd-PVP-MeOH/NaOH, was effective as a catalyst for hydrogenation of 1,3-, 1,4-, and 1,5-cyclooctadiene at 30 °C under atmospheric hydrogen pressure. As shown in Table 1, the hydrogenation rate for

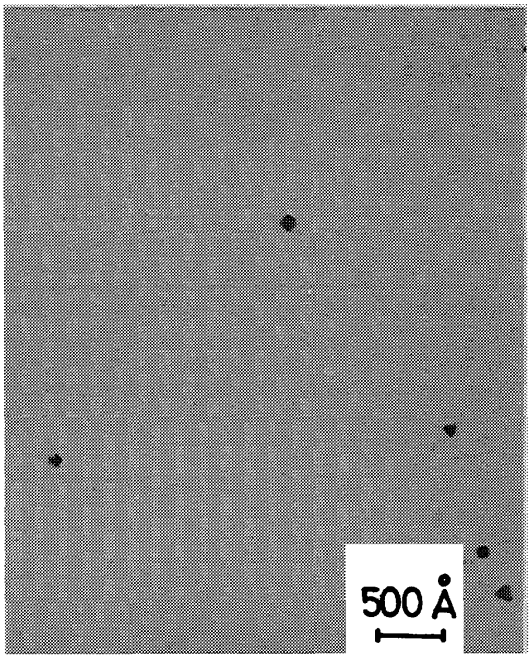

Fig. 1. Electron micrograph of colloidal palladium, Pd-PVP-MeOH/NaOH; original magnification, 100000×.

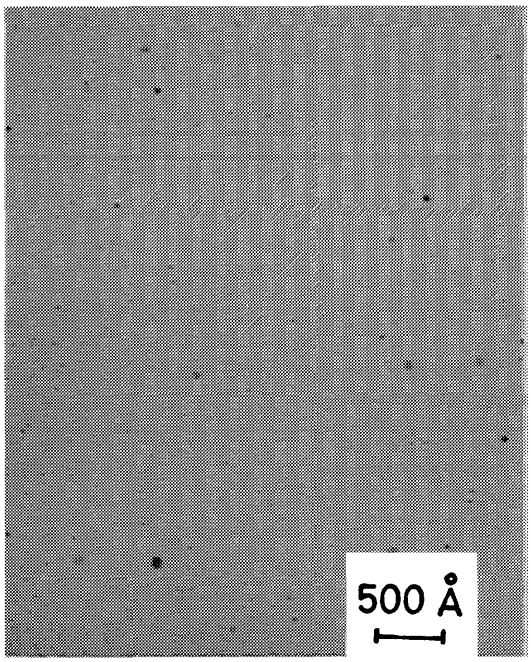

Fig. 2. Electron micrograph of colloidal palladium, Pd-PVP-MeOH/H_2O; original magnification, 100000×.

1,3-cyclooctadiene is the fastest among cyclooctadienes and the rate decreases in the order: 1,3-, 1,4-, and 1,5-isomer. For hydrogenation of 1,5-cyclooctadiene the colloidal palladium showed almost the same catalytic activity as that of 5% Pd-C. Typical curves of hydrogen uptake against time are shown in Fig. 3. In hydrogenation of 1,3-cyclooctadiene the rate of hydrogen uptake is very rapid until the amount of hydrogen uptake become equimolar to the charged amount of diene. At this point, however, the rate suddenly decreases

Table 1. Hydrogenation of cyclooctadienes with colloidal palladium[a)]

Substrate	c[b)]	r[c)]	Product composition/%[d)]			
	mol dm^{-3}	s^{-1}	1,5-COD	1,4-COD	COE	COA
1,3-COD	0.01	35	0.0	0.0	99.9	0.1
1,4-COD[e)]	0.02	4.6	1.7	3.5	94.0	0.8
1,5-COD	0.1	1.4	0.4	0.3	97.8	1.5
1,5-COD	0.1[f)]	1.2	0.4	0.2	94.2	5.2
COE	0.1	0.07				

a) Hydrogenation conditions: temperature, 30°C; total pressure, 1 atm; [substrate]=25 mmol dm^{-3}; solvent, methanol (20 cm^3); catalyst: Pd-PVP-MeOH/NaOH. COD=cycloocadiene, COE=cyclooctene, COA=cyclooctane. b) Concentration of palladium. c) Initial rate of hydrogen uptake in (H_2mol/Pd mol s). d) The composition of the reaction mixture when the amount of hydrogen uptake becomes equimolar with charged diene. e) Containing 6.9% of 1,5-COD. f) Commercial 5% Pd-C was used as a catalyst.

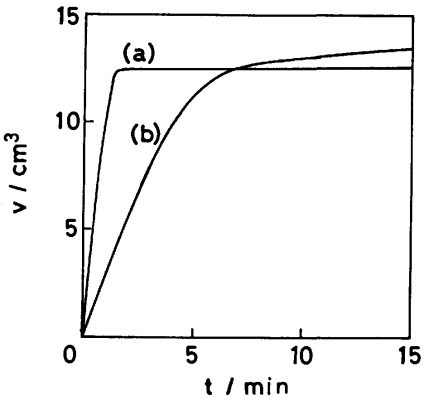

Fig. 3. Hydrogen uptake (v) in the hydrogenation of 1,3- (a) and 1,5-cyclooctadiene (b) with Pd-PVP-MeOH/NaOH. [COD]=25 mmol dm^{-3}: [Pd]= 0.01 (a) and 0.05 (b) mmol dm^{-3}.

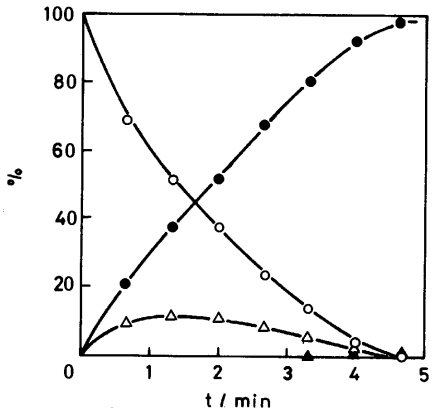

Fig. 4. Composition of the reaction mixtures on hydrogenation of 1,5-cyclooctadiene with a Pd-PVP-MeOH/NaOH catalyst in methanol at 30°C under a total pressure of 1 atm of hydrogen. [Pd]=0.1 mmol dm^{-3}: [1,5-COD]=25 mmol dm^{-3}. ○: 1,5-COD, △: 1,4-COD, ●: COE, ▲: COA.

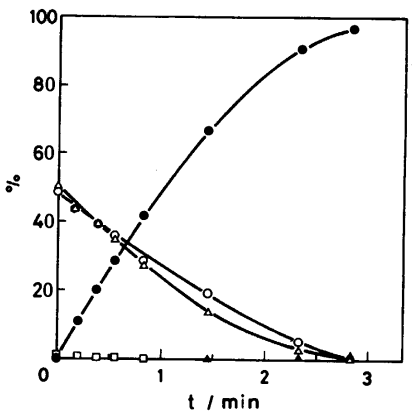

Fig. 5. Composition of the reaction mixtures on hydrogenation of 1,4- and 1,5-cyclooctadiene with a Pd-PVP-MeOH/NaOH catalyst in methanol at 30°C under a total pressure of 1 atm of hydrogen. [Pd]=0.1 mmol dm^{-3}: [1,4-COD]+[1,5-COD]=25 mmol dm^{-3}.
○: 1,5-COD, △: 1,4-COD, □: 1,3-COD, ●: COE, ▲: COA.

to 1/570 of the initial rate. The conversion of 1,3-cyclooctadiene was complete at this point and cyclooctene was produced in a 99.9% yield.

In hydrogenation of 1,5-cyclooctadiene (curve b) the change in the rate at an equimolar hydrogen uptake is rather small compared with the case of 1,3-cyclooctadiene (curve a). The yield of cyclooctene is 97.8% in hydrogenation of 1,5-cyclooctadiene. This value is considerably higher than that in the hydrogenation with 5% Pd-C (94.3%).

Initial hydrogenation rate of cyclooctene with colloidal palladium was 1/20 of that of 1,5-cyclooctadiene, and was almost the same as the rate of the second stage (after equimolar hydrogen uptake) in hydrogenation of the diene.

Formation of 1,4-cyclooctadiene in the early stage of hydrogenation of 1,5-cyclooctadiene (shown in Fig. 4) indicates that the hydrogenation is accompanied by isomerization. No other hydrogenated product than cyclooctene is observed at the initial stage of the reaction. Cyclooctane is produced after consumption of most diene.

No isomerization occurred when a methanol solution of 1,5-cyclooctadiene and the colloidal dispersion of palladium was stirred under nitrogen.

1,4-Cyclooctadiene is hydrogenated at 3.3 times the rate of hydrogenation of 1,5-cyclooctadiene (Table 1). While, in hydrogenation of equimolar mixture of 1,4- and 1,5-cyclooctadiene, initial rate of consumption of 1,4-cyclooctadiene is only 1.3 times that of 1,5-cyclooctadiene as shown in Fig. 5.

Kinetics of Hydrogenation of Cyclooctadiene. Initial rates of hydrogenation of 1,3-, 1,4-, and 1,5-

cyclooctadiene were measured as a function of catalyst concentration, substrate concentration, and hydrogen pressure. The rate for 1,3- and 1,4-cyclooctadiene increased linearly with increasing catalyst concentration and hydrogen pressure, and were independent of substrate concentration. Thus, the rate, R, is expressed in the following form:

$$R = k_1[H_2][Pd] \quad (1)$$

where k_1 is a rate constant. The value of k_1 was determined to be 4.86×10^3 and 1.06×10^3 dm^3 mol^{-1} s^{-1} for 1,3- and 1,4-cyclooctadiene, respectively.

The rate of hydrogenation of 1,5-cyclooctadiene increased linearly with increasing catalyst concentration and was independent of substrate concentration. However, dependence on hydrogen pressure deviated from linear relationship. The hydrogenation rate, R, is expressed in the following form:

$$R = k_2[H_2]^{0.7}[Pd] \quad (2)$$

where k_2 is a rate constant.

Effects of Solvents. Hydrogenation of 1,5-cyclooctadiene with colloidal palladium, Pd-PVP-MeOH/NaOH, was carried out using various solvents, as listed in Table 2. For the experiments in solvents without methanol, methanol used for the preparation of the colloid was evaporated under vacuum, and then resulting residues were re-dissolved in the solvent for hydrogenation. Catalytic activity of the colloidal palladium was confirmed not to change by the treatment of evaporation and re-dissolution.

The highest rate of hydrogenation was observed in methanol. In ethanol and 1-propanol the rates were found to be a little lower than that in methanol, but selectivities for formation of monoene were almost the same.

Colloidal palladium protected by poly(N-vinyl-2-pyrrolidone) was insoluble in ethyl acetate and tetrahydrofuran, but it became soluble in the presence of a small amount of methanol. In these mixed solvents hydrogenation rate and selectivity are considerably lower than those in methanol.

Table 2. Effect of solvents on hydrogenation of 1,5-cyclooctadiene[a)]

Solvent (cm^3)	r[b)]	Product composition/%[b)]			
	s^{-1}	1,5-COD	1,4-COD	COE	COA
Methanol(20)[c)]	1.6	0.5	0.4	96.6	2.5
Ethanol(20)[c)]	1.3	0.0	0.0	94.8	5.2
1-Propanol(20)[c)]	1.2	0.5	0.2	96.3	3.0
Ethyl acetate(17) /Methanol(3)	0.4	5.7	2.1	89.6	2.6
Tetrahydrofuran(17) /Methanol(3)	0.2	1.3	0.9	94.0	3.8

a) Hydrogenation conditions: temperature 30 °C; total pressure: 1 atm; [Pd]=0.1 mmol dm^{-3}; [COD]=25 mmol dm^{-3}; catalyst, Pd-PVP-MeOH/NaOH. b) Abbreviations: See legend of Table 1. c) The catalyst solution was evaporated and re-dissolved in the hydrogenation solvent.

Effects of Additives. As mentioned above, colloidal palladium, Pd-PVP-MeOH/NaOH, exhibits considerably higher selectivity for formation of monoene than a Pd-C catalyst. Difference in sizes of palladium particles and interaction between palladium and the protective colloid have been considered to play important roles in exhibiting high selectivity of the colloidal palladium.[5,6] In addition, base added in preparation of the colloidal palladium (Pd-PVP-MeOH/NaOH) may have some effect on the selectivity. In order to clarify this effect, hydrogenation of 1,5-cyclooctadiene was carried out in the presence of additives using colloidal palladium, Pd-PVP-MeOH/H_2O, as a catalyst. In Fig. 6 the yield of cyclooctene is plotted against the degree of hydrogenation which is calculated as [(yield of cyclooctene)+(yield of cyclooctane)×2]. In the absence of additives the yield of cyclooctene reaches a maximum value of 95—96%, which is smaller by 2% than one with the base-added colloid (Pd-PVP-MeOH/NaOH).

On addition of sodium hydroxide the yield of cyclooctene over the Pd-PVP-MeOH/H_2O catalyst increased by 0.7% at a degree of hydrogenation of 95—100%. The yield of cyclooctene also increased by addition of triethylamine instead of sodium hydroxide, while it did not change by addition of sodium chloride or hydrochloric acid.

Addition of hydrochloric acid into the solution for hydrogenation with the colloid prepared by addition of base (Pd-PVP-MeOH/NaOH) decreased the yield of cyclooctene from 96.5% to 94.5% at the degree of hydrogenation of 100%.

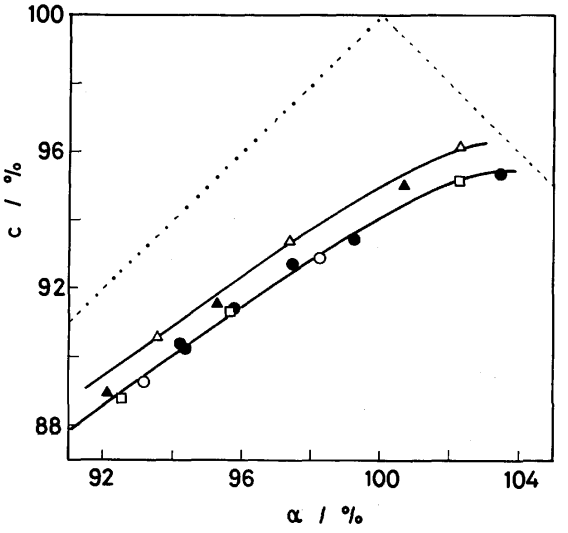

Fig. 6. Effect of additives on the hydrogenation of 1,5-cyclooctadiene with Pd-PVP-MeOH/H_2O. Yield of cyclooctene (c) is plotted as a function of degree of hydrogenation (α). The dotted line shows the yield of cyclooctene at the complete selectivity. [Pd]=0.1 mmol dm^{-3}; [1,5-COD]=25 mmol dm^{-3}. Amount of additives=10 μmol; additives: ●: none, △: NaOH, □: HCl, ▲: Et_3N, ○: NaCl.

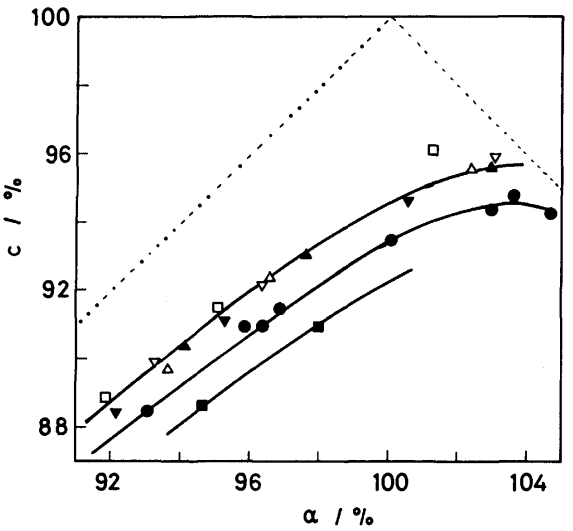

Fig. 7. Effect of additives on the hydrogenation of 1,5-cyclooctadiene with Pd-C catalyst. Yield of cyclooctene (c) is plotted as a function of degree of hydrogenation (α). Pd-C, 4.3 mg; [1,5-COD]=25 mmol dm^{-3}. Additives (amount in μmol): ●: None, △: NaOH(10), ▽: NaOH(20), □: NaOH(40), ▲: KOH(10), ▼: Et_3N(10), ■: HCl(10).

Effects of Additives on the Hydrogenation with Pd-C. Effects of addition of base and acid in the hydrogenation with 5% Pd-C are illustrated in Fig. 7. In the absence of additives the yield of cyclooctene reaches a maximum value of 94—95% at a degree of hydrogenation of 104%. This value in yield is smaller by 3% than that with the base-added colloid and by 1% than that with the water-added colloid.

The yield of cyclooctene increased by 1% on addition of a base such as sodium hydroxide, potassium hydroxide, and triethylamine, but decreased by 1% on addition of hydrochloric acid.

Discussion

Selectivity for the Formation of Cyclooctene. In the first stage of hydrogenation of 1,5-cyclooctadiene with the colloidal palladium, Pd-PVP-MeOH/NaOH, hydrogenation of cyclooctene to cyclooctane was inhibited and cyclooctene was produced in a high yield. However, after most of the diene was consumed, hydrogenation of cyclooctene occurred at an appreciable rate. This fact strongly suggests that adsorption of diene on the catalytic site is much stronger than that of monoene, and thus the adsorption of monoene is completely suppressed in the presence of diene.

Formation of 1,4-cyclooctadiene in hydrogenation of 1,5-cyclooctadiene (Fig. 4) shows that this reaction occurs with accompanying isomerization of nonconjugated dienes to conjugated diene as follows (COD, cyclooctadiene; COE, cyclooctene):

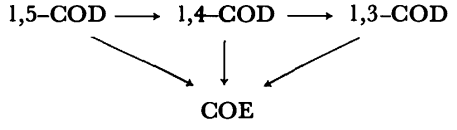

1,3-Cyclooctadiene was not detected in the reaction mixtures, probably because the rate of hydrogenation of 1,3-cyclooctadiene was much higher than that of the isomerization of 1,4-cyclooctadiene to 1,3-cyclooctadiene.

The yield of cyclooctene in hydrogenation of 1,5-cyclooctadiene was 97.8% with the colloidal palladium, and 94.2% with Pd-C. This difference in selectivity is relatively small compared with that in the hydrogenation of cyclopentadiene, in which the yield of cyclopentene is 98.7% with colloidal palladium and 82.6% with Pd-C.[5] Relatively high selectivity for cyclooctene formation in the hydrogenation of 1,5-cyclooctadiene with Pd-C may be explained by the considerably small hydrogenation rate of cyclooctene. Unusually low hydrogenation rate of cyclooctene has also been reported by Jardine *et al.*, and was related to the lower heat of hydrogenation due to the severe transannular interactions in cyclooctane.[8]

In hydrogenation of equimolar mixtures of 1,4- and 1,5-cyclooctadiene, 1,4-cyclooctadiene was consumed 1.3 times as fast as 1,5-cyclooctadiene. These rates of consumption of 1,5- and 1,4-cyclooctadiene were 0.85 and 0.3 times of the rate of the separate hydrogenation, respectively. Large inhibition effect of 1,5-cyclooctadiene in the hydrogenation of 1,4-cyclooctadiene indicates that the adsorption of 1,5-cyclooctadiene on the catalyst is stronger than that of 1,4-cyclooctadiene.

Kinetics of Hydrogenation of Cyclooctadienes. Zero order with respect to substrate and positive order with respect to hydrogen indicate that diene is more strongly adsorbed on the surface of catalysts than hydrogen, and consequently the surface coverage of diene is larger than that of hydrogen.

Dependence of the rate on the hydrogen pressure was the first order in the hydrogenation of 1, 3- and 1, 4-cyclooctadiene, but deviated from the first order in the hydrogenation of 1,5-cyclooctadiene. This divergence from linear relationship can be associated with the extent of accompanying isomerization. As shown in Fig. 4, the yield of 1,4-cyclooctadiene reaches the maximum value of 12% in hydrogenation of 1,5-cyclooctadiene at the hydrogen pressure of 728 Torr. As the hydrogen pressure was decreased from 728 to 371 Torr, the maximum value increased from 12 to 15%. This fact indicates that the proportion of the diene hydrogenated *via* the isomerization to 1,4-isomer increased by decreasing hydrogen pressure.

Effect of Additives. In the hydrogenation with the water-added colloid (Pd-PVP-MeOH/H_2O), selectivity for monoene incrcased by addition of sodium hydroxide and triethylamine. On the other hand, the selectivity decreased by addition of hydrochloric acid in the hydrogenation with the base-added colloid (Pd-PVP-MeOH/NaOH). These results suggest that hydroxide ion have some effects on the selectivity. In accordance with this assumption, addition of sodium

chloride had no effect on the selectivity. Similar effects of addition of bases were also observed with Pd-C. This suggests that bases affect the selectivity not through changes in the state of polymer which protects colloidal palladium, but through direct interactions between palladium metals and hydroxide ions.

McQuillin *et al.* have reported that hydrogenation of 2-butyne-1,4-diol, 2-butene-1,4-diol, and mesityl oxide over Pd-C in ethanol was retarded by the addition of a base such as potassium hydroxide.[9] The effect of base on the monoene selectivity in the present study is also interpreted in terms of inhibition effect of base. As a hydroxide ion is more strongly adsorbed on the catalytic site than monoene, but more weakly is than diene, addition of the ion may inhibit the adsorption of monoene more strongly than that of diene. As a result, monoene selectivity is enhanced with the addition of a base.

By the way discussed above, the base added in preparation contributes to the high selectivity of the base-added colloid (Pd-PVP-MeOH/NaOH). Other factors for the high selectivity may involve the particle size of the palladium particles and the interaction between palladium and the polymer or the support. Thus, in the hydrogenation of cyclopentadiene, the selectivity increased with decreasing size of palladium particles, and with addition of poly(*N*-Vinyl-2-pyrrolidone) to Pd-C and Pd-black.[5]

The difference in activity with solvents (Table 2) is also interpreted by the adsorption of solvent molecules on catalytic sites. On the palladium catalyst, hydrocarbon groups have been reported to be adsorbed more strongly than oxygen atoms.[10] Higher alcohols, ethyl acetate, and tetrahydrofuran act as a kind of inhibitor because of a large portion of hydrocarbon groups in a molecule. Thus, the hydrogenation rate is relatively slow in these solvents. The high hydrogenation rate in methanol can be due to a small hydrocarbon group of methanol and, therefore, a weak inhibiting character of methanol.

References

1) L. D. Rampino and F. F. Nord, *J. Am. Chem. Soc.*, **63**, 2745 (1941).

2) L. D. Rampino, K. E. Kavanagh, and F. F. Nord, *Proc. Natl. Acad. Sci., U.S.A.*, **29**, 246 (1943).

3) H. Hirai, Y. Nakao, and N. Toshima, *J. Macromol. Sci., Chem.*, **A12**, 1117 (1978).

4) H. Hirai, Y. Nakao, and N. Toshima, *J. Macromol. Sci., Chem.*, **A13**, 727 (1979).

5) H. Hirai, H. Chawanya, and N. Toshima, *Reactive Polymers*, in press.

6) H. Hirai, H. Chawanya, and N. Toshima, *Nippon Kagaku Kaishi*, **1984**, 1027.

7) This work has been published in a communication: H. Hirai, H. Chawanya, and N. Toshima, *Makromol. Chem., Rapid Commun.*, **2**, 99 (1981).

8) I. Jardine and F. J. McQuillin, *J. Chem. Soc. (C)*, **1966**, 458.

9) F. J. McQuillin, W. O. Ord, and P. L. Simpson, *J. Chem. Soc.*, **1963**, 5996.

10) J. Iijima and K. Mitsui, *Nippon Kagaku Kaishi*, **85**, 687 (1964).

The Role of Aroyloxyl Radicals in the Formation of Solvent-derived Products in Photodecomposition of Diaroyl Peroxides. The Reactivity of Substituted Cyclohexadienyl Radicals and Intermediacy of ipso Intermediates

Shigeru TAKAHARA, Toshiyuki URANO, Akihide KITAMURA,†† Hirochika SAKURAGI,* Osamu KIKUCHI, Masayuki YOSHIDA,† and Katsumi TOKUMARU

Department of Chemistry, University of Tsukuba, Sakura-mura, Ibaraki 305

†*University of Library and Information Science, Yatabe, Ibaraki 305*

(Received September 25, 1984)

Photolyses of bis(2-thiophenecarbonyl) peroxide (TPO) in benzene and toluene afforded, among free-radical products, biphenyl and dimethylbiphenyls, respectively, which were solely derived from the aromatic solvents. The yields of biphenyls depended upon the rate with which the radical intermediates were generated from the peroxides in sufficiently high concentrations for their dimerization. Photolyses of TPO and dibenzoyl peroxide in 1,3,5-trimethylbenzene afforded also a solvent-derived product, 2,3′,4,5′,6-pentamethyldiphenylmethane. Its formation provides clear evidence for participation of cyclohexadienyl radicals bearing the aroyloxyl group on the methyl-substituted ipso carbon atom.

Aroyloxyl radicals, when generated in aromatic solvents, reversibly add to the solvents to produce aroylcyclohexadienyl radicals,[1,2] which are intercepted by a suitable oxidant to give aryl esters,[3,4] and also undergo recombination with other radicals followed by elimination of arenecarboxylic acid to give arylation products.[5,6] Dimerization of the cyclohexadienyl radicals[7] and subsequent elimination of two moles of the arenecarboxylic acid could be the course leading to biphenyls on decomposition of diaroyl peroxides in aromatic solvents. However, usually in benzene which has been employed as one of "inert" solvents, photochemical and free-radical reactions do not give biphenyl. On photochemical decomposition of bis(2-

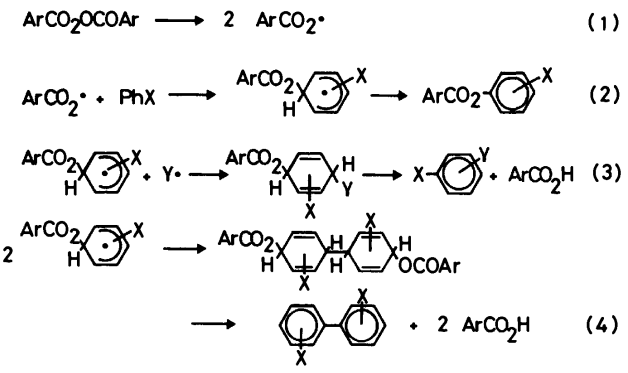

thiophenecarbonyl) peroxide (TPO) in aromatic solvents, we have found some remarkable features of the reactions of the aroylcyclohexadienyl radicals; 1) in benzene biphenyl was formed in a noticeable yield, particularly at low temperatures,[8] 2) in toluene among the possible dimethylbiphenyls 2,3′- and 3,3′-dimethyl isomers were formed together with a small amount of 2,2′-dimethyl isomer, and 3) in 1,3,5-trimethylbenzene 2,3′,4,5′,6-pentamethyldiphenylmethane was formed in a considerable yield.[9] In this paper we wish to report some new aspects of reactivities of aroyloxyl radicals with aromatic solvents and the role of ipso intermediates in the reaction.

Results

Photolysis and Thermolysis of Bis(2-thiophenecarbonyl) Peroxide in Benzene. Effects of Light Intensity and Temperature. Bis(2-thiophenecarbonyl) peroxide (TPO, 0.03 mol/dm^3) was irradiated at varying temperatures (5—60 °C) in benzene (3 cm^3) under argon and oxygen atmosphere for five times half-life periods with 313 nm light of varying intensities from a 400 W high pressure mercury lamp through a filter (85 min) or from a 1 kW high pressure mercury lamp directly (20—30 min), or with 337.1 nm laser pulses from a nitrogen laser (80 Hz, 20—30 min). TPO (0.03 mol/dm^3) was also heated in benzene at 80 °C for 2880 min (5 times half-life period) under degassed conditions. The products were determined quantitatively by GLPC except carbon dioxide, which was determined by gravimetry using an Ascarite tube. The results are summarized in Table 1.

TPO (0.03 mol/dm^3) was photolyzed in a mixture (400 cm^3) of varying fractions of benzene and styrene (1:0 to 3:1 by volume) in a nitrogen stream. The carbon dioxide evolved was absorbed with an Ascarite tube and determined by gravimetry. The results are summarized in Table 2 and depicted in Fig. 1.

Spin Trapping of 2-Thiophenecarbonyloxyl Radicals in Photolysis and Thermolysis of TPO. A solution of TPO (0.01 mol/dm^3) containing *N*-benzylidene-*t*-butylamine oxide (0.1 mol/dm^3) was irradiated at room temperature with a 1 kW high pressure mercury lamp or heated at 80 °C for several minutes in the cavity of an ESR spectrometer. The photolysis and thermolysis resulted in the same ESR signals (a_N=1.35 mT) attributable to the 2-thiophenecarbonyloxy spin adduct, *N*-{phenyl(2-thiophenecarbonyloxy)methyl}-*t*-butylaminyloxyl.[10,11]

Trapping of Phenyl Radicals Resulting from the Sol-

††Present address: Department of Chemistry, College of Arts and Sciences, Chiba University, Yayoi-cho, Chiba 260.

Table 1. Effects of light intensity and temperature on product yields in photolysis of TPO in benzene

Light source	Temp/°C	Product yield[a]				
		PhPh	2-ThPh	$ThCO_2Ph$	$ThCO_2H$	CO_2
Under deaerated conditions						
Δ[b]	80	0.02	—	0.01	0.68	0.30
Δ[c]	75—85	—	—	0.04	0.63	0.26
1 kW Hg[d]	60	0.02	trace	0.04	0.74	0.27
1 kW Hg	40	0.04	trace	0.06	0.62	0.27
1 kW Hg	29	0.07		0.05	0.48	
1 kW Hg	25	0.11	0.02	0.08	0.82	0.28
400 W Hg[e]	25	0.02	0.03	0.13	0.97	
N laser[f]	25	0.11	0.01	0.07	1.01	
1 kW Hg	15	0.11	0.01	0.06	0.45	
1 kW Hg	5	0.14	0.01	0.07	0.38	
N laser	5	0.17	trace	0.06	0.96	
Under oxygen						
1 kW Hg	60	0.01		0.28	1.06	
1 kW Hg	40	0.02		0.51	0.86	
1 kW Hg	29	0.03		0.61	0.60	
1 kW Hg	25	0.05		0.45	0.60	
1 kW Hg	15	0.06		0.45	0.60	
1 kW Hg	5	0.06		0.39	0.52	

a) Yields based on a mole of TPO. b) Thermolysis for 2880 min. c) Taken from Ref. 16. d) 20—30 min irradiation with a 1 kW high pressure mercury lamp. e) 85 min irradiation with a 400 W high pressure mercury lamp. f) 25—30 min irradiation with nitrogen laser pulses (80 Hz).

Table 2. Yields of carbon dioxide in photolysis and thermolysis of TPO in benzene-styrene mixtures

Ratio by volume		CO_2 yield[a]	
PhH	Styrene	Photolysis	Thermolysis
400	0	0.27	0.30
395	5		0.18
390	10	0.18	0.01
350	50	0.14	0.01
300	100	0.14	

a) Yields based on a mole of TPO.

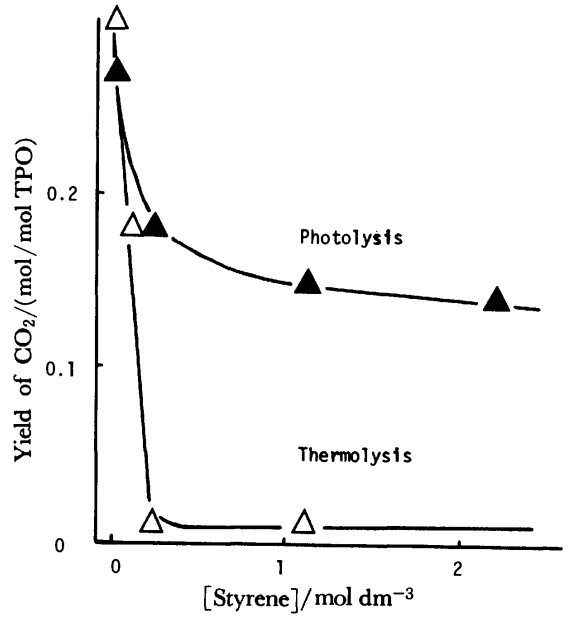

Fig. 1. Change of carbon dioxide yield with styrene concentration in thermolysis and photolysis of TPO in benzene.

Table 3. Yields of biphenyl and chlorobenzene on irradiation of TPO, bis(4-methoxybenzoyl) peroxide (MeOBPO), and benzophenone in a 1:1 mixture of benzene and carbon tetrachloride

Initiator	Product yield[a]	
	PhPh	PhCl
TPO	0.04	trace
MeOBPO	0.03	trace
Ph_2CO	trace	0.03

a) Yields based on a mole of substrate.

vent Benzene by Carbon Tetrachloride. TPO (0.03 mol/dm^3), bis(4-methoxybenzoyl) peroxide (0.03 mol/dm^3), and benzophenone (0.03 mol/dm^3) were irradiated, respectively, under nitrogen in a mixture of carbon tetrachloride and benzene (1:1 by volume, 3 cm^3) at room temperature with a 1 kW high pressure mercury lamp. The yields of biphenyl and chlorobenzene were determined by GLPC, and are listed in Table 3.

Photolysis and Thermolysis of TPO in Toluene. Effects of Wavelength and Temperature on Product Yields. TPO (0.03 mol/dm^3) was photolyzed in toluene (3 cm^3) by irradiating with 254 (low pressure mercury lamp), 313 (high pressure mercury lamp), and 337.1 nm light (nitrogen laser) at varying temperatures (5—22 °C). TPO was also thermolyzed at 80 °C in toluene. Table 4 compares the yields of 2-thiophenecarboxylates resulting from the photolysis with 313 nm light and thermolysis, and Table 5 summarizes the yields of dimethylbiphenyls afforded in the photolyses.

Photolysis of TPO and Dibenzoyl Peroxide in 1,3,5-

Table 4. Yields of isomeric methylphenyl and benzyl 2-thiophenecarboxylates in photolysis and thermolysis of TPO in toluene

	Temp /°C	Benzyl ester Yield[a]	Methylphenyl ester Total yield[a]	Isomer ratio o-	m-	p-
Photolysis	20	0.01	0.09	63	11	26
Thermolysis[b]	80	0.03	0.04	69	8	23
Thermolysis[c]	80	0.02	0.18	48	17	35

a) Yields based on a mole of TPO. b) Thermolysis under degassed conditions. c) Thermolysis under oxygen.

Table 5. Yields of isomeric dimethylbiphenyls in photolysis of TPO in toluene under nitrogen[a]

Light /nm	Temp /°C	Dimethylbiphenyl 2,2'-	2,3'-	2,4'-	3,3'-	3,4'-	4,4'-
254	5	0.02	0.10	trace	0.10	trace	0
	22	0.01	0.06	trace	0.06	trace	0
313	7-8	0.01	0.05	trace	0.05	trace	0
	22	0.01	0.03	trace	0.03	trace	0
337.1	5	0.01	0.06	trace	0.06	trace	0
	10	0.01	0.06	trace	0.06	trace	0
	20	trace	0.02	trace	0.02	trace	0

a) Yields based on a mole of TPO.

Table 6. Product yields in photolysis of TPO in 1,3,5-trimethylbenzene[a]

Temp/°C	Product[b] TMPT	DMBT	BDPE	PMDM	TCA
70	0.06	0.07	0.42	trace	1.66
60	0.07	0.07	0.34	0.05	1.56
50	0.10	0.07	0.32	0.06	1.62
40	0.12	0.07	0.21	0.10	1.59
20	0.20	0.07	0.17	0.12	1.48

a) Yields based on a mole of TPO. b) TMPT: 2,4,6-trimethylphenyl 2-thiophenecarboxylate, DMBT: 3,5-dimethylphenylmethyl 2-thiophenecarboxylate, BDPE: 1,2-bis(3,5-dimethylphenyl)ethane, PMDM: 2,3',4,5',6-pentamethyldiphenylmethane, TCA: 2-thiophenecarboxylic acid.

Table 7. Product yields in photolysis of BPO in 1,3,5-trimethylbenzene[a]

Temp/°C	Product[b] TMPB	$PhCO_2Ph$	BDPE	PMDM
65	0.00	0.06	0.32	0.00
40	0.02	0.07	0.26	0.03
30	0.02	0.08	0.24	0.04
20	0.03	0.06	0.20	0.07
10	0.06	0.09	0.15	0.09
5	0.06	0.09	0.14	0.09

a) Yields based on a mole of BPO. b) TMPB: 2,4,6-trimethylphenyl benzoate, BDPE: 1,2-bis(3,5-dimethylphenyl)ethane, PMDM: 2,3',4,5',6-pentamethyldiphenylmethane.

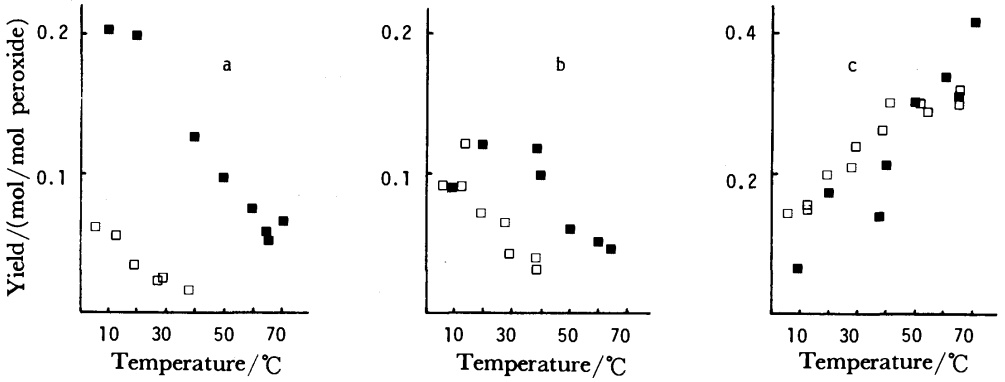

Fig. 2. Temperature dependence of product yields in photolysis of TPO (■) and BPO (□) in TMB; a) TMPT (■) and TMPB (□), b) PMDM, c) BDPE.

Trimethylbenzene. Temperature Effects on Product Yields. TPO (0.03 mol/dm^3) was irradiated in 1,3,5-trimethylbenzene (TMB, 3 cm^3) at varying temperatures (20—70 °C) under nitrogen with 313 nm light, and the products were determined by GLPC. The results are summarized in Table 6 and depicted in Fig. 2. Dibenzoyl peroxide (BPO, 0.03 mol/dm^3) was similarly photolyzed in TMB at varying temperatures (5—65 °C), and the results are summarized in Table 7 and depicted in Fig. 2. Thermolyses of TPO and BPO were carried out at 80 °C in TMB under deaerated and aerated conditions. Table 8 lists the results.

Generation of 3,5-Dimethylphenylmethyl Radicals in TMB and Temperature Effects on the Product Distribu-

Table 8. Product yields in thermolyses of BPO and TPO in 1,3,5-trimethylbenzene at 80 °C[a]

Peroxide	Conditions	Product[b]			
BPO		TMPB	$PhCO_2Ph$	BDPE	PMDM
	degassed	0.02	0.00	0.37	0.00
	air	0.06	0.00	0.03	0.03
TPO		TMPT	$ThCO_2Th$	BDPE	PMDM
	degassed	0.07	0.02	0.32	0.03
	air	0.19	0.01	0.00	0.11

a) Yields based on a mole of peroxide. d) TMPB: 2,4,6-trimethylphenyl benzoate, TMPT: 2,4,6-trimethylphenyl 2-thiophenecarboxylate, BDPE: 1,2-bis(3,5-dimethylphenyl)ethane, PMDM: 2,3',4,5',6-pentamethyldiphenylmethane, Th: thienyl.

tion. Attempts were made to generate 3,5-dimethylphenylmethyl radicals in the absence of any aroyloxyl radicals by photochemical and thermal procedures in TMB.

a) Photolysis of 1,3-Bis(3,5-dimethylphenyl)-2-propanone. 1,3-Bis(3,5-dimethylphenyl)-2-propanone (0.01 mol/dm^3) in TMB (3 cm^3) was irradiated with 313 nm light under degassed conditions. The product yields at varying temperatures (10—68 °C) are summarized in Table 9.

Table 9. Photolysis of 1,3-bis(3,5-dimethylphenyl)-2-propanone in 1,3,5-trimethylbenzene

Temp/°C	Conversion/%	Yield/%	
		PMDM	BDPE
10	95	<6	84
19	100	<6	92
30	100	<6	91
47	96	<6	73
68	84	<6	40

b) Photoreaction of Benzophenone in TMB. Degassed and sealed samples of benzophenone (0.03 mol/dm^3) in TMB (3 cm^3) were irradiated with 366 nm light at varying temperatures (30—55 °C). The results are summarized in Table 10.

c) Thermolysis of Di-t-butyl Diperoxyoxalate. Di-*t*-butyl diperoxyoxalate (0.03 mol/dm^3) was heated at 35—55 °C in TMB (3 cm^3) under degassed conditions. Table 11 summarizes the results.

MO Calculations of Some Models for Ipso- and Non-ipso-substituted Cyclohexadienyl Radicals. Open shell restricted SCF-MO calculations were performed

Table 10. Photoreaction of benzophenone in 1,3,5-trimethylbenzene

Temp/°C	Product yield/%		
	PMDM	BDPE	$Me_2C_6H_3CH_2CPh_2OH$
30	0	29	35
40	0	27	35
55	0	27	36

Table 11. Thermolysis of di-*t*-butyl diperoxyoxalate in 1,3,5-trimethylbenzene

Temp/°C	Product yield/%	
	PMDM	BDPE
35	0	75
45	0	77
55	0	77

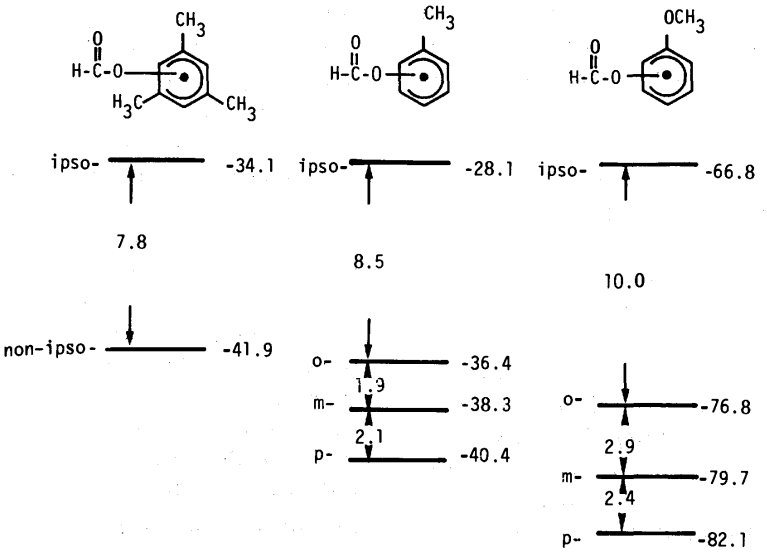

Fig. 3. Total and relative energies of substituted cyclohexadienyl intermediates (kcal/mol).

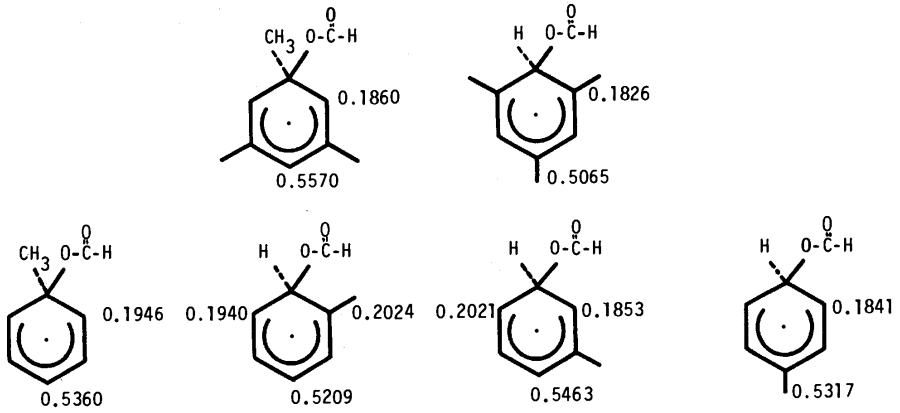

Fig. 4. Spin density of substituted cyclohexadienyl intermediates.

for cyclohexadienyl radicals derived from addition of formyloxyl radicals to toluene, anisole, and 1,3,5-trimethylbenzene by the MINDO/3 method[12] on a FACOM M-200 system. First, the structure of the unsubstituted cyclohexadienyl radical was optimized under C_{2v} constraint.[13] Then, by using this optimized planar ring structure, 6-formyloxycyclohexadienyl and 6-formyloxy-6-methylcyclohexadienyl radicals were optimized. Here, the formyloxyl group was fixed to the conformations for the C–O single bond in which the cyclohexadienyl group and carbonyl oxygen are cis and the carbonyl and *O*-cyclohexadienyl bonds are coplanar, since esters, in general, prefer strongly such a conformation.[14,15] Finally, based on these conformations, the total energies, relative energies, and spin densities of the ipso- and non-ipso-substituted cyclohexadienyl radicals were determined. The results are shown in Figs. 3 and 4. The total energy of the formyloxy-substituted cyclohexadienyl radicals decreases in the order of ipso, ortho, meta, and para isomers. The energy difference between the ipso- and ortho(non-ipso)-substituted cyclohexadienyl radicals is 7.8kcal/mol in the case of 1,3,5-trimethylbenzene, which is the smallest value among the substituted benzenes employed. The difference of energies among the substituted cyclohexadienyl radicals increases in the order of trimethyl-, methyl-, and methoxy-substitution.

Discussion

Mechanism for Formation of Biphenyls. As Table 1 shows, most of the products from the photolysis of TPO in benzene are the same as those from its thermolysis,[16] and their production can be understood in terms of the conventional free-radical pathways.[1,2] The following scheme shows the formation processes of the products except biphenyl; TPO is thermally or photochemically decomposed to give 2-thiophenecarbonyloxyl radicals (TCR) (Eq. 5), which decarboxylate to give 2-thienyl radicals (TR) and carbon dioxide (Eq. 6), add to benzene to give cyclohexadienyl radicals (CHDR) (Eq. 7),[3] or abstract a hydrogen atom to give 2-thiophenecarboxylic acid (TCA)(Eq. 8). CHDRs are oxidized by radicals or oxygen to give phenyl 2-thiophenecarboxylate (Eq. 9). TRs add to benzene to give finally 2-phenylthiophene (Eq. 10).

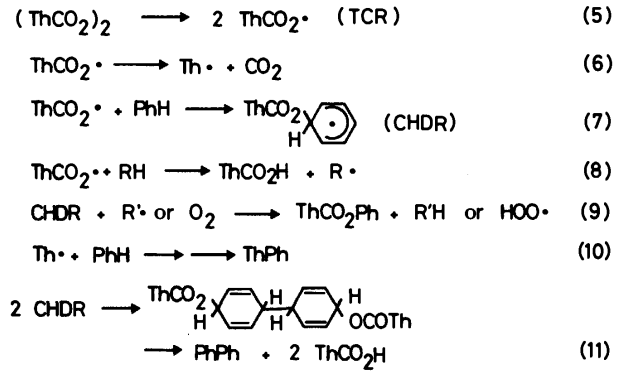

Scheme 1.

The production of biphenyl is noticeable, since decomposition of various types of radical generators except for phenyl radicals in benzene has never given such a high yield of biphenyl.[1,2] Biphenyl is not produced from phenyl radicals which could be formed from the reaction medium, since chlorobenzene was not detected in the photolysis of TPO in the presence of carbon tetrachloride as a phenyl radical scavenger in contrast with irradiation of benzophenone under similar conditions (Table 3). The formation of biphenyl in the photolysis of TPO in benzene can be reasonably understood by the following scheme; CHDRs generated from addition of TCRs to the solvent benzene undergo dimerization into tetrahydrobiphenyl derivatives[7] followed by elimination of two moles of thiophenecarboxylic acid (Eq. 11). This mechanism is supported by the results of photolyses carried out under oxygen atmosphere which gave phenyl 2-thiophenecarboxylate in a much higher yield than under argon atmosphere at the expense of biphenyl (Table 1).

Efficient production of biphenyl requires that TCRs effectively add to benzene, in competition with decarboxylation, to give CHDRs. This is in contrast with other kinds of aroyloxyl radicals which fail in production of biphenyl in benzene.[1,2] Reluctance of TCR to decarboxylation can be seen in a much lower yield of carbon dioxide (*ca.* 0.3 mol/mol TPO in Table 1) in benzene than from other diaroyl peroxides such as BPO (1.4 mol)[10] and in the efficient formation of the acyloxy spin adduct in the photolysis and thermolysis of TPO in the presence of the nitrone. Although decomposition of other diaroyl peroxides in benzene usually gives only negligible amounts of phenyl arenecarboxylates in the absence of oxidants such as oxygen,[3,17] TPO gives a non-negligible amount of phenyl 2-thiophenecarboxylate (Table 1). This fact can be taken as a piece of evidence for the higher reactivity of TCR towards benzene than other aroyloxyl radicals. The higher reactivity and stability of TCR probably arise from electronic effects of the sulfur atom.[16]

The yield of biphenyl is highly dependent on the photolysis conditions; it is very sensitive to temperature and remarkably reduced with increasing temperature. Since the yield of carbon dioxide was not varied in the temperature range examined, the effect of temperature is not due to acceleration of the decarboxylation rate of TCR. Therefore, the reduction of the yield of biphenyl indicates that TCR is in an addition equilibrium with CHDR and that at higher temperatures than 40 °C CHDR tends to decrease its stationary concentration by dissociating into TCR and benzene rather than undergoing recombination.

According to the above mechanism for biphenyl formation, the yield of biphenyl should be controlled by the stationary concentration of CHDR, and thus by the decomposition rate of the peroxide. In Table 1,

when the apparent half-life period of TPO is decreased from 80 to 25 min by use of higher light intensity, the yield of biphenyl is increased from 0.02 to 0.11 (high pressure mercury lamp) and 0.17 mol (nitrogen laser).

In the presence of styrene as a radical scavenger, carbon dioxide was produced in much higher yield (0.14 mol) in photolysis than in thermolysis (0.01 mol), as shown in Fig 1. This result exhibits the decarboxylation from photoexcited TPO is more efficient than that from vibrationally excited TPO; in the thermolysis carbon dioxide almost results from decarboxylation of out-of-cage TCRs (Eq. 6), while in the photolysis, carbon dioxide results not only from decarboxylation of the out-of-cage TCRs but also from the two-bond fission (O–O and C(α)-C(carbonyl) bonds) of photoexcited TPO in either simultaneous or successive way (Eq. 12) and/or decarboxylation of in-cage TCRs (Eq. 13).[10]

$$(ThCO_2)_2 \longrightarrow ThCO_2\cdot + CO_2 + Th\cdot \quad (12)$$

$$(ThCO_2)_2 \longrightarrow (2ThCO_2\cdot)_{cage} \longrightarrow ThCO_2\cdot + CO_2 + Th\cdot \quad (13)$$

Photolysis of TPO in toluene under similar conditions to the above resulted in the formation of dimethylbiphenyls among usual radical reaction products[1,2] (Tables 4 and 5). The isomer ratio of dimethylbiphenyls was high in meta- and ortho-substituted derivatives and very low in para-substituted ones[18] (Table 5). As discussed above on the formation of biphenyl in benzene, dimethylbiphenyls are considered to arise from recombination of cyclohexadienyl radicals formed through addition of TCR to toluene. Temperature effects on the yield of dimethylbiphenyls are consistent with this mechanism. The total yield and isomer ratio of methylphenyl 2-thiophenecarboxylates are 0.1 mol and 63:11:26 for ortho:meta:para isomers, respectively. The isomer ratio is in good agreement with that in the thermolysis of TPO in toluene. In thermolysis oxygen increased the ester yield and gave the isomer ratio which was lower in the ortho and higher in the para ratio. An intermediate isomer ratio (57:16:27) was reported for thermolysis of TPO in acetonitrile containing toluene in the presence of a copper(II) salt.[19]

The isomer ratio of dimethylbiphenyls is highly remarkable, since the ratio depends, according to the above mechanism, to the population of isomeric cyclohexadienyl intermediates (for their structures, see Fig. 4). As mentioned above, the photolysis of TPO in toluene under deaerated conditions afforded the isomer ratio of methylphenyl thiophenecarboxylates different from that given by the thermolysis under oxygen. Since the oxidants such as oxygen would scavenge the initially formed cyclohexadienyl intermediates to afford the corresponding esters, their isomer ratios would reflect the population of the isomeric cyclohexadienyl radicals.[20,21] The para-substituted derivatives among dimethylbiphenyls would arise from recombination of the meta or ipso intermediate. Therefore, if the isomer ratio of the esters under oxygen reflects the ratio of the corresponding cyclohexadienyl radicals, the absence of any para-substituted dimethylbiphenyls means that the adjacent positions to the carbon atoms substituted by a thiophenecarbonyloxyl group are almost unreactive in recombination with other acyloxycyclohexadienyl radicals, as previously discussed for photolysis of BPO in toluene.[18] However, since it is expected that the ipso intermediate could undergo recombination at the 3 position with other intermediates to give para-substituted dimethylbiphenyls, the above facts indicate that ipso intermediate would not play an important role in the dimethylbiphenyl formation.

The high ratio of methylphenyl thiophenecarboxylates in the ortho isomer in the decomposition of TPO under the deaerated conditions indicates the contribution of the rearrangement of the ipso intermediate to the ortho one, though the possibility cannot be ruled out that a selectivity in the disproportionation step determined the isomer ratio of the esters.[22]

Intermediacy of ipso Intermediates. Photolysis of TPO in 1,3,5-trimethylbenzene(TMB) at 20 °C afforded thiophenecarboxylate esters, 2,4,6-trimethylphenyl 2-thiophenecarboxylate(TMPT) and 3,5-dimethylphenylmethyl 2-thiophenecarboxylate(DMBT), dimers from the solvent, 1,2-bis(3,5-dimethylphenyl)ethane(BDPE) and 2,3′,4,5′,6-pentamethyldiphenylmethane(PMDM), and 2-thiophenecarboxylic acid (TCA) (Table 6). The formation of TMPT and BDPE can be understood in terms of the usual radical processes (Eqs. 14—17).[1,2] The yield of DMBT is rather

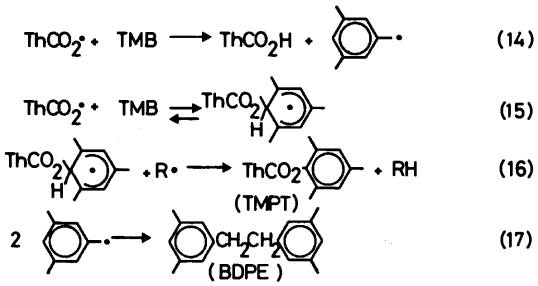

higher compared with that of the corresponding esters from other diaroyl peroxides such as BPO (Table 7). Taking into account the stability of TCR, DMBT is reasonably assumed to be formed through recombination of TCR with 3,5-dimethylphenylmethyl radicals (Eq. 18).

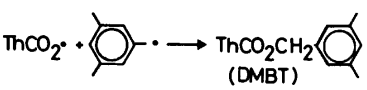

The formation of PMDM is quite unusual since, as the following control experiments show, benzyl-type radicals in general do not facilely add to aromatic rings.[1,2] Therefore, it is reasonably proposed that PMDM is formed through recombination of 3,5-di-

methylphenylmethyl radicals with cyclohexadienyl radicals generated by attack of TCR on the ipso positions of TMB, followed by elimination of TCA (Eqs. 19 and 20).

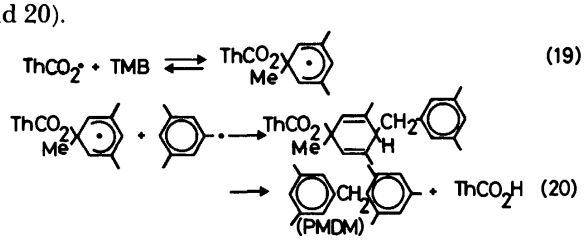

Attempts were made to eliminate the possibility of addition of benzyl-type radicals to TMB and to confirm contribution of aroyloxyl radicals to PMDM formation. Thus, 3,5-dimethylphenylmethyl radicals were generated in TMB in the absence of any aroyloxyl radicals by the following photochemical and thermal procedures; first, 1,3-bis(3,5-dimethylphenyl)-2-propanone was photolyzed at 10—50 °C to generate the dimethylphenylmethyl radicals through Norrish I cleavage.[23,24] BDPE was produced almost quantitatively and only a slight amount of PMDM was detected on GLPC at all temperatures employed (Table 9). Second, hydrogen atom abstraction by triplet benzophenone was used to generate the benzyl-type radicals.[25] Thus, benzophenone was irradiated in TMB at 25—55 °C to give BDPE and $3,5\text{-}Me_2C_6H_3CH_2CPh_2OH$ but almost none of PMDM (Table 10). Finally, di-*t*-butyl diperoxyoxalate was heated at 35—55 °C in TMB to result in the formation of BDPE (Table 11). In this case *t*-butoxyl radicals abstract a hydrogen atom from a methyl group of the solvent to generate 3,5-dimethylphenylmethyl radicals.[26] These results show that 3,5-dimethylphenylmethyl radicals can neither add to TMB by themselves (Eq. 22) nor recombine at the ring carbons, the potential radical centers of their resonance forms (Eq. 23), but undergo exclusively recombi-

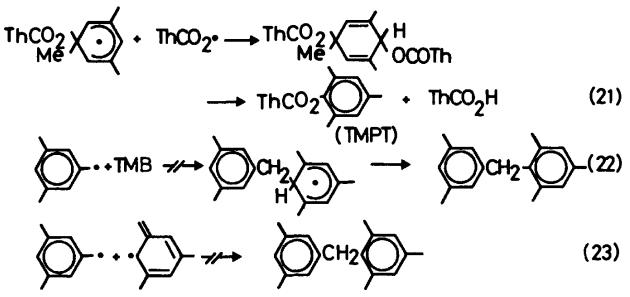

Scheme 2.

nation (dimerization) at their benzyl carbons (Eq. 17).

In order to confirm involvement of the aroyloxyl radicals in the formation of PMDM, temperature dependence of product yields in the photolysis of TPO was examined, as summarized in Table 6 and depicted in Fig. 2, since aroyloxyl radicals reversibly add to aromatic solvents. Figure 2 shows that the yield of BDPE increases but those of TMPT and PMDM decrease with increasing temperature. These results are consistent with the above mechanism; at higher temperatures the addition equilibria (Eqs. 15 and 19) tend to be shifted to the side of TCR and TMB, and thus TCR tends to abstract a hydrogen atom from a methyl group of TMB.

As to elimination of ipso substituents, products from homolytic substitution of a methyl group by TCR such as 3,5-dimethylphenyl 2-thiophenecarboxylate were not detected in the photolysis of the peroxides in TMB.

Formation of PMDM and similar temperature effects on the product yields were observed in the photolysis of BPO in TMB (Table 7 and Fig. 2). The product formation can be accounted for by processes similar to those mentioned above except phenyl benzoate, the geminate product,[10] which was not detected in the thermolysis. When the yields of products are compared between the two peroxides at the same temperatures, the yields of BDPE are almost of the same magnitude; however, the yields of PMDM and 2,4,6-trimethylphenyl esters, TMPT and $PhCO_2C_6H_2Me_3$ (TMPB), are higher from TPO than from BPO. The difference in yield is much remarkable in the esters, and this can be understood by the difference in stability between TCR and benzoyloxyl radicals, the latter decarboxylating faster.[27] That TMPT is much higher in yield and suffers more remarkable temperature effects than TMPB (Fig. 2) indicates that TMPT is formed not only through addition of TCR to TMB followed by disproportionation (Eqs. 15,16) but also through recombination of TCR with the ipso intermediate followed by acid elimination (Eq. 21).

Therefore, it is quite reasonable to conclude that the formation of PMDM in photolyses of TPO and BPO provides clear evidence for intermediacy of the ipso intermediates formed by attack of aroyloxyl radicals to TMB.

Thermolysis of the peroxides in TMB shows some intriguing trends. The formation of 2-thienyl 2-thiophenecarboxylate is noticeable, since BPO did not give any corresponding phenyl benzoate. This fact provides another piece of evidence for the stability (slow decarboxylation) of TCR. More remarkable is the increase of the PMDM yield for both peroxides under aerated conditions. Although the cause has not been clarified, it can be tentatively proposed that oxygen will contribute to elongation of a lifetime of the ipso intermediate at high temperature by an addition-elimination equilibrium (Eq. 24).[28,29]

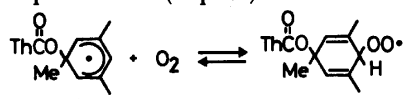

Estimation of Stability of ipso Intermediates from MO Calculations. Open shell restricted SCF-MO MINDO/3 calculations showed that the energy difference between ipso and non-ipso intermediates from TMB (7.8 kcal/mol) is smaller than that from toluene (8.5 kcal/mol) (Fig. 3). This may indicate that the ipso intermediate from TMB is relatively stabilized more

than that from toluene. For anisole as a model compound for diphenyl ether, of which the phenoxyl group has been established to be substituted by benzoyloxyl radicals,[30] the difference of the total energy between the ipso and non-ipso intermediates is much larger (10.0 kcal/mol) than the above two cases. In all three cases, the energy difference among the non-ipso intermediates is small compared with the above values. Similar results have been reported on substituted cyclohexadienyl radicals on the basis of CNDO/2[22] and *ab initio* MO calculations.[31] The relative energies of the isomeric intermediates have been similarly assessed by MINDO/3 calculations based on isodesmic reactions.[32] As discussed above, PMDM is apparently formed from the reaction of 6-aroyloxy-1,3,5-trimethylcyclohexadienyl radicals, of which the model is estimated to be higher in energy than the non-ipso intermediates. Therefore, the stability of substituted cyclohexadienyl radicals seems not to play an important role in the selectivity in the addition step of the aroyloxyl radicals, but to contribute to the ipso →ortho rearrangement as proposed in the case of toluene; the positions of the initial addition of aroyloxyl radicals to aromatic solvents can be predicted by the frontier orbital theory.[22,33]

The calculated spin density predicts that all cyclohexadienyl radicals depicted in Fig. 4 are the most reactive at the 3-position. The isomer ratio of dimethylbiphenyls indicates low reactivity of the 1- and 5-positions as discussed above. Based on the product distributions in toluene and the spin densities, the four cyclohexadienyl intermediates are considered to behave as follows; the ortho and meta intermediates are predominantly responsible for the dimethylbiphenyl formation by recombining at the 3-position, and the para intermediate reacts at the 1- or 5-position because of low reactivity of the 3-position due to the methyl substitution. On the contrary, the ipso intermediate is not responsible for biphenyl formation but rearranges to the ortho one.

Conclusion

The high reactivity of TCR towards aromatic solvents and the high stationary concentration of cyclohexadienyl radical intermediates in photolysis of TPO bring about their bimolecular reactions giving dimeric products of the solvents. Biphenyl and dimethylbiphenyls are formed in noticeable yields in benzene and toluene, respectively, through dimerization of the corresponding cyclohexadienyl radicals followed by acid elimination. In TMB PMDM arises from recombination of the ipso intermediates generated by attack of TCR and benzoyloxyl radicals to TMB with the benzyl-type radicals derived from TMB.

Experimental

Materials. Bis(2-thiophenecarbonyl) peroxide was prepared from 2-thiophenecarbonyl chloride and hydrogen peroxide (30% aqueous solution) in the presence of sodium hydroxide,[16] and dibenzoyl peroxide was commercially obtained. The peroxides were purified by precipitating from dichloromethane–methanol.

Di-*t*-butyl diperoxyoxalate was prepared by adding a pentane solution of *t*-butyl hydroperoxide to a cooled mixture of oxalyl dichloride, pyridine, and pentane, and reprecipitated from pentane.[26]

1,3-Bis(3,5-dimethylphenyl)-2-propanone was prepared by the reaction of 3,5-dimethylphenylmethyl bromide with nonacarbonyldiiron(0) in hexane,[34,35] and purified by recrystallization from petroleum ether.

2,4,6-Trimethylphenyl 2-thiophenecarboxylate was prepared by the reaction of 2,4,6-trimethylphenol and 2-thiophenecarboxylic acid in trifluoroacetic anhydride,[36] and recrystallized from hexane. Mp 89.3—89.8 °C. ^{1}H-NMR ($CDCl_3$): δ=2.12 (s, 6H), 2.24 (s, 3H), 6.79 (s, 2H), 7.06 (m, 1H), 7.50 (d, 1H), 7.86 (d, 1H). IR (KBr): $\nu_{C=O}$ 1720 cm^{-1}. Found: C, 68.13; H, 5.68%. Calcd for $C_{14}H_{14}O_2S$: C, 68.26; H, 5.72%.

3,5-Dimethylphenylmethyl 2-thiophenecarboxylate was prepared by the reaction of sodium 2-thiophenecarboxylate with 3,5-dimethylphenylmethyl bromide in acetic acid.[37] Bp 148.3—149.2 °C/1100 Pa. ^{1}H-NMR ($CDCl_3$): δ=2.32 (s, 6H), 5.29 (s, 2H), 7.0—7.3 (m, 4H), 7.58 (d, 1H), 7.86 (d, 1H). Found: C, 68.42; H, 5.82%. Calcd for $C_{14}H_{14}O_2S$: C, 68.26; H, 5.72%.

3,5-Dimethylphenyl 2-thiophenecarboxylate was prepared by the reaction of 2-thiophenecarbonyl chloride with 3,5-dimethylphenol in a mixture of benzene and pyridine. Mp 39.2—42.3 °C. ^{1}NMR ($CDCl_3$): δ=2.30 (s, 6H), 6.75 (s, 2H), 6.98 (s, 1H), 7.08 (m, 1H), 7.55 (d, 1H), 7.86 (d, 1H). Found: C, 67.21; H, 5.22%. Calcd for $C_{13}H_{12}O_2S$: C, 67.21; H, 5.20%.

2,4,6-Trimethylphenyl benzoate,[38] phenyl,[16] 2-methylphenyl,[16] 3-methylphenyl,[16] 4-methylphenyl,[16] and benzyl 2-thiophenecarboxylate[39] were prepared similarly from 2-thiophenecarbonyl chloride and the corresponding phenols.

2-Thienyl 2-thiophenecarboxylate was prepared by the thermolysis of TPO in the presence of copper(II) chloride in acetonitrile containing thiophene.[16]

2,2′-Dimethyl- and 3,3′-dimethylbiphenyl were prepared by heating 2-iodo- and 3-iodotoluene, respectively, with copper powder (Ullman reaction),[40] and 4,4′-dimethylbiphenyl was commercially obtained.

2,3′-Dimethylbiphenyl was prepared in the following way.[41,42] 3-Methyl-1-(2-methylphenyl)cyclohexanol was prepared by Grignard reaction of 2-bromotoluene with 3-methylcyclohexanone. The cyclohexanol was heated with oxalic anhydride to give a mixture of 3-methyl-1-(2-methylphenyl)cyclohexene and 5-methyl-1-(2-methylphenyl)-cyclohexene. This mixture was refluxed with sulfur in quinoline to afford 2,3′-dimethylbiphenyl.

2,4′-Dimethyl- and 3,4′-dimethylbiphenyl were prepared in a similar way from 4-bromotoluene with 2-methyl- and 3-methylcyclohexanone, respectively.

2,2′,4,4′,6,6′-Hexamethylbiphenyl was prepared by heating 2,4,6-trimethylphenylmagnesium bromide with anhydrous copper(II) chloride.[43]

2-Methyl-, 3-methyl-, and 4-methyldiphenylmethane were prepared from the corresponding methylbenzophenones by modified Wolff-Kishner reaction.[44]

2,3′,4,5′,6-Pentamethyldiphenylmethane was prepared by

Friedel-Clafts reaction of 3,5-dimethylphenylmethyl bromide with 1,3,5-trimethylbenzene in the presence of iron(III) trichloride.[45]

1,2-Bis(3,5-dimethylphenyl)ethane were prepared by heating the corresponding dimethylphenylmethylmagnesium bromide with anhydrous copper(II) chloride.[45]

Benzophenone commercially obtained was recrystallized from methanol and petroleum ether.

Toluene and 1,3,5-trimethylbenzene (special grade, Wako) were purified by distilling over calcium hydride.

Photolyses and Thermolyses of Diacyl Peroxides. A solution (3 cm^3) of a peroxide (0.03 mol/dm^3) in benzene, toluene, or 1,3,5-trimethylbenzene in a Pyrex tube was degassed by the usual freeze-thaw cycles or by bubbling with argon, and irradiated with a 1 kW or a 400 W high pressure mercury lamp using a merry-go-round type Riko Rotary Photochemical Reactor or with a nitrogen laser (Lambda Physik M100B; 337.1 nm, 3.5 mJ/pulse, 80Hz). On irradiation with 254 nm light, a peroxide solution in a quartz tube was deaerated by bubbling with nitrogen, and irradiated with a 160 W low pressure mercury lamp. Irradiation was continued for more than five times the half-life period of the peroxide determined by iodometric analysis or high-performance liquid chromatography (Shimadzu LC2; column, ODS 25cm) under the experimental conditions.

Thermolyses of peroxides were carried out in the following manner. A solution of a peroxide degassed by the usual freeze-thaw cycles or under oxygen in a Pyrex tube was heated in a thermostat for more than five times the half-life period of the peroxide determined under the experimental conditions.

Photolysis of 1,3-Bis(3,5-dimethylphenyl)-2-propanone in 1,3,5-Trimethylbenzene. A solution of 1,3-bis(3,5-dimethylphenyl)-2-propanone in 1,3,5-trimethylbenzene (0.01 mol/dm^3, 3 cm^3) was degassed by the usual freeze-thaw cycles, and irradiated by a 1 kW high pressure mercury lamp for 70 min in a thermostat.

Irradiation of Benzophenone in 1,3,5-Trimethylbenzene. A solution of benzophenone in 1,3,5-trimethylbenzene (0.03 mol/dm^3, 3 cm^3) was degassed and irradiated by a 1 kW high pressure mercury lamp for 3 h in a thermostat.

Thermolysis of Di-t-butyl Diperoxyoxalate in 1,3,5-Trimethylbenzene. A solution of di-*t*-butyl diperoxyoxalate in 1,3,5-trimethylbenzene (0.03 mol/dm^3, 3 cm^3) was degassed and heated in a thermostat for five times the half-life period (1.0 h at 55 °C, 3.5 h at 45 °, and 14.2 h at 35 °) estimated from the reported decomposition rate constants.[26]

Product Analyses. Biaryls, diphenylmethanes, diphenylethanes, and esters were determined quantitatively by GLPC analysis on a Shimadzu GC-4CM PF gas chromatograph equipped with a flame ionzation detector. Acids were determined on a Shimadzu LC2 high-performance liquid chromatograph.

Trapping of Carbon Dioxide in the Presence of Styrene. TPO (0.03 mol/dm^3) in a mixture of varying fractions of benzene and styrene was thermolyzed at 80 °C and photolyzed at room temperature with a 400 W high pressure mercury lamp through a Pyrex wall. The resulting carbon dioxide was absorbed with an Ascarite tube and determined by gravimetry.

Spin Trapping of 2-Thiophenecarbonyloxyl Radicals. A solution of TPO (0.91 mol/dm^3) containing *N*-benzylidene-*t*-butylamine oxide (0.1 mol/dm^3) was heated at 80 °C or irradiated at room temperature with a 1 kW high pressure mercury lamp in the cavity of an ESR spectrometer (JEOL JES-ME-1X) for several minutes.

References

1) O. Simamura, T. Migita, N. Inamoto, and K. Tokumaru, "Yurikihanno," Tokyo Kagaku Dozin, Tokyo (1969), Vol II, pp. 399—437.

2) M. J. Perkins, "Free Radicals," ed by J. K. Kochi, Wiley-Interscience, New York (1973), Vol II, pp. 231—271.

3) T. Nakata, K. Tokumaru, and O. Simamura, *Tetrahedron Lett.*, **1967**, 3303; *Bull. Chem. Soc. Jpn.*, **43**, 3590 (1970).

4) M. E. Kurz, P. Kovacic, A. K. Bose, and I. Kugajevsky, *J. Am. Chem. Soc.*, **90**, 1818 (1968); M. E. Kurz and M. Pellegrini, *J. Org. Chem.*, **35**, 990 (1970); P. Kovacic, C. G. Reid, and M. J. Brittain, *ibid.*, **35**, 2152 (1970).

5) T. Suehiro, S. Igeta, O. Kuwabara, and M. Hirai, *Tetrahedron*, **26**, 963 (1970).

6) H. Sakuragi, S. Ishikawa, T. Nishimura, M. Yoshida, N. Inamoto, and K. Tokumaru, *Bull. Chem. Soc. Jpn.*, **49**, 1949 (1976).

7) D. F. DeTar and R. A. Long, *J. Am. Chem. Soc.*, **80**, 4742 (1958); D. F. DeTar, R. A. Long, J. Rendleman, J. Bradley, and P. Duncan, *ibid.*, **89**, 4051 (1967).

8) T. Urano, A. Kitamura, H. Sakuragi, and K. Tokumaru, *Chem. Lett.*, **1983**, 867.

9) S. Takahara, A. Kitamura, H. Sakuragi, and K. Tokumaru, *Chem. Lett.*, **1983**, 1315.

10) A. Kitamura, H. Sakuragi, M. Yoshida, and K. Tokumaru, *Bull. Chem. Soc. Jpn.*, **53**, 1393 (1980).

11) E. G. Janzen, C. A. Evans, and Y. Nishi, *J. Am. Chem. Soc.*, **94**, 8236 (1972).

12) R. C. Bingham, M. J. S. Dewar, and D. H. Lo, *J. Am. Chem. Soc.*, **97**, 1285 (1975).

13) O. Kikuchi and S. Shimomura, *Bull. Chem. Soc. Jpn.*, **57**, 2993 (1984).

14) D. G. Lister, J. N. McDonald, and N. L. Owen, "Internal Rotation and Inversion," Academic Press, London (1978).

15) J. P. Hummel and P. J. Flory, *Macromolecules*, **13**, 479 (1980).

16) M. C. Ford and D. Mackay, *J. Chem. Soc.*, **1957**, 4620; D. Mackay, *Can. J. Chem.*, **44**, 2881 (1966).

17) K. Tokumaru, *Nippon Kagaku Kaishi*, **92**, 887 (1971).

18) Y. Sakaguchi, H. Hayashi, and S. Nagakura, *Bull. Chem. Soc. Jpn.*, **53**, 3059 (1980).

19) S. Hashimoto, W. Koike, and M. Oyama, *Nippon Kagaku Kaishi*, **1972**, 375.

20) M. K. Eberhardt, *J. Phys. Chem.*, **81**, 1051 (1977).

21) G. W. Klein, K. Bhatia, V. Madhaven, and R. H. Schuler, *J. Phys. Chem.*, **79**, 1767 (1975).

22) M. K. Eberhardt and M. Yoshida, *J. Phys. Chem.*, **77**, 589 (1973).

23) P. S. Engel, *J. Am. Chem. Soc.*, **92**, 6074 (1970).

24) W. K. Robbins and R. H. Eastman, *J. Am. Chem. Soc.*, **99**, 6076, 6077 (1977).

25) W. M. Moore, G. S. Hammond, and R. P. Foss, *J. Am. Chem. Soc.*, **83**, 2789 (1961).

26) P. D. Bartlett, E. P. Benzing, and R. E. Pincock, *J. Am. Chem. Soc.*, **82**, 1762 (1960).

27) T. Urano, Thesis, University of Tsukuba (1984).

28) J. A. Howard, "Free Radicals," ed by J. K. Kochi, Wiley-Interscience, New York (1973), Vol. II, pp. 3—62.
29) For triphenylmethyl radicals, E. G. Janzen, F. J. Johnston, and C. A. Ayers, *J. Am. Chem. Soc.*, **89**, 1176 (1976); J. A. Howard and K. U. Ingold, *Can. J. Chem.*, **46**, 2655 (1968).
30) K. Nowada, H. Sakuragi, K. Tokumaru, and M. Yoshida, *Chem. Lett.*, **1976**, 1243.
31) A. J. Birch, A. L. Hinde, and L. Radom, *J. Am. Chem. Soc.*, **102**, 4074 (1980).
32) R. D. Gandour, *Tetrahedron*, **36**, 1001 (1980).
33) K. Fukui, *Top. Current Chem.*, **15**, 1 (1970); K. Fukui, T. Yonezawa, and H. Shingu, *J. Chem. Phys.*, **20**, 722 (1952); K. Fukui, T. Yonezawa, C. Nagata, and H. Shingu, *ibid.*, **22**, 1433 (1954); K. Fukui, T. Yonezawa, and C. Nagata, *Bull. Chem. Soc. Jpn.*, **27**, 423 (1954); *idem.*, *J. Chem. Phys.*, **27**, 1247 (1957).
34) A. N. Nesmeyanov, G. P. Zol'nikova, G. M. Babakhina, I. I. Kritskaya, G. G. Yakobson, *Zh. Obshch. Khim.*, **43**, 2007 (1973); *Chem. Abstr.*, **80**, 15042r (1974).
35) I. Rhee, M. Ryang, and S. Tsutsumi, *J. Organomet. Chem.*, **9**, 361 (1967).
36) R. C. Parish and L. M. Stock, *J. Org. Chem.*, **30**, 927 (1965).
37) E. C. Horing, *Org. Synth.*, Coll. Vol. **3**, 650 (1955).
38) K. v. Auwers and W. Mauss, *Justus Liebigs Ann. Chem.*, **464**, 293 (1928).
39) B. Weinstein, *J. Am. Chem. Soc.*, **77**, 6709 (1955).
40) S. R. Sandler and W. Karo, "Organic Functional Group Preparations," Academic Press, New York (1968), p 21.
41) R. B. Carlin and D. A. Constantine, *J. Am. Chem. Soc.*, **69**, 50 (1947).
42) D. H. Hey and E. R. B. Jackson, *J. Chem. Soc.*, **1934**, 645.
43) W. Mayer and R. Adams, *J. Am. Chem. Soc.*, **51**, 630 (1929).
44) Huang-Minlon, *J. Am. Chem. Soc.*, **68**, 2487 (1946).
45) C. Serris, Jr. and E. K. Fields, *J. Am. Chem. Soc.*, **82** 4685 (1960); S. Meyerson, H. Drews, and E. K. Fields, *ibid.*, **86**, 4964 (1964).

NAD(P)$^+$-NAD(P)H Models. 53. Proximity Effect of Intramolecular Heteroatom on Reaction Rate

Atsuyoshi OHNO,* Takehiko GOTO,† Hisami KOBAYASHI, and Shinzaburo OKA
Institute for Chemical Research, Kyoto University, Uji, Kyoto 611
†*Department of Resource Chemistry, Faculty of Engineering, University of Iwate, Ueda, Morioka, Iwate 020*
(Received September 25, 1984)

NAD(P)H-model compounds that have a sulfur or oxygen substituent in the molecule have been synthesized and kinetics for the reduction of both substituted and unsubstituted α,α,α-trifluoroacetophenones with these model compounds are studied. Reduction with the heteroatom-containing model compounds proceeds at a slower rate than the reduction with a model without any heteroatom substituents. Furthermore, the dependency of the kinetic isotope effect on the electron-deficiency of the substrate differs. Kinetic parameters reveal that the retardation caused by the heteroatom is due to the loss of entropy in the initial electron-transfer process. The enthalpic term favors the reduction with the heteroatom-containing model.

Biomimetic reaction systems for reductions which are catalyzed by NAD(P)H-dependent dehydrogenases have been extensively studied for their reaction mechanisms and applications to organic syntheses.[1] Since the true reductant in this redox system is the 1,4-dihydronicotinamide moiety of NAD(P)H, almost all researches have been concentrated on the chemistry of 1,4-dihydropyridine derivatives. After we found that magnesium ion in dry acetonitrile is a good catalyst in a mimetic system,[2] the requirements for substrates that can be subjected to mimetic reduction have been lessened extensively. However, the enzymic redox system is still much superior to the corresponding mimetic one in the sense that the former system reduces a far wider variety of substrates than the latter. There is no doubt that the difference in the reactivity between enzymic and mimetic systems lies in complex constituents of the enzyme, which supply the essential functional groups for catalysis and, at the same time, construct a favorable environment for the reaction. Therefore, in order to extend the mimetic reaction system, we have to take into account not only the chemical constitution at the reaction center but also environmental effects. There are a lot of positively or negatively polarized groups around the active site of the enzyme, and these groups may assist the transfer of (net) hydride. It is also known that, for some liver alcohol dehydrogenases, a zinc ion is essential for the reaction, and this zinc ion, which is ligated by one molecule of water, is tetrahedrally ligated by cysteinyl sulfurs and histidinyl nitrogens.[3] The zinc ion is supposed to activate substrates as a Lewis acid by ligating onto the carbonyl oxygen of the substrate ketone.[4] However, there is some doubt whether the pentacoordinated zinc ion at the reaction center can retain its catalytic activity as a Lewis acid. At least in a mimetic system, a metal ion with a chelating reagent was not a catalyst.[5]

As a trial to introduce some environmental effects into a mimetic reaction system, we synthesized NAD(P)H models that have sulfur or oxygen functional groups as substituents on an alkyl chain at the N_1 position of 1,4-dihydronicotinamide and studied the effects of heteroatoms on the kinetics in the presence or absence of magnesium ion.

It should be mentioned that magnesium ion in the mimetic system is a catalyst for some substrates,[2] but an inhibitor for others.[6] For a third class of substrates, it may be a catalyst or an inhibitor depending on its concentration.[7] Such complex behavior is best interpreted in terms of a multi-step mechanism with the initial electron transfer from the dihydropyridine moiety to the substrate, and of acceleration of this electron-transfer process by magnesium ion.[8]

Results

Six 1-[(ω-methylthio)alkyl]-1,4-dihydronicotinamides (S2NAH, S3NAH, S4NAH, S5NAH, S6NAH, and S8NAH) and one 1-[(ω-methoxy)alkyl]-1,4-dihydronicotinamide (O2NAH) were synthesized as model compounds with a heteroatom in the molecule. Two 1-alkyl-1,4-dihydronicotinamides (PNAH and ONAH) were employed as standards.

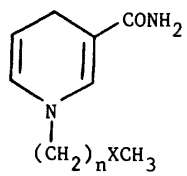

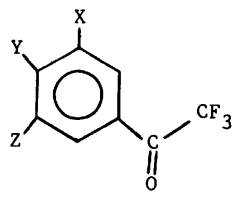

S2NAH: X = S, $n = 2$
S3NAH: X = S, $n = 3$
S4NAH: X = S, $n = 4$
S5NAH: X = S, $n = 5$
S6NAH: X = S, $n = 6$
S8NAH: X = S, $n = 8$
O2NAH: X = O, $n = 2$
PNAH: X = CH_2, $n = 1$
ONAH: X = CH_2, $n = 6$

1a: X = Y = Z = H
1b: X = Z = H, Y = Cl
1c: X = CF_3, Y = Z = H
1d: X = NO_2, Y = Z = H
1e: X = NO_2, Y = Cl, Z = H
1f: X = CF_3, Y = H, Z = NO_2

Substituted and unsubstituted α,α,α-trifluoroacetophenones (**1a—1f**) were prepared as substrates for the reduction. A compound with a free mercapto group (SHNAH) was also prepared, but could not be used in the kinetic studies because of its instability. First-order rate constants were measured by observing the decrease in the intensity at around 350 nm (an absorption characteristic of the dihydropyridine moiety) on a

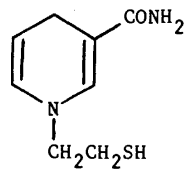

SHNAH

spectrophotometer. The observed rate constants were corrected for the rate constant for the magnesium ion-catalyzed decomposition of each model compound. The second-order rate constant, k, was calculated by dividing the corrected rate constant by the concentration of the substrate and the results are summarized in Table 1.

Kinetic parameters for some pairs of reactants were calculated from the temperature dependency of the rate constants, and the results are listed in Table 2.

Kinetics were also studied with S2NAH-4-*d*, and the kinetic deuterium isotope effect was calculated using Steffens and Chipman's equation.[9] The values are listed in Table 3. We have confirmed that the accuracy of the value obtained by this procedure is as high as that obtained from the calculation with the dideuterated compound.[8a]

Table 1. Second-order rate constants for the reduction of α,α,α-trifluoroacetophenone and its derivatives with NAD(P)H models[a]

No.	Substrate	Model	Temp °C	10k, dm^3 mol^{-1} s^{-1} without metal ion	with Mg^{2+}	with Zn^{2+}
1	**1a**	S2NAH	30	c)	0.0786±0.0010[d]	
2	**1a**	S2NAH	40	c)	0.167±0.0029[d]	
3	**1a**	S2NAH	50	b)	0.270±0.0046[d]	b)
4	**1a**	S2NAH	60	c)	0.561±0.018[d]	
5	**1b**	S2NAH	50	b)	0.660±0.013[d]	b)
6	**1c**	S2NAH	50	0.222±0.0017[d]	1.22±0.033[d]	c)
7	**1d**	S2NAH	30	c)	1.04±0.031[d]	
8	**1d**	S2NAH	40	c)	1.84±0.021[d]	
9	**1d**	S2NAH	50	0.995±0.058	3.21±0.093[d]	c)
10	**1d**	S2NAH	60	c)	5.30±0.070[d]	
11	**1e**	S2NAH	50	b)	4.74±0.0055[d]	c)
12	**1f**	S2NAH	30	c)	2.68±0.016[d]	
13	**1f**	S2NAH	40	c)	5.49±0.021[d]	
14	**1f**	S2NAH	50	15.6±0.40	6.76±0.040[d]	c)
15	**1f**	S2NAH	60	c	11.1±0.18[d]	
16	**1d**	S3NAH	50	2.03±0.054	4.38±0.090	1.77±0.065
17	**1d**	S4NAH	50	2.40±0.048	5.83±0.11	c)
18	**1d**	S5NAH	50	2.71±0.060	6.81±0.16	2.48±0.060
19	**1d**	S6NAH	50	3.35±0.040	8.01±0.053	c)
20	**1d**	S8NAH	30	c)	2.71±0.079	c)
21	**1d**	S8NAH	40	c)	4.64±0.033	c)
22	**1d**	S8NAH	50	3.39±0.045	8.20±0.11	3.38±0.050
23	**1d**	S8NAH	60	c)	14.3±0.082	c)
24	**1a**	O2NAH	50	b)	0.322[e]	
25	**1b**	O2NAH	50	b)	0.669[e]	
26	**1c**	O2NAH	50	0.295[e]	1.73[e]	
27	**1d**	O2NAH	50	1.46±0.050	4.10±0.055	c)
28	**1e**	O2NAH	50	1.46[e]	4.89[e]	
29	**1f**	O2NAH	50	1.89[e]	6.27[e]	
30	**1d**	PNAH	50	2.89±0.062[d]	6.43±0.13[d]	1.51±0.040
31	**1d**	ONAH	50	3.29±0.090	8.07±0.0789	c)

a) Errors are standard deviations. b) Too slow to be followed. c) Not observed. d) Data from ref. 8a. e) Data from one kinetic run.

Table 2. Second-order rate constants for the reduction of α,α,α-trifluoroacetophenone and its derivatives with 1-[(2-methylthio)ethyl]-1,4-dihydronicotinamide-4-*d* (S2NAH-*d*) and kinetic deuterium isotope effects[a]

Substrate	10k dm^3 mol^{-1} s^{-1}[b] without Mg^{2+}	with Mg^{2+}	k^H/k^{Dc} without Mg^{2+}	with Mg^{2+}
1a		0.178±0.0075		3.11
1c	0.157±0.0018		2.43	
1d	0.704±0.018	2.12±0.039	2.41	3.13
1e		2.92±0.023		4.31
1f	10.2±0.17	3.99±0.049	3.29	5.51

a) At 50 °C in acetonitrile. b) Errors are standard deviations. c) Error is less than ±10%.

Table 3. Kinetic parameters for the reduction of 3-nitro-α,α,α-trifluoroacetophenone with NAD(P)H model compounds[a]

Substrate	Model	$\Delta H^{\ddagger}$	$\Delta S^{\ddagger}$	$\Delta G^{\ddagger}$
		kJ mol^{-1}	J K^{-1} mol^{-1}	kJ mol^{-1}[b]
1a	S2NAH	56.0	−151.2	104.9±0.060
1d	S2NAH	48.5	−155.5	98.6±0.053
1d	S8NAH	49.2	−145.7	96.2±0.021
1f	S2NAH	40.4	−173.5	96.6±0.098

a) Values at 50°C. b) Errors are standard deviations.

Water in the solvent acetonitrile strongly influences the results in these kinetic studies. Particular attention was paid to this point and the water content of the reaction system was measured before and after each kinetic run and was always less than 0.075% v/v even in the presence of magnesium perchlorate.[10]

Discussion

Hammett plots for the reduction of various substrates with S2NAH and O2NAH in the presence and absence of magnesium ion are illustrated in Fig. 1. In the reductions with S2NAH, a straight line with ρ=2.62 (correlation coefficient r=0.998) is obtained when magnesium ion is absent, but the plot for the reduction in the presence of magnesium ion is composed of two straight lines, one of which has ρ=1.50 (r=0.999) and the other has ρ=0.768 (r=1.000).[11] The corresponding plots for the reduction with O2NAH have essentially the same tendency; ρ=2.55 (r=1.000) for the reduction without magnesium ion, and ρ= 1.59 (r=0.995) and 0.436 (r=0.990) for the reduction with magnesium ion.

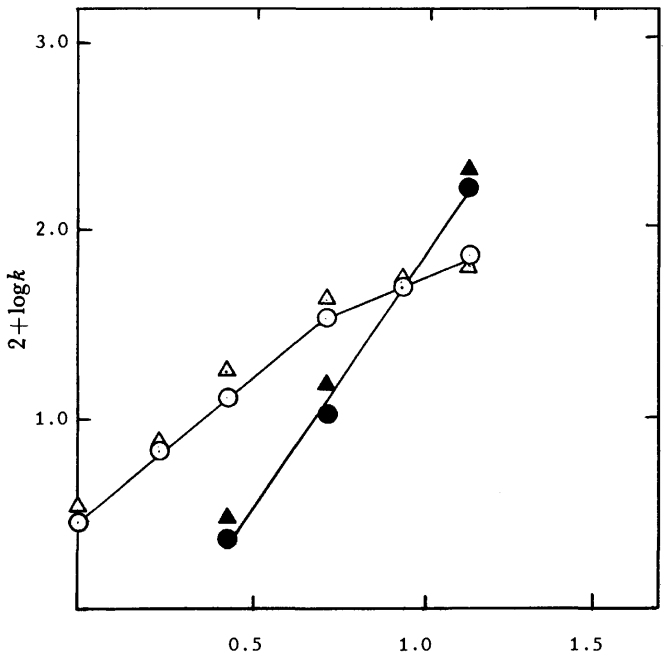

Fig. 1. Hammett plots for the reduction with S2NAH in the presence (○) and absence (●) of magnesium ion and with O2NAH in the presence (△) and absence (▲) of magnesium ion.

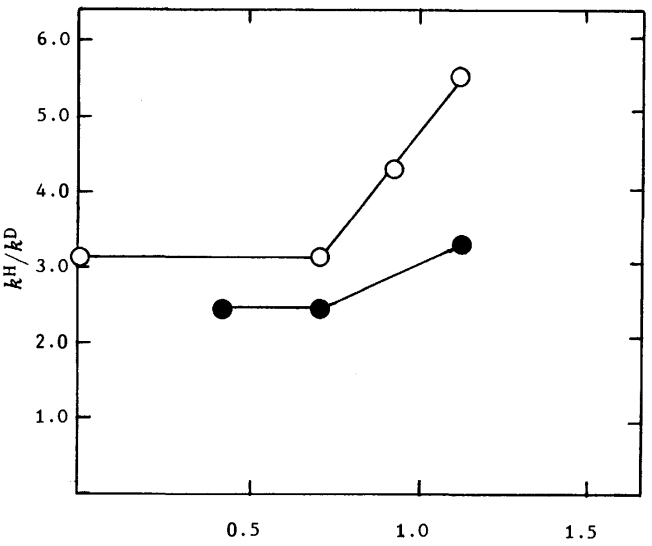

Fig. 2. Plotts of kinetic isotope effects in the reduction with S2NAH against σ-values of substituents in the presence (○) and absence (●) of magnesium ion.

The present results with heteroatom-containing models[12] are a striking contrast to the free energy relationship exerted by PNAH, where the reduction with magnesium ion gave a straight line but that without magnesium ion appeared as a bent line.[8a]

The dependency of kinetic isotope effects on the substituent σ-value for the reduction with S2NAH again differs from that with PNAH. That is, as plotted in Fig. 2, the isotope effect for the former reduction increases, regardless of the presence or absence of magnesium ion, as the electron-deficiency of the substrate becomes large. On the other hand, in the reduction with PNAH, the kinetic isotope effect remained constant when the reduction was run in the presence of magnesium ion, whereas in its absence the value increased to an asymptote.[8a] For each reductant, the σ-value where the slope of the line changes in the plot of the kinetic isotope effect corresponds exactly with the position where the change in slope is seen in the Hammett plot. Thus, it is apparent that the change in slope reveals a change in the rate-determining step, or the reduction is composed of several steps.

Comparison of activation parameters for the reductions of **1a** (a weakly electron-deficient substrate), **1d** (a moderately electron-deficient substrate), and **1f** (a strongly electron-deficient substrate) with S2NAH in the presence of magnesium ion reveals that the entropy of activation for the reduction of **1f** is much smaller than those for the reductions of **1a** and **1d**. If the reduction proceeded through a one step hydride-transfer mechanism, Hammond's posturation proposes that the transition state for a strongly electron-deficient substrate should resemble the reactant more than the transition state for a less electron-deficient substrate, or the entropy of activation for the reduction of **1f** should be larger than those for the reductions of **1a** and **1d**. On the other hand, if the electron-transfer

step constitutes a major part of the rate-determining step, the stability of the resulting radical ion pair might play an important role in determining the activation parameter, and the entropy of activation may be smaller for **1f** than for **1a** or **1d**. This is a conclusion which comes out of the fact that a strongly electron-deficient substrate in a radical ion pair can keep an electron in its own counterpart more tightly than a less electron-deficient substrate.

Nevertheless, the reduction is accompanied by a certain amount of kinetic isotope effect. Thus, the transition state of the rate-determining step of the reduction seems to be such that the transfer of an electron is accompanied by the loosening of C_4–H bond in the reductant.

Table 1 shows that the reduction with S2NAH or O2NAH is slower than the reduction with PNAH regardless the presence or absence of magnesium ion. The retardation exerted by a heteroatom, however, becomes less important as the number of methylene groups, n, becomes large, and comes to an asymptote after n=6. The asymptotic value is equivalent to the reduction rate with ONAH. Activation parameters for the reduction of **1d** with S2NAH and S8NAH, as listed in Table 3, show that the reduction with the former model is rather preferred by the enthalpic term but the larger contribution of the entropic term results in the retardation of reduction with the former model.

Consequently, the retardation of the reduction caused by the intramolecular heteroatom can be accounted for by a major contribution of the initial process, in which at least a partial positive charge is developed in the reductant without affording a large kinetic deuterium isotope effect (or without dissociating the hydrogen nucleus greatly from the carbon at the 4-position), to the rate-determining step of the reduction. The intermediate must be one which is stabilized, in terms of enthalpy, by the proximity effect of an intramolecular hetero-atom, and the stabilization becomes more important as the electron deficiency of the substrate increases. The structure of the transition state for the initial step is, therefore, best expressed as a one-electron-transfer type of complex between the model compound and a substrate, the cation radical part of which is stabilized by participation by an electron pair on the heteroatom as illustrated in Scheme I. By the participation of an electron pair on the heteroatom, the partial positive charge in the dihydropyridine ring which develops as an electron in this ring is transferred onto the substrate, is stabilized in terms of enthalpy. However, for the electron pair to stabilize the electron-deficient dihydropyridine ring, the side-chain must be kept from free rotation, which causes a decrease in entropy. As the number of spacer methylene groups becomes larger, such participation of a heteroatom becomes less important because the entropic loss becomes too large, and the rate constant for the reduction comes to an asymptotic value. Since the activation energies for the initial electron-transfer process in the reduction with the heteroatom-substituted models are higher than those with PNAH and ONAH, the priority of this process in the rate-determining step of the reduction with a heteroatom-substituted model still remains even with the catalytic assistance of magnesium ion, keeping the kinetic isotope effects for these reductions small.

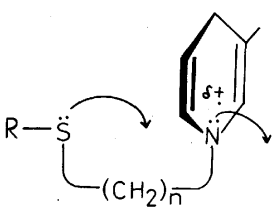

Scheme 1.

It is noteworthy that an inspection with a CPK-model shows that the sulfur or oxygen atom in S2NAH and O2NAH, respectively, is close to the dihydropyridine ring nitrogen when the dihydropyridine ring and the heteroatom are set at the *syn* position.

Table 1 shows that zinc ion retards the reduction in contrast to the catalytic effect of magnesium ion. However, the retardation diminishes as the alkyl chain becomes longer. The inhibitory effect of zinc ion can be accounted for if zinc ion has a higher efficiency than magnesium ion in stabilizing the charge-transfer ternary complex given by the initial one electron-transfer process.[6c,d] Since zinc ion is softer than magnesium ion as a Lewis acid, the former is better trapped by sulfur than the latter.[13] At the same time, the sulfur atom has a stronger affinity for the zinc ion than for the dihydropyridine ring. When the sulfur atom is set far from the reaction center as in the case of S8NAH, therefore, zinc ion is less involved in the reaction (the interaction between the dihydropyridine ring and the substrate) and the rate increases to the magnitude available without metal ion.

Although, unfortunately, it has been confirmed that intramolecular heteroatoms in the NAD(P)H model compounds decrease the reactivity, the interference is caused by the entropic term. The above conclusion, therefore, proposes that, if the heteroatom in a molecule is fixed at a proper position in the reactant, like atoms in a reaction pocket of an enzyme, there is no entropic interference and the increase in the reaction rate due to enthalpic assistance is expected. Enhanced reactivity caused by the participation of a proximate negative charge has been reported for reduction in micellar system.[14]

Experimental

Melting points were not corrected. UV spectra and VPC were recorded on a Union Giken SM-401 spectrophotometer and Hitachi 633-50 chromatograph, respectively. JEOL JNMFX-100 and Hitachi R-22 spectrometers were employed

for NMR spectroscopy.

Materials. Acetonitrile was refluxed over calcium hydride for several hours, then distilled from the refluxing pot under an argon atmosphere before use. Magnesium and zinc perchlorates were dried over phosphorus pentaoxide for 1 d under reduced pressure at 100 °C. The amount of water in kinetic solutions was determined on VPC (30% bis(2-cyanoethyl) ether, 1 m, 40 °C) before and after the kinetic measurement and was found to be less than 0.075% v/v and 0.094% v/v for the magnesium and zinc perchlorate solutions, respectively.

α,α,α-Trifluoroacetophenone (**1a**), 4-chloro-α,α,α-trifluoroacetophenone (**1b**), 3-trifluoromethyl-α,α,α-trifluoroacetophenone (**1c**), 3-nitro-α,α,α-trifluoroacetophenone (**1d**), 4-chloro-3-nitro-α,α,α-trifluoroacetophenone (**1e**), and 3-nitro-5-trifluoromethyl-α,α,α-trifluoroacetophenone (**1f**) were prepared according to procedures in the literature.[8a]

1-Propyl-1,4-dihydronicotinamide (PNAH) was prepared according to a procedure in the literature.[15] 1-Octyl-1,4-dihydronicotinamide (ONAH) was synthesized similarly. 1-[(2-Methylthio)ethyl]-1,4-dihydronicotinamide (S2NAH), 1-[(3-methylthio)propyl]-1,4-dihydronicotinamide (S3NAH), and 1-[(2-methoxy)ethyl]-1,4-dihydronicotinamide (O2NAH) were prepared in the same manner by the reduction of the corresponding pyridinium salt.[16]

1-[(8-Methylthio)octyl]-1,4-dihydronicotinamide (S8NAH). A solution of nicotinamide (0.48 g) and 10-fold excess of 1,8-dibromooctane in 10 cm³ of acetonitrile was heated at 60 °C for 1 d to obtain 1-(8-bromooctyl)-3-carbamoylpyridinium bromide in 72% yield after recrystallization from acetonitrile. The pyridinium salt was subjected to methylthiolation with sodium methanethiolate in water. The resulting 1-[(8-methylthio)octyl]-3-carbamoylpyridinium bromide (92% yield) was reduced with sodium dithionite to yield yellow crystals of S8NAH in 54% yield after recrystallization from ethanol.

1-[(4-Methylthio)butyl]-1,4-dihydronicotinamide (S4NAH), 1-[(5-methylthio)pentyl]-1,4-dihydronicotinamide (S5NAH), and 1-[(6-methylthio)hexyl]-1,4-dihydronicotinamide (S6NAH) were synthesized similarly.

UV and NMR spectra as well as the results of elemental analyses are listed in Table 4.

2-(Methoxymethylthio)ethanol. A solution of 31.3 g of 2-mercaptoethanol (0.40 mol) in 400 cm³ of ethanol was added to a solution of sodium ethoxide (0.44 mol) in 40 cm³ of ethanol under a nitrogen atmosphere. The mixture was cooled to 0 °C, and to this mixture 35.4 g of chloromethyl methyl ether (0.44 mol) was added dropwise. The reaction mixture was stirred for an hour, then the precipitate was filtered off and the solvent was evaporated from the filtrate. The residue was distilled (bp 58—60 °C/26.6 Pa) to give 35.9 g of 2-(methoxymethylthio)ethanol as an oil (73.5% yield). ^{1}H NMR in $CDCl_3$ (δ from TMS) 2.81 (t, 2H), 3.13 (bs, 1H), 3.42 (s, 3H), 3.78 (t, 2H), and 4.67 (s, 2H).

2-(Methoxymethylthio)-1-chloroethane. Into a stirred mixture of 33.0 g of 2-(methoxymethylthio)-1-ethanol (0.27 mol) and 23.7 g of pyridine (0.30 mol) at 0 °C, 33.7 g of thionyl chloride (0.28 mol) was added dropwise. It took about 1 h. After the reaction, the mixture was warmed to room temperature and organic materials were extracted with ether. The organic layer was washed with water and dried over sodium sulfate, then the solvent was evaporated. The residue was distilled (bp 43 °C/266 Pa) to give 2-(methoxymethylthio)-1-chloroethane in 64% yield (24.2 g). ^{1}H NMR in $CDCl_3$ (δ from TMS) 2.93 (t, 2H), 3.37 (s, 3H), 3.71 (t, 2H), and 4.67 (s, 2H). Found: C, 33.95; H, 6.72%. Calcd for C_4H_9OSCl: C, 34.15; H, 6.46%.

1-[2-(Methoxymethylthio)ethyl]-3-carbamoylpyridinium Chloride. A mixture of 16.9 g of 2-(methoxymethylthio)-1-chloroethane (0.12 mol) and 13.4 g of nicotinamide (0.11 mol) in 12 cm³ of ethanol was refluxed for 20 h. After the reaction, the precipitate was filtered and washed with ether and ethanol to give crude 1-[2-(methoxymethylthio)ethyl]-3-carbamoylpyridinium chloride in 95.6% yield. Recrystallization from methanol–ether gave the pure salt as white crystals in 59.8% yield (based on nicotinamide). ^{1}H NMR DMSO-d_6 (δ from TMS) 3.16 (s, 3H), 3.32 (t, 2H), 4.71 (s, 2H), 4.92 (t, 2H), 8.0—8.4 (m, 2H), 9.05 (s, 2H), and 9.18 (dd, 1H). Found: C, 44.59; H, 5.69; N, 10.25%. Calcd for $C_{10}H_{15}ClO_2S$: C, 45.70; H, 5.77; N, 10.66%.

1-(2-Mercaptoethyl)-3-carbamoylpyridinium Chloride (SHNA$^+$).[17] A solution of 26.3 g of 1-[2-(methoxymethylthio)ethyl]-3-carbamoylpyridinium chloride (0.1 mol) in 400 cm³ of water-acetonitrile (1:1 v/v) was poured into a solution of $HgCl_2$ in 400 cm³ of water-acetonitrile (1:1 v/v) to precipitate white solid. After 24 h, the solid was filtered and washed with acetonitrile and water. Thus obtained mercury-complex of the pyridinium salt was placed in 250 cm³ of water and H_2S gas was bubbled through the water layer for 3 h. The resulted HgS was filtered off, and the filtrate was freeze-dried to give 1-(2-mercaptoethyl)-3-carbamoylpyridinium chloride in 40% yield after recrystallization from methanol-ether mixture. ^{1}H NMR in DMSO-d_6 (δ from TMS) 2.8—3.4 (m, 3H), 4.87 (t, 2H), 7.9—8.4 (m, 2H), 8.92 (s, 2H), 9.18 (dd, 1H), and 9.72 (s, 1H).

1-(2-Mercaptoethyl)-1,4-dihydronicotinamide (SHNAH). A solution of 1.01 g of SHNA$^+$ (5 mmol) in 90 cm³ of water was added to a mixture of CH_2Cl_2 (400 cm³) and buffered aqueous solution of sodium dithionite (21 g of $Na_2S_2O_4$, 37 g of $NaHPO_4 \cdot 2H_2O$, 150 cm³ of 1 mol dm^{-3} aq-NaOH, and 150 cm³ of water; pH=7.5) dropwise with vigorous stirring under an argon atmosphere. After 40 min, the organic layer was separated, and the aqueous layer was extracted with CH_2Cl_2. The combined dichloromethane layer was washed with water and dried over sodium sulfate. The evaporation of the solvent from the dried solution gave 1-(2-mercaptoethyl)-1,4-dihydronicotinamide (SHNAH) as a yellow oil in 68.4% yield (0.63 g). UV in CH_3CN; λ_{max} 354 nm. When this compound was kept in a freezer at −20 °C overnight, an absorption at 303 nm appeared suggesting that the decomposition had begun under such conditions. ^{1}H NMR in $CDCl_3$ (δ from TMS) 1.40 (t, 1H), 2.70 (dt, 2H), 3.0—3.5 (m, 4H), 4.83 (dt, 1H), 5.4—5.9 (m, 3H), and 7.00 (d, 1H).

Kinetic Procedures. A kinetic solution was prepared under an atmosphere of argon and placed in a 1 cm UV cell which had a silicone rubber stopper. The compartment for UV cells was kept within ±0.05 °C of an appropriate temperature through the kinetic run.

As a general procedure, both sample and reference cells were filled with a solution of substrate (and magnesium or zinc perchlorate, when necessary) in acetonitrile to obtain a difference spectrum. Then, an acetonitrile solution of a

TABLE 4. ANALYTICAL DATA FOR NAD(P)H MODEL COMPOUNDS

Model	Mp(θ_m/°C) (decomp)	λ_{max}/nm in MeCN	Anal(%)[a]			^{1}H-NMR[b]
			C	H	N	
S2NAH	71	348	54.51 (54.29	7.13 7.21	14.13 14.37)	2.11 (s, 3H) 2.60 (t, 2H) 3.13 (m, 2H) 3.29 (t, 2H) 4.72 (dt, 1H) 5.55 (bs, 2H) 5.74 (dq, 1H)
S3NAH	oil	349				1.6—2.1 (m, 2H) 2.07 (s, 3H) 2.49 (t, 2H) 3.1—3.4 (m, 4H) 4.70 (dt, 1H) 5.55 (bs, 2H) 5.73 (dq, 1H) 6.98 (d, 1H)
S4NAH	oil	351				1.4—1.9 (m, 4H) 2.08 (s, 3H) 2.48 (t, 2H) 2.9—3.3 (m, 4H) 4.69 (dt, 1H) 5.58 (bs, 1H) 7.71 (dq, 1H) 6.97 (d, 1H)
S5NAH	oil	351				1.2—1.8 (m, 6H) 2.09 (s, 3H) 2.46 (t, 2H) 2.9—3.3 (m, 4H) 4.68 (dt, 1H) 5.47 (bs, 2H) 5.69 (dq, 1H) 6.98 (d, 1H)
S6NAH	70	351	60.87 (61.36	9.14 8.73	11.01 11.07)	1.0—1.9 (m, 8H) 2.08 (s, 3H) 2.48 (t, 2H) 2.8—3.3 (m, 4H) 4.70 (dt, 1H) 5.38 (bs, 2H) 5.70 (dq, 1H) 7.00 (d, 1H)
S8NAH	74	353	63.67 (63.77	9.17 9.30	9.82 9.92)	1.0—1.9 (m, 12H) 2.48 (s, 2H) 2.9—3.3 (m, 4H) 4.71 (dt, 1H) 5.46 (bs, 2H) 5.71 (dq, 1H) 7.01 (d, 1H)
O2NAH	91	347	59.29 (59.31	7.93 7.76	15.30 15.37)	3.0—3.6 (m, 9H) 4.71 (dt, 1H) 5.64 (bs, 2H) 5.77 (dq, 1H) 7.01 (d, 1H)
ONAH	57	351	71.18 (71.13	10.12 10.12	11.79 11.79)	0.87 (t, 3H) 0.8—1.8 (m, 12H) 2.9—3.3 (m, 4H) 4.70 (dt, 1H) 5.56 (bs, 2H) 5.72 (dq, 1H) 7.01 (d, 1H)

a) Numbers in parentheses are calculated values. b) δ from TMS in $CDCl_3$.

model compound was injected into the sample cell with a syringe to start the reaction. An appropriate concentration of the substrate (and the metal ion, when necessary) was chosen to keep at least 80-fold molarity of the substrate (and the metal ion) over the concentration of the reductant. For example, for the run in entry 9 in Table 1, the concentrations were: [**1d**]=6.59×10^{-2} mol dm^{-3}, [Mg(ClO_4)$_2$]=2.58×10^{-2} mol dm^{-3}, and [S8NAH]=3.0×10^{-4} mol dm^{-3}. It was confirmed

that the rates were first-order in the substrate, first-order in the reductant, and zero-order in the metal ion.

The kinetics was followed by observing the decrease in the intensity of absorption at around 400 nm from the reductant. The spectrometer was connected to an NEC PC-8001 computer and the intensity of absorption at appropriate times was monitored over 3 half-lives through the computer. One observed absorption was the average of 80 consecutive measurements. More than 30 points were monitored for a run. The data were automatically subjected to the least-squares treatment to give a pseudo-first order rate constant. The standard deviation and correlation coefficient for each run were better than 1% and 0.9999, respectively. More than 3 runs were averaged to obtain the rate constants listed in Table 1.

One of the authors (A. O.) wishes to thank the Ministry of Education, Japan for a Scientific Research Grant.

References

1) For example, see (a) R. J. Kill and D. A. Widdowson, "The Redox Chemistry of 1,4-Dihydronicotinic Acid Derivatives" and (b) D. S. Sigman, J. Hadju, and D. J. Creighton, "Nonenzymatic Dihydronicotinamide Reductions as Probes for the Mechanism of NAD+-Dependent Dehydrogenases," in "Bioorganic Chemistry," ed by E. E. van Tamelen, Academic Press Inc., New York, N. Y. (1978), Vol. 4, Chaps. 8 and 14, pp. 239—275 and pp. 385—407.

2) a) Y. Ohnishi, M. Kagami, and A. Ohno, *J. Am. Chem. Soc.*, **97**, 4766 (1975); b) A. Ohno, H. Yamamoto, T. Okamoto, S. Oka, and Y. Ohnishi, *Bull. Chem. Soc. Jpn.*, **50**, 2385 (1977).

3) C.-I. Brändén, H. Jörnvall, H. Eklund, and B. Furugren, "Alcohol Dehydrogenases," in "The Enzymes," ed by P. D. Boyer, Academic Press Inc., New York, N. Y. (1975), pp. 104—190.

4) a) H. Eklund, J.-P. Samama, L. Wallén, C. I. Brändén, Å. Åkeson, and T. A. Jones, *J. Mol. Biol.*, **146**, 561 (1981); b) H. Eklund, B. V. Plapp, J.-P. Samama, and C.-I. Brändén, *J. Biol. Chem.*, **257**, 14349 (1982).

5) A. Ohno, T. Kimura, H. Yamamoto, S. L. Kim, S. Oka, and Y. Ohnishi, *Bull. Chem. Soc. Jpn.*, **50**, 1535 (1977).

6) a) D. C. Dittmer, A. Lombardo, F. H. Batzold, and C. S. Greene, *J. Org. Chem.*, **41**, 2976 (1976); b) S. Shinkai, T. Ide, H. Hamada, O. Manabe, and T. Kunitake, *J. Chem. Soc., Chem. Commun.*, 848 (1977); C) A. Ohno, S. Yasui, K. Nakamura, and S. Oka, *Bull. Chem. Soc. Jpn.*, **51**, 290 (1978); d) A. Ohno, S. Yasui, H. Yamamoto, S. Oka, and Y. Ohnishi, *ibid.*, **51**, 294 (1978).

7) a) Y. Ohnishi, T. Numakunai, T. Kimura, and A. Ohno, *Tetrahedron Lett.*, 2699 (1976); b) R. A. Gase, G. Boxhoorn, and U. K. Pandit, *ibid.*, 2889 (1978); c) M. Hughs and R. H. Prince, *J. Inorg. Nucl. Chem.*, **40**, 703 (1978); d) A. Ohno, S. Yasui, R. A. Gase, S. Oka, and U. K. Pandit, *Bioorg. Chem.*, **9**, 199 (1981).

8) a) A. Ohno, H. Yamamoto, and S. Oka, *J. Am. Chem. Soc.*, **103**, 2041 (1981); b) S. Yasui, K. Nakamura, and A. Ohno, *J. Org. Chem.*, **49**, 878 (1984).

9) J. J. Steffens and D. M. Chipman, *J. Am. Chem. Soc.*, **93**, 6694 (1971).

10) A. Ohno, H. Kobayashi, G. Goto, and S. Oka, *Bull. Chem. Soc. Jpn.*, **57**, 1279 (1984).

11) A. Ohno, H. Kobayashi, S. Oka, and T. Goto, *Tetrahedron Lett.*, **24**, 5123 (1983).

12) Hereafter the word "heteroatom" is used to denote a sulfur or oxygen atom in the side chain at the N_1 position of the reductant.

13) T.-L. Ho, "Hard and Soft Acids and Bascs Principle in Organic Chemistry," Academic Press, New York, N. Y. (1977), pp. 4—25.

14) S. Shinkai, R. Ando, R.; and T. Kunitake, *Bull. Chem. Soc. Jpn.*, **49**, 3652 (1976).

15) D. Mauzerall and F. H. Westheimer, *J. Am. Chem. Soc.*, **77**, 2261 (1955).

16) S. Shiflin, *Biochemistry*, **3**, 829 (1964).

17) N. J. Curtis and R. S. Brown, *Can. J. Chem.*, **59**, 64 (1981).

Spectroscopic Studies on the Interaction of Polymeric In-chain Biguanide Biocide with Phospholipid Membranes as Probed by 8-Anilinonaphthalene-1-sulfonate

Tomiki IKEDA, Shigeo TAZUKE,* Clement H. BAMFORD,† and Anthony LEDWITH††

Research Laboratory of Resources Utilization, Tokyo Institute of Technology, 4259, Nagatsuta, Midori-ku, Yokohama 227

†*Bioengineering and Medical Physics Unit, Duncan Building, Royal Liverpool Hospital, P.O. Box 147, Liverpool L69, UK*

††*Department of Inorganic, Physical and Industrial Chemistry, University of Liverpool, P.O. Box 147, Liverpool L69 3BX, UK*

(Received September 27, 1984)

Interaction of a highly effective polymeric biocide poly(hexamethylene biguanide hydrochloride)(PHMB) with phospholipid model membranes was investigated spectroscopically by using 8-anilinonaphthalene-1-sulfonate (ANS) as a fluorescent probe. PHMB enhanced the fluorescence intensity and shifted the maximum wavelength of fluorescence of ANS embedded in the negatively-charged liposome composed of egg PC and dicetyl phosphate, while it had only small effect on the neutral liposome composed of egg PC alone. These results were interpreted in terms of preferred binding of PHMB to negatively-charged species. The Benesi-Hildebrand type plots revealed that PHMB was adsorbed to a greater extent onto the negatively-charged membrane than onto the neutral membrane: the dissociation constants for the liposome–ANS complexes derived from the plots gave quantitative evidence for the enhanced binding of PHMB to the negatively-charged membrane. Diaminohexyl biguanide (DAHB), a corresponding monomer to PHMB, was found to have no significant effect on either the neutral nor the negatively-charged liposome, a finding probably related to the fact that DAHB is practically inactive.

Poly(hexamethylene biguanide hydrochloride)(PHMB) is a polymeric biocide which exhibits highly antimicrobial activity against a wide range of microbes such as bacteria, fungi and yeasts.[1] Its mode of action was reported to be similar to that of monobiguanides and bisbiguanides.[2] The sequence of elementary events in the lethal action of those biguanide compounds can be summarized as follows:[3]

1) Adsorption on to the bacterial cell surface;
2) Diffusion through the cell wall;
3) Binding to the cytoplasmic membrane;
4) Disruption of the cytoplasmic membrane;
5) Release of K^+ ions and other cytoplasmic constituents;
6) Precipitation of cell contents and death of the cell.

Among the elementary processes described above, the binding to the cytoplasmic membrane is a very important process, as the disruption of the membrane is considered to be a crucial step in the cidal action. However, the molecular nature of the interaction of the polymeric biocide with the bacterial cytoplasmic membrane has not been fully understood at molecular level.

Fluorescence spectroscopy has been used extensively to study membrane-associated phenomena. Among the common fluorescent probes, 8-anilinonaphthalene-1-sulfonate (ANS) has been one of the most widely used probes in membrane studies.[4] It has been used as a probe for protein studies[5–7] and to study the energized state of mitochondrial membranes.[8]

In the present study, the interaction of PHMB with phospholipid membranes has been investigated by fluorescence spectroscopy with ANS as a probe to obtain insight into the adsorption behavior of the polymeric biocide on to the bacterial membranes.

Experimental

Materials. Egg yolk phosphatidylcholine (egg PC, chromatographically pure) and dihexadecyl phosphate (DCP) were obtained from Sigma and used without further purification. 8-Anilinonaphthalene-1-sulfonate (ANS, magnesium salt) was purchased from BDH (>98% pure) and used as received. PHMB and its corresponding monomer diaminohexyl biguanide (DAHB) were hydrochloride salts, and PHMB was free from contamination by starting materials, DAHB being > 99% pure. (These biguanide compounds are kind gifts from Dr. D. Pemberton of ICI, UK).

Method. Liposomal solutions were prepared by dispersing lipids in Tris-HCl buffer (20 mM Tris, 100 mM KCl, pH 7.4) with the aid of sonication (a MSE probe-type sonicator). The dispersion was then subjected to ultracentrifugation at 100000×g for 40 min (a MSE Prepspin 50). By this procedure, a transparent liposome solution was obtained. Although the preparation method of the liposome solutions was essentially the same in all experiments, two different ways of addition of ANS were employed: i) ANS was incorporated in the liposomal phase by cosonication. That is, lipid films containing ANS were prepared by mixing the lipid solution in chloroform and the ANS solution in ethanol in a flask and by removing the solvents under dry N_2 and subsequent storage in high vacuum. The Tris-HCl buffer was added to the dried lipid film and the lipid was dispersed by sonication. These liposome solutions were used in the experiments concerning Figs. 1, 2, and 3. The effect of PHMB and DAHB was studied by adding some amounts of concentrate of PHMB and DAHB to the liposome solutions. ii) For measurements of fluorescence of ANS at various ANS concentrations (experiments on Benesi-Hildebrand plots, Figs. 4 and 5), liposome solutions which consisted only of lipids were prepared first, and to 4 ml portion of the liposome solution various amounts of ANS concentrate (1.43 mM in

distilled water) were added by means of a microsyringe (up to 50 μl). The resulting solution was mixed vigorously for 30 s and fluorescence spectra were taken. It was confirmed that the fluorescence spectra did not change with time: after 1 h the same spectra were obtained. In the measurements of the ANS fluorescence in the presence of PHMB (Fig. 4, b-d and Fig. 5, b-d), PHMB concentrate was added to the liposome solution by means of a microsyringe with vigorous mixing before the ANS concentrate was added. It must be mentioned here that ANS incorporated in the liposome by cosonication method (i) followed by addition of PHMB gave similar spectra to those observed when ANS was added after PHMB was added to the liposome solution composed of lipids alone.

Emission spectra were recorded on a Perkin-Elmer Hitachi MPF-4 spectrofluorometer and the spectra were uncorrected.

Results

Figure 1 shows the fluorescence spectra of ANS incorporated in egg PC vesicles. As is well known, free ANS emits only very weak fluorescence peaking at around 530 nm in water. In our measurements, the emission spectrum of ANS in buffer alone coincided with the base line at the same sensitivity as used to measure the spectra shown in the figure. Furthermore, addition of 500 μg/ml PHMB to ANS solution (2.2 μM) in buffer alone caused no significant change in spectrum; no detectable emission at the same sensitivity as used for the spectra shown in Fig. 1. This means that increase in the intensity of fluorescence (I_F) observed on addition of PHMB occurs only in the ternary system, egg PC-PHMB-ANS.

Since the first report by Stryer on emission properties of ANS in various solvents,[9] it has been known that both λ_{max} and the fluorescence quantum yield (ϕ_F) are strongly dependent on the polarity of the solvent: with decreasing polarity, λ_{max} shifts to lower wavelengths and ϕ_F increases. Comparison of the fluorescence spectra of ANS embedded in the egg PC liposome and those in various solvents demonstrated that the binding site for ANS in the PC liposome has similar polarity to that of methanol. Similar spectra were observed when ANS molecules were incorporated in negatively-charged liposomes composed of egg PC and DCP (Fig. 2, a), though the intensity was somewhat reduced. These results indicate that the polarity of the binding site for ANS is not so different even when negatively-charged species are present in bilayer. When 210 μg/ml PHMB was added to the egg PC dispersion containing ANS prepared by the method (i), I_F of ANS was slightly increased: Increase of I_F at 460 nm was recognized, though the maximum still remained at 482 nm (Fig. 1, b). Addition of 200 μg/ml DAHB caused no change in I_F and λ_{max}.

Drastic change in spectrum was observed when PHMB was added to egg PC-DCP mixed liposome prepared by the method (i), which was negatively-charged at pH 7.4. Figure 2 shows the fluorescence spectra of ANS embedded in the egg PC-DCP mixed

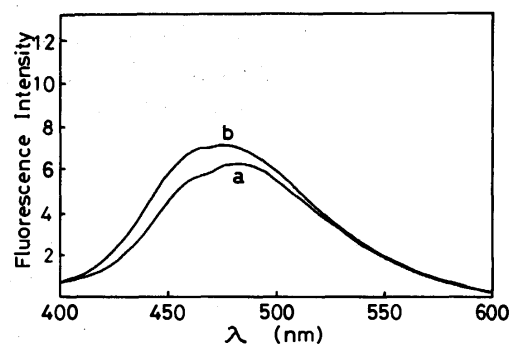

Fig. 1. Fluorescence spectra of ANS embedded in egg PC liposome in the absence and presence of PHMB: a, without PHMB; b, with 210 μg/ml PHMB added. The liposome solution was prepared by dispersing 0.8 mM egg PC in Tris-HCl buffer at pH 7.4; [ANS]= 2.2 μM, λ_{ex}=350 nm.

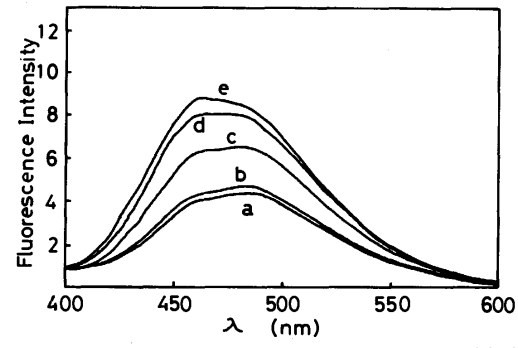

Fig. 2. Fluorescence spectra of ANS embedded in egg PC-DCP liposome in the presence of various concentrations of PHMB: [PHMB]=a, 0; b, 10.1 μg/ml; c, 50.4 μg/ml; d, 111 μg/ml; e, 170 μg/ml, λ_{ex}= 350 nm.
The liposome solution was prepared by dispersing 0.8 mM egg PC and 0.2 mM DCP in Tris-HCl buffer at pH 7.4; [ANS]=2.2 μM.

liposome ([egg PC]=0.8 mM, [DCP]=0.2 mM) in the presence of various concentrations of PHMB (0—170 μg/ml). With increasing concentration of PHMB, I_F increased gradually with gradual change in the shape of the spectrum. At 170 μg/ml of PHMB, λ_{max} is clearly changed to 460 nm. Addition of DAHB to the negatively-charged liposome composed of egg PC-DCP ([DAHB]=500 μg/ml) caused a slight increase of I_F, but to an insignificant extent. In Fig. 3 is depicted the increase of I_F as a function of the concentration of PHMB: the ratio $I_F/(I_F)_0$ at 460 nm was plotted against the concentration of PHMB, where I_F and $(I_F)_0$ are the fluorescence intensities at 460 nm in the presence and absence of PHMB, respectively. It can be readily seen from the figure that the increase of I_F at 460 nm is strongly dependent on the negative surface charge of the liposome. In the case of the neutral egg PC liposome, increase of I_F was very small and practically saturated at 50 μg/ml. On the other hand in the negatively-charged liposome composed of egg PC-DCP ([egg PC]=0.8 mM, [DCP]=0.09 mM) the $I_F/(I_F)_0$ increases with the concentration of PHMB added. Furthermore, much greater increase of I_F was ob-

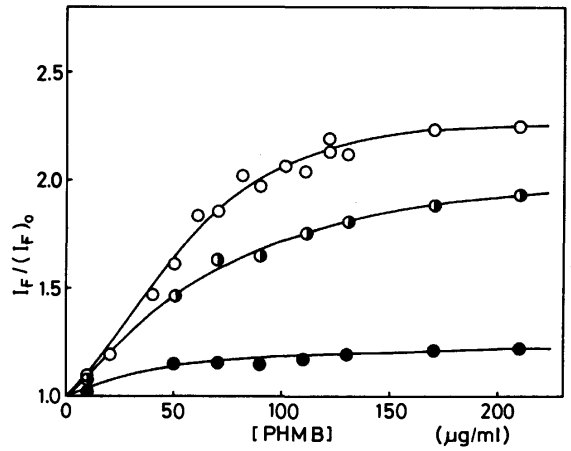

Fig. 3. Effect of PHMB on the fluorescence intensity of ANS embedded in various liposomes: (●), in egg PC liposome ([egg PC]=0.8 mM); (◑), in egg PC-DCP mixed liposome ([egg PC]=0.8 mM, [DCP]=0.09 mM); (○), in egg PC-DCP mixed liposome ([egg PC]=0.8 mM, [DCP]=0.2 mM). [ANS]=2.2 μM.

Table 1. Effect of Mg^{2+} and Ca^{2+} ions on fluorescence intensity of ANS embedded in egg PC liposome and in egg PC-DCP liposome

[ion]		I_F at 485 nm[a]	
	(μM)	egg PC	egg PC-DCP[b]
Mg^{2+}	0	1.00	1.00
	50	0.90	0.92
	99	0.89	0.91
	244	0.87	
Ca^{2+}	0	1.00	1.00
	5	0.96	0.99
	15	0.95	0.97
	49	0.94	0.99
	97	0.93	0.99
	239	0.93	0.97

a) Relative intensity; [ANS]=2.2 μM, λ_{ex}=350 nm. b) [egg PC]=0.8 mM, [DCP]=0.2 mM.

served in the more negatively-charged liposome which contained higher compositional ratio of DCP ([egg PC]=0.8 mM, [DCP]=0.2 mM).

The effects of Mg^{2+} and Ca^{2+} ions on fluorescence intensity of ANS embedded in the egg PC liposome and in the egg PC-DCP liposome were investigated ($MgSO_4$ and $CaSO_4$ were used). As seen in Table 1, unlike PHMB, these divalent cations rather lowered the intensity. These results clearly show that the enhancement of fluorescence intensity observed on adding PHMB is not just a sequence of electrostatic interaction between ANS and positive charges.

In order to investigate adsorption behavior of PHMB onto phospholipid membranes, incorporation of ANS molecules into liposomes without or with PHMB added was studied spectroscopically. In these experiments, addition of ANS was performed by the method (ii) (see Experimental). Higher concentrations of ANS gave rise to increased intensity of fluorescence, but no change in the shape of the spectrum, regardless of the presence of PHMB.

Benesi-Hildebrand type plots have been commonly used to estimate dissociation constants of complexes in many systems.[10,11] This type of plots is applicable to our system since only ANS molecules bound to liposomes contribute to the observed fluorescence intensity.[11]

$$\text{liposome}\cdot\text{ANS} \overset{K_D}{\rightleftarrows} \text{liposome} + \text{ANS}$$

$$\frac{1}{I_F} = \frac{1}{(I_F)_\infty} + \frac{K_D}{(I_F)_\infty}\cdot\frac{1}{[\text{ANS}]} \quad (1)$$

where [ANS] is the initial concentration of ANS (M); I_F, the fluorescence intensity of ANS associated with liposomes; $(I_F)_\infty$, I_F at the infinite concentration of ANS; K_D, the dissociation constant for liposome-ANS complex (M). The concentration of liposomes can be estimated from the concentration of phospholipids employed (1 mM) and the aggregation number of egg PC vesicles reported (N=2335)[12] as 0.4 μM. The concentrations of ANS used for this study were 3.6—18 μM, so that the concentration change in ANS due to association can by neglected. Thus Eq. 1 suffices for the present study. In Fig. 4 are shown $1/I_F$ *vs.* 1/[ANS] plots for the egg PC liposome-ANS system in the presence of various concentrations of PHMB. It is evident from the figure that with increasing concentration of PHMB the slope of the plots is reduced, whilst the intercept remains practically identical. Similar plots for the egg PC-DCP mixed liposome-ANS system are shown in Fig. 5. The same trend with respect to the PHMB concentration may be seen. From these plots, the dissociation constants were calculated and listed in Table 2.

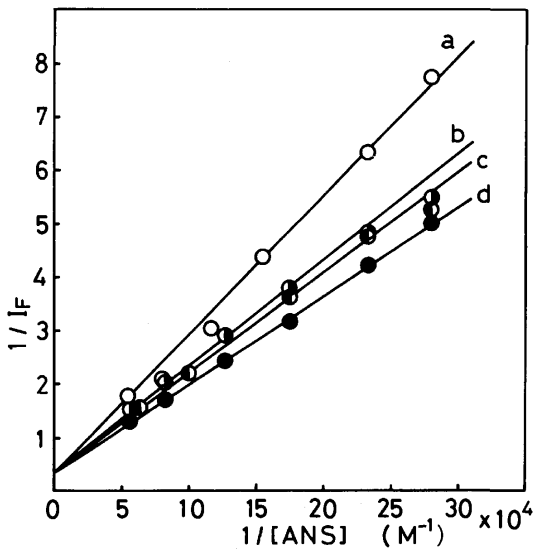

Fig. 4. $1/I_F$ *vs.* 1/[ANS] plots for egg PC-ANS complex in the presence of various concentrations of PHMB:
[PHMB]=a, 0; b, 20.3 μg/ml; c, 50.8 μg/ml; d, 102 μg/ml.
The liposome solution was prepared by dispersing 0.8 mM egg PC in Tris-HCl buffer at pH 7.4.

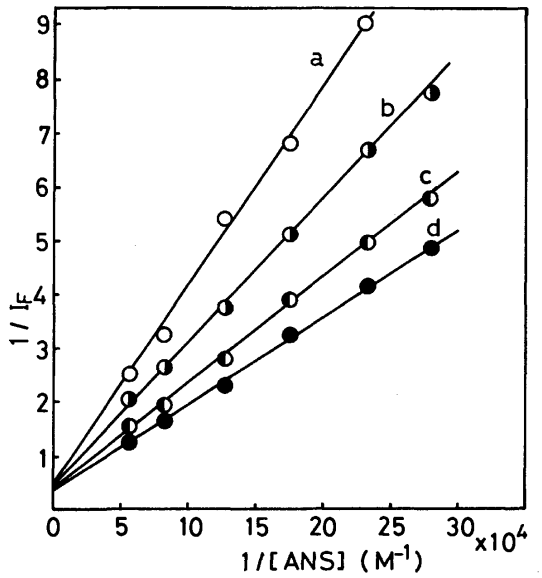

Fig. 5. $1/I_F$ *vs.* 1/[ANS] plots for egg PC-ANS complex in the presence of various concentrations of PHMB:
[PHMB]=a, 0; b, 20.3 μg/ml; c, 50.8 μg/ml; d, 102 μg/ml.
The liposome solution was prepared by dispersing 0.8 mM egg PC and 0.2 mM DCP in Tris-HCl buffer at pH 7.4.

TABLE 2. DISSOCIATION CONSTANTS FOR EGG PC-ANS AND EGG PC-DCP-ANS COMPLEXES IN THE ABSENCE AND PRESENCE OF PHMB[a)]

	[PHMB] added (μg/ml)			
	0	20.3	50.8	102
egg PC-ANS	6.7×10^{-5}	5.3×10^{-5}	5.0×10^{-5}	5.3×10^{-5}
egg PC-DCP-ANS	8.3×10^{-5}	6.3×10^{-5}	4.5×10^{-5}	3.8×10^{-5}

a) K_D (M) values obtained from the $1/I_F$ *vs.* 1/[ANS] plots shown in Figs. 4 and 5.

Discussion

The results obtained in this study clearly indicate that PHMB interacts more strongly with negatively-charged membranes than with a neutral membrane. This is quite reasonable from the fact that biguanides are strong bases (pK_1=10.5—11.5, pK_2=2—3) and are entirely monoprotonated at physiological pH.[13] Thus PHMB acts as a polyelectrolyte (polycation), and on account of the high positive charge density in its vicinity stronger interaction of PHMB with negatively-charged membranes is expected. The large difference between PHMB and DAHB in their interaction with membranes is most probably related to the great difference in their biocidal activity, DAHB being practically inactive.

NMR studies on the egg PC-ANS system have revealed that the amphipathic probe molecules are located at the interface region of the lipid dispersions where they interact with the head-groups of the lipids.[14] In the absence of PHMB, the lower intensity of fluorescence of ANS observed in the egg PC-DCP liposomes than that observed in the egg PC liposomes is evidently attributable to limited incorporation of the ANS molecules into the negatively-charged liposomes due to electrostatic repulsion. The larger K_D value estimated for the egg PC-DCP-ANS complex (at [PHMB]=0) is in support of this view quantitatively. The shift of λ_{max} observed on addition of PHMB to the egg PC-DCP liposomes can by no means be explained by simple increase in incorporation of ANS molecules in the presence of increased amount of PHMB, because the shape of the spectra remains unchanged when the concentration of ANS is varied at the fixed concentration of PHMB. Furthermore, it is evident from the control experiment already mentioned that direct interaction of ANS with PHMB does not contribute to the shift in λ_{max} and the increase in I_F under the experimental conditions employed to measure the spectra. A probable interpretation is as follows. PHMB is adsorbed on to the surface of the membranes where the sulfonato group of ANS is located. Then binding of a biguanide moiety to ANS as a counterion may take place. As a result, a less soluble complex of PHMB-ANS will be formed. This was evidenced by the formation of insoluble PHMB-ANS complex observed when 1% aqueous solutions of PHMB and ANS were mixed. The complex formation between PHMB and ANS will certainly produce less polar microenvironment around the bound ANS molecule in the membrane. The hydrophobic hexamethylene groups which link biguanide moiety in PHMB may contribute to give more hydrophobic environment to the bound ANS molecule. The effect of negatively-charged species (DCP) may be explained by two factors: (1) enhancement of surface adsorption of PHMB by electrostatic attraction and (2) endowment of additional "less polar" nature to the PHMB-ANS complex by participating in the complex as additional counterions of PHMB. These PHMB-ANS complexes are supposed to be solubilized in phospholipid bilayers.

The K_D values for the negatively-charged liposomes provide further support of the above view. The K_D values for the egg PC-DCP-ANS complex decrease with increasing concentration of PHMB added, whilst those for the egg PC-ANS complex remain nearly constant at the concentrations of PHMB higher than 20 μg/ml. These results seem to indicate that the quantity of PHMB adsorbed on to the neutral egg PC liposome is no longer increased above [PHMB]=20 μg/ml, whereas it increases with increasing concentration of PHMB added for the negatively-charged egg PC-DCP liposome. Actually, the lower values of K_D were obtained for the egg PC-DCP liposomes above [PHMB]=50 μg/ml, although below this concentration the K_D values for the negatively-charged liposomes were higher. Thus, the K_D value is a good indicator of adsorption behavior of PHMB onto the phospholipid bilayers. These results are consistent with preliminary results on electrophoretic mobility of the liposomes in

the presence of PHMB: The egg PC-DCP dispersion gave negative value of mobility and the addition of PHMB brought about reversal of the surface charge, giving positive values of mobility.[15]

In conclusion, our work has demonstrated that adsorption of PHMB takes place to a greater extent on to a negatively-charged membrane than on to a neutral membrane. This indicates that the adsorption site for PHMB is mainly negatively-charged species. In bacterial cytoplasmic membranes, there have been found many negatively-charged species such as membrane-bound proteins and acidic phospholipids.[16] Thus our work has provided reason for believing that the target sites for PHMB interaction are these negatively-charged species in intact bacterial membranes.

References

1) T. Ikeda and S. Tazuke, *Membrane*, **7**, 203 (1982).
2) A. Davies, M. Bentley, and B. S. Field, *J. Appl. Bacteriol.*, **31**, 448 (1968).
3) T. J. Franklin and G. A. Snow, "Biochemistry of Antimicrobial Action," Chapman and Hall (1981), Chapter 3.
4) G. K. Radda and J. Vanderkooi, *Biochim. Biophys. Acta*, **265**, 509 (1972).
5) R. H. Muesing and T. Nishida, *Biochemistry*, **10**, 2952 (1971).
6) H. Yoshino and O. Minari, *J. Biochem. (Tokyo)*, **87**, 1357 (1979).
7) T.-R. Hahn and P.-S. Song, *Biochemistry*, **20**, 2602 (1981).
8) G. K. Radda, "Biological Membranes," ed by D. S. Parson, Oxford University Press, London (1975), p. 96.
9) L. Stryer, *J. Mol. Biol.*, **13**, 482 (1965).
10) H. A. Benesi and J. H. Hildebrand, *J. Am. Chem. Soc.*, **71**, 2703 (1949).
11) H. Dodiuk, H. Kanety, and E.M. Kosower, *J. Phys. Chem.*, **83**, 515 (1979).
12) J. T. Mason and C. Huang, *Ann. N. Y. Acad. Sci.*, **308**, 29 (1978).
13) F. Kurzer and E. D. Pitchfork, *Fortschr. Chem. Forsch.*, **10**, 375 (1968).
14) G. L. Jendrasiak and T. N. Estep, *Chem. Phys. Lipids*, **18**, 181 (1977).
15) T. Ikeda, H. Yamaguchi, and S. Tazuke, to be published.
16) N. S. Gel'man, M. A. Lukoyanova, and D. N. Ostrouskii, *Biomembrane*, **6**, 27 (1975).

The BBGKY Equation in the Interaction Site Model for Polyatomic Molecular Fluids

Lloyd Lieh-shen LEE

School of Chemical Engineering and Materials Science, The University of Oklahoma, Norman, Oklahoma 73019, U.S.A.

(Received December 5, 1983)

We extend the atom-atom interaction site model to a fluid of polyatomic molecules in an external field by deriving the first Born-Bogoliubov-Green-Kirkwood-Yvon(BBGKY) hierarchy for a nonuniform system. It is shown that the intramolecular structure contributes to the density gradient as well as the intermolecular correlations. By invoking the mechanical equilibrium conditions for microscopic forces we also obtain new expression for the gradient of the pressure tensor in inhomogeneous fluids. The BBGKY equation provides a consistency check on any theories of the interaction site variety. An examination of the so-called RISM theory[1] of uniform fluids shows that the latter is inconsistent with respect to the BBGKY condition.

The interaction site model (ISM) for structured molecules in a uniform medium has been widely studied in literature.[1-17] It has been applied to the hard polyatomics, soft polyatomics[2-17] and to simulate real molecules (*e.g.* CO_2,[6] benzene[15,18] and water[7,11]). One of the popular theories is the so-called reference interaction site model[1] (RISM), based on certain approximation to the site-site direct correlation function (ss-dcf). Recently some inconsistencies inherent in RISM have been discovered[19-24] and modifications to it have been proposed.[23,24] It is desirable to have an alternative theoretical framework to RISM where exact relations are used. Here we present the formal results, the BBGKY hierarchy, for a nonuniform system using the ISM potential model. Applications will be postponed to a future study.

In section 2 we shall define the singlet (one-body) and pair (two-body) correlation functions in a grand canonical ensemble for polyatomic molecules (PM) in an external field. This picture may, say, correspond to the adsorption of structured molecules near a potential surface (the adsorbent phase). The first memeber of the Born-Bogoliubov-Green-Kirkwood-Yvon hierarchy is then derived. This equation is exact. We can interpret the results as specifying the linear momentum balance at the microscopic level.[25] From the equivalence of the mechanical equilibrium conditions with the BBGKY equation[26] we are able to express the pressure tensor in a nonuniform fluid in terms of the site-site correlation functions. This new expression can be contrasted with other known expressions of the pressure tensor.[27-30] Since the BBGKY equation is exact, any ISM theories concerning the correlation functions must satisfy this equation. Thus we have a consistency condition based on the BBGKY. We analyze the conventional RISM[1] theory in light of our new theoretical framework and discover that the Ornstein-Zernike-like equation given for the ss-dcf in the RISM is not exact. Its corrected form is one involving the incorporation of a Q factor (Section 5), whose form is explicitly given here.

The Grand Canonical Ensemble

In this section we give an explicit definition of the distribution function in a grand canonical ensemble. These explicit definitions will be found to be useful in the derivation of the BBGKY hierarchy.

For the simplicity in notation, we consider first a fluid of heteronuclear diatomics under the influence of an external potential, $U(.)$. There are N_a atoms of type a, and N_b, ($N_b=N_a$), atoms of type b. We distinguish the pair interaction, u $(\alpha_i\gamma_j)$, between atom α_i in molecule i and atom γ_j in a different molecule j (*i.e.* intermolecular potential) and the pair interaction, $\bar{u}$ (a_ib_j), between atom a and atom b of the same molecule i(*i.e.* intramolecular potential). We shall be brief in our descriptions.[31,32] Let V_N, ($N=N_a+N_b$), be the sum of the atom-atom potential energies,

$$V_N = \sum_{i<j}\sum_{\alpha,\gamma} u(\alpha_i\gamma_i) + \sum_k u(a_kb_k) \tag{2.1}$$

and W_N be the sum of the one-body energies,

$$W_N = \sum_k \sum_\alpha U(\alpha_k) \tag{2.2}$$

The grand canonical partition function, $\Xi[U]$, is given by

$$\Xi[U] \equiv \sum_{\underset{\sim}{N}\geq\underset{\sim}{0}} \frac{z_a^{N_a} z_b^{N_b}}{N_a!N_b!} \int_\Gamma d\{N_a\}d\{N_b\} \exp(-\beta V_N - \beta W_N), \tag{2.3}$$

where z_α is the activity of species α (α=a,b), β is the reciprocal temperature, $(kT)^{-1}$, k=the Boltzmann constant, $\{N_a\}$ is the set of position vectors, $\{a_1,a_2,..,a_{N_a}\}$, where a_i represents the distance vector, $\mathbf{r}_i^a$; and $d\{N_a\}$, the product of the differentials $da_1da_2\cdots$ Γ is the phase space appropriate for the diatomics (we exclude the regions of phase space where chemical decomposition of the diatomics takes place). The singlet density, $\rho_a^{(1)}$ $(a_1; U)$, and the pair densities, $\rho_{ab}^{(2)}$ $(a_1b_2; U)$, and $\bar{\rho}_{ab}$ $(a_1b_1; U)$ are defined as,

$$\rho_a^{(1)}(a_1;U) \equiv \frac{1}{\Xi[U]} \sum_{\underset{\sim}{N}>\underset{\sim}{1}} \frac{z_a^{N_a} z_b^{N_b}}{(N_a-1)!\,N_b!} \times \int_\Gamma d\{N_a-1\}d\{N_b-1\} \exp(-\beta V_N - \beta W_N), \tag{2.4}$$

$$\rho_{ab}^{(2)}(a_1b_2;U) \equiv \frac{1}{\Xi[U]} \sum_{\underset{\sim}{N}\geq\underset{\sim}{2}} \frac{z_a^{N_a} z_b^{N_b}}{(N_a-1)!\,N_b(N_b-2)!} \times \int_\Gamma d\{N_a-1\}d\{N_b-1\} \exp(-\beta V_N - \beta W_N) \tag{2.5}$$

and

$$\bar{\rho}^{(2)}_{ab}(a_1b_1;U) \equiv \frac{1}{\Xi[U]} \sum_{N\geq 2} \frac{z_a^{N_a} z_b^{N_b}}{(N_a-1)!\,N_b!} \times \int_\Gamma d\{N_a-1\} d\{N_b-1\} \exp(-\beta V_N - \beta W_N), \quad (2.6)$$

where the argument, $;U$, inside the functions denotes the nonuniformity (when $U=0$, we have the homogeneous case). The overbar, $\bar{}$, denotes the intramolecular quantities. We have not specified the nature of the inhomogeneity, U. It should assume the form appropriate for the problem at hand. For example, in planar adsorption U has the form of Lennard-Jones 10-4 or 9-3 interaction,[33] or of the Boltzmann averaged form.[34] For electrified walls, the Coulombic forces should be added. However, our equations are general. With these definitions at our disposal, we can proceed to the derivation of the BBGKY equation.

The BBGKY Equation

With the definition of the singlet density in (2.4), it is possible to derive the first equation in the BBGKY hierarcy for the ISM. The procedure follows the same line as in the monatomic (MA) case.[35-37] In order to avoid tedious notation we propose the following abbreviations:

$$e^{a}(\alpha_1) = \exp[-\beta U(\alpha_1)] \quad (3.1)$$

$$e^{+a}(\alpha_1) = \exp[+\beta U(\alpha_1)] \quad (3.2)$$

$$E^{ar}(\alpha_1\gamma_j) = \exp[-\beta v(\alpha_1\gamma_j)] \quad (3.3)$$

also,

$$\hat{S}_{(a_1)}(\cdots) \int db_1 da_2 db_2 \cdots da_{N_a} db_{N_b}(\cdots) \quad (3.4)$$

and

$$f^{N_a-1}_{N_b N_b-2} = \frac{z_a^{N_a} z_b^{N_b}}{(N_a-1)!N_b(N_b-2)!} \quad (3.5)$$

where v is the pair potential, which becomes $\bar{u}$ for intramolecular interaction or u for intermolecular interaction. Thus Eq. (2.4) can be written as

$$\rho^{(1)}_a(a_1;U) = \frac{1}{\Xi[U]} \sum f^{N_a-1}_{N_b} \hat{S}_{(a_1)} E^{ab}(a_1b_1) E^{ae}(a_1\varepsilon_2)\cdots e^{a}(a_1)\cdots \quad (3.6)$$

where we have exhibited three typical Boltzmann factors. Denoting the gradient operator with respect to $\mathbf{r}^1_a$ as ∇_1, we differentiate both sides of (3.6)

$$\nabla_1\rho^{(1)}_a(a_1;U) = \Xi[U]^{-1} \sum f^{N_a-1}_{N_b} \hat{S}_{(a_1)} \times \begin{bmatrix} -\nabla_1\beta\bar{u}(a_1b_1)E^{ab}(a_1b_1)\cdots \\ -\sum_\varepsilon (N_\varepsilon-1)\nabla_1\beta u(a_1\varepsilon_2)E^{ae}(a_1\varepsilon_2)\cdots \\ -\nabla_1\beta U(a_1)e^{a}(a_1)\cdots \end{bmatrix} \quad (3.7)$$

Applying the definitions of the singlet and pair densities, we obtain

$$\nabla_1\rho^{(1)}_a(a_1;U) = -\int db_1 \nabla_1\beta\bar{u}(a_1b_1)\cdot\bar{\rho}^{(2)}_{ab}(a_1b_1;U) - \sum_\varepsilon \int d\varepsilon_2 \nabla_1\beta u(a_1\varepsilon_2)\cdot\rho^{(2)}_{a\varepsilon}(a_1\varepsilon_2;U) - \nabla_1\beta U(a_1)\cdot\rho^{(1)}_a(a_1;U) \quad (3.8)$$

(BBGKY: Diatomics)

This is the first member of the BBGKY equation for heteronuclear diatomic molecules immersed in an external field. We observe the appearance of the intramolecular pair density, $\bar{\rho}^{(2)}$, as well as the usual intermolecular one, $\rho^{(2)}$. Higher members of the hierarchy can be similarly derived. Equation (3.8) similar to the monatomic case is not closed. In order to solve for the densities, a closure relation is needed. However, the relation given is exact. Any theory concerning the correlation functions must satisfy (3.8) in order to be consistent. In fact, the first member of the BBGKY hierarchy is known to express the force equilibrium among the molecules. The consistency check is then a check on the mechanical equilibrium.

The Pressure Tensor

From a microscopic linear momentum balance, one can show[25-27,38] that the mechanical equilibrium condition in a nonuniform fluid is given by

$$\sum_\nu \nabla_\nu P^{\mu\nu}(q) = -\sum \rho^{(1)}_a(q)\nabla_\mu U(q) \quad (4.1)$$

$$\mu,\nu = x, y, z$$

where $P^{\mu\nu}$ is the pressure tensor and U is the external potential. For structured molecules with non-central forces, $P^{\mu\nu}$ may be asymmetrical.[28-30] The well-known equivalence of the first BBGKY hierarchy and the mechanical equilibrium condition requires[26]

$$\sum_\nu \nabla_\nu\cdot\beta P^{\mu\nu}(q) = \sum_\alpha \nabla_\mu \rho^{(1)}_a(q;U) + \sum_\alpha\sum_\varepsilon \int d\varepsilon_1 \nabla_\mu\beta\bar{u}(q\varepsilon_1)\cdot\bar{\rho}^{(2)}_{a\varepsilon}(q\varepsilon_1;U)(1-\delta_{a\varepsilon}) + \sum_\alpha\sum_\varepsilon \int d\varepsilon_2 \nabla_\mu\beta u(q\varepsilon_2)\cdot\rho^{(2)}_{a\varepsilon}(q\varepsilon_2;U) \quad (4.2)$$

We obtain a microscopic description of the pressure tensor (*via* its gradient) in terms of the site-site correlation functions and the inter- and intramolecular potentials. (N.B. the factor $(1-\delta_{a\varepsilon})$, is to remove the one-atom autocorrelation, $\bar{\rho}^{(2)}_{aa}$.) It is obvious to see that the first term on the righthand side (RHS) is the kinetic contribution (ideal gas term), while the second term is the interaction contribution due to the internal forces, $\nabla\bar{u}(\alpha_i\gamma_j)$; and the third term due to the usual intermolecular forces, $\nabla u(\alpha_i\gamma_j)$. The pressure tensor $P^{\mu\nu}$ is known[25-27] to be not uniquely defined. Its gradient, ∇P, however, is well behaved,[26] *i.e.* the microscopic $P^{\mu\nu}$ is defined modulo a divergenceless quantity.[28] Since our system is nonuniform ($U\neq 0$), the pressure tensor is asymmetric (the singlet density is anisotropic in the orientation space and the angular velocity in general lacks local orientational rigidity.[28-30]) Even though we are in an atomic picture,[39] the intramolecular contribution (the second term) shall contribute to the asymmetry and to the so-called body torque.[26,29] In the limit $\bar{\rho}^{(2)}=0$, we recover the familiar pressure tensor expression as given by Irving and Kirkwood,[25] Bearman and Kirkwood,[40] and Davis and Scriven.[41]

Analyses of the RISM

We have mentioned in Sect. 3 that any theory on the site-site functions should satisfy the consistency conditions posed by (3.8). We now check the RISM. The original theory[1] on the site-site direct correlation function (ss-dcf), $c^{(2)}_{\alpha\gamma}(\alpha_i\gamma_j)$, $(i\neq j)$, can be written *via* a matrix form,

$$[\omega^{-1}\delta/\rho^{(1)}-c^{(2)}]_{\alpha\xi}[\delta\rho^{(1)}\omega+F^{(2)}]_{\xi\gamma}=\delta_{\alpha\gamma}\delta_D \tag{5.1}$$

(as we shall see shortly, this is not the exact Ornstein-Zernike (OZ) relation. Actually, it is an approximate form of the OZ relation). In (5.1), δ is the unit matrix (or the Kronecker delta, $\delta_{\alpha\gamma}$), $\delta_D(qr)$, is the Dirac delta function; ω is the intramolecular structure used in RISM[1] and is related to our intramolecular pair density, $\bar{\rho}^{(2)}$, *via*

$$\sum_\xi \rho^{(1)}_\alpha(\alpha)\delta_{\alpha\xi}\omega(\xi\gamma)=\rho^{(1)}_\alpha(\alpha)\delta_D(\alpha\gamma)\delta_{\alpha\gamma}+\bar{\rho}^{(2)}_{\alpha\gamma}(\alpha\gamma)(1-\delta_{\alpha\gamma}) \tag{5.2}$$

and $F^{(2)}$ is the truncated (Ursell) pair correlation function,

$$F^{(2)}(\alpha_i\gamma_j)=-\rho^{(1)}_\alpha(\alpha_j)\rho^{(1)}_\gamma(\gamma_j)+\rho^{(2)}_{\alpha\gamma}(\alpha_i\gamma_j), \tag{5.3}$$

In Eq. (5.1) the matrix multiplication conventions have been used (*i.e.* summation over repeated indices and integration over repeated arguments).

As was shown by Lebowitz and Percus[42-44] the basis of OZ is the matrix inverse properties of the two functional derivatives,

$$\frac{\delta(-\beta U)}{\delta\rho^{(1)}}\,\frac{\delta\rho^{(1)}}{\delta(-\beta U)}=\delta\delta_D \tag{5.4}$$

With the definition (2.4) for the singlet density, it is easy to show[45] that the derivative $\delta\rho^{(1)}/\delta(-\beta U)$ is

$$\frac{\delta\rho^{(1)}_\alpha(\alpha)}{\delta(-\beta U(\gamma))}=\sum_\xi \rho^{(1)}_\alpha(\alpha)\delta_{\alpha\xi}\omega(\xi\gamma)+F^{(2)}_{\alpha\gamma}(\alpha\gamma) \tag{5.5}$$

(Here we have suppressed the inhomogeneity, $;U$). Thus (5.5) accounts for the second factor on the LHS of (5.1). The first factor of (5.1) must correspond to the functional derivative $\delta(-\beta U)/\delta\rho^{(1)}$ in order to satisfy the exact mathematical condition (5.4). To estimate this so-called "compressibility" derivative,[46,47] we notice that Eq. (3.8) can be rearranged to give,

$$\begin{aligned}\nabla_1[-\beta U(a_1)] &= \nabla_1 \ln \rho^{(1)}_a(a_1)\\ &+\int db_1\nabla_1\beta u(a_1b_1)\bar{\rho}^{(2)}_{ab}(a_1b_1)/\rho^{(1)}_a(a_1)\\ &+\sum\int d\varepsilon_2\nabla_1\beta u(a_1\varepsilon_2)\rho^{(2)}_{a\varepsilon}(a_1\varepsilon_2)/\rho^{(1)}_a(a_1)\end{aligned} \tag{5.6}$$

Assuming the interchangeability of the two differential operators, ∇_1 and $\delta(.)/\delta\rho^{(1)}$ (see *e.g.* Percus[48]), we can functionally differentiate (5.6) to get,

$$\begin{aligned}\nabla_1\frac{\delta(-\beta U)}{\delta\rho^{(1)}} &= \nabla_1\frac{\delta\ln\rho^{(1)}}{\delta\rho^{(1)}}+\int db_1\nabla_1\beta\bar{u}\frac{\delta}{\delta\rho^{(1)}}\left(\frac{\bar{\rho}^{(2)}}{\rho^{(1)}}\right)\\ &+\sum_\xi\int d\xi_2\nabla_1\beta u\frac{\delta}{\delta\rho^{(1)}}\left(\frac{\rho^{(2)}}{\rho^{(1)}}\right)\end{aligned} \tag{5.7}$$

In comparison with the MA case, it is natural[49] to identify the ss-dcf which is the correlation function between atoms in different molecules as the last term on the RHS $\nabla_1 c^{(2)}_{\alpha\gamma}$ of (5.7):

$$\nabla_1 c^{(2)}_{\alpha\gamma}=-\sum_\xi\int d\xi_2\nabla_1\beta u\frac{\delta}{\delta\rho^{(1)}_\gamma}\left(\frac{\rho^{(2)}_{\alpha\xi}}{\rho^{(1)}_\alpha}\right) \tag{5.8}$$

The first term on the RHS (Eq. (5.7)) is due to the ideal gas (kinetic) contribution (see Eq. (4.2)); while the second term is due to contribution from intramolecular forces. We shall call this term $\mathcal{Q}$, *i.e.*

$$\nabla_1\mathcal{Q}\equiv\nabla_1\frac{\delta\ln\rho^{(1)}}{\delta\rho^{(1)}}+\int db_1\nabla_1\beta u\frac{\delta}{\delta\rho^{(1)}}\left(\frac{\bar{\rho}^{(2)}}{\rho^{(1)}}\right) \tag{5.9}$$

Comparing (5.7) with (5.4) and (5.1) shows that if the RISM assumption (5.1) were correct, the quantity $\mathcal{Q}$ in (5.9) should be given by

$$\mathcal{Q}\overset{?}{=}\omega^{-1}\left(\frac{\delta}{\rho^{(1)}}\right) \tag{5.10}$$

modulo a divergenceless quantity. The question mark on the " ? " sign is to question the equality of the two sides. A check of the cluster expansions[23,24] for ω shows that this equality does not hold beyond the first density term; *i.e.* the quantity in (5.9) is not the same as was assumed in RISM to be $\omega^{-1}(\delta/\rho^{(1)})$:

$$\begin{aligned}\omega^{-1}\left(\frac{\delta}{\rho^{(1)}}\right)&=\Delta^{-1}\begin{pmatrix}\frac{\delta_D}{\rho^{(1)}_a} & -\frac{\bar{\rho}^{(2)}_{ab}}{\rho^{(1)}_a\rho^{(1)}_b}\\ -\frac{\bar{\rho}^{(2)}_{ba}}{\rho^{(1)}_b\rho^{(1)}_a} & \frac{\delta_D}{\rho^{(1)}_b}\end{pmatrix}\\ &=\begin{pmatrix}\frac{\delta_D}{\rho^{(1)}_a}+\frac{\bar{\rho}^{(2)}_{ab}*\bar{\rho}^{(2)}_{ba}}{\rho^{(1)}_a\rho^{(1)}_a\rho^{(1)}_b}+\cdots & -\frac{\bar{\rho}^{(2)}_{ab}}{\rho^{(1)}_a\rho^{(1)}_b}-\cdots\\ -\frac{\bar{\rho}^{(2)}_{ba}}{\rho^{(1)}_b\rho^{(1)}_a}-\cdots & \frac{\delta_D}{\rho^{(1)}_b}+\frac{\rho^{(2)}_{ba}*\rho^{(2)}_{ab}}{\rho^{(1)}_b\rho^{(1)}_b\rho^{(1)}_a}+\cdots\end{pmatrix}\end{aligned} \tag{5.11}$$

where Δ is the normalization factor. Therefore the RISM assumption (5.1) does not satisfy the BBGKY condition. (There was an additional assumption on the ss-dcf in RISM,[50] which we shall not comment here.) We conclude that the relation (5.1) is not a true Ornstein-Zernike relation (we base our definition of OZ on Eq. (5.4)). And the conventional RISM theory is not an exact theory in more ways[19-24] than one.

Discussions

From explicit definitions of the correlation functions in the interaction site model we have derived for the first time the BBGKY equation in a nonuniform system. We specialize to the case of the heteronuclear diatomics. Higher polyatomics can be easily treated along analogous lines. Since the BBGKY equation is equivalent to the mechanical equilibrium condition, we are able to express the pressure tensor in terms of both intra- and inter-molecular correlation functions. These connections confirm that the gradients of the density and the external potential are related to microscopic force balances. Therefore any equations relating the many-body distribution functions using the ISM approach much satisfy this microscopic force balance condition. We examined the reference interaction site model and found that its proposed Ornstein-Zernike-

like equation is not consistent with the general form of the BBGKY equation.

In the monatomic case, other types of hierarchy were given for the gradient of the singlet density, *e.g.*

$$\nabla_1\rho^{(1)} = \rho^{(1)}\nabla_1(-\beta U) + \rho^{(1)}\int \mathrm{d}2\, c^{(2)}\nabla_2\rho^{(1)} \qquad (6.1)$$

as given by Lovett *et al.*[51] (See also[44,52,53]). Their implications in the polyatomic case shall also be investigated in the future.

In the MA Henderson[38] has derived the following pressure gradient relation based on the potential distribution theorem of Widom,[54]

$$\sum_\nu \nabla\beta P^{\mu\nu} = \rho^{(1)}\nabla \ln \rho^{(1)} - \rho^{(1)}\nabla c^{(1)}, \quad \text{(MA)} \qquad (6.2)$$

where $c^{(1)}$ is the one-body direct correlation function. Since the two-body dcf, $c^{(2)}$, can be obtained from $c^{(1)}$ *via* the functional differentiation[55]

$$c^{(2)}(\mathrm{r}, \mathrm{r}') = \frac{\delta c^{(1)}(\mathrm{r})}{\delta\rho^{(1)}(\mathrm{r}')}\,, \quad \text{(MA)} \qquad (6.3)$$

we could differentiate (6.2) with respect to $(\delta/\delta\rho^{(1)})$ (after interchanging the order with the gradient ∇)[48] to obtain

$$\nabla c^{(1)} = -\sum_\nu \nabla\frac{\delta}{\delta\rho^{(1)}}\left(\frac{\beta P_c^{\mu\nu}}{\rho^{(1)}}\right), \quad \text{(MA)} \qquad (6.4)$$

where $P_c^{\mu\nu}$ is the configurational part of the pressure tensor. Equation (6.4) bears striking resemblance to our Eq. (5.8) after the substitution of (4.2). In this respect the monatomics exhibit similar behavior as our diatomic case. (In fact our diatomic equations should reduce to the MA case when the intramolecular potential is set equal to the intermolecular one; or when $\bar{\rho}^{(2)}=0$). In fact Eq. (6.4) lends support to our identification (5.8). The potential distribution theorem has played an important role in the computer simulations of the chemical potential in MA.[56-62] Its extension to polyatomics is under investigation.

References

1) D. Chandler and H. C. Andersen, *J. Chem. Phys.*, **57**, 1930 (1972) and later works.
2) K. Kojima and K. Arakawa, *Bull. Chem. Soc. Jpn.*, **51**, 1977 (1978).
3) D. E. Sullivan, R. Barker, C. G. Gray, W. B. Streett, and K. E. Gubbins, *Mol. Phys.*, **44**, 597 (1981).
4) B. C. Freasier, D. Jolly, and R. J. Bearman, *Mol. Phys.*, **32**, 1463 (1976).
5) G. P. Morris, J. W. Perram, and E. R. Smith, *Mol. Phys.*, **38**, 465 (1979).
6) C. S. Murthy, K. Singer, and I. R. McDonald, *Mol. Phys.*, **44**, 135 (1981).
7) G. P. Morris and J. W. Perram, *Mol. Phys.*, **43**, 669 (1981).
8) E. Johnson and R. P. Hazoumé, *J. Chem. Phys.*, **70**, 1599 (1979).
9) A. Habenschuss, E. Johnson, and A. H. Narten, *J. Chem. Phys.*, **74**, 5234 (1981).
10) F. Hirata, P. J. Rossky, *Chem. Phys. Lett.*, **83**, 329 (1981).
11) B. M. Pettitt and P. J. Rossky, *J. Chem. Phys.*, **77**, 1451 (1982).
12) F. Hirata, P. J. Rossky, and B. M. Pettitt, *J. Chem. Phys.*, **78**, 4133 (1983).
13) F. Hirata, B. M. Pettitt, and P. J. Rossky, *J. Chem. Phys.*, **77**, 509 (1982).
14) P. A. Monson, *Mol. Phys.*, **47**, 435 (1982).
15) M. Claessens, M. Ferrario, and J.-P. Ryckaert, *Mol. Phys.*, **50**, 217 (1983).
16) G. A. Chapela and S. E. Martinez-Casas, *Mol. Phys.*, **50**, 129 (1983).
17) S. M. Thompson, K. E. Gubbins, E. E. Sullivan, and C. G. Gray, *Mol. Phys.*, **51**, 21 (1984).
18) D. J. Evans and R. O. Watts, *Mol. Phys.*, **32**, 93 (1976).
19) D. E. Sullivan and C. G. Gray, *Mol. Phys.*, **42**, 443 (1981).
20) P. T. Cummings and G. Stell, *Mol. Phys.*, **44**, 529 (1981).
21) P. T. Cummings and G. Stell, *Mol. Phys.*, **46**, 383 (1982).
22) P. T. Cummings and D. E. Sullivan, *Mol. Phys.*, **46**, 665 (1982).
23) D. Chandler, R. Silbey, and B. M. Ladanyi, *Mol. Phys.*, **46**, 1335 (1982).
24) D. Chandler, C. G. Joslin, and J. M. Deutch, *Mol. Phys.*, **47**, 871 (1982).
25) See *e.g.* J. H. Irving and J. G. Kirkwood, *J. Chem. Phys.*, **18**, 817 (1950).
26) P. Schofield and J. R. Henderson, *Proc. R. Soc. Londan, Ser A*, **379**, 231 (1982).
27) A. Harasima, *Adv. Chem. Phys.*, **1**, 203 (1958).
28) D. J. Evans, *Mol. Phys.*, **32**, 1171 (1976).
29) D. J. Evans and W. B. Streett, *Mol. Phys.*, **36**, 161 (1978).
30) D. J. Evans, *J. Stat. Phys.*, **20**, 547 (1979).
31) For details, see *e.g.* D. Chandler and L. R. Pratt, *J. Chem. Phys.*, **65**, 2925 (1976); **66**, 147 (1977).
32) E. W. Montroll and J. L. Lebowitz, ed., "The Liquid State of Matter: Fluids, Simple and Complex," Vol. 8, North Holland, Amsterdam (1982).
33) W. A. Steele, "The Interaction of Gases with Solid Surfaces," Pergamon, Oxford (1974).
34) F. F. Abraham, *J. Chem. Phys.*, **68**, 3713 (1978).
35) J. Yvon, *J. Phys., Radium*, **19**, 733 (1958).
36) R. Balescu, "Equilibrium and Nonequilibrium Statistical Mechanics" Wiley, New York (1975).
37) S. Toxvaerd, *Mol. Phys.*, **26**, 91 (1973).
38) J. R. Henderson, *Mol. Phys.*, **48**, 715 (1983).
39) R. D. Omsted and R. F. Snider, *J. Chem. Phys.*, **65**, 3407, 3423 (1976).
40) R. J. Bearman and J. G. Kirkwood, *J. Chem. Phys.*, **28**, 136 (1958).
41) H. T. Davis and L. E. Scriven, *Adv. Chem. Phys.*, **49**, 357 (1982).
42) J. L. Lebowitz and J. K. Percus, *Phys. Rev.*, **122**, 1675 (1961);
43) J. L. Lebowitz and J. K. Percus, *J. Math. Phys.*, **4**, 116, 248, 1495 (1963).
44) J. K. Percus "The Equilibrium Theory of Classical Fluids", ed by H. L. Frisch and J. L. Lebowitz, Benjamin, New York (1964).
45) D. Chandler, *J. Chem. Phys.*, **59**, 2742 (1973).
46) J. G. Kirkwood and F. P. Buff, *J. Chem. Phys.*, **19**, 774 (1951).
47) F. P. Buff and R. Brout, *J. Chem. Phys.*, **23**, 458 (1955).
48) See, *e.g.*, Eq.(6.19) in J. K. Percus, Ref. 44.
49) See, *e.g.* Section 6, Discussions; and L. L. Lee, *Physica*, **69**, 627 (1973).
50) See, *e.g.*, Eq.(5.9a), of Ref. 45.
51) R. Lovett, C. Y. Mou, and F. P. Buff, *J. Chem. Phys.*, **65**, 570 (1976).

52) M. S. Wertheim, *J. Chem. Phys.*, **65**, 2377 (1976).
53) S. Sokolowski, *Mol. Phys.*, **44**, 557 (1981).
54) B. Widom, *J. Chem. Phys.*, **39**, 2808 (1963).
55) See, *e.g.*, D. Nicholson and N. G. Parsonage, "Computer Simulation and the Statistical Mechanics of Adsorption," Academic Press, New York (1982), p. 113.
56) E. Byckling, *Physica*, **27**, 1030 (1961).
57) J. G. Powles, *Chem. Phys. Lett.*, **86**, 335 (1982).
58) J. G. Powles, W. A. B. Evans, and N. Quirke, *Mol. Phys.*, **40**, 1347 (1982).
59) D. J. Adams, *Mol. Phys.*, **28**, 1241 (1974).
60) M. Fixman, *J. Chem. Phys.*, **78**, 4223 (1983).
61) K. S. Shing and K. E. Gubbins, *Mol. Phys.*, **46**, 1109 (1982).
62) J. S. Rowlinson and B. Widom, "Molecular Theory of Capillarity," Clarendon, Oxford (1982).

Thermal Investigations of 1,4-Butanediamine Complexes of Nickel(II) in the Solid Phase

Goutam De and Nirmalendu Ray Chaudhuri*

Department of Inorganic Chemistry, Indian Association for the Cultivation of Science, Calcutta 700032, India

(Received December 8, 1983)

$[NiL_3]Cl_2 \cdot H_2O$, $[NiL_2(H_2O)_2]Br_2$, and $[NiL_2(NCS)_2]$ (L= 1,4-butanediamine) have been synthesized and their thermal investigations have been carried out. $[Ni_2L_3Cl_4]$, $[NiLCl_2]$, $[Ni_4L_3Br_8]$, and $[NiL(NCS)_2]$ have been synthesized pyrolytically in solid phase by temperature arrest technique from their corresponding parent diamine complexes. All the parent tris and bis(diamine)complexes possess O_h geometry. $[NiLCl_2]$ possesses T_d geometry, whereas, $[NiL(NCS)_2]$ possesses O_h though 1,4-butanediamine is chelated in both of these mono-(diamine) complexes. Thiocyanate is found to be bridged in $[NiL(NCS)_2]$. The probable mechanistic paths of decomposition of these diamine complexes have been propsoed.

Chelating and bridging bidentate character of 1,4-butanediamine (L) in metal complexes are well documented in literature.[1-3] Metal complex having unidentate diamine is also known.[4] Synthesis of $[NiL_3]^{2+}$ is not yet reported. But tris chelate complexes like $[CoL_3]^{3+}$ are known, where L attains seven-membered chelate rings and possesses chair conformations.[5,6] Recently, some 1,4-butanediamine complexes are being used for the preparation of macrocyclic complexes.[7]

We have recently reported a series of thermal investigations of metal 1,2-ethanediamine and 1,3-propanediamine complexes in the solid phase.[8-12] In these investigations we synthesized a good number of novel metal diamine complexes. Besides these, thermally induced structural and conformational changes in nickel(II) diamine complexes were observed by us.[13]

The purpose of this paper is to report the thermochemical studies of nickel diamine complexes having seven-membered chelate rings and to compare their decomposition patterns with those of five and six-membered chelate complexes.

Experimental

The metal salts used were all of A.R. grade purity. 1,4-Butanediamine was supplied from Fluka AG, Switzerland.

Preparation: $[NiL_3]Cl_2 \cdot H_2O$ (**1**), $[NiL_2(H_2O)_2]Br_2$ (**2**), and $[NiL_2(NCS)_2]$ (**3**).

1,4-Butanediamine (L) (3—4 mmol) was added to the ethanolic solution of nickel salt (1 mmol) dropwise with stirring. On mixing immediate separation of complex took place. The resulting heterogeneous mixture was stirred for ≈10 h and the desired complexes were collected by filtration, washed thoroughly with ethanol and dried over fused $CaCl_2$ desiccator.

$[Ni_2L_3Cl_4]$ (**1A**): This was synthesized by keeping the complex (**1**) at ≈185 °C in a nitrogen atmosphere. The thermolysis was stopped when no more diamine was lost as evident by getting a constant weight.

$[NiLCl_2]$ (**1B**): This was synthesized following the method adopted for the synthesis of complex (**1A**) from complex (**1**) at ≈245 °C.

$[NiL_2Br_2]$ (**2A**): This was synthesized by heating the complex (**2**) upto ≈135 °C.

$[Ni_4L_3Br_8]$ (**2B**): This was synthesized from complex (**2**) at ≈260 °C by the similar procedure to that adopted for the synthesis of complex (**1A**).

$[NiL(NCS)_2]$ (**3A**): This was also synthesized from complex (**3**) at ≈235 °C by the similar procedure to that adopted for the synthesis of complex (**1A**).

Molar conductance data of these complexes could not be taken since these complexes decompose in water and are insoluble in all the available solvents.

Analytical, spectral band maxima and magnetic data are shown in Table 1.

The apparatus employed for carrying out thermal analysis is the same as reported earlier.[8,9] Table 2 lists the thermal

Table 1. Analytical, magnetic and electronic spectral data of Ni^{II} 1,4-butanediamine(L) complexes

Compound		Color	Elemental analyses/%[a]			μ_{eff} (B.M.)	λ_{max} (nm)
			Nickel	Nitrogen	Halogen/Sulfur		
$[NiL_3]Cl_2 \cdot H_2O$	(**1**)	Blue	14.3(14.2)	20.5(20.4)	17.0(17.2)	3.32	600, 370
$[Ni_2L_3Cl_4]$[b]	(**1A**)	Green	22.3(22.4)	16.1(16.0)	26.9(27.1)	3.29	670, ≈470(sh), 400
$[NiLCl_2]$[b]	(**1B**)	Greenish yellow	26.9(26.9)	12.9(12.8)	32.2(32.6)	3.50	680, ≈530(sh), ≈440(sh), 400
$[NiL_2(H_2O)_2]Br_2$	(**2**)	Light blue	13.6(13.6)	12.9(13.0)	36.7(37.1)	3.20	580, 365
$[NiL_2Br_2]$[b]	(**2A**)	Light blue	14.8(14.8)	14.2(14.1)	40.2(40.5)	3.22	580, 364
$[Ni_4L_3Br_8]$[b]	(**2B**)	Greenish yellow	20.5(20.6)	7.3(7.3)	56.0(56.1)	3.56	≈740(sh), 685, ≈520(sh), ≈460(sh), 405
$[NiL_2(NCS)_2]$	(**3**)	Light blue	16.7(16.7)	23.9(23.9)	18.0(18.2)	3.23	580, 370
$[NiL(NCS)_2]$[b]	(**3A**)	Blue black	22.3(22.3)	21.1(21.3)	24.2(24.3)	3.16	≈710(sh), 580 ≈470(sh), 350

a) Figures in parentheses are the calculated values. b) Compounds synthesized in the solid state.

Table 2. Thermal parameters of Ni^{II} 1,4-butanediamine(L) complexes

Decomposition reaction	Temperature range/°C	DTA peak temperature/°C	
		Endo	Exo
$[NiL_3]Cl_2 \cdot H_2O \rightarrow [NiL_3]Cl_2$	50— 85	80	—
$[NiL_3]Cl_2 \rightarrow [NiL_2Cl_2]$	135—185	180	—
$[NiL_2Cl_2] \rightarrow [Ni_2L_3Cl_4]$	185—205	200	—
$[Ni_2L_3Cl_4] \rightarrow [NiLCl_2]$	215—245	240	—
$[NiLCl_2] \rightarrow [Ni_2LCl_4]$	285—315	—	314
$[Ni_2LCl_4] \rightarrow NiCl_2$	315—375	—	335, 360
$[NiL_2(H_2O)_2]Br_2 \rightarrow [NiL_2Br_2]$	75—130	105, 120	—
$[NiL_2Br_2] \rightarrow [Ni_4L_3Br_8]$	155—260	178, 202, 250	—
$[Ni_4L_3Br_8] \rightarrow NiBr_2$	275—345	—	284, 312 332, 340
$[NiL_2(NCS)_2] \rightarrow [NiL(NCS)_2]$	175—230	224	—
$[NiL(NCS)_2] \rightarrow Ni(SCN)_2$	280—340	—	270, 280

data.

Infrared spectra in KBr (4000—400 cm^{-1}) and in polythene discs (400—250 cm^{-1}, in some cases) were recorded using a Beckman IR-20A and Perkin-Elmer 597 IR spectrophotometers respectively and the corresponding data were given in Table 3.

Results

$[NiL_3]Cl_2 \cdot H_2O$ (**1**) becomes anhydrous at 85 °C (Fig. 1, Table 2) showing an endothermic peak at 80 °C. The blue-colored anhydrous species starts decomposition at 135 °C and transforms to $[Ni_2L_3Cl_4]$ at 205 °C through the formation of nonisolable intermediate, $[NiL_2Cl_2]$. The derived $[Ni_2L_3Cl_4]$ on further heating results $[NiLCl_2]$ at 245 °C. The unis(diamine) species is stable upto 285 °C and then decomposes to $NiCl_2$ through the formation of nonisolable intermediate, $[Ni_2LCl_4]$ at 315 °C. DTA curve shows three endotherms for the elimination of first two moles of diamine and three exotherms for the elimination of residual diamine.

$[NiL_2(H_2O)_2]Br_2$ (**2**) starts deaquation (Fig. 2, Table 2) at 75 °C and becomes deaquated completely at 130 °C showing two overlapping endotherms in the DTA profile. The deaquated species starts deamination at 155 °C and transforms to $[Ni_4L_3Br_8]$ at 260 °C, through the formation of nonisolable intermediates. The derived $[Ni_4L_3Br_8]$ starts decomposition at 275 °C and transforms to $NiBr_2$ at 345 °C. The corresponding DTA curve shows three endotherms for elimination of 1.25 mole of diamine and four exotherms overlapping to each other for the elimination of residual diamine.

$[NiL_2(NCS)_2]$ starts deamination (Fig. 2, Table 2) at 175 °C and generates thermally stable $[NiL(NCS)_2]$ at 230 °C. Unis(diamine) species starts decomposition at 280 °C and transforms to $Ni(SCN)_2$ at 340 °C. The DTA curve shows initially an endotherm followed by an exotherm for the elimination of first molecule of diamine. It shows two overlapping exotherms for the elimination of last molecule of diamine.

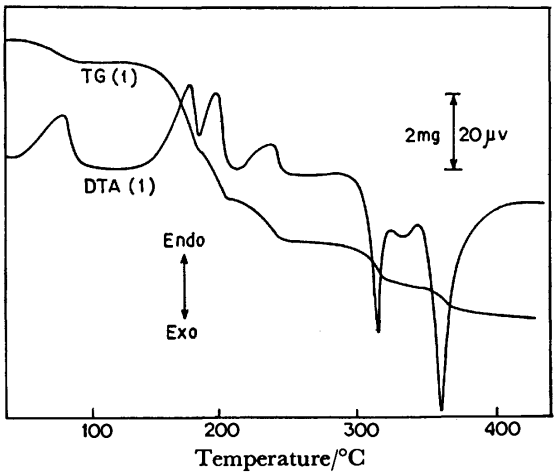

Fig. 1. Thermal curves of $[NiL_3]Cl_2 \cdot H_2O$ (**1**) sample mass, 11.60 mg.

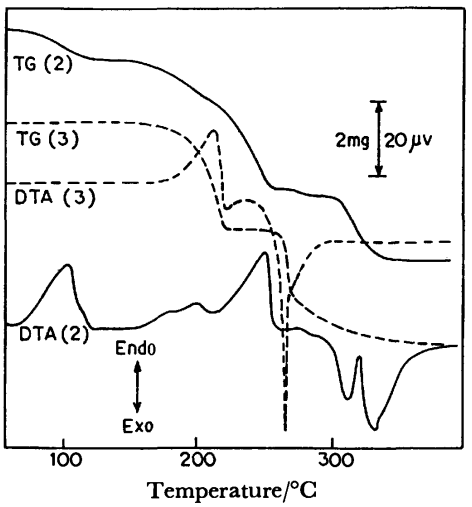

Fig. 2. Thermal curves of $[NiL_2(H_2O)_2]Br_2$ (**2**) (——), sample mass 12.86 mg and $[NiL_2(NCS)_2]$ (**3**) (- - -), sample mass 11.50 mg.

Discussion

Possession of bands at 3300, 3245, 3220, and 3140 cm^{-1} due to $\nu(NH_2)$ and at 2945, 2940, 2860, and 2850 cm^{-1} due to $\nu(CH_2)$ in IR spectrum (Table 3) of $[NiL_3]Cl_2 \cdot H_2O$ (**1**) is well consistent with chela-

Table 3. IR Spectral data (cm^{-1}) of Ni^{II} 1,4-butanediamine(L) complexes in KBr

Compound	Assignments										
	$\nu(NH_2)$	$\nu(CH_2)$	$\nu(CN)$	$\delta(NH_2)$	$\delta(CH_2)$	$\rho_w(CH_2)$	$\tau(NH_2)+\rho_w(NH_2)+\tau(CH_2)$	Stretching Vibrations of skeleton ν(C-N)+ν(C-C)	$\rho_r(CH_2)$	ν(CS)/ $\rho_r(H_2O)$	$\rho_r(CH_2)+\nu$(M-N)
$[NiL_3]Cl_2\cdot H_2O$[a]	3300m, 3245sh, 3220 s, 3140ms	2945ms, 2940ms, 2860m, 2850m	—	1595 s, 1550 sh	1458m, 1440 w, 1435sh	1370 sh, 1360 mbr	1260m, 1250 sh, 1220vw, 1176m, 1145 s	1118 s, 1090 w, 1065 sh, 1030 s	950 s, 920 w, 730 w	—	590sbr
$[Ni_2L_3Cl_4]$	3315 w, 3265 s, 3230 s, 3180sh, 3140m	2945m, 2920sh, 2910m, 2865m, 2845m	—	1590 s, 1575sh, 1550sh	1470sh, 1452m, 1445sh, 1435sh	1395 w, 1385 w, 1362 w	1335vw, 1306vw, 1250vw, 1215m, 1182m, 1158ms	1125m, 1110sh, 1092 s, 1068m, 1045 s, 1030m, 1010 s, 990sh, 965sh	950m, 920vw, 825vw, 730 w	—	630sh, 600sbr
$[NiLCl_2]$	3295m, 3250 s, 3200sh, 3160 w	2975 w, 2935 w, 2930m, 2890 w, 2862vw	—	1590 s, 1550sh	1460m, 1450sh	1360m, 1355 w	1270sh, 1175 s, 1132vs	1112sh, 1050sh, 1040 s	958 s, 720 w	—	645 w, 580sh, 550 s
$[NiL_2(H_2O)_2]Br_2$[b]	3330sh, 3296 s, 3277sh, 3240 s, 3160m	2975m, 2950m, 2930m, 2890 w, 2880sh, 2860m	—	1592 s, 1565m, 1545m, 1532sh, 1500mbr	1472sh, 1462m, 1450 w, 1435m	1390sh, 1380m, 1347m	1320sh, 1290 w, 1255m, 1235vw, 1220vw, 1200 w, 1172m, 1135 s	1110m, 1105sh, 1090m, 1056 w, 1045 w, 1010 s, 995 s, 967m	952m, 940 w, 905 w, 895 w, 855vw, 842vw, 815 w, 800 w, 755sh, 740sh	710 w	650vw, 618ms, 560m
$[NiL_2Br_2]$	3340vw, 3280 w, 3230 s, 3160m	2970sh, 2940m, 2920m, 2890sh, 2880m, 2855sh	—	1585 s, 1575m, 1562sh, 1540m, 1530 w, 1500mbr	1480sh, 1460sh, 1450m, 1445sh, 1430 w	1390sh, 1375m, 1860m, 1345sh	1335 w, 1310sh, 1255wbr, 1215m, 1188 s, 1145sh, 1140m	1100sh, 1085 s, 1044m, 1030sh, 1012m, 1000m, 980vw	955 w, 938 w, 918vw, 875 w, 815sh, 795wbr, 750sh, 735vw	—	670wbr, 605ms, 560m
$[Ni_4L_3Br_8]$	3496 w, 3290m, 3240m, 3210vw, 3190m, 3150vw, 3070wbr, 3020wbr	2965m, 2930m, 2880 w, 2860 w	—	1580 s, 1570m, 1545sh	1458m, 1438m, 1430sh	1395vw, 1363 w, 1355sh	1335 w, 1272 w, 1255m, 1160sh, 1130 s	1120sh, 1100m, 1045sh, 1038m, 1020vw, 1010vw, 960sh	955 s, 905 w, 890vw, 858m, 750vbr	—	630m, 605 w, 540 s
$[NiL_2(NCS)_2]$	3308m, 3260m, 3240sh, 3218m, 3129 w	2945sh, 2930m, 2915sh, 2870m, 2840 w	2095vs	1580 s, 1576sh, 1550sh	1450m, 1445sh, 1435vw, 1425sh	1360sh, 1350m	1235vw, 1250m, 1150sh, 1120vw	1120 s, 1075m, 1032 s	945 s, 920 w, 895vw, 722 w	770 w	595 s, 555 s
$[NiL(NCS)_2]$	3318m, 3260m, 3225sh, 3138 w	2950m, 2937m, 2920sh, 2875m, 2840 w	2160wsh, 2130 s, 2120 s, 2080sh, 2060sh	1575sh, 1560 s, 1550m,	1452m, 1445sh, 1432vw, 1425sh	1360m, 1350 w,	1245m, 1220vw, 1140sh	1100 s, 1072sh, 1067sh, 1045m, 1040sh, 1015 w	955 s, 935 w, 910vw, 898vw, 722 w	763 w	590sh, 520 s

vs=very strong, s=strong, ms=medium strong, m=meduim, br=broad, w=weak, vw=very weak, sh=shoulder. a): Compound gives bands at 3240 ms and 3360 ms for ν(OH) and at 1630 sh for δ(HOH). b): Compound gives bands at 3400 sh and 3370 sh for ν(OH) and at 1655 ms and 1645 sh for δ(HOH).

tion character of the ligand.[8-13] Literature shows less number of IR bands due to $\nu(NH_2)$ and $\nu(CH_2)$ for the complexes, where diamine acts as bridging bidentate ligand.[2] Morever, the IR spectrum of complex (**1**) is quite similar to the IR spectrum of $[Ni(tn)_3]Cl_2 \cdot 2H_2O$ (tn=1,3-propanediamine),[9] which also indicates the chelation character of the ligand in the complex.

We are not able to isolate the bis(diamine) species from complex (**1**) by temperature arrest technique owing to its thermal instability. So it is very difficult to suggest the actual configuration of the bis species. But the isolation of *cis* bis(diamine) complexes from $[M(en)_3]Cl_3$ [M=Co(III) and Cr(III)],[14,15] $[Ni(en)_3]Cl_2$ and $[Ni(tn)_3]Cl_2$[9] hint the formation of *cis* bis-(diamine) species here. Decomposition of $[NiL_3]Cl_2$ is different from the corresponding tris chelate complexes of 1,2-ethanediamine and 1,3-propanediamine as it generates $[Ni_2L_3Cl_4]$ (**1A**) upon heating. The IR spectrum (Table 3) of complex (**1A**) shows some additional bands in the regions of stretching (ν), bending (δ), wagging (ρ_w), twisting (τ) vibrations of NH_2 and CH_2 and stretching vibrations of skeleton ν(C–N) and ν(C–C) along with the other bands responsible for chelation character of diamine in comparison to the IR spectrum of complex (**1**). This observation suggests the chelating as well as bridging character of the ligand in complex (**1A**). Two probable structures are suggested (Structures 1* and 1; Scheme 1) for the complex (**1A**). It is rather difficult to say which structure actually displays here. Spectral and magnetic data of the complex cannot distinguish the structures clearly. However, electronic spectral band positions (Fig. 3) in 800—300 nm and their relative intensity difference may suggest the formation of *tbp* geometry.[16] If O_h geometry would be considered for the complex (**1A**), the relative intensity of $\nu_2[^3A_2 \rightarrow {}^3T_1(F)]$ and $\nu_3[^3A_2 \rightarrow {}^3T_1(P)]$ bands in mull spectra would not differ much.[8,9,13]

Scheme 1 clarifies that formation of $[NiLCl_2]$ (**1B**) occurs either from complex (**1A**)(O_h) or from complex (**1A**)(*tbp*). Both the cases seem to be feasible. But if we have octahedrally symmetrical $[Ni_2L_3Cl_4]$, then cleavage of bridging chlorine as well as ligand elimination (Scheme 1) would occur simultaneously during heating, which is rather complicated path. On the contrary, if the complex (**1A**) possesses *tbp* geometry then only ligand elimination would occur for affording $[NiLCl_2]$. In this context single endothermic DTA

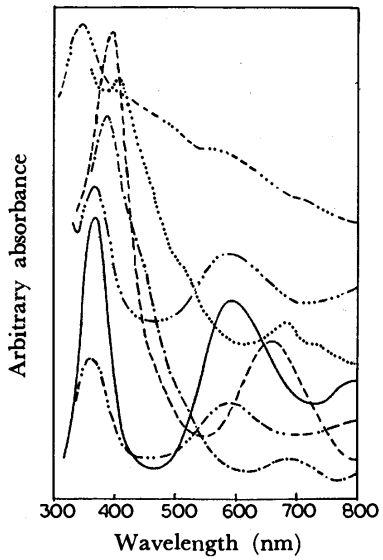

Fig. 3. Electronic mull spectra of $[NiL_3]Cl_2 \cdot H_2O$(**1**) (——), $[Ni_2L_3Cl_4]$ (**1A**) (- - -), $[NiLCl_2]$ (**1B**) (-·-·-), $[NiL_2(H_2O)_2]Br_2$ (**2**) (- ·· - ·· - ·· -), $[Ni_4L_3Br_8]$ (**2B**) (·····). $[NiL_2(NCS)_2]$ (**3**) (-·····-) and $[NiL(NCS)_2]$ (**3A**) (- - ····· - -).

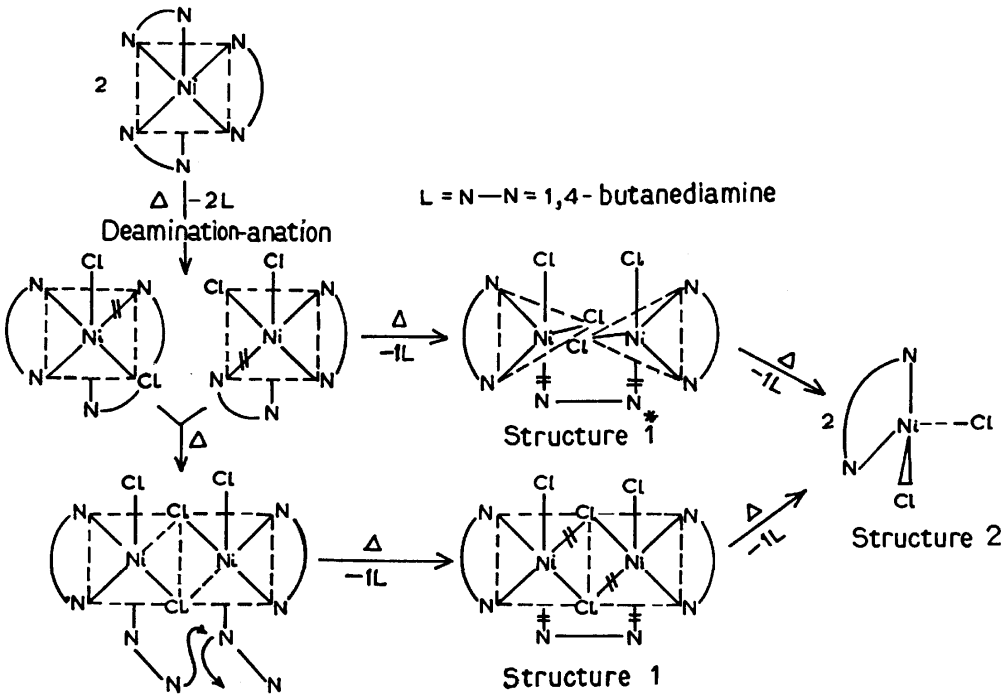

Scheme 1.

peak (Fig. 1) for the solid state reaction of $[Ni_2L_3Cl_4] \rightarrow [NiLCl_2]$ probably corroborates the *tbp* geometry in $[Ni_2L_3Cl_4]$.

The IR spectrum of $[NiLCl_2]$ suggests that the ligand is chelated here. Band appearing at 345 and 336 cm^{-1} in IR spectrum (Table 3) is well significant for terminally coordinated Cl atom in T_d geometry.[17] Higher magnetic moment (Table 1) of $[NiLCl_2]$ in comparison to other complexes is due to greater orbital contribution for loss of symmetry. The electronic spectra in mull (Fig. 3) display the characteristic band of the T_d Ni^{II} system (Structure 2, Scheme 1) at $\approx$670 nm which is tentatively assignable to the $^3T_1 \rightarrow {}^3T_1(P)$ transition (ν_3).[18,19]

In addition to the fundamental modes, we observe other modes of vibration of water molecule $\rho_r(H_2O)$ at $\approx$700 cm^{-1} and ν(MO) at $\approx$395 cm^{-1} in IR spectrum of $[NiL_2(H_2O)_2]Br_2$ (2).[20] The bands responsible for $\rho_r(H_2O)$ and ν (MO)are found to be absent in the anhydrous species. The diaquabis(1,4-butanediamine)nickel(II) bromide and dibromobis(1,4-butanediamine)-nickel(II) complexes are undoubtedly *cis* as is evident from IR assignments[21,22] in comparison to the *trans*-$[NiL_2(NCS)_2]$ (**3**). Complex (**2**) after deaquation-anation decomposes less stoichiometrically than that of its chloro analogue (*vide supra*) and generates isolable as well as nonisolable intermediates. This is probably due to anion effect. Complex (**2B**) possesses some additional bands (Table 3) in comparison to the IR spectrum of complex (**1B**) which might be due to the possession of chelating as well as bridging behavior of the diamine. Higher magnetic moment (than that of an O_h complex) and electronic spectrum of complex (**2B**) (Fig. 3) suggest that nickel(II) is probably tetracoordinated having T_d geometry.

Appearance of ν(CN) at 2095 cm^{-1} and ν(CS) at 770 cm^{-1} in the IR spectrum[23-26] (Table 3) of $[NiL_2(NCS)_2]$(**3**) clearly indicates that the compound (**3**) is actually *trans*-diisothiocyanatobis-(1,4butanediamine)-nickel(II). The IR spectrum of complex (**3**) supports the chelation character of diamine. Complex (**3**) generates $[NiL(NCS)_2]$ (**3A**) at 230 °C in single step as observed from its TG curve (Fig. 2) and corresponding DTA profile gives an endotherm followed by an exotherm. The exothermic peak may be due to some rearrangement taking place in complex (**3A**) after its formation. It is interesting to note that isolation of $[Ni(NCS)_2(en)]$ and $[Ni(NCS)_2(tn)]$ was not possible by us from their corresponding bis(diamine) complexes. Similar IR data of $[NiL(NCS)_2]$ (**3A**) with those of $[NiLCl_2]$ and $[NiL_2(NCS)_2]$ indicate that the ligand is also chelated in complex (**3A**). Magnetic moment (Table 1) of the complex (**3A**) suggests that nickel(II) is octahedrally surrounded. Although electronic spectra in mull (Table 1, Fig. 3) are not well resolved due to its dark color, the band maxima are well consistent for pseudooctahedral coordination of nickel(II) ion. ν(CN) of complex (**3A**) exhibits two intense bands at 2130 and 2120 cm^{-1} and three prominent shoulders at 2160, 2080, and 2060 cm^{-1} (Table 3). These data indicate the bridging character of thiocyanato group in the complex.[27,28] The spectroscopic and magnetic data suggest that all thiocyanato groups are bridged having

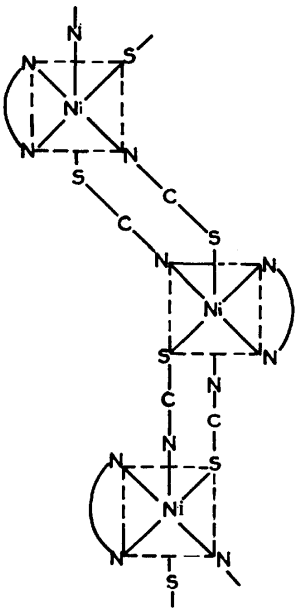

Structure 3

pseudooctahedral chromophore in complex (**3A**). Structures of $[M(NCS)_2(bipy)]$[M=Co(II) and Mn(II)] have been reported earlier by Dockum *et al.*[28] This observation suggests the probable structure of complex (**3A**) as depicted above. The occurrence of the geometrical difference in $[NiLX_2](X=Cl^-$ and $NCS^-)$ is probably due to more bridging ability of thiocyanato group although examples of similar type chloro-bridged complexes are known.[28]

Thermal studies on en and tn complexes of nickel(II) reported by us and the present investigation reflect that thermal decomposition is very much dependent on the chain length of diamine.

References

1) P. Pfeiffer, E. Schmitz, and A. Bohm, *Z. Anorg. Allg. Chem.*, **270**, 287 (1952).

2) H. L. Schläfer and O. Kling, *Z. Anorg. Allg. Chem.*, **309**, 245 (1961).

3) I. S. Ahuja and R. Singh, *J. Coord. Chem.*, **4**, 181 (1975).

4) M. A. Banares, A. Angoso, and J. J. Criado, *Synth. React. Inorg. Met. Org. Chem.*, **13**, 145 (1983).

5) F. Basolo, J. W. Palmer, and R. G. Pearson, *J. Am. Chem. Soc.*, **82**, 1073 (1960).

6) J. Fujita and H. Ogino, *Chem. Lett.*, **1974**, 57.

7) J. W. L. Martin, J. H. Timmous, A. E. Martell, and C. J. Willis, *Inorg. Chem.*, **19**, 2328 (1980).

8) S. Mitra, G. De, and N. Ray Chaudhuri, *Thermochim. Acta*, **66**, 187 (1983).

9) G. De, P. K. Biswas, and N. Ray Chaudhuri, *Bull. Chem. Soc. Jpn.*, **56**, 3145 (1983).

10) G. De and N. Ray Chaudhuri, *Thermochim. Acta*, **69**, 349 (1983).

11) S. Mitra, G. De, and N. Ray Chaudhuri, *Thermochim. Acta*, **71**, 117 (1983).

12) G. De and N. Ray Chaudhuri, *Thermochim. Acta*, **77**, 1 (1984).

13) G. De, P. K. Biswas, and N. Ray Chaudhuri, *J. Chem. Soc. Dalton Trans.* in press.

14) L. W. Collins, W. W. Wendlandt, and E. K. Gibson, *Thermochim. Acta*, **8**, 307 (1974).
15) C. L. Rollinson and J. C. Bailar, *J. Am. Chem. Soc.*, **66**, 641 (1944).
16) J. D. W. Van Voorst, and P. Hemmerich, *J. Chem. Phys.*, **45**, 3914 (1966).
17) K. Shobatake and K. Nakamoto, *J. Am. Chem. Soc.*, **92**, 3332 (1970).
18) M. Goodgame, D. M. L. Goodgame, and F. A. Cotton, *J. Am. Chem. Soc.*, **83**, 4161 (1961).
19) J. T. Donoghue and R. S. Drago, *Inorg. Chem.*, **1**, 866 (1962).
20) I. Nakagawa and T. Shimanouchi, *Spectrochim. Acta*, **20**, 429 (1964).
21) M. E. Baldwin, *J. Chem. Soc.*, **1960**, 4369.
22) J. M. Rigg and E. Sherwin, *J. Inorg. Nucl. Chem.*, **27**, 653 (1965).
23) N. F. Curtis and Y. M. Curtis, *Aust. J. Chem.*, **19**, 1423 (1966).
24) P. C. H. Mitchell and R. J. P. Williams, *J. Chem. Soc.*, **1960**, 1912.
25) A. Sabatini and I. Bertini, *Inorg. Chem.*, **4**, 1665 (1965).
26) M. M. Chamberlain and J. C. Bailar, Jr., *J. Am. Chem. Soc.*, **81**, 6412 (1959).
27) J. L. Cox, W. Marprida, H. Stockton, and J. Howatron, *J. Inorg. Nucl. Chem.*, **38**, 1217 (1976).
28) B. W. Dockum, G. A. Eisman, E. H. Wilten, and W. M. Reiff, *Inorg. Chem.*, **22**, 150 (1983).

Studies on Mixed-Ligand Complexes of Cadmium with 2,2′-Bipyridyl and Some Dicarboxylic Acids in Dioxane Medium

Rajani KUMARI, Chandra Pal Singh CHANDEL,* and Chand Mal GUPTA

Department of Chemistry, University of Rajasthan, Jaipur-302004, India

(Received January 5, 1984)

The mixed-ligand complexes of cadmium with 2,2′-bipyridyl and dicarboxylic acids (tartaric, succinic, maleic, malonic, and malic) were studied polarographically in the 50% dioxane medium. The stability constants of simple systems were calculated by Deford and Hume[1] method, and the values of stability constants of mixed-ligand complexes have been determined by the method of Schaap and McMasters.[2] The overall stability constants have been evaluated with the help of Leden's[3] graphical extrapolation method and the values of β_{11}, β_{12}, and β_{21} are (5.24, 5.80, and 8.19) for Cd-bpy-tartarate system (5.62, 6.15, and 8.34) for Cd-bpy-succinate system (5.48, 6.10, and 8.32) for Cd-bpy-maleate system (5.57, 6.15, and 8.37) for Cd-bpy-malonate system, and (5.57, 6.15, and 8.34) for Cd-bpy-malate system.

Polarography has been widely used in complex chemistry. Recently, a large number of mixed-ligand complexes have been studied by this technique. The mixed-ligand complexes of Cd have been studied in our laboratory.[4,6] The present communication is a part of our programme. The metal complexes of 2,2′-bipyridyl have been studied by many workers.[7,8] The spectrochemical studies of bipyridyl with cadmium and other metals have been reported in the literature.[9] The mixed-ligand complexes of 2,2′-bipyridyl with malonate, amino acids, and copper have been carried out by potentiometry[10] and by electrode process.[11] But the literature is quite silent about the polarographic studies of mixed-ligand complexes of cadmium with 2,2′-bipyridyl and dicarboxylates. Hence the present investigations have been undertaken to study their stability constants polarographically.

Theoretical

For a complexation reaction

$$M + iX + jY \rightleftharpoons MX_iY_j, \quad (1)$$

where i, j are stoichiometry numbers, X and Y are two different ligands and charges have been ignored for simplicity.

The overall stability constants β_{ij} for the above reaction is given by

$$\beta_{ij} = \frac{MX_iY_j}{M[X]^i[Y]^j}. \quad (2)$$

According to Schaap and McMasters mixed-ligand complex formation should be preferred over simple complexes whenever the concentration of the ligands involved are such that the products of the formation constants for the simple complexes and the concentration of the ligand raised to the appropriate power are approximately equal, *i.e.*

$$\beta_{MX_i}[X]^i = \beta_{MY_j}[Y]^j = \cdots. \quad (3)$$

$F_0[X]$ function of the Deford and Hume method may be extended to give a new function.

$$F_{00}[X, Y] = \text{antilog}\left[\frac{0.4343\,nF}{RT}E\tfrac{1}{2} + \log\frac{I_M}{I_C}\right], \quad (4)$$

where n, F, R, and T have the same meaning as in the Nernst equation, I_M and I_C are the diffusion current constants of the uncomplexed and complexed metal ion respectively.

This expression can be written in the form (assuming three bidentate ligands)

$$\begin{aligned} F_{00}[X, Y] = {} & \{\beta_{00} + \beta_{01}[Y] + \beta_{02}[Y]^2 + \beta_{03}[Y]^3\}[X]^0 \\ & + \{\beta_{10} + \beta_{11}[Y] + \beta_{12}[Y]^2\}[X] \\ & + \{\beta_{20} + \beta_{21}[Y]\}[X]^2 \\ & + \{\beta_{30}\}[X]^3 \end{aligned} \quad (5)$$

or

$$F_{00}[X, Y] = A + B[X] + C[X]^2 + D[X]^3. \quad (6)$$

Where for a given value of [Y], A, B, C, and D are constant having values defined in equation (5).

The concentration of one ligand is kept constant while that of the other is varied. In practice [Y] is kept constant and [X] is varied. The other functions were

$$F_{10}[X, Y] = \frac{F_{00} - A}{[X]} = B + C[X] + D[X]^2,$$

$$F_{20}[X, Y] = \frac{F_{10} - B}{[X]} = C + D[X],$$

and

$$F_{30}[X, Y] = \frac{F_{20} - C}{[X]} = D.$$

With the help of two values of B at two concentrations the overall stability constants β_{11}, β_{12}, and β_{21} may be calculated.

Experimental

The DME used in recording polarographic waves manually, had the following characteristics, $m = 1.96$ mg s^{-1}, $t = 4.05$ sec drop^{-1}, $h_{corr} = 40$ cm (at 303 ± 1 K in 0.1 M $NaClO_4$ in open circuit (1 M = 1 mol dm^{-3})).

The chemicals used were of AnalaR grade. 2,2′-bipyridyl and dicarboxylic acids were used as complexing agents. Potassium nitrate was used as supporting electrolyte to maintain the ionic strenght constant at 1.5 M. The presence of 0.004 % gelatin in final solution sufficed to suppress the maxima observed. All the investigations were carried out at constant temperature of 303 ± 1 K and in the 50% dioxane medium. The experimental technique was the same as described earlier.[12]

Results

The pK values, calculated by the method of Albert and Sergeant[13] and the values of stability constants of simple systems are tabulated in Table 1. All the systems were studied by keeping the concentration of weaker ligands (dicarboxylic acids) constant while varying that of bipyridyl. In all the systems a single well-defined wave was found. The plots of $-E_{de}$ *vs.* log $(i/(i_d-i))$ were linear with a slope of 30 ± 2 mV showing that two electron reduction is reversible. The reduction is diffusion-controlled as evident by the direct proportionality of the diffusion current to the square root of the effective height of mercury column.

The overall stability constants β_{11}, β_{12}, and β_{21} as calculated by the method of Schaap and McMasters are tabulated in Table 2, and are summarised in Schemes (1—5), where the numerical values indicate the logarithms of the equilibrium constants, The values of F_{ij} function for all the systems are not given in the paper to avoid the length of the paper.

TABLE 1.

	Log β_{01}	Log β_{02}	Log β_{03}
bpy	4.00	7.20	10.10
Tart.	1.40	2.20	2.94
Succ.	1.48	2.90	3.40
Male.	1.70	2.65	3.32
Malo.	1.70	2.75	3.48
Mal.	1.90	2.80	3.46

TABLE 2. MIXED-LIGAND COMPLEXES OF Cd-bpy-DICARBOXYLIC ACIDS

Systems	Log β_{11}	Log β_{12}	Log β_{21}
Cd-bpy-Tart.	5.24	5.80	8.19
Cd-bpy-Succ.	5.62	6.15	8.34
Cd-bpy-Male.	5.48	6.10	8.32
Cd-bpy-Malo.	5.57	6.15	8.37
Cd-bpy-Mal.	5.57	6.15	8.34

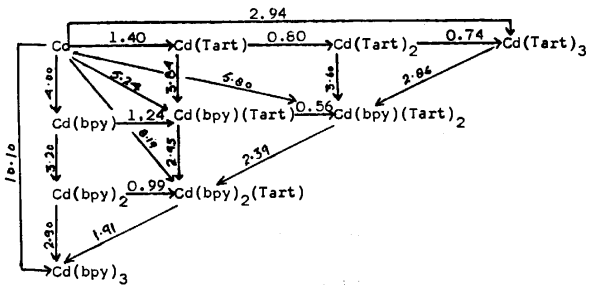

Scheme 1. Cd-bpy-Tartrate system.

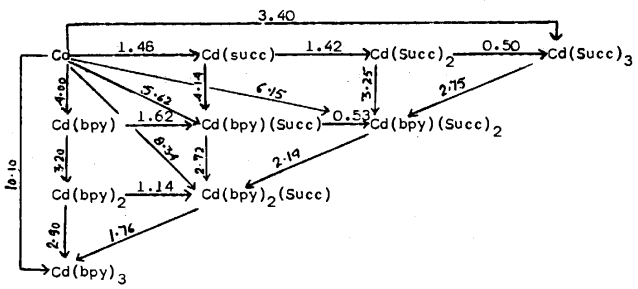

Scheme 2. Cd-bpy-succinate system.

Discussion

By considering the schemes (1—5), the formation of β_{11}, β_{12}, and β_{21} may be explained in a good manner. The tendency to add dicarboxylate to Cd(dicarboxylate), Cd(Bipyridyl) can be compared. The log K values are (0.80, 1.24), (1.42, 1.62), (0.95, 1.48), (1.05, 1.57), and (0.90, 1.57) for Cd-bpy-tartrate, Cd-bpy-succinate, Cd-bpy-maleate, Cd-bpy-malonate, and Cd-bpy-malate systems respectively. The largest part of the difference in log K must be attributed to entropy and electrostatic effect which would favour the formation of a charged complex. The addition of bipyridyl to Cd(dicarboxylate) and Cd(bpy) can also be confirmed, the mixed-ligand complex formation. The log K values are (3.84, 3.20), (4.14, 3.20), (3.78, 3.20), (3.87, 3.20), and (3.67, 3.20) for the Cd-bpy-tartrate, Cd-bpy-succinate, Cd-bpy-maleate, Cd-bpy-malonate, and Cd-bpy-malate systems respectively.

For the addition of dicarboxylate as a second ligand to [Cd(bpy)dicarboxylate)][Cd(dicarboxylate)$_2$] and [Cd(bpy)$_2$]. The log K values are (0.56, 0.74, and 0.99), (0.53, 0.50, and 1.14), (0.62, 0.67, and 1.12),

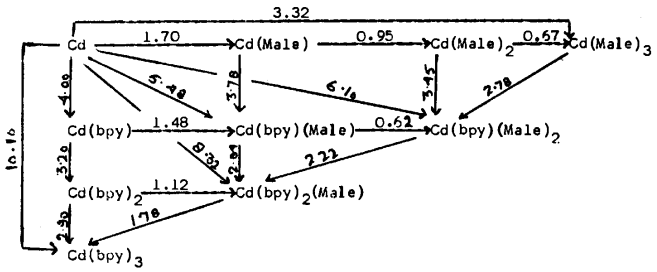

Scheme 3. Cd-bpy-Maleate system.

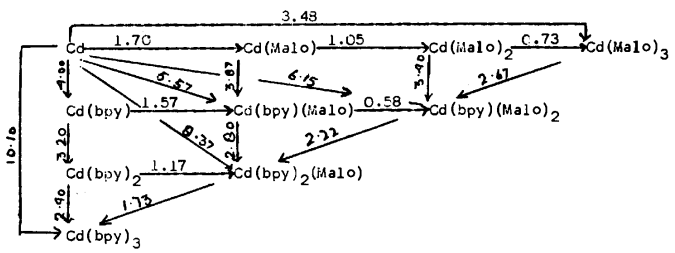

Scheme 4. Cd-bpy-Malonate system.

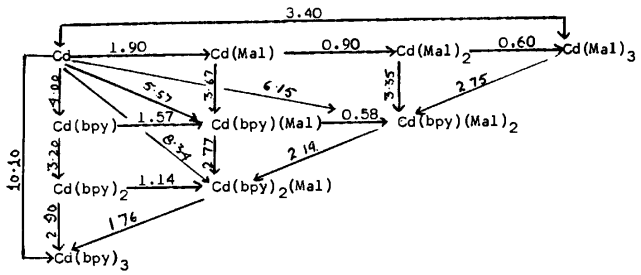

Scheme 5. Cd-bpy-Malate system.

Table 3. Values of stability constants of mixed-ligand of Cd(II) with 2,2'-bipyridyl and dicarboxylic acids by watters and dewitt equations

Systems	Log β_{11}	Log β_{12}	Log β_{21}
Cd-bpy-Tart.	5.12	5.80	8.19
Cd-bpy-Succ.	5.28	6.11	8.34
Cd-bpy-Male.	5.25	6.06	8.32
Cd-bpy-Malo.	5.30	6.16	8.37
Cd-qpy-Mal.	5.28	6.11	8.34

(0.58, 0.73, and 1.17), and (0.58, 0.60, and 1.14) for the Cd-bpy-tartrate, Cd-bpy-succinate, Cd-bpy-maleate, Cd-bpy-malonate, and Cd-bpy-malate systems respectively.

The higher log K values in the addition of dicarboxylate ion to $[Cd(bpy)_2]$ suggest that the addition or the substitution of dicarboxylate occurs easier to $[Cd(bpy)_2]$ than that to [Cd(dicarboxylate)(bpy)] or to [Cd(dicarboxylate)].

The log K values for the addition of bpy as a second ligand to [Cd(bpy)(dicarboxylate)], $[Cd(dicarboxylate)_2]$, and $[Cd(bpy)_2]$ are (2.95, 3.60, and 2.90), (2.72, 3.25, and 2.90), (2.84, 3.45, and 2.90), (2.80, 3.40, and 2.90), and (2.77, 3.55, and 2.90) respectively.

The higher log K values for the addition of bipyridyl to [Cd(dicarboxylate)] suggest that the formation of mixed-ligand complexes is favoured in the presence of weaker ligand.

According to Watters and Dewitt equations, the formation of mixed-ligand complexes may be speculated on the basis of thermodynamical considerations. The values of stability constants calculated on these equations are given in Table 3.

By comparing these values with the observed ones, it may be suggested that MX_2Y complexes are formed in an equilibrium state thermodynamically.

If we assume the following equilibria:

$$[2Cd(bpy)(dicarboxylate)] \rightleftharpoons [Cd(bpy)_2] + [Cd(dicarboxylate)_2]$$

then thermodynamically the value of log K^D is expected to be -0.60 but the observed values were -1.08, -1.14, -1.11, -1.19, and -1.14 for the Cd–bpy–tartrate, Cd–bpy–succinate, Cd–bpy–maleate, Cd–bpy–malonate, and Cd–bpy–malate systems respectively.

If we assume that the two equilibria of the disproportionation reactions, cited below should occur in dioxane medium,

$$[3Cd(bpy)(dicarboxylate)_2] \rightleftharpoons [Cd(bpy)_3] + [2Cd(dicarboxylate)_3]$$

and

$$[3Cd(bpy)_2(dicarboxylate)] \rightleftharpoons [2Cd(bpy)_3] + [Cd(dicarboxylate)_3],$$

then, the values of the disproportionation constant are calculated to be (1.42, 1.55, 1.56, 1.39, and 1.55) and (1.43, 1.42, 1.44, 1.43, and 1.42) respectively for both the equilibria of the corresponding Cd–bpy–dicarboxylate systems.

These results suggest that these mixed ligand complexes may exist more stably than those with a single ligand in an equilibrium state of 50% dioxane medium thermodynamically.

One of the authors (Rajani Kumari) is thankful to U.G.C. New Delhi for providing Junior Research Fellowship and C.P.S. Chandel is thankful to C.S.I.R. for providing Post-Doctoral fellowship.

References

1) D. D. Deford and D. N. Hume, *J. Am. Chem. Soc.*, **73**, 5321 (1951).
2) W. B. Schaap and D. L. McMasters, *J. Am. Chem. Soc.*, **83**, 4699 (1961).
3) I. Leden, *Z. Phys. Chem.*, **188**, 160 (1941).
4) N. P. Sachan, C. P. S. Chandel, and C. M. Gupta, *Chemica. Scripta*, **20**, 111 (1982).
5) C. P. S. Chandel, C. M. Gupta, and N. P. Sachan, *Chemica. Scripta*, **20**, 229 (1982).
6) Nishi Gupta, C. P. S. Chandel, P. C. Gupta, and C. M. Gupta, *Bull. Chem. Soc. Jpn.*, **56**, 3138 (1983).
7) B. E. Douglas, H. A. Laitinen, and J. C. Bailar, Jr. *J. Am. Chem. Soc.*, **72**, 2484 (1950).
8) E. I. Onstott and H. A. Laitinen, *J. Am. Chem. Soc.*, **72**, 4724 (1950).
9) K. Yamasaki, *Bull. Chem. Soc. Jpn.*, **12**, 390 (1937); **14**, 538 (1938); **15**, 130, 461 (1940); K. Yamasaki and M. Yasuda, *Proc. Jpn. Acad.*, **29**, 337 (1953).
10) H. Sigel, P. R. Huker, and R. F. Pasternack, *Inorg. Chem.*, **10**, 2226 (1971).
11) S. S. Singh, M. S. Verma, H. S. Sharma, and H. L. Nigam, *Electrochim. Acta*, 23, 1287 (1978).
12) S. C. Khurana and C. M. Gupta, *Talanta* **19**, 1235 (1972).
13) A. Albert and E. P. Sergeant, "The Determination of Ionization Constants", Chapman & Hall, London (1971).

Preparation, Properties, and Analytical Applications of Crystalline Tin(IV) Tungstoselenate

Syed Ashfaq Nabi† and Zia Mahmood Siddiqi*
Department of Chemistry, Aligarh Muslim University, Aligarh 202001, India
(Received January 5, 1984)

Synthesis of tin(IV) tungstoselenate has been done under a variety of conditions. The effects of mixing ratio of reagents and the pH of the mixture on the properties of the material have been studied. The crystalline sample of tin(IV) tungstoselenate has been chosen for detailed studies, such as chemical and thermal stabilities, chemical composition, pH-titrations, IR and X-ray analyses. On the basis of above studies a tentative formula has been proposed for tin(IV) tungstoselenate. The adsorption behaviour of metal ions in different concentrations of perchloric acid has been studied. On the basis of K_d values few analytically important separations of metal ions have been achieved on small columns of tin(IV) tungstoselenate.

It has been observed that double salts often exhibit much better ion-exchange properties than simple salts.[1-5] Most of the ion-exchange studies reported in the area of synthetic inorganic ion-exchangers are based on amorphous products. Zirconium phosphate is probably the most widely studied crystalline ion-exchange material.[6-12] Recently, synthesis and ion-exchange properties of crystalline tin(IV) selenophosphate have been reported by Nabi *et al.*[13] Crystalline inorganic ion-exchanger shows superiority over amorphous products in many respects. Amorphous materials are restricted in their application as they undergo extensive hydrolysis even in weakly alkaline or neutral solutions. Moreover, the crystalline products are rigid in their structure and reversible in nature. Synthesis of crystalline inorganic ion-exchangers is also important in order to understand the mechanism of exchange.

The present paper deals with the synthesis, ion-exchange properties, and analytical applications of tin(IV) tungstoselenate as a new inorganic ion-exchanger.

Experimental

Reagents. Tin(IV) chloride (Baker analyzed, U.S.A.), sodium selenite (BDH), and sodium tungstate (BDH) were used for the synthesis of tin(IV) tungstoselenate. All other chemicals were of analytical reagent grade.

Apparatus. EC Spectrophotometer GS 866D for spectrophotometry, Elico LI-10 pH-meter for pH measurements, Perkin Elmer model 137 spectrophotometer for IR studies, X-ray diffractometer PW 1140/90 for X-ray analysis and stanton thermobalance type H_4 for TGA, were used. A temperature controlled shaker 'SICO' was used for shaking purposes.

Synthesis. Tin(IV) tungstoselenate samples were prepared by adding an aqueous mixture which was 0.05 mol dm^{-3} in sodium selenite and 0.05 mol dm^{-3} in sodium tungstate to 0.05 mol dm^{-3} aqueous solution of tin(IV) chloride in varying volume ratios and at different pH values as indicated in Tables 1 and 2. The pH of the mixture was adjusted by adding either an acid or a base and was then kept for one day at room temperature. The white product was filtered, washed several times with demineralized water to remove excess reagents and then dried at 40 °C. The particles of 50—100 mesh size were obtained when the product was immersed in demineralized water. The material was converted to H^+ form by treating it with 1 mol dm^{-3} nitric acid for 24 h at 25±2 °C. The excess acid was removed after several washings with demineralized water. The material was finally dried at 40 °C in an oven. Tables 1 and 2 describe the conditions of synthesis and few properties of the ion-exchange material.

Ion-exchange Capacity. Ion-exchange capacities for some uni and bivalent cations are reported in Table 3. A 0.5 g exchanger in the hydrogen form was taken in the column. The hydrogen ions were then eluted by applying 1 mol dm^{-3} solutions (pH=6) of cations. The hydrogen ions in the effluent were determined after titrating against standard sodium hydroxide solution.

Chemical Stability. A 0.5 g of the material (sample SSW_4 in Table 1) was shaken with 50 cm^3 of the solvent of interest for 6 h at room temperature. Tin(IV), selenium, and tungsten in the aqueous phase were determined spectrophotometrically using hematoxylin,[14] potassium iodide[15] and potassium thiocynate[16] as colouring reagents, respectively. The results are given in Table 4.

Thermal Stability. The thermogravimetric analysis of the ion-exchanger in the hydrogen form was performed at a heating rate of 10 °C/min. The thermogram of the material is shown in Fig. 1. The effect of heating on the ion-exchange capacity of the material was also examined. The ion-exchange capacity for potassium ions is given in Table 5. The material in the hydrogen form was heated at the desired temperature for 1 h in a muffle furnace.

Chemical Composition. A 0.5 g of the sample was dissolved in hot concentrated hydrochloric acid. The solution was cooled and diluted. Tin[14] and selenium[15] were then estimated spectrophotometrically. Tungsten content was determined by gravimetric analysis.[17]

pH-Titrations. Topp and Peppers' method[18] was used for pH titrations using NaCl-NaOH system. For this purpose 0.5 g of the exchange material was treated with 50 cm^3 of the solution. Figure 2 represents the pH-titration curve of tin(IV) tungstoselenate.

IR Analysis. The infrared spectra of crystalline sample (SSW_4) dried at different temperatures were obtained by potassium bromide disc method (Fig. 3).

X-Ray Analysis. For X-ray diffraction analysis, manganese filtered Fe-$K\alpha$ radiation was used. The sample SSW_4 (dried at 40 °C) in the hydrogen form was used. Table 6 and Fig. 4 show the X-ray results.

Distribution Coefficients. Distribution coefficients for various metal ions in perchloric acid medium were determined by a published method.[19] The ion-exchange material (50—100 mesh size) was equilibrated with cation solutions at 25±1 °C. The ionic strength of Ce(IV) and Th(IV) ion solutions was 0.0041 and 0.0175 respectively whereas the

† Present address: Faculty of Education, P. O. Box. 18758, University of Sebha, Sebha, Libya.

Table 1. Synthesis and ion-exchange properties of tin(IV) tungstoselenate

Sample	Conditions of synthesis					Appearance of precipitate	Appearance after drying the material at 40 °C	Ion-exchange capacity by K^+ ions
	$SnCl_4 \cdot 5H_2O$ mol dm^{-3}	Na_2SeO_3 mol dm^{-3}	$Na_2WO_4 \cdot 2H_2O$ mol dm^{-3}	Mixing ratio (v/v/v)	pH			meq/dry g
SSW_1	0.05	0.05	0.05	1:1:1	0.0	White Upper layer-gelatinous Lower layer-granular	White opaque	0.80
SSW_2	0.05	0.05	0.05	2:1:1	0.0	White granular	White opaque	0.73
SSW_3	0.05	0.05	0.05	3:1:1	0.0	White gelatinous	Brownish shiny	0.72
SSW_4	0.05	0.05	0.05	4:1:1	0.0	White gelatinous	White shiny	0.88
SSW_5	0.05	0.05	0.05	1:1:2	0.0	White Upper layer-gelatinous Lower layer-granular	White Powdery opaque	0.91
SSW_6	0.05	0.05	0.05	1:2:1	0.0	White Upper layer-gelatinous Lower layer-granular	White powdery opaque	1.07
SSW_7	0.05	0.05	0.05	2:1:2	0.0	White Upper layer-gelatinous Lower layer-granular	Brownish opaque	0.84
SSW_8	0.05	0.05	0.05	2:2:1	0.0	White Upper layer-gelatinous Lower layer-granular	White powdery opaque	1.07

Table 2. Effect of pH on the synthesis and ion-exchange properties of tin(IV) tungstoselenate

Sample	Conditions of synthesis					Appearance of precipitate	Appearance of beads after drying at 40 °C	Ion-exchange capacity by K^+
	$SnCl_4 \cdot 5H_2O$ mol dm^{-3}	Na_2SeO_3 mol dm^{-3}	$Na_2WO_4 \cdot 2H_2O$ mol dm^{-3}	Mixing ratio (v/v/v)	pH			meq/g
SSW_4	0.05	0.05	0.05	4:1:1	0.0	White gelatinous	White shiny	0.88
SSW_9	0.05	0.05	0.05	4:1:1	1.0	White gelatinous	White shiny	0.85
SSW_{10}	0.05	0.05	0.05	4:1:1	2.0	White gelatinous	White powdery	0.84
SSW_{11}	0.05	0.05	0.05	4:1:1	3.0	White gelatinous	White powdery	0.77

Table 3. Ion-exchange capacity (Meq/g) of various ion-exchange materials with different metals ions at 25±2 °C

Metal ions	Salt used	Tin(IV) selenite[20]	Tin(IV) tungstate[21]	Tin(IV) tungstoselenate
Li^+	LiCl	1.15	—	0.71
Na^+	NaCl	0.96	0.50	0.77
K^+	KCl	0.75	0.57	0.88
Ca^{2+}	$Ca(NO_3)_2$	—	—	1.43
Sr^{2+}	$Sr(NO_3)_2$	—	0.59	1.36
Ba^{2+}	$Ba(NO_3)_2$	1.0	—	1.36

ionic strength of other ion solutions lie between 0.0006 to 0.006. The results are given in Table 7. The metal ions in the solution after and before treatment with the exchanger were determined by EDTA titrations.

Quantitative Separations. Important separations of metal ions were achieved on the columns of tin(IV) tungstoselenate. The elution curves for each set of separations are shown in Figs. 5a—5c. For each separation, 1.5 g of the exchanger (50—100 mesh size) in the hydrogen form was taken in a column of i.d. 0.6 cm with glass wool support. The mixture of the metal ions solution was adsorbed on the exchanger beads. The exchange bed was washed with demineralized water. The all metal ions loaded were eluted with suitable reagent and collected in 10 cm^3 fractions at the flow rate

Table 4. Chemical stability of some tin(IV) based ion-exchangers

Solvent	Tin(IV) selenite[20] (mg/50 cm³)		Tin(IV) tungstate[21] (mg/50 cm³)		Tin(IV) tungstoselenate (mg/50 cm³)		
	Sn released	Se released	Sn released	WO_4 released	Sn released	Se released	WO_4 released
Demineralized Water	0.0	0.03	0.065	0.00	0.00	0.0	0.0
4 mol dm^{-3} Nitric acid	1.1	5.0	—	0.0	0.54	0.25	0.0
1 mol dm^{-3} Sulfuric acid	—	—	—	4.26	0.39	0.15	2.5
1 mol dm^{-3} Hydrochloric acid	—	—	—	14.0	2.46	0.20	4.2
1% Perchloric acid	—	—	—	1.0	0.06	0.0	0.0
0.1 mol dm^{-3} Oxalic acid	—	—	—	Dissolved	0.02	0.1	1.6
0.01 mol dm^{-3} Sodium hydroxide	—	—	—	20.00	0.0	0.40	0.45
4 mol dm^{-3} Acetic acid	—	—	—	—	0.0	0.0	0.0
4 mol dm^{-3} Formic acid	—	—	—	—	0.0	0.0	0.0

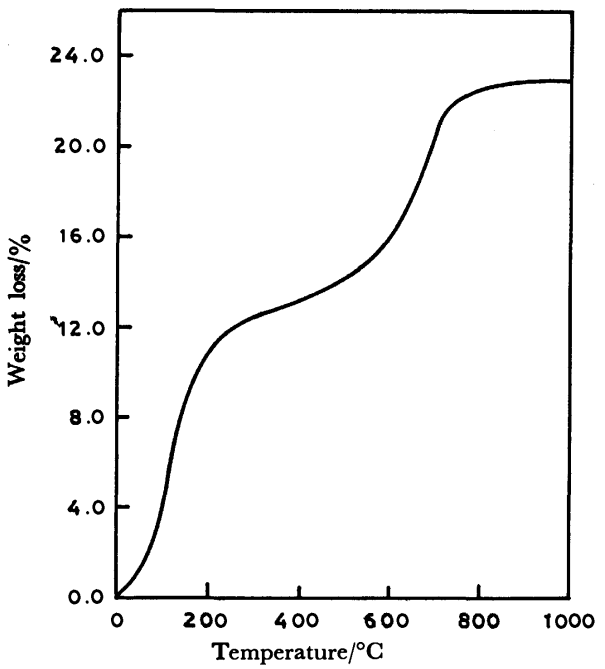

Fig. 1. Thermogram of tin(IV)tungstoselenate in H^+ form.

of 15 drops/min. The metal ions were then titrated against 0.002 mol dm^{-3} EDTA solution.

Discussion

It is apparent from Table 1 that the mixing ratio of reagents in the preparation of tin(IV) tungstoselenate is found to affect the ion-exchange capacity to some extent. The capacity is found higher for those samples which have been prepared with higher concentrations of either selenite or tungstate in the reaction mixtures. Table 2 shows the effect of pH on the mixing solutions. Between 0—2 pH the capacity remains almost constant but it reduces to 0.77 meq/g when the sample is prepared at pH 3. However, it has been observed that the capacity significantly increased (1.8 meq/g) when the preparation of tin(IV) tungstoselenate is done in highly acidic medium (negative pH).

Table 5. Effect of drying temperature on the ion-exchange capacity (Meq/g) of different material

Temperature/°C	Tin(IV) selenite[20]	Tin(IV) tungstate[21]	Tin(IV) tungstoselenate
40	0.75	0.57	0.88
100	0.75	0.13	0.62
200	0.75	0.10	0.58
300	0.75	0.10	0.48
400	0.75	0.10	0.45
500	0.70	0.10	0.34
600	0.20	0.10	0.22
700	—	0.10	0.20
800	—	—	0.00

The tin(IV) tungstoselenate sample (SSW_4) has been found to possess an ion-exchange capacity higher than tin(IV) selenite[20] and tin(IV) tungstate.[21]

It is interesting to note that tin(IV) tungstoselenate (SSW_4), prepared by mixing tin(IV) chloride sodium selenite and sodium tungstate in the ratio of 4 : 1 : 1 at pH=0, shows the crystalline character. Therefore, this sample has been chosen for detailed studies.

The data in Table 3 show that ion-exchange capacities for alkaline earths are higher than for alkali metals as expected. This is in accordance with the size of the hydrated radii of the metal. In the case of alkali metals, the capacity increases with the decrease in size of the hydrated radius of the ions. However, the capacity for alkaline earth metals remains almost constant as there is little difference in the size of hydrated radii of these metals.

Tin(IV) tungstoselenate is highly stable in water and appreciable concentrations of sulfuric acid, nitric acid,

oxalic acid, perchloric acid, and low concentrations of hydrochloric acid and sodium hydroxide. A comparison of the chemical stability of tin(IV) based ion-exchangers shows that tin(IV) tungstoeslenate is more stable than tin(IV) selenite and tin(IV) tungstate (Table 4). The order of chemical stability of various ion-exchangers are as follows: Tin(IV) tungstoeslenate >tin(IV) tungstoarsenate[22]>tin(IV) molybdoarsenate.[3]

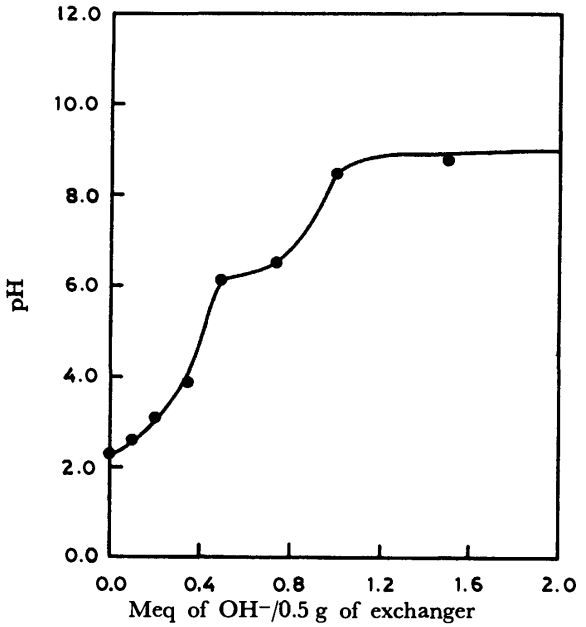

Fig. 2. pH Titration curve of tin(IV)tungstoselenate.

The ion-exchange capacity is also affected by drying temperatures of the material. The data in Table 5 indicate that tin(IV) tungstoselenate is thermally more stable than tin(IV) tungstate. Tin(IV) tungstoselenate shows considerable ion-exchange capacity (0.34 meq/g) even when the drying temperature is raised to 500 °C and can thus safely used as an ion-exchanger. On the other hand tin(IV) tungstate loses its ion-exchange capacity almost completely when a drying temperature is 100 °C.

The thermogram of tin(IV) tungstoselenate (Fig. 1) may be interpreted as follows. The material experiences a continuous loss in weight (11%) upto 200 °C which can be attributed to the loss of external water

Table 6. X-ray data of tin(IV) tungstoselenate (sample SSW_4)

Angle (θ/°)	d-Values	Intensity of peak
6.4	9.6451	S
8.3	7.457	W
16.45	3.7882	S
17.82	3.5037	W
20.5	3.0586	M
22.0	2.8576	W
23.95	2.6347	W
24.65	2.5635	W
26.05	2.4329	W
26.95	2.3563	M

S=Sharp. M=Medium. W=Weak

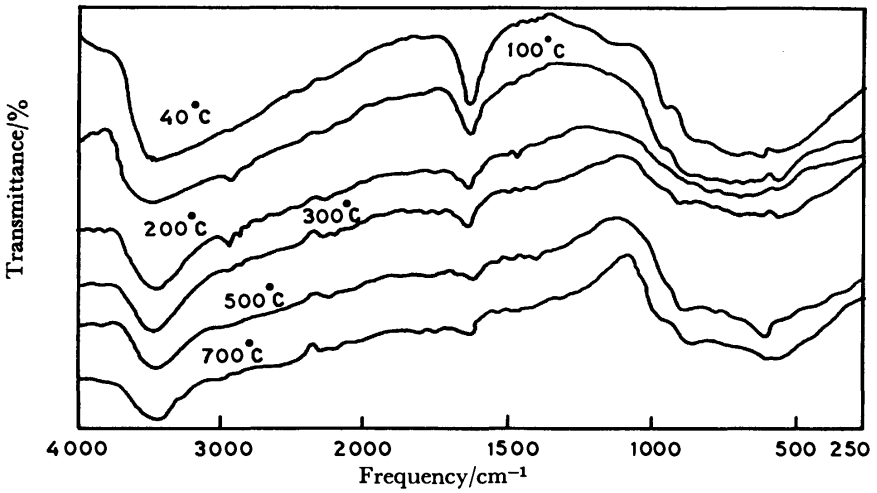

Fig. 3. Infrared spectra of tin(IV)tungstoselenate dried at different temperatures.

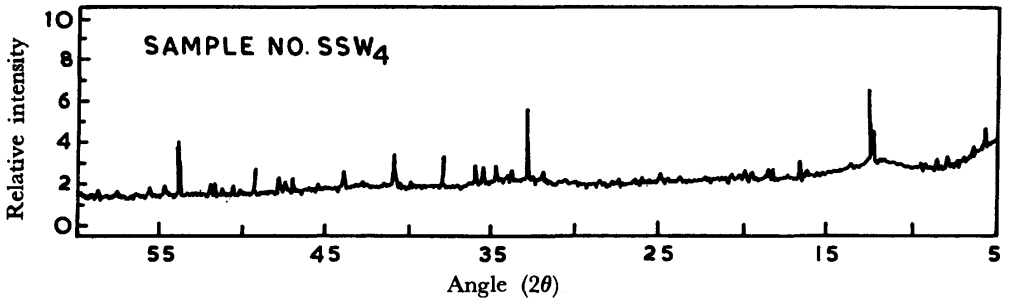

Fig. 4. X-Ray diffraction pattern of tin(IV)tungstoselenate.

molecules. The weight loss in the region 200—350 °C may be due to the removal of water molecules due to condensation of OH groups and is accompanied by loss of selenium by vaporization. No prominent weight loss is found in the small temperature range 350 °C to 400 °C which probably indicates the gradual loss of selenium by vaporization. This conclusion is also supported by the exchange capacity data at these temperatures. As the temperature is raised beyond 400 °C, decomposition of the material starts which continues upto 800 °C. The loss in weight in this region may be referred to the loss of water molecules by the condensation of the other type of OH groups and loss of tungsten. This is in good agreement of the capacity data at 400—600 °C. The capacity reduces gradually after 600 °C and vanishes completely at 800 °C. The weight becomes constant after 800 °C due to the formation of stable oxides of metals.

Table 7. Distribution coefficients of some metal ion tin(IV) tungstoselenate

Metal ion	K_d/ml/g			
	Water	$HClO_4$ 0.01 mol dm^{-3}	$HClO_4$ 0.05 mol dm^{-3}	$HClO_4$ 0.1 mol dm^{-3}
Ba^{2+}	1500±35	888±25	197±6	80±2
Ca^{2+}	1720±50	185±5	125±5	125±2
Sr^{2+}	923±30	174±5	15±2	2±1
Mg^{2+}	194±5	26±2	5±1	2±1
Zn^{2+}	3260±62	804±8	222±10	32±2
Mn^{2+}	504±8	412±6	43±2	15±2
Co^{2+}	2900±60	102±2	97±2	3±1
Hg^{2+}	2235±55	918±20	152±2	10±1
Pb^{2+}	8582±180	1011±24	404±2	84±2
Cd^{2+}	9900±200	985±20	138±2	98±2
Ni^{2+}	1724±50	560±5	89±2	8±2
Cu^{2+}	2335±52	608±6	66±2	10±2
Th^{4+}	9980±200	8906±100	989±5	722±5
Ce^{4+}	3800±64	3665±66	2742±50	909±5

The molar composition of tin(IV) tungstoselenate shows that tin(IV) selenium and tungsten are present in the ratio of 7 : 1 : 18. The pH-titration curve shows bifunctional character of tin(IV) tungstoselenate (Fig. 2) whereas tin(IV) tungstate and tin(IV) selenite are found to be mono and bifunctional respectively.[20,21]

The IR spectra of tin(IV) tungstoselenate dried up to 600 °C resemble each other and show three absorption peaks (Fig. 3). A strong and broad peak in the region 3600—3200 cm^{-1} represents the interstitial water, free water, and OH groups. Another sharp peak in the region 1700—1500 cm^{-1} with a maximum at 1620 cm^{-1} is characteristic of interstitial water. The third peak in the region 1100—250 cm^{-1} may be due to metaloxygen bonds. There is no difference in the IR spectra between hydrogen form and patassium form of the sample dried at 40 °C.

The X-ray diffraction pattern suggests that tin(IV)

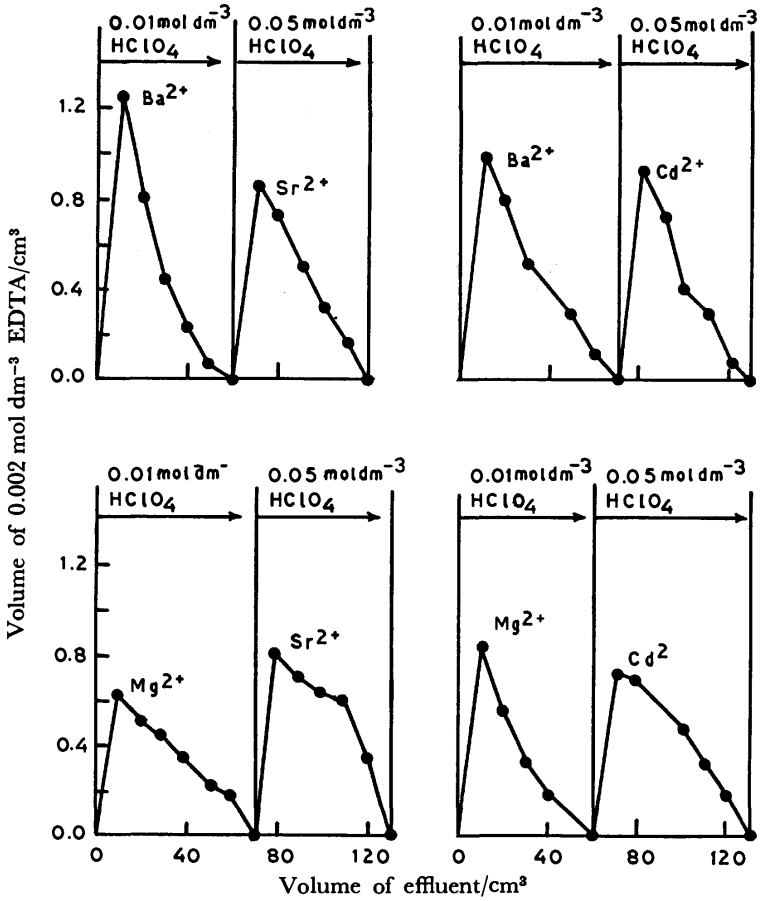

Fig. 5A Separations of Ba^{2+}–Sr^{2+}, Ba^{2+}–Cd^{2+}, Mg^{2+}–Sr^{2+}, and Mg^{2+}–Cd^{2+}.

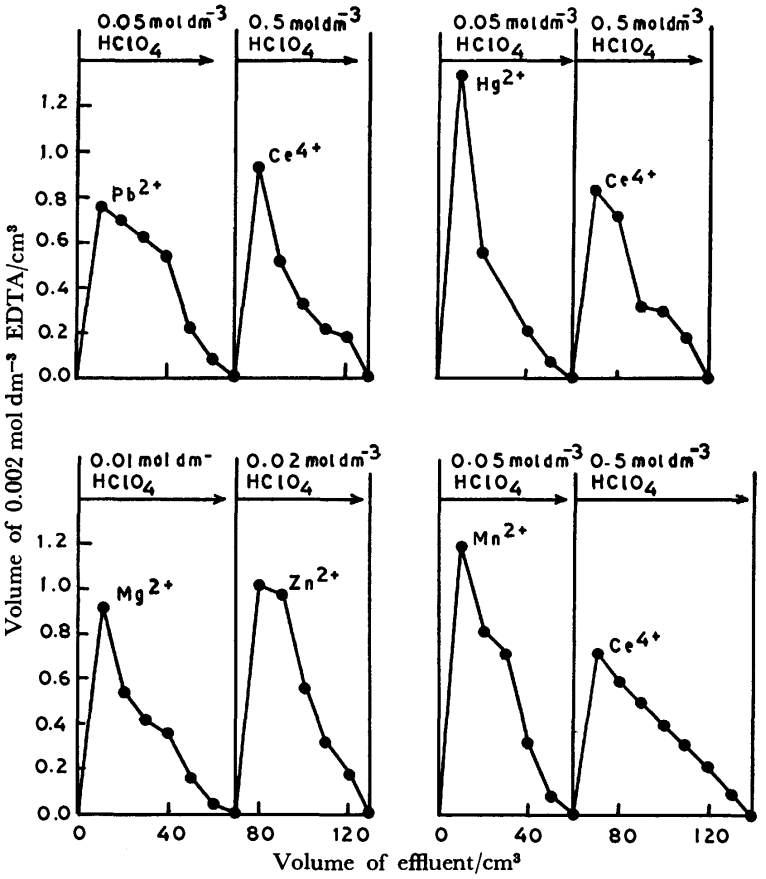

Fig. 5B Separations of Pd^{2+}–Ce^{4+}, Hg^{2+}–Ce^{4+}, Mn^{2+}–Ce^{4+}, and Mg^{2+}–Zn^{2+}.

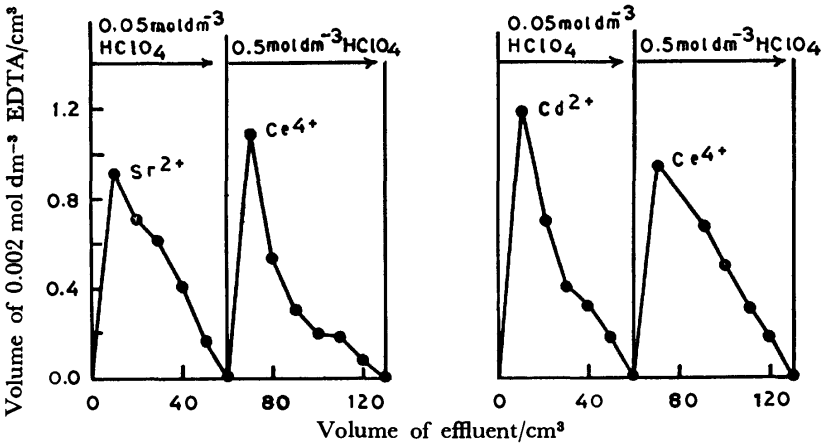

Fig. 5C Separations of Sr^{2+}–Ce^{4+} and Cd^{2+}–Ce^{4+}.

tungstoselenate (sample SSW_4) is crystalline in character. The *d*-values and other results of tin(IV) tungstoselenate are given in Table 6 and Fig. 4.

On the basis of chemical composition, pH-titration, thermogravimetric and IR studies, the following tentative formula may be assigned to tin(IV) tungstoselenate.

$$[(SnO_2)_7 \cdot HSeO_3(HWO_4)_{18}] \quad (1)$$

If all the external water molecules are lost upto 200 °C, the percentage weight loss is 11%. The number of water molecules then calculated by the method of Alberti *et al.*[23] The number of external water molecules per molecule of the exchanger is found to be 45. The formula therefore can be rewritten as

$$[(SnO_2)_7 \cdot HSeO_3(HWO_4)_{18}] \cdot 45H_2O \quad (2)$$

The molecule contains nineteen replaceable hydrogen atoms according to the above formula. If it is assumed that only $7H^+$ ions are exchanged at pH=6, then the ion-exchange capacity calculated from formula 2 is 0.91 meq/g which is very close to the experimental value (1.0 meq/g from pH-titration curve). When the pH of the mixture is increased upto 8.5, the capacity as indicated by pH-titration curve becomes 2.4 meq/g and supports the theoretical ion-exchange

capacity of the material (2.5 meq/g) when all the replaceable hydrogen ions are taken into consideration.

The data in Table 7 show that K_d values for metal ions decrease in general with the increase in the concentration of perchloric acid. K_d values of Th(IV), and Ce(IV) are exceptionally high in all concentrations of perchloric acid, whereas negligible adsorption of almost all metal ions occurs in 0.5 mol dm^{-3} $HClO_4$. The behavior of barium(II) is quite different from other alkaline earth metals and therefore can be selectively separated from a mixture of these metal ions on tin(IV) tungstoselenate.

On the basis of differential selectivity of metal ions in various concentrations of perchloric acid, a number of important separations have been achieved quantitatively using tin(IV) tungstoselenate columns. The elution curves of metal ions separated from one another are shown in Figs. 5A-5C.

The authors are thankful to Prof. W. Rahman, Chairman, for providing research facilities and to C.S.I.R. New Delhi for financial assistance.

References

1) C. B. Amphlett, "Inorganic Ion-Exchangers," Elsevier, Amsterdam; (1964).
2) M. Qureshi and R. C. Kaushik, *Anal. Chem.*, **49**, 163—168 (1977).
3) M. Qureshi, R. Kumar, and R. C. Kaushik, *Sep. Sci. Technol.*, **13**, 185 (1978).
4) H. F. Walton, *Anal. Chem.* **42**, 86R (1970).
5) V. Pekarek and V. Vesely, *Talanta*, **19**, 1245 (1972).
6) A. Clearfield and J. A. Stynes, *J. Inorg. Nucl. Chem.*, **26**, 117 (1964).
7) A. Clearfield, W. L. Daux, A. S. Medina, G. D. Smith, and J. R. Thomas, *J. Phys. Chem.*, **73**, 3424 (1969).
8) A. Clearfield, A. Oskarsson, and C. Oskarsson, *Ion Exch. Membr.*, **1**, 9 (1972).
9) A. Clearfield, L. Kullberg, and A. Oskarsson, *J. Phys. Chem.*, **78**, 1150 (1974).
10) Y. Inoue and Y. Yamada, *Bull. Chem. Soc. Jpn.*, **52** 3528 (1979).
11) Y. Inoue and Y. Yamada, *Chem. Lett.*, **1975**, 1293.
12) J. Albertsson, *Acta. Chem. Scan.*, **20**, 1689 (1966).
13) S. A. Nabi, Z. M. Siddiqi, and R. A. K. Rao, *Separ. Sci. Technol.*, Communicated.
14) F. D. Snell and C. T. Snell, "Colorimetric Methods of Analysis," Vol. IIA, p. 135, Princeton, New Jersey, (1959).
15) Ref. 14, p. 776.
16) N. H. Furman, "Standard Methods of Chemical Analysis," 6 th Edn., Vol. I, p. 1163, D. Van Nostrand Inc., Princeton, New Jersey, (1962).
17) Ref. 16; p. 1162.
18) N. E. Topp and K. W. Pepper, *J. Chem. Soc.*, **1949**, 3299.
19) H. Hamaguchi, R. Kuroda, K. Aoki, R. Sugisita, and N. Onuma, *Talanta*, **10**, 153 (1963).
20) M. Qureshi and S. A. Nabi, *Talanta*, **19**, 1033 (1972).
21) M. Qureshi and K. G. Varshney, *J. Inorg. Nucl. Chem.*, **30**, 3081 (1968).
22) M. Qureshi, R. Kumar, V. Sharma, and T. Khan, *J. Chromatogr.*, **118**, 175 (1976).
23) G. Alberti, P. C. Galli, U. Costantino, and E. Rorracca, *J. Inorg. Nucl Chem.*, **29**, 517 (1967).

The Unusually Strong Effect of a 4-Cyano Group upon Electronic Spectra and Dissociation Constants of 3-Substituted 7-Hydroxycoumarins

Otto S. Wolfbeis,* Ernst Koller, and Petra Hochmuth
Institut für Organische Chemie, Karl-Franzens-Universität, A-8010 Graz, Austria
(Received March 12, 1984)

Synthesis, absorption and fluorescence spectra as well as pK_a values of 7-hydroxycoumarins with electron-withdrawing substituents in positions 3 are described. Introduction of a 4-cyano group is achieved by oxidative cyanation of coumarins using potassium cyanide and elemental bromine. 7-Hydroxycoumarins without a 4-cyano group are useful indicators for measuring physiological pH values due to their intense fluorescences, longwave absorptions and emissions, as well as pK_a values of around 7. The presence of a 4-cyano group gives rise to a dramatic longwave shift in absorption (30—40 nm in methanol) and emission (55—80 nm). In water solution, the fluorescence maxima are at around 570—600 nm, with excitation maxima between 410 and 510 nm, depending on whether the phenol or phenolate species is excited. For all coumarins under investigation, fluorescence is from the anion form even in the pH 2—7 range. This phenomenon is interpreted in terms of excited state dissociation according to the Förster model. The interpretation is corroborated by calculations of the excited state pK_a values, which show them to be lower by 4.5—6.4 units than those of the ground state.

7-Hydroxycoumarins such as 4-methylumbelliferone (4-MU) play an important role in measuring physiological pH values by fluorimetry.[1-6] In addition, esters, ethers and glycosides of 4-MU are frequently used- and commercially available-enzyme substrates for use in clinical chemistry and enzymology. The formation of fluorescent 4-MU from practically nonfluorescent ethers and esters is a measure for the enzyme activity.[7,8]

However, 4-MU has two decisive disadvantages: (a) Its pK_a value of 7.8 is relatively high, so that under physiological pH conditions only partial dissociation to the highly fluorescent anion (fluorescence maximum 450 nm) takes place;[9] (b) its fluorescence is maximally excited between 330 and 360 nm, a spectral region where background fluorescence from biological matter such as serum or intracellular liquids is fairly high, mostly due to the presence of reduced nicotinamide adenine dinucleotide.

By introducing an electron-withdrawing substituent in position 3, we hoped to shift the excitation and emission maxima to longer wavelengths, and simultaneously to lower the pK_a values. The bathochromic effect of certain substituents in position 3 is known in the chemistry of optical brighteners derived from 7-aminocoumarins.[10]

The emission maxima of 3-substituted umbelliferones in alkaline solutions have been reported by Sherman and Robins, and fluorescence intensity was correlated with Hammett σ-constants.[11] More recently, we have reported on the photodissociation of related umbelliferones.[12] Their properties as laser dyes have also been described.[13] The effect of substituents in position 3 on spectra and pK_a values of umbelliferones has not been studied so far.

Results and Discussion

Syntheses. 7-Hydroxycoumarins with a substituent in position 3 (**1a**—**i**) can be prepared according to one of the numerous methods decribed in the literature including patents.[10,14] We found the procedure of condensing 2,4-dihydroxybenzaldehyde with an appropriate CH_2-acidic ester or acid such as ethyl 2-benzoxazolylacetate in the presence of pyridine (as a solvent) and aniline (as a catalyst, 1 mol-equiv), most suitable.[15]

Introduction of a 4-cyano group into umbelliferones was accomplished by addition of potassium cyanide to a suspension of the coumarin in *N,N*-dimethylformamide (DMF) and subsequent dehydrogenation with elemental bromine. We assume that leuko-dyes of general structure **2** are reaction intermediates, which are then oxidized to the respective cyanocoumarins **3a**—**e**.

Oxidative cyanations of dyes with activated double bonds have been described by various authors.[16-20] Oxidizing agents such as ferric ion.[16,19] lead tetra-

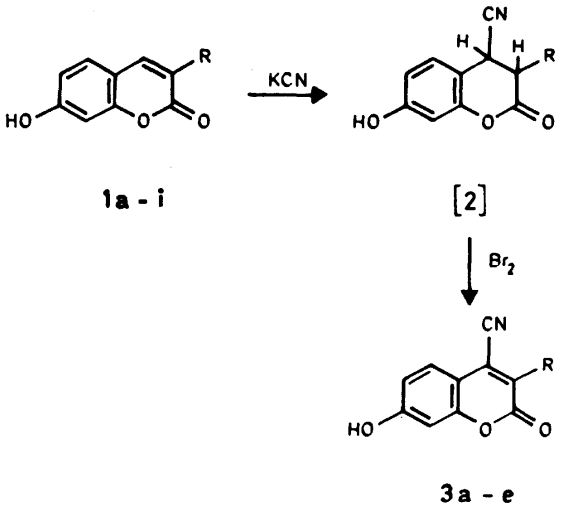

1, 3	R
a	2-Benzoxazolyl
b	2-Benzothiazolyl
c	5-Methyl-7-sulfonato-2-benzoxazolyl, potassium salt
d	5-Chloro-2-benzoxazolyl
e	2-Benzimidazolyl
f	2-Furyl
g	2-Thienyl
h	COOH
i	Phenyl

acetate,[17,18,21] bromine,[21] peroxides, and other oxidizing agents[19] have been proposed.

It should be noted that, for unknown reasons, we failed to prepare the 4-cyano derivatives of compounds **1f**—**i**. **3c** was synthesized by oxidative cyanation of the potassium phenolate **1c**, since when employing the free 7-hydroxy compound no reaction took place. **3e** could be prepared in low yield only, possibly due to competitive bromination of the imidazolyl NH.

The structures of the cyanoumbelliferones were confirmed by correct analytical and spectral data. The IR spectra are characterized by carbonyl bands in the 1710—1750 cm^{-1} range, and the lack of an intense band of the cyano group. If at all observable, the band consists of a very weak signal at around 2240 cm^{-1}.

The ^{1}H-NMR spectra are of little significance, since most of the protons come to lie in δ=6.7—8.1 range, except for the methyl group present in **3e**. The protons of the 7-hydroxy groups show no sharp signal in pure dimethyl sulfoxide. However, in the presence of traces of water a signal can be observed at around δ=11.2.

The mass spectra consist of strong signals for the molecular ion (M^+) and fragments resulting from the elimination of CN (M^+-26), HCN (M^+-27), and CO (M^+-28). In each case, the molecular ion peak is the 100 % (base) peak.

The dyes are fairly stable in neutral and acidic aqueous solutions, albeit much less than the respective cyanounsubstituted coumarins. They suffer, however, considerable decomposition at pH values above 8. The 4-cyano group is not stable under sulfonation conditions (*e.g.*, oleum). Therefore, sulfonato groups have to be introduced prior to cyanation.

Electronic Spectra. The spectra of 7-hydroxycoumarins **1a**—**i** in water-free organic solvents consist of an intense absorption band in the 365—390 nm range, and an emission maximum between 450 and 470 nm (Table 1), except for compounds **1h** and **1i**, which absorb distinctly shorter (*ca.* 340 nm).

In aqueous solution both the absorption and fluorescence spectra are highly pH-dependent in the near neutral pH range, a fact that prevents the use of 7-hydroxycoumarins as optical brighteners.[10] The absorption and fluorescence data of aqueous pH 4 and pH 9 solutions are summarized in Table 1. While the fluorescence maxima do not change significantly

Table 1. Longest-wave absorption and fluorescence maxima of 7-hydroxycoumarins **1** and **3** in various solvents[a]

Compound	Solvent[a]	Absorption maximum nm	ε M^{-1} cm^{-1}	Fluorescence maximum nm	Compound	Solvent[a]	Absorption maximum nm	ε M^{-1} cm^{-1}	Fluorescence maximum nm
1a	A	370	—	458	**1h**	A	336	—	403
	B	377	31.800	448		B	337	15.300	408
	C	377	28.200	469, 435(sh)		C	342	—	447, 405(sh)
	D	427	44.300	471[c]		D	386	—	448[c]
1b	A	378	—	462	**1i**	A	336	—	422
	B	390	29.800	465		B	342	23.000	430
	C	385	31.000	485, 465(sh)		C	338	19.700	465, 428
	D	439	47.000	490[c]		D	383	26.100	462[c]
1c	A	—[b]	—	—	**3a**	A	405	—	517
	B	380	34.400	451		B	409	25.600	516
	C	378	32.000	468, 435(sh)		C	416	24.100	575, 520(sh)
	D	431	44.000	470[c]		D	494	33.200	577[c]
1d	A	372	—	456	**3b**	A	420	—	518
	B	378	30.600	450		B	430	28.300	520
	C	378	—	470, 440(sh)		C	432	23.300	594, 520(sh)
	D	425	—	472[c]		D	505	33.100	595[c]
1e	A	—[b]	—	—	**3c**	A	—[b]	—	—
	B	387	33.000	466		B	408	23.000	519
	C	385	—	477, 435(sh)		C	416	—	574, 510(sh)
	D	427	—	479[c]		D	494	—	577[c]
1f	A	370	—	430	**3d**	A	408	—	509
	B	370	26.300	454		B	411	27.100	519
	C	368	—	468, 435(sh)		C	418	21.400	576
	D	405	—	489[c]		D	497	32.400	577[c]
1g	A	367	—	448	**3e**	A	419	—	509
	B	369	25.000	466		B	418	25.400	528[d]
	C	365	—	476, 455(sh)		C	419	—	590, 530(sh)
	D	407	—	500[c]		D	487	—	593

a) A, benzene; B, methanol; C, buffer of pH 4 (citrate); D, buffer of pH 9 (borate). b) Insoluble. c) Very intense. d) In acetone.

with pH between pH 4 and 9, the relative intensities are around two times higher in alkaline solutions than in acidic solution.

The presence of a 4-cyano group results in a considerable bathochromic shift in both absorption and emission. All cyanocoumarins are orange-red (absorption maxima 405—430 nm) and exhibit bright green fluorescence in organic solvents. The maxima suffer a longwave shift with increasing solvent polarity. The molar absorbances are somewhat lower than those of compounds **1**. The spectra of 4-cyanoumbelliferones in alkaline solutions are far red-shifted in both absorption and emission, when compared with the respective phenol species. In addition, they exhibit large Stokes shifts of 80—90 nm, which, however, in terms of wavenumbers is about the same as for coumarins **1a—i** (3000—4500 cm^{-1}).

pH Effects. The pK_a values of selected umbelliferones were determined by spectrophotometry and are listed in Table 2. As can be seen, the values are temperature dependent and decrease by 0.012—0.016 units per °C increase in temperature. Coumarins possessing a 4-cyano group display distinctly increased acidities (0.6—0.8 units lower).

It is noted that fluorescence of 7-hydroxycoumarins **1** and **3** is almost invariably from the anion form in the pH 4—9 range, despite of photoexciting the undissociated* species in acidic solutions. According to Förster,[22] this can be interpreted in terms of photodissociation due to a decrease in pK_a in the first excited singlet state (S_1-state).

We have calculated the pK_a values of the S_1-state with the help of the following equation,[22-24]

$$pK_a(S_1) = pK_a(S_0) - \frac{N \cdot h}{2.303RT}(\nu'_{BH} - \nu'_B)$$

wherein ν'_{BH} and ν'_B are the wavenumbers of the O–O transition of phenol and phenolate, respectively. The mean of the wavenumbers of absorption and fluorescence was taken as O–O transition.[23]

The results are given in Table 2. They show all coumarins to become stronger acids by 4.5—6.4 pK_a units, a fact that can explain the appearance of anion fluorescence even in weakly acidic solutions: When photoexciting a coumarin such as compound **1a** in pH 4 solution, it will dissociate during the lifetime of the S_1-state by virtue of its $pK_a(S_1)$ of 1.74 (Table 2).

It is, however, noted that shortwave shoulders are in most cases observed in the fluorescence emission bands of coumarins **1** and **3** in pH 4 solutions. These shoulders are attributed to emissions from the neutral species, occurring prior to the S_1-state dissociation step.

Concluding Remarks. We have presented here a series of fluorescent compounds with interesting spectral properties. Their pK_a values between 6 and 7 may render them useful longwave excitable and fluorescing indicators for measuring physiological pH values. Owing to their lower pK_a values, cyanocoumarins **3** are more suitable to measure pH's of weakly acidic bioliquids such as urine, whereas coumarins **1** are more useful to measure near-neutral pH's (such as in blood).

Esters of coumarins **1** and **3** with carboxylic, phosphoric and sulfuric acids, respectively, as well as ethers and glycosides are useful enzyme substrates for direct and continuous kinetic determination of hydrolyses.[25] These results will be reported elsewhere.

Experimental

Melting points are uncorrected. Spectra were recorded on the following instruments: Perkin Elmer Lambda 5 (UV/VIS); Aminco SPF 500 (fluorescence); Perkin Elmer 421 (IR); Varian A60 A (^{1}H-nmr); Varian-Mat 111 (mass spectra). Elemental analyses were performed on a Carlo-

Table 2. Ground state and first excited singlet state pK_a values of umbelliferones **1** and **3** at 22 °C

Compound	Ground state pK_a value	O-O-transition/cm^{-1} a)		Calculated Excited state pK_a	ΔpK_a
		Phenol species	Phenolate species		
1a	6.84±0.04	24.757	22.325	1.74	−5.10
1b	7.02±0.03; 6.79[b]	23.740	21.594	2.50	−4.51
1c	6.80±0.08; 6.60[b]	24.722	22.239	1.59	−5.21
1d	6.80±0.07	24.591	21.186	2.11	−4.69
1e	7.01[b]	24.481	22.148	2.11[b]	−4.90
1f	7.41[b]	25.081	22.570	2.14[b]	−5.27
1g	7.71±0.05	24.688	22.285	2.67	−5.04
1h	7.04±0.02	26.965	24.114	1.06	−5.98
1i	7.80±0.05	26.475	23.877	2.35	−5.45
3a	6.07±0.04	21.708	18.787	−0.06	−6.13
3b	6.38±0.03	21.190	18.304	0.32	−6.06
3c	6.08±0.04	21.823	18.787	−0.29	−6.37
3d	6.00±0.04	21.614	18.726	−0.06	−6.06

a) The mean of the longest-wave absorption and fluorescence maximum (in cm^{-1}) was taken as O-O-transition; the wavelength of the shortwave shoulder in pH 4 solution, which is attributed to emission from the neutral form, was used for the calculation of the values for the phenol species. b) At 37 °C.

* The expression "undissociated" refers to the phenol group, not to the sulfonato group.

Table 3. Physicochemical properties as well as spectral data for coumarins **3a—e**

Compound	Mp θ_m/°C (cryst. from)	Yield/%	IR (cm^{-1})	^{1}H-NMR (in DMSO-d_6) (δ-units, TMS=0)	Mass spectrum
3a	282—285 (Ethanol)	49	3300, 1750, 1620 1590	6.70—7.90 (m, 7H)	—
3b	336—338 (Dec.) (Ethanol)	61	3330, 1730, 1700, 1620, 1590	6.80—8.10 (m, 7H) 11.2 (s, 1H)	320 (M^+, 100%), 292 (27%)
3c	>350 (Ethanol/water, 1:1)	63	3400, 1730, 1620, 1590	2.35 (s, 3H), 6.80—7.80 (m, 5H), 11.3 (br.s, 1H)	—
3d	291—294 (Ethanol)	52	3400, 1745, 1620, 1590	6.70—7.90 (m, 6H)	338 (M^+, 100%), 310 (37%)
3e	322 (dec.) (Ethanol)	21	3340, 1710, 1620, 1555	—	303 (M^+, 100%) 275 (21%)

Erba 1106 C,H,N-analyzer. pH values were measured with a pH electrode (Metrohm, Switz.) that was calibrated against pH 7 and pH 4 standard buffers.

General Procedure for the Preparation of 4-Cyano-7-hydroxycoumarins ***3a—e***. 2.6 g (0.04 Mol) potassium cyanide, dissolved in 6 ml water, are added at room temperature to a suspension of 0.02 mol of the respective 7-hydroxycoumarin (**1a—e**) in 50 ml *N,N*-dimethylformamide. Note that **1c** should be employed as its potassium phenoxide salt. The mixture is stirred for 1 h at 40 °C. After filtration, 1 ml (0.02 mol) elemental bromine is added dropwise to the filtrate at 0 °C. The mixture is then stirred for 1 h at this temperature. The resulting precipitate is collected, washed with water and methanol and purified by double recrystallization from the solvent given in Table 3. Physicochemical and spectral data of the new compounds are given in Table 3. All compounds gave C,H, and N-analyses in agreement (deviation maximally ±0.3 %) with calculated values.

Financial support by the "Fonds zur Förderung der wiss. Forschung" (Projekt P5014) is gratefully acknowledged. We also thank Dr. H. Harnisch (Bayer AG, Leverkusen) for generous gifts of chemicals.

References

1) G. G. Guilbault, "Practical Fluorescence-Theory, Methods and Techniques," Marcel Dekker, (1973), p. 598
2) R. Robl, *Ber. Dtsch. Chem. Ges.*, **59**, 1725 (1926).
3) H. Linser, *Biochem. Z.*, **224**, 157 (1932).
4) D. W. Lübbers and N. Opitz, *Z. Naturforsch.*, *C* **30**, 532 (1975).
5) D. W. Lübbers, N. Opitz, P. P. Speiser, and H. J. Bisson, *Z. Naturforsch.*, *C* **32**, 133 (1977).
6) H. Alpes and W. G. Pohl, *Naturwiss.*, **65**, 652 (1978).
7) G. G. Guilbault, "Enzymatic Methods of Analysis," Pergamon Press, Oxford, (1970), pp. 52 and 62.
8) Ref. 1, p. 354.
9) G. J. Yakatan, R. J. Juneau, and S. G. Schulman, *Anal. Chem.* **44**, 1044 (1972).
10) H. Gold, "Fluorescent Whitening Agents," ed by F. Coulson and F. Korte, Georg Thieme Verlag, Stuttgart, 1975.
11) W. R. Sherman and E. Robins, *Anal. Chem.* **40**, 803 (1968).
12) O. S. Wolfbeis, *Z. Naturforsch.*, *A* **32**, 1065 (1977).
13) O. S. Wolfbeis, W. Rapp, and E. Lippert, *Monatsh. Chem.*, **109**, 899 (1978).
14) A. Dorlars, C. W. Schellhammer, and J. Schroeder, *Angew. Chem.*, **87**, 693 (1975); *Angew. Chem., Int. Ed. Engl.*, **25**, 665 (1975).
15) R. Adams and T. E. Bockstahler, *J. Am. Chem. Soc.* **74**, 5346 (1952).
16) P. Ehrlich and L. Benda, *Ber. Dtsch. Chem. Ges.*, **46**, 1931 (1913)
17) B. C. McKusick, R. E. Heckert, T. L. Cairns, D. D. Coffman, and H. F. Mower, *J. Am. Chem. Soc.* **80**, 2806 (1958).
18) G. N. Sausen, V. A. Engelhardt, and W. J. Middleton, *J. Am. Chem. Soc.* **80**, 2815 (1958).
19) R. Stolle, G. Bach, and I. Wolf, East German Pat. 131.178 (7. June 1978), to VEB Farbenfabrik Wolfen.
20) H. Harnisch, DOS 29.25.546 (5. June 1979), to Bayer AG.
21) P. Möckli, *Dyes and Pigments*, **1**, 3 (1980).
22) Th. Förster, *Z. Elektrochem.* **54**, 42 and 531 (1950).
23) A. Weller, *Z. Elektrochem.* **56**, 662 (1952).
24) Review: S. G. Schulman, "Acid-Base Chemistry of Excited Singlet States," in: "Modern Fluorescence Spectroscopy," ed by E. L. Wehry, Heyden & Son, London-New York-Rheine, (1976), p. 239.
25) E. Koller and O. S. Wolfbeis, *Anal. Biochem.*, in press (1984).

 © 1985 The Chemical Society of Japan Bull. Chem. Soc. Jpn., 58, 735—744 (1985)

Aromatic Systems with 10π Electrons Derived from 3a-Azapentalene. Part 40. Studies on the 1,2,4-Triazolo[4,3-*b*][1,2,4]triazole Series

Mateo ALAJARIN,† Pedro MOLINA,† Alberto TARRAGA,† Mª Jesús VILAPLANA,† Mª de la Concepción FOCES-FOCES,†† Felix HERNANDEZ CANO,†† Rosa Mª CLARAMUNT,††† and José ELGUERO*

†*Departamento de Química Orgánica, Facultad de Ciencias, Universidad de Murcia, Murcia, Spain*

††*Departamento de Rayos X, Instituto de Química Física "Rocasolano", Serrano 119, Madrid-6, Spain*

†††*Química Organica, Universidad Nacional de Educación a Distancia, Ciudad Universitaria, Madrid-3, Spain*

**Instituto de Química Médica, CSIC, Juan de la Cierva 3, Madrid-6, Spain*

(Received January 13, 1984)

The synthesis, structure, and reactivity of several 1,2,4-triazolo[4,3-*b*][1,2,4]triazole derivatives have been studied. Structures have been established throughout a careful carbon-13 NMR study, and for the most unusual one (inner salt of 2-methyl-3-methylthio-6-phenyl-7*H*-1,2,4-triazolo[4,3-*b*][1,2,4]triazolium hydroxide) by X-ray crystallography: the space group is P21/c, the cell constants are $a=12.6939(5)$, $b=16.0936(6)$, $c=12.0239(5)$ and $\beta=107.247(3)°$ and $Z=8$. The *S*-methyl group is directed towards the fusion of the five-membered rings at +/−syn conformations. The azapentalene moieties have the first atoms of the substituents on its plane and the 6-phenyl rings make an angle of −26.7 and −4.3° with it, in the two independent molecules respectively.

Continuing our interest in azapentalene derivatives[1] we have directed our attention to the 1,2,4-triazolo-[4,3-*b*][1,2,4]triazole ring. We have already obtained some results in these series,[2-4] but we want to present here a coherent view on the synthesis and reactivity of functional (oxo and thioxo) derivatives. Scheme 1 contains all the compounds and reactions studied.

The reaction of arenecarbonitriles in basic medium with 4-amino-3-methylthio-4*H*-1,2,4-triazole derivatives, **1**, **5**, and **10**, yields 6-aryl-1,2,4-triazolo[4,3-*b*]-[1,2,4]triazoles. The potassium salts lead by acidification the neutral molecules **4**, **9**, and **13**. In the first case, the cyclized form **3** was isolated and identified. In the second one, the intermediate amidine salt **6** was obtained. Thus, even in the third case, where the unstability of salts **11** and **12** prevents their isolation,

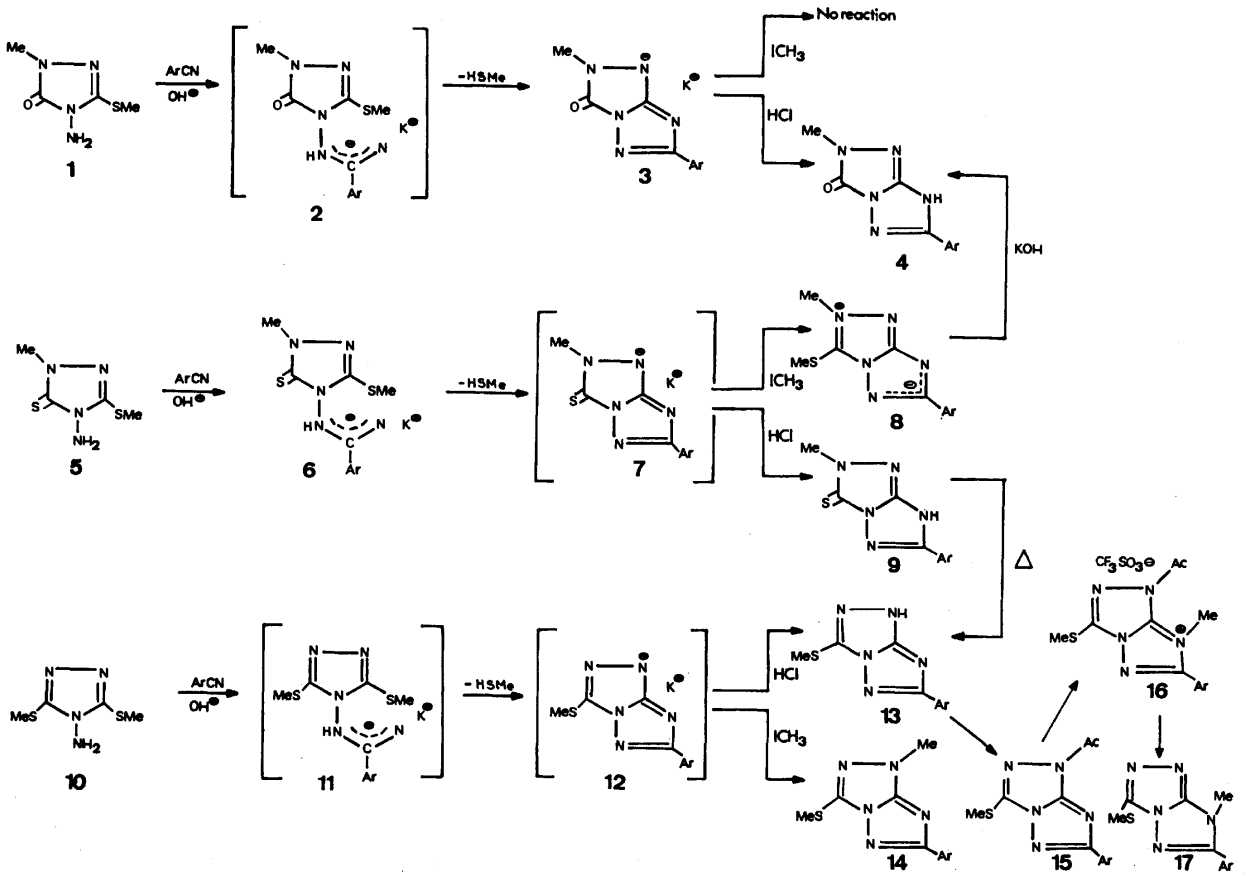

Scheme 1.

we have supposed the same mechanism. The first step is a nucleophilic addition of the *N*-amino group on the cyano group leading to the amidines **2**, **6**, and **11**. The cyclization step involves the departure of the methylthio group at position 3 with concomitant formation of the triazolotriazoles **3**, **7**, and **12**. These compounds carry at position 6 an aryl group and at position 3 an oxo **3**, thioxo **7** or methylthio group **12**. The tautomerism of the corresponding neutral molecules, **4**, **9**, and **13**, will be discussed later.

Table 1. Crystal data

Chemical formula	$C_{11}H_{11}N_5S$
Formula weight	245.3
Crystal system	Monoclinic
Space group	$P2_1/c$
a/Å	12.6939(5)
b/Å	16.0936(6)
c/Å	12.0239(5)
β/°	107.247(3)
V/Å^3	2345.9(2)
D_{calcd}/g cm^{-3}	1.389
Z	8
μ/cm^{-1}	22.82

Compound **3** did not react with methyl iodide. The potassium salt **6** leads to a new mesoionic ring system **8**. The structure of this compound was established by radiocrystallography (see later). Nitrogens N_1, N_5, and N_7 could also have reacted with methyl iodide, but no *N*,*N*'-dimethyl derivative has been isolated. The high reactivity of the sulfur atom in mercaptotriazoles[5] could explain the formation of **8**, but having carried out the reaction on salt **6** it cannot be excluded that the *S*-methylation precedes the cyclization step. The methylation of salt **12** prepared either from **10** or from **13**, can yield three different *N*-methyl derivatives, but only 1-methyl-3-methylthio-6-aryl-1*H*-1,2,4-triazolo-[4,3-*b*][1,2,4]triazole **14** was actually isolated. The N_1 nitrogen atom is also the most reactive in the parent compound.[2] An isomer of **13** can be obtained using Olofson and Kendall's method.[6] The reaction of the azolide **15** with methyl trifluoromethanesulfonate yields the 7-methyl isomer **17** through the quaternary salt

Table 2. Coordinates and thermal parameters as $U_{eq}=(1/3)\cdot\sum(U_{ij}a_i^*a_j^*a_ia_j\cos(a_ia_j))$ ($\times 10^4$)

Atom	x	y	z	U_{eq}
N(1)	0.09162(22)	−0.23634(15)	0.20103(25)	695(10)
N(2)	0.08576(22)	−0.15356(15)	0.17071(23)	668(9)
C(3)	0.01914(26)	−0.10842(16)	0.21478(26)	646(10)
N(4)	−0.01858(20)	−0.16304(13)	0.27841(22)	603(8)
N(5)	−0.08870(21)	−0.16656(13)	0.34525(23)	633(9)
C(6)	−0.08198(23)	−0.24857(16)	0.37114(26)	607(10)
N(7)	−0.01471(20)	−0.29583(13)	0.32778(24)	646(9)
C(8)	0.02561(24)	−0.23971(16)	0.26780(27)	625(10)
C(9)	0.15011(36)	−0.12439(27)	0.09608(36)	808(15)
S(10)	−0.01335(9)	−0.00411(4)	0.19132(8)	786(3)
C(11)	0.02883(37)	0.03224(22)	0.33733(35)	809(14)
C(12)	−0.14938(23)	−0.28306(17)	0.43997(26)	623(10)
C(13)	−0.18411(28)	−0.36583(19)	0.42369(36)	753(13)
C(14)	−0.25149(31)	−0.39751(23)	0.48347(39)	832(15)
C(15)	−0.28502(34)	−0.34971(26)	0.56063(38)	875(16)
C(16)	−0.25151(35)	−0.26739(26)	0.57782(35)	862(15)
C(17)	−0.18419(29)	−0.23482(21)	0.51760(30)	736(12)
N(1')	0.52857(26)	0.01220(16)	0.15301(25)	755(11)
N(2')	0.56178(26)	0.09376(17)	0.15717(27)	779(11)
C(3')	0.53118(26)	0.14014(18)	0.23462(32)	717(12)
N(4')	0.47504(20)	0.08735(14)	0.28294(22)	614(8)
N(5')	0.42056(20)	0.08536(14)	0.36437(23)	632(9)
C(6')	0.38937(22)	0.00488(16)	0.35670(26)	593(9)
N(7')	0.41809(21)	−0.04292(14)	0.27691(22)	635(9)
C(8')	0.47351(25)	0.01079(17)	0.23139(27)	637(10)
C(9')	0.62762(61)	0.11959(37)	0.08236(55)	1084(25)
S(10')	0.56202(7)	0.24384(5)	0.26831(10)	845(4)
C(11')	0.43396(43)	0.28823(28)	0.20403(79)	1552(37)
C(12')	0.32998(22)	−0.02870(17)	0.43405(26)	608(10)
C(13')	0.29265(25)	−0.11129(19)	0.42122(32)	692(11)
C(14')	0.23707(29)	−0.14268(23)	0.49441(36)	805(14)
C(15')	0.21825(31)	−0.09459(27)	0.58136(38)	852(15)
C(16')	0.25438(30)	−0.01293(26)	0.59469(36)	839(14)
C(17')	0.31025(26)	0.01932(22)	0.52234(31)	722(12)

16. In the case of the parent compound **18** a similar reaction yielded also the 7-methyl derivative **20**.[2]

Hydrolysis of the mesoionic compound **8** results in the formation of **4**. On heating compound **9** rearranges to compound **13** (this rearrangement takes place when the ^{13}C NMR spectrum of **9** is recorded at 80 °C to increase its solubility). The rearrangement **9** → **13** is another example of the well known *N* to *S* migration of alkyl groups in *N*-methylazolethiones.[7,8]

Determination of the Structure of Different Compounds

Carbon-13 NMR spectroscopy was used as the sole tool for establishing the different structures. However, due to its importance and unusual formula the structure of **8a** was determined by X-ray crystallography.

Table 1 presents the crystal data. Unit cell parameters were obtained from a least-squares refinement of 52 reflexions as measured on a Philips PW 1100 diffractometer with Cu $K\alpha$ radiation, up to 45° in θ. The intensities of 4347 reflexions with $\theta \leqslant 65°$ were measured with Cu $K\alpha$ radiation graphite monochromated and $\omega/2\theta$ scans. No deterioration of the sample was observed. Data were corrected for Lorentz and polarization factors but not for absorption. 3560 reflexions with $I \geqslant 2\sigma(I)$ were used in the analysis.

The structure was determined by direct methods[9] and refined by full matrix least-squares[10] anisotropically for all non-hydrogen atoms, leading to a final *R*-factor of 0.054 (R_w=0.058, with an empirical weighting scheme so as to give no trends in <w. Δ^2F>). All scattering factors were taken for neutral atoms.[11]

Final atomic parameters are given in Table 2.[12] There are two crystallographically independent molecules, **8a′** and **8a″**, in the unit cell, with bond lengths and angles as specified in Table 3.

Since the X-ray structures of aromatic azapentalenes are so scarce,[1] those of **8a′** and **8a″** deserve some comments, other than the fact that the mesoionic structure is established without ambiguity. The 1,2,4-triazolo-[4,3-*b*][1,2,4]triazole ring is planar in agreement with its aromatic nature. In order to make easy the discussion carbon C_{7a} has been numbered C_8 and substituents heavy atoms from C_9 to C_{17} (for the second molecule we have used dashed numbers) as represented in Fig. 1.

From the relationship between bond lengths and bond orders, it can be deduced that a canonical form, as the represented below, describes accurately the electronic structure of **8a**. Atoms C_9, S_{10}, and C_{12} lie on the plane of the azapentalene ring. The *S*-methyl group is directed towards N_5 and the dihedral angles 11–10–3–4 (11′–10′–3′–4′) are 58.9(3)° for **8a′** and −74.8(4)° for **8a″**. The 6-phenyl ring is planar. Bond distances and angles in this ring range in 1.367

Table 3. Bond distances (l/Å) and angles (ϕ/°) with the estimated standard deviations in parenthesis

Bond/Angle	Molecule **8a′**	Molecule **8a″**
S(10)-C(3)	1.732(3)	1.735(3)
S(10)-C(11)	1.776(4)	1.734(5)
C(3)-N(2)	1.338(5)	1.338(5)
C(3)-N(4)	1.343(4)	1.346(5)
N(2)-N(1)	1.377(3)	1.375(4)
N(2)-C(9)	1.479(6)	1.458(9)
N(1)-C(8)	1.322(5)	1.330(5)
C(8)-N(4)	1.377(4)	1.377(4)
C(8)-N(7)	1.348(4)	1.330(4)
N(4)-N(5)	1.366(4)	1.356(4)
N(5)-C(6)	1.353(3)	1.350(3)
C(6)-N(7)	1.358(4)	1.361(4)
C(6)-C(12)	1.465(5)	1.463(5)
C(3)-S(10)-C(11)	99.8(2)	100.1(2)
S(10)-C(3)-N(4)	128.3(2)	128.2(2)
S(10)-C(3)-N(2)	127.6(2)	127.4(3)
N(2)-C(3)-N(4)	104.1(2)	104.4(3)
C(3)-N(2)-C(9)	127.2(3)	127.5(3)
C(3)-N(2)-N(1)	114.3(3)	114.1(3)
N(1)-N(2)-C(9)	118.6(3)	118.4(3)
N(2)-N(1)-C(8)	101.9(2)	102.2(3)
N(1)-C(8)-N(7)	139.6(3)	139.1(3)
N(1)-C(8)-N(4)	111.6(3)	111.3(3)
N(4)-C(8)-N(7)	108.7(2)	109.6(3)
C(3)-N(4)-C(8)	108.1(2)	108.0(3)
C(8)-N(4)-N(5)	111.8(2)	111.2(2)
C(3)-N(4)-N(5)	140.1(2)	140.8(3)
N(4)-N(5)-C(6)	99.7(2)	100.1(2)
N(5)-C(6)-C(12)	119.5(3)	120.5(3)
N(5)-C(6)-N(7)	117.5(3)	117.1(3)
N(7)-C(6)-C(12)	123.0(2)	122.4(2)
C(8)-N(7)-C(6)	102.2(2)	102.0(2)

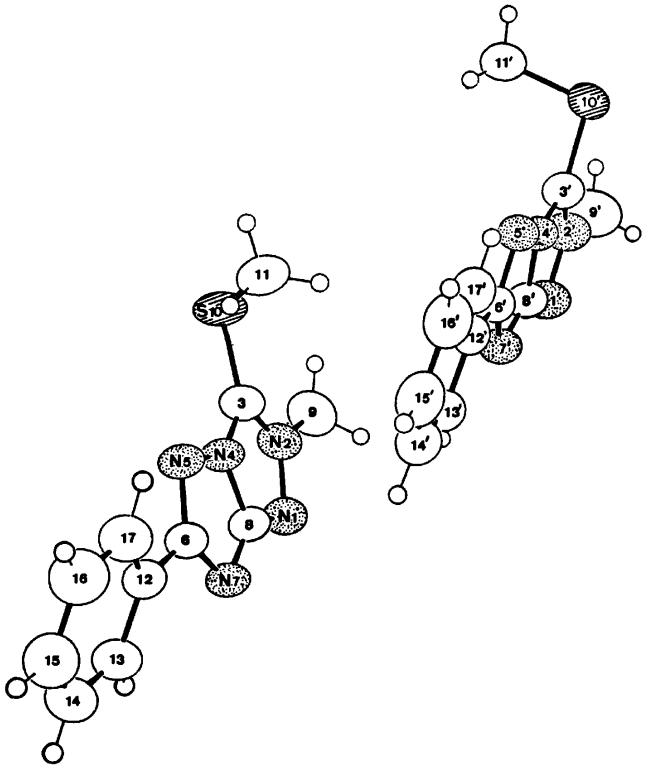

Fig. 1. Ortep drawing of the two molecules with atomic numbering.

(7)—1.404(4) Å and 118.5(3)—121.7(3)°. The dihedral angles about the 6—12 (6′—12′) bonds are −26.7 (4)° and −4.3(4)°.

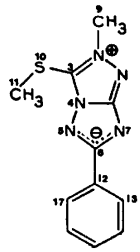

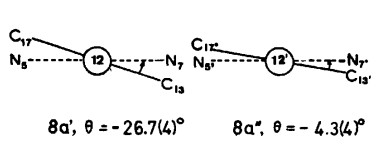

8a′, θ = −26.7(4)° 8a″, θ = −4.3(4)°

These small angles are expected[13] for a situation where hydrogen atoms on $C_{13(13')}$ and $C_{17(17')}$ are opposed to the lone pairs of $N_{5(5')}$ and $N_{7(7')}$.

To discuss the ^{13}C NMR results it is useful to divide the compounds of Scheme 1 into two classes: the 1,2,4-triazole derivatives **1**, **5** and **10** (solvent: DMSO-d_6) and the bicyclic compounds **3**, **4**, **8**, **9**, **13**, **14**, **15**, and **17**. The salts **16** have been isolated (see experimental part) but not studied due to its fragility. However, the position of the acetyl group, on N_1 and that of the methyl group, on N_7, follows from the structures of **15** and **17**. Salts **6**, 1,2,4-triazole derivatives, cyclize when dissolved in D_2O with release of methanethiol, so the ^{13}C spectrum obtained correspond to salt **7** and will be discussed together with the bicyclic compounds.

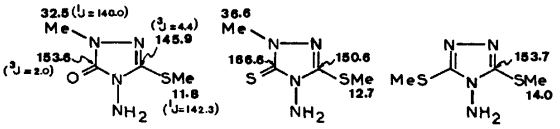

1 5 10

Compound **10** due to its symmetry shows a unique signal for carbons C_3 and C_5. The assignment of carbons C_3 (δ=150.6) and C_5 (δ=166.6) in compund **5** was straightforward from literature data.[14,15] The most difficult case was that of compound **1**, but the assignment was made unambiguous by selective proton decoupling. Irradiation of the SMe signal (δ=2.37, solvent DMSO-d_6) transforms the δ=145.9 quartet into a singlet.

The only ^{13}C NMR spectra of 1,2,4-triazolo[4,3-*b*]-[1,2,4]triazoles so far described are those of the parent compounds **18**, **19**, and **20**.[16,17]

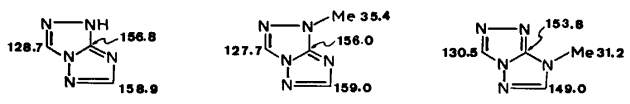

18 19 20

The assignment problems concern exclusively the quaternary carbons C_3, C_6, C_{7a}, C_1', and C_4' (X≠H). The benzene-ring carbons (C_1' and C_4') have been assigned through the known[18] effects of the X-substituent (Table 4). The carbon bearing the phenyl group (C_6) appears as a triplet in the coupled spectra due to a $^3J_{CCCH}$ coupling with protons 2′ and 6′. Methylbenzenes[19] and methylpyridines[20] show similar couplings for the methyl carbon atom. Carbons C_3 and C_{7a} were assigned by internal comparison between the different derivatives of Table 4.

The effect of SMe and phenyl substituents (see below) are almost negligible on C_{7a} and internally consistent on carbons C_3 and C_6:

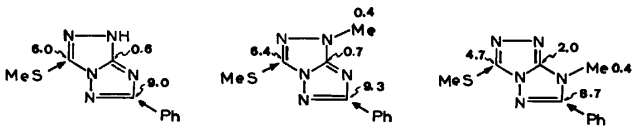

13a-18 14b-19 17a-20

In benzene derivatives[21] the effect of an SMe group on the *ipso* carbon is +9.7 ppm and that of a phenyl group +13.0 ppm. On carbon C_2 of benzoxazoles, the phenyl produces an SCS of +8.4 ppm.[22] Thus the values obtained in the triazolotriazole series are quite normal, taking into account that we have neglected the long-range effects.

The chemical shifts of *N*-CH_3 groups in compounds **14** and **17** are characteristic of their positions N_1 and N_7 (compare with **19** and **20**[16]). Moreover, the carbons C_2' and C_3' in compound **17a** have identical chemical shifts (a similar situation is observed in ^1H NMR, see experimental part). This corresponds[23] to a hindered phenyl group. Only a methyl substituent on a neighbor nitrogen atom could produce such an effect. The acetyl derivative **15** displays a spectrum close to that of **14**, which proves the 1-acetyl-substituted structure.

Finally, concerning the annular tautomerism of **13**, the similitude of chemical shifts with **14** and the large differences with **17** (see, especially, C_6 and C_1') favor the tautomer *N*(H)1. On the other side, compounds **4** and **9** seem to be *N*(H)7 tautomers (carbons C_6 and C_1' appear as in **17**). Obviously, these conclusions concern exclusively DMSO solutions.

Experimental

All melting points were determined with a Kofler hot-stage microscope and are uncorrected. Spectral characterization was performed with the following instruments: IR, Nicolet FT-5DX, ^1H-NMR (80 MHz), Varian FT-80, ^{13}C-NMR (20 MHz), Bruker WP80SY. Mass spectra (70 eV) were obtained with a Hewlett-Packard 5993 C instrument. Combustion analyses were performed with a Perkin-Elmer 240 °C instrument.

Materials. All the reagents, except those listed below were obtained from commercial sources and were used without purification. The 4-amino-1-methyl-3-methylthio-1*H*-1,2,4-triazole-5(4*H*)-thione **5**,[24] 4-amino-1-methyl-3,5-bis(methylthio)-1,2,4-triazolium iodide,[24] 6-aryl-3-methylthio-1*H*-1,2,4-triazolo[4,3-*b*][1,2,4]triazoles **13**,[3] and 6-aryl-1-methyl-3-methylthio-1*H*-1,2,4-triazolo[4,3-*b*][1,2,4]triazoles **14**[3] were prepared according to the methods described in the literature.

The previously unreported 3-methylthio-6-(*p*-nitrophenyl)-1*H*-1,2,4-triazolo[4,3-*b*][1,2,4]triazole **13h** was prepared from **10** and 4-nitrobenzonitrile. Yield, 41%; white needles, mp 280—282 °C; IR (Nujol) 3080, 1630, 1520, 1220, 980, 870, 840, 720 cm^{-1}.

*4-Amino-1-methyl-3-methylthio-1*H*-1,2,4-triazol-5(4*H*)-one* **1**. A solution of 4-amino-1-methyl-3,5-bis(methylthio)-1,2,4-triazolium iodide (6.36 g, 20 mmol) and sodium methoxide (1.35 g, 25 mmol) in methanol (200 ml), was heated under reflux for 10 h. The reaction mixture was filtered, concen-

TABLE 4. CARBON-13 CHEMICAL SHIFS (IN ppm FROM TMS) OF 1,2,4-TRIAZOLO[4,3-*b*][1,2,4]TRIAZOLE DERIVATIVES

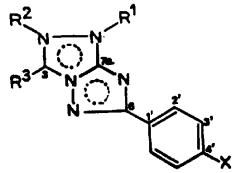

Compound	R^1	R^2	R^3	X	C_3	C_6	C_{7a}	Ar	R^1	R^2	R^3
3a[a]	⊖	Me	O	H	159.0	168.0	146.6	1′: 131.2 2′: 127.2 3′: 129.6 4′: 130.8	—	33.4	—
3b[a]	⊖	Me	O	Me	159.0	168.0	146.6	1′: 128.2 2′: 127.2 3′: 129.9 4′: 141.4 Me: 21.2	—	33.3	—
3d[a]	⊖	Me	O	OMe	c)	167.7	c)	1′: 124.1 2′: 128.8 3′: 114.7 4′: 162.1 OMe: 56.2	—	33.2	—
4a[b]	H	Me	O	H	145.2	155.2[d]	146.5	1′: 125.9 2′: 126.3 3′: 129.1 4′: 131.5	—	32.9[e]	—
4b[b]	H	Me	O	Me	145.4	155.6	146.8	1′: 123.4 2′: 126.4 3′: 129.6 4′: 141.6 Me: 21.0	—	32.9	—
4d[b]	H	Me	O	OMe	145.5	155.4	146.8	1′: 118.4 2′: 128.2 3′: 114.7 4′: 162.0 OMe: 55.5	—	32.9	—
7a[a]	⊖	Me	S	H	160.1	168.4	147.8	1′: 131.0 2′: 127.3 3′: 129.5 4′: 131.0	—	36.9	—
7b[a]	⊖	Me	S	Me	160.0	168.4	147.5	1′: 128.1 2′: 127.2 3′: 129.7 4′: 141.4 Me: 21.4	—	36.9	—
8a[b]	⊖	Me⊕	SMe	H	159.4[g]	168.9[d]	161.9	1′: 131.6 2′: 126.7 3′: 129.9 4′: 128.5	—	38.3[e]	15.5[f]
8b[b,h]	⊖	Me⊕	SMe	Me	160.8	168.9	161.7	1′: 128.7 2′: 126.4 3′: 128.7 4′: 139.2 Me: 21.0	—	37.9	15.1
8c[b]	⊖	Me⊕	SMe	Cl	c)	168.1	162.1	1′: 130.6 2′: 128.4* 3′: 128.6* 4′: 134.7	—	38.3	15.6
9a[b,h]	H	Me	S	H	154.2	156.8	149.0	1′: 125.5 2′: 126.9 3′: 129.4 4′: 132.2	—	36.6	—
9b[b]	H	Me	S	Me	153.6	157.1	149.6	1′: 122.9 2′: 126.5 3′: 129.7 4′: 142.0 Me: 21.0	—	36.3	—

Table 4. (Continued)

Compound	R^1	R^2	R^3	X	C_3	C_6	C_{7a}	Ar	R^1	R^2	R^3
9c[b]	H	Me	S	Cl	c)	156.0	149.4	1′: 124.8 2′: 128.5 3′: 129.3 4′: 136.7	—	36.4	—
9d[b]	H	Me	S	OMe	153.8	156.5	149.0	1′: 117.8 2′: 128.4 3′: 114.7 4′: 162.0 OMe: 55.5	—	36.3	—
13a[b]	H	—	SMe	H	134.7	167.9	157.4	1′: 131.1 2′: 126.2 3′: 128.1 4′: 129.3	—	—	13.5
13b[b]	H	—	SMe	Me	135.1	168.4	157.7	1′: 128.7 2′: 126.5 3′: 129.2 4′: 139.5 Me: 21.0	—	—	13.8
14a[b]	Me	—	SMe	H	c)	c)	157.1	1′: 130.9 2′: 126.6 3′: 128.7 4′: 130.3	35.8	—	14.1
14b[b]	Me	—	SMe	Me	134.1	168.3	156.7	1′: 128.3 2′: 126.4 3′: 129.2 4′: 139.7 Me: 20.9	35.5	—	13.8
15a[b]	COMe	—	SMe	H	140.4[g]	164.7[d]	155.0	1′: 130.2 2′: 126.6 3′: 128.8 4′: 130.4	168.4[g] 21.8[i]	—	13.1
15b[b]	COMe	—	SMe	Me	140.5	164.6	155.1	1′: 127.6 2′: 126.6 3′: 129.3 4′: 140.3 Me: 21.0	168.8 21.7	—	13.2
17a[b]	R^7=Me	—	SMe	H	135.2	157.7	155.8	1′: 125.3 2′: 129.1 3′: 129.1 4′: 131.4	R^7 31.6	—	15.4
17b[b]	R^7=Me	—	SMe	Me	135.1	157.8	155.8	1′: 122.4 2′: 128.9 3′: 129.6 4′: 141.5 Me: 21.0	R^7 31.5	—	15.3

a) Solvent: D_2O-dioxane; b) Solvent: DMSO-d_6; c) Not observed; d) Benzylic coupling (triplet, ^3J=3.5 Hz); e) N-CH_3 coupling (quartet, ^1J=142 Hz); f) S-CH_3 coupling (quartet, ^1J=144 Hz); g) Complex multiplet; h) At 80 °C; i) CO-CH_3 coupling (quartet, ^1J=133 Hz).

trated to one third of volume and cooled to 0 °C. The precipitated solid was filtered, dried, and recrystallized from methanol to give 4-amino-1-methyl-3-methylthio-1*H*-1,2,4-triazol-5(4*H*)-one **1** (2.78 g, 87%) as white needles, mp 175—176 °C.

IR (Nujol) 3320, 3210, 1720, 1650, 1560, 1420, 1270, 990, 970, 950, 890, 730 cm^{-1}. ^1H-NMR (DMSO-d_6) δ=5.29 (2H, s, NH_2), 3.30 (3H, s, N-CH_3), 2.37 (3H, s, S-CH_3).

Found: C, 29.91; H, 4.99; N, 34.82; S, 19.87%. Calcd for $C_4H_8N_4OS$: C, 29.99; H, 5.03; N, 34.97; S, 20.01%

General Procedure for the Preparation of Triazolotriazole Salts **3**. To a solution of 4-amino-1-methyl-3-methylthio-1*H*-1,2,4-triazol-5(4*H*)-one **1** (3.5 g, 21.8 mmol) in *t*-butyl alcohol (80 ml), equimolar amounts of potassium *t*-butoxide (2.44 g, 21.8 mmol) and the appropriate aromatic nitrile were added. The reaction mixture was heated under reflux with stirring for 6 h. After cooling, the precipitated solid was separated and recrystallized from ethanol to give the corresponding triazolotriazole salt **3** as crystalline solid in high yield (Table 5).

By this procedure, the following salts **3** were prepared:

3a as colorless prisms. IR(Nujol) 1680, 1600, 1460, 1440, 1280, 1180, 1120, 850, 830, 750 cm^{-1}.

3b as colorless prisms. IR(Nujol) 1680, 1600, 1460, 1440, 1380, 1280, 1120, 1070, 1030, 860, 780, 750, 710, 690 cm^{-1}.

3c as colorless prisms. IR(Nujol) 1680, 1600, 1520, 1460, 1430, 1380, 1200, 1125, 845, 810, 765, 740 cm^{-1}.

3d as colorless prisms. IR(Nujol) 1680, 1600, 1460, 1440,

Table 5. Triazolotriazole and amidine salts **3** and **6**

Compound	X	Yield/%	Mp θ_m/°C	Found/%				Molecular formula	Calcd/%			
				C	H	N	S		C	H	N	S
3a	H	80	>350	47.25	3.12	27.42		$C_{10}H_8N_5OK$	47.37	3.15	27.63	
3b	4-CH_3	85	>350	49.25	3.54	25.92		$C_{11}H_{10}N_5OK$	49.38	3.74	26.18	
3c	4-Cl	80	>350	41.57	2.33	24.20		$C_{10}H_7N_5ClOK$	41.72	2.43	24.33	
3d	4-OCH_3	82	>350	46.53	3.49	24.50		$C_{11}H_{10}N_5O_2K$	46.59	3.52	24.70	
3e	2-CH_3	87	>350	49.29	3.60	26.12		$C_{11}H_{10}N_5OK$	49.38	3.74	26.18	
3f	2,4-$(CH_3)_2$	75	>350	51.06	4.17	24.60		$C_{12}H_{12}N_5OK$	51.17	4.26	24.87	
6a	H	74	>350	41.48	3.83	21.94	20.25	$C_{11}H_{12}N_5S_2K$	41.62	3.81	22.06	20.19
6b	4-CH_3	69	>350	43.40	4.12	21.05	19.22	$C_{12}H_{14}N_5S_2K$	43.47	4.25	21.12	19.34
6c	4-Cl	64	>350	37.45	3.03	19.76	18.10	$C_{11}H_{11}N_5ClS_2K$	37.54	3.15	19.90	18.22
6d	4-OCH_3	61	>350	41.33	4.02	20.01	18.30	$C_{12}H_{14}N_5OS_2K$	41.47	4.06	20.15	18.45
6e	2-CH_3	58	>350	43.38	4.20	21.01	19.18	$C_{12}H_{14}N_5S_2K$	43.47	4.25	21.12	19.34
6f	2,4-$(CH_3)_2$	56	>350	45.13	4.51	10.13	18.66	$C_{13}H_{16}N_5S_2K$	45.19	4.66	20.26	18.55

Table 6. 1,2,4-triazolo[4,3-*b*][1,2,4]triazol-3-one and 1,2,4-triazolo[4,3-*b*][1,2,4]-triazole-3-thione derivatives **4** and **9**

Compound	X	Yield/%	Mp θ_m/°C	Found/%				Molecular formula	Calcd/%			
				C	H	N	S		C	H	N	S
4a	H	83	299—300	55.57	3.91	32.55		$C_{10}H_9N_5O$	55.81	4.18	32.55	
4b	4-CH_3	79	323—324	57.70	4.52	30.29		$C_{11}H_{11}N_5O$	57.64	4.80	30.56	
4c	4-Cl	81	>350	48.12	3.17	28.10		$C_{10}H_8N_5ClO$	48.09	3.20	28.05	
4d	4-OCH_3	75	327—330	53.71	4.29	28.80		$C_{11}H_{11}N_5O_2$	53.87	4.48	28.57	
4e	2-CH_3	75	278—279	57.40	4.60	30.48		$C_{11}H_{11}N_5O$	57.64	4.80	30.56	
4f	2,4-$(CH_3)_2$	70	294—296	59.17	5.14	28.70		$C_{12}H_{13}N_5O$	59.25	5.34	28.80	
9a	H	92	300—302	52.01	3.90	30.17	13.72	$C_{10}H_9N_5S$	51.93	3.92	30.28	13.86
9b	4-CH_3	95	268—270	53.77	4.50	28.44	13.10	$C_{11}H_{11}N_5S$	53.86	4.52	28.55	13.07
9c	4-Cl	98	330—333	45.09	2.97	26.18	11.92	$C_{10}H_8N_5ClS$	45.20	3.03	26.35	12.06
9d	4-OCH_3	87	287—289	50.51	4.22	26.76	12.12	$C_{11}H_{11}N_5OS$	50.56	4.24	26.80	12.27
9e	2-CH_3	85	215—217	53.76	4.40	28.49	12.99	$C_{11}H_{11}N_5S$	53.86	4.52	28.55	13.07
9f	2,4-$(CH_3)_2$	83	220—222	55.55	5.01	26.89	12.22	$C_{12}H_{13}N_5S$	55.57	5.05	27.00	12.36

1260, 1040, 860, 770 cm^{-1}.

3e as colorless prisms. IR(Nujol) 1680, 1600, 1460, 1440, 1380, 1280, 1180, 1115, 855, 830, 750 cm^{-1}.

3f as colorless prisms. IR(Nujol) 1680, 1600, 1460, 1440, 1280, 1230, 1175, 1110, 1030, 850, 830, 800, 750, 680 cm^{-1}.

*General Procedure for the Preparation of 6-Aryl-2-methyl-7*H*-1,2,4-triazolo[4,3-*b*][1,2,4]triazol-3(2*H*)-ones* **4**. To a well stirred solution of triazolotriazole salt **3** (10 mmol) in water (80 ml), 1 M† hydrochloric acid was added dropwise until pH=5. The precipitated solid was collected by filtration, dried, and recrystallized from ethanol to give pure 6-aryl-2-methyl-7*H*-1,2,4-triazolo[4,3-*b*][1,2,4]triazol-3(2*H*)-one **4** as crystalline solid in high yield (Table 6).

By this procedure, the following compounds **4** were prepared:

4a as colorless prisms. IR(Nujol) 3070, 1695, 1650, 1500, 970, 840, 780, 730, 680 cm^{-1}. ^{1}H-NMR (DMSO-d_6/D_2O) δ=7.9—7.6 (5H, m), 3.40 (3H, s), MS *m/z* (%), 215 (M^+, 100), 103 (82).

4b as colorless prisms. IR (Nujol) 3080, 1710, 1650, 970, 835, 730, 680, 640 cm^{-1}. ^{1}H-NMR (DMSO-d_6/D_2O) δ=7.60 (2H, d), 7.15 (2H, d), 3.38 (3H, s), 2.33 (3H, s). MS *m/z* (%), 229 (M^+, 100), 117 (91).

4c as colorless needles. IR (Nujol) 3090, 1710, 1660, 1500, 1470, 1100, 970, 835, 730, 700, 660 cm^{-1}. ^{1}H-NMR (DMSO-d_6/D_2O) δ=7.90 (2H, d), 7.20 (2H, d), 3.39 (3H, s). MS *m/z* (%), 249 (M^+, 100), 251 (M^++2, 31), 137 (85), 139 (25).

4d as colorless prisms. IR (Nujol) 3080, 1705, 1660, 1620, 1590, 1505, 1260, 1185, 1030, 965, 835, 735, 710, 660, 650, 630 cm^{-1}. ^{1}H-NMR (DMSO-d_6/D_2O) δ=7.88 (2H, d), 7.10 (2H, d), 3.85 (3H, s), 3.39 (3H, s). MS *m/z* (%), 245 (M^+, 100), 133 (80).

4e as colorless prisms. IR (Nujol) 3100, 1710, 1660, 1500, 970, 830, 770, 710, 680, 660 cm^{-1}. ^{1}H-NMR (DMSO-d_6/D_2O) δ=7.5—7.2 (4H, m). 3,39 (3H, s), 2.39 (3H, s). MS *m/z* (%) 229 (M^+, 100), 117 (90).

4f as colourless prisms. IR (Nujol) 3070, 1710, 1660, 1500, 1340, 970, 830, 730, 710, 680, 670 cm^{-1}. ^{1}H-NMR (DMSO-d_6/D_2O) δ=7.5—7.2 (3H, m), 3.40 (3H, s), 2.48 (3H, s), 2.34 (3H, s). MS *m/z* (%), 243 (M^+, 100), 131 (82).

General Procedure for the Preparation of Amidine Salts **6**. To a well-stirred solution of 4-amino-1-methyl-3-methylthio-1*H*-1,2,4-triazole-5(4*H*)-thione **5** (3.52 g, 20 mmol) in *t*-butyl alcohol (100 ml), equimolar amounts of potassium *t*-butoxide (2.24 g, 20 mmol) and the appropriate aromatic nitrile, were added. The reaction mixture was heated under reflux for 3 h. After cooling, the precipitated solid was separated by filtration and recrystallized from ethanol to give the cor-

† 1 M=1 mol dm^{-3}.

Table 7. Inner salt of 6-aryl-2-methyl-3-methylthio-7*H*-1,2,4-triazolo[4,3-*b*][1,2,4]-triazolium hydroxydes **8**

Compound	X	Yield/%	Mp θ_m/°C	Found/%				Molecular formula	Calcd/%			
				C	H	N	S		C	H	N	S
8a	H	82	165—167	53.74	4.50	28.41	12.93	$C_{11}H_{11}N_5S$	53.86	4.52	28.55	13.07
8b	4-CH_3	74	158—160	55.52	4.96	26.84	12.12	$C_{12}H_{13}N_5S$	55.58	5.05	27.00	12.36
8c	4-Cl	77	160—162	47.12	3.61	24.91	11.33	$C_{11}H_{10}N_5ClS$	47.23	3.60	25.03	11.46
8d	4-OCH_3	91	185—187	52.23	4.65	25.39	11.48	$C_{12}H_{13}N_5OS$	52.35	4.76	25.43	11.64
8e	2-CH_3	57	151—153	55.50	5.02	26.89	12.30	$C_{12}H_{13}N_5S$	55.58	5.05	27.00	12.36
8f	2,4-$(CH_3)_2$	61	175—177	57.01	5.47	25.49	11.56	$C_{13}H_{15}N_5S$	57.12	5.53	25.62	11.73

responding amidine salt **6**, as crystalline solid in moderated yields (Table 5).

By the above procedure, the following salts **6** were obtained:

6a as colorless prisms. IR (Nujol) 3180, 1590, 1580, 1460, 1200, 1120, 1010, 835, 750, 705 cm^{-1}.

6b as colorless prisms. IR (Nujol) 3210, 1590, 1460, 1330, 1130, 1010, 830, 755 cm^{-1}.

6c as colorless prisms. IR (Nujol) 3210, 1595, 1450, 1400, 1280, 1130, 1110, 1020, 1000, 840, 760 cm^{-1}.

6d as colorless prisms. IR (Nujol) 3200, 1590, 1580, 1460, 1255, 1175, 1030, 1000, 855, 760 cm^{-1}.

6e as colorless prisms. IR (Nujol) 3200, 1590, 1450, 1325, 1190, 1120, 1000, 830, 745, 720 cm^{-1}.

6f as colorless prisms. IR (Nujol) 3180, 1590, 1580, 1450, 1190, 1120, 1010, 835, 735, 720 cm^{-1}.

*General Procedure for the Preparation of Inner Salt of 6-Aryl-2-methyl-3-methylthio-7*H*-1,2,4-triazolo[4,3-*b*][1,2,4]triazolium Hydroxides* **8**. To a well-stirred solution of amidine salt **6** (10 mmol) in water (100 ml), methyl iodide (13 mmol) and enough ethanol (about 20 ml) were added to give a clear solution. The resulting solution was kept at room temperature for 24 h. The solvent was partially removed under reduced pressure and the separated solid was filtered, dried and recrystallized from ethanol to give pure **8** as crystalline solid in good yield (Table 7).

By this procedure the following mesoionic compounds **8** were prepared:

8a as white prisms. IR (Nujol) 1590, 1580, 1410, 1350, 1280, 1080, 990, 790, 755, 715 cm^{-1}. ^{1}H-NMR ($CDCl_3$) δ=8.3—7.4 (5H, m), 4.00 (3H, s), 2.75 (3H, s). MS *m/z* (%) 245 (M^+, 38), 212 (25), 129 (44), 103 (34), 77 (100).

8b as white prisms. IR (Nujol) 1585, 1460, 1400, 1330, 1180, 1105, 1030, 980, 830, 755, 730 cm^{-1}. ^{1}H-NMR ($CDCl_3$) δ=7.70 (2H, d), 7.40 (2H. d), 4.05 (3H, s), 2.75 (3H, s), 2.40 (3H, s). MS *m/z* (%) 259 (M^+, 26), 226 (79), 185 (30), 143 (51), 117 (43), 81 (76), 69 (100).

8c as white prisms. IR (Nujol) 1580, 1570, 1470, 1420, 1320, 1020, 990, 840, 760, 730 cm^{-1}. ^{1}H-NMR ($CDCl_3$) δ=7.80 (2H, d), 7.60 (2H, d), 4.00 (3H, s), 2.70 (3H, s). MS *m/z* (%) 281 (M^++2, 6), 279 (M^+, 18), 248 (5), 246 (15), 165 (8), 163 (8), 139 (10), 137 (30), 70 (100).

8d as white prisms. IR (Nujol) 1610, 1590, 1430, 1405, 1350, 1310, 1250, 1180, 1020, 850, 740, 680 cm^{-1}. ^{1}H-NMR ($CDCl_3$) δ=7.90 (2H, d), 7.20 (2H, d), 3.95 (3H, s), 3.80 (3H, s), 2.70 (3H, s). MS *m/z* (%) 275 (M^+, 31), 270 (12), 244 (5), 242 (8), 159 (21), 133 (13), 69 (100).

8e as white needles. IR (Nujol) 1590, 1460, 1330, 1260, 1190, 1025, 990, 820, 750, 735 cm^{-1}. ^{1}H-NMR ($CDCl_3$) δ=8.1—7.3 (4H, m), 4.00 (3H, s), 2.70 (3H, s), 2.65 (3H, s). MS *m/z* (%) 259 (M^+, 43), 226 (12), 143 (72), 117 (25), 69 (100).

8f as white needles. IR (Nujol) 1585, 1560, 1455, 1420, 1325, 1200, 1020, 980, 830, 760 cm^{-1}. ^{1}H-NMR ($CDCl_3$) δ=8.0—7.1 (3H, m), 4.00 (3H, s), 2.75 (3H, s), 2.65 (3H, s), 2.40 (3H, s). MS *m/z* (%) 273 (M^+, 70), 258 (43), 157 (33), 131 (30), 69 (100).

*General Procedure for the Preparation of 6-Aryl-2-methyl-7*H*-1,2,4-triazolo[4,3-b][1,2,4]triazole-3(2*H*)-thiones* **9**. To a well-stirred solution of amidine salt **6** (10 mmol) in water (100 ml), 1 M hydrochloric acid was added dropwise until pH=5. The precipitated solid was collected by filtration, dried, and recrystallized from ethanol to give pure **9** as crystalline solid in high yield (Table 6).

By the above procedure, the following compounds **9** were prepared:

9a as white prisms. IR (Nujol) 3080, 1655, 1605, 1465, 1430, 1380, 1120, 960, 830, 780, 690 cm^{-1}. ^{1}H-NMR (DMSO-d_6/D_2O) δ=7.9—7.3 (5H, m), 3.83 (3H, s). MS *m/z* (%) 231 (M^+, 55), 198 (11), 172 (42), 103 (100), 77 (21).

9b as white needles. IR (Nujol) 3080, 1650, 1610, 1460, 1320, 1200, 1125, 960, 830, 825, 730 cm^{-1}. ^{1}H-NMR (DMSO-d_6/D_2O) δ=7.70 (2H, d), 7.30 (2H, d), 3.80 (3H, s), 2.40 (3H, s). MS *m/z* (%) 245 (M^+, 61), 212 (8), 186 (32), 117 (100), 70 (48).

9c as white needles. IR (Nujol) 3080, 1655, 1605, 1470, 1400, 1100, 960, 840, 830, 730 cm^{-1}. ^{1}H-NMR (DMSO-d_6/D_2O)) δ=7.90 (2H, d), 7.60 (2H, d), 3.80 (3H, s). MS *m/z* (%) 267 (M^++2, 32), 265 (M^+, 100), 234 (4), 232 (12), 208 (21), 206 (63), 139 (10), 137 (30).

9d as white needles. IR (Nujol) 3070, 1650, 1605, 1490, 1460, 1250, 1175, 1025, 950, 850, 845, 810, 735 cm^{-1}. ^{1}H-NMR (DMSO-d_6/D_2O) δ=7.70 (2H, d), 7.30 (2H, d), 3.85 (3H, s), 3.75 (3H, s). MS *m/z* (%) 261 (M^+, 100), 228 (8), 202 (56), 133 (42).

9e as white prisms. IR (Nujol) 3080, 1650, 1460, 1310, 1120, 1050, 950, 825, 770, 720 cm^{-1}. ^{1}H-NMR (DMSO-d_6/D_2O) δ=8.1—7.3 (4H, m), 3.82 (3H, s), 2.65 (3H, s). MS *m/z* (%) 245 (M^+, 100), 212 (7), 186 (34), 158 (25), 143 (11), 117 (44).

9f as white prisms. IR (Nujol) 3080, 1650, 1610, 1460, 1370, 1300, 1200, 1120, 955, 830, 735, 720 cm^{-1}. ^{1}H-NMR (DMSO-d_6/D_2O) δ=8.0—7.1 (3H, m), 3.80 (3H, s), 2.65 (3H, s), 2.40 (3H, s). MS *m/z* (%) 259 (M^+, 100), 226 (13), 200 (28), 172 (36), 131 (76), 116 (62).

Basic Hydrolysis of Compounds **8**. A solution of inner salt of 6-aryl-2-methyl-3-methylthio-7*H*-1,2,4-triazolo[4,3-*b*]-[1,2,4]triazolium hydroxide **8** (5 mmol) in 10 % methanolic potassium hydroxide (75 ml) was heated under reflux until evolution of methanethiol was ceased (about 5 h). Then, the solvent was removed under reduced pressure and the residual material was dissolved in water (60 ml). The resulting solution was acidified by dropwise addition of 1 M hydrochloric acid until pH=5. The precipitated solid was collected by filtration, dried and crystallized from ethanol to give 6-aryl-2-methyl-7*H*-1,2,4-triazolo[4,3-*b*][1,2,4]triazol-

3(2*H*)-one **4** in almost quantitative yield.

*General Procedure for the Preparation of 1-Acetyl-6-aryl-3-methylthio-1,2,4-triazolo[4,3-*b*][1,2,4]triazoles* **15**. A solution of 6-aryl-3-methylthio-1*H*-1,2,4-triazolo[4,3-*b*][1,2,4]-triazole **13** (20 mmol) in acetic anhydride (100 ml) was heated under reflux for 1 h with stirring. After cooling, the precipitated solid was collected by filtration, dried under vacuum at 100 °C, and crystallized from ethanol to give pure **15** as crystalline solid in high yield (Table 4).

By this procedure the following compounds **15** were obtained:

15a as white plates. IR (Nujol) 1750, 1570, 1490, 1420, 1310, 1130, 990, 790, 740, 710, 680 cm^{-1}. ^{1}H-NMR ($CDCl_3$/CF_3CO_2H) δ=8.1—7.5 (5H, m), 2.90 (3H, s), 2.75 (3H, s).

15b as white needles. IR (Nujol) 1740, 1585, 1570, 1490, 1430, 1420, 1320, 1205, 1125, 835, 760, 745 cm^{-1}. ^{1}H-NMR ($CDCl_3$/CF_3CO_2H) δ=7.90 (2H, d), 7.50 (2H, d), 2.90 (3H, s), 2.75 (3H, s), 2.40 (3H, s).

15c as white needles. IR (Nujol) 1745, 1570, 1420, 1320, 1210, 1125, 1020, 910, 850, 745 cm^{-1}. ^{1}H-NMR ($CDCl_3$/CF_3CO_2H) δ=7.90 (2H, d), 7.60 (2H, d), 2.95 (3H, s), 2.75 (3H, s).

15e as white needles. IR (Nujol) 1730, 1585, 1570, 1480, 1410, 1380, 1325, 1125, 900, 760, 730 cm^{-1}. ^{1}H-NMR ($CDCl_3$/CF_3CO_2H) δ=8.1—7.4 (4H, m), 2.90 (3H, s), 2.75 (3H, s), 2.65 (3H, s).

15f as white needles. IR (Nujol) 1740, 1570, 1495, 1420, 1320, 1210, 1130, 990, 910, 840, 760, 730 cm^{-1}. ^{1}H-NMR ($CDCl_3$/CF_3CO_2H) δ=7.9—7.1 (3H, m), 2.90 (3H, s), 2.75 (3H, s), 2.65 (3H, s), 2.40 (3H, s).

15g as white needles. IR (Nujol) 1730, 1585, 1570, 1485, 1410, 1380, 1330, 1205, 1125, 1045, 900, 735, 710 cm^{-1}. ^{1}H-NMR ($CDCl_3$/CF_3CO_2H) δ=8.1—7.4 (4H, m), 2.95 (3H, s), 2.75 (3H, s).

15h as white plates. IR (Nujol) 1745, 1575, 1520, 1420, 1350, 1310, 1130, 990, 870, 860, 740, 720 cm^{-1}. ^{1}H-NMR ($CDCl_3$/CF_3CO_2H) δ=7.90 (2H, d), 7.60 (2H, d), 2.90 (3H, s), 2.75 (3H, s).

General Procedure for the Preparation of 1-Acetyl-6-aryl-7-methyl-3-methylthio-7H-1,2,4-triazolo[4,3-b][1,2,4]triazol-7-ium Trifluoromethanesulfonates **16**. To a solution of 1-acetyl-6-aryl-3-methylthio-1*H*-1,2,4-triazolo[4,3-*b*][1,2,4]triazole **15** (10 mmol) in dry dichloromethane (75 ml), methyl trifluoromethanesulfonate (12 mmol) was added dropwise. The reaction mixture was stirred at room temperature for 24 h. Occasionally the trifluoromethanesulfonate salt **16** precipitated in the course of the reaction. If not, the solvent was removed under reduced pressure and the residual material was crystallized from dichloromethane-diethyl ether to give the pure **16** as crystalline solid in high yield (Table 8).

By this procedure the following compounds **16** were prepared:

16a as colorless prisms. IR (Nujol) 1755, 1640, 1530, 1460, 1370, 1300, 1230, 1210, 1160, 1130, 1030, 950, 780, 730, 710, 640 cm^{-1}. ^{1}H-NMR ($CDCl_3$) δ=7.8—7.5 (5 H, m), 4.15 (3H, s), 2.85 (3H, s), 2.75 (3H, s).

16b as colorless prisms. IR (Nujol) 1770, 1620, 1520, 1310, 1270, 1230, 1160, 1030, 980, 840, 770, 740, 640 cm^{-1}. ^{1}H-NMR ($CDCl_3$) δ=8.0 (2H, d), 7.5 (2H, d), 4.15 (3H, s), 2.90 (3H, s), 2.75 (3H, s), 2.40 (3H, s).

16c as colorless prisms. IR (Nujol) 1765, 1610, 1540, 1360, 1270, 1230, 1160, 1030, 1010, 965, 910, 840, 730, 640 cm^{-1}. ^{1}H-NMR ($CDCl_3$) δ=7.90 (2H, d), 7.60 (2H, d), 4.10 (3H, s), 2.90 (3H, s), 2.75 (3H, s).

16e as colorless prisms. IR (Nujol) 1765, 1615, 1550, 1370, 1310, 1270, 1240, 1230, 1160, 1030, 970, 910, 770, 760, 740, 640 cm^{-1}. ^{1}H-NMR ($CDCl_3$) δ=8.2—7.4 (4H, m), 4.15 (3H, s), 2.85 (3H, s), 2.75 (3H, s), 2.65 (3H, s).

16f as colorless prisms. IR (Nujol) 1770, 1620, 1520, 1420, 1310, 1270, 1230, 1180, 1160, 1030, 970, 830, 780, 760, 720, 640 cm^{-1}. ^{1}H-NMR ($CDCl_3$) δ=7.9—7.0 (3H, m), 4.15 (3H, s), 2.90 (3H, s), 2.75 (3H, s), 2.65 (3H, s),

Table 8. 3-Methylthio-6-arylthio-6-aryl-1,2,4-triazolo[4,3-*b*][1,2,4]triazole derivatives **15**, **16**, and **17**

Compound	X	Yield/%	Mp θ_m/°C	Found/%				Molecular formula	Calcd/%			
				C	H	N	S		C	H	N	S
15a	H	88	193—195	52.64	4.02	25.47	11.58	$C_{12}H_{11}N_5OS$	52.73	4.06	25.62	11.73
15b	4-CH_3	68	174—175	54.21	4.49	24.19	10.98	$C_{13}H_{13}N_5OS$	54.34	4.56	24.37	11.16
15c	4-Cl	70	199—200	46.78	3.22	22.59	10.31	$C_{12}H_{10}N_5ClOS$	46.83	3.27	22.75	10.42
15e	2-CH_3	82	140—142	54.28	4.52	24.19	11.03	$C_{13}H_{13}N_5OS$	54.34	4.56	24.37	11.16
15f	2,4-$(CH_3)_2$	95	200—202	55.69	4.93	23.18	10.49	$C_{14}H_{15}N_5OS$	55.80	5.02	23.24	10.64
15g	2-Cl	67	130—131	46.85	3.21	22.62	10.33	$C_{12}H_{10}N_5ClOS$	46.83	3.27	22.75	10.42
15h	4-O_2N	47	220—222	45.14	3.12	26.33	9.93	$C_{12}H_{10}N_6O_3S$	45.28	3.17	26.40	10.07
16a	H	70	156—158	38.54	3.18	16.05	14.53	$C_{14}H_{14}N_5F_3O_4S_2$	38.44	3.23	16.01	14.66
16b	4-CH_3	81	110—112	39.83	3.51	15.39	14.07	$C_{15}H_{16}N_5F_3O_4S_2$	39.91	3.57	15.51	14.20
16c	4-Cl	89	185—186	35.52	2.69	14.73	13.40	$C_{14}H_{13}N_5ClF_3O_4S_2$	35.64	2.78	14.84	13.59
16e	2-CH_3	51	115—117	39.85	3.51	15.38	14.08	$C_{15}H_{16}N_5F_3O_4S_2$	39.91	3.57	15.51	14.20
16f	2,4-$(CH_3)_2$	81	101—103	41.18	3.85	14.94	13.66	$C_{16}H_{18}N_5F_3O_4S_2$	41.29	3.90	15.04	13.78
16g	2-Cl	63	149—150	35.59	2.69	14.72	13.43	$C_{14}H_{13}N_5ClF_3O_4S_2$	35.64	2.78	14.84	13.59
16h	4-O_2N	37	129—130	34.77	2.70	17.36	13.13	$C_{14}H_{13}N_6F_3O_6S_2$	34.86	2.72	17.42	13.29
17a	H	86	113—115	53.80	4.47	28.37	12.94	$C_{11}H_{11}N_5S$	53.86	4.52	28.55	13.07
17b	4-CH_3	91	128—129	55.44	4.96	26.83	12.19	$C_{12}H_{13}N_5S$	55.58	5.05	27.00	12.36
17c	4-Cl	96	110—112	47.12	3.52	24.89	11.29	$C_{11}H_{10}N_5ClS$	47.23	3.60	25.03	11.46
17e	2-CH_3	74	112—114	55.53	5.01	26.82	12.27	$C_{12}H_{13}N_5S$	55.58	5.05	27.00	12.36
17f	2,4-$(CH_3)_2$	81	92— 93	56.97	5.46	25.49	11.61	$C_{13}H_{15}N_5S$	57.12	5.53	26.62	11.73
17g	2-Cl	67	98— 99	47.05	3.56	24.92	11.33	$C_{11}H_{10}N_5ClS$	47.23	3.60	25.03	11.46
17h	4-O_2N	93	148—150	45.43	3.38	28.83	10.89	$C_{11}H_{10}N_6O_2S$	45.51	3.47	28.95	11.04

2.40 (3H, s).

16g as colorless prisms. IR (Nujol) 1770, 1620, 1530, 1370, 1310, 1270, 1230, 1160, 1030, 970, 910, 780, 760, 730, 640 cm^{-1}. ^1H-NMR ($CDCl_3$) δ=8.2—7.4 (4H, m), 4.10 (3H, s), 2.90 (3H, s), 2.75 (3H, s).

16h as white needles. IR (Nujol) 1770, 1620, 1550, 1520, 1360, 1320, 1270, 1160, 1040, 975, 910, 870, 860, 730, 640 cm^{-1}. ^1H-NMR ($CDCl_3$) δ=7.90 (2H, d), 7.70 (2H, d), 4.10 (3H, s), 2.85 (3H, s), 2.75 (3H, s).

General Procedure for the Preparation of 6-Aryl-7-methyl-3-methylthio-7H-1,2,4-triazolo[4,3-b][1,2,4]triazoles **17**. To a solution of 1-acetyl-6-aryl-7-methyl-3-methylthio-1*H*-1,2,4-triazolo[4,3-*b*][1,2,4]triazol-7-ium trifluoromethanesulfonate **16** (10 mmol) in water (250 ml), ethanol was added until a clear solution was obtained at 70 °C. Then a saturated aqueous solution of sodium carbonate was added dropwise with stirring, until pH=9. After cooling to 0 °C, the precipitated solid was collected by filtration, dried, and recrystallized from chloroform-hexane to give the pure **17** as crystalline solid in high yield (Table 8).

By the above procedure, the following compounds **17** were obtained:

17a as white prisms. IR (Nujol) 1590, 1470, 1330, 1320, 1170, 1045, 1020, 955, 785, 720, 710 cm^{-1}. ^1H-NMR (DMSO-d_6) δ=7.7—7.2 (5H, m), 3.80 (3H, s), 2.75 (3H, s); ($CDCl_3$) δ=7.60 (5H, s), 3.75 (3H, s), 2.65 (3H, s). The fact that the phenyl appears as a singlet is characteristic of a phenyl out-of-plane (For another example in the azapentalene series, see Ref. 25).

17b as white needles. IR (Nujol) 1590, 1480, 1460, 1270, 1175, 1070, 990, 970, 840, 730 cm^{-1}. ^1H-NMR (DMSO-d_6) δ=7.90 (2H, d), 7.65 (2H, d), 3.80 (3H, s), 2.70 (3H, s), 2.50 (3H, s).

17c as white needles. IR (Nujol) 1590, 1495, 1320, 1180, 1170, 1090, 1000, 945, 835, 720 cm^{-1}. ^1H-NMR (DMSO-d_6) δ=8.00 (2H, d), 7.80 (2H, d), 3.80 (3H, s), 2.70 (3H, s).

17e as white prisms. IR (Nujol) 1590, 1490, 1370, 1320, 1170, 1050, 1030, 950, 785, 740, 730 cm^{-1}. ^1H-NMR (DMSO-d_6) δ=7.8—7.4 (4H, m), 3.65 (3H, s), 2.70 (3H, s), 2.35 (3H, s).

17f as white prisms. IR (Nujol) 1590, 1500, 1370, 1320, 1180, 1140, 1060, 1000, 970, 840, 745, 735, 730 cm^{-1}. ^1H-NMR (DMSO-d_6) δ=7.9—7.3 (3H, m), 3.60 (3H, s), 2.75 (3H, s), 2.45 (3H, s), 2.35 (3H, s).

17g as white prisms. IR (Nujol) 1600, 1500, 1430, 1370, 1320, 1180, 1095, 1040, 970, 780, 745, 720 cm^{-1}. ^1H-NMR (DMSO-d_6) δ=8.0—7.6 (4H, m), 3.70 (3H, s), 2.75 (3H, s).

17h as yellow plates. IR (Nujol) 1590, 1540, 1530, 1470, 1350, 1170, 1060, 950, 860, 760, 720, 710 cm^{-1}. ^1H-NMR (DMSO-d_6) δ=7.90 (2H, d), 7.65 (2H, d), 3.80 (3H, s), 2.70 (3H, s).

We thank Mrs. M. D. Casado, Mrs. M. L. Jimeno, and Mrs. M. Plaza for recording the ^{13}C NMR spectra.

References

1) J. Elguero, R. M. Claramunt, and A. J. H. Summers, *Adv. Heterocycl. Chem.*, **22**, 183 (1978).
2) R. M. Claramunt, J. P. Fayet, M. C. Vertut, P. Mauret, and J. Elguero, *Tetrahedron*, **31**, 545 (1975).
3) P. Molina, M. Alajarin, and M. J. Vilaplana, *Synthesis*, **1983**, 415.
4) P. Molina and A. Tárraga, *Synthesis*, **1983**, 411.
5) K. Schofield, M. R. Grimmett, and B. T. R. Keene, "The Azoles," Cambridge University Press, Cambridge (1976).
6) R. A. Olofson and R. V. Kendall, *J. Org. Chem.*, **35**, 2246 (1970).
7) A. Maquestiau, Y. Van Haverbeke, and J. D. Vanovervelt, *Bull. Soc. Chim. Belg.*, **86**, 961 (1977).
8) C. Guimon, G. Pfister-Guillouzo, and M. Begtrup, *Can. J. Chem.*, **61**, 1197 (1983).
9) P. Main, S. J. Fiske, S. E. Hull, L. Lessinger, G. Germain, J. P. Declerq, and H. H. Woolfson, "The MULTAN-80 System," Univ. of York, England and Louvain, Belgium, (1980).
10) J. M. Stewart, P. A. Maclin, C. W. Dickinson, H. L. Ammon, H. Heck, and H. Flack, "The X RAY-76 System," Univ. of Maryland, USA, (1976).
11) "International Tables for X-Ray Crystallography," Kynoch Press, Birmingham, Vol. IV, (1974).
12) The H positions, the anisotropic model and the observed and calculated structure factors are deposited at the office of this Bulletin as Document No. 8501.
13) T. Avignon, L. Bouscasse, and J. Elguero, *Tetrahedron*, **34**, 1139 (1978).
14) H. Kristinsson and T. Winkler, *Helv. Chim. Acta*, **66**, 1129 (1983).
15) R. Faure, E. J. Vincent, G. Assef, J. Kister, and J. Metzger, *Org. Magn. Reson.*, **9**, 688 (1977).
16) R. Faure, E. J. Vincent, R. M. Claramunt, and J. Elguero, *Org. Magn. Reson.*, **9**, 508 (1977).
17) In Ref. 16 the value of carbon C_{7a} chemical shift in compound **19** was erroneously printed at δ 146.0 instead of the true value (δ 156.0).
18) J. B. Stothers, "Carbon-13 NMR Spectroscopy," Academic Press, New York (1972), p. 197.
19) M. J. Shapiro, *J. Org. Chem.*, **43**, 212 (1978).
20) Y. Takeuchi, *Org. Magn. Reson.*, **7**, 181 (1975).
21) W. W. Paudler and M. V. Jovanovic, *Org. Magn. Reson.*, **19**, 192 (1982).
22) J. Llinares, J. P. Galy, R. Faure, E. J. Vincent, and J. Elguero, *Can. J. Chem.*, **57**, 937 (1979).
23) R. N. Butler, T. McEvoy, E. Alcalde, R. M. Claramunt, and J. Elguero, *J. Chem. Soc., Perkin Trans. 1*, **1979**, 2886.
24) P. Molina and M. Alajarin, *Synthesis*, **1983**, 414.
25) E. Alcalde, R. M. Claramunt, J. Elguero, and C.P.S. Huber, *J. Heterocycl. Chem.*, **15**, 395 (1978).

The Crystal Structure of [4*R*,7*S*]-7-Isopropyl-4-methyl-2-azepanone [(−)-Menthone Lactam]

Hiroaki TAKAYANAGI, Etsuko HIROSE, Kimio FURUHATA, and Haruo OGURA*
School of Pharmaceutical Sciences, Kitasato University Shirokane, Minato-ku, Tokyo 108
(Received June 22, 1984)

Synopsis. The conformation of the title compound was determined by X-ray crystal analysis. The seven-membered lactam ring is in a quasi-chair conformation with the amide chromophore being approximately coplanar.

We proposed a sign rule (Ogura's sign rule)[1] regarding the relationship between the absolute configuration of the seven-membered lactams and the signs of the n→π* c.d. The Cotton effect of the amide chromophore, indicating that seven-membered lactam rings are classified into two types (A and B) as shown in Fig. 1. The former exibits a positive Cotton effect and the latter a negative one.

Recently, Klyne[2] reported that 7-membered lactam rings connected with a second adjacent ring at the 3,4- or 6,7 positions of the lactam ring showed abnormal CD, and Ogura rule failed to predict the signs of the Cotton effect of several of them. From the results of an X-ray analysis of 2-aza-*A*-homo-5α-cholestan-1-one[3] and ε-caprolactam[4] and on the basis of a study of Dreiding Models, they proposed the hyposesis that the lactam ring A has a positive sign of the C-NH-CO-C torsion angle corresponding to a Cotton effect of the same sign.

We carried out an X-ray analysis of the optical active monocyclic (−)-menthone lactam which obviously has the lactam ring in the conformation depicted in Type B,[5] to confirm the coplanarity of the amide chromophore on which Ogura rule is based. We also wanted to make it clear that (−)-menthone lactam really has a negative C-NH-CO-C torsion angle predicted from the Klyne's hypothesis.

Experimental

A crystal with the dimensions of 0.3×0.4×0.2 mm was used for the structure determination. The density of the crystal was measured by the flotation method using a carbon tetrachloride-light petroleum solution. The cell dimensions and the diffraction intensities were measured on a Rigaku four-circle diffractometer, using graphite monochromated Cu $K\alpha$ radiation at 23°C. Crystal data: $C_{10}H_{19}ON$, orthorhombic, space group $P2_12_12_1$, a=8.837(1), b=40.176(1), c=6.028(1) Å, Z=8. D_c=1.051 g cm^{-3}. 1121 independent reflections within the range of $2\theta<140°$ were collected by the use of the 2θ–ω scan mode with a scanning rate 4° (2θ)min^{-1}. A total 861 independent reflections with $|F_o|>3\sigma(|F_o|)$ were obtained and corrected for Lorentz and polarization factors but not for absorption factors. The structure was solved by a direct method using MULTAN.[6] The E-map of the phase set with the highest figure of merit showed the skeletons of the molecules.

The structure, thus obtained, was refined by a full-matrix least-squares method with anisotropic temperature factors. After all the hydrogen atoms except those of the methyl group had been located in the difference Fourier map, several cycles of least-squares refinement were carried out including these hydrogen atoms. The atomic scattering factors for C, O, and N were given by Cromer and Mann,[7] and that for H by Stewart *et al.*[8] The final R value was 9.5%, where $R=\sum||F_o|-|F_c||/\sum|F_o|$.

Results and Discussion

The final atomic parameters of crystallographically

Table 1. Atomic coordinates (×10⁴) and equivalent isotropic temperature factors of (−)-menthone lactam standard deviations are given in parentheses

Atom	x	y	z	B_{eq}/Å$^{2a)}$
Molecule I				
C(2)	5404(23)	1531(4)	9992(43)	4.9
C(3)	4813(21)	1671(4)	7885(32)	5.8
C(4)	4725(26)	2054(4)	7605(46)	6.2
C(5)	6336(27)	2191(4)	7313(41)	7.0
C(6)	7599(24)	2120(4)	8974(41)	6.5
C(7)	8010(19)	1750(4)	9201(34)	5.3
C(8)	3690(30)	2161(5)	5757(41)	9.3
C(9)	9634(20)	1700(5)	10287(54)	4.8
C(10)	9904(31)	1825(5)	12597(42)	10.0
C(11)	10095(28)	1356(7)	9917(50)	12.5
O(1)	4524(14)	1371(3)	11258(24)	5.7
N(1)	6854(17)	1570(3)	10540(27)	4.8
Molecule II				
C(2)	7015(18)	921(3)	5087(29)	4.7
C(3)	7782(19)	649(4)	6362(35)	4.9
C(4)	7261(24)	600(4)	8853(36)	6.1
C(5)	5704(20)	427(4)	8906(30)	5.2
C(6)	4371(23)	591(4)	7790(33)	5.5
C(7)	4518(19)	620(4)	5211(31)	4.2
C(8)	8473(19)	416(4)	10132(31)	5.9
C(9)	2995(16)	661(4)	4033(33)	5.4
C(10)	2039(19)	336(4)	4099(37)	5.7
C(11)	2057(16)	964(4)	4932(40)	4.1
O(1)	7737(12)	1167(3)	4477(20)	5.7
N(1)	5508(13)	898(3)	4529(23)	3.5

a) W.C. Hamilton, *Acta Crystallogr.*, **12**, 609 (1959).

Fig. 1. Projection of a seven-membered lactam ring.

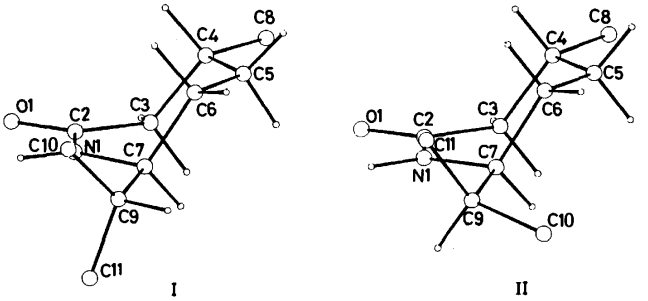

Fig. 2. Perspective view of (−)-menthone lactam (I and II).

Table 2. Bond angles(ϕ/°) and lengths(l/Å) of (−)-menthone lactam standard deviations are given in parentheses

Molecule	I	II		I	II
C(3)-C(2)-O(1)	=120(2)	120(1)	C(2)-C(3)	=1.52(3)	1.50(2)
C(3)-C(2)-N(1)	=120(2)	121(1)	C(2)-O(1)	=1.27(2)	1.23(2)
O(1)-C(2)-N(1)	=120(2)	119(1)	C(2)-N(1)	=1.33(3)	1.38(2)
C(2)-C(3)-C(4)	=117(2)	116(1)	C(3)-C(4)	=1.55(2)	1.58(3)
C(3)-C(4)-C(5)	=109(2)	110(1)	C(4)-C(5)	=1.54(3)	1.54(3)
C(3)-C(4)-C(8)	=112(2)	110(2)	C(4)-C(8)	=1.50(3)	1.51(3)
C(5)-C(4)-C(8)	=112(2)	114(1)	C(5)-C(6)	=1.53(3)	1.51(3)
C(4)-C(5)-C(6)	=122(2)	119(1)	C(6)-C(7)	=1.54(2)	1.56(3)
C(5)-C(6)-C(7)	=114(2)	114(2)	C(7)-C(9)	=1.59(3)	1.53(2)
C(6)-C(7)-C(9)	=112(1)	113(1)	C(7)-N(1)	=1.49(2)	1.48(2)
C(6)-C(7)-N(1)	=111(1)	112(1)	C(9)-C(10)	=1.50(4)	1.56(2)
C(9)-C(7)-N(1)	=110(2)	108(1)	C(9)-C(11)	=1.46(3)	1.57(2)
C(7)-C(9)-C(10)	=119(2)	112(1)			
C(7)-C(9)-C(11)	=108(2)	113(1)			
C(10)-C(9)-C(11)	=115(2)	111(1)			
C(2)-N(1)-C(7)	=126(1)	124(1)			

Table 3. Torsional angles(ϕ/°) of (−)-menthone lactam

Molecule	I	II
N(1)-C(2)-C(3)-C(4)	=−69(2)	−68(2)
O(1)-C(2)-C(3)-C(4)	=113(2)	114(2)
C(2)-C(3)-C(4)-C(5)	=74(2)	75(2)
C(2)-C(3)-C(4)-C(8)	=−162(2)	−159(1)
C(3)-C(4)-C(5)-C(6)	=−56(2)	−60(2)
C(8)-C(4)-C(5)-C(6)	=180(2)	177(2)
C(4)-C(5)-C(6)-C(7)	=63(3)	65(2)
C(5)-C(6)-C(7)-C(9)	=161(2)	158(1)
C(6)-C(7)-C(9)-C(10)	=62(2)	−71(2)
C(6)-C(7)-C(9)-C(11)	=−165(2)	55(2)
N(1)-C(7)-C(9)-C(10)	=−62(2)	164(1)
N(1)-C(7)-C(9)-C(11)	=71(2)	−70(2)
C(6)-C(7)-N(1)-C(2)	=63(2)	61(2)
C(9)-C(7)-N(1)-C(2)	=−173(2)	−173(1)
C(3)-C(2)-N(1)-C(7)	=1(3)	3(2)
O(1)-C(2)-N(1)-C(7)	=180(2)	−178(1)

independent two molecules I and II are listed in Table 1. The complete table of observed and calculated structure factors, thermal parameters and the atomic coordinates of hydrogen atoms are kept as Document No. 8509 at the Office of the Editor of the Bulletin of the Chemical Society of Japan. A perspective drawing of the molecular structure of (−)-menthone lactam is shown in Fig. 2. The bond angles and bond lengths are listed in Table 2, and torsion angles are in Table 3.

The conformation of the lactam ring of (−)-menthone lactam is a quasi-chair with the amide chromophore being approximately coplanar (Table 3). (−)-Menthone lactam belongs to type B, as shown in Fig. 2, and the mean value of the C-NH-CO-C torsion angle is +2°, whose sign is opposite to that of ε-caprolactam (−4.2°). The conformations of the two independent molecules are almost identical except the isopropyl groups. Although the C-NH-CO-C torsion angles in (−)-menthone lactam have the positive sign which is opposite to that predicted by Klyne's hypothesis, this can not be discussed in detail because the values of the torsion angles have large standard deviations.

The authors are grateful to the Ministry of Education, Science, and Culture for a financial support by a Grant-in-Aid (No. 58570883).

References

1) H. Ogura, H. Takayanagi, and K. Furuhata, *Chem. Lett.*, **1973**, 387; H. Ogura, H. Takayanagi, K. Kubo, and K. Furuhata, *J. Am. Chem. Soc.*, **95**, 8056 (1973); H. Ogura, H. Takayanagi, and K. Fukuhara. *J. Chem. Soc. Perkin Trans. 2*, **1979**, 665.

2) W. Klyne, D. N. Kirk, J. Tilley, and H. Sugimome, *Tetrahedron*, **36**, 543 (1980).

3) H. Suginome and A. Furusaki, *J. Chem. Soc., Chem. Commun.*, **1979**, 782.

4) F. K. Winkler and J. D. Dunitz, *Acta Crystallogr., Sect. B*, **31**, 268, (1975).

5) H. Ogura, H. Takayanagi, K. Kubo, and K. Furuhata, *J. Am. Chem. Soc.*, **95**, 8056 (1973).

6) G. Germain, P. Main and M. M. Woolfson, *Acta Crystallogr., Sect. A*, **27**, 368, (1971).

7) D. J. Cromer and J. B. Mann, *Acta Cryst, Sect. A*, **24**, 321 (1958).

8) R. F. Stewart, E. R. Davidson, and W. T. Simpson, *J. Phys. Chem.*, **42**, 3175 (1965).

X-Ray Photoelectron Spectroscopy of Sodium-doped Polyacetylene

Isao IKEMOTO,* Toshihide ICHIHARA, Chikashi EGAWA,† Koichi KIKUCHI,† Haruo KURODA,† Yukio FURUKAWA,†† Issei HARADA,†† and Hideki SHIRAKAWA†††

Department of Chemistry, Faculty of Science, Tokyo Metropolitan University, Fukazawa, Setagaya-ku, Tokyo 158
†*Department of Chemistry, Faculty of Science, University of Tokyo, Hongo, Tokyo 113*
††*Pharmaceutical Institute, Tohoku University, Aobayama, Sendai 980*
†††*Institute of Materials Science, University of Tsukuba, Sakura-mura, Ibaraki 305*

(Received July 28, 1984)

Synopsis. The change of the C ls peak shape in an X-ray photoelectron spectrum was studied for sodium-doped polyacetylene. The C ls peak due to negatively-charged carbon atoms was found to appear on the low-binding-energy side of a peak due to neutral carbon atoms. An electron, which is transferred to a polyacetylene chain from the sodium atom, has been determined to reside over several carbon atoms.

Previously, we studied bromine-doped polyacetylene by X-ray photoelectron spectroscopy[1] and found that the shape of the C ls peak varied markedly with the bromine content. The observed change of the peak shape suggested that the peak was composed of two components, mutually separated by 1.7—2.0 eV, and that the intensity of the higher-binding-energy component increased while that of the lower-binding-energy component decreased on increasing the bromine content. We attributed the former characteristic to the carbon atoms in the metallic domain where carbon atoms are positively charged as the result of a charge transfer to bromine to form a Br_3^- ion, and the other component to the carbon atoms in the low conductive (or undoped) domain. However, the intensity of the higher-binding-energy component continues to increase even when the bromine content exceeds the value where the conductivity shows a steep decrease because of the progress of the addition and/or substitution reaction of bromine with the polyacetylene chain.[1,2] Thus, in a heavily-doped case the higher-binding-energy component might contain a large contribution from carbon atoms which form a bond with bromine. Furthermore, a recent EXAFS study of the bromine-doped polyacetylene revealed that the C-Br bond is formed even in a lightly-doped polyacetylene.[2] Thus, there remains the question whether the higher-binding-energy component of the C ls peak is actually due to the positively-charged carbon atoms in the metallic domain.

Salaneck *et al.* studied AsF_5- and I_2-doped polyacetylene by XPS.[3,4] They also observed two components in their C ls peaks. However, they attributed a shoulder which appeared on the higher-binding-energy side of the peak upon doping with AsF_5 (or I_2), to the conduction-electron-plasmon shake-up. The main, rather sharp component on the lower-binding energy side moves to the higher-binding energies, relative to undoped polyacetylene. They concluded that all the carbon atoms in polyacetylene were uniformly charged and that the average charge per carbon atom depends on the amount of the dopant.

In the case of the sodium-doped polyacetylene where carriers are different from those in the bromine-doped polyacetylene, doped sodium atoms will change to sodium ions giving an electron to the polyacetylene chain, and none of the addition or substitution reaction can occur between sodium and polyacetylene. According to the interpretation proposed by Salaneck *et al.*, the main, rather sharp C ls peak would shift to the lower binding energy and a shoulder due to the conduction-electron-plasmon shake-up would appear on the higher-binding-energy side of the main peak. The chemical shift of the main peak may depend on the amount of the dopant. On the other hand, if we consider the presence of the doped and undoped domains in the sodium-doped polyacetylene, the component due to the negatively-charged carbon atoms in the doped domain would appear on the lower-binding-energy side of the component due to the carbon atoms of the undoped domain. The intensity of the former component would increase and the latter would decrease with the increase of sodium content.

Since the sodium-doped polyacetylene is extremely sensitive to air, we have to prepare specimens under an ultra-high vaccum condition and immediately carry out all XPS measurements without exposing the doped polyacetylene film to air. The present experiment was done by use of a VG ESCA LAB 5. A polyacetylene film, prepared by a previously described method,[5] was introduced into the sample chamber of the apparatus by keeping the film in a nitrogen atmosphere. The polyacetylene film, thus introduced into the apparatus, did not show any detectable O ls peak. Then, the film was exposed to a sodium vapor in a sample-preparation chamber, a sodium-metal dispenser by S.A.E.S. Getters S.p.A. being used as the sodium source. The C ls and Na ls peaks were measured immediately after the deposition of sodium onto the film. The same procedure was repeated in order to study the effect of an increase of the amount of the doped sodium, which means that we measured the sodium-doped polyacetylene with various dopant contents. The Na ls/C ls intensity ratio and the approximate Na/C atomic ratio derived from the intensity ratio, and the C ls peak width (f.w.h.m.) with the repetition of sodium deposition are summarized in Table 1. The Na/C atomic ratio derived from the intensity ratio might be smaller since sodium is only on the surface of the polyacetylene film. The shape of the C ls peak of the undoped polyacetylene and those of two sodium-doped polyacetylenes (after 4th and 7th depositions which correspond to $(CHNa_{0.045})_x$ and $(CHNa_{0.075})_x$, respectively) are shown in Fig. 1(a). The shape of the C ls peak varied markedly upon increasing the sodium content. The f.w.h.m. of the C ls peak increased to 2.8 eV by doping sodium from 1.5 eV of the undoped polyacetylene. However, the total intensity of the C ls

Table 1. XPS Results of sodium-doped polyacetylene

Number of Depositions	Na ls/C ls intensity ratio	Na/C atomic ratio	f.w.h.m. of C ls peaks/eV
0	0.00	0.000	1.5
1	0.04	0.005	1.6
2	0.10	0.015	1.6
3	0.28	0.035	1.9
4	0.34	0.045	2.0
5	0.45	0.055	2.5
6	0.50	0.065	2.7
7	0.60	0.075	2.8

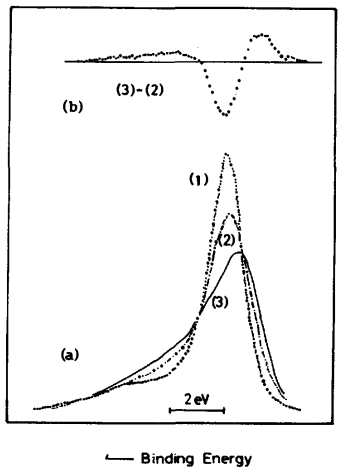

Fig. 1. (a): The C 1s peaks of (1) polyacetylene, (2) Na-doped polyacetylene (4th deposition) and (3) Na-doped polyacetylene (7th deposition).
(b): Difference spectrum of the C 1s peaks of (2) and (3).

peak was found to remain constant. We took the difference between the spectra of the doped samples which have different amounts of sodium in order to see the effect of the increase of the amount of the doped sodium. One of the difference spectrums (Fig. 1(b)) indicates that there are at least two main components in the C ls peak of the sodium-doped polyacetylene. Upon doping sodium, a lower-binding-energy peak (or shoulder) begins to appear and its intensity increases with the sodium content keeping the binding energy constant. The higher-binding-energy peak which corresponds to neutral carbon atoms decreases in intensity. That is, a part of the neutral carbon atoms changes their state upon the sodium doping. Therefore, we attribute the former to the negatively-charged carbon atoms and the latter to the neutral carbon atoms. The chemical shift between the two main components is about 1.2 eV, from which we can estimate the average negative charge per carbon atom to be about −0.2 e. This means that an electron transferred from a sodium atom spreads over at least five carbon atoms. The difference spectrum also shows that the lower-binding-energy peak has a tail on the higher-binding-energy side. This might be attributable to the conduction-electron-plasmon shake-up as suggested by Salaneck *et al.*[3,4] Including this component, there are three components in the C ls peak of the sodium-doped polyacetylene, which cannot be explained by the interpretation proposed by Salaneck *et al.* The difference between the binding energies of the higher-binding-energy component in the C1s level and the Na ls level stays almost constant while increasing of the sodium content. This means that the sodium is in the same state, that is, in the form of Na^+ irrespective of the sodium content.

In conclusion, the XPS data of the sodium-doped polyacetylene suggest that the charge transfer from sodium to polyacetylene results in the formation of negatively-charged carbon atoms and an electron transferred from a sodium atom spreads over several (possibly more than five) carbon atoms of the polyacetylene chain. Based on these facts, we conclude that in the bromine-doped polyacetylene, the higher-binding-energy component is mainly due to the positively-charged carbon atoms, at least in the lightly-doped regions. However, the small contribution of the conduction-electron-plasmon shake-up to this component cannot be excluded.

The present work was supported by a Grant-in-Aid for Scientific Research No. 58218009 from the Ministry of Education, Science and Culture.

References

1) I. Ikemoto, Y. Cao, M. Yamada, H. Kuroda, I. Harada, H. Shirakawa, and S. Ikeda, *Bull. Chem. Soc. Japn.*, **55**, 721 (1982).

2) M. Tokumoto, H. Oyanagi, T. Ishiguro, H. Shirakawa, H. Nemoto, T. Matsushita, M. Ito, H. Kuroda, and K. Kohra, *Solid State Commun.*, **48**, 861 (1983).

3) W. R. Salaneck, H. R. Thomas, C. B. Duke, A. Paton, E. W. Plummer, A. J. Heeger, and A. G. MacDiarmid, *J. Chem. Phys.*, **71**, 2044 (1979).

4) W. R. Salaneck, H. R. Thomas, R. W. Bigelow, C. B. Duke, E. W. Plummer, A. J. Heeger, and A. G. MacDiarmid, *J. Chem. Phys.*, **72**, 3674 (1980).

5) T. Ito, H. Shirakawa, and S. Ikeda, *J. Polym. Sci., Polym. Chem. Ed.*, **12**, 11 (1974); 13, 1943 (1975).

Application of Laser Flash Photolysis to Determine Association Constants between Zn-TPPS$_3$ and Viologens

Ichiro OKURA,* Shigetoshi AONO, Mikio HOSHINO,† and Akira YAMADA†
Department of Chemical Engineering, Tokyo Institute of Technology, Meguro-ku, Tokyo 152
†*The Institute of Physical and Chemical Research, Hirosawa, Wako-shi, Saitama 351*
(Received July 30, 1984)

Synopsis. The association behavior between zinc 5,10,15,20-tetraphenylporphyrintrisulfonate (Zn-TPPS$_3$) and viologens was investigated from the T-T absorption band of the triplet Zn-TPPS$_3$ by laser-flash photolysis. The association constants of Zn-TPPS$_3$ with methylviologen and propylviologen-3,3′-sulfonate (PVS) were 1.7×10^4 and 7.3×10^2 mol^{-1}·dm^3, respectively.

Water-soluble zinc meso-tetraphenylporphyrintrisulfonate (Zn-TPPS$_3$) has been found to be a suitable photosensitizer in the photoinduced hydrogen evolution system, consisting of a photosensitizer, an electron donor, an electron acceptor, and a catalyst.[1] Zn-TPPS$_3$, however, has been reported to form a complex with viologen and it has been clarified that the complex does not take part in the photoreduction of viologen, and that only the uncomplexed Zn-TPPS$_3$ plays an important role in the reaction.[2] The determination of the association constant between Zn-TPPS$_3$ and viologen provides suitable reaction conditions. As it is difficult to determine the association constant from the visible spectra (the visible spectra of the complex is very similar to that of Zn-TPPS$_3$) a laser-flash photolysis was applied to determine the association constant in this study.

Experimental

Methylviologen was purchased from Tokyo Kasei Kogyo Co., and PVS was prepared according to the literature.[3] The sample solution, which consisted of Zn-TPPS$_3$ and viologen (if included), was deaerated by repeated freeze-pump-thaw cycles. Conventional laser photolysis was carried out using a Nd-YAG Laser, Model HY-500 from JK Lasers Ltd., equipped with second, third, and fourth harmonic generators. The second harmonic (532 nm), of *ca.* 100 mJ cm^{-2} and a flash duration of 20 ns was used to excite the sample solutions throughout this study. The analyzing light beams from a xenon lamp (Ushio UXL-150 D, 150 W) were intensified by a factor of *ca.* 20 during the detection of the transient spectra. Transient spectra having a lifetime longer than 200 μs were measured without intensification of the analyzing light. The light, after passing through a sample cell, was focused onto the entrance slit of a monochromator (Model MC-20 N from Ritsu Appl. Opt. Co.). The output from a Hamamatsu photomultiplier (R 758) attached to the exit slit of the monochromator was displayed on a Tektronix oscilloscope, Model 7904.

Results and Discussion

Figure 1-(a) shows an oscilloscopic photograph monitored at 470 nm (the peak wavelength of the T-T absorption band due to the triplet Zn-TPPS$_3$) after a laser flash. In the presence of methylviologen, the decay rate of the transient spectrum measured at 470 nm increased, as shown in Fig. 1-(b) and 1-(c). The methylviologen cation radical (MV^+, λ_{max}=605 nm) initially increased and then decreased as shown in Fig. 1-(e) and 1-(f). The absorbance of the triplet spectrum at 470 nm measured immediately after the laser flash decreased with an increase in methylviologen concentration (Fig. 1-(a), 1-(b), and 1-(c)), and the T-T absorption was not detected at concentrations higher than 5.01×10^{-3} mol·dm^{-3}. As a consequence of the decrease in the absorbance at 470 nm, the concentration of MV^+ formed after the laser flash decreased, and MV^+ formation was not observed in the absence of T-T absorption as shown in Fig. 1-(g). These results can be expressed by the following reaction scheme, suggesting the 1:1 complex (PQ) formation between Zn-TPPS$_3$ (P) and MV^{2+} (Q).

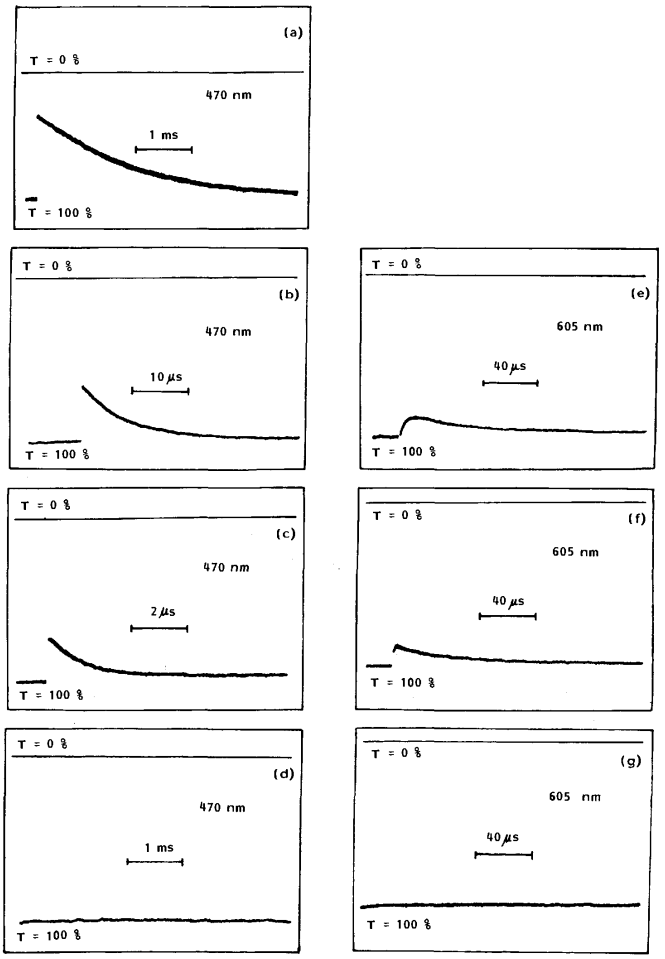

Fig. 1. Oscilloscopic photographs obtained from laser flash photolysis of aqueous solutions of (a) Zn-TPPS$_3$, (b)—(g) Zn-TPPS$_3$+MV^{2+}. Zn-TPPS$_3$: 3.03×10^{-5} mol·dm^{-3}; concentration of viologens, (a): 0, (b), (e): 1.21×10^{-5} (c), (f): 5.01×10^{-5}, (d), (g): 5.01×10^{-3} mol·dm^{-3}.

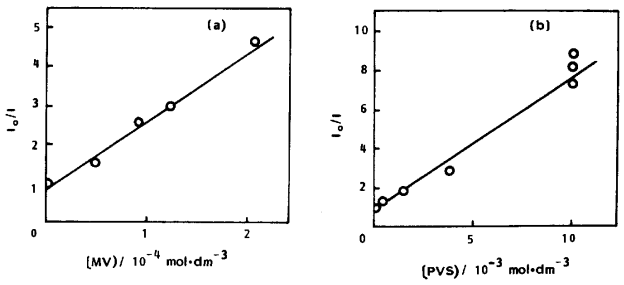

Fig. 2. Relation between I_0/I and the concentration of methylviologen or PVS.

$$P + Q \overset{K}{\rightleftharpoons} PQ$$

$$P \xrightarrow{h\nu} {}^3P^*$$

$${}^3P^* + Q \longrightarrow P^+ + Q^-$$

$$P^+ + Q^- \longrightarrow P + Q$$

$$PQ \xrightarrow{h\nu} PQ^* \xrightarrow{\text{fast}} PQ$$

where K is the association constant.

According to such a reaction scheme, the concentration of PQ increases with the increase of the Q concentration. The absorbance of the T-T absorption at 470 nm is considered to be proportional to the concentration of uncomplexed Zn-$TPPS_3$ on the assumption that the photoexcited complex (PQ*) may convert to PQ very rapidly. We, therefore, obtain,

$$I_0/I = 1 + K[Q]$$

where I_0 and I are the absorbance at 470 nm measured immediately after the laser flash in the absence and in the presence of methylviologen, respectively. This equation is the same as that reported previously[4] in the case of the static quenching of fluorescence.

As shown in Fig. 2-(a), the fairly linear relationship between I_0/I and [Q] indicates that the above proposed scheme is adequate. From the slope of the straight line, the K value was obtained as 1.7×10^4 mol^{-1}·dm^3. For propylviologen-3,3′-sulfonate(PVS), a similar linear relationship was also obtained (Fig. 2-(b)), and the K value was 7.3×10^2 mol^{-1}·dm^3. The difference in the K values between PVS and methylviologen is explained by the difference of electrostatic force between Zn-$TPPS_3$ and viologens or the redox potentials of each viologen.

The difference between the redox potential of methyl-viologen (−0.44 eV *vs* NHE) and that of PVS (−0.41 eV *vs* NHE) is so small that the larger K value of methylviologen compared with PVS may be mainly due to an electrostatic effect. Since the positively charged methylviologen is more favorable to associate with the negatively charged Zn-$TPPS_3$, the larger K value detected for methylviologen (compared with PVS) is plausible.

References

1) I. Okura, M. Takeuchi, and N. Kim-Thuan, *Chem. Lett.*, **1980**, 765; I. Okura, M. Takeuchi, and N. Kim-Thuan, *Photochem. Photobiol.*, **33**, 413 (1981).

2) I. Okura, K. Kusunoki, and S. Aono, *Inorg. Chim. Acta*, **77**, L99 (1983).

3) I. Willner, J. W. Otvos, and M. Calvin, *J. Am. Chem. Soc.*, **103**, 3203 (1981).

4) G. Oster, *Trans. Faraday Soc.*, **47**, 660 (1951).

Triphenylmethyl-substituted Arylthioaminyl Radicals. An ESR Study of *N*-(Arylthio)triphenylmethylaminyls[1)]

Yozo MIURA,* Mamoru ISOGAI, and Masayoshi KINOSHITA
Department of Applied Chemistry, Faculty of Engineering, Osaka City University, Sumiyoshi-ku, Osaka 558
(Received August 1, 1984)

Synopsis. The title radicals have been studied by ESR spectroscopy. The radicals are fairly long-lived in solution and satellite lines due to the ^{33}S atom at natural abundance could be observed in their ESR spectra.

Since the triphenylmethyl group is one of the most bulky groups, triphenylmethyl-substituted free radicals are expected to be sterically protected from reactions by which the free radicals will be destroyed.[2)] Therefore, this steric protection may make the free radicals more long-lived. From this viewpoint triphenylmethyl-substituted arylthioaminyls, **2**, are of considerable interest and the present work was initiated with the hope of isolating them. Thioaminyl radicals (RN̈SR′) are essentially long-lived in solution,[3)] but the thioaminyl radicals stable enough to be isolated as the free radical substance are rare.[4)] The results of an ESR study of **2**, however, showed that **2** were not as stable as we had expected. Interestingly, however, in their ESR spectra satellite lines due to the ^{33}S atom at natural abundance could be observed for any **2** radical. Herein we report the $a_{^{33}S}$ values for **2** and discuss their electronic structures and plausible conformations on the basis of their ESR parameters.

$Ph_3CNHSAr$ $Ph_3CN̈SAr$ t-$BuN̈SAr$
1 **2** **3**

Radicals **2** were generated in benzene from **1** by either of the two methods described in the Experimental section. A typical ESR spectrum is illustrated in Fig. 1 and the ESR parameters are listed in Table 1. The ESR spectra obtained were very clean and the signals due to impurity radicals were either very weak or absent. These clean ESR spectra are in contrast to those of *N*-(arylthio)-*t*-butylaminyl radicals (**3**)[5)] in which an impurity radical, *t*-BuN̈OBu-*t*, was simultaneously recorded with comparable intensity.[6)] This difference may be explained in terms of the steric protection by the bulky triphenylmethyl group from the reactions by which impurity radicals will be produced.

Radicals **2** were fairly long-lived in solution. For instance, the steady-state radical concentrations obtained by method **a** were $\approx 10^{-4}$ mol dm^{-3}, and on interruption of UV-irradiation, the radicals persisted for a long period (≈10 h at room temperature), although they were not stable enough to be isolated.

As can be seen from Fig. 1, the ESR spectra of **2** showed relatively narrow lines and gave well resolved splittings due to the phenylthio aromatic protons. This contrasts with the broad and poorly resolved ESR spectra of **3**.[5)] Interestingly, this line narrowing permitted us clearly to observe the satellite lines due to the ^{33}S atom at natural abundance for any **2** radical, on recording at high gain. The measured intensities heights of the satellite lines correspond to ≈0.12% of the parent peak (theoretical 0.19%). The results are listed in Table 1.

The large a_N and large $a_{^{33}S}$ values for **2** strongly suggest that in **2** the unpaired electron resides mainly

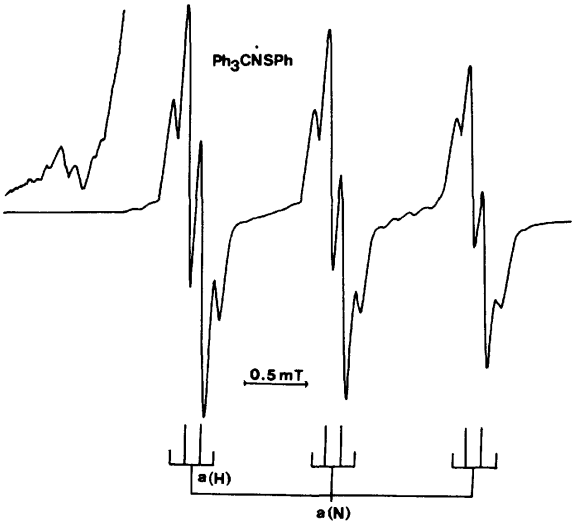

Fig. 1. ESR spectrum of **2a** recorded during photolysis of a solution of **1a** in 1:9 (v/v) di-*t*-butyl peroxide–benzene at 20°C. The left wing is shown under high amplification (100 times) and the satellite lines due to the ^{33}S atom can be clearly seen.

TABLE 1. ESR PARAMETERS FOR *N*-(ARYLTHIO)- AND *N*-(*t*-BUTYLTHIO) TRIPHENYLMETHYLAMINYL RADICALS[a-c)]

$Ph_3CN̈SR$ R		a_N	a_H[d)]	$a_{^{33}S}$	g
2a	Ph	1.171	0.119 (3)[e)]	0.683	2.0071
2b	4-ClC_6H_4	1.181	0.116 (2)[f)]	0.678	2.0071
2c	3,5-$Cl_2C_6H_3$	1.188	0.112 (3)[e)]	0.641	2.0068
2d[g)]	2,4,6-$Me_3C_6H_2$	1.209		0.740	2.0077
4	*t*-Bu	1.228			2.0076

a) Unless otherwise noted, the radicals are generated by method a (see, Experimental section). b) ESR measurements are carried out at 20°C. c) Hyperfine splitting constants are given in mT. d) Numbers in parentheses refer to the number of equivalent protons. e) One para and two ortho protons of the phenylthio benzene ring. f) Two ortho protons of the phenylthio benzene ring. g) The radical is generated by method **b** (see, Experimenatl section).

on the nitrogen and sulfur. Furthermore, their ESR parameters (except those for **2d**) are similar to those for **3** (a_N=1.170—1.189 mT, g=2.0068—2.0072).[5] Therefore, it is likely that **2** adopt a similar conformation to that of **3** which we believe to be planar.[3]

To discuss the spin density distribution in **2** in more detail, the spin density on each atom was calculated by both the standard Hückel MO method and the McLachlan perturbation treatment,[7] assuming the radicals to be planar. The parameters used are as follows: $\alpha_N=\alpha+0.6\beta$, $\alpha_S=\alpha+\beta$, $\beta_{NS}=0.7\beta$, $\beta_{CS}=0.7\beta$, $\lambda=0.7$.[3] The spin densities on the nitrogen, sulfur and ortho and para carbons of the phenylthio benzene ring calculated by the Hückel MO method are 0.554, 0.325, 0.04, and 0.04, respectively.[8] Then, the a_N, $a_{33}S$, and a_H values derived from these values by use of the simple McConnell relationship $a_x=Q_x\rho_x{}^\pi$, where Q_N=2.2, Q_{33S}=2.3, and Q_H=−2.7 mT,[3] become 1.22, 0.75, and 0.11 mT, respectively. It is seen from Table 1 that these values are in good agreement with the experimental ones.

The ESR parameters (a_N, a_{33S}, and g) for **2d** are unusually increased compared with those for the other radicals. We believed that these unusual increases in the ESR parameters could be accounted for by assuming that **2d** adopted a twisted conformation in which the phenylthio benzene ring did not lie in the nodal plane of the nitrogen $2p_z$ (and sulfur $3p_z$) orbital. In this assumed conformation the unpaired electron will be poorly delocalized over the phenylthio benzene ring.[9] To confirm this assumption, *N*-(*t*-butylthio)-triphenylmethylaminyl radical (**4**) was generated. If this assumption is correct, the ESR parameters for **2d** should come close to those for **4**. As can be seen from Table 1, the parameters for both radicals are very similar to each other. Consequently, it is concluded that the unusual increases in the ESR parameters for **2d** are attributable to the twisted conformation of **2d**.

Experimental

IR and ^{1}H NMR measurements have been described in a previous paper.[3] Di-*t*-butyl diperoxyoxalate,[10] triphenylmethylamine,[13] and alkane- and benzenesulfenyl chlorides[3,11,12] were prepared by the previously reported methods.

General Procedure for Preparation of N-(Arylthio)triphenylmethylamines (1). A benzenesulfenyl chloride (7.60 mmol) in 30 cm^3 of dry diethyl ether (ether) was added to a stirred solution of triphenylmethylamine (5.78 mmol) and triethylamine (3 cm^3) in dry ether (150 cm^3) at 0 °C. After being stirred for 1 h at 0 °C and for an additional 4 h at room temperature, the reaction mixture was filtered, evaporated, and the residue chromatographed on alumina (Merck art 1097, colum size 4×11 cm). Elution with hexane gave the diaryl disulfide and subsequent elution with 1:3 (v/v) benzene–hexane gave product **1** which was recrystallized from the appropriate solvent.

N-(Phenylthio)triphenylmethylamine (1a). Colorless prisms (from hexane); mp 116—118 °C; yield 67%; IR (KBr) 3300 cm^{-1} (NH); NMR ($CDCl_3$) δ=4.29 (s, 1H, NH, exchanged by D_2O) and 6.93—7.37 (m, 20H, aromatic). Anal. ($C_{25}H_{21}NS$) C, H, N.

N-(4-Chlorophenylthio)triphenylmethylamine (1b). Colorless prisms (from hexane–benzene); mp 151—153 °C; yield 46%; IR (KBr) 3280 cm^{-1} (NH); NMR ($CDCl_3$) δ=4.37 (s, 1H, NH, exchanged by D_2O) and 7.04—7.38 (m, 19H, aromatic). Anal. ($C_{25}H_{20}ClNS$) C, H, N.

N-(3,5-Dichlorophenylthio)triphenylmethylamine (1c). Colorless prisms (from hexane); mp 120—122 °C; yield 67%; IR (KBr) 3320 cm^{-1} (NH); NMR ($CDCl_3$) δ=4.38 (s, 1H, NH, exchanged by D_2O) and 6.87—7.34 (m, 18H, aromatic). Anal. ($C_{25}H_{19}Cl_2NS$) C, H, N.

N-(2,4,6-Trimethylphenylthio)triphenylmethylamine (1d). Colorless needles (from ethanol-benzene); mp 144—145 °C; yield 36%; IR (KBr) 3280 cm^{-1} (NH); NMR ($CDCl_3$) δ=2.21 (s, 6H, *o*-CH_3), 2.23 (s, 3H, *p*-CH_3), 3.85 (s, 1H, NH, exchanged by D_2O), and 6.78—7.35 (m, 17H, aromatic). Anal. ($C_{28}H_{27}NS$) C, H, N.

Although an attempt was made to prepare *N*-(*t*-butylthio)-triphenylmethylamine (**1e**) by the reaction of triphenylmethylamine with 2-methyl-2-propanesulfenyl chloride, it could not be isolated from the reaction mixture. For ESR measurements the concentrate of the reaction mixture was used.

ESR Measurements. Radicals **2** were produced by either of the following two methods: (a) photolysis of a solution of **1** (20 mg) in 1:9 (v/v) di-*t*-butyl peroxide—benzene (0.4 cm^3) with a high-pressure mercury lamp and (b) reaction of **1** (25 mg) with di-*t*-butyl diperoxyoxalate (8 mg) in benzene (0.4 cm^3).

ESR spectra were recorded with a JEOL JES-ME-3X spectrometer. Hyperfine splitting constants and g values were determined by comparison with those (a_N=1.309 mT, g=2.0057) for Fremy's salt in K_2CO_3 aqueous solution.

References

1) Part 23 in the series "ESR Studies of Nitrogen-Centered Free Radicals." For part 22, see: Y. Miura, A. Yamamoto, and M. Kinoshita, *Electrochim. Acta*, **29**, 1731 (1984).

2) M. Kamachi, Y. Kuwae, S. Nosakura, K. Hatada, and H. Yuki, *Polymer J.*, **13**, 919, (1981).

3) Y. Miura, H. Asada, M. Kinoshita, and K. Ohta, *J. Phys. Chem.*, **87**, 3450 (1983).

4) Y. Miura, A. Yamamoto, Y. Katsura, M. Kinoshita, S. Sato, and C. Tamura, *J. Org. Chem.*, **47**, 2618 (1982).

5) Y. Miura, H. Asada, and M. Kinoshita, *Bull. Chem. Soc. Jpn.*, **50**, 1855 (1977).

6) H. Woynar and K. U. Ingold, *J. Am. Chem. Soc.*, **102**, 3813 (1980).

7) A. D. McLachlan, *Mol. Phys.*, **3**, 233 (1960).

8) The spin densities on the same atoms calculated by the McLachlan perturbation treatment are 0.754 (N), 0.234 (S), 0.023 (*o*-C), and 0.017 (*p*-C), which are in poor agreement with experiment.

9) Such a twisted conformation has also been assumed for polysubstituted arylthioaminyl radicals; Y. Miura, Y. Katsura, and M. Kinoshita, *Bull. Chem. Soc. Jpn.*, **52**, 1121 (1979); Y. Miura and M. Kinoshita, *J. Org. Chem.*, **49**, 2724 (1984).

10) P. D. Bartlett, E. P. Benzing, and R. E. Pincock, *J. Am. Chem. Soc.*, **82**, 1762 (1960).

11) Y. Miura, N. Makita, and M. Kinoshita, *Bull. Chem. Soc. Jpn.*, **50**, 482 (1977).

12) 2,4,6-Trimethylbenzenesulfenyl chloride was prepared by the reaction of 2,4,6-trimethylbenzenethiol with two equivalents of SO_2Cl_2 and used in the following step without distillation; J. Kuyper and G. B. Street, *J. Am. Chem. Soc.*, **99**, 7848 (1977).

13) C. A. Kraus and R. Rosen, *J. Am. Chem. Soc*, **47**, 2739 (1925).

Effect of Choline Derivatives on the Critical Micelle Concentrations of Anionic and Cationic Surfactants

Masayuki NAKAGAKI and Shoko YOKOYAMA*
Faculty of Pharmaceutical Sciences, Kyoto University, Yoshida-Shimoadachi-cho, Sakyo-ku, Kyoto 606
(Received August 10, 1984)

Synopsis. The decrease of the critical micelle concentration (cmc) of sodium dodecyl sulfate (SDS) was larger, while the decrease of that of dodecyltrimethylammonium chloride (DTAC) was smaller in the presence of choline derivatives than in the presence of NaCl at the same molar concentration.

A large number of studies have been reported on the effect of various electrolytes[1-10] and alcohols[8-15] on the micellization of ionic surfactants. The association of ionic surfactant in aqueous solution is governed by two opposing forces. The hydrophobic force between the hydrophobic tails attracts the surfactant molecules or ions to the micelle core from the aqueous bulk solution. The ionic head groups, on the other hand, favour the aqueous bulk phase, because the electrostatic repulsive force between the head groups prevents the surfactant molecule to associate. In this connection, the decrease of the critical micelle concentration (cmc) by addition of inorganic salts and alcohols may be discussed. The effect of the inorganic electrolytes is explained in terms of the shielding of the electrostatic repulsion by the counterions, while the effect of alcohol is explained from the reduction of the free energy of mixing and the reduction of the surface charge density by the alcohols entering in the palisade layer of the micelle.

Moreover, it has been found that the mixed micelle composed of anionic and cationic surfactants is not formed.[16] Therefore, the effect on the micellization of the salts which have a short hydrophobic part and a polar part of the opposite sign may be interesting.

From these points of view, we studied the critical micelle concentration of anionic and cationic surfactants in aqueous solutions of choline chloride and its esters ($HOCH_2CH_2N^+(CH_3)_3\cdot Cl^-$, $CH_3COOCH_2CH_2N^+(CH_3)_3\cdot Cl^-$, $CH_2COOCH_2CH_2N^+(CH_3)_3\cdot Cl^-$ / $CH_2COOCH_2CH_2N^+(CH_3)_3\cdot Cl^-$), by the measurements of the surface tension.

Experimental

Materials. Sodium dodecyl sulfate (SDS) supplied from Nihon Emulsion Co., Ltd., Japan was extracted with petroleum benzine in a Soxlet apparatus for at least 20 h, recrystallized twice from ethanol, and dried under vacuum for a day and night. Dodecyltrimethylammonium chloride (DTAC) purchased from Nakarai Chemicals, Ltd. was extracted with petroleum ether in a Soxlet apparatus for at least 20 h, recrystallized twice from aceton, and dried under vacuum for a day and night. Choline chloride (Ch), acetylcholine chloride (Ach) and succinylcholine chloride (Sch) purchased from Nakarai Chemicals, Ltd. were of a guaranteed reagent grade and were used without further purification. All solutes were dissolved in deionized and redistilled water.

Surface Tension Measurements. The surface tension was measured by Du Nouy tensiometer. The platinum ring with diameter 23 mm was heated by oxidizing flame before use. All glass apparatus were preserved in chromate-sulfuric acid mixture and linsed well with distilled water before use. Temperature of the thermostat was maintained at 25±0.2 °C. For the calculation of the surface tension of aqueous solutions, the value of 71.96 m N·m^{-1} was used as the surface tension of pure water at 25 °C. The experimental determination of the surface tension was precise to ±0.1 m N·m^{-1}. cmc was obtained from the break point in the curve of surface tension, γ, as a function of logarithm of the concentration of SDS or DTAC, at various values of the concentration of choline derivatives.

Results and Discussion

cmc of SDS in the presence of choline chloride and its derivatives, *i.e.* Ch, Ach and Sch is shown in Fig. 1 together with the data of inorganic salts and normal alkanols quoted from the references.[13,17] cmc of DTAC in the presence of choline derivatives is shown in Fig. 2 together with the data of NaCl quoted from the reference.[17] The measured values of cmc of SDS and DTAC in the absence of additives (8.1 m mol·dm^{-3},

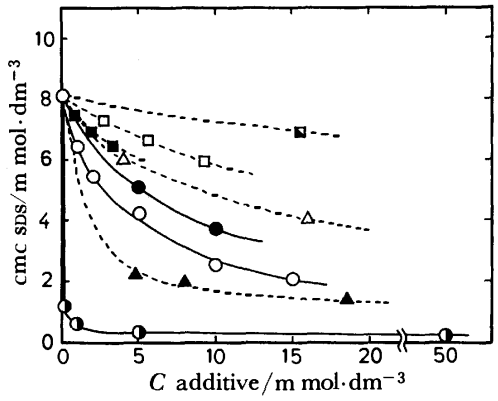

Fig. 1. Effect of Additives on the cmc of SDS at 25 °C.
●: Ch, ○: Ach, ◑: Sch, △: NaCl, ▲: $MgCl_2$,[17] ◪: 1-pentanol, □: 1-hexanol, ■: 1-heptanol,[13] ——: measured results by us, -----: reference results.

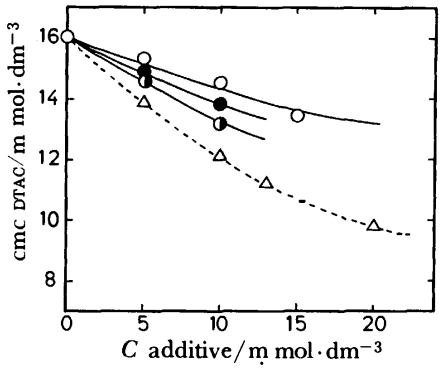

Fig. 2. Effect of Additives on the cmc of DTAC at 25 °C.
The symbols are same as Fig. 1.

16.0 m mol·dm^{-3}) and the values in the presence of NaCl of 5 m mol·dm^{-3} (6 m mol·dm^{-3}, 14 m mol·dm^{-3}) are consistent well with the values from the reference,[17] so the values obtained by us are considered to be adequate.

cmc of SDS and DTAC decreased with increase of the concentration of choline derivatives. The effectiveness of choline derivatives is larger than that of NaCl on the cmc of SDS, while the effectiveness of choline derivatives is smaller than that of NaCl on the cmc of DTAC. Furthermore, in the case of SDS, the order of effectiveness to decrease the cmc is Sch>Ach>Ch>NaCl, while in the case of DTAC, the order is NaCl>Sch>Ch>Ach. These results are considered to be due to the followings: (1) In the case of SDS, the electric charge of micelle has opposite sign to that of choline derivatives: The choline derivatives, as organic ions, may have specific interaction rather than the simple electrostatic effect of shielding by the counterions. In addition, choline derivatives lead to the reduction of the free energy of mixing by entering in the micelle. The difference of effectiveness is explained from the distribution of choline derivatives to micelle from bulk phase and the deepness of penetration, due to the hydrophobic property (Sch is more hydrophobic because Sch has the structure that two molecules of Ach have condensed). Regarding the distribution of choline derivatives between micellar and bulk phases, we have measured the distribution of Ach by means of ultrafiltration and it has been found that Ach enter indeed in the micelle. According to the result, the distribution ratio of Ach of 5 m mol·dm^{-3} in the micellar phase is 30—40% in the presence of SDS or DTAC of 30 m mol·dm^{-3}. The results of ultrafiltration will be reported in detail in a later paper. (2) In the case of DTAC, the electric charge of micelle has same sign to that of choline derivatives: The choline derivatives decrease the cmc by the shielding effect of the electrostatic repulsion by chloride ions as the effect of NaCl, while the choline derivatives entered in the micelle prevent the surfactant molecule to associate by the electrostatic repulsive force between the head groups. Therefore, the effectiveness of the choline derivatives is smaller than that of NaCl. The reason that Sch is more effective than Ch or Ach is considered mainly to be due to the counterion effect because that Sch has the structure composed of two Ach. It can, therefore, be concluded that the facts that the order of the effectiveness to decrease the cmc is Sch>Ach>Ch>NaCl for SDS, and NaCl>Sch>Ch>Ach for DTAC, are explained by the electrostatic effect and the distribution of choline derivatives between micellar and bulk phases.

References

1) G. S. Hartley, *J. Chem. Soc.*, **1938**, 1968.
2) M. M. Corrin and W. D. Harkins, *J. Am. Chem. Soc.*, **69**, 683 (1947).
3) H. Lange, *Kolloid Z.*, **121**, 66 (1951).
4) E. W. Anacker, R. D. Geer, and E. H. Eylar, *J. Phys. Chem.*, **75**, 369 (1971).
5) J. F. Voeks and H. V. Tarter, *J. Phys. Chem.*, **59**, 1190 (1955).
6) J. M. Corkill and J. F. Goodman, *Trans. Faraday Soc.*, **58**, 206 (1962).
7) M. J. Shick, *J. Phys. Chem.*, **68**, 3585 (1964).
8) H. N. Singh, S. Swarup, and S. M. Saleen, *J. Colloid Interface Sci.*, **68**, 128 (1979).
9) S. Miyagishi, *Bull. Chem. Soc. Jpn*, **47**, 2972 (1974).
10) S. H. Herzfeld, M. L. Corrin, and W. D. Harkins, *J. Phys. Colloid Chem.*, **54**, 271 (1950).
11) K. Shirahama and T. Kashiwabara, *J. Colloid Interface Sci.*, **36**, 65 (1971).
12) M. Manabe and M. Koda, *Bull. Chem. Soc. Jpn*, **51**, 1599 (1978).
13) K. Hayase and S. Hayano, *Bull. Chem. Soc. Jpn*, **50**, 83 (1977).
14) K. Hayase and S. Hayano, *J. Colloid Interface Sci.*, **63**, 446 (1978).
15) Mohammad Abu-Hamdlyyah and Chrlstiane M. El-Danab, *J. Phys. Chem.*, **87**, 5443 (1983).
16) J. Fendler and E. Fendler, "Catalysis in Micellar and Macromolecular Systems," Academic Press, New York, 1975.
17) Handbook of Surfactants, (1963) Maruzen, Tokyo, Japan.

NMR Spectra of Benzenes Containing Trifluoromethyl Groups

Kensuke TAKAHASHI,* Akihiro YOSHINO, Kenzo HOSOKAWA,† and Hiroshige MURAMATSU†
Nagoya Institute of Technology, Gokiso-cho, Showa-ku, Nagoya 466
†*Government Industrial Research Institute, Nagoya, Hirate-machi, Kita-ku, Nagoya 462*
(Received August 20, 1984)

Synopsis. The ^{1}H, ^{13}C, and ^{19}F NMR spectra of the nine title compounds were measured. The substituent effect of a trifluoromethyl group were generally additive for the ^{1}H, ^{13}C, and ^{19}F chemical shifts. The assignment of the ^{13}C signals was assisted by the observed coupling constants between the carbon and the fluorine, which were about 275, 35, and 6 Hz for the ^{1}J, ^{2}J, and ^{3}J values of these compounds.

The NMR spectral data of the title compounds have not yet been systematically reported except for the ^{19}F NMR data.[1] The aim of this study was to obtain the NMR parameters of the title compounds. The values of the coupling constants between the carbon and fluorine, ^{1}J, ^{2}J, and ^{3}J, were also helpful for the assignment of the ^{13}C signal.

Experimental

The ^{1}H and ^{19}F NMR spectra were observed with a frequency-swept Hitachi R-20B spectrometer, whose center frequencies were 60 and 56.46 MHz, respectively. The ^{13}C NMR spectra were measured using a Varian XL-200 spectrometer with a frequency of 50.3 MHz. The chemical shifts were determined in a chloroform-*d* solution using a small amount of TMS and C_6F_6 as internal references.

The benzenes containing trifluoromethyl group were prepared by the fluorination of the corresponding benzene carboxylic acids by sulfur tetrafluoride in the presence of anhydrous hydrogen fluoride.[2] The compounds studied in this article are summarized (with their reference numbers) in Table 1.

Results and Discussion

Chemical Shifts. The values of the chemical shifts for ^{1}H, ^{19}F, and ^{13}C nuclei are given in Tables 2 and 3.

The ^{1}H chemical shifts fall within a range of 7.45—8.34 ppm with respect to TMS. Therefore, the hydrogen atoms in the present compounds are less shielded than those of benzene (7.31 ppm in the $CDCl_3$ solution). The substituent chemical shift (SCS) values of the trifluoromethyl group (S_o, S_m, and S_p) were evalu-

Table 1. Compounds studied

No.	Substituents
1	1-CF_3
2	1,2-$(CF_3)_2$
3	1,3-$(CF_3)_2$
4	1,4-$(CF_3)_2$
5	1,3,5-$(CF_3)_3$
6	1-Br-2,4,6-$(CF_3)_3$
7	1,2,4-$(CF_3)_3$
8	1,2,3-$(CF_3)_3$
9	1,2,4,5-$(CF_3)_4$

Table 2. ^{1}H and ^{19}F chemical shifts of the compounds studied, ppm[a]

No.	δ(1)	δ(2)	δ(3)	δ(4)	δ(5)	δ(6)
1	99.25	7.61	7.45	7.52	7.45	7.61
2	102.57	102.57	7.84	7.67	7.67	7.84
3	98.94	7.89	98.94	7.73	7.59	7.73
4	98.71	7.75	7.75	98.71	7.75	7.75
5	98.76	8.10	98.76	8.10	98.76	8.10
6	—	99.17	8.13	98.61	8.13	99.17
7	102.22[b]	102.24[b]	8.11	98.42	7.98	8.03
8	104.23	107.24	104.23	8.10	7.83	8.10
9	101.95	101.95	8.34	101.95	101.95	8.34

a) ^{1}H and ^{19}F chemical shifts are found from 7.45 to 8.34 and from 98 to 107 ppm respectively, and referred to TMS and C_6F_6 in the $CDCl_3$ solutions. b) The assignment is tentative.

Table 3. ^{13}C Chemical shifts of the compounds studied, ppm

No.	1-C	2-C	3-C	4-C	5-C	6-C	CF_3	
1	131.28 (32)[a]	125.57	129.16	132.17	129.16	125.57	125.03 (272)	
2	b)	b)	128.46	132.79	132.79	128.46	123.82 (275)	
3	132.63 (34)	123.15	132.63 (34)	129.30	130.26	129.30	124.37 (272)	
4	134.99 (33)	126.58	126.58	134.99 (33)	126.58	126.58	124.36 (272)	
5	134.00 (35)	126.24	134.00 (35)	126.24	134.00 (35)	126.24	123.43 (272)	
6	124.28	135.18 (32)	128.60	131.52 (35)	128.60	135.18 (32)	122.77 (274)(2,6)	123.35 (273)(4)
7	b)	b)	125.83	135.51 (34)	129.77	129.56	122.88 (275)(1,2)	123.41 (273)(4)
8	130.80 (38)	128.28 (38)	130.80 (38)	131.96 (6)	132.70	131.96 (6)	123.12 (274)(1,3)	122.21 (275)(2)
9	132.78 (38)	132.78 (38)	128.32 (4)	132.78 (38)	132.78 (38)	128.32 (4)	121.63 (276)	

a) The values in parentheses are the coupling constants between the carbon and the fluorine in Hz. b) Signals are not confirmed yet.

ated from a comparison of the chemical shifts of **1** with that of benzene. They are 0.30, 0.14, and 0.21 ppm, respectively. An ortho-effect, which is an interaction effect of two adjacent substituents, was also taken into consideration. Thus, S_{abc} is used to express the ortho-effect of the a- and b-positioned substituents to the c-positioned nucleus. Then S_{123} and S_{124} can be estimated to be 0.09 and 0.01 ppm from a comparison of the observed chemical shifts of 1,2-disubstituted compounds (**2**) with its calculated ones based on the additivity. The S_{123}, which is 0.09 ppm, gives an appreciable effect to the chemical shifts while the S_{124} can be neglected. By using these SCS values, the chemical shifts of the tri- and tetra-substituted compounds can be evaluated from the additivity rule to obtain values which are in agreement with the experimental ones within 0.1 ppm. The ^{1}H NMR spectrum of **1** was previously analyzed by Kostelnik *et al.*[3] The chemical shifts of **1** in a $CDCl_3$ solution were evaluated by visual fittings of the observed spectrum to the simulated one where the calculation was performed by changing the chemical-shift values and keeping the spin couplings constant.

The ^{19}F chemical shifts of the trifluoromethyl group were similarly treated. The SCS values (S_o, S_m, and S_p) of the ^{19}F chemical shifts of the substituent CF_3 groups are 3.32, −0.31, and −0.54 ppm, respectively. These were derived from a comparison of the chemical shifts of disubstituted compounds (**2**, **3**, and **4**) with that of **1**. Typical examples of the calculated chemical shifts are given for **7** as follows:

$$\delta(\text{F-1}) = 99.25 + S_o + S_p = 102.03 \text{ (Exp. 102.22)}$$

$$\delta(\text{F-2}) = 99.25 + S_o + S_m = 102.26 \text{ (Exp. 102.24)}$$

$$\delta(\text{F-4}) = 99.25 + S_m + S_p = 98.40 \text{ (Exp. 98.42)}$$

The SCS values of the ^{13}C chemical shifts of the trifluoromethyl group were obtained from the ^{13}C chemical shifts of **1** as compared with that of benzene (128.33 ppm in $CDCl_3$). The values are 2.95, −2.76, 0.83, and 3.84 ppm, respectively, for the ipso-, ortho-, meta-, and para-carbons. The observed ^{13}C chemical shifts for tri- and tetrasubstituted compounds are consistent with the calculated ones, which were derived by using the above-mentioned SCS values, within 2 ppm with two exceptions. The large deviations are found to be 4 and 2 ppm for the C_3 of **9** and the C_3 of **2**. When an ortho-effect of S_{123}, which is assumed to be 2.0 ppm, is introduced, the observed ^{13}C chemical shifts become consistent with the calculated ones within 1 ppm.

Coupling Constants. The observed values of the coupling constants between the carbon and fluorine were about 275, 35, and 6 Hz for the ^1J, ^2J, and ^3J (Table 3). The values for **1** were previously reported.[4] These values were useful for the assignment of the ^{13}C signals of the compounds studied. However, the splitting of the ^{13}C signals was disadvantageous for finding the signals. Several signals of **2** and **7** have not yet been confirmed.

The long-range coupling constants between the hydrogen and fluorine are generally small and change in magnitude from compound to compound. An example of the ^{1}H spectra is given in Fig. 1 for **2**.

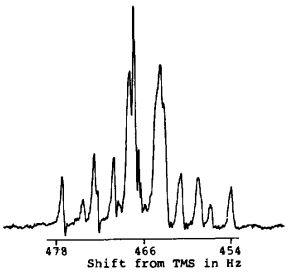

Fig. 1. An observed ^{1}H NMR spectrum of **2** at 60 MHz.

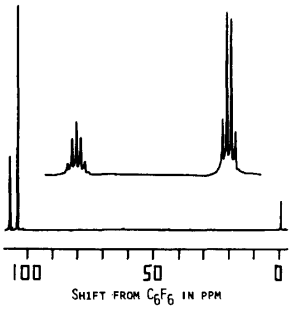

Fig. 2. An observed ^{19}F[^{1}H] NMR spectrum of **8** at 188.22 MHz with an expanded one.

This was analyzed as an AA'BB' spin system. The analysis shows that the chemical shift between the H_3 and the H_4 is 10.1 Hz at 60 MHz and the J_{34}, J_{35}, J_{36}, and J_{45} values are 8.0, 1.3, 0.5, and 7.6 Hz, respectively. The upfield spectrum is broader than the other half by about 0.2 Hz, as shown in Fig. 1. The origin of the broadening is considered to be the couplings between the hydrogens and fluorines. Therefore it is concluded that $|^5J_{HF}| > |^4J_{HF}|$. This is consistent with the analyzed values of **1**.[3] However, $|^4J_{HH}| > |^5J_{HH}|$ has been found in a similar system of toluene.[6] The ^{1}H signal of **6** appeared as a sextet whose splitting was about 0.7 Hz. The situation is also the same with the ^{1}H signals of **5**. The splitting of about 0.7 Hz is consistent with the couplings reported for **1** and **5**.[3,5]

The fluorine-fluorine couplings may be observed for the compounds (**6**, **7**, and **8**), which have unequivalent CF_3 groups. The line breadth of the ^{19}F signal of **6** is about 1.1 Hz. Therefore, the ^6J(F-F) is smaller than 1 Hz. On the other hand, the ^5J(F-F) observed for **8** is about 16 Hz. This is shown in the ^{19}F[^{1}H] spectrum as given in Fig. 2 and consistent with the reported values.[1]

References

1) G. P. Vdovin, Yu. P. Egorov, E. V. Konovalov, A. P. Krasnoshchek, V. G. Lukmanov, E. P. Saenko, L. M. Yagunol'skii, *Teoret. i Eksperim. Khimi.*, **11**, 44 (1975).

2) K. Hosokawa, T. Ueda, and H. Muramatsu, Preprint presented at the 49th National Meeting of the Chemical Society of Japan, Tokyo, April 1984, Vol. **2**, p. 917 (1H16).

3) R. J. Kostelnik, M. P. Williamson, D. E. Wisnosky, and S. M. Castellano, *Can. J. Chem.*, **47**, 3313 (1969).

4) D. Doddrell, M. Barfield, W. Adcock, M. Aurangzeb, and D. Jordan, *J. Chem. Soc., Perkin Trans. 2*, **1976**, 402.

5) J. V. Acrivos, *Mol. Phys.*, **5**, 1 (1962).

6) M. P. Williamson, R. J. Kostelnik, and S. M. Castellano, *J. Chem. Phys.*, **49**, 2218 (1968).

The Electrochemical Behavior of BR_2-linked Bis(glyoximato)nickel(II) Complexes in a Nonaqueous Solvent

Makoto AIHARA,* Yumiko NISHI, Hiroko OMATSU, and Yasuomi NONAKA†

Laboratory of Inorganic Chemistry, Faculty of Home Life Science, Fukuoka Women's University, Higashi-ku, Fukuoka 813

†*Fukuoka Jogakuin Junior College, Minami-ku, Fukuoka 816*

(Received July 4, 1984)

Synopsis. Nickel(II) complexes with dioximers replaced by BF_2 and $B(C_2H_5)_2$ groups for bridging by the hydrogen atom were investigated by electrochemical methods. The nickel(II) complexes exhibited two distinct one-electron reduction waves in *N,N*-dimethylformamide. It was found that the electron-withdrawing effect of the replaced group is exerted on the electronic states of the nickel(II) complexes.

The nickel(II) complexes of BF_2- or $B(Et)_2$- linked dioximers (Fig. 1) were synthesized and characterized by Schrauzer[1] and Gagné.[2] Schrauzer concluded that these substituents exert no effect on the ligand field around the nickel(II) ion. One of the present authors (Y. N.) reported on the effects of BF_2- and $B(Et)_2$-substitution for bridging by the hydrogen atom in the Co(II), Ni(II), and Cu(II) complexes with some oximate ligands.[3] The BF_2-substitution caused a red-shift of the d-d band, increased the $g_{//}$-value for copper(II) complexes, and caused a positive shift of the polarographic half-wave potential of nickel(II) complexes. These results suggested that the electrochemical method is useful in investigating the electronic state of the nickel(II) complexes.

The present report deals with the electrochemical behavior of nickel(II) complexes with BF_2- or $B(Et)_2$-substituted macrocyclic ligands, as is shown in Fig. 1.

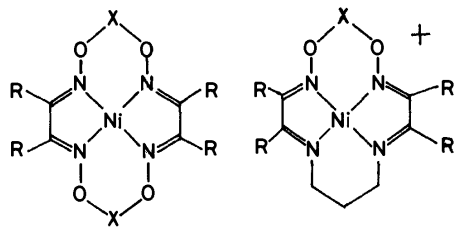

$R = CH_3$: $Ni(dmgX)_2$ $R = CH_3$: $Ni(tnomX)^+$

$R = C_6H_5$: $Ni(dpgX)_2$ $X = H$, BF_2 and $B(Et)_2$

Fig. 1. Structures and abbreviations of the complexes in this study.

Experimental

Synthesis of the Complexes. The complexes were prepared according to the method reported previously.[3]

Electrochemical Measurements. All the measurements were carried out in an 0.1 M tetraethylammonium perchlorate (TEAP) solution (1 M=1 mol dm^{-3}) of *N,N*-dimethylformamide (DMF) at 25±0.1 °C. A Fuso Model 312 polarograph and a DME (or HMDE) were employed for the polarographic and cyclic voltammetric measurements, respectively. The reference electrode was an SCE with a salt bridge.[4] Controlled-potential electrolysis was performed at a mercury pool under stirring. The other apparatus was the same as that described previously.[4]

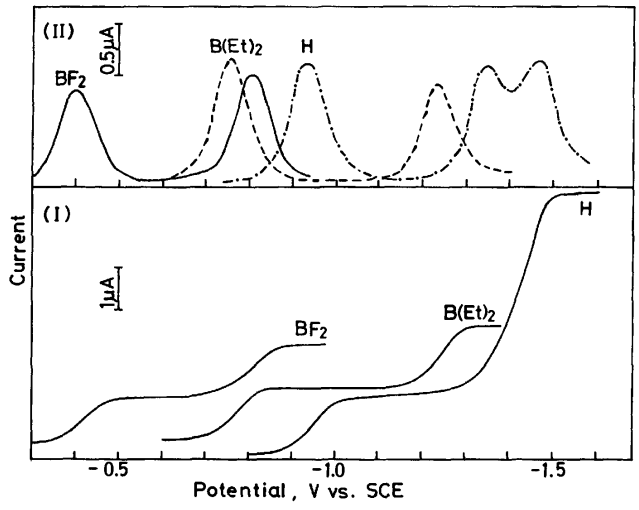

Fig. 2. Current-sampled dc polarograms(I) and differential pulse polarograms(II) of 0.5 mM Ni(dpgX)$_2$ in DMF.

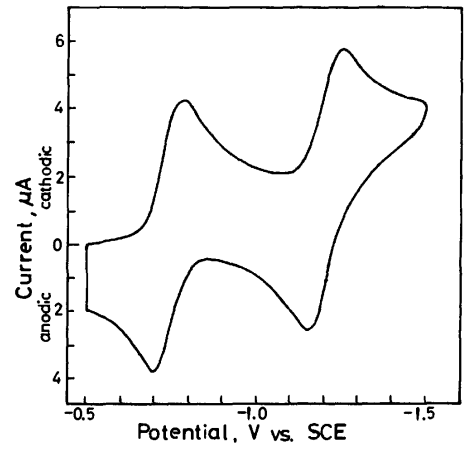

Fig. 3. Cyclic voltammogram of 0.5 mM Ni{dpgB(Et)$_2$}$_2$ in DMF at HMDE, scan rate 200 mV/sec.

Results and Discussion

Some typical current-sampled dc polarograms for the $Ni(dpgX)_2$ complexes in DMF are shown in Fig. 2. For $Ni(dmgX)_2$, the same current-sampled dc polarograms were obtained in DMF. Each complex gives a two-stepped reduction wave. The heights of the first and second waves were almost the same except in the $Ni(dmgH)_2$ and $Ni(dpgH)_2$ systems. The height of the second wave for these two systems was larger than that of the first wave. On the other hand, the second wave for the $Ni(tnomX)^+$ system split into two waves.

These systems were investigated by means of normal pulse polarography. Each system exhibited electrochemical behavior much like the current-sampled dc polarography. The relationship of the current (i, μA) of the normal pulse polarogram and the sampling time

Table 1. Polarographic data for 0.5 mM Ni(II) complexes

Complex	$E_{1/2}$	i	Slope	n	$E_{1/2}$	i	Slope	n
	V *vs.* SCE	μA	mV		V *vs.* SCE	μA	mV	
$Ni(dmgH)_2$[a]	−1.279	0.48	56		−1.608	1.56		
$Ni\{dmgB(Et)_2\}_2$	−1.119	1.10	56	1.1	−1.652	1.48	55	
$Ni(dmgBF_2)_2$	−0.729	1.15	67	1.1	−1.225	1.48	55	2.1
$Ni(dpgH)_2$	−0.962	1.18	59	1.0	−1.435	4.20		
$Ni\{dpgB(Et)_2\}_2$	−0.771	0.98	53	1.1	−1.228	1.23	53	2.0
$Ni(dpgBF_2)_2$	−0.442	0.94	53	1.1	−0.830	1.08	65	2.1
$Ni(tnomH)^+$	−0.802	0.97	40	1.0	−1.304	0.58	39	
					−1.454	0.55	41	
$Ni\{tnomB(Et)_2\}^+$	−0.723	1.09	51	1.0	−1.211	0.93	37	
					−1.364	0.29	25	2.0
$Ni(tnomBF_2)^+$	−0.559	0.63	43		−0.970	0.73	45	
					−1.146	0.40	50	

a) Measured at the concentration of the 0.3 mM Ni(II) complex.

(t, s) was determined. There exists an obvious linear relationship between i and $t^{-1/2}$. These facts indicate that each electrode reaction is diffusion-controlled.

Some typical differential pulse polarograms of $Ni(dpgX)_2$ in DMF are shown in Fig. 2. Two main peaks were observed on each differential pulse polarogram, and their shapes were found to be symmetrical. The differential pulse polarograms for $Ni(dmgH)_2$ and $Ni(dpgH)_2$ indicate that the second wave of the current-sampled dc polarogram contains two-reduction waves. Each second wave of the current-sampled dc polarogram was three times or more larger than the first wave. Therefore, the reduction at the second wave was assumed to correspond to the electron transfer to the metal and ligand in the complex.

A typical cyclic voltammogram of the $Ni\{dpgB(Et)_2\}_2$ in DMF is shown in Fig. 3. Two peaks were observed on the cathodic branch, and two peaks, on the anodic branch, suggesting reversible processes.

The results of constant potential electrolysis showed the consumption of one electron for each step to be as is summarized in Table 1.

The electrode reactions for the $Ni(dmgX)_2$ and $Ni(dpgX)_2$ systems were assumed to be as follows.

$$Ni^{II}L + e \rightleftharpoons Ni^{I}L \quad (1)$$

$$Ni^{I}L + e \rightleftharpoons Ni^{0}L \quad (2)$$

where L denotes $(dmgX)_2$ and $(dpgX)_2$.

For $Ni(tnomX)^+$, the same electrode reaction was assumed for the first wave, but the reciprocal slope of each wave was 37—50 mV. These values were assumed to suggest Ni-Ni metal intramolecular interaction. The same behavior has been observed in polynuclear metal complexes.[5]

A comparison of the half-wave potentials for the $Ni(dmgX)_2$, $Ni(dpgX)_2$, and $Ni(tnomX)^+$ systems is shown in Fig. 4. The order of the half-wave potentials is; BF_2>$B(Et)_2$>H. The Ni(II) complex with the BF_2-substituted group is more easily reduced compared with the other complexes; this is because of the electron-withdrawing effect of the BF_2 group. The electron-withdrawing effect of the BF_2 group in these complexes was observed, although Schrauzer suggested that the effect of BF_2 groups on the nickel(II) ion could not be observed in a spectrophotometric study.

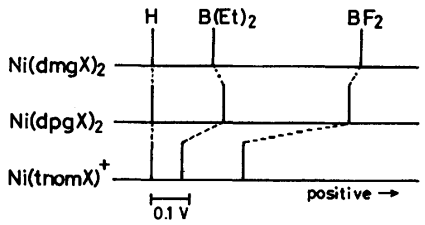

Fig. 4. Comparison of the half-wave potentials of each first wave as a criterion of that of Ni(II) complexes with hydrogen bridging.

The reduction potentials of $Ni(dpgX)_2$ are more positive than those of $Ni(dmgX)_2$. This fact may correspond to the weak electron-donating effect of the phenyl group.

On the other hand, the effect of a substituted group on the $Ni(tnomX)^+$ system is weak compared with those for $Ni(dmgX)_2$ and $Ni(dpgX)_2$. This is because of the structure of $Ni(tnomX)^+$, which has a closed ring and only one substituted group. However, the effect of Ni-Ni metal interaction on the half-wave potential should also be considered. This will be a subject for further study.

References

1) G. N. Schrauzer, *Chem. Ber.*, **95**, 1438 (1962).
2) R. R. Gagnè, *J. Am. Chem. Soc.*, **98**, 6709 (1976).
3) Y. Nonaka and K. Hamada, *Bull. Chem. Soc. Jpn*, **54**, 3185 (1981).
4) S. Misumi and M. Aihara, *Talanta*, **19**, 549 (1972).
5) M. Aihara, Y. Kubo, Y. Nishida, and S. Kida, *Bull. Chem. Soc. Jpn.*, **54**, 3207 (1981).

Stability Constants of Complex Formations between Divalent Metal Ions and Cyclic Dipeptides: Cyclo(glycyl-L-histidyl) and Cyclo(L-methionyl-L-histidyl)

Yoshitane KOJIMA,* Noriaki ISHIO, and Tetsushi YAMASHITA
Department of Chemistry, Faculty of Science, Osaka City University, Sugimoto, Sumiyoshi-ku, Osaka 558
(Received July 5, 1984)

Synopsis. The values($\log K_1$ and $\log K_2$) of the complex formations between divalent metal ions and two cyclic dipeptides of this title were determined by Bjerrum's method. It is apparent from ^{1}H NMR data that metal ions link exclusively to the nitrogen atom of the imidazolyl group of cyclo(L-methionyl-L-histidyl).

The authors[1] have studied some metal complexes with cyclic dipeptides as model compounds for metallo-proteins and -enzymes, in which the metal ions link exclusively to the functional groups of the side chains of the peptides.

This paper reports the values of the stability constants of the complex formations between divalent metal ions and cyclic dipeptides with an imidazolyl group[cyclo(glycyl-L-histidyl)=CGH and cyclo(L-methionyl-L-histidyl)=CMH].

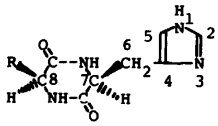

CGH; R = H

CMH; R = $CH_2CH_2SCH_3$

9 10 11

Experimental

Materials. CGH and CMH were prepared according to methods reported earlier.[1a] All metal salts obtained commercially were used without further purification.

Measurements. ^{1}H NMR data were obtained in D_2O at 45 °C with sodium 3-trimethylsilyl-1-propanesulfonate as an internal reference using a JEOL PS-100. In the measurements of the stability constants of the complex formations, the titrated solution contained 0.24—1.27 mmol of a cyclic dipeptide, 0.10—0.27 mmol of $Ni(NO_3)_2$, $CuSO_4$ or $ZnSO_4$, and 0.40—1.50 mmol of HCl in 0.50 dm^3, the ionic strength being adjusted to 0.2 mol dm^{-3} with KNO_3. The solution was titrated with a 0.943 mol dm^{-3} NaOH aqueous solution at 25 °C under a nitrogen atmosphere using a Hitachi-Horiba F-5 pH meter. The acid dissociation constants(K_a) used in calculations were determined by titration to be $10^{-6.25}$ and $10^{-6.31}$ for CGH and CMH, respectively. The free-ligand concentration(L) and the average coordination number($\bar{n}$) were calculated from the titer and the hydrogen-ion concentration on the assumption that 1:1 and 1:2 complexes formed. The stability constants, $K_1=[ML]/([M][L])$ and $K_2=[ML_2]/([ML][L])$, were obtained by linear fittings according to the following equation: $Y=K_1K_2X-K_1$, where X is $(2-\bar{n})[L]/(\bar{n}-1)$ and Y is $\bar{n}/\{(\bar{n}-1)[L]\}$.

Results and Discussion

Figure 1 shows that the ^{1}H NMR signals of imidazole-2 and -4 protons are equally broadened in CMH:Cu^{2+} (5000:1) and in CMH:Ni^{2+} (1000:1) systems, respectively, suggesting the coordination of the imidazolyl group to metal ions. The amide protons of the diketopiperazine (DKP) ring are replaced by deuterium in D_2O. Figure 1 also shows no broading or

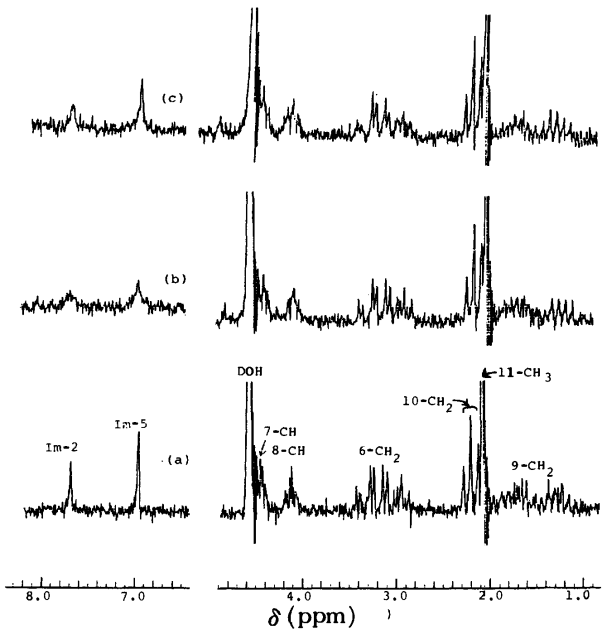

Fig. 1. ^{1}H NMR spectra of D_2O solution of the ligand (CMH) in the absence and presence of Ni^{2+} or Cu^{2+} at 45 °C. Ligand concentration = 0.052 mol dm^{-3}. (a) ligand alone, (b) ligand:Cu^{2+} = 5000:1, (c) ligand: Ni^{2+} = 1000:1. Im; imidazole.

shift of the methylene and methyl protons (C_{10} and C_{11}) adjacent to the sulfur atom and the methine protons (C_7 and C_8), though one of the methine protons (C_7) is partially overlapped by the signal of DOH. These observation suggest that both the sulfur atom[2] of the methionyl residue and the amide groups of DKP do not link with these metal ions. A similar tendency was also observed in the cyclo(L-histidyl-L-histidyl)-Cu^{2+}system reported earlier.[1b] An earlier report of X-ray analysis of a Zn^{2+} complex with CMH indicates that four 1-N atoms of each imidazole of four CMH's coordinate to Zn^{2+} ion.[1c] In the ^{1}H NMR measurement of this complex, a distinct down-field shift [δ (Zn^{2+} complex ion) $-\delta$ (free ligand)=0.33(ppm)] is observed only for the imidazole-2 proton of CMH. Thus, these metal ions(Ni^{2+}, Cu^{2+}, and Zn^{2+}) appear to interact exclusively with the imidazolyl group of CMH.

The stability constants between a divalent metal ion and monodentate ligands (CGH and CMH) were obtained by Bjerrum's method. Figure 2 shows a typical example of an *X-Y* plot. As shown in Table 1, the obtained values of $\log K_1$ and $\log K_2$ seem to be in the order of the Irving-Williams series. Table 1 also shows that the *K* values for CMH are comparable to those for CGH having no functional group except an imidazolyl one. These results suggest that the coordination mode of CMH for metal ions is similar to that of CGH. Table 2 indicates that the *K* values for divalent metal ions and

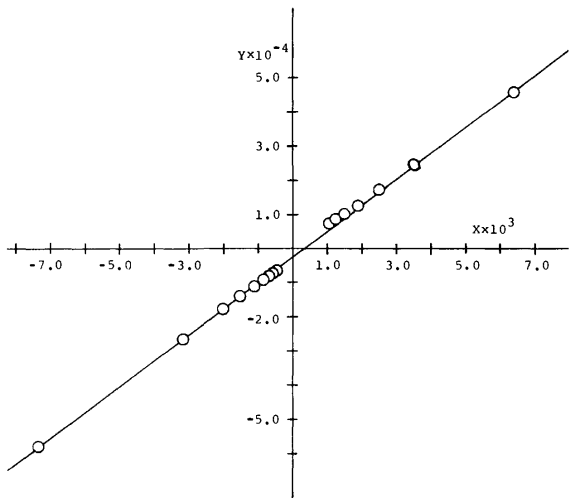

Fig. 2. A typical example of an X-Y plot. Cu: CGH=1:3.3.

TABLE 1. STABILITY CONSTANTS OF COMPLEXES BETWEEN DIVALENT METAL IONS AND CYCLIC DIPEPTIDES

Metal	M_t:L_t*	logK_1	logK_2
	cyclo(glycyl-L-histidyl)		
Ni	1:1.1	2.48	1.86
	1:2.1	2.60	1.79
	1:3.0	2.56	1.89
Cu	1:3.3	3.48	3.39
	1:4.2	3.48	3.29
Zn	1:2.1	2.28	1.65
	1:4.4	2.21	1.53
	cyclo(L-methionyl-L-histidyl)		
Ni	1:2.2	2.61	2.31
	1:3.1	2.49	2.20
Cu	1:2.4	3.37	3.19
	1:3.2	3.40	3.28
	1:3.6	3.29	3.20
Zn	1:2.0	2.50	1.48
	1:4.2	2.43	2.31

*M_t and L_t are total concentrations of each metal ion and each ligand, respectively.

cyclic dipeptides (CGH and CMH) are proportional to the strength of the basicities of ligands as compared with those for imidazole and pyridine.

In order to consider higher coordination numbers for metal ions, attempts to obtain the values of K_3 were carried out by successive approximations. However, the values were not successfully obtained because of the relatively small values of $\bar{n}$, as shown in Fig. 3. The values from K_1 to K_4 were also determined by Scatchard's method.[3] The values of logK_1 and logK_2 are shown as follows in order to make a comparison with those obtained by Bjerrum's method: CGH (Ni, 2.47, 1.33; Cu, 3.53, 2.99) and CMH (Ni, 2.38, 1.73; Cu, 3.50, 2.91; Zn, 2.34, 2.24). The stability constants between the Zn^{2+} ion and CGH were not obtained because of bad linearity. The values of logK_1 are in good agreement with those calculated using Bjerrum's method.

TABLE 2. LOGARITHMS OF STABILITY CONSTANTS[a]

Ligands		H^+	Ni^{2+}	Cu^{2+}	Zn^{2+}
Imidazole[b]	K_1	7.11	3.0	4.20	2.52
	K_2		2.5	3.42	2.32
	K_3		2.0	2.88	2.32
	K_4		1.5	2.1	2.0
CMH	K_1	6.31	2.55	3.35	2.43
	K_2		2.26	3.22	1.89
CGH	K_1	6.25	2.55	3.48	2.25
	K_2		1.85	3.34	1.59
Pyridine[b]	K_1	5.21	1.78	2.41	0.88
	K_2		1.22	1.88	0.47
	K_3		0.3	1.14	0.15
	K_4		−0.3	0.60	−0.2

a) The average values of this report (see Table 1), except b). b) The values of Ref.4).

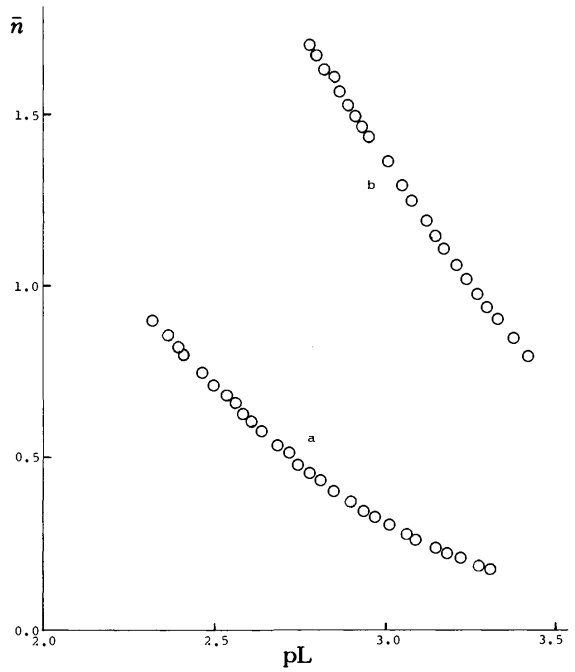

Fig. 3. Formation curves. a, Ni:CGH=1:3.0; b, Cu: CMH=1:3.6.

References

1) a) Y. Kojima, T. Yamashita, Y. Ishino, T. Hirashima, and T. Miwa, *Bull. Chem. Soc. Jpn.*, **56**, 3841(1983); b) Y. Kojima, *Transition Met. Chem.*, **4**, 269 (1979); c) Y. Kojima, N. Ishio, T. Yamashita, and K. Hirotsu, *Chem. Lett.*, **1983**, 1365.

2) R. Ettorre, V. Guantieri, A. M. Tamburro, and L. de Nardo, *Inorg. Chim. Acta*, **32**, L39 (1979). This paper showed that the sulfur atom of cyclo(L-methionyl-L-methionyl) interacts with Cu^{2+} ion.

3) J. T. Edsall, G. Felsenfeld, D. S. Goodman, and F. N. Gurd, *J. Am. Chem. Soc.*, **76**, 3054 (1954).

4) R. J. Sundberg and R. B. Martin, *Chem. Rev.*, **74**, 471 (1974).

The Magnetic Properties of the Ammonium Chloride Adducts of Copper(II) Chloroacetates

Shuji EMORI,* Nobuyuki HARAMAKI, and Yoneichiro MUTO
Department of Chemistry, Faculty of Science and Engineering, Saga University, Honjo-machi, Saga 840
(Received July 25, 1984)

Sinopsis. Various ammonium chloride adducts of copper(II) chloroacetate and copper(II) dichloroacetate were prepared. The variable-temperature magnetic susceptibilities of the dimethylammonium chloride adducts obey the Bleaney-Bowers equation, indicating the existence of the copper(II) acetate type of dinuclear moiety in their crystals. The effect of the counter cations on their magnetic moments was discussed.

A large number of dinuclear copper(II) carboxylate adducts, $[Cu(RCOO)_2 \cdot L]_2$, have been studied to elucidate the factors influencing the magnetic properties in these compounds. In particular, the effects of the carboxylate substituent R and of the axial ligand L upon the strength of the spin-exchange interaction or singlet-triplet separation($-2J$) have been extensively investigated.[1] However, both the variation of surrounding ions around the dinuclear molecule and the crystal packing must also affect the magnetic properties. Goodgame *et al.* reported the preparation and magnetic properties of some dinuclear anionic copper(II) acetate complexes, $\{(CH_3)_4N\}_2[Cu(CH_3COO)_2X]_2$ (X= NCS, NO_2, or Br).[2,3] Because the counter cation can be easily replaced, these anionic dinuclear copper(II) compounds are appropriate to examine the effect of the surrounding ions but only insufficient data have been available. Here, we report the preparation and magnetic properties of the various ammonium chloride adducts of copper(II) chloroacetate and copper(II) dichloroacetate.

The compound with the stoichiometry of $Cu(ClCH_2COO)_2 \cdot n$ACl, where n=2 for A=NH_4 and n=1 for A=$(CH_3)_2NH_2$ and CH_3NH_3, was precipitated in green crystals when an excess of ACl was added to a hot aqueous solution of copper(II) chloroacetate with a small amount of chloroacetic acid, and then the mixture was allowed to stand for a few minutes. The dichloroacetate compond $Cu(Cl_2CHCOO)_2 \cdot n$ACl, where n=5/7 for A=$(CH_3)_2NH_2$ and n=3/2 for A=$(CH_3)_3NH$, was also obtained in a similar way.

The magnetic moments of these compounds (Table 1) were evaluated from their susceptibilities observed at room temperature and the relevant Pascal constants.[4] They are low and practically the same as that of copper(II) acetate monohydrate (1.40 BM at 21 °C).[5] The temperature dependence of the magnetic susceptibilities of the dimethylammonium chloride adducts of copper(II) chloroacetate and copper(II) dichloroacetate over the temperature range of 77—300 K (Fig. 1) was also found to correspond well with the known behavior of copper(II) acetate monohydrate. A reasonably good agreement was found between the experimental results and a theoretical curve calculated from the usual expression[6] for the susceptibility of the copper(II) ions in the copper(II) acetate dimer (Bleaney-Bowers equation), using the following parameters: g=2.19 and $2J$=−278 cm^{-1} for the chloroacetate compound and g=2.21 and $2J$=−271 cm^1 for the dichloroacetate compound, respectively, and $N\alpha$=60×10^{-6} emu/mol (1 emu/mol=4π×10^{-6} m^3/mol). The result obtained is consistent with the assumption that all have the familiar bridged dimeric copper(II) acetate monohydrate structure. Although the chloride ion has a tendency to displace the bridging carboxylate, the anionic dinuclear copper(II) carboxylate is constructed by the axial coordination of a chloride ion with the exception of the dimethylammonium chloride adduct of copper(II) dichloroacetate and the tetramethylammonium chloride adduct of copper(II) chloroacetate. Garner and Senior[7] reported that the reaction of molybdenum(II) trifluoroacetate with tetraethylammonium halides resulted in the formation of the hemi- and mono-adducts, $\{(C_2H_5)_4N\}$, $[Mo_2(CF_3COO)_4X]$, and $\{(C_2H_5)_4N\}_2[Mo(CF_3COO)_2X]_2$, and suggested that the adducts are more stable than the neutral molecule, presumably due in large measure to the lattice energy of these salts. This is also the case for copper(II) carboxylate, and the $(NH_4)_2ZnCl_4$ adduct of copper(II) chloroacetate (1.41 BM at 28 °C) can be isolated easily.[8] From the Table 1 and the magnetic data of the corresponding acetate adducts,[9] the following trends in the magnetic properties can be seen. First, the magnetic moments in the series of the same ammonium chloride adducts increase as the acid strength of the parent carboxylic acids become stronger, which is attributed to the fact that the stronger carboxlylic acid has a tendency to elongate the bridging Cu-O-C-O-Cu length.[1] The IR spectra, assigned by a comparison with the spectra of the corresponding pyridine adducts, show absorption bands characteristic of Cu-Cl stretching vibrations, except for the dimethylammonium chloride adduct of copper(II)

TABLE 1. ANALYTICAL DATA AND EFFECTIVE MAGNETIC MOMENTS AT 27 °C

Compound	Cu(%)		Cl(%)		μ_{eff}(BM)
	Calcd	Found	Calcd	Found	
$Cu(ClCH_2COO)_2 \cdot 2NH_4Cl$	17.88	18.09	19.84	19.69	1.42
$Cu(ClCH_2COO)_2 \cdot CH_3NH_3Cl$	19.98	20.06	11.15	11.22	1.43
$Cu(ClCH_2COO)_2 \cdot (CH_3)_2NH_2Cl$	19.14	19.22	10.67	10.83	1.42
$Cu(ClCH_2COO)_2 \cdot 1/3(CH_3)_4NCl \cdot H_2O$	20.83	20.93	3.87	3.72	1.41
$Cu(Cl_2CHCOO)_2 \cdot 5/7(CH_3)_2NH_2Cl$	16.82	16.84	6.70	6.57	1.47
$Cu(Cl_2CHCOO)_2 \cdot 3/2(CH_3)_3NHCl$	13.73	13.74	11.49	11.35	1.50

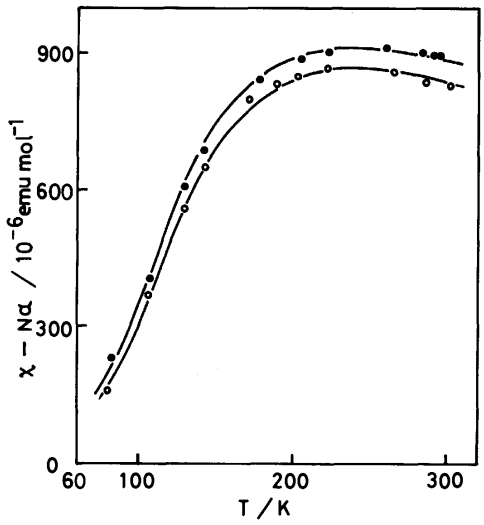

Fig. 1. Magnetic susceptibilities of the dimethylammonium chloride adducts of copper(II) chloroacetate (white circles) and copper(II) dichloroacetate (black circles). The solid curve represents the Bleaney-Bowers equation.

dichloroacetate which shows the complicated spectrum in the region of 276—317 cm^{-1} in agreement with its complicated stoichiometry. The observation of a band shift for the Cu-Cl stretching to the higher frequency, from 232—234 cm^{-1} of the acetates to 260—264 cm^{-1} of the chloroacetates suggests the stronger axial coordination in the chloroacetates. This is consistent with the fact that there is a movement of the copper atom out of the basal plane of its square pyramidal coordination polyhedron when the acid strength increases.[1,10] Secondly, since the difference in the magnetic moments between the chloride adducts (1.38—1.41 BM at 17 °C for the acetates and 1.41—1.43 BM at 27 °C for the chloroacetates, respectively) and the hydrates (1.40 BM at 21 °C for the acetate[5] and 1.45 BM at 24 °C for the chloracetate[11]) is very small, it was difficult to evaluate the effect of the axial ligands. Thirdly, even for the same carboxylate compounds, there are slight differences in the observed magnetic moments of the chloride adducts (1.39—1.41 BM for the ammonium chloride adducts and 1.38 BM for the potassium chloride adduct of copper(II) acetate[9]). This fact suggests that the hydrogen bonds to the bridging carboxylate and the cation affect the magnetic property in addition to the packing effect. The amount of the scattering seems to increase as the parent carboxylic acids become stronger.

References

1) M. Melnik, *Coord. Chem. Rev.*, **42**, 259 (1982).
2) D. M. L. Goodgame, N. J. Hill, D. F. Marsham, A. C. Skapski, M. L. Smart, and P. G. H. Thoughton, *Chem. Commun.*, **1969**, 629.
3) D. M. L. Goodgame and D. F. Marsham, *J. Chem. Soc.*, A, **1966**, 1167.
4) G. Foex, "Constants Sélectionées, Diamagnétisme et Paramagnétisme," Masson, Paris (1957).
5) B. N. Figgis and R. L. Martin, *J. Chem. Soc.*, **1956**, 3837.
6) J. Lewis, Y. C. Lin, L. K. Royston, and R. C. Thomson, *J. Chem. Soc.*, **1965**, 428.
7) C. D. Garner and R. G. Senior, *J. Chem. Soc., Dalton Trans.*, **1975**, 1171.
8) to be published.
9) S. Emori and Y. Muto, *Bull. Chem. Soc. Jpn.*, **57**, 291 (1984).
10) V. M. Rao, D. N. Sathyanarayana, and H. Manohar, *J. Chem. Soc., Dalton Trans.*, **1983**, 2167.
11) K. S. Patel, J. A. Faniran, and A. Earnshaw *J. Inorg. Nucl. Chem.*, **38**, 352 (1976).

Stereoisomers of *trans*-Dichlorocobalt(III) Complex with 1,7-Bis[(*S*)-2-pyrrolidinyl]-2,6-diazaheptane

Masahiko SABURI,* Shusei OBATA, Motowo YAMAGUCHI, and Sadao YOSHIKAWA*

Department of Synthetic Chemistry, Faculty of Engineering, The University of Tokyo, Hongo, Bunkyo-ku, Tokyo 113

(Received August 29, 1984)

Synopsis. The complex *trans*-[$CoCl_2$(SS-pyht)]$^+$ (SS-pyht=1,7-bis[(*S*)-2-pyrrolidinyl]-2,6-diazaheptane), prepared *via* the HCl treatment of *Λ*-*β*-[$CoCO_3$(SS-pyht)]$^+$, was found to take the (*R*,*R*) configuration with regard to the secondary nitrogen centers involving the central chelate. The isomer ratio of two diastereomers (trans(*R*,*S*) and trans(*R*,*R*)) was estimated at the equilibrium in methanol; (*R*,*S*)/(*R*,*R*)= 10.4±2.6.

The *trans*-dichlorocobalt(III) complex of 1,7-bis[(*S*)-2-pyrrolidinyl]-2,6-diazaheptane (SS-pyht), an optically active 2,3,2-tet derivatives having the pyrrolidine rings at the both side arms, was first reported by Jun and Liu[1] (2,3,2-tet=3,7-diazanonane-1,9-diamine). They supposed that the *trans*-[$CoCl_2$(SS-pyht)]$^+$ produced by the standard air-oxidation method takes the (*R*,*R*)[2] configuration with respect to the secondary nitrogen centers connecting the central six-membered chelate and the five membered chelates (Fig. 1a).[1] However, the true structure of the complex ion determined by an X-ray crystallographic study[3] was found to assume the trans(*R*,*S*) configuration (Fig. 1b).

In our previous report,[4] an alternative method, *i.e.*, the treatment of [$CoCO_3$(SS-pyht)]$^+$ with hydrochloric acid, was applied for preparing *trans*-[$CoCl_2$(SS-pyht)]-ClO_4. This Note describes that the above mentioned dichloro complex adopts the trans(*R*,*R*) configuration, as is expected from the observations that the HCl treatment of *β*-carbonatocobalt(III) with 2,3,2-tet[5] or its chiral derivatives[6] yields trans-dichloro complex having the C_2 symmetry (trans(*R*,*R*) and/or (*S*,*S*)).

Experimental

Materials. The ligand, 1,7-bis[(*S*)-2-pyrrolidinyl]-2,6-diazaheptane (SS-pyht), was synthesized by the reported method.[1,4] The complex *trans*(*R*,*S*)-[$CoCl_2$(SS-pyht)]ClO_4 was obtained by the air-oxidation method.[1] The *trans*(*R*,*R*)-[$CoCl_2$(SS-pyht)]ClO_4 was prepared by the reported method *via* the carbonato complex.[4]

Measurements. Visible absorption and circular dichroism (CD) spectra were obtained on a Shimadzu UV-210 spectrophotometer and JASCO J-500 spectropolarimeter, respectively. ^{13}C NMR spectra at 100 MHz were obtained on a JEOL GX-400 spectrometer in the standard manner, employing methanol-*d* as a solvent and tetramethylsilane as an external reference.

Results and Discussion

It has been demonstrated that ^{13}C NMR spectrometry is a convenient tool to determine the molecular symmetry of cobalt(III) complexes with polyamine ligand(s) which has no probe signal appropriate for ^1H NMR spectral examination.[6,7,8] As for the *trans*-[$CoCl_2$(SS-pyht)]$^+$ ion, the (*R*,*S*) isomer, which has no symmetry element (Fig. 1b), is expected to show, in principle, thirteen resonances on the spectrum, while the (*R*,*R*) isomer with the C_2 symmetry (Fig. 1a), should exhibit maximally seven resonances.

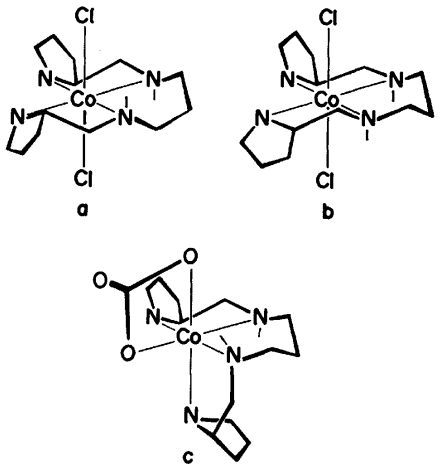

Fig. 1. Structures of *trans*(*R*,*R*)-[$CoCl_2$(SS-pyht)]$^+$ ion, (a), *trans*(*R*,*S*)-[$CoCl_2$(SS-pyht)]$^+$ ion, (b), and *Λ*-*β*-[$CoCO_3$(SS-pyht)]$^+$ ion, (c).

TABLE. ^{13}C NMR SPECTRAL DATA OF *trans*-[$CoCl_2$(SS-pyht)]$^+$ ION[a]

Chemical Shift (ppm)[b]		Assignments[c]
trans(*R*,*S*)	*trans*(*R*,*R*)	
25.44	23.35 (1)[d]	C_7
26.95	27.18 (2)	
27.65	27.83 (2)	C_2, C_3, C_{11}, C_{12}
28.39		
29.41		
48.73	44.65 (2)	
49.93	49.57 (2)	C_1, C_6, C_8, C_{13}
50.22		
50.85		
56.17	59.96 (2)	
60.80	62.44 (2)	C_4, C_5, C_9, C_{10}
61.42		
63.82		

a) Taken at 100 MHz in methanol-d solution. b) From external TMS. c) The order of each carbon atom is as

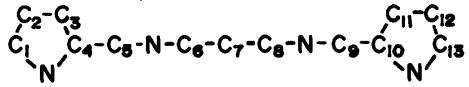

shown. d) The values in parentheses are the relative intensities of resonances.

The *trans*(*R*,*S*)-[$CoCl_2$(SS-pyht)]$^+$ ion, the structure of which has been clarified by the X-ray analysis study,[3] exhibits, in fact, thirteen resonances in the ^{13}C NMR spectrum (see Table). The ligand SS-pyht has thirteen carbon atoms so that the above spectral feature is in accord with that the tetramine in this complex ion adopts a rigid conformation without symmetry, which is anticipated for the trans(*R*,*S*) configuration. The carbon resonances can be classified into four subgroups as in Table, though it is difficult to assign every reso-

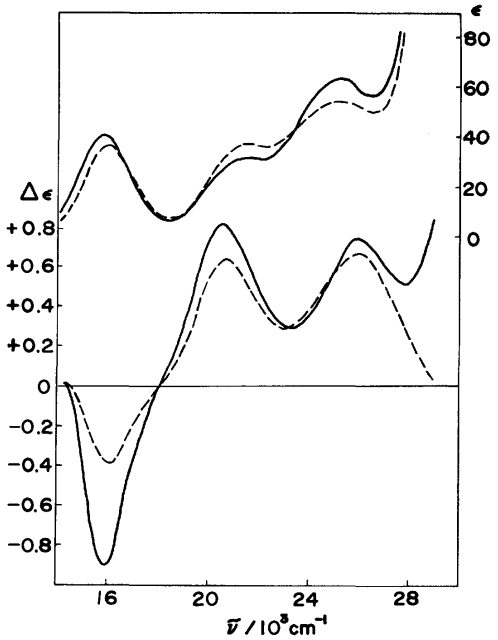

Fig. 2. Visible absorption and CD spectra of *trans*-[$CoCl_2$-(SS-pyht)]$^+$ ion; trans(*R*,*S*) isomer, (——), and trans(*R*,*R*) isomer (----).

nance to the individual carbon of SS-pyht.

We have prepared the *trans*-dichlorocobalt(III) complex of SS-pyht *via* the carbonato complex.[4] The carbonato complex [$CoCO_3$(SS-pyht)]$^+$, which was produced *in situ* by a reaction of SS-pyht with $[Co(CO_3)_3]^{3-}$, showed a dominant positive CD peak in the $^1A_{1g}\rightarrow {}^1T_{1g}(O_h)$ transition region. It has been indicated that the oxalato complex [$Co(C_2O_4)$(SS-pyht)]$^+$ adopts specifically the *Λ*-*β*(*R*,*R*) configuration,[3] and that the CD curve of this complex exhibits a positive Cotton effect in the $^1A_{1g}\rightarrow {}^1T_{1g}(O_h)$ transition. Thus, it is probable that the carbonato complex of SS-pyht also assumes the *Λ*-*β*(*R*,*R*) configuration (Fig. 1c).

The transformation from *Λ*-*β*(*R*,*R*)-[$CoCO_3$(SS-pyht)]$^+$ to trans-dichloro complex in acidic medium should proceed with retention of the configuration with regards to the secondary N centers at the central chelate ring. Thus, it was expected that the *trans*-[$CoCl_2$(SS-pyht)]ClO_4 obtained via the carbonato complex has the (*R*,*R*) configuration with C_2 symmetry (Fig. 1a). The ^{13}C NMR spectrum of the present complex actually showed seven resonances (Table), demonstrating that the complex ion has the C_2 symmetry and, therefore, is assigned to the trans(*R*,*R*) geometry. Thus, *trans*-[$CoCl_2$(SS-pyht)]$^+$ produced by two independent methods clearly differs from each other.

The CD curve of *trans*(*R*,*S*)- and *trans*(*R*,*R*)-[$CoCl_2$(SS-pyht)]$^+$, measured in methanol solution, were apparently dissimilar to each other as shown in Fig. 2. Further, it was noticed that the CD curve of trans(*R*,*S*) isomer obtained here is not identical with that reported by Jun and Liu,[1] though the complex employed are considered to have the same structure. The reason for such difference is uncertain.

It has been shown[9] that both of *trans*(*R*,*S*)- and *trans*(*R*,*R*)-[$CoCl_2$(2,10-Me_2-2,3,2-tet)]$^+$ (2,10-Me_2-2,3,2-tet=(2*S*,10*S*)-2,10-diamino-4,8-diazaundecane) give rise to an equilibrium mixture of these diastereomers by the base treatment in methanol solution, and that the isomer ratio at the equilibrium is readily determined by CD measurements when both of the chiral diastereomers are available. Thus, the CD changes of *trans*(*R*,*S*)-and *trans*(*R*,*R*)-[$CoCl_2$(SS-pyht)]ClO_4 were followed in basic methanol solution, in a similar manner to that employed for the 2,10-Me_2-2,3,2-tet complexes.[9] The curve of the trans(*R*,*R*) isomer changed remarkably, while that of the trans(*R*,*S*) varied slightly. After 2 h standing, however, the CD curves of two diastereomers became identical with each other within experimental error. The wavenumbers and intensities of the CD intersections for the two species (at 23200 and 24900 cm^{-1}) did not change during the base treatment, indicating that any isomer other than the trans(*R*,*R*) and (*R*,*S*) was not formed during the above conversion. It was determined, therefore, that the equilibrium mixture contains only two diastereomers of *trans*-[$CoCl_2$(SS-pyht)]$^+$.

Based on the CD intensities (at 625 and 351 nm) before and after the base treatment, the isomer ratio at the equilibrium is estimated to be (*R*,*S*)/(*R*,*R*)=10.4±2.6, which corresponds to $-\Delta G$=5.85±0.71 kJ·mol^{-1} (or 1.40±0.17 kcal·mol^{-1}) at 300 K. The energy difference between the diastereomers obtained here is large enough for the more stable (*R*,*S*) isomer to occupy more than 90% of the equilibrium mixture, and is the largest one observed so far between the possible diastereomers of trans-dichloro complexes with chiral 2,3,2-tet derivatives.[6,9]

The preference of the (*R*,*S*) isomer over the (*R*,*R*) has been postulated for *trans*-[$CoCl_2$(2,3,2-tet)]$^+$ ion, supposing a significant conformation energy difference between the chair and skew conformation of the central six-membered chelate ring adopted, respectively, by the (*R*,*S*) and (*R*,*R*) isomer, though the exact value has not been determined yet.[5] In line with this assumption, the (*R*,*S*) isomer is more stable than the (*R*,*R*) isomer for most trans-dichloro complexes with chiral 2,3,2-tet derivatives in spite of the destabilizing factors caused by the axially oriented substituent involved in the (*R*,*S*) isomers.[6] The present observation on the SS-pyht complex also supports a general tendency that metal complexes with six-membered chelate ring in the chair conformation is more favourable than those with the chelate in the skew conformation.

References

1) M. J. Jun and C. F. Liu, *J. Coord. Chem.*, **5**, 1 (1975).
2) The absolute configuration of the coordinated secondary nitrogen centers is indicated with *R* or *S* in parentheses.
3) W. A. Freeman, *Inorg. Chem.*, **17**, 2982 (1978).
4) M. Yamaguchi, S. Yamamatsu, T. Furusawa, S. Yano, M. Saburi, and S. Yoshikawa, *Inorg. Chem.*, **19**, 2010 (1980).
5) H. G. Hamilton and M. D. Alexander, *J. Am. Chem. Soc.*, **89**, 5065 (1967).
6) M. Saburi, Y. Ishii, S. Obata, M. Yamaguchi, and S. Yoshikawa, *Inorg. Chem.*, in press.
7) G. R. Brubaker and D. W. Johnson, *Inorg. Chem.*, **21**, 2223 (1982).
8) M. Saburi, Y. Yokowo, and S. Yoshikawa, *Bull. Chem. Soc. Jpn.*, **57**, 1235 (1984).
9) M. Goto, T. Makino, M. Saburi, and S. Yoshikawa, *Bull. Chem. Soc. Jpn.*, **49**, 1879 (1976).

Synthesis of 1-Phenylsulfonylcyclopropanecarboxylic Acid Derivatives

Masahiko TAKAHASHI,* Hideo SUZUKI, and Yoshimi KATA
Department of Industrial Chemistry, Faculty of Engineering, Ibaraki University, Hitachi, Ibaraki 316
(Received May 17, 1984)

Synopsis. Ethyl phenylsulfonylacetate was treated with 1,2-dibromoethane in the presence of benzyltriethylammonium chloride and alkali to give 1-phenylsulfonylcyclopropanecarboxylic acid, from which the carbonyl chloride, ester, carboxamide, 1,2-diacylhydrazine, carbonyl azide, carbamate, isocyanate, and γ-butyrolactone derivatives were prepared.

Cyclopropanes which are activated by geminal electron-withdrawing substituents have great potential in organic synthesis.[1] However, the synthesis and reactions of cyclopropanes that have a sulfonyl group[2] as one of the geminal activating groups are limited. Preparative approaches to these cyclopropanes include; (a) carboxylation of lithiated sulfonylcyclopropanes to **1a**;[3] (b) oxidation of arylthiocyclopropanes to the corresponding arylsulfonylcyclopropanes **1b**[4] and **1c**, which has been developed as a synthon for a propyrene 1,3-dipole;[5] (c) direct cyclopropanation of aryl bromomethyl sulfone with 1,2-dibromoethane in the presence of phase-transfer catalyst and alkali to yield **1d**.[6]

In connection with our studies on the synthesis of heterocycles using cyclopropanes[7] we became interested in the reactions of this relatively unknown class of cyclopropanes because of the possibility of their intramolecular cyclization to heterocycles, and therefore we prepared some derivatives of 1-phenylsulfonylcyclopropanecarboxylic acids.

Phenylsulfonylacetonitrile (**2a**) and -acetate (**2b**) undergo Knoevenagel condensation.[2,8] These acidic sulfones **2a** and **2b** were subjected to direct cyclopropanation in a similar manner as for **1d**[6] and other active methylene compounds.[9] Although cyclopropanecarbonitrile (**3a**) was obtained from **2a** in the presence of a catalytic amount of benzyltriethylammonium chloride (BTEA) in a 71% yield, only phenylsulfonylacetic acid was produced from **2b** under the same reaction conditions. Cyclopropanation of **2b**, however, was accomplished by the use of an equimolar quantity of BTEA to yield **3b** in a 67% yield. Treatment of **3b** with thionyl chloride gave the carbonyl chloride **4** (77%), from which the methyl ester **5** (97%), carboxamide **6** (84%), 1,2-diacylhydrazine **7** (71%), and carbonyl azide **8** (79%) were prepared in the usual manner. Heating of **8** in methanol gave the methyl carbamate **9** (92%), indicating the presence of the intermediary isocyanate **10** in the course of the Curtius rearrangement. Isolation of **10** was attempted by heating **8** in toluene but only crude **10** (73%) was obtained. The structure of **10** was ascertained by conversion to **9** on refluxing a methanolic solution of **10**. Attempts to prepare cyclopropylamine from **6** or **9** were unsuccesful.

Cyclopropanecarboxylic acids were reported to rearrange to γ-butyrolactones thermally[10] or in the presence of acids.[11] Heating of **3b** in polyphosphoric acid at 160°C for 10h gave 3-phenylsulfonyltetrahydro-2-furanone (**11**) in a 45% yields.

The structures of the products are evident on the basis of the analytical and spectral data. In particular, the NMR spectra of **3**—**10** showed the characteristic absorptions of A_2B_2 system at *ca.* δ 1.1—2.2 due to the adjacent methylene groups of the cyclopropane rings.

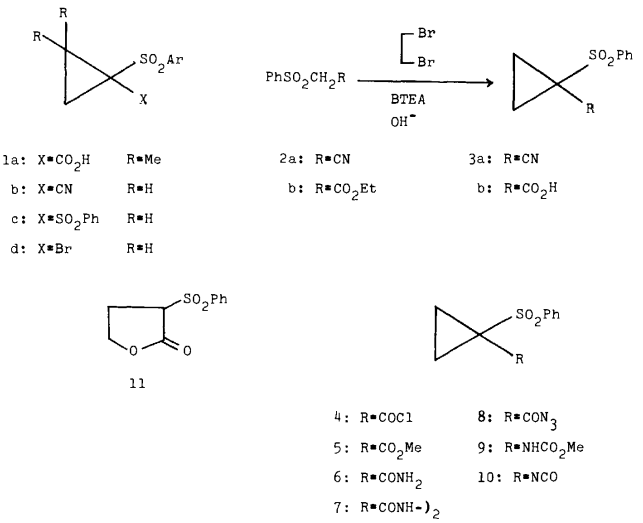

Experimental

Melting points were determined on a Yanagimoto micro-melting point apparatus and are uncorrected. ^{1}H-NMR, IR, and mass spectra were measured with a JEOL JMX-60, a JASCO A-102, and a JEOL JMS-DX300 spectrometer, respectively. Microanalysis was performed with a Shimadzu UM-3B microanalyser.

1-Phenylsulfonylcyclopropanecarbonitrile (3a). A mixture of phenylsulfonylacetonitrile[8] (4.35 g, 24 mmol), 1,2-dibromoethane (9.02 g, 48 mmol), and BTEA (270 mg, 1.2 mmol) in 50% aqueous NaOH (120 cm^3) was stirred with cooling in a water bath for 1 h. The mixture was diluted with water until all the precipitates were dissolved, and extracted with ether. The ethereal solution was dried over $MgSO_4$, and evaporated. The residue was recrystallized from AcOEt to give **3a** (3.51 g, 71%), mp 80—81 °C (lit,[4] mp 88 °C). IR (KBr): 2230 (CN), 1570, 1440, 1415 cm^{-1}. NMR ($CDCl_3$): δ=1.73 (m, 2H), 1.93 (m, 2H), 7.48—8.07 (m, 5H). Found: C, 57.97; H, 4.38%. Calcd for $C_{10}H_9O_2SN$: C, 58.25; H, 4.33%.

1-Phenylsulfonylcyclopropanecarboxylic Acid (3b). A mixture of ethyl phenylsulfonylacetate (**2b**)[8] (2.28 g, 10 mmol), 1,2-dibromoethane (3.76 g, 20 mmol), and BTEA (3.28 g, 10 mmol) in 50% aqueous NaOH (20 cm^3) was stirred in a water bath for 1 h. The mixture was diluted with water until all the precipitates were dissolved, and washed with ether. The aqueous layer was acidified with conc. HCl, and extracted with ether. The ethereal solution was dried over $MgSO_4$ and evaporated. The residue was recrystallized from AcOEt to give **3b** (1.53 g, 67%), mp 144—145 °C. IR (KBr): 3230 (OH), 1720 (CO), 1575, 1475, 1420, 1410 cm^{-1}. NMR ($CDCl_3$): δ=1.77 (m, 2H), 2.00 (m, 2H), 7.60—8.02 (m, 5H), 10.10 (s, 1H). Found: C, 53.06; H, 4.55%. Calcd for $C_{10}H_{10}O_4S$: C, 53.09; H, 4.45%.

1-Phenylsulfonylcyclopropanecarbonyl Chloride (4). Mp

62—63°C (AcOEt). IR (KBr): 3075, 1755 (CO), 1575, 1475, 1445, 1410 cm^{-1}. NMR ($CDCl_3$): δ=2.10 (m, 2H), 2.22 (m, 2H), 7.51—8.07 (m, 5H). Found: C, 49.34; H, 3.67%. Calcd for $C_{10}H_9ClSO_3$: C, 49.09; H, 3.71%.

Methyl 1-Phenylsulfonylcyclopropanecarboxylate (5). Mp 76—77°C (AcOEt). IR (KBr); 1710 (CO), 1575, 1440, 1310 cm^{-1}. NMR ($CDCl_3$): δ=1.58—1.80 (m, 2H), 1.95—2.14 (m, 2H), 3.63 (s, 3H), 7.50—8.06 (m, 5H). Found: C, 54.87; H, 5.06%. Calcd for $C_{11}H_{12}SO_4$: C, 54.99; H, 5.03%.

1-Phenylsulfonylcyclopropanecarboxamide (6). Mp 138 -140°C (MeOH). IR (KBr): 3400, 3170 (NH), 1665 (CO), 1605, 1440 cm^{-1}. NMR ($CDCl_3$): δ=1.75 (s, 2H), 1.80 (s, 2H), 6.15 (br s, 2H), 7.50—7.95 (m, 5H). Found: C, 53.68; H, 4.92%. Calcd for $C_{10}H_{11}O_3NS$: C, 53.33; H, 4.92%.

1,2-Bis[1-(phenylsulfonyl)cyclopropylcarbonyl]hydrazine (7). Mp 147—148°C (AcOEt). IR (KBr): 3250 (NH), 1730 (CO), 1580, 1480, 1445 cm^{-1}. NMR ($CDCl_3$): δ=1.58—1.80 (m, 2H), 1.97—2.18 (m, 2H), 7.50—8.03 (m, 10H), 10.20 (s, 2H). Found: C, 53.29; H, 4.64%. Calcd for $C_{20}H_{20}N_2O_6S_2$: C, 53.56; H, 4.49%.

1-Phenylsulfonylcyclopropanecarbonyl Azide (8). Mp 70—72°C. IR (KBr): 2150 (N_3), 1685 (CO), 1580, 1475, 1445, 1415 cm^{-1}. NMR ($CDCl_3$): δ=1.58—1.80 (m, 2H), 1.98—2.22 (m, 2H), 7.47—8.05 (m, 5H). Found: C, 48.11; H, 3.55%. Calcd for $C_{10}H_9O_3N_3S$: C, 47.81; H, 3.61%.

Methyl 1-(Phenylsulfonyl)cyclopropylcarbamate (9). Mp 108—111°C (AcOEt). IR (KBr): 3180 (NH), 1750 (CO), 1610, 1580, 1510, 1445, 1425 cm^{-1}. NMR ($CDCl_3$): δ=1.27—1.58 (m, 2H), 1.73—2.05 (m, 2H), 3.38 (s, 3H), 5.83 (br s, 1H), 7.53—7.98 (m, 5H). MS: *m/z* 255 (M^+). Found: C, 51.88; H, 5.12%. Calcd for $C_{11}H_{13}O_4NS$: C, 51.76; H, 5.13%.

1-Phenylsulfonylcyclopropyl Isocyanate (10). Mp 50—60°C (further purification was difficult). IR (KBr): 2250 (NCO), 1440, 1315, 1305, 1140 cm^{-1}. NMR ($CDCl_3$): δ=1.12—1.45 (m, 2H), 1.60—1.93 (m, 2H), 7.40—7.92 (m, 5H).

3-Phenylsulfonyltetrahydro-2-furanone (11). A mixture of **3b** (226 mg, 1.0 mmol) and polyphosphoric acid (2 cm^3) was heated at 160°C for 10 h. The mixture was poured into water and the precipitates were collected by filtration. Recrystallization from AcOEt-petroleum ether gave **11** (101 mg, 45%), mp 116—118°C. IR (KBr): 2920, 1750 (CO), 1575, 1475, 1440 cm^{-1}. NMR ($CDCl_3$): δ=2.45—3.20 (m, 2H), 3.98—4.55 (m, 3H), 7.53—8.02 (m, 5H). MS: *m/z* 226 (M^+). Found: C, 52.87; H, 4.47%. Calcd for $C_{10}H_{10}O_4S$: C, 53.10; H, 4.46%.

References

1) S. Danishefsky, *Accounts. Chem. Research*, **12**, 66 (1979); M. Murakami and S. Nishida, *J. Synthetic Org. Chem. Jpn.*, **41**, 22 (1983); D. Tunemoto and K. Kondo, *J. Synthetic Org. Chem. Jpn.*, **35**, 1070 (1977).

2) A review of sulfone chemistry; P. D. Magnus, *Tetrahedron*, **33**, 2019 (1977).

3) D. J. Cram and A. Ratajczak, *Ger., Offen.* 1 912 193 (1969); *Chem. Abstr.*, **72**, 12370v (1970).

4) M. Makosza, E. Bialecka, and M. Ludwikow, *Tetrahedron Lett.*, 2391 (1972).

5) B. M. Trost, J. Cossy, and J. Burks, *J. Amer. Chem. Soc.*, **105**, 1052 (1983).

6) A. Jonczyk, K. Banko, and M. Makosza, *J. Org. Chem.*, **40**, 266 (1975).

7) M. Takahashi, T. Nogami, and K. Nidaira, *Heterocycles*, **22**, 581 (1984); M. Takahashi, N. Takeshi, K. Myojoh, H. Sano, and T. Morisawa, *J. Heterocycl. Chem.*, **20**, 209 (1983).

8) H. Dressler and J. E. Graham, *J. Org. Chem.*, **32**, 985 (1967).

9) R. K. Singh and S. Danishefsky, *J. Org. Chem.*, **40**, 2969 (1975).

10) M. Matsui, T. Ohno, S. Kitamura, and M. Toyao, *Bull. Chem. Soc. Jpn.*, **25**, 210 (1952).

11) P. F. Hudrlik, L. R. Rundnick, and S. H. Korzeniowski, *J. Amer. Chem. Soc.*, **95**, 6848 (1973) and references cited therein.

Synthesis of Chiral Crown Ethers Derived from *trans, trans*- and *cis, trans*-2,2′-Spirobiindan-1,1′-diols. Their Chiral Recognition and Complexation Properties

Koichiro NAEMURA,* Iwao EBASHI, and Masao NAKAZAKI
Department of Chemistry, Faculty of Engineering Science, Osaka University, Toyonaka, Osaka 560
(Received August 22, 1984)

Synopsis. *trans,trans*-2,2′-Spirobiindan-1,1′-diol (**1**) was resolved as its (−)-ω-camphanic ester and the absolute rotation of the glycol **1** was determined. Two crown ethers and the acyclic analog were derived from (+)-**1**. Two crown ethers incorporating (+)-*cis,trans*-2,2′-spirobiindan-1,1′-diol were also prepared. Their chiral recognition properties in transport of methyl (±)-phenylglycinate hydrochloride and abilities to extract alkali metal picrates were investigated.

In the preceding paper,[1] we reported the preparation of optically active crown ethers incorporating *trans*-2,5-bis(hydroxymethyl)tetrahydrofuran as the chiral center. Our continuing interest in chiral macrocyclic polyether prompted us to incorporate 2,2′-spirobiindan-1,1′-diol with known absolute configuration into crown ether, and in this paper we report the preparation of some optically active crown ethers composed of the glycol as well as their chiral recognition properties and complexation properties.

Among three possible diastereomers of 2,2′-spirobiindan-1,1′-diol, *trans,trans*-glycol (C_2 symmetry) **1** and *cis,trans*-glycol (C_1 symmetry) **2** were isolated in optically active forms.[2-4] There is, however, no report of the determination of the absolute rotation of *trans,trans*-glycol **1**. Reduction of (±)-diketone **3** with LiAlH(OBu′)$_3$ gave (±)-**1** in 95% yield. Treatment of (±)-**1** with 1 equiv of (−)-ω-camphanic acid chloride gave half ester **4** which was recrystallized from acetone to afford (−)-**4**, $[\alpha]_D$ −144°. Reduction of (−)-**4** with $LiAlH_4$ gave (−)-**1** whose ^1H NMR spectrum was in agreement with the reported ^1H NMR spectral data for *trans,trans*-2,2′-spirobiindan-1,1′-diol (**1**).[3] Jones oxidation of (−)-**1**, $[\alpha]_D$ −15.2°, to (2*R*)-(−)-diketone 3,[4] $[\alpha]_D$ −147°, permitted to assign the (1*S*,1*S*′,2*R*) configuration to (−)-**1**. The enantiomeric excess of (−)-**3**, $[\alpha]_D$ −147°, was determined to be >98% by means of HPLC with a chiral column.[5] The antipode; (+)-**1** was also prepared from (+)-**2** as follows. (+)-*cis,trans*-glycol **2**, $[\alpha]_D$ +13.5°, prepared *via* (−)-**5**,[3] was oxidized with Jones reagent to give (2*S*)-(+)-**3**, $[\alpha]_D$ +150°, from which (+)-**1**, $[\alpha]_D$ +15.0°, was prepared by LiAlH(OBu′)$_3$ reduction.

Condensation of (+)-**1** with pentaethylene glycol ditosylate in THF-NaH gave crown ether **6** in 69% yield. Crown ether **7** was obtained in 35% yield by condensation of (+)-**1** with tetraethylene glycol ditosylate. Similarly crown ethers **8** and **9** were derived from (+)-**2**. Acyclic polyether **10** was obtained in 63% yield by condensation of (+)-**1** with diethylene glycol monomethyl ether tosylate. Table 1 lists the chiral recognition behaviour of crown ethers and acyclic polyether with methyl (±)-phenylglycinate hydrochloride. The cationbinding ability of polyethers was assessed by solvent extraction of aqueous solution of alkali metal picrates with $CHCl_3$ solution containing polyethers

Table 1. Differential transport of methyl (±)-phenylglycinate hydrochloride

Host	Time/h	Transport/%	Configuration of dominant enantiomer	Optical purity/%
(+)−**6**	2	5.9	S	5.9
(+)−**7**	22	5.5	R	5.4
(+)−**8**	4	5.5	R	13.0
(−)−**9**	70	4.7	R	4.0
(+)−**10**	90	4.9	S	8.0

Table 2. Extraction of alkali metal picrates

Host	Extractability/%[a]				
	Li^+	Na^+	K^+	Rb^+	Cs^+
6	1	1	26	11	2
7	1	4	0	0	0
8	0	0	1	0	0
9	0	1	1	0	0
10	0	0	0	0	0
18-crown-6	3	6	66	59	33

a) Defined as % picrate extracted into the organic phase.

6—**10**. The results are given in Table 2.

A number of features in these Tables deserve comment. (1) Crown ethers containing six oxygens carried the amino ester salt more rapidly than did crown ethers containing five oxygens. (2) Crown ethers incorporating *trans,trans*-glycol moiety transported the amino ester salt more rapidly than did crown ethers composed of *cis,trans*-glycol moiety. (3) The enantiomer selectivity of acyclic polyether **10** is comparable to that of crown ethers. (4) Crown ether containing six oxygens as well

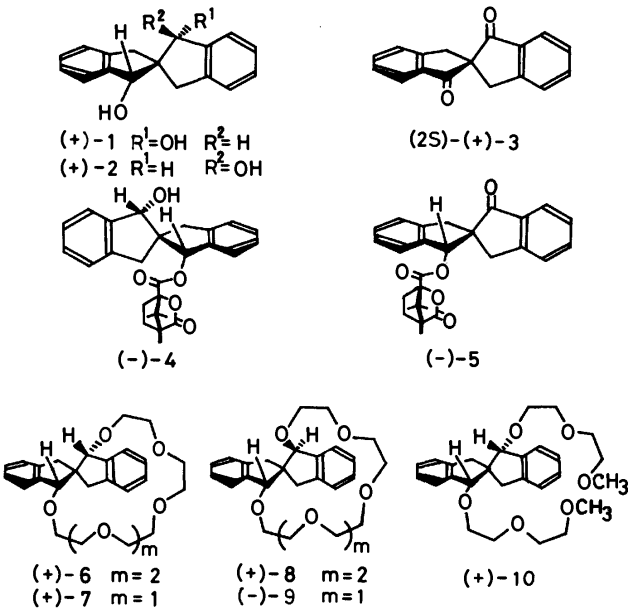

as *trans,trans*-glycol moiety showed fairly high relative selectivity for K^+ and Rb^+.

2,2′-Spirobiindan-1,1′-diols are conformationally rigid, so that complexation properties of the crown ethers incorporating these units are extremely depend on the length of polyether bridge as well as the configuration at C 1 and C 1′ of the glycol moiety.

Experimental

*(+)-*cis,trans*-2,2′-Spirobiindan-1,1′-diol (2).* This compound was prepared by Dynessen's method;[3] $[\alpha]_D^{26}$ +13.5° (*c* 0.511, THF) (lit,[3] $[\alpha]_D$ +10.9° (THF)); mp 152—154°C; Anal. ($C_{17}H_{16}O_2$) C, H.

*(±)-*trans,trans*-2,2′-Spirobiindan-1,1′-diol (1).* A solution of (±)-**3**[3] (8.13 g, 32.8 mmol) in dry THF (180 mL) was added to a solution of $LiAlH(OBu^t)_3$ (25.7 g, 98.2 mmol) in dry THF (260 mL). The mixture was refluxed for 13 h and cooled in an ice-bath. To the chilled reaction mixture was added water (80 mL), and an inorganic solid was filtered off. After filtrate was concentrated, the residue was dissolved in $CHCl_3$, washed with water, and dried. The solvent was removed to give a solid which was recrystallized from ethanol to give (±)-**1** (7.85 g, 95% yield); mp 220—222°C; Found: C, 80.89; H, 6.36%. Calcd for $C_{17}H_{16}O_2$: C, 80.92; H, 6.39%.

Optical Resolution of (±)-1. (±)-*trans,trans*-Glycol **1** (10.1 g, 39.8 mmol) was treated with (−)-ω-camphanic acid chloride (17.1 g, 39.8 mmol) by the similar procedure reported for the preparation of the ester **5**.[3] The product was recrystallized from acetone to give (−)-**4** (2.12 g); $[\alpha]_D^{25}$ −144° (*c* 0.292, $CHCl_3$); mp 158—160°C; Found: C, 75.11; H, 6.55%. Calcd for $C_{27}H_{28}O_5$: C, 74.98; H, 6.53%.

The (−)-ester **4** (2.06 g, 4.76 mmol) was refluxed with $LiAlH_4$ (2.71 g, 71.4 mmol) in dry THF (120 mL) for 8 h. After a usual workup, the product was recrystallized from acetone to give (−)-**1** (636 mg, 53% yield); $[\alpha]_D^{25}$ −15.2° (*c* 0.309, THF); mp 234—236°C; Found: C, 80.96; H, 6.40%. Calcd for $C_{17}H_{16}O_2$: C, 80.92; H, 6.39%.

(+)-2,2′-Spirobiindan-1,1′-dione (3). Oxidation of (+)-**2**, $[\alpha]_D$ +13.5° (252 mg, 1.00 mmol) with 8N Jones reagent was carried out according to literature[3] to give (+)-**3** (220 mg, 89% yield); $[\alpha]_D^{28}$ +150° (*c* 0.290, $CHCl_3$). Recrystallization from ethanol furnished colorless needles; $[\alpha]_D^{28}$+149° (*c* 0.363, $CHCl_3$) (lit,[3] $[\alpha]_D$ +151.86° ($CHCl_3$)); mp 218—219°C; Anal. ($C_{17}H_{12}O_2$) C, H.

(−)-2,2′-Spirobiindan-1,1′-dione (3). Oxidation of (−)-**1**, $[\alpha]_D$ −15.2°, (100 mg, 0.396 mmol) with 8N Jones reagent gave (−)-**3** (74 mg, 75% yield); $[\alpha]_D^{24}$ −147° (*c* 0.339, $CHCl_3$); mp 219—220°C; Found: C, 82.18; H, 4.85%. Calcd for $C_{17}H_{12}O_2$: C, 82.24; H, 4.87%.

*(+)-*trans,trans*-2,2′-Spirobiindan-1,1′-diol (1).* (+)-Diketone **3**, $[\alpha]_D$ +150°, (808 mg, 3.26 mmol) was reduced with $LiAlH(OBu^t)_3$ (3.31 g, 13.0 mmol) in dry THF (75 mL) by the same manner as described for (±)-**1** to give (+)-**1** (756 mg, 92% yield); $[\alpha]_D^{26}$ +15.0° (*c* 0.353, THF); mp 233—234°C; Found: C, 80.88; H, 6.37%. Calcd for $C_{17}H_{16}O_2$: C, 80.92; H, 6.39%.

(+)-(1S,5R,22R)-3,4:23,24-Dibenzo-6,9,12,15,18,21-hexaoxatricyclo[20.3.0.0^{1,5}]pentacosa-3,23-diene (6). To a boiling suspension of NaH (150 mg, 6.25 mmol) in dry THF (40 mL) was added a solution of (+)-**1** (528 mg, 2.00 mmol) and pentaethylene glycol ditosylate (1.15 g, 2.22 mmol) in dry THF (70 mL) dropwise over an 8 h period under N_2. The reaction mixture was refluxed for further 16 h under N_2, cooled in an ice-bath, and quenched with water (2 mL). After a usual workup, the crude product was chromatographed on alumina (benzene eluent) to give a solid which was recrystallized from hexane to furnish (+)-**6** (625 mg, 69% yield); $[\alpha]_D^{27}$ +45.3° (*c* 0.371, $CHCl_3$); mp 101—102°C; Found: C, 71.20; H, 7.51%. Calcd for $C_{27}H_{34}O_6$: C, 71.34 H, 7.54%.

(+)-(1S,5R,19R)-3,4:20,21-Dibenzo-6,9,12,15,18-pentaoxatricyclo[17.3.0.0^{1,5}]docosa-3,20-diene (7). A procedure similar to that for **6** using (+)-**1** (510 mg, 2.02 mmol) and tetraethylene glycol ditosylate (1.02 g, 2.03 mmol) gave (+)-**7** (274 mg, 35% yield) as colorless crystals from hexane; $[\alpha]_D^{25}$ +81.3° (*c* 0.200, $CHCl_3$); mp 106°C; Found: C, 73.15; H, 7.44%. Calcd for $C_{25}H_{30}O_5$: C, 73.14; H, 7.37%.

(+)-(1S,5S,22R)-3,4:23,24-Dibenzo-6,9,12,15,18,21-hexaoxatricyclo[20.3.0.0^{1,5}]pentacosa-3,23-diene (8). Condensation of (+)-**2** (816 mg, 3.11 mmol) with pentaethylene glycol ditosylate (1.78 g, 3.44 mmol) was carried out by the same procedure as described for **6**. The product was chromatographed on alumina (benzene eluent) to give (+)-**8** (465 mg, 33% yield) as a colorless oil; $[\alpha]_D^{27}$ +2.77° (*c* 0.433, $CHCl_3$); Found: C, 71.19; H, 7.48%. Calcd for $C_{27}H_{34}O_6$: C, 71.34; H, 7.54%.

(−)-(1S,5S,19R)-3,4:20,21-Dibenzo-6,9,12,15,18-pentaoxatricyclo[17.3.0.0^{1,5}]docosa-3,20-diene (9). A procedure similar to that for **6** using (+)-**2** (680 mg, 2.69 mmol) and tetraethylene glycol ditosylate (1.36 g, 2.70 mmol) gave (−)-**9** (270 mg, 24% yield); $[\alpha]_D^{27}$ −23.0° (0.390, $CHCl_3$); mp 86—87°C; Found: C, 73.09; H, 7.41%. Calcd for $C_{25}H_{30}O_5$: C, 73.14; H, 7.37%.

(+)-(1R,1′R,2S)-1,1′-Bis(5-methoxy-3-oxapentyloxy)-2,2′-spirobiindan (10). After a mixture of (+)-**1** (400 mg, 1.58 mmol), NaH (150 mg, 6.25 mmol), and DMF (30 mL) was stirred at 30°C for 2 h, to the mixture was added a solution of Methyl Carbitol tosylate (960 mg, 3.49 mmol) in DMF (20 mL). The mixture was stirred at 45°C for 24 h under N_2 and quenched with water (1 mL). Workup followed by chromatography on alumina (hexane–benzene 1:1 eluent) gave (+)-**10** (440 mg, 61% yield) as a colorless oil; $[\alpha]_D^{25}$ +46.8° (*c* 0.948, $CHCl_3$); Found: C, 71.30; H, 7.89%. Calcd for $C_{27}H_{36}O_6$: C, 71.02; H, 7.95%.

Enantiomer Differential Transport. Enantiomer differential transport was carried out in a conventional apparatus which consisted of an outer cylindrical glass vessel (24.5 mm inner diameter) and a central glass tube (15.5 mm inner diameter). The 0.005 M $CHCl_3$ solution of the host separated the inner aqueous phase (0.1 M HCl (1 M=1 mol dm^{-3})) and the outer aqueous phase (0.08 M HCl) which contained $LiPF_6$ (0.4 M) and methyl (±)-phenylglycinate hydrochloride (0.04 M). The $CHCl_3$ layer was stirred at 20°C, and transport was followed by monitoring the absorbance at 261 nm and $[\theta]_{261}$ of the inner aqueous phase.

Extraction Procedure. Aqeous solution (5 mL) of metal picrate (2.4×10^{-4} M) and a $CHCl_3$ solution (5 mL) containing the host (2.4×10^{-4} M) were placed in a screw-cap glass tube (30 mL) and the tube was shaken for 30 min at room temperature. Extraction of picrate was followed by monitoring the absorbance at 357 nm of the aqueous phase.

References

1) M. Nakazaki, K. Naemura, M. Makimura, A. Matsuda, T. Kawano, and Y. Ohta, *J. Org. Chem.*, **47**, 2429 (1982).

2) H. Falk, W. Frost, and K. Schlögl, *Tetrahedron Lett.*, **1974**, 217.

3) E. Dynessen, *Acta Chem. Scand., Ser. B*, **29**, 77 (1975).

4) N. Harada, T. Ai, and H. Uda, *J. Chem. Soc., Chem. Commun.*, **1982**, 232.

5) H. Yuki, Y. Okamoto, and I. Okamoto, *J. Am. Chem. Soc.*, **102**, 6356 (1980); Y. Okamoto, S. Honda, I. Okamoto, and H. Yuki, *ibid.*, **103**, 6971 (1981).

A Practical Synthesis of *N*-Bromo Imides by Use of Sodium Bromite

Shoji KAJIGAESHI,* Takashi NAKAGAWA, Shizuo FUJISAKI, and Akiko NISHIDA
Department of Industrial Chemistry, Faculty of Engineering Yamaguchi University, Tokiwadai, Ube 755
(Received August 27, 1984)

Synopsis. *N*-Bromo imides can be readily prepared under mild conditions by a reaction of imides with sodium bromite in the presence of hydrobromic acid in fairly good yields. The scope and limitation are also presented.

A new reagent, sodium bromite ($NaBrO_2$), has recently been noted in organic synthesis.[1-3] Durig the course of our investigation on the synthetic utilities of sodium bromite,[4] we found that the reaction of imides (**1**) with sodium bromite in the presence of hydrobromic acid under mild conditions gave *N*-bromo imides (**2**) in fairly good yields.

In general, *N*-bromo imides **2**, *e.g.*, familiar *N*-bromosuccinimide, have been prepared by the treatment of a corresponding **1** in an aqueous medium with bromine in the presence of a strong base, or with alkali hypobromite prepared separately by treatment of bromine with a strong base.[5] The derivatives **2** have been also prepared by the reaction of **1** with bromine in water by sodium bromate and sulfuric acid.[6] In our method, sodium bromite (which is available in stable crystals under an ordinary atmosphere and, hence, can be handle much more easily compared with the toxic liquid bromine) was used in place of bromine. *N*-bromo imides **2** such as *N*-bromosuccinimide[5] (**2a**), *N*-bromophthalimide[7] (**2b**), *N*-bromo-α-methylsuccinimide[6] (**2c**), *N*-bromoglutarimide[6] (**2d**), and 1,3-dibromohydantoin[6] (**2e**) were synthesized from the corresponding imides, succinimide (**1a**), phthalimide (**1b**), α-methylsuccnimide (**1c**), glutarimide (**1d**), and hydantoin (**1e**), respectively. *N*-bromo-ε-caprolactam (**3a**) was also prepared from ε-caprolactam.

When hydrobromic acid was added to an ice-cold aqueous solutuion of sodium bromite and imide under stirring, the desired **2** precipitated readily as white crystals. In the cases of syntheses of **2b**, **2c**, and **2d**, aqueous sodium hydroxide was used in order to dissolve the corresponding imides, **1b**, **1c**, and **1d**. These methods (using sodium bromite and hydrobromic acid) showed that one mole of sodium bromite was able to brominate 2 moles of **1** into **2**.

Our method could not be applied to imides which were insoluble in water or alkaline solution (*e.g.*, 1,8-naphthalimide). It was not applicable, furthermore, to imides having other active group in the molecule (*e.g.*, maleinimide) or chain imides (*e.g.*, diacetamide), because other reactions also proceeded under the conditions.

The reaction scheme for the synthesis of **2** may be presented in the following equations. That is, it can be

$$NaBrO_2 + HBr \rightleftharpoons HBrO_2 + NaBr, \quad (1)$$

$$HBrO_2 + HBr \rightleftharpoons 2HBrO, \quad (2)$$

$$2\text{>NH} + 2HBrO \rightleftharpoons 2\text{>N-Br} + 2H_2O, \quad (3)$$

overall:

$$2\text{>NH} + NaBrO_2 + 2HBr \longrightarrow 2\text{>N-Br} + NaBr + 2H_2O, \quad (4)$$

presumed that bromous acid ($HBrO_2$) produced by the reaction of sodium bromite with hydrobromic acid (Eq. 1) reacts with excess hydrobromic acid to give hypobromous acid (Eq. 2) and the subsequent reaction of **1** with the hypobromous acid give *N*-bromo imide (Eq. 3). We now postulate that a major active brominating species is the hypobromous acid derived from sodium bromite and hydrobromic acid as shown in equation 1 and 2. The overall reaction equation is shown is equation 4. Acutually, the experimental results described above concord stoichiometrically with equation 4.

Since further excess hydrobromic acid reacts with hypobromous acid to form free bromine, we can recognize the end point of *N*-bromination by a red coloration due to bromine formed in the reaction mixture. This is one of the merits of our method.

$$HBrO + HBr \rightleftharpoons Br_2 + H_2O \quad (5)$$

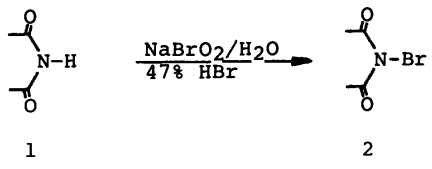

1 2

Scheme 1.

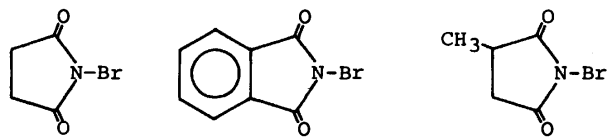

2a 2b 2c

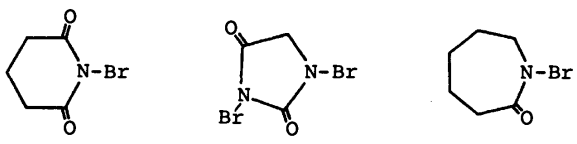

2d 2e 3a

Scheme 2.

Experimental

N-Bromosuccinimide (NBS) (2a). A solution of 94.7% sodium bromite[9] (0.95 g, 6.7 mmol) in water (2 ml) was added to a solution of **1a** (1 g, 10.1 mmol) in water (5 ml). To the cold (0—5 °C) solution was added (dropwise, slowly) 47% hydrobromic acid (1.3 ml, 11.2 mmol) under stirring,[10] and then the reaction mixture was further stirred for 10 min at

0 °C. The precipitate obtained was filtered, washed with cold water and dried at room temperature to give **2a** as white crystals. Weight 1.54 g (86% of theoretical amount). Analysis by iodometric titration[11] showed 44.8% active bromine, as compared with the theoretical value for $C_4H_4BrNO_2$ of 44.9%. Mp 175—178 °C (from water) (lit,[5] mp 173—175 °C). MS: *m/z* 177, 179 (M^+).

N-Bromophthalimide (2b). A solution of 94.7% sodium bromite (0.63 g, 4.4 mmol) in water (5 ml) was added to an aqueous solution of **1b** (1 g, 6.8 mmol) and sodium hydroxide (0.3 g, 7.5 mmol) in water (15 ml). To the ice-cold solution was added (dropwise, slowly) 47% hydrobromic acid (1.8 ml, 15.5 mmol) under stirring,[10] and then the reaction mixture was further stirred for 10 min at 0 °C. The obtained precipitate was filtered, washed with cold water and dried to give **2b** as white crystals. Weight 1.25 g (81% of theoretical amount). Analysis showed 33.6% active bromine, as compared with the theoretical value for $C_8H_4BrNO_2$ of 35.4%. Mp 227—229 °C (from water). MS: *m/z* 225, 227 (M^+).

N-Bromo-α-methylsuccinimide (2c). Compound **2c** could be obtained from **1c** (0.5 g, 4.4 mmol) in the same manner as that of **2b**. Weight 0.38 g (45% of theoretical amount). Analysis showed 38.4% active bromine, as compared with the theoretical value for $C_5H_6BrNO_2$ of 41.4%. Mp 154—157 °C. MS: *m/z* 191, 193 (M^+).

N-Bromoglutarimide (2d). Compound **2d** could be obtained from **1d** (0.6 g, 5.3 mmol) in the same manner as that of **2b**. Weight 0.31 g (30% of theoretical amount). Analysis showed 37.9% active bromine, as compared with the theoretical value for $C_5H_6BrNO_2$ of 41.6%. Mp 149—151 °C. MS: *m/z* 191, 193 (M^+).

1,3-Dibromohydantoin (2e). A 47% hydrobromic acid (1.5 ml, 12.9 mmol) was added to a solution of **1e** (0.5 g, 5.0 mmol) in water (5 ml). To the ice-cold solution was added (dropwise, slowly) a solution of 94.7% sodium bromite (1 g, 7.0 mmol) in water (2 ml) under stirring,[10] and then the reaction mixture was further stirred for 1 h at 0 °C. The precipitate obtained was filtered, washed with cold water and dried to give **2e** as white crystals. Weight 0.9 g (70% of theoretical amount). Analysis showed 59.4% active bromine, as compared with the theoretical value for $C_3H_2Br_2N_2O_2$ of 62.0%. Mp 135—136 °C. MS: *m/z* 256, 258, 260 (M^+).

N-Bromo-ε-caprolactam (3a). Compound **3a** could be obtained from ε-caprolactam (2 g, 17.7 mmol) in the same manner as that of **2a**. Weight 2.7 g (80% of theoretical amount). Analysis showed 39.5% active bromine, as compared with the theoretical value for $C_6H_{10}BrNO$ of 41.6%. Mp 60—63 °C (lit,[8] mp 64—66 °C). MS: *m/z* 191, 193 (M^+).

References

1) T. Kageyama, S. Kawahara, K. Kitamura, Y. Ueno, and M. Okawara, *Chem. Lett.*, **1983**, 1097.
2) T. Kageyama, Y. Tobito, A. Katoh, Y. Ueno, and M. Okawara, *Chem. Lett.*, **1983**, 1481.
3) T. Kageyama, Y. Ueno, and M. Okawara, *Synthesis*, **1983**, 815.
4) S. Kajigaeshi, T. Nakagawa, S. Fujisaki, A. Nishida, and M. Noguchi, *Chem. Lett.*, **1984**, 713.
5) C. Djerassi, *Chem. Revs.*, **43**, 271 (1948).
6) T. D. Waugh and R. C. Waugh, U. S. Patent 2971959 (1961); *Chem. Abstr.*, **55**, 14483 (1961).
7) A. Kergomard, *Bull. Soc. Chim. Fr.*, **1961**, 2360.
8) B. Taub and J. B. Hino, *J. Org. Chem.*, **25**, 263 (1960).
9) Commercial sodium bromite is now available from Kanto Kagaku Co. Ltd.
10) During the treatment, the mixture was instantaneously colored red owing to bromine formed (see Eq. 5) and soon decolorized. Whereupon a white precipitate was gradually deposited. The hydrobromic acid addition was done until the red color did not disappear. Thus, the amount of hydrobromic acid was employed as noted in the text.
11) E. R. Oliveto and C. Gerold, "*Org. Synthesis*," **31**, p. 18 (1951).

Synthesis of β-Alkylimino α-Cyano Dithiocarboxylic Acids, 3-Alkyl-1,3-thiazine-2,6-dithiones, and Related Compounds

Tatsuo YAMAMOTO, Shigeo HIRASAWA, and Motomu MURAOKA*

Department of Chemistry, Faculty of Science, Josai University, 1-1, Keyaki-Dai, Sakado, Saitama 350-02

(Received August 29, 1984)

Synopsis. The title compounds **2** and **5** were synthesized by the reaction of β-alkylimino nitriles with carbon disulfide.

β-Alkylimino dithiocarboxylic acids have been reported to be unstable except 2-(alkylimino)cyclopentanecarbodithioic acids.[1] No stable acyclic β-alkylimino dithiocarboxylic acids[2] and 2- and 4-(dithiocarboxymethylene)dihydropyridines[3] at room temperature are known. We have previously reported the first examples of stable acyclic imino dithiocarboxylic acids, α-cyano β-imino dithiocarboxylic acids.[4] 2-(Alkylimino)cyclopentanecarbodithioic acids have been prepared by the reaction of 2-iminocyclopentanecarbodithioic acid and alkylamines.[5] This method, however, could not be applied to the synthesis of β-alkylimino α-cyano dithiocarboxylic acids from the imino cyano dithiocarboxylic acids.

Our present finding is that β-alkylimino nitriles[6] react with carbon disulfide in the presence of a base to give β-alkylimino dithiocarboxylic acids (**2**). In some cases, 3-alkyl-2*H*-1,3-thiazine-2,6(3*H*)-dithiones (**5**) were produced.

Compounds **2a—g** were obtained as major product when β-alkylimino nitriles (**1a—g**) were treated with carbon disulfide in the presence of sodium 1,1-dimethylpropoxide in benzene. In some cases, the imino acids were accompanied by a small amount of 4-cyano-3*H*-1,2-dithiole-3-thiones (**3a—c**). 3-Methylimino-3-(*m*-tolyl)-propanenitrile gave 3,5-dicyano-2,6-di(*m*-tolyl)-1-methyl-4(1*H*)-pyridinethione (**4**) in addition to compounds **2e** and **3b**. We have reported that the same type of *N*-unsubstituted 4(1*H*)-pyridinethiones are synthesized by the reaction of 5-cyano-2*H*-1,3-thiazine-2,6(3*H*)-dithiones with β-imino nitriles.[7]

When these reactions were performed in *N*,*N*-dimethylformamide, 3*H*-1,2-dithiole-3-thiones (**3a—c**) were formed as a major product instead of the β-alkylimino dithiocarboxylic acids (**2c—g**). Furthermore, 3-(alkylimino)butanenitriles (**1a—b**) produced 3-alkyl-5-cyano-4-methyl-2*H*-1,3-thiazine-2,6(3*H*)-dithiones (**5a—b**) in addition to **2**. In the ^{13}C NMR spectrum of compound **5b** in dimethyl-d_6 sulfoxide, two quartets at δ 11.86 and 23.62 ppm were observed. Compound **5b** was easily methylated with methyl iodide to form 5-cyano-3,4-dihydro-3-ethyl-4-methylene-6-methylthio-2*H*-1,3-thiazine-2-thione (**6**). In the ^1H NMR spectrum of compound **6**, a pair of dublets appeared at δ 4.98 and 5.17 ppm suggesting the existence of a terminal methylene. From these facts, an alternative structure; 4-alkylimino-3-cyanothiane-2,6-dithiones for compounds **5** was eliminated.

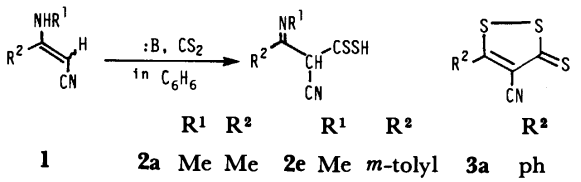

	R¹	R²		R¹	R²		R²
1	**2a**	Me	Me	**2e**	Me	*m*-tolyl	**3a** ph
	b	Et	Me	**f**	Me	*p*-tolyl	**b** *m*-tolyl
	c	Me	Ph	**g**	Et	*p*-tolyl	**c** *p*-tolyl
	d	Et	Ph				

Scheme 1.

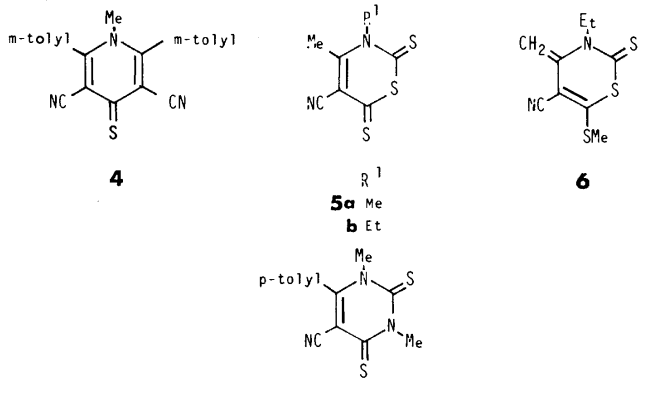

Block 1

Occasionally, 1,3-dimethyl-5-cyano-4-(*p*-tolyl)-2,6(1*H*,3*H*)-pyrimidinedithione (**7**) was obtained in very low yield besides compounds **2f** and **3c**.

Experimental

Measurements. NMR spectra were recorded with a Jeol JNM-GX-270 spectrometer. Infrared spectra were measured on Nippon Bunko IR-A-302 spectrophotometer. Mass spectra were determined with a Hitachi LKB-9000 mass spectrometer. Electronic spectra were measured with a Hitachi 557 Double Wavelength Double Beam Spectrophotometer.

2-Cyano-3-(methylimino)butanedithioic Acid (2a). A mixture of 3-(methylimino)butanenitrile (0.80 g, 8.32 mmol), sodium 1,1-dimethylpropoxide (1.40 g, 12.7 mmol), carbon disulfide (1.00 g, 13.1 mmol), and dry benzene (20 ml) was shaken at room temperature for 3 h. Water (40 ml) was added to the mixture and the aqueous layer was washed with ether. Ether (100 ml) and 2M-hydrochloric acid (10 ml (1 M=1 mol dm^{-3})) were added to the aqueous layer and extracted several times with ether. A small quantity of methanol containing piperidine was added to the combined ethereal extracts. Resulting solid was collected, dissolved in hydrochloric acid in acetone (*ca.* 0.5 M, 30 ml), and to this was added water. The yellow crystals separated were recrystallized. ν_{max}(KBr) 2850 s, 2510 s, 2200 s, 1630 vs, 1500 s, and 1270 s cm^{-1}; δ (CD_3COCD_3) 13.62 vb (s, 1H, NH or SH), 5.95 (s, 1H, NH or SH), 3.25 (d, 1.5H, *J*=3.1 Hz, $NHCH_3$), 3.23 (d, 1.5H, *J*=3.1 Hz, $NHCH_3$), and 2.48 ppm (s, 3H, CH_3). (Found: C, 42.01; H, 4.73; N, 16.20; S, 37.07. $C_6H_8N_2S_2$ requires C, 41.79; H, 4.68; N, 16.25; S, 37.22%). Other *β-alkylimino dithiocarboxylic acids (2b—g)* were prepared in the same way.

4-Cyano-5-aryl-3H-1,2-dithiole-3-thiones (3a—c). A mixture of 3-alkylimino-3-arylpropanenitrile (5 mmol), carbon disulfide (12 mmol), and *N*,*N*-dimethylformamide (5 ml) was added dropwise to a mixture of sodium 1,1-dimethylpropoxide (15 mmol) and *N*,*N*-dimethylformamide (15 ml) at 0 °C.

TABLE 1. YIELDS AND PHYSICAL PROPERTIES OF **2—7**

Compound	Yield %	Mp θ_m/°C	UV (EtOH) nm (log ε)
2a	39	73—75[a]	243 (4.12), 303 (3.83), 368 (4.35)
2b	50	117—118[a]	244 (4.12), 304 (3.72), 369 (4.35)
2c	51	131—132[a]	243 (4.06), 309 (3.72), 373 (4.34)
2d	44	110[a]	243 (4.09), 309 (3.79), 373 (4.36)
2e	45	111—112[a]	238 (4.13), 370 (4.40)
2f	42	132—133[a]	241 (4.12), 373 (4.40)
2g	42	106—110[a]	241 (4.10), 373 (4.38)
3a	38,[b] 44[c]	178[d]	223 (4.10), 292 (4.23), 312 (4.12), 430 (3.88)
3b	53	183[d]	226 (4.11), 293 (4.20), 318 (4.12), 433 (3.94)
3c	24,[e] 49[f]	210.5[d]	230 (4.13), 293 (4.16), 329 (4.20), 433 (3.93)
4	6	280[g]	263 (4.20),[h] 350 (4.36)[h]
5a	49	151—152[a]	308 (4.38), 417 (3.64) These $\lambda_{max.}$'s shifted to 268 (3.98) and 305 (4.46) in 2 h.
5b	47	161[a]	310 (3.84), 417 (3.78) These $\lambda_{max.}$'s shifted to 268 (3.84) and 308 (4.48) in 2 h.
6	85	93.5[a]	293 (4.44)
7	9	232.5[d]	293 (4.58), 303 (3.95)

a) Recrystallized from acetone–water. b) Yield from 1c. c) Yield from 1d. d) Recrystallized from ethanol. e) Yield from 1f. f) Yield from 1g. g) Recrystallized from *N,N*-dimethylformamide–water. h) Dioxane used as solvent. All compounds gave satisfactory IR and elemental analyses data.

The mixture was kept standing at room temperature for 4 h. Water was added to the mixture and the solid which separated was collected.

3,5-Dicyano-2,6-di(m-tolyl)-1-methylpyridine-4(1H)-thione (4). A mixture of 3-methylimino-3-(*m*-tolyl)propanenitrile (2.00 g, 11.6 mmol), sodium 1,1-dimethylpropoxide (2.00 g, 18.2 mmol), carbon disulfide (1.40 g, 18.4 mmol), and benzene (50 ml) was mechanically shaken at room temperature for 3 h and water (50 ml) was added to this. The solids from both layers were collected and recrystallized. ν_{max} (KBr) 2240 w, 1575 vs, 1480 m, 1260 s, and 1080 m cm^{-1}; δ (DMSO-d_6) 7.42 (m, 8H, C_6H_4), 2.99 (s, 3H, NCH_3), and 2.40 ppm (s, 6H, $C_6H_4C\underline{H}_3$); *m/z* 355 (M^+, 98%), 354 (M^+—1, 100%), and 340 (M^+—CH_3, 48%). (Found: C, 74.40; H, 4.62; N, 11.86; S, 9.17. $C_{22}H_{17}N_3S$ requires C, 74.35; H, 4.62; N, 11.86; S, 9.02%).

5-Cyano-3,4-dimethyl-2H-1,3-thiazine-2,6(3H)-dithione (5a). To a mixture of 3-(methylimino)butanenitrile (2.00 g, 20.8 mmol), sodium 1,1-dimethylpropoxide (6.88 g, 62.4 mmol), and *N,N*-dimethyl formamide (20 ml), was added dropwise carbon disulfide (4.75 g, 62.4 mmol) at −15 °C and the mixture was kept standing at −20 °C for 40 h. Ether (150 ml) and 1M-hydrochloric acid (30 ml) were added to the reaction mixture. The brown crystals insoluble in both layers were collected. ν_{max} (KBr) 2230 m, 1535 s, 1420 s, 1365 s, 1265 s, 1225 s, and 1085 s cm^{-1}; δ (C_5D_5N) 3.88 (s, 3H, NCH_3) and 2.75 ppm (s, 3H, CH_3). (Found: C, 39.01; H, 3.03; N, 13.00; S, 44.91. $C_7H_6N_2S_3$ requires C, 39.22; H, 2.82; N, 13.07; S, 44.91%).

5-Cyano-3-ethyl-4-methyl-2H-1,3-thiazine-2,6(3H)-dithione (5b) was Prepared Similarly. ν_{max} (KBr) 2980 w, 2900 w, 2220 m, 1530 s, 1525 s, 1405 s, 1300 s, 1240 s, 1200 s, and 1100 s cm^{-1}, ^{1}H NMR δ (DMSO-d_6) 4.60 (q, 2H, J=6.6 Hz, $NC\underline{H}_2CH_3$), 2.80 (s, 3H, CH_3), and 1.35 ppm (t, 3H, J=6.6 Hz, $NCH_2C\underline{H}_3$); ^{13}C NMR (DMSO-d_6) 201.70 (s), 191.96 (t, J=6.1 Hz), 158.62 (s), 114.91 (s), 110.96 (s), 47.98 (t, J=143.4 Hz), 23.63 (q, J=131.2 Hz), and 11.86 ppm (q, J=128.2 Hz); *m/z* 228 (M^+, 100%), 195 (M^+—SH, 13%), 141 (M^+—C_2H_5NCS, 4%), and 70 ($CH_3C{\equiv}N^+$—C_2H_5, 33%). (Found: C, 42.28; H, 3.38; N, 12.39; S, 42.38. $C_8H_8N_2S_3$ requires C, 42.08; H, 3.53; N, 12.27; S, 42.12%).

5-Cyano-3,4-dihydro-3-ethyl-4-methylene-6-methylthio-2H-1,3-thiazine-2-thione (6). Triethylammonium salt of **5b** was methylated by treating with methyl iodide in methanol. Water was added to this mixture and resulting solids were collected. ν_{max} (KBr) 2980 w, 2950 w, 2220 m, 1600 s, 1530 m, 1460 m, 1420 m, 1390 s, and 1375 s cm^{-1}; δ ($CDCl_3$) 5.17 (d, 1H, J=3.7 Hz, $=CH_2$), 4.98 (d, 1H, J=3.7 Hz, $=CH_2$), 4.48 (q, 2H, J=7.1 Hz, $NC\underline{H}_2CH_3$), 2.56 (s, 3H, SCH_3), and 1.38 ppm (t, 3H, J=7.1 Hz, $NCH_2C\underline{H}_3$); *m/z* 242 (M^+, 100%), 213 (M^+—C_2H_5, 82%), 195 (M^+—SCH_3, 32%), 155 (M^+—C_2H_5NCS, 26%), and 108 ($CH_2{=}C{=}C(CN)C{\equiv}S^+$, 31%). (Found: C, 44.87; H, 4.38; N, 11.72; S, 39.48. $C_9H_{10}N_2S_3$ requires C, 44.59; H, 4.16; N, 11.56; S, 39.69%).

1,3-Dimethyl-5-cyano-4-(p-tolyl)-2,4(1H,3H)-pyrimidinedithione (7). This compound was isolated on recrystallization of **3c** from the filtrate. ν_{max} (KBr) 2890 w, 2220 m, 1600 w, 1560 s, 1505 s, 1460 s, 1420 m, 1405 s, 1330 s, 1305 s, and 1275 s cm^{-1}; *m/z* 287 (M^+, 100%) and 132 ($C_7H_7C{\equiv}N^+$—CH_3, 24%). (Found: C, 58.66; H, 4.51; N, 14.33; S, 22.10. $C_{14}H_{13}N_3S_2$ requires C, 58.50; H, 4.59; N, 14.62; S, 22.32%).

References

1) T. Takeshima, N. Fukada, T. Miyauchi, M. Muraoka, T. Yamamoto, and T. Hayashi, *J. Chem. Soc., Perkin Trans. 1*, **1974**, 914.

2) R. Mayer and J. Jentzsch, *J. Prakt. Chem.*, **23**, 83, (1964).

3) R. Gompper, B. Wetzel, and W. Elser, *Tetrahedron Lett.*, **1968**, 5519.

4) M. Muraoka, T.Yamamoto, S. Yamaguchi, F. Tonosaki, T. Takeshima, and N. Fukada, *J. Chem. Soc., Perkin Trans. 1*, **1977**, 1273.

5) B. Bardas, P. Sohar, G. Matolscy, and P. Berencsi, *J. Org. Chem.*, **37**, 1727, (1972).

6) T. Yamamoto and M. Muraoka, *Org. Prep. Proced. Int.*, **16**, 130, (1984).

7) M. Muraoka and T. Yamamoto, *J. Heterocycl. Chem., in press.*

Solubilization of Alkyl *p*-Hydroxybenzoates in Hexa(oxyethylene) Dodecyl Ether Micelle

Ayako GOTO,* Fumio ENDO, and Takeo HIGASHINO
Shizuoka College of Pharmacy, 2-2-1, Oshika, Shizuoka 422
(Received May 25, 1984)

Synopsis. An experimental study was made on the effect of the alkyl-chain length of alkyl *p*-hydroxybenzoates on their solubilization in nonionic micelle. The location of alkyl *p*-hydroxybenzoate in micelle and the change in micelle structure are discussed on the basis of the experimental result.

Two subjects should be considered to elucidate the solubilization mechanism:[1] One is concerned with the variation of the overall distribution coefficient with the concentration of solubilizate in a micelle and with thermodynamic interpretation of its behavior; the other is concerned with the location of solubilizate in a micelle. The latter subject has been investigated spectrophotometrically by a number of workers, but few papers have been published in which the latter is considered in connection with the former. We[2,3] have reported on the concentration dependence for methyl and ethyl *p*-hydroxybenzoates in nonionic surfactant micelles and explained this dependence on the basis of the regular solution theory.

In the present work we have inferred the location of alkyl *p*-hydroxybenzoate in hexa(oxyethylene) dodecyl ether ($C_{12}E_6$) micelle and discussed the inference in terms of the nonideality of distribution and the change in micelle structure.

Experimental

Hexa(oxyethyelene) dodecyl ether[2] ($C_{12}E_6$) and alkyl *p*-hydroxybenzoates (alkyl=methyl, ethyl, propyl, and butyl) were of reagent grade. Gel filtration was carried out at 20°C in the same way as previously described.[2] The concentration of alkyl *p*-hydroxybenzoates was determined spectrophotometrically[2,3] and that of $C_{12}E_6$ was measured by gas chromatography.[4] Distribution coefficient (K), mole fraction in micelle phase (X_s^m) and that in aqueous phase (X_s^w), cmc, interchange energy (ω), free energy change of solubilization (ΔG), elution volume of micelle (V_m), and cloud point were evaluated in the same way as reported in our previous paper.[2] UV spectra of *p*-hydroxybenzoates in water and aqueous $C_{12}E_6$ solution were measured with a Hitachi EPS-3T spectrophotometer.

Results and Discussion

The apparent distribution coefficients of propyl and butyl *p*-hydroxybenzoates (K_a), X_s^m/X_s^w were measured at 20°C. Figure 1 shows a plot of K_a values of propyl and butyl esters against X_s^m. The values at $X_s^m=0$ corresponds to the K value.[2] ΔG values for alkyl esters obtained from K values are given in Table 1. They are linearly related with the carbon number of the alkyl group of *p*-hydroxybenzoates, and the slope of the straight line corresponds to the increment of -2.6×10^3 J/mol of ΔG per methylene unit. This value is equal to the reported values for alcohols (-2.6×10^3 J/mol) in sodium dodecyl sulfate (SDS) micelle[5] and *p*-hydroxybenzoates (-2.6×10^3 J/mol) in SDS micelle.[6] It may also be concluded that the alkyl moiety of *p*-hydroxybenzoate is incorporated in the hydrocarbon core of micelle. We[3] reported that the solubilization of ethyl *p*-hydroxybenzoate in $C_{12}E_6$ micelle results from both the enthalpy and entropy effects and that the latter effect might be due to a hydrophobic interaction, which is also compatible with the above conclusion.

A red shift was observed with UV maxima of *p*-hydroxybenzoates in $C_{12}E_6$ micelle; methyl, ethyl, propyl, and butyl esters have UV maxima at 257.9, 258.1, 258.4, and 258.9 nm in 2.0% $C_{12}E_6$ solution, respectively, whereas they all have UV maxima at 256 nm in water. The change of spectra in the nonionic surfactant micelle might be due to the following factors:[7] i) specific interactions such as hydrogen bonding; ii) change in polarity of the environment. Therefore, the above red shift suggests an increase in polarity of the environment and/or specific interactions between $C_{12}E_6$ and *p*-hydroxybenzoate. Nemethy and Ray[8] reported that phenol molecules are located in a polar environment of nonionic surfactant micelle and/or are hydrogen-bonded. Muller and Metcalf[9] described that chloroxyrenol is hydrogen-bonded in poly(oxyethylene) dodecyl ether micelle. Therefore, the hydrogen bond between the phenolic hydrogen of alkyl esters and the etheric oxygen of $C_{12}E_6$ may occupy an important position in the specific interactions. This interaction has also been proved in terms of interchange energy (ω), which is

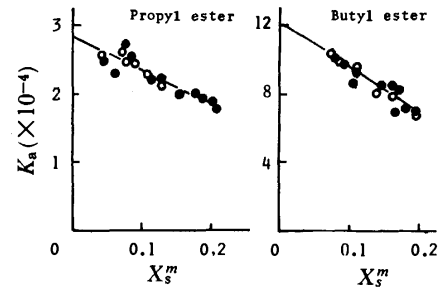

Fig. 1. Apparent Distribution Coefficient of Propyl and Butyl *p*-Hydroxybenzoates between the $C_{12}E_6$ Micellar and Aqueous Phases *vs.* Mole Fraction of the Esters in the Micelle, X_s^m.
●: 2 mM (1 M=1 mol dm^{-3}) $C_{12}E_6$, ○: 4 mM $C_{12}E_6$.

TABLE 1. FREE ENERGY CHANGE OF SOLUBILIZATION OF ALKYL *p*-HYDROXYBENZOATES IN $C_{12}E_6$ MICELLE (ΔG) AND INTERCHANGE ENERGY (w)

p-Hydroxybenzoate	ΔG/J/mol	w/J/mol
Methyl ester[4]	-2.07×10^4	-3700 ± 400
Ethyl ester[5]	-2.26×10^4	-3400 ± 500
Propyl ester	-2.49×10^4	-2800 ± 700
Butyl ester	-2.85×10^4	-3300 ± 500

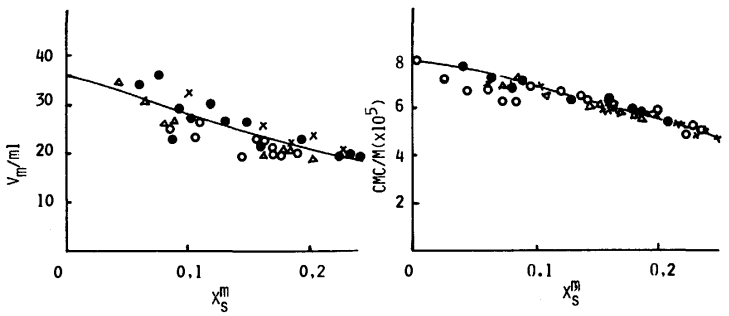

Fig. 2. Variation of the Elution Volumes of the $C_{12}E_6$ Micelles (V_m) and the cmc's of $C_{12}E_6$ Solutions in the Presence of Alkyl *p*-Hydroxybenzoates with Mole Fraction of Alkyl *p*-Hydroxybenzoates, X_s^m.
(●): Methyl ester,[2] (○): ethyl ester, (×): propyl ester, (△): butyl ester.

calculated on the basis of the regular solution theory.[2] These values (ω) are negative as shown in Table 1, corresponding to the ω value of methyl ester in hepta (oxyethylene) dodecyl ether ($C_{12}E_7$) obtained by molar volume measurements.[10] This suggests that $C_{12}E_6$ and alkyl ester in a mixed micelle become thermodynamically stable by mutual attraction. From the above results, it is concluded that solubilized esters are most likely to be located in the area spreading from the inside of hydrocarbon core to the poly(oxyethylene) mantle of micelle. Furthermore, it may also be concluded that the hydrophobic interaction and the specific interaction in a micelle reflect directly the distribution coefficient and that the nonideality of distribution is due mainly to the specific interaction.

Figure 2 shows plots of the retention volume of micelle which is a measure of the hydrated size of micelle[12] and of the cmc against X_s^m. The cmc and retention volume decrease with X_s^m and the pattern of the decrease depends little on the length of the alkyl chain of *p*-hydroxybenzoate. Therefore, Fig. 2 implies that the mixed micelle becomes thermodynamically stable[2,11] by enlarging its size and indicates that the manners of change in cmc and retention volume are nearly the same, suggesting that such a change in micellar structure is due mainly to the specific interaction, *i.e.* the hydrogen bonding between *p*-hydroxybenzoate and $C_{12}E_6$ in the mixed micelle.

Figure 3 shows a plot of cloud points against the concentration of esters added. The longer alkyl chain of *p*-hydroxybenzoates is able to depress the cloud point more deeply because of its denser distribution into the micelle phase. Kuriyama[14] has suggested that increase in micellar weight with increasing temperature is a dominant factor for the cloud formation. Therefore, the depression of cloud point by the ester added is related closely with the increase in micelle size, as shown in Fig. 2a; this effect would result from both the specific interaction favoring the retention of ester in the oxyethylene region of micelle and the structured water supported by the ester in this environment.[13]

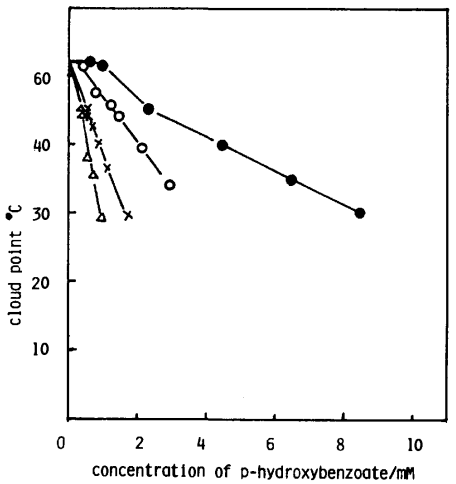

Fig. 3. Cloud Point of Aqueous $C_{12}E_6$ Solution in the Presence of Alkyl *p*-Hydroxybenzoates.
(●): Methyl ester,[2] (○): ethyl ester, (×): propyl ester, (△): butyl ester.

References

1) P. Mukerjee, *J. Pharm. Sci.*, **60**, 1531, 1538 (1971).
2) A. Goto, M. Nihei, and F. Endo, *J. Phys. Chem.*, **84**, 2268 (1980).
3) A. Goto, F. Endo, and T. Higashino, *Chem. Pharm. Bull.*, **32**, 2905 (1984).
4) A. Goto, R. Sakura, and F. Endo, *J. Colloid Interface Sci.*, **67**, 491 (1978).
5) K. Hayase and S. Hayano, *Bull. Chem. Soc. Jpn.*, **50**, 83 (1977).
6) A. Goto and F. Endo, *J. Colloid Interface Sci.*, **66**, 26, (1978).
7) L. Sepulveda, *J. Colloid Interface Sci.*, **46**, 372 (1974).
8) G. Nemethy and A. Ray, *J. Phys. Chem.*, **77**, 64 (1973).
9) B. A. Mulley and A. D. Metcalf, *J. Pharm. Pharmacol.*, **8**, 774 (1956).
10) N. Funasaki and S. Hada, *J. Phys. Chem.*, **86**, 2504 (1982).
11) K. Shirahama and T. Kashiwabara, *J. Colloid Interface Sci.*, **36**, 65 (1971).
12) a) H. Suzuki and T. Sasaki, *Bull. Chem. Soc. Jpn.*, **44**, 2630 (1971); b) H. Suzuki, *ibid.*, **49**, 375, 1470 (1976).
13) M. Donbrow and E. Azaz, *J. Colloid Interface Sci.*, **47**, 20 (1976).
14) K. Kuriyama, *Kolloid Z. Z. Polym.*, **181**, 144 (1962).

Sintered Iron (III) Oxide Photoanode Doped with Molybdenum

Shigero OISHI,* Keiko TAJIME, and Akeri HOSAKA
Sagami Chemical Research Center, Nishi-Ohnuma 4-4-1, Sagamihara, Kanagawa 229
(Received July 21, 1984)

Synopsis. Sintered iron(III) oxide electrodes which contained about 0.01 atomic% of molybdenum showed considerable improvement in generating anodic photocurrent, particularly, in a cathodic potential region. 0.01 Atomic% doping level was found to be attained by sintering at 1200 °C for 12 h using 0.2 atomic% of MoO_2 or 1.0 atomic% of MoO_3.

The photoelectrochemistry of sintered iron(III) oxide has received considerable attention in recent years, because of prospects of an efficient and low-cost photoanode in the direct photoassisted electrolysis of water using visible light.[1-8] In order to make iron(III) oxide conductive by increasing negative carriers, doping with group IVB elements has been intensively investigated, and among them silicon doped iron(III) oxide has appeared to have good properties in producing photocurrent and stability against photodissolution.[2] We report here the photoelectrochemical behavior of sintered iron(III) oxide doped with molybdenum.

Experimental

Electrodes were prepared from α-Fe_2O_3 (99.999%, Alfa Co.) by mixing with 0.02—2 atomic% of MoO_2 (99%, Mitsuwa Co.) or MoO_3 (99.999%, Aldrich Co.), pressing into pellets, sintering at 1150—1300 °C for 6—24 h in air, followed by quenching to room temperature. Dimensions of the pellets were 1.1 cm (diameter)×0.1 cm (thickness). New surfaces were obtained by polishing with emery, washed with water using ultrasonic wave, and etched with concentrated hydrochloric acid. A copper lead was attached to the back surface by ultrasonic soldering. Resistances measured across the thickness were 3—50 Ω. The electrodes were mounted into appropriate glass holders with epoxy resin.

Current-potential curves were obtained with a potentiostat HA-104 (Hokuto Denko Co.) and a regular three-electrode arrangement, in which a platinum wire as a counter electrode and a saturated calomel electrode(SCE) as a reference electrode were used. Iron(III) oxide electrodes were illuminated with a 1 kW xenon lamp through a Pyrex optical system, and a series of interference filter was employed for the measurement of spectral response.

The concentrations of molybdenum in sintered iron(III) oxide were photometrically determined by the use of 3,4-toluenedithiol.[9]

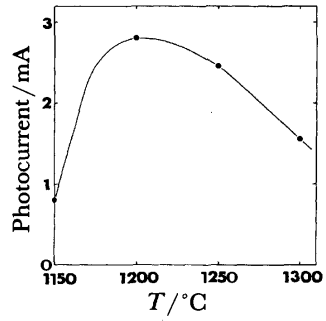

Fig. 1. The dependence of anodic photocurrent upon sintering temperature measured at 0.1 V (*vs.* SCE) in pH 10 borate buffer (0.1 M). Iron(III) oxide pellets containing 0.2 atomic% of MoO_2 were sintered for 6 h.

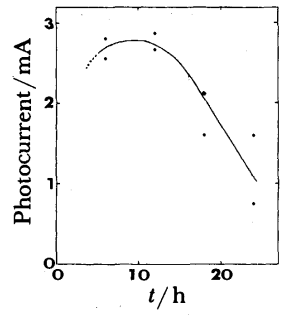

Fig. 2. The dependence of anodic photocurrent upon sintering time measured at the same conditions as Fig. 1. Iron(III) oxide pellets containing 0.2 atomic% of MoO_2 were sintered at 1200 °C.

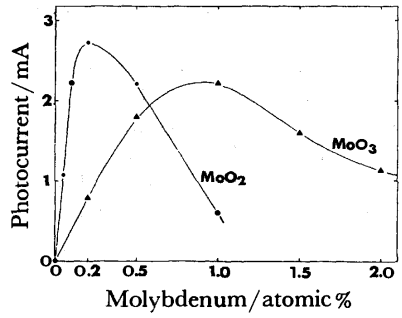

Fig. 3. The dependence of anodic photocurrent upon the amounts of dopants used, measured at the same conditions as Fig. 1. Sintering was conducted at 1200 °C for 6 h.

Results and Discussion

An alumina mortar was used for mixing ferric oxide with dopants because it was found that the use of an agate mortar, the chemical compornent of which is none other than silica, brought about contamination with silicon which concealed any effects caused by other dopants.

Figures 1, 2, and 3 show the dependencies of photocurrent upon sintering temperature, sintering time, and amounts of dopants, respectively. Sintering at 1200 °C for 12 h gave the best result. At these conditions, the concentration of molybdenum at the boundary of each grain of iron(III) oxide may be most suitable for the flow of photocurrent. In the case of electrode sintered at a higher temperature and/or for a longer time, where dopant may diffuse into the grains of iron(III) oxide, photocurrent was rather small. Attempts to know the actual concentration of molybdenum at the electrode surface by means of fluorescence X-ray analysis and ESCA were unsuccessful because of low concentration. Chemical analysis for molybdenum, however, revealed that iron(III) oxide pellets sintered at 1200 °C for 12 h contained

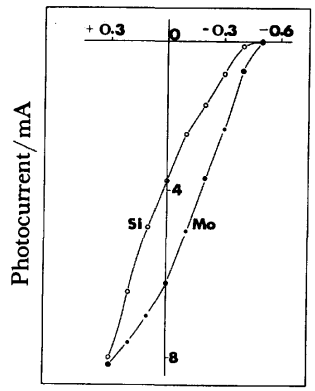

Fig. 4. Photocurrent-electrode potential curves for 0.01 atomic% of molybdenum and 2 atomic% of silicon doped iron(III) oxide electrode, measured in pH 10 borate buffer (0.1 M).

about 1/20 and 1/100 of the original amount of molybdenum when MoO_2 and MoO_3 were used as dopants, respectively. Therefore, in Fig. 3, the best results for anodic photocurrent generation are considered to be obtained at around 0.01 atomic% of doping level based on the actual concentration of molybdenum. The decrease in concentration of molybdenum is due to the oxidation of MoO_2 to volatile MoO_3.[10] Then, it can be concluded that the optimum conditions for sintering are corresponding to those in which 0.01 atomic% of doping level was attained when the sintering of iron(III) oxide was completed.

The surface of the effective electrode was revealed to be porous by means of a scanning electron microscope; one hole (around 20 μm in diameter) per $4\times10^3\,\mu m^2$. Similar microstructure of electrode surface could be observed even in the case of electrodes not containing molybdenum, but they were not effective. The presence of molybdenum is essential for producing photocurrent.

A typical polarization curve for 0.01 atomic% Mo doped iron(III) oxide is shown in Fig. 4. A considerable improvement in the cathodic potential region can be noticed as compared with the case of the best 2% Si doped iron(III) oxide electrode[2] which we could prepare. This advance is important considering the reduction at the counter electrode in the electrolysis cell.

Visible light up to around 570 nm were effective in generating photocurrent and this is in accord with the fact that a band gap of iron(III) oxide is 2.2 eV.[1]

Photodissolution of the electrode was inspected by means of bathophenanthroline photometry using hydroxylamine as a reducing agent of iron(III) to iron(II) ion. The electrode is so stable against photodisolution that detectable amount of iron(II) ion was not found in 10 cm^3 of anolyte(1 mol/dm^3 aq NaOH) when 42 coulomb of photocurrent flowed at 0.3 V (*vs.* SCE).

The electrode is also stable in generating photocurrent, indeed, about 4 mA of steady photocurrent was flowing for 6 h in a two-electrode system divided by agar-agar using a platinum wire as a counter electrode, where 1 mol/dm^3 aqueous sodium hydroxide 0.5 mol/dm^3 sulfuric acid were used as an anolyte and a catholyte, respectively. Moreover, in this case, oxygen and hydrogen could be collected in 92% current efficiency.

The authors thank the Agency of Industrial Science and Technology of MITI under the Sunshine Project contract for support of this work.

References

1) J. H. Kennedy and K. W. Frese, Jr., *J. Electrochem. Soc.*, **125**, 723 (1978).
2) J. H. Kennedy, R. Shinar, and J. P. Ziegler, *J. Electrochem. Soc.*, **127**, 2307 (1980).
3) M. Gori, H. -R. Grüniger, and G. Calzaferri, *J. Appl. Electrochem.*, **10**, 345 (1980).
4) J. H. Kennedy, M. Anderman, and R. Shinar, *J. Electrochem. Soc.*, **128**, 2371 (1981).
5) C. Leygraf, M. Hendewerk, and G. A. Somorjai, *J. Phys. Chem.*, **86**, 4484 (1982).
6) K. G. McGregor, M. Calvin, and J. W. Otvos, *J. Appl. Phys.*, **50**, 369 (1979).
7) J. H. Kennedy and M. Anderman, *J. Electrochem. Soc.*, **103**, 848 (1983).
8) J. C. Curran and W. Gissler, *J. Electrochem. Soc.*, **126**, 56 (1983).
9) K. Tanaka and N. Takagi, *Bunseki Kagaku*, **19**, 790 (1970).
10) A. N. Zelikman, N. N. Gorovits, and T. E. Prosenkova, *Zh. Neorg. Khim.*, **1**, 632 (1956).

Elimination Reaction of *Aldehydo*-D-glucurono-6,3-lactone Derivatives

Hiroshi ITOH,* Koichi AOKI,† and Takahiro MATSUMOTO†
The Noguchi Institute, 1-8-1 Kaga, Itabashi-ku, Tokyo 173
†*Department of Industrial Chemistry, Faculty of Engineering, Tokai University, Hiratsuka, Kanagawa 254*
(Received July 31, 1984)

Synopsis. D-Glucurono-6,3-lactone derivatives are converted to butenolide or dihydro-2*H*-pyran derivatives by treatment with triethylamine.

Because of the effect of the carbonyl group, uronic acid and aldonolactone derivatives readily underwent β-elimination reactions to yield unsaturated compounds.[1,2,3] D-Glucurono-6,3-lactone (**1**) derivatives were also susceptible to elimination reaction to give unsaturated compounds.[4,5] We wish to report herein the formation of butenolide or dihydro-2*H*-pyran derivatives by elimination reactions of 2,4,5-tri-*O*-acetyl-*aldehydo*-D-glucurono-6,3-lactone diacetyl acylal (**2**), *aldehydo*-D-glucurono-6,3-lactone ethylene dithioacetal (**3**),[6] or 2,4,5-tri-*O*-acetyl-*aldehydo*-D-glucurono-6,3-lactone ethylene dithioacetal (**4**) by treatment with triethylamine.

Acetolysis of methyl β-D-glucofuranosidurono-6,3-lactone with $BF_3 \cdot OEt_2$ in acetic anhydride afforded crystalline **2** in 55% yield. The compound **2** was also obtained from **1** or 1,2,5-tri-*O*-acetyl-β-D-glucurono-6,3-lactone in lower yields, 39% and 27%, respectively. The compound **2** was isolated from the mixture of **2** and 1,2,5-tri-*O*-acetyl-D-glucurono-6,3-lactone by crystallization from ethyl acetate–petroleum ether (1:4). Other acidic catalysts such as H_2SO_4, $AlCl_3$, H_3PO_4, and CF_3COOH did not afford **2**. Treatment of **2** with triethylamine afforded 3-acetoxy-5-(2,2-diacetoxyethylidene)-2(5*H*)-furanone (**5**). The results obtained with various solvents are summerized in Table 1, acetic anhydride was found to be the most suitable solvent and **5** was obtained in 91% yield.

Upon treatment of **4** with acetic anhydride-triethylamine, 3-acetoxy-5-[1-acetoxy-2-(1,3-dithiolan-2-yl) ethyl]-2(5*H*)-furanone (**6**) was obtained as a main product, together with 3-acetoxy-5-[2-(1,3-dithiolan-2-yl) ethylidene]-2(5*H*)-furanone (**7**), in 69% and 11% yields, respectively. This reaction also occurred smoothly in ethyl acetate, and **6** and **7** were also obtained in 74% and 16% yields, respectively.

On the other hand, when **3** was treated with acetic anhydride-triethylamine, the 6,3-lactone linkage rearranged to a 6,2-lactone linkage along with acetylation and elimination reactions. In this reaction, 3,5-diacetoxy-6-(1,3-dithiolan-2-yl)-5,6-dihydro-2*H*-pyran-2-one (**8**) was obtained in 83% yield, but the butenolide derivatives, **6** and **7**, and α-pyrone derivative were not obtained.

TABLE 1. CONVERSION OF **2** INTO **5** BY TREATMENT WITH TRIETHYLAMINE

Solvent	Temp/°C	Time/h	Yield/%
CH_3CN	0	4	3
CH_3CN–Ac_2O	0	2	76
DMF	0	22	0
DMF–Ac_2O	0	3	65
EtOAc	60	2	0
EtOAc–Ac_2O	60	1	50
Ac_2O	0	24	91

The dithioacetal derivatives, **3** and **4**, tend mainly to give monounsaturated product, while **2** gave the conjugated unsaturated compound.

The product **5** and **7** were a mixture of *E* and *Z* isomers. The structures of the two isomers were easily determined by ^{1}H-NMR studies, since the olefinic hydrogen in the *E* isomer is considerably deshielded by virtue of its *cis* relationship to the butenolide oxygene.[7] In the ^{1}H-NMR spectrum of **8**, the value for $J_{5,6}$ (2.4 Hz) indicated the *cis* relationship for the two protons, H-5 and H-6,[8] and the other physical data are consistent with the proposed structure for **8**. Moreover, in the pharmacological screening tests of **5**, antihypertension and bradycardia activities were observed.

Experimental

Melting points are uncorrected. The infrared spectra and ^{1}H-NMR spectra were recorded on a JASCO A-102 spectrometer and a JNM PMX-60 spectrometer, respectively, under standard conditions.

2,4,5-Tri-O-acetyl-aldehydo-D-*glucurono-6,3-lactone Diacetyl Acylal (2).* To a mixture of acetic anhydride (12 ml) and $BF_3 \cdot OEt_2$ (2 ml) was added methyl β-D-glucofuranosidurono-6,3-lactone[9] (0.3 g). After heating the mixture at 60 °C for 16 h, the reagents were distilled off under reduced pressure. The residue was extracted with ethyl acetate–water and the organic layer was washed with 5% $NaHCO_3$ aq and water, dried and evaporated under reduced pressure. The residue was extracted with 15 ml of ethyl acetate–petroleum ether (1:4) and the insoluble material was **2** (0.25 g, 55%). It was recrystallized from acetone–petroleum ether: mp 202—203 °C. ^{1}H-NMR (DMSO-d_6) δ=2.10 (6H, s), 2.30 (9H, s), 5.00 (1H, dd, J=3.0, 7.8 Hz), 5.44 (1H, dd, J=3.2, 7.8 Hz), 5.63 (1H, dd, J=3.0, 4.9 Hz), 5.95 (1H, d, J=4.9 Hz), 6.63 (1H, d, J=3.2 Hz). IR 1805, 1770, 1750 cm^{-1}. Found: C, 47.51; H, 5.11%. Calcd for $C_{16}H_{20}O_{12}$: C, 47.52; H, 5.00%.

3-Acetoxy-5-(2,2-diacetoxyethylidene)-2(5H)-furanone (5). To a solution of **2** (0.3 g) in acetic anhydride (15 ml) triethylamine (0.5 ml) was added at 0 °C. After stirring for 24 h at 0 °C, the mixture was extracted with benzene-water. The benzene layer was washed with HCl aq and water, dried and evaporated under reduced pressure. The products were separated by column chromatography on silica gel (Wako gel C-200) with ethyl acetate–petroleum ether (2:3). The first moving compound was (*E*)-**5** (0.073 g, 34%) which was recrystallized from carbon tetrachloride–petroleum ether: mp 68 °C. The second moving compound was (*Z*)-**5** (0.12 g, 57%) as oil. (*E*)-**5**; ^{1}H-NMR ($CDCl_3$) δ= 2.13 (6H, s), 2.35 (3H, s), 5.75 (1H, d, J=7.6 Hz), 7.43 (1H, d), 7.77 (1H, s). IR 1780, 1760, 1740, 1680, 1615 cm^{-1}. Found: C, 50.64; H, 4.06%. Calcd for $C_{12}H_{12}O_8$: C, 50.71; H, 4.26%. (*Z*)-**5**; ^{1}H-NMR ($CDCl_3$) δ=2.13 (6H, s), 2.37 (3H, s), 5.47 (1H, d, J=8.0 Hz), 7.40 (1H, s), 7.65 (1H, d). IR 1790, 1760, 1680, 1615 cm^{-1}.

3-Acetoxy-5-[1-acetoxy-2-(1,3-dithiolan-2-yl)ethyl]-2(5H)-furanone (6) and 3-Acetoxy-5-[2-(1,3-dithiolan-2-yl)ethylidene]-2(5H)-

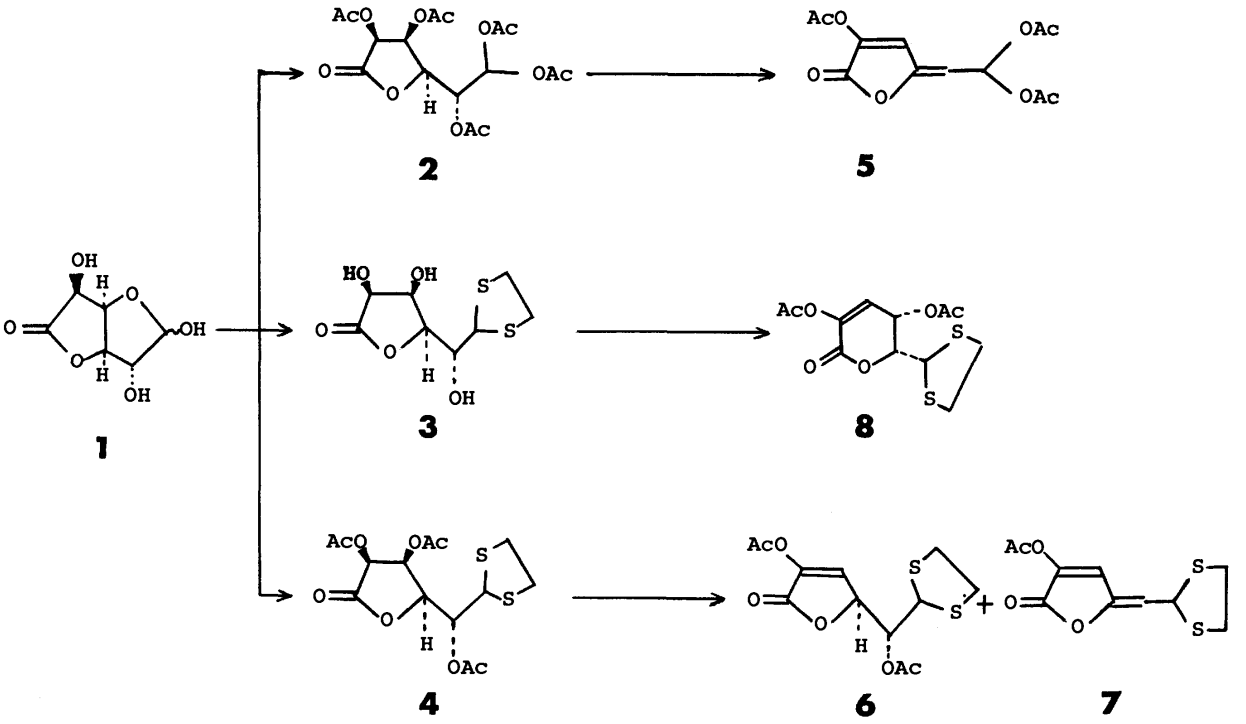

furanone (7). To a solution of **4** (0.150 g) in ethyl acetate (4 ml) triethylamine (0.4 ml) was added. After stirring for 19 h at room temperature, the solution was extracted with ethyl acetate–water. The organic layer was washed with HCl aq and water, dried and evaporated under reduced pressure. The products were separated by column chromatography on silica gel with benzene–ethanol (40:1.5). The first moving compound was **7** (0.016 g, 16%). The second moving compound was **6** (0.093 g, 74%) which was recrystallized from carbon tetrachloride–petroleum ether: mp 168—170 °C. **6**; ^{1}H-NMR ($CDCl_3$) δ=2.05 (3H, s), 2.28 (3H, s), 3.24 (4H, s), 4.83—5.00 (2H, m), 5.50—5.60 (1H, m), 7.00 (1H, d, J=2.0 Hz). IR 1775, 1750, 1650 cm^{-1}. Found: C, 44.97; H, 4.53%. Calcd for $C_{12}H_{14}O_6S_2$: C, 45.27; H, 4.43%. (*E*)-**7**; ^{1}H-NMR ($CDCl_3$) δ=2.33 (3H, s), 3.35 (4H, s), 5.30 (1H, d, J=11.0 Hz), 5.84 (1H, d), 7.69 (1H, s). (*Z*)-**7**; ^{1}H-NMR ($CDCl_3$) δ=2.33 (3H, s), 3.35 (4H, s), 5.37 (1H, d, J=10.4 Hz), 5.71 (1H, d), 7.28 (1H, s).

3,5-Diacetoxy-6-(1,3-dithiolan-2-yl)-5,6-dihydro-2H-pyran-2-one (8). To a solution of **3** (0.200 g) in acetic anhydride (3 ml) triethylamine (0.3 ml) was added. After stirring for 1 h at room temperature, the reagent were distilled off under reduced pressure. The residue was extracted with benzene–water and the organic layer washed with 5% $NaHCO_3$ aq and water, dried and evaporated under reduced pressure. The product was separated by column chromatography on silica gel with benzene–ethanol (40:1.5). Obtained **8** was recrystallized from carbon tetrachloride–petroleum ether (0.210 g, 83%): mp 91—92 °C. ^{1}H-NMR ($CDCl_3$) δ= 2.11 (3H, s), 2.35 (3H, s), 3.23 (4H, s), 4.42 (1H, dd, J=2.4, 10.0 Hz), 4.77 (1H, d, J=10.0 Hz), 5.58 (1H, dd, J=2.4, 6.4 Hz), 6.63 (1H, d, J= 6.4 Hz). IR 1770, 1660 cm^{-1}. Found: C, 45.10; H, 4.62%. Calcd for $C_{12}H_{14}O_6S_2$: C, 45.27; H, 4.43%.

References

1) J. Kiss, *Adv. Carbohydr. Chem. Biochem.*, **29**, 229 (1971).
2) R. M. De Lederkemer and M. I. Litter, *Carbohydr. Res.*, **20**, 442 (1971).
3) C. R. Nelson and J. S. Gratzl, *Carbohydr. Res.*, **60**, 267 (1978).
4) K. Dax and H. Weidman, *Adv. Carbohydr. Chem. Biochem.*, **33**, 189 (1976).
5) K. Tajima, H. Itoh, and H. Morooka, *Chem. Lett.*, **1980**, 1465.
6) R. E. Ireland and C. S. Wilcox, *J. Org. Chem.*, **45**, 197 (1980).
7) M. J. Begley, D. R. Gedge, and G. Pattenden, *J. Chem. Soc., Chem. Comm.*, **1978**, 60.
8) A. Alemany, *Tetrahedron Lett.*, **1979**, 3579.
9) E. M. Osman, K. C. Hobbs, and W. E. Walston, *J. Am. Chem. Soc.*, **73**, 2726 (1951).

Characterization of 13-Hydroxyneocembrene from Soft Corals[1)]

Mario AOKI, Tadahiro KATO,* Yasuto UCHIO,*,† Mitsuru NAKAYAMA,† and Mitsuaki KODAMA††
Department of Chemistry, Faculty of Science, Tohoku University, Aramaki-Aoba, Sendai 980
†*Department of Chemistry, Faculty of Science, Hiroshima University, Nakaku, Hiroshima 730*
††*Faculty of Pharmaceutical Science, Tokushima Bunri University, Yamashiro cho, Tokushima 770*
(Received September 6, 1984)

Synopsis. The isolation and structural elucidation of 13-hydroxyneocembrene from soft corals were carried out.

In the previous paper, some of us (Hiroshima group) have reported the characterization of a hydroxyneocembrene (**1**), named mayol, from a soft coral, *Sinularia mayi*.[2)] The structural elucidation of **1** was based on the spectral coincidence with the authentic *dl-cis*-1-hydroxyneocembrene synthesized by Tohoku group.[3)] The absolute configuration of the natural mayol, $[\alpha]_D$ +138.5° ($CHCl_3$) however, has remained unsolved because of limited amounts of the material.

In order to determine the absolute configuration, optical resolution of the synthetic *dl*-compound was performed by converting to *l*-camphanates followed by separation with high pressure liquid chromatography-(HPLC). Subsequent chemical transformation of the resultant enantiomers having $[\alpha]_D$ +156° and −156°, respectively, led to the conclusion that mayol has 1*S*,14*R* absolute stereochemistry although the value of optical rotation of the mayol is somewhat less than that of the resolved compound.[4)] For the sake of clarification of the difference of the specific rotation, the natural mayol was converted into the corresponding *l*-camphanate and subjected to HPLC analysis. It was soon made clear that the natural specimen was contaminated with minute amounts of an isomeric hydroxyneocembrene (**2**). It was found later that mayol and the isomeric hydroxyneocembrene could be separated by the repeated column chromatographies of the crude extracts. This paper concerns with the characterization of the isomeric compound.

The isomeric compound (**2**) has a molecular formula of $C_{20}H_{32}O$ (M^+ 288.2428, Calcd. MW=288.2451) having $[\alpha]_D$ −30.3° (*c* 0.93, $CHCl_3$). The gross structure was deduced from ^{1}H- and ^{13}C-NMR spectra, which were indicative of the existence of three CH=CMe- and an isopropenyl groups in addition to a secondary hydroxyl group. Oxidation of **2** with Collins' reagent afforded the corresponding ketone (**3**) having the carbonyl absorption at 1705 cm^{-1} in the IR spectrum, exhibiting that the carbonyl moiety is *not* conjugated with the double bond. This deduction was supported by the observation of only end absorption in its UV spectrum. Wolff-Kishner reduction of **3** gave a hydrocarbon, the mass fragmentation of which was completely identical with the authentic *dl*-neocembrene (**4**).[5)]

The evidence described so far demonstrates the isomeric alcohol (**2**) is 13-hydroxyneocembrene. Recently Faulkner and his co-worker reported the isolation of 2,3-epoxy derivative (**5**) of 13-hydroxyneocembrene from a marine organism.[6)]

Determination of the relative stereochemistry of the 13-hydroxyneocembrene (**2**) by the synthetic study will be the future subject. It should be noticed that the naturally occurring mayol is not enantiomerically mixed with the corresponding antipode as suspected previously.[4)]

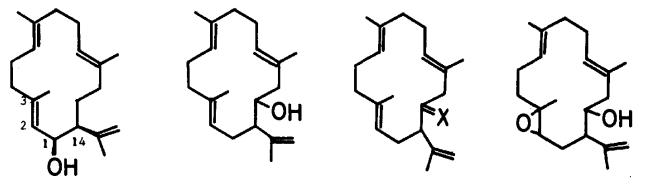

1 **2** **3** X = O **5**
4 X = H_2

Experimental

Measurements. NMR spectra were recorded with Varian EM-390 (90 MHz) and Varian XL-200 (200 MHz) spectrometers. Mass spectra were determined with a JEOL DX-300 spectrometer.

Isolation of Mayol (1) and 13-Hydroxyneocembrene (2). Crude MeOH extracts (30 g) from *Lobophytum denticulatum* Tixie-Durivault collected at coral reef of Miyako of Okinawa was eluted through a SiO_2 column with hexane–EtOAc (10:1) and the resultant fractions containing hydroxyneocembrenes (**1** and **2**) were developed on preparative TLC of 10% $AgNO_3$–SiO_2 with the same solvents. Repetition of TLC gave mayol (**1**) (37 mg) and the isomeric alcohol (**2**) (16 mg), respectively. **2** has the following physical data. IR(neat) 3400, 3070, 1660, 1640, 1050, and 890 cm^{-1}; ^{1}H-NMR ($CDCl_3$) δ= 1.54 (3H, t, 1.1 Hz), 1.58 (3H, s), 1.64 (3H, d, 0.9 Hz), 1.79 (3H, q, 0.7 Hz), 3.88 (1H, bt, 6 Hz), 4.83 (1H, bs), 4.92 (1H, bs), and 4.7—5.2 (3H, m); ^{13}C-NMR ($CDCl_3$) δ=14.9 (q), 15.3 (q), 16.7 (q), 22.8 (q), 24.2 (t), 24.8 (t), 24.9 (t), 38.7 (t), 39.9 (t), 43.9 (t), 49.9 (d), 71.6 (d), 111.6 (t), 125.4 (d), 125.9 (d), 127.2 (d), 131.1 (s), 132.9 (s), 134.0 (s), and 147.6 (s).

Purification of 13-Hydroxyneocembrene (2) by the Formation of l*-Camphanate.* To a solution of *l*-camphanyl chloride (22 mg) in pyridine (0.6 ml) was added a benzene solution (1 ml) of 13 mg of the crude mayol with $[\alpha]_D$ +138.5° (a mixture of mayol (**1**) and 13-hydroxyneocembrene (**2**)) at 0 °C. The resulting reaction mixture was stirred at 0 °C for 2 h and then at rt for an additional 1 h. The mixture was diluted with ether (20 ml) and sequentially washed with dil $CuSO_4$ and brine, and then dried over Na_2SO_4 and filtered. The filtrate was evaporated *in vacuo* to give a viscous oil. Repeated HPLC (Lichrosorb SI 100) of the oil with hexane–ether (20:1) provided *l*-camphanates of mayol (9 mg) and of 13-hyroxyneocembrene (5 mg).

l-Camphanate of **2** $[\alpha]_D$ −33.8° (*c* 0.83, $CHCl_3$); ^{1}H-NMR ($CDCl_3$) δ= 0.95 (3H, s), 1.05 (3H, s), 1.10 (3H, s), 1.49 (3H, s), 1.56 (3H, s), 1.64 (3H, s), 1.74 (3H, s), 4.73 (1H, s), 4.85 (1H, m), and 4.8—6.0 (4H, m). The *l*-camphanate of **2** (4 mg) was dissolved in 2M KOH–MeOH (2 ml (1 M=1 mol dm^{-3})). The solution was stirred at rt for 17 h, poured into water, and extracted with ether. The combined organic layers were sequentially washed with 1M HCl, sat $NaHCO_3$, and brine, dried over Na_2SO_4, and then filtered. The filtrate was evaporated *in vacuo* to afford a crude product. The crude

product was passed through a SiO_2 column eluted with hexane–EtOAc (10:1) to give pure 13-hydroxyneocembrene (1.8 mg).

Oxidation of 13-Hydroxyneocembrene (2). To a stirred solution of Collins' reagent (11 mg, 0.04 mmol) in CH_2Cl_2 (1 ml) was added a solution of the alcohol (**2**) (1.2 mg, 0.004 mmol) in CH_2Cl_2 (0.1 ml) at room temperature. The resultant mixture was stirred for 5 min and then diluted with EtOAc (3 ml). The EtOAc layer was passed through a short SiO_2 column and the solvent was evaporated to give a light brown oil. Filtration through a SiO_2 column with hexane–EtOAc (30:1) afforded a colorless oil (**3**)(0.6 mg). The ketone (**3**) has the following physical data. M^+ 286; $[\alpha]_D$ +482.4° (*c* 0.09, $CHCl_3$); IR(CCl_4) 3010, 1705, 1645, and 905 cm^{-1}, ^{1}H-NMR ($CDCl_3$) δ=1.57 (6H, s), 1.66 (3H, s), 1.69 (3H, s), 2.63 (1H, ddd, 11.0, 11.0, 7.0 Hz), 2.71 (1H, bd, 13 Hz), 3.23 (1H, d, 13 Hz), 3.30 (1H, bd, 11 Hz), 4.86 (2H, bs), and 4.8—5.2 (3H, m).

Wolff-Kishner Reduction of the Ketone (3). The ketone (**3**) (0.6 mg) was dissolved into a mixture of 80% hydrazine hydrate (18 µl), NaOH (18 mg) and diethylene glycol (0.3 ml) and gradually heated to 190°C and kept for 3 h at 190°C. After cooling, the reaction mixture was diluted with ether, washed successively with 0.5 M HCl, sat. $NaHCO_3$ and then brine and dried over Na_2SO_4. The ether solution was evaporated and the residue was passed through a SiO_2 column with hexane to afford a hydrocarbon (**4**)) (*dl*-neocembrene) (0.1 mg). M^+ 272 (30%) and *m/z* at 121 (62), 107 (66), 93 (92), 81 (80), 68 (100), and 67 (58). The fragmentation pattern was identical with that of *dl*-neocembrene (**4**).

References

1) This constitutes part 43 of the series of "Cyclization of Polyenes" of Tohoku group.

2) Y. Uchio, H. Nabeya, M. Nakayama, S. Hayashi, and T. Hase, *Tertrahedron Lett.*, **22**, 1689 (1981).

3) T. Kato, M. Suzuki, M. Takahsshi, and Y. Kitahara, *Chem. Lett.*, **1977**, 456.

4) M. Aoki, T. Uyehara, T. Kato, K. Kabuto, and S. Yamaguchi, *Chem. Lett.*, **1983**, 1121.

5) T. Kato, M. Suzuki, T. Kobayashi, and B. P. Moore, *J. Org. Chem.*, **45**, 1126 (1980).

6) B. N. Ravi and D. J. Faulkner, *J. Org. Chem.*, **43**, 2127 (1978).

Valence Isomerization between Water-soluble Norbornadiene and Quadricyclane Derivative

Kazuhiro MARUYAMA,* Hitoshi TAMIAKI, and Tetsuya YANAI
Department of Chemistry, Faculty of Science, Kyoto University, Kyoto 606
(Received September 11, 1984)

Synopsis. Photoisomerization of 3-(arylcarbamoyl)-norbornadiene-2-carboxylic acid **1** to the corresponding quadricyclane derivative **2** in an aqueous alkaline solution was clean and dependent upon the *p*-substituent of the aryl group. The exothermically reversal reaction of **2** to **1** was also clean but independent upon the substituent.

Valence isomerization between norbornadiene and quadricyclane has attracted much attention from solar energy storage.[1] This system has inherently an inevitable problem: norbornadiene cannot absorb sunlight. To overcome the great disadvantage, we have proposed introduction of substituents to norbornadiene.[2] Moreover, we first used water, safe and inexpensive, as the reacting media.[3] Usually, organic solvent had been used in similar systems. In this paper, we describe the effect of the substituents of aryl group in valence isomerization between 3-(arylcarbamoyl)norbornadiene-2-carboxylic acid **1** and 3-(arylcarbamoyl)quadricyclane-2-carboxylic acid **2** in water.

Results and Discussion

Norbornadiene-2,3-dicarboxylic anhydride and *p*-substituted aniline gave norbornadiene derivative **1** in a high yield.[2] The norbornadiene derivative **1** was highly soluble in an aqueous alkaline solution because of the carboxyl group. In an aqueous alkaline solution **1** has absorption band in longer wavelength than 400 nm and absorbs sunlight (Fig. 1). When an aqueous sodium carbonate solution of norbornadiene derivatives **1a—d** was irradiated by light of 366 or 334 nm, the corresponding quadricyclane derivatives **2a—d** were quantitatively formed even in the presence of air (Table 1). The photoisomerization by light of longer wavelength than 300 nm including sunlight was so clean that isosbestic points were observed in UV spectral changes. On irradiating light of 313 nm **1a, b** photoisomerized to **2a, b** quantitatively, but **1c, d** didn't (Table 1). This reaction is photochromic,[4] so **2** isomerizes again to **1** by light which is able to be absorbed by **2**. Under the conditions, **2c, d** isomerized to **1c, d** to attain a photostationary state. These facts may be rationalized by taking into consideration that introduction of a substituent into phenyl group to make **1** absorb light of the longer wavelength affects **2** concomitantly to absorb light of longer wavelength. Similarly, the quantum yield of the photoisomerization decreased with increasing the absorption edge of **1**. Therefore, bathochromic shift of absorption band of **1** induces decrease of both the chemical and the quantum yield of the photoisomerization. Wavelength dependency of the quantum yield is given in Table 1.

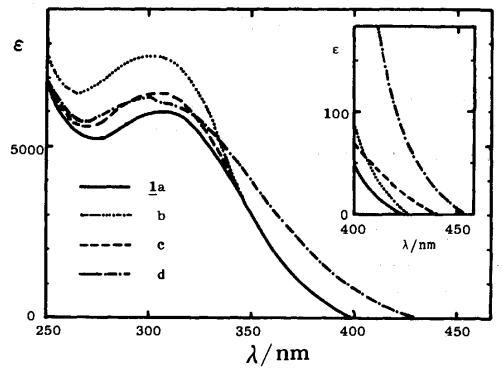

Fig. 1. Ultraviolet and visible spectra of 1 in 0.1 M Na_2CO aq (1 M = 1 mol dm^{-3}).

The isomerized **2** was so stable in a boiling aqueous sodium carbonate solution that none of **1** and other products could be produced under the conditions. However, addition of a catalytic amount of cobalt 5,10,15,20-tetrakis(*p*-carboxyphenyl)porphyrin (Co-TPPC) in the solution at room temperature induced a sudden isomerization of **2** to **1** quantitatively under release of heat. The exothermically catalytic reaction was of pseudo-first order. The rate constant was about 7 $M^{-1}s^{-1}$ and independent upon varieties of *p*-sub-

TABLE 1. PHOTO- AND CATALYTIC ISOMERIZATION OF **1** AND **2** IN Na_2CO_3 aq

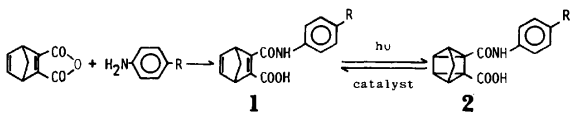

1 **2**

	R	Yield/%	Photoisomerization of **1** to **2**[a] Chemical Yield/% 313 nm	334 nm	366 nm	Quantum Yield 313 nm	334 nm	366 nm	Catalytic Isomerization of **2** to **1** k[b] $M^{-1}s^{-1}$	$-\Delta H$[c] kJ mol^{-1}
a	H	93	100	100	100	0.10	0.04	0.04	7—8	55—63
b	Cl	68	100	100	100	0.07	0.03	0.03	6—8	56—64
c	CH_3	82	95	100	100	0.06	0.01	0.01	6—7	55—65
d	OCH_3	85	77	100	100	0.03	0.01	0.003	7—8	55—63

a) These values were determined by UV spectral analysis. b) These values were measured at 25 °C by ^1H NMR technique. c) These values were measured by using a corrected copper-constantan thermocouple.

stituents of **2**. The heat of molar storage was about 60 kJ mol^{-1} and also independent upon the structure of **2a—d**. These facts may be explained as followings; a substituent introduced into phenyl group is so far from the reaction center, double bonds of **1** and so banana bonds of **2**.

From the viewpoint of the conversion efficiency in solar energy,[5] introduction of a substituent is effective little, but in view of utilizing light of longer wavelength of sun, the introduction is of some improvement. This water-soluble solar energy storage system may be promising for actual use by the following two points: i) this system can utilize the light of 450 nm; ii) this system is so clean in both photo- and catalytic reaction.

Experimental

Apparatus. All melting points were measured with a Yanagimoto micro melting point appratus and uncorrected. Ultraviolet and visible spectra were measured with a Shimadzu UV-200 spectrometer. Infrared spectra were measured with a JASCO IRA-1 spectrometer. ^{1}H NMR spectra were recorded on a JEOL JMN-PS-100 spectrometer. Mass spectra were recorded with a JEOL JMS-DX-300 spectrometer. Elemental analyses were performed at the Microanal ysis Center of Kyoto University.

Materials. Compound **1** was prepared from norbornadiene-2,3-dicarboxylic anhydride and *p*-substituted aniline, and the isomerized **2** was prepared by photoreaction of **1** in a similar manner reported previously.[2] Co-TPPC was synthesized according to the literature,[7] and purified by recrystallization from methanol and chloroform.

Physical Properties. ***1a***:[2] UV (0.1M Na_2CO_3 aq (1 M=1 mol dm^{-3})), 228 (ε 13900) and 302 nm (6570). ***1b***: yellow crystals; mp 187—189 °C (from acetonitrile); UV (0.1 M Na_2CO_3 aq) 235 (ε 14600) and 307 nm (7660); IR (KBr) 2400—3640 (br, COOH and NH) and 1685 cm^{-1} (C=O); ^{1}H NMR ($CDCl_3$) δ=2.06—2.36 (2H, m), 4.1—4.3 (2H, m), 6.85—7.05 (2H, m), 7.29 (2H, a half of ABq, J=9 Hz), 7.57 (2H, a half of ABq, J=9 Hz), and 9.3—9.5 (1H, br); Found: C, 62.15; H, 4.10; N, 5.05; Cl, 12.37%; M$^+$, 289 and 291. Calcd for $C_{15}H_{12}NO_3Cl$: C, 62.19; H, 4.17; N, 4.83; Cl, 12.24%; M, 289 and 291. ***1c***: yellow needles; mp 197—198 °C (from acetonitrile); UV (0.1 M Na_2CO_3 aq) 231 (ε 14400) and 308 nm (6070); IR (KBr) 2860—3440 (br, COOH), 3290 (NH), and 1690 cm^{-1} (C=O); ^{1}H NMR ($CDCl_3$) δ=2.13—2.40 (2H, m), 2.36 (3H, s), 4.08—4.36 (2H, m), 6.92—7.1 (m, 2H), 7.24 (2H, a half of ABq, J=8 Hz), 7.54 (2H, a half of ABq, J=8 Hz), and 8.6—8.8 (1H, br); Found: C, 71.44; H, 5.55; N, 5.16%; M$^+$, 269. Calcd for $C_{16}H_{15}NO_3$: C, 71.36; H, 5.61; N, 5.20%; M, 269. ***1d***:[2] UV (0.1 Na_2CO_3 aq) 231 (ε 14800) and 300 nm (6420). ***2a***:[2] UV (0.1 M Na_2CO_3 aq) 258 nm (ε 15900); Found: m/z 255.0901. Calcd for $C_{15}H_{13}NO_3$: M, 255.0895. ***2b***: white crystals; mp 168—172 °C (from acetonitrile); UV (0.1 M Na_2CO_3 aq) 262 nm (ε 16400); IR (KBr) 2400—3680 (br, COOH and NH), 1690, and 1640 cm^{-1} (C=O); ^{1}H NMR ($CDCl_3$) δ=2.14—2.94 (6H, m), 7.22 (2H, a half of ABq, J=8 Hz), and 7.48 (2H, a half of ABq, J=8 Hz); Found: m/z 289.0509 and 291.0474. Calcd for $C_{15}H_{12}NO_3{}^{35}Cl$ and $C_{15}H_{12}NO_3{}^{37}Cl$: M, 289.0506 and 291.0476. ***2c***: white crystals; mp 152—155 °C (from acetonitrile); UV (0.1 M Na_2CO_3 aq) 261 nm (ε 19200); IR (KBr) 2940—3640 (br,COOH), 3300 (NH), and 1690 cm^{-1} (C=O); ^{1}H NMR ($CDCl_3$) δ=2.1—2.9 (6H, m) 2.3 (3H, s), 7.05 (2H, a half of ABq, J=8 Hz), and 7.39 (2H, a half of ABq, J=8 Hz); Found: m/z 269.1041. Calcd for $C_{16}H_{15}NO_3$: M, 269.1052. ***2d***:[2] UV (0.1 M Na_2CO_3 aq) 262 nm (ε 14500). Found: m/z 285.1004. Calcd for $C_{16}H_{15}NO_4$: M, 285.1001.

Measurements. *Quantum Yield*: An apparatus and actinometer as described previously were used.[2] A Na_2CO_3–H_2O solution of **1** was irradiated at an each wavelength and absorbance of **1** at the wavelength was measured at an appropriate time interval. According to the method described by Kaupp and Prinzbach,[6] the quantum yield was determined.

Rate Constant: After a Na_2CO_3–D_2O solution of Co-TPPC was added to a Na_2CO_3–D_2O solution of **2** in a NMR sample tube, signals of **1** and **2** were integrated at an appropriate time interval. According to the method described previously,[2] the second order rate constant in the pseudo-first order reaction was determined.

Isomerization Heat: A Na_2CO_3–H_2O solution of Co-TPPC was added to a Na_2CO_3–H_2O solution of **2** in a test tube. Heat release in the solution was measured by using a corrected copper-constantan thermocouple. After correction of the heat of mixing and the radiative heat, the isomerization heat was determined.

References

1) R. R. Hautala, R. B. King, and C. Kutal, "Solar Energy; Chemical Conversion and Storage," The Humana Press, Clifton (1979); T. Toda, E. Hasegawa, T. Mukai, H. Tsuruta, T. Hasegawa, and T. Yoshida, *Chem. Lett.*, **1982**, 1551; Z. Yoshida and S. Miki, Jpn. Kokai Tokkyo Koho, JP 57 147577 (1982); H. Hirao, A. Ando, T. Hamada, and O. Yonemitsu, *J. Chem. Soc., Chem. Commun.*, **1984**, 300; K. Maruyama and H. Tamiaki, *Kagaku to Kogyo* (Osaka), **58**, 319 (1984).

2) K. Maruyama, K. Terada, and Y. Yamamoto, *J. Org. Chem.*, **46**, 5294 (1981).

3) K. Maruyama and H. Tamiaki, *Chem. Lett.*, **1982**, 1699; K. Maruyama, H. Tamiaki, and S. Kawabata, *ibid.*, **1984**, 743.

4) G. Kaupp and H. Prinzbach, *Liebigs Ann. Chem.*, **725**, 52 (1969).

5) H.-D. Scharf, J. Fleischhauer, H. Leismann, I. Ressler, W. Schlenker, and R. Weitz, *Angew. Chem. Int. Ed. Engl.*, **18**, 652 (1979).

6) G. Kaupp and H. Prinzbach, *Helv. Chim. Acta.*, **52**, 956 (1969).

7) F. R. Longo, M. G. Finarelli, and J. B. Kim, *J. Heterocyclic Chem.*, **6**, 927 (1969); A. D. Adler, F. R. Longo, F. Kampas, and J. Kim, *J. Inorg. Nucl. Chem.*, **32**, 2443 (1970).

Synthesis of Lariat Ferrocenocrown Ethers and Their Alkali Metal Complexes

Sadatoshi AKABORI,* Yoichi HABATA, and Masaru SATO†
Department of Chemistry, Faculty of Science, Toho University, Funabashi, Chiba 274
†*Chemical Analysis Center, Saitama University, Urawa, Saitama 338*
(Received August 7, 1984)

Synopsis. Lariat ferrocenocrown ethers were synthesized by the reaction of disodium salt of 1,1′-dihydroxyferrocene with *N*-substituted bis(2-chloroethyl)amines and/or by the reaction of bis(2-chloroethoxy)ferrocene with disodium salts of *N*-substituted bis(2-hydroxyethyl)amines. Crystalline 1:1 complexes of *N*-(2-methoxyethyl)-4-aza-1,7-dioxa-[7]ferrocenophane with $LiClO_4$ and $NaClO_4$ were also isolated.

Recently, the syntheses of highly functionalized crown ethers have been described,[1] and in this connection several research groups[2] reported the syntheses and physicochemical properties of ferrocenocrown ethers. We have previously reported on both syntheses and extractability for metal cations of polythia-,[3] polyoxa-,[4] and oxathia[*n*]ferrocenophanes.[5] It was found that these compounds showed high extractability for Tl^+ and Ag^+ and low extractability for alkali and alkaline earth metal cations. However, little is known concerning oxaaza[*n*]ferrocenophanes and lariat ferrocenocrown ethers. We now wish to report on the syntheses of lariat ferrocenocrown ethers and their metal complexes.

The reaction of potassium salt of **1** with **2** gave mononuclear ferrocenocrown ether **4** and its dimer **6** in 20 and 2% yields, respectively, while the reaction of **1** and **3** gave only **5** in the range from 9 to 20% yields. The reaction of **7** with **8** in the presence of NaH and 18-crown-6 as a phase-transfer catalyst[6] gave only **11** in 5% yield, while the reaction of **7** with **9** gave the cyclized products **10** and **12** in 4 and 10% yield, respectively.

The extractability of **4** and **5** for alkali metal picrates was measured by the method described in the previous paper.[4a] All of the lariat ferrocenocrown ethers showed little extractability. However, it was found that the selectivity for alkali metal cations of **4a** increased more than that of other ferrocenocrown ethers. The extractability of **4a** toward alkali metal cations was in the following order: K^+ (3%)>Rb^+=Cs^+(2%)>Na^+(0.6%)>Li^+(0.8). Also, the extractability of the crown ethers depends on the length and kind of the side arm. Compounds **5a** and **5b**, which contained an alkyl group as a side arm, showed a lower extractability compared with **4a**, which is explained in terms of the steric hindrance of a too lengthy side arm.

In contrast with the low extractability, the complex of alkali metal perchlorate with **4a**, and **4b** was isolated quantitatively. These complexes showed a higher melting point than the corresponding ligand and were confirmed by elemental analyses to be a 1:1 complex. Compound **4a** also gave a 1:1 complex with sodium

TABLE 1. MELTING POINT, MASS AND NMR SPECTRAL DATA OF LARIAT FERROCENOCROWN ETHERS AND THEIR METAL COMPLEXES

Comp	Mp θ_m/°C	Mass[a] (M^+)	^{1}H-NMR spectra/(δ values, in acetonitrile-d_3)[b]
4a	46.0—46.5	345	4.17(t, *J*=1.8Hz, 4H), 3.78(t, *J*=1.8Hz, 4H), 4.00(t, *J*=4.6Hz, 4H), 3.45(t, *J*=5.4Hz, 2H), 3.29(s, 3H), 2.91(t, *J*=4.6Hz, 4H), 2.79(t, *J*=5.4Hz, 2H)
4b	37.0—37.5	343	4.15(t, *J*=1.8Hz, 4H), 3.77(t, *J*=1.8Hz, 4H), 3.99(t, *J*=4.6Hz, 4H), 2.83(t, *J*=4.6Hz, 4H), 2.56(t, *J*=5.9Hz, 2H), 1.38(s, 4H), 1.02—0.70(m, 3H)
5a	12.5—13.5	389	4.16(t, *J*=1.8Hz, 4H), 3.77(t, *J*=1.8Hz, 4H), 3.99(t, *J*=4.6Hz, 4H), 3.60—3.40(m, 6H), 3.30(s, 3H), 2.92(t, *J*=4.6Hz, 4H), 2.80(t, *J*=6.2Hz, 2H)
5b	43.0—43.5	385	4.15(t, *J*=1.8Hz, 4H), 3.77(t, *J*=1.8Hz, 4H), 3.99(t, *J*=4.6Hz, 4H), 2.82(t, *J*=4.6Hz, 4H), 2.54(t, *J*=7.1Hz, 2H), 1.30(s, 10H), 1.02—0.70(m, 3H)
6a[c]	67.0—67.5	690	4.05(t, *J*=1.8Hz, 8H), 3.83(t, *J*=1.8Hz, 8H), 3.98(t, *J*=6.0Hz, 8H), 2.98(t, *J*=6.0Hz, 8H), 3.48(t, *J*=6.6Hz, 4H), 2.83(t, *J*=6.6Hz, 4H), 3.32(s, 6H)
6b[c]	oil	686	4.00(t, *J*=1.8Hz, 8H), 3.74(t, *J*=1.8Hz, 8H), 3.89(t, *J*=6.0Hz, 8H), 2.88(t, *J*=6.0Hz, 8H), 2.62(t, *J*=6.6Hz, 4H), 1.85—1.14(m, 8H), 1.14—0.80(m, 6H)
10[c]	oil	521	4.00(t, *J*=1.8Hz, 4H), 3.79(t, *J*=1.8Hz, 4H), 3.87(t, *J*=6.0Hz, 4H), 3.52(s, 8H), 3.30(s, 3H), 2.78(t, *J*=6.0Hz, 4H), 2.69(t, *J*=6.0Hz, 2H), 3.73—3.45(m, 10H)
11[c]	oil	477	4.15(t, *J*=1.8Hz, 4H), 3.88(t, *J*=1.8Hz, 4H), 3.85(t, *J*=6.0Hz, 4H), 3.35(s, 3H), 2.80(t, *J*=6.0Hz, 6H), 2.70(s, 1H), 3.71—3.40(m, 10H), 6.54(dd, J_{ab}=6.6Hz, J_{ac}=13.2Hz, 1H), 4.59(dd, J_{ac}=13.2Hz, J_{bc}=1.8Hz, 2H), 4.26(dd, J_{ab}=6.6Hz, J_{bc}=1.8Hz, 2H)
12[c]	oil	521	4.18(t, *J*=1.8Hz, 4H), 3.91(t, *J*=1.8Hz, 4H), 3.87(t, *J*=6.0Hz, 4H), 3.39(s, 3H), 2.88(t, *J*=6.0Hz, 6H), 3.70(s, 1H), 3.85—3.46(m, 14H), 6.67(dd, J_{ab}=6.6Hz, J_{ac}=13.2Hz, 1H), 4.57(dd, J_{ac}=13.2Hz, J_{bc}=1.8Hz, 2H), 4.28(dd, J_{ab}=6.6Hz, J_{bc}=1.8Hz, 2H)
13a	150—152		4.20(t, *J*=1.8Hz, 4H), 3.79(t, *J*=1.8Hz, 4H), 4.00(t, *J*=4.6Hz, 4H), 3.47(t, *J*=5.4Hz, 2H), 3.32(s, 3H), 2.91(t, *J*=4.6Hz, 4H), 2.79(t, *J*=6.0Hz, 2H)
13b	Dec 190		4.23(t, *J*=1.8Hz, 4H), 3.73(t, *J*=1.8Hz, 4H), 3.98(t, *J*=4.6Hz, 4H), 3.47(t, *J*=5.4Hz, 2H), 3.33(s, 3H), 2.86(t, *J*=4.6Hz, 4H), 2.75(t, *J*=6.0Hz, 2H)
14a	Dec 170		4.23(t, *J*=1.8Hz, 4H), 3.83(t, *J*=1.8Hz, 4H), 4.12(t, *J*=4.6Hz, 4H), 3.20(t, *J*=4.6Hz, 4H), 2.91(t, *J*=5.9Hz, 2H), 1.46(s, 4H), 1.02—1.80(m, 3H)

a) The mass spectra were taken on a Hitachi M-80 mass spectrometer(70eV). b) NMR spectra were recorded with tetramethylsilane as internal standard on a JEOL-FX-90Q spectrometer. c) Measured in $CDCl_3$.

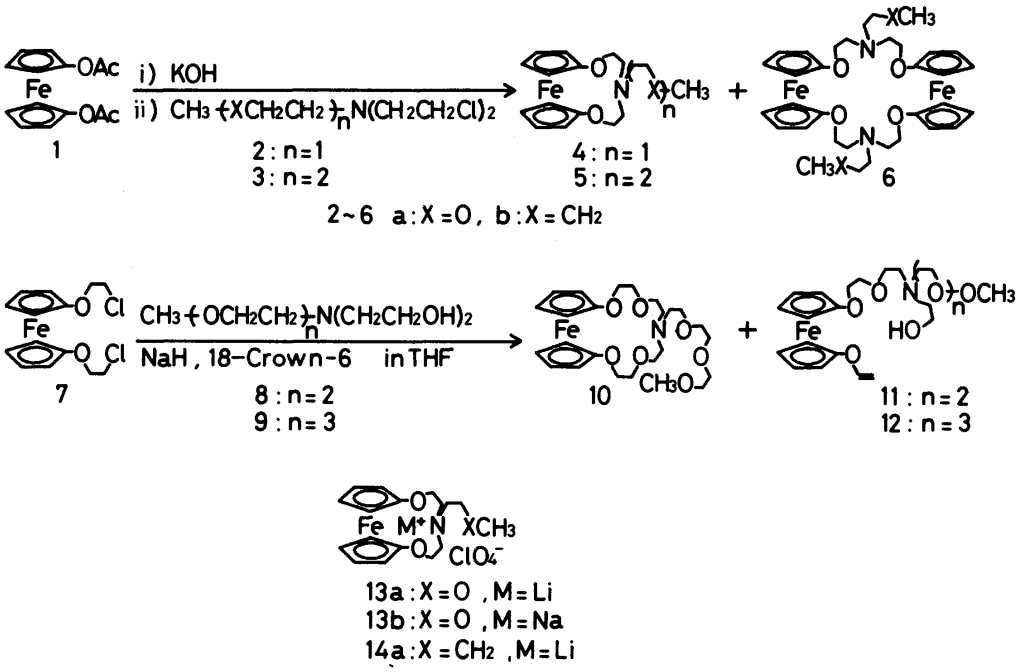

perchlorate, while **4b** gave no crystalline complex. As shown in the ^{1}H-NMR spectral data in Table 1, there was only a little difference in the chemical shift between the ligand and the corresponding complex. The signals of the α- and β-protons of the ferrocene ring and the methylene protons in the complexes shifted down field as compared with those in the free ligand. A similar trend was observed on the addition of alkali metal perchlorate to a solution of ligand in acetonitrile-d_3. The tendency for this down-field shift observed here was also similar to that shown in the ^{1}H-NMR data of the polyoxa[n]ferrocenophanes and these alkali metal thiocyanate complexes.[4b]

Experimental

Reaction of 1 with 2a. **1** (2.24 mmol) was added to potassium hydroxide (12.3 mmol) in water (10 cm^3) under nitrogen, and the mixture was stirred under reflux. After 1 h, a solution of **2a** (2.69 mmol) in 60% ethanol (70 cm^3) was added at one time and the mixture was then stirred for 5 h at reflux temperature. After the usual work-up, the reaction mixture was chromatographed on silica-gel TLC (hexane–acetone). The first band gave red oil which was crystallized from hexane to give **4a** in 26% yield. Found: C, 58.90; H, 6.91; N, 4.25%. Calcd for $C_{17}H_{23}O_3NFe$: C, 59.15; H, 6.72; N, 4.06%. The second band gave **6a** as red crystals (from hexane) in 2% yield. Found: C, 58.91; H, 6.99; N, 3.60%. Calcd for $C_{34}H_{46}O_6N_2Fe_2$: C, 59.15; H, 6.72; N, 3.47%.

Similarly, reaction of **1** (6.08 mmol) with **2b** (7.24 mmol) gave **4b** and **6b** in 20 and 3% yields, respectively. **4b** Found: C, 63.25; H, 7.30; N, 4.23%. Calcd for $C_{18}H_{26}O_2NFe$: C, 62.99; H, 7.34; N, 4.07%. **6b**, Found: C, 62.81; H, 7.63; N, 4.15%. Calcd for $C_{36}H_{50}O_4N_2Fe_2$: C, 62.99; H, 7.34; N, 4.08%.

Similarly, reaction of **1** (5.23 mmol) with **3a** (6.5 mmol) gave **5a** in 20% yield. Found: C, 58.60; H, 7.12; N, 3.85%. Calcd for $C_{19}H_{27}O_4NFe$: C, 58.61; H, 7.00; N, 3.60%.

Similarly, reaction of **1** (5.0 mmol) with **3b** (5.3 mmol) gave **5b** in 14% yield. Found: C, 65.51; H, 8.34; N, 3.69%. Calcd for $C_{21}H_{31}O_2NFe$: C, 65.44; H, 8.12; H, 3.64%.

Reaction of 7 with 9. A solution of **9** (3.46 mmol) in the presence of sodium hydride (16.2 mmol) and 18-crown-6 (3.7 mmol) in THF (150 cm^3) was stirred under reflux for 10 h and then a solution of **7** (3.19 mmol) in THF (50 cm^3) was added to the mixture all at one time. After 48 h, the mixture was chromatographed on silica-gel TLC (hexane:acetone=1:1). The first band gave **10** as red oil in 4% yield. Found: C, 57.51; H, 7.72; N, 2.85%. Calcd for $C_{25}H_{39}NO_7Fe$: C, 57.57; H, 7.55; N, 2.69%. The second band gave **12** as red oil in 10% yield. Found: C, 57.82; H, 7.41; N, 2.75%. Calcd for $C_{25}H_{39}NO_7Fe$: C, 57.57; H, 7.55; N, 2.69%.

Similarly, reaction of **7** (2.91 mmol) with **8** (3.29 mmol) gave **11** as red oil in 5% yield. Found C, 58.10; H, 7.65; N, 3.18%. Calcd for $C_{23}H_{35}NO_6Fe$: C, 57.86; H, 7.40; N, 2.93%.

General Procedure for the Alkali Metal Perchlorate Complex. A solution of **4a** or **4b** (0.1 mmol) in acetonitrile (2 cm^3) was added to an acetonitrile solution (2 cm^3) containing alkali metal perchlorate (0.1 mmol). The mixture was heated for a few minutes, and allowed to stand in an ice bath. After the precipitates had been completed, the complex was filtered and then washed with a small portion of acetonitrile. **13a**: Found: C, 45.22; H, 5.16; N, 3.11%. Calcd for $C_{17}H_{23}NO_7FeLiCl$: C, 45.21; H, 5.14; N, 3.10%. **13b**. Found: C, 43.60; H, 4.99; N, 3.05%. Calcd for $C_{17}H_{23}NO_7FeNaCl$: C, 43.65; H, 4.97; N, 3.00%. **14a**. Found: C, 48.03; H, 5.67; N, 3.13%. Calcd for $C_{18}H_{25}NO_6FeLiCl$: C, 48.07; H, 5.62; N, 3.12%.

References

1) R. E. Izatt and J. J. Christensen, "Synthetic Multidentate Macrocyclic Compound," Academic Press, New York (1977).

2) G. Oepen and F. Vogtle, *Liebigs Ann. Chem.*, **1979**, 1094. A. P. Bell and D. Hall, *J. Chem. Soc., Chem. Commun.*, **1980**, 163; B. Czech and A. Ratajczak, *Polish J. Chem.*, **54**, 767 (1980).

3) M. Sato, H. Watanabe, S. Ebine, and S. Akabori, *Chem. Lett.*, **1982**, 1753.

4) a) S. Akabori, Y. Habata, Y. Sakamoto, M. Sato, and S. Ebine, *Bull. Chem. Soc. Jpn.*, **56**, 537 (1983); b) S. Akabori, Y. Habata, and M. Sato, *Bull. Chem. Soc. Jpn.*, **57**, 68 (1984).

5) S. Akabori, S. Shibahara, Y. Habata, and M. Sato, *Bull. Chem. Soc. Jpn.*, **57**, 63 (1984); M. Sato, M. Kubo, S. Ebine, and S. Akabori, *Bull. Chem. Soc. Jpn.*, **57**, 421 (1984).

6) S. Akabori and H. Tuji, *Bull. Chem. Soc. Jpn.*, **51**, 1197 (1978).

Synthesis of Pyrazolo[3,4-*d*]thiazoles†

S. V. THIRUVIKRAMAN and S. SESHADRI*

Dyes Research Laboratory, Department of Chemical Technology, Matunga, Bombay 400019, India

(Received November 29, 1983)

Synopsis. Several 5-substituted 1-phenylpyrazolo-[3,4-*d*]thiazole derivatives have been synthesized by reaction of 5-amino-3-methyl-1-phenylpyrazole-4-thiol with different reagents.

There is little information in the literature about pyrazolothiazoles although a good deal of work has been carried out on various other fused pyrazoles. This paper reports a convenient approach to the synthesis of pyrazolo[3,4-*d*]thiazoles.

Thiocyanation of 5-amino-3-methyl-1-phenylpyrazole (**1**) gave rise to the 4-thiocyanato derivative (**2**). The thiocyanato compound was readily hydrolyzed by acid to the amino thiol (**3**). This amino thiol proved to be an excellent precursor for the synthesis of pyrazolo-[3,4-*d*]thiazoles.

Reaction of the amino thiol (**3**) with acetic anhydride gave 3,5-dimethyl-1-phenylpyrazolo[3,4-*d*]thiazole(**4**). The structure of this product (**4a**) was established by its elemental analysis, mass spectrum (*m/z* at 229) and its NMR spectrum. The compound exhibited fluorescence in UV light. It was hoped that the introduction of an aromatic ring at the 5-position of the pyrazolothiazole would shift the fluorescence into the visible region.

Reaction of the amino thiol (**3**) with benzoic acid in polyphosphoric acid at high temperature gave rise to the 5-phenyl derivative (**5a**) as shown by its elemental analysis and mass spectrum (*m/z* at 291). However, this compound also exhibited fluorescence only in UV.

The amino thiol was therefore reacted with cinnamic acid in polyphosphoric acid and the expected 5-styryl derivative (**5b**) was obtained as shown by elemental analysis and infrared spectrum (absence of -NH and amide carbonyl peaks). The 5-styryl derivative (**5b**) showed pale green fluorescence in daylight.

The amino thiol (**3**) was reacted with ethyl cyanoacetate to give 5-cyanomethyl-3-methyl-1-phenylpyrazolo[3,4-*d*]thiazole (**4b**). The structure of this product was established by elemental analysis and infrared spectrum. (Chart I).

We have earlier[1] shown that *o*-cyanoarylamidines (**6**) readily cyclize with ammonium acetate to yield 4-aminoquinazoline derivative (**7**). It was therefore anticipated that a similar heterocyclization could be achieved by reacting the *o*-thiocyanato amidine (**8**) to yield the aminothiadiazepine derivative (**10**). Accordingly the 5-amino-4-thiocyanatopyrazole (**2**) was reacted with the Vilsmeier reagent (DMF/$POCl_3$) which gave the expected amidine (**8**). Hydrolysis of the amidine (**8**) under mild acidic or alkaline conditions gave mercapto amidine (**9**). Hydrolysis of the mercapto amidine with stronger acid or alkali gave rise to the amino thiol (**3**). Reaction of the thiocyanato amidine with ammonium acetate did not proceed as anticipated but gave rise to the mercapto amidine (**9**) identified by mixed mp and TLC comparison with the authentic sample. (Chart II).

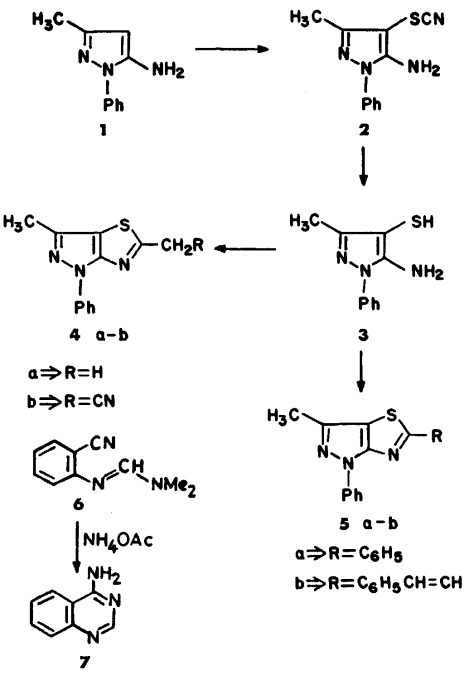

Chart I

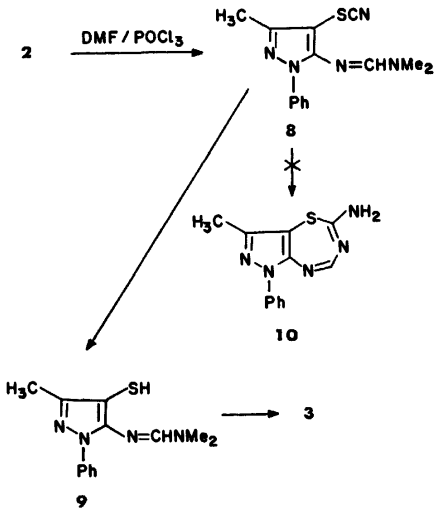

Chart II

Experimental

All melting points are uncorrected. The infrared spectra (in Nujol) were recorded on Perkin Elmer 395 spectrophotometer and ^{1}H-NMR spectra on a Varian EM-360 spectrometer. The mass spectra were recorded on Varian MAT II RS with Varian 100 e data system.

† Abstracted in part from the Ph. D. Thesis of S. V. Thiruvikraman, University of Bombay, 1981.

5-Amino-3-methyl-1-phenyl-4-thiocyanatopyrazole (2). A mixture of aminopyrazole (**1**) (0.01 mol) and potassium thiocyanate(0.03 mol) in MeOH(10 ml) was cooled to 0 °C. Under stirring Br_2(0.01 mol) in MeOH(2 ml) was added dropwise maintaining the temperature below 5 °C. The mixture was stirred for 3 h at 0—5 °C. It was then poured into ice-cold water and neutralized with Na_2CO_3 to pH 9. The yellowish brown thiocyanato compound (**2**) that separated was filtered, washed with water, and dried. The thiocyanato compound (**2**) was obtained in 89% yield and was crystallized from ethanol: mp 115 °C. Found: C, 57.4; H, 4.0, N, 24.0, S, 14.3%. Calcd for $C_{11}H_{10}N_4S$: C, 57.4; H, 4.3; N, 24.3, S, 13.9%; IR: 3300 (NH_2) and 2300 cm^{-1} (SCN).

5-Amino-3-methyl-1-phenylpyrazole-4-thiol (3). A solution of thiocyanato compound (**2**) in dilute HCl (10 ml, 10%) was stirred at room temperature for 4—5 h. The reaction mixture was neutralized with Na_2CO_3 to pH 9 and the yellowish brown compound (**3**) that separated in quantitative yield was crystallized from aqueous ethanol: mp 178 °C. Found: N, 20.4; S, 15.7%; M^+, 205. Calcd for $C_{10}H_{11}N_3S$: N, 20.5; S, 15.6%; M, 205. IR: 3300 cm^{-1} (NH_2).

3,5-Dimethyl-1-phenylpyrazole[3,4-d]thiazole (4a). A mixture of mercaptopyrazole (**3**) and Ac_2O (5 ml) was refluxed for 3 h. After pouring the reaction mixture into ice water the product (**4a**) separated in 85% yield was crystallized from ethanol: mp 148 °C. Found: N, 18.5; S, 14.0%; M^+, 229. Calcd for $C_{12}H_{11}N_3S$: N, 18.3, S, 13.9%; M, 229; ^1H NMR (TFA) $\delta=2.2$ (3H, d, 3-CH_3), 3.0(3H, d, 5-CH_3), 7.4 (5H, s, aromatic).

General Procedure for the Preparation of 5-Aryl-3-methyl-1-phenylpyrazolo[3,4-d]thiazole (5). To polyphosphoric acid (P_2O_5 7 g, H_3PO_4 3 ml) at room temperature, a mixture of 5-aminopyrazole-4-thiol (**3**) (0.005 mol) and aromatic acid (0.005 mol) was added. The reaction mixture was heated to 180 °C and maintained for 1 h. After the usual work up, the product that separated was filtered and washed with water. Thus, the 5-phenyl derivative (**5a**) was obtained in 75% yield and was crystallized from ethanol, mp 152 °C. Found: N, 14.6; S, 11.3; M^+, 291. Calcd for $C_{17}H_{13}N_3S$: N, 14.4; S, 11.0%; M, 291. Also the 5-styryl derivative (**5b**) was obtained in 80% yield and was crystallized from ethanol; mp 200 °C; Found: N, 13.5; S, 9.9%. Calcd for $C_{19}H_{15}N_3S$: N, 13.2, S, 10.1%.

5-Cyanomethyl-3-methyl-1-phenylpyrazolo[3,4-d]thiazole (4b). A mixture of 5-aminopyrazole-4-thiol (**3**) (0.005 mol) and ethyl cyanoacetate (0.005 mol) was heated in an oil bath at 150 °C for 30 minutes. The mixture was cooled, dumped into water, neutralized to pH 6 and filtered. The product was purified by passing through a short column of alumina. It was further crystallized from aqueous ethanol to give **4b** in 72% yield; mp 125 °C. Found, N, 22.1; S, 12.5%. Calcd for $C_{13}H_{10}N_4S$: N, 22.1; S, 12.5%. IR 2240 cm^{-1}(CN) and absence of NH and amide carbonyl peaks.

Vilsmeier Reaction on 5-Amino-4-thiocyanatopyrazole (2). To the Vilsmeier reagent from DMF (7 ml) and $POCl_3$(0.02 mol) at 0—5 °C, 5-amino-4-thiocyanatopyrazole(0.01 mol) was added. After half hour the temperature was raised to 70 °C and maintained for 3 h. After pouring the reaction mixture into ice water, the pH was adjusted to 9 with Na_2CO_3. The oil separated was extracted in C_6H_6 and solvent removed to obtain **8** in 80% yield. Found, N, 24.8; S, 11.2%; M^+, 260. Calcd for $C_{14}H_{15}N_5S$: N, 24.5; S, 11.2%; M^+, 260. IR 2250 cm^{-1}(SCN).

Hydrolysis of Thiocyanatoamidine (8). A mixture of thiocyanatoamidine (**8**) (1 g) and HCl (10 ml, 10%) or NaOH (10 ml, 10%) was stirred overnight. The solution was cooled and neutralized to pH 8—9, when an oil separated. The benzene extract of the oil when eluted with C_6H_6 over a neutral alumina column afforded **9** in 80% yield, crystallized as yellow crystals from ethanol; mp 110 °C. Found: N, 21.4; S, 12.4%. Calcd for $C_{13}H_{16}N_4S$: N, 21.5; S, 12.3%, IR: absence of SCN peak at 2250 cm^{-1} and presence of a weak band at 2500 cm^{-1} for SH function.

We are thankful to Dr. K Nagarajan of Ciba-Geigy Research Centre, Bombay for the mass spectra and to the Microanalytical Section for the analysis, one of us (S. V. T.) is grateful to the U. G. C., New Delhi for the award of a Junior Research Fellowship.

References

1) M. M. Deshpande and S. Seshadri, *Indian J. Chem.*, **11**, 58 (1973).

Kinetic and Mechanism of the Electrochemical Reduction of Fluoranthene in *N,N*-Dimethylformamide

Refat Abdel-Hamid

Department of Chemistry, Faculty of Science, Sohag, Egypt

(Received Januray 9, 1984)

Synopsis. Detailed mechanism of electrochemical reduction of fluoranthene has been studied by cyclic voltammetric method in *N,N*-dimethylformamide solution using 0.1 mol dm^{-3} tetraethylammonium perchlorate as a supporting electrolyte. It was found that fluoranthene undergoes a reversible diffusion-controlled one electron-transfer wave followed by an irreversible one-electron one. The reaction in the presence of proton donor such as phenol was also studied. The results reveal that the kinetics of the reaction is first-order in anion radical, zero-order in fluoranthene and first-order with respect to phenol. The overall reaction is of the ECE_h type. It is concluded that the mechanism of the electrochemical reduction of fluoranthene consists of (a) heterogeneous electron transfer to form an anion radical, (b) proton transfer reaction, (c) homogeneous electron transfer in which the neutral radical formed in (b) is reduced to the carbanion and finally (d) the rapid protonation of the carbanion.

Generally, the electrochemical reduction of aromatic hydrocarbons in aprotic solvents involves two one-electron successive steps yielding the anion radical and the dianion respectively.[1,2] Thus the typical cyclic voltammetry reduction pattern of aromatic hydrocarbons in aprotic solvents displays a one-electron reversible wave followed by a one-electron irreversible wave. In the presence of a proton donor such as phenol, a proton transfer reaction following the initial electron transfer step is common to the electrochemical reduction of these compounds. Although the electrochemical behaviour of aromatic hydrocarbons have been the subject of a large number of investigators,[3,4] very few studies have been done on the electrochemical reduction of fluoranthene. The only previous study includes fluoranthene as one of a series of investigated compounds,[5] detailed measurements were not reported.

The objective of the present study was detail electrochemical investigation of fluoranthene in *N,N*-dimethylformamide. Moreover, the study was extended to include the effect of proton-donor concentration on the reduction process. The kinetics and mechanism of the electrode process were proposed and discussed.

Experimental

A Princeton Applied Research Model 303 mercury-drop electrode system in (small) hanging-drop mode linked to a microprocessor-controlled polarograph with 16-bit DAC and three-channel Servoger 460 recorder was used for cyclic voltammetric measurements. The electrode area was 1.06×10^{-2} cm^2. The reference electrode was $Ag/AgNO_3$ (0.01 M) in 0.1 mol dm^{-3} tetraethylammonium perchlorate, TEAP, in *N,N*-dimethylformamide. The solutions were deoxygenated by passing pure nitrogen. The cell and referenced potentials were recorded simultaneously with current.

A. R. grade *N,N*-dimethylformamide was purified and dried using the method discribed previously[6] and stored over Linde type 4A Molecular Sieve under nitrogen atmosphere. Polarographic grade TEAP was dried under vacuum for at least 24 h and used as a supporting electrolyte. Fluoranthene (BDH) and phenol (BDH) were used.

Stock solutions of fluoranthene, 10^{-2} M, and phenol, 1.0 M, were prepared by dissolving the appropriate weights of each in appropriate volume of 0.1 M TEAP/DMF solution. Lower concentrations required were prepared by accurate dilution.

Results and Discussion

Cyclic voltammetric results of 5.0×10^{-4} M fluoranthene in a *N,N*-dimethylformamide solution containing 0.1 M TEAP for scan rates, v, of 14 to 308 mV s^{-1}, show two well-defined waves. A typical cyclic voltammogram is shown in Fig. 1 for fluoranthene. The peak current, i_p, of both waves varies systematically with varying scan rate. The ratio of the cathodic to the anodic currents, i_{pc}/i_{pa}, for the first wave amounts to 1.05 ± 0.05 through the scan rate range used (*c.f.* Table 1). It was found that the peak current for the first wave correlates with the square root of the scan rate, $v^{1/2}$, (correlation coefficient=0.998). The slopes of the straight line graph obtained on plotting i_p against $v^{1/2}$ amounts to 2.51 ± 0.01 μA s$^{1/2}$ V$^{-1/2}$ for 0.5 mM fluoranthene from which the diffusion coefficient, D, of 3.09×10^{-6} cm^2 s^{-1} is evaluated.[7] Furthermore, it is found that the potential separation, $E_{pa}-E_{pc}$, amounts to 59.6 ± 2.3 mV (where E_{pa} and E_{pc} are the anodic and cathodic peak potentials respectively) and the shape of the cyclic voltammetric wave as measured by its width $E_p-E_{p/2}$, is 56.00 ± 0.05 mV. These values are only slightly different than the theoritical values (59.1 and 56.5 mV at 25 °C for $n=1$ respectively[8]). This is probably due to a small uncompensated resistance. It is worthy to mention that the peak potential, E_p, receives no change on varying the scan rate. These facts reveal that the first wave is a reversible one electron transfer diffusion-controlled wave.

On the other hand, from the cyclic voltammograms covering the complete polarographic waves, one observes that for

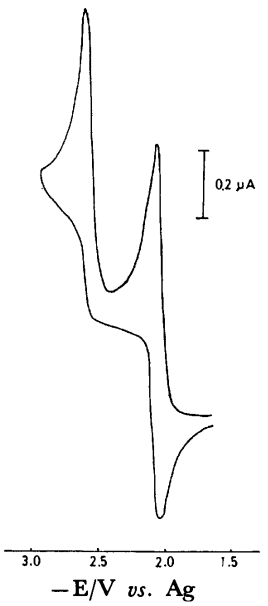

Fig. 1. Cyclic voltammogram of 5.0×10^{-4} M fluoranthene in TEAP/DMF solution at a sweep rate of 77 mV s^{-1} at HMDE.

Table 1. Cyclic voltammetric data for 5 mM fluoranthene in *N*,*N*-dimethylformamide containing 0.1 M tetraethylammonium pherchlorate solutions at 25 °C

Sweep. rate mV s^{-1}	First wave		Second wave	
	$E_p-E_{p/2}$ mV	i_{pc}/i_{pa}	i_{pc} uA	$-E_p$ mV
14	58	1.00	0.50	2612
20	58	0.98	0.46	2620
39	64	1.07	0.76	2626
77	60	1.05	1.05	2633
154	62	1.08	1.39	2640
308	62	1.12	1.90	2658

the second electrode process the anodic counterpart of the cathodic peak is lacking. This behaviour suggests that the second electron transfer is electrochemically unidirectional *i.e.* totally irreversible or is coupled to an irreversible chemical follow-up reaction. Moreover, the cathodic peak current is proportional to the square root of the scan rate (correlation coefficient=0.999) which is consistent with diffusion as the rate-limiting step.

In order to establish that the charge-transfer reaction in the cathodic reduction of fluoranthene is intrinsically slow *i.e.* the electrochemical process is totally irreversible, one can apply relation (1) between the peak potential, E_p, and the peak current, i_p, in a totally irreversible wave.[8]

$$E_p = \frac{(\ln 10)RT}{Bn_bF} \log i_p + \text{constant}. \quad (1)$$

The value of the transfer coefficient, B, obtained assuming that $n_b=1$ (0.38) bears out the total irreversibility of the second wave.

All the above results reveal that fluoranthene, *F*, undergoes a reversible one electron transfer, $E_p=2.088\pm0.003$ V, to form anion radical, $F^{\cdot-}$, followed by an irreversible second wave at higher negative potentials. The anion radicals are reasonably stable during the time of the experiments.

On the addition of proton donor, phenol, the first wave does not increase in peak current or change in the peak potential, while for the second one a change in both the peak current and the peak potential is observed.

The dependence of the peak potential, E_p on the voltage scan rate, v, during the voltammetric reduction of fluoranthene for the second wave is given by the following equation,[9]

$$dE_p/d \log v = [\ln 10/(b+1)]RT/F, \quad (2)$$

where b is the reaction order in *B*, the primary product of electron transfer reaction (3),

$$A + e \rightleftharpoons B, \quad (3)$$

the other notations are conventional. The $dE_p/d \log v$ value of fluoranthene in TEAP/DMF solutions in the presence of 50.0 mM phenol as a proton donor is measured using the linear least-square fit method of E_p *versus* $\log v$. The theoretical value of $b=1$ corresponding to the protonation reaction (4) with phenol in excess is 29.6 at 25 °C.

$$F^{\cdot-} + PhOH \longrightarrow F\cdot\text{-}H + PhO^- \quad (4)$$

It was found that value of $dE_p/d\log v$ closes to the theoretical value (30.7±3.1 mV/decade). Accordingly, one can conclude that, the reaction is first-order with respect to the primary product of the electron transfer reaction.

The dependence of E_p on the concentration of fluoranthene, C_A, is tested using equation 5, where a and i are the reaction order in A, substrate, and the products formed whice further participate in the process.[9]

$$dE_p/d \log C_A = [(a+b+i-1)/(b+1)] \ln 10(RT/F). \quad (5)$$

For the reaction (3), $a=0$, $b=1$, $i=0$, and $dE_p/d \log C_A$ is also zero. The data obtained for different concentrations of fluoranthene (5.0×10^{-4}—2.0×10^{-4} M), reveal that both a and i are zero and $dE_p/d \log C_A$ is zero as well.

It was found that E_p of the second wave depends on the concentration of the proton donor. This dependence is given by equation 6, where x is the reaction order in X(phenol) for the protonation reaction (4).

$$dE_p/d \log C_x = [(X \ln 10)/(b+1)]RT/F. \quad (6)$$

It is expected that x equals 1 and $dE_p/d \log C_x$ equals 29.6 mV/decade at 25 °C. The experimental value obtained for $dE_p/d \log C_x$ amounts to 28.4±4.3 mV/decade scan rate of 154 mV s^{-1}. This indicates that the apparent reaction order in phenol closes unity.

The rate law for the electrochemical reduction of fluoranthene on the basis of the above facts can be written as follows:

$$\text{Rate} = K_{odsd}[F^{\cdot-}][PhOH]. \quad (7)$$

The rate in equation (7) is equivalent to the following rate.[10]

$$\text{Rate} = K_{obsd}[F^{\cdot-}]^2[PhOH]/[F]. \quad (8)$$

The results obtained are consistent with the ECE_h mechanism proposed previously for the voltammetric reduction of aromatic hydrocarbons.[10] Accordingly, the electrochemical reduction reaction of fluoranthene in DMF proceeds *via* the following steps. (a) A heterogeneous reversible one electron transfer step (9) followed by (b) protonation reaction of $F^{\cdot-}$ radical anion by phenol (10), then followed by a homogeneous electron transfer (11) and finally rapid protonation of the resulting carbanion (12). The electroreduction scheme can be represented as

$$F + e \rightleftharpoons F^{\cdot-} \quad (9)$$

$$F^{\cdot-} + PhOH \longrightarrow F\cdot\text{-}H + PhO^- \quad (10)$$

$$F\cdot\text{-}H + F^{\cdot-} \rightleftharpoons F\text{-}H^- + F \quad (11)$$

$$F\text{-}H^- + PhOH \longrightarrow F\text{-}H_2 + PhO^- \quad (12)$$

This work has been performed at The University of Leeds, England. The author wishes to thank Dr. N. Taylor for the provision of facilities.

References

1) M. E. Peover, "Electroanalytical Chemistry," ed by A. J. Bard, Vol. 2, Marcel Dekker, New York (1967). pp. 1—29.

2) R. Dietz, "Organic Electrochemistry," ed by M. Baizer, Marcel Dekker, New York (1973), pp. 253—262.

3) C. Amatore and J. M. Saveant, *J. Electroanal. Chem.*, **107**, 353 (1980). and Refs. therein.

4) H. A. Sharifian and S. Park, *J. Electroanal. Chem.*, **143**, 337 (1983).

5) A. J. Fry and A. Schuettenberg, *J. Org. Chem.*, **39**, 2452 (1974).

6) D. D. Perrin, W. L. Armarego, and D. R. Perrin, "Purification of Laboratory Chemicals," Pergamon Press, Oxford, London (1966), p. 143.

7) A. J. Bard and L. R. Faulkner, "Electrochemical Methods, Fundamentals and Applications," John Wiley, Sons INC. New York, Chichester, Brishane, Toronto (1980), pp. 218, 219.

8) R. S. Nicholson and I. Shain, *Anal. Chem.*, **36**, 706 (1964).

9) V. D. Parker, *Acta Chem. Scand., Ser. B* **35**, 259 (1981).

10) V. D. Parker, *Acta Chem. Scand., Ser. B* **35**, 349 (1981).

The Fast and Selective Reduction of Organic Halides by Lithium Hydrotri-s-butylborate

Sunggak KIM* and Kyu Yang YI

Department of Chemistry, Korea Advanced Institute of Science and Technology, Seoul 131, Korea

(Received January 17, 1984)

Synopsis. Lithium hydrotri-*s*-butylborate is shown to be a powerful reducing agent in its reducing abilities toward organic halides and discriminates structurally different organic halides due to the bulkiness of the reagent. Essentially complete utilization of the hydride of the reagent for the reduction of organic halides is also of synthetic significance.

The reductive dehalogenation of organic halides, one of the most fundamental reactions in organic chemistry, is often accomplished by various hydrido complex reducing agents.[1] Among many hydrido complex reducing agents for this purpose, lithium hydrotriethylborate has enjoyed its role as a source of an exceptionally powerful nucleophilic hydride in displacement reaction with organic halides after its discovery in 1973 by Brown.[2]

Although lithium hydrotri-*s*-butylborate, belonging to hydrotrialkylborates along with lithium hydrotriethylborate, has been widely used in the stereoselective reduction of cyclic and bicyclic ketones,[3] the reactivity of lithium hydrotri-*s*-butylborate toward organic halides has not been investigated. Furthermore, it was our purpose to explore the possibility of utilizing the bulkiness of the reagent for selective reduction of a variety of structurally different organic halides.

Results and Discussion

Reductions were usually carried out in tetrahydrofuran at 25 °C under nitrogen using equimolar amounts of the reagent and the substrate and reaction mixtures were maintained at 0.25 M (1 M=1 mol dm^{-3}) in the substrate and 0.25 M in the reagent unless specified. The rate of reduction was followed by GLC at appropriate intervals of time and the yield was determined by GLC using an internal standard.

First, the reactivity of lithium hydrotri-*s*-butylborate toward 1-chlorooctane was examined in order to compare with that of lithium hydrotriethylborate. Employment of 2 molar equiv of each reagent allowed complete reduction of 1-chlorooctane into octane in 4 h, indicating that the reactivity achieved with lithium hydrotri-*s*-butylborate is comparable to lithium hydrotriethylborate.[2]

It has been known that the reaction of alkyl halides with equimolar amounts of lithium hydrotriethylborate proceeds rapidly up to 50%, with further reaction being sluggish probably due to the formation of lithium hydrotriethylborate-triethylborane complex during the reduction.[4] Thus, 2 molar equiv of lithium hydrotriethylborate are required for every molar equiv of alkyl halide for the complete reduction. This phenomenon has been observed with other hydride reducing agents such as sodium borohydride[5] and lithium hydrotrimethoxyaluminate.[6] Since it is expected that the bulkiness of lithium hydrotri-*s*-butylborate would prevent the formation of lithium hydrotri-*s*-butylborate-tri-*s*-butylborane complex, the reagent was reacted with equimolar amounts of 1-chlorooctane. Indeed, the reaction proceeded smoothly, yielding octane in 78, 85, and 94% yield in 2, 4, and 8 h, respectively.

Encouraged by these results, we examined various alkyl halides with equimolar amounts of lithium hydrotri-*s*-butylborate in tetrahydrofuran at 25 °C in order to establish its effectiveness in reduction of organic halides. Simple primary alkyl halides such as 1-iodododecane and 1-bromododecane were almost instantly reduced to dodecane, whereas 1-bromooctane was generally inert toward the reagent at −78 °C and only 5% of 1-bromooctane was reduced to octane in 4 h. Thus, the reagent may be valuable for selective reduction of other readily reducible functional groups such as ketones and esters at −78 °C without simultaneous reduction on alkyl halides including relatively reactive primary alkyl bromides. Simple primary benzylic and allylic halides were rapidly and quantitatively reduced to the corresponding hydrocarbons, whereas secondary benzylic halides required longer reaction times as shown in Table 1. The simple secondary alkyl bromide like 2-bromooctane was reduced at a reasonable rate at 25 °C, whereas 2-chlorooctane was generally inert to the reagent. More sterically hindered cycloalkyl bromides such as cyclohexyl bromide and *exo*-2-bromonorbornane were extremely resistant to reduction. The analysis revealed 11% reduction of cyclohexyl bromide and the inertness of *exo*-2-bromonorbornane at 25 °C in 24 h. Unlike lithium hydrotriethylborate,[2] the low reactivity toward sterically hindered cycloalkyl bromides is attributed to the bulkiness of the reagent. The reduction of tertiary alkyl bromides did not occur and resulted predominantly in elimination in the case of 3-bromo-3-ethylheptane. Furthermore, the reagent was inert toward aryl halide like 1-bromonaphthalene at 25 °C in 24 h.

Since essentially complete utilization of the hydride of the reagent toward relatively reactive organic halides and the low reactivity toward sterically hindered organic halides have been observed in the reduction of organic halides, it is expected that employment of a stoichiometric amount of the reagent may permit selective reduction of structurally different organic halides. For selective reductions, equimolar amounts of two different organic halides were allowed to compete for a limited quantity of the reagent (1 molar equiv) at 25 °C and the results were determined by GLC analysis. 1-Bromododecane was selectively reduced to dodecane (98%) in the presence of 1-chlorooctane (1% reduction) for 5 min, whereas 1-bromododecane was selectively reduced to dodecane (96%) in the presence of 2-bromooctane (4% reduction) under the same reaction

Table 1. Reduction of organic halides with $Li[BH(s\text{-}Bu)_3]$ in THF at 25 °C[a]

Substrate	Time	Product	Yield/%[b]
1-Iodododecane	2 min	Dodecane	100
1-Bromododecane	2 min	Dodecane	99
Benzyl bromide	2 min	Toluene	100
Cinnamyl bromide	2 min	β-Methylstyrene	99
Benzyl chloride	10 min	Toluene	98
α-Methylbenzyl bromide	30 min	Ethylbenzene	99
Benzhydryl bromide	1 h	Diphenylmethane	97
1-Chlorooctane	8 h	Octane	94
1-Chlorododecane	8 h	Dodecane	90
2-Bromooctane	24 h	Octane	56
Cyclohexyl bromide	24 h	Cyclohexane	11
2-Chlorooctane	24 h	Octane	2
3-Bromo-3-ethylheptane	24 h	3-Ethylheptane	0[c]
1-Bromoadamantane	24 h	Adamantane	0
exo-2-Bromonorbornane	24 h	Norbornane	0 (5)[d]
1-Bromonaphthalene	24 h	Napthalene	0

a) The solutions were 0.25 M in the substrate and 0.25 M in the reagent. b) The yields were determined by GLC using internal standards. c) Elimination products (60%) were observed. d) The reduction was carried out at 65 °C for 24 h.

conditions. Similarly, benzyl bromide was selectively reduced to toluene (98%) without simultaneous attack on α-methylbenzyl bromide (2% reduction) at 25 °C for 5 min. However, the selectivity was somewhat decreased in the reduction of organic halides containing two bromo substituents in a molecule. 1,2-Dibromononane was reduced to a 84 : 10 mixture of 2-bromononane and nonane along with 5% of the unreacted original halide at 25 °C in 30 min.

Experimental

Lithium hydrotri-*s*-butylborate in THF was purchased from Aldrich Chemical Co. The hydride concentration (0.90 M) was determined by removing a known aliquot with a hypodermic syringe, hydrolyzing with a THF–water–glycerol mixture (1 : 1 : 1) at room temperature and measuring the hydrogen evolved. Tetrahydrofuran was distilled from sodium benzophenone under nitrogen. All glasswares were dried in a drying oven and cooled under nitrogen. All reduction experiments were carried out under nitrogen, and hypodermic syringes were used to transfer the solutions.

GLC analysis was performed on a Varian 2800 gas chromatograph with an FID detector. All analyses were carried out on 7 ft × 0.125 in† or 4 ft × 0.125 in 5% SE-30 on Chromosorb W columns.

Since the reactions performed are all similar in many respects, typical reactions will be described as specific examples.

Reduction of 1-Chlorooctane with Equimolar Amounts of Li[BH(s-Bu)$_3$] in THF. A 25 ml oven-dried flask with a magnetic stirring bar and a rubber septum under a balloon-filled atmosphere of nitrogen was immersed in a water bath at 25 °C. Then a solution of lithium hydrotri-*s*-butylborate (2.2 ml of a 0.90 M solution, 2.0 mmol) in THF was injected into the reaction flask by a hypodermic syringe, followed by the addition of a solution of decane (2.0 mmol) in THF (2.8 ml) as an internal standard. Finally, a solution of 1-chlorododecane (2.0 mmol) in THF (3 ml) was added and the reaction mixture was stirred at 25 °C. After 30 min, the reaction mixture was withdrawn with a syringe, quenched with water, extracted with ether, and analyzed by GLC. Analysis revealed the presence of 49% of octane. Similarly, aliquots were removed after 1, 2, 4, and 8 h and analyzed by GLC. Analysis revealed the presence of octane in 61, 78, 85, and 94 %, respectively.

Selective Reduction of 1-Bromododecane in the Presence of 2-Bromooctane with Li[BH(s-Bu)$_3$] in THF. A 25 ml oven-dried flask with a magnetic stirring bar and a rubber septum under a balloon-filled atmosphere of nitrogen was immersed in a water bath at 25 °C. Then a solution of 1-bromododecane (2.0 mmol) in THF (2.8 ml) was injected, followed by the addition of a solution of 2-bromooctane (2.0 mmol) and decane (2.0 mmol) in THF (2.8 ml). A solution of lithium hydrotri-*s*-butylborate (2.2 ml of a 0.90 M solution, 2.0 mmol) in THF was slowly added to the reaction flask for 1 min and the reaction mixture was stirred for an additional 4 min at 25 °C. The reaction mixture was quenched with water, extracted with ether, and analyzed by GLC. Analysis revealed the presence of 96% dodecane and 4% octane along with 4% 1-bromododecane and 95% 2-bromooctane.

This work was financially supported by a grant from Korea Science and Engineering Foundation.

References

1) For a recent review: A. R. Pinder, *Synthesis* **1980**, 425, and references cited therein.
2) H. C. Brown and S. Krishnamurthy, *J. Am. Chem. Soc.*, **95**, 1669 (1973).
3) H. C. Brown and S. Krishnamurthy, *J. Am. Chem. Soc.*, **94**, 7159 (1972).
4) H. C. Brown, A. Khuri, and S. Krishnamurthy, *J. Am. Chem. Soc.*, **99**, 6237 (1977).
5) H. C. Brown and P. Tierney, *J. Am. Chem. Soc.*, **80**, 1552 (1958).
6) S. Krishnamurthy and H. C. Brown, *J. Org. Chem.*, **45**, 849 (1980).

† 1 ft = 0.30479 m, in = 2.54×10^{-2} m

Synthesis of 4-(1,5,9-Trimethyl-1-vinyl-4,8-decadienyl)catechol Dimethyl Ether

Ramesh Chander ANAND* and Harish RANJAN

Department of Chemistry, Indian Institute of Technology, Hauz Khas, New Delhi 110016, India

(Received January 23, 1984)

Synposis. Synthesis of 4-(1,5,9-trimethyl-1-vinyl-4,8-decadienyl)catechol dimethyl ether has been described utilizing Wittig reaction for the introduction of vinylic substituent at the quaternary carbon.

4-(1,5,9-Trimethyl-1-vinyl-4,8-decadienyl)catechol (**I**), a C_{21} terpenoid with novel structure has recently been isolated[1] from the hexane extracts of the roots and leaves of *Potomorphe umbellata (L)* Miq (Piperaceae*) by Kijjoa and coworkers. It has been assigned constitution (**I**) on the basis of spectroscopic studies.

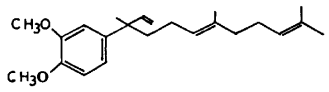

(I) R=H
(Ia) R=CH3

In the present paper we wish to report a synthesis of 4-(1,5,9-trimetyl-1-vinyl-4,8-decadienyl)catechol dimethyl ether and thus corroborate the structure assigned to (**I**).

4-(1,5,9-Trimethyl-1-vinyl-4,8-decadienyl) catechol dimethyl ether (**Ia**) could be synthesized using 2-(3,4-dimethoxyphenyl)ethanenitrile (**II**) as the suitable starting compound and Wittig reaction for the introduction of vinylic substituent at the quaternary carbon-1. The scheme of the synthesis is given below: 2-(3,4-Dimethoxyphenyl)ethanenitrile (**II**) was subjected to alkylation with 9-bromo-2,6-dimethyl-2,6-nonadiene[2] in the presence of NaH-DME. The quaternary carbon could conveniently be generated by methylation of alkylated nitrile (**III**) with CH_3I in NaH-HMPA mixture. Grignard reaction of CH_3MgI on nitrile (**IV**) followed by acid hydrolysis of the crude product afforded a complex mixture as indicated by TLC. IR also did not show any significant absorption in the carbonyl region. However, nitrile(**IV**) could be converted into vinyl group through multi-step sequence of reactions (**IV**→**Ia**).

Alkaline hydrolysis of 2-(3,4-dimethoxyphenyl)-2,6,10-trimethyl-5,9-undecadienenitrile (**IV**) furnished the acid (**V**) which was esterified with CH_3I in NaH-DMF. LAH reduction of the ester (**VI**) gave the corresponding alcohol. Pyridinechlorochromate oxidation of the alcohol (**VII**) generated the aldehyde (**VIII**) which on submission to methylenetriphenylphosphorane resulted in the formation of 4-(1,5,9-trimethyl-1-vinyl-4,8-decadienyl)catechol dimethyl ether. IR and NMR of this product is in good agreement with the data reported by Kijjoa and coworkers'.

Experimental

Boiling points are uncorrected. IR spectra were recorded on Pye Unicam SP 1200 or Perkin-Elmer IR spectrophotometer. Thin liquid films were used in NaCl or KBr optics. NMR spectra were recorded in CCl_4 or $CDCl_3$ at 60 MHz Varian A60D, 90 MHz Perkin Elmer spectrometer or 100 MHz JNM-FX 100 FT-NMR spectrometer (JEOL). TMS was used as internal standard. Anhydrous Na_2SO_4 was used as drying agent. DMSO and HMPA were dried over CaH_2 and DME was dried over LAH.

2-(3,4-Dimethoxyphenyl)ethanenitrile (II). To a suspension of $SOCl_2$ (8 ml) and powdered $CaCl_2$ (0.5 g) at 35 °C was added 3,4-dimethoxybenzyl alcohol (15.0 g, 0.083 mol) in benzene (15 ml) in 1 h whereupon ether (25 ml) and $CaCO_3$ (1 g) were added. After stirring for overnight, the excess reagent was decomposed by cold water (120 ml) and then worked up in the usual manner. The solvent was distilled off and the residue was refluxed with a mixture of benzene (20 ml), NaCN (8.5 g) and water (40 ml) for 6 h. The solvent was washed with water and dried. The solvent was distilled off and the residual oil was fractionated *in vacuo* to afford nitrile (**II**, 7.7 g) in 52.7 % yield, bp 131—132 °C/2 mm, R_f 0.59 (C_6H_6 : EtOAc 9 : 1). IR: ν_{max} 2255, 1520, 1460, 1385, 1162, 1148, 1030, 810, 768, 745 cm^{-1}. NMR: δ=3.6(2H, s), 3.84 (6H, s), 6.76 (3H, s). Found: C, 68.12; H, 6.74; N, 8.1 $C_{10}H_{11}O_2N$ requires C, 67.78; H, 6.26; N, 7.9%.

2-(3,4-Dimethoxyphenyl)-6,10-dimethyl-5,9-undecadienenitrile (III). 2-(3,4-Dimethoxyphenyl)ethanenitrile (II, 2.0 g,

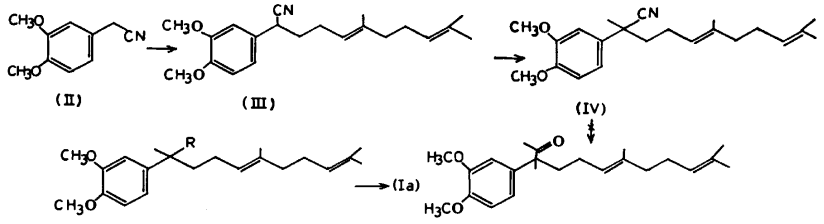

(II) (III) (IV) (Ia)

(V) R=COOH
(VI) R=COOCH3
(VII) R=CH2OH
(VIII) R=CHO

* Also known as pariparoba or Caapeba and used in Brazil as popular medicine for the treatment of liver diseases or epilepsy.

0.011 mol) dissolved in DME (5 ml) was added to a stirred suspension of NaH (50 %, 0.625, 0.013 mol) in DME (8 ml) under N_2. After stirring for 1 h, a solution of 9-bromo-2,6-dimethyl-2,6-nonadiene (2.77 g, 0.012 mol) in DME (6 ml) was added to the reaction mixture. It was stirred overnight at room temperature and then heated at 50 ° for 5h. After cooling, it was poured into ice cold water (120 ml). The reaction mixture was extracted with ether (3×40 ml). The combined organic extracts were washed with brine and dried. The solvent was evaporated and the residue chromatographed on silica gel (120 g). The desired product (**III**, 1.4 g) was obtained from the elute with benzene in 40 % yield. R_f 0.76 (C_6H_6–EtOAc 9 : 1). IR: ν_{max} 2245, 1622, 1605, 1530, 1460, 1428, 1272, 1248, 1150, 1032, 850, 810, 765, 640 cm^{-1}. NMR: δ=1.56(6H, s), 1.68(3H, s), 1.8—2.16(8H, m), 3.64(1H, t, J=7 Hz), 3.84(6H, s), 5.08—5.16(2H, m), 6.76(3H, br). Found: C, 77.40; H, 9.20; N, 3.99. $C_{21}H_{29}O_2N$ requires C, 77.02; H, 8.93; N, 4.28%.

2-(3,4-Dimethoxyphenyl)-2,6,10-trimethyl-5,9-undecadienenitrile (IV). To a stirred and cooled solution of NaH(50%, 0.145 g, 3.0 mmol) in HMPA(6 ml) under N_2 atmosphere was added alkylated nitrile (**III**, 0.8 g, 2.4 mmol) dissolved in HMPA (8 ml) dropwise. It was stirred at room temperature for 1 h followed by dropwise addition of a solution of CH_3I (0.710 g, 5.0 mmol) in HMPA (4 ml) at room temperature. After stirring overnight, it was warmed to 60 °C for 2 h. Ice cold water (50 ml) was added to the reaction mixture and extracted with ether (4×25 ml). The combined ether extracts were washed with water (3×25 ml) and dried. The solvent was distilled and residual oil chromatographed on silica gel (60 g). The desired product was obtained with petroleum ether–benzene (2 : 8) as a light yellow oil (**IV**, 0.630 g) in 77% yield; R_f 0.78 (C_6H_6–EtOAc 9 : 1). IR: ν_{max} 2248, 1612, 1530, 1460, 1428, 1398, 1272, 1250, 1155, 1032, 850, 820, 730 cm^{-1}. NMR: δ=1.49(3H, s), 1.56(6H, s), 1.6—2.12(11H, m), 3.86(6H, s), 5.02—5.16(2H, m), 6.78—6.86(3H, m). Found: C, 77.82; H, 9.20; N, 4.33. $C_{22}H_{31}O_2N$ requires C, 77.37; H, 9.15; N, 4.1%.

Reaction of 2-(3,4-Dimethoxyphenyl)-2,6,10-trimethyl-5,9-undecadienenitrile (IV) with Methylmagnesium Iodide. Methylmagnesium iodide was prepared from Mg(0.1 g, 4.2 mmol) and CH_3I(0.596 g, 4.2 mmol) in ether (30 ml). To this chilled solution was added nitrile (**IV**, 0.5 g, 1.4 mmol) in ether (8 ml) with stirring. The resulting mixture was allowed to stir at room temperature overnight and then refluxed for 6 h. The reaction mixture was cooled and acidified with HCl (10%, 25 ml). After working up in the usual manner, it was dried and solvent removed. TLC of the residual oil showed it to be a complex mixture difficult to separate and IR did not show any significant absorption in carbonyl region.

2-(3,4-Dimethoxyphenyl)-2,6,10-trimethyl-5,9-undecadienoic Acid (V). To a mixture or NaOH (1.5 g) in aqueous ethanol (60%, 8 ml) was added alkylated nitrile (**IV**, 0.6 g, 1.7 mmol). The reaction mixture was heated to reflux for 26 h with stirring. After cooling the reaction mixture was poured into ice cold water (75 ml) and unreacted nitrile was extracted with ether (3×50 ml). Aqueous phase was acidified with dil HCl (20%, 30 ml) to pH ≈2. It was saturated with NaCl and extracted with ether (5×20 ml). The combined organic phase was washed with brine (3×25 ml) and dried. The solvent was evaporated and the residual oil was chromatographed on silica gel (50 g). The pure acid (**V**, 0.530 g) was procured through benzene–ethyl acetate (8 : 2) as the eluent in 86.6% yield; R_f 0.36 (C_6H_6–EtOAc 9 : 1). IR: ν_{max}. 3520—3080, 1710, 1630, 1598, 1520, 1462, 1452, 1278, 1140, 1030, 830, 742 cm^{-1}. NMR: δ=1.34(3H, s), 1.56(6H, s), 1.62(3H, s), 1.8—2.1(6H, m), 2.64(2H, m), 3.82(6H, s), 4.98—5.0(2H, m), 6.74—6.84(3H, m), 10.79 (1H, s). Found: C, 73.40; H, 8.88. $C_{22}H_{33}O_4$ requires C, 73.30; H, 8.95%.

Methyl 2-(3,4-Dimethoxyphenyl)-2,6,10-trimethyl-5,9-undecadienoate (VI). To a stirred suspension of NaH (50%, 0.067 g, 1.4 mmol) in DMF (4 ml) was added acid (**V**, 0.450 g, 1.2 mmol) in DMF (3 ml). After 30 min, a solution of CH_3I (0.340 g, 2.4 mmol) in DMF (4 ml) was added to the resulting solution. The reaction mixture was quenched by adding it to ice cold water(60 ml). It was extracted with ether (3×50 ml) and the organic layer was washed with brine (2×30 ml) and dried. The solvent was removed and oil left behind was purified by PLC in benzene–hexane (9 : 1) to give the ester (**VI**, 0.452 g) in 96.7% yield; R_f 0.6 (C_6H_6–EtOAc 9 : 1). IR: ν_{max} 1738, 1598, 1525, 1460, 1280, 1145, 1105, 1030, 820, 805 cm^{-1}. NMR: δ=1.29(3H, s), 1.56(6H, s), 1.64(3H, s), 1.66—1.88(6H, m), 2.56(2H, br), 3.6(3H, s), 3.78(6H, s), 4.96(2H, m), 6.64(3H, m). Found: C, 74.20; H, 9.00. $C_{23}H_{34}O_4$ requires C, 73.46; H, 9.15%.

2-(3,4-Dimethoxyphenyl)-2,6,10-trimethyl-5,9-undecadien-1-ol (VII). A solution of ester (**VI**, 0.4 g, 1.0 mmol) in ether (8 ml) was added dropwise at room temperature to a slurry of LAH (0.152 g, 4.0 mmol) in ether (15 ml). After refluxing for 6 h, it was decomposed with NaOH (2%, 20 ml), and worked up in the usual way. The solvent was evaporated and the residual oil was purified by PLC in benzene–ethyl acetate (9 : 1) to get the pure alcohol (**VII**, 0.28 g) in 80.9% yield; R_f 0.39 (C_6H_6–EtOAc 9 : 1). IR: ν_{max} 3560—3240, 1615, 1525, 1480—1460, 1422, 1270, 1165, 1038, 840, 790, 770 cm^{-1}. NMR: δ=1.28(3H, s), 1.56(6H, s), 1.64(3H, s), ≈1.94(6H, br), 2.28(2H, m), ≈3.6(2H, br), 3.8(6H, s), 4.96(2H, m), 6.64(3H, m). Found: C, 76.34; H, 9.40. $C_{22}H_{34}O_3$ requires C, 76.26; H, 9.89%.

2-(3,4-Dimethoxyphenyl)-2,6,10-trimethyl-5,9-undecadienal (VIII). PCC oxidation of alcohol (**VIII**, 0.2 g, 0.57 mmol) was carried out using PCC(0.170 g), fused NaOAc (0.015 g) in CH_2Cl_2 (30 ml) to afford the aldehyde (**VIII**, 0.172 g) in 87.7% yield; R_f 0.42(C_6H_6–EtOAc 9 : 1). IR: ν_{max} 2728, 1735, 1630, 1525, 1460, 1278, 1268, 1032, 828, 805 cm^{-1}.

3-(3,4-Dimethoxyphenyl)-3,7,11-trimethyl-1,6,10-dodecatriene (Ia). Reaction of aldehyde (**VIII**) with methylenetriphenylphosphorane was carried with NaH (50%, 0.052 g, 1.1 mmol) in DMSO (2.2 ml), methyltriphenylphosphonium iodide (0.458 g, 1.2 mmol) in DMSO(4.2 ml) under N_2 atmosphere. To this solution was added aldehyde (**VIII**, 0.160 g, 0.46 mmol) in DMSO (4 ml) at 10 °C. It was worked up in the usual manner and then chromatographed over silica gel (75 g). The desired product was obtained in petroleum ether–benzene (8 : 2). This was followed by PLC in benzene–hexane (6 : 4) to afford 4-(1,5,9-trimethyl-1-vinyl-4,8-decadienyl)catechol dimethyl ether (**Ia**, 0.066 g) in 42% yield; R_f 0.71 (C_6H_6–EtOAc 9.5 : 0.5). IR: ν_{max} 3110, 1600, 1518, 1447, 1378, 1280, 1128, 1020, 920, 850, 800, 760, 660 cm^{-1}. NMR: δ=1.3 (3H, s, CH_2=CH–C–C$\underline{H}_3$), 1.58[6H, s, –CH=C(C$\underline{H}_3$)$_2$], 1.67 (3H, s, C$\underline{H}_3$–C=CH–), 1.7—2.35 [8H, m, –(C$\underline{H}_2$)$_2$–CH=C(C$\underline{H}_2$)$_2$=C(CH$_3$)$_2$], 3.86 (6H, s, 2× aromatic OCH$_3$), 5.08 [4H, br, –CH=C$\underline{H}_2$ plus –C=C$\underline{H}$–plus–C$\underline{H}$=C(CH$_3$)$_2$], 5.92 (1H, br, –C$\underline{H}$=CH$_2$), 6.72 (3H, m, aromatic protons). Found: C, 81.10; H, 10.24. $C_{23}H_{34}O_2$ requires C, 80.65; H, 10.01%.

References

1) A. Kijjoa and A. M. Giesbrecht, *Planta Medica*, **39**, 85 (1980).
2) D. Barnard and L. Bateman, *J. Chem. Soc.*, **1950**, 926.

Synthesis and Characterization of Hydrazone and Azine Derivatives of Bis(cyclopentadienyl)titanium(IV)

Brij KHERA, Anand Kumar SHARMA, and Narender Kumar KAUSHIK*
Department of Chemistry, University of Delhi, Delhi-110007, India
(Received January 25, 1984)

Synopsis. Pentacoordinated hydrazone and azine derivatives of bis(cyclopentadienyl)titanium(IV) of the type $[(OC_6H_4CR:NNHR')TiCl(Cp)_2]$ and $[(OC_6H_4CR'':NN:CR''C_6H_4O)Ti(Cp)_2]$, where R=H or CH_3, R'=H, C_6H_5 or $C_6H_3(NO_2)_2$ and R''=H or CH_3, have been prepared. The products were characterized by chemical analyses, electrical conductance, IR, ^1H NMR, and electronic spectral studies.

Some hydrazone complexes and a few azine complexes of titanium have been studied.[1-4] However, no systematic study on their organometallic derivatives is available. In view of the versatile chelating ability, widespread applications and lack of data involving organometallic derivatives of titanium, it has been considered of interest to study the reactions of Cp_2TiCl_2 with the title ligands.

Experimental

Physical Measurements. Conductance measurements were made in DMSO on a Systronic Digital Direct Reading Conductivity Meter Type 304. Solid state IR spectra were recorded in KBr pellets in the 4000—200 cm^{-1} region on a Perkin-Elmer 621 grating spectrophotometer. ^1H NMR spectra were recorded in deuterated chloroform on a JEOL JNM-FX 200 Fourier Transform NMR spectrometer. Chemical shifts are expressed relative to an internal reference of TMS (1% by volume). The electronic spectra of these complexes were run on a Perkin-Elmer 4000 Å instrument.

Preparation of the Ligands. Hydrazones of salicylaldehyde and 2'-hydroxyacetophenone were prepared by the gradual addition of salicylaldehyde/2'-hydroxyacetophenone to the ethanolic solution of hydrazine hydrate, phenylhydrazine or 2,4-dinitrophenylhydrazine in equimolar ratio. Due to insoluble nature of 2,4-dinitrophenylhydrazine in ethanol, a minimum quantity of sulfuric acid was added into its ethanolic suspension to make its homogeneous solution. The mixture was stirred under reflux for half an hour and then cooled in an ice bath. The precipitate so obtained was filtered, washed with ethanol and recrystallized from hot ethanol or glacial acetic acid in case of 2,4-dinitrophenylhydrazone derivatives.

Azines were synthesized by the condensation reaction of salicylaldehyde or 2'-hydroxyacetophenone with hydrazine hydrate in 2 : 1 molar ratio in ethanol and the products were isolated in a similar manner as described for the hydrazones.

Preparation of Complexes. To a stirred solution of bis(cyclopentadienyl)titanium(IV)dichloride, $(Cp)_2TiCl_2$ (8 mmole) in 30 ml tetrahydrofuran, a solution containing 8 mmole of appropriate hydrazone or azine in 30 ml tetrahydrofuran was added slowly and the reaction mixture was refluxed for 10—12 h. It was then filtered and the volume of the filtrate was reduced to *ca.* 20 ml by evaporating the solvent under reduced pressure. The crystals of the product were precipitated by adding 80 ml petroleum ether (60—80 °C) to the concentrated filtrate. These were filtered, washed with petroleum ether and dried under vacuum. Recrystallized from dichloromethane by adding excess of petroleum ether.

Results and Discussion

The reactions involved in the preparation of hydrazone and azine derivatives of bis(cyclopentadienyl)-titanium(IV) may be represented according to equations 1 and 2, respectively as shown below:

$$(Cp)_2TiCl_2 + (HO)C_6H_4CR:NNHR' \xrightarrow[68\,°C]{THF} [(OC_6H_4CR:NNHR')TiCl(Cp)_2] + HCl \quad (1)$$

$$(Cp)_2TiCl_2 + (HO)C_6H_4CR'':NN:CR''C_6H_4(OH) \xrightarrow[68\,°C]{THF} [(OC_6H_4CR'':NN:CR''C_6H_4O)Ti(Cp)_2] + 2HCl \quad (2)$$

where R=H or CH_3, R'=H, C_6H_5 or $C_6H_3(NO_2)_2$ and R''=H or CH_3.

Table 1 lists the analytical data and physical characteristics of the complexes. The satisfactory elemental analyses support the stoichiometry assigned to these complexes. These are moderately soluble in chloroform, dichloromethane, acetone, THF and DMSO. Electrical conductance measurements in DMSO show these complexes to be non-electrolytes.

Infrared Spectra. Absorption bands indicating the presence of cyclopentadienyl groups are found at ca. 3100 cm^{-1} ν(C–H), 1450 cm^{-1} ν(C–C), 1025 cm^{-1} ν(C–H) in plane and 810 cm^{-1} ν(C–C) out of plane.[5] Apart from this, the band at 445 cm^{-1} may be assigned to ν(Ti–C_5H_5) vibrations.[6]

A strong band (due to the azomethine, >C=N– group)[7,8] at *ca.* 1630 cm^{-1} in the spectra of free hydrazone ligands is shifted to lower wave numbers (*ca.* 1600 cm^{-1}) in the complexes studied, showing the coordination of azomethine nitrogen to the metal.[9,10] The N–N frequency found at ≈940 cm^{-1} in the free ligands is shifted to higher value (≈970 cm^{-1}).

A high intensity band at *ca.* 1265 cm^{-1} in the free hydrazone ligands may be assigned to the phenolic C–O stretching.[7,8] In the complexes this band appears at ≈1290 cm^{-1}, indicating bonding of the hydrazone ligand through oxygen. Furthermore, ν(OH) band in the 3450—3390 cm^{-1} region disappears in the hydrazone complexes.

The coordination of methine nitrogen and bonding of the phenolic oxygen to the metal is supported by the appearance of two new absorption bands in the spectra of hydrazone derivatives at *ca.* 530—550 cm^{-1} and 430—470 cm^{-1}, which may be assigned to ν(Ti←N) and ν(Ti–O) vibrations,[2] respectively. Band at *ca.* 380 cm^{-1} is the characteristic of ν(Ti–Cl) vibration.[11]

TABLE 1. ANALYTICAL DATA AND PHYSICAL CHARACTERISTICS OF $[(OC_6H_4CR:NNHR')TiCl(Cp)_2]$ AND $[(OC_6H_4CR'':NN:CR''C_6H_4O)Ti(Cp)_2]$

R, R′ or R″	Yield/%	Colour	Decomp temp °C	Found (Calcd) %				
				C	H	Ti	N	Cl
R=H, R′=H	62	Yellow	146—148	58.32 (58.55)	4.72 (4.88)	13.38 (13.75)	7.96 (8.04)	10.08 (10.19)
R=H, R′=C_6H_5	60	Yellowish brown	152—155	65.19 (65.03)	4.74 (4.95)	11.07 (11.29)	6.51 (6.60)	8.13 (8.36)
R=H, R′=$C_6H_3(NO_2)_2$	78	Red	144—145	53.82 (53.65)	3.84 (3.69)	9.04 (9.31)	10.95 (10.89)	6.73 (6.90)
R=CH_3, R′=H	70	Pinkish red	186—187	59.46 (59.60)	5.00 (5.24)	13.09 (13.22)	7.59 (7.73)	9.64 (9.79)
R=CH_3, R′=C_6H_5	68	Yellowish brown	178—181	65.48 (65.69)	5.42 (5.25)	10.62 (10.93)	6.32 (6.39)	8.16 (8.10)
R=CH_3, R′=$C_6H_3(NO_2)_2$	73	Orange	168—170	54.74 (54.50)	4.13 (3.97)	8.61 (9.06)	10.46 (10.60)	6.81 (6.72)
R″=H	68	Light brown	156—157	69.12 (69.25)	4.67 (4.81)	11.20 (11.52)	6.70 (6.73)	—
R″=CH_3	65	Yellowish brown	142—143	70.07 (70.29)	5.30 (5.41)	10.67 (10.79)	6.16 (6.31)	—

As expected, the spectra of the azine complexes do not show ν(OH), ν(NH), and ν(Ti-Cl) vibrations. The splitting and lowering of the ν(C=N) vibration suggests the coordination of one of the methine nitrogens and hence the formation of two dissimilar rings. The ν(C-O) phenolic shifts to a higher frequency and ν(Ti←N) and ν(Ti-O) vibrations appear as a result of complex formation.

Proton Magnetic Resonance Spectra. All the hydrazone compounds give four different resonance signals corresponding to (i) C_5H_5 ring protons, which appear as a sharp singlet at *ca.* δ=6.40, (ii) the -CR=N- group proton(s), appearing at *ca.* δ=8.60 (R=H); δ=3.00 (R=CH_3), show a downfield shift as compared to the corresponding free hydrazone ligands *ca.* δ=8.40 (R=H), δ=2.75 (R=CH_3), indicating deshielding as a result of coordination through the nitrogen to titanium, (iii) aromatic protons, which appear as a multiplet at ca. δ=6.70—7.80, also show a downfield shift as compared to the corresponding signals in the free ligands (observed at *ca.* δ=6.60—7.50), further supporting the coordination of nitrogen of the azomethine group to the metal, (iv) the -NH- and $-NH_2$ protons (*ca.* δ=4.85 and δ=4.30, respectively) appear at the same positions as observed for the free hydrazone ligands.

The ^{1}H NMR spectra of the azine complexes show three different resonance signals corresponding to (i) C_5H_5 ring protons, (ii) -CR″=N- group proton(s), (iii) aromatic protons, and are quite similar to the ^{1}H NMR spectra of the hydrazone complexes.

Electronic Spectra. The electronic spectra of the complexes in chloroform exhibit a single band in the region 403—412 nm in accordance to the electronic configuration (n-1)d°, ns° of titanium.[11]

Based on analytical data, general behaviour and physicochemical studies, structure I and II may be proposed to the hydrazone and azine derivatives under investigation, respectively.

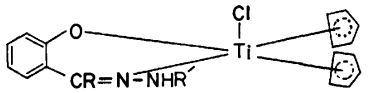

R=H or CH_3; R′=H, C_6H_5 or $C_6H_3(NO_2)_2$

I

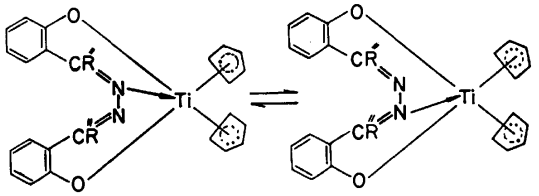

R′=H or CH_3

II

This work was supported by the Council of Scientific and Industrial Research, New Delhi as Research Fellowship awards to B. K. and A. K. S.

References

1) S. A. Pardhy, S. S. Deshpande, S. Gopinathan, and C. Gopinathan, *Indian J. Chem.* A, **21**, 173 (1982).
2) S. A. Pardhy, S. Gopinathan, and C. Gopinathan, *Synth. React. Inorg. Met. -Org. Chem.*, **13**, 385 (1983).
3) H. A. Patwardhan, S. Gopinathan, and C. Gopinathan, *Indian J. Chem.* A, **16**, 224 (1978).
4) S. A. Pardhy, S. Gopinathan, and C. Gopinathan, *Indian J. Chem.* A, **22**, 73 (1983).
5) E. R. Lippincott and R. D. Nalson, *J. Chem. Phys.*, **21**, 1307 (1953).
6) R. S. P. Coutts and P. C. Wailes, *J. Organomet. Chem.*, **84**, 47 (1975).
7) A. K. Sharma, B. Khera, and N. K. Kaushik, *Monatsh. Chem.*, **114**, 907 (1983); *Synth. React. Inorg. Met.-Org. Chem.*, **13**, 491 (1983); *Indian J. Chem. A*, **22**, 816 (1983).
8) B. Khera, A. K. Sharma, and N. K. Kaushik, *Polyhedron*, **2**, 1177 (1983).
9) R. C. Aggarwal, N. K. Singh, and R. P. Singh, *Inorg. Chim. Acta*, **32**, L87 (1979).
10) A. Braibanti, F. Dallavalle, M. A. Pellinghelli, and E. Leporati, *Inorg. Chem.*, **7**, 1430 (1968).
11) A. K. Sharma, and N. K. Kaushik, *Synth. React. Inorg. Met.-Org. Chem.*, **11**, 685 (1981).

 © 1985 The Chemical Society of Japan Bull. Chem. Soc. Jpn., 58, 795—802 (1985)

Hydrogenation of Carbon Monoxide on CO Reducing Catalyst and Solid Acid (III). The Effect of the Pore Size and Acid Properties of Zeolite on the Product Distribution

Hitoshi SAIMA,* Kaoru FUJIMOTO, and Hiro-o TOMINAGA
Department of Synthetic Chemistry, Faculty of Engineering, University of Tokyo, Hongo, Bunkyo-ku, Tokyo 113
(Received June 7, 1984)

Synthesis gas reactions over hybrid catalysts composed of Pd/SiO_2 and zeolites and methanol conversion on the same zeolites were studied. The selectivities to aromatic hydrocarbons were about 30% for the methanol conversions over ZSM-5, de-aluminated mordenite, and de-aluminated Y type zeolite (DAY), which possess strong acid sites. When ZSM-5 or mordenites were combined with Pd/SiO_2 and subjected to synthesis gas conversion, the selectivities to aromatic hydrocarbons were between 10% and 30%. However, the synthesis gas reaction over the hybrid catalyst composed of Pd/SiO_2 and DAY, gave few aromatic hydrocarbons, but aliphatic paraffins with 2 to 6 carbon atoms. Over large pore zeolites like DAY, the diffusion of olefins is so quick that most of the olefins come out of pores to be hydrogenated to paraffins on the Pd/SiO_2 catalyst. In contrast, because of the slow diffusion of olefins in the medium size pores of ZSM-5 or mordenite, olefins stay in the pores for long enough to form aromatic hydrocarbons on the strong acid sites before being hydrogenated.

It has been reported that synthesis gas is converted over a mixture of Zn-Cr oxides or Zr oxide and ZSM-5 at a temperature of 427 °C and a pressure of 83 atm to produce gaseous and liquid hydrocarbons rich in aromatics.[1]

Such synthesis gas reactions over hybrid catalysts composed of methanol synthesis catalysts and zeolites can mitigate the thermodynamic constraint of methanol formation because of the successive conversion, *in situ*, of the methanol to hydrocarbons over the zeolites. When a Cu-Zn-Al methanol synthesis catalyst was used in combination with H-ZSM-5 or H-Y at 10—20 atom and 250—380 °C, aliphatic hydrocarbons with 3 to 6 carbon atoms were obtained with a high selectivity, but few aromatic hydrocarbons were formed.[2] In the case of reactions over a hybrid catalyst composed of Pd/SiO_2 and ZSM-5, polymethylbenzenes were obtained with a high selectivity.[2-3] Similar studies of hydrocarbon synthesis from synthesis gas over several hydrid catalysts containing Cu-Zn-Pd and Zn-Cr catalysts have also been reported.[4-5]

This study attempted to clarify the charateristic feature of various zeolites as components of the hydrid catalysts containing Pd/SiO_2 from the standpoint of the direct synthesis of aromatic hydrocarbons from synthesis gas and to elucidate the effects of the zeolite catalyst on the product distributions.

Experimental

Catalyst Preparation and the Synthesis Reaction. A Pd/SiO_2 catalyst (Pd 4wt%) was prepared by impregnating a commercially available silica gel (Fuji Davison ID; specific surface area: 270 m^2; pore volume: 1.1cc/g; mean pore diameter: 140 Å) with palladium chloride from its acidic aqueous solution by a dry up method. Then the catalyst precursor was dried in an air oven at 120 °C for 20 h and reduced in flowing hydrogen at 400 °C for 4 h.

Na-ZSM-5 type zeolite was synthesized according to the method described in the literature.[6] H-ZSM-5 was prepared from Na-ZSM-5 by ion-exchanging with hydrochloric acid (1 M=1 mol dm^{-3}) at 70 °C for a week, followed by drying at 120 °C for 20 h and calcining at 500 °C for 3 h. The crystallinity of ZSM-5 was measured by X-ray diffractometry, which showed that it was high enough to use in this study. The other zeolites were commercially available substances. H-M(A) (Zeolon 100H mordenite from Norton Co.), H-M(B) (Zeolon 900H mordenite from Norton Co.), RE-Y (Linde type SK-500) and Linde type Aw-500 were activated by calcining at 400 °C for 3 h. H-Y, H-L, and H-X were prepared from Linde type SK-40, Linde type SK-45, and Na-X respectively by treating them 5 times with an aqueous NH_4Cl solution, followed by drying at 120 °C for 20 h and by calcining at 450 °C for 3 h. The DAY (de-aluminated Y type zeolite) was supplied by Shokubai Kasei, Inc. The DAM (de-aluminated mordenite) was prepared from Zeolon 100H (mordenite) by treating it with an aqueous hydrochloric acid solution (8 M) for 24 h. The physical and acidic characters of zeolites are listed in Table 1.

The hybrid catalyst was prepared and activated as follows: Portions of Pd/SiO_2 and zeolite of equal weights were mixed physically and then crushed to powder under an 80 mesh. Then they were pressed into a disk and finally crushed to granules with 20—40 mesh. About 2.0 g of the hybrid catalyst was placed in a tublar reactor (6 mm in inner diameter) and was activated in flowing hydrogen at 400 °C for 2 h. Then the synthesis gas reaction was conducted.

A pressurized flow type-reaction apparatus was used for the synthesis gas reaction. The apparatus was equipped with an electronic temperature controller, a furnace, a tublar reactor, a flow regulator-controller and a back-pressure regulator. All products were withdrawn from the reactor in the gaseous state and were and analyzed gas chromatographically.

For the methanol conversion experiment, zeolites were pressed into disks and crushed to granules with 20—40 mesh. H-M(B), RE-Y, and Aw-500 extrudates were crushed to granules with 20-40 mesh. About 1.0 g portion of

zeolite granules were placed in the tublar reactor and activated in the same way as that of the hybrid catalyst. The methanol reactions were conducted, using the same apparatus as that used for the synthesis gas reaction, by passing through a gaseous mixture of methanol vapor and hydrogen or nitrogen.

Determination of the Acidic Features of Zeolites. About a 200 mg protion of zeolite was put in a glass cell and then evacuated at 500 °C for 2 h. Then the first isotherm of ammonia adsorption was measured at room temperature. After evacuating for 1 h at room temperature, the second isotherm was determined. The difference between the two isotherms, which is defined as the ammount of ammonia chemisorbed, was defined as the "acidity" of the zeolite.

The temperature programmed desorption (TPD) of ammonia on zeolites was measured by heating the sample at the rate of 7.6 °C/min. The desorbed ammonia was measured with a mass spectrometer. (Anelva TE-150). A site which liberated ammonia above 300 °C was defined as a strong acid site.

Results

Acidic Features of the Zeolites. Figures 1,2,3, and 4 show the TPD spectra of ammonia for various zeolites, where θ is the coverage and T is the desorption temperature. It should be noted that the vertical axes $(-d\theta/dT)$ of the Figures indicate the fraction of desorbed ammonia at each temperature, therefore, the integration of each spectrum for all the temperature range is unity. The acidities of the various zeolites, as measured by means of the ammonia chemisorption, are shown in Table 1. As has previously been reported,[2] the spectrum of H-ZSM-5 has two peaks; one is at around 100 °C, and the other is at around 350 °C. The spectrum of H-M(A), similarly to H-ZSM-5, has a low temperature peak at around 100 °C and a high temperature peak at around 350 °C. In the case of DAM, the acidity is apparently smaller than that of the parent mordenite (Table 1), and both the peaks of TPD were shifted to temperatures higher by about 100 °C. These facts indicate that the acid strength of mordenite was promoted by the extraction of aluminium. Although the acidity of H-Y is large, its TPD spectrum shows only one peak, at around 100 °C, indicating that the amount of strong acid sites is quite small. RE-Y, which contains a rare earth metal ion, exhibits a spectrum

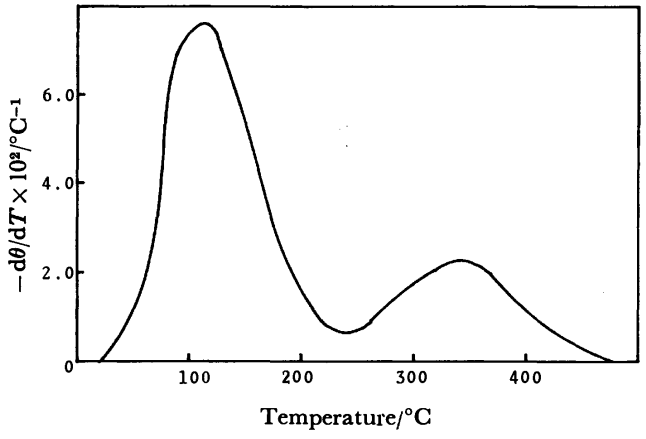

Fig. 1. TPD Profiles of NH_3 from H-ZSM-5.

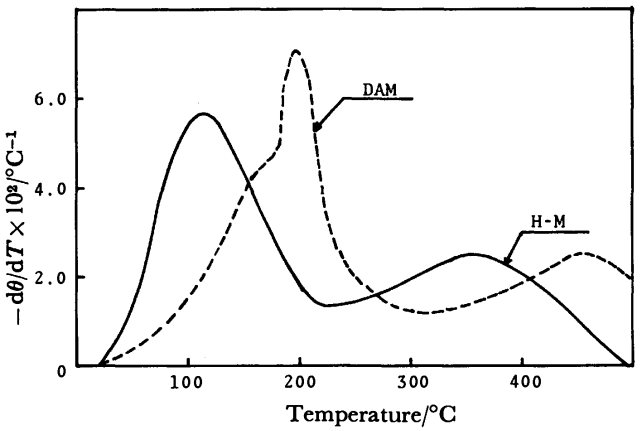

Fig. 2. TPD Profiles of NH_3 from Mordenites.

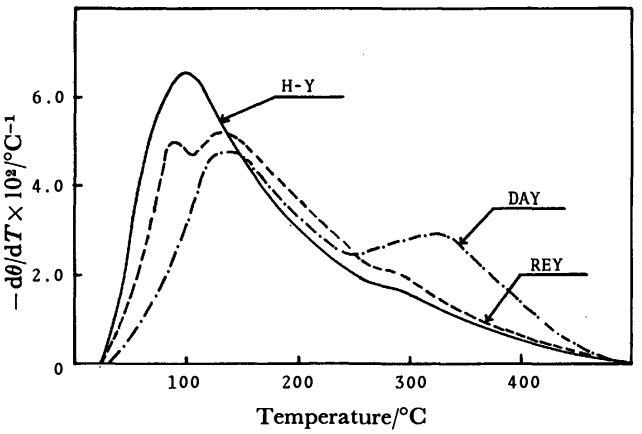

Fig. 3. TPD Profiles of NH_3 from Y Type Zeolites.

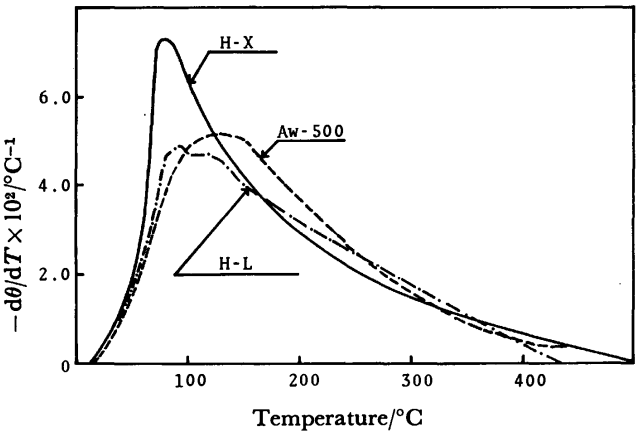

Fig. 4. TPD Profiles of NH_3 from Various Zeolites.

Table 1. Physical and acidic characteristics of zeolites used

Zeolite	Acidity (mmol/g)	Content of aluminium (mmol/g)	SiO_2/Al_2O_3 molar ratio	Fraction of strong acid sites (%)	Pore size (Å)[a]
H-ZSM-5	1.74	1.2	50.2	25.7	6
H-M(A)	3.74	2.0	14.6	32.6	6.9
H-M(B)	—	2.8	10	—	6.9
DAM	1.52	0.6	53.0	37.5	6.9
H-Y	4.63	5.1	4.8	10.2	13
DAY	4.22	3.6	7.6	27.0	13
REY	—	4.5	4.9	11.2	13
H-X	9.33	7.9	2.5	11.4	13
H-L	4.55	3.9	5.4	16.3	7.1
Aw-500	—	2.8	10	9.3	4.0

a) Data from Ref. 7.

Table 2. Results of methanol conversion over zeolite catalysts

Catalyst	H-ZSM-5	H-M(A)	DAM	DAY	H-M(B)	H-Y
Reaction conditions						
Temperature (°C)	350	350	350	332	350	350
Pressure (atm)	1	15	15	21	15	15
W/F (g-cat·h/mol)	4.6	4.4	4.9	4.6	4.8	4.9
MeOH conc. (mol%)	10.0	1.1	1.4	10	1.1	1.1
Balance Gas	N_2	H_2	H_2	H_2	H_2	H_2
Hydrocarbon yield/%	100	100	100	65	100	100
Hydrocarbon distributions (C-wt%)						
Methane	0.5	10.9	2.2	1.5	2.3	7.7
Ethane	tr.	18.8	6.7	1.3	16.0	14.6
Ethene	3.4	tr.	tr.	7.1	2.1	0.7
Propane	9.5	30.4	22.1	2.7	14.7	12.4
Propene	3.7	tr.	tr.	8.8	0.2	0.9
Butane	4.4	6.4	10.8	10.2	4.2	4.0
Isobutane	17.9	6.9	21.1		43.2	31.2
Butenes	3.6	tr.	tr.	3.8	tr.	tr.
C_5+Aliphatics	26.7	3.9	7.1	34.1	16.7	28.3
Benzene	tr.	0.3	0.6	—	—	—
Toluene	8.1	2.5	2.0	0.6	—	—
Xylenes	12.6	5.7	2.9	0.9	—	—
Trimethylbenzenes	7.6	7.2	1.2	1.8	—	—
Tetramethylbenzenes	1.3	4.9	0.2	2.3	—	0.2
Pentamethylbenzene	0.4	0.9	10.5	4.7	—	—
Hexamethylbenzene	0.1	1.1	12.3	20.1	—	—
C_{13}+Aromatics	—	—	0.4	—	—	—
Selectivity to aromatics	30.4	22.6	30.1	30.5	0	0.2
H/C ratios in products	1.9	2.5	2.3	2.0	2.6	2.8

similar to that of H-Y. DAY, whose acidity is smaller than that of H-Y, as is demonstrated in Table 1 shows a TPD spectrum with two peaks; one is at around 130 °C, and the other is at around 330 °C. It indicates that strong acid sites were generated by extracting aluminium. The TPD spectra of Aw-500, H-X, and H-L exhibit single peaks at around 100 °C.

Reaction of Methanol. Products from methanol conversion over the zeolites, which were measured at 3—4 h after the start of the reaction, are shown in Table 2 and they may be summarized as follows:

(1) Every zeolites tested except H-M(B) and H-Y gave aromatic hydrocarbons with selectivities of around 30% (carbon base).

(2) The C_2 and C_3 hydrocarbons were composed of both olefins and paraffins.

(3) De-aluminated zeolites (DAY and DAM) gave aliphatic hydrocarbons with a higher molecular weight and aromatic hydrocarbon with a higher selectivity, compared with their parent zeolites.

(4) All zeolites gave C_4 paraffins rich in iso-butane.

(5) While the major aromatic hydrocarbons obtained with H-ZSM-5 were di- or trimethylbenzenes, the main aromatics formed over DAM and DAY were C_{11} aromatics and C_{12} aromatics (mostly pentamethylbenzene and hexamethylbenzene respectively).

(6) Every zeolite tested except H-ZSM-5 lost its activity within a few hours.

TABLE 3. CONVERSION OF CO OVER Pd/SiO_2 CATALYSTS

Temperature °C	Yield[a]			
	MeOH	H.C.	CO_2	DME
250	2.3	0.02	—	—
280	4.8	0.1	—	—
300	4.2	0.2	—	—
330	1.8	0.6	0.6	0.17
350	0.8	1.1	1.0	0.23
370	0.7	1.2	1.4	0.33

a) Yield in mol% of carbon monoxide fed, 21 atm, W/F=5 g-cat·h/mol, $H_2/CO=2$,

(7) The excess hydrogen in the product hydrocarbon (H/C>2) indicates that a large amount of carbonaceous material (coke) was deposited on all the zeolites except ZSM-5 during the reaction.

(8) The facts that over DAY, which possesses a fairly large amount of strong acid sites, aromatic hydrocarbons were formed whereas H-Y, which possesses few strong acid sites, gave no aromatic hydrocarbons, are consistent with the suggestion that aromatic hydrocarbons are formed on the strong acid sites.[8]

Methanol Synthesis with Pd/SiO_2. The methanol synthesis activity of the Pd/SiO_2 used in this study is shown in Table 3. The maximum methanol yield was obtained at around 300 °C. Above 300 °C, the yield of methanol decreased markedly with increase in the temperature, presumably because of the thermodynamical limitation. The yields of oxygenates (methanol plus dimethyl ether) and hydrocarbons (90% methane, and the rest, ethane) were about 1.0% and 1.1% respectively at 350 °C, where the synthesis gas reactions were mostly studied.

Synthesis Gas Conversion over the Hybrid Catalysts. The results of synthesis gas conversion with the hybrid catalysts composed of the Pd/SiO_2 and various zeolites are shown in Table 4. The data were examined with particular attention paid to (1) the catalytic activity, (2) the carbon number distribution

TABLE 4. HYDROGENATION OF CARBON MONOXIDE OVER VARIOUS HYBRID CATALYSTS[a]

Zeolite[b]	ZSM-5	H-M(A)	H-M(B)	DAM[c]	H-Y[c]	DAY[c]	REY	Aw-500	H-L	H-X
Yields of										
Hydrocarbons	9.6	8.0	9.8	9.7	6.5	14.6	8.4	7.3	6.4	3.6
Carbon dioxide	5.4	3.3	4.2	7.2	2.7	5.9	7.7	3.4	6.1	3.3
Oxygenates	—	—	—	—	—	—	—	—	1.6	3.3
Hydrocarbon distributions (C-wt%)										
Methane	12.4	12.6	25.1	6.0	12.6	16.3	10.9	13.8	33.8	96.9
Ethane	13.3	39.7	29.7	22.7	22.3	18.2	23.4	30.3	31.8	2.4
Ethene	tr.	0.2	0.1	0.2	tr.	tr.	tr.	tr.	tr.	—
Propane	33.2	24.6	18.5	28.1	29.2	32.8	31.1	36.1	17.7	1.0
Propene	0.1	0.2	0.1	0.2	tr.	tr.	tr.	tr.	tr.	—
C-4	6.2	5.3	7.4	16.6	21.7	22.2	26.1	12.8	11.2	—
C-5	2.3	2.2	2.3	4.9	9.3	1.5	2.2	1.9	2.9	—
C-6+ Aliph.	1.9	4.2	2.0	2.3	4.9	1.5	2.2	1.9	2.9	—
Benzene	—	0.2	—	—	—	—	—	—	—	—
Toluene	—	0.1	—	—	—	—	—	—	—	—
Xylenes	0.1	0.7	—	—	—	—	—	—	—	—
Tri. M.B.[d]	1.4	0.7	0.1	0.1	—	0.1	—	—	—	—
Tetra. M.B.[d]	21.9	1.2	0.5	1.8	—	0.6	—	—	—	—
P.M.B.[d]	6.9	5.1	9.0	15.2	—	0.2	—	—	—	—
H.M.B.[d]	0.3	2.6	4.1	1.8	—	—	—	—	—	—
C-13+ Aroma.	—	0.1	1.1	—	—	—	—	—	—	—
Selectivity to aromatics	30.6	10.7	14.8	18.9	—	0.9	—	—	—	—
iso-C_4/n-C_4	0.22	0.89	0.68	0.27	1.05	0.66	0.85	tr.	0.96	—

a) Hydrogenated at 370 °C, 21 atm, W/F=10 g-cat·h/mol, $H_2/CO=2$, b) Zeolite of which hybrid catalyst composed, c) Hydrogenated at 350 °C, d) Tri. M.B.=Trimethylbenzenes; Tetra. M.B.=Tetramethylbenzenes; P.M.B.=Pentamethylbenzene; H.M.B.=Hexamethylbenzene.

of product hydrocarbon, (3) the selectivity to aromatic hydrocarbons, and (4) the content of olefin and branched products in aliphatic hydrocarbons.

The yields of hydrocarbons on the hybrid catalysts were in the range of 3—15%, much higher than those of methanol on the Pd/SiO_2 catalyst alone. For each hybrid catalyst, the main product was hydrocarbon. Small amounts of oxygenates, mainly methanol and dimethyl ether, were also formed when H-L and H-X were combined with the Pd/SiO_2 catalyst.

The selectivities of aromatic hydrocarbons lie between 0—30%, depending on the zeolites used. These results will be discussed later. There are two peaks in the carbon number distribution of the product hydrocarbons; one is at C_2 or C_3 (aliphatic hydrocarbons), while the other is at C_{10} or C_{11} (aromatic hydrocarbons). For the catalysts which contain Y type zeolite as one component, the products were mostly aliphatic hydrocarbons with 1 to 4 carbon atoms. It is worthwhile to note that the conversion of synthesis gas on the hybrid catalysts composed of DAY and Pd/SiO_2 gave few aromatic hydrocarbons, whereas the conversion of methanol on DAY gave hexamethylbenzene with fairly high selectivities.

The data of the olefin contents of C_2 and C_3 hydrocarbons shown in Table 4 indicate clearly that the formation of olefins is quite small on the hybrid catalysts. However, methanol is converted into olefins at a fairly high selectivity on the zeolites, as is exemplified in Table 2. The low selectivity of olefins in the case of synthesis gas conversion is attributed to the hydrogenation of olefins on the Pd/SiO_2 catalyst, as has already been indicated by the present authors.[3]

The *iso*-C_4/*n*-C_4 ratio, representing the degree of chain branching of aliphatic hydrocarbons, lies between 0 and 1.1, and it depends strongly on the zeolite employed.

Discussion

Formation of Lower Paraffins. A comparison of the data in Tables 2 and 4 shows that the selectivities to lower paraffins in the synthesis gas reaction over hybrid catalysts are higher than those of methanol conversion over zeolite catalysts. As has already been mentioned,[3] the products of the synthesis gas reaction over the hybrid catalysts are seriously influenced by the hydrogenation of olefins on the Pd/SiO_2 catalyst along the path shown in Fig. 5. Lower olefins, which are the key intermediates from methanol to aromatic hydrocarbons, are hydrogenated over the Pd/SiO_2 catalyst to inert paraffins, which are stable under the present reaction conditions. Thus, the selectivities to lower paraffins are higher for the synthesis gas reaction than for the methanol conversion on zeolites alone.

Formation of Branched Chain Paraffins. It is apparent from the data shown in Tables 2 and 4 that the *iso*-C_4/*n*-C_4 ratios in the products of synthesis gas reaction are smaller than those of methanol conversion. The low value of the *iso*-C_4/*n*-C_4 ratio in the products of synthesis gas reactions are also attributable to the hydrogenation of olefins on the Pd/SiO_2 catalyst. Most paraffins are formed through the hydrogenation of olefins on the Pd/SiO_2 catalyst, as has been described above. Since the skeletal isomerization of olefins can be assumed to be very fast over a zeolite catalyst, the composition of olefins should be at equilibrium. Therefore, the formations of linear and branched paraffins are on the same level if the hydrogenation reactivities of both olefins are on the same level, because the *iso*-C_4H_8/*n*-C_4H_8 ratio is not high at the equilibrium state.

In contrast, paraffins are thought to be formed, during the methanol conversion on zeolite, by hydrogen transfer,[8] that is, carbonium ions on the zeolite pick up hydride ions from other hydrocarbons during the formation of aromatics or coke. Because of the higher stability of the tertiary carbonium ion, its concentration would be higher than that of the secondary carbonium ion; thus, the formation of branched hydrocarbon would be predominant. The models of both reaction paths are shown in Fig. 6.

The ratios of *n*-C_4 to *iso*-C_4 in the products from synthesis gas *vs.* the pore diameter of zeolites or the super-cage size of faujasites (H-X, H-Y, and DAY) shown in Fig. 7 indicate that the selectivity to *iso*-C_4 is higher for the zeolite with larger pores. This fact is interpreted in terms of the shape selectivity of zeolites. That is, the formation of bulky *iso*-C_4 (5.6 Å)[9] is hard in small pore zeolite such as Aw-500, whose pore diameter is about 4 Å. It should also be noted that the ratios of *iso*-C_4 to *n*-C_4 in the C_4 paraffins obtained over the catalysts containing DAM or DAY are lower than those for the catalysts containing their parent zeolites, which possess a larger acidity.

Formation of Aromatic Hydrocarbons. Figure 8 shows how the selectivity of aromatic hydrocarbons correlates to the fraction of strong acid sites and the pore diameter of zeolite. It clearly shows that aromatic hydrocarbons are formed only with the hydrid catalysts containing the zeolites whose fractions of strong acid

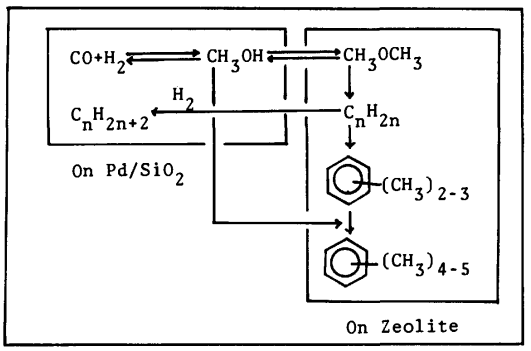

Fig. 5. Reaction Scheme on Hybrid Catalysts.

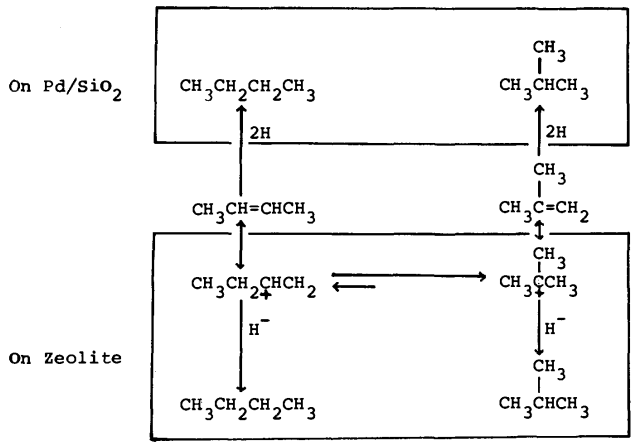

Fig. 6. Chain Branching.

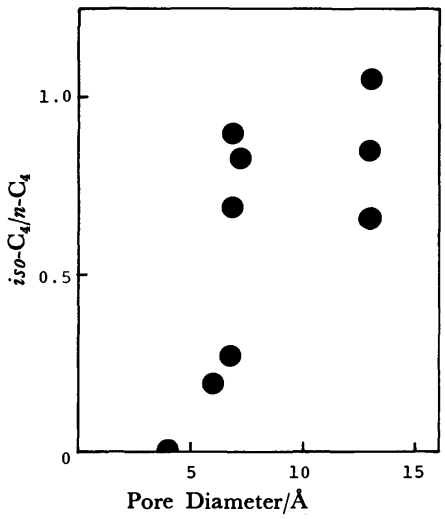

Fig. 7. A Ratio of *n*-C_4 to *iso*-C_4 *vs.* Pore Diameter.

site are higher than 20% and whose pore diameter lie between 6 and 7 Å. It should be noted that there is no relationship between the amount of strong acid sites and the selectivity to aromatic hydrocarbons. For example, the amounts of strong acid site of H-ZSM-5 and H-Y are 0.45 and 0.47 mmol/g respectively. On the hybrid catalyst containing H-ZSM-5, synthesis gas gave aromatic hydrocarbons with a high selectivity, while no aromatic hydrocarbons were formed on the H-Y containing catalyst. The hydrid catalyst containing H-M(A), whose amount of strong acid site is 1.22 mmol/g, gave aromatic hydrocarbons with a selectivity of around 10%, while the hybrid catalyst containing DAM, whose amount of strong acid sites is 0.57 mmol/g, gave aromatic hydrocarbons with a selectivity of around 20%.

Again, the formation of aromatic hydrocarbons is strongly related to the fraction of strong acid sites (Figure 8). This fact is interpreted as follows: The methanol formed on the Pd/SiO_2 is converted to olefins on both weak and strong acid sites.[10] Some of the olefins formed are converted to aromatic hydrocarbons

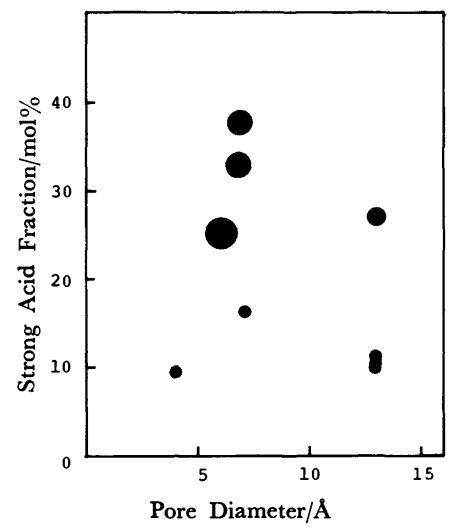

Fig. 8. Strong Acid Fraction and Selectivity to Aromatic Hydrocarbons *vs.* Pore Diameter.
●: Selectivity to Aromatics was more than 20%.
●: Selectivity to Aromatics was between 10% and 30%.
● : Selectivity to Aromatics was between 0% and 10%.
● : Selectivity to Aromatics was 0%.

on the acid site, while others are hydrogenated to the inert paraffins by means of hydrogen transfer on both weak and strong acid sites or by catalytic hydrogenation on the Pd/SiO_2. Consequently, the product distribution is controlled by the relative rate of aromatization and hydrogenation. Therefore, the fraction of strong acid sites (or the ratio of the amount of strong acid sites to that of weak acid site) is an important factor in determining the selectivity to aromatic hydrocarbons.

It is also shown the selectivity to aromatic hydrocarbons is strongly related to the pore diameter of the zeolite contained in the hybrid catalysts. It is strange that DAY gives few aromatic hydrocarbons when it is combined with Pd/SiO_2 and subjected to synthesis gas reaction although it has enough strong acid sites to produce aromatic hydrocarbons from methanol, as is shown in Table 2. This is also interpreted in terms of the diffusion of olefins from the zeolite pores to the Pd/SiO_2 and the successive hydrogenation to inert paraffins on it.

As is shown in Fig. 9, olefins formed from methanol on the zeolite can not be converted into aromatic hydrocarbons on a small pore zeolite like Aw-500, as is demonstrated in Table 4, where it is hard for even *iso*-C_4 to be formed. Thus, olefins are hydrogenated to inert paraffins on the palladium catalyst without being converted to aromatic hydrocarbons. In the case of the hybrid catalysts containing large pore zeolites, like DAY, which have the ability to form aromatic hydrocarbons, the diffusion of olefins is so quick that most of them come out of the pores before being converted into

aromatics, and they reach the palladium catalyst, where they are easily hydrogenated to paraffins. By contrast, in the case of zeolite with medium size pores (6—7 Å), like ZSM-5 or mordenites, olefins stay in the pores for long enough to be converted into aromatic hydrocarbons over the strong acid sites before being hydrogenated to paraffins, because of the slow diffusion of olefins in the pores. Although H-L has a medium size pore (7.1 Å), the fraction of strong acid sites is not enough to form aromatic hydrocarbons. Therefore, olefins formed in the pore will slowly diffuse to the Pd/SiO_2 catalyst without being converted into aromatic hydrocarbons and then hydrogenated to inert paraffins.

The product distribution obtained by methanol conversion on ZSM-5 and DAM and by synthesis gas conversion on the hybrid catalysts containing ZSM-5 and DAM are compared in Fig. 10. It is apparent that, over both catalysts, the aliphatic hydrocarbons formed from synthesis gas are lower in molecular weight than those obtained by methanol conversion and that aromatic hydrocarbons are more highly methylated in the synthesis gas conversion. These characteristics can be attributed to the hydrogenation of lower olefins and to the successive methylation of product methylbenzenes, which have previously been indicated by the present authors.[3]

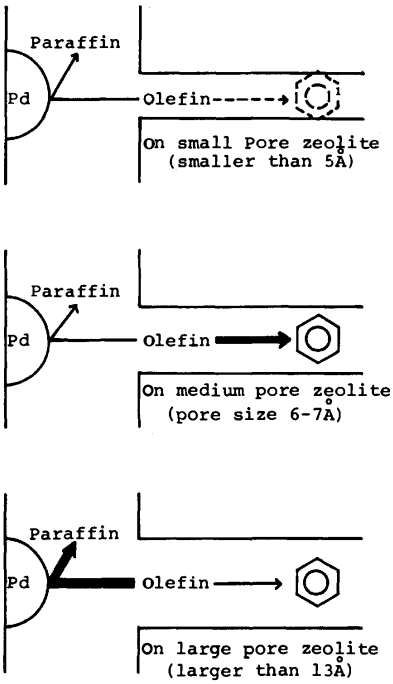

Fig. 9. Effect of Pore Diameter on Formation of Aromatic Hydrocarbons.

Conclusion

The conversion of synthesis gas over hybrid catalysts composed of Pd/SiO_2 and zeolites gave the following conclusions:

(1) The main hydrocarbons formed are C_1—C_3 paraffins and polymethylbenzenes,

(2) The ratio of linear to branched paraffins in the product hydrocarbon is higher for zeolites with larger pores and larger acidities,

(3) The extraction of aluminium in zeolites is effective for increasing strong acid sites, which is essential for the formation of aromatic hydrocarbons,

(4) Aromatic hydrocarbons are formed over the zeolites whose strong acid fraction is higher than 20% of the total acid sites and whose pore size lies between 6 and 7 Å.

References

1) C. D. Chang, W. H. Lang, and J. Silvestri, *J. Catal.*, **56**, 268 (1979).

2) K. Fujimoto, Y. Kudo, and H. Tominaga, *Nippon Kagaku Kaishi*, **1982**, 206.

3) K. Fujimoto, Y. Kudo, and H. Tominaga, *J. Catal.*, **87**, 136 (1984).

4) T. Yashima, A. Yoshimura, Y. Wakushima, and S.

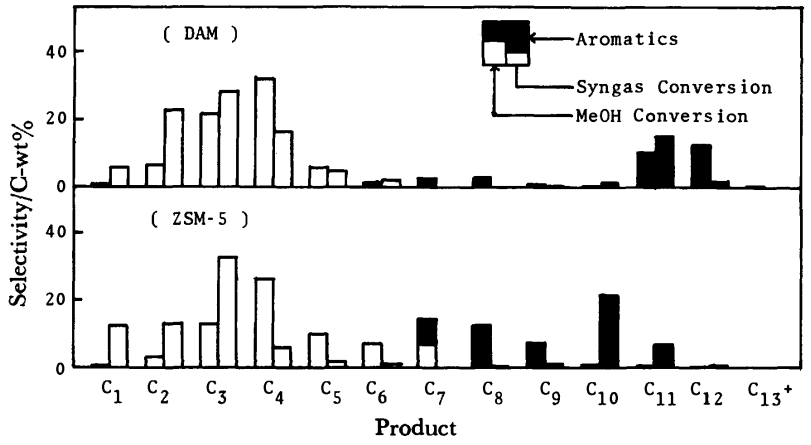

Fig. 10. Comparison of Syngas Conversion on Hybrid Catalyst and Methanol Conversion on Zeolite Catalyst alone.

Namba, Pan Pacific Synfuel Conference, Tokyo, November 1982, Preprints, No. B3.

5) T. Inui and Y. Takegami, Pan Pacific Synfuel Conference, Tokyo, November 1982, Preprints, No. B5.

6) A. Yoshimura, S. Namba, and T. Yashima, *Shokubai*, **23**, 232 (1981).

7) D. W. Breck, "Zeolite Molecular Sieves," John Wiley&Sons, New York, (1974), Chap. 2.

8) P. Dejaifve, J. C. Vedrine, V. Bolis, and E. G. Derouane, *J. Catal.*, **63**, 331 (1980).

9) N. Hara, "Zeolite To Sono-riyou," ed by H. Takahashi, Gihoudou Shuppan, Tokyo (1967), p. 144.

10) T. Imai, K. Iida, H. Fujita, T. Haruki, and N. Yokoyama, *Shokubai*, **23** (1), 99 (1981).

The Conformations of (Z)-2,3,4,7,8,9-Hexahydrooxonin and (Z)-Cyclononene. X-Ray Structure Determinations of Isolaurallene and Neolaurallene, and Force-Field Calculations

Akio FURUSAKI,* Shin-ichiro KATSURAGI, Katsunao SUEHIRO, and Takeshi MATSUMOTO
Department of Chemistry, Faculty of Science, Hokkaido University, Kita-ku, Sapporo 060
(Received August 6, 1984)

The molecular structures of isolaurallene and neolaurallene, diastereomeric nonterpenoids ($C_{15}H_{20}O_2Br_2$) from the red algae *Laurencia*, have been determined by X-ray crystallographic analysis. The crystal data are as follows: isolaurallene, orthorhombic, space group $P2_12_12_1$, a=10.393(2), b=27.824(4), c=5.397(1) Å, Z=4, D_c=1.669 g cm^{-3}; neolaurallene, monoclinic, space group $P2_1$, a=13.338(7), b=4.929(1), c=12.435(5) Å, β=98.22(4)°, Z=2, D_c=1.609 g cm^{-3}. The structures were solved by the heavy-atom method, and refined by the block-diagonal least-squares method; the final R-values were 0.076 and 0.069 respectively. The (Z)-2,3,4,7,8,9-hexahydrooxonin rings in the two substances possess essentially the same conformation. The MM2 force-field calculations have shown that this conformation is almost identical to the most stable one of the 11 minimum-energy conformations found for (Z)-2,3,4,7,8,9-hexahydrooxonin. For comparison, the conformations of (Z)-cyclononene have also been examined by the force-field calculations. Of its 10 minimum-energy conformations obtained, the asymmetric one which Favini *et al.* already studied has the lowest energy.

In the force-field calculations for (Z)-cyclononene (**2**), Favini *et al.* considered six conformations, *i.e.*, the chair-chair (CC), boat-chair (BC), chair-boat (CB), boat-boat (BB), twist chair-chair (TCC), and asymmetric (AS) conformation.[1] Since (Z)-2,3,4,7,8,9-hexahydrooxonin (**1**) can have the same molecular symmetry (C_S or C_2) as **2**, it may have conformations similar to those of **2**. We have recently carried out X-ray crystal structure analyses of two natural products, isolaurallene (**3**)[2] and neolaurallene (**4**),[3] and have found that the conformations of the nine-membered ether rings in **3** and **4** resemble each other, and that they differ essentially from any of the six conformations considered by Favini *et al.* It is of great interest to compare the stability of this new asymmetric (NAS) conformation with those of the other conformations. Thereupon, we have performed empirical force-field calculations for **1** and **2**. The present paper describes the X-ray structure determinations and molecular geometries of **3** and **4**, and discusses the results of the force-field calculations.

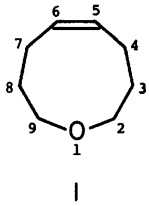

1

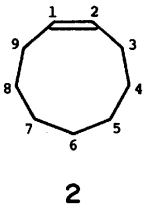

2

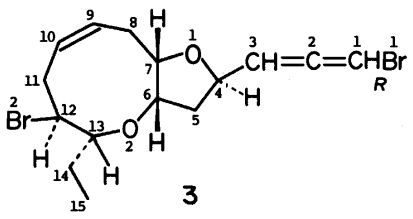

3

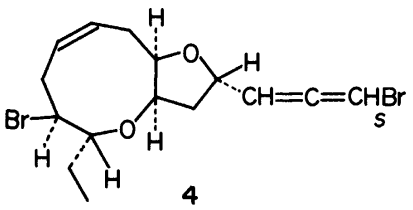

4

Experimental

X-Ray Structure Determination of Isolaurallene (3). Colorless, needle-like crystals of **3** were kindly provided by Prof. E. Kurosawa. A single crystal cut into a cube with an edge of *ca.* 0.3 mm was used for the X-ray measurement. The crystal data were as follows: $C_{15}H_{20}O_2Br_2$, mol wt 392.13, orthorhombic, space group $P2_12_12_1$, a=10.393(2), b=27.824(4), c=5.397(1) Å, Z=4, D_c=1.669 g cm^{-3}, μ(Mo $K\alpha$)=51.4 cm^{-1}. The unit-cell dimensions and reflection intensities were obtained on a Rigaku four-circle diffractometer at the Ultra High Intensity X-Ray Diffraction Laboratory of Nagoya University, using graphite-monochromated Mo $K\alpha$ radiation (λ=0.71073 Å). The θ–2θ scanning mode was employed at a θ scan rate of 6° min^{-1}; the background was measured for 5 s at each end of the scan range. Three standard reflections, measured at intervals of every 200 reflections, showed no significant decrease in intensity during the course of data collection. The intensities were corrected for the Lorentz and polarization factors, but not for the absorption or the extinction effect. In the range of 2θ values up to 50°, 1091 unique structure factors above the $3\sigma(F)$ level were selected for the structure determination.

The structure was elucidated by the heavy-atom method, and refined by the block-diagonal least-squares method with anisotropic temperature factors. The absolute configuration was determined by Hamilton's method;[4] the R-factor ratio for the two enantiomeric structures, 1.045, excluded one of them at the 99.5% confidence level. After all the hydrogen atoms had been located in a difference Fourier map, further

least-squares refinements were carried out including the hydrogen atoms with the same fixed isotropic temperature factors of 4.5 Å^2. For these refinements, the following weighting scheme was used:

$$w = 1/\{\sigma(F)^2 \exp(c_1X^2+c_2Y^2+c_3XY+c_4X+c_5Y)\},$$

where $X=|F_o|$ and $Y=\sin\theta/\lambda$. The c_1, c_2, c_3, c_4, and c_5 coefficients were evaluated from the $(\Delta F)^2$ distribution; $c_1=0.237\times10^{-5}$, $c_2=-10.3$, $c_3=-0.877\times10^{-3}$, $c_4=0.142\times10^{-2}$, and $c_5=5.69$. The final R-value was 0.076. The atomic parameters thus obtained are listed in Table 1.[5] The bond distances and angles and the ring torsion angles are given in Table 2 and Fig. 1(a) respectively.

Table 1. The final atomic parameters and estimated standard deviations for isolaurallene (**3**)

Atom	10^3x	10^4y	10^3z	B_{eq}[a]/Å^2
Br (1)	154.9 (2)	288.6 (8)	11.5 (5)	5.9
Br (2)	839.5 (2)	1219.2 (7)	−123.8 (4)	4.2
O (1)	268 (1)	2033 (4)	479 (3)	5.0
O (2)	541 (1)	1328 (3)	367 (2)	2.5
C (1)	80 (2)	503 (8)	297 (5)	7.6
C (2)	90 (2)	971 (7)	364 (4)	4.0
C (3)	108 (2)	1415 (6)	427 (4)	4.2
C (4)	221 (2)	1600 (7)	571 (4)	4.6
C (5)	337 (2)	1272 (7)	575 (3)	4.6
C (6)	403 (2)	1396 (6)	337 (3)	2.4
C (7)	361 (2)	1928 (6)	287 (3)	3.3
C (8)	470 (2)	2310 (6)	313 (4)	4.1
C (9)	543 (2)	2342 (5)	71 (3)	3.1
C (10)	664 (2)	2180 (6)	35 (4)	4.2
C (11)	744 (1)	1911 (6)	226 (4)	3.5
C (12)	744 (1)	1351 (5)	175 (3)	2.6
C (13)	604 (1)	1168 (6)	151 (4)	3.4
C (14)	593 (2)	625 (6)	132 (4)	4.2
C (15)	657 (2)	360 (7)	347 (4)	5.7

a) $B_{eq}=8\pi^2(u_1^2+u_2^2+u_3^2)/3$, where u_i is the root-mean-square deviation in the i-th principal axis of the thermal ellipsoid.

The calculations for the X-ray study were performed using our own programs. The atomic scattering factors and anomalous-dispersion corrections were taken from the International Tables.[6]

X-Ray Structure Determination of Neolaurallene (4). Colorless, needle-like crystals of **4** were also supplied by Prof. E. Kurosawa. The sample used for the X-ray experiment had dimensions of *ca.* 0.3×0.4×0.5 mm^3. The crystal data were as follows: $C_{15}H_{20}O_2Br_2$, mol wt 392.13, monoclinic, space group $P2_1$, $a=13.338(7)$, $b=4.929(1)$, $c=12.435(5)$ Å, $\beta=98.22(4)°$, $Z=2$, $D_c=1.609$ g cm^{-3}, μ(Mo $K\alpha$)=49.5 cm^{-1}. The cell dimensions and diffraction intensities were measured on a Rigaku four-circle diffractometer at the High Brilliance X-Ray Laboratory of Hokkaido University, using graphite monochromated Mo $K\alpha$ radiation (λ= 0.71073 Å). The $\theta-2\theta$ scan teachnique was applied at a θ scan speed of 4° min^{-1}; the background was counted for 10 s at each end of the scan range. The intensities of three standard reflections, measured at intervals of every 100 reflections, decreased rapidly during the course of data collection; the final-intensity/initial-intensity ratios were *ca.* 0.56—0.68. The intensities were corrected for this damage to the sample as well as for the Lorentz and polarization factors, but not for the absorption or the extinction effect.

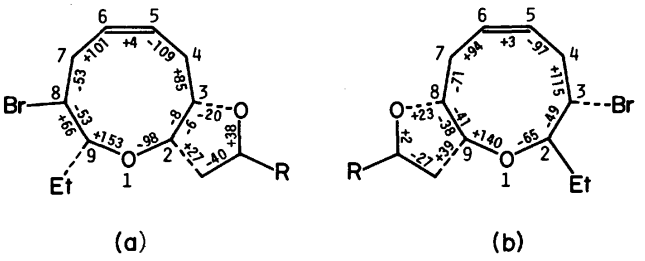

Fig. 1. The ring torsion angles (ϕ/°) in (a) isolaurallene (**3**) and (b) neolaurallene (**4**). The e.s.d.'s are 1—3°. For the sake of comparison, the numbering system for **1** is used.

Table 2. The bond distances (l/Å) and angles (θ/°) in isolaurallene (**3**)

C (1) - C (2)	1.36 (3)	C (12) - Br (2)	1.93 (2)	C (8) - C (7) - O (1)	107 (1)
C (1) - Br (1)	1.82 (2)	C (13) - C (14)	1.52 (2)	C (7) - C (8) - C (9)	109 (1)
C (2) - C (3)	1.29 (3)	C (13) - O (2)	1.41 (2)	C (8) - C (9) - C (10)	125 (2)
C (3) - C (4)	1.50 (3)	C (14) - C (15)	1.53 (3)	C (9) - C (10) - C (11)	125 (2)
C (4) - C (5)	1.51 (3)	C (2) - C (1) - Br (1)	121 (2)	C (10) - C (11) - C (12)	112 (1)
C (4) - O (1)	1.39 (2)	C (1) - C (2) - C (3)	176 (2)	C (11) - C (12) - C (13)	110 (1)
C (5) - C (6)	1.49 (2)	C (2) - C (3) - C (4)	125 (2)	C (11) - C (12) - Br (2)	110 (1)
C (6) - C (7)	1.57 (2)	C (3) - C (4) - C (5)	115 (2)	C (13) - C (12) - Br (2)	111 (1)
C (6) - O (2)	1.45 (2)	C (3) - C (4) - O (1)	113 (2)	C (12) - C (13) - C (14)	114 (1)
C (7) - C (8)	1.56 (2)	C (5) - C (4) - O (1)	104 (1)	C (12) - C (13) - O (2)	105 (1)
C (7) - O (1)	1.44 (2)	C (4) - C (5) - C (6)	103 (1)	C (14) - C (13) - O (2)	110 (1)
C (8) - C (9)	1.51 (3)	C (5) - C (6) - C (7)	104 (1)	C (13) - C (14) - C (15)	113 (2)
C (9) - C (10)	1.35 (3)	C (5) - C (6) - O (2)	109 (1)	C (4) - O (1) - C (7)	108 (1)
C (10) - C (11)	1.52 (3)	C (7) - C (6) - O (2)	115 (1)	C (6) - O (2) - C (13)	114 (1)
C (11) - C (12)	1.58 (2)	C (6) - C (7) - C (8)	115 (1)		
C (12) - C (13)	1.55 (2)	C (6) - C (7) - O (1)	105 (1)		

The e.s.d.'s given in parentheses refer to the last decimal position.

In the range of 2θ values up to 50°, 1002 independent structure factors above the $3\sigma(F)$ level were selected for the structure determination.

The structure was solved by the heavy-atom method. After the structure had been well refined by the block-diagonal least-squares method with anisotropic temperature factors, the absolute configuration was assigned by Bijvoet's method.[7] Twenty sets of hkl, $\bar{h}k\bar{l}$, $h\bar{k}l$, and $\bar{h}\bar{k}\bar{l}$ reflections having large values of $||F_c(hkl)|-|F_c(\bar{h}\bar{k}\bar{l})||/\sigma(F)$[8] were selected for this purpose. The signs of the corresponding observed and calculated values of $\{|F(hkl)|+|F(\bar{h}k\bar{l})|-|F(h\bar{k}l)|-|F(\bar{h}\bar{k}\bar{l})|\}/2$ were in agreement with each other for all the 20 sets of reflections. The absolute configuration thus determined was supported also by the R-factor ratio for the two enantiomeric structures, 1.010.[4] Since a difference Fourier map revealed all the hydrogen atoms, further least-squares refinements were performed including the hydrogen atoms with the same fixed isotropic temperature factors of 5.7 Å^2. A weighting scheme similar to that for **3** was used; $c_1=-0.107\times10^{-2}$, $c_2=32.3$, $c_3=-0.144$, $c_4=0.160$, and $c_5=-29.4$. In this manner, the R-value reached 0.069. The final atomic parameters are listed in Table 3.[5] The bond distances and angles and the ring torsion angles are given in Table 4 and Fig. 1(b), respectively.

Table 3. The final atomic parameters and estimated standard deviations for neolaurallene (**4**)

Atom	10^3x	10^3y	10^3z	B_{eq}[a]/Å^2
Br (1)	812.2 (2)	1095 (1)	279.1 (3)	12.1
Br (2)	77.8 (1)	244 (1)	440.4 (2)	5.9
O (1)	365.5 (7)	915 (3)	103.6 (9)	4.9
O (2)	279.1 (6)	720 (3)	293.0 (7)	3.6
C (1)	700 (1)	1208 (7)	188 (2)	8.0
C (2)	624 (1)	1038 (4)	160 (1)	5.3
C (3)	547 (1)	889 (4)	126 (1)	4.9
C (4)	454 (1)	861 (3)	184 (1)	2.9
C (5)	436 (1)	589 (3)	228 (1)	4.0
C (6)	322 (1)	558 (3)	214 (1)	3.1
C (7)	295 (1)	688 (3)	103 (1)	3.5
C (8)	190 (1)	800 (3)	74 (1)	4.7
C (9)	117 (1)	571 (4)	56 (1)	4.7
C (10)	64 (1)	461 (4)	130 (2)	6.1
C (11)	68 (1)	568 (4)	248 (2)	5.3
C (12)	144 (1)	402 (4)	324 (1)	3.6
C (13)	236 (1)	566 (3)	376 (1)	3.5
C (14)	317 (1)	407 (4)	448 (1)	4.2
C (15)	389 (1)	603 (5)	517 (1)	6.0

a) See Table 1.

Force-Field Calculations. The force-field calculations were performed using the MM2 program.[9] In the force-field calculations for **2**, Favini *et al.* assumed the C_S or C_2 symmetry for the whole or part of the molecule.[1] Since, however, there appeared to be no valid reason for having such symmetry, in our MM2 calculations, no symmetry was assumed for either **1** or **2**. As a result, it was found for **1** and **2** that, although the symmetric CB and BC conformations correspond to energy minima, the symmetric CC, BB, and TCC conformations correspond to energy maxima, and that, in order to reach energy minima, they must be considerably deformed. With respect to the plane which divides the molecule into two equal parts, the arrangements of the signs of the ring torsion angles in the CB, BC, CC, and BB minimum-energy conformations keep antisymmetric, while those in the AS, NAS, and TCC minimum-energy conformations are neither symmetric nor antisymmetric. Therefore, in this paper, the former four are still referred to as conformations CB, BC, CC, and BB, respectively, and the latter three are called conformations AS1, AS2, and AS3, respectively. In the course of the examination of the interconversions among the conformers of **1**, four additional minimum-energy conformations (AS4, AS5, AS6, and AS7) were obtained. As for **2**, a total of 10 minimum-energy conformations were found. Each of these conformations had the same arrangement of the signs of the ring torsion angles as the corresponding conformation of **1**. The AS6 conformation of **2** was found not to correspond to an energy minimum. When this conformation was optimized, it changed into a new minimum-energy conformation. However, because of the extremely-high strain energy (213

Table 4. The bond distances (l/Å) and angles (θ/°) in neolaurallene (**4**)

C (1) - C (2)	1.33 (3)	C (12) - Br (2)	1.96 (2)	C (8) - C (7) - O (1)	107 (1)
C (1) - Br (1)	1.83 (2)	C (13) - C (14)	1.52 (2)	C (7) - C (8) - C (9)	109 (1)
C (2) - C (3)	1.28 (2)	C (13) - O (2)	1.47 (2)	C (8) - C (9) - C (10)	127 (2)
C (3) - C (4)	1.52 (2)	C (14) - C (15)	1.54 (3)	C (9) - C (10) - C (11)	124 (2)
C (4) - C (5)	1.49 (2)	C (2) - C (1) - Br (1)	120 (2)	C (10) - C (11) - C (12)	109 (1)
C (4) - O (1)	1.45 (2)	C (1) - C (2) - C (3)	175 (2)	C (11) - C (12) - C (13)	114 (1)
C (5) - C (6)	1.51 (2)	C (2) - C (3) - C (4)	125 (2)	C (11) - C (12) - Br (2)	110 (1)
C (6) - C (7)	1.51 (2)	C (3) - C (4) - C (5)	116 (1)	C (13) - C (12) - Br (2)	108 (1)
C (6) - O (2)	1.45 (2)	C (3) - C (4) - O (1)	107 (1)	C (12) - C (13) - C (14)	116 (1)
C (7) - C (8)	1.50 (2)	C (5) - C (4) - O (1)	105 (1)	C (12) - C (13) - O (2)	110 (1)
C (7) - O (1)	1.46 (2)	C (4) - C (5) - C (6)	105 (1)	C (14) - C (13) - O (2)	111 (1)
C (8) - C (9)	1.49 (2)	C (5) - C (6) - C (7)	100 (1)	C (13) - C (14) - C (15)	110 (2)
C (9) - C (10)	1.35 (3)	C (5) - C (6) - O (2)	111 (1)	C (4) - O (1) - C (7)	109 (1)
C (10) - C (11)	1.55 (3)	C (7) - C (6) - O (2)	109 (1)	C (6) - O (2) - C (13)	115 (1)
C (11) - C (12)	1.52 (2)	C (6) - C (7) - C (8)	118 (1)		
C (12) - C (13)	1.54 (2)	C (6) - C (7) - O (1)	105 (1)		

The e.s.d.'s given in parentheses refer to the last decimal position.

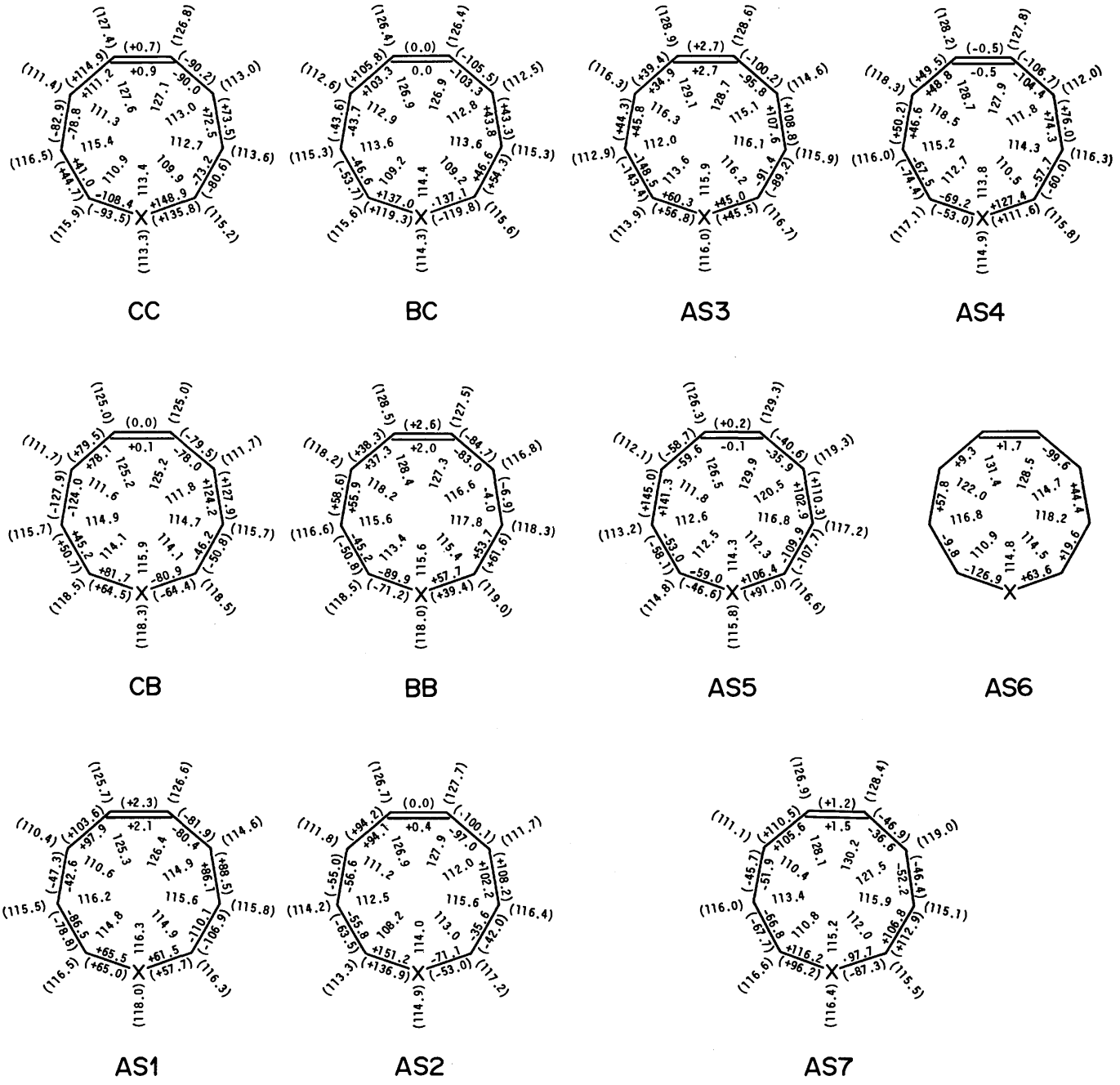

Fig. 2. The bond angles and ring torsion angles (ϕ/°) in (*Z*)-2,3,4,7,8,9-hexahydrooxonin (**1**, X=O) and (*Z*)-cyclononene (**2**, X=CH_2). The values for **2** are given in parentheses.

kJ mol^{-1} relative to AS1), this new conformation was not reckoned among minimum-energy conformations of **2**. The bond angles and ring torsion angles in the 11 different conformations are shown in Fig. 2.

Such interconversions among the conformers of **1** as could be accomplished by a change of one ring torsion angle were studied by the MM2 calculations. Each time the torsion angle used as a conversion parameter was changed by 5°, the strain energy of the molecule was minimized under the condition that this torsion angle should be fixed at the given value. From the energy profile thus obtained, the energy barrier to the conversion was estimated. The reversibility of the conversion was judged according to whether or not the energy change was continuous throughout the conversion. The results are summarized in Fig. 3.

Results and Discussion

(Z)-2,3,4,7,8,9-Hexahydrooxonin (1). The present study has revealed that there are at least 11 minimum-energy conformations of **1** (see Fig. 2). As can be seen from Table 5, the AS2 conformation is the most stable, and has a lower energy than the next most

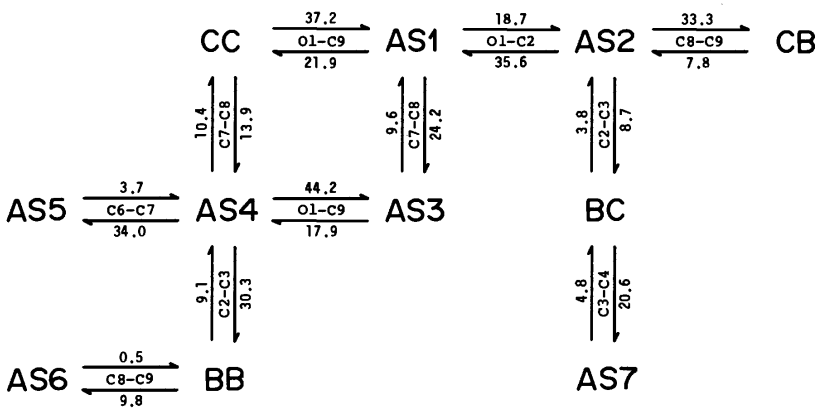

Fig. 3. The interconversions among the conformers of (Z)-2,3,4,7,8,9-hexahydrooxonin (**1**). The energy barriers (ΔE/(kJ mol^{-1})), together with the central bonds of the torsion angles used as conversion parameters, are shown.

stable CC conformation by 1.6 kJ mol^{-1}. The conformational interconversions for **1**, which can be accomplished by driving one ring torsion angle, are shown in Fig. 3. In addition to these reversible conversions, there are many irreversible conversions, *e.g.*, the AS5 →AS6→CC conversion caused by the rotation about the C8-C9 bond, the AS6→AS4 conversion caused by the rotation about the O1-C2, C2-C3, or C3-C4 bond, and the AS7→AS5*[10] conversion caused by the rotation about the C8-C9 bond. These irreversible conversions probably proceed reversibly, if they are performed by driving two or more ring torsion angles simultaneously. Accordingly, Fig. 3 should be considered to show only a part of the possible interconversions for **1**. The calculated energy barriers to the conversions shown in Fig. 3 are 44.2 kJ mol^{-1} or below, which suggests that, at room temperature, the conformations of **1** may change into one another directly or *via* one or more other conformations.

It is interesting to notice that the CB→AS2→BC transformation is accompanied by a remarkable change in torsional strain. Because of the eclipsed bond arrangements around the C7-C8 and C3-C4 bonds, the symmetric CB conformer has great torsional strains (11.6 kJ mol^{-1}) around these bonds (see Fig. 4). The changes from the CB to the AS2 conformer and from the AS2 to the BC conformer remarkably relieve these great torsional strains, respectively. However, the latter change results in an increase in the total strain energy. This is due mainly to the occurrence of great torsional strains around the O1-C2 and O1-C9 bonds.

*Isolaurallene (**3**) and Neolaurallene (**4**).* The conformations of the nine-membered rings in both **3** and **4** are substantially the same as the most stable AS2 conformation of **1** (see Figs. 1 and 2); the maximum torsion-angle deviations (28 and 15°) are observed for the junctures with the oxolane rings respectively. The diastereomeric compounds, **3** and **4**, have the same absolute configuration at each of

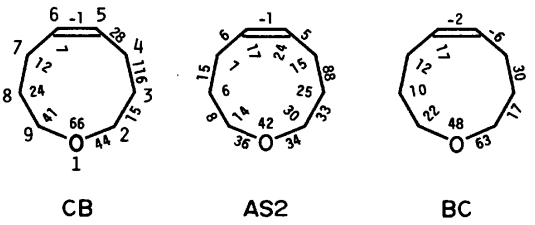

Fig. 4. The distributions of the torsional strain and bond-bending energies ($10 \times E$/(kJ mol^{-1})) in the CB, AS2, and BC conformers of (Z)-2,3,4,7,8,9-hexahydrooxonin (**1**). The torsional energy ($E_t(i-j)$) and bending energy ($E_b(i)$), defined by the following equations, are shown for each bond and each atom respectively: $E_t(i-j) = \sum_{x,y} E_t(x-i-j-y)$; $E_b(i) = \sum_{x,y} E_b(x-i-y)$.

the carbon atoms to which the ethyl group or the bromine atom is attached, while they have different absolute configurations at each of the bridgehead carbon atoms. This stereochemical difference results in a striking contrast between **3** and **4** in regard to the positions of the substituents on the nine-membered ring having the asymmetric AS2 conformation. That is, in **3**, the oxolane ring is fused at the 2- and 3-positions, and the remaining substituents are placed at the 8- and 9-positions; the reverse is the case in **4**.

Since the calculated energy difference between the AS2 and CC conformations of **1** is only 1.6 kJ mol^{-1}, in order to explain why neither **3** nor **4** adopts the CC conformation, it is necessary to examine the steric effects of the substituents in some detail. In the CC conformation of **1**, the axial hydrogen atoms at the 2- and 9-positions are very close to each other, the distance being 2.17 Å (see Fig. 5). Therefore, the replacement of one of these hydrogen atoms by an alkyl group will make the CC conformation unstable. If the nine-membered ring in **4** takes the CC conformation, one of the ethyl and methylene groups attached

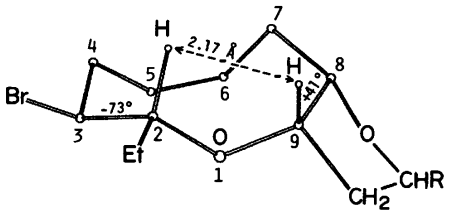

Fig. 5. The most probable arrangement of the substituents in the isolaurallene (**3**) molecule having the CC conformation.

to the C2 or C9 atom must necessarily be axial because of their trans configuration, which explains why **4** does not favor the CC conformation.

The explanation for **3** is not so easy as that for **4**. When **3** has the CC conformation, both of the ethyl and methylene groups bonded to the C2 or C9 atom will occupy the equatorial positions because of their cis configuration (see Fig. 5). If the cis fusion of the five- and nine-membered rings occurs at the C2 and C3 (or C8 and C9) atoms, the C-C2-C3-O (or O-C8-C9-C) torsion angle in the former ring should have almost the same value as the O1-C2-C3-C4 (or C7-C8-C9-O1) torsion angle. Since the magnitude of the C7-C8-C9-O1 torsion angle (41°) is much more suitable to the requirement of the oxolane ring than that of the O1-C2-C3-C4 torsion angle (−73°), it seems to be more reasonable to choose the C8-C9 bond as the junction of the two rings than to take the C2-C3 bond. In the former case, the ethyl group and the bromine atom are placed at the C2 and C3 atoms respectively. If it is assumed that the projections of the Et-C2-O1 and Br-C3-C4 bond angles along the C2-C3 bond are 120°, the Et-C2-C3-Br torsion angle is estimated to be about 47°. This value is somewhat smaller than the corresponding torsion angle (64°) in the AS2 conformation of **1** and the Et-C9-C8-Br torsion angle (66°) found actually in **3**, which would make the CC conformation of **3** more or less unstable. In the above explanation, the conformation of the oxolane ring in **3** has not been taken into consideration; for oxolane is known to be highly flexible.[11]

(Z)-Cyclononene (2). Although Favini *et al.* examined only six conformations of **2**, *i.e.*, the CC, BC, CB, BB, TCC, and AS conformations, the present study has shown that there are at least 10 minimum-energy conformations of **2** (see Fig. 2), and that the symmetric CC, BB, and TCC conformations correspond not to energy minima but to energy maxima. For the reason which has been mentioned in the preceding section, the minimum-energy conformations obtained by distorting the CC, BB, and TCC forms have been named CC, BB, and AS3 respectively, while the AS conformation has been renamed AS1. Table 5 indicates that the most stable conformation of **2** is AS1; this agrees with the result of Favini *et al.* The stability of the AS1 conformation is supported by the fact that the conformation found in the

Table 5. The relative steric energies of the conformers of (*Z*)-2,3,4,7,8,9-hexahydrooxonin (**1**) and (*Z*)-cyclononene (**2**)

Conformer	*E*/(kJ mol^{-1})	
	1	**2**
CC	1.6	0.6
BC	4.9	4.4
CB	25.5	17.0
BB	26.3	22.3
AS1	16.8	0.0
AS2	0.0	2.3
AS3	31.4	14.3
AS4	5.1	2.4
AS5	35.4	27.5
AS6	35.6	
AS7	20.7	9.8

caprylolactam hydrochloride crystal resembles it closely.[12] However, the energy differences among the four most stable conformations of **2** are less than 4 kJ mol^{-1}; especially that between the AS1 and CC conformations is only 0.6 kJ mol^{-1}. This computational result suggests that substituted derivatives of **2** may have not the AS1 but the CC, AS2, or AS4 conformation according to the positions occupied by the substituents.

The absence of the AS6 minimum-energy conformation of **2** is explained as follows. In the AS6 conformation of **1**, the O1 atom is situated near the C4, C5, C6, and C7 atoms, the distances being 2.89, 2.92, 2.85, and 2.75 Å respectively. Therefore, when the O1 atom is replaced by a methylene group (-CH_2-), one of the hydrogen atoms in this methylene group must be very close to some of those four carbon atoms. This severe steric hindrance probably makes the AS6 conformation of **2** to be so labile as to be incapable of existing as a stable minimum-energy conformation.

We would like to thank Professor Etsuro Kurosawa of this university for providing us with the samples, and Dr. Chuji Katayama of Nagoya University for measuring the X-ray diffraction intensities of isolaurallene. The calculations for the present study were done on HITAC M-200H and M-280H computers at the Hokkaido University Computing Center.

References

1) G. Favini, G. Buemi, and M. Raimondi, *J. Mol. Struct.*, **2**, 137 (1968); G. Buemi, G. Favini, and F. Zuccarello, *ibid.*, **5**, 101 (1970); F. Zuccarello, G. Buemi, and G. Favini, *ibid.*, **18**, 295 (1973).

2) K. Kurata, A. Furusaki, K. Suehiro, C. Katayama, and T. Suzuki, *Chem. Lett.*, **1982**, 1031.

3) M. Suzuki, E. Kurosawa, A. Furusaki, S. Katsuragi, and T. Matsumoto, *Chem. Lett.*, **1984**, 1033.

4) W. C. Hamilton, *Acta Crystallogr.*, **18**, 502 (1965).
5) The tables of the anisotropic temperature factors and hydrogen parameters and the F_o-F_c table are kept at the Chemical Society of Japan (Document No. 8511).
6) "International Tables for X-Ray Crystallography," Kynoch Press, Birmingham (1974), Vol. 4.
7) J. M. Bijvoet, A. F. Peerdeman, and A. J. van Bommel, *Nature*, **168**, 271 (1951).
8) A. Furusaki, "Shin Zikken Kagaku Kōza," ed by the Chemical Society of Japan, Maruzen, Tokyo (1977), Vol. 6, Chap. 4, p. 242.
9) N. L. Allinger, *J. Am. Chem. Soc.*, **99**, 8127 (1977).
10) AS5* denotes the mirror image of the AS5 conformation.
11) B. Fuchs, "Topics in Stereochemistry," ed by E. L. Eliel and N. L. Allinger, John Wiley & Sons, New York (1978), Vol. 10, p. 59.
12) F. K. Winkler and J. D. Dunitz, *J. Mol. Biol.*, **59**, 169 (1971).

The Thermal *Cis*-to-*trans* Isomerization of *N,N'*-Diacylindigos. Kinetic Pressure, Solvent, and Substituent Effects

Yoshimi SUEISHI,* Kazuo OHTANI, and Norio NISHIMURA
Department of Chemistry, School of Science, Okayama University, Okayama 700
(Received August 13, 1984)

The kinetics of the thermal *cis*-to-*trans* isomerization of *N,N'*-diacylindigos(DAI) in various solvents and under high pressures has been studied. *N,N'*-Dibenzoylindigos(DBI) isomerize about 10 times slower than molecules not having a benzene ring in the acyl groups. The values of the activation volumes were about 8.0 $cm^3\ mol^{-1}$ for the former and about 3.0 $cm^3\ mol^{-1}$ for the latter. It was suggested that the thermal isomerization proceeds *via* the biradical mechanism. The positive values of the activation volume have been interpreted in terms of the increase in the intrinsic volume upon activation. The differences in the isomerization rates and the activation parameters between DBI and the others have been ascribed to an additional interaction between the two phenyl rings in the acyl groups in the *cis*-ground state.

Recently, reaction mechanisms have been actively discussed for the thermal *cis*-to-*trans* isomerization of push-pull azobenzenes. Whitten *et al.*[1] reported that the rate of the thermal isomerization of 4-dialkylamino-4'-nitroazobenzenes is extremely sensitive to solvent polarity and that thermal isomerization proceeds *via* a dipolar rotational transition state (I).

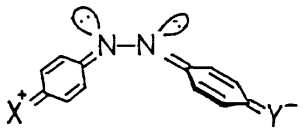

I

Asano *et al.*[2] studied the kinetic-pressure effects for the thermal isomerization of 4-dimethylamino-4'-nitroazobenzene and advocated that the mechanism changes from inversion in hexane to rotation in benzene and polar solvents. They suggested a dipolar transition state (I) in benzene and polar solvents. According to our view, the substituent, solvent, and pressure effects are in favor of the inversion mechanism and a remarkable polarity change will occur on going from the *cis* to the inversion transition state (II).[3]

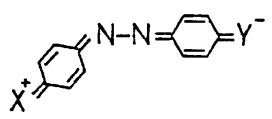

II

The thermal isomerizations of *N,N'*-diacylindigos (DAI) and push-pull stilbenes invariably proceed by the rotation mechanism around the carbon-carbon double bond. In analogy with the case of push-pull azobenzenes, charge-separated transition states (III and IV) are plausible for these compounds. However, according to Calvin and Alter,[4] push-pull stilbenes

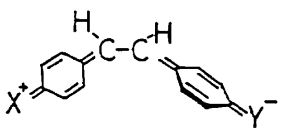

III

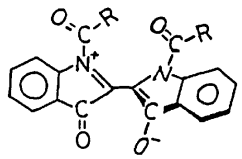

IV

thermally isomerize *via* a triplet state at 200—300 °C. Since push-pull stilbenes gradually decompose at high temperature, it is difficult to examine the solvent, substituent, and pressure effects. On the other hand, the thermal *cis*-to-*trans* isomerization of DAI readily takes place at room temperature.[5] For the thermal isomerization of DAI, two routes are possible: the isomerization *via* a double bond breaking to produce either homopolar or dipolar transient species, as indicated by IV and V.

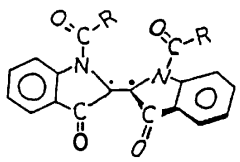

V

In connection with the recent interest regarding the mechanism of the *cis*-to-*trans* isomerization of push-pull azobenzenes, we have undertaken the investigation of the thermal isomerization of DAI in order to clarify which of these routes is more consistent with experimental observations.

Experimental

Reagents. *N,N'*-Diacetylindigo (**1**), *N,N'*-dipropionylindigo (**2**), and *N,N'*-diisobutyrylindigo (**3**) were prepared by the method reported by Blanc and Ross.[6] **1** and **2** were recrystallized from a hexane-chloroform mixture and **3** was recrystallized from hexane. **1**: mp 254—256 °C (lit,[7]

256—257 °C), **2**: mp 211—212 °C (lit,[7] 211—213 °C), **3**: mp 230—231 °C (lit,[7] 229—230 °C). *N,N'*-Distearoylindigo(**4**) was prepared by the method reported by Omote *et al.*[5] and recrystallized from petroleum ether: mp 107.5—108 °C (lit,[5] 101—102 °C). *N,N'*-Bis(cyclohexylcarbonyl)indigo (**5**), *N,N'*-dibenzoylindigo (**6**), *N,N'*-bis(p-methylbenzoyl)indigo (**7**), *N,N'*-bis(p-chlorobenzoyl)indigo (**8**), and *N,N'*-di-2-naphthoylindigo (**9**) were prepared by the method reported by Posner.[8] **5** was recrystallized from a hexane-chloroform mixture: mp 244.5—245.5 °C. **6** and **9** were recrystallized from an acetone-water mixture and **7** and **8** were recrystallized from a hexane-chloroform mixture. **6**: mp 261—262 °C (lit,[7] 256—257 °C), **7**: mp 293—294 °C, **8**: mp 271—272 °C, **9**: mp 251—252 °C.

^{1}H NMR spectra were recorded on a Hitachi R-600 High Resolution NMR spectrometer (60 MHz) with TMS as an internal standard, and IR spectra on a JASCO IRA-I spectrophotometer. **4**: IR (nujol) 1680, 1670, 1600 cm^{-1} (lit,[5] IR (KBr) 1690, 1670, 1600 cm^{-1}); ^{1}H NMR ($CDCl_3$) δ=0.73—2.02 (m, 66H), 2.60—3.09 (m, 4H), 7.00—8.37 (m, 8H). Found: C, 78.32; H, 10.01; N, 3.51%. Calcd for $C_{52}H_{78}N_2O_4$: C, 78.54; H, 9.88; N, 3.52%. **5**: IR (nujol) 1710, 1680, 1600 cm^{-1}; ^{1}H NMR ($CDCl_3$) δ=0.35—2.30 (m, 20H), 2.70—3.34 (m, 2H), 7.00—8.37 (m, 8H). Found: C, 74.79; H, 6.30; N, 5.78%. Calcd for $C_{30}H_{30}N_2O_4$: C, 74.67; H, 6.27; N, 5.81%. **6**: IR (nujol) 1700, 1660, 1590 cm^{-1} (lit,[5] IR (KBr) 1700, 1660, 1590 cm^{-1}); ^{1}H NMR ($CDCl_3$) δ=6.95—8.10(m, 18H). Found: C, 76.30; H, 3.80; N, 5.76%. Calcd for $C_{30}H_{18}N_2O_4$: C, 76.58; H, 3.86; N, 5.96%. **7**: IR (nujol) 1700, 1670, 1600, 830 cm^{-1}; ^{1}H NMR ($CDCl_3$) δ=2.43 (s, 6H), 6.90—7.49 (m, 10H), 7.49—8.14 (m, 6H). Found: C, 77.03; H, 4.24; N, 5.45%. Calcd for $C_{32}H_{22}N_2O_4$: C, 77.09; H, 4.45; N, 5.62%. **8**: IR (nujol) 1700, 1660, 1600, 830 cm^{-1}; ^{1}H NMR ($CDCl_3$) δ=6.90—7.80 (m, 8H), 7.44 (d, J=8Hz, 4H), 7.94 (d, J=8Hz, 4H). Found: C, 66.62; H, 2.86; N, 5.30%. Calcd for $C_{30}H_{16}N_2O_4Cl_2$: C, 66.80; H, 2.99; N, 5.19%. **9**: IR (nujol) 1700, 1675, 1600 cm^{-1}; ^{1}H NMR ($CDCl_3$) δ=6.50—8.65 (m, 22H). Found: C, 79.80; H, 3.77; N, 4.78%. Calcd for $C_{38}H_{22}N_2O_4$: C, 79.99, H, 3.89; N, 4.91%.

Solvents. Acetonitrile, acetone, and toluene of the reagent grade were purified by drying over calcium chloride, calcium sulfate, and sodium wire, respectively, and distillation.

Apparatus and Procedure. The high-pressure technique and the procedure for kinetic measurements were the same as those described elsewhere.[3] A solution containing an appropriate concentration of DAI (10^{-4} mol/l) in a pressure vessel was irradiated with a 650-W tungsten projection lamp through a filter of potassium dichromate solution to produce the *cis*-isomer. Then, the absorption maximum (λ_{max}=*ca.* 570 nm) of the *trans*-isomer was monitored by means of a Hitachi 100—50 spectrophotometer and the absorbance was recorded.

Results and Discussion

The thermal isomerization of DAI was carried out at various temperatures. It was found that the rate follows first-order kinetics. The rate constants are listed in Table 1, together with the activation pa-

Table 1. Rate constants and activation parameters for the thermal isomerization of DAI (probable errors in parentheses)

Compd No.	Solvent	λ_{max}^{trans} nm	$10^4 k/s^{-1}$ 30 °C	40 °C	50 °C	60 °C	70 °C	E_a kJ mol^{-1}	ΔS^*_{323K} J K^{-1} mol^{-1}
1	Acetonitrile	551		0.914(0.011)	2.85(0.01)	6.75(0.02)	17.7(0.2)	86.6(1.7)	−53.6(5.0)
1	Acetone	552	0.556(0.006)	1.58(0.02)	3.49(0.02)			74.9(3.3)	−87.9(10.0)
1	Toluene	561	0.204(0.006)	0.842(0.034)	1.67(0.02)			85.8(10.5)	−59.4(33.9)
2	Toluene	568		0.926(0.008)	2.59(0.02)	6.24(0.03)		82.8(1.7)	−66.5(4.6)
3	Toluene	577		0.550(0.006)	1.69(0.01)	4.20(0.01)		88.3(2.5)	−53.6(7.9)
4	Toluene	570		1.03(0.03)	3.17(0.02)	7.76(0.10)		87.4(2.9)	−50.2(8.8)
5	Toluene	580		0.898(0.008)	2.64(0.01)	6.90(0.07)	26.8(0.7)	99.2(4.2)	−15.1(13.0)
6	Toluene	574			0.200(0.004)	0.764(0.010)	1.80(0.01)	101(7)	−29.3(22.2)
7	Acetone[a]	575	0.0452(0.0003)	0.137(0.013)	0.533(0.007)			100(5)	−25.1(16.3)
8	Acetone[a]	578	0.0658(0.0004)	0.225(0.004)	0.533(0.011)			85.4(4.6)	−70.3(15.5)
9	Toluene	580			0.472(0.003)	1.35(0.02)	2.66(0.05)	80.0(5.9)	−89.2(17.2)

a) **7** and **8** are sparingly soluble in toluene.

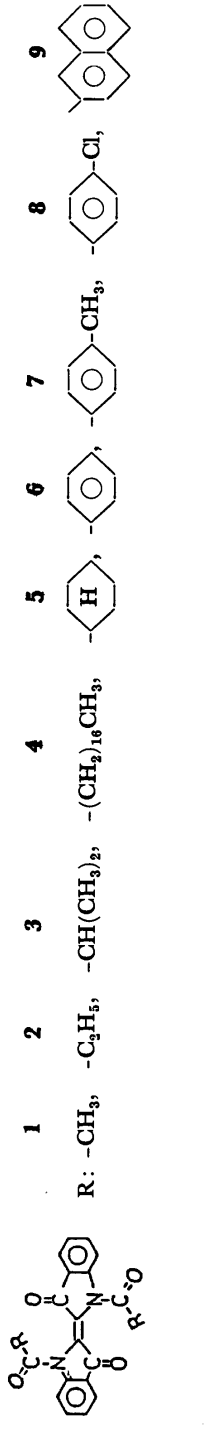

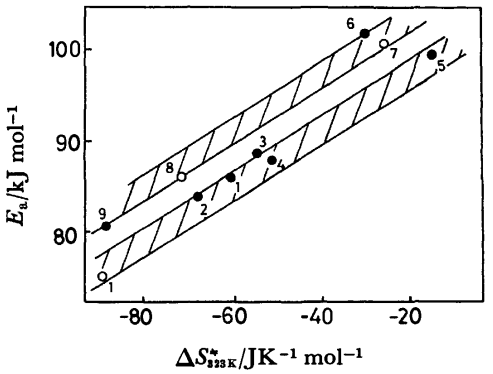

Fig. 1. Ea—$\Delta S^{\neq}_{323K}$ relationship for the thermal isomerization of DAI. ●: in toluene, ○: in acetone.

rameters. Figure 1 shows the relationship between the activation energy and entropy. It may be seen that the activation energy tends to increase with an increase in the activation entropy as a whole. From the figure, we notice the following point: the plots for **6—9** shift upward compared with the others. According to Leffler,[9] a linear enthalpy-entropy relationship suggests the simple interaction mechanism. If the activation enthalpy-entropy plots are scattered, more than two interactions must be operating. Shinkai and co-workers[2] showed that the activation enthalpy-entropy plots for the isomerization of azobenzenes give parallel straight lines and accounted the root of the parallel straight lines as the change in mechanism. In opposition to this idea, we have explained[3] that the shift is not due to a mechanism change but, rather, to the extra free-energy change. We consider that the same is true in the present case (see below).

DAI has electron-donating and -attracting groups. Therefore, there are two possible routes for the thermal isomerization (see IV and V). If a reaction starts from a nonpolar state and proceeds *via* a polar transition state (*e.g.*, IV), the reaction rate will be substantially accelerated in polar solvents. However, it was not the case (Table 1). We reported that the wavelengths(λ^{trans}_{max}) at the maximum absorption of the *trans*-isomer of push-pull azobenbenes are sensitive to the solvent polarity and are closely related to the rate of isomerization.[3] In the case of DAI, we observed that the absorption band shifts to a shorter wavelength as the solvent polarity increases (for example, **1** in Table 1). It appears, therefore, that the *trans*-ground state is somewhat more polar than the excited one. However, as far as our data are concerned, no correlation between λ^{trans}_{max} and the rate constant seems to exist. *Trans*-DAI is twisted around the central C=C double bond and the C-N bond of the acyl group and the extent of the twist may depend on the bulkiness of substituents (R). Since the twist causes a reduction in the resonance contribution (VI), the polarity of the *trans*-ground state will be diminished by the introduction of bulky substituents. Since the *trans*-ground state

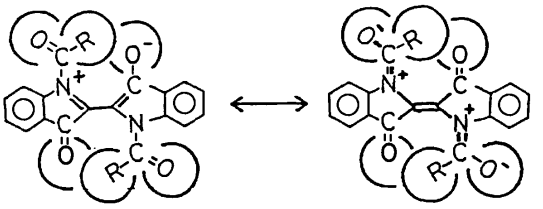

VI

may be more polar than the excited one, as described above, the decrease in the polarity of the ground state due to the bulkiness of substituent gives rise to a longer wavelength shift. This is in accord with the experimental observations (Table 1). On the other hand, *cis*-DAI is originally extremely twisted around the C=C double bond, and this might be responsible for the small substituent effect on the rate. However, it is of great interest to note that the rate constants for the isomerization of **6—9** are about 10 times smaller than those of **1—5**. A plausible reason will be given later.

Pressure Effects. Table 2 shows the pressure effects on the thermal isomerization in some solvents. The reactions are slightly retarded by external pressures. By using the data in Table 2, the activation volumes ($\Delta V^{\neq}$) at p=1 atm were estimated according to Eq 2.

$$\ln k = a + bp \tag{1}$$

$$\Delta V^{\neq} = -RT\left(\frac{\partial \ln k}{\partial p}\right)_{T,p=1} = -bRT \tag{2}$$

The activation volume ($\Delta V^{\neq}$) is usually divided into two terms:

$$\Delta V^{\neq} = \Delta V^{\neq}_{i} + \Delta V^{\neq}_{el} \tag{3}$$

where $\Delta V^{\neq}_{i}$ is the difference in the intrinsic volume of reacting molecules between the initial and the transition state and $\Delta V^{\neq}_{el}$ due to solvation or electrostriction. The values of the activation volume decrease slightly with an increase in the solvent polarity: from $\Delta V^{\neq}$(acetonitrile)=3.6 cm^3 mol^{-1} to $\Delta V^{\neq}$(toluene)=1.9 cm^3 mol^{-1} in **1**, from $\Delta V^{\neq}$(acetonitrile)=3.3 cm^3 mol^{-1} to $\Delta V^{\neq}$(toluene)=−0.6 cm^3 mol^{-1} in **5** (Table 2). The above solvent dependency indicates that the transition state is slightly more polar than the *cis*-state. In the transition state, the crowded-

ness between the two acyl groups would be relaxed compared to the *cis*-ground state. Then, a resonance contribution, such as

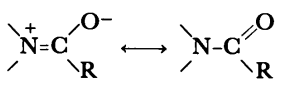

VII

Table 2. Rate constants and activation volumes for the thermal isomerization of DAI at 50 °C (probable errors in parentheses)

Compd No.	Solvent	p/kg cm^{-2} [a]	$10^4 k/s^{-1}$ 1	400	800	1200	$\Delta V^{\ddagger}$ / cm^3 mol^{-1}
1	Acetonitrile		2.85 (0.01)	2.65 (0.02)	2.53 (0.02)	2.43 (0.01)	3.6 (0.2)
1	Acetone		3.49 (0.01)	3.41 (0.01)	3.19 (0.11)	3.21 (0.05)	2.2 (0.4)
1	Toluene		1.67 (0.02)	1.63 (0.04)	1.58 (0.04)	1.54 (0.02)	1.9 (0.1)
2	Toluene		2.59 (0.02)	2.43 (0.01)	2.33 (0.02)	2.26 (0.05)	3.1 (0.2)
3	Toluene		1.69 (0.01)	1.60 (0.01)	1.53 (0.01)	1.45 (0.01)	3.5 (0.1)
4	Toluene		3.17 (0.02)	3.04 (0.02)	2.93 (0.02)	2.78 (0.02)	3.0 (0.1)
5	Acetonitrile		3.62 (0.03)	3.49 (0.05)	3.25 (0.05)	3.15 (0.01)	3.3 (0.3)
5	Toluene		2.64 (0.01)	2.67 (0.01)	2.64 (0.03)	2.73 (0.02)	−0.6 (0.3)
6	Acetone		0.366 (0.007)	0.328 (0.005)	0.273 (0.004)	0.248 (0.002)	9.3 (0.5)
6	Toluene		0.200 (0.004)	0.178 (0.002)	0.155 (0.001)	0.142 (0.002)	8.0 (0.3)
7	Acetone		0.533 (0.007)	0.488 (0.007)	0.452 (0.007)	0.396 (0.005)	6.6 (0.4)
8	Acetone		0.533 (0.011)	0.478 (0.007)	0.430 (0.005)	0.376 (0.005)	7.9 (0.2)
9	Toluene		1.35 (0.02) [b]	1.21 (0.03) [b]	1.10 (0.01) [b]	1.03 (0.01) [b]	6.4 (0.3) [b]

a) 1 kg cm^{-2} = 0.9807 bar. b) at 60 °C.

becomes greater in the transition state than in the *cis*-state. This accounts for the above observations. The volume of activation is, as a whole, small and positive. The positive values of activation volume may be explained in terms of the increase in the intrinsic volume. Since the bond character of the central carbon-carbon bond varies from the C=C double bond to the C-C single bond in the activation process, the bond length must become longer. On the assumption that the central C-C distance increment is 0.21 Å (difference in the distance between the C-C single bond and the C=C double bond) and the thickness of the molecule 3.4 Å, the increase in the van der Waals volume ($\Delta V_W^{\ddagger}$) is calculated to be about 1.5 cm^3 mol^{-1}. Hitherto, the intrinsic volume change upon activation has often been ascribed to the van der Waals volume change. Very recently, however, Yoshimura *et al.*[10] pointed out that there is a large gap between $\Delta V^{\ddagger}$ and $\Delta V_W^{\ddagger}$, and between ΔV and ΔV_W for 1,3-dipolar cycloaddition reactions. Indeed, the molar volumes of normal alkanes of short chain are about twice of their van der Waals volumes. Therefore, $\Delta V^{\ddagger}$ may be $\approx$3 cm^3 mol^{-1}, which agrees with the experimental values. Alternatively, the change in the void volume[11] around the van der Waals volume might be responsible for the gap between $\Delta V^{\ddagger}$ and $\Delta V_W^{\ddagger}$.

It is noted that in **1—5** and **6—9**, significant differences between the activation volumes as well as the rate constants were observed. Cristol and Lewis[12] showed the significant differences of ultraviolet spectra in janusene which has face-to-face rings close enough to interact. Ingraham[13] suggested that if two benzene rings are brought face-to-face (3 Å apart), the VB and LCAO methods predict that there is 4 kcal more resonance energy than for two infinitely separated benzene rings. On the other hand, Cram and Goldstein[14] reported that in the solvolysis of [9]paracyclophanyl tosylate, the interaction between the phenyl ring and a carbonium ion takes place. In the case of *cis*-DBI, the molecular structure has not been established yet. As plausible models, the following conformations may be proposed (Fig. 2). Then, the interactions just described must exist for each conformation: (a) The interaction between the two phenyl rings in the acyl groups which are held face-to-face and (b) the interaction between the phenyl ring in the acyl group and >N- group are important. It is difficult to decide which of the two conformations is more favorable. As far as $\Delta V^{\ddagger}$ is concerned, the face-to-face conformation appears more plausible. It appears that the volume change on going from conformation (b) to the activated state may be similar to those observed for **1—5** since the situation around the benzene rings in solution to the surrounding solvent molecules will not change between (b) and activated complex. Meanwhile, in the face-to-face conformation, the independent mo-

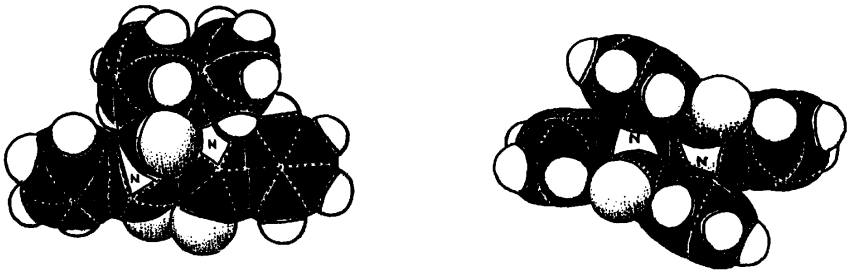

(a) (b)

Fig. 2. Plausible geometical models of *cis-N,N'*-dibenzoylindigo: (a) phenyl-phenyl interaction and (b) phenyl- >N- interaction.

tion of the two benzene rings will be partly restricted, resulting in a smaller exclusion of solvent molecules. This may be responsible for the values of $\Delta V^{\neq}$ for **6—9** compared with those for **1—5**. We tentatively consider that the *cis*-isomer of **6—9** is stabilized by the additional interaction, which is responsible for the significant differences in the rates (Table 1) and the $\Delta V^{\neq}$-values (Table 2), and the upward shift of the activation energy-entropy relationship (Fig. 1).

References

1) P. D. Wildes, J. G. Pacific, G. Irick, and D. G. Whitten, *J. Am. Chem. Soc.*, **93**, 2004 (1971); K. S. Schane, T. P. Mattox, and D. G. Whitten, *ibid.*, **104**, 1733 (1982).

2) T. Asano, *J. Am. Chem. Soc.*, **102**, 1205 (1980); T. Asano, T. Okada, S. Shinkai, K. Shigematsu, Y. Kusano, and O. Manabe, *ibid.*, **103**, 5161 (1981); T. Asano and T. Okada, *ibid.*, **104**, 4900 (1982).

3) N. Nishimura, S. Kosako, and Y. Sueishi, *Bull. Chem. Soc. Jpn.*, **57**, 1617 (1984).

4) M. Calvin and H. W. Alter, *J. Chem. Phys.*, **19**, 768 (1951).

5) Y. Omote, S. Imada, R. Matsuzaki, and K. Fujiki, *Bull. Chem. Soc. Jpn.*, **52** 3397 (1979).

6) J. Blanc and D. L. Ross, *J. Phys. Chem.*, **72** 2818 (1968).

7) H. Wakemoto, J. Setsune, K. Matsukawa, S. Ishihara, R. Yamamoto, and T. Kitao, 46rd National Meeting of the Chemical Society of Japan, Niigata, October 1982, Abstr., No. 3B13.

8) T. Posner, *Ber.*, **59B**, 1977 (1926).

9) J. E. Leffler, *J. Org. Chem.*, **31**, 533 (1966).

10) Y. Yoshimura, J. Osugi, and M. Nakahara, *J. Am. Chem. Soc.*, **105**, 5414 (1983).

11) T. Asano and W. J. Noble, *Rev. phys. Chem. Jpn.*, **43**, 82 (1973).

12) S. J. Cristol and D. C. Lewis, *J. Am. Chem. Soc.*, **89**, 1476 (1967).

13) L. L. Ingraham, *J. Chem. Phys.*, **18**, 988 (1950).

14) D. J. Cram and M. Goldstein, *J. Am. Chem. Soc.*, **85**, 1063 (1963).

The Spectrophotometric Determination of Phosphorus with *o*-Hydroxyhydroquinonephthalein and Iron(III)†

Yoshikazu FUJITA, Itsuo MORI,* Shoko KITANO, Hiroshi KAWABE, and Yozo KOSHIYAMA

Osaka College of Pharmacy, 2-10-65, Kawai Matsubara, Osaka 580

(Received August 27, 1984)

On this basis of the coloration formed with *o*-hydroxyhydroquinonephthalein, an anionic dye, and iron (III) in aqueous media, trace amounts of phosphorus(as orthophosphate ion) was determined. A sample solution containing posphorus and the reagent blank in an amber-colored test tube with a stopper were heated at 40 °C for 20 min in the presence of poly(oxyethylene)sorbitan monolaurate, a nonionic surfactant, as a dispersion agent. Beer's law was obeyed over the range of ≈1 μg/10 cm³ of phosphorus, and the apparent molar absorptivity of the complex was 2.5×10^5 dm³ mol^{-1} cm^{-1} at 610 nm. The present method was applied to the determination of total phosphorus in water — a sample solution containing small amounts of metal ions —, and the recovery percentage was satisfactory, about 95%. Other compounds containing phosphorus such as 5′-adenosine triphosphate could also be determined without a preliminary treatment.

Recently, various sensitive spectrophotometric methods for the determination of phosphorus have been reported.[1-19] Most of these methods are based upon the formation of heteropoly acids such as molybdophosphate ion, or the ionic-association complex formation with cationic dyes such as Crystal Violet,[4-7] Ethyl Violet(EV),[8,9] Malachite Green(MG),[10-14] Methylene Blue,[15] Safranin T[16,17] and Rhodamine B.[18,19] However, little work has been done on the determination of phosphorus by using an anionic dye, though an indirect method[20,21] has been studied by utilizing the coloration between molybdenum(VI) freed from heteropolyacid and Pyrocatechol Violet (PV).

Meanwhile, we noticed that the addition of micro amounts of phosphorus (as orthophosphate ion) to the reaction mixture between iron(III) and *o*-hydroxyhydroquinonephthalein(Qnph), an anionic dye, produced a different spectrum than that of the Qnph-iron(III) complex solution in a weakly basic medium.

In this paper, optimum conditions for a new spectrophotometric determination of micro amounts of phosphorus using Qnph and iron(III) were studied, and phosphorus as well as compounds containing phosphorus in water was determined.

Experimental

Reagents and Materials. A standard solution (1.0×10^{-2} mol dm^{-3}) of phosphorus was prepared by dissolving a proper quantity of potassium dihydrogenphosphate (Merck) in water, which was dried at 110 °C to a constant weight. The working solution (5.0×10^{-5} mol dm^{-3}) was made by diluting this stock solution as required. A Qnph solution (1.0×10^{-3} mol dm^{-3}) in methanol was prepared by dissolving Qnph synthesized by the published procedure.[22] An iron(III) solution (5.0×10^{-4} mol dm^{-3}) was prepared by dissolving a proper quantity of iron(III) ammonium sulfate in 5 cm³ of 1.0% sulfuric acid and diluting the mixture to 100 cm³ with water. A 5.0% poly(oxyethylene)sorbitan monolaurate (Nihon Yushi Co. Ltd., LT-221) solution was prepared by dissolving it with water. A solution (1.0×10^{-1} mol dm^{-3}) of sodium tetraborate(borax) was prepared as a buffer solution. All the other reagents and materials were of an analytical grade and were used without further purification. Doubly distilled water was used.

Apparatus. A Shimadzu Model UV-240 recording spectrophotometer with 1.0-cm quartz cells was used for the absorption spectrum and absorbance measurements. A Hitachi-Horiba Model F-7 AD glass electrode pH meter was used for the pH measurements.

Standard Procedure for the Determination of Phosphorus. To a solution containing up to 1 μg phosphorus in a 10 cm³ volumetric flask were added 1.0 cm³ of a 5.0% LT-221 solution, 0.5 cm³ of a 5.0×10^{-4} mol dm^{-3} iron(III) solution, 4.0 cm³ of a 1.0×10^{-1} mol dm^{-3} borax solution, and 0.5 cm³ of a 1.0×10^{-3} mol dm^{-3} Qnph solution. The mixture was diluted to 10 cm³ with water, and the solution was transferred to an amber-colored test tube with a stopper, kept at 40 °C for 20 min and then cooled to room temperature. The absorbance of the Qnph-iron(III)-phosphorus solution (Solution A) was measured at 610 nm against the Qnph-iron(III) solution(Solution B).

Results and Discussion

Color Reaction and Absorption Spectra. The addition of the phosphorus solution to Solution B exhibited an extreme increase in absorbance, and its absorbance at around 610 nm was proportional to the concentration of phosphorus. The reproducibility of color development of Solutions A and B without a surfactant was unfavorable. The use of a nonionic surfactant such as LT-221 was effective as a dispersion agent.

The effect of dyes in this reaction system was examined by measuring the difference of absorbance between a dye-iron(III)-phosphorus solution and a dye-iron(III) solution. The use of xanthene dyes such

† Application of Xanthene Derivatives for Analytical Chemistry. Part 45. Part 44: Y. Fujita, I. Mori, S. Kitano, and Y. Kamada, *Bunseki Kagaku*, 33, E445 (1984).

as Qnph, phenylfluorone(Phfl), Pyrogallol Red(PR) and gallein(Gall) enhanced the absorbance of the dye-iron(III) solution. The reaction sensitivity among Qnph, Phfl, PR, and Gall decreased in the sequence: Qnph≧Phfl ≫ PR and Gall. As for other dyes such as Xylenol Orange, Chromazurol S, PV, and 1-(2-pyridylazo)-2-naphthol, no difference of absorption spectra between the dye-iron(III)-phosphorus solution and the dye-iron(III) solution was observed under the standard conditions.

The effect of metal ions was also examined. Iron(III) or iron(II) ion was effective among the various metal ions tested: iron(III), iron(II), copper(II), aluminum (III), cerium(III), manganese(II), thorium(IV), molybdenum(VI), vanadium(V), cobalt(II), *etc.* Iron(III) was fairly superior to iron(II) in terms of sensitivity.

On the basis of these results, Qnph and iron(III) were chosen for the purpose of fundamental investigations on the determination of phosphorus.

The absorption spectra of Solution A, Solution B and Qnph solution under the standard conditions are shown in Fig. 1.

Effect of pH. The effect of pH on the color development was investigated with a solution containing 0.62 μg/10 cm^3 phosphorus. The maximum and nearly constant absorbance was observed at pH 9.0—9.6. A borax buffer was most effective in terms of sensitivity among the various buffer solutions, such as borax, ammonia-ammonium chloride and carbonate-hydrogencarbonate solutions. In addition, the color reaction between Qnph and various metal ions in borax solution was limited than that in the other buffer solutions, and the influence of other metal ions was relatively small. The constant absorbance was observed upon the addition of more than 3.0 cm^3 of 1.0×10^{-1} mol dm^{-3} borax in the final volume of 10 cm^3. Accordingly, 4.0 cm^3 of 1.0×10^{-1} mol dm^{-3} borax solution (pH 9.3) was used as the buffer solution.

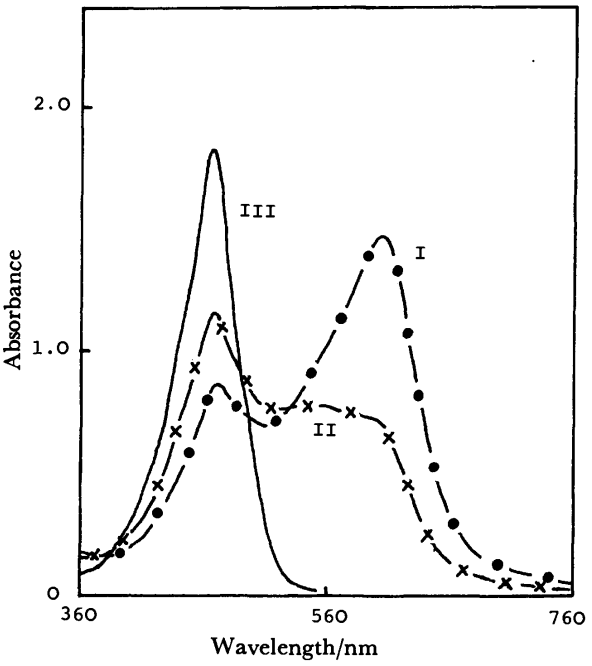

Fig. 1. Absorption spectra of Qnph-iron(III)-phosphorus, Qnph-iron(III) and Qnph solutions.
Phosphorus: 3.0×10^{-6} mol dm^{-3}; iron(III): 2.5×10^{-5} mol dm^{-3}; Qnph: 5.0×10^{-5} mol dm^{-3}; LT-221: 1.0 cm^3 of 5.0% LT-221 solution/10ml; borax: 4.0×10^{-2} mol dm^{-3}; Reference: water; curve I: Qnph-iron (III)-phosphorus solution; curve II: Qnph-iron(III) solution; curve III : Qnph solution.

Effect of Surfactants. Among various surfactants tested, LT-221, a nonionic surfactant, was best as a dispersion agent; the maximum and constant absorbance of Solution A against Solution B was observed upon the addition of more than 0.5 cm^3 of a 5.0% LT-221 solution to the final volume of 10 cm^3. The results are given in Table 1.

Effects of Qnph and Iron(III) Concentrations. The effects of the amounts of Qnph and iron(III) were examined by varying the molar ratio of iron(III) to Qnph, the amount of phosphorus being kept constant. As is shown in Fig, 2, the maximum and constant absorbance at 610 nm was observed upon the addition of a 0.4—0.6 cm^3 of 5.0×10^{-4} mol dm^{-3} iron(III) solution in the final volume of 10 cm^3. By the way, the molar ratio of iron(III) to Qnph in the reaction system was found to be 1:2 by the molar-ratio method in the presence of phosphorus. Accordingly, all further work was carried out with 2.5×10^{-5} mol dm^{-3} iron (III) and 5.0×10^{-5} mol dm^{-3} Qnph in the final volume.

Temperature and Stability. The absorbance of Solution A at 610 nm against Solution B was

Table 1. Effect of surfactants

Surfactants	Absorbance	at λ_{max}
None	0.250	610
LT-221	0.495	610
Poly(oxyethylene)sorbitan monooleate	0.475	610
Polyethylene glycol mono[*p*-(6-methylheptyl)phenyl]ether	0.490	610
Poly(vinyl alcohol)(*n*: 500)	0.465	610
Poly(*N*-vinylpyrrolidone) (K-30)	0.235	615
Gum arabic	0.028	600
Sodium dodecylsulfate	0.375	595
Sodium dodecylbenzenesulfonate	0.028	590
Hexadecyltrimethylammonium chloride	0.225	620
Benzyldimethyltetradecyl-ammonium chloride	0.180	620

P taken: 0.62 μg/10 cm^3; Fe(III): 2.5×10^{-5} mol dm^{-3}; Qnph: 5.0×10^{-5} mol dm^{-3}; surfactant: 2.0 cm^3 of 2.0% surfactant solution/10 cm^3; borax: 4.0×10^{-2} mol dm^{-3}; Reference: Solution B.

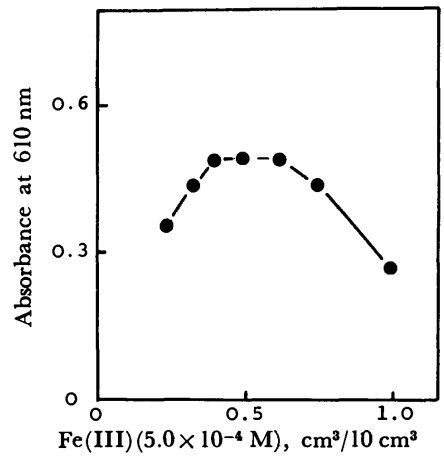

Fig. 2. Effect of iron(III) concentration.
Phosphorus: 2.0×10^{-6} mol dm^{-3}(0.62 μg/10 cm^3); Qnph: 5.0×10^{-5} mol dm^{-3}; LT-221: 1.0 cm^3 of 5.0% LT-221 solution/10 cm^3; borax: 4.0×10^{-2} mol dm^{-3}; Reference: Solution B.

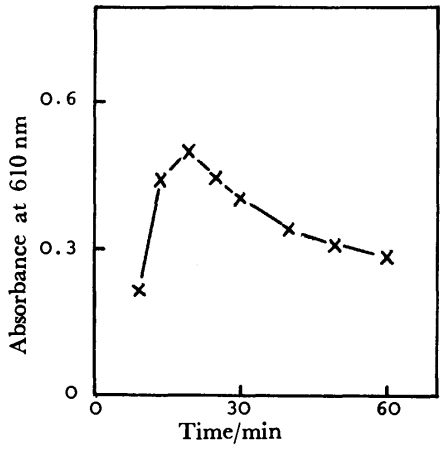

Fig. 3. Relationship between absorbance and heating time at 40 °C.
Phosphorus: 2.0×10^{-6} mol dm^{-3}; iron(III): 2.5×10^{-5} mol dm^{-3}; Qnph: 5.0×10^{-5} mol dm^{-3}; LT-221: 1.0 cm^3 of 5.0% LT-221 solution/10cm^3; borax: 4.0×10^{-2} mol dm^{-3}; Reference: Solution B.

unconstant instantaneously at room temperature (15—25 °C), and more than 6 h was required to obtain a nearly constant absorbance. The effect of the temperature was examined by heating the mixed solution for 10—60 min at various temperatures (35 °C, 40 °C, 45 °C, or 50 °C); the favorable result was obtained by heating the solution at 40 °C for 20 min and then cooling it to room temperature. The relationship between absorbance and heating time at 40 °C is shown in Fig. 3.

On the other hand, Solutions A and B were found to be fairly unstable and lacked reproducibility in diffused light. The reason was probably that Qnph in borax solution easily decomposed by light. The disadvantage is conveniently improved by the use of an amber-colored test tube.

From the results described above, the absorbance of Solution A at 610 nm against Solution B was almost constant for at least 3 h at room temperature under the standard conditions.

Calibration Curve and Repeatability. The calibration curve for phosphorus was constructed according to the standard procedure. Beer's law held in the concentration range of ≈1 μg of phosphorus in the final volume of 10 cm^3. The apparent molar absorptivity at 610 nm was estimated to be 2.5×10^5 dm^3 mol^{-1} cm^{-1}, and the Sandell sensitivity was calculated to be 0.00013 μg cm^{-2} for phosphorus. The coefficient of variation (n=8) was 2.5% for 0.62 μg of phosphorus.

Effects of Foreign Ions. The effects of foreign ions on the determination of phosphorus were examined. Among metal ions tested, small amounts of vanadium(V), zirconium(IV) and copper(II) interfered, but iron(III), aluminum(III) and arsenic(V) did not interfere in equimolar amounts with respect to phosphorus. Divalent heavy metal ions such as manganese(II), cobalt(II), zinc(II) and lead(II) did not interfere in the 5- to 10-fold excess over phosphorus, and other metal ions such as magnesium(II) and calcium(II) did not interfere in the 100-fold excess. Among various anions tested, the presence of small amounts of organic acids such as tartrate and citrate ions, and large amounts of oxalate, thiocyanate, thiosulfate and cyanide ions interfered. Other anions such as nitrate, chloride, and sulfate ions scarcely affected the determination of phosphorus. However, when strong electrolytes were present more than 5000-fold molar excess of phosphorus, it was necessary to measure the difference of absorbance between Solutions A and B containing the same ingredients. The results are summarized in Table 2.

The Composition of the Complex. The molar ratio of iron(III) to Qnph in the presence of phosphorus was estimated by the molar-ratio and continuous-variation methods. The results indicated that the molar ratio of iron(III) to Qnph was 1:2. The result obtained by the continuous-variation method is shown in Fig. 4. The phosphorus-to-iron(III) ratio obtained by the molar-ratio method was 1:2, as is shown in Fig. 5. From the results, the ternary complex formed in this reaction system is expressed as [phosphorus 1: iron(III) 2: Qnph 4].

Application for the Determination of Phosphorus in Water. The present method was applied to the determination of phosphorus in water (effluent of treated waste water and rain water). On the other hand, orthophosphate ion and total phosphorus in the same samples were determined according to the JIS method.[23] The experimental results for total phosphorus were in good agreement with the JIS method.[23] Recovery of phosphorus added to the

TABLE 2. EFFECT OF FOREGIN IONS

Ions	Added as	Added (μg/10 cm^3)	Added Mole ratio[a)]	P, Found (μg/10 cm^3)	Recovery %
—	—	—	—	0.62	100.0
Fe(III)	Iron alum	5.6	5	1.14	183.9
		0.6	0.5	0.62	100.0
Al(III)	$AlCl_3$	2.7	5	1.02	164.5
		0.5	1	0.62	100.0
As(V)	Na_2HAsO_4	3.7	2.5	0.84	135.5
		1.5	1	0.62	100.0
Cu(II)	$Cu(NO_3)_2$	1.2	1	0.87	140.3
Zr(IV)	$ZrCl_4$	1.8	1	0.51	82.3
V(V)	NH_4VO_3	0.5	0.5	0.76	122.6
Mn(II)	$MnCl_2$	5.5	5	0.62	100.0
Co(II)	$Co(NO_3)_2$	5.9	5	0.62	100.0
Zn(II)	$ZnCl_2$	5.5	5	0.62	100.0
Pb(II)	$PbCl_2$	20.7	5	0.62	100.0
Ca(II)	$CaCl_2$	80.2	100	0.62	100.0
$C_2O_4^{2-}$	$Na_2C_2O_4$	17.6	10	0.54	87.1
Citrate	Sodium citrate	3.8	1	1.28	206.5
Tartrate	Sodium tartrate	3.0	1	0.86	138.7
SCN^-	NH_4SCN	11.6	10	0.51	82.3
NO_2^-	$NaNO_2$	92.0	100	0.62	100.0
CN^-	KCN	5.2	10	0.62	100.0
$S_2O_3^{2-}$	$Na_2S_2O_3$	22.4	10	0.62	100.0
F^-	NaF	76.0	200	0.62	100.0
I^-	KI	507.6	200	0.62	100.0
Cl^-	NaCl	141.8	200	0.62	100.0
NO_3^-	KNO_3	1240.1	1000	0.62	100.0
SO_4^{2-}	Na_2SO_4	1921.0	1000	0.62	100.0

P taken: 0.62 μg/10 cm^3; Fe(III): 2.5×10^{-5} mol dm^{-3}; Qnph: 5.0×10^{-5} mol dm^{-3}; LT-221: 1.0 ml of 5.0% LT-221 solution/10 cm^3; Borax: 4.0×10^{-2} mol dm^{-3}; Reference: Solution B. a) Ion/Phosphorus.

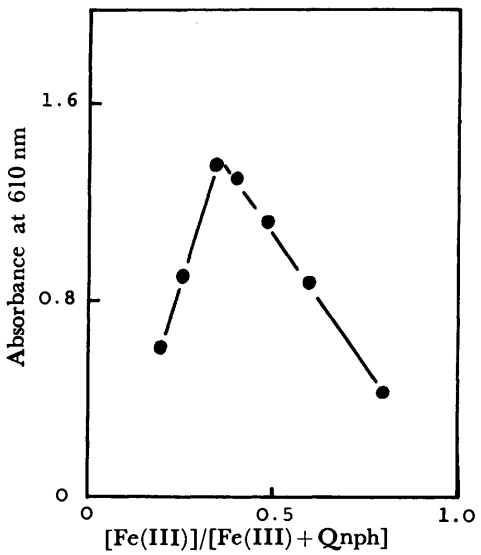

Fig. 4. Composition of [iron(III): Qnph] in the presence of phosphorus obtained by the continuous-variation method.
[iron(III)+Qnph]=5.0×10^{-5} mol dm^{-3}; phosphrus: 5.0×10^{-4} mol dm^{-3}; LT-221: 1.0 cm^3 of 5.0% LT-221 solution/10 cm^3; borax: 4.0×10^{-2} mol dm^{-3}; Reference: Solution B.

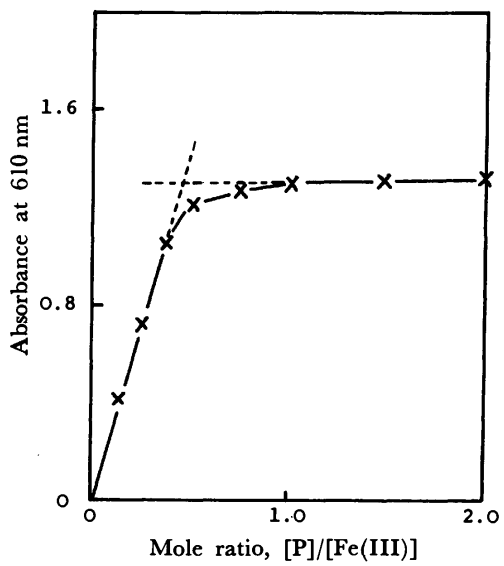

Fig. 5. Composition of [iron(III): Qnph] obtained by the molar-ratio method.
Iron(III): 2.0×10^{-5} mol dm^{-3}; Qnph: 5.0×10^{-5} mol dm^{-3}; phosphorus: 1.0×10^{-4} mol dm$^{-3}\times$X cm^3/10 cm^3; LT-221: 1.0 cm^3 of 5% LT-221 solution/10 cm^3; borax: 4.0×10^{-2} mol dm^{-3}; Reference: Solution B.

TALE 3. ANALYTICAL RESULTS OF PHOSPHORUS IN WATER

Samples	Methods[a]	P, Found[b] (ppm)		Recovery % of the proposed method[c]/%
		Proposed method	JIS method	
A	(1)[a]	0.54	0.15	96.8
	(2)[a]	1.04	0.98	94.6
B	(1)[a]	0.23	0.17	104.3
	(2)[a]	0.25	0.22	96.0

Sample A, effluent of treated waste water supplied from the Center for Conservation, Osaka College of Pharmacy (April 17, 1984); Sample B, rain water on the campus of Osaka College of Pharmacy (April 19, 1984). a) Method (1), Phosphate ion was determined according to the JIS method; a) Method (2), Total phosphorus was determined according to the JIS method. b) Mean of 5 determinations. c) P taken, 0.31 μg/10 cm³; mean of 5 determinations.

TABLE 4. APPARENT MOLAR ABSORPTIVITIES FOR VARIOUS SUBSTANCES CONTAINING PHOSPHORUS BY THE STANDARD PROCEDURE

Substances	ε/dm³ mol⁻¹ cm⁻¹
PO_4^{3-}	2.5×10^5
$P_2O_7^{4-}$	1.7×10^5
$P_3O_{10}^{5-}$	2.0×10^5
5′-Adenine triphosphate	2.3×10^5
Flavin-adenine dinucleotide	8.0×10^4
β-Nicotinamide-adenine dinucleotide	1.9×10^4
D-Glucose 6-phosphate	4.2×10^4
Inosine 5′-phosphate	1.4×10^5
Triphenyl phosphate	2.5×10^3

Fe(III): 2.5×10^{-5} mol dm⁻³; Qnph: 5.0×10^{-5} mol dm⁻³; LT-221: 1.0 cm³ of 5.0% LT-221 solution/10 cm³; Borax: 4.0×10^{-2} mol dm⁻³; Reference: Solution B.

samples was satisfactory, about 95%. The results are given in Table 3.

Application to Other Compounds Containing Phosphorus. By using the standard procedure for the determination of phosphorus, other compounds containing phosphorus were measured without a preliminary treatment. Approximate apparent molar absorptivities of these compounds were calculated from the absorbance of Qnph–iron(III)-compounds containing phosphorus solutions at 610 nm against Solution B. The results are given in Table 4.

Conclusion

The fundamental conditions for the determination of phosphorus based on the ternary complex-formation with Qnph, an anionic dye, and iron(III) were discussed, and a new spectrophotometric method for micro amounts of phosphorus has been established. This method is applicable in the concentration range of ≈1 μg phosphorus in the final volume of 10 cm³. The apparent molar absorptivity in this procedure was estimated to be 2.5×10^5 dm³ mol⁻¹ cm⁻¹ for phosphorus. In sensitivity, this method is comparable to the EV-extraction method[9] or MG-extraction method.[13] The present method is aplicable to the determination of total phosphorus in samples containing micro amounts of metal ions, and an application to the determination of organic compounds containing phosphorus without a suitable preliminary treatment may also be feasible.

Though further investigation is necessary, the method proposed here gives an important suggestion for determining phosphorus by using an anionic dye.

References

1) S. Motomizu, *Bunseki Kagaku*, **1983**, 961.
2) K. Sugawara and S. Kanamori, *Bull. Chem. Soc. Jpn.*, **34**, 258 (1961).
3) C. H. Won, *Nippon Kagaku Zasshi*, **85**, 859 (1964).
4) A. K. Babko, Yu. F. Shkaravskii, and V. I. Kulik, *Zh. Anal. Khim.*, **21**, 196 (1966).
5) A. T. Pilipenko and Yu. F. Shkaravskii, *Zh. Anal. Khim.*, **29**, 716 (1974).
6) A. G. Fogg, S. Soleymanloo, and D. T. Burns, *Anal. Chim. Acta*, **88**, 197 (1977).
7) Q. Xing-chu, Z. Yu-sheng, and Z. Ying-quan, *Bunseki Kagaku*, **32**, E 219 (1983).
8) S. Motomizu, S. Fujiwara, A. Fujiwara, and K. Tōei, *Anal. Chem.*, **54**, 392 (1982).
9) S. Motomizu, T. Wakimoto, and K. Tōei, *Anal. Chim. Acta*, **138**, 329 (1982).
10) K. Itaya and M. Ui, *Clin. Chim. Acta*, **14**, 361 (1966).
11) A. K. Babko, Yu. F. Shkaravaskii, and V. I. Kulik: *Zh. Anal. Khim.*, **21**, 196 (1966).
12) A. K. Babko, Yu. F. Shkaravskii, and E. M. Ivashkovich, *Ukr. Khim. Zh.*, **35**, 961 (1969).
13) S. Motomizu, T. Wakimoto, and K. Tōei, *Analyst (London)*, **108**, 361 (1983).
14) S. Motomizu, T. Wakimoto, and K. Tōei, *Talanta*, **31**, 235 (1984).
15) T. Matsuo, J. Shida, and W. Kurihara, *Anal. Chim. Acta*, **91**, 385 (1977).
16) L. Ducret and M. Drouillas, *Anal. Chim. Acta*, **21**, 86 (1959).
17) C. Sanchez-Pedreno, M. Hernandez Cordoba, and I. Lopez Garcia, *An. Quim., Ser. B.*, **79**, 440 (1983); *Anal. Abstr.*,

46, 5B171 (1984).
18) A. Golkowska, *Chem. Anal.(Warsaw)*, **15**, 59 (1970).
19) J. Shida, N. Iwabuchi, A. Suginoto, and T. Matsuo, *Bunseki Kagaku*, **32**, T129 (1983).
20) M. Kohara, N. Ishibashi, and K. Abe, *Bunseki Kagaku*, **19**, 48 (1970).
21) T. Fujinaga, T. Hori, and Y. Kanada, *Bunseki Kagaku*, **28**, 222 (1979).
22) C. Lieberman, *Chem. Ber.*, **37**, 1171, 2728 (1901).
23) JIS K 0102, 137 (1981).

Absorption Spectra of Tetrahedral Co(III) and Co(II) Complexes in Heteropolytungstates

Kazuo KOJIMA and Jiro MATSUDA*
Department of Chemistry, Faculty of Science and Engineering, Ritsumeikan University, Kita-ku, Kyoto 603
(Received September 1, 1984)

The absorption spectra of Co(III) and Co(II) in the single crystals of the Keggin-structure compounds, $K_5[Co^{III}W_{12}O_{40}]\cdot nH_2O$ and $K_6[Co^{II}W_{12}O_{40}]\cdot mH_2O$, have been measured at 77 K. The spectra of these complexes in aqueous solutions have also been observed. All the spectra have been interpreted using crystal-field theory by assuming that a Co(III) or Co(II) ion is in T_d symmetry. The parameters, D_q, B, and C/B can be evaluated as 780 cm^{-1}, 630 cm^{-1}, and 4.7 respectively for the Co(III) complex, and 460 cm^{-1}, 650 cm^{-1}, and 4.5 respectively for the Co(II) complex.

A few reports have been published on the absorption spectra of high-spin Co(III) complexes in the tetrahedral ligand fields; Co(III) both in garnets[1] and in xNa_2O-SiO_2 glasses ($x \geq 1.5$),[2] and 12-tungstocobaltate(III) $[Co^{III}W_{12}O_{40}]^{5-}$.[3-5] Only the solution spectra have been measured for the last complex.

We report the absorption spectra of $K_5[Co^{III}W_{12}O_{40}]\cdot nH_2O$ in single crystals at 77 K as well as in aqueous solution at room temperature. These spectra are interpreted on the basis of the crystal-field theory.

On the other hand, 12-tungstocobaltate(II) $[Co^{II}W_{12}O_{40}]^{6-}$ contains Co(II) complex with tetrahedral arrangement of oxygen atoms and the spectra of this anion have been reported only in solutions.[3,4,6,7]

The absorption spectra of $K_6[Co^{II}W_{12}O_{40}]\cdot mH_2O$ in single crystals as well as in aqueous solution are also discussed.

Experimental

$K_5[Co^{III}W_{12}O_{40}]\cdot nH_2O$ and $K_6[Co^{II}W_{12}O_{40}]\cdot mH_2O$ were prepared by the method in the literature.[8] Single crystals of both compounds were grown by slow evaporation of each aqueous solution. The shapes of crystals are hexagonal prisms. Co(III) complex prisms (light yellow) tend to grow more elongate along the hexagonal principal axis than Co(II) complex prisms (emerald green). Co(III) complex prisms are easy to break by polishing. X-Ray powder diffraction data for Co(III) compounds agree with Yanonni's data.[9]

Single-crystal spectra were measured at 77 K using a Shimadzu model MPS-50L spectrophotometer equipped with simple glass Dewars. A Nalumi RM-21 type grating monochromater with a Hamamatsu R-376 photomultiplier was also used to measure the strong band for the Co(II) complex in the visible region. Polished specimens of 0.30—0.70 mm thickness were immersed in liquid nitrogen. Filters of POLAROID HN-42T (visible region) and HR-INFRARED (near-infrared region) were used to measure preliminary polarized spectra. Spectra of aqueous solutions of 3.50×10^{-5} mol dm^{-3} were recorded both on a Hitachi 340 spectrophotometer (ultraviolet to near-infrared region) and on a Shimadzu UV-260 spectrophotometer (ultraviolet region) using 1-cm optical length quartz cells.

Energy matrices including the electrostatic[10] and crystal-field contributions were diagonalized using a HITAC M-160H computer.

Results and Discussion

Spectra of Co(III) and Co(II) Complexes in Aqueous Solutions. The absorption spectra of $K_5[Co^{III}W_{12}O_{40}]\cdot nH_2O$ and $K_6[Co^{II}W_{12}O_{40}]\cdot mH_2O$ in aqueous solutions agree well with the previous data,[3-7] except that very strong bands around 50000 cm^{-1} and shoulders around 45450 cm^{-1} are observed (Fig. 1 and Tables 1 and 2). These bands and shoulders are probably attributed to the transitions within $W_{12}O_{40}$ skeletons, because a similar band and shoulder are observed in the spectrum of aqueous solution of sodium metatungstate $Na_6[H_2W_{12}O_{40}]\cdot 29H_2O$ prepared by the method of Ref. 11 which has the Keggin-structure isopolyanion $[H_2W_{12}O_{40}]^{6-}$. The band for the Co(III) complex is shifted to lower wavenumbers than that of the Co(II) complex, likewise a 38000-cm^{-1} band in Fig. 1 due to the transition within the same skeleton.[3-5,7] It is interesting that these transition energies are

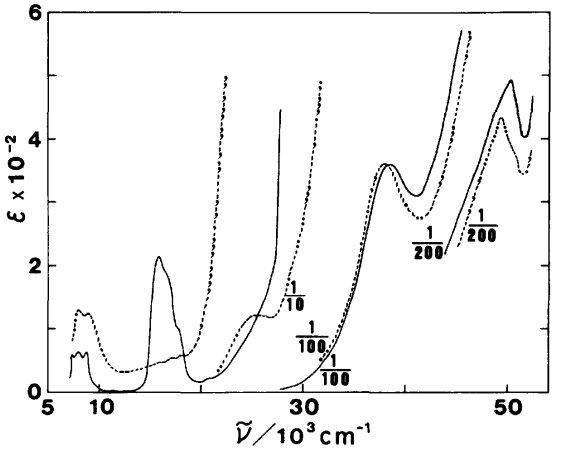

Fig. 1. Aqueous solution spectra of $K_5[Co^{III}W_{12}O_{40}]\cdot nH_2O$ (- - - -) and $K_6[Co^{II}W_{12}O_{40}]\cdot mH_2O$ (——). Fractional numbers show reduced scale for ε.

TABLE 1. OBSERVED AND CALCULATED[a] TRANSITION ENERGIES FOR $[Co^{III}W_{12}O_{40}]^{5-}$ (in 10^{-3} cm^{-1})

Observed		Calculated[b]
Solution	Single crystal[c]	
49.50		CT[e]
45.45[d]		CT[e]
38.03		CT[e]
	27.28	27.18[h] 26.90[i] 26.76[h] 26.34[j] 24.11[k] 23.53[l] 23.07[h] 22.74[m] 22.45[n] 22.01[l] 21.54[o] 19.79[l] (CT[f]) [g]
25.15		
	24.10	
	22.41	
	19.50	
	17.86[d]	17.54[p] 17.51[q]
17.12	17.21	17.38[j]
15.38		16.80[m] 16.29[h]
	15.27	15.79[l]
	14.18	14.91[l]
	10.80[d]	
9.15		9.07[l]
8.11		7.80[r]
	7.76	
	6.51	
	5.48	
	5.08	Vib[s]
	4.40	

a) Calculated higher energy levels are omitted. b) Calculation has been carried out with the parameters $D_q=780$ cm^{-1}, $B=630$ cm^{-1}, and $C/B=4.7$. c) Unpolarized spectrum. d) Shoulder. e) Charge-transfer transition within $W_{12}O_{40}$ skeleton. f) Charge-transfer transition between a ligand oxygen atom and a central Co(III) ion. g) These transitions are probably masked. h) $^5E\rightarrow{}^3T_2$. i) $\rightarrow{}^3E$. j) $\rightarrow{}^1E$. k) $\rightarrow{}^1T_1$. l) $\rightarrow{}^3T_1$. m) $\rightarrow{}^1T_2$ n) $\rightarrow{}^1A_2$. o) $\rightarrow{}^1A_1$. p) $\rightarrow{}^3A_2$. q) $\rightarrow{}^3A_1$. r) $\rightarrow{}^5T_2$. s) Vibrational peaks due to water.

TABLE 2. OBSERVED AND CALCULATED[a] TRANSITION ENERGIES FOR $[Co^{II}W_{12}O_{40}]^{6-}$ (in 10^{-3} cm^{-1})

Observed		Calculated[b]
Solution	Single crystal[c]	
50.40		CT[e]
45.45[d]		CT[e]
38.31		CT[e]
25.91[d]	26.46	26.52[i] 28.98[h] 23.57[j] 21.22[k] 22.89[k] (CT[f]) [g]
	25.84	
	20.41	19.99[l]
20.33	19.46	18.48[k]
17.79		18.07[j]
	17.39	
16.84[d]	16.81	16.51[j]
16.05	16.18	15.98[l]
15.34[d]	15.70	15.73[m]
	15.22	
		13.49[k]
	12.71	12.96[l]
8.76	8.58[d]	
8.10	7.97	7.83[n]
7.25	7.24	
	5.56	
	5.16	Vib[p] 4.60[g,o]
	4.27	

a) Calculated higher energy levels are omitted. b) Calculation has been carried out with the parameters $D_q=460$ cm^{-1}, $B=650$ cm^{-1}, and $C/B=4.5$. c) Unpolarized spectrum. d) Shoulder. e) Charge-transfer transition within $W_{12}O_{40}$ skeleton. f) Charge-transfer transition between a ligand oxygen atom and a central Co(II) ion. g) These transitions are probably masked. h) $^4A_2\rightarrow{}^2A_2$. i) $\rightarrow{}^2E$. j) $\rightarrow{}^2T_2$. k) $\rightarrow{}^2T_1$. l) $\rightarrow{}^2A_1$. m) $\rightarrow{}^4T_1(^4P)$. n) $\rightarrow{}^4T_1(^4F)$. o) $\rightarrow{}^4T_2(^4F)$. p) Vibrational peaks due to water.

affected by the oxidation state of cobalt ion in spite of the transitions within $W_{12}O_{40}$ skeletons.[5] Weak absorptions at 17120 cm^{-1} and 15380 cm^{-1} for the Co(III) complex are due to spin-forbidden d-d transitions and become well resolved in the single-crystal spectra described below.

Spectra of $K_5[Co^{III}W_{12}O_{40}]\cdot nH_2O$ in Single Crystals.[12] On the assumption that CoO_4 has T_d symmetry (it is known to be distorted[9]), the calculation of transition energies shown in Fig. 2 and Table 1 has been carried out in terms of the following estimations: (1) A band in the near-infrared region is assigned to the $^5E\rightarrow{}^5T_2$ transition, which determines the D_q value directly. (2) C/B is fitted in the vicinity of the value of 4.8.[10,15,16] (3) B is fitted in order to explain the spectra in the 13000—20000 cm^{-1} region(Figs. 2 and 3). From (1), (2), and (3), we evaluate the parameters D_q, B, and C/B as 780 cm^{-1}, 630 cm^{-1}, and 4.7 respectively. Simmons[4] has estimated the values of D_q and B as about 800 cm^{-1} and about 600 cm^{-1} respectively. Wood and Remeika[1] have reported the D_q values of 710 cm^{-1} (calculated) and 830 cm^{-1} (observed). The B value of 630 cm^{-1} is rather small compared with the value of

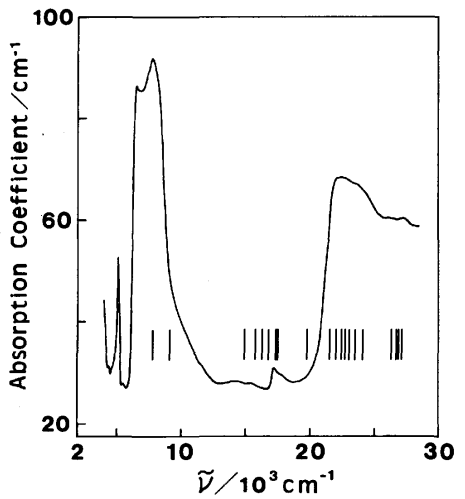

Fig. 2. Single-crystal spectrum of $K_5[Co^{III}W_{12}O_{40}]\cdot nH_2O$ at 77 K together with the calculated energy level positions (vertical lines). Details are shown in Table 1.

1053 cm^{-1} for the free Co(III) ion, which indicates the presence of a strong nephelauxetic effect. With this B

value, the bands in the visible region seem to be assigned fairly well (Fig. 2). A relatively intense band near 17500 cm^{-1} may be due to the $^5E \rightarrow {}^3A_2, \rightarrow {}^3A_1$, and $\rightarrow {}^1E$ transitions. In Fig. 3, anisotropy is observed in the 17500-, 15270-, and 14180-cm^{-1} band.

The $^5E \rightarrow {}^5T_2$ band in the solution spectrum apparently shifts to blue by about 1500 cm^{-1} compared with that of the single-crystal spectrum. It is not clear whether two peaks of this band in the former correspond directly to two peaks of the similar band in the latter, unless the single-crystal spectra are measured at higher temperatures.

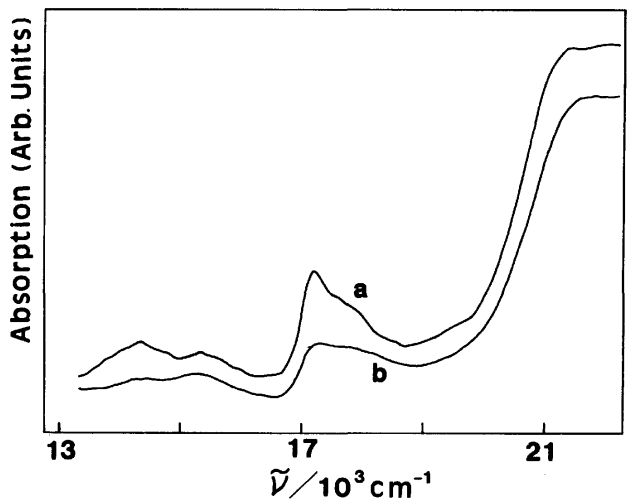

Fig. 3. Polarized single-crystal spectra of $K_5[Co^{III}W_{12}O_{40}]\cdot nH_2O$ in the visible region at 77 K. Electric vector $\boldsymbol{E}$ is perpendicular (a) and parallel (b) to the hexagonal principal axis.

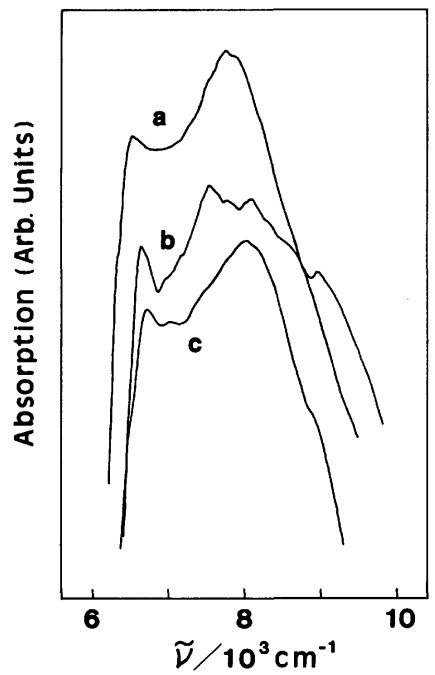

Fig. 4. Polarized single-crystal spectra of $K_5[Co^{III}W_{12}O_{40}]\cdot nH_2O$ in the $^5E \rightarrow {}^5T_2$ transition region at 77 K. The curve a is unpolarized and $\boldsymbol{E}$ is perpendicular (b) and parallel (c) to the hexagonal principal axis. The curves b and c have been shifted expediently upwards along the ordinate.

In the polarized spectra of Fig. 4, four to five peaks are observed and show anisotropy. It is of interest that the spectrum with $\boldsymbol{E}$ parallel to the hexagonal principal axis is similar to the unpolarized spectrum, unlike the $^4A_2 \rightarrow {}^4T_1$ (^4F) band for the Co(II) complex described below. Unfortunately, it is not possible to discuss the details of the reason for the splitting of this band, though the contribution of the distortion probably due to the Jahn-Teller effect[4] may be greater than that of the spin-orbit coupling. If it is possible to find out the reason for this splitting, both the D_q value and the energy of the $^5E \rightarrow {}^3T_1$ spin-forbidden transition expected to be at 9070 cm^{-1} will be confirmed.

A band around 23000 cm^{-1} in Fig. 2 is rather resolved and considerably lower both in intensity and in energy than a corresponding 25510-cm^{-1} band in the solution spectrum. These findings are of interest, though as to the intensity of the 23000-cm^{-1} band there remains some uncertainty arising from the fact that the samples are too fragile to be polished down thin specimens enough for optical measurement. Simmons[4] has proposed that this band may be due to a charge-transfer transition from a ligand oxygen atom to a central Co(III) ion, together with possibilities of other interpretations. On the other hand, the band has been assigned to a reciprocal charge-transfer transition by Dietzel and Coenen.[2] Although a number of spin-forbidden transitions are expected near this band, a charge-transfer transition between a ligand oxygen atom and a central Co(III) ion perhaps contributes mainly to this band.

Three bands at 5480 cm^{-1}, 5080 cm^{-1}, and 4400 cm^{-1} are attributed to the vibrational bands of water by referring to the previous data.[17-20]

Spectra of $K_6[Co^{II}W_{12}O_{40}]\cdot mH_2O$ in Single Crystals.[12] The transition energies calculated with the parameters D_q, B, and C/B of which values are 460 cm^{-1}, 650 cm^{-1}, and 4.5 respectively, explain the observed spectra fairly well (Fig. 5 and Table 2). The D_q value of 460 cm^{-1} is relatively large in comparison with other Co(II) tetrahedral complexes, but it agrees with that of Co(II) in yttrium gallium garnet[1] and is comparable with that of $Co(NCS)_4^{2-}$ [3,21] or $Co(NO_3)_4^{2-}$.[22] Simmons[4] has estimated the D_q and B values as 484 cm^{-1} and 672 cm^{-1} respectively. Nomiya *et al.*[7] has determined it to be 410 cm^{-1}. Likewise for the Co(III) complex, the B value of 650 cm^{-1} is rather small compared with the value of 971 cm^{-1} for the free Co(II) ion. The C/B value of 4.5 is typical for Co(II) tetrahedral complexes.

The $^4A_2 \rightarrow {}^4T_2$ transition is expected to be at 4600 cm^{-1}, but is not observed because of its low intensity[23] and of masking effect by the vibrational bands

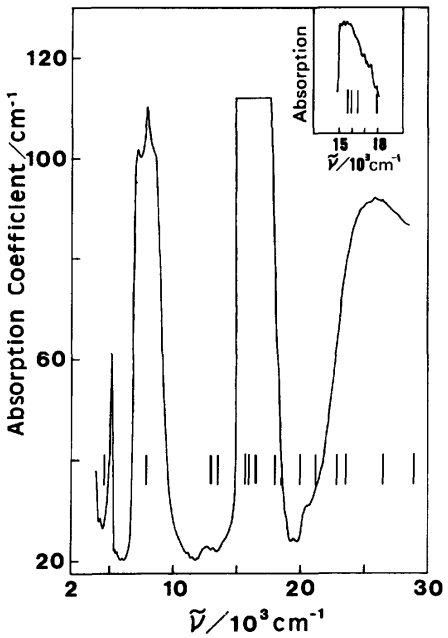

Fig. 5. Single-crystal spectrum of $K_6[Co^{II}W_{12}O_{40}]\cdot mH_2O$ at 77 K together with the calculated energy level positions (vertical lines). Details are shown in Table 2. The inset is the spectrum measured using the grating monochromater.

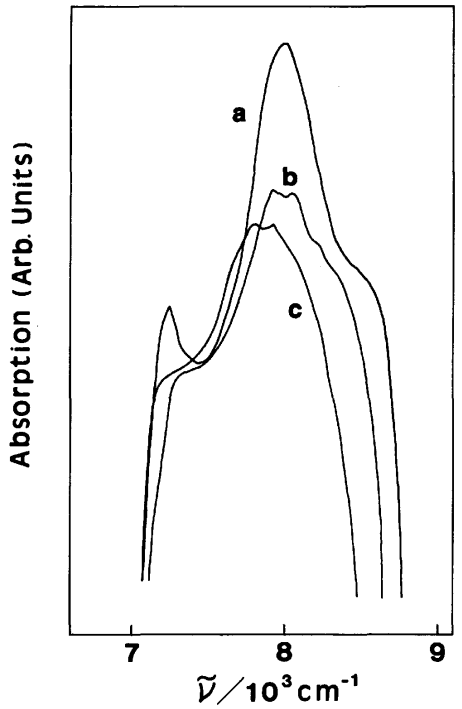

Fig. 6. Polarized single-crystal spectra of $K_6[Co^{II}W_{12}O_{40}]\cdot mH_2O$ in the $^4A_2\rightarrow{}^4T_1(^4F)$ transition region at 77 K. The curve a is unpolarized and $\boldsymbol{E}$ is perpendicular (b) and parallel (c) to the hexagonal principal axis. The curves b and c have been shifted expediently upwards along the ordinate.

due to water at 5560 cm^{-1}, 5160 cm^{-1}, and 4270 cm^{-1}.

The $^4A_2\rightarrow{}^4T_1(^4F)$ band splits into three to four peaks which show slight anisotropy (Figs. 5 and 6 and Table 2). The magnitude of the splitting by about 1340 cm^{-1} is predominantly due to the spin-orbit coupling in the excited state. The first-order value for this splitting is given by 6λ. Therefore, $|\lambda|$ is 223 cm^{-1} for this complex, the value of which is even larger than the free ion value of 178 cm^{-1}.[4,23] When the B value is decreased from the free ion value, $|\lambda|$ is also expected to be decreased. The reason for the above contradiction is probably that $|\lambda|$ is overestimated since it is evaluated primarily on the assumption that the splitting of the $^4T_1(^4F)$ band is entirely due to the spin-orbit coupling.

The $^4A_2\rightarrow{}^4T_1(^4P)$ band is too strong to be fully resolved.

A 26000-cm^{-1} band which perhaps corresponds to a 25910-cm^{-1} shoulder in the solution spectrum may be attributed to a charge-transfer transition between a ligand oxygen atom and a central Co(II) ion. This band is observed in higher wavenumbers than that of the Co(III) complex described above. The similar bands have been reported for the spectra of Co(II) in yttrium gallium garnet (26316 cm^{-1})[24] and of Ni(II) both in yttrium gallium garnet (23255 cm^{-1}) and in ZnO (22935 cm^{-1}).[25]

The authors wish to express their sincere thanks to Mr. S. Okuyama and Mr. E. Sakai for their cooperation in the experiment.

References

1) D. L. Wood and J. P. Remeika, *J. Chem. Phys.*, **46**, 3595 (1967).
2) V. A. Dietzel and M. Coenen, *Glastech. Ber.*, **34**, 49 (1961).
3) Y. Shimura and R. Tsuchida, *Bull. Chem. Soc. Jpn.*, **30**, 502 (1957).
4) V. E. Simmons, and Ph. D. Thesis, Boston University, 1963.
5) K. Nomiya, R. Kobayashi, and M. Miwa, *Bull. Chem. Soc. Jpn.*, **56**, 2272 (1983).
6) O. W. Rollins, *Inorg. Chem.*, **11**, 3114 (1972).
7) K. Nomiya, M. Miwa, R. Kobayashi, and M. Aiso, *Bull. Chem. Soc. Jpn.*, **54**, 2983 (1981).
8) L. C. W. Baker and T. P. McCutcheon, *J. Am. Chem. Soc.*, **78**, 4503 (1956).
9) N. F. Yanonni, Ph. D. Thesis, Boston University, 1961.
10) Y. Tanabe and S. Sugano, *J. Phys. Soc. Jpn.*, **9**, 753 (1954).
11) M. L. Freedman, *J. Am. Chem. Soc.*, **81**, 3834 (1959).
12) The values of n and m have been determined to be 15—17 by preliminary thermogravimetric measurement on the basis of the formula $K_5[Co^{III}W_{12}O_{40}]\cdot nH_2O$ and $K_6[Co^{II}W_{12}O_{40}]\cdot mH_2O$. The degree of hydration of this type of compound is known to vary according to the temperature of crystallization.[13] The degree of hydration of the crystals used will presumably have insignificant effects on the electronic environment of Co(III) and Co(II).[14]

13) L. C. W. Baker, V. S. Baker, K. Eriks, M. T. Pope, M. Shibata, O. W. Rollins, J. H. Fang, and L. L. Koh, *J. Am. Chem. Soc.*, **88**, 2329 (1966).
14) H. So and M. T. Pope, *J. Chem. Phys.*, **55**, 2786 (1971).
15) Y. Tanabe and S. Sugano, *J. Phys. Soc. Jpn.*, **9**, 766 (1954).
16) G. C. Allen, G. A. M. El-Sharkawy, and K. D. Warren, *Inorg. Chem.*, **10**, 2538 (1971).
17) K. Buijs and G. R. Choppin, *J. Chem. Phys.*, **39**, 2035 (1963).
18) J. D. Worley and I. M. Klotz, *J. Chem. Phys.*, **45**, 2868 (1966).
19) M. Falk and T. A. Ford, *Can. J. Chem.*, **44**, 1699 (1966).
20) W. A. P. Luck, *Diss. Fara. Soc.*, **43**, 115 (1967).
21) F. A. Cotton, D. M. L. Goodgame, M. Goodgame, and A. Sacco, *J. Am. Chem. Soc.*, **83**, 4157 (1961).
22) F. A. Cotton and T. G. Dunne, *J. Am. Chem. Soc.*, **84**, 2013 (1962).
23) H. A. Weakliem, *J. Chem. Phys.*, **36**, 2117 (1962).
24) R. Pappalardo, D. L. Wood, and R. C. Linares, Jr., *J. Chem. Phys.*, **35**, 2041 (1961).
25) R. Pappalardo, D. L. Wood, and R. C. Linares, Jr., *J. Chem. Phys.*, **35**, 1460 (1961).

Structure of Cobalt(III) Complexes with (*R,R*)- and (*R,S*)-*N,N,N',N'*-Tetrakis(2-aminoethyl)-2,4-pentanediamine and *N,N,N',N'*-Tetrakis(2-aminoethyl)-1,3-propanediamine

Toshio Ishii,† Shigeru Ohba, Masatoki Ito, Sachio Fukushi,† and Yoshihiko Saito*

Department of Chemistry, Faculty of Science and Technology, Keio University, 3-14-1, Hiyoshi Kohoku-ku, Yokohama 223

†*Department of Chemistry, Chiba Institute of Technology, 2-17-1, Tsudanuma, Narashino 275*

(Received September 6, 1984)

Crystal structures of the two isomeric Co(III) complexes with sexidentate ligands, $(NH_2CH_2CH_2)_2NC^*H(CH_3)CH_2C^*H(CH_3)N(CH_2CH_2NH_2)_2$ (hereafter abbreviated as *R,R*- and *R,S*-tptn) and of the Co(III) complex with a sexidentate ligand, $(NH_2CH_2CH_2)_2NCH_2CH_2CH_2N(CH_2CH_2NH_2)_2$ (abbreviated as ttn) were determined by an X-ray diffraction method. The crystal data and the final *R* factors are: (**1**) [Co(*R,R*-tptn)]$(ClO_4)_3\cdot H_2O$, tetragonal, $P4_22_12$, a=12.800(1), c=15.312(1) Å, V=2509(1) Å^3, Z=4, R=0.053 for 1627 observed unique reflections, (**2**) [Co(*R,S*-tptn)]$Cl_3\cdot 3H_2O$, monoclinic, $P2_1/a$, a=16.778(6), b=14.296(2), c=9.478(4) Å, β=110.99(3)°, V=2123(1) Å^3, Z=4, R=0.045 for 3583 reflections and (**3**) [Co(ttn)]$Br_3\cdot H_2O$, trigonal, $P\bar{3}c1$, a=14.436(4), c=15.718(9) Å, V=2837(2) Å^3, Z=6, R=0.096 for 1183 reflections. The equatorial preference of the methyl groups in the central six-membered chelate ring formed by Co and 2,4-pentanediamine moiety of *R,R*- and *R,S*-tptn has been recognized. In (**1**) the six-membered chelate ring adopts a twist boat form as in (**3**) with the two C-CH_3 bonds in equatorial positions. In (**2**) the six-membered chelate ring takes a largely flattened chair form with the two C-CH_3 bonds again in equatorial positions. The effect of an elongation of the Co-N bond distance on the energy of the first absorption band was discussed.

New sexidentate ligands, *R,R*- and *R,S*-tptn and their Co(III) complexes were synthesized and characterized.[1] $[Co(R,R\text{-tptn})]^{3+}$ gives the first absorption band at 20.8×10^3 cm^{-1}, whereas $[Co(R,S\text{-tptn})]^{3+}$ shows the first absorption maximum at 20.0×10^3 cm^{-1}, indicating that the ligand field exerted by the *R,S*-tptn is weaker than that by the *R,R*-tptn. A simple molecular model indicates that both isomers act as a sexidentate ligand to give metal complexes analogous to those of 1,3-propanediamine-*N,N,N',N'*-tetraacetic acid (trdta) as shown in Fig. 1. The central six-membered chelate ring in (—)$_{546}$-*ΔΔΔ*-[Co(trdta)]$^-$ takes a skew boat form.[2] The central six-membered chelate ring of $[Co(R,R\text{-tptn})]^{3+}$ is expected to adopt a skew boat form with the two C-CH_3 bonds in equatorial positions. In this connection, the absolute configuration must be skew chelate pairs *ΔΔΔ*. If the central six-membered chelate ring of $[Co(R,S\text{-tptn})]^{3+}$ takes a skew boat form, one of the two C-CH_3 bonds will be equatorial and the other axial as shown in Fig. 1. Both of the methyl groups can be in equatorial positions if the central chelate ring takes a chair form with a distorted CoN_6 octahedron. In any case, the *R,S*-complex would be much deformed owing to the nonbonded interactions. Such a strained structure may be reflected in the absorption spectrum. In order to see how the distortion of the CoN_6 chromophore affects the absorption spectra, two complexes (**1**) and (**2**) were subjected to X-ray crystal structure analysis. In addition to this, the structure of (**3**), which has no C-CH_3 bonds in the central six-membered chelate ring, was determined in order to compare the conformation with (**1**) and (**2**).

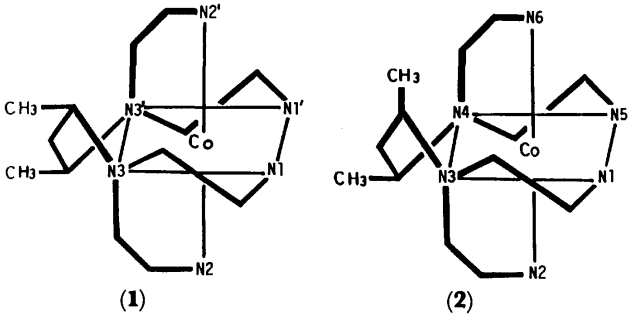

Fig. 1. Coordination of *R,R*- and *R,S*-tptn. The central six-membered chelate ring is assumed to take a skew boat form.

Experimental

Crystals of (**1**), (**2**), and (**3**) grown from aqueous solutions were kindly provided by Professor J. Fujita of Nagoya University. Experimental conditions and refinement informations are listed in Table 1. The preliminary determination of the lattice parameters and the space group of (**1**) and (**2**) was made with a Weissenberg camera. Intensities were measured using graphite monochromatized Mo *Kα* radiation (λ=0.70926 Å) on an automated Rigaku four-circle diffractometer AFC-5. The θ—2θ scan technique was employed at a scan rate of 4° min^{-1} in θ.

The usual corrections were made for Lorentz and polarization factors. The structures of (**1**) and (**2**) were solved by the heavy atom method. Positions of Co and Cl atoms were determined from the Patterson function and the other non-hydrogen atoms were located by Fourier syntheses. All the hydrogen atoms except those of the water molecule in (**1**) were found on the difference synthesis. The Laue group and systematic absences showed that the space group of (**3**) is

TABLE 1. CRYSTAL DATA, EXPERIMENTAL CONDITIONS AND REFINEMENT DETAILS

	(1)	(2)	(3)
Chemical formula	$[Co(C_{13}H_{34}N_6)]\cdot(ClO_4)_3\cdot H_2O$	$[Co(C_{13}H_{34}N_6)]\cdot Cl_3\cdot 3H_2O$	$[Co(C_{11}H_{30}N_6)]\cdot Br_3\cdot H_2O$
Formula weight	649.8	493.8	563.1
Calculated density (Mg m^{-3})	1.72	1.55	1.98
μ(Mo $K\alpha$) (mm^{-1})	1.11	1.24	7.20
Color and Habit of crystals	orange-red bipyramids	red rhomboids	orange plates(100)
Size of specimen (mm^3)	0.4×0.4×0.3	0.3×0.3×0.2	0.4×0.4×0.2
Number of reflections and 2θ range(°) used for measuring lattice parameters	20 $40<2\theta<51$	20 $40<2\theta<55$	24 $30<2\theta<40$
$2\theta_{max}$(°)	65	55	55
Range of h, k, and l	$0\leqq h,\ k\leqq 16$ $k\leqq h$ $0\leqq l\leqq 19$	$-21\leqq h\leqq 20$ $0\leqq k\leqq 17$ $0\leqq l\leqq 11$	$0\leqq h\leqq 18$ $0\leqq k\leqq 18$ $0\leqq l\leqq 20$
Systematic absences	$h00$, h odd; $00l$, l odd	$h0l$, h odd; $0k0$, k odd	$h\bar{h}l$, l odd
Number of standard reflections and variation of their $\|F_o\|$ amplitudes, $\Sigma(\|F_o\|/\|F_o\|_{initial})/n$	3 0.99—1.00	3 0.97—1.00	5 0.09—1.00
Number of reflections measured	2576	5275	2283
Number of reflections observed above the threshold $[\|F_o\|>3\sigma(\|F_o\|)]$	1627	3583	1230
Absorption correction	no	no	$1.852\leqq$correction factor, $(A^*)^{1/2}\leqq 3.748$
R	0.053	0.045	0.096
wR	0.054	0.063	0.105
Weight $w^{-1}=\sigma^2(\|F_o\|)+(c\|F_o\|)^2$	$c=0.015$	$c=0.03$	$c=0.015$
$S=[\Sigma w(\|F_o\|-\|F_c\|)^2/(m-n)]^{1/2}$	2.0	1.6	3.4
Number of observed unique reflections, m	1627	3583	1183
Number of parameters, n	230	387	106
$(\Delta/\sigma)_{max}$ for non-H atoms	1.0	0.5	0.4

P3cl or P$\bar{3}$cl. Assuming the non-centrosymmetry, the structure was solved by direct methods.[3] The possible positions of the Br and Co atoms obtained from the E map were confirmed by the Patterson function. All the non-hydrogen atoms of the sexidentate ligand were found on the Fourier synthesis. A projection of the crystal structure at this stage of the refinement suggested that the Co lies on a twofold axis perpendicular to c. It is a special position **6f** of the space group P$\bar{3}$cl. Accordingly, the space group was determined to be P$\bar{3}$cl. The general position of P$\bar{3}$cl is twelvefold and there are six formula units in a unit cell. Hence, there are 18 Br atoms in the unit cell, sixteen of which were allocated on a set of general positions **12g** and a set of special positions **4d**. It was found that the remaining two Br atoms are disordered. The difference synthesis can be most conveniently accounted for if the Br atoms are distributed randomly on the sets of special positions **2b** and **4c**, and two sets of general positions **12g** (See Table 2). The population parameters of these Br atoms were estimated by the trial and error method in such a way that each isotropic thermal parameter took nearly equal value. Positions of the hydrogen atoms in (**3**) could not be deduced from the difference synthesis so that they were obtained by calculation and not refined.

Anisotropic thermal parameters were introduced for all the non-hydrogen atoms except for the disordered Br atoms of (**3**). The function, $\Sigma w||F_o|-|F_c||^2$ was minimized by block-diagonal least squares. Complex neutral-atom scattering factors were used.[4] The calculations were carried out on a FACOM M180 computer at Keio University with the Universal Crystallographic Computation Program System UNICS III.[5] The final atomic parameters are listed in Table 2.[6]

The absolute structure of (**1**) was determined with reference to the known absolute configuration of *R,R*-tptn prepared from (*R,R*)-2,4-diaminopentane.[7]

Results and Discussion

Perspective drawings of complexes (**1**), (**2**), and (**3**) and projections of the central six-membered chelate rings of these complexes along the twofold axis or along the pseudo twofold axis are presented in Fig. 2. The bond lengths and bond angles within the com-

Table 2. Fractional coordinates ($\times 10^4$, $\times 10^5$ for Co, $\times 10^3$ for disorded Br atoms in **3**) and equivalent isotropic thermal parameters

Atom		x	y	z	B_{eq}/Å^2
(1)	Co	20688(5)	20688	100000	1.9
	Cl(1)	5000	5000	7208(1)	3.0
	Cl(2)	6127(1)	1249(1)	8671(1)	3.4
	O(1)	6460(4)	504(4)	8031(3)	5.0
	O(2)	6874(5)	2075(4)	8696(4)	6.5
	O(3)	5125(4)	1657(4)	8440(3)	6.2
	O(4)	6102(4)	752(4)	9510(3)	5.5
	O(5)	5085(5)	4084(4)	7722(3)	6.2
	O(6)	4104(4)	4924(4)	6664(4)	6.0
	N(1)	716(4)	1905(4)	9408(3)	2.9
	N(2)	2758(4)	1332(4)	9031(3)	2.5
	N(3)	2257(3)	3369(3)	9272(2)	2.0
	C(1)	467(5)	2811(6)	8837(4)	3.7
	C(2)	1158(5)	3718(5)	9077(3)	3.1
	C(3)	2669(4)	1962(5)	8200(3)	2.8
	C(4)	2838(4)	3084(4)	8444(3)	2.6
	C(5)	2827(6)	5264(5)	9222(4)	4.5
	C(6)	2837(5)	4233(4)	9736(3)	2.9
	C(7)	3958(4)	3958	10000	3.2
	OW	3575(4)	3575	5000	4.9
(2)	Co	39470(3)	20737(3)	34063(5)	1.5
	Cl(1)	6361(1)	852(1)	5139(1)	2.9
	Cl(2)	525(1)	6071(1)	2112(1)	3.2
	Cl(3)	1113(1)	795(1)	2697(1)	3.3
	O(1)	621(2)	3913(2)	1360(3)	3.4
	O(2)	5552(3)	4541(3)	−1133(5)	6.9
	O(3)	7023(6)	5915(5)	1830(9)	13.7
	N(1)	4905(2)	2197(2)	5315(3)	2.1
	N(2)	3182(2)	1561(2)	4409(3)	2.1
	N(3)	3627(2)	3332(2)	4075(3)	1.8
	N(4)	3106(2)	2003(2)	1260(3)	1.7
	N(5)	4220(2)	771(2)	3105(4)	2.1
	N(6)	4760(2)	2504(2)	2464(3)	2.1
	C(1)	5154(2)	3207(3)	5623(4)	2.7
	C(2)	4451(2)	3850(3)	4627(4)	2.3
	C(3)	2798(3)	2296(3)	5073(4)	2.4
	C(4)	3389(2)	3117(3)	5432(4)	2.2
	C(5)	2985(3)	4950(3)	3214(5)	3.3
	C(6)	2870(2)	3899(3)	3012(4)	2.0
	C(7)	2574(2)	3631(3)	1349(4)	2.1
	C(8)	2323(2)	2609(3)	987(4)	2.1
	C(9)	1666(3)	2523(3)	−607(5)	3.4
	C(10)	2869(2)	990(3)	1033(4)	2.3
	C(11)	3668(3)	418(3)	1598(5)	2.7
	C(12)	3548(3)	2263(3)	192(4)	2.5
	C(13)	4309(3)	2878(3)	920(4)	2.6
(3)	Co	62191(22)	0	75000	2.1
	N(1)	5721(11)	840(11)	6912(9)	3.1
	N(2)	5626(12)	−1130(11)	6623(7)	2.7
	N(3)	7516(11)	714(11)	6738(8)	2.9
	C(1)	6518(17)	1541(14)	6255(12)	4.2
	C(2)	7582(15)	1748(14)	6492(11)	3.4
	C(3)	6197(14)	−720(15)	5713(11)	3.3
	C(4)	7336(14)	11(15)	5958(13)	3.8
	C(5)	8520(15)	941(15)	7126(12)	3.6
	C(6)	8595(17)	0	7500	7.0
	Br(1)	3296(2)	4121(2)	1169(1)	3.9
	Br(2)	3333	6667	2236(2)	3.0
	*Br(3)	0	0	0	3.6
	*Br(4)	0	0	59(3)	3.9
	*Br(5)	30(3)	29(3)	24(1)	3.9
	*Br(6)	2(9)	29(5)	24(2)	4.3

* Population parameters of Br atoms in disorder are as follows.

Atom	Wyckoff notation of the position	Population parameter	Number of atoms in a unit cell
Br(3)	2b	0.04	0.48
Br(4)	4c	0.025	0.30
Br(5)	12g	0.065	0.78
Br(6)	12g	0.0367	0.44
			Σ 2.00

plex ions are listed in Table 3. The absolute configuration of the complex (**1**) is *ΔΔΛ* as expected. The complex has a crystallographic twofold axis through the Co and C(7) atoms. The central six-membered chelate ring takes a skew boat form with the two methyl groups in equatorial positions. The C(6)–C(5) bond axis is inclined by 6.5(5)° with respect to the coordination plane formed by Co, N(3), and N(3′) atoms, from which the C(6) is shifted by 0.67(1) Å. There are two optical isomers *ΔΔΛ* and *ΔΔΔ* in a unit cell of (**2**) and (**3**). Figure 2 depicts a *ΔΔΛ* isomer for the convenience of comparison with (**1**). The geometry of the complexes (**1**) and (**3**) is essentially identical. The difference of 0.039 Å in Co–N(1) bond lengths of (**1**) and (**3**) is not significant because of the large e.s.d. of the structural data of (**3**).

The central six-membered chelate ring of (**2**) is distorted unsymmetrically, exhibiting a largely flattened chair form with the two C–CH_3 bonds in equatorial positions. The Co, N(3), N(4), and C(6) are practically on one plane, from which the C(7) and C(8) atoms are shifted on opposite sides by 0.28(1) and 0.53(1) Å, respectively. The Co–N bond lengths in (**2**) are in the order Co-tertiary N>Co-apical primary N>Co-primary N atom which is in the trans position to the tertiary N atom. The Co–N(4) bond length of 2.021(3) Å agrees with the Co-tertiary N bond lengths of (**1**) and (**3**) [2.017(4) and 2.018(13) Å]. The Co-tertiary N bond lengths of (**2**) differ from each other, Co–N(3) being longer by 0.021(3) Å than Co–N(4). It

TABLE 3. BOND DISTANCES (l/Å) AND ANGLES (ϕ/°)

(1)			
Co-N (1)	1.966(5)	N (1)-Co-N (2)	89.8(2)
Co-N (2)	1.967(5)	N (1)-Co-N (3)	86.5(2)
Co-N (3)	2.017(4)	N (2)-Co-N (3)	85.7(2)
N (1)-C (1)	1.487(9)	Co-N (1)-C (1)	112.1(4)
N (2)-C (3)	1.511(7)	Co-N (2)-C (3)	110.2(3)
N (3)-C (2)	1.506(7)	Co-N (3)-C (2)	104.1(3)
N (3)-C (4)	1.514(6)	Co-N (3)-C (4)	108.8(3)
N (3)-C (6)	1.510(6)	Co-N (3)-C (6)	113.8(3)
C (1)-C (2)	1.505(10)	C (2)-N (3)-C (4)	111.4(4)
C (3)-C (4)	1.500(8)	C (2)-N (3)-C (6)	109.6(4)
C (5)-C (6)	1.537(8)	C (4)-N (3)-C (6)	109.2(4)
C (6)-C (7)	1.532(8)	N (1)-C (1)-C (2)	109.4(5)
		N (3)-C (2)-C (1)	111.6(5)
		N (2)-C (3)-C (4)	106.9(4)
		N (3)-C (4)-C (3)	111.6(4)
		N (3)-C (6)-C (5)	112.6(4)
		N (3)-C (6)-C (7)	114.6(4)
		C (5)-C (6)-C (7)	109.9(5)
		N (1)-Co-N (1′)	91.5(2)
		N (1)-Co-N (2′)	88.5(2)
		N (1)-Co-N (3′)	173.8(2)
		N (2)-Co-N (2′)	177.5(2)
		N (2)-Co-N (3′)	96.0(2)
		N (3)-Co-N (3′)	96.2(2)
		C (6)-C (7)-C (6′)	120.1(3)
(2)			
Co-N (1)	1.950(·3)	N (1)-Co-N (2)	92.8(1)
Co-N (2)	1.990(4)	N (1)-Co-N (3)	81.6(1)
Co-N (3)	2.042(3)	N (1)-Co-N (4)	169.9(1)
Co-N (4)	2.021(3)	N (1)-Co-N (5)	93.6(1)
Co-N (5)	1.963(3)	N (1)-Co-N (6)	85.3(1)
Co-N (6)	1.977(4)	N (2)-Co-N (3)	83.7(1)
N (1)-C (1)	1.502(5)	N (2)-Co-N (4)	97.2(1)
N (2)-C (3)	1.485(6)	N (2)-Co-N (5)	86.8(1)
N (3)-C (2)	1.488(5)	N (2)-Co-N (6)	175.9(1)
N (3)-C (4)	1.509(5)	N (3)-Co-N (4)	101.0(1)
N (3)-C (6)	1.539(4)	N (3)-Co-N (5)	169.1(1)
N (4)-C (8)	1.517(5)	N (3)-Co-N (6)	99.6(1)
N (4)-C (10)	1.497(5)	N (4)-Co-N (5)	85.5(1)
N (4)-C (12)	1.500(6)	N (4)-Co-N (6)	84.7(1)
N (5)-C (11)	1.485(5)	N (5)-Co-N (6)	89.7(1)
N (6)-C (13)	1.485(4)	Co-N (1)-C (1)	110.3(2)
C (1)-C (2)	1.526(5)	Co-N (2)-C (3)	113.2(3)
C (3)-C (4)	1.495(6)	Co-N (3)-C (2)	103.5(2)
C (5)-C (6)	1.518(6)	Co-N (3)-C (4)	105.3(2)
C (6)-C (7)	1.522(5)	Co-N (3)-C (6)	120.5(2)
C (7)-C (8)	1.525(6)	C (2)-N (3)-C (4)	107.3(3)
C (8)-C (9)	1.523(5)	C (2)-N (3)-C (6)	114.4(3)
C (10)-C (11)	1.496(6)	C (4)-N (3)-C (6)	104.9(3)
C (12)-C (13)	1.499(6)	Co-N (4)-C (8)	113.1(2)
		Co-N (4)-C (10)	104.3(2)
		Co-N (4)-C (12)	109.3(3)
		C (8)-N (4)-C (10)	111.0(3)
		C (8)-N (4)-C (12)	110.5(3)
		C (10)-N (4)-C (12)	108.2(3)
		Co-N (5)-C (11)	111.4(2)
		Co-N (6)-C (13)	111.5(2)
		N (1)-C (1)-C (2)	111.0(3)
		N (3)-C (2)-C (1)	109.4(3)
		N (2)-C (3)-C (4)	107.4(4)
		N (3)-C (4)-C (3)	108.8(3)
		N (3)-C (6)-C (5)	113.6(3)
		N (3)-C (6)-C (7)	115.6(3)
		C (5)-C (6)-C (7)	111.1(3)
		C (6)-C (7)-C (8)	115.8(3)
		N (4)-C (8)-C (7)	110.9(3)
		N (4)-C (8)-C (9)	113.5(3)
		C (7)-C (8)-C (9)	110.1(3)
		N (4)-C (10)-C (11)	108.6(3)
		N (5)-C (11)-C (10)	109.2(4)
		N (4)-C (12)-C (13)	112.3(3)
		N (6)-C (13)-C (12)	107.0(3)
(3)			
Co-N (1)	1.927(18)	N (1)-Co-N (2)	92.3(7)
Co-N (2)	1.974(12)	N (1)-Co-N (3)	86.4(7)
Co-N (3)	2.018(13)	N (2)-Co-N (3)	85.2(5)
N (1)-C (1)	1.500(22)	Co-N (1)-C (1)	110.7(12)
N (2)-C (3)	1.609(20)	Co-N (2)-C (3)	112.7(9)
N (3)-C (2)	1.498(28)	Co-N (3)-C (2)	104.0(13)
N (3)-C (4)	1.529(25)	Co-N (3)-C (4)	109.3(10)
N (3)-C (5)	1.451(27)	Co-N (3)-C (5)	115.6(11)
C (1)-C (2)	1.459(33)	C (2)-N (3)-C (4)	111.1(14)
C (3)-C (4)	1.493(23)	C (2)-N (3)-C (5)	109.0(14)
C (5)-C (6)	1.533(27)	C (4)-N (3)-C (5)	107.8(16)
		N (1)-C (1)-C (2)	109.6(17)
		N (3)-C (2)-C (1)	109.0(15)
		N (2)-C (3)-C (4)	102.2(12)
		N (3)-C (4)-C (3)	115.9(16)
		N (3)-C (5)-C (6)	117.8(13)
		N (1)-Co-N (1′)	93.1(8)
		N (1)-Co-N (2′)	86.0(7)
		N (1)-Co-N (3′)	171.2(8)
		N (2)-Co-N (2′)	177.7(5)
		N (2)-Co-N (3′)	96.4(7)
		N (3)-Co-N (3′)	95.5(7)
		C (5)-C (6)-C (5′)	118.2(20)

suggests a distortion of the CoN_6 octahedron. N(3)-Co-N(4) angle of 101.0(1)° in (**2**) is larger by 4.8 (2)° than N(3)-Co-N(3′) angle in (**1**). Edge-on view of the five-membered chelate rings are shown in Fig. 3. They adopt an envelope conformation except B ring of (**2**). N(1)-Co-N(3) angle of the chelate ring B, 81.6(1)° and N(2)-Co-N(3) angle of the ring E, 83.7(1)° are smaller than the corresponding angles in the chelate rings C and D by 3.9(1) and 1.0(1)°, respectively.

In Fig. 3 the tertiary N atoms are hatched. The conformations of the apical chelate rings D and E of

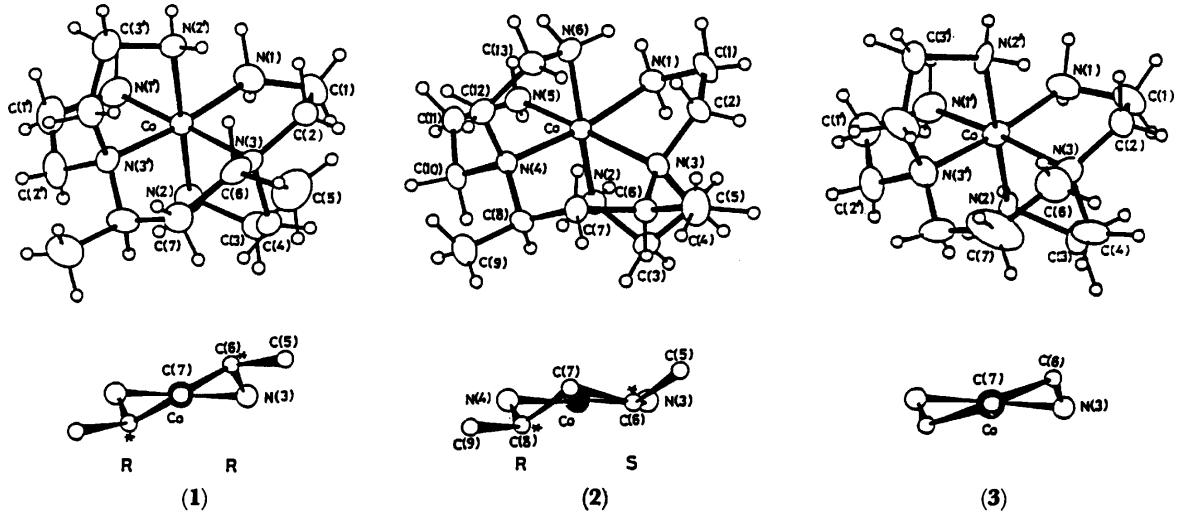

Fig. 2. Molecular structures of (**1**), (**2**), and (**3**). Projections of the central six-membered chelate rings along the midpoint of two tertiary N atoms to the Co are also shown.

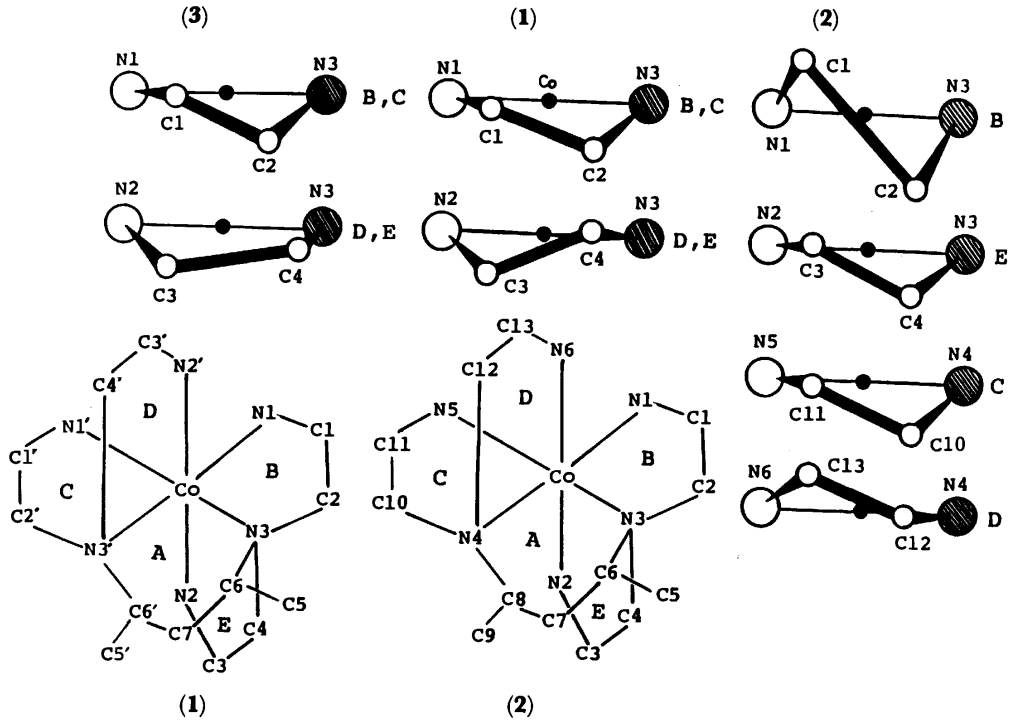

Fig. 3. Edge-on views of the five-membered chelate rings. The shaded circles stand for the tertiary N atoms, the black circles for the Co atoms.

(**1**) and (**2**) differ from each other. The simple molecular model indicates that the ring D in (1) avoids a short contact between H(C6) and one of the H atoms bonded to C(3′), and that the conformation of the ring E in (**2**) is the result of the flattened chair form of the central chelate ring, A. Table 4 lists the hydrogen bonds. The ring D in (**2**) takes a conformation which can form two hydrogen bonds, O(1)···H(N6)1-N(6) and Cl(3)···H(N6)2-N(6) in the crystal. Co-N(3)-C(6) angle of (**2**) is 120.5(2)°. It nearly equals to the mean Co-N-C angle of 122.2(2)° in $[Co(tn)_3]^{3+}$ (tn=1,3-propanediamine), which takes the C_3-chair$_3$ conformation.[8] The N-Co-N angle in the ring E of (**1**) and (**3**) agrees with that of 85.4(1)° in *lel*$_3$-$[Co(en)_3]^{3+}$ (en=1,2-ethanediamine),[9] and smaller by *ca.* 1° than that in the ring B.

The octahedral splitting parameter $10D_q$ can be easily shown to be proportional to r^{-5}, where r is the Co-N distance, if simple electrostatic model is assumed for the ligand field as a crude approximation.[10] In Fig. 4, the energy of the first absorption maxima of some Co(III) complexes with CoN_6 chromophore are plotted against the inverse fifth power of the average Co-N bond distances. A positive correlation is observed. It

Table 4. Intermolecular hydrogen bonds (distances in Å)

A···H-B (symmetry code)		A···B	A···H	H···B
(**1**)				
O(6)···H(N1)1-N(1)	(i)	3.029(7)	2.01(6)	1.02(5)
Ow···H(N1)2-N(1)	(ii)	2.952(5)	1.92(6)	1.11(6)
(**2**)				
Cl(2)···H(N1)2-N(1)	(iii)	3.213(4)	2.27(5)	0.97(5)
Cl(2)···H(N2)1-N(2)	(iii)	3.308(3)	2.45(4)	0.94(4)
Cl(1)···H(N5)2-N(5)	(iv)	3.204(4)	2.39(5)	0.83(5)
O(1)···H(N6)1-N(6)	(v)	2.893(5)	2.03(5)	0.88(5)
Cl(3)···H(N6)2-N(6)	(v)	3.281(4)	2.45(5)	0.98(4)
Cl(2)···H(O1)2-O(1)	(vi)	3.161(3)	2.33(4)	0.85(4)
(**3**)				
Br(2)···H(N1)1-N(1)	(vii)	3.420(13)	2.48	1.02
Br(1)···H(N1)2-N(1)	(viii)	3.313(16)	2.30	1.03

Symmetry codes: (i) $1/2-x$, $1/2+y$, $3/2-z$, (ii) $1/2+x$, $1/2-y$, $3/2-z$, (iii) $1/2-x$, $1/2+y$, $1-z$, (iv) $1-x$, $-y$, $1-z$, (v) $-1/2+x$, $1/2-y$, z, (vi) $-x$, $1-y$, $-z$, (vii) $1-x$, 1−y, $1-z$, (viii) $x+y$, $-y$, $-1/2+z$.

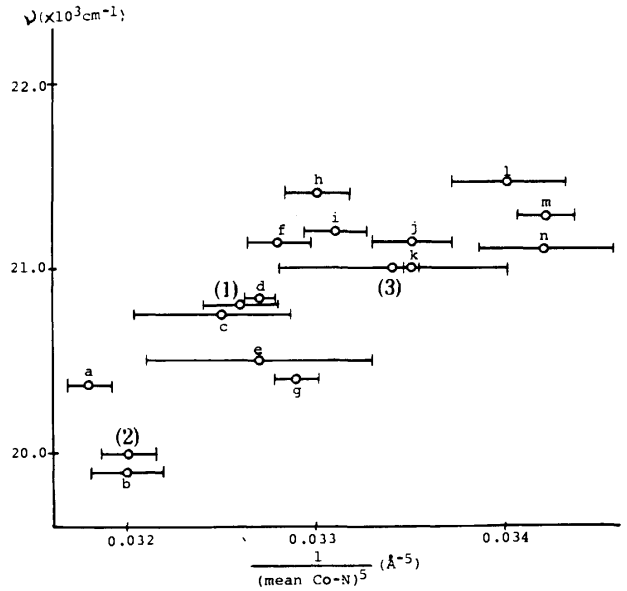

Fig. 4. Plot of the energy of the first absorption band against the inverse fifth power of the mean Co–N bond length of $Co(III)N_6$ complexes: a) $(+)_{589}$-*fac*-$[Co(R,S\text{-ptn})_3]^{3+}$,[11] b) $(+)_{589}$-$[Co(tmd)_3]^{3+}$,[12] c) $(-)_{546}$-$[Co(R,R\text{-ptn})_3]^{3+}$,[13] d) $(+)_{470}$-*cis*-$[Co(NH_3)_2(R,R\text{-ptn})_2]^{3+}$,[14] e) $(+)_{589}$-$[Co(ten)]^{3+}$,[15] f) $(+)_{589}$-(*ob*$_3$)-$[Co(chxn)_3]^{3+}$,[16] g) $(-)_{589}$-$[Co(tn)_3]^{3+}$,[8] h) $(+)_{589}$-(*lel*$_3$)-$[Co(en)_3]^{3+}$,[9] i) $(+)_{589}$-$[Co(linpen)]^{3+}$,[17] j) $(-)_{589}$-(*lel*$_2$ob)-$[Co(chxn)_3]^{3+}$,[18] k) $[Co(NH_3)_6]^{3+}$,[19] l) $(+)_{589}$-*mer*-$[Co(dien)_2]^{3+}$,[20] m) $(+)_{589}$-$[Co(en)_2(3,3'\text{-dmbpy})]^{3+}$,[21] n) $(-)_{589}$-$[Co(R,R\text{-chxn})_2(3,3'\text{-dmbpy})]^{3+}$,[22]. Error bars show ±(e.s.d.)/2.

was shown that the Co–N bond elongation in (**2**) which is caused by the nonbonded interactions is an important factor for the lower energy of the first absorption band than that of (**1**).

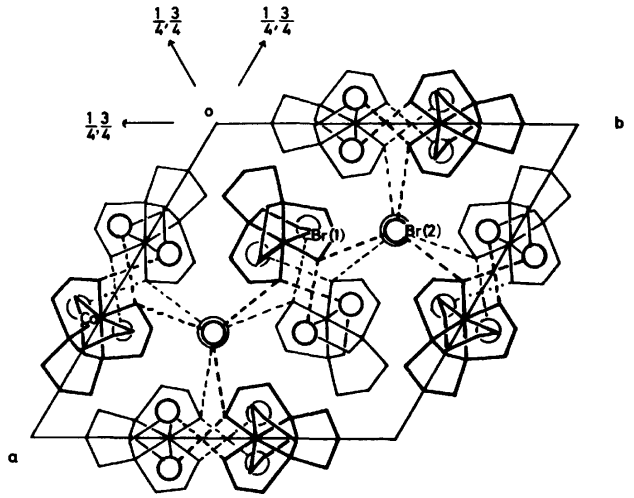

Fig. 5. A projection of the crystal structure of (**3**) along *c*. The broken lines indicate the hydrogen bonds.

A remark will be given on the disorder of the bromide ions in (**3**). The complex ions $[Co(ttn)]^{3+}$ and bromide ions Br(2) are held together by N-H···Br hydrogen bonds to form layers approximately perpendicular to *c* as shown in Fig. 5. These layers are stacked parallel to form a three-dimensional framework by attraction of Br(1) anions between the layers to the complex cations. There exists a hollow around the origin, in which the disordered bromide ions lie. The shortest interatomic distance involving Br(3) atom is 3.38 Å for Br(3)···H(C4)1 ($-y$, $1-x$, $-1/2+z$), longer than 3.05 Å, the sum of the van der Waals radius of Br and H atoms.[23]

The authors are grateful to Professor Junnosuke Fujita, Nagoya University for supplying the crystal specimen.

References

1) K. Hata, M. Doh, K. Kashiwabara, and J. Fujita, *Bull. Chem. Soc. Jpn.*, **54**, 190 (1981).

2) R. Nagao, F. Marumo, and Y. Saito, *Acta Crystallogr., Sect. B*, **28**, 1852 (1972).

3) P. Main, S. E. Hull, L. Lessinger, G. Germain, J. P. Declercq, and M. M. Woolfson, *MULTAN78*. A System of Computer Programs for the Automatic Solution of Crystal Structures from X-Ray Diffraction Data. Univs. of York, England and Louvain-la-Nerve, Belgium (1978).

4) "International Tables for X-Ray Crystallography," Birmingham, Kynoch Press (1974), Vol. IV.

5) T. Sakurai and K. Kobayashi, *Rikagaku Kenkyusho Hokoku*, **55**, 69 (1979).

6) Tables of the coordinates of hydrogen atoms, the anisotropic thermal parameters of the non-hydrogen atoms, and observed and calculated structure factors are kept as Document No. 8513 at the Chemical Society of Japan.

7) B. Bosnich and J. MacB. Harrowfield, *J. Am. Chem. Soc.*, **94**, 3426 (1972).

8) R. Nagao, F. Marumo, and Y. Saito, *Acta Crystallogr.*,

Sect. B, **29**, 2438 (1973).
9) M. Iwata, K. Nakatsu, and Y. Saito, *Acta Crystallogr., Sect B*, **25**, 2562 (1969).
10) H. Kamimura, S. Sugano, and Y. Tanabe, "Haiishibariron To Sono Oyoh," Shokabo, Tokyo (1972), Chap. 2, pp. 23—31.
11) S. Sato and Y. Saito, *Acta Crystallogr., Sect. B*, **34**, 420 (1978).
12) S. Sato and Y. Saito, *Acta Crystallogr., Sect. B*, **31**, 1378 (1975).
13) A. Kobayashi, F. Marumo and Y. Saito, *Acta Crystallogr., Sect. B*, **29**, 2443 (1973).
14) S. Ohba, H. Miyamae, S. Sato and Y. Saito, *Acta Crystallogr., Sect. B*, **35**, 321 (1979).
15) A. Muto, F. Marumo and Y. Saito, *Acta Crystallogr., Sect. B*, **26**, 226 (1970).
16) A. Kobayashi, F. Marumo and Y. Saito, *Acta Crystallogr., Sect. B*, **28**, 2709 (1972).
17) S. Sato and Y. Saito, *Acta Crystallogr., Sect. B*, **31**, 2456 (1975).
18) S. Sato and Y. Saito, *Acta Crystallogr., Sect. B*, **33**, 860 (1977).
19) M. Iwata and Y. Saito, *Acta Crystallogr., Sect. B*, **29**, 822 (1973).
20) K. Okiyama, S. Sato and Y. Saito, *Acta Crystallogr., Sect. B*, **35**, 2389 (1979).
21) S. Sato and Y. Saito, *Acta Crystallogr., Sect. B*, **34**, 3352 (1978).
22) S. Ohba, S. Sato and Y. Saito, *Acta Crystallogr., Sect. B*, **35**, 957 (1979).
23) A. Bondi, *J. Phys. Chem.*, **68**, 441 (1964).

 © 1985 The Chemical Society of Japan

Studies on the $G(Fe^{3+}\rightarrow Fe^{2+})$-value in the Radiolysis Caused by $^{6}Li(n,\alpha)T$ Reaction in Lithium Tris(oxalato)ferrate(III)

Junko Akashi, Tomoko Kojima, Yoshio Uchida, and Hirotoshi Sano*
Department of Chemistry, Faculty of Science, Tokyo Metropolitan University, Fukasawa, Setagaya, Tokyo 158
(Received October 13, 1984)

The *G*-values for the reduction of iron(III) to iron(II) state caused by $^{6}Li(n,\alpha)T$ reaction in $Li_3[Fe(C_2O_4)_3]\cdot 4.5H_2O$ and in anhydrated $Li_3[Fe(C_2O_4)_3]$ were determined by taking into account the saturation of the effect of increasing neutron fluence. The contribution of the fast neutrons and γ-rays in a nuclear reactor to the reduction was estimated by using a cadmium tube, and by using the results estimated in the ^{60}Co γ-ray irradiation, respectively. The $G(Fe^{3+}\rightarrow Fe^{2+})$-value in the radiolysis caused by $^{6}Li(n,\alpha)T$ reacation in $Li_3[Fe(C_2O_4)_3]\cdot 4.5H_2O$ is larger than that in the γ-ray radiolysis, and is also larger than the *G*-value for anhydrated $Li_3[Fe(C_2O_4)_3]$, suggesting that the radiolysis of the water of crystallization contributes to the reduction of the iron(III) species.

It has been pointed out elsewhere that the chemical effects of EC decay in several ^{57}Co-doped coordination compounds are considered to be caused by a nucleogenic local radiolysis in the compound.[1] In our previous papers,[2,3] the reduction of the iron(III) species to the iron(II) species in lithium tris(oxalato)-ferrate(III) by thermal-neutron irradiation was studied by means of Mössbauer spectroscopy. The reducing effets were attributed to a radiolytic process caused by the $^{6}Li(n,\alpha)T$ reaction.

The present paper describes the details of the effects of the $^{6}Li(n,\alpha)T$ reaction on the hydrated and anhydrated lithium tris(oxalato)ferrate(III), including an estimation of the *G*-values for reductions in those systems which are important for a better understanding of the processes caused by the $^{6}Li(n,\alpha)T$ reaction in connection to the chemical effects in the blanket materials in a fusion reactor. In order to estimate the *G*-value, the dependence of the areal intensity ratio of iron(III) to iron(II) in the Mössbauer spectra were studied on the irradiation time and on the thermal-neutron fluence rate. The effects of the fast neutrons and γ-rays concomitant in the reactor on the reduction were also determined.

Experimental

Hydrated lithium tris(oxalato)ferrate(III), $Li_3[Fe(C_2O_4)_3]\cdot 4.5H_2O$, sodium tris(oxalato)ferrate(III), $Na_3[Fe(C_2O_4)_3]\cdot 5H_2O$ and potassium tris(oxalato)ferrate(III), $K_3[Fe(C_2O_4)_3]\cdot 3H_2O$ were synthesized in the conventional ways.

The particle size of the samples was furnished to 200—300 mesh throughout the present work. Anhydrated $Li_3[Fe(C_2O_4)_3]$ was prepared by heating the $Li_3[Fe(C_2O_4)_3]\cdot 4.5H_2O$ at 400 K for 10-30 min in air.

Each 100 mg of the sample heat-sealed under nitrogen in a polyethylene envelope was irradiated either within or without a 0.5-mm thick cadmium tube in a 100-kW TRIGA MarkII reactor at the Institute for Atomic Energy, Rikkyo University.

The irradiated samples were kept in liquid nitrogen until the Mössbauer spectroscopic measurements were carried out. Mössbauer spectra were recorded with a constant-acceleration type spectrometer at 80 K. Isomer-shift values were reported with respect to metallic iron foil.

γ-Ray irradiations were carried out using a ^{60}Co-source, at the Institute of Physical and Chemical Researches, at a dose rate of 9,780 rad min^{-1} (H_2O).

Results and discussion

The Mössbauer spectrum of a sample irradiated at a thermal-neutron fluence rate of 5×10^{11} n s^{-1} cm^{-2} and at a fast-neutron fluence rate of 4.5×10^{10} n s^{-1} cm^{-2} for 2 h within the cadmium tube, which absorbs neutrons with the energy of less than 0.4 eV, is shown in Fig. 1 (b). The spectra of the sample irradiated at the same fluence rates of thermal and fast neutrons for 4 h within the cadmium tube are compared in Fig. 1 (c). A distinctive change is not found in the irradiated sample compared with the spectrum of the non-irradiated sample (Fig. 1 (a)), except for a small peak component ascribed to iron(II) species as found in Fig. 1 (c). In the spectrum shown in Fig. 1 (c), the areal intensity ratio of iron(II) to the total iron species is estimated to be less than 0.09. As shown in Fig. 1 (d), the ratio in the spectrum of the neutron-irradiated $Li_3[Fe(C_2O_4)_3]\cdot 4.5H_2O$ in the same irradiation conditions as in the case of Fig. 1(c) is estimated to be 0.67. The ratio is much larger without the cadmium tube than that obtained within the tube as found in Fig. 1(c), suggesting that the reduction of iron(III) to iron(II) observed in the neutron-irradiated $Li_3[Fe(C_2O_4)_3]\cdot 4.5H_2O$ is mainly attributed to the effect of thermal neutrons. Figures 2 (a) and (b) show the Mössbauer spectra of $Li_3[Fe(C_2O_4)_3]\cdot 4.5H_2O$ subjected to γ-rays of the total dose of 4×10^{7} rad and 1.0×10^{8} rad, respectively, at a dose rate of 9,780 rad min^{-1} (H_2O). Although the total dose in the reactor for the experiment of Fig. 2 (a) is estimated to be about 7 times larger than that in the irradiation conditions used for Fig. 1 (c), it is still not as remarkable a

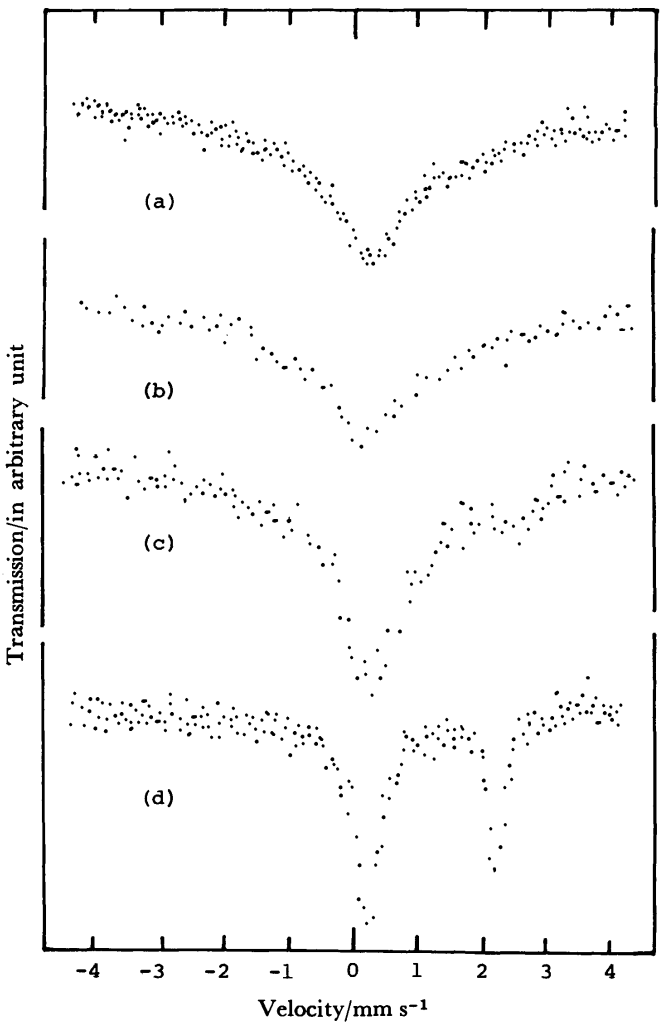

Fig. 1. Mössbauer spectra at 80 K of (a) unirradiated, (b) neutron-irradiated within a cadmium tube, (2 h), (c) neutron-irradiated within a cadmium tube, (4 h), and (d) neutron-irradiated without a cadmium tube, (4 h), $Li_3[Fe(C_2O_4)_3]\cdot 4.5H_2O$. (thermal neutron fluence rate: 5×10^{11} n s^{-1} cm^{-2} fast neutron fluence rate: 4.5×10^{10} n s^{-1} cm^{-2}).

reduction in Fig. 2 (a) as is found in Fig. 1 (c). Based on the linear dependence of the areal-intensity ratio of the iron(II) species to the total iron species in the spectra on the γ-ray irradiation time, the G-value for the reduction of iron(III) in $Li_3[Fe(C_2O_4)_3]\cdot 4.5H_2O$ caused by the γ-ray irradiation is estimated to be 8.4.

The $G(Fe^{3+}\rightarrow Fe^{2+})$-value for γ-ray-irradiated potassium, sodium and ammonium salts obtained in a similar way are listed in Table 1, together with that of the lithium salt for the sake of comparison. The value for the lithium salt is a little smaller than those for the potassium, sodium and ammonium salts.

As in the case of Fig. 1 (d), the neutron-irradiated potassium and sodium tris(oxalato)ferrate(III) at the same neutron irradiation condition also show little contribution of the iron(II) species as found in

Table 1. G-values for reduction of tris(oxalato)-ferrate(III) crystals by ^{60}Co γ-ray irradiations

Compound	$G(Fe^{3+}\rightarrow Fe^{2+})$
$Li_3[Fe(C_2O_4)_3]\cdot 4.5H_2O$	8.4
$Na_3[Fe(C_2O_4)_3]\cdot 5H_2O$	10.1
$K_3[Fe(C_2O_4)_3]\cdot 3H_2O$	15.1
$(NH_4)_3[Fe(C_2O_4)_3]\cdot 2H_2O$	16.1
$Li_3[Fe(C_2O_4)_3]$	7.3

Table 2. Areal intensity ratios of iron(III) species to total iron species in several irradiation conditions in lithium tris(oxalato)ferrate(III)

Fluence rate / n s^{-1} cm^{-2}	Irradiation time / h				
	0.5	1	2	4	6
5×10^{11}	0.82	0.64	0.44 0.45*	0.34	—
1.2×10^{12}	—	—	0.32 0.33*	0.05	0.01

* Irradiated at 200 K, others at an ambient temperature in a reactor.

Fig. 3, which is similar to the result found in ammonium salt reported in the previous result.[2] The results indicate that the G-value is negligibly small for the reduction caused by γ-rays in the lithium tris(oxalato)ferrate(III) during irradiation in the reactor for 4 h at the same neutron fluence rate as in the case of Fig. 1 (d).

The areal-intensity ratios of the iron(III) to the total iron species in several neutron-irradiation conditions for $Li_3[Fe(C_2O_4)_3]\cdot 4.5H_2O$ are listed in Table 2.

The ratio in the neutron-irradiated $Li_3[Fe(C_2O_4)_3]\cdot 4.5H_2O$ at an ambient temperature in the reactor is similar to that in the sample irradiated at 200 K (as cited in Table 2), indicating that the restoration of the iron(III) species through the thermal annealing during and after the $^6Li(n,\alpha)T$ reaction is negligibly small in the system. The ratios for neutron-irradiated $Li_3[Fe(C_2O_4)_3]\cdot 4.5H_2O$ decrease linearly neither with increased irradiation time nor with total neutron-fluence, which can be explained by assuming the presence of a saturation process in the reduction, *i.e.*, the iron(II) species produced by the $^6Li(n,\alpha)T$ reaction is practically not affected by the thermal-neutron irradiation. By simply applying the first-order reaction rate, the number of iron(III) atoms affected by the $^6Li(n,\alpha)T$ reaction is expected to follow the equations,

$$dN/d(nt) = -kN, \quad N=N_0\exp(-knt)$$

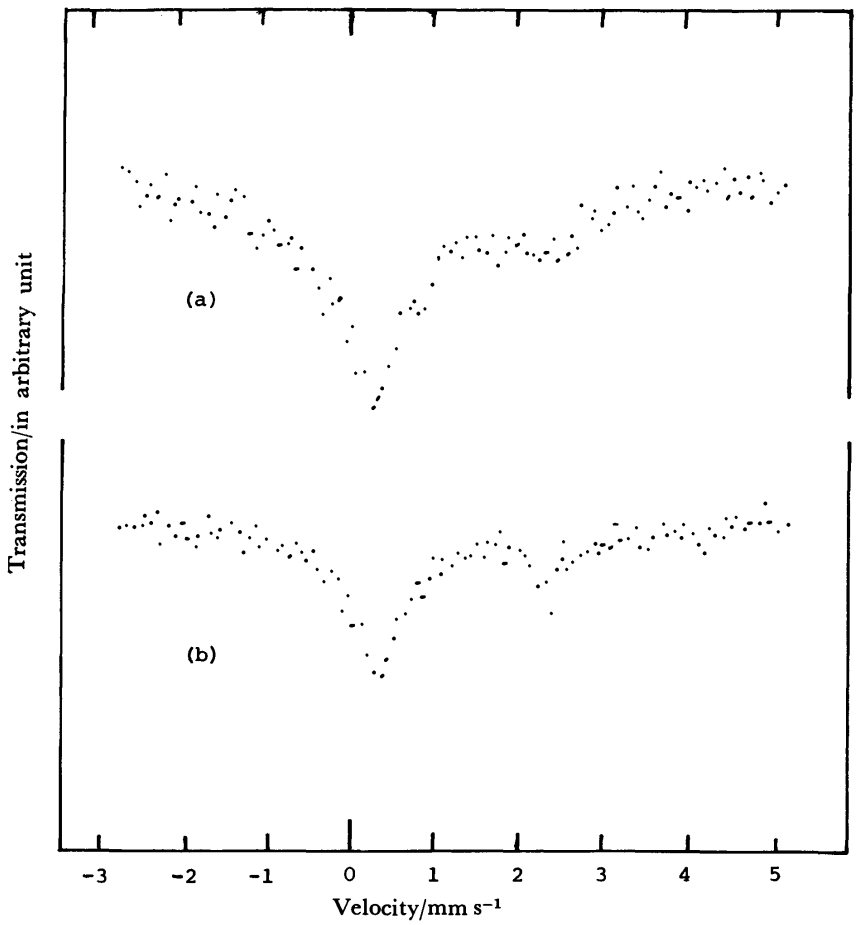

Fig. 2. Mössbauer spectra at 80 K of (a) γ-irradiated (4×10^7 rad) and (b) γ-irradiated (1.0×10^8 rad) $Li_3[Fe(C_2O_4)_3] \cdot 4.5H_2O$.

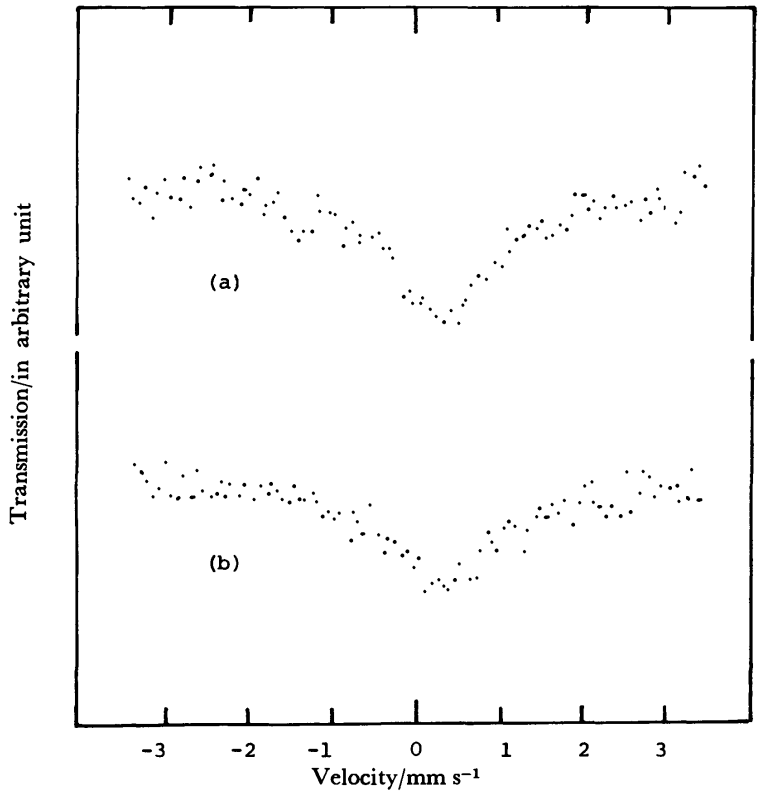

Fig. 3. Mössbauer spectra at 80 K of neutron-irradiated (5×10^{11} n s^{-1} cm^{-2}, 4 h) (a) $Na_3[Fe(C_2O_4)_3] \cdot 5H_2O$ and (b) $K_3[Fe(C_2O_4)_3] \cdot 3H_2O$.

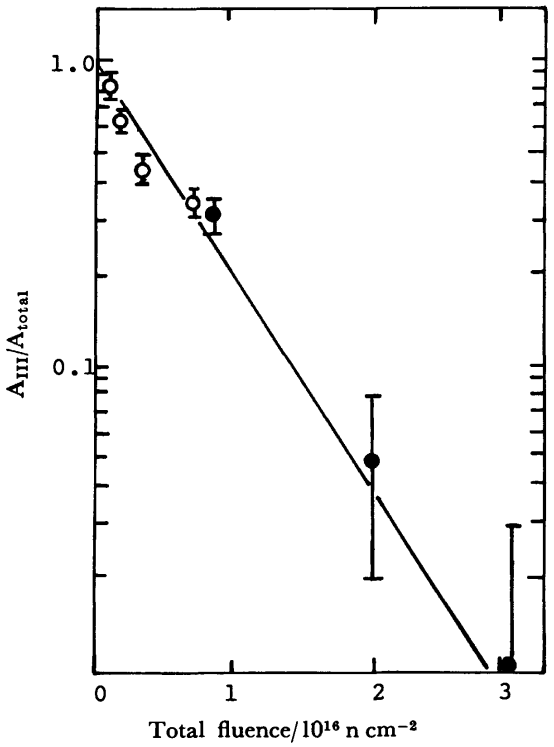

Fig. 4. Areal intensity ratio of Fe(III) to total iron species against thermal neutron fluence in Mössbauer spectra of $Li_3[Fe(C_2O_4)_3]\cdot 4.5H_2O$.

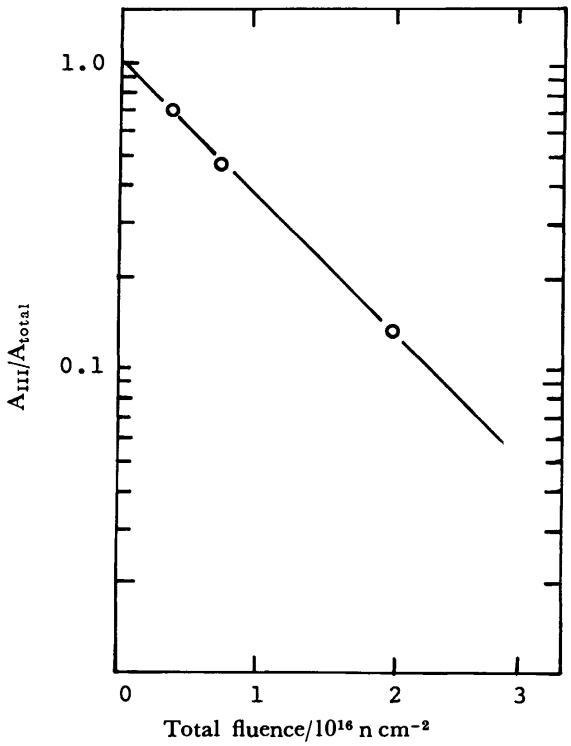

Fig. 5. Areal intensity ratio of Fe(III) to total iron species against thermal neutron fluence in Mössbauer spectra of $Li_3[Fe(C_2O_4)_3]$.

where N: the number of the iron(III) species.
n: thermal neutron fluence rate.
t: irradiation time.
k: rate constant.
N_0: initial number of the iron(III) species.

As a plot of the logarithm of the ratio of the iron(III) species to the total iron species gives practically a straight line against the increased neutron fluence, as shown in Fig. 4. The hypothetical equation seems to be useful to interpret the experimental results. The overall $G(Fe^{3+}\rightarrow Fe^{2+})$-value for the reduction in $Li_3[Fe(C_2O_4)_3]\cdot 4.5H_2O$ caused by the $^6Li(n,\alpha)T$ reaction is estimated to be 18.2 from the gradient of the line in Fig. 4. The G-value for the reduction of an anhydrated compound caused by the $^6Li(n,\alpha)T$ reaction is estimated to be 10.1 based on a similar plot, as shown in Fig. 5.

The G-value corresponds to about half of that obtained for the hydrated one, even after the small increases in the concentrations of iron and lithium compared with those in the hydrated compound. The results imply that the hydrated compound should more easily be subjected to the reduction caused by the $^6Li(n,\alpha)T$ reaction than the anhydrated one, and that the radiolytic products of water of crystallization should play an important role in the reduction of iron(III) to iron(II).

The small deviations of the experimental points from the line found in Fig. 4, may be ascribed to the possible decrease of water of crystallization in the sample during the irradiation at the accumulated fluence values. The G-value for the reduction caused by the $^6Li(n,\alpha)T$ reaction is estimated to be 19.9 from the line component derived from the data in the lower fluence region. These obtained G-values are summerized in Table 3.

Table 3. G-values for the reduction of the iron caused by the $^6Li(n,\alpha)T$ reaction in lithium tris(oxalato)ferrate(III)s

Compound	$G(Fe^{3+}\rightarrow Fe^{2+})$	
$Li_3[Fe(C_2O_4)_3]\cdot 4.5H_2O$	19.9	estimated from areal intensity of the Mössbauer spectrum in early stage of irradiation
	18.2	estimated from log plot as shown in Fig. 4
$Li_3[Fe(C_2O_4)_3]$	10.1	estimated from log plot as shown in Fig. 5

The $G(Fe^{3+}\rightarrow Fe^{2+})$-value for the hydrated lithium tris(oxalato)ferrate(III) in the $^6Li(n,\alpha)T$ reaction is about 2 times larger than that in the γ-ray-radiolysis using a ^{60}Co source, as shown in Tables 1 and 3. The difference should be attributed to the high values of

the linear energy transfer (LET) of alpha and tritium particles emitted by the $^{6}Li(n,\alpha)T$ reaction. The results reveal that a higher density of electrons and excited species, such as radicals or ions, produced by the high-energy particles is more effective in causing the reduction of the iron(III) to the iron(II) species in lithium tris(oxalato)ferrate(III).

References

1) H. Sano, M. Harada, and K. Endo, *Bull. Chem. Soc. Jpn.*, **51**, 2583 (1978).
2) J. Akashi, M. Katada, and H. Sano, *Chem. Lett.*, **1982** 785.
3) J. Akashi, Y. Uchida, T. Kojima, M. Katada, and H. Sano, *Bull. Chem. Soc. Jpn.*, **57**, 1076 (1984).

The Selective *N*-Monoalkylation of Amides with Alkyl Halides in the Presence of Alumina and KOH

Kazuaki SUKATA*
Nihon Tokushu Kagaku Kogyo Co., Ltd., 3-36, Tohda-cho, Moriguchi, Osaka 570
(Received July 27, 1984)

The effects of alumina impregnated with KOH (KOH/Al_2O_3) and a mixture of alumina and powdered KOH ($KOH+Al_2O_3$) have been examined using the alkylation of benzamide under various conditions. In each case, alkylation occurs exclusively in the pores of the alumina, the extent depending upon the alumina-pore size. For both yield and selectivity for *N*-monoalkylation, $KOH+Al_2O_3$ is superior to KOH/Al_2O_3. Dioxane is the best of the solvents employed. It is proposed that, in dioxane, an enolate-like species, $PhC(O^-K^+)=NR'$, exists as stable ion-pair aggregates, which are the true reactants in the pore. This method, using KOH/Al_2O_3 or $KOH+Al_2O_3$, has been applied to *N*-alkylation of the other amides, giving the *N*-monoalkylated products in substantial yields with extremely high selectivities. 2-Phenylacetamide is regioselectively *N*-monoalkylated in high yields. This regioselectivity is explained in terms of steric hindrance.

It has recently been reported that amides are *N*-monoalkylated in substantial yields under phase-transfer catalytic conditions.[1] In the case of propanamide, which also has a weakly acidic N-H bond, however, the yields are considerably lower than those of benzamide (**1**). When highly-reactive benzyl chloride is employed as an alkylating agent, substantial quantities of *N,N*-dibenzylated products are obtained. More recently, Watanable *et al.* have reported the *N*-alkylation of amides with alcohols using ruthenium compounds as catalysts.[2] In this process, however, the yields and the selectivities for *N*-monoalkylation were low, with only a few exceptions.

In recent years, many studies have been reported on selective organic synthesis using inorganic solids.[3] Recently, the present author has himself reported the selective monoalkylation of phenylacetonitrile (PAN) using alumina impregnated with KOH or NaOH (KOH/Al_2O_3 or $NaOH/Al_2O_3$).[4a] It was shown that the reaction of the carbanion with alkyl halide occurs in the pores of the alumina and that the selectivity can be explained in terms of steric hindrance.

It has now been found that amides are selectively *N*-monoalkylated with alkyl halides in the presence of alumina and KOH.

$$\underset{(\mathbf{1}\text{—}\mathbf{4})}{R\text{-}\overset{O}{\overset{\|}{C}}\text{-}NH_2} + \underset{(\mathbf{5})}{R'X} \xrightarrow{\text{Alumina, KOH}} R\text{-}\overset{O}{\overset{\|}{C}}\text{-}NHR'$$

(**1**), R=Ph
(**2**), R=CH_3
(**3**), R=*n*-C_3H_7
(**4**), R=$PhCH_2$

(**a**), R'=C_2H_5
(**b**), R'=*n*-C_3H_7
(**c**), R'=*n*-C_4H_9
(**d**), R'=CH_2=$CHCH_2$
(**e**), R'=$PhCH_2$

* Present address: Nihon Tokushu Kagaku Kogyo Co., Ltd., 1, Takijiri-aza-hashimoto, Izumi-cho, Iwaki, Fukushima 970-04.

Results and Discussion

The *N*-alkylation of **1** with alkyl halides (**5**) was carried out under various conditions using KOH/Al_2O_3 or a mixture of alumina and powdered KOH.

N-Alkylation of 1 Using KOH/Al_2O_3. In order to ascertain the effects of solvents, the *N*-alkylation of **1** with ethyl bromide was carried out using M-90-N alumina (Merck, Type 90, activity I, neutral, 70—230 mesh) impregnated with KOH (KOH/M-90-N) in several solvents. Table 1 shows the results. In the case of PAN, the order of the selectivities for monoalkylation has been found to be benzene>dioxane>THF>acetonitrile.[4a] In the case of **1**, however, the order of the selectivities for *N*-monoalkylation was dioxane≫benzene>THF>1,2-dimethoxyethane (DME)≈

Table 1. *N*-Ethylation of **1** using KOH/Al_2O_3 in several solvents[a]

Solvent	Time / h	Yield[b] / %	Selectivity Mono/% ; Di/%
Benzene	8	36	91 ; 9
	2[c]	45	84 ; 16
Dioxane	8	49	98.5 ; 1.5
THF	8	49	80 ; 20
DME	8	48	58 ; 42
Acetonitrile	2	52	58 ; 42
DMSO[d]	6	41	62 ; 38

a) Unless otherwise noted, the reactions were carried out with **1** (10 mmol), ethyl bromide (12 mmol), KOH (50 mmol)/Al_2O_3 (M-90-N, 10 g), and hexadecane (0.3 g) as the internal standard in a solvent (20 ml) at 60 °C. b) Mono+Di; determined by GLC. c) The reaction was carried out with **1** (10 mmol), ethyl bromide (12 mmol), finely powdered KOH (50 mmol), hexadecane (0.3 g) as the internal standard, and *n*-$Bu_4N^+Br^-$ (2 mmol) at 60 °C. d) No catalyst was used.

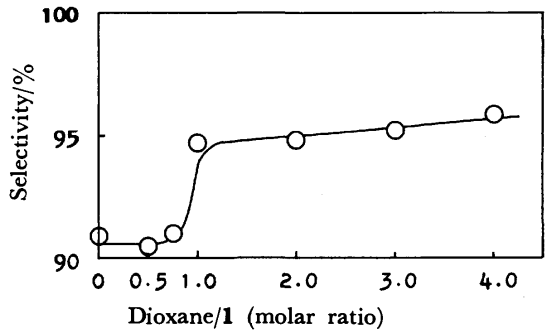

Fig. 1. The influence of the relative amount of dioxane to **1** on the selectivity for *N*-monoalkylation. The reactions were carried out with **1** (10 mmol), ethyl bromide (12 mmol), KOH (50 mmol)/M-90-N (10 g), and dioxane (0, 5, 7.5, 10, 20, 30, 40 mmol) in benzene (20 mL) at 60 °C for 8 h.

acetonitrile. An almost exclusive *N*-monoalkylation was achieved in dioxane.

In order to ascertain the specific solvent effect of dioxane, the influence of the amount of dioxane relative to that of **1** on the selectivity for *N*-monoalkylation was examined using alkylation with KOH/M-90-N and ethyl bromide in benzene (Fig. 1). At the dioxane/**1** molar ratio of *ca.* 1.0, a clear change in the selectivity was observed.

In order to establish the effect of the support pore size, the *N*-ethylation of **1** was carried out using several supports in benzene or in dioxane. Table 2 shows the results. The supports used were M-90-N, M-60-B alumina (Merck, Type 60, activity I, basic, 70—230 mesh), W-200-N alumina (Woelm, Type 200, neutral, activity super I), and Molecular Sieve 13X (MS-13X). The average pore diameters of M-90-N, M-60-B, and MS-13X are 90, 60, and 10 Å, respectively. The average pore diameter of W-200-N appears to be *ca.* 60 Å, based upon its specific surface area, which is *ca.* 200 m^2/g.[5] In the case of MS-13X, almost all of the **1** used was recovered. This resembles the alkylation of PAN.[4a] The pore diameter of MS-13X is too small for the reaction. The selectivities found in dioxane were much larger than those found in benzene in all cases examined.

Apparent differences were observed in the selectivity for *N*-monoalkylation, depending upon the kind of alumina (Table 2). The yield of *N,N*-dialkylation obviously increased with the increase in the average pore diameter. This fact, and the fact that almost no **1** is observed in the organic phase during the reaction, indicate that the *N*-alkylation occurs predominantly in the pore. Jackman *et al.* have recently shown that lithium enolates exist as tetramers or dimers in ether solvents[6] and that ion-pair aggregates are the true reactants in the methylation of lithiobutyrophenone in weakly polar aprotic solvents.[7] Similarly, an enolate-like species

Table 2. *N*-Ethylation of **1** using several supports in benzene or dioxane[a]

Solvent	Support	Yield[b] %	Selectivity Mono/% ; Di/%
Benzene	M-90-N	36	91 9
	M-60-B	42	99 1
	W-200-N	36	96 4
	MS-13X (powder)[c]	≪1	— —
	MS-13X (60—80 mesh)[c]	≪1	— —
Dioxane	M-90-N	49	98.5 1.5
	M-60-B	55	≫99 0.2
	W-200-N	51	>99 0.5
	MS-13X (powder)[c]	≪1	— —
	MS-13X (60—80 mesh)[c]	≪1	— —

a) Unless otherwise noted, the reactions were carried out with **1** (10 mmol), ethyl bromide (12 mmol), KOH (50 mmol)/support (10 g), and hexadecane (0.3 g) as the internal standard in a solvent (20 ml) at 60 °C for 8 h. b) Mono+Di; determined by GLC. c) KOH (50 mmol)/MS-13X (15 g) and a solvent (30 ml) were used.

(**6**) is also considered to exist as ion pairs or ion-pair aggregates and only in dioxane as stable ion-pair aggregates in the pore:

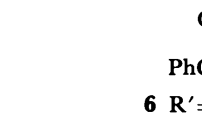

6 R′=H, Et

The clear change at the dioxane/**1** molar ratio of *ca.* 1.0 (Fig. 1) provides strong evidence for the strong interaction between dioxane and **6** of the 1:1 molar ratio, which is very compatible with the molar ratio of the solvent to solute in the structures of the tetramer and the dimer shown by Jackman *et al.*[6] This fact and the above results strongly suggest that ion-pair aggregates of **6**, a tetramer and/or a dimer, are the ture reactants in dioxane, resulting in a large steric hindrance, even in the pore of alumina, which has a relatively large pore diameter. When R′ is hydrogen in **6**, the steric hindrance to the reaction of **6** with **5** is very small.

N-Alkylation of 1 Using Nonimpregnated Alumina and Powdered KOH. Alumina and KOH were ground in a mortar. Hereafter, KOH+Al_2O_3 will represent the mixture of alumina and KOH prepared by this method. The *N*-ethylation of **1** using KOH+Al_2O_3 was carried out in several solvents. Table 3 shows the results. KOH+Al_2O_3 gave better

TABLE 3. *N*-ETHYLATION OF **1** USING KOH+Al_2O_3 IN SEVERAL SOLVENTS[a]

Solvent	Time h	Yield[b] %	Selectivity Mono/% ; Di/%
Benzene	8	36	99 1
Dioxane	8	63	≫99 ≈0.2
	8	62[c]	≫99 ≈0.1
THF	8	55	86 14
DME	6	59	75 25
Acetonitrile	2	47	80 20

a) All the reactions were carried out with **1** (10 mmol), ethyl bromide (12 mmol), KOH (50 mmol)+Al_2O_3 (M-90-N, 10 g), and hexadecane (0.3 g) in a solvent (20 ml) at 60 °C. b) Mono+Di; determined by GLC. c) Al_2O_3 (M-60-B, 10 g).

yields than KOH/Al_2O_3 in a solvent except benzene and acetonitrile, and better selectivities than KOH/Al_2O_3 for *N*-monoalkylation in all solvents. These findings are quite in contrast to the results of the alkylation of PAN, in which KOH/Al_2O_3[4a] is superior to KOH+Al_2O_3[4b] in both yield and selectivity for monoalkylation. This fact indicates that the *N*-alkylation of **1** occurs in the pores of alumina even when KOH+Al_2O_3 is employed. The difference in selectivity between KOH/Al_2O_3 and KOH+Al_2O_3 can be interpreted as follows. For KOH/Al_2O_3, KOH is present in the pores. Therefore, KOH/Al_2O_3 must deprotonate the *N*-alkylated product formed in the pores more rapidly than KOH+Al_2O_3, thus lowering the selectivity. The difference in the yield can be interpreted as follows. Since alumina was ground together with KOH in the case of KOH+Al_2O_3, the particle size of the alumina in KOH+Al_2O_3 must be smaller than the particle size in KOH/Al_2O_3. Therefore, the increase in the yield may be thought to be due to the increase in the surface area of alumina. However, as is shown in Table 4, only slight changes in yield and selectivity for *N*-monoalkylation were observed when twice as much KOH and alumina were used as in the standard. Furthermore, for both KOH/Al_2O_3 and KOH+Al_2O_3, almost no **1** was observed in the organic phase during the reaction. These facts indicate that **1** is uniformly adsorbed on both active and inactive sites. To examine the influence of pulverization of alumina, alkylation of **1** with ethyl bromide was carried out using virgin alumina or alumina ground separately from KOH. In the cases of both M-90-N and M-60-B, the results were quite similar to those obtained by using alumina ground together with KOH. These results indicate that, since KOH/Al_2O_3 contains KOH in its pores, KOH/Al_2O_3 more strongly adsorbs **1** in its pores.

Table 4 summarizes the results of the *N*-alkylation of **1** with various alkylhalides using KOH+Al_2O_3 in dioxane. Alkyl bromide was better than alkyl iodide in both yield and selectivity for *N*-monoalkylation. This finding contrasts with the results of the alkylation of PAN using KOH/Al_2O_3,[4a] where alkyl iodide was better than alkyl bromide. This indicates that the *N*-alkylation of **1** is more sterically retarded than the alkylation of PAN. This fact supports the idea that the ion-pair aggregates of **6** are the true reactants in dioxane. Alkyl iodide gave *N,N*-dialkylated products in higher yields than did alkyl bromide. *N,N*-Dialkylation should occur predominantly in the bulk organic phase and/or on the surface of KOH. The influence of the molecular size of the alkylating agents on the yield was more significant when M-60-B was employed than when M-90-N was used. This result seems surprising since the pore sizes of both M-90-M and M-60-B are much larger than the molecular sizes of **1** and **5**. However, this result can well be understood if the ion-pair aggregates of **6** are the true reactants. This result indicates that the yield and the selectivity for *N*-monoalkylation are intrinsically dependent upon the pore size.

For both KOH/Al_2O_3 and KOH+Al_2O_3, the reaction was very clean; GLC showed that the only products were *N*-mono- and *N,N*-dialkylated **1**. Almost all of the **1** was adsorbed on the alumina. Consequently, *N*-monoalkylated products were isolated in a highly pure state by filtering the solid material and removing the solvent. The unreacted **1** adsorbed on alumina was recovered in an 85—90% yield by adding a small amount of water to the alumina and by then extracting with benzene. Because of this recovery, the yields of *N*-monoalkylation were 89—92% (Table 4).

This method, using KOH/Al_2O_3 or KOH+Al_2O_3, was also utilized in the *N*-alkylation of other amides. Table 5 summarizes the results. In general, the *N*-monoalkylated products were obtained in good yields with extremely high selectivities. However, the use of highly reactive allyl bromide or benzyl bromide as an alkylating agent lowered the selectivity for *N*-monoalkylation. For selectivity in *N*-monoalkylation, KOH+Al_2O_3 and M-60-B were better than KOH/Al_2O_3 and M-90-N, respectively. Butanamide (**3**), bearing a bulkier alkyl group, gave more preferentially *N*-monoalkylated products than acetamide (**2**). For 2-phenylacetamide (**4**), the C-H bond at the α-position is also acidic, so the *C*-alkylation at the α-position is thought to accompany the *N*-alkylation.

$$\underset{\mathbf{4}}{PhCH_2\text{-}\overset{O}{\overset{\|}{C}}\text{-}NH_2} \xrightarrow{R'X} PhCH_2\text{-}\overset{O}{\overset{\|}{C}}\text{-}NHR' + PhCH(R')\text{-}\overset{O}{\overset{\|}{C}}\text{-}NH_2$$

In fact, the components of the products were more complicated than in the cases of the other amides. GLC showed the presence of several components

Table 4. *N*-Alkylation of **1** using $KOH+Al_2O_3$ in dioxane[a]

5	Al_2O_3 (g)	KOH / mmol	Yield[b] / %	Selectivity Mono/% ; Di/%
C_2H_5Br	M-90-N (10)	50	63 (92)[c]	≫99 ; ≈0.2
	M-60-B (10)	50	62	≫99 ; ≈0.1
	M-90-N (20)	100	61	>99 ; ≈0.6
C_2H_5I	M-90-N (10)	50	62	98.7 ; 1.3
n-C_3H_7Br	M-90-N (10)	50	58 (90)[c]	≫99 ; ≈0.2
	M-60-B (10)	50	32	≈100 ; ≈0
	M-90-N (20)	100	59	>99 ; ≈0.8
n-C_3H_7I	M-90-N (10)	50	33	98 ; 2
n-C_4H_9Br	M-90-N (10)	50	54 (89)[c]	≫99 ; <0.1
	M-60-B (10)	50	24	≈100 ; ≈0
	M-90-N (20)	100	50	>99 ; ≈0.4
n-C_4H_9I	M-90-N (10)	50	32	98 ; 2

a) All the reactions were carried out with **1** (10 mmol), **5** (12 mmol), and hexadecane (0.3 g) in dioxane (20 ml) at 60 °C for 8 h. b) Mono+Di; determined by GLC. c) Isolated yields based on the **1** consumed.

Table 5. *N*-Alkylation of amides using KOH/Al_2O_3 or $KOH+Al_2O_3$[a]

Amide	Alkyl bromide	Method[b]	Temp / °C	Alumina	Yield[c] / %	Selectivity for *N*-monoalkylation/%
Acetamide	C_2H_5Br	A	60	M-60-B	(61)	88.5
(**2**)		B	60	M-60-B	74[d]	97.1
	n-C_4H_9Br	A	60	M-60-B	57[d]	97.8
		B	60	M-90-N	80[d]	97.0
Butanamide	C_2H_5Br	A	60	M-60-B	80	98.9
(**3**)		B	60	M-60-B	(79)	99.2
		B	60	M-90-N	83	98.7
	n-C_4H_9Br	B	60	M-90-N	80	99.6
	CH_2=$CHCH_2Br$	B	40	M-60-B	(74)	97.0
		B	40	M-90-N	71 (81)	96.8
	$PhCH_2Br$	B	30	M-60-B	79	97.1
		B	30	M-90-N	76 (87)	95.8
2-Phenylacetamide	C_2H_5Br	A	60	M-60-B	71 (75)	97.5
(**4**)		B	60	M-60-B	(71)	97.6
	n-C_4H_9Br	A	60	M-90-N	60 (66)	99.5
		B	60	M-90-N	(57)	98.0
	CH_2=$CHCH_2Br$	A	40	M-60-B	57 (69)	82.0
		B	40	M-60-B	(66)	89.0
	$PhCH_2Br$	A	30	M-90-N	65 (69)	80.8
		B	30	M-90-N	69	86.0
Benzamide	CH_2=$CHCH_2Br$	B	40	M-90-N	(67)	93.2
(**1**)		B	40	M-60-B	56 (68)	95.5
	$PhCH_2Br$	B	30	M-90-N	71 (77)	96.5

a) All the reactions were carried out with amide (10 mmol), alkyl bromide (12 mmol), and dioxane (20 ml) for 8 h. b) A: KOH/Al_2O_3, B: $KOH+Al_2O_3$. c) Isolated yield. Unless otherwise noted, the purities were >97%. The values in parentheses are the yields determined by GLC. d) Purities were >96%.

other than *N*-monoalkylated products. In particular, when highly reactive allyl bromide or benzyl bromide was employed, GLC showed the presence of substantial quantities of several products, including the *N*-monoalkylated one.

For comparison, a solid-liquid phase-transfer alkylation of **4** was carried out using powdered KOH and tetrabutylammonium bromide (*n*-$Bu_4N^+Br^-$). Table 6 shows the results. These results indicate that the acidity of the C-H bond is similar to that of the N-H bond.[8] The regioselectivity for the alkylation of **4** using $KOH+Al_2O_3$ or KOH/Al_2O_3 must be explained

TABLE 6. ALKYLATION OF 4 USING SOLID-LIQUID PHASE-TRANSFER METHOD[a)]

Alkyl bromide	Temp °C	Time h	Yield[b)] %	Selectivity for N-monoalkylation/%
C_2H_5Br	60	2.5	35	85
$CH_2=CHCH_2Br$	40	1.5	18	47
$PhCH_2Br$	30	1.5	21	49

a) All the reactions were carried out with **4** (10 mmol), powdered KOH (50 mmol), alkyl bromide (12 mmol), and n-$Bu_4N^+Br^-$ (5 mmol) in benzene (20 ml). An almost complete conversion of **4** was observed. b) Isolated yields.

in terms of the steric hindrance as follows. Since the reaction occurs in the pore, the steric hindrance preventing the *C*-alkylation at the internal position is much larger than that preventing the *N*-alkylation at the terminal position, so the *N*-alkylation occurs predominantly.

In conclusion, amides are selectively *N*-monoalkylated by using KOH+Al_2O_3 or KOH/Al_2O_3. Even 2-phenylacetamide (**4**) is regioselectively *N*-monoalkylated in good yields. In dioxane, the enolate-like species **6** exists as stable ion-pair aggregates, which are the true reactants in the pores.

Experimental

Materials. Unless otherwise noted, reagents were obtained commercially. Benzamide (**1**), acetamide (**2**), butanamide (**3**), 2-phenylacetamide (**4**) (reagent grade, Tokyo Kasei Kogyo Co.), alumina (Merck 90 neutral, 70—230 mesh, activity I, Catalog No. 1077; Merck 60 basic, 70—230 mesh, activity I, Catalog No. 1067; Woelm 200 neutral, activity super I), Molecular Sieve 13X (for gas chromatography, 60—80 mesh), and 85% KOH were used as obtained. Alkyl halide (**5**), benzene, dioxane, THF, DME, and acetonitrile were dried with Molecular Sieve 4A. KOH/Al_2O_3 was prepared by the method previously reported.[4a)] KOH+Al_2O_3 was prepared by the method similar to that reported by Regen where reagent and alumina were ground together in a mortar.[9)] The authentic samples of *N*-ethyl- (**1a**), *N*-propyl- (**1b**), *N*-butyl- (**1c**), *N,N*-diethyl-, *N,N*-dipropyl-, and *N,N*-dibutylbenzamide were prepared by the literature method.[1)]

Typical Procedure Using KOH/Al_2O_3. N-Alkylation of Benzamide (1): A mixture of KOH/Al_2O_3 obtained from 85% KOH (3.3 g, 50 mmol) and alumina (10 g), **1** (10 mmol), **5** (12 mmol), hexadecane (0.3 g) as an internal standard, and a solvent (20 ml) was vigorously stirred at 60 °C for 8 h. After the mixture had been cooled to room temperature, water (5 ml) was added to it with vigorous stirring. The yields of *N*-mono- and *N,N*-dialkylation were determined by GLC analysis of the organic phase. When acetonitrile was employed as a solvent, hexadecane (0.3 g) as an internal standard in benzene (10 ml) was added after the reaction had finished.

N-Allyl-2-phenylacetamide (4d): A mixture of 85% KOH (3.3 g, 50 mmol)/M-60-B (10 g), **4** (1.35 g, 10 mmol), allyl bromide (1.45 g, 12 mmol), and dioxane (20 ml) was vigorously stirred at 40 °C for 8 h. GLC showed that the selectivity was 82%. The solid material was filtered off and washed with benzene (30 ml×2). Removing the solvent under reduced pressure gave 1.5 g of the crude product. Recrystallization from benzene–hexane gave 1.0 g (57% yield, 98% purity) of **4d**, mp 59—61 °C. Further recrystallization gave pure **4d** having mp 60—61 °C; IR (KBr) 3230, 1625, 1555 cm^{-1}. Found: C, 75.05; H, 7.62; N, 8.10%. Calcd for $C_{11}H_{13}NO$: C, 75.43; H, 7.43; N, 8.00%.

N-Ethyl-2-phenylacetamide (4a): A mixture of 85% KOH (3.3 g, 50 mmol)/M-60-B (10 g), **4** (1.35 g, 10 mmol), ethyl bromide (1.3 g, 12 mmol), and dioxane (20 ml) was vigorously stirred at 60 °C for 8 h. GLC showed that the selectivity was 97.5%. The same treatment as **4d** gave 1.25 g (77% yield, 97% purity) of **4a**, mp 60—68 °C. Recrystallization from ether–hexane gave 1.15 g (71% yield) of pure **4a**, mp 69—70 °C (lit,[10)] mp 69.5 °C); IR (KBr) 3290, 1635, 1555 cm^{-1}.

N-Butyl-2-phenylacetamide (4c): A mixture of 85% KOH (3.3 g, 50 mmol)/M-60-B (10 g), **4** (1.35 g, 10 mmol), butyl bromide (1.7 g, 12 mmol), and dioxane (20 ml) was vigorously stirred at 60 °C for 8 h. The same treatment as **4a** gave 1.25 g, (66% yield, 99% purity) of **4b**, mp 53—55 °C. Recrystallization from ether–hexane gave 1.15 g (60% yield) of **4b**, mp 55—56 °C (lit,[11)] mp 55—56 °C); Ir (KBr) 3250, 1630, 1560 cm^{-1}.

Typical Procedure Using KOH+Al_2O_3. N-Alkylation of 1: Alumina (10 g) and 85% KOH (3.3 g, 50 mmol)were ground together in a mortar. To this solid material was added a mixture of **1** (10 mmol), **5** (12 mmol), hexadecane (0.3 g) as an internal standard, and a solvent (20 ml). The mixture was vigorously stirred at 60 °C for 8 h. The reaction mixture was treated and GLC analyzed by the same method as described in the case of KOH/Al_2O_3.

N-Allylbutanamide (3d): A mixture of 85% KOH (3.3 g, 50 mmol)+M-90-N (10 g), **3** (0.87 g, 10 mmol), allyl bromide (1.45 g, 12 mmol), and dioxane (20 ml) was vigorously stirred at 40 °C for 8 h. The solid material was filtered off and washed with benzene (30 ml×2). After removal of the solvent, distillation gave 0.9 g (71% yield, 97% purity) of **3d**, bp 80—87 °C/1 mmHg (1 mmHg=133.322Pa). Purification by column chromatography (W-200-N, benzene and benzene-THF) gave pure **3d** having bp 88—89 °C/1 mmHg; IR (neat) 3280, 1640, 1545 cm^{-1}. Found: C, 65.68; H, 10.31; N, 10.87%. Calcd for $C_7H_{13}NO$: C, 66.14; H, 10.24; N, 11.02%.

N-Benzylbutanamide (3e): The alkylation of **3** with benzyl bromide (2.0 g, 12 mmol) similar to that with allyl bromide was performed using M-60-B. GLC showed that the selectivity was 97.1%. After the same treatment as **3d**, recrystallization from ether–hexane gave 1.4 g (79% yield) of **3e**, mp 49.5—50.5 °C; IR (KBr) 3290, 1630, 1550 cm^{-1}. Found: C, 74.34; H, 8.55; N, 7.90%. Calcd for $C_{11}H_{15}NO$: C, 74.58; H, 8.47; N, 7.91%.

N-Allylbenzamide (1d): The alkylation of **1** using 85% KOH (3.3 g, 50 mmol)+M-60-B (10 g) with allyl bromide (1.45 g, 12 mmol) similat to that of **3** with allyl bromide was performed. The solid meterial was filtered off and washed with benzene (30 ml×2). After removal of the solvent, column chromatography (W-200-N, benzene and benzene-THF)

gave 0.9 g (56% yield) of **1d** having bp 113—114 °C/0.2 mmHg (lit,[12] bp 173—174 °C/14 mmHg); IR (neat) 3300, 1640, 1535 cm^{-1}.

N-Ethylacetamide (2a): Bp 69—70 °C/2 mmHg (lit,[13] bp 140—141 °C/91 mmHg); IR (neat) 3280, 1645, 1555 cm^{-1}.

N-Butylacetamide (2c): Bp 89—90 °C/1.3 mmHg (lit,[13] bp 121—122 °C/13 mmHg); IR (neat) 3270, 1650, 1550 cm^{-1}.

N-Ethylbutanamide (3a): Bp 80—81 °C/1.2 mmHg (lit,[14] bp 101—102 °C/7 mmHg); IR (neat) 3280, 1640, 1540 cm^{-1}.

N-Butylbutanamide (3c): Bp 104—105 °C/1.2 mmHg (lit,[15] bp 138—140 °C/13 mmHg); IR (neat) 3280, 1640, 1545 cm^{-1}.

N-Benzyl-2-phenylacetamide (4e): Mp 119—120 °C (lit,[10] mp 119 °C); IR (KBr), 3280, 1635, 1545 cm^{-1}.

N-Benzylbenzamide (1e): Mp 105—106 °C (lit,[16] mp 106 °C); IR (KBr) 3280, 1640, 1550 cm^{-1}.

I wish to thank Nihon Tokushu Kagaku Kogyo Co., Ltd. for permission to publish this article, and also Dr. Nobuaki Wada for useful suggestions and discussions during this work.

References

1) T. Gajda and A. Zwierzak, *Synthesis*, **1981**, 1005.

2) Y. Watanabe, T. Ohta, and Y. Tsuji, *Bull. Chem. Soc. Jpn.*, **56**, 2647 (1983).

3) G. H. Posner, *Angew. Chem.*, **90**, 527 (1978); A. McKillop and D. W. Young, *Synthesis*, **1979**, 401, 481; G. Bram and T. Fillebeen-Khan, *J. Chem. Soc., Chem. Commum.*, **1979**, 522; G. Bram, N. Geraghty, G. Nee, and J. Seyden-Penne, *ibid.*, **1980**, 325; G. Bram, T. Fillebeen-Khan, and N. Geraghty, *Synth. Commun.*, **10**, 279 (1980); N. A. Noureldin and D. G. Lee, *Tetrahedron Lett.*, **1981**, 4889; N. A. Noureldin and D. G. Lee, *J. Org. Chem.*, **47**, 2790 (1982); G. H. Posner and M. Oda, *Tetrahedron Lett.*, **1981**, 5003; S. S. Rana, J. J. Barlow, and K. L. Matta, *ibid.*, **1981**, 5007; M. Onaka, K. Ishikawa, and Y. Izumi, *Chem. Lett.*, **1982**, 1783.

4) a) K. Sukata, *Bull. Chem. Soc. Jpn.*, **56**, 3306 (1983). b) K. Sukata, unpublished results.

5) The surface areas of M-90-N and M-60-B are *ca.* 110 and 180—200 m^2/g, respectively.

6) L. M. Jackman and N. M. Szeverenyi, *J. Am. Chem. Soc.*, **99**, 4954 (1977).

7) L. M. Jackman and B. C. Lange, *ibid.*, **103**, 4494 (1981).

8) The pK_a values of the CH_2 and NH_2 groups of **4** have not been reported.

9) S. Quici and S. L. Regen, *J. Org. Chem.*, **44**, 3436 (1979).

10) R. Delaby, P. Reynaud, and F. Lilly, *Bull. Soc. Chim. France*, **1961**, 2067.

11) O. M. Behr, G. Englinton, I. A. Lardy, and A. Raphael, *J. Chem. Soc.*, **1964**, 1147.

12) P. Kay, *Ber. Dtsch. Chem. Ges.*, **26**, 2848 (1893).

13) K. G. Wyness, *J. Chem. Soc.*, **1958**, 2934.

14) Y. K. Yur'ev, Z. V. Belyakova, P. V. Kostetskii, and A. I. Prokof'ev, *Zh. Obshch. Khim.*, **29**, 2595 (1959); *Chem. Abstr.*, **54**, 10913e (1960).

15) T. Kametani and O. Umezawa, *Chem. Pharm. Bull.*, **14**, 369 (1966).

16) T. Shingaki, *Nippon Kagaku Zasshi*, **80**, 55 (1959).

 © 1985 The Chemical Society of Japan Bull. Chem. Soc. Jpn., 58, 844—849 (1985) [Vol. 58, No. 3

Isomerization of Allylic Alcohols Catalyzed by Vanadium or Molybdenum Complexes[1)]

Seijiro MATSUBARA, Takashi OKAZOE, Koichiro OSHIMA, Kazuhiko TAKAI,* and Hitosi NOZAKI

Department of Industrial Chemistry, Faculty of Engineering, Kyoto University, Yoshida, Kyoto 606

(Received October 3, 1984)

Isomerization of primary allylic alcohols proceeds in dichloromethane at 25 °C in the presence of the catalyst prepared *in situ* from $VO(acac)_2$ or $MoO_2(acac)_2$, and $Me_3SiOOSiMe_3$ to give tertiary isomers in good yields. The catalysts are also effective for the rearrangements of *sec.*→*tert.* allylic alcohols. The isomerization of an allenyl allylic alcohol, 6-methyl-1,2,5-heptatrien-4-ol, gives either (*E*)-2-methyl-3,5,6-heptatrien-2-ol or (*E*)-6-methyl-3,5-heptadien-2-one selectively depending on the reaction conditions.

Allylic transposition reactions have been widely studied.[2)] Treatment of allylic tertiary acetates (or alcohols) with acetic anhydride produces their primary isomers.[3)] Palladium(II) complex is an effective catalyst for the isomerization of allylic tertiary acetates to primary ones.[4,5)] Rearrangements in the opposite sense (*primary*→*tertiary*) are encountered in solvolysis reactions, which are complicated by accompanying elimination, cyclization, and skeletal rearrangement.[6)] Here we wish to report the catalysts which are prepared from $VO(acac)_2$ or $MoO_2(acac)_2$ and $Me_3SiOOSiMe_3$ and are effective in (1) allylic isomerization of primary or secondary alcohols to tertiary ones and (2) regioselective isomerization of 6-methyl-1,2,5-heptatrien-4-ol into either (*E*)-2-methyl-3,5,6-heptatrien-2-ol or (*E*)-6-methyl-3,5-heptadien-2-one. Both reactions proceed in an aprotic solvent under mild conditions.

(1) Isomerization of Primary Allylic Alcohols to Tertiary Ones. Most recently, much attention has been paid on the synthetic utility of bis(trimethylsilyl) peroxide,[7,8)] which is an equivalent of 100% H_2O_2. The peroxide easily prepared from 30% H_2O_2[7)] possesses high solubility in organic solvents and thermal stability. The enhanced nucleophilicity of the oxygen by trimethylsilyl group has effectively been used for the oxidation reaction such as Baeyer-Villiger reaction[8a)] or pyridinium dichromate-catalyzed oxidation of alcohols into carbonyl compounds.[8b)] In further study of this unique reagent in combination with several transition metal catalysts, we have found that the $VO(acac)_2$ or $MoO_2(acac)_2$ catalyst activated with $Me_3SiOOSiMe_3$ effectively induces the title isomerization which is in sharp contrast to the well-known Sharpless' epoxidation of allylic alcohols (Scheme 1).[9)]

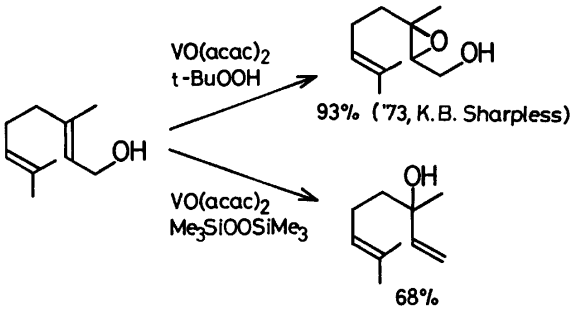

Scheme 1.

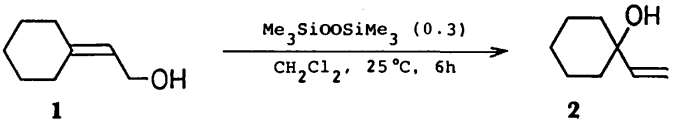

1 2

$VO(acac)_2$	(0.1)	GLPC yield	92%	(recovery 2%)
$MoO_2(acac)_2$	(0.1)		76%	(3%)
[$MoO_2(acac)_2$	(0.1) only		35%	(<2%)]

Scheme 2.

No allylic rearrangement occurs in the absence of $Me_3SiOOSiMe_3$ as far as we utilize $VO(acac)_2$ system. Meanwhile, $MoO_2(acac)_2$ catalyst has proved to be effective to bring about the isomerization with or without the peroxide, although several undesired side reactions are accompanied in the latter case. In general, $VO(acac)_2$-$Me_3SiOOSiMe_3$ system gave better yeilds of tertiary alcohol than $MoO_2(acac)_2$ one. For instance, treatment of 2-cyclohexylideneethanol (**1**) with $VO(acac)_2$-$Me_3SiOOSiMe_3$ provided the tertiary alcohol **2** in 92% GLPC yield (2% recovery of **1**), whereas $MoO_2(acac)_2$ system gave **2** in 76% or 35% yield with or without $Me_3SiOOSiMe_3$ respectively (Scheme 2).

The results of allylic isomerization with $VO(acac)_2$-$Me_3SiOOSiMe_3$ are summarized in Table 1. A general procedure is as follows. $Me_3SiOOSiMe_3$ (30 mol%) was added to a solution of $VO(acac)_2$ (10 mol%) in CH_2Cl_2 at 25 °C. The blue color of the solution turned immediately to purple. A solution of a primary alcohol in CH_2Cl_2 was added and the whole was stirred at 25 °C for 6 h. The product was purified by preparative thin-layer chromatography on silica gel. Rearrangement of primary allylic alcohols proceeded very smoothly to give tertiary ones in good yields. In contrast, isomerization of a primary into a secondary alcohol gave less satisfactory results (run 5). The resulting double bond exhibited *E* configuration in runs 3, 4,

TABLE 1. ALLYLIC ISOMERIZATION CATALYZED BY $VO(acac)_2$-$Me_3SiOOSiMe_3$ SYSTEM[a]

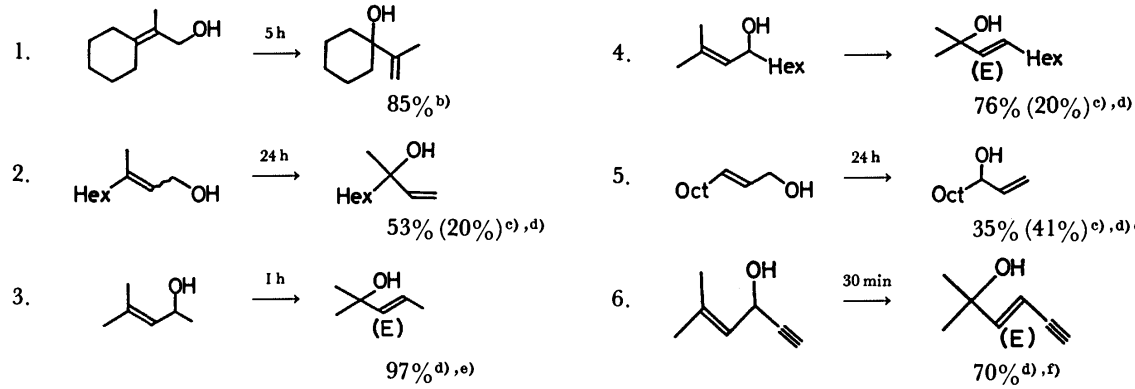

a) The substrate (2.0 mmol) was treated at 25 °C with a catalyst prepared from $Me_3SiOOSiMe_3$ (0.6 mmol) and $VO(acac)_2$ (0.2 mmol) in CH_2Cl_2. b) See Ref. 10. c) Recoveries of the unchanged materials are shown in parentheses. d) See experimental section. e) GLPC yield. f) The isomerization of this substrate was also performed in 76% yield with the $MoO_2(acac)_2$ (5 mol%) without $Me_3SiOOSiMe_3$. The reaction was complete within 10 min.

TABLE 2. ISOMERIZATION OF GERANIOL, NEROL, AND LINALOOL WITH $VO(acac)_2$–$Me_3SiOOSiMe_3$ SYSTEM[a]

	Time	Products (%)[b]			
	h	Geraniol	Nerol	Linalool	α-terpineol
geraniol	7	(10)	8	68	2
(geranyl chloride)[c]		10	0	81	7
nerol	7	11	(11)	70	3
(neryl chloride)[c]		0	2	20	72
linalool	12	8	5	(60)	2

a) Reactions were performed on 2.0 mmol scale at 25 °C in CH_2Cl_2. The catalyst was prepared by $Me_3SiOOSiMe_3$ (0.6 mmol) and $VO(acac)_2$ (0.2 mmol) in CH_2Cl_2. b) GLPC yields (10% PFG 20 M, 3% $AgNO_3$, 1.5 m, 110 °C) of these terpene alcohols were determined with hexadecane as the internal standard. c) The results of the solvolysis reaction (H_2O/acetone=95/5) of geranyl chloride or neryl chloride are cited from the literature of C. A. Bunton *et al.* (Ref. 11).

and 6.

Table 2 is concerned with the reaction of geraniol, nerol, and linalool with $VO(acac)_2$–$Me_3SiOOSiMe_3$ system. The isomer distributions of these terpene alcohols were nearly identical irrespective of the starting alcohols in the present reaction. On the other hand, the solvolysis of neryl chloride is recorded to give α-terpineol as the main product, while linalool is produced from geranyl chloride under the S_N1 conditions.[11]

Following reactions in Scheme 3 gave us some information about the mechanism of this isomerization reaction. The equilibrium between a starting allylic alcohol and the rearranged one has been examined with 1-deuterio-2-cyclohexen-1-ol (**3**). An equimolar mixture of 3-deuterio and 1-deuterio compounds was produced (Eq. 1).[12]

Treatment of (*S*)-(−)-3-methyl-2-cyclohexen-1-ol[13] (**5**, 40% e.e.) with this $VO(acac)_2$-$Me_3SiOOSiMe_3$ catalyst gave (*R*)-(+)-1-methyl-2-cyclohexen-1-ol[14] in 35% yield (**6**, 29% e.e.) and the unchanged starting material in 40% recovery as shown in Eq. 2. The hydroxyl group of the substrate **5**, therefore, resides mainly on the same side of the olefinic double bond. This suggests that the isomerization does not proceed *via* a free allylic cation.[15] The conclusion is consonant with the observed production of a trace amount of cyclized α-terpineol from nerol (Table 2).[16]

(2) Regioselective Isomerization of 6-Methyl-1,2,5-heptatrien-4-ol. The rearrangement of allenic alcohols proceeds as smoothly as allylic ones. For

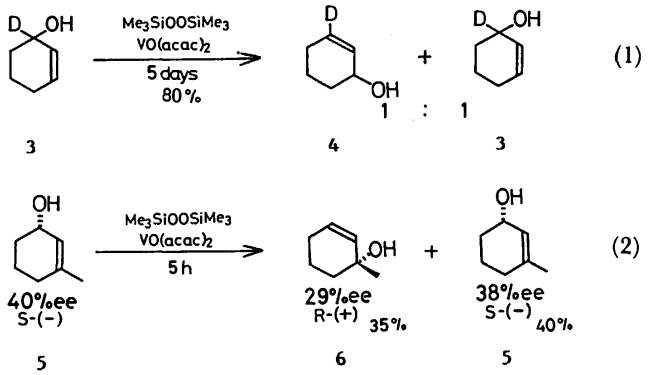

Scheme 3.

instance, (*E*)-4-phenyl-3-buten-2-one was produced from 1-phenyl-2,3-butadien-1-ol in good yields (Scheme 4) with Mo or V catalysis. Addition of $Me_3SiOOSiMe_3$ was essential for $VO(acac)_2$ catalysis, but $MoO_2(acac)_2$ turned out to be effective without $Me_3SiOOSiMe_3$. The application of this rearrangement technique to 6-methyl-1,2,5-heptatrien-4-ol (**7**) led to regioselective formation of either (*E*)-2-methyl-3,5,6-heptatrien-2-ol (**8**) and (*E*)-6-methyl-3,5-heptadien-2-one (**9**) depending on conditions (Table 3,4).

Treatment of **7** with 5 mol% of $MoO_2(acac)_2$ in dichloromethane at 25 °C for 10 min provided the enone **9** in 90% yield. The reaction temperature strongly affected the product distributions. The reaction at −78 °C gave tertiary alcohol **8** as a sole product and no trace of **9** was detected in the reaction mixture. The addition of $Me_3SiOOSiMe_3$ to $MoO_2(acac)_2$ did not alter the results dramatically. Following assumptions explain the observations. (1)

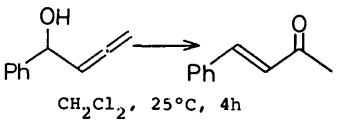

$MoO_2(acac)_2$ (0.1)	75%
$MoO_2(acac)_2$ (0.1)-$Me_3SiOOSiMe_3$ (0.3)	83%
$VO(acac)_2$ (0.1)	0%
$VO(acac)_2$ (0.1)-$Me_3SiOOSiMe_3$ (0.3)	81%

Scheme 4.

An equilibrium of Scheme 5 exists between the two alcohols **7** and **8** in the presence of the $MoO_2(acac)_2$ catalyst. (2) At lower temperature, the kinetically favored tertiary alcohol **8** is produced. (3) At 25 °C, the isomerization to the kinetically less favored trienol **10** competes with the rearrangement of **7** to **8** and the thermodynamically more stable enone **9** is produced exclusively from the tautomerization of **10**.

As shown in Table 4, $VO(acac)_2$ was less effective in

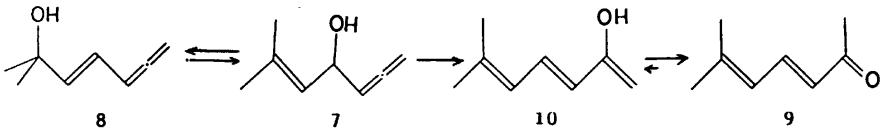

Scheme 5.

TABLE 3. ISOMERIZATION OF 6-METHYL-1,2,5-HEPTATRIEN-4-OL WITH $MoO_2(acac)_2$ SYSTEM[a)]

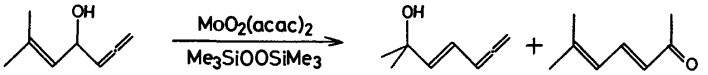

7 8 9

Run	$MoO_2(acac)_2$	$Me_3SiOOSiMe_3$	Time	Temp	Yield[b)]		
					8	9	Recov.
1	5 mol%	—	10 min	25 °C	<2%	90%	<2%
2	5 mol%	—	10 min	−78 °C	94%	<2%	<2%
3	5 mol%	5 mol%	10 min	25 °C	<2%	94%	<2%
4	5 mol%	15 mol%	10 min	25 °C	13%	82%	<2%

a) Reactions were performed on 2.0 mmol scale in CH_2Cl_2. b) Products were isolated as a mixture and the ratio was determined by nmr analysis.

TABLE 4. ISOMERIZATION OF 6-METHYL-1,2,5-HEPTATRIEN-4-OL WITH $VO(acac)_2$ SYSTEM[a)]

7 8 9

Run	$VO(acac)_2$	$Me_3SiOOSiMe_3$	Time	Temp	Yield[b)]		
					8	9	Recov.
1	5 mol%	—	10 min	25 °C	<2%	<2%	75%
2	5 mol%	—	16 h	25 °C	63%	24%	<2%
3	5 mol%	5 mol%	10 min	25 °C	68%	17%	5%
4	5 mol%	15 mol%	10 min	25 °C	80%	7%	<2%

a) Reactions were performed on 2.0 mmol scale in CH_2Cl_2. b) Products were isolated as a mixture and the ratio was determined by NMR analysis.

the isomerization of **7**. The presence of Me_3SiOO-$SiMe_3$ was essential to obtain a reasonable reaction rate. The catalyzed rearrangement provided a mixture of **8** and **9** in a 4:1 ratio (run 3). Increasing the amount of $Me_3SiOOSiMe_3$ improved the selectivity of the reaction slightly. The ratio of **8**/**9** was 11/1 with 5 mol% of $VO(acac)_2$ and 15 mol% of $Me_3SiOOSiMe_3$ (run 4).[19]

Experimental

The IR spectra were determined on a Shimadzu IR-27-G spectrometer, the mass spectra on a Hitachi M-80 machine, and the NMR spectra on a Varian EM-360 spectrometer. The chemical shifts are given in δ, with tetramethylsilane as an internal standard. The analyses were carried out by the staff at the Elemental Analyses Center of Kyoto University. Dichloromethane was dried on P_2O_5 and distilled. All the experiments were carried out under an argon atmosphere. Purification of products were performed by preparative thin-layer chromatography (TLC) or column chromatography on silica gel (Wakogel C-100). Analytical GLPC was performed with a Yanagimoto GCG-550-F and a Shimadzu GC-4CPT. Preparative GLPC was performed with a JEOL-JGC-20K apparatus.

Bis(trimethylsilyl) Peroxide: The following procedure is a modification of the method described by P. G. Cookson *et al.* too much briefly.[7] Hydrogen peroxide (30%, 11.3 g, 100 mmol) was added in less than 1 min to a stirred solution of 1,4-diazabicyclo[2.2.2]octane (DABCO, 5.6 g, 50 mmol) in diethyl ether (80 ml) at 0 °C and the resulting mixture was stirred for 15 min. Precipitated white solid was filtered through a glass filter, and dried *in vacuo* at room temperature for 5 h. This is the DABCO-hydrogen peroxide complex and is easily decomposed by a catalytical amount of metals. Danger of explosion should be taken care. This DABCO-hydrogen peroxide complex (5.9 g, 33 mmol), DABCO (3.7 g, 33 mmol), and dichloromethane (50 ml) were placed in a flame-dried flask. Chlorotrimethylsilane (12.0 g, 0.111 mol, neat) was added dropwise at 0 °C within 15 min to the solution. After being stirred for 5 h at room temperature, the resulting mixture was filtered to remove DABCO-HCl salt, and the filtrate was concentrated at room temperature under 100 Torr (1 Torr=133.322 Pa). The residue was diluted with pentane, filtered to remove the salt, and the solution concentrated at room temperature under 100 Torr. Distillation of the crude product under reduced pressure provided $Me_3SiOOSiMe_3$ in 32% yield (5.6 g, 32 mmol) as a colorless liquid, bp 40—41 °C/28 Torr: IR (neat): 2960 (s), 1250 (s), 920 (w), 840 (s), 730 (s).[20]

1-Ethenylcyclohexanol (**2**): A dichloromethane solution (5 ml) of $Me_3SiOOSiMe_3$ (0.11 g, 0.60 mmol) was added at 25 °C under an argon atmosphere to a stirred solution of $VO(acac)_2$ (53 mg, 0.20 mmol) in dichloromethane (4 ml). The blue color of the reaction mixture turned to purple immediately and the resulting mixture was stirred at 25 °C for 10 min. A solution of 2-cyclohexylideneethanol (**1**, 0.25 g, 2.0 mmol) in dichloromethane (8 ml) was added at the same temperature and the whole was stirred for an additional 6 h. The mixture was poured into brine (20 ml) and extracted with ether (2×20 ml). The separated organic layers were dried (Na_2SO_4) and concentrated. Purification by preparative thin-layer chromatography (hexane–ethyl acetate, 2:1) on silica gel gave 1-ethenylcyclohexanol (**2**) in 80% yield (0.20 g) as a colorless liquid.[21] GLPC yield 92% of **2** (10% PEG 20 M, 3% $AgNO_3$, 1.5 m, 110 °C) was determined with hexadecane as the internal standard: Bp. 70 °C (bath temp, 10 Torr); IR (neat): 3400, 1642, 1455, 960, 915 cm^{-1}; NMR (CCl_4): δ=1.00—1.80 (m, 11H), 4.88 (dd, J=10.5, 1.5 Hz, 1H), 5.12 (dd, J=17.6, 1.5 Hz, 1H), 5.87 (dd, J=17.6, 10.5 Hz, 1H); MS *m/z* (%): 126 (M^+, 6), 93 (11), 83 (100), 70 (68), 67 (21), 55 (56).

3-Methyl-1-nonen-3-ol:[22] Bp 45 °C (bath temp, 1 Torr); IR (neat): 3400, 3100, 1645, 1400, 970, 915 cm^{-1}; NMR (CCl_4): δ=0.87 (t, J=6 Hz, 3H), 1.00—1.70 (m, 10H), 1.20 (s, 3H), 1.95—2.20 (m, 1H), 4.92 (dd, J=10.5, 1.5 Hz, 1H), 5.07 (dd, J=17.5, 1.5 Hz, 1H), 5.79 (dd, J=17.5, 10.5 Hz, 1H); MS *m/z* (%): 156 (M^+, 0.3), 141 (11), 129 (8), 96 (6), 81 (10), 71 (100), 58 (16).

(E)-2-Methyl-3-penten-2-ol:[23] This compound was produced from 4-methyl-3-penten-2-ol as described above. GLPC analysis (10% PEG 20 M, 3% $AgNO_3$, 1.5 m, 45 °C) of the crude product showed a single peak having a retention time at 4.8 min ((*E*)-isomer). (*Z*)-Isomer (T_r=5.2 min), which was prepared from (*Z*)-1-bromo-1-propene and acetone, was not detected in the reaction mixture. GLPC yield 97% of (*E*)-2-methyl-3-penten-2-ol was determined with dodecane as the internal standard: Bp 70 °C (bath temp, 100 Torr); IR (neat): 3400, 3050, 1675, 970 cm^{-1}; NMR (CCl_4): δ=1.21 (s, 6H), 1.50—1.70 (m, 1H), 1.63 (d, J=5.5 Hz, 3H), 5.40—5.60 (m, 2H); MS *m/z* (%): 100 (M^+, 19), 85 (100), 67 (68), 59 (36), 43 (90).

(E)-2-Methyl-3-decen-2-ol: This compound was produced from 2-methyl-2-decen-4-ol as described above. GLPC analysis (20% PEG 6000, 1.2 m, 122 °C) of the crude product showed a single peak having a retention time at 18.5 min ((*E*)-isomer). (*Z*)-Isomer (T_r=17.2 min) was not detected. Bp 112 °C (bath temp, 2 Torr); IR (neat): 3400, 3050, 1150, 970, 910 cm^{-1}; NMR (CCl_4): δ=0.87 (t, J=6 Hz, 3H), 1.00—1.53 (m, 9H), 1.22 (s, 6H), 1.75—2.15 (m, 2H), 5.40—5.55 (m, 2H); MS *m/z* (%): 170 (M^+, 2), 155 (25), 95 (32), 85 (77), 71 (100), 68 (52); Found: C, 77.52; H, 13.02%. Calcd for $C_{11}H_{22}O$: C, 77.58; H, 13.02%.

1-Undecen-3-ol:[24] This compound was produced from (*E*)-2-undecen-1-ol as described above. GLPC yield 35% of 1-undecen-3-ol (10% PEG 20M, 3% $AgNO_3$, 1.5 m, 116 °C) was determined with hexadecane as the internal standard.

(E)-2-Methyl-3-hexen-5-yn-2-ol:[25] Bp 44 °C (bath temp, 9 Torr); IR (neat): 3250, 2070, 1605, 1140, 955 cm^{-1}; NMR (CCl_4): δ=1.30 (s, 6H), 2.00—2.35 (m, 1H), 2.68 (d, J=2.8 Hz, 1H), 5.60 (dd, J=15.6, 2.8 Hz, 1H), 6.24 (d, J=15.6 Hz, 1H); MS *m/z* (%): 110 (M^+, 1.7), 109 (12), 95 (100), 77 (10), 67 (24), 43 (54).

(S)-(−)-3-Methyl-2-cyclohexen-1-ol (**5**):[13] This compound was prepared by asymmetric reduction of 3-methyl-2-cyclohexen-1-one according to the reported procedure[26]: $[\alpha]_D^{25}$=−35.1° (c=1.86, $CHCl_3$). Enantiomeric excess (40% e.e.) of this alcohol was determined by NMR with $Eu(hfc)_3$ shift reagent.[13]

(R)-(+)-1-Methyl-2-cyclohexen-1-ol (**6**):[14] Treatment of (*S*)-(−)-3-methyl-2-cyclohexen-1-ol (**5**, 40% e.e.) with $VO(acac)_2$–$Me_3SiOOSiMe_3$ catalyst as described above gave a mixture of **5** (35% yield) and **6** (40% recovery). Yields were determined by GLPC (10% PEG 20 M, 3% $AgNO_3$, 1.5 m,

110 °C) with hexadecane as the internal standard. Purification by preparative GLPC (20% PEG 6000, 1 m, 110 °C) gave pure **5** (38% e.e.) and **6** [29% e.e., $[\alpha]_D^{25}=+15.5°$ (c=1.65, $CHCl_3$)]. Enantiomeric excess of these alcohols were determined by NMR with Eu(hfc)$_3$ shift reagent.[13]

The authentic sample of **6** [$[\alpha]_D^{25}=17.3°$ (c=2.0, $CHCl_3$)] was prepared from **5** (40% e.e.) according to the literature about stereoselective 1,3-transposition of allylic alcohols.[27] **6**: Bp 90 °C (bath temp, 50 Torr); IR (neat): 3400, 3050, 1180, 1125, 1020, 855 cm^{-1}; NMR (CCl_4): δ=1.20 (s, 3H), 1.50—2.10 (m, 7H), 5.35—5.75 (m, 2H); MS m/z (%): 112 (M^+, 9.9), 97 (100), 84 (45), 79 (43), 69 (85), 55 (32).

1-Phenyl-2,3-butadien-1-ol:[28] This compound was prepared from benzaldehyde and propargyl alcohol according to the literature.[29] Bp 72 °C (bath temp, 10 Torr); IR (neat): 3250, 1942, 1020, 846 cm^{-1}; NMR (CCl_4): δ=1.78 (bs, 1H), 4.70 (d, J=2 Hz, 1H), 4.77 (d, J=2 Hz, 1H), 5.07 (dt, J=6, 2 Hz, 1H), 5.15—5.40 (m, 1H), 6.87—7.53 (m, 5H); MS m/z (%): 146 (M^+, 2.3), 145 (10), 128 (8), 107 (100), 79 (55), 77 (23).

6-Methyl-1,2,5-heptatrien-4-ol (**7**):[30] The title compound was prepared from 3-methyl-2-butanal and propargyl alcohol according to the reported procedure:[29] Bp 47 °C (bath temp, 9 Torr); IR (neat): 3250, 1940, 1010, 840 cm^{-1}; NMR (CCl_4): δ=1.67 (s, 3H), 1,72 (s, 3H), 2.20—2.50 (m, 1H), 4.50—4.90 (m, 3H), 4.97—5.30 (m, 2H); MS m/z (%): 124 (M^+, 2), 109 (43), 91 (21), 85 (100), 81 (12), 79 (10), 67 (10), 55 (11).

(E)-2-Methyl-3,5,6-heptatrien-2-ol (**8**): A dichloromethane solution (7 ml) of 6-methyl-1,2,5-heptatrien-4-ol (**7**, 0.25 g, 2.0 mmol) was added to a solution of MoO_2(acac)$_2$ (33 mg, 0.10 mmol) in dichloromethane (4 ml) at −78 °C under an argon atmosphere. After being stirred at the same temperature for 10 min, the resulting mixture was poured into brine (20 ml) and extracted with ether (2×20 ml). The separated organic layers were dried and concentrated. Purification by preparative thin-layer chromatography (hexane–ethyl acetate, 5:1) on silica gel gave (*E*)-2-methyl-3,5,6-heptatrien-2-ol (**8**) in 94% yield (0.23 g) as a colorless liquid: Bp 70 °C (bath temp, 7 Torr); IR (neat): 3300, 1925, 1620, 1140, 965, 842; NMR (CCl_4): δ=1.30 (s, 6H), 2.15 (bs, 1H), 4.72—4.90 (m, 2H), 5.15—6.05 (m, 3H); MS m/z (%): 124 (M^+, 9.0), 109 (86), 91 (43), 85 (27), 81 (41), 65 (16), 59 (11), 55 (13), 53 (13), 43 (100); Found: C, 77.09; H, 9.98%. Calcd for $C_8H_{12}O$: C, 77.38; H, 9.74%.

(E)-6-Methyl-3,5-heptadien-2-one (**9**):[31] Treatment of 6-methyl-1,2,5-heptatrien-4-ol (**7**, 0.25 g, 2.0 mmol) with MoO_2(acac)$_2$ (33 mg, 0.10 mmol) in dichloromethane at 25 °C for 10 min as described above gave (*E*)-6-methyl-3,5-heptadien-2-one (**9**) in 90% yield (0.22 g): Bp 45 °C (bath temp, 10 Torr); IR (neat): 1654, 1620, 1580, 1260, 984, 960 cm^{-1}; NMR (CCl_4): δ=1.90 (s, 6H), 2.16 (s, 3H), 5.88 (d, J=12 Hz, 1H), 5.90 (d, J=15 Hz, 1H), 7.23 (dd, J=15, 12 Hz, 1H); MS m/z (%): 124 (M^+, 12), 109 (100), 81 (39), 79 (16), 53 (12), 43 (22).

Financial support by the Ministry of Education, Science and Culture, Japanese Government (Grant-in Aid for Special Project Research 58110005) is acknowledged.

References

1) Preliminary report, S. Matsubara, K. Takai, and H. Nozaki, *Tetrahedron Lett.*, **24**, 3741 (1983).

2) For general reviews, see: J. March, "Advanced Organic Chemistry," 2nd ed., McGraw-Hill Kogakusha, Tokyo (1977), pp. 303—307; E. A. Braude, *Q. Rev.*, **4**, 404 (1950); R. H. Dewolfe and W. G. Young, "The Chemistry of Alkenes," E. S. Patai, Ed., Interscience, New York (1964), Chapter 10.

3) J. H. Babler and D. O. Olsen, *Tetrahedron Lett.*, **1974**, 351; K. Kogami and J. Kumanotani, *Bull. Chem. Soc. Jpn.*, **47**, 226 (1974); W. G. Young and I. D. Webb, *J. Am. Chem. Soc.*, **73**, 780 (1951).

4) L. E. Overman and F. M. Knoll, *Tetrahedron Lett.*, **1979**, 321; J. Tsuji, K. Tsuruoka, and K. Yamamoto, *Bull. Chem. Soc. Jpn.*, **49**, 1701 (1976).

5) L. E. Overman, C. B. Campbell, and F. M. Knoll, *J. Am. Chem. Soc.*, **100**, 4822 (1978); B. M. Trost, J. M. Timko, and J. L. Stanton, *J. Chem. Soc., Chem. Commun.*, **1978**, 436.

6) P. Valenzuela and O. Cori, *Tetrahedron Lett.*, **1967**, 3089; K. L. Stevens, L. Jurd, and G. Manners, *Tetrahedron*, **28**, 1939 (1972); D. V. Banthorpe, P. A. Boullier, and W. D. Fordham, *J. Chem. Soc., Perkin Trans. 1.*, **1974**, 1637.

7) P. G. Cookson, A. G. Davies, and N. Fazal, *J. Organomet. Chem.*, **99**, C31 (1975).

8) a) M. Suzuki, H. Takada, and R. Noyori, *J. Org. Chem.*, **47**, 902 (1982); S. Matsubara, K. Takai, and H. Nozaki, *Bull. Chem. Soc. Jpn.*, **56**, 2029 (1983); b) S. Kanemoto, K. Oshima, S. Matsubara, K. Takai, and H. Nozaki, *Tetrahedron Lett.*, **24**, 2185 (1983); c) J. R. Hwu, *J. Org. Chem.*, **48**, 4432 (1983).

9) K. B. Sharpless and T. R. Verhoeven, *Aldrichimica Acta*, **12**, 63 (1979) and references cited therein.

10) D. Seebach, N. Meyer, and A. K. Beck, *Justus Liebigs Ann. Chem.*, **1977**, 846.

11) C. A. Bunton, O. Cori, D. Hachey, and J.-P. Leresche, *J. Org. Chem.*, **44**, 3238 (1979); C. D. Poulter and C. R. King, *J. Am. Chem. Soc.*, **104**, 1422 (1982).

12) The increased amount of the catalyst did not affect the ratio of the two allylic isomers.

13) K. Mori, S. Tamada, M. Uchida, N. Mizumachi, Y. Tachibana, and M. Matsui, *Tetrahedron*, **34**, 1901 (1978); E. L. Pummer, T. E. Stewart, K. Byrne, G. T. Pearce, and R. M. Silverstein, *J. Chem. Ecol.*, **2**, 307 (1976).

14) A. A. Renwick and P. R. Huges, *Insect Biochem.*, **5**, 459 (1975).

15) Y. Kitagawa, S. Hashimoto, S. Iemura, H. Yamamoto, and H. Nozaki, *J. Am. Chem. Soc.*, **98**, 5030 (1976).

16) A [3,3] sigmatropic rearrangement of inorganic ester such as vanadate or molybdate is considered to be one of the reasonable mechanisms. Actually, it has been reported that heating of a tertiary allylic alcohol with O=V(OR)$_3$[17a] or O=W(OR)$_4$·L[17b] at 160—200 °C gave a mixture of its primary isomer and the starting alcohol via [3,3] sigmatropic rearrangement. In our new method, the rearrangement took place in an opposite direction (primary→tertiary) under much milder conditions. These differences could be ascribed to the presence of Me_3SiOO- group attached on vanadium atom[18] in the [3,3] sigmatropic rearrangement (Scheme 6).

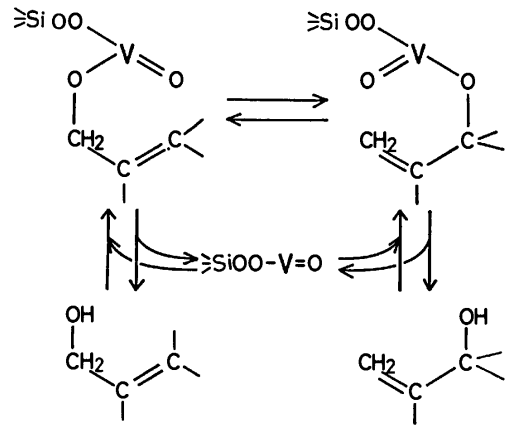

Scheme 6.

17) a) P. Chabardes, E. Kuntz, and J. Varagnat, *Tetraheron*, **33**, 1775 (1977); b) T. Hosogai, Y. Fujita, Y. Ninagawa, and T. Nishida, *Chem. Lett.*, **1982**, 357; Y. Fujita, Y. Ninagawa, T. Nishida, and K. Itoi, *J. Synth. Org. Chem. Jpn.*, **37**, 224 (1979); c) G. L. Olson, H.-G. Cheung, K. D. Morgan, R. Borner, and G. Saucy, *Helv. Chim. Acta*, **59**, 567 (1976); H. Pauling, D. A. Andrews, and N. C. Hindley, *Helv. Chim. Acta*, **59**, 1233 (1976); M. B. Erman, I. S. Aul'chenko, L. A. Kheifits, V. G. Dulova, Y. N. Novikov, and M. E. Vol'pin, *Zh. Org. Khim.*, **12**, 921 (1976).

18) IR analysis of a mixture of $Me_3SiOOSiMe_3$ and $VO(acac)_2$ indicates a new absorption at 900 cm^{-1}, while the absorption frequency of $Me_3SiOOSiMe_3$ was 840 cm^{-1}.

19) These catalysts are not effective for the rearrangements of α-acetylenic alcohols.[17c] For general review about these rearrangements, see: S. Swaminathan and K. V. Narayanan, *Chem. Rev.*, **71**, 429 (1971).

20) D. Brandes and A. Blaschette, *J. Organomet. Chem.*, **78**, 1 (1974).

21) H. J. Reich, S. K. Shah, and F. Chow, *J. Am. Chem. Soc.*, **101**, 6648 (1979).

22) F. Bohlmann and H.-G. Viehe, *Chem. Ber.*, **88**, 1245 (1955).

23) J. K. Crandall and W. R. Heitmann, *J. Org. Chem.*, **44**, 3471 (1979).

24) Y. Ueno, H. Sano, and M. Okawara, *Synthesis*, **1980**, 1011.

25) P. H. M. Schreurs, W. G. Galesloot, and L. Brandsma, *Recl. Trav. Chim. Pays-Bas*, **94**, 70 (1975).

26) S. Terashima, N. Tanno, and K. Koga, *J. Chem. Soc., Chem. Commun.*, **1980**, 1026.

27) A. Yasuda, H. Yamamoto, and H. Nozaki, *Bull. Chem. Soc. Jpn.*, **52**, 1757 (1979).

28) A. A. Petrov, K. V. Val'yan, Y. I. Kheruze, and T. V. Yakovleva, *Zh. Obshch. Khim.*, **29**, 2101 (1959).

29) M. Huche and P. Cresson, *Bull. Chem. Soc. Fr.*, **1974**, 2040.

30) L.-I. Olsson and A. Claesson, *Acta Chem. Scand. B*, **31**, 614 (1977).

31) R. Hollenstein and W. von Philipsborn, *Helv. Chim. Acta*, **55**, 2030 (1972).

Chemical Synthesis of Capped Oligoribonucleotides, $m^7G^{5'}pppAUG$ and $m^7G^{5'}pppAUGACC$

Mitsuo SEKINE, Shin-ichi NISHIYAMA, Takashi KAMIMURA, Yumi OSAKI, and Tsujiaki HATA*

Department of Life Chemistry, Tokyo Institute of Technology, Nagatsuta, Midoriku, Yokohama 227

(Received October 4, 1984)

The fully-protected pAUG (**15**) and pAUGACC (**21**) were synthesized by the phosphotriester approach where the phenylthio group was employed as the internal and 5'-terminal phosphate-protecting groups. The partially unblocked oligomers (**32**) and (**33**), obtained by alkaline treatment of (**15**) and (**21**), were condensed with a capping reagent (**1a**) in the presence of imidazole by activation with silver nitrate to afford the capped trimer and hexamer protected with the acid-labile protecting groups, *i.e.*, 4,4,'4"-trimethoxytrityl (TMTr), 4-monomethoxytrityl (MMTr), tetrahydropyran-2-yl (THP), and methoxymethylene (mM) groups. The protected capped oligomers were unblocked by a dilute HCl solution to afford $m^7G^{5'}pppAUG$ and $m^7G^{5'}pppAUGACC$, which were purified by HPLC and characterized by enzyme assays.

Chemical synthesis of capped oligoribonucleotides, $m^7G^{5'}pppNupNupNu\cdots$[1] is one of the intriguing subjects in nucleic acid chemistry, since construction of the unique cap structure will be realized by exploration of new techniques. Previously, we have reported capping reactions utilizing the arylthio group as an activatable pyrophosphate protecting group.[2-6] These studies indicate that, because of the inherent insolubility of 7-methylguanosine derivatives in organic solvents, a capping agent should be protected with sufficiently lipophilic groups so that the capping reaction proceeds homogeneously to obtain reproducible results. Therefore, we recently reported a new capping agent (**1a**) that reacted with nucleotides in the presence of silver nitrate giving rise to the cap structure with high reproducibility.[4] This silver ion-catalyzed reaction required the use of an excess amount (2 equiv) of acceptor nucleotides (**2**) to obtain $m^7G^{5'}pppNu$ (**3**) in good yields (45—60%). This is because the reaction in the reverse ratio of **1** to **2** resulted in a very complicated mixture from which **3** was isolated only in a poor yield (<5%). Similar experiences have been encountered also in the synthesis of unmethylated cap structures, $G^{5'}pppNu$, from **1b** and **2**. The silver ion-mediated reaction can hardly be applied to the synthesis of capped oligoribonucleotides, because the excess use of oligomer components is undesirable. The above complicated reaction may be rationalized by the generation of an highly active metapyrophosphate intermediate (**4**), which can react again with the product so that the P(O)-O-P(O) bond was degraded. In the case of the reaction using the excess acceptor nucleotide, **4** might be trapped mainly with the excess **2** and a little with the product **3** to give a simpler result.

Therefore, we have studied a more generally applicable method for the capping reaction. A reaction of **1b** with **2** (B=Cy, R=DMTr) was chosen to search for suitable conditions that enabled us to use excess amounts of **1b**. Consequently, it was found that coaddition of imidazole dramatically effected the silver ion-catalyzed reaction. When the reaction was carried out in the presence of 30 fold excess imidazole by using 1.7 equiv of **1b** to **2**, TLC exhibited a major spot corresponding to the protected $G^{5'}pppC$ and much less by-products. The workup gave a 61%

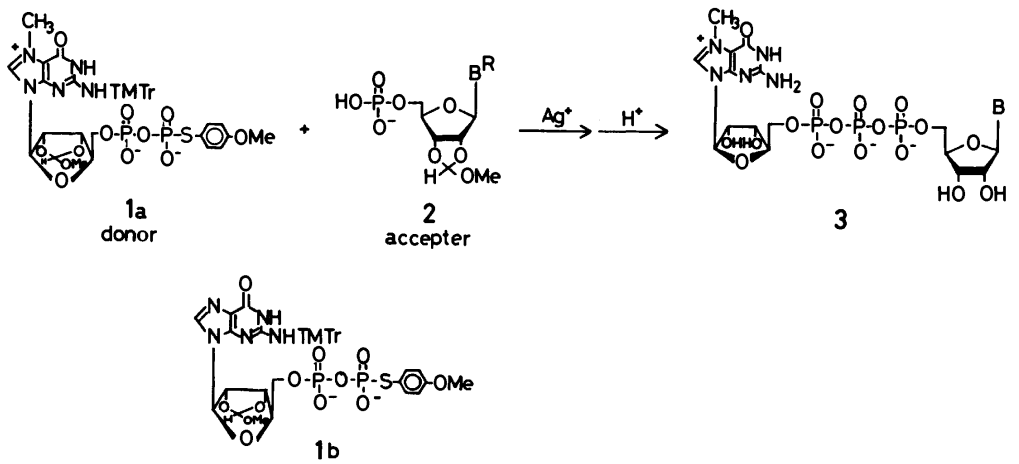

Scheme 1.

yield of G[5']pppC. This result is explained in terms of the *in situ* formation of the phosphorimidazolide (**5**)[7] capable of reacting gradually with the acceptor nucleotide and not with the product.

The protecting groups used for **2** have been reported in the previous paper.[4]

Since we could find the practical procedure for the construction of the cap structure, the fully-protected oligoribonucleotides of pApUpG and pApUpGpApCpC were synthesized by our phosphotriester method using the phenylthio group as the phosphate-protecting group. These synthetic strategies are shown in Scheme 3. All the nucleoside and nucleotide units (**6**—**11**) employed are illustrated in Scheme 4.

For the preparation of the uridine unit (**6**), an alternative to the previous route was employed. The new method involves introduction of the anisoyl group into the uracil ring[8] at an earier stage. This approach enabled us to extract the diol (**25**) easily with CH_2Cl_2, while the previous method required bothersome ion-exchange chromatography for removal of excess triethylammonium fluoride used in the conversion of the cyclic silyl ether (**28**) to 3'-*O*-(tetrahydropyran-2-yl)uridine (**29**). The uridine unit **6** was obtained *via* the six-step reaction in an overall yield of 45% from uridine. The 3'-terminal cytidine unit (**10**) was synthesized by benzoylation of the common intermediate (**30**) followed by detritylation of the resulting product (**31**). The 3'-terminal guanosine unit (**11**) was prepared by a new procedure for the methoxymethylenation catalyzed by trimethylsilyl chloride.[9]

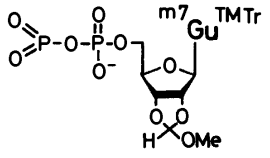

4

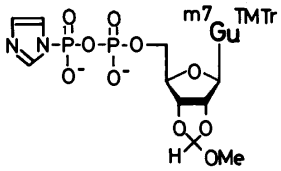

5

Scheme 2.

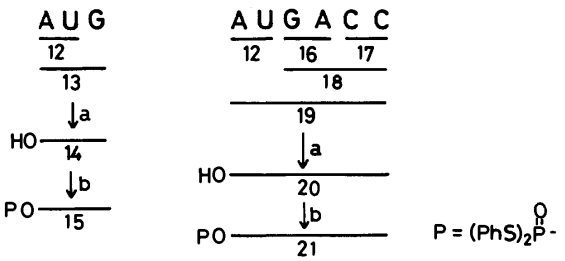

Strategy for the synthesis of the fully protected pAUG (15) and pAUGACC (21): The line (—) means fully protected oligonucleotide chains.

Scheme 3.

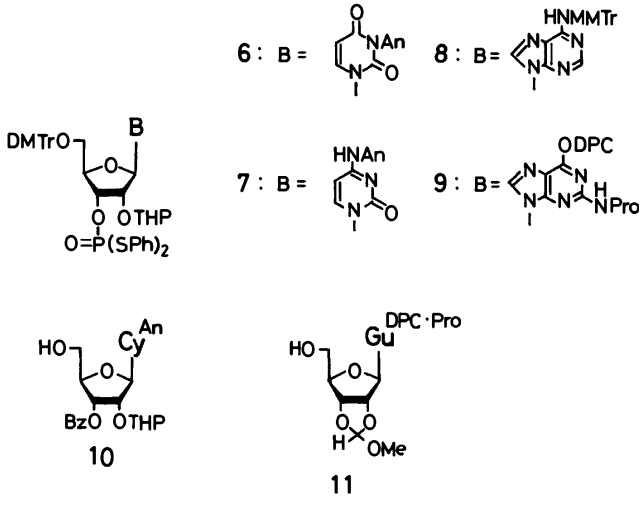

Scheme 4.

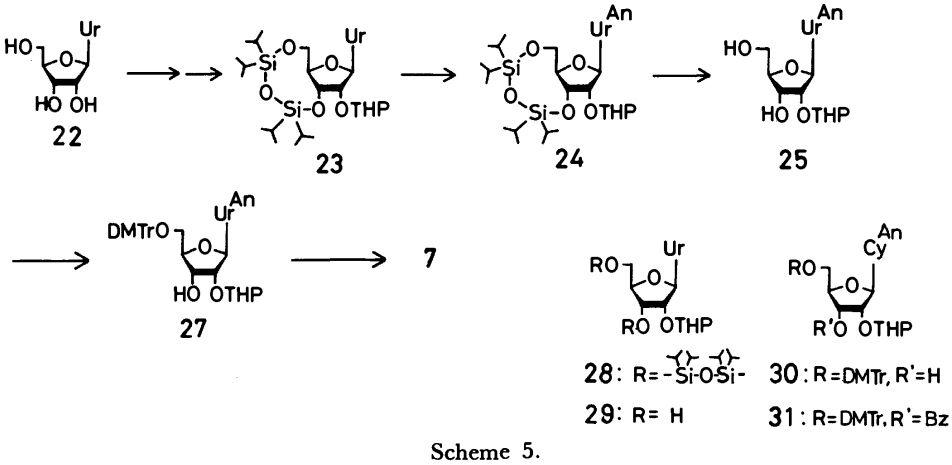

Scheme 5.

The conditions employed for the fragment condensations of oligomers were essentially the same as those reported previously.[10,11] For the construction of the triphosphate bridge, the 5′-terminal hydroxyls of compounds **14** and **20** obtained from **13** and **19** were phosphorylated with cyclohexylammonium *S,S*-diphenyl phosphorodithioate (**PSS**)[12] in the presence of mesitylene-1,3-disulfonyl dichloride (**MDS**)[13] to afford compounds (**15**) and (**21**), respectively. The phosphorylations proceeded smoothly without any side reactions. Since the cap structure was extremely labile to basic media, all the phenylthio- and acyl-protecting groups were removed by the successive treatments with 0.2 M NaOH (1 M=1 mol dm^{-3}), concentrated aqueous ammonia, and silver acetate prior to the capping reactions. This partial deprotection gave the oligomers (**32**) and (**33**) having the 2′-*O*-tetrahydropyran-2-yl and adenosine N^6-MMTr groups. The former is preserved to avoid side reactions associated with the internal phosphate groups upon the capping reaction. The latter serves as the marker for monitoring the reaction on TLC. Before the capping reactions, the roughly purified trimer **32** and hexamer **33** were treated with 0.01 M HCl to obtain the unprotected trimer pApUpG and hexamer pApUpGpApCpC, respectively. Isolation of the two oligomers was performed by HPLC as shown in Figs. 1 and 2. The yields of pApUpG and pApUpGpApCpC were 20 and 10% yields, respectively. Since these oligomers were prepared as the references in the capping reactions, no attempts to increase the yields have not been made. The enzyme treatments of the trimer and hexamer using venom phosphodiesterase resulted in mixtures of the parent 5′-mononucleotides in the correct ratios as shown in Fig. 3. Next, we examined the triphosphate bridge formation between the oligomer **32** or **33** and the unmethylated precursor (**1b**) of the capping agent **1a**. In these reactions, 5 equiv of **1b**, 20 equiv of imidazole, and 30 equiv of silver nitrate were employed. After the reactions were completed, the remaining acid-labile protecting groups were removed by treatment with 0.01 M HCl. The reaction mixtures were chromatographed on Whatman 3 MM papers and then separated by HPLC. The HPLC elution patterns are shown in Figs. 4 and 5. In the case of G^5′pppApUpG, a main peak, which appeared after pApUpG, was collected and analyzed with venom phosphodiesterase. The enzyme analysis suggested that the main peak was the desired product of G^5′pppApUpG (see Fig. 6A). This capped trimer was isolated in an overall yield of 9% from **15**. Since pApUpG was obtained in 20% yield from **15** by a similar unblocking procedure, it was estimated that the triphosphate bond formation was attained to a degree of *ca.* 45%. This means that the phos-

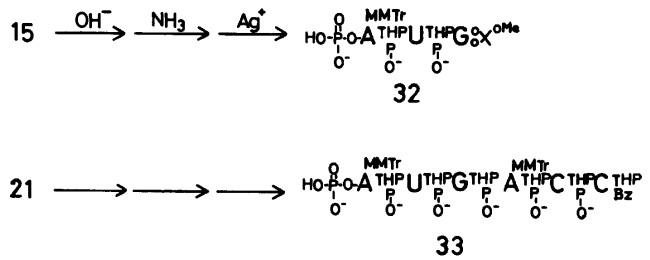

Scheme 6.

TABLE 1. CONDITIONS AND RESULTS OF FRAGMENT CONDENSATIONS OF OLIGORIBONUCLEOTIDE BUILDING BLOCKS

3′-Phosphonate component (equiv)	Removal of PhS group 4 M TEPS[a]	Time min	5′-Hydroxyl component	Removal of DMTr group Time min	Yield %	Condensation NT equiv	MDS equiv	Time min	Product	Yield %
A (1.2)	20	60	U	—	—	6	3	60	**12**	82
G (1.2)	20	40	A	—	—	6	3	45	**16**	91
AU(1.2)	20	40	G	45	86	6	3	75	**13**	69
C (1.1)	20	30	C	30	84	6(MeIm)[b]	3	30	**17**	54
GA(1.5)	20	75	CC	—	—	4	2	75	**18**	86
AU(1.6)	20	45	GACC	—	—	3	2	180	**19**	54

a) TEPS refers to triethylammonium phosphinate. b) In this reaction methylimidazole (MeIm) was employed in place of **NT**.

TABLE 2. CONDITIONS AND RESULTS OF PHOSPHORYLATION OF **14** AND **20**

Oligomer mg (μmol)	PSS mg (μmol)	MDS mg (μmol)	Pyridine mL	Time min	Yield %,	Yield mg (μmol)
14 127 (62)	28 (74)	25 (74)	2	40	73	104 (45)
15 318 (74)	39 (89)	31 (89)	0.2	70	91	305 (67)

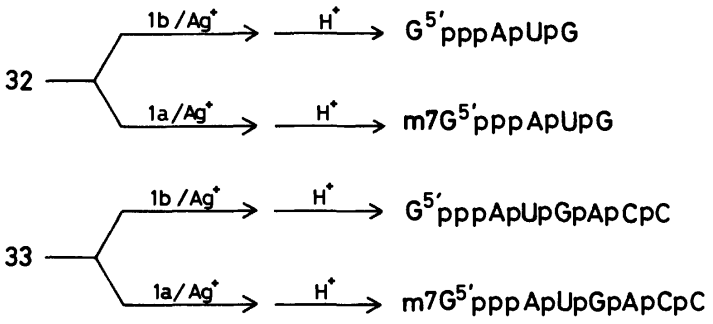

Scheme 7.

phorylation itself proceeded successfully.

In the case of the hexamer, several peaks eluted after pApUpGpApCpC were similarly collected and analyzed. As a consequence, an eminent peak was found to be composed of pA, pC, pG, and pU in the expected ratio and thereby it was determined as G5'-pppApUpGpApCpC. The isolated yield of G5'-ppppApUpGpApCpC was 5% on the basis of the fully protected hexamer **21**. The other peaks of 38 min and 48 min were derived from pG and did not contain the other nucleotides.

Finally, we tried to synthesize the capped oligoribonucleotides, m7G5'pppApUpG and m7G5'-pppApUpGpApCpC, by using G5'pppApUpG and G5'pppApUpGpApCpC as the references for HPLC analysis. In a similar manner, the capping reactions were carried out. The HPLC patterns obtained after the acid treatment are shown in Figs. 7 and 8. We expected that the capped oligomers would appear at positions near or a little behind the starting oligomers owing to the positive charge of the m7G residue. In order to detect the m7G residue, the mixtures were analyzed simultaneously by a HPLC apparatus equipped with a fluorescene detector. The detector was set up by use of the ex and em values of 279 nm and 393 nm, respectively. This double check technique has proved to be very useful for detection of the capped oligomers. On the basis of our expectation mentioned above, some prominent peaks with both UV and fluorescence were collected (Figs. 7 and 8) and characterized by enzyme assay with venom phosphodiesterase (Fig. 9). Consequently, the peaks at 27 min (Fig. 7A) and 35 min (Fig. 8A) were finally identified as the capped oligomers, m7G5'-pppApUpG and m7G5'pppApUpGpApCpC, which were isolated in 8 and 5% overall yields from the fully protected oligomers **15** and **21**, respectively. In these cases, the capping reactions were estimated to proceed to a degree of 40—50%. The enzyme assays of the capped trimer and hexamer with venom phosphodiesterase exhibited the peaks corresponding to pm7G, pA, pU, pG, and pC in the ratios of approximately 1:1:1:1:0 and 1:2:1:1:2, respectively as shown in Fig. 9. Gel electrophoresis of the isolated capped oligomers also showed the expected mobilities as shown in Fig. 10. The structures of the capped oligomers were also more clearly confirmed by digestion with nuclease P_1, which gave m7G5'-pppA and the other nucleotide monomers in the correct ratios as shown in Fig. 11. The cap structure, m7G5'pppA, formed by these enzyme degradations was completely consistent with an authentic sample by comparison with their retention times.

In these reactions the HPLC patterns detected with fluorescence were not so complicated, showing 6—7 eminent peaks. Since the two peaks were assigned as pm7G and ppm7G, the other three or four peaks contained both pm7G and oligomers. Compared with the simple fluorescence HPLC patterns, the UV HPLC patterns were very complicated. Since the UV HPLC patterns obtained in the case of G5'pppApUpG and G5'pppApUpGpApCpC were also complicated, the main reason for the relatively low isolated yields of the capped oligoribonucleotides might be ascribed to the deprotection procedure used for the preparation of **32** and **33**, where the alkaline treatment was used because of its easy post-treatment. Nevertheless sufficient amounts of the capped oligomers for biological studies were successfully obtained. We are now studing improved procedures.

Experimental

^{1}H NMR spectra were recorded at 100 MHz on a JEOL UNM PS-100 spectrometer using tetramethylsilane as an internal standard. UV spectra were obtained on a Hitachi 124 spectrophotometer. Paper chromatography was performed by use of a descending technique with Whatman 3MM papers or Toyo Roshi No. 50 papers using the following solvent system: 2-propanol–concentrated aqueous ammonia–water (Solvent I, 6:1:3, v/v/v). Column chromatography was performed with silica gel C-200 purchased from Wako Co. Ltd., and a minipump for a goldfish basin was conveniently used to gain a medium pressure for rapid chromatographic separation. Thin-layer chromatography was performed on precoated TLC plates Silica Gel 60F-254 (Merck). The R_f values of the protected nucleoside derivatives were measured after development with CH_2Cl_2–MeOH (20:1, v/v) unless otherwise noted. HPLC was performed on a JASCO TRI ROTAR Type II apparatus equipped with a GP-A30 solvent programer, a UVIDEC

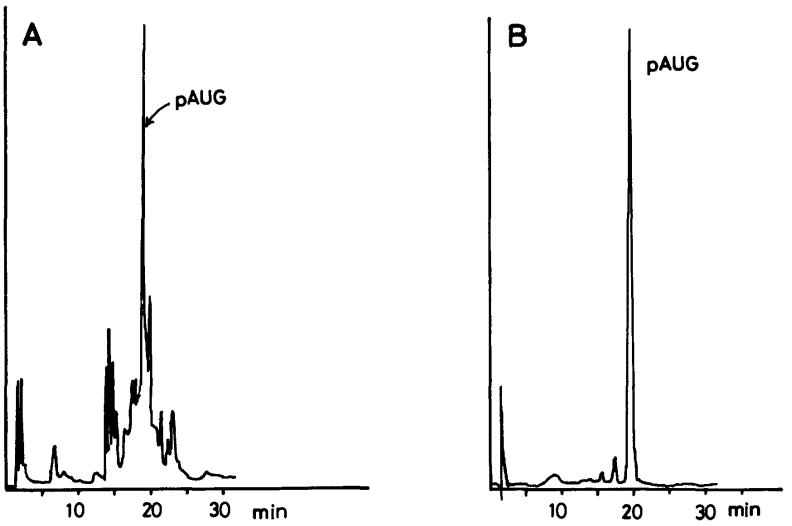

Fig. 1. A: HPLC chromatogram of the mixture after acid treatment of **32**. B: HPLC analysis of pAUG obtained by preparative HPLC shown in A. Conditions of HPLC: System B.

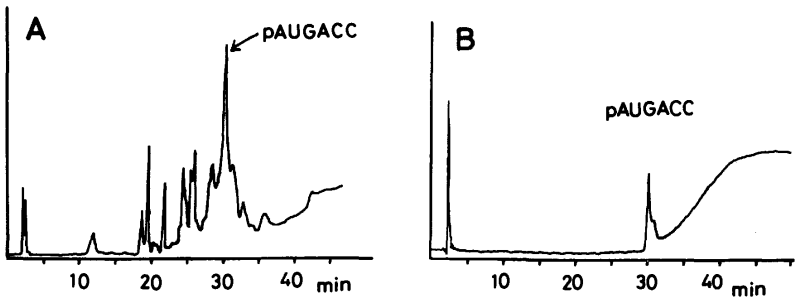

Fig. 2. A: HPLC chromatogram of the mixture after acid treatment of **33**. B: HPLC analysis of pAUGACC separated by preparative HPLC shown in A. Conditions of HPLC: System B.

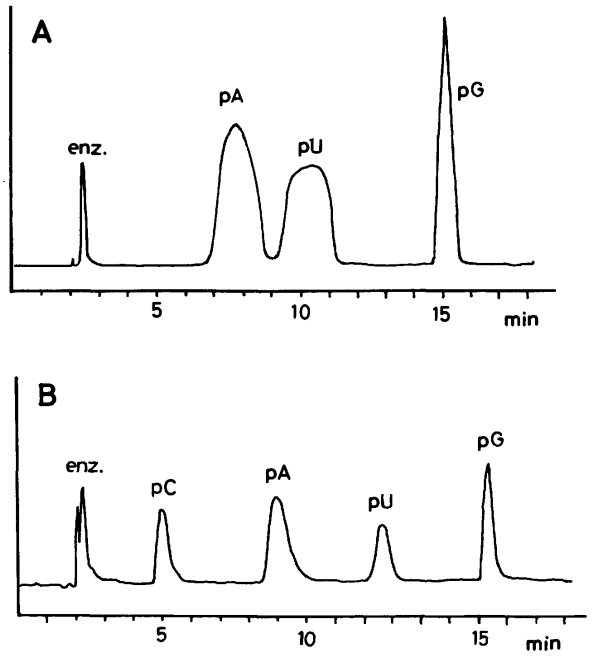

Fig. 3. HPLC analysis of the incubation mixtures of synthetic pAUG (A) and pAUGACC (B) with snake venom phosphodiesterase. Conditions of HPLC: System B.

100-II UV detecter, a FP-110 fluorescence spectrofluorometer, a RC-225 recorder, and a Ohkura Model R 7005 digital integrator. Analysis and purification of unprotected oligoribonucleotides were performed on a Whatman Partisil 10 SAX column (3.9×250 mm) using the following solvent systems: System A: a linear gradient (0—99%) starting with buffer A (0.005 M KH_2PO_4, pH 4.1) and applying buffer B (0.1 M KH_2PO_4, 1.0 M KCl, pH 4.5) at a flow rate of 2.0 mL/min for 32 min; System B: a linear gradient (0—99%) starting with buffer C (0.005 M KH_2PO_4, 20% CH_3CN, pH 4.1) and applying buffer D (0.5 M KH_2PO_4, 20% CH_3CN, pH 4.5) at a flow rate of 1.5 mL/min for 32 min. Pyridine was distilled two times from *p*-toluenesulfonyl chloride and from calcium hydride and then stored over molecular sieves (3A). DMF was distilled and stored over molecular sieves (3A). Ribonucleosides, 1,1,3,3-tetraisopropyl-1,3-dichlorodisiloxane, and DMTrCl were purchased from Yoshitomi Seiyaku Co. Ltd. Diphenylcarbamoyl chloride and the other reagents were purchased from Tokyo Kasei Co. Ltd. Venom phosphodiesterase was purchased from Boehringer Co. Ltd. and nuclease P_1 from Yamasa Shoyu Co. Ltd. Elemental analyses were performed by the Microanalytical Laboratory, Tokyo Institute of Technology, at Nagatsuta.

N^3-Anisoyl-2'-O-(tetrahydropyran-2-yl)-3',5'-O-(1,1,3,3-tetraisopropyldisiloxane-1,3-diyl)uridine (24). Compound **23**[10]

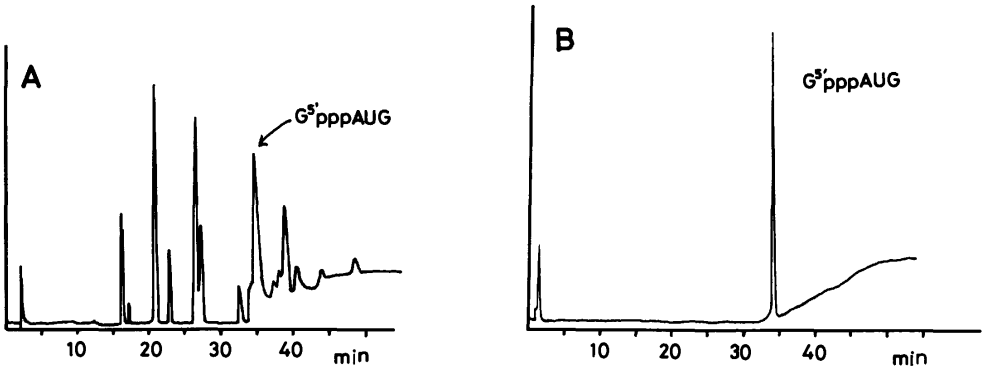

Fig. 4. HPLC chromatogram of the mixture obtained after acid treatment of the reaction mixture derived from condensation of **32** with **1b**. B: HPLC analysis of G$^{5'}$pppAUG separated by preparative HPLC shown in A. Conditions of HPLC: System B.

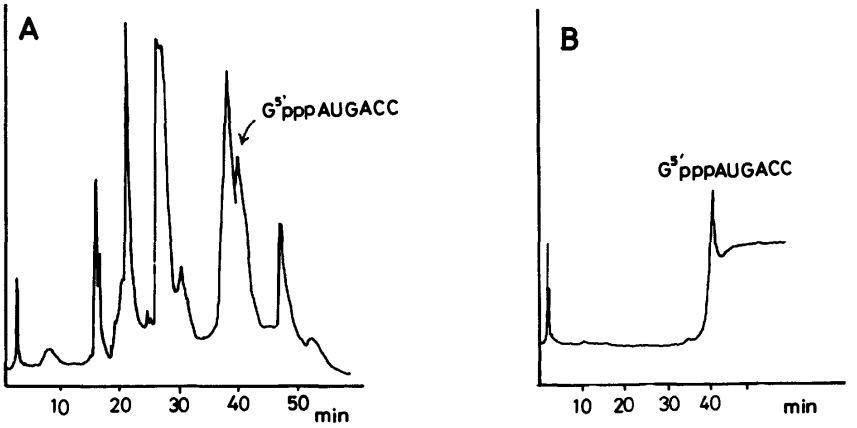

Fig. 5. A: HPLC chromatogram of the mixture obtained after acid treatment of the reaction mixture derived from condensation of **33** with **1b**. B: HPLC analysis of G$^{5'}$pppAUGACC separated by preparative HPLC shown in A. Conditions of HPLC: System B.

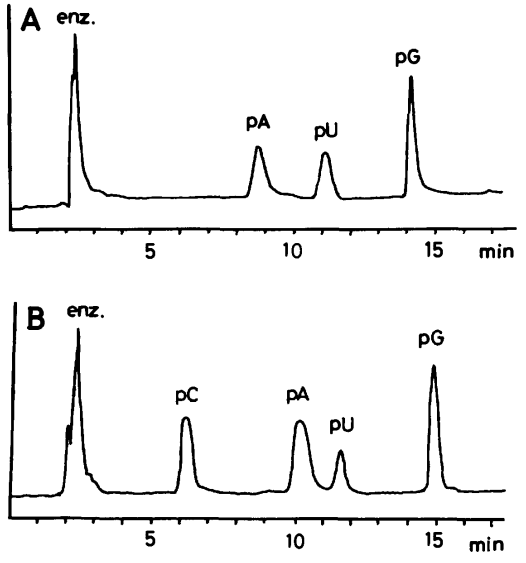

Fig. 6. HPLC analysis of the incubation mixture of synthetic G$^{5'}$pppAUG (A) and G$^{5'}$pppAUGACC (B) with snake venom phosphodiesterase. Conditions of HPLC: System A.

(10.9 g, 19.1 mmol) was rendered anhydrous by coevaporations with dry pyridine (3×20 mL) and finally dissolved in dry pyridine (56 mL). To the solution were added *N,N*-diisopropylethylamine (4.99 mL, 28.7 mmol) and anisoyl chloride (4.12 mL, 38.2 mmol). After being stirred for 10 h, the mixture was treated with ice-water. The agueous solution was extracted with CH_2Cl_2 (3×150 mL), dried over Na_2SO_4, and filtered. The filtrate was concentrated to dryness and coevaporated with toluene (3×20 mL). The residue was chromatographed on a silica-gel column to afford **24** (12.3 g, 91%): R_f 0.63 and 0.70 (benzene–ethyl acetate, 5:1, v/v); ^{1}H NMR ($CDCl_3$) δ=1.02—1.22 (24, m, $(CH_3)_2C$), 1.40—2.00 (10, m, SiCH and CH_2 of THP), 3.52 (2, m, CH_2–O of THP), 3.88 (3, s, CH_3–O), 3.95—4.42 (5, m, 2′,3′,4′,5′-H), 5.15 (1, m, O–CH–O of THP), 5.73 (1, m, 5-H), 5.94 (1, m, 1′-H), 6.92 (2, m, ArH), 7.86 (1, m, ArH), 8.00 (1, m, 6-H). Anal. Calcd for $C_{34}H_{52}N_2O_{10}Si_2$: C, 57.93; H, 7.43; N, 3.94. Found: C, 58.49; H, 7.33; N, 3.36.

N^3-Anisoyl-2′-O-(tetrahydropyran-2-yl)uridine (**25**). Compound **24** (12.3 g, 17.4 mmol) obtained in the above experiment was dissolved in acetonitrile (350 mL), and tetraethylammonium bromide (21.96 g, 104 mmol), potassium fluoride (5.86 g, 104 mmol), and water (5.22 mL) were

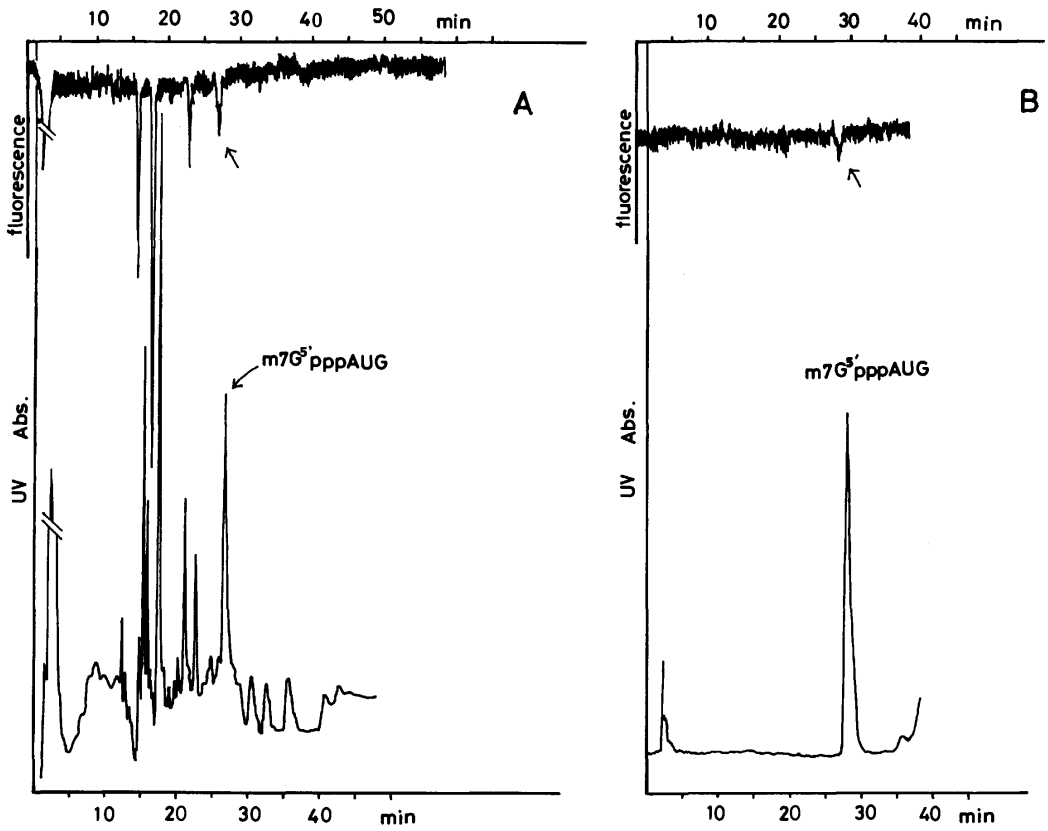

Fig. 7. A: HPLC chromatogram of the mixture obtained after acid treatment of the reaction mixture derived condensation of **32** with **1a**. B: HPLC analysis of m^{7}G^5'pppAUG separated by preparative HPLC shown in A. Conditions of HPLC: System B.

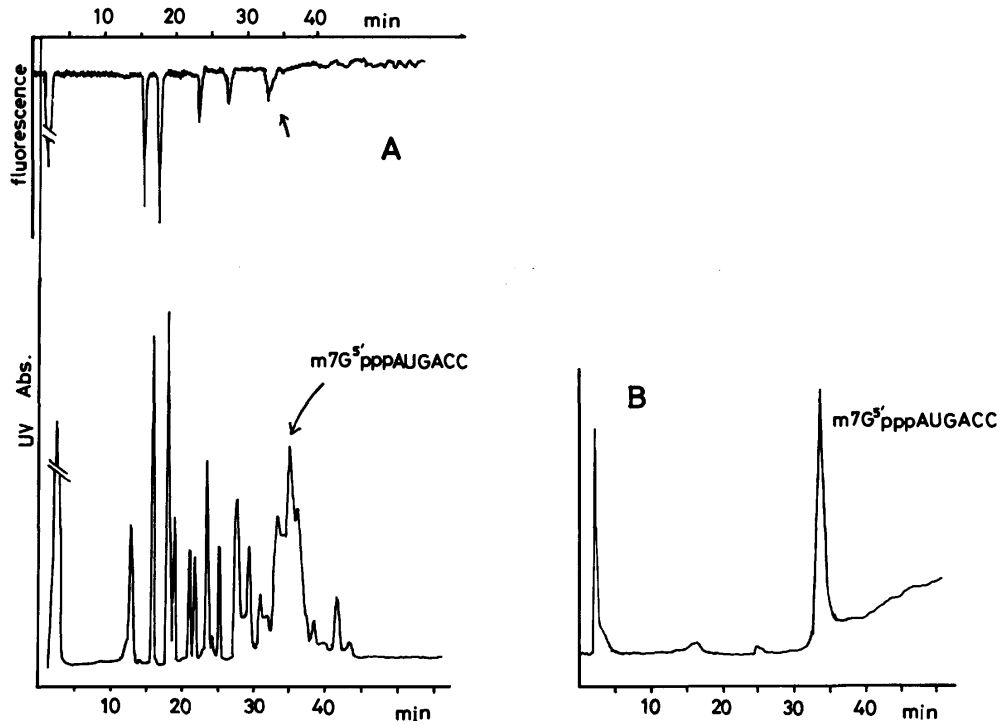

Fig. 8. A: HPLC chromatogram of the mixture obtained after acid treatment of the reaction mixture obtained by condensation of **33** with **1a**. B: HPLC analysis of m^{7}G^5'pppAUGACC preparative HPLC shown in A. Conditions of HPLC: System B.

added. The resulting mixture was stirred vigorously at 60 °C for 5.5 h. Then the precipitate was filtered and the filtrate was concentrated under reduced pressure. The residue was partitioned between CH_2Cl_2 and water. The aqueous layer was extracted further two times with CH_2Cl_2. The combined CH_2Cl_2 extracts were dried over Na_2SO_4, filtered, and evaporated. The residue was chromatographed to give **25** (7.3 g, 90%): R_f 0.11 and 0.16: ^{1}H NMR ($CDCl_3$): δ=1.10—2.05 (6, m, CH_2 of THP), 2.90 and 3.09 (2, br, OH), 3.54 (2, m, CH_2–O of THP), 3.64—4.78 (5, m, 2′,3′,4′,5′-H), 3.87 (3, s, CH_3–O), 5.77 (1, d, J=8 Hz, 5-H), 6.91 (2, d, J=8 Hz, Ar), 7.67 and 7.85 (1, d, J=8 Hz, 6-H), 7.85 (2, d, J=8 Hz, ArH). Anal. Calcd for $C_{22}H_{25}N_2O_9$: C, 57.14; H, 5.67; N, 6.06. Found: C, 56.91; H, 5.78; N, 5.71.

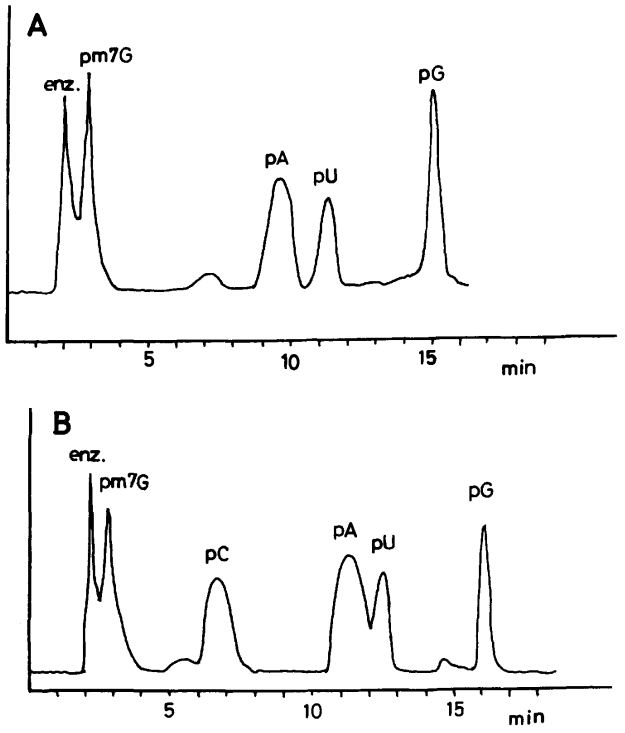

Fig. 9. HPLC analysis of the incubation mixture of synthetic m^{7}G$^{5'}$pppAUG (A) and m^{7}G$^{5'}$pppAUGACC (B) with snake venom phosphodiesterase.

N^3-Anisoyl-2′-O-(tetrahydropyran-2-yl)-5′-O-dimethoxytrityluridine (26). Compound **25** (7.3 g, 15.7 mmol) was dried by coevaporations with dry pyridine (3×20 mL) and finally dissolved in dry pyridine (47 mL). Dimethoxytrityl chloride (6.42 g, 19 mmol) was added and the mixture was stirred for 2.5 h. Then, the usual workup followed by chromatography gave **26** (74%): R_f 0.20, 0.37 ^{1}H NMR ($CDCl_3$): δ=1.38—2.00 (6, m, CH_2 of THP), 2.72 (1, br, OH), 3.52 (2, m, CH_2–O of THP), 3.78 (3, s, CH_3–O), 3.68—4.85 (5, m, 2′,3′,4′,5′-H), 5.36 (1, m, O–CH–O of THP), 5.86 and 6.11 (1, m, 1′-H), 6.68—6.96 (6, m, ArH), 7.10—7.44 (9, m, ArH), 7.82 (2, d, J=8 Hz, ArH), 8.06 (1, d, J=8 Hz, 6-H). Anal. Calcd for $C_{43}H_{44}N_2O_{11}$: C, 67.53; H, 5.80; N, 3.66. Found: C, 67.69; H, 6.27; N, 3.37.

S,S-Diphenyl N^3-Anisoyl-2′-O-(tetrahydropyran-2-yl)-5′-O-dimethoxytrityluridine 3′-Phosphorodithioate (6). Cyclohexylammonium *S,S*-diphenyl phosphorodithioate (1.15 g, 3.01 mmol) was coevaporated with dry pyridine (3×10 mL) and finally dissolved in dry pyridine (20 mL), and then **MDS** (0.97 g, 3.01) was added. After being kept for 30 min, the solution was added to **26** (1.92 g, 2.51 mmol) dried in

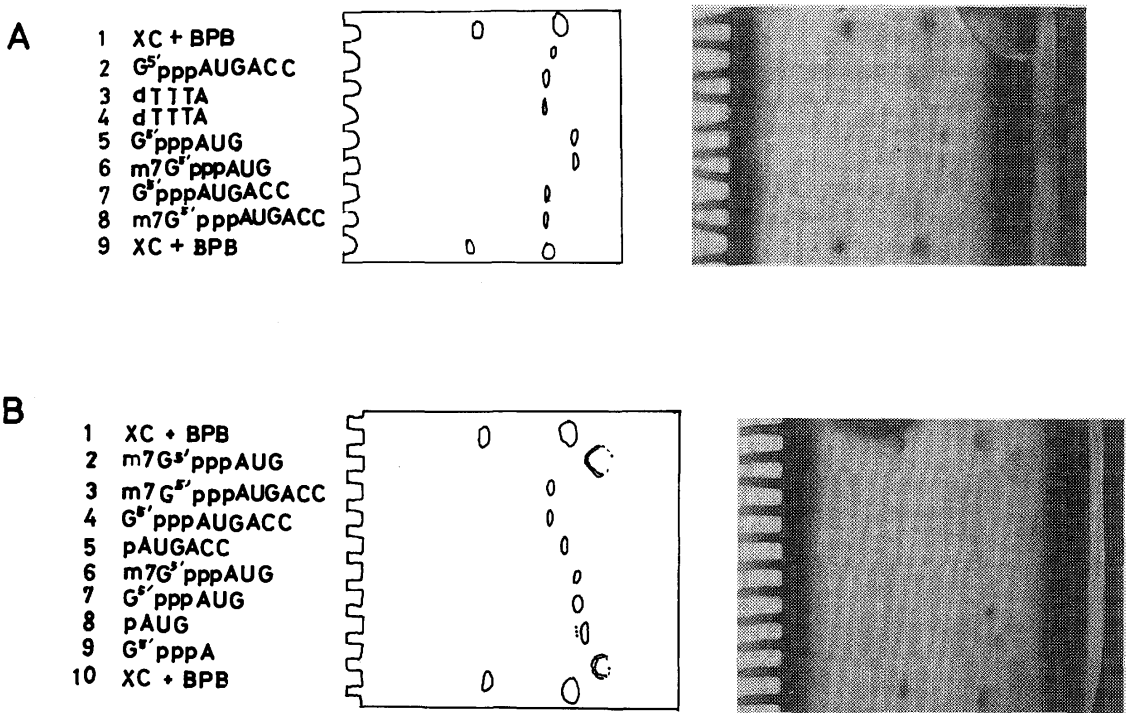

Fig. 10. 20% Polyacrylamide gel electrophoresis of the synthetic capped oligoribonucleotides and related compounds. The electrophoresis was performed at 300 V (10 mA) for 3—4 h. Markers, XC and BPB, refer to Xylene Cyanol and Bromophenyl Blue, respectively.

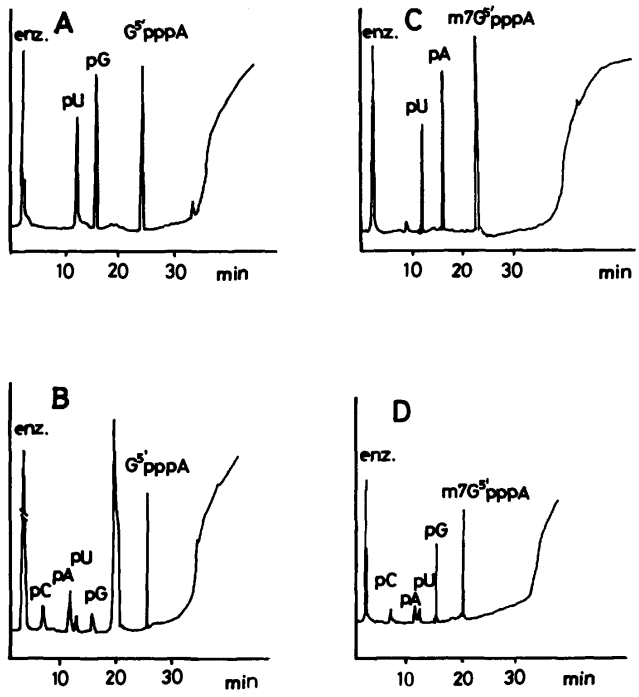

Fig. 11. HPLC analysis of the incubation mixtures of synthetic G⁵'pppAUG (A), G⁵'pppAUGACC (B), m⁷G⁵'pppAUG (C), and m⁷G⁵'pppAUGACC (D) with nuclease P_1. Conditions of HPLC: System A.

advance by coevaporations with dry pyridine. The mixture was stirred for 75 min, and then ice-water was added and extracted with CH_2Cl_2 (3×50 mL). The usual workup followed by chromatography gave **7** (1.95 g, 76%). The ^1H NMR spectrum of this compound was consistent with that of an authentic sample synthesized by the previous route.[11]

N^4-Anisoyl-2'-O-(tetrahydropyran-2-yl)-3'-O-benzoyl-5'-O-dimethoxytritylcytidine (31). Compound **30**[11] (2.29 g, 3 mmol) was coevaporated with dry pyridine (3×10 mL) and finally dissolved in dry pyridine (15 mL). Benzoyl chloride (0.42 mL, 3.6 mmol) was added and the mixture was stirred for 3.5 h. Then the usual workup involving extraction, dryness, filtration, evaporation, and chromatography gave **31** (2.19 g, 86%): R_f 0.34 and 0.37; ^1H NMR (d^6-DMSO): δ=1.20—1.88 (6, m, CH_2 of THP), 3.60 (2, br, CH_2-O of THP), 3.76 (6, s, CH_3-O of DMTr), 3.83 (3, s, CH_3-O of An), 4.53 (2, br, 5'-H), 4.72—4.92 (2, br, 3',4'-H), 5.21, (1, br, 2'-H), 5.67 (1, br, O-CH-O of THP), 6.18 (1, br, 1'-H), 6.45 (1, d, J=4 Hz, 5-H), 6.74—7.03 (6, m, ArH), 7.36—7.60 (13, m, 6-H and ArH), 7.90 (2, d, J=5 Hz, ArH), 8.05 (2, d, J=4 Hz, ArH). Anal. Calcd for $C_{50}H_{49}O_{11}N_3 \cdot 1/2H_2O$: C, 68.48; H, 5.75; N, 4.79. Found: C, 68.63; H, 5.65; N, 4.67.

N^4-Anisoyl-2'-O-(tetrahydropyran-2-yl)-3'-O-benzoylcytidine (10). Compound **31** (2.19 g, 2.58 mmol) was dissolved in CH_2Cl_2 (15 mL) and 2% trifluoroacetic acid in CH_2Cl_2 (15 ml) was added at −20 °C. After the mixture was stirred at −20 °C for 55 min, an additional amount of trifluoroacetic acid (150 μL) was added. After 2 min, pyridine was added, and then extraction was performed with CH_2Cl_2–water. The organic extract was dried over Na_2SO_4, filtered, and evaporated to dryness. The residue was chromatographed on a silica gel column to give **10** (1.02 g, 74%): R_f 0.29; ^1H NMR (d^6-DMSO): δ=1.20—1.88 (6, br, CH_2 of THP), 3.51 (2, m, CH_2-O of THP), 3.85 (3, s, CH_3-O of An), 4.02 (2, br, 5'-H), 4.50 (1, br, 4'-H), 4.72—5.12 (2, br, 2',3'-H), 5.65 (1, m, O-CH-O of THP), 5.80 (1, m, 1'-H), 6.18 (1, m, 5-H), 6.94 (2, d, J=5 Hz, ArH), 7.28—7.64 (4, m, 6-H and ArH), 7.91 (2, d, J=5 Hz, ArH), 8.07 (2, d, J=5 Hz, ArH). Anal. Calcd for $C_{29}H_{31}N_3O_9 \cdot C_6H_{14}$: C, 64.50; H, 6.96; N, 6.45. Found: C, 64.69; H, 7.23; N, 6.13.

General Procedure for the Condensation of Oligoribonucleotide Building Blocks. A fully-protected oligomer used as a diester component was treated with a 4 M pyridine solution of pyridinium phosphinate (20—30 equiv to the oligomer) and triethylamine (20—30 equiv to the oligomer), until the oligomer had been converted to a base-line material on TLC. Then, the mixture was quenched with pyridine–water (1:1, v/v) and extracted three times mith hexane–ether (1:1, v/v) to remove thiophenol. The aqueous layer was extracted three times with CH_2Cl_2. The combined CH_2Cl_2 extracts were washed with 0.2 M triethylammonium hydrogencarbonate (TEAB, pH 7.5) and water and then dried over Na_2SO_4. After the solution was filtered and evaporated, the residue was used as the diester component for the coupling reaction.

Removal of the DMTr group from oligomers was performed with 1% trifluoroacetic acid in CH_2Cl_2 at −10 °C for the times listed in Table 1. The workup was done in the same manner as described in the synthesis of **10**.

Condensation was carried out by mixing the two components, a diester and a hydroxyl components, followed by repeated coevaporations with dry pyridine, dissolving in dry pyridine (20 mL/1 mmol of the latter), and addition of **MDS** and 3-nitro-1,2,4-triazole or *N*-methylimidazole. After the condensation was complete, the mixture was quenched with pyridine–water (1:1, v/v) and extracted several times with CH_2Cl_2. The combined CH_2Cl_2 extracts were washed with 0.1 M TEAB (pH 7.5) and water. Then the usual workup followed by chromatography gave the coupling product as listed in Table 1.

5'-Phosphorylation of 14 and 20. Cyclohexylammonium *S,S*-diphenyl phosphorodithioate was coevaporated three times with dry pyridine and finally dissolved in dry pyridine (3 mL/0.1 mmol of **PSS**). **MDS** was added and the mixture was stirred for 30 min. Then the solution was added to **14** or **20** predried by repeated coevaporations with dry pyridine. The mixture was stirred for the time listed in Table 2. After the reactions was complete, the usual workup gave **15** or **21**.

Full Deprotection of 15. The trimer **15** (12.3 mg, 5 mol) was treated with 0.4 M NaOH–pyridine (1:3, v/v, 2 mL) at room temperature for 40 min. Then, the solution was passed through Dowex 50 W×2 (pyridinium form, 5 mL) and the resin was washed with pyridine–water (1:1, v/v, 50 mL). The eluent was evaporated under reduced pressure and the residue was treated with concentrated aqueous ammonia–pyridine (5:1, v/v, 18 mL) at room temperature for 12 h. Then, the solvent and ammonia were removed by evaporation and the residue was dissolved in pyridine–water (2:1, v/v, 0.5 mL). To the solution was added silver acetate (41.7 mg, 0.15 mmol). The mixture was stirred in the dark for 12 h. Then, the solution was diluted with pyridine–water (1:1, v/v, 20 mL) and hydrogen sulfide gas was bubbled into the solution at 0 °C for several minutes. The precipitate of silver sulfide was removed by centrifugation and the supernatant was concentrated to a gum. The gum was coevapo-

rated three times with methanol–toluene to remove the last traces of pyridine. The residue was dissolved in 0.02 M HCl–dioxane (1:1, v/v, 10 mL). The solution was adjusted exactly to pH 2.0 by addition of 0.1 M HCl. The resulting solution was stirred vigorously at room temperature for 48 h.

Then, concentrated aqueous ammonia (100 μL) was added and the mixture was concentrated to a gum. The gummy residue was partitioned between water (10 mL) and ether (10 mL). The ether was removed and the aqueous layer was further washed with ether (2×10 mL). The aqueous solution was concentrated to a small volume. HPLC analysis of this mixture exhibited a main peak at 19 min as seen in Fig. 1A. This peak was collected and the solvent was removed. The residue was diluted with water so as to decrease the salt concentration to less than 0.1 M, and applied to a column on DEAE-Sephadex A-25 (1×5 cm). Elution with water was performed and then elution with 1 M TEAB buffer (pH 7.5) gave fractions containing the product. Most of TEAB was removed under reduced pressure by coevaporations with water and finally the product was desalted by paper chromatography on Toyo Roshi No 51A developed with 95% ethanol. A band at the origin was eluted with water and the solution was filtered and concentrated to give pApUpG (38.0 OD, 20%): HPLC 20 min (A): UV (H_2O) λ_{max} 255 nm, λ_{min} 277 nm.

Synthesis of G⁵'pppApUpG. The fully protected trimer **15** (5 μmol) was partially deprotected as described in full deprotection of **15**. A mixture of compound **1b** (26.2 mg, 25 μmol) and imidazole (35 mg, 0.5 mmol) was rendered anhydrous by repeated coevaporations with dry pyridine and finally dissolved in dry pyridine (0.5 mL). Silver nitrate (132 mg, 0.75 mmol) was added and the solution was stirred in the dark for 3 h. Then, it was coevaporated with dry DMF (3×5 mL), dissolved in dry DMF (0.3 mL), and finally added to crude **32**, obtained from **15** after treatment with silver acetate, which had been coevaporated with dry pyridine (3×5 mL) and then DMF (3×5 mL). The resulting mixture was stirred in the dark for 48 h. Then pyridine–water (2:1, v/v, 10 mL) was added. Hydrogen sulfide gas was bubbled with stirring into the solution at 0 °C until a clear supernatant had been obtained. The supernatant was concentrated to dryness and coevaporated with methanol–toluene (1:1, v/v 3×5 mL). The residue was dissolved in a solution of 0.02 M HCL–dioxane (1:1, v/v, 10 mL) adjusted exactly to pH 2.0 by 0.1 M HCl. After being stirred for 45 h, the solution was quenched with concentrated aqueous ammonia (0.1 mL) and concentrated to a small volume. The concentrate was chromatographed on Whatman 3 MM paper with Solvent I to give crude G⁵'pppApUpG with R_f 0.09. The crude product was further purified by HPLC as shown in Fig. 4. A peak at 35 min was collected and pooled. The combined fractions were desalted by DEAE-Sephadex A-25 as described in the synthesis of pApUpG to give G⁵'-pppApUpG (25 OD, 10%): HPLC 34 min (System B); UV (H_2O): λ_{max} 255 nm, λ_{min} 232 nm.

Full Deprotection of 21. The same procedure as described in the case of **15** was employed.

The residue, obtained after the acid treatment for removal of the acid-labile protecting groups, was dissoved in water (10 ml) and washed with ether (3×10 mL). The aqueous solution was concentrated, and the residue was applied to Watman 3 MM papers and developed with Solvent I. A band at the origin was cut and eluted with water. The eluent was filtered and concentrated to a small volume. The solution was separated by HPLC. A peak at 30 min (System B) was collected and pooled. The combined fractions were evaporated under reduced pressure and diluted with water. The solution was applied to a column of DEAE-Sephadex A-25 (1×5 cm) and the column was washed with water and then eluted with 1 M TEAB. The eluent was coevaporated repeatedly with water and finally desalted by paper chromatography using Toyo Roshi developed with 95% ethanol. A UV absorbing material at the origin was eluted with water. The eluent was evaporated to give pApUpGpApCpC (22.5 OD, 10%): R_f 0.1 (Solvent I); HPLC 30 min (System B); UV (H_2O) λ_{max} 257 nm, λ_{min} 238 nm.

Synthesis of G⁵'pppApUpGpApCpC. This compound was synthesized from **33** (5 μmol) and **1b** (25 μmol) in the same manner as described in the above experiment: Purification after the acid treatment for removal of the THP, MMTr, and TMTr groups was performed as follows: The residue, obtained by evaporation after quenching of the acid solution used for removed of the acid-labile protecting groups, was dissolved in water (10 mL) and washed with ether (10 mL). The aqueous solution was filtered and separated by preparative HPLC as shown in Fig. 5. A peak at 40 min pooled and desalted by DEAE-Sephadex A-25 as described before to give G⁵'pppApUpGpApCpC (16.7 OD, 5%): R_f 0.14 (Solvent I); HPLC 40 min (System B); UV (H_2O) λ_{max} 258 nm, λ_{min} 230 nm.

Preparation of 1a from 1b. Compound **1b** (30 mg, 25 μmol) was coevaporated with dry DMF (2×5 mL) and finally dissolved in dry DMF (1.25 mL). To the solution was added methyl iodide (19 μL, 0.3 mmol). The mixture was stirred for 16 h and then evaporated under reduced pressure. The residue was coevaporated with dry pyridine (2×5 mL) and then used without further purification in the capping reactions.

Synthesis of m⁷G⁵'pppApUpG. This compound was synthesized from **1a** (5 μmol) and **32** (25 μmol) in the same manner as described in the synthesis of G⁵'pppApUpG. Purification was performed in the same manner as described in the synthesis of pApUpG: R_f 0.14 (Solvent I); HPLC 27 min (System B); UV (H_2O) λ_{max} 230 nm, λ_{min} 230 nm.

Synthesis of m⁷G⁵'pppApUpGpApCpC. This compound was synthesized from **1a** and **33** in the same manner as described in the synthesis of G⁵'pppApUpGpApCpC. Purification was performed in the same manner as described in the synthesis of pApUpG (13 OD, 5%): HPLC 33 min (System B); UV (H_2O) λ_{max} 257 nm, λ_{min} 233 nm.

Enzyme Assay. Treatment with venom phosphodiesterase. A substrate (10 OD) was incubated with venom phosphodiesterase in a mixture of 0.05 M Tris-HCl buffer (pH 8.0, 200 μL) and 1 M $MgCl_2$ (10 μL) at 37 °C for 3 h. When a less amount of substrate than 10 OD was used, the amounts of the enzyme and reagents were decreased to the same degree.

Treatment with Nuclease P_1. A substrate (0.05 OD) was incubated with nuclease P_1 (1 μL) in 0.05 M acetate buffer (pH 5.4, 9 μL) at 37 °C for 30—60 min. The mixture was analyzed by HPLC as described in the text.

We express our appreciation to Professor Kinichiro Miura for helpful discussions throughout our programs. Technical assistance was provided by Dr.

A. Kume, Mr. J. Matsuzaki, Miss K. Kohno, Mr. H. Tanimura, and is gratfully acknowledged. We also thank Mrs. C. Sugimura for typewriting this manuscript. This work was supported by the Grant-in-Aid for Scientific Research from the Ministry of Education, Science and Culture.

References

1) a) Y. Furuichi and K. Miura, *Nature (London)*, **253**, 375 (1075); b) A. J. Shatkin, *Cell*, **9**, 645 (1976); c) K. Miura, *Adv. Biophysics*, **14**, 205 (1981); d) I. Tazawa and Y. Inoue, *Nucleic Acids Res.*, **11**, 2907 (1983).

2) I. Nakagawa, S. Konya, S. Ohtani, and T. Hata, *Synthesis*, 556 (1980).

3) K. Yamaguchi, I. Nakagawa, M. Sekine, T. Hata, K. Shimotohno, M. Hiruta, and K. Miura, *Nucleic Acids Res.*, **12**, 2939 (1984).

4) T. Kamimura, Y. Osaki, M. Sekine, and T. Hata, *Tetrahedron Lett.*, **25**, 2683 (1983).

5) M. Sekine, T. Kamimura, and T. Hata, *J. Chem. Soc, Perkin Trans. 1*, in press.

6) Some papers related to the capping reaction have been published by us: a) T. Hata, I. Nakagawa, K. Shimotohno, and K. Miura, *Chem Lett.*, **1976**, 987; b) T. Hata, N. Gokita, K. Sakairi, K. Yamaguchi, M. Sekine, and Y. Ishido, *Bull. Chem. Soc. Jpn.*, **55**, 2949 (1982); c) T. Kamimura, M. Sekine, and T. Hata, *Chem. Lett.*, **1983**, 951.

7) D. E. Hoard and, D. G. Ott, *J. Am. Chem. Soc.*, **87**, 1785 (1965).

8) T. Kamimura, T. Masegi, K. Urakami, S. Honda, M. Sekine, and T. Hata, *Chem. Lett.*, **1983**, 1031.

9) A. Kume, S. Nishiyama, H. Tanimura, M. Sekine, and T. Hata, *Synthesis*, in press.

10) S. Honda, K. Urakami, K. Koura, K. Terada, Y. Sato, K. Kohno, M. Sekine, and T. Hata, *Tetrahedron*, **40**, 153 (1984).

11) T. Kamimura, M. Tsuchiya, K. Urakami, K. Koura, M. Sekine, and T. Hata, *J. Am. Chem. Soc.*, **106**, 4552 (1984).

12) a) M. Sekine, K. Hamaoki, and T. Hata, *J. Org. Chem.*, **44**, 2335 (1979); b) *idem*, *Bull. Chem. Soc. Jpn.*, **54**, 3815 (1981); c) K. Yamaguchi, S. Honda, I. Nakagawa, and T. Hata, *Chem. Lett.*, **1978**, 507.

13) M. Sekine, J. Matsuzaki, and T. Hata, *Tetrahedron Lett.*, **22**, 3209 (1980).

 © 1985 The Chemical Society of Japan Bull. Chem. Soc. Jpn., 58, 861—867 (1985)

Rearrangement Approaches to Cyclic Skeletons. II. Structural Revision and Total Synthesis of (±)-Isosesquicarene, a [3—6] Fused-Ring Sesquiterpene[1)]

Tadao UYEHARA,* Jun-ichi YAMADA, Tadahiro KATO, and Ferdinand BOHLMANN†
Department of Chemistry, Faculty of Science, Tohoku University, Aramaki-Aoba, Sendai 980
†*Institut fur Organische Chemie, Technische Universtat Berlin, Strasse des 17. Juni 135, D-1000 Berlin 12, West Germany*
(Received October 22, 1984)

The *exo*-7-(4-methyl-3-pentenyl) derivative of 3-carene (**1a**), the original structure reported for (±)-isosesquicarene, was synthesized starting from tropone, and it was found that **1a** is not identical with natural isosesquicarene. The structure of isosesquicarene was reinterpreted as *endo*-7-(4-methyl-3-pentenyl) derivative of 3-carene (**1b**). The first total synthesis of (±)-isosesquicarene, **1b**, has been accomplished on the basis of the photochemical transformation of 4-methylbicyclo[3.2.2]nona-3,6-dien-2-one into the 7-*exo*-methylbicyclo-[4.1.0]hept-2-ene.

The structure proposed for isosesquicarene, a sesquiterpenic hydrocarbon isolated from *Haplopappus tenuisectus* (Greene) Blake, is the 3-carene derivative (**1a**)[3)] which is very similar to that of sesquicarene (**2**).[4)] In connection with the stereoselective synthesis of **2** from tropone,[2)] we attempted a total synthesis of (±)-isosesquicarene, and found that **1a** is not the correct structure of isosesquicarene. In this paper we detail i) a stereoselective synthesis of **1a**, ii) proposal of the probable structure (**1b**) for isosesquicarene, and iii) the first total synthesis of (±)-isosesquicarene, **1b**.

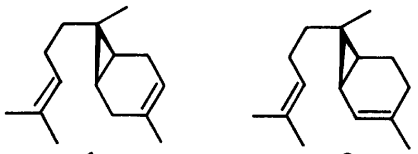

1a **2**

Results and Discussion

Synthesis of the Original Structure Reported for Isosesquicarene. Scheme 1 shows our synthetic plan along with the background.[2)] The ketone (**3**), a presumable precursor of **1a**, would be derived from the bicyclic acid (**4**) in a manner similar to the conversion of **4** into ketone **7** which is a key synthetic intermediate for sesquicarene (**2**). A practical synthetic route to **4** from tropone (**5**) has already been established *via* photochemical transformation of **6** into the acid.

The iodo lactone, derived from **4**,[2)] was transformed into the epoxide (**8**) in 95% yield from **4** by treating with sodium methoxide in methanol, as shown in Scheme 2. The stereochemistry of the epoxide followed from its ^{1}H-NMR spectra which showed $J_{1,2}$=3.6 Hz.[5)] A regioselective opening of the oxirane ring of **8** was done by heating with $LiAlH_4$ in tetrahydrofuran (THF) to give diols **9** and **10** in 76 and 19% yields, respectively. The minor product was identical with the diol obtained from the iodo lactone by treating with $LiAlH_4$.[2)] A better level of stereocontrol was obtained with diisobutylaluminium hydride (DIBAH) at 0 °C but the yield of **9** was not superior to the $LiAlH_4$ reduction; 67%, **9** and 8%, **10**.

In order to prepare an aldehyde suitable for one-

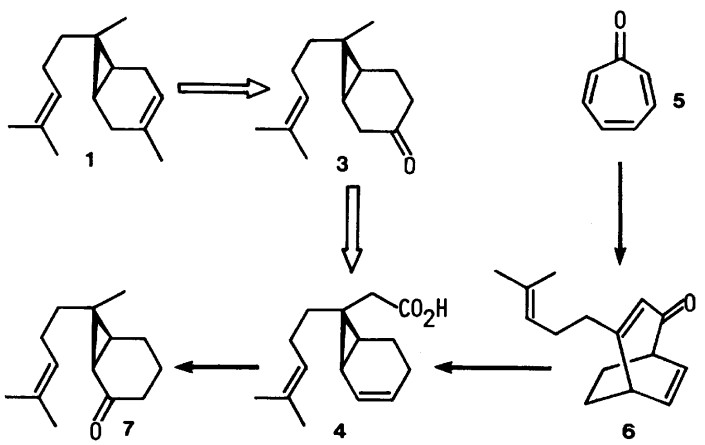

Scheme 1.

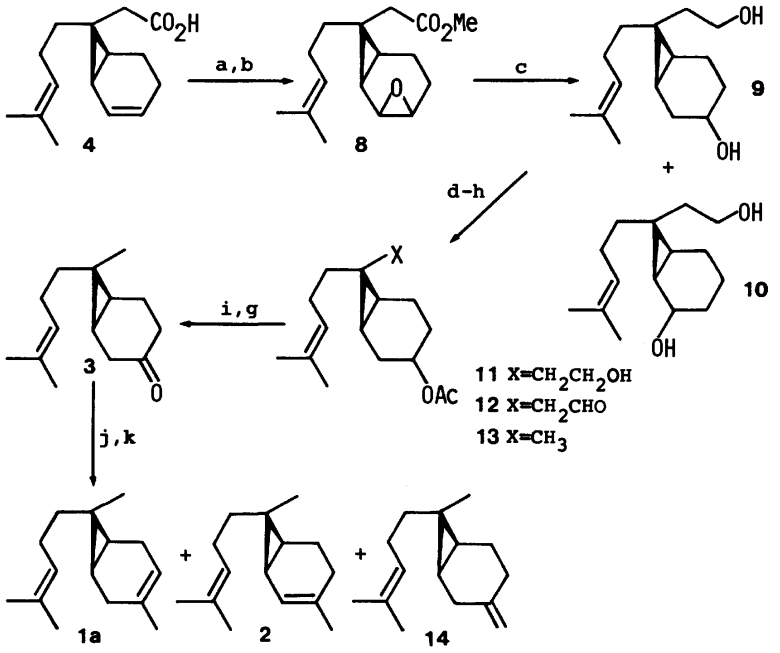

Scheme 2. Synthesis of 3,*endo*-7-Dimethyl-*exo*-7-(4-methyl-3-pentenyl)bicyclo[4.1.0]hept-3-ene (**1a**).[a)]

a) (a): I_2, $NaHCO_3$, ether, H_2O, (b): MeONa, MeOH, (c): $LiAlH_4$, THF, (d): TBDMS-Cl, DMAP, $N(CH_2CH_3)_3$, (e): Ac_2O, Py, (f): AcOH, THF, H_2O, (g): CrO_3–2Py, (h): $RhCl(PPh_3)_3$, PhCN, (i): $LiAlH_4$, ether, (j): MeLi, (k): $POCl_3$, DMAP, Py.

carbon removal from the *endo*-side chain as carbon monoxide using Wilkinson's complex,[6)] the major diol (**9**) was converted into monoacetate **11** in 78% yield. Oxidation of **11** by Collins reagent gave aldehyde **12** in 82% yield. Decarbonylation of **12** by heating with just one equivalent of Wilkinson's complex in benzonitrile at 145 °C for 8 min afforded the acetate (**13**) in 84% yield. Reduction of **13** with $LiAlH_4$ followed by oxidation with Collins reagent produced the desired ketone, **3**, in 91% yield.

Treatment of **3** with an excess of methyllitium at −78 °C gave a mixture of the tertiary alcohols in 73% yield and 22% of unchanged **3**. Dehydration of the alcohols with phosphoryl chloride, pyridine and 4-dimethylaminopyridine (DMAP) produced a 81% yield of three hydrocarbons in a ratio of 63:31:6. The second major product was identical with (±)-sesquicarene (**2**). The specimen of the minor product (**14**) was prepared from **3** by treatment with methylenetriphenylphosphorane in dimethyl sulfoxide (DMSO).

The spectral characteristics of the major product support that its structure is **1a**. However, the NMR spectral data of hydrocarbon **1a** are significantly different from those reported for natural isosesquicarene.

A Structural Revision of Isosesquicarene. It is interesting that both the ^{1}H-NMR data of **1a** and natural isosesquicarene can be arranged in the same tabular form, as shown in Table 1. The assignments of the spectrum of **1a** were performed easily starting from the largest coupling of the H_4 to one of the vicinal methylene protons. Table 1 suggests that both the compounds are the 3-carene derivatives possessing a homoprenyl side chain. A large difference between the chemical shifts of their cyclopropyl methyl protons, H_{14}, indicates that the lower-field resonance of isosesquicarene is not affected largely by the anisotropy effect of the C_3–C_4 double bond.

Thus we propose the C_7-stereoisomer of the original structure, **1b**, as the revised stereostructure of isosesquicarene. The following studies are in order to confirm our proposal.

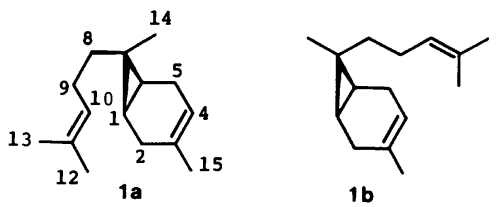

Total Synthesis of (±)-Isosesquicarene (1b). The synthesis was initiated with ketone **15** as shown in Scheme 3. The ketone has already been prepared form bicyclo[3.2.2]nona-3,6-dien-2-one.[2)] The photochemical conversion of **15** into **16** in a good yield was performed by irradiation of a methanolic solution using a high-pressure mercury lamp through a Pyrex

filter. The fact that ^{1}H-NMR of **16** shows the resonance due to the cyclopropyl methyl protons at δ=1.13 prompted us to forward the scheme.

In order to elongate the endo-side chain, **16** was reduced by $LiAlH_4$ to the alcohol, which was tosylated. Treating of the tosylate with sodium cyanide in DMSO gave nitrile **17** in 84% yield (from **16**). The silyl ether (**19**) was derived from **17** in 70% yield *via* the aldehyde (**18**) by sequential treatment with (i) DIBAH, (ii) aqueous ammonium chloride solution, (iii) $LiAlH_4$, and (iv) *t*-butyldimethylchlorosilane, triethylamine, and DMAP.

Table 1. Proton NMR data of compound **1a** and isosesquicarene (in $CDCl_3$)

	Compound **1a**			Isosesquicarene[a]	
H	δ	mult	J, Hz (coupled to)[b]	δ	mult[c]
1	0.72	dd	9.3(6), 7.2(2α)	0.66	dd
2α	2.18	bdd	18.2(2β), 7.2(1)	2.34	bdd
2β	1.81	m		2.03	m
4	5.27	bs		5.25	bs
5α	2.36	m	16.5(5β), 7.2(6), 3.5(4)	2.16	bdd
5β	1.94	m		1.86	bd
6	0.63	dd	9.3(1), 7.2(5α)	0.78	dd
8	1.19	m		(1.14	m)[d]
9	2.07	m	7.0(10)	2.03	
10	5.15	bt	9.0(9)	5.12	bt
12	1.64	bs		1.59	bs
13	1.69	d	1(10)	1.67	bs
14	0.75	s		1.02	
15	1.64	bs		1.59	bs

a) Ref. 3. b) Distinguished coupling are listed. c) $J_{5\alpha,5\beta}$=19 Hz, $J_{4,5\alpha}$=3 Hz, $J_{5\alpha,6}$=8 Hz, $J_{1,2\alpha}$=8 Hz, $J_{1,6}$=8 Hz, and $J_{9,10}$=7 Hz. d) This work.

Epoxidation of **19** with *m*-chloroperoxybenzoic acid yielded only **20**. The stereostructure of **20** was estimated on the basis of its ^{1}H-NMR spectra ($J_{1,2}$<1 Hz).[5] Treatment of **20** with DIBAH gave only the regioselective C-O cleavage product (**21**), which was converted into the benzoate (**22**) in 71% yield from **19**. This regioselective ring opening is with the assistance of the bonding between the reagent and the epoxide oxygen and due to participation of the cyclopropane to tolerate positive charge at the C_2 in the transition state. ^{1}H-NMR spectra of **22** showed the signals due to the C_3-H at δ=4.91 (b, $W_{1/2}$= 13 Hz). This half-hight width is clearly different from those of **12** and **13**: C_3-H of **12**, $W_{1/2}$=19.5 Hz; C_3-H of **13**, $W_{1/2}$=21 Hz. Thus, the 3-proton of **22** should be a pseudoequatrial one and the benzoyloxyl group should be α-configuration as illustrated. Now it is clear that the epoxidation of **19** proceeded at its less-hindered side.

After removal of the silyl group of **22**, the alcohol (**23**) was transformed into the unstable aldehyde (**24**). Immediately after isolation, **24** was treated with isopropylidenetriphenylphosphorane in ether at −30 °C to give **25** in 68% yield from **23**.

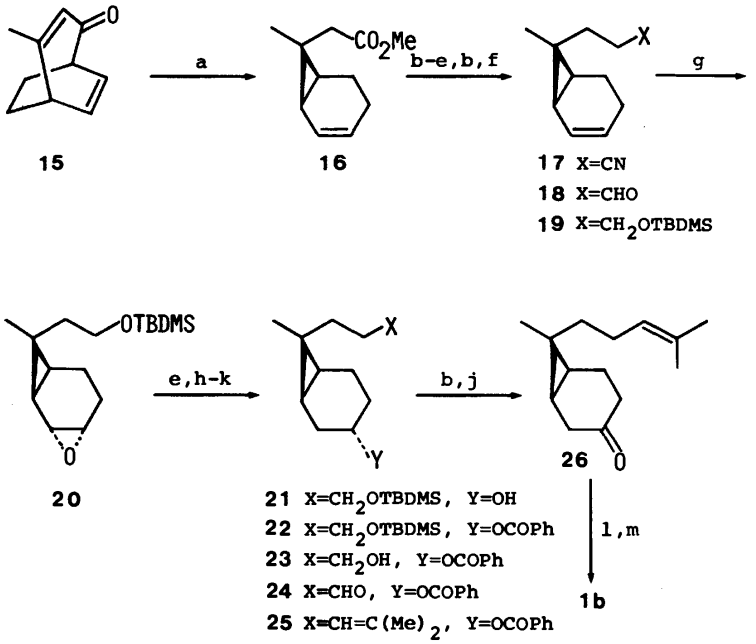

Scheme 3. Synthesis of (±)-isosesquicarene.[a]

a) (a): *hv*, MeOH, (b): $LiAlH_4$, (c): TsCl, Py, (d): NaCN, DMSO, (e): DIBAH, $PhCH_3$, (f): TBDMS-Cl, DMAP, $N(CH_2CH_3)_3$, (g): MCPBA, $NaHCO_3$, (h): $(PhCO)_2O$, DMAP, $N(CH_2CH_3)_3$, (i): AcOH, THF, H_2O, (j): CrO_3-2Py, (k): Ph_3P=CMe_2, (l): MeLi, (m): $POCl_3$, DMAP, Py.

We have examined several routes to shorten the synthetic steps but have not yet found more effective ones because of instability of the aldehydes like **24**.

Reduction of **25** with $LiAlH_4$ followed by Collins oxidation gave ketone **26** in 76% yield. Treatment of **26** with methyllithium at −95 °C yielded a mixture of tertiary alcohols in 74% yield. Dehydration of the alcohols gave a mixture of three hydrocarbons in 74% yield. The major product (**1b**) was purified by repeated preparative VPC. Thus obtained was identical spectroscopically with natural isosesquicarene.

*The stereostructure of isosesquicarene is 3,*exo*-7-dimethyl-*endo*-7-(4-methyl-3-pentenyl)bicyclo[4.1.0]hept-3-ene.*

Experimental

General. Melting and boiling points are uncorrected. IR spectra (in CCl_4, unless otherwise mentioned) were recorded on a Hitachi Model 215 spectrometer. NMR spectra (in CCl_4, unless otherwise noted) were obtained on JEOL JNM-PMX60, Varian EM-390 90 MHz, and Varian XL-200 NMR spectrometers, using tetramethylsilane as an internal standard. The mass spectral studies were conducted using a Hitachi M-52 spectrometer and a JEOL DX-300 mass spectrometer. Photochemical reactions were carried out in an immersion well through a Pyrex filter using a Ushio 300 W high pressure mercury lamp, under an inert atmosphere. THF and ether were distilled from benzophenone ketyl under argon, immediately prior to use. Dichloromethane was distilled from P_2O_5 and stored on 4A molecular sieves. Pyridine (from BaO), triethylamine, methanol (from $Mg(OCH_3)_2$), and DMSO (from BaO) were purified by distillation. Collins reagent,[7] and Wilkinson's complex[8] were prepared by using literature procedures. All reactions were monitored by analytical TLC using E. Merck precoated silica gel $60F_{254}$ plates. Column chromatography was carried out with E. Merck silica gel 60 (70—230 mesh ASTM, twenty to fifty times (w/w)). A Warters silica cartridge "Sep-Pack" was used for small scale rapid chromatography. Analytical VPC was performed on a Hitachi 663-50 gas chromatograph, outfitted with a 3 m×3 mm stainless-steel column packed with 10% FFAP on 60/80 Uniport B, and preparative VPC on a Varian Aerograph model 920 gas chromatograph with TC detector, outfitted a with 10 ft×3/8 in. aluminium column containg 10% FFAP on 60/80 Uniport B.

Preparation of Methyl endo*-2,3-Epoxy-*exo*-7-(4-methyl-3-pentenyl)bicyclo[4.1.0]heptane-*endo*-7-acetate (8).* To a solution of 262.4 mg (1.12 mmol) of **4** in 7 ml of saturated aqueous $NaHCO_3$ was added a solution of 285 mg (1.12 mmol) of iodine in 10 ml of ether over a period of 20 min at room temperature in the dark. After 1 h of stirring, the mixture was diluted with water, and extracted with several portions of ether. The extracts were combined, washed with 5% aqueous $Na_2S_2O_3$ and saturated brine, and then dried over $MgSO_4$. Evaporation of the solvent without heating from outside gave 443.3 mg of a pale yellow oil, which was supplied directly to the following reaction. To a solution of the oil in 5 ml of methanol was added a solution of sodium methoxide in methanol, prepared from 60 mg of sodium and 1.2 ml of methanol, at 0 °C. After 2 h standing at 0 °C, the mixture was diluted with water, and extracted with two portions of ether. The extracts were combined, washed with two portions of water and with saturated brine, and then dried over $MgSO_4$. Removal of the solvent gave 297.5 mg of yellow oil, which was purified by column chromatography (5:1 hexane, ethyl acetate) to yield 280.7 mg (95%) of **8**: bp 100—105 °C/2 Torr; IR 1740 (s), 1190 (m), and 1165 (m) cm^{-1}; NMR δ=5.00 (1H, tm, J=7.2 Hz), 3.62 (3H, s), 3.25 (1H, dd, J=3.6 and 3.6 Hz), 2.83 (1H, dd, J=3.6 and 2.7 Hz), 2.68 (2H, s), 1.66 (3H, bs), 1.60 (3H, bs), and 0.79 (1H, dd, J= 9.0 and 3.6 Hz); MS, m/z (rel intensity) 264 (M^+, 13) and 167 (100). Found: C, 72.67; H, 9.38%. Calcd for $C_{16}H_{24}O_3$: C, 72.69; H, 9.15%.

Reduction of Epoxide 8. Preparation of endo*-7-(2-Hydroxyethyl)-*exo*-7-(4-methyl-3-pentenyl)bicyclo[4.1.0]heptan-3-ol (9).* To a mixture of 146 mg (3.85 mmol) of $LiAlH_4$ and 5 ml of dry THF was added a solution of 398.5 mg of **8** in 30 ml of dry THF at 0 °C. The reaction mixture was heated under reflux for 1.5 h. After cooling to 0 °C, the resulting suspension was treated by successive dropwise addition of a few ml of ethyl acetate, 0.15 ml of water, 0.15 ml of 15% aqueous NaOH, and 0.45 ml of water, and then allowed to warm to room temperature with stirring. The THF solution was filtered, and the filtrate was concentrated *in vacuo* to afford 389.1 mg of a colorless oil. Separation of the products by column chromatography (1:1 hexane, ethyl acetate) gave 287.7 mg (76%) of **9** and 72 mg (19%) of **10**.[2] **9**: IR 3340 (m) and 1055 (s) cm^{-1}; NMR δ=5.00 (1H, tm, J=6.9 Hz), 4.05 (2H, bs), 1.67 (3H, s), and 1.61 (3H, s). The diacetate of **9**: C, 71.07; H, 9.51%. Calcd for $C_{19}H_{30}O_4$: C, 70.77; H, 9.38%.

Transformation of Diol 9 into endo*-7-(2-Hydroxyethyl)-*exo*-7-(4-methyl-3-pentenyl)bicyclo[4.1.0]hept-3-yl Acetate (11).* In order to protect the primary hydroxyl group selectively, a solution of 220 mg (1.2 equiv) of *t*-butyldimethylchlorosilane in 10 ml of CH_2Cl_2 was added to a solution of 287.7 mg (1.21 mmol) of **9**, 137.8 mg (0.19 ml, 1.1 equiv) of triethylamine, and a small amount of DMAP in 9 ml of CH_2Cl_2. After standing for 21 h at room temperature, the solution was washed with saturated aqueous NH_4Cl, dried over $MgSO_4$, and concentrated *in vacuo*. Chromatography (15:1 hexane, ethyl acetate) of the residue gave 341.8 mg (80%) of the monosilyl ether of **9**: IR 3620 (w), 3350 (w), 1090 (s), and 1050 (m) cm^{-1}; NMR δ=4.97 (1H, tm, J= 6.9 Hz), 3.67 (2H, m), 3.47 (1H, m), 1.64 (3H, bs), 1.58 (3H, bs), 0.90 (6H, s), and 0.05 (9H, s).

To protect the secondary hydroxyl group, 2 ml of acetic anhydride was added to a solution of 603.2 mg (1.71 mmol) of the monosilyl ether in 3 ml of dry pyridine. After standing overnight at room temperature, evaporation of the solvent *in vacuo* gave 670.5 mg of the residue, which was chromatographed (10:1 hexane, ethyl acetate) to afford 665.6 mg (98%) of the acetate: IR 1730 (s) and 1030 (m) cm^{-1}. Found: C, 70.01; H, 10.62%. Calcd for $C_{23}H_{42}O_3Si$: C, 70.00; H, 10.73%.

In order to remove the silyl group,[9] 665.6 mg (1.68 mmol) of the acetate was treated with a mixture of 3.4 ml of THF, 3.4 ml of water, and 10.2 ml of acetic acid for 7 h at room temperature. The solution was diluted with ether, washed successively with water (four times), saturated $NaHCO_3$ and brine solutions, dried over $MgSO_4$, and concentrated *in vacuo*. Chromatography (3:1 hexane, ethyl acetate) of the

residue gave 467 mg (99%) of **11**: IR 1730 (s) and 1030 (s) cm^{-1}; NMR δ=4.97 (1H, tm, J=6.9 Hz), 4.56 (1H, m, $W_{1/2}$=21.3 Hz), 3.67 (2H, m), 1.93 (3H, s), 1.65 (3H, bs), and 1.59 (3H, bs).

Preparation of endo-*7-(2-Oxoethyl)*-exo-*7-(4-methyl-3-pentenyl)bicyclo[4.1.0]hept-3-yl Acetate (12).* To a solution of 3.20 g (12.4 mmol) of Collins reagent in 40 ml of dry CH_2Cl_2 was added a solution of 578.2 mg (2.06 mmol) of the hydroxy acetate in 24 ml of CH_2Cl_2. After 6 min stirring at room temperature, the solution was decanted, and the black residue was washed with several portions of ether. The organic layers were combined, washed successively with 5% aqueous NaOH, 5% HCl, saturated $NaHCO_3$ and brine solution, dried over $MgSO_4$, and evaporated. Column chromatography (3:1 hexane, ethyl acetate) of the residue (553.1 mg) gave 529.7 mg (92%) of the unstable aldehyde, **12**: IR 2710 (w), 1730 (s), and 1245 (s) cm^{-1}; NMR δ=9.70 (1H, t, J=2.3 Hz), 4.97 (1H, tm, J=6.9 Hz), 4.58 (1H, m, $W_{1/2}$=19.5 Hz), 2.29 (2H, d, J=2.3 Hz), 1.91 (3H, s), 1.63 (3H, bs), and 1.56 (3H, s); MS, m/z (rel intensity) 218 (M^+−60, 98), 200 (74), 131 (74), and 82 (100).

Decarbonylation of 12. Preparation of endo-*7-Methyl*-exo-*7-(4-methyl-3-pentenyl)bicyclo[4.1.0]hept-3-yl Acetate (13).* A flask containing of a mixture of 155.3 mg (0.56 mmol) of **12**, 514.3 mg (0.56 mmol) of Wilkinson's complex and 2 ml of benzonitrile, prepared under argon, was immersed in a preheated oil bath at 145 °C for 8 min with stirring. The bulk of benzonitrile was removed by Kugelrohr distillation (100 °C/3 Torr), and the residue was rinsed with ethanol, filtered, and washed with ethanol. After evaporation of the solvent, chromatography (10:1 hexane, ethyl acetate) of the residue (343.3 mg) gave 117.3 mg (84%) of **13**: bp 55—60 °C/0.5 Torr (1 Torr=133.322 Pa); IR 1730 (s) and 1250 (s) cm^{-1}; NMR δ=4.98 (1H, tm, J=6.9 Hz), 4.52 (1H, m, $W_{1/2}$=21 Hz), 1.93 (3H, s), 1.65 (3H, s), 1.58 (3H, s), and 1.00 (3H, s); MS, m/z (rel intensity) 190 (M^+−60, 100), 108 (66), and 105 (51). Found: C, 76.95; H, 10.46%. Calcd for $C_{16}H_{26}O_2$: C, 76.75; H, 10.47%.

Preparation of endo-*7-Methyl*-exo-*7-(4-methyl-3-pentenyl)bicyclo[4.1.0]heptan-3-one (3).* To a suspension of 50 mg (1.32 mmol) of $LiAlH_4$ in 2 ml of dry ether was added a solution of 208.6 mg (0.83 mmol) of **13** in 10 ml of ether at 0 °C. After 20 min stirring, to the reaction mixture were added successively 0.05 ml of water, 0.05 ml of 15% aqueous NaOH, and 0.15 ml of water. After stirring until a granular precipitate was formed, $MgSO_4$ was added to the mixture and filtered. Concentration of the filtrate gave 176.3 mg of an oil. Chromatography (5:1 hexane, ethyl acetate) of the oil gave 164.7 mg (95%) of the alcohol: IR 3620 (w), 3330 (m), and 1055 (s) cm^{-1}; NMR δ=4.98 (1H, tm, J=6.9 Hz), 3.43 (1H, m, $W_{1/2}$=22.8 Hz), 1.65 (3H, bs), 1.59 (3H, bs), 1.53 (1H, s), and 0.98 (3H, s).

The alcohol (164.7 mg, 0.79 mmol) was treated with 1.14 g (4.75 mmol) of Collins reagents in 10 ml of dry CH_2Cl_2 at room temperature for 5 min. A workup similar to that employed for the synthesis of **12** gave 165.4 mg of the crude product. Chromatography on silica gel (10:1 hexane, ethyl acetate) gave 143.2 mg (96%) of pure **3**: IR 1710 (s) cm^{-1}; NMR δ=4.95 (1H, tm, J=6.9 Hz), 1.62 (3H, bs), 1.56 (3H, bs), and 0.88 (3H, s); MS, m/z (rel intensity) 206 (M^+, 11) and 82 (100). Found: C, 81.55; H, 10.89%. Calcd for $C_{14}H_{22}O$: C, 81.50; H, 10.75%.

*Preparation of 3,*endo-*7-Dimethyl*-exo-*7-(4-methyl-3-pentenyl)bicyclo[4.1.0]hept-3-ene (1a).* To a solution of 144.7 mg (0.70 mmol) of **3** in 1.5 ml of ether was added dropwise a methyllithium solution, prepared from 500 mg of methyl iodide (3.53 mmol) and 70 mg (10.1 mmol) of lithium in 3 ml of ether at 0 °C by 10 min of sonication,[10] at −78 °C. After 1 h stirring followed by addition of methanol, the mixture was diluted with ether and washed with saturated brine. The etherial solution was dried over $MgSO_4$, and concentrated. Chromatography (15:1 hexane, ethyl acetate) of the residue gave 113.2 mg (73%) of a mixture of the alcohols and 32.5 mg (22%) of **3**.

Three drops of $POCl_3$ were added to a solution of 31.0 mg (0.14 mmol) of the mixture of the alcohols and a small amount of DMAP in 2 ml of pyridine at 0 °C. After 1.5 h stirring at 0 °C, the mixture was diluted with pentane, washed successively with 5% HCl, saturated $NaHCO_3$ and NaCl solutions, and then dried over Na_2SO_4. Concentration of the solution followed by purification using a silica cartridge (pentane) gave 23.1 mg of a colorless oil. The product was shown by analytical VPC and NMR to consist of 63% **1a**, 31% **2**, and 6% **14**. Preparative VPC (10% FFAP, 150 °C) afforded **1a**: IR 2980 (s), 2920 (s), 2830 (s), 1450 (m), and 1380 (m) cm^{-1}; MS, m/z (rel intensity) 204 (M^+, 14), 161 (16), 119 (70), and 93 (100). Found: m/z 204.18590. Calcd for $C_{15}H_{24}$: M, 204.18776.

Preparation of endo-*7-Methyl-3-methylene*-exo-*7-(4-methyl-3-pentenyl)bicyclo[4.1.0]heptane (14).* Methylenetriphenylphosphorane was generated by a typical method[11] from 760 mg (2.13 mmol) of methyltriphenylphosphonium bromide in DMSO. The ylide solution was added to a solution of 76 mg (0.37 mmol) of **3** in 2 ml of DMSO at 35 °C. After 3 h standing at room temperature, the mixture was chilled by ice-water, diluted with water, and extracted with three potions of pentane. The extracts were combined washed with two portions of water and with saturated brine, and then dried over Na_2SO_4. Concentration of the solution followed by purification using a silica cartridge (pentane) gave 68.3 mg (90%) of colorless oil. **14**: IR 3085 (m), 1654 (m), and 888 (s) cm^{-1}; NMR ($CDCl_3$) δ=5.05 (1H, tm, J=6.9 Hz), 4.59 (2H, b, $W_{1/2}$=3.5 Hz), 1.68 (3H, bs), 1.62 (3H, bs), and 0.92 (3H, s); MS, m/z (rel intensity) 204 (M^+, 28), 189 (35), 161 (100), and 122 (86). Found: m/z 204.18822. Calcd for $C_{15}H_{24}$: M, 204.18776.

Photochemical Transformation of 15 into Methyl exo-*7-Methylbicyclo[4.1.0]hept-2-ene*-endo-*7-acetate (16).* A solution of 1.14 g (7.69 mmol) of **15** in 750 ml of methanol was irradiated by a 300 W Hg-lamp for 1.5 h. Evaporation of the solvent gave 1.24 g of a yellow oil. Column chromatography of the crude oil (10:1 hexane, ethyl acetate) gave 1.11 g (80%) of pure **16**: IR 1735 (s) cm^{-1}; NMR δ=5.80 (1H, dm, J=10.2 Hz), 5.60 (1H, dm, J=10.2 Hz), 3.60 (3H, s), 2.20 (2H, s), 2.2—1.4 (4H, m), 1.13 (3H, s), and 1.04 (2H, m); MS, m/z (rel intensity) 180 (M^+, 13), 106 (100), and 91 (94). Found: C, 73.40; H, 8.97%. Calcd for $C_{11}H_{16}O_2$: C, 73.30; 8.95%.

Preparation of exo-*7-Methylbicyclo[4.1.0]hept-2-ene*-endo-*7-propanenitrile (17).* Ester **16** (1.641 g, 9.88 mmol) was reduced by lithium aluminium hydride (570 mg, 15.0 mmol) in ether (120 ml) at 0 °C. A similar workup to that employed for the reduction of **13** gave the corresponding alcohol (1.677 g). To a solution of the crude alcohol in pyridine (10 ml) was added a solution of tosyl chloride (2.75 g,

14.4 mmol) in pyridine (3 ml) at 0 °C. After 2 h stirring at 0 °C, the mixture was diluted with water (50 ml), and extracted with three portions of ether. The combined extracts were washed successively with 5% HCl, saturated $NaHCO_3$ and NaCl solutions, dried over $MgSO_4$, and then concentrated. To a solution of the tosylate (2.784 g) in DMSO (20 ml) was added sodium cyanide (730 mg, 14.9 mmol), and the mixture was heated at 90 °C for 2 h under a nitrogen atmosphere. After dilution with water, the solution was extracted with three portions of CH_2Cl_2. The extracts were combined, washed with three portions of water, dried over $MgSO_4$, and concentrated *in vacuo*. Chromatography (20:1 hexane, ethyl acetate) of the residue gave pure **17** (1.327 g, 84%). **17**: bp 75 °C/15 Torr; IR 2260 (w) and 1455 (s) cm^{-1}; NMR δ=5.82 (1H, dm, J=10.5 Hz), 5.65 (1H, dm, J=10.5 Hz), 2.27 (2H, m), 1.64 (2H, m), 1.11 (3H, s), and 1.06 (3H, s); MS, m/z (rel intensity) 161 (M^+, 13), 119 (100), 107 (37), and 79 (30). Found: C, 82.24; H, 9.60; N, 8.84%. Calcd for $C_{11}H_{15}N$: C, 81.94; H, 9.38; N, 8.69%.

Preparation of exo-*7-Methylbicyclo[4.1.0]hept-2-ene*-endo-*7-propanal (18).* To a solution of 914.6 mg (5.67 mmol) of **17** in 57 ml of toluene was added 3.9 ml of a solution of DIBAH in hexane (1.76 M, 6.86 mmol (1 M=1 mol dm^{-3})) at 0 °C under an argon atmosphere. After 2 h stirring at room temperature, the mixture was cooled by ice-water. Careful addition of 50 ml of saturated aqueous NH_4Cl followed by stirring at room temperature for 30 min gave a suspension, which was filtered through a sintered-glass disk and washed with several portions of ether. The filtrates were combined, washed successively with water, saturated $NaHCO_3$ and NaCl solutions, dried over Na_2SO_4, and concentrated *in vacuo*. Column chromatography (15:1 hexane, ethyl acetate) of the residue (937.0 mg) gave 790.6 mg (85%) of **18**: IR 2815 (m) and 1725 (s) cm^{-1}; NMR δ=9.62 (1H, t, J=1.5 Hz), 5.73 (1H, dm, J=10.1 Hz), 5.62 (1H, dm, J=10.2 Hz), 2.37 (2H, m), 1.57 (2H, m), and 1.05 (3H, s). The 2,4-DNP derivative of **18**: mp 119.5—121.0 °C. Found: C, 59.44; H, 5.92; N, 16.03%. Calcd for $C_{17}H_{20}N_4O_4$: C, 59.29; H, 5.85; N, 16.27%.

Preparation of exo-*7-Methyl*-endo-*7-[3-(t-butyldimethylsiloxy)propyl]bicyclo[4.1.0]hept-2-ene (19).* To a suspension of 240 mg (6.32 mmol) of $LiAlH_4$ in 30 ml of ether was added a solution of 1.03 g (6.25 mmol) of **18** in 20 ml of ether at 0 °C. After stirring for 30 min, a similar workup to that employed for the reduction of **13** gave the corresponding alcohol. To a solution of the alcohol, 0.96 ml (6.88 mmol) of triethylamine, and a small amount of DMAP in 30 ml of dry CH_2Cl_2 was added a solution of 1.13 g (7.50 mmol) of *t*-butyldimethylchlorosilane in 30 ml of dry CH_2Cl_2 under argon. After standing for 17 h at room temperature, the solution was washed with saturated NH_4Cl solution, dried over $MgSO_4$, and evaporated. Chromatography (15:1 hexane, ethyl acetate) of the residue (1.78 g) gave 1.44 g (82%) of **19**: IR 1100 (s) and 840 (m) cm^{-1}; NMR δ=5.81 (1H, dm, J=10.5 Hz), 5.62 (1H, dm, J=10.5 Hz), 3.57 (2H, t, J=6.0 Hz), 1.10 (3H, s), 0.93 (9H, s), and 0.05 (6H, s); MS, m/z (rel intensity) 263 (16), 223 (100), and 147 (69). Found: C, 72.53; H, 11.31%. Calcd for $C_{17}H_{32}OSi$: C, 72.79; H, 11.50%.

Preparation of 2,3-Epoxy-exo-*7-methyl*-endo-*7-[3-(t-butyldimethylsiloxy)propyl]bicyclo[4.1.0]heptane (20).* To a mixture of a solution of 564.8 mg (2.01 mmol) of **19** in 9 ml of CH_2Cl_2 and 339.8 mg (4.04 mmol) of $NaHCO_3$ was added a solution of 415.9 mg (2.40 mmol) of *m*-chloroperoxybenzoic acid in 9 ml of CH_2Cl_2 at 0 °C under an argon atmosphere. After 2 h stirring at 0 °C, the mixture was diluted with water, and extracted with ether. The etherial solution was washed successively with two portions of saturated aqueous $NaHCO_3$, water, and saturated brine, dried over $MgSO_4$, and then concentrated to give 667.3 mg of an oil. An analytical sample of the epoxide (**20**) was purified by column chromatography (10:1 hexane, ethyl acetate). **20**: IR 1265 (m) and 1100 (s) cm^{-1}; NMR δ=3.80—3.61 (2H, m), 3.36—3.13 (2H, m), 1.07 (3H, s), 0.93 (9H, s), and 0.08 (6H, s); MS, m/z (rel intensity) 296 (M^+, 3), 130 (87), and 104 (100).

Preparation of exo-*7-Methyl*-endo-*7-[3-(t-butyldimethylsiloxy)propyl]bicyclo[4.1.0]hept-3-yl Benzoate (22).* A 1.76 M solution of DIBAH in hexane (2.46 ml) was added to a solution of 667.3 mg of the crude epoxide (**20**) in 20 ml of toluene at 0 °C under an argon atmosphere. After 1.5 h stirring at room temperature, the mixture was cooled by ice-water. After addition of 20 ml of saturated aqueous NH_4Cl, the mixture was stirred for 30 min at room temperature. A similar workup to that employed for the synthesis of **18** afforded 661.5 mg of a colorless oil. An analytical sample of the alcohol (**21**) was purified by column chromatography (15:1 hexane, ethyl acetate). **21**: IR 3620 (w), 3450 (w), 1110 (s), and 1095 (s) cm^{-1}; NMR δ=3.68 (1H, m), 3.63 (2H, t, J=6.0 Hz), 1.01 (3H, s), 0.94 (9H, s), 0.72 (2H, m), and 0.08 (6H, s).

Benzoic anhydride (1.20 g, 5.30 mmol) was added to a solution of 661.5 mg of the crude alcohol and a small amount of DMAP in 5 ml of triethylamine under argon. After standing for 24 h at room temperature, the solution was diluted with ether. Aqueous workup followed by chromatography (25:1 hexane, ethyl acetate) gave 573.4 mg (71%) of **22**: IR 1720 (s) and 1115 (s) cm^{-1}; NMR δ=8.5—7.83 (2H, m), 7.55—7.16 (2H, m), 4.91 (1H, m, $W_{1/2}$=13 Hz), 3.61 (2H, t, J=6.0 Hz), 1.00 (3H, s), 0.89 (9H, s), and 0.04 (6H, s). Found: C, 71.83; H, 9.51%. Calcd for $C_{24}H_{38}O_3Si$: C, 71.59; H, 9.51%.

Preparation of exo-*7-Methyl*-endo-*7-(4-methyl-3-pentenyl)bicyclo[4.1.0]heptan-3-yl Benzoate (25).* In order to remove the silyl group, 176.3 mg (0.438 mmol) of **22** was treated with a mixture of 0.88 ml of THF, 0.88 ml of water, and 2.64 ml of acetic acid[9] for 17.5 h at room temperature. A similar workup to that employed for the synthesis of **11** gave 185.4 mg of an oil. Purification by chromatography (3:1 hexane, ethyl acetate) gave 113.8 mg (90%) of the hydroxy benzoate (**23**): IR 3630 (w), 3540 (w), 1715 (s), and 1280 (s) cm^{-1}; NMR δ=8.05—7.83 (2H, m), 7.54—7.18 (3H, m), 4.93 (1H, m, $W_{1/2}$=12 Hz), 3.62 (2H, t, J=6.0 Hz), and 1.00 (3H, bs).

To a solution of 1.75 g (6.8 mmol) of Collins reagent in 20 ml of dry CH_2Cl_2 was added a solution of 324.6 mg (1.13 mmol) of **23** in 15 ml of CH_2Cl_2. The resulting mixture was stirred for 6 min at room temperature. A similar workup to that employed for the synthesis of **12** gave 272.8 mg of an oil. An analytical sample of the aldehyde (**24**) was purified by column chromatography (5:1 hexane, ethyl acetate). **24**: IR 2720 (w), 1720 (s), and 1280 (s) cm^{-1}; NMR δ=9.73 (1H, t, J=1.5 Hz), 8.02—7.82 (2H, m), 7.55—7.18 (3H, m), 4.92 (1H, m, $W_{1/2}$=13.8 Hz), 2.51 (2H, m), and 1.00 (3H, s); MS, m/z (rel intensity) 286 (M^+, 3) and 146 (100).

Isopropylidenetriphenylphosphorane[12] was generated from 1.46 g (3.38 mmol) of isopropyltriphenylphosphonium iodide and 2.1 ml of a 1.5 M solution of *n*-BuLi (hexane) in 35 ml of ether at 0 °C for 1 h under argon. To the ylide solution was added a solution of 272.8 mg of freshly pre-

pared **24** in 2 ml of ether at −30 °C, and the mixture was stirred for 15 min. The solution was diluted with wet ether, and well stirred at room temperature. After removal of the precipitate by filtration, the filtrates were combined, washed with water and saturated NaCl solution, and then dried over $MgSO_4$. Concentration of the solution followed by chromatography gave 239.2 mg (68%) of **25**: IR 1720 (s) and 715 (s) cm^{-1}; NMR δ=8.10—7.82 (2H, m), 7.55—7.12 (3H, m), 5.25—4.77 (2H, m), 1.70 (3H, bs), 1.65 (3H, bs), and 1.03 (3H, s). Found: C, 80.52; H, 9.07%. Calcd for $C_{21}H_{28}O_2$: C, 80.73; H, 9.03%.

Preparation of exo-*7-Methyl*-endo-*7-(4-methyl-3-pentenyl)bicyclo[4.1.0]heptan-3-one (26).* To a suspension of 20.0 mg (0.527 mmol) of $LiAlH_4$ in 2 ml of dry ether was added a solution of 80.0 mg (0.256 mmol) of 25 in 2.5 ml of ether at 0 °C. After 20 min stirring, a similar workup to that employed for the reduction of **13** gave 76.6 mg of an oil. Chromatography (5:1 hexane, ethyl acetate) of the oil gave 50.8 mg (95%) of the alcohol: IR 3625 (w), 3400 (w), and 1050 (m) cm^{-1}; NMR δ=5.05 (1H, tm, J=6.9 Hz), 3.53 (1H, m, $W_{1/2}$=13.5 Hz), 1.68 (3H, bs), 1.62 (3H, bs), and 0.98 (3H, s).

The alcohol (50.8 mg, 0.243 mmol) was treated with 380 mg (1.46 mmol) of Collins reagents in 3.6 ml of dry CH_2Cl_2 at room temperature for 5 min. A similar workup to that employed for the synthesis of **12** gave 42.3 mg of the crude product. Chromatography on silica gel (20:1 hexane, ethyl acetate) gave 37.4 mg (71%) of pure **26**: IR 1710 (s) cm^{-1}; NMR δ=5.05 (1H, tm, J=6.9 Hz), 1.67 (3H, bs), 1.61 (3H, bs), and 1.04 (3H, s); MS, m/z (rel intensity) 206 (M^+, 100) and 82 (84). Found: C, 81.20; H, 10.45%. Calcd for $C_{14}H_{22}O$: C, 81.50; H, 10.75%.

*Preparation of (±)-Isosesquicarene,3,*exo-*7-Dimethyl*-endo-*7-(4-methyl-3-pentenyl)bicyclo[4.1.0]hept-3-ene (1b).* To a solution of 140.0 mg (0.68 mmol) of **26** in 5 ml of ether was added dropwise a methyllithium solution (2.5 equiv) at −95 °C, and the mixture was allowed to warm to room temperature slowly. After addition of methanol–water at 0 °C, the mixture was diluted with ether, washed with saturated brine, dried over $MgSO_4$, and concentrated. Chromatography (20:1 hexane, ethyl acetate) of the residue gave 111.2 mg (74%) of a mixture of the alcohols.

Phosphoryl chloride (0.07 ml) was added to a solution of 130 mg (0.58 mmol) of a mixture of the alcohols and a small amount of DMAP in 5.8 ml of pyridine at 0 °C. After stirring 1 h at 0 °C and 30 min at room temperature, the mixture was diluted with pentane, washed successively with 5% HCl, saturated $NaHCO_3$ and NaCl solutions, dried over $MgSO_4$, and concentrated. Purification using a silica cartridge (pentane) gave 85.7 mg (74%) of a colorless oil. The product was shown by analytical VPC and NMR to consist of 63% **1b** and 28 and 9% of the isomers. Preparative VPC (10% FFAP, 150 °C) afforded pure **1b**: MS, m/z (rel intensity) 204 (M^+, 12), 133 (14), 119 (78), and 93 (100). Found: m/z 204.18840. Calcd for $C_{15}H_{24}$: M, 204.18776.

We are grateful to Mr. Toshiro Yokoyama of Government Industrial Research Institute, Tohoku, at Sendai, for the measurements of the high-resolution mass spectra. We thank Foundation for the Promotion of Research on Medical Resources for partial support of this work.

References

1) A portion of this work has been published as a preliminary communication: T. Uyehara, J. Yamada, T. Kato, and F. Bohlmann, *Tetrahedron Lett.*, **24**, 4445 (1983). Part I in this series is Ref. 2.

2) T. Uyehara, J. Yamada, K. Ogata, and T. Kato, *Bull. Chem. Soc. Jpn.*, **58**, 211 (1985).

3) F. Bohlmann, U. Fritz, H. Robinson, and R. M. King, *Phytochemistry*, **18**, 1749 (1979).

4) Y. Ohta and Y. Hirose, *Tetrahedron Lett.*, **1968**, 1251.

5) See, for example, H. Prinzbach, H.-P. Bohm, S. Kagabu, V. Wessely, and H. V. Rivera, *Tetrahedron Lett.*, **1978**, 1243.

6) K. Ohno and J. Tsuji, *J. Am. Chem. Soc.*, **90**, 99 (1968).

7) J. C. Collins and W. W. Hess, *Org. Synth.*, **52**, 5 (1972).

8) J. A. Osborn and G. Wilkinson, *Inorg. Synth.*, **10**, 67 (1967).

9) E. J. Corey and A. V. Venkateswarlu, *J. Am. Chem. Soc.*, **84**, 6190 (1972).

10) J. L. Luche and J. C. Damiano, *J. Am. Chem. Soc.*, **102**, 7926 (1980).

11) R. S. Monson, "Advanced Organic Synthesis, METHODS and TECHNIQUES," Academic Press, New York (1971), p. 106.

12) G. Wittig and D. Wittenberg, *Justus Liebigs Ann. Chem.*, **606**, 1 (1957).

Digital Derivative Spectrophotometric Determination of Micro Amounts of Iron with 1,10-Phenanthroline

Tetsuo KATSUYAMA* and Junichi SHIDA†
Department of Basic Technology, Faculty of Engineering, Yamagata University, Yonezawa, Yamagata 992
†*Department of Applied Chemistry, Faculty of Engineering, Yamagata University, Yonezawa, Yamagata 992*
(Received February 16, 1984)

Digital first-order derivative spectrophotometry was applied to the determination of iron with 1,10-phenanthroline. Under the recommended conditions, a linear relationship was confirmed between the first-derivative value and the iron concentration. The present method gives accurate results for iron, ranging from 1.6×10^{-7} to 8×10^{-5} mol dm^{-3} (8.9 μg dm^{-3}—4.5 mg dm^{-3}). The relative standard deviations for the determination of 4.8×10^{-5}, 4.8×10^{-6}, and 4.8×10^{-7} mol dm^{-3} of iron(III) were 0.37, 0.38, and 0.93%, respectively. The effects of 63 diverse ions were examined. The present method was applied to the determination of iron in practical samples, *i.e.*, river water, waste water and sea water.

There are many reagents used in the spectrophotometric determination of iron.[1-4] Among these, 1,10-phenanthroline (phen) is the most widely used. A standard procedure is usually established and the effects of diverse ions are carefully examined.[5-7] The above-mentioned reagent is not highly sensitive.

Derivative spectrophotometry, which uses a derivative spectrum, is effective for increasing sensitivity.[8-13] In the work reported in this paper derivative spectrophotometry was introduced to make the determination more sensitive.

The methods for obtaining a derivative spectrum are divided into two groups, *i.e.*, optical and electrical. The optical group includes the dual-wavelength and wavelengh-modulation methods. The electrical group includes a shift-memory method, an analogue-differentiation method, and a digital-differentiation method.[14] These methods have their individual advantages and disadvantages. In analytical applications, the digital-differentiation method (using a computer) is of interest for several reasons. (1) Absorption-spectrum data are at first stored in the main memory of the computer. Thus, it is easy to calculate a derivative spectrum from the stored data. The *S/N* ratio of the derivative spectrum can be much improved by the use of smoothing treatments. (2) An exact derivative spectrum is derived (a distorted spectrum is obtained in the case of analogue method). (3) A calibration curve (derivative value *vs.* concentration) is linear and passes through the origin even if the wavelength interval for the differentiation becomes large. (4) After a measurement of the absorption spectrum, the final results of the analysis may be obtained automatically, since all calculations are performed by the computer. Thus, in this study the digital-differentiation method was adopted.

The present method can be applied to iron existing at one-hundredth of the concentration which can be determined by ordinary spectrophotometry with phen.

Experimental

Reagents. A 1×10^{-2} M (1 M=1 mol dm^{-3}) iron(III) solution was prepared by dissolving guaranteed reagent-grade iron(III) nitrate in dilute nitric acid. The solution was standardized by edta titration using Variamine Blue B as an indicator. This solution was diluted with 0.02 M nitric acid, as required.

A 2×10^{-3} M phen solution was prepared by dissolving a weighed amount of the reagent in 0.01-M nitric acid.

The other reagents used were of a guaranteed reagent grade.

Apparatus. The absorption spectra and their derivative spectra were measured with a Hitachi 228 double-beam spectrophotometer system. This system is composed of a photometer part and a personal computer equipped with a CRT (display part) and a mini-floppy disk. With this system, the derivative spectrum is obtained as follows. The absorption spectrum measured with the photometer part (spectrum data are stored in the computer memory) is differentiated on the personal computer from one to four times (corresponding to first to fourth derivative spectrum, respectively). The derivative-spectrum data are also stored in computer memory. Then, the derivative spectrum is displayed on a CRT and on the chart of the printer of the photometer part.

In the present system, the output signals from the photometer are fed to the personal computer through an 8-bit AD converter. After the absorption-spectrum data are stored in the main memory of the computer, a most appropriate derivative spectrum can be easily calculated from the data; *e.g.*, when the ordinate of the spectrum are not suitable, the calculation is done again while changing the scale of the ordinate. The length of the time at which the derivative spectrum is calculated and shown on the CRT and the peak-to-trough value of the spectrum is recorded on the printer, was 45 s. in the present conditions (485—600 nm). Thus, the present method can be used over a wide iron-concentration range (without altering the concentration) since the scale of the ordinate of the derivative spectrum can be easily changed.

The flow chart of the present computer program is shown in Fig. 1.

Standard Procedure. A sample solution containing from 8 nmol to 4 μmol of iron is placed in a 50-cm³ volumetric flask. Then, 5 cm³ of 0.5 M hydroxylamine hydrochloride, 8 cm³ of 2×10^{-3} M phen, 5 cm³ of 0.2 M acetic acid, and 5 cm³ of 0.2 M sodium acetate are successively added to the flask. Next, water is added up to the mark of the flask; the final pH is 4.4. The flask is kept for about thirty minutes in a water bath held (thermostatically) at 25 °C. The absorption spectrum of the solution is measured in a 10-mm cell against a reagent blank as the reference. Then, the first-order derivative spectrum is calculated at around 540 nm using wavelength intervals ($\Delta\lambda$) of 10 nm. The vertical distance from the base line to a trough of the spectrum, which is written on a chart, is then determined.

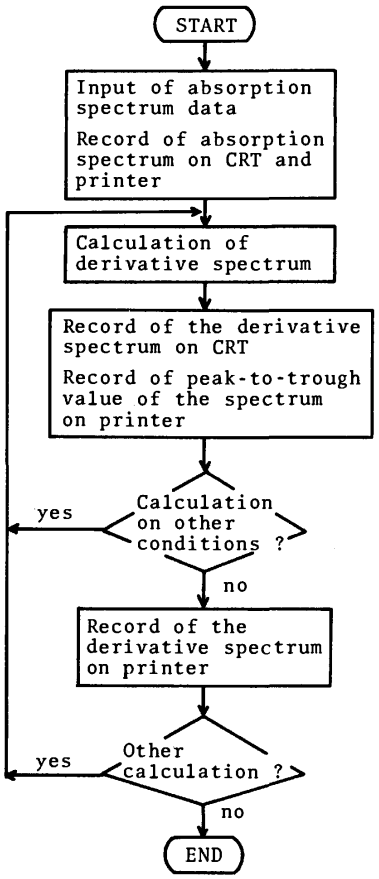

Fig. 1. Flow chart of the computer program for the derivative spectrum.

Results and Discussion

Derivative Spectrum. After the absorption spectrum of the Fe^{II}-phen complex solution was measured, the derivative spectra (first, second, third, and fourth order) were calculated from the measured absorption spectrum by use of the personal computer. Figure 2 shows a measured absorption spectrum and its first- and second-order derivative spectra (third- and fourth-order spectra are omitted). The value of the vertical distance between a peak and a trough of the derivative spectrum was greatest for a first-order derivative spectrum.

The value of the vertical distance from the base line to a trough (or a peak) of the derivative spectrum depended upon the value of $\Delta\lambda$, which can be selected between 1 to 10 nm in this program; the greater the value of $\Delta\lambda$, the longer the vertical distance (Fig. 3). Thus, in order to make the determination more sensitive, first-order derivative spectrophotometry was adopted and the value of $\Delta\lambda$ was set to 10 nm.

Reaction Time. In the color reaction, if the iron content is low, the time for a maximum color development may be long. In order to ascertain this point, the reaction time for the solution prepared by the above stated procedure was measured. When the

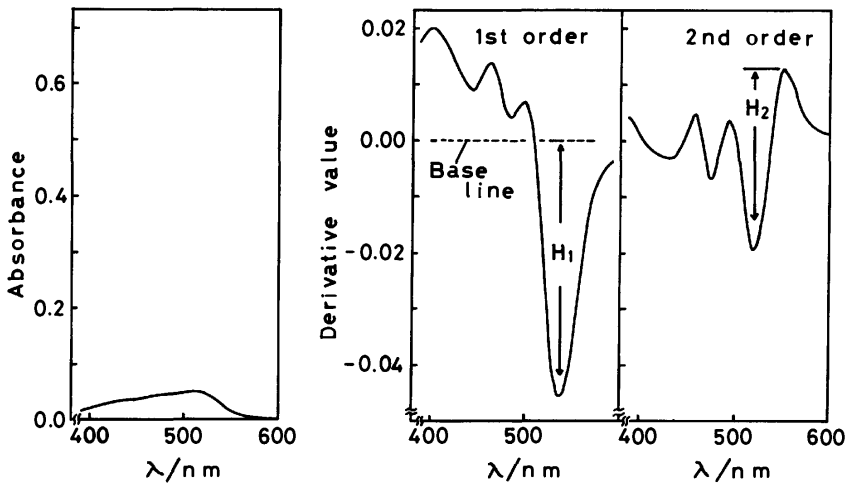

Fig. 2. Absorption spectrum and derivative spectra of Fe^{II}-phen complex solution.
Fe: 4.3×10^{-6} M, phen: 3.2×10^{-4} M, pH: 4.4, $\Delta\lambda$: 10 nm.
H_1 denotes the vertical distance from the base line to a trough of the first-order derivative spectrum and H_2 is the vertical distance between a peak and a trough of the second-order derivative spectrum.

iron content was 2 μmol, 0.2 μmol, and 0.02 μmol per 50 cm^3, the vertical distance from the base line to a trough of the first-order derivative spectrum did not vary for more than about twenty minutes at 25 °C, in respective cases. Thus, in this study, the standing time of the colored solution was set at thirty minutes for a temperature of 25 °C.

Calibration Curves. The first-order derivative spectrum of the Fe^{II}-phen complex solution at around 540 nm was recorded on a chart of the printer of the photometer by the stated standard procedure. The vertical distance from the base-line to a trough (*i.e.*, derivative value) was measured. The first-order derivative value *vs.* the iron concentration gave a straight line passing through the origin as shown in Fig. 4, where the recorder sensitivity was set so that the values of the derivatives, 1.0 in A, 0.1 in B, and 0.01 in C, gave a signal of 15 cm on the chart (full scale: 15 cm). The relative standard deviations of the first-order derivative values were 0.37, 0.38, and 0.93% for 4.8×10^{-5}, 4.8×10^{-6}, and 4.8×10^{-7} M of iron(III), respectively (11 measurements).

Effect of Diverse Ions. The effects of the 63 diverse ions were examined. The experiments were run as follows: a sample solution containing 0.202 or 0.0204 μmol of iron(III) was placed in a 50-cm^3 volumetric flask and then the ion in question was added to the flask; next, the stated standard procedure was applied.

In this study it was decided that the diverse ion concentrations for 500 times the concentration of iron should be sufficient to test for interference; *i.e.*, when this amount did not interfere, a furfher test was not undertaken. Diverse ions were added in the form of nitrate and sodium salt except for the following: K^+, Na^+, NH_4^+, Hg^{2+}, Sn^{2+}, As^{3+}, Sb^{3+}, Ce^{4+}, Sn^{4+}, Zr^{4+}, CN^-, IO_3^-, SCN^-, CrO_4^{2-}, $Cr_2O_7^{2-}$, $Mo_7O_{24}^{6-}$, and tartrate, which were added as KCl, NaCl, NH_4Cl, $HgCl_2$, $SnCl_2$, As_2O_3, $SbCl_3$, $CeSO_4$, $SnCl_4$, $ZrO(NO_3)_2$, KCN, KIO_3, NH_4SCN, K_2CrO_4, $K_2Cr_2O_7$, $(NH_4)_6Mo_7O_{24}$, and potassium sodium tartrate, respectively.

The results are summarized in Tables 1 and 2, from which it can be seen that in the determination of 4.04×10^{-6} M iron (Table 1) silver, mercury, molybdenum, and tungsten interfere with the determination when present at a concentration of 5 times that of iron, and that in the case of 4.08×10^{-7} M iron (Table 2), only mercury(II) ion interferes when present at a concentration of 5 times that of iron.

Determination of Iron in Practical Samples. Iron Ion in River Water: The water sample was collected at the Matsukawa river in Aioicho, Yonezawa, Yamagata (at August, 1983). It was instantly drawn through a membranefilter (pore size 0.45 μm), then, the determination of the iron ion of the filtrate was carried out using the stated standard procedure. The results are shown in Table 3.

Iron in Waste Water: Waste water included the following: (No. 1) water exhausted from the Faculty of Engineering, Yamagata University, and (No. 2) that from T electric company in Yonezawa, Yamagata. To these samples, concentrated hydrochloric acid was added (to become 0.1 M) to keep the iron ions from being adsorbed by the vessel.

Pretreatment of the waste water was done as follows. 100 cm^3 of the sample and 5 cm^3 of concen-

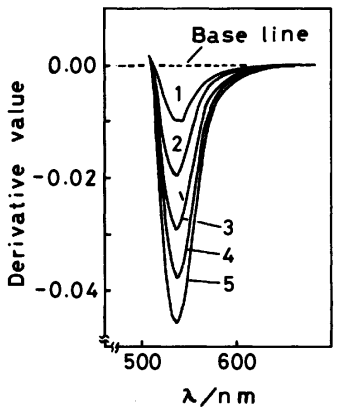

Fig. 3. Effect of $\Delta\lambda$ on the first-order derivative spectrum of Fe^{II}-phen complex solution.
Fe: 4.3×10^{-6} M, phen: 3.2×10^{-3} M, pH: 4.4.
1: $\Delta\lambda$=2, 2: $\Delta\lambda$=4, 3: $\Delta\lambda$=6, 4: $\Delta\lambda$=8, 5: $\Delta\lambda$=10.

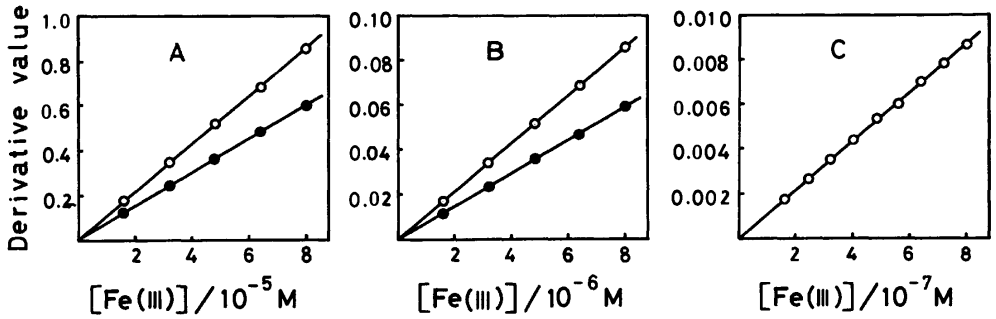

Fig. 4. Relationship between derivative value and iron(III) concentration.
phen: 3.2×10^{-4} M, pH: 4.4, reference: reagent blank, $\Delta\lambda$: 10 nm.
—○—: the results of first-order derivative spectrophotometry (base line-to-trough values are plotted).
—●—: the results of second-order derivative spectrophotometry (peak-to-trough values are plotted).[16]

Table 1. Effect of diverse ions on the determination of 4.04×10^{-6} M iron[a] at pH 4.4±0.1

Ion	Tolerable amount[b] added to 50 cm³ / μmol
K^+, Li^+, Na^+, NH_4^+, Rb^+, Tl^+, Ba^{2+}, Be^{2+}, Ca^{2+}, Mg^{2+}, Mn^{2+}, Pb^{2+}, Sr^{2+}, Al^{3+}, As^{3+} [c], Ce^{3+}, La^{3+}, Ce^{4+} [d], Zr^{4+} [e]	100
Th^{4+}	40
UO_2^{2+}, Zn^{2+}	20
Cd^{2+}, Cr^{3+}, Sb^{3+} [f]	10
Co^{2+}, Cu^{2+}, Ni^{2+}, Sn^{2+}, Sn^{4+}	4
Bi^{3+}	1
Ag^+	0.4
Hg_2^{2+}	0.2
Hg^{2+}	0.1
Br^-, CH_3COO^-, Cl^-, ClO_3^-, ClO_4^-, F^-, HSO_3^-, I^-, NO_2^-, NO_3^-, SCN^-, HPO_4^{2-}, SiO_3^{2-}, SO_4^{2-}, $S_2O_3^{2-}$, citric acid, tartrate, salicylate	100
IO_3^-, $HAsO_4^{2-}$	40
CN^-, CO_3^{2-}, $B_4O_7^{2-}$, oxalic acid	20
CrO_4^{2-}, $Cr_2O_7^{2-}$, $P_2O_7^{4-}$	4
$Mo_7O_{24}^{6-}$, WO_4^{2-}	0.4

a) Iron taken in 50 cm³ was 0.202 μmol. b) Tolerable amount was taken as that which caused an error of not more than 2%. c) pH: 4.0. d) pH: 3.8. e) pH: 4.2. f) pH: 2.8.

Table 2. Effect of diverse ions on the determination of 4.08×10^{-7} M iron[a] at pH 4.4±0.1

Ion	Tolerable amount[b] added to 50 cm³ / μmol
K^+, Li^+, Na^+, NH_4^+, Rb^+, Tl^+, Ba^{2+}, Be^{2+}, Ca^{2+}, Cd^{2+}, Mg^{2+}, Mn^{2+}, Pb^{2+}, Sr^{2+}, Zn^{2+}, Al^{3+}, As^{3+}, Ce^{3+}, La^{3+}, Ce^{4+}, Th^{4+}, Zr^{4+}	10
Sn^{4+}, UO_2^{2+}	4
Cu^{2+}, Ni^{2+}, Sn^{2+}, Cr^{3+}, Sb^{3+} [c]	2
Co^{2+}	1
Ag^+, Bi^{3+}	0.4
Hg_2^{2+}	0.1
Hg^{2+}	0.04
Br^-, CH_3COO^-, Cl^-, ClO_3^-, ClO_4^-, CN^-, F^-, HSO_3^-, I^-, IO_3^-, NO_2^-, NO_3^-, SCN^-, CO_3^{2-}, $HAsO_4^{2-}$, HPO_4^{2-}, SiO_3^{2-}, SO_4^{2-}, $S_2O_3^{2-}$, citric acid, oxalic acid, tartrate, salicylate	10
$B_4O_7^{2-}$, $P_2O_7^{4-}$	4
CrO_4^{2-}	1
$Cr_2O_7^{2-}$, $Mo_7O_{24}^{6-}$	0.4
WO_4^{2-}	0.2

a) Iron(III) taken in 50 cm³ was 0.0204 μmol. b) Tolerable amount was taken as that which caused an error of not more than 4%. c) pH: 4.2.

Table 3. Determination of iron ion in river water

Sample taken in 50 cm³ / cm³	(A) Iron added to 50 cm³ / nmol	(B) Iron found in 50 cm³ / nmol	(B)—(A)	Iron concentration in sample / mol dm⁻³
20.00	0	17.9	17.9	9.0×10^{-7} (50 ppb)
20.00	0	17.7	17.7	8.9×10^{-7} (50 ppb)
20.00	0	17.9	17.9	9.0×10^{-7} (50 ppb)
20.00	0	17.7	17.7	8.9×10^{-7} (50 ppb)
20.00	17.2	34.9	17.7	8.9×10^{-7} (50 ppb)
20.00	17.2	34.9	17.7	8.9×10^{-7} (50 ppb)

trated nitric acid was added to a 250-cm³ porcelain dish. The solution was concentrated to about 10 cm³ on a boiling-water bath. Then, 5 cm³ of concentrated nitric acid and 10 cm³ of concentrated perchloric acid were added. The solution was then heated on a hot plate until white fumes of pherchloric acid were produced. After this, the solution was cooled to room temperature, was transfered to a 100-cm³ volumetric flask and water was added up to the mark of the flask.

The determination of the iron was performed by the standard procedure, using 5 cm³ of the prepared solution. In the determination, however, 4 cm³ of 2-M sodium acetate was added in order to adjust the pH to 4.4. The analyses were run three times, starting from the pretreatment of the waste water. The results are shown in Table 4.

Iron in Sea Water: Sea water was collected at Ishinomaki bay. The collection was done at a place 200-m from the beach in Nobiru, Naruse, Miyagi. The sea water was placed in a polyethylene vessel and concentrated hydrochloric acid was added (to become 0.03 M).

4 cm³ of concentrated hydrochloric acid was added to 500 cm³ of the sea water. Then, the sea water was concentrated to about 80 cm³ on a boiling-water bath (using porcelain dish). Infrared heating was used simultaneously. After cooling, the solution was transfered to a 100-cm³ volumetric flask and then water was added up to the mark of the flask. The determination of iron was carried out by the standard procedure, using 20 cm³ of the prepared solution. In the determination, 11 cm³ of 2-M sodium acetate was added as a buffering agent. The results are shown in Table 5.

The waste water and the sea water were also ana-

TABLE 4. DETERMINATION OF IRON IN WASTE WATER

Sample number	Sample taken in 50 cm^3	Iron found in 50 cm^3	Iron concentration in waste water	Iron concentration by atomic absorption method
	cm^3	nmol	mol dm^{-3}	mol dm^{-3}
	5.00	46.6	9.3×10^{-6} (0.52 ppm)	
No. 1	5.00	45.7	9.1×10^{-6} (0.51 ppm)	9.1×10^{-6} (0.51 ppm)
	5.00	47.5	9.5×10^{-6} (0.53 ppm)	
	5.00	18.8	3.8×10^{-6} (0.21 ppm)	
No. 2	5.00	16.1	3.2×10^{-6} (0.18 ppm)	3.6×10^{-6} (0.20 ppm)
	5.00	19.7	3.9×10^{-6} (0.22 ppm)	

TABLE 5. DETERMINATION OF IRON IN SEA WATER

Sample taken in 50 cm^3	Iron found in 50 cm^3	Iron concentration in sample	Iron concentration in sea water	
			mol dm^{-3}	
cm^3	nmol	mol dm^{-3}	Present method	Atomic absorption method
20.00	193	9.7×10^{-6} (0.54 ppm)	1.9×10^{-6} (0.11 ppm)	
20.00	193	9.7×10^{-6} (0·54 ppm)	1.9×10^{-6} (0.11 ppm)	1.8×10^{-6} (0.10 ppm)
20.00	183	9.2×10^{-6} (0.51 ppm)	1.8×10^{-6} (0.10 ppm)	

lyzed for iron by atomic-absorption spectrometry (Tables 4 and 5).[15] The results agreed with those in the present method.

Characteristics of the Present Method. The base line of the absorption spectrum sometimes moved from the zero line. However, the shift of the base line of the first-order derivative spectrum from the zero line was not seen; thus, the calibration curves passed through the origin even in the case of a low iron-ion concentration as shown in Fig. 4.

In ordinary spectrophotometry, a variation of the zero point influences the results. In the present method, the results were not influenced by the deviation of the base line of the absorption spectrum. This is considered to be attributed to the fact that a determination by the derivative method does not depend directly on the absorbance (of the absorption spectrum) but mainly on the shape of the spectrum. Consequently, a derivative value may be magnified without error.

The iron ion of $1.6—8\times10^{-7}$ M (0.009—0.045 mg dm^{-3}) could be determined by the present method; this concentration level is one-hundredth of the concentration $1.6—8\times10^{-5}$ M (0.9—4.5 mg dm^{-3}) which is presented to the ordinary spectrophotometry with phen. The procedures of the present method are not complicated; thus the ppb level of an iron ion (10—50 μg dm^{-3}) can be easily determined by the present method. The concentration of iron ions in ordinary spectrophotometry when using a highly sensitive reagent, *e.g.*, 4,7-diphenyl-1,10-phenanthroline (ε of iron(II) complex: 22400 l mol^{-1} cm^{-1} at 533), 2,4,6-tris(2-pyridyl)-*s*-triazine (ε of iron(II) complex: 22600 l mol^{-1} cm^{-1} at 593) is more than about 0.1 mg dm^{-3};[4] thus, the present method can be said to be very sensitive.

References

1) "Zikken Kagaku Koza," 3rd ed, ed by the Chemical Society of Japan, Maruzen, Tokyo (1966), Vol. 15, Part II, p. 268.

2) "Shin Zikken Kagaku Koza," ed by the Chemical Society of Japan, Maruzen, Tokyo (1976), Vol. 9, Part I, p. 331.

3) "Bunseki Kagaku Binran," 2nd ed, ed by the Japan Society for Analytical Chemistry, Maruzen, Tokyo (1971), p. 102.

4) "Muki Oyo Hishoku Bunseki," Kyoritsu Shuppan, Tokyo (1974), Vol. 2, p. 323.

5) W. B. Fortune and M. G. Mellon, *Ind. Eng. Chem. Anal. Ed.*, **10**, 60 (1938).

6) J. O. Hibbits, W. F. Davis, and M. R. Meuke, *Talanta*, **8**, 163 (1961).

7) T. Hattori and T. Kuroha, *Bunseki Kagaku*, **11**, 727 (1962).

8) H. Ishii and T. Odashima, *Bunseki Kagaku*, **29**, 558 (1980).

9) H. Ishii and H. Koh, *Nippon Kagaku Kaishi*, **1980**, 203.

10) G. Talsky, S. G. Maler, and H. Betz, *Mikrochim. Acta*, **2**, 1 (1981).

11) H. Ishii, T. Odashima, and T. Imamura, *Analyst*, **107**, 885 (1982).

12) H. Ishii, K. Satoh, Y. Satoh, and H. Koh, *Talanta*, **29**, 545 (1982).

13) Y. Mori, S. Naito, and H. Matsushita, *Bunseki Kagaku*,

31, 663 (1982).
14) M. Furukawa and S. Shibata, *Bunseki*, **1980**, 608.
15) A Hitachi model 180-80 polarized Zeeman atomic absorption spectrophotometer was used.
16) Peak-to-trough values of the second-order derivative spectrum *vs.* the iron concentration also gave a straight line passing through the origin.

The Synthesis and X-Ray Structure of (L- or D-Alanine-*N*-acetato)(L-histidinato)chromium(III)

Mitsunobu SATO,[1] Masao KOSAKA, and Masatoshi WATABE*
Kogakuin University, Hachioji, Tokyo 192
(Received April 12, 1984)

The (L-alanine-*N*-acetato)(L-histidinato)chromium(III) monohydrate complex, $C_{11}H_{14}N_4O_6Cr$, has been synthesized and its crystal structure has been determined from three dimensional X-ray-diffractometer data. The crystals are orthorhombic, of the space group $P2_12_12_1$, with 4 molecules in a cell with these dimensions: a= 11.052(1), b=13.959(3), and c=9.616(2) Å. Block-diagonal least-squares refinements using 1318 independent nonzero reflections have yielded a conventional R factor of 0.033. The structure consists of monomeric [Cr(L-alama)(L-his)] units and water molecules. The L-alama ligand coordinates to the metal as of dianion, with Cr-O(acetyl), Cr-N, and Cr-O(alanine) bond lengths of 1.960(3), 2.078(5), and 1.946(4) Å respectively. The histidinate monoanion coordinates through Cr-N(amino), Cr-N(imidazole), and Cr-O bonds 2.062(4), 2.036(5), and 1.957(4) Å long respectively. The geometry at chromium is a distorted octahedron, with *cis* bond angles in the range from 80.1(2) to 99.3(2)°. Among the six possible isomers of the [Cr(L-alama)(L-his)] complex, only one isomer was prepared and crystallized; its geometry was R-L-*trans*(*O*)*cis*(*N*).

Chromium has been shown to be an essential trace element, and the hypothetical chromium(III) complex occurring in brewers yeast has been found to have outstanding biological activity.[2] Efforts to purify this factor have led to the detection of chromium, nicotinic acid, glycine, glutamic acid, and cysteine in the purified fraction.[3] Several chromium(III) complexes containing amino carboxylate have been studied.[4-6] In these reports, the monomeric tris(aminocarboxylato)complexes have been reported to have only a facial configuration. While Israily claimed the preparation of the purple meridional isomer of [Cr(gly)$_3$] (gly=glycinate ion), Gillard *et al.* showed this complex to be a dinuclear complex, [Cr(OH)$_2$(gly)$_2$]$_2$ 6H$_2$O.[5] Oki *et al.* reported a number of facial and dihydroxo-bridged dimeric (amino carboxylato)chromium(III) complexes, but their attempt at the preparation of meridional tris(amino carboxylato)chromium(III) was unsuccessful.[6] We ourselves reported the preparation of a mixed (tridentate-aminocarboxylato)chromium(III) complex[7] in the form of the [Cr(L- or D-asp)(L-his)] complex, where asp=aspartate ion and his=histidinate ion. These isomers were tentatively assigned meridional and facial structures by using the resemblance of the CD spectra and high-speed liquid chromatograms of [Cr(L- or D-asp)(L-his)] to those of [Co(L- or D-asp)(L-his)]. However, some ambiguity remains in this structural assignment because of the lack of X-ray crystallographic data. Attempts to grow crystals suitable for X-ray structural analysis were unsuccessful for the [Cr(L- or D-asp)(L-his)] complexes. This report will deal with the preparation and the assignment of [Cr(L- or D-alama)(L-his)], where alama=alanine-*N*-acetate dianion, which belongs to the same [Cr(N)$_3$(O)$_3$] type as that of [Cr(L- or D-asp)(L-his)]. As is shown in Fig. 1, this complex has six possible isomers for each L- or D-alama series because of two factors: the (S) or (R) chirality concerning the asymmetric imino nitrogen atom of alama, which occurs after coordination,[8] and the distribution of coordinated atoms (two meridional isomers and one facial isomer).

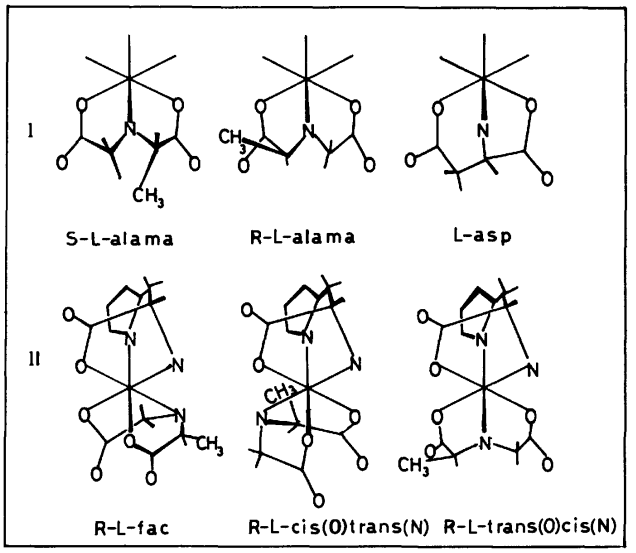

Fig. 1. I; (S) and (R) chirality of L-alama, and L-asp coordinated. II; Three possible R-type geometrical isomers of [Cr(L-alama)(L-his)]. Those of S-type are abbriviated.

Experimental

Isomers of [Cr(L- or D-alama)(L-his)]. To a concentrated ammonia solution (7 cm^3) we added $K_2Cr_2(SO_4)_4 \cdot 24H_2O$ (10 g, 0.01 mol). The precipitate was centrifuged and then suspended in 50 cm^3 of water. To this suspension we then added L-histidine (0.01 mol) and L-alanine-*N*-acetic acid (0.01 mol). After the suspension had been stirred and heated (*ca.* 80 °C) for 1 h, it was centrifuged and cooled to room temperature. One fourth of this solution was placed in a column (5×50 cm) of SP-Sephadex A-25, a strong-anion exchange resin, which was on the chloride form. The complexes in the column were eluted with water slowly. Three

bands descended; the last one contained the neutral species, which was, after having been concentrated and crystallized under room temperature, named *L*. The complex containing D-alanine-*N*-acetate was prepared in a similar way but using D-alanine-*N*-acetic acid instead of L-alanine-*N*-acetic acid; it was named *D*. Anal. Calcd for $[CrC_{11}H_{14}N_4O_6]\cdot H_2O$: C, 35.78; H, 4.64; N, 15.17%, Found (*L*): C, 35.44; H, 4.69; N, 15.24%, Found (*D*): C, 35.32; H, 4.55; N, 14.90%.

Measurements. The visible and ultraviolet absorption spectra were measured with a JASCO UVIDEC-505 spectrometer in an aqueous solution.

Data Collection. The specimens are well-developed orange-yellow prismatic crystals. A crystal with approximate dimensions of 0.20×0.23×0.33 mm was mounted on a Rigaku four-circle automatic diffractometer, AFC-6B, with its elongated axis roughly parallel to the machine axis. Automatic centering and the indexing of 23 low-angle reflections gave the preliminary conditions for data collection. Peak refinement, by which the precise cell parameters was obtained, was performed by the least-squares treatment of the 2θ values of 25 reflections measured with graphite-monochromated Mo $K\alpha_1$ radiation (λ=0.70926 Å). At this point it was clear that the crystal had an orthorhombic symmetry, with a=11.052(1) Å, b=13.959(3) Å, c=9.616(2) Å, and Z=4. Additionally, subsequent measurements of several reflections in order to examine the systematic absences suggested that the crystal belongs to the $P2_12_12_1$ space group. This result was confirmed after the data collection. With Z=4 and the molecular weight of this complex, the calculated density is 1.65 g cm^{-3}, compared with the measured density of 1.64 g cm^{-3} obtained by flotation in a 1,2-dibromoethane-carbontetrachloride mixture. The ω (2θ<30°) and 2θ–ω (2θ>30°) scan methods were employed with a scanning rate of 1°/min. A unique data set (*hkl*) was first collected in the range of $5<2\theta<55$. In order to examine the absolute configuration of the ligands, the Bijvoet-pair data set (*hkl*), with 2θ values between 17° and 27°, was then collected under the same conditions. Three standard reflections were monitored every 50 reflections; they showed only a 1—2% random variation in intensity, for which no correction was made. A total of 1472 reflections was measured, and the standard Lorentz and polarization corrections were applied. The final data set, consisting of 1472 reflections, indicated the systematic extentions of (*h*00) for *h* odd, (0*k*0) for *k* odd, and (00*l*) for *l* odd. Since the compound is optically active, the space group of the crystal was defined as $P2_12_12_1$. Of the 1472 reflections collected, 1318 had $F_o>10[\sigma(F_o)]$ and were used in the subsequent analysis. No absorption correction was made, since the μ value (7.9 cm^{-1}) was low.

Solution and Refinement of the Structure. The structure was solved by a standard heavy-atom method and refined by the block-diagonal least-squares method by the use of the Rigaku RASA SAP-2 system. An unsharpened three-dimensional Patterson function revealed the position of the chromium atom. The positions of the remaining nonhydrogen atoms were determined by successive structure-factor and electron-density-map calculations. Isotropic refinement reduced R=0.135 and R'=0.163, where $R=\Sigma||F_o|-|F_c||/|F_o|$ and $R'=(\Sigma(|F_o|-|F_c|)^2/|F_o|^2)^{1/2}$. The absolute configuration of the ligands in the complex ion was taken to be the *L* isomer. Next, the effects of the anomalous dispersion were introduced into F_c, the values of f' and f'' for Cr, O, N, and C being taken from Ref. 9. The anisotropic refinement of all the nonhydrogen atoms was performed, allowing the hydrogen atoms to vibrate isotropically. The final agreement factors, R and R', are 0.033 and 0.040 respectively. A final difference Fourier synthesis showed no significant electron density with a peak higher than 0.2 e Å.$^{-3}$ In this case, the absorption-edge technique was not sufficient to confirm the absolute configuration of the ligands; rather, the Hamilton test described above was useful.[11] The final positional parameters, along with their standard deviations, are listed in Table 1. Compilations of the anisotropic thermal parameters and of the observed and calculated structure factors are available.

Results and Discussion

Description of the Molecular Structure. The geometry of the complex is shown in Fig. 2. The coordination around the chromium(III) center is approximately octahedral, the ligand binding as the histidinate monoanion and the L-alanine-*N*-acetate dianion. The geometry of this complex was determined to be R-L-*trans*(*O*)*cis*(*N*), where R means that the chirality of the asymmetric nitrogen atom of alama is R, where L means that this complex contains L-alama, and where *trans*(*O*)*cis*(*N*) means that the coordinated oxygen atom of L-his and that of the $-CH_2COO-$ of L-alama are trans to each other (as is shown in Fig. 1, the $-CH_2COO-$ ring of L-alama corresponds to the amino acid moiety of L-asp), and the nitrogen atom of $NH_2CH(COO^-)R$ of L-his and that of L-alama are *cis* to each other. Each conformation of the four chelate rings is also presented in Fig. 3. References to chromium(III) complexes with histidine are scant, consisting of one preliminary report,[12] and one doctoral dissertation by Grouhi-Witte.[13] The histidinate ion coordinates to metal through the imidazole [N(1)] and amine [N(3)] nitrogen atoms and through a carboxyl oxygen atom [O(1)] with bond lengths of 2.036(5), 2.062(4), and 1.957(4) Å respectively. It is noted that the bond lengths of the Cr–N(amino) and Cr–O of this complex are comparable to those of [Cr(gly)$_3$] (2.068 Å for Cr–N(amino), 1.965 Å for Cr–O)[14] and that the bond lengths of Cr–N(imidazole) (2.036(5) Å) and Cr–N(amino) (2.062(4) Å) of the histidinate ligand in the present complex are longer than the corresponding bond lengths of [Co(L-his)(L-pen)],[15] where pen represents the penicilaminate ion, 1.933(3) and 1.925(3) Å respectively. The bond angles subtended the histidinate ligand at chromium N(3)–Cr–O(1)= 80.1(2)°, N(1)–Cr–N(3)=87.2(2)° and O(1)–Cr–N(1)= 89.5(2)°; the smallest angle corresponds to the smallest five-membered ring. The N(3)–Cr–O(1) bond angle, 80.1(2)°, is comparable to that of [Cr(gly)$_3$], which has an average value of 81.8°.[14] The L-alama ion, which is deprotonated at the two carboxyl ends, is coordinated to the metal through the oxygen

TABLE 1. FINAL POSITIONAL PARAMETERS AND THEIR ESTIMATED STANDARD DEVIATIONS (IN PARENTHESES)[a]

Atom	*X*	*Y*	*Z*	Atom	*X*	*Y*	*Z*
Cr	2935.8 (7)	2345.2 (5)	2294.2 (10)	C (9)	3504 (6)	2125 (5)	−1475 (7)
O (1)	3946 (3)	1309 (2)	1565 (4)	C (10)	2695 (5)	4166 (4)	859 (7)
O (2)	5484 (4)	355 (3)	2030 (5)	C (11)	2030 (5)	4220 (3)	2213 (7)
O (3)	1542 (3)	1934 (3)	1208 (4)	O (7)	1647 (4)	6427 (3)	678 (5)
O (4)	816 (3)	1794 (3)	−931 (5)	H (1)	502 (4)	297 (3)	294 (6)
O (5)	2106 (3)	3477 (2)	3031 (4)	H (2)	440 (5)	297 (4)	426 (6)
O (6)	1474 (4)	4941 (3)	2523 (5)	H (3)	401 (5)	329 (4)	41 (6)
N (1)	2462 (4)	1494 (3)	3924 (5)	H (4)	565 (6)	367 (5)	622 (7)
N (2)	1344 (5)	549 (3)	5214 (6)	H (5)	294 (6)	2 (4)	634 (6)
N (3)	4523 (3)	2621 (3)	3346 (5)	H (6)	3 (8)	464 (6)	497 (10)
N (4)	3210 (3)	3205 (3)	556 (5)	H (7)	484 (7)	91 (5)	508 (9)
C (1)	1343 (5)	1182 (4)	4155 (7)	H (8)	577 (4)	166 (3)	380 (6)
C (2)	2538 (6)	429 (4)	5605 (7)	H (9)	739 (10)	144 (7)	146 (12)
C (3)	3216 (5)	1035 (3)	4839 (6)	H (10)	174 (8)	534 (6)	524 (9)
C (4)	4559 (5)	1226 (4)	4903 (8)	H (11)	354 (6)	449 (5)	105 (8)
C (5)	5079 (4)	1677 (4)	3591 (7)	H (12)	424 (7)	240 (5)	−185 (8)
C (6)	4853 (4)	1050 (3)	2305 (7)	H (13)	312 (6)	179 (4)	−223 (7)
C (7)	2610 (5)	2739 (4)	−652 (6)	H (14)	422 (8)	153 (6)	−101 (10)
C (8)	1568 (4)	2112 (3)	−107 (7)				

a) The values have been multiplied by 10^4 for the non-hydrogen atoms and by 10^3 for the hydrogen atoms.

FINAL THERMAL PARAMETERS ($\times 10^4$) AND THEIR ESTIMATED STANDARD DEVIATIONS (IN PARENTHESES)[a]

Atom	β_{11}	β_{22}	β_{33}	β_{12}	β_{13}	β_{23}
Cr	32.8 (4)	26.3 (3)	58.4 (14)	−1.4 (4)	−2.0 (9)	3.0 (6)
O (1)	48 (3)	33 (2)	61 (7)	1 (2)	−1 (4)	−9 (3)
O (2)	74 (4)	52 (2)	93 (8)	28 (2)	−3 (5)	−2 (3)
O (3)	46 (3)	45 (2)	60 (7)	−9 (2)	−8 (4)	11 (3)
O (4)	55 (3)	69 (3)	77 (8)	−13 (3)	−26 (5)	−1 (4)
O (5)	61 (3)	37 (2)	64 (7)	8 (2)	16 (4)	10 (3)
O (6)	113 (4)	44 (2)	123 (8)	31 (3)	48 (6)	17 (4)
N (1)	47 (3)	33 (2)	62 (9)	3 (2)	16 (5)	6 (3)
N (2)	76 (4)	37 (2)	83 (9)	−7 (3)	10 (6)	18 (4)
N (3)	38 (3)	35 (2)	71 (8)	−4 (2)	−2 (4)	−11 (4)
N (4)	42 (3)	34 (2)	24 (8)	−2 (2)	−2 (4)	0 (3)
C (1)	48 (4)	40 (3)	81 (11)	−3 (3)	6 (6)	7 (5)
C (2)	85 (6)	40 (3)	58 (11)	2 (4)	−2 (7)	10 (5)
C (3)	65 (5)	29 (2)	39 (10)	9 (3)	5 (6)	1 (4)
C (4)	57 (5)	52 (3)	73 (11)	12 (3)	0 (6)	14 (5)
C (5)	32 (3)	45 (3)	58 (11)	6 (3)	−11 (5)	−7 (4)
C (6)	41 (4)	34 (2)	74 (10)	2 (2)	10 (6)	−5 (4)
C (7)	57 (4)	38 (3)	34 (9)	2 (3)	−15 (5)	0 (4)
C (8)	36 (4)	33 (3)	86 (11)	4 (3)	−9 (6)	−6 (4)
C (9)	73 (5)	63 (4)	54 (11)	−4 (4)	11 (7)	−15 (5)
C (10)	84 (6)	27 (2)	79 (11)	−5 (3)	28 (7)	4 (4)
C (11)	52 (4)	33 (2)	77 (10)	−1 (3)	9 (7)	6 (4)
O (7)	101 (4)	48 (2)	92 (8)	20 (3)	−7 (5)	14 (3)

a) Parameters have the form: $\exp[-(\beta_{11}h^2+\beta_{22}k^2+\beta_{33}l^2+2\beta_{12}hk+2\beta_{13}hl+2\beta_{23}kl)]$.

of the alaninate moiety (*O*-ala), the oxygen of the acetate moiety (*O*-ace), and imino nitrogen (*N*-imino) atoms, with bond lengths of 1.960(3), 1.947(4), and 2.078(5) Å respectively. These distances can be compared to the average (Cr-O) distance of 1.965 Å and the average (Cr-N) distance of 2.086 Å found in [Cr(gly)$_3$].[14] The bond angles of L-alama at chromium are 81.6(2)° for O(3)-Cr-N(4), 83.9(2)° for O(5)-Cr-N(4), and 93.5(2)° for O(3)-Cr-O(5). The bond angles of five-membered chelate rings can also be compared to those of [Cr(gly)$_3$], 81.8° on the average.[14] The intramolecular bond distances and angles are

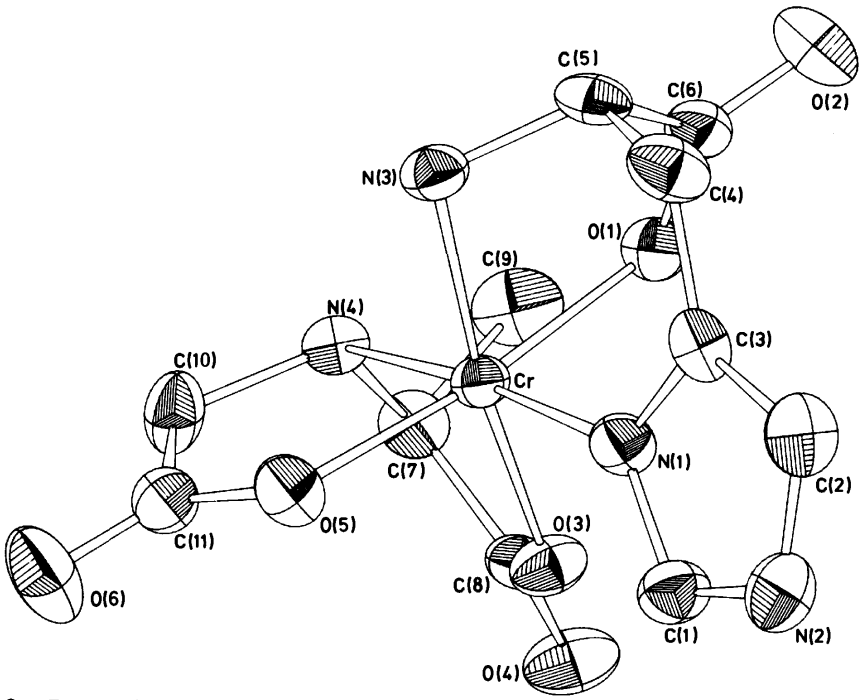

Fig. 2. Perspective drawing of the complex molecule [Cr(L-alama)(L-his)] and the numbering scheme for the atoms.

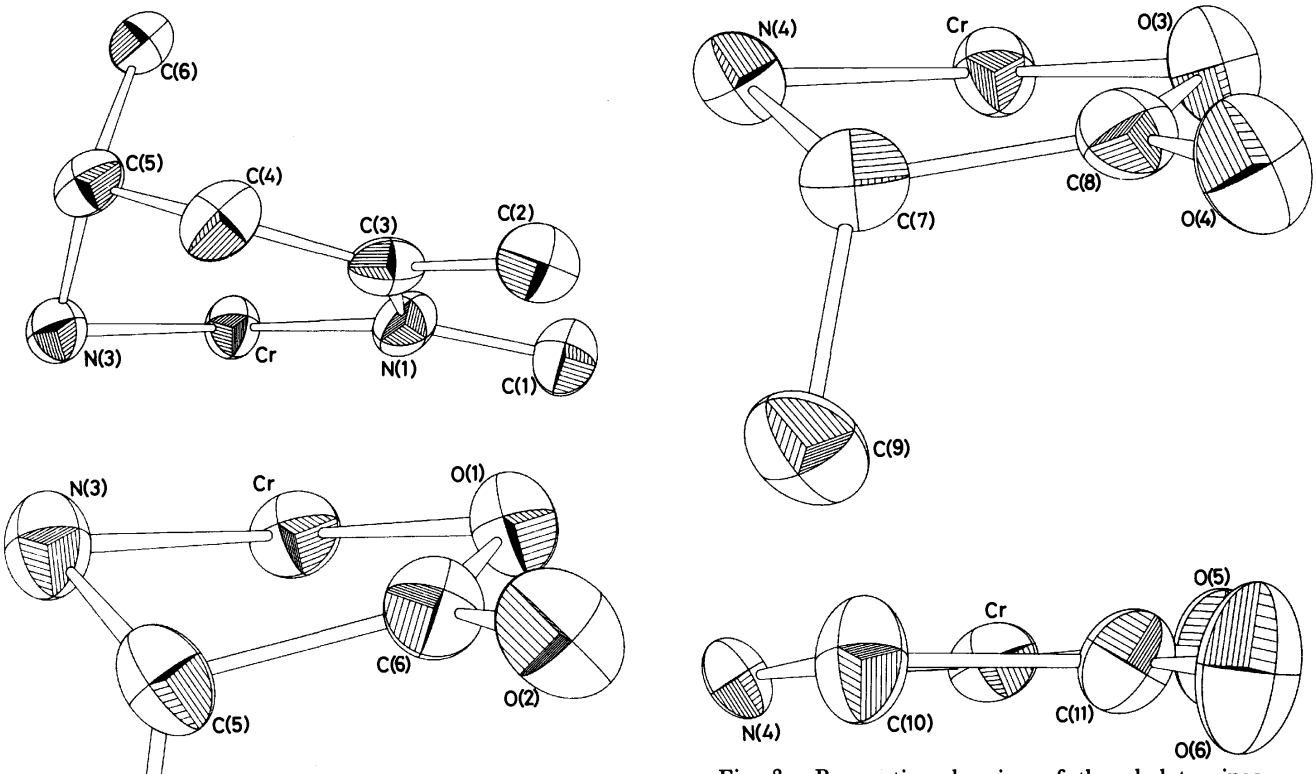

Fig. 3. Perspective drawing of the chelate rings.

summarized in Tables 2 and 3.

Description of the Unit Cell. A stereoview of the contents of one unit cell is presented in Fig. 4. The unit cell consists of 4 complex molecules and 4 waters of crystallization. Selected intermolecular interactions

TABLE 2. BOND DISTANCES (l/Å) AND THEIR ESTIMATED STANDARD DEVIATIONS (IN PARENTHESES)

Cr-O (1)	1.957 (4)	C (2)-C (3)	1.349 (8)
Cr-O (3)	1.947 (4)	C (3)-C (4)	1.509 (8)
Cr-O (5)	1.960 (3)	C (4)-C (5)	1.523 (9)
Cr-N (1)	2.036 (5)	C (5)-C (6)	1.535 (9)
Cr-N (3)	2.062 (4)		
Cr-N (4)	2.078 (5)	C (7)-C (8)	1.538 (7)
		C (7)-C (9)	1.528 (8)
N (1)-C (1)	1.329 (7)		
N (1)-C (3)	1.371 (7)	C (10)-C (11)	1.497 (9)
N (2)-C (1)	1.348 (8)		
N (2)-C (2)	1.383 (8)		
N (3)-C (5)	1.474 (7)		
N (4)-C (7)	1.488 (7)		
N (4)-C (10)	1.486 (7)		
O (1)-C (6)	1.281 (7)		
O (2)-C (6)	1.223 (6)		
O (3)-C (8)	1.289 (8)		
O (4)-C (8)	1.231 (7)		
O (5)-C (11)	1.304 (6)		
O (6)-C (11)	2.217 (6)		

TABLE 3. BOND ANGLES (ϕ/°) AND THEIR ESTIMATED STANDARD DEVIATIONS (IN PARENTHESES)

O(1)-Cr-O(3)	92.4(2)	Cr-O(1)-C(6)	117.1(4)
O(1)-Cr-O(5)	173.0(2)	O(1)-C(6)-O(2)	123.3(6)
O(1)-Cr-N(1)	89.5(2)	O(1)-C(6)-C(5)	114.5(4)
O(1)-Cr-N(3)	80.1(2)	O(2)-C(6)-C(5)	122.2(5)
O(1)-Cr-N(4)	93.2(2)		
O(3)-Cr-O(5)	93.5(2)	Cr-N(3)-C(5)	105.4(3)
O(3)-Cr-N(1)	92.2(2)	N(3)-C(5)-C(4)	110.2(5)
O(3)-Cr-N(3)	172.5(2)	N(3)-C(5)-C(6)	108.3(5)
O(3)-Cr-N(4)	81.6(2)		
O(5)-Cr-N(1)	94.1(2)	Cr-O(3)-C(8)	116.9(3)
O(5)-Cr-N(3)	94.0(2)	O(3)-C(8)-O(4)	123.2(5)
O(5)-Cr-N(4)	83.9(2)	O(3)-C(8)-C(7)	117.4(5)
N(1)-Cr-N(3)	87.2(2)	O(4)-C(8)-C(7)	119.4(6)
N(1)-Cr-N(4)	173.3(2)		
N(3)-Cr-N(4)	99.3(2)	Cr-O(5)-C(11)	117.0(4)
		O(5)-C(11)-O(6)	122.9(6)
Cr-N(1)-C(1)	124.0(4)	O(5)-C(11)-C(10)	117.0(4)
Cr-N(1)-C(3)	127.6(3)	O(6)-C(11)-C(10)	120.2(5)
N(1)-C(1)-N(2)	109.9(5)		
N(1)-C(3)-C(2)	107.8(5)	Cr-N(4)-C(7)	108.1(3)
N(1)-C(3)-C(4)	122.8(5)	Cr-N(4)-C(10)	108.0(3)
C(1)-N(1)-C(3)	107.8(5)	N(4)-C(7)-C(8)	108.4(5)
N(2)-C(2)-C(3)	107.7(5)	N(4)-C(7)-C(9)	111.2(4)
C(1)-N(2)-C(2)	106.6(5)	N(4)-C(10)-C(11)	113.8(4)
C(2)-C(3)-C(4)	129.4(6)	C(7)-N(4)-C(10)	112.1(4)
C(3)-C(4)-C(5)	114.3(5)	C(8)-C(7)-C(9)	109.9(4)
C(4)-C(5)-C(6)	111.7(4)		

are listed in Table 4. The hydrogen bond of the O-H···O type probably exists between the O(3) atom

TABLE 4. SELECTED INTERMOLECULAR INTERACTIONS

A	B	Distance/Å	Position of B
O (1)	N (3)	2.92	$1/2-x, -y, -1/2+z$
O (2)	N (3)	2.95	$1/2-x, -y, -1/2+z$
O (3)	O (7)	2.90	$1/2-x, 1-y, 1/2+z$
O (4)	N (2)	2.85	$-1/2+x, 1/2-y, -z$
O (4)	N (4)	2.90	$-1/2+x, 1/2-y, -z$
O (6)	O (7)	2.74	x, y, z

of L-alama and the water O(7) atom, the O-O distance being 2.90 Å. In the same manner, the O(6) atom of L-alama is also linked to the water O(7) atom at a distance of 2.74 Å. The N(3) atom of the L-histidine residue is associated with the O(1) and O(2) atoms of the other molecule by an N-H···O hydrogen bond at distances of 2.92 and 2.95 Å respectively. The O(4) atom of L-alama is linked to the N(2) atom of the neighboring imidazole ring and the coordinated N(4) atom in the same manner, the O-N distances being 2.85 and 2.90 Å respectively. These interactions probably assist in the formation of the stable crystal structure.

Absorption Spectra. The absorption spectra of [Cr(L- or D-alama)(L-his)] are shown in Fig. 5, along with the spectra of [Cr(L- or D-asp)(L-his)]. As for [Cr(L-alama)(L-his)], the two major peaks in the visible region are identified as $^4A_{2g} \rightarrow {}^4T_{2g}(F)$ for the 580-nm transition and $^4A_{2g} \rightarrow {}^4T_{1g}$ for the 370-nm transition. For the whole series of $[Co(O)_n(N)_{6-n}]^{3-n}$ complexes, the predicted shifts of the first and second absorption bands have been discussed by Matsuoka *et al.*[16] Their discussion is also applicable to $[Cr(O)_3(N)_3]$. The first absorption band of the third eluate isomer of [Cr(L-asp)(L-his)] and the third eluate isomer of [Co(D-asp)(L-his)] showed no splitting or only a small splitting as was predicted by the above discussion that the first absorption band of a facial isomer should not have three components. Compared with these fac isomers, the L- and D-isomers of [Cr(L- or D-alama)(L-his)], along with the first eluate isomer of [Co(L-asp)(L-his)], and the first eluate isomer of the [Co(D-asp)(L-his)] isomer, have a broad peak because of their splitting into three components. The UV spectra of the L- or D-isomers of [Cr(L- or D-alama)-(L-his)] are found to be more similar to those of the first eluate mer isomers than to those of the fac isomers of [Cr(L- or D-asp)(L-his)] by inspecting the width and peak maxma of the first-absorption band region.

Distribution of the Isomers. Though three geometrical isomers, *cis*(*N*), *trans*(*N*)(*a*), and *trans*(*N*)(*b*) (Fig. 6), are possible in the bis(iminodiacetato)chromate(III) complex, only the *cis*(*N*) isomer has been prepared.[17] Both the *cis*(*N*) and the *trans*(*N*)(*a*) isomers of $[Cr(ida)_2]^-$ seem to have no steric hindrance between two ligands. In the tris(glycinato)chromium-(III) complex, two geometrical isomers, mer and

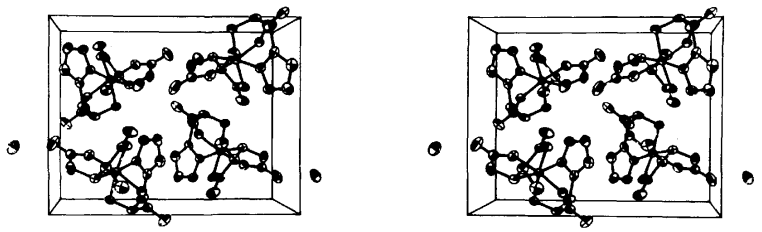

Fig. 4. Stereoscopic illustration of the unit cell contents.

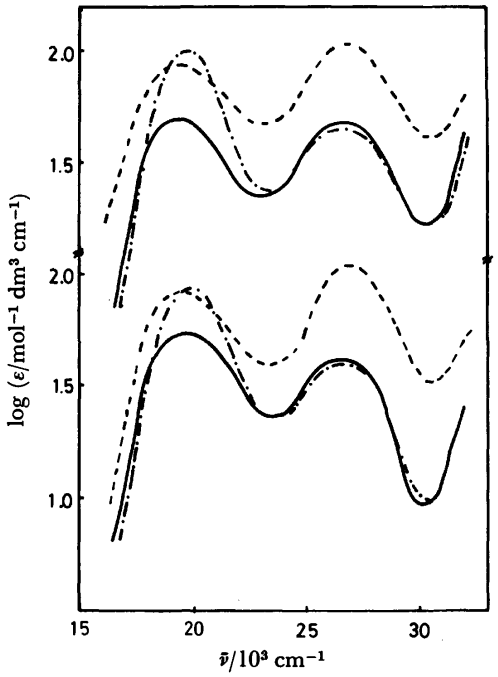

Fig. 5. Visible absorption spectra of [Cr(L- or D-alama)(L-his)] and [Cr(L- or D-asp)(L-his)]. Upper, *L* isomer (----) of [Cr(L-alama)(L-his)]. The first (——) and the third eluates (—·—·) of [Co(L-alama)(L-his)]. Lower, *D* isomer (----) of [Cr(D-alama)(L-his)]. The first (——) and the third eluates (—·—·) of [Co(D-asp)(L-his)].

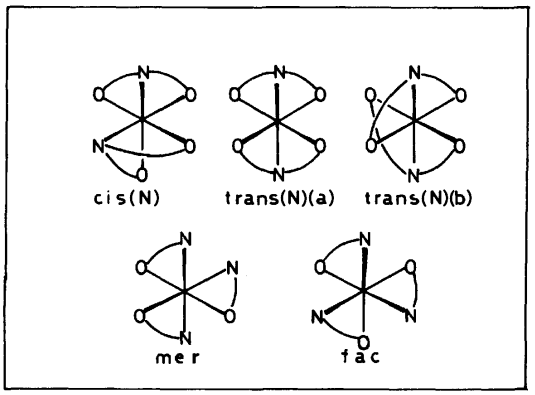

Fig. 6. Geometrical isomers of $[Cr(ida)_2]^-$ (upper) and $[Cr(gly)_3]$ (lower).

fac (Fig. 6), are possible, but only the fac isomer has been prepared. We have previously reported that, in the cobalt(III) complex having both L- or D-aspartate and L-histidinate ions the *trans*(*N*) isomers are less stable than the other isomers.[18] This suggests that the two nitrogen atoms of a five-membered chelate ring avoid the *trans* position around the chromium(III) and cobalt(III) ions. While the two isomers (one mer and one fac isomers) of [Co(L- or D-asp)(L-his)] were prepared in nearly equal amounts, only one mer isomer of [Cr(L- or D-alama)(L-his)] was prepared for each L- or D-series. This stereoselectivity is interesting because it shows the difference in coordination power between asp and alama ligands. When an asp ligand coordinates to a metal ion, it has a rigid skeleton composed of five- and six-membered chelate rings. On the other hand, an alama has two forms in chirality around the coordinated nitrogen atom ((R) and (S) configurations), in which the (R) form has less steric repulsion between methyl protons and methylene protons than does the (S) form, so that the (R) configuration may be preferable to the (S) configuration. Beside the above steric hindrance, a coordinated alama has two five-membered chelate rings which can move around the Cr–N axis. In both the R-L-*cis*(*O*)*trans*(*N*) and R-L-*fac* isomers, the methyl group of alama strikes the imidazole 2-proton or amino protons of the coordinated L-his, while the R-L-*trans*(*O*)*cis*(*N*) isomer has no such repulsion. The steric flexibility seems to be larger in the chromium(III) complex than in the cobalt(III) complex, since we could prepare both a meridional and a facial isomers of the [Co(L- or D-alama)(L-his)] complexes for each L- or D-series.[19]

References

1) Department of Engineering, National Science Museum, Ueno Park, Tokyo 110, Japan.

2) W. Y. Mertz, *Fed. Proc.*, **33**, 659 (1974).

3) W. Y. Mertz, E. W. Toepfer, E. E. Roginski, and M. M. Polansky, *Fed. Proc.*, **33**, 2275 (1974).

4) N. Israily and *C. R. Hebd. Seances. Acad. Sci.*, **C 262**, 1426 (1966).

5) R. D. Gillard, S. H. Laurie, D. C. Price, D. A. Phipps, and C. F. Weick, *J. Chem. Soc., Dalton Trans.*, **1974**, 1385.

6) a) H. Oki and K. Otuka, *Bull. Chem. Soc. Jpn.*, **49**, 1841 (1976); b) H. Oki and Y. Takahashi, *Bull. Chem. Soc. Jpn.*, **50**, 680 (1977); c) H. Oki and Y. Takahashi, *Bull. Chem. Soc. Jpn.*, **50**, 2288 (1977); d) H. Oki and H. Yoneda, *Inorg.*

Chem., **20**, 3875 (1981).
7) M. Watabe, H. Yano, Y. Odaka, and H. Kobayashi, *Inorg. Chem.*, **20**, 3623 (1981).
8) K. Okamoto, J. Hidaka, and Y. Shimura, *Bull. Chem. Soc. Jpn.*, **44**, 1601 (1971).
9) D. T. Cromer, *Acta Crystallogr.*, **18**, 17 (1965).
10) J. M. Bijvoet, A. F. Peerdeman, and A. J. Van Bommel, *Nature (London)*, **168**, 271 (1951).
11) W. C. Hamilton, *Acta Crystallogr.*, **18**, 502 (1965).
12) P. E. Hoggard, *Inorg. Chem.*, **20**, 415 (1981).
13) G. Grouhi-Witte, Dissertation, Universitat, Hamburg, 1975.
14) R. F. Bryan, D. T. Greene, D. F. Stokely, Jr., and E. Wilson, *Inorg. Chem.*, **10**,1469 (1971).
15) P. D. Meester and D. J. Hodgson, *J. Am. Chem. Soc.*, **99**, 101 (1977).
16) N. Matsuoka, J. Hidaka, and Y. Shimura, *Bull. Chem. Soc. Jpn.*, **40**, 1868 (1976).
17) J. A. Weyh and R. E. Hamm, *Inorg. Chem.*, **7**, 2431 (1968).
18) a) M. Watabe, S. Kawaai, and S. Yoshikawa, *Bull. Chem. Soc. Jpn.*, **49**, 1845 (1976); b) M. Watabe, M. Zama, and S. Yoshikawa, *Bull. Chem. Soc. Jpn.*, **51**, 1354 (1978); c) M. Watabe, H. Yano, and S. Yoshikawa, *Bull. Chem. Soc. Jpn.*, **52**, 61 (1979).
19) M. Watabe, Unpublished Data.

Solvent Extraction of Mercury(II) from Hydrochloric Acid with 1,2-Bis(hexylthio)ethane

Yoshinari BABA,* Yutaka IKEDA, and Katsutoshi INOUE
Department of Industrial Chemistry, Saga University, Honjo-machi, Saga 840
(Received August 6, 1984)

Solvent extraction of mercury(II) from hydrochloric acid with 1,2-bis(hexylthio)ethane (=BHTE=$\bar{S}$) in 1,2-dichloroethane has been studied at 30 °C. Mercury(II) was found to be extracted into pure 1,2-dichloroethane without extractants, which is due to the physical partition of the neutral species, $HgCl_2$. The partition coefficient, K_D, was evaluated as K_D=0.314. It was clarified that the extraction mechanism with BHTE can be explained in terms of solvation by BHTE and that 1:1 metal: the ligand complex is formed in the organic phase as follows.

$$\bar{S} + HgCl_2 \rightleftharpoons \overline{HgCl_2 \cdot S} \qquad K_e$$

The extraction equilibrium constant, K_e, was evaluated as K_e=1.61×10³ dm³ mol⁻¹.

Solvent extraction of metal ions is one of the effective, energy-saving and nonpolluting processes for hydrometallurgy and/or the treatment of the wastewater containing heavy metals. The most important factor in the solvent-extraction processes is the extractants selective to the specified metal ions to be recovered.

So far, a number of commercial extractants have been developed and used extensively in hydrometallurgy. The majority of them are those of the O or N atom donating ligand type. Those possessing sulfur as a donor atom are relatively few. These are interesting extractants since they have a high selectivity to special metals which are classified as "soft acids" such as copper(I), silver, mercury, gold and platinum-group metals through a so-called soft-soft interaction. Among the sulfur-possessing extractants, there have been many studies of those possessing one sulfur atom such as dialkyl sulfides and dialkyl sulfoxides acting as neutral monodentate ligands.[1-3,5] However, relatively few studies have been carried out on those possessing more than two sulfur atoms acting as polydentate ligands except for *O,O*-dialkyl hydrogenphosphorodithioate.[4]

Some Soviet investigators[6-8] studied the extraction properties of bis(alkylthio)alkanes, the bidentate neutral extractants possessing two sulfur atoms, and found that these are very selective to silver, mercury, gold, palladium and platinum although their works were merely qualitative. Ohki *et al.*[9] have conducted an investigation of the extraction of copper(I), silver(I), and gold(III) by 1,2-bis(hexylthio)ethane. They found that copper and silver are extracted as 1:2 metal:reagent complexes in the extraction from perchlorate media though a 1:1 complex becomes predominant in the region where the reagent concentration is not sufficient for silver. The same was also suggested by Artyukhin *et al.*[8] for palladium extraction from hydrochloric acid.

The present authors have conducted a quantitative investigation on the distribution equilibrium in the extraction of mercury(II) from hydrochloric acid with 1,2-bis(hexylthio)ethane in 1,2-dichloroethane in this paper to clarify the composition of the extracted species and to evaluate the extraction equilibrium constant.

Experimental

Reagents. 1,2-Bis(hexylthio)ethane (BHTE) was synthesized from 1-hexanethiol and 1,2-dibromoethane using a conventional method according to the following reaction.

$$2n\text{-}C_6H_{13}SH + CH_2BrCH_2Br + 2KOH \longrightarrow (n\text{-}C_6H_{13}S\text{-}CH_2\text{-})_2 + 2KBr + 2H_2O$$

The product was purified by vacuum distillation (bp 169—170 °C/5 mmHg (1 mmHg=133.322 Pa)). The identification of this product was carried out using IR and NMR spectra. The purity was verified to be about 97% by gas chromatography. The purified product was diluted using GR-grade 1,2-dichloroethane, the most polar diluent, to a required concentration in order to increase the solubility of the complex to be formed in the organic phase. The initial mercury concentration in the hydrochloric acids was adjusted to 0.005 mol dm⁻³.

Measurements of Extraction Equilibrium. Prior to the measurement of the extraction equilibrium, preliminary experiments were carried out in order to examine the contact time required for the attainment of equilibrium in this system

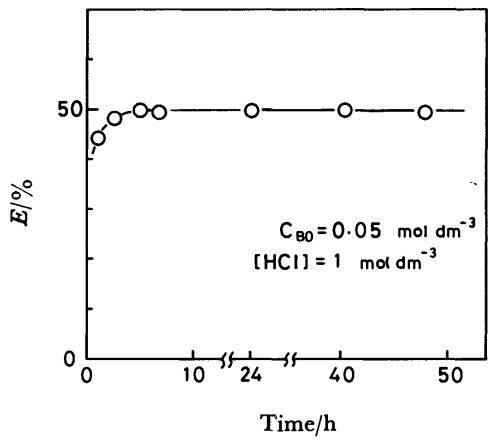

Fig. 1. Relation between the extent of extraction of mercury (II) and the contact time.

and to assure the stability of the extractant and the complex extracted into the organic phase. Figure 1 shows a typical example of the relation between the extent of extraction of mercury and the contact time. From this result, it is obvious that the extraction equilibration is attained within 5—6 h and that the extractant and the extracted complex in the organic phase are stable, at least, for 48 h. Consequently, the contact time in this system was determined as 24 h, also taking account of the convenience of the experimental operation.

Equal volumes (30 cm^3) of the aqueous and organic phases were shaken in a stoppered glass flask for 24 h at 30±0.1 °C. After equilibration, the two phases were separated and analyzed for mercury content in both phases. The mercury concentration in the aqueous phase was determined by titration with EDTA in the presence of an excess of Mg-EDTA using eriochrome black T(BT) as an indicator. That in the organic phase was determined by atomic absorption spectrochemical analysis using a Nippon Jarrell-Ash model AA-782 spectrophotometer after stripping with a 1 mol dm^{-3} aqueous ammonium thiocyanate solution.

Results and Discussion

Extraction of Mercury with Pure Diluent. First of all, mercury was found to be extracted into pure 1,2-dichloroethane without extractants as shown in Fig. 2. The extraction mechanism of mercury from a hydrochloric acid solution is considered to be caused by the physical partition of the neutral species, $HgCl_2$, as follows.

$$HgCl_2 \rightleftharpoons \overline{HgCl_2} \quad (1)$$

$$K_D = \frac{[\overline{HgCl_2}]}{[HgCl_2]} \quad (2)$$

In this case, the distribution ratio of mercury, D, is expressed as follows.

$$D = \frac{[\overline{HgCl_2}]}{C_{Hg\ aq.}} = \alpha_2 \cdot K_D \quad (3)$$

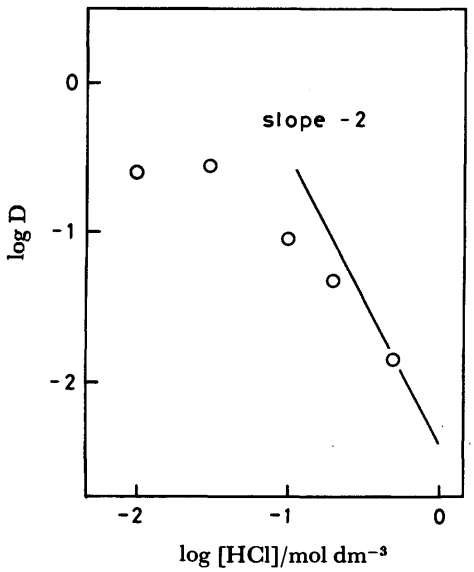

Fig. 2. Equilibrium distribution of mercury (II) from hydrochloric acid solutions with 1,2-dichloroethane.

where

$$\alpha_2 = \frac{\beta_2[Cl^-]^2}{1+\sum_1^4 \beta_i[Cl^-]^i} \quad * \quad (4)$$

The logarithm of Eq. 3 gives the following equation.

$$\log D = \log \alpha_2 + \log K_D \quad (5)$$

Figure 3 shows log-log plots of D against α_2 on the basis of Eq. 5, where the values reported by Hepler[10] were used as the stability constants of chloro complexes, β_i. The plotted points in Fig. 3 lie on a straight line of slope 1 as expected from Eq. 5. From the intercept of the straight line with the ordinate in Fig. 3, K_D was evaluated as K_D=0.314.

Extraction of Mercury from Aqueous Hydrochloric Acid Solutions with BHTE in 1,2-Dichloroethane.

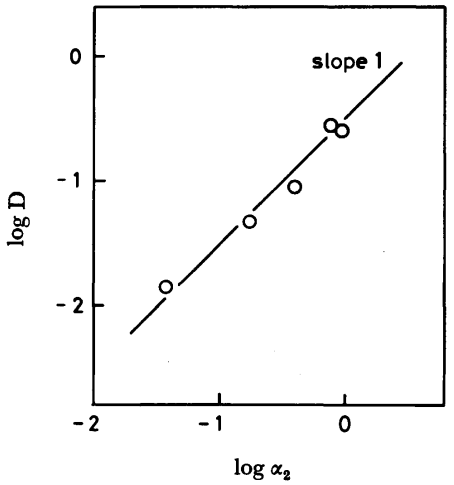

Fig. 3. Relation between logD and logα_2 for extraction of mercury(II) with 1,2-dichloroethane.

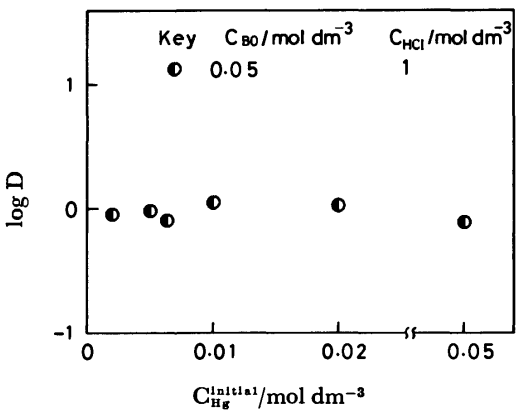

Fig. 4. Effect of the initial mercury concentration in the aqueous phase on the distribution ratio of mercury (II).

* The dimerization constant (K_d) of mercury(II) chloride in aqueous solution was reported as K_d=0.3 at 25 °C by Linhart (*J. Chem. Soc.*, **37**, 258 (1915)). This value is so small as to neglect the dimerization of mercury(II) chloride in hydrochloric acid compared with monomeric chloride complexes.

In order to investigate the species of mercury existing in both phases, the effect of the concentration of mercury on the distribution of mercury was examined. The distribution ratio was found to be independent of the mercury-ion concentration in the aqueous phase over the concentration range (2×10^{-3}—5×10^{-2} mol dm^{-3}) examined as shown in Fig. 4. This indicates that only monomeric complexes are formed in the organic phase. Figure 5 shows the effect of a hydrochloric acid concentration in the aqueous phase on the distribution ratio of mercury, where the difference between the total concentration of mercury in the organic phase and concentration of mercury extracted only by the diluent was used for the calculation of the distribution ratio. As is evident from Fig. 5, the distribution ratio decreases with an increase in the hydrochloric acid concentration. Mercury is considered to be extracted from aqueous chloride solutions according to the reaction described by

$$HgCl_2 + \bar{S} \rightleftharpoons \overline{HgCl_2 \cdot S} \qquad K_e \qquad (6)$$

$$K_e = \frac{[\overline{HgCl_2 \cdot S}]}{[HgCl_2][\bar{S}]} \qquad (7)$$

where $\bar{S}$ denotes the extractant in 1,2-dichloroethane.

In the region of a lower loading ratio of mercury, the concentration of the unreacted extractant, $[\bar{S}]$, is nearly equal to its initial concentration, C_{B0}, and is constant. Moreover, in the region of higher chloride ion concentration ($[Cl^-]>1$ mol dm^{-3}), the concentration of neutral species of mercury in the aqueous phase, $[HgCl_2]$, can be approximated as follows.

$$[HgCl_2] = \alpha_2 \cdot C_{Hg\ aq.} \simeq (\beta_2/\beta_4[Cl^-]^2) \cdot C_{Hg\ aq.} \qquad (8)$$

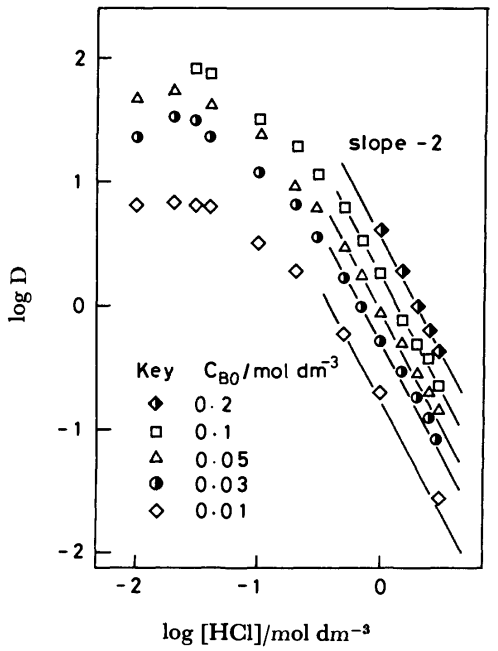

Fig. 5. Equilibrium distribution of mercury (II) from hydrochloric acid solutions with BHTE in 1,2-dichloroethane.

Therefore, the distribution ratio is approximately expressed by Eq. 9 in this region from Eqs. 7 and 8.

$$\log D = -2\log[Cl^-] + a \qquad (9)$$

where

$$a = \log(\beta_2/\beta_4) + \log C_{B0} + \log K_e \qquad (10)$$

In Fig. 5, plotted points lie on straight lines of slope −2 in the higher concentration range of hydrochloric acid as expected from Eq. 9. The values of a, defined by Eq. 10, were evaluated from the intercepts of these lines with the ordinate for each value of C_{B0} and plotted against log C_{B0} as shown in Fig. 6. As is evident from Fig. 6, the plotted points lie on a straight line of

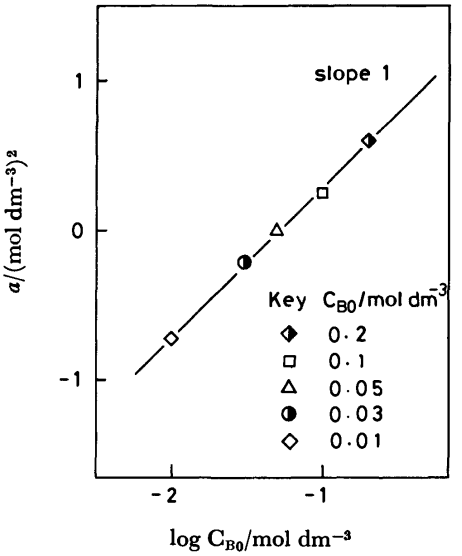

Fig. 6. Relation between a and log C_{B0}.

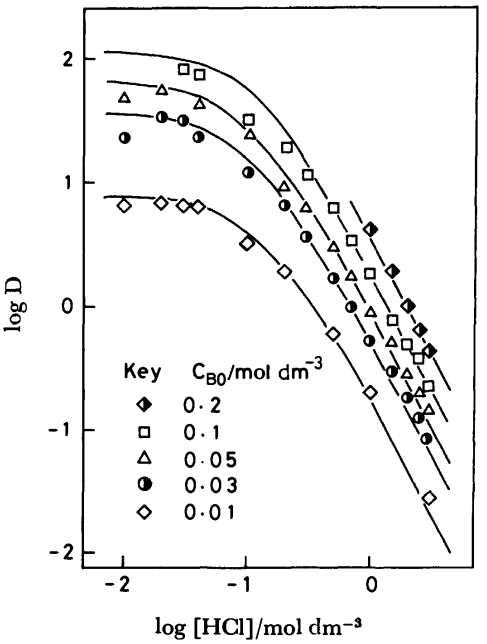

Fig. 7. Equilibrium distribution of mercury(II) from hydrochloric acid solutions with BHTE in 1,2-dichloroethane. The solid lines are the calculated results.

slope 1 as expected from Eq. 10. The extraction equilibrium constant, K_e, was evaluated from the value of the intercept of the straight line with the ordinate in Fig. 6 as $K_e=1.61\times10^3$ dm^3 mol^{-1}.

Meanwhile, in the region of the higher loading ratio of mercury to the extractant, the mass balance of the extractant gives the concentration of the unreacted extractant, [$\bar{S}$], as follows.

$$[\bar{S}] = \frac{C_{BO}}{1+K_e[HgCl_2]} = \frac{C_{BO}}{1+K_e\alpha_2 C_{Hg\ aq.}} \quad (11)$$

Substitution of Eq. 11 for Eq. 7 gives the following equation.

$$\log D = \log \alpha_2 + \log K_e + \log C_{BO} - \log(1+K_e\alpha_2 C_{Hg\ aq.}) \quad (12)$$

The solid lines in Fig. 7 are the calculated results obtained on the basis of Eq. 12 using the value of $K_e=1.61\times10^3$ dm^3 mol^{-1}. The calculated results agree satisfactorily with the experimental ones.

Infrared Spectrum of the BHTE-$HgCl_2$ Complex. The low-frequency infrared spectrum of the crystalline BHTE-$HgCl_2$ complex was measured in order to identify the bond between the metal and the reagent or that between the metal and chlorine. The crystalline complex was prepared as follows. The complex of white slime was precipitated by a dropwise addition of $HgCl_2$ in 0.01 mol dm^{-3} hydrochloric acid to BHTE dissolved in ethanol under intense agitation. It was purified by recrystallizing three times from aqueous ethanol solution to obtain the crystalline complex.

As a result, a single sharp band is observed at 273 cm^{-1} ascribable to the Hg-Cl group, on which Coats *et al.*[11] observed ν(Hg-Cl) at 288 s and 249 m cm^{-1} for the $(CH_3CH_2S\text{-}CH_2\text{-})_2HgCl_2$ complex. Therefore, also taking account of the experimental results on the effect of mercury concentration on the distribution ratio mentioned earlier, the complex extracted into the organic phase is considered to be $(n\text{-}C_6H_{13}S\text{-}CH_2\text{-})_2HgCl_2$.

Conclusion

Solvent extraction of mercury(II) with 1,2-bis(hexylthio)ethane(=BHTE) in 1,2-dichloroethane from hydrochloric acid was studied at 30 °C. It was concluded that mercury(II) can be extracted with 1,2-dichloroethane itself by the physical partition of $HgCl_2$ and that it is extracted with BHTE according to the following extraction reaction.

$$\overline{(n\text{-}C_6H_{13}S\text{-}CH_2\text{-})_2} + HgCl_2 \rightleftharpoons \overline{(n\text{-}C_6H_{13}S\text{-}CH_2\text{-})_2HgCl_2}$$

The authors are indebted to Professor M. Takagi of Kyushu University for his instruction in the synthesis of 1,2-bis(hexylthio)ethane.

The present work was supported by a Grant-in-Aid for Scientific Research from the Ministry of Education, Science, and Culture of Japan.

References

1) Yu. E. Nikitin, Yu. I. Murinov, and A. M. Rosen, *Russ. Chem. Rev.*, **45**, 1155 (1976).
2) V. A. Mikhailov, V. G. Torgov, E. M. Gil'bert, L. N. Mazolov, and A. V. Nikolaev, "Proceedings of International Solvent Extraction Conference 1971," p. 1112, Soc. Chem. Ind., London (1971).
3) V. A. Mikhailov, "Proceedings of International Solvent Extraction Conference 1977," p. 52, Con. Inst. Min. Metall., Montreal (1979).
4) K. Inoue and F. Nakashio, *Kagaku Kogaku*, **46**, 700 (1982).
5) V. A. Mikhailov, V. G. Torgov, and A. V. Nikolaev, *Izv. Sib. Otd. Akad. Nauk. SSSR, Ser. Khim. Nauk*, (3), **1973**, 3.
6) V. A. Pronin, M. V. Usol'tseva, and S. M. Shostakovskii, *Izv. Akad. Nauk SSSR, Ser. Khim.*, **1971**, 2371.
7) V. A. Pronin, M. V. Usol'tseva, Z. N. Shastina, N. K. Gusarova, E. P. Vyalykh, S. V. Amosova, and B. A. Trofimov, *Russ. J. Inorg. Chem.*, **18**, 1016 (1973).
8) P. I. Artyukhin, E. A. Startseva, L. Ya. Marochkina, V. I. Andrievskii, V. G. Marzur, L. M. Gindin, and I. L. Kotlyarevskii, *Izv. Sib. Otd. Akad. Nauk SSSR, Ser. Khim. Nauk*, (1), **1972**, 90.
9) A. Ohki, M. Takagi and K. Ueno, *Anal. Chem. Acta*, **159**, 245 (1984).
10) L. G. Hepler and G. Olofsson, *Chem. Rev.*, **1975**, 585.
11) G. E. Coates and D. Ridley, *J. Chem. Soc.*, **1964**, 166.

Preparation of $LaNi_5$ Films and Effects of Hydrogen Absorption on Electrical Resistivities of the Films

Gin-ya ADACHI,* Hiroki SAKAGUCHI, Ken-ichi NIKI, Hiroshi NAGAI, and Jiro SHIOKAWA

Department of Applied Chemistry, Faculty of Engineering, Osaka University, Yamadaoka, Suita, Osaka 565

(Received August 28, 1984)

Thin films of $LaNi_5$ have been prepared by means of a flash evaporation-deposition technique. Electric resistivity measurements on these films were carried out in an atmosphere of hydrogen. The films formed on quartz substrates were amorphous. Resistivities initially increased and then decreased during the absorption of hydrogen. During the desorption process, the reverse phenomenon was observed. The effect of the thickness of the films on the electric properties, during the hydrogen absorption-desorption process, was also studied. Sample pulverization could be avoidable by using films of less than 10 μm in thickness. The hydrogen contents of the films were determined by the quartz-crystal mass-monitoring (QCMM) method.

Technical applications of hydrogen absorption in intermetallic compounds have been eagerly pursued in some aspects,[1-8] such as energy storage, heat pumping and hydrogen purification. The $LaNi_5$ hydrides have been the most throughly investigated of all the hydrides of interest,[9-16] and the structure and phase relations have been well established.

A serious drawback regarding the practical use of $LaNi_5$ is the fact that the material pulverizes during hydrogen charging. The volume increase associated with the formation of the hydrides leads to stresses in the hydride envelope on the unhydrided core material.[9] This stress causes cracks which pulverize the hydride.[17] For $LaNi_5$ subjected to several charging-decharging cycles, the particle diameter was measured to be about 10^2 μm, though there was a broad distribution in size.[18,19]

An amorphous alloy which is prepared by rapid cooling is known to have a considerable resistance to a stress since a strain can be relaxed by the free volume existing in an alloy. The amorphous alloy is, therefore, a promising material for hydrogen storage.

A thin film of an alloy is sometimes amorphous[20] and is worth being investigated for possible applications. The preparation of a thin film of an alloy or an intermetallic compound is difficult owing to the difference in the vapour pressures of component metals. Nevertheless, the following methods have been proposed for the preparation of a thin film of an alloy: (1) ion sputtering;[21] (2) ion plating;[22] (3) vacuum vapour deposition at a temperature sufficiently high that component metals can be vaporized quickly and completely (flash evaporation-deposition).

We prepared some thin films of $LaNi_5$ by the third method and measured their electric properties under several atmospheres of hydrogen. This article is a full account of our preliminary papers.[23,24]

Experimental

Preparation of Films. $LaNi_5$ (La 32.16, Ni 67.84 wt%) powder was supplied by Santoku Metal Industry Co. Ltd., Kobe. Substrates were quartz plates, porous sintered glass discs (pore sizes; 3, 8, 50, and 100 μm) and porous sintered stainless steel discs (SUS304, pore sizes; 0.5 and 1 μm, Shoketsu Kinzoku, Tokyo). Samples for electric measurements were deposited on quartz plates. The substrates (except for a porous sintered stainless-steel discs) were first soaked in a $HCl-HNO_3$ mixed solution for 1 d and were then washed with a neutral detergent and rinsed with deionized water. The plate was cleaned with an ultrasonic washing machine filled with deionized water before drying in a desiccator. The porous sintered stainless-steel discs were first washed with acetone and next with methanol. The discs were then treated in an ultrasonic washing machine. The vacuum-deposition procedure was as follows. The $LaNi_5$ powder was placed on a tungsten boat which was preheated to a temperature of 2.3×10^3 K. Both components of $LaNi_5$ evaporated immediately (at this temperature) and were deposited onto a substrate which was placed just above the tungsten boat. The alloy powder was supplied by a conveyor belt equipped with a hopper. The vacuum during deposition was *ca.* 10^{-3} Pa. After deposition, pure helium gas was allowed into the chamber to prevent the formation of an oxide on the films. The thicknesses of the obtained films were determined by the direct observation of the cross sections of the samples using a Hitachi Scanning Electron Microscope S-405. The composition of the film bulk was determined with a Rigaku X-ray Energy Spectrometer equipped with an Si(Li) detector. The XPS measurement was carried out with a Shimazu Electron Spectrometer ESCA 650B mounted with a Mg target.

Measurements of Properties. Electric-resistivity measurements were performed under a hydrogen atmosphere. A sample with attached leads and a thermocouple were installed in a reactor which was made of 316 stainless steel (Fig. 1). The reactor was connected to a high-pressure manifold with connections to a pressure gauge, a vacuum pump and a high-pressure hydrogen gas cylinder. The resistivity of the film was measured by the four-probe technique.[25,26] The voltage drop across the film for a constant current was recorded as a function of time. Then hydrogen gas was quickly admitted to the vacuum reactor. The resulting changes in voltage drop due to absorption were monitored on a recorder.

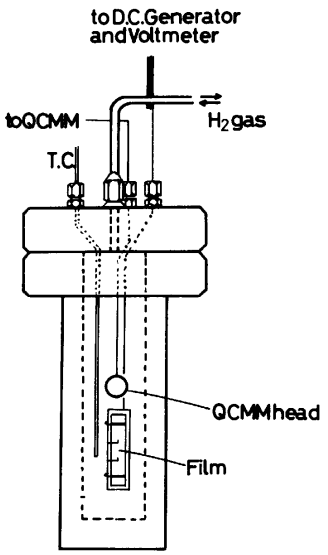

Fig. 1. The apparatus used for the electrical resistivity measurements and the QCMM frequency measurements.

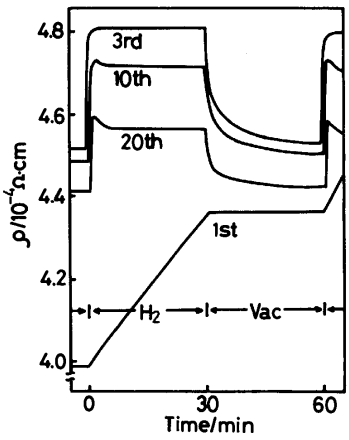

Fig. 2. Variation of resistivities as a function of time for thicker $LaNi_5$ film (thickness *ca.* 0.63 μm) in the activation process (at 313 K for lst and 2nd cycle, at 363 K for other cycle. H_2 2.5×10^6 Pa).

A QCMM apparatus (NICHIDEN ANELVA EVM 32B) was used to determine the quantity of hydrogen absorbed in the films. The apparatus and procedure were as follows. Flash vacuum evaporation was also used to form an $LaNi_5$ film. A crystal monitor head with a quartz disk was placed 0.2 m above a tungsten filament to recieve the metal vapor. The vessel for setting the $LaNi_5$ deposited QCMM head was the same one that was used to measure the electrical resistivity. All the QCMM measurements were done at 333 K. After the vacuum system had reached thermal equilibrium, hydrogen was then introduced into the vessel. The change in the frequency of the quartz was recorded as a function of pressure change.

Results and Discussion

Characterization of Deposited $LaNi_5$ Films: Obtained films were amorphous, at least as determined from X-ray diffraction results. Faint dots were observed in some electron-diffraction patterns. These dots, however, did not originally seem to be due to the presence of any crystalline phase, but due to the oxidation of the film or crystallization by the electron beam in the electron microscope.[27]

The chemical composition of the films (determined by the X-ray fluorescence method) was the same as the original $LaNi_5$ supplied in the hopper. X-ray photoelectron spectroscopy revealed that the La $3d_{2/3}$ peak was split into two components (1.367×10^{-6} and 1.372×10^{-6} J) because of the oxide.[28-33] However, the peak at 1.372×10^{-6} J disappeared after bombardment with argon ions for 30 min. Therefore, the oxide was considered to have formed only on the top surfaces of the films.

The homogeneity of the chemical composition for the whole surface of the films was confirmed by EPMA (Electron Probe Micro Analysis).

The density of the film was 4.44 g/cm³. This was estimated from the weight, area, and thickness of a film (1.33 μm thick). This value is considerably smaller than the bulk value, *i.e.* 8.28 g/cm³.[34]

Stability of the Films during Hydrogen Absorption-desorption Cycles: Intermetallic compounds, such as $LaNi_5$, are brittle materials and break up into fine particles because of their volumetric expansion during hydrogen absorption. The thin films obtained, however, do not form powders even after 150 cycles of the absorption-desorption of hydrogen. This is because that the films are amorphous, *i.e.* hydrogen enters the film just like a hand put into water.

Electric Resistivities: Figures 2, 3, and 4 show the variation in electric resistivity as a function of the time that hydrogen pressure was applied to $LaNi_5$ films of various thicknesses during the activation process.

The resistivity change in a thicker film (*ca.* 0.63 μm thick) is shown in Fig. 2. In the first cycle, the resistivity for the film keeps rising when hydrogen gas is allowed into the system. After the evacuation of the system, the resistivity maintains a constant value. In the third cycle, the resistivity of the film increases immediately and then attains a constant value during the absorption process. During the desorption process, the resistivity decreases rapidly at first and then gradually. During the tenth cycle the variation in the resistivity was almost the same as that during the third cycle. The corresponding increase and decrease was, however, quicker than that for the third cycle. After the first sudden increase, the resistivity decreased slightly. This behaviour suggests that the following steps take place during hydrogen absorption. Hydrogen molecules are adsorbed on the surface of the film and then dissociate into atoms. The dissociated hydrogen atoms reach the underlying $LaNi_5$ by diffusion in

monatomic form along the La_2O_3–Ni interface.[35] The hydrogen atoms take on the conduction electrons of $LaNi_5$ and become the hydrogen anions. This reaction is represented by the formula $H+e^- \rightarrow H^-$. The number of electrons in the conduction band of the $LaNi_5$ decreases and, consequently, the resistivity of the $LaNi_5$ film increases. The second step (the formation of a highly conductive hydride) then, occurs. For a thicker film, the resistivity is maintained at a constant value since the formation of the hydrogen anion is balanced by the formation of the highly conductive hydride. In the hydrogen-desorption process, the dissolved hydrogen anions are removed as hydrogen molecules, releasing their electrons to the conduction band of the metal. Since the number of electrons in the conduction band of the $LaNi_5$ increases, the resistivity of the film decreases. Subsequently, hydrogen which has formed the highly conductive metal hydride, slowly desorbs. The decrease in the resistivity of the film becomes slow.

Figure 3 illustrates the change in resistivity of a thinner film (*ca.* 0.20 μm thick). The behavior during the first cycle is similar to that of the third cycle for a thicker film. As the cycle is repeated, the rate of decrease in the resistivity (which occurs after the increase when hydrogen is first admitted into the system) becomes faster. This is because the quantity of the highly conductive hydride increases. When the system is evacuated (as seen from the results of the 10th cycle in the thicker film) there occurs a sudden decrease in the resistivity because of the removal of the residual hydrogen anions in the film. Then, the resistivity gradually increases due to the decomposition of the highly conductive hydride.

Figure 4 displays the resistivity change in the thinnest film (*ca.* 3.8×10^{-2} μm thick). During the 10th cycle, there was no increase caused by introduction of hydrogen into the system because all of the dissolved hydrogen anions formed highly conductive hydride. As mentioned above, the resistivity change differs depending on the thickness of the film. The thickness of the highly conductive hydride layer seems to be almost the same even though the film thickness is different. For the thicker film, the thickness of the H^- dissolved slightly conductive $LaNi_5$ layer was quite large and the effect of this layer was predominant rather than that of the highly conductive hydride layer. For the thinner film, the effect of the highly conductive hydride was forcible and the electric resistivity fell immediately.

Figure 5 shows the effect of temperature on the electric resistivity of an $LaNi_5$ film (0.3 μm thick) during a hydrogen-desorption process. The rate of released hydrogen which is formed the highly conductive hydride increases with a rise in temperature.

Hydrogen Pressure Dependence on Resistivities: Figure 6 illustrates the pressure dependence of the saturated electric resistivity for hydrogen absorption in the film. The saturated resistivity reaches a constant value at about 1.2×10^6 Pa. Regarding the effect of the temperature on the electric resistivity and the hydro-

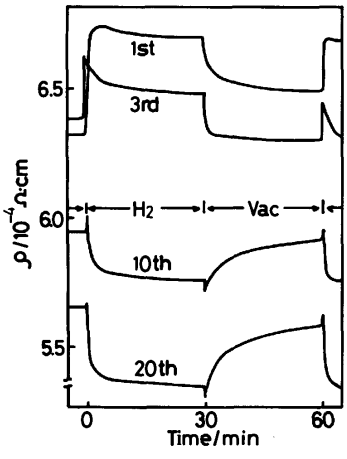

Fig. 3. Variation of resistivities as a function of time for thinner $LaNi_5$ film (thickness *ca.* 0.20 μm) in the activation process (at 313 K for lst and 2nd cycle, at 363 K for other cycle. H_2 2.5×10^6 Pa).

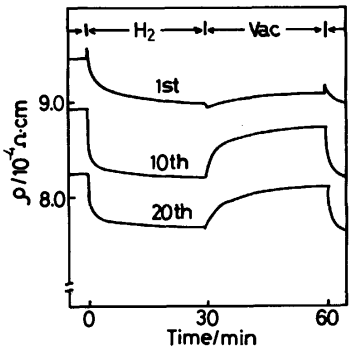

Fig. 4. Variation of resistivities as a function of time for thinnest $LaNi_5$ film (thickness *ca.* 3.8×10^{-2} μm) in the activation process (at 313 K for 1st and 2nd cycle, at 363 K for other cycle. H_2 2.5×10^6 Pa).

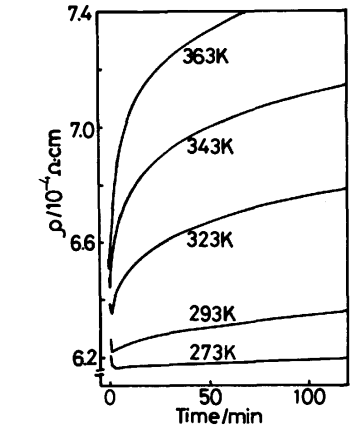

Fig. 5. Effect of temperature on electrical resistivity of an $LaNi_5$ film (thickness *ca.* 0.30 μm) in hydrogen desorption process.

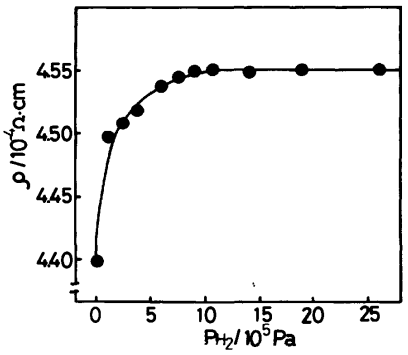

Fig. 6. Electrical resistivity *vs.* Hydrogen pressure for an $LaNi_5$ film (thickness *ca.* 0.63 μm) at 363 K.

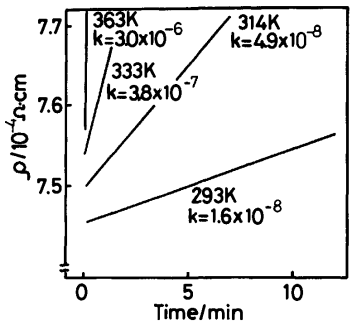

Fig. 7. Variation of resistivities *vs.* Time at various temperatures for an $LaNi_5$ film (thickness *ca.* 0.35 μm).

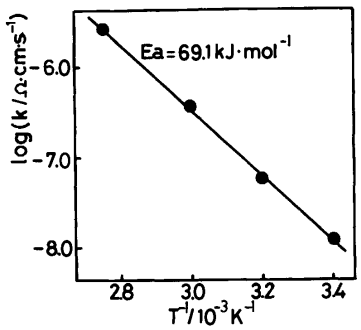

Fig. 8. Arrhenius plot of the rate constant for hydrogen absorption in an $LaNi_5$ film (thickness *ca.* 0.35 μm).

gen pressure dependence on resistivities, some typical results since the behavior of the resistivity is unrelated to the film thickness.

Activation Energy for Hydrogen Absorption: The time dependence of the resistivities for the initial stages of absorption is shown in Fig. 7. The reaction-rate constants are obtained from the slopes of straight lines in the figure.[36] Figure 8 gives an Arrhenius plot of the rate constants for the hydrogen absorption of the film. An activation energy for the absorption, E_a, is evaluated from the slope, being 69.1 kJ mol^{-1}. The E_a is related to the reaction which is the formation of a hydrogen anion. This reaction is independent of the film thickness.

Hydrogen Concentration in the Films: Figure 9 gives

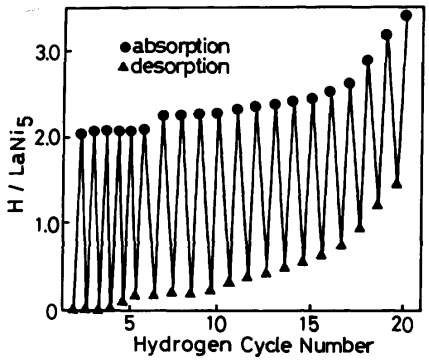

Fig. 9. Hydrogen concentration in an $LaNi_5$ film (thickness *ca.* 1.8 μm) in the hydrogen absorption-desorption cycle (in H_2 2.5×10^6 Pa—Vacuum cycle at 333 K).

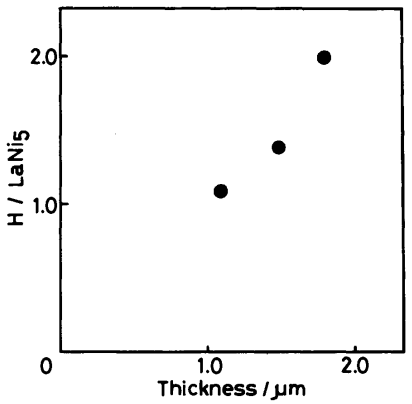

Fig. 10. Hydrogen concentration *vs.* $LaNi_5$ film thickness (in H_2 2.5×10^6 Pa—Vacuum cycle at 333 K).

the hydrogen concentration in $LaNi_5$ films measured by the QCMM method[37] while repeating the hydrogen absorption-desorption cycle. The amounts of hydrogen taken up by the $LaNi_5$ film (*ca.* 1.8 μm thick) is about 2.0 H/$LaNi_5$. It is recognized that the amount of the hydride which is not desorbed from the film increases as the cycle repeats. This agrees with the measurements of the electrical resistivity. The amounts of hydrogen for other films are 1.1 and 1.4 for films of 1.1 and 1.5 μm thickness, respectively. The hydrogen content in their films is dependent on the film thickness and, as indicated in Fig. 10, the hydrogen concentration decreases with a decrease in film thickness. The hydrogen content for thinner films is at present under investigation. For a bulk sample, it is known that the amount of hydrogen taken up by $LaNi_5$ is about 7.[9] The smallness of hydrogen uptake by the films compared with the bulk is due to the amorphous state of the film structure and to the existence of a surface oxide as a dead layer for hydrogen absorption.

Figure 11 shows a pressure-composition isotherm for the $LaNi_5$ film (*ca.* 1.5 μm thick) at 333 K. The hydrogen concentration increases with an increase in

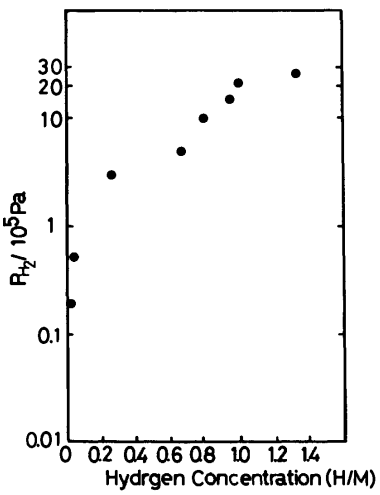

Fig. 11. Pressure-Concentration isotherm for an $LaNi_5$ film (thickness *ca.* 1.5 μm) at 333 K.

pressure. A pressure plateau (usually observed in a bulk sample) is absent. A result for an ZrNi amorphous alloy[38] is analogous to our result. It can be assumed that the absence of a pressure plateau is one of the features of an amorphous alloy.

The present work was partially supported by a Grant-in-Aid for Developmental Scientific Research No. 58850168 from the Ministry of Education, Science and Culture.

References

1) E. L. Huston and J. J. Sheridan III, "Industrial Applications of Rare Earth Elements," ed by K. A. Gschneidner, Jr., ACS Symposium Series 164, American Chemical Society, Washington, D.C., 1981, pp. 223.
2) D. P. Gregory, "The Rare Earths in Modern Science and Technology," ed by G. J. McCarthy and J. J. Rhyne, Plenum Press New York, 1977, pp. 1.
3) Y. Fukai, *Jpn. J. Appl. Phys.*, **48**, 1035 (1979).
4) I. Sheft, D. M. Gruen, and G. J. Lamich, *J. Less-Common Met.*, **74**, 401, (1980).
5) G. D. Sandrock and E. L. Huston, *Chem. Tech.*, **1981**, 754.
6) S. Ono and Y. Osumi, *Seramikkusu*, **14**, 339 (1979).
7) R. L. Cohen and J. H. Wernick, *Science*, **214**, 1081 (1981).
8) M. Nakane, *Kagaku To Kogyo*, **36**, 861 (1983).
9) J. H. N. van Vucht, F. A. Kuijpers, and H. C. A. M. Bruning, *Philips Res. Rept.*, **25**, 133 (1970).
10) K. H. J. Buschow and H. H. van Mal, *J. Less-Common Met.*, **29**, 203 (1972).
11) H. H. van Mal, K. H. J. Buschow, and A. R. Miedema, *J. Less-Common Met.*, **35**, 65 (1974).
12) A. Iandelli and A. Palenzona, "Handbook in the Physics and Chemistry of Rare Earths," ed by K. A. Gschneidner, Jr. and L. Eyring, North-Holland, Amsterdam, 1979, Vol. **2**. pp. 1.
13) J. Deporles, D. Givord, R. Lemaire, and H. Nagai, *J. Less-Common Met.*, **40**, 299 (1975).
14) A. L. Bowman, J. L. Anderson, and N. G. Nereson, "Proc. 10th Rare Earth Research Conf., Carefree, AZ, 1973," ed by C. J. Kevane and T. Moeller, U. S. Atomic Energy Commission, Oak Ridge, TN, 1973, pp. 485.
15) A. F. Andresen, *J. Less-Common Met.*, **88**, 1 (1982).
16) W. E. Wallace, *J. Less-Common Met.*, **88**, 141 (1982).
17) R. Wang, *Mater. Res. Bull.*, **11**, 281 (1976).
18) L. Belkbir, E. Joly, N. Gerard, J. C. Achard, and A. Percheron-Guégan, *J. Less-Common Met.*, **73**, 69 (1980).
19) L. Schlapbach, A. Seiler, F. Slucki, and H. C. Siegmann, *J. Less-Common Met.*, **73**, 145 (1980).
20) K. Masumoto, K. Suzuki, H. Fujimori, and K. Hashimoto, "Materials Science of Amorphous Metals," Ohmu-sha, Tokyo, 1982, p.p. 7.
21) H. Okuno and Y. Sakurai, *J. Appl. phys.*, **53**, 8245 (1982).
22) D. M. Mattox, *J. Vac. Sci. Technol.*, **10**, 47 (1973).
23) G. Adachi, K. Niki, and J. Shiokawa, *J. Less-Common Met.*, **81**, 345 (1981).
24) G. Adachi, K. Niki, H. Nagai, and J. Shiokawa, *J. Less-Common Met.*, **88**, 213 (1982).
25) B. Singh, N. A. Surplice, and J. Müller, *J. phys. D*, **9**, 2087 (1976).
26) O. Singh and A. E. Curzon, *Thin Solid Films*, **44**, 233 (1977).
27) A. E. Curzon and O. Singh, *J. Phys. F*, **8**, 1619 (1978).
28) C. K. Jorgensen and H. Berthou, *Chem. Phys. Lett.*, **13**, 186 (1972).
29) W. Y. Howng and R. J. Thorn, *Chem. Phys. Lett.*, **56**, 463, (1978).
30) S. Suzuki, T. Ishii, and T. Sagawa, *J. Phys. Soc. Jpn.*, **37**, 1334 (1974).
31) Y. Okamoto, K. Adachi, T. Imanaka, and S. Teranishi, *Chem. Lett.*, **1974**, 241.
32) K. Tatsumi, K. Kasuga, and M. Tsutsui, *J. Am. Chem. Soc.*, **101**, 486 (1979).
33) W. Y. Howng and R. J. Thorn, *J. Phys. Chem. Solids*, **41**, 75 (1980).
34) J. H. Wernick and S. Geller, *Acta Cryst.*, **12**, 662 (1959).
35) W. E. Wallace, R. F. Karllcek, Jr., and H. Imamura, *J. Phys. Chem.*, **83**, 1708 (1979).
36) M. Kitada, *Nippon Kinzoku Gakkai Shi*, **41**, 412 (1977).
37) G. A. Frazier and R. Glosser, *J. Phys. D*, **12**, L113 (1979).
38) K. Suzuki, *J. Less-Common Met.*, **89**, 183 (1983).

Ultraviolet Photoelectron Spectroscopy of Some Fundamental Vinyl Polymers and the Evolution of Their Electronic Structures

CHEN Shang Xian,† Kazuhiko SEKI,* Hiroo INOKUCHI, Shimpei HASHIMOTO,††
Nobuo UENO,††† and Kazuyuki SUGITA†††
Institute for Molecular Science, Myodaiji, Okazaki 444
††*Research Laboratory, Japan Synthetic Rubber Co., Higashi-Yurigaoka, Asao-ku, Kawasaki 215*
†††*Department of Image Science and Technology, Faculty of Engineering, Chiba University, Yayoicho, Chiba 260*
(Received May 31, 1984)

UV photoelectron spectra were measured for polypropylene (PP), poly(vinyl fluoride) (PVF), 1,2-polybutadiene (1,2-PBD), poly(vinyl chloride) (PVC), and poly(vinyl alcohol) (PVA). Their threshold ionization energies were found to be 8.5, 9.2, 7.5, 8.8, and 8.0 eV (1 eV≅0.1602 aJ), respectively. The evolution of their electronic structures (from those of small related molecules) were analyzed, mainly, by using the photoelectron spectra of these small compounds (including the new data of 1,2-propanediol). The data of previously measured polyethylene (PE) and polystyrene (PS) were analyzed together. With the results, the polymers were classified into three groups according to the increasing order of localization of the positive hole in the cationic state: (1) PE, PP, and PVF, (2) 1,2-PBD, PVC, and PVA, and (3) PS as a representative of aromatic-pendant polymers.

Ultraviolet photoelectron spectroscopy (UPS) has been developed as a powerful tool in studying the electronic structure of organic solids.[1-4] In particular, an important quantity obtainable by UPS is the threshold ionization potential of a solid, which gives the location of the top of a valence band. Together with the energy of the bottom of a conduction band, it gives a basic picture of the electronic structure of a solid. However, so far studies of organic polymers by UPS have been concentrated on polymers with aromatic groups,[5,6] polyethylene (PE) and its model compounds,[7] and some conducting polymers.[8] There seems to be no report on vinyl polymers with pendants other than aromatic rings, except for a relevant report by Vilesov *et al.*[9] on the photon-energy dependence of the photoemission quantum yield. Pireaux *et al.*[10] reported an X-ray photoelectron spectroscopy (XPS) study of vinyl polymers, but the low intensity and the broadness of the spectral features prevented a detailed study of the valence bands.

In this work, we report a UPS study regarding a series of vinyl polymers $\{CH_2CHX\}_n$ with non-aromatic pendant X, *i.e.*, polypropylene (PP, X:CH_3), poly(vinyl fluoride) (PVF, X:F), 1,2-polybutadiene (1,2-PBD, X:$CH{=}CH_2$), poly(vinyl chloride) (PVC, X:Cl), and poly(vinyl alcohol) (PVA, X:OH).

Our aims are (1) to obtain reliable experimental data regarding threshold ionization energy, and (2) to interpret the observed threshold energies (and other spectral features) in terms of intramolecular and intermolecular factors. The results of previously measured polyethylene (PE, X:H)[7a] and polystyrene (PS, X:C_6H_5)[5a] were also analyzed.

For aim (2), the electronic structure of an isolated single polymer chain is used as the base of interpretation. The intermolecular contribution can be deduced by comparing it with the observed solid state results. Unfortunately, however, the gaseous state of a polymer is not realizable, and theoretical calculations are not quantitatively reliable, either. In order to overcome this difficulty, we estimated the electronic structure of an isolated chain from the gas-phase photoelectron spectra of related small molecules by analyzing the pendant-chain and also pendant-pendant interaction. Since no information in the literature was available for 1,3-propanediol, which is related to PVA, we measured its gas-phase photoelectron spectrum. Theoretical band calculations for an isolated polymer chain[10-13] and solid XPS results[10] also helped in the interpretation for some polymers.

This method of analysis shows how the electronic structures of polymer solids evolve from those of small units. The results indicate various patterns of evolution, depending on the polymers. In particular, the degree of delocalization of the positive hole in the cationic state ranges from almost complete localization in a pendant to extensive delocalization over the principal chain. Although rather rough approximations are involved in the present treatment, we believe it gives a general viewpoint for analyzing the electronic structures of polymers.

Experimental

Standard samples of PP (isotactic), PVF, PVC, and PVA were available from Scientific Polymer Products Inc. (catalog Nos. 130, 022c, 038c, and 002, respectively). Low-crystallinity 1,2-PBD was provided by Japan Synthetic Rubber Company. PP was twice reprecipitated from a decalin solution with cyclohexane as a poor solvent; PVF twice from *N,N*-dimethyl formamide (DMF) with methanol; PVC three times from tetrahydrofuran (THF) with methanol; and 1,2-PBD once from a benzene solution with methanol. PVA was used without further purification.

† On leave from the Institute of Chemistry, Academia Sinica, Beijing, China.

The UPS spectrometer consists of a light source and a retarding-potential-type electron energy analyzer, which was reported previously.[14] Two kinds of light sources were used. One was hydrogen discharge lamp attached to a 0.5 m Seya-Namioka-type monochromator and the other was a rare-gas resonance lamp capable of He I (21.2 eV), Ne I (16.8 eV), and Ar I (11.7 eV) emissions. The same ionization energies were obtained by both two light sources.

Since these polymers are insulators, we had to use thin film samples to avoid charging. The films were prepared by putting a few drops of a hot solution (≈0.2 wt%) of a polymer on a Cu-disk (12 mm diameter) substrate, followed by the rotation of the substrate. The rotation spreaded the solution, and the solvent vaporized, leaving a thin film.[15] The temperatures of the solution and the substrate were kept at 60—70 °C except for the case of 1,2-PBD, where the film was prepared at room temperature. The solvents used for PP, PVF, 1,2-PBD, PVC, and PVA were decalin, DMF, benzene, DMF, and redistilled water, respectively.

In this sample preparation procedure, we paid close attention to the suppression of the emission from the substrate, because the threshold energy of the substrate was inferred to be smaller than those of polymers. This requires both a good uniformity of the film and a sufficient average thickness. We found that the uniformity significantly depends on the adhesive property of the solution to the substrate. For example, PVC films of poor (net-like) quality were obtained from THF solution even if a large amount of solution was used, while a uniform film was obtained by using DMF and heating the substrate and the solution. After choosing appropriate solvents, we increased the amount of deposited polymer sample until there was no further change in the spectrum. The concentration and procedures described above gave satisfactory films for getting an intrinsic spectra of the polymers without charging, although we had to use very weak light for some specimens in order to avoid charging. The nominal average thickness of a film was ≈2 μm, but the polymers tended to accumulate at the periphery of a substrate surface when the solvent vaporized away. Therefore, the real average thichness on a substrate surface should be smaller. The absence of charging was verified by the sharpness of the cut off at the low-kinetic-energy side of the spectra.

The He I gas-phase photoelectron spectrum of 1,3-propanediol was measured on the photoelectron spectrometer which was reported previously.[16]

Results and Discussion

Threshold Ionization Energies. In Figs. 1—5, the photoelectron spectra of the polymers are shown. The abscissa represents the solid ionization energy I_s, which is related to the kinetic energy of a photoelectron by $I_s=h\nu-E_k$, where $h\nu$ is the photon energy. The values of the threshold ionization energy are given by $I_s^{th}=h\nu-E_k^{max}$, where E_k^{max} is the maximum kinetic energy of photoelectrons. They are listed in Table 1. These values are the averages of at least six times measurements for each compound. The standard deviation was less than 0.2 eV. Table 1 also lists our previous data for high-density PE[7a] and PS,[5a] the

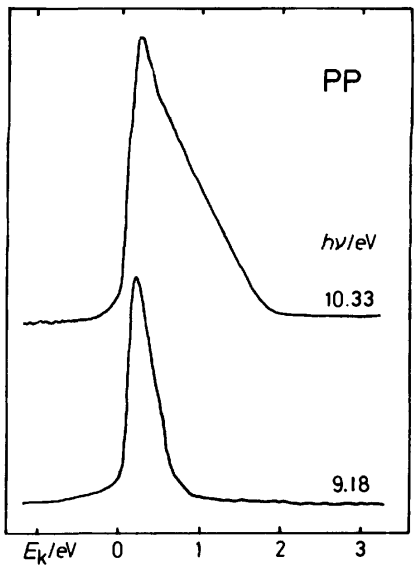

Fig. 1. Photoelectron spectra of polypropylene. The photon energy of the exciting light is shown at the side of each curve.

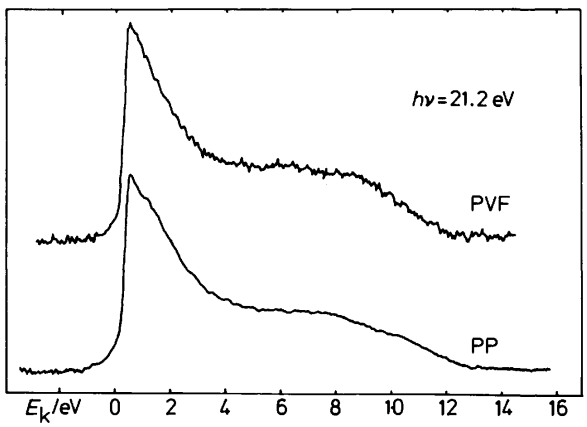

Fig. 2. Photoelectron spectra of poly(vinyl fluoride) and polypropylene by He I (21.2 eV) light source.

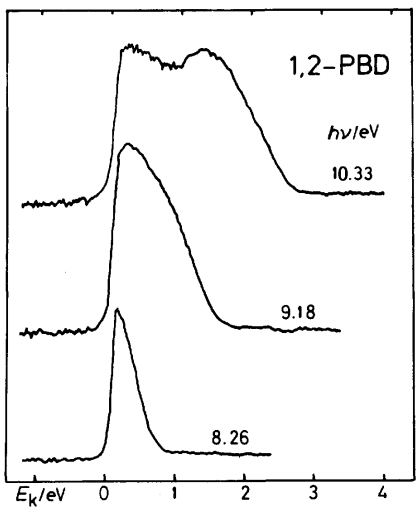

Fig. 3. Photoelectron spectra of 1,2-polybutadiene. The photon energy of the exciting light is shown at the side of each curve.

assignment of the character of the HOMO (discussed below), the threshold (adiabatic) ionization energies of the corresponding "unit" compounds CH_3CH_2X in the gas phase I_g^a(unit),[16-18] and the difference $\Delta I = I_g^a$(unit) $-I_s^{th}$. (Pireaux *et al.*[10] used $CH_2=CHX$ for the unit compound, but this is inadequate since the character of the highest occupied orbital can change from the π orbital in $CH_2=CHX$ to σ or lone pair orbitals in the polymer, as shown below).

Vilesov *et al.*[9] reported the I_s^{th} values of PVA, PVC, poly(*N*-vinylcarbazole) (PVCz), and PS to be 6.0, 6.0, 5.8, and 7.0 eV, respectively. The values for PVA and PVC are much lower than the present results, while those for PVCz and PS are in good agreement with our results (5.85 eV[5d] and 6.95 eV[5a] obtained with the present instrument). Since the preparation of uniform films was more difficult for PVA and PVC than for polymers with aromatic pendants, we may conclude that the data by Vilesov *et al.* are questionable for PVA and PVC.

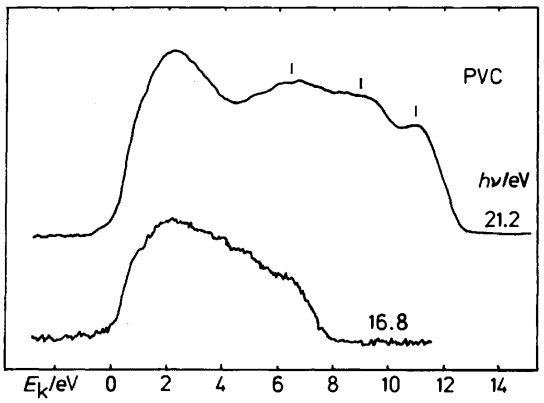

Fig. 4. Photoelectron spectra of poly(vinyl chloride) by He I (21.2 eV) and Ne I (16.8 eV) light sources.

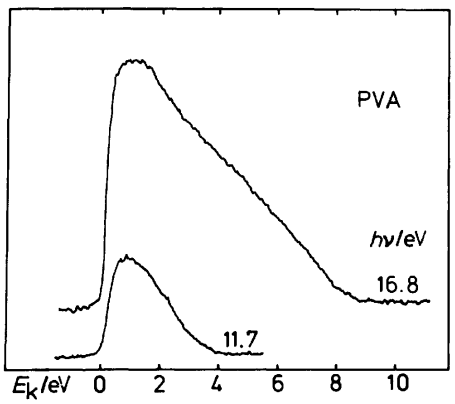

Fig. 5. Photoelectron spectra of poly(vinyl alcohol) by Ne I (16.8 eV) and Ar I (11.7 eV) light sources.

Pireaux *et al.* reported XPS data on the location of the top of the valence band for some of these polymers,[10] but threshold energies derived from their data with estimated work functions ($E_1+\phi$ in Table 6 of Ref. 10) are 0.5—2 eV larger than the present directly-measured values.

Method of Analysis. It is known that for molecular solids, a solid photoelectron spectrum resembles the gas-phase spectrum of the compound if a shift is made in the ionization-energy scale.[19] The similarity indicates the preservation of the electronic structure of a molecule in a solid, and that the photoemission from a molecular solid can be regarded as the ionization of a molecule in the solid. The shift can be attributed to the stabilization of the molecular cation by the polarization of the surrounding molecules; hence, it is called the polarization energy P.[1,4c] According to an analysis of the contribution of molecules in the bulk and at the surface, we already noted that the bulk polarization energy can be evaluated as the difference of the threshold energies of the gas and solid phases rather than the difference in the peak energies.[4c]

In the case of a polymer solid, each chain corresponds to a molecule in the above discussion. Thus, the discussion regarding a photoelectron spectrum of a polymer solid can be divided into that of (1) the electronic structure of an isolated chain and (2) the polarization energy. The character of the occupied orbitals and their relative energy difference is determined by the former factor, while both factors affect the absolute energy scale.

Figure. 6 illustrates our way of interpreting the observed thresholds and spectral features. At first we

TABLE 1. THE THRESHOLD IONIZATION ENERGIES OF VINYL POLYMERS (I_s^{th}) AND THE GAS PHASE THRESHOLD IONIZATION ENERGIES OF THEIR "UNIT" COMPOUNDS (I_g^a)

Compound	I_s^{th}/eV	Assignment	Unit compound	I_g^a (unit)/eV	ΔI/eV[g]
PE	8.5[a]	backbone	CH_3CH_3	11.7[c]	3.2
PP	8.5	backbone	$CH_3CH_2CH_3$	11.1[c]	2.6
PVF	9.2	backbone	CH_3CH_2F	11.7[d]	2.5
1,2-PBD	7.5	pendant	$CH_3CH_2CH=CH_2$	9.7[e]	2.2
PVC	8.8	pendant n_{Cl}	CH_3CH_2Cl	11.0[c]	2.2
PVA	8.0	pendant n_O	CH_3CH_2OH	10.3[c]	2.3
PS	6.9_5[b]	pendant	$CH_3CH_2C_6H_5$	8.6[f]	1.7

PP: polypropylene, PVF: poly(vinyl fluoride), 1,2-PBD: 1,2-polybutadiene, PVC: poly(vinyl chloride), PVA: poly(vinyl alcohol), PE: polyethylene, PS: polystyrene.
a) Ref. 7a). b) Ref. 5a). c) Ref. 21a). d) Ref. 16. e) Ref. 17. f) Ref. 18. g) $\Delta I \equiv I_g^a$(unit)$-I_s^{th}$.

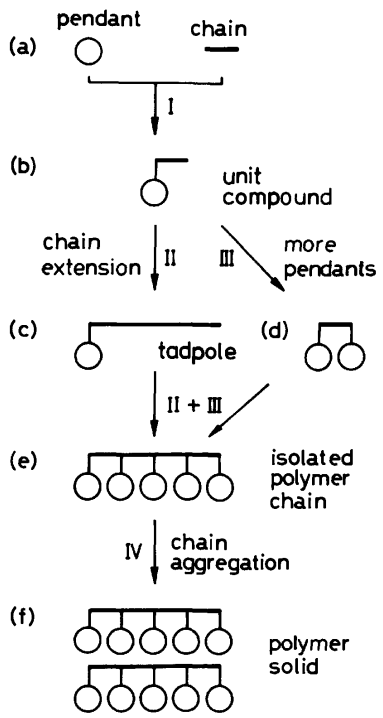

Fig. 6. Schematic representation of the evolution of the electronic structure of a vinyl polymer solid from those of small units.

estimate the electronic structure of an isolated polymer chain (e) from data for small related molecules, by analyzing the effects of the following steps.

(I) The combination of a pendant with a short alkane C_2H_6 to form a unit compound CH_3CH_2X, which is the repeating unit of a vinyl polymer.

(II) The extension of an alkyl chain to form a "tadpole" compound $CH_3(CH_2)_\infty X$.

(III) The attachment of other pendants to the chain to form an isolated polymer chain.

The remaining difference between the estimated structure of an isolated chain and the observed results for a polymer solid (f) is ascribed to the effect of

(IV) aggregation of chains to form a polymer solid.

Steps (I) and (II) jointly correspond to the interaction of a pendant and the principal (backbone) chain, (III) to the interaction among pendants through space or through the principal chain, and (IV) to the interaction among chains. For small compounds from (a) to (d) in Fig. 6, gas-phase UPS spectra are available. Further, additional information on the isolated polymer chain (e) and polymer solid (f) are available from theoretical band calculations[10-13] and XPS spectra,[10] respectively.

In this analysis, we distinguish the ionization energies for the onset and peak of a band in a photoelectron spectrum. In the gas phase, the peak energy for the ionization from a MO corresponds to ionization without a change in the molecular geometry, while the onset corresponds to the ionization to a relaxed molecular geometry.[20] When we assume Koopmans' theorem, the former corresponds to the orbital energy of the MO.[20] Thus, peak energies are more suitable for discussing the evolution of the electronic structure of a molecule. However, bands originating from different MO's often overlap and no clear peak can be observed, as in some of the compounds studied here. In such cases, we can still discuss the change in the electronic structure using onset energies, assuming that the onset-peak energy separation changes little among similar molecules. In the solid spectrum, on the other hand, the physical meaning of the peak energy is ambiguous owing to various mechanisms of peak broadening.[4b,c] Further, no clear peak can be observed for some of the polymers studied here. Fortunately, however, the polarization energy is obtained as the difference between the thresholds of gas and solid states, as described above. Thus, we don't need the peak energies in order to evaluate the intermolecular effects.

Taking account of such a situation, we will mainly use the onset energies in the following analysis, but will also use peak energies when they are available and useful. We denote the threshold (adiabatic) ionization energies of a tadpole compound and a polymer chain as I_g^a(tadpole) and I_g^a(polymer), respectively. As materials for discussion, Table 2 lists the data[21] for small alkanes with corresponding pendants, *i.e.* the ionization energies of the highest occupied orbitals among (1) orbitals localized on the pendant (I_1), and (2) orbitals delocalized over the chain (I_2).

Electronic Structure of an Isolated Chain. A difficulty in the analysis of step (I) for the small pendants studied here is the choice of a compound embodying the "pendant" X. For larger pendants such as aromatic ones, the attchment of an H atom to X has little effect on the electronic structure of the molecular orbitals, and HX is a natural choice. For small X, however, an H atom strongly affects the electronic structure of HX. Therefore, we will not discuss process (I) in detail and will start from CH_3CH_2X, although we also list the threshold ionization energies of HX[21] in Table 2. This difficulty is the reason why we listed I_g^a(unit)'s in Table 1.

The effect of chain extension (II) can be estimated by examining the dependence of the ionization energies on the carbon number n. As shown in Fig. 7, the ionization potentials of normal alkanes form a good linear relation with $1/n$. The decrease of I_2 with n is due to the delocalization of the highest σ orbital. Also the first vertical ionization energies of alkyl alcohols from C_2H_5OH ($1/n$=0.5) to n-$C_8H_{15}OH$ ($1/n$=0.125)[21i] are also linear with $1/n$ within 0.03 eV. This corresponds to a change of the inductive effect to the O_{2p} lone pair orbital. These empirical relations suggest that we can estimate the threshold ionization energy of a tadpole compound by extrapolation to $1/n$=0 with a probable error of ≈0.1 eV. Such plots are shown by

TABLE 2. IONIZATION ENERGIES OF ONSETS OF ORBITALS LOCALIZED ON PENDANT GROUP (I_1) AND DUE TO PRINCIPAL CHAIN (OR CHAIN-PENDANT BOND) (I_2) OF SUBSTITUTED ALKANES

-X		HX	CH_3CH_2X	CH_3CH_2-CH_2X	CH_3CHX-CH_3	$CH_3CH_2CH_2$-CH_2X	CH_2XCH_2-X	CH_2XCH_2-CH_2X
-H	I_2/eV	15.43[a]	11.65[a]	11.07[a]	11.07[a]	10.63[a]	11.65[a]	11.07[a]
$-CH_3$	I_2/eV	12.98[a]	11.07[a]	10.63[a]	10.55[b]	10.35[a]	10.63[a]	10.35[a]
-F	I_1/eV	16.05[c]	15.3[d]	14.7[d]	—	—	—	—
	I_2/eV	—	11.7[d]	11.3[d]	—	—	—	—
$-CH=CH_2$	I_1/eV	10.51[d]	9.7[e]	9.4[f]	9.5[g]	9.4[f]	9.3[h]	9.1[h]
	I_2/eV	—	11.3[e]	10.8[f]	—	10.6[f]	10.7[h]	10.7[h]
-Cl	I_1/eV	12.75[d]	11.0[d]	10.7[d]	10.7[d]	10.6[d]	11.1[i]	10.9[i]
	I_2/eV	—	12.5[d]	11.8[d]	12.1[d]	11.4[d]	13.1[i]	12.3[i]
-OH	I_1/eV	12.62[d]	10.3[d]	10.1[d]	10.0[d]	10.0[i]	10.3[d]	9.9
	I_2/eV	—	11.6[d]	11.3[d]	11.0[d]	11.0[i]	11.8[d]	11.4
$-C_6H_5$	I_1/eV	9.25[d]	8.6[j]	8.6[j]	8.6[j]	8.6[j]	8.7[k]	—
	I_2/eV	—	10.8[j]	10.7[j]	10.7[j]	10.4[j]	10.7[k]	—

a—j) Ref. 21. Values were read from reported photoelectron spectra unless an explicit value was given in the reference.

TABLE 3. IONIZATION ENERGIES OF NORMAL ALKANES, METHYL SUBSTITUTED ALKANES, AND CYCLOALKANES

[Normal] Compound	I_2/eV	[Branched] Compound	I_2/eV
$CH_3CH_2CH_3$	11.07[a]	CH_3CHCH_3 (CH$_3$ on 2nd C)	10.55[b]
$CH_3CH_2CH_2CH_3$	10.63[a]	$CH_3CHCH_2CH_3$ (CH$_3$ on 2nd C)	10.30[b]
$CH_3(CH_2)_3CH_3$	10.35[a]	$CH_3CHCH_2CH_2CH_3$ (CH$_3$ on 2nd C)	10.09[b]
cyclohexane	9.88[c]	methylcyclohexane	9.86[b]

a) Ref. 21a). b) Ref. 21b). c) Ref. 22.

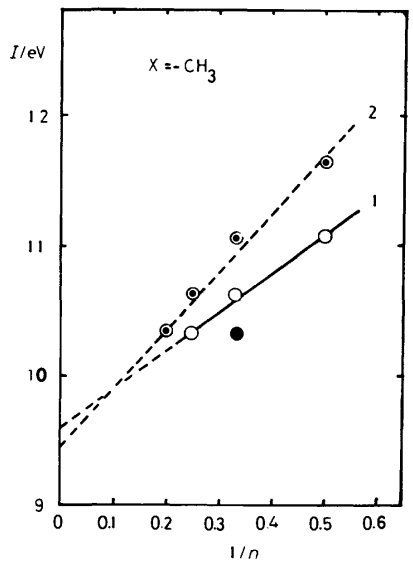

Fig. 7. Dependence of the ionization potential I_2 of normal alkanes (2, ⊙) and their methyl-substituted derivatives (1, ○) on the reciprocal of the chain carbon number n. The value of 1,3-disubstituted propane is also shown (●).

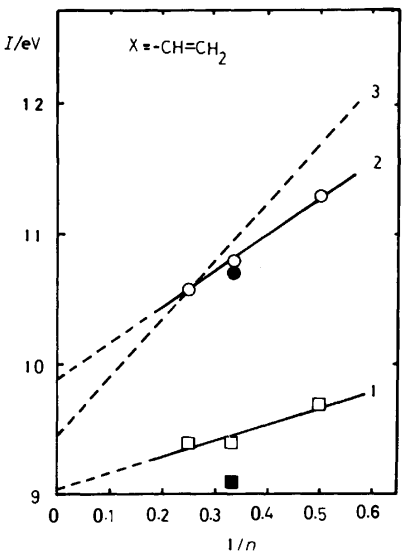

Fig. 8. Dependence of onset ionization energy I of monovinyl-substituted n-alkanes on the reciprocal of the chain carbon number n. 1: onset of π ionization (I_1, □), 2: onset of principal chain ionization (I_2, ○), and 3: I of unsubstituted alkanes from Fig. 7 as a reference. Values of I_1 (■) and I_2 (●) of 1,3-disubstituted propane are also shown.

real lines 1 in Figs. 7—10 for X=CH_3, -CH=CH_2, -Cl, and -OH, respectively. The plot for X=F was impossible owing to a lack of data. By assuming a linear relation between I_2 and $1/n$ also, we see that there will be no crossover between I_1 and I_2 in a tadpole compound, with X=Cl being a case that is a little ambiguous.

The further introduction of pendants will affect the electronic structure through (1) the inductive effect and (2) the interaction among pendants. The details of these effects depend on the polymers, so we will now discuss each polymer.

Polyethylene (PE) and Polypropylene (PP): There are

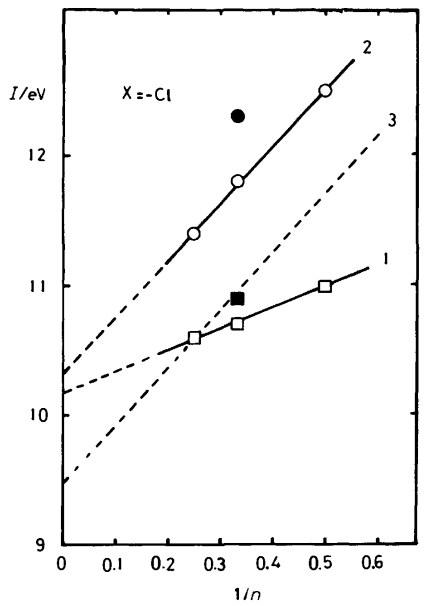

Fig. 9. Dependence of onset ionization potential I of monochloro-substituted normal alkane on the reciprocal of the chain carbon number n. 1: Cl_{3p} ionization (I_1, □), 2: principal chain ionization (I_2, ○), 3: I of unsubstituted alkanes as a reference. Values of I_1 (■) and I_2 (●) of 1,3-disubstituted propane are also shown.

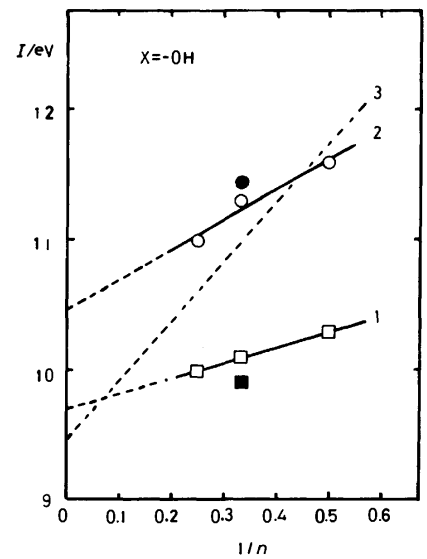

Fig. 10. Dependence of onset ionization potential I of monohydroxy-substituted normal alkanes on the reciprocal of the chain carbon number n. 1: O_{2p} ionization (I_1, □), 2: principal chain or C-O bond ionization (I_2, ○), 3: I of unsubstituted n-alkanes (----) as a reference. Values of I_1 (■) and I_2 (●) 1,3-disubstituted propane are also shown.

only σ-electrons in these polymers, and orbitals are delocalized over the principal chain.

Table 3 lists the I_2's of methyl-substituted alkanes. The values of monomethyl-substituted alkanes are also shown in Fig. 7 (○). The latter are lower than those of unsubstituted compounds (⊙), but the difference decreases with the increase in n and becomes almost zero for $n\rightarrow\infty$. Although the introduction of a second CH_3 group lowers the I_2 for $n=3$ (●) a little, band calculations of isolated chains of PE and PP give a negligible difference between the orbital energies of the HOMOs.[13] Such an insensitivity to the CH_3 substitution can be understood when we consider that (1) the attachment of a CH_3 group does not affect the range of delocalization of the HOMO on the whole chain, and (2) the CH_3 group has almost no inductive effect to alkyl chain.

Therefore, we can expect the I_g^a(polymer) of PP to be the same as I_g^a(tadpole). The latter can be estimated to be 9.6 eV from the extrapolation in Fig. 7 to $1/n=0$. A similar extrapolation for PE gives I_g^a(polymer)=9.4 eV, which is indeed similar to that of PP.

Poly(vinyl fluoride) (PVF): Band calculations[10-12] and XPS[10] show that F_{2p} orbitals have higher ionization potentials than σ orbitals derived from atomic orbitals of carbon and hydrogen. This tendency has already been seen for compounds listed in Table 2. The increase in the length of the alkyl chain seems not to change this situation because of the large difference between I_1 and I_2. Thus, we can expect that the highest occupied orbital is a delocalized one over the principal chain as in the case of PE and PP. The ionization potential of fluoroalkanes in Table 2 are higher than those of corresponding alkanes due to the inductive effect of the fluorine atom. Thus, we expect a higher I_g^a(polymer) of PVF than those of PE or PP. Unfortunately, the data of small related compounds are not sufficient for making a quantitative estimation of I_g^a(polymer).

1,2-Polybutadiene (1,2-PBD): For this polymer, there is a double bond in the side chain with π electrons localized in it. It determines the value of I_1. The right-hand peak in the spectrum for $h\nu$=10.33 eV (Fig. 3) should correspond to this orbital, since such a distinct peak does not appear in the spectra of PE.[7a]

The effect of introducing more than one vinyl group can be seen in CH_2=$CH(CH_2)_3CH$=CH_2 (■, ● in Fig. 8) in which the number of carbon atoms between the pendants is the same as in the polymer. As seen from the vertical ionization energies listed in Table 4, the interaction of the two vinyl groups results in a splitting of 0.4 eV between the π ionization energies of CH_2=$CH(CH_2)_3CH$=CH_2, while their centroid does not shift from the π ionization energy of $CH_3(CH_2)_2CH$=CH_2. This means that the inductive effect of the vinyl group is small, and only the π-π interaction is important. The change of I_2 by the inductive effect is also very small. As a result, I_1 is more decreased than I_2 and the I_g^a(polymer) is determined by the π orbitals.

The effect of π-π interaction in an isolated infinite polymer chain can be evaluated by a simple theory of a one-dimensional chain with only the nearest-neighbor

TABLE 4. VERTICAL IONIZATION ENERGIES OF $CH_3CH_2CH_2X$ AND $XCH_2CH_2CH_2X$ (IN eV)

X	CH_3CH_2CHX I_0	$XCH_2CH_2CH_2X$ I_I	I_{II}	Splitting $I_{II}-I_I$	Shift $(I_I+I_{II})/2-I_0$
$CH=CH_2$	9.7_0[a]	9.5_2[b]	9.9_3[b]	0.4_1	0.0_3
Cl	10.8_8[c]	11.1_6[d]	11.5_5[d]	0.3_9	0.4_8
OH	10.4_9[c]	10.2_4[e]	10.9_0[e]	0.6_6	0.0_8

a) Ref. 20f). b) Ref. 20h). c) Ref. 16. d) Ref. 20i). e) Present results.

interaction β among the units. According to this formalism, the splitting for a dimer is 2β and the energy spread for an infinite chain is 4β, which is symmetric with respect to the energy of one unit.[23] Therefore, the lowest ionization potential in the infinite chain should be lower than that of one unit by the amount of the splitting in the dimer. Assuming the same amount of decrease in the threshold ionization energy as that in the peak energy, we can expect that the value of I_g^a (polymer) is 0.4 eV smaller than I_g^a(tadpole), which can be estimated to be 9.1 eV from the extrapolation in Fig. 8. This gives I_g^a(polymer)=8.7 eV.

Poly(vinyl chloride) (PVC): The values of I_1 are determined by the two Cl_{3p} lone pairs. In the He I spectrum, three features at E_k=11.0, 9.0, and 6.5 eV (I_s=10.2, 12.2, and 14.7 eV) can be clearly seen. These features were also observed in the reported XPS spectrum,[10] with a good agreement of intervals. They should be due to the Cl atoms.

The effect of multiple Cl-substitution can be examined as in the case of 1,2-PBD using the ionization potentials in Table 4. Similar to 1,2-PBD, the introduction of the second Cl atom in $CH_3CH_2CH_2Cl$ gives a splitting of 0.4 eV in the Cl_{3p} lone-pair bands. Unlike 1,2-PBD, however, the large inductive effect of the Cl atoms raises the centroid of these bands by 0.5 eV from that of $CH_3CH_2CH_2Cl$. As a net result of these conflicting effects, I_1 is even increased by 0.3 eV (■ in Fig. 9). On the other hand, I_2(●) experiences only an inductive effect, and is significantly increased (≈0.5 eV).

With the simple theory described for 1,2-PBD, the interaction among the lone pairs in an infinite PVC chain will lower the Cl_{3p} ionization energy by 0.4 eV relative to that of $CH_3(CH_2)_\infty Cl$. The inductive effect will not change the centroid of the Cl 3p levels significantly from that in $Cl(CH_2)_3Cl$ by further Cl-introduction, judging from the small change of ionization energy from CH_2ClCH_2Cl (11.41 eV)[16] to $CHCl_2CH_2Cl$ (11.48 eV)[16] and CCl_3CH_2Cl (11.45 eV).[16] With these conflicting effects, we expect that I_1 will change only a little (≈0.1 eV increase) from $CH_3(CH_2)_\infty Cl$ to $\{CH_2CHCl\}_n$. The value of I_2 will be increased by an inductive effect. With these values and the extrapolation of the lines in Fig. 9 to $1/n=0$, we see that the HOMO of the polymer is derived from the Cl_{3p} lone-pair orbitals with I_g^a(polymer)≃I_g^a(tadpole)= 10.3 eV. The peak at I_s=10.2 eV in Fig. 4 should correspond to this. This assignment agrees with that from XPS.[10] For deeper levels, contributions from lone pairs, C-Cl bonds, and alkyl chains overlap and form peaks of I_s=12.2 eV and 14.7 eV. Since these peaks do not appear in the spectrum of PE, we will tentatively follow the assignments by Pireaux *et al.*[10] to lone pair and C-Cl bonds, respectively.

Poly(vinyl alcohol) (PVA): There are two O_{2p} lone pairs per oxygen atom, which determine the value of I_1.

The way of discussing the effect of the multiple introduction of OH groups is the same as those for 1,2-PBD and PVC, but we must pay attention to the effect of possible hydrogen bonding.[24] Such hydrogen bonding should lead to a larger interaction than the usual van der Waals interaction. As for the intramolecular hydrogen bond, the data of $HO(CH_2)_3OH$ in Table 4 indeed gives a large splitting of 0.6_6 eV for orbitals. The inductive effect of the new OH group is small (0.1 eV increase) for both the mean ionization energy of such a split pair and I_2 (Table 4). With a similar discussion as for 1,2-PBD and PVC, we can estimate a decrease of I_1 by 0.6 eV from $CH_3(CH_2)_\infty OH$ to $\{CH_2CHOH\}_n$.

In the case of an intermolecular hydrogen bond, the inductive effect by the OH groups in the same chain will remain small, but the intramolecular O_{2p}-O_{2p} interaction should be smaller than for the case of an intramolecular hydrogen bond. Instead, the intermolecular interaction of OH groups should cause a lowering of the ionization potential comparable to that from methanol (10.96 eV) to methanol dimer (10.42 eV).[25] Although this is not an intramolecular effect, the total difference between I_g^a (tadpole) and I_s^h should be similar to that in the case of an intramolecular hydrogen bond.

In any case, the ordering of I_1 and I_2 in a polymer chain is not changed from that in $CH_3(CH_2)_\infty OH$ estimated by the extrapolation in Fig. 10, and O_{2p} lone pairs will form the HOMO. Pireaux *et al.*[10] made the same assignment from XPS. The estimated value of I_g^a (tadpole)=9.7 eV gives I_g^a (polymer)=9.1 eV for a polymer chain with intramolecular hydrogen bonds.

Polystyrene (PS): As seen above, the highest occupied states of 1,2-PBD, PVC, and PVA are rather localized on a pendant group, in contrast to the case of PP and PVF where the highest occupied orbital is delocalized over the principal chain. A hole in the cationic state of

aromatic-pendant vinyl polymers is also known to be localized in a pendant group.[5] Therefore it is interesting to compare the present results described above with those of aromatic-pendant polymers.

We will examine polystyrene (PS) as a typical example. In PS, the highest occupied orbital gives a much smaller ionization energy (I_1) than that of the principal chain (I_2), as in most other aromatic-pendant polymers. Further, I_1 does not depend on the length of alkyl chain as shown in Fig. 11. Similar insensitivity to the size of alkyl group can be also seen in the small difference between *N*-ethylcarbazole and *N*-isopropylcarbozole.[26] Such an independence of the chain length is different from the tendency observed for the polymers studied above. This small interaction should be a result of the large difference in energy between π and σ orbitals and the small difference in electronegativity between the chain and the pendant. Another difference is an almost negligible interaction between the aromatic rings as seen in the small difference of I_1 values for ethylbenzene and bibenzyl in Table 2.

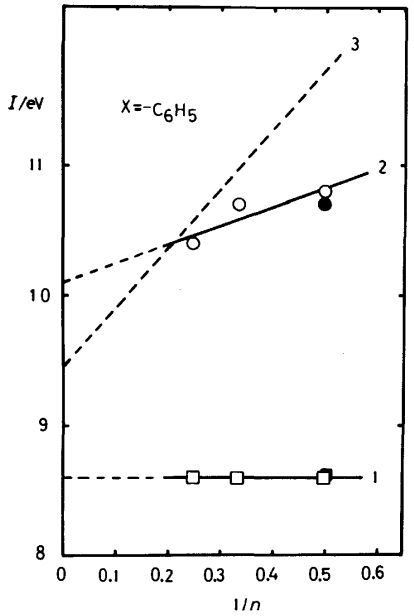

Fig. 11. Dependence of onset ionization potential I of monophenyl-substituted normal alkanes on the reciprocal of the chain carbon number n. 1: π ionization (I_1, □), 2: σ ionization (I_2, ○), 3: I of unsubstituted *n*-alkanes as a reference. Values of I_1 (■) and I_2 (●) of 1,2-disubstituted ethane are also shown.

The value of I_s^{th} is thus determined almost solely by a pendant phenyl group. In this sense, the picture of the ionization of one chromophore is more adequate in the aromatic-pendant polymers than in the other polymers studied here. As a result, both I_g^a(tadpole) and I_g^a(polymer) are expected to be the same as the threshold of ethylbenzene (8.6 eV).

Polarization Energies. Table 5 lists the estimated values of I_g^a(tadpole), I_g^a(polymer), and the polarization energy as the difference I_g^a(polymer)$-I_s^{th}$. It also lists the refractive indices n_D[29] as a guide for the polarizability. Possible errors of P is ±0.3 eV for PE, PP, and PS, while those for 1,2-PBD, PVC, and PVA should be larger (say, ±0.5 eV), mainly due to the uncertainty about the conformational dependence of the pendant-pendant interaction. Thus, we cannot discuss the latter group in detail. We only note that the value of the latter group are within the range covered by those of the former group.

On the average, these values are comparable or a little smaller than the common value of 1.7 eV for aromatic hydrocarbons,[4c] while aliphatic hydrocarbons have similar values. (Although PS has a P=1.7 eV, it is still smaller than the value 2.1 eV for benzene solid[27]). A possible factor contributing to such a trend is the polarizability of the molecules. The refractive indices in Table 5 are comparable to those of aliphatic solids,[27] but smaller than those of aromatic hydrocarbons. (*e,g*, n_D of anthracene for the three optical axes are 1.550, 1.775, and 2.04[30]).

Further, we also note two differences of polymer solids from molecular solids. (1) For some polymers, the positive charge is delocalized in a long chain in contrast to the localization in a molecule. At present there is no satisfactory theoretical method of estimating P for such a case. This situation may contribute to the small P of PE and PP. (2) Even for a localized positive charge, considerable part of the medium surrounding the charge may belong to the same molecule. Thus, the polarization effect from other molecules will be smaller than for molecular

Table 5. Estimated values I_g^a(tadpole), I_g^a(polymer) and P

Polymer	I_g^a(tadpole)/eV	I_g^a(polymer)/eV	P/eV	n_D
Polyethylene	9.4	9.4	0.9	1.545[a)]
Polypropylene	9.6	9.6	1.1	1.50[a)]
Poly(vinyl fluoride)	—	—	—	1.45[b)]
1,2-Polybutadiene	9.1	8.7	1.2	1.51[c)]
Poly(vinyl chloride)	10.3	10.3	1.5	1.54—1.55[a)]
Poly(vinyl alcohol)	9.7	9.1	1.1	1.49—1.53[a)]
Polystyrene	8.6	8.6	1.7	1.59[a)]

a—c) Ref. 29.

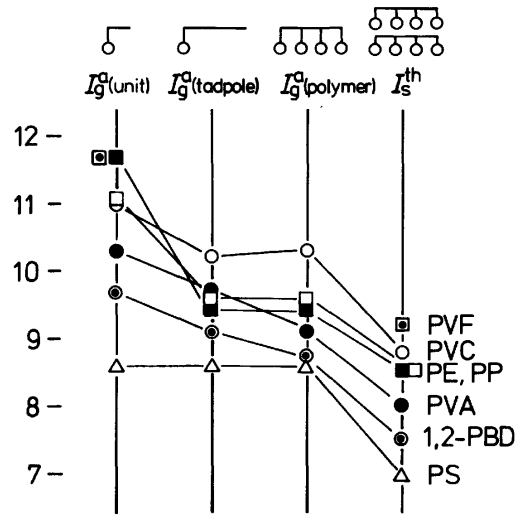

Fig. 12. Change of threshold ionization energy (in eV) from unit compounds to polymer solids.

solids. This may contribute to make the *P* of PS smaller than for benzene.

Summary of the Evolution of the Electronic Structure. Fugure 12 summarizes the change of threshold ionization energy from the unit compounds to polymer solids. As stated above, the estimated values might not be very accurate, in particular for 1,2-PBD, PVC, and PVA. Nevertheless, Fig. 12 clearly shows how a change of thresholds depends on the class of polymers.

For polymers with the HOMO delocalized over the principal chain, an extention of the chain length decreases the threshold energy effectively by delocalization, as seen in PE and PP. Although we could not make a quantitative examination, compounds related to PVF should also follow this trend. This delocalization is the reason for the larger values of ΔI for PE, PP, and PVF in Table 1 than the other polymers. The introduction of methyl groups into a polymer chain in PP does not affect the thresholds, but we can expect some inductive effect by pendants with a very different electronegativity from carbon, (*e.g.* X=F). Such an inductive effect should be the main reason of the much larger I_s^{th} of PVF than that of PE and PP. Similar large I_s^{th}'s were also found for other fluoropolymers.[31] As seen in Table 5, the polarization energies of these polymers are a little smaller than those of other polymers. It may be partly due to the extended distribution of the positive charge over the chain.

In polymers with aromatic pendants, represented by PS, neither a chain extension beyond CH_3CH_2X nor a pendant-pendant interaction affects the threshold. This fact comes from the well-localized nature of the hole, and makes ΔI smaller than those of the other polymers in Table 1, although the polarization energy is a little larger than for the other polymers.

Other polymers with small nonaromatic pendants (1,2-PBD, PVC, and PVA) show an intermediate behavior between the two classes of compounds described above. A chain extension causes a small decrease in the threshold energy, owing to the inductive effect of the alkyl chain. The introduction of many pendants also results in some change, but its magnitude and sign depend on a balance between the pendant-pendant interaction and the inductive effect.

The above discussion shows that an analysis of the change of ionization energy at the transition from a unit compound to a polymer solid is a fairly complex task. Even the inversion of the order of the threshold energies happens among different polymers. Such a situation is much more complex than for the case of simple molecular solids, where the polarization energy is the only origin of a lowering of the threshold energy from a free molecule. However, as shown above, if the analysis is properly made, it gives a deep insight into the electronic structure of polymers.

We also note that a group of polymers with an intermediate delocalization is new in UPS studies regarding polymers. The polymers so far studied could be classified into two extreme cases where the HOMO is either well delocalized (PE and fully conjugated polymers such as polyacetylene and $(SN)_x$)[8] or well localized (vinyl polymers with aromatic pendants[5] and poly(*p*-phenylene-ethylene,[6] where benzene rings are in the principal chain). The present study shows that the degree of delocalization of the cationic state covers a wide range from almost complete localization to extensive delocalization.

The authors express their sincere thanks to Dr. Y. Achiba for the measurement of the photoelectron spectrum of 1,3-propanediol, and to Dr. N. Sato, Prof. J. Delhalle, and Prof. K. Ishii for helpful discussion. Chen Shang Xian is indebted to Yamada Science Foundation for financial support.

References

1) L. E. Lyons and G. C. Morris, *J. Chem. Soc. (London) B*, 5192 (1960).

2) F. I. Vilesov, A. A. Zagrubskii, and D. F. Garbuzov, *Fiz. Tverd. Tela*, **5**, 2000 (1963).

3) M. Kochi, Y. Harada, T. Hirooka, and H. Inokuchi, *Bull. Chem. Soc. Jpn.*, **43**, 2690 (1970).

4) For recent developments, see a) W. D. Grobman and E. E. Koch, "Photoemission in Solids," Vol. 2, (Topics in Applied Physics Vol. 27) ed by L. Ley and M. Cardona, p. 261, Springer-Verlag, Berlin (1979); b) C. B. Duke, "Photon, Electron, and Ion Probes of Polymer Structure and Properties," ed by W. Dwight, T. J. Fabish, and H. R. Thomas, A. C. S. Symposium Series 162, p. 113, American Chemical Society, Washington (1981); c) N. Sato, K. Seki, and H. Inokuchi, *J. Chem. Soc., Faraday Trans. 2*, **77**, 3621 (1981).

5) a) M. Fujihira, T. Hirooka, and H. Inokuchi, *Chem. Phys. Lett.*, **19**, 584 (1973); b) W. R. Salaneck, "Photon,

Electron, and Ion Probes of Polymer Structure and Properties," ed by W. Dwight, T. J. Fabish, and H. R. Thomas, A. C. S. Symposium Series 162, American Chemical Society, Washington (1981) p. 121; d) Y. Shirota, M. Matsumoto, H. Mikawa, K. Seki, and H. Inokuchi, *Chem. Phys. Lett.*, **97**, 57 (1983).

6) a) Y. Takai, T. Mizutani, M. Ieda, K. Seki, and H. Inokuchi, *Polym. Photochem.*, **2**, 33 (1982); b) C. B. Duke, R. W. Bigelow, A. Dilks, A. Paton, W. R. Salaneck, and H. R. Thomas, *Chem. Phys. Lett.*, **83**, 255 (1981).

7) a) M. Fujihira and H. Inokuchi, *Chem. Phys. Lett.*, **17**, 554 (1972); b) K. J. Less and E. G. Wilson, *J. Phys.* **C6**, 3110 (1973); c) K. Seki, S. Hashimoto, N. Sato, Y. Harada, K. Ishii, H. Inokuchi, and J. Kanbe, *J. Chem. Phys.*, **66**, 3644 (1977); d) N. Ueno, T. Fukushima, K. Sugita, S. Kiyono, K. Seki, and H. Inokuchi, *Chem. Phys. Lett.*, **89**, 268 (1982); K. Seki, N. Sato, and H. Inokuchi, to be published.

8) a) E. E. Koch and W. D. Grobman, *Solid State Commun.*, **23**, 49 (1977); b) W. R. Salaneck, H. W. Gibson, E. W. Plummer, and B. H. Tonner, *Phys. Rev. Lett.*, **49**, 801 (1982).

9) F. I. Vilesov, A. A. Zagrubskii, and K. A. Shukov, *Fiz. Tverd. Tela*, **11**, 3409 (1969).

10) J. J. Pireaux, J. Riga, R. Caudano, J. J. Verbist, J. Delhalle, S. Delhalle, J. M. Andre, and Y. Gobillon, *Phys. Scripta*, **16**, 329 (1977).

11) J. Delhalle, *Chem. Phys.*, **5**, 306 (1974).

12) J. Delhalle, S. Delhalle, J. M. Andre, J. J. Pireaux, J. Riga, R. Caudano, and J. Verbist, *J. Electron Spectrosc.*, **12**, 293 (1977).

13) J. Delhalle, R. Montigny, C. Demanet, and J. M. Andre, *Theor. Chim. Acta*, **50**, 343 (1979); J. Delhalle, private communication.

14) T. Hirooka, K. Tanaka, K. Kuchitsu, M. Fujihira, H. Inokuchi, and Y. Harada, *Chem. Phys. Lett.*, **18**, 390 (1973).

15) N. Ueno and K. Sugita, *Jpn. J. Appl. Phys.*, **18**, 2159 (1979).

16) K. Kimura, S. Katsumata, Y. Achiba, T. Yamazaki, and S. Iwata, "Handbook of He-I Photoelectron spectra of Fundamental Organic Molecules," Japan Scientific Societies Press, Tokyo (1981).

17) R. M. White, T. A. Carlson, and D. P. Spears, *J. Electron Spectrosc.*, **3**, 59 (1974).

18) R. C. Dunber, *J. Phys. Chem.*, **83**, 2376 (1979).

19) K. Sekí, H. Inokuchi, and Y. Harada, *Chem. Phys. Lett.*, **20**, 197 (1973).

20) For example, A. D. Baker and D. Betteridge, "Photoelectron Spectroscopy," Pergamon Press, Oxford (1972).

21) a) K. Watanabe, Y. Nakayama, and J. Mottl., *J. Quant. Spectrosc. Radiat. Transfer*, **2**, 269 (1962); b) W. C. Price, R. Brailsford, P. V. Harris, and R. G. Ridlay, *Spectrochim. Acta*, **14**, 45 (1959); c) H. J. Lempka and W. C. Price, *J. Chem. Phys.*, **48**, 1875 (1968); d) Ref. 16; e) Ref, 17; f) F. S. Ashmore, Ph. D. Thesis, University of London (1975); g) P. Masclet, K. Grosjean, G. Mouvier, and J. Dubois, *J. Electron Spectrosc.*, **2**, 239 (1973); h) J. C. Buenzle, *Tetrahedron*, **29**, 3735 (1973); i) A. D. Baker, D. Betteridge, N. R. Kemp, and R. E. Kirby, *Anal. Chem.*, **43**, 375 (1971); j) Ref. 18; k) S. Pignataro, V. Mancini, J. N. Ridyard, and H. J. Lempka, *J. Chem. Soc., Chem. Commun.*, **1981**, 142.

22) K. Watanabe, *J. Chem. Phys.*, **26**, 542 (1957).

23) For example, C. Kittel "Introduction to Solid State Physics," 5th ed., Wiley, New York, 1976.

24) C. W. Bunn, *Nature*, **161**, 929 (1948); S. Murahashi, H. Yuki, T. Sano, U. Yonemura, H. Tadokoro, and Y. Chatani, *J. Polym. Sci.* **62**, S77 (1962).

25) S. Tomoda and K. Kimura, *Chem. Phys.*, **74**, 121 (1983).

26) R. W. Bigelow and G. P. Ceasar, *J. Phys. Chem.*, **83**, 1790 (1979).

27) K. Seki and H. Inokuchi, *Bull. Chem. Soc. Jpn.*, **56**, 2212 (1983).

28) K. Seki, unpublished.

29) a) J. Brandrup and E. H. Immergut, Ed., "Polymer Handbook," 2nd ed., John Wiley, New York (1975) (PE, PP, PVC, and PVA); b) V. L. Simril and B. A. Curry, *J. Appl. Polym. Sci.*, **4**, 62 (1960) (PVF); c) JSR RB Catalog of Japan Synthetic Rubber Co. (1,2-PBD).

30) I. Nakada, *J. Phys. Soc. Jpn.*, **17**, 113 (1962).

31) Chen S. X., K. Seki, H. Inokuchi, N. Ueno, and K. Sugita, *Polym. J.*, **15**, 763 (1983).

Catalytic Activity of Copper(II) Salt of Heteropolyphosphoric Acid for the Reduction of NO with Its Supporting Active Carbon

Isao MOCHIDA,* Kiyoshi YATA,† Hiroshi FUJITSU, and Yoshinobu KOMATSUBARA††
Research Institute of Industrial Science,
†*Department of Molecular Technology Graduate School of Industrial Sciences, Kyushu University 86, Kasuga 816*
††*Mitsui Mining Co., Kitakyushu Factory Hibiki, Wakamatsu-ku, Kitakyushu 808*
(Received June 4, 1984)

The catalytic activity of a copper(II) salt of polymolybdophosphoric acid ($Cu_{1.1}H_{0.8}PA$) for the reduction of NO with the supporting active carbon into N_2 and N_2O was studied at 400 °C using a fixed bed flow reactor. A considerable activity was observable at a stationary state where the spill-over of oxygen left on the active site of the acid to the carbon surface appeared to be rate-determining. The activity of the salt was much higher than for component oxides produced through its decomposition at higher temperatures. This suggested that the active site was characteristic to the salt (very probably the reduced site in the salt). The reaction mechanism in terms of the reaction paths, the N_2O/N_2 selectivity, and the roles of the supporting active carbon are discussed based on kinetic investigations.

A more efficient removal of the air pollutant, NO_x, has been explored in order to achieve a better environment at less cost.[1] The reduction of NO_x with the carbons (Eq. 1)

$$2NO + C \longrightarrow N_2 + CO_2 \quad (1)$$

can represent such a reaction and should be studied more since active carbon is an inexpensive reductant. Okuhara and Tanaka[2] and Inui *et al.*[3] have reported on the reactivities of several kinds of active carbons with NO catalyzed by alkali metal salts and complex oxides supported on them.

The present authors have reported on the reduction of NO_x on copper(II) salt of polymolybdophosphoric acid (CuHPA) which gain some reduced sites during preparation.[4] If the site oxidized by NO is properly reduced by transferring the left oxygen to the support where it is converted or liberated, the catalytic reduction of NO proceeds on the CuHPA. The soluble CuHPA can be easily recovered and regenerated when the support is greatly consumed.

In this study, the reduction of NO with some kinds of active carbon catalyzed by CuHPA was examined. The carbon can enlarge the effective surface area of CuHPA. The redox interaction of HPA with active carbon has been reported by Izumi *et al.*[5] and Baba and Ono.[6] The generation or activation of reduced sites by the carbon support can be expected through a catalyst-support interaction. The reactivity of the active carbon for such a reaction may attract other interests since the spill-over is one of the most important mechanisms regarding catalyst-support cooperation, which is a guide-line for the preparation of a better catalyst.

Experimental

Catalysts. 12-Molybdophosphoric acid ($H_3Mo_{12}PO_{40}$) was purchased from Nippon Inorganic Color and Chemical Co. The copper(II) salt in the form of $Cu_{1.1}H_{0.8}PA$ (CuHPA) was prepared using its corresponding metal carbonate according to a method described in the literature.[7] CuHPA was supported on to several kinds of active carbons (listed in Table 1 with some of their properties) from its methanol solution. The loading of the $Cu_{1.1}HPA$ was 10—33.3 wt%. Granules of 28—40 mesh (prepared by molding and crushing) were used for the catalytic reaction.

Reaction Procedure. The Reaction of NO or N_2O was carried out in a fixed bed flow reactor (8 mmϕ, Pyrex glass tube). The reactant gas contained 1.0% (1.01 kPa) of NO or 2.7% (2.74 kPA) of N_2O (Seitetsu Kagaku Co.). The catalyst weight and the total flow rate were 1.5—2.5 g and 100 $cm^3\,min^{-1}$, respectively. The gas composition was analyzed by a gas chromatograph using columns packed with Porapak (1 m) and Molecular Sieves 13X(2 m). The partial pressure of NO was varied from 1.0 (1.01 kPa) to 10 vol% (10.1 kPa) to observe the rate dependence on its pressure using a flow reactor under the conditions of the differential reactor.

TABLE 1. REDUCTION OF NO CuHPA SUPPORTED ON ACTIVE CARBON[a)]

Support	Area (m^2/g)	NO conv. (%)	Product yield(select.)(%)		
			N_2	N_2O	CO_2
DA	1200	16.7	7.2(45)	8.8(55)	11.6
		1.4[b)]	1.4(100)	0.0(00)	
SAC	1200	16.2	9.4(58)	6.8(42)	11.7
		1.2[b)]	0.5(43)	0.7(57)	
BF	210	7.6	6.3(83)	1.3(17)	6.1
		1.3[b)]	0.6(45)	0.7(55)	
PAN-ACF	595	21.2	18.7(88)	2.5(12)	13.2
		10.5[b)]	5.6(53)	4.9(47)	
CB[c)]	560	21.2	15.7(73)	5.8(27)	10.8
		1.4[b)]	1.4(100)	0.0(00)	
1.7%CuO-3.3% Fe_2O_3/SAC		21.4	21.4(100)	0.0(00)	18.8
0.7%Pt/SAC[d)]		38.0			

a) CuHPA/DA(loading: 33 wt%): 2 g, react. temp: 400 °C, feed: NO 1.0% in He carrier: 100 $cm^3\cdot min^{-1}$, b) activity of carrier alone(1.33 g), c) carbon black, d) NO: 0.63%, SV: 20000 h^{-1}.[3)]

Results

Reduction of NO over CuHPA/DA. The reactivity of NO with DA catalyzed by CuHPA (loading 33 wt%) is illustrated in Fig. 1, where the reaction temperature and the amount of carbon used were 400 °C, and 2 g, respectively. NO was reduced into N_2 and N_2O, producing carbon dioxide. Without CuHPA, the reaction rate was very slow, the conversion of NO being as low as 1.4% at the same temperature. The catalytic role of CuHPA is, thus, definite. NO of 1.2×10^{-2} mole was reduced by 3.4×10^{-4} mole of CuHPA within 20 h. The conversion of NO was initially as high as 65% and decreased, gradually, and leveled off at 17% at 6 h on stream.

The conversion after the initial 5 h was much larger than that observed with CuHPA on silica gel, indicating the favorable role of the active carbon. Carbon dioxide produced at this stage was less than expected from the conversion of NO (roughly 3/5), while the production of carbon dioxide at a steady state maintained the oxygen balance.

The yields of N_2 and N_2O at a steady state are compared to the contact time in Fig. 2. Both yields increased monotonously with an increasing contact time. However, a contact time greater than 4.7×10^{-2} min gave more N_2 at the expense of N_2O, suggesting a contribution from the consecutive reaction to the major competitive formation of N_2 and N_2O as described by Eq. 2.

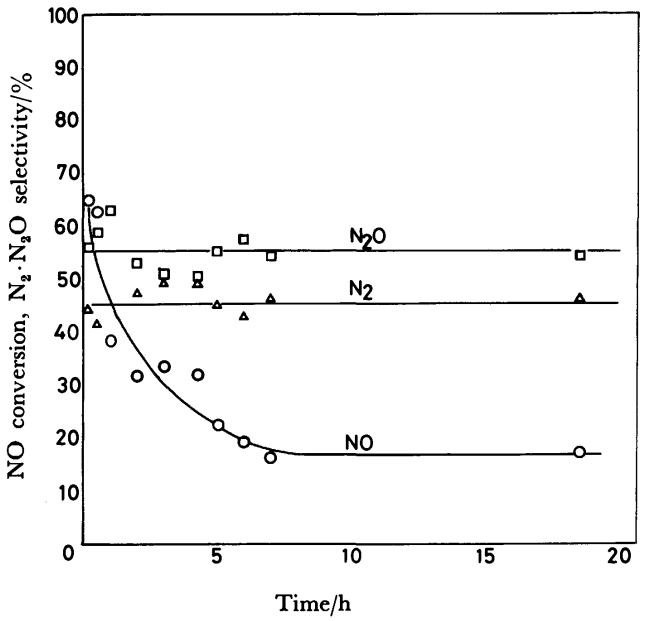

Fig. 1. Reduction of NO over CuHPA supported on DA active carbon.
○: NO conversion
△, □: N_2, N_2O selectivity
CuHPA/DA(loading: 33 wt%): 2 g, react. temp: 400 °C, feed: NO 1.0% in He carrier, 100 $cm^3 \cdot min^{-1}$.

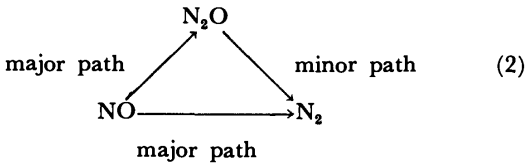

(2)

The reactivity of DA catalyzed by CuHPA at several reaction temperatures is summarized in Table 2, where the reactivity is described by the stationary conversion observed with the flow reactor. The reactivity increased with an increasing temperature (from 300 to 400 °C), the activation energies for N_2 and N_2O formations being calculated to be 1.23 and 1.83 kJ mol^{-1}, respectively. Although the selectivity of N_2 formation

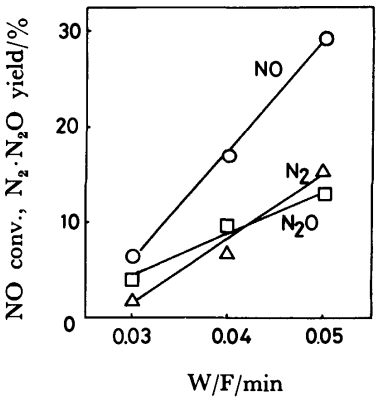

Fig. 2. Dependence of NO conversion on the contact time.
○: NO conversion
△, □: N_2, N_2O yield
CuHPA/DA(loading: 33 wt%), feed: NO 1.0% in He carrier, 100 $cm^3 \cdot min^{-1}$.

Table 2. Dependence of NO conversion on the reaction temperature[a)]

React. temp (°C)	NO conv. (%)	Product yield(select.)(%)		
		N_2	N_2O	CO_2
300	1.7	0.3 (17)	1.4 (83)	0.8
350	3.5	1.3 (38)	2.2 (62)	2.3
400	17	7.7 (45)	9.3 (55)	11.6
450	14	10.5 (75)	3.5 (25)	11.9
500	68	67 (98)	1 (2)	32
400[b)]	2.6	1.4 (51)	1.2 (49)	0.9
NO-H_2 React.[c)]	16.5	10.7 (65)	5.8 (35)	—

a) CuHPA/DA(loading: 33 wt%) 2 g, react. temp: 400 °C, feed: NO 1.0% in He carrier, 100 $cm^3 \cdot min^{-1}$, b) after the reaction at 500 °C for 28 h, c) CuHPA/DA (loading: 33 wt%) 0.5 g, react. temp: 300 °C, feed: NO 5%(H_2 5%) in He carrier, 100 $cm^3 \cdot min^{-1}$.

increased rather sharply with a rising reaction temperature, more N_2O was always produced than N_2 at these temperatures. Even if the consecutive conversion of N_2O was taken into account at a high conversion, the higher temperature appears favorable for the formation of N_2. It is very interesting that the reaction temperature of 450 °C provided a smaller conversion than that observed at 400 °C. More N_2 was produced at this temperature in spite of the smaller conversion than that at 400 °C. A higher temperature (500 °C) allow a high conversion (68%) almost exclusively into N_2. After a reaction at 500 °C for 28 h (where 22% of the carbon was consumed), the conversion became as low 3% at 400 °C. The level of the conversion was much lower than that of the same carbon at the same temperature without experiencing 500 °C. It was also noted that slightly more N_2 was produced in spite of the very low conversion. A significant change in the catalyst nature is suggested.

The reactivities of NO at different partial pressures is illustrated in Fig. 3. The reaction rates into N_2 and N_2O are plotted separately. In order to eliminate the

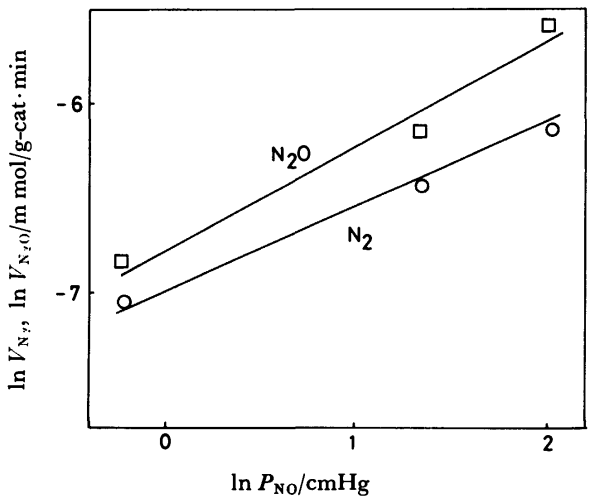

Fig. 3. The reactivity of NO of different partial pressures.
○, □: N_2, N_2O reaction rate,
CuHPA/DA(loading: 33 wt%): 2 g, react. temp: 400 °C, feed(He carrier): 100 $cm^3 \cdot min^{-1}$.

Table 3. Dependence of NO conversion on the loading level[a)]

Loading (%)	NO conv. (%)	Product yield/%	
		N_2	N_2O
5	3.0	1.9	1.1
		(63)	(37)
8	6.7	4.6	2.1
		(69)	(31)
33.3	16.7	7.2	8.8
		(45)	(55)

a) CuHPA/DA: 2 g, react. temp: 400 °C, feed: NO 1.0%. in He carrier, 100 $cm^3 \cdot min^{-1}$.

Table 4. Reduction of N_2O over CuHPA/DA[a)]

Reactant	Inlet gas (%)		Outlet gas (%)		
	N_2O	NO	N_2O	NO	N_2
N_2O	2.70	—	0.00	—	2.70
$NO+N_2O$	2.20	1.01	2.21	0.81	0.09

a) CuHPA/DA: 2 g, react. temp: 400 °C, feed: 100 $cm^3 \cdot min^{-1}$ (He carrier).

influence of a consecutive contribution, the conversions were kept below 10%. Both reaction orders in NO to produce N_2 and N_2O were *ca.* 0.5.

The stationary rate of NO reduction was proportional to the amount of supported CuHPA until the loading was 33.3% (Table 3). However, the ratio of N_2/N_2O produced decreased with the increasing loading in spite of the increased conversion where a more consecutive conversion of NO may take place. The catalyst density may influence the relative contribution of competitive reaction path which lead to N_2 and N_2O respectively.

The Reactivity of N_2O. The reactivity of N_2O against DA catalyzed by CuHPA (loading: 33.3%) is summarized in Table 4, where N_2O (2.7%) and N_2O-NO (2.2 and 1.0%, respectively) were examined. N_2O was very reactive at 400 °C, allowing its complete conversion into N_2 under similar conditions of NO reduction where the conversion of NO was 17%. The reactivity of N_2O appeared to be very much suppressed when NO was present (Table 4), while the reactivity of NO was almost unchanged by the presence of N_2O to provide an 18% conversion (NO base). To balance the N_2 produced, the conversion of N_2O was calculated to be only 2.3%.

The Reactivities of Several Kinds of Active Carbons Catalyzed by CuHPA. The conversions of several active carbons with and without the catalyst CuHPA are summarized in Table 1, where the loading and the reaction temperature were fixed at 33% and 400 °C, respectively. The reactivities of the active carbons without the catalyst were very low, the conversion being around 1.4% except for an active PAN-fiber. The conversion, when catalyzed, varied from 7.6 to 21%, carbon black showing the highest reactivity. The selectivity was also variable with the carbons, commercial active carbons of DA and SAC showing smaller selectivity for N_2 production than other carbons. The high reactivity and selectivity (to N_2) of active PAN-carbon-fiber without the catalyst needs to be noted. Details on its reactivity will be reported later.

IR Spectrum of CuHPA on DA. The IR spctra of CuHPA on DA before and after the reaction are illustrated in Fig. 4. By supporting on DA, the IR spectrum of CuHPA was slightly changed. Although the bands around 880 and 800 cm^{-1} somewhat shifted, other major bands were unchanged. The broadening

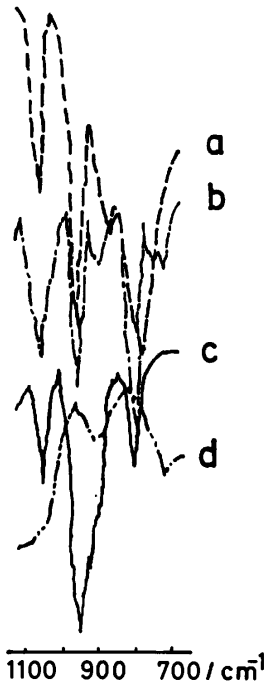

Fig. 4. IR spectra of catalysts after the reaction at several temperature.
a: CuHPA, b: CuHPA/DA, c: CuHPA/DA after the reaction at 400 °C, d: CuHPA/DA after the reaction at 500°C.

of these adsorption bands was observable after the reaction at 400 °C, but still major peaks were unchanged. In contrast, the reaction at 500 °C completely changed the spectrum and the sharp bands observable in the region became very broad or disappeared. The decomposition of CuHPA into component oxides is strongly suggested. The decomposition of CuHPA may take place between 400 and 450 °C.

Discussion

The catalytic activity of CuHPA in the reduction of NO with active carbon is comparable to those for mixed oxides[8] of copper and iron but much less than that for noble metals[3] supported on active carbon. The former catalyst has been reported to be very active for the NO-NH_3 reaction. An interesting observation is that the activity of CuHPA was much larger than that of its decomposed component oxides produced by heating to above 450 °C. Certain sites characteristic to the heteropoly acid appear to be active in this reaction.

In a previous study,[4] the acid supported on silica gel was reported to reduce NO to a limited extent (3.49×10^{-4} mole NO/mole acid within 20 h). Some reduced sites are induced in the acid during the preparation as ESR suggested. Such a reduced site may also be the active site for the present catalysis. NO is reduced by the site into N_2O and N_2, leaving oxygen. Oxygen, thus produced, may spillover to the carbon to produce carbon dioxide and to regenerate the reduced site in the acid. The high conversion during the initial 7—8 h may be partly due to the reduced sites induced prior to the catalysis, and partly due to the active portions of the carbon probably located in the vicinity of CuHPA. Because some portions of the former sites were irreversibly oxidized by NO, a smaller amount of CO_2 was produced than expected from the amount of consumed NO. The conversion decreased, corresponding to the decreasing number of the sites, to the stationary one, which is determined by the regeneration of the active site through the spill-over mechanism. It may be noted that the product from active carbon was only CO_2. Furusawa *et al.*[9] reported that CO_2 was formed by the reaction of NO with active carbon below 579 °C. The oxidation of active carbon may proceed *via* the formation of an oxygen-containing functionarity to form CO_2.[10,11]

The activity in the present reaction is much smaller than that of the reduction with hydrogen in spite of the similar mechanism.[4] This suggests that the rate of the oxygen spill-over onto the active carbon was inferior to that of the reductive regeneration of the active site. It is noted that similar product distributions were obtained in both reactions on the same support.

The reduction of NO on CuHPA supported on the active carbon proceeds into N_2O and N_2 through both competitive and consecutive paths as described in the Results. In spite of the high reactivity, N_2O remained in the product, suggesting its weaker adsorption to the active site. It can be easily converted into N_2 simply to extend the contact time.

The selectivity in the competitive paths is worth being discussed. The reaction kinetics suggest the dissociative adsorption of NO as the common intermediate for both N_2O and N_2, although the former product may require another NO molecule. Thus, the selectivity is determined by the respective rates of coupling of dissociatively adsorbed nitrogen with another nitrogen (to N_2) and NO (to N_2O), respectively. The superior formation of N_2 on the catalyst of low CuHPA loading even at the lower conversion may suggest the favorable geometry of active site for the N_2 formation. It has been reported that several reduced sites are produced in a unit cell of the heteropoly acid.[12]

The roles of active carbon are the support for the catalyst as well as the reductant. Through these two roles, the carbon influences the activity and selectivity of the present reaction. The reactivity of active carbon may be most influential on a stationary conversion, however the initial conversion, which is due to the reduced sites of CuHPA being induced during the catalyst preparation, is much higher on the active carbon than that on silica gel, suggesting a role of the

support in their generation. The redox interaction may attract for the study.[5,6,13] At present, the factors influencing the spill-over are difficult to discuss.

The selectivity is different among the used active carbons, high N_2 formation being noted on the PAN-ACF and the carbon black in spite of their similar conversions to those of the active carbons. Although the removal of N_2O is much easier than NO because of its thermodynamical unstability, such carbons may provide the better catalysts for the conversion of NO to N_2. The support may influence the geometry of the active sites in the supported CuHPA through a magnetic interaction.

References

1) T. Shikada, K. Fujimoto, T. Kunugi, and H. Tominaga, *Ind. Eng. Chem., Prod. Res. Dev.*, **20**, 91 (1981); S. Okazaki, *Hyomen*, **20**, 504 (1982).

2) T. Okuhara and K. Tanaka, *Shokubai (Catalyst)*, **20**, 251 (1978).

3) T. Inui, T. Otowa, and Y. Takegami, *Ind. Eng. Chem., Prod. Res. Dev.*, **21**, 56 (1982).

4) I. Mochida, T. Nakashima, and H. Fujitsu, *Bull. Chem. Soc. Jpn.*, **57**, 1449 (1984).

5) Y. Izumi and K. Urabe, *Chem. Lett.*, **1981**, 663.

6) T. Baba and Y. Ono, The 47th Meeting of the Chemical Society of Japan (1983), 1M44.

7) G. A. Tsigdinos, *Ind. Eng. Chem., Prod. Res. Dev.*, **13**, 267 (1974).

8) I. Maruko and F. Nozaki, *Nippon Kagaku Kaishi*, **11**, 1673 (1980).

9) T. Furusawa, T. Kunii, A. Oguma, and N. Yamada, *Kagaku Kogaku Ronbunshu*, **4**, 562 (1978).

10) G. H. Bedjai, H. K. Orbach, and F. C. Riesenteld, *Ind. Eng. Chem.*, **50**, 1165 (1958).

11) R. N. Smith, J. Swinehart, and D. Lesnini, *J. Phys. Chem.*, **63**, 44 (1959).

12) K. Eguchi, T. Toyozawa, K. Furuta, N. Yamazoe, and T. Seiyama, *Chem. Lett.*, **1981**, 1253.

13) K. Fujimoto, A. Ohno, and T. Kunugi, *J. Japan Petrol. Inst.*, **26**, 339 (1983).

Spirolactone of Xanthene. II.[1] Synthesis and Molecular Structure of 2′,5,7′-Trichlorospiro[benzofuran-3(2*H*),9′-[9*H*]xanthen]-2-one

Michio KIMURA
Niigata College of Pharmacy, 5829 Kamishin'ei-cho, Niigata, 950-21
(Received July 12, 1984)

The title compound has been synthesized by the novel condensation reaction of *p*-chlorophenol with oxalic and sulfuric acids; its crystal and molecular structures have been determined by the single crystal X-ray diffraction method. The space group is $C2/c$. There are eight molecules of the title compound in the unit cell of dimensions a=21.316(9), b=17.267(4), c=9.158(6) Å, and β=94.05(5)°. The structure was solved by the direct method and refined by the block-diagonal least-squares method to a value of 0.088 for R using 1993 independent observed reflections with $F_o > 3\sigma(F_o)$. The molecule possesses three phenyl rings fused to spirolactone and the dihedral angles between the phenyl rings are 73.60°, 83.60°, and 22.81°.

In a previous communication,[1] it has been reported that, in the studies of the reactivity of xanthene, the reaction of 1-naphthol with oxalic and sulfuric acids accompanying the loss of four molecules of water gave a novel spirolactone (**1**) of dibenzo[*c*,*h*]xanthene in excellent yield (70—75%), and the molecular structure of **1** has been established by the single crystal X-ray diffraction method (Cu $K\alpha$ radiation) as shown in Fig. 1. In order to increase the examples of this novel reaction and to get some information about the reaction mechanism, further studies concerning the synthesis of derivatives were performed by utilizing substituted phenols in place of 1-naphthol. Reaction of *p*-chlorophenol with oxalic and sulfuric acids gave the corresponding novel spirolactone (**3**), whose molecular structure could not be well established on the basis of chemical and spectroscopic data described in the experimental section. Accordingly, the X-ray analysis of **3** has been undertaken in order to elucidate the correct structure. The established molecular structure for **3** resembles the well known fluoran (**5**),[2] except for the lactone moiety, which is formed by the reaction of phenols with phthalic anhydride in the presence of dehydrating agents as in Scheme 1 (fluorescein if R is OH in **5**).

Experimental

*Preparation of 2′,5,7′-Trichlorospiro[benzofuran-3(2*H*),9′-[9*H*]xanthen]-2-one (3).* To a mixture of *p*-chlorophenol (11.0 g) and oxalic acid (8.0 g), conc. sulfuric acid (8.0 g) was added cautiously, and the resulting mixture was heated gently for 4 h at 140—145 °C in an oil bath. After cooling,

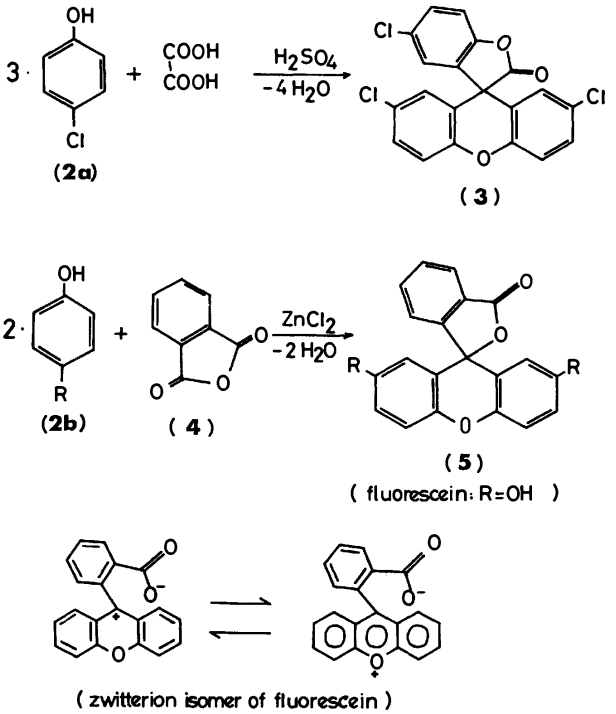

Scheme 1.

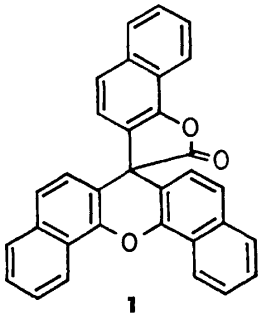

1

Fig. 1. Spiro[7*H*-dibenzo[*c*,*h*]xanthene-7,3′(2′*H*)-naphtho- [1,2-*b*]furan]-2′-one

TABLE 1. CRYSTAL DATA

Mol. formula	$C_{20}H_9O_3Cl_3$
Mol. wt.	403.64
Space group	$C2/c$
Cell dimensions	
a/Å	21.316(9)
b/Å	17.267(4)
c/Å	9.158(6)
β/°	94.05(5)
Unit cell volume/Å^3	3362.2
Z-value	8
Dc/g cm^{-3}	1.59
μ/cm^{-1} (Cu $K\alpha$)	51.96

the reaction mixture was poured into water and extracted with chloroform (100 ml). The organic layer was separated, washed with water, dried over anhydrous sodium sulfate, and concentrated under vacuum. The crude oily products were chromatographed over 300 g of silica gel (using chloroform as eluent) to give 1.5 g of **3**. Crystals suitable for X-ray analysis were obtained by slow evaporation of a xylene solution of **3** at room temperature. Mp 237 °C; IR ν_{max}^{KBr} cm^{-1} 1630, 1790 (C=O); MS *m/z* 402 (M^+), 374 (M^+—CO), 357 (M^+—CO—OH), 339 (M^+—CO—OH—H_2O). ^{1}H-NMR ($CDCl_3$) δ=7.5—6.3 (m for three aromatic ring protons).

Collection and Reduction of Crystallographic Data. The crystal selected for the measurement of the lattice parameters and intensity data was a cleaved fragment which had approximate dimensions of 0.20×0.15×0.25 mm. A preliminary examination of the crystal carried out on a Rigaku AFC diffractometer showed it to be monoclinic. Systematic absences of $h+k=2n+1$ for hkl and $l=2n+1$ for $h0l$ showed the space group to be ***Cc*** or ***C2/c***. The correct space group was later confirmed to be ***C2/c*** by the successful refinement of the structure. The unit cell parameters at room temperature were refined by the least-squares method using the Bragg angles (Cu $K\alpha$ λ=1.54178 Å) of thirty reflections ($20°<2\theta<35°$). The unit cell dimensions and other data are summarized in Table 1. Intensity data were collected at room temperature on the Rigaku AFC diffractometer utilizing nickel-filtered Cu $K\alpha$ radiation. The $2\theta-\omega$ scans were employed with a scan speed of $4°min^{-1}$ in 2θ and scan range which was varied by $1.2°+0.15°\tan\theta$. Background counts were taken at both ends of the scan with a displacement of 3.0° from the $K\alpha$ peak; the time of each measurement was one-third of the scan time. A total of 2823 unique reflections was measured in the range of $0°<2\theta<120°$. The intensities of three standard reflections were measured after every 57 reflections; three intensities dropped by an average of a few percent over the period of data collection, but no correction factor was applied because the decrease was not considered significant. Lorentz and polarization corrections were applied to convert intensities to structure amplitudes, but no absorption corrections were applied. Standard deviations in the structure amplitudes, $\sigma(F_o)$, were derived from counting statistics.

Solution and Refinement of the Structure. The structure was solved by the direct method using MULTAN[3] to calculate phases for the 300 reflections with $|E_o|>1.60$. The *E*-map computed from the phases with the largest combined figure of merit (2.59) revealed all the non-hydrogen atoms. The 1993 observed reflections for which $|F_o|$ were greater than $3\sigma(F_o)$ were used for the block-diagonal least-squares refinement of the structure. The function minimized was $\Sigma w(|F_o|-|F_c|)^2$, where w is the unit weight for $0<|F_o|\leq 20$ and $w=(20/|F_o|)^{-2}$ for $|F_o|>20$. An initial refinement using individual isotropic temperature factors for the non-hydrogen atoms led to a conventional $R=(\Sigma||F_o|-|F_c||)/\Sigma|F_o|$ of 0.143. After the successive refinement with the anisotropic temperature factors for all the non-hydrogens, all the hydrogen atoms were readily located from the difference Fourier map. In the further refinement positional and isotropic thermal parameters for the hydrogen atoms were included. The refinement, after 6 cycles of block-diagonal least-squares calculation, converged to an *R* of 0.088 and a weighted $R_w=(\Sigma w(|F_o|-|F_c|)^2/\Sigma w|F_o|^2)^{1/2}$ of 0.088. An extinction parameter was refined because extinction effects were considered significant. The refinement was completed when the largest shift in any parameters among the non-hydrogen atoms was less than 0.01% of standard deviations, while the largest shift for the hydrogen atoms was 0.09%. The final positional and thermal parameters† are given in Table 2. The largest peak in the final difference map, 0.2 eÅ^{-3}, was located near the chlorine atoms. The atomic scattering factors for Cl, O, and C were those of Cromer and Weber[4] and for H, the

TABLE 2. FINAL POSITIONAL AND THERMAL PARAMETERS OF NON-HYDROGEN AND HYDROGEN ATOMS WITH ESTIMATED STANDARD DEVIATIONS

$$B_{eq}=\frac{1}{3}(U_{11}+U_{22}+U_{33})$$

Atoms	*x*	*y*	*z*	B_{eq} or *B*/Å^2
CL1	0.2463(2)	0.1307(2)	0.5068(2)	6.71
CL2	−0.0900(2)	0.3244(2)	−0.1451(2)	7.10
CL3	0.0673(2)	0.4861(2)	0.3778(2)	7.93
C1	0.1177(5)	0.2286(6)	0.0752(5)	4.09
C2	0.0523(5)	0.2116(6)	0.0188(5)	3.91
C3	0.0153(5)	0.2706(6)	−0.0324(6)	4.78
C4	−0.0434(5)	0.2502(6)	−0.0856(6)	5.05
C5	−0.0636(5)	0.1754(7)	−0.0918(6)	5.33
C6	−0.0269(6)	0.1157(7)	−0.0407(6)	6.01
C7	0.0301(6)	0.1367(6)	0.0158(6)	5.10
O8	0.0655(4)	0.0745(4)	0.0669(5)	6.62
C9	0.1091(5)	0.0921(6)	0.1676(6)	5.09
C10	0.1272(6)	0.0291(6)	0.2525(7)	6.30
C11	0.1712(6)	0.0416(6)	0.3558(6)	5.81
C12	0.1951(5)	0.1143(6)	0.3699(6)	5.15
C13	0.1775(5)	0.1778(6)	0.2858(6)	4.51
C14	0.1338(5)	0.1646(6)	0.1795(5)	4.02
O15	0.1786(4)	0.1718(5)	−0.1354(4)	6.77
C16	0.1653(5)	0.2248(6)	−0.0557(6)	4.88
O17	0.1961(4)	0.2946(5)	−0.0682(4)	5.73
C18	0.1715(5)	0.3459(6)	0.0393(6)	4.57
C19	0.1880(6)	0.4197(7)	0.0552(7)	6.32
C20	0.1592(6)	0.4626(6)	0.1583(7)	6.45
C21	0.1085(7)	0.4297(6)	0.2500(7)	7.83
C22	0.0919(6)	0.3526(6)	0.2376(6)	5.22
C23	0.1269(5)	0.3095(6)	0.1232(5)	3.80
HC3	0.031(5)	0.330(6)	−0.032(5)	2.5
HC5	−0.108(8)	0.162(10)	−0.136(9)	3.9
HC6	−0.052(5)	0.058(6)	−0.009(6)	3.5
HC10	0.110(5)	−0.026(6)	0.245(6)	2.3
HC11	0.186(7)	−0.005(8)	0.423(8)	3.5
HC13	0.209(5)	0.232(6)	0.265(6)	2.5
HC19	0.225(6)	0.444(7)	−0.017(7)	3.4
HC20	0.172(5)	0.552(5)	0.155(5)	1.5
HC22	0.057(5)	0.328(6)	0.326(6)	2.7

† Tables of the final thermal parameters and the observed and the calculated structure factors are deposited as Document No. 8510 at the Office of the Editor of the Bulletin of the Chemical Society of Japan.

scattering factors of Stewart, Davidson, and Simpson[5] were used. Computations were performed by the crystallographic program system UNICS.[6]

Discussion

The molecular structure and the labeling sequence of **3** is presented in the ORTEP drawing of Fig. 2. The molecule of **3** has a T-like shape with the benzofuranone moiety nearly perpendicular to the xanthene plane. The gross molecular conformation and the configuration around the spiro-carbon atom (C1) of **3** are similar to the corresponding part of **1**. The bond distances and angles of **3** are presented in Table 3. The average C-C bond lengths in the benzene rings A, C, and E are 1.376, 1.391, and 1.392 Å, respectively, which are normal compared with the values usually found for the C-C distances in aromatic rings (1.395 Å). In Fig. 3 the geometry of the important parts of **3** and of fluorescein are compared. In fluorescein,[2] the bond length (1.525 Å) between the spiro-carbon and oxygen atoms (corresponding to C1-C16 in **3**) is exceptionally long and indicates weakness in the bond which is consistent with the behaviour of fluorescein in solution, where the ready cleavage of that bond yields the fluorescent zwitterion isomer (as shown in Scheme 1). On the other hand, the distance of C1-C23 in **3** (1.482 Å) is typical of C-C sp^2—sp^3 bond, and does not show comparable weakness of the bond. In comparison with related compounds with three fused rings, two C-O bond distances (C7-O8=1.411 and C9-O8=1.389 Å) in

Table 3. Bond lengths (l/Å) and angles (ϕ/°) in **3**

(a) Bond lengths for non-hydrogen atoms					
CL1-C12	1.744(6)	CL2-C4	1.732(9)	CL3-C21	1.717(8)
C1-C2	1.549(11)	C1-C14	1.516(9)	C1-C16	1.517(8)
C1-C23	1.482(11)	C2-C3	1.390(11)	C2-C7	1.379(13)
C3-C4	1.420(12)	C4-C5	1.364(15)	C5-C6	1.395(13)
C6-C7	1.402(13)	C7-O8	1.411(11)	O8-C9	1.389(8)
C9-C10	1.408(11)	C9-C14	1.365(13)	C10-C11	1.396(11)
C11-C12	1.364(14)	C12-C13	1.407(10)	C13-C14	1.414(8)
O15-C16	1.193(8)	C16-O17	1.375(12)	O17-C18	1.398(8)
C18-C19	1.334(14)	C18-C23	1.337(9)	C19-C20	1.318(10)
C20-C21	1.438(12)	C21-C22	1.385(14)	C22-C23	1.448(8)
(b) Bond lengths involving hydrogen atoms					
HC3-C3	1.08(9)	HC5-C5	1.08(13)	HC6-C6	1.16(9)
HC10-C10	1.02(9)	HC11-C11	1.08(9)	HC13-C13	1.16(9)
HC19-C19	1.08(8)	HC20-C20	1.07(9)	HC22-C22	1.15(6)

(c) Bond angles			
C23-C1-C16	100.4(6)	C23-C1-C14	117.4(4)
C23-C1-C2	114.7(7)	C16-C1-C14	107.4(7)
C16-C1-C2	107.2(4)	C14-C1-C2	108.8(7)
C7-C2-C3	118.5(8)	C7-C2-C1	120.2(7)
C3-C2-C1	121.4(8)	C4-C3-C2	118.0(9)
C5-C4-C3	122.6(8)	C5-C4-CL2	119.8(7)
C3-C4-CL2	117.6(7)	C6-C5-C4	119.9(8)
C7-C6-C5	117.1(9)	O8-C7-C6	115.0(8)
O8-C7-C2	121.0(8)	C6-C7-C2	123.9(8)
C9-O8-C7	116.9(6)	C14-C9-C10	122.8(7)
C14-C9-O8	122.3(6)	C10-C9-O8	114.9(8)
C11-C10-C9	118.6(9)	C12-C11-C10	118.6(7)
C13-C12-C11	123.4(6)	C13-C12-CL1	118.1(7)
C11-C12-CL1	118.3(5)	C14-C13-C12	117.7(8)
C13-C14-C9	118.7(6)	C13-C14-C1	120.4(7)
C9-C14-C1	120.8(5)	O17-C16-O15	122.1(6)
C1-C16-O17	108.5(6)	O15-C16-C1	129.3(8)
C18-O17-C16	110.0(5)	C23-C18-C19	124.7(6)
C23-C18-O17	108.9(7)	C19-C18-O17	126.4(6)
C20-C19-C18	120.2(8)	C21-C20-C19	119.3(9)
C22-C21-C20	121.2(7)	C22-C21-CL3	118.7(6)
C20-C21-CL3	120.1(7)	C22-C23-C1	112.1(5)
C18-C23-C1	112.1(5)		

ring D of **3** are comparable with 1.382 and 1.369 Å of 4-azaphenoxathiin,[6] 1.401 and 1.386 Å of phenoxathiin,[7] and 1.378 and 1.377 Å of fluorescein[2] within the experimental errors.

In Table 4 the best least-squares planes are given together with the displacement of the atoms from the best planes. The lactone ring B is coplanar with ring A, and its orientation is almost perpendicular to the xanthene ring, which is similar to that observed in **1**.[1] The dihedral angles between rings A—C, rings A—E, and rings C—E are 73.6°, 83.6°, and 22.81°, respectively, which may be compared with those of **1** (81.4°, 86.9°, and 5.9° in order).[1] The great difference in the butterfly angles of the xanthene rings in **1** and **3** (22.81° and 5.9°) seems to be caused by electron-withdrawing effects of the chlorine atoms and the lesser steric hindrance of the phenyl ring of **3** in comparison with the bulky naphthalene ring of **1**.

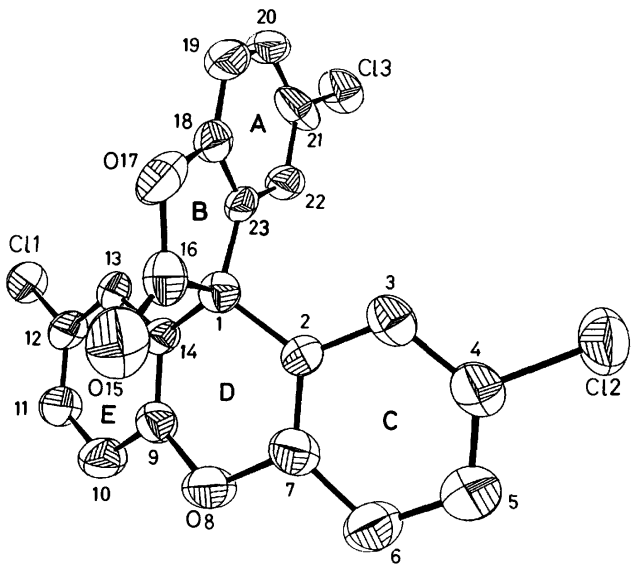

Fig. 2. ORTEP drawing of the title compound ---- Thermal ellipsoids are drawn at the 50% probability level.

TABLE 4. LEAST-SQUARES PLANES AND DEVIATIONS (d/Å) OF ATOMS FROM THE PLANES

Plane A: Defined by the atoms C18-C23
$-0.7151X+0.2669Y-0.6461Z+1.2829=0$[a]
C18 0.013; C19 0.001; C20 −0.019
C21 0.019; C22 −0.005; C23 −0.009
Plane B: Defined by the atoms C1, C16, O17, C18, and C23
$-0.7323X+0.3150Y-0.6038Z+1.0369=0$
C1 −0.008; C16 0.014; O17 −0.014
C18 0.006; C23 0.002; O15 −0.005
Plane C: Defined by the atoms C2-C7
$0.3902X-0.1095Y-0.9142Z+0.1252=0$
C2 0.008; C3 0.004; C4 −0.016
C5 0.008; C6 0.012; C7 −0.011
Plane E: Defined by the atoms C9-C14
$-0.6944X+0.2179Y+0.6859Z+0.3037=0$
C9 0.011; C10 −0.000; C11 −0.004
C12 −0.002; C13 0.007; C14 −0.013

a) Expressed in an orthogonal coordinate system in Å units.

TABLE 5. INTERMOLECULAR DISTANCES LESS THAN 4 Å

CL2···C3[a]	3.385(5)
C6···O8[b]	3.400(12)
C16···O17[c]	3.257(10)
O17···C13[c]	3.270(8)
C18···O15[c]	3.388(11)
C19···O15[c]	3.380(13)

Symmetry code	Symmetry operation
a	$-x, y, 1/2-z$
b	$-x, -y, -z$
c	$1/2-x, 1/2-y, -z$

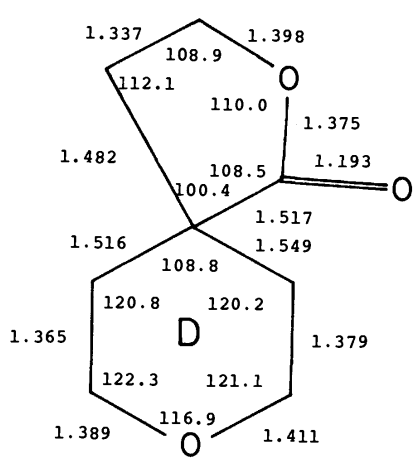

3

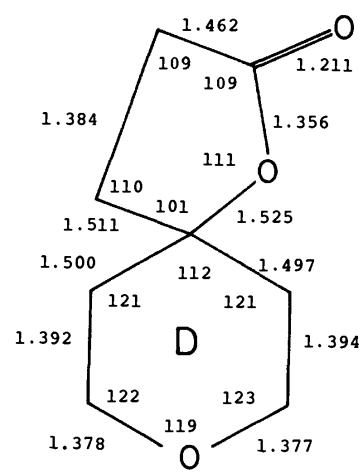

fluorescein[2]

Fig. 3. The selected bond lengths and angles around the spiro carbon atom of **3** and fluorescein. The standard deviations are described in Table 3.

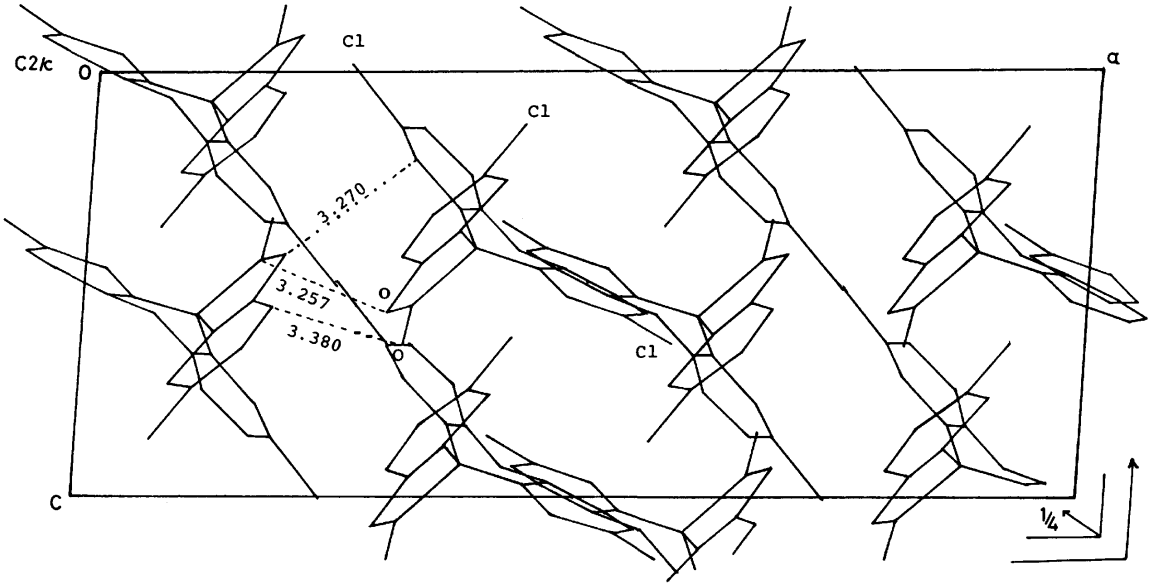

Fig. 4. Projection of the structure along the b-axis.

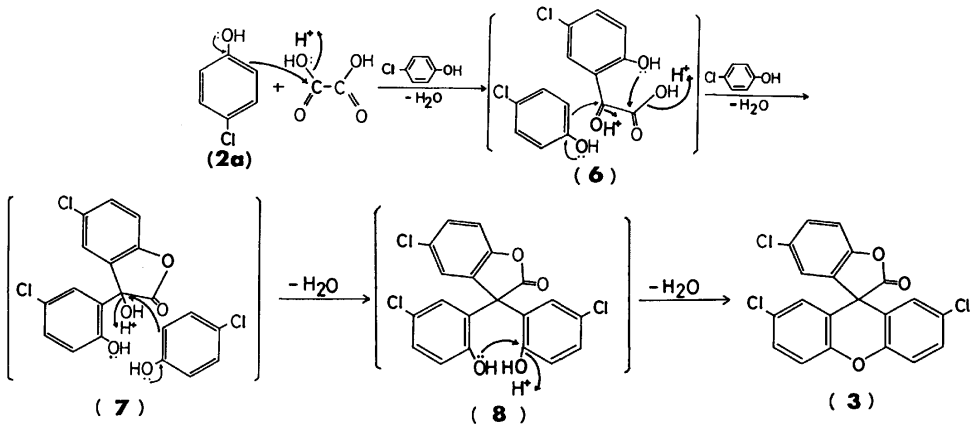

Scheme 2.

On the other hand, the corresponding value of 9.4° for fluorescein is comparable with that of **1** (5.9°). The projection of the crystal structure along the b-axis is shown in Fig. 4, and the shortest intermolecular distances are given in Table 5. There are no unusually close contacts of atoms in the unit cell, and all the intermolecular van der Waals distances are larger than 3.26 Å.

As the molecular structure of **3** has been elucidated by the X-ray diffraction method, a plausible reaction mechanism leading to the formation of **3** could be infered as shown in Scheme 2. The initial step probably involves a Friedel-Crafts type reaction between phenols (**2a**) and oxalic acid to form the oxalophenols (**6**). Subsequently, the nucleophilic attack of another phenols (**2a**) to the protonated carbonyl carbon atom of **7** forms the intermediates (**8**) with three phenol rings connected by the lactone moiety. Further, the intermediates (**8**) proceed by the intramolecular cyclization to the xanthene ring accompanying the loss of one molecule of water to reach **3**. Thus the reaction mechanism to form **3** seems to be based on the nucleophilic approach of the electron localized ortho-position of phenols to the carbonyl carbon atom, which results in the loss of four molecules of water.

The author is grateful to Professor M. Kakudo, Dr. N. Yasuoka, and the staff of Crystallographic Research Center, Institute for Protein Research, Osaka University, for use of the diffractometer and computing facilities. The author is also grateful to Professor I. Okabayashi for valuable discussion and Dr. A. Kato, Niigata College of Pharmacy, for mass spectral measurement.

References

1) Part I: M. Kimura and I. Okabayashi, *Chem. Pharm. Bull.*, **31**, 3357 (1983).
2) R. S. Osborn and D. Rogers, *Acta Crystallogr., Sect. B,*

31, 359 (1975).
3) G. Germain, P. Main, and M. M. Woolfson, *Acta Crystallogr., Sect. A*, **27**, 368 (1971).
4) D. T. Cromer and J. B. Mann, *Acta Crystallogr., Sect. A*, **24**, 321 (1968).
5) R. F. Stewart, E. R. Davidson, and W. T. Simpson, *J. Chem. Phys.*, **42**, 3175 (1965).
6) T. Ashida and N. Yasuoka, UNICS-Osaka, Computation Center, Osaka University, 1979.
7) C. H. Womack, J. C. Turley and G. E. Martin, and M. Kimura and S. H. Simonsen, *J. Heterocycl. Chem.*, **18**, 1173 (1983).
8) S. Hosoya, *Acta Crystallogr., Sect. A*, **20**, 429 (1966).

Identification of the Adsorbate Formed on a Platinum Electrode from Methanol

Hiroshi MATSUI,* Takeo HISANO, and Toshio TERAZAWA
Department of Applied Chemistry, Faculty of Engineering, The University of Tokushima, Minami-josanjima-cho, Tokushima 770
(Received August 3, 1984)

The kind of carbon-containing adsorbate formed on a platinum electrode from methanol in an acid medium was identified by an electrochemical method. Certain improvements were made in view of the harmful effects of the following factors on the Q^F value, the quantity of electricity required to form adsorbate. The factors: a) The amounts of dissolved oxygen in both solution and electrode itself; b) the concurrent oxidation of the adsorbate in the adsorption process; and c) the presence of by-products of the methanol oxidation, formaldehyde and formic acid. By appropriate procedures, these effects could be minimized or corrected. The ratio Q^F/Q^{ox}, where Q^{ox} was an electric quantity required to oxidize completely that amount of adsorbate corresponding to the Q^F, was found to be 1.8—2.0 when the potential was 0.30—0.54 V, and the methanol concentration 0.005—1 mol dm^{-3}. It was thus concluded that the adsorbate was almost exclusively CO_{ad}.

Different conclusions have been reported about the kind of carbon-containing adsorbate (M_{ad}) formed on a Pt electrode from methanol in acid media. The adsorbates proposed are COH_{ad},[1-7] CO_{ad},[8] a mixture of COH_{ad} and $COOH_{ad}$,[9] *etc.*,[10-11] but most investigators[12] seem to support the conclusion that COH_{ad} is, at least, the dominant species. Most of these conclusions were drawn from electrochemical data, such as the quantities of electricity participating in the formation (Q^F) and subsequent oxidation (Q^{ox}) of the adsorbate. More recently, B. Beden *et al.*[13,14] have identified CO_{ad} as the adsorbate by means of their newly developed technique[14,15] capable of observing *in situ* the vibrational IR spectra of an adsorbate on a Pt electrode. They claimed that there was no spectroscopic evidence for COH_{ad} under their experimental conditions.

Although such spectra would directly indicate the molecular structure of an adsorbate, the traditional electrochemical procedures seem to have an advantage of permitting wider experimental conditions.

The disagreement among investigators about the kind of adsorbate could have resulted from some small but decisive differences in their experimental electrochemical methods. D. Pletcher *et al.*,[16] for example, emphasized recently that the pretreatment of a Pt electrode surface crucially determined the experimental data about the methanol oxidation.

The present paper describes the disturbing effects of the following factors on the value of Q^F. a) Dissolved oxygen present in solution and inside the Pt electrode itself. b) Oxidation of the adsorbate accompanying the adsorption. c) Formaldehyde or formic acid, a possible by-product in the methanol oxidation. By using appropriate procedures in which these disturbing effects on Q^F were minimized or corrected, an electrochemical identification of the adsorbate in question was carried out. It was concluded that the adsorbate was almost exclusively CO_{ad} when the electrode potential was 0.30—0.54 V, the methanol concentration 0.005—1 mol dm^{-3}, and the temperature 0 °C.

Experimental

Test Electrodes. Q^F values were determined by the graphical integration of current-time curves for the M_{ad} formation process, and Q^{ox} values by the anodic pulse method of Breiter *et al.*[17,18] immediately after the adsorption process.

Generally, a large surface area is suitable for measuring small current densities in M_{ad} formation, but a very large pulse current is required to oxidize the M_{ad}. In order to facilitate the measurements of Q^F and Q^{ox} at a single electrode, one of the three test electrodes with roughness factors of about 1, 6, and 44 was used depending on the methanol concentration ranges of 2—1, 0.5—0.3, and below 0.2 mol dm^{-3}, respectively.

To prepare these roughened electrodes, platinum wires of 99.99% purity and 3×10^{-5} m^2 geometrical surface area each were platinized, then heat-treated at 300 or 500 °C in a hydrogen stream. The heat-treatment was necessary in order a) to remove oxygen in the metal itself; b) to prevent the coated Pt black from falling off; and c) to smooth the sharp regions of the Pt-black so that the distribution of currents might not become too uneven.

Electrolysis Cell. The cell consisted of three compartments. The first had a test electrode, around which a spiral platinum wire was concentrically placed as a counter electrode. This pair of electrodes was used to measure Q^{ox} by the pulse method. In the second compartment connected to the first by a narrow glass tube, another counter electrode was placed to keep the test electrode at a desired potential in co-operation with a potentiostat. The narrow tube served to suppress the migration of products formed at the counter electrode toward the test electrode. A palladium-hydrogen reference electrode[19] was in the third compartment connected to the first by way of a Teflon stopcock, which was closed during the deoxygenation of the solution in the other compartments under reduced pressure.

All the potentials described here were referred to a reversible hydrogen electrode in the same solutions.

Potential-pulse Sequence. A potential sequence used for the measurement of Q^F and Q^{ox} is shown in Fig. 1,

differing mainly in the pretreatment of the electrode from those used by Bagotzky[3,20] and Biegler.[8,11]

Effects of dissolved oxygen were serious as shown in Fig. 2, where the electrode had a roughness factor of about 44. In the normal experiments, the solutions were deoxygenated under reduced pressure for 1 min and subsequently by nitrogen-gas bubbling for 30 min through fritted-glass disks (Step A in Fig. 1). Most of the dissolved oxygen remaining in the vicinity of the test electrode was removed during Step B, in which the potential was kept at 0.06 V for 5 min. By this procedure the current for oxygen reduction in the base solution, 0.5 mol dm^{-3} sulfuric acid, was confirmed to have diminished to about 10^{-4} A m^{-2} with a roughened electrode. For a smooth electrode, the effect of oxygen was difficult to minimize to this extent as is indicated in Curve 4 of Fig. 2. Consequently, the electrode was used only when the observed current for M_{ad} formation was larger than the residual reduction current of the dissolved oxygen remaining. In other words, it was used only when the methanol

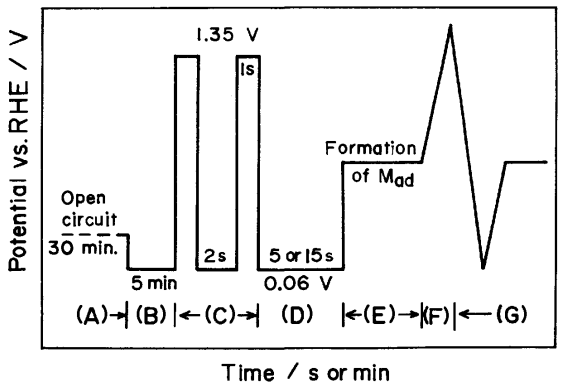

Fig. 1. Potential sequence for measurements of Q^F and Q^{ox}, A) Deoxygenation under reduced pressure and sudsequent N_2 bubbling, B) Reduction of remaining oxygen, C) Cleaning of electrode surface, D) Reduction of surface oxides and removal of oxidation products, E) M_{ad} formation and Q^F measurement, F) Q^{ox} measurement, G) for next run.

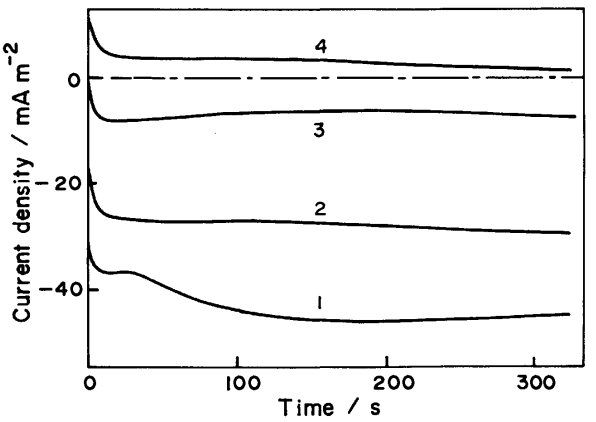

Fig. 2. Current decay on roughened electrode at 0.30 V in 0.03 mol dm^{-3} CH_3OH+0.5 mol dm^{-3} H_2SO_4 solution containing dissolved oxygen, Solution was saturated with air, oxygen was removed by degassing under reduced pressure and subsequent N_2 bubbling for: 1) 0; 2) 5; 3) 7; 4) 30 min.

concentration was higher than 1 mol dm^{-3}. The test electrode underwent final cleaning-up at Step C and D. At 1.35 V, platinum oxides were formed, and most of the M_{ad} were removed by oxidation; at 0.06 V the platinum oxides were reduced without evolution of free hydrogen. The double rectangular pulses in Step C served to remove M_{ad} completely and to prevent the formation of a deep layer of surface oxides. A small amount of by-products, which might be formed at 1.35 V and at high concentrations of methanol, were allowed to diffuse away during Step D (0.06 V), the duration of which was 5 or 15 s. The longer duration was favorable for the complete disappearance of a non-steady current produced in the transit from C into D Steps. The shorter one, however, was superior at methanol concentrations above 0.3 mol dm^{-3}, because the amount of M_{ad} formed even at this low potential became perceptible at longer times. To diminish such concomitant events, all the measurements were made at a low temperature of 0 °C.

The potential sequence was generated by means of a LB-75 M Wenking potentiostat and a handmade pulse generator. In the measurement of Q^F, the currents at Step E were stored in a HR-1200 transient converter (Kawasaki Electronics), which had a decimal 12-bit resolution, and recorded on a WX-4401 XY recorder (Watanabe Instruments Corp.,).

All the current densities described are for a unit true area of electrode surface, determined by the conventional hydrogen deposition method. In the measurement of Q^{ox} (Step F), the scan rates were 263, 99.4, and 27.6 V/s in the methanol concentration ranges of 2—1, 0.5—0.3, and below 0.2 mol dm^{-3}, respectively. Under these conditions, the observed currents were almost exclusively due to the oxidation of M_{ad}.

Results and Discussion

As most investigators[1-5,8,11] approve, the formation of an experimentally perceptible adsorbate from methanol in acid solution and the oxidation of the adsorbate may well be written as

$$M_{ad} \text{ formation: } CH_3OH = M_{ad} + n_1H^+ + n_1e \quad (1)$$

$$M_{ad} \text{ oxidation: } M_{ad} + H_2O = CO_2 + n_2H^+ + n_2e \quad (2)$$

M_{ad} denotes a carbon-containing adsorbate, n_1 and n_2 are the number of participating electrons. It should be noted that the equations do not necessarily represent the only path for methanol oxidation. According to the Eqns., $n_1+n_2=6$. If M_{ad} is, *e.g.*, CO_{ad} or COH_{ad}, n_2 should be 2 or 3, respectively. The ratio $n_1/n_2=Q^F/Q^{ox}$, where Q^F is a quantity of electricity required to form an amount of M_{ad}, and Q^{ox} is that required to oxidize this amount of M_{ad} to carbon dioxide.

Determination of Q^F *by Experimental* i-t *and* Q^{ox}-t *Relationships.* It is no doubt a prerequisite for obtaining a correct value of Q^F by integration of an experimental *i-t* relationship in the adsorption process that the *i* is solely due to the adsorption. As the criterion, previous investigators[3,8,11] employed either of the following theoretical *i-t* relationships:

$$i = k_1/t \quad (3)$$

$$1/i = 1/i_0 + k_2 t \quad (4)$$

where k_1 and k_2 are constants. Equation 3 was derived by Bagotzky *et al*,[3,8,11] by using the next relation.

$$\theta_M = a + b \ln t \quad (5)$$

where a and b are constants, and θ_M is a surface coverage with M_{ad}. They assumed that θ_M was in direct proportion to the number of M_{ad} species. The assumption, however, is not always correct, because every M_{ad} might not always occupy the same number of sites on the electrode surface; the details of which will be reported later. Thus, we prefer to use Q^{ox} instead of θ_M,

$$Q^{ox} = a' + b' \log t \quad (6)$$

where a' and b' are constants. When the values of Q^{ox}/Q_H^0 are within the range about 0.1 to 0.9, Eq. 6 is valid as shown in Fig. 3. Instead of Q^{ox}, Q^{ox}/Q_H^0 is used for convenience of comparison with other data, Q_H^0 being a quantity of electricity required fully to cover the surface with a monolayer of adsorbed hydrogen atoms. According to Eq. 6 or 5, Q^{ox} approaches minus infinity as t approaches zero, while it is required for the derivation of Eq. 4 that Q^{ox} approaches zero. It thus appears that Eq. 3 is preferable to Eq. 4.

Figure 4 shows typical *i-t* relations observed for the adsorption process under the same conditions as in Fig. 3. A linear part with a slope of −0.99 is seen in any curve obtained at a potential within the limits of 0.30—0.48 V, *e.g.*, the latter parts of curves 4 and 5, indicating the validity of Eq. 3. On the other hand, the former parts of the curves at low potentials show considerable deviations from that linear relation, and the lower the potential, the larger becomes the deviation. Although it might be ascribed to a change in the kinetics of adsorbate formation, the nature of the currents remains unknown. However the contributions of the currents to the value of Q^{ox} were so small that treating them as genuine adsorption currents brought no serious errors in obtaining the Q^F—Q^{ox} relationship (Fig. 6).

At potentials above 0.48 V, appreciable and stationary currents were observed even after 30 min from the start of adsorption. If adsorption on a electrode surface is completed, the adsorption current should fall to zero. Consequently, these stationary currents might be considered to be due to both the stationary oxidation of the adsorbate and, in some cases, the formation of by-products. Thus, the net adsorption currents at every moment were estimated by subtracting the stationary current still flowing at 30 min after the start of adsorption from the observed current.

Effects of Formaldehyde and Formic Acid on Q^F *and* Q^{ox}. Breiter *et al.*[21,22,23] reported that appreciable amounts of formaldehyde and formic acid were formed during the oxidation of methanol in acid so-

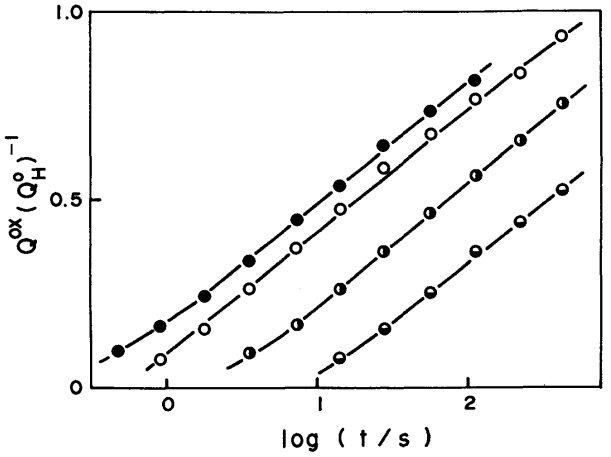

Fig. 3. Variation in Q^{ox} with time, M_{ad} was formed in 0.03 mol dm^{-3} CH_3OH+0.5 mol dm^{-3} H_2SO_4 at constant potentials: ◒ 0.36; ◑ 0.42; ○ 0.48; ● 0.57 V.

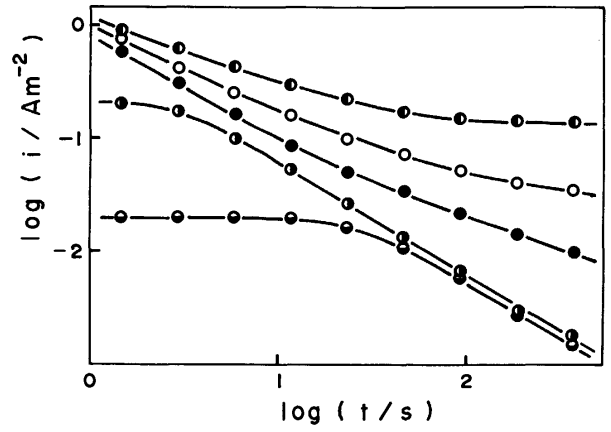

Fig. 4. Variation in current density at constant potential with time, 0.03 mol dm^{-3} CH_3OH+0.5 mol dm^{-3} H_2SO_4, Potential: 1) 0.65; 2) 0.60; 3) 0.55; 4) 0.45; 5) 0.35 V.

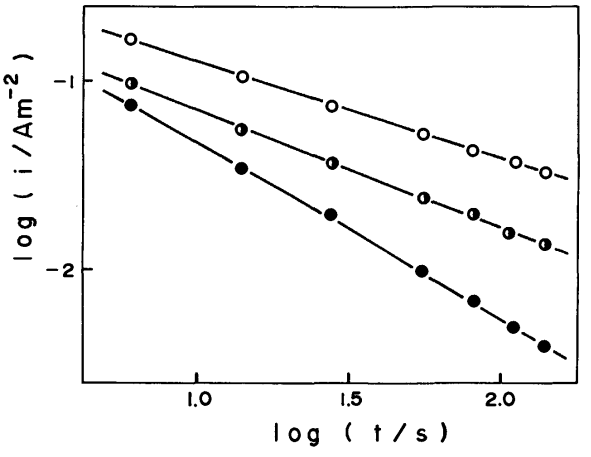

Fig. 5. Variation in M_{ad} formation current with concentration of formaldehyde in 0.03 mol dm^{-3} CH_3OH+0.5 mol dm^{-3} H_2SO_4+HCHO, Concn. of HCHO: ● 0; ◑ 0.01; ○ 0.03 mol dm^{-3}.

lution in which the concentration of methanol was relatively high. The effects of these substances on the *i-t* curves for M_{ad} formation process were significant even in their very low concentrations. Figure 5 shows how the presence of formaldehyde increases both the currents and the slopes of the log *i*—log *t* curves. The resulting Q^F were obviously larger than those in the absence of the aldehyde. Its presence, on the other hand, had only a small effect on the values of Q^{ox}, thus resulting in an increase in the Q^F/Q^{ox} values. The effects of formic acid were similar to those of formaldehyde. These contaminants originally present in methanol reagent can readily be removed. However there is no way of removing the substances that are unavoidably formed during the pretreatment for cleaning the electrode surface by potential pulses. Consequently, it seems best to design a pulse sequence which produces only as small amounts of these substances as possible. Such is the case with the sequence described in the experimental section. In addition, it was confirmed that[23] regardless of the potential the formation of these by-products only became perceptible, when the methanol concentration was above about 1 mol dm^{-3}. Their formation at a constant potential should be accompanied by a stationary current. Therefore, the background-current correction to obtain the net adsorption current would also eliminate that stationary current so long as the amount of by -products are not too large.

Q^F-Q^{ox} *Relationship.* Figure 6 shows the typical Q^F-Q^{ox} relations for the adsorption process under the same conditions as those in Figs. 3 and 4. There is a straight line relationship with a slope, Q^F/Q^{ox}, close to 2. In spite of the background-current corrections, upward deviations from linearity took place when the potential was above 0.48 V, while at the same time the Q^{ox} value was large. The cause of such deviation remains unknown. Figure 7 shows the variation in the slope of the linear part with potential. Within the potential range of 0.30—0.54 V, the slope varied only slightly, the average being 1.84. Biegler *et al.*[11] had reported that the slope depended on the potential. The virtual invariance of the slope value can be largely attributed to the current correction, which Biegler *et al.* did not made. The effects of methanol concentration on the slope value are illustrated in Fig. 8. In this instance the potential was 0.42 V, at which no background current was observed. The slope varied only slightly over a wide range of methanol concentration, 0.005—1 mol dm^{-3} the average being 1.89. Higher potentials resulted in slightly larger slopes. Lower potentials also led to slightly smaller values, and moreover narrowed the methanol-concentration range in which the slope remained practically constant.

As described above, the slope is almost constant over the considerably wide ranges of M_{ad}-formation time, potential, and methanol concentration. This fact indicates that only one kind of M_{ad} species is formed. As the M_{ad}, CH_3O_{ad}, CH_2O_{ad}, COH_{ad}, CO_{ad}, or $COOH_{ad}$ is to be expected from Eqs. 1 and 2, if the slope is 1/5, 1/2, 1, 2, and 5, respectively. Because the slope is close to 2, it is concluded that the adsorbate should almost exclusively be CO_{ad}, at least, under those conditions which have hitherto been specified. A slight deviation of the

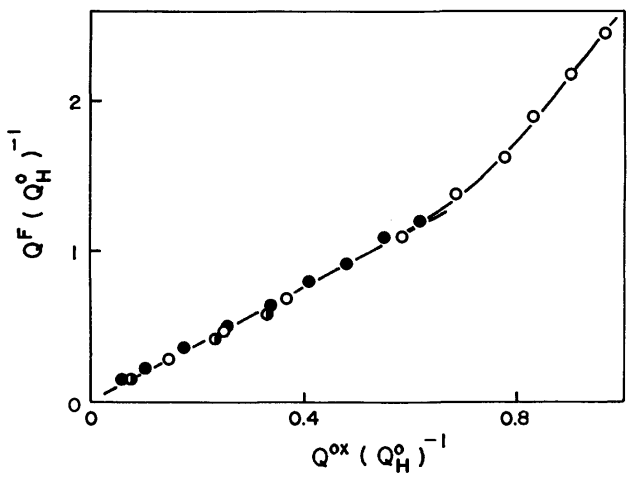

Fig. 6. Variation in Q^F with Q^{ox} in 0.03 mol dm^{-3} CH_3OH+0.5 mol dm^{-3} H_2SO_4, Constantials: ◑ 0.33; ● 0.42; ○ 0.51 V.

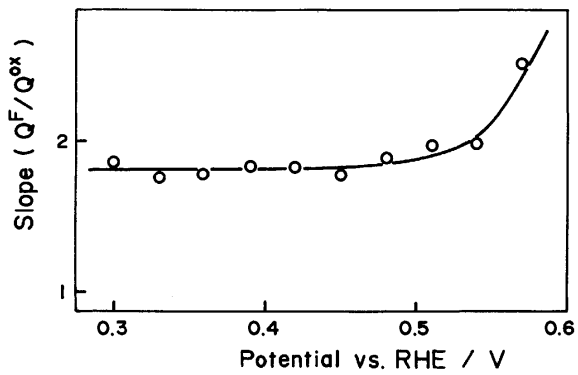

Fig. 7. Variation in slope (Q^F/Q^{ox}) with potential in 0.03 mol dm^{-3} CH_3OH+0.5 mol dm^{-3} H_2SO_4.

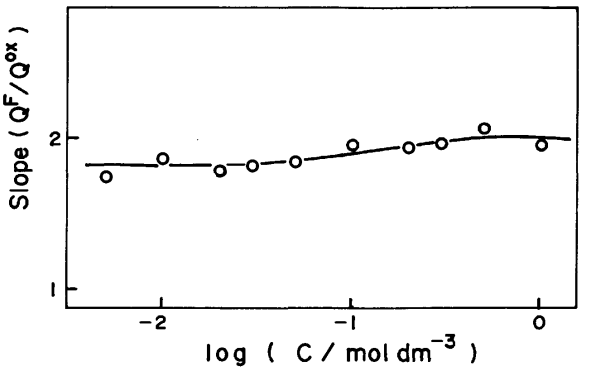

Fig. 8. Variation in slope (Q^F/Q^{ox}) with methanol concentration at 0.42 V in CH_3OH+0.5 mol dm^{-3} H_2SO_4.

slope value from 2 might have been caused by the coexistence of some other adsorbate such as COH_{ad}.

References

1) O. A. Petrii, "Adsorption of Organic Compounds on Electrodes," ed by B. B. Damaskin, O. A. Petrii, and V. V. Batrakov, Plenum press, New York, (1971) p. 324.
2) O. A. Petrii, B. I. Podlovchenko, A. N. Frumkin, and Hira Lal, *J. Electroanal. Chem.*, **10**, 253 (1965).
3) V. S. Bagotzky and Yu. B. Vassiliev, *J. Electroanal. Chem.*, **12**, 1323 (1967).
4) P. Sidheswaran and Hira Lal, *J. Electroanal. Chem.*, **34**, 173 (1972).
5) V. E. Kazarinov, G. Ya. Tysyachnaya, and V. N. Andrew, *J. Electroanal. Chem.*, **65**, 391 (1975).
6) V. F. Stenin, V. E. Kazarinov, and B. I. Podlovchenko, *Elektrokhimya*, **5**, 442 (1969).
7) B. I. Podlovchenko and E. P. Gorgonova, *Dokl. Akad. Nauk, SSSR*, **156**, 673 (1964).
8) T. Biegler and D. F. A. Koch, *J. Electrochem. Soc.*, **114**, 904 (1967).
9) M. W. Breiter, *J. Electroanal. Chem.*, **14**, 407 (1967); M. W. Breiter, *ibid.*, **15**, 221 (1967).
10) A. Wieckowski and J. Sobkowski, *J. Electroanal. Chem.*, **63**, 365 (1975); A. Wieckowski and J. Sobkowski, *ibid.*, **73**, 317 (1976).
11) T. Biegler, *J. phys. Chem.*, **72**, 1571 (1968).
12) M. W. Breiter, "Modern Aspects of Electrochemistry," ed by J. O'M. Bockris and B. E. Conway, Vol. 10, Plenum press, New York, (1975) p. 161.
13) B. Beden, C. Lamy, A. Bewick, and K. Kunimatsu, *J. Electroanal. Chem.*, **121**, 343 (1981).
14) K. Kunimatsu, A. Bewick, and J. Russel, *Shokubai*, **23**, 266 (1981); K. Kunimatsu, *Hyomen*, **20**, 197 (1982).
15) B. Bewick, K. Kunimatsu, and B. S. Pons, *Electrochim. Acta*, **25**, 465 (1980).
16) D. Pletcher and V. Solis, *Electrochim. Acta*, **27**, 775 (1982).
17) M. W. Breiter and S. Gilman, *J. Electrochem. Soc.*, **109**, 622 (1962).
18) S. Gilman, "Electroanalytical Chemistry," ed by A. J. Bard, Vol. 2, Marcel Dekker, New York (1967) p. 166.
19) H. Shiratori, *Denki Kagaku*, **29**, 457 (1971).
20) V. S. Bagotzky and Yu. B. Vassilyev, *Electrochim. Acta*, **11**, 1439 (1966).
21) M. W. Breiter, *Discuss. Faraday Soc.*, **45**, 79 (1968).
22) Y. Nakagawa, K. Ota, and M. Takahashi, The 23 rd Battery Symposium in Japan, Yokohama, November (1982).
23) H. Matsui, T. Hisano, and T. Terazawa, 50 th Meeting of Electrochemical Society of Japan, Tokyo, May (1983).

A Relation between Oxidation State of Sulfur and Acidic Property of Iron Oxide Containing Sulfur

Yoshinori NAGASE, Tuo JIN, Hideshi HATTORI, Tsutomu YAMAGUCHI, and Kozo TANABE*

Department of Chemistry, Faculty of Science, Hokkaido University, Sapporo 060

(Received August 13, 1984)

Five kinds of iron oxide catalysts promoted with sulfur were prepared by impregnating $Fe(OH)_3$ with $(NH_4)_2SO_4$ and by treating Fe_2O_3 and $Fe(OH)_3$ with H_2S and SO_2. Changes in acidic properties of the catalysts with changes in oxidation states of sulfur were investigated by test reactions such as isomerization of cyclopropane and dehydration of 2-propanol over the oxidized or reduced catalysts. It has been found that the generation of acidic properties of the catalysts was independent of the kinds of the starting sulfur compounds, but dependent on the oxidation states of the sulfur. The sulfur in the highest oxidation state was responsible for the strongly acidic property of the catalyst.

It has been reported recently that the iron oxide catalyst promoted with SO_4^{2-} ion exhibited high catalytic activities for the isomerization of cyclopropane and the dehydration of 2-butanol.[1] It was also found that this type of catalyst was quite effective for a coal liquefaction under a high hydrogen pressure and at a high temperature.[2] High catalytic activities in the former reactions were attributed to the enhanced acidic properties of the promoted catalysts, which originated from a strongly electrophilic nature of S=O bonds of sulfur species bound on the surface.[1] In the latter reaction, however, the Fe_2O_3–SO_4^{2-} catalyst is considered to be reduced with hydrogen to lose the high acidic property as well as the catalytic activity. Therefore, it is necessary to examine the influence of the oxidation state of sulfur on the acidic property of Fe_2O_3 containing sulfur. This report deals with whether H_2S and SO_2, besides SO_4^{2-}, as sulfur sources are effective for enhancing the acidic property and how such a property changes when the oxidation state of sulfur is controlled.

Experimental

Catalyst Preparation. Iron oxide and hydroxide were prepared by the hydrolysis of $Fe(NO_3)_3$ with aqeous ammonia. The sulfur promoted catalysts were prepared by adsorbing inorganic sulfur compounds on iron hydroxide or oxide, followed by calcination, reduction, and oxidation. The Fe_2O_3 (A)–SO_4^{2-} catalyst was prepared by immersing $Fe(OH)_3$ in an aqueous solution of $(NH_4)_2SO_4$, followed by drying at 110 °C and calcining at 500 °C. The amount of sulfur loaded was adjusted to about 2 wt% as SO_3. The Fe_2O_3 (A)–H_2S and Fe_2O_3 (A)–SO_2 catalysts were obtained by treating $Fe(OH)_3$ with 1200 Pa of H_2S and SO_2. The Fe_2O_3 (B)–H_2S and Fe_2O_3 (B)–SO_2 catalysts were obtained by treating Fe_2O_3 instead of $Fe(OH)_3$ similarly as above. Treating temperature is denoted as Fe_2O_3 (A)–H_2S-400 (Fe_2O_3 (A) treated with H_2S at 400 °C). When the catalyst was oxidized with O_2 at 500 °C, it is denoted as Fe_2O_3 (A)–H_2S-400–O_2-500. Catalyst nomenclature is illustrated in Table 1. Prior to the reaction, some of the catalysts treated with H_2S and SO_2 were oxidized with O_2 at 400 to 500 °C for 10 min and evacuated at 500 °C, and some of the Fe_2O_3 (A)–SO_4^{2-} catalysts were reduced with hydrogen at 350—500 °C.

Table 1. Catalysts treated with sulfur compounds by different methods

Catalyst nomenclature	Source of sulfur	Supporting method	Temperature of gas treatment/°C
Fe_2O_3	None	—	Untreated[a]
Fe_2O_3(A)-SO_4^{2-}	$(NH_4)_2SO_4$	Impregnation	Untreated[a]
Fe_2O_3(A)-SO_4^{2-}-H_2-350	$(NH_4)_2SO_4$	Impregnation	350 with H_2
Fe_2O_3(A)-SO_4^{2-}-H_2-400	$(NH_4)_2SO_4$	Impregnation	400 with H_2
Fe_2O_3(A)-SO_4^{2-}-H_2-500	$(NH_4)_2SO_4$	Impregnation	500 with H_2
Fe_2O_3(A)-H_2S-400	H_2S	Gas treatment	400 with H_2S
Fe_2O_3(A)-H_2S-400-O_2-500	H_2S	Gas treatment	400 with H_2S and 500 with O_2
Fe_2O_3(B)-H_2S-400	H_2S	Gas treatment	400 with H_2S
Fe_2O_3(B)-H_2S-400-O_2-500	H_2S	Gas treatment	400 with H_2S and 500 with O_2
Fe_2O_3(A)-SO_2-400	SO_2	Gas treatment	400 with SO_2
Fe_2O_3(A)-SO_2-400-O_2-500	SO_2	Gas treatment	400 with SO_2 and 500 with O_2
Fe_2O_3(B)-SO_2-400	SO_2	Gas treatment	400 with SO_2
Fe_2O_3(B)-SO_2-400-O_2-500	SO_2	Gas treatment	400 with SO_2 and 500 with O_2

a) Untreated with any gas, but calcined in air at 500 °C.

The Fe_2O_3 (B)-SO_4^{2-} was prepared by the hydrolysis of iron alum with urea as described in our previous paper.[1] The amount of sulfur loaded was 6 wt% as SO_3. The Fe_2O_3 (B)-SO_4^{2-} catalyst was used for 2-propanol dehydration. For a series of the experiments, the catalyst was evacuated at 500 °C, reduced with a stream of hydrogen at different temperatures, and then evacuated again at the same temperature of reduction. In the case of the catalyst reduced below 200 °C, the final evacuation was performed at 200 °C. For the other series of experiments, the catalysts were treated as in the cases of the first series of experiments and then oxidized with flowing air at 500 °C for 1 h, followed by evacuation at 500 °C.

Measurement of Surface Area. Specific surface area was determined by the BET method using nitrogen.

Measurement of Sulfur Content. The atomic ratios of S/Fe in the catalysts reduced at different temperatures were determined by X-ray fluorescent spectroscopy on the basis of the samples of known S/Fe ratios.

Reaction Procedure. Isomerization of cyclopropane was carried out at 150 °C by use of 0.2 g of catalyst in a closed recirculation apparatus of 800 ml capacity which was equipped with a sampling manifold. A 6,670 Pa of cyclopropane was used. The reaction of 2-propanol was carried out at 200 °C in a closed recirculation apparatus of 266 ml capacity, 4,000 Pa of 2-propanol being passed through 0.2 g of a Fe_2O_3-SO_4^{2-} catalyst. The product was only propene.

Results and Discussion

Isomerization of Cyclopropane. Isomerization of cyclopropane to yield propene is known to be one of the best reactions for examining acidic properties of solid acid catalysts.[3,4] The rates of the isomerization over the Fe_2O_3 catalysts treated with $(NH_4)_2SO_4$, H_2S or SO_2 and then with H_2 or O_2 are summarized in Table 2. The Fe_2O_3 catalyst was inactive, but became active when treated with $(NH_4)_2SO_4$ in accordance with our previous work.[1] However, the activity of Fe_2O_3 (A)-SO_4^{2-} decreased on reduction with H_2 at 400 °C and lost the activity completely when reduced with H_2 at 500 °C. Thus, the oxidized state of SO_4^{2-} is considered to be essential for the generation of acidity of the catalyst.

Table 2. Catalytic activities for isomerization of cyclopropane

Catalyst	Rate of reaction 10^{-5} mol min^{-1} g^{-1}
Fe_2O_3	0
Fe_2O_3(A)-SO_4^{2-}	30
Fe_2O_3(A)-SO_4^{2-}-H_2-350	34
Fe_2O_3(A)-SO_4^{2-}-H_2-400	15
Fe_2O_3(A)-SO_4^{2-}-H_2-500	0
Fe_2O_3(A)-H_2S-400	0
Fe_2O_3(A)-H_2S-400-O_2-500	30
Fe_2O_3(B)-H_2S-400	0
Fe_2O_3(B)-H_2S-400-O_2-500	28
Fe_2O_3(A)-H_2S-500	0
Fe_2O_3(A)-H_2S-500-O_2-500	7
Fe_2O_3(B)-H_2S-500	0
Fe_2O_3(B)-H_2S-500-O_2-500	6
Fe_2O_3(A)-SO_2-400	0
Fe_2O_3(A)-SO_2-400-O_2-500	44
Fe_2O_3(B)-SO_2-400	0
Fe_2O_3(B)-SO_2-400-O_2-500	35
Fe_2O_3(A)-SO_2-500	0
Fe_2O_3(A)-SO_2-500-O_2-500	32
Fe_2O_3(B)-SO_2-500	0
Fe_2O_3(B)-SO_2-500-O_2-500	32

In the case of Fe_2O_3 treated with H_2S or SO_2 at 400 °C, no catalytic activity was observed. However, the Fe_2O_3-H_2S and Fe_2O_3-SO_2 catalysts exhibited almost the same activity as that of Fe_2O_3-SO_4^{2-} when oxidized with O_2. The difference between Fe_2O_3-H_2S and Fe_2O_3-SO_2 was that Fe_2O_3 treated with H_2S at 500 °C followed by oxidation with O_2 showed a low activity ($6—7\times10^{-5}$ mol min^{-1} g^{-1}), whereas Fe_2O_3 treated with SO_2 at 500 °C followed by oxidation with O_2 showed almost the same activity (32×10^{-5} mol min^{-1} g^{-1}) as that of Fe_2O_3 (A)-SO_4^{2-}. Thus, the temperature of treatment with H_2S is important to generate the activity after the oxidation in the case of H_2S-treated catalysts.

The data of Table 2 clearly indicate that the introduction of any kinds of sulfur compounds causes the enhancement of the activity for the acid-catalyzed reaction, provided that the sulfur-treated catalysts are oxidized, whatever the source of sulfur is. Since the high catalytic activities of Fe_2O_3-SO_4^{2-} for the acid type reactions were attributed to strong acid sites created by the electron-attracting property of S=O bonds of a sulfur species like $>S\lesssim^{O}_{O}$ on the surface,[1] H_2S and SO_2 are considered to be converted into the sulfur species by oxidation. In other words, the highest oxidation state of sulfur (S^{6+} in the $>S\lesssim^{O}_{O}$) is necessary to show high catalytic activity.

Dehydration of 2-Propanol. An iron oxide catalyst containing SO_4^{2-} ions was highly active for the dehydration of 2-butanol.[1] The dependency of the catalytic activity on the temperature of H_2 treatment was examined over the catalyst, Fe_2O_3 (B)-SO_4^{2-}, prepared by a urea method by use of the dehydration of 2-propanol as a test reaction. As shown by open circles in Fig. 1, when the catalyst was reduced with flowing H_2 below 100 °C, no detectable change in the activity was observed. The activity, however, abruptly decreased with increase in the reduction temperature from 100 to 150 °C. By raising the temperature from 150 °C to 400 °C, the catalytic activity decreased gradually to zero. The activities of the catalysts reoxidized at 500 °C are also shown by solid circles in Fig. 1. Recovery of the activity by oxidation was observed for all the catalysts. The extent of recovery varied

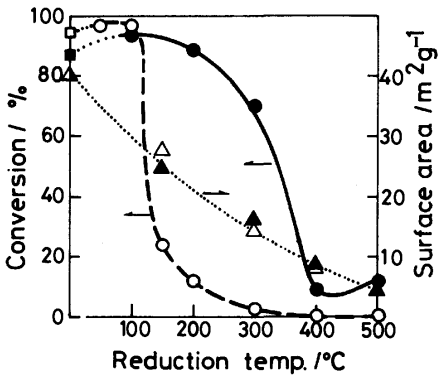

Fig. 1. Decomposition of 2-propanol at 200°C over Fe_2O_3 (B)-SO_4^{2-} △,○; Fe_2O_3 (B)-SO_4^{2-} evacuated at 500°C for 2 h was reduced with hydrogen for 2 h, followed by evacuation for 1 h at each temperature indicated in the figure. In the case of below 200°C of reduction temperature, the catalyst was evacuated at 200 °C for 1 h.
▲,●; The above catalyst was oxidized with air at 500 °C for 2 h, followed by evacuation at 500 °C for 2 h.
□; Fe_2O_3 (B)-SO_4^{2-} evacuated at 500 °C for 2 h was oxidized with air at 500 °C for 2 h.
■; Fe_2O_3 (B)-SO_4^{2-} evacuated at 500 °C for 2 h was oxidized with air at 500 °C for 2 h, followed by evacuation at 500 °C for 2 h.
Δ; Fe_2O_3 (B)-SO_4^{2-} evacuated at 500 °C for 2 h.

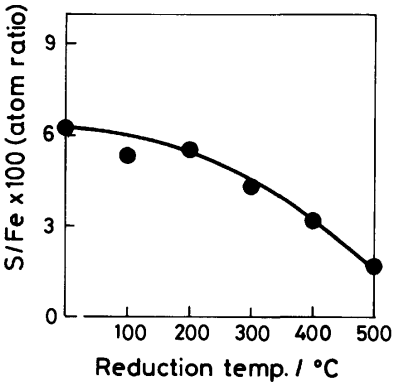

Fig. 2. Variation of S/Fe ratio in Fe_2O_3 (B)-SO_4^{2-} with reduction temperature.

with the reduction temperatures. A catalyst reduced at 200 °C recovered the original activity after the reoxidation and a catalyst reduced at 300 °C recovered about 80% of its original activity. The catalysts reduced above 400 °C, however, restored the activity to a small extent. Recovery by the oxidation indicates that the active sites are related with a higher oxidation state of sulfur.

State of Sulfur. It is pointed out that the activity loss by reduction at lower temperatures may arise from the removal of surface oxygens. An X-ray diffraction analysis revealed that the reduction of Fe_2O_3 took place to yield Fe_3O_4 phase around 250 °C.[5] Therefore, below 300 °C, the reduction may occur *via* a removal of the oxygens bridged to both S and Fe. Such a removal of the oxygens will result in the loss of the catalytic activity in the low temperature range and the lost activity is easily restored by reoxidation in agreement with the case of the isomerization of cyclopropane.

Figure 2 shows the change in the sulfur contents measured by X-ray fluorescent spectroscopy with reduction temperature. The amount of sulfur gradually decreased with an increase in the reduction temperature. Loss of sulfur by raising the reduction temperature from 300 to 400 °C was not significant as compared with a large decrease in the activity. Thus, the marked decrease in catalytic activity observed when reduction temperature was raised from 300 to 400 °C can not be attributed to the removal of the sulfur.

Changes in the surface area by reduction and reoxidation at various temperatures are also shown in Fig. 1. Although this changes are not coincide with the changes in the catalytic activities, poor recovery of the activity for the catalyst reduced at 400 °C is considered to be partly due to a decrease in surface area.

XPS results indicated the reversible change between S^{2-} and S^{6+} states by reduction and reoxidation above 400 °C.[6] This suggests that catalytically inactive iron sulfide is formed by reduction and it is changed to catalytically active sulfate complex by reoxidation. Thus, another reason for the poor recovery is considered to be due to the decrease in the number of sulfur species on the surface by its migration to the bulk on reduction above 400 °C.

This work was supported by Grant-in-Aids for Special Research (No. 58108005 and 57040002) of Ministry of Education, Science and Culture, Japan.

References

1) A. Kayo, T. Yamaguchi, and K. Tanabe, *J. Catal.*, **83**, 99 (1983).
2) K. Tanabe, H. Hattori, T. Yamaguchi, S. Yokoyama, J. Umematsu, and Y. Sanada, *Fuel*, **61**, 399 (1982).
3) J. W. Hightower and W. K. Hall, *J. Phys. Chem.*, **72**, 4555 (1968).
4) B. H. Bartley, H. W. Habgood, and Z. M. George, *J. Phys. Chem.*, **72**, 1689 (1968).
5) T. Jin, H. Hattori, and K. Tanabe, *Bull. Chem. Soc. Jpn.*, **56**, 3208 (1983).
6) T. Jin, M. Machida, T. Yamaguchi, and K. Tanabe, *Shokubai*, **26**, 336 (1984).

Studies on Salt Hydrates for Latent Heat Storage. VII. The Relation between Activation Process of Crystal Nucleation Catalysts for Sodium Acetate Trihydrate and Their Deactivation Temperatures

Takahiro WADA* and Hiroshi YONENO
Central Research Laboratory, Matsushita Electric Industrial Co. Ltd., 1006 Kadoma, Osaka 571
(Received August 31, 1984)

Influences of preheating temperature were studied on crystallization of $CH_3CO_2Na \cdot 3H_2O$ from its melts containing a small amount of $Na_4P_2O_7$ or Na_2HPO_4 as a crystal nucleation catalyst. The relation between the activation process of these nucleation catalysts and their deactivation temperatures was investigated in detail. Aging of nucleation catalyst which was preceded by forced crystallization of $CH_3CO_2Na \cdot 3H_2O$ from its melt containing the catalyst, largely affects the catalyst's deactivation temperature. Whenever $Na_4P_2O_7$ or Na_2HPO_4 was used as a nucleation catalyst, the deactivation temperature was raised by lengthening aging time at a constant aging temperature. When the catalysts were aged for 4 d at 20 °C, the aging effect on them was almost saturated. At lower temperatures, longer aging times were required for saturation of the effect. The results obtained are discussed with a modified adsorption model, which takes into account commensurate-incommensurate phase transition of solid adsorbate.

Sodium acetate trihydrate ($CH_3CO_2Na \cdot 3H_2O$) has attracted attention as a useful heat storage material because of its large latent heat of fusion (264 J/g).[1,2] Pure $CH_3CO_2Na \cdot 3H_2O$ melt supercools to a considerably lower temperature than its melting point (58.4 °C).[3,4] Its practical application has been impaired by this supercooling phenomenon.[5] Wada and Yamamoto[6] first found that addition of $Na_4P_2O_7 \cdot 10H_2O$ is very effective for preventing this supercooling. Afterward, Kimura[7] reported that addition of a mixture of Na_2HPO_4 and anhydrous CH_3CO_2Na also is effective for prevention of the supercooling.

Recently, Wada *et al.*[8,9] studied the influence of preheating on the crystallization of $CH_3CO_2Na \cdot 3H_2O$ from aqueous solutions containing a nucleation catalyst ($Na_4P_2O_7$[10] or Na_2HPO_4[11]). They found that these nucleation catalysts were deactivated at an elevated temperature above the melting point of $CH_3CO_2Na \cdot 3H_2O$ and that temperatures at which the catalysts began to get deactivated were raised with increasing CH_3CO_2Na concentration in the solution. They explained these results on the basis of the crystalline adsorption model proposed by Richards.[12] This model is illustrated in Fig. 1. Adsorbed crystalline layers (crystalline adsorbate) are retained on the nucleation catalyst (adsorbent) surface under such condition as preclude the existence of bulk crystals.

In our previous studies[8,9] the deactivation temperature of nucleation catalysts sometimes varied widely, and the reason for this variation has not yet been understood. In order to elucidate the cause of the variation, we investigated in detail the relation between the activation process of a nucleation catalyst and its deactivation temperature. This paper reports that aging of a nucleation catalyst preceded by forced crystallization of $CH_3CO_2Na \cdot 3H_2O$ from a melt containing the catalyst, largely affects its deactivation temperature. The results obtained are discussed with a modified adsorption model, which takes into account commensurate-incommensurate phase transition of solid adsorbate.

Experimental

$CH_3CO_2Na \cdot 3H_2O$, $Na_4P_2O_7$, and Na_2HPO_4 were guaranteed grade reagents from Wako Pure Chemical Industries Ltd. Eight grams of $CH_3CO_2Na \cdot 3H_2O$ and 0.16 g of nucleation catalyst were placed in a container, about 3 mm in thickness, made of four-layered laminate film: Polyethylene terephthalate (12 μm)/nylon (15 μm)/aluminium film (9 μm)/polyethylene (70 μm). The sample temperature was measured by a chromel-alumel thermocouple attached to the outer wall of the container. The container was placed between plate heaters.

Experimental runs were performed according to the temperature program shown in Fig. 2. Eight containers, each containing 8 g of $CH_3CO_2Na \cdot 3H_2O$ and 0.16 g of nucleation catallyst, were heated at 95 °C for 1 h (D→E) in order to deactivate the nucleation catalyst completely. Then, they were cooled to room temperature (E→F), and the supercooled melts were seeded (F); this is forced crystallization of $CH_3CO_2Na \cdot 3H_2O$. Immediately, the temperature was raised to the freezing point (F→G→H). Then they were cooled to the aging temperature in a thermostat (H→I) and kept there for the aging time (I→J). After that, the containers were heated to a predetermined temperature (J→M), kept there for 1 h (M→N), and then cooled to 40 °C at a rate of 30 °C/h (N→R). In this cooling process, crystallization of $CH_3CO_2Na \cdot 3H_2O$ was detected by a sudden rise in the temperature of the sample (O→P→Q). This process was repeated with the preheating temperature raised stepwise. In some of the eight containers preheated at a certain temperature, $CH_3CO_2Na \cdot 3H_2O$ failed to crystallize on cooling to 40 °C. The nucleation catalyst in such containers must have been deactivated or degraded to lose nucleation ability. The percentage of the containers with

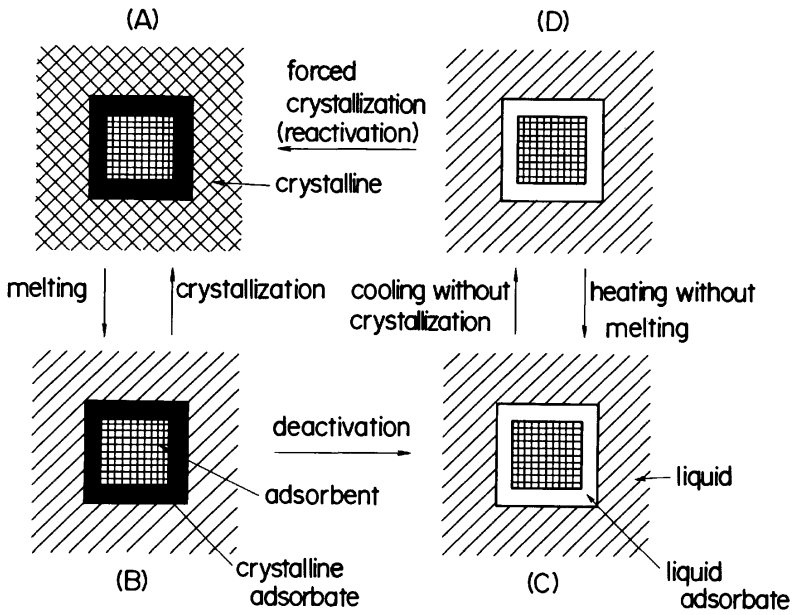

Fig. 1. The crystalline adsorption model for heterogeneous nucleation. (A): Crystalline state, (B): melting state with crystalline adsorbate, (C): melting state with liquid adsorbate, (D): supercooled state.

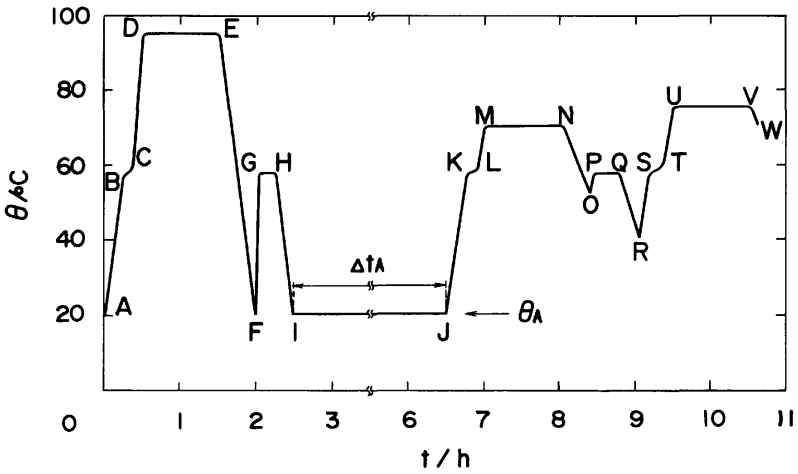

Fig. 2. The temperaure program of a typical sample. The nucleation catalyst is activated during the first crystallization of $CH_3CO_2Na \cdot 3H_2O$.

such deactivated nucleation catalysts was plotted against the difference ($\Delta\theta$) between the preheating temperature (θ) and the melting point of $CH_3CO_2Na \cdot 3H_2O$ (58.4 °C), the results being shown in Figs. 3—6.

Results

$Na_4P_2O_7$ as a Nucleation Catalyst. It is clear from Fig. 3 that the nucleation catalyst which was aged for 0.5 h at 20 °C began to get deactivated at 69 °C, higher by about 10 °C than the melting point of $CH_3CO_2Na \cdot 3H_2O$, and that all of the catalysts were deactivated at about 80 °C. The nucleation catalysts which were aged for 4, 20, and 96 h began to get deactivated at 74, 84, and 86 °C, and all of them were deactivated at 86, 92, and 93 °C, respectively. It is understood from Fig. 3 that the deactivation temperature of nucleation catalyst is raised with lengthening aging time at a constant aging temperature. The deactivation behavior of the nucleation catalyst aged for 500 h at 20 °C, which is not shown in Fig. 3, is almost the same as that of the nucleation catalyst aged for 96 h at 20 °C. It is evident that the aging effect at 20 °C is almost saturated within 96 h.

It can be seen from Fig. 4 that the nucleation catalyst aged for 96 h at −20 °C began to get deactivated at 76 °C and that all of them were deactivated at about 83 °C. The deactivation temperature of the nucleation catalyst aged for 96 h at −20 °C is about 10 °C lower than that of the nucleation catalyst aged for 96 h at 20 °C. With the 8 samples which

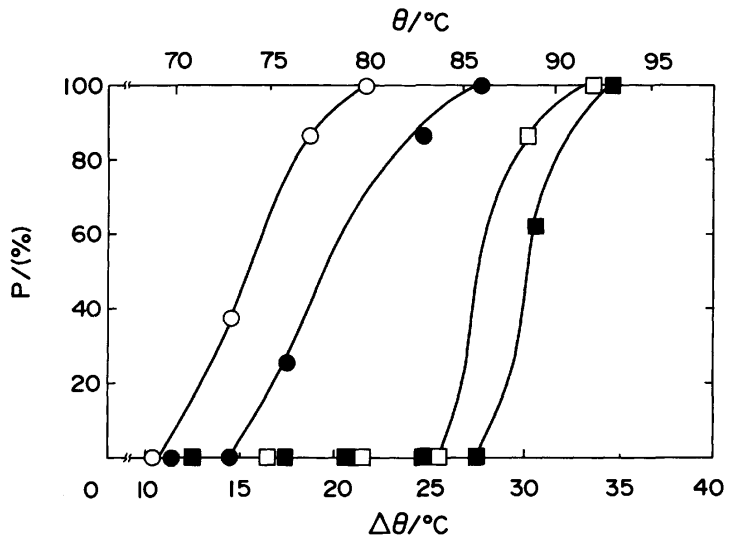

Fig. 3. The influence of preheating temperature on the crystallization of $CH_3CO_2Na \cdot 3H_2O$ from the melts containing a small amount of $Na_4P_2O_7$ as a nucleation contalyst, which were aged at 20 °C. ○: Δt_A(aging time)$=0.5$ h, ●: $\Delta t_A=4.0$ h, □: $\Delta t_A=20$ h, ■: $\Delta t_A=96$ h.

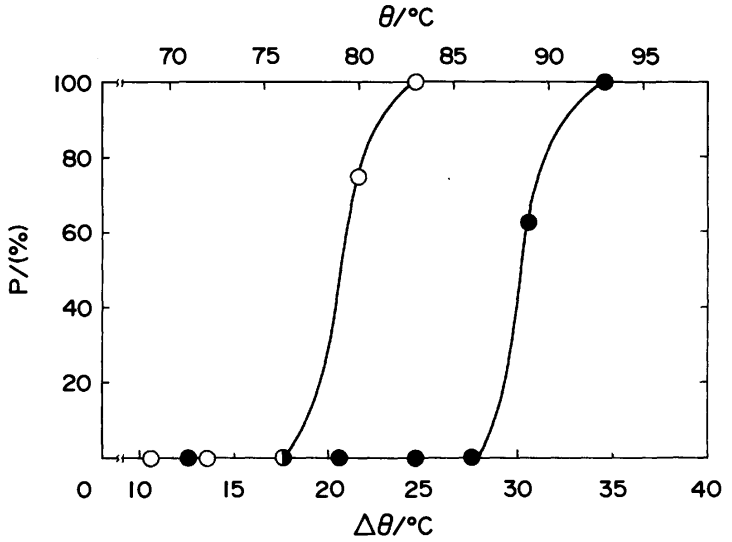

Fig. 4. The influence of preheating temperature on the crystallization of $CH_3CO_2Na \cdot 3H_2O$ from the melts containing a smal amount of $Na_4P_2O_7$, which were aged for 96 h. ○: θ_A(aging temperature) $=-20$ °C, ●: $\theta_A=20$ °C.

were aged for 96 h in liquid N_2, the cooling to 40 °C preceded by the preheating at 65 °C for 1 h caused no $CH_3CO_2Na \cdot 3H_2O$ to crystallize. It is evident that at lower temperatures, longer aging times are required for the full aging effect on nucleation catalyst.

Na_2HPO_4 as a Nucleation Catalyst. It is clear from Fig. 5 that the nucleation catalyst aged for 0.5 h at 20 °C began to get deactivated at 81 °C and that all of them were deactivated at about 88 °C. The nucleation catalyst aged for 20 h or 96 h began to get deactivated at 84 or 86 °C and all of them were deactivated at 89 or 91 °C, respectively. It is understood from Fig. 5 that the deactivation temperature of nucleation catalyst is a little raised with lengthening aging time. The deactivation behavior of the nucleation catalyst aged for 500 h at 20 °C, which is not shown in Fig. 5, is almost the same as that of the nucleation catalyst aged for 96 h at 20 °C. These phenomena are similar to those observed with $Na_4P_2O_7$ as a nucleation catalyst. The time required for saturation of the aging effect is much shorter than in the case of $Na_4P_2O_7$.

It can be seen from Fig. 6 that the nucleation catalyst aged for 96 h at −20 °C began to get deactivated at 84 °C and that all of them were deactivated at 89 °C. This deactivation temperature of the nucleation catalyst is a little lower than that of the nucleation catalyst aged for 96 h at 20 °C. These phenomena are also similar to those observed with $Na_4P_2O_7$. However, the

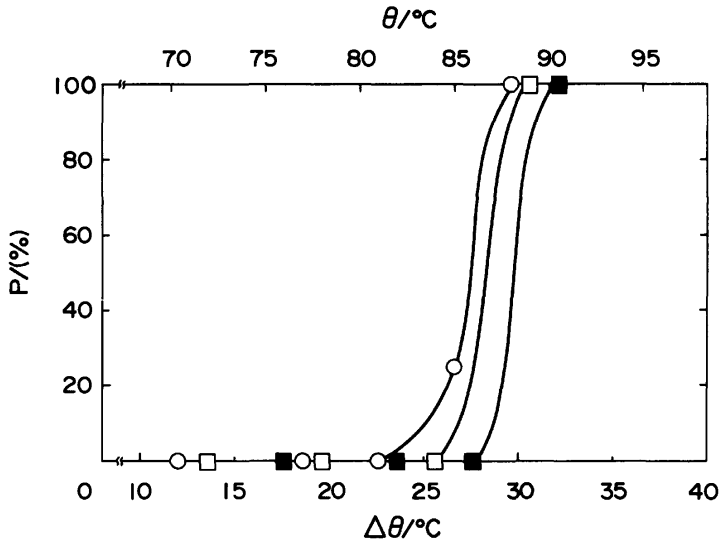

Fig. 5. The influence of preheating temperature on the crystallizaiton of $CH_3CO_2Na \cdot 3H_2O$ from the melts containing a small amount of Na_2HPO_4, which were aged at 20 °C.
○: $\Delta t_A = 0.5$ h, □: $\Delta t_A = 20$ h, ■: $\Delta t_A = 96$ h.

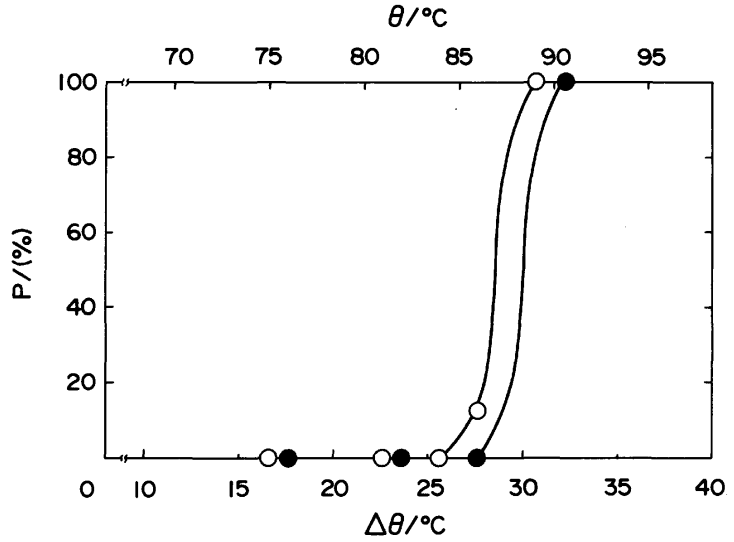

Fig. 6. The influence of preheating temperature on the crystallizaiton of $CH_3CO_2Na \cdot 3H_2O$ from the melts containing a small amount of Na_2HPO_4, which were aged for 96 h.
○: $\theta_A = -20$ °C, ●: $\theta_A = 20$ °C.

aging-temperature dependence of the deactivation temperature is not so pronounced as in the case of $Na_4P_2O_7$.

Discussion

Previously, we investigated the preheating effect on crystallization of $CH_3CO_2Na \cdot 3H_2O$ from a solution containing a small amount of nucleation catalyst ($Na_4P_2O_7$ or Na_2HPO_4).[8,9] In that investigation we did not fully take into account the aging effect on nucleation catalysis. However, in every experiment previously reported, we kept the coagulum containing a nucleation catalyst for more than one week at room temperature, in order to obtain some steady, reproducible deactivation temperature. Therefore, the reported deactivation temperatures are considered to corresponde to fully aged nucleation catalysts.

Two general explanations have been applied to the thermal history of heterogeneous nucleation. One is that crystalline germs are retained in fissures or cavities in the nucleation catalyst surface as a result of a (postulated) concave crystalline meniscus under such condition as preclude the existence of bulk crystals.[13] The other is that adsorbed crystalline layers are retained on the nucleation catalyst surface, as illustrated in Fig. 1 (B). The first explanation has received most attention because, when certain assumptions are given concerning the size of fissures and the contact angle of the crystal thereon, estima-

tion of the activated nucleation temperature (*i.e.*, the temperature at which crystallization is initiated) can be made.[14] However, we are not satisfied with this explanation because high, sharp deactivation temperatures of fully activated nucleation catalysts would require a very small associated fissure and a sharp limit to its geometry. The relation between the degree of supercooling and the preheating temperature for the nucleation catalysts, $Na_4P_2O_7$ and Na_2HPO_4, which will be reported in the near future, is not in agreement with the relation which is expected from the cavity model. In any cases of $Na_4P_2O_7$ and Na_2HPO_4 as nucleation catalysts, the degree of supercooling is not directly proportional to the difference between preheating temperature and bulk melting point, but is kept almost constant, about 6 °C, until catalysts begin to get deactivated. Furthermore, the theory is considered to be unable to explain the aging effect on nucleation catalyst as observed in the present experiment.

The second explanation, that is, the crystalline adsorption model, has received little consideration because thermodynamic properties of adsorbed layer have hitherto been speculative. Evans *et al.*[15–17] have studied the ability of a solid substrate to nucleate ice in supercooled water under high pressure, and explained results on the basis of an assumption that on certain substrates the heterogeneous nucleation of ice is preceded by a change of state (order-disorder transition) of the water monolayer adsorbed on the substrate.

Recently, the monolayer adsorbed on substrate has been studied extensively. From this study, possible phase diagrams of the adsorbed monolayer on substrate, such as that shown in Fig. 7,[18] are postulated.[19,20] The competition of adsorbate-adsorbate interaction with adsorbate-substrate lateral periodic potential can produce a structure which is either commensurate or incommensurate with the substrate, depending on the fitness between substrate and natural adsorbate lattice spacing; the fitness depends on both temperature and chemical potential (two-dimensional pressure). In Fig. 7, the low-dimensional (where the ratio of the periodicity of substrate to that of adsorbed monolayer is very simple) commensurate solid adsorbate is transformed directly into the fluid (liquid) adsorbate with rise in temperature (order-disorder transition), and the high-dimentional commensurate solid adsorbate is transformed into the fluid adsorbate through the incommensurate solid adsorbate with rise in temperature. Jaubert *et al.* evidenced the existence of a uniaxial commensurate-incommensurate transition in a solid monolayer of xenon adsorbed on the (110) face of copper by low-energy electron diffraction and Auger electron spectroscopy. The crystalline adsorption model, shown in Fig. 1, may be modified by considering the commensurate-incommensurate transition into solid adsorbate, as shown in Fig. 8. The results obtained in the present experiment will be dicussed on the basis of this modified crystalline adsorption model.

In a pervious paper, we considered that the crystalline adsorbate is formed on the nucleation catalyst as soon as $CH_3CO_2Na \cdot 3H_2O$ is forced to crystallize from a supercooled melt. However, $CH_3CO_2Na \cdot 3H_2O$ solid adsorbate which is formed as soon as $CH_3CO_2Na \cdot 3H_2O$ is forced to crystallize from a supercooled melt containing a nucleation catalyst (adsorbent), is considered to be incommensurate with the adsorbent. The negative heat of adsorption of metastable incommensurate solid adsorbate on the nucleation catalyst is not so large as that of liquid (fluid) adsorbate. Therefore, the incommensurate solid adsorbate melts near the bulk melting point of $CH_3CO_2Na \cdot 3H_2O$ and thus the deactivation temperature of the nucleation catalyst in this state is not so high.

The incommensurate solid adsorbate is transformed into the commensurate solid adsorbate (crystalline adsorbate) with elapse of time, because incommensurate solid adsorbate is considered to be a metastable phase. The negative heat of adsorption

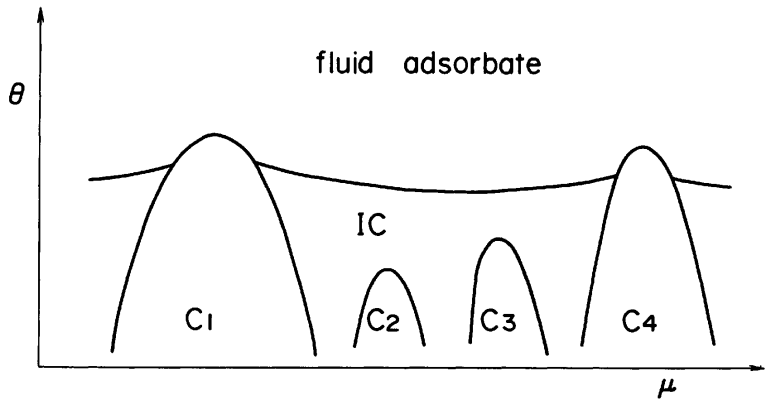

Fig. 7. The shematic phase diagram of the monolayer on the substrate as a function of temperature (ordinate) and chemical potential (abscissa).
C_n: commensurate solid adsorbate (crystalline adsorbate), IC: incommensurate solid adsorbate.

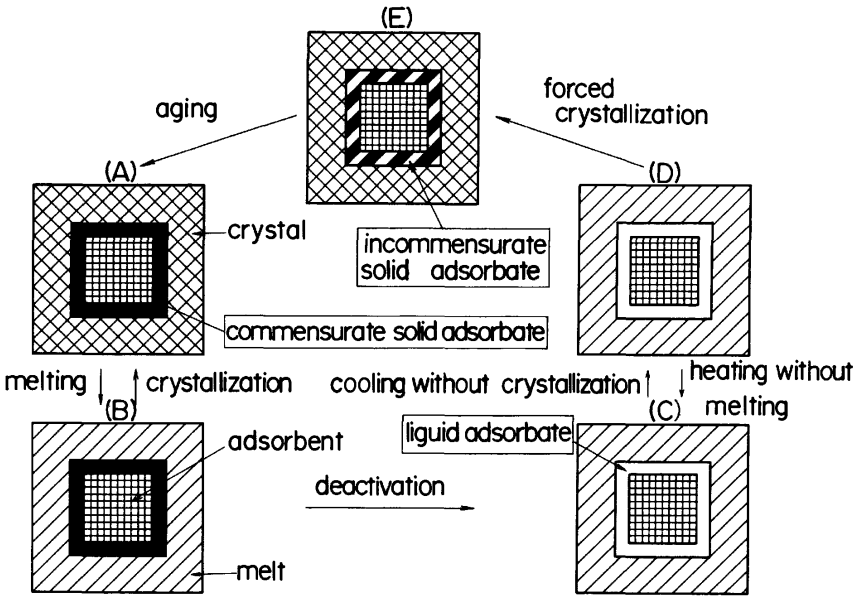

Fig. 8. The modified adsorption model for heterogeneous nucleation. (A): crystalline state with commensurate solid adsorbate, (B): melting state with commensurate solid adsorbate, (C): melting state with fluid adsorbate, (D): supercooled state, (E): crystalline state with incommensurate solid adsorbate.

of commensurate solid adsorbate on the adsorbent is considered to be much larger than that of liquid adsorbent. Therefore, the commensurate solid adsorbate does not melt near the bulk melting point of $CH_3CO_2Na \cdot 3H_2O$ and thus the deactivation temperature of the fully aged nucleation catalyst is much higher.

The transformation of incommensurate into commensurate solid adsorbate is considered to proceed with atomic (ionic) diffusion, because the rate of transformation is dependent on aging temperature. In the modified adsorption model illustrated in Fig. 8 as well as the crystalline adsorption model shown in Fig. 1, the commensurate solid adsorbate is transformed directly into the liquid adsorbate at elevated temperatures.

According to the modified crystalline adsorption model, a satisfactory, though qualitative, explanation has been given to the obserbations on the heterogeneous nucleation of $CH_3CO_2Na \cdot 3H_2O$, including the aging effect on nucleation catalyst. The modified crystalline adsorption model is expected to apply to heterogeneous nucleation of other salt hydrates such as $CaCl_2 \cdot 6H_2O$. Some quantitative explanation of these crystal nucleation catalytic actions remains to be given.

The authors wish to express their thanks to Dr. Ryoichi Kiriyama for his helpful discussion and to Drs. Eiichi Hirota, Tsuneharu Nitta, and Masanari Mikoda and Mr. Yukihiko Ise for their continuous encouragements. They are also grateful to Drs. Yoshihiro Matsuo and Ryoichi Yamamoto for their discussions throughout this work.

References

1) M. Telkes, "Solar Materials Science," ed by L. E. Murr, Academic Press, New York (1980), Chap. 11.
2) A. Pebler, *Thermochim. Acta*, **13**, 109 (1975).
3) F. de Winter, *Solar Energy*, **17**, 379 (1975).
4) K. Narita and J. Kai, *Denki Gakkai*, (in Japanese) **101**, 15 (1981).
5) M. Telkes, *Ind. Eng. Chem.*, **44**, 1308 (1952).
6) T. Wada and R. Yamamoto, *Bull. Chem. Soc. Jpn.*, **55**, 3603 (1982).
7) H. Kimura, *Nippon Kessho Seicho Gakkaishi*, **9**, No. 3, 73 (1982).
8) T. Wada, K. Matsumaga, and Y. Matsuo, *Bull. Chem. Soc. Jpn.*, **57**, 557 (1984).
9) T. Wada and Y. Matsuo, *Bull. Chem. Soc. Jpn.*, **57**, 561 (1984).
10) T. Wada, F. Yokotani, and Y. Matsuo, *Bull. Chem. Soc. Jpn.*, **57**, 1671 (1984).
11) T. Wada, F. Yokotani, and Y. Matsuo, *Bull. Chem. Soc. Jpn.*, **57**, 2021 (1984).
12) W. T. Richards, *J. Am. Chem. Soc.*, **54**, 478 (1932).
13) D. Turnbull, *J. Chem. Phys.*, **18**, 198 (1950).
14) M. E. Fine, "Introduction to Phase Transformations in Condensed System," The Macmillan Co., New York (1964), Chap. 2.
15) L. F. Evans, *Trans. Faraday Soc.*, **63**, 1 (1967).
16) G. R. Edwards, L. F. Evans, and A. F. Zipper, *Trans. Faraday Soc.*, **66**, 220 (1970).
17) G. R. Edwards and L. F. Evans, *J. Atmos. Sci.*, **28**, 1443 (1971).
18) H. Shiba, *Kotai Butsuri* (in Japanese), **7**, 504 (1981).
19) S. Sugano and N. Hamada "Hyomen no Bishiteki

Kozo" in "Butsurigaku no Saizensen," ed by Y. Otsuki, Kyoritsu Shuppan, Tokyo (1984), Vol. 6, Chap. 1, pp. 50—55.
20) D. R. Nelson and B. I. Halperin, *Phys. Rev. B*, **19**, 2457 (1979).
21) M. Jaubelt, A. Glachant, M. Bienfait, and G. Boato, *Phys. Rev. Lett*, **46**, 1679 (1981).

Resonance Raman and ^{129}I Mössbauer Spectroscopic Study of Iodine Doped in Poly(thienylene)s

Hiroshi SAKAI,* Manabu MIZOTA, Yutaka MAEDA, Takakazu YAMAMOTO,† and Akio YAMAMOTO†

Research Reactor Institute, Kyoto University, Kumatori-cho, Sennan-gun, Osaka 590-04
†*Research Laboratory of Resources Utilization, Tokyo Institute of Technology, Nagatsuta, Midori-ku, Yokohama 227*

(Received August 31, 1984)

Resonance Raman and ^{129}I Mössbauer spectroscopy have been used in a study of iodine doped poly(thienylene)s, which are chemically synthesized by the polymerization of dibromothiophenes. It is shown that the iodine species in the polymers are present predominantly in the form of a polyiodide which consists of unsymmetrical I_3^- and I_2 units. That is, the iodine molecule doped is reduced by taking electrons from the polymer in a similar manner to iodine doped in polyacetylene. This result is consistent with the fact that poly(thienylene)s undergo an increase in electrical conductivity upon doping with iodine.

Extensive studies have been made of electrically conducting organic polymers doped with either strong electron acceptors or donors. Polyacetylene especially, the simplest linear conjugated polymer, has attracted attention because the electrical conductivity can be varied over 12 orders of magnitude from insulator to semiconductor and metal by doping with arsenic pentafluoride (AsF_5) or iodine (I_2).[1] Polymers containing a phenylene ring in the polymer chain, poly(*p*-phenyline),[2,3] poly(phenylene vinylene),[4] and poly(phenylene sulfide),[5-7] also undergo a large increase in electrical conductivity upon doping with AsF_5. This behavior is similar to that of polyacetylene. However, when these polymers are exposed to iodine vapor, a relatively weak electron acceptor, the conductivities do not increase as is observed for polyacetylene. ^{129}I Mössbauer studies have revealed that iodine doped in poly(*p*-phenylene) exists as an almost free iodine molecule, whereas iodine doped in poly(phenylene sulfide) interacts weakly with the sulfur atoms of the polymer chain.[8,9]

Recently poly(thienylene), which consists of a linear sequence of thiophene rings, as shown in Fig. 1, has been found to exhibit a high conductivity ($\approx 10^{-1}$ S/cm) upon exposure of I_2 vapor at room temperature.[10] This is the second polymer which exhibits a high conductivity with the iodine doping. It is important for the understanding of the conduction mechanism to determine the chemical form and the electronic structure of the iodine species present in the polymer. Resonance Raman and ^{129}I Mössbauer spectroscopy are useful methods for investigating the chemical and electronic structures of iodine, and have been successfully applied for iodine-doped polyacetylenes.[11-14] In the present work we report on resonance Raman and ^{129}I Mössbauer spectroscopic studies of the iodine species in poly(2,5-thienylene) and in poly(3-methyl-2,5-thienylene).

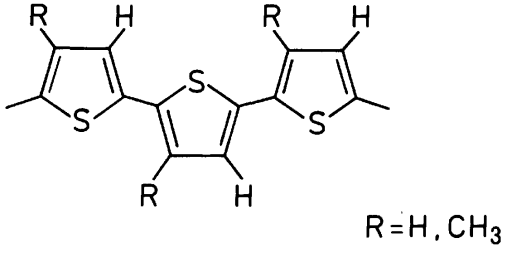

Fig. 1. Idealized chemical structure of poly(2,5-thienylene) or poly(3-methyl-2,5-thienylene).

Experimental

Poly(2,5-thienylene) and poly(3-methyl-2,5-thienylene) were synthesized by the polymerization of 2,5-dibromothiophene and 3-methyl-2,5-dibromothiophene, according to the method described previously.[10] Both powdery polymers used in this work were $CHCl_3$-insolvable fractions. The iodine-doping was carried out by immersing the polymer in a CCl_4 solution of iodine at room temperature for 1 d. The iodine content of the specimen used for the resonance Raman measurement was determined to be 43 wt-% for poly(2,5-thienylene) and 52 wt-% for poly(3-methyl-2,5-thienylene) by gravimetric analysis. Radioactive $^{129}I_2$ ($t_{1/2}=1.7\times10^7$ y), which was prepared by oxidizing Na ^{129}I in Na_2SO_3 solution with 6 M-H_2SO_4 (1 M=1 mol dm^{-3}) and 10%-H_2O_2 and extracting with CCl_4, was used for the Mössbauer sample. The iodine content was found to be 24 wt-% for poly(2,5-thienylene) and 12 wt-% for poly(3-methyl-2,5-thienylene). The sample thickness for the Mössbauer measurement was about 20 mg $^{129}I/cm^2$.

Laser Raman spectra were measured with Ar^+ (514.5 nm) excitation by using a JEOL-JRS-400T triple monochromator. The data were obtained with compressed pellets of the powdery samples by the front surface reflection method using 60 mW of laser power and a spinning cell, in order to prevent decomposition of the iodine species. No decomposition was observed within this laser power, though the scans were made repeatedly for each iodine-doped sample.

^{129}I Mössbauer effect measurements were performed in a transmission geometry by cooling the source and the absorber sample at 16 K with a closed cycle helium refrigerator "Cryodyne 1020." The Mössbauer source, $^{66}Zn^{129}Te$ ($t_{1/2}$=70 min) was prepared by neutron irradiation

of a 140 mg $^{66}Zn^{128}Te$ compound at flux of 2×10^{13} neutrons/cm^2·s for 1 h in the Kyoto University Reactor (KUR). The source was used repeatedly. The constant acceleration drive was calibrated with an Fe foil.

Results and Discussion

A. Resonance Raman Spectroscopic Study. In Fig. 2 are presented resonance Raman spectra of iodine-doped poly(2,5-thienylene) (iodine content 43 wt-%) and iodine-doped poly(3-methyl-2,5-thienylene) (52 wt-%) excited by the Ar^+ 514.5 nm line. Both spectra (170 s, 145 w, 108 m, 63 w, cm^{-1}) are very similar to each other, indicating that the iodine species in both polymers has a similar chemical form. The possibility for the presence of free iodine molecules is clearly ruled out by finding no Raman band around 210 cm^{-1}. It is of interest to compare these spectra with those of iodine-doped polyacetylene. The Raman band at 108 cm^{-1}, also observed for iodine-doped polyacetylene at 105—107 cm^{-1},[11,12] can be assigned to the symmetric stretching vibration of a linear triiodide anion (I_3^-). Isolated and symmetrical I_3^- ions in methanol[15] and $(C_6H_5)_4As^+I_3^-$[16] show the Raman bands at 112 and 113 cm^{-1}, respectively, while the bands for unsymmetrical I_3^- ions and I_3^- units in polyiodides are observed in the 100 to 120 cm^{-1} region.[16,17] The latter distorted I_3^- ions give rise to a second weak band around 150 cm^{-1}, assigned to the antisymmetric stretching vibration. Therefore, the relatively weak band at 145 cm^{-1} observed in iodine-doped poly(thienylene)s is assigned to the antisymmetric vibration band of the distorted I_3^- ion.

On the other hand, the strong Raman band at 170 cm^{-1} seems to be due to an iodine molecule coordinated to the I_3^- ion. It is well known that molecular I_2 acts as a Lewis acid and coordinates to Lewis bases such as I^- and I_3^-. The coordination weakens the I-I bonding and shifts the I-I stretching band to lower frequency. Actually a few polyiodides which consist of I_3^- and I_2 units show the strong Raman bands for the I-I stretching vibration; 172 cm^{-1} for Cs_2I_8[16] and 173 cm^{-1} for $(\alpha\text{-CD})_2Li^+I_5^-8H_2O$.[17] The bands for I_3^- unit in these polyiodides are observed in the 105—110 cm^{-1} region as described previously. Notably the resonance Raman spectra of iodine-doped poly(thienylene)s are similar to the spectrum observed for the $(\alpha\text{-CD})_2Li^+I_3^-I_2 8H_2O$ inclusion compound, in which the iodine chain, constructed of alternate I_3^- and I_2 units, is slightly zigzagged and is included in the cavity of the α-cyclodextrin dimer.[18] Another example of the polyiodide is found in the perylene-iodine complex, which exhibits a high electrical conductivity ($\approx10^{-1}$ S/cm) at room temperature. This complex shows resonance Raman bands at 115 m and 145 w cm^{-1} assigned to the unsymmetrical I_3^- unit and at 175 s cm^{-1} to the weakly coordinated I_2 unit.[16] The agreement between the Raman spectra of this complex and of iodine-doped poly(thienylene)s is extremely close.

These results suggest strongly that iodine doped in poly(thienylene)s exists predominantly as a polyiodide

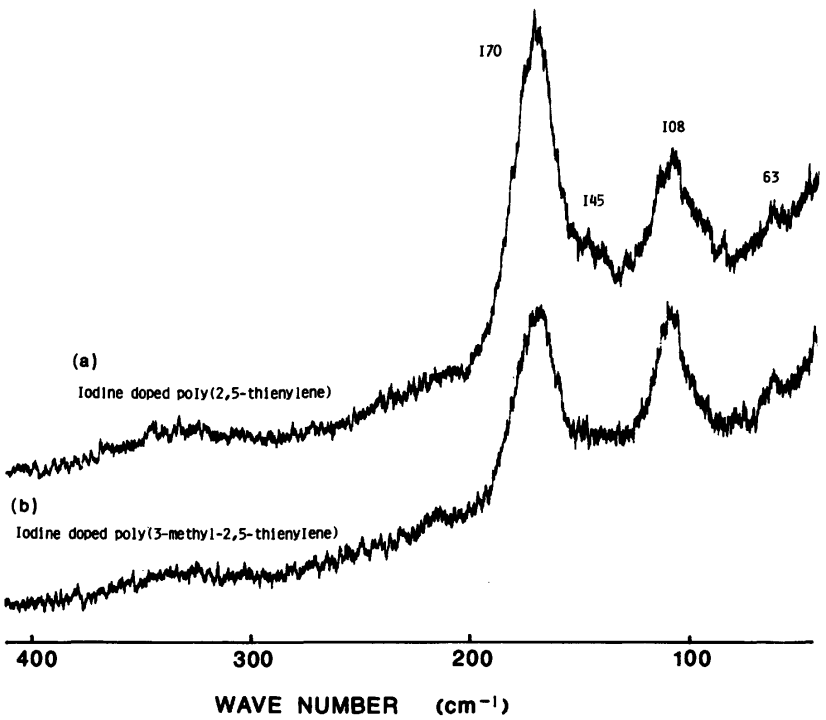

Fig. 2. Resonance Raman spectra of (a) iodine-doped poly(2,5-thienylene) and (b) iodine-doped poly(3-methyl-2,5-thienylene), observed with the 514.5 nm excitation.

made up of alternate I_3^- and I_2 units. In polyacetylene heavily doped with iodine, the strong Raman band is not observed at 170 cm^{-1} but another band appears at 150—160 cm^{-1}.[11,12] The intensity of this band is relatively weak compared to the intensity of the 105—107 cm^{-1} band and depends on the sample treatment. This band, different obviously from the 170 cm^{-1} band observed in iodine-doped poly(thienylene)s, is assigned to the linear I_5^- ion, because of the similarity of the Raman frequency (162 cm^{-1}) of (trimesic acid $H_2O)_{10}$ $H^+I_5^-$, which contains the linear and symmetrical I_5^- chain.[19] That is, the iodine species are present in polyacetylene heavily doped with iodine as the I_3^- chain and the linear I_5^- chain. Both iodine molecules doped in poly(thienylene)s and in polyacetylene act as electron acceptors and form polyiodides, though the chemical forms of these polyiodides differ slightly from each other.

Resonance Raman spectroscopy is obviously useful for the identification of the chemical form of the iodine species in the polymers, but there is a limitation with regard to the quantification of the relative amount of each iodine species, because the relative intensites of the resonance Raman bands are strongly dependent on the excitation wavelength. Furthermore, information about the electronic structure such as the charge distribution and the charge density can not be obtained in this method. ^{129}I Mössbauer spectroscopy can compensate for such disadvantages and has been actually applied to the iodine species in polyacetylene,[13,14] poly(*p*-phenylene),[8] or poly(phenylene sulfide).[9]

B. Mössbauer Spectroscopic Study. ^{129}I Mössbauer spectra of iodine doped in poly(2,5-thienylene) (iodine content 24 wt-%) and in poly(3-methyl-2,5-thienylene) (12 wt-%) are presented in Figs. 3 and 4, respectively. In spite of the different iodine contents, both spectra are similar to each other, which agrees with the result of the resonance Raman spectra. The Mössbauer spectra clearly rule out the presence of the isolated I^- ion, which is inactive and undetectable by Raman spectroscopy. The presence of the I^- ion, observed in polyacetylene extremely lightly doped with iodine,[13] would show the single absorption peak at −0.5 mm/s in the spectrum. Since the spectra are complicated, the presence of the free iodine molecule is not clear. However, the resonance Raman spectra of more heavily doped samples do not indicate the presence of any free iodine molecules.

We attempted first to analyze the spectra in terms of three different iodine sites, *i.e.*, the superposition of three quadrupole octet patterns, assuming those asymmetry parameters to be zero. In the case of the spectrum of iodine-doped poly(3-methyl-2,5-thienylene) (Fig. 4), the fitting analysis indicated acceptable agreement between observed and calculated spectra, though the line-width of the intermediate quadrupole split pattern was broadened considerably. This broadening is presumed to be due to an overlap of the spectra originated from two iodine sites which have slightly different values of the quadrupole coupling constant (e^2Qq) and the isomer shift (δ). The best fitted subspectra of each component and their peak positions for the three unequivalent iodine sites are represented

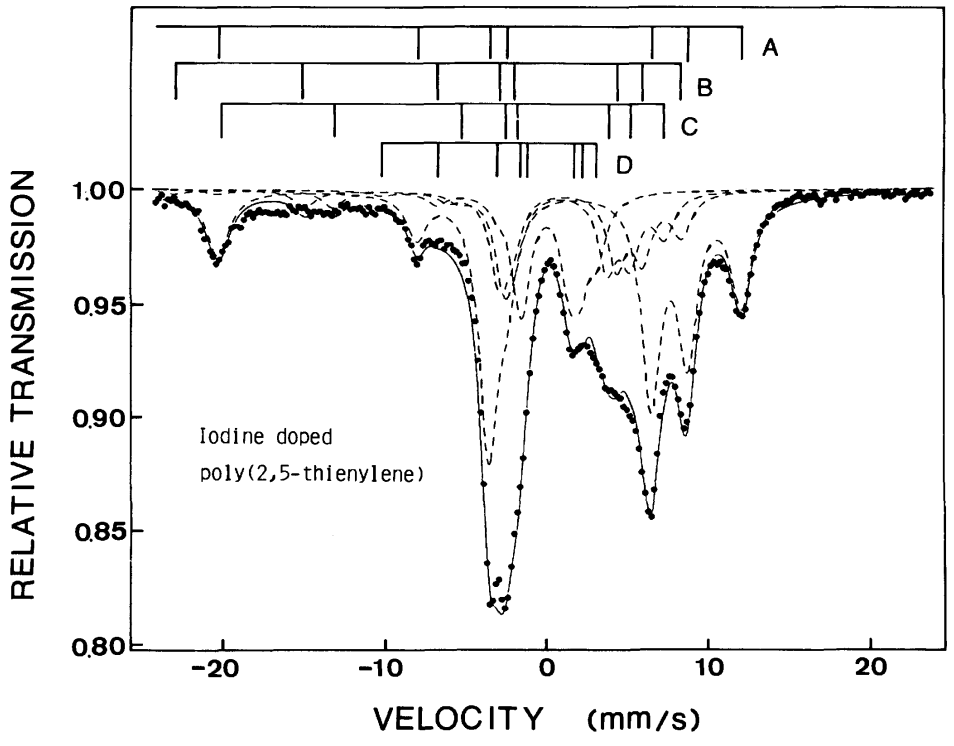

Fig. 3. ^{129}I Mössbauer spectrum of iodine doped in poly(2,5-thienylene) at 16 K.

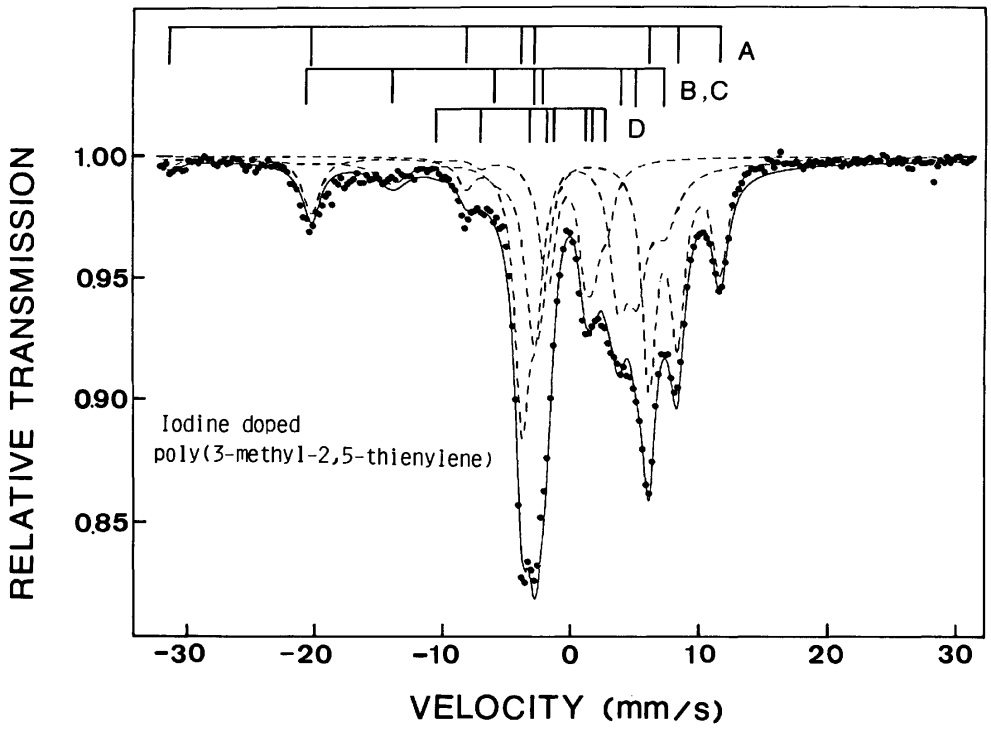

Fig. 4. ^{129}I Mössbauer spectrum of iodine doped in poly(3-methyl-2,5-thienylene) at 16 K.

by dashed curves and stick diagrams, respectively, as shown in Fig. 4. Since the sub-spectrum with the intermediate quadrupole splitting is expected to consist of two slightly different iodine sites, the notations B and C are used for these two iodine sites. On the other hand, for the more expanded spectrum of iodine-doped poly(2,5-thienylene) (Fig. 3), a satisfactory agreement was not obtained by the analysis with three different iodine sites. The analysis of the spectrum with four unequivalent iodine sites gave rise to a reasonable agreement, as shown in Fig. 3. The dashed curves represent the best fitted sub-spectra for each iodine site and the stick diagrams indicate the peak positions of the sub-spectra, where the four iodine sites are symbolized with A, B, C, and D. The obtained Mössbauer parameters, such as the quadrupole coupling constant (e^2Qq), isomer shift (δ), full-width at half-maximum (2Γ), and relative area, are summarized in Table 1.

The e^2Qq and δ values for site A are larger than those for the free iodine molecule in inert matrices (e^2Qq=−1587 MHz, δ=+0.98 mm/s for I_2 in hexane[20]), which indicates that the iodine atom of site A has a slightly positive charge density. Such an iodine atom is observed in the central iodine of linear triiodide anions (I_3^-); e^2Qq=−1750 MHz, δ=+1.40 mm/s for the central iodine of CsI_3:[21] e^2Qq=−1725 MHz, δ=+1.48 mm/s for $[Ru(cp)_2I]I_3$.[22] It is therefore reasonable to assign site A to the central iodine atom in an I_3^- ion. The e^2Qq values for the terminal iodine atoms of the unsymmetrical I_3^- in CsI_3 are found to be −1025 MHz and −580 MHz from the ^{129}I Mössbauer measurement.[21] These values are in good agreement with those obtained from the ^{127}I NQR method;[23] 1007 MHz and 574 MHz at 77 K, converted to ^{129}I using the ratio $^{129}Q/^{127}Q$=0.7013. For the symmetrical I_3^- in $[Ru(cp)_2I]I_3$, the e^2Qq value is −808 MHz for both terminal iodine atoms[22], and indicates the average of two e^2Qq values for the terminal iodines in the unsymmetrical I_3^-. Since each e^2Qq value for site C or D is comparable to that for each terminal iodine of CsI_3, we assign site C and site D to the two terminal iodine atoms in the unsymmetrical I_3^- ion.

These assignment are consistent with the resonance Raman spectra (108 cm^{-1} and 145 cm^{-1} bands), indicating the presence of an unsymmetrical I_3^- ion, as previously described. Since the unsymmetrical I_3^- ion consists of three unequivalent iodine sites with relative populations of 1:1:1, the relative absorption areas of the sub-spectra corresponding to sites A, C, and D are expected to be 1:1:1. However, the absorption area obtained for the sub-spectrum of the site A is 2.7 to 2.8 times that of site D, as shown in Table 1. This result predicts the presence of another iodine atom (designated as site A′) with the same charge density as the central iodine atom in the I_3^- ion. The strong Raman band at 170 cm^{-1} suggests that the I_2 unit interacting with the I_3^- unit exists in iodine-doped poly(thienylene)s. Therefore, the iodine atom of site A′ and an iodine atom of site B seem to constitute this I_2 unit. It is appropriate to assign site A′ to the iodine atom coordinating to one (site D) of the unsymmetrical I_3^- ion and site B to the terminal iodine atom of the I_2 unit, because

TABLE 1. ^{129}I MÖSSBAUER PARAMETERS FOR IODINE DOPED IN POLY(2,5-THIENYLENE) AND POLY(3-METHYL-2,5-THIENYLENE)

	Site	e^2Qq / MHz	δ[a] / mm·s^{-1}	2Γ[b] / mm·s^{-1}	Relative[c] area	U_p[d]	h_p[e]
Iodine-doped poly(2,5-thienylene)	A	−1750±20	1.27±0.04	1.35±0.06	2.8	1.09	1.21
	B	−1262±20	0.63±0.04	1.32±0.06	1.0	0.78	0.78
	C	−1111±20	0.52±0.04	1.32±0.06	1.0	0.69	0.71
	D	−539±20	−0.05±0.04	1.24±0.06	1.0	0.33	0.33
Iodine-doped poly(3-methyl-2,5-thienylene)	A	−1726±20	1.29±0.04	1.38±0.06	2.7	1.07	1.22
	B, C	−1156±20	0.57±0.04	1.75±0.06	1.9	0.72	0.74
	D	−533±20	−0.04±0.04	1.34±0.06	1.0	0.33	0.33

a) Isomer shifts (δ) are relative to the ZnTe source. b) Line-widths (2Γ) are full-width at half-maximum. c) Relative areas are normalized with respect to the D site. d) $U_p = e^2Qq/e^2Qq_{atom}$, $e^2Qq_{atom} = -1608$ MHz. e) $\delta = 1.5\,h_p - 0.54$ (mm/s).

the values of e^2Qq and δ suggest that the former (the bridging iodine atom) is positively charged and the latter is negatively charged.

Consequently the iodine species present in poly(thienylene)s have the following structure:

$$[I\text{——}I\text{——}I\cdots\cdots I\text{——}I]^-$$
site C A D A′ B

Taking into account the above structure of the iodine species, the absorption area for the sites A and A′ is still large compared with those for each site B, C, or D. The enhanced absorption area is explained on the basis of the difference in the recoilless fraction. That is, the recoilless fractions of sites A and A′ are larger than those of sites B, C, and D, because the central and bridging iodine atoms are bound to two neighboring iodine atoms. This effect is often observed for the I_3^- ions in $[Ru(cp)_2I]I_3$[22] and a β-carotene-iodine complex,[24] in which the central atom indicates stronger absorption intensity than each terminal atom. The fit achieved by assuming the asymmetry parameters to be zero gave rise to a satisfactory result. Accordingly even if they would not be zero, they may be small. This suggests that the iodine species made up of the I_3^- and I_2 units possesses a nearly linear arrangement.

The charge density localized on each iodine atom is calculated from the values of e^2Qq and δ by the usual procedure;[25,26]

$$e^2Qq = -U_p \cdot e^2Qq_{atom},$$
$$\delta(\text{mm/s}) = 1.5\,h_p - 0.54 \text{ (ZnTe source)},$$

where e^2Qq_{atom}, the atomic iodine quadrupole coupling constant, is equal to 1608 MHz for ^{129}I, and U_p, the number of unbalanced p electrons, is proportional to the difference of $5p_\sigma$ and $5p_\pi$ electron populations; h_p is the number of p electrons removed from the $5s^25p^6$ (I^-) configuration. Therefore, when the bonding of iodine is formed by only $5p_\sigma$ electrons, one expects the relationship $U_p = h_p = 1 \pm i$ to be valid, where i is the ionic character. When $5p_\pi$ electrons take part in bond formation, in addition to $5p_\sigma$ electrons, the relationship that $U_p < h_p$ is generally observed. On the other hand, the contribution of 5s electrons leads to the relationship that $U_p > h_p$ because of the decrease in the s electron density at the nucleus. The values of U_p and h_p obtained from the above expressions are given in Table 1. They are in good agreement with each other for the terminal iodine atoms of sites B, C, and D, indicating that the bonding is mainly due to $5p_\sigma$ electrons. The charge densites localized on sites B, C, and D are evaluated to be −0.22, −0.30, and −0.67 respectively, for the iodine species present in poly(2,5-thienylene). For the iodine species in poly(3-methyl-2,5-thienylene), the iodine atoms at sites B and C are negatively charged by about 0.27, and iodine at site D by 0.67.

On the other hand, it is evident that the U_p value is smaller than h_p for the central (site A) and bridging (site A′) iodine atoms. This tendency is generally observed for the central iodine atom in the I_3^- ions[21,22,24] and for the bridging iodine atom in amine-iodine charge transfer complexes.[27,28] In our previous paper[28] it was proposed that the tendency was explained in terms of the contribution of $4d_\sigma$ electrons to the bond formation rather than the participation of the π-bonding. That is, the chemical bond of the I_3^- ion is described by a mixture of a four-electron three-center bond and a covalent bond of the $d_\sigma p_\sigma$ hybrid orbitals. The contribution of the $4d_\sigma$ electrons remarkably increases the isomer shift but hardly increases the quadrupole coupling constant. The charge densities localized on the central and bridging iodine atoms are consequently evaluated to be +0.07 to +0.09 from the U_p values.

The total charge densities are close to unity for the iodine species present in both polymers, as can be seen below.

charge −0.30 +0.09 −0.67 +0.09 −0.22
I——I——I ····· I——I
site C A D A′ B
[iodine species in poly(2,5-thienylene)]

charge −0.27 +0.07 −0.67 +0.07 −0.27

I———I———I ..... I———I

site C A D A′ B

[iodine species in poly(3-methyl-2,5-thienylene)]

The charge densities for sites B and C are not rigorously equal because of the broad line-width of the corresponding sub-spectrum for iodine-doped poly(3-methyl-2,5-thienylene), then the value of −0.27 represents the average value of sites B and C. The iodine species observed in this polymer is essentially identical to that in poly(2,5-thienylene). The charge densities for sites A′ and B of the I_2 unit are close to those for sites A and C in the I_3^- unit, which suggests that the intermolecular $I_D \cdots I_{A'}$ bonding is considerably strong. This result is also supported by the fact that the I_2 unit shows the stretching vibration band at 170 cm^{-1}, largely shifted from 210 cm^{-1} of the isolated I_2 molecule.

In summary, resonance Raman and ^{129}I Mössbauer spectroscopy have revealed the chemical forms and the electronic structures of the iodine species in poly(2,5-thienylene) and in poly(3-methyl-2,5-thienylene). The iodine species are found to be present predominantly in the polymers as polyiodides consisting of unsymmetrical I_3^- and I_2 units. That is, the iodine molecule doped acts as an electron acceptor and produces the positive holes in the polymers, in a similar manner to iodine doped in polyacetylene. This result strongly suggests that poly(thienylene)s undergo an increase in electrical conductivity upon doping with iodine.

We wish to thank Professor Takenobu Higashimura (Research Reactor Institute, Kyoto University) for his encouragement. We are greateful to Professor Masamichi Kobayashi (Department of Polymer Chemistry, Osaka University) for his valuable discussion on the Raman spectra. We are also indebted to Mr. Shuichi Muraishi (JEOL Ltd.) for the measurements of the Raman spectra.

References

1) See, for example, Y.-W. Park, A. J. Heeger, M. A. Druy, and A. G. MacDiarmid, *J. Chem. Phys.*, **73**, 946 (1980) and the references cited therein.

2) D. M. Ivory, G. G. Miller, J. M. Sowa, L. W. Shacklette, R. R. Chance, and R. H. Baughman, *J. Chem. Phys.*, **71**, 1506 (1979).

3) L. W. Shacklette, R. R. Chance, D. M. Ivory, G. G. Miller, and R. H. Baughman, *Synthetic Metals*, **1**, 307 (1979).

4) G. E. Wnek, J. C. W. Chien, F. E. Karasz, and C. P. Lillya, *Polymer*, **20**, 1441 (1979).

5) J. F. Rabolt, T. C. Clarke, K. K. Kanazawa, J. R. Reynolds, and G. B. Street, *J. Chem. Soc., Chem. Commun.*, **1980**, 347.

6) R. R. Chance, L. W. Shacklette, G. G. Miller, D. M.Ivory, J. M. Sowa, R. L. Elsenbaumer, and R. H. Baughman, *J. Chem. Soc., Chem. Commum.*, **1980**, 348.

7) L. W. Skacklette, R. L. Elsenbaumer, R. R. Chance, H. Eckhardt, J. E. Frommer, and R. H. Baughman, *J. Chem. Phys.*, **75**, 1919 (1981).

8) H. Sakai, T. Matsuyama, H. Yamaoka, and Y. Maeda, *Bull. Chem. Soc. Jpn.*, **56**, 1016 (1983).

9) H. Sakai, T. Matsuyama, H. Yamaoka, and Y. Maeda, *Chem. Phys. Lett.*, **101**, 490 (1983).

10) T. Yamamoto, K. Sanechika, and A. Yamamoto, *Chem. Lett.*, **1981**, 1079; *Bull. Chem. Soc. Jpn.*, **56**, 1503 (1983).

11) S. L. Hsu, A. J. Signorelli, G. P. Pez, and R. H. Baughman, *J. Chem. Phys.*, **69**, 106 (1978).

12) I. Harada, Y. Furukawa, M. Tasumi, H. Shirakawa, and S. Ikeda, *J. Chem. Phys.*, **73**, 4746 (1980).

13) T. Matsuyama, H. Sakai, H. Yamaoka, Y. Maeda, and H. Shirakawa, *Solid State Commun.*, **40**, 563 (1981); *J. Phys. Soc. Jpn.*, **52**, 2238 (1983).

14) G. Kaindl, G. Wortmann, S. Roth, and K. Menke, *Solid State Commun.*, **41**, 75 (1982).

15) K. Kaya, N. Mikami, Y. Udagawa, and M. Ito, *Chem. Phys. Lett.*, **16**, 151 (1972).

16) R. C. Teitelbaum, S. L. Ruby, and T. J. Marks, *J. Am. Chem. Soc.*, **101**, 7568 (1979).

17) R. C. Teitelbaum, S. L. Ruby, and T. J. Marks, *J. Am. Chem. Soc.*, **100**, 3215 (1978); *ibid.*, **102**, 3322 (1980).

18) M. Noltemeyer and W. Saenger, *Nature*, **259**, 629 (1976).

19) F. H. Herbstein and M. Kapon, *Acta Crystallogr., Sect. A*, **28**, 74 (1972).

20) S. Bukshpan, C. Goldstein, and T. Sonnino, *J. Chem. Phys.*, **49**, 5477 (1968).

21) B. S. Erhlich and M. Kaplan, *J. Chem. Phys.*, **51**, 603 (1969).

22) M. J. Potasek, P. G. Debrunner, W. H. Morrison, Jr, and D. N. Hendrickson, *J. Chem. Phys.*, **60**, 2203 (1974).

23) A. Sasane, D. Nakamura, and M. Kubo, *J. Phys. Chem.*, **71**, 3249 (1967).

24) T. Matsuyama, H. Sakai, H. Yamaoka, and Y. Maeda, *J. Chem. Soc., Dalton Trans.*, **1982**, 229.

25) N. N. Greenwood and T. C. Gibb, "Mössbauer Spectroscopy," Chapman and Hall, London (1971).

26) S. L. Ruby and G. K. Shenoy, "Mössbauer Isomer Shifts," ed by G. K. Shenoy and F. E. Wagner, North-Holland, Amsterdam (1978), Chapter 9b.

27) C. H. W. Jones, *J. Chem. Phys.*, **62**, 4343 (1975).

28) H. Sakai, Y. Maeda, S. Ichiba, and H. Negita, *J. Chem. Phys.*, **72**, 6192 (1980).

Solvation and Protonation of 1,10-Phenanthroline in Aqueous Dioxane Solutions

Shin-ichi ISHIGURO, Hideo WADA, and Hitoshi OHTAKI*
Department of Electronic Chemistry, Tokyo Institute of Technology at Nagatsuta, 4259, Nagatsuta-cho, Midori-ku, Yokohama 227
(Received October 6, 1984)

Solvation and protonation of 1,10-phenanthroline (phen) have been studied by potentiometry and calorimetry in various aqueous dioxane solutions. Protonation reactions were studied in the mixtures (the dioxane content x=0—0.4 mole fraction) containing 0.3 mol dm^{-3} NaCl as a constant ionic medium at 25 °C. Potentiometric and calorimetric titration curves obtained in the range of $-\log[H^+]$=2—7 were well explained in terms of the formation of Hphen$^+$ and H(phen)$_2^{2+}$, and the formation constants, enthalpies and entropies of formation of the species were determined. The formation constants of the both species gradually decreased with increasing x, and then the formation of H(phen)$_2^{2+}$ became negligibly small at x>0.1, while the enthalpy and entropy of formation of Hphen$^+$ first decreased and then increased with increasing x and thus minima were found at x=0.05. Enthalpies of solution of anhydrous 1,10-phenanthroline were also determined in both neutral (x=0—1) and acidic (0.1 mol dm^{-3} HCl, x=0—0.4) aqueous dioxane solutions. By knowing enthalpies of solution of 1,10-phenanthroline in acidic solutions and of formation of Hphen$^+$ in the mixed solvents, enthalpies of solution of 1,10-phenanthroline in neutral solutions (ΔH_s°(phen)) were evaluated and compared with those directly obtained in the neutral solutions ($\Delta H_{s,\text{neutral}}^\circ$). A significant difference was found between ΔH_s°(phen) and $\Delta H_{s,\text{neutral}}^\circ$ in the range x<0.3, which could be ascribed to the formation of stacked species of 1,10-phenanthroline molecules, (phen)$_n$. The variation of ΔH_s°(phen) with x was explained in terms of the enhanced solvation of dioxane to phenanthroline molecules owing to breaking of the hydrophobic water structure around them. Solvent effects on the formation of Hphen$^+$ and H(phen)$_2^{2+}$ were discussed in terms of different solvation behavior of 1,10-phenanthroline and proton with x.

Protonation reactions of 1,10-phenanthroline (phen) in aqueous solutions have so far been studied by potentiometry and calorimetry, and it has been reported that Hphen$^+$ and H(phen)$_2^{2+}$ were formed in the range of $-\log[H^+]$=2—7 and H$_2$phen^{2+} was also found in a solution of [H$^+$]>1 mol dm^{-3}.[1-5]

A proton NMR study of 1,10-phenanthroline solutions containing various concentrations of hydrochloric acid also suggested the formation of Hphen$^+$ and H(phen)$_2^{2+}$ and, in fact, the Hphen·ClO$_4$ and H(phen)$_2$·ClO$_4$ crystals were isolated.[6]

Due to the hydrophobicity of aromatic rings of 1,10-phenanthroline, the solubility of the neutral species is low in water, but remarkably increases in organic solvents and also in aqueous organic mixtures. With this point of view, protonation reactions of 1,10-phenanthroline have been studied in various aqueous alcohol solutions.[7]

Solvent effects on protonation reactions of 1,10-phenanthroline is very different from those of amines and amino acids. The protonation constant of Hphen$^+$ decreases with increasing concentration of an organic component in aqueous organic solutions, in contrast to protonation constants of amino and carboxyl groups which are practically invariable and remarkably increases, respectively, in the solutions.

The formation of H(phen)$_2^{2+}$ and different solvent effects on the formation of Hphen$^+$ from those on the formation of protonated amines or amino acids suggested an importance of solvation at aromatic rings of 1,10-phenanthroline in the course of protonation reactions of 1,10-phenanthroline. In order to elucidate the solvation phenomenon of 1,10-phenanthroline, enthalpies of solution of anhydrous 1,10-phenanthroline were determined both in neutral aqueous dioxane solutions (x=0—1) and in acidic ones containing 0.1 mol dm^{-3} HCl (x=0—0.4). Thermodynamic quantities, ΔG_n°, ΔH_n°, and ΔS_n°, for protonation reactions of 1,10-phenanthroline in various aqueous dioxane solutions will be discussed in connection with changes in solvation of the neutral and protonated species.

Experimental

Reagents. All chemicals used were of reagent grade. *1,10-Phenanthroline monohydrate* was recrystallized three times from water and then dried in a vacuum desiccator over P_2O_5 to prepare anhydrous 1,10-phenanthroline. *Sodium hydroxide* was prepared by electrolysis of an aliquot of a sodium chloride solution under an atmosphere of nitrogen gas in a polyethylene bottle. *Hydrochloric acid* and *sodium chloride* of super special grade were used without further purification. *Dioxane* was dried with metallic sodium and then distilled.

Method of Measurements and Analysis of Data. All potentiometric and calorimetric measurements were carried out in thermostated baths at (25.00±0.02) °C and (25.000±0.007) °C, respectively, which were placed in a room thermostated at (25.0±0.2) °C.

Throughout potentiometric and calorimetric titrations, 0.3 mol dm^{-3} NaCl was used as an ionic medium, except for the 0.4 mole fraction dioxane–water mixture in which a lower ionic medium of *ca.* 0.05 mol dm^{-3} NaCl was used because of the phase separation in a solution of a higher salt concentration. In the course of potentiometric titrations,

values of $-\log[H^+]$ in solutions were measured by using a glass electrode and an Ag–AgCl electrode as reference over the range 2 to 7. In calorimetric titrations, 1,10-phenanthroline solutions were titrated with a hydrochloric acid solution of *ca.* 0.3 mol dm^{-3}. The method of measurements were similar to those described elsewhere.[8]

Enthalpies of solution of anhydrous 1,10-phenanthroline were measured by dissolving a given amount of crystals of the anhydrous species in either neutral or acidic (0.1 mol dm^{-3} HCl) aqueous dioxane solution in which no medium salt was contained. Procedures of the measurements and analysis of data were described in a previous paper.[9]

Results and Discussion

The formation curves experimentally obtained, $\bar{n}_{H,obsd}=(C_H-[H^+])/C_L$, where C_H and C_L denote the total concentrations of proton and 1,10-phenanthroline in the solution, respectively, at each point of titration are depicted in Fig. 1. We found that experimental points systematically deviated from the theoretical curve (curve A in Fig. 1) calculated by assuming the formation of only Hphen$^+$. Thus we assumed the formation of other species such as H(phen)$_2^+$ and H(phen)$_3^+$ which may be expected to be formed at $-\log[H^+]=4$—6. As shown in Table 1, the introduction of H(phen)$_2^+$ (case 2) significantly improved the error square sum, $U=\sum\{(C_{H,obsd}-C_{H,calcd})^2+(C_{L,obsd}-C_{L,calcd})^2\}$, while further introduction of H(phen)$_3^+$ (case 3) did not improve the result anymore. Experimental points well fell on the curve (curve B in Fig. 1) calculated by assuming the formation of Hphen$^+$ and H(phen)$_2^+$. Therefore, we concluded that the Hphen$^+$ and H(phen)$_2^+$ species were formed in the solutions under the present experimental conditions.

Table 1. The least-squares refinement of formation constants of H(phen)$_n^+$ in aqueous solution containing 0.3 mol dm^{-3} NaCl at 25 °C

Species	$\log\beta_n$		
	Case 1	Case 2	Case 3
Hphen$^+$	4.97(0.0061)	4.96(0.0032)	4.97(0.0025)
H(phen)$_2^+$	—	6.65(0.019)	6.63(0.10)
H(phen)$_3^+$	—	—	7.90(0.045)
U	8.3×10^{-7}	9.2×10^{-8}	9.1×10^{-8}

The values in parentheses refer to standard deviations.

Calorimetric titration curves are illustrated in Fig. 2 as the heat evolved, $\Delta H^\circ=q/vC_{H,tit}$, at the addition of a potion of a standard hydrochloric acid solution against the ratio C_H/C_L in the solution, where q, v, and $C_{H,tit}$ stand for heat measured and volume of the titrant added at each point of titration and concentration of hydrochloric acid in the titrant solution, respectively. The ΔH° curves obtained in the aqueous dioxane solutions depended on the ratio C_H/C_L, and the curves were well reproduced by assuming the formation of Hphen$^+$ and H(phen)$_2^+$ (the solid lines in Fig. 2).

The formation constants and enthalpies finally obtained by the least-squares procedure for the formation of Hphen$^+$ and H(phen)$_2^+$ in the aqueous dioxane solutions examined are summarized in Table 2. With increasing mole fraction of dioxane in the mixtures, the formation of H(phen)$_2^+$ became unfavorable and practically negligible in mixtures of $x>0.1$. It should

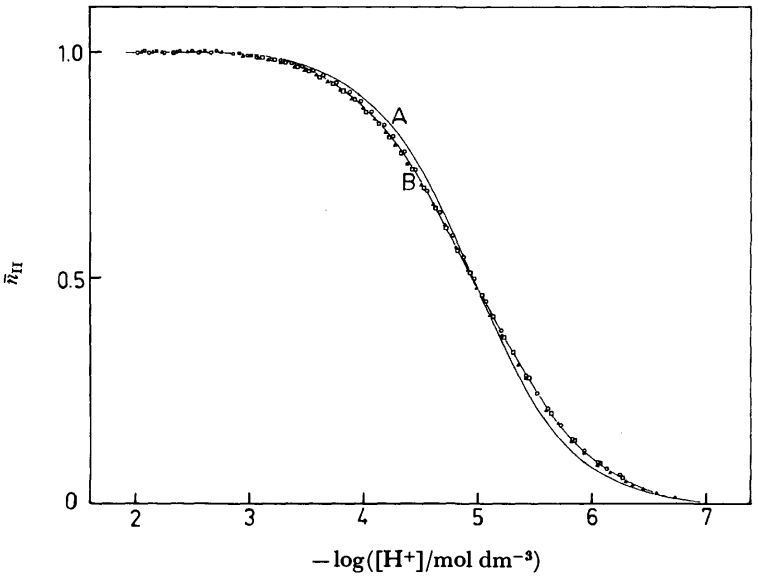

Fig. 1. Formation curves of protonated species of 1,10-phenanthroline (phen) in aqueous solution.
C_L(phen)/mmol dm^{-3}=7.215 (○), 10.84 (△), and 13.00 (□). The solid lines A and B were calculated in case 1 (Hphen$^+$ only) and case 2 (Hphen$^+$ and H(phen)$_2^+$), respectively.

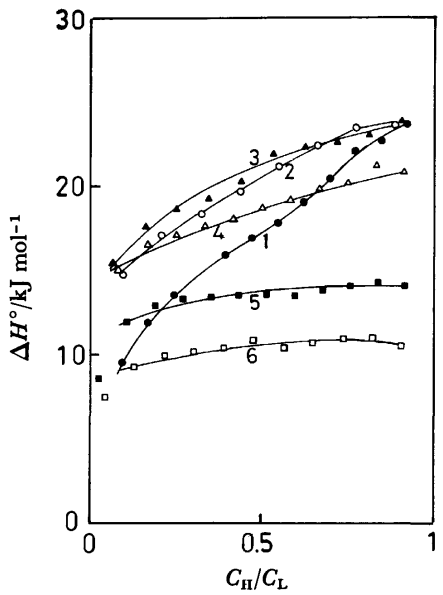

Fig. 2. Calorimetric titration curves of 1,10-phenanthroline aqueous dioxane solutions.
Curve 1: mole fraction of dioxane x=0.0; 2: 0.025; 3: 0.05; 4: 0.1; 5: 0.2; 6: 0.3. The solid lines show the curves calculated by using the constants obtained in Table 2.

be noted that the dependence of ΔH° on the ratio C_H/C_L became less pronounced with x in the mixtures (see Fig. 2). This reflected that the formation of $H(phen)_2^+$ became insignificant in the mixture of higher x.

The thermodynamic quantities, log (K_n/mol^{-1} dm^3), ΔG_n°/kJ mol^{-1}, ΔH_n°/kJ mol^{-1}, and ΔS_n°/JK^{-1} mol^{-1}, for the stepwise reactions, $H(phen)_{n-1}^+ + phen = H(phen)_n^+$ (n=1 and 2), are summarized in Table 3.

Enthalpies of solution of anhydrous 1,10-phenanthroline were determined in both neutral ($\Delta H^\circ_{s,neutral}$, x=0—1) and acidic ($\Delta H^\circ_{s,acid}$, x=0—0.4) aqueous dioxane solutions. In the neutral solvents, the formation of protonated species of 1,10-phenanthroline were negligible. In solutions involving 0.1 mol dm^{-3} HCl, 1,10-phenanthroline was fully converted into $Hphen^+$, but not into $H(phen)_2^+$ in such a highly acidic solution. Thus, the enthalpy of solution measured in an acidic solution at a given solvent composition was given as the sum of enthalpies of solution of 1,10-phenanthroline (ΔH_s°(phen)) and of formation of $Hphen^+$ (ΔH_1°), the latter value having been determined in the calorimetric titration experiment as described in the previous section. Thus ΔH_s°(phen)

Table 2. The formation constants, β_n/mol^{-n} dm^{3n}, and enthalpies, $\Delta H^\circ_{\beta n}$/kJ mol^{-1}, for the reaction, $H^+ + nL = HL_n^+$; $\beta_n = [HL_n^+]/[H^+][L]^n$ (L=phen) in aqueous dioxane containing 0.3 mol dm^{-3} NaCl at 25 °C

Concentration of dioxane / mole fraction	$\log \beta_1$	$\log \beta_2$	$\Delta H^\circ_{\beta 1}$	$\Delta H^\circ_{\beta 2}$
0	4.96(0.01)	6.65(0.06)	−16.6(0.3)	−34.3(1.4)
0.0125	4.83(0.02)	6.52(0.17)	—	—
0.025	4.71(0.02)	6.16(0.24)	−19.7(0.3)	−35.9(2.3)
0.05	4.57(0.02)	6.02(0.20)	−20.7(0.3)	−30.6(1.8)
0.1	4.33(0.01)	5.71(0.25)	−18.7(0.4)	−25.3(0.2)
0.2	4.10(0.01)	5.32(0.25)	−13.9(0.3)	—
0.3	3.86(0.01)	—	−10.7(0.2)	—
0.4	3.86(0.01)	—	−10.2(0.2)	—

The values in parentheses refer to three standard deviations.

Table 3. The formation constants, K_n/mol^{-1} dm^3, and thermodynamic quantities, ΔG_n°/kJ mol^{-1}, ΔH_n°/kJ mol^{-1}, and ΔS_n°/JK^{-1} mol^{-1}, for the stepwise reaction, $H(phen)_{n-1}^+ + phen = H(phen)_n^+$ (n=1 and 2) in dioxane-water mixtures containing 0.3 mol dm^{-3} NaCl as a constant ionic medium at various mole fractions x of dioxane

x	$Hphen^+$				$H(phen)_2^+$			
	$\log K_1$	ΔG_1°	ΔH_1°	ΔS_1°	$\log K_2$	ΔG_2°	ΔH_2°	ΔS_2°
0.0	4.96	−28.3	−16.6	39	1.69	−9.6	−17.7	−27
0.0125	4.83	−27.6	—	—	1.69	−9.6	—	—
0.025	4.71	−26.9	−19.7	24	1.45	−8.3	−16.2	−27
0.05	4.57	−26.1	−20.7	18	1.45	−8.3	−9.9	−5
0.1	4.33	−24.7	−18.7	20	1.38	−7.4	−6.6	+4
0.2	4.01	−22.9	−13.9	30				
0.3	3.86	−22.0	−10.7	38				
0.4	3.86	−22.0	−10.2	40				

TABLE 4. ENTHALPIES OF SOLUTION OF 1,10-PHENANTHROLINE MEASURED IN ACIDIC ($\Delta H^\circ_{s,acid}$/kJ mol^{-1}) AND NEUTRAL ($\Delta H^\circ_{s,neutral}$/kJ mol^{-1}) AQUEOUS DIOXANE SOLUTIONS, AND CALCULATED ENTHALPIES OF SOLUTION OF MONOMERIC 1,10-PHENANTHROLINE (ΔH°_s(phen)/kJ mol^{-1}) IN THE MIXTURES

Dioxane content / mole fraction	$\Delta H^\circ_{s,acid}$	$\Delta H^\circ_{s,neutral}$	ΔH°_t	ΔH°_s(phen)	$\Delta H^\circ_{s,neutral} - \Delta H^\circ_s$(phen)
0.0	−11.6	−0.3	−16.6	5.0	−5.3
0.025	−10.2	—	−19.7	9.5	—
0.05	−9.4	3.9	−20.7	11.3	−7.4
0.10	−5.0	5.7	−18.7	13.7	−8.0
0.20	−0.6	11.3	−13.9	13.3	−2.0
0.30	−1.2	10.0	−10.7	9.5	0.5
0.40	0.2	10.8	−10.2	10.4	0.4
0.60		11.9			
0.70		11.4			
0.80		11.7			
0.90		13.4			
1.0		17.7			

was calculated according to Eq. 1.

$$\Delta H^\circ_s(\text{phen}) = \Delta H^\circ_{s,acid} - \Delta H^\circ_t \quad (1)$$

Values of ΔH°_s(phen), $\Delta H^\circ_{s,acid}$, and $\Delta H^\circ_{s,neutral}$ obtained in various aqueous dioxane solutions are summarized in Table 4.

Enthalpies of Solution of 1,10-Phenanthroline. If only monomeric 1,10-phenanthroline molecules were present in a neutral solution $\Delta H^\circ_{s,neutral}$ should be equal to ΔH°_s(phen). However, as seen in Fig. 3, ΔH°_s(phen) was appreciably different from $\Delta H^\circ_{s,neutral}$ in the dioxane-water mixtures of $x<0.3$. The difference may be ascribed to the formation of stacked neutral species of 1,10-phenanthroline, $(\text{phen})_n$, in the neutral solvent mixtures, as suggested by an NMR study in water.[10] The value of $\Delta H^\circ_{s,neutral}$ was always positive but smaller than ΔH°_s(phen) in the mixtures of $x<0.3$, which suggested that the enthalpy of formation of the stacks should be negative if such stacks of 1,10-phenanthroline are formed in the mixtures. Negative enthalpies for the formation of stacked species were also reported for Methylene Blue in aqueous mixtures of various alcohols.[11]

The value of ΔH°_s (phen) was practically the same as $\Delta H^\circ_{s,neutral}$ in the dioxane-water mixtures at $x=0.3$ and 0.4, and the results suggested that the stacks did not form in the solutions due, probably, to destruction of the hydrogen-bonded structure of water in the bulk, which led to the decomposition of the hydrophobic hydration sphere around the aromatic rings of 1,10-phenanthroline. Observations by means of X-ray diffraction[12] suggested the destruction of the hydrogen-bonded structure of bulk water at $x>0.3$.

Values of ΔH°_s(phen) were obtained in aqueous dioxane solutions at $x=0$—0.4, but not in solutions at $x>0.4$ on account of experimental difficulties for determination of ΔH°_t and $\Delta H^\circ_{s,acid}$. However, since self-

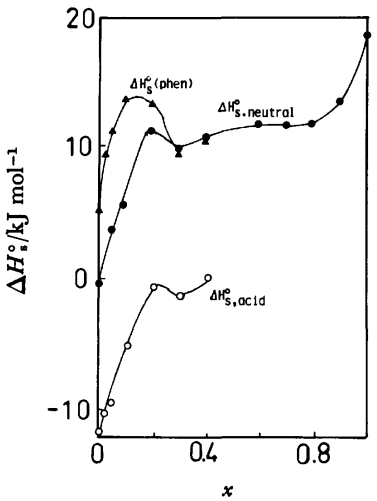

Fig. 3. Enthalpies of solution of 1,10-phenanthroline in neutral ($\Delta H^\circ_{s,neutral}$) and acidic ($\Delta H^\circ_{s,acid}$) solutions and ΔH°_s(phen) plotted against x.

stacking of 1,10-phenanthroline molecules was hardly expected in aqueous dioxane solutions at $x>0.4$ and, in fact, practically the same values of ΔH°_s(phen) as those of $\Delta H^\circ_{s,neutral}$ were found in the mixtures at $x=0.3$ and 0.4, we can reasonably assume that $\Delta H^\circ_s(\text{phen}) = \Delta H^\circ_{s,neutral}$ in aqueous dioxane solutions at $x>0.4$.

The value of ΔH°_s(phen) steeply increased with increasing x up to 0.1, and then slightly decreased in the range $x=0.1$—0.3. The sharp increase in ΔH°_s was also reported for the solution of 2,2′-bipyridyl in aqueous alcohol solutions with increasing alcohol content.[13] A further increase in x did not appreciably affect the ΔH°_s(phen) value until $x=0.8$. In the range $x>0.8$, ΔH°_s(phen) again steeply increased with x, and ΔH°_s(phen) in pure dioxane was more positive by about 13 kJ mol^{-1} than that in pure water. It is well known that the solubility of 1,10-phenanthroline markedly increases in organic solvents. Therefore,

the result that ΔH_s°(phen) was more endothermic in pure dioxane than in pure water indicated that the high solubility of 1,10-phenanthroline in dioxane was essentially owing to the contribution of a large entropy of solution of the species.

The variation of ΔH_s°(phen) in the range x=0—0.1 may be explained in terms of enhanced solvation of dioxane due to the breaking of the hydrophobic hydration structure around the aromatic rings of 1,10-phenanthroline molecules. A slight decrease of ΔH_s°(phen) in the range x=0.1—0.3 may be ascribed to the enhanced hydration of hydrophilic nitrogen atoms within 1,10-phenanthroline due to the breaking of the hydrogen-bonded water structure in the bulk. The enhancement of hydration of cations in aqueous dioxane solutions than in water has been suggested in a previous paper.[9]

The solvation structure of 1,10-phenanthroline with water at the sites of nitrogen atoms and with dioxane at the aromatic part may be practically remained unchanged in the range x=0.3—0.8, so that ΔH_s°(phen) was almost independent of solvent composition.

In solutions of the highest dioxane content x>0.8, water molecules solvating the nitrogen atoms within 1,10-phenanthroline may be replaced with dioxane molecules.

Solvent Effects on the Formation of Hphen$^+$.

The solvent effect on thermodynamic quantities for the formation of Hphen$^+$ was shown in Fig. 4, where the increments of ΔG_1°, ΔH_1°, and $T\Delta S_1^\circ$ in an aqueous dioxane solution from those in water, $\Delta\Delta G_1^\circ = \Delta G_1^\circ(\text{mix}) - \Delta G_1^\circ(\text{w})$, $\Delta\Delta H_1^\circ = \Delta H_1^\circ(\text{mix}) - \Delta H_1^\circ(\text{w})$, and $T\Delta\Delta S_1^\circ = T\Delta S_1^\circ(\text{mix}) - T\Delta S_1^\circ(\text{w})$, are plotted against x in the range x<0.4.

$\Delta\Delta G_1^\circ$ monotonously increased with increasing x, while $\Delta\Delta H_1^\circ$ and $T\Delta\Delta S_1^\circ$ first decreased and then increased after passing through minima at x=0.05 with increasing x. The change in $\Delta\Delta H_1^\circ$ can be expressed in terms of enthalpies of transfer, $\Delta H_t^\circ = \Delta H_s^\circ(\text{mix}) - \Delta H_s^\circ(\text{w})$, of the related species from water to the dioxane-water mixtures as follows:

$$\Delta\Delta H_1^\circ = \Delta H_t^\circ(\text{Hphen}^+) - \Delta H_t^\circ(\text{H}^+) - \Delta H_t^\circ(\text{phen}). \quad (2)$$

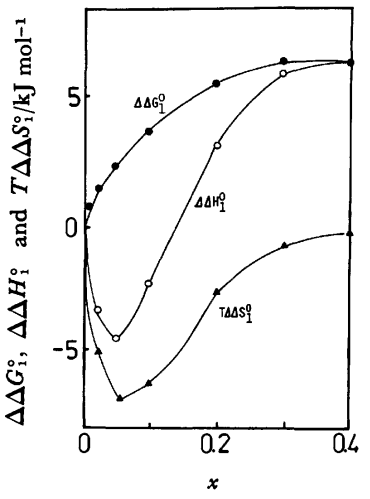

Fig. 4. Gibbs energies, enthalpies and entropies of formation of Hphen$^+$ in aqueous dioxane solutions relative to those in water.

By knowing values of $\Delta\Delta H_1^\circ$ and ΔH_t°(phen), the value of $\Delta H_t^\circ(\text{Hphen}^+) - \Delta H_t^\circ(\text{H}^+)$ was calculated according to Eq. 2, and the values of ΔH_1°, ΔH_t°(phen) and $\Delta H_t^\circ(\text{Hphen}^+) - \Delta H_t^\circ(\text{H}^+)$ thus calculated are summarized in Table 5. Since the enthalpy of transfer of proton $\Delta H_t^\circ(\text{H}^+)$ from water to the 0.2 mole fraction dioxane-water mixture was already reported in a previous paper,[9] $\Delta H_t^\circ(\text{Hphen}^+)$ from water to the mixture was also calculated and the values are also listed in Table 5.

Hphen$^+$ involves a hydrophilic $\gtrless$NH$^+$ group solvated with water and hydrophobic aromatic rings preferentially solvated with dioxane in aqueous dioxane solutions. The enthalpy of transfer of Hphen$^+$ from water to an aqueous dioxane solution should thus involve contributions of those of $\gtrless$NH$^+$ ($\Delta H_t^\circ(\gtrless\text{NH}^+)$) and aromatic rings ($\Delta H_t^\circ$(Ar)) within Hphen$^+$. The enthalpy of transfer of the $\gtrless$NH$^+$ group may be assumed to be similar to that of H$^+$, because it has been found that the enthalpy of transfer of the protonated ethylenediamine (Hen$^+$) from water to the 0.2 mole fraction dioxane-water mixture was very close to that of proton, *i.e.*, $\Delta H_t^\circ(\text{Hen}^+) \cong \Delta H_t^\circ(\text{H}^+)$.[9]

Table 5. Changes in enthalpy of formation of Hphen$^+$ relative to that in water and enthalpies of transfer ΔH_t°/kJ mol^{-1} of relevant species from water to aqueous dioxane solutions at 25 °C

x	$\Delta\Delta H_1^\circ$	ΔH_t°(phen)	$\Delta H_t^\circ(\text{Hphen}^+) - \Delta H_t^\circ(\text{H}^+)$	$\Delta H_t^\circ(\text{Hphen}^+)$	$\Delta H_t^\circ(\text{H}^+)$[a]
0.025	−3.1	4.5	1.4		
0.05	−4.1	6.3	2.2		
0.1	−2.1	8.7	6.6		
0.2	2.7	8.3	11.0	−11.7	−22.7
0.3	5.9	4.5	10.4		
0.4	6.4	5.4	11.8		

a) Ref. 9.

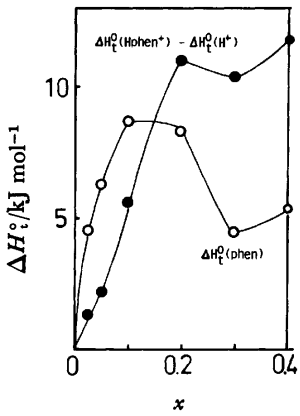

Fig. 5. Enthalpies of transfer, ΔH_t°(phen) and ΔH_t°(Hphen$^+$)$-\Delta H_t^\circ$(H$^+$), from water to aqueous dioxane solutions plotted against x.

If we assume that solvation of the protonated nitrogen atom $\gtrless$NH$^+$ within Hphen$^+$ with water varies in a similar manner to that of H$^+$ in the range x= 0—0.4, ΔH_t°(Hphen$^+$)$-\Delta H_t^\circ$(H$^+$) should approximately reflect the change in solvation of the aromatic rings within Hphen$^+$. Variations of ΔH_t°(Hphen$^+$)$-$ ΔH_t°(H$^+$) and ΔH_t°(phen) plotted against x (Fig. 5) show that they have a similar trend in the range x= 0—0.2. The result thus suggested that the aromatic rings within Hphen$^+$ was also significantly solvated with dioxane in the range of x up to 0.2. In the range x=0.2—0.3, ΔH_t°(phen) more steeply decreased with x than ΔH_t°(Hphen$^+$)$-\Delta H_t^\circ$(H$^+$), which may be caused by enhanced hydration at the sites of nitrogen atoms within 1,10-phenanthroline as discussed in a previous section.

The value ΔH_t°(Hphen$^+$) from water to the 0.2 mole fraction dioxane-water mixture was -11.7 kJ mol^{-1}, which should be represented as the sum of ΔH_t°($\gtrless$NH$^+$) and ΔH_t°(Ar). If we simply assume that ΔH_t°($\gtrless$NH$^+$)=ΔH_t° (H$^+$) in the range x=0—0.2, the value of ΔH_t°(Ar) from water to the 0.2 mole fraction dioxane-water mixture was estimated to be about 11 kJ mol^{-1}, which was slightly larger than ΔH_t°(phen) (8.3 kJ mol^{-1}). The slightly larger value of ΔH_t°(Ar) than ΔH_t°(phen) suggests that the hydration at the sites of nitrogen atoms within 1,10-phenanthroline was enhanced in the 0.2 mole fraction dioxane-water mixture relative to water.

Solvent Effects on the Formation of H(phen)$_2^+$. The formation of H(phen)$_2^+$ could be detected only in aqueous dioxane solutions of x<0.1, where the hydrogen-bonded structure of water in the bulk might still significantly remain and the stacks of 1,10-phenanthroline were expected to be formed.

Mitchell[14] suggested from measurements of the concentration dependence of the proton NMR spectrum of 1,10-phenanthroline in acidic solutions that considerable self-stacking occurred among 1,10-phenanthroline molecules to form the H(phen)$_2^+$ species. Considering that the H(phen)$_2^+$ species was not formed in aqueous dioxane solutions of relatively higher dioxane content in which the hydrogen-bonded structure of water in the bulk may be almost destructed, 1,10-phenanthroline molecules within H(phen)$_2^+$ may have a stacked structure. A suggested form for the structure of H(phen)$_2^+$ is illustrated in Fig. 6.

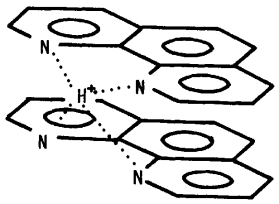

Fig. 6. The suggested structure of the H(phen)$_2^+$ species.

The values of ΔH_2° pertaining to the reaction, Hphen$^+$+phen=H(phen)$_2^+$, were negative in all aqueous dioxane solutions examined. The result can be expected because of negative enthalpies of formation of stacked oligomers of 1,10-phenanthroline (phen)$_n$.

The work has partially been supported by the Grant-in-Aid for Scientific Research No. 57470054 from the Ministry of Education, Science and Culture and Asahi Glass Foundation for Industrial Technology.

References

1) T. S. Lee, I. M. Kolthoff, and D. L. Leussing, *J. Am. Chem. Soc.*, **70**, 2348 (1948).
2) M. J. Fahsel and C. V. Banks, *J. Am. Chem. Soc.*, **88**, 878 (1966).
3) P. Paoletti, A. Dei, and A. Vacca, *J. Chem. Soc. (A)*, **1971**, 2656.
4) A. A. Schilt and W. E. Dunbar, *Tetrahedron*, **30**, 401 (1974).
5) R. D. Alexandar, A. William L. Dudeney, and R. J. Irving, *J. Chem. Soc., Faraday Trans. 1*, **74**, 1075 (1978).
6) J. V. Rund and P. C. Keller, *J. Chem. Soc. (A)*, **1970**, 2827.
7) S. Bandyopadhyay, A. K. Mandal, and S. Aditya, *J. Indian Chem. Soc.*, **LVIII**, 467 (1981).
8) S. Ishiguro, Y. Oka, and H. Ohtaki, *Bull. Chem. Soc. Jpn.*, **56**, 2426 (1983).
9) S. Ishiguro and H. Ohtaki, *Bull. Chem. Soc. Jpn.*, **57**, 2622 (1984).
10) P. R. Mitchell, *J. Chem. Soc. Dalton*, **1980**, 1079.
11) S. L. Fornili and G. Sgroi, *J. Chem. Soc., Faraday Trans. 1*, **79**, 1085 (1983).
12) V. I. Korsunskii and Y. I. Naberukhin, *Zh. Strukt. Khim.*, **18**, 587 (1977).
13) J. Burgess and R. Sherry, *J. Chem. Soc., Perkin Trans. 2*, **1981**, 366.
14) P. R. Mitchell, *J. Am. Chem. Soc.*, **102**, 1180 (1980).

Oxygen-17 NMR Study of the Uranyl Ion. II.[1] Correlation between ^{17}O NMR Chemical Shifts and Wavelengths of UV-Visible Absorption Bands of Uranyl Complexes

Woo-Sik JUNG, Hiroshi TOMIYASU, and Hiroshi FUKUTOMI*
Research Laboratory for Nuclear Reactors, Tokyo Institute of Technology, O-okayama, Meguro-ku, Tokyo 152
(Received October 20, 1984)

^{17}O NMR chemical shifts, UV-visible and IR spectra of a series of $[UO_2L_n](ClO_4)_2$ (L=unidentate oxygen-donor ligand; n=coordination number) complexes in nonaqueous solvents have been measured. The electronic transition bands of the UO_2^{2+} entity shift toward lower energies with the increase in base strength of ligands in the equatorial plane. The asymmetric stretching frequencies of U=O bands are also affected by the base strength of equatorial ligands and correlated with the lowest electronic transition energies of uranyl complexes with the same geometry. The ^{17}O chemical shifts are shown to be related to the lowest electronic transition energies of uranyl complexes. It appears that oxygen isotope shifts in ^{17}O NMR spectra of the uranyl ion are predominantly attributed to the increase in the lowest electronic transition energies.

The electronic structure of dioxouranium(VI) (uranyl) ions has been extensively studied by UV-visible, infrared, and Raman spectroscopy.[2] In particular, much attention has been paid to ligation effects on the vibrational spectrum of the uranyl ion. Recently Bray and Kramer[3] showed that there are some correlations between spectroscopic parameters and ligand(L) basicity for UO_2(hexafluoroacetylacetonato)$_2$L. They reported that the asymmetric stretching frequencies of U=O bonds decrease with increasing the base strength of ligands L in the vapor phase and benzene solution.

Our interest in ligation effects on U=O bonds has led to the study of UV-visible, infrared, and ^{17}O NMR spectra of $[UO_2L_n](ClO_4)_2$,[4] in which the base strength of ligand L in the equatorial plane may be characterized by its donor number.[5] Electronic spectra of uranyl complexes exhibit a remarkable similarity, which implies that UV-visible absorption bands arise from electronic transitions within the UO_2^{2+} entity. The absorption bands could be divided into three groups with origins at 22050, 24150, and 27000 cm^{-1} representing the three components of the triplet state which is split by the equatorial field.[2a] Furthermore, the vibronic fine structure is superimposed on these absorption bands. We investigated the variation in the position of electronic transition bands by changing ligand L. It is also of interest to see whether the position of the bands is correlated with the uranyl asymmetric stretching frequency.

From the study of ^{17}O NMR spectroscopy of oxygen-containing compounds, it is evident that ^{17}O NMR chemical shifts are very sensitive to a change in the nature of oxygen bonding.[6] In this connection it is interesting to study ligation effects on the ^{17}O NMR spectrum of oxygen in the uranyl ion (uranyl oxygens hereafter). There are a few ^{17}O NMR studies of uranyl complexes,[7] but no systematic study has been carried out. In this paper ^{17}O chemical shifts of uranyl oxygens of some uranyl complexes are reported and interpreted in terms of the lowest electronic transition energies in UV-visible spectra. Oxygen isotope shifts in ^{17}O NMR spectra of enriched uranyl oxygens in aqueous solution[1] may also be interpreted in terms of the lowest electronic transition energies.

Experimental

Preparation of Uranyl Complexes. Methods in the literature[8] were used to prepare all the uranyl complexes used in this study. Hydrated uranyl perchlorate was refluxed with triethyl orthoformate at 50—60 °C for 1 h, followed by the addition of dried nonaqueous solvent L at room temperature. The resulting crystals of $[UO_2L_n](ClO_4)_2$ were filtered, washed with diethyl ether and dried under reduced pressure. In the case of DEF a yellow oil was formed at the bottom of the flask. The supernatant fraction was decanted and the residual oil was stirred with successive portions of diethyl ether. The resulting oil was dried under reduced pressure. Synthesized complexes, which are listed in Table 1, were identified by elemental analyses and/or ^1H NMR measurements.

NMR Measurements. ^{17}O NMR measurements of uranyl oxygens in natural abundance were carried out at 13.46 MHz on a JEOL JNM-FX 100 FT-NMR spectrometer. A spectral width of 20 kHz, 8 K data points, and a 90° pulse width of 10 μs were used. One hundred and fifty thousand transients were usually collected. All measurements were made at 20 °C and all chemical shifts were downfield relative to $H_2{}^{17}O$ in natural abundance. No bulk susceptibility correction was made.

Sample solutions for NMR measurements were prepared by dissolving uranyl complexes in nonaqueous solvent-(L)-CD_2Cl_2 (CD_3CN for LNO complex) mixture, where $5[UO_2L_n(ClO_4)_2]<$[free ligand]. An additional measurement was carried out in the case of TMU complex, where [free TMU]=0. The concentration of complexes was about 0.1 M (1 M=1 mol dm^{-3}), and less soluble complexes were studied in saturated solutions. Sample solutions were introduced into NMR microcells (Wilmad). The microcell was inserted in a 10 mm o.d. NMR tube (Wilmad) containing reference water.

^{17}O NMR measurements of uranyl oxygens enriched by

using $H_2{}^{17}O$ (Merck, ^{17}O, 42.1; ^{18}O, 31.7 atom%) were carried out at 54.10 MHz on a JEOL JNM-GX 400 FT-NMR spectrometer. Detailed procedure for preparation of enriched uranyl oxygens is described in a previous paper.[1] The temperature of the solution was maintained at 24.4±0.1 °C.

UV-Visible and IR Spectra Measurements. UV-visible spectra (350—550 nm) were measured on a Shimadzu UV-365 spectrophotometer using 1 cm quartz cells. IR spectra in the region 4000—400 cm^{-1} were taken on a Hitachi 270-30 IR spectrophotometer using KRS-5 cells (Horiba). Sample solutions for UV-visible and IR measurements were prepared by dissolving each uranyl complex in the solvent corresponding to the equatorial ligand. An additional measurement was carried out for the TMU complex, where [free TMU]=0. The concentrations of sample solutions for UV-visible and IR spectra measurements were usually 0.01 and 0.3 M, respectively, and less soluble complexes were measured by using saturated solutions.

Results and Discussion

UV-Visible and IR Spectra. The electronic spectra of most uranyl complexes in this study exhibited three band groups with a well-defined vibronic structure, which are characteristic of uranyl complexes. On the other hand, no vibronic structure was observed in the third band group with the origin at 27000 cm^{-1} for TMU, LNO, and HMPT complexes. This arises from the fact that the third band group is overshadowed by an intense ligand-to-uranyl charge-transfer band when the base strength of equatorial ligands is considerably high. Assignment of the electronic states involved in the electronic absorption spectrum of the uranyl ion is still a matter of controversy, but the interpretation by McGlynn and Smith[2a] is generally accepted. They suggested that the absorption band between 20500 and 30000 cm^{-1} results from excitation of an electron from the highest filled π-orbital to a nonbonding orbital on uranium (ϕ_u or δ_u).

It was found that an increase in base strength of equatorial ligands results in a bathochromic shift of the electronic transition bands. As shown in Fig. 1, 0′←0″ band in the first electronic transition (band number I_0 after De Jaegere and Görller-Walrand's notation[9]) shifts toward lower energies with the increase in base strength of equatorial ligands. The same trend was observed for 2′←0″ band in the second transition (band number II_2[9]) except for the HMPT complex. Belford *et al.*[10] reported the similar results, in which absorption bands in visible region shifted toward higher energies with successive fluorination of acetylacetone in the bis(acetylacetonato)dioxouranium(VI), *i.e.* with decreasing the base strength of ligands.

These ligation effects on UV-visible spectra can be explained by McGlynn and Smith's suggestion.[2a] According to the suggestion, the electron density of the ϕ_u or δ_u atomic orbitals of uranium might be enhanced by σ(L-M) electron donation of equatorial

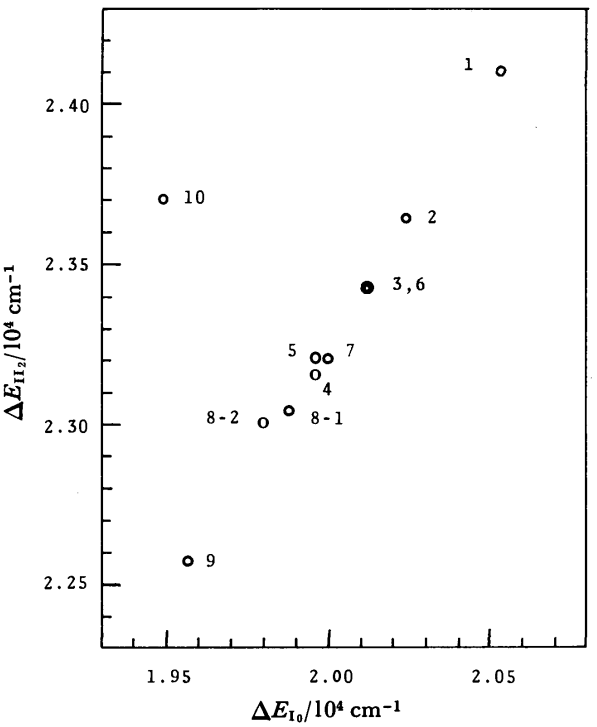

Fig. 1. Correlation of energies (ΔE_{II_2}) of 2′←0″ bands in the second electronic transition with energies (ΔE_{I_0}) of 0′←0″ bands in the first electronic transition. The figures correspond to those in Table 1.

ligands. This may result in stabilization of energy levels of nonbonding orbitals, thus lowering the electronic transition energies. The enhanced electron density on the uranium also causes a loosening of the U=O bond because of increased electrostatic repulsion with the highly negative axial uranyl oxygens.[2b] This is reflected in the asymmetric stretching frequency ν_{as} of the U=O bonds. It was observed, therefore, that the uranyl asymmetric stretching frequency is lowered by increasing base strength of equatorial ligands. These ligation effects on both UV-visible and infrared spectra give a good correlation between ν_{as} and the energy of 0′←0″ band in the first electronic transition (ΔE_{I_0}), as shown in Fig. 2. The fact that the results for four-coordinated HMPT and TMU complexes deviated from the correlation line in Fig. 2 may be explained in terms of the difference in geometry between four-coordinated complexes (D_{4h}) and the other complexes (D_{5h}), by considering that absorption spectra of uranyl complexes can be affected by difference in the number and geometric disposition of equatorial ligands.[2f] However, this explanation requires further study.

In addition to the electronic interaction as mentioned above, the uranyl asymmetric stretching frequency is also affected by vibrational interaction, which is attributed to the coupling between the U=O stretching and the bending of bonds between uranium and equatorial ligands. Jones[11] estimated

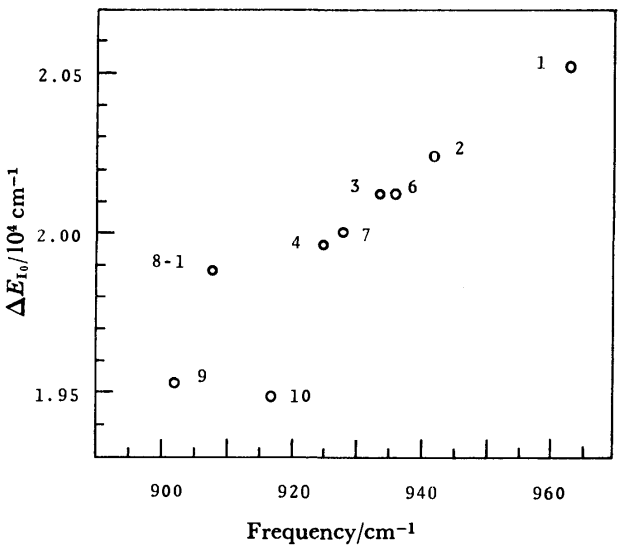

Fig. 2. Correlation of energies (ΔE_{I_0}) of 0′←0″ bands in the first electronic transition with the asymmetric stretching frequencies of the U=O bonds. The figures correspond to those in Table 1.

that the maximum alteration would be 3%. Furthermore, the effect of intermolecular interaction on ν_{as} can not be neglected when ν_{as} is measured in liquid sample. In the case of hydrated uranyl perchlorate, for example, ν_{as} measured in D_2O solution at pH 2.5 is about 10 cm^{-1} lower than that in H_2O solution at pH 2.5, while no variation in UV-visible spectra was observed in both the solutions. This phenomenon is ascribed to the solvent effect, where hydrogen bonds between uranyl oxygens and D_2O are stronger than those between uranyl oxygens and H_2O. It is known that the hydrogen bond contributes to weakening the U=O bond strength.[12] However, the solvent effect in aprotic solvents employed in this study is considered to be negligible.

From our results of ligation effects on both UV-visible and infrared spectra, we propose that ΔE_{I_0} in UV-visible spectra and ν_{as} in infrared spectra can be used as parameters of the complexing ability (or base strength) of equatorial ligands toward the uranyl ion. The parameters may be compared to the donor number,[5] which is defined as the enthalpy of complex formation between the given solvent and antimony pentachloride in 1,2-dichloroethane solutions. Figures 1 and 2 show that the base strengths of DEA and DEF toward the uranyl ion are almost equal to those of DMA and DMF, respectively, although there are considerable differences in the donor numbers each other. Fukutomi *et al.*[13] showed that the donor property of ligands is correlated with the E_B parameter[14] in equilibrium study on the anation reaction of uranyl complexes.

^{17}O NMR Chemical Shifts. ^{17}O chemical shifts ($\delta^{17}O$) measured in this study are summarized in Table 1. It is noted that ^{17}O resonances of uranyl oxygens shift downfield with increasing the base strength of equatorial ligands of the uranyl ion. This ligation effect on ^{17}O chemical shifts can be explained in terms of the electronic transition energy.

TABLE 1. SPECTROSCOPIC PARAMETERS FOR $[UO_2L_n](ClO_4)_2$ COMPLEXES IN SOLUTION

L[a]	C.N.[b]	λ_{I_0}[d] nm	λ_{II_2}[d] nm	ν_{as}(U=O)[e] cm^{-1}	$\delta(^{17}O)$[h] ppm
1. H_2O	5	487	415	963	1119.0[f]
2. TMP	5	494	423	942	1122.5
3. DMF	5	497	427	934	1131.5
4. DMA	5	501	432	925	1133.3
5. DMSO	5	501	431	g)	1129.7
6. DEF	5	497	427	936	1131.2
7. DEA	5	500	431	928	1133.7
8-1. TMU	4[c]	503	434	908	1138.8
8-2. TMU	5	505	435	g)	1138.4
9. LNO	5	512	443	902	1137.7
10. HMPT	4	513	422	917	1138.8

a) Ref. 4. b) Coordination number in the equatorial plane of uranyl ion in solution, where $5[UO_2L_n(ClO_4)_2]$ <[free ligand]. See Ref. 8. c) C.N., where [free TMU]=0. d) Precision of measurement: ±1 nm. Band numbers I_0 and II_2 refer to 0′←0″ band in the first electronic transition and 2′←0″ band in the second electronic transition, respectively. e) Precision of measurement: ±1 cm^{-1}. f) At pH 2.5. g) Unmeasurable due to masking by the absorption of ligand. h) Precision of measurement: ±0.5 ppm.

The nuclear shielding of ^{17}O nuclei can be approximated as the sum of diamagnetic (σ_d) and paramagnetic (σ_p) terms, $\sigma=\sigma_d+\sigma_p$.[15] It has been shown[16] that the paramagnetic term is principally responsible for the total shielding constant in ^{17}O nuclear shieldings. This paramagnetic term can be expressed as follows[17]:

$$\sigma_p^A = -\frac{2e^2\hbar^2}{3m^2c^2\Delta E}\langle r^{-3}\rangle_{2p}\sum_B Q_{AB},$$

where A is the nucleus under investigation, B represents all the other nuclei in the molecule, m is the electron mass, $\langle r^{-3}\rangle_{2p}$ is the average value of the reciprocal cube of the 2p orbital radius, and ΔE is the "mean" excitation energy of the molecule. $\sum Q_{AB}$ is related to the electronic charges and bond orders. To a first approximation, the ΔE can be equated to the excitation energy of the lowest excited state. Figgis *et al.*[18] established a linear relationship between the ^{17}O chemical shifts for oxyanions of the transition metals and the reciprocal of their lowest electronic transition energies. Kazanskii[19] also showed the correlation between the ^{17}O chemical shifts of both the terminal and bridge oxygen atoms in polyoxometalates and the wavelength of the first charge transfer. The data for the uranyl ion in aque-

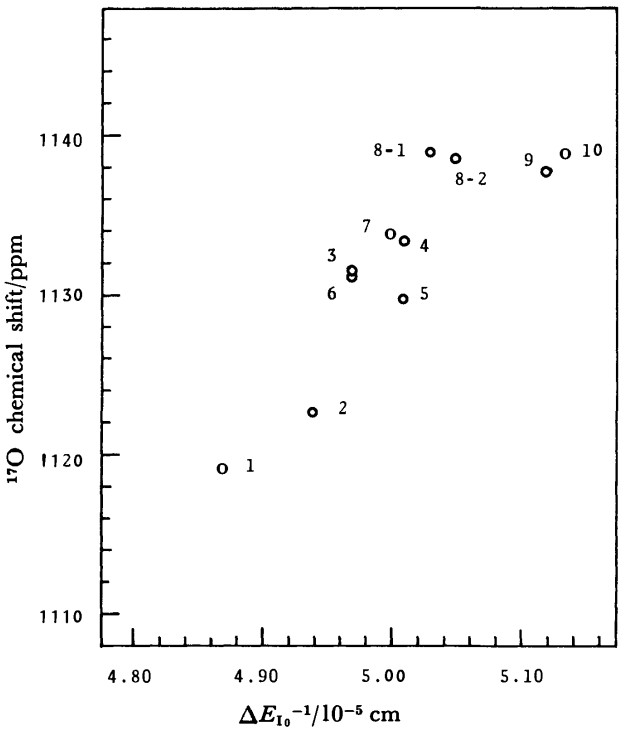

Fig. 3. Correlation of ^{17}O chemical shifts with the reciprocal of the lowest electronic transition energies. The figures correspond to those in Table 1.

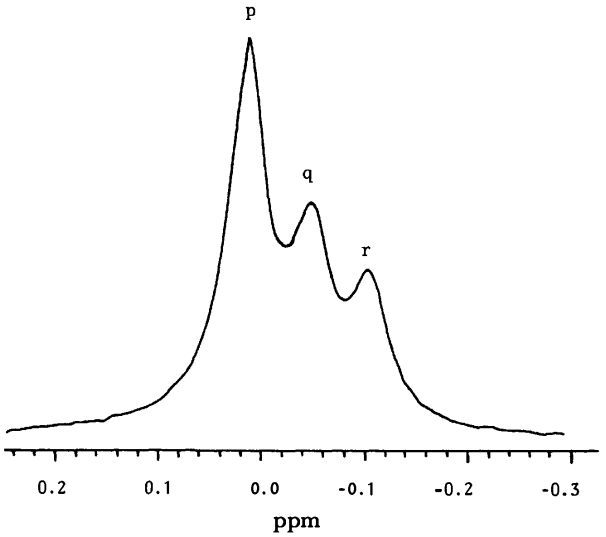

Fig. 4. ^{17}O NMR spectrum of the uranyl oxygens measured at 54.10 MHz. The uranyl oxygens were enriched by using $H_2{}^{17}O$ (42.1 atom%). $[UO_2{}^{2+}]$= 0.098 m and $[H^+]$=0.23 m (1 m=1 mol kg^{-1}). Typical ^{17}O spectral parameters are as follows: spectral width=1000 Hz, data points=16 K, scans=200, pulse width=10 μs. Peaks p, q, and r correspond to $[^{16}O{=}U{=}^{17}O]^{2+}$, $[^{17}O{=}U{=}^{17}O]^{2+}$, and $[^{18}O{=}U{=}^{17}O]^{2+}$, respectively.

ous solution (at pH 2.5, δ=1119.0 ppm; λ_{I_0}=487 nm) fall on the correlation line obtained by Figgis *et al.* This indicates that ΔE is the dominant factor in determining ^{17}O nuclear shielding of uranyl oxygens in uranyl complexes.

As shown in Fig. 3, a good correlation is observed between the ^{17}O chemical shifts and the reciprocal of the lowest electronic transition energies ($1/\Delta E_{I_0}$) of uranyl complexes. Besides the lowest electronic transition energy, the other factors such as U=O distance and the other electronic transition must be considered as minor factors. As mentioned above, the uranyl asymmetric stretching frequency, which can be a measure of the U=O bond distance,[20] changes with equatorial ligands. The variation in bond distance can affect ^{17}O nuclear shielding. Since an increase in U=O bond distance is expected to lead to an increase in ^{17}O nuclear shielding,[21] the ^{17}O chemical shift for the LNO complex may be lower than that expected from its lowest electronic transition energy (see Fig. 3). On the other hand, ΔE_{II_2} value for the HMPT complex is significantly higher than that expected from ΔE_{I_0} value, as shown in Fig. 1. Therefore, the contribution from the second electronic transition in the HMPT complex will be considerably smaller than in the other complexes, resulting in a low ^{17}O chemical shift.

Oxygen Isotope Shifts in ^{17}O NMR Spectra. In the previous paper[1] we assigned three peaks of ^{17}O-enriched uranyl oxygens to the signals of three isotopomers, *i.e.*, $[^{16}O{=}U{=}^{17}O]^{2+}$, $[^{17}O{=}U{=}^{17}O]^{2+}$, and $[^{18}O{=}U{=}^{17}O]^{2+}$. In order to support our previous results further, we measured the ^{17}O NMR spectrum of enriched uranyl oxygens at 54.10 MHz. As shown in Fig. 4, three peaks were much better resolved than those at 13.46 MHz. Chemical shifts for the signals of $[^{17}O{=}U{=}^{17}O]^{2+}$ and $[^{18}O{=}U{=}^{17}O]^{2+}$ isotopomers were observed to be -0.059 ± 0.004 and -0.117 ± 0.004 ppm, respectively, relative to $[^{16}O{=}U{=}^{17}O]^{2+}$, which are more accurate than values reported previously.[1] A few data on the isotope shift through two bonds have been reported,[22] but no data are available for the isotope shift through two bonds in ^{17}O NMR except for the oxygen isotope shifts in the uranyl ion. It may be, therefore, of interest to interpret these isotope shifts.

Heavy substitution of the molecule commonly leads to the reduction of the zero point vibrational energies.[23] Since this reduction is larger in the ground state than in the electronically excited state, the electronic transition energies of substituted molecules are generally shifted toward higher energies. In view of this fact the lowest electronic transition (0′←0″ band in the first electronic transition) of heavier isotopomers of the uranyl ion is expected to occur at higher energies. The increase in the lowest electronic transition energy, which is a dominant factor in determining the ^{17}O nuclear shielding of uranyl oxygens, will result in an increase in ^{17}O nuclear shielding. It is estimated from the correlation in Fig. 3 that the difference in chemical shifts between $[^{16}O{=}U{=}^{17}O]^{2+}$ and $[^{18}O{=}U{=}^{17}O]^{2+}$ at 24.4 °C corresponds to the difference of *ca.* 6.6 cm^{-1} in the lowest electronic transi-

tion energies. Unfortunately no experimental results are found for oxygen isotope shifts in the electronic absorption spectrum of the uranyl ion in aqueous solution. This small difference may be compared to the experimental value in $[UO_2Cl_4]^{2-}$, where the difference in the lowest electronic transition energies between $[^{16}O{=}U{=}^{16}O]^{2+}$ and $[^{18}O{=}U{=}^{18}O]^{2+}$ was observed to be 10 cm^{-1} at 4.2 K.[24]

Heavy substitution also leads to the change in U=O bond distance, but the contribution of this change to the ^{17}O nuclear shielding will be less important than that of the change in the lowest electronic transition energies, as indicated above. Mamayev *et al.*[25] demonstrated that, in a semi-empirical calculation of the isotope shifts in ^{13}C, ^{14}N, and ^{17}O NMR, the variation in the "mean" excitation energy cannot be left out of account on isotopic substitution of the molecule. It is considered that oxygen isotope shifts in ^{17}O NMR spectra of enriched uranyl oxygens can be explained only in terms of the change in the lowest electronic transition energies by isotopic substitution.

^{235}U-^{17}O Spin-Spin Coupling. Taking account of the fact that ^{17}O resonance of uranyl oxygens is very sharp, we intended to observe $^{235}U(I=7/2)$-^{17}O spin-spin coupling of enriched $^{235}UO_2^{2+}$ (*ca.* 90% ^{253}U) ion in aqueous solution. No fine structure was observed even at 65 °C. It appears that this is associated with a very small magnetic moment of ^{235}U nucleus. Oxygen isotope shifts measured at 65 °C for $^{235}UO_2^{2+}$ solution were somewhat lower than for $^{238}UO_2^{2+}$ solution at room temperature.

The authors wish to express their thanks to Messrs. Tohru Himoto and Naoyuki Fujii of JEOL, Ltd. for running some NMR spectra. This work was partially supported by a Grant-in-Aid for Scientific Research No. 5470035 from the Ministry of Education, Science and Culture.

References

1) Part I: W.-S. Jung, Y. Ikeda, H. Tomiyasu, and H. Fukutomi, *Bull. Chem. Soc. Jpn.*, **57**, 2317 (1984).

2) a) S. P. McGlynn and J. K. Smith, *J. Mol. Spectrosc.*, **6**, 164 (1964); b) S. P. McGlynn, J. K. Smith, and W. C. Neely, *J. Chem. Phys.*, **35**, 105 (1961); c) J. I. Bullock, *J. Chem. Soc. (A)*, **1969**, 781; d) J. P. Day and L. M. Venanzi, *J. Chem. Soc. (A)*, **1966**, 1363; e) J. M. Haigh and D. A. Thornton, *J. Mol. Struct.*, **8**, 351 (1971); f) C. Görller-Walrand and S. De Jaegere, *Spectrochim. Acta*, **28A**, 257 (1972).

3) R. G. Bray and G. M. Kramer, *Inorg. Chem.*, **22**, 1843 (1983).

4) Ligand abbreviations: TMP=trimethyl phosphate; DMF=*N*,*N*-dimethylformamide; DEF=*N*,*N*-diethylformamide; DMA=*N*,*N*-dimethylacetamide; DEA=*N*,*N*-diethylacetamide; DMSO=dimethyl sulfoxide; TMU=1,1,3,3-tetramethylurea; LNO=2,6-lutidine *N*-oxide; HMPT=hexamethylphosphoric triamide.

5) V. Gutmann, "Coordination Chemistry in Non-Aqueous Solutions," Springer-Verlag, Berlin (1968).

6) W. G. Klemperer, *Angew. Chem., Int. Ed. Engl.*, **17**, 246 (1978).

7) S. W. Rabideau, *J. Phys. Chem.*, **71**, 2747 (1967); L. G. Mashirov, D. V. Suglobov, and V. A. Shcherbakov. *Radiokhimiya*, **17**, 881 (1975).

8) A. M. Hounslow, S. F. Lincoln, P. A. Marshall, and E. H. Williams, *Aust. J. Chem.*, **34**, 2543 (1981) and references cited therein.

9) S. De Jaegere and C. Görller-Walrand, *Spectrochim. Acta*, **25A**, 559 (1969).

10) R. N. Belford, A. E. Martell, and M. Calvin, *J. Inorg. Nucl. Chem.*, **14**, 169 (1960).

11) L. H. Jones, *Spectrochim. Acta*, **10**, 395 (1958).

12) G. V. Sidorenko, R. B. Dushin, E. K. Legin, and D. N. Suglobov, *Radiokhimiya*, **23**, 407 (1981).

13) H. Doine, Y. Ikeda, H. Tomiyasu, and H. Fukutomi, *Bull. Chem. Soc. Jpn.*, **57**, 1021 (1984).

14) R. S. Drago and R. B. Wayland, *J. Am. Chem. Soc.*, **87**, 3571 (1965); R. S. Drago, *Coord. Chem. Rev.*, **33**, 251 (1980).

15) N. F. Ramsey, *Phys. Rev.*, **78**, 699 (1950).

16) K. A. Ebraheem and G. A. Webb, *J. Magn. Reson.*, **25**, 399 (1977).

17) M. Karplus and J. A. Pople, *J. Chem. Phys.*, **38**, 2803 (1954).

18) B. N. Figgis, R. G. Kidd, and R. S. Nyholm, *Proc. R. Soc. London, Ser. A.*, **269**, 469 (1962).

19) L. P. Kazanskii, *Koord. Khim.*, **3**, 327 (1977).

20) L. H. Jones, *Spectrochim. Acta*, **11**, 409 (1959).

21) K. F. Miller and R. A. D. Wentworth, *Inorg. Chem.*, **18**, 984 (1979); R. G. Kidd, *Can. J. Chem.*, **45**, 605 (1967).

22) G. V. D. Tiers, *J. Chem. Phys.*, **29**, 963 (1958); R. A. Bell, C. L. Chan, and B. G. Sayer, *J. Chem. Soc., Chem. Commun.*, **1972**, 67; R. A. Bernheim and B. J. Lavery, *J. Chem. Phys.*, **42**, 1464 (1965).

23) G. Herzberg, "Molecular Spectra and Molecular Structure," Vol. III, D. Van. Nostrand, Princeton (1966).

24) R. G. Denning, T. R. Snellgrove, and D. R. Woodwark, *Mol. Phys.*, **32**, 419 (1976).

25) V. M. Mamayev, N. M. Sergeev, and K. A. Orazberdiev, *J. Struct. Chem.*, **18**, 38 (p. 31 English ed.) (1977); V. M. Mamayev and N. M. Sergeyev, *Chem. Phys. Lett.*, **34**, 317 (1975).

 © 1985 The Chemical Society of Japan Bull. Chem. Soc. Jpn., 58, 943—947 (1985)

The Raman Spectra of Cobalt(III) Complexes. V.[1] Differentiation between Two *cis*(a) Isomers of [Coa$_2$(NH$_3$)$_2$(en)] Type Complexes (a=NO$_2^-$ and CN$^-$)

Kan KANAMORI,* Ikuko BANSHO, Kiyoyasu KAWAI, Keiji AKAMATSU,† and Yoichi SHIMURA†

Department of Chemistry, Faculty of Science, Toyama University, Gofuku, Toyama 930
†*Department of Chemistry, Faculty of Science, Osaka University, Toyonaka, Osaka 560*

(Received June 16, 1984)

Three geometrical isomers of [Co(NO$_2$)$_2$(NH$_3$)$_2$(en)]$^+$ were newly prepared. Two *cis*(NO$_2$) isomers (*trans*-(NH$_3$) and *cis,cis*) were clearly differentiated on the basis of the polarizabilities of the Raman bands due to Co-N(NH$_3$ and en) stretching vibrations. The Raman polarization measurement was also applied successfully to the determination of the geometrical configurations of two [Co(CN)$_2$(NH$_3$)$_2$(en)]$^+$ isomers. The structural assignments were substantiated by optical resolution of the *cis,cis* isomers of [Coa$_2$(NH$_3$)$_2$(en)]$^+$ (a=NO$_2^-$ and CN$^-$).

Three geometrical isomers (*trans*(a), *trans*(NH$_3$), and *cis,cis*) of [Coa$_2$(NH$_3$)$_2$(en)] type complex were first prepared by Bailar and Peppard[2] for a=Cl$^-$. In general, it is difficult to distinguish the two *cis*(a) isomers (*trans*(NH$_3$) and *cis,cis*) of [Coa$_2$(NH$_3$)$_2$(en)] type complexes on the basis of their electronic absorption spectra, since no definite difference could be expected between the spectra of the two *cis*(a) isomers because of the similarity in the ligand field strengths of NH$_3$ and ethylenediamine. Bailar and Peppard[2] distinguished the two *cis*(Cl) isomers of [CoCl$_2$(NH$_3$)$_2$(en)]$^+$ on the basis of their preparative method. Their assignment was confirmed later by optical resolution of the *cis,cis* isomer by Hawkins *et al.*[3] It is of interest to find a reliable spectroscopic method for differentiating the two *cis*(a) isomers of [Coa$_2$(NH$_3$)$_2$(en)] type complexes.

Raman spectra in the skeletal vibration region have been applied successfully to the differentiation of geometrical isomers of cobalt(III) complexes.[1,4,5] The Raman criteria established for the cobalt(III) complexes are expected to be profitably applied to the determination of the geometry of other metal analogs, whereas NMR method, although widely used in the stereochemistry of cobalt(III) complexes, would incur some difficulties in application to paramagnetic complexes such as chromium(III) complexes. In this paper, we report the preparation of three geometrical isomers of [Co(NO$_2$)$_2$(NH$_3$)$_2$(en)]$^+$ complex for the first time and the Raman method for differentiation between the two *cis*(a) isomers of [Coa$_2$(NH$_3$)$_2$(en)] type complexes.

Experimental

Three Geometrical Isomers of [Co(NO$_2$)$_2$(NH$_3$)$_2$(en)]ClO$_4$.

Method I: To a green solution of 0.9 g (3.5 mmol) of *trans*-(Cl)-[CoCl$_2$(NH$_3$)$_2$(en)]Cl[2] in 20 cm^3 of water containing a few drops of glacial acetic acid was added a solution of 0.9 g (13 mmol) of NaNO$_2$ in 10 cm^3 of water. After being stirred for 12 h, the color of the solution changed to yellowish brown. The solution was diluted to 2 dm^3 with water and poured onto a cation-exchange column (SP-Sephadex, C-25, Na$^+$ form; 3×50 cm). By eluting with 0.03 M NaClO$_4$ (1 M=1 mol dm^{-3}), two colored bands, both yellowish brown, descended. Each eluate was concentrated to a small volume in a rotary evaporator and ethanol was added to induce a precipitation of a yellowish brown powder. This powder was recrystallized from a small amount of warm water by adding ethanol. From the electronic absorption and Raman spectra the complex which was obtained from the first eluate was identified to be the *trans*(NO$_2$) isomer and that from the second eluate the *cis,cis* isomer. Yield: 0.3 g for the *trans*(NO$_2$) isomer and 0.2 g for the *cis,cis* one. Absorp. max. σ/10^3 cm^{-1} (log ε/mol^{-1} dm^3 cm^{-1}): 22.8 (2.28), 29.1 (3.54), 39.8 (4.22) for the *trans*(NO$_2$) isomer; 22.8 (2.24), 31.2 (3.65), 42.2 (4.30) for the *cis,cis* isomer. Found: C, 6.96; H, 4.16; N, 24.23% for the *trans*(NO$_2$) isomer. C, 6.96; H, 4.05; N, 24.42% for the *cis,cis* isomer. Calcd for [Co(NO$_2$)$_2$(NH$_3$)$_2$(en)]ClO$_4$=CoC$_2$ClH$_{14}$N$_6$O$_8$: C, 6.97; H, 4.10; N, 24.39%.

Method II: The *cis,cis* isomer was also prepared in a high yield by this method. To a solution of 3 g (10 mmol) of *cis*-[Co(CO$_3$)(NH$_3$)$_2$(en)]ClO$_4$[2] in 100 cm^3 of 3% HClO$_4$ was added 6.0 g (100 mmol) of NaNO$_2$. The mixture was kept at 60 °C for half an hour, then cooled in a refrigerator. The yellowish brown crystals which deposited were collected by filtration and recrystallized from a small amount of warm water. Yield: 2.0 g.

Method III: The remaining isomer, *trans*(NH$_3$), was obtained by this method. To a bluish violet solution of 1.5 g (6 mmol) of *trans*(NH$_3$)-[CoCl$_2$(NH$_3$)$_2$(en)]Cl[2] in 20 cm^3 of water was added a solution of 1.5 g (22 mmol) of NaNO$_2$ in 10 cm^3 of water. The mixture was stirred at 25 °C for 12 h, whereupon the color of the solution turned to yellowish brown. Addition of a large amount of solid NaClO$_4$ to this solution induced the precipitation of a yellowish brown solid. This solid was recrystallized from a small amount of warm water. Yield: 1.2 g. Absorp. max. σ/10^3 cm^{-1} (log ε/mol^{-1} dm^3 cm^{-1}): 23.0 (2.22), 31.0 (3.71), 41.9 (4.49). Found: C, 6.93; H, 4.09; N, 24.42%. Calcd for [Co(NO$_2$)$_2$(NH$_3$)$_2$(en)]-ClO$_4$=CoC$_2$ClH$_{14}$N$_6$O$_8$: C, 6.97; H, 4.10; N, 24.39%.

trans(*CN*)- *and* cis,cis-[*Co(CN)$_2$(NH$_3$)$_2$(en)*]*ClO$_4$*.

These had been obtained by Maki and Sakuraba.[6] The complexes were obtained more conveniently, however, by

the following methods. Powdered *trans*(Cl)-[$CoCl_2(NH_3)_2$(en)]Cl (4 g; 15 mmol) was added to a solution of KCN (2 g; 30 mmol) in 300 cm^3 of dimethyl sulfoxide (DMSO). After being stirred continuously at 80 °C for 3 h, the reaction mixture consisted of an orange yellow solution and a small amount of orange precipitate. The mixture was diluted to 2 dm^3 with water and poured onto a cation-exchanger column (SP-Sephadex, C-25, Na^+ form; 3×60 cm). By eluting with 0.03 M $NaClO_4$, two colored bands, orange and yellow, descended in that order. Each eluate was concentrated to dryness by a rotary evaporator and the residue washed with ethanol to remove the contaminated $NaClO_4$. The crude compound thus obtained was recrystallized from warm water. The electronic absorption spectra of the orange and yellow isomers coincide respectively with those of *trans*(CN)- and *cis*(CN)-[$Co(CN)_2(NH_3)_2$(en)]$^+$ reported by Maki and Sakuraba.[6] The *cis*(CN) isomer was identified to be *cis,cis* from the Raman spectrum. Yield: 1.7 g for the *trans*(CN) isomer and 0.2 g for the *cis,cis* one.

The *cis,cis* isomer was also prepared in a high yield by the following method.

To a solution of *trans*(Cl)-[$CoCl_2(NH_3)_2$(en)]Cl (2.6 g; 10 mmol) in 60 cm^3 of DMSO was added a solution of $AgNO_3$ (1.7 g; 10 mmol) in a small amount of DMSO. The silver chloride deposited was filtered off. To the filtrate was added 5.4 g (40 mmol) of AgCN and the resulting suspension was stirred continuously at 80 °C for 5 h. During this time, the color of the liquid phase changed from bluish violet to brownish yellow. To the suspension 1 dm^3 of water was added and the insoluble product filtered off. The filtrate was chromatographed in a similar manner as above. In this case, only one band, *cis,cis*, descended. Yield: 1.1 g. Absorp. max. $\sigma/10^3$ cm^{-1} (log ε/mol^{-1} dm^3 cm^{-1}): 21.5 sh (1.48), 24.2 (1.76), 31.9 (1.88), 47.4 (4.61) for the *trans*(CN) isomer; 23.5 sh (1.84), 25.1 (1.87), 32.2 (1.94), 47.7 (4.32) for the *cis,cis* one. Found: C, 15.72; H, 4.64; N, 27.63% for the *trans*(CN) isomer. C, 15.72; H, 4.67; N, 27.57% for the *cis,cis* one. Calcd for [$Co(CN)_2(NH_3)_2$(en)]ClO_4=$CoC_4ClH_{14}N_6O_4$: C, 15.77; H, 4.63; N, 27.59%.

Attempts to obtain the *trans*(NH_3) isomer from *trans*-(NH_3)-[$CoCl_2(NH_3)_2$(en)]Cl were not successful; the reaction with AgCN yielded only the *cis,cis* isomer and with KCN only the *trans*(CN) and *cis,cis* ones.

Optical Resolution of cis,cis *Isomers of [Coa$_2$(NH_3)$_2$(en)]$^+$ (a=NO_2^- and CN^-).* $(+)^{CD}_{450}$-cis, cis-*[Co(NO_2)$_2$(NH_3)$_2$(en)]Cl*: A solution of racemic *cis,cis*-[$Co(NO_2)_2(NH_3)_2$(en)]ClO_4 was passed through an anion-exchange resin column (Dowex 1×8, Cl^- form) and the eluate was evaporated to dryness. The crude product was recrystallized from a minimun amount of hot water and dried in air. Found: C, 8.27; H, 5.01; N, 29.76%. Calcd for [$Co(NO_2)_2(NH_3)_2$(en)]Cl= $CoC_2ClH_{14}N_6O_4$: C, 8.56; H, 5.01; N, 29.96%.

The chloride of the *cis,cis* isomer (0.5 g; 1.8 mmol) was dissolved in 10 cm^3 of water and to the solution was added solid $(+)_{546}$-K[Co(edta)]·$2H_2O$[7] (0.7 g; 1.8 mmol) at 40 °C with stirring. The resulting reddish violet solution was evaporated to half the initial volume below 20 °C and kept standing in a refrigerator overnight. The reddish violet crystals which deposited were collected by filtration and recrystallized from a small amount of warm water (at *ca.* 40 °C) to give crystals of the less-soluble diastereomer with a needle-like shape. Found: C, 23.54; H, 4.62; N, 18.36%. Calcd for [$Co(NO_2)_2(NH_3)_2$(en)][Co(edta)]·H_2O=$Co_2C_{12}H_{28}N_8O_{13}$: C, 23.61; H, 4.63; N, 18.36%.

The less-soluble diastereomer was converted into the chloride salt by passing a solution through an anion-exchange resin (Dowex 1×8, Cl^- form) and evaporating the eluate to dryness. CD $\sigma_{ext}/10^3$ cm^{-1} ($\Delta\varepsilon$/mol^{-1} dm^3 cm^{-1}): 21.6 (+0.34), 24.4 (−0.18), 29.7 (−1.49), 35 sh (+1.80), 38.6 (+2.56), 43.2 (−14.6). Found: C, 8.30; H, 5.10; N, 29.76%. Calcd for [$Co(NO_2)_2(NH_3)_2$(en)]Cl=$CoC_2ClH_{14}N_6O_4$: C, 8.56; H, 5.01; N, 29.96%.

$(+)^{CD}_{450}$-cis,cis-[Co(CN)$_2$(NH_3)$_2$(en)]ClO_4: A solution of racemic *cis,cis*-[$Co(CN)_2(NH_3)_2$(en)]ClO_4 (0.46 g; 1.5 mmol) in 20 cm^3 of warm water was passed through a Cl^- form ion-exchange resin. To the filtrate was added $(-)_{546}$-Ag[Co(edta)][8] (0.69 g; 1.5 mmol) with stirring and the silver chloride deposited was filtered off. The filtrate was evaporated to dryness and a small amount of methanol was added to the residue. The crude brownish violet powder of the less-soluble diastereomer was recrystallized from warm water; the dark reddish violet crystals which deposited were recrystallized from a minimum amount of warm water. Found: C, 27.72; H, 5.31; N, 18.35%. Calcd for [$Co(CN)_2$-(NH_3)$_2$(en)][Co(edta)]·$3H_2O$=$Co_2C_{14}H_{32}N_8O_{11}$: C, 27.73; H, 5.33; N, 18.48%.

The less-soluble diastereomer was converted to the perchlorate salt by adding $NaClO_4$ to a chloride solution obtained by means of a chromatographic method. CD $\sigma_{ext}/10^3$ cm^{-1} ($\Delta\varepsilon$/mol^{-1} dm^3 cm^{-1}): 20.5 (−0.01), 23.2 (+0.22), 26.6 (−0.22), 32.0 (+0.06), 35.5 sh (−0.01), 41.1 (−1.7), 45.4 (+9.7). Found: C, 15.62; H, 4.64; N, 26.98%. Calcd for [$Co(CN)_2(NH_3)_2$(en)]ClO_4=$CoC_4ClH_{14}N_6O_4$: 15.77; H, 4.64; N, 27.59%.

Measurements. Electronic absorption spectra were recorded on a Hitachi 220 spectrophotometer. Raman spectra were recorded in water on a JASCO R-800 Laser Raman spectrophotometer, using a He-Ne laser (632.8 nm; 50 mW) as an excitation source. A spinning sample cell was employed to avoid decomposition of the sample induced by laser illumination. Polarization measurements were carried out by employing a half-wave plate for incident light and a polarization analyzer for scattered light. Infrared spectra were recorded on a JASCO IRA-3 as Nujol mulls. Circular dichroism (CD) spectra were recorded on a JASCO MOE-1 spectropolarimeter in aqueous solution.

Results and Discussion

Electronic Absorption Spectra. Figure 1 shows the configurations of geometrical isomers of [$Coa_2(NH_3)_2$(en)] type complex (a denotes a monodentate ligand). The *trans*(a) and *cis*(a) (*trans*(NH_3) or

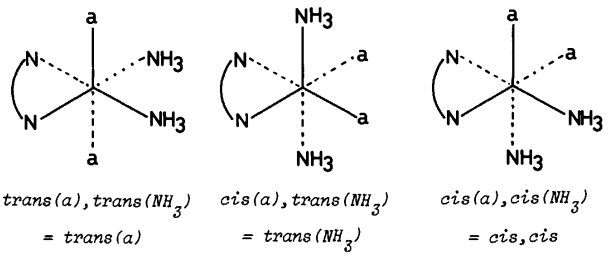

Fig. 1. Three geometrical isomers of [$Coa_2(NH_3)_2$(en)] type complex (a denotes a monodentate ligand).

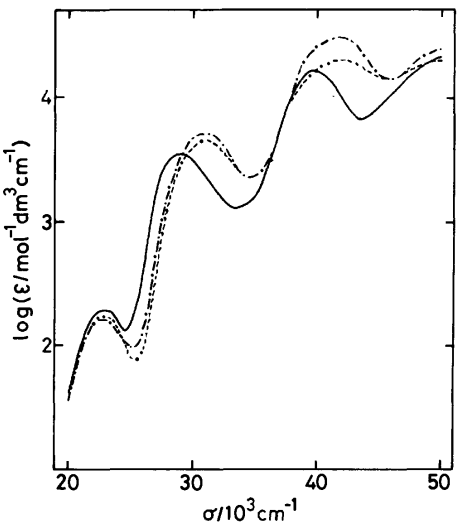

Fig. 2. Electronic absorption spectra of the three geometrical isomers of $[Co(NO_2)_2(NH_3)_2(en)]^+$ (——); *trans*(NO_2), (----); *trans*(NH_3), and (– – –); *cis,cis*.

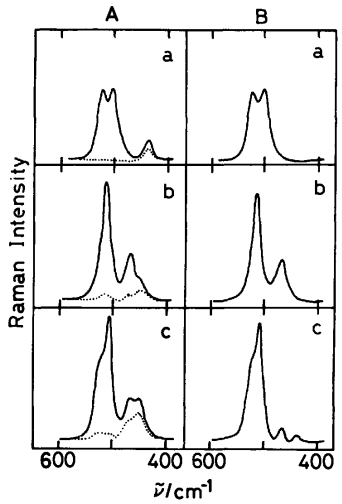

Fig. 3. Polarized Raman spectra (A) [(——), ∥; (----), ⊥] and difference Raman spectra (B) [$I_\parallel - I_\perp \times 4/3$] of the three isomers of $[Co(NO_2)_2(NH_3)_2(en)]^+$: a; *trans*($NO_2$), b; *trans*($NH_3$), and c; *cis,cis*.

cis,cis) isomers can be differentiated on the basis of their electronic absorption spectra in a similar manner as for the corresponding isomers of $[Coa_2(en)_2]$ or $[Coa_2(NH_3)_4]$ type complexes. Figure 2 shows the electronic absorption spectra of the three isomers of $[Co(NO_2)_2(NH_3)_2(en)]^+$. It has been shown for dinitro cobalt(III) complexes that the "nitro-specific" band of the *trans* isomer is always more bathochromic than the band of the *cis* isomer.[9] Therefore, the isomer which exhibits the "nitro-specific" band in the lower energy region (29100 cm^{-1}) than those of the other two isomers (31000 and 31200 cm^{-1}) can be unambiguously assigned to the *trans*(NO_2) isomer. It is difficult to differentiate the two *cis*(NO_2) isomers by their electronic absorption spectra, since their absorption bands are similar.

Maki and Sakuraba[6] obtained the two (orange and yellow) of the three geometrical isomers of $[Co(CN)_2(NH_3)_2(en)]^+$ complex. By comparing their absorption curves with those of the *trans* and *cis* isomers of $[Co(CN)_2(en)_2]^+$ and $[Co(CN)_2(NH_3)_4]^+$ complexes in the first d-d absorption band region, the orange isomer was assigned to the *trans*(CN) one and the yellow *cis*(CN). However, they did not mentioned further assignment for the *cis*(CN) isomer (*trans*(NH_3) or *cis,cis*). Also in this case, it is difficult to determine which *cis*(CN) isomer was obtained only from its absorption spectrum.

Raman Spectra. We examined what difference exists between the Raman spectra of the two *cis*(NO_2) isomers of $[Co(NO_2)_2(NH_3)_2(en)]^+$. The most striking difference was found in the polarizabilities of the Raman bands due to Co-N(NH_3 and en) stretching vibrations. Figure 3-A shows the polarized Raman spectra of the three isomers of $[Co(NO_2)_2(NH_3)_2(en)]^+$ in the 400—600 cm^{-1} region, where Co-N(NH_3 and en) stretching vibrations are expected.[4] If it is assumed that the molecular symmetry of the *trans*(a) isomer of $[Coa_2(NH_3)_2(en)]$ type complex is C_{2v}, that of the *trans*(NH_3) is C_{2v}, and that of the *cis,cis* is C_1, the Co-N(NH_3 and en) stretching vibrations are reduced to ($2A_1+2B_1$), ($2A_1+B_1+B_2$), and (4A), respectively. Although the apparent difference can be recognized in the number of the observed Raman bands between the two *cis*(NO_2) isomers (Fig. 3-A-b and -c), no explicit differences could be expected in the number of Raman bands, because of all the modes being Raman active. However, some differences would be expected in the polarizabilities of the Raman bands. Thus, a Raman band due to a totally symmetric vibration (A_1 or A mode) should be observed as a polarized band ($I_\perp/I_\parallel<3/4$), whereas that due to a non-totally symmetric vibration (B_1 or B_2 mode) as a depolarized band ($I_\perp/I_\parallel=3/4$). Therefore, the *trans*(a) and *trans*-(NH_3) isomers should have one or more depolarized bands in their Raman spectra, while all the Raman bands should be observed as polarized bands for the *cis,cis* isomer. Unfortunately, the accurate depolarization ratio, $\rho=I_\perp/I_\parallel$, can not be obtained directly from the Raman spectra of the three isomers of $[Co(NO_2)_2(NH_3)_2(en)]^+$, since the observed bands are partially overlapped (Fig. 3-A). Therefore, we calculated the difference spectra ($I_\parallel - I_\perp \times 4/3$) as shown in Fig. 3-B. The depolarized band would vanish completely in the difference spectra since $I_\perp=I_\parallel \times 3/4$. On the other hand, the polarized band would leave some trace in the difference spectra. A weak band at *ca.* 450 cm^{-1} completely disappeared in each of the difference spectra of the *trans*(NO_2) (Fig. 3-a) and one of the *cis*(NO_2) isomer (Fig. 3-b), *i.e.*, these bands can be regarded as depolarized. On the other hand, all the bands leave some traces in the difference

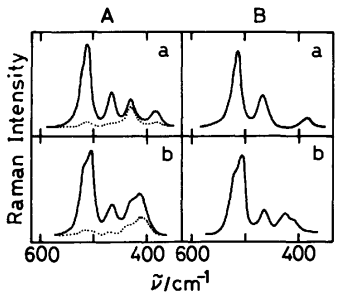

Fig. 4. Polarized Raman spectra (A) [(——), ∥; (----), ⊥] and difference Raman spectra (B) [$I_{\parallel} - I_{\perp} \times 4/3$] of the two isomers of $[Co(CN)_2(NH_3)_2(en)]^+$: a; *trans*(CN) and b; *cis,cis*.

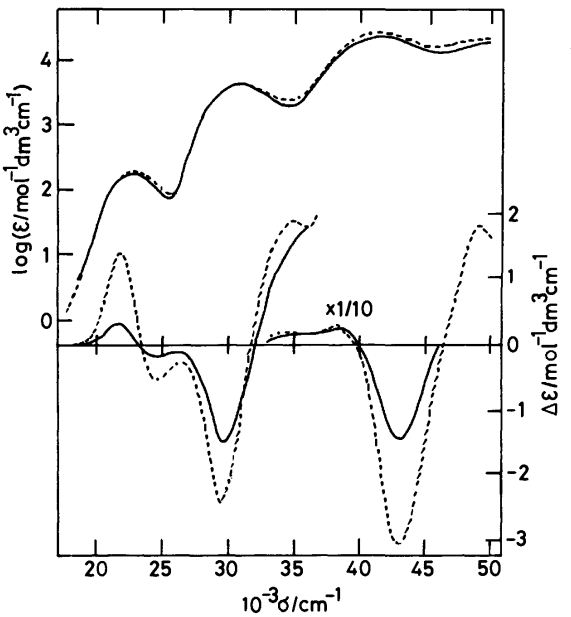

Fig. 5. Electronic absorption and CD spectra of $(+)^{CD}_{480}$-*cis-cis*-$[Co(NO_2)_2(NH_3)_2(en)]Cl$ (——) and *Λ*-$[Co(NO_2)_2(en)_2]Cl$ (----).

spectrum of another *cis*(NO_2) isomer (Fig. 3-c), *i.e.*, all can be regarded as polarized. It is concluded, therefore, that the *cis*(NO_2) isomer which has a depolarized band in its Raman spectrum has a *trans*(NH_3) configuration and that another *cis*(NO_2) isomer whose Raman bands are all polarized has a *cis,cis* configuration. The other Raman active depolarized bands of the *trans*(NO_2) and *trans*(NH_3) isomers would be very weak, and hidden by the strong polarized bands. An infrared band was observed at 491 cm^{-1} for the *trans*(NO_2) isomer and also at 496 cm^{-1} for the *trans*(NH_3) isomer, they being counterparts of the hidden Raman bands.

Figure 4 shows the polarized Raman spectra (A) and the difference spectra (B) of the two isomers of $[Co(CN)_2(NH_3)_2(en)]^+$. The bands around 400 cm^{-1} can be assignable to the Co-CN stretching vibrations. By a similar argument as above, it is concluded that the present *cis*(CN) isomer has the *cis,cis* configura-

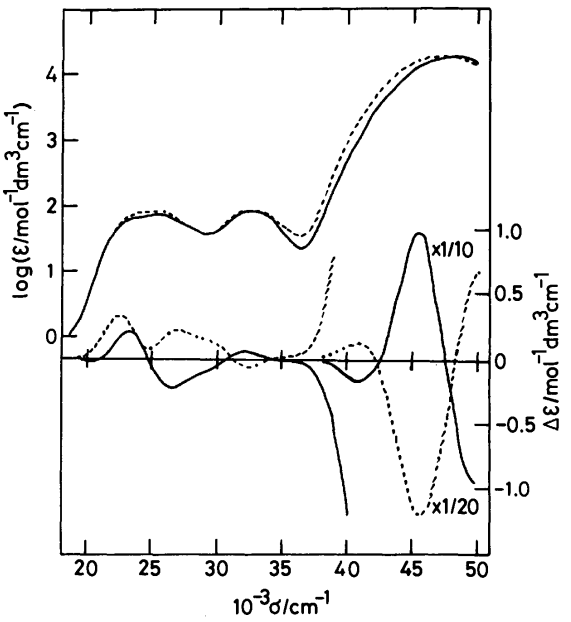

Fig. 6. Electronic absorption and CD spectra of $(+)^{CD}_{480}$-*cis,cis*-$[Co(CN)_2(NH_3)_2(en)]ClO_4$ (——) and *Λ*-$[Co(CN)_2(en)_2]Cl$ (----).

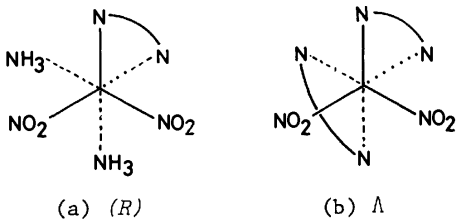

Fig. 7. Absolute configurations of $(+)^{CD}_{480}$-*cis,cis*-$[Co(NO_2)_2(NH_3)_2(en)]^+$ (a) and *Λ*-$[Co(NO_2)_2(en)_2]^+$ (b).

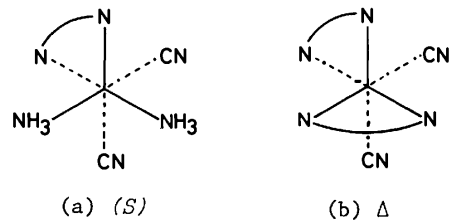

Fig. 8. Absolute configurations of $(+)^{CD}_{480}$-*cis,cis*-$[Co(CN)_2(NH_3)_2(en)]^+$ (a) and *Δ*-$[Co(CN)_2(en)_2]^+$ (b).

tion, since all the Raman bands are polarized.

Optical Resolution. The differentiation among the geometrical isomers of $[Coa_2(NH_3)_2(en)]$ type complexes (a=NO_2^- and CN^-) based upon the Raman spectra was confirmed by the optical resolution of the *cis,cis* isomers. Figure 5 shows the absorption and CD spectra of $(+)^{CD}_{480}$-*cis,cis*-$[Co(NO_2)_2(NH_3)_2(en)]^+$ complex which was obtained from the less-soluble diastereomer with *Λ*$(+)_{546}$-[Co(edta)]$^-$ and Fig. 6 those of $(+)^{CD}_{480}$-*cis,cis*-$[Co(CN)_2(NH_3)_2(en)]^+$ which was obtained from the less-soluble diastereomer with *Λ*$(-)_{546}$-[Co(edta)]$^-$. These figures also show the absorption

and CD spectra of Λ-$[Co(NO_2)_2(en)_2]^+$ and Λ-$[Co(CN)_2(en)_2]^+$, respectively, for comparison. The absolute configurations of these bis(ethylenediamine) complexes have been determined by previous CD[10] and X-ray[11,12] studies. The CD spectral pattern of $(+)^{CD}_{450}$-$[Co(NO_2)_2(NH_3)_2(en)]^+$ is similar to that of Λ-$[Co(NO_2)_2(en)_2]^+$ not only in the visible but also in the ultraviolet region, though the CD intensity of the former complex is about half that of the latter. Therefore, the absolute configuration of $(+)^{CD}_{450}$-$[Co(NO_2)_2(NH_3)_2(en)]^+$ corresponds to the Λ configuration of bis(chelate) complexes, being assigned to the (*R*) configuration by Cahn, Ingold, and Prelog's Nomenclature[13] (Fig. 7). Since the $(+)^{CD}_{450}$-$[Co(CN)_2(NH_3)_2(en)]^+$ isomer shows a reversed CD pattern with respect to Λ-$[Co(CN)_2(en)_2]^+$ except for the lowest energy region, the absolute configuration corresponds to the Δ configuration as is shown in Fig. 8 and can be assigned to the (*S*) configuration.

References

1) Part IV of this series: K. Kanamori, H. Ichinose, and K. Kawai, *Bull. Chem. Soc. Jpn.*, **55**, 1315 (1982).

2) J. C. Bailar and D. F. Peppard, *J. Am. Chem. Soc.*, **62**, 105 (1940).

3) C. J. Hawkins, J. A. Stark, and C. L. Wong, *Aust. J. Chem.*, **25**, 273 (1972).

4) K. Kanamori and K. Kawai, *Bull. Chem. Soc. Jpn.*, **53**, 2520 (1980); K. Kanamori, T. Morikawa, and K. Kawai, *Bull. Chem. Soc. Jpn.*, **53**, 2787 (1980); K. Kanamori and K. Kawai, *Bull. Chem. Soc. Jpn.*, **55**, 764 (1982).

5) T. F. Maruyama, K. Okamoto, J. Hidaka, and H. Einaga, *Bull. Chem. Soc. Jpn.*, **56**, 2610 (1983).

6) N. Maki and S. Sakuraba, *Bull. Chem. Soc. Jpn.*, **42**, 1908 (1969).

7) F. P. Dwyer and F. L. Garvan, *Inorg. Synth.*, **6**, 192 (1960).

8) W. T. Jordan, B. J. Brennan, L. R. Froebe, and B. E. Douglas, *Inorg. Chem.*, **12**, 1827 (1973).

9) Y. Shimura, *J. Am. Chem. Soc.*, **73**, 5079 (1951); K. Akamatsu, J. Hidaka, and Y. Shimura, *Bull. Chem. Soc. Jpn.*, **50**, 533 (1977).

10) A. J. McCaffery, S. F. Mason, and B. J. Norman, *J. Chem. Soc.*, **1965**, 5094.

11) K. Matsumoto and H. Kuroya, *Bull. Chem. Soc. Jpn.*, **45**, 1755 (1972).

12) K. Matsumoto, S. Ooi, and H. Kuroya, *Bull. Chem. Soc. Jpn.*, **44**, 2721 (1971).

13) R. S. Cahn, C. K. Ingold, and V. Prelog, *Angew. Chem. Int. Ed. Engl.*, **5**, 385 (1966).

Phase Equilibria in the Ln_2O_3-V_2O_3-V_2O_5 (Ln=Pr, Tb, and Y) Systems at 1200 °C

Kenzo KITAYAMA* and Takashi KATSURA
Department of Chemistry, Faculty of Science, Tokyo Institute of Technology, Ookayama, Meguro-ku, Tokyo 152
(Received July 27, 1984)

The phase equilibria in the systems, Pr_2O_3-V_2O_3-V_2O_5, Tb_2O_3-V_2O_3-V_2O_5, and Y_2O_3-V_2O_3-V_2O_5, were established at 1200 °C by changing the oxygen partial pressure from −1.20 (in the CO_2) to 7.50 in $-\log(P_{O_2}/\text{Pa})$ for Pr_2O_3 and Tb_2O_3 systems, and from −4.32 (in the air) to 7.50 in $-\log(P_{O_2}/\text{Pa})$ for Y_2O_3 system. In the first system $0.81Pr_2O_3 \cdot 0.19V_2O_5$ (A) and $3Pr_2O_3 \cdot V_2O_5$ (B), in the second $0.81Tb_2O_3 \cdot 0.19V_2O_5$ (A′), and in the last one $4Y_2O_3 \cdot V_2O_5$ (A″) were stable in addition to Ln_2O_3, $LnVO_4$, $LnVO_3$, V_nO_{2n-1} (n= 2—7, and Ln means Pr, Tb, and Y), and VO_2 under the present experimental conditions. On the basis of the established phase diagrams, the standard Gibbs energies ($\Delta G°$) of reactions appeared in the systems were calculated. Compounds A, B, $PrVO_3$, A′, A″, and $LnVO_4$ have nonstoichiometric compositions. $\Delta G°$ values for the reactions and crystallographic values of the compounds were represented as a function of the ionic radius of lanthanoid (including Y) elements.

Phase equilibria in the Ln_2O_3-V_2O_3-V_2O_5 systems (Ln=Sm, Lu, Er, Gd, La, Nd, Tm, Eu, Yb, Dy, and Ho) at 1200 °C have been established[1-9] by changing the oxygen partial pressure from −4.32 to 7.50 or 9.00 in terms of $-\log(P_{O_2}/\text{Pa})$. The standard Gibbs energy of the reactions appeared in the established systems and the crystallographic data of the ternary compounds and the activities of the components in the solid solutions were also successfully obtained.

In the present study, Pr_2O_3, Tb_2O_3, and Y_2O_3 were chosen as Ln_2O_3. It was well known that Pr_2O_3 and Tb_2O_3 were unstable in air. They change compositions to Pr_6O_{11} and Tb_4O_7 or other compositions depending upon the oxygen partial pressure and the temperature.[10-14] Recently, the oxygen partial pressure ranges in which Pr_2O_3 and Tb_2O_3 are stable have been determined at 1000°, 1100°, and 1200 °C by Sugihara.[15] According to his results, Pr_2O_3 is stable in the log P_{O_2} range from 4.30 to −11.00 and Tb_2O_3 in the log P_{O_2} range from 3.25 to −11.00 at 1200 °C. Thus the oxygen partial-pressure range in the present experiments was confined to pressures lower than $10^{1.20}$ Pa (in the CO_2) for both systems. On the other hand, Y_2O_3 is stable in air and, thus, the experimental atmosphere was extended to an air atmosphere from a CO_2 atmosphere.

Livin[16] studied Y_2O_3-V_2O_5 in the temperature range from 650° to 1800 °C and found three compounds $4Y_2O_3 \cdot V_2O_5$, $5Y_2O_3 \cdot V_2O_5$, and YVO_4 with a melting point 1810±25 °C. He also pointed out that the Y_2O_3-YVO_4 subsystem is probably pseudo-binary because of oxygen losses from the 4:1 and 5:1 phases. Brusset *et al.*[17] studied three systems, Pr_2O_3-V_2O_5, Tb_2O_3-V_2O_5, and Y_2O_3-V_2O_5, in the temperature range from 600° to 1500 °C. $4Pr_2O_3 \cdot V_2O_5$, $6Pr_2O_3 \cdot V_2O_5$, $4Tb_2O_3 \cdot V_2O_3$, $5Tb_2O_3 \cdot V_2O_5$, $4Y_2O_3 \cdot V_2O_5$, and $5Y_2O_3 \cdot V_2O_5$ were found in addition to $LnVO_4$.

In the Pr_2O_3-V_2O_3, Tb_2O_3-V_2O_3, and Y_2O_3-V_2O_3[18] systems, $PrVO_3$, $TbVO_3$, and YVO_3 were well known, but these systems have not yet been completely studied, because V_2O_3 is unstable in the air. The crystallographic properties of these $LnVO_3$ have been investigated by McCarthy *et al.*[19] and Shin-ike *et al.*[20] and it has been confirmed that these compounds are orthorhombic.

The objectives of the present experiments were: (1) to establish the detailed phase equilibria in the systems at 1200 °C in order to confirm which compounds are stable under the present experimental conditions, (2) to calculate the standard Gibbs energies of reactions which appear in the established phase diagrams, and (3) to examine the fitness of the present data on the linear relationship between $\Delta G°$ values for the reaction, $LnVO_3 + 1/2\ O_2 = LnVO_4$ and the ionic radius of the lanthanoid elements, including Y.

Experimental

Pr_2O_3, Tb_2O_3, and Y_2O_3 (99.9%), V_2O_5 were used as starting materials. V_2O_5 was prepared by heating a guaranteed grade of NH_4VO_3 at 500 °C in air for about 24 h. Pr_2O_3 and Tb_2O_3 were prepared by reducing the commercial Pr_6O_{11} (99.9%) and Tb_4O_7 (99.9%) in an atmosphere of log (P_{O_2}/Pa)=−5.00 at 1200 °C for about 5 h. The hexagonal, light-green Pr_2O_3 and white Tb_2O_3 with C-form were confirmed by the powder X-ray diffraction method[21,22] and the compositions were determined to be $Pr_2O_{3.00}$ and $Tb_2O_{3.00}$ by EDTA titration. Desired Pr_2O_3/V_2O_5, Tb_2O_3/V_2O_5, and Y_2O_3/V_2O_5 mole ratios of samples were obtained by thoroughly mixing appropriate quantities in an agate mortar under ethyl alcohol. The mixtures, thus obtained, were treated by the same procedures in the previous paper.[1] The apparatus and procedures for controlling the oxygen partial pressure and keeping a constant temperature, the method of thermogravimetry, the criterion for an equilibrium establishment, and the method of the chemical analysis for the mixtures of Y_2O_3 and V_2O_5 were the same as those described in previous reports.[1,23-27] The vanadium content of the mixtures of V and Pr and of V and Tb was volumetrically determined after confirming that the consumption of the $KMnO_4$ standard solution by the coexisting Pr and Tb was within the experimental errors. Samples used for analysis

were prepared in the atmosphere, in which the stoichiometric V_2O_3, $LnVO_3$, and Ln_2O_3 were stable at 1200 °C. Pr_2O_3 and Tb_2O_3 contents were determined as a difference between the V_2O_3 weight and the total weight.

Results and Discussion

Phase Equilibria. Nine samples with Pr_2O_3/V_2O_5 mole ratios of 85/15, 8/2, 77/23, 7/3, 65/35, 1, 4/6, 3/7, and 15/85 were prepared to be used in the thermogravimetric experiments. In Figs. 1a and 1b the relationships between the oxygen partial pressure, $-\log(P_{O_2}/Pa)$, on the ordinate and the weight change, W_{O_2}/W_T, on the abscissa are shown as representative cases with four samples, 85/15, 77/23, 65/35, and 15/85. Here, W_{O_2} is the weight gain of the samples from the reference weight in an atmosphere of log P_{O_2}=−7.50, and W_T is the calculated total weight increase of samples which might be obtainable if V_2O_3 in the samples at the reference state would change to V_2O_5 in the higher oxygen pressures. The W_{O_2}/W_T ratio was usually shown in the range from 0.995 to 1.00. From Fig. 1 the oxygen partial pressure in equilibrium 6.75, 4.56, 4.14, and 4.02 in -log P_{O_2} were found in addition to those in the V_2O_3-VO_2 subsystem.[1]

The identification of the phases was performed with the quenched samples using a powder X-ray diffractometer with Cu $K\alpha$ radiation. The following phases and two-phase combinations are present under the present experimental conditions: $0.81Pr_2O_3 \cdot 0.19V_2O_5$(A), $3Pr_2O_3 \cdot V_2O_5$(B), Pr_2O_3(R), $PrVO_4$(T), $PrVO_3$(O), and VO_2(J) in addition to six compounds in the V_2O_3-VO_2 system,[1] and Pr_2O_3+A, A+B, B+$PrVO_4$, Pr_2O_3+$PrVO_3$, A+$PrVO_3$, B+$PrVO_3$, V_2O_3+$PrVO_3$, V_2O_3+$PrVO_4$, V_nO_{2n-1}(n=2—7)+$PrVO_4$, and VO_2+$PrVO_4$.

Based upon the above experimental results from the thermogravimetry and the identification of phases, a phase diagram of the system at 1200 °C was drawn and is shown in Fig. 2. As is apparent from Fig. 2, $6Pr_2O_3 \cdot V_2O_5$ is not stable but a new compound $3Pr_2O_3 \cdot V_2O_5$(Pr_3VO_7) was found. The compounds, $3La_2O_3 \cdot V_2O_5$ and $3Nd_2O_3 \cdot V_2O_5$ had been found in the La_2O_3-,[5] and Nd_2O_3-system[6] which have the same phase diagram pattern as that of the present system. $3Eu_2O_3 \cdot V_2O_5$ was known to be stable[28] although it could not be found in the Eu_2O_3-V_2O_3-V_2O_5 system[8] at 1200 °C. An X-ray powder pattern of Pr_3VO_7 is similar to those of La_3VO_7 and Nd_3VO_7. The crystal system of the compounds has not been determined yet. The spacing and relative intensities of the compound were determined and are shown in Table 1.

Compound A might be $4Pr_2O_3 \cdot V_2O_5$ reported by Brusset *et al.*[17] However, this compound does not have such a round mole ratio in the present case. This kind of compound has been found in La,[5] Nd,[6] Eu,[8] and Gd[4] systems, and will be found in a Tb system. It is interesting that these elements have a lower atomic

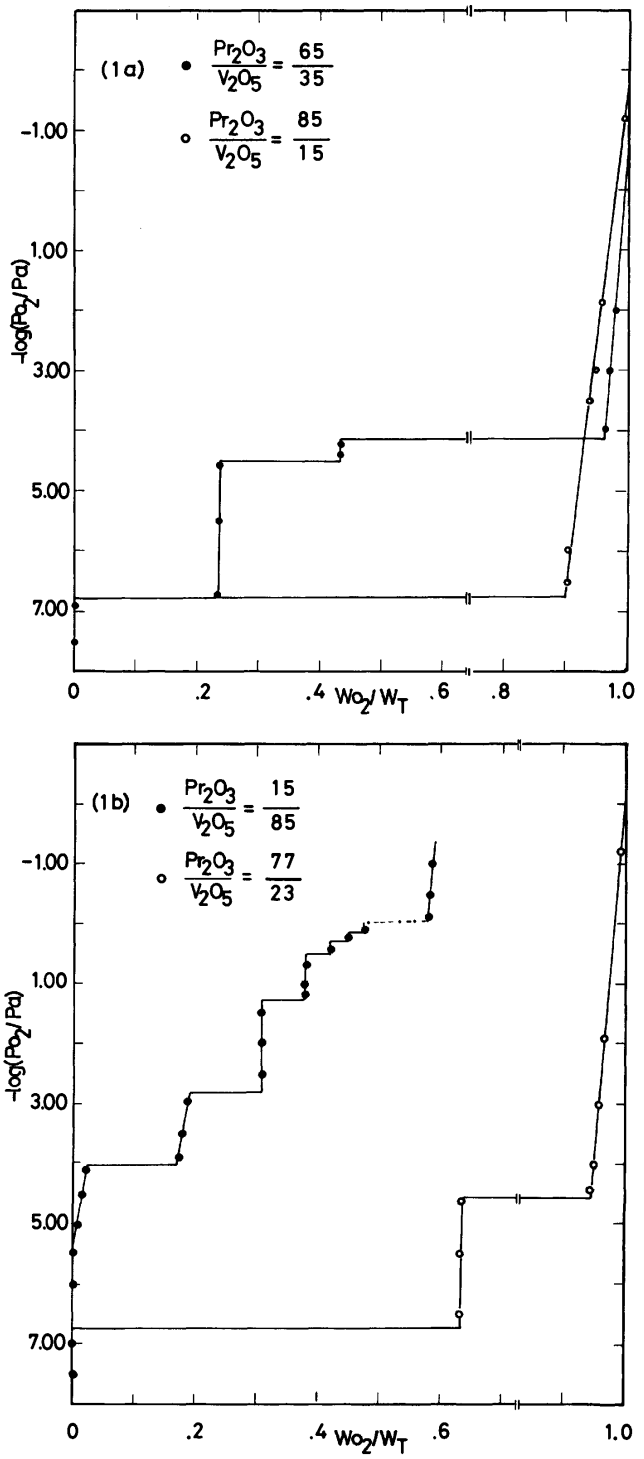

Fig. 1. The relationship between $-\log(P_{O_2}/Pa)$, and the composition, W_{O_2}/W_T, of samples. (1a) ●: Pr_2O_3/V_2O_5=65/35, ○: Pr_2O_3/V_2O_5=85/15, (1b) ●: Pr_2O_3/V_2O_5=15/85, ○: Pr_2O_3/V_2O_5=77/23.

number in the lanthanoid elements except for Sm in which system $5Sm_2O_3 \cdot V_2O_5$ was stable at 1200 °C. Since $4Ln_2O_3 \cdot V_2O_5$ was not detectable by our techniques, it might be nonstoichiometric toward the Ln_2O_3 side and mole ratio, Ln_2O_3/V_2O_5=81/19, might be rewritten to the ratio 4/1.

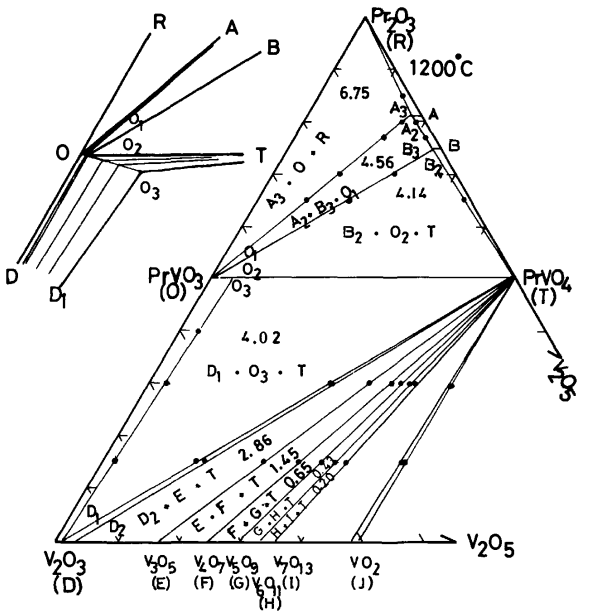

Fig. 2. Phase equilibria in the Pr_2O_3–V_2O_3–V_2O_5 system at 1200°C. Numerical values in the three-phase regions are the oxygen partial pressure in $-\log(P_{O_2}/Pa)$ in equilibrium. Symbols are the same as those in Table 3. A tentative, enlarged diagram near $PrVO_3$ was drawn on the left side with a little exaggeration.

Table 1. Spacings and relative intensities of $3Pr_2O_3 \cdot V_2O_5$ ($\log(P_{O_2}/Pa) = -4.30$, 47 h)

d/Å	I/I_o	d/Å	I/I_o
3.28	.83	2.161	.14
3.161	.74	1.983	.37
3.127	1.00	1.967	.29
3.056	.23	1.927	.26
3.014	.23	1.875	.23
2.933	.40	1.718	.17
2.808	.49	1.678	.14
2.719	.43		

Compounds A, Pr_3VO_7, $PrVO_4$, and $PrVO_3$ have nonstoichiometric compositions. The relationship between the composition and the oxygen partial pressure is represented by a linear equation, $N_O/N_A = a \log P_{O_2} + b$. Here, N_O is the mole fraction of the oxygen atom and N_A is the mole fraction of component A in the compound. The a and b values obtained from the results of the thermogravimetry are tabulated in Table 2. However, those values for $PrVO_4$ were not obtained because of the shortness of the solid-solution range.

Log $P_{O_2} = -4.14$ is the oxygen partial pressure in equilibrium with $Pr_3VO_7(B_2)$, $PrVO_4(T_1)$, and $PrVO_3(O_2)$, and on the other hand, log $P_{O_2} = -4.02$ is that in equilibrium with $V_2O_3(D_1)$, $PrVO_4(T_1)$, and $PrVO_3(O_3)$. This sort of the difference of the pattern was not found in the other systems reported by us. The

Table 2. a and b values for the solid solutions ($N_O/N_X = a \log P_{O_2} + b$)

X	a	b
$PrVO_3$	0.0122	0.069
$0.81Pr_2O_3 \cdot 0.19V_2O_5$	4.00×10^{-3}	−0.018
$3Pr_2O_3 \cdot V_2O_5$	9.80×10^{-3}	−0.0124
$TbVO_4$	4.71×10^{-3}	2.07×10^{-3}
$0.81Tb_2O_3 \cdot 0.19V_2O_5$	7.00×10^{-3}	−0.015
$Y_8V_2O_{17}$	0.619	−0.124

solid-solution ranges for $PrVO_3$ with a mole ratio $Pr_2O_3/V_2O_5 \geqq 1$ and that for $PrVO_3$ with a mole ratio $Pr_2O_3/V_2O_5 < 1$ were apparently different. This phenomenum may be understood considering that $PrVO_3$ had a solid solution range toward the V_2O_3 and V_2O_5 side. A tentative phase diagram near $PrVO_3$ is depicted with a little exaggeration in the left side of Fig. 2.

Seven samples with Tb_2O_3/V_2O_5 mole ratio of 84/16, 8/2, 72/28, 65/35, 1, 3/7, and 15/85 were prepared to be used in thermogravimetric experiments. In Figs. 3a and 3b, the relationships between W_{O_2}/W_T and log (P_{O_2}/Pa) of samples, 84/16, 8/2, 72/28, and 15/85, are shown as representatives. Two oxygen partial pressures, 5.27 and 3.95 in $-\log P_{O_2}$, in equilibrium with three solid phases were obtained in addition to those in the V_2O_3–VO_2 subsystem. A phase diagram was depicted with the results of the thermogravimetry and the identification of phases and is shown in Fig. 4. The following phases are present; Tb_2O_3(R′), $0.81Tb_2O_3 \cdot 0.19V_2O_5$(A′), $TbVO_3$ (O′), and $TbVO_4$(T′) in addition to the compounds in the V_2O_3–VO_2 system.[1] The $5Tb_2O_3 \cdot V_2O_5$ was not stable. Using the quench method, the following two-phase combinations were confirmed; Tb_2O_3+A′, A′+$TbVO_4$, A′+$TbVO_3$, Tb_2O_3+$TbVO_4$, V_2O_3+$TbVO_3$, $TbVO_4$+V_nO_{2n-1} (n=2—7), and $TbVO_4$+VO_2. The pattern of Fig. 4 is similar to those of Eu_2O_3[8] and Gd_2O_3[4] systems which had been established.

Compounds A′ and $TbVO_4$ have nonstoichiometric compositions, but $TbVO_3$, on the other hand, is stoichiometric. a and b values for A′ and $TbVO_4$ are shown in Table 2 together with values for other compounds.

It has been confirmed that Y_2O_3 is stable under the present experimental conditions.[25] Seven samples with Y_2O_3/V_2O_5 mole ratios of 85/15, 8/2, 75/25, 65/35, 1, 25/75, and 1/9 were used for the establishment of the phase diagram in the thermogravimetry. The variation of the weight with log P_{O_2} for four samples, 85/15, 65/35, 1, and 1/9, were shown in Fig. 5 as representative cases. Two oxygen partial pressure, 4.62 and 3.98 in -log P_{O_2}, in equilibrium with three solid phases were found in addition to six values in the V_2O_3–VO_2 system. Compounds Y_2O_3(R″), $4Y_2O_3 \cdot V_2O_5$(A″), YVO_4(T″), and YVO_3-

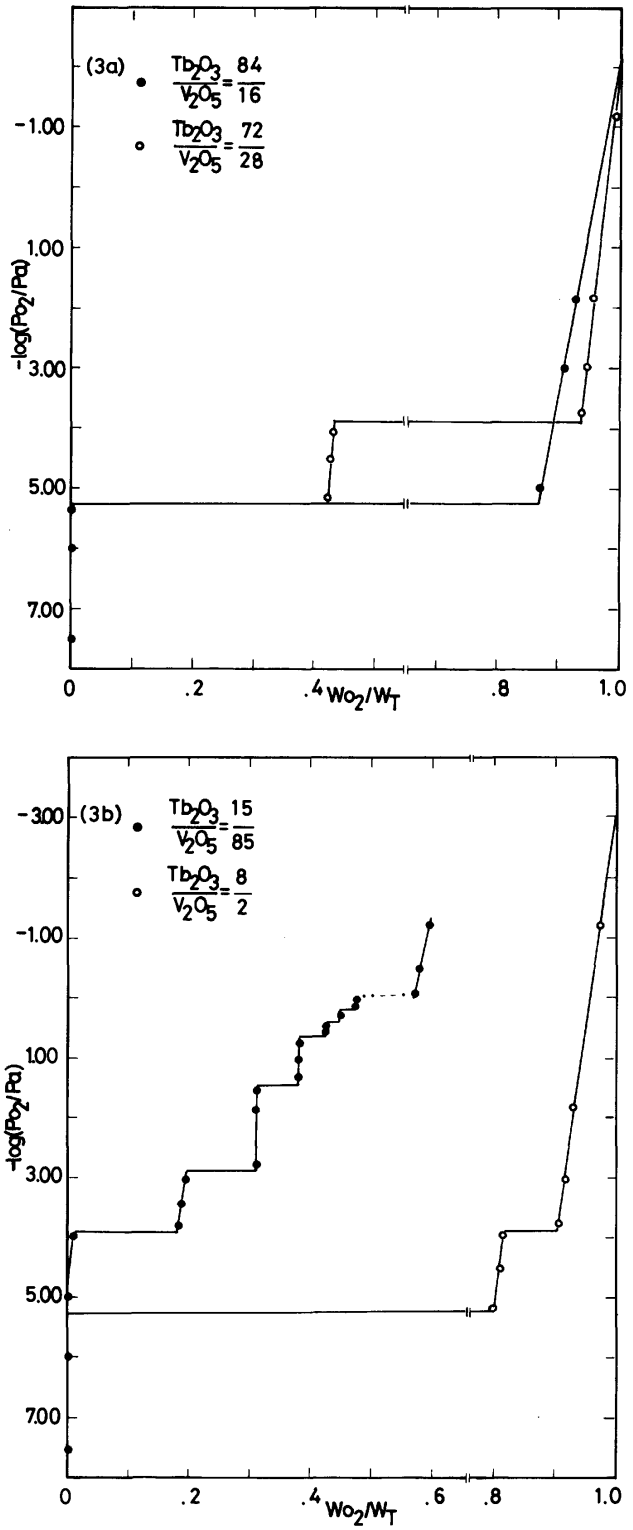

Fig. 3. The realtionship between $-\log(P_{O_2}/Pa)$ and the composition, W_{O_2}/W_T, of samples. (3a) ●: $Tb_2O_3/V_2O_5=84/16$, ○: $Tb_2O_3/V_2O_5=72/28$, (3b) ●: $Tb_2O_3/V_2O_5=15/85$, ○: $Tb_2O_3/V_2O_5=8/2$.

(O″) were confirmed to be stable by the quench method. Two-phase combinations are: Y_2O_3+A″, A″+YVO_4, A″+YVO_3, Y_2O_3+YVO_3, YVO_3+V_2O_3, YVO_4+V_{2n-1} (n=2—7), and VO_2+YVO_4. The $5Y_2O_3 \cdot V_2O_5$ was not found in the present system.

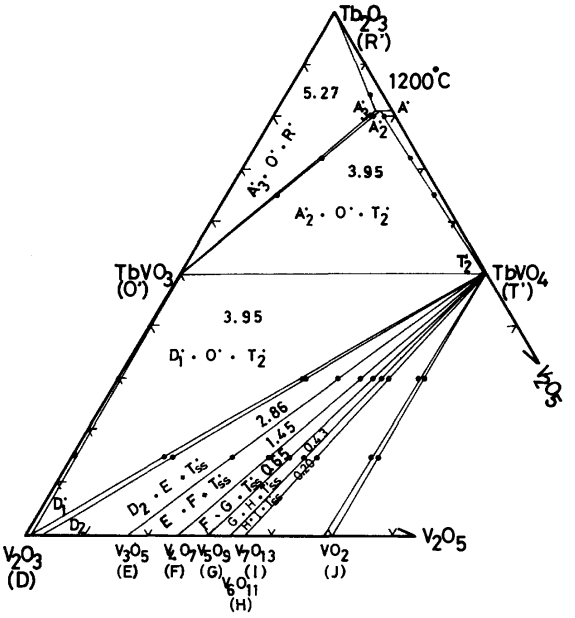

Fig. 4. Phase equilibria in the Tb_2O_3-V_2O_3-V_2O_5 system at 1200°C. Numerical values in the three-phase regions are the oxygen partial pressure in $-\log(P_{O_2}/Pa)$ in equilibrium. Symbols are the same as those in Table 3.

Compounds A″ and YVO_4 have nonstoichiometric compositions, and composition *vs.* $\log P_{O_2}$ for A″ is also tabulated in Table 2. The relation for YVO_4 could not determined because the non-stoichiomeric range is too narrow. Levin's report[16] regarding the pseudobinary of Y_2O_3-YVO_4 described above might imply the nonstoichiometry of $4Y_2O_3 \cdot V_2O_5$ and YVO_4.

Using the thermogravimetry results and the phase identification, a phase diagram at 1200 °C was drawn and is shown in Fig. 6. This diagram is a popular type and has one ternary compound, Ln_2O_3/V_2O_5= 4/1, in the Ln_2O_3-$LnVO_4$ subsystem. This diagram is similar to those of Dy_2O_3, Ho_2O_3, and Er_2O_3.

The activities of each components in a solid-solution were calculated using the Gibbs-Duhem equation and applying the relation between N_O/N_x and $\log P_{O_2}$ obtained above. The detailed method of the calculation has been discussed in a paper by Kimizuka and Katsura.[27] The results of the calculation are tabulated in Table 3 together with a composition of the compounds obtained by thermogravimetry, symbols of compounds, and the stability ranges of the compounds in terms of $\log P_{O_2}$. The activity of the $PrVO_3$ component at the composition O_2 was chosen as unity. The activity of the $PrVO_3$ component at the composition O_3 was not determined.

The lattice constants of the compounds A, A′, and A″ were successfully determined with the data of the assigment of $4Tm_2O_3 \cdot V_2O_5$[29] although errors were still large compared with the data of others. The values of the lattice constant of $LnVO_3$ and $LnVO_4$

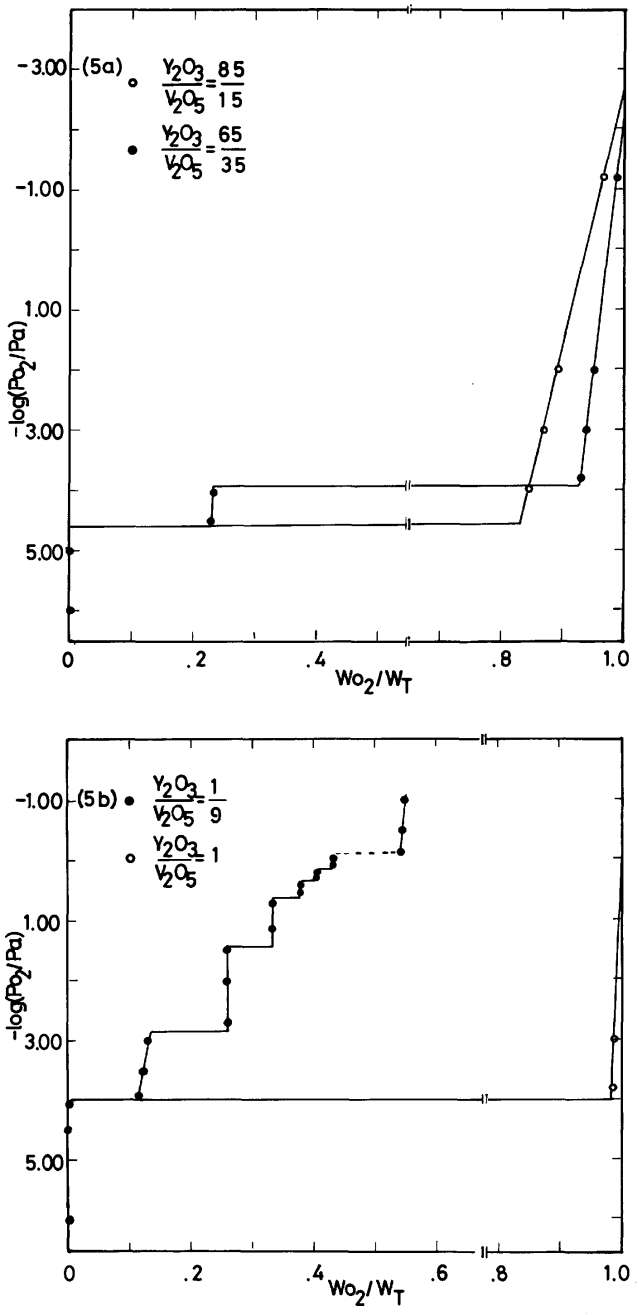

Fig. 5. The relationship between $-\log(P_{O_2}/Pa)$ and the composition, W_{O_2}/W_T, of samples. (5a) ○: $Y_2O_3/V_2O_5=85/15$, ●: $Y_2O_3/V_2O_5=65/35$, (5b) ●: $Y_2O_3/V_2O_5=1/9$, ○: $Y_2O_3/V_2O_5=1$.

were also determined by the powder X-ray diffractometer and tabulated in Table 4 together with previous values. The ternary compounds which were made in the different conditions of the oxygen partial pressure show no considerable difference in lattice constant. Instrumental errors were calibrated by measuring the diffraction angles of a standard specimen of silicon.

Calculation of the Standard Gibbs Energies of Reactions. On the basis of the established phase diagrams, the standard Gibbs energies of the reactions which are

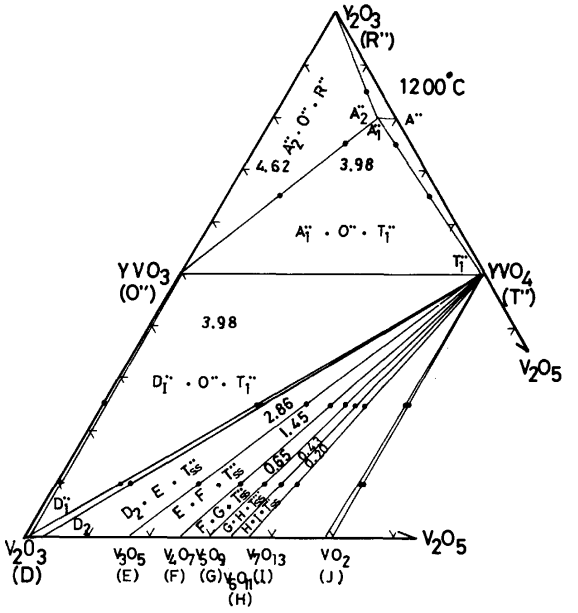

Fig. 6. Phase equilibria in the Y_2O_3-V_2O_3-V_2O_5 system at 1200 °C. Numerical values in the three-phase regions are the oxygen partial pressure in $-\log(P_{O_2}/Pa)$ in equilibrium. Symbols are the same as those in Table 3.

found in the phase diagrams can be calculated by the equation, $\Delta G°=-RT \ln K$, where the R is the gas constant, the T the absolute temperature, and the K the equilibrium constant of a reaction. Reactions and $\Delta G°$ values calculated are shown in Table 5 together with the oxygen partial pressures in equilibrium. The activities necessary for the calculation are shown in Table 3. The standard state can be arbitrarily chosen and, as described above, the activity of the $PrVO_3$ component at the composition O_2 was chosen as unity in this case. If the standard state are changed to that of the $PrVO_3$ component at the composition O_3, the $\Delta G°$ values for the reaction (3) is 127.2 kJ. The difference in $\Delta G°$ values is about 2 kJ.

The Relationship between $\Delta G°$ and Ionic Radius. In a previous report,[7] the relationship between the $\Delta G°$ value for the reaction, $LnVO_3+1/2\ O_2=LnVO_4$, and the ionic radius of lanthanoid elements in 8 coordination had been shown graphically. According to the result, the lanthanoid group is divided into two groups and the relation is linear within each of groups. After the report[7] was published, the values for Eu, Yb, Dy, and Ho systems have also been confirmed to fit well to the previous linear relation. The present values are plotted in Fig. 7 with open circles together with solid circles of the previous data. The present values for Pr and Tb fit well to the previous line, but the value for Y is widely different from what was anticipated. The reason for this difference could not be elucidated. Perhaps it might be one of the reasons why Y

has no property similar to lanthanoid contraction.

In the series of this study, a reaction, $3Ln_2O_3+2LnVO_3+O_2=4Ln_2O_3\cdot V_2O_5(Ln_8V_2O_{17})$, is often found although $0.8|Ln_2O_3\cdot 0.19V_2O_5$ is stable instead of $4Ln_2O_3\cdot V_2O_5$ for La, Nd, Pr, Eu, Gd, and Tb. As described above, the composition $0.8|Ln_2O_3\cdot 0.19V_2O_3$ is still unplausible and questionable, but the oxygen partial pressure in equilibrium with Ln_2O_3, $LnVO_3$, and $4Ln_2O_3\cdot V_2O_5$ or $0.8|Ln_2O_3\cdot 0.19V_2O_5$ are valid within experimental errors. Thus, the relation be-

Table 3. Compositions, symbols, stability ranges in the oxygen partial pressures, and activities of the solid solutions

Component	Composition	Symbol	$-\log(P_{O_2}/Pa)$	$-\log a_i$
$Pr_{1.62}V_{0.38}O_{3.38}$	$Pr_{1.62}V_{0.38}O_{3.33}$	A_3	6.75	0
	$Pr_{1.62}V_{0.38}O_{3.34}$	A_2	4.56	0.045
	$Pr_{1.62}V_{0.38}O_{3.37}$	A_1	−1.20(CO_2)	0.116
Pr_3VO_7	$Pr_3VO_{6.94}$	B_3	4.56	0
	$Pr_3VO_{6.95}$	B_2	4.14	0.0116
	$Pr_3VO_{6.995}$	B_1	−1.20	0.0831
$PrVO_3$	$PrVO_{3.07}$	O_3	4.02	Not determined
	$PrVO_{3.02}$	O_2	4.14	0
	$PrVO_{3.01}$	O_1	4.56	3.35×10^{-3}
	$PrVO_{3.00}$	O	6.75—7.50[a]	3.36×10^{-3}
$Tb_{1.62}V_{0.38}O_{3.38}$	$Tb_{1.62}V_{0.38}O_{3.33}$	A_3'	5.27	0
	$Tb_{1.62}V_{0.38}O_{3.34}$	A_2'	3.95	0.0318
	$Tb_{1.62}V_{0.38}O_{3.38}$	A_1'	−1.20	0.0951
$TbVO_3$	$TbVO_{3.00}$	O′	3.95—7.50[a]	0
$TbVO_4$	$TbVO_{3.98}$	T_2'	3.95	0
	$TbVO_{4.00}$	T_1'	−1.20	0.0138
$Y_8V_2O_{17}$	$Y_8V_2O_{16.59}$	A_2''	4.62	0
	$Y_8V_2O_{16.65}$	A_1''	3.98	0.125
	$Y_8V_2O_{17.00}$	A″	−2.00—−4.32	0.679

a) This value is the lowest oxygen partial pressure in the present experiment. $PrVO_3$, $TbVO_3$, and YVO_3 may be stable in the lower oxygen partial pressure range than this value.

Table 4. Unit cell dimensions of compounds

Sample	$-\log(P_{O_2}/Pa)$	a/Å	b/Å	c/Å	β/°	V/Å^3	Ref.
$PrVO_4$	−1.20	7.363±0.001		6.464±0.001		350.5±0.1	Present
	3.50	7.364±0.001		6.465±0.001		350.6±0.1	Present
		7.364±0.002		6.465±0.003			17)
$PrVO_3$	5.00[a]	5.470±0.004	5.531±0.004	7.763±0.004		234.9±0.3	Present
	7.50	5.472±0.009	5.561±0.009	7.779±0.010		236.7±0.6	Present
		5.472±0.003	5.529±0.003	7.774±0.003		235.2±0.1	19)
		5.487	5.562	7.751			31)
A	−1.20	11.01±0.05	8.92 ±0.04	16.70±0.22	99.4±0.5	1618±24	Present
	6.50	11.01±0.06	8.91 ±0.05	16.67. ±0.24	99.3±0.6	1615±25	Present
$TbVO_4$	−1.20	7.183±0.002		6.332±0.002		326.7±0.2	Present
		7.179±0.003		6.324±0.003			30)
$TbVO_3$	5.00	5.334±0.001	5.610±0.001	7.627±0.001		228.2±0.1	Present
		5.325±0.002	5.606±0.002	7.614±0.002		227.3±0.05	19)
A′	−1.20	10.71±0.04	8.45 ±0.06	15.80±0.11	97.9±0.3	1433±15	Present
	5.00	10.70±0.10	8.67 ±0.07	15.30±0.20	94.7±0.7	1410±28	Present
YVO_4	−4.32	7.115±0.012		6.327±0.013		320±1	Present
		7.119		6.290			16)
YVO_3	6.00	5.282±0.002	5.589±0.002	7.576±0.002		223.6±0.2	Present
		5.274±0.002	5.590±0.002	7.574±0.002		223.3±0.05	19)
		5.284	5.605	7.587			31)
A″	−4.32	10.52±0.06	8.32 ±0.03	15.78±0.13	97.6±0.5	1369±14	Present
	4.00	10.70±0.07	8.37 ±0.07	15.83±0.25	98.9±0.7	1402±27	Present

a) This sample, which has a starting mole ratio $Pr_2O_3/V_2O_5=4/6$, coexists with V_2O_3.

TABLE 5. THE STANDARD GIBBS ENERGIES OF REACTIONS

	Reaction	$-\log(P_{O_2}/\mathrm{Pa})$	$-\Delta G^\circ$/kJ
(1)	$31/50Pr_2O_3+19/50PrVO_3+19/100O_2=Pr_{1.62}V_{0.38}O_{3.38}$	6.75±0.08	62.9±1.0
(2)	$50/31Pr_{1.62}V_{0.38}O_{3.38}+12/31PrVO_3+6/31O_2=Pr_3VO_7$	4.56±0.05	50.1±0.5
(3)	$PrVO_3+1/2O_2=PrVO_4$	4.14±0.03	128.9±0.5
(4)	$31/50Tb_2O_3+19/50TbVO_3+19/100O_2=Tb_{1.62}V_{0.38}O_{3.38}$	5.27±0.03	55.0±1.0
(5)	$TbVO_3+1/2O_2=TbVO_4$	3.95±0.03	126.2±0.5
(6)	$3Y_2O_3+2YVO_3+O_2=Y_8V_2O_{17}$	4.62±0.02	271 ±1
(7)	$YVO_3+1/2O_2=YVO_4$	3.98±0.02	126.6±0.5

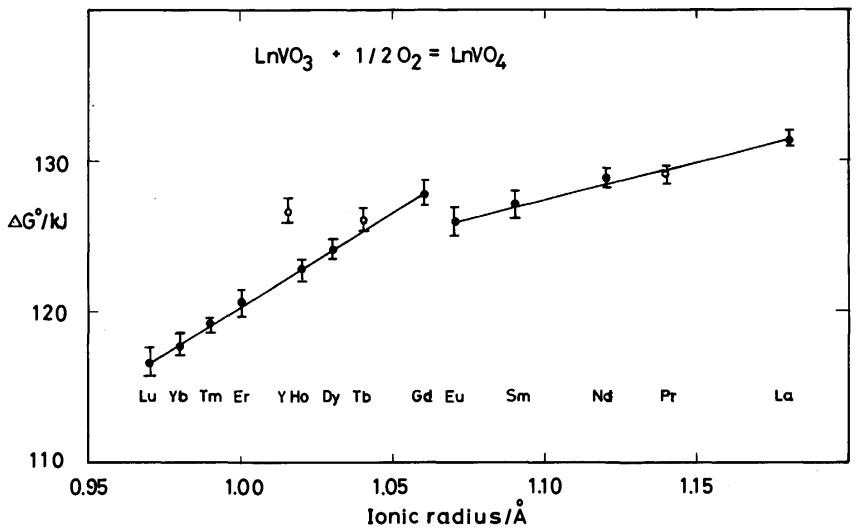

Fig. 7. The relationship between the ionic radius of lanthanoid elements in 8 coordination and the ΔG° values of reaction, $LnVO+1/2O_2=LnVO_4$.

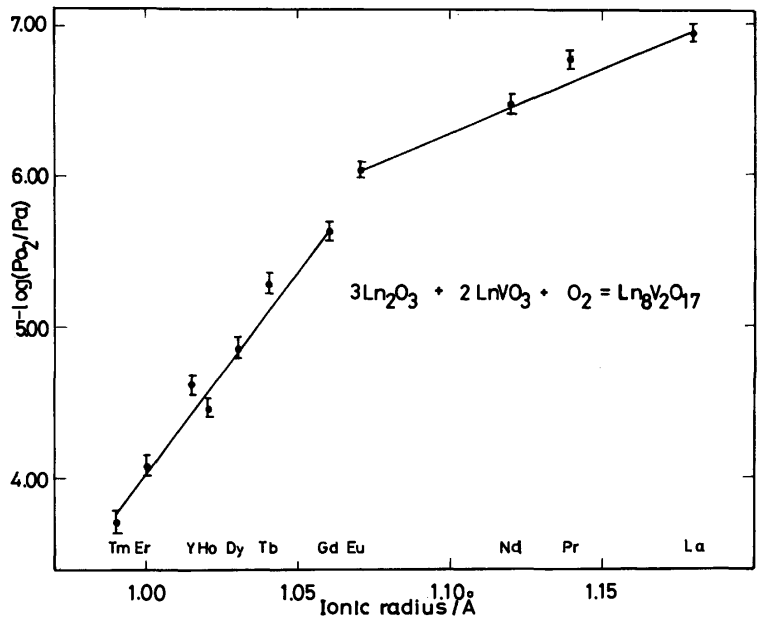

Fig. 8. The relationship between the ionic radius of lanthanoid elements in 8 coordination and the ΔG° values of reaction, $3Ln_2O_3+2LnVO_3+O_2=Ln_8V_2O_{17}$.

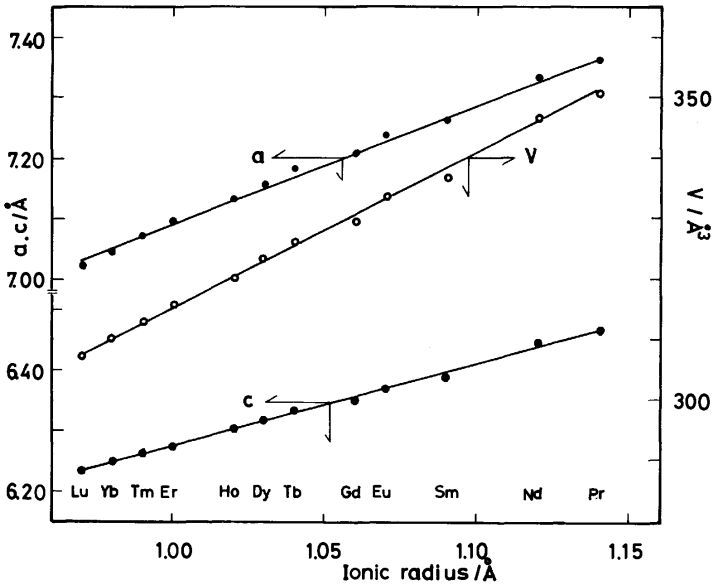

Fig. 9. Variations of the lattice parameter and the volume of $LnVO_4$ with Ln^{3+} radius (Å) in 8 coordination.

tween the oxygen partial pressure and the ionic radius of elements in the 8 coordination is plotted in Fig. 8. Comparing this with the previous case, the points are in a less linear fashion, but the same trend appears; that is, the lanthanoid elements are divided into two groups and in each group the relation is nearly linear.

Variations with Lattice Parameters with Ionic Radius. The lattice parameters and the volumes of $LnVO_4$ with a zircon structure are plotted as a function of the ionic radius in the 8 coordination in Fig. 9. Lattice parameters for other compounds have already been presented.[1-9] A smooth decreases in the *a*, *c*, and *V* values with atomic number is noted as would be expected from the lanthanoid contraction. The relation between lattice parameters and volumes of $LnVO_3$ and the ionic radius in 12 coordination is shown in Fig. 10. The *a*, *c*, and *V* values decrease with increasing atomic number and these values seem to form *a* gap at Gd. On the other hand, the *b* values show a gentle curve with a maximum near the intermeadiate atomic number. These characteristics were already pointed out by McCarthy *et al.*[19]

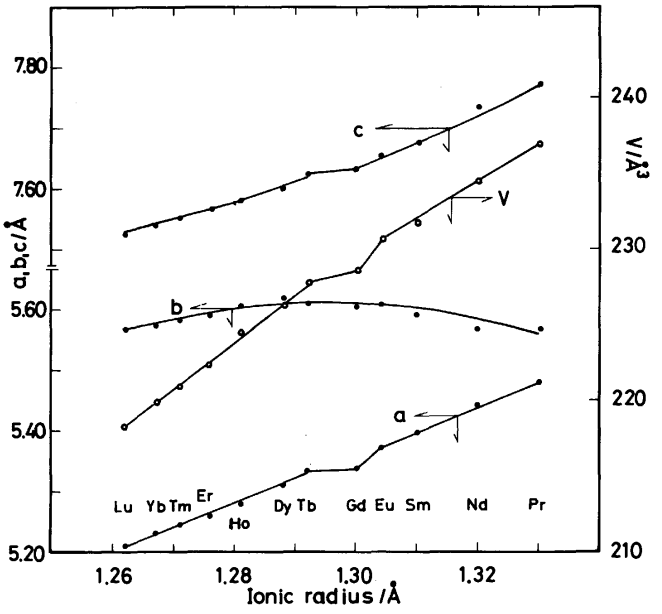

Fig. 10. Variations of the lattice parameter and the volume of $LnVO_3$ with Ln^{3+} radius (Å) in 12 coordination.

Classification of the Phase Diagram Pattern. According to a study of this series, systems at 1200 °C could be clssified into six groups with respect to the assemblages of ternary compounds. The La_2O_3–V_2O_3–V_2O_5 system belongs to the A-type in which three ternary compounds are stable in the Ln_2O_3–$LnVO_4$ subsystem, the (Pr and Nd)$_2O_3$–V_2O_3–V_2O_5 systems belong to the B-type in which two ternary compound, $0.8lLn_2O_3 \cdot 0.19V_2O_5$ and Ln_3VO_7, are stable in the subsystem, the (Sm, Eu, Gd, Tb, Dy, Ho, and Er)$_2O_3$–V_2O_3–V_2O_5 systems belong to the C-type in which one ternary compound, $4Ln_2O_3 \cdot V_2O_5$ or $0.8lLn_2O_3 \cdot 0.19V_2O_5$ or $5Ln_2O_3 \cdot V_2O_5$, is stable in the subsystem, the Tm_2O_3–V_2O_3–V_2O_5 system belongs to the D-type in which two ternary compounds, $4Tm_2O_3 \cdot V_2O_5$ and $Tm_7V_3O_{16}$, are stable, the Yb_2O_3–V_2O_3–V_2O_5 system belongs to the E-type in which one compound $Yb_7V_3O_{16}$ is stable, and the Lu_2O_3–V_2O_3–V_2O_5 system belongs to the F-type in which three ternary compounds, $Lu_7V_3O_{16}$, $Lu_2V_2O_7$, and LuV_4O_8, are stable.

It would be interesting to know whether the ternary compound assemblages change or not upon changing the experimental temperature.

References

1) K. Kitayama and T. Katsura, *Bull. Chem. Soc. Jpn.*, **50**, 889 (1977).
2) K. Kitayama and T. Katsura, *Bull. Chem. Soc. Jpn.*, **51**, 1358 (1978).
3) K. Kitayama, T. Sugihara, and T. Katsura, *Bull. Chem. Soc. Jpn.*, **52**, 458 (1979).
4) K. Kitayama and T. Katsura, *Bull. Chem. Soc. Jpn.*, **55**, 1820 (1982).
5) K. Kitayama, D. Zoshima, and T. Katsura, *Bull. Chem. Soc. Jpn.*, **56**, 689 (1983).
6) K. Kitayama, C. Mizokuchi, and T. Katsura, *Bull. Chem. Soc. Jpn.*, **56**, 695 (1983).
7) K. Kitayama and T. Katsura, *Bull. Chem. Soc. Jpn.*, **56**, 1084 (1983).
8) K. Kitayama, H. Sou, and T. Katsura, *Bull. Chem. Soc. Jpn.*, **56**, 3415 (1983).
9) K. Kitayama and T. Katsura, *Bull. Chem. Soc. Jpn.*, **57**, 1222 (1984).
10) R. L. Martin, *Nature*, **165**, 202 (1950).
11) R. Ferguson, E. D. Guth, and L. Eyring, *J. Am. Chem. Soc.*, **76**, 3890 (1954).
12) R. P. Turcotte, J. M. Warmkessel, R. J. D. Tilley, and L. Eyring, *J. Solid State Chem.*, **3**, 265 (1971).
13) E. D. Guth and L. Eyring, *J. Am. Chem. Soc.*, **76**, 5242 (1954).
14) N. C. Baenziger, H. A. Eick, H. Schulett, and L. Eyring, *J. Am. Chem. Soc.*, **83**, 2219 (1961).
15) T. Sugihara, Theses, Tokyo Institute of Technology 1978.
16) E. M. Levin, *J. Am. Ceram. Soc.* **50**, 381 (1967).
17) H. Brusset, F. Madaule-Aubry, B. Blanck, J. P. Glaziou, and J. P. Laude, *Can. J. Chem.*, **49**, 3700 (1971).
18) T. Shinike, G. Adachi, and J. Shiokawa, *Nippon Kagaku Kaishi*, **1974**, 1038.
19) G. J. McCarthy, C. A. Sipe, and K. E. McIlvried, *Mat. Res. Bull.*, **9**, 1279 (1974).
20) T. Shinike, G. Adachi, and J. Shiokawa, *Denki Kagaku*, **48**, 258 (1980).
21) J.C.P.D.S. Card, No. 6-410.
22) J.C.P.D.S. Card, No. 23-1418.
23) T. Katsura and H. Hasegawa, *Bull. Chem. Soc. Jpn.*, **40**, 561 (1967).
24) T. Katsura and A. Muan, *Trans. AIME*, **230**, 77 (1964).
25) N. Kimizuka and T. Katsura, *J. Solid State Chem.*, **13**, 176 (1975).
26) N. Kimizuka and T. Katsura, *J. Solid State Chem.*, **15**, 151 (1975).
27) N. Kimizuka and T. Katsura, *Bull. Chem. Soc. Jpn.*, **47**, 1801 (1974).
28) S. S. Kiparisov, R. A. Belyaev, V. V. Bondarenko, and V. P. Vyskubov, *Izv. Akad. Nauk SSSR, Neorg. Mat.*, **9**, 68 (1973).
29) H. Brusset, R. Mahe, and J. P. Laude, *Bull. Soc. Chim. Fr.*, 495 (1973).
30) H. Schwartz, *Z. Anorg. Allgem. Chem.*, **323**, 44 (1963).
31) B. Reuter, *Col. Inst. C.N.R.S.*, 1053 (1965).
32) J.C.P.D.S. Card, No. 17-341.

Reduction of Nitrobenzenes on Thin Aluminium Oxide Utilized in Inelastic Electron Tunneling Spectroscopy

Hideaki MONJUSHIRO,* Katsuo MURATA, and Shigero IKEDA
Department of Chemistry, Faculty of Science, Osaka University, Toyonaka, Osaka 560
(Received September 22, 1984)

Chemical interactions between aromatic nitro compounds and thin aluminium oxide grown on aluminium film were studied by the combined use of inelastic electron tunneling spectroscopy (IETS) and X-ray photoelectron spectroscopy (XPS). IET spectra of nitrobenzoic acids and nitrophenols show that nitro groups of these compounds are reduced on the oxide and result in the corresponding amino compounds. In this conversion reaction, oxygen atoms of nitro group are consumed for the growth of the oxide layer and hydrogen atoms of the surface hydroxyl groups are used for the amidation reaction. The intermediate of the reaction is identified to the corresponding nitroso compounds from the XPS analysis.

Inelastic electron tunneling spectroscopy (IETS) is a useful technique to obtain a vibrational spectrum of trace amounts of chemical species adsorbed on aluminium oxide. In certain cases, vibrational spectra obtained by IETS partly differ from IR or Raman spectra of parent molecules. This is induced by chemical interaction between the sample molecules and aluminium oxide surface. Therefore the elucidation of the mechanism for the interactions between various samples and aluminium oxide surface is the present interest, in order to establish IETS as a useful analytical tool. The major chemicals whose IET spectra have been investigated are carboxylic acids,[1-4] alcohols,[5,6] amines,[7,8] sulfonic acids,[9] phenols,[10] unsaturated hydrocarbons,[11] and esters.[12]

Tremendous difference is found in the molecular vibrational spectra of nitro compounds between IETS and IR spectroscopy and we focussed a study on the isomers of nitrobenzoic acids and nitrophenols. The interactions between these aromatic nitro compounds and aluminium oxide surface are observed by both methods of IETS and X-ray photoelectron spectroscopy (XPS). We chose to study mainly on *p*-nitrobenzoic acid (PNBA), because the vibrational spectra of adsorbed PNBA on various substrates have been measured by other spectroscopic techniques such as surface enhanced Raman scattering,[13-15] surface picosecond Raman gain[16] and Fourier transform infrared emission spectroscopy.[17]

Experimental

The sample-loaded tunneling junctions for IETS measurements were prepared using procedures as described elsewhere.[18] Briefly, the aluminium oxide layer was formed on a vacuum deposited aluminium film (*ca.* 300 nm thick) by exposing the film to atmospheric pressure of oxygen containing H_2O or D_2O vapor for 5 min. Samples were then loaded with 0.1 and 1 mg cm^{-3} acetone solutions. Tunnel junctions of Al–AlO_x–sample–Pb sandwich structure were completed by depositing the top lead electrode (*ca.* 300 nm thick).

Usually, for single ring compounds, IET spectra were successfully obtained from 1 mm×1 mm junctions. In the case of nitrobenzene derivatives, however, 2 mm×3 mm junctions were employed to obtain the spectra of sufficient quality. Because the junctions loaded with nitrobenzene derivatives showed large resistance and junctions of large resistance result in the spectra of poor signal to noise ratio. IET spectra were recorded at 4.2 K with a modulation voltage of 1.2 mV rms using the circuit described previously.[18] The observed peak positions were converted from millivolt to wavenumber with correlation of 1 mV=8.065 cm^{-1}. And a correction of -7 cm^{-1} was made to cancel out the superconducting energy gap of lead electrode.

X-ray photoelectron spectra were measured at room temperature on a Shimadzu Hips-70 spectrometer with Mg $K\alpha$ radiation. In XPS measurement, samples were prepared in a similar manner as above but without lead top electrode. Loaded samples were washed with fresh acetone to remove multilayer physisorbed sample molecules. Binding energy of Al2p(metal) peak was taken to be 72.8 eV[19] and used as the energy standard.

Chemicals used were obtained from Wako Pure Chemical Ind. or Nakarai Chemical Co. They were recrystallized from water, ethanol or toluene before use. D_2O(99.85%) for preparing deuterated oxide, was purchased from Commissariat a l'Enerqie Atomique.

Results and Discussion

IET Spectra. IET spectrum of PNBA adsorbed on aluminium oxide is shown in Fig. 1-A. Since there observed a peak due to the symmetric stretching mode of carboxylato group at 1424 cm^{-1}, PNBA is considered to be adsorbed on the oxide by dissociating a proton of carboxyl group to form surface carboxylate. In the IET spectrum of PNBA, the most remarkable feature is that the peaks attributed to the vibrational modes of nitro substituent are all absent. Instead, there appear unexpected peaks for PNBA at 3340 cm^{-1} and at 3445 cm^{-1}. These peaks could be assigned to the symmetric and antisymmetric stretching modes of amino group respectively. Further, twisting mode of amino group is observed at 1058 cm^{-1}. This spectrum is essentially identical to the IET spectrum of *p*-aminobenzoic acid (PABA) shown in Fig. 1-B. The observed peak positions and their tentative assignments are listed in Table 1.

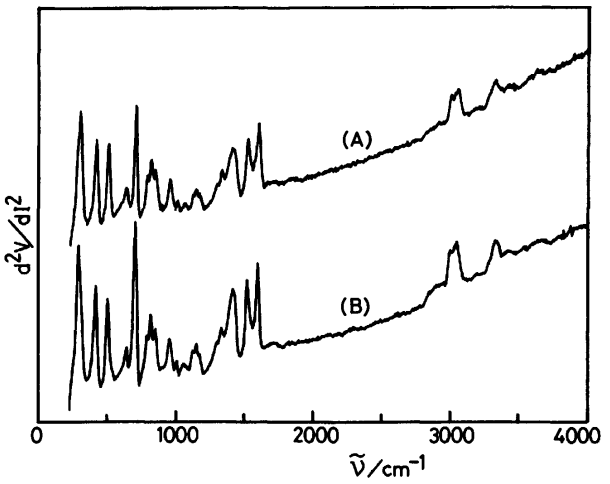

Fig. 1. IET spectra of *p*-nitrobenzoic acid(A) and *p*-aminobenzoic acid(B) adsorbed on aluminium oxide.

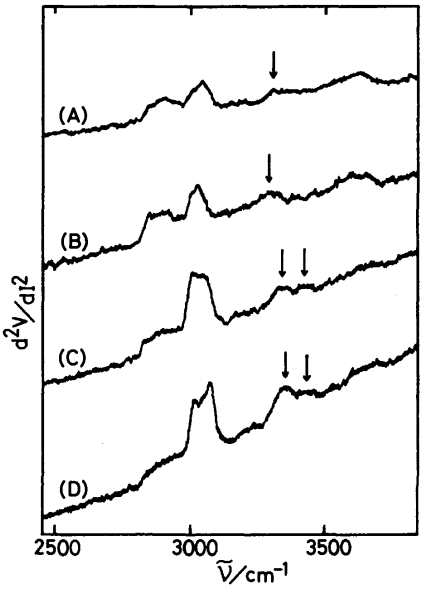

Fig. 2. Expanded IET spectra of *p*-nitrophenol(A), *o*-nitrophenol(B), *m*-nitrobenzoic acid(C) and *p*-nitrobenzoic acid(D) on aluminium oxide. Peaks due to N-H stretching modes are indicated by arrows.

These facts indicate that nitro group of PNBA is converted to amino group on the oxide, and PNBA and PABA give same adsorbed species. The similarity of the IET spectrum of PNBA to that of PABA has been suggested by Tsang *et al.*[15] But detailed analysis of the spectra and the conversion reaction was not cited in their study. Korman and Coleman[20] have also studied the IET spectrum of PNBA and assigned the peaks at 1343 cm^{-1} and at 1532 cm^{-1} to the symmetric and antisymmetric stretching modes of nitro group (in our observation 1337 cm^{-1} and 1527 cm^{-1}). However, these peaks are also observed in the IET spectrum of PABA. Thus these peaks should be assigned to the ring modes or modes of amino group and not to the modes of nitro group.

Table 1. IET spectral data of *p*-nitrobenzoic acid and *p*-aminobenzoic acid on aluminium oxide

Peak position[a] /cm^{-1}			Approximate description[b]
PABA	PNBA	PNBA on deuterated oxide	
3638 w-b	3638 w-b		ν(OH)
3445 w-b	3445 w-b		ν_a(NH$_2$)
		3380 w-b	ν(NHD)
3342 m-b	3340 m-b		ν_s(NH$_2$)
3060 m	3060 m	3061 m	ν(CH)
3009 m	3007 m	3009 m	ν(CH)
		2687 w-b	ν(OD)
		2570 w-b	ν_a(ND$_2$)
		2496 w-b	ν(NHD)
		2429 m-b	ν_s(ND$_2$)
1605 s	1604 s	1605 s	ν(CC)
1528 s	1527 s	1527 s	ν(CC)
1421 s-b	1424 s-b	1425 s-b	ν(CC), ν_s(COO)
1342 w	1337 w		?
1307 w	1304 w	1318 w	β(CH)
1182 w	1180 w	1180 w	X-sens.
1158 w	1157 w	1150 w	β(CH)
1129 w	1129 w	1116 w	β(CH), X-sens.
1061 w-b	1058 w-b		twist(NH$_2$)
1012 w	1011 w	1011 w	β(CH)
958 w-b	958 w-b	958 w-b	γ(CH)
852 m	851 m	852 m	γ(CH), δ(COO)
818 m	818 m	818 m	γ(CH), X-sens.
		796 m	twist(ND$_2$)
791 m	788 m		X-sens.
704 vs	705 vs	704 vs	ϕ(CC)
640 w	639 w	639 w	α(CCC)
616 sh	614 sh	610 sh	X-sens.
505 s	504 s	507 s	ϕ(CC)
417 s	416 s	417 s	ϕ(CC), X-sens.
296 vs	295 vs	293 vs	X-sens.

a) Peak positions corrected as in the text, relative intensity also shown; s=strong, m=medium, w=weak, v=very, sh=shoulder, b=broad. b) Assignment based on IR and Raman spectra of *p*-disubstituted benzenes; Ref. 29, alkali metal benzoate; Ref. 30 and anilines; Ref. 31.

In the IET spectra of other nitrobenzene derivatives also there observed the peaks due to N-H stretching modes instead of the peaks corresponding to nitro substituent. Figure 2 shows the expanded IET spectra of several nitro compounds in 2500 to 4000 cm^{-1} region. In each spectrum, one or two peaks corresponding to N-H stretching modes are observed around 3300 cm^{-1} as disignated in arrows. Therefore the conversion reaction on the aluminium oxide is thought to be common for aromatic nitro compounds.

XPS Spectra. In order to obtain an IET spectrum, lead metal must be deposited on the sample as a

counter electrode. To investigate the effect of the lead cover electrode for the conversion reaction, X-ray photoelectron spectra were measured on the similar system discussed above without lead electrode.

Figure 3 shows Nls photoelectron spectra of PNBA and PABA on the aluminium oxide. As the spectrum of PNBA changed with the time-course, spectra were recorded at regular time interval. In the spectrum of PNBA immediately after loading (Fig. 3-a), there observed two peaks at 406.9 eV and at 401.6 eV. With the elapse of time, the relative intensity of the two peaks reverses and the low energy peak is shifted to lower binding energy. But the total intensity of the two peaks is kept constant. One hundred minutes after loading (Fig. 3-f), the peak at 406.9 eV is completely missing and only single peak at 400.6 eV is observed in the spectrum. The resultant spectrum well agrees with that of PABA on the oxide (Fig. 3-g).

The peak at 406.9 eV is considered to be attributed to nitro group and the peak at 400.6 eV is to be due to amino group from analogy with the XPS results[21,22] of nitrobenzenes and anilines. Therefore it is clear that the conversion reaction of nitro to amino group takes place without lead cover electrode and the conversion proceeds rather slowly after adsorption reaction.

The peak at 401.6 eV initially appears in the spectrum is considered to be transient intermediate. It is known that nitrosobenzene radical is produced as an intermediate species of electrochemical reduction of nitrobenzene.[23] And the observed binding energy is in good agreement with that of nitrosobenzene in solid state.[22,24] Thus the intermediate is considered to be nitrosobenzoate on the oxide. However, we cannot rule out the possibility of phenyl-hydroxyl amine like species as an intermediate, because this species is also proposed as an intermediate of the reduction of nitrobenzene.[25]

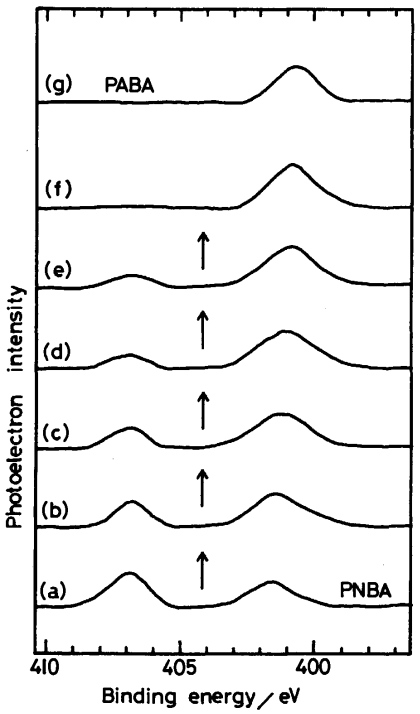

Fig. 3. Nls photoelectron spectra of PNBA on aluminium oxide measured 10 min(a), 25 min(b), 40 min(c), 55 min(d), 70 min(e), and 100 min(f) after loading, and that of PABA(g) on aluminium oxide.

Analysis of the Conversion Reaction. Although PNBA and PABA give the same adsorbed species on the oxide and the obtained IET spectra show similar intensities (indicating that the surface concentration of both compounds is comparable), the tunneling resistance of the junction loaded with PNBA is about 10 times that of the junction with PABA. This difference in tunnel resistance is considered to reflect the difference in the thickness of the insulating oxide layer. To obtain more precise information, the thickness of the oxide layer has been calculated from the XPS data as follows.

Figure 4 shows the schematic view of the surface layers of aluminium-aluminium oxide-adsorbate system and its XPS Al2p spectrum. By assuming that the oxide and the adsorbate layers are uniform, the Al2p photoelectron intensity from the metal substrate, I_m, can be expressed by

$$I_m = I_m^0 \exp(-d/\lambda_o \sin\theta) \exp(-l/\lambda_a \sin\theta), \quad (1)$$

where I_m^0 is the Al2p photoelectron intensity of the clean aluminium metal film, d is the thickness of the oxide layer, λ_o is the electron mean free path value in the oxide layer for the Al2p metal peak, θ is the photoelectron collection angle with respect to the sample plane, l is the thickness of the adsorbate layer and λ_a is the electron mean free path value in the adsorbate for the Al2p metal peak. As the kinetic energy of electrons for Al2p metal peak is nearly equal to that for Al2p oxide peak, the mean free path values for the two peaks are considered to be equal. Thus the intensity of the photoelectron from the oxide layer I_o can be expressed

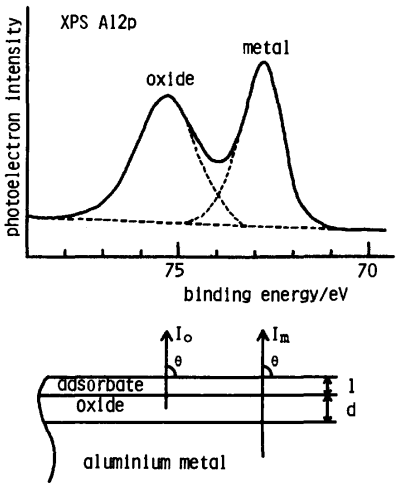

Fig. 4. Schematic view of surface layers and XPS Al2p spectrum.

Table 2. Resistance of tunnel junction and thickness of the oxide for various treatment

	Wet O_2 5 min (A)	(A) + acetone	(A) + PABA	(A) + PNBA
Junction resistance[a]/Ω	0—5	0—10	100—450	1400—8000
Oxide thickness[b]/nm	1.26±0.07	1.31±0.04	1.34±0.05	1.59±0.08

a) Resistance of 1 mm × 1 mm junction. b) Estimated from XPS Al2 p metal to oxide intensity ratio, see text.

as

$$I_o = I_o^0[1-\exp(-d/\lambda_o \sin\theta)]\exp(-l/\lambda_a \sin\theta), \quad (2)$$

where I_o^0 is the photoelectron intensity of the thick oxide layer without covering layer. By dividing Eq. 1 by Eq. 2, the terms including the effects of the adsorbate layer can be cancelled out and we obtain an equation:

$$\frac{I_m}{I_o} = \frac{I_m^0 \exp(-d/\lambda_o \sin\theta)}{I_o^0[1-\exp(-d/\lambda_o \sin\theta)]}. \quad (3)$$

Thus the thickness of the oxide layer, d, is given by

$$d = \lambda_o \sin\theta \ln[1+(I_m^0/I_o^0)(I_o/I_m)]. \quad (4)$$

In the present experiment, $\theta=\pi/2$ and the observed value of I_m^0/I_o^0 is 1.33 for Al2p photoelectron. And with assuming λ_o=1.50 nm for about 1180 eV kinetic energy electron,[26] the thickness of the oxide layer in nm can be expressed by

$$d = 1.50 \ln[1+1.33(I_o/I_m)]. \quad (5)$$

With Eq. 5, the thickness of the oxide layer can be estimated from the Al2p photoelectron intensity ratio, I_o/I_m, even if the surface is covered with unknown amounts of adsorbates.

In Table 2, junction resistance and estimated oxide thickness for various treatment are listed. The oxide thickness is little affected by the adsorption of PABA, while the adsorption of PNBA causes apparent enlargement of the thickness. This is also revealed in the difference of tunneling resistance. These facts imply that the conversion reaction results in the increase of the oxide thickness. Thus it is clear that the oxygen atoms of the nitro group are consumed for the growth of the oxide layer with conversion reaction.

The hydrogen required for the conversion is thought to be present on the substrate surface as hydroxyl group. If surface hydroxyl groups are deuterated, we can elucidate the mechanism of the conversion reaction. Figure 5 shows the expanded IET spectrum of PNBA on the oxide grown with oxygen containing D_2O vapor. Treatment with D_2O is expected to give the surface OD group. The observed peak positions are listed in Table 1. In the spectrum, characteristic peaks due to N-D stretcing modes are observed at 2500 cm^{-1} region. This observation indicates that the hydrogen atom or the surface hydroxyl group is used for the conversion

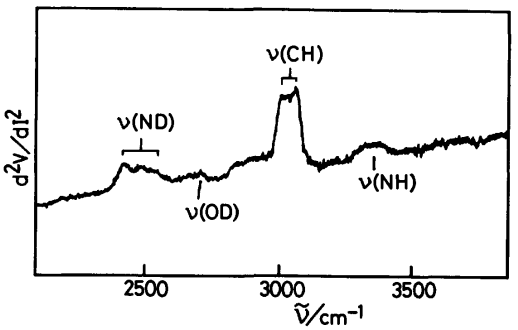

Fig. 5. Expanded IET spectrum of *p*-nitrobenzoic acid adsorbed on deuterated aluminium oxide.

reaction of nitro to amino group. The small peak at 3380 cm^{-1} is thought to appear by the reaction with residual surface OH group to form -NHD species.

On bulk alumina, it is concluded from ESR study[27] that nitrobenzene and their derivatives were adsorbed as anion radicals, and the conversion of nitro group to amino group has not been reported. Thus the conversion is thought to be specific reaction on the oxide utilized for IETS. This phenomena can be explained as follows. The oxide formed on aluminium metal is known to reach a limiting thickness of 4.5 nm after one month in air,[28] whereas the thickness of the oxide layer utilized for IETS is only *ca.* 1.3 nm (Table 2). So the oxide layer can easily grow by the reaction with oxidizing chemicals (in this case, nitro substituent). In the case of bulk alumina, this reaction cannot take place.

In previous paper,[18] we indicated that the oxide surface used in IETS behaves as base (OH donor) against acidic functional group such as -COOH, -OH, and -SH. In the case of conversion reaction reported here, however the surface hydroxyl group acts as hydrogen donor. Thus the oxide surface exhibits various properties in accordance with the property of the adsorbate and the reactivity is quite different from bulk alumina.

From the results obtained by this study, it is found that IETS cannot be used to distinguish between nitro group and amino group. It is a serious problem to apply IETS to the identification of unknown compounds containing amino or nitro group. Further studies on the property of the oxide used in IETS and the modification of the oxide are needed in order to solve this problem.

References

1) B. F. Lewis, M. Mosesman, and W. H. Weinberg, *Surf. Sci.*, **41**, 142 (1974).
2) J. T. Hall and P. K. Hansma, *Surf. Sci.*, **76**, 61 (1978).
3) N. M. D. Brown, R. B. Floyd, and D. G. Walmsley, *J. Chem. Soc., Faraday Trans. 2*, **75**, 17 (1979); N. M. D. Brown, W. J. Nelson, and D. G. Walmsley, *ibid.*, **75**, 32 (1979); N. M.D. Brown, R. B. Floyd, and D. G. Walmsley, *ibid.*, **75**, 261 (1979).
4) S. De Cheveigne, S. Gauthier, J. Klein, A. Leger, C. Guinet, M. Belin, and D. Defourneau, *Surf. Sci.*, **105**, 377 (1981).
5) H. E. Evans and W. H. Weinberg, *J. Chem. Phys.*, **71**, 1537, 4789 (1979).
6) A. Bayman and P. K. Hansma, *Nature*, **285**, 97 (1980).
7) N. M. D. Brown, R. B. Floyd, W. J. Nelson, and D. G. Walmsley, *J. Chem. Soc., Faraday Trans. 1*, **76**, 2335 (1980).
8) S. D. Williams and K. W. Hipps, *J. Catal.*, **78**, 96 (1982).
9) J. T. Hall and P. K. Hansma, *Surf. Sci.*, **71**, 1 (1978).
10) I. W. N. McMorris, N. M. D.Brown, and D. G. Walmsley, *J. Chem. Phys.*, **66**, 3952 (1977).
11) N. M. D. Brown, W. E. Timms, R. J. Turner, and D. G. Walmsley, *J. Catal.*, **64**, 101 (1980).
12) A. Bayman, P. K. Hansma, and L. H. Gale, *Surf. Sci.*, **125**, 613 (1983).
13) R. Dornhaus, R. E. Benner, and R. K. Chang, *Surf. Sci.*, **101**, 367 (1980).
14) C. A. Murray and D. L. Allara, *J. Chem. Phys.*, **76**, 1290 (1982).
15) J. C. Tsang, Ph. Avouris, and J. R. Kirtley, *J. Chem. Phys.*, **79**, 493 (1983).
16) J. P. Heritage and D. L. Allara, *Chem. Phys. Lett.*, **74**, 507 (1980).
17) D. L. Allara, D. Teicher, and J. F. Durana, *Chem. Phys. Lett.*, **84**, 20 (1981).
18) H. Monjushiro, K. Murata, and S. Ikeda, *Bull. Chem. Soc. Jpn.*, **57**, 2428 (1984).
19) C. D. Wagner, *Faraday Discuss. Chem. Soc.*, **60**, 291 (1976).
20) C. S. Korman and R. V. Coleman, *Phys. Rev. B.*, **15**, 1877 (1977).
21) K. Kishi, K. Chinomi, Y. Inoue, and S. Ikeda, *J. Catal.*, **60**, 228 (1979).
22) F. P. Colonna, G. Distefano, D, Jones, A. Modelli, and V. Galasso, *Z. Naturforsch.*, **36a**, 385 (1981).
23) C. Nishihara and M. Kaise, *J. Electroanal. Chem.*, **149**, 287 (1983).
24) G. Distefano, G. Spunta, F. P. Colonna, and S. Pignataro, *Z. Naturforsch.*, **31a**, 856 (1976).
25) M. Kijima, Y. Nambu, T. Endo, and M. Okawara, *J. Org. Chem.*, **48**, 2407 (1983).
26) F. L. Battye, J. G. Jenkin, J. Liesegang, and R. C. G. Leckey, *Phy. Rev. B.*, **9**, 2887 (1974).
27) B. D. Fockhart, I. R. Leith, and R. C. Pink, *Trans. Faraday Soc.*, **66**, 469 (1970).
28) G. Haas, *Z. Analog. Chem.*, **254**, 96 (1947).
29) J. H. S. Green, *Spectrochim. Acta Part A*, **26**, 1503 (1970).
30) J. H. S. Green, *Spectrochim. Acta Part A*, **33**, 575 (1977).
31) J. C. Evans, *Spectrochim. Acta*, **16**, 428 (1960).

The Reaction of [CoL_2] (L=5-Chloro- or 5-Nitro-8-quinolinolate Ion) with Nitrogen Monoxide

Eiichi Miki,* Kazuomi Ishimaru, Kunihiko Mizumachi, Tatsujiro Ishimori, and Mikio Tanaka†

Department of Chemistry, College of Science, Rikkyo University, Nishi-Ikebukuro, Toshima-ku, Tokyo 171

†*Laboratory of Chemistry, Nippon Medical School, Kosugi, Nakahara-ku, Kawasaki 211*

(Received September 22, 1984)

[CoL_2]·$n$$H_2O$ (L=5-chloro-8-quinolinolate ion, n=4; L=5-nitro-8-quinolinolate ion, n=5) reacted with nitrogen monoxide in CH_2Cl_2 at *ca.* 253 K to give [CoL_2(NO)] with NO^- group. [CoL_2(NO)] reacted further with nitrogen monoxide in 10 v% pyridine–DMF at room temperature to give [$CoL_2(NO_3)$(py)]·nDMF·0.5py (L=5-chloro-8-quinolinolate ion, n=0; L=5-nitro-8-quinolinolate ion, n=1) with liberation of dinitrogen oxide. [CoL_2]·$n$$H_2O$ also reacted with nitrogen monoxide in the pyridine–DMF to give the same nitrato complexes. In pyridine, [CoL_2]·$n$$H_2O$ gave [$CoL_2(NO_3)$(py)]. In DMF, [CoL_2]·$n$$H_2O$ reacted with nitrogen monoxide at room temperature to give [CoL_2(NO)]·0.5H_2O (L=5-chloro-8-quinolinolate ion) or [$CoL_2(NO_2)$(DMF)]·2H_2O (L=5-nitro-8-quinolinolate ion).

Transition-metal complexes react with nitrogen monoxide, NO, causing the NO to disproportionate, or to give the nitrosyl or hyponitrito complexes. NO also reacts with transition-metal nitrosyls to bring about electrophilic attack by the NO on the coordinating NO or disproportionation of the NO, or to give the hyponitrito or further nitrosylated complexes. These reactions proceed separately or simultaneously, as the case may be.[1-3] Of the products obtained from the disproportionation, the product with most oxidized nitrogen atom has been reported to be nitrite ion. Recently, we reported that the reactions of NO with [Co(qn)$_2$] (qn=8-quinolinolate ion) and [Co(2mqn)$_2$]·H_2O (2mqn=2-methyl-8-quinolinolate ion) in CH_2Cl_2 at room temperature caused disproportionation of the NO in the presence of the cobalt ion; $Co^{2+}+9NO \rightarrow Co^{3+}+NO^++NO_2^-$(coord)$+NO_3^-$(coord)$+3N_2O$ (coord=coordinating), and $Co^{2+}+11NO \rightarrow Co^+ + 3NO^+ + NO_2^-$(coord)$+NO_3^-$(coord)$+3N_2O$, respectively.[4,5] One of the features of the reactions is that the NO disproportionates to produce nitrate ion and nitrosyl cation.

In this paper, we report the reaction of [Co(5cqn)$_2$]·4H_2O (5cqn=5-chloro-8-quinolinolate ion, $C_9H_5NOCl^-$), [Co(5nqn)$_2$]·5H_2O (5nqn=5-nitro-8-quinolinolate ion, $C_9H_5N_2O_3^-$), or their nitrosyl complexes with NO in CH_2Cl_2, DMF, 10 v% pyridine–DMF, or pyridine. The reactions were characterized by NMR (^{13}C and ^{15}N), IR (including ^{15}N-isotopic shifts), and MS measurements.

Experimental

Materials. Dichloromethane was distilled and stored under argon over Zeorum A-4. DMF was purified by distilling under reduced pressure after dried over barium oxide, and stored under argon over Zeorum A-4. JIS-GR pyridine dried over Zeorum A-4 and JIS-GR diethyl ether were used without further purification. ^{15}NO was derived from $K^{15}NO_3$ (^{15}N atom%=99—99.7). Starting materials, [Co(5cqn)$_2$]·4H_2O (Found: Co, 12.4. Calcd: Co, 12.1%) and [Co(5nqn)$_2$]·5H_2O (Found: Co, 11.2. Calcd: Co, 11.1%) were prepared by the ordinary method.

Measurements. The C, H, N, and Cl contents of the products were analyzed by the Organic Analysis Center of the Institute of Physical and Chemical Research. The magnetic susceptibilities were measured by the Gouy method at room temperature.

The IR spectra in the solid state were measured as Nujol and poly(chlorotrifluoroethylene) oil mulls on a JASCO A-202 and a JASCO IR-F spectrometers in the region 200—4000 cm^{-1}. Since the solid products showed a number of the bands due to the coordinating quinolinolate ions, the isotopic shifts upon ^{15}N-substitution were carefully measured at 80 K using a Liquid Nitrogen Cooling Unit-DN 70 (Oxford Instruments) in many cases.

The gaseous products from the reaction of the cobalt or nitrosylcobalt complex with NO were identified by a Hitachi M-80 double-focusing mass spectrometer equipped with a Hitachi M-003 data processing system and by the IR bands and their ^{15}N-isotopic shifts.[6] A relative molar ratio of the residual NO to the produced N_2O was measured by the mass spectrometer for examining stoichiometry of the reaction.

Nitrogen-15 NMR spectra of the obtained nitrato and nitro complexes were measured at 308—353 K in the Fourier transform mode with proton decoupling using a JEOL FX-90Q spectrometer operating at 9.04 MHz. For measuring the ^{15}N NMR spectra were used the samples with $^{15}NO_2^-$ and $^{15}NO_3^-$ (^{15}N atom%=99—99.7). Chemical shifts were referenced to the NH_4^+ signal of a saturated aqueous $^{15}NH_4{}^{15}NO_3$ solution employed as the external standard, and were converted to the liquid ammonia scale by addition of 20.68 ppm.[7] The saturated solutions in DMSO-d_6 were placed in egg-shaped sample tubes, and a sweep width of 5.0 kHz over 8 K data points was used. A pulse width corresponding to a tip angle of 30° and a repetition time of 4 s was used; 1—2 K transients were required for an adequate signal-to-noise ratio. Carbon-13 NMR spectra were recorded on the same spectrometer at 308—353 K at 22.5 MHz using the same solution. The chemical shifts were referenced to internal TMS. The spectral width was typically 5000 Hz with 8 K data points for acquisition. A pulse width of 15 μs (45°) and a delay of 3 s were used; 500—1000 transients were accumulated in the region where

the resonances of the quinolinolato and py ligands were observed.

The UV spectra were run on a Hitachi 340 spectrometer.

Reaction with Nitrogen Monoxide. All reactions were carried out in a vacuum line equipped with greaseless valves and O-ring joints. The organic solvents were carefully degassed by three cycles of freeze-pump-thaw or deaerated with argon or dinitrogen before use.

Reaction of [Co(5cqn)$_2$]·4H$_2$O or [Co(5nqn)$_2$]·5H$_2$O with NO in CH$_2$Cl$_2$: The starting cobalt(II) complexes (0.5—1 mmol) suspended in CH_2Cl_2 (20 cm^3) was brought into contact with NO (5—10 mmol) and stirred for 7 d at *ca.* 253 K to obtain [Co(5cqn)$_2$(NO)], **1**, or [Co(5nqn)$_2$(NO)], **2**. The product was collected by filtration, washed with diethyl ether, and then dried under vacuum.

Reaction of [Co(5cqn)$_2$]·4H$_2$O or [Co(5cqn)$_2$(NO)] with NO in DMF, 10 v% Pyridine-DMF, or Pyridine: NO (5 mmol) was trapped into a reaction vessel containing [Co(5cqn)$_2$]·4H$_2$O (0.25 mmol) dissolved in DMF (10 cm^3), and the solution was stirred at room temperature for 1 d. A small amount of **3** was obtained.

When the pyridine-DMF (10 cm^3) were used instead of DMF, **4** was precipitated by dropping deoxygenated diethyl ether (200 cm^3) in a clear reddish brown solution obtained by the reaction of NO (5 mmol) with [Co(5cqn)$_2$]·4H$_2$O or [Co(5cqn)$_2$(NO)] (0.25 mmol). The elementary analyses and the IR spectra for the product from [Co(5cqn)$_2$]·4H$_2$O were the same as those for the product from [Co(5cqn)$_2$(NO)]. In pyridine (10 cm^3), [Co(5cqn)$_2$]·4H$_2$O (0.25 mmol) reacted with NO (5 mmol) to give a clear reddish brown solution, to which **5** was precipitated by adding deoxygenated diethyl ether.

Reaction of [Co(5nqn)$_2$]·5H$_2$O or [Co(5nqn)$_2$(NO)] with NO in DMF, 10 v% Pyridine-DMF, or Pyridine: The reactions were carried out on the same scale as described in the preceding paragraph. A clear reddish brown solution obtained from the reaction of [Co(5nqn)$_2$]·5H$_2$O with NO in DMF for 1—4 d was dropped in deoxygenated diethyl ether (100 cm^3) to precipitate **6**. When the pyridine-DMF (10 cm^3) was used instead of DMF, reddish brown suspention was obtained from the reaction of [Co(5nqn)$_2$]·5H$_2$O or [Co(5nqn)$_2$(NO)] with NO. The precipitated **7** was collected by filtration. The elementary analyses and the IR spectra for the product from [Co(5nqn)$_2$]·5H$_2$O were the same as those for the product from [Co(5nqn)$_2$(NO)]. From the reaction of [Co(5nqn)$_2$]·5H$_2$O with NO in pyridine, **8** was obtained as precipitate.

Results and Discussion

Characterization of the Solid Products. Elementary analyses and chemical formulae for the obtained complexes, **1—8**, are shown in Table 1. The complexes were diamagnetic, suggesting that all the solid products are low-spin type cobalt(III) complexes since the formal oxidation number of the coordinating NO group for the nitrosyl complexes is −I as mentioned later.

The nitrosyl complexes in the solid state were stable in air, but unstable in deoxygenated organic solvents such as CH_2Cl_2 and DMF to gradually decompose with liberation of NO. The nitro and nitrato complexes were stable in common organic solvents such as CH_2Cl_2, pyridine, DMF, and DMSO.

Reactions in CH$_2$Cl$_2$: The nitrosyls, **1** and **2**, were prepared at 253 K, but could not be isolated at above 273 K. Upon ^{15}N-substitution, the IR band at 1669 cm^{-1} (vs)[8] for **1** shifted to 1636 cm^{-1}, and the 1720 cm^{-1}

Table 1. Elementary analyses and yields of the solid products

Compound (Color)	Yield/%		Co(%)	C(%)	H(%)	N(%)	Cl(%)
1 [Co(5cqn)$_2$(NO)]	90	Found	13.2	48.4	2.3	9.4	16.1
(Dark green)		Calcd	13.2	48.5	2.3	9.4	15.9
2 [Co(5nqn)$_2$(NO)]	90	Found	11.9	45.7	2.2	14.2	
(Dark brown)		Calcd	12.6	46.3	2.2	15.0	
3 [Co(5cqn)$_2$(NO)]·0.5H$_2$O	Very low	Found		47.5	2.1	9.1	
(Dark green)		Calcd		47.5	2.4	9.2	
4 [Co(5cqn)$_2$(NO$_3$)(py)]·0.5 py	10	Found (from **A**)	9.5	50.8	3.1	10.5	
(Khaki)	50	Found (from **1**)	9.6	51.1	3.0	10.4	11.9
		Calcd	9.8	51.3	3.0	10.6	11.8
5 [Co(5cqn)$_2$(NO$_3$)(py)]	90	Found		49.5	3.0	9.8	
(Khaki)		Calcd		49.6	2.7	10.1	
6 [Co(5nqn)$_2$(NO$_2$)(DMF)]·2H$_2$O	50	Found	9.9	42.7	3.4	14.0	
(Brown)		Calcd	10.0	42.6	3.6	14.2	
					(3.3)[a]		
7 [Co(5nqn)$_2$(NO$_3$)(py)]·DMF·0.5 py	40	Found (from **B**)		49.3	3.5	15.4	
(Brown)	50	Found (from **2**)	8.5	49.3	3.5	15.4	
		Calcd	8.5	49.5	3.6	15.2	
8 [Co(5nqn)$_2$(NO$_3$)(py)]·py	60	Found		50.9	3.1	14.2	
(Brown)		Calcd		51.2	3.1	14.2	

A, [Co(5cqn)$_2$]·4H$_2$O; **B**, [Co(5nqn)$_2$]·5H$_2$O; 5cqn, 5-chloro-8-quinolinolate ion; 5nqn, 5-nitro-8-quinolinolate ion. a) The hydrogen content on the assumption that H$_2$O of **6** leaves during the preliminary treatments of the elementary analysis.

(vs) band for **2** shifted to 1688 cm^{-1}. These bands were assigned to the N-O stretching vibrations.[9] Difference in wave numbers of the N-O stretching vibrations for **1** and **2** arise from that electron-attractive power of the nitro group in the quinoline ring is larger than that of the chloro group. Of nitrosyl-cobalt complexes, the N-O stretching vibration of the NO^- complexes are observed in the region 1570—1710 cm^{-1}, while that of the NO^+ complex at *ca.* 1850 cm^{-1}.[1,5] Thus, the present nitrosyls are the NO^- complexes, which is also supported from an empirical rule in the value of the N-O stretching bands for transition-metal nitrosyl complexes proposed by Haymore and Ibers.[9] The reaction in CH_2Cl_2 can be regarded as an oxidative addition of NO to the Co^{2+}, $Co^{2+}+NO \rightarrow Co^{3+}+NO^-$(coord).

Reactions in DMF: The yield of **3** was very low. The IR spectrum was quite similar to that of **1**; the N-O stretching vibration was observed at 1667 cm^{-1}. The reaction over more than 2 d at room temperature made **3** decompose to uncharacterized product with liberation of N_2O.

The 3400(br) and the 1655 cm^{-1}(vs) bands for **6** could be assigned to the O-H stretching vibration of the water of crystallization and the C-O stretching one for the coordinating DMF, respectively.[10] The bands characteristic of the coordinating nitro group could be clearly observed; upon ^{15}N-substitution, the 792(w), 606(w), and 428 cm^{-1}(w) bands shifted to 787, 598, and 424 cm^{-1}, respectively, and were assinged to the NO_2 symmetric deformation, NO_2, wagging, and Co-NO_2 stretching vibrations, respectively.[4-6,11] However, the N-O stretching bands characteristic of the nitro group could not be observed because these bands were hidden under many strong bands due to the 5-nitro-8-quinolinolate ions. The reaction giving **6** was broken off halfway, and the obtained solution was poured into deoxygenated diethyl ether to precipitate a dark brown product. The IR spectrum showed the characteristic bands of **6** together with the 1720 cm^{-1} band assignable to the N-O stretching vibration of **2**. This suggests that [Co(5nqn)$_2$] reacts with NO to yield **2** followed by the further reaction of NO with the coordinating NO group of **2** to give the nitrite ion. Thus, the reaction may be shown as follows; $Co^{2+}+NO \rightarrow Co^{3+}+NO^-$(coord), NO^-(coord)$+2NO \rightarrow NO_2^-$(coord)$+N_2O$. Such electrophilic attack of NO on the coordinating NO group has already been reported by Gwost and Caulton.[12]

Reactions in 10 v% Pyridine-DMF or Pyridine: [Co(5cqn)$_2$]·4H_2O reacted with NO in the pyridine-DMF or in pyridine to give **4** or **5**, respectively, with liberation of N_2O. **1** gave also the same nitrato complex, **4**, in the pyridine-DMF. Table 2 shows wave numbers and the assignments of the bands on which ^{15}N-isotopic shifts were observed in the region 200—4000 cm^{-1}. The bands characteristic of a coordinating nitrate ion were observed for **4**. Separation of two N-O stretching bands due to the nitrate ion was less than 100 cm^{-1}, suggesting that the nitrate ion coordinates to the cobalt atom as a unidentate ligand.[4,5,13] **5** also showed one of the N-O stretching bands due to the coordinating nitrate ion at 1404 cm^{-1}(m). Upon ^{15}N-substitution, the another N-O stretching band could be observed at 1295 cm^{-1}(m, sh).

Table 2. Wave numbers and the assignments of coordinating nitrate ion for [Co(5cqn)$_2$(NO_3)(py)]·0.5 py and [Co(5nqn)$_2$(NO_3)(py)]·DMF·0.5 py at 80 K

[Co(5cqn)$_2$(NO_3)(py)]·0.5 py

^{14}N-compound	^{15}N-compound	Assignment
1414 m	1385 sh[a]	N-O antisym str of NO_3^-
1330 m[a]	1300 m	N-O sym str of NO_3^-
832 sh[a]	820 s	Out-of-plane bend of NO_3^-
596 w	584 w	NO_2 sym bend or NO_2 antisym bend of NO_3^-

[Co(5nqn)$_2$(NO_3)(py)]·DMF·0.5 py

^{14}N-compound	^{15}N-compound	Assignment
1421 m	1393 m	N-O antisym str of NO_3^-
1328 m	1308 sh[a]	N-O sym str of NO_3^-
820 vs[a]	810 vs[a]	Out-of-plane bend of NO_3^-
600 vs[a]	591 w	NO_2 sym bend or NO_2 antisym bend of NO_3^-
579 vs[a]	576 s, br[a]	

a) The bands due to the nitrate ion and the strong bands due to the coordinating 5-chloro- or 5-nitro-8-quinolinolate ions partially overlapped.
Abbreviations: str=stretching, bend=bending, sym=symmetric, antisym=antisymmetric, vs=very strong, s=strong, m=medium, w=weak, sh=shoulder, br=broad.

Both [Co(5nqn)$_2$]·5H_2O and **2** gave the same nitrato-complex, **7**, in the pyridine-DMF. In Table 2 are also shown the IR bands characteristic of a unidentate nitrate ion for **7** with their ^{15}N-isotopic shifts. The strong band at 1670 cm^{-1} could be assigned to the C-O stretching vibration due to the uncoordinating DMF.[10] **8** obtained from the reaction in pyridine also showed two N-O stretching bands at 1425(m) and 1326 cm^{-1}(m) due to the unidentate nitrate ion.

The reaction of [CoL_2] and [CoL_2(NO)] with NO can be shown as follows; $Co^{2+}+5NO \rightarrow Co^{3+}+NO_3^-$(coord)$+2N_2O$, and $Co^{3+}+NO^-$(coord)$+4NO \rightarrow Co^{3+}+NO_3^-$(coord)$+2N_2O$, respectively.

DMF in **6** and **7** could be also confirmed by the ^{13}C NMR measurements as mentioned later. The IR measurements could not confirm pyridine in **4**, **5**, **7**, and **8**, but the ^{13}C NMR ones suggest that **4** and **5** contain pyridine.

UV Measurements: The electronic spectra for the nitro and nitrato complexes are shown in Table 3.

Table 3. Electronic spectra of the solid products

Compound[a]	Solvent	σ/nm(ε/mol^{-1} dm^3 cm^{-1})
4	CH_2Cl_2	330(4.93×10^3), 346(5.14×10^3)
		428(7.68×10^3), 560 sh(4.9×10^2)
6	CH_2Cl_2	340(1.63×10^4)
		438(5.06×10^4), 580 sh(5.7×10^2)
7	CH_2Cl_2	344(1.59×10^4)
		442(4.35×10^4), 560 sh(3.5×10^2)
8	10 v% py-DMF	342(1.76×10^4)
		438(4.35×10^4), 560 sh(2.9×10^2)
A	10 v% py-DMF	352(5.78×10^3), 418(7.65×10^3)
B	10 v% py-DMF	344(1.26×10^4), 444(4.30×10^4)

a) Abbreviations of the compounds are the same as those shown in Table 1.

The bands at 330—440 nm may be assigned to the charge transfer absorption between the coordinating 8-quinolinolate ion and the cobalt(III) ion as compared with the absorption maxima and intensities for the spectra of [Co(5cqn)$_2$] or [Co(5nqn)$_2$]. The shoulder bands at 560—580 nm may be due to *d–d* absorption in the cobalt(III) ion.[14]

NMR Measurements: Since the obtained nitrosyl complexes, **1** and **2**, were unstable in deoxygenated common organic solvents, the NMR spectra could not be measured. The ^{15}N and ^{13}C NMR measurements of the nitro and nitrato complexes, **4**—**8**, were tried in DMSO-d_6 at 308—353 K to alleviate their sparing solubility to DMSO and the high viscosity of the solution at room temperature (the solubility is less than 10^{-3} mol dm^{-3} at room temperature).

The ^{15}N NMR spectra of the nitrato complexes, **4**, **5**, **7**, and **8**, showed a single resonance at 379.34, 388.06, 379.72, and 375.56 ppm, respectively. These values were comparable to 376.25 ppm of $^{15}NO_3^-$ in a saturated aqueous solution of $^{15}NH_4{}^{15}NO_3$, and 380.26 ppm of a DMSO-d_6 solution of $K^{15}NO_3$ (0.28 mg/0.35 cm^3) at 333 K. The ^{15}N NMR resonance of the nitro complex, **6**, was also observed at 371.12 ppm and the coordinating nitro ion showed a high-field resonance by 240 ppm compared with 610 ppm of free nitrite ion. Such a phenomenon has been found for [RhCl(NO_2)(NO)L_2](L=phosphine derivatives).[15] On the other hand, the ^{15}N resonance of the coordinating nitrate ion was found in the same region as that of free nitrate ion. Because the coordination of the nitrate ion to the cobalt(III) ion is through the oxygen atom, the shifts are small as observed for nitrato complexes of various metals.[16]

The ^{13}C NMR spectra of **4** and **5** were very complicated (see Fig. 1), and thus could not be clearly assigned. The resonances were observed in the region 112—166 ppm which coincided with the regions, 111—153 ppm for 5-chloro-8-quinolinol and 123—150 ppm for pyridine.[17] Number of the observed signals for **4** was 25, and that for **5** was 22. Assuming

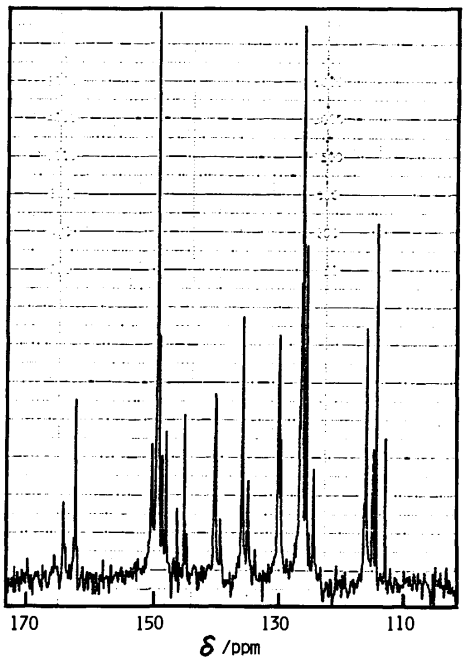

Fig. 1. ^{13}C NMR spectrum of [Co(5cqn)$_2$(NO_3)(py)]·0.5py in DMSO-d_6; standard, internal TMS.

that **4** contains two kinds of the coordinating 5-chloro-8-quiolinolate ions, a coordinating pyridine, and a free pyridine, number of the expected resonances becomes 24. Also, assuming that **5** consists of two kinds of the coordinating 5-chloro-8-quinolinolate ions and a coordinating pyridine, number of the expected signals becomes 21. The NMR data suggest that among **4** and **5**, the nitrato ligand is in *cis*-position to the pyridine. The ^{13}C NMR spectra of **6**, **7**, and **8** could not be measured clearly due to their solubilities, but two kinds of 5-nitro-8-quinolinolate ions seems to exist. The resonances due to DMF in **6** and **7** could be observed. The resonances at 28.97 and 33.90, and at 160.96 ppm for **6** could be assinged to the methyl carbons, and the carbonyl carbon, respectively.[17] The resonances at 30.66, 35.65, and 162.20 ppm for **7** were almost equal to those at 31.17, 36.27, and 162.39 ppm for free DMF, respectively.[17]

Gaseous Products. Gaseous product from the reaction in DMF, the pyridine-DMF, or pyridine was only N_2O. It has been reported that N_2 together with N_2O was liberated on disproportionation of NO in the presence of transition-metal complex.[3] N_2 was not liberated under the present experimental conditions.

For the reaction giving **4**, **5**, or **8**, the stoichiometry was examined by measuring the relative molar ratio of the residual NO to the produced N_2O. The molar ratio of NO to the cobalt complex was 20.0, and the cobalt complex and the organic solvent used were 0.25 mmol and 10 cm^3, respectively. The ratio observed was generally larger than that calculated on the assumption that the reaction proceeded completely, and the repro-

ducibility was not always good. The yield of the solid product calculated from the observed ratio was smaller than the yield obtained actually. These suggest that the total reaction with NO is not simple, and side reactions which could not be identified may consume the produced N_2O.

Effects of Organic Solvents on the Reactions. On the reaction of $[Co(qn)_2(NO)]$ (qn=8-quinolinolate ion) with NO in CH_2Cl_2 having very poor coordinating ability to metal ion, NO attacks the coordinating nitrosyl group, NO^-, electrophilically to give NO_2^- with retention of the Co-NO bond; the nitrogen atom in the nitro group comes from the nitrosyl group. This was confirmed by ^{15}N-labelled experiments.[4]

For examining the mechanism of the reaction of the nitrosyl complex, **1**, or **2**, with NO in the pyridine-DMF, the following combinations of nitrogen isotopes were used; A, (^{14}NO-complex)-(^{15}NO gas) and B, (^{15}NO-complex)-(^{14}NO gas). The molar ratio of the NO to the nitrosyl complex was *ca.* 6—7. In the case of A, the mass analysis showed that the relative molar ratio of ^{14}NO to ^{15}NO in the residual NO was almost equal to that of the ^{14}NO-complex to the ^{15}NO gas. The experiment using the isotopes suggests that the ^{14}NO-complex decomposes almost perfectly to liberate ^{14}NO and the liberated ^{14}NO together with ^{15}NO, original reactant, reacts with the resulting cobalt(II) complex to give the nitrato complex. In the case of B was also found the same phenomena as observed for the case A. The ^{14}N-^{15}N scramble was observed for the reaction of the nitrosyl complex with NO, hence the reaction mechanism could not be elucidated from the isotopic experiments. In solution containing strong σ-donor Lewis base such as pyridine, after the Co-NO bond in the original nitrosyl complex was broken and the resulting cobalt(II) complex was nitrosylated again, NO reacts with the NO^- group to give NO_2^- and N_2O with cleavage of the Co-NO bond, and the NO_2^- reacts further with NO to give NO_3^- and N_2O. Coordination of pyridine to the cobalt ion seems to unstabilize the Co-NO bond. The proposed mechanism for the reaction is pictured (Scheme 1).

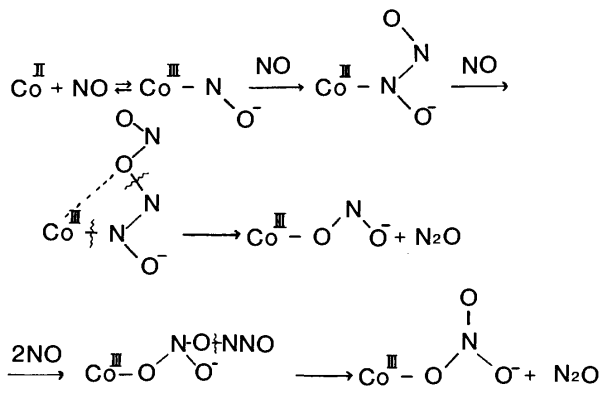

Scheme 1. Proposed reaction mechanism.

The reaction of the nitrosyl complex with NO in DMF could not be elucidated. Since coordinating ability of DMF to metal ion is weaker than that of pyridine, the complicated reactions may proceed.

On the reaction of $[CoL_2]$ with NO in pyridine and 10 v% pyridine-DMF, the disproportionation of NO to NO_3^- and N_2O involving an oxidation of cobalt(II) to cobalt(III) was observed. The reaction is considered to be initiated from a nitrosylation of $[CoL_2]$ followed by the reaction of the resulting nitrosyl complex with NO as mentioned above. The reaction giving **6** is considered as follows; after $[Co(5nqn)_2]$ was nitrosylated, the resulting NO^- group seems to react further with NO to give NO_2^- without cleavage of the Co-NO bond, because DMF is not so strong Lewis base as break the Co-NO bond.

On metal-induced NO disproportionations which has been reported so far, the product with most oxidized nitrogen atom is nitrite ion.[3] In a series of our reaction system[4,5] including the present study, nitrate ion was produced. This phenomenon is considered to be usual on the disproportionation, especially in solvent with strong coordinating ability such as pyridine.

A number of studies on the disproportionation of NO have been reported,[3] but the stoichiometry of the reaction has been mentioned for only a few examples.[2,18] Since this type of the reaction is very complicated, it seems likely that stoichiometry of the total reaction can not be elucidated in many cases.

The authors wish to express their thanks to Professor Yoshito Takeuchi of the University of Tokyo, Assistant Professor Reiko Hirota of Rikkyo University, and Professor Minoru Hirota of Yokohama National University, for measuring the NMR spectra. The authors also would like to thank Professor Yoshito Takeuchi of the University of Tokyo for his kindhearted discussion of the NMR data, and Mr. Shigeaki Oyama of Rikkyo University for his technical assistance.

References

1) J. H. Enemark and R. D. Feltham, *Coord. Chem. Rev.*, **13**, 339 (1974).

2) K. G. Caulton, *Coord. Chem. Rev.*, **14**, 317 (1975).

3) J. A. McCleverty, *Chem. Rev.*, **79**, 53 (1979); K. K. Pandey, *Coord. Chem. Rev.*, **51**, 69 (1983).

4) E. Miki, *Chem. Lett.*, **1980**, 835.

5) E. Miki, K. Saito, K. Mizumachi, and T. Ishimori, *Bull. Chem. Soc. Jpn.*, **56**, 3515 (1983).

6) S. Pinchas and I. Laulight, "Infrared Spectra of Labelled Compounds," Academic Press, London (1971), Chap. 6; J. Laane and J. R. Ohlsen, "Characterization of Nitrogen Oxides by Vibrational Spectroscopy," in "Progress in Inorganic Chemistry" ed by S. J. Lippard, An Interscience

Publication by John Wiley & Sons, Inc., New York (1980), Vol. 27, pp. 465—513.

7) G. C. Levy and R. L. Lichter, "Nitrogen-15 Nuclear Magnetic Resonance Spectroscopy," Wiley-Interscience, New York (1979), Chap. 3.

8) The signs in parentheses indicate the abbreviations of the strength and shape of the IR bands; vs=very strong, s=strong, m=medium, w=weak, sh=shoulder, br=broad.

9) B. L. Haymore and J. A. Ibers, *Inorg. Chem.*, **14**, 3060 (1975).

10) M. L. Larson and F. W. Moore, *Inorg. Chem.*, **5**, 801 (1966); E. Miki, M. Motonaga, K. Mizumachi, T. Ishimori, and M. Katada, *Bull. Chem. Soc. Jpn.*, **55**, 2858 (1982).

11) E. Miki, unpublished work for the IR spectra of $[Co(NO_2)(NH_3)_5](NO_3)_2$ and its ^{15}N-nitro analog.

12) D. Gwost and K. G. Caulton, *Inorg. Chem.*, **13**, 414 (1974).

13) B. M. Gatehouse, S. E. Livingstone, and R. S. Nyholm, *J. Chem. Soc.*, **1957**, 4222; *J. Inorg. Nucl. Chem.*, **8**, 75 (1958).

14) L. E. Orgel, "An Introduction to Transition-Metal Chemistry: Ligand Field Theory," Methuen & Co. Ltd., London (1959), pp. 99—102.

15) L. K. Bell, J. Mason, D. M. P. Mingos, and D. G. Tew, *Inorg. Chem.*, **22**, 3497 (1983).

16) K. F. Chew, M. A. Healy, M. I. Khalil, and N. Logan, *J. Chem. Soc., Dalton Trans.*, **1975**, 1315.

17) L. B. Beach, "Selected ^{13}C Nuclear Magnetic Resonance Spectra Data," Thermodynamics Research Center, Texas A & M University, College Station, Texas, (1975).

18) R. D. Feltham, *Inorg. Chem.*, **3**, 119 (1964); R. D. Feltham and J. T. Carriel, *ibid.*, **3**, 121 (1964); M. Rossi and A. Sacco, *J. Chem. Soc., Chem. Commun.*, **1971**, 694.

Structural, Magnetic and IR Spectroscopic Characterization of Dimeric Copper(II) Trichloroacetate Adduct with Benzonitrile. Nature of the Copper(II)-Bezonitrile Bond

Michio NAKASHIMA, Masahiro MIKURIYA,† and Yoneichiro MUTO*
Department of Chemistry, Faculty of Science and Engineering, Saga University, Saga 840
†*Department of Chemistry, Faculty of Science, Kyushu University, 33, Hakozaki, Higashi-ku, Fukuoka 812*
(Received October 8, 1984)

The benzonitrile adduct of copper(II) trichloroacetate, $[Cu(Cl_3CCOO)_2(PhCN)]_2$, was prepared and characterized. The dimeric structure was confirmed by an X-ray structural determination. This compound crystallizes in the triclinic space group $P\bar{1}$ with a=12.780(1), b=16.064(1), c=10.130(1) Å; α=108.39(1), β=113.34(1), γ=81.07(1)°. The crystal consists of two crystallographically independent dimeric units. Both units have the familiar dimeric copper(II) acetate monohydrate structure with Cu–Cu distances of 2.731(1) and 2.732(1) Å. Magnetic susceptibility data in the range of 80—300 K are well represented by the usual dimer equation with a singlet-triplet energy separation of $-2J$=224 cm^{-1}. The C≡N stretching frequency of benzonitrile in the compound shows an increase by 31 cm^{-1} from the free ligand value. On the basis of the X-ray crystallographic and IR spectroscopic results, the nature of the copper(II)–benzonitrile bond is discussed. For discussion magnetic and spectroscopic properties of some analogous nitrile adducts of copper(II) chloroacetates were also studied.

Studies on a number of dimeric copper(II) carboxylate adducts, $[Cu(RCOO)_2 \cdot L]_2$, have revealed some of the factors which determine the extent of antiferromagnetic interaction in these complexes. On the effect of addend ligand L, Jotham *et al.*[1] have stated that the singlet-triplet separation ($-2J$, a measure of the magnitude of the magnetic interaction) in $[Cu(RCOO)_2 \cdot L]_2$ complexes tends to increase as L becomes a stronger electron donor. On the other hand, Hibdon *et al.*[2] have reported that the magnetic interaction in a series of dimeric copper(II) acetate adducts with 4-substituted pyridine N-oxides becomes stronger as the π-back-donation from the metal ion to the addend ligand increases. However, Muto *et al.*[3] have recently found that, in a series of $[Cu(RCOO)_2 \cdot L]_2$ complexes, where R=CH_3, $ClCH_2$, and Cl_2CH, and L=pyridine analogues, the value of $-2J$ increases as the basicity of the addend ligands becomes weaker. Then a larger $-2J$ has been attributed to a weaker σ-donation of the addend ligand. These apparent discrepancies prompted us to investigate the bonding nature between Cu-L in $[Cu(RCOO)_2 \cdot L]_2$ complexes.

In the present study five complexes, $Cu(ClCH_2COO)_2(PhCN)$, $Cu(ClCH_2COO)_2(4\text{-}CH_3C_6H_4CN)$, $Cu(Cl_2CHCOO)_2(4\text{-}CH_3C_6H_4CN)$, $Cu(Cl_3CCOO)_2(PhCN)$, and $Cu(Cl_3CCOO)_2(4\text{-}CH_3C_6H_4CN) \cdot 1/2bz$, where PhCN=benzonitrile, $4\text{-}CH_3C_6H_4CN$=4-methylbenzonitrile and bz=benzene, have been prepared and characterized by means of magnetic susceptibility and IR spectroscopy measurements. The structure of the benzonitrile adduct of copper(II) trichloroacetate has been determined by a single-crystal X-ray structural analysis to obtain accurate information about the coordinating mode of the addend ligand. In particular relations of the stretching frequency of the C≡N group with its bond length have been studied.

Experimental

Syntheses. $Cu(ClCH_2COO)_2 \cdot L$(L=PhCN and $4\text{-}CH_3C_6H_4CN$): A solution of L (10 mmol) in benzene (10 ml) was added to a solution of $Cu(ClCH_2COO)_2$ (2 mmol) in acetone (20 ml). The resulting solution was filtered and then concentrated to one-third of its volume. When petroleum ether was added to the solution, green crystals precipitated. The crystals were collected, washed with a 1:2 benzene-petroleum ether mixture and dried *in vacuo* at room temperature.

$Cu(Cl_2CHCOO)_2(4\text{-}CH_3C_6H_4CN)$: This compound was prepared from $Cu(Cl_2CHCOO)_2$ and $4\text{-}CH_3C_6H_4CN$ in the same manner as with $Cu(ClCH_2COO)_2 \cdot L$.

$Cu(Cl_3CCOO)_2(PhCN)$: $Cu(Cl_3CCOO)_2 \cdot 3H_2O$ (2 mmol) and PhCN (10 mmol) were suspended in a mixture of benzene (30 ml) and 2,2-dimethoxypropane (1 ml). The mixture was warmed gently with stirring and then filtered. After the solution had been concentrated to one-third of its volume, it was allowed to stand overnight at *ca.* 5 °C in a refrigerator. The separated green crystals were collected, washed with a 1:2 benzene–petroleum ether mixture and dried *in vacuo* at room temperature.

$Cu(Cl_3CCOO)_2(4\text{-}CH_3C_6H_4CN) \cdot 1/2bz$: This compound was prepared from $Cu(Cl_3CCOO)_2 \cdot 3H_2O$ and $4\text{-}CH_3C_6H_4CN$ as described above.

The results of the elemental analyses are given in Table 1.

X-Ray Crystal Structure Determination of $Cu(Cl_3CCOO)_2(PhCN)$. A Rigaku AFC-5 automated four-circle diffractometer was used for all measurements. Crystal data and details of the data collection are summarized in Table 2. Lattice constants were determined by the least-squares refinement based on 35 reflections with $20° < 2\theta < 30°$. The intensity data were corrected for the Lorentz-polarization effects, but not for absorption.

Table 1. Analytical data

Complex	Found (Calcd) (%)			
	C	H	N	Cu
$Cu(ClCH_2COO)_2$-(PhCN)	37.63 (37.36)	2.61 (2.57)	4.14 (3.96)	17.76 (17.97)
$Cu(ClCH_2COO)_2$-(4-$CH_3C_6H_4CN$)	39.03 (39.20)	3.01 (3.01)	3.72 (3.81)	17.34 (17.28)
$Cu(Cl_2CHCOO)_2$-(4-$CH_3C_6H_4CN$)	33.15 (33.01)	2.09 (2.08)	3.06 (3.21)	14.60 (14.56)
$Cu(Cl_3CCOO)_2(PhCN)$	26.88 (26.51)	0.94 (1.03)	2.94 (2.85)	12.88 (12.93)
$Cu(Cl_3CCOO)_2$-(4-$CH_3C_6H_4CN$)·1/2bz	32.86 (33.09)	1.66 (1.85)	2.61 (2.57)	11.61 (11.67)

Table 2. Crystal data and data collection details

Formula	$C_{22}H_{10}Cl_{12}Cu_2N_2O_8$
fw	982.86
Temp/K	292±1
Cryst syst	triclinic
Space group	$P\bar{1}$
a/Å	12.780(1)
b/Å	16.064(1)
c/Å	10.130(1)
α/°	108.39(1)
β/°	113.34(1)
γ/°	81.07(1)
V/Å^3	1810.9(2)
Z	2
D_m/g cm^{-3}	1.78
D_c/g cm^{-3}	1.80
Radiation	graphite-monochromated Mo $K\alpha$ (λ=0.71073 Å)
μ(Mo $K\alpha$)/cm^{-1}	21.1
Cryst dimens/mm	0.23×0.23×0.40
Scan type	θ–2θ
Scan speed/° min^{-1}	3
Scan width/°	1.4+0.5 tan θ
Standard reflcns	($\bar{1}$, $\bar{3}$, 0) ($\bar{2}$, 0, 1) (0, $\bar{1}$, 2)
Decay of standard	±4%
2θ range/°	2.5—45.0
Total no. of obsd Reflcns	4989
no. of unique reflcns with $\|F_o\|>3\sigma(\|F_o\|)$	3694
Final no. of variables	456
Final residuals	
R	0.058
R_w	0.086

Table 3. Fractional positional parameters (×10^4) and thermal parameters of non-hydrogen atoms with their estimated standard deviations in parentheses

Atom	x	y	z	B_{eq}/Å^2
Cu(A)	−912(1)	180(1)	439(1)	4.2
Cu(B)	4088(1)	5181(1)	−1170(1)	4.2
Cl(A1)	1352(2)	2933(2)	3033(3)	7.9
Cl(A2)	−847(3)	3186(2)	846(4)	9.9
Cl(A3)	1142(5)	2796(2)	53(5)	14.1
Cl(A4)	1560(3)	221(2)	5485(3)	8.7
Cl(A5)	3452(2)	−153(3)	4564(3)	9.1
Cl(A6)	1894(4)	−1473(2)	3676(4)	11.2
Cl(B1)	3645(2)	2066(2)	−1260(3)	7.8
Cl(B2)	5838(3)	1811(2)	−1501(5)	9.9
Cl(B3)	3860(5)	2204(2)	−3886(3)	13.8
Cl(B4)	3441(3)	4776(2)	3702(3)	8.8
Cl(B5)	1552(2)	5154(3)	1264(3)	9.3
Cl(B6)	3115(4)	6475(2)	3260(5)	11.2
O(A1)	−485(5)	1397(4)	944(7)	5.7
O(A2)	1004(5)	1098(4)	243(7)	6.1
O(A3)	256(5)	65(4)	2358(6)	5.8
O(A4)	1751(4)	−231(4)	1638(6)	5.3
O(B1)	3989(5)	3893(4)	−1874(6)	6.1
O(B2)	5488(5)	3604(4)	40(6)	5.6
O(B3)	3258(4)	5238(4)	131(6)	5.4
O(B4)	4753(4)	4936(4)	2046(6)	5.6
N(A)	−2317(6)	538(5)	1175(8)	5.9
N(B)	2686(5)	5541(5)	−2950(7)	5.7
C(A1)	306(7)	1593(5)	714(9)	5.0
C(A2)	465(9)	2573(6)	1113(11)	6.4
C(A3)	1279(6)	−139(5)	2543(8)	4.5
C(A4)	2009(7)	−359(5)	4023(8)	4.7
C(A5)	−3048(6)	817(5)	1532(8)	4.5
C(A6)	−4010(6)	1180(6)	1966(8)	5.1
C(A7)	−4743(8)	613(9)	1909(11)	7.5
C(A8)	−5695(10)	963(14)	2244(13)	13.3
C(A9)	−5846(12)	1813(17)	2651(14)	17.6
C(A10)	−5147(14)	2395(11)	2798(14)	13.8
C(A11)	−4177(10)	2077(8)	2371(12)	8.6
C(B1)	4701(7)	3403(5)	−1174(8)	4.8
C(B2)	4544(9)	2421(6)	−1930(10)	6.6
C(B3)	3743(6)	5150(5)	1414(8)	4.2
C(B4)	2986(7)	5362(5)	2362(9)	4.9
C(B5)	1943(6)	5816(5)	−3767(8)	4.4
C(B6)	986(6)	6178(6)	−4797(9)	4.8
C(B7)	265(8)	5608(8)	−6032(10)	7.4
C(B8)	−701(10)	5986(13)	−6974(14)	12.6
C(B9)	−858(12)	6822(14)	−6688(21)	14.8
C(B10)	−137(14)	7420(11)	−5500(25)	14.6
C(B11)	855(10)	7086(8)	−4437(15)	8.5

The structure was solved by the heavy-atom method. Refinements were carried out by the block-diagonal least-squares method. Hydrogen atoms were inserted in their calculated positions and included in the refinement. The final R values were $R=\sum||F_o|-|F_c||/\sum|F_o|=0.058$, $R_w=[\sum w(|F_o|-|F_c|)^2/\sum w|F_o|^2]^{1/2}=0.086$. The weighting scheme was $w=(6.5+|F_o|+0.007|F_o|^2)^{-1}$. The final difference Fourier synthesis showed no peaks higher than 0.84 e Å^3.

The atomic scattering factors for Cu, Cl, O, N, C, and H and the anomalous dispersion corrections, $\Delta f'$ and $\Delta f''$

TABLE 4. INTERATOMIC DISTANCES (l/Å) AND BOND ANGLES (ϕ/°) WITH THEIR ESTIMATED STANDARD DEVIATIONS IN PARENTHESES

(1) Binuclear molecule A			
(a) Copper coordination spheres			
Cu(A)-Cu(A)^{1} [a]	2.731(1)	Cu(A)-O(3A)	1.967(5)
Cu(A)-O(A1)	1.965(6)	Cu(A)-O(A4)^{1}	1.969(5)
Cu(A)-O(A2)^{1}	1.955(6)	Cu(A)-N(A)	2.141(9)
O(A1)-Cu(A)-O(A3)	90.1(3)	O(A3)-Cu(A)-O(A4)^{1}	165.6(3)
O(A1)-Cu(A)-O(A4)^{1}	88.0(3)	O(A1)-Cu(A)-N(A)	94.4(3)
O(A1)-Cu(A)-O(A2)^{1}	165.0(3)	O(A2)^{1}-Cu(A)-N(A)	100.6(3)
O(A2)^{1}-Cu(A)-O(A3)	88.4(3)	O(A3)-Cu(A)-N(A)	97.2(3)
O(A2)^{1}-Cu(A)-O(A4)^{1}	89.8(3)	O(A4)^{1}-Cu(A)-N(A)	97.3(3)
(b) Trichloroacetate ion			
C(A1)-O(A1)	1.228(13)	C(A3)-O(A3)	1.250(10)
C(A1)-O(A2)	1.238(11)	C(A3)-O(A4)	1.245(12)
C(A1)-C(A2)	1.522(13)	C(A3)-C(A4)	1.538(11)
C(A2)-Cl(A1)	1.775(9)	C(A4)-Cl(A4)	1.741(9)
C(A2)-Cl(A2)	1.775(11)	C(A4)-Cl(A5)	1.756(9)
C(A2)-Cl(A3)	1.761(15)	C(A4)-Cl(A6)	1.729(9)
Cu(A)-O(A1)-C(A1)	123.1(5)	Cl(A1)-C(A2)-Cl(A3)	108.0(6)
Cu(A)-O(A2)^{1}-C(A1)^{1}	123.2(7)	Cl(A2)-C(A2)-Cl(A3)	109.2(6)
Cu(A)-O(A3)-C(A3)	123.8(6)	O(A3)-C(A3)-O(A4)	127.3(7)
Cu(A)-O(A4)^{1}-C(A3)^{1}	123.2(4)	O(A3)-C(A3)-C(A4)	115.7(8)
O(A1)-C(A1)-O(A2)	128.4(8)	O(A4)-C(A3)-C(A4)	116.8(7)
O(A1)-C(A1)-C(A2)	115.2(8)	C(A3)-C(A4)-Cl(A4)	112.8(6)
O(A2)-C(A1)-C(A2)	116.3(10)	C(A3)-C(A4)-Cl(A5)	111.2(7)
C(A1)-C(A2)-Cl(A1)	108.2(7)	C(A3)-C(A4)-Cl(A6)	106.2(5)
C(A1)-C(A2)-Cl(A2)	112.2(7)	Cl(A4)-C(A4)-Cl(A5)	108.5(4)
C(A1)-C(A2)-Cl(A3)	111.1(7)	Cl(A4)-C(A4)-Cl(A6)	109.8(6)
Cl(A1)-C(A2)-Cl(A2)	108.0(5)	Cl(A5)-C(A4)-Cl(A6)	108.1(5)
(c) Benzonitrile			
N(A)-C(A5)	1.113(12)	C(A8)-C(A9)	1.303(33)
C(A5)-C(A6)	1.445(12)	C(A9)-C(A10)	1.326(32)
C(A6)-C(A7)	1.378(17)	C(A10)-C(A11)	1.440(26)
C(A7)-C(A8)	1.381(17)	C(A11)-C(A6)	1.375(15)
Cu(A)-N(A)-C(A5)	171.9(9)	C(A8)-C(A9)-C(A10)	125.6(16)
N(A)-C(A5)-C(A6)	178.9(9)	C(A9)-C(A10)-C(A11)	118.4(15)
C(A5)-C(A6)-C(A7)	118.6(8)	C(A10)-C(A11)-C(A6)	115.7(13)
C(A6)-C(A7)-C(A8)	118.3(13)	C(A11)-C(A6)-C(A7)	122.8(10)
C(A7)-C(A8)-C(A9)	119.0(18)	C(A11)-C(A6)-C(A5)	118.6(10)
(2) Binuclear molecule B			
(a) Copper coordination spheres			
Cu(B)-Cu(B)^{II}	2.732(1)	Cu(B)-O(B3)	1.968(7)
Cu(B)-O(B1)	1.972(6)	Cu(B)-O(B4)^{II}	1.965(7)
Cu(B)-O(B2)^{II}	1.959(5)	Cu(B)-N(B)	2.138(6)
O(B1)-Cu(B)-O(B3)	90.1(3)	O(B3)-Cu(B)-O(B4)^{II}	165.6(2)
O(B1)-Cu(B)-O(B4)^{II}	88.3(3)	O(B1)-Cu(B)-N(B)	100.4(2)
O(B1)-Cu(B)-O(B2)^{II}	165.5(2)	O(B2)^{II}-Cu(B)-N(B)	94.1(3)
O(B2)^{II}-Cu(B)-O(B3)	87.7(3)	O(B3)-Cu(B)-N(B)	97.6(3)
O(B2)^{II}-Cu(B)-O(B4)^{II}	90.3(3)	O(B4)^{II}-Cu(B)-N(B)	96.8(3)
(b) Trichloroacetate ion			
C(B1)-O(B1)	1.252(10)	C(B3)-O(B3)	1.242(10)
C(B1)-O(B2)	1.224(8)	C(B3)-O(B4)	1.241(8)
C(B1)-C(B2)	1.526(12)	C(B3)-C(B4)	1.551(14)
C(B2)-Cl(B1)	1.782(14)	C(B4)-Cl(B4)	1.753(10)
C(B2)-Cl(B2)	1.755(11)	C(B4)-Cl(B5)	1.745(8)
C(B2)-Cl(B3)	1.760(9)	C(B4)-Cl(B6)	1.732(8)
Cu(B)-O(B1)-O(B1)	122.0(4)	Cl(B)-C(B2)-Cl(B3)	107.7(6)
Cu(B)-O(B2)^{II}-C(B1)^{II}	123.4(6)	Cl(B)-C(B2)-Cl(B3)	109.7(6)

TABLE 4. Continued

Cu(B)-O(B3)-C(B3)	122.6(5)	O(B3)-C(B3)-O(B4)	128.9(9)
Cu(B)-O(B4)^{ii}-C(B3)^{ii}	122.5(6)	O(B3)-C(B3)-C(B4)	115.2(6)
O(B1)-C(B1)-O(B2)	128.9(7)	O(B4)-C(B3)-C(B4)	115.9(7)
O(B1)-C(B1)-C(B2)	115.1(6)	C(B3)-C(B4)-Cl(B4)	112.3(6)
O(B2)-C(B1)-C(B2)	115.9(7)	C(B3)-C(B4)-Cl(B5)	112.5(5)
C(B1)-C(B2)-Cl(B1)	107.4(8)	C(B3)-C(B4)-Cl(B6)	105.3(7)
C(B1)-C(B2)-Cl(B2)	112.4(7)	Cl(B4)-C(B4)-Cl(B5)	108.5(6)
C(B1)-C(B2)-Cl(B3)	111.3(7)	Cl(B4)-C(B4)-Cl(B6)	109.4(4)
Cl(B1)-C(B2)-Cl(B2)	108.2(6)	Cl(B5)-C(B4)-Cl(B6)	108.7(5)
(c) Benzonitrile			
N(B)-C(B5)	1.122(9)	C(B8)-C(B9)	1.283(30)
C(B5)-C(B6)	1.440(10)	C(B9)-C(B10)	1.374(23)
C(B6)-C(B7)	1.371(11)	C(B10)-C(B11)	1.457(22)
C(B7)-C(B8)	1.415(18)	C(B11)-C(B16)	1.388(15)
Cu(B)-N(B)-C(B5)	172.2(6)	C(B8)-C(B9)-C(B10)	124.9(16)
N(B)-C(B5)-C(B6)	179.1(8)	C(B9)-C(B10)-C(B11)	118.1(16)
C(B5)-C(B6)-C(B7)	118.1(8)	C(B10)-C(B11)-C(B6)	114.7(10)
C(B6)-C(B7)-C(B8)	116.6(12)	C(B11)-C(B6)-C(B7)	125.0(9)
C(B7)-C(B8)-C(B9)	120.7(12)	C(B11)-C(B6)-C(B5)	116.8(7)

a) Superscripts (i) and (ii) refer to the equivalent positions $(-x, -y, -z)$ and $(1-x, 1-y, -z)$, respectively.

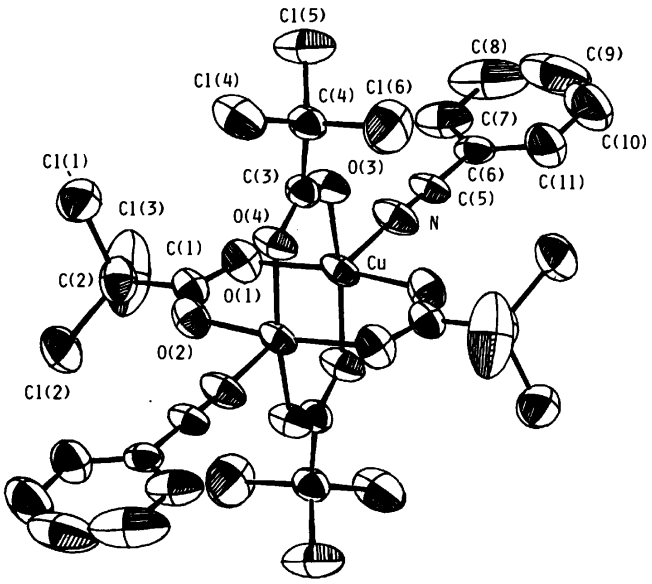

Fig. 1. Molecular structure of $[Cu(Cl_3CCOO)_2(PhCN)]_2$ with thermal ellipsoids (50% probability level).

for Cu, Cl, O, N, and C, were taken from the International Tables for X-Ray Crystallography.[4] All the calculations were carried out on the FACOM-200 computer in the Computer Center of Kyushu University by use of a local version[5] of the UNICS-II and the ORTEP programs. The final positional and thermal parameters with their estimated standard deviations are given in Table 3. The coordinates and isotropic temperature factors of the hydrogen atoms, the anisotropic thermal parameters of the non-hydrogen atoms, and the F_o-F_c tables have been deposited as Document No. 8514 at the Office of the Editor. A perspective drawing of the dimeric molecule and numbering system are illustrated in Fig. 1. The bond distances and angles are tabulated in Table 4.

Magnetic Measurement. Magnetic susceptibilities in the temperature range of 80—300 K were determined by the Faraday method. The correction for diamagnetic contribution (χ_{dia}) was made by use of Pascal's constants.[6] The cryomagnetic data were fitted to the Bleaney-Bowers equation (1) allowing for the presence of paramagnetic impurity,[7]

$$\chi_A = \frac{Ng^2\beta^2}{3kT}\left[1+\frac{1}{3}\exp\left(\frac{-2J}{kT}\right)\right]^{-1}(1-P) + \frac{Ng_i^2\beta^2}{4kT}\cdot P + N\alpha, \quad (1)$$

where P is the mole fraction of the noncoupled copper(II) impurity, g_i is the average g factor for the impurity, and the other symbols have their usual meanings. The values of $g_i=2.2$ and $N\alpha=60\times10^{-6}$ cgs emu (1 cgs emu$=4\pi\times10^{-6}$ m^3) were used throughout the present study. The best-fit parameters, $-2J$, g, and P, were obtained by using a non-linear least-squares program, SALS (model D).[3] As a convenient statistical indicator of the quality of the least-squares fits, the discrepancy index σ_{dis} ($\sigma_{dis}=[\Sigma(\chi_{obsd}-\chi_{calcd})^2/\Sigma\chi_{obsd}^2]^{1/2}$) was employed. The thermal magnetic data are shown in Figs. 2 and 3 as plots of χ_A *vs.* T. The values of χ_{dia}, g, P, $-2J$, and σ_{dis} are summarized in Table 5.

IR Measurement. IR spectra were recorded on a Hitachi 260-10 IR Spectrophotometer as Nujol mulls. The C≡N stretching frequencies observed for the complexes and those for the free nitriles are given in Table 6.

Results and Discussion

The crystal structure of the copper(II) trichloroacetate adduct with benzonitrile contains two independent centrosymmetric $[Cu(Cl_3CCOO)_2(PhCN)]_2$ molecules; they are abbreviated as A and B. The two

independent molecules are quite similar to each other in shape, although there are small differences in their interatomic distances and bond angles. As shown in Fig. 1, each molecule has the well-known dimeric copper(II) acetate monohydrate structure. The benzonitrile is bound to the copper atom in a linear fashion through the terminal nitrogen atom. The coordination geometry around each copper atom is best described as a distorted square pyramid with four carboxylato oxygen atoms in the basal plane (Cu-O 1.955—1.969 Å for A and 1.959—1.972 Å for B) and a nitrile nitrogen atom in the apical position (Cu-N 2.141(9) Å for A and 2.138(6) Å for B), in a similar way to that observed in $[Cu(Cl_3CCOO)_2(2\text{-chloropyridine})]_2$.[8] The basal

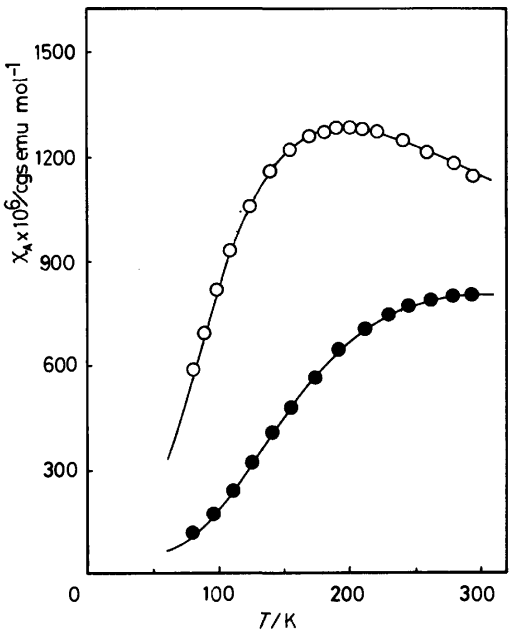

Fig. 2. Variation of magnetic susceptibilities with temperature.
(●): $Cu(ClCH_2COO)_2(PhCN)$, (○): $Cu(Cl_3CCOO)_2(PhCN)$.
The solid curves were obtained as described in the text.

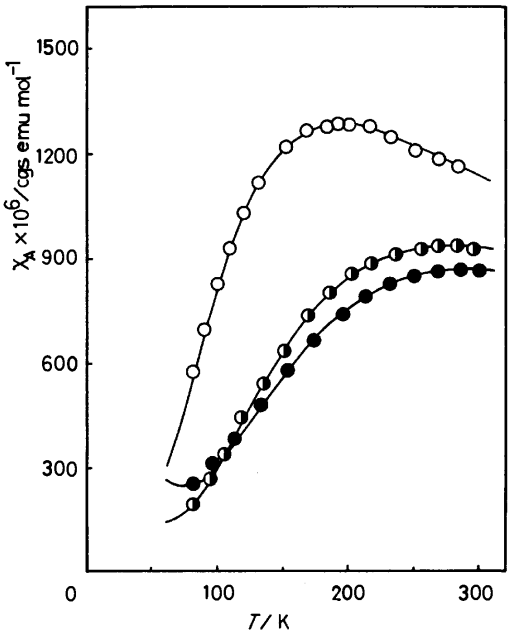

Fig. 3. Variation of magnetic susceptibilities with temperature.
(●): $Cu(ClCH_2COO)_2(4\text{-}CH_3C_6H_4CN)$, (◑): $Cu(Cl_2CHCOO)_2(4\text{-}CH_3C_6H_4CN)$, (○): $Cu(Cl_3CCOO)_2(4\text{-}CH_3C_6H_4CN)_2 \cdot 1/2$ bz.
The solid curves were obtained as described in the text.

TABLE 5. MAGNETIC DATA

Complex	$\frac{\chi_{dia} \times 10^6}{\text{cgs emu}}$	g	$P \times 10^2$	$\frac{-2J}{cm^{-1}}$	$\sigma_{dis} \times 10^3$
$Cu(ClCH_2COO)_2(PhCN)$	−165	2.23_5	0.33	352	4.96
$Cu(ClCH_2COO)_2(4\text{-}CH_3C_6H_4CN)$	−177	2.25_8	2.60	339	7.43
$Cu(Cl_2CHCOO)_2(4\text{-}CH_3C_6H_4CN)$	−211	2.28_2	0.90	314	3.56
$Cu(Cl_3CCOO)_2(PhCN)$	−234	2.26_1	2.11	224	3.23
$Cu(Cl_3CCOO)_2(4\text{-}CH_3C_6H_4CN) \cdot 1/2bz$	−273	2.23_6	0.90	216	6.18

TABLE 6. C≡N STRECHING VIBRATIONS (cm^{-1}) FOR NITRILE ADDUCTS OF COPPER(II) CHLOROACETATES

Complex	Coordinated	Free[a]	$\Delta\bar{\nu}C{\equiv}N$[b]
$Cu(ClCH_2COO)_2(PhCN)$	2257	2231	26
$Cu(ClCH_2COO)_2(4\text{-}CH_3C_6H_4CN)$	2264	2230	34
$Cu(Cl_2CHCOO)_2(4\text{-}CH_3C_6H_4CN)$	2262	2230	32
$Cu(Cl_3CCOO)_2(PhCN)$	2262	2231	31
$Cu(Cl_3CCOO)_2(4\text{-}CH_3C_6H_4CN) \cdot 1/2$ bz	2264	2230	34

a) Ref. 17. b) Change in $\bar{\nu}C{\equiv}N$ on coordination.

atoms in both A and B are almost coplanar with the largest deviation of 0.004 Å. The copper atoms in A and B are shifted from the basal planes toward the apical nitrogen atoms by 0.251 and 0.247 Å, respectively. The Cu-Cu separation (2.731(1) Å for A and 2.732(1) Å for B) is slightly shorter than that in the 2-chloropyridine adduct (2.766(3) Å).[8] The other bond distances and angles about the coordination sphere (*cf.* Table 4) are comparable to those found for the 2-chloropyridine adduct. A noteworthy feature of the coordinated benzonitrile is the C-N distances of 1.113(12) Å (A) and 1.122(9) Å (B), which are significantly shorter than that in the free molecule (1.159(2) Å).[9] This apparent shortening indicates that the C≡N bond strength increased upon formation of the CN→metal coordination bond.[10,11]

The magnetic susceptibility data of the complexes prepared in the present study are well represented by Eq. 1 (*cf.* Figs. 2 and 3), indicating that all the complexes have a dimeric structure similar to that found for $[Cu(Cl_3CCOO)_2(PhCN)]_2$. The $-2J$ values found for the respective benzonitrile adducts are larger than those found for the corresponding 4-methylbenzonitrile adducts. This fact is in accord with the previous conclusion that the antiferromagnetic interaction in dimeric copper(II) carboxylate adducts becomes stronger as the basicity of the addend ligands becomes weaker,[3] because benzonitrile must be less basic than 4-methylbenzonitrile. From Table 5, we can also see that the $-2J$ values in both the benzonitrile and 4-methylbenzonitrile adducts decrease as the pK_a values of the parent carboxylic acids become smaller. This trend can be explained in terms of weakening of the ligand field strength of the four carboxylato oxygen atoms.[3,12,13]

A remarkable feature of the IR spectra of the present complexes is that, in each case, the C≡N stretching absorption appears at a higher wavenumber by 30—40 cm^{-1} than that of the free nitrile (*cf.* Table 6). Such an increase in $\tilde{\nu}$C≡N has been attributed to an increase in the C≡N bond strength resulting from a hybridization change in the coordinated CN group or a greater contribution of the donor atom N_{2s} orbital to the CN σ-bonding system upon σ-donation of the lone pair of electrons on the nitrile nitrogen atom.[14,15] Thus, both of the shortening of the CN bond and the increase of the $\tilde{\nu}$ C≡N observed for $[Cu(Cl_3CCOO)_2(PhCN)]_2$ can be ascribed to the formation of a CN→metal σ-donating bond. On the other hand, if the metal—addend ligand bond is, on the whole, the type of C≡N← metal π-back bonding, the CN bond order should decrease; consequently, the $\tilde{\nu}$C≡N is expected to decrease.[11,16,17]

Thus, the X-ray crystallographic, magnetic and IR spectroscopic results indicate that the nitriles in the present complexes act as the σ-donor ligands. This conclusion is in accord with the recent claim by Rao *et al.* that the pyridine molecule in $[Cu(CH_3COO)_2(py)]_2$ complex functions as a σ-donor base.[18]

References

1) R. W. Jotham, S. F. A. Kettle, and J. A. Marks, *J. Chem. Soc., Dalton Trans.*, **1972**, 428.

2) D. Hibdon and J. H. Nelson, *Inorg. Chim. Acta*, **7**, 629 (1973).

3) Y. Muto, T. Tokii, K. Chijiwa, and M. Kato, *Bull. Chem. Soc. Jpn.*, **57**, 1008 (1984).

4) "International Tables for X-Ray Crystallography," Kynoch Press, Birmingham (1974), Vol. IV.

5) S. Kawano, Rep. Comp. Cent. Kyushu Univ., **16**, 113 (1983); T. Sakurai and K. Kobayashi, *Rep. Inst. Phys. Chem. Res.*, **55**, 69 (1979); C. K. Jhonson, Report No. 3794, Oak Ridge National Laboratory, Oak Ridge, Tennessee (1965).

6) P. W. Selwood, "Magnetochemistry," Interscience Publishers, New York (1956), pp. 78 and 91.

7) A. P. Ginsberg, *Inorg. Chim. Acta Rev.*, **5**, 45 (1971).

8) J. A. Moreland and R. J. Doedens, *Inorg. Chem.*, **17**, 674 (1978).

9) B. Bak, D. Christensen, W. B. Dixon, L. Hansen-Nygaard, and J. Pastrup-Andersen, *J. Chem. Phys.*, **37**, 2027 (1962).

10) B. S. Swanson, D. F. Shriver, and J. A. Ibers, *Inorg. Chem.*, **8**, 2182 (1969).

11) B. N. Storhoff, *Coord. Chem. Rev.*, **23**, 1 (1977).

12) L. Dubicki and R. L. Martin, *Inorg. Chem.*, **5**, 2203 (1966).

13) T. Tokii and Y. Muto, *Bull. Chem. Soc. Jpn.*, **49**, 1849 (1976).

14) K. F. Purcell and R. S. Drago, *J. Am. Chem. Soc.*, **88**, 919 (1966).

15) K. F. Purcell, *J. Am. Chem. Soc.*, **89**, 247 (1967).

16) R. E. Clarke and P. C. Ford, *Inorg. Chem.*, **9**, 227 (1970).

17) P. C. Ford, *Coord. Chem. Rev.*, **5**, 75 (1970).

18) V. M. Rao, D. N. Sathyanarayana, and H. Manobar, *J. Chem. Soc., Dalton Trans.*, **1983**, 2167.

Untersuchungen von Diiodogermylen und Triphenylphosphindiiodogermylen und die Kristallstruktur von Triphenylphosphindiiodogermylen

Yoshio INOGUCHI, Shuko OKUI, Kunio MOCHIDA,* und Akiko ITAI†
Chemisches Departement, Naturwissenshaftliche Fakultät, Gakushuin Universität, 1-5-1 Mejiro, Toshima-ku, Tokyo 171
†*Pharmazeutische Fakultät, Tokyo Universität, 7-3-1 Hongo, Bunkyo-ku, Tokyo 113*
(Eigegangen am August 2, 1984)

Reaktivitäten und chemische Eigenschaften von Diiodogermylen und Triphenylphosphindiiodogermylen wurden durch ihre Reaktionen mit Organolithium-Verbindungen oder Butadienen untersucht. Die Kristallstruktur von Triphenylphosphindiiodogermylen wurde röntgenographisch aufgeklärt.

Diorganogermylene, GeR_2, sind für metallorganische Synthesen als Carbenanaloge ebenso wie die homologen Silylene und Stannylene von großem Interesse; zahlreiche Arbeiten über diese Verbindungsklasse wurden in den letzten Jahren publiziert.[1] Diorganogermylene sind sehr instabil und konnten mit wenigen Ausnahmen nicht isoliert werden.[2] Wir haben durch Umsetzung von Diiodogermylen bzw. Triphenylphosphindiiodogermylen mit Organolithium-Verbindung untersucht, ob Diorganogermylen als Zwischenprodukt entsteht und eventuell durch das phosphankoordination stabilisiert werden kann:

$$:GeI_2 + RLi \longrightarrow [:GeR_2],$$
$$LGeI_2 + RLi \longrightarrow [LGeR_2] \quad (L=PPh_3).$$

Durch röntgenographische Aufklärung der Struktur von Triphenylphosphindiiodogermylen sollte es untersucht werden, wie Triphenylphosphan an Diiodogermylen koordiniert ist. Sie sollte außerdem Anhaltspunkte für die Reaktivität dieser Verbindung geben.

Ergebnisse und Diskussion

Diiodogermylen, GeI_2, reagiert mit Phenyllithium in Ether zu Tetraphenylgerman, Ph_4Ge, Triphenylgerman, Ph_3GeH, und polymeren Produkten[3]:

$$:GeI_2 + PhLi \xrightarrow[2)\ H_2O]{1)\ \text{Ether}} Ph_4Ge,\ Ph_3GeH,\ \text{Polymer.} \quad (1)$$

Die Umsetzung von Triphenylphosphindiiodogermylen, Ph_3PGeI_2, mit Phenyllithium in Ether nach anschließender Hydrolyse ergibt Ph_4Ge, Ph_3GeH und Polymer:

$$Ph_3PGeI_2 + PhLi \xrightarrow[2)\ H_2O]{1)\ \text{Ether}} Ph_4Ge,\ Ph_3GeH,\ \text{Polymer.} \quad (2)$$

In Tabelle 1 sind die Einzelheiten der durchgeführten Reaktionen zusammengestellt. Phenyllithium wurde bezogen auf zu GeI_2 bzw. Ph_3PGeI_2 in den Stöchiometrien 1:1, 2:1 und 4:1 verwendet. Je größer das Molarverhältnis von Phenyllithium zu GeI_2 ist, desto höher sind die Ausbeuten an Ph_4Ge. Ph_3GeH entsteht durch Hydrolyse von Triphenylgermyllithium, das als Zwiechenprodukt der dritten Stufe über PhGeI und Ph_2Ge aus GeI_2 und Phenyllithium gebildet wird.[3] Andere germaniumhaltige Produkte zersetzen sich wahrscheinlich zu den aufgefundenen Polymeren. Die Ausbeute an Ph_4Ge bei der Reaktion von Ph_3PGeI_2 mit Phenyllithium ist vom zugegebenen Phenyllithium abhängig. Auch freies Triphenylphosphan fiel in größeren Mengen an. Bei 1:1 und 1:2 in den beiden Reaktionen erschien kein Unterschied der Ausdeuten. Nur bei 1:4 trat ein Unterschied auf. Die hohe Ausbeute von 39% an Ph_3GeH

TABELLE 1. REAKTIONEN VON GeI_2 ODER Ph_3PGeI_2 MIT PHENYLLITHIUM

Verbindung[a]		Bedingungen	Produkte/%[b]			
GeI_2	: PhLi		PhI	Ph-Ph	Ph_3GeH	Ph_4Ge
1	: 1	5 d, Ether	4.9	3.8	1.9	1.6
1	: 2	5 d, Ether	7.3	13	0.6	11
1	: 4	5 d, Ether	40	62	0.7	32

Verbindung[a]		Bedingungen	Produkte/%[b]				
Ph_3PGeI_2	: PhLi		PhI	Ph-Ph	Ph_3GeH	Ph_4Ge	Ph_3P
1	: 1	5 d, Ether	2.9	2.9	1.9	14	82
1	: 2	5 d, Ether	7.7	9.6	1.3	19	79
1	: 4	5 d, Ether	10	13	39	36	100

a) Molarverhältnisse. b) Gerechnet aus der Konzentration von GeI_2 bzw. Ph_3PGeI_2.

in der Reaktion von Ph_3PGeI_2 mit PhLi bedeutet, daß Ph_3GeLi in größeren Mengen entsteht, das mit PhI zu Ph_4Ge nicht umsetzt wird. Daher könnte Ph_3GeLi oder GeR_2 bei Triphenylphosphan in dieser Reaktion stabilisiert werden.

Umsetzungen von GeI_2 mit Butadienen in Heptan sollte eigentlich die entsprechenden Addukte ergeben:[4]

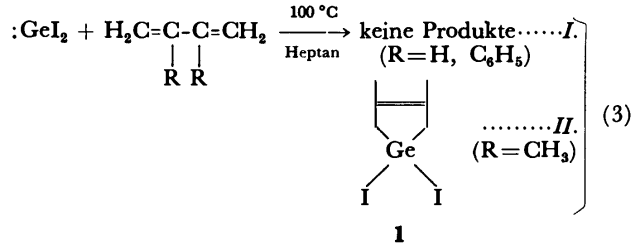

(3)

1

In dieser Untersuchung gelang nur *3II*, das Addukt 1,1-diiodo-3,4-dimethylgermacyclopent-3-en **1** zu ergeben. Dieser Unterschied der Addition hängt vielleicht von der Donatoreigenschaft der Doppelbindung von Butadien gegen Germanium ab. Im Fall *3I* wird die Doppelbindung wegen Wasserstoff bzw. Phenylgruppe nicht genug aktiviert, um an Germanium zu addieren. Nur die Methylgruppe bei *3II* gelang, die Elektronendichte an der Doppelbindung für Addition zu aktivieren. Umsetzungen von Ph_3PGeI_2 mit Butadienen unter denselben Bedingungen wie für GeI_2 ergeben keine Addukte:

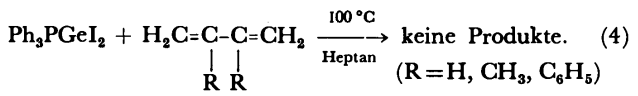

Bei GeI_2 ist die Donatorfunktion der Doppelbindung zu leerem Orbital an Germanium möglich. Im Gegensatz dazu, kann die Doppelbindung bei Ph_3PGeI_2 wegen der Besetzung desselben Orbitals an Germanium durch Koordination von Triphenylphosphan keine Donatorfunktion ausüben.

Die Umsetzungen von GeI_2 mit Phenyllithium in Gegenwart von Butadienen ergeben Ph_4Ge und erst bei *5II* ein zweites Produkt, das von der Phenylgruppe substituierte Addukt 3,4-Dimethyl-1,1-diphenylgermacyclopent-3-en **2**:

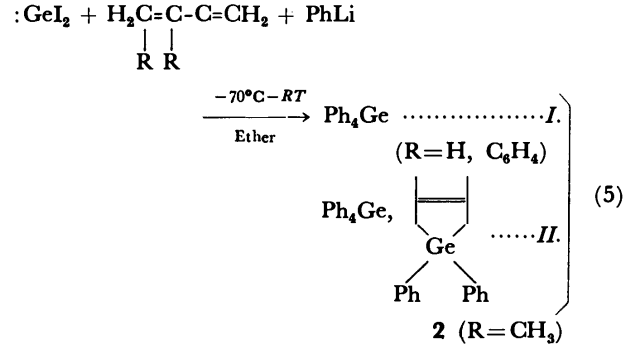

(5)

Ph_4Ge entsteht in dieser Reaktion aus der direkten Umsetzung von GeI_2 mit Phenyllithium wie *Gl. 1*. **2** entsteht aus der Reaktion von Phenyllithium und **1**, das nach *3II* aus GeI_2 und Butadien ergeben wird.

Die Reaktionen von Ph_3PGeI_2 mit Phenyllithium und Butadienen wurden auch für Vergleich mit *Gl. 5* durchgeführt:

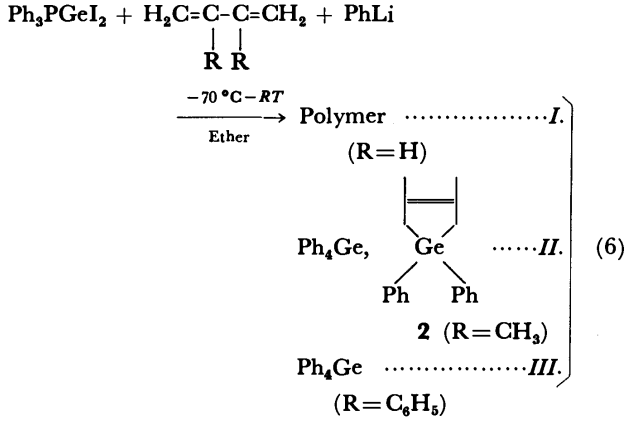

(6)

Die Polymerisation bei *6I* kommt aus Butadien mit Phenyllithium, weil es kein Produkt aus Ph_3PGeI_2 mit Butadien ergibt (s. *3II*) und weil Ph_4Ge aus Ph_3PGeI_2 mit Phenyllithium entstehen soll (s. *Gl. 2*). Bei *6II* ergab es zwei Produkte, Ph_4Ge und Addukt **2**. Ph_4Ge entsteht aus der direkten Reaktion von Ph_3PGeI_2 mit Phenyllithium. Aber die Bildung von **2** erregte uns eine große Interesse. Die Umsetzung von Ph_3PGeI_2 mit Butadien (*Gl. 4*) ergibt Produkt **1** nicht, das sich mit Phenyllithium zu der Verbindung **2** überführen läßt. Mit anderen Worten entsteht die Verbindung **2** nicht über **1**. Ein möglicher Weg zu **2** in der Reaktion *6II* ist die Umsetzung von Butadien mit Ph_2Ge, das letzte Germylen, das als Zwischenprodukt in der Reaktion von Ph_3PGeI_2 mit Phenyllithium entstehen soll. Die Bildung von **2** bei *6II* ist ein Beweis für das Auftreten von Diphenylgermylen Ph_2Ge. Bei *6III* wird nur Ph_4Ge wie bei *5I* gegeben und das Butadien hat keinen Einfluß auf die Umsetzung von Ph_3PGeI_2 mit Phenyllithium.

Röntgenkristallstrukturanalyse von Ph_3PGeI_2. Die Kristallstruktur von Ph_3PGeI_2 wurde röntgenographisch untersucht. Ph_3PGeI_2 kristallisiert aus Xylol in monoklinen Würfeln in der Raumgruppe $P2_1/n$, $Z=8$, $a=11.858\,(3)$, $b=38.569\,(8)$, $c=9.304\,(2)$ Å, $\beta=111.217\,(4)°$, $R=10.0$ (Abb. 1, Tabelle. 2). Zwei verschiedene Strukturen von Ph_3PGeI_2 wurden gegeben. Jeder Bindungswinkel (P-Ge-I, I-G-I) von 90—99° an dem Germaniumatom ist kleiner als der von 109° in allgemeinem sp^3-Orbital. Die zwei Elektronen des Germaniums lokalisieren sich als ein Elektronenpaar an dem Germaniumatom in gegenseitigem Lappen von den zwei Iodatome und dem Phosphoratom. Triphenylphosphan ist an dem Germaniumatom einfach koordiniert und darum erscheint keine Rückbindung aus Germaniumatom zu Phosphoratom. Aus dieser Lokalisierung der Elektronen an Germaniumatom und dem Abstand von 2.503 bzw. 2.510 Å zwischen

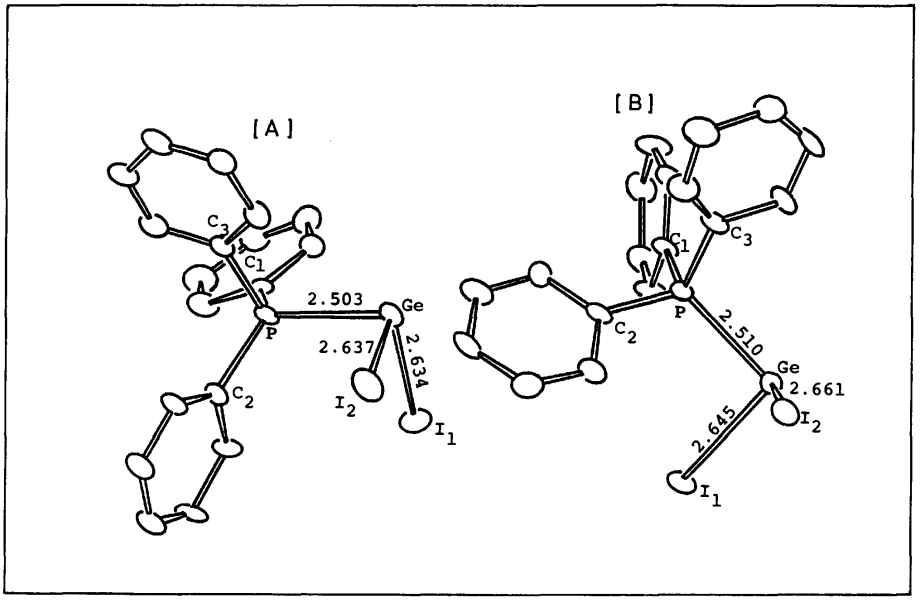

Abb. 1. Kristallstruktur von Ph_3PGeI_2.

TABELLE 2. ABSTÄNDE/Å UND WINKEL/° IN Ph_3PGeI_2

	[A]	[B]
Ge-I_1	2.634(2)	2.645(2)
Ge-I_2	2.637(3)	2.661(3)
Ge-P	2.503(4)	2.510(5)
P-C_1	1.811(19)	1.813(19)
P-C_2	1.813(17)	1.777(17)
P-C_3	1.824(19)	1.813(15)
I_1-Ge-I_2	99.0(1)	99.0(1)
I_1-Ge-P	90.4(1)	94.5(1)
I_2-Ge-P	93.0(1)	93.8(1)
Ge-P-C_1	108.8(6)	108.2(6)
Ge-P-C_2	118.7(6)	120.6(6)
Ge-P-C_3	108.6(6)	112.0(6)
C_1-P-C_2	109.4(8)	104.8(8)
C_2-P-C_3	105.5(8)	105.5(8)
C_1-P-C_3	104.9(8)	104.5(8)

dem Germaniumatom und Phosphoratom ist es deutlich, daß die Phosphor-Germanium Bindung keinen Doppelbindungscharakter hat.

Experimenteller Teil

Alle Arbeiten wurden zum Ausschluß von Sauerstoff und Feuchtigkeit unter Stickstoff durchgeführt. Lösungsmittel und Glasgeräte waren entsprechend vorbehandelt. GeI_2 wurde aus GeO_2 und HI nach dem Verfahren in Lef. 6 hergestellt. Ph_3PGeI_2 wurde aus GeI_2 mit Triphenylphosphan nach der Methode von King[7] dargestellt. NMR Spektren wurden mit einem Varian FT-80 und einem Jeol FX-90Q aufgenommen.

Spektroskopische Daten von Ph_3PGeI_2. ^{13}C NMR ($CDCl_3$) δ=126.12 (d, ^1J (PC)=40.9 Hz, C-1), 133.47 (d, ^2J (PC)=8.8 Hz, C-2,6), 129.34 (d, ^3J (PC)=10.3 Hz, C-3,5) und 132.17 (s, C-4); ^{31}P NMR ($CDCl_3$) δ=10.89 (br).

Reaktionen von GeI_2 mit Phenyllithium (Gl. 1). Zu einer Suspension von 0.40 g (1.23 mmol) GeI_2 in 5 cm^3 Ether wurde bei Raumtemperatur 2.8 cm^3 (1.23 mmol) Phenyllithium (0.44 M† Lösung in Ether) langsam zugetropft. Nach einem Rühren im Lauf von 5 Tagen beim Erwärmen unter Rückfluß wurde die Reaktionlösung hydrolysiert. Die Produkte wurden mit GLC untersucht. Zwei- und vierfach Phenyllithium wurden auch mit GeI_2 umgesetzt. Die Ausbeuten der Produkte sind in Tabelle 1 aufgenommen.

Reaktionen von Ph_3PGeI_2 mit Phenyllithium (Gl. 2). Zu einer Suspension von 1.16 g (1.97 mmol) Ph_3PGeI_2 in 5 cm^3 Ether wurde 1.97 mmol Phenyllithium bei RT zugetropft (zwei- und vierfach Phenyllithium wurden auch verwendet). Nach einem fünf tägigen Rühren beim Erwärmen unter Rückfluß wurde die Lösung hydrolysiert und getrocknet. Die erzeugte Verbindungen wurden mit GLC untersucht. Die Daten der Ausbeuten sind in Tabelle 1 dargestellt.

Reaktionen von GeI_2 mit Butadienen (Gl. 3). *3I*: Die Umsetzung von 3.0 g (9.2 mmol) GeI_2 mit 1.0 g (18.5 mmol) 1,3-Butadien bzw. 18.5 mmol 2,3-Diphenyl-1,3-butadien in 5 cm^3 Heptan nach dreitägigem Erwärmen bei 100 °C in einer Druckflasche ergab kein Produkt.[4,8]

3II: Die Umsetzung von 2.0 g (6.13 mmol) mit 0.51 g (6.21 mmol) 2,3-Dimethyl-1,3-butadien in 5 cm^3 Heptan bei 110 °C ergab nach 1 Tag 0.2 g (0.49 mmol) 1,1-Diiodo-3,4-dimethylgermacyclopent-3-en **1**. Ausbeute 8%.

Reaktionen von Ph_3PGeI_2 mit Butadienen (Gl. 4). Die Reaktionen von Ph_3PGeI_2 mit den Butadienen in Heptan unter den in *Gl. 3* bezeichnet Bedingungen ergaben keine Produkte.

Reaktionen von GeI_2 mit Phenyllithium und Butadienen (Gl. 5). *5II*: Zu einer Suspension von 2.0 g (6.13 mmol) GeI_2 und 0.51 g (6.21 mmol) 2,3-Dimethyl-1,3-butadien in 10 cm^3 Ether wurde bei −70 °C 25 cm^3 (12.3 mmol) Phenyllithium (0.49 M Lösung in Ether) zugetropft. Nach 1 Stunde wurde die Reaktionlösung bis Zimmertem-

†1 M=1 mol dm^{-3}

peratur langsam erwärmt, wobei sie sich von gelb zu braun änderte. Die Lösung wurde nach dem Rühren im Lauf von 2 Tagen bei RT hydrolysiert und mit Na_2SO_4 getrocknet. Das Produkt wurde mit GLC isoliert. 3,4-Dimethyl-1,1-diphenylgermacyclopent-3-en **2** ist ein farbloser Kristall mit einem Schmelzpunkt von 46—49 °C (Lit,[4,9] 40—41 °C). Ausbeute 19%. Spektroskopische Daten von **2**: ^1H NMR ($CDCl_3$) δ=1.78 (s, CH_3), 2.00 (s, CH_2) und 7.37 (m, C_6H_5). Ph_4Ge wurde mit einer Ausbeute von 3% ergeben.

5I: Umsetzung von 2.0 g (6.13 mmol) GeI_2 und 1.0 g (18.5 mmol) 1,3-Butadien mit 12.3 mmol Phenyllithium in Ether bei −70 °C ergab Ph_4Ge 5%. Reaktion von 0.65 g (1.99 mmol) GeI_2 und 0.41 g (1.99 mmol) 2,3-Diphenyl-1,3-butadien mit 4 mmol Phenyllithium ergab Ph_4Ge 6%.

Reaktionen von Ph_3PGeI_2 mit Phenyllithium und Butadienen (Gl. 6). *6I*: Die Reaktion von 2.6 g (4.42 mmol) Ph_3PGeI_2 und 1.0 g (18.5 mmol) 1,3-Butadien mit 8.87 mmol Phenyllithium in Ether bei −70 °C polymerisierte nach Erwärmen bis 0 °C.

6II: Zu einer Suspension von 0.85 g (1.45 mmol) Ph_3PGeI_2 und 0.12 g (1.46 mmol) 2,3-Dimethyl-1,3-butadien in 5 cm^3 Ether wurde bei −70 °C 6.5 cm^3 (2.95 mmol) Phenyllithium (0.45 M Lösung in Ether) zugetropft. Nach 1 Stunde wurde die Lösung bis RT erwärmt. Nach Hydrolyse und Vertrocken wurden die Produkte mit GLC untersucht. Es ergab 3,4-Dimethyl-1,1-diphenylgermacyclopent-3-en **2** 14% und Ph_4Ge 5%.

6III: Die Umsetzung von 0.75 g (0.93 mmol) Ph_3PGeI_2 und 0.19 g (0.92 mmol) 2,3-Diphenyl-1,3-butadien mit 18.5 mmol Phenyllithium in Ether bei −70 °C ergab Ph_4Ge 5%.

Röntgenstrukturanalyse von Ph_3PGeI_2. Einkristall mit der Größe von *ca.* 0.2×0.3×0.3 mm wurde aus einer langsamen Kühlung von warmem Xylol dargestellt. Der gelbe Kristall wurde in der abgeschmolzenen Kapillare unter Stickctoff röntgenographisch aufgenommen.

Wir danken dem Kultusministerium für finanzielle Unterstützung für naturwissenschaftliche Forschung (Nr. 58740286).

Literatur

1) K. H. Scherping und W. P. Neuman, *Organometallics*, **1**, 1017 (1982); A. Bacceiredo, G. Bertrand, und P. Mazerolles, *Tetrahedron Lett.*, **22**, 2553 (1981); G. Dousse und J. Sátge, *Helv. Chim. Acta*, **60**, 1381 (1977); J. Sátge, M. Massol, und P. Riviere, *J. Organomet. Chem.*, **56**, 1 (1973).

2) D. H. Harris und M. F. Lappert, *J. Chem. Soc., Chem. Commun.*, **1975**, 895 D. E. Goldberg, D. H. Harris, und M. F. Lappert, *ibid.*, **1976**, 261 P. J. Davidson, D. H. Harris, und M. F. Lappert, *J. Chem. Soc., Dalton Trans.*, **1976**, 2268.

3) F. Glockling und K. A. Hooton, *J. Chem. Soc.*, **1973**, 1849.

4) P. Mazerolles, G. Manuel, und F. Thoumas, *C. R. Acad. Sci. Paris, Ser. C*, **267**, 619 (1968); P. Mazerolles und G. Manuel, *Bull. Soc. Chim. Fr.*, 327 (1966); G. Manuel und P. Mazerolles, *ibid.*, 2447 (1965).

5) N. G. Bokii, Y. T. Struchkov, S. P. Kolesnikov, I. S. Rogozhin, und O. M. Nefedov, *Izv. Akad. Nauk SSSR, Ser Khim*,**1975**, 812.

6) L. S. Foster und A. F. Williston, *Inorg. Synth.*, **2**, 112 (1946); L. S. Foster, *ibid.*, **3**, 63 (1950).

7) R. B. King, *Inorg. Chem.*, **2**, 199 (1963).

8) P. Mazerolles, G. Manuel und F. Thoumas, *C. R. Acad. Sci. Paris*, **1968**, 619.

9) G. Manuel, P. Mazerolles, M. Lesbre, und J. P. Pradel, *J. Organomet. Chem.*, **61**, 147 (1973); P. Mazerolles und G. Manuel, *Bull. Soc. Chim. Fr.*, **1966**, 327.

The Syntheses of the Corticoid Side Chain. I. An Improved Method for the Preparation of 17α-Hydroxyprogesterone from Androst-4-ene-3,17-dione

Issei NITTA,* Shinichiro FUJIMORI, and Hiroaki UENO
Biosciences Laboratory, Research Center, Mitsubishi Chemical Industries Limited, 1000 Kamoshida-cho, Midori-ku, Yokohama, Kanagawa 227
(Received August 9, 1984)

The 17β-cyano-17α-hydroxyandrost-4-en-3-one can be prepared from androst-4-ene-3,17-dione in an excellent yield. This derivative can be converted into 17α-hydroxyprogesterone, an intermediate of corticosteroids.

Since the microbial degradation of the side chain of cholesterol or sitosterol had been developed,[1] the transformation of androstan-17-one derivatives into corticoids became very important and recently, several efficient methods for partial synthesis of corticoid side chain from 17-oxo steroids have been published.[2]

We present here an improved method for converting androst-4-ene-3,17-dione (**1**) into 17α-hydroxyprogesterone (**6**), an intermediate of corticoids, featuring a stereoselective one-step formation of 17β-cyano-17α-hydroxy group at the C-17 position of **1**.[3]

Results and Discussion

The methods employed in this conversion are summerized in Scheme 1.

The first step is the regio- and stereoselective addition of hydrogen cyanide to 17-keto function of **1**. According to the conventional procedure, the dione **1** was treated with alcoholic hydrogen cyanide.[4a] Many products were formed and it was expected that 17α-cyano and 17β-cyano compounds were formed in addition to 3,17-bis(cyanohydrin)s. The use of acetone cyanohydrin (in an exchange reaction in acetone cyanohydrin in the presence of a small amount of amine) afforded 17-monocyanohydrin **2b** quantitatively. In order to determine the configuration of the cyano group of **2b**, 3,3-ethylene acetal 17-silyl ether of **2b** was treated with excess methylmagnesium chloride at 70 °C, followed by deprotection of the 3-acetal. The isolated product was 17α-acetyl-17β-hydroxyandrost-4-en-3-one. This result indicated that the configuration of the cyano group at C-17 was α-configuration, which meant that an undesirable epimer was formed.

On the other hand, when acetic acid (5 equiv of **1**) was added to a suspension of **1** and KCN (10 equiv of **1**) in methanol at 25 °C, the poorly soluble isomer **2a** crystallized out. The HPLC analysis of the crystal showed that **2a**, having a retention time of 9.1 min, was formed as almost the sole product (the retention time of **2b** is 8.4 min). By means of NMR and IR, **2a** was identified as 17β-cyano-17α-hydroxyandrost-4-en-3-one. This process gives the required cyanohydrin **2a** in pure form yielding about 95%. This may be attributed to the fact that the 17α-cyanohydrin **2b** which was formed by the cyanide anion attack on C-17 from the least hindered side was converted to **2a** under equilibrium conditions (in the presence of KCN) and the poorly soluble **2a** crystallized out preferentially. We have also found that this procedure could be applica-

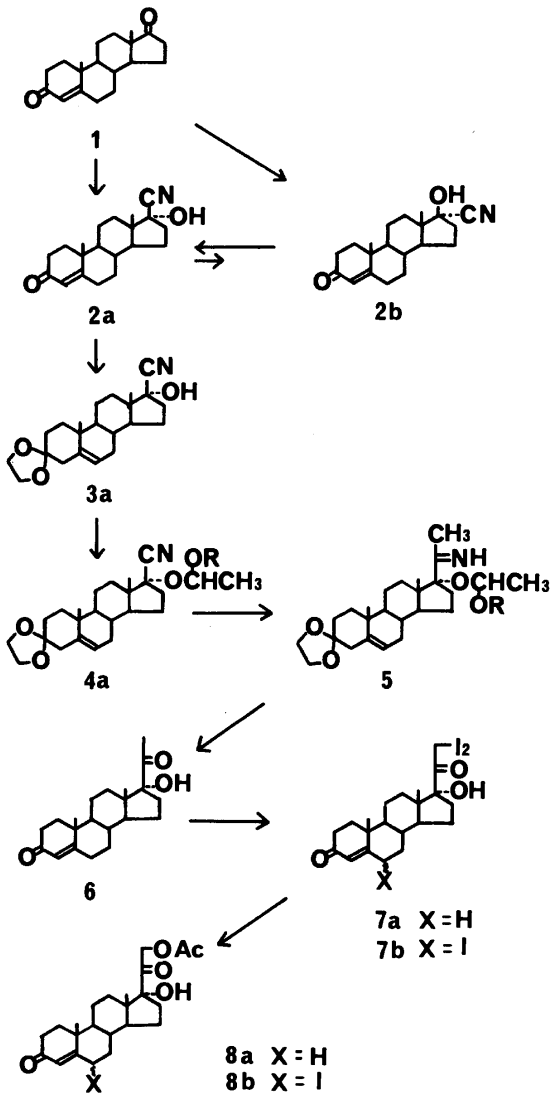

Scheme 1.

ble to the preparation of 17β-cyanohydrins of various androstanes. (see Experimental)

For the following step of the synthesis, it is necessary to protect the carbonyl and hydroxyl functions of **2a**. Treatment of **2a** in ethylene glycol with trimethyl orthoformate in the presence of TsOH led to the expected acetal **3a**. Without further purification, **3a** was treated with butyl vinyl ether in THF containing a small amount of TsOH to give **4a**. Without isolation, **4a** was treated with a 1 M† solution of methyllithium (1.2 equiv of **2a**). Aqueous acetic acid was added and the solution was heated to 110 °C for 1 h. 17α-hydroxyprogesterone, a versatile intermediate for the synthesis of corticoids, was obtained from **2a** with an overall yield of about 70%.

The 21-acetoxy introduction into **6** was accomplished by Stork's iodination procedure.[4b] Iodination of **6** in THF–methanol with excess iodine in the presence of calcium oxide gave the 21,21-diiodosteroid **7a**, which was converted directly to **8a** by treating it with potassium acetate in acetone. The HPLC analysis of the product showed that 17α,21-dihydroxypregn-4-ene-3,20-dione 21-acetate (about 60%) and a by-product (about 35%) were formed. The by-product was isolated by TLC on silica gel developed with ethyl acetate–benzene (1:2). From NMR spectra, it was assumed to be 17α,21-dihydroxy-6-iodopregn-4-ene-3,20-dione 21-acetate (**8b**), and **8a** was recovered from **8b** by treating it with zinc powder in acetic acid in a satisfactory yield.

Transformation of **8a** into hydrocortisone, a typical corticoid, was followed by microbilological process.

Experimental

Melting points were determined with a Mettler FP 61. Preparative TLC was accomplished with silica gel 60 F-254 plates (2 mm thick, E. Merck). HPLC was performed with a Shimadzu LC-2 liquid chromatograph instrument equipped with a Shimadzu Zorbax-ODS column (4.6 mm×25 cm) and a UV detector, and operated at flow rate of 2 ml min^{-1} by using a solvent consisting of MeOH–H_2O (8:2). Optical rotations were determined with a Jasco model DIP-digital polarimeter. NMR spectra were determined with a JEOL JNM-PS-100 spectrometer, with TMS as the internal standard. GLC analyses were performed on a Shimadzu GC-6A gas chromatograph equipped with a flame-ionization detector, using a column packed with 1% Silicone DC-QF-1 on Gaschrom Q (3 mm×0.5 m; column temp, 220 °C; carrier gas, N_2 60 ml/min; injector temp., 250 °C).

Materials. Androst-4-ene-3,17-dione (**1**) was obtained from Sigma. Androsta-4,9(11)-diene-3,17-dione was prepared according to the procedure in the literature[2f] from 9α-hydroxyandrost-4-ene-3,17-dione.

17β-Cyano-17α-hydroxyandrost-4-en-3-one (2a). Acetic acid (17.6 ml, 0.293 mol) was added over a period of 20 min at 25 °C to a stirred mixture of androst-4-ene-3,17-dione (**1**) (52.3 g, 0.182 mol) and potassium cyanide (50.0 g, 0.769 mol) in methanol (400 ml). The mixture was stirred at 25 °C. The starting material was completely dissolved within 1 h and product began to crystallize after reaction for 2 h. The mixture was kept overnight at room temp and then acetic acid (30 ml) was added. After dilution with water, the precipitated product was collected by filtration, washed with water and dried to give crude **2a** (57.5 g). The HPLC analysis indicated that the purity of **2a** (t_r: 9.1 min) was 95%, and 2% of **2b** and 2.5% of **1** were contained. Recrystallization from ethanol afforded the analytically pure sample: mp 169—172 °C dec.; $[\alpha]_D^{28}$ +120.3° (*c* 0.66, dioxane); IR (KBr) 3250 (OH), 2220 (C≡N) and 1640 cm^{-1} (C=O); NMR ($CDCl_3$) δ=0.98 (3H, s, 13-CH_3).

Found: C, 76.59; H, 8.72; N, 4.48%. Calcd for $C_{20}H_{27}O_2N$: C, 76.64; H, 8.68, N, 4.46%.

In a similar procedure, 17β-cyano-17α-hydroxyandrosta-4,9(11)-dien-3-one (**9a**), 3,3-ethylenedioxy-17β-cyanoandrosta-5,9(11)-dien-17α-ol (**10a**) were prepared.

(**9a**): Mp 199—201 °C dec.; $[\alpha]_D^{28}$ +95.6° (*c* 0.83, dioxane); NMR ($CDCl_3$) δ=0.95 (3H, s, 13-CH_3). Found: C, 77.17; H, 8.01; N, 4.45%. Calcd for $C_{20}H_{25}O_2N$: C, 77.13; H. 8.09: N, 4.50%.

(**10a**): Mp 202—205 °C; $[\alpha]_D^{28}$ +17.8° (*c* 0.53, dioxane); NMR ($CDCl_3$) δ=0.91 (3H, s, 13-CH_3). Found: C, 74.52; H, 8.28; N, 3.72%. Calcd for $C_{22}H_{29}O_3N$: C, 74.33; H, 8.23; N, 3.94%.

17α-Cyano-17β-hydroxyandrost-4-en-3-one (2b). Androst-4-ene-3,17-dione (**1**) (20.0 g) was dissolved by gentle warming in 30 ml of acetone cyanohydrin. Stirring was continued for 8 h at room temp, but the crystallization did not begin. Two drops of DBU was added. After five minutes crystallization began and was completed within 1 h at room temp. The resulting precipitated product was collected by filtration, washed with ether and dried to give 17-cyanohydrin **2** (23.0 g). The HPLC analysis showed that 17α-cyano-17β-hydroxyandrost-4-en-3-one (**2b**) (t_R: 8.4 min) formed as an almost sole product and no 17β-cyano-17α-hydroxyandrost-4-en-3-one (**2a**) (t_R: 9.1 min) was detected. Recrystallization from ethanol afforded the analytically pure sample, mp 153—155 °C (pre-melting point), 171—172 °C dec.; $[\alpha]_D^{28}$ +45.5° (*c* 0.72, dioxane); IR (KBr) 3250 (OH), 2230 (C≡N), and 1640 cm^{-1} (C=O); NMR ($CDCl_3$) δ=0.91 (3H, s, 13-CH_3).

Found: C, 76.87; H, 8.52; N, 4.43%. Calcd for $C_{20}H_{27}O_2N$: C, 76.64; H, 8.68: N, 4.46%.

According to the previous procedure,[5] 3,3-ethylenedioxy-17α-cyanoandrost-5-en-17β-ol (**3b**), 17α-cyano-17β-hydroxyandrosta-4,9(11)-dien-3-one (**9b**), 3,3-ethylenedioxy-17α-cyanoandrosta-5,9(11)-dien-17β-ol (**10b**) were also prepared.

(**3b**): Mp 194—195 °C dec.; $[\alpha]_D^{28}$ −71.4° (*c* 0.95, dioxane); NMR ($CDCl_3$) δ=0.83 (3H, s, 13-CH_3). Found: C, 73.72; H, 8.63; N, 3.82%. Calcd for $C_{22}H_{31}O_3N$: C, 73.91; H, 8.74; N, 3.92%.

(**9b**): Mp 201—204 °C dec.; $[\alpha]_D^{28}$ +20.8° (*c* 0.76, dioxane); NMR ($CDCl_3$) δ=0.88 (3H, s, 13-CH_3). Found: C, 77.07; H, 7.99; N, 4.31%. Calcd for $C_{20}H_{25}O_2N$: C, 77.13; H, 8.09; N, 4.50%.

(**10b**): Mp 185—186 °C; $[\alpha]_D^{28}$ −44.7° (*c* 0.49, dioxane); NMR ($CDCl_3$) δ=0.85 (3H, s, 13-CH_3). Found: C, 74.50; H,

† 1 M=1 mol dm^{-3}.

8.14; N, 3.95%. Calcd for $C_{22}H_{29}O_3N$: C, 74.33; H, 8.23; N, 3.94%.

*3,3-Ethylenedioxy-17β-cyanoandrost-5-en-17α-ol (**3a**).* *p*-Toluenesulfonic acid (1.5 g) was added to a suspension of **2a** (57.5 g) in trimethyl orthoformate (50 ml) and ethylene glycol (350 ml) and the mixture was stirred at 40 °C for 6 h. The solution was poured into water containing pyridine (1.5 ml). The resulting precipitated product was collected by filtration, washed with water and dried to give 3,3-ethylenedioxy-17β-cyanoandrost-5-en-17α-ol (**3a**) containing about 10% of 3,3-ethylenedioxy-17β-cyanoandrost-4-en-17α-ol (60.3 g). Without further purification, crude **3a** was used in the next step. Recrystallization from methanol afforded the analytically pure sample; mp 227—229 °C dec.; $[\alpha]_D^{28}$ −15.3 °C (*c* 1.00, dioxane); IR (KBr) 3450 (OH) and 2240 cm^{-1} (C≡N); NMR ($CDCl_3$) δ=0.94 (s, 3H, 13-CH_3).

Found: C, 73.90; H, 8.51; N, 3.88%. Calcd. for $C_{22}H_{31}O_3N$: C, 73.91; H, 8.74; N, 3.92%.

*17α-Hydroxyprogesterone (**6**).* To the crude **3a** (2.00 g), butyl vinyl ether (1.27 ml) and *p*-toluenesulfonic acid soln. (0.2% in THF, 3.0 ml) were added. After stirring for 20 min at room temp, methyllithium (1 M solution in ether, 10 ml) was added and stirred for 2 h at room temp. Acetic acid (8.0 ml) and water (4.0 ml) were added and heated at 110 °C for 1 h. After dilution with water containing sodium carbonate, the precipitated product was collected by filtration, washed with water and dried to give 17α-hydroxyprogesterone (**6**) (1.77 g, purity 72% which was determined by HPLC analysis, yield 69%). Recrystallization from ethyl acetate afforded the analytically pure sample. The NMR and IR spectrum were identical to that of an authentic specimen of 17α-hydroxyprogesterone and the melting point was undepressed on admixture with authentic specimen.

References

1) M. Nagasawa, H. Hashiba, N. Watanabe, M. Bae, G. Tamura, and K. Arima, *Agric. Biol. Chem.*, **34**, 801 (1970); Y. Imada and I. Nitta, *Hakko To Kogyo*, **38**, 1117 (1980).

2) a) A. R. Daniewski and W. Wojciechowska, *J. Org. Chem.*, **47**, 2993 (1982); b) D. H. R. Barton, W. B. Motherwell, and S. Z. Zard, *J. Chem. Soc., Chem. Commun.*, **1981**, 774; c) G. Neef, U. Eder, A. Seeger, and R. Wiechert, *Chem. Ber.*, **113**, 1184 (1980); d) V. V. Rheenen and K. P. Shephard, *J. Org. Chem.*, **44**, 1582 (1979); e) R. W. Freerksen, M. L. Raggio, C. A. Thoms, and D. S. Watt, *ibid.* **44**, 702 (1979); f) H. Hofmeister, K. Annen, H. Laurent, and R. Wiechert, *Chem. Ber.*, **111**, 3086 (1978); g) M. Biollaz, W. Haefliger, E. Velarde, P. Crabbe, and J. H. Fried, *Chem. Commun.*, **1971**, 1322.

3) The major part of the work described in this paper forms the basis of Japan. Kokai 57-062296, 57-062298, 57-062299, and 57-062300 (15 Apr 1982, Appl. 1 Oct 1980). After the completion of our work, DD-147-669 (15 Apr 1981) disclosed the synthesis of 17β-cyano-17α-hydroxyandrostane and estrane derivatives, which was very similar to our procedure.

4) a) J. Fried and J. A. Edwards, "Organic Reactions in Steroid Chemistry", Van Nostrand Reinhold Company, (1972), vol II, p. 133); b) *ibid.* pp. 206—209.

5) A. Ercoli and P. D. Ruggieri, *J. Am. Chem. Soc.*, **75**, 650 (1953).

The Syntheses of the Corticoid Side Chain. III. A New Synthesis of 17α,21-Dihydroxypregna-1,4-diene-3,20-dione 17,21-Diacetate from Androsta-1,4-diene-3,17-dione

Issei NITTA,* Shinichiro FUJIMORI, Toshio HARUYAMA, Shinya INOUE, and Hiroaki UENO

Biosciences Laboratory, Research Center, Mitsubishi Chemical Industries Limited, 1000 Kamoshida-cho, Midori-ku, Yokohama, Kanagawa 227

(Received August 9, 1984)

An efficient synthesis of 17α,21-dihydroxypregna-1,4-diene-3,20-dione 17,21-diacetate (**10**) from androsta-1,4-diene-3,17-dione (**1**), a biodegradation product of cholesterol, is described, which involves the ethynylation of the 17-ketone, the epimerization of the 17α-ethynyl group and conversion of the ethynyl group to the 20-keto pregnane. Overall yield is relatively high (about 54%) and **10** will be a potential intermediate for prednisolone.

Corticosteroids are produced commercially from deoxycholic acid *via* a chemical process comprising many steps or from diosgenin and stigmasterol *via* a process involving a microbiological oxidation step at C-11.[1] Recent advances in the microbial degradation of cholesterol and abundant soya sterols allowed the production of androst-4-ene-3,17-dione and androsta-1,4-diene-3,17-dione,[2] from which various steroidal drugs such as estrone, testosterone, spironolactone, *etc.* have been produced. These 17-oxo steroids may be potentially useful starting materials for the synthesis of progestins and corticoids. Especially, androsta-1,4-diene-3,17-dione may be a useful starting material for prednisolone because the A ring is fully functionalized as 1,4-dien-3-one system and the 17-ketone provides a handle to elaborate the corticoid side chain.

Recently, efficient methods for partial synthesis of dihydroxyacetone side chain from 17-oxo steroids were published,[3] but most of them need protection of the 3-oxo group on ring A. Then they can not be simply applied for androsta-1,4-diene-3,17-dione because the protection of 3-carbonyl group of 1,4-diene-3,17-dione system is difficult. We present here an improved conversion of androsta-1,4-diene-3,17-dione into 17α, 21-dihydroxypregna-1,4-diene-3,20-dione 17,21-diacetate, an intermediate of artificial corticoids, especially prednisolone.

The methods employed in this conversion are summarized in Scheme 1.

The first step in the present conversion is the selective addition of a two-carbon fragment to the 17-keto function in androsta-1,4-diene-3,17-dione (**1**), *via* reaction with acetylene. Thus, by treating **1** with potassium acetylide in THF, 17α-ethynyl-17β-hydroxyandrosta-1,4-dien-3-one (**2**) was obtained in a quantitative yield, but this ethynyl compound **2** had the opposite configuration at C-17 to that required for the corticosteroids. Recently, a novel epimerization for converting 17α-ethynyl group into 17β-ethynyl group was reported,[4] which can be accomplished by the Ag^+-catalyzed hydrolysis of 17β-mesylate of 17α-ethynyl steroids.

However, the 17β-mesylate of **2** is extremely unstable and can be synthesized only in a very poor yield by limited procedure. Therefore, we examined various 17β-esters of **2** and selected 17α-ethynyl-17β-(nitro-

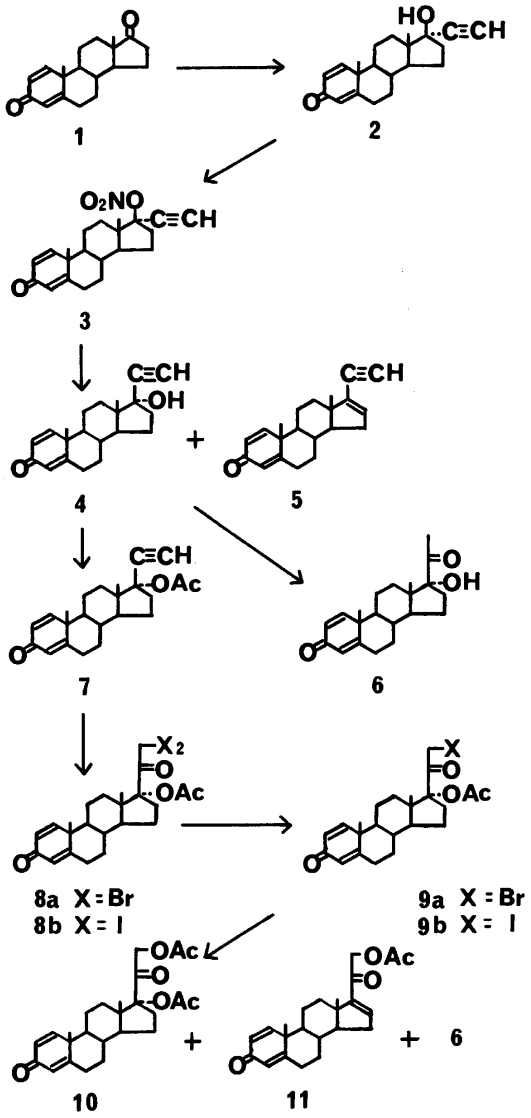

Scheme 1.

oxy)androsta-1,4-dien-3-one as the preferable one. Treatment of **2** with fuming nitric acid in acetic anhydride at −20 °C afforded 17α-ethynyl-17β-(nitrooxy) androsta-1,4-dien-3-one (**3**) in a high yield. The advantages of **3** were that the preparation was easy and the yield was very high.

Subsequently, **3** was stirred with $AgNO_3$ (0.2 mol equiv based on **3**) in a mixture of THF and distilled water for 72 h at 20 °C. The resulting reaction mixture was then poured into an aqueous NH_4Cl solution containing NaCN. The desired epimer **4** was obtained in an excellent yield (88.9%), together with a small amount of the enyne **5** (6.5%). Compound **4** could be easily purified from **5** by recrystallization from heptane–dichloromethane. The assignment of the configuration of **4** was conducted as follows. The desired epimer **4** was treated with mercury(II) chloride in benzene–water in the presence of aniline at 60 °C for 13 h to give 17α-hydroxypregna-1,4-diene-3,20-dione which was identified with the authentic sample prepared from 17α-hydroxypregn-4-ene-3,20-dione by treatment with 2,3-dichloro-5,6-dicyano-*p*-benzoquinone. NMR signals of the 13-CH_3 proton in **4** showed an upfield shift and that of the ethynylic proton showed a downfield shift when compared with **2**. Similar shifts of the signals have already been observed for the epimeric 17-ethynyl-17-hydroxy steroids.[5] Under the conditions in the absence of silver nitrate, the nitrate **3** was recovered quantitatively. Besides silver nitrate, copper(I) chloride also catalyzed the hydrolysis of **3** to give **4** in about 63% yield and **5** in about 30% yield. Then, many additives were examined in order to increase the yield of **4** and it became apparent that the addition of thiourea improved it to about 74%. (Table 1.)

In order to elucidate the mechanism of these silver ion and copper(I) ion-catalyzed solvolyses, we examined the solvolysis of the epimeric nitrate, 17β-ethynyl-17α-(nitrooxy)androsta-1,4-dien-3-one in the presence of copper(I) chloride. Main product was 17β-ethynyl compound **4** and 17α-ethynyl compound **2** was less than 2%. (Table 2.) That is to say, the substitution reaction of epimer of **3** proceeded with retention of configuration compared with the reaction of **3** proceeded with inversion of configuration. Hofmeister *et al.* reported the formation of 17β-ethynyl-17α-formyloxyandrost-4-en-3-one (yield 15%) in Ag-catalyzed solvolysis of 17α-ethynyl-17β-(nitrooxy)androst-4-en-3-one in the mixture of formic acid and hexamethylphosphoramide and proposed the mechanism which involve the S_N2 type attack of nucleophile to the intermediate (I), in which the silver ion that makes a bridged ion structure between metal ion and acetylenic bond electrons, can interact with the oxygen atom of nitrooxy group and weaken the bond between C-17 and the leaving nitrooxy group. However, this mechanism can not be applied to our reaction because the reaction of epimer of **3** dose not proceed with inversion.

Hence, we are forced to suggest the formation of a carbonium ion stabilized by the silver or copper(I) ion (II) (S_N1 mechanism). That is , if we assume that the hydroxide ion or water attacks the carbonium ion (II) derived from both epimeric nitrates and that

TABLE 1. EFFECTS OF ADDITIVES ON THE COPPER(I) CHLORIDE-CATALYZED SOLVOLYSIS OF THE NITRATE **3**[a]

Additive	Reaction condition			Product (%)	
	Molar ratio		Solvent		
	Additive /CuCl	CuCl/**3**	H_2O vol%	**4**	**5**
None		0.7	15	63.2	28.2
Pyridine	1.2	0.7	15	26.2	65.8
Ethylene-diamine	1.2	0.7	15	58.5	35.5
Acetonitrile	1.0	0.6	30	61.4	24.6
Acetone-oxime	1.5	0.8	30	55.3	18.5
None		0.8	30	65.4	18.5
Thiourea	0.2	0.8	30	70.1	16.5
Thiourea	0.4	0.8	30	74.0	18.4
Thiourea	0.7	0.8	30	70.5	15.8

a) The reaction was carried out at 60 °C in THF–H_2O.

TABLE 2. COPPER(I) CHLORIDE-CATALYZED SOLVOLYSIS OF THE NITRATE **3** AND ITS EPIMER[a]

Substrate	Molar ratio CuCl/Substrate	Product (Yield/%)		
		2	**4**	**5**
3	0.7	1	63	28
Epimer of **3**[b]	0.7	2	43	36

a) The reaction was carried out at 60 °C for 3 h in THF containing 15% water. In the absence of copper(I) chloride, the nitrate **3** was recovered quantitatively.
b) 17β-Ethynyl-17α-(nitrooxy)androsta-1,4-dien-3-one.

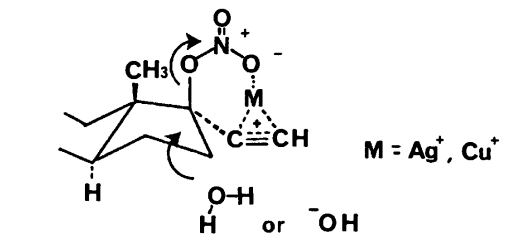

I

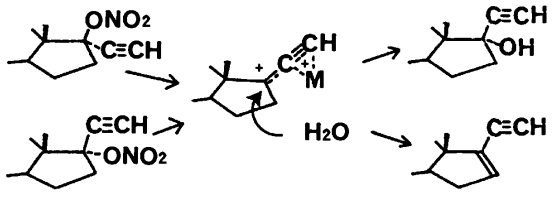

II

the attack occurs only from the least hindered side, opposite to the C-18 methyl group, formation of 17β-ethynyl compound **4** as the main product could be interpreted. As examples of metal-stabilized carbonium ions, cationic propargyl complexes $(RC{\equiv}CCR_2)$-$Co_2(CO)_6^+$ were reported.[6] But further study is required to elucidate a precise mechanism for these silver or copper(I) ion-catalyzed solvolysis.

The conversion of **4** into dihydroxyacetone side chain was accomplished as follows. Reaction of **4** with acetic anhydride in the presence of triethylamine and a catalytic amount of 4-(dimethylamino)pyridine in toluene gave the 17-acetate **7** in 96.7% yield. Treatment of 17-acetate **7** with *N*-bromoacetamide in buffered aqueous acetic acid furnished the dibromo ketone **8a**. This was converted to monobromo ketone **9a** in high yield (about 90% from **7**) on treatment with trimethyl phosphite in nitromethane at room temperature according to the "Perkow reaction."[7] According to conventional procedures for the acetoxylation of 21-bromo-17-hydroxy- or 21,21-dibromo-17-hydroxypregnane derivatives, the dibromide **8a** and monobromide **9a** were treated with potassium acetate in the presence or the absence of sodium iodide[8] in refluxing acetone, or with triethylammonium acetate in acetone.[9] But only unreacted **8a** or **9b** was recovered. Then, some dipolar aprotic solvents such as *N*,*N*-dimethylformamide, *N*,*N*-dimethylacetamide, dimethyl sulfoxide or acetonitrile were examined and it was found that on treatment with potassium acetate in *N*,*N*-dimethylformamide at around 60 °C the corresponding 21-acetate **10** was given from **9a** in moderate yield (50—70%). The major by-product was unsaturated product **11** and its amount increased when heating time or temperature was increased.

Next, the preparation of monoiodide **9b** was examined. Ogata and Urasaki reported the iodoacetoxylation of acetylenic compounds with a mixture of iodine and peracetic acid at 50 °C and suggested a mechanism involving slow formation of acetyl hypoiodite followed by its rapid addition to the triple bond to give α-iodo enol acetate[10] which may be converted to α-iodo ketone by hydrolysis.

$$I_2 + CH_3CO_3H + CH_3CO_2H \xrightarrow[\text{slow}]{\text{rate-determining step}} 2CH_3COOI + H_2O$$

$$R\text{-}C{\equiv}C\text{-}R' + CH_3COOI \xrightarrow[\text{fast}]{} \begin{matrix} I \\ R \end{matrix}\!\!>\!C{=}C\!<\!\!\begin{matrix} R' \\ OCOCH_3 \end{matrix}$$

17-Acetate **7** was treated with a mixture of iodine and peracetic acid in 10% aqueous acetic acid at room temperature (mole ratio; **7**:I_2:CH_3CO_3H=1:1:1). This reaction was completed in 2 h at room temperature. In contrast, the rate of formation of acetyl hypoiodite was very slow, the second-order rate constant for the consumption of iodine k_2 being *ca.* $2{\times}10^{-5}\,M^{-1}\,s^{-1}$ at 25 °C, and the consumption of iodine was less than 2% in the reaction of iodine and peracetic acid alone in the absence of 17-acetate **7** in 2 h at room temperature. The product was not enol acetate but diiodo ketone **8b** which was afforded in quantitative yield. When the molar ratio of iodine and peracetic acid to **7** was reduced to one-half, **8b** and unreacted **7** yielded at about 50% each, instead of the enol acetate. Here we could say that the reaction of **7** with a mixture of iodine and peracetic acid did not involve the formation of acetyl hypoiodite, because the rate of the whole reaction was faster than that of the rate-determining acetyl hypoiodite formation.

These observations lead to a hypothetical mechanism involving a rapid complex formation between the triple bond and iodine followed by a rate-determining attack of peracetic acid on the π-complex (IV), which was discussed as an alternative mechanism of iodoacetoxylation by Ogata and Urasaki.[10] The initially formed π-complex (IV) can be converted to cyclic iodonium ion (V) by peracetic acid. Carbonium ion (V) reacts with acetate ion to form enol acetate (VI) and is successively attacked by hypoiodous acid to give diiodo ketone (VII).

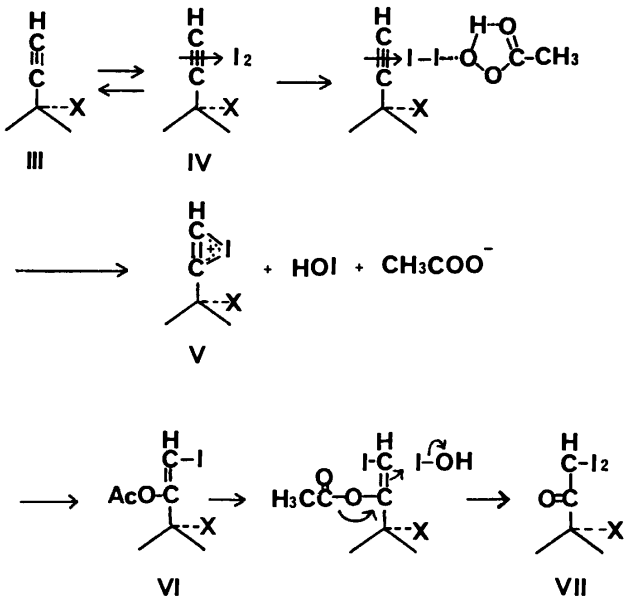

When the acetoxyl group at C-17 position in **7** was replaced with a hydroxyl group, the reaction was significantly slow and many products were formed. (When X=OAc, conversion after 1 h at room temperature 100%. When X=OH, conversion after 2 h was 20%.) These observations also indicate that the present reaction involves a carbonium ion as an intermediate. That is, the neighboring acetoxyl group can delocalize the positive charge of the carbonium ion center, stabilize the carbonium ion and accelerate the reaction involving the carbonium ion. The proposed carbonium ion is (VIII).

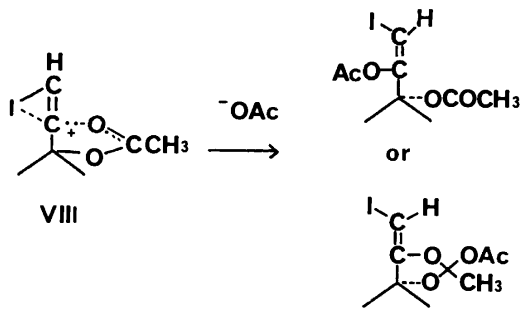

Diiodo ketone **8b** could be converted to monoiodo ketone **9b** on treatment with sodium acetate or triethylammonium acetate in refluxing acetone in 94.4% yield from **7**. Moreover, **8b** was treated with pyridine *p*-toluenesulfonate in refluxing acetone to give 17α-hydroxypregna-1,4-diene-3,20-dione 17-acetate (**6**) in about 90% yield.

Monoiodo ketone **9b** resisted acetoxylation to give a diacetate **10** and gave large amounts of **11** and **6** by conventional methods. The use of tetramethylammonium acetate afforded **10** in 79% yield under optimum conditions (in *N*-methylpyrrolidone at 21 °C for 7 h). Crude **10** of 80% purity was obtained in 60% overall yield from **1** and was subsequently recrystallized from acetone-water to give practically pure **10** (94% purity) in 91% yield. (54% yield from **1**).

Transformation of **10** into a typical corticoid, prednisolone, was followed by microbiological C-11 hydroxylation process. In such a process, **10** was a more suitable substrate than 17α,21-dihydroxypregna-1,4-diene-3,20-dione or 17α,21-dihydroxypregna-1,4-diene-3,20-dione 21-acetate, because introduction of the acetoxyl group into C-17 prevented the hydroxylation at C-14 and could bring a higher yield of prednisolone.

From the above, we concluded that the overall yield was relatively high and this sequence could be applied to other 17-keto steroids to provide useful pregnane steroids such as 17α,21-dihydroxypregn-4-en-3-one 17,21-diacetate, possible intermediate of hydrocortisone, or 17α-hydroxyprogesterone acetate.

Experimental

Melting points were determined with a Mettler FP61. Preparative TLC was accomplished with silica gel 60 F-254 plates (2 mm thick, E. Merck). HPLC was performed with a Shimadzu LC-2 liquid chromatograph instrument equipped with a Shimadzu Zorbax-ODS column (4.6 mm×25 cm) and a UV detector, and operated at a flow rate of 2 ml/min by using a solvent consisting of MeOH–H_2O (8:2).

Optical rotations were determined with a Jasco model DTP-4 digital polarimeter. NMR spectra were determined with a JEOL JMN-PS-100 spectrometer, with TMS as the internal standard. GLC analyses were performed on a Shimadzu GC-6A gas chromatograph equipped with a flame-ionization detector, using column packed with 1% Silicone DC-QF-1 on Gaschrom Q (3 mm×0.5 m; column temp 220 °C; carrier gas, N_2 60 ml/min; injector temp 250 °C).

17α-Ethynyl-17β-hydroxyandrosta-1,4-dien-3-one (2). In a three-necked flask, 95% potassium hydroxide (200 g), tetrahydrofuran (1000 ml) and ethanol (120 ml) were stirred at 50 °C for 1 h under a nitrogen atmosphere and then cooled to 3 °C. Into the mixture prepared as above, pure dry acetylene was passed at 3 °C for 2 h. A solution of androsta-1,4-diene-3,17-dione (**1**) (100 g) in 200 ml of dry tetrahydrofuran was added and stirred for 2 h. The mixture was acidified with 10% aqueous HCl solution, stirred under reflux for half an hour and diluted with water. The resulting precipitated product was collected by filtration, washed with water and dried to give 17α-ethynyl-17β-hydroxyandrosta-1,4-dien-3-one (**2**) (110.3 g, purity 92.9%, yield 96.6%), which was satisfactorily pure for the subsequent reaction. Recrystallization from acetone-hexane afforded the analytically pure sample, mp 218.9—219.1 °C; IR (KBr) cm^{-1}: 3330, 3250, 1660, 1615, 1605; NMR ($CDCl_3$) δ=0.92 (s, 3H), 1.23 (s, 3H), 2.54 (s, 1H), 6.05 (d, 1H), 6.20 (q, 1H), 7.03 (d, 1H).

Found: C, 81.48; H, 8.43%. Calcd for $C_{21}H_{26}O_2$: C, 81.25; H, 8.44%.

17α-Ethynyl-17β-(nitrooxy)androsta-1,4-dien-3-one (3). To 17α-ethynyl-17β-hydroxyandrosta-1,4-dien-3-one (**2**) (8.00 g) was added acetic anhydride (64 ml) and the mixture was cooled to −20 °C. Thereafter, fuming nitric acid (6.4 ml) was added dropwise and stirred for 1 h at −20 °C. The reaction mixture was poured into 500 g of ice water and stirred. The resulting precipitated product was filtered off and then dissolved in ethyl acetate. The ethyl acetate solution was washed with water, dried and concentrated to give 17α-ethynyl-17β-(nitrooxy)androsta-1,4-dien-3-one (8.9 g, purity 98.1%, yield 96.1%). The product could be used as the starting material in the subsequent hydrolysis step without further purification. Recrystallization from benzene afforded the analytically pure sample, mp 137—139 °C; NMR ($CDCl_3$) δ=1.02 (s, 3H), 1.26 (s, 3H), 2.72 (s, 1H), 6.03 (s, 1H), 6.18 (q, 1H), 7.00 (d, 1H); IR (KBr) 1660, 1625, 1295 cm^{-1}; MS *m/z* 355 (M^+).

Found: C, 71.23; H, 7.06; N, 4.03%. Calcd for $C_{21}H_{25}O_4N$: C, 70.96; H, 7.09; 3.94%.

17β-Ethynyl-17α-hydroxyandrosta-1,4-dien-3-one (4).
(A) Silver Nitrate-catalyzed Hydrolysis. 17α-Ethynyl-17β-(nitrooxy)androsta-1,4-dien-3-one (**3**) (2.50 g) was dissolved in tetrahydrofuran (17 ml). Subsequently distilled water (3.0 ml) and silver nitrate (9.55 g) were added and the mixture was stirred for 24 h at 25 °C. The reaction mixture was poured into saturated ammonium chloride solution (70 ml) containing sodium cyanide (0.7 g). After stirring for 15 min, the reaction mixture was extracted with dichloromethane and the separated organic layer was washed with water and dried to give 2.40 g of white crystals. The crude crystals thus obtained were recrystallized from a mixture of tetrahydrofuran (20 ml) and hexane (140 ml) to give 17β-ethynyl-17α-hydroxyandrosta-1,4-dien-3-one (**4**) (1.10 g). Recrystallization from ethyl acetate twice afforded the analytically pure sample, mp 218—219 °C; $[\alpha]_D^{24}$ +90.9° (c: 1.02, tetrahydrofuran); IR (KBr) 1660, 1620 cm^{-1}; NMR ($CDCl_3$) δ=0.96 (s, 3H), 1.26 (s, 3H), 2.52 (s, 1H), 6.09 (s, 1H), 6.25 (q, 1H), 7.08 (d, 1H); MS *m/z* 310 (M^+).

Found: C, 81.79; H, 8.33%. Calcd for $C_{21}H_{26}O_2$: C, 81.25; H, 8.44%.

To 17α-ethynyl-17β-hydroxyandrosta-1,4-dien-3-one (**2**)

(100.2 g, purity 94.1%) was added acetic anhydride (250 ml) and cooled to −20 °C. Fuming nitric acid (55 ml) was added and stirred for 1 h at −20 °C. The reaction mixture was poured into ice water and the resulting precipitated product was filtered off. The wet product (153.5 g) was dissolved in tetrahydrofuran (3000 ml). Distilled water (2960 ml) and silver nitrate (11.6 g) were added and stirred for 72 h at room temperature. After tetrahydrofuran was distilled off, 150 ml of 60% nitric acid was added, and the mixture was extracted with dichloromethane, washed with water and concentrated to give crude 17β-ethynyl-17α-hydroxyandrosta-1,4-dien-3-one (100.7 g, purity 81.2%, yield 86.7% from **2**). The crude crystals were recrystallized from a mixture of dichloromethane and heptane to give 17β-ethynyl-17α-hydroxyandrosta-1,4-dien-3-one (84.2 g, purity 92.0%, yield 95.0%).

(B) Copper(I) Chloride-catalyzed Hydrolysis. To a mixture prepared by adding tetrahydrofuran (6.2 ml) and water (15.8 ml) to 17α-ethynyl-17β-(nitrooxy)androsta-1,4-dien-3-one (**3**) (2.50 g) was added copper(I) chloride (0.2 g), and the resulting mixture was stirred for 4 h at 65 °C in a nitrogen atmosphere. Benzene and saturated saline were added to the reaction mixture to extract the product into benzene. The separated benzene layer was further washed three times with saturated saline, dried over anhydrous sodium sulfate and concentrated to get crystals. HPLC analysis of the crystals showed that 17β-ethynyl-17α-hydroxyandrosta-1,4-dien-3-one (**4**) and 17-ethynylandrosta-1,4,16-trien-3-one (**5**) were formed in yields of 63 mole% and 32 mole%, respectively.

17α-Hydroxypregna-1,4-diene-3,20-dione (6). To 17β-ethynyl-17α-hydroxyandrosta-1,4-dien-3-one (**4**) (0.680 g) were added benzene (40 ml), distilled water (8 ml), murcury(II) chloride (1.12 g), and aniline (0.2 ml). The mixture was stirred at 60 °C for 13 h. The insoluble matters were filtered off and they were thoroughly washed with chloroform. The chloroform washings were combined with the filtrate (reaction mixture) and the aqueous layer was separated. The organic layer was washed successively with 5% hydrochloric acid and saturated sodium hydrogencarbonate solution and then dried over sodium sulfate. The solvent was then distilled off to give 17α-hydroxypregna-1,4-diene-3,20-dione (**6**) (0.616 g). Recrystallization from a mixture of tetrahydrofuran (40 ml) and octane (10 ml) gave analytically pure 17α-hydroxypregna-1,4-diene-3,20-dione (**6**) (0.499 g). High speed liquid chromatogram, thin layer chromatogram and infrared absorption, NMR and mass spectra of the product were all in agreement with those of an authentic sample, mp 258.0—258.7 °C; NMR ($CDCl_3$) δ=0.8 (s, 3H), 1.26 (s, 3H), 2.28 (s, 3H), 2.96 (s, 1H), 6.08 (s, 1H), 6.22 (d, 1H, J=10 Hz), 7.06 (d, 1H, J=10 Hz).

Found: C, 76.95; H, 8.48%. Calcd for $C_{21}H_{28}O_3$: C, 76.79; H, 8.59%.

17β-Ethynyl-17α-hydroxyandrosta-1,4-dien-3-one 17-Acetate (7). To 17β-ethynyl-17α-hydroxyandrosta-1,4-dien-3-one (**4**) (2.00 g) were added acetic anhydride (2.0 ml), triethylamine (2.0 ml), 4-(dimethylamino)pyridine (0.114 g) and toluene (5.0 ml) and the mixture was heated at 80—90 °C for 11 h. Upon cooling, the reaction product was extracted into dichloromethane. The organic layer was washed successively with 5% hydrochloric acid and 5% sodium hydrogencarbonate solution and the separated organic layer was dried over anhydrous sodium sulfate and concentrated. The liquid chromatograph analysis of the extract showed that 17β-ethynyl-17α-hydroxyandrosta-1,4-dien-3-one 17-acetate was formed in 96.7% yield. The concentrate was passed through a column filled with 250 g of alumina and eluted with 500 ml of a mixture of benzene and ethyl acetate (9:1) to give 2.3 g of crystals. Recrystallization of the crystals from octane-tetrahydrofuran (20:1), heptane–ethanol (5:1) and octane–tetrahydrofuran (30:7) gave 17β-ethynyl-17α-hydroxyandrosta-1,4-dien-3-one 17-acetate (**7**), mp 171.8—172.6 °C; NMR ($CDCl_3$) δ=1.00 (s, 3H), 1.26 (s, 3H), 2.02 (s, 3H), 2.56 (s, 1H), 6.04 (d, 1H), 6.15 (q, 1H), 6.98 (d, 1H).

Found: C, 79.02; H, 8.01%. Calcd for $C_{23}H_{28}O_3$: C, 78.38; H, 8.01%.

21-Bromo-17α-hydroxypregna-1,4-diene-3,20-dione 17-Acetate (9a). A mixture of 17β-ethynyl-17α-hydroxyandrosta-1,4-dien-3-one 17-acetate (**7**) (0.786 g), *N*-bromoacetamide (0.644 g), anhydrous sodium acetate (0.735 g), water (1.3 ml) and acetic acid (13 ml) was left at 0 °C for 1 h, then poured into ice–water and the resulting precipitate was collected by filtration, washed with water and dried to give crude 21,21-dibromo-17α-hydroxypregna-1,4-diene-3,20-dione 17-acetate (**8a**) (1.158 g). To this crude dibromide **8a** (0.134 g) in nitromethane (2.5 ml), trimethyl phosphite (0.2 ml) was added and stirred at room temp for 50 min. The reaction mixture was diluted with ether and washed with water. The separated organic layer was dried over anhydrous sodium sulfate and concentrated to give crude 21-bromo-17α-hydroxypregna-1,4-diene-3,20-dione (**9a**) (0.112 g). Recrystallization from octane–tetrahydrofuran gave an analytically pure sample (0.083 g). MS m/z 448, 450 (M^+).

Found: C, 61.59; H, 6.61; Br, 17.77%. Calcd for $C_{23}H_{29}O_4Br$; C, 61.47; H, 6.50; Br, 17.78%.

17α-Hydroxy-21-iodopregna-1,4-diene-3,20-dione 17-Acetate (9b). To a mixture prepared by adding iodine (0.408 g), acetic acid (4.5 ml), and water (0.5 ml) to 17β-ethynyl-17α-hydroxyandrosta-1,4-dien-3-one 17-acetate (**7**) (0.571 g), a mixture of 40% peracetic acid (0.26 ml), acetic acid (16 ml) and water (2 ml) was added dropwise and stirred at room temp for 2 h. The reaction mixture was poured into water (150 ml) and the resulting precipitate was collected with filtration, washed with water and dissolved in dichloromethane. The solution was washed successively with 7% aqueous KI solution, 10% aqueous sodium thiosulfate solution and water, dried over anhydrous sodium sulfate and concentrated to give crude 21,21-diiodo-17α-hydroxypregna-1,4-diene-3,20-dione 17-acetate (**8b**) (0.961 g), NMR ($CDCl_3$) δ=0.89 (s, 3H), 1.24 (s, 3H), 2.09 (s, 3H), 5.52 (s, 1H), 6.11 (d, 1H), 6.26 (q, 1H), 7.10 (d, 1H); MS m/z 496 (M^+).

To this crude iodide **8b** (0.200 g), triethylamine (0.83 ml), acetic acid (0.53 ml), and acetone (5 ml) were added and stirred under reflux for 1 h. The reaction mixture was poured into water (100 ml) and the resulting precipitate was collected by filtration and dried to give 17α-hydroxy-21-iodopregna-1,4-diene-3,20-dione 17-acetate (**9b**) (0.142 g). Without further purification, crude iodide was used for the next step. Recrystallization from acetone–heptane affored the analytically pure sample, mp 156.9—157.2 °C, NMR ($CDCl_3$) δ=0.78 (s, 3H), 1.26 (s, 3H), 2.12 (s, 3H), 3.92 (d, 2H), 6.10 (d, 1H), 6.26 (q, 1H), 7.09 (d, 1H); MS m/z 496 (M^+).

Found: C, 55.74; H, 5.92; I, 25.45%. Calcd for $C_{23}H_{29}O_4I$: C, 55.65; H, 5.89; I, 25.57%.

17α,21-Dihydroxypregna-1,4-diene-3,20-dione 17,21-Diacetate (10). To 17α-hydroxy-21-iodopregna-1,4-diene-3,20-dione 17-acetate (**9b**) (2.01 g), *N*-methylpyrrolidone (6.0 ml),

and tetramethylammonium acetate (0.80 g) were added and stirred at 21 °C for 7 h. Thereafter, 60 ml of water was slowly dropped while agitating. The resulting crystal was filtered off, washed with water, and dried to obtain 1.64 g of crystals. Recrystallization from ethanol (16 ml) yielded 17α,21-dihydroxypregna-1,4-diene-3,20-dione 17,21-diacetate (**10**), mp 207.7—208.0 °C; NMR ($CDCl_3$) δ=0.80 (s, 3H), 1.26 (s, 3H), 2.08 (s, 3H), 2.16 (s, 1H), 4.74 (q, 2H), 6.04 (broad, 1H), 6.18 (q, 1H), 7.02 (d, 1H), MS *m/z* 428 (M^+).

Found: C, 70.14; H, 7.56%. Calcd for $C_{25}H_{32}O_6$: C, 70.07; H, 7.53%.

References

1) a) A. Applezweig, "Steroid Drugs," McGraw-Hill, New York (1962), pp 41—86; b) L. F. Fieser and M. Fieser, "Steroids," Reinhold, New York (1959), Chapter 19.

2) a) M. Nagasawa, H. Hashiba, N. Watanabe, M. Bae, G. Tamura, and K. Arima, *Agric. Biol. Chem.*, **34**, 801 (1970); b) Y. Imada and I. Nitta, *Hakko To Kogyo*, **38**, 1117 (1980).

3) a) D. H. R. Barton, W. B. Motherwell, and S. Z. Zard, *Bull. Soc. Chim. Fr.*, **1983**, 61; b) A. R. Daniewski and W. Wojciechowska, *J. Org. Chem.*, **47**, 2993 (1982); c) D. H. R. Barton, W. B. Motherwell, and S. Z. Zard, *J. Chem. Soc., Chem. Commun.*, **1981**, 774; d) R. M. Moriarty, L. S. John, and P. C. Du, *J. Chem. Soc., Chem. Commun.*, **1981**, 641; e) G. Neef, U. Eder, A. Seeger, and R. Wiechert, *Chem. Ber.*, **113**, 1184 (1980); f) V. V. Rheenen and K. P. Shephard, *J. Org. Chem.*, **44**. 1582 (1979); g) R. W. Freerksen, M. L. Raggio, C. A. Thoms, and D. S. Watt, *ibid.*, **44**, 702 (1979); h) H. Hofmeister, K. Annen, H. Laurent, and R. Wiechert, *Chem. Ber.*, **111**, 3086 (1978); i) M. Biollaz, W. Haefliger, E. Velarde, P. Crabbe, and J. H. Fried, *J. Chem. Soc., Chem. Commun.*, **1971**, 1322.

4) H. Westmijze, H. Kleijn, P. Vermeer, and L. A. Van Dijck, *Tetrahedron Lett.*, **1980**, 2665.

5) L. A. Van Dijck, B. J. Lankwerden, and J. G. C. M. Vermeer, *Recl. Trav. Chim. Pays-Bas*, **96**, 200 (1977).

6) K. M. Nicholas and R. Pettit, *Tetrahedron Lett.*, **1971**, 3475; H. D. Hodes and K. M. Nicholas, *ibid.*, **1978**, 4349.

7) F. W. Lichtenthaler, *Chem. Rev.*, **61**, 607 (1961).

8) F. A. Cuther, Jr., L. Mandell, J. F. Fisher, D. Shew, and J. M. Chermerda, *J. Org. Chem.*, **24**, 1629 (1959).

9) W. T. Moreland, Jr., *J. Org. Chem.*, **21** 820 (1956).

10) Y. Ogata and I. Urasaki, *J. Org. Chem.*, **36**, 2164 (1971).

Electrocatalytic Oxidation of Chlorpromazine in Phosphate Solution

Kiyoko TAKAMURA,* Satoshi INOUE, Fumiyo KUSU, and Noboru OYAMA†
Tokyo College of Pharmacy, Hachioji, Tokyo 192-03
†*Department of Applied Chemistry for Resources, Tokyo University of Agriculture and Technology, Koganei, Tokyo 184*
(Received August 13, 1984)

The kinetics of electrocatalytic oxidation process of chlorpromazine (CPZ) at a pyrolytic graphite electrode in a phosphate solution was investigated by rotating disk voltammetry. The reactions involving regeneration process of CPZ through the disproportionation of reaction intermediates are proposed and the rate constants of the chemical reaction (k_{obsd}), following the electrochemical oxidation of CPZ to the CPZ cation radical, were evaluated from the electrode rotation-rate dependence of the limiting currents obtained in the CPZ solution with and without phosphate. The proportional relations between the logarithm of k_{obsd} and pH, and between k_{obsd} and the concentration of $H_2PO_4^-$ were obtained.

In a previous paper,[1] we proposed an electrochemical oxidation mechanism of chlorpromazine (CPZ) involving the regeneration processes of CPZ through the disproportionation of reaction intermediates at the electrode surface, as given by Eqs. 1—4,

$$CPZ \underset{+e}{\overset{-e}{\rightleftharpoons}} CPZ^{\cdot+} \quad (1)$$

$$CPZ^{\cdot+} + H_2PO_4^- \overset{K_1}{\rightleftharpoons} [CPZ(HPO_4)]^{\cdot-} + H^+ \quad (2)$$

$$[CPZ(HPO_4)]^{\cdot-} + CPZ^{\cdot+} \underset{k_{-2}}{\overset{k_2}{\rightleftharpoons}} [CPZ(HPO_4)]^0 + CPZ \quad (3)$$

$$[CPZ(HPO_4)]^0 + H_2O \xrightarrow{k_3} CPZO + H_2PO_4^- + H^+ \quad (4)$$

where $CPZ^{\cdot+}$ and CPZO are the CPZ cation radical and CPZ S-oxide, respectively. Chlorpromazine is a well-known drug in phenothiazines and frequently used as a major tranquilizer. Thus, further confirmation of the oxidation mechanism of CPZ may give more significant informations for determination of the best conditions for highly sensitive electrochemical analysis of CPZ and understanding of the drug metabolic pathway.

In this paper, we examine in detail the mechanism of the electrocatalytic oxidation of CPZ in phosphate media. Although our proposed reaction mechanism of CPZ is somewhat complicated, it is reported that the following simplified expression, so-called "half-generation reaction";

$$A \xrightarrow{e} B$$

$$2B \xrightarrow{k} A + C$$

suffices Eqs. 1—4 and the k value can be obtained from the voltammetric limiting current, using a rotating disk electrode (RDE) according to the procedure of Holub.[2]

Experimental

Chemicals. Chlorpromazine hydrochloride was obtained from Sigma Chemical Co. All other chemicals were of analytical grade and were used without further purification. A perchlorate salt of the chlorpromazine cation radical was prepared electrochemically according to the procedure of McCreery *et al.*[3] Phosphate buffers, prepared by mixing of H_3PO_4 and NaOH solutions, were used as supporting electrolyte solution and the pH's of the buffers were measured at 25 °C with a Toa pH meter HM-5ES.

Apparatus. Measurements of current-potential curves and controlled potential electrolysis were carried out using an HA-301 potentiostat (Hokuto Denko Ltd.) and a function generator HB-104 (Hokuto Denko Ltd.). In these experiments, a pyrolytic graphite disk was chosen as a working electrode so as to render the adsorption of CPZ on the electrode surface negligibly small.[4] To prepare the rotating disk electrode, the pyrolytic graphite disk (Union Carbide Co.) was sealed with the heat shrinkable teflon tubing. The graphite disk was connected to a stainless steel shaft attached to rotating disk rotor RRDE-1 (Nikko Keisoku Ltd.) and motor speed controller SC-5 (Nikko Keisoku Ltd.). A fresh electrode surface with an area of 0.19 cm^2 was produced by cleaving the disk with a stainless steel cutter. The potentials are quoted with respect to a saturated calomel electrode (SCE). The electrolysis solution was deaerated by bubbling nitrogen gas. During the experiment, the solutions were shielded from light and air, and the temperature was maintained at 25 °C.

Measurements of ^{31}P-NMR spectra were carried out using a FX-200 spectrometer (JEOL). The crystallized $CPZ^{\cdot+}$ perchlorate was directly dissolved in methanol containing 7.8% D_2O with 1.0×10^{-2} mol dm^{-3} NaH_2PO_4 and the spectra of NaH_2PO_4–$CPZ^{\cdot+}$ solution were measured immediately.

Results and Discussion

The current-potential (i-E) curves of 1.0×10^{-3} mol dm^{-3} CPZ obtained by using the stationary graphite electrode are shown in Figs. 1 and 2. The oxidation peaks appear clearly on the anodic scan, and the peak current (i_p) at 0.65 V *vs.* SCE becomes large at higher pH and higher phosphate concentrations. This trend is essentially the same as that observed previously by using a stationary glassy carbon electrode.[1] Thus, the electrochemical oxidation of CPZ is also catalyzed by phosphate anion at the graphite electrode.

The anodic current-potential curves of 1.0×10^{-3} mol dm^{-3} CPZ obtained by RDE are shown in Figs. 3 and 4. A well-defined oxidation wave is observed with a half-wave potential of 0.60 V *vs.* SCE. The limiting current, i_{lim}, of the oxidation increases with increasing the phosphate concentration, whereas the half wave potential is independent of the phosphate concentration (Fig. 3). The value of i_{lim} also depends on pH. A larger i_{lim} is observed at higher pH (Fig. 4).

Figure 5 shows the Levich plot, *i.e.*, the reciprocal of the limiting current (i_{lim}^{-1}) *vs.* that of the square root of the rotation rate ($\omega^{-1/2}$) obtained for the CPZ oxidation wave. At a pH lower than 3, i_{lim}^{-1} is in proportion to $\omega^{-1/2}$, but not so at higher pH. This indicates that the limiting current is diffusion-controlled at lower pH, but kinetic in nature at higher pH. The contribution of chemical reactions to the overall electrode process of CPZ thus becomes apparent.

From the plot of log $(i/(i_{lim}-i))$ *vs.* E (Fig. 6), the number of electrons, n, involved in the oxidation process of CPZ (Eq. 1) is estimated to be unity.

The electrolysis products were produced by controlled potential electrolysis and detected by UV-visible absorption spectroscopy, and thin-layer chromatography. Electrolysis was carried out in a 0.1 mol dm^{-3} phosphate solution (pH 2—7) at a fixed potential of 0.72 V *vs.* SCE, until the limiting current dropped below 0.5% of the initial value. When the solution showed below pH 3, it was tinged red during the electrolysis. The solution showed an absorption peak due

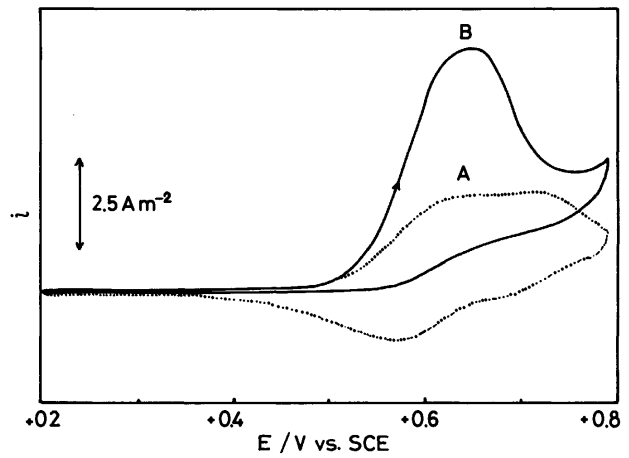

Fig. 1. Current-potential curves of 1.0×10^{-3} mol dm^{-3} CPZ in a 0.1 mol dm^{-3} CF_3COONa solution using the stationary graphite electrode.
Phosphate concentration: (curve A): 0 mol dm^{-3}, (curve B): 0.1 mol dm^{-3}.
Scan rate: 100 mV s^{-1}.

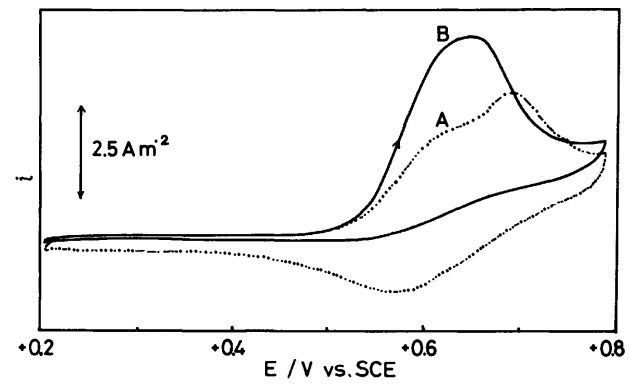

Fig. 2. Current-potential curves of 1.0×10^{-3} mol dm^{-3} CPZ in a 0.1 mol dm^{-3} phosphate solution using the stationary graphite electrode.
(curve A): pH 3.10, (curve B): pH 6.90.
Scan rate: 100 mV s^{-1}.

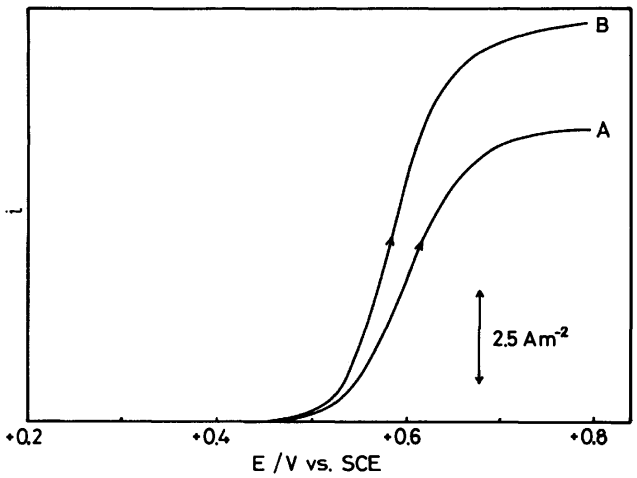

Fig. 3. Current-potential curves of 1.0×10^{-3} mol dm^{-3} CPZ in a 0.1 mol dm^{-3} CF_3COONa solution using the rotating disk electrode.
Phosphate concentration: (curve A): 0 mol dm^{-3}, (curve B): 0.1 mol dm^{-3}.
Scan rate: 2 mV s^{-1}.
Rotation rate: 2500 min^{-1}.

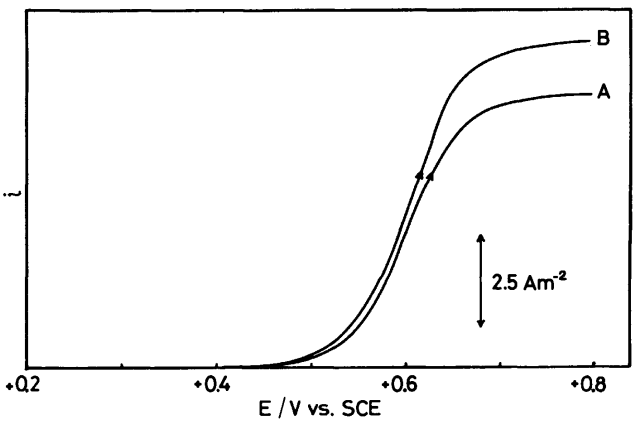

Fig. 4. Current-potential curves of 1.0×10^{-3} mol dm^{-3} CPZ in a 0.1 mol dm^{-3} phosphate buffer using the rotating disk electrode.
(curve A): pH 3.10, (curve B): pH 6.90.
Scan rate: 2 mV s^{-1}.
Rotation rate: 2500 min^{-1}.

to $CPZ^{\cdot+}$ at 524 nm. The final electrolysis product was found to be CPZO on the basis of a comparison with an authentic sample.

The above findings are important in regard to the validity of our assumption previously proposed for the electrode processes of CPZ.[1] The presence of an intermediary adduct between $CPZ^{\cdot+}$ and phosphate given in Eq. 2 is suggested from the data of ^{31}P-NMR of the $CPZ^{\cdot+}$-$H_2PO_4^-$ system. The ^{31}P-NMR spectra were measured in methanol containing 7.8% D_2O at pH 3.75 to avoid rapid decomposition of $CPZ^{\cdot+}$. A distinct peak can be seen in the ^{31}P-NMR spectrum of a 1.0×10^{-2} mol dm^{-3} NaH_2PO_4 solution (pH 3.75) without $CPZ^{\cdot+}$ (Fig. 7A). When 1.0×10^{-2} mol dm^{-3} $CPZ^{\cdot+}$ coexists with NaH_2PO_4, the peak of NaH_2PO_4 shifts upfield (Fig. 7B) and is little affected by the presence of 1.0×10^{-2} mol dm^{-3} CPZ (Fig. 7C). This implies an interaction between $CPZ^{\cdot+}$ and $H_2PO_4^-$.

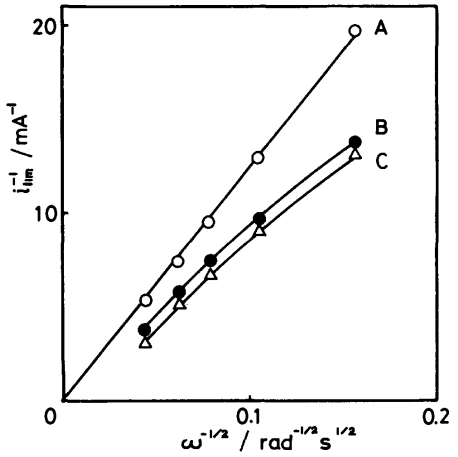

Fig. 5. Plots of reciprocal of the limiting current (i_{1lm}^{-1}) *vs.* reciprocal of square root of rotation rate of RDE ($\omega^{-1/2}$) for the oxidation of 1.0×10^{-3} mol dm^{-3} CPZ in a 0.1 mol dm^{-3} phosphate solution.
(curve A): pH 3.0, (curve B): pH 5.9, (curve C): pH 6.9.

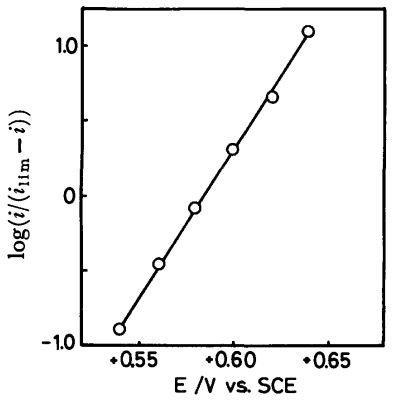

Fig. 6. Plot of $\log(i/(i_{1lm}-i))$ *vs.* E.
1.0×10^{-3} mol dm^{-3} CPZ in a 0.1 mol dm^{-3} phosphate solution (pH 6.9).
Rotation rate: 900 min^{-1}.

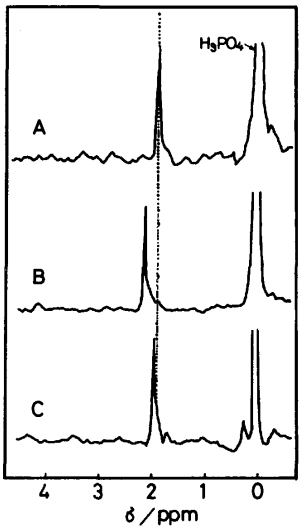

Fig. 7. ^{31}P-NMR spectra of $H_2PO_4^-$ with and without $CPZ^{\cdot+}$ and CPZ in methanol containing 7.8% D_2O at pH 3.75.
(A): 1.0×10^{-2} mol dm^{-3} NaH_2PO_4, (B): 1.0×10^{-2} mol dm^{-3} NaH_2PO_4 with 1.0×10^{-2} mol dm^{-3} $CPZ^{\cdot+}$, (C): 1.0×10^{-2} mol dm^{-3} NaH_2PO_4 with 1.0×10^{-2} mol dm^{-3} CPZ.

Assuming the reaction given by Eq. 2 always to be in equilibrium and the reactions expressed by Eqs. 3 and 4 to be of comparable rate,[5] the observed rate constant, k_{obsd}, for a series of reactions expressed by Eqs. 2—4 may be written as

$$k_{obsd} = \frac{2K_1k_3(k_2/k_{-2})[H_2O][H_2PO_4^-]}{([CPZ]+k_3[H_2O]/k_{-2})[H^+]} \quad (5)$$

Provided the concentration of CPZ is virtually constant at the electrode surface, the following two relations can be expected to hold.

$$k_{obsd} \propto [H^+]^{-1} \quad (6)$$

$$k_{obsd} \propto [H_2PO_4^-] \quad (7)$$

The values of k_{obsd} can be calculated from the ratio of the kinetic current to diffusion current, according to Holub's analysis of the half-generation mechanism.[2] First, the quantity J, defined as $(i_c-i_0)/i_0$, is calculated, where i_c and i_0 are the limiting currents obtained in the CPZ solution with and without phosphate, respectively. It is then possible to obtain κ by using Holub's table which tabulates the relation between J and κ. The κ is expressed as

$$\kappa = (2k_{obsd}\,a^*/(0.51^{2/3}\omega))(\nu/D)^{1/3} \quad (8)$$

where a^* is the bulk concentration of CPZ, ν the kinematic viscosity and D the diffusion coefficient of CPZ. From the slope of the Levich plot, the value of D is obtained as 6.53×10^{-10} m^2 s^{-1}. The value of ν is then assumed to be 1.0×10^{-6} m^2 s^{-1}, the viscosity of water.

The plot of log k_{obsd} *vs.* pH and k_{obsd} *vs.* $H_2PO_4^-$ concentration are shown in Figs. 8 and 9, from which the relations 6 and 7 are found to hold except at pH

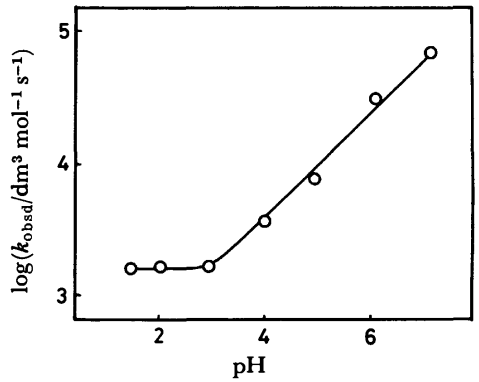

Fig. 8. Plot of the log k_{obsd} *vs.* pH.
1.0×10^{-3} mol dm^{-3} CPZ in a 0.1 mol dm^{-3} phosphate solution.

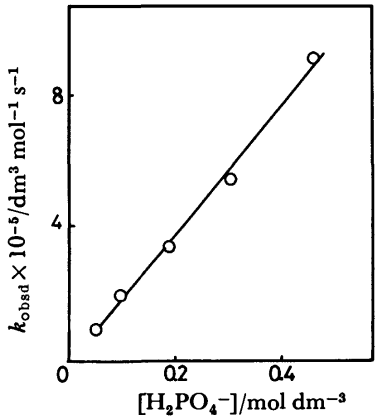

Fig. 9. Plot of k_{obsd} *vs.* $H_2PO_4^-$ concentration.
1.0×10^{-3} mol dm^{-3} CPZ; pH 6.8.

lower than 3. The deviation from the relation 6 at pH lower than 3.0 may attributed to the fact that the reaction expressed by Eqs. 2—4 is not established in the strong acidic solution and that other unknown regeneration processes of CPZ occur. Since the solubility of CPZ greatly decreases at pH higher than 7, the measurement of k_{obsd} cannot be made in such a pH region. Thus the kinetics of the electrocatalytic oxidation processes of CPZ described above is valid in the pH range 3—7.

McCreery *et al.*[3] studied the degradation of CPZ$^{\cdot+}$ in bulk solution by spectrophotometric technique and obtained the value of 177 dm^3 mol^{-1} s^{-1} for the rate constant (k_{obsd}) in a 0.1 mol dm^{-3} phosphate solution at pH 3.99 in the presence of 2.0×10^{-3} mol dm^{-3} CPZ, assuming the same reaction sequence as Eqs. 2—4. Under the same conditions, determination of k_{obsd} was made by the present method for comparison and the value of 142 dm^3 mol^{-1} s^{-1} was obtained. This value is essentially the same as above, indicating the validity of the electrode processes of CPZ presented by Eqs. 1—4.

The results presented in this paper confirm the mechanism previously proposed for the anodic oxidation processes of CPZ.[1]

References

1) K. Takamura, S. Inoue, F. Kusu, M. Otagiri, and K. Uekama, *Chem. Pharm. Bull.*, **31**, 1821(1983).
2) K. Holub, *J. Electroanal. Chem.*, **30**, 71 (1971).
3) H. Y. Cheng, P. H. Sackett, and R. L. McCreery, *J. Am. Chem. Soc.*, **100**, 962 (1978).
4 This expectation is realized by means of chronocoulometry.
5) P. H. Sackett and R. L. McCreery, *J. Med. Chem.*, **22**, 1447 (1979).

Nonacarbonyldiiron-, Pentacarbonyliron-, or Hexacarbonylmolybdenum-induced Reactions of 4,5-Polymethylene-substituted 2-Isoxazolines[1)]

Makoto NITTA,* Akihiro YI, and Tomoshige KOBAYASHI
Department of Chemistry, School of Science and Engineering, Waseda University, Shinjuku-ku, Tokyo 160
(Received September 26, 1984)

The reaction of 4,5-polymethylene-substituted 2-isoxazolines, 3-phenyl-3a,5,6,7a-tetrahydro-4*H*-pyrano-[3,2-*d*]isoxazole or 3-phenyl-3a,4,5,6a-tetrahydrofuro[3,2-*d*]isoxazole, with [$Fe_2(CO)_9$], [$Fe(CO)_5$], or [$Mo(CO)_6$] resulted in the formation of 5-hydroxy-1-phenyl-1-pentanone or 4-hydroxy-1-phenyl-1-butanone, *via* the N–O and C–C bond cleavage of the 2-isoxazoline ring and the subsequent hydrolysis. The similar reaction of 7a-morpholino- and 7a-(1-pyrrolidinyl)-3-phenyl-3a,4,5,6,7,7a-hexahydro-1,2-benzoisoxazoles undergoes the N–O bond cleavage and, the subsequent elimination of the amino group or the C-3a–C-7a bond fission. Although the reaction of 6a-morpholino- and 6a-(1-pyrrolidinyl)-3-phenyl-3a,4,5,6a-tetrahydro-4*H*-cyclopent[*d*]isoxazoles with [$Mo(CO)_6$] undergoes the N–O bond cleavage, and the subsequent elimination of the amino group or the C-3a–C-6a bond fission, the reaction of those 2-isoxazolines with [$Fe_2(CO)_9$] proceeds very slowly. The mechanisms are proposed for these reactions.

The 2-isoxazoline ring systems have been a subject of great synthetic interest, and they have been used for the synthesis of β-amino alcohol,[2)] α,β- or β,γ-unsaturated oximes,[3)] and β-hydroxy ketones.[4)] The versatility of 2-isoxazolines as precursors for a number of classes of compounds was also demonstrated recently.[5)] Previously, it has been shown that the reaction of 3,5-disubstituted 2-isoxazolines **1** with [$Fe(CO)_5$] under photoirradiation, or with [$Fe_2(CO)_9$] under thermal conditions undergoes the N–O bond and C-4–C-5 bond cleavage to give aldehydes **2** and ketones **3**, which are derived from reduction and the subsequent hydrolysis of the postulated vinylnitrene complexes.[6)] Furthermore, 2-isoxazolines bearing substituent such as an acetoxy or ethoxy group at C-5, undergo the N–O bond cleavage and the concomitant elimination of the acetoxy or ethoxy group leading to β-amino enones **4**.[6)] However, in the case of 2-isoxazolines bearing 1-pyrrolidinyl group at C-5, the N–O and C-4–C-5 bond cleavage giving **2** and **3** predominates over elimination of the C-5-substituent giving **4**.[6)] The facile metal carbonyl-induced N–O bond cleavage of 2-isoxazolines has a strong resemblance to the photochemically[7)] induced N–O bond fission of the various 2-isoxazolines. This fact seems to suggest the p-d electron delocalization from the central metal to the π* (LUMO) orbital of the C=N–O moiety of the complexed 2-isoxazolines.[6)] This effect would weaken the N–O bond to undergo a facile cleavage.

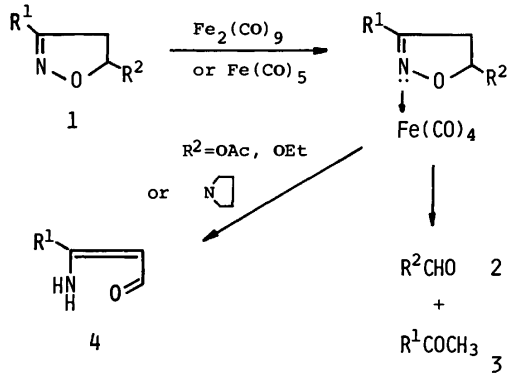

Scheme 1.

In search for further synthetic utilities of the 2-isoxazoline ring system and in connection with the previous studies,[6)] we have investigated the reaction of 4,5-polymethylene-substituted 2-isoxazolines in the presence of [$Fe_2(CO)_9$], [$Fe(CO)_5$], or [$Mo(CO)_6$]. The results are presented in this paper.

The thermal reaction of 2-isoxazolines **5a**[8)] and **5b**[8)] with 1.2 molar equivalent amounts of [$Fe_2(CO)_9$] in anhydrous methanol for 24 h and separation by TLC afforded 5-hydroxy-1-phenyl-1-pentanone (**9a**) and 4-hydroxy-1-phenyl-1-butanone (**9b**) in moderate yields. The photoirradiation of **5a,b** with [$Fe(CO)_5$] also afforded the similar results. In addition, the reaction of **5a,b** with [$Mo(CO)_6$] in anhydrous methanol was also found to result in the formation of **9a** and **9b**. The yields and the reaction conditions are listed in Table 1. The products are known compounds and were identified by comparison of the spectral properties with those reported in the literature.[9)]

The reaction seems to be selective and no other product was detected. The products obtained in these reactions correspond to those formed by the N–O and C–C bond cleavage of the 2-isoxazoline ring. Free or solvated [$Fe(CO)_4$] species is generally assumed to be the common intermediate in thermolysis (≥80 °C) or photolysis of [$Fe(CO)_5$] and thermolysis of [$Fe_2(CO)_9$] (≥20 °C).[10)] [$Mo(CO)_6$] has also been shown to give an N-donor complex of isoxazoles.[11)] Therefore the initial step is N-donor complexation of **5a,b** to give **6**. The following ring cleavage of **6** gives the complexed nitrene **7**, the reduction of which gives enamine **8**.[12)] The enamine moiety of **8** as well as the ester moiety would be hydrolyzed to give **9a,b** under the reaction conditions in the presence of stray water or under workup condi-

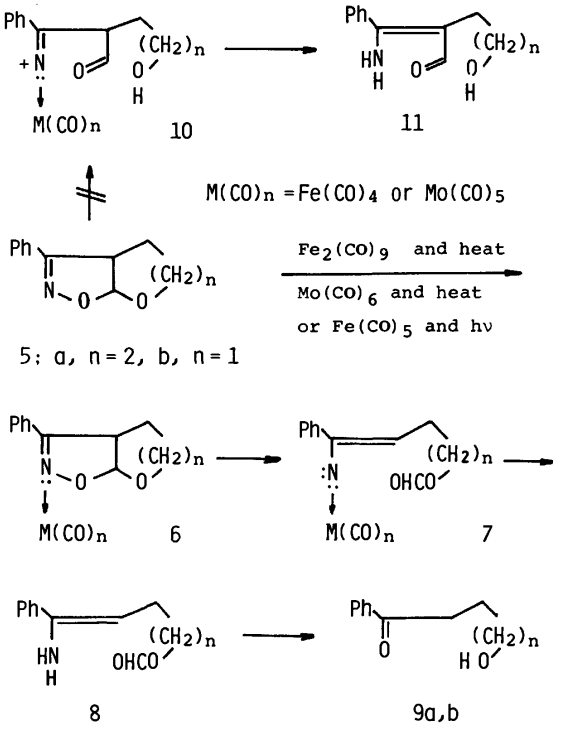

Scheme 2.

tions.[6,12] The N-O and C-O bond cleavage giving β-amino enone **11** *via* **10** did not occur, unlike in the case of **1** (R^2=OEt or OAc).[6]

The reaction of 7a-morpholino- and 7a-(1-pyrrolidinyl)-3-phenyl-3a,4,5,6,7,7a-hexahydro-1,2-benzoisoxazole (**12a** and **12b**)[13] with [$Fe_2(CO)_9$] at the refluxing temperature, or with [$Fe(CO)_5$] under photoirradiation, afforded the β-amino enone **15** and the ester **17**, in addition to the unreacted starting materials **12a,b** (Scheme 3). On the other hand, treatment of **12a** or **12b** with [$Mo(CO)_6$] in methanol resulted in the complete consumption of the starting material and gave **15** and **17**, in addition to the small amount of **16a** or **16b**. The reaction conditions and the yields of the products are listed in Table 2. The products **15**[11] and **17**[14] are known compounds. Furthermore, the structures of new compounds **16a,b** were confirmed by the independent preparations of the corresponding samples (see Experimental). The complexed 2-isoxazoline **13** undergoes the N-O bond cleavage and the concomitant elimination of morpholino or 1-pyrrolidinyl group to give β-amino enone **15**. The complex **13** also undergoes the N-O and C-3a-C-7a bond cleavage to give **18**, the reduction of which and the subsequent hydrolysis under the reaction conditions in the presence of stray water or under workup conditions gives **16a,b**. The compound **17** may be derived from the methanolysis of the amide group of **16** in the presence of oxidized-metal carbonyl species.

On the other hand, the reaction of 6a-morpholino- and 6a-(1-pyrrolidinyl)-3-phenyl-3a,4,5,6a-tetrahydro-4*H*-cyclopent[*d*]isoxazoles (**20a** and **20b**),[15] with

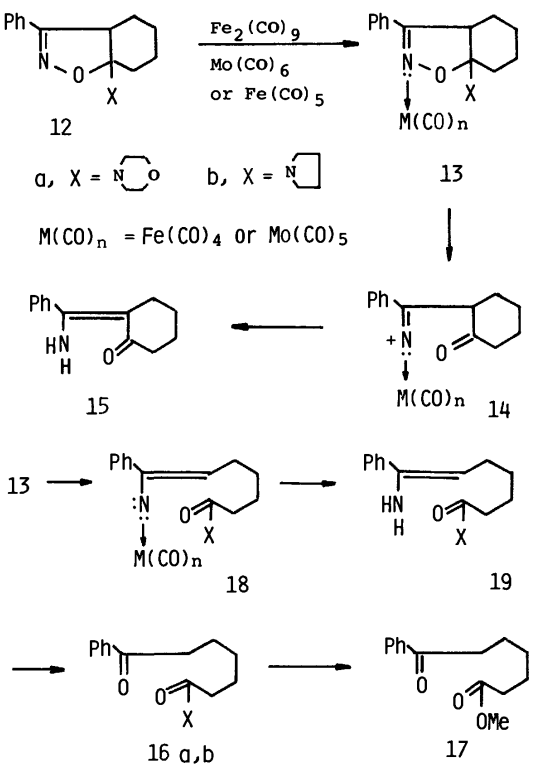

Scheme 3.

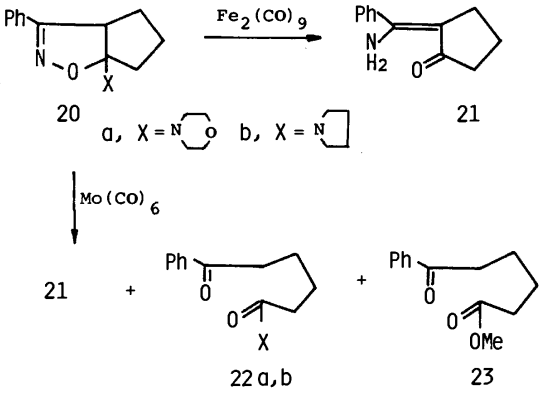

Scheme 4.

[$Fe_2(CO)_9$] is very slow, and β-amino enones **21**[11] were obtained in addition to the large amount of unreacted **20a,b**. However, [$Mo(CO)_6$] effects the complete reaction of **20a,b** to give β-amino enones **21**, the amide **22a,b**, and ester **23**[14,16] (Scheme 4). The yields and the reaction conditions are also listed in Table 2 (entries 7—10). The structures of new compounds **22a,b** were also confirmed by independent preparations of the corresponding samples (see Experimental). The formation of the products are explained by the pathways, which are similar to those of **12a,b**.

Regarding the product composition for the reaction of **12a,b**, the substituent such as morpholino or 1-pyrrolidinyl groups does not affect the reaction pathways giving **15**, **16**, and **17**. However, the size of the 4,5-polymethylene chain seems to affect the reaction

pathways. The N-O bond cleavage and the concomitant elimination of the morpholino or 1-pyrrolidinyl group giving β-amino enones become the major pathway for **20a,b**. The details for the ring size effect are ambiguous. Furthermore, $[Mo(CO)_6]$ is found to be more efficient for the ring cleavage of the 2-isoxazolines **12a,b** and **20a,b**, as compared to $[Fe_2(CO)_9]$.

In summary, these results demonstrate that $[Fe_2(CO)_9]$, $[Fe(CO)_5]$, and $[Mo(CO)_6]$ are useful reagents for the ring cleavage reaction of the appropriately substituted 2-isoxazoline ring system. Furthermore, the ring cleavage of the present 2-isoxazolines affords a series of interesting compounds, such as **9a,b**, **16a,b**, and **17** in modest yields.

Experimental

The IR spectra were recorded on a Shimadzu IR-400 spectrometer. The mass spectral studies were conducted using Shimadzu GCMS-QP1000 spectrometer. The NMR spectra were recorded on a Hitachi R-24 spectrometer, using tetramethylsilane as the internal standard. $[Mo(CO)_6]$ and $[Fe(CO)_5]$ (Strem Chemical, Inc.) were commercial samples. $[Fe_2(CO)_9]$ was prepared by the standard method.[17] Methanol was purified and dried by the standard method. All of the reactions were carried out under a dry nitrogen atmosphere. The desired 2-isoxazolines, **5a,b**,[8] **12a,b**,[13] and **20a,b**[14] were synthesized by the 1,3-dipolar cycloadditions of benzonitrile oxide with the corresponding olefins according to the literatures.

*General Procedure for the Reaction of 2-Isoxazolines **5a,b**, **12a,b**, or **20a,b** with $[Fe_2(CO)_9]$ or $[Mo(CO)_6]$.* A solution of **5**, **12**, or **20** (1 mmol) and $[Fe_2(CO)_9]$ (436 mg, 1.2 mmol) or $[Mo(CO)_6]$ (264 mg, 1 mmol) in anhydrous methanol (20 cm^3) was refluxed for an adequate period. After evaporation of the methanol, hexane–benzene (1/1, 20 cm^3) was added to the residue and the mixture was filtered through Celite to remove insoluble material. The filtrate was concentrated, and the resulting residue was separated by TLC on silica gel using the CH_2Cl_2–AcOEt (3/1) mixture as the eluent to give the products, which are summarized in Table 1 (entries 1, 3, 4, and 6) and Table 2 (entries 1, 3, 4, and 6—10). The products **9a,b**,[9] **15**,[11] **17**,[16] **21**,[11] and **23**[14,16] are known compounds and were identified by comparison of the physical properties with those reported in the literatures. The spectral data of the products, **16a,b**, **22a,b** were identical with those of the samples which were prepared independently by the following procedures.

*General Procedure for the Photoirradiation of **5a,b** or **12a,b** with $[Fe(CO)_5]$.* A solution of **5** or **12** (1 mmol) and $[Fe(CO)_5]$ (471 mg, 2.4 mmol) in anhydrous methanol (20 cm^3) was irradiated in a Pyrex vessel with RPR-350 nm lamps for an adequate period at an ambient temperature. The reaction mixture was filtered through Celite to remove insoluble material, and the filtrate was concentrated. The residue was separated by TLC on silica gel using CH_2Cl_2–AcOEt (3/1) as the eluent to give the products **9a,b**, **15**, **16a,b**, and **17** (Table 1, entries 2 and 5; Table 2, entries 2 and 5).

*Independent Preparation of **16a**.* To a stirred dichloromethane (4 cm^3) solution of 6-benzoylhexanoyl chloride, which was prepared from 6-benzoylhexanoic acid[16] (440 mg, 2 mmol) and thionyl chloride (1.29 g, 10 mmol), morpholine (4.35 g, 50 mmol) was added. After the reaction mixture was stirred for 1 h, water was added to the reaction mixture. The product was extracted with CH_2Cl_2 and the extract was dried over Na_2SO_4. After evaporation of the CH_2Cl_2, the resulting residue was distilled to give **16a** (301 mg, 52%): bp

Table 1. Reaction of 2-isoxazolines **5a,b** with $[Fe_2(CO)_9]$, $[Fe(CO)_5]$, or $[Mo(CO)_6]$[a]

Entry	Compound	Conditions[b]	Reaction time/h	Product (Yield/%)
1	**5a**	A	24	**9a** (57)
2	**5a**	B	24	**9a** (51)
3	**5a**	C	24	**9a** (61)
4	**5b**	A	24	**9b** (65)
5	**5b**	B	24	**9b** (70)
6	**5b**	C	24	**9b** (71)

a) Reactions were carried out in anhydrous methanol. b) A: 1.2 molar equivalent amounts of $[Fe_2(CO)_9]$ were used under reflux; B: 2.4 molar equivalent amounts of $[Fe(CO)_5]$ were used under photoirradiation; C: An equivalent amount of $[Mo(CO)_6]$ was used under reflux.

Table 2. Reaction of 2-isoxazolines, **12a,b** and **20a,b** with $[Fe_2(CO)_9]$, $[Fe(CO)_5]$, or $[Mo(CO)_6]$[a]

Entry	Compound	Conditions[b]	Reaction time/h	Recovery/%	Product (Yield/%)					
1	**12a**	A	24	31	**15**	(26)	**16a**	(—)	**17**	(19)
2	**12a**	B	81	29	**15**	(29)	**16a**	(—)	**17**	(26)
3	**12a**	C	24	—	**15**	(14)	**16a**	(7)	**17**	(28)
4	**12b**	A	24	21	**15**	(32)	**16b**	(—)	**17**	(26)
5	**12b**	B	67	40	**15**	(38)	**16b**	(—)	**17**	(21)
6	**12b**	C	24	—	**15**	(44)	**16b**	(3)	**17**	(22)
7	**20a**	A	24	77	**21**	(22)	**22a**	(—)	**23**	(—)
8	**20a**	C	22	—	**21**	(69)	**22a**	(10)	**23**	(—)
9	**20b**	A	24	65	**21**	(32)	**22b**	(—)	**23**	(—)
10	**20b**	C	23	—	**21**	(55)	**22b**	(9)	**23**	(4)

a) Reactions were carried out in anhydrous methanol. b) A: 1.2 molar equivalent amounts of $[Fe_2(CO)_9]$ were used under reflux; B: 2.4 molar equivalent amounts of $[Fe(CO)_5]$ were used under photoirradiation; C: An equivalent amount of $[Mo(CO)_6]$ was used under reflux.

130—140 °C/20.0 Pa; IR ($CHCl_3$), 1679, 1625 cm^{-1}; NMR (CCl_4), δ=1.22—1.90 (6H, m), 2.05—2.47 (2H, m), 2.74—3.07 (2H, m), 3.27—3.70 (8H, m), 7.23—7.57 (3H, m), 7.75—8.04 (2H, m); MS, *m/z* (rel intensity), 289 (M^+, 11) 105 (100). Found: C, 70.94; H, 7.87; N, 4.81%. Calcd for $C_{17}H_{23}N_3$: C, 70.56; H, 8.01; N, 4.84%.

Independent Preparation of ***16b***. The similar procedure described above was applied using 6-benzoylhexanoic acid (440 mg, 2 mmol), thionyl chloride (1.298 g, 10 mmol), and pyrrolidine (3.55 g, 50 mmol) to give **16b** (475, 87%): bp 110—120 °C/13.3 Pa; IR ($CHCl_3$), 1672, 1616 cm^{-1}; NMR ($CDCl_4$), δ=1.16—2.41 (12H, m), 2.70—3.06 (2H, m), 3.16—3.52 (4H, m), 7.18—7.57 (3H, m), 7.70—7.98 (2H, m); MS, *m/z* (rel intensity), 273 (M^+, 10), 70 (100). Found: C, 74.86; H, 8.32; N, 5.33%. Calcd for $C_{17}H_{23}NO_2$: C, 74.69; H, 8.48; N, 5.12%.

Independent Preparation of ***22a***. To a stirred CH_2Cl_2 (4 cm^3) solution of 5-benzoylpentanoyl chloride, which was prepared from 5-benzoylpentanoic acid[18] (380 mg, 2 mmol) and thionyl chloride (1.29 g, 10 mmol) at an ambient temperature, morpholine (4.3 g, 50 mmol) was added. After the reaction mixture was stirred for 1 h at an ambient temperature, water was added to the reaction mixture. The product was then extracted with CH_2Cl_2 and the extract was dried over Na_2SO_4 and concentrated. The resulting residue was purified by column chromatography on alumina using benzene as the eluent to give the crude crystalline solid, which was recrystallized from a benzene–hexane (1/1) mixture to give **22a**: mp 74—75 °C; IR ($CHCl_3$), 1675, 1620 cm^{-1}; NMR (CCl_4), δ=1.50—1.97 (4H, m), 2.10—2.43 (2H, m), 2.83—3.13 (2H, m), 3.33—3.73 (8H, m), 7.40—7.63 (3H, m), 7.87—8.01 (2H, m); MS, *m/z* (rel intensity), 289 (M^+, 10), 105 (100). Found: C, 70.12; H, 7.58; N, 5.18%. Calcd for $C_{14}H_{21}NO_3$: C, 69.79; H, 7.69; N, 5.09%.

Independent Preparation of ***22b***. The similar procedure described above was applied using 5-benzoyl-pentanoic acid (380 mg, 2 mmol), thionyl chloride (1.29 g, 10 mmol), and pyrrolidine (3.55 g, 50 mmol). The similar workup afforded **22b**: mp 69—71 °C (from benzene–hexane, 1/1); IR ($CHCl_3$), 1682, 1620 cm^{-1}; NMR (CCl_4), δ=1.47—2.38 (10H, m), 2.74—3.12 (2H, m), 3.12—3.57 (4H, m), 7.23—7.58 (3H, m), 7.74—8.05 (2H, m); MS, *m/z* (rel intensity), 259 (M^+, 9), 113 (100). Found: C, 74.14; H, 8.04; N, 5.05%. Calcd for $C_{16}H_{21}NO_2$: C, 74.10; H, 8.16; N, 5.40%.

References

1) This paper was presented at the National Meeting of Chemical Society of Japan, April, 1983.

2) V. Jäger, W. Buβ, and W. Schwab, *Tetrahedron Lett.*, **1978**, 3133; V. Jäger, W. Schwab, and V. Buβ, *Angew. Chem. Int. Ed. Engl.*, **20**, 601 (1981); A. P. Kozikowski and Y. Y Chan, *J. Org. Chem.*, **46**, 5248 (1981).

3) V. Jäger and H. Grund, *Angew. Chem. Int. Ed. Engl.*, **15**, 50 (1976); V. Jäger, H. Grund, and W. Schwab, *ibid.*, **17**, 78 (1978).

4) O. P. Curran, *J. Am. Chem. Soc.*, **104**, 4024 (1982); M. Asaoka, T. Murata, and H. Takei, *Tetrahedron Lett.*, **22**, 735 (1981); A. P. Kozikowski and M. Adamezyk, *ibid.*, **23**, 3123 (1982).

5) S. Andersen, N. B. Das, R. D. Jorgensen, G. Kjeldesen, J. S. Knudsen, S. C. Sharma, and K. B. G. Torssell, *Acta Chem. Scand. Ser. B*, **36**, 1 (1982); N. B. Das and K. B. G. Torssell, *Tetrahedron*, **39**, 2247 (1983) and references cited therein.

6) M. Nitta and T. Kobayashi, *Chem. Lett.*, **1983**, 51; M. Nitta and T. Kobayashi, *J. Chem. Soc., Perkin Trans. 1*, **1984**, 2103.

7) P. Claus, P. Gilgen, H.-J. Hansen, H. Heimgartner, B. Jackson, and H. Schmid, *Helv. Chim. Acta*, **57**, 2173 (1974); Y. Itoh and T. Matsuura, *Tetrahedron*, **31**, 1373 (1975); T. Kumagai, K. Shimizu, Y. Kawamura, and T. Mukai, *ibid.*, **37**, 3365 (1981) and references cited therein.

8) I. Adachi and H. Kano, *Chem. Pharm. Bull.*, **16**, 117 (1968).

9) J. Golonge and G. Descotes, *C. R. Acad Sci. Paris*, **254**, 887 (1962); G. Descotes and J. C. Soula, *Bull. Soc. Chim. F.*, **10**, 2636 (1964); P. J. Wagner and A. E. Kemppainen, *J. Am. Chem. Soc.*, **94**, 7495 (1972).

10) R. C. Kreber, "The Organic Chemistry of Iron," ed by F. W. Grevels and I. Fishler, Academic Press, New York, (1981), p. 1.

11) M. Nitta and T. Kobayashi, *J. Chem. Soc., Chem. Commun.*, **1982**, 878.

12) M. Nitta and T. Kobayashi, *Bull. Chem. Soc. Jpn.*, **57**, 1035 (1984).

13) M. E. Kuehne and S. J. Weaver, *J. Org. Chem.*, **29**, 1582 (1964).

14) S. Hauptmann and F. Brandes, *J. Prakt. Chem.*, **25**, 56 (1964).

15) M. E. Kuehne and T. Garbacik, *J. Org. Chem.*, **35**, 1555 (1970).

16) H. Saiki, Ph. D. Thesis, Tohoku Univ., **1977**.

17) E. H. Braye and W. Hübel, *Inorg. Synth.*, Vol. VIII, 1966, p. 178.

18) L. F. Somerville and C. F. H. Allen, *Org. Synth.*, Coll. Vol. II, 81 (1943).

Convenient Preparations of 3,5-Disubstituted 1,2,4-Thiadiazoles by Oxidative Dimerization of Thioamides

Yuji TAKIKAWA,* Kazuaki SHIMADA, Katsuyuki SATO, Shinichi SATO, and Saburo TAKIZAWA

Department of Applied Chemistry, Faculty of Engineering, Iwate University, Morioka, Iwate 020

(Received October 8, 1984)

3,5-Disubstituted 1,2,4-thiadiazoles **2** were prepared by reaction of thioamides **1** with DMSO in the presence of such an electrophilic reagent as 1-methyl-2-chloropyridinium iodide, benzoyl chloride, acetyl chloride, hydrochloric acid, or trimethylsilyl chloride in organic solvents at room temperature in high yields. Thiadiazoles **2** were also obtained by reaction of **1** with NBS at room temperature in high yields. Thioamide *S*-oxides reacted with electrophilic reagents at room temperature to give the corresponding thiadiazoles **2** in high yields.

Thiadiazoles are useful for bactericides,[1-3] fungicides,[1-4] herbicides,[5,6] antibiotics,[7-9] *etc.*, and a number of preparations for them have been reported. The preparation of 3,5-disubstituted 1,2,4-thiadiazoles can be roughly divided into three methods; intermolecular cyclization,[10,11] intermolecular cyclization of two different molecules,[12,13] and oxidative dimerization of the same molecules.[14-17] Some of the methods by the oxidative dimerization of thioamides, however, suffer disadvantages that substituents in 3,5-positions are limited mainly to aryl groups[14] and that by-products such as nitriles and isothiocyanates are formed.[5,18]

It is known well that the sulfur atom in thioamide easily reacts with electrophilic reagents and that resulting sulfonium salts[19-21] are very reactive with nucleophilic reagents to give various products. When an electrophilic reagent is constructed of a pair of a soft electrophile such as X^+ and a counter anion having a low nucleophilicity, the resulting sulfonium salt would eliminate HX immediately to form unstable thiazirine[17] or nitrile sulfide[22] equivalent, which is regarded as an oxidized form of thioamides and a precursor of thiadiazoles. On the basis of such a view, thioamide **1** was allowed to react with DMSO in the presence of an electrophilic reagent in organic solvent at room temperature to obtain thiadiazole **2** in high yields. In this paper, we report convenient preparations of 3,5-disubstituted 1,2,4-thiadiazoles by oxidative dimerization of thioamides using DMSO–electrophilic reagent systems and NBS. A preparation of thiadiazoles by reaction of thioamide *S*-oxides with electrophilic reagents is also described.

Results and Discussion

The conversion of thioamides **1** to 3,5-disubstituted 1,2,4-thiadiazoles **2** using DMSO–electrophilic reagent systems is shown in Table 1. These conversions do not occur in the absence of either DMSO or such electrophilic reagents as 1-methyl-2-chloropyridinium iodide **3** (Runs 1 and 2 in Table 1), and do not necessarily need one equivalent of **3** (Run 3 in Table 1). Moreover, the conversion to thiadiazole **2a** is successful in most organic solvents (Runs 3—7 in Table 1). The arenecarbothioamides **1a—g** could be converted to the corresponding thiadiazoles **2a—g** in high yields. The conversion of 2-(substituted phenyl)ethanethioamides **1h—j** to thiadiazoles **2h—j** was also achieved in moderate yield (Runs 18—20 in Table 1). When benzoyl chloride, acetyl chloride, 36% HCl, or trimethylsilyl chloride was used as electrophilic reagent thiadiazole **2a** was also obtained in high yield (Runs 21—24 in Table 1). However, thiobenzamide **1a** reacted with such sulfoxides as dibutyl sulfoxide and dibenzyl sufoxide in the presence of **3** at room temperature in CH_2Cl_2 giving thiadiazole **2a** in high yield (Runs 9 and 10 in Table 1). However, in the reaction with diphenyl sulfoxide having a low nucleophilicity, thiadiazole **2a** was obtained only in 9% yield at reflux for 6 h (Run 11 in Table 1). The corresponding sulfides were obtained in a series of these reactions. In the reaction of **3** with DMSO, 1-methyl-2(1*H*)-pyridineone was hardly obtained at room temperature, but it was quantitatively formed at 80 °C for 2 h along with iodine.

On the other hand, thiadiazoles **2** were obtained in high yields by the reaction of thioamide *S*-oxides **4** with an electrophilic reagent such as **3**, trimethylsilyl chloride, benzoyl chloride, acetic anhydride, or 36% HCl. It is interesting that the yields of 3,5-dibenzyl-1,2,4-thiadiazoles **2h—k** were enhanced. These results are shown in Table 2. No thiadiazole **2a** was obtained by stirring at room temperature for 24 h in CH_2Cl_2 in the absence of electrophilic reagent (Run 1 in Table 2), apparently implying that thiobenzamide *S*-oxide **4a** was activated by electrophilic reagent (Run 2 in Table 2). Consequently, the formation of thiadiazoles **2** may be as illustrated in Scheme 1.

As shown in Table 1, the reaction of thiobenzamide **1a** with DMSO gave quantitatively thiadiazole **2a** even with an addition of 0.03 equivalent of pyridinium salt **3** at 60 °C for 2.5 h. Thiobenzamide **1a** reacted also with 36% HCl in DMSO at room tem-

35 TABLE 1. CONVERSION TO 3,5-DISUBSTITUTED 1,2,4-THIADIAZOLES USING DMSO-ELECTROPHILIC REAGENTS[a]

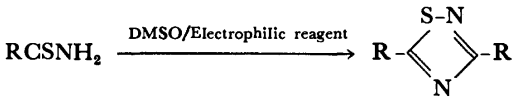

1 2

Run	Thioamide R		Solvent	DMSO equiv	Electrophilic reagent	equiv	Temp °C	Time h	Product	Yield %
1	C_6H_5	**1a**	DMSO	—	—		60	2	**2a**	0
2	C_6H_5	**1a**	CH_2Cl_2	0	Py salt[b]	1.0	Reflux	4	**2a**	0
3	C_6H_5	**1a**	DMSO	—	Py salt	0.03	60	2.5	**2a**	quant.
4	C_6H_5	**1a**	CH_2Cl_2	0.5	Py salt	0.5	r.t.	14	**2a**	48
5	C_6H_5	**1a**	CH_2Cl_2	1.0	Py salt	0.5	r.t.	4	**2a**	94
6	C_6H_5	**1a**	C_6H_6	1.0	Py salt	0.5	r.t.	4	**2a**	90
7	C_6H_5	**1a**	EtOH	1.0	Py salt	0.5	r.t.	4	**2a**	84
8[c]	C_6H_5	**1a**	CH_2Cl_2	1.1	Py salt	0.5	r.t.	13	**2a**	83
9	C_6H_5	**1a**	CH_2Cl_2	1.0[d]	Py salt	1.0	r.t.	18	**2a**	86
10	C_6H_5	**1a**	CH_2Cl_2	1.0[e]	Py salt	1.0	r.t.	18	**2a**	78[f]
11	C_6H_5	**1a**	CH_2Cl_2	1.0[g]	Py salt	1.0	Reflux	6	**2a**	9
12	4-$CH_3C_6H_4$	**1b**	DMSO	—	Py salt	0.5	40	1.5	**2b**	93
13	4-ClC_6H_4	**1c**	DMSO	—	Py salt	0.5	r.t.	6	**2c**	91
14	4-$CH_3OC_6H_4$	**1d**	DMSO	—	Py salt	0.5	35	24	**2d**	quant.
15	4-$(CH_3)_2NC_6H_4$	**1e**	CH_2Cl_2	1.0	Py salt	0.5	r.t.	7	**2e**	52
16	1-Naphthyl	**1f**	CH_2Cl_2	1.0	Py salt	0.5	r.t.	6	**2f**	52[h]
17	2-Naphthyl	**1g**	CH_2Cl_2	1.0	Py salt	1.0	r.t.	7	**2g**	79
18	$C_6H_5CH_2$	**1h**	CH_2Cl_2	1.0	Py salt	0.25	r.t.	5 d	**2h**	36
19	4-$CH_3C_6H_4CH_2$	**1i**	CH_2Cl_2	1.0	Py salt	0.25	r.t.	29	**2i**	48
20	4-$ClC_6H_4CH_2$	**1j**	CH_2Cl_2	1.0	Py salt	0.25	r.t.	4 d	**2j**	26
21	C_6H_5	**1a**	CH_2Cl_2	1.1	PhCOCl	0.5	r.t.	0.5	**2a**	99[i]
22	C_6H_5	**1a**	CH_2Cl_2	1.1	CH_3COCl	0.5	r.t.	0.5	**2a**	94
23	C_6H_5	**1a**	CH_2Cl_2	1.1	$(CH_3)_3SiCl$	(Excess)	r.t.	0.5	**2a**	65
24	C_6H_5	**1a**	DMSO	—	36% HCl	0.5	r.t.	8	**2a**	quant.
25	C_6H_5	**1a**	CH_2Cl_2	1.1	$(CH_3CO)_2O$	1.2	Reflux	2	**2a**	2[j]
26	C_6H_5	**1a**	CH_2Cl_2	1.1	CH_3I	1.2	r.t.	5 d	**2a**	0

a) Thioamide: 1 mmol; solvent: 2 ml. b) Py salt: 1-methyl-2-chloropyridinium iodide. c) 20 mmol of phenylacetylene was added. d) Dibutyl sulfoxide. e) Dibenzyl sulfoxide. f) Dibenzyl sulfide was obtained in 71% yield. g) Diphenyl sulfoxide. h) 1-Naphthonitrile was obtained in 44% yield. i) Benzoic acid was obtained in 93% yield. j) 89% of thiobenzamide **1a** was recovered.

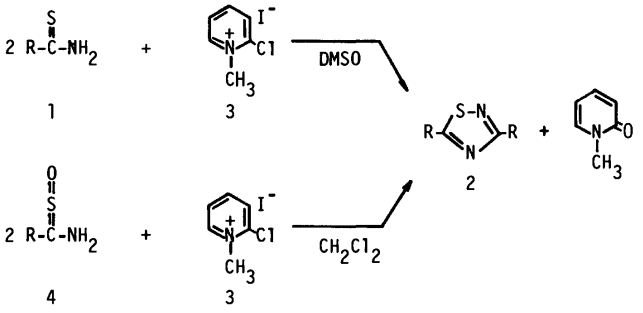

Scheme 1.

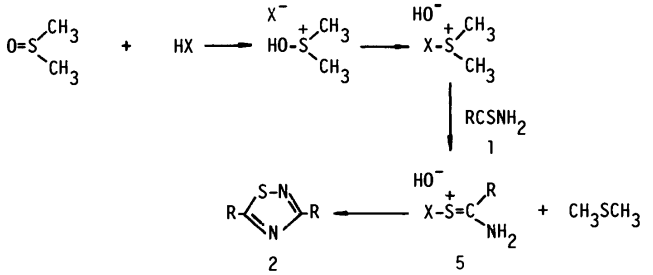

Scheme 2.

perature for 8 h giving quantitatively thiadiazole **2a** (Run 24 in Table 1), which suggests that both HCl and HI generated in the reaction of thiobenzamide **1a** with DMSO in the presence of **3** also participate in the formation of thiadiazole **2a**.[23-26] Therefore, the conversion to thiadiazoles **2** by the reaction of thioamides **1** with DMSO in the presence of electrophilic reagent may proceed as shown in Scheme 2.[27]

If thiadiazoles **2** are formed *via* sulfonium salt **5**, they must be obtained by the reaction of thioamides **1** with NBS. As had been expected, various thioamides **1** reacted with NBS at room temperature to give the cor-

Table 2. Conversion of thioamide *S*-oxides to 3,5-disubstituted 1,2,4-thiadiazoles using electrophilic reagents[a)]

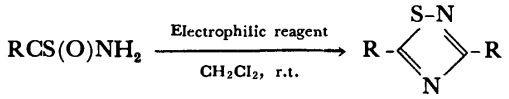

4 2

Run	Thioamide *S*-oxide/R		Electrophilic reagent/equiv		Time/h	Product	Yield/%
1	C_6H_5	**4a**	—		24	**2a**	0
2	C_6H_5	**4a**	Py salt	0.27	0.5	**2a**	97
3	4-$CH_3C_6H_4$	**4b**	Py salt	0.5	1	**2b**	70
4	4-$CH_3OC_6H_4$	**4d**	Py salt	0.5	0.5	**2d**	72
5	1-Naphthyl	**4f**	Py salt	0.5	24	**2f**	63
6	$C_6H_5CH_2$	**4h**	Py salt	0.5	1.25	**2h**	70
7	4-$CH_3C_6H_4CH_2$	**4i**	Py salt	0.5	24	**2i**	70
8	4-$ClC_6H_4CH_2$	**4j**	Py salt	0.5	24	**2j**	70
9	4-$CH_3OC_6H_4CH_2$	**4k**	Py salt	0.5	24	**2k**	64
10	C_6H_5	**4a**	$(CH_3)_3SiCl$	(Excess)	2	**2a**	69
11[b)]	4-ClC_6H_4	**4c**	36% HCl	0.5	9	**2c**	quant.
12	4-$ClC_6H_4CH_2$	**4j**	PhCOCl	1.3	10	**2j**	73
13	4-$ClC_6H_4CH_2$	**4j**	$(CH_3CO)_2O$	1.3	2.5	**2j**	68

a) Thioamide *S*-oxide: 1 mmol; CH_2Cl_2: 2 ml. b) 5 ml of EtOH was added.

Table 3. Conversion to 3,5-disubstituted 1,2,4-thiadiazoles using NBS[a)]

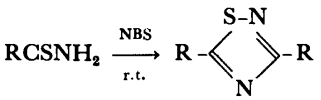

1 2

Run	Thioamide/R		Solvent	Time/h	Product	Yield/%
1[b)]	C_6H_5	**1a**	$CHCl_3$	13	**2a**	39[c)]
2	C_6H_5	**1a**	$CHCl_3$	21	**2a**	quant.
3	4-$CH_3C_6H_4$	**1b**	$CHCl_3$	20	**2b**	93
4	4-$CH_3OC_6H_4$	**1d**	$CHCl_3$	1	**2d**	83
5	1-Naphthyl	**1f**	CH_2Cl_2	0.5	**2f**	82
6	$C_6H_5CH_2$	**1h**	$CHCl_3$	26	**2h**	78
7	4-$CH_3C_6H_4CH_2$	**1i**	CH_2Cl_2	1	**2i**	79
8	4-$ClC_6H_4CH_2$	**1j**	$CHCl_3$	23	**2j**	72
9	4-$CH_3OC_6H_4CH_2$	**1k**	CH_2Cl_2	1	**2k**	86

a) Thioamide: 1 mmol; NBS: 1.1 mmol; solvent: 2 ml. b) NBS: 0.5 mmol. c) 37% of thiobenzamide **1a** was recovered.

responding thiadiazoles **2** in high yields. These results are shown in Table 3.

A few mechanisms have been reported for the formation of 3,5-disubstituted 1,2,4-thiadiazoles by the oxidative dimerization of thioamides. One of them[28)] comprises a route *via* dithiazoline, which is formed by the reaction of thioamide-bromine adduct with thioamide. Another mechanism[22)] resorts to the 1,3-dipolar adduct of nitrile sulfide, which is formed by way of photooxidation through extrusion of thioamide hydrogens under aerobic conditions. The conversion of thioamide into 3,5-disubstituted 1,2,4-thiadiazole *via* dithiazoline by bromine proceeds through the reaction of thioamide-bromine adduct with one more molecule of thioamide and accompanies loss of hydrogen sulfide. In a series of these reactions, however, the use of equimolar amounts of thioamide and NBS or DMSO–electrophilic reagent was needed for bringing the reaction to completion and no hydrogen sulfide but elemental sulfur was obtained in all reaction systems (Runs 4 and 5 in Table 1, and Runs 1 and 2 in Table 3). Consequently, the mechanism *via* dithiazoline is unlikely. On the other hand, the mechanism *via* thiazirine[17)] or nitrile sulfide[22)] also is considered infeasible for the following reason. Benzonitrile *N*-sulfide is known to undergo 1,3-dipolar cycloaddition with such a dipolarophile as dimethyl acetylenedicarboxylate,[29)] phenylacetylene,[22)] or benzonitrile[22)] to give dimethyl 3-phenylisothiazole-4,5-dicarboxylate, 3,4-diphenylisothiazole, or 3,5-diphenyl-1,2,4-thiadiazole, respectively. Thiobenzamide **1a** reacted with DMSO–pyridinium salt **3** in the presence of phenylacetylene in CH_2Cl_2 at room temperature for 13 h to give 3,5-diphenyl-1,2,4-thiadiazole **2a** and 1-methyl-2(1*H*)-pyridinethione in 83 and 18% yields, respectively, and no adduct with phenylacetylene was obtained. (Run 8 in Table 1). A solution of *p*-(methyl)thiobenzamide **1c** (1 mmol), *p*-methoxybenzonitrile (3 mmol), DMSO (1 mmol), and **3** (0.5 mmol) in CH_2Cl_2 (2 ml) was stirred at room temperature for 8 h to give only 3,5-di-*p*-tolyl-1,2,4-thiadiazole **2c** in 88% yield, and *p*-methoxybenzonitrile was quantitatively recovered. Both of these results suggest that the mechanism through thiazirine or nitrile sulfide is unlikely.

N-(methyl)thiobenzamide reacted with iodine in the presence of Et_3N in CH_2Cl_2 at room temperature for 1 d to give N^1-benzoyl-N^1,N^2-dimethylbenzamidine in

41% yield along with a trace amount of N^1-thiobenzoyl-N^1,N^2-dimethylbenzamidine and elemental sulfur

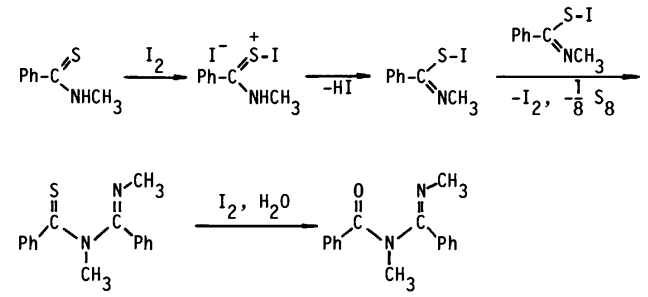

Scheme 3.

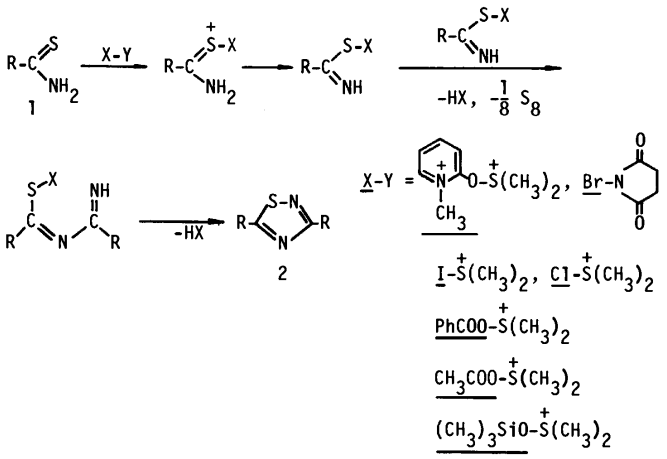

Scheme 4.

in 70% yield. N^1-thiobenzoyl-N^1,N^2-dimethylbenzamidine reacts with H_2O in the presence of iodine to give N^1-benzoyl-N^1,N^2-dimethylbenzamidine quantitatively. The pathway for this sequence would be given in Scheme 3.

It is apparent that the sulfonium intermediate **5** (X=I, Br, Cl, CH_3COO, PhCOO, $(CH_3)_3SiO$, or 1-methyl-2-pyridiniooxy) is present in a series of these reactions as judged from the reaction of thioamide *S*-oxides **4** with electrophilic reagents and of thioamides **1** with NBS. Therefore, conversion of thioamides **1** to 3,5-disubstituted 1,2,4-thiadiazoles **2** using DMSO-electrophilic reagents or NBS would proceed as shown in Scheme 4.

Experimental

General. The thioamides[30] and thioamide *S*-oxides[31] were prepared according to the literatures. The other reagents were commercial reagent grade materials and were purified by recrystallization or by distillation prior to use. IR spectra were recorded with a Hitachi 295 infrared spectrophotometer. ^{1}H NMR spectra were recorded with a Hitachi R-22 (90 MHz) spectrometer in carbon tetrachloride or deuteriochloroform solution containing tetramethylsilane as an internal standard. Mass spectra were recorded with a Hitachi RMU-6M spectrometer, with a direct inlet system, operating at 20 eV. For column chromatography Wakogel C-300 was used.

Preparation of 3,5-Diphenyl-1,2,4-thiadiazole **2a** *by DMSO-1-Methyl-2-chloropyridinium Iodide* **3**. A solution of

TABLE 4. PHYSICAL AND ANALYTICAL DATA OF THIADIAZOLES

Product	Mp θ_m/°C	^{1}H NMR spectra δ, $CDCl_3$	MS (20 eV) m/z (M^+)	Found (Calcd)/%			
				C	H	N	S
2a	91—91.5(EtOH) (lit,[32] 89—90)	7.41—7.79(6H, m), 7.91—8.03(2H, m), 8.31—8.41(2H, m)	238				
2b	130.5—131(EtOH) (lit,[33] 135—137)	2.40(6H, s), 7.21(2H, s), 7.30(2H, s), 7.89(2H, d, J=9 Hz), 8.24(2H, d, J=9 Hz)	266				
2c	161.5—162(EtOH-$CHCl_3$) (lit,[32] 161—162)	7.42(2H, d, J=9 Hz), 7.44(2H, d, J=9 Hz), 7.92(2H, d, J=9 Hz), 8.26(2H, d, J=9 Hz)	306				
2d	139—139.5(EtOH-$CHCl_3$) (lit,[32] 139—140)	3.85(6H, s), 6.96(4H, d, J=9 Hz), 7.93(2H, d, J=9 Hz), 8.30(2H, d, J=9 Hz)	298				
2e	223(EtOH-$CHCl_3$) (lit,[14] 223)	3.04(12H, s), 6.46, 6.81(4H, m) 7.88(2H, d, J=9 Hz), 8.24(2H, d, J=9 Hz)	324				
2f	99—100(MeOH-$CHCl_3$)	7.40—7.80(6H, m), 7.80—8.10(5H, m) 8.40—8.60(1H, m), 8.80—9.00(1H, m), 9.10—9.30(1H, m)	338	77.88 (78.08)	4.05 (4.17)	8.11 (8.28)	9.43 (9.47)
2g	180—180.5(EtOH-$CHCl_3$)	7.24—7.60(4H, m), 7.79—8.13(7H, m), 8.39—8.54(2H, m), 8.91(1H, s)	153 (B.p.)	77.55 (78.08)	3.94 (4.17)	7.89 (8.28)	9.62 (9.47)
2h	Oil(lit,[32] 39)	4.28(2H, s), 4.31(2H, s), 7.31(10H, s)	266				
2i	59(EtOH)	2.29(3H, s), 2.39(3H, s), 4.23(2H, s) 4.26(2H, s), 7.03—7.26(8H, m)	294	72.72 (73.43)	6.14 (6.16)	9.26 (9.52)	11.08 (10.89)
2j	60—62(EtOH)	3.75(3H, s), 3.78(3H, s), 4.20(2H, s), 4.24(2H, s), 6.79—6.93(4H, m), 7.17—7.28(4H, m)	326	65.23 (66.23)	5.49 (5.56)	8.19 (8.58)	10.15 (9.82)
2k	87(EtOH-$CHCl_3$)	4.23(2H, s), 4.28(2H, s), 7.28(8H, s)	334	56.86 (57.32)	3.50 (3.61)	8.11 (8.36)	9.55 (9.56)

thiobenzamide **1a** 137 mg (1 mmol), DMSO 78 mg (1 mmol), and **3** 128 mg (0.5 mmol) in CH_2Cl_2 (2 ml) was stirred at room temperature for 4 h, and the reaction mixture was filtered. After removal of CH_2Cl_2, the residue was purified by silica-gel column chromatography using $CHCl_3$ as an eluent to afford thiadiazole **2a** in 94% yield. The preparation of 3,5-disubstituted 1,2,4-thiadiazoles **2** by DMSO–**3** also was carried out in a similar manner as above. The physical properties and elemental analyses of thiadiazoles **2** are shown in Table 4.

Preparation of 3,5-Disubstituted 1,2,4-Thiadiazoles 2 by DMSO–Electrophilic Reagents (Benzoyl Chloride, Acetyl Chloride, 36% HCl, Trimethylsilyl Chloride, Acetic Anhydride, and Methyl Iodide). A typical procedure is described below for the preparation of 3,5-diphenyl-1,2,4-thiadiazole **2a** by DMSO–benzoyl chloride. A solution of thiobenzamide **1a** 137 mg (1 mmol), DMSO 86 mg (1.1 mmol), and benzoyl chloride 78 mg (0.5 mmol) in CH_2Cl_2 (2 ml) was stirred at room temperature for 30 min, and the reaction mixture was filtered. After removal of CH_2Cl_2, the residue was purified by silica-gel column chromatography using $CHCl_3$ as an eluent to afford thiadiazole **2a** and benzoic acid in 100 and 93% yields, respectively.

Preparation of 3,5-Disubstituted 1,2,4-Thiadiazoles 2 by NBS. A typical procedure is described below for the preparation of 3,5-bis(*p*-methoxybenzyl)-1,2,4-thiadiazole **2k**. A solution of (*p*-methoxyphenyl)thioacetamide **1k** 181 mg (1 mmol) and NBS 196 mg (1.1 mmol) in CH_2Cl_2 (2 ml) was stirred at room temperature for 1 h. To this reaction mixture was added 2 ml of 10% NaOH and an extraction with $CHCl_3$ was applied. After removal of $CHCl_3$, the residue was purified by silica-gel column chromatography using $CHCl_3$ as an eluent to give thiadiazole **2k** in 88% yield.

Conversion of Thioamide S-Oxides 6 to 3,5-Disubstituted 1,2,4-Thiadiazoles 2 by Electrophilic Reagents (Pyridinium Salt 3, Benzoyl Chloride, Trimethylsilyl Chloride, Acetic Anhydride, and 36% HCl). A typical procedure is described below for the preparation of 3,5-bis(*p*-chlorophenyl)-1,2,4-thiadiazole **2c** by the reaction of *p*-(chloro)thiobenzamide *S*-oxide **4c** with 36% HCl. A solution of **4c** 188 mg (1 mmol) and 36% HCl 51 mg (0.5 mmol) in EtOH (5 ml) was stirred at room temperature for 9 d, and a large amount of water was added to the reaction mixture to precipitate white crystals. The crude crystals were collected and purified by silica-gel column chromatography using $CHCl_3$ as an eluent to afford thiadiazole **2c** quantitatively.

References

1) H. Sumi and Y. Takahi, *Japan Kokai*, **74**, 29697 (1974).
2) S. Kamada, K. Nishio, and K. Takita, *Japan Kokai*, **74**, 04241 (1974).
3) A. B. George and E. M. Craig, U. S. Patent 4209522 (1980).
4) E. K. Lamrence, U. S. Patent 4263312 (1981).
5) B. Muefit, N. Siegfried, P. Harun, and K. Friedhelm, *J. Agric. Food Chem.*, **27**, 815 (1979).
6) A. G. Walter, U. S. Patent 4207089 (1980).
7) H. Rene and L. Andre, Fr. Demande 2381053 (1979).
8) T. Teraji, K. Sakane, and J. Goto, *Eur. Pat. Appl.* 13762 (1980).
9) T. Teraji, K. Sakane, and J. Goto, *Eur. Pat. Appl.* 27599 (1981).
10) F. Kurzer and S. A. Taylor, *J. Chem. Soc.*, **1958**, 379.
11) C. P. Joshva and V. K. Verma, *J. Indian Chem. Soc.*, **38**, 988 (1961).
12) J. Goerder, H. Gvoschopp, and U. Sommerlad, *Chem. Ber.*, **90**, 182 (1952).
13) E. Rothgery and H. J. A. Schroeder, U. S. Patent 4143044 (1979).
14) K. Shibuya, *Nippon Kagaku Kaishi*, **1979**, 389.
15) M. W. Cronyn and T. W. Nakagawa, *J. Am. Chem. Soc.*, **74**, 3693 (1952).
16) I. Yusuf and P. Harun, *Chem.-Ztg.*, 104, 365 (1980).
17) W. T. M. El-Wassimy, K. A. Jorgensen, and S.-O. Lawesson, *Tetrahedron*, **39**, 1729 (1983).
18) M. Bahadin, S. Nitz, H. Parlar, and F. Korte, *Z. Naturforsch., B*, **34B**, 1651 (1979).
19) S. A. Okecha and F. Stansfield, *J. Chem. Soc., Perkin Trans. 1*, **1977**, 1811.
20) T. Harada, Y. Tamaru, and Z. Yoshida, *Tetrahedron Lett.*, **1979**, 3525.
21) T. Harada, Y. Tamaru, and Z. Yoshida, *Chem. Lett.*, **1979**, 1353.
22) M. Machida, K. Oda, and Y. Kanaoka, *Tetrahedron Lett.*, **25**, 409 (1984).
23) A. J. Mancuso and D. Swern, *Synthesis*, **1981**, 165.
24) K. Omura and D. Swern, *Tetrahedron*, **34**, 1651 (1978).
25) A. J. Mancuso, D. S. Brownfain, and D. Swern, *J. Org. Chem.*, **44**, 4148 (1979).
26) A. J. Mancuso, S. -L. Huang, and D. Swern, *J. Org. Chem.*, **43**, 2480 (1978).
27) The reaction of thiobenzamide **1a** (1 mmol) with DMSO (1.1 mmol) in the presence of benzoic acid (1.1 mmol) at room temperature for 6 d did not give thiadiazole **2a** and the substrate was recovered in 88% yield.
28) A. Corsaro, A. Compagnini, G. Perrini, and G. Purrello, *J. Chem. Soc., Perkin Trans. 1*, **1984**, 897.
29) P. K. Howe, T. A. Gruner, L. G. Carter, L. L. Black, and J. E. Franz, *J. Org. Chem.*, **43**, 3736 (1978).
30) E. E. Gilbert, E. J. Rumanowski, and P. E. Newallis, *J. Chem. Eng. Data.*, **13**, 130 (1968).
31) R. Kitamura, *Yakugaku Zasshi*, **58**, 809 (1938).
32) G. Kresze, A. Horn, R. Philippson, and A. Trede, *Chem. Ber.*, **98**, 3401 (1965).
33) M. Komatsu, J. Shibata, Y. Oshiro, and T. Agawa, *Bull. Chem. Soc. Jpn.*, **56**, 180 (1983).

Optically Active *Anti* Head-to-head Coumarin Dimer. Resolution, Absolute Configuration, and Molecular Structure

Kazuhiko SAIGO,* Noriyuki YONEZAWA, Kazuhiro SEKIMOTO, Masaki HASEGAWA, Katsuhiko UENO,† and Hachiro NAKANISHI*†

Department of Synthetic Chemistry, Faculty of Engineering, The University of Tokyo, Hongo, Bunkyo-ku, Tokyo 113

†*Research Institute for Polymers and Textiles, Yatabe-higashi, Tsukuba, Ibaraki 305*

(Received October 11, 1984)

(±)-*Anti* head-to-head coumarin dimer was successfully resolved into a pair of optically active forms in good yields and in high optical purity by the fractional crystallization of both lactone-opened diamides with optically active 1-phenylethylamine followed by hydrolysis and relactonization. The absolute configuration of $(-)_{589}$-*anti* head-to-head coumarin dimer was confirmed to be (3*R*,3′*R*,4*R*,4′*R*) by X-ray crystal structure analysis, which showed puckering of the cyclobutane ring (32.5°) and some short nonbonded distances (2.15—2.60 Å).

In the previous papers it was shown that the lactone rings in *anti* head-to-head coumarin dimer, which can be easily prepared by the photochemical dimerization of coumarin,[1] are susceptible to nucleophilic ring-opening,[2] and the reaction was successfully applied to ring-opening polyaddition.[3] Although the optically active dimer may be useful as an optically active reagent with high reactivity and as an optically active diacid component in organic and polymer syntheses, respectively, no attempt at optical resolution of the dimer was reported. We have now optically resolved the dimer and determined the absolute configurations as reported in the preliminary paper.[4] This paper describes the optical resolution in detail and the absolute configuration on the basis of X-ray crystal structure analysis.

Results and Discussion

Optical Resolution of Anti *Head-to-head Coumarin Dimer (1).* It is known that *anti* head-to-head coumarin dimer (**1**) and the lactone-ring-opened derivative, *t*-3,*c*-4-bis(2-hydroxyphenyl)-*r*-1,*t*-2-cyclobutanedicarboxylic acid, are interconvertible.[1] The fractional crystallization of the salts of the cyclobutanedicarboxylic acid with chiral amines such as 1-phenylethylamine, brucine, strychnine, and quinidine has been carried out in an attempt to obtain optically active **1**, but all the trials resulted in failure. On the other hand, in our laboratory the relactonization of mono(lactone-ring-opened) *N*-butylamide of **1** has been found to occur smoothly on heating in solution.[5] The optical resolution of the diamide, prepared from **1** and an optically active amine by ring-opening reaction, was tried with the expectation that the diamide would be easily converted to the dimer (**1**).

When **1** was allowed to react with two molar amounts of (*S*)-(−)-1-phenylethylamine in dioxane at room temperature, white precipitate deposited. On the basis of elemental analysis, and ^{1}H NMR and IR spectral data, the precipitate was found to be one (**2a**) of a pair of diastereomeric diamides (79% yield). The residue, obtained from the filtrate on concentration, was crystallized from acetone/methanol (10/1 v/v) to give the other diastereomer (**2b**) in 81% yield. HPLC analyses of **2a** and **2b** thus-obtained each showed one peak only. The peak corresponding to the other diastereomer could not be detected, indicating that both of **2a** and **2b** were almost diastereomerically pure. Consequently both of the diastereomeric diamides could be obtained in good chemical yields and in high diastereomeric purity by crystallization from dioxane or acetone/methanol without recrystallization since their solubilities were extremely different.

Hydrolysis of **2** in ethanol/concd hydrochloric acid under refluxing proceeded without difficulty, and **2** was shown to be hydrolyzed completely within 20 h by TLC check. On heating the reaction mixture in acetic acid as described in the literature,[1] relactonization took place easily to give optically active **1**. The relactonization also proceeded efficiently on heating a toluene solution of the reaction mixture in the presence of a catalytic amount of *p*-toluenesulfonic acid.

Thus, $(+)_{589}$- and $(-)_{589}$-**1** were obtained from **2a** and **2b**, respectively. They were found to be almost optically pure since HPLC analyses of the diamides produced by the reaction of (+)- and (−)-**1** thus-obtained with (*S*)-(−)-1-phenylethylamine showed only one peak of the corresponding diastereomeric diamide. The result indicates that no racemization nor epimerization occurs in the course of the hydrolysis, the relactonization, and the nucleophilic ring-opening with an amine.

Absolute Configuration of (−)-1 Determined by X-Ray Crystal Structure Analysis. To determine the absolute configuration of optically active **1**, an X-ray crystal structure analysis of (−)-**1** was carried out. Differences of the calculated structure factors of ten selected Friedel pairs, *i.e.*, $\Delta F_c = |F_c(hkl)| - |F_c(\bar{h}\bar{k}\bar{l})|$ are compared in Table 1 with those of the observed

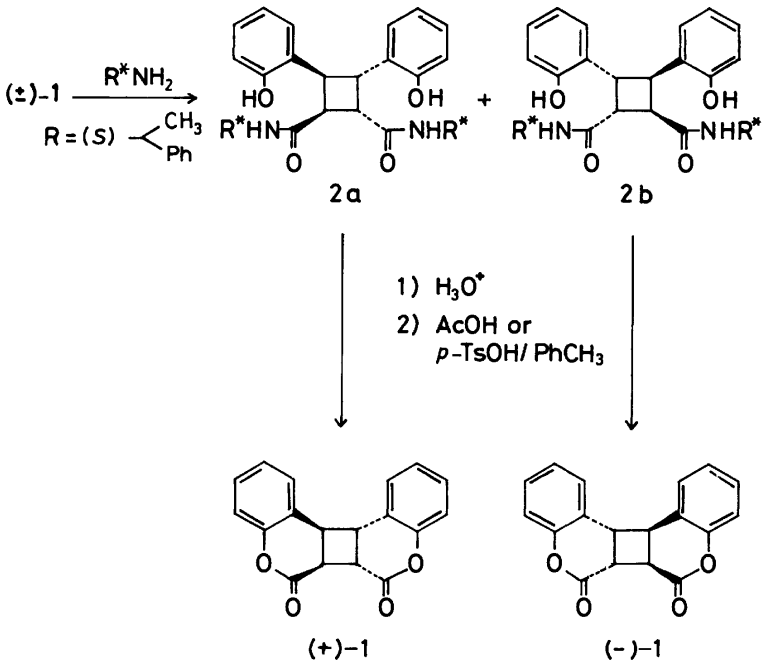

Table 1. Relation of $|F|$ in Friedel pairs

h	k	l	$\langle F_c \rangle$	$\langle F_o \rangle$	ΔF_c	ΔF_o	$\sigma(\Delta F_o)$
6	8	1	12.5	16.4	0.6	2.1	0.9
1	11	1	20.3	24.1	0.4	0.4	0.4
5	5	2	23.8	16.3	0.8	1.9	0.8
3	5	2	21.1	23.2	0.7	1.1	0.4
2	1	3	24.9	20.2	−0.7	−0.7	0.3
9	8	3	14.0	12.2	−0.3	−1.4	0.7
1	8	6	16.9	21.3	−0.8	−1.0	0.8
2	5	6	49.8	51.1	−1.0	−1.2	0.5
1	4	9	33.5	26.7	0.6	1.1	0.6
1	7	9	36.1	41.2	0.7	0.7	0.6

All $|F_c|$s are multiplied by 10.0 in the absolute scale.

ones, $\Delta F_o = |F_o(hkl)| - |F_o(\bar{h}\bar{k}\bar{l})|$. All the signs of ΔF_o are consistent with those of ΔF_c, indicating that the absolute configuration of (−)-**1** is correctly expressed by the atomic coordinates in Table 2 referred to a right-handed coordinate system. The configuration is drawn in Fig. 1, where the numbering system is also shown. From Fig. 1 the absolute configuration of (−)-**1** is concluded to be (3*R*, 3′*R*, 4*R*, 4′*R*).

Molecular Structure of (−)-1. The bond distances and angles are listed in Table 3. The dihedral angles between planes C(3′)-C(3)-C(4) and C(3′)-C(4′)-C(4), and between C(3)-C(4)-C(4′) and C(3)-C(3′)-C(4′) are the same value of 32.5°, showing that the cyclobutane ring in **1** crystal is puckered.

Some short nonbonded distances are found for C(2)···C(3′) (2.602(5) Å), C(3)···C(2′) (2.579(5) Å), C(4)···C(10′) (2.565(4) Å), and C(10)···C(4′) (2.515(4) Å), in addition to short ones in the cyclobutane ring, *i.e.*, C(3)···C(4′) (2.150(4) Å) and C(4)···C(3′) (2.152(4) Å), resulting from the puckering of the cyclobutane ring. This puckering and subsequent short contacts might be the reason for the instability and/or the high reactivity of lactones in **1**.

Table 2. Fractional atomic coordinates with their estimated deviations in parentheses and equivalent isotropic temperature factors (B/Å^2) of non-hydrogen atoms

	x	y	z	B_{eq} [a)]
O (1)	0.5802(3)	−0.0163(2)	0.8124(2)	5.5
C (2)	0.4660(3)	−0.0947(3)	0.7404(3)	4.7
C (3)	0.3448(3)	−0.0134(2)	0.7624(2)	4.6
C (4)	0.3098(3)	0.0180(3)	0.8773(2)	4.1
C (5)	0.4664(5)	0.0616(3)	1.0378(2)	5.9
C (6)	0.6038(5)	0.0571(3)	1.0950(3)	7.1
C (7)	0.7250(5)	−0.0016(3)	1.0572(3)	7.2
C (8)	0.7168(4)	−0.0555(3)	0.9625(3)	6.3
C (9)	0.5786(4)	−0.0491(3)	0.9071(3)	4.9
C (10)	0.4527(4)	0.0088(3)	0.9420(2)	4.5
O (11)	0.4721(3)	−0.1494(2)	0.6624(2)	5.9
O (1′)	0.2094(3)	0.1882(2)	0.6193(2)	5.1
C (2′)	0.3506(4)	0.1481(3)	0.6361(3)	5.1
C (3′)	0.3881(3)	0.1064(3)	0.7424(2)	4.2
C (4′)	0.2869(3)	0.1351(2)	0.8381(2)	4.0
C (5′)	0.0026(4)	0.1602(2)	0.8716(3)	5.3
C (6′)	−0.1454(4)	0.1880(3)	0.8373(3)	5.9
C (7′)	−0.1674(4)	0.2157(3)	0.7338(3)	6.1
C (8′)	−0.0480(4)	0.2171(3)	0.6627(3)	5.4
C (9′)	0.0968(4)	0.1870(3)	0.6991(3)	4.5
C (10′)	0.1265(3)	0.1598(2)	0.8031(2)	4.3
O (11′)	0.4369(3)	0.1464(3)	0.5634(2)	7.6

a) The equivalent isotropic temperature factors were computed using the following expression; $B_{eq} = 4/3(B_{11}a^2 + B_{22}b^2 + B_{33}c^2)$. The B_{ij}'s are defined by; $\exp[-(h^2B_{11} + k^2B_{22} + l^2B_{33} + klB_{23} + hlB_{13} + hkB_{12})]$.

^1H NMR Study of (−)-1. ^1H NMR spectrum of (−)-**1** (Fig. 2a) showed a singlet of four protons (Ha, Hb, Hc, Hd) on the cyclobutane ring at δ 3.86. But, in ^1H NMR spectra of the both lactone-ring-opened derivatives, such as (−)-*t*-3,*c*-4-bis(2-hydroxyphenyl)-*r*-1,*t*-2-cyclobutanedicarboxylic acid (Fig. 2b) and its dimethyl and diethyl esters, two *pseudo* doublets were observed at δ 3.5—3.6 and 4.6—4.7. As the signal of methine protons adjacent to an aryl group is known to appear at lower region in a magnetic field than that of methine protons adjacent to a carboxyl group, the lower signal is assigned to the signal of Hb′ and Hd′, and the higher one to that of Ha′ and Hc′, respectively (see Fig. 2). The large up-field shift of the signal of Hb and Hd in comparison with that of Hb′ and Hd′ would be explained by the shielding effect of the facing aryl group. HGS molecular models show that Hb and Hd are in the shielding zone of the facing aryl group on the assumption of some puckering of the cyclobutane ring.

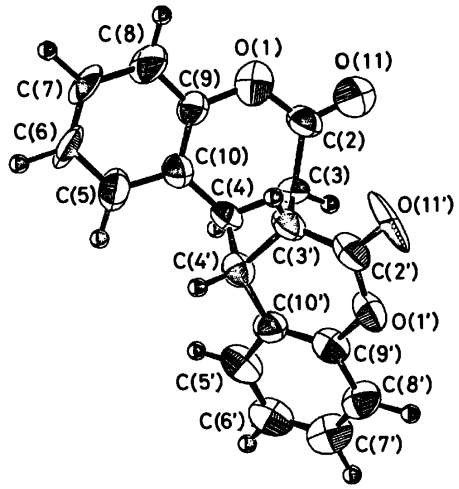

Fig. 1. Computer drawing of (−)-**1**.

The puckering, which would exist in a solution as well as in the crystalline state, conforms well to the up-field shift of Hb and Hd signals in the ^1H NMR spectrum of (−)-**1**.

CD Study of (+)-1. The absolute configuration of (+)-**1** was considered to be determinable on the basis of the CD exciton chirality theory,[6] if two phenolic

Table 3. Bond distances (l/Å) and angles (θ/°)

O(1)-C(2)	1.361(4)	O(1′)-C(2′)	1.345(4)
O(1)-C(9)	1.401(4)	O(1′)-C(9′)	1.412(4)
C(2)-C(11)	1.206(4)	C(2′)-C(11′)	1.193(5)
C(2)-C(3)	1.491(4)	C(2′)-C(3′)	1.485(5)
C(3)-C(4)	1.545(4)	C(3′)-C(4′)	1.546(4)
C(4)-C(10)	1.497(4)	C(4′)-C(10′)	1.499(4)
C(10)-C(5)	1.399(5)	C(10′)-C(5′)	1.387(5)
C(5)-C(6)	1.396(6)	C(5′)-C(6′)	1.406(5)
C(6)-C(7)	1.373(6)	C(6′)-C(7′)	1.375(6)
C(7)-C(8)	1.383(6)	C(7′)-C(8′)	1.379(5)
C(8)-C(9)	1.397(5)	C(8′)-C(9′)	1.395(5)
C(9)-C(10)	1.387(5)	C(9′)-C(10′)	1.391(4)
C(3)-C(3′)	1.564(4)		
C(4)-C(4′)	1.558(4)		
C(2)-O(1)-C(9)	121.2(3)	C(2′)-O(1′)-C(9′)	121.1(3)
O(1)-C(2)-C(3)	117.6(3)	O(1′)-C(2′)-C(3′)	118.5(3)
O(1)-C(2)-O(11)	117.5(3)	O(1′)-C(2′)-O(11′)	117.3(3)
C(3)-C(2)-O(11)	124.9(3)	C(3′)-C(2′)-O(11′)	124.2(3)
C(2)-C(3)-C(4)	119.4(3)	C(2′)-C(3′)-C(4′)	120.7(3)
C(3)-C(4)-C(10)	109.7(2)	C(3′)-C(4′)-C(10′)	110.2(3)
C(4)-C(10)-C(5)	121.3(3)	C(4′)-C(10′)-C(5′)	122.6(3)
C(4)-C(10)-C(9)	121.4(3)	C(4′)-C(10′)-C(9′)	121.4(3)
C(5)-C(10)-C(9)	117.3(3)	C(5′)-C(10′)-C(9′)	116.9(3)
C(10)-C(5)-C(6)	120.5(3)	C(10′)-C(5′)-C(6′)	121.3(3)
C(5)-C(6)-C(7)	120.0(3)	C(5′)-C(6′)-C(7′)	119.2(3)
C(6)-C(7)-C(8)	121.7(3)	C(6′)-C(7′)-C(8′)	121.8(3)
C(7)-C(8)-C(9)	117.2(3)	C(7′)-C(8′)-C(9′)	117.4(3)
C(8)-C(9)-C(10)	123.3(3)	C(8′)-C(9′)-C(10′)	123.4(3)
O(1)-C(9)-C(10)	123.3(3)	O(1′)-C(9′)-C(10′)	123.9(3)
C(2)-C(3)-C(3′)	116.8(3)		
C(4)-C(3)-C(3′)	87.6(3)		
C(10)-C(4)-C(4′)	110.7(3)		
C(3)-C(4)-C(4′)	87.7(3)		

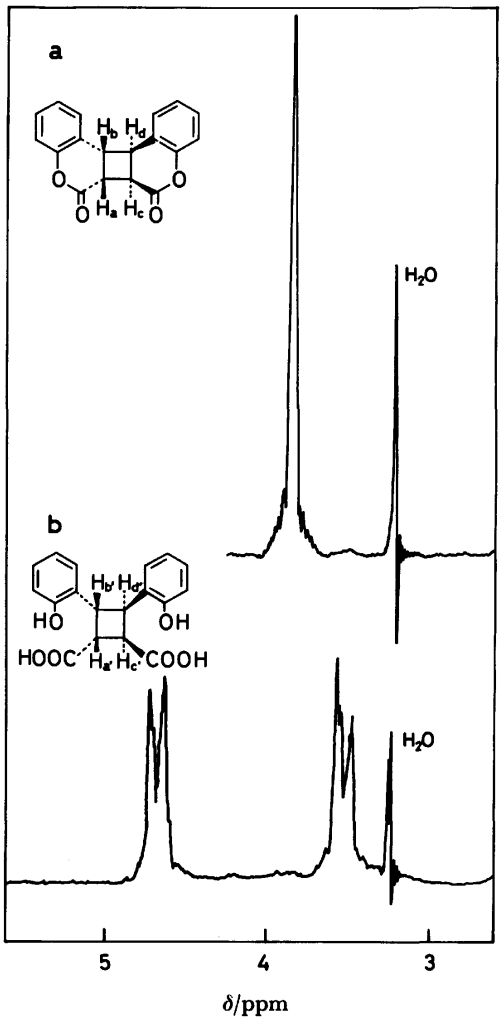

Fig. 2. The partial ^1H NMR spectra of (a) *anti* head-to-head coumarin dimer and (b) its both lactone-ring-opened derivative, *t*-3, *c*-4-bis(2-hydroxyphenyl)-*r*-1,*t*-2-cyclobutanedicarboxylic acid.

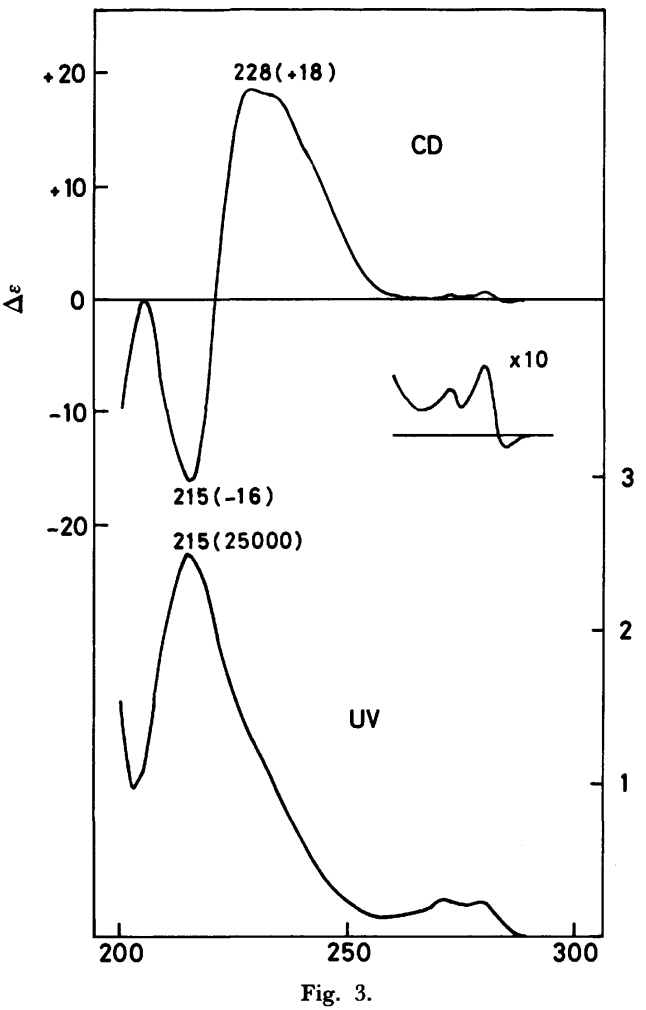

Fig. 3.

carbon–oxygen bonds in (+)-**1** are non-parallel. The UV spectrum of (+)-**1** in acetonitrile (Fig. 3) showed an absorption maximum at 215 nm, which would be attributable to $^1L_a \leftarrow {}^1A$ transition directed along the long axis of the acyloxyphenyls, namely, along the phenolic carbon–oxygen bonds.[6,7] The CD spectrum of (+)-**1** in acetonitrile (Fig. 3) showed a strong positive first Cotton effect at 228 nm and a negative second one at 215 nm, indicating a right-handed screw of the carbon–oxygen bonds.[6] Assuming that the predominant conformation of the lactone rings of (+)-**1** in a solution is a *pseudo*-boat form as well as that in the crystalline state (Fig. 1), an HGS molecular model constracted on the basis of a right-handed screw of the carbon–oxygen bonds shows that the absolute configuration of (+)-**1** is (3*S*, 3′*S*, 4*S*, 4′*S*), which is in good agreement with the result of the X-ray crystal structure analysis.

In the previous paper[4] the absolute configuration of (+)-**1** has been reported to be (3*R*,3′*R*,4*R*, 4′*R*), which is the opposite of that indicated above. The erroneous conclusion would result from the mistaken assumption that the predominant conformation of the lactone rings of (+)-**1** is a *pseudo*-chiar form.

Experimental

Melting points were determined on a Laboratory Devices Mel-Temp apparatus and are uncorrected. The IR spectra were measured on a JASCO IRA-1 Spectrophotometer. The ^1H NMR and UV spectra were recorded on a Hitachi R-40 Spectrometer (90 MHz) and on a Hitachi Model 100-60 Spectrophotometer, respectively. The specific rotations were measured on a JASCO DIP-181 digital polarimeter. The HPLC analyses were carried out on a LiChrosorb SI-60 column (4×250 mm, 0.5 ml/min) using a UV detector (280 nm).

Materials. (±)-*Anti* head-to-head coumarin dimer (**1**) was prepared by the method described in the literature.[1] Optically active 1-phenylethylamine (Yamakawa Chemical Industrial Co. Ltd.) was used without purification.

*Synthesis and Separation of Diastereomeric Diamides (**2a** and **2b**).* To a solution of (±)-**1** (58.46 g, 0.20 mol) in dry dioxane (870 ml) was added (*S*)-(−)-1-phenylethylamine (48.47 g, 0.40 mol). On stirring the mixture at room tem-

perature, a white precipitate appeared gradually. After stirring for 12 h at the temperature, the precipitate was collected by filtration, washed thoroughly with dioxane (70 ml×2), and dried over P_2O_5 to give 42.29 g (79%) of one of diastereomeric diamides (**2a**): mp 237—238 °C; $[\alpha]_D^{21}$ −19.0° (*c* 0.50, 99% MeOH); IR (KBr) 3360, 3200, 1635, 1520, 1450, 750, and 695 cm^{-1}; ^{1}H NMR (DMSO-d_6) δ 1.26 (6H, d, *J*=7 Hz), 3.74 (2H, *pseudo* d, *J*=7 Hz), 4.5—4.9 (4H, m), 6.4—7.2 (18 H, m), 7.64 (2H, d, *J*=7 Hz), and 9.42 (2H, s).

Found: C, 76.54; H, 6.27; N, 5.17%. Calcd for $C_{34}H_{34}N_2O_4$: C, 76.38; H, 6.40; N, 5.23%.

The filtrate was concentrated to dryness under reduced pressure, and the residue was crystallized from acetone/methanol (1,500 ml/150 ml), giving 35.54 g (67%) of the other diastereomeric diamide (**2b**): mp 246—247 °C; $[\alpha]_D^{21}$ −177.3° (*c* 0.51, 99% MeOH); IR (KBr) 3360, 3200, 1630, 1520, 1445, 750, and 695 cm^{-1}; ^{1}H NMR (DMSO-d_6) δ 0.85 (6H, d, *J*=7 Hz), 3.72 (2H, *pseudo* d, *J*=7 Hz), 4.5—4.9 (4H, m), 6.6—7.3 (18H, m), 7.43 (2H, d, *J*=7 Hz), and 9.56 (2H, s).

Found: C, 76.66; H, 6.16; N, 5.19%. Calcd for $C_{34}H_{34}N_2O_4$: C, 76.38; H, 6.40; N, 5.23%.

The evaporation of the filtrate followed by crystallization from acetone/methanol (600 ml/60 ml) gave 7.66 g (14%) of **2b** as a second crop. The total yield of **2b** was 43.20 g (81%). The diastereomeric purities of **2a** and **2b** were found to be more than 99% on the basis of HPLC analysis (eluent: benzene/ethyl acetate=60/40 v/v).

*Hydrolysis and Relactonization of **2a** and **2b**.* The suspension of **2b** (5.35 g, 0.01 mol) in 99% ethanol/concd hydrochloric acid (100 ml/50 ml) was refluxed for 20 h to give a clear solution. After concentration, water (200 ml) was added to the residue and it was extracted with ethyl acetate (150 ml×3). The extracts were dried over anhydrous sodium sulfate and concentrated under reduced pressure. To the remaining oil acetic acid (150 ml) was added, and the solution refluxed for 20 h. After evaporation of the solvent to dryness, purification of the crude product by silica-gel chromatography (eluent: benzene then benzene/ethyl acetate=90/10 v/v) followed by recrystallization from ethyl acetate/hexane (60/40 v/v) gave 1.92 g (66%) of (−)-**1**: mp 168.5—169 °C; $[\alpha]_D^{21}$ −9.0°, $[\alpha]_{435}^{21}$ −65.8° (*c* 1.00, benzene); IR (KBr) 1760, 1490, 1450, 775, and 765 cm^{-1}; ^{1}H NMR (DMSO-d_6) δ 3.86 (4H, s) and 6.9—7.4 (8H, m).

Similar treatment of **2a** gave (+)-**1** in 64% yield: mp 168—169 °C; $[\alpha]_D^{21}$ +9.0°, $[\alpha]_{435}^{21}$ +66.0° (*c* 1.00, benzene); IR (KBr) 1760, 1490, 1450, 775, and 765 cm^{-1}; ^{1}H NMR (DMSO-d_6) δ 3.86 (4H, s) and 6.9—7.4 (8H, m).

The relactonization also proceeded in toluene in the presence of *p*-toluenesulfonic acid. A toluene solution (120 ml) of the crude product, obtained by the similar hydrolysis of **2a** (5.35 g, 0.01 mol), and *p*-toluenesulfonic acid (156 mg, 1 mmol) was refluxed for 48 h. After cooling, the mixture was washed with water (100 ml×2), dried over anhydrous sodium sulfate, and concentrated under reduced pressure. Chromatographic purification followed by recrystallization in a similar manner gave 1.48 g (51%) of (+)-**1**.

To determine the optical purities of (+)- and (−)-**1**, small quantities of the dimers were again converted into both lactone-ring-opened diamides by the reaction with (*S*)-(−)-1-phenylethylamine in dioxane; they were found to be almost optically pure since the HPLC analyses of the diamides derived from them showed the sole formation of **2a** or **2b**, respectively.

Optically active **1** melting at 193—193.5 °C was sometimes obtained, while its ^{1}H NMR spectrum, HPLC retention time, and $[\alpha]_D$ value were identical with those of optically active **1** melting at 168—169 °C.

X-Ray Crystal Structure Determination. Colorless plate-shaped crystals of (−)-**1** (mp 168.5—169 °C) were grown from an acetone solution by slow evaporation at room temperature. The space group was determined from Weissenberg photographs. The precise lattice constants and intensity data were derived from measurements on an Enraf-Nonius CAD-4 diffractometer with graphite-monochromated Cu-$K\alpha$ radiation. The specimen used was a fragment of a plate, 0.20×0.20×0.20 mm. The density was measured by the floatation method in a mixture of cyclohexane and carbon tetrachloride. All reflections within the range of $\theta<75°$ were collected by use of the $\omega-2\theta$ scan mode with variable scan rate from 1.43 to 5°/min, of which 1593 were greater than $3\sigma(|F_o|)$ and were used for structure determination. No correction was made for absorption. Crystallographic data of (−)-**1**: $C_{18}H_{12}O_4$, M.W. 292.3. Orthorhombic, $P2_12_12_1$, a=8.711(1), b=12.493(4), c=12.728(3) Å, V=1385.1 Å^3. Z=4, D_x=1.407, D_m=1.40 g/cm^3.

The structure was solved by the direct method and was refined by the block-diagonal least-squares method.[8] The final refinement including isotropic hydrogen atoms reduced the R value to 0.055.[9] Atomic scattering factors were taken from International Tables for X-Ray Crystallography (1974). The final atomic coordinates are given in Table 2.

To determine the absolute configuration of (−)-**1**, structure factors of all the Friedel pairs (hkl and $\overline{hkl}$) were calculated using the parameters in Table 2. Among them, ten Friedel pairs were selected manually in order of difference in the intensities, and their intensities were measured on the diffractometer under the same conditions as those of the data collection described above.

UV and CD Measurements. The UV spectrum of a solution of (+)-**1** in acetonitrile (1.00×10^{-4} mol dm^{-3}) was recorded on a Shimadzu UV-260 Spectrophotometer. The CD spectrum of a solution of (+)-**1** in acetonitrile (3.23×10^{-4} mol dm^{-3}) was measured on a JASCO J-500 Automatic Spectropolarimeter under the following conditions using a 1 mm quartz cell: sensitivity 2m° cm^{-1}; time constant 8 s; wave length expansion 5 nm cm^{-1}; chart speed 2 cm min^{-1}; integration time 8 times.

The CD spectra of solutions of (+)-**1** in acetonitrile (4.04×10^{-5}, 8.07×10^{-5}, 8.07×10^{-6} mol dm^{-3}) were also measured, giving similar results to that shown in Fig. 3.

The authors wish to thank Miss Junko Umezawa of the University of Tokyo for the preparation of optically active *anti* head-to-head coumarin dimers and Dr. Noriaki Hirayama at Tokyo Research Laboratories of Kyowa Hakko Kogyo Co. Ltd. for the X-ray data collection. This work was partially supported by a Grant-in-Aid for Scientific Research (No. 58550557) from the Ministry of Education, Science and Culture.

References

1) C. H. Krauch, S. Farid, and G. O. Schenck, *Chem. Ber.*, **99**, 625 (1966).

2) a) M. Hasegawa, Y. Suzuki, and N. Kita, *Chem. Lett.*, **1972**, 317; b) N. Yonezawa and M. Hasegawa, *Bull. Chem. Soc. Jpn.*, **56**, 367 (1983).

3) a) Y. Suzuki, M. Hasegawa, and N. Nishikawa, *J. Polym. Sci., Polym. Lett. Ed.*, **11**, 173 (1973); b) M. Hasegawa, N. Yonezawa, T. Kanoe, and Y. Ikebe, *J. Polym. Sci., Polym. Lett. Ed.*, **20**, 309 (1982); c) M. Hasegawa, K. Saigo, H. Katsuki, N. Yonezawa, and T. Kanoe, *J. Polym. Sci., Polym. Chem. Ed.*, **21**, 2345 (1983).

4) K. Saigo, K. Sekimoto, N. Yonezawa, and M. Hasegawa, *Tetrahedron Lett.*, **24**, 5381 (1983).

5) N. Yonezawa, Y. Ikebe, T. Yoshida, T. Hirai, K. Saigo, and M. Hasegawa, *Bull. Chem. Soc. Jpn.*, **57**, 1608 (1984).

6) N. Harada and K. Nakanishi, "Circular Dichroic Spectroscopy-Exciton Coupling in Organic Stereochemistry," University Science Books, California (1983).

7) H. H. Jaffé and M. Orchin, "Theory and Applications of Ultraviolet Spectroscopy," John Wiley and Sons, Inc, New York (1962).

8) G. M. Sheldrick, SHELX (program for crystal structure determination), University of Cambridge, England.

9) Thermal parameters and a list of the observed and calculated structure factors are deposited at the Office of the Chemical Society of Japan (Document No. 8517).

Optically Active *Anti* Head-to-head Coumarin Dimer. A New Agent for the Determination of Enantiomeric Excess of Amines and Alcohols

Kazuhiko SAIGO,* Kazuhiro SEKIMOTO, Noriyuki YONEZAWA, Fumio ISHII, and Masaki HASEGAWA

Department of Synthetic Chemistry, Faculty of Enginnering, The University of Tokyo, Hongo, Bunkyo-ku, Tokyo 113

(Received October 11, 1984)

The enantiomeric excess of chiral amines was successfully determined by ^{1}H NMR spectral and/or HPLC analysis of the diastereomeric diamides derived from optically active *anti* head-to-head coumarin dimer and the amines by lactone-ring-opening reaction without any condensing agent. This procedure also proved to be applicable to chiral alcohols.

Methods for determining the enantiomeric excess of a chiral amine or alcohol include NMR spectral analysis using a chiral lanthanoid shift reagent[1] and chromatographic or NMR spectral analysis of a mixture of the diastereomeric amides or esters obtained by the reaction of an amine or alcohol with an optically active derivatizing agent such as 2-methoxy-2-phenyl-2-(trifluoromethyl)acetic acid,[2] 1-(1-naphthyl)ethyl isocyanate,[3] and 2-[1-(9-anthryl)-2,2,2-trifluoroethoxy] acetic acid.[4] The latter method gives more accurate values than the former and is applicable to the chromatographic separation of the diastereomers. The former method is more convenient and advantageous in the recovery of the amine or alcohol.

In the previous paper[5] it was shown that *anti* head-to-head coumarin dimer can be easily resolved into pure enantiomers by fractional crystallization of the lactone-ring-opened diastereomeric diamides with (*S*)-(−)-1-phenylethylamine followed by hydrolysis and relactonization. The optically active dimer reacts with two molar equivalents of (*S*)-(−)-1-phenylethylamine to give the corresponding diamides, which are diastereomeric and thus show different chemical shifts in the ^{1}H NMR spectra and retention time in HPLC. Accordingly, the optically active dimer was considered to be useful as a chiral derivatizing agent. We report here the use of the optically active dimer in the determination of the enantiomeric excess of a chiral amine or alcohol on the basis of ^{1}H NMR spectral and/or HPLC analysis.

Results and Discussion

The reaction of (*R,R,R,R*)-(−)$_{589}$-*anti* head-to-head coumarin dimer ((−)-**1**) with two molar equivalents of a racemic primary amine (**2**) at 60 °C for 3 h was effected smoothly to give a mixture of three diastereomeric diamides (**3**, **4**, and **5**) in high yield. For example, when 1-phenylethylamine (**2a**) was used as the racemic amine substrate, a mixture of diastereomeric diamides (**3a**, **4a**, and **5a**) was obtained in 99% yield. The diastereomer distribution was based on the ^{1}H NMR spectral data. The methyl proton signals of the diastereomer mixture appeared at two isolated magnetic fields, δ 0.7—1.0 ppm (one doublet) and δ 1.1—1.4 ppm (two doublets), and the area ratio of these two distinct regions was 1:1 as shown in Fig. 1. On the basis of the chemical shifts of methyl protons of **3a** and the enantiomer of **5a** as reported in our previous paper,[5] it is concluded that the methyl proton signal of **3a** appeared at a higher magnetic field than that of **5a** by virtue of the shielding by the cis-oriented hydroxyphenyl group. The two methyl proton signals arising from (*S*)- and (*R*)-1-phenylethylamino moieties in **4a** might be observed in almost the same regions of the magnetic field as those in **3a** and **5a**, respectively. Similarly, methyl proton signals were observed in two regions with an area ratio of 1:1 when either 1-(4-isopropylphenyl)ethylamine (**2b**), 1-phenylpropylamine (**2c**), *s*-butylamine (**2d**), norephedrine (**2e**), or 2-amino-1-butanol (**2f**) were employed as the primary amine substrate. The results from the synthesis of diastereomer mixtures and the chemical shifts of their methyl proton signals are shown in Table 1.

For amino alcohols such as **2e** and **2f**, the preferred reaction of the amino functions with **1** was established

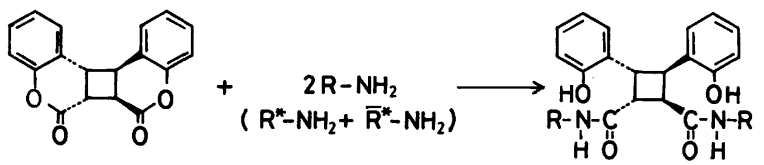

1 (*R,R,R,R*) **2** **3**: R*-(*R,R,R,R*)-R̄* **4**: R̄*-(*R,R,R,R*)-R* **5**: R̄*-(*R,R,R,R*)-R̄*

by the exclusive formation of diastereomeric diamides, and no ester formation was detected in their IR spectra. The low reactivity of the alcohol under these conditions was confirmed by the separate reactions of (−)-**1** with methanol and ethanol, which gave no esters and resulted in the quantitative recovery of (−)-**1**. The versatility of **1** as an optically active derivatizing agent is enhanced by the observation that the β-methyl protons in the amine having an α-asymmetric carbon such as **2c** and **2f** are also shielded by the cis-oriented hydroxyphenyl group, yielding methyl proton signals of the diastereomer mixtures in two distinct regions. Moreover, it is advantageous that the amide formation requires no condensing agent.

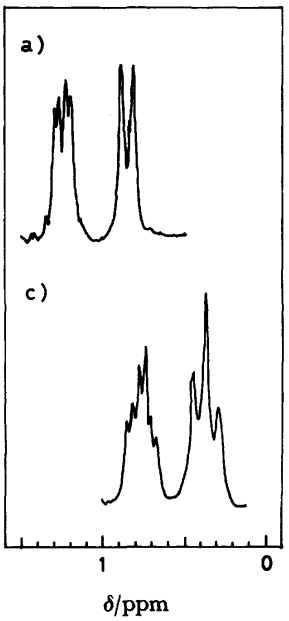

Fig. 1. ^{1}H NMR spectra of methyl protons of diastereomeric diamide mixtures: a) of **3a**, **4a**, and **5a**; c) **3c**, **4c**, and **5c**.

The HPLC of the diastereomer mixture (**3**, **4**, and **5**) showed three base-line separated peaks. Typical examples are shown in Fig. 2. The area ratio of **3a**, **4a**, and **5a** obtained from (−)-**1** and racemic **2a** was 25.4:49.7:24.9, giving the enantiomer ratio of 50.3:49.7. Moreover, the HPLC analysis of minus-enantiomer-enriched **2a** (49.4% optical purity based on its specific rotation) showed the area ratio of 56.7:40.4:2.9, representing 53.8% of enantiomeric excess. The ratios are in good agreement with those predicted. Similarly, the distribution of **3**, **4**, and **5**

Table 1. Yield and chemical shifts of diastereomeric diamide mixture (**3**, **4**, and **5**)

Amine	Yield/%	Methyl proton/δ, ppm (DMSO-d_6)	
2a	99	0.85	1.25 1.27
2b	97	0.83	1.15
2c	97	0.35	0.76
2d	95	0.42	0.90
2e	95	0.34	0.72
2f	96	0.32	0.75 0.78

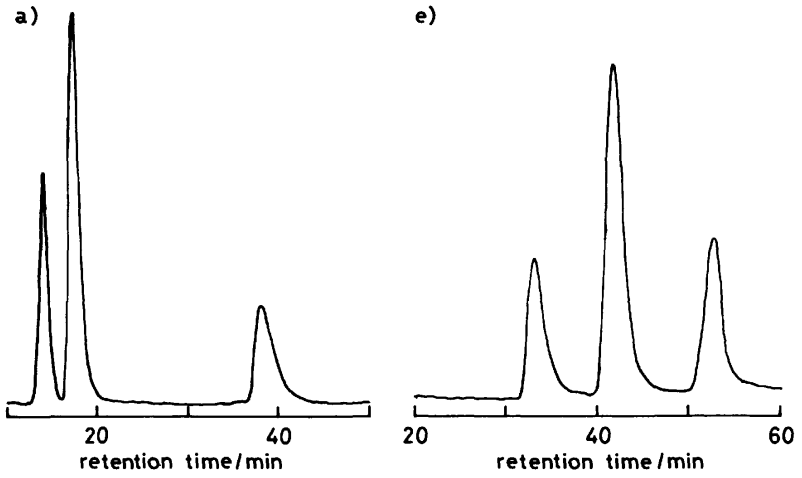

Fig. 2. HPLC of diastereomeric diamide mixtures: a) **3a**, **4a**, and **5a**; e) **3e**, **4e**, and **5e**.

Table 2. HPLC of diastereomeric diamide mixture (**3**, **4**, and **5**)

Diamide	Retention Time/min			Area ratio/%			Eluent
a	13.9	17.7	38.4	25.4	49.7	24.9	C_6H_6/AcOEt = 60/40
b	12.1	15.9	47.3	26.0	48.3	25.7	70/30
c	43.8	62.1	126.4	23.9	53.7	22.4	80/20
d	22.6	28.3	39.4	24.9	50.4	24.7	50/50
e	32.8	41.5	52.3	22.6	52.0	25.4	50/50
f	14.2	19.3	35.6	24.9	47.1	28.0	MeOH/AcOEt = 8/92

prepared from **2b—2f** was in nearly 1:2:1 area ratio as shown in Table 2. These results indicate that the HPLC analysis of the diastereomeric diamides prepared from optically active **1** and a given chiral amine is also useful for the determination of enantiomeric excess of the amine. No measurable kinetic resolution was considered to occur during the course of the ring-opening reaction since the reactions of racemic **1** with racemic amines (**2a—2f**) gave the corresponding diastereomer mixtures in high yields and in the area ratio of 1:2:1 as determined by HPLC.

The HPLC of the reaction mixture of (−)-**1** and **2a**, obtained without work-up, also showed three peaks of **3a**, **4a**, and **5a** in the area ratio of nearly 1:2:1. Small peaks due to impurities in different regions from the main peaks were also noted. The result indicates that the work-up is not always necessary for the HPLC analysis.

The reaction of **1** with an alcohol was reexamined to see if **1** can also be used as an optically active derivatizing agent for alcohols, since the reaction did not take place under the conditions of 60 °C for 3 h as mentioned above. After some elaboration, two equimolar amounts of lithium alcoholate were found to effect the reaction smoothly with (−)-**1** at room temperature to give a mixture of three diastereomeric esters (**7**, **8**, and **9**) in good yield. In the case of the diastereomeric diesters derived from alcohols having an α-asymmetric carbon and an α-methyl such as 1-phenylethanol (**6a**) and 2-butanol (**6b**), the methyl proton signals were also observed at two regions in the area ratio of 1:1 in their ^{1}H NMR spectra, respectively. However those of the diastereomer mixture obtained from 2-phenyl-1-propanol (**6c**) having a β-asymmetric carbon and a β-methyl were observed with difficulty in almost the same region. HPLC analysis of the diastereomer mixtures, obtained not only with **6a** and **6b** but also with **6c** gave satisfactory results. In all cases, three peaks were observed with base-line separation, and the area ratios of the peaks approximated to 1:2:1. The results are shown in Tables 3 and 4.

Table 3. Yield and chemical shifts of diastereomeric diester mixture (**7**, **8**, and **9**)

Alcohol	Yield/%	Methyl proton/δ, ppm (DMSO-d_6)		
6a	99	0.83	1.21	1.23
6b	99	0.52	0.97	
6c	99	1.01		

Experimental

The ^{1}H NMR and IR spectra were recorded on a Hitachi R-40 Spectrometer (90 MHz) and a JASCO IRA-1 Spectrophotometer, respectively. The HPLC analyses were carried out on a LiChrosorb SI-60 column (4×250 mm) under the conditions of 70 kg/cm^2 and 0.5 ml/min using a Shimadzu SPD-2A UV detector (280 or 285 nm).

Materials. Optically active coumarin dimer (**1**) was prepared by the method reported in the previous paper.[5] The racemic amines (**2a—2d** and **2f**) were dried overnight with NaOH pellets and distilled carefully under an argon atmosphere or under reduced pressure in the presence of NaOH pellets. Norephedrine (**2e**) was regenerated from its hydrochloric acid salt, dried overnight, and used without recrystallization. The alcohols (**6a—6c**) were predried with molecular sieves 3A for 1 d and distilled before use.

General Procedure for the Preparation of Diastereomeric Diamide Mixture. A mixture of (−)-**1** (1.0 mmol) and the racemic amine (2.0 mmol) in dry dioxane (4.5 ml) was warmed at 60 °C for 3 h under an argon atmosphere. The residue, left after evaporation of the solvent, was dissolved in chloroform or ethyl acetate (150—200 ml) and washed successively with 1 M HCl solution (50 ml×2, 1 M=1 mol dm^{-3}), 4% $NaHCO_3$ solution (50 ml), and sat. NaCl solution (50 ml). After drying over anhydrous Na_2SO_4, evaporation of the solvent followed by drying under reduced pressure at about 45 °C for 1 d gave a mixture of three diastereomeric diamides (**3**, **4**, and **5**).

General Procedure for the Preparation of Diastereomeric Diester Mixture. To a solution of the alcohol (2.0 mmol) in dry dioxane (4 ml) was added a hexane solution of butyllithium (2.1 mmol) on cooling, and the mixture was stirred at room temperature for 1 h. A solution of (−)-**1** (1.0 mmol) in dry dioxane (4 ml) was added at room temperature dropwise during a period of 20 min. After stirring at the temperature for 24 h, the solvent was removed under reduced pressure. The remaining residue was dissolved in ethyl acetate (100 ml), washed successively with 0.2 M HCl solution (15 ml) and water (50 ml), and dried over anhydrous Na_2SO_4. Evaporation of the solvent to dryness gave the corresponding mixture of diastereomeric diesters (**7**, **8**, and **9**).

The present work was supported by a Grant-in-Aid for Scientific Research No. 58550557 from the Ministry of Education, Science and Culture.

References

1) a) H. L. Goering, J. N. Eikenberry, and G. S. Koermen, *J. Am. Chem. Soc.*, **93**, 5913 (1971); b) G. M. Whitesides and W. D. Lewis, *J. Am. Chem. Soc.*, **93**, 5915 (1971); c) G. R. Sullivan, *Topics Stereochem.*, **10**, 287 (1978).

Table 4. HPLC of diastereomeric diester mixture (**7**, **8**, and **9**)

Diester	Retention Time/min			Area ratio/%			Eluent
a	11.2	12.9	14.9	27.4	47.4	25.2	C_6H_6/AcOEt = 90/10
b	29.1	33.1	37.8	26.4	48.0	25.6	93/7
c	37.0	40.8	45.3	25.6	46.9	27.5	C_6H_6/CH_3CN = 96/4

2) a) J. A. Dale, D. L. Dull, and H. S. Mosher, *J. Org. Chem.*, **34**, 2543 (1969); b) B. Halpern, "Handbook of Derivatives for Chromatography," Heyden, London (1977).
3) W. H. Pirkle and M. S. Hoekstra, *J. Org. Chem.*, **39**, 3904 (1974).
4) W. H. Pirkle and K. A. Simmons, *J. Org. Chem.*, **46**, 3239 (1981).
5) K. Saigo, N. Yonezawa, K. Sekimoto, M. Hasegawa, K. Ueno, and H. Nakanishi, *Bull. Chem. Soc. Jpn.*, **58**, 1000 (1985).

Determination of Formal Potentials of Multihemoprotein, Cytochrome c_3 by ^{1}H Nuclear Magnetic Resonance

Keisaku KIMURA,* Shinsuke NAKAJIMA,† Katsumi NIKI,† and Hiroo INOKUCHI
Institute for Molecular Science, Myodaiji, Okazaki 444
†*Department of Electrochemistry, Yokohama National University, Tokiwadai, Hodogaya-ku, Yokohama 240*
(Received November 2, 1984)

Macroscopic redox potentials of tetrahemoprotein, cytochrome c_3 from *D.* vulgaris, Miyazaki strain, were derived from 400 MHz ^{1}H NMR measurements. The formal potential, $E_1^{\circ\prime}$, was determined to be -0.245 ± 0.005 V *vs.* NHE compared with a value of -0.240 V obtained electrochemically. The distributions of the intermediate states from the NMR spectra during a redox titration are in good agreement with those previously determined by electrochemistry.

Cytochrome c_3 (cyt. c_3) has four hemes within a single polypeptide chain and functions as an electron carrier in the sulfate reducing bacteria, *Desulfovibrio vulgaris*. The oxidoreduction of cyt. c_3 is regulated by the catalytic action of hydrogenase, an iron-sulfur enzyme. The physicochemical properties of the cyt. c_3 have been well studied by Mössbauer spectroscopy,[1] photoelectron spectroscopy,[2] electrical conductivity,[3] electrochemical methods,[4,5] ESR,[6] and NMR.[7] These studies have revealed that this protein has unusual properties such as a very low ionization potential, high electrical conductivity, and a rapid and reversible redox reaction owing to its multiheme structure. It also has been suggested that the redox potentials of the hemes are connected with these properties.

The macroscopic redox potentials of this multihemeprotein derived from 400 MHz ^{1}H NMR measurements are reported. These potentials have previously been obtained by the simulation of the differential pulse voltammetric response during redox titrations. The redox potential, E, of cyt. c_3 is defined by

$$E = E^{\circ\prime}_{i+1} + (RT/F)\ln[f_i]/[f_{i+1}] \quad (1)$$

where $E^{\circ\prime}_{i+1}$ is the macroscopic formal potential for the $f_i \rightleftharpoons f_{i+1}$ equilibrium and where f_i is the ith oxidation state as shown in Fig. 1. It should be noted in this figure that there is an unity (one electron) difference for each oxidation state. There are five states corresponding to n=0, 1, 2, 3, and 4 electrons (designated by f_0 to f_4) while states f_1—f_3 can have multiplicities arising from the multicomponent electron sites.

Experimental

D. vulgaris cyt. c_3 was purified by a method previously reported.[8] The purity index $[A_{552}(Fe^{2+})/A_{280}(Fe^{3+})]$ was 3.0. The protein was lyophilized twice from 99.95% D_2O. Hydrogenase was also purified according to the method described by Yagi *et al.*[9] The lyophilized powder of cyt. c_3 and a trace amount of deuterized hydrogenase were dissolved into the deuterized phosphate buffer solution (pD=7.0), giving a final cyt. c_3 concentration of 5 mM (1 M=1 mol m^{-3}). The pD values were measured by a pH meter. The NMR spectra were recorded and analyzed using a JEOL GX 400 spectrometer. After measurements on the ferricytochrome c_3, it was reduced to the ferro-form by hydrogen. The samples of various intermediate oxidation states were prepared by the reoxidation of the fully reduced sample with air. All measurements were conducted at (25±0.5) °C, and the chemical shifts were quoted in part per million, down field from sodium 3-(trimethylsilyl) propionate-2,2,3,3-d_4(TSS).

The optical absorption spectra of the *ca.* 0.1 mM cyt. c_3 of an intermediate oxidation state were measured in the NMR tube before and after NMR measurement. We confirmed that there were no significant differences in the optical spectra taken before and after NMR measurement. In the case of the 0.1 mM cyt. c_3 solution, the number of accumulation of free induction decay was 10,000 in order to increase the signal to noise ratio. However, this acquisition number was still not large enough for a good signal to noise ratio and a smoothing technique was used to analyze the NMR lineshape.

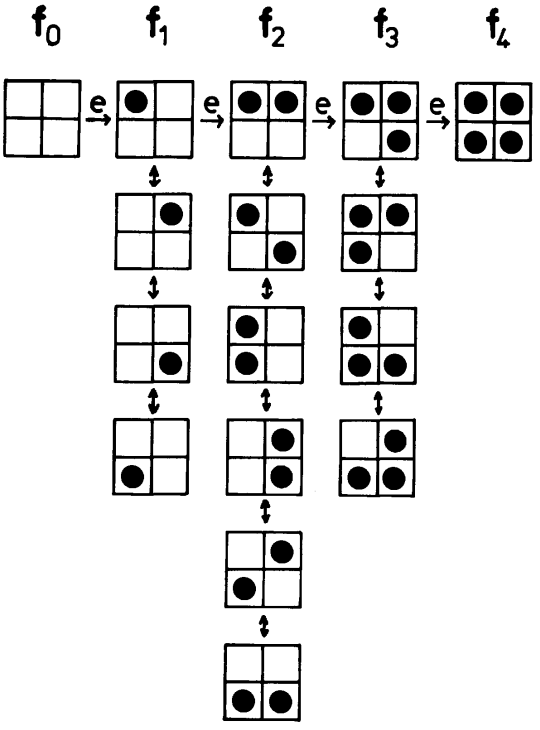

Fig. 1. Microscopic oxidation states of cyt. c_3. Solid circles indicate the reduced sites. f_0—f_4 indicate macroscopic oxidation states.

Results and Discussion

Figure 2 shows the NMR spectra in the lower field region for a redox titration of cyt. c_3. The sharp singlet peaks (A—P) with three-proton intensity in the region of 31—8 ppm were assigned to the heme methyl resonances of the f_0 state.[7,10] As the amount of reduction is incrementally increased, (spectra # 1—9 in Fig. 2) new peaks are seen to appear at the expense of the f_0 intensity. The height of all f_0 peaks decreased simultaneously. This is due to the fact that the intramolecular electron-exchange rate of cyt. c_3 is so rapid on the NMR time scale that the microscopic states in each intermediate oxidation state, f_1, f_2, and f_3, are indistinguishable, so it is the average fraction of each intermediate state that is determined by the NMR. From the intensity of five well-isolated peaks (A,B,C,F,I), the reduction ratio of the f_0 state was obtained. The new peaks that appeared at 27.7, 20.0, 19.55, and 18.0 ppm were assigned to f_1, and those at 15.36, 14.1, and 13.8 ppm were assigned to f_2. The assignment was done by the saturation transfer method.[7]

From the peak area of each of the oxidation states, one can calculate the fractions of the f_0, f_1, and f_2 states. The macroscopic formal potential, $E_1^{\circ\prime}$ for the equilibrium between f_0 and f_1, can be determined from the ratio of the f_0 state to the f_1 state and was estimated to be (-0.245 ± 0.005) V, which is in good agreement with that determined by the electrochemical method, -0.239 V, in D_2O. Similarly, one can calculate the macroscopic formal potentials of the intermediate states from the fraction of each intermediate state.

The macroscopic formal potentials of cyt. c_3 from *D. vulgaris* determined by electrochemical method in both H_2O and D_2O are given in Table 1. On the basis of the macroscopic formal potentials given in Table 1, we can calculate the relative concentrations of the five redox states defined in Fig. 1 as a function of the electrochemical potential as shown in Fig. 3. In the upper part of this figure, arrows designate the points at which UV and redox titration measurements were conducted. At the bottom of the figure, the four macroscopic formal potentials are shown. The broken line indicates the average fraction of the ferri-heme in cyt. c_3, which is observed by optical absorption spectroscopy. The ratios, f_1/f_0 and f_2/f_0, calculated from

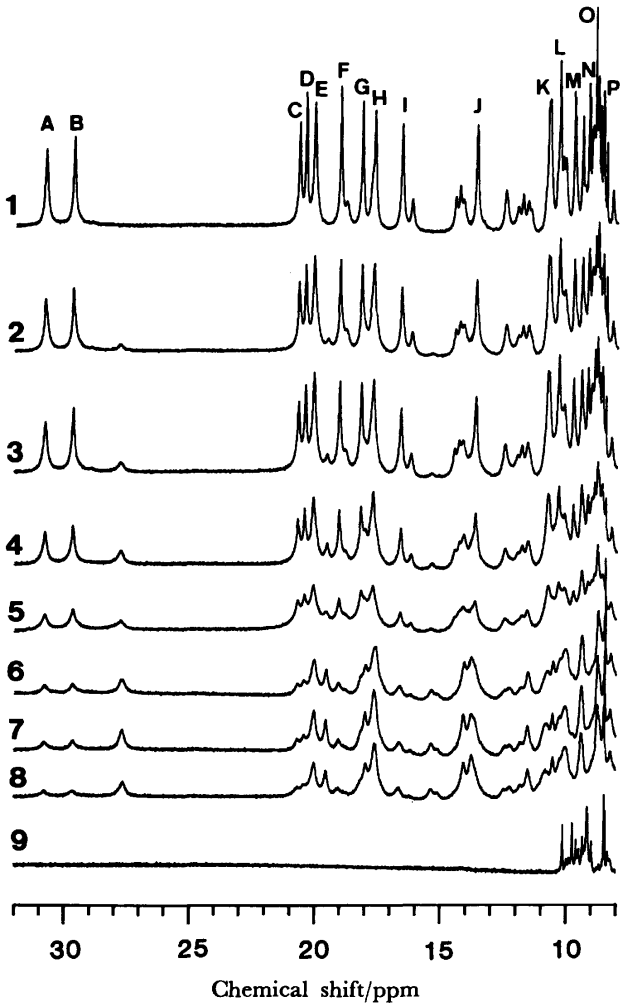

Fig. 2. NMR spectra for a redox titration of cyt. c_3 recorded on a 400 MHz NMR: spectrum (1) is fully oxidized cytochrome c_3, (2) $f_0=0.94$, (3) $=0.93$, (4)$=0.665$, (5)$=0.42$, (6)$=0.22$, (7)$=0.16$, (8)$=0.10$, and (9) is fully reduced cyt. c_3.

Table 1. Macroscopic formal potentials of cytochrome c_3, *D. vulgaris*, Miyazaki strain (V *vs.* NHE)

	in D_2O (pD=7.1)	in H_2O (pH=7.1)
$E_1^{\circ\prime}$	−0.239	−0.240
$E_2^{\circ\prime}$	−0.293	−0.297
$E_3^{\circ\prime}$	−0.310	−0.315
$E_4^{\circ\prime}$	−0.352	−0.357

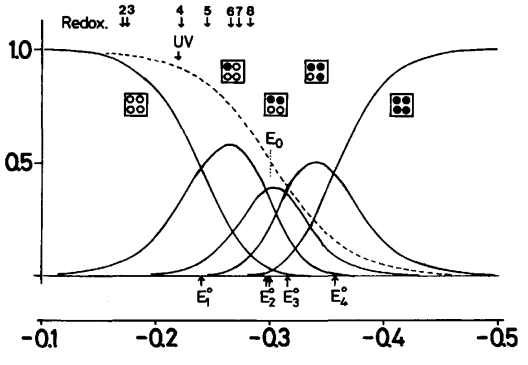

Fig. 3. Population of five macroscopic oxidation states calculated from the electrochemical data as a function of electrochemical potentials. Arrows on the top of the figure designate the intermediate oxidation states (2) to (8) shown in Fig. 2.

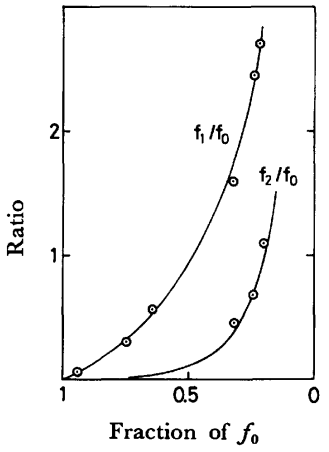

Fig. 4. The f_1/f_0 and f_2/f_0, as a function of the fraction of the f_0 state. Open circles are calculated from NMR data; solid lines, from electrochemical data.

the NMR data (open circles) and those from the data shown in Fig. 3 (solid lines) are plotted in Fig. 4 as a function of the fraction of the f_0 state. The NMR data fit well with the curve calculated from electrochemical methods. These results strongly suggest that the four macroscopic formal potentials of the cyt. c_3 are a unique set of formal potentials. The well resolved spectra in the present study gave the rigid foundation to assign the absorption lines, many of which were compatible with the early work.[7] Based upon their poorly resolved spectra.[11] Santos *et al.* derived four redox potentials of *D.* gigas which were quite different from the present study.

With respect to the reaction scheme between the microscopic states as shown in Fig. 1, we should emphasize that the intramolecular and intermolecular electron exchange rates and the microscopic formal potentials of cyt. c_3 must be studied. Further NMR studies are now in progress.

This work was supported by Grant-in-Aid for Special Project Research from the Ministry of Education, Science and Culture of Japan (No. 57102011) for which the authors would like to express their sincere thanks. Many useful discussions with Professor Ted Kuwana and Mrs. Jane Kuwana are greatefully acknowledged. The authors wish to acknowledge the kindly supply of sulfate reducing bacteria by Ajinomoto Co. as well as their continuous interest and help.

References

1) K. Ono, K. Kimura, T. Yagi, and H. Inokuchi, *J. Chem. Phys.*, **63**, 1640 (1975); M. Utuno, K. Ono, K. Kimura, H. Inokuchi, and T. Yagi, *ibid*, **72**, 2264 (1980).

2) K. Kimura, N. Sato, S. Hino, T. Yagi, and H. Inokuchi, *J. Am. Chem. Soc.*, **100**, 6564 (1978); N. Sato, K. Kimura, H. Inokuchi, and T. Yagi, *Chem. Phys. Lett.*, **73**, 35 (1980).

3) Y. Nakahara, K. Kimura, H. Inokuchi, and T. Yagi, *Chem. Lett.*, **1979**, 877; K. Kimura, Y. Nakahara, T. Yagi, and H. Inokuchi, *J. Chem. Phys.*, **70**, 3317 (1979); K. Kimura and H. Inokuchi, *J. Phys. Soc. Jpn.*, **51**, 2218 (1982).

4) K. Niki, T. Yagi, H. Inokuchi, and K. Kimura, *J. Am. Chem. Soc.*, **101**, 3335 (1979).

5) W. Sokol, D. H Evans, K. Niki, and T. Yagi, *J. Electroanal. Chem.*, **108**, 107 (1980); K. Niki, Y. Kobayashi, and H. Matsuda, *J. Electroanal. Chem.* in press.

6) J. LeGall, M. H. Bruschi and D. V. DerVartanian, *Biochim. Biophys. Acta*, **234**, 499 (1971); D. V. DerVartanian and J. LeGall, *ibid*, **346**, 79 (1974).

7) J. J. G. Moura, H. Santos, I. Moura, J. LeGall, G. R. Moore, R. J. P. Williams, and A. V. Xavier, *Eur. J. Biochem.*, **127**, 151 (1982).

8) T. Yagi and K. Maruyama, *Biochim. Biophys. Acta*, **234**, 214 (1971).

9) T. Yagi, K. Kimura, H. Daidoji, F. Sakai, S. Tamura, and H. Inokuchi, *J. Biochem.*, **79**, 661 (1976).

10) In Ref. 7), only five of the sixteen heme methyls were assigned.

11) H. Santos, J. J. G. Moura, I. Moura, J. LeGall, and A. V. Xavier, *Eur. J. Biochem.*, **141**, 283 (1984).

 © 1985 The Chemical Society of Japan Bull. Chem. Soc. Jpn., 58, 1013—1018 (1985)

Reaction of Leucocrystal Violet with Tetracyanoethylene and Chloranil II.[1] Solvent Effects

Norio NISHIMURA* and Takushi MOTOYAMA
Department of Chemistry, School of Science, Okayama University, Tsushima, Okayama 700
(Received July 2, 1984)

The proton/deuteron transfer reaction of Leucocrystal Violet(LCV) with tetracyanoethylene(TCNE) and chloranil(CA) in various solvents has been followed spectrophotometrically. It was found that the reaction proceeds slower in polar solvents such as acetonitrile and acetone than in less polar solvents such as chloroform and 1,2-dichloroethane. The rate is remarkably accelerated by pressure indicating probably a substantial polarity increase in the rate processes. The formation of CT complexes was observed at low temperatures. Their nature is presumed to be similar to that of a complex formed by the reaction of CA with *N,N*-dimethyl-*p*-toluidine(DMT), and the latter is discussed in connection with the reaction rate of the LCV–TCNE and LCV–CA systems. A possible reaction path is proposed.

In a previous paper,[1] the rate of reaction of Leucocrystal Violet(LCV) with tetracyanoethylene(TCNE) and chloranil(CA), and the kinetic pressure and isotope effects were reported. For both reaction systems, it was found that the reaction follows the second-order rate law: first-order with respect to each reactant. In the LCV–CA system, a very large kinetic isotope effect ($k_H/k_D \approx 11$) was observed suggesting that the so-called proton tunneling is involved, while in the LCV–TCNE system, it was not so large ($k_H/k_D \approx 5$). From large kinetic pressure effects, it was suggested that the reaction proceeds *via* very polar transition states for both reactions. At low temperatures, the formation of CT complexes in equilibrium with the reactants was observed. From the above findings, the following alternative reaction schemes have been proposed:

$$\mathrm{LCV} + \mathrm{CA(TCNE)} \rightleftarrows \mathrm{X_1} \rightleftarrows \mathrm{X_2}$$
$$\mathrm{X_1\ or\ X_2} \xrightarrow{\text{slow}} \mathrm{CV^+} + \cdots\cdots$$

Scheme 1.

$$\begin{array}{l} \mathrm{LCV} + \mathrm{CA(TCNE)} \rightleftarrows \mathrm{X_1} \rightleftarrows \mathrm{X_2} \\ \quad\quad\quad\

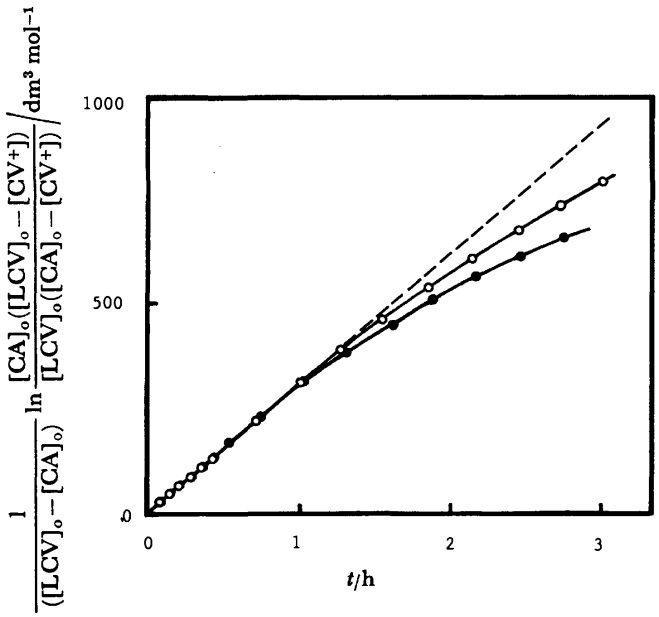

Fig. 1. Second-order plots for the reaction between LCV and CA in acetonitrile at 20 °C. ○: $[LCV]_o = 2.86\times10^{-5}$ mol dm^{-3}, $[CA]_o = 9.51\times10^{-4}$ mol dm^{-3}; ●: $[LCV]_o = 5.73\times10^{-4}$ mol dm^{-3}, $[CA]_o = 4.80\times10^{-5}$ mol dm^{-3}.

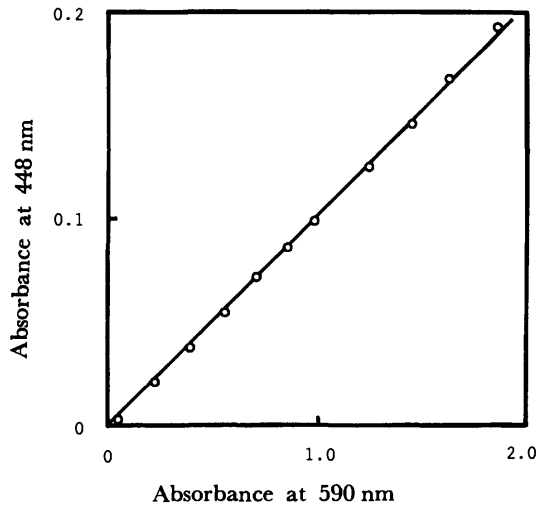

Fig. 2. Relationship between the absorbance at $\lambda_{max}=$ 448 nm and the absorbance at $\lambda_{max}=590$ nm at various times.

polar solvents. The rate is, however, faster in less polar solvents than in more polar solvents. The second notable point is the solvent dependency of the kinetic isotope effect. According to Isaacs *et al.*[3] and Sugimoto *et al.*,[4] if the atom (H or D) being transferred is strongly coupled with solvent molecules, the probability of tunneling will diminish, because the effective mass of the proton and deuteron should increase. In Scheme 2, a highly polarized transition state was assumed[1] in accordance with the large negative $\Delta V^{\neq}$-values. Substantial solvent effects on the ratio k_H/k_D can be expected in this case. However, the ratios are almost independent of solvent polarity.

TABLE 1. RATE CONSTANTS FOR THE REACTION BETWEEN LEUCOCRYSTAL VIOLET AND CHLORANIL AT 25 °C

Solvent	k_H	k_D	k_H/k_D
	10^{-2} dm^3 mol^{-1} s^{-1}	10^{-2} dm^3 mol^{-1} s^{-1}	
CH_3CN	11.0	1.01	10.9
CH_3COCH_3	5.28	0.502	10.5
CH_2ClCH_2Cl	24.3	2.11	11.5
CH_2Cl_2	25.6	2.31	11.1
$CHCl_3$	31.0	2.67	11.6
CH_3CCl_3	21.5	1.82	11.8

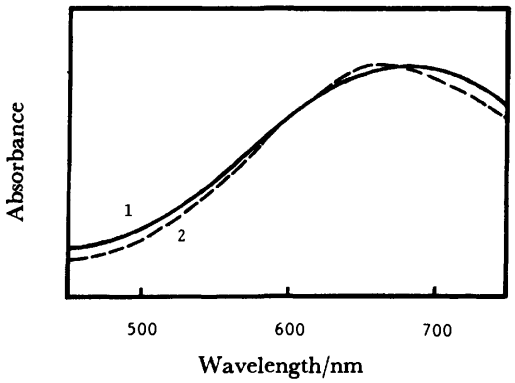

Fig. 3. Absorption spectra of the CT band appeared in the LCV+CA (1) and DMT+CA (2) systems; in EPA, 77K.

These two remarkable points have led us to the question about the single-step hydride ion shift mechanism[3] (Scheme 2). On the other hand, if Scheme 1 is the case, information about X_1 and X_2 is required. As reported previously, the formation of the outer CT complex between LCV and CA was observed at temperatures as low as below −50 °C, as identified by its characteristic spectrum. This made the spectrophotometric measurement of the CT band and hence, the assessment of the equilibrium constant in various solvents difficult. However, the CT band is very similar to that observed in the DMT-CA system (Fig. 3), as can be expected from the structural similarity between LCV and DMT. Hence, X_3 will not be so bad a model for X_1. We expected that informations about X_3 might shed light on the reaction mechanism we are interested in.

Table 2 shows the CT band of X_3 in various solvents. In Fig. 4, $\bar{\nu}_{max}$ is plotted against the E_T-value of the solvents. It appears that the plots can be divided into two groups: Group A containing an electronegative oxygen or nitrogen atom within a molecule, and Group B belonging to the other kind. Since CT complexes are more polar in the excited state than in the ground state, the red shift of the CT band can be expected. For Group A, however, $\bar{\nu}_{max}$ is scarcely sensitive to the solvent polarity parameters such as the E_T-value and Brownstein's *S*-value. Aihara *et al.*[5] investigated Aromatic-TCNE complexes in vari-

Table 2. Absorption maxima, λ_{max}/nm of the CT band formed in the DMT-CA system in various solvents

	Solvent	λ_{max}/nm		Solvent	λ_{max}/nm
1	Hexane	689	9	CH_2Cl_2	718
2	Cyclohexane	692	10	CH_2ClCH_2Cl	716
3	CCl_4	706	11	Diethyl ether	688
4	Toluene	704	12	THF	686
5	Benzene	709	13	Acetone	687
6	CH_3CCl_3	706	14	DMSO	693
7	Chlorobenzene	716	15	CH_3CN	694
8	$CHCl_3$	720	16	Ethanol	688

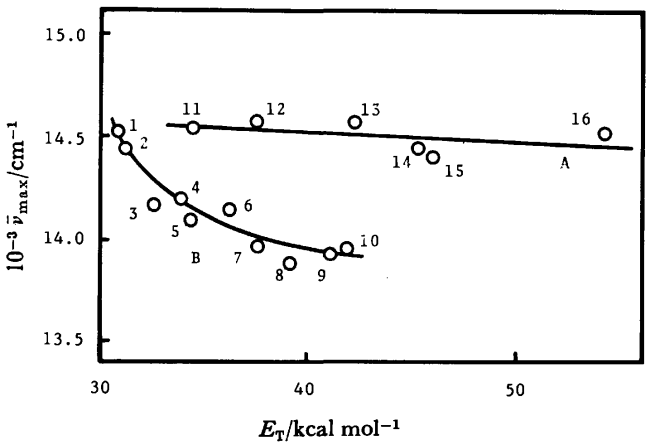

Fig. 4. Plots of $\bar{\nu}_{max}$ of the CT band of X_3 against the E_T-value. Key is shown in Table 2.

ous solvents and interpreted the spectral shift in terms of McRae's formula. They found that a series of solvents except for oxygen-containing solvents behave normally, and suggested that these solvents might change the nature of complexes. Relevant discussion will be made later.

In Fig. 5, ln k_H is plotted, on trial, against $\bar{\nu}_{max}$ in Table 2. It appears that there exists an affirmative correlation in spite of the fact that solvents are classified into two groups. Further, the equilibrium constants for the formation of X_3 in various solvents were estimated by means of the Benesi-Hildebrand plot (Fig. 6), and the results are given in Table 3. In Fig. 7, k_H is plotted against K, giving a fair correlation.

In Scheme 1, the reaction proceeds *via* X_1 and therefore, the equilibrium constant must be involved in the numerator of the second-order rate constant expressed in a composite form. If the values of the equilibrium constant for DMT-CA system in the solvents we used are related to those for LCV-CA system, this may be responsible for the above finding. On the other hand, the existence of the equilibria in Scheme 2 must scarcely affect the rate, since the equilibrium constant for the LCV-CA system must be small at the vicinity of room temperature(*vide supra*). Although the situation has not been clarified sufficiently, the above observations and considerations support the involvement of X_1 in the reaction process.

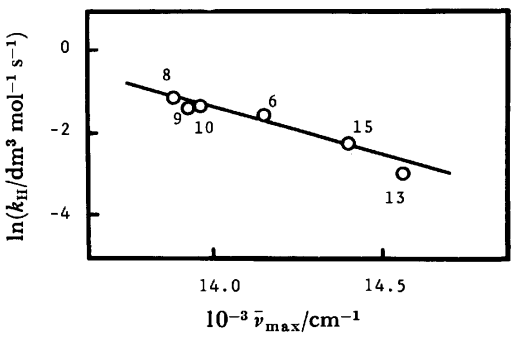

Fig. 5. Relationship between $\ln k_H$ and $\bar{\nu}_{max}$ of X_3. Key is shown in Table 2.

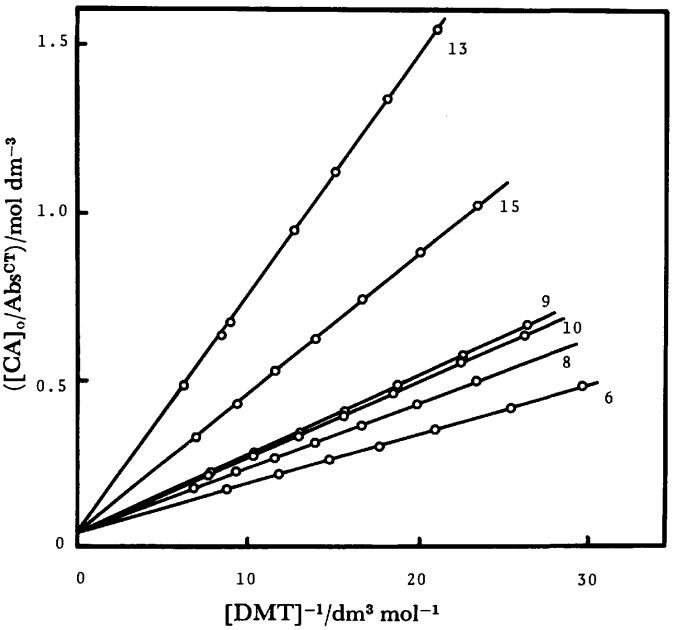

Fig. 6. Benesi-Hildebrand plots in various solvents. Key is shown in Table 2.

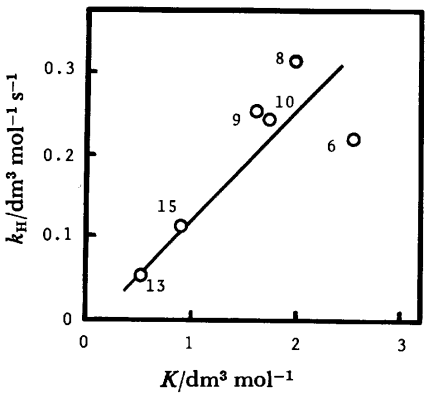

Fig. 7 Relationship between k_H and the equilibrium constant for the formation of X_3.

LCV-TCNE System. In the preceding paper, we reported the pressure dependence of the rate constant for this system. In order to examine the pressure effects in polar solvents, acetonitrile was chosen as representative, and the rate was followed under high pressures. The results are given in Table 4. The rate

was also followed in various solvents under atmospheric pressure, and the results are given in Table 5, together with the activation parameters. By inspection of these data, we notice some points. (1) The application of external pressure remarkably accelerates the rate in acetonitrile as well as in chloroform. It is generally accepted that a large polarity increase of reacting species gives rise to a large volume shrinkage of surrounding solvent molecules as exemplified by the pressure effect on the rate. It appears that during the course of reaction from the initial to the transition state, there exists a step in which a large polarity increase is involved. When we remember that the products in our systems are ionic ones, this presumption may be accepted. (2) The kinetic isotope effect(k_H/k_D) in acetonitrile is a little smaller than that in chloroform. This might be ascribed to the solvent-coupled proton transfer as stated above. The isotope effect is far smaller than that in the LCV–CA system. Therefore, the proton tunneling would, if any, be very small. (3) Much more remarkable kinetic solvent effects are observed in this system than in the LCV–CA system, *i.e.*, in polar solvents the rate is reduced greatly and the activation energy increased. This is apparently inconsistent with the fact stated in (1) by the reason explained in the previous section.

In this respect, we considered that the kinetic study in binary mixtures might afford useful informations about the solvent effect. Kondo *et al.*[6] have developed a theory of bimolecular reactions in binary mixed solvents 1 and 4. If one of the reactants is solvated by, say, 4, to form a kind of addition product, the simplified rate equation can be given by

$$\ln k_{mix} = x_1 \ln k_1 + x_4 \ln k_4 + x_4 \ln(K_x+1) - \ln(x_4 K_x + 1)$$

where K_x denotes the association constant expressed in terms of mole fractions for the formation of the addition product; x_1 and x_4 are the mole fractions of 1 and 4, respectively. This equation predicts that the ln k_{mix} *versus* x_1 plot should deviate downward from a straight line expected for ideal binary mixed solvents, the extent of the deviation depending on the value of K_x. On the other hand, according to the theory, if none of the reactants are solvated, but the activated complex is solvated, with one of the solvents, the upward deviation can be expected. In Table 6, the rate constants in chloroform–acetonitrile mixtures are given. By using these data, ln k_{mix} is plotted against the mole fraction of chloroform as shown in Fig. 8. It is seen that the plots constitute a curve shifted downward from the ideal line. Previously,[7] we reported that this type of curve was realized in the reaction of 2,2-diphenyl-1-picrylhydrazyl with phenols in dioxane–2,2,4-trimethylpentane, and cyclohexane–acetone mixed solvents. In that case, a special interaction through hydrogen bonding between phenols and the oxygen-containing solvents was assumed. Marrifield and Philipps reported[8] that the equilibrium constant for the π-complex formation between TCNE and various kinds of aromatic compounds is remarkably affected by variation of the solvent. According to them, this effect is due to the formation of a complex between TCNE and the solvent, as exemplified by a new weak band at 335 nm when TCNE is dissolved in diethyl ether. Although, owing to the experimental difficulties, conclusive evidence for the formation of

TABLE 3. EQUILIBRIUM CONSTANTS FOR THE REACTION CA + DMT $\rightleftarrows$ X_3 AT 25 °C IN VARIOUS SOLVENTS

Solvent	$K\varepsilon$/dm³ mol⁻¹	K*/dm³ mol⁻¹
CH_3CN	2394	0.921
CH_3COCH_3	1398	0.538
CH_2ClCH_2Cl	4401	1.69
CH_2Cl_2	4225	1.63
$CHCl_3$	5174	1.99
CH_3CCl_3	6982	2.69

* Calculated as $\varepsilon = 2600$.

TABLE 4. PRESSURE DEPENDENCE OF THE RATE CONSTANT FOR THE REACTION BETWEEN LCV AND TCNE IN ACETONITRILE AT 35 °C

P/10⁵ Pa	$10^2 k$/dm³ mol⁻¹ s⁻¹			
	1	300	600	900
H	6.41	8.91	11.4	14.9
D	1.25	1.67	2.21	2.93

TABLE 5. RATE CONSTANTS FOR THE REACTION BETWEEN LCV AND TCNE AT 25 °C AND ACTIVATION PARAMETERS

	Solvent	$10^2 k_H$ / dm³ mol⁻¹ s⁻¹	E_a[b] / kJ mol⁻¹	ΔS^*[b] / JK⁻¹ mol⁻¹	ΔV^* / cm³ mol⁻¹
H	Acetonitrile	3.78	43.1	−135	−29.9
	Acetone	4.66			
	1,2-Dichloroethane	52.2			
	Chloroform[a]	173	30.0	−148	−28.6
D	Acetonitrile	0.78	46.8	−137	−26.9
	Chloroform[a]	29.5	34.1	−149	−29.2

a) Cited from Ref. 1. b) Estimated from the k_H-values at 25—45 °C.

Table 6. Rate constants for the reaction between LCV and TCNE in acetonitrile–chloroform mixtures at 30 °C

Mole fraction of $CHCl_3$	$10^2 k_{mix}$ / $dm^3\ mol^{-1}\ s^{-1}$
0	5.20
0.304	7.70
0.495	11.9
0.724	32.2
0.880	84.4
1.00	213

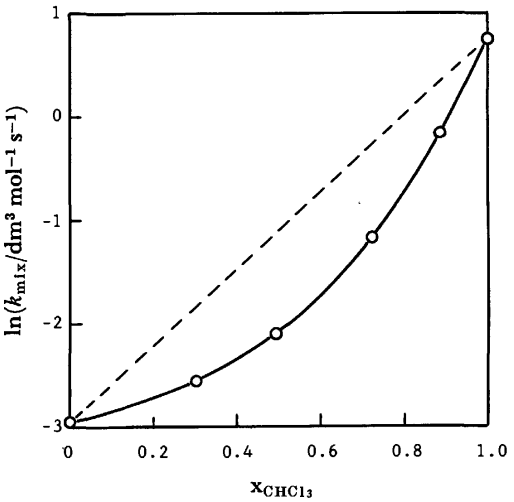

Fig. 8. Relationship between $\ln k_{mix}$ and the mole fraction of $CHCl_3$ in $CHCl_3$–CH_3CN binary mixtures.

such TCNE/solvent complexes has not been obtained yet in the solvent we used, a special interaction between TCNE(CA) and the solvents belonging to Group A may be assumed to exist. The interaction with the TCNE as a reactant must be the greatest, intermediate with the TCNE in the ground CT complex, and the smallest with the TCNE in the excited CT complex, since the interaction between TCNE and LCV must increase in this order. If this is the case, the reactivity of "solvated" TCNE will diminish and this may be responsible for the decreased rate of reaction, the enhanced activation energy, the blue shift of the CT band of X_3 in acetonitrile and acetone, and the kinetic behavior in the binary mixtures.

Reaction Mechanism From the point of view of the kinetic solvent effects, and the correlation of the rate of reaction with the nature of X_3 chosen as a model of X_1, it may be concluded that the reaction proceeds probably *via* X_1. Although the processes thereafter have not necessarily been fully elucidated, we could presume probable reaction routes on the basis of the informations obtained so far: The second-order kinetics and simultaneous formation of CV^+ and semiquinone anion radicals and available informations on reactions which proceed through inner and outer CT complexes.[9–13] The following chart for the LCV–CA system may be proposed:

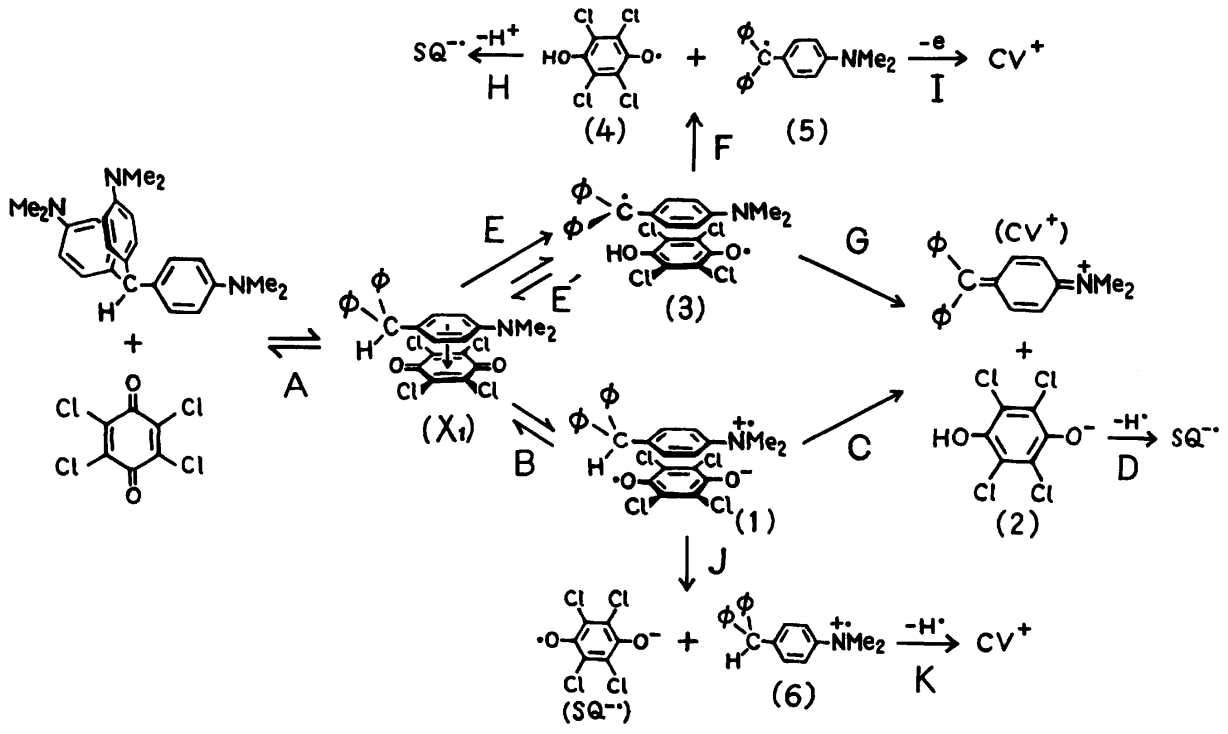

In accordance with this chart, the possible reaction routes are summarized as follows:

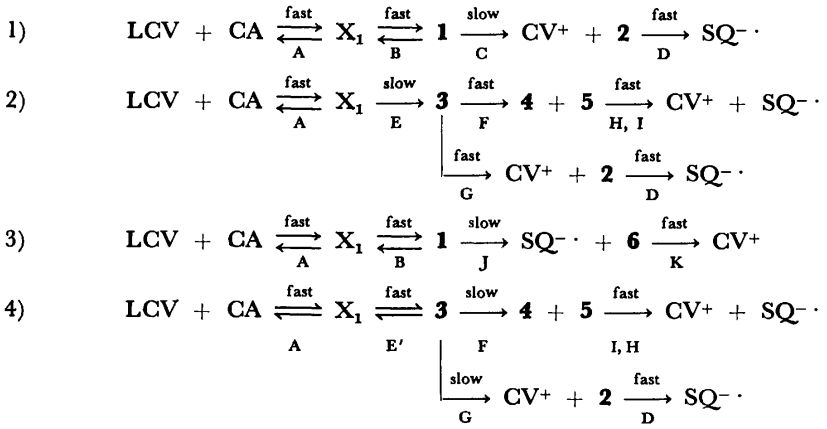

Of these reaction paths, the kinetic isotope effect precludes the possibility of 3) and 4), since proton transfer is not involved in the rate-determining steps. The volume change in Step A may be 0—−14 cm³/mol observed for most cases for the formation of CT complexes.[14] The volume change in step E in which hydrogen atom transfer is involved, will be no more than few cm³. Hence, the large negative value of $\Delta V^{\neq}$ obtained for our systems could eliminate the possibility of 2). We have noticed that X_3 decomposes gradually to produce $SQ^{-\cdot}$ in polar solvents, suggesting the existence of **1** instead of **3**. In the remaining possibility 1), Step C is assumed to be the rate-determining one. Proton transfer is involved in this step and this is in accord with the observed large isotope effect. A remarkable volume change can be expected in Step B where electron transfer is involved, and this is responsible for the large kinetic pressure effect. We have observed the correlation between $\ln k_H$ and $\bar{\nu}_{max}$. It could be assumed that $\bar{\nu}_{max}$ is proportional to the energy difference between **1** and X_1. As for the kinetic isotope effect, we consider as follows. Owing to the bulkiness of CA skeleton, the hydrogen atom being transferred is blocked from the surrounding solvent molecules. The effective mass of the hydrogen (and deuteron) is then not affected substantially by solvent polarity, thus accounting for the constant k_H/k_D-value in various solvents. This is in accord with the appreciable tunneling effect, too. In the LCV-TCNE system, the ratio is considerably smaller, and the tunneling effect, if any, so small. We tentatively consider that the difference would arise from the difference in the ability of protecting the hydrogen atom from the surrounding solvent molecules during its transfer. We conclude that the reactions of LCV-CA and LCV-TCNE systems probably proceed *via* Route 1).

References

1) Part I, N. Nishimura and T. Motoyama, *Bull Chem. Soc. Jpn.*, **57**, 1 (1984).
2) Y. Sueishi and N. Nishimura, *Bull. Chem. Soc. Jpn.*, **56**, 2598 (1983).
3) N. S. Isaacs, K. Javaid, and E. Rannala, *J. Chem. Soc., Perkin Trans. 2*, **1978**, 709.
4) N. Sugimoto, M. Sasaki, and J. Osugi, *J. Am. Chem. Soc.*, **105**, 7676 (1983).
5) J. Aihara, M. Tsuda, and H. Inokuchi, *Bull. Chem. Soc. Jpn.*, **42**, 1824 (1969).
6) Y. Kondo, K. Uosaki, and N. Tokura, *Bull. Chem. Soc. Jpn.*, **44**, 2548 (1971), and references cited therein.
7) N. Nishimura, T. Moriya, Y. Okino, K. Tanabe, K. Kawabata, and T. Watanabe, *Bull. Chem. Soc. Jpn.*, **50**, 1969 (1977).
8) R. E. Merrifield and W. D. Phillips, *J. Am. Chem. Soc.*, **80**, 2778 (1958).
9) A. H. Ewald, *Trans. Faraday Soc.*, **64**, 733 (1968).
10) A. H. Ewald and J. A. Scudder, *J. Phys. Chem.*, **76**, 249 (1968).
11) T. Nakayama, M. Sasaki, and J. Osugi, *Rev. Phys. Chem. Jpn.*, **46**, 57 (1976).
12) A. Ohno and N. Kito, *Chem. Lett.*, **1972**, 369.
13) S. Fukuzumi and T. Tanaka, *Chem. Lett.*, **1982**, 1513.
14) T. Asano and J. leNoble, *Chem. Rev.*, **78**, 407 (1978).

 © 1985 The Chemical Society of Japan Bull. Chem. Soc. Jpn., 58, 1019—1022 (1985)

Calorimetric Investigation of *N*-Acyl Amino Acids

Shigeyoshi MIYAGISHI,* Seiichi MATSUMURA, Kazuhiko MURATA, Tsuyoshi ASAKAWA, and Morie NISHIDA

Department of Industrial Chemistry, Faculty of Technology, Kanazawa University, Kanazawa 920

(Received September 12, 1984)

The melting characteristics of *N*-acyl amino acids were examined using a differential scanning calorimeter (DSC). The melting-point temperature of *N*-dodecanoyl L-amino acid increased with the size of its amino acid residue, while the order was opposite for the DL-amino acids. The racemic derivatives formed racemic compounds in their solid states. Each *N*-dodecanoyl L-amino acid had a larger enthalpy and entropy-of-fusion than its racemic isomer. Differences in the thermodynamic quantities between the optically active and racemic isomers were larger for *N*-dodecanoylvaline and -leucine compared with those of *N*-dodecanoylalanine. A mixture of these molecules were also studied. Each racemic isomer of *N*-dodecanoylalanine and -leucine partly formed a racemic pair in the liquid state.

Attention is presently being given to the stereochemical effects not only of micelle-catalyzed reactions but also to condensed systems of long hydrocarbon chain compounds. Tachibana and his coworkers[1-4] have investigated chiral and racemic 12-hydroxyoctadecanoic acids in their crystal aggregate and monolayer states. Iwahashi, *et al.*[5] studied the thermodynamic and structual relationship between optically active α-monostearin and its racemic isomer in their crystalline, molten, and dissolved states. They suggested that (*R*)- and (*S*)-molecules in the (*RS*)-form interacted to form a racemic pair not only in the crystalline state, but also in the molten state. Miyagishi and Nishida[6] reported that the smaller critical micelle concentration for a sodium salt of the optically active *N*-acyl amino acid resulted from a difference in the micellization enthalpy. The object of this paper is to describe the chirality effect on the melting characteristics of *N*-acyl amino acids.

Experimental

N-Acyl amino acids were prepared according to a procedure described before[6,7] and are tabulated in Table 1. The recrystallization of *N*-acyl amino acids was repeated until the DSC curve and a peak temperature became constant. A differential scanning calorimeter (Daini Seikosha DSC, model SSC/560S) was used for the measurement of the heat-of-fusion and melting temperature. A sample (about 5 mg) was sealed in an aluminium vessel (50 mm^3). The scanning rate was 5 K min^{-1}. Standard samples of phenanthrene and indium were used for calibration. A mixed sample was prepared as follows. A mixture of a known composition was dissolved in methanol and the resulting solution was allowed to stand for several hours. After the methanol was evaporated, a part of the mixture was used for the DSC measurement.

In the mixed systems, two peaks appeared on the DSC curve and each was detected as a separated peak. When the peaks approached each other, they began to overlap and became one broad peak with two peaks superimposed on it. The temperature at each peak was measured.

Results and Discussion

Melting Temperature. The melting temperatures of *N*-acyl amino acids are shown in Table 1 along with the heats-of-fusions. The melting-point temperature increased with the size of the amino acid residue in an L-series, while the order was opposite in a DL-series. The branched isomers of *N*-dodecanoylvaline all had similar melting-point temperatures. The same tendency was observed among the branched isomers of *N*-dodecanoylleucine. *N*-Acylglycine and -alanine each showed a tendency for the melting-point temperature to increase with the chain length of an acyl group. *N*-Acyl-DL-norleucine, however, gave melting-point temperatures scattered between 354—360 K and had no regular tendency.

Latent Heat of Fusion. The latent heat ΔH_f and entropy-of-fusion ΔS_f for *N*-dodecanoyl amino acids are plotted against the carbon number of their amino

Table 1. Properties of *N*-acyl amino acids

	Mp/K	ΔH_f/KJ mol^{-1}	[α]
N-Dodec-Gly	393.1	48.4	
N-Dodec-L-Ala	353.1	37.6	−18.7
N-Dec-DL-Ala	365.6	37.5	
N-Dodec-DL-Ala	379.1	44.7	
N-Tetradec-DL-Ala	381.3	54.0	
N-Hexadeca-DL-Ala	387.1	58.4	
N-Dodec-Abu[a]	389.1	41.4	
N-Dodec-L-Val	378.6	33.1	−2.6
N-Dodec-DL-Val	364.5	64.4	
N-Dodec-DL-*n*-Val[b]	362.1	59.5	
N-Dodec-L-Leu	381.1	33.5	−14.5
N-Dodec-L-Ile	380.1	30.6	+4.6
N-Dodec-DL-Leu	354.6	59.9	
N-Oct-DL-*n*-Leu[c]	359.1	33.9	
N-Dec-DL-*n*-Leu	355.3	29.9	
N-Dodec-DL-*n*-Leu	350.4	55.2	
N-Tetradec-DL-*n*-Leu	360.1	57.7	

a) *N*-dodecanoyl-2-aminobutanoic acid. b) *N*-dodecanoyl-DL-norvaline. c) *N*-Octanoyl-DL-norleucine.

acid part in Fig. 1. The values of ΔH_f and ΔS_f depended on the size and optical isomerism of the acyl amino acid (see also Fig. 2). We did not find a significant difference of thermodynamic quantity among the branched isomers.

Racemic compounds always had larger ΔH_f and ΔS_f values than the corresponding chiral isomers. For the optically active series, ΔH_f and ΔS_f decreased with the carbon number of the amino acid part, while for the racemic series, there were abrupt increases of ΔH_f and ΔS_f above a carbon number of 5. The difference of ΔH_f between the optically active and racemic isomers was 31.3 and 23.0 KJmol^{-1} for *N*-dodecanoylvaline and -leucine, and the difference of ΔS_f was 92 and 72 Jmol^{-1} K^{-1}, respectively. These values were very large compared to 7.1 KJmol^{-1} and 12 Jmol^{-1} K^{-1} for *N*-dodecanoylalanine.

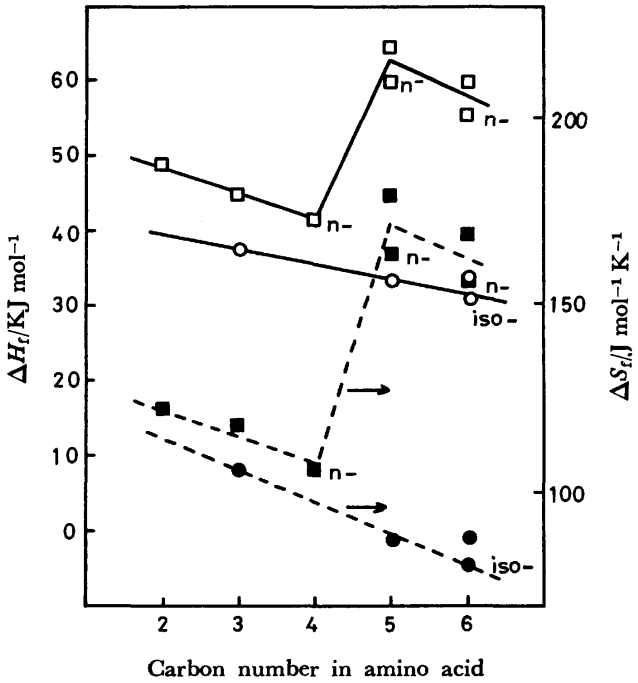

Fig. 1. Enthalpies and entropies of fusion of *N*-dodecanoyl amino acids. (○,●); L-form, (□,■); DL-form.

Figure 2 shows that the enthalpy and entropy-of-fusion depend on the size of an acyl group. For the alanine compounds, ΔH_f and ΔS_f increased linearly with the number of the methylene group in the acyl group. The enthalpy-of-fusion per methylene group was 4 KJmol^{-1}, which was identical with a figure found for normal alkane,[8] and monoglyceride.[9] The entropy-of-fusion increased by a factor 9 Jmol^{-1} K^{-1} for each additional methylene group added to the acyl chain. This value also agreed with that of normal alkane[8] and monoglyceride.[9] It can be concluded from the above results that the acyl group of the *N*-acyl DL-alanines behaves in the same manner as a normal alkane when it melts, and is hardly affected by the amino acid residue.

On the contrary, the theromodynamic quantities of *N*-acyl DL-norleucine varied, irregularly, with the size of the acyl group. It is suggested that the acyl group of the *N*-acyl DL-norleucines may interact somewhat with their amino acid residue, or at least perturbs the melting process.

Melting of Mixture. The temperatures cited in Figs. 3—6 are the peak temperatures on a DSC curve since it was difficult to determine the point at which the DSC curve started to deviate from the base line.

The melting-point temperatures of mixtures of *N*-

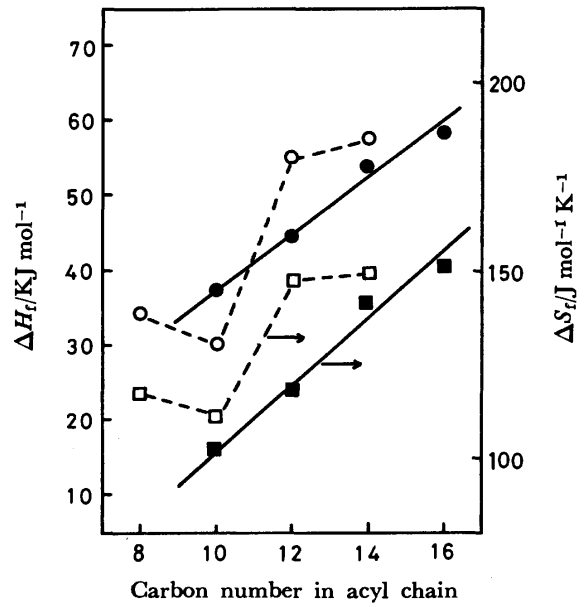

Fig. 2. Enthalpies and entropies of fusion of *N*-acyl DL-alanines and -DL-norleucines. (●,■); the alanines, (○,□); the leucines.

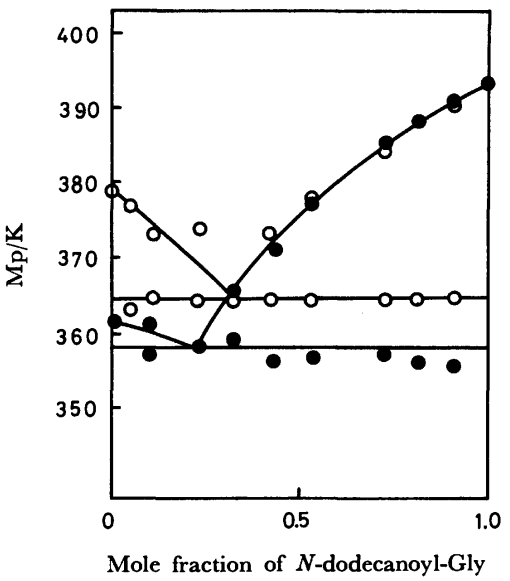

Fig. 3. Phase diagrams of mixtures of *N*-dodecanoylglycine and -valines. (○); L-form, (●); DL-form. The solid lines are the calculated values on the assumption of ideal mixing.

dodecanoylglycine and *N*-dodecanoyl-L-valine are shown in Fig. 3. This system has a single eutectic point and is a typical system with equilibrium between unmixed solid and mixed liquid states.

In a previous paper,[7] it was reported that a mixture of sodium salts of *N*-dodecanoylglycine and -L-valine could be treated as an ideal mixture in a micelle state. We attempted to apply the assumption of ideal mixing to the present system. The solid curves in Fig. 3 were calculated from Eq. 1[10] and are in good agreement with the experimental points.

$$\ln x = (\Delta H_0/R)(1/T_0 - 1/T) \quad (1)$$

where x is mole fraction of the first component and ΔH_0 and T_0 are the latent heat-of-fusion and melting point.

The system, where racemic *N*-dodecanoylvaline was used instead of the optically active isomer, was also examined. We considered a system composed of A moles of *N*-dodecanoylvaline (1 mole is a mole of an optically active isomer) and B moles of *N*-dodecanoylglycine (mole fraction in Fig. 3 is equal to $B/(A+B)$). If the racemic *N*-dodecanoylvaline formed a racemic compound in the liquid state, the mole fraction of *N*-dodecanoylglycine would be $B/(A/2+B)$ in the liquid mixture (which differs from the mole fraction used in Fig. 3). Consequently, this phase diagram should be different in all regions from one containing the optically active isomer. The experimental results did not agree with such a prediction. When *N*-dodecanoyl-DL-valine is a racemic mixture in a liquid state, the mole fraction of the glycine derivative is given as $B/(A+B)$ in the liquid mixture. The results calculated from this mole fraction and Eq. 1 are given in Fig. 3. This figure indicates that the racemic *N*-dodecanoylvaline is a racemic mixture in a liquid state rather than a racemic compound, although it forms a racemic compound in the solid state (described later).

Mixture of Optically Active and Racemic Isomers. The systems shown in Figs. 4—6 were examined. In all of them, the formation of racemic compounds occured. These results reflect the fact shown in Fig. 1, that the ΔH_f and ΔS_f values of a racemic isomer are always larger than those of a corresponding optically active one. The difference may correspond to the formation energy of a racemic compound.

We could not assume ideal mixing in these systems, but could roughly estimate an interaction parameter between two corresponding chiral isomers in a liquid state. The excess thermodynamic potential of the first

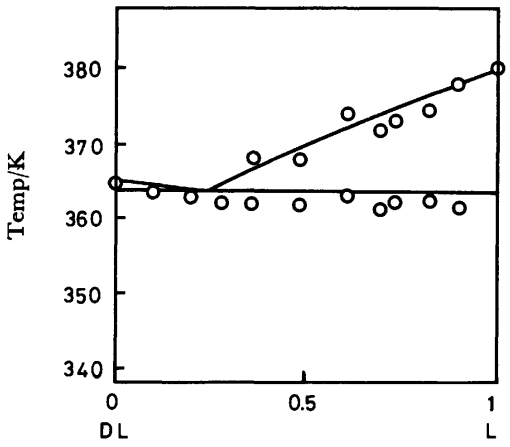

Mole fraction of dodec-L-Val

Fig. 5. Melting-point temperatures of mixture of *N*-dodecanoyl-L-valine and -DL-valine. The plotted points are experimental data, the solid and broken lines correspond the values calculated with β of 0.06 and 0, respectively, but two curves were almost overlapped.

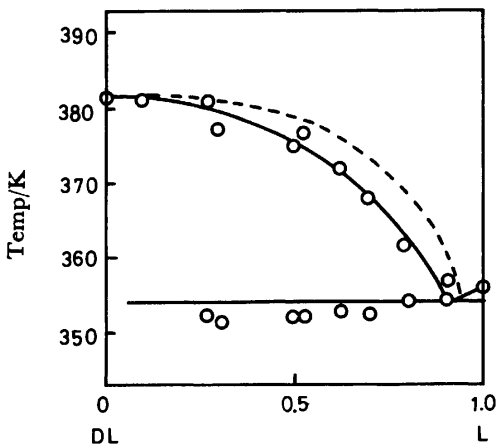

Mole fraction of *N*-dodec-L-Ala

Fig. 4. Melting-point temperatures of mixture of *N*-dodecanoyl-L-alanine and -DL-alanine. The plotted points are experimental data, the solid and broken lines correspond the values calculated with β of -1.08 and 0, respectively.

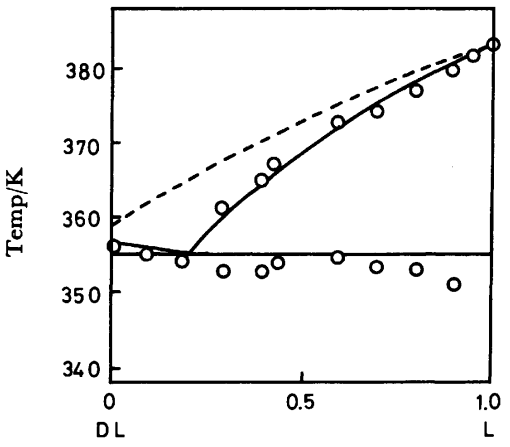

Mole fraction of dodec-L-Leu

Fig. 6. Melting-point temperatures of mixture of *N*-dodecanoyl-L-leucine and -DL-leucine. The plotted points are experimental data, the solid and broken lines correspond the values calculated with β of -1.91 and 0, respectively.

component, $\mu^e(T,x)$ is in the most simple form[10]

$$\mu^e(T, x) = RT \ln f_1 = A(1-x_1)^2. \quad (2)$$

When we assume $A=RT\beta$, an activity coefficient f_1 is given by Eq. 3.

$$\ln f_1 = \beta(1-x_1)^2 \quad (3)$$

Substitution of Eqs. 2 and 3 into the following equation[11]

$$-\int_{T_1}^{T} \Delta S_f dT + RT \ln x_1 + \mu^e(T, x) = 0 \quad (4)$$

and a rearrangement gives:

$$T = \frac{\Delta H_1/R}{\Delta H_1/RT_1 - \ln x_1 - \beta(1-x_1)^2} \quad (5)$$
$$(0 \leqq x_1 \leqq x_{eu1}, \text{ and } x_{eu2} \leqq x_1 \leqq 1)$$

where x_1 and T_1 are the mole fraction and melting point of the first component. ΔS_f is its fusion entropy and is equal to $\Delta H_1/RT_1$. ΔH_1 is the latent heat-of-fusion. Our systems contain two components of L- and D-isomers, and the L-isomer corresponds to the first component. By using Eq. 3 and the method described by Oonk,[12,13] we obtain Eq. 6.

$$T = \frac{\Delta H_c}{\Delta H_c/T_c - R/2[\ln 4x_1(1-x_1) + \{x_1^2 + (1-x_1)^2 - 1/2\}\beta]} \quad (x_{eu1} < x_1 < x_{eu2}) \quad (6)$$

Here, T_c is the melting temperature of the racemic isomer, ΔH_c is its latent heat-of-fusion and x_{eu1} and x_{eu2} are the compositions at the eutectic points ($x_{eu1} < x_{eu2}$). The melting-point temperature can be calculated from Eqs. 5 and 6.[15]

The interaction parameter (β) was estimated from the experimental values using Eqs. 2—6. The value of β was −1.08, 0, and −1.91 for *N*-dodecanoylalanine, -valine, and -leucine, respectively. These values suggest that the L- and D-isomers interact with each other to form at least a racemic pair in the systems of the alanine and leucine derivatives.

References

1) T. Tachibana and H. Kambara, *J. Colloid Interface Sci.*, **28**, 173 (1968).

2) T. Tachibana and H. Kambara, *Bull. Chem. Soc. Jpn.*, **42**, 3422 (1969).

3) T. Tachibana and K. Hori, *J. Colloid Interface Sci.*, **61**, 398 (1977).

4) T. Tachibana, T. Yoshizumi, and K. Hori, *Bull. Chem. Soc. Jpn.*, **52**, 34 (1979).

5) M. Iwahashi, Y. Watanabe, T. Watanabe, and M. Muramatsu, *Bull. Chem. Soc. Jpn.*, **57**, 1446 (1984).

6) S. Miyagishi and M. Nishida, *J. Colloid Interface Sci.* **65**, 380 (1978).

7) S. Miyagishi, Y. Ishibai, T. Asakawa, and M. Nishida, *J. Colloid Interface Sci.*, in press.

8) R. H. Aranow, L. Witten, and D. H. Andrews, *J. Phys. Chem.*, **62**, 812 (1958).

9) T. Maruyama, I. Niiya, M. Imamura, and T. Matsumoto, *Yukagaku*, **26**, 104 (1977).

10) H. A. J. Oonk, "Phase Theory (Studies in modern thermodynamics: 3)," Elsevier, Amsterdam (1981) p. 172.

11) Ref. 10), p. 171.

12) Ref. 10), p. 176.

13) Equation 6 can also be derivated from equation 23.10 in reference 14 on the assumption of Eq. 3.

14) I. Prigogine and R. Defay, "Thermodynamique Chimique," (1950), Japanese ed by Misuzu Shobo (1966) p. 385—388.

15) The values calculated in the region between x_1=0.5 and 1.0 are given Figs. 4—6 and the left side of the figures (mole fraction of DL- isomer is 1) corresponds to x_1=0.5 in Eqs. 5—6.

Solution Properties of Low Molecular Weight Fractions of Poly(2-vinylpyridine)

Masafumi YOSHIDA, Shinsuke YAMAGUCHI,† Noriyuki SAKAMOTO, and Shizuo ARICHI*
Department of Chemistry, Faculty of General Education, Kumamoto University, Kurokami 2-40-1, Kumamoto 860
(Received September 19, 1984)

The relationships between the weight-average molecular weight M_w and the intrinsic viscosity $[\eta]$ of poly(2-vinylpyridine) [P2VP] in benzene and methyl alcohol at 25 °C, were investigated by the use of fractions with molecular weights ranging from 2.1×10^3 to 2.3×10^4. The exponent ν in the Mark-Houwink-Sakurada equation, $[\eta]=K_0M_w^{\nu}$, was 0.5 in both solvents when M_w was lower than about 10^4. A constant K_0 was approximately in accord with Flory's $K\theta$ value for ordinary high-molecular-weight P2VP, obtained earlier in respective solvents. By measuring $[\eta]$ for these low-molecular-weight fractions in several solvents at different temperatures, the temperature coefficients of an unperturbed dimension, $d\ln\bar{r}^2_0/dT$, of this polymer were estimated and averaged to be $-2.3\times10^{-3}\,K^{-1}$. These are quite different from the positive values calculated from the $K\theta$'s by Dondos *et al.* which were estimated using the extrapolation method for non-θ-solvents. Our results were further corroborated after adding a $K\theta$ value which was directly determined at another θ-state; *i.e.* in toluene at 63.7 °C, to that in benzene at 16.2 °C published earlier, which was found from phase-separation experiments in this work.

Extensive theoretical and experimental investigations regarding the temperature coefficient of the unperturbed dimension, $d\ln\bar{r}^2_0/dT$, have been made for linear polymers because they offer important information on the hindrance potential affecting rotation around bonds in the main chain.[1] The value of $d\ln\bar{r}^2_0/dT$ can be evaluated by measuring the stress-temperature coefficient for a cross-linked network,[2] or more directly by measuring the unperturbed mean-square end-to-end dimension,[3] $\bar{r}^2_0$, or the intrinsic viscosity,[4] $[\eta]_\theta$ in several θ-solvents with different θ-temperatures distributed within a certain temperature range. Naturally, the Stockmayer-Fixman plot, as an indirect method, is frequently used to evaluate $d\ln\bar{r}^2_0/dT$, for Flory's $K\theta$ values can be calculated from the $[\eta]$ values for different molecular-weight fractions in non-θ-solvents at several temperatures.[5,6] Flory *et al.* also proposed a method in which the temperature coefficient of $[\eta]$ of linear polymer is measured in athermal solvents.[7,8]

In general, it is often impossible to find the θ-solvent and/or θ-temperature for some polymers, since the elimination of the long-range interactions of a polymer in non-θ-solvent is troublesome, especially for polar polymers.[9] The method proposed by Bianchi *et al.* is effective in such cases.[9-11] According to them, the coil-expansion factor α, is essentially unity in many solvents when the molecular weight of the polymer is sufficiently low. Consequently, the temperature coefficient of the intrinsic viscosity of such low-molecular-weight fraction is equal to that of the unperturbed dimension. As for poly(2-vinylpyridine), P2VP, it is very difficult to determine a single component θ-solvent. Only values for benzene have been reported; 16.2 °C or 15 °C for this polymer.[12,13] Most of the reported values for the unperturbed dimension of P2VP were evaluated in non-θ-solvents and at very limited temperatures. In addition, even the sign of the temperature coefficients of the unperturbed dimension estimated from these literature values differs with each other.

The main purpose of this study was to determine the $d\ln\bar{r}^2_0/dT$ of P2VP according to the method of Bianchi *et al.* Moreover, the experimental evidence supporting the results was complementarily shown by the estimation of $d\ln\bar{r}^2_0/dT$ using the $K\theta$ values which were directly observed in θ-solvents, benzene and toluene. The latter was proved to be a θ-solvent at 63.7 °C.

Experimental

The monomer of 2-vinylpyridine was kindly supplied by Tokyo Yukigosei Co., and was distilled under a reduced pressure (bp 55 °C/15 Torr (1 Torr=133.322 Pa)) immediately before use. Polymerization was carried out either by the anionic method (Samples denoted below by BL and C) using butyllithium in tetrahydrofuran(THF) under a reduced pressure at −27 °C, or by the radical method (Samples denoted by A) with azobisisobutyronitrile in benzene at 50 °C. Fractionation of the polymer was carried out by the successive precipitation method using benzene and hexane as a solvent-precipitant pair, as outlined elsewhere.[14]

The phase separation was carried out in a thick glass capillary tube as described by Cowie *et al.*[15] After being measured with modified Ubbelohde-type dilution viscometers in a water bath (thermostatically controlled within ±0.01 °C), the intrinsic viscosity $[\eta]$ was calculated in dl/g with the Huggins plot.

Light scattering was carried out with a Fica 50 automatic light-scattering photometer with vertically polarized incident light of 436 nm. The vertically polarized component of the scattered light was measured for scattering angles of 30°—150° in methyl alcohol at 25 °C. The optical purification of each solution and solvent was achieved by filtration

† Present address: Technical Center, Bridgestone Co., Ogawahigashi-machi 2800-1, Kodaira 187.

Table 1. Light-scattering and viscosity data for poly(2-vinylpyridine) at 25 °C

Fraction	$M_w \times 10^{-3}$	$[\eta]$		dn/dc
		MeOH	Benzene	MeOH
BL6-2	22.9	0.170	0.111	0.263
BL6-3	13.1	0.117	0.089	0.262
BL6-4	9.4_6	0.099	0.075	—
BL6-5	7.4_9	0.086	0.065	0.261
BL6-6	5.4_6	0.074	0.057	—
BL6-7	4.9_5	0.073	0.055	0.262
BL6-8	3.5_5	0.057	0.043	—
BL6-9	2.1_0	0.043	0.039	0.259

through Millipore membrane filters "FG"(pore size: 0.2 μm). An antifluorescence filter of 436 nm was also used to remove the effect of the fluorescence which was confirmed not to be negligible. The weight-average molecular weight M_w was calculated using the double-extrapolation plots of Zimm.

The specific refractive-index increment dn/dc was measured in methyl alcohol at 25 °C with a Shimadzu DR-3 type refractometer.

Results and Discussion

Table 1 summarizes the $[\eta]$ results obtained in methyl alcohol and benzene and, also, those of M_w and dn/dc in methyl alcohol (all measured at 25 °C for the low-molecular-weight fractions of P2VP).

Concerning the molecular weight dependence of dn/dc, Kamata *et al.*[16] found considerable fluctuations for oligostyrene in an ethyl methyl ketone when the molecular weight was lower than 2000. As can be seen in Table 1, dn/dc for P2VP is essentially in accordance with each other for all the fractions measured in this study. Also, the average value of 0.262 is close to that of 0.270, reported for ordinary high-molecular-weight P2VP fractions in the same solvent.[17] Therefore, the value of 0.262 was used in the calculation of M_w from light-scattering data in this study.

In Figs. 1 and 2, the $[\eta]$'s for methyl alcohol and benzene are plotted against M_w, respectively. The points for the ordinary high-molecular-weight P2VP fractions (reported by one of the authors[12]) are represented by filled circles for comparison. As can be seen in both Figs., the points can be represented by two distinct straight lines. These are the so-called Mark-Houwink-Sakurada empirical equation:

$$[\eta] = KM_w^{\nu}, \quad (1)$$

where K and ν are constants. The point for the fraction BL6-2 in methyl alcohol, for example, is on the line for the higher molecular-weight fractions, however, the remaining points are on a different straight line. Using a least-squares method, the constants K_0 and ν of the lines for the lower-molecular-weight

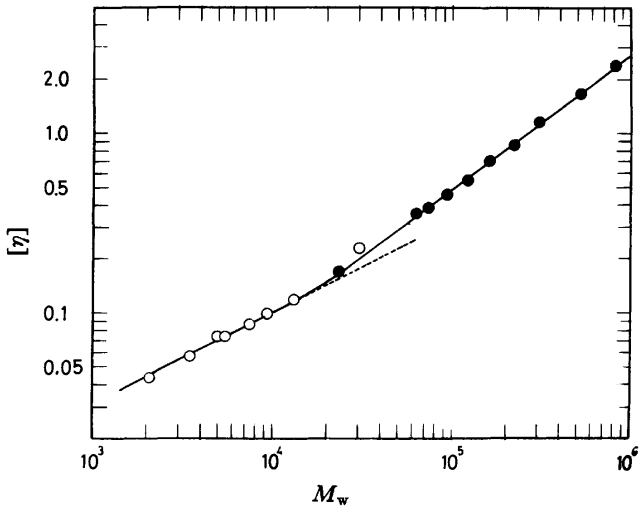

Fig. 1. Double logarithmic plot of $[\eta]$ against M_w for poly(2-vinylpyridine) in methyl alcohol at 25 °C. Filled circles represent the relationship obtained earlier.[12]

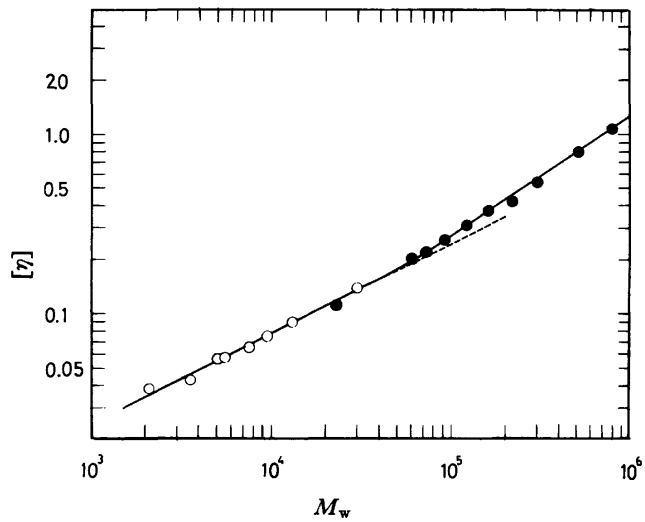

Fig. 2. Double logarithmic plot of $[\eta]$ against M_w for poly(2-vinylpyridine) in benzene at 25 °C. Filled circles represent the relationship obtained earlier.[12]

fractions were determined as follows:

$$[\eta] = 10.0 \times 10^{-4} M_w^{0.5} \quad \text{in methyl alcohol,} \quad (2)$$

$$[\eta] = 7.5 \times 10^{-4} M_w^{0.5} \quad \text{in benzene.} \quad (3)$$

The breaks for these two lines in Figs. 1 and 2 occur in the vicinity of $M_w \approx 1.5 \times 10^4$ in methyl alcohol, and 4×10^4 in benzene, respectively. The existence of such breaks has been reported for many polymers.[11,18-21] Hirai *et al.*[22] reported two distinct sections in $\log[\eta]$–$\log M_n$ plots for poly(4-vinylpyridine) fractions in *t*-butyl alcohol, methyl alcohol, and ethyl methyl ketone–isopropyl alcohol mixture (85:15 by wt.) at 30 °C, where M_n is the number-average molecular weight. They also found that the slope of the lines is 0.5 for all solvents in the region of molecular weight below 10^4.

According to Bianchi *et al.*,[10,11,23,24] when the molecular weight is sufficiently low, there is a molecular-weight range for many polymers where the expansion coefficient α is practically undistinguishable from unity. Hence, the K_0 constant of the Mark-Houwink-Sakurada equation in such a molecular-weight range is almost equal to K_θ, which is defined as follows:

$$[\eta]_\theta = K_\theta M^{1/2}, \tag{4}$$

$$K_\theta = \Phi_0(\bar{r}^2_0/M)^{3/2}. \tag{5}$$

Φ_0 is Flory's viscosity constant, and M is the polymer molecular weight. It is, therefore, interesting to compare the K_0 values in Eqs. 2 and 3 with K_θ reported in the literature for each corresponding P2VP-solvent system at 25 °C. In fact, the above-mentioned values of K_0=10.0×10^{-4} in methyl alcohol and 7.5×10^{-4} in benzene agreed fairly well with those of K_θ=9.3×10^{-4} and 7.9×10^{-4} in each solvent, derived from the Stockmayer-Fixman plot by one of the authors.[12]

From these results, it may be concluded that when the molecular weight of P2VP is lower than *ca.* 1×10^4 at least, the excluded volume effect can be considered negligible even in a very good solvent such as methyl alcohol. This was similarly reported for many other linear polymers. Thus, we can evaluate $d\ln\bar{r}^2_0/dT$ by measuring the temperature coefficient of $[\eta]$ in any solvent with a low molecular-weight fraction by means of the following equation:

$$d\ln \bar{r}^2_0/dT = (2/3)d\ln [\eta]/dT. \tag{6}$$

The intrinsic viscosities for P2VP fractions, BL6-7 (M_w=4.9$_5$×10^3) and Al-V (M_w=7.8$_7$×10^3) were measured in ethyl alcohol, chloroform, dioxane, THF, ethyl methyl ketone, and benzene in the temperature range of 14.9° to 60 °C. In Figs. 3 and 4, the $\ln[\eta]$ for the above two fractions was plotted against temperature, respectively. All plotted points fall on straight

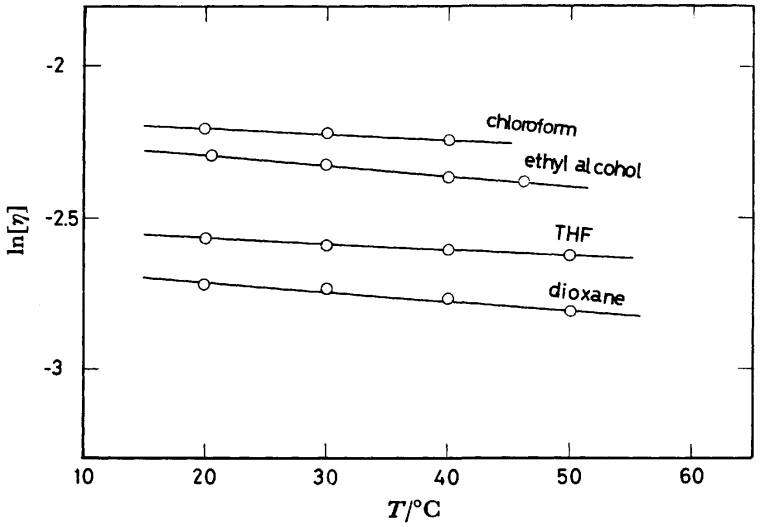

Fig. 3. Plots of $\ln[\eta]$ *vs.* temperature for poly(2-vinylpyridine) fraction A-1-V in various solvents.

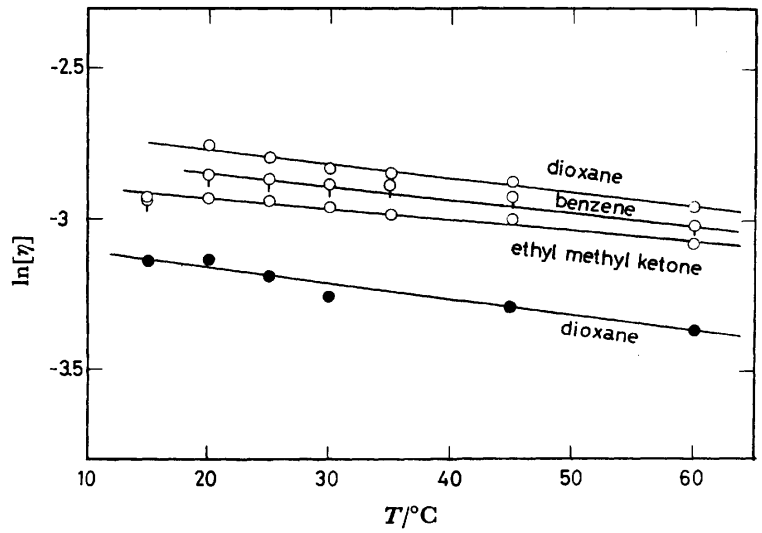

Fig. 4. Plots of $\ln[\eta]$ *vs.* temperature for poly(2-vinylpyridine) fractions BL6-7 (○) and BL6-9 (●) in various solvents.

Table 2. Temperature coefficient of unperturbed dimension of poly(2-vinylpyridine) estimated from intrinsic viscosity in various solvents

Fraction	$M_w \times 10^{-3}$	Solvent	$[d\ln \bar{r}^2_0/dT] \times 10^3$	
			This work	Lit,[25,26]
A-1-V	7.8_7	Ethyl alcohol	−2.4	0.6
A-1-V	7.8_7	Chloroform	−1.2	−0.2
A-1-V	7.8_7	Dioxane	−1.9	—
A-1-V	7.8_7	Tetrahydrofuran	−1.2	6.7
BL6-7	4.9_5	Dioxane	−3.0	—
BL6-7	4.9_5	Ethyl methyl ketone	−2.6	—
BL6-7	4.9_5	Benzene	−2.4	3.4
BL6-9	2.1_0	Dioxane	−3.4	—
—	—	Methyl alcohol	—	4.3
—	—	Isopropyl alcohol	—	2.6
—	—	Cyclohexanol	—	1.8

lines for each solvent except the one at 14.9 °C in benzene. This deviation may be explained by the fact that a temperature of 14.9 °C is slightly lower than the θ-temperature, 16.2 °C for the P2VP–benzene system.[12]

The temperature coefficients of $d\ln[\eta]/dT$ were analyzed by a least-squares method, and the values of $d\ln\bar{r}^2_0/dT$ were calculated according to Eq. 6 and are summarized in Table 2. As shown in the Table, the values of $d\ln\bar{r}^2_0/dT$ estimated in this study were explicitly negative for all solvents used and were averaged to be $-2.3(\pm 1.1)\times 10^{-3}$ K^{-1}. Concerning those of P2VP, there has been no value in the literature except for the data on K_θ obtained at only two or three different temperatures. Our estimated values of $d\ln\bar{r}^2_0/dT$ from such data on K_θ reported by Dondos *et al.*[13,25,26] are cited in the last column of Table 2. Though a practical estimation of these values is indeed a delicate problem, it is noted that even the signs of $d\ln\bar{r}^2_0/dT$ (for the latter) are reverse to those obtained in this work (except in chloroform). This may, perhaps, be due to the inevitable ambiguity in the K_θ values of Dondos *et al.*, which were indirectly determined in non-θ-solvents with an extrapolation method based on the two-parameter theory for dilute polymer solutions.

Strictly, it will be better, therefore, to estimate $d\ln\bar{r}^2_0/dT$ from the K_θ obtained for an ordinary high-molecular-weight polymer in more than two single θ-solvents with different θ-temperatures. One of us has reported that benzene is the θ-solvent for P2VP at 16.2 °C and that the value of K_θ directly deduced by measuring the viscosity at the state is 9.1×10^{-4} (after a correction due to the molecular-weight heterogeneity in samples)[12] is different from the above-quoted value indirectly determined at 25 °C. However, no other single θ-solvent has been reported. We did find in this investigation that toluene is expectative. As is well

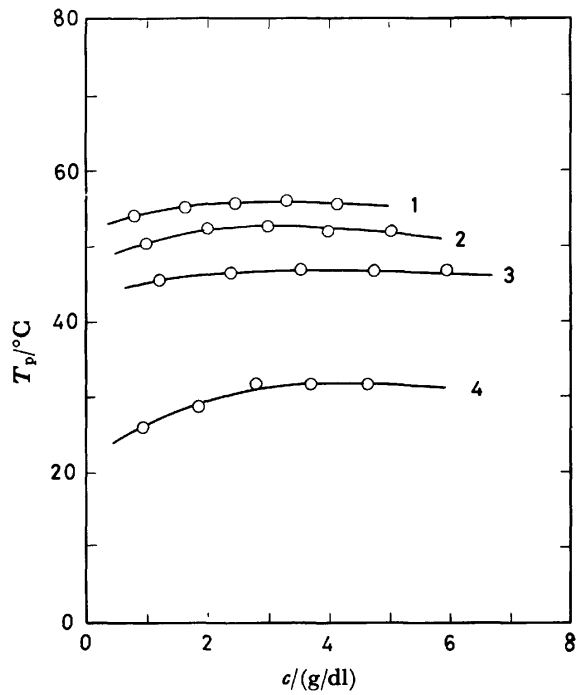

Fig. 5. Phase diagram for poly(2-vinylpyridine) fractions in toluene, whose weight-average molecular weights are respectively; 1: $50.0\cdot 10^4$, 2: $35.9\cdot 10^4$, 3: $12.1\cdot 10^4$, 4: $3.0\cdot 10^4$.

known, the unperturbed dimension of a linear polymer is often affected by the specific solvent effect, but benzene and toluene are homologous nonpolar solvents and the specific solvent effect on the unperturbed dimension of P2VP is considered to be the same and not so large. Hence, an estimation of $d\ln\bar{r}^2_0/dT$ from K_θ for these solvents will be useful.

The phase-separation experiments were, therefore, carried out for the P2VP–toluene system and the phase diagrams obtained are depicted in Fig. 5, where the numbers 1 and 2 denote the results for fractions BL21-1 and BL21-3 (in Table 3) and the other numbers, for fractions which were ionically polymerized at the same time (though not given in this Table). The reciprocal of the critical temperature, T_c^{-1}, was plotted in Fig. 6 against $M_w^{-1/2}$, according to the well known equation:[27]

$$1/T_c = (1/\theta)[1 + b/M_w^{1/2}], \quad (7)$$

where b is a constant and θ is the temperature at the theta state. The value of θ determined from the intercept of the line was 63.7 °C.

In Table 3, the M_w evaluated by light scattering in methyl alcohol at 25 °C and the $[\eta]$ in toluene at 63.7 °C for six fractions of P2VP, are summarized. In Fig. 7, $[\eta]$ is plotted against M_w on a double-logarithmic scale, from which the following equation was derived:

$$[\eta]_\theta = 7.54 \times 10^{-4} M_w^{0.5}. \quad (8)$$

The fact that the exponent of M_w is 0.5, indicates

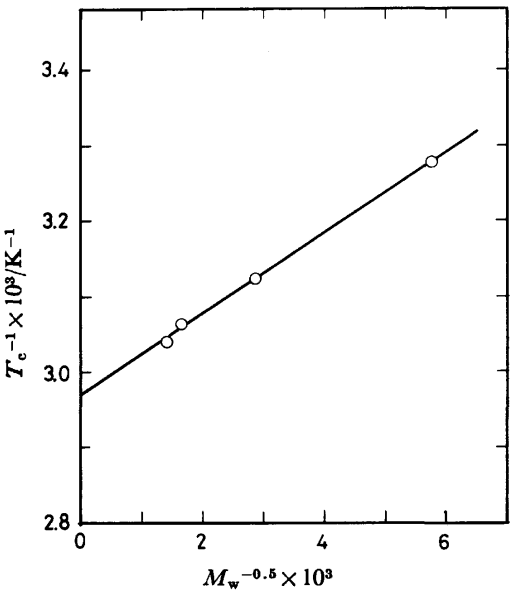

Fig. 6. Plot of reciprocal critical precipitation temperature of poly(2-vinylpyridine) in toluene, $1/T_c$, against $M_w^{-0.5}$.

Table 3. Light-scattering and viscosity data in toluene at 63.7 °C

Fraction	$M_w \times 10^{-4}$	M_w/M_n a)	$[\eta]_\theta$	$([\eta]_\theta/M_w^{0.5}) \times 10^4$
C-22	101.4	1.35	0.77	7.65
C-11	62.4	1.23	0.62	7.72
BL21-1	50.0	1.10	0.54	7.63
BL21-3	35.9	1.07	0.44	7.26
C-14	11.8	1.20	0.26	7.48
C-21	3.0	1.15	0.13	7.51
			(average)	7.54

a) Estimated by gel permeation chromatography.

that toluene is a θ-solvent at 63.7 °C for P2VP as predicted from the phase-separation method. Accordingly, the proportionality constant in the above equation was regarded as the K_θ for P2VP at 63.7 °C. The correct value of 7.66×10^{-4} was finally obtained by applying the polydispersity correction of molecular weight in the same manner as before,[12] using the M_w/M_n of each fraction (in Table 3). Here M_n was evaluated by GPC with the DMF solutions. As a result, the value of $d\ln\bar{r}^2_0/dT$ was estimated to be $-2.4(\pm1.0) \times 10^{-3}$ K^{-1} with the K_θ (both in benzene at 16.2 °C and in toluene at 63.7 °C) being expressed as in the following equation:

$$d\ln \bar{r}^2_0/dT = (2/3)d\ln K_\theta/dT. \quad (9)$$

This is almost the same as the average value, $-2.3(\pm1.1) \times 10^{-3}$ K^{-1}, obtained above from the temperature dependence of $[\eta]$ for low-molecular-weight P2VP fractions.

One more additional datum supporting the results obtained in this study was reported earlier by one of us[28]. The distinct negative temperature coefficient of K_θ for P2VP in ethyl alcohol (corresponding to $d\ln\bar{r}^2_0/dT = -2.1 \times 10^{-3}$ K^{-1}, estimated by the Stockmayer-Fixman plot for data of an intrinsic viscosity and molecular weight of ordinary high-molecular-weight P2VP fractions at temperatures from 10° to 65 °C) was noted. It agreed very closely with that of -2.4×10^{-3} K^{-1} presented here for the same solvent.

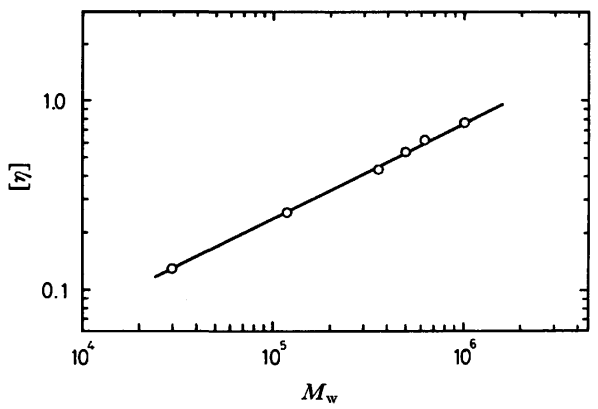

Fig. 7. Double logarithmic plot of $[\eta]_\theta$ against M_w for poly(2-vinylpyridine) in toluene at 63.7 °C.

Thus, we may conclude that the $d\ln\bar{r}^2_0/dT$ value for P2VP is negative, and its absolute value is considerably larger than those reported for many other polymers; *e.g.*, -0.17×10^{-3} K^{-1} for polyisobutylene,[9] -1×10^{-3} K^{-1} for polystyrene[10], $0.48(\pm0.3) \times 10^{-3}$ K^{-1} for poly(*p*-chlorostyrene).[4] However, the larger absolute values of $d\ln\bar{r}^2_0/dT$ have also been reported in the literature; *e.g.*, -24×10^{-3} K^{-1} for poly(ethylene oxide)[29] and $-4.7(\pm0.91) \times 10^{-3}$ K^{-1} for polystyrene.[3] A theoretical investigation of $d\ln\bar{r}^2_0/dT$ for P2VP has not yet been reported, but our results indicate that the extended conformation of P2VP must be associated with lower energies.

References

1) P. J. Flory, "Statistical Mechanics of Chain Molecules," Interscience, New York (1969).
2) P. J. Flory, C. A. J. Hoeve, and A. Ciferri, *J. Polym. Sci.*, **34**, 337 (1959).
3) A. Bazuaye and M. B. Huglin, *Polymer*, **20**, 44 (1979).
4) Y. Izumi and Y. Miyake, *Polym. J.*, **4**, 205 (1973).
5) G. Moraglio, G. Gianotti, and U. Bonicelli, *Eur. Polym. J.*, **9**, 623 (1973).
6) O. Quadrat and L. Mrkvicková, *Eur. Polym. J.*, **17**, 1155 (1981).
7) P. J. Flory, A. Ciferri, and R. Chiang, *J. Am. Chem. Soc.*, **83**, 1023 (1961).
8) J. E. Mark and P. J. Flory, *J. Am. Chem. Soc.*, **86**, 138 (1964).
9) U. Bianchi, E. Patrone, and M. Dalpiaz, *Makromol. Chem.*, **84**, 230 (1965).
10) E. Patron, C. Cuniberti, and U. Bianchi, *Makromol. Chem.*, **100**, 282 (1967).
11) U. Bianchi and A. Peterlin, *J. Polym. Sci., A-2*, **6**, 1759

(1968).
12) S. Arichi, *Bull. Chem. Soc. Jpn.*, **39**, 439 (1966).
13) A. Dondos, *Makromol. Chem.*, **135**, 181 (1970).
14) S. Arichi, M. Y. Pedram, and J. M. G. Cowie, *Eur. Polym. J.*, **15**, 107 (1979).
15) J. M. G. Cowie, A. Maconnachie, and R. J. Ranson, *Macromolecules*, **4**, 57 (1971).
16) T. Kamata, H. Nakahara, and S. Hattori, *Bull. Chem. Soc. Jpn.*, **50**, 2558 (1977).
17) S. Arichi, M. Yoshida, and Y. Ogawa, *Bull. Chem. Soc. Jpn.*, **48**, 1417 (1975).
18) E. T. Cohn-Ginsburg, T. G. Fox, and H. F. Mason, *Polymer*, **3**, 97 (1962).
19) B. J. Cottam, J. M. G. Cowie, and S. Bywater, *Makromol. Chem.*, **86**, 116 (1965).
20) T. Miyamoto and H. Inagaki, *J. Polym. Sci., Part A-2*, **7**, 963 (1969).
21) S. Arichi, M. Y. Pedram and J. M. G. Cowie, *Eur. Polym. J.*, **15**, 113 (1979).
22) Y. Hirai and T. Yanagida, *Bull. Chem. Soc. Jpn.*, **51**, 2421 (1978).
23) U. Bianchi, M. Dalpiaz, and E. Patrone, *Makromol. Chem.*, **80**, 112 (1964).
24) E. Patrone and U. Bianchi, *Makromol. Chem.*, **94**, 52 (1966).
25) A. Dondos and H. Benoit, *Makromol. Chem.*, **129**, 35 (1969).
26) A. Dondos and H. Benoit, *Macromolecules*, **4**, 279 (1971).
27) A. R. Shultz and P. J. Flory, *J. Am. Chem. Soc.*, **74**, 4760 (1952).
28) S. Arichi, *Bull. Chem. Soc. Jpn.*, **41**, 548 (1968).
29) T. C. Amu, *Polymer*, **23**, 1775 (1982).

Comparative Studies of Anionic Molecular Assemblies as Mediums for Electron Transfer Quenching of Excited Ru[(bpy)$_3$]$^{2+}$ by Cationic Quenchers

Hiroshi SHIOYAMA, Akihiro TAKAMI, and Noboru MATAGA*
Department of Chemistry, Faculty of Engineering Science, Osaka University, Toyonaka, Osaka 560
(Received November 5, 1984)

Behaviors of excited [Ru(bpy)$_3$]$^{2+}$ bound to anionic molecular assemblies such as polymer electrolytes, vesicles and micelles together with electron-acceptor quencher MV^{2+} have been investigated by measurements of [Ru(bpy)$_3$]$^{2+}$ luminescence quenching and radical yields in electron-transfer quenching using a dye laser photolysis apparatus. Quenching behavior characteristic to each molecular assembly has been observed. A remarkable enhancement of quenching was observed in the presence of poly(vinyl sulfate). Such an effect was observed also in sodium dihexadecyl phosphate solution though it is less pronounced. However, no such specific quenching behavior was observed in sodium dodecyl sulfate micellar solution.

The photochemical and photophysical properties of [Ru(bpy)$_3$]$^{2+}$ and related metal complexes are the subject under lively investigations from the viewpoint of solar energy conversion.[1] The electron-transfer and energy-transfer phenomena of these complexes in the excited state have been studied in some details both in bulk and heterogeneous systems.[2-4] In relation to the photoinduced electron transfer and excitation transfer in heterogeneous systems involving molecular assemblies, it is important to elucidate the nature of these systems as microenvironments on which those reaction processes take place. For example, luminescence quenching of ruthenium complex by Cu^{2+} and methylviologen cation (MV^{2+}) bound to anionic micelles was used as a probe to investigate the nature of the micelle as a microenvironment.[5]

However, our recent studies of excitation transfer among dye ions adsorbed on various molecular assemblies indicate clearly that the mode of excitation transfer and trapping is very characteristic to each kind of molecular assembly,[6,7] which seems to reflect the different adsorbed state of dyes characteristic to each molecular assembly. This result suggests the importance of the comparative studies of various molecular assemblies as mediums for photochemical reactions by using a common photochemical probe system. Along this line, we have examined the luminescence quenching reactions of excited [Ru(bpy)$_3$]$^{2+}$ due to electron transfer to MV^{2+} in solutions containing various anionic molecular assemblies such as polymer electrolyte, vesicles and micelles.

Results of these investigations shows very clearly the different microenvironmental characteristics of these molecular assemblies as the mediums for photochemical electron transfer reactions between cations.

Experimental

[Ru(bpy)$_3$]$^{2+}$ was synthesized according to the standard method[8] and was recrystallized several times from water. MV^{2+} (G. R. Grade, Tokyo Kasei) was purified by repeated recrystallization from methanol. Purified propylviologen sulfonate (PVS°) was kindly supplied by Dr. M. Furue of this University and used as received. *p*-Benzoquinone (BQ) was purified by recrystallization from ethanol and subsequent sublimation. $CuCl_2 \cdot 2H_2O$ (G. R. Grade, Nakarai) was used as received.

Sodium dodecyl sulfate (SDS) (S. U. Grade, Nakarai) and three kinds of polyelectrolyte; potassium poly(vinyl solfate) (PVSK) (G. R. Grade, Nakarai), poly(vinyl alcohol) (PVA) (E. P. Grade, Nakarai) and poly(methacrylic acid) sodium salt (PMAS) (Polysciences, Inc.) were used without further purification. Sodium dihexadecyl phosphate (NaDHP) was obtained by treating dihexadecyl hydrogen phosphate, which was synthesized according to Ref. 9, with NaOH in ethanol solution. To prepare the vesicle, NaDHP was sonicated in water at 60 °C for 30 min., using a sonifier set (Branson, model 185).

Water was purified by distillation with a nonboiling type distillation apparatus. All solutions for measurements were deoxygenated by flushing with N_2 gas for at least 20 min. All measurements were carried out at room temperature.

Spectra and relative yields of [Ru(bpy)$_3$]$^{2+}$ emission were measured with an Aminco-Bowman spectrophotofluorometer. Radical yields in electron-transfer quenching of excited [Ru(bpy)$_3$]$^{2+}$ were measured by using a dye laser photolysis apparatus:[10] the lasing dye was Coumarin 503 (Phase-R Company), whose lasing wavelength, output power and fwhm were 498 nm, 35 mJ and 250 ns, respectively. The luminescence decay curves were determined by exciting the sample with the second harmonic of a mode locked Nd^{3+}:YAG laser and by observing the decay curve with a highspeed microchannel plate photomultiplier (HTV R-1194UX)-fast storage oscilloscope (Tektronix 7834) combination.

Results and Discussion

Luminescence Quenching of [Ru(bpy)$_3$]$^{2+}$ in Molecular Assemblies. It is well-known that the luminescence of [Ru(bpy)$_3$]$^{2+}$ (λ_{max}=610 nm, τ_0=650 ns) is quenched by MV^{2+} with a quenching rate constant of

$k_q \approx 5\times10^8\ M^{-1}\ s^{-1}$ (1 M=1 mol dm^{-3}) in water with a controlled ionic strength. However, when 0.01 M (in monomer unit) of PVSK was added to solution, a peculiar curves with a lump as shown in Figure 1 was obtained instead of the simple Stern-Volmer straight line. I_0/I shows a peak at 1.5×10^{-3} M of MV^{2+} where 98% of the $[Ru(bpy)_3]^{2+}$ emission is quenched, and the luminescence is restored with further addition of the quencher. When MV^{2+} concentration is higher than 5×10^{-3} M, the quenching is very similar to that in bulk solution.

Above results can be explained in terms of a limited capability of the anionic molecular assembly to adsorb cations. All $[Ru(bpy)_3]^{2+}$ cations may be adsorbed on PVSK when MV^{2+} concentration is low. Under these conditions, because both $[Ru(bpy)_3]^{2+}$ and MV^{2+} are concentrated by adsorption on PVSK, the luminescence is effectively quenched. With increase of the MV^{2+} concentration, all adsorption sites may be occupied by $[Ru(bpy)_3]^{2+}$ and MV^{2+}. With further increase of MV^{2+}, $[Ru(bpy)_3]^{2+}$ seems to be expelled into bulk solutions. Eventually, almost all of $[Ru(bpy)_3]^{2+}$ ions appear to be removed from the vicinity of PVSK, where the concentration of MV^{2+} is very high. The expelled $[Ru(bpy)_3]^{2+}$ ions undergo simple Stern-Volmer type of luminescence quenching quite similar to that in bulk solution.

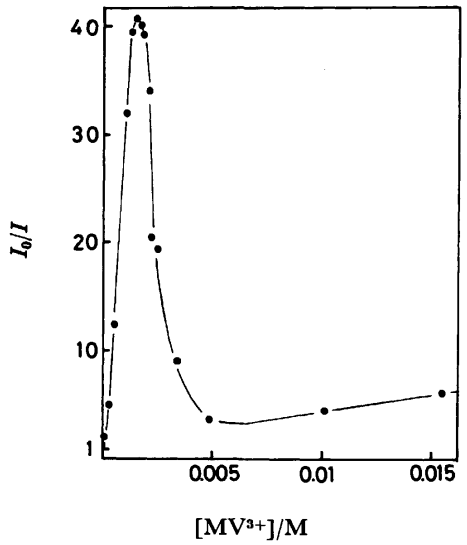

Fig. 1. $(I_0/I)\sim$[quencher] relation for the luminescence quenching of $[Ru(pby)_3]^{2+}$–MV^{2+} system in aqueous solution containing PVSK.
$[[Ru(bpy)_3]^{2+}]=6\times10^{-5}$ M. [PVSK]$=1\times10^{-2}$ M (in monomer unit)

We have examined the effect of PVSK concentration as indicated in Table 1. The MV^{2+} concentration that gives the peak value of I_0/I is proportional to the concentration of PVSK. This result suggests that PVSK is able to bind MV^{2+} at a ratio of *ca.* one MV^{2+} for 6 monomer units of PVSK. Another cationic quencher Cu^{2+} also causes the similar effect, but the extent of the quenching (the peak value of I_0/I) in this case is much smaller. The neutral quencher BQ or PVS°, however, does not give such a peculiar quenching. Moreover, when the anionic PVSK is replaced by neutral PVA, the lump in I_0/I *vs.* [quencher] relation disappears. After the completion of the present work we found similar report[11] on $[Ru(bpy)_3]^{2+}$–Cu^{2+}–PVSK system. However, the object of the present work is the comparative studies of various anionic molecular assemblies as microenvironment for the photochemical electron transfer quenching reaction between adsorbed cations. For this purpose, MV^{2+} which shows far greater quenching ability than Cu^{2+} in the ad-

Table 1. Peak value $(I_0/I)_{peak}$ of the lump in I_0/I *vs.* $[MV^{2+}]$ relation as a function of added PVSK concentration

[PVSK]/M	$[Ru(bpy)_3]^{2+}$/M	$[MV^{2+}]$ which gives $(I_0/I)_{peak}$/M	$(I_0/I)_{peak}$
1×10^{-3}	6×10^{-5}	1.5×10^{-4}	≈40
5×10^{-3}	6×10^{-5}	7×10^{-4}	≈50
1×10^{-2}	6×10^{-5}	1.5×10^{-3}	≈40
1×10^{-2}	3×10^{-5}	1.5×10^{-3}	≈55

Table 2. Results for various molecular assembly-quencher systems

Molecular assembly	[molecular assembly]/M[a]	Quencher	[quencher] which gives $(I_0/I)_{peak}$/M	$(I_0/I)_{peak}$
PVSK	1×10^{-2}	MV^{2+}	1.5×10^{-3}	≈40
PVSK	1×10^{-2}	Cu^{2+}	2.2×10^{-3}	≈10
PVSK	1×10^{-2}	BQ	— [b]	—
PVSK	1×10^{-2}	PVS°	— [b]	—
PVA	1×10^{-2}	MV^{2+}	— [b]	—
PMAS	2×10^{-3}	MV^{2+}	2.5×10^{-5}	≈1.4
SDS	8×10^{-2}	MV^{2+}	— [b]	—
NaDHP	2.6×10^{-4}	MV^{2+}	3.4×10^{-5}	≈3
NaDHP	1.3×10^{-3}	MV^{2+}	4.1×10^{-4}	≈5

a) Concentrations are given in monomer unit. b) No lump was observed in I_0/I *vs.* [quencher] plot.

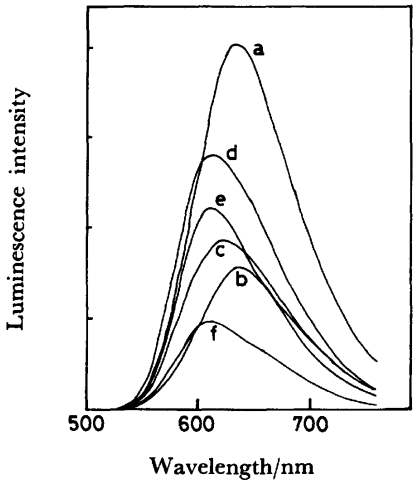

Fig. 2. Effect of the addition of MV^{2+} upon the luminescence spectrum of $[Ru(bpy)_3]^{2+}$ in aqueous solution containing NaDHP.
[NaDHP]$=2.6\times10^{-4}$ M.
[MV^{2+}]: a; 0, b; 1.0×10^{-5}, c; 6.1×10^{-5}, d; 1.3×10^{-4}, e; 5.4×10^{-3}, f; 1.1×10^{-2} M.

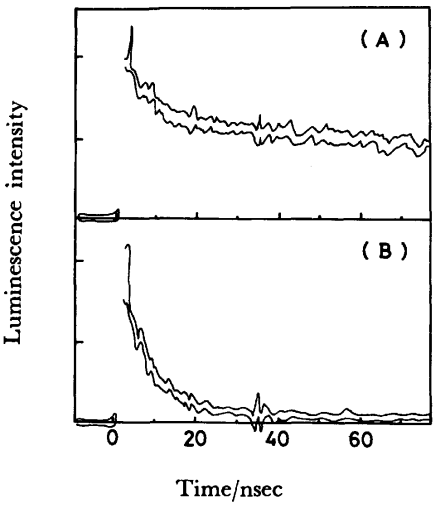

Fig. 3. Decay curves of $[Ru(bpy)_3]^{2+}$ emission in aqueous solution containing PVSK.
$[[Ru(bpy)_3]^{2+}]=6\times10^{-5}$ M. [PVSK]$=1\times10^{-2}$ M (in monomer unit). [MV^{2+}]: A; 4×10^{-3}, B; 2×10^{-3} M.

sorbed state is much better system.

Above experimental results are summarized in Table 2, which suggests that the electrostatic force plays an important role for the adsorption of $[Ru(bpy)_3]^{2+}$ and MV^{2+} onto the molecular assemblies. Table 2 also indicates that each anionic molecular assembly shows characteristic behavior in the adsorption of cations. Not only the MV^{2+} concentration at $(I_0/I)_{peak}$ but also the luminescence quenching itself is characteristic to each kind of molecular assembly. Moreover, SDS micellar solution does not show such a peculiar behavior in luminescence quenching as observed in PVSK solution in the present experimental conditions. However, it should be noted here that there is some kind of specific interaction between SDS micelle and $[Ru(bpy)_3]^{2+}$ because a slight broadening of the absorption spectrum and a bathochromic shift of *ca.* 20 nm of the luminescence spectrum occurs by adsorption. We have observed similar spectral shift also in the case of NaDHP vesicle solution. As shown in Figure 2, the emission maximum of $[Ru(bpy)_3]^{2+}$ without MV^{2+} or with low concentration MV^{2+} lies at *ca.* 630 nm, in which case $[Ru(bpy)_3]^{2+}$ is supposed to be adsorbed on the NaDHP vesicle.

By adding more MV^{2+}, the emission intensity is a little recovered and the peak wavelength becomes the same as in pure water solution. Further increase of MV^{2+} concentration results in the simple Stern-Volmer type quenching in bulk solution. Contrary to these spectral shifts in SDS and NaDHP solutions which indicate more or less specific interaction between $[Ru(bpy)_3]^{2+}$ and detergent molecules, no such shift caused by adsorption was observed in the case of PVSK solution, where, although the adsorption due to electrostatic attraction is the strongest among the molecular assemblies used here, the environmental state for $[Ru(bpy)_3]^{2+}$ is very close to that in pure aqueous solution.

Emission Decay Curve. Figure 3 shows that the emission of $[Ru(bpy)_3]^{2+}$ -MV^{2+} system in PVSK solution does not show single exponential decay; the decay curves are composed of at least two components. The fast decay component corresponds to the quenching of excited $[Ru(bpy)_3]^{2+}$ on PVSK chain by the MV^{2+} which is also adsorbed on PVSK chain in the vicinity of the quencher. The slow one corresponds to the decay of $[Ru(bpy)_3]^{2+}$ in the bulk. The intensity of the slow component emission of sample A is higher than that of sample B, since the large part of $[Ru(bpy)_3]^{2+}$ of the former is expelled into bulk.

Laser Photolysis Experiments. In Table 3, the absorbances of transient MV^+ radical obtained with a dye laser photolysis system are listed. In simple aqueous solution, the absorbance of the transient radical observed in the samples with different quencher concentrations was proportional to the degree of quenching. This is in agreement with the result in our previous report.[10]

In the case of PVSK solution, however, the radical formation is strongly suppressed at the MV^{2+} concentration of 1.5×10^{-3} M, where I_0/I shows the peak of lump. In general, the radical yield is determined by the competition between the dissociation into free radicals and deactivation by back electron transfer in the geminate radical pair formed by the photoinduced electron transfer. When both radical ions are bound to PVSK in close proximity to each other, the back electron transfer will dominate in

TABLE 3. TRANSIENT ABSORBANCE OF MV^+ GENERATED BY AN ELECTRON TRANSFER FROM EXCITED $[Ru(bpy)_3]^{2+}$ TO MV^{2+}

Solvent	$[MV^{2+}]$/M	Degree of quenching /%	Transient absorbance of MV^+ observed at 603 nm
H_2O	0.0015	22	0.064
H_2O	0.007	66	0.177
H_2O	0.012	78	0.216
H_2O with 0.01 M PVSK	0.0015	98	0.026
H_2O with 0.01 M PVSK	0.007	71	0.076
H_2O with 0.01 M PVSK	0.012	80	0.150

TABLE 4. CHANGE OF $(I_0/I)_{peak}$ VALUE AND $[MV^{2+}]$ WHICH GIVES $(I_0/I)_{peak}$ DEPENDING UPON THE IONIC STRENGTH OF SOLUTION[a)]

Ionic strength	$(I_0/I)_{peak}$	$[MV^{2+}]$ which gives $(I_0/I)_{peak}$ /M
0.0045	40	0.0015
0.01	25	0.0013
0.023	9.5	0.0010
0.045	4.5	0.0009

a) In each measurement of $(I_0/I)_{peak}$, the ionic strength was kept constant by adjusting the NaCl concentration.

the pair leading to a very small free radical yield. With increase of MV^{2+} concentration, $[Ru(bpy)_3]^{2+}$ may be expelled into bulk solutions, where the free radical yield is considerably higher than in adsorbed state. We have observed analogous effect of adsorption upon free radical yield also in the case of NaDHP solution.

Effect of the Addition of Salt upon the Luminescence Quenching Behavior in PVSK Solution. In order to examine in a more detail the adsoprtion on molecular assembly and the luminescence quenching behaviors of $[Ru(bpy)_3]^{2+}$–MV^{2+} system, we have investigated the effect of addition of NaCl on the luminescence of PVSK solution. The results are summarized in Table 4, which shows that the MV^{2+} concentration that gives $(I_0/I)_{peak}$ and the $(I_0/I)_{peak}$ value itself decrease with increase of the ionic strength of the solution. This result means that, when NaCl is added into the solution, Na^+ may be attracted to the polymer electrolyte, shielding its electrostatic fields and preventing adsorption of $[Ru(bpy)_3]^{2+}$ and MV^{2+} on polymer electrolyte.

Concluding Remarks. In the present work, we have demonstrated the luminescence-quenching behaviors of $[Ru(bpy)_3]^{2+}$–MV^{2+} system adsorbed on anionic molecular assemblies. The remarkable enhancement of quenching observed when both $[Ru(bpy)_3]^{2+}$ and quencher cations are adsorbed on anionic moelcular assembly was the largest in PVSK solution. Such effect was observed also in NaDHP vesicle solution though it is less pronounced compared with PVSK solution. However, no such specific quenching behavior was observed in SDS micellar soluton. These results show clearly the difference among these anionic molecular assemblies in the capability to keep $[Ru(bpy)_3]^{2+}$-cationinc quencher pair in sufficiently close proximity to undergo photoinduced electron transfer. In this respect, SDS micelle seems to have the most disordered structure among these three molecular assemblies, which can be concluded also from several other experimental results.[6,7,12,13]

The present work was partly supported by the Grant-in-Aid from the Japanese Ministry of Education, Science and Culture to NM (58045097).

References

1) See for example, M. Grätzel, *Acc. Chem. Res.*, **14**, 376 (1981).
2) W. H. Elfring, Jr. and G. A. Crosby, *J. Am. Chem. Soc.*, **103**, 2683 (1981).
3) R. Ballardini, G. Varani, M. T. Indelli, F. Scandola, and V. Balzani, *J. Am. Chem. Soc.*, **100**, 7218 (1978).
4) K. Mandal, T. D. L. Pearson, W. P. Krug, and J. N. Demas, *J. Am. Chem. Soc.*, **105**, 701 (1983).
5) T. K. Foreman, W. M. Sobol, and D. G. Whitten, *J. Am. Chem. Soc.*, **103**, 5333 (1981); J. B. S. Bonilha, T. K. Foreman, and D. G. Whitten, *ibid.* **104**, 4215 (1982).
6) S. Takaya, N. Ikeda, and N. Mataga, to be submitted for publication.
7) N. Tamai, A. Mizuma, I. Yamasaki, and N. Mataga, to be submitted for publication.
8) I. Fujita and H. Kobayashi, *Ber. Bunsenges. Phys. Chem.*, **76**, 115 (1982).
9) T. Kunitake and Y. Okahata, *Bull. Chem. Soc. Jpn.*, **51**, 1877 (1978).
10) H. Shioyama, H. Masuhara, and N. Mataga, *Chem. Phys. Lett.*, **88**, 161 (1982).
11) D. Meisel and M. S. Matheson, *J. Am. Chem. Soc.*, **99**, 6577 (1977).
12) Y. Waka, K. Hamamoto, and N. Mataga, *Photochem. Photobiol.*, **32**, 27 (1980).
13) Y. Waka, N. Mataga, and F. Tanaka, *Photochem. Photobiol.*, **32**, 335 (1980).

Formation Constants of Cyclodextrin Inclusion Complexes with Iodine in Aqueous Solutions

Isao SANEMASA,* Toyohisa KOBAYASHI, and Toshio DEGUCHI
Department of Chemistry, Faculty of Science, Kumamoto University, Kurokami 2-39-1, Kumamoto 860
(Received May 28, 1984)

Formation constants of cyclodextrin (CyD) inclusion complexes with iodine were determined by measuring solubilities of iodine vapor in water. The formation constants at 25 °C are 8.3×10^3 (α-CyD), 1.0×10^2 (β-CyD), and 13 $dm^3\,mol^{-1}$ (γ-CyD). The temperature dependence of α-CyD–I_2 complexation was studied. ΔH and ΔS, being 9.52 kJ mol^{-1} and 107 J K^{-1} mol^{-1} at 25 °C, respectively, are both largely dependent on temperature even within a rather small temperature range 15—35 °C studied. For the complexation with α-CyD, contribution of dehydration of iodine was estimated. The method proposed here is useful to study the formation of CyD association complexes with such substrates as are slightly soluble in water and easily vaporize from the aqueous phase.

The complex formation of cyclodextrin (CyD) with iodine has been studied with a view to understanding the far more complicated starch systems.[1,2] The molecular geometry of α-CyD–I_2 inclusion crystals has been determined by X-ray analysis as follows:[3] (a) The iodine molecule is coaxial with the host molecule, (b) one iodine atom of I_2 is situated near the opening on the primary alcohol side with a van der Waals contact with the cavity and the other is surrounded by six O(4) atoms with a contact greater than the van der Waals contact, and (c) the cavity is deep enough to enclose the whole iodine molecule. An iodine molecule can thus be suitably fitted with the α-CyD cavity. This may be responsible for giving the formation constant as large as 9.35×10^4 $dm^3\,mol^{-1}$ at 24 °C, the only data available so far in the literature.[2]

In our preceding paper[4] we reported a method of preparing an aqueous iodine solution saturated with its vapor. An important characteristic of this method is that the equilibrium solubility of iodine at a desired concentration can be obtained by adjusting the temperature of a solid iodine which is held separately isolated in space from an aqueous phase. The method seems to be suitable for studying possible interactions between iodine and a particular substance in an aqueous medium.

Here we have applied the method to aqueous CyD solutions. The equilibrium solubility of iodine vapor is increased by the presence of α-, β-, or γ-CyD, from which formation constants of inclusion complexes can be determined.

Experimental

Materials. Solid iodine of analytical reagent grade and cyclodextrins (α-, β-, and γ-CyD form Nakarai Chemicals) of guaranteed grade were used without further purification. A suitable amount of CyD, which had been dried over phosphorus pentaoxide, was weighed and dissolved in 1.0×10^{-3} mol dm^{-3} $HClO_4$ to prepare a CyD solution of known concentration. Perchloric acid was used instead of pure water to prevent hydrolysis of iodine.

Apparatus and Procedures. The apparatus used for preparing aqueous iodine solutions saturated with iodine vapor was essentially the same as that previously reported.[4] A 50 cm^3 aqueous CyD solution was placed in a separation funnel designated as the "solubility flask," and iodine crystals were packed in a column (ϕ 8 mm×200 mm) designated as the "solute reservoir." The temperatures of the solubility flask and the solute reservoir were held constant with water flows from separate thermostated baths circulating through their surrounding jackets. The assembled apparatus was placed in a chamber, where the temperature was kept higher than that of the solute reservoir. The iodine vapor, generated by a flow of air through the solute reservoir, was introduced into the solubility flask *via* a sintered glass ball and circulated by means of a Viton diaphragm air-pump. The circulation rate was set at 0.8 $dm^3\,min^{-1}$. At this rate, concentrations of iodine in CyD solutions had been found in advance to reach constant values after 60 min aeration. After attainment of solubility equilibrium, 10 cm^3 samples were withdrawn and the iodine concentrations were determined by solvent extraction-spectrophotometry at 514 nm. The solvent extraction was repeated twice for the same sample solution with a successive addition of 20 cm^3 of CCl_4.

Results and Discussion

Equilibrium Solubilities of Iodine Vapor in the Presence and Absence of Cyclodextrins. Solubility runs were made under the condition that the temperature of the solute reservoir was lower than that of the solubility flask, with the latter maintained constant. The vapor pressure of iodine at a given temperature of the solute reservoir was estimated from the equation, derived based on Ref. 5, $\log PT^{3/2}=16.945-3464/T$, where P is the vapor pressure in Pa and T is absolute temperature. At first, equilibrium solubilities were measured in the absence of CyD, and Henry's law constant, K_H, at each temperature of the aqueous phase was determined from the equation $K_H=P/X_2$, where X_2 is the mole fraction of dissolved iodine. The results are shown in Table 1, in which the K_H value obtained in iodic acid solution is also given since the use of HIO_3 was recommended in view of protecting iodine in aqueous medium from reduction.[2] If the reduction of iodine does occur in $HClO_4$ solution, an increase in

TABLE 1. HENRY'S LAW CONSTANTS OF IODINE VAPOR IN $HClO_4$ SOLUTIONS[a]

Temperature of aqueous phase / °C	Henry's law constant[b] / 10^6 Pa	ΔG_{dehyd}[c] / kJ mol^{-1}
15.00	1.08±0.04 (0.995)	−5.67
20.00	1.36±0.02 (0.999)	−6.33
25.00	1.81±0.03 (0.999)	−7.15
	1.72±0.02 (0.999)[d]	
30.00	2.32±0.02 (0.999)	−7.89
35.00	3.01±0.02 (0.999)	−8.69

a) The concentration of $HClO_4$ is 1.0×10^{-3} mol dm^{-3}. b) In parentheses are indicated the correlation coefficients derived from $K_H = P/X_2$. c) Estimated from K_H in atom units by using $\Delta G_{dehyd} = -RT \ln K_H$, where "dehyd" refers to the dehydration of iodine dissolved in the aqueous phase. ΔH_{dehyd} and ΔS_{dehyd} are estimated to be 38.2 kJ mol^{-1} and 152 J K^{-1} mol^{-1}, respectively, in the temperature range studied. d) Obtained in HIO_3 solutions of 0.20 mol dm^{-3}.

the apparent solubility of iodine would be expected from the equilibrium $I^- + I_2 \rightleftarrows I_3^-$. Yet, as seen from Table 1, the K_H value observed in HIO_3 solution is rather small compared with that in $HClO_4$ at the same temperature of the aqueous phase. There was observed an increase by *ca.* 5% in the solubility of iodine in iodic acid medium of 0.2 mol dm^{-3} relative to that in perchloric acid of 1.0×10^{-3} mol dm^{-3}. The reason for this is not clear, but some interaction between IO_3^- and I_2 may be responsible.

Equilibrium solubilities of iodine vapor were measured in α-, β-, or γ-CyD solutions and the results expressed as S_{obsd} are shown in Table 2, where are also listed the equilibrium solubilities in the absence of CyD, expressed as S_o.

Iodine molecules dissolved in a CyD solution are equilibrated with CyD molecules to form associated complex(es), while those in the free form are equilibrated with iodine vapor in the gaseous phase. If it is assumed that the solubility of *free* iodine is little affected by the presence of CyD in the aqueous medium, the S_o value at a given temperature of the aqueous phase can be estimated from Henry's law constant provided the temperature of solid iodine is known.

Estimation of Formation Constants. α-CyD is reported to from a 1:1 complex with iodine,[1] but there are no experimental data concerning the stoichiometry of β- and γ-CyD complexes. We have measured absorption spectra of iodine in CyD solutions of various concentrations; A clear isosbestic point was observed at 460 nm for α-CyD and a hardly recognizable one near 460 nm for β-CyD, but for γ-CyD the spectra appeared too closely superimposed to reveal any isosbestic point.

It may be valid to assume that, at the most, one CyD molecule is able to accept two iodine molecules, since even with γ-CyD the cavity is not large enough to receive more than three iodine molecules. Complex formation can then be written as

$$CyD + I_2 \rightleftharpoons CyD\cdot I_2, \quad K_1, \tag{1}$$

$$CyD\cdot I_2 + I_2 \rightleftharpoons CyD\cdot (I_2)_2, \quad K_2, \tag{2}$$

where K_1 and K_2 are stepwise formation constants. The total concentration of iodine present in the aqueous phase, C_{I_2}, and the total concentration of CyD, C_{CyD}, are expressed as

$$C_{I_2} = [I_2] + [CyD\cdot I_2] + 2[CyD\cdot (I_2)_2]$$
$$= [I_2](1 + K_1[CyD] + 2K_1K_2[CyD][I_2]), \tag{3}$$

$$C_{CyD} = [CyD] + [CyD\cdot I_2] + [CyD\cdot (I_2)_2]$$
$$= [CyD](1 + K_1[I_2] + K_1K_2[I_2]^2), \tag{4}$$

where $[I_2]$ and $[CyD]$ denote free concentrations of I_2 and CyD, respectively. Here, $[I_2]$ and C_{I_2} are equal to S_o and S_{obsd}, respectively. Combining Eqs. 3 and 4, we have

$$(S_{obsd} - S_o)/C_{CyD} = K_1S_o(1 + 2K_2S_o)/\{1 + K_1S_o(1 + K_2S_o)\}. \tag{5}$$

Suppose, as a first approximation, $1 + 2K_2S_o \approx 1 + K_2S_o$, that is, the product K_2S_o is small compared with unity, and Eq. 5 becomes

$$(S_{obsd} - S_o)/S_o(C_{CyD} - S_{obsd} + S_o) = K_1 + nK_1K_2S_o, \tag{6}$$

where n takes the value of 1 or 2. It can be seen from Table 2 that for a particular type of CyD the left-hand side of Eq. 6 is almost constant independently of S_o at a given temperature of the aqueous phase. This means that the K_2 term need not be considered, *i.e.*, α-, β-, and γ-CyD form 1:1 complexes with iodine.

The formation constants K_f ($=K_1$)$=[CyD\cdot I_2]/([CyD][I_2])$ are summarized in Table 3. The K_f value obtained for α-CyD at 25 °C in 0.20 mol dm^{-3} HIO_3 solution is in good agreement with the literature value included in Table 3 despite different experimental approaches employed in these two studies. The reason that the K_f value observed in $HClO_4$ solution is somewhat smaller than that in HIO_3 is not clear at present, but may be due to an inhibition effect of perchloric acid. It is agreed that $HClO_4$ can enter the α-CyD cavity, the formation constant being reported to be 40 dm^3 mol^{-1}.[6]

It can be seen from Table 3 that the formation constant of the complex with iodine decreases drastically on going from α- to γ-CyD. This is probably due to the size of the CyD cavity; β- and γ-CyD, especially the latter, have too large cavities to accommodate an iodine molecule tightly.

Thermodynamic Considerations of α-Cyclodextrin Complexation with Iodine. A striking feature of complex formation of α-CyD with iodine is the

temperature dependence of the formation constant. Table 3 shows that with rising temperature the K_f value increases at first, and then decreases. The thermodynamic parameters of the complexation were estimated from the temperature dependence of K_f with the aid of the equations $\Delta G=-RT \ln K_f=\Delta H-T\Delta S$ and $dH/dT=\Delta C_p=A+BT$, where ΔC_p is the heat capacity change, A and B are constants, and the other symbols have their usual meanings. We can express K_f as a function of T as

$$\ln K_f = (A/B) \ln T + (B/2R)T - (C/R)T^{-1} + C' - A/R, \quad (7)$$

where C and C' are integration constants. The data shown in Table 3 are best fitted by the equation

$$\ln K_f = 140.0 \ln T - 1.441\ T - 87500\ T^{-1} - 65.60. \quad (8)$$

The result is shown in Fig. 1 by a solid curve. The ΔH and ΔC_p are expressed, respectively, by $\Delta H=87500\ R+140.0\ RT-1.441\ RT^2$ and $\Delta C_p=140.0\ R-2.882\ RT$. The thermodynamic parameters thus estimated for the α-CyD-I_2 complex are summarized in Table 3. It is noteworthy that ΔH and ΔS values are both strongly temperature dependent, changing from positive to negative.

A large number of ΔH and ΔS data concerning CyD

Table 2. Solubilities of iodine vapor in the presence of cyclodextrins

Temperature of aqueous phase/°C	Temperature of solid iodine/°C	Vapor pressure of iodine/Pa	C_{CyD}[a] / 10^{-3} mol dm^{-3}	Solubility of iodine / 10^{-3} mol dm^{-3}		K_f[d] / dm^3 mol^{-1}
				S_o[b]	S_{obsd}[c]	
α-Cyclodextrin in 1.0×10^{-3} mol dm^{-3} $HClO_4$ solutions						
15.00	10.17	10.97	0.9786	0.564	1.24	3.96×10^3
15.00	10.85	11.69	1.141	0.601	1.43	4.42×10^3
15.00	14.49	16.36	1.005	0.842	1.67	5.56×10^3
20.00	9.90	10.70	1.137	0.438	1.31	7.51×10^3
20.00	12.35	13.44	1.073	0.550	1.39	6.55×10^3
20.00	15.36	17.71	1.026	0.724	1.60	8.07×10^3
20.00	19.38	25.36	1.011	1.04	1.94	7.80×10^3
25.00	10.31	11.11	0.9971	0.340	1.09	8.93×10^3
25.00	14.89	16.97	1.005	0.519	1.35	9.20×10^3
25.00	17.96	22.36	1.040	0.684	1.56	7.80×10^3
25.00	19.43	25.47	1.053	0.779	1.69	8.24×10^3
25.00	19.43	25.47	1.527	0.779	2.10	8.24×10^3
25.00	19.50	25.63	1.217	0.784	1.83	7.80×10^3
25.00	23.67	36.80	1.059	1.13	2.08	7.71×10^3
30.00	19.93	26.61	1.040	0.636	1.50	7.72×10^3
30.00	23.48	36.05	1.024	0.861	1.75	7.65×10^3
30.00	28.30	54.32	1.001	1.30	2.20	6.85×10^3
35.00	10.12	10.91	1.005	0.201	0.813	7.75×10^3
35.00	18.58	23.63	1.046	0.436	1.21	6.53×10^3
35.00	24.40	39.16	1.001	0.723	1.54	6.14×10^3
35.00	29.65	60.71	1.201	1.12	2.17	6.21×10^3
α-Cyclodextrin in 0.20 mol dm^{-3} HIO_3 solutions						
25.00	14.75	16.75	1.071	0.540	1.45	1.05×10^4
25.00	17.99	22.42	1.065	0.723	1.64	8.57×10^3
25.00	21.88	31.54	1.036	1.02	1.96	9.60×10^3
β-Cyclodextrin in 1.0×10^{-3} mol dm^{-3} $HClO_4$ solutions						
25.00	10.40	11.21	1.454	0.343	0.386	88.8
25.00	16.28	19.24	1.827	0.589	0.700	110
25.00	19.30	25.18	2.007	0.771	0.900	89.1
γ-Cyclodextrin in 1.0×10^{-3} mol dm^{-3} $HClO_4$ solutions						
25.00	14.78	16.80	10.10	0.514	0.587	14.2
25.00	14.55	16.45	14.89	0.505	0.589	11.3
25.00	14.55	16.45	18.00	0.505	0.598	10.4
25.00	22.75	34.00	10.04	1.04	1.19	14.6

a) Concentration of CyD prepared by adding a known amount of dried CyD to the aqueous phase. b) The solubility of iodine in the absence of CyD. c) The solubility of iodine in the presence of CyD. d) $K_f=(S_{obsd}-S_o)/S_o(C_{CyD}-S_{obsd}+S_o)$, *i.e.*, the left-hand side of Eq. 6 in the text.

TABLE 3. FORMATION CONSTANTS OF CYCLODEXTRIN-IODINE COMPLEXES AND THERMODYNAMIC PARAMETERS

Temperature / °C	Formation constant / $dm^3\ mol^{-1}$	ΔG / kJ mol^{-1}	ΔH / kJ mol^{-1}	ΔS / J K^{-1} mol^{-1}	ΔC_p / J K^{-1} mol^{-1}
α-Cyclodextrin in 1.0×10^{-3} mol dm^{-3} $HClO_4$ solution					
15.00	$(4.6\pm0.7)\times10^3$	−20.1	68.1	306	−5.74
20.00	$(7.5\pm0.6)\times10^3$	−21.7	39.1	207	−5.86
25.00	$(8.3\pm0.5)\times10^3$	−22.4	9.52	107	−5.98
30.00	$(7.4\pm0.4)\times10^3$	−22.5	−20.7	5.94	−6.10
35.00	$(6.7\pm0.7)\times10^3$	−22.6	−51.5	−93.8	−6.22
α-Cyclodextrin in 0.20 mol dm^{-3} HIO_3 solution					
25.00	$(9.6\pm0.8)\times10^3$				
α-Cyclodextrin in 0.08 mol dm^{-3} HIO_3 solution[a]					
24	9.3×10^3				
β-Cyclodextrin in 1.0×10^{-3} mol dm^{-3} $HClO_4$ solution					
25.00	100 ± 10				
γ-Cyclodextrin in 1.0×10^{-3} mol dm^{-3} $HClO_4$ solution					
25.00	13 ± 2				

a) Taken from Ref. 2.

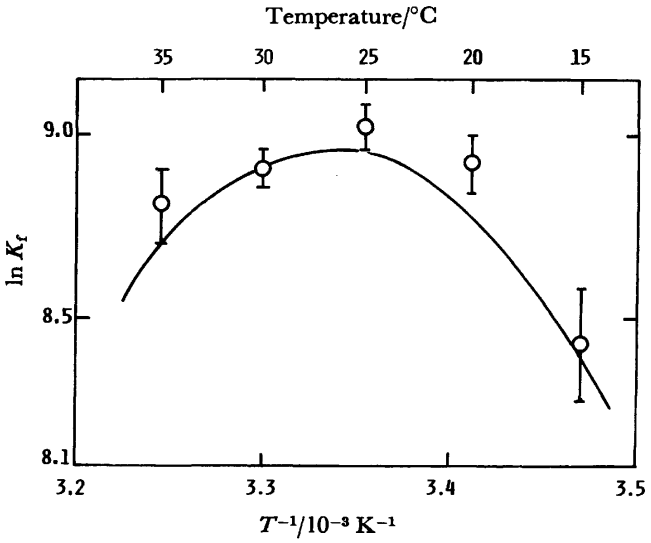

Fig. 1. Temperature dependence of α-cyclodextrin-iodine complex formation constant.
The smoothed curve is drawn by using Eq. 8 given in the text.

complexation have been obtained for a wide variety of substrates, and it has now become evident that ΔH takes usually negative value, whereas ΔS can be positive or negative.[7] Theoretical approaches have been made to elucidate the mechanism of CyD complexation with substrates,[8,9] but there are still some arguments in detail. It is now generally accepted that both the dehydration of a guest molecule on entering the CyD cavity and the interaction between a guest and CyD inside the cavity play an important role. The guest being hydrophobic, the interaction decreases with increasing temperature. On the other hand, the guest being a gaseous nonelectrolyte molecule, the dehydration increases with rising temperature, and in this case thermodynamic parameters can be easily determined by measuring the temperature dependence of the aqueous solubility of the guest in the absence of CyD. The results for iodine are shown in Table 1. Substracting the free energy change of dehydration from that of the overall process yields −14.4 (15 °C), −15.4 (20 °C), −15.3 (25 °C), −14.6 (30 °C), and −13.9 kJ mol^{-1} (35 °C). If it is assumed that these values provide a rough measure of iodine-CyD interaction, the order of the above figures at lower temperatures is not consistent with the view that the interaction can be explained by considering only hydrophobic interaction.

To shed light on what is really responsible for the present unusual temperature dependence of K_f observed for iodine, it seems desirable to study CyD complexations with nonelectrolytes, only sparingly soluble in water and volatile. For such a purpose the experimental technique proposed here is useful which utilizes vapor of nonelectrolyte.

References

1) J. A. Thoma and D. French, *J. Am. Chem. Soc.*, **80**, 6142 (1958).
2) J. A. Thoma and D. French, *J. Phys. Chem.*, **62**, 1603 (1958).
3) R. K. McMullan, W. Saenger, J. Fayos, and D. Mootz, *Carbohydr. Res.*, **31**, 37 (1973).
4) I. Sanemasa, T. Kobayashi, C. Y. Piao, and T. Deguchi, *Bull. Chem. Soc. Jpn.*, **57**, 1352 (1984).
5) G. P. Baxter, C. H. Hickey, and W. C. Holmes, *J. Am. Chem. Soc.*, **29**, 127 (1907); H. Chihara and N. Nakamura, *Bull. Chem. Soc. Jpn.*, **41**, 1787 (1968).
6) E. A. Lewis and L. D. Hansen, *J. Chem. Soc., Perkin Trans. 2*, **1973**, 2081.
7) W. Saenger, *Angew. Chem., Int. Ed. Engl.*, **19**, 344 (1980).
8) I. Tabushi, Y. Kiyosuke, T. Sugimoto, and K. Yamamura, *J. Am. Chem. Soc.*, **100**, 916 (1978).
9) K. Harata, *Bull. Chem. Soc. Jpn.*, **49**, 2066 (1976).

Solubility and Synergistic Extraction Equilibria for [4-(2-Pyridylazo)resorcinolato] Nickel(II) Complexes

Hitoshi HOSHINO and Takao YOTSUYANAGI*
Department of Applied Chemistry, Tohoku University, Aoba, Aramaki, Sendai 980
(Received September 14, 1984)

The nickel(II) complex of 4-(2-pyridylazo)resorcinol (PAR, H_2L) is known to show somewhat anomalous and complicated behavior in solution. In this regard, the solubility and the synergistic extraction equilibria of the above complex are studied in connection with acid dissociation reactions. The intrinsic solubility and the acid dissociation constants are determined to be, $S_0=[[Ni(HL)_2]]=10^{-6.2\pm0.1}$ mol dm^{-3}, $K_{a1}=[[Ni(HL)L^-][H^+][[Ni(HL)_2]]^{-1}=10^{-6.2\pm0.1}$, and $K_{a2}=[[NiL_2]^{2-}][H^+][[Ni(HL)L]^-]^{-1}=10^{-7.1\times0.1}$, respectively in the solution with the ionic strength of 0.10 (Na_2SO_4) at 298 K. Using the above constants, the extraction constant of the neutral complex with trioctylphosphine oxide (TOPO) into chloroform is evaluated as $K_{ex}=[[Ni(HL)_2(TOPO)_2]]_o[[Ni(HL)_2]]^{-1}[TOPO]_o^{-2}=10^{3.1\pm0.2}$, where the subscript o denotes the organic phase. An equilibrium diagram for the nickel(II)-PAR complexes is proposed.

A well-known sensitive reagent, 4-(2-pyridylazo)-resorcinol (PAR, H_2L) has been used for the trace determination of nickel(II) ion.[1-4] In our previous studies[5-8] of the ion pair extraction of anionic PAR complexes with a quaternary ammonium salt (QCl),[9] it was shown that the nickel(II) ion yields the PAR complex having somewhat unusual properties in sharp contrast to those of other divalent ions, Fe(II), Cu(II), Zn(II), and Cd(II). (1) The ion pair of the mononegative complex, Q[Ni(HL)L] has much poorer extractability than that of the dinegative one, $Q_2[NiL_2]$. This seems to be contrary to the general rule found in ion pair extraction, *i.e.*an increase in the charge number of the anion leads to a decrease in the extractability. (2) The neutral complex, $[Ni(HL)_2]$ is slightly soluble in water as well as in chloroform or nitrobenzene, whereas the correponding iron(II) complex is partly distributed into these solvents. The neutral nickel(II) complex can be extracted synergistically with trioctylphosphine oxide (TOPO) as $[Ni(HL)_2(TOPO)_2]$, which is not an unusual matter as compared with the other neutral PAR complexes.[7,10]

These observations have prompted a more thorough investigation of the solubility, acid dissociation, and synergistic extraction equilibria of the nickel(II)-PAR complexes. This was expected to be an approach to interpret the somewhat anomalous and complicated behavior of the complexes in solutions, especially in the solvent extraction systems.

In this paper is established the equilibrium relation between nickel(II)-PAR complexes which has been sometimes ambiguous and inconsistent,[6,11-13] and the results are discussed in comparison with those of the other metal ion complexes.

Experimental

Apparatus and Reagents. A Hitach model 124 double beam recording spectrophotometer with 1 cm glass cells and a Horiba M-5 pH meter were used. In extraction procedures, samples were shaken in an Iwaki KM-type reciprocating shaker. A Yamato Coolnics Circulator model CTR200/CTE220 water bath was used at a constant temperature of 298 K.

TOPO, as obtained from Dojindo Lab. (Kumamoto, Japan) was dissolved in chloroform which was purified by distillation and saturated with water. Nickel(II)-PAR complex ($[Ni(HL)_2]\cdot2H_2O$) was prepared as described by Corsini *et al.*[14] The concentration of the PAR complex stock solution (pH 8) was determined spectrophotometrically.

All other reagents used were of analytical grade.

Procedure. Solubility Measurements: About 50 cm^3 of a phosphate buffer solution (2×10^{-3} mol dm^{-3}) containing nickel(II)-PAR complex (initially 10^{-3}—10^{-4} mol dm^{-3}) and sodium sulfate (0.033 mol dm^{-3}, I=0.10) with 5 cm^3 of chloroform was allowed to stand at 298 K for at least 5 h with occasional shaking. Sodium sulfate was used to maintain a constant ionic strength in conformity with the ion pair extraction study.[6] The initial pH of the solution was roughly adjusted with the buffer, dilute sulfuric acid and sodium hydroxide solutions. The pH range of 6 to 8 was chosen in order to prevent the decomposition of the complex due to protolysis and hydrolysis reactions. The concentration of the nickel complex in aliquots of the saturated solutions was determined spectrophotometrically after filtration through a G-4 sintered glass filter. The pH of the filtrate solution was measured. Because of the inert nature of the nickel(II)-PAR complexes, sulfate and phosphate ions in the solution had no significant effect on the above experiments. Partition of the neutral and the anionic complexes into chloroform phase occurs to a slight extent. However, such a phenomenon has no effect on the solubility measurements under the conditions where the precipitate is present in the system.

TOPO Extraction: Ten cm^3 of an aqueous solution containing phosphate buffer (2.5×10 mol dm^{-3}), sodium sulfate (I=0.10), and nickel(II)-PAR complex were equilibrated by shaking with an equal volume of chloroform containing an appropriate concentration of TOPO in a glass sample tube (50 cm^3), and allowed to stand in a thermostated bath at 298 K for more than 5 h with occasional shaking. Aliqouts of the organic phase were taken and the absorbance at 535 nm was measured (the molar absorption coefficient is 3.57×10^4 dm^3 mol^{-1} cm^{-1}).

Results and Discussion

The equilibrium saturation with respect to the nickel(II)–PAR complex was attained after 4 h; this was confirmed by the solubility-time curve obtained by heating the samples to 313—323 K followed by rapid cooling to the final temperature, 298 K.

The solubility-pH curve for the nickel(II)–PAR complex in water saturated with chloroform is shown in Fig. 1. Above pH 6, the complex is in part soluble as the anionic species of $[Ni(HL)L]^-$ and $[NiL_2]^{2-}$. Decomposition of the complex was negligible. The solubility equilibria can be expressed by the following reactions; the intrinsic solubility S_0 of the neutral complex is given by

$$[Ni(HL)_2]_s \rightleftharpoons [Ni(HL)_2], \quad S_0 = [[Ni(HL)_2]] \tag{1}$$

where the subscript s denotes the solid phase, and the acid dissociation constants are represented as

$$[Ni(HL)_2] \rightleftharpoons [Ni(HL)L]^- + H^+, \quad K_{a1} = \frac{[[Ni(HL)L]^-][H^+]}{[[Ni(HL)_2]]} \tag{2}$$

$$[Ni(HL)L]^- \rightleftharpoons [NiL_2]^{2-} + H^+, \quad K_{a2} = \frac{[[NiL_2]^{2-}][H^+]}{[[Ni(HL)L]^-]} \tag{3}$$

The solubility, S of the complexes is given by

$$S = [[Ni(HL)_2]] + [[Ni(HL)L]^-] + [[NiL_2]^{2-}] \tag{4}$$

From Eqs. 1—4 the following equation is obtained,

$$\left(\frac{S}{S_0} - 1\right)[H^+]^2 = K_{a1}[H^+] + K_{a1}K_{a2} \tag{5}$$

The intrinsic solubility, S_0 was obtained by extrapolation on the solubility-pH curve shown in Fig. 1 (dashed line).

$$\log S_0(\text{mol dm}^{-3}) = -6.2 \pm 0.1 \quad [I=0.10(Na_2SO_4),\ 298\ K]$$

From the plots of Eq. 5 given in Fig. 2, the values of K_{a1} and K_{a2} were determined to be

$$pK_{a1} = 6.2 \pm 0.1, \quad pK_{a2} = 7.1 \pm 0.1 \quad [I=0.10(Na_2SO_4),\ 298\ K]$$

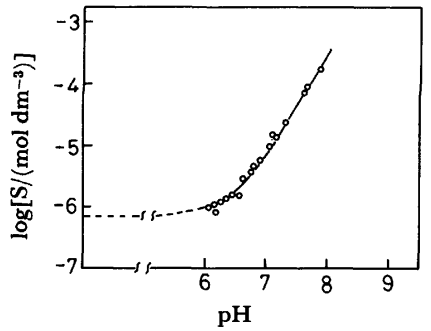

Fig. 1. Solubility *vs.* pH curve for Ni(II)–PAR complex at 298 K.
I=0.10 (Na_2SO_4), $C_{Phosphate}=2.0\times10^{-3}$ mol dm^{-3}.

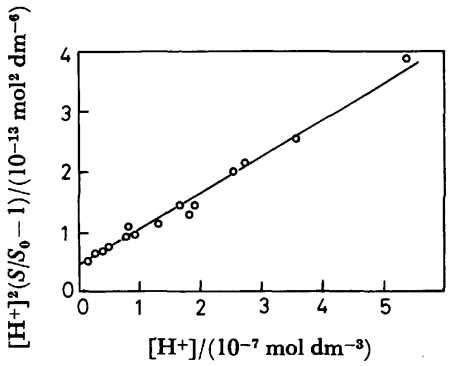

Fig. 2. Plots of Eq. 5.

The calculated log S *vs.* pH curve shown in Fig. 1 as the solid line is in good agreement with the experimental points.

The value of S_0 for the nickel(II)–PAR complex is very small. Although no quantitative solubility data of the other metal–PAR complexes are available, there is no evidence for the precipitation of the complexes at concentrations below 5×10^{-6} mol dm^{-3} in a similar medium. The iron(II) complex, $[Fe(HL)_2]$ was partly distributed into chloroform and still more so into nitrobenzene.[8] This fact demonstrates an interesting contrast between the nickel and iron PAR complexes.

The acid dissociation constants of 1-hydroxyl groups (para position to azo group) in the nickel(II)–PAR complex in 50% aqueous dioxane solution were reported by Corsini *et al.*[15] as pK_{a1}=7.7 and pK_{a2}=9.2. As these values were obtained in quite a different medium, these are not considered in greater detail. The values obtained here agree within a similar order of magnitude with those of the PAR complexes of divalent ions, iron(II); pK_{a1}=6.47, pK_{a2}=7.66 (I=0.10, 293 K),[8] copper(II); 6.54, 7.64 (I=0.10, 298 K),[16] zinc(II); 6.45, 7.55 (I=0.10, 298 K),[17] and cadmium(II); 6.67, 7.84 (I=0.10, 298 K),[18] respectively. The parallel order between the acidity of 1-hydroxyl groups and the stability of PAR complexes suggested by Corsini *et al.*[15] does not seem to be valid in the light of these data as the stability order may be $Fe^{II}>Ni^{II}>Cu^{II}>Zn^{II}>Cd^{II}$.[8,16–18]

At the pH condition for the photometric determination of nickel (pH 9.2, borate buffer)[2,3] the predominant species (99%) is, thus, the dianion, $[NiL_2]^{2-}$ which has the largest molar absorption coefficient of $(7.2—7.8)\times10^4$ dm^3 mol^{-1} cm^{-1} at 495 nm as compared with the other protonated ones.

Besides TOPO, typical monodentate adduct formers such as pyridine, pyridine *N*-oxide, and tributyl phosphate are effective for the extraction of the neutral complex $[Ni(HL)_2]$, while the bidentate ones, 1,10-phenanthroline, 2,2′-bipyridine, and ethylenediamine, fail to work.

The extraction with TOPO is represented by

$$[Ni(HL)_2] + 2TOPO_{(o)} \rightleftharpoons [Ni(HL)_2(TOPO)_2]_{(o)} \tag{6}$$

$$K_{ex} = \frac{[[Ni(HL)_2(TOPO)_2]]_o}{[[Ni(HL)_2]][TOPO]_o^2} \quad (7)$$

where the subscript o is used for the species in the organic phase. Using the total concentration of the complex species in the aqueous phase, $C_{a,Ni}$, Eq. 7 is rewritten as

$$K_{ex} = \frac{[[Ni(HL)_2(TOPO)_2]]_o}{C_{a,Ni}[TOPO]_o^2}\left(1+\frac{K_{a1}}{[H^+]}+\frac{K_{a1}K_{a2}}{[H^+]^2}\right) \quad (8)$$

where the aqueous concentration of $[Ni(HL)_2(TOPO)_2]$ is neglected. When the precipitate is present, $C_{a,Ni}$ is equal to the solubility, S(Eq. 4). At constant pH, the plots of $\log\{[[Ni(HL)_2(TOPO)_2]]_o(C_{a,Hi})^{-1}\}$ *vs.* $\log\{[TOPO]_o\}$ give a straight line of a slope 2 as shown in Fig. 3. Because of the upward deviation at low organic concentration of TOPO (<0.05 mol dm^{-3}, curve 1 in Fig. 3), the calculation of the K_{ex} value was made using the experimental points on the straight line portion. Under the conditions where the precipitate is in the system at pH≤7.05, the concentration of $[Ni(HL)_2]$ is held constant according to Eq. 1, thus,

$$K_{ex} = \frac{[[Ni(HL)_2(TOPO)_2]]_o}{S_0[TOPO]_o^2} \quad (9)$$

Under higher pH conditions (pH≥7.40) where no precipitate is in the system, Eq. 8 is used for calculation of the K_{ex} value, where $C_{a,Ni}$ is given by $C_{a,Ni}=C_{Ni}-[[Ni(HL)_2(TOPO)_2]]_o$, ($C_{Ni}$ is the total concentration of the nickel(II)-PAR complexes). The calculated values of log K_{ex} at various pH and TOPO concentrations are shown in Table 1. The mean value was determined to be,

$$\log K_{ex} = 3.1\pm0.2 \quad [I=0.10(Na_2SO_4),\ 298\ K]$$

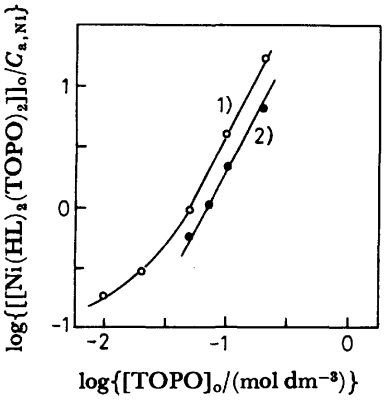

Fig. 3. Extraction of Ni(II)-PAR complex with TOPO. $C_{Ni}=2.08\times10^{-5}$ mol dm^{-3}, I=0.10 (Na_2SO_4), at 298 K.
1) pH 6.0±0.1, 2) pH 6.9±0.1.

Table 1. Logarithmic extraction constant (log K_{ex}) of nickel(II)-PAR complex with TOPO into chloroform

$[TOPO]_o$ / mol dm^{-3}	pH						
	6.00	6.18	6.41	6.50	6.71	6.80	6.81
0.05	2.9		2.9		3.0	3.1	
0.10	2.9	3.2		3.3			3.2
0.20	2.9						
$[TOPO]_o$ / mol dm^{-3}	pH						
	6.90	7.05	7.40	7.42	7.47	7.50	
0.05	3.3	3.2	3.1	3.2			
0.07	3.3						
0.10	3.2				3.2	3.2	
0.20	3.0						

log K_{ex}=3.1±0.2 [I=0.10 (Na_2SO_4), at 298 K] (averaged value of 18 runs).

A few reports have dealt with this type of extraction of neutral PAR complexes.[7,19,20] Only one comparable datum is the extraction constant for the vanadium(V)-PAR-TOPO complex, $K_{ex}=[[VO_2(HL)(TOPO)]]_o[[VO_2(HL)]]^{-1}[TOPO]_o^{-1}=10^{2.17}$.[7] In general, in TOPO synergistic extraction systems, over-all extraction constants (including formation of parent complexes) and adduct formation constants in the organic phase have been most frequently used to describe the extraction processes.[21] However, they can not be directly compared with the data obtained in this work. The adduct formation constant in chloroform, $\beta_2=[[Ni(HL)_2(TOPO)_2]]_o[[Ni(HL)_2]]_o^{-1}[TOPO]_o^{-1}$ was roughly estimated as follows: when the distribution ratio, D_{Ni} is defined as $D_{Ni}=\{[[Ni(HL)_2]]_o+[[Ni(HL)_2(TOPO)_2]]_o\}(C_{a,Ni})^{-1}$, by extrapolating the $[TOPO]_o$ term (curve 1 in Fig. 3, pH 6.0) to zero, $D_{Ni}\approx[[Ni(HL)_2]]_o(C_{a,Ni})^{-1}\approx10^{-1}$ is obtained, and from Eq. 8, $\beta_2=K_{ex}\{D_{Ni}(1+K_{a1}/[H^+]+K_{a1}K_{a2}/[H^+]^2)\}^{-1}\approx10^{3.9}$. It is clearly recognized that this β_2 value is smaller by some order of magnitude than those for the other TOPO adducts in chloroform, in which TOPO molecules are directly bound to the central metal ions replacing aqua ligands, *i.e.* mixed ligand complex (for example, some β-diketone complex systems).[21,22] In the nickel(II)-PAR system, therefore, there is a little doubt about the possibility of a mixed ligand complex. It is also likely that two TOPO molecules are bound to each of two 1-hydroxyl groups on the PAR ligands *via* hydrogen bonding, which causes an increase in hydrophobicity of the parent PAR complex. This possibility seems to be supported by the fact that the complex is well distributed into some polar solvents having hydrogen bonding ability, alcohols, esters, and ketones. It is important to observe that the coordination mode of the PAR ligands (bidentate or tridentate) would decide between the alternative possibilities depending upon whether the complex is "coordinatively saturated" with two tridentate HL^- or "unsaturated" having two bidentate HL^- and two aqua ligands. Kawamoto *et al.* re-

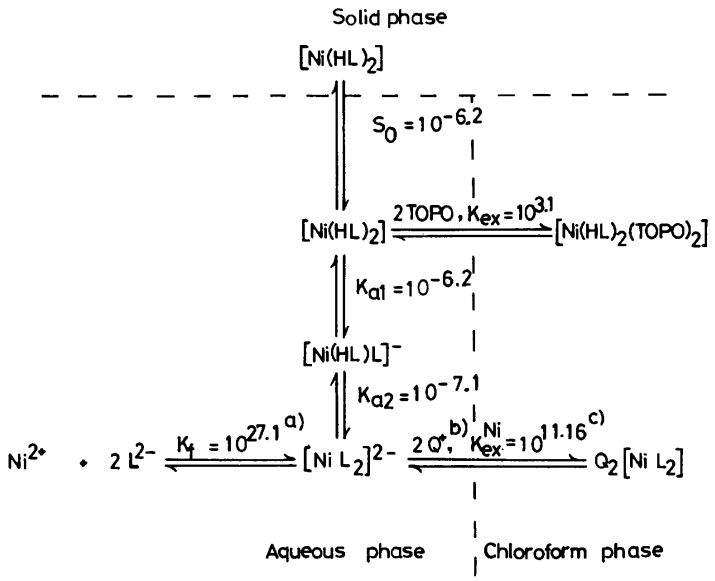

Fig. 4. Equilibrium diagram of Ni(II)–PAR system.
a) Ref. 3), b) Q^+, Ref. 9), c) Ref. 6), $K_{ex}^{Ni}=[Q_2[NiL_2]]_o[Q^+]^{-2}[[NiL_2]^{2-}]^{-1}$.

cently found the nickel(II)–PAR complex having the 1:3 stoichiometry in the ion pair extraction system with a highly lipophilic quaternary ammonium salt.[11] Detailed discussion of the extraction mechanism, in all events, will be the emphasis of a future study which will provide valuable information on the chemistry of PAR complexes.

Finally, several nickel(II)–PAR complex species in solutions and their equilibrium constants were verified as summarized in Fig. 4. These data serve as a quantitative basis for understanding and designing of the conventional spectrophotometric systems and the ion pair solvent extraction for the nickel determination.

References

1) S. Shibata, in A. J. Barnard and H. Flaschka, Ed. "Chelates in Analytical Chemistry," M. Dekker, Vol. 3, New York (1972), pp. 132.

2) Y. Shijo and T. Takeuchi, *Bunseki Kagaku*, **14**, 511 (1965).

3) L. Sommer, V. Kubán and M. Langová, *Fresenius'Z. Anal. Chem.*, **310**, 51 (1982).

4) T. Yotsuyanagi, R. Yamashita, H. Hoshino, K. Aomura, H. Satoh, and N. Masuda, *Anal Chim. Acta*, **82**, 431 (1976).

5) T. Yotsuyanagi and H. Hoshino, *Bunseki*, **1976**, 743.

6) H. Hoshino, T. Yotsuyanagi, and K. Aomura, *Anal. Chim. Acta*, **83**, 317 (1976).

7) M. Tajika, H. Hoshino, T. Yotsuyanagi, and K. Aomura, *Nippon Kagaku Kaishi*, **1979**, 85.

8) H. Hoshino and T. Yotsuyanagi, *Talanta*, **31**, 525 (1984).

9) Benzyldimethyltetradecylammonium chloride (Zephiramine) commercially available from Dojindo Lab., Kumamoto, Japan.

10) T. Ebina, *Doctoral Thesis*, Tohoku University, Sendai, **1984**.

11) H. Kawamoto, T. Takenouchi, and H. Akaiwa, *Nippon Kagaku Kaishi*, **1983**, 358.

12) D. Nonova and B. Evtimova, *Anal. Chim. Acta*, **49**, 103 (1970).

13) D. Nonova and B. Evtimova, *Anal. Chim. Acta*, **62**, 456 (1972).

14) A. Corsini, I.M. Yih, Q. Fernando, and H. Freiser, *Anal Chem.*, **34**, 1090 (1962).

15) A. Corsini, Q. Fernando, and H. Freiser, *Inorg. Chem.*, **2**, 224 (1963).

16) A. Hrdlicka and M. Langová, *Collect. Czech. Chem. Commun.*, **45**, 1502 (1980).

17) M. Tanaka, S. Funahashi, and K. Shirai, *Inorg. Chem.*, **7**, 573 (1968).

18) S. Vlcková, L. Jancár, V. Kubán, and J. Havel, *Collect. Czech. Chem. Commun.*, **47**, 1086 (1982).

19) H. Tomioka and K. Terashima, *Bunseki Kagaku*, **16**, 698 (1967).

20) B. Subrahmayan and M. C. Eshwar, *Anal. Chem.*, **47**, 1692 (1975).

21) Y. Marcus and A. S. Kertes, "Ion-exchange and Solvent Extraction of Metal Complexes," Wiley-Interscience, New York (1969), Chap. 11.

22) T. Sekine and D. Dyrssen, *J. Inorg. Nucl. Chem.*, **29**, 1475 (1967).

Basic Properties of MgO Doped with Alkaline Metal Compounds

Tsuneo MATSUDA,* Yo SASAKI,† Hiroshi MIURA, and Kazuo SUGIYAMA
Department of Applied Chemistry, Faculty of Engineering, Saitama University, Shimo-ohkubo, Urawa 338
†*Tokyo Institute of Technology, Nagatsuda, Midoriku, Yokohama 227*
(Received August 24, 1984)

Synopsis Basic properties of MgO doped with NaOH, KOH, and Li_2CO_3 which was calcined at 550, 700, and 900 °C in air were examined. The basicity of the catalysts was determined from the irreversible amount of adsorption of phenol and BF_3, followed by evacuation at room temperature (for both adsorbates), 100, 200, and 300 °C (for phenol) after adsorption at room temperature. A good correlation was observed between the amount of phenol remained after evacuation at higher temperature than 200 °C and that of BF_3. By doping of 1 wt% of alkali metal compounds in MgO the isomerization activity of 1-butene was enhanced, but by 10 wt% the activity remarkably decreased.

The studies on the addition effects of sodium hydroxide on the physicochemical properties of MgO were reported by Malinowski *et al.*[1] in which any change in the acidic or basic strength of MgO was not found. In the literature[2] the basicity of the catalysts containing 0 to 0.82 mmol Na^+/g MgO were examined. However, there is no report on the studies of the catalysts containing more than 0.82 mmol and other alkali metal compounds except NaOH. In this study the effect of the addition of KOH, Li_2CO_3, and also NaOH on the basicity of MgO was examined in connection with 1-butene isomerization and, in part, reexamined the results of Malinowski *et al.*[2]

Experimental

Catalysts Preparation. Magnesium hydroxide was first prepared by precipitating with aqueous ammonia (6 mol dm^{-3}) from the saturated aqueous solution of magnesium nitrate. Thus prepared $Mg(OH)_2$ was impregnated into the aqueous solution of NaOH, KOH, and Li_2CO_3 of different concentration which was arranged to be 1 and 10 wt% as M^+ per MgO (M^+ is alkali metal ion) after calcination and then evaporated to dryness on the water bath. The dry $Mg(OH)_2$ doped with the each alkali metal compound (abbreviated simply as dopant) was arranged to the granule of 20 to 60 mesh, which were calcined at 550, 700, and 900 °C for 3 h in air. Magnesium oxide not doped with the dopants was prepared by the calcination of $Mg(OH)_2$ at 550, 700, and 900 °C for 20 h in air.

Measurement of Basicity. Basicity was determined from the irreversible amount of adsorption of phenol or BF_3 according to the spring balance method, *i.e.*, after the adsorption of phenol or BF_3 was attained to equilibrium at room temperature, the sample in the quartz basket was evacuated at room temperature (for both adsorbates) and at 100, 200, and 300 °C (for phenol) until the change of the reading of the quartz spring balance ceased. The strength of the basicity was qualitatively examined with the color change of indicators.[2]

Isomerization of 1-Butene. The isomerization of 1-butene was carried out at 0 °C in a closed vessel (dead volume=*ca.* 180 cm^3) equipped with a circulation system. The reaction products were analyzed by gas chromatography on a column of VZ-7 (4 m) at 0 °C.

Results and Discussion

The irreversible amounts of adsorption of phenol and BF_3, surface area, and basic strength of various samples are shown in Table 1. The adsorbed amounts of phenol decreased as the evacuation temperature of the adsorbed samples increased. The molecular sizes of both phenol and BF_3 were calculated to be 8.24×10^{-20} and 9.62×10^{-20} m^2, from the excluded volumes of the van der Waals equation estimated from the critical points. From the sizes and the adsorbed amounts of each adsorbate the adsorption of phenol can be calculated to be more than monolayer (for instance, 1.27 and 2.7 molecular layer on MgO–KOH (10) treated at 550 °C (evacuated at r.t.) and 900 °C (at 100 °C), respectively) and, on the other hand, BF_3 adsorbed less than monolayer. By the evacuation at higher temperature than 200 °C, the adsorbed amount of phenol was reduced to less than monolayer. At the temperature of lower than 100 °C phenol of physical adsorption seems to be still remained on the surface. Tanabe[3] reports that phenol adsorbs not only on the basic site but also on the acidic one, indicating that phenol is not necessarily suitable for the measurement of basicity. As shown in Fig. 1, however, a good correlation between the basicity obtained from the adsorption of BF_3 and that from phenol evacuated at 200 and 300 °C was obtained. The measurement of basicity by BF_3 adsorption is also reported by Niiyama and Echigoya.[4] Accordingly, it is possible to measure the basicity by phenol adsorption, if the evacuation treatment at 200 or 300 °C, is followed after the adsorption.

The surface areas of MgO–alkali metal system decrease as increasing the content of the dopants, indicating that they exert the shrinking effect on the surface by any kind of interaction with MgO. As shown in the case of Al_2O_3–$NaNO_3$ system,[5] the dopants will also interact with surface OH groups MgO, causing the decrease of the surface area. This effect was also found in other alkali compounds except those used in this study.[6] In doping of 10 wt% the strength of the basicity decreased, which would be difficult to ascribe to the interaction of the dopants with the OH groups on the surface. The OH groups on MgO will be of weak basic sites as those on CaO.[7] Therefore the dopants will interact with or block over Lewis base site on MgO, resulting to the reduction of the basic strength.

The results of the isomerization of 1-butene over the catalysts doped with the alkali compounds followed with calcination at 550°C are shown in Fig. 2. By doping of 1 wt% of the dopants the isomerization activity was enhanced, but the doping to 10 wt% caused the remarkable decrease of the activity. As shown in Fig. 2 the activity of the catalyst doped with Li_2CO_3 by 1 wt% was the highest, which might be due to both the higher surface area and suitable basicity produced by the interaction with MgO and Li_2CO_3.

Table 1. Results of basicity measurements and surface area

Catalyst	Temp[a] °C	Adsorbed amount of phenol (mmol/g) r.t.[b,c]	100[c]	200[c]	300[c]	Adsorbed amount of BF_3 (mmol/g)	Surface area (m^2/g)	Basic strength (H_-)
MgO-NaOH (1)	550	1.11	0.700	0.548	0.479	1.58	131	35
	700	0.494	0.400	0.303	0.281	0.759	61	35
	900	0.269	0.231	0.179	0.142	0.451	30	35
MgO-NaOH (10)	550	1.34	0.688	0.501	0.347	1.36	78	27
	700	0.483	0.243	0.167	0.142	0.449	36	15.0
	900	0.105	0.080	0.069	0.036	—	4.6	15.0
MgO-KOH (1)	550	0.983	0.619	0.492	0.442	1.23	105	27
	700	0.403	0.290	0.213	0.199	0.589	41	22.3
MgO-KOH (10)	550	1.40	0.557	0.375	0.328	0.907	56	22.3
	700	1.10	0.438	0.307	0.212	0.535	26	17.2
	900	0.226	0.191	0.188	0.156	—	3.5	17.2
$MgO-Li_2CO_3$ (1)	550	1.19	0.371	0.504	0.474	1.02	144	35
$MgO-Li_2CO_3$ (10)	550	1.12	0.810	0.534	0.484	1.15	109	27
MgO	500	1.19	0.792	0.653	0.568	1.79	188	27
	700	0.602	0.418	0.373	0.313	1.06	93	27
	900	0.431	0.344	0.269	0.215	0.580	47	27

a) Treatment temperature. b) Room temperature. c) Evacuation temperature (°C) after adsorption. The values of parenthesis in catalyst column indicate the doped amount (wt.%) of alkali metal.

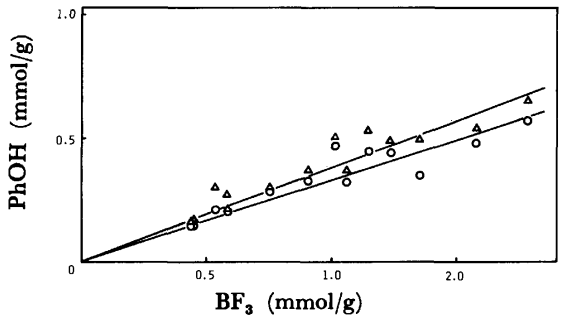

Fig. 1. The relationship between the irreversible amounts of adsorption of phenol and BF_3.
△: Evacuation at 200 °C, ○: at 300 °C.
Each points in the figure were obtained from the results of Table 1.

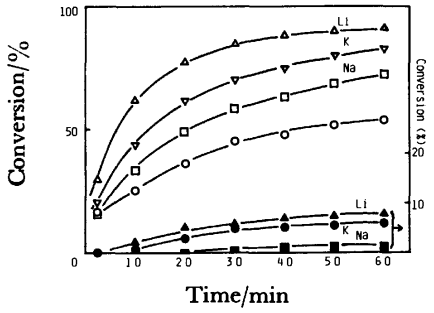

Fig. 2. Conversion *vs.* reaction time plot in 1-butene isomerization.
Open symbols 1 wt% doping.
Closed symbols 10 wt% doping.
○: no doping.

As Li_2CO_3 can be decomposed releasing CO_2 at lower temperature (618 °C) than the decomposition temperature of NaOH and KOH, a parts of Li_2CO_3 may be decomposed with the treatment at 550 °C, by which the suitable active sites may be formed. Anyway, by the doping of 1 wt% of the dopants the active sites of the suitable basic strength of H_-=22.3 and 27 for the isomerization[6] will be increased. Deactivation by the addition of 10 wt% of dopants may be ascribed to the considerable decrease in the surface area of the catalysts except the case of $MgO-Li_2CO_3$ and in the sites related with the suitable basic strength. The ratios of cis to trans isomers at the initial stage of the isomerization are shown in Table 2. The ratios exhibited the characteristic values[8] for the basic catalysts, but the correlation between the ratios and basicity including the basic strength could not be found, indicating that it is impossible to evaluate the basic strength of the catalysts from the ratios.

Table 2. Initial *cis* to *trans* ratio in 1-butene isomerization

Catalyst[a]	*cis*/*trans*
MgO-NaOH (1)	5.7
MgO-NaOH (10)	10.5
MgO-KOH (1)	5.7
MgO-KOH (10)	13.9
$MgO-Li_2CO_3$ (1)	5.8
$MgO-Li_2CO_3$ (10)	7.4
MgO	6.8

a) All catalysts were calcined at 550 °C for 3 h in air except MgO.

References

1) S. Szczepanska and S. Malinowski, *J. Catal.*, **15**, 68 (1969); *ibid*, **27**, 1 (1972).
2) J. Kijenski and S. Malinowski, *Bull. Acad. Polon Asci., Ser. Sci. Chim.*, **25**, 329 (1977).
3) K. Tanabe, *Yūkigōsei Kyōkaishi*, **33**, 842 (1975).
4) H. Niiyama and E. Echigoya, *Kōgyō Kagaku Zasshi*, **74**, 560 (1971).
5) A. Lycourghiotis, C. Defosse, F. Delannay, and B. Delmon, *J. Chem. Soc., Faraday Trans. 1*, **76**, 1677 (1980).
6) T. Matsuda, J. Tanabe, N. Hayashi, Y. Sasaki, H. Miura, and K. Sugiyama, *Bull. Chem. Soc. Jpn.*, **55**, 990 (1982).
7) T. Iizuka, H. Hattori, Y. Ohno, J. Sohma, and K. Tanabe, *J. Catal.*, **22**, 130 (1971).
8) H. Hattori, N. Yoshii, and K. Tanabe, 5th Inter. Congr. Catal., **10**, 233 (1971).

An Inspection of the Purity of Helium Used as the Carrier Gas in Pulse-adsorption Experiments

Hiroshi MIURA,* Toshiyuki NARITA, Makoto HARUTA, Kazuo SUGIYAMA, and Tsuneo MATSUDA

Department of Applied Chemistry, Faculty of Engineering, Saitama University, Shimo-ohkubo, Urawa 338

(Received September 4, 1984)

Synopsis. A novel method is proposed to inspect the oxygen content of the helium used as the carrier gas in pulse-adsorption experiments. The oxygen is first adsorbed on Pt/SiO_2 catalyst and then titrated by CO pulses. This method is very simple and requires only a conventional pulse-adsorption system.

The measurement of the metal surface area —dispersion— of supported metal catalysts is one of the most important techniques in the characterization of catalysts. The selective chemisorption of such gases as hydrogen, carbon monoxide, and oxygen is very frequently used for this purpose. This method is, however, based on the correspondence of the numbers of surface atoms and adsorbed molecules, and so the stoichiometry of chemisorption must be stable. Hydrogen chemisorption is believed to be most satisfactory[1] because the stoichiometry is stable for many metals, even when the dispersion is relatively high. On the other hand, CO adsorbs on noble metals very rapidly and attains the equilibrium of adsorption very easily at room temperature because of its strong affinity to metals, although the stoichiometry is sometimes complex.[2] Such behavior of CO is very advantageous for chemisorption using a pulse appararus, which is a very simple and convenient method of chemisorption. Thus, hydrogen adsorption is preferred by laboratories doing basic research, whereas CO adsorption is often selected by the researchers of catalysts for practical applications.

One of the most serious technical problems which we encounter when we try to perform pulse-adsorption experiments is that a very high purity is required for the carrier gas. For example, if helium carrier gas contains 1 ppm of oxygen and is passed through a Pt/SiO_2 catalyst (0.1 wt% Pt, 0.3 g) at a rate of 30 ml/min for 1 h (the time required to desorb H_2 and to cool it down to room temperature after pretreatment), then the number of oxygen atoms adsorbed on the catalyst surface is 10% of the total Pt atoms. Therefore, the oxygen content of helium must be less than 0.1 ppm for exact experiments. Obviously, it is important to inspect whether or not the carrier gas has a purity high enough of satisfy the demand. However, it is not easy to determine such a very low concentration of oxygen. Because the advantage of using the pulse-adsorption of CO is convenience, the inspection of the carrier gas is of no value unless the method is also very simple and convenient.

The reason why such a high purity of the carrier gas is required is that the reduced metal surface has a strong function to capture gaseous oxygen. Therefore, we tried to determine the oxygen content by utilizing the ability of metal catalysts to capture oxygen; *i.e.*, first flowing the carrier gas through a Pt catalyst to collect the small amount of oxygen on the Pt surface, and second analyzing the adsorbed oxygen by means of O_2–CO titration.

This method is based on the following surface reactions on supported Pt catalysts;[3]

$$1/2 \cdot O_2 + Pt(s) \rightarrow Pt\text{-}O(a), \quad (1)$$

$$2CO + Pt\text{-}O(a) \rightarrow Pt\text{-}CO(a) + CO_2, \quad (2)$$

$$CO + Pt(s) \rightarrow Pt\text{-}CO(a). \quad (3)$$

When the carrier gas is passed through the Pt catalyst for a period longer than in the pulse-adsorption experiment, the gaseous oxygen contained in the helium is captured on the Pt surface as in Eq. 1. The adsorbed oxygen easily reacts with CO pulses at room trremperature, and CO_2 is evolved following Eq. 2, so we can estimate the amount of adsorbed oxygen by measuring the amount of CO_2. If the Pt surface is only partly covered with oxygen, Reaction (3) also takes place on the surface. Because Reaction (2) occurs in preference to Reaction (3), CO_2 is easily detected, even if its amount is small.

Figure 1 illustrates the apparatus. Helium was purified by being passed through a reduced copper trap (500 K) and molecular sieves. CO was pulsed by means of a six-port valve with a sampling tube of 0.352 ml attached. This apparatus is similar to a conventional pulse-adsorption system except that an active carbon column is attached between the sample

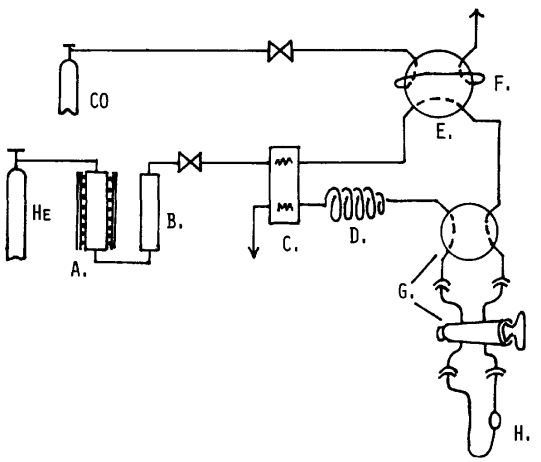

Fig. 1. Experimental apparatus both for purity check of carrier gas and pulse adsorption of CO. A. Oxygen trap (activated copper; normally kept at 500 K), B. Water trap (molecular sieves), C. Detector, D. Active carbon column, E. 6-port valve, F. Sampling tube, G. 4-port valve, H. Catalyst sample.

and the detector in order to separate the CO and CO_2. After the carrier-gas inspection is finished, experiments on CO adsorption or O_2–CO titration may be carried out using this apparatus unchanged.

The probe catalyst, Pt/SiO_2, was prepared by impregnating SiO_2 (aerosil 380) with an aqueous solution of hydrogen chroloplatinate(IV). The metal loading was 0.15 mmol/g (2.8 wt%). The pretreatment procedure was the same as in our previous studies of O_2–CO titration over $Pt–Ru/SiO_2$.[3,4] That is, after the catalyst had been evacuated at room temperature for 10 min, it was heated to 400 K and then evacuated for 1 h. In a flow of hydrogen, the temperature was increased to 600 K at a rate of 10 K/min. The catalyst was subsequently reduced at 600 K for 3 h, evacuated at 720 K for 30 min, and then cooled slowly to room temperature. After the pretreatment, the reactor was removed from the pretreatment apparatus to the pulse apparatus, keeping a vacuum. Such a pretreatment minimized the period (less than 30 min) during which the catalyst was in contact with the carrier gas compared with the case of desorbing hydrogen in a flow of helium.

Figures 2-A and B show typical examples of chromatograms resulting from this experiment. When the heating of reduced Cu was stopped and helium was passed through the catalyst without removing the oxygen for 1 h, we obtained the chromatogram shown in Fig. 2-A. CO was consumed almost completely in the first three pulses. A significant amount of CO_2 was evolved in the first pulse, but only a trace was evolved in the following pulses. Residual CO was detected after the fourth pulse. Because CO_2 is evolved as a single peak, as a result of the character of the Pt surface in preferring Reaction (2) to Reaction (3), it is easy to determine CO_2 even when the amount is very small. In this case, the oxygen content of helium was concluded to be 9.7 ppm.

When the Cu trap was working at 500 K, and when the system was in the same condition as in the CO adsorption experiments, we obtained the chromatogram shown in Fig. 2-B. In this case, no evolution of CO_2 was observed after the helium had flowed for 1.5 h. Supposing the peak height of CO_2 to be less than 1 mm (the same order as the baseline perturbation), the oxygen content of helium was calculated to be less than 0.1 ppm. Such a calculation is based on the assumption that all of the oxygen molecules are captured on the Pt surface. However, when the oxygen content is very low, the adsorption of oxygen (Reaction (1)) may be reversible and not all the oxygen may be captured. Thus, this method may be incomplete as a means of determining the oxygen content. Even so, it is sufficient as a means to judge whether or not the carrier gas is pure enough for pulse-adsorption experiments, because if the oxygen concentration is so small that oxygen is not captured on the metal surface, then the impurity can not affect the CO-adsorption experiments.

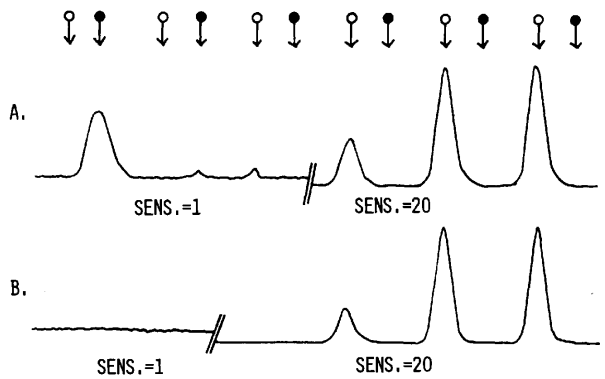

Fig. 2. Examples of chromatograms resulting from the CO titration of adsorbed oxygen contained in the helium carrier gas. ⚲: CO, ⚲: CO_2.
A. Heating of oxygen trap was stopped, B. Oxygen trap was kept at 500 K.

In this way, we could estimate the effect of oxygen impurity in the carrier gas on CO adsorption using a conventional pulse-adsorption system with quite a simple procedure.

References

1) J. R. Anderson, "Structure of Metallic Catalysts," Academic Press, London (1975), p. 295.
2) T. Keii, "Shokubai Kagaku," Tokyo Kagaku Dohjin, Tokyo (1981), p. 149.
3) H. Miura and R. D. Gonzalez, *J. Catal.*, **74**, 216 (1982).
4) H. Miura, T. Suzuki, Y. Ushikubo, K. Sugiyama, T. Matsuda, and R. D. Gonzalez, *J. Catal.*, **85**, 331 (1984).

General Formulas for Evaluating Ring Currents Induced in a Polycyclic Conjugated System

Jun-ichi AIHARA
Department of Chemistry, Faculty of Science, Shizuoka University, Oya, Shizuoka 422
(Received September 13, 1984)

Synopsis. Two apparently different but physically identical formulas were presented to evaluate bond currents (*i.e.*, ring currents in popular terminology) induced in a polycyclic conjugated system. They are applicable to all kinds of planar conjugated systems.

It was in 1979 that we reported a graph-theoretical formula for London susceptibility (*i.e.*, magnetic susceptibility attributable to ring currents) of a planar polycyclic hydrocarbon with no bond alternation.[1] It was later modified to estimate London susceptibility of a bond-alternate hydrocarbon.[2] In fact, this modified formula proved to be applicable to all kinds of planar conjugated systems, including heterocycles. In 1983, we formulated ring currents induced magnetically in a carbocyclic system with no bond alternation.[3] It is now easy to formulate ring currents induced in a heterocycle whose conjugated system is depicted with a variety of Coulomb and resonance integrals.

The term "ring current" has been used by many chemists. However, we hereafter use the term "bond current" instead of the term "ring current" since the latter term has so far borne some different meanings.[3-7] A bond current is defined as an entire current which is induced magnetically in a given π bond and passes through it. Mallion has once used this term in the same sense.[8]

We start with the modified graph-theoretical formula for London susceptibility.[2] It is expressed as

$$\chi_G = 9\chi_0 \sum_{i=1}^{M} \left(\frac{S_i}{S_0}\right)^2 \prod_{(lm)}^{r_i} k_{lm} \sum_{j=1}^{N} \frac{g_j P_{G-r_i}(X_j)}{P_G'(X_j)}. \quad (1)$$

Here, G stands for an entire conjugated system of a planar monocyclic or polycyclic molecule; r_i is the ith π-electron circuit in G,[9] which has been referred to as the ith π-electron ring in our previous papers;[1-3,10-13] G is assumed to have M conjugated atoms and N π-electron circuits; $G-r_i$ is the subsystem of G, obtained by deleting from G the ith π-electron circuit and all π bonds incident to it; $P_G(X)$ is the characteristic polynomial for G; $P_G'(X)$ is its first derivative with respect to X; $P_{G-r_i}(X)$ is the characteristic polynomial for $G-r_i$; X_j is the energy of the jth π-electron molecular orbital, obtained by solving the equation $P_G(X)=0$; g_j is the occupation number for the jth π-electron molecular orbital; S_i is the area of the ith π-electron circuit; S_0 is the area of the benzene ring; k_{lm} is the resonance integral parameter for the $l-m$ π bond, the resonance integral itself being expressed as $k_{lm}\beta$; (lm) runs over all π bonds constituting the ith π-electron circuit; and χ_0 is London susceptibility of benzene. π-Electron circuits denoted by r_i are nothing other than ring components defined in Sachs' graph theory.[14-17]

According to the same procedure as shown in a previous paper,[3] the circuit current induced in the ith π-electron circuit is expressible in the form:

$$I_i = 9I_0 \frac{S_i}{S_0} \prod_{(lm)}^{r_i} k_{lm} \sum_{j=1}^{N} \frac{g_j P_{G-r_i}(X_j)}{P_G'(X_j)}, \quad (2)$$

where I_0 is the circuit current induced in benzene under the same experimental condition. I_0 is equal to the bond current induced in benzene. Both I_0 and I_i are proportional to the intensity of the external magnetic field. The bond current induced in the $l-m$ π bond of G is then given by adding up all circuit currents passing through it. It is expressed as

$$J_{lm} = \sum_{i(lm)} I_i, \quad (3)$$

where i runs over all π-electron circuits with the $l-m$ π bond in common. Since Eq. 1 is applicable to all kinds of planar conjugated systems, Eq. 3 is again applicable to them all.

Equation 3 can be written explicitly in terms of χ_G. The signed area of the triangle formed by the origin of the coordinates and the $l\rightarrow m$ π bond, s_{lm}, can be defined in such a manner that it satisfies the following two conditions:[4,5]

$$s_{lm} = -s_{ml} \quad (4)$$

and

$$S_i = \sum_{(lm)}^{r_i} s_{lm}, \quad (5)$$

where (lm) runs over all π bonds constituting the ith π-electron circuit. By substituting S_i in Eq. 1 by Eq. 5 and then by differentiating Eq. 1 with respect to s_{lm}, we obtain the formula for a quantity proportional to the bond current induced in the $l-m$ π bond. This relationship can be written formally as

$$J_{lm} = \frac{S_0 I_0}{2\chi_0} \frac{\partial \chi_G}{\partial s_{lm}}. \quad (6)$$

This expression is necessarily identical with Eq. 3.

On the other hand, Veillard formulated the total π-electron energy of a heterocyclic conjugated system as a function of the external magnetic field.[18] By differentiating the energy twice with respect to the field strength, we obtain the following expression for London susceptibility of a heterocyclic system:

$$\chi_G = \frac{9\chi_0}{S_0^2}\left[\sum_{(lm)}^{G} k_{lm} p_{lm} s_{lm}^2 + \sum_{(lm)}^{G}\sum_{(l'm')}^{G} k_{lm}k_{l'm'}\bar{\pi}_{lm,l'm'}s_{lm}s_{l'm'}\right]. \quad (7)$$

Here, p_{lm} is the bond order for the $l-m$ π bond; $\bar{\pi}_{lm,l'm'}$ is what McWeeny defined as the imaginary bond-bond

polarizability of the $l-m$ and $l'-m'$ π bonds;[4,20] and both (lm) and $(l'm')$ run over all π bonds in G. Eq. 7 is applicable to bond-alternate hydrocarbons alike. In fact, Gayoso and Boucekkine reported a similar formula for bond-alternate hydrocarbons.[19]

Equation 7 is mathematically identical with Eq. 1 since these two formulas have been derived from the same field-dependent secular determinant.[2,18,19] They manifest two different physical features of London susceptibility. Accordingly, Eq. 6 can be applied to Eq. 7 to formulate the bond currents. By substituting χ_G in Eq. 6 by Eq. 7 and with the equality $\overline{\pi}_{lm,l'm'}=\overline{\pi}_{l'm',lm}$ in mind,[20] the following expression is obtained for the bond current induced in the $l-m$ π bond:

$$J_{lm}=\frac{9I_0}{S_0}\left[k_{lm}p_{lm}s_{lm}+k_{lm}\sum_{(l'm')}^{G}k_{l'm'}\overline{\pi}_{lm,l'm'}s_{l'm'}\right], \quad (8)$$

where $(l'm')$ runs over all π bonds in G. Equation 8 is again applicable not only to bond-alternate hydrocarbons but also to heterocycles as long as they are planar in shape. According to Mallion,[8] Haigh devised in 1971 a formula analogous to Eq. 8 to calculate bond currents in a hydrocarbon with no bond alternation. Equation 8 is a generalized form of it.

It is to be noted that both Eqs. 3 and 8 are general, in the sense that they can be applied to any planar cyclic conjugated system. All modifications of the Hückel molecular orbital method can be used to evaluate such quantities as k_{lm}, p_{lm}, and $\overline{\pi}_{lm,l'm'}$ which appear in Eqs. 3 and 8. Gayoso and Mallion recommended the iterative $\beta\omega'\omega''$ Hückel method for evaluating London susceptibility and bond currents.[19,21-23] Both Eqs. 3 and 8 naturally gave the same numerical results for naphthalene, biphenylene, anthracene, azulene, and pyracylene,[22,23] all with realistic carbon-carbon bond lengths.[19,21-23] The bond currents calculated by one of these formulas can be confirmed numerically by means of the other formula. Eq. 8 is much simpler in appearance than Eq. 3. If there is no need to obtain individual circuit currents, the former formula is best suited for evaluation of bond currents by computer.

References

1) J. Aihara, *J. Am. Chem. Soc.*, **101**, 5913 (1979).
2) J. Aihara, *Bull. Chem. Soc. Jpn.*, **54**, 1245 (1981).
3) J. Aihara and T. Horikawa, *Bull. Chem. Soc. Jpn.*, **56**, 1853 (1983). Equation 10 in this paper is erroneous. It should read:

$$\frac{I_i}{I_0}=18\frac{S_i}{S_0}\sum_{j=1}^{n}\frac{P_{G-r_i}(X_j)}{P_G'(X_j)}.$$

4) J. A. Pople, *Mol. Phys.*, **1**, 175 (1958).
5) R. McWeeny, *Mol. Phys.*, **1**, 311 (1958).
6) C. A. Coulson, J. A. N. F. Gomes, and R. B. Mallion, *Mol. Phys.*, **30**, 713 (1975).
7) C. W. Haigh and R. B. Mallion, *J. Chem. Phys.*, **76**, 4063 (1982).
8) R. B. Mallion, *Mol. Phys.*, **25**, 1415 (1973).
9) N. Mizoguchi, *Chem. Phys. Lett.*, **106**, 451 (1984).
10) J. Aihara, *J. Am. Chem. Soc.*, **103**, 5704 (1981).
11) J. Aihara and T. Horikawa, *Chem. Phys. Lett.*, **95**, 561 (1983).
12) T. Horikawa and J. Aihara, *Bull. Chem. Soc. Jpn.*, **56**, 1547 (1983).
13) J. Aihara, *Pure Appl. Chem.*, **54**, 1115 (1982).
14) H. Sachs, *Publ. Math. (Debrecen)*, **11**, 119 (1964).
15) A. Graovac, I. Gutman, N. Trinajstić, and T. Živković, *Theor. Chim. Acta*, **26**, 67 (1972).
16) A. Graovac, O. E. Polansky, N. Trinajstić, and N. Tyutyulkov, *Z. Naturforsch., Teil A*, **30**, 1696 (1975).
17) J. Aihara, *J. Am. Chem. Soc.*, **98**, 6840 (1976).
18) A. Veillard, *J. Chim. Phys.*, **59**, 1056 (1962).
19) J. Gayoso and A. Boucekkine, *C. R. Hebd. Seaces Acad. Sci., Ser. C*, **272**, 184 (1971).
20) R. B. Mallion, *Proc. R. Soc. London, Ser. A*, **341**, 429 (1975).
21) A. Boucekkine and J. Gayoso, *C. R. Hebd. Seances Acad. Sci., Ser. C*, **274**, 358 (1972).
22) C. A. Coulson and R. B. Mallion, *J. Am. Chem. Soc.*, **98**, 592 (1976).
23) J. A. N. F. Gomes and R. B. Mallion, *J. Org. Chem.*, **46**, 719 (1981).

Mössbauer Spectroscopic Study of Danalite, $Fe_4(BeSiO_4)_3S$

Yonezo MAEDA,* Yoshimasa TAKASHIMA, and Kiyotake ISHIDA†
Department of Chemistry, Faculty of Science, Kyushu University, Hakozaki, Higashiku, Fukuoka 812
†*Institute of Earth Science, College of General Education, Kyushu University, Ropponmatsu, Fukuoka 810*
(Received July 2, 1984)

Synopsis. The Mössbauer spectra for danalite have been examined in the temperature range 4.2 to 321 K. The strong temperature dependencies of the Mössbauer parameters are explained on the basis of a ligand field at a tetrahedral site for iron.

The helvite group is a general term of the mineral consisting of (Mn, Fe, Zn)$_4$(BeSiO$_4$)$_3$S in which the cations of the end members are manganese (helvite), iron (danalite), and zinc (genthelvite).[1-3] Metal ions are located in a tetrahedra made of three oxygen atoms and one sulfur atom. An iron(II) ion at a tetrahedral site has been found in spinel-type oxides[4,5] and $MFeCl_4$ type complexes.[6] Their Mössbauer spectra are usually temperature dependent since quadrupole splittings are sensitive to a splitting of the dγ-orbital. There has been no discussion so far regarding the distribution of the splittings of the dγ-orbital, except one paper.[5] In this paper the splitting of the dγ-orbital and its distribution in danalite are examined in terms of Mössbauer spectroscopy.

Experimental

Danalite and helvite occur in the Hirako mine, Hiroshima prefecture[7] and in the Yagisawa mine, Gunma Prefecture,[8] respectively. The apparatus used to carry out the Mössbauer measurements has been reported elsewhere.[9] Every spectrum was fitted to Lorentzian line shapes using a least-squares method at the Computer Center, Kyushu University. The velocity scale was normalized with respect to the center of the spectrum of an iron foil at 297 K.

Results and Discussion

The chemical composition of the danalite used in this study was measured using an X-ray microanalyzer. The distribution of cations was $Fe_{1.94}Mn_{1.58}Zn_{0.39}Ca_{0.09}$.

The Mössbauer spectra for the danalite at three different temperatures are shown in Fig. 1. The value of the quadrupole splitting for the danalite is small (QS=0.369 mm/s) at 321 K, but increases with a decrease in temperature (QS=2.740 mm/s at 4.2 K). The electric field gradient for a high-spin iron(II) ion may be considered as follows.

$$q = (1-R)q_{val} + (1-\gamma)q_{lat}.$$

The subscript *"val"* refers to the charge distribution of an aspherical 3d "valence" electron. The subscript *"lat"* refers to the charge distribution of the neighboring ions in a crystalline lattice. The Sternheimer factors (1-R) and (1-γ) were added to correct for the polarization of an iron(III)-like core. The large temperature dependence of quadrupole splitting of danalite indicates that the splitting of the

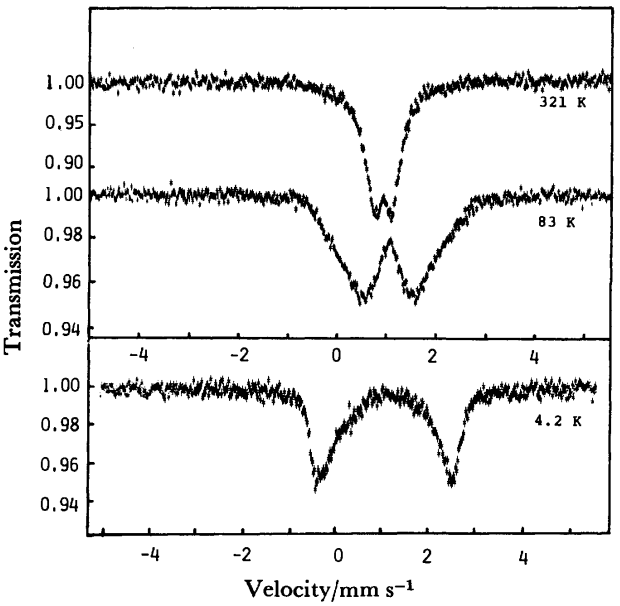

Fig. 1. Mössbauer spectra of the danalite at various temperatures.

dγ-orbitals of an iron(II) ion is small and the small quadrupole-splitting values at high temperatures confirm that the contribution of q_{lat} to the electric field gradient is small, although an iron(II) ion is located in an elongated tetrahedral site (one sulfur and three oxygens, "S3O"). From the crystallographic data for helvite, the bond length for Mn–S was found to be 0.2432 nm, and that for Mn–O 0.2082 nm. The bonding angle for S–Mn–O was 116.1 degrees, and that for O–Mn–O was 102.1 degrees.[2] If an electric field gradient $q_{lat}=(Z_i/r_i^3)(3\cos^2\theta_i-1)$ is applied for the 1-st nearest "S3O" core with the point charge model, a quadrupole splitting QS=−1.93 mm/s can be calculated using the values of Q=0.29 barn and 1−γ=−7.17. The calculated value of q_{lat} is large, due to the elongated tetrahedral structure. Values of q_{lat} are temperature independent on the first approximation and influences the QS value at high temperatures. However, the observed values of QS are smaller at high temperatures than the calculated values. This disagreement may result from the fact that the charge density at a sulfur atom is not the same as that for an oxygen atom and that the contributions to QS from the second nearest neighbor atoms and a further neighbor atoms are important. The splitting of the dγ-orbitals(Δ) may be calculated theoretically.[6]

$$QS = QS_0 \times \frac{1-\exp(-\Delta/kT)}{1+\exp(-\Delta/kT)},$$

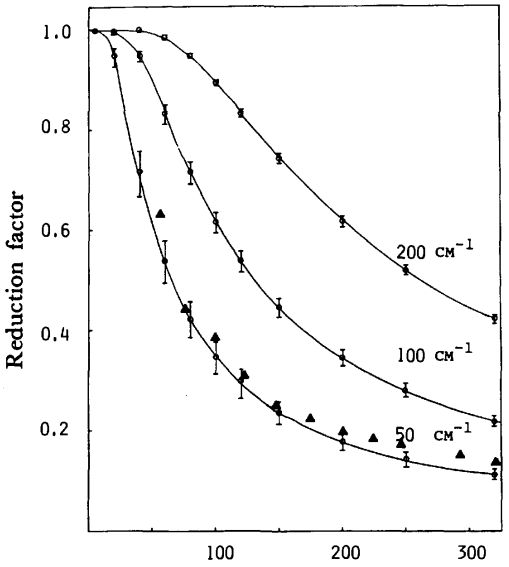

Fig. 2. Temperature dependence of the quadrupole splitting for $\Delta=50$, 100, 200 cm^{-1} and the experimental values. The bars on the circles show the difference of $\Delta\pm5$ cm^{-1}. Triangles show the QS values observed for the danalite. The value at 4.2 K is reduced to 1.00.

where k is the Boltzmann constant and QS_0 is taken to be 2.74 mm/s (the value at 4.2 K). Figure 2 shows the plots of the observed values of QS and some theoretical curves. A $\Delta=50$ cm^{-1} was calculated for the danalite by fitting the theoretical value to experimental measurements. This value seems to be so small for an iron(II) ion located in an elongated tetrahedral site.

The temperature dependence of the full widths at half maximum (FWHM) is plotted in Fig. 3. The differences of QS values between $\Delta=45$ cm^{-1} and $\Delta=55$ cm^{-1} at a certain temperature are also plotted as a solid line in the Figure. The difference becomes maximum at a particular temperature. The small geometrical distortion of a tetrahedra brings about the difference of the crystal field strength. This determines the distribution of quadrupole splittings and consequently causes the line width to broaden. The plots of the observed FWHM *vs.* T are similar to the shape of a theoretical curve. A gaussian distribution of Δ with a half width of 5 cm^{-1} explains the observed line broadening, if a gaussian distribution of it is postulated. The observed broad FWHM may come from the nonrandom distribution of cations in danalite.

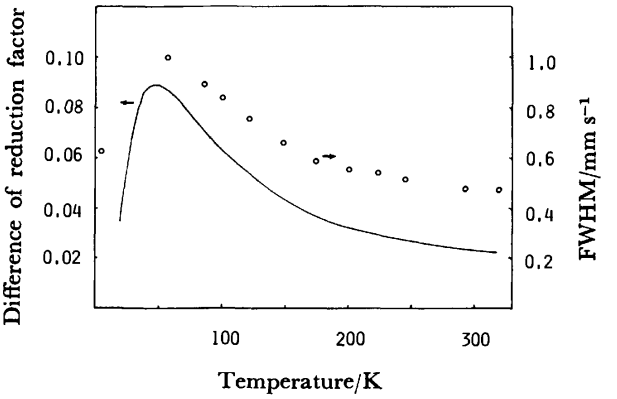

Fig. 3. Temperature dependence of the full width at half maximum for the danalite (open circles) and the differences of the theoretical reduction factors at $\Delta=50\pm5$ cm^{-1} (solid line).

The isomer shifts values are 1.13 (4.2), 1.08 (57), 1.07 (83), 1.06 (100), 1.06 (122), 1.04 (149), 1.03 (175), 1.01 (201), 0.999 (224), 0.986 (246), 0.959 (293), and 0.944 mm/s (at 321 K). The *IS* values decrease linearly with an increase in temperature and any changes in chemical bonding may not occur in the temperature range from 83 to 321 K. The discovery of the existence of a crystal-field distribution in one compound is due to the existence of a very small splitting of the dγ-orbitals of iron(II) in danalite. Similar QS values and line broadening were also observed for the helvite. This observation supports the idea that a nonrandom distribution of cations brings about such a wide broadening of a spectral line.

References

1) J. J. Glass, R. H. Jahns, and R. E. Stevens, *Am. Mineral.*, **29**, 163 (1944).
2) E. M. Holloway, Jr, T. J. Giordano, and D. R. Peacor, *Acta Cryst.*, **B28**, 114 (1972).
3) D. M. Burt, *Am. Mineral.*, **65**, 355 (1980).
4) T. Mizoguchi and M. Tanaka, *J. Phys. Soc. Jpn.*, **18**, 1301 (1963).
5) K. Ono, A. Ito, and Y. Syono, *Phys. Lett.*, **A19**, 621 (1966).
6) P. R. Edwards, C. E. Johnson, and R. J. P. Williams, *J. Chem. Phys.*, **47**, 2074 (1967).
7) Y. Aoki and N. Hida, *Mining Geology*, **24**, 201 (1974).
8) M. Yoshinaga, *Mem. Fac. Sci., Kyushu Univ., Ser. D, Geology Vol.*, **IX**, 47 (1959).
9) H. Ohshio, Y. Maeda, and Y. Takashima, *Inorg. Chem.*, **22**, 2684 (1983).

Thermodynamic Studies of Halogenocadmium Complexes in Nonaqueous Solvents

Yukio SASAKI,* Kazuya ABE, and Masao TAKIZAWA
Faculty of Engineering, Tokyo Institute of Polytechnics, Iiyama, Atsugi, Kanagawa 243-02
(Received August 4, 1984)

Synopsis. The thermodynamic constants for the formation of halogenocadmium complexes in *N,N*-dimethylformamide (DMF) and propylene carbonate (PC) were calculated by potentiometric titration. The differences in the order of the stability among the halide ions (X^-) for CdX_4^{2-} in nonaqueous solvents and water were found to be dependent mainly on the enthalpy changes of transfer from water to DMF and PC for the formation of CdX_4^{2-}.

Earlier studies on the stability of metal halide complexes (halogenocadmium, -lead and -copper complexes[1-3]) proved that the classification of metals by Ahrland[4] according to their complexation with halide ions in water was different from that in dipolar aprotic solvents. In the nonaqueous solvents the stability of the halogeno complexes on the metals described above decreases in the order of $Cl^->Br^->I^-$, which is the reversed order in water.

The purpose of the present paper is to investigate from the thermodynamic constants of the formation of halogenocadmium complexes the difference of the stability on metal halide complexes in *N,N*-dimethylformamide, propylene carbonate and water.

Experimental

Materials. The purification of *N,N*-dimethylformamide (DMF) and propylene carbonate (PC), the preparation and purification of tetraehylammonium perchlorate, tetraethylammonium halides, and the preparation of the saturated cadmium amalgam have been described elsewhere.[2,5] As a cadmium salt, cadmium perchlorate (Found: C, 28.8 ; H, 5.6 ; N, 11.2%. Calcd for $Cd(ClO_4)_2 \cdot 6DMF$: C, 28.3; H, 6.2; N, 11.5%.) obtained by twice recrystallization of the commercial reagent $[Cd(ClO_4)_2 \cdot 6H_2O)$ in DMF was used. The $Cd(ClO_4)_2 \cdot 6DMF$ was dried in a vacuum oven for two days at 30 °C.

Procedure. The experimental device for measuring the potential was described in the previous papers.[6,7] A solution of 10^{-3} mol dm^{-3} of $Cd(ClO_4)_2 \cdot 6DMF$ was titrated with a solution of 5×10^{-2} mol dm^{-3} of tetraethylammonium halides in 0.1 mol dm^{-3} tetraethylammonium perchlorate. Each temperature was controlled to an accuracy of 0.1 °C.

Results and Discussion

The titration curves for Cd^{2+} with Cl^- in PC at 15, 20, and 25 °C are shown in Fig. 1. The higher-order halogenocadmium complexes produced in DMF and PC are found to be CdX_4^{2-}, as shown in the previous paper.[2] The method for calculating the overall formation constants (β_4) of CdX_4^{2-} is described elsewhere.[2,8] The enthalpy changes ($\Delta H^\circ_{(CdX_4^{2-})}$) for the formation of CdX_4^{2-} were obtained graphically from the slope of the log β_4 *vs.* $1/T$ plot (Vant Hoff plot, Eq. 1).

$$\log \beta_4 = -\frac{\Delta H^\circ_{(CdX_4^{2-})}}{2.303R}\frac{1}{T} + \text{const.} \quad (1)$$

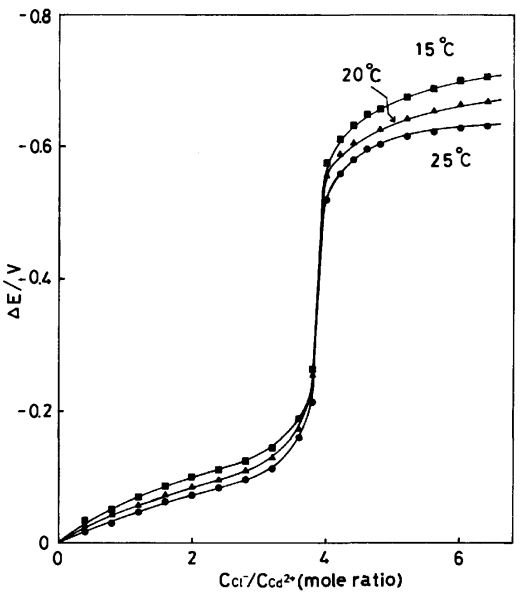

Fig. 1. Potentiometric titration curves for Cd^{2+} with Cl^- in PC at 15, 20 and 25 °C.
ΔE : potential shift caused by addition of Cl^-.

The free energy changes ($\Delta G^\circ_{(CdX_4^{2-})}$) for the formation of CdX_4^{2-} can be correlated to log β_4 with the temperature in Eq. 2, and

$$\Delta G^\circ_{(CdX_4^{2-})} = -2.303RT \log \beta_4 \quad (2)$$

the entropy changes ($T\Delta S^\circ_{(CdX_4^{2-})}$) were calculated from the $\Delta H^\circ_{(CdX_4^{2-})}$ and $\Delta G^\circ_{(CdX_4^{2-})}$. These thermodynamic constants in water have already been reported by many authors.[9] The overall formation constants in 0.1 mol dm^{-3} tetraethylammonium perchlorate and these thermodynamic constants in DMF, PC, and water at 25 °C are given in Table 1. These data in water were quoted from the literature.[9-12] The formation of $CdCl_4^{2-}$ in water is recognized polarographically by Marple.[10] However, its formation is not observed by calorimetric measurement.[11,12] In Table 1, the order of the stability of CdX_4^{2-} with $\Delta G^\circ_{(CdX_4^{2-})}$ in DMF and PC is found to be $CdCl_4^{2-}>CdBr_4^{2-}>CdI_4^{2-}$, while it is the reversed order in water. These thermodynamic constants in DMF were compared with those in dimethyl sulfoxide (DMSO).[13,14] The values of $-\Delta G^\circ_{(CdX_4^{2-})}$ in DMF are larger than those values in DMSO. It seems reasonable to consider that donicity of DMF is smaller than that of DMSO. The values of $\Delta H^\circ_{(CdX_4^{2-})}$ and $T\Delta S^\circ_{(CdX_4^{2-})}$ in DMF differ fairly from those in DMSO. The difference in $\Delta H^\circ_{(CdX_4^{2-})}$ and $T\Delta S^\circ_{(CdX_4^{2-})}$ in these solvents will be based on that of the measurements, because the calorimetric measurement takes account of the

Table 1. Thermodynamic constants for formation of halogenocadmium complexes(CdX_4^{2-}) in DMF, PC, and water at 25 °C

Solvent	CdX_4^{2-}	$\log \beta_4$	$\Delta G^\circ_{(CdX_4^{2-})}$ / kJ mol^{-1}	$\Delta H^\circ_{(CdX_4^{2-})}$ / kJ mol^{-1}	$T\Delta S^\circ_{(CdX_4^{2-})}$ / kJ mol^{-1}
DMF	$CdCl_4^{2-}$	21.3±0.4	−121	−288	−167
	$CdBr_4^{2-}$	17.7±0.3	−101	−206	−105
	CdI_4^{2-}	14.1±0.1	−81	−129	−48
PC	$CdCl_4^{2-}$	32.3±0.6	−184	−400	−216
	$CdBr_4^{2-}$	29.9±0.8	−171	−306	−135
	CdI_4^{2-}	26.6±0.5	−152	−269	−117
Water	$CdCl_4^{2-}$ [a]	1.7	−9.4		
	$CdBr_4^{2-}$ [b,c]	3.7	−21.0	+2.0	+23.0
	CdI_4^{2-} [b,c]	6.5	−37.1	−29.3	+7.8

a) Ref. 10. b) Ref. 11. c) Ref. 12.

Table 2. Thermodynamic constants for formation of halogenocadmium complexes(CdX_4^{2-}) of transfer from water to DMF and PC at 25 °C

Transfer	CdX_4^{2-}	$\Delta G^\circ_{tr(CdX_4^{2-})}$ / kJ mol^{-1}	$\Delta H^\circ_{tr(CdX_4^{2-})}$ / kJ mol^{-1}	$T\Delta S^\circ_{tr(CdX_4^{2-})}$ / kJ mol^{-1}
From water to DMF	$CdCl_4^{2-}$	−112		
	$CdBr_4^{2-}$	−80	−208	−128
	CdI_4^{2-}	−44	−100	−56
From water to PC	$CdCl_4^{2-}$	−175		
	$CdBr_4^{2-}$	−150	−308	−158
	CdI_4^{2-}	−115	−240	−125

state of the bulk in solution and the potentiometric titration considers the state of the vicinity of the electrode. However, considering the fact that the difference in the enthalpy changes for free Cd^{2+} in DMF and DMSO is very small,[15] and that the difference in solvation of X^- is not so large between DMF and DMSO,[16] it is difficult to elucidate the reason of the large difference for $\Delta H^\circ_{(CdX_4^{2-})}$ in DMF and DMSO.

The thermodynamic constants for the formation of CdX_4^{2-} of the transfer from water to DMF and PC are listed in Table 2. From the values of $\Delta G^\circ_{tr(CdX_4^{2-})}$ it is manifest that $CdCl_4^{2-}$ becomes the most stable complex for transfer among the CdX_4^{2-} complexes. The difference in $\Delta H^\circ_{tr(CdX_4^{2-})}$ between the $CdBr_4^{2-}$ and CdI_4^{2-} complexes is larger than that in $T\Delta S^\circ_{tr(CdX_4^{2-})}$ as shown in Table 2. Therefore, it was found that the enthalpy changes in transfer from water to DMF and PC contribute much to the free-energy changes of the transfer. It may be concluded that the differences in the order of the stability for metal halogeno complexes in DMF, PC, and water depend mainly on the enthalpy changes ($\Delta H^\circ_{tr(CdX_4^{2-})}$) for the formation of CdX_4^{2-} complexes.

References

1) Y. Sasaki, M. Takizawa, and N. Matsuura, *Nippon Kagaku Kaishi*, **1976**, 1414.
2) N. Matsuura, M. Takizawa, and Y. Sasaki, *Nippon Kagaku Kaishi*, **1976**, 1495.
3) Y. Sasaki, M. Takizawa, K. Umemoto, and N. Matsuura, *Nippon Kagaku Kaishi*, **1977**, 983.
4) S. Ahrland, *Acta Chem. Scand.*, **10**, 723 (1956).
5) N. Matsuura and K. Umemoto, *Bull. Chem. Soc. Jpn.*, **47**, 806 (1974).
6) Y. Sasaki, M. Takizawa, K. Umemoto, and N. Matsuura, *Bull. Chem. Soc. Jpn.*, **54**, 65 (1981).
7) Y. Sasaki, M. Takizawa, K. Umemoto, and N. Matsuura, *Electrochimica Acta*, **26**, 185 (1981).
8) M. Aihara and S. Misumi, *Bull. Chem. Soc. Jpn.*, **46**, 1674 (1973).
9) L. G. Sillen, "Stability Constants Supplement No. 1," Special Publication 25, The Chemical Society, London (1971).
10) L. W. Marple, *J. Inorg. Nuclear Chem.*, **27**, 1693 (1965).
11) P. Gerding, *Acta Chem. Scand.*, **20**, 79 (1966).
12) P. Gerding and B. Johansson, *Acta Chem. Scand.*, **22**, 2255 (1968).
13) S. Ahrland and N.-o. Bjork, *Acta Chem. Scand.*, **A,30**, 257 (1976).
14) S. Ahrland, *Pure Appl. Chem.*, **51**, 2019 (1979).
15) G. R. Hedwig and A. J. Parker, *J. Am. Chem. Soc.*, **96**, 6589 (1974).
16) J. F. Coetzee and C. D. Ritchie, "Solute-solvent Interactions," Marcell Dekker, New York and Basel (1976), Vol. 2, pp. 348.

Preparation and Properties of the New High Pressure Phase β-$Zr(OH)PO_4$

Akira ONO* and Fujio Peter OKAMURA
National Institute for Research in Inorganic Material, Namiki, Ibaraki 305
(Received September 19, 1984)

Synopsis. A new phase with chemical formula $Zr(OH)PO_4$ was prepared above 1.5 GPa using a high pressure apparatus. Stability field of the compound was investigated, and X-ray study for a single crystal revealed that it is orthorhombic with space group Cmca or C2ca. The X-ray data are similar to those of $Zr_2O(PO_4)_2$.

Phosphate compounds in the system ZrO_2–P_2O_5–H_2O have been studied in relation to the inorganic ion exchanger, $Zr(HPO_4)_2 \cdot H_2O$[1] and the ceramic material with low thermal expansion, $Zr_2O(PO_4)_2$.[2,3] Other crystalline phases in this system are $Zr_{0.25}Zr_2(PO_4)_3$,[4] ZrP_2O_7 and $Zr(OH)PO_4$.[5] We have prepared a new high pressure compound isochemical with $Zr(OH)PO_4$ reported by Chernorukov *et al.*[9] Hereafter, the low and high pressure phases will be called α-$Zr(OH)PO_4$ and β-$Zr(OH)PO_4$, respectively. Preparation and properties of the new phase will be described below.

Experimental

Starting Materials. Reagents used for synthesis were $NH_4H_2PO_4$, ZrO_2, and $ZrOCl_2 \cdot 8H_2O$ of a high purity. Three kinds of starting materials were used. First one was prepared from a mixture of ZrO_2 and $NH_4H_2PO_4$ with the Zr/P ratio equal to 1/2. The mixture was dried at 473 K for 24 h and then heated at 873 K for 5 h, and crystalline ZrP_2O_7 was obtained. A mixture of ZrP_2O_7 and water was used as a starting material for obtaining single crystals large enough for X-ray studies. Second starting material was an equimolar mixture of ZrP_2O_7 and ZrO_2, which was used for most of the experiments carried out above 1 GPa. Third starting material was a gel prepared by mixing equimolar solutions of $ZrOCl_2 \cdot 8\ H_2O$ and H_3PO_4. The gel dried at 323 K was used as a starting material for experiments below 0.2 GPa.

High Pressure Experiments. A piston cylinder type high pressure apparatus was used for experiments above 1 GPa. A pressure cell consists of a concentric assemblage of NaCl with 10% MoS_2, a carbon heater and pure NaCl. A platinum capsule containing the starting material and water (10—50 wt%) was put in the center of the pressure cell. Sizes of the cell are 12.7 mm in diameter and 400 mm in length. Temperature was measured by an alumel-chromel thermocouple in contact with the Pt capsule. Pressure was gradually raised up to a desired value at a given temperature. Pressure is a nominal value not corrected for friction. Run durations are 48 to 72 h.

Experiments below 0.2 GPa were performed using a cold seal high pressure vessel in order to establish the stability range of α-$Zr(OH)PO_4$. Temperature was measured by an internal thermocouple, and pressure by a calibrated Heise Bourdon tube pressure gauge. Pressure medium is pure water. The third starting material was sealed in a gold capsule together with water.

Characterization of the Products. After washing with distilled water, experimental products were examined using an optical microscope, an X-ray diffractometer, a Weissenberg camera, an infrared spectrometer and a differential thermal analyzer. X-Ray powder patterns taken with a Toshiba ADG 301 diffractometer were obtained at room temperature in the range 2θ=7 to 60° using Cu $K\alpha$ radiation. Weissenberg photographs for a single crystal of β-$Zr(OH)PO_4$ were obtained using Ni-filtered Cu $K\alpha$ radiation. Infrared (IR) spectra recorded on a Hitachi model EPI-G3 IR spectrometer were measured in the frequency range 400 to 4000 cm^{-1} by using the normal KBr disk method. Thermal analyses were performed in air with an ULVAC TA-1500 at a heating rate of 10 K min^{-1}.

Synthetic crystals were analyzed using an electron probe microanalyzer, JXA 5A. Single crystals of ZrO_2, ZrP_2O_7, and $Zr_2O(PO_4)_2$ were used as standards. Apparent concentration was corrected after the Bence-Albee method.[6]

Results and Discussion

1) β-Zr(OH)PO₄. This phase was obtained above 1.5 GPa as shown by open circle in Fig. 1. Single crystals up to 100 μm were prepared together with $Zr(HPO_4)_2 \cdot H_2O$ when ZrP_2O_7 and water were used as the starting material. From Weissenberg photographs it was seen that β-$Zr(OH)PO_4$ crystallized in the orthorhombic system, the following reflexions being systematically absent, $hkl: h+k=2n$ (n: integer), $0kl: k=2n$, $h0l: l=2n$, $hk0: h=2n$, $00l: l=2n$. These extinctions indicate the space group to be Cmca or C2ca. Lattice constants are: a=0.6607, b=0.8657, c=1.1718 (nm). These are similar to those of $Zr_2O(PO_4)_2$: a=0.6624, b=0.8637, c=1.1872 (nm).[7]

Weight loss for β-$Zr(OH)PO_4$ took place in the temperature range 683 to 943 K. Amount of the water loss is 4.2 wt%, which is consistent with the theoretical value of 4.4%. The X-ray diffraction pattern of the final product is the same as that of $Zr_2O(PO_4)_2$. The X-ray data for β-$Zr(OH)PO_4$ and $Zr_2O(PO_4)_2$ obtained here are listed in Table 1.

An IR spectrum of β-$Zr(OH)PO_4$ illustrated in Fig. 2 A exhibits an absorption band at 3560 cm^{-1} which may be attributed to the OH stretching vibration and is absent for $Zr_2O(PO_4)_2$. Analytical result of β-$Zr(OH)PO_4$ using an electron probe microanalyzer is; Found: ZrO_2,60.32; P_2O_5,35.26; Total,95.58; H_2O,4.42

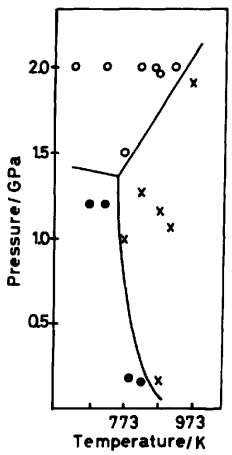

Fig. 1. Stability field of β-$Zr(OH)PO_4$.
○: β-$Zr(OH)PO_4$, ●: α-$Zr(OH)PO_4$, ×: $Zr_2O(PO_4)_2$.

TABLE 1. X-RAY POWDER DIFFRACTION DATA

	β-$Zr(OH)PO_4$				$Zr_2O(PO_4)_2$		α-$Zr(OH)PO_4$	
	d	d_{cal}			d		d	
$h\ k\ l$	10^{-1} nm	10^{-1} nm	I_{obsd}	$h\ k\ l$	10^{-1} nm	I_{obsd}	10^{-1} nm	I_{obsd}
0 0 2	5.86	5.859	55	0 0 2	5.94	50	5.88	44
0 2 0	4.33	4.328	40	0 2 0	4.33	60	5.48	23
0 2 1	4.06	4.060	66	0 2 1	4.06	74	5.08	23
1 1 2	3.91	3.910	38	1 1 2	3.94	50	4.83	23
0 2 2	3.49	3.481	33	0 2 2	3.49	43	4.53	100
2 0 0	3.30	3.303	100	2 0 0	3.31	100	4.37	92
1 1 3	3.14	3.134	36	1 1 3	3.16	52	4.27	77
0 0 4	2.95	2.929	17	0 0 4	2.96	13	4.08	23
0 2 3	2.90	2.899	36	0 2 3	2.92	32	3.94	77
2 2 0	2.62	2.626	7	2 2 0	2.63	15	3.69	34
1 3 1	2.58	2.579	39	1 3 1	2.58	88	3.66	74
1 1 4	2.56	2.558	55	1 1 4			3.62	23
1 3 2	2.41	2.410	28	1 3 2	2.41	33	3.31	53
2 0 4	2.19	2.192	9	2 0 4			3.17	84
0 4 0	2.167	2.164	5	0 4 0			3.12	61
0 4 1	2.130	2.128	14	0 4 1	2.125	16	3.10	30
3 1 1	2.100	2.099	7	3 1 1			2.91	16
0 2 5	2.060	2.061	15	0 2 5	2.03	15	2.85	54
3 1 2	2.004	2.005	20	3 1 2	2.01	38	2.78	43
3 2 0	1.960	1.962	11	3 2 0	1.97	22	2.74	30
0 0 6	1.956	1.953	17	0 0 6			2.69	17
0 4 3	1.896	1.893	24	0 4 3	1.897	31	2.65	33
3 1 3	1.874	1.873	8	3 1 3	1.886	9	2.59	23
1 1 6	1.833	1.830	14	1 1 6	1.853	28	2.56	38
0 2 6	1.782	1.780	6	0 2 6	1.801	18		
3 3 1	1.728	1.725	38	3 3 1	1.735	66		
3 1 4		1.731		3 1 4				
3 3 2	1.679	1.677	8	3 3 2	1.682	16		
1 5 1	1.657	1.658	29	1 5 1	1.657	50		
0 4 5	1.589	1.590	22					

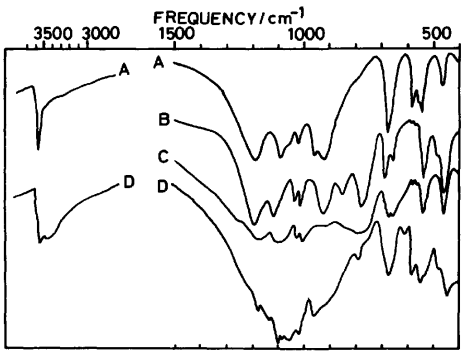

Fig. 2. IR spectra.
A: β-$Zr(OH)PO_4$, B: $Zr_2O(PO_4)_2$ prepared by heating β-Zr $(OH)PO_4$ at 973 K, C: $Zr_2O(PO_4)_2$ prepared at 1.15 GPa, D: α-$Zr(OH)PO_4$ obtained at 1.2 GPa.

[100-Total]. Calcd for $Zr(OH)PO_4$: ZrO_2,60.64; P_2O_5,34.93 (wt%).

2) α-Zr(OH)PO₄. This phase was prepared below 1.2 GPa and represented by solid circle in Fig. 1. The X-ray powder pattern of α-$Zr(OH)PO_4$ obtained at 1.2 GPa is similar to that given in the literature.[5] Figure 2 D shows an IR spectrum for this material. An absorption band near 3560 cm^{-1} is attributed to the OH stretching vibration.

3) $Zr_2O(PO_4)_2$. An IR spectrum of this material prepared at 873 K, 1.15 GPa is illustrated in Fig. 2C. The X-ray powder pattern of this phase is the same as that listed in Table 1.

The structure of dizirconium diorthophosphate[7] consists of chains composed of edge sharing ZrO_7 polyhedra which are connected by the P atoms in tetrahedral coordination. The chains are, however, partly bonded directly with each other by sharing an oxygen atom. If hydration of $Zr_2O(PO_4)_2$ takes place at the site of this oxygen atom, Zr_1–O–Zr_2 may change to Zr_1–OH+Zr_2–OH where Zr_1 and Zr_2 represent different chains. We propose that the structure of β-$Zr(OH)PO_4$ is similar to that of $Zr_2O(PO_4)_2$, but each chain is not joined directly. A structure similar to the proposed one is known for $Hf(OH)_2SO_4$.[8] $Hf(OH)_2SO_4$ contains chains of $[Hf(OH)_2]_n^{2+}$ which are joined by sulfate groups. The chains do not share any oxygen atom with each other.

References

1) A. Clearfield and J. A. Stynes, *J. Inorg. Nucl. Chem.*, **26**, 117 (1964).
2) D. E. Harrison, H. A. McKinstry, and F. A. Hummel, *J. Am. Ceram. Soc.*, **37**, 277 (1954).
3) I. Yamai, T. Oota, and S. Kawaminami, *Ann. Rep. Ceram. Engin. Res. Lab. Nagoya Inst. Techn.*, **9**, 23 (1982).
4) J. Alamo and R. Roy, *J. Am. Ceram. Soc.*, **78**, 80 (1984).
5) N. G. Chernorukov, I. A. Korshunov, and M. I. Zhuk, *Russ. J. Inorg. Chem.*, **28** (7), 934 (1984).
6) A. E. Bence and A. L. Albee, *J. Geol.*, **93**, 500 (1970).
7) V. W. Gebert and E. Tillmanns, *Acta Crystallogr., Sect. B* **31**, 1768 (1975).
8) M. Hansson, *Acta Chem. Scand.*, **27**, 2455 (1973).

The Structure of Diaquatris[(methylthio)acetato]-ytterbium(III), $[Yb(CH_3SCH_2CO_2)_3(H_2O)_2]_n$

Akira Ouchi,* Mamoru Shimoi, and Satoshi Kondo
Department of Chemistry, College of Arts and Sciences, the University of Tokyo, Komaba, Meguro-ku, Tokyo 153
(Received October 8, 1984)

Synopsis. The crystal and molecular structure of the title complex has been determined by the use of single-crystal X-ray diffraction. The crystal of $YbC_9H_{19}O_8S_3$, $F.W.$= 524.48, was monoclinic, with a space group of $P2_1/a$; a= 12.501(6), b=25.096(9), c=10.788(2) Å, β=90.25(3)°, U=3384 (2) Å^3, Z=8, D_m=2.07(3), D_x=2.06 Mg m^{-3}, and μ(Mo $K\alpha$)= 6.20 mm^{-1}. Both Yb(1) and Yb(2) are octa-coordinated and are in a dodecagedral geometry. They are in a linear polymer form, parallel to the c axis; Yb(1) and Yb(2) are arrayed in a line alternatively, bridged by one carboxylate ligand.

In a previous paper,[1] the present authors showed the structure of the neodymium(III) complex of (methylthio)acetic acid (Hmesa), $[Nd_2(mesa)_6(H_2O)_3]_n$, which is isostructural to its cerium(III), praseodymium(III), and europium(III) salts.

In that paper, the dysprosium(III) and ytterbium(III) complexes of the same ligand were found to have the $[M(mesa)_3(H_2O)_2]$ formula (where M=Dy or Yb).[1] Therefore the crystal and molecular structures of the ytterbium(III) complex have now been determined by the single-crystal X-ray diffraction technique.

Experimental

Single-crystal X-Ray Analysis. The title complex is obtained as described in the previous paper[1] and is recrystallized from water. However, as the crystals thus obtained were mostly in thin plates and poor in the b-axis direction and as, moreover, many of them were twin crystals, we chose the best one from among the about 30 samples tested.

A 0.3×0.3×0.1 mm^3 crystal was used, without shaping. The reflections whithin the range of $3°<2\theta<55°$ were collected on a Rigaku AFC-6A four-circle automated X-ray diffractometer with graphite-monochromated Mo $K\alpha$ radiation by means of the ω-scan technique. From the 8019 independent reflections observed, 4046 $|F_o|>3\sigma(|F_o|)$ reflections were used for the refinement. The intensities were corrected for the Lorentz and polarization factors, but no correction was made for the absorption or extinction. All the calculations were carried out on a HITAC M-200H computer at the Computer Center of The University of Tokyo, using the local version of the UNICS.[2] The scattering factors were taken from the tables.[3]

The structure was solved by the heavy-atom method. All the non-hydrogen atoms were found; the final R-value was 0.086,[4] with anisotropic temperature factors for all atoms.

Results and Discussion

The selected interatomic distances and bond angles are shown in Table 1.[5] A perspective drawing of the complex with the numbering scheme is given in Fig. 1, and a schematic presentation to show the positions of the ligating atoms around Yb(1) and Yb(2), in Fig. 2.[5]

As is shown in the figures, both the central metal atoms of the complex are octa-coordinated, and they are in a deformed dodecahedral geometry; their coordi-

Table 1. Selected inter-atomic distances and bond angles, with estimated standard deviations in parentheses

Bond length	l/Å	Bond length	l/Å
Yb(1)-O(11W)	2.28(1)	Yb(1)-O(12W)	2.29(2)
Yb(1)-O(13)	2.38(1)	Yb(1)-O(14)	2.40(2)
Yb(1)-O(15)	2.38(1)	Yb(1)-O(16)	2.39(1)
Yb(1)-O(17)	2.24(1)	Yb(1)-O(27^i)	2.22(1)
Yb(2)-O(21W)	2.28(1)	Yb(2)-O(22W)	2.31(1)
Yb(2)-O(23)	2.41(1)	Yb(2)-O(24)	2.34(2)
Yb(2)-O(25)	2.36(1)	Yb(2)-O(26)	2.42(1)
Yb(2)-O(28)	2.25(1)	Yb(2)-O(18)	2.19(2)
Yb(1)···Yb(2)	5.573(2)	Yb(1)···Yb(2^i)	5.777(2)
Bond angle	ϕ/°	**Bond angle**	ϕ/°
Yb(1)-O(13)-C(11)	93.2(15)	Yb(1)-O(14)-C(11)	91.5(15)
Yb(1)-O(15)-C(14)	95.2(15)	Yb(1)-O(16)-C(14)	94.7(15)
Yb(2)-O(23)-C(21)	90.7(16)	Yb(2)-O(24)-C(21)	94.0(17)
Yb(2)-O(25)-C(24)	94.7(15)	Yb(2)-O(26)-C(24)	95.4(16)
Yb(1)-O(17)-C(17)	169.9(16)	Yb(2)-O(18)-C(17)	143.4(17)
Yb(1)-O(27^i)-C(27^i)	140.0(16)	Yb(2)-O(28)-C(27)	168.8(19)
O(13)-C(11)-O(14)	120(2)	O(25)-C(24)-O(26)	117(2)
O(17)-C(17)-O(18)	126(2)	O(27)-C(27)-O(28)	121(2)

Key to the symmetric operations: i, x, y, $-1.0+z$.

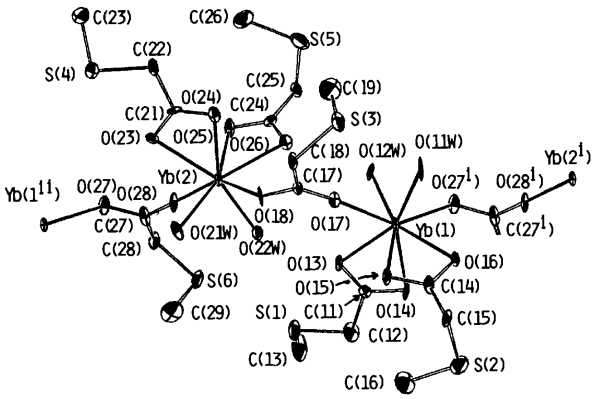

Fig. 1. The perspective drawing of the complex and the numbering scheme of atoms. (Key to the symmetry operations; i, x, y, $-1.0+z$; ii, x, y, $1.0+z$)

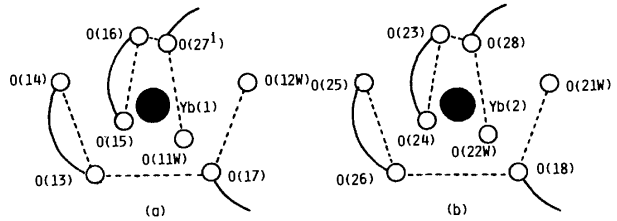

Fig. 2. Schematic presentation of the bonding modes of the ligands around (a) Yb(1) and (b) Yb(2) atoms (●, ytterbium ; and ○, oxygen atoms).

nation number is smaller than that of the neodymium(III) complex of the same ligand, where both types of metal atoms are ennea-coordinated.[1] Although lanthanoid(III) carboxylates, such as *m*-hydroxybenzoates[6] and nicotinates,[7] are also in octa-coordination, they are rather in a square-antiprism geometry. The deviations of the atomic positions of the four oxygen atoms and the central metal atom from each average trapezium plane are relatively large: 0.316 Å at the maximum (O(17)) and 0.124 Å on the average. The dihedral angles between the two trapezia around the same metal atom are 83.9 and 87.2° respectively.

The arrangements of the ligated atoms around both metal atoms are about the same; as is shown in Fig. 2, two oxygen atoms of one carboxylate occupy both the apexes of an oblique edge of each trapezium, forming a four-membered chelate ring. On the other oblique edge of each trapezium, the oxygen atom of the coordinated water takes the bottom-end position, and the oxygen atom of the bridging ligand, the other-end one.

The Yb–O bond lengths of the complex are classified into three groups. The shortest ones are those of the bridging ligand oxygen atoms (2.223 Å on the average), the second ones are those of the water oxygen atoms (2.293 Å on the average), and the longest ones are those of the chelating oxygen atoms (2.383 Å on the average). As the ionic radii of Yb^{III} and of O^{2-} are 0.985 and 1.38 Å respectively,[8] the bridging oxygen atoms bond to the metal atoms strongly, consequently, the bridges are likely to be stable. As shown in Table 1, Yb(1)···Yb(2), and Yb(1)···Yb(2^{i}) are 5.573(2) and 5.777(2) Å respectively, not much different from one another. Both of the bridges are of the *Z–E* type,[9] where the Yb–O–C angles of the *Z*-side (O(17) and O(28) sides) are 169.9(16) and 168.8(19)°, while those of the *E*-side (O(18) and O(27) sides) are 143.4(17) and 140.0(16)° respectively. None of the sulfide sulfur atoms are coordinated to any metal atoms, as in the case of the neodymium(III) complex.

Thus, the complex chains in a zig-zag form lie nearly parallel to the c-axis, and there is almost no interaction between the chains.

The authors are greatly obliged to the Shin-Etsu Chemical Ind. Co., Ltd., for aiding this study by presenting the highly pure ytterbium(III) oxide. The present work was partially supported by a Grant-in-Aid for Scientific Research (No. 57430011) from the Ministry of Education, Sciences, and Culture.

References

1) S. Kondo, M. Shimoi, A. Ouchi, and T. Takeuchi, *Bull. Chem. Soc. Jpn.*, **55**, 2840 (1982).
2) "The Universal Crystallographic Computation Program System (UNICS)," ed by T. Sakurai, Crystallographic Society of Japan, Tokyo (1967).
3) "International Tables for Crystallography," Kynoch Press, Birmingham (1974), Vol. IV, pp. 72, 150.
4) $R=\Sigma||F_o|-|F_o||/\Sigma|F_o|$.
5) The crystal packing diagram, the final atomic coordinates, and their thermal parameters, the final F_o-F_c values, and some additional data about the bond lengths and bond angles are deposited as Document No. 8512 at the Office of the Editor of Bull. Chem. Soc. Jpn.
6) Y. Koizumi, H. Sawase, Y. Suzuki, T. Takeuchi, M. Shimoi, and A. Ouchi, *Bull. Chem. Soc. Jpn.*, **57**, 1809 (1984).
7) J. W. Moore, M. D. Glick, and W. A. Baker, Jr., *J. Am. Chem. Soc.*, **94**, 1858 (1972).
8) R. D. Shannon, *Acta Crystallogr., Sect A*, **32**, 751 (1976).
9) H. Sawase, Y. Koizumi, Y. Suzuki, M. Shimoi, and A. Ouchi, *Bull. Chem. Soc. Jpn.*, **57**, 2730 (1984).

Reaction of Azobenzene with Dichlorocarbene in Phase-transfer-catalyzed System

Tomohisa FUJIU, Kazuo IZUMI, and Shizen SEKIGUCHI*
Department of Synthetic Chemistry, Gunma University, Kiryu, Gunma 376
(Received August 4, 1984)

Synopsis. Azobenzene (**2**) reacted with dichlorocarbene at 40 °C in the presence of several phase-transfer catalysts in a binary solvent ($CHCl_3$–aqueous KOH), giving 2,2,3,3-tetrachloro-1-phenylaziridine (**3**), 1-phenyl-1,3-dihydro-2*H*-benzimidazol-2-one (**4b**), dichloroacetanilide (**6**), *N*,*N*′-diphenylurea (**7**), and trace amounts of 2-chloro-1-phenylbenzimidazole (**8**).

We have recently reported the reaction of azoxybenzene (**1**) with dichlorocarbene (DC) in the presence of a phase-transfer-catalyst (PTC 18-crown-6 or tributylamine) in the binary solvent ($CHCl_3$-aq KOH), in which azobenzene (**2**), 2,2,3,3-tetrachloro-1-phenylaziridine (**3**), and 1-phenyl-1,3-dihydro-2*H*-benzimidazol-2-one (**4b**) were formed[1] (Eq. 1).

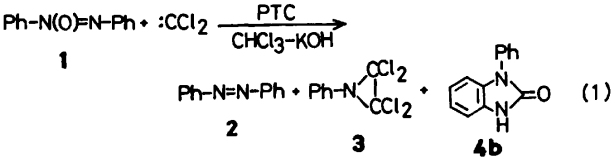

These results are very different from those of Seyferth *et al.*,[2] who reported the reaction of **1** with DC generated from $PhHgCCl_2Br$ in benzene, giving **2**, **3**, and 1,1-dichloro-*N*-phenylmethanimine (**5**) as products. Especially, the formation of **4b** in the reaction (Eq. 1) led us to study the reaction of **2** with DC, where **3**, **4b**, dichloroacetanilide (**6**), *N*,*N*′-diphenylurea (**7**), and 2-chloro-1-phenylbenzimidazole (**8**) (trace amounts) were formed (Eq. 2).

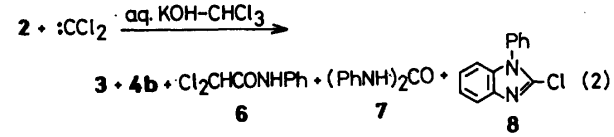

The results are summarized in Table 1. The compound (**8**) was produced in trace amounts in every run. The results that **4**, **6**, **7**, and **8** were obtained are conspicuously different from those of Seyferth *et al.*[2] and Sasaki *et al.*[3] With TBA the product yields are higher than with 18-crown-6: The higher catalytic activity of the former is atrributed to the intermediate formation of trialkyl(dichloromethyl)-ammonium trichloromethanide (Eq. 4), as represented in Eqs. 3—5.[4]

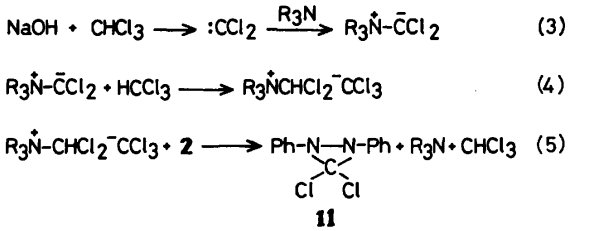

Table 1. Reactions of azobenzene (**2**) with dichlorocarbene[a]

Run	Reaction time / h	Product/%[b] 4b	6	7	3	Conversion[c] / %
1	0.5	14.7	5.3	1.2	6.2	37.1
2	1	13.7	5.8	1.0	7.6	58.7
3	2	13.0	5.1	0.8	9.4	67.3
4	4	10.2	3.8	0.3	10.8	72.0
5	7	6.5	2.8	0.1	10.2	74.0
6[d]	0.5	34.9	7.6	3.1	10.9	49.3
7[d]	1	21.6	7.6	trace	12.7	70.6
8[d]	2	22.3	5.5	trace	14.8	75.5
9[d]	4	15.5	4.2	0.4	31.0	76.7
10[d]	7	11.7	3.7	0.3	29.0	78.7
11[e]	4	13.2	3.7	trace	29.0	81.0
12[f]	4	4.6	4.0	trace	—	20.7

a) Reaction conditions: **2** 15.0 mmol; $CHCl_3$ 226 mmol; aq KOH (50%) 223 mmol; temperature 40 °C; 18-crown-6 0.39 mmol. b) Based on **1** consumed. c) Conversion of **2**. d) Tributylamine (TBA, 0.39 mmol) used in the place of 18-crown-6. e) Benzyltriethylammonium chloride (0.38 mmol) used in the place of 18-crown-6. f) Benzyltributylphosphonium chloride (0.39 mmol) used in the place of 18-crown-6.

The PTCs other than 18-crown-6 and TBA were tested (Runs 11 and 12). Although benzyltriethylammonium chloride is reported to be very effective,[5] its activity is quite similar to TBA under the present conditions. However, benzyltributylphosphonium chloride is much less effective: the poor migratory aptitude of the corresponding ion pair (Eq. 5) from the aqueous to the organic layer may be responsible for it.

The reaction path is shown in Scheme 1.

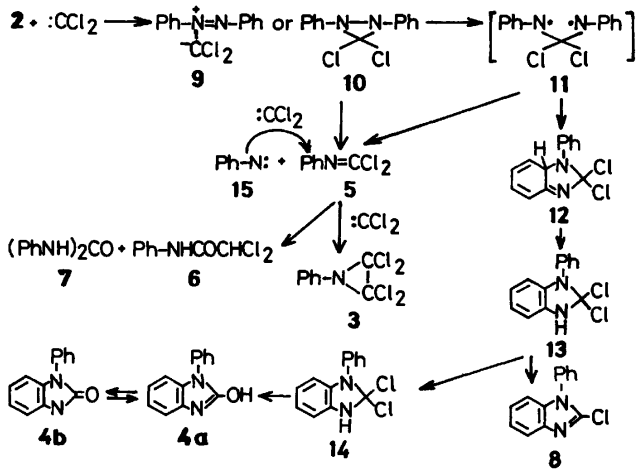

Scheme 1.

The formation of **15** and **5** may be formed *via* an acylic (9) or a cyclic (**10**) intermediate.[2] Further, the intermediacy of **10** is required, because the benzimidazole derivatives (**4** and **8**) are expected to be formed from **11**.[3]

The reaction sequences (**5**+**15**→**3**+**6**+**7**) are proposed from the following results (see Experimental): First, **6** was not formed in the reaction of **3** with DC under the conditions (PTC TBA, reaction time 4 h) similar to those described in Table 1, whereas the reaction of carbanilides with sodium hypochlorite giving 1,3-dihydro-2*H*-benzimidazol-2-ones was reported by Rosanti[6] and Oftedahl *et al.*;[7] second, **6** was not formed in the reaction of **7** with DC under the same conditions to those described in the first item; third, in the reaction of **5** with DC under the same conditions as those described in the first item except for the absence of TBA, **7** and **6** were formed in only 2.0 and 0.1% yields, respectively, which indicated that **7** and **6** are formed *via* the reaction of **5** not with DC but with OH^- (see Scheme 2): fourth, **3** was formed in a 30% yield in the reaction of **5** with DC under the conditions similar to those described in the first item.

The products (**6** and **7**) are presumed to be formed *via* the reaction shown in Scheme 2 from the following experimental results: First, Seyferth *et al.* reported that 1-chloro-1-trichloromethyl-*N*-phenylmethanimine hydrolyzes to produce trichloroacetanilide [$Cl_3C(O)NHPh$] in a 95% yield;[2] second, **6** was formed in a 2% yield in the reaction of aniline with DC under the conditions similar to those described in Table 1 (PTC TBA, reaction time 1 h),[8] during the course of which the disagreeable isocyanide-like odor evolved, indicating the possibility of the production of Ph-NC.[9]

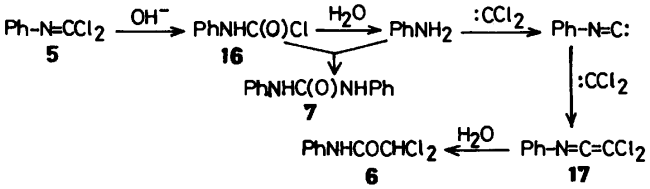

Scheme 2.

In conclusion it is found that the kind of products depends largely on reaction conditions-especially polarities of solvents.

Experimental

General Comments. The products were identified by using NMR and Mass spectrometers, UV and IR spectrophotometer, and elemental analyses. The boiling point of ligroin used was 80—100 °C. All the capillary melting points were uncorrected.

Reaction of Azobenzene (2) with Dichlorocarbene for Isolation of the Products. The reaction and the isolation of products were carried out according to the procedure described in the revious work,[1] where the physical and chemical properties of **3** and **4b** were indicated.

2-Chloro-1-phenylbenzimidazole (8); mp 67—68 °C; IR (KBr) 1600, 1450, 760, 740, 690 cm^{-1}; NMR (DMSO-d_6) δ=7.7 (s, 1-phenyl 5H), 7.2—7.5 (m, phenyl 4H); Found: C, 68.66; H, 4.11; N, 12.43%; M^+ 228. Calcd for $C_{13}H_9ClN_2$: C, 68.27; H, 3.94; N, 12.25%; M, 228.

Dichloroacetanilide (6); mp 117—118.5 °C; IR (KBr) 3260, 1670, 1550, 1240, 860, 810, 760, 730, 690, 670 cm^{-1}; NMR (DMSO-d_6) δ=10.5 (s, NH 1H), 7.1—7.7 (m, phenyl 5H), 6.6 (s, CH 1H); Found: C, 47.51; H, 3.31; N, 7.08%; M^+, 203. Calcd for $C_8H_7Cl_2NO$: C, 47.17; H, 3.44; N, 6.88%, M, 203.

N,N'-Diphenylurea (7); mp 238—239 °C; IR (KBr) 3300, 1650, 1590, 1230, 750, 690 cm^{-1}; NMR (DMSO-d_6) δ=8.6 (s, NH 2H), 6.8—7.8 (m, phenyl 10H); Anal. ($C_{13}H_{12}N_2O$) C. H. N.

The NMR and IR spectra show that 2-hydroxy-1-phenylbenzimidazole (**4a**) considerably tautomerizes to **4b**.

Reaction of 2,2,3,3-Tetrachloro-1-phenylaziridine (3) or N,N'-diphenylurea (7) with Dichlorocarbene. To an 18 ml chloroform solution containing 18 mmol of **3** (3.85 g) or **7** (3.18 g) and 0.076 g (0.41 mol) of TBA was added a 25 g (223 mmol) aqueous KOH (50 wt%) solution. After the mixture was stirred for 4 h at 40 °C, it was processed according to the method described in the reaction of **2** with DC. In the both reactions **6** was not obtained but the substrate was recovered.

Reaction of 1,1-Dichloro-N-phenylmethanimine (5) with Dichlorocarbene. In the reaction of **5** (2.61 g, 15 mmol), prepared according to the method of Seyferth *et al.*,[2] with DC under the same conditions as those in the reaction of **3** with DC except for the absence of TBA, **7** and **6** were obtained 0.031 g (2%) and 0.0016 g (0.1%), respectively [both yields are based on **5** consumed (60% conversion)].

Reaction of Aniline with Dichlorocarbene. In the reaction of aniline (1.38 g, 15 mmol) with DC under the same conditions as those in the reaction of **3** with DC, **6** was obtained in a 2% yield (0.06 g).

The determination of products was carried out according to the method described in the previous paper.[1]

References

1) S. Sekiguchi, T. Fujiu, and K. Izumi, *Bull. Chem. Soc. Jpn.*, **57**, 3337 (1984).

2) D. Seyferth, W. Tronich, and H.-m.Shin, *J. Org. Chem.*, **39**, 158 (1974).

3) T. Sasaki, S. Eguchi, and T. Ogawa, *Heterocycles*, **3**, 193 (1975).

4) M. Mokosza, A. Kacprowicz, and M. Fedorynski, *Tetrahedron Lett.*, **1975**, 2119.

5) a) C. M. Starks and C. Liotta, "Phase Transfer Catalysis," Academic Press, New York (1978); b) M. Jones, Jr. and R. A. Moss, "Carbenes," Wiley-Interscience, New York (1973), Vol. 1 and (1975), Vol. 2; c) W. P. Weber and G. W. Gokel, "Phase Transfer Catalysis in Organic Synshesis," Springer-Verlag, Berlin (1977).

6) R. Rosanti, *Gass. Chim. Ital.*, **86**, 1089 (1956).

7) M. L. Oftedahl, R. W. Radue, and M. W. Dietrich, *J. Org. Chem.*, **28**, 578 (1963).

8) R. Bacaloglue and C. A. Bunton, *Tetrahedron*, **29**, 2721, 2725 (1973).

9) A. P. Krapcho, *J. Org. Chem.*, **27**, 1089 (1962).

The Reaction of (*Z*)-2-(3-Oxo-1-propenyl)-2*H*-azirine Derivative with Molybdenum Carbonyl Complexes

Tomoshige KOBAYASHI and Makoto NITTA*

Department of Chemistry, School of Science and Engineering, Waseda University, Shinjuku-ku, Tokyo 160

(Received August 17, 1984)

Synopsis. The thermal reaction of (*Z*)-2,3-diphenyl-2-(2,3-diphenyl-3-oxo-1-propenyl)-2*H*-azirine with [Mo(CO)$_6$] or [Mo(CO)$_3$(MeCN)$_3$] was reinvestigated to afford 2,3,5,6-tetraphenylpyridine along with the pyrroles and 1,3-oxazepine derivative. The formation of 1,3-oxazepine was demonstrated to be the purely thermal process. The 1,2,4,5-tetraphenyl-5-oxo-1,3-pentadienylnitrene complex was shown to give the pyridine and the pyrrole derivatives.

It has previously been shown that [Mo(CO)$_6$] effects a reaction of isoxazoles **1** to undergo a novel insertion of acetylenic esters across the C-4–C-5 bond and elimination of an oxygen atom to give pyridine derivatives.[1] Complex **2** and the complexed nitrene **3** were proposed as the intermediates. Independent reaction of 3-phenyl-2-oxa-3-azabicyclo[3.2.0]hepta-3,6-diene (**5**) with [Mo(CO)$_6$] giving 2-phenylpyridiene (**7**) *via* the nitrene complex **6** (R^1=Ph, R^2=E=E′=H in **3**) supports the proposed mechanism.[1] The facile N–O and C-1–C-5 bond cleavage of the complexed **5** (or **2**) giving **6** (or **3**) is similar to the photochemical reaction of **5** to give 3-(3-phenyl-2*H*-azirin-2-yl)acrylaldehyde,[2] suggesting the delocalization of the p-d electron from the molybdenum atom to the π^* orbital of the C=N–O moiety in the complex such as **2**.[1b,3]

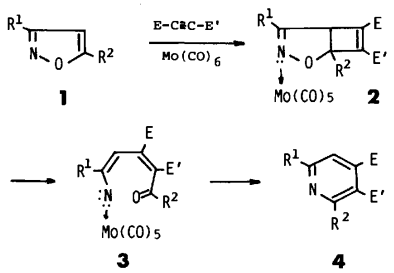

1 **2** **3** **4**

R^1, R^2 = Phenyl or Alkyl

E = CO_2Me; E′ = CO_2Me or H

On the contrary, the complexed nitrene **15**, which is similar to **3** or **6**, has been proposed as an intermediate in the reaction of (*Z*)-2-(3-oxo-1-propenyl)-2*H*-azirine derivative **8** with [Mo(CO)$_6$] leading to the 1,3-oxazepine **9** and the pyrroles **10**, **11**, and **12**. The yields of the products are not mentioned, and no pyridine is obtained.[4] We report here the reaction of **8** with [Mo(CO)$_6$] or [Mo(CO)$_3$(MeCN)$_3$] giving 2,3,5,6-tetraphenylpyridine **13**, in addition to the 1,3-oxazepine **9** and the pyrroles **10**—**12**. The reaction conditions and the yields of the products are summarized in Table 1.

The reaction of **8**[5] with [Mo(CO)$_6$] in tetrahydrofuran (THF) at an ambient temperature, or in boiling benzene, gave the 1,3-oxazepine **9** and the pyridine **13**, along with the pyrroles **10**—**12** (entry 1 or 3 in Table 1). However, the thermal reaction of **8** without [Mo(CO)$_6$] in THF or in benzene afforded only **9** (entry 2 or 4). Thus **9** seems to have been derived by the purely thermal process which involves a C-2–C-3 bond fission of the azirine ring.[4,5] The reaction of **9** with [Mo(CO)$_6$] under the similar conditions to the [Mo(CO)$_6$]-induced reaction of **8** gave no product, and **9** was recovered quantitatively. Therefore, the pyridine **13** and the pyrroles **10**—**12** are supposed to be the primary products of the reaction of **8** with [Mo(CO)$_6$].

It has been shown that the ligand exchange of [Mo(CO)$_3$(MeCN)$_3$] with **5** proceeded under mild conditions to afford **7**.[1b] The reaction of **8** with [Mo(CO)$_3$(MeCN)$_3$] (prepared *in situ*, see Experimental) in acetonitrile also proceeded very fast even at an ambient temperature giving the pyrroles **10** and **11** as well as the pyridine **13**, in addition to the small amount of 1,3-oxazepine **9** (entry 5). The purely thermal reaction giving **9** is reduced under these conditions.

The formation of the pyrroles **10**—**12** is explained as follows. The n-donor complexation of the azirine ring of **8** seems to give the complexed nitrene **15** *via* **14**.[4,7,8] A ring-annelation of **15** and the subsequent decomplexation gives an intermediate **16**. In **16**, the benzoyl migration to the adjacent carbon atom and the subsequent hydrogen migration gives **10**, while benzoyl

Table 1. Reaction of the azirine **8** in the presence or absence of [Mo(CO)$_6$]

Entry	Reaction Conditions		Time/h	Products (Yield/%)					
	[Mo(CO)$_6$]	Solvent		**8**	**9**	**10**	**11**	**12**	**13**
1	Added[a]	THF[b]	65	—	54	39	0.8	0.7	1.3
2	None	THF	65	39	49	—	—	—	—
3	Added[a]	PhH[c]	1	—	71	17	1.5	1.7	2.6
4	None	PhH	1	—	99	—	—	—	—
5	Added[d]	MeCN	0.5	—	3	53	2	—	4

a) 1.0 Molar equivalent amount of [Mo(CO)$_6$] was used. b) Stirred at an ambient temperature. c) Stirred at the refluxing temperature. d) [Mo(CO)$_3$(MeCN)$_3$], prepared from 2.0 molar equivalent amount of [Mo(CO)$_6$], was used at an ambient temperature.

migration to the adjacent nitrogen atom leads to **11**.[4] The attempted reaction of the pyrrole **11** with [Mo(CO)$_6$] in anhydrous or moist benzene gave no **12**, and **11** was recovered quantitatively. Furthermore, **12** was not obtained in the reaction of entry 5 in Table 1. Thus the possibility for the formation of **12** may be ascribed to a stray water-assisted debenzoylation (elimination of benzoyl group as benzoic acid) of the intermediate **16**. The pyridine **13** can be obtained by a cyclization of **15** to give **17**, followed by a ligand migration giving **18**, which would collapse to **13**.[1,8]

In conclusion, the complexed nitrene **15** was shown to give the pyrroles **10**—**12** along with the pyridine **13**, the formation of which was not observed in the previous study.[4] The complexed nitrene **3** or **6** was found to give only pyridine.[1] The steric and/or the electronic effect of the tetraphenyl-substituted derivative, **15**, may be reflected in the pathway giving the pyrroles and the pyridine derivative.

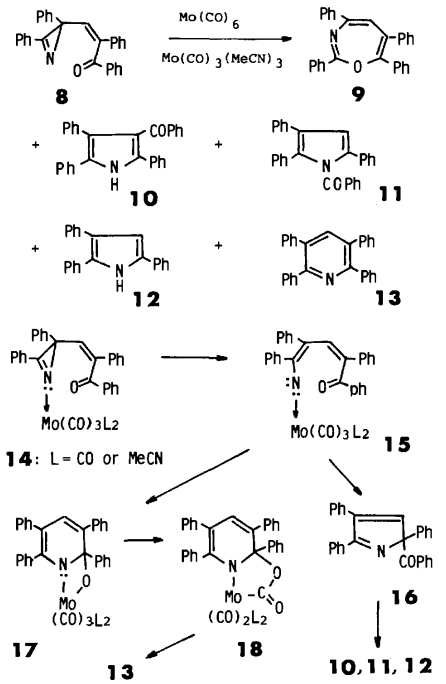

Experimental

All of the reactions were carried out under a dry nitrogen atmosphere. Solvents were purified and dried by the standard methods. All of the melting points were uncorrected.

Reaction of 8 with [Mo(CO)$_6$]. The reaction of **8** (399 mg, 1 mmol) and [Mo(CO)$_6$] (264 mg, 1 mmol) was carried out in 10 cm^3 of THF at an ambient temperature for 65 h, in boiling benzene for 1 h. After the solvent was evaporated, the residue was separated by TLC on silica gel using CCl_4 as an eluent to give **9**, **10**, **11**, **12**, and **13** (Table 1, entries 1 and 3). For **9**: mp 138—139 °C (from EtOH) (lit,[5] 146—147 °C). For **10**: mp 198—199 °C (from EtOH) (lit,[5] 200—201 °C). For **11**: mp 152—153 °C (from EtOH) (lit,[9] 154—155 °C). For **12**: mp 137—139 °C (from CCl_4) (lit,[10] 137—138 °C). For **13**: mp 228—230 °C (from AcOEt) (lit,[11] 228.5—229.5 °C).

Reaction of 8 with [Mo(CO)$_3$(MeCN)$_3$]. A solution of [Mo(CO)$_3$(MeCN)$_3$] was prepared from [Mo(CO)$_6$] (528 mg, 2 mmol) in 10 cm^3 of acetonitrile under reflux for 4 h[6] After this solution was cooled to an ambient temperature, **8** (399 mg, 1 mmol) was added to the solution, and it was stirred for 0.5 h. A similar workup as described above gave **9**, **10**, **11**, and **13** (Table 1, entry 5).

Reaction of 8 in the Absence of [Mo(CO)$_6$]. A solution of **8** (150 mg, 0.37 mmol) in THF (5 cm^3) was stirred at an ambient temperature for 65 h and the subsequent separation by TLC on silica gel using benzene as the eluent gave **9** and **8**. A similar reaction of **8** (150 mg, 0.37 mmol) in boiling benzene (10 cm^3) for 1 h gave only **9** (Table 1, entries 2 and 4).

Reaction of 1,3-Oxazepine 9. A solution of **9** (100 mg, 0.25 mmol) and [Mo(CO)$_6$] (66 mg, 0.25 mmol) in THF (3 cm^3) was stirred at an ambient temperature for 65 h. After the evaporation of the THF, the residue was purified by TLC on silica gel using benzene as the eluent to recover **9** (89 mg, 89%). A similar reaction of **9** (150 mg, 0.37 mmol) and [Mo(CO)$_6$] (98 mg, 0.37 mmol) in boiling benzene 10 cm^3) for 1 h also gave the unreacted **9** (142 mg, 95%).

Reaction of 11 with [Mo(CO)$_6$]. A solution of **11** (100 mg, 0.25 mmol) and [Mo(CO)$_6$] (66 mg, 0.25 mmol) in 5 cm^3 of anhydrous or moist benzene was refluxed for 1 h. After the evaporation of the benzene, the residue was purified by TLC on silica gel to give **11** in 96% (in anhydrous benzene) or in 94% (in moist benzene).

References

1) a) T. Kobayashi and M. Nitta, *Chem. Lett.*, **1983**, 1233; b) T. Kobayashi and M. Nitta, *Bull. Chem. Soc. Jpn.*, **58**, 152 (1985).

2) T. Mukai, T. Kumagai, and O. Seshimoto, *Pure Appl. Chem.*, **49**, 287 (1977); T. Kumagai, H. Sawaura, C. Kabuto, and T. Mukai, *Nippon Kagaku Kaishi*, **1984**, 158.

3) M. Nitta and T. Kobayashi, *Chem. Lett.*, **1983**, 51; *J. Chem. Soc., Perkin Trans., 1*, **1984**, 2103.

4) F. Bellamy, *Tetrahedron Lett.*, **1978**, 4577.

5) J. -P. LeRoux, J. -C. Cherton, and P.-L. Desbens, *Compt. Rend. Ser. C*, **280**, 37 (1975).

6) D. P. Tate, W. R. Knipple, and J. M. Augle, *Inorg. Chem.*, **1**, 433 (1962).

7) H. Alper, J. E. Prickett, and S. Wollowitz, *J. Am. Chem. Soc.*, **99**, 4330 (1977).

8) F. Bellamy, *J. Chem. Soc., Chem. Commun.*, **1978**, 998.

9) C. L. Pederson and O. Buchardt, *Acta. Chem. Scand.*, **27**, 271 (1973).

10) M. Takahashi, N. Inada, H. Kirihara, and S. Watanabe, *Bull. Chem. Soc. Jpn.*, **51**, 3321 (1978).

11) A. R. Katritzky, K. Hornath, and B. Plan, *J. Chem. Soc., Perkin Trans. 1*, **1980**, 2554.

Synthesis and Properties of a New Photoresponsive Crown Ether with a Fluorescent Stilbene-cap[1)]

Seiji SHINKAI,* Kiminori MIYAZAKI, Mikio NAKASHIMA, and Osamu MANABE*
Department of Industrial Chemistry, Faculty of Engineering, Nagasaki University, Nagasaki 852
(Received October 13, 1984)

Synopsis. A new photoresponsive crown ether **2** with a stilbene-cap was synthesized. The crown *trans*-**2** could extract Li^+ and Na^+ into the organic phase, and UV light irradiation which produces photoisomerized *cis*-**2** enhanced the extractability. Thus, the stilbene-cap induces the conformational change in the crown ether moiety by photoirradiation.

Macrocyclic polyethers contain intramolecular cavities delineated with molecular segments capable of binding cations. Previously, we synthesized an azobenzene-capped crown ether *trans*-**1**[2,3)] which was one of the early examples of photoresponsive crown ethers.[4—6)] In **1**, the azobenzene-cap undergoes photoinduced reversible interconversion between the trans- and cis-configuration, and thus the three-dimensional cavity structure changes in response to photoirradiation. Here, we wish to address a new photoresponsive crown ether, **2** which has a photoresponsive stilbene-cap on the N_2O_4 crown ether. We used **3** as a reference compound.

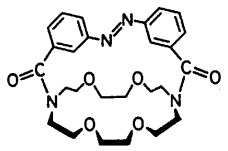

trans-1

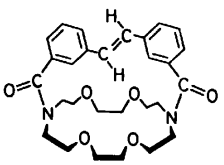

trans-2

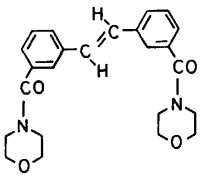

trans-3

Experimental

Materials. Stilbene-3,3′-dicarboxylic acid was prepared according to the method of Toland *et al.*[7)] This was treated with thionyl chloride to yield 3,3′-bis(chloroformyl)-stilbene: mp 179—181 °C, yield 73%. Found: C, 62.64; H, 3.30%. Calcd for $C_{16}H_{10}O_2Cl_2$: C, 62.98; H, 3.30%.

The crown *trans*-**2** was prepared in chlorobenzene from equimolar amounts of 1,4,10,13-tetraoxa-7,16-diazacyclooctadecane(N_2O_4 crown) and 3,3′-bis(chloroformyl)stilbene according to the high-dilution method. The basic operation is similar to that described for the preparation of *trans*-**1**.[3)] The raw product was subjected to the TLC separation (silica gel, chloroform–ethyl acetate (1:1 v/v) and finally recrytallized from benzene: mp 193.5—195 °C, yield 8.8%. IR (KBr) $\nu_{C=O}$ 1625 cm^{-1} and $\nu_{C=C}$ 1600 cm^{-1}; ^1H NMR ($CDCl_3$) δ=3.08—3.35 (8H, m), 3.65—4.32 (16H, m), 7.07 (2H, s), and 7.41—7.58 (8H, m); M^+ (*m/z*) 494. Found: C, 68.02; H, 7.02; N, 5.63%. Calcd for $C_{28}H_{34}N_2O_6$: C, 68.00; H, 6.93; N, 5.66%.

The compound *trans*-**3** was prepared by treatment of 3,3′-bis(chloroformyl)stilbene with excess morpholine in chlorobenzene. Recrystallization from benzene gave white crystals: mp 198—200 °C, yield 93%. IR (KBr) $\nu_{C=O}$ 1625 cm^{-1}; ^1H NMR ($CDCl_3$) δ=3.68 (16H, s), 7.07 (2H, s), and 7.20—7.51 (8H, m). Found: C, 70.28; H, 6.47; N, 6.83%. Calcd for $C_{24}H_{26}N_2O_4$: C, 70.92; H, 6.45; N, 6.89%.

Results

Absorption Spectra, Fluorescence Spectra, and Photoisomerization. Absorption maxima of *trans*-**2** and *trans*-**3** were 290 nm (ε_{max} 21900) and 297 nm (ε_{max} 26800) in acetonitrile at 30 °C, respectively. The light-mediated trans-to-cis isomerization was carried out by using a 100 W high-pressure Hg-lamp through a color glass filter (330 nm<λ<380 nm). The lamp and a N_2-substituted Thunberg cuvette containing 1-butanol solution of *trans*-**2**(or *trans*-**3**)(1.12×10^{-5} M (1 M=1 mol dm^{-3})) were immersed in a thermostated (30 °C) water bath. The absorption maxima decreased with photoirradiation time and finally reached equilibrium values: *cis*%'s at the photostationary state were 52% for **2** and 48% for **3**. The time-dependence could be approximated by a first-order rate equation with r>0.99: k_1 (first-order rate constant)= 3.25×10^{-3} s^{-1} for **2** and 1.15×10^{-3} s^{-1} for **3**. In the trans-to-cis photoisomerization of **1** and its reference compound, 3,3′-bis-(morpholinocarbonyl)azobenzene, we could not find a significant rate difference between these two compounds.[3)] The larger rate constant for **2** relative to **3** suggests, therefore, that *trans*-**2** in the initial state should be somewhat destabilized.

Fluorescence maxima of *trans*-**2** and *trans*-**3** appeared at 373 nm and 365 nm in acetonitrile at 30 °C, respectively (excitation 320 nm). The absolute fluorescence intensity of *trans*-**3** was greater by about 4-fold than that of *trans*-**2**.[8)] We found, interestingly, that fluorescence emission of *trans*-**2** is quenched by LiI and NaI more efficiently than that of *trans*-**3** (Fig. 1). Such a large difference was not observed for KI, RbI, and CsI. As described below, Li^+ and Na^+ are bound to the crown ether moiety of *trans*-**2**, while other alkali metal ions are not. The finding suggests, therefore, that the metal-crown interaction is responsible for the efficient fluorescence quenching observed for *trans*-**2**. The efficiency of fluorescence quenching was similar between Li^+ and Na^+ in spite of the efficient binding of Li^+ relative to Na^+ (*vide post*). This reason is not clear yet. Conceivably, the quenching can occur through the weak metal-crown interaction in dehydrated acetonitrile.

Two-Phase Solvent Extraction of Alkali Metal Ions. The ionophoric functions of *trans*-**2** and *cis*-**2** were evaluated through solvent extraction. We used the mixture containing 44% *cis*-**2** for solvent extraction. First, we employed extraction conditions used for **1**[3)]

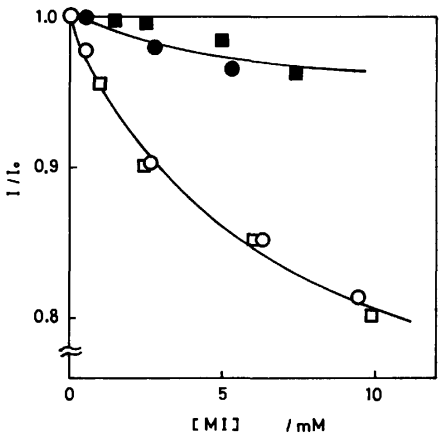

Fig. 1. Relative fluorescence intensity of *trans*-**2** and *trans*-**3** (3.20×10^{-5} M) plotted against the concentration of alkali iodides. ○: *trans*-**2**+LiI, □: *trans*-**2**+NaI, ●: *trans*-**3**+LiI, ■: *trans*-**3**+NaI.

Table 1. Solvent extraction of alkali picrates from water to the organic phase(*o*-dichlorobenzene: 1-butanol=50 : 50 v/v) at 30 °C[a]

Metal	Ex(%)	
	trans-**2**	Photoirradiated-**2**[b]
Li^+	11	13
Na^+	4	11
K^+	1	6
Rb^+	(<1)	(<1)
Cs^+	(<1)	(<1)

a) Organic phase: $[2]=2.70\times10^{-3}$ M. Aqueous phase: [MCl]=0.50 M, [MOH]=7.00×10^{-3} M, [picric acid]=5.00×10^{-3} M. b) *Cis*-form 44%.

but none of alkali metal salts was extracted into the benzene phase. This indicates that the stilbene-cap has some negative effect on the metal-binding ability of the N_2O_4 crown moiety. We thus changed the extraction conditions as recorded in a footnote to Table 1.

Examination of Table 1 reveals that in contrast to the ion selectivity of *trans*-**1** for Na^+ and K^+,[3] *trans*-**2** shows the highest selectivity for Li^+ having the smallest ion radius. It extracts K^+ only by 1%. Interestingly, the extractabilities for Na^+ and K^+ are efficiently improved by photoirradiation. The finding suggests that apparently, the size of the crown ether ring is enlarged upon photoinduced *trans*-to-*cis* isomerization of the stilbene-cap.

Discussion

The crown *trans*-**2**, in comparison with *trans*-**1** or *trans*-**3**, can be characterized by (i) low yield in the high-dilution synthesis, (ii) low fluorescence intensity, (iii) fast light-mediated trans-to-cis isomerization, and (iv) specific ion-selectivity for Li^+. These results consistently suggest that *trans*-**2** should be destabilized by some steric strain. Two possible explanations emerge. According to X-ray crystallographic studies and theoretical calculations,[9,10] the C=C bond of *trans*-stilbene (1.453 Å) is longer than the N=N bond of *trans*-azobenzene (1.23 Å) by 0.22 Å. One possible explanation is, therefore, that the distance between two carbonyl groups of 3,3′-bis(chloroformyl)stilbene is a little too longer to intramolecularly react with 7-*N* and 16-*N* of N_2O_4 crown. If so, this explanation can readily accommodate the low yield and the inferior ion-binding ability of *trans*-**2**. N_2O_4 crown ether itself shows the K^+-selectivity.[11] The previous X-ray studies on an analogue of *trans*-**1** showed that the crown ether ring is oval-shaped,[12] and the N_2O_4 crown ether moiety in *trans*-**1** showed the Na^+-selectivity.[3] The result implies that when the crown ether is stretched and enforced to adopt the oval-shaped conformation, the crown ether ring would favorably bind smaller alkali metal ions. The Li^+-selectivity observed for *trans*-**2** suggests that the N_2O_4 crown of *trans*-**2** is more stretched than that of *trans*-**1**.

Examination of Corey-Pauling-Koltun (CPK) molecular models of *trans*-**2** offers another possible explanation: one of the olefin protons in the CH=CH bond, which are absent in the azo linkage, deeply penetrates into the crown cavity and seems to interfere metal-binding. The low metal-affinity of *trans*-**2** relative to *trans*-**1** may be related to this steric disadvantage. On the other hand, CPK models of *cis*-**2** show that the olefinic protons in the *cis*-stilbene-cap exist apart from the crown ether plane. This favorable configuration would largely improve the metal-binding ability (especially, for large metal ions).

In conclusion, the present study indicates that the N_2O_4 crown with a fluorescent stilbene-cap acts as a new photoresponsive crown ether. Furthermore, the stilbene unit which apparently seems to be sterically equivalent to the azobenzene unit brought forth several marked differences in ion-binding ability, isomerization process, *etc.* The efforts to modify *trans*-**2** as a metal-selective fluorescence probe are now continued in this laboratory.

References

1) Photoresponsive Crown Ethers. 15. Part 14: S. Shinkai, M. Ishihara, K. Ueda, and O. Manabe, *J. Chem. Soc., Parkin Trans. 2*, in press.
2) S. Shinkai, T. Ogawa, T. Nakaji, Y. Kusano, and O. Manabe, *Tetrahedron Lett.*, **1979**, 4569.
3) S. Shinkai, T. Nakaji, Y. Nishida, T. Ogawa, and O. Manabe, *J. Am. Chem. Soc.*, **102**, 5860 (1980).
4) I. Yamashita, M. Fujii, T. Kaneda, S. Misumi, and T. Otsubo, *Tetrahedron Lett.*, **1980**, 541.
5) M. Shiga, M. Takagi, and K. Ueno, *Chem. Lett.*, **1980**, 1021.
6) J.-P. Desvergne and H. Bouas-Laurent, *J. Chem. Soc., Chem. Commun.*, **1978**, 403.
7) W. G. Toland, Jr., J. B. Wilkes, and F. J. Brutschy, *J. Am. Chem. Soc.*, **75**, 2262 (1953).
8) The correction for the optical density at the excitation wavelength (320 nm) was not made. The ε_{320}'s were 11200 cm^{-1} M^{-1} for *trans*-**2** and 16400 cm^{-1} M^{-1} for *trans*-**3**.
9) G. C. Hampson and J. M. Robertson, *J. Chem. Soc.*, **1941**, 409.
10) M. J. S. Dewar and N. Trinajstic, *J. Chem. Soc. (A)*, **1971**, 1220.
11) S. Shinkai and Y. Honda, unpublished results.
12) H. L. Ammon, S. K. Bhattacharijee, S. Shinkai, and Y. Honda, *J. Am. Chem. Soc.*, **106**, 262 (1984).

Sterically Controlled Synthesis of Aspartic Acid by Addition of Dialkyl Malonate to *N*-Benzyloxycarbonyl-L-alanyl-2-chloroglycine Methyl Ester

Shozo SHIONO and Kaoru HARADA*

Department of Chemistry, University of Tsukuba, Sakura-Mura, Niihari, Ibaraki 305
(Received September 12, 1984)

Synopsis. Aspartic acid was synthesized stereoselectively by addition of dialkyl malonate to *N*-benzyloxycarbonyl-L-alanyl-2-chloroglycine methyl ester, followed by hydrolysis. Substituent effect of the alkyl group of dialkyl malonate on the stereoselectivity was observed. Higher optical purity of aspartic acid was obtained as the alkyl group of dialkyl malonate became bulkier.

Several studies on the asymmetric addition reactions of malonic acid ester have been reported.[1-3] Recently, the preparation of *N*-benzyloxycarbonyl-3-carboxyaspartic acid derivatives from *N*-benzyloxycarbonyl-2-chloroglycine methyl ester was reported.[4] In the present paper, we describe a sterically controlled synthesis of aspartic acid by the addition of dialkyl malonate to *N*-benzyloxycarbonyl-L-alanyl-2-chloroglycine methyl ester (Z-L-Ala-Cl-Gly-OMe)(**2**), which was obtained from *N*-benzyloxycarbonyl-L-alanyl-2-hydroxyglycine methyl ester (Z-L-Ala-OH-Gly-OMe) (**1**) by treatment with thionyl chloride, followed by hydrolysis (Scheme 1).

The results are summarized in Table 1. Dimethyl malonate reacted with compound **2** in THF at −10 °C and aspartic acid was obtained with 29% enantiomeric excess after hydrolysis (Table 1, entry 1). Substituent effect of the ester residue of malonic acid on the stereoselectivity was observed. As the ester residue of malonic acid became bulkier, the optical purity of aspartic acid obtained became higher. When di-*t*-butyl malonate was used, the optical purity of the resulting aspartic acid reached 48% enantiomeric excess (Table 1, entry 6).

The sterically controlled synthesis of aspartic acid shown in Scheme 1 involves three stereochemical steps in which the configuration of the product would be controlled by each reaction. These are: 1) the condensation reaction between *N*-benzyloxycarbonyl-L-alaninamide with methyl glyoxylate hemiacetal to form compound **1**, 2) the chlorination reaction of compound **1** to form compound **2**, and 3) the coupling reaction of compound **2** with dialkyl malonate.

In order to examine the asymmetric induction in the condensation reaction between *N*-benzyloxycarbonyl-L-alaninamide with methyl glyoxylate hemiacetal, the diastereomeric ratio of synthesized compound **1** was determined by HPLC. Though the configuration of each diastereomer, which was separated by HPLC, was unknown, the diastereomer eluted first on HPLC ver-

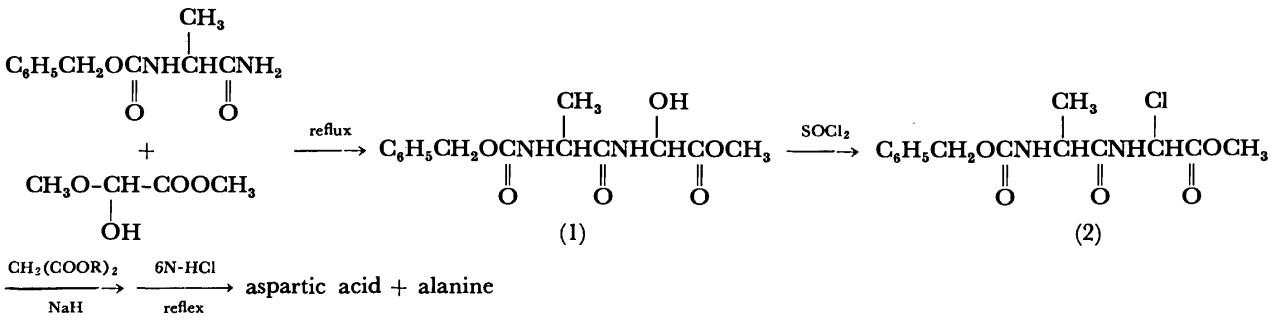

Scheme 1.

TABLE 1. ASPARTIC ACID OBTAINED BY SUCCESSIVE REACTIONS FROM **1**

Entry	d.r.[a]	Ester residue[b]	Temp/°C[c]	Solvent[d]	c.y./%[e]	e.e/%[f]	Confign.[g]
1	56 : 44	Me	−10	THF	48	29	S
2	74 : 26	Me	−10	THF	37	32	S
3	56 : 44	Me	−30	THF	57	32	S
4	56 : 44	Me	−10	diglyme	65	37	S
5	56 : 44	Et	−10	THF	41	33	S
6	56 : 44	*t*-Bu	−10	THF	37	48	S

a) Diastereomeric ratio of Z-L-Ala-OH-Gly-OMe. b) Ester residue of malonic acid. c) Reaction temperature in the addition reaction of dialkyl malonate. d) Solvent used in the addition reaction of dialkyl malonate. e) Chemical yield based on Z-L-Ala-OH-Gly-OMe. f) Enantiomeric excess of aspartic acid obtained. g) Configuration of aspartic acid.

sus that eluted second was 54:46. Compound **1** was recrystallized twice, and the diastereomeric ratios after first and second recrystallization were found to be 56:44 and 74:26, respectively. These were converted to compound **2**, and **2** was allowed to react with sodium salt of dimethyl malonate without purification to avoid diastereomeric fractionation. The enantiomeric excess of the resulting aspartic acid was 29% and 32%, respectively (Table 1, entry 1 and 2). These results indicate that the enantiomeric ratio of aspartic acid does not depend strongly on the diastereomeric ratio of Z-L-Ala-OH-Gly-OMe.

The stereochemistry of the chlorination reaction of compound **1** was not examined. The chemical property of compound **2** was too labile to determine the diastereomeric ratio by using HPLC. Therefore, the stereochemical relation between compound **2** and aspartic acid was unknown.

The substituent effect of the alkyl group of dialkyl malonate on the stereoselectivity shown in Table 1 indicates that the reaction with dialkyl malonate could be an important stereochemical step in the synthesis of optically active aspartic acid.

Experimental

All the melting points were uncorrected. NMR spectra were obtained with a Hitachi R-24A spectrometer and the chemical shifts were given in δ values (ppm) from tetramethylsilane (TMS). All the gas chromatographic analyses were carried out with a Hitachi 163 gas chromatograph. HPLC was carried out on a Jasco component consisting of a TRI ROTAR-V pump and a UVIDEC-100-IV UV spectrometer using a OA-1000 column. Amino acid analyses were carried out with a Hitachi 835-50 instrument.

Preparation of Z-L-Ala-OH-Gly-OMe (1). *N*-Benzyloxycarbonyl-L-alaninamide (0.88 g, 4×10^{-3} mol) was suspended in 10 ml of benzene, and methyl glyoxylate hemiacetal (0.48 g, 4×10^{-3} mol) was added to the suspension. The reaction mixture was refluxed for 3 d and then concentrated *in vacuo*. The residue was purified by column chromatography on silica gel using $CHCl_3$-MeOH (19:1 v/v) as an eluent. The solid obtained was recrystallized from hexane–ethyl acetate, yield 0.77 g (62%), mp 105—110 °C, ^{1}H NMR (CD_3OD): δ=1.33 (d, 3H), 3.69 (s, 3H), 4.12 (q, 1H), 5.02 (s, 2H), 5.53 (s, 1H), 7.24 (s, 5H). Found: C, 53.98; H, 5.86; N, 9.04%. Calcd for $C_{14}H_{18}N_2O_6$: C, 54.18; H, 5.84; N, 9.02%. Diastereomeric ratio of compound **1** was determined by HPLC using hexane-2-propanol (12:1 v/v) as an eluent.

Preparation of Z-L-Ala-Cl-Gly-OMe (2). Z-L-Ala-OH-Gly-OMe (**1**)(783 mg, 2.53×10^{-3} mol) was suspended in 10 ml of CH_2Cl_2, and 1 ml of thionyl chloride was added to the suspension. The reaction mixture was refluxed for 1 h and then concentrated *in vacuo*. The crude product obtained was recrystallized from CH_2Cl_2–hexane, yield 671 mg (81%), mp 120—124 °C, ^{1}H NMR ($CDCl_3$): δ=1.37 (d, 3H), 3.81 (s, 3H), 4.27 (m, 1H), 5.10 (s, 2H), 5.42 (d, 1H), 6.35 (d, 1H), 7.29 (s, 5H), 7.60 (d, 1H). Found: C, 51.20; H, 5.20; N, 8.40%. Calcd for $C_{14}H_{17}N_2O_5Cl$: C, 51.14; H, 5.21; N, 8.52%.

Reaction of Z-L-Ala-OH-Gly-OMe with Thionyl Chloride Followed by Addition of Dialkyl Malonate. General Procedure: Z-L-Ala-OH-Gly-OMe (**1**)(31 mg, 1×10^{-4} mol) was suspended in 1 ml of CH_2Cl_2, and 1 ml of thionyl chloride was added to the suspension. The reaction mixture was refluxed for 1 h and then concentrated *in vacuo*. The residue was dissolved in 1 ml of THF, and a suspension of sodium salt of dimethyl malonate in 1 ml of THF (prepared from 13 mg of dimethyl malonate and 4 mg of NaH (60%)) was added to the solution at −10 °C. After stirring for 2 h at −10 °C, 3 ml of MeOH saturated with hydrogen chloride was added to the mixture, and the mixture was concentrated *in vacuo*. The residue was refluxed with 6 M HCl (1 M=1 mol dm^{-3}) for 10 h and the hydrolyzate was concentrated *in vacuo*. A part of the residue was diluted appropriately and analyzed with an amino acid analyzer to determine the chemical yield of aspartic acid (48%, based on **1**). A part of the resulting aspartic acid was converted to *N*-(trifluoroacetyl)aspartic acid diisopropyl ester in the usual manner and then subjected to gas chromatographic analysis employing a chiral stationary phase (Chirasil-Val[5]).

References

1) G. Tsuchihashi, S. Mitamura, S. Inoue, and K. Ogura, *Tetrahedron Lett.*, **1973**, 323.

2) S. Hashimoto, N. Komeshima, S. Yamada, and K. Koga, *Tetrahedron Lett.*, **1977**, 2907.

3) S. Hashimoto, N. Komeshima, S. Yamada, and K. Koga, *Chem. Pharm. Bull.*, **27**, 2437 (1979).

4) D. H. Rich and M. K. Dhaon, *Tetrahedron Lett.*, **1983**, 1671.

5) H. Frank, G. J. Nicolson, and E. Bayer, *J. Chromatogr.*, **146**, 197 (1978).

The Use of *N,N*-Dimethylformamide-Sulfonyl Chloride Complex for the Preparation of Thiophenesulfonyl Chlorides

Tyo SONE,* Yukio ABE, Norio SATO, and Manabu EBINA

Department of Applied Chemistry, Faculty of Engineering, Yamagata University, Yonezawa 992

(Received September 14, 1984)

Synopsis. A 1:1 *N,N*-dimethylformamide-SO_2Cl_2 complex was found to be a useful agent for the one-step preparation of thiophenesulfonyl chlorides.

Thiophenesufonyl chlorides, key intermediates of the syntheses of sulfur derivatives of thiophene, have been mostly prepared by the chlorosulfonation of thiophenes with chlorosulfuric acid.[1] In the reaction of acid-sensitive thiophenes, however, polymerization and the rearrangement and/or elimination of the substituent such as halogen on the thiophene ring disturb the formation of the desired sulfonyl chlorides. In addition, the thiophenesulfonic acids are formed as the main products in some cases, and further tedious procedures are needed for converting the sulfonic acids to the sulfonyl chlorides. It is also the case with an alternative method *via* sulfonation using SO_3-organic compound adducts.[2]

It has been briefly reported by Kojtcheff *et al.* that a 1:1 *N,N*-dimethylformamide (DMF)-SO_2Cl_2 complex serves as a chlorosulfonating agent depending on the substrate.[3] Despite the potential utility, little systematic study of the direct chlorosulfonation using DMF-SO_2Cl_2 complex seems to have been made. On searching for a simple and convenient procedure for the preparation of thiophenesulfonyl chlorides, we studied the reactions of some thiophene derivatives with the complex.

The reaction procedure simply consits of heating a mixture of the thiophene derivatives and the complex at an appropriate temperature for 1—3 h.

The results are summarized in Table 1.

By this procedure, all thiophene derivatives examined, except 2-methoxy- (**1d**), 2-(1-cyclohexenyl)- (**1j**), and 2-acetylthiophenes, gave the corresponding sulfonyl chlorides as the main products. It is noteworthy

TABLE 1. REACTION OF THIOPHENE DERIVATIVES WITH DMF-SO_2Cl_2 COMPLEX

Substituent R	Reaction Conditions[a]	Product	Yield/%[b]	Bp, °C/mmHg or Mp, °C(lit,)
1a: H	A	**2a**: 2-SO_2Cl	79	bp 88—93/2.5(123—124/14[1a]), 82—84/2[1b]) amide mp 141—142(146—147[2a]), 141—142[1a])
1b: 2-CH_3	A	**2b**: 2-CH_3, 5-SO_2Cl	56	bp 105—110/4(96—98/3[1d]) amide mp 117—118(119—119.5[1d])
1c: 3-CH_3	A	**2c**: 3-CH_3, 2-SO_2Cl } c) **2'c**: 4-CH_3, 2-SO_2Cl }	78	bp 100—108/5(98—99/0.5 for **2c**[1e]) amide mp 120—143(146 for **2c**[1e])
1d: 2-CH_3O	B	**3d**: 2-CH_3O, 5-CHO	47	bp 97—99/4(79—81/0.9[7]) acid mp 161.5—162.5(162—163[7])
1e: 2-Cl	A	**2e**: 2-Cl, 5-SO_2Cl	60	bp 101—102/3(mp 28[1g]) amide mp 113—114(116[1c])
1f: 2-Br	A	**2f**: 2-Br, 5-SO_2Cl	60	bp 105—110/4(mp 44—46[1h]) amide mp 138—139(144[1g], 141[2b])
1g: 2-I	A	**2g**: 2-I, 5-SO_2Cl	43	mp 49—50(51—52[1h]) amide mp 162—163 (165[1h], 163—164[2a])
		2a: 2-SO_2Cl	8	
1h: 2-$C_6H_5CH_2$	C	**2h**: 2-$C_6H_5CH_2$, 5-SO_2Cl	54	oil; amide mp 98—99
		3h: 2-$C_6H_5CH_2$, 5-CHO	10	mp 25—26(27.5—28[8]) acid mp 128.5—129.5 (129[8])
1i: 2-C_6H_5	A	**2i**: 2-C_6H_5, 5-SO_2Cl	41	mp 86—86.5; amide mp 221—222
		3i: 2-C_6H_5, 5-CHO	21	mp 93.5—94(93—93.5[9])
1j: 2-C_6H_9[d]	B	**3j**: 2-C_6H_9, 5-CHO	7	mp 65.5—66
1k: 2-$COOCH_3$	D	**2k**: 2-$COOCH_3$, 5-SO_2Cl } e) **2'k**: 2-$COOCH_3$, 4-SO_2Cl }	9	oil; amide mp 149—151
1l: 2,5-$(CH_3)_2$	A	**2l**: 2,5-$(CH_3)_2$, 3-SO_2Cl	66	bp 106—108/3(115—130/2.5[1f]) amide mp 138—139(138.5—140.5[1f])
7: 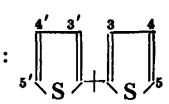	E	**8**: 5-SO_2Cl	23	mp 69—70; amide mp 61.5—62.5
		9: 5,5'-$(SO_2Cl)_2$	30	mp 118—119; amide mp 164—165
		10: 5,5'-$(CHO)_2$	4	mp 86.5—87.5
		11: 5-CHO, 5'-SO_2Cl	12	mp 52.5—53.5; anilide mp 125—126

a) Unless otherwise noted, substrate/DMF-SO_2Cl_2 = 1/1.3(mole ratio). A: 95—98 °C, 1 h. B: 50—60 °C, 1h. C: 80—85 °C, 1 h. D: 115—120 °C, 3 h. E: 65—70 °C, 1.5 h, substrate/DMF-SO_2Cl_2 = 1/2.6. b) Isolated yield based on the substrate used. c) 2c/2'c = 90/10 (NMR). Amide, Anal. ($C_5H_7O_2NS_2$) C, H. d) 1-cyclohexenyl. e) Amide, Anal. ($C_6H_7NO_4S_2$) C, H.

that methylthiophenes (**1b** and **1c**), which were expected to be much more reactive than anisole[4] and to yield the aldehydes,[3] afforded the sulfonyl chlorides. With 2-iodothiophene (**1g**), a replacement of the iodine atom by a chlorosulfonyl group was observed, but to a lesser extent than by the chlorosulfuric acid procedure.[1h] In some cases, the corresponding aldehydes were produced as the by-products in yields of up to *ca.* 20%, which could be easily separated from the sulfonyl chlorides by usual methods. The reaction of methyl 2-thiophenecarboxylate (**1k**) was attained only with difficulty, affording a mixture of the two isomeric sulfonyl chlorides (**2k** and **2'k**) in low yield.

Repeated attempts to chlorosulfonate **1d** and **1j** with the complex gave only tars, and when the reactions were carried out under mild conditions, only the aldehydes (**3d** and **3j**) were isolated from the reaction products. The results offer a sharp contrast with those of anisole[3] and styrene,[5] which were chlorosulfonated with the complex in the ring and in the side chain, respectively. 2-Acetylthiophene reacted easily with the complex to give unidentified materials. In this case DMF-SO_2Cl_2 complex probably functioned as a chloroformylating agent, and 2-acetylthiophene underwent the reaction in the side chain as in the Vilsmeier reaction.[6,10] Actually, the reaction of cyclohexanone with the complex was found to afford 2-chlorocyclohex-1-enecarbaldehyde in *ca* 40% yield.

In conclusion, the DMF-SO_2Cl_2 procedure is particularly useful for the preparation of several thiophenesulfonyl chlorides. The yields are approximately equal or superior to the previously reported ones. The principal advantages of this procedure over the conventional ones are the operational simplicity, one-step procedure, and the use of easy-to-handle reagents.

Experimental

All melting and boiling points are uncorrected. The IR spectra were obtained on a Hitachi EPI-S2 spectrometer, and the NMR spectra on Hitachi R-22 spectrometer at 90 MHz using TMS as an internal reference.

*Reaction of Thiophene (**1a**) with DMF-SO_2Cl_2 Complex (Typical Procedure).* Freshly distilled SO_2Cl_2 (17.6 g, 0.13 mol) was added dropwise with shaking to ice-cooled DMF (9.5 g, 0.13 mol); the temperature was kept below 25 °C during the addition. The hygroscopic solid complex, thus formed within 10 min, was held at the same temperature for additional 30 min. Thiophene (**1a**; 8.4 g, 0.1 mol) was added to the complex and the mixture was heated on a water-bath at 95—98 °C for 1 h with occasional shaking. The viscous brown mixture was cooled, poured into ice-water, and then extracted with $CHCl_3$. The $CHCl_3$ solution was washed successively with water, 5% $NaHCO_3$ solution, and water and dried. Evaporation of the solvent left a liquid, which was distilled *in vacuo* to give 2-thiophenesulfonyl chloride (**2a**; 13.5 g, bp 88—93 °C/2.5 mmHg (1 mmHg≈133.322 Pa)).

*Reaction of 2-Phenylthiophene (**1i**) with DMF-SO_2Cl_2 Complex (Typical Procedure).* 2-Phenylthiophene (**1i**; 3.2 g, 0.02 mol) was heated with 1.3 molar equivalent of DMF-SO_2Cl_2 complex at 95—98 °C on a water-bath for 1 h. Water was added to the cooled reaction mixture. The products were extracted with $CHCl_3$. The combined extracts were washed with water and dried. After evaporating the solvent, the residue was chromatographed (silica gel/hexane-$CHCl_3$ (1:3)) to give 5-phenyl-2-thiophenesulfonyl chloride (**2i**; 2.1 g, mp 86—87 °C) and 5-phenyl-2-thiophenecarbaldehyde (**3i**; 0.3 g, mp 93—94 °C). The aqueous layers were concentrated under reduced pressure to *ca* 10 ml and extracted with ether. Evaporation of the solvent from the extracts gave another crop of **3i** (0.5 g, mp 91—93 °C) **2i**: IR (CCl_4) 1175, 1385 cm^{-1} (ν_{SO_2}). NMR (CCl_4) δ=7.23 and 7.75 (1H, d each, $J_{3,4}$=4.0 Hz, 3-H and 4-H), 7.3—7.7 (5H, m, phenyl). Anal. ($C_{10}H_7ClO_2S_2$) C, H. Sulfonamide: Anal. ($C_{10}H_9NO_2S_2$) C, H.

*5-Benzyl-2-thiophenesulfonyl Chloride (**2h**)*: IR ($CHCl_3$) 1175, 1385 cm^{-1} (ν_{SO_2}). NMR (CCl_4) δ=6.86 and 7.70 (1H, d each, $J_{3,4}$=3.9 Hz, 3-H and 4-H), 7.1—7.5 (5H, m, phenyl), 4.20 (2H, s, CH_2). Sulfonamide: Anal. ($C_{11}H_{11}NO_2S_2$) C, H.

*5-(1-Cyclohexenyl)-2-thiophenecarbaldehyde (**3j**)*: IR (CCl_4) 1680 cm^{-1} (ν_{CO}). NMR ($CDCl_3$) δ=9.75 (1H, s, CHO), 7.02 and 7.60 (1H, d each, $J_{3,4}$=4.1 Hz, 3-H and 4-H), 6.42 (1H, m, cyclohexenyl CH), 1.5—2.6 (8H, m, cyclohexenyl CH_2). Anal. ($C_{11}H_{12}OS$) C, H.

*2-(5-Chlorosulfonyl-2-thienyl)-2-(2-thienyl)propane (**8**)*: IR (KBr) 1175, 1380 cm^{-1} (ν_{SO_2}). NMR ($CDCl_3$) δ=7.76 (1H, d, $J_{3,4}$=4.0 Hz, 4-H), 7.92 (1H, ABXq, 5'-H), 6.9—7.1 (3H, m, 3-H, 3'-H and 4'-H), 1.88 (6H, s, $C(CH_3)_2$). Anal. ($C_{11}H_{11}ClO_2S_3$) C, H. Sulfonamide: Anal. ($C_{11}H_{13}NO_2S_3$) C, H.

*2,2-Bis(5-chlorosulfonyl-2-thienyl)propane (**9**)*: IR (KBr) 1170, 1380 cm^{-1} (ν_{SO_2}). NMR ($CDCl_3$) δ=7.76 and 7.00 (2H, d each, $J_{3,4}$=4.0 Hz, 4-H and 4'-H, and 3-H and 3'-H), 1.93 (6H, s, $C(CH_3)_2$). Anal. ($C_{11}H_{10}Cl_2O_4S_4$) C, H. Sulfonamide: Anal. ($C_{11}H_{14}N_2O_4S_4$) C, H.

*2,2-Bis(5-formyl-2-thienyl)propane (**10**)*: IR (KBr) 1660 cm^{-1} (ν_{CO}). NMR ($CDCl_3$) δ=9.86 (2H, s, CHO), 7.71 and 7.08 (2H, d each, $J_{3,4}$=4.2 Hz, 4-H and 4'-H, and 3-H and 3'-H), 1.89 (6H, s, $C(CH_3)_2$). Anal. ($C_{13}H_{12}O_2S_2$) C, H.

*2-(5-Formyl-2-thienyl)-2-(5-chlorosulfonyl-2-thienyl)-propane (**11**)*: IR (KBr) 1180, 1385 cm^{-1} (ν_{SO_2}), 1670 cm^{-1} (ν_{CO}). NMR ($CDCl_3$) δ=9.91 (1H, s, CHO), 7.82 and 7.74 (1H, d each, $J_{3,4}$=4.0 Hz, 4-H and 4'-H), 7.11 and 7.03 (1H, d, $J_{3,4}$=4.0 Hz, 3-H and 3'-H), 1.91 (6H, s, $C(CH_3)_2$). Anal. ($C_{12}H_{11}ClO_3S_3$) C, H. Sulfonanilide: Anal. ($C_{18}H_{17}NO_3S_3$) C, H.

References

1) For example, a) W. Steinkopf and T. Höpner, *Ann.*, **501**, 174 (1933); b) W. E. Truce, B. Van Gemert, and W. W. Brand, *J. Org. Chem.*, **43**, 101 (1978); c) A. Buzas and J. Teste, *Bull. Soc. Chim. Fr.*, **1960**, 793; d) T. Sone and Y. Matsuki, *Nippon Kagaku Zasshi*, **83**, 138 (1962); e) F. Challenger, S. A. Miller, and G. M. Gibson, *J. Chem. Soc.*, **1948**, 769; f) O. Dann and W. Dimmling, *Chem. Ber.*, **87**, 373 (1954); g) W. Steinkopf and W. Köhler, *Ann.*, **532**, 250 (1937); h) W. Steinkopf, H. Jacob, and H. Penz, *Ann.*, **512**, 1136 (1934).

2) For example, a) A. P. Terent'ev and G. M. Kadatskii, *Zhur. Obshch. Khim.*, **23**, 251 (1953); b) A. P. Terent'ev and G. M. Kadatskii, *Zhur. Obshch. Khim.*, **21**, 1524 (1951).

3) T. Kojtscheff, F. Wolf, and G. Wolter, *Z. Chem.*, **6**, 148 (1966).

4) Ya. L. Gol'dfarb, V. P. Litvinov, and V. E. Shvedov, *Zhur. Obshch. Khim.*, **30**, 534 (1959).

5) B. M. Culbertson and S. Dietz, *J. Chem. Soc., C*, **1968**, 992.

6) K. Bodendorf and R. Mayer, *Chem. Ber.*, **98**, 3554 (1965).

7) J. Sicé, *J. Am. Chem. Soc.*, **75**, 3697 (1953).

8) Y. Matsuki and T. Yoshinari, *Bull. Chem. Research Institute Non-Aqueous Solutions, Tohoku Univ.*, **9**, 221 (1963).

9) N. Gjos and S. Gronowitz, *Acta Chem. Scand.*, **26**, 1851 (1972).

10) J. M. Gagan, A. G. Lane, and D. Lloyd, *J. Chem. Soc., C*, **1970**, 2484.

Tetrabromooxomolybdate(V) Complex. The Catalytic Reactivity for the Reaction of *t*-Butyl Hydroperoxide

Yasuhiko KURUSU,* Yoshiro MASUYAMA, and Mikio SAITA
Department of Chemistry, Faculty of Sciencae and Technology, Sophia University, 7-1, Kioicho, Chiyoda-ku, Tokyo 102
(Received September 21, 1984)

Synopsis. The nature of an ammonium counter cation of tetrabromooxomolybdate complex influences the rate of decomposition of *t*-butyl hydroperoxide(*t*-BuOOH) and oxidation with *t*-BuOOH. The catalytic activity of the ammonium for the decomposition of *t*-BuOOH decreased as the following order; benzyltrimethylammnium, -*N*-methyl pyridinium, -trimethylene bispyridinium, ≫pyridinium, -quinolinium, >1,3-propanediammonium, -1,6-hexanediammonium. However, the reverse order was observed in the catalytic activity for the epoxidation by *t*-BuOOH, and the rate of oxidation of alcohol by *t*-BuOOH was independent of the nature of ammonium cation.

In the synthetic applications of catalytic oxygen transfer process a metal catalyst mediates the selective transfer of an oxygen atom from alkyl hydroperoxides to the substrate.[1] A few examples of this application are epoxidation and other oxidation with alkyl hydroperoxides. For epoxidation of olefin with hydroperoxides molybdenum compounds are effective well-known catalysts.

We have investigated the epoxidation of olefin with *t*-butyl hydroperoxide(*t*-BuOOH) in the presence of various molybdenum compounds.[2] In the process, we found that oxomolybdate complex showed an interesting character for the reaction of *t*-BuOOH; the reactivity of *t*-BuOOH was dependent on the counter cation of the tetrabromooxomolybdate-(V) complex. In order to clarify this tendency, we prepared tetrabromooxomolybdate(V) complexes containing benzyltrimethylammonium(**1**), *N*-methylpyridinium(**2**), trimethylene bispyridinium(**3**), pyridinium(**4**), quinolinium(**5**), 1,3-propanediammonium(**6**), and 1,6-hexanediammonium(**7**) as a counter cation.

The decomposition of *t*-BuOOH in the presence of various complexes mentioned above was examined.

TABLE. DECOMPOSITION OF *t*-BuOOH, EPOXIDATION OF CYCLOHEXENE, AND OXIDATION OF 2-OCTANOL IN THE PRESENCE OF AMMONIUM TETRABROMOOXOMOLYBDATE(V) COMPLEX

Mo complex	Decomposition of *t*-BuOOH conversion/%	Epoxidation of cyclohexene yield of/% cyclohexene oxide	Oxidation of 2-octanol yield of/% 2-octanone[a]
1	85	0	80
2	96	0	44
3	91	0	46
4	37	66	78
5	35	68	—
6	10	78	77
7	6	85	—

a) The residue compound is only 2-octanol unreacted.

The results are shown in Table. **1** shows the highest activity in the decomposition of *t*-BuOOH. When an ammonium cation of tetrabromooxomolybdate(V) complex has no hydrogen on the nitrogen atom such as **1**, **2**, and **3**, decomposition of *t*-BuOOH and oxidation of alcohols to carbonyl compounds took place smoothly, but the epoxidation of olefins with *t*-BuOOH did not proceed. On the other hand, the decomposition is rarely found in **6** and **7**. The decomposition of *t*-BuOOH is essentially free-radical-induced decomposition initiated by metal-hydroperoxide interaction,[3] since the addition of 2,6-xylenol, 2,6-xylidine or *N*-phenyl-2-naphthylamine as a radical scavenger depressed the decomposition of *t*-BuOOH. For example, only 4% of *t*-BuOOH were decomposed when a mole of four of 2,6-xylenol to one of **4** was used.

The epoxidation of cyclohexene with *t*-BuOOH was carried out in the presence of a catalytic amount of various ammonium tetrabromooxomolybdate(V) complexes. As can be seen from Table, the tendency in the rate of decomposition of *t*-BuOOH reversely relates to that of the epoxidation, that is, in the case of high activity for epoxidation, decomposition activity is low. For example, **6** and **7** are effective for epoxidation with *t*-BuOOH but not for decomposition. On the other hand, oxidation activity for alcohol is independent of the decomposition activity for *t*-BuOOH. **1**, **2**, and **3** show no activity for epoxidation but have high effectivity for oxidation of 2-octanol. Also, we have already reported that unsaturated alcohols were oxidized to unsaturated carbonyl compounds.[4]

It is worth noting that *t*-BuOOH shows no activity for olefinic compound in the presence of **1**, **2**, and **3**, thus unsaturated alcohol can be oxidized selectively by *t*-BuOOH with **1**, **2**, and **3** without disturbing carbon-carbon double bond. It is interesting that ammonium as a counter-cation of tetrabromooxomolybdate(V) complex profoundly affects the reactivity of *t*-BuOOH.

Experimental

Materials. Pyridinium tetrabromooxomolybdate(V) (**4**) and quinolinium tetrabromooxomolybdate(V)(**5**) were prepared according to the procedure of Allen and Newmann.[5] Similar procedures were used with a little modification for the preparation of other ammonium tetrabromooxomolybdate(V) complexes. These complexes were identified by the elemental analysis (Mo:EDTA method and Br: Volhard method), and spectral measurements. Benzyltrimethylammonium tetrabromooxomolybdate(V)(**1**): Found: Mo, 15.8; Br, 54.6%. Calcd for $C_{10}H_{16}Br_4MoNO$: Mo, 16.5; Br, 54.9%. *N*-Methylpyridinium tetrabromooxomo-

lybdate(V)(**2**): Found: Mo, 18.2%. Calcd for $C_6H_8Br_4MoNO$: Mo, 18.3%. Trimethylenebispyridinium tetrabromoxomolybdate(V)(**3**): Found: Mo, 18.3%. Calcd for $C_{13}H_{16}Br_8Mo_2N_2O_2$: Mo, 18.0%. 1,3-propanediammonium tetrabromooxomolybdate(V)(**6**): Found: Mo, 20.0; Br, 64.0%. Calcd for $C_3H_{12}Br_8Mo_2N_2O_2$: Mo, 20.4; Br,68.1%. 1,6-hexanediammonium tetrabromooxomolybdate(V)(**7**): Found Mo, 19.0; Br, 63.8%. Calcd for $C_6H_{18}Br_8Mo_2N_2O_2$: Mo, 19.6; Br, 65.1%. *t*-BuOOH supplied by Nippon Oils & Fats Co. was used after the purification by vacuum distillation.

General Procedure for Decomposition. In a test tube with a screw cap, benzene(50 cm^3) and *t*-BuOOH(0.05 mol) were mixed with a catalytic amount of molybdenum complex(0.2 meq). Then the tube contents were stirred at 60 °C for 60 min in an aluminum block thermostat. The products were analyzed by GC; column packing material was DOP/Chromosorb PNAW, carrier gas was hydrogen.

General Procedure for Epoxidation. Cyclohexene (0.05 mol) was dissolve in benzene(50 cm^3) and the mixture was stirred at 60 °C. Then molybdenum catalyst(0.2 meq) and *t*-BuOOH (0.05 mol) were added to the solution. The stirring was continued at 60 °C for 60 min. Cyclohexene oxide was separated by GC (DOP/Chromosorb PNAW, carrier gas; nitrogen or helium) and identified by NMR and IR.

General Procedure for Oxidation of 2-Octanol. Molybdenum catalyst(0.15 meq), *t*-BuOOH(5 mmol), and 2-octanol(3 mmol) were added into benzene(3 cm^3) and stirred at 60 °C for 24 h. After evaporation, the product, 2-octanone, was separated by column chromatography(Wako gel C-200/hexane; ethyl acetate (3:1)) and identified by NMR and IR.

References

1) R. A. Sheldon, "Synthesis and Uses of Alkyl Hydroperoxides and Dialkyl Peroxides" in "The Chemistry of Peroxides" ed by S. Patai, John Wiley & Sons, Chichester-New York-Brisbane-Toronto-Singapore (1983) pp. 161—200.

2) M. Yamazaki, H. Endo, M. Tomoyama, and Y. Kurusu, *Bull. Chem. Soc. Jpn.*, **56**, 3523 (1983).

3) R. Hiatt, T. Mill, K. C. Irwin, and J. Castleman, *J. Org. Chem.*, **33**, 1421 (1968).

4) Y. Masuyama, M. Takahashi, and Y. Kurusu, *Tetrahedron Lett.*, **25**, 4417 (1984).

5) J. F. Allen and H. M. Newmann, *Inorg. Chem.*, **3**, 1612 (1964).

A Facile Displacement of Tertiary Nitro Group by Hydrogen with Sodium Hydrogentelluride

Hitomi SUZUKI,* Koji TAKAOKA, and Atsuhiro OSUKA†
Department of Chemistry, Faculty of Science, Ehime University, Bunkyo-cho, Matsuyama 790
(Received September 25, 1984)

Synopsis. Sodium hydrogentelluride is a useful reagent for replacement of a class of tertiary nitro group by hydrogen.

In recent years, reductive removal of nitro group from nitroalkanes has been the subject of extensive investigation in connection with the versatile utilities of nitroalkanes in organic syntheses, which have been well demonstrated in the last two decades.[1] As a result, several methods have been developed to bring about such a conversion — a) sodium salt of methanethiol in dipolar aprotic solvents,[2] b) potassium hydroxide in ethylene glycol,[3] c) *N*-benzyl-1,4-dihydronicotinamide,[4] and d) tributyltin hydride in the presence of azobis-isobutyronitrile.[5] However, these methods have certain drawbacks such as the necessity of high temperature (method a, b, and c), long reaction time (method a), and chromatographic separation (method d), the formation of side products (method a), or the incompatibility of other functional groups (method b).

Herein we disclose the results of our new procedure for the replacement of tertiary nitro group by hydrogen through the use of sodium hydrogentelluride (NaHTe).[6] The experimental procedure is marked by its simplicity in that it involves just the treatment of nitro compounds with NaHTe in ethanol for 15 min at room temperature.

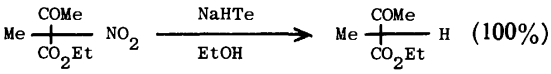

(100%) (1)

1 **2**

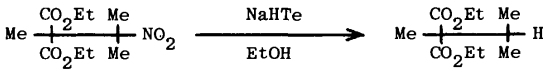

(98%) (2)

3 **4**

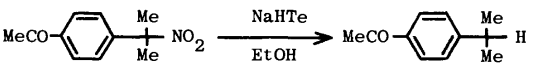

9 **10** (85%) (3)

Tertiary nitro group at α or β-position of ketone and ester was readily replaced by hydrogen (Eqs. 1 and 2). Similarly, α-nitrocumene derivative **9** was transformed into the corresponding 4-substituted cumene **10** in 85% yield (Eq. 3). Other examples were listed in Table 1. It should be noted that the isolated yields were excellent, the chromatographic separation was unnecessary, and other functional groups such as keto, cyano, ester, and sulfonyl groups remained unaffected under the present conditions.

However, to our surprise, nitro compounds, **17**, **18**, and **19** in which nitro group is situated at γ-position of ketone, ester, and nitrile, were quantitatively recovered after prolonged treatment with NaHTe even at refluxing conditions in ethanol. Finally, the reaction of 1-nitro-1-(phenylsulfonyl)cyclohexane **20** with NaHTe gave rise to the replacement of phenylsulfonyl group, instead of nitro group, by hydrogen (Eq. 4).

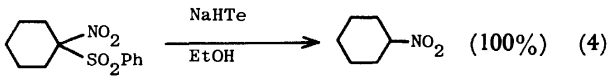

(100%) (4)

20 **21**

Although the reaction mechanism has not been studied yet, it appears to involve one-electron transfer to the nitro compound from NaHTe and the subsequent detachment of nitrite anion from the resulting nitro compound anion radical. Thus, in the case of compound **20**, phenylsulfonyl group which is a better leaving group than nitro group, was preferentially cleaved from the anion radical intermediate over nitro group.[8] In addition, the reluctance of nitro compounds **17**, **18**, and **19** toward NaHTe might be ascribed to the failure of the initial electron transfer from NaHTe to these compounds.

TABLE 1. REPLACEMENT OF TERTIARY NITRO GROUP BY HYDROGEN WITH SODIUM HYDROGENTELLURIDE (NaHTe)[a]

Reactant		Product		Yield/%[b]
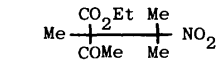	**5**	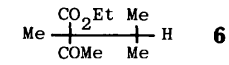	**6**	96
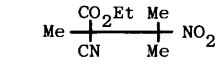	**7**	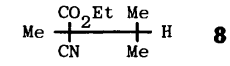	**8**	95
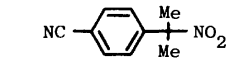	**11**	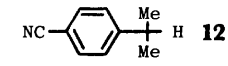	**12**	80
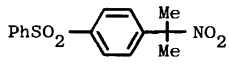	**13**	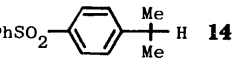	**14**	81
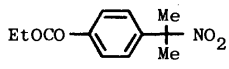	**15**	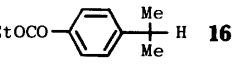	**16**	87

a) All reactions were performed as described in detail in the text. b) Values reported are isolated ones.

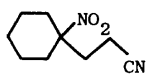

17

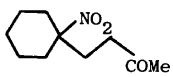

18

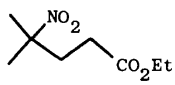

19

Experimental

Tertiary nitro compounds were prepared according to

† Present address: Department of Chemistry, Faculty of Science, Kyoto University, Kyoto 606.

the reported procedure.[7]

General Procedure for the Replacement of Tertiary Nitro Group by Hydrogen with Sodium Hydrogentelluride (NaHTe). A solution of tertiary nitro compound (4 mmol) in ethanol (4 ml) was added at room temperature under nitrogen atmosphere to a solution of NaHTe,[6] prepared *in situ* by reacting tellurium powder (1.30 g, 10 mmol) and sodium borohydride (0.90 g, 24 mmol) for 1 h in refluxing ethanol (40 ml). An instantaneous reaction occurred and the color of the reaction mixture changed to deep black. After 15 min, water (50 ml) was added, and the resulting mixture was left open to air with stirring. The solution became clear after 1 h with the deposition of tellurium powder. It was then filtered through Celite 545 and the filtrate was extracted with three portions of dichloromethane (30 ml). The combined extracts were washed with water, dried over Na_2SO_4, and evaporated to give the crude product, which was purified by Kugelrohr distillation or recrystallization. The products were identified by comparison with authentic samples.

The present work was partially supported by a Grant-in-Aid for Scientific Research No. 59740251 from the Ministry of Education, Science and Culture.

References

1) N. Ono and A. Kaji, *J. Synth. Org. Chem. Jpn.*, **38**, 115 (1980).
2) N. Kornblum, S. C. Carlson, and R. G. Smith, *J. Am. Chem. Soc.*, **101**, 647 (1979).
3) A. Łytko-Krasuska, H. Piotrowska, and T. Urbański, *Tetrahedron Lett.*, **1979**, 1243.
4) N. Ono, R. Tamura, and A. Kaji, *J. Am. Chem. Soc.*, **102**, 2851 (1980).
5) N. Ono, H. Miyake, R. Tamura, and A. Kaji, *Tetrahedron Lett.*, **1981**, 1705.
6) D. H. R. Barton and S. W. McCombie, *J. Chem. Soc., Perkin Trans. 1*, **1975**, 1574.
7) a) N. Kornblum, L. Cheng, R. C. Kerber, M. M. Kestner, B. N. Newton, H. W. Pinnick, R. G. Smith, and P. A. Wade, *J. Org. Chem.*, **41**, 1560 (1976); b) N. Kornblum, S. D. Boyd, and N. Ono, *J. Am. Chem. Soc.*, **96**, 2580 (1974).
8) N. Ono, R. Tamura, R. Tanikaga, and A. Kaji, *J. Chem. Soc., Chem. Commun.*, **1981**, 71.

A New Preparation of Aliphatic Nitro Compounds by S_H2' Reactions of *gem*-Halo Nitro Compounds with Allyltributylstannane

Noboru ONO,* Klaus ZINSMEISTER, and Aritsune KAJI*
Department of Chemistry, Faculty of Science, Kyoto University, Kyoto 606
(Received October 3, 1984)

Synopsis. α-Nitroalkyl radicals generated from *gem*-halo nitro compounds are reactive enough to undergo the carbon-carbon bond forming reaction with allyltributylstannane *via* radical chain processes, which provides a new method for the introduction of an allyl group into nitroalkanes.

The chemistry of aliphatic nitro compounds has recently recieved much attention because of their importance in organic synthesis.[1] Although aliphatic nitro compounds can be prepared by numerous methods, a new method is still desired. The method *via* the carbon–carbon bond formation at the α-position of the nitro function is particularly useful among them. This has be done so far mainly by Michael addition reactions of nitroalkanes,[1] nitro-aldol condensation reactions,[1] or single-electron transfer reactions involving α-nitroalkyl radicals as intermediates.[2] However, it is very difficult to introduce alkyl groups such as methyl, ethyl, or allyl groups at the α-position of the nitro function, for reactions of alkyl halides with the α-anions of nitroalkanes give exclusive *O*-alkylation products in general,[1] and the inverse reactions using *gem*-halo nitro compounds and alkyl anions such as Grignard reagents or alkyllithium reagents fail to give the alkylated products.[3] In this paper we wish to report a simple method for the introduction of an allyl group at the α-position of the nitro function by application of S_H2' reactions of allyltin compounds developed by Migita and his coworkers[4] to the reaction of *gem*-halo nitro compounds (**1**) with allyltributylstannane (**2**).

Various *gem*-halo nitro compounds (**1**) were allowed to react with **2** in the presence of a radical initiator (azobisisobutyronitrile, AIBN) at 100 °C. The reaction was also initiated by light, which was achieved by using a conventional medium-pressure mercury lamp equipped with a pyrex filter at 25 °C. Monoallylated products (**3**) were isolated from the reaction mixture by distillation and further purified by chromatography. The results are summarized in the Table.

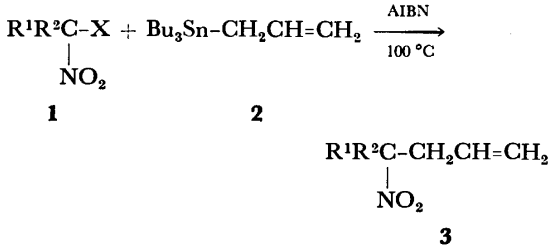

1 **2** **3**

Thus, *gem*-bromo nitro or *gem*-chloro nitro compounds undergo S_H2' reactions, but the reactions of *gem*-iodo nitro compounds with **2** proceed in the different way from S_H2' reactions. Although it is reported that simple alkyl halides such as isopropyl bromide react with **2** to give the allylated products in good yields,[4] **1** is much more reactive than simple alkyl halides in the present S_H2' reactions. For example, treatment of a mixture of 2-bromo-2-nitropropane and isopropyl bromide with **2** resulted in selective formation of **3a** was recovered unchanged.

Table. Preparation of 4-nitro-1-alkenes

R^1	R^2	X	Time/h	Yield of **3**/%[a]
Me	Me	Br	24	**3a**, 67 (65)[b]
Me	Me	Cl	24	**3a**, 65
Me	Me	I	24	**3a**, 0[c]
Me	Et	Br	24	**3b**, 45
$-(CH_2)_4-$		Br	24	**3c**, 55
Me	H	Br	15	**3d**, 70
Et	H	Br	15	**3e**, 60
H	H	Br	15	**3f**, 35

a) Yields refer to pure and isolated products. b) Photoinitiation at 25 °C. c) Allyl iodide was formed.

Although the reactions of various organic halides with **2** have been already reported,[4] the present alkylation of **1** with **2** may find its synthetic value, because compounds **3** cannot be prepared by ordinary S_N2 reactions of allyl bromides with the α-carbanions of nitroalkanes,[5] and also **3** can be converted into various important compounds such as ketones, aldehydes, carboxylic acids, nitriles, oximes, or amines through the manipulation of the nitro function.[1]

Experimental

Materials. Allyltributylstannane was prepared by the reaction of allymagnesium bromides with tributyltin chloride in diethyl ether.[4] *gem*-Halo nitro compounds were prepared according to the literature method; 2-bromo-2-nitropropane[6] (bp 72—75 °C/50 mmHg, 1 mmHg=133.32 Pa), 2-bromo-2-nitrobutane[7] (bp 65—68 °C/30 mmHg), 1-bromo-1-nitrocyclopentane[7] (bp 100—103 °C/20 mmHg), 1-bromo-1-nitroethane[8] (bp 70 °C/50 mmHg), 1-bromo-1-nitropropane[8] (bp 70—74 °C/50 mmHg), bromonitromethane[9] (bp 143—145 °C), 2-chloro-2-nitropropane[6] (bp 57 °C/50 mmHg), 2-iodo-2-nitropropane.[6]

Preparation of 4-Methyl-4-nitro-1-pentene (3a). Method A: A mixture of 2-bromo-2-nitropropane (1.7 g, 10 mmol), **2** (6.5 g, 15 mmol), and AIBN (0.5 g, 3 mmol) was heated at 100 °C for 24 h. In the course of the reaction, AIBN was added in three portions. The products were distilled off by Kugelrohr distillation and purified by column chromatography on silica gel with hexane to give pure **3a** (0.86 g, 67% yield). IR (neat) 3040, 1610, 1540, 1380 cm^{-1}; ^1H-NMR ($CDCl_3$) δ=1.56

(s, 6H), 2.66 (d, 2H, J=7.5 Hz), 4.9—5.2 (m, 2H), 5.5—5.8 (m, 1H). Found: C, 55.72; H, 8.76; N, 10.92%. Calcd for $C_6H_{11}NO_2$: C, 55.72; H, 8.53; N, 10.86%. Method B: The same procedures of method A using 2-chloro-2-nitropropane (1.3 g, 10 mmol) gave **3a** in 65% yield. Method C: A solution of 2-bromo-2-nitropropane (0.51 g, 3 mmol) and **2** (2 g, 4.5 mmol) in 100 ml of benzene was internally irradiated for 10 h with a 300 W medium-pressure mercury lamp using a Pyrex filter. The same work-up as described in method A have pure **3a** in 65% yield.

Following compounds were prepared by the method A.

4-Methyl-4-nitro-1-hexene (3b): IR (neat) 3040, 1610, 1535, 1375 cm^{-1}; ^{1}H-NMR ($CDCl_3$) δ=0.88 (t, 3H, J=7.0 Hz), 1.52 (s, 3H), 1.6—2.1 (m, 2H), 2.5—2.7 (m, 2H), 4.9—5.2 (m, 2H), 5.5—5.8 (m, 1H). Found: C, 58.38; H, 9.14; N, 9.63%. Calcd for $C_7H_{13}NO_2$: C, 58.76, H, 9.09; N, 9.78%.

1-Allyl-1-nitrocyclopentane (3c): IR (neat) 3040, 1610, 1540, 1380 cm^{-1}; ^{1}H-NMR ($CDCl_3$) δ=1.2—1.4 (m, 8H), 2.50 (d, 2H, J=7.2 Hz), 4.9—5.2 (m, 2H), 5.4—5.8 (m, 1 H). Found: C, 61.74; H, 8.13; N, 9.16%. Calcd for $C_8H_{13}NO_2$: C, 61.95; H, 8.39; N, 9.03%.

4-Nitro-1-pentene (3d): IR (neat) 3040, 1610, 1540, 1380 cm^{-1}; ^{1}H-NMR ($CDCl_3$) δ=1.54 (d, 3H, J=7.0 Hz), 2.4—2.8 (m, 2H), 4.4—4.8 (m, 1H), 5.0—5.2 (m, 2H), 5.5—5.9 (m, 1H). Found: C, 52.19; H, 8.12; N, 12.35%. Calcd for $C_5H_9NO_2$: C, 52.16; H, 7.88; N, 12.17%.

4-Nitro-1-hexene (3e): IR (neat) 3030, 1610, 1540, 1380 cm^{-1}; ^{1}H-NMR ($CDCl_3$) δ=0.98 (t, 3H, J=7.0 Hz), 1.7—2.1 (m, 2H), 2.4—2.8 (m, 2H), 4.2—4.6 (m, 1H), 5.0—5.2 (m, 2H), 5.4—5.8 (m, 1H). Found: C, 55.63; H, 8.83; N, 11.04%. Calcd for $C_6H_{11}NO_2$: C, 55.79; H, 8.53; N, 10.86%.

4-Nitro-1-butene (3f): IR (neat) 3030, 1610, 1540, 1380 cm^{-1}. ^{1}H-NMR ($CDCl_3$) δ=2.8 (q, 2H), 4.6 (t, 2H), 5.2—5.5 (m, 2H), 5.6—6.2 (m, 1H). These spectral data are in good agreement with those of authentic sample of **3a** which is prepared from 4-bromo-1-butene.[1)]

References

1) D. Seebach, E. W. Colvin, F. Lehr, and T. Weller, *Chimia*, **33**, 1 (1979); N. Ono and A. Kaji, *Yuki Gosei Kagaku Kyokai Shi*, **38**, 115 (1980).

2) N. Kornblum, *Angew. Chem., Int. Ed. Engl.*, **14**, 734 (1975).

3) G. A. Russell, M. Jawdosiuk, and M. Makosza, *J. Am. Chem. Soc.*, **101**, 2355 (1979).

4) T. Migita, K. Nagai, and M. Kosugi, *Bull. Chem. Soc. Jpn.*, **56**, 2480 (1980), and references therein.

5) D. Seebach and F. Lehr, *Helv. Chim. Acta*, **62**, 2239 (1979), in which the dianions derived from primary nitroalkanes are carbon-allylated with allyl bromides. Thus, **3d** and **3e** can be prepared by the method using dianions of nitroalkanes.

6) L. W. Seigle and H. B. Hass, *J. Org. Chem.*, **5**, 102 (1940).

7) D. C. Iffland and G. X. Criner, *J. Am. Chem. Soc.*, **75**, 4047 (1953).

8) A. S. Erickson and N. Kornblum, *J. Org. Chem.*, **42**, 3764 (1977).

9) J. Tscherniak, *Justus Liebigs Ann. Chem.*, **180**, 123 (1876).

Stereochemistry on the Catalytic Hydrogenation of 1-*t*-Butyl-4-methylenecyclohexane over Modified Raney Ni, Co, and Fe Catalysts

Shin IMAIZUMI,* Hitoshi MURAYAMA, Jun-ichi ISHIYAMA, and Yasuhisa SENDA
Department of Engineering Science (Chemistry), Faculty of Engineering, Tohoku University, Aoba, Sendai 980
(Received October 12, 1984)

Synopsis. Contrary to a fresh catalyst, aged Raney Ni in ethanol provided exclusively a less stable product in the hydrogenation of the title compound. A similar stereoselectivity was observed over a catalyst which was refluxed in ethanol as well as that treated with carbon monoxide. These results indicate that the catalyst stored in ethanol is modified with carbon monoxide generated by the decomposition of the solvent.

Mitsui and his coworkers found that the Raney Ni catalyst stored in ethanol shows; i) a different stereoselectivity to Pt, Rh, and Pd catalysts in the hydrogenation of alkylmethylenecyclohexanes[1] and alkylmethylcyclohexenes,[2] ii) the appreciable anchor effect of a hydroxyl group in the hydrogenation of substituted cyclohexanols.[3] They suggested that the product-controlling step of the hydrogenation over Raney Ni is the adsorption of the substrate on the catalyst.[1-3] Tyman reported that the hydrogenation of 1-methyl-3- and 4-methylenecyclohexane over Raney Ni aged in methanol preferably gave the thermodynamically less stable of two possible products, while alternatives were obtained over a new catalyst.[4]

In order to examine the characteristics of the Raney Ni catalyst aged in ethanol, 1-*t*-butyl-4-methylenecyclohexane (**1**) and 4-*t*-butyl-1-methylcyclohexene (**3**) were hydrogenated under various selected conditions.

Results and Discussion

The stereoselectivity on the hydrogenation of **1** over Raney Ni varied appreciably depending on the origin of the catalysts and the reaction conditions (Tables 1 and 2). A thermodynamically more stable product, *trans*-1-*t*-butyl-4-methylcyclohexane (**2e**), was predominantly obtained over fresh Raney Ni. The amount of **2e** decreased in an atmosphere of hydrogen, and increased with the amount of the catalyst. This suggests that the amount of hydrogen available on the catalyst surface is also responsible for the stereochemistry on the hydrogenation of a reactive substrate such as **1**.[5,6] When Raney Ni which had been stored in ethanol for 40 d was used, a thermodynamically less-stable product, *cis*-1-*t*-butyl-4-methylcyclohexane (**2a**), was selectively yielded regardless of the amount of the catalyst and pressure of the hydrogen. Contrary to this, the stereoselectivity over a catalyst aged in water or cyclohexane was not as high as that over a catalyst aged in ethanol (Table 1).

The proportion of products over a catalyst modified under various conditions are shown in Table 2. The catalyst refluxed in methanol and ethanol under a nitrogen atmosphere showed a similar stereoselectivity to that aged in ethanol, while **2e** was still predominant over the catalyst refluxed in 2-propanol, 2-methyl-2-propanol, tetrahydrofuran or cyclohexane. The catalyst which was stirred in ethanol or cyclohexane under an atmosphere at room temperature for 2 h showed a stereoselectivity analogous to the aged catalyst in the respective solvent for 40 d. Moreover, **2a** was selectively formed over a fresh catalyst which was treated with carbon monoxide in cyclohexane as well as in ethanol. It has been shown that ethanol is decomposed to carbon monoxide and methane by refluxing over Raney Ni.[7] Consequently, it is clear that the high selectivity of the axial methyl product on use of the catalyst stored in ethanol is attributed to

TABLE 1. EFFECT OF STORAGE ON THE STEREOSELECTIVITY IN THE HYDROGENATION OF 1-*t*-BUTYL-4-METHYLENECYCLOHEXANE (1)[a]

Catalyst	Weight[b] (mg)	H_2 (kg/cm²)	Solvent	Initial	Products (a-Me %)[c] Period of storage (days)			
					10	20	30	40
Raney Ni	30	1	EtOH	46 (7)[d]	56 (7)	69 (3)	81 (3)	94 (1)
	100	1	EtOH	35 (7)	44 (8)	60 (6)	84 (3)	93 (2)
	500	1	EtOH	23 (11)	27 (13)	43 (8)	87 (3)	95 (1)
	500	25	EtOH	42 (4)				
	500	100	EtOH	47 (3)	57 (5)	71 (6)	80 (3)	96 (1)
	500	1	H_2O	23 (13)		27 (13)		46 (8)
	500	1	C_6H_{12}[e]	14 (14)		46 (8)		63 (5)
Raney Co	50	1	EtOH	33 (0)		35 (0)		39 (0)
	500	1	EtOH	29 (0)		30 (0)		39 (0)
	500	100	EtOH	46 (0)				
Raney Fe	50	1	EtOH	55 (2)	72 (2)			
	500	1	EtOH	35 (5)	50 (5)	54 (5)	71 (4)	
	500	100	EtOH	58 (2)	69 (2)	75 (2)	80 (2)	

a) Substrate; 0.5 mmol, Solvent; Ethanol 5 ml, Ambient temperature. b) Weight of wet state containing about 40% of solvent. c) a-Me% = **2a**/**2a** + **2e** × 100. d) Is% = **3**/**2a** + **2e** + **3** × 100, given in parentheses. e) Cyclohexane 5 ml.

Table 2. Effect of modification of fresh catalyst on the stereoselectivty in the hydrogenation of 1-*t*-butyl-4-methylenecyclohexane (**1**)[a]

Catalyst	Solvent	Untreated	Products (a-Me %)[b] Modification			
			Reflux[c]	Air[d]	CO[e]	*n*-$BuNH_2$[f]
Raney Ni	MeOH	20 (13)[g]	87 (3)			
	EtOH	23 (11)	94 (1)	96 (1)	98 (1)	49 (0)
	2-PrOH	16 (14)	23 (14)			
	2-Me-2-PrOH	15 (15)	27 (34)			
	THF	12 (14)	26 (11)			
	C_6H_{12}	14 (14)	24 (47)	60 (4)	88 (2)	60 (0)
Raney Co	EtOH	29 (0)	32 (0)	48 (0)	51 (0)	17 (0)
	C_6H_{12}	29 (0)	35 (0)	40 (0)	44 (0)	14 (0)
Raney Fe	EtOH	35 (5)	83 (3)	53 (5)	80 (3)	38 (0)
	C_6H_{12}	32 (8)	41 (8)	53 (5)	84 (3)	39 (0)

a) Substrate; 0.5 mmol, Catalyst; 0.5 g (wet), Solvent; 5 ml, Ambient temperature and pressure. b) See Table 1, footnote c. c) Refluxed in given solvent for 2 h under N_2 atmosphere. d) Stirred gently in given solvent for 2 h at ambient temperature under air. e) Introduced 100 μmol of CO, then stirred for 0.5 h at ambient temperature under hydrogen atmosphere. f) Added 100 μmol of *n*-$BuNH_2$, then stirred for 0.5 h at ambient temperature under hydrogen atmosphere. g) See Table 1, footnote d.

carbon monoxide formed from ethanol rather than the partial oxidation of the catalyst.

The hydrogenation of **1** over Raney Ni aged in ethanol for a long time gave exclusively **2a** irrespective of the hydrogen pressure and the amount of catalyst. This indicates the following: i) The interaction between the catalyst and the substrate plays a major role in determining the product distribution, ii) the hydrogen available on a catalyst surface does not directly contribute to the determination of the product distribution. These results indicate that the product-controlling step is the adsorption of the substrate on the catalyst in the hydrogenation over Raney Ni which is poisoned by carbon monoxide. On the other hand, the product-controlling step is not primarily defined to be the adsorption of the substrate on fresh Raney Ni.

3, which is generated by the double-bond migration of **1** during the hydrogenation, was also hydrogenated. No appreciable stereoselectivity was observed and the apparent rate of reaction was very slow compared to that of **1**. This means that the stereoselectivity which appears in Tables 1 and 2 is primarily the results from the direct hydrogenation of **1**.

The thermodynamically more stable product (**2e**) was preferred in the hydrogenation of **1** over fresh Raney Co. No effect of a storing period as well as refluxing under a nitrogen atmosphere was observed on the product ratio. The effects of air and carbon monoxide on Raney Co were not appreciable compared to those on Raney Ni. When the catalysts were treated with *n*-$BuNH_2$, the amount of **2a** increased over Raney Ni compared to that over the parent catalyst, while more than 80% of **2e** was yielded over Raney Co (Table 2). No endocyclic olefin which was derived from the starting material by the double bond migration was detected in the hydrogenation (Tables 1 and 2). Such differences in the effects regarding the modification of Raney Ni and Raney Co give important information to elucidate the characteristics of both Ni and Co catalysts.

Experimental

Catalyst. Raney Ni was prepared from Raney Ni NDH (Kawaken Fine Chemicals Co.) by the W-4 method.[8] The catalyst was stored at room temperature. Raney Co and Fe were prepared from Raney Co OD and Fe ND (Kawaken Fine Chemicals Co.) by an analogous method as Raney Ni.

Catalytic Hydrogenation. 0.5 mmol of substrate and a known amount of catalyst (contains *ca.* 40 wt% of solvent) in a solvent (5 ml) were stirred with hydrogen at an atmospheric or a high pressure and room temperature. The reaction was followed gas chromatographically by analyzing aliquots of the reaction mixture at appropriate time intervals.

The present work was partially supported by a Grant-in-Aid for Scientific Reseach No. 56550601 from the Ministry of Education, Science and Culture, Japan.

References

1) Mitsui, K. Gohke, H. Saito, A. Nanbu, and Y. Senda, *Tetrahedron*, **29**, 1523 (1973).
2) S. Mitsui, S. Imaizumi, A. Nanbu, and Y. Senda, *J. Catal.*, **36**, 333 (1975).
3) S. Mitsui, M. Ito, A. Nanbu, and Y. Senda, *J. Catal.*, **36**, 119 (1975).
4) J. H. P. Tyman and S. W. Wilkins, *Tetrahedron Lett.*, 1773 (1973).
5) H. O. House, R. G. Carlson, H. Müller, A. W. Noltes, and C. D. Slater, *J. Am. Chem. Soc.*, **84**, 2614 (1962).
6) R. L. Augustine, *J. Org. Chem.*, **28**, 152 (1963); *Adv. Catal.*, **25**, 63 (1976).
7) T. Kubomatsu, S. Kishida, and K. Hotta, *Kagaku to Kogyo*, **40**, 504 (1966).
8) A. A. Pavlic and H. Adkins, *J. Am. Chem. Soc.*, **68**, 1471 (1946); H. Adkins and A. A. Pavlic, *J. Am. Chem. Soc.*, **69**, 3039 (1947).

Preparation and Conversion of Aminodiphenylcyclopropenium Salts to 1,2,3-Triazines

Hiroshi YOSHIDA.* Kohnosuke YAGI, Tomoji TAMAI, Hiroe SANO, Tsuyoshi OGATA, and Kiyoshi MATSUMOTO†

Department of Applied Chemistry, Faculty of Engineering, Shizuoka University, Hamamatsu 432

†*College of Liberal Arts and Sciences, Kyoto University, Kyoto 606*

(Received October 18, 1984)

Synopsis. Diphenylcyclopropenone gave aminodiphenylcyclopropenium fluorosulfate (**3**) by ethylation with ethyl fluorosulfate, followed by treating with secondary amine in one-pot operation. The salt **3** reacted with sodium azide to afford 1,2,3-triazine in a good yield.

In a continuation of our studies of the monoalkylthiocyclopropenium salts,[1] we have become interested in the chemistry of monoaminocyclopropenium compounds.

Some aminodiphenylcyclopropenium salts have been prepared by the reaction of diphenylcyclopropenone with triethyloxonium tetrafluoroborate (Meerwein reagent), followed by treating with secondary amines.[2,3]

In this communication we report an improved one-pot synthesis of 1-amino-2,3-diphenylcyclopropenium salts using commercially available ethyl fluorosulfate and its application to the synthesis of 5-amino-1,2,3-triazines.

Since the Meerwein reagent decomposes in atmospheric moisture, we used ethyl fluorosulfate (Aldrich Chem. Co.) which is easy to handle. The reagent reacted with diphenylcyclopropenone (**1**) in dry dichloromethane to yield the cyclopropenium salt **2**. The salt was *in situ* treated with equimolar amount of secondary amines to give 1-amino-2,3-diphenylcyclopropenium fluorosulfates (**3**) in moderate yields. The structure of **3** was elucidated on the basis of their IR (at around 1900 cm^{-1}) and ^1H-NMR data (Table 1).

It has been reported that cyclopropenium salts substituted with triamino[4] or triaryl[5] groups react with azide ion to yield 3-azidocyclopropenes which gave 1,2,3-triazines on heating. Although the reaction of 1-bis(1-methylethyl)amino-2,3-diphenylcyclopropenium perchlorate (**3b** analogue) and potassium azide has been reported[4] to give 5-bis(1-methylethyl)amino-4,6-diphenyl-1,2,3-triazine (**4b**), the structure elucidation seems to be uncertain. The reaction of **3** with sodium azide gave 5-amino-1,2,3-triazines **4**

TABLE 1. YIELDS AND PHYSICAL PROPERTIES OF **3**

	Yield /%	Mp θ_m/°C	^1H-NMR($CDCl_3$)	Anal/% Found(Calcd) C	H	N	IR(KBr)/cm^{-1}
3a	74	164—165	1.41(6H, t, J=7 Hz, CH_3), 3.94(2H, q, CH_2), 7.5—8.1(10H, m, Ph)	63.06 (63.14)	5.47 (5.58)	3.91 (3.88)	1900
3b	16	197—202	1.65(12H, d, J=7 Hz, CH_3), 4.46(2H, sept, CH), 7.6—8.3(10H, m, Ph)	64.97 (64.76)	6.20 (6.21)	3.73 (3.60)	1890
3c	65	200—202	2.00(6H, bs, CH_2), 4.16(4H, bs, $(CH_2)_2N$), 7.6—8.3(10H, m, Ph)	64.20 (64.33)	5.39 (5.40)	3.67 (3.75)	1900
3d	57	217—218	4.18(8H, bs, $(CH_2CH_2)_2$), 7.1—8.2(10H, m, Ph)	60.62 (60.79)	4.69 (4.83)	3.70 (3.73)	1900
3e	43	188—190	3.75(6H, s, CH_3), 7.4—8.3(10H, m, Ph)	61.09 (61.25)	4.98 (4.84)	4.26 (4.20)	1900
3f	83	161—162	4.21(3H, s, CH_3), 7.4—8.5(15H, m, Ph)	66.66 (66.82)	4.50 (4.59)	3.49 (3.54)	1900

TABLE 2. YIELDS AND PHYSICAL PROPERTIES OF **4**

	Reaction time/h	Yield /%	Mp θ_m/°C	^1H-NMR($CDCl_3$)	MS (M+)	Anal/% Found(Calcd) C	H	N
4a	16	89	216—217	0.90(6H, t, J=7 Hz, $CH_2\underline{CH_3}$), 2.68(4H, q, CH_2), 7.2—8.0(10H, m, Ph)	304	75.21 (74.97)	6.73 (6.62)	18.24 (18.41)
4b	20	73	200—201[a]	0.82(12H, d, J=7 Hz, $\underline{Me_2}CH$), 3.26 (2H, sept, CH), 7.2—7.8(10H, m, Ph)	332	75.74 (75.87)	7.20 (7.28)	16.58 (16.85)
4c	19	81	256—272	1.35(6H, bs, $(CH_2)_3$), 2.65(4H, bs $N(CH_2)_2$), 7.59(10H, bs, Ph)	316	75.68 (75.92)	6.30 (6.37)	17.54 (17.71)
4d	82	82	250—252	2.70(4H, t, J=5 Hz, $N(CH_2)_2$), 3.45(4H, t, $O(CH_2)_2$), 7.4—7.9(1H, m, Ph)	318	71.21 (71.68)	5.69 (5.70)	17.00 (17.60)
4e	33	89	217—219	2.52(6H, s, Me), 7.4—8.0(10H, m, Ph)	276	74.01 (73.89)	5.81 (5.84)	20.39 (20.27)
4f	16	93	231—235	2.93(3H, s, Me), 6.4(15H, m, Ph)	338	77.78 (78.08)	7.21 (7.36)	16.44 (16.56)

a) Lit,[4] mp 186—188 °C.

Table 3. Preparation and physical properties of triazine derivatives

	Reaction conditions		Yield /%	Mp θ_m/°C	^{1}H-NMR($CDCl_3$)	Anal/% Found(Calcd)		
	Temp/°C	Time/h				C	H	N
5a	25	17	68	217—219	1.04(6H, t, J=7 Hz, CH_3), 3.44(4H, q, CH_2), 4.52(3H, s, NCH_3), 7.2—7.8(10H, m, Ph)	53.77 (53.82)	5.08 (5.19)	12.64 (12.55)
5e	25	9	76	100—101	2.95(6H, s, 5-NMe_2), 4.45(3H, s, 2-NMe), 7.1—7.8(10H, m, Ph)	51.47 (51.69)	4.36 (4.58)	13.25 (13.39)
5f	60	67	31	98—101	3.20(3H, s, PhNMe), 4.61(3H, s, 2-NMe), 6.7—7.6(15H, m, Ph)	57.58 (57.51)	4.62 (4.41)	11.54 (11.66)
6			52	118	4.03(3H, s, Me), 6.7—8.1(10H, m, Ph)	73.22 (72.99)	5.05 (4.98)	15.91 (15.96)

Table 4. ^{13}C-NMR spectra of some triazine derivatives

4a	12.8(q, Me), 46.1(t, CH_2), 128.4(d), 128.7(d), 129.4(d), 137.0(s), 153.0(s)
4e	43.6(q, Me), 128.2(d), 128.5(d), 129.2(d), 136.4(s), 138.9(s), 150.0(s)
5a	10.8(q, CH_2Me), 49.3(t, CH_2), 50.4(q, 2-NMe), 127.4(d), 128.7(d), 130.2(d), 132.4(s), 139.9(s), 142.0(s)
5e	49.0(q, 5-NMe_2), 50.5(q, 2-NMe), 127.9(d), 129.2(d), 130.5(d), 132.6(s), 139.6(s), 143.6(s)
6	50.7(q, Me), 128.0(d), 128.4(d), 130.1(d), 132.4(s), 151.7(s), 161.4(s)

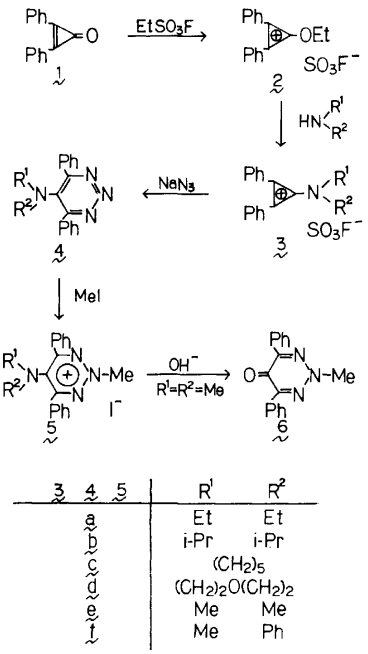

whose structures were confirmed unambiguously by their ^{13}C-NMR spectra and chemical transformations. The ^{13}C-NMR spectra of **4a** and **4e** showed the symmetric structure for these compounds. Physical properties of **4** are shown in Table 2.

The reactions of **4a** and **4e** with methyl iodide took place easily to give 2-methyl derivatives **5a** and **5e**, respectively. Hydrolysis of **5e** with aqueous sodium hydroxide afforded 4,6-diphenyl-1,2,3-triazin-5(2*H*)-one (**6**). The structures of **5a**, **5e**, and **6** were confirmed on the basis of ^{1}H- and ^{13}C-NMR data (Tables 3 and 4).

Experimental

Preparation of 3: General Procedure. A mixture of **1** (4.8 mmol) and ethyl fluorosulfate (5.3 mmol) in dry CH_2Cl_2 (10 cm^3) was stirred at room temperature for 1 h. To the resulting solution was added a dichloromethane solution of an amine (4.8 mmol in 5 cm^3) under nitrogen. After 30 min to the solution was added 25 cm^3 of ethanol and the mixture was condensed to 30 cm^3. The precipitated salt was recrystallized from CH_3CN (or $CHCl_3$) and ethanol to afford pure salt **3**.

The Reaction of 3 with Sodium Azide: General Procedure. A suspension of **3** (0.9 mmol) and sodium azide (2.7 mmol) in CH_2Cl_2 was stirred at room temperature for 16 h. The mixture was evaporated and benzene-soluble product was separated. Recrystallization from chloroform–ethanol gave pure triazine **4**.

Reaction of 4a, e, and 4f with Methyl Iodide. A mixture of **4a** (1 mmol) and MeI (10 mmol) in CH_2Cl_2 (5 cm^3) was stirred at room temperature for 12 h. Then the solution was evaporated and benzene-insoluble salt **5a** was separated. Similar treatment of **4e** and **4f** gave **5e** and **5f**.

Hydrolysis of 5e. A mixture of **5e** (1 mmol) in benzene (10 cm^3) and 5 cm^3 of aq NaOH (10%) was stirred at room temp for 2 h, the organic layer was separated, and dried under reduced pressure. Recrystallization from ethanol afforded faint yellow needles **6** in 52% yield.

References

1) H. Yoshida, M. Nakajima, T. Ogata, and K. Matsumoto, *Bull. Chem. Soc. Jpn.*, **55**, 1973 (1982); H. Yoshida, M. Nakajima, T. Ogata, K. Matsumoto, R. M. Acheson, and J. D. Wallis, *Chem. Lett.*, **1983**, 155; *Bull. Chem. Soc. Jpn.*, **56**, 3015 (1983); H. Yoshida, M. Nakajima, T. Ogata, and K. Matsumoto, *Heterocycles*, **20**, 1013 (1983); *Bull. Chem. Soc. Jpn.*, **57**, 734 (1984).

2) R. Breslow, T. Eicher, A. Krebs, R. A. Peterson, and J. Posner, *J. Am. Chem. Soc.*, **87**, 1320 (1965).

3) R. C. Kerber and C. Hsu, *J. Am. Chem. Soc.*, **95**, 3239 (1973).

4) R. Gompper and K. Schoenfinger, *Chem. Ber.*, **112**, 1514 (1979).

5) R. J. Kobylecsi and A. Mckillop, *Adv. Heterocycl. Chem.*, **19**, 215 (1976).

Palladium Catalyzed Coupling Reaction of α-Bromo Ketones with Hexabutylditin

Masanori KOSUGI,* Mamoru KOSHIBA, Hiroshi SANO, and Toshihiko MIGITA*
Department of Chemistry, Faculty of Technology, Gunma University, Kiryu, Gunma 376
(Received October 23, 1984)

Synopsis. Palladium-catalyzed reaction of α-bromo ketones with hexabutylditin in the presence of trimethylsilyl chloride gave enol trimethylsilyl ether in moderate to good yields.

There have been so far known two methods for the preparation of tributyltin enolates (α-tributylstannyl ketones and/or enol tributylstannyl ethers).[1] The one is the reaction of enol acetates with tributyltin methoxide, and the other is the addition of tributyltin hydride to α,β-unsaturated ketones.

$$RHC{=}CHOAc + Bu_3SnOMe \longrightarrow RHC{=}CHOSnBu_3 + AcOMe$$

$$RHC{=}CH\text{-}COR' + Bu_3SnH \longrightarrow RCH_2CH{=}CR'OSnBu_3$$

For the preparation of organotin compounds, the coupling reaction between hexabutylditin and organic halides in the presence of palladium complexes is recently developped.[2]

$$RX + Bu_3SnSnBu_3 \xrightarrow{[Pd]} RSnBu_3 + Bu_3SnX$$

In order to develop another route for preparation of tributyltin enolates, we applied the above coupling reaction to α-bromo ketones.

$$BrCH_2COR + Bu_3SnSnBu_3 \xrightarrow{[Pd]} CH_2{=}CROSnBu_3 + Bu_3SnBr$$

Initially we carried out the reaction of α-bromoacetophenone with hexabutylditin in the presence of a catalytic amount of tetrakis(triphenylphosphine)palladium. However, isolated products were tributyltin bromide and acetophenone. This means that tin enolate was not produced or was not stable enough under the reaction conditions. According to Lutsenko *et al.*[3] addition of trimethylsilyl chloride into tin enolate gave stable enol trimethylsilyl ether in good yield as the result of tin-silicon exchange. Then we tried to convert the tin enolate produced into enol silyl ether, by carring out the reaction in the presence of trimethylsilyl chloride. Results are shown in Table 1.

TABLE 1. Pd-CATALYZED REACTION OF α-BROMO KETONES WITH HEXABUTYLDITIN IN THE PRESENCE OF TRIMETHYLSILYL CHLORIDE

$$\underset{12\ mmol}{Bu_3SnSnBu_3} + \underset{10\ mmol}{R\text{-}Br} + \underset{12\ mmol}{Me_3SiCl} \xrightarrow[80\,^\circ C,\ 20\,h\ in\ tetralin\ 10\,cm^3]{[Pd]\ 0.1\ mmol}$$

R-Br	Catalyst[a]	Product	Yield/%[b]
$BrCH_2COEt$	A	$CH_2{=}CEtOSiMe_3$	69
$BrCH_2COBu^t$	A	$CH_2{=}CBu^tOSiMe_3$	81
$MeCHBrCOMe$	A	$MeCH{=}CMeOSiMe_3$	77
$Me_2CBrCOMe$	A	$Me_2C{=}CMeOSiMe_3$	75
$BrCH_2COPh$	A	$CH_2{=}CPhOSiMe_3$	65
$BrCH_2CO_2Et$	B[c]	$Me_3SiCH_2CO_2Et$	79
$MeCHBrCO_2Et$	B[c]	$Me_3SiCHMeCO_2Et$	49
$BrCH_2CN$	B	Me_3SiCH_2CN	61
$BrCH_2NO_2$	B	$Me_3SiCH_2NO_2$	—

a) A: $Pd(PPh_3)_4$, B: $PdCl_2[P(o\text{-tolyl})_3]_2$. b) Isolated yield based on R-Br. c) HMPA was used as solvent.

As Table 1 shows, moderate to good yields of enol silyl ethers were obtained. From the reaction of α-bromo carboxylates, α-trimethylsilyl carboxylates were produced, but not ketene silyl acetals, even when the reaction was carried out in the presence of trimethylsilyl iodide.[3] Similarly, from the α-bromoacetonitrile, trimethylsilylacetonitrile was obtained, but (trimethylsilyl)nitromethane could not be obtained from the reaction of bromonitromethane.

The following three possible reaction sequences can be considered for the formation of the enol silyl ether from this reaction system.

The first:

$$2Me_3SiCl + Pd(PPh_3)_4 \longrightarrow Me_3SiSiMe_3 + PdCl_2(PPh_3)_2$$[4]

$$Me_3SiSiMe_3 + BrCH_2COR \xrightarrow{[Pd]} CH_2{=}CROSiMe_3 + Me_3SiBr$$[5]

The second:

$$Bu_3SnSnBu_3 + Me_3SiCl \xrightarrow{[Pd]} Bu_3SnSiMe_3 + Bu_3SnCl$$

$$Bu_3SnSiMe_3 + BrCH_2COR \xrightarrow{[Pd]} CH_2{=}CROSiMe_3 + Bu_3SnBr$$[6]

The third:

$$Bu_3SnSnBu_3 + BrCH_2COR \xrightarrow{[Pd]} CH_2{=}CROSnBu_3 + Bu_3SnBr$$

$$CH_2{=}CROSnBu_3 + Me_3SiCl \longrightarrow CH_2{=}CROSiMe_3 + Bu_3SnCl$$

Since the reaction in the absence of hexabutylditin did not give the enol silyl ether, and the reaction of hexamethyldisilane with α-bromo ketone in the presence of palladium complex did not occur, the first possibility is excluded. The second one is also unlikely, because the reaction of hexabutylditin with trimethylsilyl chloride in the presence of palladium catalyst also did not produce the (trimethylsilyl)tributyltin. Thus, the third one is most plausible, that is, the coupling between hexabutylditin and α-bromo ketone is thought to actually occur, forming the tin enolates. In the absence of trimethylsilyl chloride, the tin enolate seemed to collapse to the corresponding ketone.

Other trial for trapping tin enolates also shows the formation of tin enolates in this reaction, although trapping efficiency was not so high. For example, the palladium-catalyzed reaction of α-bromoacetophenone with hexabutylditin in the presence of benzaldehyde gave 1,3-diphenyl-2-propen -1- one[7] in 30% yields.

Experimental

IR spectra were recorded on a Jasco A-100 spectrophotometer. ^{1}H NMR spectra were recorded on a Varian EM-360 instrument. GLC analyses were carried out with Ohkura 802 instrument, using columns (1.5 m) packed with 10% Silicone SF-96 and SE-30 on Celite 545.

Materials. α-Bromo ketones and palladium complexes were used reported previously.[6] Ethyl bromoacetate, ethyl 2-bromopropionate, and bromoacetonitrile were commercially available. Bromonitromethane was prepared by the method described in literature.[8]

Reaction Procedure. The mixture of hexabutylditin (12 mmol), bromide (10 mmol), trimethylsilyl chloride (12 mmol), palladium complex (0.1 mmol), and tetralin (10 cm^3) as solvent is heated under argon at 80 °C for 20 h. Products were collected in cold trap by vacuum distillation under room temperature.

Products. All the products were known. Enol trimethylsilyl ethers were reported previously.[6] ^{1}H NMR and IR data using in identification of ethyl trimethylsilylacetate, ethyl 2-(trimethylsilyl)propionate, and trimethylsilylacetonitrile were recorded here.

Ethyl Trimethylsilylacetate; ^{1}H NMR (CCl_4) δ=0.15 (s, 9H), 1.24 (t, J=7 Hz, 3H), 1.78 (s, 2H), and 4.02 (q, J=7 Hz, 2H). IR (neat): 1720 (C=O), 1365, 1245, 1240, 1100, and 850 cm^{-1}.

Ethyl 2-(Trimethylsilyl)propionate; ^{1}H NMR (CCl_4) δ=0.05 (s, 9H), 1.20 (t, J=7 Hz, 3H), 1.25 (d, J=7 Hz, 3H), 1.87 (q, J=7 Hz, 1H), and 4.07 (q, J=7 Hz, 2H). IR (neat): 1730 (C=O), 1350, 1245, 1235, 1095, and 870 cm^{-1}.

Trimethylsilylacetonitrile; ^{1}H NMR (CCl_4) δ=0.15 (s, 9H) and 1.44 (s, 2H). IR (neat): 2220 (CN), 1390, 1255, and 850 cm^{-1}.

The gift of tributyltin oxide by Kohriyama Kasei Co. is gratefully acknowledged.

References

1) M. Pereyre and J-C Pommier, "New Applications of Organometallic Reagents on Organic Synthesis," *J. Organomet. Chem. Library* **1**, ed by D. Seyferth, Elsevier Scientific Publishing Co., Amsterdam, 1976, p. 196.

2) M. Kosugi, T. Ohya, and T. Migita, *Bull. Chem. Soc. Jpn.*, **56**, 3855 (1983) and references cited therein.

3) Y. I. Baukov, G. S. Burlachenko, and I. F. Lutsenko, *J. Organomet. Chem.*, **3**, 478 (1965).

4) H. Gilman, K. Shiina, D. Aoki, B. J. Gaj, D. Wittenberg, and T. Bremnan, *J. Organomet. Chem.*, **13**, 323 (1968).

5) H. Urata, H. Suzuki, Y. Moro-oka, and T. Ikawa, *J. Organomet. Chem.*, **234**, 367 (1982).

6) M. Kosugi, T. Ohya, and T. Migita, *Bull. Chem. Soc. Jpn.*, **56**, 3539 (1983).

7) J. G. Noltes, H. M. J. C. Creemers, and G. J. M. Van Der Kerk, *J. Organomet. Chem.*, **11**, 21 (1968).

8) J. Tscherniak, *Justus Liebigs Ann. Chem.*, **180**, 129 (1876).

Catalytic Functionalities of Molybdenum Catalysts Supported on Brazilian Bentonites

Gerhard W. SCHULTZ,† Hiromichi SHIMADA,* Yuji YOSHIMURA, Toshio SATO, and Akio NISHIJIMA

National Chemical Laboratory for Industry, Yatabe, Ibaraki 305

(Received August 16, 1984)

Synopsis. Two kinds of Brazilian bentonites were applied to supports of molybdenum catalysts to improve the catalytic selectivities of the hydrotreating catalysts. Separate model tests reactions showed that bentonite-supported molybdenum catalysts have higher activities for hydrocracking and hydrodesulfurization as compared to a standard Al_2O_3 supported catalyst, while the Al_2O_3 was superior to the bentonites for hydrogenation activity.

Some kinds of natural clays such as bentonite, have been recognized as suitable for cracking catalysts. In fact, acid-treated clays of montmorillonite type were the first fluid cracking catalysts widely employed by the industry, though the clays were abandoned in favor of synthetic alumina and silica-alumina. Then zeolites came to dominate the petroleum refining industry. Recently, an application of molybdenum catalysts to hydrotreating of petroleum residue or coal derived oil has rekindled interest in these clays as the catalyst supports because of their large pores.

Sakata and Hamrim[1] reported hydrodesulfurization(HDS) and hydrodenitrogenation(HDN) over several clays found in coal mineral matter. Takeuchi *et al.*[2] showed that sepiolite-supported molybdenum catalysts are applicable to the hydrotreating of petroleum residue. Mochida *et al.*[3] also mentioned roles of sepiolite as the support of nickel-molybdenum catalysts in the selective hydrotreating of solvent refined coal. With other clays as the support for molybdenum catalyst, catalytic functionalities of hydrotreating catalysts such as hydrocracking or hydrogenation, still remain unresolved, although a lot of patents were applied in this field. In the present paper, Brazilian bentonites were used as supports of molybdenum catalysts to improve the catalytic selectivity of hydrotreating catalyst. Hydrocracking of diphenylmethane(DPM), HDS of dibenzothiophene(DBT) and hydrogenation of 1-methylnaphtalene(1-MN) were performed under a high pressure of H_2 using bentonite-supported catalysts and a standard alumina-supported catalyst to elucidate their catalytic functionalities.

Experimental

Catalyst supports used in this experiment were two kinds of Brazilian bentonites (Bentonite S and V, Somipal S/A. Co.). These natural minerals were activated chemically with H_2SO_4 (35%), followed by washing until no sulfur could be detected. Then, the samples were heated at 500 °C for 3 h in a presence of air. A commercial type of γ-Al_2O_3 (Sumitomo Aluminium Co.), which was selected as a standard support in our work, was also used. Properties of the bentonites and the alumina are given in Table 1. A 10 wt% of MoO_3 catalysts were prepared by impregnating the carriers with a solution of ammonium heptamolybdate. After drying at 100 °C for 8 h, the samples were calcined at 500 °C for 1 h. Then the catalysts were presulfided in a stream of 10 vol% of H_2S (balance H_2) at 430 °C for 1 h before reaction.

For hydrocracking, HDS and hydrogenation, the reactions were carried out in a stainless steel microreactor (50 cm^3) charged with 10 cm^3 of the commercial reagent and 0.5 g of the catalyst. The unit was pressurized with H_2 to an initial pressure of 70 kg/cm^2 and then injected into an oven heated at 430 °C. Hydrocracking and HDS reactions were performed at 400 °C for 60 min, while 90 min of reaction were selected for hydrogenation. At least the reactions were done twice, and values given in Table 2 are averaged. Reaction products were analyzed by a gas cromatography (Shimadzu GC-6AM). More thorough analyses were done by obtaining mass spectra (Shimadzu GC-MS QP-1000) of the individual products.

Results and Discussion

The catalytic functionalities obtained on the various supports are summarized in Table 2.

Hydrocracking, HDS and hydrogenation activities for the sulfided molybdenum catalysts are given in Runs 1—4. MoS_2 catalyst supported on bentonite gave higher hydrocracking activities as compared to that on γ-Al_2O_3. Among the bentonite supports examined, hydrocracking activities of the catalysts increased after acid treatment of the bentonites. Bentonite S was superior to Bentonite V for hydrocracking of DPM.

TABLE 1. PROPERTIES OF THE SUPPORTS

Sopport	Chemical composition/wt%								S.A.[a]	P.V.[b]
	SiO_2	Al_2O_3	Fe_2O_3	TiO_2	K_2O	Na_2O	MgO	CaO	$m^2\,g^{-1}$	$ml\,g^{-1}$
Bentonite S[c]	69.6	14.4	8.0	1.38	2.16	3.39	0.15	0.52	95	0.15
Bentonite AS[d]	93.6	3.7	0.7	0.69	0.41	0.25	0.18	0.01	194	0.45
Bentonite V[c]	55.2	20.6	9.5	1.69	3.64	1.10	0.56	1.26	92	0.16
γ-Al_2O_3	tr.[e]	99	0.01	0.0	0.0	0.01	0.0	0.0	184	0.53

a) Surface area. b) Pore volume. c) For details refer to the text. d) Bentonite S after acid treatment. e) Less than 0.5.

† Present address: Produquimica Ind. E Com. LTDA., Rua Serra do Japi, 84—03309, Sao Paulo, Brazil.

Table 2. Catalytic activities for HC, HDS, and HY

Run	Support	HC of DPM				HDS of DBT		HY of 1-MN
		Conv./%[a]	HC/%[b]	HY/%[c]	Others/%[d]	HDS/%[e]	HY/%[f]	HY/%[g]
1	MoS_2/Al_2O_3	1.9	1.3	0.6	0	8.8	6.7	41.5
2	MoS_2/Bentonite AS	84.1	83.3	0	1.1	37.8	5.6	16.6
3	MoS_2/Bentonite AV	43.8	43.2	0	0.6	7.1	6.1	—
4	MoS_2/Bentonite S	30.0	21.8	0	8.2	6.0	1.2	—
5	MoO_3/Al_2O_3	0.3	0.3	0	0	13.5	3.1	18.5
6	MoO_3/Bentonite AS	80.0	78.4	0	1.6	34.7	1.5	7.0
7	MoO_3/Bentonite AV	44.1	37.2	0	6.9	9.1	0	—
8	γ-Al_2O_3	0	0	0	0	0	0	0
9	Bentonite AS	81.9	73.6	0	8.3	0	0	0.2
10	Bentonite AV	42.6	33.8	0	8.8	0	0	—

a) Total conversion. b) Yields of benzene and toluene. c) Yields of cyclohexylphenylmethane. d) Mainly polymerized products. e) Yields of biphenyl. f) Yields of cyclohexylbenzene, bicyclohexyl and tetrahydrodibenzothiophene. g) Yields of 1-methyltetralin and 5-methyltetralin.

Acid treated Bentonite S was the most effective to achieve maximum hydrocracking and HDS activities. In contrast to these results, presulfided molybdenum catalyst supported on γ-Al_2O_3 showed the highest hydrogenation activity.

Runs 5—7 shows the results obtained on oxide catalysts. Similar trends were observed for hydrocracking and hydrogenation in the case of MoO_3 supported catalyst. Higher hydrocracking and HDS activities were given on the bentonite supports. While, higher hydrogenation activity was obtained on the Al_2O_3 support, though hydrogenation activities of the oxide catalyst were lower than those of the sulfided catalyst. HDS activity obtained on MoO_3/Al_2O_3 catalyst was higher than that on MoS_2/Al_2O_3 catalyst. This may be due to the sulfiding of MoO_3. XPS analyses showed that after HDS reactions, MoO_3 changed to MoS_2 to some extent.

Large differences in hydrocracking activities were also obtained for the reactions over the support. The bentonites were found to contribute to hydrocracking activity by itself, as shown in Runs 8—10. This is the most evident in the results obtained in the present work, where the bentonite-supported catalysts gave high hydrocracking performances, in line with the known high activities of these protonic acid supports for cracking reactions.[4] Almost no hydrogenation activity was observed on the Al_2O_3 and the bentonite supports.

From these results it is considered that the role of molybdenum ions in bentonite-supported molybdenum catalyst is to give the activities for HDS and hydrogenation. Molybdenum ions also seem to improve the selectivity of the catalysts, because polymerization products decreased after impregnating MoO_3 on the bentonite. On the other hand, presulfurization seems to enhance hydrogenation activities of the catalysts, by comparing Run 2 with Run 6. In the case of the alumina-supported molybdenum catalyst, molybdenum ions gave the hydrocracking activity as well as HDS and hydrogenation activities. The presulfurization was found to contribute to the enhancement of the hydrogenation activity.

References

1) Y. Sakata and C. E. Hamrin, *Ind. Eng. Chem., Prod. Res. Dev.*, **22**, 250 (1983).
2) C. Takeuchi, M. Nakamura, and Y. Shiroto, *Prep. Div. Pet. Chem., Am. Chem. Soc.*, **24**, 666 (1979).
3) I. Mochida. T. Oishi, Y. Korai, and H. Fujitsu, *Ind. Eng. Chem., Prod. Res. Dev.*, **23**, 203 (1984).
4) M. L. Occelli, *Ind. Eng. Chem., Prod. Res. Dev.*, **22**, 553 (1983).

The Thermal Properties of Liquid Crystalline Materials Incorporating Piperazine Skeleton

Shunsuke TAKENAKA,* Toshiro HIROHATA, and Shigekazu KUSABAYASHI
Department of Applied Chemistry, Faculty of Engineering, Osaka University, Suita, Osaka 565
(Received August 24, 1984)

Synopsis. The thermal and electric properties of the homologous series of liquid crystalline materials incorporating a piperazine skeleton have been examined. Some piperazine compounds having a cyano group as the terminal function give rise to a wide-range nematic phase. On the other hand, the homologous series of α,α′-bis(4-alkyl-1-piperadinylimino)-*p*-xylenes and 1,4-bis-(4-alkylbenzylideneamino)piperazines show strong smectic properties.

Liquid crystalline materials incorporating a saturated cyclic system such as cyclohexane,[1] and 1,3-dioxane[2] are currently of interest for applications involving optical devices. Piperazine is a saturated six-membered ring incorporating two nitrogen atoms at the 1 and 4 positions. Some piperazine compounds are known to exhibit mesomorphic properties.[3,4] In this paper, we describe the thermal properties of a new homologous series of liquid cyrstalline materials incorporating piperazine.

Experimental

The preparation of *N*-alkylpiperazine compounds has been described in a previous paper.[3]

Results and Discussion

The transition temperatures and latent heats of series **1**, **2**, **3**, and **4** are summarized in Tables 1, 2, 3, and 4, respectively.

One of the characteristics of the piperazine core is that a tautomerization around the nitrogen atoms at the 1 and 4 positions gives rise to cis and trans isomers in which the former would be very unfavorable for mesophase stability. However, we can assume that the cis isomer should be energetically very unstable because of a relatively strong repulsive interaction between both substituents at the 1 and 4 positions.

As a whole, the piperazine compounds show apparent smectic properties compared with the corresponding phenyl and cyclohexyl compounds, as shown in Table 5.

Series **1** reveals the nematic and smectic phases, though the thermal stability of the nematic phase is lower than that of compound **5**. Series **2** reveals only highly stable smectic phases, while the phenyl and cyclohexyl compounds **6** and **7** show a nematic phase. A similar trend is observed in series **3**, and also **4**, having alkyl groups at the terminals. Furthermore, these compounds tend to reveal relatively tight smectic phases such as the smectic B modification. For series **1** and **2**, the smectic-isotropic transition temperatures tend to decrease while increasing the carbon number in the alkyl or the alkoxyl chains (similar to usual nonpolar mesogens). The nonpolar interaction around the piperazine and phenyl cores along the lateral direction of the molecules would facilitate a layer arrangement of the molecules, increasing the smectic properties.

When the terminal function is replaced by a cyano group, series **3** and **4** tend to exhibit highly stable nematic phase. The effective order for the nematic stability is benzene>cyclohexane>piperazine, though the difference is quite small. In general, mesogens having a cyano group at a terminal function tend to show strong nematic properties, *e.g.*, **8** and **9**. Opposite to the general trend, the butyl homolog of series **3** and thereafter show a smectic B phase and the hexyl homolog also shows a smectic A phase, while these

TABLE 2. THE TRANSITION TEMPERATURES FOR SERIES **2**(T/°C)

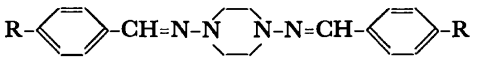

R	C	S[a]	S_B	I
n-C_3H_7	150.9	236.4	239.9	
n-C_4H_9	104.0	211.6	256.1	
n-C_5H_{11}	100.1	204.6	241.6	
n-C_6H_{13}	87.1	193.6	237.1	
n-C_7H_{15}	92.4	185.8	231.2	
n-C_8H_{17}	79.9	170.5	219.6	

a) The smectic phase has not been characterized.

TABLE 1. THE TRANSITION TEMPERATURES (T/°C) AND LATENT HEATS FOR SERIES **1**

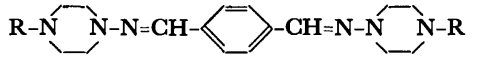

R	C	S_1[a]	S_B	N	I	ΔH_{N-I} (kJ/mol)
CH_3	159.5	—	—	211.3		
n-C_3H_7	188.6	—	—	206.1		1.3
n-C_4H_9	171.3		(167.3)	195.6		1.8
n-C_5H_{11}	50.5	151.1	174.1	197.6		2.3
n-C_6H_{13}	114.2	173.0	182.8	186.1		3.4

The value in parenthes indicates a monotropic transition.
a) The smectic phase has not been characterized.

Table 3. The transition temperatures (T/°C) and latent heats for series **3**

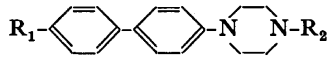

R_1	R_2	C		S_B		S_A		N		I	ΔH_{N-I}
n-C_2H_5	-C_2H_5(n-)	.	174.3	.	193.8	—		—		.	
	C_4H_9(n-)	.	187.2	.	202.1	—		—		.	
n-C_6H_{13}	C_4H_9(n-)	.	157.3	.	199.6	—		—		.	
CN	C_4H_9(n-)	.	145.1	.	159.9	—		.	214.1	.	0.8
	C_5H_{11}(n-)	.	114.7	.	160.7	—		.	210.6	.	0.6
	C_6H_{13}(n-)	.	116.6	.	160.5	.	183.1	.	203.1	.	1.0

Table 4. The transition temperatures (T/°C) and latent heats for series **4**

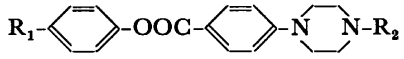

R_1	R_2	C		S_A		N		I	ΔH_{N-I} (kJ/mol)
n-C_3H_7	C_3H_7(n-)	.	96.3	.	118.8	.	157.8	.	0.9
	C_5H_{11}(n-)	.	104.7	.	162.5	.	175.3	.	2.0
n-C_4H_9O	C_4H_9(n-)	.	100.0	.	165.0	.	194.3	.	3.7
CN	C_3H_7(n-)	.	124.6	—		.	202.4	.	0.7
	C_4H_9(n-)	.	110.3	—		.	202.4	.	0.8
	C_5H_{11}(n-)	.	92.9	—		.	204.3	.	0.5
	C_6H_{13}(n-)	.	84.5	—		.	184.8	.	0.6
	C_7H_{15}(n-)	.	85.7	—		.	180.6	.	0.5

Table 5.

5	n-C_4H_9-Ph-N=CH-Ph-CH=N-Ph-C_4H_9(n-)[5]	C-59.8-S-143-S_C-171-S_A-198-N-260-I
6	n-C_3H_7O-Ph-CH=N-Ph-N=CH-Ph-OC_3H_7(n-)[6]	C-210-N-220-I
7	n-C_3H_7-Ph-CH=N-Ph-N=CH-Ph-C_3H_7(n-)[6]	C-125-N-247-I
8	n-C_5H_{11}-Ph-Ph-Ph-CN[7]	C-130-N-239-I
9	n-C_5H_{11}-Ph-Ph-Ph-CN[8]	C-95-N-219-I
10	n-C_4H_9O-Ph-COO-Ph-Pyrazine-C_5H_{11}(n-)[9]	C-98-N-198-I
11	NC-Ph-COO-Ph-Pyrazine-C_5H_{11}(n-)[9]	C-96-S_B-119-S_A-129-N-221-I

homologs have a cyano group at the terminal function. In series **4**, the butoxy homolog shows a smectic A phase in addition to a nematic one, while compound **10** shows only a nematic phase. On the other hand, the cyano compounds in series **4** show only a nematic phase, while compound **11** shows smectic A and B phases in addition to a nematic one. The opposite trend indicates that an electric circumstance around the piperazine cores is very important in determining the mesomorphic properties of these compounds.

References

1) R. Eidenschink, D. Erdmann, J. Krause, and L. Pohl, *Angew. Chem.*, **89**, 105 (1977), and **90**, 133 (1978).

2) D. Demus and H. Zaschke, *Mol. Cryst. Liq. Cryst.*, **63**, 129 (1981).

3) K. Kinashi, S. Takenaka, and S. Kusabayashi, *Mol. Cryst. Liq. Cryst.*, **67**, 49 (1981).

4) H. Schubert, W. Schulze, H.-J. Deutscher, V. Uhlig, and R. Kuppe, *J. Phys.*, **Cl-36**, Cl-379 (1975).

5) M. E. Neubert and L. J. Maurer, *Mol. Cryst. Liq. Cryst.*, 43, 313 (1977).

6) D. Demus, H. Demus, and H. Zaschke, "Flüssige Kristalle in Tabellen" VEB Deutscher Verlag für Grundstoff Industries, Leipzig (1974).

7) G. W. Gray, K. J. Harrison, and S. A. Nash, *J. Chem. Soc., Chem. Commun.*, **1974**, 431.

8) B. Granwehr and R. Anehm, *Chem. Abstr.*, **92** (15), 128592n (1980).

9) H.-J. Deutscher, H.-M. Vorbrodt, and H. Zaschke, *Z. Chem.*, **21**, 9 (1981).

The Syntheses of the Corticoid Side-chain. II. A New Synthesis of 17α,21-Dihydroxypregna-1,4-diene-3,20-dione 21-Acetate from 21-Hydroxy-20-methylpregna-1,4-dien-3-one

Issei NITTA,* Toshio HARUYAMA, Shinichiro FUJIMORI, Shinya INOUE, and Hiroaki UENO

Biosciences Laboratory, Research Center, Mitsubishi Chemical Industries Limited, 1000 Kamoshida-cho, Midori-ku, Yokohama-city, Kanagawa 227

(Received August 9, 1984)

Synopsis. 17α,21-Dihydroxypregna-1,4-diene-3,20-dione, a potentially useful intermediate of prednisolone, can be prepared from 21-hydroxy-20-methylpregna-1,4-dien-3-one, a biodegradation product of cholesterol.

Corticosteroids are commercially produced from deoxycholic acid, stigmasterol or diosgenin. Recently, it was reported that cholesterol could be degraded to 21-hydroxy-20-methylpregna-1,4-dien-3-one (**1**) by a mutant of *Mycobacterium* sp.[1] Compound **1** may be one of the ideal starting materials for prednisolone synthesis. We present here a new conversion of **1** into 17α,21-dihydroxypregna-1,4-diene-3,20-dione 21-acetate (**10**), a precursor of prednisolone.

Results and Discussion

The methods employed in this conversion are summerized in Scheme 1. The first step is the oxidation of **1** to the aldehyde **2**. The oxidation of **1** was conducted by using the complex obtained from dimethyl sulfide and *N*-chlorosuccinimide[2] in toluene–dichloromethane to give **2** in 90% yield. The conversion of **2** into the ketone **3** was followed by a known oxidative decarboxylation procedure.[3] By bubbling air through a mixture of **2**, DBU and copper (II) acetate-2,2′-bipyridyl complex in DMF, the ketone **3** was obtained in 90% yield. The ketone **3** was converted to the oxime **4** easily in 92% yield.

Modifying the synthetic method of 3-acetylamino-5α-cholest-2-ene,[4] the oxime **4** was heated in acetic anhydride–pyridine for 40 h. The resulting solution was evaporated to dryness and the black tarry residue was partitioned into benzene and aqueous sodium hydrogencarbonate solution layers. Further processing including chromatography on silica gel yielded the enamide **5**. The NMR spectra of **5** showed that **5** was a 4:1 mixture of E and Z isomers. The hydrolysis of **5** in aqueous potassium hydrogencarbonate–methanol gave the enamide **6** as an amorphous product. Without further purification, **6** was treated with peracetic acid in the presence of sodium acetate in dichloromethane in the usual way.[5] After usual treatment, **8** was obtained in 43% yield from **4**. This was identified with the authentic sample which was derived from 17α-hydroxyprogesterone by the dehydrogenation with 2,3-dichloro-5,6-dicyano-*p*-benzoquinone.

The 21-acetoxy introduction into **8** was accomplished by Stork's iodination procedure.[6] Iodination of **8** in THF–methanol with an excess of iodine in the presence of calcium oxide gave the iodide **9**, which was converted directly to **10** by treatment with triethylammonium acetate in acetone. Overall yield of **10** was 88% from **8** and 28% from **1**. The transformation of **10** into prednisolone can be followed by a microbiological process.

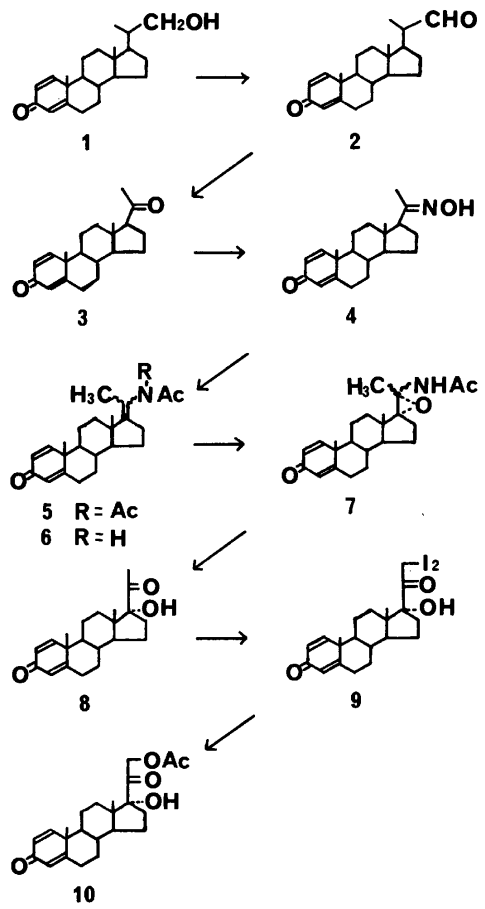

Scheme 1.

Experimental

20-Methyl-3-oxopregna-1,4-dien-21-al (2). To a stirred solution of *N*-chlorosuccinimide (8.0 g) in toluene (150 ml), dimethyl sulfide (6.0 ml) in toluene (50 ml) was added at 0 °C under nitrogen atmosphere. The mixture was cooled to −25 °C and a solution of 21-hydroxy-20-methylpregna-1,4-dien-3-one (**1**) (6.0 g) in dichloromethane (100 ml) was added dropwise. The stirring was continued for 2 h at −25 °C and then a solution of triethylamine (3.0 g) in dichlomethane (5.0 ml) was added dropwise. The cooling bath was removed and after 5 min, ether was added. The organic layer was

washed with 1% hydrochloric acid and then with water. Removal of dried (sodium sulfate) solvents produced **2** in 90% yield. Recrystallization from ethyl acetate–hexane afforded the analytically pure sample; mp 154.4—154.8 °C dec., NMR ($CDCl_3$) δ=0.91 (s, 3H), 1.14 (d, 3H, J=4 Hz), 1.24 (s, 3H), 6.08 (s, 1H), 6.22 (d, 1H, J=10 Hz), 7.06 (d, 1H, J=10 Hz), 9.54 (d, 1H, J=4 Hz); m/z 326 (M^+).

Found: C, 81.03; H, 9.25%. Calcd for $C_{22}H_{30}O_2$: C, 80.98; H, 9.20%.

Pregna-1,4-diene-3,20-dione (3). Through a rapidly stirring mixture of **2** (0.5 g), DBU (0.1 g), $Cu(OAc)_2 \cdot H_2O$ (8 mg), and 2,2′-bipyridyl (7 mg) in *N,N*-dimethylformamide (10 ml), air was bubbled at 20 °C for 14 h. The reaction mixture was extracted with chloroform and the organic layer was washed with 1% hydrochloric acid and then with water. Removal of solvents afforded **3** in 89.6% yield. Recrystallization from tetrahydrofuran-octane provided the analytically pure sample; mp 152.0—152.3 °C; NMR ($CDCl_3$) δ=0.7 (s, 3H), 1.24 (s, 3H), 2.12 (s, 3H), 6.08 (s, 1H), 6.24 (d, 1H, J=10 Hz), 7.06 (d, 1H, J=10 Hz).

Found: C, 80.93; H, 9.03%. Calcd for $C_{21}H_{28}O_2$: C, 80.73; H, 9.03%.

Pregna-1,4-diene-3,20-dione 20-Oxime (4). To a stirred solution of **3** (10.0 g) and sodium acetate (5.0 g) in aqueous methanol (90%, 150 ml), hydroxylamine hydrochloride (2.3 g) was added at 3—5 °C and stirred for 1.5 h. Water was added and the resultant precipitate was separated by filtration to give **4** (10.3 g) in 91.9% yield. Recrystallization from tetrahydrofuran-octane afforded the analytically pure sample; NMR ($CDCl_3$) δ=0.72 (s, 3H), 1.24 (s, 3H), 1.88 (s, 3H), 6.08 (s, 1H), 6.24 (d, 1H), 7.06 (d, 1H); m/z 327 (M^+).

Found: C, 77.24; H, 8.83; N. 4.28%. Calcd for $C_{21}H_{29}NO_2$: C, 77.02; H, 8.93; N, 4.28%.

20-(Diacetylamino)pregna-1,4,17(20)-trien-3-one (5). The oxime **4** (2.91 g) in dry pyridine (75 ml) and acetic anhydride (50 ml) was refluxed under nitrogen atmosphere for 40 h. The solvent was evaporated off under reduced pressure, the resultant black tar was taken up in benzene and saturated sodium carbonate solution.

The mixture was shaken and then filtered through a Celite pad, which was washed thoroughly with benzene. The benzene layer was separated, washed with water, dried and evaporated. The product in benzene was chromatographed on silica gel (Wakogel C-100, 15 g). The elution with benzene afforded **5** (3.77 g). This product was a mixture of E:Z=4:1, which was determined by NMR. NMR ($CDCl_3$) δ(E-form)=1.00 (s, 3H), 1.24 (s, 3H), 2.28 (s, 3H), 2.32 (s, 3H), 6.06 (s, 1H), 6.22 (d, 1H, J=10 Hz), 7.06 (d, 1H, J=10 Hz), δ(Z-form)=0.88 (s), 1.24 (s), 2.26 (s), 2.38 (s), 6.04 (s), 6.20 (d, J=10 Hz), 7.04 (d, J=10 Hz); m/z 395 (M^+).

20-(Acetylamino)pregna-1,4,17(20)-trien-3-one (6). Diacetylamino compound **5** (3.77 g) was added to methanol (60 ml) and potassium hydrogencarbonate (3.5 g) and refluxed for 1.5 h. The reaction mixture was extracted with dichloromethane and the organic layer was washed with water, dried and evaporated to give **6** (3.14 g). NMR ($CDCl_3$) δ(E-form)=0.96 (s, 3H), 1.24 (s, 3H), 2.00 (s, 6H), 6.06 (s, 1H), 6.22 (d, 1H, J=10 Hz), 6.56 (broad, 1H), 7.06 (d, 1H, J=10 Hz), δ(Z-form)=0.94 (s), 1.22 (s), 1.98 (s), 6.06 (s), 6.20 (d, J=10 Hz), 6.76 (broad), 7.04 (d, J=10 Hz); m/z 353 (M^+).

17α-Hydroxypregna-1,4-diene-3,20-dione (8). To a mixture of **6** (1.54 g) and sodium acetate (0.22 g) in dichloromethane (5 ml), 40% peracetic acid (0.99 g) in dichloromethane (15 ml) was added dropwise at 3—5 °C. After 1 h, sat. sodium hydrogencarbonate solution was added and the organic layer was separated, washed successively with 5% potassium iodide solution, sodium thiosulfate solution and water, dried and evaporated. To the residue, methanol (20 ml) and 0.3 M(1M=1 mol dm^{-3}) sodium hydroxide solution (20 ml) were added and the mixture was heated under reflux for 1.5 h. After cooling, the mixture was neutralized with acetic acid and then concentrated. The products were extracted with dichloromethane and the organic layer was washed with water and dried. Removal of solvents afforded crude **8** (1.39 g), which was chromatographed on a column of silica gel with benzene–methanol (85:15) to give **8** (0.61 g) in 43% yield from **4**. Recrystallization from octane–tetrahydrofuran (1:1) afforded the analytically pure sample; mp 258.0—258.7 °C, NMR ($CDCl_3$) δ=0.8 (s, 3H), 1.26 (s, 3H), 2.28 (s, 3H), 2.96 (s, 1H), 6.08 (s, 1H), 6.22 (d, 1H, J=10 Hz), 7.06 (d, 1H, J=10 Hz).

Found: C, 76.95; H, 8.48%. Calcd for $C_{21}H_{28}O_3$: C, 76.79; H, 8.59%.

References

1) a) Y. Imada and K. Takahashi, Japan. Kokai 54-67094, 54-67095 (30 May 1979, Appl. 14 Oct 1977); b) Y. Imada and I. Nitta, *Hakko To Kogyo*, **38**, 1117 (1980).

2) E. J. Corey and C. U. Kim, *J. Am. Chem. Soc.*, **94**, 7586 (1972).

3) V. V. Rheenen, *Tetrahedron Lett.*, **1969**, 985.

4) R. B. Boar, J. F. McGhie, M. Robinson, D. H. R. Barton, D. C. Horwell, and R. V. Stick, *J. Chem. Soc., Perkin Trans 1*, **1975**, 1237.

5) H. Ruschig, W. Fritsch, J. Schmidt-Thomé, and W. Haede, *Chem. Ber.*, **88**, 883 (1955).

6) H. J. Ringold and G. Stork, *J. Am. Chem. Soc.*, **80**, 250 (1958).

 © 1985 The Chemical Society of Japan Bull. Chem. Soc. Jpn., 58, 1083—1087 (1985)

Nonadiabatic Transitions in Photochemical Electrocyclic Reaction of Acrylaldehyde to Form 2*H*-Oxete

Kenji MORIHASHI,* Hiroshi KUBOTA, and Osamu KIKUCHI*
Department of Chemistry, The University of Tsukuba, Sakura, Ibaraki 305
(Received July 16, 1984)

The photochemical electrocyclic reaction of *s-cis*-acrylaldehyde to form 2*H*-oxete was examined on the basis of the nonadiabatic interaction between potential energy surfaces. The nonadiabatic coupling *g* terms were calculated by the reduced classical-trajectory method along two postulated reaction paths, the concerted path and the step-by-step path. The calculated *g* terms were characteristic of the avoided crossing between the potential energy surfaces. The calculated *g* terms and the transition probabilities indicated that the step-by-step path was very efficient in the formation of 2*H*-oxete from the π-π^* state of acrylaldehyde.

The photochemical electrocyclic reaction of *s-cis*-butadiene, **1**→**2**, has been investigated theoretically by several researchers.[1,2] During the disrotatory mode of

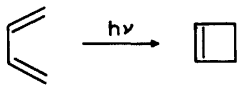

1 2

this isomerization reaction, there is an avoided crossing[3,4] between the ground state (S_0) and the lowest excited singlet state (S_1) surfaces. This avoided crossing plays a significant role in the isomerization reaction, and its existance can be easily predicted from an MO correlation diagram.[4] In the case of a formal electrocyclic reaction of *s-cis*-acrylaldehyde, **3**→**4**, such

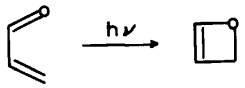

3 4

a simple prediction is impossible because of a lack of symmetry in the molecular structure.

Since the **3**→**4** system is isoelectronic with the **1**→**2** system, the **3**→**4** reaction may be considered to proceed along the concerted reaction path as is expected for the **1**→**2** reaction. However, a recent analysis of the potential energy surfaces of the **3**→**4** reaction[5] has given evidence of the existance of another reaction path, a step-by-step path in which the ring closing occurs after a rotation of the methylene group. In this path, the Z_+

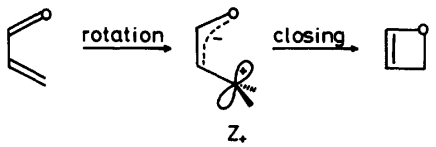

Z_+

zwitterion, in which the positive charge is localized on the terminal carbon atom, can undergo the ring closing very easily because of the strong attraction between the positive charge and the in-plane lone-pair electrons on the oxygen atom. It is thus very interesting to compare the efficiencies of the two reaction paths, the concerted path and the step-by-step path.

Since a photochemically-excited reactant molecule decays to the ground state of the reaction product *via* some nonadiabatic transitions, the transition-probability calculation as well as the potential-energy-surface analysis is necessary in order to understand the photochemical reaction processes. This is especially true for the **3**→**4** system, in which the symmetry argument of the MO correlation diagram is not effectively used. In our previous paper,[5] the **3**→**4** reaction paths were discussed on the basis of the potential energy surfaces obtained by the MINDO/3[6] CI calculations. In this paper, the nonadiabatic coupling term between the electronic states and the transition probability were calculated using the reduced classical-trajectory method,[2] and the efficiencies of the two postulated reaction paths, the concerted path and the step-by-step path, were examined on the basis of the nonadiabatic interaction between the potential energy surfaces.

Method

The method employed here is the reduced classical-trajectory method.[2] This method has been demonstrated to be a simple method for estimating nonadiabatic transition probabilities in polyatomic systems where transitions between the Ψ_1 and Ψ_2 states are induced, mainly, by the reaction-coordinate-coupling term:

$$g = \langle \Psi_2 | \partial/\partial s | \Psi_1 \rangle. \tag{1}$$

The reaction coordinate, *s*, is defined as the mass-weighted distance along the postulated reaction path A:[7]

$$s = \int_A ds. \tag{2}$$

The coupling term can be written as a sum of the CI and MO terms.[8] These terms were calculated by means of the finite-difference method for the reaction coordinate:[2]

$$g = g_{CI} + g_{MO}, \tag{3}$$

$$g_{CI} = \sum_m B_m(\partial A_m/\partial s),$$

$$g_{MO} = \sum_{\substack{m \\ (m \neq n)}} \sum_n B_m A_n \langle \Phi_m | \partial/\partial s | \Phi_n \rangle,$$

where A_m and B_m are the coefficients of configurations Φ_m in each each state function, *i.e.*,

$$\Psi_1 = \sum_m A_m \Phi_m$$
$$\Psi_2 = \sum_m B_m \Phi_m.$$

The transition probability from the Ψ_2 state to the Ψ_1 state, $P_{2\to1}=|a_1|^2$, was obtained from the solution of the reduced classical-trajectory equations:[2b]

$$\dot{a}_1 = +g\dot{s}\exp\left[-(i/\hbar)\int^t \Delta E\,dt\right]a_2,$$
$$\dot{a}_2 = -g\dot{s}\exp\left[+(i/\hbar)\int^t \Delta E\,dt\right]a_1, \quad (4)$$

where ΔE is the energy gap between Ψ_1 and Ψ_2, *i.e.*, $\Delta E=E_2-E_1>0$. Thus the reduced classical-trajectory equations have a one-dimensional form for nuclear motions, and are derived by neglecting all of the 3N-7 vibrational-coupling terms in the N-atom system.[2b] The transition probability was estimated from the Landau-Zener model:[9]

$$P_{2\to1} = \exp\left[-(\pi/4)\xi\right], \quad (5)$$

with the Massey parameter,[10]

$$\xi = \Delta E(s_c)/\hbar\,\dot{s}_c\,g(s_c). \quad (6)$$

ξ was calculated for the s_c point where the g value becomes maximum. The velocity $\dot{s}_c$ was obtained from knowledge of the kinetic energy in the direction of the reaction coordinate, $T_s=(\dot{s}_c)^2/2$.

Linear reaction paths were assumed for the concerted and step-by-step paths of the **3**→**4** reaction. For the concerted path, all geometrical variables were varied simultaneously between the structures of acrylaldehyde and 2*H*-oxete. These values were first optimized using the MINDO/3 SCF calculation.[5] The step-by-step path was expressed by two linear paths. In the first linear path, only the twisting angle of the methylene group was varied to make the methylene CH_2 plane become perpendicular to the C-C-C-O skeleton. In the second linear path, all the geometrical variables, except for that of the methylene rotation, were simultaneously varied between the structures of the twisted acrylaldehyde and of 2*H*-oxete molecules.

Although the MINDO/3 parameters had been determined so as to well reproduce the ground-state properties of molecules, the MINDO/3 CI calculations gave reasonable results for several photochemical reaction processes.[5,11,12] We thus feel that the nonadiabatic coupling terms calculated with the MINDO/3 CI wavefunctions can be employed for the qualitative consideration regarding a decay process from the excited state.

Results and Discussion

Concerted Path. The total distance between the optimized structures of acrylaldehyde and 2*H*-oxete is **10.47** (atomic mass unit)$^{1/2}$ (bohr). This value was obtained by numerical integration of Eq. 2. The three lowest singlet states along this reaction path are shown in Fig. 1. The S_1 and S_2 states correspond to the n→π^* and $\pi\to\pi^*$ states of acrylaldehyde, respectively. Two avoided crossings were observed along the reaction path, *i.e.*, the A1 avoided crossing between the S_2 and S_1 state and the A2 avoided crossing between the $S_1$and S_0 states. The reaction proceeds from the n→π^* state of acrylaldehyde and reaches the ground state of 2*H*-oxete through the two avoided crossings. On the other hand, the 2*H*-oxete formation from the $\pi\to\pi^*$ is inefficient due to a potential barrier on the S_1 state. This agrees well with the experimental evidence reported by Friedrich and Schuster.[13] Therefore, the efficiency of the concerted path, which starts from the $\pi\to\pi^*$ state of acrylaldehyde, depends on the transition probabilities at the two avoided crossing regions.

The nonadiabatic coupling terms calculated along the concerted path are shown in Fig. 2. The coupling term between S_2 and S_1, which is related to the A1 avoided crossing, has a narrow shape and the CI term is dominant. On the other hand, a broad shape is observed for the coupling term between S_1 and S_0, which is related to the A2 avoided crossing; the MO term is dominant for the g shape. A remarkable observed feature in the concerted path is the overlapping between the two coupling regions. This overlapping indicates that nonadiabatic transitions are expected to occur over a wide range of the two coupling regions. Thus, the shape of the coupling term clearly reflects the property of the nonadiabatic interaction which is not directly observed from the potential energy curves.

Step-by-step Path. The total distance, 3.76(amu)$^{1/2}$

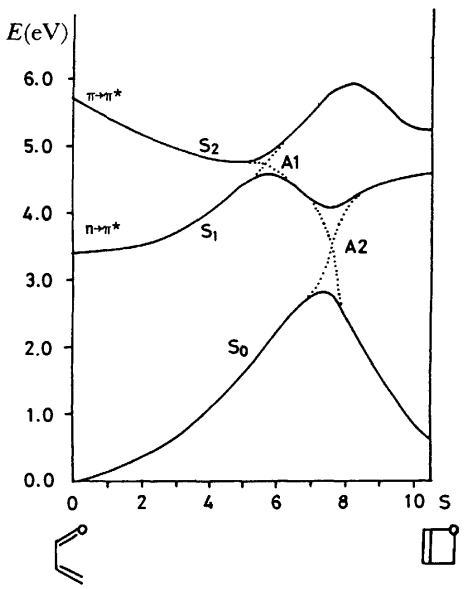

Fig. 1. Potential energy curves along the concerted path for the acrylaldehyde-2*H*-oxete system. Two avoided crossings, A1 and A2, are involved in the process. Unit of reaction coordinate is (amu)$^{1/2}$-(bohr).

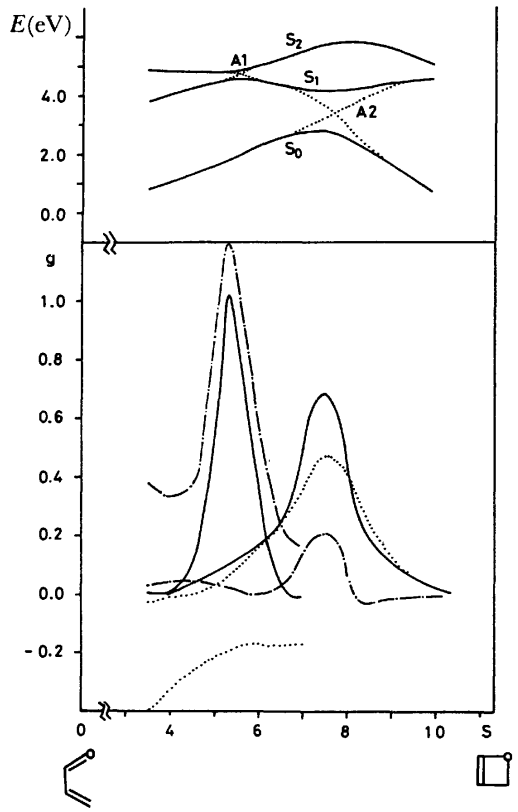

Fig. 2. Nonadiabatic coupling terms calculated along the concerted path(lower part) and the corresponding potential energy curves(upper part).
The lower part; (—·—): g_{CI}(CI term); (·····): g_{MO}(MO term); (——): $g=g_{CI}+g_{MO}$. Unit of g: $(amu)^{-1/2}(bohr).^{-1}$

(bohr), of the reaction coordinate in the first step is very short, since only hydrogen atoms with small masses move along the path. In the second step, the total distance, 9.62 $(amu)^{1/2}$ (bohr), is longer than that of the first step, since the heavy carbon and oxygen nuclei move. Figure 3 shows the potential energy curves along the step-by-step path. The rotation of the methylene group easily occurs in the $\pi\rightarrow\pi^*$ state of acrylaldehyde to give the twisted structure through the A3 avoided crossing between the S_1 and S_2 surfaces.

In the ring-closing step, the symmetry property with respect to the molecular plane is preserved. The S_1 and S_0 states are allowed to intersect since they belong to different symmetry representations.[5] If the symmetry property is destroyed, even slightly, an intersection between S_0 and S_1 is avoided. Such an intersection is called the conical intersection.[14] In order to investigate the nonadiabatic property of the conical intersection, the reaction path, in which the symmetry property was slightly destroyed, was adopted for the ring-closing step. The twisting angle of methylene group was fixed at 87.5° (not at 90°). The potential energy curves along this step-by-step path, therefore, involve two avoided crossings, A3 and A4, as shown in Fig. 3.

The calculated nonadiabatic coupling terms for the two avoided crossing regions are shown in Fig. 4. The

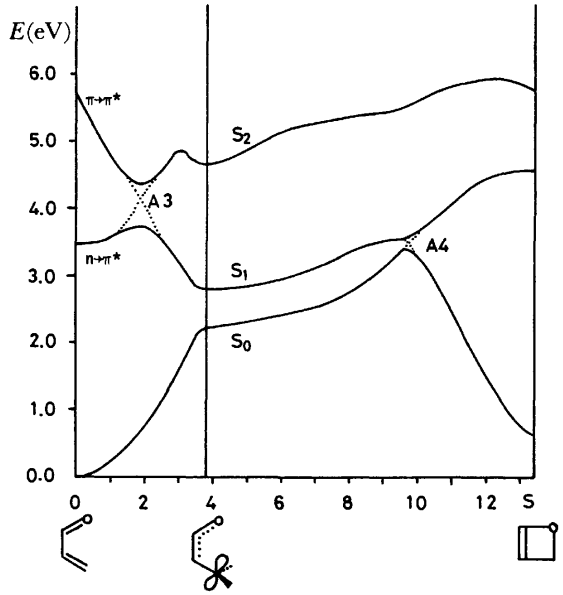

Fig. 3. Potential energy curves along the step-by-step path for the acryaldehyde-2*H*-oxete system. Two avoided crossings, A3 and A4, are involved in the process.

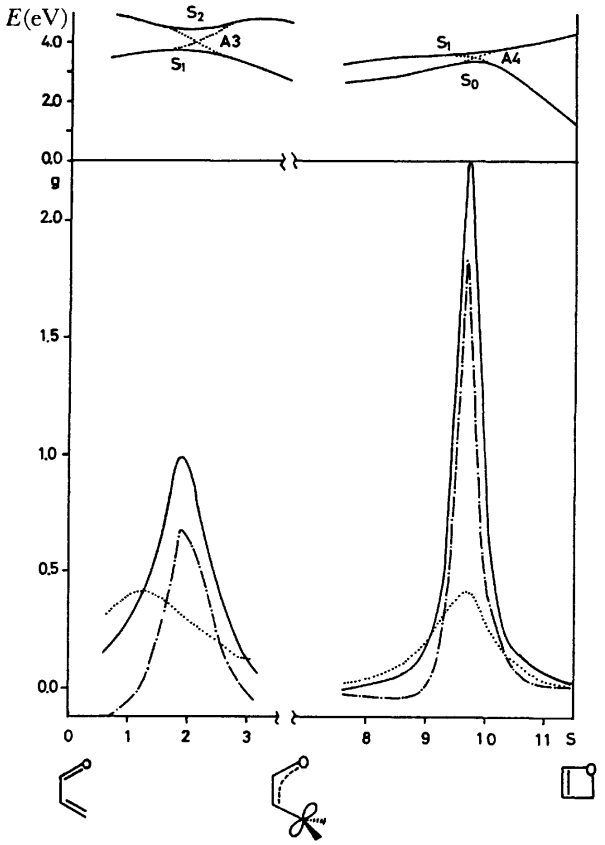

Fig. 4. Nonadiabatic coupling terms calculated along the step-by-step path(lower part) and the corresponding potential energy curves (upper part).
The lower part; (—·—): g_{CI}; (·····): g_{MO}; (——): $g=g_{CI}+g_{MO}$. Unit of g: $(amu)^{-1/2}(bohr).^{-1}$

total g shape for the A3 avoided crossing is similar to that of the A1 avoided crossing in the concerted path, although the shape of the MO and CI components are

TABLE 1. TRANSITION PROBABILITIES AND THEIR RELATED QUANTITIES FOR THE CONCERTED AND STEP-BY-STEP PATHS IN THE ACRYLALDEHYDE-2*H*-OXETE SYSTEM.

Avoided crossing		T_s[a]	$\Delta E(s_c)$	$g(s_c)$[b]	ξ	P
		eV	eV	R		
Concerted	A1	1.25	0.25	0.980	1.32	0.35
	A2	1.95	1.32	0.686	7.96	0.0019
Step-by-step	A3	1.63	0.66	0.974	3.07	0.090
	A4	2.46	0.18	2.23	0.30	0.79

a) T_s is the nuclear kinetic energy. The velocity $\dot{s}_c$ in the Massey parameter ξ was obtained from T_s by the equation. $\dot{s}_c=(2T_s)^{1/2}$. b) $g(s_c)$ indicates the maximum value of coupling term in each avoided crossing region, and the unit, (R), is equal to $(\text{amu})^{-1/2}$ $(\text{bohr})^{-1}$.

quite different between the A1 and A3 regions. A very sharp peak is observed in the variation of the coupling term between S_0 and S_1. The character of the conical intersection is clearly reflected in the *g* shape. It can be seen from the *g* shape that the nonadiabatic interaction suddenly increases near the allowed crossing, and the nonadiabatic transition occurs, effectively, in the very narrow region. If the symmetry property with respect to the molecular plane is preserved during the ring-closing step, the *g* shape would be that of a delta function at the crossing point.

Figure 3 may indicate that the $S_1 \rightarrow S_0$ transition occurs, effectively, at the twisted form of acrylaldehyde ($s=3.76$). This transition is induced by the rotation of the terminal methylene group and can be understood by the analogy of the photochemical *cis-trans* isomerization process of simple olefins.[15] The nonadiabatic coupling for this transition was not calculated, since this process is not important for the 2*H*-oxete formation.

Transition Probability. The reaction was assumed to start from the $\pi \rightarrow \pi^*$ state of acrylaldehyde, and the transition probability was calculated for each avoided crossing according to Eq. 5. The results are summarized in Table 1. The kinetic energy, T_s, was calculated from the difference between the energies of the upper state at each avoided crossing point and of the $\pi \rightarrow \pi^*$state of acrylaldehyde. The excitation energy of acrylaldehyde was assumed to be 6 (eV); this value was determined so as to be slightly higher than that of the calculated $\pi \rightarrow \pi^*$ state of acrylaldehyde.

Let us compare the possibility of the step-by-step path with that of the concerted path. If the reaction starts from the $\pi \rightarrow \pi^*$ state of acrylaldehyde, two nonadiabatic transitions are involved in each reaction path. In the first transition from the S_2 state to the S_1 state, the probability of the A1 avoided crossing in the concerted path is higher than that of the A3 avoided crossing in the step-by-step path. In the second transition from S_1 to S_0, however, the A4 avoided crossing has a much higher transition probability than that of the A2 avoided crossing. By the large difference in the probabilities of the second transition, the step-by-step path is considered to be the more effective reaction path in the two postulated paths.

It is noted that some shortcomings are involved in the above consideration. One of them involves the estimation of the kinetic energies employed in the transition-probability calculation. The kinetic energy along the reaction coordinate was estimated from the $\pi \rightarrow \pi^*$ excited-state energy, and the energy distribution among several degrees of nuclear freedom was not taken into account. This may be unrealistic and more reliable statistical methods[16] are necessary to determine the decay-rate constant.

The efficiencies of the two postulated reaction paths were compared on the basis of the nonadiabatic interaction, and the effect of the potential energy barriers on the S_0 and S_1 surfaces was not quantitatively considered. The discussion is, thus, a qualitative one and the most probable reaction path was not determined by the present treatment, although the step-by-step path was expected to be involved in the isomerization reaction.

The possibility of the existance of the step-by-step path in the photochemical electrocyclic reaction of acrylaldehyde was supported by means of the reduced classical-trajectory method. The step-by-step path *via* a zwitterion has been proposed not only for the **3**→**4** reaction but also for the various types of hetero-atom conjugated systems.[11] The present study indicates the importance of this reaction path in the photochemical electrocyclic reaction of heteroatom conjugated systems.

References

1) W. Th. A. M. van der Lugt, and L. J. Oostehoff, *J. Am. Chem. Soc.*, **91**, 6042 (1969); O. Kikuchi, *Bull. Chem. Soc. Jpn.*, **47**, 1551 (1974); D. Grimbert, G. Segal, and A. Devaquet, *J. Am. Chem. Soc.*, **97**, 6629 (1975).

2) a) K. Morihashi, O. Kikuchi, and K. Suzuki, *Chem. Phys. Lett.*, **90**, 346 (1982); b) K. Morihashi and O. Kikuchi, *Theor. Chim. Acta*, in press.

3) R. B. Woodward and R. Hoffmann, "The Conservation of Orbital Symmetry," Academic Press, New York (1970).

4) L. Salem, C. Leforestier, G. Segal, and R. Wetmore, *J. Am. Chem. Soc.*, **97**, 479 (1975).

5) O. Kikuchi, H. Kubota, and K. Suzuki, *Bull. Chem. Soc. Jpn.*, **54**, 1126 (1981).

6) R. C. Bingham, M. J. S. Dewar, and D. H. Lo, *J. Am. Chem. Soc.*, **97**, 1285 (1975).

7) The infinitesimal distance, d*s*, can be given by $ds^2=\sum_i$

dx_i^2, if the reaction path is represented with the mass-weighted Cartesian coordinates of the N-atom system, $A=(x_1, x_2, \ldots, x_{3N})$. For a more general definition of reaction coordinate, see A. Tachibana and K. Fukui, *Theor, Chim. Acta*, **49**, 321 (1978); P. G. Mezey, *ibid.*, *54*, 95 (1980).

8) C. Galloy and J. C. Lorquet, *J. Chem. Phys.*, **67**, 4672 (1977).

9) L. Landau, *Phy. Z. Sowjetunion*, **2**, 46 (1932); C. Zener, *Proc. Roy. Soc. Ser, A*, **137**, 696 (1932); E. E. Nikitin, in "Chemishe Elementarprozesse," ed by H. Hartmann, Springer-Verlag, Berlin, 1968, p. 43.

10) M. Desouter-Lecomte and J. C. Lorquet, *J, Chem. Phys.*, **71**, 4391 (1979).

11) O. Kikuchi, K. Morihashi, and K. Suzuki, *Bull. Chem. Soc. Jpn.*, **55**, 1133 (1982); O. Kikuchi, *ibid.*, **55**, 1669 (1982); O. Kikuchi, *Tetrahedron Lett.*, **22**, 859 (1981).

12) O. Kikuchi and H. Yoshida, *Bull. Chem. Soc. Jpn.*, **58**, 131 (1985).

13) L. E. Friedrich and G. B. Schuster, *J. Am. Chem. Soc.*, **93**, 4602 (1971).

14) E. Teller, *J. Phys. Chem.*, **41**, 109 (1937); T. Carrington, *Acc. Chem. Res.*, **7**, 20 (1974).

15) M. Persico, *J. Am. Chem. Soc.*, **102**, 7839 (1980); M. Persico and V. Bonacic-Koutecky, *J. Chem. Phys.*, **76**, 6018 (1982).

16) A. J. Lorquet, J. C. Lorquet and W. Forst, *Chem. Phys.*, **51**, 241 (1980); *ibid.*, **51**, 253 (1980); *ibid.*, **51**, 261 (1980).

The Photochemical Magnetic Field Effect of Isoquinoline *N*-Oxides

Norisuke HATA
Department of Chemistry, College of Science and Engineering, Aoyama Gakuin University, Chitosedai, Setagaya-ku, Tokyo 157
(Received August 2, 1984)

The irradiation of isoquinoline *N*-oxide in ethanol resulted in the formation of lactam in a *ca.* 67% yield *via* the S_1 state (Process I). When the photochemical isomerization was carried out in the presence of a magnetic field, the chemical yield of lactam was found to show a minimum at approximately 1T. In order to interpret this new phenomenon, Process I was assumed to be initiated by electron transfer from the excited singlet *N*-oxide to the hydrogen-bonded ethanol (the formation of a singlet hydrogen-bonded radical ion pair). Thus, the new type of magnetic-field effect was excellently explained in terms of an electron-nuclear hyperfine interaction mechanism including the electron-exchange interaction in the radical-ion pair (the magnetic-field effect due to HFI-J mechanism). This implies that the magnetic-field effect is unambiguous evidence that Process I (*N*-oxide→lactam) does not involve the oxaziridine intermediate, but proceeds *via* the singlet hydrogen-bonded radical-ion pair (radical-ion-pair mechanism of Process I). The irradiation of 1-cyanoisoquinoline *N*-oxide in ethanol resulted in the formation of 1,3-oxazepine in a *ca.* 66% yield *via* the S_1 state (Process II). The photochemical isomerization was not affected at all by an external magnetic field. This is consistent with the idea that Process II (*N*-oxide→oxazepine) does not involve a field-sensitive intermediate, but occurs with the intervention of oxaziridine (the oxaziridine mechanism of Process II).

It is one of the most interesting and challenging problems in chemistry to determine whether or not a magnetic field has an effect on chemical reactions. Although a number of studies of this subject had been made over a long period, corroborating evidence for the existence of an external magnetic-field effect upon chemical reactions in a liquid solution had never been obtained until 1970.[1] In 1971, on the basis of the radical-pair model of CIDNP (Chemically Induced Dynamic Nuclear Polarization),[2,3a] Lawler and Evans predicted the influence of a magnetic field on radical-pair reactions in solution.[4] In 1972 and later, as was expected from the radical-pair model, the magnetic-field effect arising from electron-nuclear hyperfine interaction (HFI mechanism) or electronic Zeeman interaction (Δg mechanism) was observed by Molin's group in the thermal reaction of pentafluorophenylmethyl chloride or decafluorodiphenylchloromethane with butyllithium.[5] Such magnetic-field effects (HFI and Δg mechanisms) were also observed in several photochemical systems by Tanimoto *et al.*,[6a] Schulten *et al.*,[6b] and Michel-Beyerle *et al.*,[6c] in 1976.

In that same year (1976), the present author found a very interesting and unexpected effect of the magnetic field which was quite different from the above two types of magnetic-field effects;[7] when the photochemical isomerization of isoquinoline *N*-oxide in ethanol was carried out in either the absence or presence of a magnetic field, the chemical yield of the product (1-isoquinolone) was observed to show a minimum at approximately 1T. In 1978 this new phenomenon was successfully interpreted in terms of a hyperfine interaction mechanism including an electron-exchange interaction in the singlet hydrogen-bonded radical-ion pair assumed to be a transient intermediate of this reaction;[8] thus, it has been termed the magnetic-field effect due to the HFI-J mechanism. These studies were partly reported in preliminary form.[7-10] The purpose of the present and succeeding papers is to present further details of the new type of external magnetic-field effect, together with a novel mechanism of the photochemical isomerization of isoquinoline *N*-oxide.

Experimental

The isoquinoline *N*-oxide **1** used as a sample was synthesized by treating isoquinoline with 35% aqueous hydrogen peroxide and acetic anhydride according to the method given in the literature;[11] it was then purified by vacuum distillation, followed by alumina-column chromatography (the eluent, chloroform–ethanol (40:1)); mp 103—105 °C. The 1-cyanoisoquinoline *N*-oxide **4** used as the other sample was prepared from 1-isoquinolinecarbonitrile according to Ochiai's method[12] and recrystallized from ethanol three times; mp 205—206 °C.

A 50-cm^3 portion of ethanolic solution containing 35 mg of isoquinoline *N*-oxide **1** (or 20 mg of 1-cyanoisoquinoline *N*-oxide **4**) in a quartz vessel was placed in an electromagnet (EEO-1815) supplied by the Maezumi Electric Company and subsequently, illuminated with a 500W Ushio Super-high-pressure Mercury Lamp (USH-500D) equipped with a Toshiba filter UV-31 (or a Toshiba filter UV-35) for 10 min (or 15 min) at room temperature while nitrogen was being bubbled in. The ethanol used as the reaction medium was a reagent-grade product (99.5%) of Wako Pure Chemical Industries. The photoproduct **2** (or **5**) and unreacted *N*-oxide **1** (or **4**) were separated by means of silica-gel TLC (Merck silica-gel plate $60F_{254}$; layer thickness, 2 mm; the eluent, benzene–ethanol–diethyl ether (5:1:2) for **1** and **2**, or hexane–diethyl ether (1:2) for **4** and **5**), and the amounts were determined spectrophotometrically. The UV absorption spectra were taken with a Shimadzu recording spectrophotometer, UV-220.

Results

The irradiation of isoquinoline *N*-oxide **1** in ethanol resulted in the formation of lactam **2** (1-isoquinolone)[13] in a *ca.* 67% yield (Eq. 1). Figure 1 shows the results when the reaction was carried out

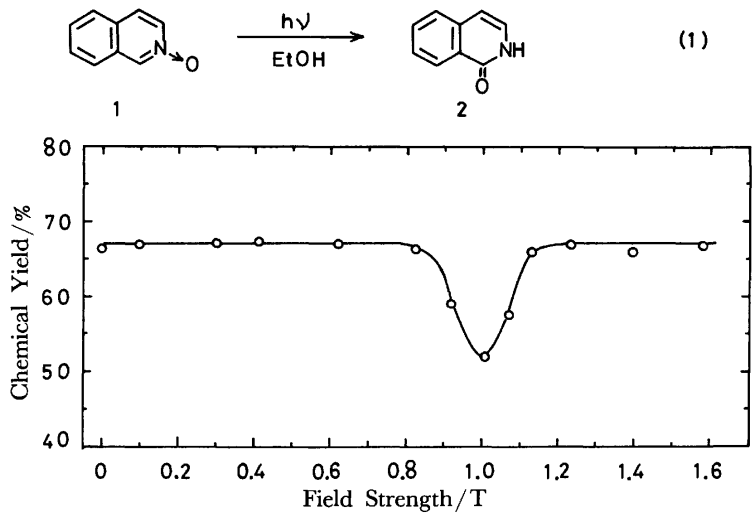

Fig. 1. The magnetic-field dependence of the chemical yield of lactam **2** in the photochemical reaction of isoquinoline *N*-oxide **1**. [*N*-oxide **1**]=4.82×10^{-3} mol dm^{-3}. Conversion: *ca.* 17%. Solvent: 50 cm^3 of ethanol.

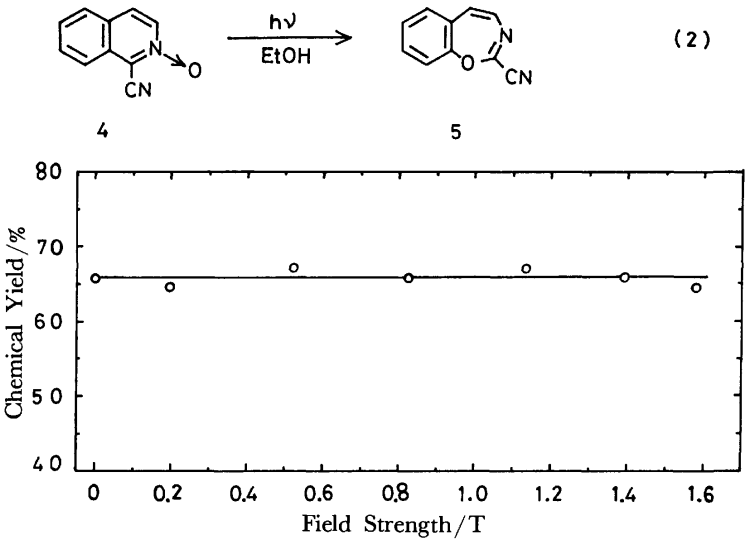

Fig. 2. The chemical yield of oxazepine **5** *vs.* magnetic-field strength in the photochemical reaction of 1-cyanoisoquinoline *N*-oxide **4**. [*N*-oxide **4**]=2.35×10^{-3} mol dm^{-3}. Conversion: *ca.* 30%. Solvent: 50 cm^3 of ethanol.

in the absence and in the presence of a magnetic field; the chemical yield of lactam **2** was determined as a function of the field strength. As can be seen from the figure, the chemical yield of lactam **2** was *ca.* 67% at a magnetic field below 0.8T, but it decreased steeply with an increase in the field strength to be *ca.* 52% at about 1T. A further increase in the magnetic field resulted in a steep increase in the chemical yield until it approached an approximately constant value (*ca.* 67%). The conversion remained almost constant (*ca.* 17%).

In the case of 1-cyanoisoquinoline *N*-oxide **4**, unlike the case of isoquinoline *N*-oxide **1**, the oxazepine **5** (2-cyano-1,3-benzoxazepine)[14] was obtained in the yield of *ca.* 66% (Eq. 2). Figure 2 shows a plot of the chemical yield of oxazepine **5** against the field strength, from which the chemical yield was proved to be independent of an external magnetic field. Here, also, the conversion remained almost constant (*ca.* 30%).

Discussion

It is well known that, the irradiation of isoquinoline *N*-oxide as well as that of quinoline *N*-oxide in solution results in the formation of a lactam and/or 1,3-oxazepine, depending on the nature of the reaction medium or the substituent group;[15] the photochemical isomerization of the *N*-oxides into lactam and oxazepine are referred to as Process I and Process II respectively. In non-hydroxylic solvents, the *N*-oxide is predominantly transformed into its oxazepine (Process II), whereas in hydroxylic solvents (ROH), Process I

(*N*-oxide→lactam) becomes much more important than Process II (*N*-oxide→oxazepine). When *N*-oxide has a CN or CF_3 group at the carbon atom adjacent to the ring nitrogen, however, only Process II occurs to yield the 1,3-oxazepine, independent of the nature of the reaction medium. Both Processes I and II have been revealed to proceed through the lowest excited singlet state (S_1), whereas the deoxygenation products (the parent amines) are formed from the lowest triplet state (T_1) in only a trace or in a yield of a few percent.[15-17]

Reactive Intermediate. In order to account for Processes I and II, oxaziridine **3a** has been custamarily postulated as the primary photoproduct (reactive intermediate) from which all the products (lactam **2** and oxazepine **3**) are derived[15a] (*cf.* Scheme 1). Since 1972, however, several experimental data conflicting with this idea have been documented in the literature.[11,15b,15c,16-18] We ourselves have demonstrated that the photochemical isomerizations are closely related to whether or not the *N*-oxide oxygen atom forms hydrogen bond with a solvent molecule;[18] that is, such a hydrogen-bonding interaction turns out to be essential for the photochemical rearrangement to the lactam **2** (Process I), but not for the photoisomerization into the oxazepine **3** (Process II). On the basis of these facts, as is shown in Scheme 1, Process I has been assumed to proceed *via* the hydrogen-bonded ion pair **2b** which is formed by the protonation of the N→O group with the hydrogen-bonded solvent molecule (EtOH) in the S_1 state (ion-pair mechanism of Process I), whereas Process II occurs with the formation of the oxaziridine intermediate **3a** from the S_1 state (oxaziridine mechanism of Process II). Such reaction mechanisms have been strongly supported by the studies of quenching by inorganic anions.[19] However, there has still been considerable doubt as to the ion-pair mechanism of Process I; the formation of the ion-pair **2b** through the hydrogen-bonding interaction was not considered to be favorable from the S_1 state, because a hydrogen-bonding ability of the oxygen atom of the N→O group was much lower in the S_1 state than in the S_0 state.[20]

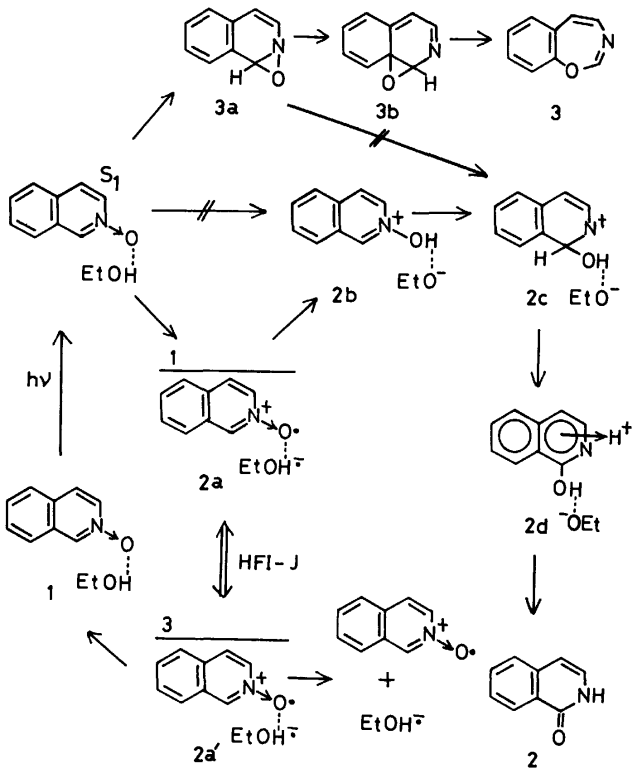

Scheme 1.

As a general rule, if a chemical reaction in solution is subject to a magnetic-field effect, then it may be taken as definite evidence that the reaction proceeds *via* a radical-pair intermediate.[3] As has been described in the Experimental section, the photochemical rearrangement of isoquinoline *N*-oxide **1** to the lactam **2** (Process I) showed an unexpected magnetic-field effect (Fig. 1), whereas the photoisomerization of 1-cyanoisoquinoline *N*-oxide **4** into the 1,3-oxazepine **5** (Process II) was not at all affected by an external magnetic field (Fig. 2). The results indicate unambiguously that Process I involves a field-sensitive radical pair as a reactive intermediate, while Process II does not. Hence, as will be described below, some modifications are required for the ion-pair mechanism of Process I.

Isoquinoline *N*-oxide molecule has two pairs of 2p non-bonding electrons on the oxygen atom of the N→O group; one of them is in conjugation with the π-electron system of the isoquinoline ring (πO:), while the other remains as a nonbonding pair (σO:). The photoelectron spectrum of this molecule shows the first band at 7.98 eV to be due to πO:,[21] indicating that the *N*-oxide cation radical is a π-radical with a radical center at the oxygen atom of the N→O group. Therefore, as is shown in Scheme 1, if an electron (πO:) is transferred from the excited singlet *N*-oxide (S_1) to the hydrogen-bonded ethanol to form the singlet hydrogen-bonded radical-ion-pair **2a** in a solvent cage, the following reactions will take place between the two radical ions constituting the pair; the *N*-oxide cation radical attributable to an odd π-electron on the oxygen atom will abstract hydrogen from the hydrogen-bonded ethanol anion radical, resulting in the formation of the hydrogen-bonded ion-pair **2b** responsible for Process I. This idea makes it possible to explain clearly not only the formation of the ion-pair **2b** which is not explicable by the ion-pair mechanism, but also the observed magnetic field effect. Hereafter, the above reaction mechanism postulated the initial formation of hydrogen-bonded radical ion pair **2a** will be termed the radical ion pair mechanism of Process I.

Magnetic-field Effect. An external magnetic-field effect can generally be expected for chemical reactions proceeding *via* radical-pair intermediates in solution, becuase an external magnetic field may influence the rate of the intersystem crossing of a radical pair.[3]

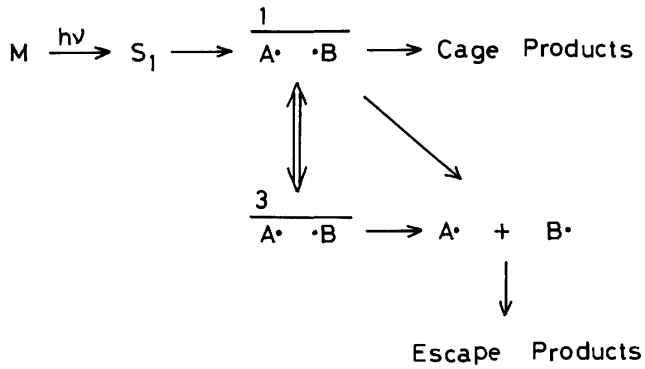

Scheme 2.

Scheme 2 shows the case of a compound M in solution absorbing light and so being exctied into the S_1 state, thus forming a singlet radical-pair intermediate. The radical pair, because of its singlet character, mostly undergoes recombination or disproportionation within a solvent cage to give a cage product. The transition of the singlet radical pair to the triplet, however, results in the formation of an escape product. If the intersystem crossing undergoes an external magnetic perturbation, the chemical yield of the cage product or the escape product can be expected to show a magnetic-field dependence.

If the exchange interaction between the unpaired electrons in a radical pair is disregarded, the following two mechanisms are currently accepted for the magnetic-field effect upon the rate of the intersystem crossing of a radical pair:[3] (i) The external magnetic field causes the intersystem crossing of a radical pair by virtue of the different *g*-values of the component radicals; therefore, the chemical yield of the cage product (or of the escape product) decreases (or increases) quadratically with an increase in the field strength (the magnetic-field effect due to the Δg mechanism). (ii) The external magnetic field results in a reduction in the number of effective working channels for the hyperfine-induced intersystem crossing of a radical pair. As a result, the chemical yield of the cage product (or of the escape product) increases (or decreases) remarkably at a very low field (the magnetic-field effect due to the HFI mechanism).

The magnetic-field effect observed in the present photochemical system (Fig. 1) is quite different from the above two cases; it can not be interpreted in terms of either the Δg or the HFI mechanism. As is shown in Scheme 1, however, if we assume the singlet hydrogen-bonded radical-ion pair **2a** as a reactive intermediate of Process I, the observed magnetic-field effect can be reasonably explained as follows:

The exchange interaction between the unpaired electrons in the radical ion-pair **2a** may be considered to be much greater than the electron-nuclear hyperfine energy because the radical centers are in close proximity as a result of hydrogen-bonding interaction between the two radical ions; as is shown in Scheme 3,

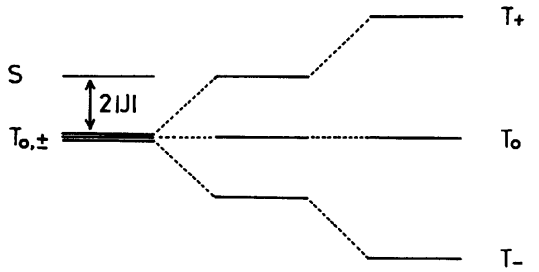

Scheme 3.

the singlet (S) and triplet ($T_{0,\pm}$) levels of the pair are nondegenerate, having an energy gap of $2|J|$, where J denotes the electron-exchange integral. Therefore, the singlet-triplet mixing due to hyperfine interaction does not occur in the zero field. However, the triplet level is resolved into three sublevels, T_0, T_+, and T_-, by the application of the magnetic field to this system; the T_+ level approaches the S level as the field strength increases. Consequently, the S–T_+ mixing becomes possible at the field strength in which the S–T_+ energy gap is of the order of the hyperfine interaction. The S–T_+ mixing is maximal at the magnetic field in which the singlet level (S) is in resonance with the T_+ level. A further increase in the field strength results in an increase in the separation between the levels of S and T_+; consequently, the mixing of S and T_+ decreases steeply. Thus, the chemical yield of lactam **2** comes to show a minimum at the resonance magnetic field (*ca.* 1T) in which the intersystem crossing of the singlet radical ion-pair **2a** is most favorable.

As has been mentioned above, the new type of magnetic-field effect observed in the present investigation was proved to be explicitly accounted for by an electron-nuclear hyperfine interaction mechanism including electron-exchange interaction in the singlet hydrogen-bonded radical ion-pair **2a** assumed as a reactive intermediate. Hereafter, this will be referred to as the "magnetic-field effect due to the HFI-J mechanism." Needless to say, if the electron-exchange interaction in a pair is neglected (J=0), the magnetic-field effect due to the HFI or Δg mechanism can be expected in lieu of the HFI-J magnetic-field effect.

The magnetic-field effect due to the HFI-J mechanism is thought to be particularly interesting and important from the viewpoint of mechanistic photochemistry, because it can be expected when a photoexcited molecule in solution undergoes chemical interaction with the hydrogen-bonded species to form an appropriate hydrogen-bonded radical pair or radical ion-pair intermediate in a solvent cage.[22]

Reaction Mechanism. An examination of the photochemical magnetic-field effect of isoquinoline *N*-oxide **1** or 1-cyanoisoquinoline *N*-oxide **4** in ethanol leads to the conclusion that Process I (*N*-oxide→lactam) is initiated by the formation of the singlet hydrogen-bonded radical ion-pair **2a** from

the S_1 state, while Process II (*N*-oxide→oxazepine) proceeds through the formation of oxaziridine **3a** (or **5a**) from the S_1 state, as is shown in Schemes 1 and 4.

In the case of isoquinoline *N*-oxide **1** (Scheme 1), the primary photochemical step is an electron (πO:) transfer from the excited singlet *N*-oxide (S_1) to the hydrogen-bonded ethanol to produce the singlet hydrogen-bonded radical ion-pair **2a** which is sensitive to the external magnetic field. Subsequently, hydrogen transfer takes place from the ethanol anion radical to the hydrogen-bonded *N*-oxide cation radical, the hydrogen-bonded ion-pair **2b** responsible for Process I being produced. The oxaziridine intermediate **3a** which is involved in Process II is also formed from the S_1 state in competition with the formation of the radical ion-pair **2a**. The conversion of the ion-pair **2b** to the lactam **2** may be supposed to follow the carbonium-ion rearrangement mechanism proposed by Kaneko,[23] because the *N*-oxide bearing a CN or CF_3 group at the carbon atom adjacent to the ring nitrogen does not undergo Process I. Kaneko has assumed the oxaziridine **3a** to be a precursor of the ion-pair **2c** and proposed the oxaziridine mechanism (**3a**→**2c**→**2d**→**2**) for Process I.[23] However, it is now clear, from the observation of HFI-J magnetic-field effect, that Process I does not involve the oxaziridine intermediate **3a**, but proceeds according to the radical ion-pair mechanism (**2a**→**2b**→**2c**→**2d**→**2**). This mechanism has been also supported by the examination of the quenching of the photochemical isomerization of 4-methylquinoline *N*-oxide by inorganic anions.[19]

In the case of 1-cyanoisoquinoline *N*-oxide **4** (Scheme 4), the formation of the oxaziridine intermediate **5a** occurs first from the S_1 state, followed by isomerization into the oxazepine **5** (Process II). Unlike the case of isoquinoline *N*-oxide **1**, no electron transfer occurs between the excited singlet *N*-oxide (S_1) and the solvent molecule; therefore, Process I does not occur. This is probably because the strong electron-withdrawing CN group at the 1-position of an isoquinoline nucleus may cause a lowering of the hydrogen-bonding ability of the oxygen atom of the N→O group and an increase in the ionization potential; also, it may render the carbonium-ion rearrangement unfeasible, even though a radical ion-pair responsible for Process I is formed. The intervention of an oxaziridine in Process II has been demonstrated, in the case of 2-cyanoquinoline *N*-oxide, from the quenching studies using inorganic anions.[19]

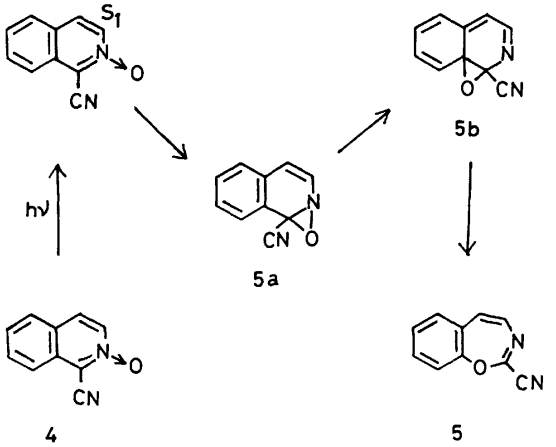

Scheme 4.

The author wishes to thank Professor Saburo Nagakura of the Institute for Molecular Science for his kind discussion.

References

1) See, for example, P. W. Atkins, and T. P. Lambert, *Annu. Rep. Prog. Chem., Sect. A*, **72**, 67 (1975).

2) See, for example, "Chemically Induced Magnetic Polarization," ed by A. P. Leply and G. L. Closs, John Wiley & Sons, New York (1973); L. T. Muus, P. W. Atkins, K. A. McLauchlan, and J. B. Pedersen, eds., "Chemically Induced Magnetic Polarization," D. Reidel, Dordrecht (1977).

3) a) "Spin Polarization and Magnetic Effects in Radical Reactions," ed by Yu. N. Molin, Elsevier, Amsterdam (1984); b) N. J. Turro and B. Kraeutler, "Diradicals," ed by W. T. Borden, John Wiley & Sons, New York (1982), Chapter 6.

4) R. G. Lawler and G. T. Evans, *Ind. Chim. Belg.*, **36**, 1087 (1971).

5) R. Z. Sagdeev, K. M. Salikhov, T. V. Leshina, M. A. Kamkha, S. M. Shein, and Yu. N. Molin, *JETP Letters*, **16**, 422 (1972); R. Z. Sagdeev, Yu. N. Molin, K. M. Salikhov, T. V. Leshina, M. A. Kamkha, and S. M. Shein, *Org. Mag. Resonance*, **5**, 603 (1973); A. V. Podoplelov, R. Z. Sagdeev, T. V. Leshina, Yu. A. Grishin, and Yu. N. Molin, *Dokl. Akad. Nauk. SSSR*, **225**, 866 (1975).

6) a) Y. Tanimoto, H. Hayashi, S. Nagakura, H. Sakuragi, and K. Tokumaru, *Chem. Phys. Lett.*, **41**, 267 (1976); b) K. Schulten, H. Staerk, A. Weller, H.-J. Werner, and B. Nickel, *Z. Phys. Chem. N. F.*, **101**, 371 (1976); c) M. E. Michel-Beyerle, R. Haberkorn, W. Bube, E. Steffens, H. Schröder, H. J. Neusser, E. W. Schlag, and H. Seidlitz, *Chem. Phys.*, **17**, 139 (1976).

7) N. Hata, *Chem. Lett.*, **1976**, 547.

8) N. Hata, *Chem. Lett.*, **1978**, 1359.

9) N. Hata, Y. Ono, and F. Nakagawa, *Chem. Lett.*, **1979**, 603.

10) N. Hata and A. Yagi, *Chem. Lett.*, **1983**, 309.

11) C. Lohse, *J. Chem. Soc. Perkin Trans. 2*, **1972**, 229.

12) E. Ochiai, "Aromatic Amine Oxides," Elsevier, Amsterdam (1967), p. 24.

13) M. Ishikawa, S. Yamada, H. Hotta, and C. Kaneko, *Chem. Pharm. Bull.*, **14**, 1102 (1966).

14) O. Buchardt, C. Lohse, A. M. Duffield, and C. Djerassi, *Tetrahedron Lett.*, **1967**, 2741.

15) See, for example, a) G. G. Spence, E. C. Taylor, and O. Buchardt, *Chem. Rev.*, **70**, 231 (1970); b) F. Bellamy and J. Streith, *Heterocycles*, **4**, 1391 (1976); c) A. Albini and M. Alpegiani, *Chem. Rev.*, **84**, 43 (1984).

16) K. B. Tomer, N. Harrit, I. Rosenthal, O. Buchardt, P. L. Kumler, and D. Creed, *J. Am. Chem. Soc.*, **95**, 7402 (1973).

17) I. Ono and N. Hata, *Bull. Chem. Soc. Jpn.*, **46**, 3658 (1973).

18) N. Hata and I. Ono, *Bull. Chem. Soc. Jpn.*, **49**, 1794 (1976).

19) N. Hata, *Nippon Kagaku Kaishi*, **1984**, 44; Preliminary report, N. Hata and T. Oguro, *Chem. Lett.*, **1978**, 597. The effect of such inorganic anions as $SeCN^-$, I^-, SCN^-, and Br^- upon the photochemical isomerization of 4-methylquinoline *N*-oxide into the lactam (Process I) or of 2-cyanoquinoline *N*-oxide into the oxazepine (Process II) in aqueous ethanol was examined. Both Processes, I and II, were quenched by the addition of inorganic anions, resulting in the formation of a deoxygenation product; the quenching was more pronounced in the order of the redox potential of these anions. Even more noticeable was the fact that the irradiation of 2-cyanoquinoline *N*-oxide (Process II) in the presence of I^- brought about the liberation of iodine, while in the case of 4-methylquinoline *N*-oxide (Process I) no such iodine liberation was observed. The lifetimes of the transient intermediates responsible for the quenching were estimated, from the Stern-Volmer quenching constant, to be *ca.* 1.4 ns in the case of Process I and *ca.* 370 ns in the case of Process II; these values correspond to the lifetime of the S_1 state and the oxaziridine respectively. The quenching studies by inorganic anions led to the conclusion that Process II proceeds *via* the oxaziridine intermediate, while Process I does not involve such an intermediate.

20) See, for example, N. Mataga, and T. Kubota, "Molecular Interaction and Electronic Spectra," M. Dekker (1970), Chapter 7.

21) J. P. Maier, J.-F. Muller, T. Kubota, and M. Yamakawa, *Helv. Chim. Acta*, **58**, 1641 (1975).

22) The second example of an HFI-J magnetic-field effect was found in the photoinduced substitution reaction of 4-methyl-2-quinolinecarbonitrile in ethanol; N. Hata and M. Hokawa, *Chem. Lett.*, **1981**, 507.

23) C. Kaneko, S. Hayashi, and Y. Kobayashi, *Chem. Pharm. Bull.*, **22**, 2147 (1974) and the references cited therein.

 © 1985 The Chemical Society of Japan Bull. Chem. Soc. Jpn., 58, 1094—1099 (1985) [Vol. 58, No. 4

Conductivity and Ion Association of Some Diastereoisomeric Salts in Water. II. Ion Association between the Δ(−)$_{589}$- or Λ(+)$_{589}$-*cis*-Bis(ethylenediamine)dinitrocobalt(III) Ion and the Δ(+)$_{589}$-(Ethylenediamine)bis(malonato)cobaltate(III) Ion and Its Temperature Dependence

Haruhiko YOKOYAMA* and Michio NISHIMURA
Department of Chemistry, Yokohama City University, 22-2 Seto, Kanazawa-ku, Yokohama 236
(Received October 6, 1984)

The electric conductivities of aqueous solutions of the diastereoisomeric salts, Δ(−)$_{589}$-*cis*-[Co(NO$_2$)$_2$(en)$_2$]Δ(+)$_{589}$-[Co(mal)$_2$(en)] and Λ(+)$_{589}$-*cis*-[Co(NO$_2$)$_2$(en)$_2$]Δ(+)$_{589}$-[Co(mal)$_2$(en)](en=ethylenediamine and mal=malonate ion), have been measured at several temperatures from 15 to 35 °C. From the analysis of the conductivity data using the Pitts equation, it was found that the Δ- or Λ-*cis*-[Co(NO$_2$)$_2$(en)$_2$]$^+$ and Δ-[Co(mal)$_2$(en)]$^-$ ions are appreciably associated in spite of the large monovalent ions and that the ion association is almost nonstereoselective and is endothermic in contrast to the exothermic ion association between Δ- or Λ-*cis*-[Co(NO$_2$)$_2$(en)$_2$]$^+$ and Δ-[Co(edta)]$^-$ (edta=ethylenediaminetetraacetate ion). By considering the obtained values of thermodynamic parameters of ion association and the significantly large Stokes radius of Δ-[Co(mal)$_2$(en)]$^-$ compared to the effective radius estimated from its partial molar volume, this complex anion was presumed to have two hydration water molecules and to release one of them by associating with the complex cations. Possible short-range interactions between the complex ions were also discussed by considering the structures of the complex ions and the chemical properties of the ligands.

In a previous conductivity study[1] of the diastereoisomeric salts, Δ(−)$_{589}$-*cis*-[Co(NO$_2$)$_2$(en)$_2$]Δ(+)$_{546}$-[Co(edta)] and Λ(+)$_{589}$-*cis*-[Co(NO$_2$)$_2$(en)$_2$]Δ(+)$_{546}$-[Co(edta)], we have found that the Δ- or Λ-*cis*-[Co(NO$_2$)$_2$(en)$_2$]$^+$ and Δ-[Co(edta)]$^-$ ions are appreciably associated in water in spite of being large and monovalent. The ion association, though not stereoselective, was an exothermic reaction entirely unable to be explained by the usual electrostatic theories of ion association,[2-4] suggesting the presence of short-range interactions which are operative on the surface of the complex ions and which are almost independent of the dielectric constant of the medium. Such interactions are considered to be of interest in connection with the problem of the stereoselectivity in the ion association of optically active complex ions, and of importance for the elucidation of the ion-ion and ion-solvent interactions in solutions containing complex ions and also for that of the mechanisms of various reactions of dissolved complex ions involving ion-pair formation in the reaction process.

In the present study, in order to accumulate information about the short-range interactions and make this nature clearer, the electric conductivities of aqueous solutions of the diastereoisomeric salts, Δ(−)$_{589}$-*cis*-[Co(NO$_2$)$_2$(en)$_2$]Δ(+)$_{589}$-[Co(mal)$_2$(en)] and Λ(+)$_{589}$-*cis*-[Co(NO$_2$)$_2$(en)$_2$]Δ(+)$_{589}$-[Co(mal)$_2$(en)], were measured at several temperatures from 15 to 35 °C and the ion association between Δ- or Λ-*cis*-[Co(NO$_2$)$_2$(en)$_2$]$^+$ and Δ-[Co(mal)$_2$(en)]$^-$ was examined. The reasons for the use of these diastereoisomeric salts are as given below.

We can expect to obtain exact thermodynamic information about the short-range interactions, if present, between the complex ions, because such a system containing only monovalent complex ions of large size can be treated almost without considering the Bjerrum-type ion association[2-4] and the usual Born-type hydration[5a] of ions. The absolute configuration and structure of Δ(−)$_{589}$-*cis*-[Co(NO$_2$)$_2$(en)$_2$]Δ(+)$_{589}$-[Co(mal)$_2$(en)], less soluble in water than the other diastereoisomeric salt, have been determined by an X-ray diffraction study.[6] This can help the stereochemical consideration of the ion pairs formed. Further, it is of interest what differences are present between the ion associations of Δ- or Λ-*cis*-[Co(NO$_2$)$_2$(en)$_2$]$^+$ with Δ-[Co(mal)$_2$(en)]$^-$ and Δ-[Co(edta)]$^-$, since the Δ-[Co(mal)$_2$(en)]$^-$ ion is similar to Δ-[Co(edta)]$^-$ in having four carboxyl groups and two coordinated nitrogen atoms.

Experimental

Materials. *Δ- and Λ-cis-[Co(NO$_2$)$_2$(en)$_2$]X(X=Br and I)*: These salts were prepared in the manner described previously.[1] The [α]$_{589}$ values of Δ- and Λ-*cis*-[Co(NO$_2$)$_2$(en)$_2$]Br were −44°±1° and +44°±1° respectively, while those of the iodides of Δ- and Λ-complexes were −38°±1° and +39°±1° respectively.

KΔ-[Co(mal)$_2$(en)]·2H$_2$O: This salt was prepared following the method of Dwyer *et al.*[7] The recrystallization was effected from water by the addition of ethanol and repeated until a constant value of the optical rotation was reached. After air-drying at room temperature, the [α]$_{589}$ and [α]$_{546}$ values of the salt were +1530°±30° and +1260°±30° respectively.

Δ-cis-[Co(NO$_2$)$_2$(en)$_2$]Δ-[Co(mal)$_2$(en)] and Λ-cis-[Co(NO$_2$)$_2$(en)$_2$]Δ-[Co(mal)$_2$(en)]: These diastereoisomeric salts were prepared as follows. The Δ- or Λ-*cis*-[Co(NO$_2$)$_2$(en)$_2$]I salt was transformed to the acetate by shaking silver acetate in warm water (*ca.* 40°C). After the removal of the silver iodide, an equimolar amount of KΔ-[Co(mal)$_2$(en)]·2H$_2$O was dissolved in the filtrate and ethanol was added to precipitate the diastereoisomeric salt. The recrystallization was carried out several times from water by the addition of ethanol. After air-drying, both salts were ascertained to be anhydrous by the use of an Abderhalden dryer and by the Kahl-Fischer method. The [α]$_{589}$ and [α]$_{546}$ values of Δ-*cis*-[Co-

$(NO_2)_2(en)_2]\Delta$-[Co(mal)$_2$(en)] were +1010°±20° and +780° ±20° respectively. The $[\alpha]_{589}$ and $[\alpha]_{546}$ values of Λ-*cis*-[Co-$(NO_2)_2(en)_2]\Delta$-[Co(mal)$_2$(en)] were +1060°±20° and +900° ±20° respectively.

ORD and Electronic Absorption Spectra of Diastereoisomeric Salts in Dilute Aqueous Solution. Measurements of the ORD and the absorption spectra were carried out with a JASCO ORD/UV-5 spectropolarimeter and a Hitachi 139 spectrophotometer. The molar rotation of Δ-*cis*-[Co$(NO_2)_2$-$(en)_2]\Delta$-[Co(mal)$_2$(en)] in water was identical with the sum of those of Δ-*cis*-[Co$(NO_2)_2$(en)$_2$]Br and KΔ-[Co(mal)$_2$(en)] at any wavelength from about 370 to 700 nm, within the limits of experimental error. A similar additivity was observed for Λ-*cis*-[Co$(NO_2)_2(en)_2]\Delta$-[Co(mal)$_2$(en)]. The absorption spectra of both diastereoisomeric salts in the same wavelength region as above agreed with each other and with the sum of those of *cis*-[Co$(NO_2)_2$(en)$_2$]Br and K[Co(mal)$_2$(en)], within the limits of experimental error.

Conductivity Measurements. Conductivity measurements were made at 15.0, 20.0, 25.0, 30.0, and 35.0°C using a Fuso 360 linear-bridge conductometer in the manner described previously.[1] The cell constant of the cell used in the present study was 0.11400 cm^{-1}.

The observed conductivity data were corrected for the conductivity of water, lower than 2.1×10^{-7} S cm^{-1} at 25°C, and for the minor conductivity change due to the aquation of *cis*-[Co$(NO_2)_2$(en)$_2]^+$.[8] Each solution was completely measured within about 3.5 h after the preparation of the solution. Throughout the measurements, the solution was protected from light. The reproducibility of the conductivity measurements was about ±0.1%. The precision of the temperature measurements was ±0.003°C.

Densities and Concentrations of Solutions. The solutions used for the conductivity measurements were made up by weight. The concentration, c, at each temperature was calculated from the molality, m, by the use of the density data. The densities, d, at (25.00±0.02)°C were measured for all solutions by using an Ostwald-type pycnometer with capacity of 50 cm^3. Approximately linear relationships were found between m and d (25°C):

for Δ-*cis*-[Co$(NO_2)_2(en)_2]\Delta$-[Co(mal)$_2$(en)],

$$d(25°\text{ C})/\text{g cm}^{-3} = (0.99703\pm0.00002) + (0.284\pm0.003)m, \quad (1)$$

and for Λ-*cis*-[Co$(NO_2)_2(en)_2]\Delta$-[Co(mal)$_2$(en)],

$$d(25°\text{ C})/\text{g cm}^{-3} = (0.99704\pm0.00002) + (0.283\pm0.003)m. \quad (2)$$

The densities at the other temperature, t, were measured only for the most concentrated solution. The observed $d(t)$ values agreed, within the limits of experimental error, with those calculated by assuming:

$$d(t)/\text{g cm}^{-3} = d(H_2O, t) + pm, \quad (3)$$

where $d(H_2O, t)$ is the density of water and where p is identical with the coefficient of m given in Eq. 1 or 2. The $d(t)$ values of the other solutions were estimated by using Eq. 3.

The concentrations of solutions at the temperature, t, could be reproduced within the limits of experimental error by the use of the following equation:

$$c(t) = c(25°\text{ C}) \times f, \quad (4)$$

where $c(t)$ and $c(25°C)$ are concentrations at t and 25°C respectively and where f is equal to the ratio of $d(H_2O, t)/d(H_2O, 25°C)$: $f=1.00206$, 1.00116, 0.99860, and 0.99698 for $t=15$, 20, 30, and 35°C respectively.[9]

Results and Discussion

Molar Conductivities of Diastereoisomeric Salts. The observed values of the molar conductivity, Λ(obsd), are summarized in Tables 1 and 2 and are plotted against $\sqrt{c}$ for each salt in Fig. 1. No appreciable difference in the plot is found between the two diastereoisomeric salts at any temperature. This relation is similar to that found between Δ-*cis*-[Co$(NO_2)_2(en)_2]\Delta$-[Co(edta)] and Λ-*cis*-[Co$(NO_2)_2$(en)$_2]\Delta$-[Co(edta)].[1]

Analysis of Conductivity Data. The conductivity data were analyzed by assuming an ion association between Δ- or Λ- *cis*-[Co$(NO_2)_2$(en)$_2]^+$ and Δ-[Co(mal)$_2$-(en)]$^-$. The analysis was made in terms of the Pitts conductivity equation,[10] modified by considering the obstruction effect in the manner described previously.[1,11]

The ion-association constant, K, and the limiting molar conductivity, Λ^∞, were calculated by the least-squares procedure minimizing $\sum[\Lambda(\text{obsd})-\Lambda(\text{calcd})]^2$. The values of the closest distance of approach of the ions, a, involved in the theoretical equations of conductivity and activity coefficient were estimated by considering the effective ionic radii of the dissolved complex ions to be reported in the following section.

Effective Ionic Radii of Complex Ions. The partial molar volume of a salt at an infinite dilution, V^∞(salt), can be estimated to be 176±2 $cm^3\,mol^{-1}$ for K[Co-(mal)$_2$(en)] according to the conventional manner[12] from d (0.008745 mol dm^{-3}, 25°C)=0.99868 g cm^{-3}. The partial molar volume, V^∞(ion), for [Co(mal)$_2$(en)]$^-$ is, therefore, evaluated to be 172±2 $cm^3\,mol^{-1}$, taking V^∞-(K^+, 25°C)=3.6 $cm^3\,mol^{-1}$.[12,13] By substituting the obtained value for V^∞(ion) into Glueckauf's expression of the partial molar volume of an ion,[1,12,14] the ionic radius, r, corresponding to the crystallographic radius, can be estimated to be 3.5$_9$ Å for [Co(mal)$_2$(en)]$^-$ on the assumption that the shape of the complex ion is spherical.

The A^∞ values of Δ-*cis*-[Co$(NO_2)_2(en)_2]\Delta$-[Co(mal)$_2$-(en)] and Λ-*cis*-[Co$(NO_2)_2(en)_2]\Delta$-[Co(mal)$_2$(en)] at 25°C were determined to be 50.52±0.04 and 50.55± 0.02 S cm^2mol^{-1} respectively, from an analysis assuming that a=7.0 Å. Both values of A^∞, in accord with each other within the limits of experimental error, were almost independent of the assumed value of a. The limiting molar conductivity, A^∞(ion), for [Co-(mal)$_2$(en)]$^-$ can be calculated to be 23.7±0.1 S cm^2 mol^{-1} by using A^∞(ion)=26.8±0.1 S cm^2mol^{-1} for *cis*-[Co$(NO_2)_2$(en)$_2]^+$.[1] The Stokes radius, r_s, is thus obtained to be 3.8$_9$ Å for [Co(mal)$_2$(en)]$^-$.

The values of r and r_s for *cis*-[Co$(NO_2)_2$(en)$_2]^+$ and [Co(edta)]$^-$ were as follows: r=3.3$_7$ Å and r_s=3.4$_4$ Å for the former ion and r=3.6$_3$ Å and r_s=3.5$_2$ Å for the latter

Table 1. Molar conductivities of Λ-*cis*-$[Co(NO_2)_2(en)_2]\Lambda$-$[Co(mal)_2(en)]$ in water

c(25 °C)[a]	Λ(obsd)/S cm^2 mol^{-1}				
10^{-3} mol dm^{-3}	at 15 °C	at 20 °C	at 25 °C	at 30 °C	at 35 °C
0.9929	37.72	42.85	48.19	53.67	59.35
1.5072	37.37	42.40	47.63	53.07	58.65
2.0019	36.93	41.91	47.11	52.51	58.04
2.4931	36.64	41.58	46.73	52.08	57.56
2.9687	36.43	41.34	46.46	51.75	57.22
3.9217	35.94	40.78	45.78	51.03	56.40
5.0278	35.46	40.25	45.18	50.32	55.61
6.4901	34.92	39.61	44.48	49.52	54.74
8.0476	34.35	38.97	43.71	48.71	53.79
9.9821	33.77	38.30	43.01	47.84	52.85

a) Concentrations at the other temperatures can be obtained by using Eq. 4.

Table 2. Molar conductivities of Λ-*cis*-$[Co(NO_2)_2(en)_2]\Lambda$-$[Co(mal)_2(en)]$ in water

c(25 °C)[a]	Λ(obsd)/S cm^2 mol^{-1}				
10^{-3} mol dm^{-3}	at 15 °C	at 20 °C	at 25 °C	at 30 °C	at 35 °C
1.4976	37.38	42.43	47.66	53.11	58.68
2.0156	37.01	41.98	47.19	52.54	58.07
2.4942	36.74	41.66	46.81	52.14	57.64
2.9824	36.40	41.30	46.42	51.68	57.11
3.9840	35.91	40.75	45.80	50.98	56.35
4.9958	35.46	40.22	45.18	50.30	55.59
6.4758	34.91	39.59	44.46	49.52	54.72
7.9951	34.40	39.01	43.81	48.76	53.86
9.9628	33.80	38.33	43.05	47.88	52.86

a) Concentrations at the other temperatures can be obtained by using Eq. 4.

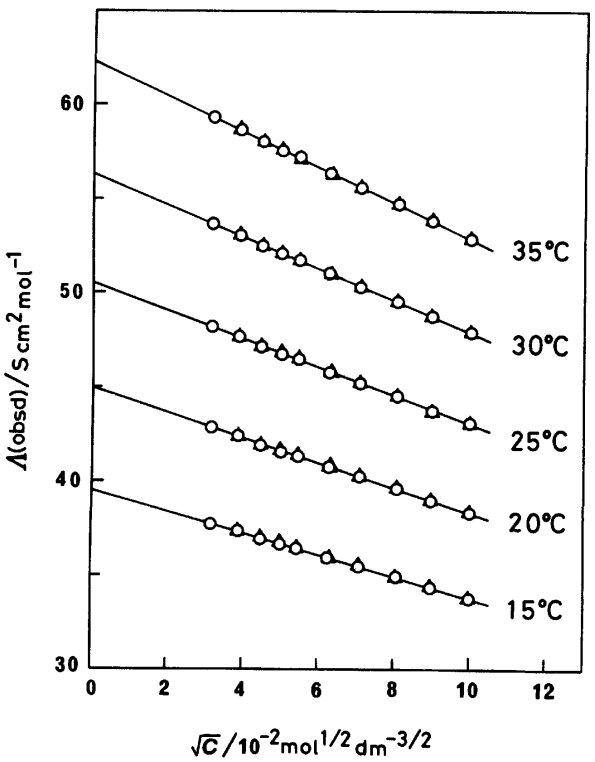

Fig. 1. Plot of Λ(obsd) against $\sqrt{c}$.
O: Λ-*cis*-$[Co(NO_2)_2(en)_2]$ Λ-$[Co(mal)_2(en)]$, Δ: Λ-*cis*-$[Co(NO_2)_2(en)_2]$ Λ-$[Co(mal)_2(en)]$.
Solid lines are theoretical curves reproduced with the Λ^∞ and K values given in Table 3; the curves at a given temperature are close and overlapped to each other between the two diastereoisomeric salts and between a=7.0 and 7.3 Å.

ion.[1] It is obvious that the r and r_s values are close to each other for these complex ions. On the other hand, a significant difference is found between the r and r_s values for $[Co(mal)_2(en)]^-$. Considering the closeness between the r values of $[Co(mal)_2(en)]^-$ and $[Co(edta)]^-$, the r_s value of the former complex ion seems to be significantly large. This may imply that the $[Co(mal)_2(en)]^-$ ion is hydrated. That is, the Stokes radius of $[Co(mal)_2(en)]^-$ can be well explained by assuming that this complex ion has two hydration water molecules, because an r value of 3.85 Å close to that of 3.89 Å for r_s, can be obtained for the hydrated complex ion from its partial molar volume, $V^\infty([Co(mal)_2(en)]^- \cdot 2H_2O)$=208±2 cm^3 mol^{-1}, where the molar volume of the hydration water molecule was assumed to be 18.1 cm^3 mol^{-1}, equal to the partial molar volume of water.[9] Further discussion about the hydration of $[Co(mal)_2(en)]^-$ will be made later.[15]

In a previous study,[1] the value of a between *cis*-$[Co(NO_2)_2(en)_2]^+$ and $[Co(edta)]^-$ was taken to be 7.0 Å, equal to the sum of the r or r_s values of the complex ions. The sums of the ionic radii of *cis*-$[Co(NO_2)_2(en)_2]^+$ and $[Co(mal)_2(en)]^-$ become 7.0 Å with r and 7.3 Å with r_s. The results obtained by assuming both a=7.0 Å and a=7.3 Å will be discussed below.

Ion Association. In Table 3, the ion-association constants (K) and the limiting molar conductivities (Λ^∞) obtained by assuming a=7.0 and 7.3 Å are summarized, together with the standard deviations, σ.[16] The values of Λ^∞ are almost the same between a=7.0 and 7.3 Å at a given temperature, while those of K are

TABLE 3. Λ^{∞} AND K VALUES OBTAINED FOR THE DIASTEREOISOMERIC SALTS BY ASSUMING a=7.0 AND 7.3 Å WITH THE PITTS EQUATION

Temp	a=7.0 Å			a=7.3 Å		
	Λ^{∞}	K	σ	Λ^{∞}	K	σ
°C	S cm² mol⁻¹	dm³ mol⁻¹	S cm² mol⁻¹	S cm² mol⁻¹	dm³ mol⁻¹	S cm² mol⁻¹
			Δ-cis-[Co(NO₂)₂(en)₂]*Δ*-[Co(mal)₂(en)]			
15	39.55±0.04	5.4±0.6	0.0332	39.55±0.04	5.5±0.6	0.0331
20	44.92±0.04	5.5±0.4	0.0326	44.92±0.04	5.6±0.4	0.0325
25	50.52±0.04	5.8±0.4	0.0351	50.51±0.04	5.9±0.4	0.0351
30	56.31±0.03	5.9±0.3	0.0274	56.31±0.03	6.0±0.3	0.0271
35	62.27±0.05	6.0±0.3	0.0404	62.27±0.04	6.1±0.3	0.0401
			Λ-cis-[Co(NO₂)₂(en)₂]*Δ*-[Co(mal)₂(en)]			
15	39.62±0.02	5.6±0.2	0.0204	39.62±0.02	5.7±0.2	0.0206
20	44.97±0.02	5.7±0.2	0.0200	44.96±0.02	5.8±0.2	0.0202
25	50.55±0.02	5.8±0.2	0.0206	50.55±0.02	5.9±0.2	0.0208
30	56.33±0.03	6.0±0.2	0.0254	56.33±0.03	6.1±0.2	0.0256
35	62.30±0.03	6.1±0.2	0.0279	62.30±0.03	6.2±0.2	0.0279

TABLE 4. THERMODYNAMIC PARAMETERS OF ION ASSOCIATION, $\Delta G°$, $\Delta H°$, AND $\Delta S°$, AT 25 °C OBTAINED BY ASSUMING a=7.0 Å WITH THE PITTS EQUATION

Salt	$\Delta G°$	$\Delta H°$	$\Delta S°$
	kJ mol⁻¹	kJ mol⁻¹	J mol⁻¹ K⁻¹
Δ-cis-[Co(NO₂)₂(en)₂]*Δ*-[Co(mal)₂(en)]	−4.35±0.15	4.0±1.0	28±4
Λ-cis-[Co(NO₂)₂(en)₂]*Δ*-[Co(mal)₂(en)]	−4.36±0.07	3.2±0.7	25±3
Δ-cis-[Co(NO₂)₂(en)₂]*Δ*-[Co(edta)]	−6.13±0.13[a)]	−5.7±0.3[a)]	1.4±1.4[a)]
Λ-cis-[Co(NO₂)₂(en)₂]*Δ*-[Co(edta)]	−6.17±0.12[a)]	−5.3±0.7[a)]	3.0±2.8[a)]

a) Cited from Ref. 1.

slightly changed, depending on the assumed value of a, but still within the limits of experimental error.

No appreciable difference in the obtained K values is found between *Δ-cis*-[Co(NO₂)₂(en)₂]*Δ*-[Co(mal)₂(en)] and *Λ-cis*-[Co(NO₂)₂(en)₂]*Δ*-[Co(mal)₂(en)] at any temperature, considering the experimental error. A similar relation has also been obtained between *Δ-cis*-[Co(NO₂)₂(en)₂]*Δ*-[Co(edta)] and *Λ-cis*-[Co(NO₂)₂(en)₂]*Δ*-[Co(edta)]. The ion-association constants of these diastereoisomeric salts were as follows: K/dm³ mol⁻¹= 12.9±0.4 (15 °C), 11.9±0.6 (25 °C), and 11.1±0.8 (35 °C) for the former salt and 13.2±0.7 (15 °C), 12.0±0.5 (25 °C), and 11.4±0.5 (35 °C) for the latter.[1)]

The K values obtained in the present study are about half of those for the ion association between *cis*-[Co(NO₂)₂(en)₂]⁺ and [Co(edta)]⁻. However, they are considerably larger than the previously reported theoretical ion-association constants: K (25 °C, a=7.0 Å)/dm³ mol⁻¹=0 (by Bjerrum[2)]), 2.41 (by Fuoss[3)]), and 0.24 (by Ebeling[17)] and Yokoyama-Yamatera[4)]).[1)] This implies that interactions other than the simple electrostatic one are also present between *cis*-[Co(NO₂)₂(en)₂]⁺ and [Co(mal)₂(en)]⁻.

The ion association of *cis*-[Co(NO₂)₂(en)₂]⁺ with [Co(mal)₂(en)]⁻ is endothermic, since the K value increases with an increase in the temperature, as is shown in Table 3. This temperature dependence is the opposite of that observed for the ion association of this complex cation with [Co(edta)]⁻,[1)] but it is seemingly similar to that observed for such 2:2 electrolytes as MgSO₄[18)] or that predicted from the ion-association theories.[1,3,4,17)]

The standard enthalpy and entropy of ion association, $\Delta H°$ and $\Delta S°$, were estimated from the temperature dependence of the ion-association constant. The values of $\Delta H°$, $\Delta S°$, and the standard Gibbs free energy, $\Delta G°$, at 25 °C are shown in Table 4 with a=7.0 Å; the $\Delta H°$ and $\Delta S°$ values obtained with a=7.3 Å were the same as those given in Table 4 within 1%. Slight differences in the $\Delta H°$ and $\Delta S°$ values might seem to be present between *Δ-cis*-[Co(NO₂)₂(en)₂]*Δ*-[Co(mal)₂(en)] and *Λ-cis*-[Co(NO₂)₂(en)₂]*Δ*-[Co(mal)₂(en)], but the situation is ambiguous because of the experimental error.

In Table 4, the $\Delta H°$ and $\Delta S°$ values are also shown for the ion association between *Δ-* or *Λ-cis*-[Co(NO₂)₂(en)₂]⁺ and *Δ*-[Co(edta)]⁻. In the previous paper,[1)] by considering the small $\Delta S°$ value to be close to zero and the $\Delta H°$ value to be negative, these ion associations were interpreted as being caused by short-range interactions between the complex ions, almost independent of the dielectric constant of the medium, and to be performed without any release of hydration water molecules. The last argument was consistent with the presumption, based on the likeness between the r and r_s values, that the ions of both *cis*-[Co(NO₂)₂(en)₂]⁺ and [Co(edta)]⁻ are not appreciably hydrated.

The $\Delta H°$ and $\Delta S°$ values for the ion association between *cis*-[Co(NO₂)₂(en)₂]⁺ and [Co(mal)₂(en)]⁻ are in contrast with those between this complex cation and [Co(edta)]⁻, as is to be expected from the temperature dependence of the ion-association constant. The

present results can be explained well by assuming that the $[Co(mal)_2(en)]^-$ ion is hydrated. That is, the large positive $\Delta S°$ value implies that the ion association is accomplished by the release of hydration water molecules of the complex anion. The positive $\Delta H°$ value is considered to result from the energy requirement for the release of hydration water molecules. The assumption of the hydration of $[Co(mal)_2(en)]^-$ is consistent with the presumption from its Stokes radius described in the preceding section.

The most effective short-range interaction of *cis*-$[Co(NO_2)_2(en)_2]^+$ with $[Co(edta)]^-$ was considered to be hydrogen-bonding between the amino group in the complex cation and the carboxyl group in the complex anion.[1] The ion association of *cis*-$[Co(NO_2)_2(en)_2]^+$ with $[Co(mal)_2(en)]^-$ may also be caused mainly by the hydrogen-bonding between the above two groups as well as by that between the nitro ion in the complex cation and the amino group in the complex anion. The possibility of the presence of the former hydrogen-bonding between the complex cation and anion in the *Δ-cis*-$[Co(NO_2)_2(en)_2]$*Δ*-$[Co(mal)_2(en)]$ crystal has been revealed by an X-ray diffraction study.[6]

The hydration of $[Co(mal)_2(en)]^-$ is thought to be due to specific interactions of the complex ion with water molecules, since the usual Born-type hydration[5a] of such a large monovalent complex ion is considered to be very weak. The most effective interaction is probably also hydrogen-bonding. Both the carboxyl and amino groups of $[Co(mal)_2(en)]^-$ can contribute to the hydrogen bonding with water molecules. Especially, the amino groups may play an important part, together with the carboxyl groups, considering the difference in the degree of hydration between $[Co(mal)_2(en)]^-$ and $[Co(edta)]^-$. The two hydration water molecules of the former anion, estimated from the deviation between the r and r_s values, may be related to the fact that this complex anion has two amino groups. From the structural point of view, two spaces favorable for accepting such water molecules exist on the surface of $[Co(mal)_2(en)]^-$. Each space is adjacent to an amino group of the ethylenediamine and two coordinated oxygen atoms of different malonate ions, and is located on the side opposite another one across the central cobalt(III) ion.

The entropies of ion association between *cis*-$[Co(NO_2)_2(en)_2]^+$ and $[Co(mal)_2(en)]^-$ were more positive by about 20—30 $J\,mol^{-1}K^{-1}$ than those between this complex cation and $[Co(edta)]^-$, as is shown in Table 4. Assuming that the difference in the entropy is mainly attributable to that in the number of hydration water molecules released on the ion association, and that the entropy of hydration is to be regarded as -25 $J\,mol^{-1}K^{-1}$, according to Ulich's treatment,[19] the difference in the number of released hydration water molecules can be estimated to be about one. Since the *cis*-$[Co(NO_2)_2(en)_2]^+$ and $[Co(edta)]^-$ ions probably have no hydration water molecule, only one of the two hydration water molecules of $[Co(mal)_2(en)]^-$ comes to be released on the ion association of this complex anion with *cis*-$[Co(NO_2)_2(en)_2]^+$. This is conceivable, because it is geometrically difficult for the associated *cis*-$[Co(NO_2)_2(en)_2]^+$ ion to occupy simultaneously the two spaces situated apart from each other on the surface of $[Co(mal)_2(en)]^-$, described above, by removing the two hydration water molecules from these spaces. In other words, this implies that the occupation of one of the two spaces by *cis*-$[Co(NO_2)_2(en)_2]^+$ is required for the short-range interactions between these complex ions.

The stereoselectivity in the formation of the diastereoisomeric ion pairs, *Δ-cis*-$[Co(NO_2)_2(en)_2]^+$*Δ*-$[Co(mal)_2(en)]^-$ and *Λ-cis*-$[Co(NO_2)_2(en)_2]^+$*Δ*-$[Co(mal)_2(en)]^-$, seemed to be absent or slight, if present, with respect to the thermodynamic parameters of ion association given in Tables 3 and 4. This implies that the ease of approaching the complex cation and anion to interact and the strength of the interactions are not so very different between the two diastereoisomeric ion pairs.

The present work was partially supported by a Grant-in-Aid for Scientific Research (No. 564197) from the Ministry of Education, Science and Culture.

References

1) H. Yokoyama, *Bull. Chem. Soc. Jpn.*, **57**, 1304 (1984).
2) N. Bjerrum, *Kgl. Danske Videnskab. Selskab.*, **7**, No. 9 (1926).
3) R. M. Fuoss, *J. Am. Chem. Soc.*, **80**, 5059 (1958).
4) H. Yokoyama and H. Yamatera, *Bull. Chem. Soc. Jpn.*, **48**, 1770, 3002 (1975).
5) R. A. Robinson and R. H. Stokes, "Electrolyte Solutions," 2nd Ed, Butterworths, London (1959); a) Chap. 3, p. 69; b) Chaps. 6 and 9.
6) K. Matsumoto and H. Kuroya, *Bull. Chem. Soc. Jpn.*, **45**, 1755 (1972).
7) F. P. Dwyer, I. K. Reid, and F. L. Garvan, *J. Am. Chem. Soc.*, **83**, 1285 (1961).
8) The rate of increase in the conductivity was about 0.02%/h at 25 °C. The increase per molar conductivity of *cis*-$[Co(NO_2)_2(en)_2]^+$ is, therefore, calculated to be about 0.04%/h. This value is in agreement with that obtained in the case of *cis*-$[Co(NO_2)_2(en)_2][Co(edta)]$.[1]
9) For the density of water, see the monograph of D. Eisenberg and W. Kauzmann: "The Structure and Properties of Water," Oxford-Clarendon Press, London (1969).
10) E. Pitts, *Proc. R. Soc. London, Ser. A*, **217**, 43 (1953); E. Pitts, B. E. Tabor, and J. Daly, *Trans. Faraday Soc.*, **65**, 849 (1969).
11) The analysis was also made by the use of the Fuoss-Hsia equation,[20] as in a previous study.[1] However, only the results obtained by the modified Pitts equation will be shown in this paper.
12) F. J. Millero, *Chem. Rev.*, **71**, 147 (1971); "The Partial Molal Volumes of Electrolytes in Aqueous Solutions," in "Water and Aqueous Solutions," ed by R. A. Horne, Wiley-Interscience, New York (1972), Chap. 13.

13) R. Zana and E. Yeager, *J. Phys. Chem.*, **71**, 521 (1967).
14) E. Glueckauf, *Trans. Faraday Soc.*, **61**, 914 (1965).
15) The information about the interaction of $[Co(mal)_2(en)]^-$ with water can also be obtained from the temperature dependence of the Walden product, $\Lambda^\infty(ion)\eta_0$, where η_0 is the viscosity of the solvent. The values of $\Lambda^\infty(ion)\eta_0/10^{-5}$ S Ns mol^{-1} [21] for *cis*-$[Co(NO_2)_2(en)_2][Co(mal)_2(en)]$ can be estimated to be 0.450, 0.450, 0.450, 0.449, and 0.448 at 15, 20, 25, 30, and 35 °C respectively, from the Λ^∞(salt) values given in Table 3. Hence, the temperature coefficient of the Walden product at 25 °C, $d\{\Lambda^\infty(salt)\eta_0\}/dT/10^{-5}$ S Ns mol^{-1} K^{-1}, becomes -1×10^{-4}, which is larger than the value of -3×10^{-4} obtained for *cis*-$[Co(NO_2)_2(en)_2][Co(edta)]$.[1] This means that the temperature coefficient for $[Co(mal)_2(en)]^-$ is more positive by 2×10^{-4} than that for $[Co(edta)]^-$. Considering that the temperature coefficient of the Walden product usually becomes more positive with an increase in the strength of the hydration, as is seen in the case of alkali metal or halide ions,[5b,22] the hydration of $[Co(mal)_2(en)]^-$ seems more likely than that of $[Co(edta)]^-$.
16) Almost the same values of K and Λ^∞ as those given in Table 3 were obtained from the analysis using the Fuoss-Hsia equation.[20]
17) W. Ebeling, *Z. Physik. Chem. (Leipzig)*, **238**, 400 (1968); H. Falkenhagen and W. Ebeling, "Ionic Interactions," Vol. 1, ed by S. Petrucci, Academic Press, New York (1971), Chap. 1.
18) S. Katayama, *Bull. Chem. Soc. Jpn.*, **46**, 106 (1973); S. Katayama, *J. Solution Chem.*, **5**, 241 (1976); H. Yokoyama and H. Yamatera, *Bull. Chem. Soc. Jpn.*, **54**, 2286 (1981).
19) H. Ulich, *Trans. Faraday Soc.*, **23**, 388 (1927); J. O'M. Bockris and B. E. Conway, "Modern Aspects of Electrochemistry," Butterworths, London (1954), Chap. 2, p. 63; B. E. Conway, "Ionic Hydration in Chemistry and Biophysics," Elsevier, Amsterdam (1981), Chap. 29, p. 596.
20) R. M. Fuoss and K.-L. Hsia, *Proc. Natl. Acad. Sci. U. S. A.*, **57**, 1550 (1967); **58**, 1818 (1968).
21) The unit of 10^{-5} S Ns mol^{-1} for $\Lambda^\infty(salt)\eta_0$ is equal to the conventional unit of P S cm^2 mol^{-1} because 1 P (poise)= 0.1 Pa s=0.1 N m^{-2} s. The description of 10^{-4} S Ns mol^{-1} in our previous paper[1] was erroneous.
22) R. L. Kay, "Ionic Transport in Water and Mixed Aqueous Solvents," in "Water," ed by F. Franks, Plenum Press, New York (1973), Vol. 3, Chap. 4.

 © 1985 The Chemical Society of Japan Bull. Chem. Soc. Jpn., 58, 1100—1104 (1985) [Vol. 58, No. 4

Decomposition of Crystalline Potassium Hexacyanoferrate(II) Trihydrate by Incident Energetic Argon Ions†

Shin-ichi OHNO* and Katsutoshi FURUKAWA
Department of Chemistry, Japan Atomic Energy Research Institute, Tokai-mura, Ibaraki 319-11
(Received November 9, 1984)

Ar^+ ions in the energy range of 0.4 to 2 MeV was found to induce a chemical reaction in solid potassium hexacyanoferrate(II) trihydrate giving rise to Fe^{3+}-ion clusters which have been evidenced by EPR observations. γ-Irradiations at high doses ($>10^9$ rad) followed by heating (>150 °C) were found to induce the same reaction. Irradiations with γ-rays, protons, or low-energy (<40 keV) Ar^+ ions alone did not induce this reaction, nor did a thermal activation. A possible mechanism for this reaction is discussed mainly from a qualitative point of view on the basis of experimental observations and results of atomic collision physics. It is concluded that the reaction is caused by a highly inelastic excitation of iron(II) in the complex which is accompanied with a simultaneous momentum transfer.

Radiation chemical reactions in matter due to energetic ion passage, and different from those due to γ-irradiations, are generally interpreted in terms of an LET (linear rate of energy transfer per unit length) effect.[1,2] An LET value itself for an energetic ion traversing a given medium increases with decreasing ion velocity and different LET radiations generally produce different spatial distributions of the initial products of radiolysis.[1,2]

On the other hand, recent results in atomic collision physics,[3-5] suggest that slow-moving particle collisions (in the energy range of 10 to 1000 keV) may result in such primary processes as inner shell or multiple excitations of an atom or molecule, which would involve an energy transfer per event much larger than outer-shell or single excitations. Thus, low-energy particle collisions may induce chemical reactions different from those induced by γ- and UV-irradiations. The importance of these highly inelastic processes in chemical or biological effectiveness was pointed out a long time ago,[6,7] and the processes themselves have been studied rather extensively[3-5] since then, but their chemical or biological consequences remain unexploited except for a few cases.[5,7,8] Atomic displacements in a collision cascade zone may also be important for possible chemical reactions in a material bombarded with energetic ions.[7]

In this paper we report that Ar^+ ions of a certain energy range induce a chemical reaction in solid cyanide complexes giving rise to Fe^{3+}-ion clusters, which have been evidenced by EPR observations. γ-Irradiations at doses higher than 10^9 rad (1 rad=10^{-2} J kg^{-1}) followed by heating (>150 °C) were found to induce the same reaction. Irradiations with γ-rays, protons, or helium ions alone did not induce this reaction, nor did a thermal activation. It seems that the reaction is caused through electronic excitations of the iron(II) in the complex which are accompanied by a simultaneous momentum transfer.

Experimental

Sample Preparation. Single crystals of potassium hexacyanoferrate(II) trihydrate (Koso Chemicals Co., Inc.) were grown from aqueous solutions. In some cases powders were pressed into disks of the diameter of 1 cm.

For comparison of the EPR spectra of the irradiated sample, some EPR spectra of solid solutions of aluminum oxide containing various amount of iron(III) were recorded. These solid solutions were prepared from aqueous solutions of $KAl(SO_4)_2 \cdot 12H_2O$ containing varing concentrations of iron(III) sulfate, reacted with NH_3+NH_4Cl to form precipitate, and then fired in a crucible for 20 min at 1000 °C.

Irradiations. The samples to be irradiated were mounted onto the sample holder by means of clamps or with the aid of adhesives and were irradiated at ambient temperatures in vacuum (*ca.* 10^{-5} Pa) with energetic ion beams or γ-rays.

i) Van de Graaf accelerator: Ar^+ ions in the energy range of 0.4 to 2 MeV were from a Van de Graaf accelerator equipped with PIG- and RF-type ion sources. Other ions like H^+, N^+, and O^+ were also used in the present study.

ii) Low-energy ion accelerator: Ions with lower energies were from a small accelerator[9] which has been constructed in our laboratory. The Ar^+ ions were extracted from a Duoplasma-type source operated at a pressure of 20 to 50 Pa and further accelerated to a desired energy (10—100 keV), focussed by an electrostatic lens system, and analyzed electromagnetically before impinging on the target.

iii) Beam intensity: The intensity of the beam was from 0.1 to 10 μA depending on the ion used, and typically ≈10^{12} ions s^{-1} through an aperture of 0.4 cm^2.

iv) γ-Irradiation: γ-Irradiations were performed with a 4.5 kCi ^{60}Co source in aerated conditions. Irradiations were also done in vacuum for analysis of the evolved gases.

EPR Measurement. EPR spectra of irradiated samples were obtained with a JP-1 X-band (9.5 GHz) spectrometer (Japan Electron Optics Co., Ltd.) with a modulation of 100 kHz using a polycrystalline DPPH as a magnetic field marker and Mn^{2+} in MgO as a reference for the magnetic field strength.

The signal intensity of the absorption was measured by using an approximation $h \cdot \Delta H_m^2$, where h is the peak-to-peak height and ΔH_m the peak-to-peak linewidth of the first derivative of the spectrum, respectively.

Secondary Ion Mass Spectrometry. Secondary ions emitted from the surface of the sample during ion bombardment were mass analyzed with a quadrupole mass filter (MSQ-300, Ulvac Co., Tokyo). Bombardment were performed through an aperture of 2 mmφ. Current densities were adjusted to 0.1 μA cm^{-2} for the convenience of getting relative yields of the emitted ions due to different kind of bombarding ions with

† Chemical Reactions Induced by Energetic Particles. I.

different energies.

Results

EPR Measurements. Potassium hexacyanoferrate(II) trihydrate, a low spin Fe(II) complex, is a diamagnetic compound and shows no EPR signals. On exposure to a beam of 1.8 MeV Ar^{2+} or 450 keV Ar^+ ion the bombarded (010) surface of a single crystal of the sample was decomposed to give EPR-absorption spectra. In Fig. 1 are shown some of the spectra thus obtained.

The signal intensities of the central absorption at $g=2.0$ as a function of irradiation time are shown in Fig. 2, together with the values of the linewidth. As may be seen in Fig. 2, the signal grows linearly with irradiation time up to 2—3 min and then levels off. The linewidths are also dependent on irradiation time, ranging from 140 at the beginning to 300 G in cases of 1.8 MeV Ar^{2+} bombardment, and from 100 to 150 G in cases of 450 keV Ar^+ bombardment.

It should be noted that (i) these spectra were obtained at 300 K and stable for several months at room temperature, (ii) the central absorption at $g=2.0$ with a large width has a Lorentzian shape, and (iii) the ratio of the signal intensities taken at 300 and 77 K, I_{300}/I_{77}, for this absorption is remarkably large compared with the corresponding ratio for the absorption lines of Mn^{2+} in MgO.

Irradiations of the sample with 40 or 20 keV Ar^+ ions at the beam intensity of 0.3 and 10 $\mu A\,cm^{-2}$ produced no remarkable EPR signal and, only after prolonged irradiations over 10 min at the intensity of 10 $\mu A\,cm^{-2}$, yielded the spectra which are shown in Fig. 3 (a) and (b). Besides the distinct line at the lower field, the central portion of the spectrum became gradually with irradiation time like that which would be obtained from the sample pre-heated at temperatures higher than 200 °C.

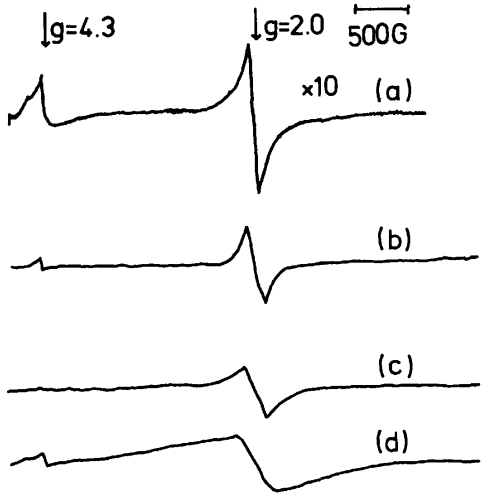

Fig. 1. EPR spectra of 1.8 MeV Ar^{2+}-irradiated (010) surface of $K_4[Fe(CN)_6]\cdot 3H_2O$. Current density: 0.75 $\mu A\,cm^{-2}$; irradiation time: (a) 10 s, (b) 1 min, (c) 5 min, and (d) 15 min.

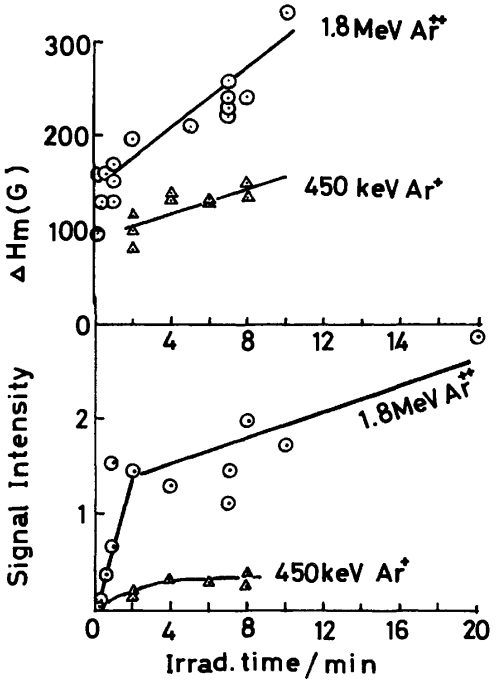

Fig. 2. Irradiation time dependence of signal intensity and linewidth ΔH_m of EPR spectrum of Fe^{3+} clusters formed in 1.8 MeV Ar^{2+}- and 450 keV Ar^+-ion bombarded (010) surface of $K_4[Fe(CN)_6]\cdot 3H_2O$. Ion current density: 0.75 $\mu A\,cm^{-2}$.

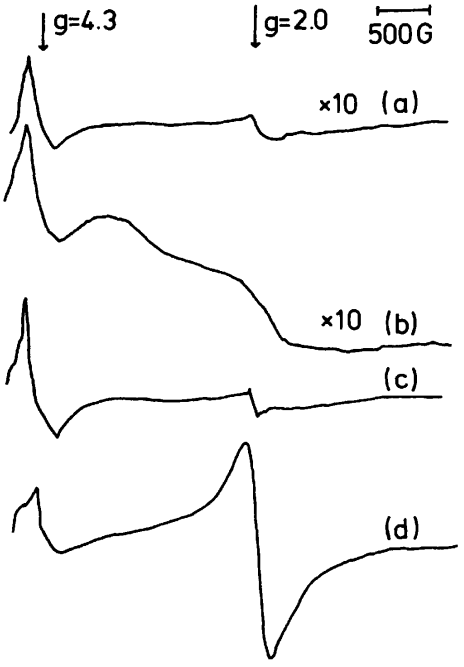

Fig. 3. EPR spectra of irradiated pellets of $K_4[Fe(CN)_6]\cdot 3H_2O$.
(a) 40 keV Ar^+-bombarded at 10 $\mu A\,cm^{-2}$ for 10 min,
(b) 40 keV Ar^+-bombarded at 10 $\mu A\,cm^{-2}$ for 30 min,
(c) 1.45 MeV H^+-bombarded at 1.5 $\mu A\,cm^{-2}$ for 10 min, (d) ^{60}Co-γ irradiated at 4×10^9 rad followed by heating at 150 °C for 30 min.

Irradiations with 0.4 or 1.6 MeV H^+ ions were also performed at the intensity of 0.6 $\mu A\,cm^{-2}$ with the results of Fig. 3 (c), similar to those obtained in the 20

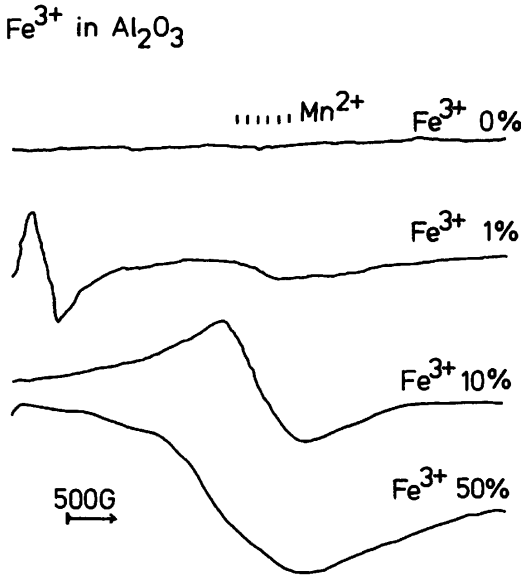

Fig. 4. EPR spectra of solid solutions of iron(III) oxide in aluminum oxide. The concentration of Fe^{3+} (*vs.* Al^{3+}): (a) 0, (b) 1, (c) 10, (d) 50%.

or 40 keV Ar^+-ion case.

γ-Irradiations at room temperature of the powder sample at doses below 10^9 rad were found to produce a line at g=4.3 alone and no other signals near at g=2.0. Further irradiations of the sample with γ-rays up to 10^{10} rad produced a single absorption line at g=2.06 of the linewidth ≈5 G at room temperature. This spectrum remained unchanged when treated at temperatures below 100 °C for an hour or so. When treated at higher temperatures, however, it disappeared to produce a strong absorption at g=2.0 with a large width as is shown in Fig. 3(d).

EPR spectra of solid solutions of aluminum oxide containing various amount of Fe^{3+} are shown in Fig. 4. Main features of the spectrum are as follows: (i) The sample of the low iron concentrations (≈1% with respect to Al) reveals an EPR absorption due to isolated Fe^{3+} ions at g=4.3, and (ii) at higher iron concentrations this spectrum is replaced by a Lorentzian signal which behaves as the absorption at g=2.0 in Fig. 1 and which has been attributed by Gesumundo *et al.*[10-12] to clusters of Fe^{3+} ions coupled by a strong exchange interaction.

Anisotropic Nature of the Line at g=2.0. The crystal type of potassium hexacyanoferrate(II) trihydrate is monoclinic, pseudo-tetragonal with lattice constants a=c=9.3 Å, b=16.8 Å, β=90°, four molecules in unit cell and space group C_{2h}^6.[13] The crystals grow in flat rectangular plates parallel to the ac plane, thus having well developed (010) faces. Energetic ions were bombarded onto a (010) plane. The EPR-absorption line at g=2.0 thus obtained was found to have an anisotropy of g factor. When the applied magnetic field is parallel to the direction of the incident beam, hereafter, denoted by b, g factor, $g(H//b)$, is around 1.98—1.99 and when the field is in the (010) plane, g factor, $g(H\perp b)$, is 2.02—2.03. The results are included in Table 1. We have verified that this anisotropic feature of the g factor is due to the direction of the Ar^+ beam and not to crystallographic anisotropy by having examined various factors which might be responsible for this anisotropy, *e.g.*, changes in the direction of the Ar^+ beam and the sizes and geometries of the sample to be bombarded, employment of the disk sample made from powders and as well as possible effects of the orientation of the specimen in the EPR cavity.

Table 1. EPR g factors and linewidths, and the relative yields of Fe^{3+} clusters from ion-bombarded $K_4[Fe(CN)_6]\cdot 3H_2O$.

Ion	Energy	$g(H//b)$[a]	$g(H\perp b)$[a]	ΔH_m	Relative yields
Ar^{2+}	1.8 MeV	1.98	2.03	140-300 G[b]	2.9
Ar^+	450 keV	1.99	2.02	100-150 G	0.23
Ar^+	20—40 keV	—	—	—	0
H^+	0.4—1.6 MeV	—	—	—	0

a) H=magnetic field; b=axis of irradiation beam. b) G=10^{-4} T.

It must be noted that the absorption at g=2.0 appearing in the sample which has been γ-irradiated at doses higher than 10^9 rad and then heated at 100—200 °C shows no anisotropy of g factor.

Secondary Ion Mass Spectrometry. When crystals of potassium hexacyanoferrate(II) trihydrate were bombarded with energetic ions, various secondary ions were emitted from the bombarded surface. Positive secondary ions were mainly composed of H^+, C^+, O^+, K^+, and Fe^+. Such ions as C^{2+}, N^+, K_2^+, and probably K_2O^+ and KFe^+ in small yields were also included. Negative secondary ions were H^-, C^-, CH^-, O^-, and a small amount of OH^-, C_2^-, and KO^-. Effects of the kinetic energy of bombarding particle were examined in the case of Ar^+ ion in the energy range of 10 keV to 1.8 MeV. The yields of emitted ions were nearly unchanged when the energy of the bombarding Ar^+ ion varied from 1.8 MeV down to 70 keV, though increased as the Ar^+-ion energy decreased to 10—30 keV. In Fig. 5 are shown the results of changing the bombarding ion while the bombarding energy and the beam intensity were maintained at 450 keV and 0.3 μA cm^{-2}, respectively.

Gas Analysis. The gas evolved by the irradiation of the complex with ^{60}Co-γ rays at the dose of 3×10^7 rad was submitted to mass analysis. While the main peaks in the mass spectrum were due to the water molecule, other peaks at mass number of 14 (N_2^{2+}), 28 (N_2^++CO^+), and 44 (CO_2^+) were remarkably significant, indicating that the ligand CN^- had been decomposed by γ-irradiation.

Discussion

When potassium hexacyanoferrate(II) trihydrate are subjected to ionizing radiations, *e.g.*, γ-rays or high-energy charged particles, many electronic processes will

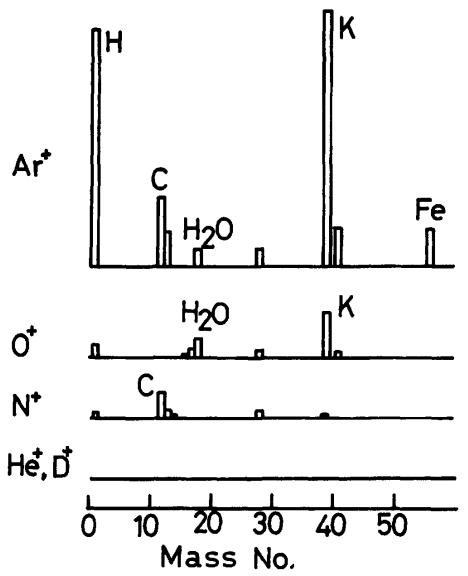

Fig. 5. Emitted positive ion spectrum from $K_4Fe(CN)_6]\cdot 3H_2O$ bombarded by various ions. Bombarding energy: 450 keV, Ion current density: 0.3 μA cm^{-2}.

occur. Among them only those processes which require a relatively small energy transfer per event have been studied from the viewpoint of chemical consequence of the initial process, the electronic transitions between d orbitals of Fe which induce the dissociation of the metal(Fe)–ligand(CN) bond and the electron transfer from metal(Fe) to ligand(CN) which results in oxidation of the Fe.[14] The oscillator strength for these electronic processes amounts only to 0.6.[15] The chemical consequence of the many other processes including inner shell and multiple excitations with a big energy transfer per event remain unstudied. In cases of the energetic particle penetrating a solid, the energy is also deposited into atomic motion, thus giving rise to a collision cascade or a thermal spike. A chemical effectiveness of the atomic motion is not clear for the present moment.[7,16,17]

Comparing the EPR spectra of Figs. 1 and 3 with those of Fig. 4, it is suggested that the spectrum at $g=4.3$ observed in the irradiated sample can be attributed to the isolated Fe^{3+} ions and that the strong absorption at $g=2.0$ to Fe^{3+}-ion clusters. The EPR spectrum of Fe^{3+}-ion clusters have been studied by many workers[10–12,18,19] and it is known that their linewidth depends on two features, the dipole–dipole interaction which produces a broadening of the line and the exchange interaction which produces a narrowing.[10,18]

γ-Irradiations. It is expected that a single and isolated electronic excitation of the complex will be annealed at the ambient temperature without any effect of radiations, since the electronic system relaxes quickly while the atoms are still at rest.[20] The results of analyzing the evolved gas, however, indicate that γ-irradiation *does* decompose the ligand or crystalline water of the sample. Two possible processes may be assumed: (i) The electron ejected in the ionization event and having kinetic energy larger than 6 eV may be captured by H_2O molecule to form H^- and OH.[21] (ii) Ionizations of inner-shell orbital followed by the Auger process and double ionization and/or excitations of cyanides would result in the atomic displacement by Coulomb explosion mechanism.[8,22,23] In either processes the decomposition of the ligands may occur. The *G* value of these processes may be estimated to be 0.1.[24]

Further irradiations at doses of 10^9 rad may produce isolated Fe^{3+} ions (≈50% ligand decomposed) the d-shell electrons of which are now free from being quenched by the presence of the ligand and are responsible for an EPR signal at $g=4.3$.

However, γ-irradiations up to 4×10^{10} rad did not produce an EPR signal due to Fe^{3+} clusters, indicating that the distances between Fe^{3+} ions in the γ-irradiated sample were too large to interact with each other by an exchange process. By heating at *e.g.* 150 °C, displacement of Fe^{3+} ions in the irradiated solid may occur to aproach each other within the distances smaller than 7 or 8 Å.[10] It is interesting that a *g* factor of an EPR absorption of the Fe^{3+} clusters thus formed is isotropic in contrast to an EPR signal of Fe^{3+} clusters formed by the Ar^+-ion bombardment.

Proton Irradiations. Most of the energy of fast protons (0.4—1.6 MeV) goes into electronic excitations, though energetic recoil atoms (C, N, and O) with kinetic energies of 10 keV or less may be created.[7] Thus, the action of a fast proton is essentially the same as that of γ-rays. The present results may be understood as such.

Ar^+-ion Bombardment. An Ar^+ ion in the energy range below *ca.* 40 keV loses most of its energy to create energetic recoil atoms (C, N, and O)[7] which in turn form collision cascades or thermal spikes. The results of Fig. 5 indicate that, among the various incident ions examined, the Ar^+ ion is most effective for the atomic displacement. Moreover, the further results showed that displacement by the energetic Ar^+ ion is most effective in the energy range of 10 to 30 keV.

By 40 keV Ar^+-ion bombardment of the complex, an EPR signal due to isolated Fe^{3+} ions alone has been observed. Further irradiations with 40 keV Ar^+ ions modified the spectrum to a one similar to that observed when the complex was heated at temperatures higher than 200 °C (Fig. 3; b).

At higher bombarding energies, the kinetic energy of Ar^+ ion goes more and more into electronic excitations.[7] Moreover, many collisions between Ar^+ ions and atoms in the solid will be highly inelastic due to inner-shell or multiple excitations which are pronounced in the energy range from 50 keV to 1 MeV.[3,5] As examples of this type of collisions, it should be mentioned: Collision of two Ar atoms (≈100 keV) produced a number of highly charged particles like Ar^{2+}, Ar^{4+}, and Ar^{5+}, apparently due to successive processes of autoionization and electron shake off after

the deposition of some 1000 eV energy into electron cloud of two Ar atoms.[25] Probably C, N, and O atoms, and especially Fe atoms will show the same effects in the case of Ar^+ bombardment at the energy higher than 100 keV. This could lead to a violent destruction of the complex, as has been discussed by Stöcklin in the case of biological compounds.[8]

In fact, the present results at Ar^+-ion bombarding energies of 450 keV or 1.8 MeV demonstrate that an EPR absorption due to Fe^{3+} clusters was obtained even at the lowest doses examined, *i.e.* 5 s irradiation at the ion current density of 0.3 $\mu A\,cm^{-2}\,s^{-1}$ which corresponds to 10^{13} Ar^+ ions cm^{-2}. At this dose, the tracks of incident Ar^+ ions probably do not overlap each other (radius of track $\approx$3 Å). Thus, one may conclude that Fe^{3+} clusters are formed even in a single track of an incident Ar^+ ion.

It should be further noted that an EPR absorption of Fe^{3+} clusters thus formed has an anisotropic g factor which is axially symmetric with respect to the direction of the incident beam (Table 1), in remarkably contrast to that obtained by thermal decomposition of heavily γ-irradiated complex.

In cases of Ar^+-ion collisions, highly inelastic excitations of Fe may be accompanied with a simultaneous momentum transfer from the incident Ar^+ ion. This would cause a production of a Fe^{3+} cluster, the structure of which retains some axially symmetric feature with respect to the direction of an incident beam.

The authors wish to thank Mr. Chiaki Kobayashi and Mr. Susumu Kanda for their kind operation of the 2 MV Van de Graaff accelerator.

References

1) J. W. T. Spinks and R. J. Woods, "An Introduction to Radiation Chemistry," John Wiley, New York (1964); A. Mozumder, "Advances in Radiation Chemistry," ed by M. Burton and J. L. Magee, John Wiley, New York (1969), Vol. 1, p. 1.

2) ICRU, "Linear Energy Transfer," Report No. 16, International Commission on Radiation Units and Measurements, Washington, DC (1970).

3) J. B. Hasted, "Physics of Atomic Collisions," Butterworths, London (1972).

4) Q. C. Kessel and B. Fastrup, "Case Studies in Atomic Physics III," ed by E. W. McDaniel *et al.*, North-Holland, Amsterdam (1974), p. 140.

5) F. T. Smith and A. Salop, "Radiation Research," ed by O. F. Nygaard *et al.*, Academic Press, New York (1975), p. 242.

6) R. L. Platzman, "Symposium on Radiobiology," ed by J. J. Nickson, John Wiley, New York (1952), Chs. 7 and 9.

7) J. Kistemaker, F. J. De Heer, J. Sanders, and C. Snoek, "Radiation Research," ed by G. Silini, North-Holland, Amsterdam (1967), p. 68.

8) G. Stöcklin, "Radiation Research," ed by S. Okada *et al.*, Tokyo (1980), p. 382.

9) K. Furukawa and S. Ohno, To be published in JAERI-M.

10) F. Gesmundo and C. De Asmundis, *J. Phys. Chem. Solids*, **35**, 1007 (1974).

11) F. Gesmundo and C. De Asmundis, *J. Phys. Chem. Solids*, **33**, 1861 (1972).

12) A. F. Reid, H. K. Perkins, and M. J. Sienco, *Inorg. Chem.*, **7**, 119 (1968).

13) K. Yamazaki and B. Inoue, "Mukikagaku-zensho," Maruzen, Tokyo (1959), Vol. 15 (2), p. 219.

14) S. Ohno, *Bull. Chem. Soc. Jpn.*, **40**, 1765, 1770, 1779 (1967).

15) H. B. Gray and N. A. Beach, *J. Am. Chem. Soc.*, **85**, 2922 (1963).

16) O. Puglisi, G. Marletta, and A. Torrisi, *Radiat. Eff.*, **65**, 251 (1982).

17) R. W. Ollerhead, J. Bøttiger, J. A. Davies, J. L'ecuyer, H. K. Haugen, and N. Matsunami, *Radiat. Eff.*, **49**, 203 (1980).

18) F. Gesmundo and C. De Asmundis, *J. Phys. Chem. Solids*, **34**, 637 (1973).

19) F. Galembeck, N. F. Leite, L. C. M. Miranda, H. R. Rechenberg, and H. Vargas, *Phys. Stat. Solidi* (a), **60**, 63 (1980).

20) F. Seitz and J. S. Koehler, "Solid State Physics," ed by F. Seitz and D. Turnbull, Academic Press, New York (1956).

21) R. N. Compton and L. G. Cristophorou, *Phys. Rev.*, **154**, 110 (1967).

22) J. Durup and R. L. Platzman, *Discuss. Faraday Soc.*, **31**, 156 (1961); *Int. J. Radiat. Phys. Chem.*, **7**, 121 (1975).

23) P. Williams, *Surface Science*, **90**, 588 (1979).

24) K. Okazaki, S. Sato, and S. Ohno, *Bull. Chem. Soc. Jpn.*, **48**, 1411 (1975); *ibid.*, **49**, 174 (1976).

25) A. Russek, *Phys. Rev.*, **132**, 246 (1963).

 © 1985 The Chemical Society of Japan Bull. Chem. Soc. Jpn., 58, 1105—1108 (1985)

Molecular Dynamics Using Internal Coordinates. I. Infrared Spectra of Sulfur Dioxide

Soichi HAYASHI,* Motohisa OOBATAKE, Tatsuo OOI, and Katsunosuke MACHIDA†

Institute for Chemical Research, Kyoto University, Uji, Kyoto 611

†*Faculty of Pharmaceutical Sciences, Kyoto University, Sakyo-ku, Kyoto 606*

(Received November 17, 1984)

A simulation method of molecular dynamics using internal coordinates for polyatomic molecule is described. The method permits intramolecular interaction to be expressed in terms of the internal coordinate, and produces translation, rotation, and vibration of molecule. As the first application, infrared spectra of sulfur dioxide both at gas and liquid phases are simulated by the method with an aid of the techniques proposed by Berens and Wilson. The spectrum at gas phase exhibits the pure rotational band and the vibrational-rotational bands for fundamental modes. The ν_1 and ν_2 vibrations show B-type band shape, and the ν_3 mode shows A-type band shape, in accord with the experimental result and the selection rule for a prolate symmetrical top which may practically represent the molecule. At liquid phase, multiple peaks due to rotational structure disappeared, and single-peaked bands are simulated as expected. The method can be extended so as to describe more realistic intermolecular interactions than pairwise atom-atom potentials.

Molecular dynamics simulation has become a powerful tool for the study of average structures and dynamic properties of molecular systems. Except for the simplest molecules,[1,2] however, molecules have been usually dealt with as rigid or partially flexible ones.[3] In order to perform a more physically realistic simulation, it may be necessary to make molecules flexible, that is, all degrees of freedom of atomic motion should be included. Because it is hard to describe the intramolecular potential by Cartesian coordinates for polyatomic molecules, it is desirable to express explicitly the potential in terms of the internal coordinates such as bond stretching, valence angle bending, out-of-plane bending, and torsion. We describe, in this paper, a simulation method satisfying the above requirements for polyatomic molecules. The method permits the calculation of molecular dynamics including all degrees of freedom, and produces translation, rotation and vibration of molecule.

As the first application of the method, infrared spectra are simulated of sulfur dioxide, which has two stretching and one bending coordinates, both at gas and liquid phases. The spectra are obtained with the aid of the techniques proposed by Berens and Wilson[1,2] who have reproduced surprisingly accurate infrared and Raman spectra of diatomic molecules from classical molecular dynamics, classical linear response theory and classical statistical mechanical ensemble averaging, with the use of simple quantum corrections. The spectrum obtained by the molecular dynamics simulation is compared with the experimental one.[4-6]

Method and Model

Molecular Dynamics. We consider a system of N atoms interacting through intra- and intermolecular potentials at a given energy and density. The force $\boldsymbol{F}_i$ on the ith atom is assumed to be the sum of the intra- and intermolecular forces, $\boldsymbol{F}_i^{\text{intra}}$ and $\boldsymbol{F}_i^{\text{inter}}$.

$$\boldsymbol{F}_i = \boldsymbol{F}_i^{\text{intra}} + \boldsymbol{F}_i^{\text{inter}} = -\frac{\partial V^{\text{intra}}}{\partial \boldsymbol{r}_i} - \frac{\partial V^{\text{inter}}}{\partial \boldsymbol{r}_i}, \quad i = 1, \cdots, N, \tag{1}$$

where V^{intra} and V^{inter} are the intra- and intermolecular potential energies, respectively, and $\boldsymbol{r}_i$ is the position expressed for each atom i by a vector whose components are along the three Cartesian coordinates.

The intramolecular potential energy V^{intra} is expressed in terms of the internal coordinates as

$$V^{\text{intra}} = \frac{1}{2}\sum_{tt'} f_{tt'} \cdot S_t \cdot S_{t'} + \frac{1}{6}\sum_{tt't''} g_{tt't''} \cdot S_t \cdot S_{t'} \cdot S_{t''} + \cdots \tag{2}$$

in which $f_{tt'}$ and $g_{tt't''}$ are the quadratic and cubic force constants, respectively, and S_t, $S_{t'}$, and $S_{t''}$ are tth, t'th, and t''th internal coodinates, respectively. The internal coordinate is related to the Cartesian displacement vector $\Delta \boldsymbol{r}_i$ by

$$S_t = \sum_{i=1}^{L} \boldsymbol{s}_{ti} \cdot \Delta \boldsymbol{r}_i \tag{3}$$

where the coefficient $\boldsymbol{s}_{ti}$ is the well known $\boldsymbol{s}$-vector determined by the geometry of the internal coordinate,[7] L is the number of the constituent atoms for the coordinate, and the dot represents the scalar product of the two vectors. Consequently one can write the intramolecular force as follows,

$$\boldsymbol{F}_i^{\text{intra}} = -\sum_{tt'} f_{tt'} \cdot \boldsymbol{s}_{ti} \cdot S_{t'} - \frac{1}{2}\sum_{tt't''} g_{tt't''} \cdot \boldsymbol{s}_{ti} \cdot S_{t'} \cdot S_{t''} + \cdots \tag{4}$$

Internal coordinates written in our program of molecular dynamics are increases in bond lengths Δr, in valence bond angles $\Delta\varphi$, in angles between a bond and a plane defined by two bonds $\Delta\theta$, and in torsion $\Delta\tau$. The $\boldsymbol{s}_{ti}$ vectors for these coordinates are calculated for every instantaneous structure of each molecule so as to take account of the higher-order terms omitted in Eq. 3 implicitly.

For the intermolecular part, we use the sum of the pairwise atom-atom potential terms of the two types,

$$V_1^{\text{inter}} = \sum_{ij} [-Ar_{ij}^{-6} + B \exp(-Cr_{ij})] \tag{5}$$

and

$$V_2^{\text{inter}} = \sum_{ij} e_i e_j / r_{ij} \tag{6}$$

where r_{ij} is the distance between the atoms i and j the index i runs over a single molecule and j over the others, and A, B, and C are parameters for the potential. The potential V_1^{inter} represents the exchange repulsion and dispersion interaction for atom pairs, and V_2^{inter} arises from the Coulomb interaction between the atomic charges e_i and e_i.

The classical trajectories $r_1(t)$, $\cdots$, $r_N(t)$ are obtained by integrating Newton's second law

$$F_i = m_i \frac{d^2 r_i}{dt^2}, \quad i = 1, \cdots, N \tag{7}$$

where m_i is the mass of the ith atom. A modified Verlet integration algorithm[8] was used with a periodic boundary condition.

Infrared Spectra. We use the same approach presented by Berens and Wilson[1] who calculated the pure rotational and vibrational-rotational absorption bands of carbon monoxide from the time history of dipole moment computed using the trajectories, classical linear response theory and classical statistical mechanical ensemble averaging, with the use of simple quantum corrections. We modified the approach so as to be applicable to oriented system. The dipole moment time history of the system $\mu_d(t)$ for the d direction is calculated by using the trajectories of the atoms and $(\partial\mu/\partial Q_i)$, where d is x, y, or z Cartesian coordinate, μ the molecular dipole moment, and Q_i is the ith normal coordinate.

The absorption spectrum for a system at equilibrium is obtained from the linear response equations:

$$\alpha_d(\omega) = \frac{4\pi^2\omega^2\beta}{3cn} I_d(\omega), \quad d = x, y, z, \tag{8}$$

and

$$I_d(\omega) = \frac{3}{2\pi}\left[\lim_{\tau\to\infty} \frac{1}{2\tau}\left|\int_{-\tau}^{\tau} dt \exp(-i\omega t)\mu_d(t)\right|^2\right], \quad d = x, y, z \tag{9}$$

in which $\alpha_d(\omega)$ is the absorption cross section as a function of angular frequency ω, $\beta=(k_BT)^{-1}$ in which k_B is Boltzmann's constant and T is the temperature, c is the velocity of light, and n is the refractive index of the medium. $I_d(\omega)$ is defined as the absorption band shape, and may be computed in the form of the power spectrum by fast Fourier-transform techniques. The equations are written in the form applicable to oriented systems and can be used for isotropic systems by taking an average of the three $\alpha_d(\omega)$.

For the comparison with an experimental spectrum, it is necessary to obtain an ensemble average of spectra computed from very small system consisting of an order of several hundreds atoms, from very short time period, and especially from weakly interacting system such as low pressure gas phase. Therefore, for gas phase, many sets of the initial values are chosen randomly from the Maxwell-Boltzmann distribution. In order to satisfy a thermal equilibrium condition under a given temperature with the Maxwell-Boltzmann distribution, initial values of translational velocity and angular momentum of molecule and amplitude of each fundamental vibrations are chosen from normal random numbers. On the other hand, initial translational and rotational coordinates of molecule and phase of each fundamental vibrations are chosen from uniform random numbers. For liquid phase where intermolecular interaction must be dominant, the final values in one period of the time history are used as the initial values of the next.

Quantum correction for the pure rotational band contour is usually small and is

$$I^Q(\omega)/I^C(\omega) = \frac{\sinh(\beta\hbar\omega/2)}{\beta\hbar\omega/2} \tag{10}$$

in which the superscripts Q and C indicate quantum and classical, respectively, and $\hbar=h/2\pi$ where h is Planck's constant. The correction for the vibrational band is the frequency shift of $-4\pi r_e x_e$ due to anharmonicity in the potential. The rotational lineshape correction for a rotational-vibrational band is achieved by multiplying the classical band by $\exp[\beta\hbar(\Delta\omega)/2]$, in which $\Delta\omega$ is the frequency measured from the center of the vibrational band. For the liquid phase spectrum, no quantum corrections were applied.

Resolution and Frequency Range. As the resolution, we employed the most popular criterion of the full-width at half-height (FWHH). The minimum value of the FWHH ($\tilde{\nu}_{1/2}$), *i.e.* resolution, in a calculated spectrum depends on the time of one period of the time history (Δ) as follows:

$$\tilde{\nu}_{1/2} = \frac{1}{c\Delta}. \tag{11}$$

In practice, however, the resolution is lowered by an apodization (window) function,[9] which must be used to avoid distortion of the spectra caused by the use of finite time history.

Frequency range (0—$\tilde{\nu}_{\max}$) depends on the sampling time interval (Δt) and is given by

$$\tilde{\nu}_{\max} = \frac{1}{2c\Delta t}. \tag{12}$$

For example, when Δt is 1/1024 psec, $\tilde{\nu}_{\max}$ is 17067 cm^{-1}.

Model. As the first application of the molecular dynamics method using internal coordinates, a simple model of gaseous and liquid systems was adopted. The systems consist of 125 sulfur dioxide molecules, periodic in three dimensions (x, y, z). The box sizes are 3.322^3 nm^3 for gas phase, and 0.419^3 nm^3 for liquid phase. The SO bond length and OSO bond angles were assumed to be 1.43 Å and 119.05°, respectively.[10] The atomic charges on the S and O atoms were estimated from the observed values of the dipole moment;[10] $e_s=-2e_o=0.46$ in the electronic charge unit.

For the SO stretching and OSO bending harmonic force constants (k_{st} and k_{bend}/l^2) of 9.97 and 0.81 mdyne/Å respectively, were taken from the literature values.[11]

Table 1. Parameters of the nonbonded atom–atom interaction

Atomic pair	A (kcal·Å^6·mol^{-1})	$B\times10^{-3}$ (kcal·mol^{-1})	C (Å^{-1})
S···S	1430	220.8	3.62
O···O	800	745.9	4.55
S···O	1070	405.9	4.09

The parameters A, B, and C used in the Eq. 5 for the S···S, O···O, and S···O intermolecular atom-atom interactions were listed in Table 1.[11] The summation limit is placed at the distance of 8.15, 7.35, and 6.85 Å for the V_1^{inter} of the S···S, S···O, and O···O, respectively, and 16 Å for the V_2^{inter}. To reduce the error in the use of truncated potentials, the shifted force potentials were adopted.[12]

Although V_2^{inter} was calculated by the fixed charge model, the dipole moment time history of the system is evaluated by using the $(\partial\mu/\partial Q_i)$ of 0.780, −0.820, and 2.138 for ν_1, ν_2, and ν_3, respectively, in the unit of D amu$^{1/2}$Å^{-1}.[13] Normal coodinates are obtained from the following relation,

$$\boldsymbol{Q} = \tilde{\boldsymbol{L}}_x \boldsymbol{M} \boldsymbol{X}_p \qquad (13)$$

where $\tilde{\boldsymbol{L}}_x$ denotes the inverse matrix of the transformation matrix, $\boldsymbol{M}$ is a diagonal matrix consisting of the mass of constituting atoms, and $\boldsymbol{X}_p$ is a matrix of Cartesian displacement coordinates with respect to the coordinate system of principal axes of moment of inertia. The calculation was carried out using a FACOM M-180 II AD computer of the Institute for Chemical Research, Kyoto University. The calculations for one psec time history of the gaseous and liquid systems required 85 and 107 min of the computer, respectively.

Results and Discussion

Figure 1 demonstrates the simulated infrared spectra for the gas phase sulfur dioxide at 320 K from classical molecular dynamics using internal coordinates, and the technique proposed by Berens and Wilson.[1] The spectra were obtained by averaging over 7500 single-molecule 8 psec time histories. Ensemble average were taken over 15 runs of 42 psec duration in which initial coordinates and velocities were different and first 10 psec are discarded for thermal equilibrium. The value of the resolution is 4.17 cm^{-1} from Eq. 11, and becomes to be 6.15 cm^{-1} by using the Gaussian apodization function.[9] As one of the moment of inertia (I_A) is quite smaller than the other two (I_B and I_C), as listed in Table 2, the molecule may be regarded as a prolate symmetrical top molecule. The ν_1 and ν_2 vibrations, whose directions of transition moments are parallel to the B axis, show B-type band shape, and the ν_3 mode, whose direction of the transition moment is parallel to the A axis, shows A-type band shape, in accord with the experimental result.[5] This is consistent with the selection rule for symmetrical top molecule. The band shape and the frequency of about 50 cm^{-1} for the pure rotational band are quite similar to those of the observed spectrum.[14] The integrated intensities and standard deviations for the simulated spectrum are 24.8±5.0, 30.5±9.6, and 180.8±47.5 km mol^{-1} for ν_1, ν_2, and ν_3, fundamental bands of gaseous sulfur dioxide, respectively, and agree with the corresponding values observed of 20.6—26, 25.2—28, and 188—197 km mol^{-1}.[15–17]

Figure 2 shows the simulated infrared spectra of liquid phase sulfur dioxide at 230 K on average. The spectra were obtained by averaging over 7500 single molecule 4 psec time histories. The value of the resolution is 8.34 cm^{-1} from Eq. 11, and 12.3 cm^{-1} from the Gaussian appodization function.[9] The spectrum shows that the multiple peaks observed at gas phase disappear at liquid phase, and single-peaked bands are found at 1172, 521, and 1359 cm^{-1} for ν_1, ν_2, and ν_3 respectively. Statistical noises appeared typically at peaks of the lowest bands seen in Figs. 1 and 2, are due

Table 2. Moment of inertia of sulfur dioxide[a]

I_A	I_B	I_C
1.38	8.13	9.53

a) in 10^{-43}·g·m^2

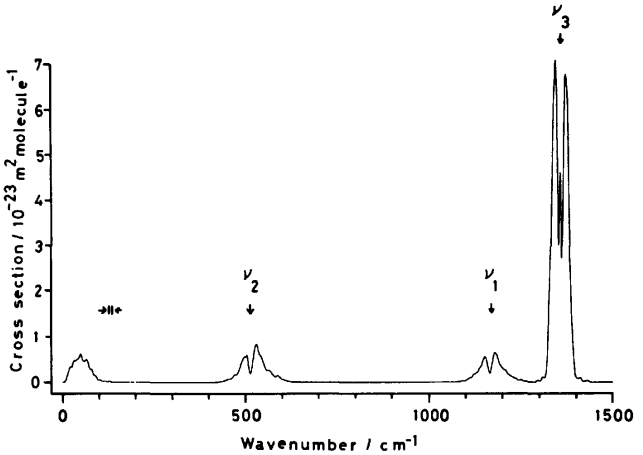

Fig. 1. Infrared spectrum for gas phase sulfur dioxide at 320 K on average.

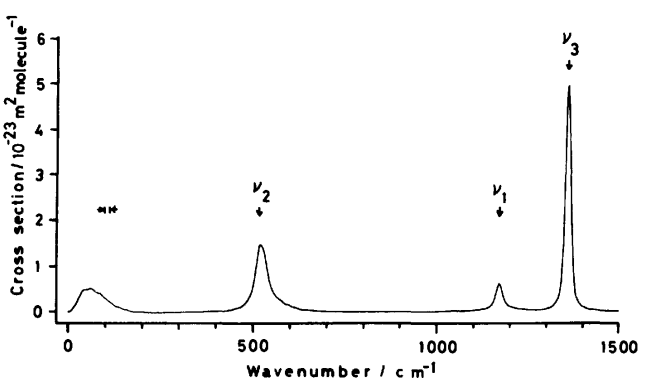

Fig. 2. Infrared spectrum for liquid phase sulfur dioxide at 230 K on average.

to ensemble sampling with only 60 runs for gas and liquid phases. Much more prolonged computation will improve the shapes of peakes, thus enabling the more detailed analysis.

Conclusion

A simulation method of molecular dynamics using internal coordinates for polyatomic molecule is proposed, and was applied to a simulation of the infrared spectra of sulfur dioxide both at gas and liquid phases. The frequencies of the fundamental vibrations of the spectra agree with those calculated by normal coordinate analysis. The bands of the ν_1 and ν_2 vibrations show B-type band shape, while that of the ν_3 mode shows A-type band shape in accordance with the selection rule. At liquid phase, the multiple peaks due to rotational structure disappeared, and single peaked bands are simulated.

The method using internal coordinates can be extended so as to describe more realistic intermolecular interactions containing multibody effects, as well as intramolecular potential, than pairwise atom-atom potentials. Although potential surfaces of multibody systems, especially in chemical reaction systems, are usually complicated, these are able to be expressed by using the four kinds of coordinates, Δr, $\Delta\varphi$, $\Delta\theta$, and $\Delta\tau$.

The authors wish to thank Dr. Y. Kataoka and Dr. K. Ishizuka of this university for their valuable discussions.

References

1) P. H. Berens and K. R. Wilson, *J. Chem. Phys.*, **74**, 4872 (1981).
2) P. H. Berens, S. R. White, and K. R. Wilson, *J. Chem. Phys.*, **75**, 515 (1981).
3) For example, P. von der Ploeg, and H. J. C. Berendsen, *J. Chem. Phys.*, **76**, 3271 (1982).
4) T. Nakanaga, S. Kondo, and S. Saëki, *J. Mol. Spectrosc.*, **81**, 413 (1980).
5) R. D. Shelton, A. H. Nielsen, and W. H. Fletcher, *J. Chem. Phys.*, **21**, 2178 (1953).
6) R. H. Maybury, S. Gordon, and J. J. Katz, *J. Chem. Phys.*, **23**, 1277 (1955).
7) E. B. Wilson, Jr., J. C. Decius, and P. C. Cross, "Molecular Vibrations," McGraw-Hill, New York (1955).
8) D. Beeman, *J. Comp. Phys.*, **20**, 130 (1976).
9) F. J. Harris, *Proc. IEEE*, **66**, 51 (1978).
10) B. Post, R. S. Schwartz, and I. Fankuchen, *Acta Cryst.*, **5**, 372 (1952).
11) Y. Kuroda, and K. Machida, *Bull. Chem. Soc. Jpn.*, **49**, 1475 (1976).
12) W. B. Street, D. J. Tildesley, and G. Saville, "Computer Modeling of Matter," by P. Lykas, ACS Symposium series (1978), p. 144.
13) G. C. Tejwani, K. Fox, and R. J. Corice, Jr., *Chem. Phys. Letters*, **18**, 365 (1973).
14) R. J. Larkin, R. W. Lovejoy, P. M. Silvaggio, and R. W. Boese, *J. Quant. Spectrosc. Radiat. Transfer*, **25**, 25 (1981).
15) K. Kim and W. T. King, *J. Chem. Phys.*, **80**, 969 (1984).
16) A. J. Von Straten and W. M. A. Smit, *J. Mol. Spectrosc.*, **62**, 297 (1976).
17) C. Secroun, A. Barbe, and P. Jouve, *J. Mol. Spectrosc.*, **45**, 1 (1973).

Synthetic Inorganic Ion-exchange Materials. XXXVIII. Acid-base Properties of a Cryptomelane-type Hydrous Manganese(IV) Oxide and Some Chromatographic Applications

Masamichi Tsuji* and Mitsuo Abe
Department of Chemistry, Faculty of Science, Tokyo Institute of Technology, 2-12-1, Ookayama, Meguro-ku, Tokyo 152
(Received July 12, 1984)

The pH titration curves of a cryptomelane-type hydrous manganese(IV) oxide(CRYMO) apparently showed a dibasic Brönsted-acid towards Li^+, Na^+, K^+, and Rb^+ ions and a monobasic Brönsted-acid towards Cs^+ ions, instead of an amphoteric character, using a mixed solution of alkali metal nitrate and nitric acid or each hydroxide with the ionic strength of 0.1. The apparent ion-exchange capacities(meq/g) of alkali metal ions increased in this order: $Li^+(0.50)<Na^+(0.55)<Cs^+(0.85)<Rb^+(1.00)<K^+(1.10)$ at pH 2 and $Cs^+(1.20)<Rb^+(1.72)<Na^+(1.78)<Li^+(1.80)<K^+(1.81)$ at pH 10. The point of zero charge(PZC) of CRYMO was estimated to be much lower than 2. The unusual selectivity for K^+ and Rb^+ ions can be successfully applied to some ion-exchange separations: *e.g.*, the removal of K^+ ions from $NaNO_3$ and $NaMnO_4$ solutions, the removal of Rb^+ ions from a $CsNO_3$ solution, and the selective uptake of K^+ ions from seawater.

An ion-exchange property has been known for a long time in manganese(IV)-oxide minerals.[1-3] Hydrous manganese(IV) oxide is considered to be a multifunctional ion-exchanger with an amphoteric nature.[4] The colloid-chemical properties of synthesized hydrous manganese(IV) oxides have been investigated by many authors.[5-9] The PZC or isoelectric points (IEP) of hydrous manganese(IV) oxides have been reported to change depending on the modifications.:[10] Mn(II)-manganite(1.8 ± 0.5)<δ-type(2.8 ± 0.3)<α-type(4.5 ± 0.5)<γ-type(5.5 ± 0.2)<β-type(7.3 ± 0.2). Of these modifications, α- and γ-type manganese(IV)-oxide minerals exhibit a relatively large ion-exchange capacity (0.6 meq/g of MnO_2 at pH 11).[4] Hydrous manganese(IV) oxides show only cation-exchange properties at pH>1.[11]

Recently, much attention has been paid to manganese(IV) oxides as scavengers in analytical chemistry and nuclear-waste processing; they have attracted this attention because of their high selectivities towards certain elements and their stability against various chemicals or the strong fields of various radiations.[11-17]

The present authors have reported that a cryptomelane-type hydrous manganese(IV) oxide behaves as a so-called ion-exchange material. It shows an excellent selectivity towards alkali and alkaline earth metal ions with an effective ionic radius (EIR)[18] of about 1.4 Å (1 Å=0.1 nm).[19] The ion-exchange selectivity for micro-amounts increased in this order: $Li^+<Na^+<Cs^+\ll Rb^+$, K^+ for the alkali metal ions and $Mg^{2+}<Ca^{2+}<Sr^{2+}<Ba^{2+}$ for the alkaline earth metal ions. This performance could be successfully utilized for the separation of micro-amounts of Ca^{2+} or Sr^{2+} ions from large amounts of K^+ or Rb^+ ions respectively.[20] This behavior is very different from that of the hydrous manganese(IV) oxides reported by other authors.[4]

This paper will describe the acid-base properties of the CRYMO and some chromatographic applications.

Experimental

Ion-exchange Materials and Characterization. The CRYMO in the H^+ form was prepared as has been described previously.[19] The CRYMO was identified by an X-ray powder analysis and thermal studies (TG and DTA). The X-ray powder diffraction and the thermal studies were carried out by using a JEOL-7E diffractometer and a Rigaku Denki thermal analyzer, Model 8001, with a heating rate of 20 °C/min respectively. The characteristics of the product obtained showed a good agreement with those reported previously:[19] the chemical composition was $MnO_2 \cdot 0.28H_2O \cdot 0.003K_2O$, and the lattice constants (a_o and c_o) were 9.77 Å and 2.85 Å respectively in the tetragonal system.

pH Titration Curve. An aliquot of the sample solution(12.5 cm^3), adjusted to the ionic strength of 0.1 with MNO_3 and HNO_3 or MOH (M=Li, Na, K, Rb, and Cs), was equilibrated with the CRYMO in the H^+ form (0.125 g) at 30 ± 0.5 °C. After the equilibration, the metal ion concentration and the pH of the solution were determined. The metal concentration was determined as follows: A 10 cm^3-aliquot of the equilibrated solution was neutralized with the standardized 0.05 M (1 M=1 mol dm^{-3}) NaOH or HNO_3; it was then percolated through a Dowex 50W-X8 cation-exchange resin column in the H^+ form. After the column had been washed with demineralized water (>10^6 S cm^{-1}) until the effluent was neutral, the amount of H^+ ions liberated by the CRYMO was determined. Thus, the equilibrium concentration of the M^+ ions was deduced by subtracting the amount of NaOH used for neutralization from the amount of H^+ ions titrated. The amount of M^+ ions exchanged was determined from the difference between the initial and equilibrated concentrations.

Preparation of CRYMO in the Na^+ Form. The CRYMO in the H^+ form was converted into the Na^+ form by charging a 0.1 M $NaNO_3$ solution onto the top of a CRYMO column in the H^+ form until the pH of the effluent attained that of the feed (pH 7). The column was washed with water and used in the subsequent experiments.

Column Experiment. A relatively small column (4.6 cm×0.5 cm I.D. or 3 cm×0.4 cm I.D.) of the CRYMO in the H^+ or Na^+ form was used at the ambient temperature. The flow rate was regulated by means of a high pressure pump (Nihon Seimitsu Kagaku, Model NSP-800-5UDX). The effluent was collected by using a drop-counting type fraction collector (Ohtake Works, Model UM-200).

Determination of Alkali and Alkaline Earth Metals. The alkali and alkaline earth metal ions were determined by

emission and absorption spectrophotometries respectively by means of a Varian-Techtron atomic absorption spectrometer, Model 1100. The standard addition method was used in both cases.

Optical Spectrophotometry. A Shimadzu double beam optical spectrophotometer, Model UV-150-02, was used for the identification of the Mn(VII) ions.

Reagents. All the chemicals were of an analytical grade from Wako Pure Chemical Ind. Ltd. (Japan), except for Rb_2CO_3, Cs_2CO_3, and $NaMnO_4 \cdot H_2O$. The two carbonates (>99%) and $NaMnO_4 \cdot H_2O$ (>97% purity) were obtained from Soekawa Chemicals (Japan) and Aldrich Chemical Company, Inc. (USA) respectively. They were employed without further purification. Rubidium and cesium hydroxide solutions were prepared by percolating the nitrate solution through a Dowex2-X4 anion-exchange resin column in the OH^- form(2.5 cmϕ×20 cm) with bubbling N_2 gas. The seawater used was collected 1 km off shore at Takamatsu, Kagawa Prefecture, Japan, and filtered through a membrane filter (0.45 μm pore). The chemical composition of the seawater sample was 0.464 M Na^+, 0.00995 M K^+, 0.0492 M Mg^{2+}, and 0.00983 M Ca^{2+} ions.

Results and Discussion

pH Titration Curves. The pH titration curves on the CRYMO in the H^+ form showed a break point at pH 7, except in the case of the Cs^+ ions(Fig. 1). It behaves apparently as a dibasic acid towards these alkali metal ions, while apparently as a monobasic acid for Cs^+ ions. A purple color was observed in a small amount of Mn(VII) ions when the H^+ ions in the CRYMO were exchanged with any alkali metal ions except Cs^+ ions at pH values higher than 10. The CRYMO was broken into fine particles when the H^+ ions in the CRYMO were exchanged with Cs^+ ions at pH values higher than 10. The pH titration curves indicate that there are stronger Brönsted-acid sites in the CRYMO than those of hydrous oxides of other quadrivalent metals, such as Si, Ti, Sn, and Zr.[11]

The amounts of the replaceable protons responsible for the ion-exchange reactions can be estimated by the differences between the blank run (the dotted line) and each titration curve. The apparent capacity thus determined agreed well with the amount estimated from the titration curve (Fig. 2). These results indicate that the cation uptake obeys the ion-exchange reaction in the pH range studied. The ion-exchange capacity increases in this order: $Li^+ < Na^+ < Cs^+ < Rb^+ < K^+$ at pH values lower than 5. The affinity sequence agrees well with our earlier results in acidic media.[19] The apparent capacity of Cs^+ ions almost reaches a saturated value at pH 5. It results in a different sequence of the affinity: $Cs^+ < Rb^+ < Na^+ < Li^+ < K^+$ at pH 10 because of the large steric effect for large cations. The largest ion-exchange capacity (2.4 meq/g) was obtained for Li^+ ions at pH> 11. This value is quite large compared with those of the α- and γ-types hydrous manganese(IV) oxide (0.6 meq/g) reported by other authors.[4]

This ion-exchange behavior can be well understood on the basis of the crystal structure of a cryptomelane.[21] It has been considered that the unit cell contains eight manganese ions (chiefly quadrivalent), with vacancies at two positions of (0, 0, 1/2) and (1/2, 1/2, 0), and sixteen oxygen ions. The two sites are surrounded by eight oxygen ions at a distance of 2.74 Å, forming a cube, and by four oxygen ions at a greater distance of 3.31 Å, forming a square at the same z level as the vaca-

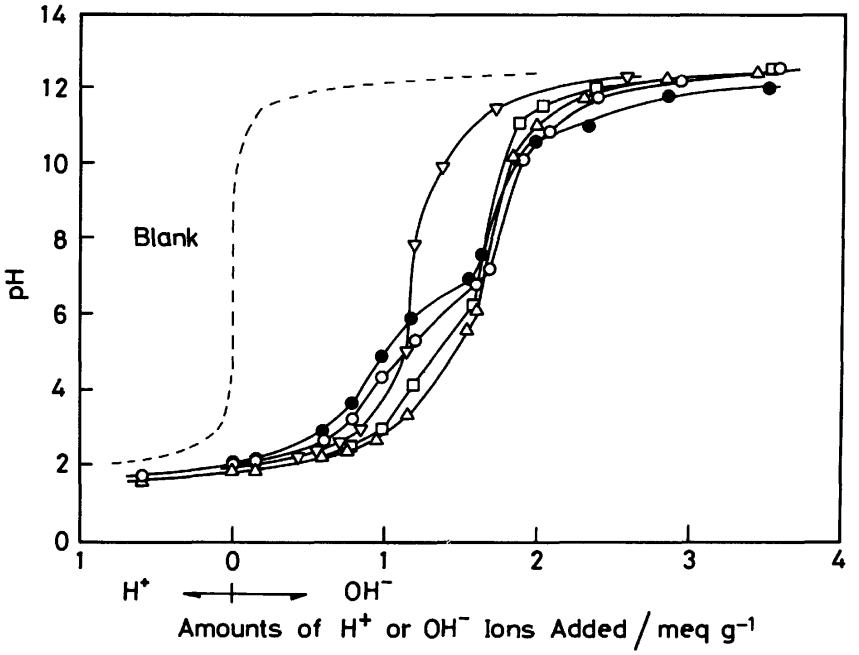

Fig. 1. pH Titration curves of the CRYMO in the H^+ form by various bases. CRYMO: 0.125 g, Soln.: 0.1 mol dm^{-3} (MNO_3+HNO_3) or (MNO_3+MOH) (M=Li(●), Na(○), K(△), Rb(□), and Cs(▽)), Total vol. of soln.: 12.5 cm^3, Temp.: 30±0.5°C.

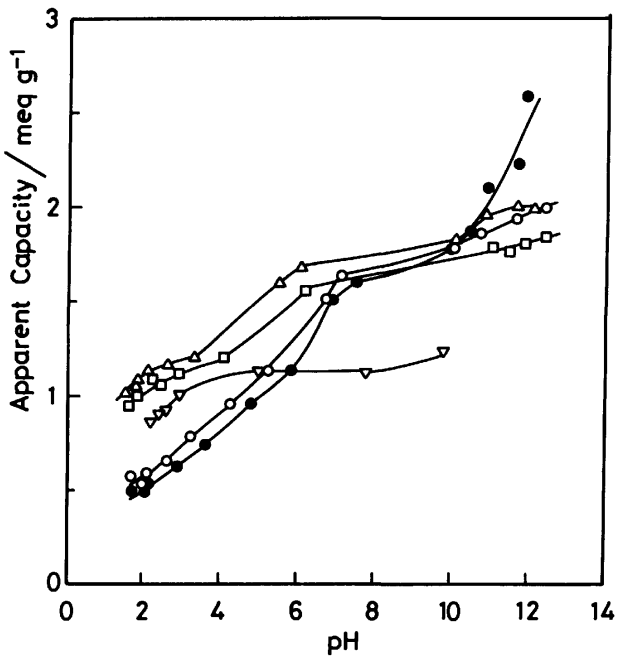

Fig. 2. pH Dependence of the apparent capacity for the alkali metal ions on the CRYMO. The experimental conditions and the marks are the same as in Fig. 1.

ncy. Both ion-exchange sites have the same electrostatic field and are 7.05 Å apart. The sites are estimated to be 2.68 Å long along the a axis and 2.84 Å long along the c axis, based on r ($^{VI}O^{2-}$)=1.40 Å. Hence, because of the electrostatic repulsion, Cs^+ ions with a radius of 1.88 Å cannot occupy all the ion-exchange sites, while Li^+ ions with a radius of 0.74 Å can enter almost all the ion-exchange sites.

The electron configuration of alkali metal ions as well as of alkaline earth metal ions is represented by s^2p^6. The metal ions of this group are less polarized under the influence of the electrical field of the crystal. For this reason, K^+ and Rb^+ ions, with about the same dimentions as the size of the ion-exchange site, are selectively exchanged.

It has been considered that the charges of the entering cations are compensated for by this reaction:[22]

$$V_2Mn_8O_{16} + M^{n+} \rightleftharpoons (V_{2-x}, M_x)Mn^{IV}_{8-y}Mn^{II}_yO_{16}$$

In fact, however, the sorptions of alkali, alkaline earth, and divalent transition-metal ions obey the stoichiometric ion-exchange reaction.[19,23] No such reduction occurs when these metal ions are sorbed. Instead, equivalent amounts of H^+ ions are released. Therefore, H^+ ions lie at the positions of the vacancy considered above.

The strength of hydrous oxide as an acid or base can be well described by the corresponding dissociation constants:[24,25] at a high pH:

$$RH \rightleftharpoons R^- + H^+,$$

$$K_{R^-} = \frac{[R^-][H^+]}{[RH]}$$

and
at a low pH:

$$R'OH \rightleftharpoons R'^+ + OH^-,$$

$$K_{R'^+} = \frac{[R'^+][OH^-]}{[R'OH]}$$

or

$$R'OH + H^+ \rightleftharpoons R'OH_2^+,$$

$$K_{R'OH_2^+} = \frac{[R'OH_2^+]}{[R'OH][H^+]}$$

where R or R′ denote the framework of the exchanger. The densities of the "surface" charges, $[R^-]$, $[R'^+]$, and $[R'OH^+_2]$, are often determined by titrating with alkali metal nitrates, and the corresponding hydroxide having less complexing.[6] The PZC is defined by a pH value yielding a zero-charge surface,[25,26] *i.e.*, giving the following relation:

$$[R^-] = [R'^+] + [R'OH_2^+]$$

The pH titration curve shows that the CRYMO releases H^+ ions equal in amount to the alkali metal ions exchanged. Even at pH 2, no appreciable uptake of nitrate ions was observed. Therefore, $[R'^+]$ or $[R'OH^+_2]$ is nearly null at a pH value of 2, and the PZC of the CRYMO can be estimated to be considerably lower than 2.

Healy *et al.* have reported that a cryptomelane-type hydrous manganese(IV) oxide showed a PZC value of 4.5±0.5.[10] Their specimen showed an X-ray pattern corresponding exactly with that given by Butler and Thirsk,[27] whose samples have larger lattice constants (a_o 9.85 Å, c_o 2.852 Å) than those reported by the present authors. The K^+ ions in this specimen cannot be removed by washing with water alone. When a considerable amount of K^+ ions is present in the material, increased lattice constants can be observed.[19] Hence, in their sample, a considerable amount of the dissociable protons can be inferred to be replaced by K^+ ions. For this reason, their sample probably showed a larger PZC value.

Selective Uptake of a Small Amount of Alkali Metal Ions from a Large Amount of Alkali Metal Salts by Using the Batch Technique. Generally, the synthetic inorganic ion-exchange materials are more stable against an attack of oxidizing reagents than the organic ion-exchange resins. The CRYMO was stable for a week in such oxidizing reagents as Cr(VI) and Mn(VII) salts solution containing a 1 M H_2SO_4 solution at room temperature. The K^+ impurity in a 0.5 M $NaMnO_4$ solution containing 1 M H_2SO_4 could be removed using the CRYMO (Fig. 3). An X-ray diffraction pattern of the CRYMO used showed no change in the crystalline modification, and repeated use is possible by removing the K^+ ions sorbed.

The uptake of alkali and alkaline-earth metal ions from seawater was determined by changing the ratios of the volume of seawater to the weight of CRYMO (*R* value) (Table 1). The total uptake (Na^+, K^+, Mg^{2+}, and

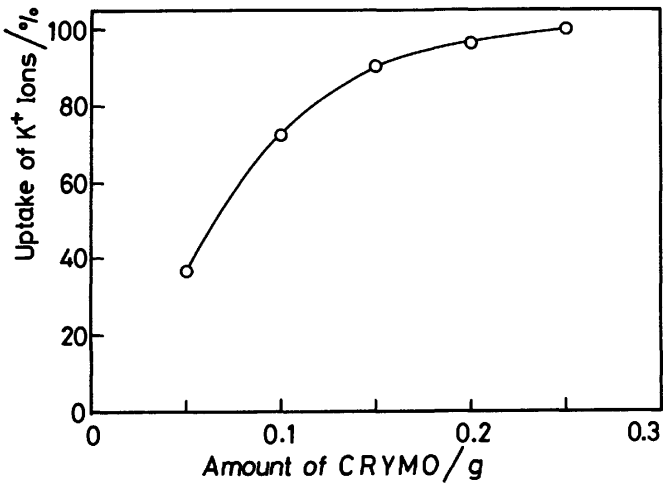

Fig. 3. Selective removal of K^+ ions from 0.5 mol dm^{-3} $NaMnO_4$ containing 1 mol dm^{-3} H_2SO_4 using the CRYMO by the batch technique. Concn. of K^+ ions: 3.65×10^{-3} mol dm^{-3}, Total vol: 25.0 cm^3. Temp: 30±0.5 °C. Immersing time: 4 d.

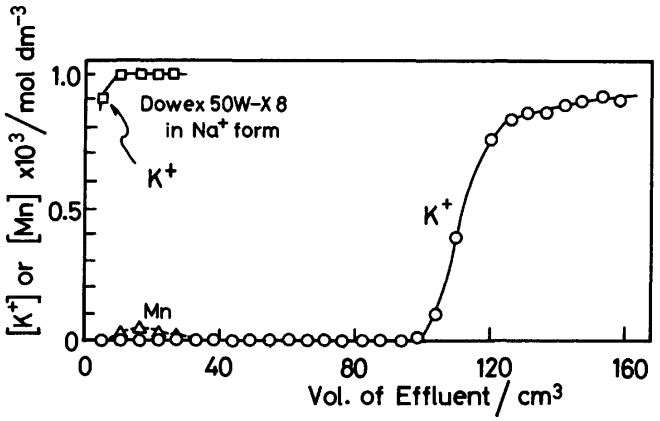

Fig. 4. Selective removal of K^+ ions from $NaNO_3$ solution with the CRYMO column in the Na^+ form. Column: 3×0.4 cm I.D. (100—200 mesh size, 0.50 g), Feed: (1 mol dm^{-3} $NaNO_3$+10^{-3} mol dm^{-3} KNO_3) mixed solution. Flow rate: 0.5—0.6 cm^3/min. □, ○: K^+ ion concn. in the effluent from Dowex 50W-X8 and CRYMO columns, respectively. △: Total manganese ions released to the soln.

Ca^{2+}), 1.3—1.6 meq/g, is nearly equal to the cation content of the CRYMO in the Na^+ form (1.32 meq $(Na^+ + K^+)$/g). Hence, a decreased amount of Na^+ ions in the CRYMO is compensated for by the K^+, Mg^{2+}, and Ca^{2+} ions through the ion-exchange process with Na^+ ions. The uptake of K^+ ions increases with an increase in the R values and attains about a constant value of 0.65 meq/g at the R value of 167.

The concentration factor was estimated by using the following equation by Abe and Hayashi[28] (Table 1):

$$f^{M}_{Na} = \frac{[(M)/(Na)]_{CRYMO}}{[(M)/(Na)]_{seawater}}$$

where M denotes K, Mg, and Ca.

The value of f^{K}_{Na} attains about 85 at the R value of 167, while f^{Ca}_{Na} gives the maximum of 55 at the R value of 100. At the pH values and metal concentrations studied, small f^{Mg}_{Na} values were obtained; hence, the selectivity for Mg^{2+} ions is slightly larger than for Na^+ ions. The results are in good agreement with those of our earlier report.[19]

Selective Removal of Alkali Metal Impurities from Salts of Alkali Metals by Using the Column Technique. The frontal chromatographic technique is one of the simplest procedures for the separation of a small amount of an element from a large amount of other elements. However, this technique is not very useful for the separation of a small amount of K^+ ions from a high concentration of Na^+ ions on a Dowex50W-X8 column because of its low selectivity. It is, however, evident from the selectivity studies of the CRYMO in our earlier report[19] that the separation of K^+ ions from Na^+ ions is feasible. The separation can be achieved with a much larger volume of the $NaNO_3$ solution containing 10^{-3} M K^+ ions on the CRYMO than that on Dowex 50W-X8 (Fig. 4).

K^+ ions in the feed solution were retained quantitatively on the column up to 97 cm^3. A faint purple color was observed in the effluent at the early stage of the injection of the feed. The chemical species of the colored component could be assigned spectrophotometrically as Mn(VII) ions. In the final stage, a large gas bubble generated by an unknown cause did not allow the percolation of the feed.

An unusual selectivity for Rb^+ ions on the CRYMO was applied to the separation of a micro-amount of Rb^+ ions from a 1 M $CsNO_3$ solution (Fig. 5). A trace amount of Rb^+ ions ($<10^{-6}$M) leaked out from the column up to 107 cm^3 of the effluent. The purified cesium nitrate (effluent up to 107 cm^3) showed an impurity level lower than 10^{-6} M for both Rb^+ ions and the total manganese. At 110 cm^3 of the effluent,

Table 1. Uptake of metal ions from seawater[a] by the CRYMO[b]

R[c]	Equil.	Uptake(meq/g)				Total uptake	Concentration factor		
Value	pH	Na^+	K^+	Mg^{2+}	Ca^{2+}	(meq/g)	f^{K}_{Na}	f^{Mg}_{Na}	f^{Ca}_{Na}
25	6.33	0.740	0.289	0.206	0.203	1.43	18.2	2.62	13.8
50	6.32	0.501	0.445	0.095	0.439	1.47	41.4	1.78	41.3
100	6.38	0.436	0.612	0.111	0.512	1.67	65.5	2.40	55.6
125	6.70	0.381	0.650	0.088	0.199	1.32	79.7	2.17	24.7
167	6.70	0.361	0.656	0.052	0.220	1.29	84.9	1.35	28.8

a) Initial pH of seawater used: 7.74. b) Cation contents of the CRYMO in the Na^+ form used: Na^+; 1.29 meq/g, K^+; 0.034 meq/g. c) R value: ratio of volume of seawater to weight of exchanger in cm^3/g.

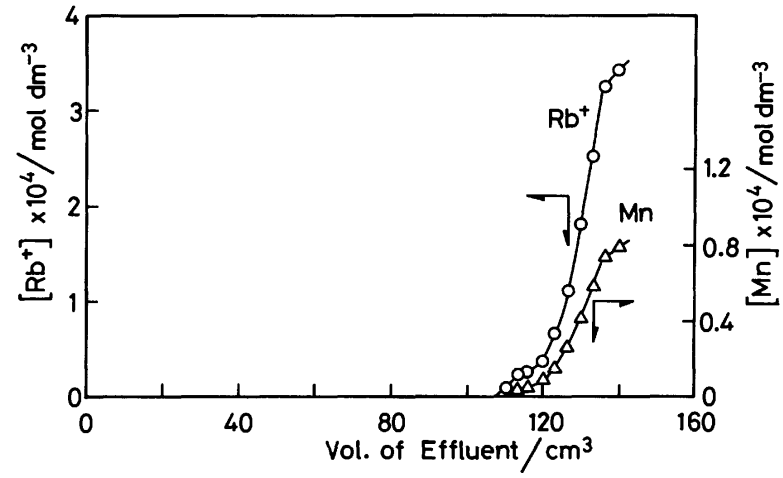

Fig. 5. Selective removal of Rb^+ ions from 1 mol dm^{-3} $CsNO_3$ solution by using the CRYMO column in the H^+ form. Column: 4.6×0.5 cm I.D. (100—200 mesh size, 1.0 g). Feed: 1 mol dm^{-3} $CsNO_3$+8.8× 10^{-4} mol dm^{-3} $RbNO_3$. Flow rate: 0.2 cm^3/min. △: Total manganese ions released to the solution by the CRYMO.

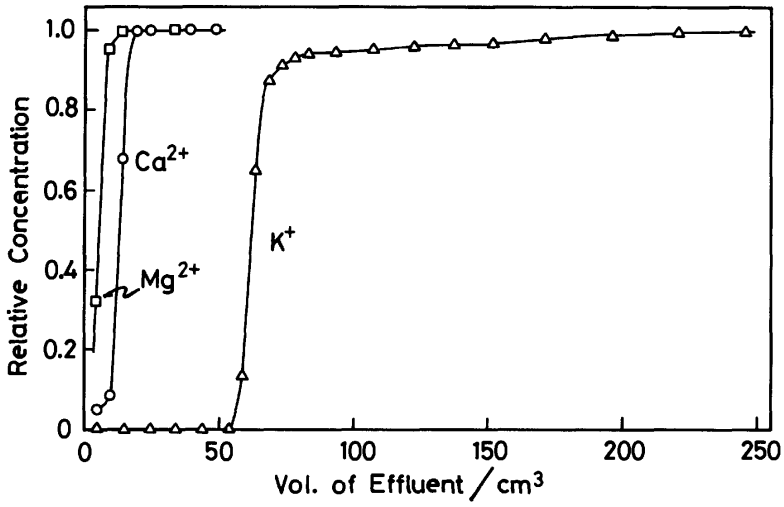

Fig. 6. Breakthrough behavior of metal ions in seawater on the CRYMO column. Column: 4.6×0.5 cm I.D. (100—200 mesh size, 1.0 g). Flow rate: 0.2 cm^3/min. The ordinate shows the concentration in the effluent relative to each metal ion concentration in seawater.

Mn(VII) ions were released from the column. Thus, commercial Cs salts can be very effectively purified by the use of the CRYMO column.

An effective separation of K^+ ions from seawater using a commercial cation-exchange resin is usually difficult because of the relatively low separation factor for K^+ to Na^+ ions, as has been pointed out above. The K^+ ions in seawater were collected batchwise as insoluble organic or inorganic compounds.[29,30] However, an effective separation cannot be expected using such a method. The separation technique using the CRYMO may give a better one.

The ion-exchange column technique allows a continuous operation, which is much superior to the batchwise process in terms of time and space. The breakthrough behavior for K^+, Mg^{2+}, and Ca^{2+} ions was studied by charging seawater continuously onto the top of the column of CRYMO in the Na^+ form (Fig. 6). Metal ions were eluted in this order: Mg^{2+}< Ca^{2+}<K^+. The breakthrough capacity showed 0.54 meq/g. The amount (0.65 meq/g) of K^+ ions sorbed up to 167 cm^3 of the feed solution is in good agreement with that of K^+ ions recovered in the batch equilibration technique at the R value of 167 cm^3/g.

By taking advantage of the large difference in the selectivity for K^+ and other ions, a more selective concentration of K^+ ions in seawater can be achieved by washing out Na^+ ions in the CRYMO column with an appropriate eluent. A 30-cm^3 aliquot of seawater was charged onto the column, and the column was washed with 250 cm^3 of a 1 M HNO_3 solution at a flow rate of 0.2 cm^3/min. By this operation, less concentration of

K^+ ions than 10^{-6} M was eluted, while almost all of the Mg^{2+} and Ca^{2+} ions and a considerable amount of Na^+ ions were eluted. Then, the K^+ ions exchange-adsorbed could be eluted by 250 cm^3 of a 13 M HNO_3 solution with an average yield of 90—95% in three runs. The concentration factor, f_{Na}^{K}=480—500, was obtained in the effluent by this once-through processing. The Mg^{2+} and Ca^{2+} ions in the effluent were less than 10^{-6} M.

References

1) B. L. Sreenivas and R. Roy, *Econ. Geol.*, **56**, 198 (1961).
2) J. W. Gruner, *Am. Mineral.*, **28**, 497 (1943).
3) A. McL. Mathieson and A. D. Wadsley, *Am. Mineral.*, **35**, 99 (1950).
4) Gmelin Handbuch der Anorganischen Chemie, Mangan Teil C 1, Springer-Verlag, Berlin (1973), pp. 345—355.
5) M. H. Kurbatov, G. B. Wood, and J. D. Kurbatov, *J. Phys. Colloid Chem.*, **55**, 1170 (1951).
6) J. J. Morgan and W. Stumm, *J. Colloid Sci.*, **19**, 347 (1964).
7) D. J. Murray, T. W. Healy, and D. W. Fuerstenau, *Adv. Chem. Ser.*, **79**, 74 (1968).
8) J. W. Murray, *J. Colloid Interf. Sci.*, **46**, 357 (1974).
9) J. W. Murray, *Geochim. Cosmochim. Acta*, **39**, 505 (1975).
10) T. W. Healy, A. P. Herring, and D. W. Fuerstenau, *J. Colloid Interf. Sci.*, **21**, 435 (1966).
11) M. Abe, *Bunseki Kagaku*, **23**, 1254 (1974).
12) C. B. Amphlett, "Inorganic Ion Exchangers," Elsevier, Amsterdam (1964).
13) V. Veselý and V. Pekárek, *Talanta*, **19**, 219 (1972).
14) G. Svehla (Ed.), "Comprehensive Analytical Chemistry," Vol. XIV, Elsevier, Amsterdam (1982), p. 388.
15) C. Bigliocca, F. Girardi, J. Pauly, E. Sabbioni, S. Meloni, and A. Provasoli, *Anal. Chem.*, **39**, 1634 (1967).
16) "Radionuclide Generator," ed by F. F. Knapp, Jr. and T. A. Butler ACS Symposium Series No. 241, *Am. Chem. Soc.*, Washington, D.C. (1984).
17) M. Tsuji and M. Abe, *Radioisotopes*, **31**, 29P (1982).
18) R. D. Shannon and C. T. Prewitt, *Acta Crystallogr., Sect. B*, **25**, 925 (1969).
19) M. Tsuji and M. Abe, *Solv. Extr. Ion Exchange*, **2**, 253 (1984).
20) M. Tsuji and M. Abe, *Radioisotopes*, **33**, 218 (1984).
21) A. Byström and A. M. Byström, *Acta Crystallogr.*, **3**, 146 (1950).
22) C. Frondel, U. B. Marvin, and J. Ito, *Am. Mineral.*, **45**, 871 (1960).
23) M. Tsuji, M. Abe, and T. Toriyama, 28th National Meeting on Radiochemistry, Kobe, Oct., 1984, 3C06.
24) P. Schindler and H. R. Kamber, *Helv. Chim. Acta*, **51**, 1781 (1968).
25) H. P. Boehm, *Discuss. Faraday Soc.*, **52**, 264 (1971).
26) "Chemical Oceanography," ed by J. P. Riley and G. Skirrow Academic Press, London, 2nd Ed. (1975). Vol. 1, Chap. 4 by G. A. Parks.
27) G. Butler and H. R. Thirsk, *J. Electrochem. Soc.*, **100**, 297 (1953).
28) M. Abe and K. Hayashi, *Hydrometallurgy*, **12**, 83 (1984).
29) Ref. 26, 2nd Ed. Academic Press, London (1975), Vol. 4, Chap. 21 by W. F. McIlhenny.
30) J. A. Epstein, *Chem. Ind.*, **1977**, 572.

 © 1985 The Chemical Society of Japan Bull. Chem. Soc. Jpn., 58, 1115—1118 (1985)

Atomic Absorption Spectrophotometric Determination of Copper(I) After Extraction of Its Ternary Complex with 3-(4-Phenyl-2-pyridyl)-5,6-diphenyl-1,2,4-triazine and Tetraphenylborate into Molten Naphthalene

Tohru NAGAHIRO,* Katsuya UESUGI, Masatada SATAKE,† and Bal K. PURI††
Department of Chemistry, Himeji Institute of Technology, 2167, Shosha, Himeji 671-22
†*Faculty of Engineering, Fukui University, Fukui 910*
††*Department of Chemistry, Indian Institute of Technology, Hauz Khas, New Delhi-110016, India*
(Received July 23, 1984)

A preferable atomic absorption spectrophotometric method has been established for trace determination of copper(I) *via* extraction of its ion-associated complex with 3-(4-phenyl-2-pyridyl)-5,6-diphenyl-1,2,4-triazine and tetraphenylborate into molten naphthalene. The optimum pH range for the extraction is 1.6—8.2. Solid naphthalene containing the copper(I) complex is separated by filtration and dissolved in *N,N*-dimethylformamide. The absorbance is measured at 324.7 nm. Beer's law is obeyed in the concentration range 2.5—80 μg of copper in 10 cm^3 *N,N*-dimethylformamide solution. Ten repeat analyses on a sample containing 35 μg of copper give a mean absorbance of 0.205 with a standard deviation of 0.0017 and a relative standard deviation of 0.83%. The method has been successfully applied to determination of copper in standard reference materials and biological samples.

Numerous chromogenic reagents like 2,2′-dipyridyl- and 3-(2-pyridyl)-5,6-diphenyl-1,2,4-triazine have been used for determination of copper(I) in various methods.[1-8] These reagents react with copper(I) to form water-soluble, colored complex cations, which in turn form water-insoluble, stable, ternary complexes with anions such as ClO_4^-, SCN^-, HgI_4^{2-}, $HgBr_4^{2-}$, and CdI_4^{2-}. Ternary complexes formed can be extracted into suitable organic solvents, and some metal ions or anions can thus be determined spectrophotometrically.[9]

In the present paper, 3-(4-phenyl-2-pyridyl)-5,6-diphenyl-1,2,4-triazine (PPDT) will be recommended as a reagent for extraction of copper(I) with naphthalene. PPDT forms a light brown complex with copper(I) which is partially soluble in water.[7] Perchlorate species of this complex is extremely insoluble in water and many nonaqueous solvents. Though it can be extracted into isopentyl alcohol, the color of the complex fades in a short time[7] and it is inconvenient to work with this solvent due to its unpleasant odor. These difficulties have been overcome by means of extraction with molten naphthalene.[10-14] In the presence of tetraphenylborate (TPB) anion, the Cu(I)—PPDT complex cation mentioned above forms a thermally stable, water-insoluble, ion-associated complex. This complex cannot be extracted into any organic solvents, but can easily be extracted into molten naphthalene. The extracted mixture is soluble in *N,N*-dimethylformamide, dimethyl sulfoxide, propylene carbonate, or acetonitrile, which are all miscible with water. Various conditions have been tested and a preferable method has been applied to determination of copper in some standard reference materials and biological samples.

Experimental

Reagents. Standard copper(II) solution of 5 ppm was prepared by diluting an aliquot of 1000 ppm standard copper(II) solution with distilled water. PPDT solution of 0.04% was prepared in ethanol. TPB solution of 1% was prepared in distilled water. Hydroxylammonium chloride solution of 2% was prepared in distilled water. Buffer solutions were prepared by mixing 1 M acetic acid (1 M=1 mol dm^{-3}) and 1 M ammonium acetate solution for pH 3—6 and 1 M aqueous ammonia and 1 M ammonium acetate solution for pH 8—11. *N,N*-dimethylformamide (DMF), naphthalene, and all the other reagents were of analytical-reagent grade.

Apparatus. All absorbance measurements were made with a Perkin-Elmer Model 403 atomic absorption spectrophotometer with an air-acetylene burner head. A hollow-cathode lamp for copper was obtained from Hamamatsu Photonics Ltd. Atomic absorption data were obtained in an air-acetylene mode at 324.7 nm. Measurements of pH were carried out with a Beckmann Model G pH meter.

General Procedure. To an about 25 cm^3 sample solution containing 2.5—80 μg copper(II) in a 100 cm^3 tightly stoppered Erlenmeyer flask are added 2.0 cm^3 of 2% hydroxylammonium chloride solution, 3.0 cm^3 of 1 M ammonium acetate solution, 2.0 cm^3 of 0.04% PPDT solution, and 2.0 cm^3 of a buffer (pH 5.8). The solution is stirred well and 2.0 cm^3 of 1% TPB solution added. After warming the solution on a water bath at about 60 °C for 5 min, 0.7 g naphthalene is added and the mixture is heated on a water bath at 85 °C to melt naphthalene completely. The solution is then shaken vigorously until naphthalene solidifies forming very fine crystals. The crystals are filtered out on a filter paper (No. 5A), washed with water and dried in an oven at 50—60 °C. The solid is dissolved in *N,N*-dimethylformamide and diluted to 10 cm^3. The solution is aspirated into an air-acetylene flame to be subjected to a measurement at 324.7 nm with a copper hollow-cathode lamp.

Results and Discussion

Effect of pH. To a copper solution was added 3 cm^3 of 1 M ammonium acetate solution and complex extractions were carried out at different pH with the other conditions kept the same. The optimum pH range was 1.6—8.2 (Fig. 1). Addition of 1.5—5.0 cm^3

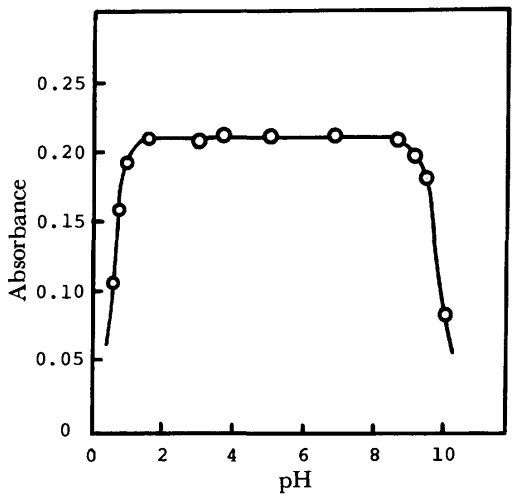

Fig. 1. Effect of pH.
Cu: 35μg; wavelength: 324.7 nm; 0.04% PPDT: 2.0 cm^3; 1% TPB: 2.0 cm^3; naphthalene: 0.7 g; 2% hydroxylammonium chloride: 2.0 cm^3; digestion time: 5 min; shaking time: 30 s; solvent: *N,N*-dimethylformamide.

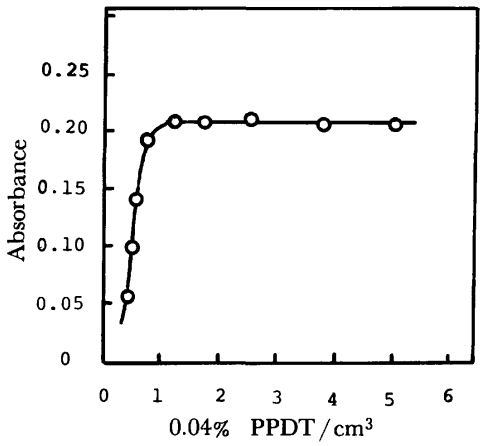

Fig. 2. Effect of PPDT concentration.
pH: 5.8; Conditions were the same as those in Fig. 1.

buffer (pH 5.8) caused virtually no variation in absorbance. Subsequent studies were conducted at pH 5.8 using 2.0 cm^3 of buffer solution.

Effect of Hydroxylammonium Chloride Concentration. Varying volumes of 2% hydroxylammonium chloride solution were added to sample solutions containing 35 μg of copper. Copper(II) was completely reduced to copper(I) by addition of 0.5—5.0 cm^3 of the 2% solution. For assured functioning, 2.0 cm^3 of the 2% solution of reducing agent was selected.

Effect of PPDT and TPB Concentrations. Extractions were carried out at fixed pH but different PPDT concentrations. It was observed that extractions were quntitative for 1.2—5.0 cm^3 of 0.04% PPDT solution. Similar studies with sodium tetraphenylborate showed that the absorbance remained constant for 0.8—4.0 cm^3 of 1% TPB solution. Thus 2.0 cm^3 of 0.04% PPDT solution and 2.0 cm^3 of 1% TPB solution were selected for the extraction of complex (Figs. 2—3).

Effect of Addition of Naphthalene. The amount of

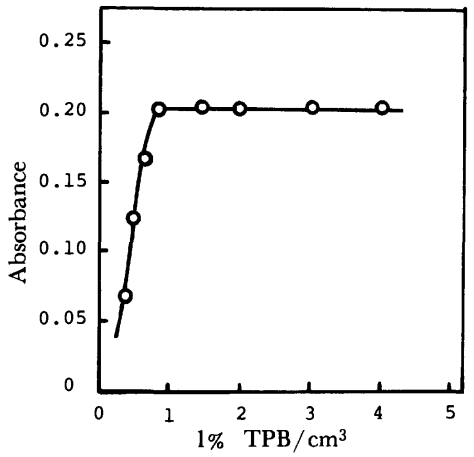

Fig. 3. Effect of TPB concentration.
Conditions were the same as those in Fig. 2.

naphthalene was varied from 0.2 to 1.5 g and extractions were carried out by the general procedure. The extraction was quantitative in the range 0.3—1.5 g of naphthalene, but beyond this range, naphthalene interfered with the determination of copper due to its deposition on the burner head. Hence 0.7 g naphthalene was selected as a suitable amount.

Effect of Digestion and Shaking Times. A solution containing the Cu(I)-PPDT-TPB complex at pH 5.8 was digested at 50—60 °C. The digestion time is not critical, 1 min being sufficient for completion of the complex formation. The extraction of complex into molten naphthalene (81—85 °C) was found to be very rapid and no change was observed when the shaking time was varied from 3 to 120 s.

Effect of Electrolytes. The extraction of complex was carried out in the presence of sodium chloride, potassium nitrate, sodium acetate, ammonium acetate, ammonium chloride, or sodium sulfate (0.02—1.0 M). It was found that ammonium acetate is the most suitable for the formation and extraction of complex when its ionic strength is in the range 0.05—1.0 M. In the absence of ammonium acetate, the pH range for extraction was 3.1—8.2 and the absorbance was low, indicating a salting-out effect.

Effect of the Volume of Aqueous Phase. Since the organic/aqueous phase ratio is an important factor in such procedures, the effect of the latter on the extraction of complex was studied. The extraction is quantitative when the volume of aqueous phase does not exceed 50 cm^3 (Fig. 4).

Choice of Solvent. Various organic solvents were tried to dissolve an extracted mixture of complex and naphthalene. The complex is insoluble in benzene, toluene, xylene, chlorobenzene, *o*-dichlorobenzene, nitrobenzene, chloroform, carbon tetrachloride, 1,2-dichloroethane, isopentyl acetate, diethyl ether, 1-pentanol, dioxane or isobutyl methyl ketone (IBMK), but it is soluble in dimethyl sulfoxide, propylene carbonate, acetonitrile, or *N,N*-dimethylformamide, which are miscible with water. Dimethyl sulfoxide and propyl-

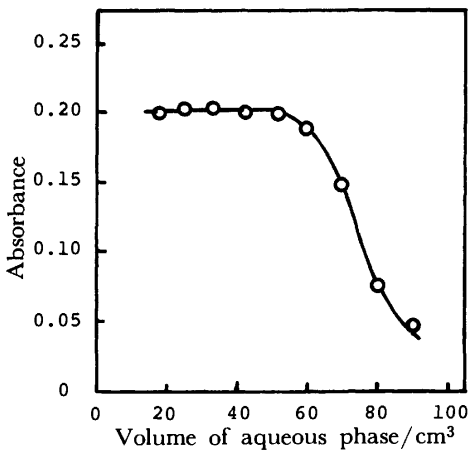

Fig. 4. Effect of volume of aqueous phase.
Cu: 35 μg; 0.04% PPDT: 3.0 cm³; Conditions were the same as those in Fig. 2.

Table 1. Effect of diverse ions and salts[a)]

Ion/Salt	Tolerance limit
NaI	1.5 g
NaF, Cd^{2+}	1.0 g
KSCN	300 mg
Pb^{2+}	200 mg
Mo^{6+}	40 mg
Zn^{2+}	35 mg
Ca^{2+}	25 mg
Mn^{2+}	8 mg
Mg^{2+}, W^{6+}	7 mg
Cr^{6+}	5 mg
V^{5+}	4 mg
Al^{3+}	3.5 mg[b)]
Sodium tartrate	2 mg
Sodium citrate	1.5 mg
$Na_2C_2O_4$, Hg^{2+}, Ag^{+}, Bi^{3+}	1 mg
KCN	700 μg
Fe^{3+}	500 μg
Co^{2+}	300 μg
Ni^{2+}	30 μg
Disodium EDTA	10 μg
Pd^{2+}	2 μg

a) pH: 5.8; 0.04% PPDT: 3.0 cm³; 1% TPB: 2.0 cm³; naphthalene: 0.7 g; 1 M CH_3COONH_4: 3.0 cm³; 2% hydroxylammonium chloride: 2.0 cm³. b) Extraction at pH 3.0.

ene carbonate are better solvents, but they are expensive and viscous. Acetonitrile may be used but the absorbance is rather low in this solvent. Hence *N,N*-dimethylformaide is preferable for dissolving the metal complex and naphthalene.

Calibration Curve. For the optimum conditions specified above, a calibration curve was constructed at 324.7 nm. It was found to be linear over the concentration range 2.5—80.0 μg of copper in 10 cm³ of *N,N*-dimethylformamide solution. Ten repeat analyses on a sample solution containing 35 μg of copper gave a mean absorbance of 0.205 with a standard deviation of 0.0017 and a relative standard deviation of 0.83%.

Effect of Diverse Ions. Sample solutions containing 35 μg of copper and various amounts of different alkali metal salts or metal ions were prepared, and the determination of copper was carried out by the general procedure. Tolerance limits of diverse ions are given in Table 1. Naturally the method is fairly selective and may be applied to determination of copper in various complex materials.

Determination of Copper in Standard Reference Materials. A 0.05—0.5 g sample of alloy was completely dissolved in 20—30 cm³ of hydrochroric acid (1+1) on a water bath. Then 3—5 cm³ of 30% hydrogen peroxide were added to it. The excess of peroxide was decomposed by heating the solution on a water bath. The mixture was cooled and filtered through a filter paper. The filtrate was diluted to 500 cm³ with distilled water in a flask. An appropriate volume of this solution was taken and the copper was determined by the general procedure. The results are given in Table 2.

Determination of Copper in Human Hair. A 10.0 g sample of human hair was taken and dissolved in 30 cm³ of concentrated nitric acid and 3.0 cm³ of concentrated perchloric acid by heating. This solution was cooled, filterd, and diluted to 200 cm³ with distilled water in a standard flask. An aliquot of this solution was taken and the copper was determined by the general procedure. The results in Table 2 are in reasonable agreement with those obtained by the standard

Table 2. Analysis of copper in samples

Sample	Composition/%	Copper certified value/%	Copper content/%[a)]	
			Present method	DDTC–IBMK method
N.B.S., SRM-85b Aluminium alloy	Ni: 0.084, Mg: 1.49 Mn: 0.61, Cr: 0.21 Si: 0.18, Fe: 0.24 Zn: 0.03, Ti: 0.022 Pb: 0.021, Ga: 0.019 V: 0.006,	3.99	4.07±0.06	—
N.B.S., SRM-94c Die Casting alloy	Mn: 0.014, Ni: 0.006 Sn: 0.006, Al: 4.13 Cd: 0.002, Fe: 0.018 Pd: 0.006, Mg: 0.042	1.01	0.983±0.013	—
Human hair (male)	—	—	0.00156±0.00004	0.00161±0.00002
Human hair (female)	—	—	0.00253±0.00003	0.00258±0.00003

a) Mean of 5 individual determinations.

DDTC-IBMK method.[15]

References

1) A. A. Schilt, "Analytical Applications of 1,10-Phenanthroline and Related Compounds," Pergamon Press, New York (1969).
2) G. Trabanelli, *Atti Accad. Sci. Ferarra*, **35**, 133 (1957—58); *Chem. Abstr.*, **55**, 12153 (1961).
3) B. Zak and N. Nessler, *Anal. Chem.*, **28**, 1158 (1956).
4) J. W. Lander and B. Zak, *Am. J. Clin. Pathol.*, **29**, 590 (1958).
5) D. Banerjea and K. K. Tripathi, *Anal. Chem.*, **32**, 1196 (1960).
6) D. H. Wilkins and G. F. Smith, *Anal. Chim. Acta*, **9**, 538 (1953).
7) A. A. Schilt, *Talanta*, **13**, 895 (1966).
8) A. A. Schilt and W. C. Hoyle, *Anal. Chem.*, **39**, 114 (1967).
9) K. Kotsuji, *Bull. Chem. Soc. Jpn.*, **38**, 402 (1965).
10) B. K. Puri and M. Gautam, *Talanta*, **84**, 484 (1978).
11) T. Fujinaga, M. Satake, and T. Yonekubo, *Bull. Chem. Soc. Jpn.*, **48**, 899 (1975).
12) A. Wasey, R. K. Bansal, and B. K. Puri, *Mikrochim. Acta*, **I**, 211 (1984).
13) A. Wasey, R. K. Banzal, M. Satake, and B. K. Puri, *Bull. Chem. Soc. Jpn.*, **56**, 3603 (1983).
14) A. Wasey, R. K. Banzal, B. K. Puri, and A. L. J. Rao, *Talanta*, **31**, 205 (1984).
15) JIS K 0102, 153 (1981).

 © 1985 The Chemical Society of Japan Bull. Chem. Soc. Jpn., 58, 1119—1124 (1985)

Preparation and Some Properties of Bis(trimethylenediamine)cobalt(III) Complexes with a Bidentate-*N,S* or -*N,Se* Ligand

Takumi KONNO,* Ken-ichi OKAMOTO, Hisahiko EINAGA,† and Jinsai HIDAKA
Department of Chemistry, University of Tsukuba, Sakura, Ibaraki 305
†*Institute of Materials Science, University of Tsukuba, Sakura, Ibaraki 305*
(Received August 3, 1984)

Seven optically active cobalt(III) complexes of [Co(bidentate-*N,S* or -*N,Se*)$(tn)_2$] type were prepared for the first time; bidentate-*N,S* or -*N,Se* denotes 2-aminoethanethiolato (aet), 2-aminoethaneselenolato (aes), 2-aminoethanesulfenato (aese), 2-aminoethanesulfinato (aesi), 2-(methylthio)ethylamine (mea), and 2-(methylseleno)ethylamine (mseea). These complexes were characterized from their absorption, CD, and ^{1}H NMR spectra. All complexes obtained were assigned to the *Λ* configuration. The $(+)^{CD}_{550}$ mea isomer took selectively the *Λ*-(*R*) configuration in solution, while the $(+)^{CD}_{550}$ mseea isomer a mixture of the *Λ*-(*R*) and *Λ*-(*S*) ones. The absorption and CD spectra of the complexes are discussed in comparison with those of the corresponding bis(ethylenediamine)cobalt(III) complexes. The *Λ*-(*R*)- and *Λ*-(*S*)-[Co(aese)$(tn)_2$]$^{2+}$ isomers showed the CD spectral change with time and it was suggested that the epimerization at sulfur was accompanied by the racemization of the skew pair of chelate rings.

Bis(ethylenediamine)cobalt(III) complexes with a bidentate-*N,S* or -*N,Se* ligand have extensively been investigated,[1–12] and these complexes showed some unique spectrochemical and stereochemical properties.[4–9] However, it has not been clarified whether the properties depend on the sulfur- or selenium-containing ligand itself or on the ethylenediamine chelate ring. Therefore, it is worthwhile to study the corresponding cobalt(III) complexes with six-membered trimethylenediamine chelate ring, [Co(bidentate-*N,S* or -*N,Se*)$(tn)_2$]. No report has been presented for the trimethylenediamine complexes up to now.

In this paper, the bis(trimethylenediamine)cobalt(III) complexes with 2-aminoethanethiolato, [Co(aet)$(tn)_2$]$^{2+}$, and 2-aminoethaneselenolato, [Co(aes)$(tn)_2$]$^{2+}$, were prepared and optically resolved. The other optically active cobalt(III) complexes, $(+)^{CD}_{550}$·$(+)^{CD}_{370}$- and $(+)^{CD}_{550}$·$(-)^{CD}_{370}$-[Co(aese)$(tn)_2$]$^{2+}$, $(+)^{CD}_{500}$-[Co(aesi)$(tn)_2$]$^{2+}$, and $(+)^{CD}_{550}$-[Co(mea)$(tn)_2$]$^{3+}$, were derived from $(+)^{CD}_{600}$-[Co(aet)$(tn)_2$]$^{2+}$, and $(+)^{CD}_{550}$-[Co(mseea)$(tn)_2$]$^{3+}$ was derived from $(+)^{CD}_{600}$-[Co(aes)$(tn)_2$]$^{2+}$.[13] The absorption and CD spectra of these complexes were discussed in comparison with those of the corresponding bis(ethylenediamine)cobalt(III) complexes. The rate constants of the epimerization at sulfur and the racemization of the skew pair of chelate rings of the complex were estimated for $(+)^{CD}_{550}$·$(+)^{CD}_{370}$- and $(+)^{CD}_{550}$·$(-)^{CD}_{370}$-[Co(aese)$(tn)_2$]$^{2+}$.

Experimental

1) Preparation and Resolution of the Complexes. a) $(+)^{CD}_{600}$*-[Co(aet)$(tn)_2$]$(ClO_4)_2$*: To a deoxygenated solution containing 4.0 g of $CoCl_2 \cdot 6H_2O$ in 15 cm^3 of water were successively added with stirring deoxygenated solutions containing 1.9 g of $(NH_2CH_2CH_2S\text{-})_2 \cdot 2HCl$ in 15 cm^3 of water and 4.0 g of $NH_2(CH_2)_3NH_2$ in 40 cm^3 of water. The mixture was continuously stirred under nitrogen atmosphere for 40 min in an ice bath. The dark brown solution was filtered and to the filtrate was added a solution containing 15 g of NaI in 50 cm^3 of ice-cold water. The solution was kept in a refrigerator overnight. The resultant dark brown crystals were collected by filtration and washed with ice-cold ethanol and ether. Found: C, 17.86; H, 4.89; N, 13.03%. Calcd for [Co(aet)$(tn)_2$]I_2=$C_8H_{26}N_5SCoI_2$: C, 17.88; H, 4.87; N, 13.03%.

One point five gram of [Co(aet)$(tn)_2$]I_2 was dissolved in 70 cm^3 of ice-cold water. To this were added with stirring a solution containing 1.0 g of $K_2[Sb_2(d\text{-}tart)_2] \cdot H_2O$ in 20 cm^3 of water and 20 cm^3 of ethanol. The solution was stirred for 20 min in an ice bath, though fine reddish brown crystals began to appear after a few minutes. The crystals were collected by filtration and washed with ethanol and ether. Found: C, 22.60; H, 3.88; N, 8.26%. Calcd for [Co(aet)$(tn)_2$][Sb_2(d-tart)$_2$]·$1.5H_2O$=$C_{16}H_{30}N_5O_{12}SCoSb_2 \cdot 1.5H_2O$: C, 22.72; H, 3.93; N, 8.28%.

Zero point seven gram of $(+)^{CD}_{600}$-[Co(aet)$(tn)_2$][Sb_2(d-tart)$_2$]·$1.5H_2O$ was dissolved in 20 cm^3 of an aqueous solution containing 4.0 g of $NaClO_4$ with stirring in an ice bath. When the solution was continuously stirred for 10 min, fine dark brown crystals appeared. The resultant crystals were collected by filtration and washed with ice-cold ethanol and ether. The concentration of this isomer was evaluated from the extinction coefficient of the racemic iodide salt.

b) $(+)^{CD}_{600}$*-[Co(aes)$(tn)_2$]$(ClO_4)_2$*: This complex was prepared by a procedure similar to that used for $(+)^{CD}_{600}$-[Co(aet)$(tn)_2$]$(ClO_4)_2$ described in *a)*, using $(NH_2CH_2CH_2Se)_2 \cdot H_2SO_4$[14] instead of $(NH_2CH_2CH_2S\text{-})_2 \cdot 2HCl$. The concentration of this isomer was evaluated from the extinction coefficient of the racemic iodide salt. Found: C, 15.69; H, 4.91; N, 11.86%. Calcd for [Co(aes)$(tn)_2$]$I_2 \cdot H_2O$=$C_8H_{26}N_5CoSeI_2 \cdot H_2O$: C, 15.96; H, 4.69; N, 11.63%. Found: C, 21.19; H, 3.73; N, 7.72%. Calcd for [Co(aes)$(tn)_2$][Sb_2(d-tart)$_2$]·$2H_2O$=$C_{16}H_{30}N_5O_{12}CoSeSb_2 \cdot 2H_2O$: C, 21.31; H, 3.80; N, 7.77%.

c) $(+)^{CD}_{550}$·$(+)^{CD}_{370}$*-[Co(aese)$(tn)_2$]$(ClO_4)_2$ and* $(+)^{CD}_{550}$·$(-)^{CD}_{370}$*-[Co(aese)$(tn)_2$]I_2*: The preparation procedure was operated without light. To a solution containing 0.2 g of $(+)^{CD}_{600}$-[Co(aet)$(tn)_2$]$(ClO_4)_2$ in 2 cm^3 of ice-cold water was added a calculated amount of 2% H_2O_2 (0.6 cm^3). The mixture was stirred for 20 min in an ice bath and the resultant precipitate of the $(+)^{CD}_{550}$·$(+)^{CD}_{370}$ aese isomer was collected by filtration. To the filtrate was soon added 0.5 g of NaI and the solution was stirred for 10 min in an ice bath. The resultant precipitate, which was found from the CD measurement to be the $(+)^{CD}_{550}$·$(-)^{CD}_{370}$ aese isomer containing a small amount of the $(+)^{CD}_{550}$·$(+)^{CD}_{370}$ one, was filtered off. To the filtrate were added 1.0 g of NaI and a large amount of 2-propanol–ether (2:1), and

then the solution was stood in a refrigerator overnight. The resultant orange-red precipitate of the $(+)^{CD}_{550}\cdot(-)^{CD}_{370}$ aese isomer was collected by filtration. The formation ratio of the two isomers, $(+)^{CD}_{550}\cdot(+)^{CD}_{370}$:$(+)^{CD}_{550}\cdot(-)^{CD}_{370}$, was about 6:5, which was evaluated from the CD spectra of the reaction solution. Found for $(+)^{CD}_{550}\cdot(+)^{CD}_{370}$ isomer: C, 19.31; H, 5.23; N, 14.03%. Calcd for $[Co(aese)(tn)_2](ClO_4)_2=C_8H_{26}N_5O_9SCl_2Co$: C, 19.28; H, 5.26; N, 14.05%. Found for $(+)^{CD}_{550}\cdot(-)^{CD}_{370}$ isomer: C, 16.61; H, 4.60; N, 12.04%. Calcd for $[Co(aese)(tn)_2]I_2\cdot H_2O=C_8H_{26}N_5OSCoI_2\cdot H_2O$: C, 16.83; H, 4.94; N, 12.26%.

d) $(+)^{CD}_{600}$*-[Co(aesi)(tn)$_2$](ClO$_4$)$_2$*: To a solution containing 0.1 g of $(+)^{CD}_{600}$-$[Co(aet)(tn)_2](ClO_4)_2$ in 2 cm^3 of ice-cold water was added an excess amount of 10% H_2O_2 (0.6 cm^3), followed by the addition of 0.3 cm^3 of 60% $HClO_4$. The solution was stirred for 20 min in an ice bath and stood in a refrigerator for 2 d. The solution was poured onto a column of QAE-Sephadex A-25 (ClO_4^- from, 2 cm×20 cm) and the adsorbed band was eluted with water. The eluate was concentrated to a small volume with a rotary evaporator and to this was added an appropriate amount of ethanol. The solution was kept in a refrigerator for several days and the resultant crystals were collected by filtration. Found: C, 18.59; H, 5.12; N, 13.51%. Calcd for $[Co(aesi)(tn)_2](ClO_4)_2=C_8H_{26}N_5O_{10}SCl_2Co$: C, 18.68; H, 5.09; N, 13.61%.

e) $(+)^{CD}_{550}$*-[Co(mea)(tn)$_2$](NO$_3$)$_3$*. To a solution containing 0.1 g of $(+)^{CD}_{600}$-$[Co(aet)(tn)_2](ClO_4)_2$ in 2 cm^3 of ice-cold water was added 2 cm^3 of ice-cold dimethyl sulfate. When the mixture was allowed to stand in a refrigerator overnight, it was separated into two layers. The red upper layer was poured onto a column of QAE-Sephadex A-25 (NO_3^- form, 2 cm×20 cm) and the adsorbed band was eluted with water. The eluate was concentrated to a small volume with a rotary evaporator and to this was added a small amount of ethanol. After cooling in a refrigerator overnight, the resultant crystals were collected by filtration and washed with ethanol and ether. Found: C, 22.01; H, 6.09; N, 22.77%. Calcd for $[Co(mea)(tn)_2](NO_3)_3\cdot0.5H_2O=C_9H_{29}N_8O_9SCo\cdot0.5H_2O$: C, 21.91; H, 6.13; N, 22.71%.

f) $(+)^{CD}_{550}$*-[Co(mseea)(tn)$_2$](NO$_3$)$_3$*. This complex was prepared by a procedure similar to that used for $(+)^{CD}_{550}$-$[Co(mea)(tn)_2](NO_3)_3$ described in *e)*, using $(+)^{CD}_{600}$-$[Co(aes)(tn)_2](ClO_4)_2$ instead of $(+)^{CD}_{600}$-$[Co(aet)(tn)_2](ClO_4)_2$. Found: C, 19.10; H, 5.74; N, 19.61%. Calcd for $[Co(mseea)(tn)_2](NO_3)_3\cdot2H_2O=C_9H_{29}N_8O_9CoSe\cdot2H_2O$: C, 19.05; H, 5.86; N, 19.75%.

g) Λ*-[Co(aet)(en)$_2$](ClO$_4$)$_2$,* Λ*-(R)- and* Λ*-(S)-[Co(aese)(en)$_2$](ClO$_4$)$_2$,* Λ*-[Co(aesi)(en)$_2$](ClO$_4$)$_2$, and* Λ*-(R)-[Co(mea)(en)$_2$](NO$_3$)$_3$.* These bis(ethylenediamine)cobalt(III) complexes were prepared by the methods described in previous papers.[8,11]

2) Measurements. The electronic absorption spectra were recorded with a JASCO UVIDEC-1 spectrophotometer, and the CD spectra with a JASCO J-20 spectropolarimeter. All measurements were carried out in an aqueous solution at room temperature. The ^1H NMR spectra were recorded in deuterium oxide on a JEOL JNM-FX-100 NMR spectrometer at probe temperature. Sodium 2,2-dimethyl-2-silapentane-5-sulfonate (DSS) was used as an internal reference. The absorption and CD spectral changes for the epimerization and racemization were followed at 24 °C in the room light which was (4.7±0.3)×10^2 lx with a lux-meter ANA-999 of Tokyo Photo-electric Co., Ltd.

Results and Discussion

Absorption and CD Spectra. Figures 1—4 and Tables 1 and 2 show the absorption and CD spectra of the bis(trimethylenediamine)cobalt(III) complexes. The absorption spectral behavior of the present complexes with a sulfur- or selenium-containing ligand is quite similar to that of the corresponding [Co(bidentate-*N,S* or -*N,Se*)(en)$_2$] type complexes.[4-11] All com-

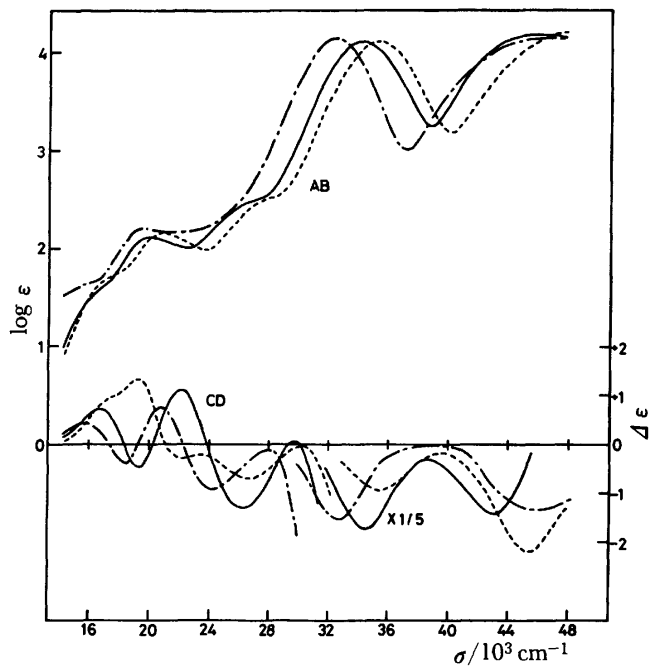

Fig. 1. Absorption and CD spectra of $(+)^{CD}_{600}$-$[Co(aet)(tn)_2]^{2+}$ (——), $(+)^{CD}_{600}$-$[Co(aes)(tn)_2]^{2+}$ (—·—), and Λ-$[Co(aet)(en)_2]^{2+}$ (-----).

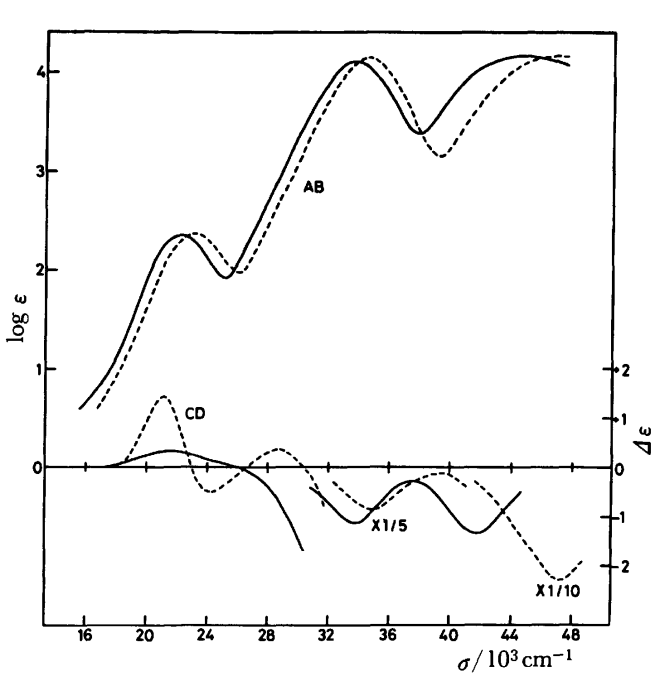

Fig. 2. Absorption and CD spectra of $(+)^{CD}_{500}$-$[Co(aesi)(tn)_2]^{2+}$ (——), and Λ-$[Co(aesi)(en)_2]^{2+}$ (-----).

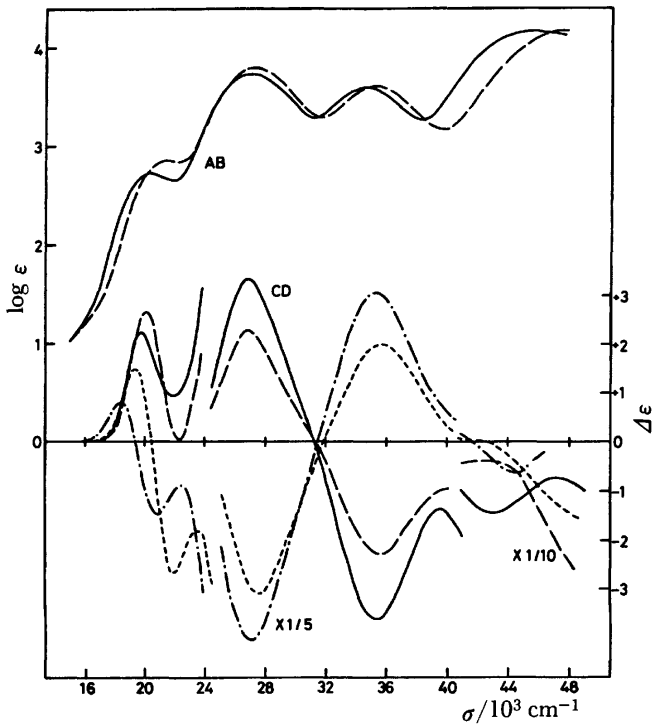

Fig. 3. Absorption and CD spectra of $(+)^{CD}_{550}$·$(+)^{CD}_{370}$-[Co(aese)(tn)$_2$]$^{2+}$ (——), $(+)^{CD}_{550}$·$(-)^{CD}_{370}$-[Co(aese)(tn)$_2$]$^{2+}$ (—·—), *Λ*-(*S*)-[Co(aese)(en)$_2$]$^{2+}$ (———), and *Λ*-(*R*)-[Co-(aese)(en)$_2$]$^{2+}$ (-----).

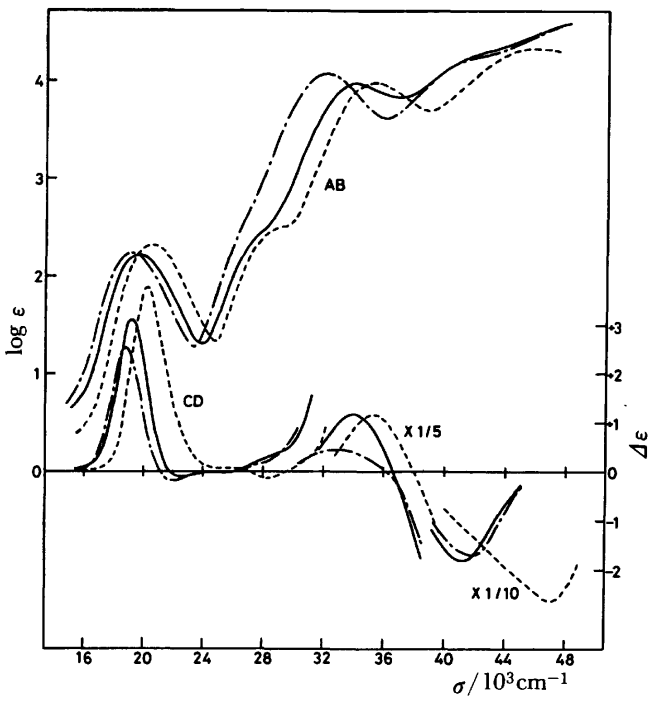

Fig. 4. Absorption and CD spectra of $(+)^{CD}_{550}$-[Co-(mea)(tn)$_2$]$^{3+}$ (——), $(+)^{CD}_{550}$-[Co(mseea)(tn)$_2$]$^{3+}$ (—·—), and *Λ*-(*R*)-[Co(mea)(en)$_2$]$^{3+}$ (-----).

plexes show the chalcogen-to-metal charge transfer band at 32—35×10^3 cm^{-1}, which shifts to lower energy than that of the corresponding bis(ethylenediamine) complexes. As for [Co(aese)(tn)$_2$]$^{2+}$, another characteristic charge transfer band appears at *ca.* 27×10^3 cm^{-1}, as in the case for [Co(aese)(en)$_2$]$^{2+}$.[6,8-10] The first absorption band of the [Co(bidentate-*N,S* or -*N,Se*)(tn)$_2$] type complexes shifts to lower energy than that of the corresponding [Co(bidentate-*N,S* or -*N,Se*)(en)$_2$] ones,[4-11] in analogous with the fact that the [Co(L)-(tn)$_2$] type complexes show the first absorption band at lower energy as compared with that of the corresponding [Co(L)(en)$_2$] ones; L denotes a bidentate ligand such as glycinate and oxalate.[15,16]

The *Δ* and *Λ* isomers are possible for each of [Co-(aet)(tn)$_2$]$^{2+}$, [Co(aes)(tn)$_2$]$^{2+}$, and [Co(aesi)(tn)$_2$]$^{2+}$. As shown in Fig. 1, the CD spectrum of $(+)^{CD}_{600}$-[Co(aet)-(tn)$_2$]$^{2+}$ agrees well with that of *Λ*-[Co(aet)(en)$_2$]$^{2+}$,[4,8] except for the two bands at higher energy in the first absorption band region (*ca.* 19 and 22×10^3 cm^{-1}). Furthermore, the stoichiometric oxidation of $(+)^{CD}_{600}$-[Co-(aet)(tn)$_2$]$^{2+}$ generated *Λ*-(*R*)- and *Λ*-(*S*)-[Co(aese)(tn)$_2$]$^{2+}$ (*vide infra*), as in the oxidation reaction of *Λ*-[Co(aet)-(en)$_2$]$^{2+}$.[7-9] These facts suggest that the starting thiolato complex, $(+)^{CD}_{600}$-[Co(aet)(tn)$_2$]$^{2+}$, takes the *Λ* configuration. As shown in Fig. 1, $(+)^{CD}_{600}$-[Co(aes)(tn)$_2$]$^{2+}$ exhibits a CD spectra quite similar to that of *Λ*-$(+)^{CD}_{600}$-[Co(aet)(tn)$_2$]$^{2+}$ over the whole region, and then can be assigned to the *Λ* configuration. The $(+)^{CD}_{500}$ aesi isomer, which is the oxidation product from *Λ*-$(+)^{CD}_{600}$-[Co(aet)(tn)$_2$]$^{2+}$, shows a positive CD band in the first absorption band region (Fig. 2), being also assigned to the *Λ* configuration. These facts indicate that the oxidation reaction for the starting thiolato complex proceeded with retention of its absolute configuration, as in the case for the bis(ethylenediamine) cobalt-(III) complexes.[7-9,11] In the present bis(trimethylenediamine)cobalt(III) complexes, *Λ*-[Co(aet) (tn)$_2$]$^{2+}$, *Λ*-[Co(aes)(tn)$_2$]$^{2+}$, and *Λ*-[Co(aesi)(tn)$_2$]$^{2+}$, which have no chirality due to the coordinated chalcogen atom, commonly show a negative CD band in the chalcogen-to-metal charge transfer band region similar to that of the corresponding bis(ethylenediamine) complexes, though the CD spectra in the first absorption band region are different from one another (Fig. 1 and 2).[4,7,8,11] This may suggest that the configurational chirality due to the skew pair of chelate rings can be deduced from the CD pattern in the chalcogen-to-metal charge transfer band region as for the bis-(diamine)cobalt(III) complexes with the aet, aes or aesi ligand.

Taking the asymmetric chalcogen donor atom, (*R*) and (*S*), into consideration, four isomers, *Δ*-(*R*), *Δ*-(*S*), *Λ*-(*R*), and *Λ*-(*S*), are possible for each of [Co(aese)-(tn)$_2$]$^{2+}$, [(Co(mea)(tn)$_2$]$^{3+}$, and [Co(mseea)(tn)$_2$]$^{3+}$. The two isomers, $(+)^{CD}_{550}$·$(+)^{CD}_{370}$- and $(+)^{CD}_{550}$·$(-)^{CD}_{370}$-[Co(aese)-(tn)$_2$]$^{2+}$, which are formed by the stoichiometric oxidation reaction of $(+)^{CD}_{600}$-[Co(aet)(tn)$_2$]$^{2+}$ with aqueous H_2O_2, show the CD spectra quite similar to those of *Λ*-(*S*)- and *Λ*-(*R*)-[Co(aese)(en)$_2$]$^{2+}$, respectively, over the whole region (Fig. 3).[8,9] This fact suggests that the $(+)^{CD}_{550}$·$(+)^{CD}_{370}$ and $(+)^{CD}_{550}$·$(-)^{CD}_{370}$ aese isomers take the

TABLE 1. ABSORPTION DATA OF [Co(bidentate-*N*,*S* or -*N*,*Se*)(tn)$_2$] TYPE COMPLEXES

Complex	First band	Second band	Charge transfer band
$(+)^{CD}_{600}$-[Co(aet)(tn)$_2$]$^{2+}$	16.9 (1.61 sh)	27.3 (2.51 sh)	34.13 (4.12)
	19.92 (2.11)		45.35 (4.20)
$(+)^{CD}_{600}$-[Co(aes)(tn)$_2$]$^{2+}$	16.0 (1.64 sh)		32.36 (4.16)
	19.70 (2.21)		46.30 (4.16)
$(+)^{CD}_{500}$-[Co(aesi)(tn)$_2$]$^{2+}$	22.15 (2.36)		33.67 (4.12)
			44.64 (4.17)
$(+)^{CD}_{550}\cdot(-)^{CD}_{370}$-[Co(aese)(tn)$_2$]$^{2+}$	20.68 (2.66)		26.95 (3.81)
			34.48 (3.62)
			44.15 (4.63)
$(+)^{CD}_{550}\cdot(+)^{CD}_{370}$-[Co(aese)(tn)$_2$]$^{2+}$	20.20 (2.73)		26.88 (3.74)
			34.42 (3.61)
			45.15 (4.19)
$(+)^{CD}_{550}$-[Co(mea)(tn)$_2$]$^{3+}$	19.67 (2.22)	28.3 (2.52 sh)	34.07 (3.97)
			43.9 (4.33 sh)
			49.02 (4.60)
$(+)^{CD}_{550}$-[Co(mseea)(tn)$_2$]$^{3+}$	19.16 (2.24)		32.15 (4.07)
			43.1 (4.28 sh)
			48.78 (4.57)

Wave numbers and logε values (in parentheses) are given in 10^3 cm^{-1} and mol^{-1} dm^3 cm^{-1}, respectively. Sh denotes a shoulder.

TABLE 2. CD DATA OF [Co(bidentate-*N*,*S* or -*N*,*Se*)(tn)$_2$] TYPE COMPLEXES

Complex	First band	Second band	Charge transfer band
$(+)^{CD}_{600}$-[Co(aet)(tn)$_2$]$^{2+}$	16.67 (+0.70)	30.21 (−1.30)	34.42 (−8.72)
	19.23 (−0.46)		43.1 (−7.0)
	22.08 (+1.13)		
$(+)^{CD}_{600}$-[Co(aes)(tn)$_2$]$^{2+}$	15.70 (+0.43)	24.21 (−0.89)	32.68 (−7.56)
	18.45 (−0.36)		45.5 (−6.6)
	20.79 (+0.76)		
$(+)^{CD}_{500}$-[Co(aese)(tn)$_2$]$^{2+}$	21.51 (+0.33)		33.56 (−5.45)
			41.67 (−6.6)
$(+)^{CD}_{550}\cdot(-)^{CD}_{370}$-[Co(aese)(tn)$_2$]$^{2+}$	18.38 (+0.85)		27.03 (−20.18)
	20.70 (−1.48)		35.27 (+15.26)
			44.3 (−6.1)
$(+)^{CD}_{550}\cdot(+)^{CD}_{370}$-[Co(aese)(tn)$_2$]$^{2+}$	19.67 (+2.25)		26.81 (+16.71)
			35.34 (−17.95)
			44.76 (−14.2)
$(+)^{CD}_{550}$-[Co(mea)(tn)$_2$]$^{3+}$	19.23 (+3.14)	29.4 (−0.43 sh)	34.13 (+5.68)
	22.47 (−0.11)		41.32 (−18.4)
$(+)^{CD}_{550}$-[Co(mseea)(tn)$_2$]$^{3+}$	18.80 (+2.57)		32.15 (+2.31)
	21.98 (−0.18)		41.59 (−17.2)

Wave numbers and $\Delta\varepsilon$ values (in parentheses) are given in 10^3 cm^{-1} and mol^{-1} dm^3 cm^{-1}, respectively. Sh denotes a shoulder.

Λ-(*S*) and *Λ*-(*R*) configurations, respectively. This assignment is confirmed by comparing the vicinal CD due to the asymmetric sulfur atom and the configurational CD due to the skew pair of chelate rings for [Co(aese)(tn)$_2$]$^{2+}$ with those for [Co(aese)(en)$_2$]$^{2+}$. Figure 5 shows the (*S*) vicinal and the *Λ* configurational CD curves calculated from the observed CD curves of *Λ*-(*R*)- and *Λ*-(*S*)-[Co(aese)(tn)$_2$]$^{2+}$, together with those calculated from *Λ*-(*R*)- and *Λ*-(*S*)-[Co(aese)(en)$_2$]$^{2+}$. The (*S*) vicinal CD curve for [Co(aese)(tn)$_2$]$^{2+}$ is quite similar to that for [Co(aese)(en)$_2$]$^{2+}$, showing two bands, (−) and (+), from lower energy in the first absorption band region, and two bands, (+) and (−), from lower energy in the sulfur-to-metal charge transfer band region. A similar relation is also observed for the *Λ* configurational CD curves; the dominant positive CD band is observed at the lower energy side of the first absorption band region and a negative band in the sulfenato charge transfer band region (*ca.* 28× 10^3 cm^{-1}), though the CD intensity for [Co(aese)(tn)$_2$]$^{2+}$ is weaker than that for [Co(aese)(en)$_2$]$^{2+}$ in the first absorption band region. The formation ratio of the two isomers, *Λ*-(*R*):*Λ*-(*S*), is about 5:6 for [Co(aese)(tn)$_2$]$^{2+}$ and this ratio is in contrast to the case for [Co(aese)(en)$_2$]$^{2+}$ (*Λ*-(*R*):*Λ*-(*S*)=3:1).[8] This may be due to the absence of the effective intramolecular hydrogen bond between the sulfenato oxygen atom and the adjacent amine proton in [Co(aese)(tn)$_2$]$^{2+}$, because of the flexibility of the six-membered trimethylenediamine cheate ring.

Each of $(+)^{CD}_{550}$-[Co(mea)(tn)$_2$]$^{3+}$ and $(+)^{CD}_{550}$-[Co(mseea)(tn)$_2$]$^{3+}$, which is the methylation product of *Λ*-[Co(aet)(tn)$_2$]$^{2+}$ and *Λ*-[Co(aes)(tn)$_2$]$^{2+}$, respectively, shows a major positive CD band in the first absorp-

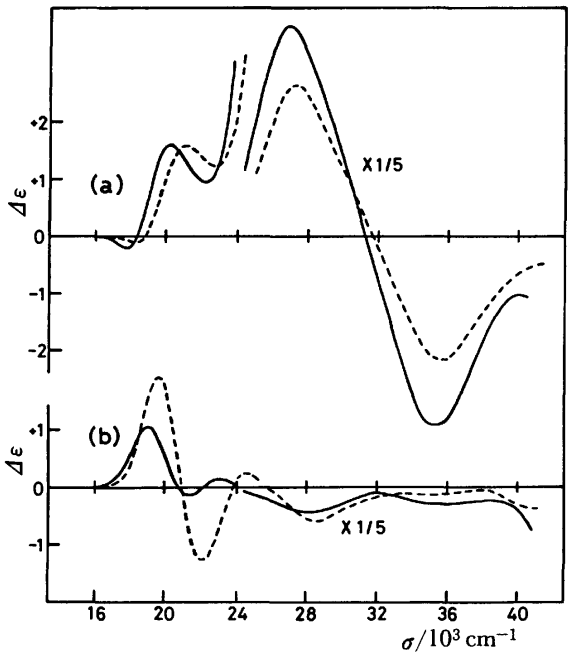

Fig. 5. (a): Vicinal CD curves ($\Delta\varepsilon(S)=1/2\{\Delta\varepsilon[\Lambda\text{-}(S)]-\{\Delta\varepsilon[\Lambda\text{-}(R)]\}$) of [Co(aese)(tn)$_2$]$^{2+}$ (——) and [Co(aese)(en)$_2$]$^{2+}$ (-----).
(b): Configurational CD curves ($\Delta\varepsilon(\Lambda)=1/2\{\Delta\varepsilon[\Lambda\text{-}(S)]+\{\Delta\varepsilon[\Lambda\text{-}(R)]\}$) of [Co(aese)(tn)$_2$]$^{2+}$ (——) and [Co(aese)(en)$_2$]$^{2+}$ (-----).

tion band region, as well as Λ-(+)$^{CD}_{500}$-[Co(mea)(en)$_2$]$^{3+}$ and Λ-(+)$^{CD}_{500}$-[Co(mseea)(en)$_2$]$^{3+}$ (Fig. 4).[4,7,8] Therefore, it is suggested that no isomerization occurs during the methylation procedure and the (+)$^{CD}_{550}$ mea and mseea isomers take the Λ configuration. The ^{1}H NMR spectrum of Λ-(+)$^{CD}_{550}$-[Co(mea)(tn)$_2$]$^{3+}$ exhibits a single peak in the methyl protons region (2.26 ppm from DSS), suggesting that the (+)$^{CD}_{550}$ mea isomer takes either the (*R*) or (*S*) configuration in solution. It is probable that the Λ-(+)$^{CD}_{550}$ mea isomer prefers to the (*R*) configuration as Λ-(+)$^{CD}_{500}$-[Co(mea)(en)$_2$]$^{3+}$,[4,8] because there is a nonbonded interaction between the methyl group and the adjacent diamine chelate ring when Λ-[Co(mea)(tn)$_2$]$^{3+}$ takes the (*S*) configuration. In the sulfur-to-metal charge transfer band region, Λ-(+)$^{CD}_{550}$-[Co(mea)(tn)$_2$]$^{3+}$ shows a positive CD band similar to that of Λ-(*R*)-[Co(mea)(en)$_2$]$^{3+}$ (Fig. 4). The CD band in this region is closely related to the chirality due to the chalcogen donor atom.[8] From these facts, it is suggested that (+)$^{CD}_{550}$-[Co(mea)(tn)$_2$]$^{3+}$ takes selectively the Λ-(*R*) configuration in solution. For Λ-(+)$^{CD}_{550}$-[Co(mseea)(tn)$_2$]$^{3+}$, the ^{1}H NMR spectrum shows two peaks in the methyl protons region (2.19 and 2.32 ppm, in the ratio 4:1). This indicates that the Λ-(+)$^{CD}_{550}$ mseea isomer takes a mixture of the Λ-(*R*) and Λ-(*S*) configurations in solution, contrary to the case of Λ-(+)$^{CD}_{550}$-[Co(mea)(tn)$_2$]$^{3+}$, although the (*R*) configuration seems to be dominant for the Λ-(+)$^{CD}_{550}$ mseea isomer. It is considered that the nonbonded interaction between the methyl group and the adjacent diamine chelate ring in Λ-(*S*)-[Co(mseea)(tn)$_2$]$^{3+}$ is not so conspicuous as that in Λ-(*S*)-[Co(mea)(tn)$_2$]$^{3+}$, because of the longer bond lengths of Co–Se and Se–C than those of Co–S and S–C.[8] The CD spectrum of Λ-(+)$^{CD}_{550}$-[Co(mseea)(tn)$_2$]$^{3+}$ shows a positive band in the chalcogen-to- metal charge transfer band region (*ca.* 32×10^3 cm^{-1}) as well as Λ-(*R*)-[Co(mea)(tn)$_2$]$^{3+}$, though the CD intensity of the former is weaker than that of the latter (Fig. 4). This supports that the Λ-(+)$^{CD}_{550}$ mseea isomer has dominantly the (*R*) configuration, because a negative CD band will appear in the chalcogen-to-metal charge transfer band region if not so.[8,12] The Λ-(+)$^{CD}_{550}$ mseea isomer chromatographed on SP-Sephadex column gave only one adsorbed band and all of its fractions showed the same CD spectra in the whole region. This suggests that the inversion at selenium in Λ-(+)$^{CD}_{550}$-[Co(mseea)(tn)$_2$]$^{3+}$ occurs as in the case for thioether or selenoether cobalt(III) complexes.[17–19]

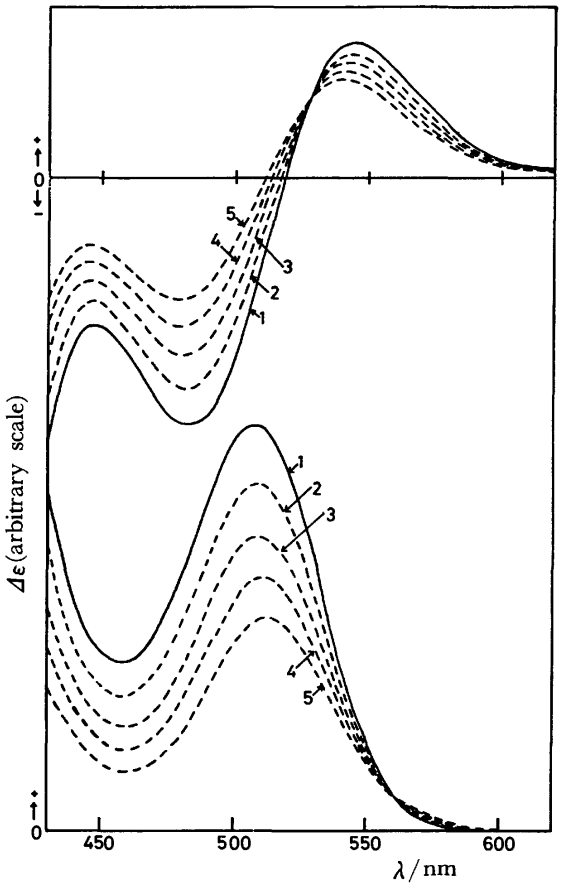

Fig. 6. CD spectral change with time for Λ-(*R*)-[Co(aese)(tn)$_2$]$^{2+}$ (upper) and Λ-(*S*)-[Co(aese)(tn)$_2$]$^{2+}$ (lower) in water at 24 °C. The curves 1—5 were measured at 0, 60, 120, 180, and 240 min, respectively.

Epimerization and Racemization of Λ-(R)- *and* Λ-(S)-*[Co(aese)(tn)$_2$]$^{2+}$.* Of the bis(trimethylenediamine)-cobalt(III) complexes in the present work, Λ-(*R*)- and Λ-(*S*)-[Co(aese)(tn)$_2$]$^{2+}$ exhibited the CD spectral change with time in water. Figure 6 shows the CD spectral change of Λ-(*R*)-[Co(aese)(tn)$_2$]$^{2+}$ (2.72×10^{-3} mol dm^{-3}) and Λ-(*S*)-[Co(aese)(tn)$_2$]$^{2+}$ (3.05×10^{-3} mol dm^{-3}) at 24 °C in the room light. Though the absorption spectral change was also observed for the isomers, the change

was negligibly small as compared with the CD spectral change. The isodichroic point was recognized at 528 nm for the *Λ*-(*R*) isomer and at 561 nm for the *Λ*-(*S*) one for at least 1.5 half-lives. These facts indicate that not only the epimerization at sulfur but the racemization of the skew pair of chelate rings takes place for these isomers under these conditions. The CD intensity change was also observed in the dark. However, this change was only 15% in the room light at the same intervals, and the rate constant could not be obtained because of the decomposition for the complex. Thus, the rate constants for the epimerization and racemization were tentatively estimated from the CD spectral change in the room light. The CD intensity change at 455 nm or 483 nm ($\Delta\varepsilon[\Lambda\text{-}(R)]=-\Delta\varepsilon[\Lambda\text{-}(S)]$) should be regarded as being caused by the epimerization at sulfur and that at 543 nm ($\Delta\varepsilon[\Lambda\text{-}(R)]=\Delta\varepsilon[\Lambda\text{-}(S)]$) by the racemization of the skew pair of chelate rings (Fig. 3). At these wavelengths, the plots of the logarithmic CD intensity change against time gave a straight line, from which the first-order rate constant was obtained; $4.9\times10^{-5}\,s^{-1}$ for the *Λ*-(*R*) isomer and $6.7\times10^{-5}\,s^{-1}$ for the *Λ*-(*S*) one at 455 nm, and $5.0\times10^{-5}\,s^{-1}$ for the *Λ*-(*R*) isomer and $7.2\times10^{-5}\,s^{-1}$ for the *Λ*-(*S*) one at 483 nm. These values may be taken as about the same, considering that the epimerization is affected by the light. The rate constant for the racemization obtained from the CD spectral change at 543 nm is $2.4\times10^{-5}\,s^{-1}$ for both of the *Λ*-(*R*) and *Λ*-(*S*) isomers. This value is smaller than that of the epimerization at sulfur and it is suggested that the epimerization at sulfur was accompanied by the racemization of the skew pair of chelate rings.

References

1) C. A. Stein, P. E. Ellis, Jr., R. C. Elder, and E. Deutsch, *Inorg. Chem.*, **15**, 1618 (1976).

2) B. A. Lange, K. Libson, E. Deutsch, and R. C. Elder, *Inorg. Chem.*, **15**, 2985 (1976).

3) R. H. Lane, F. A. Sedor, M. J. Gilroy, P. E. Eisenhardt, J. P. Bennett, Jr., R. X. Ewall, and L. E. Bennett, *Inorg. Chem.*, **16**, 93 (1977).

4) K. Yamanari, J. Hidaka, and Y. Shimura, *Bull. Chem. Soc. Jpn.*, **50**, 2299 (1977).

5) R. C. Elder, G. J. Kennard, M. D. Payne, and E. Deutsch, *Inorg. Chem.*, **17**, 1296 (1978).

6) I. K. Adzamli, K. Libson, J. D. Lydon, R. C. Elder, and E. Deutsch, *Inorg. Chem.*, **18**, 303 (1979).

7) T. Konno, K. Okamoto, and J. Hidaka, *Chem. Lett.*, **1982**, 535.

8) T. Konno, K. Okamoto, and J. Hidaka, *Bull. Chem. Soc. Jpn.*, **57**, 3104 (1984).

9) M. Kita, K. Yamanari, and Y. Shimura, *Bull. Chem. Soc. Jpn.*, **55**, 2873 (1982).

10) M. Kojima and J. Fujita, *Bull. Chem. Soc. Jpn.*, **56**, 139 (1983).

11) K. Okamoto, T. Konno, M. Nomoto, H. Einaga, and J. Hidaka, *Bull. Chem. Soc. Jpn.*, **57**, 1494 (1984).

12) T. Konno, K. Okamoto, H. Einaga, and J. Hidaka, *Chem. Lett.*, **1983**, 969.

13) Abbreviation used for ligands are as follows: aet, 2-aminoethanethiolate $NH_2CH_2CH_2S^-$; aes, 2-aminoethane selenolate $NH_2CH_2CH_2Se^-$; aese, 2-aminoethanesulfenate $NH_2CH_2CH_2SO^-$; aesi, 2-aminoethanesulfinate $NH_2CH_2CH_2SO_2^-$; mea, 2-(methylthio)ethylamine $NH_2CH_2CH_2SCH_3$; mseea, 2-(methylseleno)ethylamine $NH_2CH_2CH_2SeCH_3$.

14) D. L. Klayman, *J. Org. Chem.*, **32**, 3929 (1967).

15) G. R. Brubaker and D. P. Schaefer, *Inorg. Chem.*, **10**, 968 (1971).

16) G. R. Brubaker and D. P. Schaefer, *Inorg. Chem.*, **10**, 2170 (1971).

17) W. G. Jackson and A. M. Sargeson, *Inorg. Chem.*, **17**, 2165 (1978).

18) K. Okamoto, T. Isago, M. Ohmasa, and J. Hidaka, *Bull. Chem. Soc. Jpn.*, **55**, 1077 (1982).

19) K. Nakajima, M. Kojima, and J. Fujita, *Chem. Lett.*, **1982**, 925.

 © 1985 The Chemical Society of Japan Bull. Chem. Soc. Jpn., 58, 1125—1129 (1985)

Rate and Mechanism of Ligand Exchange of Several Tris(β-diketonato)-iron(III) Complexes with 4-Isopropyltropolone in Carbon Tetrachloride

Tatsuya SEKINE* and Kazuho INABA
Department of Chemistry, Science University of Tokyo, Kagurazaka, Shinjuku-ku, Tokyo 162
(Received September 12, 1984)

The rate of ligand exchange of seven tris(β-diketonato)iron(III) in carbon tetrachloride with 4-isopropyltropolone was measured by a spectrometric method in order to determine the effect of the chemical properties of the leaving ligand on the reaction mechanism. It was found from the dependence of the rate on the leaving and entering ligands and also from the values of $\Delta H^{\neq}$ and $\Delta S^{\neq}$ that the exchange reaction of iron(III) complexes with acetylacetone and its two phenyl-substituted derivatives proceeds by a dissociative mechanism. It was also found that reactions with trifluoroacetylacetone and its phenyl- and 2-thienyl-substituted derivatives proceeds by an associative mechanism. An hexafluoroacetylacetonato complex formed an intermediate with the entering ligand in the first stage of the reaction and then a ligand exchange occured. It was concluded from these results that the ligand exchanges of more stable complexes were controlled by the break of a leaving ligand. Less stable ones were controlled by bond formation with the entering ligand.

In previous studies,[1-3] it was found that the ligand-exchange reaction producing a less stable complex of tris(β-diketonato)iron(III) in carbon tetrachloride proceeded by a dissociative mechanism while the one producing a more-stable complex proceeded by an interchange mechanism. In the present paper, the ligand exchange is further studied with seven tris(β-diketonato)iron(III) using only one entering ligand, 4-isopropyltropolone, which forms a complex more stable than any of these starting compounds. The effect of the nature of the leaving ligand on the reaction mechanism is also considered.

Experimental

All procedures were similar to ones described previously.[1] Iron(III) complexes with acetylacetone (2,4-pentanedione; Hacac), benzoylacetone (1-phenyl-1,3-butanedione; Hbza), dibenzoylmethane (1,3-diphenyl-1,3-propanedione; Hdbm), trifluoroacetylacetone (1,1,1-trifluoro-2,4-pentanedione; Htfa), benzoyltrifluoroacetone (1-phenyl-4,4,4-trifluoro-1,3-butanedione; Hbfa), and 2-thenoyltrifluoroacetone (1-(2-thienyl-)-4,4,4-trifluoro-1,3-butanedione; Htta) were synthesized by a conventional method.[4] The iron(III) complex with hexafluoroacetylacetone (1,1,1,5,5,5-hexafluoro-2,4-pentanedione; Hhfa) was supplied by Tokyo Kasei Co., Tokyo. The 4-isopropyltropolone (Hipt) was supplied by Takasago Perfumery Co., Tokyo. It was dissolved in an aqueous dilute sodium hydroxide solution and then precipitated by a small excess of acetic acid. The precipitates were filtered off and further purified by recrystallization from benzene–petroleum ether. Carbon tetrachloride was purified and dehydrated in the same manner as described previously.[1] A carbon tetrachloride solution containing one of the iron(III) complexes (FeA_3) and β-diketone (HA) in concentration ratios of two to ten FeA_3 to HA was mixed with a portion of the same solvent containing a certain amount of Hipt. The concentration of the complex in the resultant solution was 1×10^{-5} to 2×10^{-4} mol dm^{-3} and that of Hipt was 1×10^{-4} to 1×10^{-1} mol dm^{-3}. In each run, the optical absorption at a certain wavelength of the sample was measured as a function of time.

Data Treatment. When the ligand exchange of FeA_3 with Hipt is controlled by the first exchange reaction and the whole iron(III) species may be exchanged to $[Fe(ipt)_3]$ as under the conditions of the present study, the rate of the ligand-exchange reaction may be expressed from the decrease in the FeA_3 concentration as:

$$V = -\mathrm{d}[FeA_3]/\mathrm{d}t = k_{obsd}[FeA_3]. \quad (1)$$

The concentration of the unexchanged species may be given by:

$$[FeA_3] = [E-\varepsilon_3\times[Fe(III)]](\varepsilon_0-\varepsilon_3)^{-1} \quad (2)$$

where ε_0 and ε_3 give the molar absorption coefficients of the FeA_3 and $[Fe(ipt)_3]$ species and [Fe(III)] gives the total concentration of the iron(III) complex in the solutions.

Results

Under the conditions employed, it was found that the spectrum of the sample solution containing one of the starting complexes and Hipt always completely changed to that of $[Fe(ipt)_3]$ when an equilibrium was established. For this reason, the data analysis was achieved using Eq. 2. The molar absorption coefficient used for the data analysis was as follows: 160 for $[Fe(acac)_3]$ at 550 nm; 530 for $[Fe(bza)_3]$ at 550 nm; 220 for $[Fe(dbm)_3]$ at 590 nm; 270 for $[Fe(tfa)_3]$ at 550 nm; 130 for $[Fe(bfa)_3]$ at 590 nm; 360 for $[Fe(tta)_3]$ at 590 nm; 140 for $[Fe(hfa)_3]$ at 590 nm; and 3180 and 2130 for $[Fe(ipt)_3]$ at 550 and 590 nm.

Rate of Ligand Exchange of [Fe(acac)$_3$], [Fe(bza)$_3$], and [Fe(dbm)$_3$]. The rate of ligand exchange of $[Fe(acac)_3]$, $[Fe(bza)_3]$, and $[Fe(dbm)_3]$ with Hipt was first order with respect to the starting complex. The rate was independent of the leaving ligand but in all cases first order in Hipt in the higher and lower concentration regions. However, it was also found that the rate was independent of the entering ligand in the intermediate concentration region. Figure 1 gives the results as a function of the Hipt concentration at 298 K. The kinetic data in Fig. 1 may generally be represented by the following equation:

$$k_{obsd} = \frac{k_A(1+k_C[Hipt])[Hipt]}{k_B+[Hipt]}. \quad (3)$$

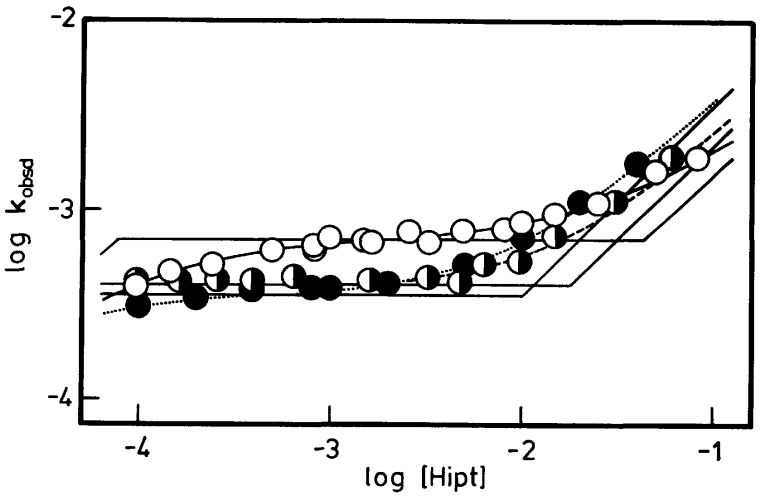

Fig. 1. Rate of [Fe(acac)$_3$] (-○-), [Fe(bza)$_3$] (--◑--), and [Fe(dbm)$_3$] (···●···) reaction with Hipt as a function of the entering ligand concentration at 298 K. The curves are calculated by introducing the constants in Table 1 into Eq. 3. The straight lines are the asymptotes for the curves.

Table 1. Summary of rate constants and activation parameters

	[Fe(acac)$_3$]	[Fe(bza)$_3$]	[Fe(dbm)$_3$]	[Fe(tfa)$_3$]	[Fe(bfa)$_3$]	[Fe(tta)$_3$]
log (k_A/s^{-1})	−3.16±0.06	−3.41±0.10	−3.45±0.05	—	—	—
log (k_B/mol dm^{-3})	*ca.* −4.5	<−5.0	*ca.* −4.9	—	—	—
log (k_C/mol^{-1} dm^3 s^{-1})	1.36±0.27	1.75±0.40	1.99±0.12	—	—	—
log (k_D/mol^{-1} dm^3 s^{-1})	—	—	—	0.16±0.09	−0.46±0.06	−0.53±0.05
ΔH^*/kJ mol^{-1}	82±2	88±2	85±2	47±1	52±1	52±1
ΔS^*/J K^{-1} mol^{-1}	−29±5	−12±5	−25±5	−84±2	−81±2	−81±2

The constants k_A, k_B, and k_C obtained from these data by a least-squares program are listed in Table 1.

Rate of Ligand Exchange of [Fe(tfa)$_3$], [Fe(bfa)$_3$], and [Fe(tta)$_3$]. The rate of ligand exchange between these complexes with Hipt was first order with respect to the starting complex and independent of the leaving ligand. However, in all cases, it was first order with respect to the entering ligand. Figure 2 gives the results as a function of the Hipt concentration at 298 K. These results may be represented by the following equation:

$$k_{obsd} = k_D[\text{Hipt}]. \quad (4)$$

The values of the constant k_D obtained from these data are listed in Table 1.

Rate of Ligand Exchange of [Fe(hfa)$_3$]. In the course of the study of the ligand exchange of [Fe(hfa)$_3$] with Hipt, it was found that the color of a sample solution changed rather rapidly from orange to green after mixing the complex and ligand solutions. The color then gradually changed due to the ligand exchange until the solution became completely that of [Fe(ipt)$_3$]. It was concluded from the absorption of the mixed solutions at equilibrium, that this change was not due to the formation of mixed complexes, [Fe(hfa)$_2$(ipt)] and [Fe(hfa)(ipt)$_2$], but due to an association between the [Fe(hfa)$_3$] and Hipt. However, the data in these experiments were not accurate enough to allow a further data analysis of such an association

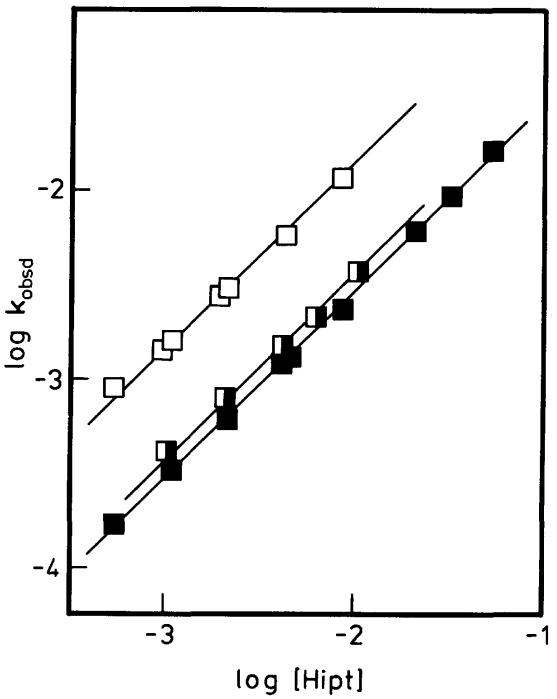

Fig. 2. Rate of [Fe(tfa)$_3$] (□), [Fe(bfa)$_3$] (◨), and [Fe(tta)$_3$] (■) reaction with Hipt as a function of the entering ligand concentration at 298 K. The straight lines are calculated by introducing the constants in Table 1 into Eq. 4.

reaction and no final conclusions regarding the mechanism of the ligand exchange reaction of [Fe(hfa)$_3$]

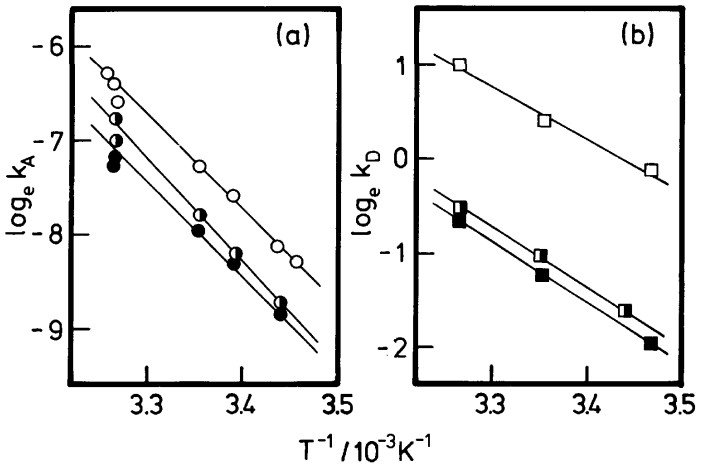

Fig. 3. Arrhenius plot of the ligand exchange reactions.
(a) Dependence of k_A for [Fe(acac)$_3$] (○), [Fe(bza)$_3$] (◑), and [Fe(dbm)$_3$] (●) reaction as a function of temperature.
(b) Dependence of k_D for [Fe(tfa)$_3$] (□), [Fe(bfa)$_3$] (◨), and [Fe(tta)$_3$] (■) reaction as a function of temperature.

could be drawn.

Effect of Temperature. The ligand-exchange rate was also determined at various temperatures. Figures 3(a) and (b) give the $\log_e k_A$ or k_D *vs.* $1/T$ plot. As seen from Fig. 3(a), the results with [Fe(acac)$_3$], [Fe(bza)$_3$], and [Fe(dbm)$_3$] seems to be somewhat erroneous at high temperatures for some unknown reasons. This kind of inaccuracy was also observed in a previous study.[1] However, it can also be seen from the figure that the values of ΔH^* and ΔS^* obtained from the slope of the lines are reasonable. The values of the activation enthalpy and entropy obtained from these data are listed in Table 1.

Discussion

Since the ligand-exchange data for [Fe(acac)$_3$], [Fe(bza)$_3$], and [Fe(dbm)$_3$] with Hipt could be represented by Eq. 3, the reaction should proceed through a dissociative or an interchange mechanism. The values of the activation parameters of the ligand exchange of [Fe(acac)$_3$] with Hipt are similar to those when the entering ligand was Htfa or Htta in the previous paper.[1] For this reason, the mechanism of this reaction was concluded to be dissociative. The values of the activation parameters (ΔH^* and ΔS^*) of the reactions of [Fe(bza)$_3$] and [Fe(dbm)$_3$] with Hipt also indicate a dissociative nature of the mechanism and this seems to be reasonable because the leaving ligand from the complexes are chemically similar to that of [Fe(acac)$_3$]. Thus, it was assumed that the reaction mechanism for these three complexes should be similar to that found in the previous paper:[1]

$$FeA_3 \underset{k_{-1}}{\overset{k_1}{\rightleftharpoons}} FeA_3^* \xrightarrow[+Hipt]{k_2} [FeA_2(ipt)] + HA. \quad (5)$$

Here FeA_3^* gives a complex one of whose chelate ring is open. When the chemical species FeA_3^* is assumed to be in a steady-state, the rate may be written as:

$$V = \frac{k_1[Hipt]}{k_{-1}/k_2 + [Hipt]}[FeA_3]. \quad (6)$$

As seen from Eq. 3, k_1 in Eq. 6 corresponds with k_A and k_{-1}/k_2 with k_B. The k_C value was calculated from data obtained in a higher Hipt concentration region where the rate is dependent on the entering ligand. This dependence should be due to a catalytic reaction by Hipt.[1]

The first-order dependence on the entering ligand found with the three complexes of the β-diketones having one trifluoromethyl group, indicates that the reaction proceeds by an associative mechanism:

$$FeA_3 + Hipt \xrightarrow{k} [FeA_3(Hipt)] \xrightarrow{fast} [FeA_2(ipt)] + HA. \quad (7)$$

Thus the rate should be represented by:

$$V = k[Hipt][FeA_3]. \quad (8)$$

The value of k in Eq. 8 is naturally identical to the value of k_D in Table 1, which was obtained on the basis of Eq. 4. As seen from Table 1, the value k_D of [Fe(tfa)$_3$] is somewhat different from those of [Fe(tta)$_3$] and [Fe(bfa)$_3$]. This could be caused by various factors such as the difference in the ability of the complexes to accept an entering ligand and as the difference in the steric hindrance by these ligands.

Among complexes of a certain metal ion with homologous ligands such as β-diketones, the order of the ability as an acceptor of several neutral ligands to form adducts in nonpolar organic solvents is usually

opposit to that of their stability. In other words, less stable complexes tend to form more stable adducts. This has been observed in the "synergistic" solvent extraction of metal β-diketonates.[5] The replacement of a methyl group of a β-diketone with a trifluoromethyl group increases the acid-dissociation constant. This, consequently, causes a decrease in the ability to form complexes with metal ions. For example, the values of pK_a is about $10^{9.0}$, $10^{6.1}$, and $10^{4.3}$, respectively, for Hacac, Htfa, and Hhfa in a 1 mol dm^{-3} sodium perchlorate solution.[6] The values of β_3 are about 10^{27}, 10^{20}, and 10^{10}, respectively, for $[Fe(acac)_3]$,[7] $[Fe(tfa)_3]$,[8] and $[Fe(hfa)_3]$.[9] From these data, it can reasonablly be assumed that $[Fe(hfa)_3]$ should be the strongest acceptor for neutral ligand to form adducts and $[Fe(acac)_3]$ should be the weakest among these three.

In separate experiments, the absorption spectra of $[Fe(acac)_3]$, $[Fe(tfa)_3]$, and $[Fe(hfa)_3]$ in carbon tetrachloride and in 4-methyl-2-pentanone (MIBK) were measured. It was observed that each spectrum of $[Fe(acac)_3]$ and $[Fe(tfa)_3]$ was not affected by the solvents. However, that of $[Fe(hfa)_3]$ in the visible region was much lower in MIBK than in carbon tetrachloride. This change in the spectrum seems to be caused by stronger interactions between the MIBK molecules and the complex. The fact that this occured only with $[Fe(hfa)_3]$ also illustrates the higher ability of $[Fe(hfa)_3]$ to act as an acceptor of a neutral ligand than the other two complexes.

In previous studies[10,11] it was suggested that a reaction in aqueous solutions could be represented as $Fe^{3+}+HX \rightarrow FeX^{2+}+H^+$ where HX was an acid to form a chelate complex proceeded by an associative interchange mechanism. When this assumption is also valid with β-diketones, the order of complex formation ($V=k_{CF}[Fe^{3+}][HA]_{enol}$: log k_{CF} for Hipt is 1.3,[10] for Hacac is 0.7,[12] for Htfa is 0.8,[13] and for Htta is 0.1[14]) should indicates the order of nucleophilic tendency of these ligands. Furthermore, if the order of nucleophilic tendency would be similar to the order of the nucleophilic tendency of the ligands in nonpolar solvents, Hipt should be a stronger donor than any of the β-diketones studied in the previous paper, Hacac, Htfa, and Htta.[1]

The mechanism of the ligand-exchange reactions treated in this study may be written as follows. (1) The nature of the mechanism of the ligand-exchange reactions of $[Fe(acac)_3]$, $[Fe(bza)_3]$, and $[Fe(dbm)_3]$ whose ability to accept a donor was smaller than the other tris(β-diketonato)iron(III), was dissociative. (2) The ligand-exchange reaction of $[Fe(hfa)_3]$, whose ability to accept a donor was the greatest among the complexes studied here, proceeded after an association of the complex with the entering ligand. (3) The ligand-exchange reactions of $[Fe(tfa)_3]$, $[Fe(bfa)_3]$, and $[Fe(tta)_3]$ who had intermediate ability as an acceptor proceeded by an associative mechanism. In the previous paper,[1] it was assumed from the activation parameters that the exchange reactions of $[Fe(tfa)_3]$ with Hacac and Htta which are weaker donors than Hipt proceeded by an interchange mechanism. Those of $[Fe(tta)_3]$ with Hacac and Htfa also proceeded by a mechanism of the same type. These reactions indicate that the mechanism is very much affected by the nature of the bonds between the metal ion and leaving ligands.

Gutmann[15] pointed out that the rate of dissociation of a ligand from a complex is higher if the donecity of the other ligands is greater. A tendency of this type has been suggested by the present study though the complexes treated here contained only one kind of ligand. The mechanism of the ligand exchange of the three iron(III) chelates with the β-diketones having no trifluoromethyl group were always dissociative. On the other hand, those of the other complexes were in all cases not dissociative. This may be explained in terms of the fact that the donecity of the ligands in the latter complexes is lower than of the ligands in the former. At the same time, the latter complexes are better acceptors of the entering ligand to form associates.

Ishihara, Funahashi, and Tanaka[16] measured the activation volume of the complex formation of iron(III) with Hipt in water, *N,N*-dimethylformamide, and dimethyl sulfoxide. They interpreted the data of activation volume in terms of the bulkiness of both the entering ligand and the coordinated solvent molecules. The present results indicate that the ability of the complex as an acceptor and the ability of the entering ligand as a donor are also important factors which affect the type of the reaction mechanism.

The rate of ligand exchange of $[Fe(bza)_3]$ in hexane with Hacac and the effect of butanol as a catalyst for this reaction was studied using a spectrometric method.[17]

Kido and Saito[4] concluded that the ligand-exchange reaction of $[Fe(acac)_3]$ with Hacac in undiluted acetylacetone proceeds by an associative mechanism. Since the medium and the entering ligand in our study are different, no direct comparison of the results from the two studies is possible.

The authors are grateful to Miss Chiaki Mizuno and Mr. Eiji Yokose for their experimental help during this study. They are also grateful to Dr. Shigeru Suzuki of the Tokyo College of Pharmacy, for the elementary analysis of the complexes.

References

1) T. Sekine and K. Inaba, *Bull. Chem. Soc. Jpn.*, **57**, 3083 (1984).

2) T. Sekine and K. Inaba, *Chem. Lett.*, **1983**, 1669.

3) T. Sekine, H. Honda, M. Kokiso, and T. Tosaka, *Bull. Chem. Soc. Jpn.*, **52**, 1046 (1979).

4) H. Kido and K. Saito, *Bull. Chem. Soc. Jpn.*, **53**, 424 (1980).

5) T. Sekine and Y. Hasegawa, "Solvent Extraction Chemistry," Marcel Dekker, New York (1977).

6) T. Sekine, Y. Hasegawa, and N. Ihara, *J. Inorg. Nucl.*

Chem., **35**, 3968 (1973).

7) L. G. Sillén and A. E. Martell, "Stability Constants," spec. pub. No. 17, The Chemical Society, London (1964).

8) T. Sekine and K. Inaba, *Bunseki Kagaku*, **31**, E291 (1982).

9) K. Inaba, N. Itoh, Y. Matsuno, and T. Sekine, *Bull. Chem. Soc. Jpn.*, submitted.

10) K. Ishihara, S. Funahashi, and M. Tanaka, *Inorg. Chem.*, **22**, 194 (1983).

11) S. Funahashi, K. Ishihara, and M. Tanaka, *Inorg. Chem.*, **22**, 2070 (1983).

12) D. P. Fay, A. R. Nichols, Jr., and N. Sutin, *Inorg. Chem.*, **10**, 2096 (1971).

13) T. Sekine and K. Inaba, *Bull. Chem. Soc. Jpn.*, **55**, 3773 (1982).

14) M. R. Jaffe, D. P. Fay, M. Cefola, and N. Sutin, *J. Am. Chem. Soc.*, **93**, 2878 (1971).

15) V. Gutmann, "The Donor-Acceptor Approach to Molecular Interactions," Chapter 12, pp. 183—184, Plenum Press, New York (1978).

16) K. Ishihara, S. Funahashi, and M. Tanaka, *Inorg. Chem.*, **22**, 3589 (1983).

17) V. M. Nekipelov, V. A. Ivanchenko, and K. I. Zamaraev, *Kinet. Katal.*, **24**, 591 (1983).

Inversion at Selenium in $[M^{III}(RSeCH_2CH_2NH_2)\{N(CH_2CH_2NH_2)_3\}]^{3+}$ (M^{III}=Co, Rh; R=CH_3, CH_3CH_2, $C_6H_5CH_2$) and $[Co(CH_3SeCH_2COO)\{N(CH_2CH_2NH_2)_3\}]^{2+}$

Kiyohiko NAKAJIMA, Katsuhiko TOZAKI, Masaaki KOJIMA, and Junnosuke FUJITA*
Department of Chemistry, Faculty of Science, Nagoya University, Nagoya 464
(Received October 17, 1984)

The selenoether (selenide) complexes, *t*-[Co(RSeCH$_2$CH$_2$NH$_2$)(tren)]$^{3+}$ (*t*=*trans*(*tertiary amine nitrogen, Se*); R=CH_3, CH_3CH_2, $C_6H_5CH_2$; tren=tris(2-aminoethyl)amine), *p*-[Rh(CH$_3$SeCH$_2$CH$_2$NH$_2$)(tren)]$^{3+}$ (*p*=*cis*-(*tertiary amine nitrogen, Se*)), and *t*-[Co(CH$_3$SeCH$_2$COO)(tren)]$^{2+}$ were prepared and resolved for the first time by the chemical or SP-Sephadex column chromatographic method. Racemization of these complexes in aqueous solutions was studied at an ionic strength of 0.25 ($NaClO_4$) in the pH and temperature ranges of 4.00—6.91 and 0.25—33.50 °C, respectively. The racemization rates were independent of pH and an intramolecular inversion mechanism was suggested. The $\Delta G^{\neq}_{25\,°C}$ values for inversion of *t*-[Co(RSeCH$_2$CH$_2$NH$_2$)-(tren)]$^{3+}$ decreases in the order of CH_3 (95.2 kJ mol^{-1})>CH_3CH_2 (89.4)>$C_6H_5CH_2$ (87.7), while the $\Delta H^{\neq}$ values are almost the same (95—97 kJ mol^{-1}). The variable-temperature ^{13}C NMR study of *p*-[Co(CH$_3$SeCH$_2$CH$_2$NH$_2$)-(tren)]$^{3+}$ yielded the inversion rate constant, 10 s^{-1} at the coalescence temperature (*ca.* 60 °C), which is much larger than that of the corresponding *t*-isomer (8.5×10^{-3} s^{-1} at 60 °C). The difference in inversion rate between the isomers seems to be related to the steric crowding around the Se-R group of the complex. The rhodium(III) complex racemizes slower than the corresponding cobalt(III) complex. The values of thermodynamic parameters for *t*-[Co(CH$_3$SeCH$_2$COO)(tren)]$^{2+}$ are nearly the same as those for *t*-[Co(CH$_3$SeCH$_2$CH$_2$NH$_2$)(tren)]$^{3+}$.

Many sulfonium ions have been resolved and the racemization can be followed in solution by conventional techniques such as polarimetry.[1] The activation energy for inversion has been reported to be 105—120 kJ mol^{-1}, and larger values are to be expected for inversion at selenium in analogous selenonium ions.[1] It is known that both thioethers (sulfides) and selenoethers (selenides) form metal complexes formally analogous to sulfonium and selenonium ions, respectively. However, activation energy for inversion at the sulfur and selenium donor atoms in metal complexes is much smaller than that for their organic counterparts.[2] For example, the rates of inversion at sulfur and selenium in the Pd^{II}, Pt^{II}, and Pt^{IV} complexes have been reported to be in the range of 10^4—10^{-1} s^{-1} by the ^1H or ^{13}C dynamic NMR method.[2] Thus, neither optically active thioether nor selenoether complexes, in which the sulfur or selenium atom is the sole source of optical activity, have been reported.

Studies on chiral cobalt(III)–thioether complexes,[3,4] on the other hand, suggest that the rate of inversion at sulfur in these complexes is slower than those for the Pd^{II}, Pt^{II}, and Pt^{IV} complexes. Since inversion at a coordinated selenoether site will be slower than that at a corresponding thioether site,[1] a selenoether ligand coordinated to cobalt(III) would be fairly stable toward inversion and might permit optical activity.

This paper reports resolution, characterization, and kinetic studies on inversion of *p*-[M^{III}(CH$_3$SeCH$_2$-CH$_2$NH$_2$)(tren)]$^{3+}$ [5] (M^{III}=Co, Rh; tren=tris(2-aminoethyl)amine), *t*-[Co(RSeCH$_2$CH$_2$NH$_2$)(tren)]$^{3+}$ [5] (R=CH_3, CH_3CH_2, $C_6H_5CH_2$), and *t*-[Co(CH$_3$SeCH$_2$-COO)(tren)]$^{2+}$ (Fig. 1). In these complexes, the configuration of the selenium atom is the sole source of chirality. A preliminary report on [Co(CH$_3$SeCH$_2$CH$_2$NH$_2$)-(tren)]$^{3+}$ has been published.[6]

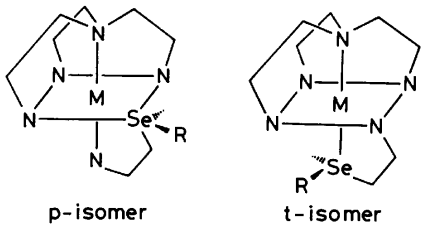

Fig. 1. Two geometrical isomers of [M(RSeCH$_2$-CH$_2$NH$_2$)(tren)]$^{3+}$.

Experimental

Materials. *p*-[Co(SeCH$_2$CH$_2$NH$_2$)(tren)](ClO$_4$)$_2$,[6,7] *t*-[Co(SeCH$_2$CH$_2$NH$_2$)(tren)]ZnCl$_4$·2H$_2$O,[6,7] and *p*-[Rh(Se-CH$_2$CH$_2$NH$_2$)(tren)](ClO$_4$)$_2$[7] were prepared as described earlier.

p-[Co(CH$_3$SeCH$_2$CH$_2$NH$_2$)(tren)]Cl$_3$·2.5H$_2$O. This complex was prepared by methylating *p*-[Co(SeCH$_2$CH$_2$NH$_2$)-(tren)](ClO$_4$)$_2$ according to the procedure analogous to that for *p*- and *t*-[Co(CH$_3$SCH$_2$CH$_2$NH$_2$)(tren)]$^{3+}$.[3] To a dimethyl sulfoxide (DMSO) solution (50 cm^3) of *p*-[Co(SeCH$_2$CH$_2$-NH$_2$)(tren)](ClO$_4$)$_2$ (2.64 g, 5 mmol) was added CH_3I (7.10 g, 50 mmol). Within a few minutes the color of the solution changed from dark brown to orange-red. The solution was allowed to stand for 5 h at room temperature, diluted with 1×10^{-3} mol dm^{-3} HCl (500 cm^3), and the excess CH_3I was extracted with $CHCl_3$ (150 cm^3×2). The orange-red aqueous layer was applied on a column (ϕ1.5 cm×2 cm) of SP-Sephadex C-25. The adsorbed product was washed with water, and then eluted with 1 mol dm^{-3} $NaClO_4$. The effluent was evaporated under reduced pressure to yield red crystals of the perchlorate of the complex (2.5 g). The complex was converted into the chloride by use of a column (ϕ1.5 cm× 6 cm) of Dowex 1X8 (Cl^- form). The effluent containing the chloride was evaporated to a small volume. On addition of ethanol the concentrate yielded red fine crystals, which were collected by filtration and recrystallized from water by adding ethanol. Yield: 0.8 g. Found: C, 21.84; H, 6.69; N, 14.36%. Calcd for $C_9H_{32}N_5Cl_3CoO_{2.5}Se$: C, 21.85; H, 6.52; N, 14.16%.

t-[Co(CH$_3$SeCH$_2$CH$_2$NH$_2$)(tren)]Br$_3$·H$_2$O, *t-[Co(CH$_3$CH$_2$-*

$SeCH_2CH_2NH_2$)(tren)]$Br_3 \cdot 4H_2O$, and t-*[Co($C_6H_5CH_2SeCH_2$-CH_2NH_2)(tren)]$Cl_3 \cdot 2H_2O$.* These complexes were prepared from *t*-[Co($SeCH_2CH_2NH_2$)(tren)]$ZnCl_4 \cdot 2H_2O$ and an appropriate alkylating reagent (CH_3I, CH_3CH_2I, and $C_6H_5CH_2Br$) by a method similar to that for *p*-[Co(CH_3-$SeCH_2CH_2NH_2$)(tren)]$Cl_3 \cdot 2.5H_2O$. The CH_3-, CH_3CH_2-, and $C_6H_5CH_2$-substituted complexes adsorbed on SP-Sephadex C-25 were eluted with 1 mol dm^{-3} NaBr, LiBr, and LiCl, respectively. Each eluate was concentrated to a small volume, and then mixed with ethanol, yielding crystals of the complex. Yields: 80—98%. Found: C, 17.95; H, 5.04; N, 11.99%. Calcd for $C_9H_{29}N_5Br_3CoOSe$: C, 17.98; H, 4.86; N, 11.65%. Found: C, 17.71; H, 4.93; N, 10.32%. Calcd for $C_{10}H_{37}N_5Br_3CoO_4Se$: C, 17.95; H, 5.57; N, 10.46%. Found: C, 32.11; H, 5.92; N, 12.85%. Calcd for $C_{15}H_{35}N_5Cl_3CoO_2Se$: C, 32.07; H, 6.28; N, 12.47%.

p-*[Rh($CH_3SeCH_2CH_2NH_2$)(tren)]X_3 (X=Br, ClO_4).* This complex was prepared from *p*-[Rh($SeCH_2CH_2NH_2$)(tren)]-$(ClO_4)_2$ and CH_3I by the same method as that described for *p*-[Co($CH_3SeCH_2CH_2NH_2$)(tren)]$^{3+}$, and isolated as the bromide and the perchlorate. Yields: 80—85%. Found: C, 17.43; H, 4.37; N, 11.14%. Calcd for $C_9H_{27}N_5Br_3RhSe$: C, 17.24; H, 4.34; N, 11.17%. Found: C, 15.67; H, 4.30; N; 10.50%. Calcd for $C_9H_{27}N_5Cl_3O_{12}RhSe$: C, 15.77; H, 3.97; N, 10.22%.

t-*[Co($SeCH_2COO$)(tren)]Cl and* t-*[Co(CH_3SeCH_2COO)(tren)]-$(ClO_4)_2$.* The *t*-[Co($SeCH_2COO$)(tren)]Cl complex was prepared by a method analogous to that for [Co($SeCH_2$-COO)$(en)_2$]$^{+}$[8] (en=ethylenediamine). Time required for the oxidation of Co^{II}-N_4 (N_4=tren or $(en)_2$) species with the diselenide, ($HOOCCH_2Se$-)$_2$[9] was longer for the tren complex than that for the en complex. To a deoxygenated aqueous solution (5 cm^3) of $CoCl_2 \cdot 6H_2O$ (2.20 g, 6.0 mmol) was added a deoxygenated aqueous solution (9 cm^3) containing tren·3HCl (1.53 g, 6.0 mmol) and NaOH (0.72 g, 18.0 mmol). The color of the solution changed from light red to violet. Then a deoxygenated aqueous solution (10 cm^3) containing ($HOOCCH_2Se$-)$_2$ (0.828 g, 3.0 mmol) and NaOH (0.24 g, 6.0 mmol) was added to the solution and the mixture was allowed to stir for 5 days under a nitrogen atmosphere. The color of the solution changed from violet to dark brown and brown fine crystals were deposited. The crystals were collected by filtration, washed with ethanol, and air dried. Yield: 0.18 g. No evidence indicative of the presence of the other isomer was obtained either in the ^1H NMR spectrum of the isolated complex or by column chromatography (column: SP-Sephadex C-25; eluent: 0.05 mol dm^{-3} Na_2SO_4) of the reaction mixture. The complex was used for the subsequent reaction without any purification.

The complex was methylated by the same method as that for *p*-[Co($CH_3SeCH_2CH_2NH_2$)(tren)]$^{3+}$, and the product was isolated as the perchlorate. Yield: 65%. Found: C, 19.44; H, 4.17; N, 10.08%. Calcd for $C_9H_{23}N_4Cl_2CoO_{10}Se$: C, 19.37; H, 4.16; N, 10.10%. The bromide of the complex was obtained from the perchlorate by means of Dowex 1X8 (Br^- form).

Resolution of the Complexes. All the complexes except for *p*-[Co($CH_3SeCH_2CH_2NH_2$)(tren)]$^{3+}$ were partially resolved. Complete resolution of the complexes was not attempted because they are likely to racemize.

$(-)^{CD}_{480}$-t-*[Co($CH_3SeCH_2CH_2NH_2$)(tren)]$Br_3 \cdot 1.5H_2O$.* To an aqueous solution (2 cm^3) of *t*-[Co($CH_3SeCH_2CH_2NH_2$)-(tren)]$Br_3 \cdot H_2O$ (0.21 g, 3.43 mmol) was added $Ag_2[Sb_2(d\text{-tart})_2]$ (0.258 g, 3.43 mmol, *d*-tart=(*R,R*)-tartrate ion). The silver bromide precipitated was removed by filtration, and the filtrate was slowly evaporated to dryness over P_2O_5 in a vacuum desiccator to yield a glassy material, which was broken up, suspended in ethanol, filtered, and washed with ethanol. The product was dissolved in a small amount of cold water. To the solution was added sodium tetraphenylborate to give a precipitate immediately. It was filtered, washed with water, and dissolved in a small amount of acetone. To this solution was added excess LiBr followed by addition of ethanol to yield an orange-red precipitate. It was collected by filtration, washed with ethanol, and air dried. Yield: 0.10 g. Found: C, 17.37; H, 4.85; N, 11.62%. Calcd for C_9H_{30}-$N_5Br_3CoO_{1.5}Se$: C, 17.19; H, 5.04; N, 11.99%.

t-[Co($CH_3SeCH_2CH_2NH_2$)(tren)]$^{3+}$ was also partially resolved by column chromatography. An aqueous solutoin of the complex (*ca.* 70 mg) was charged on the top of an SP-Sephadex C-25 column (ϕ2 cm×30 cm). By elution with 0.15 mol dm^{-3} $Na_2[Sb_2(d\text{-tart})_2]$, the column showed a single band, however, the front and the tail fractions of the band showed enantiomeric CD patterns.

$(-)^{CD}_{480}$-t-*[Co($CH_3CH_2SeCH_2CH_2NH_2$)(tren)]$^{3+}$*, $(-)^{CD}_{475}$-t-*[Co-($C_6H_5CH_2SeCH_2CH_2NH_2$)(tren)]$^{3+}$, and $(-)^{CD}_{330}$*-p-*[Rh(CH_3-$SeCH_2CH_2NH_2$)(tren)]$^{3+}$.* The racemic complexes were resolved by the same method as that for $(-)^{CD}_{480}$-*t*-[Co($CH_3SeCH_2CH_2NH_2$)(tren)]$^{3+}$ except that AgBCS·H_2O (BCS=(*1R,3S,4S,7R*)-3-bromo-9-camphorsulfonate ion) was used ([complex]:[BCS^-]=1:1) instead of $Ag_2[Sb_2(d\text{-tart})_2]$ for the former two complexes. The BCS^- and $[Sb_2(d\text{-tart})_2]^{2-}$ ions were not converted into achiral anions such as Cl^-, because these complexes racemize rather fast in solution.

$(-)^{CD}_{475}$- *and* $(+)^{CD}_{475}$-t-*[Co(CH_3SeCH_2COO)(tren)]$^{2+}$.* The racemic complex was resolved with AgBCS·H_2O([complex]:[BCS^-]=1:2) by a method similar to that for $(-)^{CD}_{480}$-*t*-[Co(CH_3-$SeCH_2CH_2NH_2$)(tren)]$^{3+}$. The silver bromide precipitated was filtered off, and the filtrate was evaporated over P_2O_5 in a vacuum desiccator to yield fine crystals consisting of two different colors, pink and deep orange-red. The two kinds of crystals which show enantiomeric CD patterns were separated by hand picking. The pink $(-)^{CD}_{475}$-isomer was converted into the perchlorate by the same method as that for $(-)^{CD}_{480}$-*t*-[Co($CH_3SeCH_2CH_2NH_2$)(tren)]$Br_3 \cdot 1.5H_2O$ except that $LiClO_4 \cdot 3H_2O$ was used instead of LiBr.

Racemization Studies. Rates of racemization were determined by monitoring the change in CD strength at 480 nm (*t*-[Co($RSeCH_2CH_2NH_2$)(tren)]$^{3+}$; R=CH_3, CH_3-CH_2), 475 nm (*t*-[Co($C_6H_5CH_2SeCH_2CH_2NH_2$)(tren)]$^{3+}$ and *t*-[Co(CH_3SeCH_2COO)(tren)]$^{2+}$), and 330 nm (*p*-[Rh(CH_3-$SeCH_2CH_2NH_2$)(tren)]$^{3+}$) as a function of reaction time. The complex concentrations were *ca.* 10^{-3} mol dm^{-3}, and the measurements were made at an ionic strength of 0.25 ($NaClO_4$) and in the pH and temperature ranges of 4.00—6.91 and 0.25—33.50 °C, respectively. The inversion rate of *p*-[Co-($CH_3SeCH_2CH_2NH_2$)(tren)]$^{3+}$ was determined by monitoring the change in the ^{13}C NMR spectrum in the temperature range of 30—60 °C.

Measurements. Absorption and circular dichroism (CD) spectra were recorded on a Hitachi 323 spectrophotometer and a JASCO J-40CS spectropolarimeter, respectively. ^{13}C NMR spectra were obtained in D_2O with a JEOL FX-60 FT NMR spectrometer using dioxane as an internal reference.

Results and Discussion

Preparation, Partial Resolution, and Characterization

TABLE 1. ABSORPTION SPECTRAL DATA OF THE COMPLEXES

Complex	$\tilde{\nu}_{max}/cm^{-1}$	$\log(\varepsilon/mol^{-1}\,dm^3\,cm^{-1})$
p-[Co($CH_3SeCH_2CH_2NH_2$)(tren)]$^{3+}$	20120	2.29
	32700	4.01
	42550	4.14
t-[Co($CH_3SeCH_2CH_2NH_2$)(tren)]$^{3+}$	20280	2.17
	32800	4.15
	45500	4.16[a]
t-[Co($CH_3CH_2SeCH_2CH_2NH_2$)(tren)]$^{3+}$	20240	2.16
	32700	4.14
	44500	4.14[a]
t-[Co($C_6H_5CH_2SeCH_2CH_2NH_2$)(tren)]$^{3+}$	20140	2.24
	31950	4.22
	44250	4.33
t-[Co(CH_3SeCH_2COO)(tren)]$^{2+}$	20160	2.14
	33000	4.09
	44800	4.09
p-[Rh($CH_3SeCH_2CH_2NH_2$)(tren)]$^{3+}$	31650	2.87
	41500	4.09

a) Shoulder.

of the Complexes. The selenoether complexes of cobalt(III) and rhodium(III) were prepared by alkylating the corresponding selenolato complexes with the appropriate alkyl halides. The reactions proceeded almost quantitatively. Column chromatography of the reaction mixtures showed a single band, and the selenoether complexes thus obtained should have the same geometrical configurations as those of the respective parent selenolato complexes. The geometrical configurations of [Co($SeCH_2CH_2NH_2$)(tren)]$^{2+}$ have been assigned on the basis of the elution order in column chromatography.[6,7] The structure of the rhodium(III) complex, *p*-[Rh($SeCH_2CH_2NH_2$)(tren)](ClO_4)$_2$ has been determined by the X-ray method.[7]

The first d-d absorption band of *t*-[Co($RSeCH_2CH_2NH_2$)(tren)]$^{3+}$ shifts to lower energy as R is changed from CH_3 through CH_3CH_2 to $C_6H_5CH_2$ (Table 1).

Both *p*- and *t*-isomers of [Co($RSeCH_2CH_2NH_2$)(tren)]$^{3+}$ exhibit a strong Se to Co^{III} charge-transfer (CT) band at 32000—33000 cm^{-1}, while the rhodium(III) complex gives the corresponding band at 41500 cm^{-1}. The positions of the CT bands are nearly the same as those for the parent selenolato complexes.[7]

The [Co(CH_3SeCH_2COO)(tren)]$^{2+}$ complex forms one geometrical isomer as confirmed by chromatography and ^1H NMR spectroscopy. The corresponding thioether complex, [Co(CH_3SCH_2COO)(tren)]$^{2+}$ and analogous [Co{$CH_3SCH(CH_3)COO$}(tren)]$^{2+}$ also form one geometrical isomer,[10] and the structure of the latter complex has been determined to have the *t*-configuration by X-ray analysis.[11] These thioether complexes show the first absorption band ([Co(CH_3SCH_2COO)(tren)]$^{2+}$: 20620 cm^{-1}, [Co{$CH_3SCH(CH_3)COO$}(tren)]$^{2+}$: 20640 cm^{-1}) between those of the *p*-(20530 cm^{-1}) and *t*-isomer (20790 cm^{-1}) of [Co($CH_3SCH_2CH_2NH_2$)(tren)]$^{3+}$.[10] The first absorption band (20160 cm^{-1}) of [Co(CH_3SeCH_2COO)(tren)]$^{2+}$ is also observed between the *p*-(20120 cm^{-1}) and *t*-isomer (20280 cm^{-1}) of [Co($CH_3SeCH_2CH_2NH_2$)(tren)]$^{3+}$. Selective formation of the thio and selenoether complexes

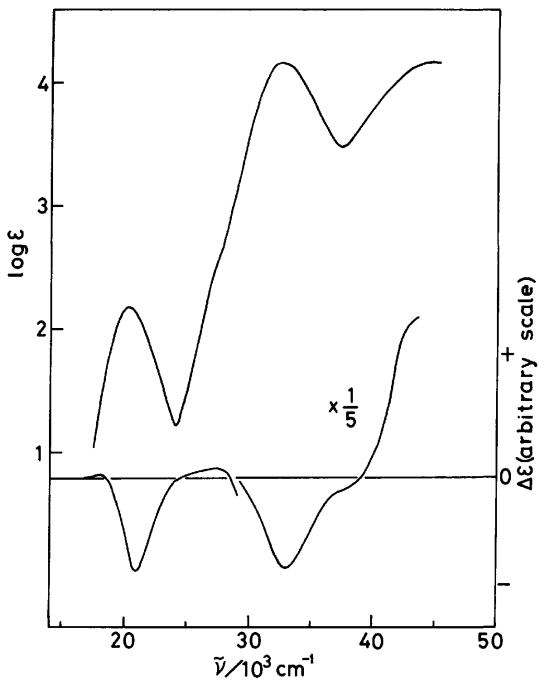

Fig. 2. Absorption and CD spectra of $(-)^{CD}_{480}$-*t*-[Co($CH_3SeCH_2CH_2NH_2$)(tren)]$Br_3 \cdot 1.5H_2O$ in water.

and similarities in absorption spectra between these complexes will strongly support that the present [Co(CH_3SeCH_2COO)(tren)]$^{2+}$ complex is the *t*-isomer.

The *t*-[Co($RSeCH_2CH_2NH_2$)(tren)]$^{3+}$ and *p*-[Rh($CH_3SeCH_2CH_2NH_2$)(tren)]$^{3+}$ complexes were partially resolved with [Sb_2(*d*-tart)$_2$]$^{2-}$ or BCS^-. The crystalline or glassy product obtained by slow evaporation of an aqueous solution containing the complex and the resolving agent shows strong CD in the d-d transition region when dissolved in water. The result indicates that the inversion occurs at selenium to form a less soluble diastereomer during slow evaporation. However, rates of inversion are moderately slow as discussed below. In the case of [Co(CH_3SeCH_2COO)(tren)]($BCS)_2$, the pair of diastereomeric salts crystallized in different forms, which can be separated by hand picking.

All the resolved complexes show CD spectra similar or almost enantiomeric to that of $(-)^{CD}_{480}$-*t*-[Co($CH_3SeCH_2CH_2NH_2$)(tren)]$^{3+}$ (Fig. 2). At present, the absolute configurations of selenium atoms in these tren complexes can not be assigned on the basis of the CD spectra. An analogous thioether complex, $(-)_{589}$-*S*(S),*R*(C)-*t*-[Co{$CH_3SCH(CH_3)COO$}(tren)]$^{2+}$, whose absolute configuration has been determined by the X-ray method,[11] exhibits a positive CD band in the S to Co^{III} CT band region (34000 cm^{-1}). On the other hand, *Δ*-[Co($CH_3SCH_2CH_2NH_2$)(en)$_2$]$^{3+}$[12] and *Λ*-[Co($CH_3SCH_2CH_2CH_2NH_2$)(en)$_2$]$^{3+}$[13] (en=ethylenediamine), in which both sulfur donor atoms are considered to have the same *R* configuration to reduce nonbonded interactions between the methyl group and the en chelate ring, also show a positive CD band in the corresponding CT region (35000 cm^{-1}). These results make

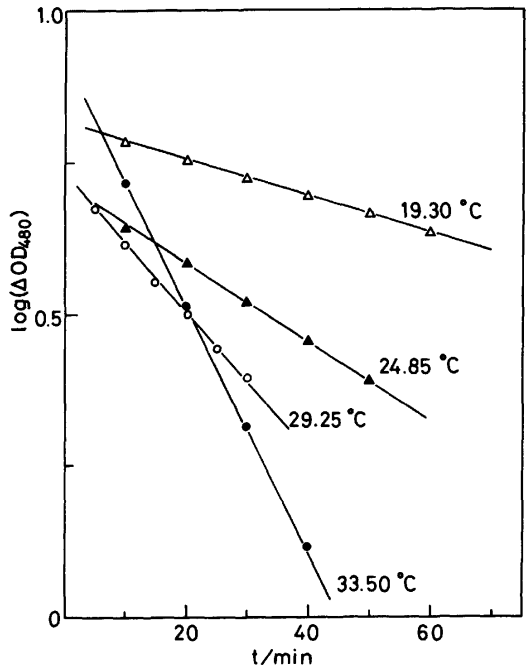

Fig. 3. Plot of $\log(\Delta OD_{480})$ against time for $(-)^{CD}_{480}$-*t*-$[Co(CH_3SeCH_2CH_2NH_2)(tren)]Br_3 \cdot 1.5H_2O$ in water (I=0.25, $NaClO_4$) at 19.30, 24.85, 29.25, and 33.50°C.

the assignment of the absolute configurations for chiral selenium donor atoms difficult.

Inversion at the Coordinated Selenium Atom. Rates of inversion at selenium of the resolved complexes were determined by monitoring the change in CD strength as a function of time. Measurements were carried out over the temperature range of 0.25 to 33.50°C in the pH region of 4.00 to 6.91. The CD strength at 480 nm of $(-)^{CD}_{480}$-*t*-$[Co(CH_3SeCH_2CH_2NH_2)(tren)]Br_3$ in water (I=0.25, $NaClO_4$) at a constant temperature decreases with time, and the plot of $\log(\Delta OD_{480})$ against time gave a straight line (Fig. 3), from which the first-order rate constants of racemization, k_r and inversion, $k_{inv}=k_r/2$ were obtained. No detectable change in the absorption spectra was observed during the measurements.

Except for *t*-$[Co(CH_3SeCH_2CH_2NH_2)(tren)]^{3+}$ and *t*-$[Co(CH_3SeCH_2COO)(tren)]^{2+}$ the optically active complexes were obtained as the diastereomeric salt with a resolving agent, and conversion into salts with achiral counter ions. was difficult because of racemization. Therefore, the effect of resolving agent on the rate of inversion should be taken into consideration. The inversion rate of $(-)^{CD}_{480}$-*t*-$[Co(CH_3SeCH_2CH_2NH_2)(tren)]$ $Br[Sb_2(d\text{-tart})_2]$ was compared with that of the bromide salt. The $Br^-[Sb_2(d\text{-tart})_2]^{2-}$ salt in water shows the same CD pattern as the bromide in the d-d transition region, and the CD strength decreases with passage of time. However, the solution shows weak CD (residual CD) even after the reaction attained equilibrium, and the pattern of the CD spectrum is almost the same as that of the starting solution. On the other hand, a solution of racemic $[Co(CH_3SeCH_2CH_2NH_2)(tren)]Br_3$ in 0.15 mol dm^{-3} $Na_2[Sb_2(d\text{-tart})_2]$ exhibits very weak CD (induced CD) immediately after dissolution of the complex, and the spectral pattern differs from that of the above residual CD. However, the spectrum gradually changes and finally gives the same pattern as that of the residual CD. These results indicate that the residual CD arises primarily from a shift of equilibrium between the (*R*)- and (*S*)-isomers caused by the presence of $[Sb_2(d\text{-tart})_2]^{2-}$, contribution of the induced CD being very small. For the reaction of $(-)^{CD}_{480}$-*t*-$[Co(CH_3SeCH_2CH_2NH_2)(tren)]Br[Sb_2(d\text{-tart})_2]$, a plot of log $(\Delta OD_{obsd} - \Delta OD_{res})$ against time gave a straight line, where ΔOD_{obsd} and ΔOD_{res} denote the observed and residual CD strengths, respectively, from which the rate of inversion was obtained (Fig. 4 and Table 2). The rate agrees with that of the corresponding bromide within the experimental error. The CD data for *p*-$[Rh(CH_3SeCH_2CH_2NH_2)(tren)]Br[Sb_2(d\text{-tart})_2]$ were analyzed in the same way. For kinetic studies on racemization of *t*-$[Co(RSeCH_2CH_2NH_2)(tren)]^{3+}$ ($R=CH_3CH_2$, $C_6H_5CH_2$) and *t*-$[Co(CH_3SeCH_2COO)(tren)]^{2+}$, the BCS^- salts were used. No CD remained after the reaction attained equilibrium, and the inversion rate was obtained from a straight line given by a plot of $\log(\Delta OD)$ *vs.* time.

Attempts to resolve *p*-$[Co(CH_3SeCH_2CH_2NH_2)(tren)]^{3+}$ by the chemical method with several resolving agents and by SP-Sephadex column chromatography were all unsuccessful. However, the complex exhibits nine signals in the ^{13}C NMR spectrum as shown in Fig. 5. The diastereotopic carbon resonances of the tren ligand (1,3 and 4,6 carbons in Fig. 5) arising from the presence

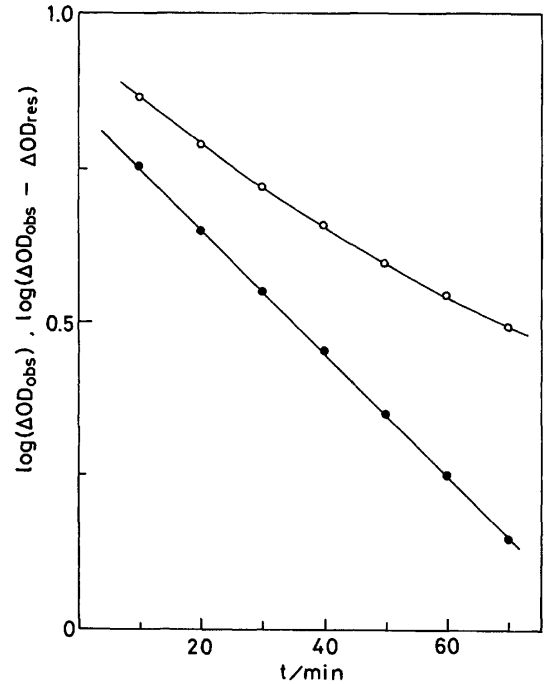

Fig. 4. Plots of $\log(\Delta OD_{obsd})$ *vs.* *t* (○) and $\log(\Delta OD_{obsd} - \Delta OD_{res})$ *vs.* *t* (●) for $(-)^{CD}_{480}$-*t*-$[Co(CH_3SeCH_2CH_2NH_2)(tren)]Br[Sb_2(d\text{-tart})_2]$ in water (I=0.25, $NaClO_4$) at 28.25°C.

TABLE 2. RATE CONSTANTS FOR INVERSION OF THE COMPLEXES

Complex	t/°C	k_{inv}/s^{-1}
t-[Co($CH_3SeCH_2CH_2NH_2$)(tren)]$^{3+}$	19.30	(0.58±0.01)×10^{-4}
	24.85	(1.25±0.03)×10^{-4}
	29.25	(2.19±0.05)×10^{-4}
	33.50	(3.86±0.03)×10^{-4}
t-[Co($CH_3CH_2SeCH_2CH_2NH_2$)(tren)]$^{3+}$	4.37	(0.73±0.01)×10^{-4}
	8.10	(1.24±0.01)×10^{-4}
	12.25	(2.31±0.02)×10^{-4}
	15.80	(3.84±0.02)×10^{-4}
t-[Co($C_6H_5CH_2SeCH_2CH_2NH_2$)(tren)]$^{3+}$	0.25	(0.75±0.02)×10^{-4}
	4.15	(1.40±0.02)×10^{-4}
	8.15	(2.44±0.03)×10^{-4}
	12.10	(4.58±0.04)×10^{-4}
t-[Co(CH_3SeCH_2COO)(tren)]$^{2+}$	19.10	(0.59±0.01)×10^{-4}
	24.12	(1.16±0.01)×10^{-4}
	28.80	(2.13±0.01)×10^{-4}
	32.83	(3.62±0.02)×10^{-4}
p-[Rh($CH_3SeCH_2CH_2NH_2$)(tren)]$^{3+}$	0.45	(0.94±0.05)×10^{-4}
	4.10	(1.80±0.04)×10^{-4}
	7.90	(3.18±0.06)×10^{-4}
	11.90	(5.51±0.08)×10^{-4}
p-[Co($CH_3SeCH_2CH_2NH_2$)(tren)]$^{3+}$	*ca.*60	10±1

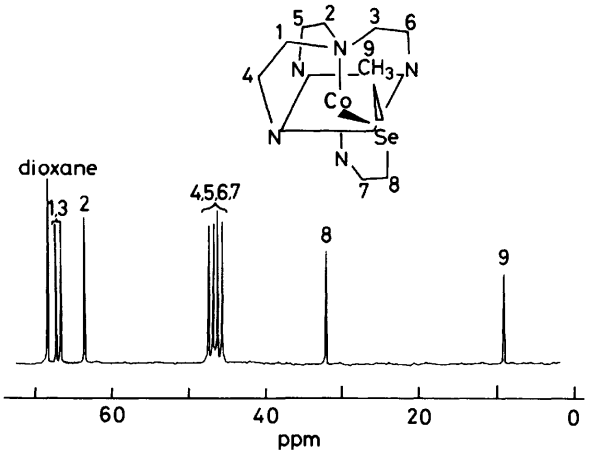

Fig. 5. ^{13}C NMR spectrum of p-[Co($CH_3SeCH_2CH_2NH_2$)(tren)]$^{3+}$ in D_2O at room temperature.

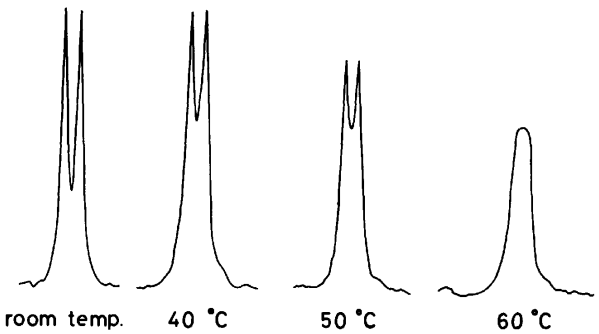

Fig. 6. Variable-temperature ^{13}C NMR spectra of the 1,3-carbon absorption region of p-[Co($CH_3SeCH_2CH_2NH_2$)(tren)]$^{3+}$ in D_2O (See Fig. 5 for carbon numbers).

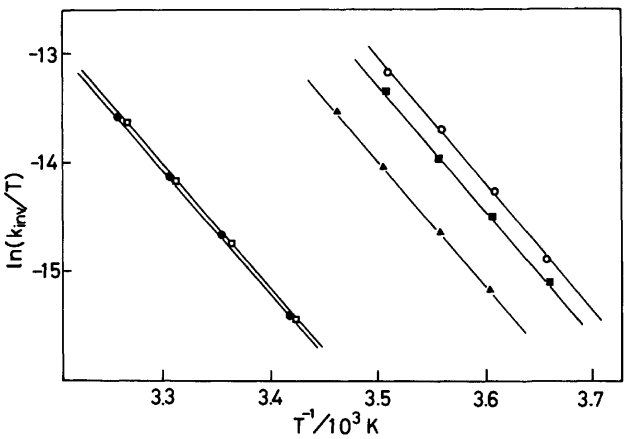

Fig. 7. Plot of $\log(k_{inv}/T)$ against T^{-1} for t-[Co($CH_3SeCH_2CH_2NH_2$)(tren)]$^{3+}$ (●), t-[Co(CH_3SeCH_2COO)(tren)]$^{2+}$ (◇), t-[Co($CH_3CH_2SeCH_2CH_2NH_2$)(tren)]$^{3+}$ (▲), t-[Co($C_6H_5CH_2SeCH_2CH_2NH_2$)(tren)]$^{3+}$ (■), and p-[Rh($CH_3SeCH_2CH_2NH_2$)(tren)]$^{3+}$ (○).

of the chiral selenoether group are clearly resolved at room temperature, demonstrating the stability toward inversion on the NMR time scale. Thus it can be concluded that the inversion at selenium in the p-isomer is slow on the NMR time scale , but not so slow as to be resolved by conventional techniques. With a rise in temperature, the two signals of 1 and 3 carbons broaden and coalesce at *ca.* 60 °C (Fig. 6). Although activation parameters of the inversion could not be obtained because of the instability of the complex at elevated temperatures, the rate at the coalescence temperature (*ca.* 60 °C) is roughly estimated to be *ca.* 10 s^{-1}.

Eyring treatments of $\log(k_{inv}/T)$ *vs.* T^{-1} yielded activation parameters (Fig. 7 and Table 3). The rate constant of t-[Co($CH_3SeCH_2CH_2NH_2$)(tren)]$^{3+}$ at 60 °C is calculated from the $\Delta H^{\ddagger}$ and $\Delta S^{\ddagger}$ values to be 8.5×10^{-3} s^{-1}. The value is smaller by a factor of 10^3 than that of the p-isomer at the same temperature. Jackson and Sargeson[3] studied the rates of sulfur inversion in t-[Co($CH_3SCH_2CH_2NH_2$)(tren)]$^{3+}$ and related complexes by the NMR method, and revealed that the rates are slow ($k_{inv}<10$ s^{-1}) on the NMR time scale at 25 °C, but

TABLE 3. THERMODYNAMIC PARAMETERS FOR INVERSION OF THE COMPLEXES

Complex	ΔS^*/J mol^{-1} K^{-1}	ΔH^*/kJ mol^{-1}	$\Delta G^*_{25°C}$/kJ mol^{-1}
t-[Co($CH_3SeCH_2CH_2NH_2$)(tren)]$^{3+}$	3.1±2.2	96.1±0.6	95.2±0.9
t-[Co($CH_3CH_2SeCH_2CH_2NH_2$)(tren)]$^{3+}$	19.4±3.4	95.2±0.6	89.4±1.4
t-[Co($C_6H_5CH_2SeCH_2CH_2NH_2$)(tren)]$^{3+}$	26.9±5.6	95.7±1.5	87.7±2.2
t-[Co(CH_3SeCH_2COO)(tren)]$^{2+}$	−0.2±2.2	95.1±1.7	95.1±1.0
p-[Rh($CH_3SeCH_2CH_2NH_2$)(tren)]$^{3+}$	35±13	97.6±4.4	87.2±5.9
p-[Co($CH_3SeCH_2CH_2NH_2$)(tren)]$^{3+}$			*ca.* 76 (60 °C)

exceeds 0.1 s^{-1}. For example, the ^{13}C NMR spectrum of *t*-[Co($CH_3SCH_2CH_2NH_2$)(tren)]$^{3+}$ showed clearly resolved diastereotopic carbon signals at 25 °C. On the other hand, the corresponding signals for the *p*-isomer were not resolved under the same conditions. These observations are consistent with our results that the inversion rate of the coordinated selenium atom is faster in the *p*-isomer than in the *t*-isomer. A similar trend was reported for sulfur inversion in *p*- and *t*-[Co{S(O)$CH_2CH_2NH_2$}(tren)]$^{2+}$.[14]

Studies of the variable-temperature NMR spectra of Pt^{II}–thioether and –selenoether complexes revealed the presence of coupling between ^{195}Pt and ^1H even above the coalescence temperature.[15,16] The result suggests that the inversion does not involve breaking of the Pt–S and Pt–Se bonds; pyramidal inversion mechanism is proposed, which proceeds *via* a trigonal planar intermediate.[17] Although such argument on couplings may not be applied on the present selenoether Co^{III} and Rh^{III} complexes, the facts that the rates of racemization are independent of pH and the presence of resolving agent strongly suggest that the racemization takes place intramolecularly by pyramidal inversion at the selenium atom. If the racemization would proceed by this mechanism, the difference in rate of inversion between the two isomers of [Co($CH_3SeCH_2CH_2NH_2$)(tren)]$^{3+}$ seems to stem from a difference in structure around the Se–R group. Molecular models of [Co($CH_3SeCH_2CH_2NH_2$)(tren)]$^{3+}$ show that the *p*-isomer involves fairly large steric interactions between the methyl group and the tren chelate ring, whereas the *t*-isomer does not have such large steric interactions around the Se–CH_3 group. In the trigonal planar transition state, on the other hand, both *p*- and *t*-isomers seem to have a similar structural situation involving no particular steric interaction around the Se–CH_3 group. Accordingly, the *p*-isomer will have a lower energy barrier for the inversion than that of the *t*-isomer, and racemizes faster than does the *t*-isomer.

The ΔG^* values for inversion of *t*-[Co($RSeCH_2CH_2NH_2$)(tren)]$^{3+}$ decrease in the order $CH_3 > CH_3CH_2 > C_6H_5CH_2$. The decrease in ΔG^* value comes from an increase in positive ΔS^*, the ΔH^* values being almost constant (95—97 kJ mol^{-1}) in these complexes. It seems that the entropy change associated with inversion arises from the gain of ratational freedom of the substituent on selenium upon going from the ground state to the transition state. Although the *t*-isomer is

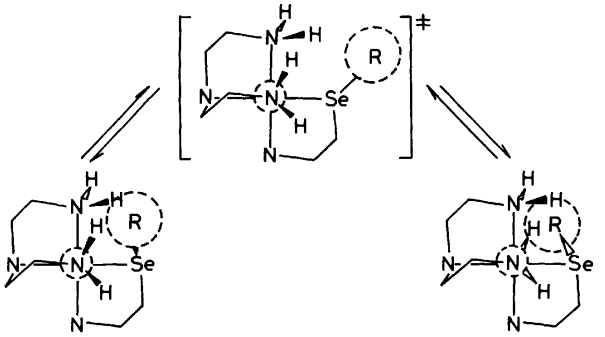

Fig. 8. A proposed mechanism for inversion of *t*-[Co($RSeCH_2CH_2CH_2NH_2$)(tren)]$^{3+}$ viewed from the *p*-N–Co–*p*-N bond axis.

sterically preferred in the ground state, the steric interaction in this isomer increases with an increasing size of the substituent, $CH_3 < CH_3CH_2 < C_6H_5CH_2$ to reduce the degree of rotational freedom of the substituent on the selenium atom in the ground state (Fig. 8). In the transition state, however, the substituent is far away from the tren chelate ring, and can rotate more easily than in the ground state (Fig. 8). Thus, the difference in degree of freedom between the ground and the transition states becomes larger with an increasing size of the substituent, which is reflected on the ΔS^* values (Table 3).

It is to be noted that the activation parameters of *t*-[Co(CH_3SeCH_2COO)(tren)]$^{2+}$ are nearly the same as those of *t*-[Co($CH_3SeCH_2CH_2NH_2$)(tren)]$^{3+}$. The effect of nature of the donor atom cis to selenium on the inversion barriers (cis effect) seems to be small in the present complexes. Similarly equivocal results for the cis effect on sulfur and selenium inversion barriers have been reported on *fac*-[$Pt^{IV}XMe_3${MeE(CH_2)$_n$EMe}] (X=Cl, Br, I; E=S, Se; n=2, 3).[18]

The inversion rate of *p*-[Rh($CH_3SeCH_2CH_2NH_2$)(tren)]$^{3+}$ is calculated to be *ca.* 2.3×10^{-1} s^{-1} at 60 °C from the ΔH^* and ΔS^* values, the rate being much smaller than that of the corresponding cobalt(III) complex (*ca.* 10 s^{-1}) at the same temperature. The difference can be explained by both steric and electronic factors. The M–Se and M–N bond distances should be longer in the Rh^{III} complex than in the Co^{III} complex,[2] and thus smaller steric interactions are expected for the Rh^{III} complex between the ligands to increase the activation energy for the inversion. The inversion is also related with the M–Se bond strength; the weaker the bond becomes, the faster the inversion occurs.[16] *p*-[M($CH_3SeCH_2CH_2NH_2$)(tren)]$^{3+}$ (M=Co, Rh) seems to

be the case; the Rh–Se bond is expected to be stronger than the Co–Se bond because a soft selenium donor atom will prefer Rh^{III} to Co^{III}.

The authors wish to thank the Ministry of Education for Scientific Research Grant-in-Aid No. 58470032.

References

1) J. B. Lambert, *Top. Stereochem.*, **6**, 19 (1971).
2) S. G. Murray and F. R. Hartley, *Chem.Rev.*, **81**, 365 (1981) and references cited therein.
3) W. G. Jackson and A. M. Sargeson, *Inorg. Chem.*, **17**, 2165 (1978).
4) K. Yamanari, J. Hidaka, and Y. Shimura, *Bull. Chem. Soc. Jpn.*, **50**, 2451 (1977).
5) The *p*- and *t*-isomers have the Se (S) atom at the trans position to the primary (*p*) and tertiary (*t*) amine nitrogens of tren, respectively.
6) K. Nakajima, M. Kojima, and J. Fujita, *Chem. Lett.*, **1982**, 925.
7) K. Nakajima, M. Kojima, J. Fujita, T. Ishii, S. Ohba, M. Ito, and Y. Saito, *Inorg. Chim. Acta*, **99**, 143 (1985).
8) C. Y. Stein, P. E. Ellis, Jr., R. C. Elder, and E. Deutsch, *Inorg. Chem.*, **15**, 1618 (1976).
9) H. J. Backer and W. Van Dam, *Recl. Trav. Chim. Pays-Bas*, **49**, 482 (1930).
10) M. Kojima and J. Fujita, *Bull. Chem. Soc. Jpn.*, **56**, 2958 (1983).
11) S. Ohba and Y. Saito, *Acta Crystallogr., Sect. C*, **40**, 398 (1984).
12) K. Yamanari, J. Hidaka, and Y. Shimura, *Bull. Chem. Soc. Jpn.*, **50**, 2299 (1977).
13) M. Kojima and J. Fujita, unpublished data.
14) M. Kojima and J. Fujita, *Bull. Chem. Soc. Jpn.*, **56**, 139 (1983).
15) P. Haake and P. C. Turley, *J. Am. Chem. Soc.*, **89**, 4611 (1967).
16) E. W. Abel, G. W. Farrow, K. G. Orrell, and V. Šik, *J. Chem. Soc., Dalton Trans.*, **1977**, 42.
17) W. G. Jackson and A. M. Sargeson, "Rearrangements in Ground and Excited States," ed by P. de Mayo, Academic Press, New York (1980), Vol. 2, p. 273.
18) E. W. Abel, A. R. Khan, K. Kite, K. G. Orrell, and V. Šik, *J. Chem. Soc., Dalton Trans.*, **1980**, 1175.

 © 1985 The Chemical Society of Japan Bull. Chem. Soc. Jpn., 58, 1137—1142 (1985)

Flavin Mononucleotide Chemiluminescence for Determination of Traces of Copper(II) by Continuous Flow and Flow Injection Methods

Masaaki YAMADA,* Hideshi KANAI, and Shigetaka SUZUKI
Department of Industrial Chemistry, Faculty of Technology, Tokyo Metropolitan University, Tokyo 158
(Received November 7, 1984)

Flow injection analysis, with chemiluminescence detection, is used to determine traces of copper(II) by means of the flavin mononucleotide-hydrogen peroxide-phosphate buffer system. This permits the determination of copper(II) more selectively than any other chemiluminescence system with a detection limit of 0.03 ng(20-μl sample injection) or 0.06 ng ml^{-1} (continuous sample flow). The linear range is 3 orders of magnitude, the sampling rate is 120 h^{-1}, and the relative standard deviation is 3.1% for 1 ng Cu(II)(n=10). Iron(II) and chromium(III and VI), the strongest enhancer after copper(II), provide signals 2—3% of that for copper(II). Effect of surfactant micelles on the signal for copper is also discussed. The method is successfully applied to real samples.

Chemiluminescence (CL) methods have been recognized as a valuable approach to sensitive analyses. In particular, the use of solution CL in analyses for inorganic and organic species at trace levels has received considerable attention because of the simplicity of instrumentation, the wide dynamic range, and the short analysis time as well as high sensitivity. An alkaline hydrogen peroxide solution of luminol, lucigenin, lophine, or gallic acid has mainly been utilized for trace metals, cobalt(II) being the most effective catalyst.[1] Copper(II) can be detected by means of its catalytic effect on the oxidation of CL reagent; its detection limit is 0.2 ppm in the lophine system,[2] 1×10^{-7} M (1 M=1 mol dm^{-3}) in the luminol system,[3] and 0.1 ppm in the lucigenin system.[4] These CL systems, however, suffer from lack of selectivity for copper determination. For instance, in the luminol system there are at least 30 different species that enhance light emission.[5]

Flow injection analysis(FIA) is very suitable for the determination of various kinds of analytes based on CL measurements. Cobalt(II) in the pg to sub-pg range has been detected by the gallic acid[6] or luminol system,[7] cadmium(II) and zinc(II) in the sub-ng range by their inhibiting effects on the luminol system,[8] hydrogen peroxide in the 10^{-8} to 10^{-9} M range by the oxalic ester[9] or luminol system,[10] iodine in the sub-ng range by the hypochlorite system,[11] sulfite in the ng range by the permanganate system,[12] fluorescent compounds in the fmol range by the oxalic ester system,[13] and albumin in the 10^{-8} M range by its inhibiting effect on the luminol system.[14]

In the preliminary work, we have made it clear that flavin mononucleotide (FMN) is usable as a CL reagent for sensitive, selective, and rapid determination of copper(II) by FI method.[15] It is based on the measurement of CL arising from the copper-catalyzed oxidation of FMN by hydrogen peroxide under nearly neutral conditions. The object of this paper is to further explore the combination of FIA and CL method and its analytical characteristics, and to verify the utility of the present FI-CL method in copper determination by applying to real samples.

Experimental

Apparatus. Prior to flow experiments, a batch system as shown in Fig. 1 was assembled in order to obtain CL decay curves, that is, to know how fast the present CL reaction proceeds. Each 0.2 ml of FMN, hydrogen peroxide, and copper(II) solutions is transferred in that order to a reaction vessel by a peristaltic pump. The light emitted is observed *via* a fiber optics by a photomultiplier tube (PMT, Hamamatsu Photonics R453) with no wavelength discrimination.

A schematic diagram of the flow system for FIA is given in Fig. 2. An aqueous solution containing FMN and phosphate

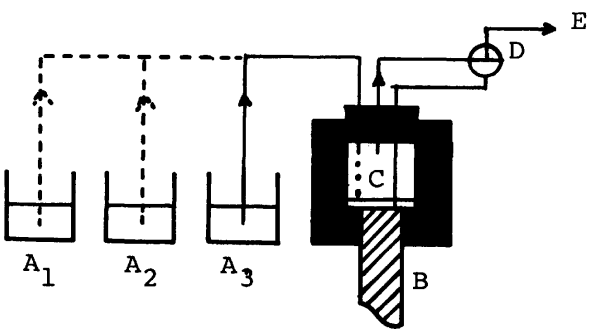

Fig. 1. Batch system for obtaining CL decay curves. A_1: 2.8×10^{-3} M FMN (phosphate buffer), A_2: 10% H_2O_2, A_3: 10^{-4} M Cu(II), B: fiber optics, C: reaction cell, D: 3-way cock, E: to peristaltic pump.

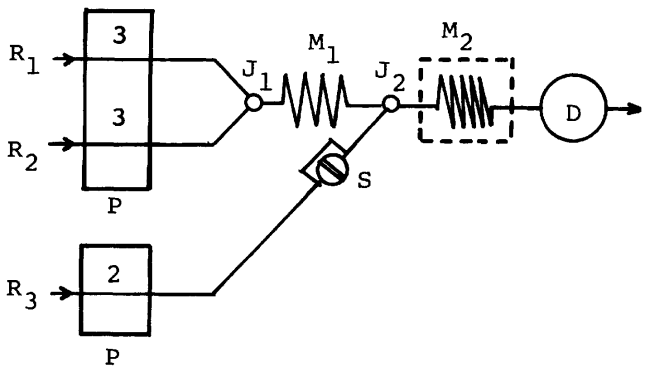

Fig. 2. Schematic diagram of the flow system for FIA (for key, see text).
Recommended conditions: 1.4×10^{-3} M FMN (pH 5.8) for R_1; 5% H_2O_2 for R_2; water for R_3. Flow rates are given as ml min^{-1}. Coil M_2 is held in a heating bath at 60°C.

buffer is supplied through R_1 and hydrogen peroxide through R_2. A flow line R_3, which is newly placed in this experiment, represents a carrier stream for copper(II) and others. This is an aqueous copper(II) solution for the continuous flow method, or pure water when copper(II) and other species are injected by means of a 20-μl rotary valve injector S (injection method). The streams are delivered by peristaltic pumps P and mixed at Y-joints J_1 and J_2. For adequate mixing of R_1 and R_2, a 0.5-m mixing coil M_1 is placed between J_1 and J_2; a second 1-m mixing coil (reaction coil) M_2 is placed in a heating bath controlled to ±0.5 °C between J_2 and D. Teflon tubing (1-mm i.d.) is used for flow lines except the pump tubes and detection flow cell D. The distance between J_2 and D is about 5 cm (the minimum distance achieved). For D a spiral flow cell is assembled as described previously.[16] The light emitted, which has an maximum emission between 500 and 600 nm similar to the fluorescence emission of FMN (λ_{max}=*ca.* 540 nm), is observed directly by a PMT (Hamamatsu Photonics R268) with no wavelength discrimination. The signal from the PMT is fed to an electrometer and then recorded *via* a laboratory-built low-pass active filter, whose frequency cut-off is *ca.*0.1 Hz.

Fluoresecence spectra were measured by a fluorescence spectrophotometer (Hitachi MPF-4). The measurements were performed with respect to the waste solution in the flow system in Fig. 2, in which the stream of hydrogen peroxide solution was substituted by that of water.

Reagents. Chemicals of reagent grade were used as received. The water used was prepared by distillation of Millipore (milli-R) water from an all Pyrex glass apparatus. FMN (monosodium riboflavin 5′-phosphate), phosphate buffer (M/15 KH_2PO_4–M/15 Na_2HPO_4), and hydrogen peroxide solutions were prepared daily.

Analysis of Real Samples. Each 0.7 g of Pepperbush and Pond Sediment (standard reference materials) from NIES (National Institute for Environmental Studies) and of Yabukita tea leaf from National Chemical Laboratory for Industry was boiled with *ca.* 20 ml of concentrated nitric acid on a hot plate until the appearance of white fumes, and with concentrated sulfuric acid until the solution became colorless. After cooling, the solution was diluted to 100 ml. A 40-ml portion of the acid-digested sample was neutralized to about pH 6 with 2 M sodium hydroxide and diluted to 100 ml. A 10-ml portion was added to each of several 100-ml volumetric flasks for standard addition of copper before dilution to volume, and copper was determined as described above.

Results and Discussion

Total Flow Rate and Reaction Temperature. Determinations of the total flow rate in the system and of the reaction temperature in the heating bath are very important for the FI-CL method in sensitivity and rapidity, although both are closely related to each other. At too low or too high total flow rate, most of the CL reaction, the speed of which is considerably slow at room temperature (see Fig. 3), proceeds outside the flow cell, resulting in low signal or low sampling throughput. In the previous work,[15] they were determined to be 8 ml min^{-1} and 60 °C, respectively. These are also employed in the present system, *i.e.*, 3 ml min^{-1} for R_1 and R_2, 2 ml min^{-1} for R_3, and 60 °C for M_2.

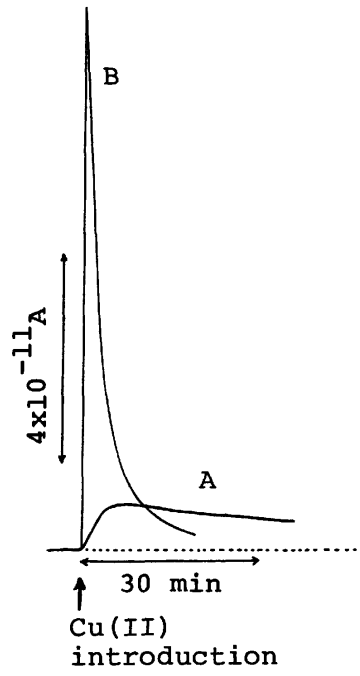

Fig. 3. CL decay curves.
A: room temperature, B: 60 °C (Each 0.2 ml of reagent solution warmed to 60 °C was introduced into the reaction cell.).

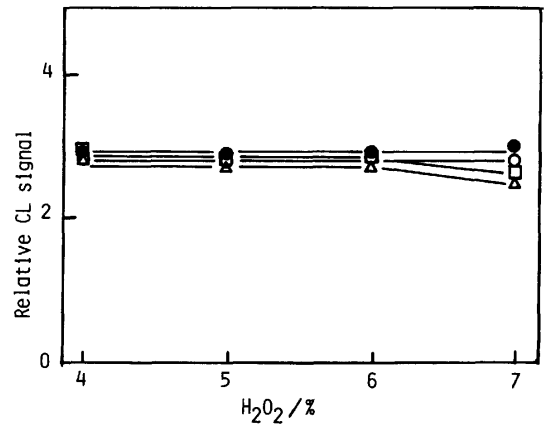

Fig. 4. Effect of the concentrations of hydrogen peroxide and FMN.
FMN concentration (10^{-3} M): △ 0.8; □ 1.0; ○ 1.2; ● 1.4, pH: 6.0, 20-μl injections of 5×10^{-7} M Cu(II), Other conditions as in Fig. 2.

Reagent Concentrations and pH of R_1. Three reaction variables, the concentrations of FMN and hydrogen peroxide and the pH of FMN solution were optimized. Figure 4 shows that the CL signal is almost independent of the reagent concentrations. The concentrations of 1.4×10^{-3} M for FMN and of 5% for hydrogen peroxide were chosen for further experiments, which were slightly higher than those in the previous system because of the dilution of reagent solution with water of R_3.

The effect of pH is shown in Fig. 5, indicating that the optimum pH is about 5.8. The nature of the buffer

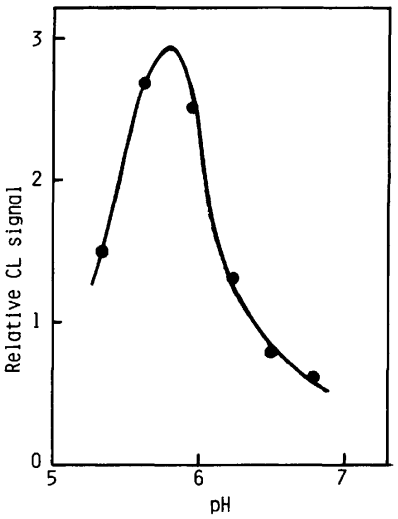

Fig. 5. Effect of pH.
1.4×10^{-3} M FMN, 6% H_2O_2, Other conditions as in Fig. 4.

components also influenced the signal, the phosphate buffer exhibiting maximum sensitivity. In sodium dihydrogencitrate-sodium tetraborate and disodium hydrogenphosphate-citric acid buffers the signals for 20-μl injections of 5×10^{-7} M copper solution were only *ca.*10 and 20% of that in the phosphate buffer, respectively; the use of sodium citrate-sodium hydroxide and sodium acetate-acetic acid buffers gave rise to no emission.

Effect of Surfactants. Over a narrow range of concentration (called the critical micelle concentration, cmc), amphiphilic surfactant molecules dynamically associate in aqueous solution to form aggregates called micelles, in which there is a sudden transition in the physical properties of aqueous surfactants. It is known that the local microenvironment in micellar media leads to significant increase in CL quantum yield.[17] We already found that the copper-catalyzed CL of 1,10-phenanthroline[18] and the FMN-sensitized CL of sulfur dioxide[19] were enhanced by some cationic and nonionic surfactant molecules, respectively.

In order to investigate whether micellar media function effectively for the present CL system, hexadecyltrimethylammonium bromide (CTAB) as a cationic surfactant, sodium dodecyl sulfate(SDS) as an anionic surfactant, and polyoxyethylene (20) sorbitan trioleate (Tween 85) as a nonionic surfactant were added to the carrier stream (R_3). However, no CL enhancement was observed, regardless of the presence or absence of buffer reagent, its components, and the reaction temperature. These surfactants, except Tween 85 at lower concentrations, suppressed the signal as shown in Table 1. In the table; the effect of surfactants on the fluorescence intensity of FMN is also represented; the micellar solution of CTAB causes decreased fluorescence intensity but those of SDS and Tween 85 increased fluorescence. It can be said from the table that the suppression of CL signal, especially for SDS,

Table 1. Effect of surfactants on CL signal for copper(II)

Surfactant[a]	Concentration	Relative CL signal	Relative fluorescence intensity of FMN
none		1.0	1.0
CTAB	1×10^{-4} M	0.88	
	1×10^{-3} M	0.29	0.72
	8×10^{-3} M	ND[b]	0.47
SDS	1×10^{-3} M	0.74	
	1×10^{-2} M	0.17	1.1
	8×10^{-2} M	0.04	2.9
Tween 85	0.5 g l^{-1}	1.0	
	7 g l^{-1}	1.0	2.1
	20 g l^{-1}	0.91	3.2

a) cmc: 9×10^{-4} M for CTAB, 8×10^{-3} M for SDS, unknown for Tween 85, b) Not detected.

is mainly ascribable to the inhibition of CL reaction due to the addition of surfactant, although for CTAB it is due in part to the decreased fluorescence yield of emitter (the similarity of CL spectrum to the FMN fluorescence spectrum indicates that the emitter has the flavin residue, *i.e.*, the isoalloxazine ring). At the CTAB and SDS concentrations over their cmcs, the signals are suppressed completely or markedly. In contrast, Tween 85 does not suppress the signal or the suppression is not so rigorous as the ionic surfactants even in the addition of large amount of surfactant over its cmc. These are rationalized in terms of the micellar effect that one of the ionic reactants (Cu^{2+} and FMN^-) is repelled electrostatically from the charged micellar surface which the ionic surfactant forms, while the other is attracted, resulting in an inhibition of the CL reaction. On the contrary, the ionic reactants are not influenced by the noncharged micellar surface which the nonionic surfactant forms. This is supported by the finding that the signal for chromium(VI) with a charge of the same sign as that of FMN is enhanced by CTAB, while it is suppressed by SDS and not changed by Tween 85. Other surfactants tested like zephiramine, didodecyldimethylammonium bromide, sodium oleate, Brij-35, and Triton X-100 also did not enhance the signal for copper.

Characteristics of the System. Under the recommended conditions (as specified in Fig. 2), the analytical characteristics of the system were investigated. The background and noise currents were 1.6×10^{-11} and 2.4×10^{-13} A, respectively. The detection limit is defined by the noise level, which depends on the background signal arising presumably from copper as an impurity in the reagents and water used. Accordingly, an improvement of the detection limit would be expected with decreased background. Thus, EDTA or tetraethylenepentamine was added to the reagent stream R_1 in an attempt to mask copper as the impurity. However, no decreased background signal was observed. This indicates that the background comes from noncatalyzed CL of FMN which can not be

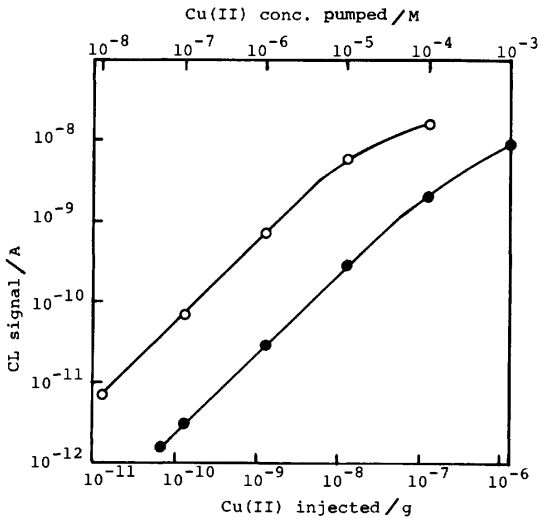

Fig. 6. Calibration graphs.
○: Continuous flow; ●: 20-μl injection.

eliminated.

Logarithmic calibration graphs were linear over three decades for 20-μl sample injections and for continuous sample flow (2 ml min^{-1}) (Fig. 6). The detection limit for a signal-to-noise ratio of 3 is 0.06 ng ml^{-1} for continuous sample flow and 0.03 ng for 20-μl sample injections. This is much lower than the 30 ng (30 ng ml^{-1}) achieved by the flash-photolytically initiated riboflavin CL[20] and the 6 ng ml^{-1} by the luminol electrochemiluminescence.[3] The relative standard deviation is 3.1% when 20-μl of the 1×10^{-6} M solution (*ca.* 1 ng) is successively injected ten times. The sampling rate is 120 h^{-1}.

Effect of Other Substances. Most solution CL methods suffer from poor selectivity. The luminol, lucigenin, and lophine systems permit 30, 20, and 11 species, respectively, to enhance the luminescent reaction.[5] In contrast, the FMN system is fairly selective and only iron(II) and chromium(III,VI) provide CL signals 2—3% of that for copper(II); other species enhance the emission very weakly, or give rise to no emission (Table 2). The signals which S^{2-}, SCN^-, and $S_2O_3^{2-}$ provide seem to derive from the FMN-sensitized CL produced by the energy transfer from excited sulfur molecules (max. emission wavelength= *ca.* 440 nm) to FMN molecules in such a way that the CL based on the hydrogen peroxide-oxidation of sulfide is sensitized by fluorescein (max. fluorescence wavelength λ_{fl}=535 nm) or rhodamine B (λ_{fl}=575 nm).[21] This is supported by the fact that the emission from these species are also sensitized by brilliant sulfoflavine (CI=56205, λ_{fl}=*ca.* 520 nm), another efficient sensitizer used in a previous work.[12] For ascorbic acid, cyanide, and EDTA, the emission may arise from the CL process involving singlet oxygen molecules as in the gallic acid-,[22] pyrogaroll-,[23] tannic acid-,[24] or formaldehyde-hydrogen peroxide CL system[25] and in the urea-, gelatin-, or guanidine-hypochlorite CL system.[25] The background suppression due to iodide is ascribable to the decreased fluorescence yield of emitter because the presence of 10^{-3} M iodide decreases the FMN fluorescence intensity by *ca.* 20%.

To check the effect of concomitant species on the signal for copper, 20 μl of a 10^{-4} to 10^{-6} M solution of each common species was injected into the stream R_3 of 2×10^{-8} M copper(II) solution. The results are

TABLE 2. SELECTIVITY OF THE FMN CL SYSTEM

Species[a]	Relative molar signal	Species[a]	Relative molar signal
Cu(II)	1000		
Cr(VI)	34	S^{2-}	8.7
Fe(II)	28	SCN^-	3.6
Cr(III)	18	Ascorbic acid	2.1
Pb(II)	1.7	$S_2O_3^{2-}$	0.9
Co(II)	1.6	CN^-	0.03
Fe(III)	1.2	EDTA	0.01
Mn(II)	0.1	I^-	−0.02

a) 20-μl injection of 10^{-3} M solution of chloride or nitrate, or sodium or potassium salt except ammonium sulfate for Fe(II,III), and of 10^{-4} M solution of nitrate for Cu(II). Mg(II), Ca(II), Ba(II), Al(III), Sn(II), Ni(II), Zn(II), Cd(II), Ag(I), Hg(II), As(V), NH_4^+, F^-, Cl^-, Br^-, NO_2^-, NO_3^-, CO_3^{2-}, SO_3^{2-}, SO_4^{2-}, $S_2O_8^{2-}$, ClO_4^-, IO_3^-, $B_4O_7^{3-}$, $[Fe(CN)_6]^{3-}$, acetate, citrate, oxalate, and urea give rise to no emission.

TABLE 3. INTERFERENCE STUDY FOR CATIONIC SPECIES

Species	Relative error[a] /%		
	10^{-4}M	10^{-5}M	10^{-6}M
Co(II)	370(80)	40(12)	ND
Cr(VI)	320(500)	50	ND
Cr(III)	260(300)	35	ND
Fe(II)	190(240)	50	ND
Zn(II)	110(ND)	58(ND)	12(ND)
Mn(II)	100(40)	15(ND)	ND
Fe(III)	71(12)	27(ND)	ND
Hg(II)	60(9)	15(ND)	ND
Pb(II)	55(ND)	10(ND)	ND
Cd(II)	30(ND)	ND	
Ni(II)	15(ND)	ND	
Sn(II)	−15(ND)	ND	

a) Values in parentheses: For the carrier solution containing 10^{-4} M Zn(II), ND: Not detected. 10^{-4} M Mg(II), Ca(II), Ba(II), Al(III), Ag(I), and As(V) do not interfere.

TABLE 4. INTERFERENCE STUDY FOR ANIONIC SPECIES

Species	Relative error/%	
	10^{-4}M	10^{-5}M
S^{2-}	85	ND
Ascorbic acid	64	
CN^-	35	ND
$C_2O_4^{2-}$	23	ND
SCN^-	15	ND
$S_2O_3^{2-}$	9	ND
I^-	−10	ND
$[Fe(CN)_6]^{3-}$	−20	ND
EDTA	−100	−100

10^{-4} M F^-, Cl^-, Br^-, ClO_4^-, IO_3^-, NO_2^-, NO_3^-, SO_3^{2-}, SO_4^{2-}, $S_2O_8^{2-}$, CO_3^{2-}, NH_4^+, $B_4O_7^{3-}$, acetate, citrate, and urea do not interfere.

shown in Tables 3 and 4.

Interesting features which appear in Table 3 are that species (Zn, Hg, Cd, Ni, Sn) eliciting no emission *per se* enhance the copper(II)-catalyzed emission (Sn suppresses it) and that species which elicit emission *per se* provide larger signal than those which they provide in the absence of copper. Such interferences are reduced or eliminated by the addition of zinc(II) to the carrier stream as shown in parentheses in the table. On the other hand, the addition of zinc(II) slightly increases the signals for chromium(III,VI) and iron(II) (and also for copper). Although these phenomena can not be readily interpreted, it may be correlated with the stability of FMN–metal complex which is likely to be formed during the CL reaction;[26] the stability of the complex decreasing in the order Cu>Zn>Co>Mn>Ni[27] may account for the reduction and elimination of interference owing to the addition of zinc(II). For anionic species, oxalate which does not chemiluminesce by itself provides signal, in addition to the emissive species (Table 4). Although the interference due to oxalate is not fully explainable, it is closely related to the fact that the oxalate–hydrogen peroxide system emits weak light which is easily sensitized by an appropriate fluorescent compound.[28] It is conceivable that the presence of copper enhances the sensitized-emission which can not be detected in the absence of copper.

Application to Real Samples. The applicability of the proposed method was evaluated by assaying NIES standard reference materials (Pepperbush[29] and Pond Sediment[30]) and Yabukita tea leaf.[31] Standard additions of copper to the acid-digested samples indicated that the results obtained for Pepperbush (12, 13, 13 $\mu g\,g^{-1}$), Pond Sediment (220, 213, 222 $\mu g\,g^{-1}$), and Yabukita tea leaf (9.1, 9.0 $\mu g\,g^{-1}$) by the continuous sample flow method were within the certified values (12±1, 210±12, and 9.09±0.97 $\mu g\,g^{-1}$, respectively).

Conclusion

The above results indicate that ultratrace amounts of copper(II) can be selectively and rapidly determined by FIA based on the FMN CL system. This provides a lower detection limit (0.03 ng or 0.06 $ng\,ml^{-1}$) for copper(II) than that by any other method, the detection limit being lower than those for flame atomic-absorption (18 $ng\,ml^{-1}$) and -fluorescence methods (1.5 $ng\,ml^{-1}$)[32] and neutron activation analysis (0.1 ng),[33] and comparable to those for flameless atomic absorption and inductively coupled plasma emission methods (0.04 $ng\,ml^{-1}$).[32]

Although no micellar enhanced CL is observed here, CL in oriented systems like micelles is very attractive in the analytical point of view because there is much possibility of enhancing quantum efficiency or energy transfer efficiency and because they permits the use of CL reagents and sensitizers insoluble in water. Furthermore, electrostatic interaction between charged analytes and the ionic micellar surface serves to improve selectivity. In the present CL system, for instance, cationic surfactant micelles may enable selective detection of chromium (anionic analytes) because the micellar effect works to suppress emission for cationic analytes like copper and iron, the emission for copper being completely suppressed by the presence of CTAB micelles as shown in Table 1.

The authors thank S. Nakamura (National Chemical Laboratory for Industry) for providing a tea leaf sample.

References

1) M. Yamada and S. Suzuki, *Bunseki*, **1980**, 57.
2) D. F. Marino, F. Wolff, and J. D. Ingle, Jr., *Anal. Chem.*, **51**, 2051 (1979).
3) K. E. Haapakka and J. J. Kankare, *Anal. Chim. Acta*, **118**, 333 (1980).
4) L. A. Montano and J. D. Ingle, Jr., *Anal. Chem.*, **51**, 919 (1979).
5) A. MacDonald, K. W. Chan, and T. A. Nieman, *Anal. Chem.*, **51**, 2077 (1979).
6) M. Yamada, T. Komatsu, S. Nakahara, and S. Suzuki, *Anal. Chim. Acta*, **155**, 259 (1983).
7) M. Yamada and S. Suzuki, *Chem. Lett.*, **1983**, 783.
8) J. L. Burguera, M. Burguera, and A. Townshend, *Anal. Chim. Acta*, **127**, 199 (1981).
9) G. Scott, W. R. Seitz, and J. Ambrose, *Anal. Chim. Acta*, **115**, 221 (1980).
10) B. Olsson, *Anal. Chim. Acta*, **136**, 113 (1982).
11) J. L. Burguera and M. Burguera, *An. Quim.*, **78, B**, 307 (1982).
12) M. Yamada, T. Nakada, and S. Suzuki, *Anal. Chim. Acta*, **147**, 401 (1983).
13) K. Honda, J. Sekino, and K. Imai, *Anal. Chem.*, **55**, 940 (1983).
14) T. Hara, M. Toriyama, and K. Tsukagoshi, *Bull. Chem. Soc. Jpn.*, **57**, 289 (1984).
15) M. Yamada and S. Suzuki, *Chem. Lett.*, **1982**, 1747.
16) S. Nakahara, M. Yamada, and S. Suzuki, *Anal. Chim. Acta*, **141**, 255 (1982).
17) C. M. Paleos, G. Vassilopoulos, and J. Nikokavouras, *J. Photochem.*, **18**, 327 (1982).
18) M. Yamada and S. Suzuki, *Anal. Lett.*, **17**, 251 (1984).
19) M. Kato, M. Yamada, and S. Suzuki, *Anal. Chem.*, **56**, 2529 (1984).
20) E. L. Wehry and A. W. Varnes, *Anal. Chem.*, **45**, 848 (1973).
21) J. L. Burguera and A. Townshend, *Talanta*, **27**, 309 (1980).
22) D. Slawinska and J. Slawinski, *Anal. Chem.*, **47**, 2101 (1975).
23) R. J. Miller and J. D. Ingle, Jr., *Talanta*, **29**, 303 (1982).
24) D. Slawinska, J. Slawinski, K. Polewski, and W. Pukacki, *Photochem. Photobiol.*, **30**, 71 (1979).
25) J. Stauff and G. Rümmler, *Z. Physik. Chem. Neue Folge*, **34**, 67 (1962).
26) J. E. Vorhaben and R. H. Steele, *Biochemistry*, **6**, 1404 (1967).
27) M. M. Taqui Khan and M. S. Mohan, *J. Inorg. Nucl.*

Chem., **35**, 1749 (1973).
28) I. Kamiya, "Kagakuhakko," Kodansha, Tokyo (1972), 177.
29) K. Okamoto, Y. Yamamoto, and K. Fuwa, *Anal. Chem.*, **50**, 1950 (1978).
30) Y. Iwata, K. Matsumoto, H. Haraguchi, K. Fuwa, and K. Okamoto, *Anal. Chem.*, **53**, 1136 (1981).
31) Kagakurengobukai-Bunsekibunkakai of Kogyogijutsukyodokaigi, "Chaba no Bunseki (the 23rd Bunsekigijutsukyodokenkyu Sogoshiryo)," National Chemical Laboratory for Industry and Industrial Research Institute of Kanagawa Prefecture (1980).
32) H. Haraguchi, *Kagaku no Ryoiki*, **32**, 313 (1978).
33) K. Terada, *Bunseki*, **1981**, 848.

 © 1985 The Chemical Society of Japan Bull. Chem. Soc. Jpn., 58, 1143—1148 (1985)

Calorimetric and Spectrophotometric Studies on Formation of Copper(II) Chloride Complexes in *N,N*-Dimethylformamide

Shin-ichi ISHIGURO, Bojana G. JELIAZKOVA,† and Hitoshi OHTAKI*

Department of Electronic Chemistry, Tokyo Institute of Technology at Nagatsuta, 4259, Nagatsuta-cho, Midori-ku, Yokohama 227

†*Department of Analytical Chemistry, Sofia University, Anton Ivanov 1, Sofia, Bulgaria*

(Received November 7, 1984)

Formation of copper(II) chloride complexes has been studied by calorimetric and spectrophotometric titrations in *N,N*-dimethylformamide (DMF) containing different ionic media, 0.1 and 0.2 mol dm^{-3} $(C_2H_5)_4NClO_4$ and 1 mol dm^{-3} $LiClO_4$ at 25 °C. In all the DMF solutions examined, calorimetric and spectrophotometric titration curves were well explained in terms of formation of a series of four mononuclear complexes, $[CuCl_n]^{(2-n)+}$ (n=1—4), and formation constants, enthalpies and entropies of formation of the complexes were determined. Formation constants were determined by both calorimetry and spectrophotometry and most of the values obtained by the different methods were in good agreement each other. Calorimetric titration curves obtained in 0.1 and 0.2 mol dm^{-3} $(C_2H_5)_4NClO_4$ ionic media were practically the same, but they significantly differed from those obtained in 1 mol dm^{-3} $LiClO_4$ ionic medium, the result indicating that the formation of copper(II) chloride complexes was more favored in the former ionic media than in the latter. Stepwise enthalpies of formation were positive for $[CuCl]^+$, $[CuCl_2]$, and $[CuCl_3]^-$, but negative for $[CuCl_4]^{2-}$ in the $(C_2H_5)_4NClO_4$ DMF solutions, while the values in the 1 mol dm^{-3} $LiClO_4$ DMF solution were more negative by 6—8 kJ mol^{-1} than the respective values in the $(C_2H_5)_4NClO_4$ solutions. A significant difference was also found for stepwise entropies of formation of copper(II) chloride complexes between the ionic media. The ionic medium effect on the formation of the complexes found was ascribed to ion pairing of LiCl in the 1 mol dm^{-3} $LiClO_4$ DMF solution, ion pairing of $(C_2H_5)_4NCl$ being insignificant in the $(C_2H_5)_4NClO_4$ DMF solutions used. A largely negative ΔH_4° and a small ΔS_4° values in the $(C_2H_5)_4NClO_4$ DMF solutions suggested that solvation of the $[CuCl_3]^-$ complex was not strong, and thus, release of solvent molecules from the $[CuCl_3]^-$ complex did not play an important role for the formation of $[CuCl_4]^{2-}$. Therefore, the enthalpy and entropy of formation of $[CuCl_4]^{2-}$ were mainly attributable to those of desolvation of chloride ions and of bond formation between Cl^- and $[CuCl_3]^-$. The $[CuCl_4]^{2-}$ complex may have no DMF molecules in the primary coordination sphere of the central metal ion within the complex. Electronic spectra of individual copper(II) chloride complexes were determined from spectra at various concentrations of chloride ions by using the formation constants obtained.

Although a number of studies have so far been carried out for electronic spectra of copper(II) chloride complexes in both crystalline and solution states, only a few quantitative investigations were examined for the formation of the complexes in solutions. Khan and Schwing-Weill[1] reported the formation constants and electronic spectra of $[CuCl_n]^{(2-n)+}$ (n=1—4) in aqueous solution containing 5 mol dm^{-3} $Na(ClO_4,Cl)$ as a constant ionic medium. Ellev *et al.*[2,3] also spectrophotometrically studied the complex formation reactions in *N,N*-dimethylformamide (DMF) and dimethyl sulfoxide (DMSO) containing 1 mol dm^{-3} $LiClO_4$ and in propylene carbonate containing 0.1 mol dm^{-3} $(C_2H_5)_4NClO_4$. Manahan and Iwamoto[4] investigated the formation and electronic spectra of the copper(II) chloride complexes in acetonitrile by a combination of spectrophotometric and electrochemical methods. In weaker donor solvents such as acetonitrile and propylene carbonate, a series of four mononuclear complexes, $[CuCl_n]^{(2-n)+}$ (n=1—4), were found. However, the only formation of $[CuCl]^+$, $[CuCl_3]^-$, and $[CuCl_4]^{2-}$ were concluded in stronger donor solvents such as DMSO and DMF.

The formation of copper(II) chloride complexes was more favorable in aprotic solvents than in water, and it was more enhanced in weaker donor solvents. Although the formation constants of the $[CuCl_n]^{(2-n)+}$ (n=1—4) complexes have been determined by some authers,[1-4] no values of enthalpy and entropy of formation of the complexes have been reported.

The aim of our present study is to elucidate interactions between copper(II) and chloride ions and between the ions and solvent molecules in *N,N*-dimethylformamide from enthalpic and entropic points of view. The complex formation reactions of copper(II) with chloride ions in DMF containing various inert ionic media were investigated by calorimetry and formation constants, and enthalpies and entropies of formation of the complexes were determined. Spectrophotometric measurements were also carried out to determine the formation constants and electronic spectra of the individual copper(II) chloride complexes.

Experimental

Reagents. *Copper(II) perchlorate* was prepared from copper(II) oxide and perchloric acid of super special reagent grade. The copper(II) perchlorate thus prepared was recrystallized three times from water. The copper(II) perchlorate hexahydrate, $Cu(ClO_4)_2 \cdot 6H_2O$, thus obtained were dried in a vacuum oven at 70 °C for 48 hours.

Copper(II) perchlorate DMF solvates, $Cu(ClO_4)_2(DMF)_x$, were prepared by dissolving copper(II) perchlorate hexahydrate crystals in DMF and recrystallized six times from DMF and finally from a DMF–acetone mixture. The crystals thus obtained involved four to six DMF molecules per copper(II) ion, as already noted by Schneider,[5] and were dried at 40 °C in a vacuum oven for several days and kept in a vacuum desiccator over P_2O_5. Electrogravimetrical analysis showed that the copper(II) perchlorate DMF solvate crystals finally obtained were $Cu(ClO_4)_2(DMF)_4$.

Lithium perchlorate and *lithium chloride* were recrystallized from water and dried as described elsewhere.[6]

Tetraethylammonium perchlorate and *tetraethylammonium chloride* of reagent grade were used without further purification and dried at 100 °C.

N,N-*Dimethylformamide* was dried for several weeks over molecular sieves 4A 1/16, and then distilled at 40 °C under a reduced pressure (2 mmHg) and stored over the molecular sieves in a dark bottle with a P_2O_5 guard-tube. The residual water determined by Karl Fisher tests was less than 220 ppm.

As *N,N*-dimethylformamide is hygroscopic, all test solutions were prepared in a dry box over P_2O_5 and under an atmosphere of dried nitrogen gas.

Measurements. Calorimetric measurements were carried out in a thermostated bath controlled at (25.000±0.007) °C placed in a room thermostated at (25.0±0.2) °C. Throughout the calorimetric titrations, an ionic medium was kept constant by using either $(C_2H_5)_4NClO_4$ (0.1 and 0.2 mol dm^{-3}) or $LiClO_4$ (1 mol dm^{-3}). A 100 cm^3 of copper(II) perchlorate solution was first placed in a Dewar vessel, which was filled with nitrogen gas and prevented from moisture with a P_2O_5 guard-tube, and then titrated with a relevant chloride solution. The titrants employed were $(C_2H_5)_4NCl$ (0.1 and 0.2 mol dm^{-3}) and LiCl (1 mol dm^{-3}) solutions. The heat of dilution of chloride ions was separately determined by titrating either $(C_2H_5)_4NClO_4$ or $LiClO_4$ solution without copper(II) perchlorate with the relevant titrant solutions. The values were 0.06, 0.08, and 0.28 J cm^{-3} per the addition of a unit volume of the titrants, 0.1 and 0.2 mol dm^{-3} $(C_2H_5)_4NCl$ and 1 mol dm^{-3} LiCl, respectively. A heat q of reaction evolved at each point of titration was ranged −5 to 5 J with a certainty ±0.05 J. Calorimetric measurements were carried out by using a fully automatic on-line system as described in a previous paper.[6]

Spectrophotometric measurements were carried out in DMF solutions containing the same ionic media as those employed in calorimetric measurements. A flow cell with a light-path length of 0.5 cm was connected with a titration vessel through teflon and glass tubes. A 15 cm^3 of $Cu(ClO_4)_2$ DMF solution was placed in a vessel under a nitrogen atmosphere and then titrated with either a tetraethylammonium or a lithium chloride solution. Electronic spectra were measured with a HITACHI 340 spectrophotometer (HITACHI) equipped with a JEC 6 electronic computer (JEOL) which recorded data at selected wavelengths.

Analysis of Calorimetric and Spectrophotometric Data. A heat q_i evolved at a titration point i is represented by Eq. 1 by using formation constants β_n and overall enthalpies $\Delta H^\circ_{\beta n}$ of formation of the $[CuCl_n]^{(2-n)+}$ complexes.

$$q_i = -(V_i \sum_n \beta_n \Delta H^\circ_{\beta n} m_i x_i^n - V_{i-1} \sum_n \beta_n \Delta H^\circ_{\beta n} m_{i-1} x_{i-1}^n), \quad (1)$$

where V denotes the volume of a test solution, and m and x stand for concentrations of free copper(II) and chloride ions, respectively, which are related to their total concentrations C_M and C_X according to the mass-balance equations 2 and 3:

$$C_M = \sum_n \beta_n m_i x_i^n + m \quad (2)$$

$$C_X = \sum_n n\beta_n m_i x_i^n + x. \quad (3)$$

The formation constants and enthalpies were determined by minimizing the error-square sum, $U = \sum_i (q_{i,obsd} - q_{i,calcd})^2$ by using the program KALORI.[7]

Absorbance A_{ij} at a titration point i and a selected wavelength λ_j is represented by Eq. 4 by using the formation constants and molar extinction coefficients $\varepsilon_n(\lambda_j)$ of the $[CuCl_n]^{(2-n)+}$ complexes.

$$A_{ij} = \sum_n \varepsilon_n(\lambda_j) \beta_n m_i x_i^n \quad (\beta_0 = 1), \quad (4)$$

where the wavelengths λ_j selected in the present work were 262, 270, 280, 290, 300, 310, 320, 370, 410, and 440 nm. The formation constants and molar extinction coefficients were determined by minimizing the error-square sum, $U = \sum_i \sum_j (A_{ij,obsd} - A_{ij,calcd})^2$ by using the program SPEC.

Results and Discussion

Calorimetric titration curves obtained in 1 mol dm^{-3} $LiClO_4$ ionic medium are depicted in Fig. 1. The enthalpy ΔH°/kJ mol^{-1} per the addition of a unit mole of chloride ions at each titration point was plotted against the ratio C_X/C_M, where C_X and C_M denote total concentrations of chloride and copper(II) ions, respectively, in a solution. In DMF solution with the same ionic medium, Ellev *et al.*[2] reported the only formation of $[CuCl]^+$, $[CuCl_3]^-$, and $[CuCl_4]^{2-}$ from spectrophotometric measurements. Therefore, the formation constants and enthalpies were first optimized by assuming the formation of the three copper(II) chloride complexes. The theoretical curves calculated by using the constants thus obtained are illustrated by broken lines in Fig. 1, which appreciably deviated from experimental curves, especially in the range C_X/C_M=0.5—2. This indicated that the formation of the $[CuCl_2]$ complex can not be neglected in the DMF solution. Subsequently, we assumed the formation of four complexes, $[CuCl_n]^{(2-n)+}$ (n=1—4), and then the experimental points fit well the curves (solid lines) calculated by using the constants of the four complexes. A comparison for the formation constants and enthalpies obtained by different assumptions of three (case 1, n=1, 3, and 4) and four (case 2, n=1, 2, 3, and

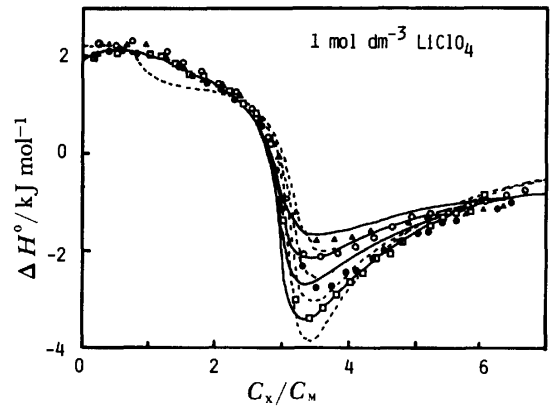

Fig. 1. Calorimetric titration curves of copper(II) chloride DMF solutions containing 1 mol dm^{-3} $LiClO_4$. Initial concentrations of copper(II) perchlorate (C_M/mmol dm^{-3}): 25.40 (▲), 35.63 (○), 48.36 (●) and 74.73 (□).

Table 1. The least-squares refinement of formation constants, β_n/mol^{-n}dm^{3n} and enthalpies, $\Delta H^\circ_{\beta n}$/kJ mol^{-1}, of copper(II) chloride complexes in DMF containing 1 mol dm^{-3} $LiClO_4$ at 25 °C

	Case 1	Case 2
β_1	(1.86±1.5)×10^4	(6.20±1.3)×10^3
β_2	—	(1.25±0.01)×10^7
β_3	(1.85±1.6)×10^{10}	(3.54±0.5)×10^{10}
β_4	(2.66±2.4)×10^{11}	(2.60±0.3)×10^{11}
$\Delta H^\circ_{\beta_1}$	(2.2±0.1)	(1.84±0.05)
$\Delta H^\circ_{\beta_2}$	—	(5.41±0.25)
$\Delta H^\circ_{\beta_3}$	(4.8±0.2)	(4.42±0.06)
$\Delta H^\circ_{\beta_4}$	−(6.5±0.9)	−(9.90±0.6)
U[a]	13.1	1.1
N[b]	92	92

a) Error-square sum, b) The number of calorimetric data points.

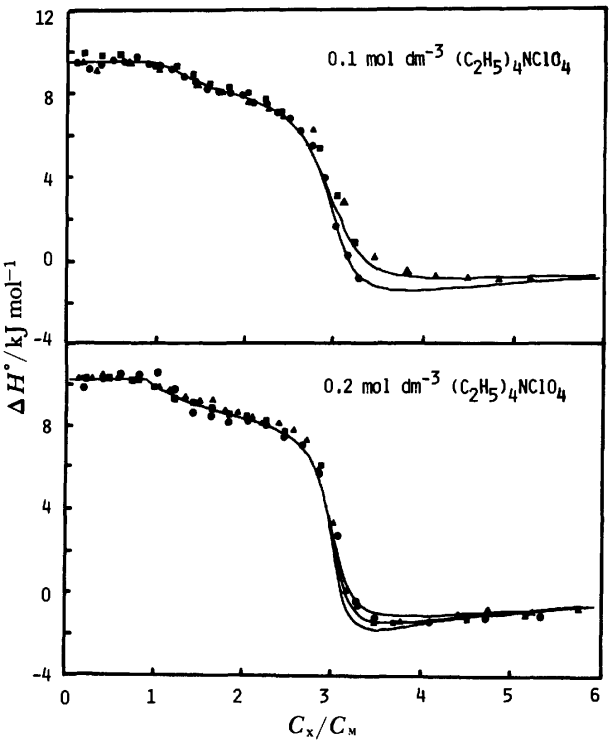

Fig. 2. Calorimetric titration curves of copper(II) chloride DMF solutions containing 0.1 and 0.2 mol dm^{-3} $(C_2H_5)_4NClO_4$. Initial concentrations of copper(II) perchlorate (C_M/mmol dm^{-3}): 7.30 (■), 15.20 (▲) and 20.25 (●) in 0.1 mol dm^{-3} $(C_2H_5)_4NClO_4$ DMF solution, and 9.80 (●), 14.66 (■) and 19.93 (▲) in 0.2 mol dm^{-3} $(C_2H_5)_4NClO_4$ DMF solution.

4) copper(II) chloride complexes is shown in Table 1. The error-square sum U and standard deviations were much smaller in case 2 than in case 1. Thus, we concluded that a series of four mononuclear complexes, $[CuCl_n]^{(2-n)+}$ (n=1—4), were formed in the 1 mol dm^{-3} $LiClO_4$ DMF solution.

Calorimetric titration curves obtained in DMF solutions containing 0.1 and 0.2 mol dm^{-3} $(C_2H_5)_4NClO_4$ are depicted in Fig. 2. Experimental points well fell on the curves (solid lines) calculated by using the formation constants in Table 2 and the enthalpies in Table 3 of the four mononuclear copper(II) chloride complexes in each $(C_2H_5)_4NClO_4$ DMF solution.

The stepwise formation constants obtained by calorimetry and spectrophotometry in each ionic medium are compared in Table 2. In all cases, the error-square sum U became small enough to explain experimental data in terms of the formation of $[CuCl_n]^{(2-n)+}$ (n=1—4). Standard deviations for each constant were not well evaluated because the product of diagonal elements of the error matrix exceeded 10^{-75}, which was the lowest limit of the computer ability employed. However, a reasonable agreement was obtained between the formation constants determined by calorimetry and spectrophotometry.

The overall enthalpies of formation of the complexes obtained by calorimetry are listed in Table 3, together with the enthalpy values obtained by employing the formation constants determined by spectrophotometry for the analysis of the calorimetric data. Except for the $\Delta H^\circ_{\beta_4}$ value in the 0.1 mol dm^{-3} $(C_2H_5)_4NClO_4$ ionic medium, all enthalpy values obtained by the both estimations were in good agreement. In the 0.1 mol dm^{-3} $(C_2H_5)_4NClO_4$ ionic medium, test solutions were titrated with a 0.1 mol dm^{-3} $(C_2H_5)_4NCl$ solution, and thus, the formation of the $[CuCl_4]^{2-}$ complex might be insufficient even after the addition of a large volume of the titrant. Therefore, the $\Delta H^\circ_{\beta_4}$ value thus estimated may involve a rather large uncertainty.

Formation of Copper(II) Chloride Complexes in $(C_2H_5)_4NClO_4$ Ionic Media. It is obvious from similar calorimetric titration curves in Fig. 2 that thermodynamic quantities in the 0.1 mol dm^{-3} $(C_2H_5)_4NClO_4$ ionic medium were not appreciably different from those in the 0.2 mol dm^{-3} $(C_2H_5)_4NClO_4$ ionic medium.

Thermodynamic quantities, ΔG°_n/kJ mol^{-1}, ΔH°_n/kJ mol^{-1}, and ΔS°_n/J K^{-1} mol^{-1}, for stepwise reactions, $CuCl_{n-1}^{(3-n)+} + Cl^- = CuCl_n^{(2-n)+}$ (n=1—4), in the 0.2 mol dm^{-3} $(C_2H_5)_4NClO_4$ ionic medium are summarized in Table 4, together with those in the 1 mol dm^{-3} $LiClO_4$ ionic medium.

Copper(II) ions are more strongly solvated in DMF than in water,[8] as is expected from a stronger donor property of DMF (the donor number (D_N)=26.6) than that of water (D_N=18.0).[9] On the other hand, chloride ions are less strongly solvated in DMF than in water.[10] The change in enthalpy of solvation of Cl^- between the solvents is much less significant than that of Cu^{2+}. Therefore, the formation of copper(II) chloride complexes should be less favored in DMF than in water from the enthalpic point of view. However, the reverse was the case, that is, the formation of copper(II) chloride complexes was more favorable in DMF than in water. The facts indicated that the formation of the complexes was more favored by the entropy term in DMF than in water, although the enthalpies and entropies of formation of the complexes in water have not been known.

According to Ahrland,[11] such a more favorable en-

Table 2. Stepwise formation constants, K_n/mol^{-1}dm^3, for the reactions, $CuCl_{n-1}^{(3-n)+}+Cl^- = CuCl_n^{(2-n)+}$ (n=1—4), obtained in N,N-dimethylformamide containing various ionic media at 25 °C

	0.1 mol dm^{-3} $(C_2H_5)_4NClO_4$		0.2 mol dm^{-3} $(C_2H_5)_4NClO_4$		1 mol dm^{-3} $LiClO_4$	
	Cal[a]	Spec[b]	Cal[a]	Spec[b]	Cal[a]	Spec[b]
$\log K_1$	7.60	7.16	6.79	5.72	3.79	4.26
$\log K_2$	3.95	4.15	4.54	4.19	3.31	3.44
$\log K_3$	3.67	3.92	4.00	4.02	3.45	4.14
$\log K_4$	1.12	1.35	1.52	1.60	0.86	0.98
U[c]	0.25	0.238	0.52	0.084	1.13	0.131
N[d]	56	210	73	210	92	340

a) Calorimetry, b) Spectrophotometry, c) Error-square sum, d) The number of data points.

Table 3. The overall enthalpies, $\Delta H^\circ_{\beta n}$/kJ mol^{-1}, for the reactions, $Cu^{2+}+nCl^- = CuCl_n^{(2-n)+}$ (n=1—4), obtained in N,N-dimetylformamide containing various ionic media at 25 °C

	0.1 mol dm^{-3} $(C_2H_5)_4NClO_4$		0.2 mol dm^{-3} $(C_2H_5)_4NClO_4$		1 mol dm^{-3} $LiClO_4$	
	Cal[a]	Spec[b]	Cal[a]	Spec[b]	Cal[a]	Spec[b]
$\Delta H^\circ_{\beta 1}$	9.5	9.6(0.07)	10.3	10.3(0.1)	1.84	1.99(0.04)
$\Delta H^\circ_{\beta 2}$	19.3	19.4(0.15)	20.0	20.4(0.2)	5.41	4.32(0.07)
$\Delta H^\circ_{\beta 3}$	25.4	25.1(0.13)	27.3	27.4(0.1)	4.42	4.67(0.05)
$\Delta H^\circ_{\beta 4}$	6.5	15.0(0.9)	19.7	19.8(0.2)	−9.89	−8.60(0.11)

Values in parentheses refer to standard deviations. a) Calorimetry, b) Enthalpy values evaluated by using formation constants obtained by spectrophotometry in Table 2.

Table 4. Thermodynamic quantities, ΔG°_n/kJ mol^{-1}, ΔH°_n/kJ mol^{-1} and ΔS°_n/J K^{-1} mol^{-1}, for stepwise reactions, $CuCl_{n-1}^{(3-n)+}+Cl^- = CuCl_n^{(2-n)+}$ (n=1—4), in N,N-dimethylformamide solution at 25 °C

	0.2 mol dm^{-3} $(C_2H_5)_4NClO_4$	1 mol dm^{-3} $LiClO_4$
ΔG°_1	−38.8	−21.6
ΔG°_2	−25.9	−18.9
ΔG°_3	−22.8	−19.7
ΔG°_4	−8.7	−5.0
ΔH°_1	10.3	1.8
ΔH°_2	9.7	3.6
ΔH°_3	7.3	−1.0
ΔH°_4	−8.1	−14.3
ΔS°_1	165	79
ΔS°_2	120	75
ΔS°_3	101	63
ΔS°_4	2	−31

tropy of complex formation reactions of metal ions in DMF than in water is not unexpected and it can be interpreted in terms of both different solvation structure of metal ions and different solvent structure between solvent molecules in DMF from those in water. In water, water molecules leave a hydrate structure and then enter another fairly well-ordered structure of bulk water. The entropy changes at the two stages compensate each other to yield a modest entropy gain, or even a net loss if the entropy change connected with the coordination of the ligand is not so favorable. In DMF, solvent molecules leave a solvate structure which may be more strictly ordered than the corresponding hydrate and then enter a bulk solvent that is fairly unstructured. Thus, a very large entropy gain may result.

Largely positive entropies ΔS°_n of formation were observed for the formation reactions of the $[CuCl_n]^{(2-n)+}$ (n=1—3) complexes in DMF containing 0.2 mol dm^{-3} $(C_2H_5)_4NClO_4$, which therefore suggested that the metal and chloride ions in the solution were extensively desolvated in the course of the formation of the complexes.

On the other hand, the ΔS°_4 value for the reaction, $CuCl_3^- + Cl^- = CuCl_4^{2-}$, was almost zero and remarkably smaller than the ΔS°_n (n=1—3) values in the 0.2 mol dm^{-3} $(C_2H_5)_4NClO_4$ DMF solution, indicating that the entropy gain due to desolvation of the $[CuCl_3]^-$ complex in the course of the formation of $[CuCl_4]^{2-}$ may not be significant if the extent of entropy loss accompaning the coordination of the ligand is similar at each consecutive step of the formation reactions, $CuCl_{n-1}^{(3-n)+}+Cl^- = CuCl_n^{(2-n)+}$ (n=1—4).

A large difference between the enthalpies of formation of the copper(II) chloride complexes was also observed. The ΔH°_4 value was negative in contrast to the ΔH°_n (n=1—3) values which were all positive. The $[CuCl_3]^-$ complex may not be strongly solvated in DMF, and thus, DMF molecules weakly solvating the complex may be exothermically replaced with a chloride ion in the course of the formation of the $[CuCl_4]^{2-}$ complex. Consequently, it was suggested that the $[CuCl_4]^{2-}$ complex has no solvent molecules in the primary coordination sphere of copper(II) ion within the complex.

Formation of Copper(II) Chloride Complexes in $LiClO_4$ Ionic Medium. In the 1 mol dm^{-3} $LiClO_4$ DMF solution, the ΔH°_n value of formation of the $[CuCl_n]^{(2-n)+}$

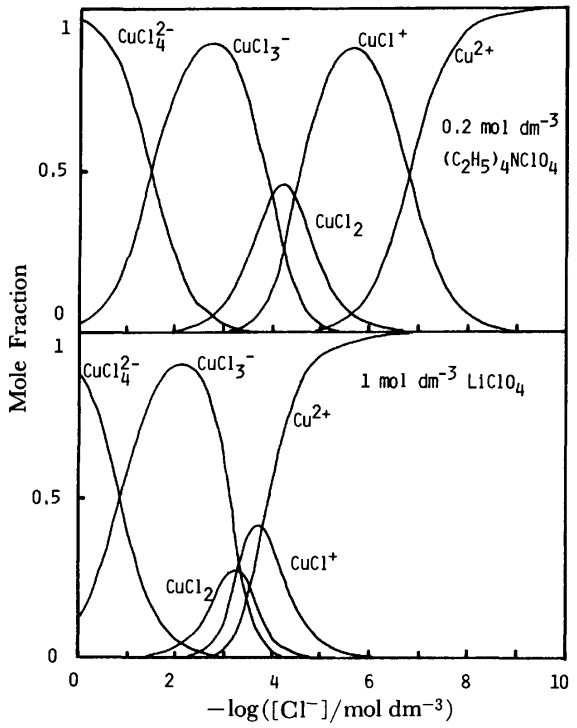

Fig. 3. Distribution of the copper(II) chloride complexes in 0.2 mol dm^{-3} $(C_2H_5)_4NClO_4$ and 1 mol dm^{-3} $LiClO_4$ DMF solutions, calculated by using the formation constants obtained by calorimetry.

complex was slightly positive for n=1 and 2, slightly negative for n=3 and largely negative for n=4, all the enthalpy values being more negative by 6—8 kJ mol^{-1} than the respective values in the 0.2 mol dm^{-3} $(C_2H_5)_4NClO_4$ DMF solution. As to the entropy of formation of $[CuCl_n]^{(2-n)+}$ in the 1 mol dm^{-3} $LiClO_4$ DMF solution, the ΔS_n° value was positive for n=1—3, but was negative for n=4, and all the values were significantly smaller than the respective entropy values in the 0.2 mol dm^{-3} $(C_2H_5)_4NClO_4$ DMF solution. Consequently, the formation of copper(II) chloride complexes was less favored in the 1 mol dm^{-3} $LiClO_4$ than in the $(C_2H_5)_4NClO_4$ DMF solutions as illustrated by the distribution curves in Fig. 3.

It has been reported that lithium ions associate with perchlorate[12] and chloride[13-15] ions to form solvent-shared and contact ion pairs in DMF solutions. Since it is expected that lithium ions are strongly solvated with DMF molecules,[16] ionic association of $LiClO_4$ may not be significant in solutions less than 2 mol dm^{-3} of the salt.[12] However, LiCl forms ion pairs even in relatively dilute solutions, the K_1 value for the formation of the ion pairs being reported to be 35 by conductivity[14] and 4 by emf measurements.[15] From these constants, we can estimate that 25—85% of chloride ions in the 1 mol dm^{-3} LiCl DMF solution may form ion pairs.

Enthalpies of solution of $(C_2H_5)_4NCl$ crystals measured in DMF solutions of various ionic media are listed in Table 5. The enthalpy of solution of $(C_2H_5)_4NCl$ in 1 mol dm^{-3} $LiClO_4$ DMF solution was more positive by 8—9 kJ mol^{-1} than the values in 0.1 and

Table 5. Enthalpies of solution of $(C_2H_5)_4NCl$ crystals in *N,N*-dimethylformamide solution at 25 °C

Ionic Medium	ΔH_S°/kJ mol^{-1}
Pure DMF	7.3
0.1 mol dm^{-3} $(C_2H_5)_4NClO_4$	9.7
0.2 mol dm^{-3} $(C_2H_5)_4NClO_4$	10.3
1 mol dm^{-3} $LiClO_4$	18.7

0.2 mol dm^{-3} $(C_2H_5)_4NClO_4$ DMF solutions. The difference may be mainly attributable to the enthalpy of formation of ion pairs between lithium and chloride ions in the 1 mol dm^{-3} $LiClO_4$ DMF solution, although enthalpies of solution of the crystals may vary depending on ionic media of the solutions examined. In fact, the enthalpy of solution of $(C_2H_5)_4NCl$ in the 0.1 mol dm^{-3} $(C_2H_5)_4NClO_4$ DMF solution was slightly more positive than that in pure DMF solution, but was practically the same as that in the 0.2 mol dm^{-3} $(C_2H_5)_4NClO_4$ DMF solution. The positive enthalpy of formation of the LiCl ion pair has also been suggested from concentration dependence of heat of solution of LiCl in DMF.[13]

Considering that $K_1>1$ and $\Delta H_{ip}^\circ>0$ for the formation of ion pairs between lithium and chloride ions in DMF, we can expect the relations between the thermodynamic quantities, ΔG_{ip}°, ΔH_{ip}°, and ΔS_{ip}°, for the ion pairs formation reaction, $Li^+ + Cl^- = LiCl$, in DMF as follows: $\Delta G_{ip}^\circ<0$ and $T\Delta S_{ip}^\circ>\Delta H_{ip}^\circ>0$. Therefore, the entropy of formation which may be mainly owing to desolvation of DMF molecules from lithium ions plays an important role for the formation of LiCl ion pairs in DMF.

Accordingly, the complex formation reactions between copper(II) and chloride ions should be accompanied by dissociation of LiCl ion pairs in 1 mol dm^{-3} $LiClO_4$ DMF solution. The enthalpy of dissociation of LiCl was negative, which led to more negative ΔH_n° (n=1—4) values of formation of $[CuCl_n]^{(2-n)+}$ in the 1 mol dm^{-3} $LiClO_4$ than in the 0.2 mol dm^{-3} $(C_2H_5)_4NClO_4$ where $(C_2H_5)_4NCl$ does not appreciably form ion pairs. The smaller entropies ΔS_n° of formation of $[CuCl_n]^{(2-n)+}$ (n=1—4) in the 1 mol dm^{-3} $LiClO_4$ than in the 0.2 mol dm^{-3} $(C_2H_5)_4NClO_4$ may be also ascribed to the ion pairing of LiCl in the former DMF solution.

Electronic Spectra of Copper(II) Chloride Complexes. Electronic spectra of copper(II) chloride at various concentrations of chloride ions were measured in 0.2 mol dm^{-3} $(C_2H_5)_4NClO_4$ and 1 mol dm^{-3} $LiClO_4$ DMF solutions. Each spectrum obtained was resolved into spectra of individual copper(II) chloride complexes by knowing the formation constants of the complexes in the solutions. Molar extinction coefficients of individual copper(II) chloride complexes at various wavelengths thus obtained in the 0.2 mol dm^{-3} $(C_2H_5)_4NClO_4$ and 1 mol dm^{-3} $LiClO_4$ DMF solutions are depicted in Fig. 4.

The calculated spectra of the $[CuCl]^+$, $[CuCl_3]^-$, and $[CuCl_4]^{2-}$ complexes in the 1 mol dm^{-3} $LiClO_4$ DMF solu-

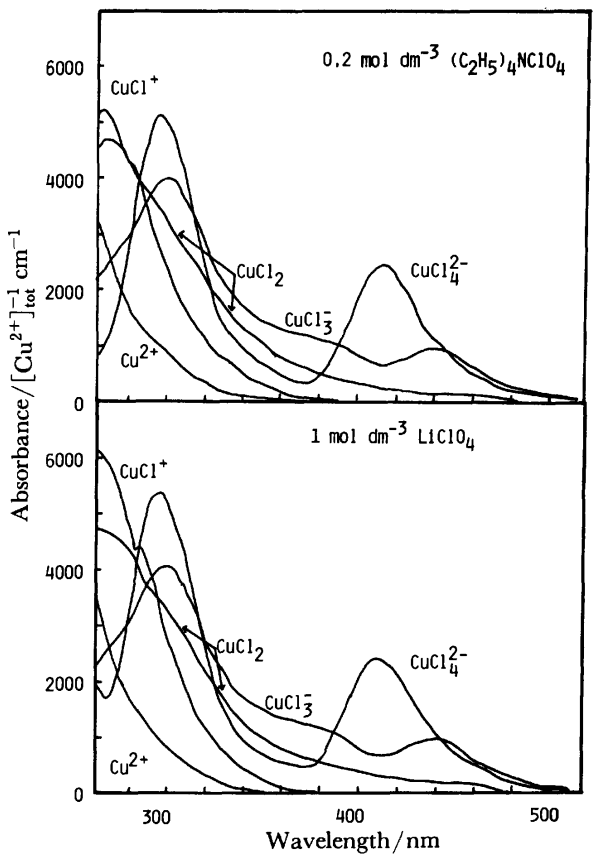

Fig. 4. Molar extinction coefficients of individual copper(II) chloride complexes at various wavelengths in 0.2 mol dm^{-3} $(C_2H_5)_4NClO_4$ and 1 mol dm^{-3} $LiClO_4$ DMF solutions.

tion were similar to those obtained in the same DMF solution by Ellev *et al.*[2] who neglected the formation of the $[CuCl_2]$ complex in the solution. Although the formation of the $[CuCl_2]$ complex was less significant in the 1 mol dm^{-3} $LiClO_4$ DMF solution than in the 0.2 mol dm^{-3} $(C_2H_5)_4NClO_4$ DMF solution as seen in Fig. 3, the formation of the complex was still appreciable even in the former solution. Thus, the spectrum of the $[CuCl_2]$ complex could be determined in both the 0.2 mol dm^{-3} $(C_2H_5)_4NClO_4$ and 1 mol dm^{-3} $LiClO_4$ DMF solutions, the spectra of the complex thus obtained in the solutions being practically the same. No absorption peak in the range of wavelength 300—500 nm was observed for the $[CuCl_2]$ complex as well as the $[CuCl]^+$ complex.

Molar extinction coefficients of individual copper(II) chloride complexes calculated were not appreciably different between the 0.2 mol dm^{-3} $(C_2H_5)_4NClO_4$ and 1 mol dm^{-3} $LiClO_4$ DMF solutions over the whole range of wavelengths measured, and therefore, structures of the copper(II) chloride complexes formed in the solutions might not essentially be affected by the inert ionic medium salts within the concentration range examined in the present study.

From electronic spectra measured in various nonaqueous solvents and in crystals, Furlani and Morpurgo[17] suggested a flattened tetrahedral structure with D_{2d} symmetry for the $[CuCl_4]^{2-}$ complex. However, structures of the copper(II) chloride complexes in DMF have not been directly determined by a diffraction method. Fergusson[18] suggested that the presence of an absorption peak between 435 and 455 nm of a copper(II) chloride complex was indicative of the D_{2d} form of the complex. If the consideration by Fergusson would be acceptable for the $[CuCl_3]^-$ complex in DMF, the complex should have the D_{2d} form with a DMF molecule solvating copper(II) ion within the complex, since the spectrum of the $[CuCl_3]^-$ complex showed an absorption peak at *ca.* 440 nm. However, the copper(II)-DMF bond within the $[CuCl_3]^-$ complex may not be so strong, as already discussed in a previous section. On the other hand, the spectrum of the $[CuCl]^+$ and also that of the $[CuCl_2]$ complex did not show any peak at the region of wavelength 435—455 nm.

The work has been supported by the Grant-in-Aid for Scientific Research No. 59540386 from the Ministry of Education, Science and Culture.

References

1) M. A. Khan and M. J. Schwing-Weill, *Inorg. Chem.*, **15**, 2202 (1976).
2) M. Ellev, J. Meullemeestre, M. J. Schwing-Weill, and F. Vierling, *Inorg.Chem.*, **19**, 2699 (1980).
3) M. Ellev, J. Meullemeestre, M. J. Schwing-Weill, and F. Vierling, *Inorg. Chem.*, **21**, 1477 (1982).
4) S. E. Manahan and R. T. Iwamoto, *Inorg. Chem.*, **4**, 1409 (1965).
5) W. Schneider, *Helv. Chim. Acta*, **46**, 1842 (1963).
6) S. Ishiguro, Y. Oka, and H. Ohtaki, *Bull. Chem. Soc. Jpn.*, **56**, 2426 (1983).
7) R. Karlsson and L. Kullberg, *Chem. Scr.*, **9**, 54 (1976).
8) S. Ishiguro, B. G. Jeliazkova, and H. Ohtaki, *Bull. Chem. Soc. Jpn.*, in press.
9) V. Gutmann, "The Donor-Acceptor Approach to Molecular Interactions," Prenum, New York and London (1978).
10) Y. Marcus, *Pure & Appl. Chem.*, **55**, 977 (1983).
11) S. Ahrland, *Pure & Appl. Chem.*, **51**, 2019 (1979).
12) D. W. James and R. E. Mayes, *J. Phys. Chem.*, **88**, 637 (1984).
13) R. P. Held and C. M. Criss, *J. Phys. Chem.*, **71**, 2487 (1967).
14) J. E. Prue and P. J. Sherrington, *Trans. Faraday Soc.*, **57**, 1795 (1961).
15) J. N. Bulter and J. C. Synnott, *J. Am. Chem. Soc.*, **92**, 2602 (1970).
16) C. V. Krishnan and H. L. Friedman, *J. Phys. Chem.*, **75**, 3606 (1971).
17) C. Furlani and G. Morpurgo, *Theor. Chim. Acta*, **1**, 102 (1963).
18) J. Fergusson, *J. Chem. Phys.*, **40**, 3406 (1964).

 © 1985 The Chemical Society of Japan Bull. Chem. Soc. Jpn., 58, 1149—1155 (1985)

The Structure–Reactivity–Chemoselectivity Relationship on the Reactions of 1-Unsubstituted Tautomeric 2-Pyridones with Benzyne

Masayuki KUZUYA,* Akihiro NOGUCHI, Ei-ichi MANO, and Takachiyo OKUDA
Gifu Pharmaceutical University, 6-1, Mitahora-higashi, 5-Chome, Gifu 502
(Received September 20, 1984)

The reactions of 2-pyridones with benzyne were investigated in order to gain some insight into the structure–reactivity–chemoselectivity relationship involved in the tautomeric systems. All reactions examined have resulted in the formation of Diels-Alder and Michael-type adducts. It has been shown that the Diels-Alder reactivities were well correlated with the HOMO energy levels of the 2-pyridone form and the yields of the Michael-type adduct were closely associated with the tautomeric equilibria. In summary, the chemoselectivities of 2-pyridones in the reaction with benzyne were largely affected by the tautomeric properties.

The tautomerism, 2-pyridone⇌2-pyridinol (**1a**), is one of the most frequently investigated tautomeric equilibria present in many heterocyclic systems. It has been well established experimentally and theoretically that there is no significant difference in the fundamental stabilities of the unimolecular state of the tautomers, **1A** and **1B**.[1] Most of 2-pyridone derivatives, however, are known to exist largely in the 2-pyridone form (**A**) as the self-associated dimer in the crystalline state[2] and in solution[3] due to the greater association ability of the 2-pyridone form (**A**), whereas derivatives bearing a 6-polar substituent exist predominantly in the 2-pyridinol form (**B**) in solution.[4]

A delicate balance of such tautomeric properties and/or aggregation forms in solution can be expected to exert an influence upon the chemical reactivity, and such reactions could provide some insight into the structure–reactivity–chemoselectivity relationship involved in the tautomeric systems. Thus, a study of the reaction of these compounds with benzyne will be interesting in connection with a variety of reactions, [*i. e.* Diels-Alder reaction and Michael-type addition].

However, in contrast to the substantial amount of experimental work on the Diels-Alder reaction of 1-substituted 2-pyridones with a variety of dienophiles in recent years,[6] similar reactions of 1-unsubstituted 2-pyrdiones have received only limited attention, and most of such reactions have been concerned only with the Michael-type addition to the oxygen and/or nitrogen atom.[6a,7] The only example of the formation of a Diels-Alder adduct to be found in the literature is the reaction with *N*-phenylmaleimides,[8] and the formation of Diels-Alder adduct with benzyne was not known prior to our preliminary publication.[9]

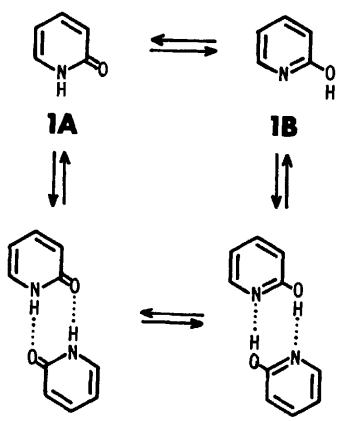

Scheme 1.

In view of these points of interest, we have studied the reactions of various substituted 2-pyridones with benzyne. In the present paper, we show that the product composition varied with the effect of the tautomeric properties exerted by a substituent, and discuss the structure–reactivity–chemoselectivity relationship observed in such reactions.

Experimental

Measurement of the Relative Diels-Alder Reactivity of 1-Methyl-2-pyridones (2) with Benzyne by Competitive Reactions. Two 2-pyridones (**2x**) and (**2y**) (0.001 mol of each) and isopentyl nitrite (0.53 g, 0.0045 mol) were dissolved in dry chloroform (80 ml). Then, anthranilic acid (0.38 g, 0.0028 mol) in a mixed solvent of acetone (20 ml) and dry chloroform (30 ml) was added dropwise to the solution over a period of 2 h under nitrogen bubbling at 70 °C. The whole was allowed to heat for an additional 2 h at 70 °C and the solvent evaporated under reduced pressure. The yields of the Diels-Alder adduct (**3x**) and (**3y**) were determined from the comparison of the integrated intensity of the peak between the product and the corresponding unreacted starting pyridones, respectively, in the ^{1}H NMR spectra of the reaction mixtures. None of the other product derived from 2-pyridones was observed. Based on the ^{1}H NMR inspection of authentic samples of the Diels-Alder adduct (**3**), the combination of two 2-pyridones (**2x**) and (**2y**) for the competitive reactions was selected so as to permit such a determination of the yield in the ^{1}H NMR spectrum of the reaction mixture. The yields(%) (Y(**3x**) and Y(**3y**)) in each set of competitive reactions are summarized in Table 1.

Reactions of 1-Unsubstituted 2-Pyridones (1) with Benzyne. The reactions were performed on 2-pyridones (**1a—j**, **1l—q**, and **1s—u**) in a similar manner as above. The Diels-Alder adduct (**4**), 2-phenoxypyridine (**5**), and 1-phenyl-2-pyridone (**6**) were isolated by chromatographic separation of the products on alumina in chloroform. The residue of each fraction was weighed after evaporation of the solvent.

Effects of Concentration on the Reactivity and Chemoselectivity. The procedures are essentially identical to those described above. For the reactions in 0.00625 mol dm^{-3} solution, each of 2-pyridones (**1h**), (**1i**), (**1m**), (**1n**), and

Table 1. Product yields in various pairs of competition reactions.

Pair of pyridones (2x) and (2y)	Yield/% Y(3x) and Y(3y)	Pair of pyridones (2x) and (2y)	Yield/% Y(3x) and Y(3y)
2a—2e	14—19	2d—2e	19—21
2a—2u	15—77	2e—2f	19—54
2b—2e	21—19	2e—2m	15—44
2b—2g	19—19	2i—2k	32—15
2b—2h	17—29	2i—2q	29—59
2b—2i	15—39	2i—2s	27—18
2b—2j	10—60	2i—2v	37—24
2b—2m	14—41	2j—2n	67—54
2b—2r	36—24	2k—2l	31—38
2b—2t	36— 9	2m—2n	47—67
2c—2i	10—34	2n—2o	55—73
2c—2k	24—38	2o—2p	79—85

(**1o**) (0.004 mol of each) and isopentyl nitrite (1.06 g, 0.009 mol) in dry chloroform (640 ml) were treated with anthranilic acid (0.76 g, 0.0056 mol) in a mixed solvent of acetone (160 ml) and dry chloroform (320 ml). On a similar workup as above, the product yields of 2-phenoxypyridine (**5**), the Diels-Alder adduct (**4**) and the unreacted 2-pyridone (**1**) were determined from the integrated intensities of the peak characteristic of each compound in the ^{1}H NMR spectra except for **1o**. The crude mixture obtained from **1o** did not show the well defined ^{1}H NMR spectrum. The crude mixture of **1o**, therefore, was chromatographed on alumina in chloroform as an eluent and the product yield then determined from the isolated yield of each of the compounds (**4o**), (**5o**), and (**1o**). For the reactions in 0.1 mol dm^{-3} solution, each of 2-pyridones (**1h**), (**1i**), (**1m**), (**1n**), and (**1o**) (0.004 mol of each) and isopentyl nitrite (1.06 g, 0.009 mol) in dry chloroform (40 ml) were treated with anthranilic acid (0.76 g, 0.0056 mol) in a mixed solvent of acetone (10 ml) and dry chloroform (20 ml), and the product composition analyzed as above.

Molecular Orbital Calculations. The CNDO/2 calculations for methylated 2-pyridones and self-associated dimeric form of 2-pyridone and 2-pyridinol were described in a previous paper.[10] For the comparison of the relative energetics with the same level of approximation, the CNDO/2 calculations of benzyne were performed with the standard parametrizations.[11] The geometric parameters were taken from the *ab initio* (4-31G) study with geometry optimization for singlet benzyne.[12]

Results and Discussion

Substituent Effect on Diels-Alder Reactivity of 1-Methyl-2-pyridones with Benzyne. In order to evaluate the substituent effect on the Diels-Alder reactivity of the 2-pyridone tautomer, we have first studied the reactions of 1-methyl-2-pyridones (**2**) with benzyne to afford 1-methyl-5,6-benzo-2-azabarrelen-3(2*H*)-one derivatives (**3**), several members (**2a—e**) of which were initially studied under somewhat different conditions by Sheinin *et al.*[6a] (Scheme 2). The structural assignment and physicochemical properties of the products (**3**) will be published in a separate paper.[13]

The Diels-Alder reaction of **2** with benzyne is sensitive to the reaction conditions. In fact, the yields

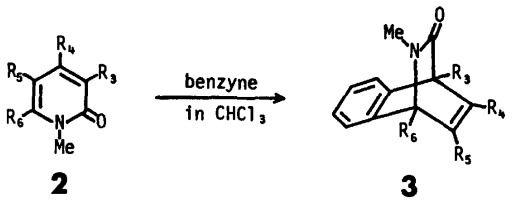

2 **3**

a[14] : $R_3=R_4=R_5=R_6=H$
b[15] : $R_3=Me$, $R_4=R_5=R_6=H$
c[16] : $R_3=R_5=R_6=H$, $R_4=Me$
d[16] : $R_3=R_4=R_6=H$, $R_5=Me$
e[17] : $R_3=R_4=R_5=H$, $R_6=Me$
f[13] : $R_3=R_5=Me$, $R_4=R_6=H$
g[14] : $R_3=R_5=H$, $R_4=R_6=Me$
h[6d] : $R_3=R_4=H$, $R_5=R_6=Me$
i[13] : $R_3=H$, $R_4=R_5=R_6=Me$
j[18] : $R_3=R_4=R_5=R_6=Me$
k[6d] : $R_3=R_5=R_6=H$, $R_4=Ph$
l[6d] : $R_3=R_5=H$, $R_4=Ph$, $R_6=Me$
m[13] : $R_3=R_6=Me$, $R_4=Ph$, $R_5=H$
n[13] : $R_3=H$, $R_4=Ph$, $R_5=R_6=Me$
o[13] : $R_3=R_5=R_6=Me$, $R_4=Ph$
p[13] : $R_3=Me$, $R_4=Ph$, R_5–$R_6=-(CH_2)_3-$
q[13] : $R_3=R_4=R_6=Me$, $R_5=Ph$
r[13] : $R_3=CN$, $R_4=H$, $R_5=R_6=Me$
s[13] : $R_3=Me$, $R_4=R_6=H$, $R_5=Br$
t[4a] : $R_3=R_4=R_5=H$, $R_6=Cl$
u[4c] : $R_3=H$, $R_4=Me$, R_5–$R_6=-CH_2CH_2O-$
v[19] : $R_3=R_4=R_5=H$, $R_6=OMe$

Scheme 2.

of Diels-Alder adducts of 1-methyl-2-pyridones with benzyne were rather poorly reproduced. Accordingly the relative reactivities were determined by the competition reactions between two 1-methyl-2-pyridones (**2x**) and (**2y**). In a competitive reaction, the concentration of highly reactive benzyne to which the two pyridones (**2x**) and (**2y**) are exposed at any time is the same for both, since they are present in the same reaction mixture. So, from the yields(%) (Y(**3x**) and Y(**3y**)) obtained by the competition reaction of **2x** and **2y** (*vide supra*), the competition constant was calculated by

$$\frac{k_{2y}}{k_{2x}} = \frac{\ln([2y]/[2y]_0)}{\ln([2x]/[2x]_0)} = \frac{\ln(1-0.01Y(3y))}{\ln(1-0.01Y(3x))}$$

where $[2x]_0$ and $[2y]_0$ are the initial concentrations of **2x** and **2y**, respectively. From these competition constants, the relative reactivities (k_r) against the parent 1-methyl-2-pyridone (**2a**) were determined, and summarized in Table 2.

The reliability of this competition method was checked on several sets of the competition constants: the reactivity ratio of **2x** and **2x′** was calculated from the competition constants of two pairs of 2-pyridones (**2x**, **2y** and **2x′**, **2y**), and this value was checked against that obtained in a direct competition experiment of **2x** and **2x′**. The scrutinized results are as follows: k_{2k}/k_{2i}(=0.42) was calculated as 0.44 from k_{2i}/k_{2c} and k_{2k}/k_{2c}; k_{2m}/k_{2e}(=3.6) as 3.9 from k_{2e}/k_{2b} and k_{2m}/k_{2b}; k_{2n}/k_{2m}(=1.7) as 1.7 from k_{2m}/k_{2b}, k_{2j}/k_{2b} and k_{2n}/k_{2j}. Thus, the probable errors for the relative reactivities obtained are considered to be within ±10%.

Table 2. The relative Diels-Alder reactivity (k_r) of 1-methyl-2-pyridones with benzyne

Substrate	k_r	Substrate	k_r
2a	1.0	**2l**	2.6
2b	1.6	**2m**	5.4
2c	1.2	**2n**	9.2
2d	1.3	**2o**	15
2e	1.5	**2p**	18
2f	5.2	**2q**	12
2g	1.6	**2r**	0.96
2h	2.8	**2s**	3.0
2i	4.8	**2t**	0.33
2j	14	**2u**	9.0
2k	2.0	**2v**	2.8

Table 2 shows that on the whole the Diels-Alder reactivities were raised as the number of substituents increased. From the comparison of the results between 3,5-dimethyl (**2f**) and 4,6-dimethyl derivatives (**2g**), and between the two 4-phenyl derivatives (**2l**) and (**2o**), introduction of the substituent into the 3- and 5-position seems to exert the greater influence on enhancement of the reactivity; the 4-phenyl substituent also exhibited further enhancement of the reactivity in a series of 5,6-dimethyl derivatives (**2n**) and (**2o**).

Reaction of 1-Unsubstituted Derivatives with Benzyne. In order to discuss the reactivity and chemoselectivity observed with 1-unsubstituted 2-pyridone derivatives (**1**), the reactions of 1-unsubstituted 2-pyridones (**1**) with benzyne have been carried out according to the procedure similar to those for 1-methyl derivatives (**2**) (Scheme 3). The structural proof of the products (**4**), (**5**), and (**6**) will be published in a separate paper.[13]

The product composition in such reactions was listed in Table 3.

It can be seen from Table 3 that the reactivity and chemoselectivity apparently varied with the substituents. Special features disclosed include the following facts; the most favored reaction is the formation of 2-phenoxypyridine (**5**) which is one of the Michael-type adducts. In all cases, the Diels-Alder reaction also proceeded to give 5,6-benzo-2-azabarrelen-3(2*H*)-ones (**4**), and the polysubstitutions apparently raised the yields of the Diels-Alder adduct, this tendency is in accord with that observed for the 1-methyl derivatives (**2**).

Interestingly, the formation of 1-phenyl-2-pyridones (**6**), another Michael-type adduct, was not observed or occured only in a very low yield for the derivatives which exist in the 2-pyridone form in solution. However, in the case of the derivatives (**1s**) and (**1t**) which tend to exist in the 2-pyridinol form in solution, appreciable amounts of the 1-phenyl-2-pyridones (**6**) were obtained as well as the Diels-Alder adduct (**4**) and the 2- phenoxypyridine (**5**). These facts seem to indicate that the formation of **5** and **6** is derived from the reac-

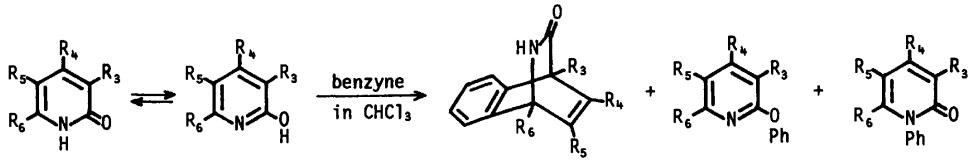

1 **4** **5** **6**

Scheme 3.

Table 3. Reactions of 2-pyridones with benzyne

2-Pyridones	Substituents				Product composition (%)				Total recovery (%)[c]
	R_3	R_4	R_5	R_6	**4**	**5**	**6**	**1**	
1a	H	H	H	H	7[a]	35	4	1	46
1b[20]	Me	H	H	H	4[a]	48	0	2[a]	54
1c[21]	H	Me	H	H	12[a]	29	0	12[a]	53
1d[20]	H	H	Me	H	17[a]	45	0	31[a]	93
1e[22]	H	H	H	Me	4[a]	74	0	17[a]	95
1f[23]	Me	H	Me	H	15[a]	45	0	27[a]	87
1g[24]	H	Me	H	Me	4	79	0	13[a]	96
1h[6d]	H	H	Me	Me	6	73	0	19	98
1i[24]	H	Me	Me	Me	5	75	0	19	99
1j[25]	Me	Me	Me	Me	8	77	0	11	96
1l[26]	H	Ph	H	Me	8	75	0	15	98
1m[26]	Me	Ph	H	Me	7	69	0	13	89
1n[13]	H	Ph	Me	Me	14	74	0	10	98
1o[25]	Me	Ph	Me	Me	26	66	0	7	99
1p[25]	Me	Ph	$-(CH_2)_3-$		30	41	0	11	82
1q[13]	Me	Me	Ph	Me	14	78	0	7	99
1s[4a]	Me	H	Br	H	7	35	7	0	49
1t[19]	H	H	H	Cl	1	33	11	0	45
1u[26]	H	Me	$-CH_2-CH_2-O-$		30[b]	0	0	0	30

a) Yields with a small amount of contamination. b) Based on a naphthalene derivative derived from a spontaneous retro Diels-Alder reaction. c) The low values are mainly due to the difficulty in recovery of the starting 2-pyridones.

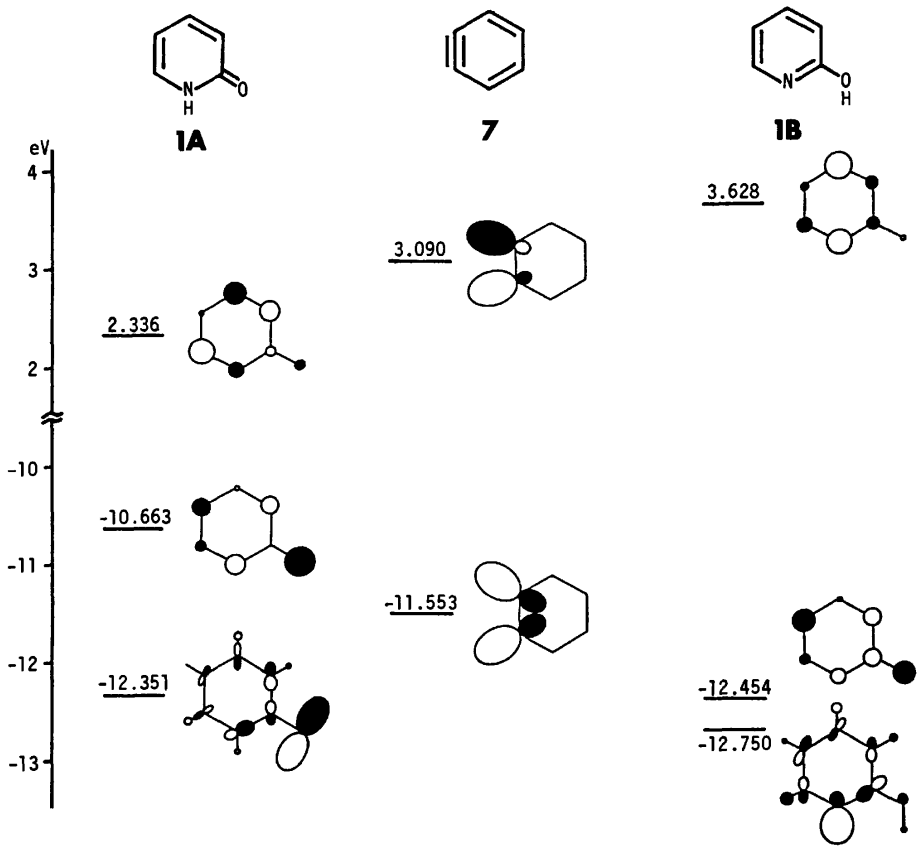

Fig. 1. Frontier molecular orbitals of 2-pyridone–2-pyridinol and benzyne calculated by the CNDO/2 method.

tion of the 2-pyridone form and the 2-pyridinol form with benzyne, respectively.

Another interesting feature is that there is a distinct difference in the yield of **5** between 6-methyl-substituted derivatives and 6-unsubstituted ones, that is, 6-methyl substitution leads to increase in the yield of **5**.

Molecular Orbital Consideration of the Structure–Reactivity–Chemoselectivity Relationship. In order to assess the substituent perturbation on the reactivity and to gain a fundamental insight into the factors controlling the chemoselectivity of this type reactions, the frontier molecular orbital (FMO) interactions were examined based on the CNDO/2 wavefunctions previously calculated.[10]

The FMO energies and the coefficient distributions of 2-pyridone (**1A**) and 2-pyridinol (**1B**) are presented in Fig. 1, together with those of benzyne (**7**).

Special features of these FMO are that the HOMO–LUMO energy separation of 2-pyridinol (**1B**) is larger than that of 2-pyridone (**1A**) and that of benzyne (**7**). This implies that the FMO interaction of **1B** with benzyne is smaller than that of **1A**. Thus, provided the reaction proceeds in accord with the FMO theory, the latter form may be more reactive with benzyne.

Figure 1 also shows that the LUMO of benzyne and the HOMO of 2-pyridone (**1A**) has a smaller separation in energy (13.753 eV) than the reverse pair (13.889 eV). Although the difference in the energy separation

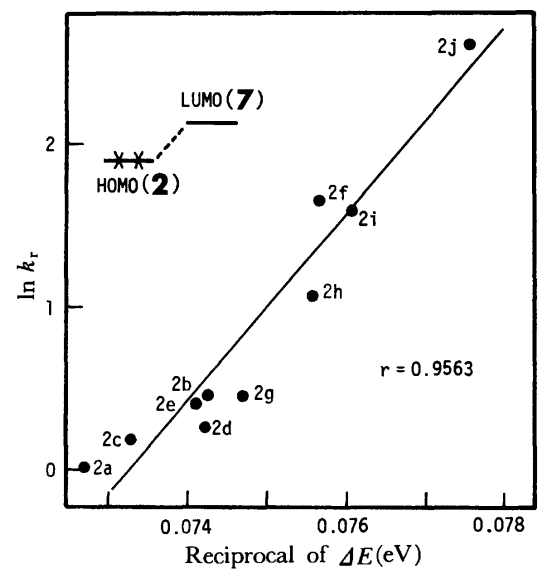

Fig. 2. Plots of the relative Diels-Alder reactivities (k_r) against the reciprocal of the FMO energy separations (ΔE).

between the two pairs is small, plots of the logarithms of relative Diels-Alder reactivities (ln k_r) of 1-methyl derivatives (**2a—j**) against the reciprocal of the FMO energy separation between the HOMO of 2-pyridones and the LUMO of benzyne displayed a good correlation as shown in Fig. 2. Thus, the dominant HOMO–LUMO interaction for the Diels-Alder reaction should involve the LUMO of benzyne and the HOMO of the 2-pyridione, *i. e.* normal electron demand for a Diels-

Alder reaction.

Little improvement in the correlation was obtained by additional consideration of the orbital interactions of the reverse pair, due to the relatively small difference in the LUMO energies among 2-pyridones.

For reactions of the 1-unsubstituted derivatives which exist largely as self-associated dimers, the FMO of such dimers should be considered. However, the relevant orbital energy diagrams for the formation of the respective dimer in the 2-pyridone (**1A**) and 2-pyridinol (**1B**) calculated by the CNDO/2 method[10] indicated that the π-type orbitals have been little affected, although the σ-type orbitals have undergone a large energy perturbation. Therefore, the essential reactivity of Diels-Alder reaction of 1-unsubstituted 2-pyridones (**1**) would be similarly interpreted as that for the 1-methyl derivatives (**2**).

It should be noted that the formation of 2-phenoxypyridine (**5**) involves the ring structural conversion from the 2-pyridone form (**A**) to the 2-pyridinol form (**B**) and includes an abstruction of the NH proton which locates in the plane of the 2-pyridone ring. Likewise, the formation of 1-phenyl-2-pyridone (**6**) involves an abstruction of the OH proton of 2-pyridinol form as well as the reverse ring structural conversion. Such characteristic features should be associated with the tautomeric properties. It seems unlikely that π-type orbital interaction in the transition state is involved for such reactions and it can be rather otherwise considering that the reaction is charge controlled in view of the electrophilic nature of benzyne; the transition state may be better represented as shown in Scheme 4 for **1a** as an example.

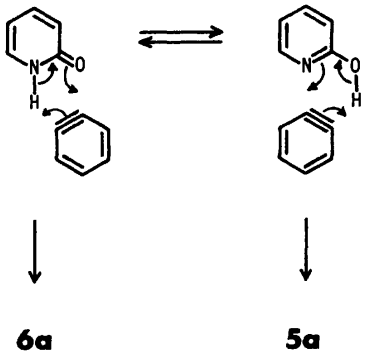

Scheme 4.

We have shown previously, based on the quantum chemical calculations, that the tautomeric equilibria of 6-methyl derivatives were labile to the molecular environment. This is true particularly for 5,6-dimethyl derivatives due to an additional buttressing effect of the 5,6-dimethyl substituents.[10] Futhermore these derivatives are very effective catalysts for the mutarotation of TMG.[15] Also, our recent fluorescence study of various substituted 2-pyridones indicated that the tautomeric equilibria of 6-methyl derivatives were very sensitive to the solvent polarity and concentration. This results in a facile shift in the tautomeric equilibria leading to predominance of the 2-pyridinol form (**B**) over the 2-pyridone form (**A**) in less polar solvent and in diluted solution.[27] The above mentioned tautomeric properties of the 6-methyl derivatives account clearly for the higher yield of the formation of 2-phenoxypyridines (**5**) from the 2-pyridone form (**A**).

A similar rationalization may also be applicable for the 4-phenyl substituent effect on further enhancement of the Diels-Alder reactivity observed with 5,6-dimethyl derivatives. The Diels-Alder reactions involve the destruction of diene character of the pyridone form as the reaction proceeds. This ring structural modification bears some resembrance to the tautomeric conversion to the 2-pyridinol form. Thus, one explanation is the greater buttressing effect of the

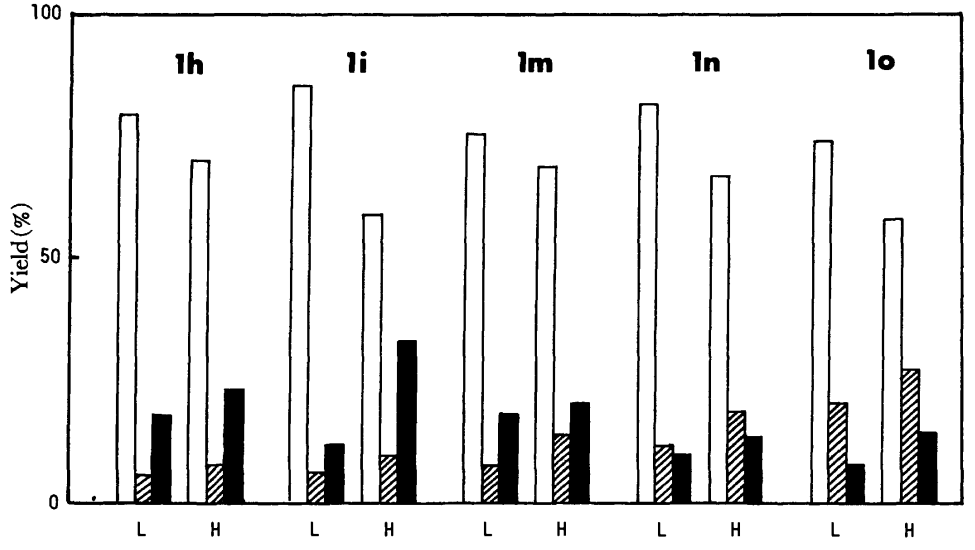

Fig. 3. Effect of concentration on the reactivity and chemoselectivity.
The products (**5**, **4**) and the unreacted 2-pyridone (**1**) were represented by □, ▨, and ■, respectively. L and H denote the reaction in 6.25×10^{-3} mol dm^{-3} solution and 0.1 mol dm^{-3} solution, respectively.

5,6-dimethyl substituents induced by the adjacent 4-phenyl group on lowering the activation energy of the transition state of the Diels-Alder reaction.

Concentration Dependency in Reactions of 1-Unsubstituted 2-Pyridones. Based on the foregoing facts and discussions, it can be considered that the factors determining the tautomeric equilibria [*i.e.* concentration, temperature and solvent] significantly affect the reactivity and the chemoselectivity of the reaction with benzyne. The concentration-dependencies for the reactions of several selected 2-pyridones such as **1h**, **1i**, **1m**, **1n**, and **1o** have been investigated and the results are illustrated in Fig. 3.

As shown in Fig. 3, the yields of 2-phenoxypyridines (**5**) were considerably lowered for the reactions in higher concentration. The recoveries of the starting 2-pyridones (**1**) were inversely raised to a similar extent and the yields of the Diels-Alder adducts (**4**) were slightly raised. Similar results were also obtained in the reaction of **1o** using a hydrogen-accepting solvent (dioxane) and in the reaction at lower temperature. It appears likely that the observed reversal in the yield of products was caused by the tautomeric properties, and indicated the importance of the abundance of the nonassociated forms for the formation of **5**. The observed chemoselectivity, therefore, could be rationalized for the formation of the Diels-Alder adduct (**4**) concomitantly increased as the major reaction (formation of **5**) was suppressed. These reaction schemes are summarized in Scheme 5 for **1a** as an example.

Thus, we have shown a novel example in which the tautomeric properties significantly affect the chemical reactivity and the chemoselectivity; it is of interest in connection with a widely accepted concept that the tautomeric equilibria are closely related to some biologically important properties of nucleic acids such as RNA transcription and DNA replication.

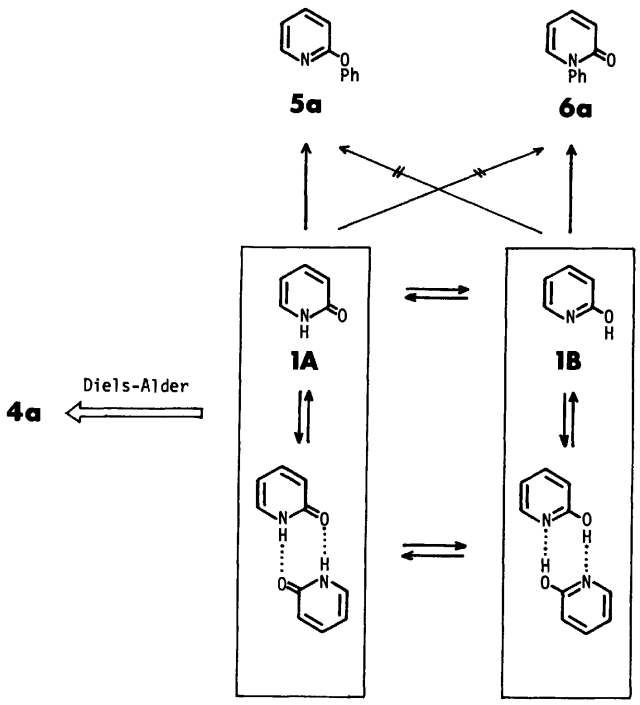

Scheme 5.

References

1) P. Beak and F. S. Fry, Jr., *J. Am. Chem. Soc.*, **95**, 1700 (1973); P. Beak, F. S. Fry, Jr., J. Lee, and F. Steele, *ibid.*, **98**, 171 (1976); P. Beak, J. B. Covington, and S. G. Smith, *ibid.*, **98**, 8284 (1976); P. Beak, *Acc. Chem. Res.*, **10**, 186 (1977); C. Guimon, G. Garrabe, and G. Pfister-Guillouzo, *Tetrahedron Lett.*, **1979**, 2585.

2) B. R. Penforld, *Acta Crystallogr.*, **6**, 591 (1953); J. Almlof, A. Kvick, and I. Olovsson, *Acta Crystallogr., Sect. B*, **27**, 1201 (1971); A. Kvick and S. S. Booles, *Acta Crystallogr., Sect. B*, **28**, 3405 (1972).

3) J. Elguero, C. Marzin, A. R. Katritzky, and P. Linda, "The Tautomerism of Heterocycles. Advances in Heterocyclic Chemistry, Suppl. 1," ed by A. R. Katritzky and A. J. Boulton, Academic Press, New York (1976), pp. 87—102.

4) a) A. R. Katritzky, J. D. Rowe, and S. K. Roy, *J. Chem. Soc. (B)*, **1967**, 758; b) G. Simchen, *Chem. Ber.*, **103**, 407 (1970); c) E. Spinner and G. B. Yeoh, *J. Chem. Soc (B)*, **1971**, 289, 279.

5) I. Tabushi, "Carbene, Yilide, Nitrene, and Benzyne," ed by T. Goto, Hirokawa Publishing Co., Tokyo (1976), p. 341.

6) a) E. B. Sheinin, G. E. Wright, C. L. Bell, and L. Bauer, *J. Heterocycl. Chem.*, **5**, 859 (1968); b) U. Heep, *Tetrahedron*, **31**, 77 (1975); c) H. Tomosawa, H. Hongo, R. Fujita, and H. Kato, *Heterocycles*, **6**, 1765 (1977); d) H. Tomisawa, H. Hongo, H. Kato, R. Fujita, and A. Sato, *Chem. Pharm. Bull*, **26**, 2312 (1978); e) K. Somekawa, T. Watanabe, and S. Kumamoto, *Nippon Kagaku Kaishi*, **1978**, 412; f) P. S. Mariano, P. L. Huesman, and R. L. Beamer, *Tetrahedron*, **34**, 2617 (1978); g) G. P. Gisby, S. E. Royall, and P. G. Sammes, *J. Chem. Soc., Chem. Comm.*, **1979**, 501; h) K. Matsumoto, Y. Ikemi-Kono, T. Uchida, and R. M. Acheson, *J. Chem. Soc., Chem. Comm.*, **1979**, 1091; i) R. Gompper and A. Schmidt, *Angew. Chem., Int. Ed. Engl.*, **19**, 463 (1980); j) H. Tomisawa, H. Hongo, H. Kato, K. Sato, and R. Fujita, *Heterocycles*, **16**, 1947 (1981); k) G. P. Gisby, S. E. Royall, and P. G. Sammes, *J. Chem. Soc., Perkin Trans. 1*, **1982**, 169; l) K. Matsumoto, Y. Ikemi, S. Nakamura, T. Uchida, and R. M. Acheson, *Heterocycles*, **19**, 499 (1982).

7) a) L. Bauer, C. L. Bell, and G. E. Wright, *J. Heterocycl. Chem.*, **3**, 393 (1966); b) B. Weinstein and D. N. Bratlesani, *J. Org. Chem.*, **32**, 4107 (1967); c) N. P. Schusherina, O. V. Slavyanova, G. N. Rodionova, and R. Ya Levina, *Khim. Geterotsikl. Soedin*, **1970**, 489; *Chem. Abstr.*, **73**, 109639y (1970); d) R. M. Acheson, N. D. Wright, and P. A. Tastker, *J. Chem. Soc., Perkin Trans. 1*, **1972**, 2918; e) N. P. Schusherina and L. V. Betaneli, *Khim. Geterotsikl. Soedin.*, **1974**, 1247; *Chem. Abstr.*, **82**, 16664y (1975).

8) I. Matsuura, Japan Patent, 14698, 25594 (1975); *Chem. Abstr.*, **83**, 43295f, 131563x (1975); L. V. Vetaneri, N. P. Schusherina, A. V. Stepanyants, and E. A. Tarkhanova, *Zh. Org. Khim.*, **13**, 1926 (1977).

9) M. Kuzuya, E. Mano, M. Adachi, A. Noguchi, and T. Okuda, *Chem. Lett.*, **1982**, 475.

10) M. Kuzuya, A. Noguchi, and T. Okuda, *Bull. Chem. Soc. Jpn.*, **57**, 3454 (1984).

11) J. A. Pople and G. A. Segal, *J. Chem. Phys.*, **44**, 3289 (1966).

12) J. O. Noell and M. D. Newton, *J. Am. Chem. Soc.*, **101**, 51 (1979).
13) M. Kuzuya, A. Noguchi, S. Kamiya, and T. Okuda, *Chem. Pharm. Bull.* (in press).
14) J. A. Elvidge and L. M. Jackman, *J. Chem. Soc.*, **1961**, 859.
15) R. Adams and A. W. Schrecker, *J. Am. Chem. Soc.*, **71**, 1186 (1949).
16) D. J. Cook, R. E. Bowen, P. Sorter, and E. Daniels, *J. Org. Chem.*, **26**, 4949 (1961).
17) M. Shamma and P. D. Rosenstock, *J. Org. Chem.*, **26**, 2586 (1961).
18) H. Hart, D. A. Dickson, and W. Y. Li, *Tetrahedron Lett.*, **1975**, 2253.
19) A. R. Katritzky, F. D. Popp, and J. D. Rowe, *J. Chem. Soc. (B)*, **1966**, 562.
20) B. M. Bain and J. E. Saxton, *J. Chem. Soc.*, **1961**, 5216.
21) O. Seide, *Ber.*, **57**, 793 (1924).
22) Y. Murakami and J. Sunamoto, *Bull. Chem. Soc. Jpn.*, **42**, 3350 (1969).
23) G. F. Rooyen, C. V. D. M. Brink, and P. A. Villier, *Tydskr. Naturwetenskappe*, **4**, 182 (1964); *Chem. Abstr.*, **63**, 13202e (1965).
24) H. Ohmori, S. Nakai, and M. Masui, *Chem. Pharm. Bull.*, **28**, 2247 (1980).
25) M. Kuzuya, A. Noguchi, and T. Okuda, *Bull. Chem. Soc. Jpn.*, **57**, 3461 (1984).
26) C. R. Hauser and C. J. Eby, *J. Am. Chem. Soc.*, **79**, 728 (1957).
27) M. Kuzuya, A. Noguchi, and T. Okuda, *J. Chem. Soc., Chem. Commun.*, **1984**, 435.

Inclusion Complex Formation of γ-Cyclodextrin. One Host-Two Guest Complexation with Water-soluble Dyes in Ground State

Hidefumi Hirai,* Naoki Toshima, and Satoshi Uenoyama
Department of Industrial Chemistry, Faculty of Engineering, The University of Tokyo, Hongo, Bunkyo-ku, Tokyo 113
(Received October 4, 1984)

β-Cyclodextrin forms the 1:1 inclusion complex with Crystal Violet, Methylene Blue, Methyl Orange, or Congo Red in water. On the other hand, γ-cyclodextrin forms the 1:2 complex with Crystal Violet, Methylene Blue, or Methyl Orange, while the 1:1 complex is given with Congo Red. The one host-two guest complexations are shown on the bases of the changes of the electronic spectra, dependence of induced circular dichroisms on the concentrations of dyes, and the continuous variation methods with induced circular dichroism. The dissociation constants for the 1:2 complexes are determined with the improved Benesi-Hildebrand equation. Alternation between the 1:1 and 1:2 complexation is discussed in terms of the cavity size of cyclodextrin and the aggregation character of dye.

Cyclodextrin, to be denoted here as CyD, forms the inclusion complex with a large number of organic or inorganic molecules and anions in an aqueous solution.[1,2] The internal diameters of hydrophobic cavities of α-CyD (cyclohexaamylose), β-CyD (cycloheptaamylose), and γ-CyD (cyclooctaamylose) are 4.5, 7.0, and 8.5 Å, respectively, and the depths of the cavities are given by the same value of 6.7—7.0 Å.[1] The inclusion complex of CyD has been vigorously investigated for a potential model of the enzyme in biomimetic chemistry[1,2] and also for the pharmaceutical application.[3] The stability of the inclusion complex depends mainly on the size and hydrophobicity of the CyD cavity. Since the cavity diameter of γ-CyD is nearly twice of that of α-CyD, γ-CyD seems to be able to include a large molecule. However, the stability of the complex of γ-CyD remains equivocal since the cavity diameter of γ-CyD is much larger than that of α- or β-CyD in spite of their common depths.

Recently, attentions have been paid for inclusion of two guest molecules in a cavity of CyD[4-14] from the viewpoint of conformational regulation of two molecules or as a model of CyD-catalyzed bimolecular reactions.[15,16] Ueno *et al.*[4] have shown the complexation of two molecules with one γ-CyD by enhancement of the excimer fluorescence. The enhancement gave the evidence for the inclusion of two molecules in the excited state, and gave the suggestion for the inclusion of two molecules in the ground state. We have separately communicated that a γ-CyD molecule forms the 1:2 complex in the ground state with three kinds of water-soluble dye molecules.[5] The present paper is a full paper of the previous letter. We would like to present here not only the detailed data but also the analytical methods supporting the 1:2 complexation.

Experimental

Materials. α- and β-CyD (Nakarai Chemicals) and dyes are used as received. γ-CyD used is also commercially available and its purity is more than 98%.

Sample Preparation. The aqueous solution of CyD or dyes are prepared by using the distilled water and phosphate buffer (pH=7.0, ion strength, μ=0.1). Stirring for 2 d at room temperature is performed for preparation of the aqueous solution of dye for the aggregated dye to come to equilibrium with its monomer form. The concentrations mainly used are 2.5×10^{-3} and 5×10^{-5} mol dm^{-3} for CyD and dyes, respectively.

Spectral Measurement. Electronic absorption spectra were measured by using a Hitachi 340 automatic spectrophotometer. Spectra of circular dichroism were obtained at 20°C with a JASCO J-20 automatic spectropolarimeter. The magnitude of circular dichroism induced by inclusion of a dye with CyD is presented by Eq. 1.

$$\theta_{tr} = \frac{c \cdot \Delta E_c}{x} \quad (1)$$

Here, θ_{tr}, ΔE_c, and x are the molar ellipticity of the complex, the circular dichroism measured, and the concentration of the complex, respectively. The term c is the constant. In the present paper, however, the initial concentration of dye is used instead of the concentration of the compelx, x, since x is unknown. Consequently, the apparent molar elipticity, θ, is used as the measure of the induced circular dichroism instead of θ_{tr}.

Determination of Dissociation Constant, K_d, for CyD–Dye Complex with Visible Spectral Measurement. The absorption spectra of dyes change with the concentration of CyD. For the 1:1 complex, the Benesi-Hildebrand equation can be applied for determination of K_d by plotting $(ab/\Delta E)$ against a, where a, b, and ΔE are initial concentrations of CyD and the dye, and difference of absorbance in the visible spectra, respectively. For the 2:1 complex, K_d must be determined from the intercept of the ordinate of the straight line obtained by a method of least squares for the plot of $(ab^2/\Delta E)$ against a. The details for providing the expression are shown in Appendix A.

Spectral Change Depending on the Concentration of Dyes. Induced circular dichroism changes with the concentration of dyes at the constant concentration of CyD. The measured magnitude of induced circular dichroism was plotted against the concentration of a dye under the conditions that the concentration of CyD is much larger than that of the dye. For the system of the 1:1 complexation, the straight line obtained passes through the point of the origin. For the 2:1 complex, on the other hand, no linear relationship exists between the concentration of dye and the magnitude of the induced circular dichroism as shown in Appendix B. Therefore, the linearities have been examined for four dyes by plotting ΔE_c of induced circular dichroism against the

concentration of the dye (5×10^{-6}—5×10^{-5} mol dm^{-3}) in order to determine the molar ratio of the inclusion complex.

Continuous Variation Method. Continuous variation method was also applied to determine the molar ratio of the inclusion complex by assuming the equilibrium 2 as described in Appendix C.

$$n\cdot\text{Dye} + \text{CyD} \rightleftharpoons \text{Complex} \qquad (2)$$

The kinds of aqueous solutions of CyD and the dye at various molar ratio were prepared with keeping the total concentration constant at 6×10^{-4} mol dm^{-3}. The apparent ellipticities, ΔE_c's, of the mixed solutions at different ratio were measured with a spectropolarimeter with a 1 mm-cell. The molar ratio with the maximum ellipticity indicates the ratio of the inclusion complex.

Results

Electronic Spectra and Induced Circular Dichroism in the Presence of CyD. Inclusions of Crystal Violet (**1**, CV), Methylene Blue (**2**, MB), Methyl Orange (**3**, MO), and Congo Red (**4**, CR) with CyDs have been examined in the aqueous solutions by the electronic spectra and the circular dichroisms. Generally, the absorption band of the guest molecule shifts by inclusion with CyD and the new circular dichroism is induced by the inclusion. Results are shown in Figs. 1—4.

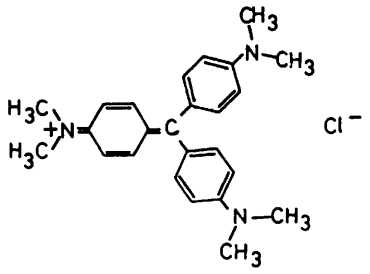

CRYSTAL VIOLET (1)

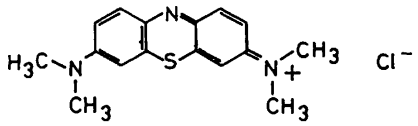

METHYLENE BLUE (2)

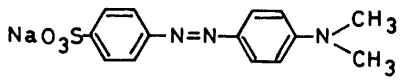

METHYL ORANGE (3)

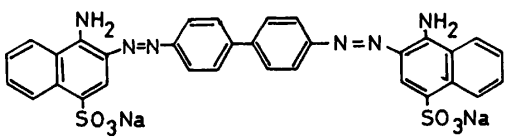

CONGO RED (4)

The aqueous solution of CV at the concentration of 5×10^{-5} mol dm^{-3} had the absorption peak at 580 nm and no circular dichroism was observed. When γ-CyD were introduced to this solution at the concentration of 6.4×10^{-3} mol dm^{-3}, the absorption maximum shifted to 548 nm and the new circular dichroism appeared. Continuous change of the concentration of CyD indicated that the original absorption peak at 580 nm disappeared and the new peak at 548 nm appeared with increase of the concentration of CyD, as shown in Fig. 1a. The Silimar changes in the electronic spectra were observed in the case of MB and MO in the presence of γ-CyD (Figs. 2a and 3a). On the other hand, the small shift of the absorption band of CR was observed with addition of γ-CyD while the large circular dichroism were induced in this case (Fig. 4a).

When β-CyD was used as an additive instead of γ-CyD, the wavelength of the maximum absorption of CV shifted slightly to the longer wavelength (red shift by 5 nm) although γ-CyD provided large blue shift (32 nm). Similar small shift of the maximum wavelength as well as increase of the absorption coefficient was observed in the case of MB, MO, and CR with β-CyD as shown in Figs. 2b, 3b, and 4b, respectively. In these cases the circular dichroisms were also induced with the different shape from those with γ-CyD.

Addition of α-CyD resulted in no significant change in the electronic spectra of CV, MB, and CR and no circular dichroism were induced as well. In the case of MO, however, wavelength of the maximum absorption shifted from 462 nm to 454 nm with addition of α-CyD and the circular dichroism was induced. These effects of α-CyD on the spectra of MO is similar to those of β-CyD.

Change of Induced Circular Dichroism with Concentration of Dye. The magnitude of the induced circular dichroism increased with the concentration of the dye in the presence of large excess of CyD, so long as the circular dichroism was induced by addition of CyD. The apparent ellipticity of the solution was plotted against the concentration of the dye in the presence of 2.5×10^{-3} mol dm^{-3} of CyD as shown in Figs. 5 and 6. The linear relationships were clear in the cases of CR-γ-CyD (in Fig. 5) and MO-β-CyD (in Fig. 6), but the nonlinearly increasing curves were obtained in the cases of CV-γ-CyD, MB-γ-CyD, and MO-γCyD (Fig. 5).

Continuous Variation Method. Apparent ellipticity of the mixed solution of the dye and CyD was plotted against the molar fraction of the dye in the solution keeping the total concentration of the dye and CyD to be constant at 6.0×10^{-4} mol dm^{-3}. Here the fraction f is defined as molar ratio of dye to the sum of dye and CyD. In the solution of CR and γ-CyD, where

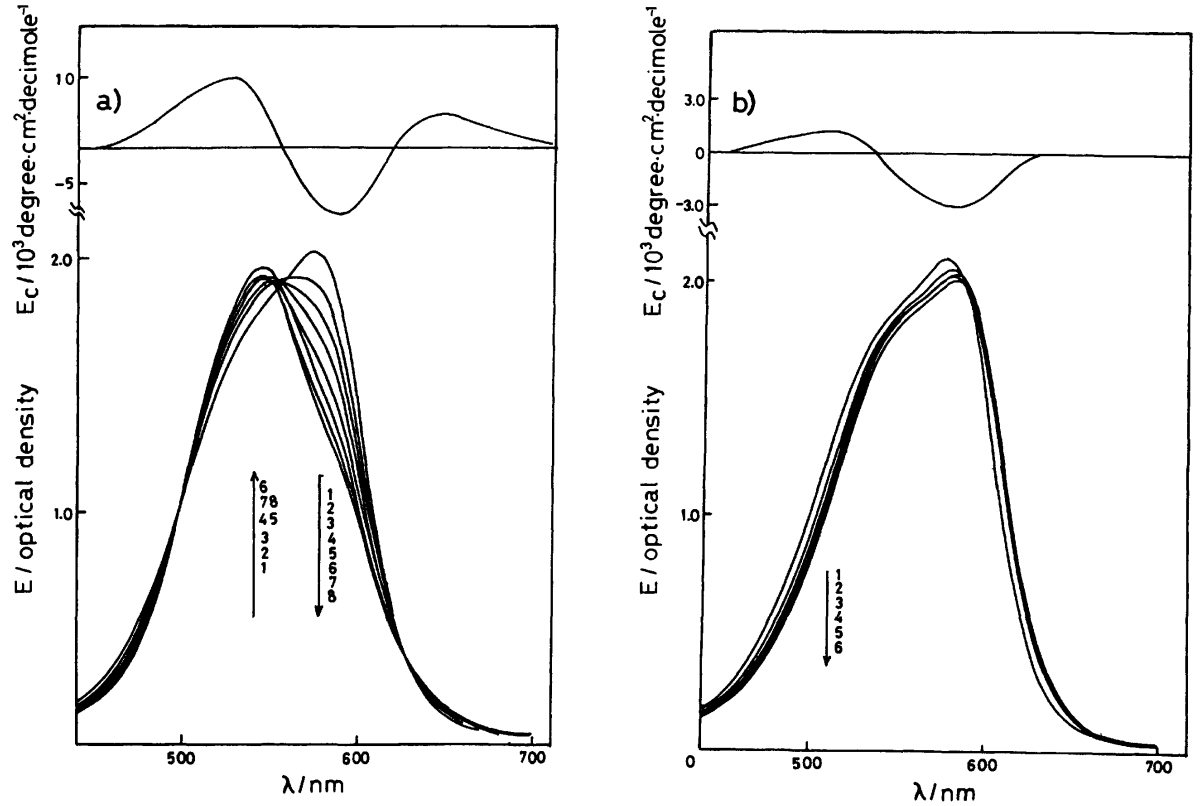

Fig. 1. Induced circular dichroism and absorption spectra of Crystal Violet (5×10^{-5} mol dm^{-3}) at various concentrations of γ-cyclodextrin (a: ICD, [γ-CyD]=2.5×10^{-3} mol dm^{-3}; AB, 1, 0.0; 2, 0.1; 3, 0.2; 4, 0.4; 5, 0.8; 6, 1.6; 7, 3.2; 8, 6.4×10^{-3} mol dm^{-3}) and β-cyclodextrin (b: ICD, [β-CyD]=2.5×10^{-3} mol dm^{-3}; AB, 1, 0.0; 2, 0.25; 3, 0.5; 4, 1.6; 5, 2.0; 6, 4.0×10^{-3} mol dm^{-3}).

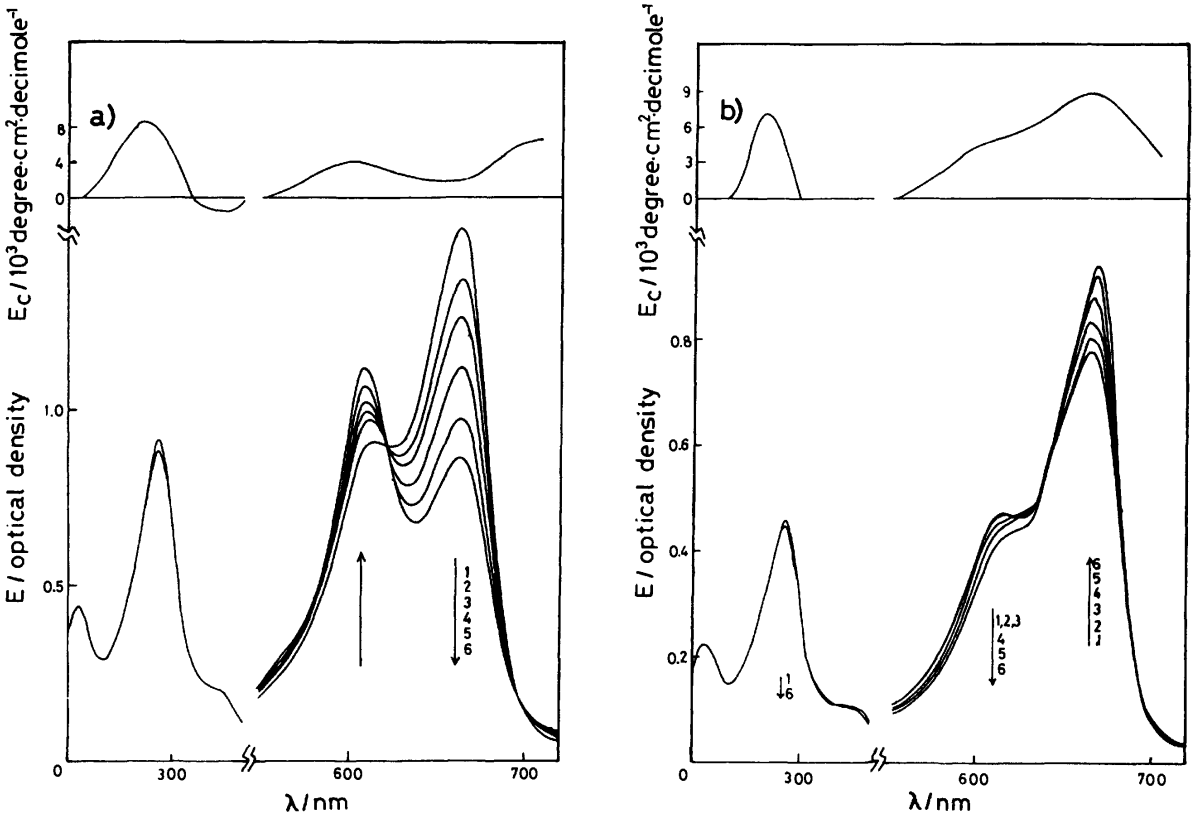

Fig. 2. Induced circular dichroism and absorption spectra of Methylene Blue (2.5×10^{-5} mol dm^{-3}) at various concentrations of γ-cyclodextrin (a: ICD, [γ-CyD]=2.5×10^{-3} mol dm^{-3}; AB, 1, 0.0; 2, 0.4; 3, 0.8; 4, 1.6; 5, 3.2; 6, 6.4×10^{-3} mol dm^{-3}) and β-cyclodextrin (b: ICD, [β-CyD]=2.5×10^{-3} mol dm^{-3}; AB, 1, 0.0; 2, 0.25; 3, 0.5; 4, 1.0; 5, 2.0; 6, 4.0×10^{-3} mol dm^{-3}).

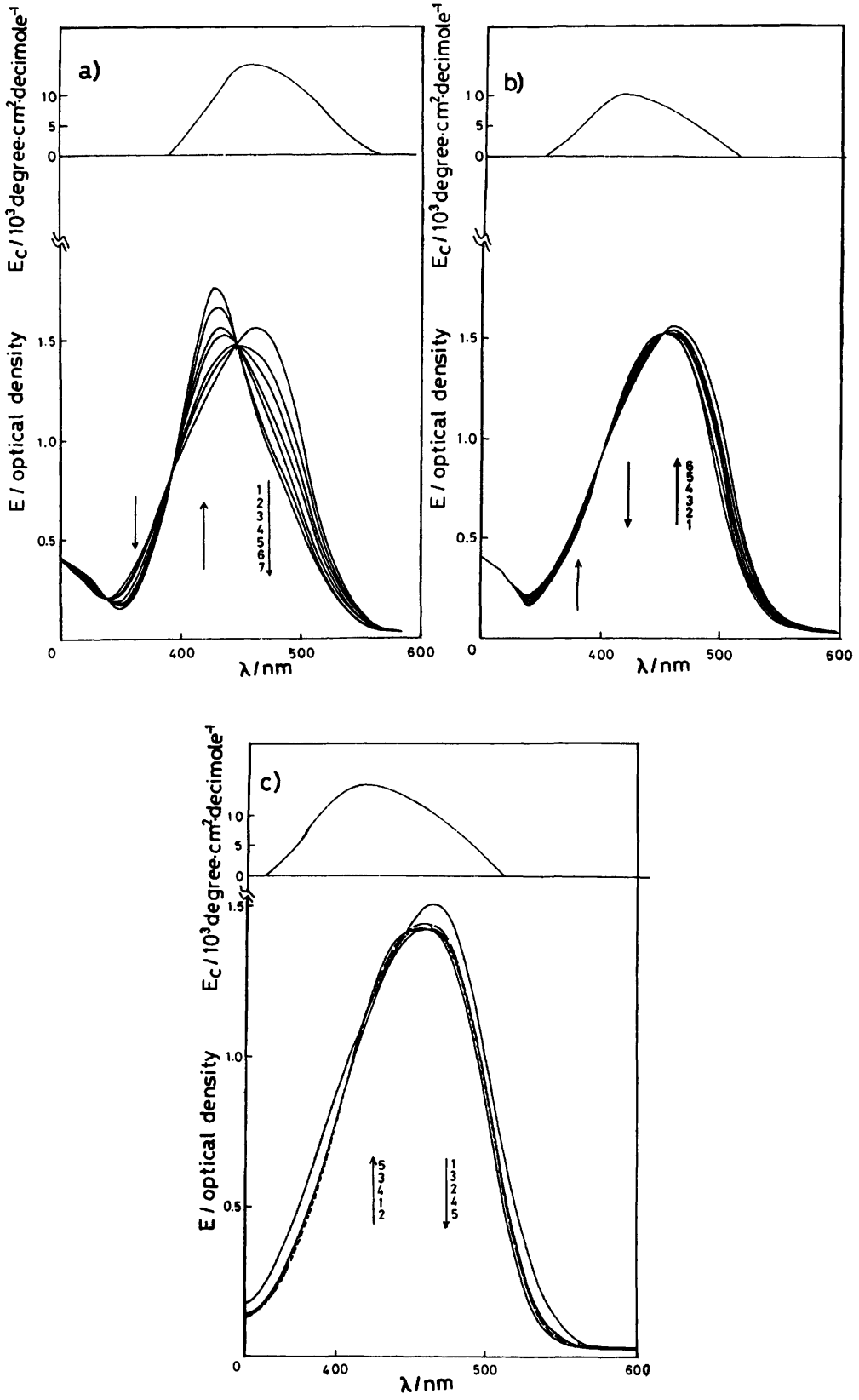

Fig. 3. Induced circular dichroism and absorption spectra of Methyl Orange (5×10^{-5} mol dm^{-3}) at various concentrations of γ-cyclodextrin (a: ICD, [γ-CyD]= 2.5×10^{-3} mol dm^{-3}; AB, 1, 0.0; 2, 0.25; 3, 0.5; 4, 1.0; 5, 2.0; 6, 4.0; 7, 8.0×10^{-3} mol dm^{-3}), β-cyclodextrin (b: ICD, [β-CyD]=2.5×10^{-3} mol dm^{-3}; AB, 1, 0.0; 2, 0.25; 3, 0.5; 4, 1.0; 5, 2.0; 6, 4.0×10^{-3} mol dm^{-3}) and α-cyclodextrin (c: ICD, [α-CyD]= 2.5×10^{-3} mol dm^{-3}; AB, 1, 0.0; 2, 0.25; 3, 0.5; 4, 2.0; 5, 4.0×10^{-3} mol dm^{-3}).

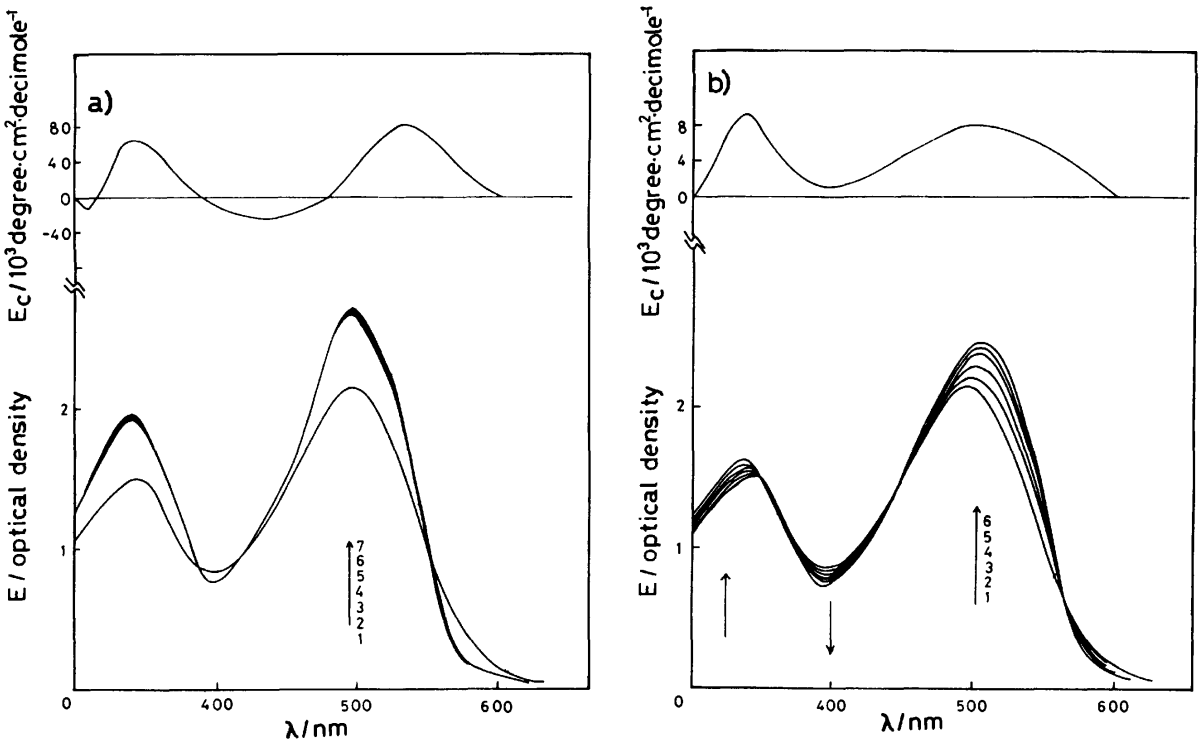

Fig. 4. Induced circular dichroism and absorption spectra of Congo Red (5×10^{-5} mol dm^{-3}) at various concentrations of γ-cyclodextrin (a: ICD, [γ-CyD]=2.5×10^{-3} mol dm^{-3}; AB, 1, 0.0; 2, 0.25; 3, 0.5; 4, 1.0; 5, 2.0; 6, 4.0; 7, 8.0×10^{-3} mol dm^{-3}) and β-cyclodextrin (b: ICD, [β-CyD]=2.5×10^{-3} mol dm^{-3}; AB, 1, 0.0; 2, 0.25; 3, 0.5; 4, 1.0; 5, 2.0; 6, 4.0×10^{-3} mol dm^{-3}).

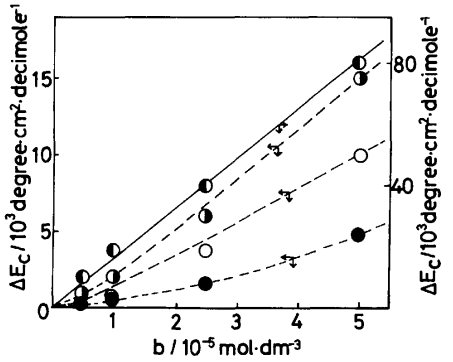

Fig. 5. The plot of the initial concentration of the dye (*b*) *vs.* the magnitude of circular dichroism (ΔE_c) induced by the complexes between the γ-cyclodextrin (2.5×10^{-3} mol dm^{-3}) and dyes (○, Crystal Violet, CD at 530 nm; ●, Methylene Blue, at 600 nm; ◑, Methyl Orange, at 456 nm; ◐, Congo Red, at 533 nm) in water. The broken curves follow the Eq. B-10, and the solid straight line follows the Eq. B-1.

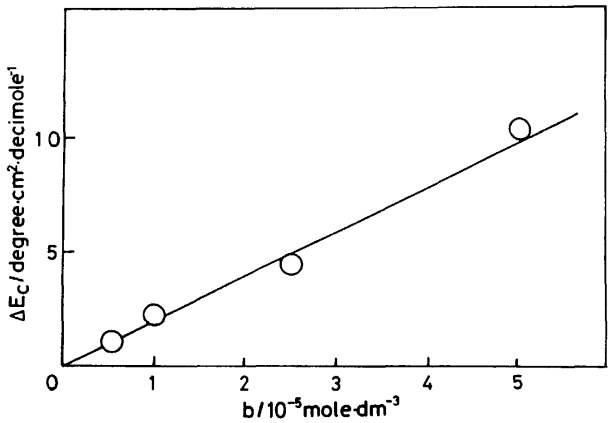

Fig. 6. The plot of the initial concentration of Methyl Orange (*b*) *vs.* the magnitude of circular dichroism (ΔE_c) induced by the Methyl Orange–β-cyclodextrin complex. [β-CyD]=2.5×10^{-3} mol dm^{-3} in water. ICD at 418 nm. The straight line follows Eq. B-1.

the linear relationship was shown in Fig. 5, the maximum ellipticity was obtained at the point of $f=1/2$ (Fig. 7), indicating the 1:1 complex formation of CR and γ-CyD. On the other hand, the peak was observed at $f=2/3$ in the case of the mixed solution of CV, MB, or MO (Fig. 7) with γ-CyD, suggesting the 1:2 complex formation of these three dyes with γ-CyD according to the Appendix C.

Dissociation Constant of the Inclusion Complex. The general Benesi-Hildebrand equation was applied to determine the dissociation constant of the 1:1 inclusion complex. For the complex of CV, MB, and MO with γ-CyD, the improved Benesi-Hildebrand equation shown in Appendix A was used for calculating the dissociation constant by assuming the 1:2 complex formation. These results are summerized in Table 1 as well as the electronic spectral data and the maximum apparent molar ellipticities of the circular dichroisms.

Discussion

Electronic Spectral Change of Dye by Addition of Cyclodextrin. Change in the electronic spectrum of

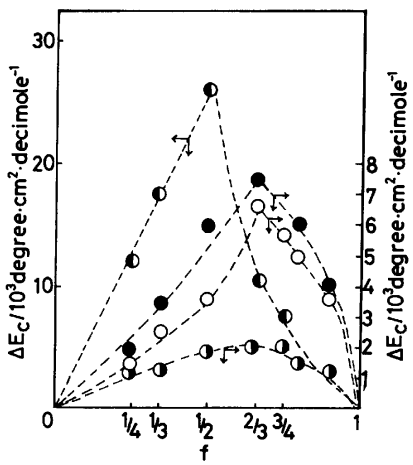

Fig. 7. Continuous variation method with induced circular dichroism (ΔE_c) for the complexes between γ-cyclodextrin and dyes (●, Crystal Violet, ◑, Methylene Blue, ○, Methyl Orange, ◐, Congo Red). [CyD]+[Dye]=6.0×10^{-4} mol dm^{-3}.

TABLE 1. DISSOCIATION CONTANTS OF THE COMPLEXES BETWEEN CYCLODEXTRINS AND DYES[a)]

Dye	$K_d\times10^5$ [b)]	
	β-CyD	γ-CyD
Congo Red	60	5.7
Methyl Orange	26	0.0062[c)]
Crystal Violet	38	0.0046[c)]
Methylene Blue	110	0.019[c)]

a) [Cyclodextrin (CyD)]=2.5×10^{-3} mol dm^{-3}, [Dye]=5×10^{-5} mol dm^{-3} in H_2O. b) Dissociation constant of the 1:1 complex (mol dm^{-3}) except c). c) Dissociation constant of the 1:2 complex (mol^2 dm^{-6}).

a guest molecule by inclusion with CyD is generally explained by the effect of environment around the guest molecule, *i.e.*, so-called solvent effect. Among the present investigations, the small shifts, observed by addition of α- or β-CyD and by addition of γ-CyD to CR could take place due to the similar effect of the hydrophobic cavity of CyD. However, the spectral change observed by addition of γ-CyD to CV, MB, or MO is too large to be explained by the similar effect and must be caused by the completely different effect.

Dye can exist in a monomer form in a very dilute aqueous solution like 10^{-5} mol dm^{-3}. In a more concentrated solution, however, dye can aggregate each other. For example, the direct dye like CR forms the large ionic micelle,[17] whereas the basic dye like CV and MB stays as a stable dimer in a usual aqueous solution. The absorption peak of the dimer in an aqueous solution is well investigated. For example, the dimer peaks appear at 532 nm and 605 nm for CV and MB, respectively.[18,19] In the absence of CyD, CV, and MB stay mostly as a monomer form and some fractions as a dimer form in the present experimental conditions (5 or 2.5×10^{-5} mol dm^{-3}) as shown in curves 1 of Figs. 1 and 2. With addition of β-CyD, the absorbance at the wavelength of the dimer peak slightly decreases, as indicated in Figs. 1 and 2. On the other hand, the addition of γ-CyD increases the absorbance at the dimer peak and decreases the monomer peak dramatically to result in an appearance of a new peak. These spectral changes strongly suggest that γ-CyD includes the dimer forms of CV and MB while β-CyD does the monomer forms.

In case of MO, any sharp peak has not clearly been assigned as the dimer peak in literatures, but the peak at 462 nm has been reported to be the overlap peak of two bands of monomer and dimer forms.[20] The large blue shift observed with addition of γ-CyD is considered due to the inclusion of the species which have the absorption maximum at the shorter wavelength between the two species. Consequently, the unique change in the electronic spectra suggests that γ-CyD forms the 1:2 complex with MO as well as CV and MO.

Relationship between the Magnitude of the Induced Circular Dichroism and the Concentration of the Inclusion Complex. The dyes examined in the present paper do not indicate any circular dichroism by themselves. CyDs also have no circular dichroic absorption in the visible region. When the dye is included by CyD to form the inclusion complex, the circular dichroism is induced in the visible region where the complex has the electronic absorption. The magnitude of the induced circular dichroism is proportional to the amount of the complex produced. In case of the 1:1 complex formation, the amount of the complex is expected to increase with charged concentration of the dye. If the charged concentration of CyD is kept constant and is large excess compared with that of the dye, the linear relationship is expected as shown in Appendix B. Therefore, when the magnitude of the circular dichroism, ΔE_c, is plotted against the charged concentration of the dye, b, the linear relationship between ΔE_c and b is observed as shown in Eq. B-1 in Appendix B. Thus, the linear relationship is often used as the evidence of the 1:1 complex formation.[20] In the 1:n complex, however, ΔE_c is not proportional to b but the correlation is more complicated than that for the 1:1 complex as shown in Eq. B-10 of Appendix B.

The present results about the dependence of induced ellipticity on the initial concentration of the dye shown in Figs. 5 and 6 are well consistent with the above consideration. The linear relationship was observed indeed for the case of the 1:1 complex formation which had been suggested from the electronic spectral changes (solid lines in Figs. 5 and 6). Nonlinear relationship was observed for the case of the 1:2 complex formation (broken curves in Fig. 5). In the latter case, the induced ellipticity increased at the rate proportional to b^2 when the charged concentration of the dye, b, was small enough as estimated from Eq. B-10. In fact, the data plotted in Fig. 5 are considerably well fit to the broken curves calculated from Eq. B-10.

The 1:2 Complex Formation. Recently much attention has been paid to the inclusion of two guest molecules with the large cavity of γ-CyD. Enhance-

ment of excimer fluorescence by addition of γ-CyD has suggested the 1:2 complex formation.[4,6] However, no direct evidence for the 1:2 complexation had not been reported before the preliminary communication.[5] In the present investigation, the large blue shift in the electronic absorption spectrum and nonlinear relation between the ellipticity and the concentration of the dye suggest the complexation between two dye molecules (CV, MB, and MO) and one γ-CyD. The 1:2 complex formation is strongly supported by the continuous variation method by using the induced circular dichroism. As shown in Fig. 7, the maximum ellipticity was observed at the point that the molar fraction of the dye, f, equals to 2/3 for CV, MB, and MO. In the case of CR, the maximum appeares at f=0.5.

From the present results, CV, MB, and MO are concluded to form the 1:2 complex with γ-CyD, while CR results in the 1:1 complexation. These differences could be explicable from the viewpoint of aggregation character of the water-soluble dye, because the former three dyes are known to form the corresponding dimers by aggregation in water, while no report on dimer formation has been presented in case of CR. The fitness of the size of the guest molecules to the cavity of CyD is also an important factor for complexation, which will be discussed in the next section.

These observations could also suggest the complexation mechanism. The 1:2 complex could be produced not by including one more dye molecule with the 1:1 complex, but by directly including the dimer of the dye with γ-CyD (as Eq. A-3 in Appendix A).

Fitness of the Size for Inclusion Complex. The molecular size of the guest molecule has to fit to the size of the cavity of the host molecule for the inclusion complex formation.[1] Here the fitness of the molecular size is considered based on the CPK model.

Congo Red contains the naphthyl moiety having the large sulfonato group. The CPK model shows that CR is too large to pass through the small cavity of α-CyD. This result is consistent with the fact that CR cannot be included by α-CyD. In case of β-CyD, the CR molecule is still unable to be included completely within the cavity according to the CPK model. Thus, the induction of the circular dichroism in this case suggests the partial inclusion of CR by β-CyD.[21] On the other hand, γ-CyD can include a CR molecule completely. The sulfonato groups of CR could interact with the hydroxyl groups of γ-CyD and could lock the CyD molecule from both sides by a hydrogen bond. The model structure of the inclusion complex seems to suggest the very strong complex formation. This consideration is supported by the small dissociation constant observed for the complex of CR with γ-CyD.

Methyl Orange is an enough small molecule to be included with α-CyD.[22-24] The electronic spectra of MO with different concentrations of α-CyD have not an isosbestic point. This fact could be explicable by the simultaneous formation of both the 1:1 complex and the 2:1 complex (two molecules of α-CyD and one molecule of MO).[25-26] The CPK models of MO and CyDs suggest that β-CyD includes one molecule of MO, while γ-CyD does two molecules but never three molecules of MO. The apparent isosbestic point was observed in the electronic spectra of MO with different concentrations of γ-CyD as shown in Fig. 3a. This fact suggests the direct formation of a single complex, *i.e.*, the 1:2 complex of γ-CyD with MO.

With regard to MB and CV, the CPK molecular model indicates that (1) the cavity of α-CyD is too small to include these dyes, (2) β-CyD has an enough large cavity to include one molecule of MB or CV but not to include two molecules, and (3) the cavity size of γ-CyD does well fit to the two molecules of MB or CV. These demonstrations with a CPK model are completely consistent with the experimental results. The difference in the dissociation constants of CV and MB cannot arise from the molecular size, but from another character of the molecules.

Appendix A.

Improved Benesi-Hildebrand Equation for Determination of Dissociation Constant, K_d, of the 1:2 Inclusion Complex. The dissociation constant for the 1:1 complex has been determined by the Benesi-Hildebrand equation (A-1)[27] where a and b are the concentrations of CyD and the dye, respectively, l is the length of a cell, and ΔE and $\Delta\varepsilon$ present the differences of absorbance and molar absorption coefficient between the complex and the dye, respectively. It is assumed in the equation that all the dye molecules in the solution

$$\frac{a \cdot b \cdot l}{\Delta E} = \frac{K_d}{\Delta\varepsilon} + \frac{a}{\Delta\varepsilon} \qquad \text{(A-1)}$$

form the complexes with CyD if the concentration of CyD is large excess to that of the dye.

For the 1:2 complex, there are two way of formation. One case is the direct equilibrium between two molecules of the dye and a molecule of CyD (Eq. A-2) and the other is the coexistance of two equilibriums shown in Eq. A-3.

$$\mathrm{CyD} + 2\,\mathrm{Dye} \overset{K_d}{\rightleftharpoons} \mathrm{Complex} \qquad \text{(A-2)}$$

$$\left.\begin{aligned} 2\,\mathrm{Dye} &\overset{k_1}{\rightleftharpoons} (\mathrm{Dye})_2, \\ (\mathrm{Dye})_2 + \mathrm{CyD} &\overset{k_2}{\rightleftharpoons} \mathrm{Complex} \end{aligned}\right\} \qquad \text{(A-3)}$$

When a and b are used as the initial concentrations of CyD and the dye, respectively, and x is the concentration of the complex, the dissociation constant, K_d, for the former Eq. A-2, is presented by the following Eq. A-4.

$$K_d = \frac{(a-x)(b-2x)^2}{x} \qquad \text{(A-4)}$$

Even though the separate equations A-5 and A-6 exist instead of Eq. A-2 among these species, the overall dissociation constant from Eqs. A-5 and A-6 is the same with that of Eq. A-4.

$$\text{Dye} + \text{CyD} \rightleftharpoons (\text{Dye–CyD}) \quad \text{(A-5)}$$

$$\text{Dye} + (\text{Dye–CyD}) \rightleftharpoons (\text{Dye}_2\text{–CyD}) \quad \text{(A-6)}$$

In other words, the dissociation constant does not depend on whether the two molecules of the dye are included stepwise or at once.

On the other hand, the latter case (Eq. A-3) gives the little different results. The dissociation constants for dimer of the dye, k_1, and for the ternary complex, k_2, are given by the following by using y as the concentration of the dimer.

$$k_1 = \frac{(b-2y-2x)^2}{y}, \quad k_2 = \frac{y(a-x)}{x} \quad \text{(A-7)}$$

Thus, the over-all dissociation constant, K_d', is led as follows.

$$K_d' = \frac{(a-x)(b-2x-2y)^2}{x} \quad \text{(A-8)}$$

The difference between K_d and K_d' is very small since the concentration of the free dimer, y, is very small under the experimental conditions. Moreover, it is not so easy to determine the concentration of the free dimer of the dye or the dissociation constant, k_1. Therefore, K_d has been used in the present paper for the practical discussion. When a is much larger than b, $(a-x)$ and x can be replaced with a and $b/2$, respectively. So, the Eq. A-4 can be rewritten as follows:

$$K_d = \frac{ab^2}{x} - 4ab + 4ax = \frac{ab^2}{x} - 2ab \quad \text{(A-9)}$$

Since the concentration of the complex, x, is proportional to $\Delta E/(\Delta\varepsilon \cdot l)$, the Eq. A-9 can be rearranged as Eq. 10 like the Benesi-Hildebrand equation.

$$\frac{a \cdot b^2 \cdot l}{\Delta E} = \frac{K_d}{\Delta\varepsilon} + \frac{2b}{\Delta\varepsilon}a \quad \text{(A-10)}$$

Thus, the dissociation constant, K_d, for the 1:2 complex can be obtained from the intercept of the straight line by plotting $(a \cdot b^2 \cdot l)/\Delta E$ against a under the conditions that a is much larger than b and that b is constant.

Appendix B.

Nonlinear Relationship between the Concentration of Dye and the Induced Circular Dichroism for the 1:n Complex. The magnitude of induced circular dichroism changes with the concentration of the dye, when the concentration of CyD is much larger than that of the dye for the 1:1 complex, the linear relationship is given between ΔE_c and b according to Eq. B-1, where a and b are the initial concentration of CyD and the dye, respectively, and ΔE_c, θ_{tr}, and K_d are the measured magnitude of induced circular dichroism, the molar ellipticity of the complex, and the dissociation constant for the complex, respectively.

$$\Delta E_c = \frac{\theta_{tr}a}{100 \cdot (K_d + a)}b \quad \text{(B-1)}$$

For 1:n complex formation, the following equilibriums would be kept.

$$n\,\text{Dye} \overset{k_1'}{\rightleftharpoons} (\text{Dye})_n \quad \text{(B-2)}$$

$$(\text{Dye})_n + \text{CyD} \overset{k_2'}{\rightleftharpoons} \text{Complex} \quad \text{(B-3)}$$

Here,

$$k_1' = \frac{(b-ny-nx)^n}{y} \quad \text{(B-4)}$$

$$k_2' = \frac{y(a-x)}{x} \quad \text{(B-5)}$$

The term x and y present the concentrations of the CyD complex and of the n-mer of the dye, respectively.

When the concentration of CyD is much larger than that of the dye, ny is negligible small compared with b and nx. Therefore, the Eq. B-4 can be rewritten as Eq. B-6.

$$k_1' = \frac{1}{y}(b^n - {}_nC_1 \cdot nx \cdot b^{n-1} + {}_nC_2 \cdot (nx)^2 \cdot b^{n-2} - \cdots) \quad \text{(B-6)}$$

By using Eq. B-5, Eq. B-6 is rearranged as follows.

$$k_1' = \frac{(a-x)}{x \cdot k_2'}(b^n - {}_nC_1 \cdot nx \cdot b^{n-1} + {}_nC_2 \cdot (nx)^2 \cdot b^{n-2} - \cdots) \quad \text{(B-7)}$$

When the first and the second terms of the development equation are used, and $(a-x)$ is replaced with a since the concentration of CyD is very large, the overall dissociation constant for the CyD complex of the n-mer is presented as follows.

$$K_d'' = k_1' \cdot k_2' = \frac{a \cdot b^n}{x} - n^2 \cdot a \cdot b^{n-1} \quad \text{(B-8)}$$

Rearrangement of Eq. B-8 leads Eq. B-9.

$$x = \frac{a \cdot b^n}{K_d'' + n^2 \cdot a \cdot b^{n-1}} \quad \text{(B-9)}$$

Since the magnitude of the induced circular dichroism is proportional to the concentration of the complex, x can be replaced with $100 \cdot \Delta E_c/\theta_{tr}$. Then, Eq. B-9 can be rewritten as Eq. B-10.

$$\Delta E_c = \frac{\theta_{tr} \cdot a \cdot b^n}{100(K_d'' + n^2 \cdot a \cdot b^{n-1})} \quad \text{(B-10)}$$

One can compare Eq. B-10 for the 1:n complex with Eq. B-1 for the 1:1 complex to find the difference.

Appendix C.

Continuous Variation Method to Determine the Molar Ratio of the Inclusion Complex. When more than two equilibrium exist under experimental conditions, the continuous variation method is complicated. Therefore, one equilibrium (Eq. C-1) is considered in place of n equilibriums since the concentration of the intermediate $(\text{Dye})_n$ is thought negligible.

$$n\,\text{Dye} + \text{CyD} \rightleftharpoons \text{Complex} \quad \text{(C-1)}$$

The continuous variation method in the equilibrium C-1 is led as follows. When the concentrations of the dye, CyD, and the complex in the equilibrium are represented as c_1, c_2 and c_3, respectively, and the sum of the initial concentrations of the dye and CyD is constant equaling to m, then the following relations are obtained.

$$c_1 = m \cdot f - n \cdot c_3 \quad \text{(C-2)}$$

$$c_2 = m(1-f) - c_3 \quad \text{(C-3)}$$

$$K_d = \frac{c_1^n \cdot c_2}{c_3} \quad \text{(C-4)}$$

Here, f indicates the molar fraction of the dye.

The value f, that makes the concentration of the complex, c_3, maximum, can be obtained from the condition of $(dc_3/df)=0$. Differentiation of Eqs. C-2, C-3, and C-4 with f gives the following Eqs.

$$\frac{dc_1}{df} = m - n\frac{dc_3}{df} \quad \text{(C-5)}$$

$$\frac{dc_2}{df} = -m - \frac{dc_3}{df} \quad \text{(C-6)}$$

$$K_d \cdot \frac{dc_3}{df} = c_1{}^n \cdot \frac{dc_2}{df} + c_2 \cdot \frac{dc_1}{df} n \cdot c_1{}^{(n-1)} \quad \text{(C-7)}$$

Substitution of the condition $(dc_3/df)=0$ for the Eqs. C-5, C-6, and C-7, and rearrangement give the Eq. C-8.

$$n = \frac{f}{1-f} \text{ or } f = \frac{n}{1+n} \quad \text{(C-8)}$$

Therefore, if the concentration of the intermediate $(\text{dye})_n$ is assumed negligible, the concentration of the complex becomes maximum at the condition satisfying the Eq. C-8.

The fraction at the maximum induction of the circular dichroism observed gives the composition of the complex.

References

1) M. L. Bender and M. Komiyama, "Cyclodextrin Chemistry," Springer-Verlag, New York, 1978; Japanese translation by H. Hirai and M. Komiyama, Japan Scientific Societies Press, 1979.

2) W. Saenger, *Angew. Chem. Int. Ed.*, **19**, 344 (1980).

3) K. Uekama, *Kagaku to Yakugaku no Kyoshitsu*, **59**, 43 (1978).

4) A. Ueno, K. Takahashi, and T. Osa, *J. Chem. Soc., Chem. Commun.*, **1980**, 921.

5) H. Hirai, N. Toshima, and S. Uenoyama, *Polymer J.*, **13**, 607 (1981).

6) K. Kano, I. Takenoshita, and T. Ogawa, *Chem. Lett.*, **1980**, 1035.

7) R. Breslow, M. F. Czaruiecki, J. Emert, and H. Hamaguchi, *J. Am. Chem. Soc.*, **102**, 762 (1980).

8) A. Ueno, K. Takahashi, Y. Hino, and T. Osa, *J. Chem. Soc., Chem. Commun.*, **1981**, 194.

9) N. Kobayashi, A. Ueno, and T. Osa, *J. Chem. Soc., Chem. Commun.*, **1981**, 340.

10) N. Kobayashi, R. Sato, Y. Hino, A. Ueno, and T. Osa, *J. Chem. Soc., Chem. Commun.*, **1982**, 706.

11) K. Kano, I. Takenoshita, and T. Ogawa, *Chem. Lett.*, **1982**, 321.

12) K. Kano, I. Takenoshita, and T. Ogawa, *J. Phys. Chem.*, **86**, 1833 (1982).

13) J. Emert, D. Kodali, and R. Catena, *J. Chem. Soc., Chem. Commun.*, **1981**, 758.

14) K. Takemura, S. Inoue, and F. Kusu, *Chem. Lett.*, **1983**, 233.

15) I. Tabushi, *Yuki Gosei Kagaku Kyokai Shi*, **40**, 892 (1982).

16) M. Komiyama and H. Hirai, *J. Am. Chem. Soc.*, **105**, 2018 (1983); **106**, 174 (1984).

17) S. Ando, "Development of Modern Colloidlogy," Vol. 1, p. 138 (1948) Gakujutsu Tosho.

18) W. H. J. Stock, G. J. M. Lippits, and M. Mandel, *J. Phys. Chem.*, **76**, 1372 (1972).

19) K. Bergmann and C. T. O'Konski, *J. Phys. Chem.*, **67**, 2169 (1963).

20) R. T. Reeves and R. S. Kaiser, *Can. J. Chem.*, **51**, 628 (1973).

21) K. Takeo and T. Kuge, *Stärke*, **24**, 281 (1972).

22) K. Harata, *Bull. Chem. Soc. Jpn.*, **49**, 1493 (1976).

23) K. Yamada and J. Morimoto, *Research Report of Chiba Univ.*, **24-47**, 71 (1973).

24) W. Brocer and W. Lantsch, *Z. Naturforsch.*, **86**, 711 (1953).

25) F. Cramer, W. Saenger, and H.-Ch. Spatz *J. Am. Chem. Soc.*, **89**, 14 (1967).

26) R. L. VanEtten, J. F. Sebastian, G. A. Cloorves, and M. L. Bender, *J. Am. Chem. Soc.*, **89**, 3242 (1967).

27) T. Fujinaga, *Kagaku (Kyoto)*, **26**, 91 (1970).

 © 1985 The Chemical Society of Japan Bull. Chem. Soc. Jpn., 58, 1165—1170 (1985)

The Syntheses and Absolute Configurations of Nellionol and 5-Dehydronellionol

Takashi MATSUMOTO,* Sachihiko IMAI, and Takashi YOSHINARI
Department of Chemistry, Faculty of Science, Hiroshima University, Higashisenda-machi, Naka-ku, Hiroshima 730
(Received October 24, 1984)

To determine the absolute configurations of C-15 in natural nellionol and 5-dehydronellionol, (15*R*)-8,11,13-abietatriene-12,16-diol was converted into (15*R*)-6α,11,12,16-tetrahydroxy-8,11,13-abietatrien-7-one (**3a**) and (15*R*)-6,11,12,16-tetrahydroxy-5,8,11,13-abietatetraen-7-one (**4a**), which were identical with natural products. For direct comparisons with **3a** and **4a**, (15*S*)-6α,11,12,16-tetrahydroxy-8,11,13-abietatrien-7-one (**3b**) and (15*S*)-6,11,12,16-tetrahydroxy-5,8,11,13-abietatetraen-7-one (**4b**) were also synthesized from (15*S*)-8,11,13-abietatriene-12,16-diol. The synthetic **3b** and **4b** were not identical with the natural products. From the present study, the absolute configurations of nellionol and 5-dehydronellionol were conclusively assigned as 5*S*,6*R*,10*S*,15*R* (**3a**) and 10*R*,15*R* (**4a**), respectively.

Nellionol and 5-dehydronellionol have been isolated from the root bark of *Premna latifolia* Roxb. by Rao *et al.*[1] On the basis of chemical and spectroscopic studies they deduced the structures of nellionol and 5-dehydronellionol to be 6α,11,14,16-tetrahydroxy-8,11,13-abietatrien-7-one (**1**) and 6,11,14,16-tetrahydroxy-5,8,11,13-abietatetraen-7-one (**2**), respectively. However, our examination on the published ^{1}H NMR spectral data[1] suggested alternate structures, 6α,11,12,16-tetrahydroxy-8,11,13-abietatrien-7-one (**3**) and 6,11,-12,16-tetrahydroxy-5,8,11,13-abietatetraen-7-one (**4**), for nellionol and 5-dehydronellionol respectively. The correctness of these revised structures was supported by the syntheses of C-15 epimeric mixtures of **3** and **4**,[2] whereas the precise stereochemistry of C-15 in these natural products could not be determined. Burnell *et al.*[3] also reported independently the same revised structures, **3** and **4**, for nellionol and 5-dehydronellionol, but the stereochemistry of C-15 still remained unsettled. In order to determine the absolute configurations of C-15 in these natural products we have now attempted the syntheses of (15*R*)-6α,11,-12,16-tetrahydroxy-8,11,13-abietatrien-7-one (**3a**), (15*R*)-6,11,12,16-tetrahydroxy-5,8,11,13-abietatetraen-7-one (**4a**), and their (15*S*)-epimers (**3b** and **4b**). For this purpose, (15*R*)-8,11,13-abietatriene-12,16-diol (16-hydroxyferruginol) (**5a**) and its (15*S*)-isomer (**5b**) were chosen as convenient relay intermediates, because these compounds have recently been synthesized in our laboratory by an unambiguous method starting from (*R*)-(−)-α-cyclocitral.[4]

In the present study, however, new preparations of **5a** and **5b** using natural dehydroabietic acid (**6**) were carried out as follows. Dehydration of 12-methoxy-8,11,13-abietatrien-15-ol (**7**)[2] prepared from **6**, with refluxing acetic anhydride, followed by hydroboration-oxidation of the resulting tetraene (**8**),[2] afforded a mixture of the C-15 epimeric alcohols. The mixture was separated by repeated column chromatography on silica gel to give (15*R*)-12-methoxy-8,11,13-abietatrien-16-ol (**9a**) and its (15*S*)-epimer (**9b**). The alcohols, **9a** and **9b**, were demethylated respectively with anhydrous aluminium chloride, sodium iodide, and

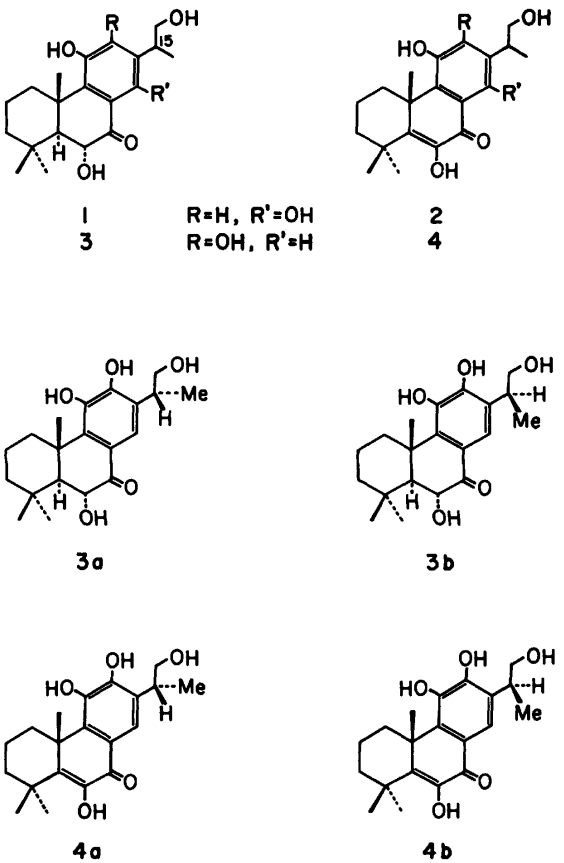

acetonitrile in dichloromethane[5] at 35—40 °C under a stream of nitrogen to give the crystalline diols, which were shown to be identical with authentic **5a** and **5b**[4] by physical and spectral comparisons. Oxidation of the diol **5a** with benzoyl peroxide in refluxing chloroform, followed by reduction with lithium aluminium hydride in ether and subsequent acetylation with acetic anhydride in pyridine, afforded (15*R*)-11,12,16-triacetoxy-8,11,13-abietatriene (**10a**: 49.5%) along with (15*R*)-12,16-diacetoxy-8,11,13-abietatriene[4] (**11a**: 26.7%). Similar treatment of the diol **5b** also produced the corresponding (15*S*)-triacetate (**10b**: 47.0%) and (15*S*)-diacetate[4] (**11b**: 29.8%). The triacetates, **10a** and **10b**, were oxidized respectively with chromium trioxide in acetic acid at room temperature to give (15*R*)-11,12,16-

triacetoxy-8,11,13-abietatrien-7-one (**12a**: 73.2%) and its (15*S*)-isomer (**12b**: 76.1%). The 7-oxo compound **12a** was refluxed with isopropenyl acetate in the presence of *p*-toluenesulfonic acid to give an enol acetate (**13a**: 95.0%). This was converted into (15*R*)-6α,11,12,16-tetraacetoxy-8,11,13-abietatrien-7-one (**14a**: 91.3%), mp 185—187 °C, by oxidation with *m*-chloroperbenzoic acid in dichloromethane and subsequent acetylation with acetic anhydride in pyridine. Hydrolysis of **14a** with dilute hydrochloric acid in refluxing ethanol gave **3a** (77.3%), mp 222—224 °C. The synthetic **3a** and **14a** were identical with natural nellionol (mp 226—227 °C) and its tetraacetate (mp 185—186 °C). Subsequently the 7-oxo compound **12a** was reduced with sodium borohydride in methanol to give a mixture of C-7 epimeric alcohols, which was immediately converted into (15*R*)-11,12,16-triacetoxy-6,8,11,13-abietatetraene (**15a**: 75.5%) by refluxing with *p*-toluenesulfonic acid in dry benzene. The tetraene **15a** was further converted into (15*R*)-11,12,16-triacetoxy-8,11,13-abietatrien-6-one (**16a**: 85.5%) by a series of reactions: oxidation with *m*-chloroperbenzoic acid in dichloromethane at room temperature, refluxing with dilute hydrochloric acid in methanol, and acetylation with acetic anhydride in pyridine. Oxidation of **16a** with Jones reagent, followed by refluxing with sodium acetate in acetic anhydride, afforded (15*R*)-6,11,12,16-tetraacetoxy-5,8,11,13-abietatetraen-7-one (**17a**: 68.7%), mp 149—153 °C. Hydrolysis of **17a** with dilute hydrochloric acid in refluxing methanol afforded **4a** (82.3%), mp 211—213 °C. The synthetic **4a** and **17a** were identical with natural 5-dehydronellionol (mp 210—212 °C) and its tetraacetate (mp 141—142 °C). The specific rotation of **3a**, **14a**, and **17a** showed positive values, which were also in the same direction as those of the corresponding natural products.

For direct comparisons with **3a** and **4a**, the syntheses of (15*S*)-isomers (**3b** and **4b**) were also carried out starting from **12b** in the same manner to that described for the preparation of **3a** and **4a**. The synthetic **3b** (mp 216—217 °C) and **4b** (mp 187—189 °C) were not identical with natural nellionol and 5-dehydronellionol.

From the present study, the absolute configurations of nellionol and 5-dehydronellionol were conclusively assigned as 5*S*, 6*R*, 10*S*, 15*R* (**3a**) and 10*R*, 15*R* (**4a**), respectively.

Experimental

All melting points are uncorrected. The IR spectra and optical rotations were measured in chloroform, and the ^1H NMR spectra in deuteriochloroform at 90 MHz, with tetramethylsilane as an internal standard, unless otherwise stated; s: singlet, bs: broad singlet, d: doublet, dd: double doublet, m: multiplet. The column chromatography was performed using Merck silica gel (0.063 mm).

12-Methoxy-8,11,13,15-abietatetraene (8). A solution of 12-methoxy-8,11,13-abietatrien-15-ol (**7**)[2] (18.6 g) in acetic anhydride (80 ml) was refluxed for 1 h. After removal of the

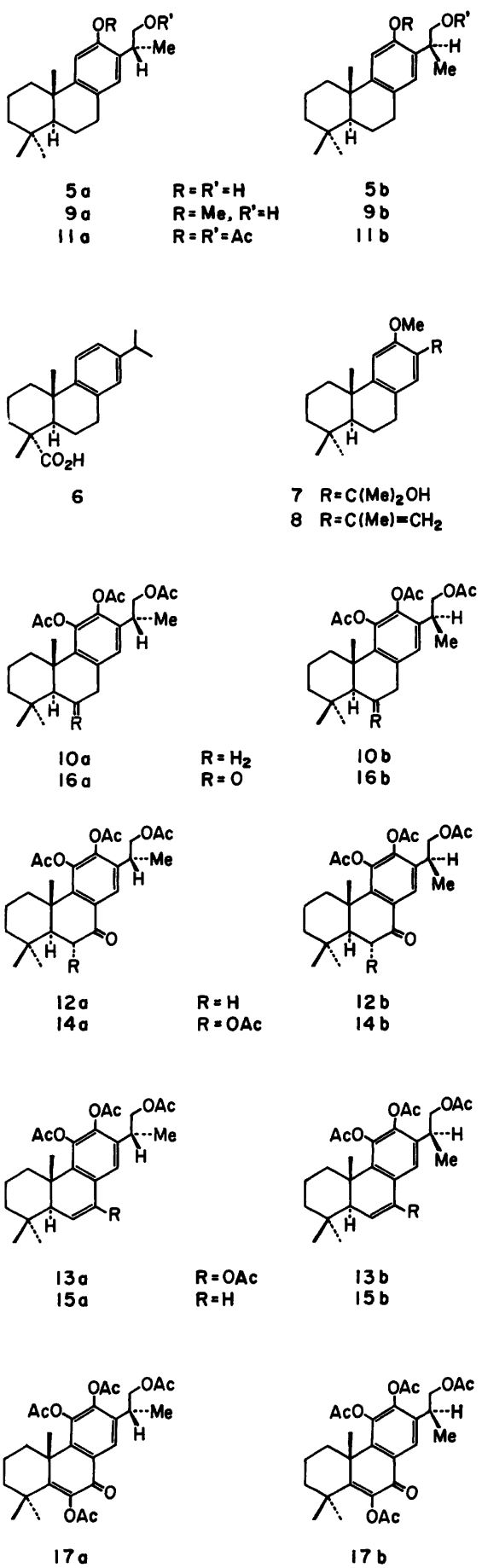

acetic anhydride *in vacuo*, the residue was chromatographed on silica gel (250 g), using hexane–benzene (7:3) as the eluent, to give **8** (16.0 g: 91.4%). The IR and ^{1}H NMR spectra of **8** were identical with those of the authentic sample.[2]

*(15R)-12-Methoxy-8,11,13-abietatrien-16-ol (**9a**) and Its (15S)-Epimer (**9b**).* A solution of borane–tetrahydrofuran complex (1 mol dm^{-3}: 18.1 ml) was added to a stirred solution of **8** (6.748 g) in dry tetrahydrofuran (67 ml) at −10 °C for 10 min under a stream of nitrogen. After the mixture had been stirred at −10—0 °C for 25 min and at 0—5 °C for 3 h, there were added successively aqueous tetrahydrofuran (50%: 7.8 ml), aqueous sodium hydroxide (12%: 7.8 ml), and hydrogen peroxide (30%: 7.8 ml) at −10—−4 °C. The mixture was stirred at −5—0 °C for 30 min and then at room temperature for 1 h, diluted with water, and extracted with ether. The ether extract was washed with brine, dried over sodium sulfate, and evaporated *in vacuo*. The residue was chromatographed on silica gel (250 g), using ether–benzene (1:99 and then 8.5:91.5) as the eluent, to give a mixture of C-15 epimers (**9a** and **9b**)[2] (6.873 g: 96.1%). The mixture was carefully separated by repeated column chromatography on silica gel to give **9a** and **9b**, by monitoring of doublet signal due to C-15 methyl group in the ^{1}H NMR spectra (60 MHz: δ in CCl_4, 1.17 for **9a** and 1.16 for **9b**)[2] of fractions.

*(15R)-8,11,13-Abietatriene-12,16-diol (**5a**) and Its (15S)-Epimer (**5b**).* *a)*: Anhydrous aluminium chloride (2.237 g), sodium iodide (2.514 g), and a solution of **9a** (265 mg, containing a small amount of **9b**) in dichloromethane (5.5 ml) were added in this order to acetonitrile (11.0 ml) with stirring at −5—5 °C under a stream of nitrogen over a 20 min period. The mixture was stirred at this temperature for 10 min and then at 35—40 °C for 5 h, poured into water, and extracted with ether. The ether extract was washed successively with aqueous sodium thiosulfate and brine, dried over sodium sulfate, and evaporated *in vacuo*. The residue was chromatographed on silica gel (15 g), using ether–benzene (3:97) as the eluent, to give the demethylated diol (242 mg: 95.6%). This was recrystallized from ether–hexane to give **5a**, mp 139—140 °C, $[\alpha]_D$ +64.5° (*c* 2.79), whose IR and ^{1}H NMR spectra were identical with those of the authentic sample.[2] Found: C, 79.29; H, 10.27%. Calcd for $C_{20}H_{30}O_2$: C, 79.42; H, 10.00%.

b): Anhydrous aluminium chloride (1.073 g), sodium iodide (1.206 g), and a solution of **9b** (127 mg, containing a small amount of **9a**) in dichloromethane (4.0 ml) were added in this order to acetonitrile (8.0 ml) with stirring at −5—5 °C under a stream of nitrogen over a 16 min period. The mixture was stirred at this temperature for 15 min and then at 35—40 °C for 5 h. After the work-up as described in *a)*, the crude product was chromatographed on silica gel (8.0 g), using ether–benzene (3:97) as the eluent, to give the demethylated diol (87 mg: 71.2%). This was recrystallized from ether–hexane to give **5b**, mp 178—179 °C, $[\alpha]_D$ +45.5° (*c* 2.18), whose IR and ^{1}H NMR spectra were identical with those of the authentic sample.[2] Found: C, 79.25; H, 10.13%. Calcd for $C_{20}H_{30}O_2$: C, 79.42; H, 10.00%.

*(15R)-11,12,16-Triacetoxy-8,11,13-abietatriene (**10a**) and Its (15S)-Epimer (**10b**).* *a)*: A solution of **5a** (215 mg) and benzoyl peroxide (269 mg) in chloroform (6.0 ml) was refluxed for 5 h, cooled, and diluted with ether (9.0 ml). After addition of acetic acid (1.26 ml) and aqueous potassium iodide (20%: 6.3 ml), the mixture was stirred at room temperature for 2 h and then washed successively with water, aqueous sodium thiosulfate, aqueous sodium hydrogencarbonate, and brine. The dried solution was evaporated *in vacuo* to give the crude product, which was used, without purification, in the next reaction.

A stirred suspension of the above crude product and lithium aluminium hydride (130 mg) in dry ether (20 ml) was refluxed for 80 min. The mixture was cooled, poured into ice-dilute hydrochloric acid, and extracted with ether. The ether extract was washed with brine, dried over sodium sulfate, and evaporated *in vacuo*. The residue was acetylated with acetic anhydride (2.0 ml) in pyridine (2.0 ml) at 75—80 °C for 2 h. After the usual work-up, the crude product was chromatographed on silica gel (20 g), using ether–benzene (1:99) as the eluent, to give a diacetate (**11a**) (73 mg: 26.7%), $[\alpha]_D$ +56.9° (*c* 3.59). The IR and ^{1}H NMR spectra of **11a** were identical with those of (15*R*)-12, 16-diacetoxy-8,11,13-abietatriene.[2] Found: C, 74.84; H, 9.01%. Calcd for $C_{24}H_{34}O_4$: C, 74.57; H, 8.87%.

Further elution with ether–benzene (1:9) gave **10a** (157 mg: 49.5%), $[\alpha]_D$ +61.3° (*c* 2.76); IR: 1765, 1730 cm^{-1}; ^{1}H NMR (60 MHz, CCl_4): δ=0.95 (6H, bs, $-\underset{|}{C}(CH_3)_2$), 1.19 (3H, d, *J*= 7 Hz, C_{15}–CH_3), 1.21 (3H, s, C_{10}–CH_3), 1.94 (3H, s, C_{16}–$OCOCH_3$), 2.21 (6H, s, C_{11}–$OCOCH_3$ and C_{12}–$OCOCH_3$), 3.92 (2H, d, *J*=7 Hz, $-C\underline{H}_2OAc$), 6.77 (1H, s, C_{14}–H).

b): A solution of **5b** (204 mg) and benzoyl peroxide (255 mg) in chloroform (6.0 ml) was refluxed for 5 h. The crude product was reduced with lithium aluminium hydride (130 mg) in dry ether (20 ml) and then acetylated with acetic anhydride (2.0 ml) in pyridine (2.0 ml) as described in *a)*. The product was purified by column chromatography on silica gel (20 g), using ether–benzene (1:99) as the eluent, to give a diacetate (**11b**) (78 mg: 29.8%), $[\alpha]_D$ +33.7° (*c* 3.29). The IR and ^{1}H NMR spectra of **11b** were identical with those of (15*S*)-12,16-diacetoxy-8,11,13-abietatriene.[2] Found: C, 74.79; H, 9.17%. Calcd for $C_{24}H_{34}O_4$: C, 74.57; H, 8.87%.

Further elution with ether–benzene (1:9) gave **10b** (141 mg: 47.0%), $[\alpha]_D$ +43.9° (*c* 4.00); IR: 1768, 1733 cm^{-1}; ^{1}H NMR (60 MHz, CCl_4): δ=0.95 (6H, bs, $-\underset{|}{C}(CH_3)_2$), 1.17 (3H, d, *J*= 7 Hz, C_{15}–CH_3), 1.22 (3H, s, C_{10}–CH_3), 1.95 (3H, s, C_{16}–$OCOCH_3$), 2.22 (6H, s, C_{11}–$OCOCH_3$ and C_{12}–$OCOCH_3$), 3.98 (2H, d, *J*=7.5 Hz, $-C\underline{H}_2OAc$), 6.78 (1H, s, C_{14}–H). Found: C, 70.45; H, 8.42%. Calcd for $C_{26}H_{36}O_6$: C, 70.24; H, 8.16%.

*(15R)-11,12,16-Triacetoxy-8,11,13-abietatrien-7-one (**12a**) and Its (15S)-Epimer (**12b**).* *a)*: A mixture of **10a** (965 mg) and chromium trioxide (413 mg) in acetic acid (20 ml) was stirred at room temperature for 23.5 h. The mixture was diluted with water and extracted with ether. The ether extract was washed successively with water, aqueous sodium hydrogencarbonate, and brine, dried over sodium sulfate, and evaporated *in vacuo*. The residue was chromatographed on silica gel (50 g), using ether–benzene (5:95) as the eluent, to give the starting **10a** (88 mg). Further elution with ether–benzene (5:95 and then 15:85) afforded **12a** (729 mg: 73.2%), $[\alpha]_D$ +66.8° (*c* 4.40); IR: 1775, 1734, 1687, 1608 cm^{-1}; ^{1}H NMR (60 MHz, CCl_4): δ=0.98 (6H, s, $-\underset{|}{C}(CH_3)_2$), 1.29 (3H, s, C_{15}–CH_3), 1.32 (3H, s, C_{10}–CH_3), 1.94 (3H, s, C_{16}–$OCOCH_3$), 2.25 (6H, s, C_{11}–$OCOCH_3$ and C_{12}–$OCOCH_3$), 3.95 (2H, d, *J*=7 Hz, $-C\underline{H}_2OAc$), 7.93 (1H, s, C_{14}–H). Found: C, 68.09; H, 7.51%. Calcd for $C_{26}H_{34}O_7$: C, 68.10; H, 7.47%.

b): A solution of **10b** (957 mg) in acetic acid (21 ml) was oxidized with chromium trioxide (409 mg) at room temperature for 22 h as described in *a)*. The crude product was

chromatographed on silica gel (50 g), using ether–benzene (5:95) as the eluent, to give **10b** (162 mg) and **12b** (667 mg: 67.6%), $[\alpha]_D$ +8.6° (*c* 14.35); IR: 1776, 1732, 1686, 1608 cm^{-1}; ^1H NMR (60 MHz, CCl_4): δ=1.00 (6H, s, $-C(CH_3)_2$), 1.27 (3H, d, *J*=7 Hz, C_{15}–CH_3), 1.34 (3H, s, C_{10}–CH_3), 1.96 (3H, s, C_{16}–$OCOCH_3$), 2.27 (6H, s, C_{11}–$OCOCH_3$ and C_{12}–$OCOCH_3$), 4.02 (2H, d, *J*=7 Hz, $-CH_2OAc$), 7.93 (1H, s, C_{14}–H). Oxidation of the recovered **10b** (162 mg) with chromium trioxide (69 mg) in acetic acid (3.5 ml) was then carried out as described above. The crude product was purified by column chromatography on silica gel (10 g) to give some additional **12b** (84 mg: 8.5%).

*(15R)-7,11,12,16-Tetraacetoxy-6,8,11,13-abietatetraene (**13a**) and Its (15S)-Epimer (**13b**).* *a)*: A mixture of **12a** (220 mg) and *p*-toluenesulfonic acid (20 mg) in isopropenyl acetate (5.0 ml) was refluxed for 18 h. The mixture was cooled and diluted with ether. The ether solution was washed with brine, dried over sodium sulfate, and evaporated *in vacuo*. The residue was chromatographed on silica gel (20 g), using ether–benzene (1:9) as the eluent, to give a mixture of **12a** and **13a** (61 mg). Further elution gave **13a** (176 mg: 73.3%), which was recrystallized from methanol, mp 140.5—141.5 °C, $[\alpha]_D$ +28.6° (*c* 3.40); IR: 1768, 1737sh, 1668, 1610 cm^{-1}; ^1H NMR: δ=0.94 (3H, s) and 1.02 (3H, s) ($-C(CH_3)_2$), 1.22 (3H, d, *J*=7 Hz, C_{15}–CH_3), 1.27 (3H, s, C_{10}–CH_3), 2.01 (3H, s, C_{16}–$OCOCH_3$), 2.25 (3H, s) and 2.28 (6H, s) (C_7–$OCOCH_3$, C_{11}–$OCOCH_3$, and C_{12}–$OCOCH_3$), 2.39 (1H, d, *J*=3 Hz, C_5–H), 3.15 (1H, m, C_{15}–H), 4.03 (2H, d, *J*=7 Hz, $-CH_2OAc$), 5.68 (1H, d, *J*=3 Hz, C_6–H), 7.01 (1H, s, C_{14}–H). Found: C, 67.05; H, 7.45%. Calcd for $C_{28}H_{36}O_8$: C, 67.18; H, 7.25%. The above mixture of **12a** and **13a** (61 mg) was then treated with *p*-toluenesulfonic acid (10 mg) in refluxing isopropenyl acetate (2.5 ml) for 15.5 h to give some additional **13a** (52 mg: 21.7%).

b): A mixture of **12b** (312 mg) and *p*-toluenesulfonic acid (30 mg) in isopropenyl acetate (7.0 ml) was refluxed for 18 h. After the work-up as described in *a)*, the crude product was chromatographed on silica gel (30 g), using ether–benzene (7:93) as the eluent, to give **13b** (285 mg, containing a small amount of **12b**: *ca.* 83.5%). This was recrystallized from methanol, mp 203—204 °C, $[\alpha]_D$ −7.8° (*c* 7.66); IR: 1765, 1738 sh, 1668, 1610 cm^{-1}; ^1H NMR (60 MHz): δ=0.93 (3H, s) and 1.01 (3H, s) ($-C(CH_3)_2$), 1.19 (3H, d, *J*=7 Hz, C_{15}–CH_3), 1.27 (3H, s, C_{10}–CH_3), 1.99 (3H, s, C_{16}–$OCOCH_3$), 2.25 (3H, s) and 2.29 (6H, s) (C_7–$OCOCH_3$, C_{11}–$OCOCH_3$, and C_{12}–$OCOCH_3$), 4.08 (2H, dd, *J*=7 and 3.5 Hz, $-CH_2OAc$), 5.65 (1H, d, *J*=3 Hz, C_6–H), 6.95 (1H, s, C_{14}–H). Found: C, 67.45; H, 7.34%. Calcd for $C_{28}H_{36}O_8$: C, 67.18; H, 7.25%.

*(15R)-6α,11,12,16-Tetraacetoxy-8,11,13-abietatrien-7-one (**14a**) and Its (15S)-Epimer (**14b**).* *a)*: A mixture of **13a** (67.0 mg) and *m*-chloroperbenzoic acid (80%: 40.4 mg) in dichloromethane (1.5 ml) was stirred at room temperature for 22.5 h. The mixture was diluted with ether and washed successively with aqueous potassium iodide, aqueous sodium thiosulfate, aqueous sodium hydrogencarbonate, and brine. The dried solution was evaporated *in vacuo* to give a mixture of 6α-acetoxy and 6α-hydroxy derivatives, which was immediately acetylated with acetic anhydride (0.7 ml) in pyridine (0.7 ml) at 75—80 °C for 2 h. After the usual work-up, the crude product was purified by column chromatography on silica gel (8.0 g), using ether–benzene (1:9) as the eluent, to give **14a** (63.1 mg: 91.3%). This was recrystallized from acetone–hexane, mp 185—187 °C, $[\alpha]_D$ +103.5° (*c* 2.54); IR: 1778, 1740, 1705, 1610 cm^{-1}; ^1H NMR: δ=1.05 (3H, s) and 1.14 (3H, s) ($-C(CH_3)_2$), 1.27 (3H, s, C_{15}–CH_3), 1.50 (3H, s, C_{10}–CH_3), 2.00 (3H, s, C_{16}–$OCOCH_3$), 2.24 (3H, s) and 2.30 (6H, s) ($C_{6\alpha}$–$OCOCH_3$, C_{11}–$OCOCH_3$, and C_{12}–$OCOCH_3$), 2.27 (1H, d, *J*=13 Hz, C_5–H), 3.20 (1H, m, C_{15}–H), 4.06 (2H, d, *J*=7 Hz, $-CH_2OAc$), 5.83 (1H, d, *J*=13 Hz, $C_{6\beta}$–H), 8.00 (1H, s, C_{14}–H). Found: C, 64.93; H, 7.04%. Calcd for $C_{28}H_{36}O_9$: C, 65.10; H, 7.03%. The synthetic **14a** was identical with natural nellionol tetraacetate (mp 185—186 °C).[1]

b): Oxidation of **13b** (245 mg, containing a small amount of **12b**) with *m*-chloroperbenzoic acid (80%: 148 mg) in dichloromethane (5.0 ml), followed by acetylation with acetic anhydride (1.5 ml) in pyridine (1.5 ml), were carried out as described in *a)*. The crude product was chromatographed on silica gel (10 g), using ether–benzene (5:95) as the eluent, to give **14b** (203 mg: *ca.* 80.3%) (67.1% from **12b**). This was recrystallized from acetone–hexane, mp 142.5—143 °C, $[\alpha]_D$ +35.4° (*c* 0.91); IR: 1778, 1740, 1705, 1610 cm^{-1}; ^1H NMR: δ=1.06 (3H, s) and 1.13 (3H, s) ($-C(CH_3)_2$), 1.23 (3H, d, *J*=7 Hz, C_{15}–CH_3), 1.51 (3H, s, C_{10}–CH_3), 2.00 (3H, s, C_{16}–$OCOCH_3$), 2.23 (3H, s) and 2.30 (6H, s) ($C_{6\alpha}$–$OCOCH_3$, C_{11}–$OCOCH_3$, and C_{12}–$OCOCH_3$), 3.18 (1H, m, C_{15}–H), 4.07 (2H, d, *J*=7 Hz, $-CH_2OAc$), 5.83 (1H, d, *J*=13 Hz, $C_{6\beta}$–H), 7.98 (1H, s, C_{14}–H). Found: C, 64.86; H, 7.05%. Calcd for $C_{28}H_{36}O_9$: C, 65.10; H, 7.03%.

*(15R)-6α,11,12,16-Tetrahydroxy-8,11,13-abietatrien-7-one (Nellionol) (**3a**) and Its (15S)-Epimer (**3b**).* *a)*: A mixture of **14a** (60.0 mg) and dilute hydrochloric acid (15%: 0.5 ml) in ethanol (3.0 ml) was refluxed for 6 h. After removal of the ethanol *in vacuo*, the residue was extracted with ether. The ether extract was washed with brine, dried over sodium sulfate, and evaporated *in vacuo*. The residue was chromatographed on silica gel (Mallinckrodt CC-4, 10 g), using hexane–chloroform (35:65) as the eluent, to give **3a** (31.3 mg: 77.3%). This was recrystallized from benzene, mp 222—224 °C, $[\alpha]_D$ +47.2° (*c* 0.36); IR (KBr): 3500, 3390, 1675, 1613 cm^{-1}; ^1H NMR (DMSO-d_6–D_2O): δ=1.13 (3H, s) and 1.16 (3H, s) ($-C(CH_3)_2$), 1.17 (3H, d, *J*=7 Hz, C_{15}–CH_3), 1.46 (3H, s, C_{10}–CH_3), 1.66 (1H, d, *J*=13 Hz, C_5–H), 3.0—3.4 (2H, m, $C_{1\beta}$–H and C_{15}–H), 3.53 (2H, d, *J*=6 Hz, $-CH_2OH$), 4.44 (1H, d, *J*=13 Hz, $C_{6\beta}$–H), 7.31 (1H, s, C_{14}–H). Found: C, 69.10; H, 8.20%. Calcd for $C_{20}H_{28}O_5$: C, 68.94; H, 8.10%. The synthetic **3a** was identical with natural nellionol (mp 226—227 °C).[1]

b): A mixture of **14b** (186.7 mg) and dilute hydrochloric acid (15%: 2.0 ml) in ethanol (10 ml) was refluxed for 6 h. After the work-up as described in *a)*, the crude product was chromatographed on silica gel (Mallinckrodt CC-4, 15 g), using hexane–chloroform (35:65) as the eluent, to give **3b** (79.4 mg: 63.1%). This was recrystallized from benzene, mp 216—217 °C, $[\alpha]_D$ +75.7° (*c* 0.52); IR (KBr): 3490, 3375, 3275, 1675, 1615 cm^{-1}; ^1H NMR (DMSO-d_6): δ=1.14 (3H, s) and 1.17 (3H, s) ($-C(CH_3)_2$), 1.18 (3H, d, *J*=7 Hz, C_{15}–CH_3), 1.48 (3H, s, C_{10}–CH_3), 1.68 (1H, d, *J*=13 Hz, C_5–H), 3.54 (2H, d, *J*=6 Hz, $-CH_2OH$), 4.47 (1H, d, *J*=13 Hz, $C_{6\beta}$–H), 7.32 (1H, s, C_{14}–H). Found: C, 69.13; H, 8.28%. Calcd for $C_{20}H_{28}O_5$: C, 68.94; H, 8.10%.

*(15R)-11,12,16-Triacetoxy-6,8,11,13-abietatetraene (**15a**) and Its (15S)-Epimer (**15b**).* *a)*: A mixture of **12a** (330 mg) and sodium borohydride (55 mg) in methanol (4.0 ml) was stirred at 0—5 °C for 30 min and then at room temperature for 1 h. The mixture was acidified with dilute hydrochloric acid and

extracted with ether. The ether extract was washed with brine, dried over sodium sulfate, and evaporated *in vacuo*. The residual oil was dissolved in dry benzene (3.5 ml) and then refluxed with *p*-toluenesulfonic acid (20 mg) for 1 h. The mixture was cooled, diluted with ether, and washed with brine. The dried solution was evaporated *in vacuo*. The residue was chromatographed on silica gel (18 g), using ether–benzene (5:95) as the eluent, to give **15a** (241 mg: 75.5%); IR: 1767, 1733 cm^{-1}; ^1H NMR (60 MHz, CCl_4): δ=0.97 (3H, s), 1.02 (3H, s), and 1.10 (3H, s) (–C(CH$_3$)$_2$ and C_{10}–CH$_3$), 1.22 (3H, d, J=7 Hz, C_{15}–CH$_3$), 1.93 (3H, s, C_{16}–OCOCH$_3$), 2.18 (3H, s) and 2.21 (3H, s) (C_{11}–OCOCH$_3$ and C_{12}–OCOCH$_3$), 3.92 (2H, d, J=7 Hz, –CH$_2$OAc), 5.89 (1H, dd, J=9.5 and 3 Hz, C_6–H), 6.44 (1H, dd, J=9.5 and 3 Hz, C_7–H), 6.77 (1H, s, C_{14}–H).

b): Reduction of **12b** (138 mg) with sodium borohydride (23 mg) in methanol (2.0 ml), followed by dehydration with *p*-toluenesulfonic acid (10 mg) in dry benzene (2.0 ml), were carried out as described in *a*). The crude product was chromatographed on silica gel (5.0 g) to give **15b** (112 mg: 84.0%); IR: 1766, 1735 cm^{-1}; ^1H NMR (60 MHz, CCl_4): δ=0.98 (3H, s), 1.03 (3H, s), and 1.12 (3H, s) (–C(CH$_3$)$_2$ and C_{10}–CH$_3$), 1.20 (3H, d, J=7 Hz, C_{15}–CH$_3$), 1.96 (3H, s, C_{16}–OCOCH$_3$), 2.20 (3H, s) and 2.23 (3H, s) (C_{11}–OCOCH$_3$ and C_{12}–OCOCH$_3$), 4.00 (2H, d, J=7 Hz, –CH$_2$OAc), 5.91 (1H, dd, J=9.5 and 2.5 Hz, C_6–H), 6.45 (1H, dd, J=9.5 and 2.5 Hz, C_7–H), 6.78 (1H, s, C_{14}–H).

(15R)-11,12,16-Triacetoxy-8,11,13-abietatrien-6-one (16a) and Its (15S)-Epimer (16b). *a*): A mixture of **15a** (219 mg) and *m*-chloroperbenzoic acid (80%: 160 mg) in dichloromethane (4.0 ml) was stirred at 0—5 °C for 1 h and then at room temperature for 14.5 h. The mixture was diluted with ether and washed successively with aqueous potassium iodide, aqueous sodium thiosulfate, aqueous sodium hydrogencarbonate, and brine. The ether solution was dried over sodium sulfate and evaporated *in vacuo*. The residual oil was refluxed with dilute hydrochloric acid (15%: 0.5 ml) in methanol (4.0 ml) for 1 h. The mixture was evaporated *in vacuo*, diluted with water, and extracted with ether. The ether extract was washed with brine, dried over sodium sulfate, and evaporated *in vacuo* to give an oil. This oil was acetylated with acetic anhydride (1.0 ml) in pyridine (1.0 ml) at 75—80 °C for 2 h. After the usual work-up, the crude product was chromatographed on silica gel (10 g), using ether–benzene (5:95) as the eluent, to give **16a** (194 mg: 85.5%), $[\alpha]_D$ +112.8° (*c* 3.13); IR: 1769, 1717 cm^{-1}; ^1H NMR (60 MHz): δ=1.03 (3H, s), 1.20 (3H, s), and 1.32 (3H, s) (–C(CH$_3$)$_2$ and C_{10}–CH$_3$), 1.22 (3H, d, J=7 Hz, C_{15}–CH$_3$), 2.00 (3H, s, C_{16}–OCOCH$_3$), 2.29 (6H, s, C_{11}–OCOCH$_3$ and C_{12}–OCOCH$_3$), 2.57 (1H, s, C_5–H), 3.20 (1H, m, C_{15}–H), 3:57 (2H, bs, –CH$_2$CO–), 4.02 (2H, d, J=7 Hz, –CH$_2$OAc), 6.85 (1H, s, C_{14}–H).

b): Oxidation of **15b** (112 mg) with *m*-chloroperbenzoic acid (80%: 82 mg) in dichloromethane (2.5 ml), followed by treatment with dilute hydrochloric acid (15%: 0.25 ml) in methanol (2.5 ml) and subsequent acetylation with acetic anhydride (0.7 ml) in pyridine (0.7 ml), were carried out as described in *a*). The crude product was chromatographed on silica gel (5.0 g) to give **16b** (82 mg: 70.8%), $[\alpha]_D$ +39.5° (*c* 2.99); IR: 1770, 1725 cm^{-1}; ^1H NMR (60 MHz): δ=1.05 (3H, s), 1.22 (3H, s), and 1.33 (3H, s) (–C(CH$_3$)$_2$ and C_{10}–CH$_3$), 1.21 (3H, d, J=7 Hz, C_{15}–CH$_3$), 2.02 (3H, s, C_{16}–OCOCH$_3$), 2.32 (6H, s, C_{11}–OCOCH$_3$ and C_{12}–OCOCH$_3$), 2.58 (1H, s, C_5–H), 3.21 (1H, m, C_{15}–H), 3.60 (2H, bs, –CH$_2$CO–), 4.07 (2H, d, J=7 Hz, –CH$_2$OAc), 6.90 (1H, s, C_{14}–H).

(15R)-6,11,12,16-Tetraacetoxy-5,8,11,13-abietatetraen-7-one (17a) and Its (15S)-Epimer (17b). *a*): A solution of **16a** (194 mg) in acetone (4.0 ml) was oxidized with Jones reagent (2.5 mol dm^{-3}: 0.26 ml) at 0—5 °C for 10 min and then at room temperature for 2 h. The mixture was diluted with water and extracted with ether. The ether extract was washed with brine, dried over sodium sulfate, and evaporated *in vacuo*. The residue was refluxed with acetic anhydride (6.0 ml) in the presence of anhydrous sodium acetate (350 mg) for 2.5 h with stirring. The mixture was cooled and diluted with ether. The ether solution was washed with water, dried over sodium sulfate, and evaporated *in vacuo*. The crude product was chromatographed on silica gel (10 g), using ether–benzene (1:9) as the eluent, to give **17a** (137 mg: 68.7%). This was recrystallized from hexane–benzene, mp 149—153 °C, $[\alpha]_D$ +88.0° (*c* 2.41); IR: 1778, 1730 sh, 1660, 1613 cm^{-1}; ^1H NMR: δ=1.29 (3H, d, J=7 Hz, C_{15}–CH$_3$), 1.40 (6H, s, –C(CH$_3$)$_2$), 1.64 (3H, s, C_{10}–CH$_3$), 2.00 (3H, s, C_{16}–OCOCH$_3$), 2.32 (3H, s) and 2.36 (6H, s) (C_6–OCOCH$_3$, C_{11}–OCOCH$_3$, and C_{12}–OCOCH$_3$), 3.25 (1H, m, C_{15}–H), 4.08 (2H, d, J=7 Hz, –CH$_2$OAc), 8.12 (1H, s, C_{14}–H). Found: C, 65.53; H, 6.91%. Calcd for $C_{28}H_{34}O_9$: C, 65.36; H, 6.66%.

b): Oxidation of **16b** (130 mg) in acetone (3.0 ml) with Jones reagent (2.5 mol dm^{-3}: 0.18 ml), followed by treatment with anhydrous sodium acetate (210 mg) in acetic anhydride (4.0 ml), were carried out as described in *a*). The crude product was purified by column chromatography on silica gel (5.0 g) to give **17b** (100 mg: 68.8%). This was recrystallized from hexane–benzene, mp 249—252 °C, $[\alpha]_D$ +43.0° (*c* 0.54); IR: 1778, 1733 sh, 1660, 1613 cm^{-1}; ^1H NMR: δ=1.27 (3H, d, J=7 Hz, C_{15}–CH$_3$), 1.39 (6H, s, –C(CH$_3$)$_2$), 1.64 (3H, s, C_{10}–CH$_3$), 2.01 (3H, s, C_{16}–OCOCH$_3$), 2.32 (3H, s) and 2.36 (6H, s) (C_6–OCOCH$_3$, C_{11}–OCOCH$_3$, and C_{12}–OCOCH$_3$), 3.23 (1H, m, C_{15}–H), 4.10 (2H, d, J=7 Hz, –CH$_2$OAc), 8.11 (1H, s, C_{14}–H). Found: C, 65.61; H, 6.82%. Calcd for $C_{28}H_{34}O_9$: C, 65.36; H, 6.66%.

(15R)-6,11,12,16-Tetrahydroxy-5,8,11,13-abietatetraen-7-one (5-Dehydronellionol) (4a) and Its (15S)-Epimer (4b). *a*): A mixture of **17a** (115.3 mg) and dilute hydrochloric acid (15%: 1.5 ml) in methanol (10 ml) was refluxed for 3 h. After removal of the methanol *in vacuo*, the residue was extracted with ether. The ether extract was washed with brine, dried over sodium sulfate, and evaporated *in vacuo*. The crude product was chromatographed on silica gel (Mallinckrodt CC-4, 10 g), using hexane–chloroform (35:65) as the eluent, to give **4a** (63.9 mg: 82.3%). This was recrystallized from hexane–benzene, mp 211—213 °C, $[\alpha]_D$ 0° (*c* 0.55); IR: 3600, 3500, 3370, 3150, 1633, 1597, 1565 cm^{-1}; ^1H NMR: δ=1.38 (3H, d, J=7 Hz, C_{15}–CH$_3$), 1.45 (6H, s, –C(CH$_3$)$_2$), 1.66 (3H, s, C_{10}–CH$_3$), 2.91 (1H, br, C_{16}–OH), 3.0—3.4 (2H, m, $C_{1\beta}$–H and C_{15}–H), 3.80 (1H, dd, J=8 and 10 Hz) and 4.08 (1H, dd, J=3 and 10 Hz) (–CH$_2$OH), 7.58 (1H, s, C_{14}–H), 6.36 (1H, s), 7.08 (1H, s), and 9.56 (1H, br) (C_6–OH, C_{11}–OH, and C_{12}–OH). Found: C, 69.61; H, 7.67%. Calcd for $C_{20}H_{26}O_5$: C, 69.34; H, 7.57%. The synthetic **4a** was identical with natural 5-dehydronellionol (mp 210—212 °C).[1]

b): A solution of **17b** (143.0 mg) in methanol (16 ml) was hydrolyzed with dilute hydrochloric acid (15%: 2.5 ml) as described in *a*). The crude product was purified by column chromatography on silica gel (Mallinckrodt CC-4, 15 g) to

give **4b** (59.9 mg: 62.2%). This was recrystallized from hexane–benzene, mp 187—189 °C, $[\alpha]_D$ +52.4° (*c* 0.52); IR: 3610, 3500, 3375, 3150, 1633, 1598, 1565 cm^{-1}; ^1H NMR: δ=1.37 (3H, d, *J*=7 Hz, C_{15}-CH_3), 1.44 (6H, s, $-\underset{|}{C}(CH_3)_2$), 1.68 (3H, s, C_{10}-CH_3), 2.9—3.45 (3H, m, $C_{1\beta}$-H, C_{15}-H, and C_{16}-OH), 3.80 (1H, dd, *J*=8 and 10 Hz) and 4.07 (1H, dd, *J*=3 and 10 Hz) ($-C\underline{H}_2OH$), 7.58 (1H, s, C_{14}-H), 6.38 (1H, s), 7.07 (1H, s), and 9.60 (1H, br) (C_6-OH, C_{11}-OH, and C_{12}-OH). Found: C, 69.56; H, 7.64%. Calcd for $C_{20}H_{26}O_5$: C, 69.34; H, 7.57%.

References

1) CH. B. Rao, T. N. Rao, and E. K. S. Vijayakumar, *Curr. Sci.*, **47**, 455 (1978); *Indian J. Chem.*, **18B**, 513 (1979).

2) T. Matsumoto, S. Imai, S. Takeda, and M. Mitsuki, *Bull. Chem. Soc. Jpn.*, **56**, 2013 (1983).

3) R. H. Burnell, M. Jean, D. Poirier, and S. Savard, *Synth. Commun.*, **13**, 63 (1983).

4) T. Matsumoto, S. Imai, S. Miuchi, and H. Sugibayashi, *Bull. Chem. Soc. Jpn.*, **58**, 340 (1985).

5) M. Node, K. Ohta, T. Kajimoto, K. Nishide, E. Fujita, and K. Fujita, *Chem. Pharm. Bull.*, **31**, 4178 (1983).

 © 1985 The Chemical Society of Japan Bull. Chem. Soc. Jpn., 58, 1171—1173 (1985)

An Improved Method for Synthesis of L-Homoglutamic Acid *via* Epsilon-*N*-deamination of L-Lysine Derivative

Michio KONDO,* Koujiro MIYAZAKI, Hiroaki KODAMA, and Hideaki HORIMOTO
Department of Chemistry, Faculty of Science and Engineering, Saga University, Honjo-machi, Saga 840
(Received November 9, 1984)

A convenient procedure to prepare L-homoglutamic acid (L-2-aminoadipic acid; L-Aad) is described. Chlorination of ε-amino group in acetyl-L-lysine ethyl ester with *t*-butyl hypochlorite (*t*-BuOCl) followed by dehydrochlorination with pyridine gave ethyl 5-cyanovalerate which on acid hydrolysis afforded L-Aad in good yield.

2-Aminoadipic acid (Aad) is an intermediate in lysine metabolism and has been found in peptide antibiotics precursor of penicillin and cephalosporin biosynthesis. The absolute configuration of Aad from *penicillium chrysogenum* was determined to be the L-configuration by Chan *et al.*[1] Chemical synthesis of L-Aad has proceeded under optical resolution of DL-hydantoin derivative[2] or 2-(hydroxyimino)adipic ester.[3] In recent years Scott and Wilkinson[4] reported an alternative procedure based on the conversion of ε-amino group of N^{α}-benzyloxycarbonyl-L-lysine to the corresponding acid using NaOCl and a strong base, such as 1,8-diazabicyclo[5.4.0]undec-7-ene. L-Aad was obtained in 35% overall yield from the lysine derivative.

In a previous paper,[5] we reported a new method for the detection of intramolecularly hydrogen-bonded peptide NH by chlorine replacement reaction, which was initiated by adding a peptide to a solution containing Cl_2 or by adding *t*-BuOCl to a solution of peptide. The rate of chlorination measured by ^1H NMR showed that intramolecularly hydrogen-bonded peptide NH's were much more susceptible to the chlorination than solvent-exposed NH's in the peptide antibiotics, gramicidin S and tuberactinamin N. To make sure these new findings, substituent effects of alkyl (R-) or aryl (Ar-) group of CH_3CONHR (or -Ar) on H–Cl replacement reaction were also examined by ^1H NMR. The results well explained the differences in the reactivity of the amide NH protons: the more easily the amide nitrogen releases the proton (*viz.*, the more downfield NH proton signal appears), the more susceptible the NH proton is to chlorination. We postulated a mechanism to account for the H–Cl replacement reaction.[6]

We report here an improved method for the synthesis of L-Aad in optical form from N^{α}-acetyl-L-lysine ethyl ester by a deamination procedure. The procedure consists of chlorination of ε-amino group in the lysine derivative with *t*-BuOCl, dehydrochlorination of the *N,N*-dichloro amine derivative with pyridine, and hydrolysis of the nitrile. The overall yield was 60% from the lysine derivative. The present method provides a superior procedure for the synthesis of L-Aad to previously reported procedures[2–4] in high yield and in ease of operation.

Results and Discussion

Synthesis of L-*Glutamic Acid from* L-*Ornithine.* In the course of study on structure-activity relationship of gramicidin S, we found that amino acid analysis of the hydrolysis products of chlorinated gramicidin S gave three unknown peaks except ones of constituent amino acids in gramicidin S. Among the three peaks, one which appeared in the acidic region seemed to be glutamic acid derived from ornithine during chlorination of gramicidin S followed by acid hydrolysis. To confirm the results, we carried out chlorination of Ac-L-Orn-OEt and acid hydrolysis of the dichloro amine derivative. The preliminary experiments using the model compound, Ac-L-Orn-OEt, showed that the δ-NH_2 group was not susceptible to chlorination with Cl_2, but that in the case of *t*-BuOCl a chlorinated product having δ-NHCl or δ-NCl_2 group was detected by ^1H NMR and mass spectrometers. After a methanol solution of the dichloro amine derivative was tightly stoppered and stored in the dark for a month, the δ-NCl_2 group remained without decomposition, which was ascertained by appearance of its absorption band (310 nm, λ_{max}) in UV spectrum and by thin-layer chromatography. The dichloro amine derivative chlorinated with *t*-BuOCl was hydrolyzed with 6 mol dm^{-3} hydrochloric acid. Amino acid analysis of the products gave two peaks. One was ascertained to be ornithine and the other to be glutamic acid from the data of paper chromatography (PPC) and paper electrophoresis. In the above procedure, glutamic acid was obtained only in a small amount.

Nitrile synthesis from amine *via* *N,N*-dihalo amine followed by dehydrohalogenation was carried out by several procedures.[7–9] For example, the dehydrohalogenation was carried out by heating dihalo amine with cesium fluoride. In the conversion of 1,6-hexanediamine into adiponitrile the fluorinated derivative was successfully isolated.[9] Therefore, to obtain a high yield of glutamic acid, formation of nitrile by dehydrochlorination was carried out with triethylamine and pyridine. However, use of triethylamine as a base was no advantage to the yield of glutamic acid. On the other hand, application of excess pyridine gave a good yield of glutamic acid as a main product. Amino acid analysis and the value of $[\alpha]_D$ of the glutamic acid thus

Table 1. Reaction products of Ac-L-Lys-OEt with *t*-BuOCl under various conditions and acid hydrolysis of nitrile

Chlorination conditions		Chlorinated[a] NH/%		Acid hydrolysis of nitrile		
t-BuOCl[b]	time	α-NH	ε-NH_2	Aad[c]:	Lys:	insoluble
10 eq	3.5 h	60	100	15	20	65
10 eq	5 min	5	100	52	18	30
5 eq	5 min	0	100	75	7	18

a) Data from ^{1}H NMR. b) In MeOH at 0 °C and then room temperature. c) Weight ratio.

obtained were in fair agreement with those of an authentic sample. These results suggest that L-ornithine is converted into L-glutamic acid without racemization *via* the dichloro amine derivative in good yield.

Synthesis of L-Aad from L-Lysine. We are very interested in the preparation of L-homoglutamic acid (L-Aad) which is not easily available in large quantities. The above results prompted us to study for a convenient and practical synthesis of L-Aad from L-lysine derivative.

In order to find out suitable reaction conditions, chlorination of Ac-L-Lys-OEt (**2**) with *t*-BuOCl was carried out under various conditions shown in Table 1. The most satisfactory result was obtained by using 5 equivalents *t*-BuOCl for 5 min, and also acid hydrolysis of the nitrile derived from the dichloro amine under these conditions showed the best yield of L-Aad. After chlorination with *t*-BuOCl (5-equiv) in methanol for 5 min, the reaction mixture was concentrated *in vacuo* to give an oil (**3**). This oil was used in the next reaction without further purification because of its unstableness. The formation of the dichloro amine derivative was detected by ^{1}H NMR and UV spectra. As shown in Fig. 1, compound **3** was dehydrochlorinated by excess pyridine for 20 h at room temperature, the reaction mixture was concentrated *in vacuo*, and the oily residue was dissolved in chloroform. The solution was washed successively with 0.5 mol dm^{-3} sodium hydrogencarbonate, 0.5 mol dm^{-3} citric acid, and water to give the nitrile (**4**). The formation of **4** was detected by the 2260 cm^{-1} ν C≡N band of the product in the IR spectrum and further confirmed by ^{1}H NMR and mass spectra. The nitrile was refluxed with 6 mol dm^{-3} hydrochloric acid to yield L-Aad, lysine, and insoluble material. After filtering off the insoluble material, these products were subjected to ion-exchange column chromatography to afford L-Aad in 60% yield from Ac-L-Lys-OEt (**2**) which was easily obtained by catalytic hydrogenolysis of Ac-L-Lys(ε-Z)-OEt (**1**). Amino acid analysis, CD, and $[\alpha]_D$ data of the synthetic L-Aad (**5**) thus obtained were identical with those of an authentic sample.

By the above results, the deamination procedure proved to be a facile and convenient method for the synthesis of L-homoglutamic acid in optical form from L-lysine derivative.

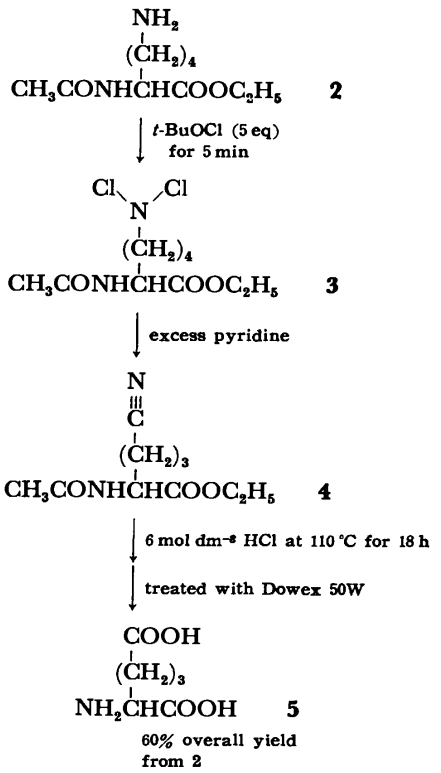

Fig. 1. Synthetic Procedure of L-2-Aminoadipic Acid.

Experimental

The melting point is uncorrected. All chemicals used for preparative experiments were of reagent grade and solvents were distilled before use. An authentic sample of L-Aad was obtained from Calbiochem-Behring Corp., La Jolla., Calf., U.S.A. Thin-layer chromatography was carried out on silica gel GF_{254} (Merck) with the following solvent system: R_f^1, $CHCl_3$-MeOH-AcOH (8:1:1, v/v). Compounds with protected amino groups were detected by spraying with 50% hydrochloric acid followed by ninhydrin. Chlorinated compounds were detected by spraying with the mixed solution (1:1, v/v) of 0.1 mol dm^{-3} potassium iodide in water and 2.1 mmol dm^{-3} *o*-tolidine in 2% AcOH. Paper chromatography was performed on Toyo Roshi No. 50 paper with the following solvent systems: R_f^2, *n*-BuOH-AcOH-H_2O (4:1:2, v/v) and R_f^3, *n*-BuOH-AcOH-pyridine-H_2O (4:1:1:2, v/v). Optical rotations were measured on a Yanagimoto polarimeter OR-50 and CD spectra with a Jasco J-20 spectropolarimeter. Mass spectra were taken on an ESCO EMD-05A and NMR spectra on a JEOL JNM-MH-100. Infrared spectra were recorded on a Hitachi 260-10 instrument using KCl plate. Amino acid analysis was carried out by amino acid analyzer model, JLC-6AH.

Ac-L-Lys(ε-Z)-OEt (1). To a solution of L-Lys(ε-Z)-OEt·*p*-TosOH[10] (7.21 g, 15 mmol) in pyridine (35 mL) was added acetic anhydride (7.1 mL, 75 mmol) at 0 °C. The mixture was stirred for 18 h at room temperature and then evap-

orated *in vacuo*. The residue was diluted with ethyl acetate (400 mL). The ethyl acetate solution was washed successively with 0.5 mol dm^{-3} citric acid, 0.5 mol dm^{-3} $NaHCO_3$, and water. The solution was dried over anhydrous Na_2SO_4 and evaporated under reduced pressure. The product was obtained as an oil; yield 4.73 g (90%); R_f^1 0.65; ^1H NMR ($CDCl_3$): δ 7.32 (s, 5H, aromatic), 6.33 (d, 1H, -NH-), 5.00 (m, 1H, -NH-), 4.52 (q, 1H, -CH), 4.16 (q, 2H, $-CH_2-$), 3.16 (q, 2H, $-CH_2-$), 1.98 (s, 3H, $-CH_3$), 1.26 (t, 3H, $-CH_3$); Found: *m/z* 350. Calcd for $C_{18}H_{26}N_2O_5$: M, 350.

Ac-L-Lys-OEt (2). Compound **1** (3.8 g, 10.8 mmol) was hydrogenated in EtOH (35 mL) in the presence of palladium black for 4.5 h. The solution filtered from the catalyst was evaporated to dryness *in vacuo*. The oily product weighed 2.3 g (98%); R_f^2 0.57, R_f^3 0.61; ^1H NMR (DMSO-d_6): δ 8.38 (d, 1H, -NH-), 4.32 (m, 1H, -CH), 4.22 (q, 2H, $-CH_2-$), 2.60 (m, 2H, $-NH_2$), 1.91 (s, 3H, $-CH_3$), 1.23 (t, 3H, $-CH_3$); Found: *m/z* 216. Calcd for $C_{10}H_{20}N_2O_3$: M, 216.

N^{ε}-Dichloro-N^{α}-acetyl-L-lysine Ethyl Ester (3). To a solution of **2** (2.3 g, 10.6 mmol) in MeOH (30 mL) was added *t*-butyl hypochlorite (5.96 mL, 53 mmol) at 0 °C. After 5 min at room temperature, the solution was evaporated to dryness *in vacuo* at 5 °C. The compound was obtained as an oil. All experimental procedures were carried out in the dark; yield 3.0 g (99%); R_f^1 0.64; ^1H NMR (DMSO-d_6): δ 8.28 (d, 1H, -NH-), 4.10 (q, 2H, $-CH_2-$), 3.00 (t, 2H, $-CH_2-$), 1.88 (s, 3H, $-CH_3$), 1.20 (t, 3H, $-CH_3$).

Ethyl 2-Acetamido-5-cyanovalerate (4). To a solution of **3** (1.51 g, 5.3 mmol) in MeOH (15 mL) was added excess pyridine (93 mL) at 0 °C in the dark. After 20 h at room temperature, the reaction mixture was evaporated and dissolved in $CHCl_3$ (200 mL). The solution was washed with 0.5 mol dm^{-3} citric acid and aq NaCl, dried over anhydrous Na_2SO_4, and then concentrated under reduced pressure to an oil. The formation of nitrile **4** by dehydrochlorination was confirmed with the 2260 cm^{-1} ν C≡N band of the product in the IR spectrum. It weighed 1.04 g (93%); R_f^1 0.67; ^1H NMR ($CDCl_3$): δ 6.52 (d, 1H, -NH-), 4.60 (m, 1H, -CH), 4.22 (q, 2H, $-CH_2-$), 2.42 (t, 2H, $-CH_2-$), 2.04 (s, 3H, $-CH_3$), 1.31 (t, 3H, $-CH_3$); Found: *m/z* 212. Calcd for $C_{10}H_{16}N_2O_3$: M,212.

L-2-Aminoadipic Acid (5). Compound **4** (1.04 g, 4.9 mmol) was refluxed with 6 mol dm^{-3} HCl (150 mL) for 18 h. The cooled solution was evaporated to give an oil, which was dissolved in water (100 mL). After filtering off a small amount of insoluble material, the solution was applied on a column (2.1×25 cm) of Dowex 50 W (H^+ form). The column was washed with water (200 mL) and was eluted with 2 mol dm^{-3} aqueous ammonia (200 mL). The collected effluents were evaporated to leave an oily product, which was dissolved in water (90 mL). Chromatography of this solution with Dowex 50 W (NH_4^+ form) separated Aad by elution with water (200 mL) and lysine was successively recovered with 2 mol dm^{-3} aqueous ammonia (200 mL). The effluent containing Aad from the column (NH_4^+ form) was evaporated to a small volume and precipitated by the addition of EtOH. The crude product was dissolved in dil HCl and the solution was adjusted to pH 3.5 with 1 mol dm^{-3} aqueous ammonia and then crystallized by the addition of EtOH; yield 525 mg (60% from **2**); R_f^2 0.27, R_f^3 0.16; mp 199—200 °C; $[\alpha]_D^{21}$ +24.4° (*c* 2, 5 mol dm^{-3} HCl). Authentic L-Aad: R_f^2 0.27, R_f^3 0.16; mp 200—201 °C; $[\alpha]_D^{21}$ +24.6° (*c* 2, 5 mol dm^{-3} HCl). Amino acid analysis and CD spectrum of L-Aad were in fair agreement with the authentic L-Aad.

Found: C, 44.54; H, 7.07; N, 8.65%. Calcd for $C_6H_{11}NO_4$: C, 44.72; H, 6.88; N, 8.69%.

Electrophoresis. Electrophoresis of compound **5**, using Toyo Roshi No. 51A paper, was carried out with the following solvent systems: Ep^1, pyridine–AcOH–H_2O (1:10:89, v/v, pH 3.6) and Ep^2, pyridine–AcOH–H_2O (25:1:225, v/v, pH 6.5) at 500 V/30 cm for 2 h. Compound **5** and L-homoglutamic acid (Aad) showed the equal mobilities, which migrated towards the cathode, 0.4 cm in Ep^1 and the anode, 2.8 cm in Ep^2, respectively.

References

1) J. A. Chan, F. Huang, and C. J. Shin, *Biochemistry*, **15**, 177 (1976).
2) M. Takehara and R. Yoshida, *Nippon Kagaku Zasshi*, **90**, 101 (1969).
3) W. Dieckmann, *Chem. Ber.*, **38**, 1656 (1905).
4) A. I. Scott and T. J. Wilkinson, *Synth. Commun.*, **10**, 127 (1980).
5) M. Kondo, K. Okamoto, I. Nishi, M. Yamamoto, T. Kato, and N. Izumiya, *Chem. Lett.*, **1980**, 703.
6) M. Kondo, I. Nishi, K. Okamoto, T. Kato, and N. Izumiya, "PEPTIDES: Synthesis-Structure-Function," ed by D. H. Rich and E. Gross, Pierce Chemical Company, Rockford (1981), p. 291.
7) T. E. Stevens, *J. Org. Chem.*, **26**, 2531 (1961).
8) L. L. Jackson, G. N. R. Smart, and G. F. Wright, *J. Am. Chem. Soc.*, **69**, 1539 (1947).
9) C. M. Sharts, *J. Org. Chem.*, **33**, 1008 (1968).
10) T. Kato, S. Makisumi, M. Ohno, and N. Izumiya, *Nippon Kagaku Zasshi*, **83**, 1151 (1962).
11) Abbreviations for amino acids are according to the IUPAC-IUB Commission on Biochemical Nomenclature, *J. Biol. Chem.*, **247**, 977 (1972).

The Photolysis of *N,O*-Diacyl-*N*-phenylhydroxylamines[1)]

Tadamitsu SAKURAI,* Hirofumi YAMAMOTO, Shuichi YAMADA, and Hiroyasu INOUE
Department of Applied Chemistry, Faculty of Technology, Kanagawa University, Rokkakubashi, Kanagawa-ku, Yokohama 221
(Received November 9, 1984)

The photochemical decomposition of the title compounds yielded the rearrangement products derived from 1,3- and 1,5-aroyloxyl migrations in addition to the fragmentation products typical of the aroyloxyl and amido radicals, while only 1,3-aroyloxyl migration was observed on thermolysis. The results of crossover experiments indicate an intramolecular rearrangement, probably involving homolysis of the N-O bond in the excited states. Triplet quenching studies demonstrate that the rearrangement and fragmentation proceed exclusively *via* the first excited singlet state. No formation of the rearrangement products on triplet sensitization was explained on the basis of the spin multiplicity effects on a radical-radical recombination process within a solvent cage.

The elegant and pioneering works of Ochiai and his coworkers in the field of the chemistry of heteroaromatic amine *N*-oxides have greatly stimulated mechanistic investigations of the reactions between these *N*-oxides and acylating agents.[2)] The devotion of many workers to this mechanistic study has resolved many questions concerning the mechanism of the reactions, which heteroaromatic and aromatic amine *N*-oxides undergo, and led to the syntheses of many biochemically and pharmaceutically important compounds.[3)] In connection with the rearrangements of *O*-acylated amine *N*-oxides, the acyloxyl migration of *N,O*-diacyl-*N*-arylhydroxylamines has attracted much attention mainly because these *N*-arylhydroxylamines have a closely related structure to "anhydrobase" which is a key intermediate for the rearrangement reactions of tertiary amine *N*-oxides.[4)]

In addition, mechanistic studies of *N,O*-diacyl-*N*-arylhydroxylamines[5)] have contributed to clarifying the mode of the N-O bond cleavage that has been a question of controversy for a long time in the rearrangement of heteroaromatic *N*-oxides and related compounds.[6)] Based on both kinetic and oxygen-18 tracer studies it was suggested that the electronic effects on the heterolysis of the N-O bond play a crucial role in determining the mechanism of 1,3-rearrangement.[5)] However, it is difficult to exclude completely the possibility of a radical rearrangement *via* the homolysis of the N-O bond although the rearrangement is now believed to proceed *via* the exclusive heterolytic cleavage of the N-O bond.[6,7)]

On the other hand, Walling and Naglieri have found that the photolysis of *N,O*-diacylhydroxylamines gives the products derived from the homolysis of the N-O bond.[8)] Their work suggested us that a systematic study of the photolysis of *N,O*-diacyl-*N*-arylhydroxylamines would lead to a new information on the mechanism of acyloxyl migrations of these hydroxylamines and related compounds. Because there are only a few investigations of the photochemical rearrangement of hydroxamic acid derivatives,[9)] we have prepared *N,O*-diacyl-*N*-phenylhydroxylamines (**Ia—d**) and examined their photochemical behavior, hoping to gain further insight into the mechanism of acyloxyl migration. In this paper we present the first observation of photorearrangements of **Ia—d** and discuss the mechanism of the photolysis of these hydroxylamines.

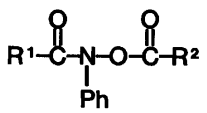

Ia-d

Ia: R^1=1-naphthyl (1-Np), R^2=p-tolyl (p-Tl)
Ib: R^1=p-Tl, R^2=1-Np
Ic: R^1=R^2=1-Np
Id: R^1=R^2=p-Tl

Results and Discussion

*Products from the Photolyses of **Ia—d**.* An oxygen-free acetonitrile solution of **I** was irradiated with Pyrex-filtered light. The irradiation was done in a water bath so that the reaction temperature was maintained constant during the photolysis (23±1 °C). Each of reactions gave two rearrangement products **II** and **III** together with arenecarboxanilide **IV**, carboxylic acid **V**, and hydrocarbon **VI** as summarized in Table 1.

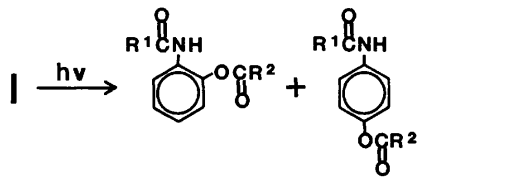

II **III**

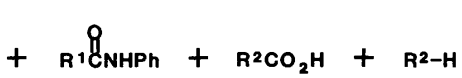

IV **V** **VI**

These products were identified by comparing their HPLC behavior at two different wavelengths (230 and 270 nm) with that of independently prepared authentic samples. In addition to the HPLC peaks of **II—VI** one can see some unknown peaks on the chromatogram, which will be discussed in a later section. Starting

Table 1. Photolysis of **Ia—d** (0.0066 M) in acetonitrile

Compound	Irradiation time/min	Conversion/%	HPLC yield[a] of product/% II	III	IV	V	VI
Ia	15	40.0	4.4	1.5	1.5	10.0	—[b]
	60	85.5	7.3	2.1	5.5	24.0	—[b]
	240	98.4	9.0	2.4	10.2	29.6	8[c]
Ib	15	43.2	0.3	0.1	2.8	11.0	—[b]
	60	71.9	1.1	1.6	8.6	31.5	—[b]
	240	97.3	0.8	0.5	28.4	64.8	3
Ic	15	27.3	1.5	1.5	2.3	17.7	—[b]
	30	48.6	3.0	2.5	5.5	33.5	—[b]
	180	94.7	2.8	2.1	21.2	70.2	3
Id	30	33.4	5.2	3.2	3.3	13.5	—[b]
	60	45.9	7.4	2.7	6.2	22.1	—[b]
	240	75.6	10.2	2.8	15.2	53.3	7[c]

a) Based on starting hydroxylamines. b) Not determined. c) GLC yield.

Table 2. Crossover experiments in acetonitrile[a]

Compound	Conversion/%	Rearrangement product and its HPLC yield[b]/% IIc	IIIc	IId	IIId	IIa	IIIa	IIb	IIIb
		crossover product							
Ia	94.8	0.03	—[c]	0.01	0.01	4.2	—[d]	1.7	—[e]
Ib	79.9								
						crossover product			
Ic	78.9	—[f]	2.4	1.5	2.4	0.03	—[f]	0.02	0.03
Id	60.8								

a) The initial concentrations of **Ia—d** were all 0.0066 M. Deaerated solutions were irradiated for 2 h with Pyrex-filtered light in a water bath (20±1 °C). b) Based on starting hydroxylamines. c) Could not be determined because of overlapping with the HPLC peak of starting **Ia**. d) The HPLC peak of starting **Ib** made this yield determination impossible. e) Could not be determined because of overlapping with unknown HPLC peak(s) derived from **Ia**. f) The HPLC peak of starting **Id** interfered with exact evaluation of this yield.

hydroxylamines **Ia—d** were recovered quantitatively without the irradiation, of course. To get more unambiguous proof of the structure for the photoproducts, irradiation of one of the starting hydroxylamines **Ia** was continued under the same conditions as above until disappearance of **Ia** was complete (monitored by TLC). Chromatography of the photolyzate allowed isolation and identification of **IIa** (4%, isolated yield), **IIIa** (8%), **IVa** (20%), **Va** (10%), and **VIa** (9%, GLC yield) except carbon dioxide (about 30%) which was characterized as barium carbonate. This product distribution is qualitatively consistent with that obtained by HPLC analysis of the photolyzate. We obtained also tarry product mixtures from which attempts to isolate any crystalline materials were not fruitful.

Independent irradiation of the photoproducts clearly shows that the rearrangement and fragmentation products undergo undesirable photodecompositions to different extent depending on the structure of the products (**IIa**, **IId**, and **IIIb**, 30% decomposition on 2 h irradiation; **IIIa** and **IIId**, 40—50%; **IIb**, **IIc**, and **IIIc**, 70—80%; **IV**, **V**, and **VI**, 2—7%). The decomposition of the fragmentation products during the irradiation is minor, whereas that of the rearrangement products takes place remarkably. Thus the low yields of **II** and **III**, especially **IIb**, **IIc**, and **IIIc**, may be ascribed in part to this low photostability.

Crossover Experiment and Thermolysis. To ascertain the intra- or intermolecularity of this interesting photorearrangement, an equimolar mixture of **Ia** and **Ib** in acetonitrile was irradiated with Pyrex-filtered light in the same manner. Careful HPLC analysis of the photolyzate indicates the formation of negligible amounts of the crossover products (**IIc**, **d**, and **IIIc**, **d**) in addition to the noncrossover rearrangement products (**IIa**, **b**, and **IIIa**, **b**) (see Table 2). A similar finding was obtained also on irradiation of a mixture of **Ic** and **Id**. These findings demonstrate that the photorearrangements proceed by an exclusively intramolecular aroyloxyl shift.

Since the photoreactions of **Ia—d** are formally analogous to the photo-Fries reactions that proceed through a caged radical mechanism in solution,[10] it is reasonable to assume that the photolysis of these hydroxylamines involves homolytic cleavage of the N–O bond in an excited state forming the amido and aroyloxyl radicals, which either recombine within a solvent cage to afford the rearrangement products or escape out of the cage to give the fragmentation products by hydrogen abstraction from the solvent or otherwise as shown in Scheme 1. The homolysis of the N–O bond is supported by the facts that the products derived from the amido and aroyloxyl radicals were identified, and that *N,O*-diacylhydroxylamines, whose structure is very similar to that of **Ia—d**, undergo the homolytic photolysis.[8]

In order to examine possible involvement of hetero-

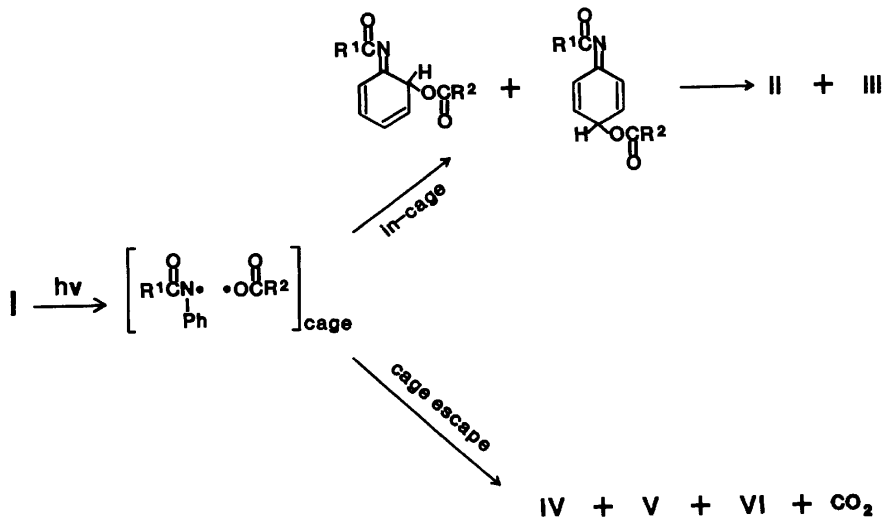

Scheme 1.

lysis of the N–O bond, **Ia—d** were heated at 120—130 °C in dimethyl sulfoxide. If participation of an ionic mechanism would be responsible for the formation of **II** and **III**, the same rearrangement products should be obtained thermally because the rearrangement of closely related *N,O*-diacyl-*N*-arylhydroxylamines is well known to proceed through the heterolytic scission of the N–O bond.[5] As seen from Table 3 the thermolyses gave only the ortho-migrated products **II** accompanied by the recovered starting materials, whereas neither fragmentation nor migration of an aroyloxyl group to the para-position could be observed. Clearly the products of the photolysis are quite different from those of the thermal decomposition, indicating that at least the para-migrated rearrangement and fragmentation products originate from the homolytic cleavage of the N–O bond. The fact that the N–O bond of diacylhydroxylamines readily undergoes homolytic cleavage in the excited states[8] allows us to propose a radical mechanism to account for the formation of **II** as well as **III—VI**.

*Solvent Effects on the Photolysis of **Ia**.* A free radical mechanism requires that anilide **IV** and carboxylic acid **V** should be found in comparable amounts because of the minor process of decarboxylation giving eventually either toluene or naphthalene. Table 1 shows, however, that there are always lower yields of **IV** than those of **V** at any conversion irrespective of the structure of starting hydroxylamines. This observation leads us to speculate that hydrogen abstraction to yield **IV** is not the only reaction pathway for the amido radical in acetonitrile. It is likely that hydrogen abstraction of the photochemically generated amido radical competes with such processes as dimerization, disproportionation, and addition[11] owing to the relatively low reactivity of acetonitrile toward hydrogen abstraction. These competing pathways might be responsible for the observation of some unknown HPLC peaks. We felt that solvent effects on the rearrangement and fragmentation pathways may clarify this point. The hydroxylamine **Ia** was chosen for this purpose. The results are given in Table 4. As expected the fragmentation products **IV** and **V** are found in comparable yields in 1,2-dichloroethane whose hydrogen atoms seem much more reactive to hydrogen abstraction compared with other two solvents used. In addition, some unknown HPLC peaks, which were observed in the photolysis in acetonitrile and benzene, could not be detected on the HPLC chromatogram of the photolyzate in 1,2-dichloroethane, supporting the view mentioned above.

TABLE 3. THERMOLYSIS OF **Ia—d** IN DIMETHYL SULFOXIDE AT 120—130 °C

Compound	Reaction time/h	Conversion/%	Yield[a] of product/% II	III
Ia	9	16	11	—[b]
Ib	10	88	65	—[b]
Ic	9	49	39	—[b]
Id	9	57	48	—[b]

a) Based on starting hydroxylamines. b) Not detected.

Quenching and Sensitization Experiments. *N,O*-Diacyl-*N*-phenylhydroxylamines used in this work exhibit a fluorescence with maxima between 370 and 390 nm except **Id** whose fluorescence is too weak to be observed. We estimated the first singlet excitation energy (E_S) of **Ia—c** from the absorption and fluorescence spectral data to tabulate in Table 5. The phosphorescence of **Ia—c** with 0,0 bands around 490 nm could be detected in acetonitrile at 77 K, while **Id** shows a broad phosphorescence at 422 nm. Table 5 also includes the first triplet excitation energy (E_T) estimated from the 0,0 bands of **Ia—c** and the emission maximum of **Id**. In Fig. 1 are typically shown the absorption and emission spectra of **Ia** in acetonitrile.

The phosphorescence of **Ia—d** (2×10^{-4} M, 1 M=1 mol dm^{-3}) is quenched by 1,3-cyclohexadiene (0.01 M), showing that this diene becomes a good triplet quencher in view of endothermicity of singlet-singlet energy transfer from **I** to the diene. Sensitization of the phosphorescence of **Ia—d** (2×10^{-4} M) by benzo-

TABLE 4. SOLVENT EFFECTS ON THE PHOTOLYSIS OF **Ia**

Solvent	Irradiation time/min	Conversion/%	HPLC yield[a] of product/%			
			IIa	**IIIa**	**IVa**	**Va**
Benzene	15	42.8	5.3	1.3	3.0	18.1
	30	71.6	7.3	2.4	7.6	37.6
	120	99.9	7.0	3.2	24.3	56.4
CH_2ClCH_2Cl	15	42.7	5.1	1.2	22.0	20.1
	30	80.9	7.4	1.8	41.7	42.7
	120	100	7.8	2.0	55.8	61.0

a) Based on starting hydroxylamines.

TABLE 5. THE FIRST SINGLET (E_S) AND TRIPLET (E_T) EXCITATION ENERGIES OF **Ia—d**, 1,3-CYCLOHEXADIENE, AND BENZOPHENONE

(1 kcal=4.18 kJ)

Compound	E_S/kcal mol^{-1}	E_T/kcal mol^{-1}
Ia	90	59
Ib	86	58
Ic	85	58
Id	<97[a]	68
1,3-Cyclohexadiene	97[b]	52.4[b]
Benzophenone	74.4[b]	69.2[b]

a) Estimated from a comparison of the absorption spectrum of **Id** with that of 1,3-cyclohexadiene. b) S. L. Murov, "Handbook of Photochemistry," Marcel Dekker, New York, N. Y. (1973), p. 3.

phenone (2×10^{-3} M) was observed accompanying the quenching of sensitizer's phosphorescence (Fig. 2). This finding indicates benzophenone to be an excellent triplet sensitizer. Also in this case singlet-singlet energy transfer from sensitizer to **I** is endothermic. In order to decide whether the photolysis occurs from the excited singlet or triplet state, triplet quenching (313-nm light) and sensitization (mostly 366-nm light) experiments were performed. The results are summarized in Tables 6 and 7. Evidently, neither product formation nor disappearance of starting hydroxylamines was affected by 1,3-cyclohexadiene within the limits of experimental accuracy (Table 6), suggesting that the rearrangement and fragmentation products come from the reaction in the excited singlet state.[12]

The diacylhydroxylamines **Ia—d** undergo greatly accelerated photodecompositions in the presence of benzophenone (Table 7). The fragmentation products are formed by the sensitized photolysis in which no benzophenone was consumed within the experimental error, whereas benzophenone does not sensitize the rearrangement. The finding that the triplet state photolysis gives the rearrangement products in a negligible yield is compatible with the result of triplet quenching experiment. Irradiation of the photoproducts **II—VI** with 366-nm light resulted in their negligible decomposition (less than 5% on 15 min irradiation) in the presence of the sensitizer (0.05 M). Another prominent facet in this triplet sensitization is that the yields of **IVa—c** are much low even at high conversion of **Ia—c**. The increased intensity of unknown HPLC peaks compensates for this decreased yield of anilide **IV**. Thus the fragmentation products including **IV** are undoubtedly formed by the sensitized photolysis.

Mechanism of the Photolyses. The triplet quenching and sensitization results establish that the rearrangement takes place *via* the excited singlet state, whereas the fragmentation products are obtained from both the excited singlet and triplet state reactions. As already noted the direct photolysis of **I** causes the homolytic scission of the N-O bond in the molecule

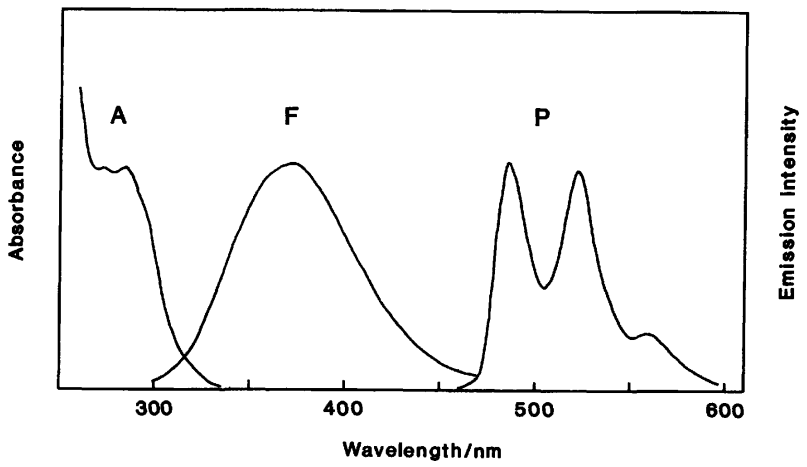

Fig. 1. UV absorption and emission spectra of **Ia** (2×10^{-4} M) in acetonitrile. (A): Absorption at room temperature; (F): Fluorescence at room temperature, excitation wavelength=315 nm; (P): Phosphorescence at 77 K, excitation wavelength=310 nm. Intensities have been adjusted for the sake of clarity.

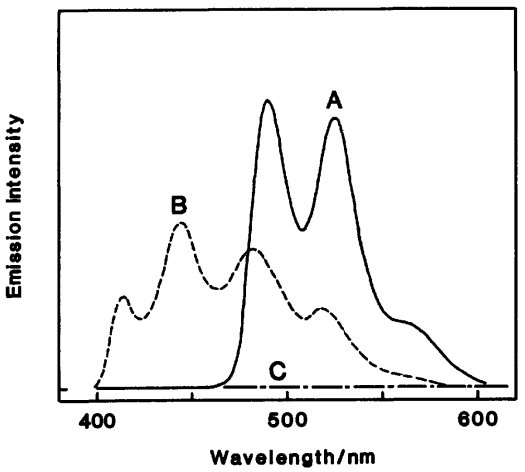

Fig. 2. Sensitization of the phosphorescence of **Ia** by benzophenone in acetonitrile at 77 K. (A): Sensitized phosphorescence of **Ia**, excitation wavelength=380 nm; [**Ia**]=2×10^{-4} M, [benzophenone]=2×10^{-3} M; (B) and (C): Phosphorescence of benzophenone (B) and **Ia** (C) under the same conditions.

affording the caged singlet radical pairs which undergo efficient cage reactions to give the rearranged products **II** and **III**, in competition with escape from the solvent cage (Scheme 2).

Since the rate of escape of the triplet radical pairs from the cage should be faster than the rate of the triplet→singlet intersystem crossing in the radical pairs,[13,14] no rearrangement products are formed by the triplet sensitized photolysis of **I**. Thus the sensitized reaction leads to the exclusive formation of "out-of-cage" reaction products as shown in Scheme 2, being consistent with the conviction that triplet radical pairs, in general, undergo very inefficient cage reactions.[15]

Experimental

All melting points were uncorrected. IR spectra were recorded on a Hitachi EPI-G3 infrared spectrometer. ^{1}H NMR spectra were obtained on a JEOL model PS-100 100 MHz spectrometer with TMS as an internal standard. UV and emission spectral data were collected with a Shimadzu UV-210A spectrophotometer and a Shimadzu RF-500 spectrophotofluorimeter, respectively. Phosphorescence spectra were taken with a cylindrical rotating sector at 77 K. GLC analysis was carried out on a Hitachi 063 gas chromatograph using 2-m column packed with 10% Silicone SE-30 on Uniport B (60/80 mesh, Gasukuro Kogyo Inc.). HPLC separation of the photoproducts was performed on a Hitachi 638-50 high performance liquid chromatography apparatus with a 2.6×500-mm ODS (Hitachi gel #3050) column.

TABLE 6. QUENCHING OF THE PHOTOLYSIS OF **Ia—d** BY 1,3-CYCLOHEXADIENE (CHD) IN ACETONITRILE

Compound	Irradiation time/min	Quencher	Conversion/%	HPLC yield[a] of product/% II	III	IV	V
Ia	60	none	13.9	4.2	1.2	0.5	3.9
	60	CHD	11.5	3.5	1.1	—[b]	2.0
	120	none	22.4	6.4	1.8	1.1	6.4
	120	CHD	26.2	6.2	1.8	—[b]	3.9
Ib	120	none	16.3	0.9	0.9	3.2	8.5
	120	CHD	17.9	1.2	1.2	2.9	6.8
	240	none	24.0	2.6	1.2	4.3	13.5
	240	CHD	26.8	2.9	1.4	5.6	13.1
Ic	60	none	11.3	0.3	0.5	1.2	8.2
	60	CHD	11.5	0.3	0.8	—[b]	6.5
	120	none	23.6	2.3	0.6	2.4	17.5
	120	CHD	18.7	2.6	1.2	—[b]	14.3
Id	60	none	10.2	2.1	1.5	1.2	5.3
	60	CHD	9.7	2.4	1.5	1.8	3.0
	120	none	19.1	4.0	2.3	2.4	6.7
	120	CHD	21.0	3.4	2.0	3.0	4.1

a) Based on starting hydroxylamines. b) Could not be determined because of overlapping with the HPLC peak of the quencher. No attempt to determine the yield of **VI** was made.

TABLE 7. SENSITIZATION OF THE PHOTOLYSIS OF **Ia—d** BY BENZOPHENONE (BP) IN ACETONITRILE

Compound	Irradiation time/min	Sensitizer	Conversion/%	HPLC yield[a] of product/% II	III	IV	V	VI
Ia	15	none	10.3	1.0	1.0	1.3	7.3	—[b]
	15	BP	96.1	<1[c]	<1[c]	3.3	33.5	10[d]
Ib	15	none	9.6	0.8	0.5	2.1	6.7	—[e]
	15	BP	65.3	0.2	<0.5[c]	2.1	44.8	—[e]
Ic	15	none	22.3	1.1	0.6	1.0	12.3	—[b]
	15	BP	83.1	<1.1[c]	<0.6[c]	1.9	55.1	1
Id	15	none	4.0	1.5	0.9	0.6	1.9	—[e]
	15	BP	43.0	0.2	<0.9[c]	14.4	10.0	—[e]

a) Based on starting hydroxylamines. b) Could not be detected. c) Could not be determined accurately because of either too small HPLC peak or of overlapping with unknown small peak(s) arising from the sensitized photolysis. d) GLC yield. e) Not determined.

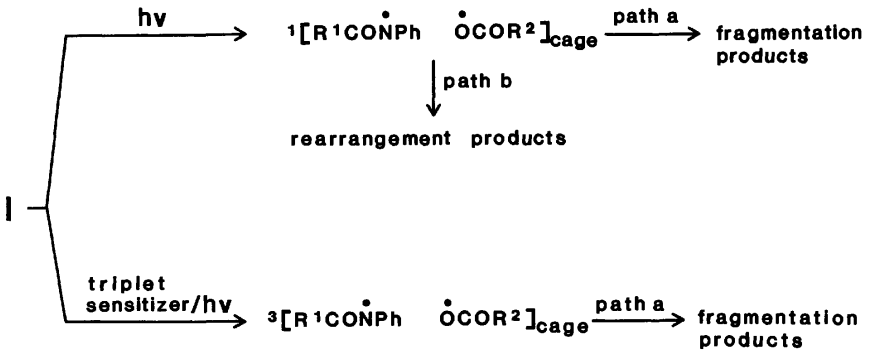

path a, 'out-of-cage' reaction; path b, 'in-cage' reaction

Scheme 2.

Materials. Acetonitrile was purified according to the modified procedure of Walden and Birr.[16] Benzene and 1,2-dichloroethane (spectrograde from Dojin Chemical Inc.) were used without further purification. Acetonitrile and water (HPLC grade from Wako Pure Chemical Industries, Ltd.) were used as received for HPLC analysis. 1,3-Cyclohexadiene (Aldrich Chemical Co.) was fractionally distilled prior to use and stored in a refrigerator. Benzophenone (reagent grade, Wako) was purified by column chromatography over silica gel (70/230 mesh) followed by repeated recrystallization from aqueous ethanol. 1-Naphthoic and *p*-toluic acids (reagent grade, Wako) were recrystallized from benzene and aqueous ethanol, respectively. Naphthalene (reagent grade, Wako) was purified by sublimation at reduced pressure. Toluene (spectrograde, Dojin) was used as received.

Preparation of Starting N,O-*Diacyl*-N-*phenylhydroxylamines* (***Ia—d***). *N*-Phenylhydroxylamine was prepared by the reduction of nitrobenzene with zinc dust in water containing ammonium chloride, then recrystallized from hexane, mp 80.5—81.5 °C (lit,[17] 81 °C). *N*-(*p*-Toluoyl)-*N*-phenylhydroxylamine was obtained from the reaction of *p*-toluoyl chloride with two equiv of *N*-phenylhydroxylamine in ether with stirring in an ice bath. After the usual workup which consisted of washing the reaction mixture with water, drying the ethereal solution over $MgSO_4$, and removing the solvent on a rotary evaporator, recrystallization of the crude product from benzene-hexane gave colorless crystals, mp 121—122 °C; IR (KBr) 3200 and 1610 cm^{-1}. *N*-(1-Naphthoyl)-*N*-phenylhydroxylamine was prepared similarly from the reaction of 1-naphthoyl chloride with two equiv of *N*-phenylhydroxylamine, then recrystallized from benzene-hexane, mp 129—130 °C; IR (KBr) 3220 and 1620 cm^{-1}. The reactions of these *N*-aroyl-*N*-phenylhydroxylamines with the corresponding aroyl chlorides in the presence of pyridine in dichloromethane gave **Ia—d** whose physical properties are the followings.

N-(*1-Naphthoyl*)-O-(p-*toluoyl*)-N-*phenylhydroxylamine* (***Ia***). Mp 134.5—135.5 °C (from benzene-hexane); NMR ($CDCl_3$) δ=2.36 (3H, s), 7.08—7.90 (15H, m), and 8.36 (1H, d, J=8 Hz); IR (KBr) 1750 and 1680 cm^{-1}. Found: C, 79.19; H, 4.94; N, 3.73%. Calcd for $C_{25}H_{19}NO_3$: C, 78.74; H, 4.99; N, 3.67%.

N-(p-*Toluoyl*)-O-(*1-naphthoyl*)-N-*phenylhydroxylamine* (***Ib***). Mp 164—165 °C (from benzene-hexane); NMR ($CDCl_3$) δ=2.30 (3H, s), 7.00—8.22 (15H, m), and 8.74 (1H, d, J=8 Hz); IR (KBr) 1775 and 1690 cm^{-1}. Found: C, 79.11; H, 4.99; N, 3.71%. Calcd for $C_{25}H_{19}NO_3$: C, 78.74; H, 4.99; N, 3.67%.

N,O-*Di*(*1-naphthoyl*)-N-*phenylhydroxylamine* (***Ic***). Mp 116—117 °C (from benzene-hexane); NMR ($CDCl_3$) δ=7.12—8.02 (17H, m), 8.40 (1H, d, J=8 Hz), and 8.70 (1H, d, J=8 Hz); IR (KBr) 1740 and 1670 cm^{-1}. Found: C, 80.99; H, 4.59; N, 3.37%. Calcd for $C_{28}H_{19}NO_3$: C, 80.58; H, 4.56; N, 3.36%.

N,O-*Di*(p-*toluoyl*)-N-*phenylhydroxylamine* (***Id***). Mp 122—123 °C (from benzene-hexane); NMR ($CDCl_3$) δ=2.26 (3H, s), 2.36 (3H, s), 6.96 (2H, d, J=8 Hz), 7.14—7.48 (9H, m), and 7.90 (2H, d, J=8 Hz); IR (KBr) 1760 and 1660 cm^{-1}. Found: C, 76.82; H, 5.52; N, 4.03%. Calcd for $C_{22}H_{19}NO_3$: C, 76.52; H, 5.51; N, 4.06%.

Photolyses of ***Ia—d***. A nitrogen purged solution of **I** (0.0066 M) in acetonitrile, benzene, or 1,2-dichloroethane (10 mL), which was placed in a sealed Pyrex tube, was irradiated for a given period of time with a 400 W high pressure mercury lamp set in a Pyrex cooling jacket. Parallel irradiations of the solutions were done on a merry-go-round apparatus (Riko model RH400-10W) immersed into a water bath (23±1 °C). The photolyzate thus obtained were subjected to the HPLC analysis. The yields of the products were determined by employing the linear calibration curves made for each product under the same analytical conditions. For the purpose of isolating the photoproducts a solution of **Ia** (0.0087 M) in acetonitrile (300 mL), placed in a Pyrex vessel, was irradiated for 70 min under purified and dried nitrogen with a Pyrex-filtered 400 W high pressure mercury lamp. After evaporation of the solvent, the resulting residue was chromatographed on silica gel (230 mesh, Merck) eluting with benzene and then with chloroform. This separation procedure allowed isolation and identification of **IIa**, **IIIa**, and **IVa**, whose structures were determined by comparing their physical properties with those of authentic samples prepared independently. In another experiment the photolyzate concentrated *in vacuo* was extracted with a 5% sodium hydrogencarbonate solution (50 mL). The extract was washed with dichloromethane twice and then acidified to pH 2 with 4M HCl giving *p*-toluic acid as a white solid. The carbon dioxide formed by this photolysis was introduced into a 0.1 M $Ba(OH)_2$ (150 mL) after having been passed through a cold trap by a nitrogen stream. The precipitate $BaCO_3$ was removed by quick filtration and the filtrate was titrated with 0.1 M HCl. The failure to avoid contamination with carbon dioxide in the air during this procedure resulted in overestimation of the yield of photochemically generated carbon dioxide. In order to detect toluene as a product a nitrogen purged acetonitrile solution of **Ia** (0.052 M) in a sealed Pyrex

tube was irradiated for 4 h. The photolyzate was submitted for the GLC analysis that led to identification of toluene whose yield was estimated by a linear calibration curve.

Thermolyses of ***Ia—d.*** A nitrogen purged dimethyl sulfoxide solution of **I** (2 mmol) in a sealed ampule was heated at 120—130 °C in an oil bath for a given period of time. The reaction mixture was poured onto water (100 mL) and extracted three times with chloroform. The combined chloroform extracts were washed twice with water and then dried over Na_2SO_4. Removal of the solvent on a rotary evaporator gave the solid residue from which **II** was isolated along with the starting **I** by column chromatography over silica gel (70/230 mesh, Merck) with benzene–chloroform (1:1 v/v) as eluent.

Preparation of Authentic Samples (II, III, and IV). *N*-(*p*-Toluoyl)-*o*-aminophenol and *N*-(1-naphthoyl)-*o*-aminophenol were prepared by *N*-aroylation of two equiv of *o*-aminophenol with *p*-toluoyl and 1-naphthoyl chlorides in dichloromethane, respectively. Recrystallization of the crude products from aqueous ethanol gave colorless crystals, mp (the former anilide) 157.5—158.5 °C; IR (KBr) 3410, 3080 (broad), and 1640 cm^{-1}. Mp (the latter anilide) 194.5—195.5 °C; IR (KBr) 3400, 3100 (broad), and 1640 cm^{-1}. *N,O*-Diacyl-*o*-aminophenols (**IIa—d**) were derived from the reactions between *N*-acyl-*o*-aminophenols and the corresponding acyl chlorides in the presence of triethylamine in dichloromethane or ether. Physical properties are the followings. *N*-(1-Naphthoyl)-*O*-(*p*-toluoyl)-*o*-aminophenol (**IIa**), mp 168—170 °C (from benzene–hexane); IR (KBr) 3180, 1730, and 1650 cm^{-1}. Found: C, 79.02; H, 4.96; N, 3.65%. Calcd for $C_{25}H_{19}NO_3$: C, 78.74; H, 4.99; N, 3.67%. *N*-(*p*-Toluoyl)-*O*-(1-naphthoyl)-*o*-aminophenol (**IIb**), mp 137—138 °C (from benzene–hexane); IR (KBr) 3430, 1735, and 1675 cm^{-1}. Found: C, 78.87; H, 4.92; N, 3.67%. Calcd for $C_{25}H_{19}NO_3$: C, 78.74; H, 4.99; N, 3.67%. *N,O*-Di(1-naphthoyl)-*o*-aminophenol (**IIc**), mp 177.5—178.5 °C (from benzene–hexane); IR (KBr) 3200, 1730, and 1640 cm^{-1}. Found: C, 80.95; H, 4.54; N, 3.36%. Calcd for $C_{28}H_{19}NO_3$: C, 80.58; H, 4.56; N, 3.36%. *N,O*-Di(*p*-toluoyl)-*o*-aminophenol (**IId**), mp 108.5—109.5 °C (from benzene–hexane); IR (KBr) 3270, 1735, and 1640 cm^{-1}. Found: C, 76.58; H, 5.53; N, 4.07%. Calcd for $C_{22}H_{19}NO_3$: C, 76.52; H, 5.51; N, 4.06%.

N-(*p*-Toluoyl)-*p*-aminophenol and *N*-(1-naphthoyl)-*p*-aminophenol were prepared by the reactions of two equiv of *p*-aminophenol with *p*-toluoyl and 1-naphthoyl chlorides in dichloromethane, respectively. These reactions were heterogeneous because of the low solubility of *p*-aminophenol so that vigorous stirring was required during the course of these acylations. The crude products were recrystallized from aqueous ethanol affording colorless crystals, mp (the former anilide) 212.5—214 °C; IR (KBr) 3380, 3320, and 1650 cm^{-1}. Mp (the latter anilide) 198.5—199 °C; IR (KBr) 3240, 3190, and 1605 cm^{-1}. *N,O*-Diacyl-*p*-aminophenols (**IIIa—d**) were prepared by treatment of *N*-acyl-*p*-aminophenols with the corresponding acyl chlorides in the presence of triethylamine in dichloromethane. These reactions were also heterogeneous. Physical properties are the followings. *N*-(1-Naphthoyl)-*O*-(*p*-toluoyl)-*p*-aminophenol (**IIIa**), mp 214—215 °C (from ethyl acetate); IR (KBr) 3270, 1730, and 1645 cm^{-1}. Found: C, 79.04; H, 5.03; N, 3.69%. Calcd for $C_{25}H_{19}NO_3$: C, 78.74; H, 4.99; N, 3.67%. *N*-(*p*-Toluoyl)-*O*-(1-naphthoyl)-*p*-aminophenol (**IIIb**), mp 235.5—236.5 °C (from ethyl acetate); IR (KBr) 3300, 1730, and 1650 cm^{-1}. Found: C, 78.95; H, 4.98; N, 3.67%. Calcd for $C_{25}H_{19}NO_3$: C, 78.74; H, 4.99; N, 3.67%. *N,O*-Di(1-naphthoyl)-*p*-aminophenol (**IIIc**), mp 190—191 °C (from ethyl acetate); IR (KBr) 3260, 1720, and 1645 cm^{-1}. Found: C, 80.85; H, 4.56; N, 3.38%. Calcd for $C_{28}H_{19}NO_3$: C, 80.58; H, 4.56; N, 3.36%. *N,O*-Di(*p*-toluoyl)-*p*-aminophenol (**IIId**), mp 245.5—246.5 °C (from ethyl acetate); IR (KBr) 3320, 1725, and 1645 cm^{-1}. Found: C, 76.71; H, 5.46; N, 4.10%. Calcd for $C_{22}H_{19}NO_3$: C, 76.52; H, 5.51; N, 4.06%.

1-Naphthanilide (**IVa, c**) and *p*-toluanilide (**IVb, d**) which were prepared by the reactions of 1-naphthoyl and *p*-toluoyl chlorides with two equiv of aniline in dichloromethane under usual conditions, respectively, had the following physical properties: **IVa, c**, mp 162—163 °C (from benzene); IR (KBr) 3270 and 1650 cm^{-1}. Found: C, 82.95; H, 5.26; N, 5.88%. Calcd for $C_{17}H_{13}NO$: C, 82.59; H, 5.26; N, 5.67%. **IVb, d**, mp 145—146 °C (from benzene); IR (KBr) 3330 and 1645 cm^{-1}. Found: C, 79.77; H, 6.19; N, 6.71%. Calcd for $C_{14}H_{13}NO$: C, 79.62; H, 6.16; N, 6.64%.

Triplet Quenching and Sensitization. Ten milliliters of an acetonitrile solution of **I** (0.0066 M) and either quencher (0.1 M) or sensitizer (0.05 M) was placed in a Pyrex tube, degassed by bubbling purified nitrogen through it for 10 min, and sealed. Deaerated solutions with and without these additives were irradiated in parallel for the same period of time on a merry-go-round apparatus with either 313- or 366-nm light through a Pyrex-cylindrical solution filter (1-cm in length, 6-cm in diameter, and 22-cm in height) from a 400 W high pressure mercury lamp. All the irradiations were carried out in a water bath whose temperature was kept constant during the photolysis by circulating water through it. The 313-nm light for quenching experiment was isolated with a potassium chromate (0.002 M) in a 1% aqueous solution of potassium carbonate. A solution of copper sulfate pentahydrate (250 g dm^{-3}) was used as the filter for sensitization experiment. The band passed had a 90% transmittance (T) at 366 nm and a 9% T at 313 nm. Molar absorption coefficients of **Ia**, **Ib**, **Ic**, and **Id** were estimated to be 1940, 6740, 9180, and 290 ($M^{-1}cm^{-1}$) at 313 nm, respectively, and 2.6, 2.8, 3.3, and 0.5 ($M^{-1}cm^{-1}$) at 366 nm, respectively, in acetonitrile at room temperature.

References

1) For a preliminary report on this work see: T. Sakurai, S. Yamada, and H. Inoue, *Chem. Lett.*, **1983**, 975.

2) E. Ochiai, "Aromatic Amine Oxides," Elsevier, Amsterdam (1967).

3) A. R. Katritzky and J. M. Lagowski, "Chemistry of the Heterocyclic *N*-Oxides," Academic Press, London (1971), Chap. 4; R. A. Abramovitch and J. G. Saha, "Advances in Heterocyclic Chemistry," ed by A. R. Katritzky and A. J. Boulton, Academic press, New York, N. Y. (1966), Vol. 6, p. 229; V. J. Traynelis, "Rearrangement of *O*-Acylated Heterocyclic *N*-Oxides," in "Mechanisms of Molecular Migrations," ed by B. S. Thyagarajan, Interscience, New York, N. Y. (1969), Vol. 2, p. 1.

4) S. Oae and K. Ogino, *Heterocycles*, **6**, 583 (1977).

5) a) D. B. Denny and D. Z. Denny, *J. Am. Chem. Soc.*, **82**, 1389 (1960); b) J. R. Cox, Jr. and M. F. Dunn, Abstracts of papers, 152nd National Meeting of the American Chemical Society, New York, N. Y., 1966, Abstr., No 162; c) G. T. Tisue,

M. Grassman, and W. Lwowski, *Tetrahedron*, **24**, 999 (1968); d) K. Ogino and S. Oae, *ibid.*, **27**, 6037 (1971); e) D. Gutschke and A. Heesing, *Chem. Ber.*, **106**, 2379 (1973); f) S. Oae and T. Sakurai, *Tetrahedron*, **32**, 2289 (1976); g) T. Ohta, K. Shudo, and T. Okamoto, *Tetrahedron Lett.*, **1978**, 1983; h) D. Gutschke, A. Heesing, and U. Heuschkel, *ibid.*, **1979**, 1363; i) U. Gessner, A. Heesing, L. Keller, and W. K. Homann, *Chem. Ber.*, **115**, 2865 (1982).

6) V. Boekelheide and D. L. Harrington, *Chem. Ind. (London)*, **1955**, 1423; V. J. Traynelis and A. I. Gallagher, *J. Am. Chem. Soc.*, **87**, 5710 (1965); S. Oae, Y. Kitaoka, and T. Kitao, *Tetrahedron*, **20**, 2685 (1964); S. Kozuka, S. Tamagaki, T. Negoro, and S. Oae, *Tetrahedron Lett.*, **1968**, 923; H. Iwamura, M. Iwamura, T. Nishida, and S. Sato, *J. Am. Chem. Soc.*, **92**, 7476 (1970); T. Cohen and G. L. Deets, *ibid.*, **89**, 3939 (1967); R. Bodalski and A. R. Katritzky, *Tetrahedron Lett.*, **1968**, 257; V. J. Traynelis, K. Yamauchi, and J. P. Kimball, *J. Am. Chem. Soc.*, **96**, 7476 (1974).

7) S. Oae, N. Asai, and K. Fujimori, *Bull. Chem. Soc. Jpn.*, **52**, 2409 (1979).

8) C. Walling and A. N. Naglieri, *J. Am. Chem. Soc.*, **82**, 1820 (1960).

9) H. Furrer, *Tetrahedron Lett.*, **1974**, 2953; A. R. Katritzky, A. V. Chapman, M. J. Cook, and G. H. Millet, *J. Chem. Soc., Perkin Trans. 1*, **1980**, 2743.

10) H. Shizuka and I. Tanaka, *Bull. Chem. Soc. Jpn.*, **41**, 2343 (1968); H. Shizuka, *ibid.*, **42**, 52, 57 (1969); D. Bellus, *Adv. Photochem.*, **8**, 109 (1971); K. Schwetlick, J. Stumpe, and R. Noack, *Tetrahedron*, **35**, 63 (1979) and references cited therein.

11) E. Hedaya, R. L. Hinman, V. Schomaker, S. Theodoropulos, and L. M. Kyle, *J. Am. Chem. Soc.*, **89**, 4875 (1967); D. Touchard and J. Lessard, *Tetrahedron Lett.*, **1973**, 3827; T. C. Joseph, J. N. S. Tam, M. Kitadani, and Y. L. Chow, *Can. J. Chem.*, **54**, 3517 (1976); R. Sutcliffe, M. Anpo, A. Stolow, and K. U. Ingold, *J. Am. Chem. Soc.*, **104**, 6064 (1982); P. S. Skell, R. L. Tlumak, and S. Seshadri, *ibid.*, **105**, 5125 (1983).

12) The formation of carboxylic acid **V** is seen to be slightly suppressed in the presence of 1,3-cyclohexadiene. This difference in the yields of **V** with and without the diene becomes larger at higher conversion of **I**, whereas the extent of disappearance of **I** is not influenced by the diene at any stage of the reaction. The observation that no reaction of **V** with the diene takes place in the ground state implies that the generated aroyloxyl radical is scavenged by the diene in competition with hydrogen abstraction and decarboxylation processes. Because of the presence of this triplet quencher in large excess, the reaction with the aroyloxyl radical resulted in negligible decrease in the quencher concentration.

13) T. Koenig and H. Fischer, "Free Radicals," ed by J. K. Kochi, Wiley-Interscience, New York, N. Y. (1973), Vol. 1, p. 179.

14) N. J. Turro and G. L. Weed, *J. Am. Chem. Soc.*, **105**, 1861 (1983).

15) J. R. Fox and G. S. Hammond, *J. Am. Chem. Soc.*, **86**, 4031 (1964); P. D. Bartlett and N. A. Porter, *ibid.*, **90**, 5317 (1968).

16) J. A. Riddick and W. B. Bunger, "Organic Solvents," in "Techniques of Chemistry," 3rd ed. ed by A. Weissberger, Wiley-Interscience, New York, N. Y. (1970), Vol. 2, p. 798.

17) O. Kamm, *Org. Synth.*, Coll. Vol. I, 445 (1941); S. R. Sandler and W. Karo, "Organic Functional Group Preparations," Academic Press, New York, N. Y. (1972), Vol. 3, p. 356.

Preparation and Enzymatic Hydrolysis of Polymers Anchoring Biphenyl-2-ol

Tomomichi ISHIKAWA* and Youji TANAKA
Department of Chemistry, Faculty of Technology Tokyo Metropolitan University, Fukasawa, Setagaya-ku, Tokyo 158
(Received October 24, 1984)

Polymers anchoring fungicidal biphenyl-2-ol(BPOL) were prepared by the polymerization and copolymerization of 2-biphenylyl methacrylate(BPMA) with various comonomers such as styrene, vinyl acetate, 2-hydroxyethyl methacrylate, *N*-methacryloylglycine, and *N*-methacryloyl-DL-alanine. The reactivity ratios of BPMA with the comonomers were evaluated. The α-chymotrypsin-catalyzed hydrolysis of the polymers was also studied. The release of BPOL from the polymers was represented by means of the Michaelis constant K_m and the catalytic-rate constant k_{cat}. The BPMA homopolymer gave higher K_m and k_{cat} values than the copolymers, and the copolymers with a higher content of substrate units underwent cleavage more readily. It was found that the hydrolysis of the polymeric substrates is affected by the structure and character of the comonomer rather than the arrangement order of the repeating monomer units in the polymer sequence.

Recently, the usefulness of biodegradable poly(α-amino acid)s in drug delivery systems has been reported. The rate of *in vivo* enzymatic degradation of the polymers can be controlled, and the drugs stored in matrix rods and capsules[1,2] or covalently bonded to polymer matrixes[3] are released with nearly zero-order kinetics. Nakajima and co-workers[4] studied the hydrolysis of poly(*N*-hydroxyalkyl-L-glutamine) by papain to simulate the *in vivo* degradation. On the other hand, Kopecek and co-workers[5–8] reported the cleavage of free 4-nitroaniline from amino acid 4-nitroanilide terminal groups in the origopeptidic side chains of the copolymers by α-chymotrypsin. In a previous paper[9] we reported on the hydrolytic process of homopolymer and copolymers of 2-biphenylyl acrylate under physiological conditions. If the polymers are attacked by a microorganism such as fungus, the ester gruops linking fungicidal biphenyl-2-ol (BPOL) will also be hydrolyzed enzymatically. In this work we describe the polymerization and copolymerization of 2-biphenylyl methacrylate (BPMA) and a study of the hydrolytic release of BPOL from the polymers by α-chymotrypsin. It is known that α-chymotrypsin effectively cleaves ester linkages as well as peptide linkages, but no data are available about the hydrolysis of a polymeric substrate such as poly(2-biphenylyl methacrylate) anchoring bulky and hydrophobic biphenyl groups.

Experimental

Materials. 2-Hydroxyethyl methacrylate (HEMA), styrene (St), vinyl acetate (VAc), and BPOL were distilled under reduced pressure prior to use. α-Chymotrypsin (51 ATEE units, Tokyo Chem. Ind. Co.) was used without further recrystallization. Solvents were dried by the usual methods and distilled. Other chemicals were of reagent grade.

Monomer Preparation. BPMA was prepared by the reaction of BPOL with methacryloyl chloride in the presence of triethylamine in benzene by a method similar to that described in a previous paper.[9] Purification was achieved by distillation under reduced pressure in the presence of 4-*t*-butylcatechol to yield BPMA (71.1%): bp 123 °C (133Pa); ^{1}H-NMR ($CDCl_3$) δ=1.85 (3H, s, CH_3), 5.51 (1H, d, CH=); 6.06 (1H, d, CH=) and 6.93—7.53 (9H, m, Aromatic).

N-Methacryloylglycine (MAG) was obtained by the reaction of glycine with methacryloyl chloride in an aqueous sodium hydroxide solution according to Ref.[5] Yield 60.8%: mp 101—102 °C (lit, 101—102 °C); ^{1}H-NMR(DMSO-d_6) δ= 1.85 (3H, s, CH_3), 3.78 (2H, d, CH_2), 5.35 (1H, d, CH=), 5.70 (1H, d, CH=), 7.70—8.30 (1H, t, NH) and 10.80—12.40 (1H, s, OH); IR (KBr) 3330 (NH), 1715 (C=O), 1640 (C=O) and 1570 (C=C).

N-Methacryloyl-DL-alanine (MAA) was obtained from DL-alanine with methacryloyl chloride according to Ref.[5] Yield 84.5%; mp 116—117.5 °C (lit, 117—118 °C); IR (KBr) 3290 (NH), 1695, 1640 (C=O) and 1600 (C=C); ^{1}H-NMR (DMSO-d_6) δ=1.32 (3H, d, CH_3), 1.85 (3H, s, CH_3), 4.17 (1H, m, CH), 5.33 (1H, d, CH=), 5.70 (1H, d, CH=), 7.70—8.20 (1H, d, NH) and 9.00—10.00 (1H, broad, OH).

General Procedure for Polymerization. All the polymerization experiments were carried out using a solution polymerization technique at 60 °C in the presence of 1 mol% AIBN. The polymers obtained were purified by repeated precipitation from a solvent system into a non-solvent system. The purified polymers were dried at 40 °C (under vaccum) to constant weight. Analyses of the copolymers obtained were carried out using ^{1}H-NMR and an elemental analysis.

General Procedure for Hydrolysis with α-Chymotrypsin. All the hydrolysis experiments were carried out in 50 cm^3 of a buffer solution (0.08 mol dm^{-3} 2-amino-2-hydroxymethyl-1,3-propanediol (Tris) and 0.1 mol dm^{-3} $CaCl_2$ adjusted with HCl to pH=8.0) in the presence of α-chymotrypsin. The temperature was maintained at 25 °C with a regulated water bath. The progress of the hydrolysis was followed by recording any increase in the absorbance at 240.0 nm. The activity of α-chymotrypsin was checked by the hydrolysis of a model compound, 2-biphenylyl propionate[9] at the beginning and the end of the experiments. They gave the same value.

Results and Discussion

Copolymerization. The solution copolymerization of VAc with BPMA was carried out in toluene. St, HEMA, MAG, and MAA were copolymerized with BPMA in ethanol. The contents of each component in the monomer and the compositions of the copolymers obtained by ^{1}H-NMR or elemental analysis are summarized in Tables 1—5. The monomer reactivity ratios

Table 1. Copolymerization of VAc with BPMA in toluene at 60 °C in the presence of AIBN

Molar fraction BPMA in monomers	Molar fraction[a] BPMA in copolymer	Time min	Yield %
0.100	0.656	60	4.8
0.300	0.863	28	2.5
0.500	0.934	27	10.0
0.700	0.970	25	11.6
0.900	0.992	25	9.1

a) Determined by ^{1}H-NMR.

Table 2. Copolymerization of St with BPMA in ethanol at 60 °C in the presence of AIBN

Molar fraction BPMA in monomers	Molar fraction[a] BPMA in copolymer	Time min	Yield %
0.100	0.271	190	6.0
0.300	0.455	75	5.0
0.500	0.589	73	6.6
0.700	0.743	70	8.0
0.900	0.908	70	6.3

a) Determined by elemental analysis.

Table 3. Copolymerization of HEMA with BPMA in ethanol at 60 °C in the presence of AIBN

Molar fraction BPMA in monomers	Molar fraction[a] BPMA in copolymer	Time min	Yield %
0.300	0.398	23	4.5
0.500	0.642	17	14.9
0.700	0.842	14	9.0
0.900	0.960	15	2.9

a) Determined by ^{1}H-NMR.

Table 4. Copolymerization of MAG with BPMA in ethanol at 60 °C in the presence of AIBN

Molar fraction BPMA in monomers	Molar fraction[a] BPMA in copolymer	Time min	Yield %
0.300	0.465	52	1.7
0.500	0.683	54	2.6
0.700	0.851	25	2.9
0.900	0.963	56	4.8

a) Determined by ^{1}H-NMR.

Table 5. Copolymerization of MAA with BPMA in ethanol at 60 °C in the presence of AIBN

Molar fraction BPMA in monomers	Molar fraction[a] BPMA in copolymer	Time min	Yield %
0.100	0.214	45	3.2
0.300	0.531	45	5.7
0.500	0.718	21	2.4
0.700	0.869	20	2.8
0.900	0.962	40	3.2

a) Determined by ^{1}H-NMR.

of these compounds were estimated (using the Fineman-Ross equation) from these data. The results are given in Table 6.

From Table 6 it appears that the polymer derived from BPMA with St shows a tendency towards alternation since r_1r_2 is relatively small (0.22). On the other hand, from the very high r_2 and low r_1 values, BPMA shows a homopropagation tendency in the copolymerization with VAc. In the copolymerization of HEMA, MAG, and MAA with BPMA, the r_1r_2 values were larger than unity. In any case, BPMA shows a random-propagation tendency. The copolymers of St with BPMA are perhaps the most interesting of the series. When the copolymers are used as coating films, the above results suggest that the fungicidal BPOL residues are distributed equally on the films.

Table 6. Reactivity ratios of BPMA

Monomer M_1	Monomer M_2	r_1	r_2	r_1r_2
VAc	BPMA	0.04	14	0.56
St	BPMA	0.22	1.0	0.22
HEMA	BPMA	1.0	2.8	2.8
MAG	BPMA	0.72	2.9	2.1
MAA	BPMA	0.42	2.7	1.1

Table 7. Polymeric substrates anchoring BPOL

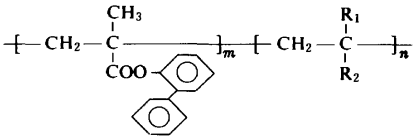

Substrate	R_1	R_2
1	CH_3	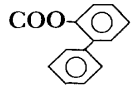
2a, 2b	H	$OCOCH_3$
3a, 3b	H	C_6H_5
4a, 4b	CH_3	$COOCH_2CH_2OH$
5a, 5b	CH_3	$CONHCH_2COOH$
6a, 6b	CH_3	$CONHCHCOOH$ $\vert$ CH_3

Hydrolysis with α-Chymotrypsin. Polymeric substrates **1—6** anchoring BPOL were obtained by homopolymerization and copolymerization of BPMA. We have chosen hydrophobic and hydrophilic comonomers. The two classes of copolymers containing about 30 and 50 mol% BPOL residues were prepared for each comonomer. All the polymers were water insoluble. Kopecek and co-workers[5] reported on the water-soluble copolymers of various 4-nitroanilides of *N*-methacryloylorigopeptides with *N*-(2-hydroxypropyl)methacrylamide. In this paper, however, even the BPMA-HEMA copolymer contained 72 mol% of HEMA units was water insoluble. The polymeric substrates prepared are shown in Table 7. It is expected from the structure of the polymers **1—6** that the complete hydrolysis of the homopolymer and copolymers other than the St-BPMA copolymer gives a water-soluble polymer which can more readily be remove from biological systems.

The polymeric substrates were hydrolyzed with α-chymotrypsin in Tris-buffer solution (pH 8). The amount of BPOL released was determined periodically using UV. When the homopolymeric substrates were

Table 8. Hydrolysis of BPMA homopolymer and opolymers with α-chymotrypsin

Substrate[a]	Comonomer	Mol% of BPOL residue[b]	Yield %	$[\eta]$[c] $dm^3 g^{-1}$	$K_m 10^3$ mol l^{-1}	k_{cat} h^{-1}	k_{cat}/K_m l $mol^{-1} h^{-1}$
1	—	100.0	61.9	1.38	1.9	7.4	3830
2a	VAc	27.7	73.5	0.10	1.8	1.4	753
2b	VAc	54.4	30.0	0.13	1.9	2.2	1140
3a	St	23.5	76.6	0.24	0.38	0.64	1670
3b	St	46.0	88.3	0.52	0.47	1.0	2130
4a	HEMA	27.8	79.2	0.25	9.1	7.4	810
4b	HEMA	45.3	79.2	0.48	3.1	7.4	2350
5a	MAG	29.7	34.3	1.14	1.8	3.2	1740
5b	MAG	59.0	56.8	4.22	1.9	4.2	2250
6a	MAA	39.6	24.3	1.27	1.8	1.3	700
6b	MAA	63.8	58.4	2.60	1.9	2.3	1200

a) Prepared by using a solution polymerization technique at 60 °C in the presence of AIBN. b) Determined by ^{1}H-NMR and elemental analysis. c) Measured in $CHCl_3$ for substrates **1**—**4b** and in DMF for substrates **5a**—**6b** at 25 °C.

hydrolyzed for 3 and 24 h in the presence of 0.4 mol% α-chymotrypsin, the conversion was 0.9 and 7 mol%, respectively. In the case of a model compound such as 2-biphenylyl propionate, the conversion reached 13 mol% after 3 h of reaction under the same conditions. The release rate of BPOL from the copolymers was slower than that for the homopolymer. The enzymatic catalyzed hydrolysis was evaluated from Michaelis constant K_m and the catalytic rate constant k_{cat} determined by a method developed by Lineweaver and Burke.[10] The enzymatic hydrolysis data for the polymeric substrates were summarized in Table 8.

It can be seen from Table 8 that the k_{cat} for the polymer **1** indicates the highest value of the series, and that the copolymers with higher contents of the substrate units undergo cleavage more readily. The K_m values for the copolymers **3a** and **3b** are smaller than those for any other of the polymers. As described above, the values of the reactivity ratios of both BPMA and St indicate that the monomers in these pairs tend to alternate during its copolymerization. Therefore, these results suggest that the hydrophobic phenyl group adjacent to the BPOL ester group is contributed to the formation of chymotrypsin-substrate complex. However, the lower k_{cat} values for the copolymers **3a** and **3b** indicate that the reaction of the complex is slow, and that the BPOL is released very slowly from the St-BPMA copolymers. This is in agreement with the results of a study of the hydrolytic release rate of drugs made from copolymers containing 5-fluorouracil.[11] It can also be seen that both the K_m and k_{cat} for the St-BPMA copolymers decrease with an increase in the content of St units. This must be due to a dilution effect of the substrates with the St units, because of cross-propagation tendency in its copolymerization.

In the copolymers of VAc, HEMA, MAG, and MAA with BPMA, α-chymotrypsin cleaves the ester linkages in VAc or HEMA units and the amide linkages in MAG or MAA units as well as the ester linkages in BPMA units. In these cases, the comonomer units may act as inhibitors in the enzymatic hydrolysis of the substrate. The hydrolysis is affected by the intensity of affinity of α-chymotrypsin towards the inhibitor. For the copolymers **4a** and **4b** derived from HEMA and BPMA, the K_m value increases with an content increased of the HEMA units, while the k_{cat} values for the copolymers are similar to the value for the BPMA homopolymer. These results indicate that the hydroxyethyl ester groups and the substrate groups compete for the enzyme. Therefore, the hydroxyethyl ester groups become a competitive inhibitor in this reaction. On the other hand, the K_m values for the copolymers of VAc, MAG, and MAA with BPMA are similar to that for the BPMA homopolymer. However, the values of k_{cat} for the copolymers of same BPMA content are in the order, BPMA homopolymer>MAG-copolymer>VAc-copolymer>MAA-copolymer. The hydrolysis of these copolymers gives glycine, alanine and acetic acid, respectively. It is well known that chymotrypsin-catalyzed reaction rate decreases with an addition of various carboxylic acids, and that carboxylic acids with higher hydrophobic groups undergo a greater decrease.[12,13] Brot and co-workers[14] reported that a more suitable substrate exhibits a higher k_{cat}/K_m value. According to this conclusion, the BPMA homopolymer is the most suitable substrate of the series, and the copolymers with VAc are unsuitable substrates for chymotrypsin-catalyzed hydrolysis. As described above, BPMA shows a homopropagation tendency during copolymerization with VAc. Nevertheless, the values of k_{cat}/K_m for the copolymers **2a** and **2b** are smaller to those for the polymer **1**. These facts can be explained in terms of the product inhibition which is caused by the by-product in the hydrolysis of the copolymeric substrate.

From the above results, it is concluded that the chymotrypsin-catalyzed hydrolysis of polymeric substrates is affected by the structure and character of the comonomer rather than the arrangement order of the monomer unit in a polymer sequence.

References

1) K. R. Sidman, A. D. Schwope, W. D. Steber, S. E.

Rudolph, and S. B. Poulin, *J. Membrane Sci.*, **7**, 277 (1980).
2) M. Asano, M. Yoshida, I. Kaetsu, K. Nakai, H. Yamanaka, H. Yuasa, K. Shida, K. Suzuki, and M. Oya, *Makromol. Chem.*, **184**, 1761 (1983).
3) J. Feijen, D. Gregonis, C. Anderson, R. V. Petersen, and J. Anderson, *J. Pharm. Sci.*, **69**, 871 (1980).
4) T. Hayashi, Y. Tabata, and A. Nakajima, *Rep. Pro. Polym. Phys. Jpn.*, **26**, 578 (1983).
5) J. Drobnik, J. Kopecek, J. Labsky, P. Rejmanova, J. Exner, V. Saudek, and J. Kalal, *Makromol. Chem.*, **177**, 2833 (1976).
6) J. Kopecek, P. Rejmanova, and V. Chytry, *Makromol. Chem.*, **182**, 799 (1981).
7) P. Rejmanova, B. Obereigner, and J. Kopecek, *Makromol. Chem.*, **182**, 1899 (1981).
8) J. Pato, M. Azori, K. Ulbrich, and J. Kopecek, *Makromol. Chem.*, **185**, 231 (1984).
9) T. Ishikawa, and S. Asai, *Bull. Chem. Soc. Jpn.*, **56**, 2177 (1983).
10) H. Lineweaver, and D. Burk, *J. Am. Chem. Soc.*, **56**, 658 (1934).
11) P. Umrigar, S. Ohashi, and G. Butler, *J. Polym. Sci., Polym. Chem. Ed.*, **17**, 351 (1979).
12) W. W. Cleland, *Biochim. Biophys. Acta*, **67**, 173 (1963).
13) R. Y. Hsu, W. W. Cleland, and L. Anderson, *Biochem.*, **5**, 799 (1966).
14) F. E. Brot, and M. L. Bender, *J. Am. Chem. Soc.*, **91**, 7187 (1969).

 © 1985 The Chemical Society of Japan Bull. Chem. Soc. Jpn., 58, 1186—1195 (1985) [Vol. 58, No. 4

Multiple Substituent Effects on ^{13}C Chemical Shifts of *N*-Benzylideneanilines. Evidence for Substituent-Substituent Interactions and Their Implications of Conformational Changes with Substituents

Ryoichi AKABA, Hirochika SAKURAGI, and Katsumi TOKUMARU*
Department of Chemistry, University of Tsukuba, Sakura-mura, Ibaraki 305
(Received October 31, 1984)

Carbon-13 chemical shifts are reported for series of *N*-benzylideneanilines; 4-$YC_6H_4CH{=}NC_6H_4NMe_2$-4, 4-$NO_2C_6H_4CH{=}NC_6H_4X$-4, 4-$YC_6H_4CH{=}NC_6H_4NO_2$-4, and 4-$YC_6H_4CH{=}NC_6H_3(CH_3)_2$-2,6. Multiple substituent effects on the azomethine carbon chemical shifts were examined, and nonadditivity observed for 4-$YC_6H_4CH{=}NC_6H_4NMe_2$-4 and 4-$NO_2C_6H_4CH{=}NC_6H_4X$-4 is interpreted in terms of substituent-substituent interactions accompanied by conformational changes with substituents in these *N*-benzylideneanilines. Effects of the substituents Y (on the benzylidene benzene ring) on the azomethine carbon chemical shifts were also studied in detail. The results suggest that there are two competetive electronic factors responsible for chemical shift variation, and that the substituent effects should be treated separately between electron-releasing and electron-withdrawing groups. The latter groups always exert inverse (the chemical shifts undergo upfield shifts with increase in the electron-withdrawing properties of the substituents) substituent effects, whereas the former exhibit normal (the chemical shifts undergo upfield shifts with increase in the electron-releasing properties of the substituents) or inverse substituent effects depending on the degree of electron demand developed on the azomethine carbons.

It is well-known that *N*-benzylideneaniline (NBA) takes a conformation in which the benzene ring on the nitrogen atom (ring A) is twisted from the molecular plane containing the C=N bond.[1] However, only a few studies have been made on the role of electronic effects of substituents on the molecular conformations of *N*-benzylideneanilines in solution.[2] We have recently shown that *N*-benzylidene-4-nitroaniline takes a more twisted conformation than NBA itself in solution and in gas phase by UV[1] and photoelectron spectroscopy.[2a] On the other hand, Zollinger[2b] and Kubota[2c] reported that *N*-(4-nitrobenzylidene)-4-dimethylaminoaniline takes a nearly planar conformation in solution. They suggested that the planar conformation of the disubstituted NBA would be ascribed to a through-conjugative interaction of the dimethylamino group with the nitro group. These studies suggest that electronic effects of a 4′-substituent on the benzylidene benzene ring (ring B) as well as those of a 4-substituent on the ring A will play an important role to determine the molecular conformations of NBAs.

In a previous paper, we demonstrated the anomalous substituent effects on the azomethine proton chemical shift of 4-substituted *N*-benzylideneanilines that the

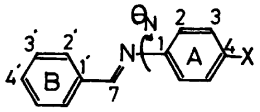

1

1a, X=NMe_2; **1b**, OCH_3; **1c**, CH_3; **1d**, H; **1e**, F; **1f**, Cl; **1h**, CO_2Et; **1j**, NO_2.

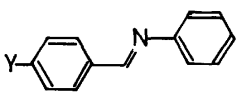

2

2a, Y=NMe_2; **2b**, OCH_3; **2c**, CH_3; **2d**, H; **2f**, Cl; **2g**, Br; **2i**, CN; **2j**, NO_2.

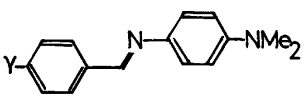

3

3a, Y=NMe_2; **3b**, OCH_3; **3c**, CH_3; **3d**, H; **3f**, Cl; **3g**, Br; **3i**, CN; **3j**, NO_2.

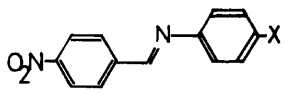

4

4a, X=NMe_2; **4b**, OCH_3; **4c**, CH_3; **4d**, H; **4e**, F; **4f**, Cl; **4h**, CO_2Et; **4j**, NO_2.

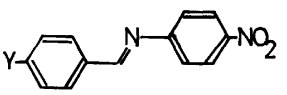

5

5a, Y=NMe_2; **5b**, OCH_3; **5c**, CH_3; **5d**, H; **5f**, Cl; **5i**, CN; **5j**, NO_2.

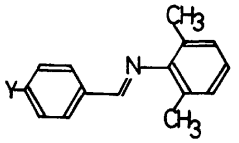

6

6a, Y=NMe_2; **6b**, OCH_3; **6c**, CH_3; **6d**, H; **6f**, Cl; **6g**, Br; **6i**, CN; **6j**, NO_2.

Scheme 1.

azomethine proton of the 4-nitro derivative resonates at a higher field than that of NBA, and interpreted them in terms of the change of molecular conformations induced by the 4-nitro group.[3] In order to get deeper insight into the conformational change with substituents in *N*-benzylideneanilines, we have undertaken a detailed study of multiple substituent effects on carbon-13 chemical shifts in several *N*-benzylideneanilines.

In the present paper, ^{13}C NMR data are presented for series of multiply substituted *N*-benzylideneanilines, **3**—**6**. Special attention is paid to additivity of the multiple substituent effects on the azomethine carbon chemical shifts in these *N*-benzylideneanilines. Effects of the substituents Y on the ring B are also analyzed and discussed in detail.

Results and Discussion

Assignment of the ^{13}C NMR Spectra. For analysis of the ^{13}C NMR chemical shifts of **3**—**6** ^{13}C NMR data of the corresponding monosubstituted NBA derivatives, series **1** and **2**, are necessary. The ^{13}C NMR spectra of **1** and **2** are already reported by Inamoto *et al.*[4] Since reinvestigation on the ^{13}C NMR spectra of some of the monosubstituted derivatives was found to give the same chemical shifts as reported within the experimental error, only the derivatives of X=NMe_2, F, and CO_2Et, Y=Br and CN were measured in the present study. The results are summarized in Table 1. The results of the multiply substituted derivatives **3**—**6** are listed in Table 2.

Assignment of the chemical shifts of some derivatives of **1** and **2** was already described.[4] Assignment of the chemical shifts in **3**—**6** has been made maily by using substituent-induced chemical shifts (SCS) of **1**, **2**, and substituted benzenes.[5] Consideration of the signal intensities also permitted to distinguish the ortho and meta carbons from the ipso carbons, the carbons attached directly to the substituents. In some cases, off-resonance decoupled spectra were used to differentiate the carbons bearing a hydrogen.

Aromatic Carbons. The SCS values of the aromatic carbons of **1** and **2** are not considered here since they were already analyzed and discussed.[4] For **3**—**6**, the Hammett relationship was examined. The results are shown in Table 3.

Generally, good correlations were found for the ipso carbons except those attached directly to the variable substituents X or Y. For example, C-1, C-1′, and C-4 in V exhibit a good correlation with Hammett σ constants; however, C-4′, which is directly attached to Y, does not show any good correlation. Furthermore,

Table 1. ^{13}C NMR Chemical shifts (ppm from TMS) of monosubstituted derivatives, **1** and **2** in $CDCl_3$[a]

No.	Substituent Y	Substituent X	C-1	C-2	C-3	C-4	C-1′	C-2′	C-3′	C-4′	C-7
1a[b]	H	NMe_2	141.29	122.03	113.08	149.70	137.29	128.34	128.53	130.20	155.52
			(+10.66)	(−1.27)	(+15.89)	(−23.91)	(−1.18)	(+0.34)	(+0.05)	(+0.88)	(+4.45)
1b[c]	H	OCH_3	144.96			158.55	136.81			131.04	157.95
			(+6.99)			(−32.76)	(−0.70)			(+0.13)	(+2.12)
1c[c]	H	CH_3	149.53			135.41	136.61			130.91	158.81
			(+2.42)			(−9.62)	(−0.50)			(+0.26)	(+1.26)
1d	H	H	152.18[c]			125.94	136.48			131.24	160.01
			151.95[b]	120.76	128.97	125.79	136.11	128.68	128.58	131.17	160.07
1e[b]	H	F	147.89	122.25	115.65	161.07	136.06	128.68*	128.58*	131.17	159.60
			(+4.06)	(−1.49)	(+13.32)	(−35.28)	(+0.05)	(0.00)	(0.00)	(0.00)	(+0.47)
1f[c]	H	Cl	150.59			131.57	136.21			131.57	160.40
			(+1.36)			(−5.78)	(−0.10)			(−0.40)	(−0.33)
1h[b]	H	CO_2Et	156.06	120.56	130.73	127.70	135.82	128.97*	128.73*	131.71	161.34
			(−4.11)	(+0.20)	(−1.76)	(−1.91)	(+0.29)	(−0.29)	(−0.15)	(−0.54)	(−1.27)
1j	H	NO_2	158.08[a]			145.69	135.68			132.56	162.79
			157.82[b]	121.15	124.87	145.50	135.53	129.27	128.88	132.25	162.46
			(−5.87)	(−0.39)	(+4.10)	(−19.71)	(+0.58)	(−0.59)	(−0.30)	(−1.08)	(−2.39)
2a[c]	NMe_2	H	152.65			125.07	124.74			153.24	160.00
			(−0.70)			(+0.72)	(+11.37)			(−22.07)	(+0.07)
2b[c]	OCH_3	H	152.58			125.60	129.52			162.39	159.41
			(−0.63)			(+0.19)	(+6.59)			(−31.22)	(+0.66)
2c[c]	CH_3	H	152.45			125.73	134.02			141.58	159.87
			(−0.50)			(+0.06)	(+2.09)			(−10.41)	(+0.20)
2f[c]	Cl	H	151.65			126.14	134.88			137.20	158.28
			(+0.30)			(−0.35)	(+1.23)			(−6.03)	(+1.79)
2g[b]	Br	H	151.41	120.76	129.07	126.09	135.03	130.00	131.86	125.70	158.55
			(+0.44)	(0.00)	(−0.10)	(−0.30)	(+1.08)	(−1.32)	(−3.28)	(+5.47)	(+1.52)
1i[b]	CN	H	150.87	120.86	128.97*	126.82	139.88	129.17*	132.34	114.26	157.63
			(+1.08)	(−0.10)	(0.00)	(−1.03)	(−3.77)	(−0.49)	(−3.76)	(+16.91)	(+2.44)
2j[c]	NO_2	H	151.06			127.26	141.78			149.40	157.38
			(+0.89)			(−1.47)	(−5.67)			(−18.23)	(+2.69)

a) The asterisk means that the assignment may be reversed. Values in parentheses indicate the SCS. The positive values mean upfield shifts. b) The present work. c) Ref. 4.

Table 2. ^{13}C NMR Chemical shifts (ppm from TMS) of disubstituted derivatives, **3**, **4**, **5**, and **6** in $CDCl_3$[a)]

No.	Substituent		C-1	C-2	C-3	C-4	C-1′	C-2′	C-3′	C-4′	C-7
	Y	X									
3a	NMe_2	NMe_2	142.27	121.88	113.18	148.87	125.21	129.85	111.67	152.00	156.59
			(−0.98)	(+0.15)	(−0.10)	(+0.83)	(+12.08)	(−1.51)	(+16.86)	(−21.71)	(−1.07)
3b	OCH_3	NMe_2	141.59	122.03	113.08	149.36	130.14	129.90	114.11	161.68	155.42
			(−0.30)	(0.00)	(0.00)	(+0.34)	(+7.15)	(−1.56)	(+14.42)	(−31.39)	(+0.10)
3c	CH_3	NMe_2	141.39	122.08	112.98	149.46	134.49	128.29	129.27	140.61	155.81
			(−0.10)	(−0.05)	(+0.10)	(+0.24)	(+2.80)	(+0.05)	(−0.74)	(−10.32)	(−0.29)
3d	H	NMe_2	141.29	122.23	113.08	149.70	137.29	128.34	128.53	130.29	155.52
3f	Cl	NMe_2	140.90	122.32	113.08	149.94	135.82	129.46	128.88	136.36	153.86
			(+0.39)	(−0.09)	(0.00)	(−0.24)	(+1.47)	(−1.12)	(−0.35)	(−6.07)	(+1.66)
3g	Br	NMe_2	140.61	122.32	112.94	149.85	136.11	129.60	131.81	124.62	153.76
			(+0.68)	(−0.29)	(+0.14)	(−0.15)	(+1.18)	(−1.26)	(−3.28)	(+5.67)	(+1.76)
3i	CN	NMe_2	139.68	122.76	112.74	150.39	141.05	128.49	132.30	113.33	152.05
			(+1.61)	(−0.73)	(+0.34)	(−0.69)	(−3.76)	(−0.15)	(−3.77)	(+16.96)	(+3.47)
3j	NO_2	NMe_2	139.56	122.83	112.67	150.46	142.71	128.62	123.84	b)	151.46
			(+1.73)	(−0.80)	(+0.41)	(−0.76)	(−5.42)	(−0.28)	(+4.69)		(+4.06)
4a	NO_2	NMe_2	139.56	122.83	112.67	150.46	142.71	128.62	123.84	b)	151.46
			(+11.50)			(−23.20)	(−0.93)				(+5.92)
4b	NO_2	OCH_3	143.69	122.57	114.62	159.33	142.03	128.99	123.84	149.10	154.52
			(+7.37)			(−32.07)	(−0.25)			(+0.30)	(+2.86)
4c	NO_2	CH_3	148.46	120.98	129.88	137.11	141.95	129.17	123.79	149.38	155.94
			(+2.60)			(−9.85)	(−0.17)			(+0.02)	(+1.44)
4d[c)]	NO_2	H	151.06			127.26	141.78			149.40	157.38
4e	NO_2	F	146.91	122.69	116.04	161.85	141.53	129.31	123.84	149.31	156.81
			(+4.15)			(−34.59)	(+0.25)			(+0.09)	(+0.57)
4f	NO_2	Cl	149.33	122.30	129.36	132.64	141.32	129.36	123.86	149.46	157.43
			(+1.73)			(−5.38)	(+0.46)			(−0.06)	(−0.05)
4h	NO_2	CO_2Et	154.93	120.61	130.88	128.88	141.14	129.60	123.99	149.70	158.65
			(−3.87)			(−1.62)	(+0.64)			(−0.30)	(−1.27)
4j	NO_2	NO_2	156.21	121.20	125.06	146.35	140.58	129.90	124.09	150.09	159.89
			(−5.15)			(−19.09)	(+1.20)			(−0.69)	(−2.51)
5a	NMe_2	NO_2	158.89	121.19	124.84	144.71	123.61	131.09	111.49	153.15	161.81
			(−1.07)	(−0.04)	(+0.03)	(+0.79)	(+11.92)	(−1.82)	(+17.39)	(−20.90)	(+0.65)
5b	OCH_3	NO_2	158.21	121.25	124.91	145.20	128.49	131.90	114.40	163.10	161.73
			(−0.39)	(−0.10)	(−0.04)	(+0.30)	(+7.04)	(−2.63)	(+14.48)	(−30.85)	(+0.73)
5c	CH_3	NO_2	158.02	121.15	124.87	145.30	132.88	129.27*	129.60*	143.05	162.37
			(−0.20)	(0.00)	(0.00)	(+0.20)	(+2.65)	(0.00)	(−0.72)	(−10.80)	(+0.09)
5d	H	NO_2	157.82	121.15	124.87	145.50	135.53	129.27	128.88	132.25	162.46
5f	Cl	NO_2	157.45	121.18	124.97	145.64	133.88	130.36*	129.27*	138.51	161.07
			(+0.37)	(−0.03)	(−0.10)	(−0.14)	(+1.65)	(−1.09)	(−0.39)	(−6.26)	(+1.39)
5i	CN	NO_2	156.74	121.20	125.01	146.20	139.05	128.53	132.62	115.60	160.36
			(+1.08)	(−0.05)	(−0.14)	(−0.70)	(−3.52)	(+0.74)	(−3.74)	(+16.65)	(+2.10)
5j	NO_2	NO_2	156.21	121.20	125.06	146.35	140.58	129.90	124.09	150.09	159.89
			(+1.61)	(−0.05)	(−0.19)	(−0.85)	(−5.05)	(−0.63)	(+4.79)	(−17.84)	(+2.57)
6a	NMe_2		151.85	127.21	127.80	122.86	124.13	129.80	111.37	152.29	161.68
			(−0.73)	(−0.34)	(+0.15)	(+0.74)	(+11.88)	(−1.17)	(+16.97)	(−21.02)	(+0.69)
6b	OCH_3		151.41	127.04	127.95	123.33	129.04	130.00	114.06	162.22	161.46
			(−0.29)	(−0.17)	(0.00)	(+0.27)	(+6.97)	(−1.37)	(+14.28)	(−30.95)	(+0.91)
6c	CH_3		151.31	126.87	127.95*	123.45	133.57	128.34*	129.36	141.53	162.12
			(−0.19)	(0.00)	(0.00)	(+0.15)	(+2.44)	(+0.29)	(+1.02)	(−10.26)	(+0.25)
6d	H		151.12	126.87	127.95	123.60	136.01	128.63	128.34	131.27	162.37
6f	Cl		150.78	126.67	128.00	123.69	134.40	129.41	128.82	137.18	160.80
			(+0.34)	(+0.20)	(−0.05)	(−0.09)	(+1.61)	(−0.78)	(−0.48)	(−5.91)	(+1.57)
6g	Br		150.68	126.58	127.95	123.64	134.69	129.56	131.71	125.65	160.85
			(+0.44)	(+0.29)	(0.00)	(−0.04)	(+1.32)	(−0.93)	(−3.37)	(+5.62)	(+1.52)
6i	CN		150.39	126.67	128.14	124.18	139.58	128.73	132.40	114.50	160.70
			(+0.73)	(+0.20)	(−0.19)	(−0.58)	(−3.57)	(−0.10)	(−4.06)	(+16.77)	(+1.67)
6j	NO_2		150.33	126.67	128.19	124.28	141.20	128.97	123.79	149.31	160.39
			(+0.79)	(+0.20)	(−0.24)	(−0.68)	(−5.19)	(−0.34)	(+4.55)	(−18.04)	(+1.98)

a) Values in parentheses indicate the SCS from the corresponding parent compounds in each series. The asterisk means that the assignment may be reversed. b) Not observed. c) Ref. 4.

among these ipso carbons, C-1′, which is situated at the para position of the carbon bearing Y, is highly sensitive to substituent electronic effects, as indicated by a ρ value exceeding 10 (Table 3). Similar high sensitivity of the substituent effects is also noticed for C-1 in **4**, C-1′ in **3** and **6**. Poor correlations (the results

Table 3. Hammett ρ values and correlation coefficients for aromatic carbons[a,b]

Carbon	Series			
	3	**4**	**5**	**6**
C-1	−1.77	10.70	−1.63	−1.02
	(0.978)	(0.942)	(0.988)	(0.988)
C-4	1.03	−8.84	1.03	0.87
	(0.996)	(0.318)	(0.995)	(0.990)
C-1′	10.54	−1.32	10.28	10.20
	(0.965)	(0.994)	(0.963)	(0.960)
C-4′	−29.20	0.83	−14.40	−15.48
	(0.827)	(0.954)	(0.513)	(0.517)

a) Calculated with σ values. b) Absolute values of the chemical shifts were employed for the regression analyses.

not shown) for C-2, C-3, C-2′, and C-3′ on the rings bearing the substituent X or Y, that is, C-2′ and C-3′ in **3**, **5**, and **6**, and C-2 and C-3 in **4**, may be attributed to predominance of secondary perturbations such as anisotropy and/or neighboring effects over the substituent electronic effects.

Substituent-Substituent Interactions in Disubstituted N-Benzylideneanilines. For disubstituted *N*-benzylideneanilines, 4-$YC_6H_4CH{=}NC_6H_4X$-4, if the effects of both substituents on the chemical shifts are additive as expressed by a simple addition of the effects of the substituents X in **1** and Y in **2**, the chemical shift of the azomethine carbon of a disubstituted NBA can be calculated according to Eq. 1, where ΔX and ΔY are differences in the chemical shifts between the unsubstituted NBA, δH, and the monosubstituted compounds with substituents X, δX, and Y, δY, respectively. The value of 160.07 denotes the chemical shift of the unsubstituted NBA. The $(\Delta X+\Delta Y)$ corresponds to a calculated SCS (Eq. 2), and the observed SCS is given by Eq. 3, where δ C_{obsd} X–Y refers to the chemical shift observed for the disubstituted NBA. For **3** and **4** δ C_{calcd} X–Y and SCS_{calcd} X–Y are obtained according to Eqs. 1 and 2, and are listed in Table 4 together with the corresponding observed values. If the additivity holds for **3** and **4**, SCS_{calcd} X–Y should be the same as SCS_{obsd} X–Y. However, Table 4 shows a large difference between them. This may reflect a strong interaction between the two substituents X and Y. This situation can well be visualized by plotting SCS_{obsd} X–Y against SCS_{calcd} X–Y, as shown

$$\delta C_{calcd}X\text{–}Y = 160.07 + (\Delta X+\Delta Y) \quad (1)$$

$$SCS_{calcd}X\text{–}Y = \Delta X + \Delta Y \quad (2)$$

$$SCS_{obsd}X\text{–}Y = 160.07 - \delta C_{obsd}X\text{–}Y \quad (3)$$

$$\Delta X = \delta H - \delta X$$

$$\Delta Y = \delta H - \delta Y$$

in Figs. 1 and 2 for **3** and **4**, respectively, in which SCS values for the corresponding monosubstituted NBAs are also plotted to provide a scaling for the deviation.[7] As shown in Fig. 1, the discrepancy between SCS_{calcd} X–Y and SCS_{obsd} X–Y is noticed for NBAs with an electron-releasing or an electron-withdrawing substituent. Thus, the actual azomethine carbon chemical shifts deviate to the downfield from the calculated values for **3** with the electron-releasing groups. In a striking contrast, the deviations are to the upfield for **3** with the electron-withdrawing groups. On the other hand, Fig. 2 shows that the observed values accord well with the calculated ones for **4** with the electron-withdrwaing groups whereas significant deviations are noticed for **4** with the electron-releasing groups such as a dimethylamino and a methoxyl.

The Hammett treatment with σ values[6] of these deviations, $\Delta\delta$ (defined by SCS_{obsd} X–Y−SCS_{calcd} X–Y), for **3** gives a fairly good linear relationship with a correlation coefficient of 0.967 as shown in Fig. 3a. A similar plot for **4** gives a relationship with a correlation coefficient of 0.900; however, a plot with σ^+ values[6] affords a better linear relationship with a correlation coefficient of 0.957 (Fig. 3b). No significant trend of $\Delta\delta$ can be found for **5**.

Multiple substituent effects have been extensively studied on reaction rates, thermal and spectroscopic parameters in various organic π-systems.[8] Although nonadditivity has been observed in the multiple substi-

Table 4. Additivity for azomethine carbon chemical shifts of **3** and **4**

No.	Substituent Y	Substituent X	$\delta C_{calcd}X$–Y	$\delta C_{obsd}X$–Y	$SCS_{calcd}X$–Y	$SCS_{obsd}X$–Y	$\Delta\delta$[a]
3a	NMe_2	NMe_2	155.55	156.59	+4.52	+3.48	−1.04
3b	OCH_3	NMe_2	154.96	155.42	+5.11	+4.65	−0.46
3c	CH_3	NMe_2	155.42	155.81	+4.65	+4.26	−0.39
3f	Cl	NMe_2	153.83	153.86	+6.24	+6.21	−0.03
3g	Br	NMe_2	154.10	153.76	+5.97	+6.31	+0.34
3i	CN	NMe_2	153.18	152.05	+6.89	+8.02	+1.13
3j (=**4a**)	NO_2	NMe_2	152.93	151.46	+7.14	+8.61	+1.47
4b	NO_2	OCH_3	155.26	154.52	+4.81	+5.55	+0.74
4c	NO_2	CH_3	156.12	155.94	+3.95	+4.13	+0.18
4e	NO_2	F	156.91	156.81	+3.16	+3.26	+0.10
4f	NO_2	Cl	157.71	157.43	+2.36	+2.64	+0.28
4h	NO_2	CO_2Et	158.65	158.65	+1.42	+1.42	0.00
4j	NO_2	NO_2	159.77	159.89	+0.30	+0.18	−0.12

a) $\Delta\delta = SCS_{obsd}X\text{–}Y - SCS_{calcd}X\text{–}Y$.

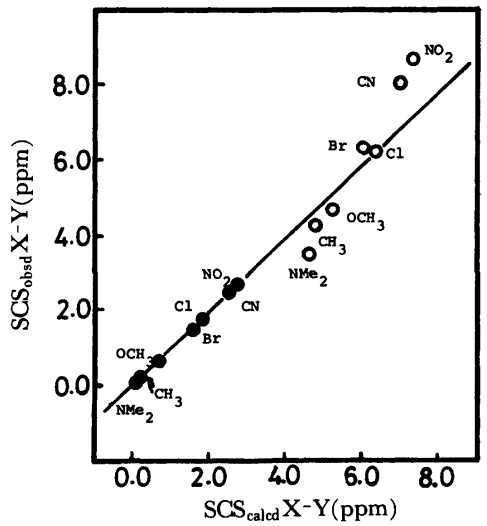

Fig. 1. Nonadditivity of multiple substituent effects on the azomethine carbon chemical shifts in **3**. The open circles denote the SCS in **3** and the closed circles denote the SCS in **2**.

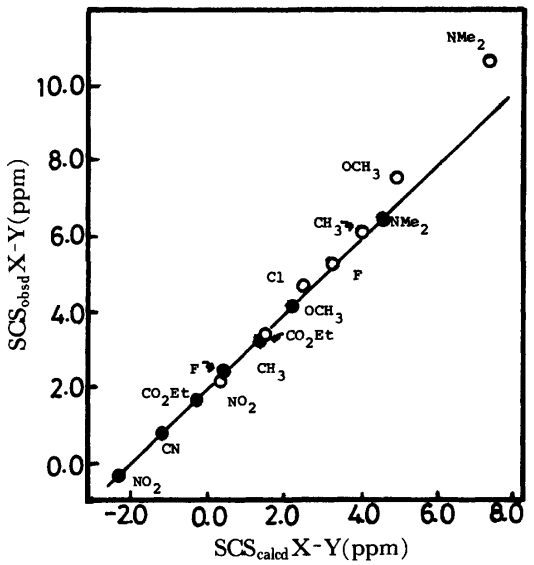

Fig. 2. Nonadditivity of multiple substituent effects on the azomethine carbon chemical shifts in **4**. The open circles denote the SCS in **4** and the closed circles denote the SCS in **1**.

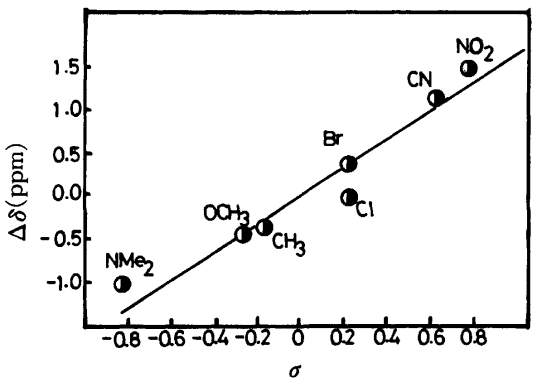

Fig. 3a. Plot of $\Delta\delta$ *vs.* Hammett σ constants in **3**.

tuent effects on bromination rates of 1,1-diphenylethylene,[8h] α-methylstilbenes,[8o] and polysubstituted

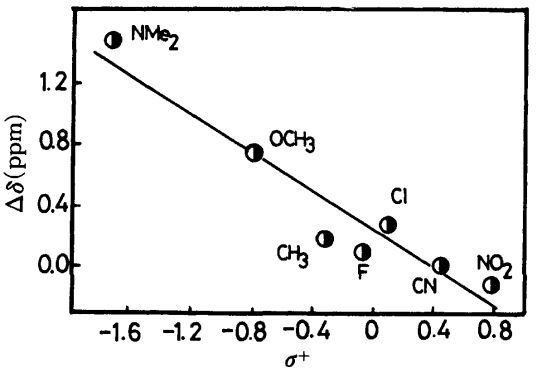

Fig. 3b. Plot of $\Delta\delta$ *vs.* Hammett σ^+ constants in **4**.

benzenes,[8i] on stabilization energies of trityl cations[8c] and anions,[8b] and on proton and carbon chemical shifts of several conjugated π-systems,[8f,g,j,l,m] few reports have appeared on the systems in which substituent–substituent interactions may lead to conformational changes of molecules.

We interpret the nonadditivity of multiple substituent effects on the azomethine carbon chemical shifts in **3** and **4** as a consequence of the substituent–substituent interaction which may be accompanied by conformational changes of the NBA derivatives. The downfield deviation of $\Delta\delta$ for NBAs with the electron-releasing groups in **3** may be reasonably interpreted in terms of suppression of the electron donation from the 4-dimethylamino group on the ring A toward the azomethine carbon by strongly electron-donating groups such as a 4′-dimethylamino and a 4′-methoxyl. In contrast, strongly electron-withdrawing groups such as 4′-cyano and a 4′-nitro enhances the electron donation resulting in an upfield deviation of $\Delta\delta$ as observed for **3** (Fig. 1). Thus, the net electron-releasing ability of the 4-dimethylamino group depends on the electronic properties of the 4′-substituents. Actually, $\Delta\delta$'s for **3** give a good linear elationship with Hammett σ constants with a correlation coefficient of 0.967 as shown above (Fig. 3a). The degree of the variable electronic effect of the 4-dimethylamino group may be evaluated by $\Delta\Delta\delta$ (defined by a difference in $\Delta\delta$'s) among the 4′-substituents. For example, for **3** $\Delta\delta(NMe_2)-\Delta\delta(NO_2)$ gives $\Delta\Delta\delta$ of 2.51 in a chemical shift unit, indicating that the net variation of the electronic effect of the 4-dimethylamino group corresponds to 2.51 ppm. This seems to be significant since the magnitude is as large as SCS of the methoxyl group in **1**. The systematic change in $\Delta\delta$ clearly indicates the interaction between the 4-dimethylamino group and the 4′-substituents. Such substituent–substituent interactions have often been observed by other workers.[8] With respect to the multiple substituent effects on the chemical shifts, Dubois, Doucet and their coworkers undertook a detailed study on electronic structures of diarylcarbenium ions.[8l,j] They observed a clear nonadditivity of the effects of two methoxyl groups on the α-carbon chemical shift. For example, for bis(4-

methoxyphenyl) carbenium ions, the first methoxyl group induces a change of 20.3 ppm in the α-carbon chemical shift whereas the second one induces only a 5.5 ppm change. Apparently, as the authors describe, saturation of the electronic effect occurs. Our own observation that the electron-donating effect of the 4-dimethylamino group is strongly suppressed by the 4'-dimethylamino and 4'-methoxyl groups is consistent with that by Dubois *et al.*, and will represent an example of a neutral system in which the electronic effect of a substituent will depend on another substituent in the molecule.

In the case of **4**, the discrepancy may also be explained similarly in terms of the interactions between the 4'-nitro group and the variable substituents, especially the electron-releasing groups on the ring A. The through-conjugative interaction between the 4'-nitro group and the electron-releasing groups will give the upfield deviations of $\Delta\delta$'s. A better correlation of $\Delta\delta$'s with σ^+ than with σ values also supports this interpretation (Fig. 3b).

We point out here that the substituent-substituent interactions in **3** and **4** may be accompanied by conformational change in these disubstituted NBAs. It is well-known that besides the π-π conjugation throughout the π-systems the n-π conjugation, which involves delocalization of the lone pair electrons on the nitrogen atom to the ring A and thus favors a highly twisted conformation, plays an important role in determining the molecular conformation of NBAs in solution.[2b,9] Since the through-conjugative interaction in the whole π-system will lead to a less twisted conformation,[2] it is reasonable to consider that the decrease in the electron donation from the 4-dimethylamino group in **3** will give rise to a less planar conformation.

Consider first the case of **4**. It is quite reasonable to assume that *N*-(4-nitrobenzylidene)-4-nitroaniline, **4j**, takes a conformation twisted as much as *N*-benzylidene-4-nitroaniline, **1j**, in solution,[1] since it is not likely that the 4'-nitro group may change the twist angle θ_N. If, for example, *N*-(4-nitrobenzylidene)-4-dimethylaminoaniline, **4a**, also adopts a considerably twisted conformation, the enhanced electron donation from the 4-dimethylamino group toward the azomethine carbon should not be observed since such electron donation must be greatly suppressed by the twisting of the conjugated π-system. Therefore, the electron donation from the 4-dimethylamino group in **4a** will be accompanied by a certain decrease in the twist angle θ_N in going from **4j** to **4a** Actually, it is reported by Zollinger[2b] and Kubota[2c] that **4a** will take a nearly planar conformation in solution as revealed by the UV and ESR spectra. A Hammett correlation of the azomethine carbon chemical shifts in **4** may also be supporting evidence. As illustrated in Fig. 4, treatment of SCS_{obsd} of the azomethine carbon chemical shifts with Hammett σ^+ constants shows an excellent linear

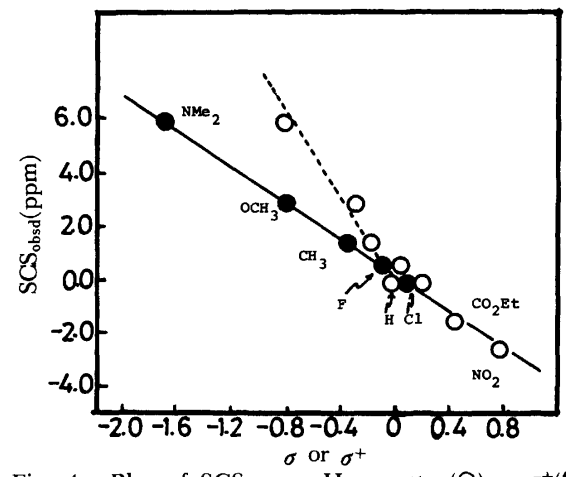

Fig. 4. Plot of SCS_{obsd} *vs.* Hammett σ(○) or σ^+(●) constants in **4**.

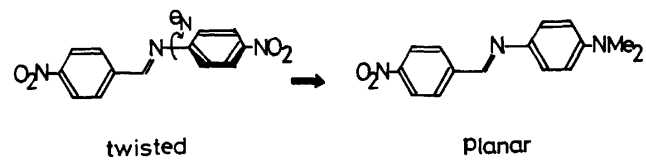

Scheme 2.

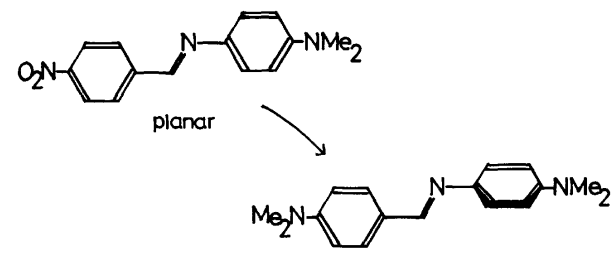

Scheme 3.

relationship with a correlation coefficient of 0.999 (correlation coefficient with σ values is 0.978). This can be best interpreted in terms of the enhanced electron donation from the electron-donating groups toward the azomethine carbon, and thus, in terms of a certain decrease in the twist angle θ_N in going from **4h** and **4j** to **4b** and **4a** (Scheme 2). A Similar concept can also be advanced to account for $\Delta\delta$'s in **3**. As already pointed out, the *N*-lone pair delocalization may be suppressed by the electron-releasing effect of the 4-substituents resulting in less twisted conformations. In other words, the more electron-donating the 4-substituent, the smaller twist angle θ_N would result. Since the electron donation from the 4-dimethylamino group is considerably suppressed in **3a** and **3b**, as shown by the larger $\Delta\delta$'s, resulting in the decrease in the through-conjugative interaction, it is reasonable to consider that **3a** and **3b** will take less planar conformations compared with a nearly planar conformation of **3j**. A feature of such a conformational change with the substituents based on the above discussion is illustrated in Scheme 3.

It is of interest noting that Freedman and his coworkers[8d] reported a substituent dependence of

rotational barriers of *N*-aryl bonds in 4′-substituted 4-dimethylaminotrityl cations. Our study may represent a new example that the change of molecular conformation can be induced by the substituent-substituent interactions.

Effects of Substituents Y on the Azomethine Carbon Chemical Shifts. Examination of the SCS data of the azomethine carbon chemical shift indicates that the modes of the substituent effects are different between the 4-substitution and 4′-substitution. Thus, in **1** and **4** which carry the variable substituents X on the ring A, the electron-releasing groups cause significant upfield shifts, whereas the electron-attracting groups generate appreciable downfield shifts. Accordingly, the substituent effect is normal in these cases. In contrast, in the series of **2**, **3**, **5**, and **6** in which the variable substituents Y are on the ring B, the electron-withdrawing groups cause upfield shifts, whereas the variation of SCS values remain small (≈1 ppm) with the electron-releasing groups. The overall SCS variation ia smaller (2—5 ppm) in **2**, **3**, **5**, and **6** than in **1** and **4** (7—8 ppm). Thus, the azomethine carbon chemical shift is more sensitive to the electronic effect of the substituents on the ring A than to that on the ring B.

However, careful examination of the SCS values in **2**, **3**, **5**, and **6** reveals that the electron-donating and electron-attracting groups behave in different ways to transmit the electronic effect on the azomethine carbon as illustrated in Figs. 5 to 8 which show plots of the azomethine carbon chemical shifts against the C-1′ chemical shifts which remarkably suffer the electronic effect of the 4′-substituents as mentioned in a previous section (halogen atoms are omitted from the consideration since they apparently deviate from the lines). Figures 5—8 clearly indicate that in all the series studied the electron-withdrawing groups on the ring B generally cause upfield shifts, whereas the effects of the electron-releasing groups are different from each other, and seem to depend on electron demand on the azomethine carbon induced by the fixed substituent on the ring A. Thus, the chemical shifts are not very sensitive to the electron-releasing groups in **2**. However, the azomethine carbon suffers a roughly inverse substituent effect (the NMe_2 derivative resonates at a lower field than the unsusbtituted derivative) in **3** which carry the 4-dimethylamino group. In a striking contrast, opposite trends can well be seen in **5** and **6**, where the azomethine carbon chemical shift suffers a roughly normal substituent effect with the electron-releasing groups to give rise to the V-shape correlation with the C-1′ chemical shifts (Figs. 7 and 8).

The above finding that 4′-substituents exert a relatively small electronic effect on the azomethine carbon chemical shift seems to be in keeping with reported results on the α-carbon chemical shifts in styrenes,[10,11] acetophenones,[12] and benzaldehydes.[13] These have been interpreted in terms that the 4-substituents do not change significantly the electron densities on the α-carbons as dipicted for 4-substituted

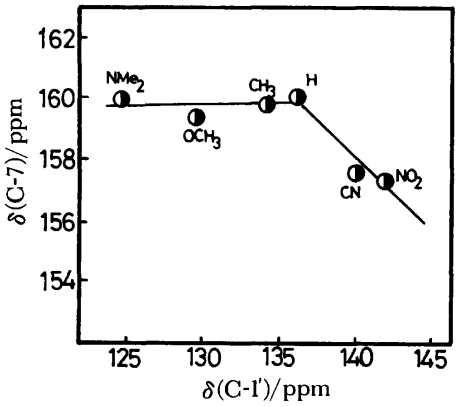

Fig. 5. Plot of δ(C-7) *vs.* δ(C-1′) in **2**.

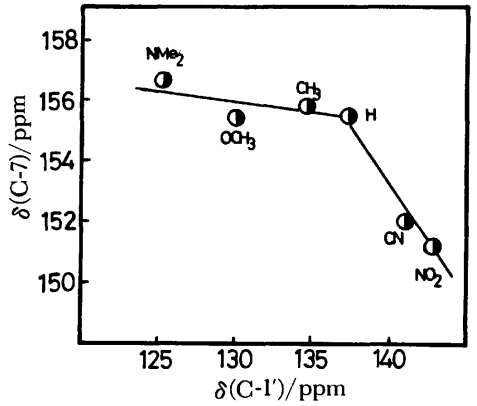

Fig. 6. Plot of δ(C-7) *vs.* δ(C-1′) in **3**.

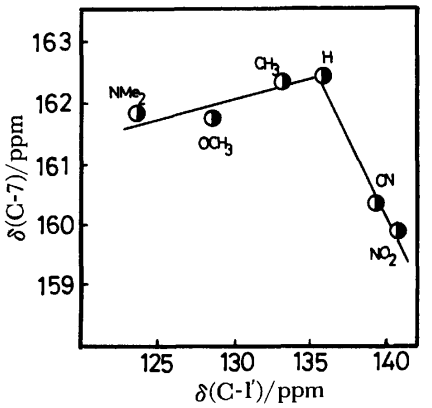

Fig. 7. Plot of δ(C-7) *vs.* δ(C-1′) in **5**.

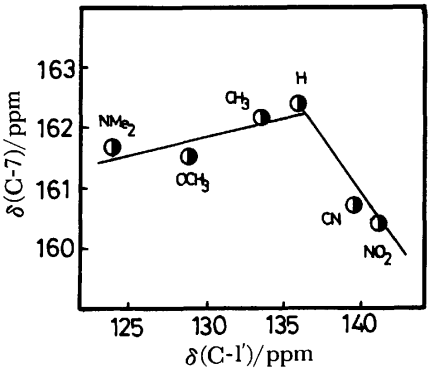

Fig. 8. Plot of δ(C-7) *vs.* δ(C-1′) in **6**.

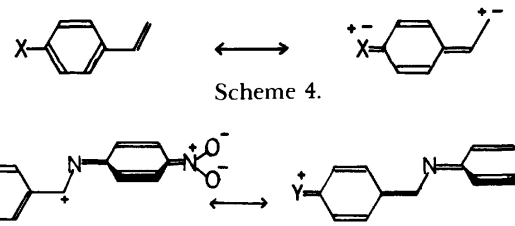

Scheme 4.

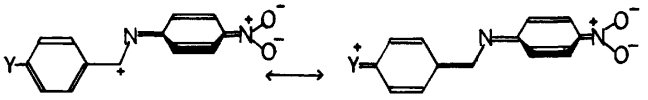

Y: electron-releasing groups

Scheme 5.

styrenes in Scheme 4 as an example. However, lack of systematic studies as well as the relatively minor variation of the chemical shifts and their poor correlation with structural parameters such as Hammett constants have made it difficult to get deeper insight into the substituent effects on the α-carbon chemical shifts in benzilidene-type conjugated systems. In this respect, the correlation of the azomethine carbon chemical shifts with the C-1′ chemical shifts is of particular interest. The present study with systematic changes of the substituents on the ring A clearly indicates that 4′-substituent effects should be treated separately between the electron-releasing and the electron-withdrawing groups. Thus, the electron-withdrawing groups cause the inverse substituent effects in all the series, whereas the effects with the electron-releasing groups may be normal, inverse, or even absent depending on the electron demand developed on the azomethine carbons by the structural and/or electronic effects of the substituents on the ring A.

As depicted in Figs. 7 and 8, the effects with the electron-releasing groups is normal in **5** and **6** in which the electron demand on the azomethine carbons seems to increase compared with **2**. In **5**, the 4′-nitro group will generate significant electron deficiency on the azomethine carbons compared with those of **2**. Likewise, the *N*-lone pair delocalization in **6** to the ring A enhanced by twisting of the C–N bond by the 2,6-dimethyl groups will result in the increase in electron demand on the azomethine carbon.[3] Under these circumstances, the electron-releasing groups will donate electrons more efficiently toward the azomethine carbon resulting in the normal upfield shift, as shown in Scheme 5. Actually, the normal substituent effect on the α-carbon chemical shift was observed in methyldiphenylcarbenium and hydroxydiphenylcarbenium ions by Doucet and his coworkers, [81] in which the strong electron demand on the cationic carbons enhances the electron donation from the electron-releasing groups to give rise to the normal upfield shift. The proposed concept can be further supported by examining available data for 4-substituted β,β-dichloro-,[14] **7**, and β,β-dicyanostyrenes,[15] **8**. We treated the results in a similar manner to that employed for the present study, and the correlations for these two series are illustrated in Figs. 9 and 10. In the case of the dichlorostyrenes, the α-carbon chemical shift suffers a inverse substitu-

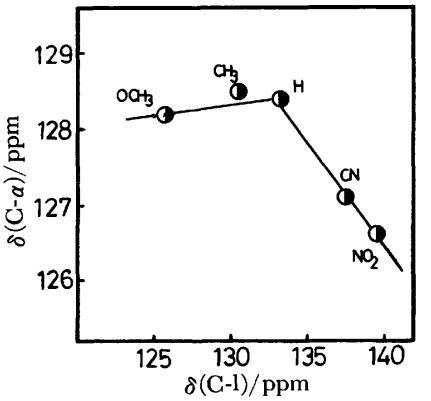

Fig. 9. Plot of δ(C-α) *vs.* δ(C-1) in **7**.

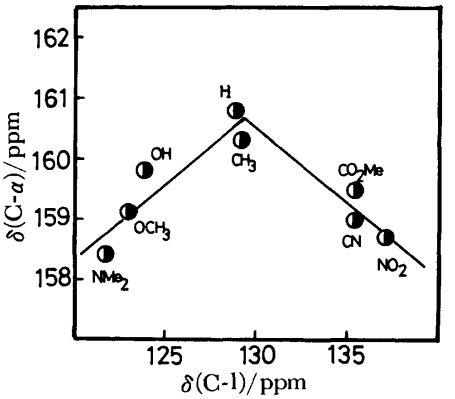

Fig. 10. Plot of δ(C-α) *vs.* δ(C-1) in **8**.

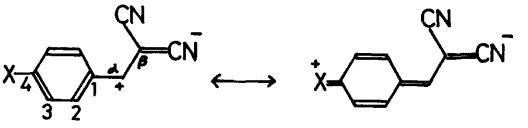

X: electron-releasing groups

Scheme 6.

ent effect with the electron-withdrawing groups, whereas the chemical shifts remain roughly constant with the electron-releasing groups, as found for **2**. This indicates that the substituent effects must also be treated separately between the electron-releasing and electron-withdrawing groups. Such a situation can well be seen in the dicyanostyrenes in which a clear V-shape correlation was observed. The normal substituent effect with the electron-releasing groups can be reasonably interpreted in terms of the proposed concept that the electron demand on the α-carbon plays an important role in determining the mode of the substituent effect (Scheme 6).

The inverse substituent effects on the proton and carbon chemical shifts have been occasionally observed by other workers. For example, Reynolds *et al.*[11] reported that introduction of a 4-nitro group caused an upfield shift of the α-carbon chemical shift in 4-substituted styrenes. Inamoto and his coworkers also reported[4] the inverse substituent effect on the azomethine carbon chemical shifts in **2**, and attributed this phenomenon to the effect of charge alternation

originally proposed by Pople.[16,17] The similar observation in the present study may also be explicable by the same effect. It should be pointed out, however, that this explanation cannot be advanced for the effect of the electron-releasing groups on the azomethine carbons. Even for **2** originally reported by Inamoto *et al.* and for **3** which carry the 4-dimethylamino group on the ring A, it is clear that the correlations cannot be treated in a single line. Whether the substituent effect is normal or inverse must depend on the degree of the electron demand developed on the azomethine carbons.

In summary, the present study revealed importance of two competetive factors responsible for the 4′-substituent effects on the azomethine carbon chemical shifts in *N*-benzylideneanilines. It should be also pointed out that similar mode of the substituent effects may be extended to the α-carbon chemical shifts in other benzylidene-type conjugated systems.

Conclusion

Multiple substituent effects on the azomethine carbon chemical shift were examined for a few series of disubstituted *N*-benzylideneanilines. Nonadditivity of the multiple substituent effects was observed for **3**, 4-$YC_6H_4CH{=}NC_6H_4NMe_2$-4, and **4**, 4-$NO_2C_6H_4CH{=}NC_6H_4X$-4. It is pointed out that the observed nonadditivity can be understood in terms of the substituent–substituent interactions accompanied by the conformational changes with the substituents in these NBAs. The present study also revealed that there are two modes of the 4′-substituent (on the ring B) effects on the azomethine carbon chemical shift. Depending on the degree of the electron demand developed on the azomethine carbons, the effects with the electron-releasing groups may be normal or inverse; the former effects result from the efficient electron donation from the substituents and the latter can be explained in terms of the charge alternation on the carbon frameworks induced by the substituents.

Experimental

Materials. *N*-benzylideneaniline, *N*-benzylidene-4-nitroaniline, and *N*-benzylidene-2,6-dimethylaniline were available from the previous work.[1] All other *N*-benzylideneanilines were similarly prepared, and fully characterized by physical constants, spectral data, and/or elemental analyses. All new compounds gave satisfactory elemental analyses. To our knowledge, the physical constants of the following compounds are not reported previously; **3b**, mp 141.5—143 °C (uncorrected), **3d**, mp 144—145 °C, **3f**, mp 162—163 °C, **3g**, mp 170.5—171 °C, **3i**, mp 194.5—195.5 °C, **4e**, mp 109—110 °C, **4h**, mp 177—178 °C, **5c**, mp 137—138 °C, **5f**, mp 164.5—165.5 °C, **5i**, mp 183—183.5 °C, **6a**, mp 74.5—76 °C, **6b**, mp 40—41 °C, **6c**, mp 162—163 °C, **6f**, mp 157—158 °C, **6g**, mp 152—153 °C, **6i**, mp 68-69 °C, **6j**, mp 98—100 °C.

^{13}C NMR Spectra. ^{13}C NMR spectra were recorded on a JEOL FX-60 spectrometer operating in a Fourier Transform mode with complete proton decoupling as described previously.[3] Off-resonance decoupled spectra were also recorded in some cases. The spectra were usually taken at room temperature; however, samples of **4** were run at *ca.* 40—55 °C of the probe temperature at saturated concentrations. Solvent was $CDCl_3$ in all cases.[18]

References

1) R. Akaba, K. Tokumaru, and T. Kobayashi, *Bull. Chem. Soc. Jpn.*, **53**, 1993 (1980), and references cited therein.

2) a) R. Akaba, K. Tokumaru, T. Kobayashi, and C. Utsunomiya, *Bull. Chem. Soc. Jpn.*, **53**, 2002 (1980); b) P. Skrabal, J. Steiger, and H. Zollinger, *Helv. Chim. Acta*, **58**, 800 (1975); c) K. Ezumi, H. Nakai, S. Sakata, K. Nishikida, M. Shiro, and T. Kubota, *Chem. Lett.*, **1974**, 1393.

3) R. Akaba, H. Sakuragi, and K. Tokumaru, *Bull. Chem. Soc. Jpn.*, **58**, 301 (1985).

4) N. Inamoto, K. Kushida, S. Masuda, H. Ohta, S. Satoh, Y. Tamura, K. Tokumaru, K. Tori, and M. Yoshida, *Tetrahedron Lett.*, **1974**, 3617.

5) G. C. Levy and G. L. Nelson, "Carbon-13 Nuclear Magnetic Resonance for Organic Chemists," Wiley-Interscience, New York (1972), Chapter 4.

6) O. Exner, "Advances in Linear Free Energy Relationship," ed by N. B. Chapman and J. Shorter, Plenum Press, London (1972), Chapter 1.

7) B. Ancian, F. Membrey, and J. P. Doucet, *J. Org. Chem.* **43**, 1509 (1978).

8) a) E. D. Jenson and R. W. Taft, *J. Am. Chem. Soc.*, **86**, 116 (1964); b) R. W. Taft and L. D. Mckeever, *ibid.*, **87**, 2489 (1965); c) L. D. Mckeever and R. W. Taft, *ibid.*, **88**, 4544 (1966); d) J. W. Rakshys, Jr., S. V. McKinley, and H. H. Freedman, *J. Chem. Soc., Chem. Commun.*, **1969**, 1180; e) R. T. C. Brownlee, D. G. Cameron, R. D. Topsom, A. R. Katritsky, and A. F. Pozharsky, *J. Chem. Soc., Perkin Trans. 2*, **1974**, 247; f) B. M. Lynch, *Can. J. Chem.*, **55**, 541 (1977); g) J. Bromilow, R. T. C. Brownlee, R. D. Topsom, and R. W. Taft, *J. Am. Chem. Soc.*, **98**, 2022 (1976); h) J. E. Dubois, A. F. Hegarty, and E. D. Bergman, *J. Org. Chem.*, **37**, 2218 (1971); i) J. E. Dubois, J. J. Aaron, P. Alcais, J. P. Doucet, F. Rothenberg, and R. Uzan, *J. Am. Chem. Soc.*, **94**, 6823 (1972); j) B. Ancian, J. P. Doucet, and J. E. Dubois, *ibid.*, **98**, 4764 (1976); k) G. Goethals, F. Membrey, B. Ancian, and J. P. Doucet, *J. Org. Chem.*, **43**, 4944 (1978); l) B. Ancian, F. Membrey, and J. P. Doucet, *ibid.*, **43**, 1509 (1978); m) F. Membrey, B. Ancian, and J. P. Doucet, *Org. Magn. Reson.*, **11**, 580 (1978); n) F. Membrey, B. Ancian, and J. P. Doucet, *J. Chem. Soc., Perkin Trans. 2*, **1980**, 1399; o) A. Argile and M.-F Ruasse, *J. Org. Chem.*, **48**, 209 (1983); p) A. J. Hoefnagel, M. A. Hoefnagel, and B. M. Wepster, *J. Am. Chem. Soc.*, **98**, 6194 (1976).

9) See, for example, T. Bally, E. Haselbach, S. Lanyiova, F. Marschner, and M. Rossi, *Helv. Chim. Acta*, **59**, 486 (1976).

10) K. S. Dhami and J. B. Stothers, *Can. J. Chem.*, **43**, 510 (1965).

11) G. K. Hamer, I. R. Peat, and W. F. Reynolds, *Can. J. Chem.*, **51**, 897 (1973).

12) K. S. Dhami and J. B. Stothers, *Can. J. Chem.*, **43**, 479 (1965).

13) J. B. Stothers and P. C. Lauterber, *Can. J. Chem.*, **42**, 1563 (1964).

14) H. O. Krabbenhoft, *J. Org. Chem.*, **43**, 1830 (1978).

15) T. B. Posner and C. D. Hall, *J. Chem. Soc., Perkin Trans. 2*, **1976**, 729.
16) J. A. Pople and M. Gordon, *J. Am. Chem. Soc.*, **89**, 4253 (1967).
17) O. Kajimoto and T. Fueno, *Tetrahedron Lett.*, **1972**, 3329.
18) The authors express their sincere thanks to Mr. T. Hinomoto of JEOL for his recording the ^{13}C NMR spectra.

Synthesis of Homoallylic Alcohols from Allylic Phosphates and Aldehydes with Organoaluminum Reagent Containing Al-Sn Linkage[1)]

Seijiro MATSUBARA, Kuni WAKAMATSU, Yoshitomi MORIZAWA, Noriyuki TSUBONIWA, Koichiro OSHIMA,* and Hitosi NOZAKI

Department of Industrial Chemistry, Faculty of Engineering, Kyoto University, Yoshida, Kyoto 606

(Received November 27, 1984)

Treatment of allylic phosphates with the reagent prepared from *n*-Bu_3SnLi and Et_2AlCl or from SnF_2 and Et_2AlCl affords allyltin compounds which react with aldehydes to produce homoallylic alcohols in good yields. The formation of allyltin compounds requires the catalytic amount of $Pd(PPh_3)_4$ and proceeds with inversion of the stereochemistry predominantly.

The addition of allylmetal species[2)] to carbonyl compounds is one of the most important methods for C–C bond formation. The stereoselectivity of the reaction as well as the yields of products depend on the nature of the element such as Si,[3)] Sn,[4)] Cr,[5)] Sm,[6)] Y,[6)] Mn,[7)] Ti,[8)] and Zr.[8)] Among them the organotin compounds are widely used because of their easiness of handling and high reactivity. For instance, the reaction of allylstannanes with carbonyl compounds in the presence of Lewis acid provides erythro homoallylic alcohols with high stereoselectivity.[4b)] The allylation of carbonyl compounds also proceeds effectively with allylstannanes generated from allylic halides and tin metal[4c)] or divalent tin compounds.[4d)] Limitations associated with availability of the allylic halides[4c,d)] in these reactions have led us to examine allylic phosphates[9)] as an alternative starting material.

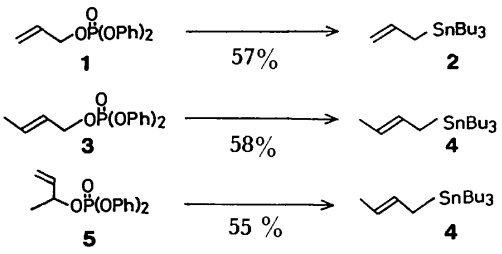

n-Bu_3SnLi (2 eq), Et_2AlCl (2 eq), $Pd(PPh_3)_4$ (0.1 eq)

Scheme 1.

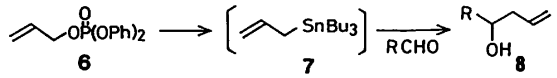

Scheme 2.

An organoaluminum reagent produced from *n*-Bu_3SnLi[10)] and Et_2AlCl, is considered to have an aluminum–tin single bond[11)] and has proved to be useful for synthetic reactions.[1)] Treatment of allyl diphenyl phosphate **1** with this reagent in the presence of $Pd(PPh_3)_4$ catalyst gave allylstannane **2** in 57% yield,[12)] and (*E*)-2-butenyl diphenyl phosphate **3** produced (*E*)-2-butenyltributylstannane **4** in 58% yield. Diphenyl 1-methyl-2-propenyl phosphate **5** also afforded (*E*)-2-butenyltributylstannane **4** contaminated by a small amount of its *Z* isomer in a 55% combined yield (Scheme 1). The yields of these products could not be improved over 70% in spite of various attempts because of the difficulty in isolating allylic stannane in a pure form.

The presence of an equimolar amount of aldehyde in this reaction system resulted in the direct formation of homoallylic alcohol **8** in good yields (Scheme 2). For example, the treatment of a mixture of allyl diphenyl phosphate and benzaldehyde with *n*-Bu_3Sn–$AlEt_2$ in the presence of $Pd(PPh_3)_4$ provided 1-phenyl-3-buten-1-ol in 82% yield after aqueous work-up. The results are summarized in Table 1.

The high reaction temperature (200 °C) is neces-

TABLE 1. SYNTHESIS OF HOMOALLYLIC ALCOHOLS FROM ALLYLIC PHOSPHATES AND ALDEHYDES WITH *n*-Bu_3SnLi–Et_2AlCl SYSTEM

Run	Phosphates	Aldehydes	Products[a)]	Yields[b)]	*E*/*T*
1	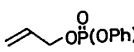	PhCHO	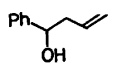	82%	—
2	〃	Hexanal	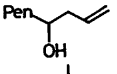	70%	—
3	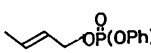	PhCHO	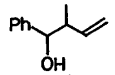	70%	(41/59)[c)]
4	〃	Hexanal	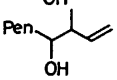	65%	(47/53)[d)]
5	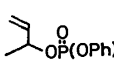	PhCHO	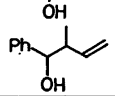	82%	(38/62)[c)]

a) All compounds gave satisfactory spectra data. See Ref. 5. b) Isolated yields. c) Ratios of the stereoisomers (erythro and threo) were determined by the examination of ^1H-NMR signal of the methine (H–C–OH) proton. See experimental section. d) A ratio of the stereoisomer was determined by GLPC analysis. See experimental section.

Table 2. Synthesis of homoallylic alcohols from allylic phosphates and aldehydes with SnF_2–Et_2AlCl system

Run	Phosphates	Aldehydes	Products[a]	Yields[b]	*E*/*T*
1	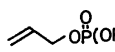	PhCHO	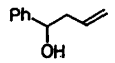	95%	—
2	〃	Hexanal	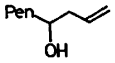	69%	—
3	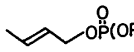	PhCHO	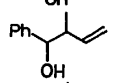	96%	(33/67)[c]
4	〃	Hexanal	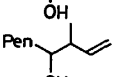	80%	(50/50)[d]
5	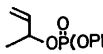	PhCHO	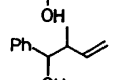	78%	(25/75)[c]
6	〃	Hexanal	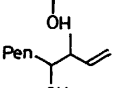	77%	(55/45)[d]

a) All compounds gave satisfactory spectra data. See Ref. 5. b) Isolated yields. c) Ratios of the stereoisomers (erythro and threo) were determined by the examination of ^{1}H-NMR signal of the methine (H–C–OH) proton. See experimental section. d) Ratios of the stereoisomers were determined by GLPC analysis. See experimental section.

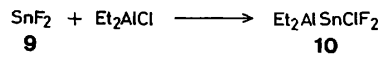

Scheme 3.

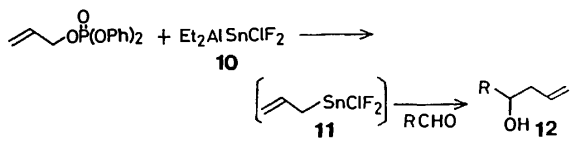

Scheme 4.

sary for the allylation of benzaldehyde with allyltributylstannane in the absence of Lewis acid.[4e] In contrast, the reaction proceeds at room temperature in the presence of Lewis acid. The stereoselectivity of the reaction between allylstannane and aldehyde depends on the nature of Lewis acids employed.[4f] In our case, Et_2Al–OP(O)(OPh)$_2$(compound **18** in Ref. 15) could behave as a Lewis acid giving poor selectivity.

Treatment of SnF_2 with an equimolar amount of Et_2AlCl in CH_2Cl_2 gave a dark red homogeneous solution. The reagent **10** thus prepared is assumed to have an aluminum–tin single bond (Scheme 3), and proved to be effective in the homoallylic alcohol synthesis from allylic phosphate and aldehyde. The results are summarized in Table 2.

The reaction is expected to involve an allylstannane **11** (Scheme 4) which has failed to be isolated. The threo stereoselectivity in the reaction with SnF_2–Et_2AlCl is slightly superior (run 3, 4) to that observed in *n*-Bu_3Sn–$AlEt_2$ reagent system.

The stereochemistry of the allylstannane synthsis from $R_3SnAlEt_2$ and allylic phosphate is shown in Scheme 5. Treatment of cis allylic phosphates **13** with Me_3Sn–$AlEt_2$ in the presence of a catalytic amount of $Pd(PPh_3)_4$ provided a mixture of cis and trans allylic stannanes **14a,b** and **15a,b** in 28:72 ratio. Both ratios of **14a**:**14b** and **15a**:**15b** were 1:1. Similar reaction of the trans isomer **16** gave **14a,b** and **15a,b** in 78:22 ratio, the ratios of **14a**:**14b** and **15a**:**15b** being 1:1 again. The stereochemistry of the allylstannanes was determined

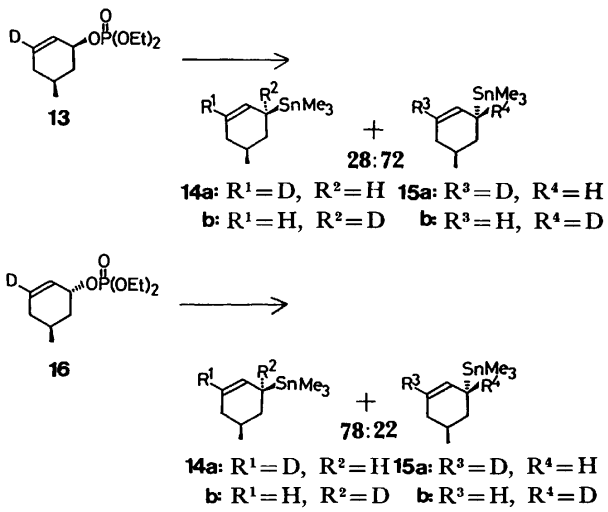

Scheme 5.

by the examination of ^{119}Sn NMR spectra.[13] These results showed that the reaction has proceeded predominantly with the net inversion of the phosphates stereochemistry[14,15,16]

Experimental

The IR spectra were determined on a Shimadzu IR-27-G spectrometer, the mass spectra on a Hitachi M-80 machine, and the proton NMR spectra on a Varian EM-390 spectrometer and a Varian XL-200 spectrometer. The ^{119}Sn NMR and ^{13}C NMR spectra were determined on a JEOL-FX 90Q spectrometer. The chemical shifts of the proton NMR and the ^{13}C NMR are given in δ, with tetramethylsilane as an internal standard, and those of the ^{119}Sn NMR are given in δ, with tetramethylstannane as an internal standard. Tetrahydrofuran was freshly distilled from sodium benzophenone ketyl. Dichloromethane was dried over P_2O_5 and distilled. All the experiments were carried out under an argon atmosphere. Purification of products was performed by preparative thin-layer chromatography (PLC), or column chromatography on silica gel (Wakogel C-100) or alumina (Merck,

Art. 1077 Aluminiumoxid 90 aktiv neutral, 70—230 mesh). Analytical GLPC was performed with a Yanagimoto GCG-550-F and a Shimadzu GC-4CPT. Preparative GLPC was performed with a JEOL-JGC-20K apparatus.

Preparation of Allyltributylstannane with the Reagent Derived from n-*Bu*$_3$*SnLi and Et*$_2$*AlCl.* A hexane solution of butyllithium (1.6 M,† 3.8 ml, 6.0 mmol) was added to a suspension of anhydrous tin(II) chloride (0.38 g, 2.0 mmol) in THF (4.0 ml) at 0 °C. After being stirred for 20 min, the reaction mixture was treated with a hexane solution of diethylaluminum chloride (1.0 M, 2.0 ml, 2.0 mmol) at 0 °C. The resulting mixture was stirred for another 20 min, and a mixture of allyl diphenyl phosphate (0.29 g, 1.0 mmol) and Pd(PPh$_3$)$_4$ (0.12 g, 0.1 mmol) in THF (4 ml) was added. The whole was stirred for 1 h, then the reaction mixture was poured into 5% NaOH (70 ml) and extracted with ether (30 ml×3). The combined organic layers were washed with 5% NaOH (60 ml×2), dried over anhydrous sodium sulfate and concentrated. The crude product was purified by alumina column chromatography (hexane) followed by distillation (bp 120 °C/0.1 Torr,†† bath temp) to give allyltributylstannane in 57% yield as a colorless oil. This compound was identical with the authentic sample.[12a]

(E)-2-Butenyltributylstannane:[12a] The title compound was produced stereospecifically in 58% yield from (*E*)-2-butenyl diphenyl phosphate. Treatment of diphenyl 1-methyl-2-propenyl phosphate with *n*-Bu$_3$SnAlEt$_2$ as described above gave the *E* and *Z* isomeric mixture of 2-butenyltributylstannane in 55% yield. The stereochemistry was determined by ^{13}C NMR spectra.[17] The ratio of the intensity of olefinic carbon for *E*:*Z* was 10:1.

The Synthesis of Homoallylic Alcohols with the n-*Bu*$_3$*SnLi–Et*$_2$*AlCl Reagent.* A mixture of diphenyl 1-methyl-2-propenyl phosphate (0.61 g, 2.0 mmol), benzaldehyde (0.11 g, 1.0 mmol), and Pd(PPh$_3$)$_4$ (0.12 g, 0.1 mmol) was added at 0 °C to a THF solution of *n*-Bu$_3$SnAlEt$_2$ (2.0 mmol) prepared following the procedure described above. After being stirred for 1 h at room temperature, the reaction mixture was poured into 1 M hydrochloric acid (40 ml) and extracted with ether. The combined organic layers were washed with saturated NaHCO$_3$ aqueous solution, dried over anhydrous sodium sulfate, and concentrated. The purification by PLC (hexane–ethyl acetate, 5:1) gave 2-methyl-1-phenyl-3-buten-1-ol[5] in 68% yield: Bp 110 °C (bath temp, 4 Torr); IR (neat): 3400, 1635, 1492, 1011, 908, 758, 698 cm^{-1}; NMR (CCl_4): δ= 0.83 (d, J=7.2 Hz, 1.8 H, threo isomer), 0.94 (d, J=6.6 Hz, 1.2 H, erythro isomer), 2.15 (bs, 1H), 2.3—2.5 (m, 1H), 4.26 (d, J=6.8 Hz, 0.59 H, threo isomer), 4.43 (d, J=5.8 Hz, 0.41 H, erythro isomer), 4.9—5.2 (m, 2H), 5.5—5.9 (m, 1H), 7.23 (s, 5H); MS *m/z* (%): 162 (M$^+$, 0.5), 145 (10), 107 (99), 105 (36), 79 (100), 77 (96), 51 (16).

The Synthesis of Homoallylic Alcohol with SnF$_2$*–Et*$_2$*AlCl Reagent.* A hexane solution of diethylaluminum chloride (1.0 M, 2.0 ml, 2.0 mmol) was added to a suspension of anhydrous tin(II) fluoride (0.31 g, 2.0 mmol) in CH_2Cl_2 (5 ml) at 0 °C. The solution turned to red immediately. After the resulting mixture was stirred for 20 min, a mixture of diphenyl 1-methyl-2-propenyl phosphate (0.61 g, 2.0 mmol), hexanal (0.10 g, 1.0 mmol), and Pd(PPh$_3$)$_4$ (0.12 g, 0.1 mmol) was added, and the whole was stirred for 2 h at 20 °C. The reaction mixture was poured into 1 M hydrochloric acid and extracted with ether. The combined organic layers were washed with saturated NaHCO$_3$ aqueous solution, dried over anhydrous Na$_2$SO$_4$, and concentrated. The Purification by PLC (hexane–ethyl acetate, 5:1) gave an isomeric mixture of 3-methyl-1-nonen-4-ol[5] as a colorless oil (0.12 g, 80%). The isomeric ratio of the product (erythro/threo=1/1) was determined by GLPC [PEG 20 M 5%, on Celite 545, 1.5 m, 110 °C, T_r (threo)=9.0 min, T_r (erythro)=10.6 min]: Bp 90 °C (bath temp, 10 Torr); IR (CCl_4): 3380, 1638, 1260, 1081, 1000, 911 cm^{-1}, NMR (CCl_4): δ=0.92 (t, J=7.5 Hz, 3H), 1.04 (d, J=6.6 Hz, 3H), 1.0—1.6 (m, 8H), 1.80 (bs, 1H), 2.0—2.4 (m, 1H), 3.2—3.5 (m, 1H), 5.01 (dd, J=17.1, 2.7 Hz, 1H), 5.18 (dd, J=10.8, 2.7 Hz, 1H), 5.6—5.9 (m, 1H); MS *m/z* (%): 156 (M$^+$, 1.0), 133 (3), 101 (12), 83 (53), 56 (100), 55 (89), 43 (20), 41 (41).

The Stereochemical Study on the Allylic Stannane Synthesis. An ether solution of methyllithium (1.8 M, 5.0 ml, 9.0 mmol) was added to a suspension of anhydrous tin(II) chloride (0.57 g, 3.0 mmol) in THF (4 ml) at 0 °C. After being stirred for 20 min, the reaction mixture was treated with a hexane solution of Et$_2$AlCl (1.0 M, 3.0 ml, 3.0 mmol) at 0 °C. The resulting mixture was stirred for 20 min, and a mixture of *cis*- or *trans*-3-deuterio-5-methyl-2-cyclohexen-1-yl diethyl phosphate[18] (0.37 g, 1.5 mmol) and Pd(PPh$_3$)$_4$ (0.17 g, 0.15 mmol) was added. The whole was stirred for another 2 h at 20 °C, then the solution was poured into 5% NaOH (70 ml) and extracted with ether (30 ml×3). The combined organic layers were washed with 5% NaOH (60 ml×2), dried over anhydrous Na$_2$SO$_4$, and concentrated. The ratio of four isomers, **14a**, **14b**, **15a**, **15b**, was determined by the examination of ^{119}Sn NMR spectra of crude products.[13]

cis- *and* trans-*5-Methyl-2-cyclohexen-1-ol:*[18] According to the previously reported procedure,[18] *cis* isomer of the title compound was prepared from 5-methyl-2-cyclohexen-1-one[19] by reduction with lithium aluminum hydride. The aluminum triisopropoxide reduction of 5-methyl-2-cyclohexen-1-one gave the mixture of *cis* and *trans* isomers in 4:3 ratio, which was transformed into *p*-nitrobenzoates with *p*-nitrobenzoyl chloride and pyridine. Recrystallization from ethanol gave *trans* isomer which was hydrolyzed to give *trans*-5-methyl-2-clohexen-1-ol.[20] The ^{1}H NMR spectra in $CDCl_3$ for both isomers are shown as follows.

cis-*5-Methyl-2-cyclohexenyl* p-*Nitrobenzoate*: δ=1.05 (d, J= 6.4 Hz, 3H), 1.15—2.25 (m, 6H), 5.65—5.75 (m, 2H), 5.80—5.95 (m, 1H), 8.10—8.35 (m, 4H).

tans-*5-Methyl-2-cyclohexenyl* p-*Nitrobenzoate*: δ= 1.04 (d, J= 6.5 Hz, 3H), 1.15—2.25 (m, 6H), 5.49—5.60 (m, 1H), 5.80—5.95 (m, 1H), 6.05—6.20 (m, 1H), 8.10—8.35 (m, 4H).

References

1) Another reports using these reagents, see, S. Matsubara, N. Tsuboniwa, Y. Morizawa, K. Oshima, and H. Nozaki, *Bull. Chem. Soc. Jpn.*, **57**, 3242 (1984); J. Hibino, S. Matsubara, Y. Morizawa, K. Oshima, and H. Nozaki, *Tetrahedron Lett.*, **25**, 2151 (1984).

2) Y. Yamamoto and K. Maruyama, *Heterocycles*, **18**, 375 (1982); P. A. Bartlett, *Tetrahedron*, **36**, 3 (1980); G. Courtois and L. Miginiac, *J. Organomet. Chem.*, **69**, 1 (1974).

3) E. W. Colvin, "Silicon in Organic Synthsis," Butterworths, London (1981), pp. 97—124; W. P. Weber, "Silicon for Organic Synthsis," Springer-Verlag, New York (1983), pp. 114—128; T. H. Chan and I. Fleming, *Synthesis*, **1979**, 761.

† 1 M=1 mol·dm^{-3}.

†† 1 Torr=133.322 Pa.

4) a) Y. Yamamoto, "Kagaku Zokan," No. 96, ed by H. Nozaki, T. Mukaiyama, H. Yamamoto, Kagaku Dojin, Kyoto (1982), pp. 155—164; b) Y. Yamamoto, H. Yatagai, Y. Naruta, and K. Maruyama, *J. Am. Chem. Soc.*, **102**, 7107 (1980); c) J. Nokami, J. Otera, T. Sudo, and R. Okawara, *Organometallics*, **2**, 193 (1983); J. Nokami, S. Wakabayashi, and R. Okawara, *Chem. Lett.*, **1984**, 869; T. Mukaiyama and T. Harada, *ibid.*, **1981**, 1527; d) T. Mukaiyama, T. Harada, and S. Shoda, *ibid.*, **1980**, 1507; T. Harada and T. Mukaiyama, *ibid.*, **1981**, 1109; e) K. König and W. P. Neumann, *Tetrahedron Lett.*, **1967**, 495; f) G. E. Keck, D. E. Abboff, E. P. Boden, and E. J. Enholm, *ibid.*, **25**, 3927 (1984).

5) T. Hiyama, Y. Okude, K. Kimura, and H. Nozaki, *Bull. Chem. Soc. Jpn.*, **55**, 561 (1982).

6) P. Girard, J. L. Namy, and H. B. Kagan, *J. Am. Chem. Soc.*, **102**, 2693 (1980).

7) T. Hiyama, M. Sawahata, and M. Obayashi, *Chem. Lett.*, **1983**, 1237; J. F. Normant and G. Cahiez, "Modern Synthetic Methods, Transition Metal in Organic Synthesis," ed by R. Scheffald, Otto Salle Verlag, Frankfurt am Main (Coedition by John Wiley and Son, New York), (1983), pp. 173—216.

8) D. Seebach, B. Weidmann, and L. Widler, "Modern Synthetic Methods, Transition Metal in Organic Synthesis," ed by R. Scheffald, Otto Salle Verlag, Frankfurt am Main (Coedition by John Wiley and Son, New York), (1983), pp. 217—354.

9) The allylations of aldehydes are also performed with the Cr(II) reagent[5] and allylic phosphates. The results will be published.

10) C. Tamborski, F. E. Ford, and E. J. Soloski, *J. Org. Chem.*, **28**, 237 (1963); W. C. Still, *J. Am. Chem. Soc.*, **99**, 4836 (1977) and 1481 (1978); W. Kitching, H. A. Olszowg, and J. Harvey, *J. Org. Chem.*, **47**, 1893 (1982).

11) Many compounds which have tin-metal single bond were reported. For, Sn-Mg: H. M. J. C. Creemers, J. G. Noltes, and J. M. Van Der Kerk, *J. Organomet. Chem.*, **14**, 217 (1968); Sn-Zn: F. J. A. Des Tambe and G. J. M. Van Der Kerk, *ibid.*, **43**, 323 (1972); Sn-Al: L. Rösch and W. Erb, *Angew. Chem. Int. Ed. Engl.*, **17**, 604 (1978); general review, see K. M. Mackay and B. K. Nicholson, "Comprehensive Organometallic Chemistry," ed by G. Wilkinson, Pergamon Press, Oxford, (1982) Vol. 6, pp. 1043—1114.

12) a) E. Matarasso-Tchiroukhine and P. Cadiot, *J. Organomet. Chem.*, **121**, 155 and 169 (1976); b) K. Maruyama, H. Yatagai, Y. Yamamoto, Abstract of 26th Symposium on Organometal Chemistry, Japan, 112 (1979); c) S. J. Hannon, T. G. Traylor, *J. Chem. Soc., Chem. Commun.*, **1975**, 630; d) Y. Ueno, M. Okawara, *J. Am. Chem. Soc.*, **101**, 1893 (1979); Y. Ueno, S. Aoki, M. Okawara, *ibid.*, **101**, 5414 (1979).

13) M. Pereyre and J.-P. Quintard, *Pure and Appl. Chem.*, **53**, 2401 (1981); J.-P. Quintard, M. Degueil-Castaing, G. Dumartin, A. Rahm, and M. Pereyre, *J. Chem. Soc., Chem. Commun.*, **1980**, 1004.

14) J. Tsuji, "Organic Synthesis with Palladium Compounds," Springer-Verlag, Berlin (1980); B. M. Trost, *Chem. Br.*, **20**, 315 (1984); B. M. Trost, J. Yoshida, and M. Lautens, *J. Am. Chem. Soc.*, **105**, 4494 (1983).

15) The Scheme 6 is consonant with the observation. The attack of Pd(O) on allylic phosphate provides π-allylpalladium having phosphoryloxy group as a ligand. The transmetalation of trialkylstannyl group on aluminum to palladium followed by reductive elimination gives aluminum compounds **18**, allylstannane **19**, and Pd(O).

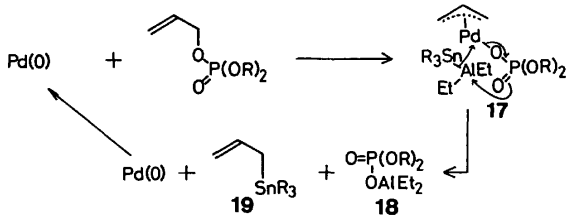

Scheme 6.

16) Allylstannane synthesis by means of aluminum-tin reagent has been reported after submitting this paper. B. M. Trost and J. W. Herndon, *J. Am. Chem. Soc.*, **106**, 6835 (1984).

17) A. Gambaro, D. Marton, V. Peruzzo, and G. Tagliavini, *J. Organomet. Chem.*, **204**, 191 (1981).

18) H. L. Goering and J. P. Blanchard, *J. Am. Chem. Soc.*, **76**, 5407 (1954).

19) J. P. Blanchard and H. L. Goering, *J. Am. Chem. Soc.*, **73**, 5863 (1951).

20) A. Itoh, S. Ozawa, K. Oshima, S. Sasaki, H. Yamamoto, T. Hiyama, and H. Nozaki, *Bull. Chem. Soc. Jpn.*, **53**, 2357 (1980).

Copper(II)-Catalyzed Transamination between Pyruvate and Hydrophobic Pyridoxamine Embedded in Synthetic Bilayer Membranes†

Yukito MURAKAMI,* Jun-ichi KIKUCHI, and Kazunari AKIYOSHI
Department of Organic Synthesis, Faculty of Engineering, Kyushu University, Hakozaki, Higashi-ku, Fukuoka 812
(Received December 7, 1984)

The copper(II)-catalyzed transamination of 4-aminomethyl-5-[(dihexadecylamino)methyl]-2-methyl-3-pyridinol [(PM)2C_{16}] with sodium pyruvate was investigated in an aqueous medium at pH 6.9, μ 0.10 (KCl), and 30.0±0.1 °C in the presence of single-walled bilayer vesicles of *N,N*-dihexadecyl-*N*$^{\alpha}$-[6-(trimethylammonio)-hexanoyl]-L-alaninamide bromide [N^+C_5Ala2C_{16}] and *N,N*-dihexadecyl-*N*$^{\alpha}$-[6-(trimethylammonio)hexanoyl]-L-histidinamide bromide [N^+C_5His2C_{16}]. The binding mode of the pyridoxamine moiety in the vesicles was clarified by comparing the reaction behavior of the (PM)2C_{16}-pyruvate-Cu^{II} system with that of the 4-aminomethyl-5-dodecylthiomethyl-2-methyl-3-pyridinol [(PM)C_{12}]-pyruvate-Cu^{II} system. The pyridoxamine moiety of (PM)2C_{16} was more tightly anchored in the hydrogen-belt domain of the membranes than that of (PM)C_{12} as confirmed by fluorescence polarization spectroscopy. The difference in binding mode between (PM)2C_{16} and (PM)C_{12} is reflected on the copper(II)-coordination equilibria for the formation of the copper(II)-ketimine intermediates. The copper(II)-catalyzed transamination of (PM)2C_{16} with pyruvate in the N^+C_5His2C_{16} vesicle was most enhanced among related reaction systems treated here. The rate enhancement was attributed to the favorable formation of the reactive 2:1 ketimine-copper(II) chelate and the general-base catalysis by the coordination-free imidazolyl group of the lipid.

Bilayer membranes have been utilized as effective media for various organic reactions, exhibiting marked functional assistance.[1-5] The interior hydrophobic domain of bilayer membranes may provide a microenvironment favorable for such reactions due to the following effects: (i) desolvation of reacting species to a significant extent relative to those in homogeneous media; (ii) proximal alignment of reacting species, which is forced by the hydrophobic interactions with organized lipid molecules; (iii) catalytic assistance by some functional groups substituted on lipid molecules. In this regard, the functional simulation of a holoenzyme system composed of an apoprotein and a relevant coenzyme is expected to be made by utilizing a combination of a synthetic bilayer membrane and the corresponding coenzyme factor modified with some hydrophobic substituents.

We have previously reported that the single-walled vesicles composed of synthetic peptide lipids, *N,N*-ditetradecyl-*N*$^{\alpha}$-[6-(trimethylammonio)hexanoyl]-L-alaninamide bromide [N^+C_5Ala2C_{14}] and *N,N*-ditetradecyl-*N*$^{\alpha}$-[6-(trimethylammonio)hexanoyl]-L-histidinamide bromide [N^+C_5His2C_{14}], provide reaction environments favorable for functional simulation of the vitamin B_6-dependent transaminase.[6,7] For the transamination of a hydrophobic pyridoxamine derivative, (PM)C_{12}, with pyruvate in the molecular aggregates, the copper(II) ion effectively catalyzed the isomerization of the ketimine Schiff-base to the corresponding aldimine Schiff-base, and the subsequent addition of ethylenediaminetetraacetate afforded the corresponding pyridoxal analogue and alanine as the final products. The kinetic analysis has shown the following characteristic features. (i) The 2:1 and 1:1 ketimine-copper(II) chelates are present during the reaction, and the reactivity of the former chelate is much larger than that of the latter in the N^+C_5Ala2C_{14} vesicle. (ii) The N^+C_5His2C_{14} vesicle allowed the formation of the 1:1 chelate in preference to that of the 2:1 chelate, and the coordination-free imidazolyl group of the lipid molecule effectively catalyzes the isomerization as a general base.

In order to improve the catalytic function of such an artificial transaminase, we prepared a pyridoxamine derivative bearing a hydrophobic double-chain, (PM)-2C_{16}, which is able to interact with matrix membranes more tightly than (PM)C_{12} having only a single hydrophobic chain.[8] We report in this article the reaction behavior of (PM)2C_{16} with pyruvate in the individual vesicles of N^+C_5Ala2C_{16} and N^+C_5His2C_{16} as effected by the copper(II) ion. A kinetic feature observed by anchoring the pyridoxamine moiety in the so-called hydrogen-belt domain[9] of the vesicles is to be discussed in terms of the proximity and orientation effects.

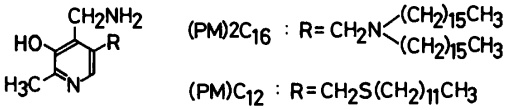

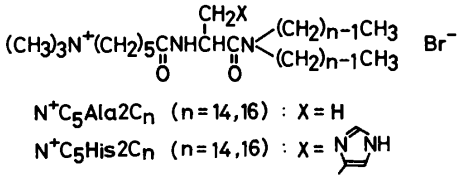

Experimental

General Analyses and Measurements. Elemental analyses were performed at the Microanalysis Center of Kyushu University. ^{1}H-NMR spectra were taken on a Hitachi R-24B spectrometer. A Beckman Φ 71 pH meter equipped with a Beckman 39505 combined electrode was used for pH-measurements after calibration with a combination of appropriate standard aqueous buffers. Electronic absorption spectra were taken on a Union Giken SM-401 high-sensitivity spec-

†Contribution No. 761 from this Department.

trophotometer. Fluorescence polarization measurements were made on a Union Giken FS-501A spectrophotometer equipped with a Sord M200 Mark II microcomputer. The steady-state fluorescence anisotropy (r_s) originated from the pyridoxamine moiety of (PM)2C_{16} or (PM)C_{12} was calculated by Eq. 1, where I is the fluorescence intensity, and the subscripts v and h refer to the orientations, vertical and horizontal, respectively, for the excitation and analyzer polarizers in this sequence. C_f is the grating correction factor, given by I_{hv}/I_{hh}.

$$r_s = (I_{vv} - C_f I_{vh})/(I_{vv} + 2C_f I_{vh}) \quad (1)$$

Materials. Preparation and characterization of hydrophobic pyridoxamines, (PM)C_{12}[7] and (PM)2C_{16},[8] and a peptide lipid having the L-alanine residue, N^+C_5Ala2C_{16},[10] have been described elsewhere. A peptide lipid having the L-histidine residue, N^+C_5His2C_{16}, was prepared by the method adopted for the synthesis of N^+C_5His2C_{14}:[6] a colorless glassy solid, $[\alpha]_D^{20}$ −9.5° (*c* 0.84, EtOH); ^{1}H-NMR ($CDCl_3$, Me_4Si) δ= 0.85 [6H, t, $(CH_2)_{15}\underline{CH_3}$], 1.23 [56H, m, $CH_2(\underline{CH_2})_{14}CH_3$], 1.90 [6H, m, $N^+CH_2(\underline{CH_2})_3CH_2CO$], 2.20 [2H, br t, $N^+(CH_2)_4\underline{CH_2}CO$], 2.80—3.50 [8H, m, N^+CH_2, NCH_2, and $CHC\underline{H_2}Im$], 3.30 [9H, s, $(CH_3)_3N^+$], 5.00 [1H, m, $NHC\underline{H}CO$], 6.91 [1H, s, Im-5H], 7.60 [1H, d, NH], 7.95 [1H, s, Im-2H].

Found: C, 66.60; H, 10.85; N, 8.03%. Calcd for $C_{47}H_{92}BrN_5O_2\cdot(1/2)H_2O$: C, 66.56; H, 11.05; N, 8.26%.

Kinetic Measurements. The copper(II)-catalyzed transamination reaction of (PM)2C_{16} with pyruvate in the single-walled vesicles was monitored spectrophotometrically in an aqueous 2-[4-(2-hydroxyethyl)-1-piperazinyl]ethanesulfonate (HEPES) buffer (2.5×10^{-3} mol dm^{-3}, pH 6.9) containing 0.10 mol dm^{-3} potassium chloride at 30.0±0.1 °C. The experimental details are analogous to those reported previously for the copper(II)-catalyzed reaction of (PM)C_{12} with pyruvate in the individual vesicles of N^+C_5Ala2C_{14} and N^+C_5His2C_{14}.[7]

Results and Discussion

Microenvironments Around the Pyridoxamine Moiety in Vesicles. The peptide lipids, N^+C_5Ala2C_{16} and N^+C_5His2C_{16}, form single-walled vesicles in aqueous media upon sonication as confirmed by electron microscopy.[10] The amino acid residues of the lipids are placed in the so-called hydrogen-belt domain[9] interposed between the hydrophobic region formed with aliphatic double chains and the hydrophilic zone with ionic head groups. In order that an effective catalytic assistance is performed by the imidazolyl group of N^+C_5His2C_{16} in the transamination, it is desirable that the pyridoxamine moiety is anchored in the hydrogen-belt domain so tightly as to interact with the imidazolyl group. The microenvironmental polarity around the pyridoxamine moiety of (PM)C_{12} incorporated into the individual vesicles of N^+C_5Ala2C_{14} and N^+C_5His2C_{14} was evaluated from its electronic absorption spectra, and found to be equivalent to that provided by dioxane-water (1:1 v/v); Kosower's *Z*-value,[11] 87.[7] This polarity value is in good agreement with that for the hydrogen-belt domain of the vesicle composed of *N,N*-dihexadecyl-*N*$^\alpha$-[1-(6-trimethylammoniohexyl)-1,4-dihydro-3-pyridylcarbonyl]-L-alaninamide bromide (*Z*-value, 89);[3] evaluated with attention to the 1,4-dihydronicotinamide moiety which is inevitably fixed in the vicinity of the domain. The pyridoxamine moiety of (PM)2C_{16} is also placed in the similar microenvironment within the vesicles of N^+C_5Ala2C_{16} (*Z*-value, 87).[8]

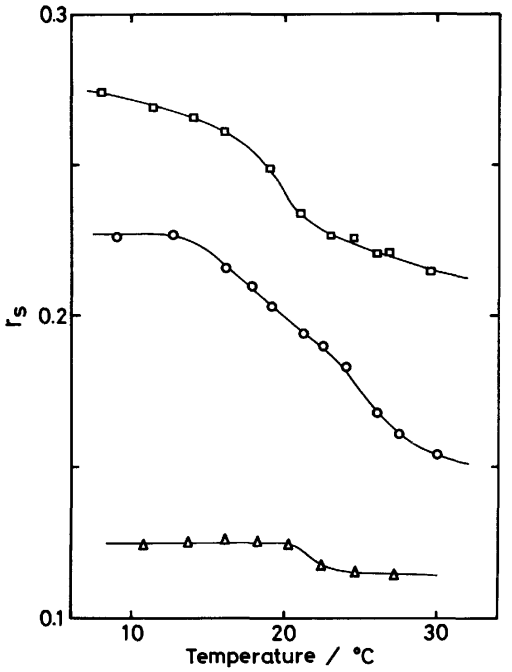

Fig. 1. Correlations between temperature and steady-state fluorescence anisotropy (r_s) for the pyridoxamine moiety (5.0×10^{-5} mol dm^{-3}) in an aqueous HEPES buffer (2.5×10^{-3} mol dm^{-3}) at pH 6.9 and μ 0.10 (KCl) in the presence of single-walled vesicles of peptide lipids (1.0×10^{-3} mol dm^{-3}): ○, (PM)2C_{16} in N^+C_5Ala2C_{16} (taken from Ref. 8); □, (PM)2C_{16} in N^+C_5His2C_{16}; △, (PM)C_{12} in N^+C_5Ala2C_{16}. Excitation and emission wavelengths: 360 and 450 nm for (PM)2C_{16}; 335 and 390 nm for (PM)C_{12}, respectively.

The parameters for steady-state fluorescence anisotropy (r_s) originated from the pyridoxamine moieties of (PM)2C_{16} and (PM)C_{12} in the vesicles were much different from each other. As shown in Fig. 1, the r_s values for (PM)2C_{16} in the individual vesicles of N^+C_5Ala2C_{16} and N^+C_5His2C_{16} are large relative to the corresponding values for (PM)C_{12} in the N^+C_5Ala2C_{16} vesicle over the whole temperature range studied here. The single-walled N^+C_5Ala2C_{16} vesicle shows a broad phase transition range (20±5 °C) as confirmed by differential scanning calorimetry[10] as well as by fluorescence polarization spectroscopy with 1,6-diphenyl-1,3,5-hexatriene embedded in the vesicle.[8] The r_s values for (PM)2C_{16} in the individual vesicles of N^+C_5Ala2C_{16} and N^+C_5His2C_{16} are more sensitive to the phase transition than that for (PM)C_{12} in the N^+C_5Ala2C_{16} vesicle. The result strongly suggests that the pyridoxamine moiety of (PM)2C_{16} is tightly anchored in the hydrogen-belt domain in the vesicles through the hydrophobic interaction of its double-chain portion with the hydrophobic domain of the vesicles. On the other

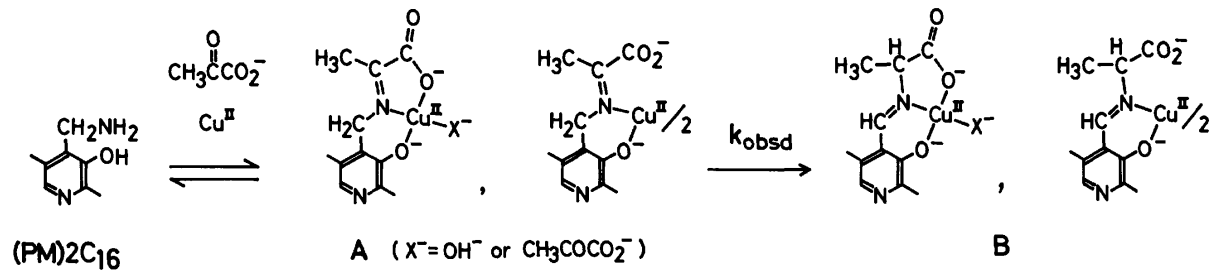

Scheme 1.

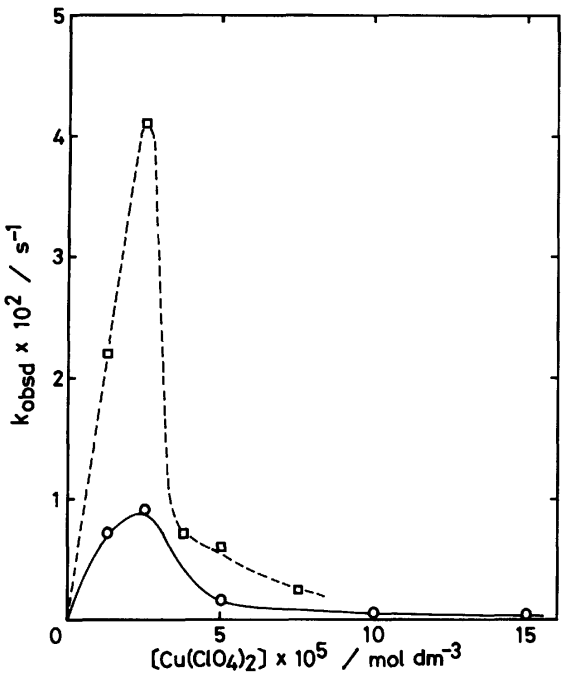

Fig. 2. Correlations between total concentration of $Cu(ClO_4)_2$ and first-order rate constant for the isomerization of Cu^{II}-ketimine to Cu^{II}-aldimine in an aqueous HEPES buffer (2.5×10^{-3} mol dm^{-3}) at pH 6.9, μ 0.10 (KCl), and 30.0±0.1 °C in the presence of $N^+C_5Ala2C_{16}$ (○, 1.0×10^{-3} mol dm^{-3}) and $N^+C_5His2C_{16}$ (□, 1.0×10^{-3} mol dm^{-3}) with initial concentrations: $(PM)2C_{16}$, 5.0×10^{-5} mol dm^{-3}; sodium pyruvate, 5.0×10^{-3} mol dm^{-3}. A solid line refers to the calculated data on the basis of Scheme 2 and evaluated kinetic parameters (Table 1).

hand, the pyridoxamine moiety of $(PM)C_{12}$ is more mobile in the vesicles than that of $(PM)2C_{16}$, although the equilibrium locations of the pyridoxamine moieties of both pyridoxamine derivatives are nearly identical. In addition, the larger r_s values for $(PM)2C_{16}$ in the $N^+C_5His2C_{16}$ vesicle relative to the corresponding values in the $N^+C_5Ala2C_{16}$ vesicle over the whole temperature range may reflect the associative interactions, hydrogen-bonding and π-π interactions, between the pyridoxamine moiety and the imidazolyl group of the former lipid. Such interactions result in repression of the molecular motion of $(PM)2C_{16}$.

Transamination Reaction in $N^+C_5Ala2C_n$ Vesicles. The reaction was initiated by adding copper(II) perchlorate and sodium pyruvate to the covesicles of $N^+C_5Ala2C_{16}$ and $(PM)2C_{16}$, and the progress of the transamination was monitored by spectrophotometric

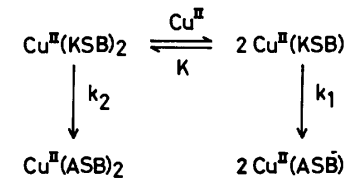

KSB: ketimine Schiff-base
ASB: aldimine Schiff-base

Scheme 2.

means. In a manner as observed for the copper(II)-catalyzed transamination of $(PM)C_{12}$ with pyruvate in the $N^+C_5Ala2C_{14}$ vesicle,[7] the reaction proceeded through the fast equilibrated formation of the copper(II) complexes of ketimine Schiff-base (**A** in Scheme 1), followed by much slower conversion into the copper(II) complexes of aldimine Schiff-base (**B** in Scheme 1). The isomerization was followed by monitoring an absorption increase at 390 nm, attributable to the formation of the copper(II)-aldimine chelates, and consistent with the first-order kinetics for each run. The observed rate constant, k_{obsd}, was plotted against the total concentration of $Cu(ClO_4)_2$ as shown in Fig. 2. The rate constant reaches a maximum and then falls down as the copper(II) concentration further increases. This kinetic feature is similar to that observed for the copper(II)-catalyzed reaction of $(PM)C_{12}$ with pyruvate in the $N^+C_5Ala2C_{14}$ vesicle.[7] The kinetic analysis was performed on the basis of Scheme 2 in a manner as reported previously[7] under conditions that both of the 2:1 and 1:1 (ketimine:Cu^{II}) chelate species are present. The kinetic parameters thus obtained for the isomerization are listed in Table 1, and the calculated molar distributions of the individual chelate species are shown in Fig. 3 against the copper(II) concentration. The reactivity of the 2:1 chelate is much larger than that of the 1:1 chelate in each reaction system, and the effective charge on the copper(II) atom seems to exert much effect on the reactivity as discussed previously.[7]

The formation of all the copper(II)-ketimine species, evaluated from the amounts of the copper(II)-aldimine chelates produced by the isomerization, is more pronounced in the $(PM)2C_{16}$-pyruvate-Cu^{II} system than in the $(PM)C_{12}$-pyruvate-Cu^{II} system: 88 and 78% mole fractions of the pyridoxamine moiety are transformed into the copper(II)-ketimine chelates for the former and the latter, respectively, at 2.5×10^{-5}

Table 1. Specific rate constants for isomerization reaction of Cu^{II}–ketimine to Cu^{II}–aldimine and stability constants for Cu^{II}–ketimine chelates in $N^+C_5Ala2C_n$ (1.0×10^{-3} mol dm^{-3}) vesicles at 30.0 ± 0.1 °C[a)]

Parameter	(PM)2C16 in $N^+C_5Ala2C_{16}$[b)]	(PM)C12 in $N^+C_5Ala2C_{14}$[c)]
k_1/s^{-1}	2.7×10^{-4}	6.8×10^{-4}
k_2/s^{-1}	1.0×10^{-2}	1.2×10^{-2}
K	170	20

a) In an aqueous HEPES buffer (2.5×10^{-3} mol dm^{-3}) at pH 6.9 and μ 0.10 (KCl). b) Initial concentrations in mol dm^{-3}: (PM)2C16, 5.0×10^{-5}; sodium pyruvate, 5.0×10^{-3}; $Cu(ClO_4)_2$, 1.3×10^{-5}—1.5×10^{-4}. c) Ref. 7.

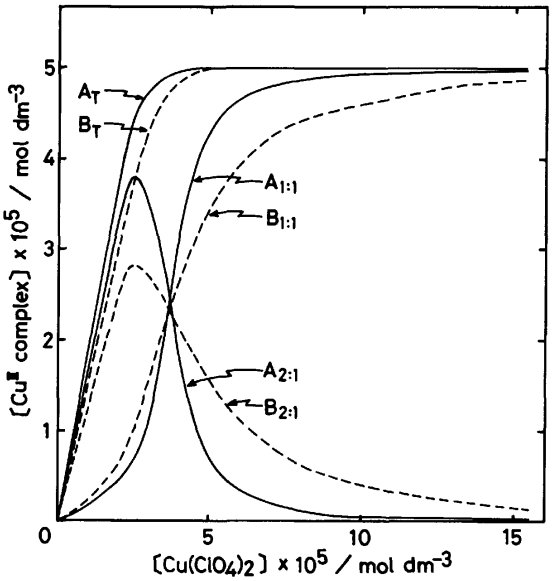

Fig. 3. Distributions of Cu^{II}-ketimine chelates in an aqueous HEPES buffer (2.5×10^{-3} mol dm^{-3}) at pH 6.9, μ 0.10 (KCl), and 30.0 ± 0.1 °C in the presence of $N^+C_5Ala2C_n$ (1.0×10^{-3} mol dm^{-3}): A, (PM)2C16 (5.0×10^{-5} mol dm^{-3})-pyruvate (5.0×10^{-3} mol dm^{-3})-Cu^{II} in $N^+C_5Ala2C_{16}$; B, (PM)C12 (5.0×10^{-5} mol dm^{-3})-pyruvate (5.0×10^{-3} mol dm^{-3})-Cu^{II} in $N^+C_5Ala2C_{14}$ (taken from Ref. 7). Subscripts T, 1:1 and 2:1 denote the total, 1:1 and 2:1 (ketimine:Cu^{II}) chelate species, respectively; [Cu^{II} complex] is given in terms of the Schiff-base unit.

mol dm^{-3} of $Cu(ClO_4)_2$ where the maximum rates were observed for the respective systems (Fig. 3). This clearly indicates that the tight fixation of the pyridoxamine moiety of (PM)2C16 in the hydrogen-belt domain entropically favors the formation of the copper(II)-ketimine chelates and further enhances the formation of the 2:1 ketimine-copper(II) chelate, as compared with the corresponding reaction system involving (PM)C12, in a lower concentration range of the copper(II) ion ([$Cu(ClO_4)_2$]<3.8×10^{-5} mol dm^{-3}): *i.e.*, molar ratios of the 2:1 chelate to the 1:1 chelate (in terms of the Schiff-base unit) at 2.5×10^{-5} mol dm^{-3} $Cu(ClO_4)_2$ are 6.3 and 2.5 for the (PM)2C16 and (PM)-C12 systems, respectively (Fig. 3).

Comparison of the stability constants for the formation of the 1:1 ketimine-copper(II) complex, as defined by Eq. 2, provides another important information.

$$K = [Cu^{II}(KSB)]^2/[Cu^{II}(KSB)_2][Cu^{II}] \quad (2)$$

The K value for the (PM)2C16 system is larger than that for the (PM)C12 system, and this requires some explanation. The efficient hydrophobic interaction of the two double-chain segments of the 2:1 ketimine-copper(II) chelate derived from (PM)2C16 with the hydrophobic vesicle domain acts to anchor the pyridoxamine moieties tightly in the intramembrane region, and consequently mobility of the pyridoxamine moieties are much repressed relative to those of the corresponding complex of (PM)C12. The resulting side-by-side arrangement of the pyridoxamine moieties of (PM)2C16 molecules with the lipid molecules in the hydrogen-belt domain induces a large steric strain within the chelate molecule since the copper(II) ion is forced to take some distorted coordination geometry away from its favorite square-planar one under such circumstances. The strain energy released upon formation of the 1:1 chelate must be greater than that for the corresponding chelate derived from (PM)C12. The steric strain effect is reflected on the activation entropy values observed above the phase transition temperature of $N^+C_5Ala2C_{16}$: for the 2:1 chelate, −2.43; for the 1:1 chelate, +23.3 J K^{-1} mol^{-1}.[8)]

Transamination Reaction in $N^+C_5His2C_n$ Vesicles. The reaction behavior of the copper(II)-catalyzed transamination in the $N^+C_5His2C_n$ vesicles is much influenced by the nature of coenzyme factors. In the (PM)2C16–pyruvate–Cu^{II}–$N^+C_5His2C_{16}$ system, the rate constant reaches a maximum at a 1:2 molar ratio of copper(II) to (PM)2C16 and then falls down sharply as the copper(II) concentration further increases (Fig. 2). The conversions to the aldimine-copper(II) chelate are 50 and 100% on the pyridoxamine base at the 4:1 and 2:1 molar ratios of (PM)2C16 to copper(II), respectively, as confirmed by electronic absorption spectroscopy. This clearly indicates that the copper-(II) ion is quantitatively converted into the 2:1 ketimine-copper(II) chelate under such conditions. On this basis, the specific rate constant evaluated for the 2:1 ketimine-copper(II) chelate in the $N^+C_5His2C_{16}$ vesicle, 0.041 s^{-1}, is 4 times larger than that for the same complex in the $N^+C_5Ala2C_{16}$ vesicle, indicating that the catalytic assistance is performed by the imidazolyl group of $N^+C_5His2C_{16}$ as a general base.

In the copper(II) concentration range higher than the 1:2 molar ratio of copper(II) *vs.* (PM)2C16, the reactivity is sharply reduced. This behavior is presumably originated from the two factors: transformation of the 2:1 ketimine-copper(II) chelate into the 1:1 chelate, which has lower reactivity relative to the former; coordination of the imidazolyl group to the copper(II) atom which results in masking of its catalytic activity.

As for the (PM)C12–pyruvate–Cu^{II}–$N^+C_5His2C_{14}$ system, conversion to the aldimine-copper(II) chelate reaches a value of 50% on the pyridoxamine base at

the 2:1 molar ratio of (PM)C_{12} to copper(II), indicating that the 1:1 ketimine–copper(II) chelate is present as the predominant species.[7] Even though the 2:1 chelate may be more reactive than the 1:1 complex in the light of the above observations, the larger fractional distribution of the 1:1 chelate over the whole copper(II) concentration range studied seems to be responsible for the lower reactivity relative to the reaction system involving (PM)2C_{16}.

In conclusion, it became apparent that the binding mode of the pyridoxamine moiety of the coenzyme analogues in the synthetic bilayer membranes appreciably controls the reaction behavior of the copper(II)-catalyzed transamination with pyruvate. The tight anchoring of the pyridoxamine moiety in the hydrogen-belt domain of the vesicles as observed with (PM)-2C_{16} results in the favorable formation of the reactive 2:1 ketimine–copper(II) chelate, and consequently the transamination reaction is much accelerated. The holoenzyme model system composed of (PM)2C_{16}, N^+-C_5His2C_{16}, and the copper(II) ion showed the extremely large reactivity for the transamination with pyruvate, which is originated from the bifunctional assistance by the copper(II) ion and the coordination-free imidazolyl group of N^+C_5His2C_{16}; the former acts to produce the reactive 2:1 chelate while the latter catalyzes the reaction as a general base.

The present work was supported in part by Grant-in-Aid for Scientific Research No. 58430016 from the Ministry of Education, Science, and Culture.

References

1) M. F. Czarniecki and R. Breslow, *J. Am. Chem. Soc.*, **101**, 3675 (1979).
2) Y. Murakami, A. Nakano, A. Yoshimatsu, and K. Fukuya, *J. Am. Chem. Soc.*, **103**, 728 (1981).
3) Y. Murakami, J. Kikuchi, K. Nishida, and A. Nakano, *Bull. Chem. Soc. Jpn.*, **57**, 1371 (1984).
4) T. Kunitake, H. Ihara, and Y. Okahata, *J. Am. Chem. Soc.*, **105**, 6070 (1983); and references cited therein.
5) R. C. Petter, J. C. Mitchell, W. J. Brittain, T. J. McIntosh, and N. A. Porter, *J. Am. Chem. Soc.*, **105**, 5700 (1983).
6) Y. Murakami, A. Nakano, and K. Akiyoshi, *Bull. Chem. Soc. Jpn.*, **55**, 3004 (1982).
7) Y. Murakami, J. Kikuchi, A. Nakano, K. Akiyoshi, and T. Imori, *Bull. Chem. Soc. Jpn.*, **57**, 1116 (1984).
8) Y. Murakami, J. Kikuchi, and K. Akiyoshi, *Chem. Lett.*, **1984**, 1185.
9) Y. Murakami, A. Nakano, and H. Ikeda, *J. Org. Chem.*, **47**, 2137 (1982).
10) Y. Murakami, A. Nakano, A. Yoshimatsu, K. Uchitomi, and Y. Matsuda, *J. Am. Chem. Soc.*, **106**, 3613 (1984).
11) E. M. Kosower, *J. Am. Chem. Soc.*, **80**, 3253 (1958).

 © 1985 The Chemical Society of Japan Bull. Chem. Soc. Jpn., 58, 1205—1209 (1985)

Phase Transition Behavior and Membrane Structure of Monoalkyl Amphiphiles

Atsushi KUMANO, Tisato KAJIYAMA,* Motowo TAKAYANAGI,
Toyoki KUNITAKE,** and Yoshio OKAHATA†
*Department of Applied Chemistry and **Organic Synthesis, Faculty of Engineering, Kyushu University 36, Hakozaki 6-10-1, Higashi-ku, Fukuoka 812*
(Received March 31, 1984)

Membrane structure and crystal-liquid crystal phase transition behaviors were investigated for two kinds of artificial amphiphiles with single alkyl chain and *N*-benzylideneaniline moiety. These artificial amphiphiles showed both thermotropic and lyotropic mesomorphisms in a similar manner to biological lipids. Artificial amphiphile with one polar head group formed the multilayer liposome even in a low concentration region of amphiphile/water system. Artificial amphiphile with two polar head groups at both ends of the molecule does not form the multilayer liposome but forms monomolecular lamellae. Addition of cholesterol to the two polar-headed amphiphile changed its aggregated structure drastically from monomolecular lamellae to large single liposomes composed of monomolecular layer. In the case of two polar-headed amphiphile/water system, two endothermic peaks were observed, which were assigned to gel I to gel II and gel II to mesophase transitions. These transitions may correspond to meltings of partial and whole part of hydrophobic portion in amphiphilic molecule, respectively.

Biological membranes are mainly composed of phospholipids which are composed of one polar head group and two alkyl chains. It has been extensively discussed on the reason why phospholipids form the bimolecular-layered membrane in water at a low concentration region, instead of globular micells or two-dimensional lamellae.[1] Many artificial amphiphiles were synthesized by Kunitake *et al.*[2-5] For some of these amphiphiles, membrane structures and permeation properties were investigated on the basis of X-ray diffraction, differential scanning calorimetry and osmosis experiments.[6-9] It was concluded that existence of two alkyl chains played an important role for formation of the stabler bilayer structure. Also, it was confirmed that these artificial amphiphiles with two alkyl chains exhibited similar characteristics with respect to molecular aggregation states, thermal properties and permeation properties of water and metal cations to those of biological phospholipids.

Ordinary amphiphiles with single alkyl chain such as soap or detergent form bimolecular lamellae in water only at a high concentration region, while they do not form bimolecular layers but form cylindrical or globular micelles at a low concentration.[10] A series of ammonium amphiphiles composed of *N*-benzylideneaniline moiety and single alkyl chain were synthesized.[11-13] It is well known that *N*-benzylideneaniline moiety is capable of forming liquid crystalline structures due to its additional intermolecular interaction and rigid character.[14] Therefore, it is interesting to investigate the effect of *N*-benzylideneaniline moiety on the formation of single- or bimolecular-layered membrane in water at a low concentration region.

The purpose of this paper is to investigate the membrane structure and the crystal-liquid crystal phase transition behavior of artificial amphiphiles in water system, which are composed of single alkyl chain, mesogenic group and one or two polar head groups.

Experimental

Materials. Figure 1 shows the chemical structures of artificial amphiphiles studied in this paper. *N*-[*p*-(trimethylammonio)benzylidene]-*p*-dodecylaniline bromide ($C_{12}BBN^+3C_1$: sample 1) was prepared by reaction of *p*-dodecylaniline and (*p*-formylphenyl)trimethylammonium bromide.[11] *N*-[*p*-[10-(trimethylammonio)decyloxy]]-*p*-[10-(trimethylammonio)-decyloxy]aniline dibromide ($N^+C_{10}BBC_{10}N^+$: sample 2) was prepared by condensation reaction of [10-(*p*-formylphenoxy)-decyl]trimethylammonium bromide and [10-(*p*-aminophenoxy)-decyl]trimethylammonium bromide in refluxing ethanol for 1 h in the presence of a small amount of acetic acid.[13] These artificial amphiphiles are designated as monoalkyl-monocation ($C_{12}BBN^+3C_1$) and monoalkyl-dication ($N^+C_{10}BBC_{10}N^+$).

Electron Microscopic Observation. Several mg of amphiphiles were dissolved in deionized water and subjected to ultrasonic treatment. Almost equal volume of 2 wt% aqueous solution of uranyl acetate was added to the resulting suspension. A drop of the solution was placed and dried on a carbon grid for an electron microscopic observation (TEM).

Differential Scanning Calorimetry. The thermal behavior of the crystal-liquid crystal phase transition in the amphiphile/water system was studied with differential scanning calorimeter (DSC).

X-Ray Analysis. The membrane structure in the amphiphile/water system was studied by wide and small angle X-ray measurements. X-Ray diffraction photographs

1. N-[p-(trimethylammonio)benzylidene]-p-dodecylaniline bromide($C_{12}BBN^+3C_1$)

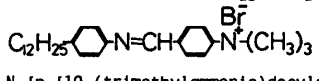

2. N-[p-[10-(trimethylammonio)decyloxy]]-p-[10-(trimethylammonio)decyloxy]aniline dibromide($N^+C_{10}BBC_{10}N^+$)

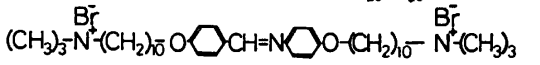

Fig. 1. Chemical structures of totally artificial lipids and their abbreviations.

†Present address: Department of Polymer Science, Tokyo Institute of Technology, Ookayama, Meguro-ku, Tokyo 152.

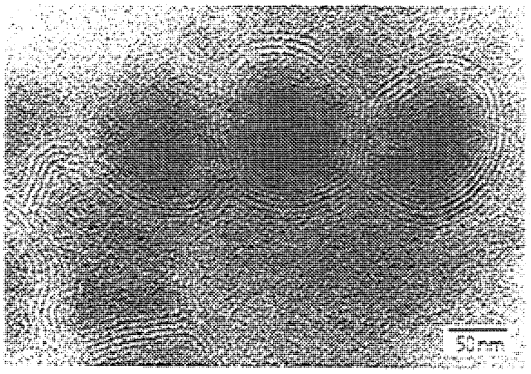

Fig. 2. Electron micrograph of $C_{12}BBN^{+}3C_1$ negatively stained with uranyl acetate.

were obtained with Ni-filtered Cu $K\alpha$ radiation.

Results and Discussion

Membrane Structure and Phase Transition of $C_{12}BBN^{+}3C_1$. Figure 2 shows the electron micrograph of $C_{12}BBN^{+}3C_1$ negatively stained with uranyl acetate. $C_{12}BBN^{+}3C_1$ favorably forms multilayer liposomes in a similar fashion to those of biological lipids. An apparent mean distance between dark striations was 5.8—6.0 nm which nearly corresponds to the bimolecular length of $C_{12}BBN^{+}3C_1$ (5.9—6.0 nm) calculated by the CPK molecular model. Since the deposition of uranyl acetate for negative staining amounts to 1—2 nm thick,[8,9] the exact repeating distance was evaluated from the small angle X-ray scattering (SAXS) measurement as mentioned later.

The multilamellar liposome was observed even in a fairly dilute aqueous solution of C=0.001 (weight fraction of amphiphile in water system) by means of an electron microscopy. This concentration is quite lower in comparison with the case for ordinary surfactants with monoalkyl chain which form the bimolecular lamellar structure at a higher concentration range above $C\simeq0.6$.[10] The stable liposome formation at an extremely low concentration in the case of $C_{12}BBN^{+}3C_1$ must be due to introduction of the rigid segment of *N*-benzylideneaniline moiety which enhances the intermolecular interaction.

Figure 3 shows the phase diagram and the concentration, (C: weight fraction) dependence of the long spacing, (L) for $C_{12}BBN^{+}3C_1$. Thermal analytical studies of $C_{12}BBN^{+}3C_1$ were carried out over the concentration range of $0.1<C\leq1.0$. The endothermic transition due to melting of alkyl chains was observed over whole concentration range studied here. The endothermic peak due to melting of ice was observed at 273 K in the concentration range lower than about C=0.83. In the concentration range of $0.83<C\leq1.0$, no endothermic transition due to melting of ice was observed in heating curve. Water molecules hydrated to the polar head groups did not form ice on cooling the $C_{12}BBN^{+}3C_1$/water mixture below 273 K.[6] The critical concentration at which nonhydrated (free) water appeared was determined by extrapolating the

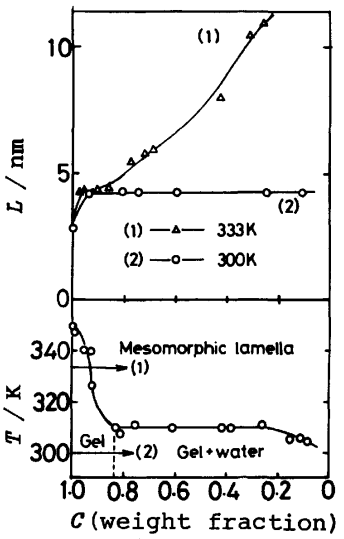

Fig. 3. Variation of the phase transition temperature (lower) and the long spacing (upper) with the concentration of $C_{12}BBN^{+}3C_1$.

magnitude of the heat of fusion of ice at 273 K *vs.* the concentration of $C_{12}BBN^{+}3C_1$ to zero. The critical concentration between gel and gel+water phases was determined to be 0.83, where the gel phase means the crystalline phase with bound water hydrated to the hydrophilic polar head groups. This value of the critical concentration indicates that on an average, five water molecules hydrate to one polar head group of $C_{12}BBN^{+}3C_1$ and these bound water molecules do not form ice on cooling even to 220 K.[8] The gel to mesophase transition temperature decreases steadily with a decrease of $C_{12}BBN^{+}3C_1$ concentration to the limiting value of 310 K over the concentration range of $0.83<C\leq1.0$. The phase diagram of the $C_{12}BBN^{+}3C_1$/water system has a very similar behavior to those of biological lipids[15] and artificial amphiphiles with two alkyl chains.[6,7,9] It is apparent from the phase transition behavior that $C_{12}BBN^{+}3C_1$ has characteristics of both thermotropic and lyotropic liquid crystals in a similar fashion to phospholipids or artificial lipids with two alkyl chains. L measured at 300 K increases with decreasing the $C_{12}BBN^{+}3C_1$ concentration down to C=0.83, where free water appears in the $C_{12}BBN^{+}3C_1$/water mixture. As mentioned before, the hydrophilic polar head group can incorporate limited amount of water and therefore, the bimolecular lamellae of $C_{12}BBN^{+}3C_1$ were gradually spread with an increase in the water concentration up to C=0.83.

The formation of lamellar structure was confirmed by the result that the ratio of reciprocal of long spacing for higher order scatterings were 1:2:3. The long spacing of the lamellar layer in a gel state is approximately one-half of the bimolecular length estimated from the CPK molecular model on the assumption of planar zigzag conformation of hydrocarbon chains. This result may be explained by the following two possible models for the assembly of $C_{12}BBN^{+}3C_1$

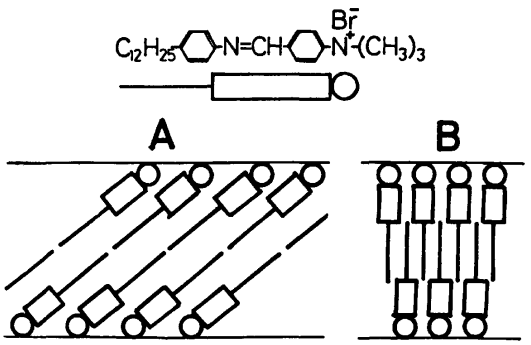

Fig. 4. Schematic assembly models for $C_{12}BBN^+3C_1$ bilayer.

molecules as shown in Fig. 4. Figure 4A is the model that hydrocarbon chains tilt with an angle of 30° to the lamellar surface. Figure 4B shows the mutual insertion of hydrocarbon chains from the opposite directions. Structure amplitudes were calculated for the two models of Figs. 4A and 4B and compared with an observed relative structure amplitude. The most plausible packing model for the $C_{12}BBN^+3C_1$/water system was determined to be the latter one (the mutual insertion of hydrocarbon chains) on the basis of the electron density distribution obtained by means of SAXS measurement.[16,17] In this case, the alkyl chains are almost perpendicular to the membrane surface. The detailed results will be reported elsewhere.[17]

Membrane Structure and Phase Transition of $N^+C_{10}BBC_{10}N^+$. $N^+C_{10}BBC_{10}N^+$ has the two polar head groups at both ends and *N*-benzylideneaniline moiety of a rigid segment in hydrocarbon chains at the para-position. In general, chemical substances containing a rigid segment such as *N*-benzylideneaniline moiety can form liquid crystalline phase. Therefore, amphiphile of monoalkyl-dication type makes us expect that the monomolecular membrane can be easily formed in a dilute aqueous solution owing to existence of the two polar head groups at both ends of molecule.

Figure 5 (a) shows the electron micrograph of $N^+C_{10}BBC_{10}N^+$ negatively stained with uranyl acetate. $N^+C_{10}BBC_{10}N^+$ amphiphile could not form multilayer liposome, but the parallel aggregation of lamellae. Taking into account the deposition of uranyl acetate, the thickness of parallel aggregated lamellae (5.3—6.4 nm) is considered to correspond to the one molecular length of $N^+C_{10}BBC_{10}N^+$ (4.4—4.5 nm) calculated by use of the CPK model. Figure 5(b) exhibits that incorporation of cholesterol to $N^+C_{10}BBC_{10}N^+$ induces a transformation from monomolecular lamellae to single- or multi-layer liposome. The diameter of vesicles are 100—200 nm and their membrane thickness is 5—20 nm. It is reasonably expected that cholesterol molecules mostly locate in the outer half of the layer, creating suitable curvature for the vesicle formation as shown in Fig. 5 (c). Figure 5(c) represents schematic speculations with respect to formation of monolayer liposome for $N^+C_{10}BBC_{10}N^+$ with

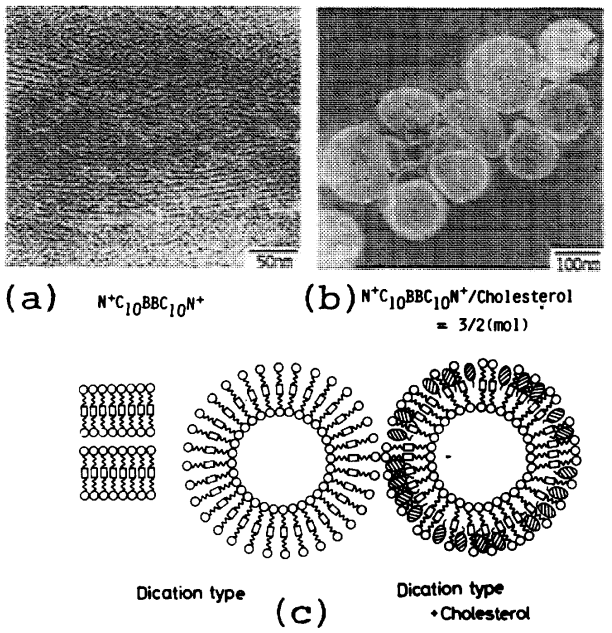

Fig. 5. (a) Electron micrograph of $N^+C_{10}BBC_{10}N^+$ negatively stained with uranyl acetate. (b) Electron micrograph of $N^+C_{10}BBC_{10}N^+$+cholesterol (3:2 molar mixture). (c) Schematic packing model of $N^+C_{10}BBC_{10}N^+$ and possible formation of monolayer liposome.

and without cholesterol. In the case of bimolecular membrane of dialkyl- or monoalkyl-monocation artificial amphiphiles, then number of molecules must be different in the outer and the inner layers because of the different spherical surface area for the inner and the outer shells. On the other hand, $N^+C_{10}BBC_{10}N^+$ forms monomolecular layer due to existence of dication groups at the both ends of the molecule as shown in the left assembly model of Fig. 5 (c). Considering the liposome formation of $N^+C_{10}BBC_{10}N^+$ in the case of this assembly, however, a large amount of vacancy or defect is produced especially in the outer half of spherical shell as shown by the middle aggregation model of Fig. 5 (c). These vacancies or defects may be reduced by addition of the second components such as cholesterol as shown in the right assembly model of Fig. 5 (c). Therefore, the monomolecular liposome of $N^+C_{10}BBC_{10}N^+$ was stably formed by addition of cholesterol.

Figure 6 shows the variation of the phase transition temperature with the weight fraction of $N^+C_{10}BBC_{10}N^+$. This phase diagram shows that $N^+C_{10}BBC_{10}N^+$ has characteristics of both thermotropic and lyotropic liquid crystals in a similar manner to those of phospholipids in biomembrane or other artificial amphiphiles. In the case of $N^+C_{10}BBC_{10}N^+$, the two endothermic peaks were recognized by DSC measurement. These were assigned to the gel I to gel II and the gel II to mesophase transitions with consideration of the wide angle X-ray diffraction as discussed later. Also, the critical concentration of C=0.84 between gel I and gel I+water (shown by the brokenline in Fig. 6)

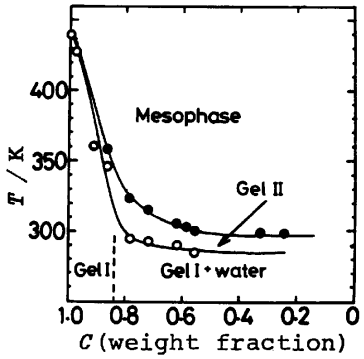

Fig. 6. Variation of the phase transition temperature with the concentration of $N^+C_{10}BBC_{10}N^+$.

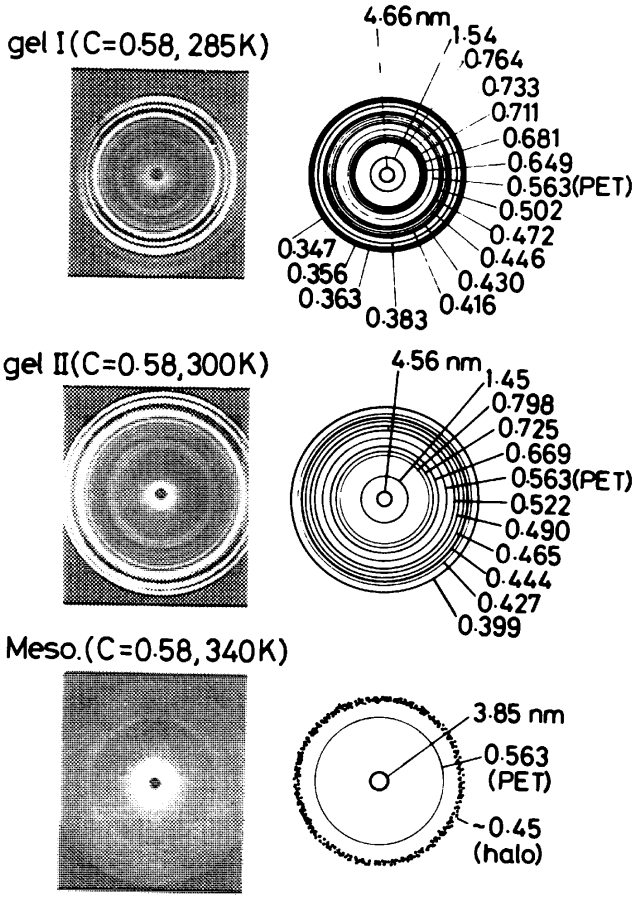

Fig. 7. Wide angle X-ray diffraction patterns for gel I, gel II and mesophase of $N^+C_{10}BBC_{10}N^+$.

was decided in a similar manner to that for $C_{12}BBN^+3C_1$ as mentioned before.

In the case of gel I (C=0.58 at 285 K), many sharp Debye rings were observed as shown in Fig. 7. A spacing of 0.563 nm is due to poly(ethylene terephthalate) (PET) film used as a window of the cell for X-ray measurements. The most inner ring corresponds to the long spacing of $N^+C_{10}BBC_{10}N^+$ (4.66 nm). This value is nearly equal to the single molecular length. In the intermediate range of gel II (C=0.58 at 300 K), the almost all diffraction rings became broader in comparison with those of gel I and their spacings were slightly changed. Also, some diffraction rings corresponding to the short spacing between alkyl chains disappeared, for example, 0.711, 0.649 and 0.416 nm spacings in gel I. Furthermore, the long spacing in gel II became slightly shorter (4.56 nm) than that in gel I. The crystallographic analysis of $N^+C_{10}BBC_{10}N^+$ will be reported in detail elsewhere. The variation of the X-ray diffraction patterns indicates the partial melting of hydrocarbon chains which locate between the polar head and the *N*-benzylideneaniline moiety. Since many fairly sharp diffraction rings were yet remained, it seems that the lateral order of the hydrophobic chains in a gel II state still remained considerably. In the case of mesophase (C=0.58 at 340 K), the sharp Debye rings corresponding to the interchain distance among the hydrophobic chains changed into diffuse ones but the scattering ring in small angle region still retained (3.85 nm), indicating the existence of the layer structure in the mesomorphic phase. These results apparently indicate that the lateral order in the interchain distance among the hydrophobic chains, was lost by melting of the whole part of the hydrophobic portion in $N^+C_{10}BBC_{10}N^+$ molecule without disappearance of layered structure of dication artificial amphiphile in a mesomorphic state as shown in Fig. 8.

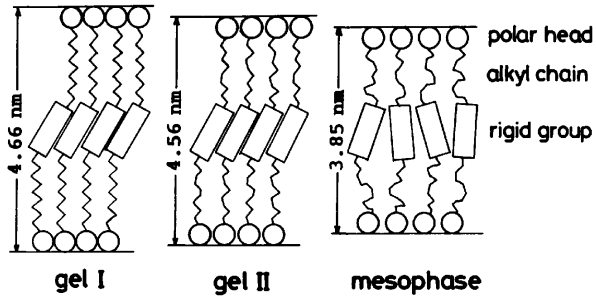

Fig. 8. Schematic representation of molecular membrane structures of $N^+C_{10}BBC_{10}N^+$ for gel I, gel II, and mesophase.

The membrane structures or the aggregation states of $N^+C_{10}BBC_{10}N^+$ for gel I, gel II, and mesomorphic phases were schematically represented in Fig. 8, although they are not clarified yet by the detailed structural analysis. In gel I phase, the alkyl chain has all trans conformation in a crystalline state. In gel II phase, the alkyl chain partially melts, but the lateral order of polar head and rigid *N*-benzylideneaniline moiety remains. In the mesophase, the alkyl chain and the rigid group are in a disordered state but the layer structure are retained.

Conclusion

The artificial amphiphiles which have one or two polar head groups and *N*-benzylideneaniline moiety as a rigid segment in hydrocarbon chains at the para-position formed bimolecular or monomolecular liposomes in an extremely low concentration, depending on the number of the polar heads. The rigid segment is required for inducing an ordered packing

of amphiphilic molecules in a dilute solution. The aggregated structure of the two polar-headed amphiphile (monoalkyl-dication type) is varied drastically from parallel aggregation of monomolecular lamellae to monomolecular or multilayered liposome by adding cholesterol.

The phase transition temperatures of $C_{12}BBN^{+}3C_1$ and $N^{+}C_{10}BBC_{10}N^{+}$ in water system decreased to the limiting value with an increase in water concentration in a concentration range of C=1.0—0.85. Since the long spacing corresponding to the thickness of lamellae was clearly observed above phase transition temperature, it is apparent that melting of hydrocarbon chains is not accompanied by appearance of isotropic phase but the mesomorphic one. The phase diagrams of the amphiphile/water system exhibited that the amphiphiles had characteristics of both thermotropic and lyotropic mesomorphisms.

References

1) C. Tanford, "The Hydrophobic Effect: Formation of Micelle and Biological Membranes," Wiley, New York (1973).

2) T. Kunitake, Y. Okahata, K. Tamaki, F. Kumamaru, and M. Takayanagi, *Chem. Lett.*, **1977**, 387; T. Kunitake, *J. Macromol. Sci., Chem.*, **A13**, 587 (1979).

3) T. Kunitake and Y. Okahata, *Bull. Chem. Soc. Jpn.*, **51**, 1877 (1978).

4) Y. Okahata, R. Ando, and T. Kunitake, *Ber. Bunsenges. Phys. Chem.*, **85**, 789 (1981).

5) Y. Okahata, S. Tanamachi, M. Nagai, and T. Kunitake, *J. Colloid Interface Sci.*, **82**, 401 (1981).

6) T. Kajiyama, A. Kumano, M. Takayanagi, Y. Okahata, and T. Kunitake, *Contemporary Topics in Polym. Sci.*, **4**, 829 (1984).

7) T. Kajiyama, A. Kumano, M. Takayanagi, Y. Okahata, and T. Kunitake, *Chem. Lett.*, **1979**, 645.

8) T. Kajiyama, *Membrane*, **4**, 229 (1979), **6**, 265 (1981).

9) A. Kumano, T. Kajiyama, M. Takayanagi, T. Kunitake, Y. Okahata, *Ber. Bunsenges. Phys. Chem.*, **88**, 1216 (1984).

10) V. Luzzati, H. Mustacchi, and A. Skoulios, *Nature (London)* **180**, 600 (1957), *Disc. Faraday Soc.*, **25**, 43 (1958).

11) T. Kunitake and Y. Okahata, *J. Am. Chem. Soc.*, **102**, 549 (1980).

12) T. Kunitake, Y. Okahata, M. Shimomura, S. Yasunami, and K. Takarabe, *J. Am. Chem. Soc.*, **103**, 5401 (1981).

13) Y. Okahata and T. Kunitake, *J. Am. Chem. Soc.*, **101**, 5231 (1979).

14) "Liquid Crystals and Plastic Crystals," ed by G. W. Gray and P. A. Winsor, Vol. 1 and 2. Wiley, New York (1974).

15) D. Chapman. R. M. Williams, and B. D. Ladbrooke, *Chem. Phys. Lipids*, **1**, 445 (1967).

16) A. Harada, A. Kumano, K. Okuyama, T. Kajiyama, M. Takayanagi, and T. Kunitake, *Rept. Progr. Polym. Phys. Jpn.*, **25**, 789 (1982).

17) A. Harada, K. Okuyama, A. Kumano, T. Kajiyama, M. Takayanagi, and T. Kunitake, submitted to *Polym. J.*

Conformation Analyses of Poly(L-lysine) Induced by Various Surfactants

Kunio TAKEDA

Department of Applied Chemistry, Faculty of Science, Okayama University of Science, 1-1 Ridai-cho, Okayama 700

(Received June 29, 1984)

The relative proportion of α-helix, β, and random-coil structures in each conformation of poly(L-lysine) (PLL) caused by surfactants was computed by simulating a mixed spectrum of typical circular dichroism(CD) spectra for these structures to the experimentally obtained spectrum. Simulation was done in both the 190—250 nm and 200—250 nm regions at 1-nm intervals. The results show that PLL assumed 52 and 75% α-helix (at largest) in sodium octyl sulfate (SOS) and sodium 1-octanesulfonate solutions, respectively. The α-helical structure was found to coexist with considerable amounts of β and random-coil structures in these surfactant solutions. For instance, 51% α-helical structure coexisted with 29% β-structure and 20% random-coil structure in 6.0 mmol dm^{-3} SOS. In contrast, PLL did not assume any α-helical structure in the concentration range of 0 to 10 mmol dm^{-3} sodium dodecyl sulfate(SDS). Rather, the random-coil structure was transformed to a β-structure when SDS was added to PLL. The effects of NaCl and of 1-octanol on the relative proportions of the three structures in PLL were also examined.

Conformational changes of homopolypeptides have been extensively studied using circular dichroism (CD) measurements. Poly(L-lysine) (PLL) has been frequently selected as a typical polypeptide because of its diversity in conformations.[1-8] The conformational change of PLL induced by surfactants has been studied by a number of investigators.[3-8] The conformation of PLL transforms to α-helix and then β-structure with an increase of sodium octyl sulfate (SOS)[3,7], while it transforms to the β-structure and then to the α-helical structure with an increase of sodium 1-octanesulfonate.[6] The PLL assumes a β-structure in solutions of sodium alkyl sulfates with hydrophobic chains longer than ten carbons.[3-5,8] However, few attempts have been made quantitatively to estimate the relative proportions of α-helix, β, and random-coil structures in the conformations of homopolypeptides induced by surfactants.

The CD spectra of the various structural conformations in a polypeptide chain are assumed to be additive.[9-18] This is now commonly accepted even for proteins which have more complex conformations than the homopolypeptides.[9-18] The relative proportion of α-helix, β, and random-coil structures can be estimated from the experimentally obtained spectrum of a polypeptide with known reference spectra of the three structures. In the present study, the relative proportion of the three structures in PLL has been computed at various concentrations of the three surfactants, SOS, sodium 1-octanesulfonate, and sodium dodecyl sulfate (SDS). This has been achieved by simulating a mixed spectrum of the typical CD spectra for these structures to the experimentally obtained spectrum according to the method of Greenfield and Fasman.[9]

Experimental

The source of PLL has been described elsewhere.[7] The SOS and SDS used were the same samples as used before.[8,19] The 1-octanol was purchased from Aldrich Chemical Co. (purity: 99%).

CD measurements were made with a JASCO J-500A spectropolarimeter equipped with a DP-501 data processor. Details of the CD measurements have been described previously.[7] All measurements were carried out at 20 °C and at a neutral pH.

Results and Discussion

The CD spectrum is a curve of continuous values of the residue ellipticity of structural elements averaged over a certain wavelength region. By examining the shape and strength of the CD spectrum over the region of π-π* and n-π* transitions,[9] the relative proportions of α-helix, β, and random-coil structures could be obtained on each conformation of PLL which was considered to partially assume these three structures in surfactant solutions.[3-8]

It has been found that PLL assumes an α-helical structure only in solutions of SOS[3,7] and sodium 1-

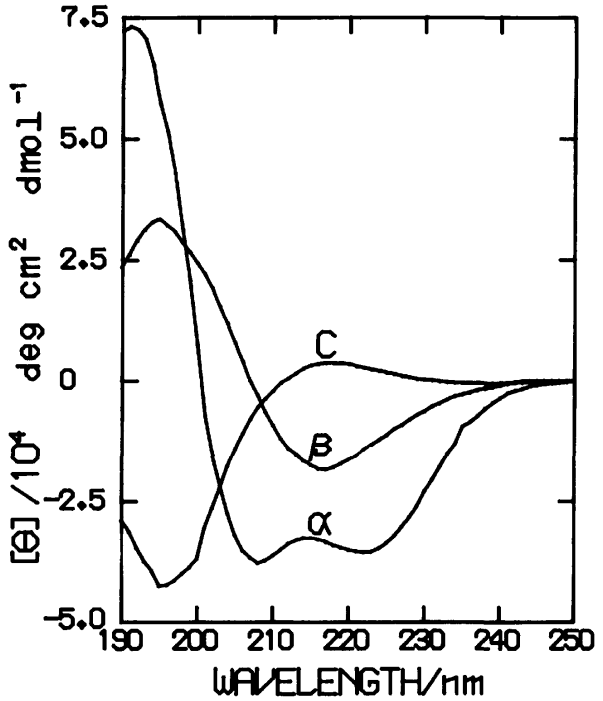

Fig. 1. Three reference spectra of α-helix (α), β-structure (β), and random coil structure (C) of PLL. Preparations of the three forms were described in text.

octanesulfonate[6] which have the same hydrophobic chain of 8 carbons. The CD spectra of PLL, in SOS concentrations between 4 and 6 mM (1 M=1 mol dm^{-3}), show a double-negative maximum which is indicative of the α-helix.[7] PLL also displays two types of CD spectra which characterize random-coil and β structures below and above the concentration range of SOS, respectively.[7] In sodium 1-octanesulfonate solutions, the CD spectra of PLL are dependent on the concentration. At concentrations of the surfactant below 6 mM, they are characteristic of a random conformation, of the β-structure between 6 and 8 mM, and of the α-helix structure above 8 mM.[6]

Figure 1 shows three reference CD spectra[9] corresponding to the three structures. The reference spectra were used to analyse the experimentally obtained spectrum of PLL. The spectrum of the α-helical structure was determined at a concentration of 0.56 mM PLL (residue) at pH 11.6. The same sample of PLL was heated to 52 °C for 15 min and then cooled to obtain the spectrum of the β-structure.[20] The spectrum of PLL obtained at a neutral pH in the absence of a surfactant was used as a typical spectrum of the random-coil structure. The negative intensities of the π-π* and n-π* transitions of the α-helical PLL in surfactant solutions (Fig. 1 in Ref. 3 and Fig. 1 in Ref. 7) are considerably smaller than that of the polypeptide in the alkaline pH range (Fig. 1). This was first observed by Grourke and Gibbs with a CD spectrum of poly(L-ornithine) in the α-helical state in SDS.[21] It is not clear whether this is due to an environmental effect of the surfactant ions on the rotational strength of the two transitions or due to an incomplete α-helix formation. However, when PLL adopts a β-structure in SDS, the positive intensity of the π-π* transition becomes larger[8] than that of a typical reference spectrum (Fig. 1). The intensities of both transitions are somewhat less in β-structured PLL in SOS[7] than in SDS[3,8] in spite of the fact that SOS has a shorter chain length than SDS. The environmental effect is expected to decrease with a decrease in the chain length of the surfactant. Furthermore, the CD spectra of α-helical PLL shows stronger negative intensities in sodium 1-octanesulfonate[6] than in SOS,[7] although both have the same chain length. These facts are not sufficient to conclude that there is no appreciable environmental effect on the two transitions, but lead us to suspect that the low intensities of the CD spectra are due to an incomplete formation of the ordered structures in these surfactant solutions. Then, it is assumed that surfactant ions have little effect on the rotational strengths of the transitions. This assumption is also supported by the results of the present computation on the relative proportions of the three structures. This will be discussed further.

If PLL takes either of the three structures—α-helix, β, and random-coil structures, the observed residue ellipticity, $[\theta]_{obsd}$, is represented by

$$[\theta]_{obsd} = f_\alpha[\theta]_\alpha + f_\beta[\theta]_\beta + f_c[\theta]_c$$

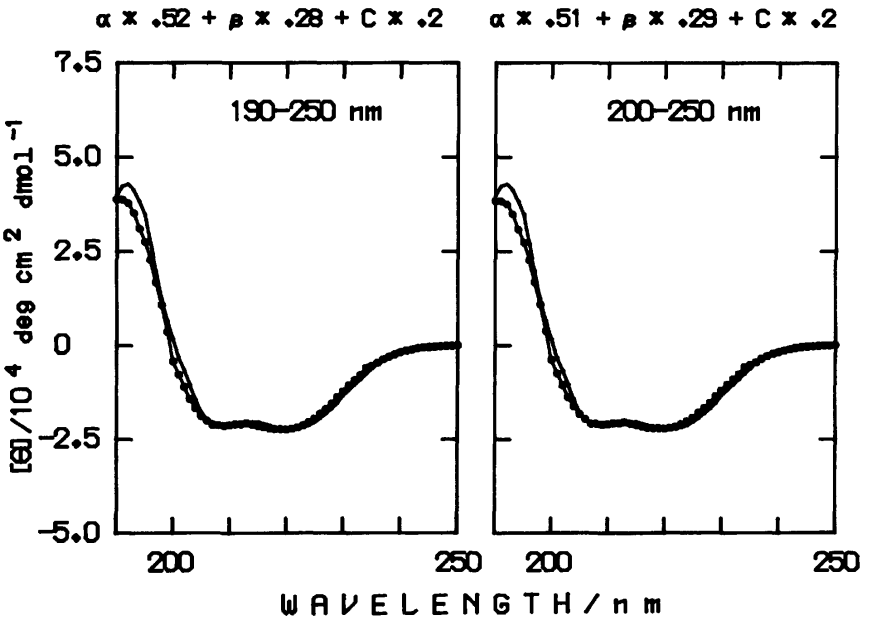

Fig. 2. The computed (—●—) and the experimental (——) CD spectra of PLL in 6.0 mM SOS. The concentration of PLL was 0.56 mM (residue). The simulation was done in two wavelength regions of 190—250 nm (left) and 200—250 nm (right). In the simulation done in 200—250 nm (right), the spectrum was calculated also in the range of 190—200 nm using the relative proportions of the three structures determined in 200—250 nm. The formula on each figure indicate that the computed spectrum consists of the three structural elements with given fractions.

where $[\theta]_\alpha$, $[\theta]_\beta$, and $[\theta]_c$ are the residue ellipticities of the reference spectra of the α-helix, β, and random-coil structures, respectively and f_α, f_β, and f_c are the relative proportions of the corresponding structures. No constraints are imposed on the relative proportions, f_i, except that they add up to unity: $\sum f_i = 1$. The computation was done in the 190—250 nm and 200—250 nm regions at 1-nm intervals by varying the amounts of each structure at 1% intervals. Figure 2 shows simulations of CD spectra of PLL which had a double-negative maximum indicative of the α-helical structure. The results indicate that the PLL contains 51—52% α-helix, 28—29% β-structure, and 20% random-coil structure. Figures 3 and 4 present the simulated spectra when PLL adopted predominantly β and random-coil structures, respectively. There is a considerable difference between the relative proportions obtained by the simulations in the 190—250 nm and 200—250 nm regions in Fig. 4. In this case, the greatest difference appeared between the two simulated spectra over the wavelength regions of this investigation. This might be due to the assumption used here that only the three structures are adopted. It appears possible that PLL may also contain slight amounts of structures other than these three since the cationic PLL is not fully neutralized in low concentrations of the surfactant. The simulation was conducted in the two wavelength regions stated above. It is well known that the signal-to-noise ratio decreases with a decrease in wavelength, especially below 200 nm. Therefore, if possible, the simulation should be done above 200 nm. However, when PLL predominantly assumes a random-coil structure, it shows a distinct spectrum only in the region below 210 nm. The values computed in the 190—250 nm region were useful in the case of PLL rich in the random-coil structure. When PLL assumes α-helix and β-structure (both of which show characteristic CD curves in the 200—250 nm region), the relative proportions computed in this wavelength region are considered to be reliable.

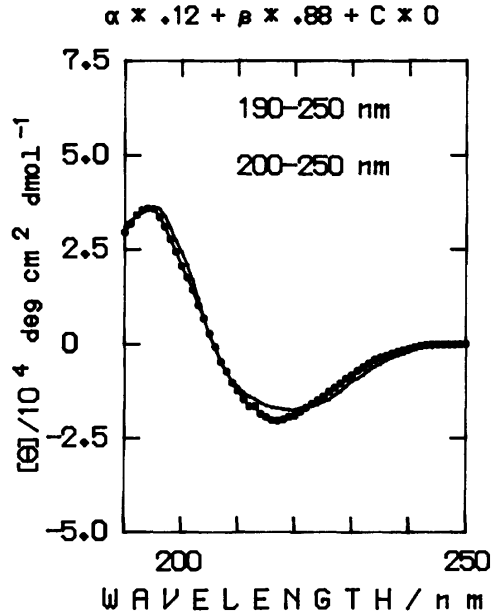

Fig. 3. The computed (—●—) and the experimental (——) CD spectra of PLL in 8.0 mM SOS. The simulations in both wavelength regions of 190—250 nm and 200—250 nm gave the same relative proportions in SOS of this concentration.

Figure 5 shows changes in the relative proportions of the three structures as a function of SOS concentration. As can be seen, PLL assumes an α-helical structure between 2 and 9 mM SOS. The α-helix content was around 52% in 4 to 6 mM SOS. The content of the β-structure increased with an increase in SOS concentration, while that of the random-coil structure decreased with an increase in surfactant concentra-

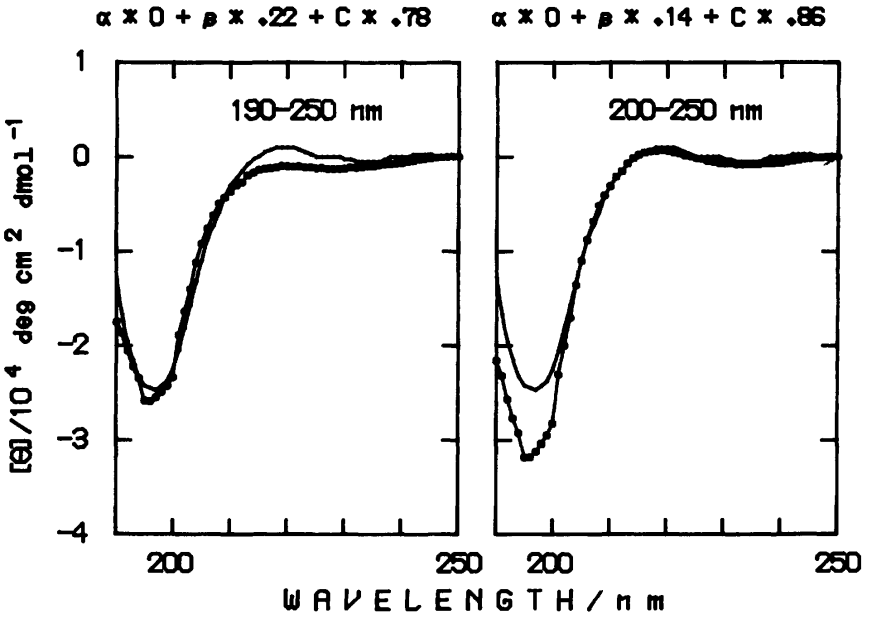

Fig. 4. The computed (—●—) and the experimental (——) CD spectra of PLL in 2.0 mM SOS.

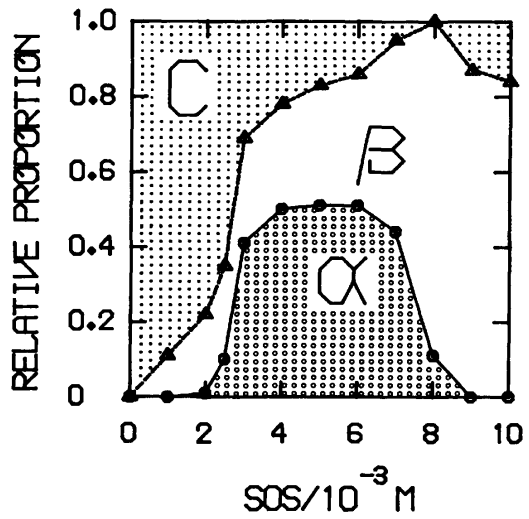

Fig. 5. The relative proportions of α-helix (α), β-structure (β), and random coil structure (C) of PLL as a function of SOS concentration. The boundary between the α-helix and the β-structure is plotted (—○—) and that between the β-structure and the random coil done (—△—). Then each area gives the fraction of the corresponding structure. The same method was used in following figures.

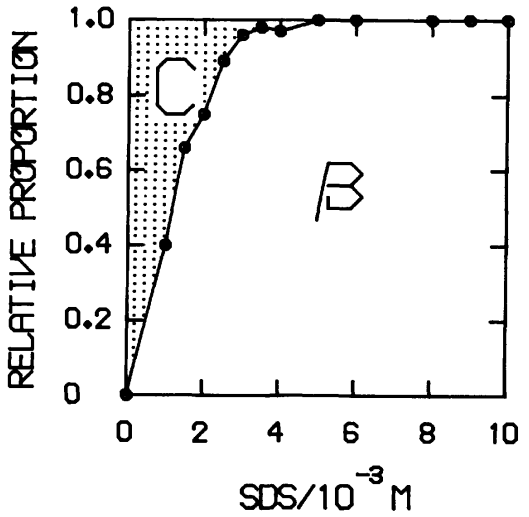

Fig. 6. The relative proportions of β-structure (β) and random coil structure (C) of PLL as a function of SDS concentration. The simulation was done by the same program as applied to the case of PLL in SOS solutions. The α-helix fraction was zero over the entire SDS concentrations in both the computations in 190—250 and 200—250 nm.

tion. The relative proportion of the β-structure and the random-coil structure was 29—35% and 26—14%, respectively in an SOS concentration range of 4 to 6 mM, while PLL assumed predominantly the α-helix structure in this range. Simulation was done for the CD spectra measured in 0.14 to 0.79 mM PLL (residue). However, a change in the concentration of PLL did not have any effect on the relative proportions of the three structures.

PLL assumes a β-structure in solutions of sodium decyl sulfate[5] and SDS.[3,4,8] Figure 6 shows changes in the relative proportions of the α-helix, β, and random-coil structures in an SDS solution. The computation was carried out by a similar simulation method as was done for the PLL conformation in SOS to obtain the relative proportions of the three structures. The α-helix content was negligible over the entire range of SDS concentration. The β-structure content increased with an increase in SDS concentration upto 5.0 mM and finally attained 100%. If there is an environmental effect of surfactant ions to decrease the CD intensities,[21] we cannot estimate 100% proportion of the ordered structure in surfactant solutions without taking into account the fading of the CD spectra. Nevertheless, the present simulation shows that PLL assumes a 100% β-structure in SDS solutions. This result also indicates that there is no appreciable environmental effect of surfactant ions on the CD intensities.

Simulation was also done on the CD spectra of PLL in sodium 1-octanesulfonate solutions containing 21.3 mM NaCl measured by Hayakawa *et al.*[6] Table 1 presents the relative proportions of the three structures in conformations of PLL caused by sodium 1-octanesulfonate. The result shows that the random-coil structure of PLL is sharply transformed to the β-structure between 5.57 and 6.07 mM of the surfactant and the β-structure content decreased above 8.30 mM. The α-helical structure is formed above 8.10 mM of the surfactant. At a surfactant concentration of 10.1 mM where the residue ellipticity at 222 nm becomes constant (see Fig. 2 in Ref. 6), 75% α-helix coexists with 11% β-structure and 14% random-coil. It is interesting to note that the coil to β-structure transition occurs predominantly in lower concentrations of sodium 1-octanesulfonate and the coil to α-helix transition in higher concentrations, in contrast to the transitions in

Table 1. Relative proportion of α-helix, β-structure, and random-coil structure of PLL in sodium 1-octanesulfonate solutions[a]

Concentration of sodium 1-octanesulfonate/mM	α-Helix	β-Structure	Random-coil	Simulated region of wavelength/nm[b]
5.57	0	0.04	0.96	205—250
6.07	0	0.70	0.30	205—250
7.79	0	0.71	0.29	207—250
8.10	0.20	0.68	0.12	205—250
8.30	0.52	0.40	0.08	204—250
10.1	0.75	0.11	0.14	198—250

a) Computed for CD spectra measured by Hayakawa *et al.*[6] b) Restricted by wavelength region presented in Ref. 6.

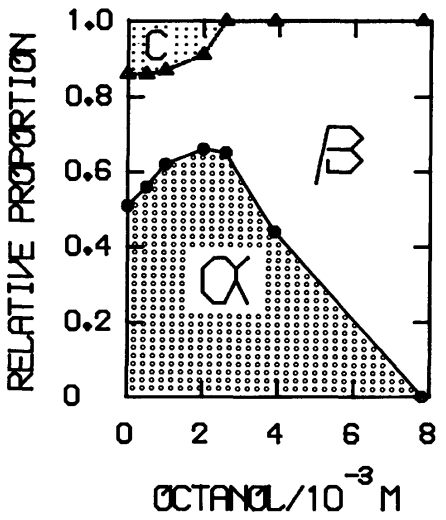

Fig. 7. The relative proportions of α-helix (α), β-structure (β), and random coil structure (C) of PLL as a function of 1-octanol concentration in the presence of 6.0 mM SOS. The concentration of PLL was 0.56 mM (residue).

Table 2. Change in relative proportion of α-helix, β-structure, and random-coil structure of PLL by addition of NaCl[a)]

Concentration of NaCl/mM	α-Helix	β-Structure	Random-coil
0	0.51	0.26	0.23
5.0	0.50	0.27	0.23
10.0	0.35	0.42	0.23
15.0	0.32	0.47	0.21
20.0	0.25	0.58	0.17
25.0	0.26	0.59	0.15
30.0	0.02	0.68	0.30

a) Values simulated in 200—250 nm region.

SOS. It has been reported that PLL assumes an α-helical structure only in SOS[7)] and sodium 1-octanesulfonate[6)] solutions of a neutral pH. However, it is not clear to what degree the α-helical structure is formed. An important result of the present simulation is the knowledge that the α-helical structure coexists with the other two structures in both the surfactant solutions.

The effect of the addition of 1-octanol on the relative proportions of the three structures was examined on the conformation of PLL in 6.0 mM SOS. Figure 7 shows the changes in relative proportions of the three structures as a function of 1-octanol concentration. The α-helix content increased until 2.0 mM octanol and abruptly decreased beyond 2.6 mM. A small amount of octanol seems to provide the best condition to form the α-helical structure, but a greater hydrophobic atmosphere enhances the β-structure. The content of the random-coil structure decreased from 14% to 0% upto 2.6 mM octanol. Therefore, only the α-helix and β-structure exist above 2.6 mM octanol in the presence of 6.0 mM SOS.

We have previously found that the double-negative maximum of PLL, which is a characteristic of the α-helical structure, fades out with an increase in the added NaCl concentration in an SOS solution (Fig. 4 in Ref. 8). These fading CD spectra of PLL by the addition of NaCl were simulated in the same manner. The results are shown in Table 2. The presence of 20—25 mM NaCl reduces the α-helix content to approximately half of that found in the absence of the electrolyte. The content of the random-coil structure was essentially constant below 25 mM of NaCl. Therefore, it appears that the addition of NaCl changes the relative proportions of only the α-helix and β-structure. In the presence of about 20 mM NaCl, the α-helix content of PLL in SOS is one third of that in sodium 1-octanesulfonate. The present result indicates that in addition to the chain length of the hydrophobic group and charge of the hydrophilic group of surfactant, the structural features of the hydrophilic group are also important for the induction of the α-helical structure.

References

1) G. Holzwarth and P. Doty, *J. Am. Chem. Soc.*, **87**, 218 (1965).
2) R. Townend, T. F. Kumosinski, S. N. Timasheff, G. D. Fasman, and B. Davidson, *Biochem. Biophys. Res. Commun.*, **23**, 163 (1966).
3) I. Satake and J. T. Yang, *Biochem. Biophys. Res. Commun.*, **54**, 930 (1973).
4) I. Satake and J. T. Yang, *Biopolymers*, **14**, 1841 (1975).
5) I. Satake and J. T. Yang, *Biopolymers*, **15**, 2263 (1976).
6) K. Hayakawa, K. Ohara, and I. Satake, *Chem. Lett.*, **1980**, 647.
7) K. Takeda, A. Iba, and K. Shirahama, *Bull. Chem. Soc. Jpn.*, **54**, 1793 (1981).
8) K. Takeda, A. Iba, and K. Shirahama, *Bull. Chem. Soc. Jpn.*, **55**, 985 (1982).
9) N. Greenfield and G. D. Fasman, *Biochemistry*, **8**, 4108 (1969).
10) V. P. Saxena and D. B. Wetlaufer, *Proc. Natl. Acad. Sci. U.S.A.*, **68**, 969 (1971).
11) H. Rosenkranz and W. Scholtan, *Hoppe-Seyler's Z. Physiol. Chem.*, **352**, 896 (1971).
12) Y. H. Chen, J. T. Yang, and H. M. Martinez, *Biochemistry*, **11**, 4120 (1972).
13) Y. H. Chen, J. T. Yang, and K. H. Chau, *Biochemistry*, **13**, 3350 (1974).
14) C. T. Chang, C. S. C. Wu, and J. T. Yang, *Anal. Biochem.*, **91**, 13 (1978).
15) S. Brahms and J. Brahms, *J. Mol. Biol.*, **138**, 149 (1980).
16) S. W. Provencher and J. Glöckner, *Biochemistry*, **20**, 33 (1981).
17) J. P. Hennessey and W. C. Johnson, *Biochemistry*, **20**, 1085 (1981).
18) A. M. Labhardt, *J. Mol. Biol.*, **157**, 331 (1982).
19) K. Takeda, M. Miura, and T. Takagi, *J. Colloid Interface Sci.*, **82**, 38 (1981).
20) N. Greenfield, B. Davidson, and G. D. Fasman, *Biochemistry*, **6**, 1630 (1967).
21) M. J. Grourke and J. H. Gibbs, *Biopolymers*, **5**, 586 (1967).

 © 1985 The Chemical Society of Japan Bull. Chem. Soc. Jpn., 58, 1215—1219 (1985)

Structure Model for Liquid Carbon Tetrachloride

Keiko NISHIKAWA* and Takao IIJIMA
Department of Chemistry, Faculty of Science, Gakushuin University, Mejiro, Toshima-ku, Tokyo 171
(Received April 25, 1984)

The X-ray scattering intensity for the visualized structure model of a liquid is formulated. It is ascertained that by the bcc model for liquid carbon tetrachloride the experimental intensity has been simulated well.

The structures of gases and crystals have been studied extensively by diffraction methods. For liquids, however, the structure analysis is rather difficult. The fundamental difficulty is that there is no idealized abstraction of the liquid state such as an ideal gas or a perfect crystal. In the gaseous state, the interaction between molecules can be neglected in many cases and only one molecule is taken into consideration for the structure analysis. Crystals are characterized by the regularity in their configuration. So, we know the crystal structure only by studying the arrangement of molecules or atoms within a unit cell. However, in the liquid state which is a condensed phase and has no such regularity in the arrangement of molecules in crystals, it is difficult to obtain the information about the molecular arrangement immediately from experimental diffraction intensities or from radial distribution functions.

One approach to overcome the difficulty is to construct a model in which we visualize a structure of liquids,[1,2] and to calculate the diffraction intensity for the structure model, which is to be tested against the experimental intensity. In constructing a model we may describe the structure of the liquid as follows. We assume a certain nearest-neighbor configuration around a central molecule and repeat this structural unit by some specified rule. According to this model the average molecular positions, as viewed from the location of a given central molecule, conform to a certain lattice structure. Unlike the crystalline case, however, repetition of the structure unit is imperfect and therefore is accompanied by rapid loss of positional correlation as the distance between the central molecule and surrounding ones increases. This loss of correlation may be embodied in the model in the form of mean-square amplitudes of distribution of the separation between atoms which increase rapidly with the distance. At least beyond a few molecular radii away from any starting point, the structure can be regarded as a continuum. This relative distribution must obviously be independent of the choice of the central molecule. Such a structure model for liquids may be called the "local lattice structure model." Some investigators have denied such crystalline-like model for the liquids,[3] but there are in fact some examples in which diffraction intensities are explained by the "local lattice structure model." Moreover, such a lattice model may be useful in serving to keep away from the inherent difficulty of statistical theories of liquids, because such local structure of the liquid reflects directly the strong molecular interactions, which are essential to the properties of the liquid.

The analysis of the diffraction intensity for liquids by constructing a structure model has been made by several authors.[4-8] However, there has been some confusion in formulating the scattering intensities from structure models. So, we feel it necessary to reproduce the correct formulation of the scattering intensity for the visualized structure model of liquids originally put forward by Narten and Levy.[2,4]

In a preceding paper we reported improved X-ray diffraction data of liquid carbon tetrachloride.[9] So, we determine a structure model for liquid carbon tetrachloride on the basis of the correct formulation of the scattering intensity. Among the various models which have so far been suggested for the structure of liquid carbon tetrachloride,[6-8] the bcc model is confirmed to be the one that gives the best agreement between theory and experiment.

Scattering Intensity from Liquids[2,4]

In the following, we consider X-ray scattering intensity from a liquid sample. The region denoted by C in Fig. 1 shows the effective volume radiated by X-rays. The total coherent intensity scattered from this region which contains N molecules is given by[10]

$$I' = \sum_{j}^{N}\sum_{i}^{N} f_i f_j \frac{\sin sr_{ij}}{sr_{ij}} \exp\left(-\frac{l_{ij}^2}{2}s^2\right), \qquad (1)$$

where f_i is the atomic scattering factor of the i-th atom and s is the scattering parameter defined by $4\pi\sin\theta/\lambda$, λ: wavelength, 2θ: scattering angle. The notation l_{ij} is the root mean-square amplitude due to the dis-

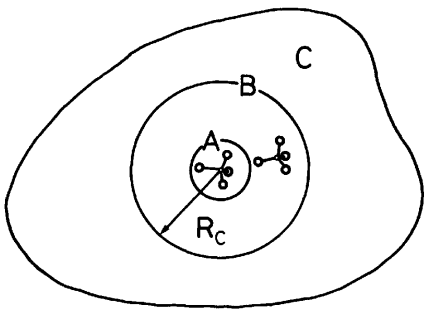

Fig. 1. Schematic model of a liquid. The region A shows a molecule or one stoichiometric unit of the liquid. The molecule "feels" the "structure" around itself up to the distance R_c. This structure region is denoted by B. The region C shows the effective volume irradiated by X-rays, and the region (C-B) is viewed as continuous from A.

tribution averaged over both time and space around the mean interatomic distance r_{ij}. The summation is over all atoms in the volume C. Here, we can define by I the scattering intensity per molecule or one stoichiometric unit in the liquid. Namely,

$$I = I'/N = \sum_{j\subset C}\sum_{i\subset A} f_i f_j \frac{\sin sr_{ij}}{sr_{ij}} \exp\left(-\frac{l_{ij}^2}{2}s^2\right), \quad (2)$$

where the summation is now over the stoichiometric unit A (Fig. 1) for i and over all atoms in the sample for j. The region A shows a central molecule or a unit as is mentioned in the introductory section. It is noted that any molecule or any stoichiometric unit in the liquid except for surface molecules is eligible to be this central unit.

In Eq. 2, however, it is hardly possible to perform the summation for j for the assumed liquid structure. For such a model of the liquid structure to be tractable, Narten and Levy terminated the series of terms of j at a distance R_c from a central molecule, and assumed a continuous distribution beyond this distance.[2,4] The sphere with the radius R_c is shown by the region B. Namely, a molecule or one stoichiometric unit (region A) "feels" the "structure" around itself up to the distance R_c and the region beyond R_c is regarded as a continuum in the distribution of the molecules. So, the scattering intensity per molecule in a liquid is given by

$$I = I_d + I_c, \quad (3)$$

where I_d is the contribution from the interference of a central molecule and those in the region of discrete structure B around it, given by

$$I_d = \sum_{j\subset B}\sum_{i\subset A} f_i f_j \frac{\sin sr_{ij}}{sr_{ij}} \exp\left(-\frac{l_{ij}^2}{2}s^2\right). \quad (4)$$

The summation for j is over all atoms in the region B. The contribution from the interference of a molecule and the continuous region is given by

$$I_c = \sum_{i\subset A} f_i \langle F\rangle \rho_0 \int_{R_c}^{\infty} 4\pi r^2 \frac{\sin sr}{sr} dr, \quad (5)$$

where ρ_0 is the bulk number density of molecules of the liquid and the mean scattering amplitude of the molecule $\langle F\rangle$ is given by

$$\langle F\rangle = \sum_{i\subset A} f_i. \quad (6)$$

On integration of Eq. 5 we obtain[11]

$$I_c = \sum_{i\subset A} f_i \langle F\rangle 4\pi\rho_0 \frac{sR_c\cos(sR_c) - \sin(sR_c)}{s^3} \exp\left(-\frac{l_c^2}{2}s^2\right) = \sum_{i\subset A} f_i \langle F\rangle n \frac{3\{sR_c\cos(sR_c) - \sin(sR_c)\}}{(sR_c)^3} \exp\left(-\frac{l_c^2}{2}s^2\right). \quad (7)$$

A "temperature factor" l_c is included in Eq. 7 in order to connect the continuous region to the discrete region as smoothly as possible. The notation n is the number of molecules included in region B. Using Eqs. 4 and 7, we can calculate the scattering intensity for any structure model of the liquid.

Sometimes there was confusion in making the summation for Eq. 4 in previous papers on the simulation study of the liquid structure. In some papers, the summation is taken over all the atoms in the region B, namely for i and j. The intensity thus calculated will not be the intensity of the liquid but that of a cluster floating in a continuous medium. For example, Narten and Levy described the theory correctly in deriving the scattering intensity for the model structure of water.[2,4] In the meantime, however, they gave a different expression for the scattering intensities for liquid carbon tetrachloride[6] and liquid benzene,[5] as if they had calculated the intensities of their "clusters." For the case of the simulation studies for liquid carbon tetrachloride, Reichelt *et al.*[7] and Nishikawa and Murata[8] took the summation over all the atoms in the discrete structure. Recently Arakawa *et al.* criticized[12] the correct summation of Narten and Levy.[2,4]

There is also some other confusion about the formulation of the scattering intensity mentioned in this section. Powles stated that the contribution from the continuous region diverged,[13] namely, the integration given by Eq. 5 in the present paper diverged. So he asserted that the "local lattice structure model" was inadequate for the description of the liquid structure. However, the integration of Eq. 5 coverges[14] as given by Eq. 7 excluding the term of $\exp(-l_c^2 s^2/2)$. Powles also remarked that the term of $\exp(-l_c^2 s^2/2)$ was introduced in order to circumvent the divergence of the integration.[13] However, this explanation is not correct. The problem in the "local lattice structure model" is the discontinuity between the discrete region and the continuous region. The introduction of the term $\exp(-l_c^2 s^2/2)$ in Eq. 7 is only to smear this discontinuity.

The Structure Models for Liquid Carbon Tetrachloride

Many diffraction experiments for liquid carbon tetrachloride have been carried out.[6-8,15-19] However, the visualized structure models were proposed by Narten and Levy,[6] by Egelstaff *et al.*,[18] by Reichelt *et al.*,[7] and by Nishikawa and Murata.[8] Also, Lowden and Chandler proposed a model for liquid carbon tetrachloride on the basis of their RISM (reference interaction site model) calculation,[20] although it is not the result of diffraction experiments. These models have been summarized briefly in Ref. 21.

For these models, namely, the Pa3 model,[6] the monoclinic model[7] and the bcc model,[8] the respective scattering intensities were calculated, though all the calculations were imperfect as noted in the previous section. However, the imperfection did not cause any serious defect, because the calculated intensities were those for respective clusters and they are different from

the correct intensities of the liquid in the weight for each atomic distance. Although some errors may have been contained in the intensities or the estimated root mean square amplitudes, the main features, especially the phases for the intensity curve, are reproduced. These three models are different from each other in three-dimensional packing, but the one dimensional scattering intensity curves happen to be similar to each other.

One cause of the difficulty in the structure analysis of liquids is that there is no general method to determine the structure of the liquid uniquely from the scattering intensity. Even if we are lucky enough to obtain a model whose calculated intensity agrees well with the experimental one, there is no assurance that the model is correct. Especially for molecular liquids, we must determine the molecular orientation and the intermolecular distances from a halo-pattern.

In the case of carbon tetrachloride, there exist plastic crystal phases. The plastic crystal can be regarded as an intermediate state between the ordered crystal and the liquid. The result of the structure analysis of the plastic crystal of carbon tetrachloride gives a helpful suggestion for the structure of the liquid carbon tetrachloride, as was mentioned in a previous paper.[21] In the structure analysis of the plastic phase Ia of carbon tetrachloride, the following result has been obtained.[21] Namely, the intermolecular distance between carbon tetrachloride molecules is 5.90 Å and the orientational correlation of neighboring molecules is explained by the head-tail head-tail packing.

Simulation of the Weighted Structure Function by the bcc Model

As is mentioned above, the most probable packing for the molecules of liquid carbon tetrachloride is the head-tail head-tail packing. By the repetition of this head-tail head-tail packing with eclipsed form for the off-axis chlorine atoms, we obtain a bcc lattice. Accordingly, we calculate here the scattering intensity from the bcc model and compare it with the experimental one.[9]

We examine how many molecules are suitable to be arranged around a central molecule with the nearest neighbor distance R of 5.9 Å.[22] For the values of the intramolecular distances $r_{C\text{-}Cl}$ and $r_{Cl\text{-}Cl}$ and their root mean square amplitudes $l_{C\text{-}Cl}$ and $l_{Cl\text{-}Cl}$, the results obtained by gas electron diffraction[23] are used. They are almost the same as the recent result for the liquid by neutron scattering experiments.[24]

Using Eqs. 4 and 7, we calculated the total coherent intensity and derived the weighted structure function $si(s)$,

$$si(s) = s(I - \sum_{i \subset A} f_i^2) = s(I_d - \sum_{i \subset A} f_i^2 + I_c) \quad (8)$$

for the bcc lattice where eight molecules are arranged as the first nearest neighbors around one molecule ($n=9$) and the distribution of molecules is assumed to be continuous beyond the distance R_c. The critical radius R_c is determined by the relationship

$$n = \frac{4}{3}\pi R_c^3 \rho_0, \quad (9)$$

where ρ_0 is the bulk number density of carbon tetrachloride molecules in the liquid phase. The mean square amplitudes are determined according to the "structural diffusion" model[1]

$$l_{ij}^2 = Dr_{ij}. \quad (10)$$

The calculated structure function reproduces main peaks and valleys of the experimental $si(s)$ curve, but their heights and depths can not be simulated even if the value D in Eq. 10 is changed. So, we repeat the same procedure one after another with the increase of the number n contained in B region (Fig. 1). At the number of $n=51$ (up to the fourth nearest neighbors around the central molecule), the experimental curve is simulated satisfactorily and further increase of n no longer changes the feature of the calculated curve.

Next, we investigate the root mean square amplitude l_{ij} in detail. Until now, we use the Prins relation (Eq. 10) for estimating the value of l_{ij} in relation to its interatomic distance r_{ij}. A value 0.0716 for D is suitable. This means that the root mean square variation of the distance between the nearest neighbor molecules is about 0.65 Å, which is about 11% of the equilibrium separation of the two molecules (5.9 Å). However, by only one value for D, the third peak of $si(s)$ curve at $s \approx 3.2$ Å^{-1} shifts to about 3 Å^{-1}, so we use two constants for the relation of Eq. 10. Namely,

$D_1 = 0.0716$ for the 1-st nearest neighbor molecules.
$D_2 = 0.1224$ for the 2-nd, 3-rd, and 4-th nearest neighbor molecules.

The result is shown in Fig. 2 by the solid curve with the experimental $si(s)$ curve[9] denoted by circles. The region from $s=0$ to 6 Å^{-1} is shown, because the $si(s)$ curve in the region of s larger than 6 Å^{-1} is approximately represented by a free carbon tetrachloride molecule and is hardly affected by intermolecular interference.

By theoretical investigations on the quasi-crystalline model for liquids, Medvedev *et al.*[25] and Baer[26] proposed a further modified "structural diffusion" relation

$$l_{ij}^2 = D(r_{ij} - r_0) \quad (11)$$

in place of the equation given by Eq. 10. Using this relation, we carried out the least-squares analysis for the parameters R, D, r_0, R_c, and l_c, with the number n fixed at 51. The result is shown in Table 1. The $si(s)$ curve calculated by using these parameters is in slightly poorer agreement with the experimental one in the

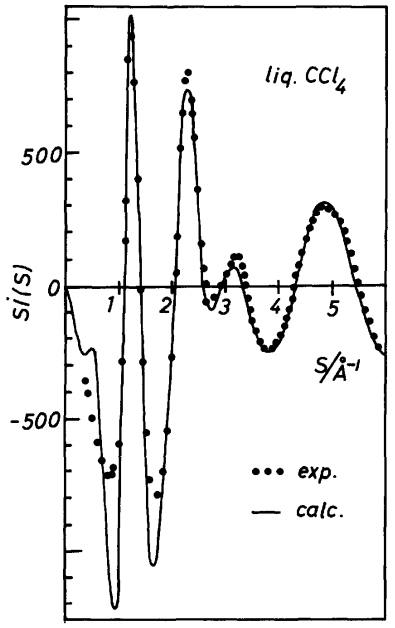

Fig. 2. The weighted structure functions $si(s)$ for liquid carbon tetrachloride. The solid curve is the calculated one for the bcc model with two D coefficients. The circles are experimental values.[9]

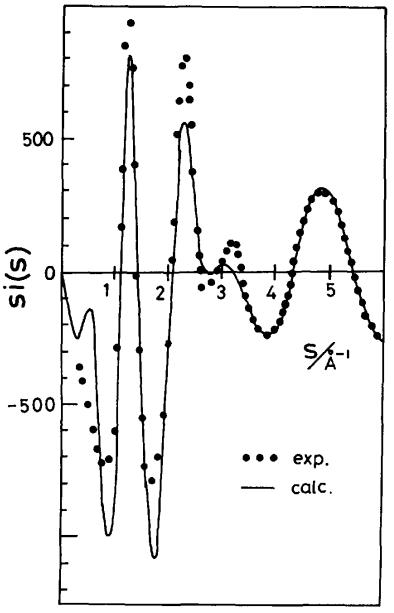

Fig. 3. The weighted structure functions $si(s)$ for liquid carbon tetrachloride. The solid curve is the calculated one for the bcc model with the relation of the root mean square amplitudes given by Eq. 11.

TABLE 1. THE REFINED PARAMETERS FOR THE BCC MODEL[a]

R/Å 5.90 (2)	R_c/Å 12.41 (3)
D/Å 0.158 (23)	l_c/Å 1.76 (76)
r_0/Å 2.46 (74)	

a) The values in the parenthesis are standard deviations.

peak height of the first and second peak as is shown in Fig. 3, than the case of the calculated $si(s)$ curve using the two D_1 and D_2 coefficients. The result in Table 1 shows that the parameters for the distances converge very well, but not for the mean square amplitudes. This may indicate that the theoretical expression for the loss of positional correlation of the molecules from the equilibrium position in the liquid is not satisfactory. In the least squares analysis, R_c is changed as a fitting parameter, and its value has converged exactly to the value obtained by Eq. 9.

Discussion

In Fig. 2, the circles are the experimental intensities which are obtained by the improved and revised analysis of the energy-dispersive X-ray diffractometry.[9] This experimental result is in good agreement with Narten's result obtained by the angle-dispersive method.[19] In the previous work, one of the present authors (K. N.) reported that there were fine structures in the diffraction pattern of liquid carbon teterachloride,[8] but it has been proved that they are not fine structures from the liquid but are the parasitic scattering from Myler windows of the sample holder.

As is shown in Fig. 2, the calculated intensity for the bcc model is in good agreement with the experimental one except for the depth of the valley at $s=1.7$ Å^{-1} and the intensity ranging from 0 to 1.2Å^{-1}. The disagreement in the intensity at $s=1.7$Å^{-1} has not been explained. We could not simulate the depth of the valley by changing the value of D without disturbing the balance of the other peaks and valleys in the intensity curve.

The discrepancy of the intensity ranging from 0 to 1.2Å^{-1} between the calculated and experimental intensities is explained by the unreasonable connection of the discrete structure region (B in Fig. 1) and the continuum region. In order to connect the two regions as smoothly as possible, we introduce the "temperature factor" intentionally in Eq. 7 in the form of $\exp(-l_c^2 s^2/2)$, but there is is no physical reason for this expression. In other words, l_c is not the root mean square amplitude of the radius R_c.

In the case of liquid carbon tetrachloride, the success in modeling the structure by the "local lattice structure model" may be due to the long range correlation of the liquid; that is, the discrete region is comparably large, so the ghost peaks in the scattering curve caused by an unreasonable connection appear at small s-values and are easily distinguishable from the relevant peaks of the liquid.

The method of structure simulation of the scattering intensity mentioned above can be called "real space expansion," where we calculate the scattering intensity by summing up the contributions from each atomic distance in the liquid described by a real space. It is concluded that for the simulation method of the "real space expansion" the convergence is very poor in the small s-region of the intensity curve. To achieve a much better convergence of the simulation for the scattering intensity at the small s-region, a different formulation called "reciprocal space expansion" seems

to be promising.[27]

In order to express the structural diffusion of the liquid, we tried two methods, namely, one introducing two D coefficients for Eq. 10 and the other using the relation described by Eq. 11. The former leads to a more satisfactory simulation. However, it has been reported that the latter expression is more suitable to describe the temperature factor of monoatomic liquid than the expression of Eq. 10.[25,26] In the case of a molecular liquid such as carbon tetrachloride, the shape of the molecules itself seems to play an important role. Especially for liquid carbon tetrachloride, the gear-like packing of tetrahedral molecules may be important in determining the structure. We have therefore derived a more sophisticated formulation for the mean square amplitudes for liquid carbon tetrachloride, taking into account the shape of the molecules; the result is reported in a succeeding paper.[28]

In conclusion the bcc model for liquid carbon tetrachloride explains well the scattering intensity. Of course, the bcc model may not be the only one model representing the experimental intensity. However, few other arrangements seem to be left for the structure model, because almost all the fundamental packings acceptable for tetrahedral molecules were checked in the structure study of the plastic crystal phase.[21] The head-tail head-tail packing shows that the octopole interaction is important in determining the structure of the liquid. The head-tail head-tail packing is highly stabilized for the molecules with an octopole moment.[29]

References

1) J. Frenkel "Kinetic Theory of Liquid" Dover, New York (1955).

2) A. H. Narten and H. A. Levy, *Science*, **165**, 447 (1969).

3) J. F. Karnicky and C. J. Pings, *Adv. Chem. Phys.*, **34**, 157 (1976).

4) A. H. Narten, M. D. Danford, and H. A. Levy, *Discuss. Faraday Soc.*, **43**, 97 (1967).

5) A. H. Narten, *J. Chem. Phys.*, **48**, 1630 (1968).

6) A. H. Narten, M. D. Danford, and H. A. Levy, *J. Chem. Phys.*, **46**, 4875 (1967).

7) G. Reichelt, J. U. Weidner, and H. W. Zimmermann, *Ber. Bunsenges. Phys. Chem.*, **78**, 1050 (1974).

8) K. Nishikawa and Y. Murata, *Bull. Chem. Soc. Jpn.*, **52**, 293 (1979).

9) K. Nishikawa and T. Iijima, *Bull. Chem. Soc. Jpn.*, **57**, 1750 (1984).

10) P. Debye and H. Menke, *Phys. Z.*, **31**, 797 (1930).

11) Narten and Levy used the respective distance r_{cij} in place of the radius R_c.[2,4]

12) N. Ohtomo, K. Tokiwano, and K. Arakawa, *Bull. Chem. Soc. Jpn.*, **54**, 1802 (1981).

13) J. G. Powles, *Adv. Phys.*, **22**, 1 (1973).

14) B. E. Warren, *Phys. Rev.*, **45**, 657 (1934).

15) A. Eisenstein, *Phys. Rev.*, **63**, 304 (1943).

16) E. E. Bray and N. S. Gingrich, *J. Chem. Phys.*, **11**, 351 (1943).

17) R. W. Gruebell and G. T. Clayton, *J. Chem. Phys.*, **46**, 639 (1967).

18) P. A. Egelstaff, D. I. Page, and J. G. Powles, *Mol. Phys.*, **20**, 881 (1971).

19) A. H. Narten, *J. Chem. Phys.*, **65**, 573 (1976).

20) L. J. Lowden and D. Chandler, *J. Chem. Phys.*, **61**, 5228 (1974).

21) K. Nishikawa, K. Tohji, and Y. Murata, *J. Chem. Phys.*, **74**, 5817 (1981).

22) This distance is slightly longer than 5.77 Å, the one reported in the previous work,[8] but it is poved in the present work that the value of 5.9 Å is better to simulate the experimental intensity. Moreover, this value is consistent with the density of liquid carbon tetrachloride at room temperature.

23) Y. Morino, Y. Nakamura, and T. Iijima, *J. Chem. Phys.*, **32**, 643 (1960).

24) J. H. Clarke, J. R. Granada, and J. C. Dore, *Mol. Phys.*, **37**, 1263 (1979).

25) N. N. Medvedev and Yu. I. Naberukhin, *Phys. Chem. Liquids*, **6**, 137 (1977); *ibid.*, **8**, 167 (1978).

26) S. Baer, *Chem. Phys.*, **39**, 159 (1979).

27) T. Iijima and K. Nishikawa, *Chem. Phys. Lett.*, in press.

28) K. Nishikawa and T. Iijima, *Bull. Chem. Soc. Jpn.*, **58**, 1220 (1985).

29) T. Kihara, "Intermolecular Forces," Wiley, New York (1977).

 © 1985 The Chemical Society of Japan Bull. Chem. Soc. Jpn., 58, 1220—1224 (1985) [Vol. 58, No. 4

Mean Square Deviations of Interatomic Distances in Liquid Carbon Tetrachloride

Keiko NISHIKAWA* and Takao IIJIMA
Department of Chemistry, Faculty of Science, Gakushuin University, Mejiro, Toshima-ku, Tokyo 171
(Received July 10, 1984)

In simulating the X-ray scattering intensity of liquid carbon tetrachloride, the structural diffusion model for the bcc local structure has been refined by formulating the mean square deviations of interatomic distances by dividing them into two parts, namely, translational and rotational contributions. By this treatment, the simulation has not been improved in comparison with the modified Prins relation, but the description of the motion of carbon tetrachloride molecules in the liquid becomes clear. The degree of depolarization of the ν_1 Raman line is well accounted for by the use of the translational mean square deviations determined.

The structure of liquids has long been the least understood among those of the three phases of matter, and it still is. Nevertheless, it is fair to say that many works, especially recent diffraction experiments[1-5] and computer simulations,[6,7] have made it clear to a great extent.

From the stand-point of diffraction studies, it is convenient to use a visualized structure model for a liquid and calculate the diffraction intensity for the strùcture model, which is to be tested against the experimental intensity. In order to calculate the diffraction intensity of the structure model, it is necessary to construct a local lattice structure around a molecule and to express the structural diffusion by the width of atomic pair distribution. This will increase with the increase of the interatomic separations. Even in a molecular liquid, the expression for the diffraction intensity becomes more tractable if it is based on the atomic pair distribution, than on the molecular pair correlation function which is usually expanded in terms of Wigner rotation matrices.[8]

The mean square deviation of the interatomic distances due to the width of the pair distribution is often called the mean square amplitude,[2] by analogy with atomic distances in a free molecule where the distribution is caused exclusively by vibrational motion. If the local lattice structure is determined and the mean square deviation is given to each atomic pair by the use of a reasonably small number of parameters, the structure of a liquid may be said to be elucidated.

In previous papers,[2,3] it has been shown that the experimental X-ray scattering intensity of liquid carbon tetrachloride[4] is simulated in good approximation by the bcc model for the local lattice structure. In this model a chlorine atom of one molecule lies in a hollow formed by three chlorine atoms of the adjacent molecule, and the threefold axes of these molecules are aligned (see Fig. 2). This packing is called head-tail head-tail packing. By the repetition of this head-tail head-tail packing with the eclipsed arrangement for the off-axis chlorine atoms a bcc lattice is obtained. Accordingly our model for the local structure of liquid carbon tetrachloride is called a bcc model. The head-tail head-tail packing is highly stabilized for molecules with an octopole moment.[9] Moreover, this packing is known to be the fundamental orientational correlation in the plastic phase (Ia) of carbon tetrachloride.[5] It is scarcely to be doubtful that the bcc structure is the best and physically reasonable model for the local lattice structure of liquid carbon tetrachloride.

However, our knowledge about the mean square deviation to express the structural diffusion has not been satisfactory.[2] Usually, the mean square deviation l_{pq}^2 is related to the distance between the p-th and q-th atoms, r_{pq}, by the Prins relation,[10]

$$l_{pq}^2 = Dr_{pq},$$

or a modified structural diffusion relation proposed by Baer,[11]

$$l_{pq}^2 = D(r_{pq}-r_0).$$

However, it has been found that these relationships are not adequate expressions to simulate the X-ray scattering intensity from a molecular liquid such as carbon tetrachloride.[2] In this case, the distribution of the orientational fluctuation of each molecule as well as the distribution of the distance between molecular centers must be taken into account. On the basis of this inference, we derive in the present work a more sophisticated formulation for the mean square deviations for liquid carbon tetrachloride.

Mean Square Deviations

The reduced scattering intensity per molecule of liquid carbon tetrachloride is given by[2]

$$\begin{aligned} i(s) = {} & [8f_C f_{Cl} j_0(sr_{C\text{-}Cl}) \exp(-l_{C\text{-}Cl}^2 s^2/2) \\ & + 12 f_{Cl}^2 j_0(sr_{Cl\text{-}Cl}) \exp(-l_{Cl\text{-}Cl}^2 s^2/2)] \\ & + \sum_{p \neq q} f_p f_q j_0(sr_{pq}) \exp(-l_{pq}^2 s^2/2) + I_e \end{aligned} \quad (1)$$

where $j_0(x)$ is the 0-th order spherical Bessel function, *i.e.*, $\sin x/x$; f_p is the atomic scattering factor of the p-th atom, and s is the scattering parameter defined by $4\pi\sin\theta/\lambda$, λ: wavelength, 2θ: scattering angle. The first bracketed term expresses the intensity of the atomic interference in the representative or central molecule itself, and $r_{C\text{-}Cl}$, $r_{Cl\text{-}Cl}$, $l_{C\text{-}Cl}$, and $l_{Cl\text{-}Cl}$ are interatomic distances and respective root mean-square deviations of a molecule, for which the values obtained by gas electron diffraction[12] are used. l_{pq} is the root mean-square deviation for the distance r_{pq}, and I_e is the inten-

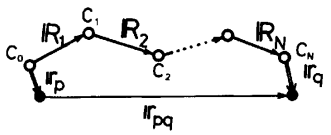

Fig. 1. The interatomic distance vector r_{pq}. The notation C_i shows the center of the i-th molecule; C_0 is the center of the representative or central molecule.

sity due to the interference of a central molecule and the continuum region. For the second term the summation for p is taken over atoms in the central molecule and for q over all atoms in the discrete structure region except for the central molecule.

We assume as a first approximation that the translational and rotational intermolecular motions are mutually independent. Then the mean square deviation l_{pq}^2 is divided into two parts, the translational contribution which reflects the distribution of the distance between molecular centers and the rotational contribution which is due to the orientational fluctuation, namely,

$$\begin{aligned} l_{pq}^2 &= \langle \Delta r_{pq}^2 \rangle \\ &= \langle \Delta r_{pq}^2 \rangle^{\mathrm{tr}} + \langle \Delta r_{pq}^2 \rangle^{\mathrm{rot}}, \end{aligned} \tag{2}$$

where Δr_{pq} is the displacement from the equilibrium distance r_{pq}. We neglect the intramolecular vibrational contribution to Δr_{pq}, which is smaller than those from the intermolecular translational and rotational motions.

Translational Contribution. Let $\boldsymbol{R}_i$ be the vector which links the centers of the $(i-1)$-th and i-th molecules that are the nearest neighbors to each other as is shown in Fig. 1. The vector $\boldsymbol{r}_p$ is the positional vector of the p-th atom from the center of the central molecule. The q-th atom belongs to the N-th molecule. The translational displacement $\Delta r_{pq}^{\mathrm{tr}}$ is given by

$$\Delta r_{pq}^{\mathrm{tr}} = \boldsymbol{\lambda}_{pq} \cdot (\Delta \boldsymbol{R}_1 + \Delta \boldsymbol{R}_2 + \cdots + \Delta \boldsymbol{R}_N) \tag{3}$$

where $\Delta \boldsymbol{R}_i$ is the displacement vector of $\boldsymbol{R}_i$ and $\boldsymbol{\lambda}_{pq}$ is the unit vector parallel to $\boldsymbol{r}_{pq}$, namely

$$\boldsymbol{\lambda}_{pq} = (-\boldsymbol{r}_p + \boldsymbol{R}_{1N} + \boldsymbol{r}_q)/|-\boldsymbol{r}_p + \boldsymbol{R}_{1N} + \boldsymbol{r}_q|. \tag{4}$$

The vector $\boldsymbol{R}_{1N}$ is given by

$$\boldsymbol{R}_{1N} = \boldsymbol{R}_1 + \boldsymbol{R}_2 + \cdots + \boldsymbol{R}_N. \tag{5}$$

In general there are many choices for the path connecting the central molecule to the N-th molecule. In the present treatment the shortest possible path is chosen in considering that Eq. 6 below is exact only when the contributions from the translational motion perpendicular to $\boldsymbol{R}_i$ can be ignored, in other words, when all $\boldsymbol{R}_i$ are on a straight line (see Appendix).

Let the unit vector along the average direction of $\boldsymbol{R}_i$ be $\boldsymbol{t}_i$. Then Eq. 3 becomes approximately

$$\Delta r_{pq}^{\mathrm{tr}} = \boldsymbol{\lambda}_{pq} \cdot (\Delta R_1 \boldsymbol{t}_1 + \Delta R_2 \boldsymbol{t}_2 + \cdots + \Delta R_N \boldsymbol{t}_N) \tag{6}$$

where ΔR_i is the component of $\Delta \boldsymbol{R}_i$ along the vector $\boldsymbol{t}_i$. Now we make assumptions as follows;

$$\langle \Delta R_i^2 \rangle = A \quad \text{for all } i, \tag{7}$$

and

$$\langle \Delta R_i \Delta R_j \rangle = \begin{cases} a & \text{for neighboring } i \text{ and } j, \\ 0 & \text{otherwise.} \end{cases} \tag{8}$$

The assumptions mean that the mean square deviation of the intermolecular separation of the neighboring molecules is A, the magnitude of the effect of coupling of adjacent intermolecular distances is described by the parameter a, and that the direct interference to the mean square deviation from the non-neighboring intermolecular distances is neglected. We obtain the following relation by using the assumptions described above,

$$\langle \Delta r_{pq}^2 \rangle^{\mathrm{tr}} = [\sum_{i=1}^{N} (\boldsymbol{\lambda}_{pq} \cdot \boldsymbol{t}_i)^2] A + [2 \sum_{i,j}{}' (\boldsymbol{\lambda}_{pq} \cdot \boldsymbol{t}_i) \cdot (\boldsymbol{\lambda}_{pq} \cdot \boldsymbol{t}_j)] a \tag{9}$$

where $\sum_{i,j}{}'$ shows the summation for i and j only when the i-th and j-th intermolecular distances are in neighbors. The coefficients for A and a can be determined when the equilibrium position and orientation for each molecule are given by a visualized structure model of the liquid.

Rotational or Librational Motion in the Liquid. The rotational displacement $\Delta \boldsymbol{r}_p$ for the p-th atom in a molecule is approximately given by

$$\Delta \boldsymbol{r}_p = \boldsymbol{r}_p \times \Delta \boldsymbol{\Omega} \tag{10}$$

where $\Delta \boldsymbol{\Omega}$ is the rotational vector with the components $\Delta \Omega_x$, $\Delta \Omega_y$, and $\Delta \Omega_z$, which are the angles of rotation around the temporarily chosen space-fixed x, y, and z-axes, respectively. Equation 10 is exact to the first order of $\Delta \boldsymbol{\Omega}$, that is, when the magnitude of $\Delta \boldsymbol{\Omega}$ is small. The displacement of the p-th and q-th atoms due to the rotational or librational motion becomes

$$\Delta r_{pq}^{\mathrm{rot}} = \boldsymbol{\lambda}_{pq} \cdot (\Delta \boldsymbol{r}_p - \Delta \boldsymbol{r}_q). \tag{11}$$

Now we also assume that for a molecule

$$\langle \Delta \Omega_s \Delta \Omega_t \rangle = W \delta_{st} \tag{12}$$

and for the neighboring i-th and j-th molecules

$$\langle \Delta \Omega_s^i \Delta \Omega_t^j \rangle = w \delta_{st}, \tag{13}$$

where

$$s \text{ or } t = x, y, \text{ or } z$$

and δ is Kronecker's delta. For non-neighboring molecules, w is assumed to be zero. When we use the components x_p, y_p, and z_p for the vector $\boldsymbol{r}_p$, we rewrite Eq. 10 as

$$\Delta \boldsymbol{r}_p = X_p \cdot \Delta \boldsymbol{\Omega} \tag{14}$$

where

$$X_p = \begin{pmatrix} 0 & -z_p & y_p \\ z_p & 0 & -x_p \\ -y_p & x_p & 0 \end{pmatrix}$$

TABLE 1. THE COEFFICIENTS OF A, a, W, AND w FOR THE BCC MODEL[a)]

	r_{pq}/Å	Trans 1	Trans 2	Rot 1	Rot 2	l_{pq}^2/Å^2
C_0-C_1	5.90	1.0	0.0	0.0	0.0	0.203
C_0-C_2	6.813	0.667	0.667	0.0	0.0	0.291
C_0-Cl_{11}	7.670	1.0	0.0	0.0	0.0	0.203
C_0-Cl_{12}	5.566	0.910	0.0	3.129	0.0	0.501
C_0-Cl_{21}	7.967	0.689	0.601	1.527	0.0	0.434
C_0-Cl_{22}	5.968	0.628	0.628	2.721	0.0	0.549
Cl_{01}-Cl_{11}	5.90	1.0	0.0	0.0	0.0	0.203
Cl_{01}-Cl_{12}	3.914	0.818	0.0	3.671	2.658	0.361
Cl_{01}-Cl_{21}	6.813	0.667	0.667	4.177	0.0	0.713
Cl_{01}-Cl_{22}	5.188	0.667	0.460	5.690	0.0	0.817

a) Trans 1 and Trans 2 are the coefficients of A and a, in Eq. 9, respectively. Similarly, Rot 1 and Rot 2 are the coefficients of W and w, in Eq. 19, respectively.

From Eq. 11, we obtain the following relation

$$\langle \Delta r_{pq}^2 \rangle^{\mathrm{rot}} = \langle (\boldsymbol{\lambda}_{pq}\cdot\Delta\boldsymbol{r}_p)^2 \rangle + \langle (\boldsymbol{\lambda}_{pq}\cdot\Delta\boldsymbol{r}_q)^2 \rangle - 2\langle (\boldsymbol{\lambda}_{pq}\cdot\Delta\boldsymbol{r}_p)(\boldsymbol{\lambda}_{pq}\cdot\Delta\boldsymbol{r}_q) \rangle. \quad (15)$$

Here,

$$\boldsymbol{\lambda}_{pq}\cdot\Delta\boldsymbol{r}_p = \tilde{\boldsymbol{\lambda}}_{pq}\cdot X_p\cdot\Delta\boldsymbol{\Omega} \quad (16)$$

where $\tilde{\boldsymbol{\lambda}}_{pq}$ is the transposed vector of $\boldsymbol{\lambda}_{pq}$. Therefore, we have

$$\langle (\boldsymbol{\lambda}_{pq}\cdot\Delta\boldsymbol{r}_p)^2 \rangle = \langle \tilde{\boldsymbol{\lambda}}_{pq} X_p \Delta\boldsymbol{\Omega} \Delta\tilde{\boldsymbol{\Omega}} \tilde{X}_p \boldsymbol{\lambda}_{pq} \rangle = W \tilde{\boldsymbol{\lambda}}_{pq} X_p \tilde{X}_p \boldsymbol{\lambda}_{pq}. \quad (17)$$

In the same way, we obtain the following relation,

$$\langle (\boldsymbol{\lambda}_{pq}\cdot\Delta\boldsymbol{r}_p)(\boldsymbol{\lambda}_{pq}\cdot\Delta\boldsymbol{r}_q) \rangle = \langle \tilde{\boldsymbol{\lambda}}_{pq} X_p \Delta\boldsymbol{\Omega}^p \Delta\tilde{\boldsymbol{\Omega}}^q \tilde{X}_q \boldsymbol{\lambda}_{pq} \rangle = w \tilde{\boldsymbol{\lambda}}_{pq} X_p \tilde{X}_q \boldsymbol{\lambda}_{pq}. \quad (18)$$

By using Eqs. 17 and 18, Eq. 15 becomes

$$\langle \Delta r_{pq}^2 \rangle^{\mathrm{rot}} = [\tilde{\boldsymbol{\lambda}}_{pq}(X_p\tilde{X}_p + X_q\tilde{X}_q)\boldsymbol{\lambda}_{pq}]W + [-2\tilde{\boldsymbol{\lambda}}_{pq} X_p \tilde{X}_q \boldsymbol{\lambda}_{pq}]w. \quad (19)$$

According to the assumptions, the second term vanishes except for the case that the p-th and q-th atoms belong to the neighboring molecules, respectively.

Results and Discussion

In our previous papers,[2,3] it was shown that the bcc model for the local lattice structure of liquid carbon tetrachloride was the best model for simulating the experimental X-ray scattering intensity. So we use the bcc model for the calculation of the bracketed coefficients in Eqs. 9 and 19.

After the calculation of the coefficients for all pairs p and q, we can set up an equation for the weighted structure function $si(s)$ with the parameters A, a, W, and w for the bcc model, where $i(s)$ is the reduced intensity (Eq. 1). The values for the structure parameters of the bcc model are the same as the ones in the previous paper,[2] namely, the first nearest neighbor distance R is 5.9 Å, the molecules up to the fourth nearest neighbors are included in the discrete structure region, and the radius of this structure region is 12.41 Å with the intentional damping factor l_c of 1.76 Å. In Table 1, the values of the coefficients of A and a in Eq. 9, and W and w in Eq. 19 for main atomic pairs are shown. The numbering of atoms is shown in Fig. 2.

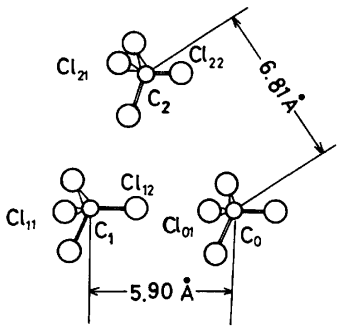

Fig. 2. The arrangement of the first and second nearest neighbor molecules in the bcc local lattice structure model for liquid carbon tetrachloride.

TABLE 2. THE REFINED PARAMETERS[a)]

A/Å^2	0.203 (0.041)	W/rad^2	0.101 (0.023)
a/Å^2	0.233 (0.122)	w/rad^2	−0.066 (0.023)

a) The values in the parentheses are standard deviations.

Carrying out a least-squares analysis by the use of our experimental $si(s)$ of the liquid carbon tetrachloride,[4] we determine the values of the fitting parameters A, a, W, and w. The s-region ranging from 1.5 to 6 Å^{-1} is used for the least-squares analysis. The result is shown in Table 2. The reliability factor defined by

$$R = \left[\sum |si(s)_{\mathrm{exp}} - si(s)_{\mathrm{calcd}}|^2 / \sum |si(s)_{\mathrm{exp}}|^2 \right]^{1/2} \quad (20)$$

is 0.23. The calculated $si(s)_{\mathrm{calcd}}$ curve using these refined parameters is shown by the solid curve in Fig. 3, with the experimental values denoted by circles.

As is shown in Fig. 3, the agreement between the experimental and calculated $si(s)$ curves has not been improved by the present treatment, in comparison with the case of using the modified Prins relation with two D constants as described in Ref. 2. By comparing the mean square amplitudes of the present treatment with respective ones obtained by the latter treatment,[2] it has proved that the values for chlorine-chlorine atomic pairs are very similar to each other, while the values

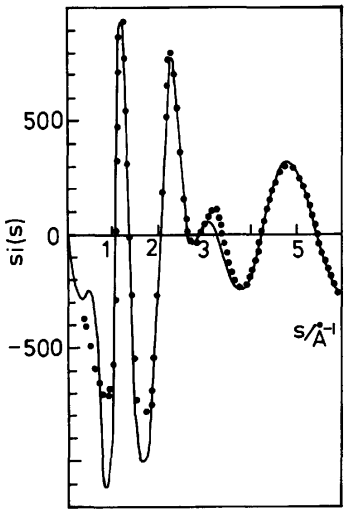

Fig. 3. The weighted structure functions $si(s)$ for liquid carbon tetrachloride. The solid curve is the calculated one and circles are experimental values.[4]

for carbon–carbon atomic pairs are significantly different. The smaller scattering power of carbon–carbon pairs makes no difference in the agreement of the $si(s)$ curves. From the point of view of only simulating the experimental $si(s)$ curve, the modified Prins relation with two D constants and the present treatment are in fair agreement. However, the physical meaning of the parameters is clear and the description of the motion of carbon tetrachloride molecules in the liquid becomes considerably clear by the present analysis.

From the value of A, 0.203 Å^2, the translational root mean-square deviation between the central and the first nearest-neighbor molecules (pair C_0–C_1) becomes 0.45 Å. The translational root mean-square deviation between the central molecule and the second nearest neighbors (pair C_0–C_2) becomes 0.54 Å. For the chlorine atoms in neighboring molecules (Cl_{01}–Cl_{11}), the value l_{pq} becomes 0.60 Å.

From the magnitude of W, 0.101 rad^2, we obtain

$$\sqrt{\langle\Delta\Omega^2\rangle} = \sqrt{\langle\Delta\Omega_x^2+\Delta\Omega_y^2+\Delta\Omega_z^2\rangle} = 0.551 \text{ rad} = 31.5\,^\circ \quad (21)$$

This value shows that the root mean-square of the librational or the orientational fluctuation of a molecule is 31.5°. The error caused by using the approximated equation (Eq. 10) is estimated to be about 10% in the worst case for this considerably large amplitude of $\sqrt{<\Delta\Omega^2>}$.

The negative sign of w shows that the rotational motion is gear-like. When a molecule rotates, the nearest molecules rotate in the reverse direction, being dragged by the first molecule. Since the magnitude of $|w/W|$ is less than unity, the rotation of the first molecule is not conveyed to the nearest molecules in the perfectly coherent phase. This incoherence causes the disturbance in rotation of the molecules, *i.e.*, the rotational diffusion. However, the ratio of $|w/W|$ amounts to 0.66, which shows that by the direct effect of the rotation of a molecule the nearest neighboring molecules are dragged about 0.66× (the rotational amplitude of the molecule). It may be said that carbon tetrachloride molecules have a tendency to keep the most stabilized orientational correlation, namely, the head-tail head-tail packing in the liquid even if the molecules are vigorously moving.

Bartoli and Litovitz discussed the motion of carbon tetrachloride molecule in the liquid[13] from an analysis of the orientational broadening of Raman bands. However, it is difficult to relate the present results to their values, because both analyses are based on different theoretical points of view; in the present work a time-averaged quantity is looked for, while in the Raman studies time-correlation is the main concern.

Steinhauser and Neuman carried out molecular dynamics study for liquid carbon tetrachloride.[14] According to their result about the velocity autocorrelation function, the period of the vibratory motion of the reference particle in the cage of its neighbors was roughly 0.3 ps. If we assume that the molecules move translationally with a velocity determined by the thermal energy, half of the mean free path for the collision, which is the distance corresponding to a fourth of the period of the vibratory motion mentioned above, can be estimated as 0.10 Å, which agrees in order of magnitude with our value of 0.45 Å for the translational root mean-square deviation of the neighboring molecules. However, we are somewhat uncertain about the extent to which the correspodence between the two quantities can be physically meaningful.

Hyodo and Fujiyama ascribed the small but significant depolarization degree of the ν_1 Raman line of liquid carbon tetrachloride to the fluctuation of the local field which is felt by each molecule in the condensed phase, and formulated the expression for the degree of depolarization in terms of the mean square amplitudes of the distances between molecular centers.[15] Calculating the degree of depolarization by the use of their formula (Eq. 25 in Ref. 15) and the present translational amplitudes, we obtain the value of 0.0042. The magnitude is in good agreement with the experimental value of 0.0039.[16]

The present study suggests that by the detailed analysis of the mean square deviations of interatomic distances in liquids obtained by diffraction methods we can obtain information on the dynamics of liquids, which may be complementary to that obtained by spectroscopic techniques.

The authors wish to thank Professor Toshiko Kato of Seibo Women's Junior College for directing their attention to the papers on Raman scattering studies of liquid carbon tetrachloride.

Appendix

Expressions where Perpendicular Displacements are Included. Let s_i be the unit vector perpendicular to t_i and on the plane

formed by t_i and λ_{pq}, and ΔP_i the displacement along s_i. The motion perpendicular to both t_i and s_i has no effect at all. Then we have in place of Eq. 6,

$$\Delta r_{pq}^{tr} = \lambda_{pq}\cdot(\Delta R_1 t_1+\Delta P_1 s_1+\Delta R_2 t_2+\Delta P_2 s_2+\cdots) \quad (A.1)$$

The following assumptions are reasonably made in addition to Eqs. 7 and 8;

$$\begin{aligned}
&\langle \Delta P_i^2\rangle = B \\
&\langle \Delta P_i \Delta P_j\rangle = 0 \qquad \text{for } i \neq j \\
&\langle \Delta P_i \Delta R_i\rangle = 0 \\
&\langle \Delta P_i \Delta R_j\rangle = \begin{cases} b & \text{for } j = i+1 \\ 0 & \text{otherwise.} \end{cases}
\end{aligned} \quad (A.2)$$

Then we have

$$\begin{aligned}
\langle \Delta r_{pq}^2\rangle^{tr} = &\sum_{i=1}^{N}(\lambda_{pq}\cdot t_i)^2 A + \sum_{i=1}^{N}(\lambda_{pq}\cdot s_i)^2 B \\
&+ 2\sum_{i,j}'(\lambda_{pq}\cdot t_i)\cdot(\lambda_{pq}\cdot t_j)a \\
&+ 2\sum_{i,j}'(\lambda_{pq}\cdot s_i)\cdot(\lambda_{pq}\cdot t_j)b
\end{aligned} \quad (A.3)$$

corresponging to Eq. 9 in the text.

In comparing Eqs. 9 and A.3, we must regard the parameter A in the text as the effective value of

$$A + \frac{\sum(\lambda_{pq}\cdot s_i)^2}{\sum(\lambda_{pq}\cdot t_i)^2}B \quad (A.4)$$

and a as that of

$$a + \frac{\sum'(\lambda_{pq}\cdot s_i)\cdot(\lambda_{pq}\cdot t_j)}{\sum'(\lambda_{pq}\cdot t_i)\cdot(\lambda_{pq}\cdot t_j)}b. \quad (A.5)$$

In the case of the present study, the maximum value of $(\lambda_{pq}\cdot s_i)$ is about 1/2 and the minimum value of $(\lambda_{pq}\cdot t_i)$ is $\sqrt{3}/2$, and most of the $(\lambda_{pq}\cdot s_i)$ terms are nearly zero, so the coefficient of B in Eq. A.5 is much smaller than 1/3. In the same way, the coefficient of b is much smaller than $1/\sqrt{3}$. The averaged quantity B is probably of the same order of magnitude as A, but it is ignored because of the small coefficients that appear in the practical computation for the case of carbon tetrachloride. Little is known about a and b, which must be strongly dependent on the angle between R_i and R_j. At the present stage of investigations, we should be content with the fact that only the effective value of Eq. A.5 can be determined.

References

1) J. F. Karnicky and C. J. Pings, *Adv. Chem. Phys.*, **34**, 157 (1976); S. I. Sandler, M. G. Lombardo, D. S. H. Wong, A. Habenschuss, and A. H. Narten, *J. Chem. Phys.*, **77**, 2144 (1982); W. E. Thiessen and A. H. Narten, *J. Chem. Phys.*, **77**, 2656 (1982).

2) K. Nishikawa and T. Iijima, *Bull. Chem. Soc. Jpn.*, **58**, 1215 (1985).

3) K. Nishikawa and Y. Murata, *Bull. Chem. Soc. Jpn.*, **52**, 293 (1979).

4) K. Nishikawa and T. Iijima, *Bull. Chem. Soc. Jpn.*, **57**, 1750 (1984).

5) K. Nishikawa, K. Tohji, and Y. Murata, *J. Chem. Phys.*, **74**, 5817 (1981).

6) K. Heinzinger, "Diffraction Studies on Non-crystalline Substances," ed by I. Hargittai and W. J. Orville-Thomas, Elsevier Scientific Publishing Co., Amsterdam, (1981).

7) K. Nakanishi, K. Ikari, S. Okazaki, and H. Touhara, *J. Chem. Phys.*, **80**, 1656 (1984).

8) L. Blum and A. H. Narten, *Adv. Chem. Phys.*, **34**, 203 (1976).

9) T. Kihara, "Intermolecular Forces," Wiley, New York (1977).

10) J. Frenkel, "Kinetic Theory of Liquids," Oxford, London (1946).

11) S. Baer, *Chem. Phys.*, **39**, 159 (1979).

12) Y. Morino, Y. Nakamura, and T. Iijima, *J. Chem. Phys.*, **32**, 643 (1960).

13) F. J. Bartoli and T. A. Litovitz, *J. Chem. Phys.*, **56**, 413 (1972).

14) O. Steinhauser and M. Neumann, *Mol. Phys.*, **40**, 115 (1980).

15) S. Hyodo and T. Fujiyama, *Bull. Chem. Soc. Jpn.*, **53**, 2456 (1980).

16) W. F. Murphy, M. V. Evans, and P. Bender, *J. Chem. Phys.*, **47**, 1836 (1967).

 © 1985 The Chemical Society of Japan Bull. Chem. Soc. Jpn., 58, 1225—1227 (1985)

Temperature Effect on Transference Numbers for KCl in Ethanol-Water Mixtures

Masakatsu UENO,* Shōgo I, and Kiyoshi SHIMIZU
Department of Applied Chemistry, Faculty of Engineering, Doshisha University, Karasuma Imadegawa, Kamigyo-ku, Kyoto 602
(Received October 4, 1984)

Cation-transference numbers were determined by the moving boundary method for 0.02 mol dm^{-3} KCl in 5-, 10-, 15-, 20-, and 30 mol% ethanol-water mixtures at 15 and 35 °C. The cation-transference number has a maximum around 10 mol% of ethanol at each temperature studied, and becomes larger with decreasing temperature in the solvent of the same composition. From the temperature dependence of the transference number, the differences in the activation energy of transport between K^+ and Cl^- ions were estimated, and it was found that the activation energy of the K^+ ion is less than that of the Cl^- ion and the difference becomes larger in the range of 5—20 mol% of ethanol. These results are discussed in terms of structural effects and ion-solvent interactions.

Transference number measurement is a matter of considerable importance in the study of electrolyte solutions by the conductivity method since individual ionic conductances can be determined without any assumptions by combining transference numbers with electrolyte conductances. Such a single-ion property at infinite dilution is closely related to the ion-solvent interaction. The investigation of the temperature and pressure dependence of limiting ionic conductances and correlated quantities in water has led to the important concept on the ion-solvent interaction in relation to the unique structure properties of water.[1-4] Since a small addition of alcohols to water increases the degree of structure of solution,[5] it is interesting to measure the transference numbers and conductances of electrolytes in these mixtures as a function of temperature and pressure. However, a few papers have been published for the temperature[6] and pressure[7] effects on transference numbers in alcohol-water mixtures. In a previous paper,[7] we reported transference numbers for KCl in ethanol-water mixtures up to 30 mol% of ethanol under high pressure at 25 °C and discussed specific interactions between the ions and solvent. Here the temperature effect on transference numbers for KCl in ethanol-water mixtures is reported.

Experimental

Potassium chloride of high purity was obtained from Merck and dried above 130 °C prior to use. Purification of ethanol and water was the same as described before.[7] The solutions of 0.02 mol dm^{-3} KCl were prepared by weighing on the assumption that the densities of the solutions were equal to those of the solvent.[8]

Cation-transference numbers t_+ were determined by the autogenic moving-boundary method using a cadmium anode and a silver-silver chloride cathode. The velocity of the moving boundary formed by KCl and $CdCl_2$ solutions was detected by measuring a change in resistance between two platinum probe electrodes. The volume between the probe electrodes was determined by calibration runs at each temperature using 0.02 mol dm^{-3} KCl aqueous solution and the values of t_+=0.4924 at 15 °C and 0.4885 at 35 °C by Allgood *et al.*[9] The calibrated volume had a standard deviation better than 0.2%. Details of cell construction, other apparatus, and the procedure for calculating the apparent and final transference numbers have been described previously.[7]

Results and Discussion

The cation-transference numbers t_+ obtained are listed in Table 1. The variation of t_+ with the ethanol content is similar at various temperatures studied as seen in Fig. 1. The cation-transference number initially increases up to about 10 mol% of ethanol and then decreases. The characteristic features for the temperature effect on t_+ are the following: The cation-transference number in the solvent of the same composition becomes larger at lower temperature, and the initial increase and the following decrease in t_+ with increasing ethanol content become more rapid with decreasing temperature. These features will be maintained for the limiting cation-transference number t_+° since there is very little concentration dependence in t_+ in the case of t_+ which is close to 0.5 as shown by the following Kay-Dye equation:[10]

$$t_+^\circ = t_+ + (0.5 - t_+)\Lambda_e/\Lambda^\circ, \quad (1)$$

where Λ_e is the electrophoretic contribution to conductance and Λ° is the limiting molar conductance of KCl. In Fig. 1, the data at 5 °C by Erdey-Grúz and Majthényi[6] are also shown. The initial increase in

TABLE 1. CATION-TRANSFERENCE NUMBERS FOR 0.02 mol dm^{-3} KCl IN ETHANOL–WATER MIXTURES AT 15-, 25-,[a] AND 35 °C

t	Mol% of ethanol					
°C	0[b]	5	10	15	20	30
15	0.4924	0.5078(6)[c]	0.5137(4)	0.5099(5)	0.5053(4)	0.4879(6)
25	0.4901	0.5025(4)	0.5060(7)	0.5052(6)	0.5004(5)	0.4856(5)
35	0.4885	0.4976(6)	0.5014(5)	0.4986(7)	0.4933(7)	0.4809(7)

a) Ref. 7. b) Ref. 9. c) The numbers in parentheses are 10^4 times the standard deviation of repeated runs.

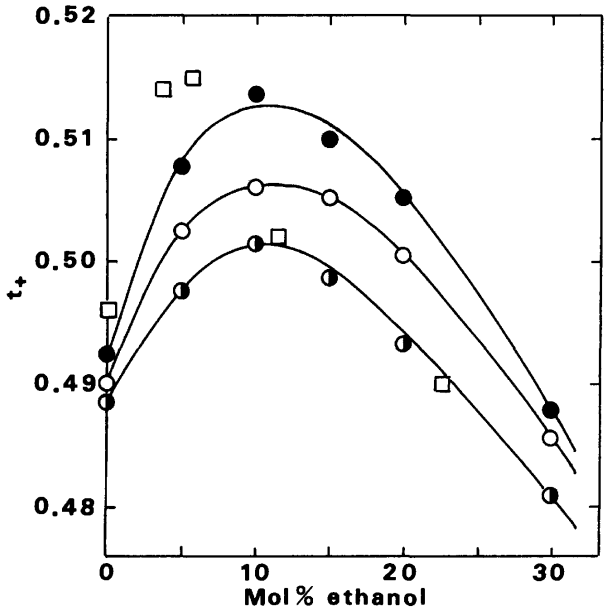

Fig. 1. Variation of the transference number for the K^+ ion with mol% of ethanol at various temperatures. ●: 15 °C, ○: 25 °C, ◑: 35 °C, □: 5 °C, Ref. 6.

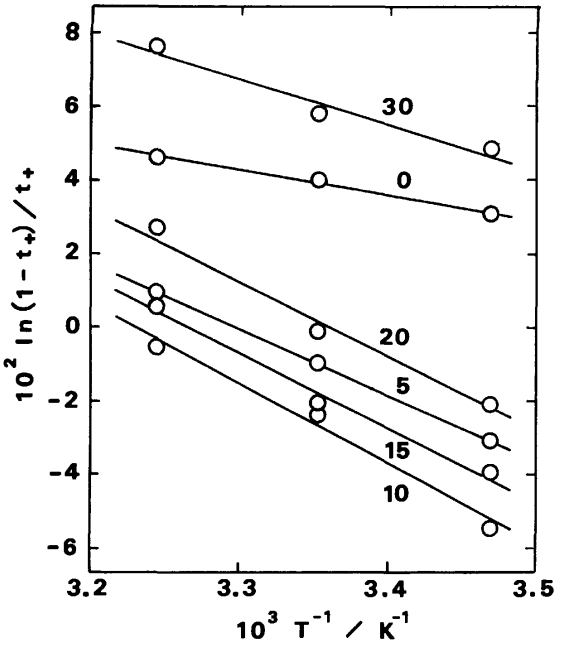

Fig. 2. A logarithmic plot of the ratio of anion- to cation-transference number against the reciprocal of the absolute temperature. Mol% of ethanol is shown in the plot.

t_+ at 5 °C is larger than that at 15 °C obtained by us, although the values above 10 mol% of ethanol at 5 °C in Ref. 6 appear to be fairly small just as those at 25 °C.

In the previous paper,[7] it has been shown that the Zwanzig dielectric friction theory[11] could not account for the variation of the transference number with the ethanol content. One of the reasons for it could be due to the neglect of the delicate difference in the ion-solvent interaction between K^+ and Cl^- ions although it is considered from a wide variety of thermodynamic and transport data that the influence of K^+ and Cl^- ions on the solvent structure is similar and almost equal in magnitude: The B-coefficients of the viscosity for K^+ and Cl^- ions were assumed to be equal in water.[1] However, the variation of the transference number with solvent composition as well as temperature and pressure sensitively reflects the relative difference in the ion-solvent interaction between these ions.

The slope of $\ln(1-t_+^\circ)/t_+^\circ$ plotted against the reciprocal of the absolute temperature $1/T$ should yield the difference in the activation energy of transport between K^+ and Cl^- ions at infinite dilution. Figure 2 shows such a plot where the concentration dependence of the transference number is neglected. The difference in the activation energy, $E(K^+)-E(Cl^-)$, was roughly estimated by assuming the linearity between $\ln(1-t_+)/t_+$ and $1/T$. The values obtained in 0-, 5-, 10-, 15-, 20-, and 30 mol% of ethanol are −0.6, −1.5, −1.8, −1.7, −1.7, and −1.0 kJ mol^{-1}, respectively: The activation energy for the K^+ ion is less than that for the Cl^- ion and the difference becomes larger in the water-rich region, 5—20 mol%. In ethanol-water mixtures, selective solvation would arise. It is considered that both the K^+ and the Cl^- ions interact more strongly with water molecules than with ethanol molecules because the dipole moment of a water molecule is larger than that of an ethanol molecule. The ion-solvent interaction of the Cl^- ion also involves the additional contribution of a hydrogen bond with water molecules.[12] In ethanol-water mixtures, the interaction of the Cl^- ion with water molecules would be weaker than in pure water, while that of the K^+ ion with water molecules would be stronger because of the enhanced basicity of water molecules.[13] Therefore, the radius of the solvated K^+ ion would be expected to be larger than that of the solvated Cl^- ion in the mixtures. According to the Eyring theory of transport process in solution,[14] the activation energy corresponds to the energy required to provide a hole in the liquid for an ion to migrate and is anticipated to be larger for a larger ion. However, it is contrary to the prediction of the theory that the activation energy for the larger solvated ion K^+ is less than that for the smaller solvated ion Cl^-. This would suggest that the structure-breaking effect of the K^+ ion is greater than that of the Cl^- ion in the mixtures as well as in water.[15]

A small addition of ethanol to water enhances the structure of the solvent.[5] If the structure-breaking effect of the K^+ ion is greater than that of the Cl^- ion, the K^+ ion obtains the larger structural excess mobility than the Cl^- ion and the mobility of the K^+ ion becomes larger relative to the Cl^- ion in the mixtures. The intial increase in t_+ up to about 10 mol% of ethanol, where the slope of the viscosity of the mixtures plotted against the ethanol content shows a maximum,[16] would be primarily ascribed to the relative structure-breaking properties of these two ions. The concept mentioned above is readily applied to the temperature effect on transference numbers for KCl. Since the structure of

the solvent is more enhanced at lower temperature, the difference in the structure-breaking effect between K^+ and Cl^- ions would become greater. Accordingly, the K^+ ion would obtain the larger structural excess mobility relative to the Cl^- ion and t_+ increases with decreasing temperature.

In addition to the structural effect, the sorting effect may be taken into consideration.[16] Since the viscosity of ethanol–water mixtures increases up to about 25 mol% of ethanol,[8,16] the effective viscosity around a solvated ion would become smaller than the bulk viscosity by selective enrichment of water molecules around a solvated ion, and the ion would have an excess mobility. This effect is larger for K^+ than for Cl^- ions since the crystallographic radius of a K^+ ion is smaller than that of a Cl^- ion. Hence the initial increase in t_+ would be also attributed to the difference in the sorting effect between these two ions. The sorting effect is expected to become greater at lower temperature since the sharper maximum of the bulk viscosity appears at lower temperature.[8,16]

References

1) R. W. Gurney, "Ionic processes in Solution," McGraw-Hill, New York (1953).

2) R. L. Kay, "Water, a Comprehensive Treatise," ed by F. Franks, Plenum Press, New York (1973), Vol. 3, Chap. 4.

3) K. Shimizu and N. Tsuchihashi, *Rev. Phys. Chem. Jpn.*, **49**, 18 (1979).

4) M. Nakahara, T. Török, N. Takisawa, and J. Osugi, *J. Chem. Phys.*, **76**, 5145 (1982); N. Takisawa, J. Osugi, and M. Nakahara, *ibid.*, **78**, 2951 (1983).

5) F. Franks and D. J. G. Ives, *Quart. Rev. London*, **20**, 1 (1966).

6) T. Erdey-Grúz and L. Majthényi, *Acta. Chim. Hung.*, **20**, 73 (1959).

7) M. Ueno, S. I, and K. Shimizu, *Bull. Chem. Soc. Jpn.*, **56**, 846 (1983).

8) M. Kikuchi and E. Oikawa, *Nippon Kagaku Zasshi*, **88**, 1259 (1967).

9) R. W. Allgood, D. J. LeRoy, and A. R. Gordon, *J. Chem. Phys.*, **8**, 418 (1940).

10) R. L. Kay and J. L. Dye, *Proc. Natl. Acad. Sci. U. S. A.*, **49**, 5 (1963).

11) R. Zwanzig, *J. Chem. Phys.*, **52**, 3625 (1970).

12) M. Nakahara, K. Shimizu, and J. Osugi, *Nippon Kagaku Zasshi*, **92**, 785 (1971).

13) D. Feakins, "Pysico-Chemical Processes in Mixed Aqueous Solvents," ed by F.Franks, Heinemann Educational Books Ltd., London (1967), pp. 71—90.

14) H. S. Taylor, *J. Chem. Phys.*, **6**, 331 (1938).

15) R. L. Kay and G. A. Vidulich, *J. Phys. Chem.*, **74**, 2718 (1970).

16) R. L. Kay and T. L. Broadwater, *J. Solution Chem.*, **5**, 57 (1976).

The Arrhenius Parameters for the Reactions of O Atoms with Ethene and Five Fluoroethenes

Hironobu UMEMOTO,* Koichiro SUGIYAMA, Shigeru TSUNASHIMA, and Shin SATO†
Department of Applied Physics, Tokyo Institute of Technology, Ookayama, Meguro-ku, Tokyo 152
†*Research Laboratory for Nuclear Reactors, Tokyo Institute of Technology, Ookayama, Meguro-ku, Tokyo 152*
(Received October 11, 1984)

The rate constants for the reactions of ground-state oxygen atoms with ethene and five fluoroethenes have been measured over the temperature range of 240—450 K, using a pulse radiolysis-resonance absorption technique. The rate constants were well expressed by the following Arrhenius expressions: $k(O+C_2H_4)=8.4\times10^6\exp(-712/T)$; $k(O+C_2H_3F)=3.1\times10^6\exp(-622/T)$; $k(O+CH_2=CF_2)=2.4\times10^6\exp(-638/T)$; $k(O+cis\text{-}CHF=CHF)=1.9\times10^6\exp(-500/T)$; $k(O+C_2HF_3)=3.0\times10^6\exp(-544/T)$; $k(O+C_2F_4)=8.1\times10^6\exp(-634/T)$, in units of $m^3mol^{-1}s^{-1}$. The change in the preexponential factors with the degree of fluorination is discussed in terms of the conventional transition-state theory.

The temperature dependence of the rate constant for the reactions of ground-state oxygen atoms with simple olefins has been widely investigated over the last two decades.[1] Especially, the rate constants for ethene have been measured extensively.[2-10] On the other hand, only a limited number of data are available for the reactions of O(^{3}P) with fluoroethenes.[11-19] The room-temperature rate constants for the reactions of O(^{3}P) with fluoroethenes have been measured by several groups, including the members of our laboratory.[12-19] It has been found that the rate constants do not change monotonously with the number of the substituted fluorine atoms.[12,14] Ethene and tetrafluoroethene are more reactive than the others, while difluoroethene has the lowest reactivity. According to the competitive experiments by Jones and Moss,[12] this change in reaction rate is due to the change in activation energies. However, their conclusion is based only on the rate measurements at two temperatures, 298 and 423 K. It is hard, we believe, to estimate the Arrhenius parameters from only two points of data. In order to make it clear if the change in the room-temperature rate constants is due to the change in the preexponential factors or to that in the activation energies, we measured the temperature dependence of the rate constants for the reactions of O(^{3}P) with ethene and five fluoroethenes.

Experimental

The experimental apparatus and the procedure were similar to those described previously.[20-22] Briefly, a mixture of CO_2 (70—140 Pa) and ethene or fluoroethenes (7—31 Pa) diluted with excess Ar (90 kPa) was irradiated with an electron pulse generated by a Febetron 706 (Hewlett Packard Co.). Oxygen molecules were not used as the O-atom source, since O_2 molecules are reactive to O atoms and disturb the estimation of the rate constants.[21] After the pulse, the concentration of the ground-state oxygen atoms was monitored by the light absorption of resonance triplet lines around 130 nm. As the source of the resonance radiation of oxygen atoms, a microwave-powered lamp with a flow of He and a trace amount of O_2 was used. Ar (Jonan Kyodo Sanso), He (Japan Helium Center), and O_2 (Nihon Sanso) were used from cylinders without further purification. The sources of the other materials were: Takachiho Kako: CO_2 and C_2H_4, Daikin Co.: C_2H_3F and C_2HF_3, Japan Halon Co.: $CH_2=CF_2$, and PCR: *cis*-CHF=CHF. The C_2F_4 was prepared by the thermal decomposition of Teflon. These gases were used after purification through several freeze-thaw cycles. The purity of the C_2H_4, C_2H_3F, and C_2HF_3 has been checked in a previous work.[14] The purity of the $CH_2=CF_2$, *cis*-CHF=CHF, and C_2F_4 was checked mass-spectroscopically. There was no detectable impurity, except that C_2F_4 contained about 1% of C_3F_6, which is much less reactive than C_2F_4.[11]

Results

The first-order rate constants were determined by a procedure similar to that described in previous papers.[21,22] Although the room-temperature rate constant for O+C_2H_4 did not change systematically with the partial pressure of C_2H_4 over 15 Pa, it did increase with the decrease in the partial pressure of ethene below 12 Pa. Similar results have also been reported by Sugawara *et al.*[21] This increase in the apparent rate constant has been considered to be the result of secondary processes, such as reactions between O atoms and the CH_3 radicals formed in the reaction of O and C_2H_4.[21] Such secondary reactions seem less important in the cases of O+fluoroethenes. For example, in the case of C_2HF_3, no increase in the apparent rate constants could be observed at pressures higher than 7 Pa at 295 K. In general, secondary reactions are considered to become more important at low temperatures. Therefore, at low temperatures, more attention was paid and the experiments were performed with partial pressures of over 21 Pa. Although the scatter of the data was more severe at low temperatures, no systematic partial pressure dependence of the rate constants could be observed. The rate constants at each temperature are summarized in Table 1 and plotted in Fig. 1 in the form of Arrhenius plots. All the data are well characterized by Arrhenius equations. The Arrhenius parameters, as determined by the least-squares method, are listed in Table 2.

Discussion

Comparison with Literature Values. A number of measurements have been performed on the temperature dependence for the reaction of atomic oxygen with

TABLE 1. RATE CONSTANTS OF O-ATOM ADDITION TO ETHENE AND FLUOROETHENES. UNCERTAINTIES ARE STANDARD DEVIATIONS

Reactant	T/K	$k_r \times 10^{-6}$/m^3 mol^{-1} s^{-1}
C_2H_4	454	1.68±0.28
	375	1.29±0.12
	330	0.99±0.11
	296	0.70±0.11
	270	0.54±0.13
	239	0.46±0.09
C_2H_3F	452	0.76±0.10
	369	0.58±0.05
	325	0.44±0.04
	297	0.39±0.04
	266	0.30±0.05
	240	0.23±0.04
$CH_2=CF_2$	446	0.59±0.03
	375	0.43±0.01
	322	0.31±0.02
	293	0.26±0.03
	268	0.22±0.01
	241	0.17±0.01
cis-CHF=CHF	448	0.64±0.06
	376	0.54±0.06
	333	0.41±0.03
	297	0.37±0.07
	273	0.31±0.03
	243	0.26±0.04
C_2HF_3	454	0.91±0.09
	387	0.73±0.12
	322	0.57±0.09
	295	0.46±0.07
	266	0.38±0.04
	241	0.32±0.03
C_2F_4	446	1.91±0.18
	375	1.52±0.12
	325	1.16±0.02
	296	0.91±0.10
	265	0.70±0.09
	243	0.63±0.10

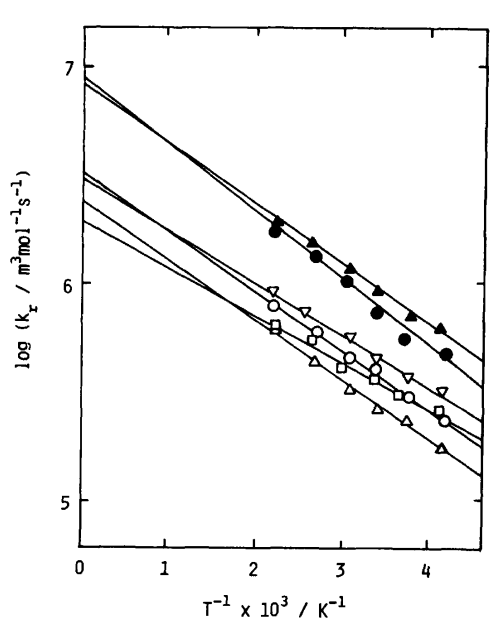

Fig. 1. Arrhenius plots for O+C_2H_4 (●), O+C_2H_3F (○), O+$CH_2=CF_2$ (△), O+*cis*-CHF=CHF (□), O+C_2HF_3 (▽), and O+C_2H_4 (▲).

TABLE 2. ARRHENIUS PARAMETERS FOR THE REACTIONS OF O ATOMS WITH ETHENE AND FLUOROETHENES. UNCERTAINTIES ARE STANDARD DEVIATIONS

Reactants	$A \times 10^{-6}$/m^3 mol^{-1} s^{-1}	E/kJ mol^{-1}
C_2H_4	8.40±1.25	5.92±0.41
C_2H_3F	3.06±0.23	5.17±0.21
$CH_2=CF_2$	2.36±0.14	5.30±0.17
cis-CHF=CHF	1.92±0.25	4.15±0.35
C_2HF_3	3.00±0.15	4.53±0.12
C_2F_4	8.13±0.67	5.27±0.24

C_2H_4. The Arrhenius parameters previously obtained for this reaction are summarized in Table 3. The agreement among the activation energies is rather good. However, the agreement among the preexponential factors is rather poor. The present value of the preexponential factor seems to be a little large, but this discrepancy is not considered to be serious, since these values were all obtained by extrapolation.

The room-temperature rate constants for ethene and fluoroethenes are listed in Table 4. Unfortunately, for $CH_2=CF_2$ and C_2F_4 there is some disagreement between the present values and those of Sugawara *et al.*, who used the same technique and the same apparatus.[14] The only difference is that they used a He/O_2 mixture as the O atom source, while we used Ar/CO_2. Since O atoms react with O_2, Sugawara *et al.* had to correct their data to estimate the reaction rates. The rate for the O+O_2 reaction under the conditions of Sugawara *et al.* was comparable to or larger than the rates for the O+fluoroethenes reactions. This may be the cause of the discrepancy. Apart from the values of Sugawara *et al.*, the present values seem to be a little larger than those obtained with different techniques. This cannot be accounted for by secondary reactions, as has been discussed in detail in a previous paper, since no partial-pressure dependence could be observed.[21] Figure 2 compares the Arrhenius plot obtained by Atkinson and Pitts for C_2H_3F[13] and the present one. The rate constants obtained in this work are larger than those of Atkinson and Pitts by a factor of 2. The cause of this discrepancy is not certain. Figure 2 also shows the results of the competitive work by Jones and Moss.[12] Since their values are relative ones, they were placed on an absolute basis using the rate constants for ethene determined in the present work.

Effect of the Substitution by F Atoms on the Arrhenius Parameters. As is shown in Table 2, the activation energies do not change greatly with the number of substituted fluorine atoms. This is not unexpected since the ionization potentials of ethene and fluoroethenes are not very different.[23] It is now well established that there is a good correlation between the activation energies and the ionization potentials in the reactions of O(^{3}P) with alkenes and alkynes.[24] On the other hand, the preexponential factors change by a factor of 4. It should also be noted that this factor first decreases upon fluorine substitution, and then increases again, so that the values for ethene and tetrafluoro-

TABLE 3. ARRHENIUS PARAMETERS FOR THE REACTION OF O WITH C_2H_4

Author(Ref.)	Method[a]	T/K	$A\times10^{-6}$/m^3 mol^{-1} s^{-1}	E/kJ mol^{-1}
Elias(2)	DF-CL	223—465	10.8±3.6	6.7±0.8
Elias(3)	DF-CL	223—613	8.4	6.7
Westenberg(4)	DF-ESR	195—715	5.0	6.3[b]
Davis(5)	FP-RF	232—500	3.3±0.2	4.7±0.1
Atkinson(6)	HgS-CL-PS	301—392	3.4	5.3±0.8
Singleton(7)	HgS-CL-PS	298—486	7.0±0.9	7.0±0.4
Atkinson(8)	FP-CL	298—439	5.6	6.2±0.8
Nicovich(9)	FP-RF	298—944	7.3±3.7	7.2±1.6[c]
Perry(10)	LP-CL	294—820	6.5±0.3	6.5±0.1[d]
This work	PR-RA	239—454	8.4±1.2	5.9±0.4

a) DF: discharge flow; CL: chemiluminescence; ESR: electron-spin resonance; FP: flash photolysis; RF: resonance fluorescence; HgS: Hg-photosensitization; PS: phase-shift; LP: laser photolysis; PR: pulse radiolysis; RA: resonance absorption. b) Deduced from the data between 226 K and 381 K, because of the nonlinearity in the Arrhenius plot at high temperatures. c) Deduced from the data between 298 K and 438 K. d) Deduced from the data between 294 K and 445 K.

TABLE 4. ROOM-TEMPERATURE RATE CONSTANTS FOR THE REACTIONS OF O ATOMS WITH ETHENE AND FLUOROETHENES IN UNITS OF 10^5 m^3 mol^{-1} s^{-1}

Author(Ref.)	Method[a]	C_2H_4	C_2H_3F	CH_2=CF_2	*cis*-CHF=CHF	C_2HF_3	C_2F_4
Jones(12)[b]	PA	(1.00)	(0.41)	(0.22)	(0.31)	(0.57)	(1.70)
Huie(15)	DF-MS	5.1[c]	2.6	2.2			
Atkinson(16)	HgS-CL-PS	4.0[d]	1.6				
Atkinson(13)	FP-CL	4.6[e]	1.6				
Gutman(17)	DF-MS	4.8[f]	2.1[f]	1.9	2.2	5.0	
Koda(19)	HgS-CL	4.3				1.9	4.3
Sugawara(14)	PR-RA	6.0	3.1	1.2		3.8	4.9
this work	PR-RA	7.0	3.9	2.6	3.7	4.6	9.1
this work[b]		(1.00)	(0.56)	(0.37)	(0.53)	(0.66)	(1.30)

a) PA: product analysis; MS: mass spectroscopy; for other abbreviations, see Table 3. b) Relative values. c) Ref. 5. d) Ref. 6. e) Ref. 8. f) Ref. 18.

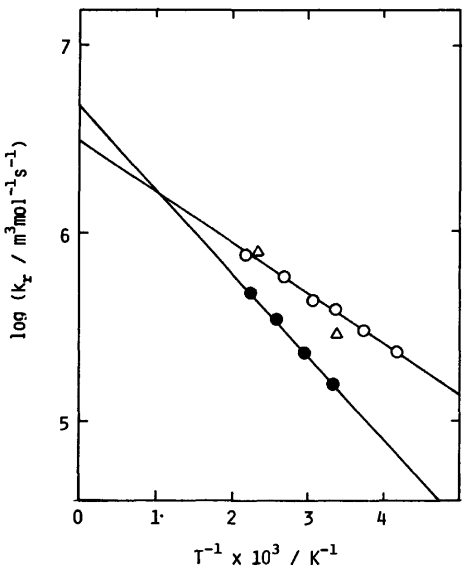

Fig. 2. Arrhenius plot for O+C_2HF_3 reaction; ●: Atikinson and Pitts, △: Jones and Moss, and ○: this work. Values of Jones and Moss were placed on an absolute basis using the present results for ethene.

ethene are nearly the same. Sugawara *et al.* tried to interpret the change in the room-temperature rate constants in terms of "approachability," the reactivity index calculated by the INDO method.[14] However, approachability is a conception correlated to the activation energy and cannot be employed to explain the change in the preexponential factors. Any correlation between the approachability and the room-temperature rate constants must be fortuitous.

The temperature dependence of the rate constant for the O+C_2H_4 reaction, including the nonlinearity in the Arrhenius plot at high temperatures, has been successfully explained by the conventional transition-state theory.[7,10] According to this theory, the rate constant is expressed by:

$$k_r = \kappa L \frac{kT}{h} \frac{F_t^{\dagger}}{F_t^{O} F_t^{R}} \frac{f_r^{\dagger}}{f_r^{R}} \frac{f_v^{\dagger}}{f_v^{R}} \frac{f_e^{\dagger}}{f_e^{O}} \exp(-E/kT). \quad (1)$$

Here, the symbols have their ordinary meanings; κ is the transmission coefficient, L is the path degeneracy, and F_t, f_r, f_v, and f_e are the translational, rotational, vibrational, and electronic partition functions respectively. Symmetry numbers are not included in the rotational partition functions. The superscripts, O, R, and †, are used to designate O atoms, reactant molecules (ethene or fluoroethene), and the transition states respectively. If we restrict the present discussion to the relative values of the rate constants, the common terms for all reactions of O+ethene or fluoroethenes, such as the partition functions for O atoms, may not be taken into account. The electronic states of the transition states are correlated to the spin-orbit states of the O(^3P_J) atoms. Since the spin-orbit splittings of the O(^3P_J) atoms are small, 1.89 and 0.82 kJ/mol, it can be assum-

ed that the energy separations of the electronic states of the transition states are small and that the electronic partition functions, $f_e^{\dagger}$, are almost the same. Singleton and Cvetanović have postulated that, in the reaction of O(^{3}P) with aliphatic olefins, the two new vibrations of the bending mode of the transition state are harmonic and have equal frequencies, ν, and that the partition functions for all the other vibrations in the transition state and the reactant cancel each other out.[7] If we employ this assumption, the temperature-dependent preexponential term in Eq. 1, A_T according to the notation of Singleton and Cvetanović,[7] can be written as:

$$A_T = C\kappa L\left[\frac{m^{\dagger}}{m^{R}}\right]^{3/2}\left[\frac{I^{\dagger}}{I^{R}}\right]^{1/2} T^{-1/2}\{1-\exp(-h\nu/kT)\}^{-2}. \quad (2)$$

Here, C is a constant independent of the nature of the reactant or the temperature, while m and I stand for the masses and the products of the three principal moments of inertia of the reactant or the transition state. The superscripts have the same meanings as in Eq. 1. The value of ν in Eq. 2 for ethene has been estimated by Singleton and Cvetanović[7] and by Perry[10] to be between 100 and 300 cm^{-1}, judging from the curvature in the Arrhenius plot. Substituting these values, it can easily be shown that the temperature dependence of the preexponential factor cannot be ignored compared to that of the exponential term. Since the experimentally obtained A factors listed in Table 2 are deduced under the assumption that the rate constants can be characterized by a simple Arrhenius equation, $k_r=A\exp(-E/kT)$, it is not fair to compare the values in Table 2 with those calculated by Eq. 2 at a certain temperature. Therefore, we re-analyzed the present results using the following equation:

$$k_r = A'T^{-1/2}\{1-\exp(-h\nu/kT)\}^{-2}\exp(-E/kT). \quad (3)$$

Here, A' is the temperature independent part of the preexponential factor:

$$A' = C\kappa L\left[\frac{m^{\dagger}}{m^{R}}\right]^{3/2}\left[\frac{I^{\dagger}}{I^{R}}\right]^{1/2}. \quad (4)$$

In order to estimate the magnitude of A' from the experimental results, it is necessary to know the value of ν. It was impossible, however, to determine the three parameters, A', ν, and E, uniquely from the present data alone. For the first step, we assumed that ν is independent of the degree of fluorination; we used the value for ethene determined by Singleton and Cvetanović and by Perry, between 100 and 300 cm^{-1}. The present experimental results could also be well characterized by Eq. 3 under such assumptions, and it was found that the relative values of A' are essentially the same as those of A listed in Table 2. The value of $(m^{\dagger}/m^{R})^{3/2}$, can easily be calculated. The results are shown in Table 5. In order to calculate the ratio of the rotational partition functions, $(I^{\dagger}/I^{R})^{1/2}$, it is necessary to know the geometry of the reactant molecule and the transition state. The structural parameters for the ground-state fluoroethene molecules have been determined experimentally by Carlos *et al.*[25] The geometry of the transition state of the C_2H_4O complex has been theoretically calculated,[26] but those of the fluoroethenes are not known. Therefore, for the first step, we assumed that the geometry of the intermediate complexes for all the fluoroethenes is analogous to that for ethene; *i.e.*, the C-O internuclear distance and the C-C-O angles are the same. The results are shown in Table 5. Both $(m^{\dagger}/m^{R})^{3/2}$ and $(I^{\dagger}/I^{R})^{1/2}$ decrease with the number of the substituted F atoms. As for C_2H_3F and $C_2H_2F_2$, the relative values of the products of $(m^{\dagger}/m^{R})^{3/2}$ and $(I^{\dagger}/I^{R})^{1/2}$ are comparable to the relative preexponential factors, A and A'. Therefore, the decrease in the preexponential factors from C_2H_4 to $C_2H_2F_2$ can be explained by assuming that the geometry of the transition states and the frequencies of the newly formed vibrations are similar for these reactants. However, it is difficult to explain the increase in the preexponential factors from $C_2H_2F_2$ to C_2F_4. In other words, it is hard to interpret why the preexponential factors for ethene and tetrafluoroethene are nearly the same under the assumptions that: 1) the geometries of the transition states are similar; 2) the newly formed vibrational frequencies of the transition states are the same, and 3) the transmission coefficients are the same. The identity of the A factors for C_2H_4 and C_2F_4 can not be accounted for by the change in the geometry of the transition states alone. For example, even if we assume

Table 5. Comparison of the relative A factors and the products of $(m^{\dagger}/m^{R})^{3/2}$ and $(I^{\dagger}/I^{R})^{1/2}$

Reactants	A or A'[a] (experimental)	$\left[\frac{m^{\dagger}}{m^{R}}\right]^{3/2}$	$\left[\frac{I^{\dagger}}{I^{R}}\right]^{1/2}$	$\left[\frac{m^{\dagger}}{m^{R}}\right]^{3/2}\times\left[\frac{I^{\dagger}}{I^{R}}\right]^{1/2}$[a]
C_2H_4	1.00	1.97	7.29	1.00
C_2H_3F	0.36	1.56	4.36	0.48
$CH_2=CF_2$	0.28	1.40	2.50	0.24
cis-CHF=CHF	0.23	1.40	2.59	0.25
C_2HF_3	0.36	1.31	1.94	0.18
C_2F_4	0.97	1.25	1.59	0.14
			2.98[b]	
			3.14[c]	

a) Values relative to that for ethene; the differences between A and A' are less than 5% when ν is a certain value between 100 and 300 cm^{-1}. b) Calculated by assuming that r(C-O) is twice as long as that for the transition state of C_2H_4O. c) Calculated by assuming that r(C-C) is twice as long as that for the transition state of C_2H_4O.

that the C-O or C-C internuclear distance of the transition state for C_2F_4 is twice as long as that for C_2H_4, the value of $(I^{\dagger}/I^{R})^{1/2}$ changes only by a factor of 2, as is shown in Table 5. The path degeneracy, L, must be 4 in both cases. Therefore, there remain only two possibilities. One is a change in κ; the other, one in ν. The present results for C_2H_4 and C_2F_4 can be explained if we assume that the degenerate vibrational frequencies of the bending mode of the transition states are 300 cm^{-1} and 110 cm^{-1} respectively. However, in this interpretation, it is necessary to assume that the vibrational frequencies of the transition states suddenly change from $C_2H_2F_2$ to C_2HF_3, which sounds unrealistic. The next problem is, then, to see if it is reasonable to assume that the values of κ for C_2HF_3 and C_2F_4 are larger than those for ethene or the other fluoroethenes. This will be discussed in the next section.

Detailed Mechanism of the Reaction. With regard to the change in κ, tunneling effects cannot be expected in the present cases, but the contribution of the reverse reaction from the intermediate diradical to its initial components may be expected. In the reaction of oxygen atoms with ethene, it is known that there are two main exit channels: the fragmentation into CH_2CHO+H and that into CH_3+HCO.[1,27] Under the beam conditions, only the CH_2CHO fragment could be detected,[28] while both could be detected in comparable yields under the bulk conditions.[27] In order to explain these experimental results, the following reaction mechanism was considered; it is similar to that proposed by Hunziker *et al.*:[27]

$$O + C_2H_4 \longrightarrow {}^3C_2H_4O^*, \quad (5)$$

$$O + C_2H_4 \rightleftarrows {}^3C_2H_4O^{**}, \quad (6)$$

$${}^3C_2H_4O^* \longrightarrow CH_2CHO + H, \quad (7)$$

$${}^3C_2H_4O^{**} + M \rightleftarrows {}^1C_2H_4O^* + M, \quad (8)$$

$${}^1C_2H_4O^* \longrightarrow CH_3 + HCO, \quad (9)$$

$${}^1C_2H_4O^* + M \longrightarrow C_2H_4O + M. \quad (10)$$

Here, ${}^3C_2H_4O^*$ and ${}^3C_2H_4O^{**}$ represent two different types of electronic states of the initial triplet diradicals, the (π,π) and (π,σ) states, following the nomenclature of Yamaguchi *et al.*[29] ${}^1C_2H_4O^*$ stands for the singlet-state diradical, which is isoenergetic to ${}^3C_2H_4O^{**}$. Although Hunziker *et al.* mention nothing about the precursor of CH_3 and HCO, this singlet state may be the precursor.[18] Now, if the rate for the reverse reaction of Reaction 6 is large enough compared to the rates for Reactions 9 and 10, the apparent value of κ will be less than unity. It is necessary to assume an equilibrium between the singlet and the triplet diradicals, Reaction 8, in order to explain the constancy of the yields of HCO at high pressures.[27] It should also be noted that the precursor of CH_3 and HCO may not necessarily be the singlet diradical. The important point in this discussion is that there must be a reverse reaction to reproduce atomic oxygen, even at high pressures. Gutman and his co-workers have studied the reactive routes for the O+fluoroethenes reactions by using mass-spectrometric detection.[17,18] They have found that the reactions for C_2H_4 and C_2H_3F do not proceed by C-C bond breakage, while those for C_2F_4 and C_2HF_3 appear to proceed exclusively by this route. This conclusion for C_2F_4 is consistent with the finding of other experimental work that the only exit channel is the decomposition to CF_2 and CF_2O:[19,30]

$$O + C_2F_4 \longrightarrow {}^3C_2F_4O^*, \quad (11)$$

$${}^3C_2F_4O^* \longrightarrow CF_2 + CF_2O. \quad (12)$$

Gorry *et al.* have shown that the triplet diradical, ${}^3C_2F_4O^*$, is very short-lived because of its great exoergicity and that it decomposes to $CF_2({}^3B_1)$ and CF_2O.[30] If the reverse reaction of Reaction 11 is minor, then the value of κ should be larger than that for the O+ethene reaction. The situation for C_2HF_3 must be similar to that for C_2F_4, while that for C_2H_3F must be similar to that for C_2H_4. As for the reactions of O+difluoroethenes, many reactive routes, including the C-C bond rupture, are possible, although the production of CH_2O and CF_2 from $O+CH_2=CF_2$ seems minor.[17] The present results imply that the values of κ for the reactions of O+difluoroethenes are similar to that for ethene. Therefore, if C-C bond rupture occurs in these cases, that process must be slow. Further experimental studies to determine the initial products of these reactions, as well as their yields, are to be desired.

The authors wish to express their thanks to Professor Soji Tsuchiya of Tokyo University and Professor Nobuo Ishikawa of this Institute for the supply of fluoroethenes. The present work was partially supported by a Grant-in-Aid for Scientific Research from the Ministry of Education.

References

1) R. J. Cvetanovic and D. L. Singleton, *Rev. Chem. Intermed.*, **5**, 183 (1984).
2) L. Elias and H. I. Schiff, *Can J. Chem.*, **38**, 1657 (1960).
3) L. Elias, *J. Chem. Phys.*, **38**, 989 (1963).
4) A. A. Westenberg and N. deHaas, *12th Symp. Combust.*, Poitiers, France 1968, 289 (1969).
5) D. D. Davis, R. E. Huie, J. T. Herron, M. J. Kurylo, and W. Braun, *J. Chem. Phys.*, **56**, 4868 (1972).
6) R. Atkinson and J. N. Pitts, Jr., *Chem. Phys. Lett.*, **27**, 467 (1974).
7) D. L. Singleton and R. J. Cvetanović, *J. Am. Chem. Soc.*, **98**, 6812 (1976).
8) R. Atkinson and J. N. Pitts, Jr., *J. Chem. Phys.*, **67**, 38 (1977).
9) J. M. Nicovich and A. R. Ravishankara, *19th Symp. Combust.*, Haifa, Israel 1982, 23 (1982).
10) R. A. Perry, *J. Chem. Phys.*, **80**, 153 (1984).
11) D. Saunders and J. Heicklen, *J. Phys. Chem.*, **70**, 1950 (1966).
12) D. S. Jones and S. J. Moss, *Int. J. Chem. Kinet.*, **6**, 443

(1974).
13) R. Atkinson and J. N. Pitts, Jr., *J. Chem. Phys.*, **67**, 2488 (1977).
14) K. Sugawara, K. Okazaki, and S. Sato, *Bull. Chem. Soc. Jpn.*, **54**, 358 (1981).
15) R. E. Huie, J. T. Herron, and D. D. Davis, *Int. J. Chem. Kinet.*, **4**, 521 (1972).
16) R. Atkinson and J. N. Pitts, Jr., *Int. J. Chem. Kinet.*, **8**, 475 (1976).
17) J. R. Gilbert, I. R. Slagle, R. E. Graham, and D. Gutman, *J. Phys. Chem.*, **80**, 14 (1976).
18) J-Y. Park, P. F. Sawyer, M. C. Heaven, and D. Gutman, *J. Phys. Chem.*, **88**, 2821 (1984).
19) S. Koda, *J. Phys. Chem.*, **83**, 2065 (1979).
20) H. Umemoto, S. Tsunashima, S. Sato, N. Washida, and S. Hatakeyama, *Bull. Chem. Soc. Jpn.*, **57**, 2578 (1984).
21) K. Sugawara, Y. Ishikawa, and S. Sato, *Bull. Chem. Soc. Jpn.*, **53**, 1344 (1980).
22) N. Washida, S. Hatakeyama, H. Takagi, T. Kyogoku, and S. Sato, *J. Chem. Phys.*, **78**, 4533 (1983).
23) R. C. Weast, ed., "CRC Handbook of Chemistry and Physics," CRC Press, 61st ed., Florida (1980/81), pp. E76—82.
24) R. E. Huie and J. T. Herron, *Prog. React. Kinet.*, **8**, 1 (1975).
25) J. L. Carlos, Jr., R. R. Karl, Jr., and S. H. Bauer, *J. Chem. Soc., Faraday Trans. 2*, **70**, 177 (1974).
26) M. Dupuis, J. J. Wendoloski, T. Takada, and W. A. Lester, Jr., *J. Chem. Phys.*, **76**, 481 (1982).
27) H. E. Hunziker, H. Kneppe, and H. R. Wendt, *J. Photochem.*, **17**, 377 (1981).
28) R. J. Buss, R. J. Baseman, G. He, and Y. T. Lee, *J. Photochem.*, **17**, 389 (1981).
29) K. Yamaguchi, S. Yabushita, T. Fueno, S. Kato, and K. Morokuma, *Chem. Phys. Lett.*, **70**, 27 (1980).
30) P. A. Gorry, R. J. Browett, J. H. Hobson, and R. Grice, *Mol. Phys.*, **40**, 1325 (1980).

The Structure of the Cyclodextrin Complex. XVIII. Crystal Structure of β-Cyclodextrin-Benzyl Alcohol (1:1) Complex Pentahydrate

Kazuaki HARATA,* Kaneto UEKAMA,† Masaki OTAGIRI,†
Fumitoshi HIRAYAMA,† and Yoshiro OHTANI††

Research Institute for Polymers and Textiles, 1-1-4 Yatabe-Higashi, Tsukuba, Ibaraki 305
†*Faculty of Pharmaceutical Sciences, Kumamoto University, 5-1 Oe-honmachi, Kumamoto 862*
††*Kaken Pharmaceutical Co., Ltd., 2-28-8 Honkomagome, Bunkyo-ku, Tokyo 113*

(Received October 23, 1984)

The crystal structure of the β-cyclodextrin-benzyl alcohol (1:1) complex pentahydrate was determined by the X-ray diffraction method. The crystal is monoclinic with the space group $P2_1$, $Z=2$, $a=15.356(3)$, $b=10.101(2)$, $c=20.869(3)$Å, and $\beta=109.90(1)°$. The structure was solved by an inspection of a Patterson map and a trial-and-error method combined with a rigid-body least-squares technique. The structure was refined using the block-diagonal least-squares method to an R-value of 0.066 for 5290 reflections ($\sin\theta/\lambda<0.63$). The β-cyclodextrin molecule is somewhat elliptically distorted from the regular heptagonal symmetry because of the inclusion of a planar molecule. One primary hydroxyl group shows a *gauche-trans* conformation, while the others are in a *gauche-gauche* conformation. The secondary hydroxyl groups form intramolecular O(2)-H···O(3′) or O(3′)-H···O(2) hydrogen bonds, which maintain the round structure of β-cyclodextrin. The guest benzyl alcohol molecule is fully enclosed within the host cavity. Water molecules are distributed in intermolecular spaces between β-cyclodextrin molecules. The phenyl group of the guest is located at the primary hydroxyl side of the cavity. The hydroxyl group occupies a position at the secondary hydroxyl side of the cavity, and forms hydrogen bonds with adjacent β-cyclodextrin molecules. β-Cyclodextrin molecules are stacked along the b axis to form a typical cage-type structure with a herringbone-like packing pattern.

Inclusion complexes of cyclodextrins with many pharmaceuticals, aromas, *etc.* have been successfully utilized in pharmaceutical and food industries.[1-4] Aralkyl alcohols are widely used antiseptics in pharmaceutical preparations. We have previously reported that aralkyl alcohols form inclusion complexes with cyclodextrins in water and in the solid state, using various techniques such as the solubility method, UV, CD, and ^{1}H-NMR spectroscopies, and powder X-ray diffractometry.[5] In this study, we carried out a crystal- and molecular-structure determination of the β-cyclodextrin complex with benzyl alcohol to gain insight into the detailed geometry of the host-guest interaction in the solid state.

Experimental

Materials and Measurements. β-Cyclodextrin and benzyl alcohol with a 1:1 molar ratio were dissolved in hot water. The solution was kept at room temperature. Then, the β-cyclodextrin-benzyl alcohol (1:1) complex pentahydrate was crystallized to a rod-like form. The crystal used in the X-ray diffraction experiment was sealed in a quartz capillary with a drop of mother liquor to prevent deterioration in air. Lattice parameters and diffraction intensities were measured on a Nicolet P3/F diffractometer with graphite-monochromated Cu $K\alpha$ radiation. The lattice constants were determined by a least-squares method using 25 reflections in the 2θ range 40—45°. By using a θ—2θ scan mode, 5290 independent reflections with $|F_o|\geqq 3\sigma(F)$ were collected up to 150° in 2θ. No correction was made for an absorption or extinction effect.

Crystal Data: $C_{42}H_{70}O_{35}\cdot C_7H_8O\cdot 5H_2O$, F.W.=1333.2, monoclinic, space group $P2_1$, $Z=2$, $a=15.356$ (3), $b=10.101$ (2), $c=20.869$ (3)Å, $\beta=109.90$ (1)°, $V=3043.6$ (9)Å^3, $D_x=1.455$ g·cm^{-3}.

Determination and Refinement of the Structure. The orientation of the *pseudo* heptagonal axis of β-cyclodextrin was easily deduced from a Patterson map. The rotation around the *pseudo* heptagonal axis and the molecular position in the unit cell was determined from an R-map, which was calculated using a model structure of β-cyclodextrin with a seven-fold symmetry. The orientational and positional parameters of each glucose unit were corrected by a rigid-body least-squares method. After the refinement of the β-cyclodextrin structure by the block-diagonal least-squares method, benzyl alcohol and water molecules were found on Fourier and difference-Fourier maps. The block-diagonal least-squares refinement of the structure, including 85 hydrogen atoms, achieved an R-value of 0.066. The quantity minimized was $\sum\omega(|F_o|-|F_c|)^2$, with $\omega=1.0$ for all the reflections. Final atomic parameters and B_{eq} values are given in Table 1. Tables of observed and calculated structure

Table 1. Atomic coordinates (×10^4) and B_{eq} values (B/Å^2) of non-hydrogen atoms

	x	y	z	B_{eq}/Å^2
C(1,G1)	−1361(5)	568(8)	3589(4)	3.39
C(2,G1)	−2030(6)	207(8)	2879(4)	3.64
C(3,G1)	−1950(5)	1162(8)	2353(4)	3.03
C(4,G1)	−2049(5)	2599(8)	2564(4)	2.89
C(5,G1)	−1414(5)	2873(8)	3286(4)	3.38
C(6,G1)	−1602(7)	4209(9)	3560(5)	4.87
O(2,G1)	−1804(4)	−1116(6)	2725(3)	4.06
O(3,G1)	−2665(4)	934(6)	1694(3)	3.67
O(4,G1)	−1807(3)	3390(5)	2099(3)	3.12
O(5,G1)	−1545(4)	1910(6)	3747(3)	3.61
O(6,G1)	−2597(5)	4248(8)	3445(4)	6.72
C(1,G2)	2188(5)	−1119(9)	4687(4)	3.71
C(2,G2)	1352(5)	−2125(8)	4469(4)	3.59
C(3,G2)	488(5)	−1505(9)	3947(4)	3.52
C(4,G2)	282(5)	−138(8)	4213(4)	3.16
C(5,G2)	1134(5)	719(9)	4493(4)	3.45
C(6,G2)	960(7)	1901(10)	4894(5)	5.41
O(2,G2)	1601(4)	−3263(6)	4157(3)	4.23
O(3,G2)	−299(4)	−2383(6)	3812(3)	4.28
O(4,G2)	−414(3)	485(6)	3628(3)	3.33
O(5,G2)	1925(4)	3(6)	4977(3)	3.62
O(6,G2)	1824(7)	2706(8)	5189(5)	8.30
C(1,G3)	4749(5)	−495(9)	3632(4)	3.63
C(2,G3)	4279(6)	−1885(9)	3574(4)	3.82

TABLE 1. (Continued)

	x	y	z	B_{eq}/Å²
C(3,G3)	3253(5)	−1705(8)	3514(4)	3.56
C(4,G3)	3317(5)	−916(8)	4149(4)	3.23
C(5,G3)	3748(6)	442(9)	4137(4)	3.83
C(6,G3)	3837(7)	1252(11)	4747(5)	5.12
O(2,G3)	4339(5)	−2602(6)	3014(3)	4.78
O(3,G3)	2851(4)	−2984(6)	3504(3)	4.50
O(4,G3)	2356(3)	−779(6)	4105(3)	3.22
O(5,G3)	4705(4)	200(6)	4179(3)	4.29
O(6,G3)	4216(5)	583(8)	5368(3)	5.62
C(1,G4)	5124(5)	2168(8)	1637(4)	3.30
C(2,G4)	4919(5)	686(8)	1497(4)	3.23
C(3,G4)	4361(5)	224(8)	1912(4)	3.27
C(4,G4)	4876(5)	520(8)	2646(4)	3.05
C(5,G4)	5091(5)	2038(8)	2745(4)	3.32
C(6,G4)	5632(7)	2465(10)	3449(5)	4.72
O(2,G4)	4442(4)	467(6)	791(3)	3.72
O(3,G4)	4219(4)	−1198(6)	1835(3)	4.13
O(4,G4)	4304(3)	137(6)	3009(3)	3.26
O(5,G4)	5591(3)	2425(6)	2330(3)	3.22
O(6,G4)	6527(4)	1839(7)	3752(3)	5.31
C(1,G5)	2758(5)	5970(8)	268(4)	2.77
C(2,G5)	2942(5)	4889(8)	−159(4)	3.14
C(3,G5)	3265(5)	3627(8)	287(4)	2.95
C(4,G5)	4096(5)	3928(8)	924(3)	2.63
C(5,G5)	3951(5)	5168(8)	1308(4)	2.83
C(6,G5)	4878(5)	5678(9)	1835(4)	3.75
O(2,G5)	2133(4)	4643(6)	−772(3)	3.69
O(3,G5)	3508(4)	2628(6)	−96(3)	3.44
O(4,G5)	4216(3)	2817(5)	1360(3)	2.95
O(5,G5)	3572(3)	6245(5)	839(3)	3.04
O(6,G5)	5485(4)	6126(6)	1512(3)	4.33
C(1,G6)	−493(5)	6951(8)	515(4)	3.07
C(2,G6)	−493(5)	6681(9)	−178(4)	3.34
C(3,G6)	372(5)	5862(8)	−133(4)	3.25
C(4,G6)	1261(5)	6453(8)	382(4)	3.13
C(5,G6)	1197(5)	6641(8)	1065(4)	3.04
C(6,G6)	2028(5)	7310(9)	1605(4)	3.95
O(2,G6)	−1351(3)	6063(7)	−608(3)	4.04
O(3,G6)	483(4)	5790(7)	−756(3)	4.52
O(4,G6)	2016(3)	5534(5)	457(3)	3.01
O(5,G6)	387(3)	7494(6)	967(3)	3.36
O(6,G6)	2231(4)	8557(7)	1369(4)	5.41
C(1,G7)	−2346(5)	4563(9)	1833(4)	3.60
C(2,G7)	−2760(5)	4484(8)	1079(4)	3.49
C(3,G7)	−2018(5)	4558(8)	769(4)	3.09
C(4,G7)	−1386(5)	5758(9)	1070(4)	3.19
C(5,G7)	−960(5)	5643(8)	1829(4)	3.11
C(6,G7)	−259(5)	6712(9)	2221(4)	3.94
O(2,G7)	−3316(3)	3275(6)	861(3)	3.75
O(3,G7)	−2401(4)	4563(7)	45(3)	4.25
O(4,G7)	−670(3)	5747(5)	790(3)	2.92
O(5,G7)	−1732(4)	5685(6)	2069(3)	3.35
O(6,G7)	−610(4)	8028(6)	2005(3)	4.38
C(1,BA)	1333(6)	1878(10)	2512(4)	4.67
C(2,BA)	1908(8)	2021(11)	2144(6)	6.21
C(3,BA)	2392(8)	3212(2)	2186(6)	7.11
C(4,BA)	2336(10)	4218(13)	2612(7)	8.62
C(5,BA)	1723(11)	4092(13)	2957(8)	9.39
C(6,BA)	1197(9)	2888(13)	2900(6)	7.43
C(7,BA)	829(9)	528(12)	2489(6)	7.01
O(1,BA)	783(5)	−241(6)	1949(3)	4.98
O(W1)	6037(5)	−100(9)	5702(4)	7.56
O(W2)	7193(5)	119(7)	4837(4)	6.50
O(W3)	3494(7)	1487(10)	6233(5)	9.49
O(W4)	3286(7)	2486(13)	7379(5)	11.84
O(W5)	5083(4)	3107(6)	−413(3)	4.31

factors, anisotropic temperature factors of non-hydrogen atoms, atomic parameters of hydrogen atoms, bond distances, angles, conformation angles, and plane equations with atomic deviations from the plane are kept at The Chemical Society of Japan (Document No. 8520). The computation was carried out on a FACOM M-380 computer at the Center of the Research Information Processing System (RIPS), Agency of Industrial Science and Technology, Tsukuba.

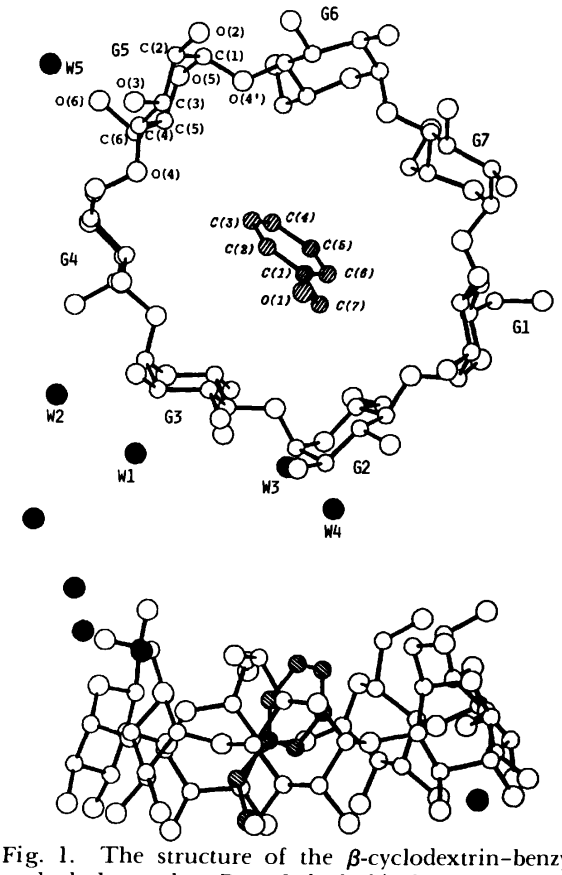

Fig. 1. The structure of the β-cyclodextrin-benzyl alcohol complex. Benzyl alcohol is shown by shaded circles. Water molecules are shown by full circles.

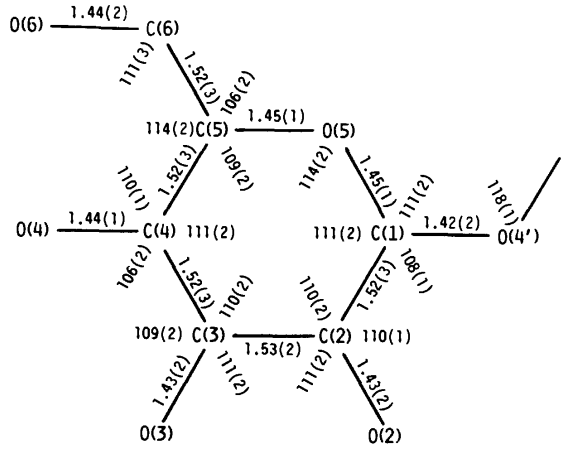

Fig. 2. Average bond distances and angles over seven glucose residues in β-cyclodextrin. Standard deviations in parentheses were estimated according to the equation:

$$\sigma = [\sum_{i=1}^{7} (x_i - \bar{x})^2/6]^{1/2}$$

where x_i refers to the bond distance or angle of the i-th residue and $\bar{x}$ is the average value.

Description and Discussion of the Structure

The structure of the β-cyclodextrin–benzyl alcohol complex is shown in Fig. 1. Average bond distances and angles of β-cyclodextrin are given in Fig. 2. Except for the orientation of C(6)–O(6) bonds, no significant structural difference was found among the seven glucose residues. The C(6)–O(6) bond in the G2 residue showed a *gauche-trans* conformation, while the other C(6)–O(6) bonds were in a *gauche-gauche* conformation. The average value of the glycosidic oxygen angles, 118 (1)°, is in good agreement with those of other β-cyclodextrin complexes.[6-8] The torsion-angle indices (Table 2), being in the range 109—140°, show a strong linear correlation with O(4)···O(4′) distances between adjacent glucose residues. Such a linear correlation is commonly observed in α- and β-cyclodextrin complexes.[7,9]

The β-cyclodextrin ring is somewhat elliptically distorted from the regular heptagonal symmetry. The radius and side length of the heptagon composed of seven O(4) atoms are in the range 4.71—5.28 Å and 4.17—4.55 Å, respectively. The radius (5.28 Å) measured from the O(4,G2) atom is 0.57 Å longer than the radius measured from the O(4,G4) atom. The largest values of radius and side length are found in a direction parallel to the plane of the guest molecule; O(4,G2)···center of the O(4) heptagon and O(4,G3)···O(4,G4), respectively. In spite of such elliptical distortion of the β-cyclodextrin ring, the average value of the radius (5.02 Å) and the side length (4.36 Å) of the O(4) heptagon are in good agreement with the corresponding values (5.05 and 4.38 Å, respectively) of the β-cyclodextrin complex with hexamethylenetetramine,[8] in which β-cyclodextrin shows a round structure owing to the inclusion of a spherically-shaped molecule. The

TABLE 2. GEOMETRICAL DATA FOR β-CYCLODEXTRIN

I. Radius of the O(4) heptagon[a]

Residue	Radius *l*/Å	Residue	Radius *l*/Å
G1	4.97	G5	5.26
G2	5.28	G6	5.18
G3	4.97	G7	4.78
G4	4.71	Average	5.02

a) The radius is measured from the center of gravity of seven O(4) atoms to each O(4) atom.

II. O(4)···O(4) distance between adjacent glucose residues

Distance *l*/Å		Distance *l*/Å	
O(4,G1)···O(4,G2)	4.29	O(4,G5)···O(4,G6)	4.20
O(4,G2)···O(4,G3)	4.17	O(4,G6)···O(4,G7)	4.45
O(4,G3)···O(4,G4)	4.55	O(4,G7)···O(4,G1)	4.50
O(4,G4)···O(4,G5)	4.39	Average	4.36

III. Tilt-angle[a] and torsion-angle index[b]

Residue	Tilt-angle ϕ/°	Torsion-angle index ϕ/°
G1	6.6	126
G2	20.5	140
G3	17.4	116
G4	−2.2	118
G5	11.4	132
G6	25.2	109
G7	17.0	105
Average	13.7	121

a) The tilt-angle is defined as the angle made by the O(4) plane and the plane through C(1), C(4), O(4), and O(4′) of each glucose residue. b) The torsion-angle index is defined as follows: $\phi=|\phi(C(1)\text{-}C(2))|+|\phi(C(2)\text{-}C(3))|-|\phi(C(3)\text{-}C(4))|-|\phi(C(4)\text{-}C(5))|+|\phi(C(5)\text{-}O(5))|+|\phi(O(5)\text{-}C(1))|$, where $\phi(C(1)\text{-}C(2))$ is the conformation angle of O(5)-C(1)-C(2)-C(3).

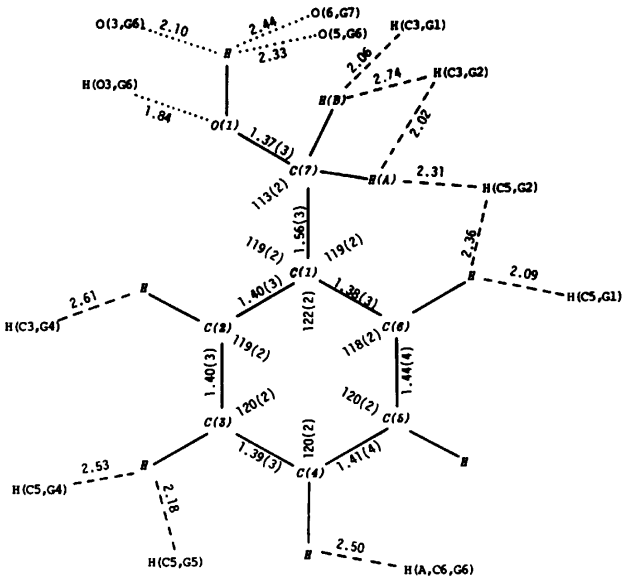

Fig. 3. Bond distances and angles in benzyl alcohol and host-guest distances less than 2.8 Å. Intermolecular contacts with adjacent β-cyclodextrin molecules are shown by dotted lines.

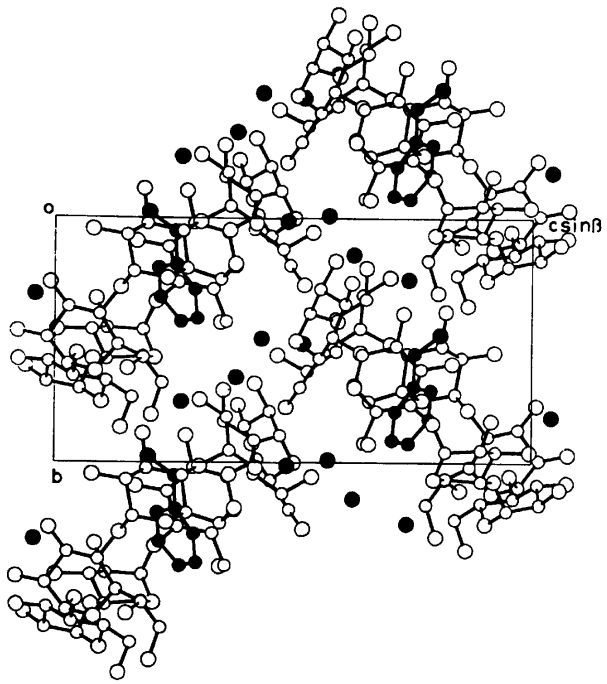

Fig. 4. The crystal structure viewed along the a axis. Benzyl alcohol and water molecules are shown by full circles.

TABLE 3. HYDROGEN-BOND DISTANCES AND ANGLES

		Distance (l/Å)		Angle (ϕ/°)	
		O-H	H···O	O···O	O-H···O
O(2,G1)·····H-O(3,G2)		1.09	1.82	2.86	158
O(2,G1)·····H-O(6,G7)	(c)	0.83	2.12	2.94	170
O(2,G1)-H·····O(W4)	(i)	0.98	2.20	2.61	104
O(3,G1)·····H-O(2,G7)		0.95	2.04	2.89	148
O(3,G1)-H·····O(2,G5)	(h)	1.04	1.80	2.72	145
O(5,G1)·····O(6,G4)	(b)			2.97	
O(6,G1)·····O(6,G4)	(b)			2.97	
O(6,G1)-H·····O(W3)	(f)	1.40	1.99	2.87	115
O(6,G1)-H·····O(5,G2)	(f)	1.40	2.02	3.02	123
O(2,G2)·····H-O(3,G3)		1.04	1.80	2.79	158
O(6,G2)·····H(B)-O(W3)		1.29	2.15	2.93	114
O(6,G2)·····O(W2)	(g)			2.88	
O(2,G3)-H·····O(3,G4)		1.02	1.89	2.83	152
O(3,G3)·····H(B)-O(W1)	(k)	0.97	2.33	2.85	113
O(6,G3)·····O(W1)				2.69	
O(6,G3)-H·····O(W3)		1.22	1.53	2.65	149
O(2,G4)·····H-O(3,G5)		1.07	1.92	2.88	147
O(2,G4)·····O(W5)	(j)			2.71	
O(2,G4)·····H-O(3,G7)	(h)	0.79	2.68	3.08	113
O(3,G4)-H·····O(6,G6)	(c)	0.90	2.08	2.83	140
O(6,G4)·····O(W2)				2.75	
O(2,G5)-H·····O(3,G6)		0.76	2.12	2.81	151
O(3,G5)·····H(A)-O(W5)		0.82	2.07	2.80	148
O(6,G5)-H·····O(W5)	(e)	1.00	2.08	2.94	143
O(6,G5)·····H(B)-O(W4)	(g)	0.96	1.82	2.75	162
O(2,G6)-H·····O(3,G7)		0.99	2.01	2.93	154
O(3,G6)-H·····O(1,BA)	(d)	0.98	1.84	2.74	151
O(3,G6)·····H-O(1,BA)	(d)	1.00	2.10	2.74	121
O(5,G6)·····H-O(1,BA)	(a)	1.00	2.33	3.00	123
O(2,G7)·····H(B)-O(W5)		1.07	1.85	2.87	158
O(W1)-H(A)·····O(W2)		1.00	2.11	3.02	150
O(W3)-H(A)·····O(W4)		1.18	1.86	2.77	130

Symmetry Code

None	x,	y,	z	f	$-x$,	$1/2+y$,	$1-z$
a	x,	$1+y$,	z	g	$1-x$,	$1/2+y$,	$1-z$
b	$-1+x$,	y,	z	h	$-x$,	$-1/2+y$,	$-z$
c	x,	$-1+y$,	z	i	$-x$,	$-1/2+y$,	$1-z$
d	$-x$,	$1/2+y$,	$-z$	j	$1-x$,	$-1/2+y$,	$-z$
e	$1-x$,	$1/2+y$,	$-z$	k	$1-x$,	$-1/2+y$,	$1-z$

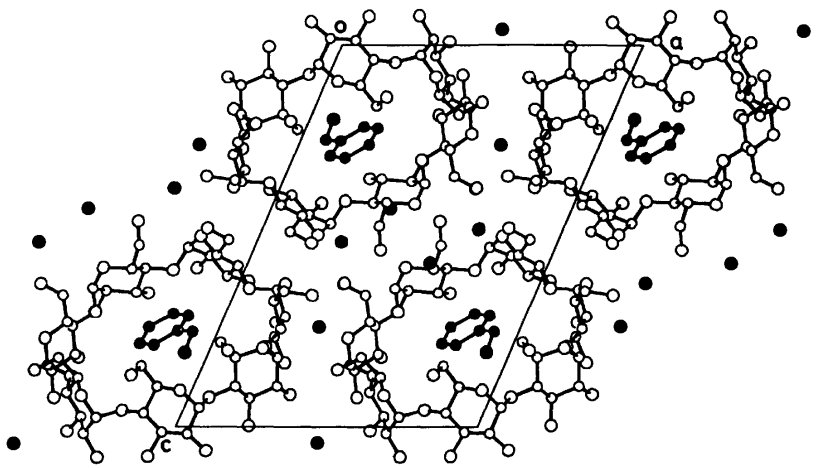

Fig. 5. The crystal structure viewed along the b axis. Benzyl alcohol and water molecules are shown by full circles.

seven O(4) atoms are coplanar within the maximum deviation of 0.228 Å.

The secondary hydroxyl groups form intramolecular hydrogen bonds, which may maintain the round shape of the β-cyclodextrin ring: four O(2)-H···O(3′) and three O(2)···H-O(3′) hydrogen bonds are found, as shown in Table 3. The O(2)···O(3′) distances are in the range 2.79—2.93 Å with the average value of 2.87

Å. The glucose residues are not perpendicular to the O(4) plane, but are inclined with their primary hydroxyl sides nearer to each other. The tilt-angles of glucose residues are in the range from −2.2 to 25.2°. The average value of 13.7° is greater than those found in the β-cyclodextrin dodecahydrate[6] and the β-cyclodextrin–hexamethylenetetramine complex[8] (12.5° and 11.4°, respectively). These larger tilt angles suggest that the glucose residues incline so as to make the shape and size of the host cavity more suitable for the accommodation of the guest molecule.

The guest benzyl alcohol molecule is fully enclosed within the β-cyclodextrin cavity. The phenyl group is located at the primary hydroxyl side of the cavity, and occupies the same position as that which the pyridyl group occupies in the β-cyclodextrin complex with nicotinamide.[10] Although in the nicotinamide complex the carbamoyl group protrudes outward from the primary hydroxyl side of the cavity, the hydroxyl group of benzyl alcohol is include within the cavity. The phenyl group has short contacts with C(5)–H methine groups of β-cyclodextrin: the C(3,BA)–H···H–C(5,G5) contact of 2.18 Å and the C(6,BA)–H···H–C(5,G1) contact of 2.09 Å, as shown in Fig. 3. The phenyl plane is not perpendicular to the O(4) plane, but makes an angle of 69.6°. As a result, the methylene group of benzyl alcohol has short contact with C(3)–H methine groups of the G1 and G2 residue: the C(7,BA)–H(A)···H–C(3,G2) contact of 2.02 Å and the C(7,BA)–H(B)···H–C(3,G1) contact of 2.06 Å. The hydroxyl group of benzyl alcohol forms hydrogen bonds with adjacent β-cyclodextrin molecules, as shown by dotted lines in Fig. 3.

β-Cyclodextrin molecules are stacked along the b axis (Figs. 4 and 5). As the O(4) plane of β-cyclodextrin makes an angle of 44.9° with the b axis, β-cyclodextrin molecules make a herringbone-like pattern along the bc plane. Adjacent β-cyclodextrin molecules block both ends of the β-cyclodextrin cavity. The isolated "cage", thus created, accommodates the guest molecule. Water molecules are not included within the host cavity, but fill intermolecular spaces between β-cyclodextrin molecules. As shown in Table 3, water molecules are involved in the formation of many hydrogen bonds. The W1 and W2 water molecules are linked to each other by the O(W1)–H···O(W2) hydrogen bond. The W3 water molecule forms the O(W3)–H···O(W4) hydrogen bond with the W4 water molecule. The W5 water molecule is isolated and forms hydrogen bonds with β-cyclodextrin molecules.

In many β-cyclodextrin complexes,[11–15] two β-cyclodextrin molecules are coupled to form a head-to-head dimer with the secondary hydroxyl sides facing each other. The cylindrical cavity formed by the dimerization can include a guest molecule with its size larger than the depth of a single β-cyclodextrin cavity. On the other hand, the shape and size of the guest molecule are quite restricted in the typical cage-type structure because of the limited space of the host cavity. In α-cyclodextrin complexes with the cage-type structure, for example, the host molecule includes only small molecules such as water,[16] iodine,[17] and alcohols,[18] *etc.* However, the present crystal structure demonstrates that the cage of β-cyclodextrin is sufficiently large to accommodate benzene derivatives. This is a first observation of the cage-structure in the β-cyclodextrin complex with benzene derivatives, although a similar structure was observed in the complex with nicotinamide having a pyridine ring.[10]

References

1) M. L. Bender and M. Komiyama, "Cyclodextrin Chemistry," Springer-Verlag, Berlin (1978).
2) W. Saenger, *Angew. Chem. Int. Ed. Engl.*, **19**, 344 (1980).
3) K. Uekama, *Yakugaku Zasshi*, **101**, 857 (1981).
4) J. Szejtli, "Cyclodextrins and their Inclusion Complexes," Academiai Kiado, Budapest (1982).
5) K. Uekama, K. Oh, F. Hirayama, M. Otagiri, M. Shibata, Y. Ohtani, Y. Yamada, and Y. Sugiyama, *Yakugaku Zasshi*, **102**, 1141 (1982).
6) K. Lindner and W. Saenger, *Carbohydr. Res.*, **99**, 103 (1982).
7) K. Harata, *Bull. Chem. Soc. Jpn.*, **55**, 2315 (1982).
8) K. Harata, *Bull. Chem. Soc. Jpn.*, **57**, 2596 (1984).
9) K. Harata, *Bull. Chem. Soc. Jpn.*, **50**, 1416 (1977).
10) K. Harata, K. Kawano, K. Fukunaga, and Y. Ohtani, *Chem. Pharm. Bull.*, **31**, 1428 (1983).
11) M. M. Harding, J. M. Maclennan, and R. M. Paton, *Nature*, **274**, 621 (1978).
12) J. J. Stezowski, K. H. Jogun, E. Eckle, and K. Bartels, *Nature*, **274**, 617 (1978).
13) R. Tokuoka, T. Fujiwara, and K. Tomita, *Acta Crystallogr. Sect. B*, **37**, 1158 (1981).
14) J. A. Hamilton and M. N. Sabesan, *Carbohydr. Res.*, **102**, 31 (1982).
15) K. Uekama, F. Hirayama, T. Imai, M. Otagiri, and K. Harata, *Chem. Pharm. Bull.*, **31**, 3363 (1983).
16) P. C. Manor and W. Saenger, *J. Am. Chem. Soc.*, **96**, 3630 (1974).
17) R. K. McMullan, W. Saenger, J. Fayos, and D. Mootz, *Carbohydr. Res.*, **31**, 211 (1973).
18) W. Saenger, R. K. McMullan, J. Fayos, and D. Mootz, *Acta. Crystallogr. Sect. B*, **30**, 2019 (1974).

 © 1985 The Chemical Society of Japan Bull. Chem. Soc. Jpn., 58, 1239—1250 (1985)

CO_2 Laser-induced Decomposition of 1,2-Dichloro-1-fluoroethane

Hiroo OGURA* and Takayuki YANO†

The Institute of Space and Astronautical Science, Komaba, Meguro-ku, Tokyo 153

†*Laboratory of Chemistry, Hitotsubashi University, Kunitachi, Tokyo 186*

(Received November 1, 1984)

$CH_2ClCHFCl$ was photolyzed with a TEA CO_2 laser at 1033.5 cm^{-1}. The infrared multiphoton dissociation mechanism of $CH_2ClCHFCl$ was investigated under various conditions: Sample gas pressure, additive gas pressure, pulse number, pulse energy, and pulse duration. It is concluded that primary process of the IRMPD is direct elimination of molecular HCl and HF, HCl elimination being predominant channel. Primary HCl elimination products *cis*-and *trans*-CHF=CHCl, and CH_2=CFCl are formed at high vibrational levels, from which additional photon absorption occurs in the secondary photolysis to give rise to CH≡CCl, CH≡CF, and CH_2=CHF. All of the secondary products are concluded to be derived from mainly CH_2=CFCl among the chlorofluoroethene isomers. CH_2=CFCl decomposes *via* HF and HCl elimination channels together with the C-Cl bond-rupture channel. CH≡CH appears to be generated by the H atom abstraction reaction of $C_2H\cdot$ radical, which may result from further decomposition of CH≡CCl and/or CH≡CF. The neat IRMPD at higher pressures gives quite similar primary product distribution, but markedly different secondary product distribution from those in shock tube pyrolysis.

Polyatomic molecules under the action of intense infrared laser radiation field can absorb a sufficient number of photons to undergo unimolecular decomposition. In generally accepted theoretical framework for infrared multiphoton excitation and dissociation (IRMPE and MPD) of polyatomic molecules,[1] the molecule is considered to be pumped through three distinct energy regions: In region I where the density of states is very low, the discrete vibrational states are excited by coherent pumping processes. After the absorption of several photons, the density of states increases dramatically, the molecule has entered region II. In this quasicontinuum region, the molecule can absorb the photons of eventually any frequency by incoherent single-photon processes. As the molecular energy increases beyond some dissociation threshold, the molecule has excited into the true continuum region, where unimolecular reactions can compete with the up-pumping processes.

A number of studies have been made of the IRMPD processes in which multiple unimolecular dissociation channels are accessible. The branching ratio between the various unimolecular pathways has been observed to be a strong function of the laser intensity or fluence, which has been explained in terms of the competition between the rates of optical pumping and the individual unimolecular reactions. The experimental advantage of such intramolecular competition together with the laser pumping processes is to probe the internal energy distribution of the excited molecule in comparison with the rates of the individual reaction channels.

Conventional end-product analysis,[2-11] infrared emission spectroscopic technique,[12-14] and molecular beam technique[15] have been employed to measure the branching ratios between the competing unimolecular dissociation channels, and have been analyzed by the RRKM unimolecular reaction theory or simulated on the basis of energy grained master equation.[16,17]

In the IRMPD processes, the energy required to overcome the reaction threshold for the unimolecular decomposition is, at least initially, deposited exclusively in the vibrational modes, while in thermal excitation both the internal and external degrees of freedom of the molecule are in the Boltzmann equilibrium distribution or very close to it. In many molecules studied, the products resulting from the IRMPD have been reported to be similar to those found in the thermal excitation. The product distribution, however, can be different from each other, reflecting the difference in the internal energy distribution of the excited molecule.

Gas cell experiments with focused geometry are valuable to study the unimolecular dissociation and subsequent reactions, because they are easier and more complete in the analysis of stable products than other techniques. Presented below are the results of the IRMPD of 1,2-dichloro-1-fluoroethane, which is expected to undergo unimolecular dissociation *via* at least two pathways, HCl and HF molecular elimination. In the present study, the final products of the photolysis were observed and the mechanisms for unimolecular decomposition and subsequent reactions are determined in as much detail as possible. Several single-pulse shock tube experiments were also carried out to compare the results with those of the IRMPD.

Experimental

A schematic drawing of the experimental arrangement is shown in Fig. 1. A multimode CO_2 TEA laser (Lumonics 103-2) which could be tuned over the various rotational lines of both vibrational bands of CO_2, was used with N_2 added to the lasing gas mixture. The output pulse was considered to consist of an initial sharp spike of 80—100 ns FWHM, followed by a low intensity tail of 1—2 μs.[9,18] The principal line used in these experiments was the P (34) line of the 9.6 μm CO_2 band at 1033.5 cm^{-1}. Determination of the laser transition line was performed with a calibrated grating monochromator blazed at 7.5 μm (JASCO model CT-50). The laser beam passed through a 14-mm circular aperture, could be attenuated selectively with CaF_2 flats, and was focused at the center of the photolysis cell by a 12.7-cm focal length antireflection coated germanium lens. All irradiations were carried out in a 22-cm long×46-mm diameter Pyrex glass cell

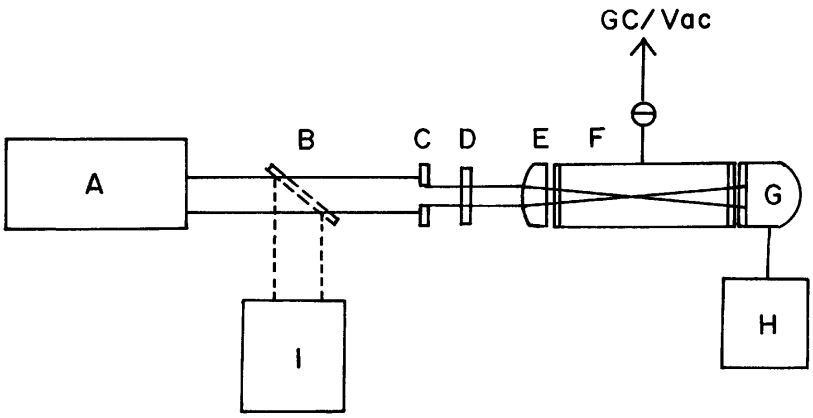

Fig. 1. Schematic diagram of experimental setup.
A: TEA CO_2 laser, B: mirror, C: aperture, D: CaF_2 flat, E: Ge lens, F: photolysis cell, G: pyroelectric detector, H: memory scope, I: monochromator.

with NaCl entrance and exit windows. The windows were compression fit to the Pyrex glass cell with Viton O-rings. The energy output per pulse was measured with a calibrated thermopile (Gen Tec ED-200). The laser was operated at 1 Hz repetition frequency for all runs. The shot-to-shot variation of the pulse energy was found to be within 5%. During the laser irradiation, the pulses were counted by an electronics of our own design.

A conventional glass vacuum system with an oil diffusion pump was used for sample preparation, greaseless stopcocks being used in the sampling manifolds. The pressures in the photolysis cell were measured with MKS Baratron Type 222BHS (0—10 Torr, 1 Torr=133.322 Pa) and 222AHS (0—1000 Torr) pressure transducers with a digital display (Iwatsu Electronics, VOAC 747).

After the focused irradiation of the test gas for 600 shots, the gas sample was analyzed by gas chromatography. The irradiated sample was directly introduced into the sampling loop of the gas chromatograph (Yanaco model G80), or was once condensed in an evacuated bulb of small volume cooled at liquid nitrogen temperature, and then transferred into the sampling loop. To insure the products are completely trapped, the freezeout times ran about 15 min. After the freezeout, the bulb was allowed to warm to room temperature, and to stand at least one hour for complete mixing.

The photolysis products were seperated on a Porapak N column (80—100 mesh, 3-m long) with helium as a carrier gas, and detected with flame ionization detector. The products were identified by comparing their retention times with those of authentic samples. When no authentic gases were available, the unknown products, being fractionated by gas chromatograph, were identified with a FT-IR spectometer (JEOL model JIR 10) and/or with a mass spectometer (Hitachi model RM 50) with library spectrum search.

The amount of each product was determined from its peak area relative to that of standard mixture. Quantitative calibrations were obtained empirically from the standard mixture made to approximate the actual photolysis samples, analytical errors being within 5—10%. The samples were run with temperature programming. In typical gas chromatographic analysis, initially the oven temperature was 60 °C for 18 min, then raised at the rate of 20 °C/min to 110 °C and maintained for 36 min, followed by a final increase to 160 °C.

The reactant $CH_2ClCHFCl$ (PCR min. 94% pure) was purified by using preparative gas chromatographic technique, and was further purified by low temperature distillation under vacuum. *trans*- and *cis*-CHCl=CHCl, and $CH_2=CCl_2$ were obtained from Tokyo Kasei Co. Ltd., and were purified by bulb-to-bulb distillation. Other gases were purchased from Takachiho Shoji Co. Ltd., and were used without further purification. The standard gases which were not available commercially, were prepared from appropriate gases by the IRMPD at high pressures (≈20 Torr), and were fractionated twice by gas chromatograph, and then were distilled several times at low temperatures under vacuum.

The experimetal details of single-pulse shock tube were fully described previously,[19] the analytical procedure being the same as that in the photolysis experiments.

Results

The infrared absorption spectrum of $CH_2ClCHFCl$ shows a maximum at 1033.2 cm^{-1}. No normal vibrational assignment has been made yet, but this band can be assigned to be the C–C stretching vibration in analogy to that in CHFClCHFCl and CH_2ClCF_2Cl.[14] The P (34) line of the 9.6 μm CO_2 band (1033.5 cm^{-1}) was used as the irradiation line for $CH_2ClCHFCl$ for all runs. The first step in the analysis of the stable species produced in the IRMPD of $CH_2ClCHFCl$ was to identify each particular species and to characterize this species in terms of gas chromatographic retention times: A large amount of the photolyzed sample gas was introduced into the gas chromatograph, and the products were isolated from the effluents and were analyzed by mass and FT-IR spectrometry. CH≡CF, CH≡CCl, $CH_2=CHF$, $CH_2=CFCl$, *trans*-, and *cis*-CHF=CHCl were idetified in this way.[20–23] These gases except for $CH_2=CFCl$ were prepared for the quantitative analysis by the IRMPD of $CH_2=CF_2$, $CH_2=CCl_2$, and $CH_2ClCHFCl$, $CH_2=CHF$ being obtained in smaller amounts from the photolysis of $CH_2=CF_2$. CH≡CF has the same retention time as $CH_2=CH_2$ at 60 °C, which could be seperated below 30 °C. No $CH_2=CH_2$ was found in the IRMPD of $CH_2ClCHFCl$.

Dependence on Reactant Pressure. The product

Table 1. Pressure dependence of product yields

P/Torr	0.10	0.20	0.50	1.0	3.0
a)					
CH≡CF	0.516	0.593	0.663	0.637	0.984
CH≡CH	0.205	0.266	0.330	0.280	0.444
CH_2=CHF	0.108	0.131	0.139	0.166	0.196
CH≡CCl	2.45	2.41	2.38	1.96	1.87
CH_2=CFCl	0.220	0.289	0.583	1.48	3.77
t-CHF=CHCl	2.27	2.30	2.67	3.84	5.86
c-CHF=CHCl	4.60	4.86	4.79	6.56	9.28
t-CHCl=CHCl	0.553	0.513	0.457	0.483	0.421
c-CHCl=CHCl	0.632	0.531	0.567	0.567	0.491
b)					
CH≡CF	11.2	12.2	13.8	9.71	10.6
CH≡CH	4.46	5.47	6.89	4.27	4.78
CH_2=CHF	2.35	2.70	2.90	2.53	2.11
CH≡CCl	53.3	49.6	49.7	29.9	20.2
CH_2=CFCl	4.78	5.95	12.2	22.6	40.6
t-CHF=CHCl	49.4	47.3	55.7	58.5	63.2
c-CHF=CHCl	100	100	100	100	100
t-CHCl=CHCl	12.0	10.6	9.54	7.36	4.54
c-CHCl=CHCl	13.7	10.9	11.8	8.64	5.29

a) Yields in % conversion per 600 shots at E_0= 0.144 J/pulse. b) Relative yields as compared to the yield of *c*-CHF=CHCl. c) *t* and *c* denote *trans* and *cis*, respectively.

yields as a function of $CH_2ClCHFCl$ pressure have been investigated with the same number of pulses, constant laser energy, same excitation line, and same geometry. Although no dielectric breakdown was observed, visible luminescence streaks were observed with a dark adapted eye around the focus of the lens at higher reactant pressures. The yields together with relative yields are shown in Table 1 in the sequence of their elution times. Major products are *cis*- and *trans*-CHF=CHCl, CH_2=CFCl, *cis*- and *trans*-CHCl=CHCl, CH≡CCl, and CH≡CF. Two lessrer, yet relatively important products are CH≡CH and CH_2=CHF. As minor products, CH_2=CF_2, *trans*- and *cis*-CHF=CHF, and *trans*- and *cis*-CHCl=CFCl are formed, their yields being about one order of magnitude smaller than those listed in Table 1.

At $CH_2ClCHFCl$ pressures below 0.2 Torr, the yields as well as relative yields appear to be relatively constant. As the reactant pressure is increased, each product yield changes in particular way: The yields of *cis*-, *trans*-CHF=CHCl, and CH_2=CFCl increase remarkably, and those of CH≡CF, CH≡CH, and CH_2=CHF slightly with increasing pressure, while the yields of *cis*-, *trans*-CHCl=CHCl, and CH≡CCl decrease. In particular, the yield of CH_2=CFCl increases more rapidly than those of CHF=CHCl isomers with higher $CH_2ClCHFCl$ pressure, while those of *cis*-, *trans*-CHCl=CHCl, and CH≡CCl show an opposite trend. In the case of CH≡CF, CH≡CH, and CH_2=CHF relative yields, there appear to be little pressure dependence.

Dependence on He and H_2 Pressure. The product yields as a function of He and H_2 pressure up to 10 Torr were examined, other photolysis parameters being same or constant. The $CH_2ClCHFCl$ pressure were constant at 0.5 and 1.0 Torr for He and H_2, respectively.

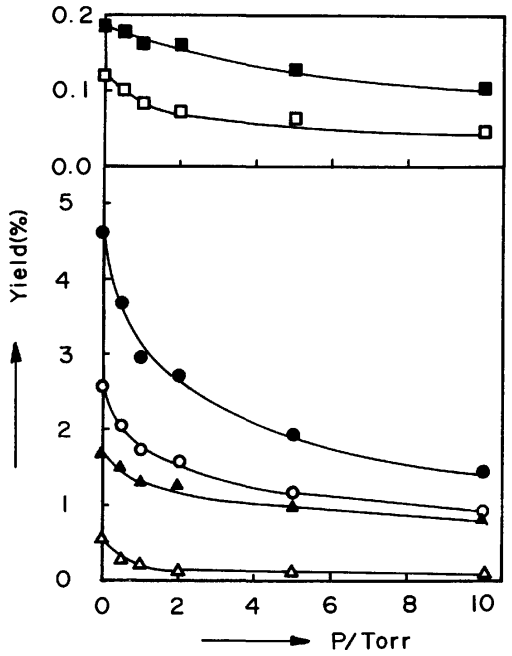

Fig. 2. Product yields as a function of He pressure. ●: *c*-CHF=CHCl, ○: *t*-CHF=CHCl, ▲: CH≡CCl, △: CH_2=CFCl, ■: CH≡CH, □: CH_2=CHF.

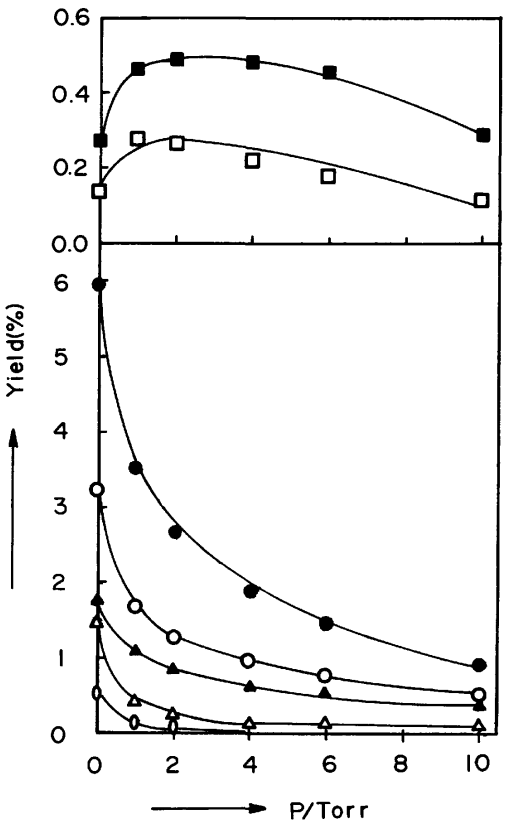

Fig. 3. Product yields as a function of H_2 pressure. ●: *c*-CHF=CHCl, ○: *t*-CHF=CHCl, ▲: CH≡CCl, △: CH_2=CFCl, (): *c*-CHCl=CHCl, ■: CH≡CH, □: CH_2=CHF.

The product yields with increasing He and H_2 pressure are shown in Figs. 2 and 3, the product distributions being summarized in Tables 2 and 3, respectively. Major products such as *cis*-, *trans*-CHF=CHCl,

Table 2. Dependence of relative yields[a] on He pressure

P/Torr	0.0	0.50	1.0	2.0	5.0	10.0
CH≡CF	10.0	11.5	12.3	13.6	16.1	17.4
CH≡CH	4.03	4.90	5.38	5.89	6.53	6.98
CH_2=CHF	2.55	2.64	2.83	2.70	3.09	3.36
CH≡CCl	36.3	41.9	44.4	48.3	53.5	57.0
CH_2=CFCl	12.2	8.98	8.56	7.79	7.93	7.29
t-CHF=CHCl	54.9	55.6	57.0	56.5	60.2	59.9
c-CHF=CHCl	100	100	100	100	100	100
t-CHCl=CHCl	9.26	11.6	12.0	12.8	14.1	15.6
c-CHCl=CHCl	11.2	12.7	12.9	14.7	16.2	19.4

a) Reactant pressure was 0.5 Torr for these runs, incident laser energy being 0.141±0.003 J/pulse.

Table 3. Dependence of relative yields[a] on H_2 pressure

P/Torr	0.0	1.0	2.0	4.0	6.0	10.0
CH≡CF	9.39	9.49	9.37	10.5	11.7	12.0
CH≡CH	3.78	13.0	18.2	25.1	30.0	30.7
CH_2=CHF	2.23	7.85	9.87	11.3	11.8	12.2
CH≡CCl	28.9	31.3	32.0	36.5	40.7	41.9
CH_2=CFCl	24.9	12.4	10.2	8.70	8.45	8.67
t-CHF=CHCl	54.3	47.8	49.6	51.4	53.6	57.8
c-CHF=CHCl	100	100	100	100	100	100
t-CHCl=CHCl	7.72	11.1	11.2	11.7	14.8	15.0
c-CHCl=CHCl	9.15	12.6	12.9	13.6	15.3	17.6

a) Reactant pressure was 1.0 Torr for these runs, incident laser energy being 0.141±0.003 J/pulse.

Table 4. Effcts of additives on products yields[a]

Additives	pure	He	Ar	H_2	N_2	CH_4	CF_4
CH≡CF	0.546	0.458	0.432	0.296	0.415	0.455	0.490
CH≡CH	0.211	0.198	0.185	0.482	0.179	0.299	0.222
CH_2=CHF	0.162	0.0972	0.108	0.262	0.0968	0.106	0.0829
CH≡CCl	1.52	1.34	1.24	0.848	1.17	1.36	1.31
CH_2=CFCl	1.51	0.573	1.19	0.269	0.812	0.196	0.813
t-CHF=CHCl	3.80	2.22	2.61	1.31	2.05	1.56	1.48
c-CHF=CHCl	6.50	3.75	4.84	2.65	3.67	2.40	2.69
t-CHCl=CHCl	0.482	0.370	0.287	0.296	0.262	0.242	0.226
c-CHCl=CHCl	0.597	0.370	0.385	0.341	0.333	0.311	0.277
E_0(J/pulse)	0.145	0.143	0.142	0.146	0.138	0.144	0.149

a) Yields in % conversion per 600shots. The pressures of added gases are 2.0 Torr for these runs, reactant pressure being 1.0 Torr.

CH_2=CFCl, *cis*-, *trans*-CHCl=CHCl, CH≡CCl, and CH≡CF decrease rapidly in their yields with increasing He and H_2 pressure. Therefore, rotational hole-filling effect, which has been observed for small molecules,[24,25] is not important for the IRMPD of $CH_2ClCHFCl$ due to its higher density of vibrational-rotational states. Upon the addition of H_2, two lesser products in the neat IRMPD, CH≡CH and CH_2=CHF, increase in their yields at lower pressures, and then decrease at higher pressures, whereas their yields decrease monotonically by the addition of He gas.

In view of relative yields, those for all major products show an increase with higher pressure, but CH_2=CFCl yield shows an opposite trend. The realtive yield of CH_2=CFCl at reactant pressure of 1.0 Torr appears to decrease more quickly than that at 0.5 Torr, both approaching to similar values at higher bath gas pressures. In contrast to the neat IRMPD of $CH_2ClCHFCl$, the rapid decrease of CH_2=CFCl relative yield seems to be accompanied by the rapid increase of CH≡CCl relative yield with higher bath gas pressure. Similarly, the relative yields of CHCl=CHCl isomers show an opposite trend in the absence and presence of bath gases. The relative yield of *trans*-CHF=CHCl increases slowly in the presence of He and H_2. The relative yields of CH≡CH and CH_2=CHF increase much more rapidly in the presence of H_2 than those in the presence of He.

Effects of Additives. Three pairs of gases of 2.0 Torr were added into the parent gas of 1.0 Torr, each pair of gases being considered to have similar efficiency of vibrational energy transfer.[26] The other parameters of photolysis were kept same or constant. The results on the product yields are tabulated in Table 4. Each pair shows a quite different effect on the yield of CH_2=CFCl: He, H_2, and CH_4 reduce the yield of CH_2=CFCl significantly compared with Ar, N_2 and CF_4. At the same time, upon the addition of H_2 and CH_4 the yields of CH≡CH and CH_2=CHF increase, but in the case of CH_4 addition the increase is smaller than that of H_2

addition. The yields of CH≡CF and CH≡CCl appear to be smaller in the presence of H_2 than those on the addition of N_2. The yields of *cis*- and *trans*-CHF=CHCl decrease upon the addition of He and H_2 in relation to those in the presence of Ar and N_2, while in the CH_4–CF_4 pair they show no significant difference. Remarkable reduction in the yield of CH_2=CFCl were also observed on the addition of C_2H_6, C_3H_8, and C_2H_4, which hardly absorb IR photons at the excitation line. Effects of NO were quite similar to those of N_2.

Dependence on Pulse Energy. The dependence of total yield on pulse energy at $CH_2ClCHFCl$ pressure of 0.2 Torr is shown in a log-log plot in Fig. 4. The plots are linear and obey the relationship: Y (yield)$\propto E_0^n$ (pulse energy). From the slope the value of the exponent is found to be n=1.62 and very close to 1.5, of which fluence dependence has been observed in many systems with focused geometry.[27] The 3/2 power dependence can be readily interpreted in terms of a simple threshold model[28,29] which is based on the assumption that all molecules contained in a conical zone where the laser fluence is above some threshold, decompose with unit probability, and neglects any reactions outside this zone. The relative yields as a function of pulse energy are given in Table 5. The relative yields appear to be rather insensitive to the laser energy: About 10 fold increase in energy affected, as an example, the relative yield of *trans*-CHF=CHCl by only 33%. Such insensitivity to the laser energy can be attributed to the focused geometry employed in the present experiments.[6,17]

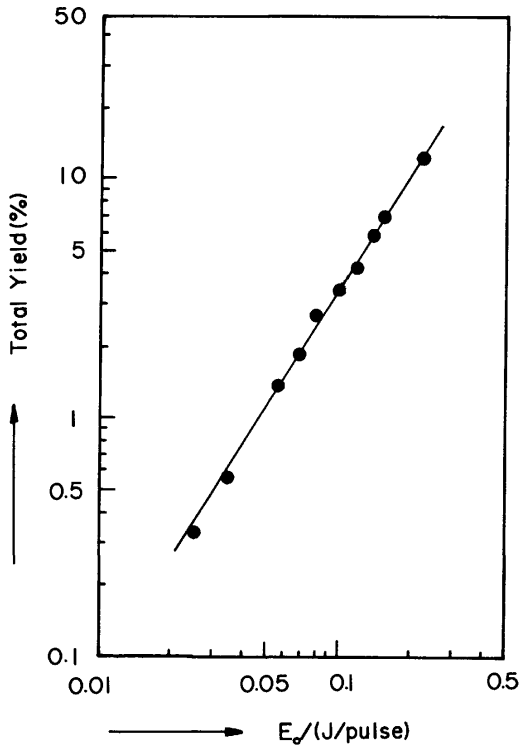

Fig. 4. Total product yield as a function of incident laser energy.

Secondary Photolysis. To investigate the formation pathways to haloethynes, primary HCl elimination products from $CH_2ClCHFCl$, CHF=CHCl isomers and CH_2=CFCl were photolyzed. The sample gas pressures were kept at 0.2 Torr, and the laser energy was the same as that in the neat IRMPD of $CH_2ClCHFCl$ at various pressures. The irradiation lines were so chosen to match their normal absorption spectrum maxima. The results together with that of *trans*-CHCl=CHCl are summarized in Table 6. Table 6 shows that CH≡CCl, CH≡CF, and CH≡CH are generated from the chlorofluoroethene isomers, in particular from CH_2=CFCl, which has no strong absorption at 1033.5 cm^{-1}. Major channels of *trans*-, *cis*-CHF=CHCl, and *trans*-CHCl=CHCl are the isomerization to the other isomers. *cis*-CHCl=CHCl has no absorption band in the CO_2 laser range, but in analogy to *trans*-CHCl=CHCl, the major channel would be also isomerization. It has been recognized that decomposition reaction is markedly reduced in the IRMPD of *trans*-CHCl=CHCl, since the isomerization reaction has lower energy threshold than that of decomposition.[30] This may be also the case for the IRMPD of CHF=CHCl isomers.

At $CH_2ClCHFCl$ pressure of 3.0 Torr, the absolute yield of CH_2=CFCl is about 0.1 Torr. Assuming CH≡CCl, CH≡CF, and CH≡CH be derived entirely from CH_2=CFCl, the % conversions of CH≡CCl, CH≡CF, and CH≡CH would be 26.5, 14.0, and 6.3, respectively, in the IRMPD of $CH_2ClCHFCl$ at the same laser energy. These % conversions are at least 50 times greater in the IRMPD of $CH_2ClCHFCl$ than those in the

Table 5. Pulse energy dependence of relative yields[a]

E_0(J/pulse)	0.220	0.153	0.140	0.118	0.0994	0.0799	0.0682	0.0503	0.0352	0.0253
CH≡CF	13.5	12.6	12.7	13.5	13.0	12.9	13.4	13.7	13.9	11.5
CH≡CH	6.35	5.88	5.57	6.59	6.11	6.10	4.98	5.49	2.87	—
CH_2=CHF	2.54	2.37	2.48	2.02	2.58	2.21	1.95	2.44	—[b]	—
CH≡CCl	56.2	54.4	53.1	56.2	54.1	59.0	53.9	50.1	47.1	41.4
CH_2=CFCl	7.25	6.10	5.96	5.32	5.00	5.66	6.20	5.34	—	—
t-CHF=CHCl	49.1	51.8	52.6	55.4	57.4	54.5	61.2	63.4	66.4	65.3
c-CHF=CHCl	100	100	100	100	100	100	100	100	100	100
	(4.77)	(2.72)	(2.28)	(1.64)	(1.32)	(0.990)	(0.707)	(0.451)	(0.244)	(0.152)
t-CHCl=CHCl	11.4	13.2	13.2	11.5	11.3	14.0	12.6	—	—	—
c-CHCl=CHCl	13.8	13.6	13.0	14.1	12.1	11.4	10.0	—	—	—

a) The yield of *c*-CHF=CHCl in % conversion per 300 shots is in parenthesis, being taken equal to 100. The reactant pressure is 0.20 Torr for these runs. b) Too small for quantitative analysis.

TABLE 6. PRODUCT YIELDS[a] IN IRMPD OF PRIMARY PRODUCTS

CH≡CF	0.0708	—	0.0390	—
CH≡CH	0.0389	—	—	—
CH_2=CHF	—[c]	—	—	—
CH≡CCl	0.495	—	0.163	—
CH_2=CFCl	reactant	—	—	—
t-CHF=CHCl	—	reactant	2.45	—
c-CHF=CHCl	—	1.15	reactant	—
t-CHCl=CHCl	—	—	—	reactant
c-CHCl=CHCl	—	—	—	4.63
E_0(J/pulse)	0.140	0.137	0.147	0.141
ν(cm^{-1})[b]	953	1029	1072	923

a) The reactant pressure is 0.20 Torr, the yields being expressed in % conversion per 600 shots. b) Irradiation wave number used. c) Yields are too small to be quantitatively determined.

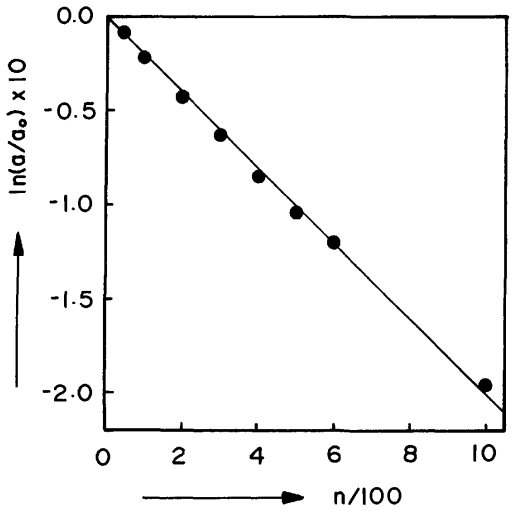

Fig. 5. Total conversion as a function of pulse number.

IRMPD of CH_2=CFCl at the maximum absorptoion wave number of CH_2=CFCl. This suggests that CH≡CCl and CH≡CF are not formed consecutively by the secondary photolysis of primarily generated chlorofluoroethenes accumulating in the system during the laser irradiation.

Dependence on Pulse Number. The product yields as a function of pulse number were tested at the reactant pressure of 0.2 Torr. The results are shown in Fig. 5. Unreacted fraction (a/a_0), where a and a_0 denote final and initial reactant pressures, respectively, deceases exponentially with the increase in pulse number n, indicating pseudo-first order decay over a wide range of pulse number up to 1000. $(a/a_0)=\exp(-dn)$, where d corresponds to the slope and can be regarded to be an apparent dissociation rate constant for $CH_2ClCHFCl$. Each yield versus n is plotted in Fig. 6. As can be seen from Fig. 6, each product yield is proportional to pulse number up to 400 in the lower conversion range, which suggests that the formation of each product is one shot event. This does not necessarily mean that each product is formed during the pulse duration, but formed within the time interval between pulses.

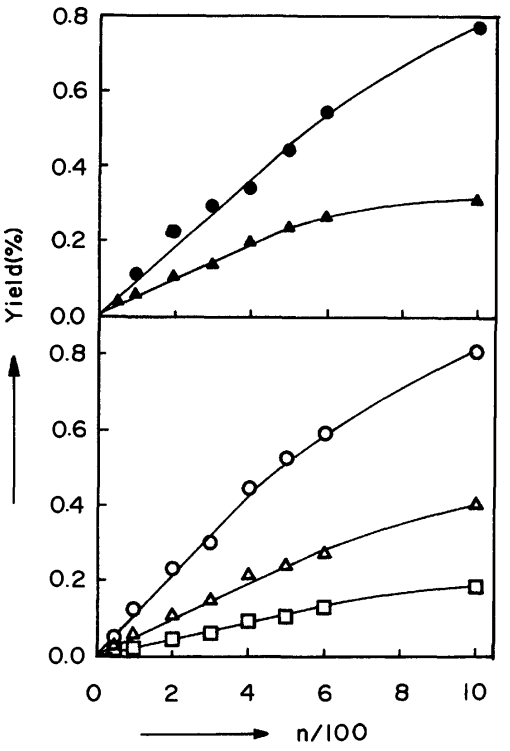

Fig. 6. Individual product yields as a function of pulse number.
●: *c*-CHF=CHCl, ▲: CH≡CCl, ○: *t*-CHF=CHCl, △: CH=CFCl, ■: CH≡CH.

TABLE 7. PRODUCT YIELD DEPENDENCE ON PULSE DURATION

duration	short pulse		long pulse	
CH≡CF	0.0712[a]	15.3[b]	0.0647[a]	17.0[b]
CH≡CH	0.0213	4.58	0.0206	5.24
CH_2=CHF	0.0107	2.30	0.0111	2.82
CH≡CCl	0.240	51.6	0.187	47.6
CH_2=CFCl	0.0658	14.2	0.0520	13.2
t-CHF=CHCl	0.293	63.0	0.254	64.6
c-CHF=CHCl	0.465	100	0.393	100
E_0(J/pulse)	0.0273		0.0299	

a) Yields in % conversion per 600 shots, reactant pressure being 0.2 Torr. b) The yield of *c*-CHF=CHCl is taken equal to 100.

Dependence on Pulse Duration. The effects of Pulse duration on the product yields were examined by two different pulses with the same pulse energy. The laser pulse duration can be varied by changing the ratio of N_2 in lasing gas mixture. In the present experiments two pulses of different duration were generated by shutting or adding N_2 into the lasing gas mixture. The pulse with N_2 added consists of a sharp spike of about 100 ns FWHM with a low intensity tail of about 1 μs,[9] while the pulse without N_2 consists of a sharp spike of about 80 ns FWHM without tailing.[13] The results are given in Table 7. Table 7 shows that the yields of the chlorofluoroethenes, CH≡CCl, and CH≡CF are increased slightly by the irradiation of the short pulse, but the yields of CH≡CH and CH_2=CHF are little affected by the duration of pulse. It is also shown that there

TABLE 8. RELATIVE PRODUCT YIELDS IN PYROLYSIS

T_5/K[a]	1060	1115	1222	1325
CH≡CF	—[c]	1.31	1.63	17.8
CH≡CH	—	—	—	3.24
CH≡CCl	—	—	—	4.39
CH_2=CFCl	42.1	43.9	40.8	36.5
t-CHF=CHCl	49.3	63.7	66.3	69.9
c-CHF=CHCl[b]	100	100	100	100
	(1.55)	(8.72)	(33.8)	(40.8)
t-CHCl=CHCl	—	3.36	4.05	3.90
c-CHCl=CHCl	—	3.92	4.23	4.63

a) Temperature behind reflected shock wave. b) The yield of *c*-CHF=CHCl in % conversion(in parenthesis) is taken to be 100. c) Product yield is too small to be quantitatively determined.

are little effects of the pulse duration on the relative yields. Since almost the same energy is contained in the two pulses, the short pulse has higher intensity than the long pulse with the same fluence. However, the increase of the product yields is very small, at most 18%, and that of the relative yields among competing channels is not observed. Thus intensity is not an important factor in the IRMPD of $CH_2ClCHFCl$.

Pyrolysis. Several pyrolysis experiments were carried out with a single-pulse shock tube. A reaction mixture of 0.285% $CH_2ClCHFCl$ diluted with argon was used. Reaction temperatures ranged from 1060 to 1325 K, the dwell times, total pressures, and reactant pressure being about 840 μs, 660 Torr, and 1.9 Torr, respectively. Under these conditions the decomposition yields ranged from about 3 to 98% (Table 8). All major products found in the IRMPD of $CH_2ClCHFCl$ were also obtained. At the lowest conversions, only chlorofluoroethene isomers are formed. HF elimination channel to produce CHCl=CHCl isomers opens up at higher temperatures. At highest temperature, secondary reactions of the chlorofluoroethenes become significant to give rise to CH≡CCl and CH≡CF together with CH≡CH. The relative yields of the chlorofluoroethene and CHCl=CHCl isomers are similar to those obtained in the IRMPD of $CH_2ClCHFCl$ at higher temperatures. The most remarkable difference is in the relative yields of CH≡CCl and CH≡CF, *viz*, CH≡CF formation is more important than that of CH≡CCl in the high temperature shock tube pyrolysis.

Discussion

Mechanism of Primary Photolysis. The elimination of molecular hydrogen halide from the parent molecule is in line with previous IRMPD studies of halogenated ethanes[31,32] together with thermal[33] and chemical activation studies.[34,35] The intersting feature in chlorofluoroethanes is that a number of competitive dissociation channels seem to be possible:

$$CH_2ClCHFCl \longrightarrow CHF{=}CHCl + HCl \qquad \Delta H^\circ \simeq 19.0 \text{ kcal/mol}^{36}$$

$$\longrightarrow CH_2{=}CFCl + HCl \qquad \Delta H^\circ \simeq 21.1 \text{ kcal/mol}$$

$$\longrightarrow CHCl{=}CHCl + HF \qquad \Delta H^\circ \simeq 10.3 \text{ kcal/mol}$$

$$\longrightarrow \cdot CH_2CHFCl + Cl$$

$$CH_2ClCHF\cdot + Cl \qquad \Delta H^\circ \simeq 80\text{—}90 \text{ kcal/mol}$$

$$\longrightarrow CH_2Cl\cdot + CHFCl\cdot \qquad \Delta H^\circ \simeq 85\text{—}90 \text{ kcal/mol}$$

$$\longrightarrow CH_2{=}CHF + Cl_2 \qquad \Delta H^\circ \simeq 45.0 \text{ kcal/mol}$$

Heats of reaction ΔH° (kcal/mol, 1 cal_{th}=4.184 J) were evaluated at 298 K. The observed product distributions under various conditions in the photolysis and pyrolysis that the chlorofluoroethene isomers are by far the major products, strongly suggest that the principal mode of reaction in the IRMPD of $CH_2ClCHFCl$ is direct elimination of molecular HCl. Similarly, the products CHCl=CHCl isomers formed in lower, yet significant yields, can be ascribed to the molecular elimination of HF:

$$CH_2ClCHFCl + nh\nu \longrightarrow \textit{cis}\text{-}CHF{=}CHCl + HCl \quad (1)$$

$$\longrightarrow \textit{trans}\text{-}CHF{=}CHCl + HCl \quad (2)$$

$$\longrightarrow CH_2{=}CFCl + HCl \quad (3)$$

$$\longrightarrow \textit{cis}\text{-}CHCl{=}CHCl + HF \quad (4)$$

$$\longrightarrow \textit{trans}\text{-}CHCl{=}CHCl + HF \quad (5)$$

IR emission of HCl and HF was observed in related systems,[13] which suggests the HCl and HF formed in Reactions 1—5 are also in their vibrationally excited states. In chemical activation studies coupled with isotopic labelling technique,[37] it has been shown clearly that three-center reaction ($\alpha\alpha$ elimination) competes with four-center reaction ($\alpha\beta$ elimination), if two halogen atoms are located at the same carbon atom. It is thought that the carbene such as CH_2XCX: (X=Cl, F) is thermodynamically more stable than CH_2XCH: due to π bonding between the halogen and the vacant p orbital of the carbene.[38] By analogy with the chemical activation studies of CH_2XCHX_2, $CH_2ClCHFCl$ could eliminate HCl and HF *via* three-center reaction together with more common four-center reaction:

$$CH_2ClCHFCl + nh\nu \longrightarrow CH_2ClCF: + HCl \quad (6)$$

$$\longrightarrow CH_2ClCCl: + HF \quad (7)$$

Three-center reaction is followed by a rapid rearrangement of the carbene. Thus CHF=CHCl and CHCl=CHCl geometrical isomers may be formed by $\alpha\alpha$ elimination processes. $CH_2ClCHFCl$, however, does not permit to distinguish $\alpha\alpha$ elimination from $\alpha\beta$ elimination by their poroducts, the contribution of $\alpha\alpha$ elimination being estimated to be much smaller than $\alpha\beta$ elimination process.[37]

The products expected from the C–C and C–Cl bond scissions of $CH_2ClCHFCl$, *e.g.*, CH_3Cl, CH_2=CHCl, and CH_3CHFCl, were found in trace amounts or not

detected at all. The contribution of the C–C and C–Cl bond scissions could be concluded to be very small under the present conditions. Molecular elimination of halogen was proposed for the IRMPD of $CHCl=CCl_2$,[5] but recent study shows that $CHCl=CCl_2$ decomposes by consecutive Cl atom elimination.[39] If $CH_2=CHF$ were formed directly *via* Cl_2 elimination, its yield would have decreased upon the addition of H_2 as CHF=CHCl and CHCl=CHCl yields did. On the contrary, the increase of $CH_2=CHF$ yield was observed in the presence of H_2 (Fig. 3). Summing up the above considerations, the primary processes in the IRMPD of CH_2Cl-CHFCl under our conditions are direct eliminations of HCl and HF molecules, $\alpha\beta$ elimination of HCl being the predominant channel.

Mechanism of Secondary Photolysis. CH≡CCl, CH≡CF, and CH≡CH were found in the IRMPD of the chlorofluoroethene isomers, which can be interpreted that they result from the secondary photolysis of the primary products in the IRMPD of $CH_2ClCHFCl$. Furthermore, the IRMPD results of chlorofluoroethene isomers (Table 6) may suggest that CH_2CFCl contributes primarily to the formation of CH≡CCl, CH≡CF, and CH≡CH, in which there is no isomerization channels with lower threshold energy among the isomers. CH_2≡CFCl has a number of competing decomposition channels:

$$CH_2=CFCl \longrightarrow CH{\equiv}CCl + HF \qquad \Delta H^\circ \simeq 19.4 \pm 10 \text{ kcal/mol}$$
$$\longrightarrow CH{\equiv}CF + HCl \qquad \Delta H^\circ \simeq 41.3 \pm 15 \text{ kcal/mol}$$
$$\longrightarrow CH_2{=}CF\cdot + Cl \qquad \Delta H^\circ \simeq 80\text{—}90 \text{ kcal/mol}$$
$$\longrightarrow CH{\equiv}CH + FCl \qquad \Delta H^\circ \simeq 75.5 \text{ kcal/mol}$$

Vinylidenecarbene CH_2=C: has very low barrier for the rearrangement,[40,41] and rapidly isomerizes to CH≡CH. In the IRMPD study of deterium labelled chloroethenes, it has been shown that HCl elimination proceeds mainly *via* three-center reaction.[5] In CH_2=CFCl molecule there are no three-center elimination reactions of HCl and HF but for that of FCl.

As mentioned earlier (Table 6), the chlorofluoroethene isomers in their vibrational ground states give rise to much smaller yields of CH=CCl and CH≡CF in their IRMPD even at their maximum absorption bands than those in the IRMPD of $CH_2ClCHFCl$ at 1033.5 cm^{-1}. In addition, the dependence of CH≡CCl and CH≡CF yields on pulse number (Fig. 6) shows that CH≡CCl and CH≡CF are generated within the time period between pulses. Furthermore, it has been shown that longer pulse does not increase the yields of CH≡CCl and CH≡CF in relation to the chlorofluoroethene isomers. Markedly enhanced secondary photolysis in one pulse points to the change in states of the primary photolysis products. Primarily formed chlorofluoroethenes must be excited into the quasicontinuum region or very close to it, in order to readily absorb many photons which are not resonant with the absorption lines of the chlorofluoroethenes;

$$CH_2=CFCl^{\#} + mh\nu \longrightarrow CH{\equiv}CCl + HF \quad (8)$$
$$\longrightarrow CH{\equiv}CF + HCl \quad (9)$$
$$trans\text{-}CHF=CHCl^{\#} + mh\nu \longrightarrow cis\text{-}CHF=CHCl \quad (10)$$
$$\longrightarrow CH{\equiv}CCl + HF \quad (11)$$
$$\longrightarrow CH{\equiv}CF + HCl \quad (12)$$
$$cis\text{-}CHF=CHCl^{\#} + mh\nu \longrightarrow trans\text{-}CHF=CHCl \quad (13)$$
$$\longrightarrow CH{\equiv}CCl + HF \quad (14)$$
$$\longrightarrow CH{\equiv}CF + HCl \quad (15)$$

where $CH_2=CFCl^{\#}$ stands for the CH_2=CFCl molecule vibrationally excited into its quasicontinuum levels. Vibrational excitation of the chlorofluoroethene isomers in line with the chemical activation studies of CH_2XCHX_2:[34,35] The *trans*- and *cis*-CHX=CHX produced from chemically activated CH_2XCHX_2 undergo isomerization, decomposition to CH≡CX being unobserved. Chemically activated $CH_2ClCHCl_2$ and CH_2FCHF_2 are estimated to have average energies of 89.5 and 95 kcal/mol, nearly equal to bond dissociation energies of the C–C bond, respectively. In the IRMPD of $CH_2ClCHFCl$ the contribution of the C–C bond-rupture channel is concluded to be very small. The average energy of $CH_2ClCHFCl$ excited by IRMPE would be smaller than those by chemical activation. Therefore, $CH_2=CFCl^{\#}$, at least, would absorb additional photons in order to decompose to CH≡CCl and CH≡CF, although *cis*- and *trans*-CHF=CHCl might isomerize without absorbing any additional photons.

In a similar manner to CHF=CHCl isomers, major channels of CHCl=CHCl isomers would be isomerization to the other isomers. Smaller yields of CHCl=CHCl isomers in the IRMPD of $CH_2ClCHFCl$ indicates smaller contribution to the formation of CH≡CCl by HCl elimination:

$$trans\text{-}CHCl=CHCl + mh\nu \longrightarrow cis\text{-}CHCl=CHCl \quad (17)$$
$$cis\text{-}CHCl=CHCl + mh\nu \longrightarrow trans\text{-}CHCl=CHCl \quad (18)$$

Activation energies for the isomerization of *cis*-CHF=CHCl and *cis*-CHCl=CHCl are reported to be 58.3 and 56.9 kcal/mol, *cis*-forms being thermodynamically more stable than *trans*-forms by 0.780 and 0.650 kcal/mol, respectively.[42,43]

The increase in the yield of CH_2=CHF upon the addition of H_2 strongly suggests that the C–Cl bond rupture is occurring in the secondary photolysis of the chlorofluoroethenes, in particular, of CH_2=CFCl. In our study of the IRMPD of CF_2ClCH_2Cl,[44] we found that the yield together with relative yield of $CH_2=CF_2$ increased upon the addition of H_2 (D_2), a large amount of $CDF=CF_2$ being observed by mass spectrometry. It is proposed that the observed $CH_2=CF_2$ is produced

primarily *via* H atom abstraction by CF_2=CH· radical, which, in turn, originates from the secondary photolysis of the primary product CF_2=CHCl. This seems to be also the case for the IRMPD of $CH_2ClCHFCl$:

$$CH_2=CFC^{\#} + mh\nu \longrightarrow CH_2=CF\cdot + Cl \quad (19)$$

$$CH_2=CF\cdot + RH \longrightarrow CH_2=CHF + R\cdot \quad (20)$$

where RH denotes any H atom donors, $CH_2ClCHFCl$ molecule itself being RH in the absence of any additives.

Molecular elimination of FCl from CH_2=CFCl to generate CH≡CH seems to be possible in view of smaller heat of reaction than that of the C–Cl bond rupture. However, due to very rapid rearrangement of CH_2=C: to CH≡CH, the formation reaction of CH≡CH is unimolecular in nature, and the addition of H_2 would have resulted in the decrease in its yield with increasing H_2 pressure as that of He did (Figs. 2 and 3).

In a similar manner to the CH_2=CHF formation, CH≡CH may be generated by H atom abstraction reaction of some radical produced during the photolysis. Possible radical would be CH≡C· radical resulting from the decomposition of CH≡CCl and/or CH≡CF. In previous study it was shown that the haloetynes dissociate to give rise to halogen atoms, instead of hydrogen halides,[45] F atom requiring about 20 kcal/mol more energy than Cl scission. CH≡CCl appears to be responsible for the generation of CH≡C· radical, but we will return to this point later. Vibrationally excited haloetynes were observed in the IRMPD of related systems.[13] Therefore, it might be possible that the haloetynes formed in the secondary photolysis are excited to high vibrational levels and dissociate by further photon absorption as in the case of the secondary photolysis:

$$CH{\equiv}CCl^{\#} + m'h\nu \longrightarrow CH{\equiv}C\cdot + Cl \quad (21)$$

$$CH{\equiv}CF^{\#} + m'h\nu \longrightarrow CH{\equiv}C\cdot + F \quad (22)$$

$$CH{\equiv}C\cdot + RH \longrightarrow CH{\equiv}CH + R\cdot \quad (23)$$

Effects of Pressure on Mechanism. As shown in Table 1, all product yields increase linearly with higher pressure up to 0.2 Torr, above which they show nonlinear behaviors. In the primary photolysis direct elimination of HCl and HF is apparently dominant mechanism of dissociation at both lower and higher pressures. However the mechanism operative at lower pressures may not be the same as that at higher pressures. In the high pressure region, true MPD still can occur, but here there are several factors which may influence the dissociation mechanism.

One of the factors which might result in a different dissociation mechanism is the collisions between the laser excited species prior to dissociation. These collisions may serve to randomize the energy among the laser excited collision partners, resultant radomization will show an effective distribution which may be different at higher pressures from that at lower pressures. These randomizations come in the form of energy gain/loss collisions, energy-pooling process, where one molecule gains and the other molecule loses energy.

The chlorofluoroethene yields increase remarkably with increasing reactant pressure, while higher channel product yields of CHCl=CHCl isomers are insensitive to the increase of $CH_2ClCHFCl$ pressure. At higher pressures energy-pooling process mentioned above can take place between two excited parent molecules with the energy below the lower energy threshold, one gaining energy beyond the lower critical energy:

$$2CH_2ClCHFC^{\#} \longrightarrow CH_2ClCHFCl^{*} + CH_2ClCHFCl \quad (24)$$

where $CH_2ClCHFCl^{\#}$ and $CH_2ClCHFCl^{*}$ represent the $CH_2ClCHFCl$ molecules excited below and above the critical energy for HCl elimination, respectively. The insensitivity of the CHCl=CHCl yields to the reactant pressure indicates that $CH_2ClCHFCl^{*}$ does not gain energy by the collision beyond the higher energy threshold:

$$CH_2ClCHFCl^{*} \longrightarrow cis\text{-}CHF{=}CHCl + HCl \quad (25)$$

$$\longrightarrow trans\text{-}CHF{=}CHCl + HCl \quad (26)$$

$$\longrightarrow CH_2{=}CFCl + HCl \quad (27)$$

In a gas cell IRMPD experiment with a focused geometry, the irradiation zone becomes optically inhomegeneous, and the results on the yields are average over the fluence distribution of the focused laser beam. As noted earlier, the dependence of total yield on laser energy at lower reactant pressures (Fig. 6) was rationalized by a simple threshold model. As the pressure is increased, this model is not applicable, since in high pressure range molecular collisions cannot be neglected. The simple extended threshold model presented by Hackett *et al.*[6] will be convenient to discuss the pressure dependence observed in the present study. In this model for a two-channel system, the conical beam is divided into three volume elements: The lower decomposition channel is induced for all molecules with unit efficiency at some threshold fluence F_1. At some higher fluence F_2, the irradiation field is sufficiently intense to derive all molecules to internal energies where upper decomposition channel predominates. The irradiated volume which is subjected to fluence between F_0 and F_1 is inhomogeneously excited by the field, where F_0 denotes incident fluence. When reactant pressure is low enough, the excited molecules would be cooled without any chance to collide with other excited molecules. At these pressures, the relative yields from various processes are equal to the ratios of volumes defined by the threshold fluence contours which describe them, being shown to be insensitive to pulse energy in this model. Our results on the relative yields versus pulse energy (Table 5) are consistent with the prediction based on this extended threshold model. The molecules outside the reaction

zone are excited by laser to an energy level not enough to decompose haloethene and HCl spontaneously. At higher reactant pressures, collision-induced decomposition by energy-pooling process can take place efficiently outside the reaction zone. It is not unreasonable that the collision-induced dissociation exits preferentially by the lower channels, increasing HCl elimination product yields with increasing pressure. The relative yields of HF elimination products CHCl=CHCl decrease with higher reactant pressure: The branching ratio between HCl and HF elimination channels is about 100:11 and 100:4 at 0.1 and 3.0 Torr reactant pressure, respectively. The yields of CHCl=CHCl isomers appear decrease slightly at higher pressures. IRMPD *via* HF elimination channels will take place efficiently only inside the inner reaction zone, where the laser fluence is higher than the threshold fluence F_2. At higher reactant pressures the energy absorption along the laser beam reduces the volume of the inner reaction zone, which results in the decrease of the CHCl=CHCl yields.

The yield of CH≡CCl does not increase but decrease to the same extent as those of CHCl=CHCl isomers with increasing substrate pressure. This strongly suggests that secondary photolysis is occurring primarily inside the outer reaction zone with the fluence between F_1 and F_2, and that the chlorofluoroethenes generated by the collision-induced decomposition outside the reaction zone remain undecomposed by the secondary photolysis. The relative yield of CH_2=CFCl increases by about 8.5 times more rapidly than that of *trans*-CHF=CHCl with increasing reactant pressure. This rapid increase of CH_2=CFCl relative yield with higher reactant pressure can be ascribed to the formation of CH_2CFCl outside the reaction zone *via* collision-induced decomposition, and indicates that decomposition of the chlorofluoroethene isomers occurs predominantly from CH_2=CFCl inside the reaction zone. Curiously, the yield of CH≡CF increases slightly with higher pressure. Other mechanism for the formation of CH≡CF may be operative at higher pressures.

Another intermolecular energy transfer process is collisional deactivation. This is the collision between vibrationally hot and cold molecules. When buffer gas is added to the reactant, energy pooling between excited parent molecules is suppressed by the buffer gas. In the presence of buffer gas, collision-induced decomposition is markedly reduced by collisional deactivation. As shown in Figs. 2 and 3, even the yields of CHCl=CHCl and CH≡CCl, which are thought to be formed primarily inside the reaction zone, decrease rapidly even at low He and H_2 pressures. Therefore, the collisional vibrational deactivation of the excited parent molecules inside the reaction zone starts even at low buffer gas pressure in the IRMPD of CH_2ClCHFCl. However, quenching of energy-pooling process is revealed in the relative yield of CH_2=CFCl: As discussed above, the increase of CH_2=CFCl relative yield with rising substrate pressure results from the energy-pooling processes outside the reaction zone. Therefore, more rapid decrease in the relative yield of CH_2=CFCl at 1.0 Torr CH_2ClCHFCl at lower buffer gas pressures than that at 0.5 Torr could be ascribed to the quenching of energy-pooling processes by the buffer gases outside the reaction zone.

An opposite trend of the relative yields of CHCl=CHCl, CH≡CCl, and CH_2=CFCl observed in the absence and presence of buffer gas indicates that the collisional deactivation derives the energy distribution of the dissociating parent molecules to higher energy distribution with higher buffer gas pressure, resulting in greater relative yields for most products. However, at higher energy distribution more CH_2=CFCl is decomposed to CH≡CCl and CH≡CF, the decrease in CH_2=CFCl and increase in CH≡CCl and CH≡CF relative yields being observed. Very slight increase of *trans*-CH=FCHCl relative yield as compared with that of CH_2=CFCl with rising He a H_2 pressure will support our finding that the decomposition channels of CHF=CHCl isomers contribute to smaller extent for the formation of secondary products. By the same reason as CH≡CCl and CH≡CF, the relative yields of CH≡CH and CH_2=CHF increase slightly upon the addition of He, being much enhanced by the presence of H_2: In the presence of H_2, much more H atom donors are available than in the presence of He, in which only the substrate molecule acts as H atom donor.

By the addition of buffer gases with similar energy transfer efficiency, the excited molecules would be quenched collisionally, and the products yields would be suppresses to a similar extent. Actually, no significant difference is observed in the yields of *trans*- and *cis*-CHF=CHCl, CH≡CCl, and CH≡CF upon the addition of CH_4 and CF_4. On the other hand, there appear to be remakable difference in the yield of CH_2=CFCl between CH_4 and CF_4. In our mechanism, CH≡CCl and CH≡CF are formed primarily from CH_2=CFCl. Therefore, the C–Cl bond-scission channel Reaction 19 will cause the difference in the yield of CH_2=CFCl. The radicals formed *via* a bond-scission reaction will recombine initially inside the reaction zone:

$$CH_2{=}CF\cdot + Cl \xrightarrow{M} CH_2{=}CFCl \qquad (28)$$

Other recombination reactions such as

$$2CH_2{=}CF\cdot \xrightarrow{M} CH{\equiv}CF + CH_2{=}CHF,\ CH_2{=}CFCF{=}CH_2$$

$$2Cl + M \longrightarrow Cl_2$$

are slower processes than Reaction 28. In the presence of H atom donor RH, abstraction reactions of the radicals become competitive with the recombination reaction, and CH_2=CF· radical and/or Cl atom are lost, being unrecovered as CH_2=CFCl by Reaction 28:

$$CH_2{=}CF\cdot + RH \longrightarrow CH_2{=}CHF + R\cdot \qquad (20)$$

$$Cl + RH \longrightarrow HCl + R\cdot \quad (29)$$

Upon the addition of H_2, $CH_2=CF\cdot$ radical is lost, while upon the addition of CH_4, Cl atom is lost by Reaction 29. The rate constant of Cl with CH_4 is about one order of magnitude greater that that with H_2.[46] In the IRMPD of CF_3I, the yield of I atom is observed to be much smaller than the real yield due to the recombination reaction between I atom and $CF_3\cdot$ radical.[47] This is in line with our observation that the C-Cl bond-scission channel is masked by the recombination reaction. In the case of Ar and He pair, there will be no chemical reaction with the rare gases added. Collisional quenching is only possible process to affect the product yields. Similar effects of collisional quenching and chemical reactions on the yields of *trans*- and *cis*-CHF=CHCl are observed to smaller extent in the presence of monoatomic and diatomic pairs (Table 4). CH≡CCl and CH≡CF are supposed to further decompose to generate CH≡C· radical by Reactions 21 and 22. Similar effects of the additives can be expected for these decomposition reactions, since these reactions generate radicals. These effects appear to be demonstrated in H_2 and N_2 pair: The yields of CH≡CCl and CH≡CF are decreased upon the addition of H_2 as compared with those on N_2 addition, probably due to the abstraction reaction of CH≡C· radical from H_2. Relatively significant decrease is observed for CH≡CF yield, indicating that a large fraction of CH≡CF is decomposed to CH≡C· and F. The observed increase of CH≡CF yield with higher reactant pressure in the neat IRMPD (Table 1), may be interpreted in terms of the enhanced recombination rate with higher substrate pressure. The effect of the recombination reaction may be very small for the yield of CH≡CCl, since the yield of CH≡CCl is much greater than that of CH≡CF.

Comparison with Thermal Excitation. As can be seen from Tables 1 and 8, the primary product distribution obtained in the shock tube pyrolysis bears a strong resemblance to that of the neat IRMPD of $CH_2ClCHFCl$ at 3.0 Torr. According to the simple extended threshold model, the volume of the reaction zone in which the fluence exceeds the lowest critical fluence value is constant at a given pulse energy, the absorption along the laser beam being neglected. The difference of the % conversions between 0.1 Torr and 3.0 Torr could be ascribed to the contribution from the collision-induced decomposition outside the reaction zone. Therefore, the similarity of the primary product distribution between the shock tube pyrolysis and the neat IRMPD at 3.0 Torr might not be surprising, since at 3.0 Torr more than one halves of CHF=CHCl and almost all $CH_2=CFCl$ molecules are generated by the collision-induced decomposition outside the reaction zone where the laser excited $CH_2ClCHFCl$ molecules are rapidly being thermalized by collisions, and the collision-induced decomposition *via* energy pooling resembles intrinsically the dissociation processes in a thermal excitation system such as shock tube pyrolysis. However, the relative yields of the haloethenes derived from the the collision-induced decomposition are estimated to be *cis*-CHF=CHCl:*trans*-CHF=CHCl:$CH_2=CFCl \simeq 100:72:59$ at 3.0 Torr, assuming that the % conversions inside the reaction zone be unchanged and corrected for the absorption along the laser beam to the same extent as those of CH≡CF and CHCl=CHCl yields. The estimated relative yields are much greater than those of shock tube pyrolysis at 1060 K, where the decomposition *via* upper channel is not appreciable as well as outside the reaction zone. This may suggest that the initial energy distribution created by the laser pulse outside the reaction zone is transferred by the energy-pooling process to a new energy distribution which has more enhanced tail between the lower and upper energy thresholds than that of corresponding Boltzmann thermal distribution.

In the shock tube pyrolysis at higher temperatures, the Boltzmann thermal distribution has a higher energy tail which crosses the upper HF elimination channels. At lower reactant pressures, where the contribution of the decomposition outside the reaction zone is negligible, the relative yields of CHCl=CHCl isomers are about three times greater in the IRMPD than those in the shock tube pyrolysis. In the present model, all molecules contained inside the outer and inner reaction zone are excited to internal energies above the lower and higher critical energies for the decomposition, respectively. Therefore, the internal energy distribution inside the reaction zone, in a similar manner to that outside the reaction zone, has also more enhanced tail above the higher energy threshold than that of the Boltzmann distribution corresponding to the temperatures examined in the shock tube pyrolysis. In a thermal excitation system, the energy distribution is an explicit function of temperature, while the energy distribution inside the reaction zone with a focused laser beam is not affected by the incident laser energy. Consequently, the comparison of the energy distribution inside the reaction zone with that in the pyrolysis remains superficial, and the fluence effect on the energy distribution would not be persued properly by such a bulk IRMPD experiment with a focused geometry as mentioned above.

In contrast to the primary product distribution, the seconary product distributions are quite different from each other in the IRMPD and shock tube pyrolysis of $CH_2ClCHFCl$. IR emission investigation on the $CH_2=CFCl$ IRMPD by Jalenak and Nogar[12] also shows that the intensity of HF emission is much greater than that of HCl. The branching ratio between CH≡CCl and CH≡CF formation channels observed in the IR emission study is in line with that obtained by gas chromatographic analysis of CH≡CCl and CH≡CF in the present IRMPD study of $CH_2ClCHFCl$, where CH≡CCl and CH≡CF are derived mainly from the primary product $CH_2=CFCl$. In the shock tube pyro-

lysis, CH_2=CHF was found in very small amounts, which might suggest some mechanistic change to give rise to CH≡CCl and/or CH≡CF in the shock tube pyrolysis.

The authors wish to express their thanks to Professor Kenji Kuratani, the Insitute of Space and Astronautical Science, for his encouragement and interest in this work. One of the authors (T. Y) is grateful to Professor Tschuikow-Roux, University of Calgary, for valuable discussions.

References

1) See for example, a) P. A. Schultz, Aa. S. Sudbø, D. J. Krajnovich, H. S. Kwok, Y. R. Shen, and Y. T. Lee, *Ann. Rev. Phys. Chem.*, **30**, 379 (1979); b) J. Jortner and R. D. Levine, *Adv. Chem. Phys.*, **50**, 70 (1982); c) M.Quack, *ibid.*, **50**, 395 (1982); d) D. S. King, *ibid.*, **50**, 105 (1982).

2) T. H. Richardson and D. W. Setser, *J. Phys. Chem.*, **81**, 2301 (1977).

3) D. M. Brenner, *Chem. Phys. Lett.*, **57**, 357 (1978).

4) A. V. Baklanov, Yu. N. Molin, and A. K. Petrov, *Chem. Phys. Lett.*, **68**, 329 (1979).

5) C. Reiser, F. M. Lussier, C. C. Jensen, and J. I. Steinfeld, *J. Am. Chem. Soc.*, **101**, 350 (1979).

6) P. A. Hackett, C. Wills, M. Drouin, and E. Weinberg, *J. Phys. Chem.*, **84**, 1873 (1980).

7) R. J. S.Morrison, R. F. Loring, R. L. Farley, and E. R. Grant, *J. Chem. Phys.*, **75**, 148 (1981).

8) P. J. Papagiannakopoulos, K. Kosnik, and S. W. Benson, *Int. J. Chem. Kinet.*, **14**, 327 (1982).

9) Y. Makide, S. Kato, T. Tominaga, and K. Takeuchi, *Appl. Phys. B*, **28**, 341 (1982).

10) W. E. Farneth and M. W. Thomsen, *J. Phys. Chem.*, **87**, 3207 (1983).

11) J. L. Buechele, E. Weitz, and F. D. Lewis, *J. Phys. Chem.*, **88**, 868 (1984).

12) W. A. Jalenak and N. S. Nogar, *J. Chem. Phys.*, **79**, 816 (1983).

13) Y. Ishikawa and S. Arai, *Chem. Phys. Lett.*, **103**, 68 (1983).

14) Y.Ishikawa and S.Arai, *Bull. Chem. Soc. Jpn.*, **57**, 681 (1983).

15) D. Krajnovich, F. Huisken, Z. Zhang, Y. R. Shen, and Y. T. Lee, *J. Chem. Phys.*, **77**, 5977 (1982).

16) J. R. Barker, *J. Chem. Phys.*, **72**, 3686 (1980).

17) R. E. Weston,Jr., *J. Phys. Chem.*, **86**, 4864 (1982).

18) Y. Ishikawa, K. Sugita, and S. Arai, *Chem. Phys. Lett.*, **109**, 264 (1984).

19) H. Ogura, *Bull. Chem. Soc. Jpn.*, **50**, 1044 (1977).

20) G. R. Hunt and M. K. Wilson, *J. Chem. Phys.*, **34**, 1301 (1961).

21) D. C. Mann, N. Acquista, and E. K. Plyler, *J. Chem. Phys.*, **23**, 2122 (1955).

22) P. Torkington and H. W. Thompson, *Trans. Faraday Soc.*, **41**, 236 (1945).

23) N. C. Craig, Y.-S. Lo, L. G. Piper, and J. C. Wheeler, J. Phys. Chem., **74**, 1712 (1970).

24) K. Takeuchi, I. Inoue, Y. Makide, S. Kato, and T. Tominaga, *J. Chem. Phys.*, **76**, 398 (1982).

25) K. Sugita, Y. Ishikawa, and S. Arai, *J. Phys. Chem.*, **87**, 3469 (1983).

26) H. Hippler, J. Troe, and H. J. Wendelken, *J. Chem. Phys.*, **78**, 6718 (1983).

27) Y. Makide, S. Hagiwara, T. Tominaga, K. Takeuchi, and R. Nakane, *Chem. Phys. Lett.*, **82**, 18 (1981).

28) S. Speiser and J. Jortner, *Chem. Phys. Lett.*, **44**, 399 (1976).

29) J. L. Lyman, S. D. Rockwood, and S. M. Freund, *J. Chem. Phys.*, **67**, 4545 (1977).

30) K. Nagai and M. Katayama, *Chem. Phys. Lett.*, **51**, 329 (1977).

31) C. R. Quick and C. Wittig, *J. Chem. Phys.*, **72**, 1694 (1980).

32) Aa. S. Sudbø, P. A. Shultz, Y. R. Shen, and Y. T. Lee, *J. Chem. Phys.*, **69**, 2312 (1978).

33) M. V. C. Sekhar and E. Tschuikow-Roux, *J. Phys. Chem.*, **78**, 472 (1974).

34) K. C. Kim and D. W. Setser, *J. Phys. Chem.*, **78**, 2166 (1974).

35) B. E. Holmes, D. W. Setser, and G. O. Pritchard, *Int. J. Chem. Kinet.*, **8**, 215 (1976).

36) The heats of formation for $CH_2ClCHFCl$, CHF=CHCl, and CH_2=CFCl are estimated to be −76.6, −35.5, and −33.4 kcal/mol, respectively, based on the group additivity method of Benson and assuming the relationship such as ΔH_f° ($CH_2ClCHFCl$)=ΔH_f° (CH_2ClCH_2Cl+CH_2ClCF_2Cl)/2. S. W. Benson, "Thermochemical Kinetics," 2nd ed., John Wiley and Sons, New York (1976). The heat of formation for CHCl=CHCl (−1.3 kcal/mol) is the average of *trans*-and *cis*-CHCl=CHCl. P. Goldfinger and G. Marteus, *Trans. Faraday Soc.*, **57**, 2220 (1961). Other values used are taken from the "JANAF Thermochemical Tables," 2nd ed., National Bureau of Standards NSRDS-NBS 37, U. S. Government Printing Office, Washington D. C.(1971).

37) K. C. Kim, D. W. Setser, and B. E. Holmes, *J. Phys. Chem.*, **77**, 725 (1973).

38) J. F. Harrison, *J. Am. Chem. Soc.*, **93**, 4112 (1971).

39) K. Y. Choo, T. J. Kang, and Q. W. Choi, *Chem. Phys. Lett.*, **102**, 321 (1983).

40) C. E. Drykstra and J. I. Steinfeld, *J. Am. Chem. Soc.*, **100**, 1378 (1978).

41) M. D. Conrad and J. I. Steinfeld, *J. Am. Chem. Soc.*, **100**, 7820 (1978).

42) N. C. Craig, L. P. Pipper, and V. L. Wheeler, *J. Phys. Chem.*, **75**, 1453 (1971).

43) P. M. Jeffers, *J. Phys. Chem.*, **78**, 1469 (1974).

44) T. Yano, S. Ozaki, H. Ogura, and E. Tschuikow-Roux, *J. Phys. Chem.* (submitted 1984).

45) C. S. Sloane and W. L. Hase, *J. Chem. Phys.*, **66**, 1523 (1977).

46) D. D. Davis, W. Braun, and A. M. Bass, *Int. J. Chem. Kinet.*, **2**, 101 (1970).

47) I. A. Boriev, E. B. Gordon, A. A. Nadeikin, A. I. Nikitin, V. L. Talrode, and A. M. Velichko, *Chem. Phys. Lett.*, **96**, 407 (1983). *ibid.*, **105**, 555 (1984).

 © 1985 The Chemical Society of Japan Bull. Chem. Soc. Jpn., 58, 1251—1254 (1985)

The Magnetic Field Effects on the Electrolysis of Hexacyanoferrate(II) Oxidation and Hexacyanoferrate(III) Reduction

Takeshi WATANABE, Yoshifumi TANIMOTO,† Tadayoshi SAKATA, Ryoichi NAKAGAKI, Mitsuo HIRAMATSU,†† and Saburo NAGAKURA*

Institute for Molecular Science, Myodaiji, Okazaki 444

(Received November 2, 1984)

The effects of a magnetic field on electrolytic currents in hexacyanoferrate(II) and hexacyanoferrate(III) solutions were studied under various conditions by means of potentiometry. These effects were observed for a wide range of current densities (10^{-6}—10^{-3} A/cm^2). The results were interpreted in terms of the magnetohydrodynamic effect, including a change in the solution density during electrolysis. The present observation suggests that a magnetohydrodynamic flow strongly affects the electrochemical processes on an electrode surface.

Studies regarding magnetic field effects on chemical reactions have attracted the attention of many chemists because of their novelity as a phenomenon and their wide utility and potentiality such as for the regulation of reaction products, the elucidation of a reaction mechanism, and isotope separation.[1] Some of the present authors have studied the magnetic field effect on various photochemical reactions taking place in solutions.[2] As an extension of our research program, we have undertaken to study magnetic field effects on electrochemical reactions in solutions.

A number of studies has, hitherto, been carried out on magnetic field effects on electrolytic properties,[3] electrolytic mass transport,[4] electrode kinetics,[5] and others.[6] However, only a few papers have been published concerning magnetic field effects upon electrochemical reactions, including the electron transfer processes in which we are much interested.

In this paper, we report several electrochemical reactions which were undertaken by means of potentiometry in the presence and absence of an external magnetic field. The magnetic field is known to remarkably affect the electrolytic reduction of Fe^{3+} and the oxidation of Fe^{2+} in the high current-density region where the reaction is diffusion-controlled.[5] We have succeeded in observing the magnetic field effect even in a low current-density region (10^{-5}—10^{-6} A/cm^2), where the process is usually believed to be reaction-controlled. All the results have been interpreted in terms of the magnetohydrodynamic effect.

Experimental

Figure 1 is a schematic diagram of the present experimental set-up. An electrolytic cell and electrodes were placed between the poles of an electromagnet (Tohoku Kinzoku Kogyo Co., model SEE-15). A magnetic field did not affect the potential of a saturated calomel electrode (SCE) used as a reference electrode.

Two orientations of the magnetic field with respect to the working electrode were employed for electrolysis as schematically shown in Figs. 2, 3, and 4. One side of the working electrode (5×10 mm Pt plate) was covered with

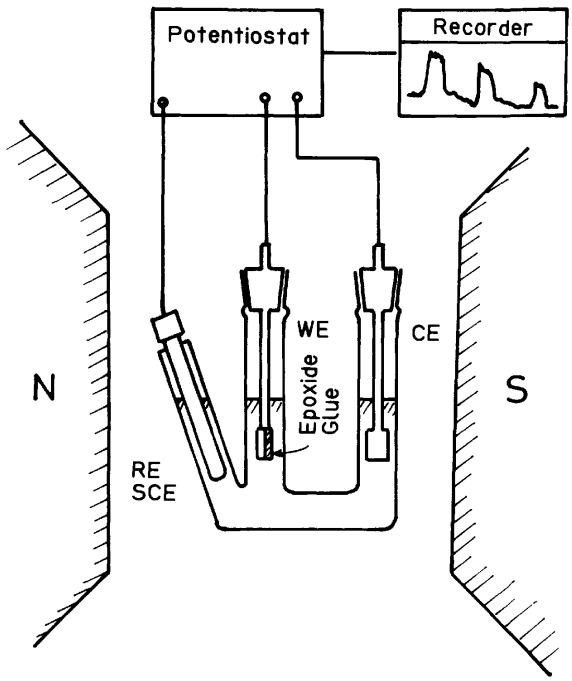

Fig. 1. Schematic diagram of experimental set-up. RE (reference electrode, SCE), WE (working electrode), and CE (counter electrode).

epoxide glue. The electrode plate was always kept parallel to the magnetic flux, and only the polarity of the magnetic field was changed (by alternating the direction of the electromagnet's current).

The electrolysis was carried out without stirring using a potentio/galvano stat (Hokuto Denko, model HA-102). Values of electrolytic current in the presence and absence of a magnetic field (represented hereafter I_H and I_O, respectively) were measured at a controlled potential of the working electrode. Argon gas was passed through the electrolytic solution to purge any dissolved oxygen before electrolysis took place.

Special grade $K_4[Fe(CN)_6]$ and $K_3[Fe(CN)_6]$, and a nonfluorescent grade glycerol were used without further purification. Potassium sulfate, which was used as a supporting electrolyte, was recrystallized from water. All the chemicals were obtained from Katayama Chemical Industries Co., Ltd.

Results

The effects of a magnetic field upon the potential/current curves of hexacyanoferrate(II) oxidation and hexacyanoferrate(III) reduction in a 1.0×10^{-1} mol/dm^3

†Adjunct Associate Professor of IMS, 1983—1984. Faculty of Pharmaceutical Sciences, Kanazawa University.

††Visiting Research Fellow from Hamamatsu Photonics K.K.

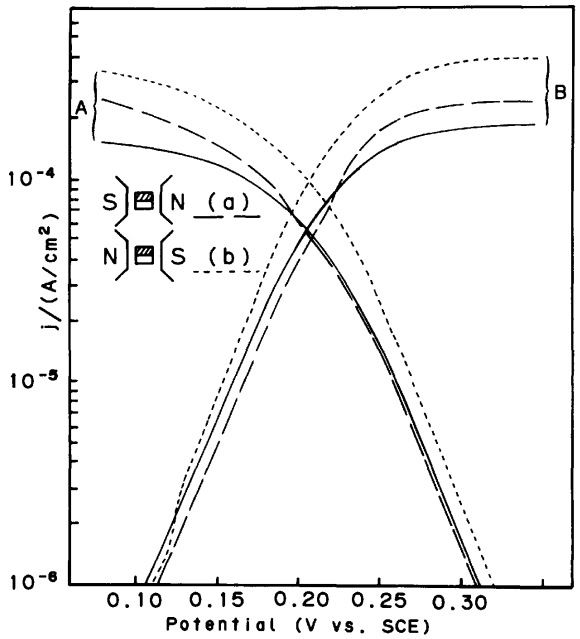

Fig. 2. Potential/current curves for (A) reduction of $K_3[Fe(CN)_6]$ (1.0×10^{-2} mol/dm^3) and (B) oxidation of $K_4[Fe(CN)_6]$ (1.0×10^{-2} mol/dm^3). Concentration of K_2SO_4 supporting electrolyte is 1.0×10^{-1} mol/dm^3). (——), at the residual magnetic field (6.2 mT); (— —), magnetic field orientation-(a) at 1.7 T; (·····), magnetic field orientation-(b) at 1.7 T. Top view of two magnetic field orientations with respective to the working electrode are also illustrated in the figure. ▨ and ▭ indicate epoxide glue and platinum plate of the electrode, respectively.

potassium sulfate aqueous solution were measured. The results are shown in Fig. 2. When a magnetic field was applied, the electrolytic current gradually changed for several tens of minutes and then reached a constant value. The magnetic field effects were observed in a limiting current (diffusion-controlled) region as have been reported in the literature.[4,5] The same is true for the low current density (reaction-controlled) region.

The effect of hexacyanoferrate(II) concentrations on a magnetic field-induced change in a limiting current is shown in Fig. 3. As the concentration increases, the ratio $R(=I_H/I_0)$ increases in magnetic field orientation-(b), while in orientation-(a) it decreases gradually to 0.8, and then increases rapidly up to 2.5. At the higher concentration, the ratio seems to become almost constant. In order to investigate the influence of the viscosity of a solution upon the current in the presence and absence of a magnetic field, a measurement was made with a 1.0×10^{-2} mol/dm^3 hexacyanoferrate(II) aqueous solution containing 3.0 mol/dm^3 glycerol. The results are also shown in Fig. 3.

The influences of the external magnetic field on the anodic current in various concentrations of hexacyanoferrate(II) are presented in Fig. 4. The curves for 3.0×10^{-2} mol/dm^3 or 1.0×10^{-2} mol/dm^3 in Fig. 4 are very similar in their shapes to the corresponding ones with regard to the magnetic field orientations in Fig. 3B. This means that the dependence of R upon the concentration is similar to that upon the magnetic field.

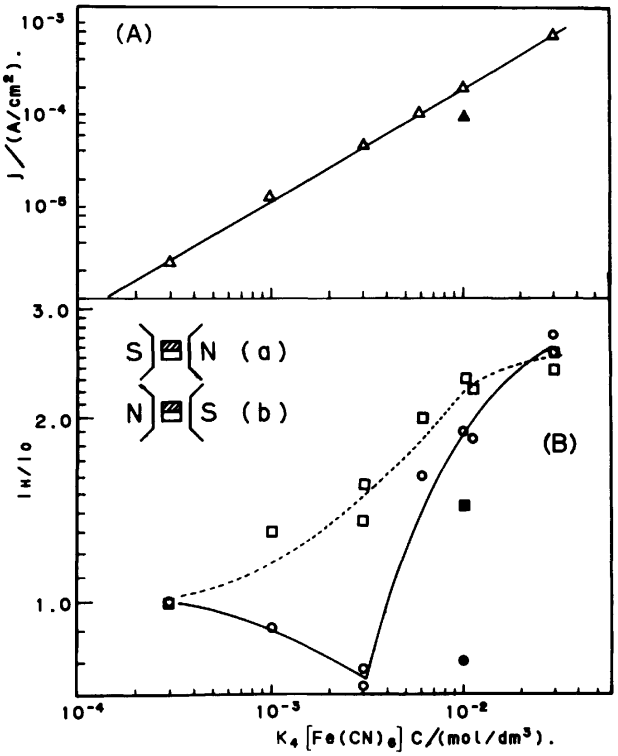

Fig. 3. Concentration dependence of $K_4[Fe(CN)_6]$ in the prssence of 1.0×10^{-1} mol/dm^3 K_2SO_4 at 0.45 V *vs.* SCE.
(A) Limiting current density in the absence of a magnetic field; (—△—). ▲ shows the value of j for the solution containing 3.0 mol/dm^3 glycerol, 1.0×10^{-2} mol/dm^3 $K_4[Fe(CN)_6]$ and 1.0×10^{-1} mol/dm^3 K_2SO_4.
(B) Ratio of limiting currents. I_H and I_0 show intensities of limiting currents in the presence and absence of magnetic field, respectively. (—○—), magnetic field orientation-(a) at 1.7 T, (···□···), magnetic field orientation-(b) at 1.7 T. ● and ■ represent the ratios I_H/I_0 with orientation-(a) and -(b) for the solution containing glycerol, respectively.

Discussion

An increase in the electrolytic current in the presence of a magnetic field has already been interpreted in terms of a magnetohydrodynamic model where the magnetohydrodynamic force induces a flow of the solution and enhances the rate of diffusional mass transfer.[4,5]

According to Aogaki *et al.*[7] under the conditions where the magnetohydrodynamic flow is mostly predominant, the ratio R is proportional to the 1/3 power of the magnetic field strength B and to the 1/3 power of the electrolyte concentrations. The concentration dependence of R in Fig. 3B and the magnetic field dependence of R in Fig. 4 seem to agree with this theoretical prediction in the high concentration region ($\geq5\times10^{-2}$ mol/dm^3) and in the strong magnetic field strength ($\geq$ 0.5 T), respectively.

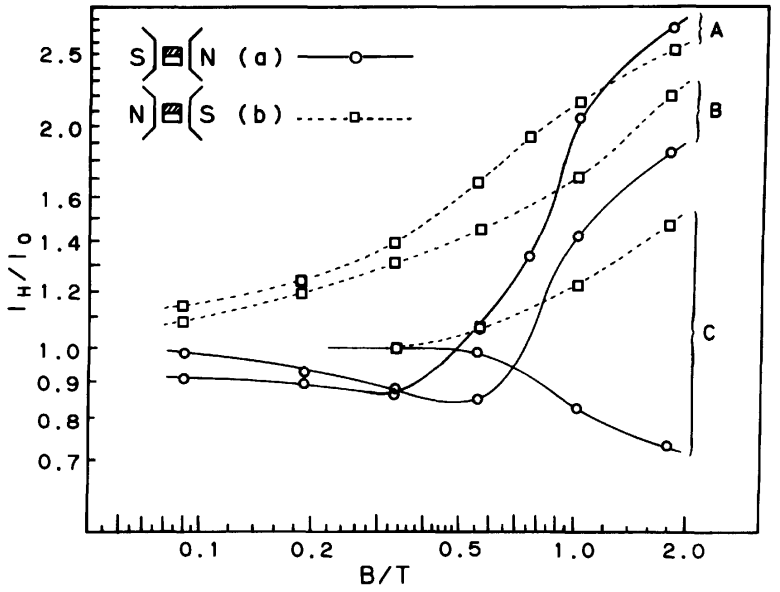

Fig. 4. Magnetic field dependence for $K_4[Fe(CN)_6]$ aqueous solution at 0.45 V *vs.* SCE. The concentration of K_2SO_4 is 1.0×10^{-1} mol/dm^3. (A), 3.0×10^{-2} mol/dm^3 $K_4[Fe(CN)_6]$ (B), 1.0×10^{-2} mol/dm^3 $K_4[Fe(CN)_6]$ and (C), 3.0×10^{-3} mol/dm^3 $K_4[Fe(CN)_6]$. (—○—) magnetic field, orientation-(a) (···□···), magnetic field orientation-(b).

Thus, under these conditions, the magnetic field effect on the electrolytic current can be explained in terms of the magnetohydrodynamic mechanism.

On the other hand, in the low concentration region or in a weak magnetic field, we observed not only an increase in the current under the magnetic field but also its decrease (shown in Figs. 2, 3, and 4).

In the case of hexacyanoferrate(II) oxidation in Fig. 2, upon electrolysis a density of the electrolyte solution localized near the working electrode may become smaller than that of the bulk solution, because the specific gravities of potassium hexacyanoferrate(III) and potassium hexacyanoferrate(II) aqueous solution are 1.002_4 at 3.0×10^{-2} mol/dm^3 and 1.003_9 at 2.7×10^{-2} mol/dm^3, respectively.[8] Therefore, the solution on the surface of the electrode may flow upward. On the other hand, the direction of the magnetohydrodynamic force is downward in magnetic field orientation-(a). This means that the magnetohydrodynamic force prevents a natural convection flow under these conditions, and the anodic current may decrease under the field in the low current density region (10^{-5}—10^{-6} A/cm^2), where the magnetohydrodynamic force is smaller than the natural convection force. In the high current density region ($>10^{-4}$ A/cm^2), the magnetic field increases the current density because the flow due to the magnetohydrodynamic force is much stronger than for convective flow. The magnetic field in orientation-(b) always increases the electrolytic current, because the direction of a magnetohydrodynamic force is parallel to that of the natural convective flow. Thus, we can explain the magnetic field effects upon the potential/current curves of hexacyanoferrate(II) oxidation as shown in Fig. 2. This interpretation is supported by the slow response of the electrolytic current to an applied magnetic field.

The potential/current curves of hexacyanoferrate(III) reduction in Fig. 2 are explained in a manner similar to that of the hexacyanoferrate(II) oxidation mentioned above. In this case, both the directions of the magnetohydrodynamic force and the natural convection flow become opposite. This can be compared with the case for hexacyanoferrate(II) oxidation. Therefore, a decrease in the electrolytic current density in the presence of a magnetic field was observed also for magnetic field orientation-(a).

According to the relation $\boldsymbol{F}=j\times\boldsymbol{B}$ (where $\boldsymbol{F}$ is a magnetohydrodynamic force and j is a electrolytic current density), the concentration dependence and the magnetic field dependence of R should resemble each other. As shown in Figs. 3B and 4, our observations are in good agreement with this prediction. This confirms our interpretation that all results presented here can be explained in terms of magnetohydrodynamics.

A magnetohydrodynamic flow velocity is affected by the viscosity of a solution. Figure 3 shows the measured results for a solution containing 1.0×10^{-2} mol/dm^3 hexacyanoferrate(II) and 3.0 mol/dm^3 glycerol, the viscosity of which is higher than that of the glycerol-free solution by a factor of 2.3. From this figure we can see that the limiting current density and R decrease for a viscous solution containing glycerol compared with a corresponding glycerol-free solution.

References

1) Yu. N. Molin, ed., "Spin Polarization and Magnetic Effects in Radical Reactions," Elsevier, Amsterdam (1984).
2) Y. Tanimoto, H. Hayashi, S. Nagakura, H. Sakuragi,

and K. Tokumaru, *Chem. Phys. Lett.*, **41**, 267 (1976); Y. Sakaguchi, H. Hayashi, and S. Nagakura, *Bull. Chem. Soc. Jpn.*, **53**, 39 (1980); Y. Sakaguchi, H. Hayashi, and S. Nagakura, *J. Phys. Chem.*, **86**, 3177 (1982); Y. Tanimoto, H. Udagawa, Y. Katsuda, and M. Itoh, *J. Phys. Chem.*, **87**, 3976 (1983).

3) J. Lielmezs and H. Aleman, *Thermochim. Acta*, **15**, 63 (1976); E. Tronel-Peyroz, A. Olivier, T. Z. Fahidy and D. Laforgue-Kantzer, *Electrochim. Acta*, **25**, 441 (1980); J. B. Hubbard and P. G. Wolynes, *J. Chem. Phys.*, **75**, 3051 (1981).

4) S. Mohanta and T. Z. Fahidy, *Can. J. Chem. Eng.*, **50**, 248 (1972); D. Guerin-Ouler and C. Nicollin, *Electrochim. Acta*, **27**, 909 (1982); R. Aogaki and K. Fueki, *J. Electrochem. Soc.*, **131**, 1295 (1984).

5) S. Fujiwara, H. Haraguchi and Y. Umezawa, *Anal. Chem.*, **40**, 249 (1968); E. J. Kelly, *J. Electrochem. Soc.*, **124**, 987 (1977); F. Takahashi, Y. Sakai, and T. Tamura, *Electrochim. Acta*, **28**, 1147 (1983).

6) J. O'M. Bockris and F. Gutmann, *Appl. Phys. Commun.*, **1**, 121 (1981); T. Z. Fahidy, *J. Appl. Electrochem.*, **13**, 553 (1983); C. Iwakura, M. Kitayama, T. Edamoto, and H. Tamura, *Chem. Lett.*, **1984**, 809.

7) R. Aogaki, K. Fueki, and T. Mukaibo, *Denki Kagaku*, **43**, 509 (1975).

8) E. W. Washburn, ed., "International Critical Tables," McGraw-Hill Vol. 3, New York, (1928), p. 54.

 © 1985 The Chemical Society of Japan Bull. Chem. Soc. Jpn., 58, 1255—1258 (1985)

Photocatalytic Oxidation of Sulfur on the Doped TiO_2 Catalysts

Yasumichi MATSUMOTO,* Yasuhide YAMAGUCHI, and Ei-ichi SATO
Department of Industrial Chemistry, Faculty of Engineering, Utsunomiya University, Ishi-icho 2753, Utsunomiya 321
(Received November 5, 1984)

TiO_2(anatase) doped with various elements was used as the photocatalyst in the production of sulfuric acid from sulfur in water into which O_2 was bubbled. The catalysts doped with typical elements having one and two valencies showed high catalytic activity, but some doped with typical elements having four and five valencies showed low activity. The intermediate, *i.e.*, O_2H radical, in the O_2 reduction produced by photoproduced electrons will probably play an important part in the production of sulfuric acid. Therefore, it was suggested that the Ti^{3+} ion in the TiO_2 lattice which contribute to direct O_2 reduction will inhibit sulfuric acid production. In the case of transition metal dopants, the transition metal cation in the TiO_2 lattice will directly affect the O_2 reduction. The catalyst doped (deposited) with Pt shows the highest catalytic activity of all the catalysts used in the present study.

Photocatalytic reactions are very important when using solar energy as a substitute for activation energy (downhill reaction), and in the chemical storage of solar energy (uphill reaction). We have discovered that sulfur is directly oxidized to SO_4^{2-}, *i.e.*, sulfuric acid, on a TiO_2 photocatalyst in water into which O_2 is bubbled.[1] This is a downhill reaction. Solar energy is used as a substitute for activation energy in this process. The direct production of sulfuric acid from sulfur by a photocatalyst is very important to the chemical industry.

However, the prodution rate of the sulfuric acid is very slow, if TiO_2 is used as the photocatalyst.[1] It is well known that the photocatalytic activity of TiO_2 is enhanced significantly by doping or deposition of some elements onto the TiO_2 surface.[2-11] Therefore, doped TiO_2 was used as the catalyst in the photocatalytic oxidation of sulfur in the present study. Some of the dopants gave higher activity, but others gave lower activity in this catalysis. In the present paper, we have discussed the catalysis bv doped TiO_2 as well as the mechanism for the photocatalytic oxidation of sulfur.

Experimental

Solid sulfur (99.99%, Rare Metallic Co. Ltd.,) and TiO_2 powder (99.6%, anatase, Merck) were used as the reactant and the catalyst, respectively. Unless otherwise stated, the doping was done by thermal decomposition of metal salts (nitrate, acetate, oxalate and chloride) on TiO_2 powder at 500 °C for 3 h, since the maximum catalytic activity was obtained at a heat treatment temperature of about 500 °C. Only TiO_2 (anatase) was detected for 1 atm% doped TiO_2 except for Pt doped TiO_2 by X-ray analysis. In the case of the latter sample, Pt metal as well as TiO_2 were detected. Pt probably is not doped into the TiO_2 lattice but is instead deposited on the surface.

Sulfur (0.4 g) was mixed with the doped TiO_2 (0.02 g) and water (50 ml). This suspension was poured into a quartz vessel and magnetically stirred with bubbling O_2 gas. It was then illuminated with an ultrahigh-pressure mercury lamp (500 W). A cutoff filter which transmits 50% of 290 nm of light, but completely cuts off light shorter than 240 nm was used in order to suppress the photoreaction of the sulfur itself, unless otherwise stated. The products were analyzed in the same manner as described in the previous paper.[1] When SO_4^{2-} ion could not be gravimetrically determined as $BaSO_4$ because it was present in a very small amount, the SO_4^{2-} was calculated from the pH value of the solution.

Results

Figure 1 shows the production rates of SO_4^{2-} and H_2S on the doped TiO_2 as a function of the concentration of the dopants. Similar tendencies to those in this figure were observed for other dopants. The production rates of SO_4^{2-} and H_2S show the maximum and the minimum at about 1 atm% concentration of the dopants, respectively. This result suggests that the elements, except for Pt, are doped into anatase lattice up to about 1 atm% but not above this range, as described in the latter section. No other products, for example $S_2O_3^{2-}$ or SO_3^{2-}, were detected for all catalysts. Photoreaction products were scarcely detected when doped rutile powder was used as the catalyst. Therefore, the anatase structure is very important for catalysis in the photooxidation of sulfur in the case of the doped TiO_2 as well as nondoped TiO_2.[1]

Figure 2 shows the relationship between the production rate of SO_4^{2-} and the ionic valency of the dopant in the TiO_2 lattice. The ionic valencies of the dopants used in this figure are those of their oxides which are the most stable under ordinary conditions. Pt was classified for convenience as a zero value, because Pt metal was detected by X-ray analysis as stated above. In general, the catalytic activity decreases with the increase in the ionic valency of the dopant. This tendency is especially clear for the typical element. Typical element dopants, having ionic valencies of one, two and three, will lead to a decrease in the amount of Ti^{3+}, while those having an ionic valency of five will lead to an increase of Ti^{3+} in the TiO_2 lattice, if the amounts of the oxygen anion vacancies are constant in the lattice. The catalytic activity of the nondoped anatase (SO_4^{2-} production rate=0.2×10^{-4} mol h^{-1}) is almost the same as those doped with typical elements having ionic valencies of three and four. This will be in agreement with the fact that the Ti cation exists as Ti^{3+} or Ti^{4+} in the TiO_2 lattice. It may be concluded from the above results that the existence of Ti^{3+} in the TiO_2 lattice will inhibit the produc-

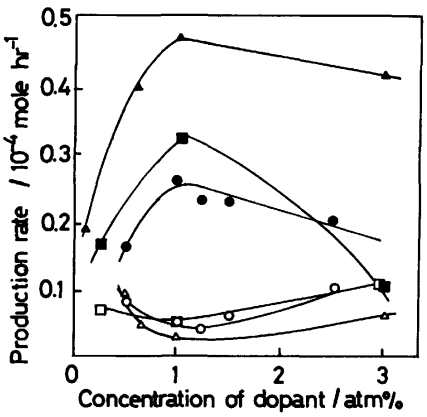

Fig. 1. Production rates of SO_4^{2-} and H_2S as a function of the concentration of dopants. Closed symbols represent the production rates of SO_4^{2-}, while open symbols represent the production rates of H_2S. Circles, squares and triangles represent TiO_2 catalysts doped with Ru, Na, and Pt, respectively.

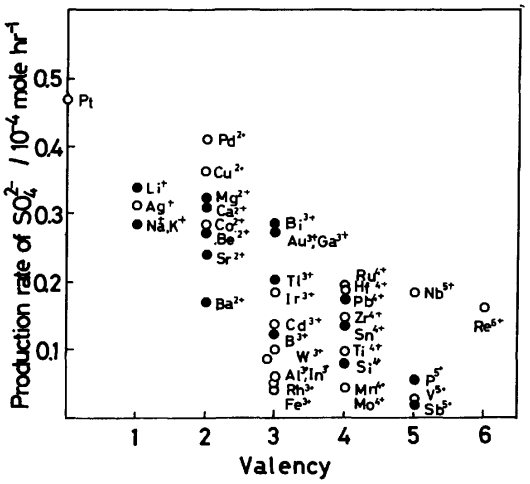

Fig. 2. Relationship between the production rate of SO_4^{2-} and the ionic valency of the dopant. Closed symbols represent typical elements and open symbols represent transition metals.

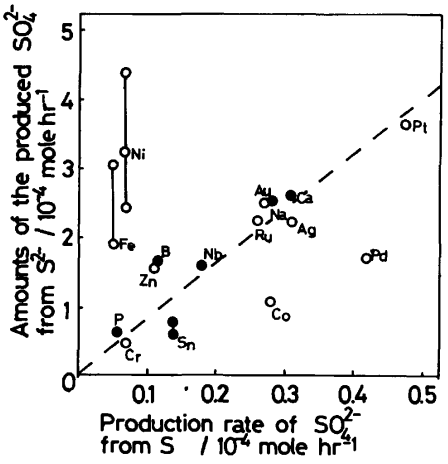

Fig. 3. Relationship between the production rate of SO_4^{2-} from sulfur and the amounts of SO_4^{2-} produced from S^{2-}.

TABLE 1. PHOTOPRODUCTS FROM S, S^{2-}, $S_2O_3^{2-}$, AND SO_3^{2-} ON TiO_2/Pt

Reactants	Products/10^{-4} mole				
	H_2S	S^{2-}	$S_2O_3^{2-}$	SO_3^{2-}	SO_4^{2-}
S(0.4 g)	0.05	0	0	0	0.47
S^{2-}(1×10^{-3} mol)	0.03	—	1.10	2.12	3.64
$S_2O_3^{2-}$(1×10^{-3} mol)	0.08	0	—	0	4.16
SO_3^{2-}(1×10^{-3} mol)	0.01	0	0	—	9.93
SO_3^{2-}(10×10^{-3} mol)	0.04	0	0	—	76.70

tion of SO_4^{2-}.

Figure 3 shows the relationship between the production rate of SO_4^{2-} from sulfur and the amount of photoproduced SO_4^{2-} from S^{2-} (Na_2S) in one hour. The initial concentration of S^{2-} in the solution was 10^{-3} mol/50 ml in this test. With the exceptions of Ni and Fe dopants, it was found that catalytic activity of the doped anatase for both reactions had almost the same tendency. Other ions, for example $S_2O_3^{2-}$ and SO_3^{2-}, were also produced when the S^{2-} ion was used as the starting reactant. On the other hand, amounts of less than 50% $S_2O_3^{2-}$ ($Na_2S_2O_3$) were also photooxidized to SO_4^{2-} on doped TiO_2 under illumination, but the tendency of the activity did not agree with that from sulfur to SO_4^{2-}, and no SO_3^{2-} was detected. When SO_3^{2-} (Na_2SO_3) was used as the reactant, large amount of SO_4^{2-} were obtained even in the dark. Under illumination, 90—100% of the SO_3^{2-} was changed to SO_4^{2-}, but no $S_2O_3^{2-}$ was detected. Table 1 shows typical results for the above tests on Pt-doped TiO_2. Thus, S^{2-} and $S_2O_3^{2-}$ will not be the intermediates in the mechanism of photocatalytic oxidation of sulfur on TiO_2, because no $S_2O_3^{2-}$ was detected in this process.

Figure 4 shows the wavelength dependencies of the photocatalytic production rate of SO_4^{2-} from sulfur on the doped TiO_2. These results show that the photocatalytic oxidation in this process is based on the hole and the electron produced by the bandgap photon of anatase (<390 nm). Figure 5 shows the photocatalytic production rate of SO_4^{2-} from sulfur on the Pt-doped TiO_2 as a function of the light intensity. Linear relationships of $\log V/\log I$ were observed, and the slope was about 1.0, where I denotes the light intensity. The same dependencies of the photoproduction of SO_4^{2-} from S^{2-} and from $S_2O_3^{2-}$ on the wavelength and the light intensity were also observed for the doped TiO_2.

Discussion

Figure 6 illustrates the process of photooxidation of sulfur to SO_4^{2-} on a TiO_2 catalyst. Sulfur is directly converted to $S_2O_3^{2-}$, SO_4^{2-}, and H_2S (S^{2-}) by the catalyst under illumination, and a small amount of S^{2-} in the solution are oxidized to $S_2O_3^{2-}$, SO_3^{2-}, and SO_4^{2-} as described in the previous section. In practice, a large portion of the produced S^{2-} is evolved from the solution as H_2S gas, because the solution changes to the acid due to the production of SO_4^{2-}. Therefore, neither $S_2O_3^{2-}$ nor SO_3^{2-} is detected in the solution. If SO_3^{2-}

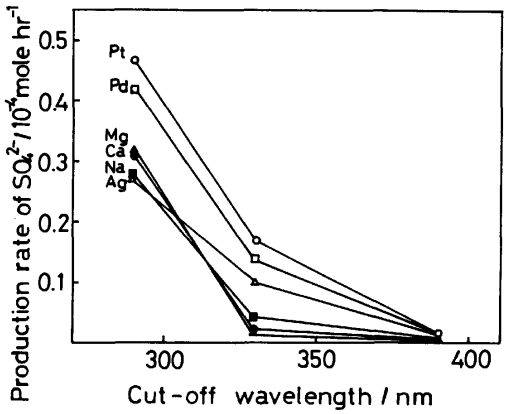

Fig. 4. Wavelength dependence of the photoproduction ate of SO_4^{2-} from sulfur.

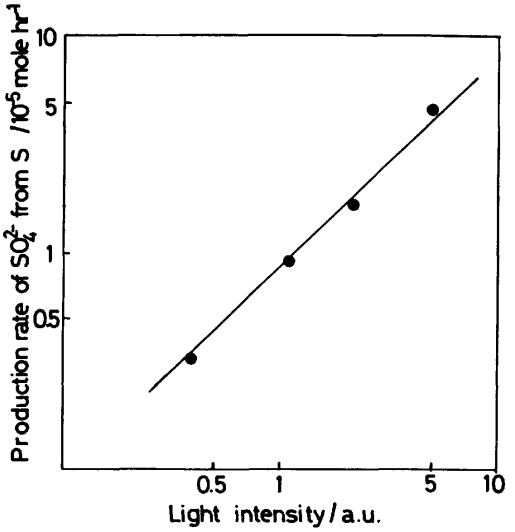

Fig. 5. Photocatalytic production rate of SO_4^{2-} from sulfur on the Pt-doped TiO_2 as a function of light intensity.

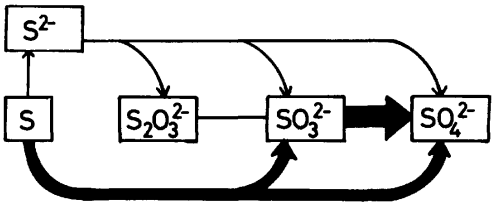

Fig. 6. Photocatalytic oxidation process of sulfur on TiO_2 catalyst.

is photoproduced in the solution, this is immediately oxidized to SO_4^{2-}.

Figure 7 shows the ratio of the rate/H_2S production rate as a function of the SO_4^{2-} production rate in the photocatalytic oxidation of sulfur on the doped TiO_2. It was found that the ratio increases with the increase in the production rate of SO_4^{2-}. If we assume the linear relationship in the figure, it can be seen that the production rate of H_2S (about 0.05×10^{-4} mol h^{-1}) is constant for all samples. It should also be noted that the minimum value of the ratio is about one.

The following reaction will proceed on the catalyst surface under illumination:

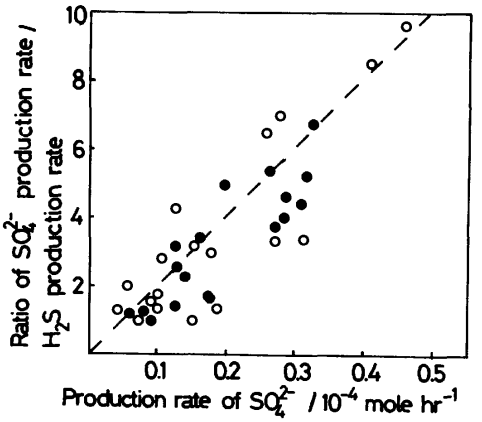

Fig. 7. Relationship between the ratio of SO_4^{2-} production rate/H_2S production rate and the production rate of SO_4^{2-}.

$$H_2O + h^+ \longrightarrow \dot{O}H + H^+ \quad (1)$$

$$O_2 + 2H_2O + 4e^- \longrightarrow 4OH^- \quad (2)$$

$$OH^- + h^+ \longrightarrow \dot{O}H \quad (3)$$

$\dot{O}H$ will be produced from both H_2O and OH^-, which are produced from the direct reduction process of O_2 (Eq. 3). After all, sulfur reacts with $\dot{O}H$ as follows, leading to unity as the value of the ratio of the SO_4^{2-} production rate/H_2S production rate:

$$2S + 4\dot{O}H \longrightarrow H_2S + H_2SO_4 \quad (4)$$

This reaction process is suitable for the catalysts which give unity for the value of the above ratio. If a relatively stable intermediate, for example $\dot{O}_2H$ is produced in the O_2 reduction process, this species will contribute to the direction production of SO_3^{2-} or SO_4^{2-} as follows:

$$O_2 + e^- \longrightarrow O_2^- \quad (5)$$

$$O_2^- + H_2O \longrightarrow \dot{O}_2H + OH^- \quad (6)$$

$$\dot{O}H + \dot{O}_2H + S \longrightarrow H_2SO_3 \quad (7)$$

$$3\dot{O}H + \dot{O}_2H + S \longrightarrow H_2SO_4 + H_2O \quad (8)$$

Many other reaction processes in which the intermediate $\dot{O}_2H$ is contained, will exist in the photocatalytic oxidation process of sulfur as a matter of course. However, this intermediate must surely contribute to the reaction process on the catalysts which gives values of more than unity in the ratio of the SO_4^{2-} production rate/H_2S production rate. Because the values of the ratio are always unity, if only the process (4) occurs in the photocatalytic oxidation of sulfur. In conclusion, only small amounts of SO_4^{2-} will be produced on the catalysts on which O_2 is immediately reduced to OH^-, but large amounts of SO_4^{2-} will be produced on the catalysts on which O_2 is not immediately reduced to OH^-.

The former catalysts are TiO_2 doped with the typical elements having ionic valences of five; therefore, relatively large amount of Ti^{3+} exist in the lattice. On

the other hand, the latter catalysts have only small amounts of Ti^{3+} in the lattice, because the catalysts are doped with the typical elements having valencies of one, two and three. That is, the Ti^{3+} ion probably will take part in the immediate reduction of O_2. In the case of doping with a transition metal, the transition metal cations in the TiO_2, as well as the titanium cations, will directly affect the O_2 reduction.

This doped area which affects the O_2 reduction will be dotted on the TiO_2 surface. When the amounts of the dopants increase beyond about 1 atm%, the dopants will deposit on the doped area as oxides. Therefore, the doped area decreases and the doped TiO_2 becomes like that of the nondoped TiO_2. The results shown in Fig. 1 are explained by this phenomenon. In the case of the Pt dopant, Pt metal on the TiO_2 will act as the site which produces the intermediate $\dot{O}H$ in the O_2 reduction. However, the increase of the deposited Pt metal will bring about inhibition of the illumination on the TiO_2 surface, leading to a decrease in the production rate of SO_4^{2-} as shown in Fig. 1. As a matter of course, the deposited oxides will cause the light passing to the TiO_2 surface to be disturbed as in the case of the other dopants.

References

1) Y. Matsumoto, H. Nagai, and E. Sato, *J. Phys. Chem.*, **86**, 4664 (1982).
2) B. Kraeutler and A. J. Bard, *J. Am. Chem. Soc.*, **100**, 2239 (1978).
3) H. Reiche and A. J. Bard, *J. Am. Chem. Soc.*, **101**, 3127 (1979).
4) C. D. Jaeger and A. J. Bard, *J. Phys. Chem.*, **83**, 3146 (1979).
5) I. Izumi and F. R. F. Fand, and A. J. Bard, *J. Phys. Chem.*, **85**, 218 (1981).
6) S. Sato and J. M. White, *J. Phys. Chem.*, **85**, 336 (1981).
7) M. Gräzel, *Ber. Bunsenges. Phys. Chem.*, **84**, 981 (1980).
8) R. H. Baker, J. Lilie, and M. Gräzel, *J. Am. Chem. Soc.*, **104**, 442 (1982).
9) J. M. Lehn, J. P. Sauvage, and R. Ziessel, *Nouveau Journal de Chimie* **4**, 623 (1980).
10) T. Kawai and T. Sakata, *Nature*, **286**, 474 (1980).
11) K. Domen, S. Naito, M. Soma, T. Onishi, and K. Tamaru, *J. Chem. Soc., Chem. Commum.*, **543**, (1980).

 © 1985 The Chemical Society of Japan Bull. Chem. Soc. Jpn., 58, 1259—1261 (1985)

A Conductance Study of Benzo-18-crown-6- and Its Analogs-Alkali Metal Ion Complexes in Various Solvents

Yasuyuki TAKEDA

Department of Chemistry, Faculty of Science, Chiba University, Yayoi-chō, Chiba 260

(Received November 10, 1984)

Limiting ionic molar conductivities of benzo-18-crown-6 (B18C6)-alkali metal ion complexes in various nonaqueous solvents were determined at 25 °C. The mobilities of the B18C6 complexes were compared with those of 18-crown-6 (18C6)- and dibenzo-18-crown-6 (DB18C6)-alkali metal ion complexes. Regardless of varieties of alkali metal ions held in the crown ether cavity, the larger is the size of the crown ether complex, the less mobile the complex is. For aprotic solvents (acetonitrile, DMF, DMSO, propylene carbonate), the mobility of the B18C6-K^+ complex is smaller than that of $(n\text{-}C_4H_9)_4N^+$; however, for the protic solvent (methanol), they are almost the same. Walden product value of the B18C6-K^+ complex as well as 18C6- and DB18C6-K^+ complexes somewhat changes with the variation of solvents. For these three crown ether-K^+ complexes, Walden product values of acetonitrile and propylene carbonate are larger than or nearly equal to those of DMF and DMSO. This may indicate that, for the aprotic solvents, donicity is a very important factor in determining the magnitude of mobility of the crown ether-K^+ complexes. The B18C6-K^+ complex as well as 18C6- and DB18C6-K^+ complexes seems to act as a structure breaker in a hydrogen-bonding solvent.

In a previous paper,[1] solvation behavior of 1:1 complexes of benzo-18-crown-6 (B18C6) with alkali metal ions in various nonaqueous solvents was studied by transfer activity coefficients. The B18C6-alkali metal ion complex is more strongly solvated in DMF and DMSO than in acetonitrile and propylene carbonate. In methanol, owing to hydrogen bonds between ether oxygen atoms of B18C6 and methanol, the B18C6 complex is more strongly solvated than the corresponding free alkali metal ion, compared to the case of the aprotic solvents.

In this work, in order to investigate solvation property for B18C6-alkali metal ion complexes from the viewpoint of transport phenomena, limiting ionic molar conductivities of B18C6-alkali metal ion complexes in various nonaqueous solvents were determined at 25 °C. The limiting ionic molar conductivities of the B18C6 complexes were compared with those of 18-crown-6 (18C6)- and dibenzo-18-crown-6 (DB18C6)-alkali metal ion complexes, and, moreover, Walden products of these three crown ether complexes were discussed in detail.

Experimental

Most of the reagents, solvents, and procedures were the same as those described previously.[1-5] The conductivities of final products of acetonitrile, propylene carbonate, methanol, DMF, and DMSO were less than 2×10^{-7}, 6×10^{-8}, 3×10^{-7}, 3×10^{-7}, and 6×10^{-8} $\Omega^{-1}cm^{-1}$, respectively. Alkali metal chlorides were used for the methanol system and perchlorates for the other solvent systems. The conductance measurements were made on a Fuso conductivity apparatus, model 362A, in a water bath thermostated at 25±0.005 °C. Two cells were used with cell constants of 0.059709 and 0.097766 cm^{-1}.

Results and Discussion

Limiting ionic molar conductivities ($\lambda°$) of B18C6 complexes with alkali metal ions were obtained in the same way as previously described.[2] In this study, it is assumed that the association between a cation and an anion is negligible (total concentration of an alkali metal ion $\approx6\times10^{-4}$ M; 1 M=1 mol dm^{-3}) and that B18C6 forms a 1:1 complex with an alkali metal ion. Corrections for viscosity changes were neglected (total concentration of B18C6$<2.5\times10^{-3}$ M). The $\lambda°$ values of B18C6 complexes with alkali metal ions in various solvents are listed in Table 1.

It is seen from Table 1 that, for acetonitrile and propylene carbonate, B18C6-alkali metal ion complexes, where the alkali metal ions closely fit into the

TABLE 1. $\lambda°$ VALUES IN VARIOUS SOLVENTS AT 25 °C

	$\lambda°/\Omega^{-1}cm^2mol^{-1}$				
	CH_3OH	CH_3CN	DMF	DMSO	PC[a]
18C6-K^+	39.9[5]	59[5]	24.6[4]	10.0[5]	8.91[2]
		61.1[6]			
B18C6-Na^+	—	53.1	—	—	7.29
B18C6-K^+	38.4	56.5	23.0	8.7	7.90
B18C6-Rb^+	—	56.1	—	—	8.16
B18C6-Cs^+	—	54.3	—	—	7.88
DB18C6-K^+	35.5[5]	53[5]	22.3[5]	8.2[5]	7.3[5]
	35.63[7]	54.2[6]			
	36.69[7]				
$(n\text{-}C_4H_9)_4N^+$	38.94[8]	61.4[9]	26.9[10]	11.29[10]	9.32[10]
Cl^-	52.36[8]	—	—	—	—
ClO_4^-	—	103.7[9]	52.83[4]	24.52[11]	18.28[10]

a) Propylene carbonate.

TABLE 2. WALDEN PRODUCTS AT 25 °C

	C_2H_5OH	CH_3OH	$C_6H_5NO_2$	CH_3CN	DMF	DMSO	PC[a]	H_2O
η_0/mP* (at 25 °C)[b]	10.84	5.42	18.11	3.39	7.96	19.6	25.3	8.903
DN**[13]	20	19	4.4	14.1	26.6	29.8	15.1	18.0
ε_r*** (at 25 °C)[b]	24.3	32.6	34.82	35.95	36.71	46.6	64.4	78.54
18C6-K^+[5]	—	0.21_6	—	0.20	0.19_5	0.19_6	0.22_5	0.22_5
B18C6-K^+	—	0.20_8	—	0.19_1	0.18_3	0.1_7	0.19_9	—
DB18C6-K^+[5]	0.1995	0.19_2	0.17	0.18	0.17_7	0.16	0.18	—
$(n\text{-}C_4H_9)_4N^+$[5]	0.2132	0.211	0.216	0.208	0.214	0.221	0.236	0.1719

* η_0 denotes viscosity and 1 P=0.1 Pa s. ** DN denotes donor number. *** ε_r denotes dielectric constant. a) Propylene carbonate. b) G. J. Janz and R. P. T. Tomkins, "Nonaqueous Electrolytes Handbook," Academic Press, New York and London (1972), Vol. 1.

B18C6 cavity, have larger mobilities. Mobilities of free alkali metal ions in acetonitrile and propylene carbonate increase in the order $Na^+<K^+<Rb^+<Cs^+$.[2,12] This indicates that the central alkali metal ion, which has the optimum size for the B18C6 cavity, is effectively screened by the B18C6 from surrounding solvent molecules; for a smaller or larger alkali metal ion than the B18C6 cavity, the interaction between the ion trapped in the B18C6 cavity and solvent molecules may decrease the mobility of the B18C6-alkali metal ion complex.

The size sequences of the three crown ethers are 18C6<B18C6<DB18C6. For the same solvent, the λ° value series of the K^+-crown ether complexes are given in the order DB18C6<B18C6<18C6. This indicates that the mobility sequences of the K^+-crown ether complexes are determined completely by the size ones of the complexes (*i.e.*, the larger is the complex size, the less mobile it is). Limiting ionic molar conductivities at 25 °C of 18C6-Na^+, Rb^+, Cs^+ complexes in propylene carbonate[2] and DB18C6-Na^+, Rb^+ complexes in acetonitrile[6] are 8.5_1, 8.8_6, 8.7_8 and 52.7, 55.5, respectively. It can be seen from these data and Table 1 that a B18C6-alkali metal ion complex is less and more mobile than the corresponding 18C6 complex in propylene carbonate and the corresponding DB18C6 complex in acetonitrile, respectively. This shows that, regardless of varieties of central alkali metal ions, the smaller crown ether-alkali metal ion complex is more mobile than the corresponding larger one.

It is interesting to compare the mobility of a B18C6-K^+ complex with that of $(n\text{-}C_4H_9)_4N^+$. For aprotic solvents (acetonitrile, DMF, DMSO, and propylene carbonate), the λ° value of the B18C6-K^+ complex is smaller than that of $(n\text{-}C_4H_9)_4N^+$; however, for the protic solvent (methanol), they are almost the same. A similar tendency was observed for the case of a 18C6-K^+ complex and $(n\text{-}C_4H_9)_4N^+$ and that of a DB18C6-K^+ complex and $(n\text{-}C_5H_{11})_4N^+$.[5] The size of a 18C6-$K^+$ complex is nearly identical with that of $(n\text{-}C_4H_9)_4N^+$.[2] Thus, it can be considered that the B18C6-K^+ complex is larger than $(n\text{-}C_4H_9)_4N^+$ by a benzene ring. For $(n\text{-}C_4H_9)_4N^+$, it is symmetrical and the charge of the nitrogen atom is well shielded; while, for the B18C6-K^+ complex, it is unsymmetrical and there exists a possible interaction of the central K^+ with solvent molecules on two axial sides of the B18C6 plane. From the above discussion, the fact that the B18C6-K^+ complex is less mobile than $(n\text{-}C_4H_9)_4N^+$ in the aprotic solvents may be attributed to the differences in the size and the structure between the B18C6-K^+ complex and $(n\text{-}C_4H_9)_4N^+$. From the results for methanol, it seems that enforcement of the hydrogen-bonded structure for the B18C6-K^+ complex is weaker than that for $(n\text{-}C_4H_9)_4N^+$.

Walden products at 25 °C of the B18C6-K^+ complex for various solvents are compiled in Table 2, together with those from the literature. From the more detailed examination of the data in Table 2, it was concluded that $\lambda^\circ\eta_0$ value of the same crown ether-K^+ complex as well as $(n\text{-}C_4H_9)_4N^+$ somewhat changes with the variation of solvents. For the same crown ether-K^+ complex, $\lambda^\circ\eta_0$ value of DMSO is the smallest and that of DMF is smaller than those of the other solvents except DMSO and nitrobenzene of the DB18C6-K^+ system; $\lambda^\circ\eta_0$ values of acetonitrile and propylene carbonate are larger than or nearly equal to those of DMF and DMSO. Dimethyl sulfoxide and DMF have extremely strong donicity compared to the other solvents listed in Table 2.[13] It thus appears that, for the aprotic solvents (CH_3CN, PC, DMF, DMSO), donicity is a very important factor in determining the magnitude of mobility of the crown ether-K^+ complexes. For $(n\text{-}C_4H_9)_4N^+$, the $\lambda^\circ\eta_0$ value of the aprotic solvent increases with an increase in dielectric constant except nitrobenzene (Table 2). The dielectric constant of nitrobenzene, however, is nearly equal to those of acetonitrile and DMF; the $\lambda^\circ\eta_0$ value of nitrobenzene is smaller than those of propylene carbonate and DMSO, and is slightly larger than that of DMF. Consequently, for the aprotic solvents, the magnitude of mobility of $(n\text{-}C_4H_9)_4N^+$ is considered to be governed largely by the dielectric constant. The difference in factors influencing mobilities of the crown ether-K^+ complexes and $(n\text{-}C_4H_9)_4N^+$ in the aprotic solvents may be attributed to the difference in structures of the cations as mentioned above. For the B18C6-alkali metal ion complex other than the B18C6-K^+ complex, $\lambda^\circ\eta_0$ value of propylene carbonate is larger than or nearly equal to that of acetonitrile. This is the same tendency for the B18C6-K^+ complex.

Generally, mobilities of 18C6-, B18C6-, and DB18C6-K^+ complexes in protic solvents are greater than those in aprotic solvents, and contrary holds for $(n\text{-}C_4H_9)_4N^+$

(Table 2). These results may be caused by the effect of hydrogen-bonded structure of the protic solvents. Methanol and ethanol have larger donicities than propylene carbonate, acetonitrile, and nitrobenzene, and have the smallest dielectric constants of all the solvents; hydrogen bonds between protic solvent molecules and ether oxygen atoms of these crown ethers would decrease the mobility of the crown ether–K^+ complexes; however, for B18C6- and DB18C6–K^+ complexes, $\lambda^\circ\eta_0$ values of the protic solvents are the largest of all the solvents. This suggests that the crown ether–K^+ complexes act as a structure breaker in the protic solvents. For the 18C6–K^+ complex, $\lambda^\circ\eta_0$ value of methanol is smaller than that of propylene carbonate, and on the contrary for B18C6- and DB18C6–K^+ complexes. For B18C6- and DB18C6–K^+ complexes, the difference in $\lambda^\circ\eta_0$ value between methanol and propylene carbonate increases on moving from B18C6 to DB18C6. A possible explanation for this is as follows. On account of lower basicity of aromatic ether oxygen atoms compared to aliphatic ones and steric hindrance caused by a benzo group, the interaction between ether oxygen atoms and methanol molecules may decrease in the order 18C6–K^+>B18C6–K^+> DB18C6–K^+. Thus, the mobility of the 18C6–K^+ complex in propylene carbonate is greater than that in methanol, and the reverse is true for B18C6- and DB18C6–K^+ complexes; moreover, the difference in the mobility of the K^+ complex between methanol and propylene carbonate increases on going from B18C6 to DB18C6. The fact that $\lambda^\circ\eta_0$ value of the 18C6–K^+ complex for water is higher than that for methanol may reflect the difference in characteristics of hydrogen bonds for water (three-dimentional structure) and methanol (one-dimentional structure). The 18C6–K^+ complex seems to act as a structure breaker more effectively in water than in methanol, resulting in the excess mobility in water.

The author would like to thank Professor Sadatoshi Akąbori of Toho University for the generous gift of benzo-18-crown-6.

References

1) Y. Takeda, Y. Ohyagi, and S. Akabori, *Bull. Chem. Soc. Jpn.*, **57**, 3381 (1984).
2) Y. Takeda, H. Yano, M. Ishibashi, and H. Isozumi, *Bull. Chem. Soc. Jpn.*, **53**, 72 (1980).
3) Y. Takeda and H. Yano, *Bull. Chem. Soc. Jpn.*, **53**, 1720 (1980).
4) Y. Takeda, *Bull. Chem. Soc. Jpn.*, **54**, 3133 (1981).
5) Y. Takeda, *Bull. Chem. Soc. Jpn.*, **56**, 866 (1983).
6) M. D. Monica, A. Ceglie, and A. Agostiano, *Electrochim. Acta*, **28**, 529 (1983).
7) L. Tušek-Božić and B. Božić, *Croat. Chem. Acta*, **57**, 119 (1984).
8) R. L. Kay and D. F. Evans, *J. Phys. Chem.*, **70**, 2325 (1966).
9) C. H. Springer, J. F. Coetzee, and R. L. Kay, *J. Phys. Chem.*, **73**, 471 (1969).
10) N. Matsuura, K. Umemoto, and Y. Takeda, *Bull. Chem. Soc. Jpn.*, **48**, 2253 (1975).
11) R. Gopal and J. S. Jha, *J. Phys. Chem.*, **78**, 2405 (1974).
12) R. L. Kay, B. J. Hales, and G. P. Cunningham, *J. Phys. Chem.*, **71**, 3925 (1967).
13) V. Gutmann, "Coordination Chemistry in Nonaqueous Solutions," Springer-Verlag, Berlin (1968).

Cathodic Cleavage of Some Aryl Phenacyl Sulfides

Akira KUNUGI,* Akinori MUTO,† and Taketsugu HIRAI
Department of Applied Chemistry, Faculty of Engineering, Osaka City University, Sugimoto, Sumiyoshi-ku, Osaka 558
(Received November 12, 1984)

The electrolytic reduction of some aryl phenacyl sulfides in aqueous ethanol and anhydrous acetonitrile solutions has been investigated by means of polarography and controlled potential electrolysis. Dc polarograms of these compounds exhibit two waves in all solutions studied, the first of which corresponds to a one-electron and a two-electron transfer depending upon the absence and presence of proton donor. The electrode reaction taking place at the first reduction step involves cleavage of the carbon-sulfur bond, resulting in formation of acetophenone and the corresponding thiols in good yields even in an acetonitrile solution containing no proton donor. The second reduction step corresponds to the reduction of the acetophenone produced.

The electrolytic desulfurization of organosulfur compounds has attracted considerable attention because most of them are valuable synthetic precursors. β-Keto sulfoxides,[1-3] for instance, are electrochemically reduced by cleavage of a carbon–sulfur bond with formation of methyl ketones and thiol derivatives. The other organosulfur compounds such as β-hydroxy sulfones,[4,5] sulfoxides,[6] and sulfides,[7] vinyl sulfones,[8] sulfoxides,[9] and sulfides,[10] and alkyl imidazolyl sulfoxide[11] and sulfides[11,12] are also electrochemically reduced to afford the corresponding desulfurated compounds.

With the consumption of small quantities of electricity compared with the case of electrolytic reduction of β-keto sulfoxides, β-keto sulfides will be expected to undergo the cathodic cleavage of the carbon–sulfur bond to yield the desulfurated compound, methyl ketones. Therefore, it is considered of interest to investigate electrolytic reduction of β-keto sulfides from the standpoint of the conversion of carboxylic esters to the corresponding methyl ketones, which contain one more carbon atom than the starting esters:

$$\mathrm{Ar\text{-}S\text{-}CH_2^-\ Li^+ + PhCO_2C_2H_5 \longrightarrow Ar\text{-}S\text{-}CH_2COPh} \xrightarrow{\text{electrolysis}} \mathrm{PhCOCH_3 + ArSH}$$

In the present work, the electrolytic reduction of some aryl phenacyl sulfoxides was investigated in both aqueous ethanol and anhydrous acetonitrile solutions by means of polarography, coulometry, and macroelectrolysis.

Experimental

Chemicals. Phenacyl *p*-tolyl sulfide (**1a**), phenacyl phenyl sulfide (**1b**), and *p*-methoxyphenyl phenacyl sulfide (**1c**) were prepared from the corresponding lithiomethyl aryl sulfides and ethyl benzoate on the basis of the procedure described for the synthesis of aryl phenacyl sulfoxides,[13] which were identified by their physical properties and ^{1}H NMR spectra.[14] **1a**; mp 32—34°, NMR ($CDCl_3$) δ 2.29 (3H, s, $-CH_3$), 4.21 (2H, s, $-CH_2-$), 7.04—8.09 (9H, m, aromatic). **1b**; mp 51—52° (lit,[15] 52—53°), NMR ($CDCl_3$) δ 4.24 (2H, s, $-CH_2-$), 7.14—7.99 (10H, m, aromatic). **1c**; NMR ($CDCl_3$) δ 3.73 (3H, s, CH_3O-), 4.14 (2H, s, $-CH_2-$), 6.77—8.07 (9H, m, aromatic).

The aqueous alcoholic buffer solutions contained 40% (v/v) ethanol and their ionic strengths were adjusted to 0.6 M (1 M=1 mol dm^{-3}) with KCl. All buffer compounds were of reagent grade. The pH reading was taken in the aqueous alcoholic buffer solutions with a pH-meter standardized against aqueous buffer solutions. A 95% (v/v) ethanol buffer solution of pH 5.8 contained 0.12 M lithium acetate, 0.08 M acetic acid, and 0.5 M lithium chloride. Anhydrous acetonitrile solutions were prepared from the pre-deoxygenated acetonitrile (MeCN) and tetrabutylammonium perchlorate (TBAP) or tetrabutylammonium tetrafluoroborate (TBAB) which were purified and dried as described previously.[16] The concentrations of the supporting electrolytes were 0.1 M.

Controlled potential macroelectrolysis and coulometry as well as polarography were carried out in both aqueous ethanol and anhydrous acetonitrile solutions, using the same experimental set-up and type of procedure as in the previous papers.[2,16] A saturated calomel electrode (SCE) and a Ag/0.1 M $AgNO_3$ in MeCN electrode (Ag/Ag^+) were used as the reference electrodes in aqueous and nonaqueous solutions, respectively.

Results

Polarography. Results of polarography with **1a**,

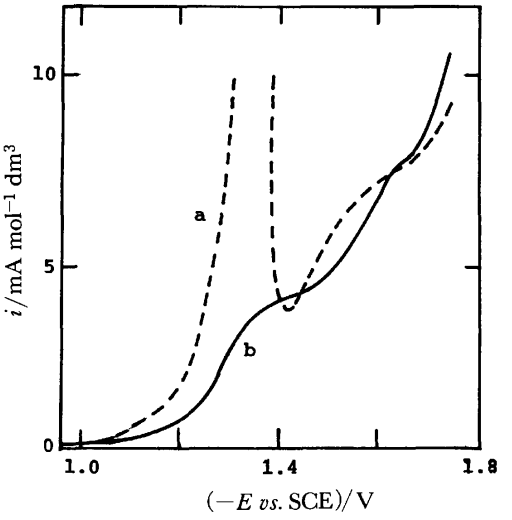

Fig. 1. Tast polarograms of phenacyl *p*-tolyl silfide (**1a**) in 40% ethanol buffer solution of pH 7.4 at 27 °C. (a) Without maximun suppressor, (b) in presence of 0.008% Triton X-100.

†Present adress: Department of Chemical Engineering, College of Engineering, University of Osaka Prefecture, Sakai, Osaka 591.

Table 1. Polarographic data for some aryl phenacyl sulfides in 40% ethanol buffer solution of pH 7.4 in presence of 0.008% Triton X-100 at 27 °C

Substrate[a)]	First wave		Second wave	
	Half-wave potential (V *vs.* SCE)	Limiting current (mA mol^{-1})	Half-wave potential (V *vs.* SCE)	Limiting current (mA mol^{-1})
1a	−1.29	3.7	−1.56	3.4
1b	−1.29	3.8	−1.56	3.4
1c	−1.29	3.7	−1.56	3.3

a) **1a**: phenacyl *p*-tolyl sulfide, **1b**: phenacyl phenyl sulfide, **1c**: *p*-methoxyphenyl phenacyl sulfide.

1b, and **1c** in a 40% ethanol buffer solution of pH 7.4 are presented in Fig. 1 and Table 1. Figure 1 shows Tast polarograms of **1a** as a representative example. The polarogram exhibited two waves with a large maximum in the absence of maximum suppressors. The addition of 0.008% Triton X-100 essentially eliminated the maximum and resulted in two well-defined waves. As can be seen from Table 1, the half-wave potentials ($E_{1/2}$) of both the first and second reduction waves of **1a**, **1b**, and **1c** are independent of the Ar group of aryl phenacyl sulfides (Ar-S-CH_2COPh). The $E_{1/2}$ of each second wave coincides with that of acetophenone in the same solution, the height of the second wave being somewhat smaller than the height of the polarographic wave of an equimolar solution of acetophenone. These suggest that the second wave is ascribed to the reduction of the acetophenone produced during the polarographic reduction. The above suggestion was confirmed by controlled potential coulometry and macroelectrolysis as will be shown later.

The ratio of the first wave-height to the second one for all three sulfides are approximately 1, indicating that each first wave corresponds to a two-electron transfer process. This was also supported from the polarographic result of phenacyl phenyl sulfoxide[2)]: This sulfoxide gives two waves with the wave-height of approximately 2:1, $E_{1/2}$ of the second wave coincides with that of **1b**, and the ratio of the first wave-height of the sulfoxide to that of **1b** is approximately 2. Furthermore, a two-electron transfer process was supported by the coulometric experiment as will be shown later. The first wave for **1a** was found to be diffusion-controlled as evidenced from the linear plots of the limiting current (i_l) against the square root of the height of the mercury head. Moreover the average temperature coefficient was of the order of 2%/°C as for a diffusion-controlled process. The other substrates, **1b** and **1c**, are also inferred to give diffusion-controlled waves from analogy with **1a** with regard to the polarographic behavior.

Figure 2 shows the dependence of $E_{1/2}$ and i_l, on pH for the first wave of **1a**, where polarograms were measured in 40% ethanol buffer solutions containing 0.008% Triton X-100. The values of i_l were substantially pH-independent. On the other hand, a plot of $E_{1/2}$ against pH gave two straight-line segments, the intersection of which corresponded to approximately

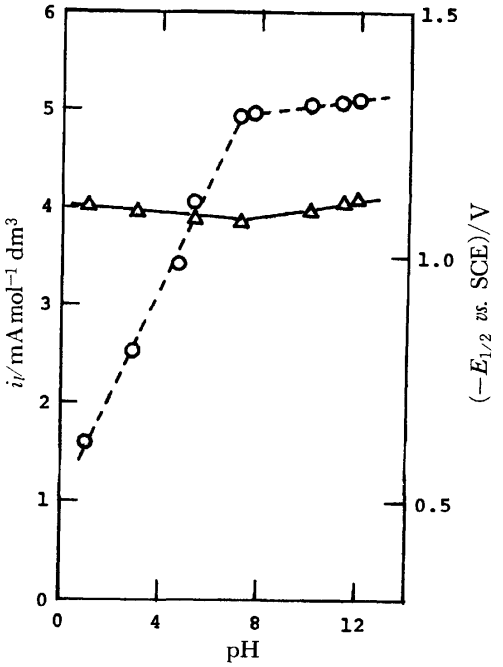

Fig. 2. Dependence of limiting current (——) and half-wave potential (----) on pH for first wave of **1a** in 40% ethanol buffer solution containing 0.008% Triton X-100 at 27 °C.

pH 7. Similarly the pH-dependence of $E_{1/2}$ and i_l of the second wave is shown in Fig. 3, together with that of acetophenone in the same solutions. The $E_{1/2}$ of the second wave of **1a** coincided with that of acetophenone over the whole pH region, but i_l of the second wave was significantly smaller than that of acetophenone.

Figure 4 shows typical Tast polarograms of **1a** in MeCN containing 0.1 M TBAP, in the absence and presence of phenol as a proton donor. In the absence of the proton donor, **1a** gave two waves with the wave-height ratio of approximately 3:1, the value of $E_{1/2}$ of the first wave indicating that **1a** is easier to reduce than alkyl phenyl sulfides bearing no carbonyl group.[17)] The addition of phenol caused both wave-heights to increase. The dependence $E_{1/2}$ and i_l of the first wave on phenol concentration is presented in Fig. 5, in which the values of i_l of di-*p*-tolyl disulfide also is included. As shown in Fig. 5, the $E_{1/2}$ was independent of the phenol concentration, but the i_l increased with an increase in the phenol concentration and reached twice of the original value when the molar ratio of phenol

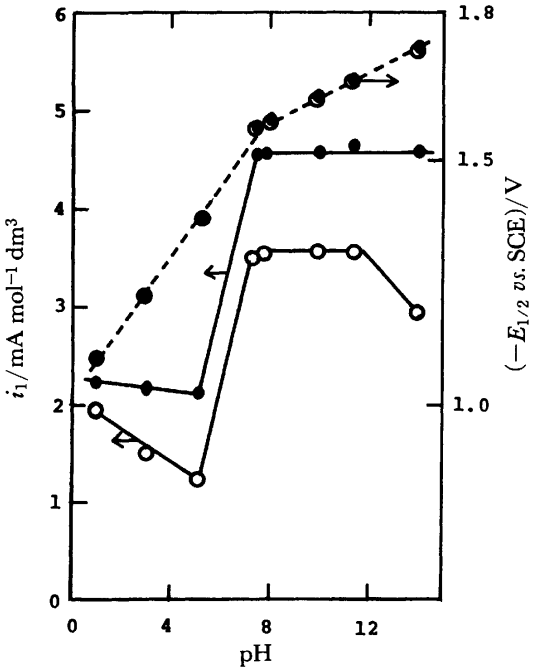

Fig. 3. Dependence of limiting current (——) and half-wave potential (----) on pH in dc polarography in 40% ethanol buffer solution containing 0.008% Triton X-100 at 27 °C.
O: Second wave of **1a**, ●: Wave of acetophenone.

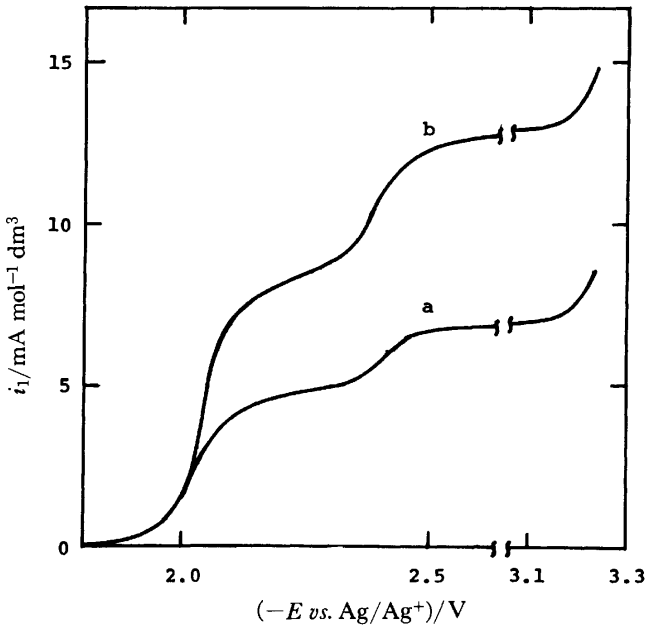

Fig. 4. Effect of phenol on Tast polarogram of **1a** in acetonitrile containing 0.1 mol dm^{-3} TBAP at 27 °C. Molar ratio of phenol/**1a**: (a) 0, (b) 2.0.

to the substrate was more than approximately 1. The electrode reaction taking place at the first wave of **1a** in anhydrous acetonitrile containing sufficient phenol is estimated to be a two-electron transfer process from comparison with the values of i_l of **1a** and di-*p*-tolyl disulfide. Thus, the first wave of **1a** in the absence of proton donors corresponds to a one-electron transfer process. Both values of $E_{1/2}$ and i_l for the second wave

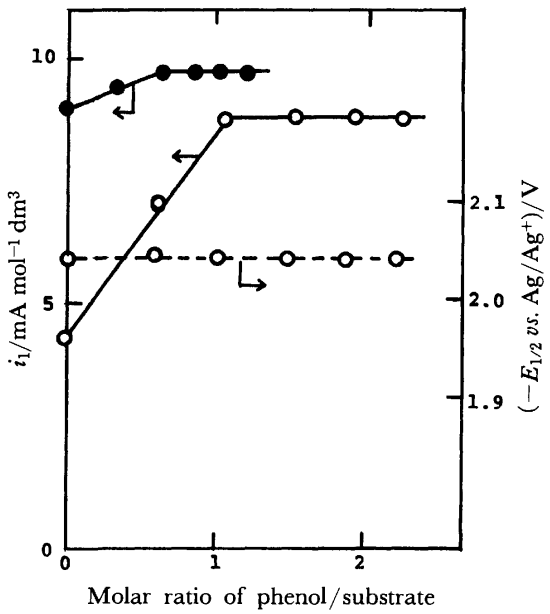

Fig. 5. Dependence of limiting current (——) and half-wave potential (----) on phenol concentration. O: First wave of **1a**, ●: Wave of di-*p*-tolyl disulfide.

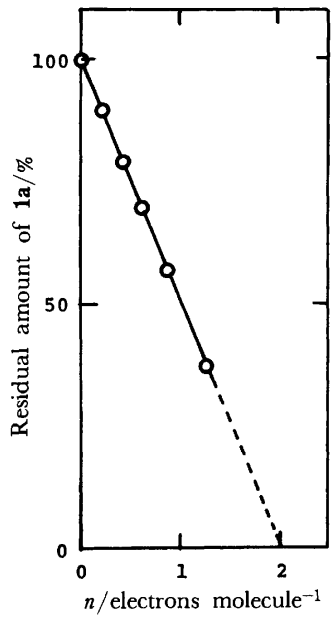

Fig. 6. Coulometric n-value of **1a** at Hg cathode of −1.35 V *vs.* SCE in 40% ethanol buffer solution of pH containing 0.008% Triton X-100 at 27 °C.

were dependent on the phenol concentration in the same fashion with acetophenone.

Coulometry. To determine the apparent number of electrons transfered (n-value) for the reduction of **1a**, **1b**, and **1c** under different electrolytic conditions, a series of controlled potential coulometric experiments were performed. The substrate concentrations were within the range, in which a linear i_l *vs.* concentration behavior is observed. The electrolyses were interrupted at several points and then the exhausted amounts of the substrate were monitored by means of polarography as a function of the quantity of electricity passed. Figure 6

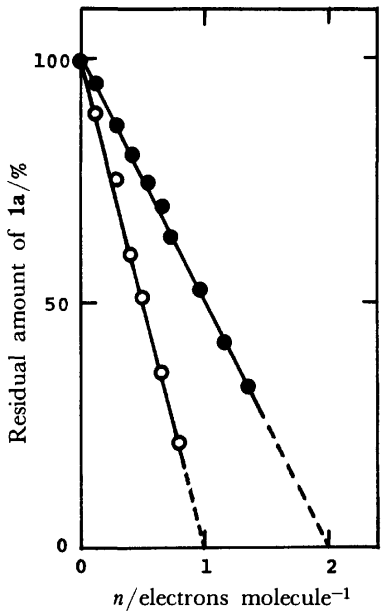

Fig. 7. Coulometric n-values of **1a** in acetonitrile containing 0.1 mol dm^{-3} TBAB at Hg cathode of −2.1 V *vs.* Ag/Ag$^+$. Molar ratio of phenol/**1a**: (○) 0, (●) 2.5.

shows a typical result of the coulometric experiment with **1a** in 40% ethanol buffer solution of pH 7.4 in the presence of Triton X-100 at a stirred mercury pool cathode. The coulometric n-value was estimated by extrapolation to be 2 electrons per molecule, which is agreement with the polarographic n-value.

Similarly typical coulometric results of **1a** at a stirred mercury pool cathode in MeCN containing 0.1 M TBAB are presented in Fig. 7, which also illustrates the effect of phenol on the n-value. Figure 7 definitely shows that the coulometric n-values in the absence and presence of phenol are 1 and 2 electron (s) per molecule, respectively. When a platinum plate electrode in place of the mercury pool was used, the same n-values were obtained.

Macroelectrolysis. Controlled potential macroelectrolyses of some β-keto sulfides were carried out at the plateau potential of the first wave of their polarograms, in 40% ethanol buffer solution of pH 7.4, 95% ethanol buffer solution of pH 5.8, and MeCN containing 0.1 M TBAB with and without phenol. These results are summarized in Table 2, with the coulometric n-values. In a series of macroelectrolyses, the amounts of acetophenone formed were almost equivalent to the sum of the diaryl disulfides and arenethiols and the yields of the isolated acetophenone were 66—76% under all conditions studied. As can be seen from Table 2, in aqueous ethanol solutions and anhydrous acetonitrile solution containing sufficient phenol, coulometric n-values all were close to 2 electrons per molecule, whereas the n-value was 1 electron per molecule in the acetonitrile with no proton donor. Namely, Table 2 shows the curious result that the yields of acetophenone are essentially invariable, no matter whether the n-values are 1 or 2 electrons per molecule. This implies that there is a difference between the reduction mechanisms of aryl phenacyl sulfides to acetophenone in the absence or presence of sufficient proton donor.

The data in Table 2 also show that, with regard to the yields and the coulometric n-values, the electrolytic reduction of aryl phenacyl sulfides is independent of the nature of the electrode material.

Discussion

As shown in Fig. 3, the second wave of **1a** in 40% ethanol buffer solutions gave somewhat underestimated values in wave-height over the whole pH region. This may be interpreted as follows: The electrode reaction taking place at the first wave leads to formation of phenacyl anion ($PhCOCH_2^-$) which is electroinactive. Of course, acetophenone, produced by protonation of the phenacyl anion, is electroactive so that it gives the second wave. Therefore, if all phenacyl anions produced are not protonated within a period of the polarograpic measurement, the second wave will result in a somewhat underestimated wave-height. This idea was supported by the following polarography in a 95% ethanol buffer solution of pH 5.8. As shown in Fig. 8, the polarogram of **1a** exhibited two waves, but the ratio of the second wave-height to the first one was small compared to that in the 40% ethanol buffer solu-

Table 2. Controlled potential macroelectrolyses of some aryl phenacyl sulfides (Ar-S-CH_2 COPh) at the plateau potential of the first wave

Substrate	Solvent	Cathode material	Mole ratio of phenol/substr.	Coulometric n-value	Products (mol%) PhCOCH$_3$	ArSH	ArSSAr[a)]	Yield[b)] of PhCOCH$_3$ (%)
Ar= p-$CH_3C_6H_4$	40% C_2H_5OH	Hg	0	1.9	50	50	0	66
	95% C_2H_5OH	Hg	0	2.0	56	40	4	66
	CH_3CN	Hg	0	1.0	48	15	37	69
	CH_3CN	Hg	2.6	2.0	51	10	39	67
	CH_3CN	Pt	0	1.0	47	9	44	72
	CH_3CN	Pt	2.5	2.1	55	0	45	76
Ar=C_6H_5	CH_3CN	Hg	2.3	1.8	47	5	48	67
Ar= p-$CH_3OC_6H_4$	CH_3CN	Hg	2.7	2.0	55	0	45	67
	CH_3CN	Pt	0	1.0	44	15	41	74
	CH_3CN	Pt	2.4	1.8	53	0	47	76

a) Calculated on the basis of sulfur content. b) Isolated yield.

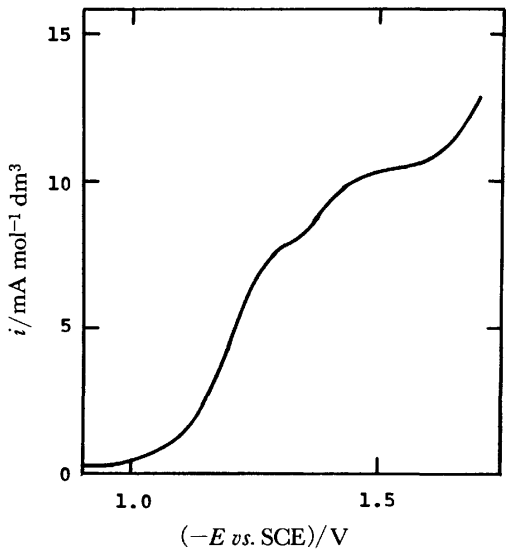

Fig. 8. Tast polarogram of **1a** in 95% ethanol buffer solution of pH 5.8 in presence of 0.008% Triton X-100 at 27 °C.

tion (curve b in Fig. 1). This can be attributed to the weakness of proton donor of the 95% ethanol solution compared to the 40% ethanol solution.

In Table 2, one is faced with the apparent paradox of the isolation of diaryl disulfides in spite of the fact that they are easily reduced to arenethiols at the potential at which the macroelectrolysis was to be run.[18] This may be resolved in terms of an air oxidation of arenethiols, *i.e.*, the thiols easily undergo an air oxidation, particularly in anhydrous media during the work-up procedure after electrolysis, resulting in formation of diaryl disulfides.

The electrolytic reduction of aryl phenacyl sulfides in the absence of proton donors afforded acetophenone and the corresponding thiols in good yields despite of the coulometric n-value of 1, suggesting that such β-keto sulfides undergo a one-electron reduction to yield phenacyl radical ($PhCOCH_2\cdot$) and the corresponding thiolate anions (ArS^-). However, the following results suggest formation of phenacyl anion rather than its radical: (1) The dimer of phenacyl radical was not detected under the present reaction conditions. (2) Phenacyl anion seems to be more stable than its radical because the phenacyl anion is stabilized through the acetyl anion in which the charge is highly delocalized onto the oxygen atom of the carboxyl group. In view of the above reasons, at the present stage, it cannot be concluded whether the electrode reaction taking place at the first wave of aryl phenacyl sulfides in MeCN containing no proton donor, involving a one-electron uptake, leads to formation of phenacyl anion or its radical.

In the sufficiently proton-donor-containing solutions such as aqueous ethanol solutions and anhydrous acetonitrile solutions containing excess phenol, the electrolytic reduction of aryl phenacyl sulfides at the first wave potential, involving a two-electron transfer, will yield phenacyl anion and the corresponding thiolate anions. Hence a plausible mechanism may be illustrated as follows:

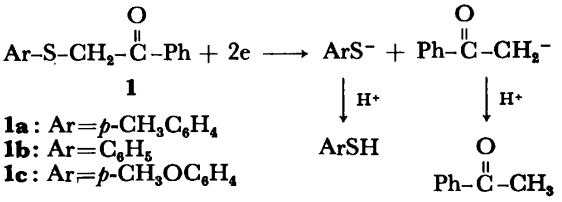

References

1) B. Lamm and B. Samuelsson, *Acta Chem. Scand.*, **23**, 691 (1969).

2) A. Kunugi and N. Kunieda, *Electrochim. Acta*, **28**, 715 (1983).

3) A. Kunugi, N. Muto, and N. Kunieda, *Denki Kagaku*, **51**, 137 (1983).

4) T. Shono, Y. Matsumura, and S. Kashimura, *Chem. Lett.*, **1978**, 69.

5) S. Gambino, P. Martigny, G. Moisset, and J. Simonet, J. Electroanal. Chem., **90**, 105 (1978).

6) A. Kunugi, N. Muto, and T. Hirai, *Nippon Kagaku Kaishi*, **1984**, 1821.

7) T. Shono, Y. Matsumura, S. Kashimura, and H. Kyutoku, *Tetrahedron Lett.*, **1978**, 2807.

8) K. Ankner, B. Lamm, and J. Simonet, *Acta Chem. Scand., Ser. B*, **31**, 742 (1977).

9) A. Kunugi and K. Abe, *Chem. Lett.*, **1984**, 159.

10) M. M. Baizer, *J. Org. Chem.*, **31**, 3847 (1966).

11) B. Johansson and S. Wendsjo, *J. Electroanal. Chem.*, **147**, 123 (1983).

12) B. Johansson and S. Wendsjo, *J. Electroanal. Chem.*, **123**, 151 (1981).

13) a) H. D. Becker, G. T. Mikol, and G. A. Russel, *J. Amer. Chem. Soc.*, **85**, 3410 (1963); b) N. Kunieda, A. Suzuki, and M. Kinoshita, *Bull. Chem. Soc. Jpn.*, **54**, 1143 (1981).

14) The NMR spectra were determined with a Hitachi-Perkin-Elmer R-20 spectrometer in $CDCl_3$ and chemical shifts are reported in parts per million (δ) from internal tetramethylsilane.

15) M. Ohta and K. Sato, *J. Pharm. Soc. Jpn.*, **68**, 160 (1948).

16) A. Kunugi, T. Hagi, T. Hirai, and K. Abe, *Electrochim. Acta*, in press.

17) C. K. Mann and K. K. Barnes, "Electrochemical Reactions in Nonaqueous System," Marcel Dekker Inc., New York (1970), pp. 385—387.

18) For example, $E_{1/2}$ of di-*p*-tolyl disulfide is 1.27 V *vs.* Ag/Ag^+ in MeCN containing 0.1 M TBAP in the presence of excess phenol.

Environment Effects on the ESR Spectrum of the Cation Radical of Dimethylketene in Low Temperature Matrices

Jun FUJISAWA, Shin SATO,* Kazuo SHIMOKOSHI,† and Tadamasa SHIDA††
Research Laboratory for Nuclear Reactors, Tokyo Institute of Technology, Ookayama, Meguro-ku, Tokyo 152
†*Department of Chemistry, Tokyo Institute of Technology, Ookayama, Meguro-ku, Tokyo 152*
††*Department of Chemistry, Kyoto University, Sakyo-ku, Kyoto 606*
(Received December 4, 1984)

The cation radical of dimethylketene produced in γ-irradiated solid solutions of various halocarbons has been investigated by ESR over a temperature range from 77 K to the melting point of each matrix. The cation radical in CCl_4 was stable up to about 180 K and the spectrum was well resolved to allow the determination of the anisotropic ESR parameters. In CCl_2FCClF_2 and CCl_2FCCl_2F, a series of irreversible spectral changes was observed with an increase in temperature. This process was interpreted in terms of the formation of the dimer cation. In the matrix of CCl_3F, the ESR spectrum exhibited extra structure, which varied reversibly with temperature. The analyses of the spectra suggested that the cation radical in CCl_3F weakly interacts with surrounding matrix molecules to form adducts.

The employment of a CCl_3F matrix for the radiolytic generation and stabilization of molecular cation radicals has been established and proved to yield ESR spectra with no serious interference by the matrix radicals.[1] Since a theoretical analysis of the spectrum without any consideration of the matrix usually gives satisfactory results, little attention has been paid to the matrix effect.

Other media such as SF_6,[2] CCl_2FCClF_2,[3] and CCl_3CF_3[4] have subsequently been found to also be useful. Use of these compounds along with CCl_3F revealed that the behavior of some cation radicals depends upon the matrix employed. For example, two types of thermal reactions of alkane cations occur depending upon the matrix.[5–7] It seems that in general, unimolecular reactions occur preferentially in CCl_3F and CCl_3CF_3, while bimolecular reactions through molecular diffusion are easy in SF_6 and CCl_2FCClF_2.[5–10]

Recently, we have examined the ESR spectra of dimethylketene cation radicals in several matrices over a wide range of temperatures, and found a drastic dependence of the spectrum upon the matrices. In the present contribution, we describe the results of detailed analyses of these ESR spectra and discuss the reactions occurring in the matrices to gain an insight into the matrix effect at low temperatures.

Experimental

Dimethylketene was kindly supplied by Dr. N. Washida of National Institute of Environmental Studies. After the purity was checked by gas chromatography, the compound was kept in liquid nitrogen to avoid polymerization. Other reagents including halocarbons (CCl_4, CCl_3F, CCl_2FCClF_2, and CCl_2FCCl_2F) from Tokyo Kasei Co. were used without further purification.

For the ESR measurement, dimethylketene was dissolved in each halocarbon to a concentration of 10^{-1}—10^{-3} in mole ratio, then degassed and sealed off in a Suprasil quartz tube. The samples, thus prepared, were γ-irradiated at 77 K to a dose of about 0.8 Mrad (1 Mrad=10^4 Jkg^{-1}) to generate the cation radicals. The ESR spectra were recorded on a JES FE-2XG spectrometer at 77 K and higher temperatures. The ESR parameters of cation radicals were determined using a proton magnetic-resonance probe and a digital frequency counter (Takeda Riken Co. TR 5211C).

Results and Discussion

Determination of Anisotropic ESR Parameters. As was briefly described in a previous paper,[11] singly occupied molecular orbitals of cation radicals of ketenes are characterized mainly by $\pi_{C=C}$ (π orbital on C=C bond), similar to olefin cation,[8] rather than by $n_{C=O}$ (lone pair orbital on C=O bond) as in the case of aldehyde and ketone cations.[12–14] The dimethylketene cation showed a nearly isotropic septet spectrum by the hyperfine interactions of six equivalent methyl protons (23.0 G (1 G=1×10^{-4} T)). In this section, the results of our further investigations with the use of CCl_4 as matrix are presented.

Though the CCl_4 matrix has been employed for the optical absorption study of various radical cations,[15] it is not generally used for ESR studies because the concomitantly produced radicals such as CCl_3 and CCl_4^+ are bothersome.[16] However, the spectrum of dimethylketene cation obtained for the solution in CCl_4 at 153 K (Fig. 1a) is not interfered with by the by-products and is highly resolved. This indicates that the local magnetic environment of the cation radical in CCl_4 varies little from site to site and that the line width of the underlying absorption of the by-products is much broader than that of the septet lines.

The spectral pattern of the septet is essentially the same as that found in our previous results,[11] but it may be noticed that there are slight splittings due to an anisotropy in the outermost component at low field. Thus, we performed a simulation of the ESR line shape for powder samples.[17] Figure 1b represents the best fit spectrum calculated by the use of the parameters listed in Table 1. From the excellent agreement between Figs. 1a and 1b, it is concluded that the hyperfine interaction of methyl protons in dimethylketene cation is slightly anisotropic. The parameters determined in this way are also applicable to the cation radicals in other matrices, which will be discussed later.

Dimerization Reaction. The ESR spectra of a

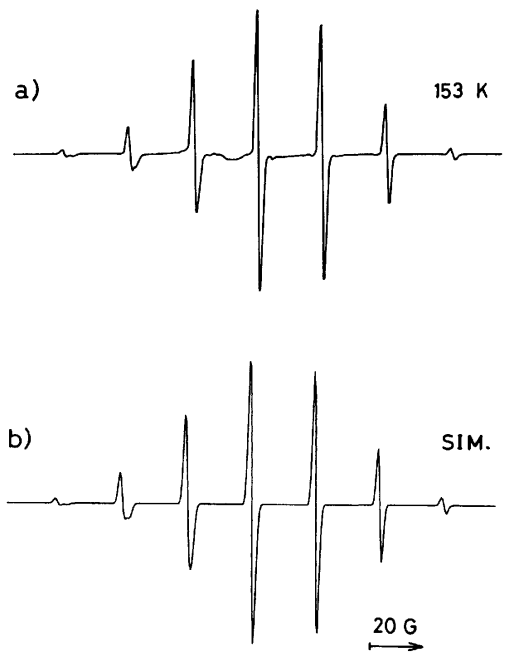

Fig. 1. (a) ESR spectrum of dimethylketene cation in CCl_4 at 153 K; (b) Simulation for (a) using the parameters given in Table 1 and a line width, ΔH_{msl}=1.6 G, of Gaussian line.

TABLE 1. ESR PARAMETERS FOR THE DIMETHYLKETENE RADICAL CATION IN CCl_4 AT 153 K

components of g tensor and g_{iso}	^1H hyperfine couplings, G
$g_{\parallel}$=2.0028	$A_{\parallel}$=22.75
$g_{\perp}$=2.0037	$A_{\perp}$=23.62
g_{iso}=2.0034	A_{iso}(6H)=23.33

dimethylketene cation in CCl_2FCClF_2 or CCl_2FCCl_2F exhibited additional small subpeaks even at 77 K.[11] The intensities were dependent upon the concentration. Figures 2a and 2b demonstrate the spectra observed for CCl_2FCClF_2 solutions with $10^{-3}$and 10^{-2} mole ratio of dimethylketene, respectively. These figures show that at lower concentrations the subpeaks are suppressed. Even in this case, however, strong subpeaks appeared by keeping the sample at 77 K overnight after γ-irradiation. These results suggest that subpeaks are due to the species formed by a reaction of dimethylketene cation with a neutral molecule of dimethylketene. Figure 2c represents the simulated spectrum for Fig. 2b. The simulation was obtained by assuming a composite of a septet (I) of dimethylketene cation and a nonet (II) as indicated by the stick diagram. The good agreement indicates the coexistence of the nonet (II) whose g factor and sum of the coupling constants are identical to those of septet (I) (17.3 G×8= 23.1 G×6).

Upon warming, the spectral feature of this system changed completely; *i.e.*, a series of irreversible change was observed. Figure 2d shows the observed spectrum at 98 K, which again can be decomposed into two components demonstrated by the stick diagrams under Fig. 2e. One is the nonet (II) mentioned above and the other is a new septet (III) with a splitting of 20.5 G which is slightly smaller than that of (I). It is noteworthy that this septet shows a considerably large positive shift of g factor. Further elevation of temperature results in the disappearence of the nonet

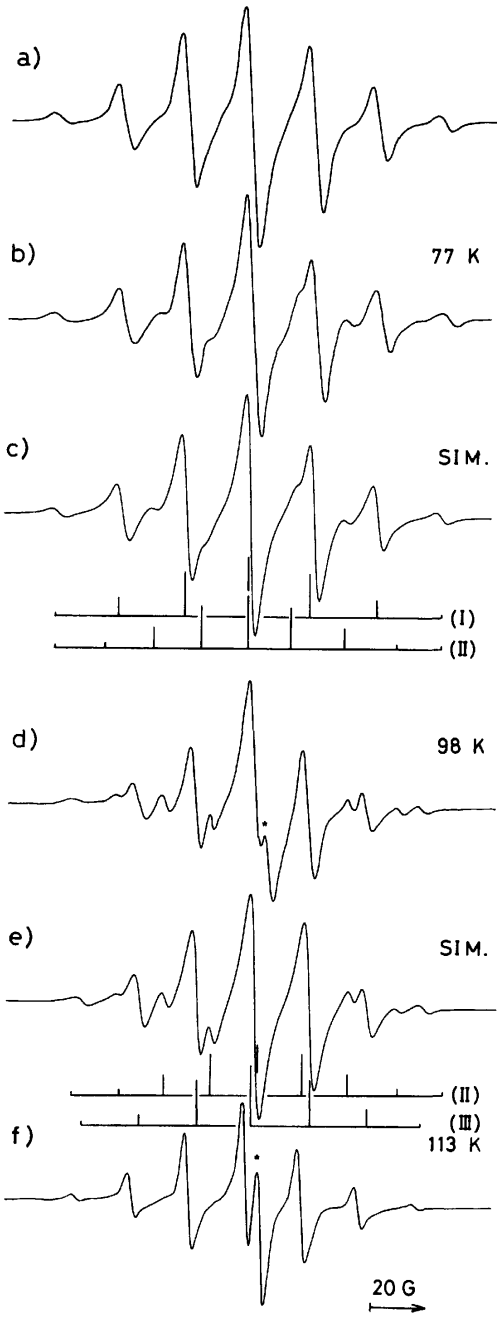

Fig. 2. ESR spectra of (a) 0.1 mol%; (b), (d), (f) 1.0 mol% solutions of dimethylketene in CCl_2FCClF_2 at (a), (b) 77 K; (d) 98K; (f) 133K after γ-irradiation at 77 K; (c) Simulation for (b) assuming the abundance ratio of 1.00 to 0.15 for $(CH_3)_2CCO^+$ (I) and $((CH_3)_2CCO)_2^+$ (II) respectively; (e) Simulation for (d) assuming the abundance ratio of 0.20 to 1.00 for $((CH_3)_2CCO)_2^+$ (II) and $(CH_3)_4C_4O_2^+$ (III) respectively. The ESR parameters of (I)—(III) are listed in Table 2. The asterisk indicates the transition due to the matrix radicals.

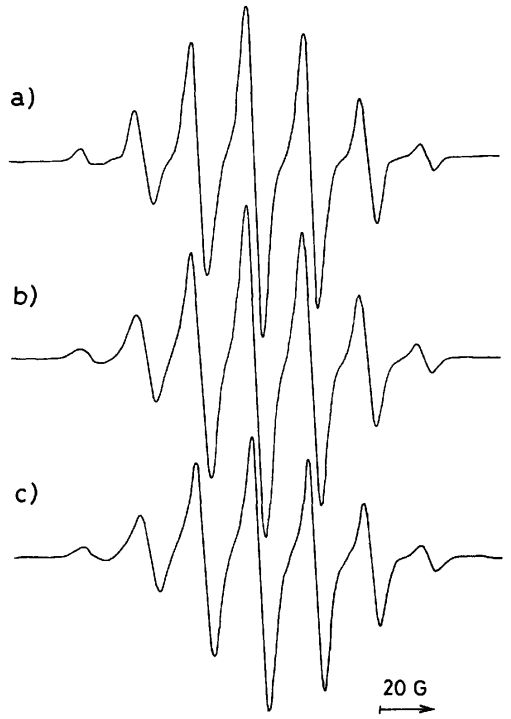

Fig. 3. ESR spectra of (a) CCl_3F; (b) CCl_2FCClF_2; (c) CCl_2FCCl_2F solutions of dimethylketene dimer measured at 77 K after γ-irradiation at 77 K, showing features assigned to $(CH_3)_4C_4O_2^+$.

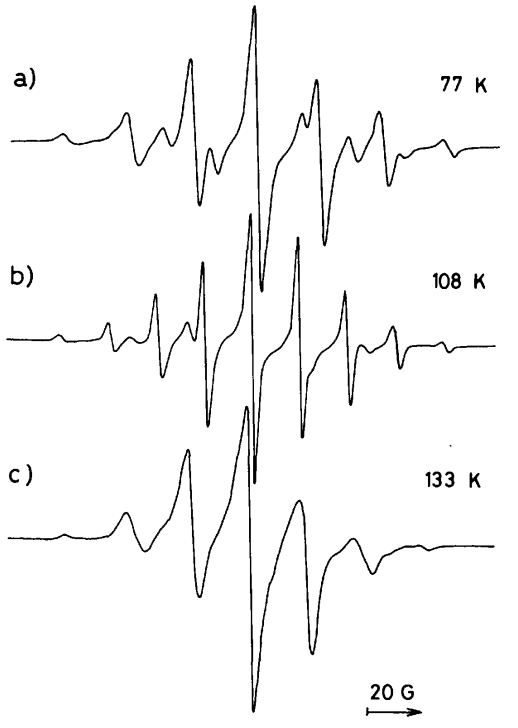

Fig. 4. ESR spectra of CCl_2FCCl_2F solution of dimethylketene measured at (a) 77 K; (b) 108 K; (c) 133 K after γ-irradiation at 77 K. Main features of these spectra are assigned to $(CH_3)_2CCO^+$ (I) $((CH_3)_2CCO)_2^+$ (II), and $(CH_3)_4C_4O_2^+$ (III), respectively.

(II) to give exclusively the septet spectrum (III) (Fig. 2f). In order to elucidate the mechanism for the sequence

Table 2. ESR parameters for the observed spectra in CCl_2FCClF_2 and CCl_2FCCl_2F

Spectrum	Species	Matrix	g_{iso}	A_{iso}(G)
(I)	$(CH_3)_2CCO^+$	CCl_2FCClF_2	2.0034	23.1 (6H)
		CCl_2FCCl_2F	2.0034	23.0 (6H)
(II)		CCl_2FCClF_2	2.0034	17.3 (8H)
		CCl_2FCCl_2F	2.0034	17.3 (8H)
(III)		CCl_2FCClF_2	2.0043	20.5 (6H)
		CCl_2FCCl_2F	2.0044	20.4 (6H)
	[a] $(CH_3)_4C_4O_2^+$	CCl_2FCClF_2	2.0041	20.4 (6H)
		CCl_2FCCl_2F	2.0041	20.4 (6H)

a) Formed from dimethylketene dimer by positive charge transfer.

of spectral changes, it is necessary to identify (II) and (III). We carefully examined a variety of candidates for the septet (III) in Fig. 2f in literatures, but no one agreed with the observed spectrum. On the other hand, we found (experimentally) a system which gives a very similar spectrum to (III). The system is the γ-irradiated Freon solution of dimethylketene dimer (2,2,4,4-tetramethyl-1,3-cyclobutanedione), $(CH_3)_4C_4O_2$. The spectra observed for the three Freon solutions are shown in Fig. 3 (see also, Fig. 4c). The ESR parameters of this spectrum are comparable with those obtained from the spectrum (III) (Table 2), although the line width of the septet in Fig. 2f is slightly smaller than those in Figs. 3 and 4c.

On the basis of above assignment, the spectral change observed in Fig. 2 may be explained in the following manner. Septet (I) is associated with the isolated dimethylketene cation, which is presumed to have a C_{2v} symmetry with six magnetically equivalent rapidly rotating methyl protons (Structure I). Upon the elevation of temperature from 77 to 98 K, molecular diffu-

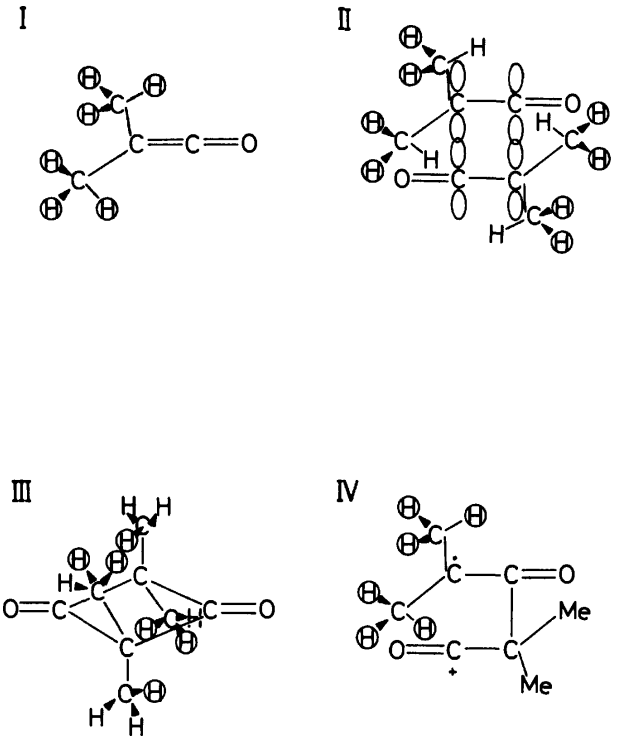

sion and/or reorientation may take place to produce a dimer cation, a possible conformation being shown in Structure II. If the rotation of the methyl groups is hindered to make the eight encircled protons in Structure II magnetically equivalent, we may associate the nonet (II) underlying in Figs. 2b and 2d with this dimer cation of dimethylketene. Such a dimer cation has been observed for tetramethylethylene;[18] the spectrum is characterized by a 25-line pattern, the splitting constant of which is one half that of the 13-line pattern of the monomer cation. Since the spectrum changed from a septet to a nonet in the present case, it is provisionally assumed that the methyl groups in the dimer cation are fixed in a restricted conformation and only eight protons participate in the revelation of the 9-line hyperfine structure. The fact that the g factor and the sum of coupling constants are common to both spectra (I) and (II) indicates the similarity of electronic structure between the two species and suggests that the spectral change from (I) to (II) corresponds only to the change in the number of the protons giving rise to the observed hyperfine splitting.

Further elevation of temperature yields another septet (III) in Fig. 2f which is attributed to a cation radical of dimethylketene dimer. As for the structure of the cation radical, there are two possibilities; one is the symmetric structure III in which six encircled protons are assumed to be magnetically equivalent. The other is the ring opened structure IV.[19]

Essentially the same spectral change as in Figs. 2a—f was observed for the matrix of CCl_2FCCl_2F as shown in Fig. 4. In this case, the nonet associated with the dimer cation was observed unambiguously at 108 K. The observed ESR parameters in CCl_2FCCl_2F are summarized in Table 2 along with those obtained in CCl_2FCClF_2.

Cation-matrix Interaction. Different behavior of dimethylketene cation was found in the case of CCl_3F matrix. Figure 5a shows the observed spectrum of the cation in CCl_3F at 77 K. The overall features of the septet due to the monomer cation of dimethylketene are similar to those observed in other matrices, except for the small peaks flanking each component of the septet.

The extra structure might be considered as due to the anisotropy of the proton hyperfine splitting. However, any reasonable set of parameters of anisotropy for the protons could not yield comparable simulation spectra. On the other hand, we found that, if the extra structure in Fig. 5a is ignored, the rest of the spectrum can be reproduced by using the anisotropic parameters determined in the previous section. Figure 5b shows the spectrum thus calculated. The variation of line widths for individual components is well reproduced. The substructure, therefore, cannot be attributed to the anisotropy of the spectrum. Moreover, the warming of the system caused a drastic and reversible change of the substructure as shown in Fig. 6. Such a change cannot be associated with a simple motional averaging

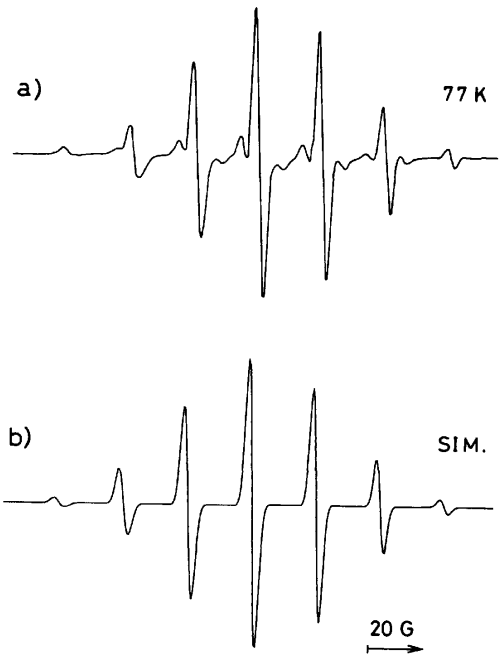

Fig. 5. (a) ESR spectrum of dimethylketene cation in CCl_3F at 77 K; (b) Simulation for (a) using the parameters given in Table 1 and a line width, ΔH_{msl}= 3.0 G.

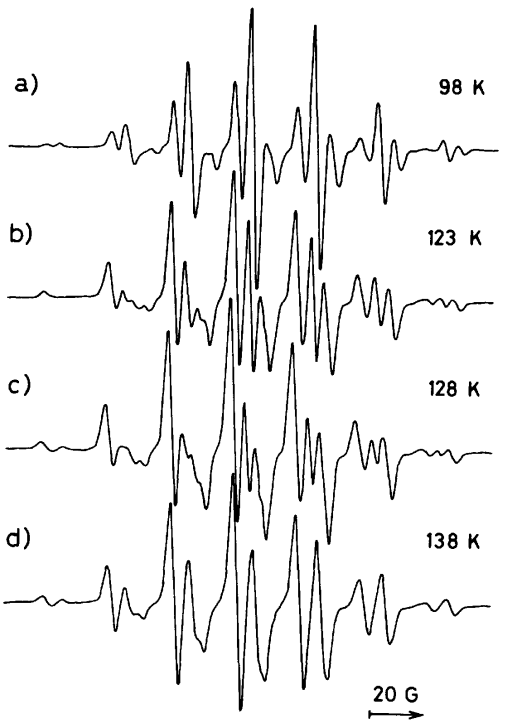

Fig. 6. ESR spectra of dimethylketene cation in CCl_3F at (a) 98 K; (b) 123 K; (c) 128 K; (d) 138 K after γ-irradiation at 77 K, showing the reversible change of substructures with temperature.

of anisotropy. Examination of Fig. 6 reveals that the substructure which is barely seen at 77 K is emphasized on warming, and the triplet feature of each component of the septet changes to a doublet (see also, Fig. 7).

Thus, the temperature dependence of the spectra observed in CCl_3F is quite different from that observed

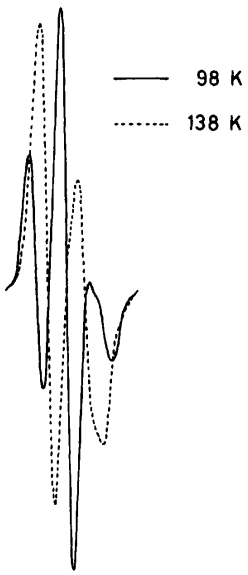

Fig. 7. The central part of the spectra of dimethylketene cation in CCl_3F recorded at 98 K (solid line) and 138 K (dotted line).

in CCl_2FCClF_2 or CCl_2FCCl_2F and evidently cannot be explained in terms of the bimolecular reaction. In addition, the perturbation causing the extra structure should not be strong, because the proton ESR parameters previously determined in the CCl_4 matrix are applicable to the present system with a good accuracy. A weak interaction between the cation and surrounding matrix molecules is conceivable. In the case of CCl_3F, the chlorine ($I=3/2$) or the fluorine ($I=1/2$) atom can cause a superhyperfine interaction. The latter seems to be more probable from the spectral features and the fact that no substructure was observed with CCl_4. Since the fluorine nucleus has a large hyperfine coupling ($A_{iso}=17160$ G for $\rho_{2s}=1$),[20] a very small spin density is enough to give the observed extra structure.

From this point of view, we attempted to simulate the observed spectra using ESR parameters in Table 1 plus the assumption that there are additional nuclei with $I=1/2$ in the system. In Figs. 8 and 9, we show the spectra obtained after repeated curve fittings to those observed at 98 and 138 K, respectively. The existence of two equivalent nuclei with splitting constants of $A_{\parallel}=8.0$ G and $A_{\perp}=4.2$ G for Fig. 8b and one nucleus with $A_{\parallel}=12.0$ G and $A_{\perp}=3.5$ G for Fig. 9b was assumed. The agreement between each pair of spectrum is satisfactory. Such a large anisotropy of the extra interaction is compatible with the involvement of the fluorine atom.

We tested various values of the g factor and the proton anisotropic hyperfine coupling constant. However, a slight change in the parameters (from those listed in Table 1) caused a remarkable deviation from the observed spectra and no improved spectra could be obtained. This indicates that the proton ESR parameters in Table 1 are valid whether there is a superhyperfine interaction or not, which, in turn, allows us to estimate

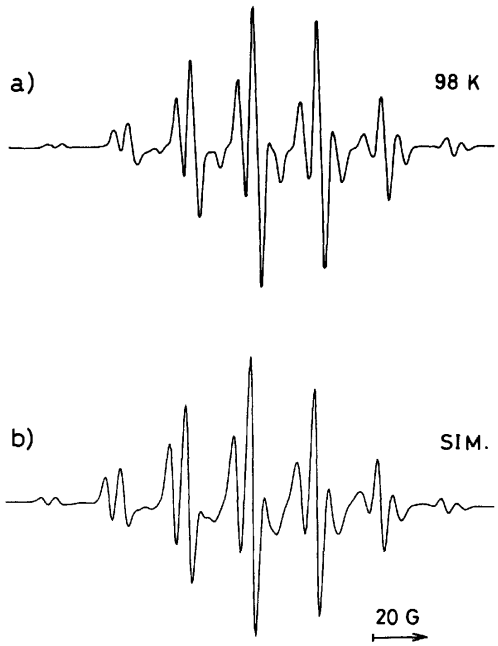

Fig. 8. (a) ESR spectrum of dimethylketene cation in CCl_3F at 98 K; (b) Simulation for (a) using the parameters given in Table 1 for protons in the cation and $A_{\parallel}=8.0$ G, $A_{\perp}=4.2$ G for two fluorine nuclei in the matrix molecules interacting with the cation.

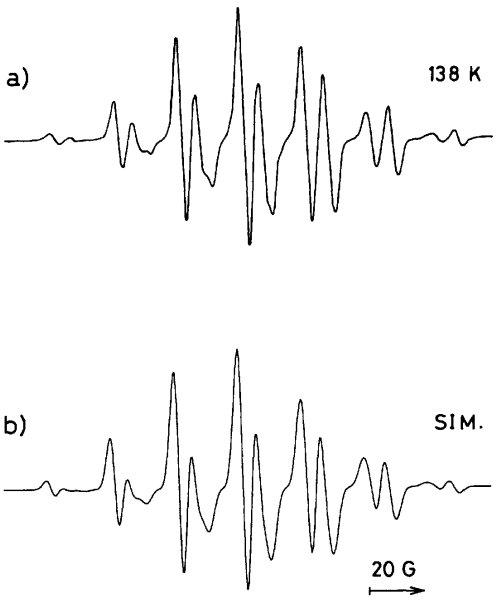

Fig. 9. (a) ESR spectrum of dimethylketene cation in CCl_3F at 138 K; (b) Simulation for (a) using the parameters given in Table 1 for protons and $A_{\parallel}=12.0$ G, $A_{\perp}=3.5$ G for one fluorine nucleus.

the superhyperfine coupling constants. The fact that we needed two sets of the superhyperfine parameters for the different temperatures may indicate that either the intermolecular complex or the mechanism of the interaction is different between the two temperatures. However, the attempt to reproduce the spectra observed in the intermediate range of the temperature by a simple superposition of the three spectra (Figs. 5b, 8b, and 9b), was not successful. Some dynamic process such as

the line alternation effect resulting from the spin exchange[21] might be related to the observed spectral change.

The superhyperfine interaction has been discussed for several cations in the matrix, in particular, in CCl_3F.[22-29] In most cases, the cations exhibit superhyperfine structures which change reversibly with the temperature. For example, the cation radical of acetaldehyde shows such behavior. Two different interpretations have been proposed for this reversibility. One is the motional averaging of the anisotropy[25] and the other is a reversible thermal dissociation.[14,26] The complete analysis of the spectral change with temperature in relation to the dynamical process is subject to further study.

References

1) T. Shida, H. Kubodera, and Y. Egawa, *Chem. Phys. Lett.*, **79**, 179 (1981).
2) M. Iwasaki, K. Toriyama, and K. Nunome, *J. Am. Chem. Soc.*, **103**, 3591 (1981).
3) K. Toriyama, K. Nunome, and M. Iwasaki, *J. Phys. Chem.*, **85**, 2149 (1981).
4) M. Tabata and A. Lund, *Z. Naturforsch.*, **38a**, 428 (1983).
5) K. Toriyama, K. Nunome, and M. Iwasaki, *J. Chem. Phys.*, **77**, 5891 (1982).
6) M. Iwasaki, K. Toriyama, and K. Nunome, *Rad. Phys. Chem.*, **21**, 147 (1983).
7) K. Nunome, K. Toriyama, and M. Iwasaki, *Chem. Phys. Lett.*, **105**, 414 (1984).
8) T. Shida, Y. Egawa, H. Kubodera, and T. Kato, *J. Chem. Phys.*, **73**, 5963 (1980).
9) K. Ushida and T. Shida, *J. Am. Chem. Soc.*, **104**, 7332 (1982).
10) M. Tabata and A. Lund, *Rad. Phys. Chem.*, **23**, 545 (1984).
11) K. Shimokoshi, J. Fujisawa, K. Nakamura, S. Sato, and T. Shida, *Chem. Phys. Lett.*, **99**, 483 (1983).
12) M. C. R. Symons and P. J. Boon, *Chem. Phys. Lett.*, **89**, 516 (1982).
13) L. D. Snow and F. Williams, *J. Chem. Soc., Chem. Commun.*, **1983**, 1090.
14) P. J. Boon, M. C. R. Symons, K. Ushida, and T. Shida, *J. Chem. Soc., Perkin Trans. 2*, 1213 (1984).
15) T. Shida and W. H. Hamill, *J. Chem. Phys.*, **44**, 2369 (1966).
16) T. Shida and Y. Takemura, *Rad. Phys. Chem.*, **21**, 157 (1983).
17) K. Shimokoshi, *Bull. Chem. Soc. Jpn.*, **51**, 635 (1978).
18) T. Ichikawa and P. K. Ludwig, *J. Am. Chem. Soc.*, **91**, 1023 (1969).
19) Our preliminary experiment at 4 K seems to favor the second possibility.
20) J. R. Morton and K. F. Preston, *J. Magn. Res.*, **30**, 577 (1978).
21) C. A. McDowell and K. Shimokoshi, *J. Chem. Phys.*, **60**, 1619 (1974).
22) A. Hasegawa and M. C. R. Symons, *J. Chem. Soc., Faraday Trans. 1*, **79**, 93 (1983).
23) D. Becker, K. Plante, and M. D. Sevilla, *J. Phys. Chem.*, **87**, 1648 (1983).
24) L. D. Snow and F. Williams, *Chem. Phys. Lett.*, **100**, 193 (1983).
25) L. D. Snow and F. Williams, *Chem. Phys. Lett.*, **100**, 198 (1983).
26) M. C. R. Symons and P. J. Boon, *Chem. Phys. Lett.*, **100**, 203 (1983).
27) G. W. Eastland, D. N. R. Rao, J. Rideout, M. C. R. Symons, and A. Hasegawa, *J. Chem. Res (S).*, 258 (1983).
28) M. Iwasaki, H. Muto, K. Toriyama, and K. Nunome, *Chem. Phys. Lett.*, **105**, 586 (1984).
29) J. Rideout and M. C. R. Symons, *J. Chem. Res (S).*, 268 (1984).

 © 1985 The Chemical Society of Japan Bull. Chem. Soc. Jpn., 58, 1273—1278 (1985)

Studies of Quenching Processes in NE-213 and Insta-Gel Liquid Scintillators by Using Pulse Shape Discrimination Technique

Kazutoyo ENDO,* Tadafumi SAOTOME, Keiko TANAKA, and Hiromichi NAKAHARA
Department of Chemistry, Faculty of Science, Tokyo Metropolitan University, Fukasawa, Setagaya, Tokyo 158
(Received September 12, 1984)

Quenching processes for different excitation sources such as alpha-particles and electrons in NE-213 and Insta-Gel were studied by the use of the pulse shape discrimination technique and pulse height analysis. The dependence on electron energies of time spectra due to the difference in pulse shape was observed for NE-213 by setting energy windows to Compton scattered electrons. The results were interpreted on the basis of the linear energy transfer of electrons in liquid scintillator solution. The chemical and oxygen quenchings in Insta-Gel were compared with each other by using conversion electrons and alpha-particles. Quenching constants for those particles were found to be the same for each organo halogen compound used, irrespective of the excitation sources used. Paramagnetic quenchings were also examined for such agents as oxygen, Gd^{3+} ($4f^7$), and Yb^{3+} ($4f^{13}$) by using the above two excitation sources in Insta-Gel. Possible mechanisms of their effects on the quenching processes were discussed in terms of the spin conversion between the paramagnetic quencher and the excited solvent.

The liquid scintillation counting technique has been widely used for the determination of soft beta-emitting nuclides such as tritium, carbon-14 and calcium-45 because of its excellent detection efficiency and of its simplicity in sample preparation.[1-5] In addition, this technique has been found to be very useful for the determination of low level radon in the environment.[6-10] However, quenching phenomena caused by various impurities often make the observable pulse heights lower. On the other hand, several studies have been made on quenching mechanisms in liquid scintillation systems by using monochromatic photons in the UV region,[11,12] but only a few by using radioactive nuclides for excitation of the scintillation system.[13-15]

Quenching effects have so far been classified into three categories; chemical quenching, color quenching, and oxygen quenching. The chemical quenching is caused by some energy transfer reactions between solvents or between the solvent and fluorescent molecules that do not take part in the emission of fluorescence. The color quenching is the process due to the absorption of fluorescence by quenching molecules. This process is caused by the superposition of the emission spectrum of the scintillator and the absorption spectrum of the quenching molecules. The oxygen quenching is considered to be the process related to the strong electron affinity and paramagnetism of oxygen, but details remain unknown.

It is known that the mean life time of fluorescence emission is affected by the chemical and oxygen quenchings. Hence, the pulse shape discrimination is a useful technique to get information regarding variation of such life times. The technique has been successfully applied to neutron spectroscopy, separating gamma-rays and recoil protons in inorganic[16-19] and organic scintillation countings.[20-21] Recently, this has been also effectively applied to alpha- and beta-countings by using liquid scintillator solution.[22-24]

In the present work, we studied the chemical and oxygen quenching processes in NE-213 (a product of Nuclear Enterprises) and Insta-Gel (a trade name of Packard Co., Inc.), using the pulse shape discrimination technique and pulse height analysis, and laid stress on the following points. Firstly, the relative resolving power of pulse shape discrimination between alpha-particles and electrons was examined as a function of electron energy. Secondly, the oxygen quenchings for different excitation sources such as alpha-particles and electrons were compared with each other by using the pulse shape discrimination technique. Thirdly, the effects of these different excitation sources on the chemical and oxygen quenching were studied by means of pulse height analysis. Lastly, the paramagnetic effects of oxygen, Gd^{3+} ($4f^7$), and Yb^{3+} ($4f^{13}$) were studied in order to clarify their quenching processes by the pulse shape discrimination technique. Among lanthanoid ions, Gd^{3+} shows high paramagnetic moments whereas Yb^{3+} does the least. The comparative study by the use of such ions as quenchers will make the quenching mechanism clear. The results will be discussed in terms of possible spin conversion mechanisms. In the present study, the alpha-particles from ^{210}Po and the conversion electrons from ^{139}Ce were used in order to compare the quenching effects for their excitation sources. It is expected that the quenching reactions involved will be simple for the electrons with a simple energy spectrum.

Experimental

Chemicals. *a) Sources for Insta-Gel.* For an alpha-ray source, ^{210}Po in 1 M[†] hydrochloric acid solution was used, and for a conversion electron source, ^{139}Ce in the cerium-(III) chloride form was used. The 1 M hydrochloric acid solution (1 ml) of these radioisotopes was put into a standard vial containing Insta-Gel (15 ml). The content was deoxygenated by argon gas bubbling, unless otherwise stated.

Gadolinium and ytterbium chlorides were prepared from their oxides. After dissolving the oxides into small amounts of nitric acid, their salts were converted to chlorides by repeated addition of hydrochloric acid and heating. Finally, the chlorides were obtained by evaporating the solution to

[†] 1 M=1 mol dm^{-3}.

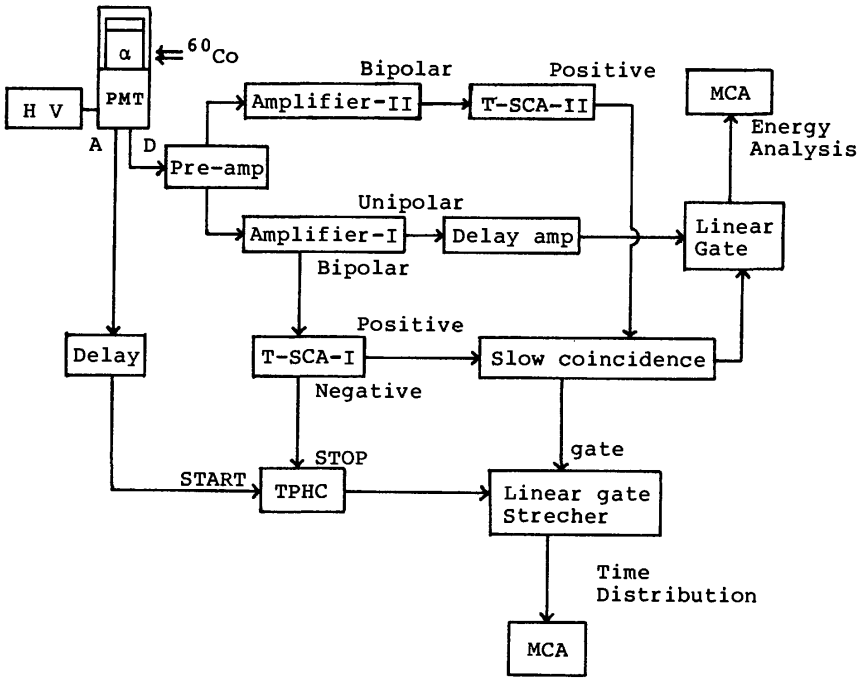

Fig. 1. A block diagram of a zero-crossing pulse shape discrimination system.

dryness.

b) Sources for NE-213. Polonium-210 and cerium-139 were extracted from each 1 M hydrochloric acid solution with a toluene solution of di(2-ethylhexyl)phosphoric acid (volume ratio of 1:1). For investigation of the electron energy dependence on the zero-crossing time, a vial containing the ^{210}Po source (the extracted solution, 1 ml) and 15 ml of NE-213 was externally irradiated with gamma-rays of ^{60}Co. The alpha-ray source was used to generate a standard zero-crossing time of alpha-rays on a time spectrum.

Measurements of Dissolved Oxygen. An oxygen analyzer manufactured by Beckman Instrument Inc. was used to measure the partial pressure of oxygen dissolved in Insta-Gel. We used the value for the partial pressure of oxygen in atmosphere, *i.e.*, 21% as the standard partial pressure of oxygen dissolved in Insta-Gel, assuming that the oxygen in solution is in equilibrium with that in air. In the case of oxygen quenching experiments, the gel was bubbled by oxygen through a glass capillary and the oxygen contents were measured before and after the pulse height and pulse shape measurements.

Measurement System. The schematic counting system used in this experiment is shown in Fig. 1. The vial was surrounded by an aluminium foil and directly connected at the bottom with optical greese to a RCA 8575 photomultiplier. All the electric instruments used were ORTEC NIM modules. In order to measure normal pulse shape distributions of alpha-particles and electrons, we used a simple system of a time pick-off at the zero-crossing point of slow bipolar signals. Anode pulses shaped with the constant fraction discriminator inside the ORTEC 270 photomultiplier base were used as start signals for a time-to-pulse height convertor (TPHC). The voltage signals from the dynode were passed through the pre-amplifier, and shaped with the main amplifier-I. The resulting bipolar signals were fed to a timing SCA-I and the fast negative signals were used as stop signals for the TPHC. In order to reduce the shifts of zero-crossing time due to pulse height variation, the range of the pulse height to be measured was kept constant by timing SCA-I and -II. The lower level of the pulse height range was selected with the timing SCA-I. For selecting the upper level of the specified range, the upper level discriminator of the timing SCA-II was used, and the lower level discriminator was set to be zero. The gain of the amplifier-I was changed to adjust the pulse height of a given electron energy to the window selected by the above two SCA.

Results and Discussion

Dependence of Zero-crossing Time Distribution on Electron Energy. Dependence of the time spectrum on the energy of electrons was examined by using Compton scattered electrons of various energies and alpha-particles of ^{210}Po in NE-213. The latter was used as a standard source for the time distribution of alpha-particles. The time spectrum of the alpha-particles from ^{210}Po and the Compton scattered electrons from ^{60}Co in NE-213 is shown in Fig. 2. The resolving power of zero-crossing time distribution between the electrons and alpha-particles was analyzed by a figure of merit, $M_{\alpha,e}$, defined as

$$M_{\alpha,e} = \frac{\Delta S}{T_1 + T_2}$$

where ΔS is the separation between two peaks, T_1 and T_2 are the full widths at half maximum (fwhm) of electrons and alpha-particles, respectively. For the present experiment, the T_2 value was constant for alpha-particles of ^{210}Po. The $M_{\alpha,e}$ values for the electrons of selected energy ranges were evaluated from the observed ΔS, T_1, and T_2 values as shown in Fig. 3. As the electron energy decreases, the $M_{\alpha,e}$ value becomes smaller. A similar trend has been reported

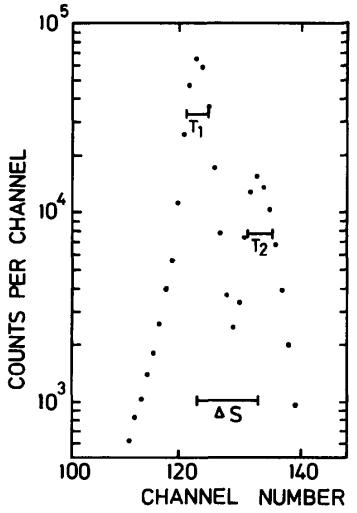

Fig. 2. Time spectrum of alpha-particles from ^{210}Po and of Compton scattered electrons in oxygen-free NE-213 irradiated with gamma-rays of ^{60}Co. T_1 and T_2 indicate the full widths at half maximum of electrons and alpha-particles, respectively.

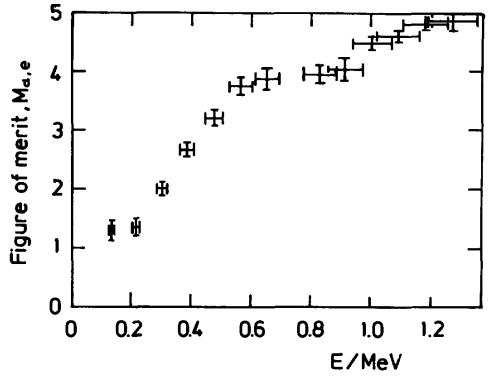

Fig. 3. Figure of merit, $M_{\alpha,e}$, of alpha-particles from ^{210}Po and of Compton scattered electrons in oxygen-free NE-213 irradiated with gamma-rays of ^{60}Co as a function of electron energy.

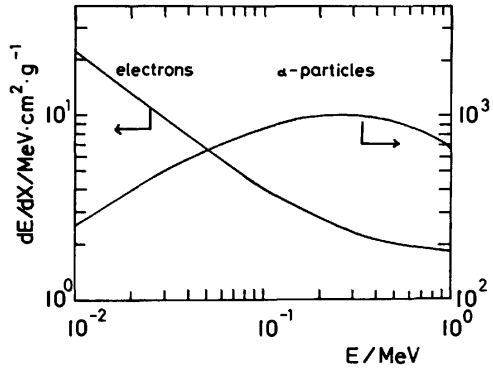

Fig. 4. Stopping powers of alpha-particles and electrons calculated by using Bethe's equation in a system of PPO (4 g), POPOP (0.1 g), and toluene (10^3 ml).

for neutron and gamma-ray separation.[19,27] The energy loss of electrons can be calculated by using Bethe's equation.[28] Although the exact chemical composition of NE-213 is not available, the energy loss of electron for an analogous material, toluene-

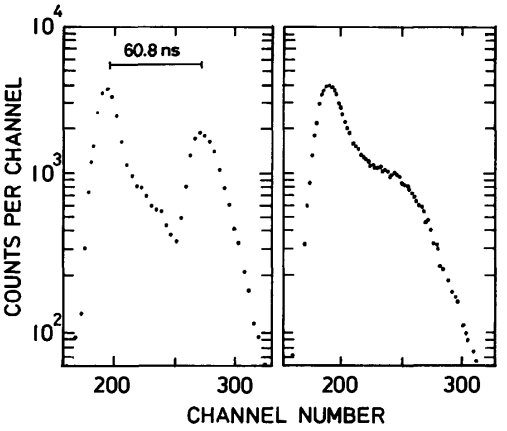

Fig. 5. Time spectra of conversion electrons from ^{139}Ce and alpha-particles from ^{210}Po in NE-213 liquid scintillator under oxygen-free (left side) and oxygen-saturated (right side) conditions.

PPO system, is shown in Fig. 4, together with that of alpha-particles.[29] The chemical compositions used for calculation are 4 g of PPO ($C_{15}H_{11}NO$, 2,5-diphenyloxazole), 0.1 g of POPOP ($C_{24}H_{16}N_2O_2$, 1,4-bis-2-(5-phenyloxazole)-benzene), and 10^3 ml of toluene. The stopping power becomes greater as the electron energy decreases. On the other hand, the value corresponding to the 5.3 MeV alpha-particles of ^{210}Po is calculated to be 2.20×10^2 MeV/cm^{2}g^{-1} in the system by using Bethe's equation,[29] which is at least two order of magnitude greater than that of electrons of the same energy. The high linear energy transfer causes localized ionization, molecular damages, and free radical formation along the path, which are closely related to the overall fluorescence conversion efficiency. The highly ionized species in a small limited spur recombine with electrons, resulting in the excited triplet state of a neutral molecule in the absence of spin correlation between the ion and an electron. The neutralization into a triplet state is favored by spin statistics. The present result of the $M_{\alpha,e}$ dependence on electron energy suggest that the energy loss processes of electrons in liquid scintillation system is similar to those of alpha-particles as the electron energy decreases.

Effects of Oxygen for Pulse Shape Discrimination. Since the time spectra of electrons were found to be dependent upon the energy in the preceding section, we used conversion electrons from ^{139}Ce as an electron source of simple energy spectrum. The time spectra of the conversion electrons and the alpha-particles from ^{210}Po in NE-213 are shown in Fig. 5. Although the center of the pulse shape distribution due to conversion electrons was not affected by oxygen, that of alpha-particles was shifted to shorter direction. The time difference of peaks was found to be 60.8 ns for oxygen-free NE-213, and to be 42 ns for oxygen saturated one. Diamagnetic compounds such as chloroform, carbon tetrachloride, bromoform, dibromomethane, and aniline did not cause variations in the time spectrum for

alpha-particles and electrons within the experimental errors, compared with those of NE-213 containing no quenching agents. The results obtained on Insta-Gel were similar to those on NE-213, except that the separation of two peaks on the time spectrum was inferior to that of the latter.

It is known in radiation chemistry that a large number of excited molecules generated through decomposition or ionization, followed by recombination of an ion and an electron, are in a triplet state as described in the preceding section. Such a triplet state will subsequently be quenched through the spin conversion process between the excited solvent and paramagnetic oxygen to the singlet state, which results in a shortening of the decay time of scintillation. The excited molecules due to the recombination of an ion and an electron will be produced in much larger quantities by alpha-particles than electrons because of the greater linear energy transfer of the former.

Shifts of the Pulse Height by Chemical and Oxygen Quenchers. The chemical and oxygen quenchings were examined by means of the pulse height analysis. Relative pulse heights (I_0/I) are plotted in Fig. 6 against the concentration of each quencher, where I and I_0 are the peak channels of the pulse height spectra observed with a given quencher and without the quencher, respectively. The linear relationship between I_0/I and the concentration was observed for each quencher. Hence, the relation can be analyzed by the following equation:

$$I_0/I = 1 + \gamma[C]$$

where γ is the quenching constant, and [C] the quencher concentration. The quenching constant was evaluated from the slope in Fig. 6, and the results are listed in Table 1. The constants were the same for alpha-particles and conversion electrons for given halogeno compounds. This would suggest that there are no remarkable differences between the chemical reactions due to the halo methanes and the excited solvents produced through the energy loss processes of alpha-particles and electrons.

Takiue and Ishikawa reported quenching constants for a series of organo halogen compounds in the toluene-PPO system using conversion electrons from ^{113}Sn.[14] For the same quencher, the quenching constant for the Insta-Gel system was found to be roughly one-half of the value in the toluene-PPO system as seen in Table 1. The quenching constant should be inversely proportional to the viscosities of the solvent from the bimolecular reaction theory.[30] The observed values, however, are not consistent with this. The discrepancy seems to be ascribed to the reasons that the scintillator solution is a mixtured solution containing PPO and a surface-active agent.

Effects of Paramagnetic Species on Time Spectrum. In order to examine in greater details the effects of paramagnetic species revealed in the time spectrum of alpha-particles and conversion electrons, we studied the effects of $GdCl_3$ ($4f^7$, S=7/2) and $YbCl_3$ ($4f^{13}$, S=1/2) in Insta-Gel. The time spectra of alpha-rays of ^{210}Po and conversion electrons of ^{139}Ce in Insta-Gel (containing 50 mM $GdCl_3$ used as a quenching agent) are shown in Fig. 7a, and the time difference between the peak channels was plotted against the concentration of $GdCl_3$ as shown in Fig. 7b. The results on $YbCl_3$ used as a quenching agent were the same as those obtained on $GdCl_3$. The oxygen effect in the foregoing arguments raises an expectation that a time spectrum of alpha-particles from ^{210}Po would be affected by the lanthanoid ions through spin conversion process. The experimental results, however, failed to show this. Unlike oxygen, paramagnetic lanthanoid ions did not shift the time spectrum for alpha-particles and conversion electrons. In order to find a reasonable explanation, the shortening process of the time distribution by paramagnetic quenchers may be considered as follows.

When the spin conversion process takes place between an unpaired electron of a paramagnetic quencher and the excited triplet state of a solvent molecule, a spin pairing will occur in the paramagnetic quencher if the partly filled electron shell has more than one electron or hole. Therefore, for the spin

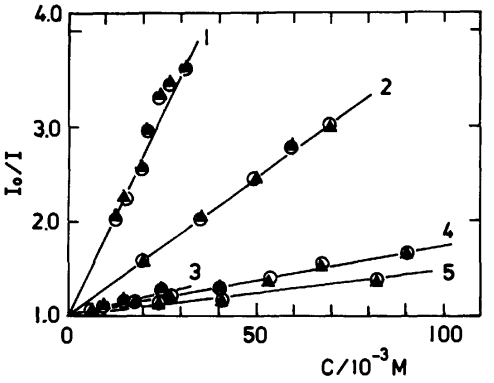

Fig. 6. Values of I_0/I plotted against the quencher concentration; 1: CBr_4, 2: $CHBr_4$, 3: CCl_4, 4: CH_2Br_2, 5: $CHCl_3$. ○: alpha-particles, ▲: electrons.

Table 1. Quenching constants of halomethanes and oxygen observed in Insta-Gel excited with conversion electrons from ^{139}Ce and alpha-particles from ^{210}Po

Compound	Quenching constant $10^3\gamma_1/M^{-1}$ (in Insta-Gel)	$10^3\gamma_2/M^{-1}$ [a] (in toluene-PPO)	(γ_1/γ_2)
CBr_4	88.7	164.0	0.54
$CHBr_3$	30.2	57.0	0.53
CCl_4	26.3	50.8	0.52
CH_2Br_2	7.39	13.3	0.56
$CHCl_3$	3.95	6.83	0.58
O_2	57.8[b]	—	—

a) The data of toluene-PPO system were cited from Ref. 14. b) In the case of oxygen, the value was obtained by the least squares method on seven data points (up to 8 mM).

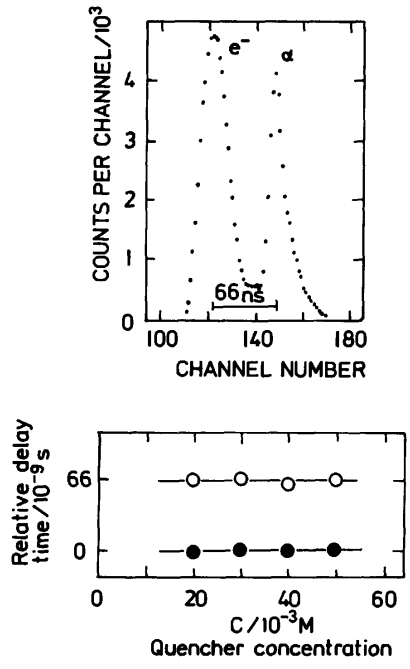

Fig. 7. (a) Time spectra of conversion electrons from ^{139}Ce and alpha-particles from ^{210}Po in oxygen-free Insta-Gel containing 50 mM $GdCl_3$. (b) Relative peak delay on the time spectra of conversion electrons and alpha-particles against the concentration of $GdCl_3$; open and full circles show the peak positions due to alpha-particles and conversion electrons, respectively.

conversion to occur, the spin pairing energy of the quenching molecule or ion must be at least lower than the energy of the lowest excited triplet state of the solvent molecule. The spin pairing energies of low lying states of oxygen are reported to be 1.46 and 0.98 eV.[31] The lowest excited triplet states of such solvents as xylene, toluene, and benzene are reported to be 3.49, 3.57, and 3,65 eV, respectively.[32–34] Thus, the spin conversion process is energetically allowed for the oxygen quencher. However, the energy balance between the solvent molecule and the paramagnetic quencher is not a sole dominant factor for the process. The lowest spin pairing energy of trivalent gadolinium ions is estimated to be 3.9 eV ($^6P_{7\,2} \leftarrow {}^8S_{7\,2}$), while trivalent ytterbium ions require no spin pairing energy with the electric confiration of $4f^{13}$,[35] so that the latter would be expected to act as a good paramagnetic quencher. However, no meaningful difference in quenching effect was found between the above two lanthanoid ions. This observation may be explained if we recall that trivalent lanthanoid ions have unpaired electrons of 4f-orbitals inside the filled 5s–5p orbitals, and probably have little overlap with an orbital of an unpaired electron of an excited solvent molecule. The spin conversion in the scintillation process is, therefore, forbidden for lanthanoid ions not only because of the energy balance but also because of the inertness of 4f-electrons. These results may lead us to conclude that the spin conversion process for oxygen is allowed from two reasons of the energy balance and the overlap of orbitals.

Conclusion. 1) The time spectra of electrons were affected by electron energies. The results may be explained in terms of the energy loss of electrons in liquid scintillator solutions as follows. As the electron energy decrease, the stopping power increases. The increased energy loss per unit length causes localized ionizations, radiation decompositions, and radical formations. The ionized species recombine in a short time with electrons, and subsequently lead to the formation of an excited triplet state in the absence of spin correlation between a positive ion and an electron. The energy transfer from the decay of a long-lived triplet state and the subsequent fluorescence of PPO will result in the delayed distribution on the time spectrum.

2) The chemical quenching constants for alpha-particle and electron excitations were found to be identical with the same organo halogen compound. The results suggest that the chemical reactions of organo halogen compounds with the excited solvents lead to practically the same reduction of the fluorescence yields for alpha-particles and electrons.

3) The time spectra of alpha-particles were shifted by oxygen, whereas those of electrons were not. In addition, they were not also affected by lanthanoid ions. The facts may be explained in terms of spin conversion mechanism. For the spin conversion to occur, the molecule must be excited at least to an excited state whose spin multiplicity is smaller by two than that of the ground state. In the case of spin doublet state, the process is expected to be allowed energetically. However, the results on the lanthanoid ions showed that the overlap of an unpaired electron of the paramagnetic quencher and that of the excited solvent is also important for the process.

The authors are grateful to Dr. H. Ishikawa of Radioisotope Nuclear Reactor School at Japan Isotope Research Institute for the use of an oxygen analyzer, and to Prof. Y. Murakami at Kitasato University for kind suggestions throughout this work.

References

1) T. Kato, *Int. J. Appl. Radiat. Isoto.*, **30**, 349 (1979).
2) T. Kato and T. Hashimoto, *Anal. Chem.*, **52**, 586 (1980).
3) R. Dyer, "An Introduction to Liquid Scintillation Counting," ed by Heyden Pergamon Press, (1974), p. 65.
4) H. Jeffay, "Advances in Tracer Methodology," Plenum Press (1963) Vol. 1, p. 113.
5) H. Jeffay and J. Alvarez, *Anal, Chem.*, **33**, 612 (1961).
6) T. Aburai, M. Takiue, and H. Ishikawa, *Radioisotopes*, **30**, 678 (1981).
7) M. Yanokura, K. Horiuchi, H. Nakahara, and Y. Murakami, *Chem. Lett.*, **1978**, 1131.
8) K. Horiuchi and Y. Murakami, *Chem. Lett.*, **1979**, 449.
9) Y. Murakami and K. Horiuchi, *J. Radioanal. Chem.*,

52, 275 (1979).
10) K. Horiuchi and Y. Murakami, *Int. J. Appl. Radiat. Iso.*, **32**, 291 (1981).
11) J. B. Birks and J. C. Conte, *Proc. R. Soc. London, Ser. A*, **303**, 85 (1968).
12) T. A. King and R. Voltz, *Proc. R. Soc. London, Sor. A*, **287**, 424 (1965).
13) M. Takiue and H. Ishikawa, *Nucl. Instrum. and Methods*, **118**, 51 (1974).
14) M. Takiue and H. Ishikawa, *Radioisotopes*, **27**, 74 (1978).
15) H. Ishikawa, M. Takiue, and S. Tanaka, *Int. J. Appl. Radiat. Isot*, **31**, 703 (1980).
16) G. T. Wright, *Proc. Phys. Soc.*, **B49**, 358 (1956).
17) D. H. Wilkinson, *Rev. Sci. Instr.*, **23**, 414 (1952).
18) W. Daehnick and R. Sherr, *Rev. Sci. Instr.*, **32**, 666 (1961).
19) R. A. Winyard, J. E. Lutkin, and G. W. McBeth, *Nucl. Instrum. Methods*, **95**, 141 (1971).
20) G. W. McBeth, J. E. Lutkin, and R. A. Winyard, *Nucl. Instr. and Meth.*, **93**, 99 (1971).
21) R. E. Howe, *Nucl. Instrum. Methods*, **190**, 309 (1981).
22) H. H. Seliger, *Int. J. Appl. Radiat. Isot.*, **8**, 29 (1960).
23) J. H. Thorngate, W. J. Farrar, and D. J. Christian, *Health Phys.*, **27**, 123 (1974).
24) W. J. McDowell, D. T. Farrar, and M. R. Billings, *Talanta*, **24**, 1232 (1974).
25) J. W. McKlveen and W. R. Johnson, *Health Phys.*, **28**, 5 (1975).
26) P. Cross and G. W. McBeth, *Health Phys.*, **30**, 306 (1976).
27) R. A. Winyard and G. W. McBeth, *Nucl. Instrum. Methods*, **98**, 525 (1972).
28) L. Pages, E. Bertel, H. Jeffre, and L. Sklavenitis, *At. Data Nucl. Data Tables* , **4**, 1 (1972).
29) J. F. Janni, *At. Data Nucl. Data Tables* , **27**, 147 (1982).
30) See for example, A. A. Frost, and R. G. Peason, "Kinetics and Mechanism," 2nd ed, John Wiley and Sons, Inc., New York and London (1961) p. 268.
31) R. J. Myers, "Molecular Magnetism and Magnetic Resonance Spectroscopy," Prentice-Hall, Inc., New Jersey (1972).
32) L. A. Blackweel, Y. Kanda, and H. Sponer, *J. Chem. Phys.*, **32**, 1465 (1960).
33) D. S. McClure, *J. Chem. Phys.*, **17**, 231 (1949).
34) R. Zemerli, *J. Chem. Phys.*, **30**, 405 (1959).
35) W. T. Carnall, P. R. Fields, and K. Rajnak, *J. Chem. Phys.*, **49**, 4412 (1968).

Preparation and Structural Studies of Tris[(1*R*,2*R*)- or (1*R*,2*S*)-2-(Aminomethyl)cyclohexylamine]cobalt(III) Complexes

Masahide Noji,* Haruo Toida, and Yoshinori Kidani
Faculty of Pharmaceutical Sciences, Nagoya City University, 3-1 Tanabe-dori, Mizuho-ku, Nagoya 467
(Received September 25, 1984)

New cobalt(III) complexes containing (1*R*,2*R*)- or (1*R*,2*S*)-2-(aminomethyl)cyclohexylamine(=amcha) have been synthesized and separated into diastereoisomers. $[Co(1R,2R\text{-amcha})_3]^{3+}$ gives two diastereoisomers, structures of which were deduced to be *mer*-Δ and *fac*-Δ based upon their ^{13}C-NMR and CD spectra. $[Co(1R,2S\text{-amcha})_3]^{3+}$ gives three diastereoisomers, structures of which were determined to be *mer*-Λ, *mer*-Δ, and *fac*-Λ. The conformations of the six-membered chelate rings were investigated in the absence or presence of sulfate ions.

The structural study of antitumor Pt(II) complexes of 2-(aminomethyl)cyclohexylamine(=amcha) isomers showed that the chelate ring of (1*R*,2*R*)-amcha is interconvertible between the two chair forms through a λ-skew form, and that of (1*R*,2*S*)-amcha exists in the fixed-chair form, as shown in Fig. 1.[1,2] Since tris(amcha)Co(III) complexes have an octahedral structure, they are expected to form crowded structures rather than square planar Pt(II) complexes. Therefore, the influence of steric interactions among the adjacent ligands is considered to contribute greatly to the conformation of the ligands. In order to investigate the conformation of the six-membered chelate rings of tris(amcha)Co(III) complexes, the authors prepared and separated them into diastereoisomers.

In this paper, the authors will discuss the structures of Co(III) complexes of amcha isomers and the conformations of the chelate rings, based upon their electronic absorption, circular dichroism, and ^{13}C-NMR spectra. This information should be useful in understanding antitumor Pt(IV) complexes of amcha isomers, which are now under investigation.

Experimental

Ligand. A synthesis of *cis*- and *trans*-2-(aminomethyl)cyclohexylamine: These ligands were synthesized from corresponding 1,2-cyclohexanedicarboxylic acids according to a method reported by Armarego *et al.*[3] Resolution of *cis*- and *trans*-amcha was achieved to give (1*R*,2*R*)- and (1*R*,2*S*)-amcha, respectively, according to a method described in the literature.[1]

Preparation of Tris[(1R,2R)- or (1R,2S)-amcha]cobalt(III) Complexes. *trans*-$[CoCl_2(1R,2R\text{- or }1R,2S\text{-amcha})_2]Cl$. To an aqueous solution (15 cm³) containing 2.42 g of $Na_3[Co(NO_2)_6]$ was added an aqueous suspension (20 cm³) of (1*R*,2*R*)- or (1*R*,2*S*)-amcha (1.5 g). The mixture was heated for 4 h at 70 °C with continuous agitation. To the resultant orange solution were added 25 cm³ of conc HCl and stirred for 2 h at 70 °C. Deposited green crystals were collected, washed with ethanol and dried *in vacuo*. Yield: 1.5 g for $[CoCl_2(1R,2R\text{-amcha})_2]Cl$ and 2.3 g for $[CoCl_2(1R,2S\text{-amcha})_2]Cl \cdot 1.5\ H_2O$.

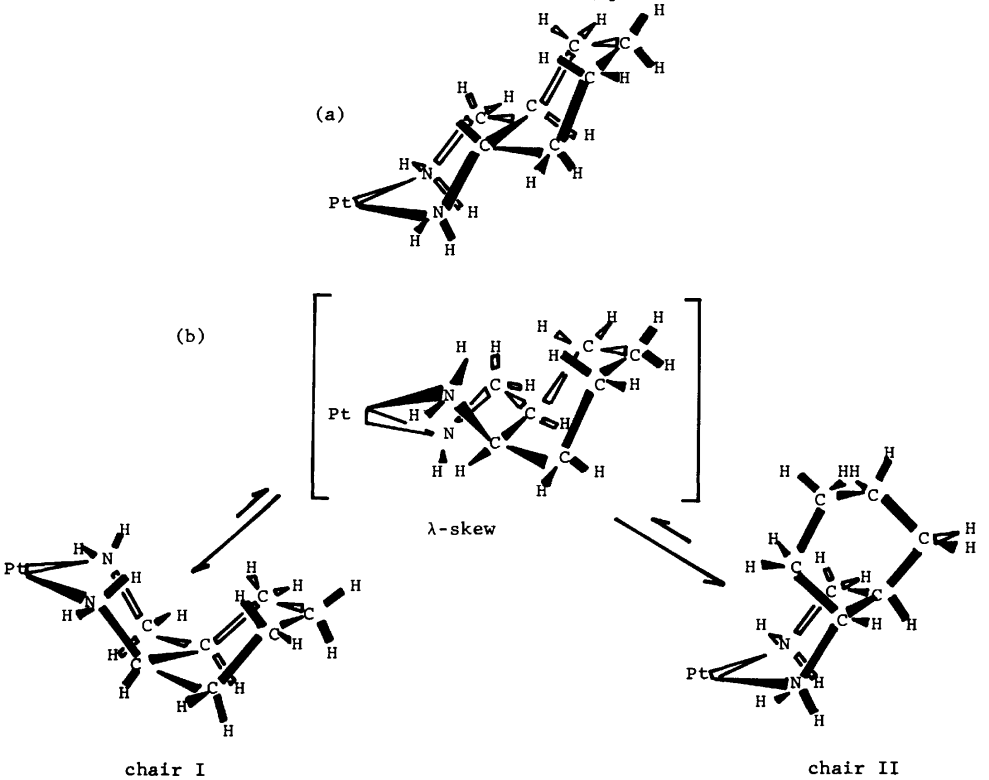

Fig. 1. Conformations of Pt(II) complexes of amcha isomers.
(a) 1*R*,2*S*-amcha, (b) 1*R*,2*R*-amcha.

Table 1. Elemental analyses of cobalt(III) complexes of 2-(aminomethyl)cyclohexylamine

Complex	H (%)		C (%)		N (%)	
	Found	Calcd	Found	Calcd	Found	Calcd
trans-$[CoCl_2(1R,2R\text{-amcha})_2]Cl$	7.92	7.66	39.69	39.86	13.17	13.29
trans-$[CoCl_2(1R,2S\text{-amcha})_2]Cl\ 1.5H_2O$	7.57	7.74	38.93	39.03	13.43	13.01
mer-Δ-$[Co(1R,2R\text{-amcha})_3](ClO_4)_3$	6.26	6.53	33.91	33.98	10.98	11.32
fac-Δ-$[Co(1R,2R\text{-amcha})_3](ClO_4)_3$	6.22	6.53	33.87	33.98	11.14	11.32
mer-Λ-$[Co(1R,2S\text{-amcha})_3](ClO_4)_3\ HClO_4\cdot 7H_2O$	6.65	6.57	25.95	26.03	8.73	8.67
mer-Δ-$[Co(1R,2S\text{-amcha})_3](ClO_4)_3\ HClO_4\cdot 2H_2O$	6.29	6.09	28.95	28.70	9.67	9.57
fac-Λ-$[Co(1R,2S\text{-amcha})_3](ClO_4)_3\ HClO_4\cdot 7H_2O$	6.35	6.57	25.76	26.03	8.69	8.67

Tris(amcha)cobalt(III) Complexes. To a DMSO solution (20 cm^3) of *trans*-$[CoCl_2(1R,2R\text{-amcha})_2]Cl$ (or *trans*-$[CoCl_2(1R,2S\text{-amcha})_2]Cl$)(1.0 g) was added a methanol solution (5 cm^3) of (1*R*,2*R*)- (or 1*R*,2*S*-)amcha (0.3 g). The mixture was stirred overnight at 60°C. A reddish-orange solution was diluted with 3 dm^3 of water and was adsorbed on SP-Sephadex C-25. These adsorbed complexes were separated by the following procedures.

a) Separation of Tris(1R,2R-amcha)Co(III) Complexes. The complexes adsorbed on the resin were placed on a column (3.0 IDX120 cm) of SP-Sephadex C-25 and were developed with 0.2 mol dm^{-3} sodium(+)$_{589}$-tartratoantimonate(III). The complexes were separated into two bands, $F_{C\text{-}1}$ and $F_{C\text{-}2}$, in the order of eluation. The fractions were diluted with water as many as ten times, followed by adsorption in an SP-Sephadex column.

mer-Δ-$[Co(1R,2R\text{-}amcha)_3](ClO_4)_3$. The $F_{C\text{-}1}$ fraction loaded in an SP-Sephadex column was washed with a large volume of 0.005 mol dm^{-3} $HClO_4$ solution and was then eluated with a 0.5 mol dm^{-3} $HClO_4$ solution. The eluate was concentrated in a desiccator *in vacuo* over P_4O_{10} and NaOH. Deposited orange crystals were collected and dried in a desiccator over P_4O_{10} and NaOH. Yield: 20 mg

fac-Δ-$[Co(1R,2R\text{-}amcha)_3](ClO_4)_3$. This complex was obtained from the $F_{C\text{-}2}$ fraction by the same procedure as that for the *mer*-Δ isomer. Yield: 50 mg.

b) Separation of Tris(1R,2S-amcha)Co(III) Complexes. The adsorbed band of tris(1*R*,2*S*-amcha)Co(III) complexes was placed on an SP-Sephadex column and was developed with 0.2 mol dm^{-3} sodium(+)$_{589}$-tartratoantimonate(III). The band split into two bands, $F_{T\text{-}1}$ and $F_{T\text{-}2}$, in the order of eluation. The $F_{T\text{-}1}$ fraction was diluted with water as many as ten times and was loaded on an SP-Sephadex column (2.0 IDX110 cm) and rechromatographed with 0.2 mol dm^{-3} Na_2SO_4. The band split into two bands, $F_{T\text{-}1\text{-}1}$ and $F_{T\text{-}1\text{-}2}$.

mer-Λ *and* mer-Δ-$[Co(1R,2S\text{-}amcha)_3](ClO_4)_3\cdot nH_2O$. The *mer*-Λ *and mer*-Δ complexes were obtained from the $F_{T\text{-}1\text{-}1}$ and $F_{T\text{-}1\text{-}2}$ fractions, respectively, by a similar procedure to that of *mer*-Δ-$[Co(1R,2R\text{-amcha})_3](ClO_4)_3$. Yield: 30 mg for *mer*-Λ and 50 mg for *mer*-Δ.

fac-Λ-$[Co(1R,2S\text{-}amcha)_3](ClO_4)_3\cdot 2H_2O$. The complex was obtained from the $F_{T\text{-}2}$ fraction by a similar procedure to that indicated above. Yield: 140 mg.

The results of elemental analyses of the Co(III) complexes, thus obtained, are shown in Table 1.

Measurements. Absorption and circular dichroism spectra were measured with a Hitachi 557 spectrophotometer and a JASCO J-40 spectropolarimeter. FT ^{13}C-NMR spectra were obtained with a JEOL JNM-FX-100 spectrometer.

Results and Discussion

^{13}C-NMR Spectra. There are two geometrical isomers, *i.e.*, *mer* and *fac*, for tris(1*R*,2*R*-amcha)Co(III) complexes. The $F_{C\text{-}1}$ and $F_{C\text{-}2}$ fractions separated through an SP-Sephadex column exhibited ^{13}C-NMR spectra (Fig. 2). The ^{13}C-NMR spectrum of the $F_{C\text{-}2}$ fraction showed 7 singlet resonance lines, indicating the *fac*-isomer, where the three coordinated amcha are chemically equivalent. The $F_{C\text{-}1}$ fraction showed a similar ^{13}C-NMR pattern to that of the *fac*-isomer, except that each resonance peak was composed of a doublet or triplet, indicating a lower symmetric *mer*-isomer with unequivalent ligands. Assignments of the resonance lines were tentatively made based on the assignments for [Pt(en)(1*R*,2*R*-amcha)]Cl_2.

Tris(1*R*,2*S*-amcha)Co(III) complexes were separated into three fractions, *i.e.*, $F_{T\text{-}1\text{-}1}$, $F_{T\text{-}1\text{-}2}$, and $F_{T\text{-}2}$, typical two ^{13}C-NMR spectra of which are illustrated in Fig. 2. The $F_{T\text{-}2}$ fraction exhibited 7 singlet resonance lines in the ^{13}C-NMR spectrum and was assigned to the symmetric *fac*-isomer. The $F_{T\text{-}1\text{-}1}$ and $F_{T\text{-}1\text{-}2}$ fractions showed a similar ^{13}C-NMR spectral pattern to that of $F_{T\text{-}2}$, except that each resonance peak was composed of a doublet or triplet, suggesting the *mer* configuration. The assignments of the resonance lines for these Co(III) complexes were made as shown in Fig. 2, based upon the assignments of [Pt(en)(1*R*,2*S*-amcha)]Cl_2.[1]

Absorption Spectra. The absorption maxima of the first absorption bands of Co(III) complexes containing 1,3-diamines were reported to shift depending upon the configurations of the complexes. For example, the tris(meso-ptn)Co(III) complex was reported to have *fac*- and *mer*-isomers with a chair conformation. The interaction among the ligands was larger in the *mer*-isomer than the *fac*-isomer and the absorption maximum of the former shifted 2 nm toward a longer-wavelength region compared to that of the latter.[4]

a) Tris(1R,2R-amcha)Co(III) Complexes. Comparing the absorption maxima of the *fac*- and *mer*-isomers of tris(1*R*,2*R*-amcha)Co(III), the maximum of the *fac*-isomer was at 489 nm and that of the *mer*-isomer

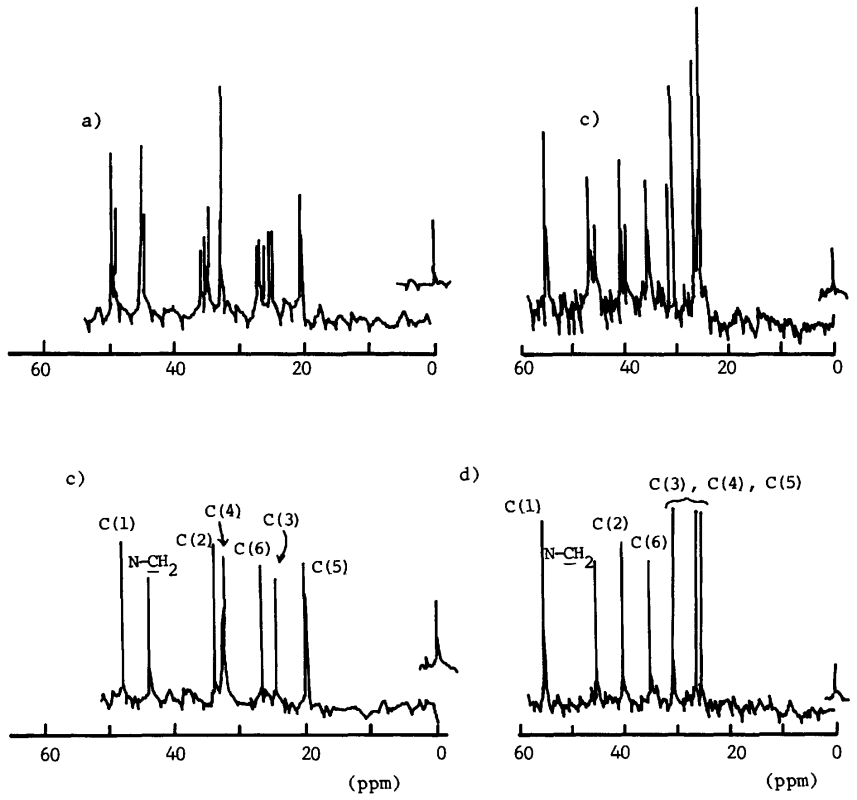

Fig. 2. ^{13}C-NMR spectra of tris(amcha)cobalt(III) complexes.
(a): F_{C-1}; *mer*-Δ-[Co(1*R*,2*R*-amcha)$_3$]$^{3+}$, (b): F_{C-2}; *fac*-Δ-[Co(1*R*,2*R*-amcha)$_3$]$^{3+}$, (c): F_{T-1-2}; *mer*-Δ-[Co(1*R*,2*S*-amcha)$_3$]$^{3+}$, (d): F_{T-2}; *fac*-Λ-[Co(1*R*,2*S*-amcha)$_3$]$^{3+}$.

Table 2. Numerical data of absorption(AB) and cicular dichroism(CD)

Complex	AB λ_{max}/nm (log ε/mol^{-1} dm^3 cm^{-1})	CD λ_{max}/nm (Δε/mol^{-1} dm^3 cm^{-1})
mer-Δ-[Co(1*R*,2*R*-amcha)$_3$](ClO$_4$)$_3$	495.0 (1.97)	517.0 (−0.853)
		530.0 (−0.365)[a]
		475.0 (+0.436)[a]
fac-Δ-[Co(1*R*,2*R*-amcha)$_3$](ClO$_4$)$_3$	489.0 (2.09)	521.0 (−0.666)
		458.5 (+0.089)
		535.0 (−0.239)[a]
		478.0 (+0.749)[a]
mer-Λ-[Co(1*R*,2*S*-amcha)$_3$](ClO$_4$)$_3$ HClO$_4$·7H$_2$O	485.0 (1.97)	505.0 (+0.749)
		505.0 (+0.632)[a]
mer-Δ-[Co(1*R*,2*S*-amcha)$_3$](ClO$_4$)$_3$ HClO$_4$·2H$_2$O	485.0 (2.01)	505.0 (−0.890)
		507.0 (−0.721)[a]
fac-Λ-[Co(1*R*,2*S*-amcha)$_3$](ClO$_4$)$_3$ HClO$_4$·7H$_2$O	485.0 (1.97)	495.0 (+1.025)
		497.0 (+0.437)[a]

a) CD data in 0.2 mol dm^{-3} Na_2SO_4 solutions.

at 495 nm. This shift can be explained by the fact that the *mer*-isomer is stereostructurally more crowded than the *fac*-isomer.

b) Tris(1R,2S-amcha)Co(III) Complexes. All three isomers showed absorption maxima at 485 nm, indicating little interaction among the ligands. The fact that the absorption maximum observed for *fac*-[Co(1*R*,2*S*-amcha)$_3$] shifted 4 nm towaed a longer-wavelength region compared to that of the corresponding *fac*-[Co(1*R*,2*R*-amcha)$_3$] may be explained by a more crowed structure of the former than of the latter.

Circular Dichroism Spectra. In tris(diamine)Co(III) complexes with five-membered chelate rings, there exists a good correlation between the signs of the CD bands corresponding to the E component of the first absorption bands and the configurations. However, in tris(diamine)Co(III) complexes with six-membered chelate rings, the correlation between the signs of the CD bands and the configurations has not been well established. A typical example was found for [Co(tn)$_3$]$^{3+}$.[5-9] However, in the case of tris(*S*-bn)(bn=1,3-butanediamine) complexes, the correlation was well maintain-

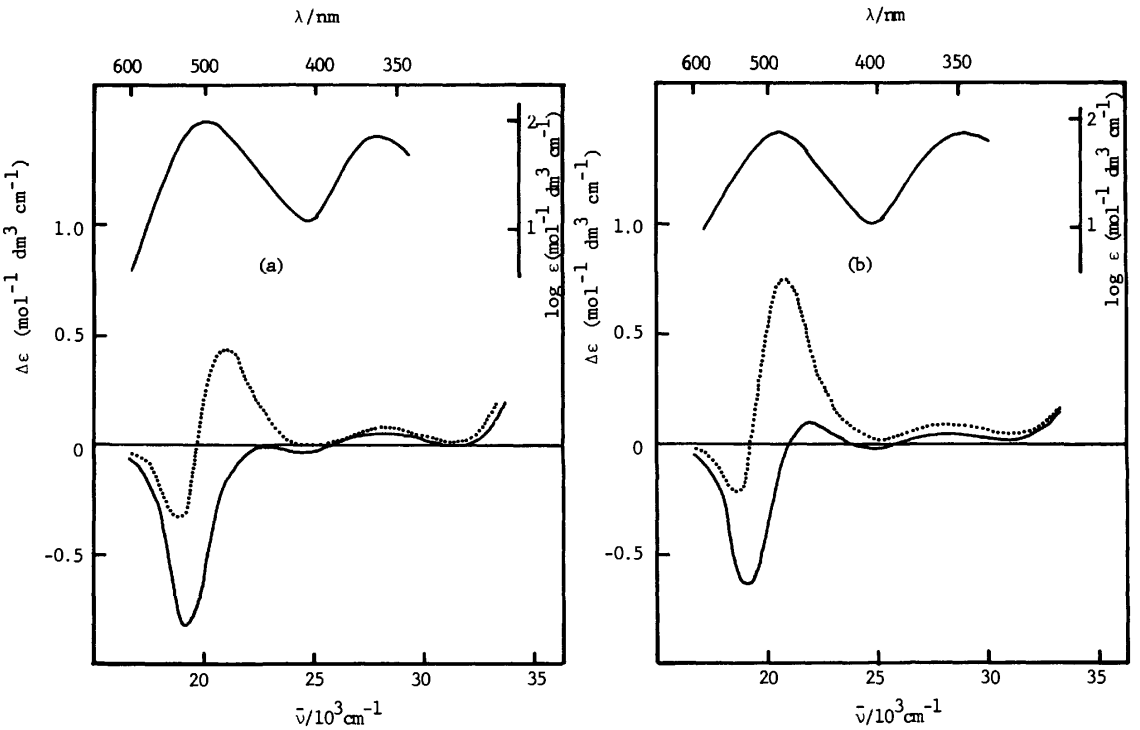

Fig. 3. Absorption and CD spectra of tris(1*R*,2*R*-amcha)cobalt(III) complexes.
(a): *mer*-Δ-[Co(1*R*,2*R*-amcha)$_3$]$^{3+}$, CD spectra of 3.4×10^{-3} mol dm^{-3} in water (——) and 1.7×10^{-3} mol dm^{-3} in 0.2 mol dm^{-3} Na_2SO_4 (·····), (b): *fac*-Δ-[Co(1*R*,2*R*-amcha)$_3$]$^{3+}$, CD spectra of 2.7×10^{-3} mol dm^{-3} in water (——) and 1.7×10^{-3} mol dm^{-3} in 0.2 mol dm^{-3} Na_2SO_4 (·····).

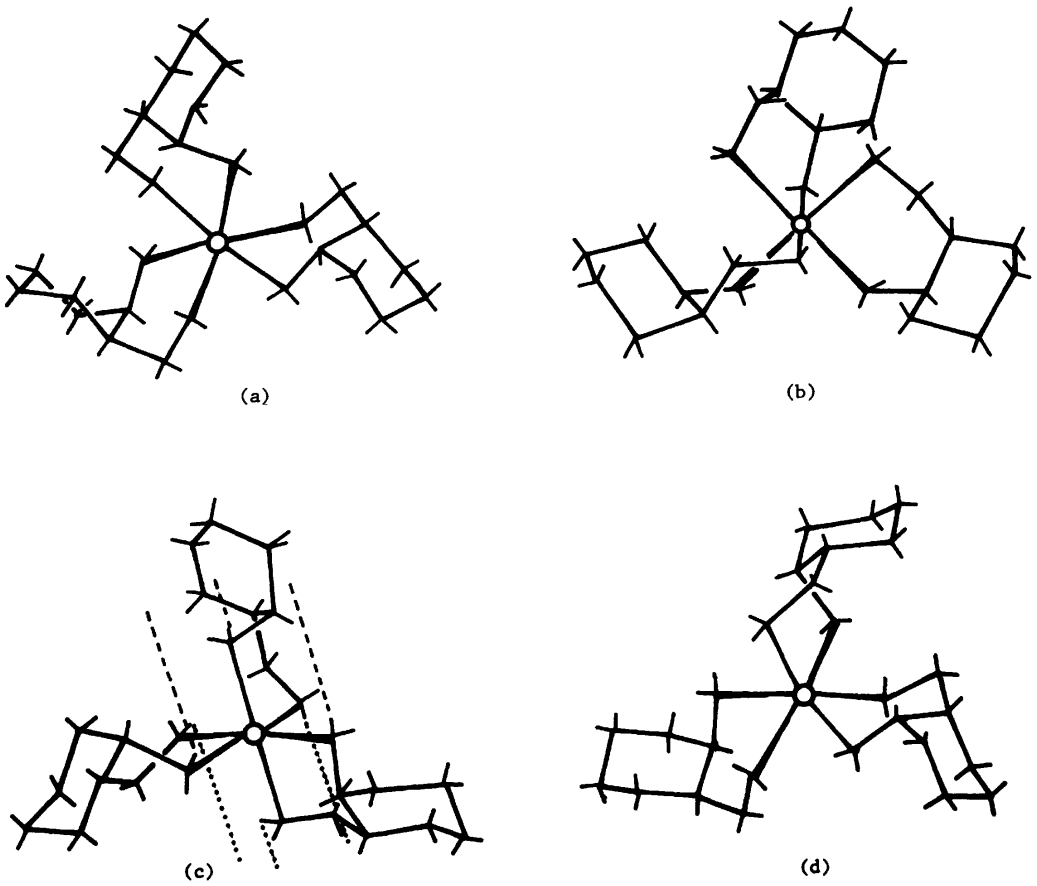

Fig. 4. Schematic structures of *fac*-Δ-[Co(1*R*,2*R*-amcha)$_3$]$^{3+}$.
(a): (chair I)$_3$, (b): (chair II)$_3$, (c): (λ-skew)$_3$, (d): (chair I)$_2$ (λ-skew).

ed, giving positive CD bands for *mer*-Λ and *fac*-Λ isomers and negative ones for the *mer*-Δ and *fac*-Δ isomers.[10]

The CD spectral behavior of tris(1*R*,2*R*- or 1*R*,2*S*-amcha) Co(III) complexes resembles that of tris(*S*-bn)Co(III) complexes, and the configurations of the former were elucidated based on the correlations found in the latter ones.

*a) Tris(1*R,2R*-amcha)Co(III) Complexes.* As shown in Fig. 3, both *mer*- and *fac*-isomers of tris-(1*R*,2*R*-amcha)Co(III) complexes showed negative CD bands at 517 and 521 nm with $\Delta\varepsilon$ values of −0.853 and −0.666 in the first absorption region, respectively. Their configurations were deduced to be Δ. The *fac*-Δ isomer also showed a small positive CD band at 458 nm ($\Delta\varepsilon$=+0.089). In a 0.2 mol dm^{-3} sodium sulfate solution, the CD band of the *mer*-Δ isomer split into two bands, giving negative and positive bands at 530 and 475 nm with $\Delta\varepsilon$ values of −0.365 and +0.436, respectively. The increment of the positive band was also observed for the *fac*-Δ isomer (Fig. 3(b)). The occurrence of the positive CD bands can be explained by taking account of the λ-gauche conformation due to a hydrogen bond formation between sulfate ions and the amino protons. This was confirmed by the molecular model speculations.

As shown in Fig. 1, 1*R*,2*R*-amcha has the possibility to assume chair conformations, one of which has an axial amino group and an equatorial aminomethyl group (chair I). The other has a reverse orientation-(chair II). As to the *fac*-Δ isomer, a (chair I)$_3$ conformer is advantageous over a (chair II)$_3$ conformer, which has a large steric hindrance than the former. However, an interconversion between the chair conformers is possible. Therefore, the small positive CD band in H_2O which was observed for the *fac*-Δ isomer may suggest the existence of a (chair I)$_2$ (λ-skew) conformer. The molecular models of (chair I)$_3$, (chair II)$_3$, and (λ-skew)$_3$ conformers indicate that a (λ-skew)$_3$ conformer can be stabilized by ion-pairs between sulfate ions and amino protons. That is, in the presence of sulfate ions, the (λ-skew)$_3$ form is more stable than other forms.

Concerning the *mer*-Δ isomer, the (chair I)$_3$ conformer is the most stable form and the (chair II)$_3$ conformer was not considered due to its steric hindrances. The other possible structure is a (chair I)$_2$ (chair II) conformer. Thus, an equilibrium between (cahir I)$_3$ and (chair I)$_2$ (chair II) is probable, but the frequency of the interconversion, which can take place through the λ-skew, is low compared to that between (chair I)$_3$ and (chair II)$_3$ for the *fac*-Δ isomer. The model of a *mer*-Δ(λλλ) conformer indicates that two ion-pairs are also possible similar to the *fac*-Δ isomer, giving an enhanced intensity of the positive CD band in the presence of sulfate ions.

*b) Tris(1*R,2S-amcha)Co(III) Complexes.* CD spectra of the mer isomers exhibited a positive and a negative CD band at 505 nm in H_2O for $F_{T\text{-}1\text{-}1}$ and $F_{T\text{-}1\text{-}2}$ fractions, respectively. The *fac*-isomer showed positive CD band at 505 nm. From these CD data, the configurations of $F_{T\text{-}1\text{-}1}$ and $F_{T\text{-}1\text{-}2}$, and $F_{T\text{-}2}$ complexes were deduced to be *mer*-Λ, *mer*-Δ, and *fac*-Λ, respectively. Their CD spectra are illustrated in Fig. 5.

In the presence of sulfate ions, the *fac*-Λ isomer exhibited a significant decrease in $\Delta\varepsilon$ (from +1.02 to +0.43). On the other hand, both the *mer*-Λ and *mer*-Δ isomers showed only a little decrease in $\Delta\varepsilon$ in 0.2 mol dm^{-3} sodium sulfate solutions. These CD spectra are also illustrated in Fig. 5. The CD spectral behavior of tris(1*R*,2*S*-amcha)Co(III) complexes suggested different conformations to those of the tris(1*R*,2*R*-amcha)-Co(III) complexes. The differences may arise due to the fact that the conformations of 1*R*,2*S*-amcha were restricted to the chair and λ-skew forms, as shown in [Pt(en)(1*R*,2*S*-amcha)]$^{2+}$.

From the molecular models of the tris(1*R*,2*S*-amcha) Co(III) complexes the following conclusions were obtained concerning the stereostructures of the three isomers. For the *fac*-Λ isomer, (chair)$_3$ and (λ-skew)$_3$ conformers are stable and in the former ion-pairs can be formed between sulfate ions and amino protons, while in the latter ion-pair formation is not possible due to its (ob)$_3$-type structure. That is, in H_2O the *fac*-Λ isomer exists as a (Λ-skew)$_3$ conformer, which changes conformations and the (chair)$_3$ conformer becomes stable in a 0.2 mol dm^{-3} sodium sulfate solution by ion-pair formation. This explains the observed decrease in $\Delta\varepsilon$.

For the *mer*-Λ isomer, a (λ-skew)$_3$ conformer is more stable than (chair)$_3$, in which steric hindrance exists between ligand A and B as shown in Fig.7. The presence of sulfate ions brought about a slight decrease in $\Delta\varepsilon$ (from +0.749 to +0.632), suggesting a partial conformational change among the three ligands. Among the three possibe (λ-skew)$_2$(chair) conformers, the one involving ligand C in a chair conformation stabilized with less steric hindrance and was able to form ion-pairs. Another conformer, containing ligand B in a chair conformation, was also stable but it could not form the ion-pairs. The other conformer containing ligand A in chair was less stable than the other two conformers due to its steric hindrance. The molecular models indicate that *mer*-Λ isomer exists as a (λ-skew)$_3$ conformer in H_2O and in the presence of sulfate ions a (λ-skew)$_2$ (chair) conformer with ligand C in a chair conformation is stabilized by the ion-pair formation with a slight decrease in $\Delta\varepsilon$.

The molecular models of the last isomer, *mer*-Δ indicate that it can also exist as a (λ-skew)$_3$ or (λ-skew)$_2$ (chair) conformer, in the latter of which ligand A or B in the chair conformation. Its CD spectral behavior in H_2O and a 0.2 mol dm^{-3} sodium sulfate solution seems to indicate that a partial conformational change from chair to λ-skew takes place with a decreased absolute $\Delta\varepsilon$ in the latter solution. That is, the *mer*-Δ isomer exists in a (λ-skew)$_2$(chair) form in H_2O and a (λ-skew)$_3$ form in the presence of sulfate ions. How-

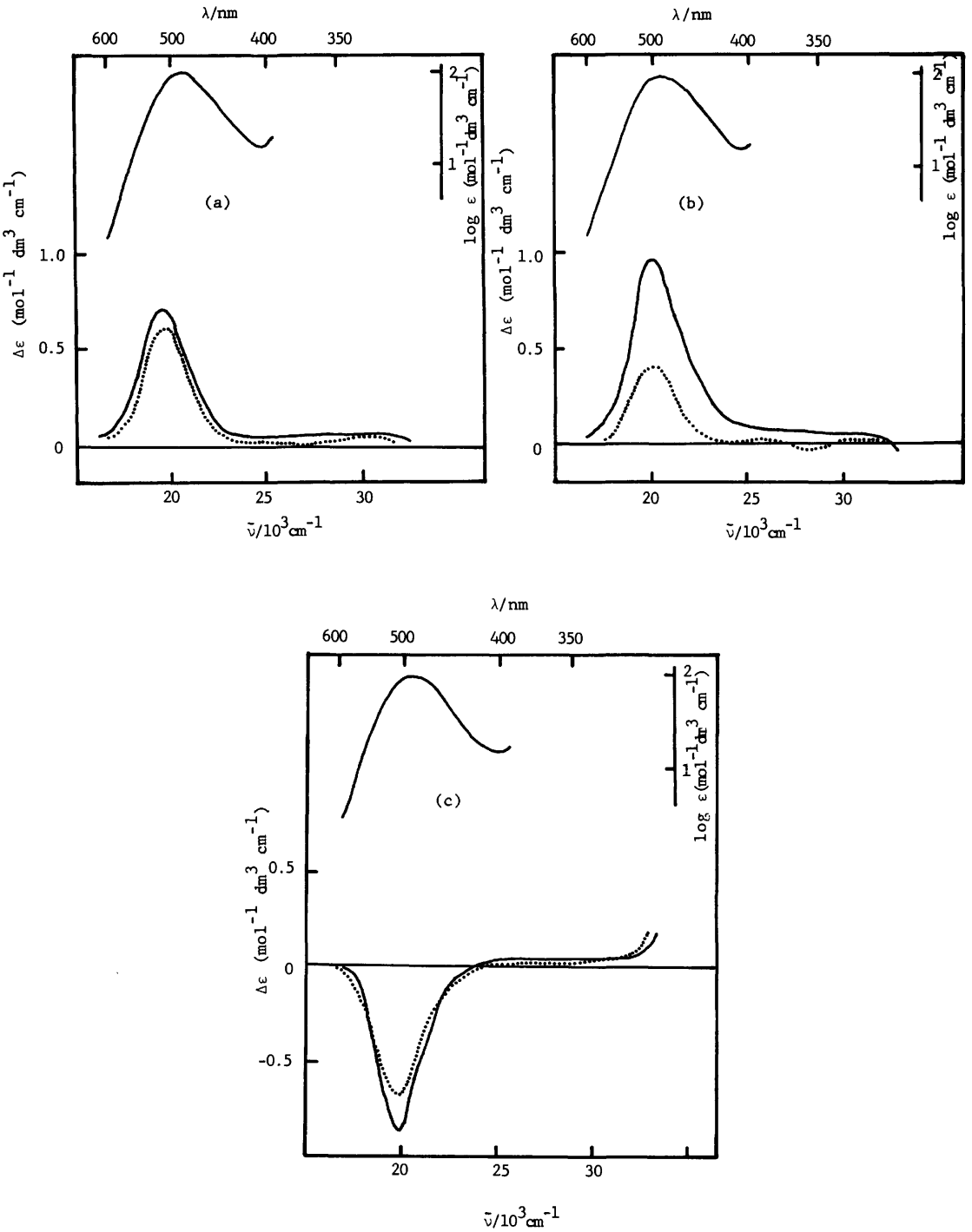

Fig. 5. Absorption and CD spectra of tris(1*R*,2*S*-smcha)cobalt(III) complexes.
(a): *mer*-Λ-[Co(1*R*,2*S*-amcha)$_3$]$^{3+}$, CD spectra of 5.19×10^{-3} mol dm^{-3} in water (——) and 0.2 mol dm^{-3} Na_2SO_4 (·····), (b): *fac*-Λ-[Co(1*R*,2*S*-amcha)$_3$]$^{3+}$, CD spectra of 5.16×10^{-3} mol dm^{-3} in water (——) and 0.2 mol dm^{-3} Na_2SO_4 (·····), (c): *mer*-Δ-[Co(1*R*,2*S*-amcha)$_3$]$^{3+}$, CD spectra of 5.73×10^{-3} mol dm^{-3} in water (——) and 0.2 mol dm^{-3} Na_2SO_4 (·····).

ever, this explanation is in conflict with the $\Delta\varepsilon$ value of −0.89 in H_2O for the *mer*-Δ isomer, because the combination of a Δ configuration and λ conformations would be expected to give a somewhat smaller absolute $\Delta\varepsilon$ than the value of +0.749 observed for the *mer*-Λ isomer with (λ-skew)$_3$ conformations. Therefore, the conformation of *mer*-Δ was not possible to determine with the present CD spectral data.

This work was supported in part by Grant-in-Aids for Cancer Research from the Ministry of Education, Sceince and Culture (No. 59015085) and from the

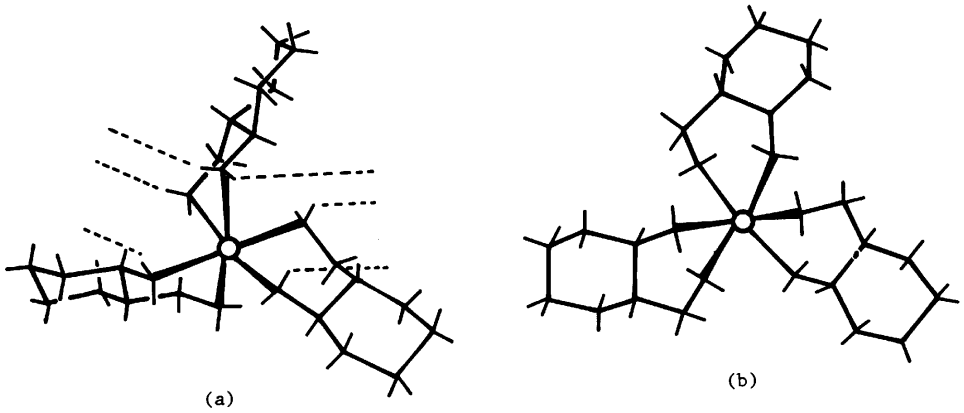

Fig. 6. Schematic structures of *fac*-Δ-[Co(1*R*,2*S*-amcha)$_3$]$^{3+}$.
(a): (chair)$_3$, (b): (λ-skew)$_3$.

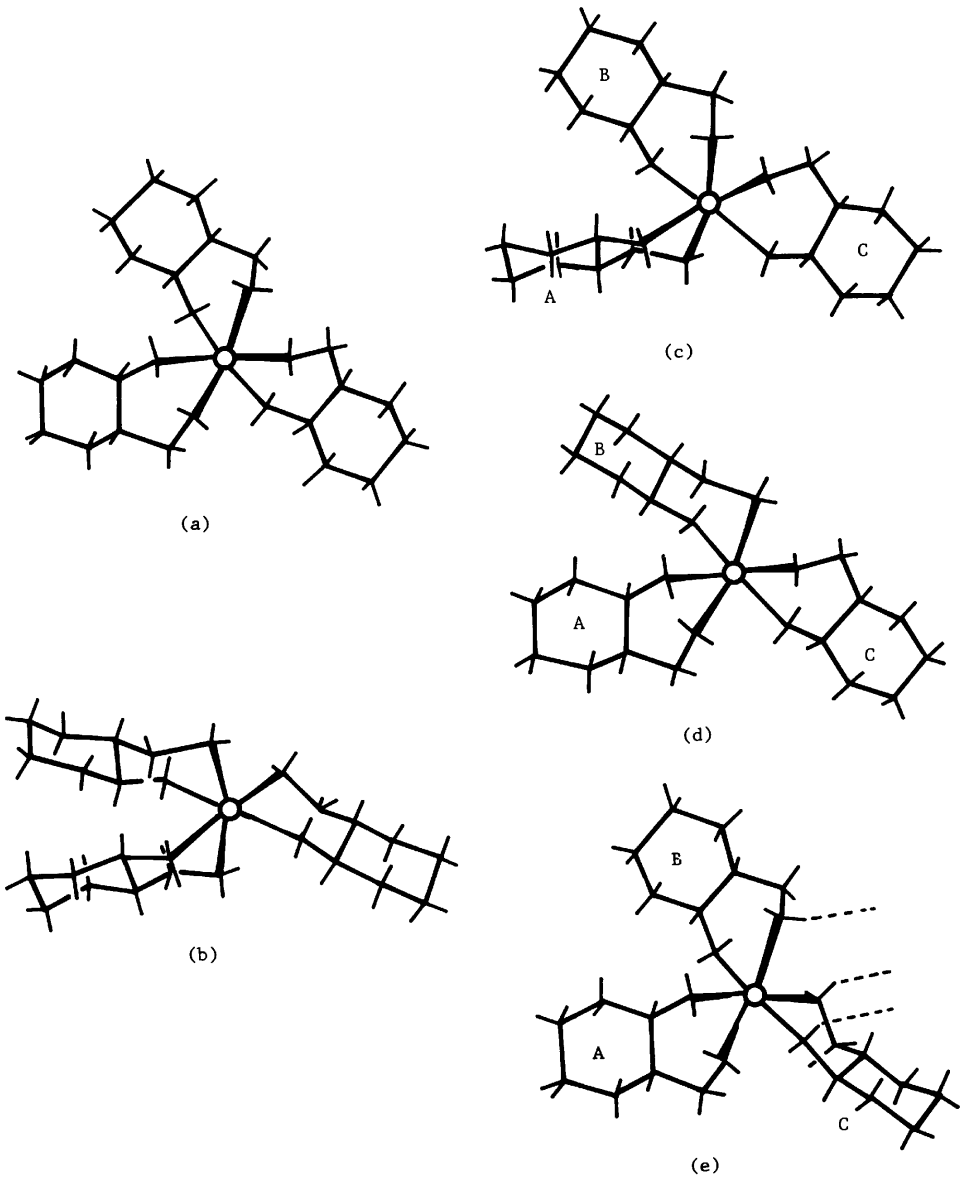

Fig. 7. Schematic structures of *mer*-Λ-[Co(1*R*,2*S*-amcha)$_3$]$^{3+}$.
(a): (λ-skew)$_3$, (b): (chair)$_3$, (c): (λ-skew)$_2$ (chair A), (d): (λ-skew)$_2$ (chair B), (e): (λ-skew)$_2$ (chair C).

Ministry of Health and Welfare of Japan.

References

1) K. Okamoto, M. Noji, and Y. Kidani, *Bull. Chem. Soc. Jpn.*, **54**, 713 (1981).
2) M. Noji, K. Okamoto, and Y. Kidani, *J. Med. Chem.*, **24**, 508 (1981).
3) W. L. F. Armarego and T, Kobayashi, *J. Chem. Soc.*, **1969**, 1635; 1970, 1597.
4) M. Kojima and J. Fujita, *Chem. Lett.*, **1976**, 429.
5) P. G. Beddoe and S. F. Mason, *Inorg. Nucl, Chem. Lett.*, **4**, 433 (1968).
6) J. R. Gollogy and C. J. Hawkins, *Chem. Commun.*, **1968**, 689.
7) K. R. Butler and M. R. Snow, *Inorg. Chem.*, **10**, 1838 (1971).
8) P. G. Beddoe. M. J. Harding, S. F. Mason, and B. S. Peart. *J. Chem. Soc., D*, **1971**, 1283.
9) R. R. Judlings and D. J. Royer, *Inorg. Nucl. Chem, Lett.*, **6**, 305 (1970).
10) M. Kojima, M. Fujita, and J. Fujita, *Bull. Chem, Soc. Jpn.*, **50**, 3237 (1977).

 © 1985 The Chemical Society of Japan Bull. Chem. Soc. Jpn., 58, 1287—1291 (1985)

Relative Acidity of Bis(2,4-pentanedionato)(diamine)cobalt(III) Complexes in Lower Dielectric Solvents

Kazuaki ITO,† Etsuro IWAMOTO, Kazuko HASEGAWA, Manabu YAMAMOTO, and Yuroku YAMAMOTO*
Department of Chemistry, Faculty of Science, Hiroshima University, Naka-ku, Hiroshima 730
(Received October 30, 1984)

The conductances of bis(2,4-pentanedionato)(diamine)cobalt(III) complexes ([Co(acac)$_2$(diamine)]X, diamine: ethylenediamine (en) and *N,N'*-dimethylethylenediamine (*N,N'*-dmen), X=Br^- and ClO_4^-) were measured in aprotic solvents covering the approximate range of dielectric constant 5—28 at 25 °C. It was found that a) in spite of the larger size of the methyl derivative the ionic association constants (K_a) for [Co(acac)$_2$(*N,N'*-dmen)]$^+$ complexes are larger than those for [Co(acac)$_2$(en)]$^+$ complexes in all the composition of nitrobenzene ($PhNO_2$)–carbon tetrachloride (CCl_4) mixtures (wt % CCl_4: 20, 40, 60, 70). b) The reverse trend was obtained in dichloromethane (DCM), 1,1,2,2-tetrachloroethane (1,1,2,2-TCE), and chloroform ($CHCl_3$). These results were explained in terms of hydrogen bonding between the NH protons in the chelate cations and the anions ClO_4^- and Br^-, selective solvation of the NH group side by nitrobenzene, and the desolvation due to the introduction of the *N*-methyl groups. The relative acidity of NH protons which is controlled by solvation plays an important role in ionic association for the chelate cations with NH protons.

It is known that when *N*-alkyl groups are introduced into some amines coordinated to a metal ion, the acidity of the residual NH protons increases.[1,2] For example, the acid dissociation constant (pK_a=7.2) of $[Pt(NH_3)_6]^{4+}$ in water increases with the replacement of ammonia (NH_3) by ethylenediamine (en) (pK_a: 5.5 for $[Pt(en)_3]^{4+}$). However, the source of the increasing acidity is not clear although the basicity of *N*-methyl-substituted amines and polyamines has been examined in great deal by vapor pressure, EMF, calorimetry, UV, NMR measurements, and *ab initio* calculation.[3]

In our previous studies,[4-6] we have employed a series of bis(β-diketonato)(diamine)cobalt(III) complexes as probes to obtain the information on solute-solvent interactions in electrolyte solutions. It is interesting to note that the ionic association constants (K_a) for [Co(acac)$_2$(*N,N'*-dmen)]X (X=ClO_4^- and Br^-) in $PhNO_2$ are larger than those for [Co(acac)$_2$(en)]X in spite of decreasing the number of the NH protons capable of hydrogen bonding with the anions. We have proposed that the results can be interpreted in terms of the difference in acidities of the NH protons owing to an ion–solvent dipole interaction. Therefore, it is considered that the properties of mixed solvents become much clear using the ion association processes of [Co(acac)$_2$(en)]$^+$ and [Co(acac)$_2$(*N,N'*-dmen)]$^+$ complexes.

In this study, we applied these ideas to the mixed solvents of nitrobenzene ($PhNO_2$) and carbon tetrachloride (CCl_4), and pure solvents dichloromethane (DCM), 1,1,2,2-tetrachloroethane (1,1,2,2-TCE), and chloroform ($CHCl_3$). Carbon tetrachloride is nonpolar aprotic and the properties of $PhNO_2$–CCl_4 mixtures (dielectric constant, viscosity, and specific gravity) change linearly with the increase in a fraction of CCl_4, so carbon tetrachloride acts only as a diluent.[7]

Experimental

The metal chelate electrolytes, [Co(acac)$_2$(en)]X and [Co(acac)$_2$(*N,N'*-dmen)]X (X=Br^- and ClO_4^-) were prepared and purified as described previously.[4,5] All the solvents employed were commercial products (Wako Pure Chemical Industries, Ltd.). Reagent grade carbon tetrachloride (CCl_4) was distilled under nitrogen atmosphere, after being shaken with $NaHCO_3$ solution, then with water, and dried over $CaCl_2$. The middle fraction was collected. Dichloromethane (DCM) was washed with $NaHCO_3$ solution and then with water, dried over $CaCl_2$, and fractionally distilled. The method of purification of nitrobenzene ($PhNO_2$) has been described previously.[5] Spectrograde chloroform was washed with water and passed through a molecular sieve (4A) ($CHCl_3$: Density 1.4799 g cm^{-3}, viscosity 0.5470 mPa s at 25 °C). Reagent grade 1,1,2,2-tetrachloroethane was used without further purification (1,1,2,2-TCE: Density 1.5866 g cm^{-3}, viscosity 1.610 mPa s at 25 °C).

Conductance measurements were carried out by a LCR-type bridge (Ando Electric Company Ltd.) having a frequency of 1592 Hz. The procedure used for the conductance measurements and other measurements (viscosity and density of solvent) have been described previously.[5] The solvent mixtures of nitrobenzene and carbon tetrachloride were prepared by weight (corrected to vaccum) under nitrogen atmosphere in a dry box. The dielectric constant (ε) and viscosity (η in mPa s) of the solvent mixtures used for analysis were obtained from interpolation of those determined by Fuoss *et al.*;[7] wt % CCl_4 20, ε=27.9, η=1.612; 40, ε=21.2, η=1.400; 60, ε=14.5, η=1.201; 70, ε=11.4, η=1.105. The dielectric constant[8] and viscosity of pure solvents are as follows: DCM, ε=8.90, η=0.416; 1,1,2,2-TCE, ε=8.01, η=1.610; $CHCl_3$, ε=4.72, η=0.5470.

Results and Discussion

The measured molar conductances Λ (S cm^2 mol^{-1}) and corresponding electrolyte concentrations C (mol dm^{-3}) at 25 °C were given in Tables 1 and 2 for [Co(acac)$_2$(diamine)]Br in $PhNO_2$–CCl_4 mixtures and [Co(acac)$_2$(diamine)]ClO_4 in chloroalkane solvents and $PhNO_2$–CCl_4 (wt % 70) mixture, respectively. The data were analyzed by using the expanded Fuoss-Hsia equation with $E=E_1\Lambda_0-2E_2$ as in the following[9]

$$\Lambda = \Lambda_0 - S(C\gamma)^{1/2} + EC\gamma \log C\gamma + J_1C\gamma - J_2(C\gamma)^{3/2} - K_aC\gamma f_\pm^2\Lambda \quad (1)$$

† Present address: Department of Environmental Science, Faculty of Engineering, Hiroshima University, Higashi-Hiroshima 724.

Table 1. Molar concentrations, C/mol dm^{-3}, and molar conductances, Λ/S cm^2 mol^{-1} of [Co(acac)$_2$(diamine)]Br in nitrobenzene–carbon tetrachloride (wt% CCl_4) mixtures at 25 °C

20 %				60 %	
[Co(acac)$_2$(en)]Br		[Co(acac)$_2$(N,N'-dmen)]Br		[Co(acac)$_2$(en)]Br	
C×10^4	Λ	C×10^4	Λ	C×10^4	Λ
3.866	26.36	4.407	23.73	3.400	12.50
2.627	27.85	3.101	24.99	1.694	15.99
1.924	28.89	2.201	26.50	0.9079	19.55
1.406	29.78	1.633	27.73	0.4258	24.11
0.9600	30.69	1.205	28.86	0.2069	28.24
0.6072	31.57	0.8105	30.11	0.1222	30.95

40 %			
[Co(acac)$_2$(en)]Br		[Co(acac)$_2$(N,N'-dmen)]Br	
C×10^4	Λ	C×10^4	Λ
3.327	22.89	4.350	18.35
1.877	25.84	3.130	20.04
1.529	26.83	2.262	21.79
1.185	27.96	1.548	23.78
0.9316	28.96	1.104	25.97
0.6368	30.38	0.6751	27.96
0.3981	31.87	0.4101	30.16

Table 2. Molar concentrations, C/mol dm^{-3}, and molar conductances, Λ/S cm^2 mol^{-1} of [Co(acac)$_2$(diamine)]ClO_4 in aprotic solvents at 25 °C

DCM				1,1,2,2-TCE			
[Co(acac)$_2$(en)]ClO_4		[Co(acac)$_2$(N,N'-dmen)]ClO_4		[Co(acac)$_2$(en)]ClO_4		[Co(acac)$_2$(N,N'-dmen)]ClO_4	
C×10^4	Λ	C×10^4	Λ	C×10^4	Λ	C×10^4	Λ
2.329	22.34	2.519	30.27	1.009	9.662	1.024	12.03
1.147	29.71	1.216	39.44	0.4224	12.95	0.7411	13.26
0.7128	35.86	0.7432	46.77	0.2365	15.31	0.4333	15.43
0.4006	44.52	0.4122	56.56	0.1156	18.04	0.2263	17.99
0.1952	57.24	0.2399	66.37	0.0545	20.33	0.1083	20.61
0.0867	73.38	0.1228	78.95			0.0311	22.73
0.0536	82.69						

$PhNO_2$–CCl_4 (wt% 70)				$CHCl_3$			
[Co(acac)$_2$(en)]ClO_4		[Co(acac)$_2$(N,N'-dmen)]ClO_4		[Co(acac)$_2$(en)]ClO_4		[Co(acac)$_2$(N,N'-dmen)]ClO_4	
C×10^4	Λ	C×10^4	Λ	C×10^4	Λ	C×10^4	Λ
2.306	16.29	3.843	13.26	4.140	0.222	54.86	0.230
1.563	18.40	2.465	15.38	3.006	0.245	45.56	0.227
1.030	20.76	1.720	17.23	1.895	0.290	33.46	0.225
0.6914	23.05	1.269	18.88	1.221	0.340	14.93	0.248
0.4782	25.12	0.8714	20.99	0.618	0.447	11.23	0.263
0.3206	27.28	0.5611	23.51	0.246	0.669	6.533	0.307
0.2168	29.12	0.3688	25.84			3.883	0.363
		0.2154	28.65			2.437	0.433
		0.1413	30.48			0.731	0.700

where K_a is the ionic association constant and Λ_0 is the limiting conductance. The molar conductances of [Co(acac)$_2$(N,N'-dmen)]ClO_4 in $CHCl_3$ indicated a minimum conductance Λ_{min} at *ca.* 3.5×10^{-3} mol dm^{-3} (Table 2). The Fuoss-Kraus theory[10] of triple ion formation showed that the position C_{min} of Λ_{min} is the product of K_{a3} by electrostatic theory and Λ_0/Λ_{03}. This relation coincides with the empirical rule, $C_{min} \simeq (\varepsilon^3/3) \times 10^{-4}$, discoverd by Walden.[10] The solubility of [Co(acac)$_2$(en)]ClO_4 is too small to obtain a minimum

Table 3. Conductance results for [Co(acac)$_2$(diamine)]Br in nitrobenzene–carbon tetrachloride mixtures at 25 °C

CCl_4 (wt %)	Electrolyte	Λ_0 / S cm^2 mol^{-1}	K_a / dm^3 mol^{-1}	d / Å	K_a(en)[a] / K_a(N,N'-dmen)
0	[Co(acac)$_2$(en)]Br[b]	32.23±0.03	449±7	18.1	0.60
	[Co(acac)$_2$(N,N'-dmen)]Br[b]	32.34±0.08	749±65	8.4	
20	[Co(acac)$_2$(en)]Br	33.62±0.08	840±140	11	0.57
	[Co(acac)$_2$(N,N'-dmen)]Br	33.79±0.29	1480±360	11	
40	[Co(acac)$_2$(en)]Br	35.28±0.19	2610±320	13	0.60
	[Co(acac)$_2$(N,N'-dmen)]Br	34.85±0.73	4310±960	12	
60	[Co(acac)$_2$(en)]Br	37.38±0.36	20500±900	17	—

a) Ratio of K_a for [Co(acac)$_2$(en)]Br to that for [Co(acac)$_2$(N,N'-dmen)]Br. b) From Ref. 4.

Table 4. Conductance results for [Co(acac)$_2$(diamine)]ClO_4 in aprotic solvents at 25 °C

Solvent	Electrolyte	Λ_0 / S cm^2 mol^{-1}	K_a / dm^3 mol^{-1}	d / Å	K_a(en)[a] / K_a(N,N'-dmen)
1,2-DCE	[Co(acac)$_2$(en)]ClO_4[b]	64.85±0.40	16600±600	20.2	1.50
	[Co(acac)$_2$(N,N'-dmen)]ClO_4[b]	64.33±0.40	11100±900	20.4	
1,1,2,2-TCE	[Co(acac)$_2$(en)]ClO_4	24.60±0.18	46000±800	—	1.82
	[Co(acac)$_2$(N,N'-dmen)]ClO_4	24.84±0.38	25300±1500	—	
DCM	[Co(acac)$_2$(en)]ClO_4	120.6±1.5	130100±3000	25	2.40
	[Co(acac)$_2$(N,N'-dmen)]ClO_4	113.0±2.9	54100±3600	23	
$CHCl_3$	[Co(acac)$_2$(en)]ClO_4	—	(6.92±0.18)×10^8[c] 950±70[d]	—	3.66
	[Co(acac)$_2$(N,N'-dmen)]ClO_4	—	(1.89±0.07)×10^8[c] 280±10[d]	—	
$PhNO_2$	[Co(acac)$_2$(en)]ClO_4[b]	31.770±0.007	56±1	12.0	0.95
	[Co(acac)$_2$(N,N'-dmen)]ClO_4[b]	31.90±0.02	59±1	11.7	
$PhNO_2$–CCl_4 (70 %)	[Co(acac)$_2$(en)]ClO_4	36.74±0.10	15000±400	32	0.93
	[Co(acac)$_2$(N,N'-dmen)]ClO_4	36.50±0.22	16200±500	19	

a) Ratio of K_a for [Co(acac)$_2$(en)]ClO_4 to that for [Co(acac)$_2$(N,N'-dmen)]ClO_4. b) From Ref. 5. c) Values were obtained from Fuoss-Kraus theory. d) Values of triple ion formation constant, K_{a3}.

conductance. The data were analyzed by using the Fuoss-Kraus equation[10]

$$\Lambda C^{1/2}g(C) = \Lambda_0/K_a^{1/2} + (\Lambda_{03}K_{a3}/K_a^{1/2})(1-\Lambda/\Lambda_0)C \quad (2)$$

where $g(C)$ is given by $g(C)=\exp[-2.303A_f(C\Lambda/\Lambda_0)^{1/2}]/[1-A_\lambda(C\Lambda/\Lambda_0)^{1/2}/\Lambda_0]$ $(1-\Lambda/\Lambda_0)^{1/2}$, K_{a3} is the triple ion formation constant and Λ_{03} is the sum of the limiting conductances of the two kinds of triple ions. A_f and A_λ are the limiting slopes of the Debye-Hückel theory and of the Onsager theory, respectively. In this study, $\Lambda_{03}/\Lambda_0=1/2$[11] was assumed and Λ_0 was estimated from the average Walden product of each chelate electrolyte in 1,2-DCE, DCM, and 1,1,2,2-TCE. The conductance parameters are given in Table 3 ([Co(acac)$_2$(en)]Br and [Co(acac)$_2$(N,N'-dmen)]Br in $PhNO_2$–CCl_4 mixtures) and Table 4 ([Co(acac)$_2$(en)]ClO_4 and [Co(acac)$_2$(N,N'-dmen)]ClO_4 in chloroalkane solvents and $PhNO_2$–CCl_4 (wt%70) mixture).

Figure 1 shows that the K_a values for [Co(acac)$_2$(diamine)]Br in $PhNO_2$–CCl_4 mixtures are much larger than those for n-Bu_4NBr,[7] this being attributed to hydrogen bonding between the NH protons of the chelate cations and the Br^- ion. However, the K_a values for [Co(acac)$_2$(N,N'-dmen)]Br are larger than those for [Co(acac)$_2$(en)]Br in spite of decreasing the number of the NH protons from four to two. Similar results were

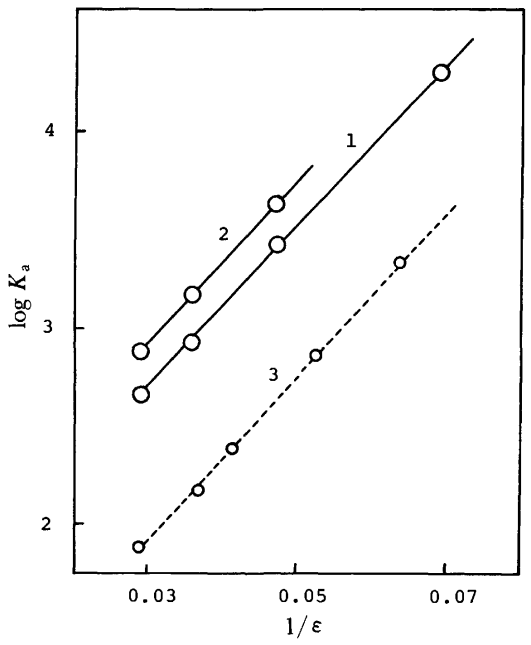

Fig. 1. Dependence of ionic association constant on dielectric constant in $PhNO_2$–CCl_4 mixtures at 25 °C. 1, [Co(acac)$_2$(en)]Br; 2, [Co(acac)$_2$(N,N'-dmen)]Br; 3, n-Bu_4NBr.[7]

obtained for $[Co(acac)_2(en)]ClO_4$ and $[Co(acac)_2(N,N'\text{-dmen})]ClO_4$ in $PhNO_2$–CCl_4 (wt% 70) mixture although the difference is small owing to the weakness of hydrogen bonding ability of the ClO_4^- ion.[5,6] On the other hand, in chloroalkane solvents (1,2-DCE, DCM, 1,1,2,2-TCE, and $CHCl_3$) the K_a values for $[Co(acac)_2(en)]ClO_4$ are all larger than those for $[Co(acac)_2(N,N'\text{-dmen})]ClO_4$ (Table 4).

The dipole moment of $PhNO_2$ (μ=4.22) is larger than that of 1,2-DCE, DCM, 1,1,2,2-TCE, and $CHCl_3$ (1,40, 1.60, 1.32, and 1.01, respectively).[8] The NH protons of the $[Co(acac)_2(en)]^+$ ion in $PhNO_2$ are solvated by an ion–solvent dipole interaction and the introduction of *N*-methyl groups removes partly the solvation sheath of the residual protons by steric hindrance, resulting in the increasing K_a.[5] This view is valid in $PhNO_2$–CCl_4 mixtures in which CCl_4 acts only as a diluent. Thus, the significant difference in K_a between $PhNO_2$–CCl_4 mixtures and the chloroalkane solvents is attributed to the selective solvation by nitrobenzene molecules. For the ionic association of *n*-Bu_4NBr and *n*-Bu_4NI in $PhNO_2$–CCl_4 mixtures,[7] the selective solvation of the cation by nitrobenzene was not observed. In addition, the ion pair extraction of R_4NI (R=Et, *n*-Pr, *n*-Bu, and *i*-C_5H_{11} from water to $PhNO_2$–CCl_4 mixtures can be interpreted mainly in terms of the dielectric constant and solubility parameter.[12] These are because of the long-range ion–solvent interaction between the cation R_4N^+ and nitrobenzene molecules. On the other hand, the selective solvation of the chelate cations by nitrobenzene molecules is due to the active NH groups in the coordinated diamine.

In $PhNO_2$–CCl_4 mixtures, the ratios of K_a for $[Co(acac)_2(en)]Br$ to that for $[Co(acac)_2(N,N'\text{-dmen})]Br$ (Table 3) are almost equal and the plots of $\log K_a$ *vs.* $1/\varepsilon$ for these two salts are linear (Fig. 1), suggesting the similar effective size (5.9 Å, ionic distance parameter from the Fuoss equation).[13] In the chloroalkane solvents, the correlation of plots for $[Co(acac)_2(en)]ClO_4$ and $[Co(acac)_2(N,N'\text{-dmen})]ClO_4$ is not good (Fig. 2). However, the ratios of K_a for the en complex to the *N*,*N*′-dmen complex in each solvent are increased with the increase in K_a (Table 4). The K_a values for each salt in 1,1,2,2-TCE are smaller than those in DCM although the bulk dielectric constants of both solvents are nearly equal, suggesting that the effective dielectric constant of 1,1,2,2-TCE is larger than that of DCM. This is due to that the effective dielectric constant of 1,2-DCE[14] and 1,1,2,2-TCE in the vicinity of an ion is appreciably greater than the macroscopic dielectric constant due to the conversion of gauche to trans molecules. The ionic distance parameters obtained tentatively from the slopes between 1,2-DCE and $CHCl_3$ are 6.1 Å for $[Co(acac)_2(en)]ClO_4$ and 6.5 Å for $[Co(acac)_2(N,N'\text{-dmen})]ClO_4$. This result indicates that the effective size of $[Co(acac)_2(N,N'\text{-dmen})]^+$ is larger than that of $[Co(acac)_2(en)]^+$ by the volume of two methyl groups in the chloroalkane solvents whcih

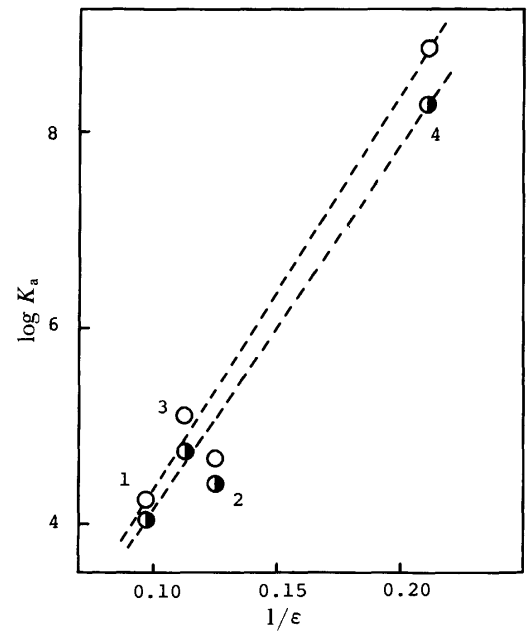

Fig. 2. Dependence of ionic association constant on dielectric constant in chloroalkane solvents at 25 °C.
○, $[Co(acac)_2(en)]ClO_4$; ◑, $[Co(acac)_2(N,N'\text{-dmen})]ClO_4$.
1, 1,2-DCE; 2, 1,1,2,2-TCE; 3, DCM; 4, $CHCl_3$.

have lower solvation ability.

In conclusion, the increasing acidity of the residual NH protons due to *N*-methylation in $PhNO_2$–CCl_4 mixtures is attributed to the appearance of the naked nitrogen protons by the steric hindrance rather than to the reduction in electron density of the protons. Thus, this leads to the results that the K_a values for $[Co(acac)_2(N,N'\text{-dmen})]X$ are larger than those for $[Co(acac)_2(en)]X$ in solvents with stronger solvation ability for the NH protons, in spite of the larger size and the decrease in the number of the protons for the former salt.

References

1) F. Basolo and R. G. Pearson, "Mechanisms of Inorganic Reactions," 2nd ed, Wiley, New York (1967).

2) a) D. A. Buckingham, B. M. Foxman, and A. M. Sargeson, *Inorg. Chem.*, **9**, 1790 (1970); b) D. A. Buckingham, C. R. Clark, and T. W. Lewis, *ibid.*, **18**, 2041 (1979).

3) a) A. Reyes and R. M. Scot, *J. Phys. Chem.*, **84**, 3600 (1980); b) A. Mucci, R. Domain, and R. L. Benoit, *Can. J. Chem.*, **58**, 953 (1980); c) R. Barbucci and V. Barone, *J. Phys. Chem.*, **85**, 64 (1981); d) R. A. Eadas, D. A. Well, D. A. Dixon, and C. H. Douglass, Jr., *ibid.*, **85**, 981 (1981); e) J. Yperman, J. Mullens, J.-P. Franqois, and L. C. Van Poucke, *ibid.*, **86**, 298 (1982).

4) K. Ito, E. Iwamoto, and Y. Yamamoto, *Bull. Chem. Soc. Jpn.*, **55**, 3190 (1982).

5) K. Ito, *Inorg. Chem.*, **22**, 2872 (1983).

6) K. Ito, H. Isono, E. Iwamoto, and Y. Yamamoto, *Inorg. Chem.*, **23**, 850 (1984).

7) a) H. Sadek and R. M. Fuoss, *J. Am. Chem. Soc.*, **76**, 5905 (1954). The data were recalculated by using the Fuoss-Hsia equation. ; b) E. Hirsch and R. M. Fuoss, *ibid.*, **82**, 1018

(1960).

8) "Handbook of Chemistry and Physics," 64th ed, ed by R. C. West CRC press: Florida, (1983).

9) a) R. M. Fuoss and K. L. Hsia, *Proc. Natl. Acad. Sci., USA*, **57**, 1550 (1967); b) R. Fernández-Prini, *Trans Faraday Soc.*, **65**, 3311 (1969).

10) a) H. S. Harned and B. B. Owen, "The Physical Chemistry of Electrolytic Solutions," 3rd ed, Reinhold (1958), Chapter 7; b) R. M. Fuoss and C. A. Kraus, *J. Am. Chem. Soc.*, **55**, 2387 (1933).

11) A larger value of Λ_{03}/Λ_0 gives a smaller K_{a3} value (*vice versa*), but it does not change a K_a value.

12) E. Iwamoto, H. Ohmori, and Y. Yamamoto, *J. Phys. Chem.*, **87**, 1776 (1983).

13) R. M. Fuoss, *J. Am. Chem. Soc.*, **80**, 5059 (1958).

14) Y. H. Inami, H. K. Bodenseh, and J. B. Ramsey, *J. Am. Chem. Soc.*, **83**, 4745 (1961).

Studies of the Hydrous Tin(IV) Oxide Ion Exchanger. IV. The Effect of Heat Treatment

Yasushi INOUE,* Hiromichi YAMAZAKI, and Hiroshi NAKAMIZO
Department of Nuclear Engineering, Faculty of Engineering, Tohoku University, Aramaki, Sendai 980
(Received November 1, 1984)

The effects of heat treatments in air or water at high pressure have been studied regarding the properties of a hydrous tin(IV) oxide ion exchanger. The exchanger in a H^+ form was stable against heat treatments in both air and water up to around 80 °C; thereafter the exchange capacity progressively decreased with temperature until 300 °C, at which point it was reduced to about a quarter of the initial value. The exchanger began to crystallize at 300 °C, and formed nearly-complete cassiterite crystals at 500 °C,(where the capacity disappeared). In contrast, the exchanger in a Na^+ form was more stable against heat treatment than the H^+ form; at 400 °C, the Na^+ form retained 40 per cent of the initial exchange capacity. An examination of the uptake curves showed that more acidic exchange sites were stronger than less acidic sites against heat treatment. The existence of three kinds of water in the exchanger (adherent, zeolitic, and bound) has been suggested on the basis of the ion-exchange capacity, the thermal-analysis curves, and the recovery of water brought about by humidifying.

In a previous paper, the acid-base property, the ion-exchange selectivity for various cations and other important properties were studied on an hydrous tin(IV) oxide ion exchanger prepared by a method previously proposed by the present authors.[1] The study on the effect of heating regarding ion-exchange properties is also important since most inorganic ion exchangers are expected to be superior to ion-exchange resins regarding thermal stability. As hydrous tin(IV) oxide has an amorphous structure, this investigation may be helpful in considering the structure of this exchanger by adding some strong circumstantial evidence. As to the effect of thermal treatment, there have been many studies regarding the composition and the physical properties,[2-7] while there have been few reports on the ion-exchange properties.

The present paper describes the effect of heat treatment in both air and water with regards to the composition and ion-exchange properties of hydrous tin(IV) oxide. Furthermore, a classification of various water forms present in the exchanger is discussed.

Experimental

Reagents and Apparatus. The hydrous tin(IV) oxide ion exchanger was prepared by a method described previously[1] and then converted into a H^+ or Na^+ form. The other chemicals were of the highest purity (Wako Pure Chemical Industries, Ltd.).

A thermal analysis was undertaken using a Shimadzu micro thermal analyzer, Model DT-20B, connected to a thermal balance, Model TGC-20H, for thermogravimetric analysis (TGA), and a high-temperature sample holder, Model MDH-20, for differential thermal analysis (DTA). The reference material for DTA was α-alumina. The measurement was performed in air at a heating rate of 10 °C/min.

X-Ray diffraction patterns were obtained by means of a Shimadzu X-ray diffraction unit, Model XD-3A, using Ni-filtered Cu $K\alpha$-radiation. The diffraction angle was calibrated using silicon powder.

The infrared (IR) absorption spectra were measured with a Nihon Bunko infrared spectrometer, Model IR-G, using the KBr disk method. The wave number was calibrated using polystyrene.

Heat Treatment. About 7 g of the exchanger in a desired ionic form was heated in air to a constant weight at a constant temperature (controlled with an accuracy of 1% by using an automatic temperature controller; Chino Workers, Ltd.). After cooling, a sample in the Na^+ form was converted into the H^+ form by conditioning with a 0.1-mol dm^{-3} HCl solution; that in the H^+ form was immersed in water. Thereafter, they were both subjected to the humidifying operation described previously.[1]

The hydrothermal treatment was carried out in a Sakashita autoclave, Model SR-100 (inner volume, 1 dm^3), by controlling the temperature whthin an accuracy of 5 °C. In this autoclave, 5 g of the exchanger in the H^+ form was immersed in 400 cm^3 of distilled water; this was treated at temperatures from 100 to 250 °C for 6 h under a pressure of 100 atm, which was regulated by pressurized N_2 gas. After cooling, a portion of the sample was conditioned with 0.1 mol dm^{-3} HCl. The rest was washed with only water. Thereafter, they were both subjected to the humidifying operation.

The other experimental procedures were the same as those described previously.[1]

Results and Discussion

Thermal Stability of the Exchanger in the H^+ Form. The results for the H^+ form exchanger are shown in Table 1. It should be noted that values at the left of the two columns (showing the exchange capacity) were those normalized to the capacity per 1 mole of tin. The right-hand values (marked C) show the amount of water per 1 mole of tin that is liberated by the condensation of the hydroxyl groups (which may act as ion-exchange sites). In the case of the exchanger without heat treatment (designated as sample R. T.), the dissolution of a part of the exchanger in strong basic solutions limits the maximum cation-exchange capacity to the value at pH 11.3.

The maximum cation-exchange capacity did not change up to 80 °C, and then it decreased with temperature; at 500 °C it was reduced to a tenth of the value of the sample R. T. The amount of water contained in the exchanger immediately after the heat treatment (marked A) at 80 °C was reduced to 37% of the original value; then, it gradually decreased with

TABLE 1. EFFECT OF HEAT TREATMENT OF H^+-FORM EXCHANGER ON THE COMPOSITION AND THE ION-EXCHANGE CAPACITY

No.	Temp of treatment °C	Weight loss wt%	Composition A[1] mol H_2O / mol Sn	Composition B[2] mol H_2O / mol Sn	Recovery of water (B-A) mol H_2O / mol Sn	Exchange capacity[3] mol Na^+ / mol Sn	Exchange capacity[3] C mol H_2O / mol Sn	C/A
1	R.T.	—	2.15±0.02	2.15±0.02	—	0.230±0.003[4]	0.115±0.002	—
2	80	12.85	0.80±0.02	1.64±0.01	0.84±0.03	0.227±0.003	0.113±0.002	0.14±0.01
3	150	15.14	0.56±0.02	1.45±0.01	0.89±0.03	0.166±0.003	0.083±0.002	0.15±0.01
4	200	16.59	0.40±0.02	1.29±0.01	0.89±0.03	0.138±0.003	0.069±0.002	0.17±0.01
5	300	18.17	0.24±0.02	1.00±0.01	0.76±0.03	0.066±0.003	0.033±0.002	0.14±0.02
6	400	19.56	0.096±0.02	0.66±0.01	0.56±0.03	0.030±0.003	0.015±0.002	0.16±0.05
7	500	20.34	0.010±0.02	0.11±0.01	0.10±0.03	0.023±0.003	0.012±0.002	1.2±0.6
8	850	20.43	0	≈0	≈0	≈0	≈0	—

1): Immediately after heat treatment. 2): Immersed in water, dried over saturated NH_4Cl. 3): 0.1 mol dm^{-3} NaOH batch exchange capacity. 4): Exchange capacity at pH 11.3.

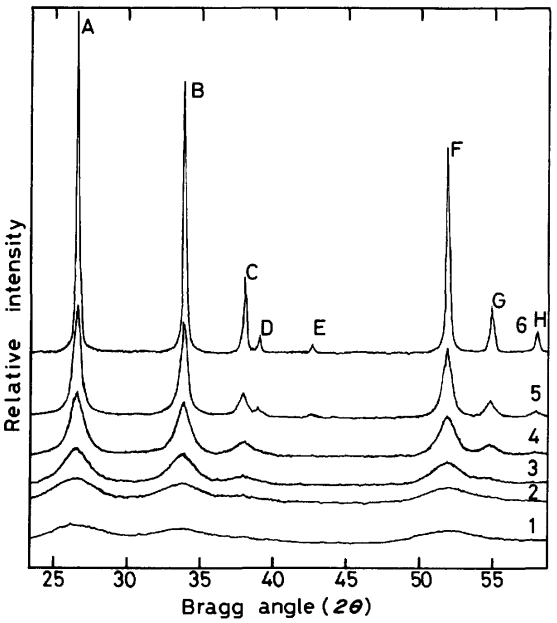

Fig. 1. X-Ray diffraction pattern of H^+-form exchanger.
Temperature of treatment; 1: R.T., 2: 200°C, 3: 300°C, 4: 400°C, 5: 500°C, 6: 600°C. Interplanar distance/nm; A: 0.335, B: 0.264, C: 0.237, D: 0.231, E: 0.212, F: 0.176, G: 0.167 H: 0.159.

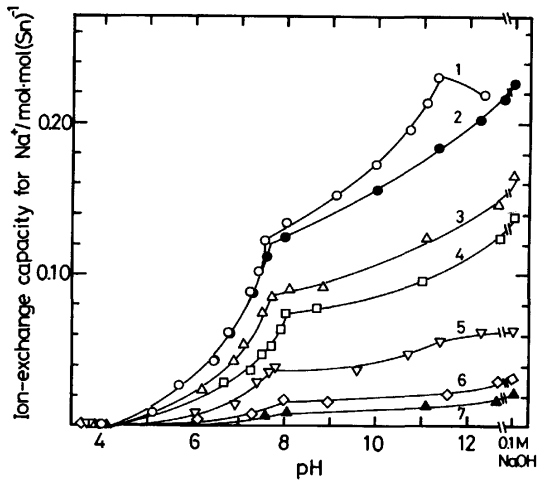

Fig. 2. Uptake curves for Na^+ (Heat treatment in H^+ form, followed by humidiation).
Temperature of treatment; 1: R.T., 2: 80°C, 3: 150°C, 4: 200°C, 5: 300°C, 6: 400°C, 7: 500°C.

temperature, and finally reached zero at 500°C. The ratio of the water originated from the exchange sites (OH groups) to the total water remaining in the exchanger immediately after the heat treatment, C/A, did not change up to 400°C, while at 500°C it suddenly increased to around unity. Hence it is considered that the water molecules remaining in the exchanger immediately after the heat treatment were liberated cooperatively with the condensation of the OH groups, so that the water molecules might be fixed in the exchanger by OH groups through some kind of interaction such as a hydrogen bond (bound water). This bound water was completely liberated at 500°C.

Next, let us consider the relation between the water content immediately after the heat treatment (marked A) and that of the exchanger subjected to the humidifying operation (marked B). For the exchangers heated up to 300°C, the amount of water recovered by humidifying was nearly constant, while for samples heated over 400°C it decreased suddenly; the exchanger heated at 500°C recovered water only slightly. Figure 1 shows the X-ray diffraction patterns of the samples subjected to the humidifying operation. The samples heated up to 300°C, together with the sample R. T., show three weak broad peaks (d=0.335, 0.264, 0.176 nm) and, hence, have poor crystallinity. The peaks sharpened with increasing temperature, indicating an enhanced crystallization. When a sample was heated at 500°C, it reflected most of the peaks characteristic of cassiterite. At 850°C, the exchanger completely crystallized as cassiterite. Therefore, the sudden decrease of water recovery at a temperature above 400°C may be associated with the crystallization of the exchanger. This brings about a decrease in the space which can hold water molecules.

In order to examine the effect of a heat treatment on the acid-base property of the exchanger, the uptake curves for Na^+ and Cl^- were measured as a function of pH. Figure 2 shows the change in the cation-exchange behavior. For the sample heated at 80°C, the exchange

capacity in a pH range higher than the breaking point in the curve decreased slightly, while in a pH range lower than that point, the curve was the same as that of the sample R. T. When the exchangers were heat-treated at 150 °C or higher, the capacity decreased in the whole pH range with the temperature; the main part of the exchange capacity remaining after the heat treatment as 300 °C was in a pH region lower than the breaking point. The exchange sites were almost completely destroyed at 500 °C. The uptake curves for Cl^- are shown in Fig. 3, which reveals that the highest pH of anion uptake was lowered with the increase in temperature. This means that basic exchange sites are liable to be destroyed. From the above observations it is considered that the resistance to thermal decomposition is greater for more acidic rather than for less acidic ion-exchange sites.

Figure 4 shows the TGA and the DTA curves for the exchangers in the H^+ form. The TGA curve of the sample heat-treated at 80 °C was similar to that of the sample R. T. except the amount of the water released below 150 °C; the sample lost weight suddenly up to around 150 °C and then, gradually, up to about 650 °C, where the weight became constant. In contrast, the weight of the sample heat-treated at 300 °C decreased sharply below 80 °C, then became constant between 150 and 300 °C, and gradually decreased again up to 650 °C. In the DTA curves, large endothermic peaks appearing in the range lower than 200 °C sharpened as the temperature for heat treatment became higher. The position of the peak, observed at 70 °C for the samples heated below 200 °C, shifted to 40 °C and its area became very small when the sample was heated at 500 °C. Apparently, this observation is compatible with the change in the exchange capacity and in the degree of the recovery of water with the temperature for heat treatment, if the peak is considered to correspond mainly to the release of water recoverable by humidifying, that is, a certain kind of zeolitic water. The shoulders observed at the high- and low-temperature sides, respectively, of the peak for the samples heat-treated at temperatures below 200 °C are attributable to the bound water liberated by the condensation of the hydroxyl groups and to the adherent water in the exchanger matrix. Mikhail *et al.* observed a small broad exothermic peak at 470 °C,[2] and Durand and Masdupuy observed a large sharp exothermic peak at 300 °C and three small ones at 400, 500, and 620 °C.[8] The DTA curves were measured at varying heating rates, but these high-temperature peaks were not observed in the present experiment.

Figure 5 shows the IR spectra of the exchangers in the H^+ form heat-treated at different temperatures. The asymmetric absorption band near 3400 cm^{-1} is attributable to the sum of the contribution from water and hydroxyl-group bonding to tin; the former at the lower, and the latter at the higher, wave-number sides. The absorption band near 1630 cm^{-1} is due

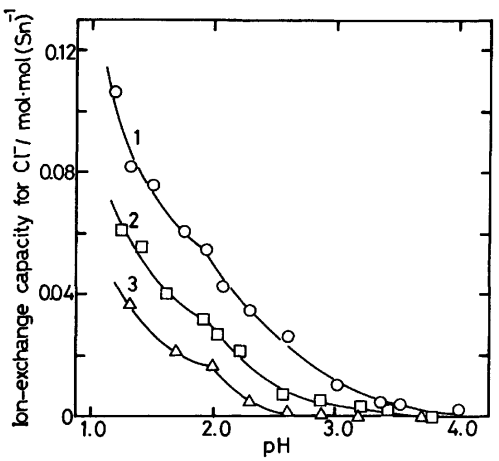

Fig. 3. Uptake curves for Cl^- (Heat treatment in H^+ form, followed by humidiation).
Temperature of treatment; 1: R.T., 2: 150 °C, 3: 300 °C.

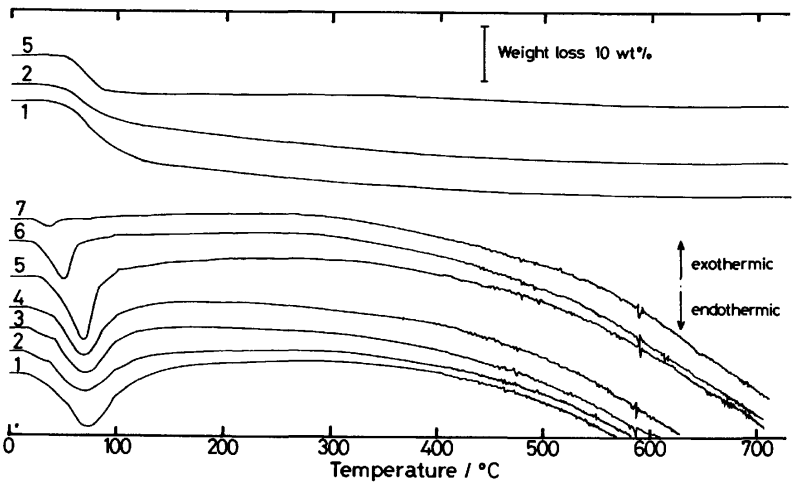

Fig. 4. TGA and DTA curves (Heat treatment in H^+ form, followed by humidiation).
Temperature of treatment; 1: R.T., 2: 80 °C, 3: 150 °C, 4: 200 °C, 5: 300 °C, 6: 400 °C, 7: 500 °C.

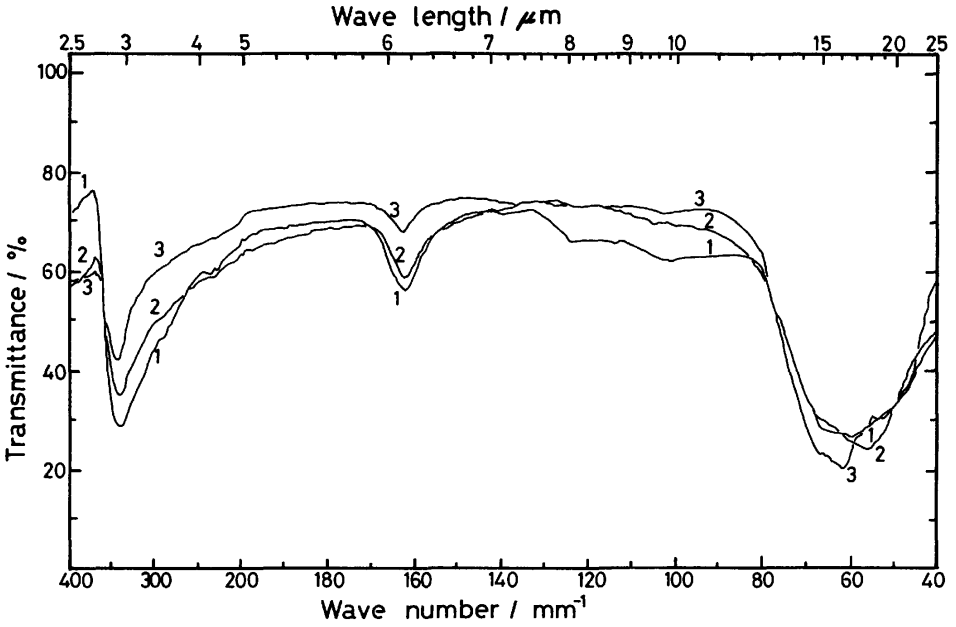

Fig. 5. IR spectra of hydrous tin(IV) oxide (Heat treatment in H^+ form).
Temperature of treatment; 1: R.T., 2: 300°C, 3: 500°C.

TABLE 2. EFFECT OF HEAT TREATMENT OF Na^+-FORM EXCHANGER ON THE COMPOSITION AND THE ION-EXCHANGE CAPACITY

No.	Temp of treatment °C	Weight loss wt%	Composition A[1] Molar ratio of H_2O/Sn	Composition A[1] Molar ratio of Na/Sn	Composition B[2] Molar ratio of H_2O/Sn	Composition B[2] Molar ratio of Na/Sn	Exchange capacity mol Na^+/mol Sn	Exchange capacity pH
1	R.T	—	1.794±0.013	0.233±0.002	2.13±0.02	$<1\times10^{-3}$	0.230±0.003	11.3
2	150	11.60	0.594±0.008	0.233±0.002	1.13±0.03	5.1×10^{-3}	0.169±0.003	11.3
3	200	12.96	0.405±0.006	0.233±0.002	1.05±0.03	6.8×10^{-3}	0.130±0.003	11.0
4	300	14.77	0.215±0.008	0.233±0.002	0.92±0.03	1.3×10^{-2}	0.111±0.003	11.1
5	400	15.65	0.122±0.009	0.233±0.002	0.89±0.03	3.2×10^{-2}	0.099±0.003	11.4

1): Immediately after heat treatment. 2): Converted to H^+ form. 3): After volatilization of tin with Br_2/HBr, measured by the atomic absorption spectrophotometric method.

to the bending mode of water and the absorption in the $<900\,cm^{-1}$ range, to Sn–O band.[9,10] The comparison of the spectra for the exchangers heat-treated at different temperatures shows that the water and hydroxyl bands were weaken with increasing temperature, while the Sn–O band was intensified. Accordingly, it is considered that the exchanger dried at room temperature contains a Sn–O band, a OH group, and water. Thus the formula of the exchanger may be written as $SnO_{2-x}(OH)_{2x}\cdot nH_2O$ in analogy with the formula proposed by Vivien *et al.*[9]

The observations described above can be summarized as follows. When the exchanger in the H^+ form is heated to 80°C, the release of adherent water is accompanied by the stabilization of a network structure. By the heat treatment at temperatures between 150 and 300°C the irreversible release of the bound water proceeds gradually and, thereby, the exchange capacity decreases with the increasing temperature of the treatment. However, the network structure remains essentially unchanged and the stabilized matrix can accommodate an approximately constant amount of a zeolitic water when humidified. The further release of the bound water at temperatures higher than 300°C leads to the partial crystallization of the exchanger. At 500°C the crystallization proceeds to an extreme and the structure changes completely. Therefore, almost all the water is not recovered by the humidifying operation.

Thermal Stability of the Exchanger in the Na^+ Form in Air. The effect of the heat treatment on the Na^+ form is shown in Table 2. The water content of the exchangers immediately after heat treatment (composition A) appears to be nearly the same as that of the exchangers heat-treated in the H^+ form as shown in Table 1. To make the comparison valid, however, the values for the Na^+ form should be corrected by adding 0.115±0.002 mol H_2O/mol Sn, which corresponds to the amount of the hydroxyl groups fixed by sodium ions. Thus, the water content of the exchanger heat-treated is larger in the Na^+ form than in the H^+ form, and it is considered that Na^+ in the exchanger hinders the release of water by heat treatment. Next, let us consider the composition of the samples converted to the H^+ form after being heat-treated in the Na^+ form (composition B). The composition of the exchanger without heat treatment became that of the original exchanger in the H^+ form. This observa-

tion is compatible with the reversibility of the exchange reaction between Na^+ and H^+, as reported previously.[1] The decrease of the water content with increasing temperature for heat treatment showed a tendency similar to the exchanger heat-treated in the H^+ form except for the exchanger heat-treated at 400 °C, which recovered nearly the same amount of water as the exchanger heat-treated at 300°C.

On the other hand, the decrease of the exchange capacity was less for the Na^+- than for the H^+ form; even at 400°C, the former still had exchange capacity five times as large as the latter. This tendency can be seen from Fig. 6, which shows the acid-base property of the exchangers heat-treated in the Na^+ form; the exchange groups in the Na^+ form appears resistant to the heat treatment especially at such high temperature as 400°C.

Figure 7 shows the DTA and the TGA curves of the exchanger heat-treated in the Na^+ form. These curves show general features similar to those for the exchangers heat-treated in the H^+ form. The amount of water released up to 150°C, however, was less for the Na^+- than for the H^+ form, which is a natural result of the difference of water content of the exchangers between the H^+ and Na^+ form. Furthermore, the curves for the samples heat-treated at 300 and 400°C do not differ from each other. It was consequently concluded that the sodium ion in the exchanger retards the release of water at temperatures beyond 300°C.

Figure 8 shows the X-ray diffraction patterns of the

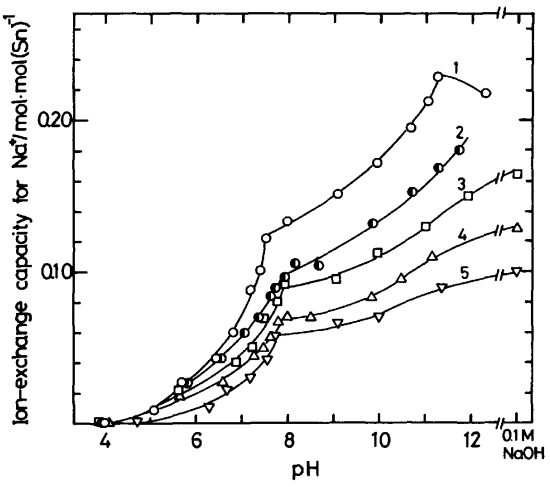

Fig. 6. Uptake curves for Na^+ (Heat treatment in Na^+ form, followed by conditioning to H^+ form).
Temperature of treatment; 1: R.T., 2: 150°C, 3: 200°C, 4: 300°C, 5: 400°C.

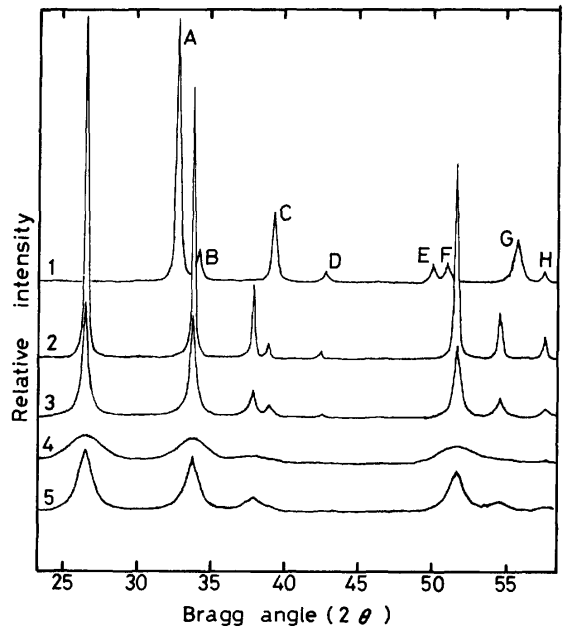

Fig. 8. X-Ray diffraction pattern of Na^+-form exchanger.
Sample 1: Na_2SnO_3 ($Na_2SnO_3 \cdot 3H_2O$, 850°C), 2: SnO_2 (H^+ form, 850°C), 3: Na^+ form, 850°C, 4: Na^+ form, 400°C, 5: H^+ form, 400°C. Temperature: Temp. of heat treatment.

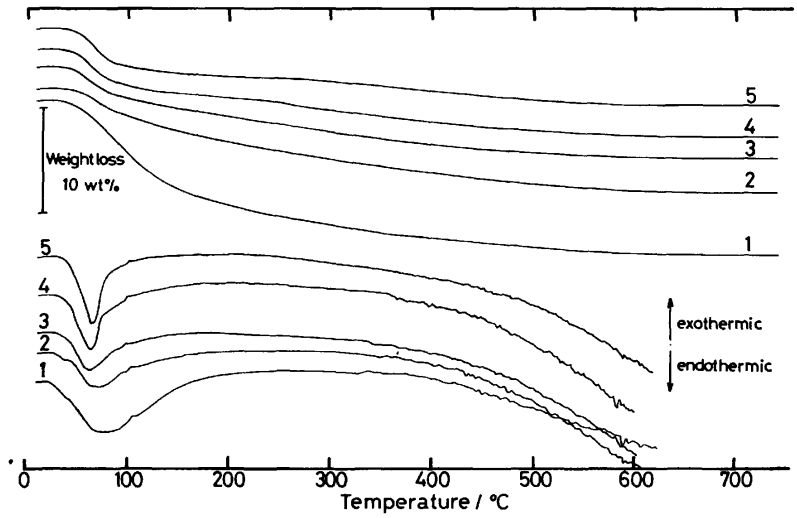

Fig. 7. TGA and DTA curves (Heat treatment in Na^+ form, followed by conditioning to H^+ form).
Temperature of treatment; 1: R.T., 2: 150°C, 3: 200°C, 4: 300°C, 5: 400°C.

samples heat-treated as the Na^+ form. It is apperent from a comparison with the H^+ form that the exchangers in the Na^+ form do not crystallize as disodium tin(IV) trioxide but as cassiterite. In addition, the broadness of the peaks indicates that the rate of the crystallization is slower for the Na^+- than for the H^+ form.

The observations described above can be summarized as follows. Although the substitution of the hydrogen ions by sodium ions is considered to stabilize the exchanger against the condensation of hydroxyl groups by a heat treatment, the matrix of the exchanger changes into a thermally stable phase by the irreversible release of water, ultimately to crystallize into cassiterite. Accordingly, the water content and the ion-exchange capacity of the exchanger decrease with the heat treatment temperature. However, the sodium ions in the exchange sites retard the change and stabilize the exchanger considerably. The difference in the thermal stability of the exchangers between the H^+- and the Na^+ form became prominent in a temperature range higher than 300 °C.

Thermal Stability in Water. The effect of a hydrothermal treatment on the properties of the exchanger in the H^+ form was studied under a pressure of 100 atm as is shown in Table 3 and Fig. 9. The symbols

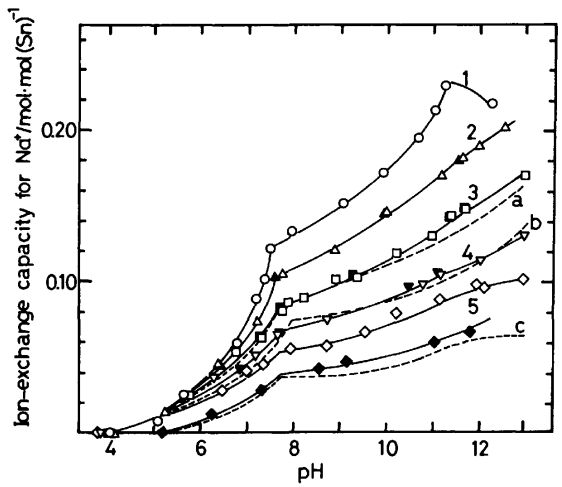

Fig. 9. Uptake curves for Na^+ (Hydrothermal treatment in H^+ form).
Temperature of treatment; 1: R.T., 2: 104 °C, 3: 150 °C, 4: 206 °C, 5: 251 °C. Solid mark: Without conditioning. ----: Heat treatment in air, temperature of treatment/°C; a: 150, b: 200, c: 300.

A and B, respectively, in Table 3 indicate the exchangers subjected to only the humidifying operation and to both the conditioning and humidifying operations. Obviously, the change in the uptake curves for sodium ions with temperature followed a tendency similar to that of the exchanger heat-treated in air. The degree of crystallization (examined by the X-ray analysis) also shows a similarity to the exchanger heated in air. On the other hand, decreases of water content with thermal treatment were less in water than in air.

Figure 10 shows the TGA and the DTA curves of the exchangers treated hydrothermally. These curves indicate the similar behavior of dehydration to the sample heat-treated in air. The amount of water released (up to 100 °C) was, however, larger with a hydrothermal treatment than with a heat treatment in air. For the exchanger heat-treated in air, most of the adherent water and the zeolitic water were lost below 100 °C and the release of the bound water occurred mainly at temperatures higher than 80 °C. Accordingly, the amount of the adherent and the zeolitic water was not reduced by the hydrothermal treatment in spite of the irreversible release of the bound water.

The conditioning did not affect the composition and the exchange capacity except for the sample heat treated at 250 °C; the conditioning increased the water content and the exchange capacity by an amount 0.2 mol H_2O/mol Sn and 0.03 mol Na^+/mol Sn, respectively. The reason for this observation is not clear, but may be due to a slight increase in the recovery of bound water, which can be seen from the increase in the area of endothermic peak higher than 72 °C.

The observations described above can be summarized as follows. When the exchanger in a hydrogen form is heat treated in water at 100 atm, the matrix crystallizes to cassiterite along with the loss of the bound water which cannot be recovered only by the humidifying operation, and the exchange capacity decreases by an amount about the same as in the case of heat treatment in air. The amount of the adherent and the zeolitic water is maintained at the original value. Thus, the loss of water is smaller in this case than in the case of heat treatment in air.

The authors wish to express their thanks to Professor Wataru Suëtaka and to Yoshio Matsumoto, Depart-

Table 3. Effect of hydrothermal treatment of H^+-form exchanger on the composition and the ion-exchange capacity

No.	Conditions of treatment: Pressure kgw/cm²	Temperature °C	Time h	Composition: A[1] mol H_2O/mol Sn	B[2] mol H_2O/mol Sn	Exchange capacity: A mol Na^+/mol Sn	pH	B mol Na^+/mol Sn	pH
1	1	R.T.	—	2.16±0.02	—	0.230±0.003	11.3	—	
2	94	104±4	6	2.14±0.02	2.15±0.02	0.192±0.003	11.6	0.190±0.003	11.6
3	102	150±3	6	2.05±0.02	2.07±0.02	0.148±0.003	11.5	0.146±0.003	11.4
4	92	206±5	6	1.90±0.02	1.86±0.02	0.104±0.003	11.2	0.106±0.003	11.2
5	98	251±2	6	1.60±0.02	1.40±0.02	0.097±0.003	11.9	0.067±0.003	11.8

1): Conditioned by 0.1 mol dm^{-3} HCl. 2): Without conditioning.

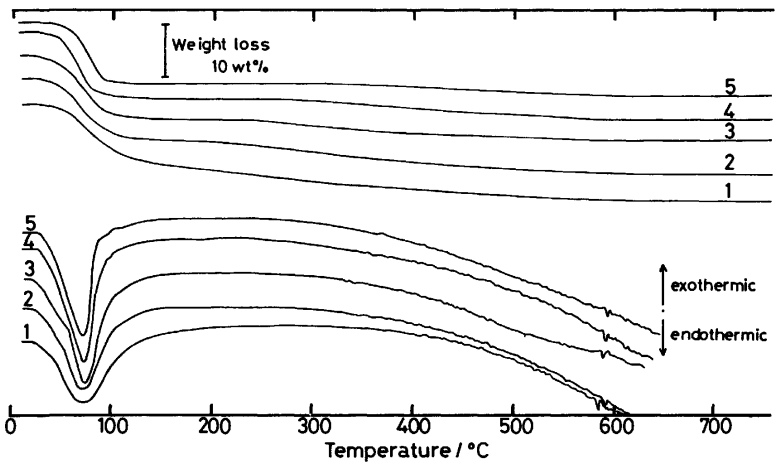

Fig. 10. TGA and DTA curves (Hydrothermal treatment in H^+ form, followed by conditioning with 0.1 mol dm^{-3} HCl). Temperature of treatment; 1: R.T., 2: 104 °C, 3: 150 °C, 4: 206 °C, 5: 251 °C.

ment of Metal Processing and Mechanical Metallurgy, Faculty of Engineering, Tohoku University, for their valuable suggestions on the measurement of IR spectra.

References

1) Y. Inoue and H. Yamazaki, *Bull. Chem. Soc. Jpn.*, **55**, 3782 (1982); **57**, 1534, 3437 (1984).

2) R. S. Mikhail, S. A. Selim, and F. I. Zeidan, *J. Appl. Chem. Biotechnol.*, **26**, 23, 191 (1976).

3) J. F. Goodman and S. J. Gregg, *J. Chem. Soc.*, **1960**, 1162.

4) M. J. Fuller, M. E. Warwick, and A. Walton, *J. Appl. Chem. Biotechnol.*, **28**, 396 (1978).

5) J. Sautereau, M. Baverez, and J. M. Bloch, *Bull. Soc. Chim. Fr.*, **1977**, 207.

6) H. B. Weiser and W. O. Milligan, *J. Phys. Chem.*, **36**, 3030 (1932).

7) T. N. Perekhozheva, L. M. Sharygin, T. G. Malykh, and V. F. Gonchar, *Radiokhimiya*, **20**, 414 (1978).

8) S. Durand and É. Masdupuy, *Bull. Soc. Chim. Fr.*, **1974**, 1844.

9) D. Vivien, J. Livage, and C. Mazieres, *J. Chim. Phys. Phys. -Chim. Biol.*, **67**, 199 (1970).

10) N. T. McDevitt and W. L. Baum, *Spectrochim. Acta*, **20**, 799 (1964).

Immunoassay Using a Metal-complex Compound as a Chemiluminescent Catalyst. V. Continuous Immunoassay by the Use of CLCCIA

Tadashi HARA,* Motohiro TORIYAMA, and Masakatsu IMAKI†
Department of Chemical Engineering, Faculty of Engineering, Doshisha University, Karasuma Imadegawa, Kamigyo-ku, Kyoto 602
†*Horiba Ltd., Kisshoin, Minami-ku, Kyoto 601*
(Received November 13, 1984)

Immunoassay, using as a labeling reagent a synthesized metal-complex compound having catalytic activity for a chemiluminescence reaction, was continuously carried out by the sandwich method. The time necessary for all the processes (including: an immune reaction, B/F separation, a sandwich reaction, and a chemiluminescence reaction) was reduced to 50 min. Human serum albumin in the range of 5 ng to 1 μg could be determined (continuously) up to 5 times by the use of the same column (immobilized with an antibody).

In order to determine a trace amount of the component in a biological sample, immunoassay is an important method. So far, enzyme immunoassay and radioimmunoassay have been used for practical purposes. Unfortunately, they have necessitated a tedious batchwise operation. Accordingly, studies regarding automatic and continuous immunoassay have been made for nonlabeled immunoassay such as laser nephelometry and latex-photometric immunoassay. However, few such attempts have been made for a labeled immunoassay, which is theoretically suitable for a very sensitive assay. This is attributed to the instability of labeling reagents such as enzymes and radioactive materials.

Chemiluminescence complex catalyst immunoassay (CLCCIA),[1-4] in which a synthesized metal-complex compound acting as a catalyst for a chemiluminescence reaction between 5-amino-2,3-dihydro-1,4-phthalazinedione (luminol) and hydrogen peroxide (H_2O_2) was used as a labeling reagent, was reported by the authors for the determination of human serum albumin (HSA) as a model compound for the protein. In a previous paper,[3] the immune complex after the immune reaction could be dissociated in a liberating solution(pH 11.4) without losing its catalytic activity for the chemiluminescence reaction since the synthesized metal-complex as a labeling reagent in CLCCIA was stable. Then, the measurement of the catalytic activity of the dissociated labeling reagent resulted in a rapid and accurate immunoassay. However, the method was far from the immunoassay in which all the processes (including: an immune reaction, B/F separation, a chemiluminescence reaction, and the cyclic use of the immobilized antibody) could be continuously carried out.

The present study deals with a method and a support suitable for the immobilization of an antibody and with an immune reaction in order to establish continuous CLCCIA in which all the immunoassay processes (including: an immune reaction, B/F separation, a sandwich reaction, a chemiluminescence reaction, and the cyclic use of the immobilized antibody) are continuously carried out.

Experimental

Preparation of a Labeled Antibody. [1,8,15,22-tetrakis-(chloroformyl)phthalocyaninato]iron(III) ([Fe(tccp)]) as a labeling reagent was synthesized as described in a previous paper.[2] 500-mm³ of a phosphate buffer solution was added to 2 cm³ of an immunoglobulin G(IgG) fraction of anti-human serum albumin(TAGO) so as to maintain the mixed solution at pH 7.2. Five mg of [Fe(tccp)] was dissolved in the above mixed solution, and the resulting solution was then reacted for 1 h at room temperature. Then, the mixed solution was incubated for 18 h at 4 °C. After the reaction, 2.5 cm³ of a potassium dihydrogenphosphate–disodium hydrogenphosphate buffer solution (0.01 mol/dm³, pH 7.2) (Buffer A) was added to the mixture. The mixture was centrifuged at 6000 min^{-1}, and the supernatant liquid was separated from the precipitate. The precipitate was treated with 2.5 cm³ of Buffer A and the supernatant liquid was again obtained by centrifuge. To the combined supernatant liquid, 5 cm³ of saturated ammonium sulfate solution was added and it was left standing at 4 °C overnight. The precipitate was separated by centrifuging and then dissolved in 2 cm³ of Buffer A. After the obtained solution was dialysed against Buffer A, the contents were separated on a column (160 cm³) charged with TOYOPEARL HW-50, and a 20-cm³ fraction corresponding to IgG was collected.

Preparation of Glass Beads Immobilized with Antibody. Five g of porous glass beads (CPG-3000, 120/200 mesh, 31250 nm mean pore diameter, ELECTRO-NUCLEONICS, INC.) were heated at 100 °C for 1 h on a water bath in 75 cm³ of a 1 mol/dm³ hydrochloric acid solution and a nitric acid solution. The beads were filtered, washed with water, and dried at 60 °C in an oven. The purified porous glass beads were suspended in 200 cm³ of 1% [3-(glycidyloxy)propyl]trimethoxysilane solution. The slurry was degassed under vacuum in an ultrasonic bath and then was heated at 90 °C for 2 h with stirring. The pH of the mixture was adjusted to 3 with a 1 mol/dm³ hydrochloric acid solution, and the mixture was heated again at 90 °C for 1 h. The diol-bonded porous glass beads, thus obtained, were washed with water and dried. Two g of the porous glass beads were placed in 20 cm³ of 6 mmol/dm³ of sodium periodate solution. A vacuum was applied for about 2 min to degas the slurry. The slurry was stirred for 1 h at room temperature, and then was washed with 100 cm³ of Buffer A. A 500-mm³ of phosphate buffer solution was added to 2 cm³ of IgG fraction of anti-human serum

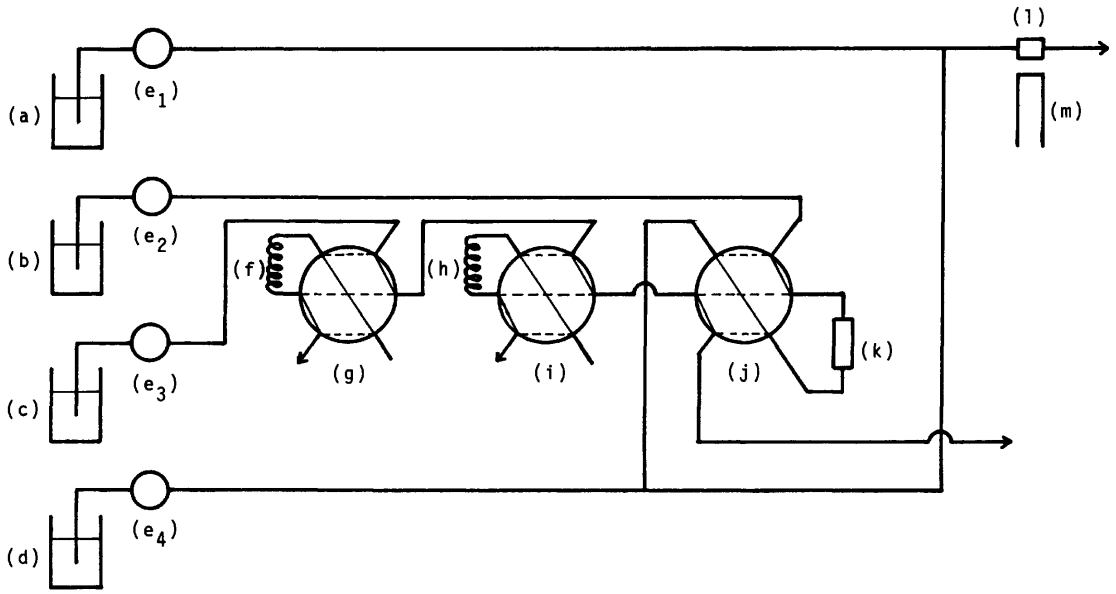

Fig. 1. Schematic flow diagram.
a: Luminol solution, b: liberating solution, c: Buffer A, d: H_2O_2 solution, e_1, e_2, e_3, e_4: pump, f,h: sampling loop, g,i,j: six-way cock, k: immobilized antibody column, 1: flow-cell, and m: photomultiplier.

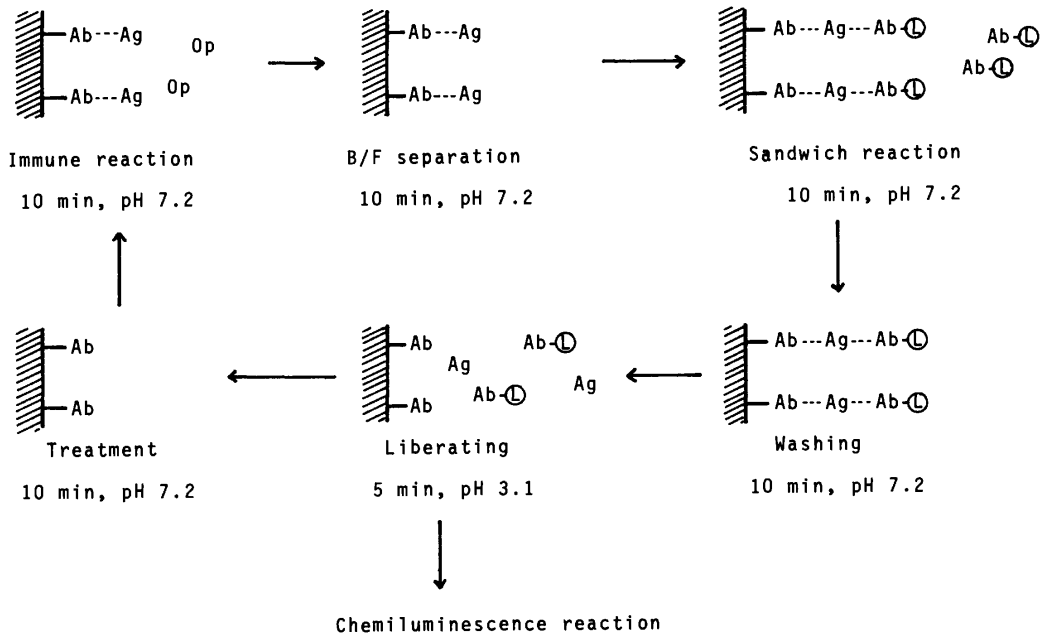

Scheme 1. Operating procedure for the continuous CLCCIA.
Ab: Antibody, Ag: antigen, Op: other protein, and L: [Fe(tccp)].

albumin(TAGO) to adjust the pH at 8.8. The aldehyde-type porous glass beads recovered from the above slurry were added to the mixed antibody solution and were reacted with the antibody for 50 h at 4 °C. After the reaction, the porous glass beads were washed with Buffer A, and were suspended in 200 cm^3 of Buffer A. Each 100-mm^3 of 40 mg/cm^3 sodium borohydride solution was added four times to the suspended solution every 30 min, and then the mixed solution was reacted for 2 h. The porous glass beads immobilized with the antibody were washed and stored in Buffer A at 4 °C.

Apparatus and Procedure. A schematic flow diagram of the apparatus used for the continuous CLCCIA is shown in Fig. 1. Its operating procedure is shown in Scheme 1.

Each bottle in Fig. 1 was filled with (a) a 1.0×10^{-3} mol/dm^3 luminol solution (pH 10.4, 0.4 mol/dm^3 boric acid-0.4 mol/dm^3 potassium hydroxide buffer solution), (b) a tartrate buffer solution (pH 3.1, 4.45×10^{-3} mol/dm^3 tartaric acid- 1.11×10^{-3} mol/dm^3 sodium tartrate buffer solution) as a liberating solution, (c) Buffer A, and (d) a 7.5×10^{-3} mol/dm^3 H_2O_2 solution. Each solution, except Buffer A(c), was fed at a flow rate of 1.65 cm^3/min by the pump (e_1, e_2, e_4) (Atto,

SJ1211). Buffer A in Fig. 1(c) was fed at a flow rate of 1.65 cm^3/min or 0.24 cm^3/min by the pump(e_3)(Atto, SJ1211). The porous glass beads immobllized with antibody were charged into a 88 mm^3 column(k).

The capacity of the sampling loop(h) was 200 mm^3, and each definite volume of HSA solution as an analyte model was injected into a flow line by the use of a sample injection six-way cock(i). Injected sample(antigen) was introduced into the column(k) at a flow rate of 0.24 cm^3/min and was made to react with the immobilized antibody. After the immune reaction, the six-way cock(i) was operated and B/F separation was accomplished by washing the column with Buffer A for 10 min at a flow rate of 1.65 cm^3/min. Then, 200 mm^3 of labeled antibody fraction(which was 50 times diluted with Buffer A) was taken in a sampling loop(f) and was injected at a flow rate of 0.24 cm^3/min by operating a six-way cock(g) into a flow line. The injected labeled antibody was subjected to a sandwich-type reaction in the column. After the reaction, a labeled antibody which was adsorbed unspecifically was eliminated by washing the column with Buffer A for 5 min at the flow rate of 1.65 cm^3/min by operating again the six-way cock(g). By operating the six-way cock(j), a tartrate buffer solution was fed into the column and the immune complex was liberated from the column. The liberated labeled antibody was mixed with H_2O_2 and luminol, and the chemiluminescence intensity of the mixture was measured by a system consisting of a flow-cell, a photomultiplier, and a photon counter as described in a previous paper.[2]

Results and Discussion

Preparation of Labeled Antibody. In order to label efficiently [Fe(tccp)] to antibody, the conditions of labeling reaction were investigated.

Labeling reactions were produced at various pH of buffer solutions, and the labeled HSAs were obtained by the procedure discussed in the experimental section. By assuming that the molar absorptivity of HSA at 280 nm and of [Fe(tccp)] at 639 nm does not change upon labeling, the approximate mole ratio of [Fe(tccp)] to HSA was obtained by the use of the calibration curves for [Fe(tccp)] and HSA. Here, the mole ratio is referred to as a labeling ratio, and HSA is used as a antibody model only in this part of the present study (to make the experiment easier). The relationship between the pH of a solution in the labeling reaction and a labeling ratio of HSA was studied. The results are shown in Fig. 2.

As can be seen from Fig. 2, the reaction between an acyl chloride group of [Fe(tccp)] and an amine group of HSA proceeded efficiently in a reacting solution at pH 7 to 8. Therefore, the labeling of the antibody was carried out in Buffer A (pH 7.2).

Preparation of Immobilized Antibody. The three methods (glutaraldehyde method, cyanogen bromide method, and periodate method) as an immobilization procedure of antibody were compared with each other.

The glutaraldehyde method by which an immobilization reaction can be easily produced, has been applied to the immobilization of many kinds of enzymes[5] and antibodies.[6] In the previous CLCCIA an

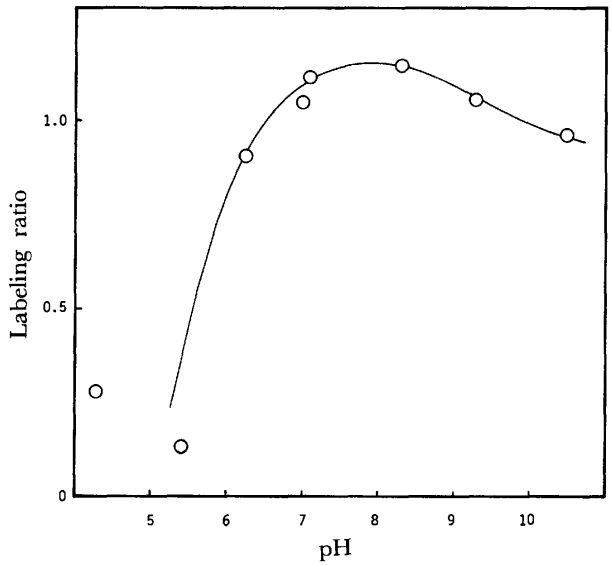

Fig. 2. Relationship between pH of solution in labeling reaction and labeling ratio of HSA.

antibody was immobilized on a glass bead of 4-mm diam. by the glutaraldehyde method. The antibody was combined with the support through an imine-type bond by the use of glutaraldehyde. As this imine-type bond is relatively weak, it dissociates easily in an acidic solution. Therefore, the immobilized antibody glass bead could not be used again after the dissociation of the immune complex on the glass bead with an acidic liberating solution.

There have been many reports in which various kinds of enzymes and proteins were immobilized on activated cellulose with cyanogen bromide. The authors were also able to immobilize albumin and galactose oxidase with good results[7] by the cyanogen bromide method. Immobilization of an antibody onto cellulose beads (Cellulofine, GC-700m, Chisso) by the cyanogen bromide method was further attempted, but the immobilized antibody, thus obtained, did not react with an antigen. This seemed to be due to the fact that the distance between the support and the antibody was too short to allow the antibody to react with the antigen.

Finally, the immobilization of an antibody on glass beads (CPG-3000) was attempted by the periodate method.[8] Glycosil bonded glass beads were converted to their aldehydic form by oxidation with sodium periodate. This formyl group and an amino group of antibodies were made to react. An imine-type bond was formed. The imine-type bond was reduced to amine-type bond with sodium borohydride, and the bond between the antibody and the support was strengthened. The immobilized antibodies, thus obtained by the periodate method, could not only be used repeatedly for an immune reaction, but also they showed little unspecific adsorption of other proteins.[9] In the present study, the periodate method was chosen as the immobilization method of the antibody.

An attempt was made to reduce an antibody im-

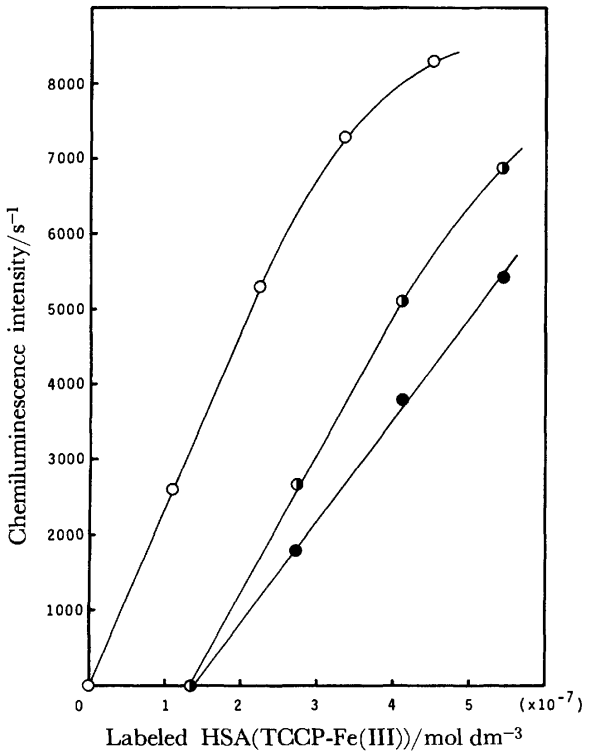

Fig. 3. Effect of volume of immobilized antibody in column.
○: 88 mm^3, ◑: 177 mm^3, and ●: 357 mm^3.

mobilized by the glutaraldehyde method with sodium borohydride, but the immobilized antibody did not show an effective immune reaction.

Immunoassay. There are competitive and sandwich methods as labeled immunoassay. A competitive immunoassay technique was used in a previous CLCCIA because the operation of the immunoassay was simple. However, the conditions of an immune reaction (the mixing ratio of a sample antigen to a labeled antigen, the desired amount of immobilized antibody, *etc.*) must be closely controlled. The control of these conditions of immune reaction is easy in the case of batchwise immunoassay, but it is difficult for continuous immunoassay in which an immobilized antibody is repeatedly used because the activity of an immobilized antibody for an immune reaction may be changed. Therefore, use was made, for immunoassay in this investigation, of the sandwich method which could be expected to be highly sensitive, though it was accompanied with a number of steps.

In order to determine the optimum volume of an immobilized antibody column, the following experiment was carried out. An immune reaction was carried out by passing labeled HSA with [Fe(tccp)] as a sample through the immobilized antibody column (Fig. 1 (k)). Here, three kinds of immobilized antibody columns were used. The catalytic activity of the labeled HSA in a liberating solution was measured for the chemiluminescence reaction between luminol and H_2O_2. The results are shown in Fig. 3. The chemiluminescence intensity increased with a decrease in the volume of the immobilized antibody column, that is, the labeled HSA liberated from the immobilized antibody column increased. Much labeled HSA was found to be unspecifically adsorbed with an increase of the column volume. On the basis of this experimental result, the volume of the immobilized antibody column was determined to be 88 mm^3.

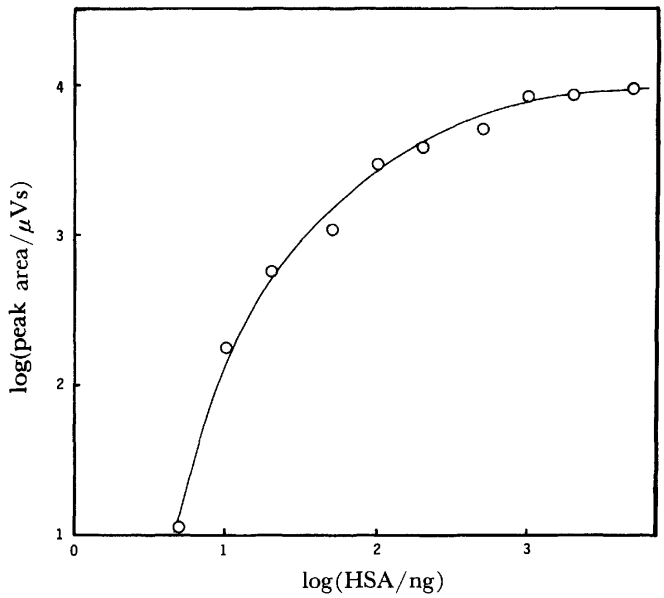

Fig. 4. Standard curve of HSA.

The relationship between the immune reaction time in the immobilized antibody column and a peak area of chemiluminescence was examined. The experiment was made as follows: 1) labeled HSA was used as a sample, 2) the flow rate of Buffer A, which was used to feed labeled HSA into the column was changed so as to give various immune reaction times. The immune reaction time was defined as the residence time of a sample in the column. The peak area of chemiluminescence increased with an increasing immune reaction time. The capacity of pump (e_3) allowed the flow rate of the sample solution to be brought to 0.24 cm^3/min, and the immune reaction time became 11 s.

To determine the washing time necessary for the removal of an excess labeled antibody from the immobilized antibody column, the relationship between washing time and intensity of chemiluminescence blank was examined. The intensity of the chemiluminescence blank was found to be almost constant at a washing time of more than 4 min. Hereafter, the immobilized antibody column was washed with Buffer A for 5 min after the sandwich reaction.

In accordance with the procedure shown in Scheme 1, a standard curve of HSA was obtained (Fig. 4). A peak area of a sample was presented by subtracting the blank peak area of unspecifically adsorbed labeled antibody from the peak area of experimental data. According to the present method, HSA in the range from 5 ng to 1 μg could be determined. The detection limit became a

much smaller value than that in the previous competitive CLCCIA (20 ng). Further, the time necessary for all the immunoassay processes (including: an immune reaction, B/F separation, a sandwich reaction, and a chemiluminescence reaction) could be reduced to 50 min from 10 h or more in the previous CLCCIA. The immunoassay of 20 ng HSA as a sample was by the use of the same immobilized antibody column. The coefficient of variation was 17% for 5 replicate analyses while 40% for 10 replicate analyses. Since the coefficient of variation up to about 20% for the immunoassay of the present level had been generally allowed, it was concluded that a continuous CLCCIA of up to 5 times could be carried out by the use of the same immobilized antibody column. In order to make continuous CLCCIA a practical automatic method of immunoassay, the immobilized antibody has to be further improved so as to increase the number of continuous analyses.

References

1) T. Hara, M. Toriyama, and K. Tsukagoshi, *Bull. Chem. Soc. Jpn.*, **56**, 2267 (1983).
2) T. Hara, M. Toriyama, and K. Tsukagoshi, *Bull. Chem. Soc. Jpn.*, **56**, 2965 (1983).
3) T. Hara, M. Toriyama, and K. Tsukagoshi, *Bull. Chem. Soc. Jpn.*, **57**, 587 (1984).
4) T. Hara, M. Toriyama, H. Miyoshi, and S. Syogase, *Bull. Chem. Soc. Jpn.*, **57**, 3009 (1984).
5) I. Chibata, T. Tosa, R. Matuno, T. Sato, and T. Mori, "Kotei-ka Kohso," Kodansha, Tokyo (1975), pp. 36—37.
6) I. Karube, T. Matsunaga, T. Satoh, and S. Suzuki, *Anal. Chim. Acta*, **156**, 283 (1984).
7) M. Toriyama, M. Inoue, and T. Hara, *Sci. Eng. Rev. Doshisha Univ.*, **25**, 109 (1984).
8) S. Ohlson, L. Hansson, P. Larsson, and K. Mosbach, *FEBS Lett.*, **93**, 5 (1978).
9) F. E. Regnier and R. Noel, *J. Chromatogr. Sci.*, **14**, 316 (1976).

The Crystal and Molecular Structure of Tetrakisthiocyanatobis-(triphenylphosphine)cobalt(II)mercury(II) in Dimer Form, $[CoHg(SCN)_4\{(C_6H_5)_3P\}_2]_2$

Hisashi KINOSHITA,* Mamoru SHIMOI,† and Akira OUCHI†

Department of Chemistry, Faculty of Liberal Arts, Shizuoka University, Ohya, Shizuoka-shi 422

†*Department of Chemistry, College of Arts and Sciences, The University of Tokyo, Komaba, Meguro-ku, Tokyo 153*

(Received November 15, 1984)

The crystal and molecular structure of the title metal complex was determined by the X-ray diffraction method. The crystal is triclinic, with the space group $P\bar{1}$, $Z=1$, $a=11.934(2)$, $b=14.642(9)$, $c=11.801(6)$Å, $\alpha=90.41(5)$, $\beta=94.04(2)$, and $\gamma=83.82(2)°$. The final R value for 6928 reflections is 0.065. The cobalt(II) atom is in a tetrahedral geometry, ligated by four nitrogen atoms of the thiocyanato (SCN) ligands, while the mercury(II) atom is in a trigonal-bipyramidal geometry, where two phosphorus atoms of both the triphenylphosphine ligands bond axially and three sulfur atoms of SCN's equatorially; however, these Hg-S bonds are very long. Thus, the pairs of cobalt(II) and mercury(II) atoms are linked by one SCN bridge, forming a sixteen-membered ring of $Co_2Hg_2(SCN)_4$, and this ring is linked with the next ones on both sides in the a-axis direction with two longer bondings.

Tetrakisthiocyanatocobalt(II)mercury(II), $CoHg(SCN)_4$ (**1**), is known as a "diamond-like" three-dimensional polymeric type of complex where each metal atom is linked with four metal atoms of another kind by thiocyanate (SCN) bridges. Its structure was clarified by Jeffery,[1] and its characteristic structure was discussed by Wells.[2a] Some of its Lewis-base adducts were also synthesized,[3,4] and the structures of the pyridine (py) adduct, $CoHg(SCN)_4(py)_2$,[5] and of *N,N*-dimethylformamide (dmf), $CoHg(SCN)_4(dmf)_2$,[6] were also elucidated. In both of the adducts, the cobalt(II) atom is in the octahedral geometry, and the mercury(II) atom, in the tetrahedral configuration, although the three-dimensional network by the SCN bridges was retained. Because of the octahedral geometry of cobalt(II) in the adducts, they are reddish in color. On the other hand, Makhija has also obtained the title complex, which is deep blue in color; this fact shows that it contains tetrahedral cobalt(II) atoms.[4] Mainly on the base of infrared absorption spectral considerations, Makhija proposed a monomer structure for it, where a cobalt atom and a mercury atom are bridged by two SCN ligands. According to his formula, the cobalt(II) atom is bonded with two phosphorus atoms of triphenylphosphine (Ph_3P) ligands as well as two nitrogen atoms of SCN ions while the mercury(II) atom is ligated by four sulfur atoms of SCN ions. This formula was not yet been proved by the single crystal X-ray diffraction method, and the former concept receives some support even now.[3,7,8] Although cobalt(II) complexes including phosphine derivatives have been reported elsewhere,[9-11] as the ligands are soft ones, they may prefer to bond with the mercury(II) atom, which is softer than cobalt(II).[12] The observed affinity of Ph_3P in the title complex seems to be higher than those of dmf or *N,N*-dimethylacetamide (dma). When the dmf or dma adduct $CoHg(SCN)_4L_2$ (where L=dmf or dma) in its solid phase was left standing in an acetonitrile solution of Ph_3P, they turned into the title Ph_3P adduct rapidly and the base was removed, on the other hand, when the title complex was stirred in an acetonitrile solution of dmf or dma, no substitution reaction occurred. Therefore, we were not able to believe the traditional formula; we have now determined its structure by the single-crystal X-ray diffraction method.

Experimental

Synthesis of Tetrakisthiocyanatobis(triphenylphosphine)-cobalt(II)mercury(II) (2). Although the title complex was synthesized by Makhija from the tetrahydrofuran (thf) adduct of **1**, $CoHg(SCN)_4(thf)_2$, which had itself been obtained from cobalt(II) and mercury(II) thiocyanates and thf, we could obtain the title complex **2**, easier by the following method.

The complex, **1**, obtained by Figgis' method,[13] was finely powdered (2.0 g, 4.1 mmol) and then poured into 20 cm^3 of an acetonitrile solution containing Ph_3P (2.4 g, 9.2 mmol), after which the mixture was stirred for 6 h at the ambient temperature. The addition reaction occurred rapidly, and the solid product thus obtained was filtered off, washed by acetonitrile, and dried on silica-gel in a vacuum desiccator. Yield, 3.5 g, (85%). By the gradual evaporation of the filtrate, some additional crop was obtained in larger-crystal grains, some of which were used for the X-ray diffraction measurement. Anal. of the main and the additional crops: ($Co_2Hg_2C_{80}H_{60}N_8P_4S_8$) Co, C, H, N. The infrared and visible absorption spectra of the product were similar to those reported by Makhija.[4]

Intensity-data Collection. A crystal with the dimensions of 0.3×0.3×0.4 mm^3 was used for the measurement without shaping. The crystallographic data are: $Co_2Hg_2C_{80}H_{60}N_8P_4S_8$, F.W.=2032.87, triclinic, space group $P\bar{1}$, $Z=1$, $a=11.934(2)$, $b=14.642(9)$, $c=11.801(6)$ Å, $\alpha=90.41(5)$, $\beta=94.04(2)$, $\gamma=83.82(2)°$, $V=2045(1)$ Å^3, $D_m=1.64(3)$, $D_x=1.65$ g cm^{-3}, $\mu(Mo\,K\alpha)=4.56$ mm^{-1}. The reflections within the range of $3°<2\theta<50°$ were collected on a Rigaku AFC-6A automated four-circle X-ray diffractometer with graphite monochromated Mo $K\alpha$ radiation, the θ—2θ scan technique being employed (scan speed, 4° min^{-1} in 2θ; scan width, $1.20+0.5\tan\theta$). The crystal was stable during the exposure to X-rays. Of the 7243 independent reflections thus obtained, 6928 with $|F_o|>3\sigma(|F_o|)$ were selected and used for the structure determination. The intensities were corrected for the Lorentz and polarization factors, but no correction was

made for absorption and extinction.

Structure Determination. The structure was solved by the heavy-atom method. The positions of the cobalt(II), mercury(II), and some sulfur and phosphorus atoms were deduced from a three-dimensional Patterson map, while the other non-hydrogen atoms were located by means of successive Fourier syntheses. Their positional, isotropic, and then anisotropic thermal parameters were refined by the block-diagonal least-squares method. The positions of all the non-hydrogen atoms were found. All the hydrogen atoms were fixed at calculated positions with B_{iso}=10.0 (the C–H length was assumed to be 1.08 Å). In the last cycle of the refinement, all the parameter-shifts of the non-hydrogen atoms were less than $\sigma/3$.

All the calculations were carried out on a HITAC M-200H computer at the Computer Center of The University of Tokyo, using the local version of the UNICS program system.[14] The atomic scattering factors were taken from the tables.[15]

Results and Discussion

The final atomic parameters of non-hydrogen atoms are listed in Table 1,[16] while the bond lengths and bond-angles are tabulated in Table 2.[16] The perspective drawings around the cobalt(II) and mercury(II) atoms, together with the numbering scheme, are shown in Figs. 1 and 2. The crystal packing diagram is shown in Fig. 3, while the schematic drawing to show the bondings in a unit cell is in Fig. 4.

The cobalt(II) atom is tetra-coordinated and is in a tetrahedral geometry, where four nitrogen atoms of four SCN ions are ligated. Although S(3) of the SCN does not bond with any metal atom, the other three SCN ligands bridge to three mercury(II) atoms, as is shown in Fig. 4. The average Co–N bond length is 1.954 Å, which is not much different from the sum of the respective atomic radii (Co=1.25, N=0.70 Å).[17] The average Co–N–C angle is 173.48°, and these atoms are almost collinear, although the deviation from 180° is a little larger than that of **1** (178.66°).[1]

The mercury(II) atom is bonded with two phosphorus atoms of the respective Ph_3P ligands in an approximately collinear geometry (P–Hg–P=166.63(10)°), and the average Hg–P bond length is 2.430 Å, which is about the same as the sum of the two atomic radii (Hg=1.50, P=1.10 Å).[17] Three sulfur atoms of the SCN ligands take their positions about perpendicular to the P–Hg–P axis, and the sulfur atoms as well as the central metal atom are almost on one plane: the average positional deviation of the atoms from the plane is 0.043 Å (maximum 0.085 Å for Hg). The S–Hg–P angles are between 81.4 to 100.2° (90.6° on the average). The S(1)–Hg–S(2^i) angle (101.0°) is a little smaller than the other two (133.6 and 125.0°). From these angular observations, the geometry around the mercury(II) atom is thought to be trigonal-bipyramidal; however, the bond lengths of Hg–S are long (Hg–S(1)=2.990(3), Hg–S(2^i)=2.745(4), and Hg–S(4^{ii})=3.323(4) Å), while the atomic radii of the two atoms are Hg=1.50 and S=1.04 Å.[17] In many mercury(II) compounds where the sulfur atom is ligated to the metal atom, the Hg–S bond length is found to be about 2.5 Å. Even in the related complexes, the normal values are shown to be writen

Table 1. Final atomic coordinates ($\times 10^4$) and equivalent isotropic temperature factors (B_{eq}/Å^2), with estimated standard deviations in parentheses

Atom	x	y	z	B_{eq}/Å$^{2a)}$
Co	7995(1)	3149(1)	6016(1)	4.5
Hg	3340.2(4)	2493.7(3)	4400.1(4)	3.6
S(1)	5286(3)	1097(2)	5071(3)	4.7
S(2)	5638(3)	5914(2)	5423(4)	6.0
S(3)	9320(4)	2648(4)	9816(4)	8.3
S(4)	10704(3)	2349(3)	3365(3)	5.4
C(1)	6183(9)	1832(7)	5379(9)	4.0
C(2)	6605(10)	5043(8)	5656(10)	4.4
C(3)	8851(10)	2812(8)	8532(11)	5.0
C(4)	9813(9)	2641(7)	4306(10)	3.9
N(1)	6829(8)	2332(6)	5620(9)	5.1
N(2)	7241(8)	4410(7)	5807(9)	5.1
N(3)	8528(8)	2926(8)	7586(9)	5.8
N(4)	9186(8)	2863(7)	4980(8)	4.9
P(1)	2687(2)	2414(2)	6297(2)	3.3
P(2)	3692(2)	2306(2)	2403(2)	3.6
C(11)	3274(9)	3344(7)	1591(9)	3.9
C(12)	2410(10)	3972(8)	1948(9)	4.4
C(13)	2131(11)	4799(9)	1383(11)	5.5
C(14)	2710(12)	5004(8)	490(11)	5.5
C(15)	3548(12)	4384(10)	105(11)	5.9
C(16)	3839(11)	3559(9)	678(10)	5.4
C(21)	5196(9)	2035(9)	2224(10)	4.8
C(22)	5884(11)	2720(11)	2477(13)	6.8
C(23)	7041(12)	2545(13)	2322(14)	8.3
C(24)	7464(11)	1729(11)	1941(14)	7.4
C(25)	6792(13)	1048(11)	1685(14)	7.9
C(26)	5625(10)	1206(9)	1840(11)	5.5
C(31)	2962(9)	1381(7)	1805(9)	3.9
C(32)	3038(10)	564(8)	2385(11)	5.0
C(33)	2474(11)	−167(9)	1987(11)	5.6
C(34)	1827(12)	−56(9)	962(12)	6.2
C(35)	1726(12)	734(10)	395(12)	6.5
C(36)	2289(11)	1478(9)	796(10)	5.2
C(41)	1896(9)	1440(7)	6407(8)	3.6
C(42)	2236(11)	644(8)	5841(11)	5.2
C(43)	1622(12)	−119(9)	5876(12)	6.2
C(44)	656(11)	−33(9)	6438(13)	6.4
C(45)	316(11)	767(10)	6966(14)	7.1
C(46)	909(10)	1504(9)	6980(12)	5.8
C(51)	1857(8)	3437(7)	6717(9)	3.8
C(52)	1656(10)	3586(9)	7832(10)	5.2
C(53)	1045(11)	4402(10)	8174(11)	6.3
C(54)	677(11)	5063(9)	7389(13)	6.1
C(55)	886(11)	4926(9)	6278(13)	6.0
C(56)	1472(10)	4119(8)	5935(10)	4.4
C(61)	3891(9)	2288(8)	7345(8)	3.9
C(62)	4575(10)	2996(9)	7420(9)	5.2
C(63)	5516(11)	2923(11)	8182(11)	6.6
C(64)	5766(11)	2164(11)	8867(11)	6.4
C(65)	5078(13)	1477(10)	8799(11)	6.9
C(66)	4109(11)	1529(8)	8036(10)	5.1

a) The isotropic temperature factors were computed using the following expression: $B_{eq}=4/3(B_{11}a^2+B_{22}b^2+B_{33}c^2+B_{12}ab\cos\gamma+B_{13}ac\cos\beta+B_{23}bc\cos\alpha)$. The B_{ij}'s are defined by: $\exp[-(h^2B_{11}+k^2B_{22}+l^2B_{33}+2klB_{23}+2hlB_{13}+2hkB_{12})]$.

TABLE 2. SELECTED BOND LENGTHS AND BOND ANGLES WITH ESTIMATED STANDARD DEVIATIONS IN PARENTHESES

Bond length	l/Å	Bond length	l/Å
Co-N(1)	1.962(10)	Co-N(2)	1.975(9)
Co-N(3)	1.934(14)	Co-N(4)	1.948(11)
Hg-S(1)	2.991(3)	Hg-S(2^{i})	2.745(4)
Hg-S(4^{ii})	3.322(4)	Hg-P(1)	2.429(4)
Hg-P(2)	2.432(4)	Co···Hg	5.920(2)
Co···Co^{i}	8.699(4)	Hg···Hg^{i}	8.768(4)
Co···Hg^{i}	6.421(4)	Hg···Co^{ii}	6.754(2)
S(1)-C(1)	1.619(11)	S(2)-C(2)	1.637(11)
S(3)-C(3)	1.589(16)	S(4)-C(4)	1.615(13)
C(1)-N(1)	1.140(15)	C(2)-N(2)	1.139(14)
C(3)-N(3)	1.16(2)	C(4)-N(4)	1.152(17)
P(1)-C(41)	1.804(11)	P(1)-C(51)	1.791(11)
P(1)-C(61)	1.823(12)	P(2)-C(11)	1.808(12)
P(2)-C(21)	1.822(11)	P(2)-C(31)	1.800(12)
Bond angle	**ϕ/°**	**Bond angle**	**ϕ/°**
N(1)-Co-N(2)	105.8(4)	N(1)-Co-N(3)	108.1(5)
N(1)-Co-N(4)	106.9(5)	N(2)-Co-N(3)	111.0(5)
N(2)-Co-N(4)	112.3(4)	N(3)-Co-N(4)	112.3(5)
S(1)-Hg-P(1)	89.58(10)	S(1)-Hg-P(2)	91.26(10)
P(1)-Hg-P(2)	166.65(12)	S(1)-Hg-S(2^{i})	101.01(9)
S(2^{i})-Hg-P(1)	100.22(11)	S(2^{i})-Hg-P(2)	92.71(11)
S(4^{ii})-Hg-P(1)	88.36(10)	S(4^{ii})-Hg-P(2)	81.41(10)
S(4^{ii})-Hg-S(1)	133.53(8)	S(4^{ii})-Hg-S(2^{i})	125.02(9)
Hg-S(1)-C(1)	95.8(4)	Hg-S(2^{i})-C(2^{i})	108.6(4)
Hg-S(4^{ii})-C(4^{ii})	111.2(5)	Hg-P(1)-C(41)	110.1(4)
Hg-P(1)-C(51)	113.8(4)	Hg-P(1)-C(61)	110.0(4)
Hg-P(2)-C(11)	112.5(4)	Hg-P(2)-C(21)	111.0(4)
Hg-P(2)-C(31)	109.8(4)	Co-N(1)-C(1)	177.4(10)
Co-N(2)-C(2)	165.4(9)	Co-N(3)-C(3)	178.5(13)
Co-N(4)-C(4)	173.0(10)	S(1)-C(1)-N(1)	178.0(11)
S(2)-C(2)-N(2)	176.9(10)	S(3)-C(3)-N(3)	178.7(15)
S(4)-C(4)-N(4)	178.9(12)		

Key to the symmetric operations: i, 1.0−x, 1.0−y, 1.0−z; ii, −1.0+x, y, z.

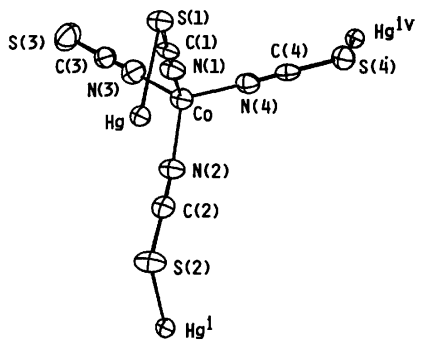

Fig. 1. Perspective drawing of the complex around the cobalt(II) atom with the numbering scheme (Key to the symmetric operations; i, 1.0−x, 1.0−y, 1.0−z; iv, 1.0+x, y, z).

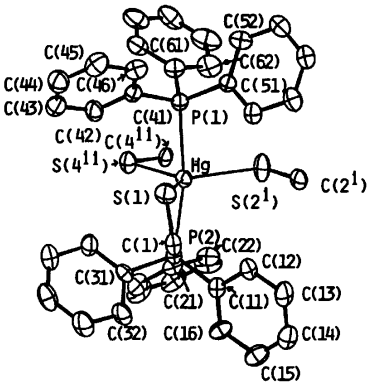

Fig. 2. Perspective drawing of the complex around the mercury atom with the numbering scheme (Key to the symmetric operations; i, 1.0−x, 1.0−y, 1.0−z; ii, −1.0+x, y, z).

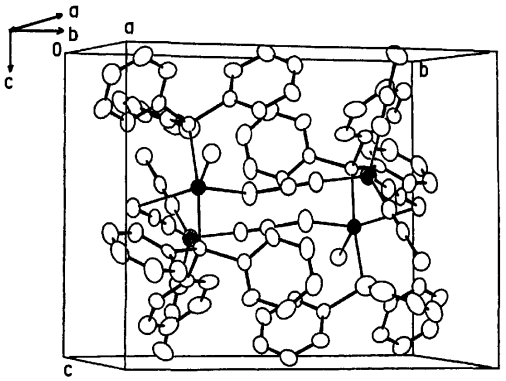

Fig. 3. Crystal packing diagram of the complex.

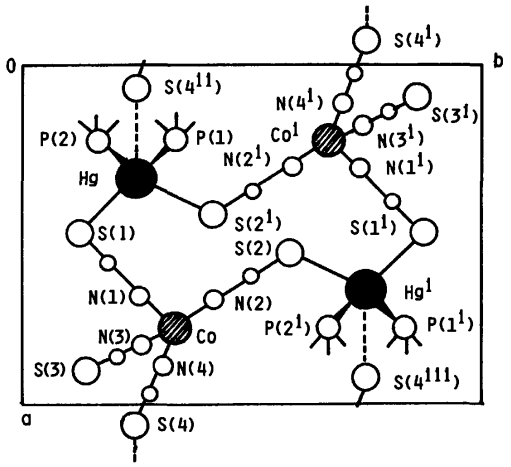

Fig. 4. Schematic presentation to show the bondings in a unit cell (Key to the symmetric operations; i, 1.0−x, 1.0−y, 1.0−z; ii, −1.0+x, y, z; iii, 2.0−x, 1.0−y, 1.0−z).

as follows: $CoHg(SCN)_4$, 2.558(4) Å;[1] $CoHg(SCN)_4(dmf)_2$, 2.539 Å on the average,[5] $CoHg(SCN)_4(py)_2$, 2.525 Å on the average;[6] and $Hg(SCN)_2(Ph_3P)$, 2.503 Å[18] and 2.528 Å[19] on the average.

Although there has been no report about such an elongated Hg-S bond as is found in this complex, it is a well-known fact that, in some multi-coordinated mercury(II) complexes, several groups of bond lengths are found;[2b] for example, in $HgSO_4 \cdot H_2O$, which is in about an octahedral geometry around the central metal atom, two Hg-O bond lengths of one axis are normal, while the other four equatorial Hg-O lengths are much longer.[20] As Ph_3P is a base which is softer than SCN,[12] it is not impossible that the Hg-P bonds take priority over the Hg-S bonds in the title complex; however, as the Hg-S bond has commonly been thought to be a typically strong bond, this kind of the long Hg-S bond has rarely been reported.

The trigonal-bipyramidal configuration of the ligating atoms around the central mercury(II) atom in its complexes has been reported in only a few cases, such as $(CH_3)_3SHgI_3$[23] and $Hg(SCN)_2(Ph_3P)$.[18,19] In these complexes, however, the axially ligating atoms take abnormally far positions: Hg-I=3.52 and 3.69 Å in the former, and Hg-N=2.74 and 2.89 Å in the latter complex. On the other hand, in the title complex, the equatorially bonded atoms are still farther apart; such a type of mercury(II) complex has not previously been reported.

The Hg-S-C angles in the title complex are 95.79 (S(1)), 108.65 ($S(2^i)$), and 111.14° ($S(4^{ii})$). In comparison with the other thiocyanato complexes of mercury(II), where the angles are about 95—98°, and where even the large one in $Hg(SCN)_2(Ph_3P)$ is only 104.5°,[18] these angles in the title complex, especially the latter two, are exceptionally large.

As Hg-$S(4^{ii})$ is longer than the other two Hg-S bonds, a sixteen-membered ring including two mercury(II) and two cobalt(II) atoms which are linked by four SCN^- ions, as is shown in Fig. 4, is considered to be the unit structure, which is linked to the next ones on both sides by means of two relatively long bondings (Hg-$S(4^{ii})$); they lie parallel to the a-axis as a ladder lying perpendicular to the bc-plane. No bridgings are found in either the b- or the c-axis direction between the rings. This type of structure is unique and has never been reported for the thiocyanate-bridged metal complexes.

As Porai-Koshits has already shown, the mixed complex $CoHg(SCN)_4(tu)_4$ (where tu=thiourea) consists of discrete $[Hg(tu)_4]^{2+}$ and $[Co(SCN)_4]^{2-}$ ions, and both of them are bonded only electrostatically; all thiocyanato sulfur atoms are far from the mercury(II) atoms.[24] Therefore, the title complex is thought to belong to an intermediate group between the three-dimensional polymeric-type complexes such as **1** and those consisting of discrete anionic and cationic complexes such as the thiourea adduct of **1**.

References

1) J. W. Jeffery and K. M. Rose, *Acta Crystallogr., Sect B*, **24**, 653 (1968).

2) A. F. Wells, "Structural Inorganic Chemistry," 5th ed, Clarendon Press, Oxford, U. K.,(1984), a) pp. 63—140, b) p. 1158.

3) P. P. Singh, *Coord. Chem. Rev.*, **32**, 33 (1980), and the references cited in it.

4) R. Makhija, L. Pazdernik, and R. Rivest, *Can. J. Chem.*, **51**, 438 (1973).

5) A. L. Beauchamp, L. Pazdernik, and R. Rivest, *Acta Crystallogr., Sect B*, **32**, 650 (1976).

6) M. R. Udupa and B. Krebs, *Inorg. Chim. Acta*, **42**, 37 (1980).

7) R. Makhija, L. Pazdernik, and R. Rivest, *Can. J. Chem.*, **51**, 2987 (1973).

8) P. P. Singh and A. K. Gupta, *Inorg. Chem.*, **17**, 1 (1978).

9) W. E. Hatfield, M. Rowley, and R. Swindells, *J. Chem. Soc., A*, **1966**, 950.

10) J. Bradburg, K. P. Forest, R. G. Nuttall, and D. W. A. Sharp, *Spectrochim. Acta, Part A*, **23**, 2701 (1967).

11) M. Shimoi, A. Ouchi, T. Uehiro, Y. Yoshino, S. Sato, and Y. Saito, *Bull. Chem. Soc. Jpn.*, **55**, 2371 (1982).

12) R. G. Pearson, *Science*, **151**, 172 (1966).

13) B. N. Figgis and R. S. Nyholm, *J. Chem. Soc.*, **1958**, 4190.

14) "Universal Crystallographic Computation Program System (UNICS)," ed by T. Sakurai, Crystallographic Society of Japan, Tokyo (1967).

15) "International Tables for X-Ray Crystallography," Kynoch Press, Birmingham (1974), Vol. IV, pp. 72, 150.

16) The positions of the hydrogen atoms, the final thermal parameters, the final F_o—F_c table, and some supplemental bond length and bond angle data are deposited as Document No. 8519 at the office of the Editor of the *Bull. Chem. Soc. Jpn.*

17) L. Pauling," The Nature of the Chemical Bond," 3rd ed, Cornell University Press, N. Y. (1960), pp. 246, 256.

18) C. Gagnon and A. L. Beauchamp, *Acta Crystallogr., Sect B*, **35**, 166 (1979).

19) R. C.M akhija, R. Rivest, and A. L. Beauchamp, *Can. J. Chem.*, **57**, 2555 (1979).

20) C. Stahlhandske, *Acta Crystallogr., Sect B*, **36**, 23 (1980).

21) G. A. Barclay and A.Cooper, *J. Chem. Soc.*, **1965**, 3741.

22) D. Hall, A. J. McKinnon, and T. N. Waters, *J. Chem. Soc., A*, **1966**, 615.

23) R. H. Fenn, *Acta Crystallogr.*, **20**, 20 (1966).

24) A. Korczynski and M. A. Porai-Koshits, *Rocz. Chem.*, **39**, 1567 (1965).

 © 1985 The Chemical Society of Japan Bull. Chem. Soc. Jpn., 58, 1308—1314 (1985) [Vol. 58, No. 4

A New Calibration Method for the Measurement of CCl_4 Concentration at 10^{-10} v/v Level and the Behavior of CCl_4 in the Atmosphere

Akihito YOKOHATA, Yoshihiro MAKIDE,* and Takeshi TOMINAGA
Department of Chemistry, Faculty of Science, The University of Tokyo, Hongo, Bunkyo-ku, Tokyo 113
(Received November 27, 1984)

A new technique was developed for the accurate determination of atmospheric CCl_4 at about 100 pptv ($=10^{-10}$ v/v) concentration level, since at such extremely low concentration CCl_4 was found to be adsorbed readily and strongly on clean metal surfaces under dry conditions. The analysis of CCl_4 by gas chromatography/electron-capture detector and the preparation of CCl_4 primary calibration standard were improved by introducing water vapor into the system to prevent the adsorption of CCl_4 and to obtain stable and reproducible results. The total amount of CCl_4 in the atmosphere was studied on the basis of our newly calibrated data of CCl_4 concentration, and a reasonable lifetime of CCl_4 was obtained assuming that its sink is only the UV photodissociation in the stratosphere.

The release of chlorine atoms following UV photodissociation of man-made halocarbons (CCl_2F_2, CCl_3F, CCl_4, *etc.*) in the stratosphere is believed to change equilibria among chemical species in the stratosphere, which have been maintained for a long time.[1-9] In particular, the dissociation of ozone by Cl-induced chain reactions and the consequent change in the vertical profile of ozone in the stratosphere may end up affecting severely the earth's environment. Accumulated amounts of man-made CCl_2F_2 and CCl_3F in the atmosphere have been sharply increasing since 1950's due to their growing uses as aerosol propellants and refrigerants. Therefore, extensive efforts have been made to estimate the Cl-atom effect on the stratospheric ozone layer. While carbon tetrachloride (similar to CCl_2F_2 and CCl_3F) is almost of anthropogenic origin as well, its behavior in the atmosphere has not been understood well. During 1920 through 1940's, all the produced CCl_4 was released into the atmosphere after its uses as industrial solvent, dry cleaning agent, fire extinguisher, and grain fumigant. Since 1950's, however, CCl_4 has been mostly used as starting chemicals in the production of CCl_2F_2 and CCl_3F and its release into the atmosphere has been considered to be limited.[10-13] Accordingly its concentration in the atmosphere had been believed to remain nearly constant. The recent estimation, however, has suggested much larger release of CCl_4 in 1970's, and it has been increasing as well with the growing production of CCl_2F_2 and CCl_3F.[14] Since the reported atmospheric concentrations of CCl_4 vary among investigators, the distribution, annual change and absolute amount of CCl_4 in the atmosphere are not completely known yet. Carbon tetrachloride is an ultratrace constituent in the atmosphere at about 100 pptv (pptv=10^{-12} v/v) and tends to be strongly adsorbed or decomposed on the internal surface of sample canisters, which results in poor precision and accuracy in its analysis as compared with the analyses of CCl_2F_2 and CCl_3F.[15,16] Therefore we have improved the procedure of CCl_4 analysis with a gas chromatograph/electron-capture detector (GC-ECD) and also established a new method of preparation of CCl_4 standard by adding water vapor to prevent the CCl_4 adsorption. In this paper we report a new method of preparation of CCl_4 primary standards at 100 pptv level and discuss the behavior of CCl_4 in the atmosphere based on the background atmospheric concentrations determined by our new measurements.

Experimental

Sampling Procedures. A 2-dm^3 stainless steel (SS) canister equipped with an all SS bellows valve (Nupro SS-4H) was mainly used for atmospheric sampling. The canister was made by welding a 2-dm^3 beaker and a top plate with a welded tube, all of which had been washed carefully with neutral detergent and then with acetone in an ultrasonic cleaner. Electropolishing was not used because it chemically activates the surface. After the installation of the bellows valve, the canister was evacuated overnight to below 10^{-3} Pa at elevated temperatures from 50 to 300 °C. After the evacuation, ambient air was temporarily introduced into the canister at room temperature and pumped out again in order to deactivate the internal surface with adsorbable ingredients (probably H_2O). The canisters once used for sampling in remote areas were used after only the evacuation at room temperature. Sample air was introduced into the evacuated canister up to the ambient pressure by simply opening the valve at sampling locations. Background air samples were collected on the coast of Hokkaido and west Tohoku area (in 40—45 °N) when the wind was blowing from the sea in order to avoid the pollution from industrialized areas and local sources in Japan.[17-20]

Analysis. Atmospheric samples were analyzed in the laboratory with a gas chromatograph (Varian GC3700) equipped with an ECD (8 mCi ^{63}Ni). The experimental set-up for analysis and the procedure were described in detail previously.[19,20] The vacuum line for handling of the sample and the flow path in the gas chromatograph are all made of stainless steel to avoid contaminations with halocarbons from organic polymers such as silicone and Teflon. An atmospheric sample was introduced into the 50 cm^3 sample loop to about 200 Torr (1 Torr=133.3 Pa) (≈13 cm^3 STP) measuring the pressure precisely with a metal diaphragm pressure gauge and was injected to the GC. Eluted halocarbons were detected by the ECD and recorded with an analog recorder (Shimadzu R-12) and a degital integrator (Shimadzu C-R2AX). The precision in the pressure measurement was about 0.3% and the reproducibility in CCl_4 measurement was better than 1%. Pure nitrogen (Nippon Sanso, grade B) was further purified successively with mole-

cular sieve 5A, activated charcoal, and molecular sieve 13X, and was used as the carrier gas at a flow rate of 80 cm^3 min^{-1}. Methane was added (6 cm^3 min^{-1}) to the carrier gas nitrogen at just before ECD in order to improve the stability, sensitivity and signal-to-noise ratio of the detector. Halocarbons were separated by the temperature programming of the column (4.25 mm i.d. ×3 m, packed with 10% Silicone OV-101 on Chromosorb-W HP) from −40 to 70 °C at 5 °C min^{-1}. The ECD was usually purged with the purified nitrogen at a flow rate of 80 cm^3 min^{-1} and was connected to the separation column by switching a four-way valve only when the halocarbons were eluted: air was by-passed to avoid the sensitivity change of ECD. After the elution of CCl_2CCl_2 at about 25 min, the column temperature was raised to 150 °C for 10 min to purge other high boiling components.

Preparation of the Calibration Standards of Halocarbons. An all SS vacuum line installed in a temperature controlled room was used for preparation of the calibration standards of halocarbons. Internal volume of each part of the line was determined at a precision below 1%. Calibration standards were prepared by static dilution of pure materials with purified nitrogen or zero air which had been purified in the same manner as carrier gas nitrogen. Since the atmospheric concentration of CCl_4 is about 100 pptv, the calibration standards with similar concentrations were prepared by 3-step dilutions (to about 100 ppmv, 100 ppbv, and 100 pptv). In preparation of pptv-level calibration standards of CCl_4 and CH_3CCl_3, zero air saturated with water vapor at 23 °C (H_2O saturated zero air) was introduced into the flask before the dilution so that the water vapor pressure in the standards finally becomes about 10 Torr.

Results and Discussion

Difficulty in CCl_4 Measurement. Previous data of CCl_4 measurements reported by several groups[14,21–38] are plotted in Fig. 1. Most measurements were made with GC-ECD by comparing the corresponding peaks with prepared calibration standards. As shown in Fig. 1 the reported values are widely scattered over 100—170 pptv in 1975—1980. Such a large fluctuation (≈50%) cannot be attributed to natural variation in CCl_4 concentration in view of the chemical inertness (long lifetime) of CCl_4 in the atmosphere. The measurements made by a group with the common method and secondary standard, however, showed only a small variation, indicating that the CCl_4 concentration increases by about 2% per year.[14,27,28] Therefore, the poor accuracy of CCl_4 measurements must be ascribed to the difficulty in the preparation of calibration standards. Another calibration method with GC-ECD-coulometry[12] based on several premises has produced widely scattered values due to poor reproducibility. The measurement of CCl_4 in the stratosphere has been limited only to the lower stratosphere, and it has suffered from severe problem of the decomposition of CCl_4 in metal canisters.[15,16,24,30–33,36,37] We have found that even in dry tropospheric samples (dew point below −5 °C) the CCl_4 concentrations decrease after stored in the metal canisters. On the other hand, in relatively humid surface level samples, the CCl_4 concentrations remain unchanged over a long storage time, probably due to the contained water vapor. Water can be strongly adsorbed on the metal surface of the canister and cover the active sites on it. We have confirmed this assumption experimentally; when a dry sample was introduced into a stainless steel

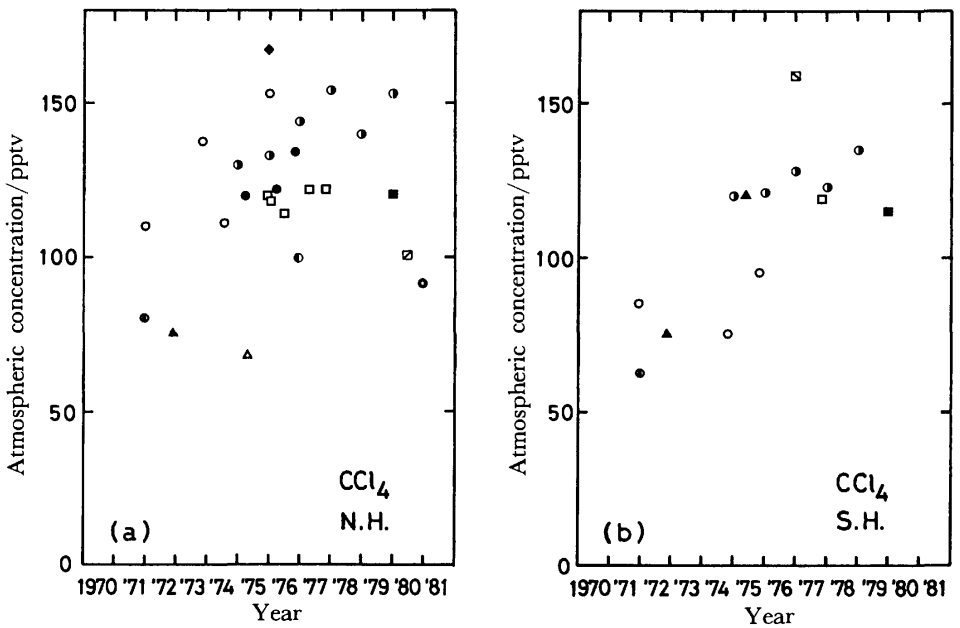

Fig. 1. Reported values of atmospheric concentrations of CCl_4 in (a) the Northern Hemisphere and (b) the Southern Hemisphere (pptv = 10^{-12} v/v). ◉: Lovelock *et al.* (Ref. 21), ○: Lovelock *et al.* (Ref. 24 and 25), ▲: Wilkniss *et al.* (Ref. 23, 34, and 35), △: Krey *et al.* (Ref. 37), ●: Robinson *et al.* (Ref. 30 and 36), Cronn *et al.* (Ref. 31), Pierotti *et al.* (Ref. 33), ◑: Rasmussen *et al.* (Ref. 28), □: Singh *et al.* (Ref. 27), ◆: Tyson *et al.* (Ref. 26), ■: Simmonds *et al.* (Ref. 14), ▨: Brice *et al.* (Ref. 29), ◐: Seiler *et al.* (Ref. 32), ▧: Fraser *et al.* (Ref. 38), ◎: This work.

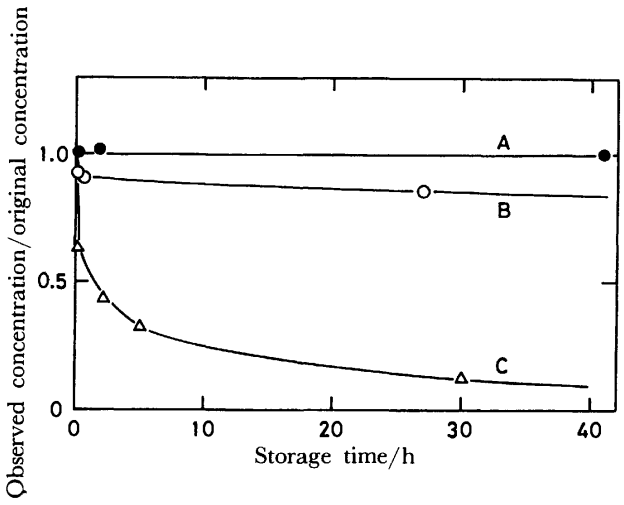

Fig. 2. Recovery of CCl_4 in dry samples stored in metal canisters: **A**, previously used for sample of background air and evacuated at room temperature; **B**, evacuated at 200 °C for 1 d; **C**, evacuated at 300 °C for 1 d.

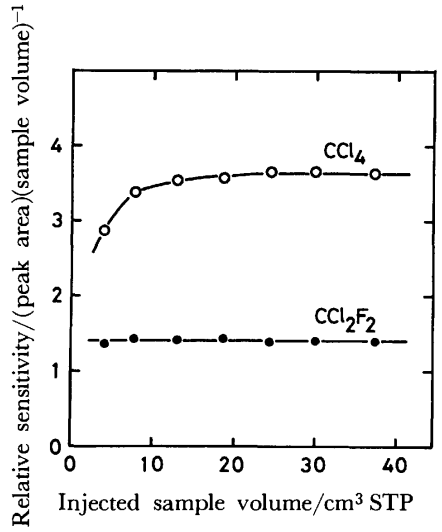

Fig. 3. Dependency of the relative sensitivity (peak area/injected sample amount) for CCl_4 and CCl_2F_2 on the injected volume of a dry sample (absolute humidity: ≈3 Torr).

canister baked at a higher temperature (300 °C, 1 d), much larger decrease in the CCl_4 concentration was observed as shown in Fig. 2. Furthermore, when the primary standards of CCl_4 at 100 pptv concentration level were prepared by dilution of 100 ppbv level standards in the metal canister with extremely purified dry air or nitrogen, the CCl_4 concentration found in the prepared standards was sometimes lower than expected even immediately after dilution, or often decreased drastically during the storage and completely diminished within a few days. These results must be explained in terms of the quick adsorption of CCl_4 on the inner surface (1) at the moment of introduction of the higher cocentration standard into the highly evacuated metal container to about several Torr, and (2) after the dilution with a water-free extremely pure dilution gas (air or nitrogen) which cannot cover the active sites on the metal surface.

Improvement of Analytical Procedures. Since we adopted the temperature-programming for the separation of 6 compounds (CCl_2F_2, CCl_3F, CH_3CCl_3, CCl_4, $CHClCCl_2$, and CCl_2CCl_2) with a single column, the commercially available high-pure grade nitrogen was further purified with purification columns for use as carrier gas. The concentrations of halocarbons in the purified nitrogen and in the purified zero air (processed with the same procedure) were: CCl_2F_2<0.01 pptv, CCl_3F<0.003 pptv, CCl_4<0.003 pptv, and CH_3CCl_3< 0.01 pptv. The separation column was therefore thoroughly cleaned by flowing the purified carrier gas nitrogen continuously for more than 5 years and by heating up to 150 °C after every run of analysis. Under these extremely clean conditions, CCl_4 in dry samples tended to be adsorbed on the column packing material during analysis and its recovery from the column was incomplete. Figure 3 shows the dependence

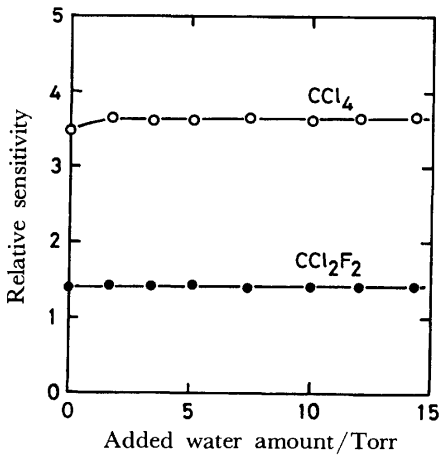

Fig. 4. The effect of preaddition of water-saturated zero air to the separation column during the analysis on the observed peak area of CCl_4 and CCl_2F_2. Water amount is shown by the corresponding vapor pressure of H_2O in the atmospheric sample.

of the relative sensitivity of CCl_4 and CCl_2F_2 (peak area/sample amount) upon the injected amount of a dry sample (dew point −5 °C, *i.e.*, absolute humidity is about 3 Torr). While the sensitivity of CCl_2F_2 was virtually independent of the injected sample amount, the CCl_4 sensitivity decreased at below 10 cm^3 STP sample injected. In order to avoid such problem, water vapor present in the purified zero air was introduced intentionally into the column at −40 °C just before the sample injection. The amount of the water-containing zero air was adjusted so as to keep the humidity in the sample constant at 15 Torr; the difference in the retention behavior of halocarbons in the GC column can also be canceled out. Each halocarbon concentration in the water saturated zero air was confirmed to be below the detection limit by GC-ECD. Figure 4 shows the change of the sensitivity of CCl_4 in the atmospher-

ic sample (13 cm^3 STP, absolute humidity 3 Torr) with preaddition of the water-saturated zero air. Since water is introduced into the column prior to the sample injection in this case, the amount of water-containing air necessary to deactivate the reactive sites was much less than in the case of Fig. 3. The recovery of CCl_4 at plateau regions in Figs. 3 and 4 agreed well and can be considered to be complete.

Preparation of Calibration Standard. The calibration standards of CCl_2F_2 and CCl_3F prepared with dry purified zero air were stored more than 2 years without change of their concentrations (<0.5%) in the 2-dm^3 SS canister equipped with a SS bellows valve. In the dry CCl_4 calibration standards prepared in the SS canister with concentrations at and below ppbv, however, the concentration decreased rapidly (*e.g.*, 80% loss in 1 d), much more rapidly at pptv levels. In a Pyrex glass flask (2—5 dm^3) equipped with the same SS bellows valve, the dry CCl_4 calibration standards at ppbv levels were stable (<0.3%) for more than 3 months, but dry CCl_4 standards at pptv levels decreased to half in a day, probably due to the metal part connected to the glass flask (*i.e.*, SS tube and the valve). Therefore, we prepared CCl_4 calibration standards at pptv levels in the Pyrex flask using water-containing zero air. More than ten calibration standards of CCl_4 at about 100 pptv were prepared by changing the water vapor pressure. The peak area of CCl_4 observed for these standards is plotted in Fig. 5 against the water vapor pressure, where the injected pressure, the presumed CCl_4 concentration, and the detector sensitivity have been normalized. The peak area of CCl_3F diluted at the same time in the same standards showed a constant value over the whole range of water pressure. While the observed CCl_4 peak area was also constant in the presence of sufficient humidity (≥6 Torr), it became unstable (*i.e.*, poor reproducibility) and decreased with the decrease in the water vapor pressure below 5 Torr. The CCl_4 peak area without addition of water vapor in the standard was about half of that with addition of water. Therefore, the CCl_4 calibration standard was prepared hereafter in the glass flask so that the water vapor pressure became about 10 Torr. The CCl_4 calibration standard prepared by this method was very stable and reproducible (<1.5%). The reliability of the concentration value in the prepared standard (*i.e.*, accuracy) was estimated to be within 6% considering all the possible systematic and random errors involved in the system and during the procedure. By using our new calibration standards and the improved analytical method, we are now able to discuss the observed concentrations of CCl_4 and the behavior of CCl_4 in the atmosphere.

The Source and Sink of CCl_4. Carbon tetrachloride has been believed to be of anthropogenic origin and no natural sources have been known.[10-14] Before 1950, most CCl_4 was used as industrial solvent, fire extinguisher and grain fumigant and eventually

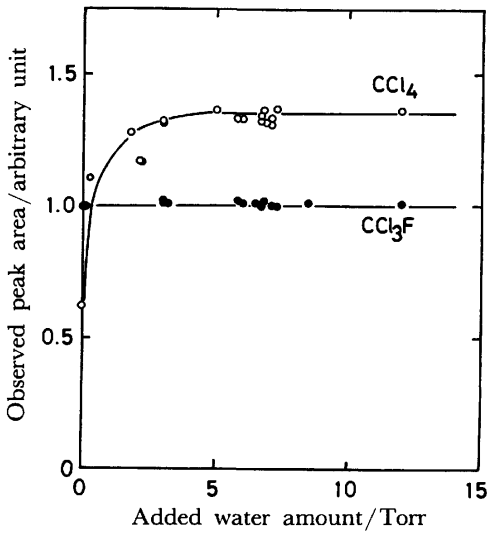

Fig. 5. The effect of water vapor pressure precedently introduced into the calibration standard at about 100 pptv concentration level prepared in a Pyrex glass flask. The peak areas of CCl_4 and CCl_3F observed in the standards are normalized for the presumed CCl_4 concentration, the injected pressure, and the ECD sensitivity.

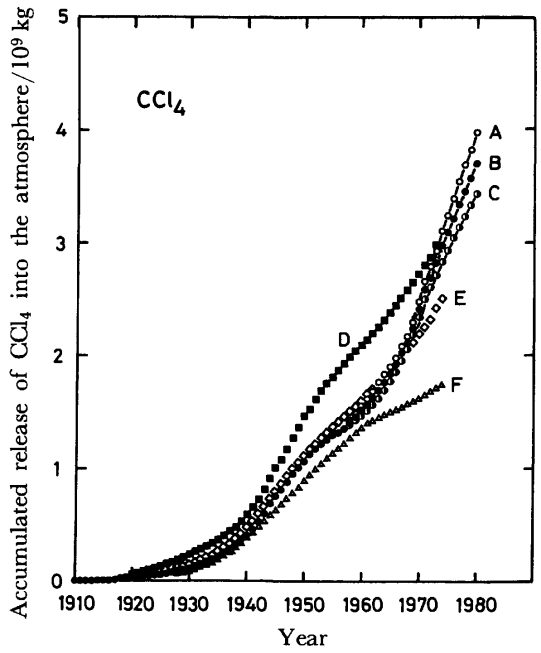

Fig. 6. Esimation of annual release of CCl_4 made by several groups: **A** (○) upper limit, **C** (◑) lower limit, **B** (●) the average of **A** and **C** by Simmonds *et al.* (Ref. 14); **D** (◆) by Galbally (Ref. 12); **E** (◇) by Singh *et al.* (Ref. 11); **F** (△) by Altshuller (Ref. 10).

released to the atmosphere. However, since 1950's, CCl_4 for solvent has been replaced by other solvents such as CH_3CCl_3, CCl_2CCl_2, and $CHClCCl_2$. On the other hand, CCl_4 has mainly been consumed as starting chemicals for the production of CCl_2F_2 and CCl_3F, so that its release into the atmosphere was estimated to be only several percent of its production.[10-14] The estimates of the total release of anthropogenic CCl_4 made by several groups are shown in Fig. 6. While these

estimates vary in amounts, they are similar in trend with the first release peak in 1940's as solvent and the recent increase accompanying the increase of the production of CCl_2F_2 and CCl_3F. Since the estimation by Simmonds *et al.* (curves **A**, **B**, and **C** in Fig. 6: **A**, upper limit; **C**, lower limit; and **B**, the average of **A** and **C**) is the most recent one and appears to be most reliable at present, we have compared our measurement data with their release estimation. The most effective sink of the atmospheric CCl_4 has been proved to be stratospheric UV photodissociation, and its lifetime in the atmosphere was calculated by Molina and Rowland as 30—50 years assuming vertical atmospheric transport parameters and solar flux at each altitude.[39] On the basis of recent values for such parameters (*i.e.*, about 10% lower UV-absorption cross-section of CCl_4 in 190—220 nm region,[6] and the increase of estimated solar flux due to the revised 30% lower absorption cross section of O_2[40,41]), the lifetime of CCl_4 in the atmosphere may become slightly shorter than the previous estimate. Other dissociation mechanisms of CCl_4 such as reactions with active species like OH, $O(^1D)$ in the atmosphere, or the hydrolysis in the ocean have been neglected because of their small reaction rates.[3,12,21,42,43] If the estimated lifetime based on the observed concentration is significantly shorter than the calculated ones based on the stratospheric photodissociation alone, we may have to reexamine or search for other dissociation mechanisms of CCl_4.

Observed Concentration and Lifetime of CCl_4 in the Atmosphere. The background concentration is defined here as the concentration observed in remote areas far enough from local emission sources. Because each halocarbon is released continuously in specified regions on the earth, the balance of its emission, diffusion, mixing, and removal processes will give a stationary concentration in remote areas, which is considered to be the background concentration at that location. As for the halocarbons, their emission has been limited to urban areas in highly industrialized countries, predominantly in the Northern Hemisphere (N. H.) such as the United States of America, Western Europe, and Japan. Table 1 shows our data of CCl_4 concentration measured in January 1981 on the coast of Hokkaido and west Tohoku area (40—45°N). The concentration is given as in dry air. The background concentration representing the mid-latitude N. H. thus obtained was 91 pptv in January 1981. For the estimation of the total amount of CCl_4 in the global atmosphere, the concentration of CCl_4 in the Southern Hemisphere (S. H.) was obtained by referring to the S. H./N. H. ratio reported in Ref. 14; while absolute concentration values are different from ours, the latitudinal distribution profile should be free from the calibration problem as discussed before. The CCl_4 concentration in the S. H. is nearly uniform due to the absence of large source in the S. H.. The S. H./N. H. ratio of the CCl_4 concentrations at mid latitudes in

TABLE 1. OBSERVED CONCENTRATION OF CCl_4 IN THE ATMOSPHERIC SAMPLES COLLECTED ON THE COAST OF HOKKAIDO AND WEST TOHOKU AREA IN JANUARY 1981

Sampling location		Sampling Date	CCl_4 concentration (pptv)[a]
Setana	(42.5°N, 139.9°E)	Jan. 13, 1981	91.4
Nosappu	(43.4°N, 145.8°E)	Jan. 14, 1981	89.3
Nosappu	(43.4°N, 145.8°E)	Jan. 15, 1981	90.7
Era	(41.6°N, 140.0°E)	Jan. 17, 1981	92.0
Nyudozaki	(40.0°N, 139.7°E)	Jan. 18, 1981	92.1
Nyudozaki	(40.0°N, 139.7°E)	Jan. 19, 1981	92.1
		Average	91.3
		σ_{n-1}	1.1

a) pptv=10^{-12} v/v in dry air.

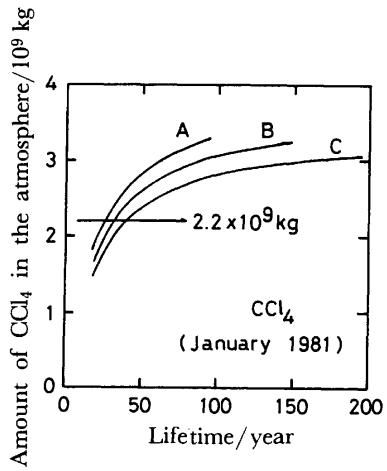

Fig. 7. Expected total amount of CCl_4 in the atmosphere in January 1981 against supposed atmospheric lifetime of CCl_4 for each emission scenario (**A**, **B**, and **C** corresponds to that in Fig. 6). The value of 2.2×10^9 kg calculated from our observation gives 33-year lifetime for the most probable emission scenario **B**.

January 1981 was thus calculated from Ref. 14 as $(S.H./N.H.)_{mid\text{-}lat.}$=(Tasmania data+American Samoa data)/(Cape Mears data+Adrigole data)=0.92. The CCl_4 concentration at the low-lat. N. H. (represented by Barbados data[14]) was calculated as 0.96 of that at the mid-lat. N. H. Since the amount of air in high and mid latitudes (>30°) is nearly equal to that in low latitude (0—30°), the global tropospheric average concentration of CCl_4 was estimated as 0.95 (=(1.0+0.96+0.92+0.92)/4) times the mid-lat. N. H. concentration. The average mixing ratio of CCl_4 in the stratosphere (where about 20% of air exists) was calculated as 60% of the global average tropospheric mixing ratio (mixing ratio denotes pressure-normalized concentration) as in the case of CCl_3F (same with Ref. 14). Since the amount of dry air on the earth is about 5.12×10^{18} kg, the total amount of CCl_4 in the whole atmosphere was calculated to be 2.2×10^9 kg in January 1981. On the other hand, the total amount remaining in the atmosphere $S(t_1)$ at time t_1 is calculated from the worldwide CCl_4 release data $I(t)$ and

CCl_4 atmospheric lifetime τ by

$$S(t_1) = \int_{t_0}^{t_1} I(t) \exp(-(t_1-t)/\tau)dt.$$

Figure 7 shows the expected total amount of CCl_4 in the atmosphere in January 1981 with the supposed lifetime of CCl_4 for each case of the emission scenario (*i.e.*, curves **A**, **B**, and **C** in Fig. 6). By comparing with the amount of 2.2×10^9 kg calculated from our measurement data, the lifetime of CCl_4 in the atmosphere is estimated as 33 years for the most probable emission scenario **B**, or 27 and 42 years for the emission scenarios **A** and **C**, respectively. These values are close to or slightly shorter than the lifetime of 30—50 years calculated by Molina and Rowland[39] assuming the UV photodissociation in the stratosphere as the only sink. For the global atmospheric concentration of CCl_4 118 pptv in January 1980 previously reported by Simmonds *et al.* in their Atmospheric Lifetime Experiment (ALE) program,[14] the calculated lifetime for CCl_4 should be about 70, 100, and 200 years for emission scenarios **A**, **B**, and **C**, respectively.[44] These lifetimes are even longer than those for CCl_3F and CCl_2F_2; this is unreasonable in view of their UV absorption cross-sections or their chemical reactivities. Furthermore, the larger atmospheric concentrations reported by other groups (Ref. 14, 21—38,45) and/or other scenarios with smaller emission (Ref. 10—13) will give much longer lifetime for CCl_4 and cannot be reasonably explained. We therefore suppose that such higher CCl_4 concentrations must have been based on inaccurate (unstable and overestimated) calibration standards.

Conclusion

Since CCl_4 was found to be readily and strongly adsorbed on clean metal surface under dry conditions, we developed new methods for analysis of CCl_4 and preparation of CCl_4 primary calibration standards by introducing water vapor into the system. This method is also effective for analysis and preparation of standards of high-boiling-point and readily-adsorbable compounds such as CH_3CCl_3, $CHCl{=}CCl_2$, and $CCl_2{=}CCl_2$. The absolute amount, distribution and lifetime of CCl_4 in the atmosphere were studied based on our newly calibrated measurement data.

References

1) M. J. Molina and F. S. Rowland, *Nature*, **249**, 810 (1974).

2) F. S. Rowland and M. J. Molina, *Rev. Geophys. Space Phys.*, **13**, 1, (1975).

3) R. Stolarski and R. Cicerone, *Can. J. Chem.*, **52**, 1610 (1974).

4) "Halocarbons: Effects on Stratospheric Ozone," National Academy of Sciences, Washington, D. C., 1976.

5) "The Stratosphere: Present and Future," National Aeronautics and Space Administration, Washington, D. C., 1979.

6) "The Stratosphere 1981, Theory and Measurements," World Meteorological Organization, Geneve (1982).

7) L. T. Gidel and P. J. Crutzen, *J. Geophys. Res.*, **88**, 6622 (1983).

8) P. J. Crutzen and L. T. Gidel, *J. Geophys. Res.*, **88**, 6641 (1983).

9) D. J. Wuebbles, *J. Geophys. Res.*, **88**, 1433 (1983).

10) A. P. Altshuller, *Environ. Sci. Technol.*, **10**, 596 (1976).

11) H. B. Singh, D. P. Fowler, and T. O. Peyton, *Science*, **192**, 1231 (1976).

12) I. E. Galbally, *Science*, **193**, 573 (1976).

13) W. B. Neely, *Science Total Environ.*, **8**, 267 (1977).

14) P. G. Simmonds, F. N. Alyea, C. A. Cardelino, A. J. Crawford, D. M. Cunnold, B. C. Lane, J. E. Lovelock, R. G. Prinn, and R. A. Rasmussen, *J. Geophys. Res.*, **88**, 8427 (1983).

15) A. Volz, D. H. Ehhalt, and H. Cosatto, *Pure Appl. Geophys.*, **116**, 545 (1978).

16) A. L. Schmeltekopf, P. D. Goldan, W. J. Harrop, T. L. Thompson, D. L. Albritton, M. MacFarland, A. E. Sapp, and W. R. Henderson, *Rev. Sci. Instrum.*, **47**, 1479 (1976).

17) Y. Makide, T. Tominaga, and F. S. Rowland, *Chem. Lett.*, **1979**, 355.

18) Y. Makide, Y. Kanai, and T. Tominaga, *Bull. Chem. Soc. Jpn.*, **53**, 2681 (1980).

19) Y. Makide, Y. Kanai, and T. Tominaga, *Nippon Kagaku Kaishi*, **1981**, 133.

20) Y. Makide, A. Yokohata, and T. Tominaga, *J. Trace Microprobe Techniques*, **1**, 265 (1982).

21) J. E. Lovelock, R. J. Maggs, and R. J. Wade, *Nature*, **241**, 194 (1973).

22) A. J. Murray and J. P. Riley, *Nature*, **242**, 37 (1973).

23) P. E. Wilkniss, R. A. Lamontagne, R. E. Larson, J. W. Swinnerton, C. R. Dickson, and T. Thompson, *Nature*, **245**, 45 (1973).

24) J. E. Lovelock, *Nature*, **252**, 292 (1974).

25) D. H. Pack, J. E. Lovelock, G. Cotton, and C. Curthoys, *Atmos. Environ.*, **11**, 329 (1977).

26) B. J. Tyson, J. C. Arvesen, and D. O'Hara, *Geophys. Res. Lett.*, **5**, 535 (1978).

27) H. B. Singh, L. J. Salas, H. Shigeishi, and E. Scribner, *Science*, **203**, 899 (1979).

28) R. A. Rasmussen, M. A. K. Khalil, and R. W. Dalluge, *Science*, **211**, 285 (1981).

29) K. A. Brice, R. G. Derwent, A. E. Eggleton, and S. A. Penkett, *Atmos. Environ.*, **16**, 2543 (1982).

30) E. Robinson, R. A. Rasmussen, and J. Krasnec, *Atmos. Environ.*, **11**, 215 (1977).

31) D. R. Cronn, R. A. Rasmussen, E. Robinson, and D. E. Harsch, *J. Geophys. Res.*, **82**, 5935 (1977).

32) W. Seiler, F. Mueller, and H. Oeser, *Pure Appl. Geophys.*, **116**, 554 (1978).

33) D. Pierotti, R. A. Rasmussen, and R. Dalluge, *J. Geomag. Geoelectr.*, **32**, 181 (1980).

34) P. E. Wilkniss, J. W. Swinnerton, D. J. Bressan, R. A. Lamontague, and R. E. Larson, *J. Atmos. Sci.*, **32**, 158 (1975).

35) P. E. Wilkniss, R. A. Lamontague, R. E. Larson, and J. E. Swinnerton, *J. Geophys. Res.*, **83**, 3672 (1978).

36) E. Robinson, R. Rasmussen, J. Krasnec, D. Pierotti, and M. Jakubovic, *Geophys. Res. Lett.*, **3**, 323 (1976).

37) P. W. Krey, R. J. Lagomarsino, and L. E. Toonkel, *J. Geophys. Res.*, **82**, 1753 (1977).

38) P. J. B. Fraser and G. I. Pearman, *Atmos. Environ.*, **12**,

839 (1978).
39) M. J. Molina and F. S. Rowland, *Geophys. Res. Lett.*, **1**, 309 (1974).
40) J. R. Hermann and J. E. Mentall, *J. Geophys. Res.*, **87**, 8967 (1982).
41) G. Brasseur, A. DeRudder, and P. C. Simon, *Geophys. Res. Lett.*, **10**, 20 (1983).
42) J. Hine, *J. Am. Chem. Soc.*, **72**, 2438 (1950).
43) R. A. Cox, R. G. Derwent, A. E. J. Eggleton, and J. E. Lovelock, *Atmos. Environ.*, **10**, 305 (1976).
44) Although ALE group reported CCl_4 lifetimes of 37, 57, and 120 years based on their data of 118 pptv for the same emission scenarios (**A**, **B**, and **C**, respectively), we could not reproduce these lifetimes using nearly the same calculation procedure. However, we could reproduce their results for lifetimes of CCl_2F_2 and CCl_3F by our calculation procedure and their reported concentrations.[46,47] While the reason for such discrepancy is not clear, results similar to ours have been suggested by F. S. Rowland *et al.* (private communication).
45) R. A. Rasmussen, M. A. K. Khalil, A. J. Crawford, and P. J. Fraser, *Geophys. Res. Lett.*, **9**, 704 (1982).
46) D. M. Cunnold, R. G. Prinn, R. A. Rasmussen, P. G. Simmonds, F. N. Alyea, C. A. Cardelino, and A. J. Crawford, *J. Geophys. Res.*, **88**, 8401 (1983).
47) D. M. Cunnold, R. G. Prinn, R. A. Rasmussen, P. G. Simmonds, F. N. Alyea, C. A. Cardelino, A. J. Crawford, P. J. Fraser, and R. D. Rosen, *J. Geophys. Res.*, **88**, 8379 (1983).

Thermodynamic Study for Complexation Reactions of Dibenzo-24-crown-8 with Alkali Metal Ions in Acetonitrile

Yasuyuki TAKEDA,*Yasuki KUDŌ, and Shizuo FUJIWARA
Department of Chemistry, Faculty of Science, Chiba University, Yayoi-chō, Chiba 260
(Received May 30, 1984)

Synopsis. Formation constants for 1:1 complexes of dibenzo-24-crown-8 with alkali metal ions in acetonitrile have been determined by conductometry at different temperatures. Enthalpy ($\Delta H°$) and entropy changes ($\Delta S°$) were calculated. All the $\Delta H°$ and $\Delta S°$ values are negative. The $-\Delta H°$ and $-\Delta S°$ sequences are $Na^+>Cs^+>Rb^+>K^+$ and $Na^+\geq Cs^+>Rb^+>K^+$, respectively.

In the previous papers,[1,2] enthalpy ($\Delta H°$) and entropy changes ($\Delta S°$) of a 1:1 dibenzo-24-crown-8 (DB24C8) complex with an alkali metal ion in propylene carbonate and methanol, and transfer activity coefficients of the complex among nonaqueous solvents were determined. Behavior of the DB24C8–alkali metal ion complexes in nonaqueous solvents was discussed from a thermodynamic point of view. For further study on factors affecting stabilities of the DB24C8 complexes, more data on $\Delta H°$ and $\Delta S°$ are required. However, there are few data on $\Delta H°$ and $\Delta S°$ at present for complexation reactions between DB24C8 and alkali metal ions.[3,4]

In the present work, formation constants for 1:1 complexes of DB24C8 with alkali metal ions in acetonitrile have been determined by conductometry at different temperatures in order to obtain $\Delta H°$ and $\Delta S°$ values. The results were compared with those of other solvents. Solvent effect were elucidated.

Experimental

Materials. Most of the reagents were the same as those described previously.[1,2] Acetonitrile was allowed to stand in contact with molecular sieves for several days. The acetonitrile was then distilled twice. The middle 70% of the distillate was used. The water content of the purified acetonitrile, as determined by means of Karl Fischer titration, was less than 0.01%. The conductivity of the final product was less than $2\times10^{-7}\ \Omega^{-1}cm^{-1}$.

Apparatus and Procedure. Conductance measurements were conducted on a Fuso conductivity apparatus, model 362A, in a thermostated water bath 17, 21, 25, 29, 33, and 37±0.02°C. Two cells were used with cell constants of 0.059701 and 0.093938 cm^{-1}. The experimental procedure to obtain formation constants of DB24C8–alkali metal ion complexes in acetonitrile was the same as those described in the previous paper.[1]

Results

The molar conductivity (Λ) *vs.* $[L]_t/[M]_t$ plots for caesium perchlorate at 17, 21, 25, 29, 33, and 37°C in acetonitrile are illustrated in Fig. 1, $[L]_t$ and $[M]_t$ being total concentrations of DB24C8 and alkali metal ion respectively. The Λ *vs.* $[L]_t/[M]_t$ plots show a monotonous decrease in Λ with an increase in the DB24C8 concentration. The Λ *vs.* $[L]_t/[M]_t$ plots for the other alkali metal perchlorates are similar to those for $CsClO_4$. In this work, it is assumed that the association between a cation and a perchlorate ion is negligible and that DB24C8 forms 1:1 complexes with the alkali metal ions. Corrections for viscosity changes caused by the addition of DB24C8 were neglected. The procedure for obtaining formation constant (K_{ML^+}) of a DB24C8–alkali metal ion complex was just the same as that mentioned in the previous paper,[1] where $K_{ML^+}=[ML^+]/[M^+][L]$, and M^+ and L denote an alkali metal ion and DB24C8 respectively. For each alkali metal system, K_{ML^+} values decrease with an increase in temperature, and the log K_{ML^+} *vs.* T^{-1} plot shows a linear relationship. Values of $\Delta H°$ and $\Delta S°$ calculated from these results are listed in Table 1, together with log K_{ML^+} values at 25°C. It is seen from Table 1 that, except for methanol, values of $\Delta H°$ and $\Delta S°$ for a DB24C8–Cs^+ complex obtained by us using conductometry are in good agreement with those by the NMR method.[4]

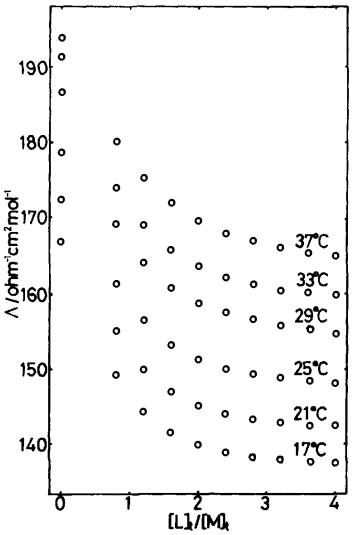

Fig. 1. Λ *vs.* $[L]_t/[M]_t$ plots for caesium perchlorate in acetonitrile at different temperatures. $[M]_t=5\times10^{-4}$ M.

Discussion

Table 1 shows that all the $\Delta H°$ and $\Delta S°$ values for complexation reactions of DB24C8 with alkali metal ions in acetonitrile are negative as well as in propylene carbonate and methanol. Since DB24C8 is a large crown ether and has a great ligand-ring flexibility, the negative $\Delta S°$ values may be primarily due to large conformational changes when a complexation reaction occurs. For the DB24C8–acetonitrile system, the $-T\Delta S°$ value is much smaller than the $-\Delta H°$ value; thus, the magnitude of log K_{ML^+} value of the alkali metal ion complex is determined largely by the $\Delta H°$ value.

TABLE 1. log (K_{ML}^+/mol^{-1}dm^3), $\Delta H°$, AND $T\Delta S°$ VALUES FOR THE COMPLEXATION OF DB24C8 WITH ALKALI METAL IONS IN NONAQUEOUS SOLVENTS

Crown ether	Cation	Solvent	log K_{ML}^+ (at 25 °C)	$-\Delta H°$ / kJ mol^{-1}	$-T\Delta S°$ / kJ mol^{-1} (at 25 °C)
DB24C8	Na^+	AN[a]	4.1_2	34.9	11.4
		PC[b, 1]	4.1_6	37.7	13.7
	K^+	AN[a]	3.8_4	27.7	5.5
		PC[b, 1]	3.7_3	34.5	13.2
		CH_3OH[1]	3.5_7	35.3	14.7
	Rb^+	AN[a]	3.8_0	30.7	8.4
		PC[b, 1]	3.5_5	32.9	12.6
		CH_3OH[1]	3.8_6	39.4	17.2
	Cs^+	AN[a]	3.9_5	33.1	10.7
				34.0[4]	10.8[4]
		PC[b]	3.4_6[1]	32.3[1]	12.6[1]
				33.9[4]	14.21[4]
		CH_3OH	3.8_4[1]	36.8[1]	14.6[1]
				41.3[4]	20.08[4]

a) Acetonitrile. b) Propylene carbonate.

For DB24C8 complexes, there is no large difference in both $\Delta H°$ and $\Delta S°$ among alkali metal ions except $\Delta S°$ value of a DB24C8–K^+ complex for acetonitrile. A sodium ion is the smallest and has the highest charge density of all the alkali metal ions (Na^+, K^+, Rb^+, Cs^+). If the sodium ion has the most suitable size for favorable arrangement of ether oxygen atoms of DB24C8 for the metal ion held in the cavity, the strongest interaction of the metal ion with the ether oxygen atoms and the largest ligand-ring conformational change would be observed for the Na^+–DB24C8 complex among all the alkali metal ion–DB24C8 complexes. The following data may support the above discussion. For acetonitrile and propylene carbonate, both $-\Delta H°$ and $-\Delta S°$ values of the Na^+–DB24C8 complex are the greatest of all the alkali metal ion complexes (Table 1), and also is $-\Delta S°$ value of the Na^+–DB24C8 complex for 70 wt% CH_3OH in H_2O.[3]

Generally, for a given DB24C8–alkali metal ion complex, both $\Delta H°$ and $\Delta S°$ values are somewhat dependent on the variation of solvent; unexpectedly, the $-\Delta H°$ value increases with an increase in the donicity of solvent (acetonitrile (14.1), propylene carbonate (15.1), methanol (19.0)[5]). For the same DB24C8–alkali metal ion complex, both $-\Delta H°$ and $-\Delta S°$ values of acetonitrile are the smallest of all the solvents except $-\Delta H°$ value of acetonitrile for a Cs^+ complex; although acetonitrile and propylene carbonate are non-structural solvents, the difference in $\Delta S°$ between the solvents is comparable to that between propylene carbonate and methanol, which has a hydrogen-bonded structure. This may be attributed to the specific interaction between uncomplexed DB24C8 and acetonitrile.[4,6] The reason why, for a given DB24C8–alkali metal ion complex, the $-\Delta H°$ value of methanol is the largest of all the solvents cannot be explained at the present time.

References

1) Y. Takeda and H. Yano, *Bull. Chem. Soc. Jpn.*, **53**, 1720 (1980).
2) Y. Takeda, *Bull. Chem. Soc. Jpn.*, **56**, 3600 (1983).
3) R. M. Izatt, R. E. Terry, D. P. Nelson, Y. Chan, D. J. Eatough, J. S. Bradshaw, L. D. Hansen, and J. J. Christensen, *J. Am. Chem. Soc.*, **98**, 7626 (1976).
4) M. Shamsipur, G. Rounaghi, and A. I. Popov, *J. Solution Chem.*, **9**, 701 (1980).
5) V. Gutmann, "Coordination Chemistry in Nonaqueous Solutions," Springer-Verlag, Berlin (1968).
6) H. S. Gold and M. R. Rice, *Talanta*, **29**, 637 (1982).

Hydrogenation of Carbon Monoxide to Form Light Olefins over an Iron-modified Crystalline Silica

Tsuneji SANO,* Hiroshi YANAGISAWA,† Kiyomi OKABE, Hideo OKADO,†† Hiroyuki HAGIWARA, Yoshiroh YASUMOTO, and Haruo TAKAYA

Catalysis Division, National Chemical Laboratory for Industry, Yatabe, Ibaraki 305

†*Ube Industries Co., Ltd*

††*Maruzen Petrochemical Co., Ltd*

(Received August 2, 1984)

Synopsis. Iron-modified crystalline silicas prepared from an Fe(II) compound were more active than those prepared from an Fe(III) compound. The (C_2H_4+C_3H_6) selectivity of the former was lower than that of the latter. By the addition of alkaline earth metals, the (C_2H_4+C_3H_6) selectivity of the catalysts prepared from the Fe(II) compound increased remarkably.

An intensive research effort is now being directed towards the development of highly selective Fischer-Tropsch catalysts. Recently, there has been considerable interest involving the use of zeolites supports for such catalysts.[1-3] Among these zeolite-based catalysts are the modified crystalline silica catalysts in which a portion of the silicon atoms in the crystal lattice were replaced by iron, ruthenium *et al.*[4-7] These catalysts have improved the product distribution.

From this point of view, the authors have also prepared zeolite-based catalysts modified with iron.[8] In this paper the hydrogenation of CO over such modified crystalline silica catalysts prepared from Fe(II), $FeSO_4$, and Fe(III), $Fe(NO_3)_3$ compounds is discussed.

The syntheses conditions regarding the various crystalline silica catalysts are shown in Table 1 together with some analytical data determined by atomic-absorption spectrophotometry.

The synthetic iron-modified crystalline silica catalyst had a well defined crystalline ZSM-5 type structure, as demonstrated by an X-ray powder diffraction pattern and a scanning electron micrograph. Peaks corresponding to iron oxide were not observed. The iron may have been highly dispersed in the catalysts.

These catalysts were used for the hydrogenation of CO after being reduced under hydrogen at 450°C for 15 h. Hydrogenation of CO was carried out in a flow reactor at 420°C and 10 kg/cm² (H_2:CO:Ar=45:45:10). Conversion and carbon-based selectivity (excluding CO_2 yield) were calculated on the basis of argon as an internal standard. Figure 1-(A) shows the CO conversion plotted against the Fe/Si atomic ratio. On the other hand, Fig. 1-(B) shows the selectivity to CH_4, (C_2H_4+C_3H_6) and (C_2H_4+C_2H_6+C_3H_6+C_3H_8) plotted against the selectivity to total gaseous hydrocarbons (C_1—C_5). It should be noted that both the catalytic activity and the product selectivity are affected by the source of iron. The catalysts prepared from an Fe(II) compound are more active than those prepared from an Fe(III) compound. The selectivity to total gaseous hydrocarbons decreased much after using the Fe(II) compound instead of the Fe(III) compound as a source of iron and by increasing the amount of the Fe(II) compound. However, a linear relationship exists between the selectivity to CH_4, (C_2H_4+C_3H_6) and (C_2H_4+C_2H_6+C_3H_6+C_3H_8) and the selectivity to gaseous hydrocarbons. This suggests that each selectivity in the gaseous hydrocarbons is constant. It may be concluded that the C_1 to C_5 hydrocarbons are produced over the same active sites.

In order to elucidate these differences involving the activity and the selectivity, X-ray powder diffraction patterns of various catalysts (after preparation) were measured using silicon as an internal standard. As shown in Fig. 2, in the case of the crystalline silica catalysts prepared from the Fe(III) compound, the d(084)-spacing sharply increased with the Fe/Si atomic ratio. On the other hand, in the case of the catalysts

TABLE 1. PREPARATION OF THE VARIOUS IRON-MODIFIED CRYSTALLINE SILICA CATALYSTS[a]

Cat. No.	Source of Fe	Atomic ratios of reaction mixture[b]		Atomic ratios of product		BET
		Si/Fe	Si/M[c]	Si/Fe	Si/M[c]	Surface area (m^2/g)
1	$Fe(NO_3)_3$	25		56		351
2		15		34		
3		7.5		20		
4		25	25(Mg)	58	58	
5		25	10(Ca)	52	19	
6		25	10(Sr)	78	21	353
7		25	10(Ba)	54	14	
8	$FeSO_4$	25		60		
9		15		32		361
10		7.5		18		352
11		3.5		9		
12		7.5	150(Mg)	18	180	361
13		7.5	150(Ca)	19	210	354
14		7.5	150(Sr)	25	244	352
15		7.5	150(Ba)	19	183	356

a) Crystallization was carried out in a 300 ml stainless steel autoclave at 150—160°C for 20—40 h. b) OH^-/SiO_2=0.2, H_2O/SiO_2=40, (n-C_3H_7)$_4$NBr/SiO_2=0.10. c) An alkaline earth metal acetate.

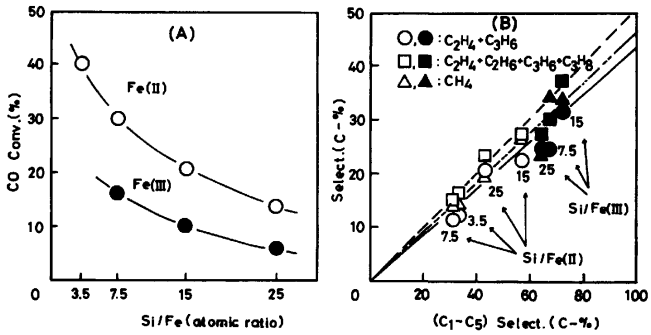

Fig. 1. Results of CO hydrogenation over the iron-modified crystalline silica catalysts prepared from Fe(II) and Fe(III) compounds as a source of iron.
Reaction conditions: Temp=420°C, SV=1000 h^{-1}, P=10 Kg/cm^2, CO/H_2=1.
Arabic number denotes Si/Fe atomic ratio of reaction mixture in Table 1.

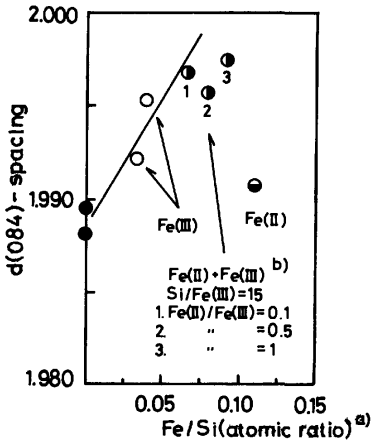

Fig. 2. Spacing d(084) of the various catalysts.
a) Determined by atomic absorption spectrophotometry, b) atomic ratios of reaction mixture in preparing catalysts.

prepared from the Fe(II) compound, the spacing remained unchanged.

From these results, it may be concluded that only Fe(III) can replace a portion of the silicon atoms in the crystal lattice and that Fe(II) is present in an enveloped form with the crystalline silica. The differences of both the catalytic activity and the product selectivity may be attributed to the amount of iron which does not replace a portion of the silicon atoms.

This concept can be supported by the following fact. The crystalline silica catalyst prepared from the Fe(III) compound was treated with 3 M HCl (1 M=1 mol dm^{-3}) at room temperature for 2 d with vigorous stirring. The catalyst, thus obtained, did not show any activity in spite of a considerable amount of iron present in the catalyst.

It may also be considered that a part of the iron enveloped with crystalline silica can easely be moved to the external surface of a crystal upon treatment with hydrogen. This iron will produce higher carbon-

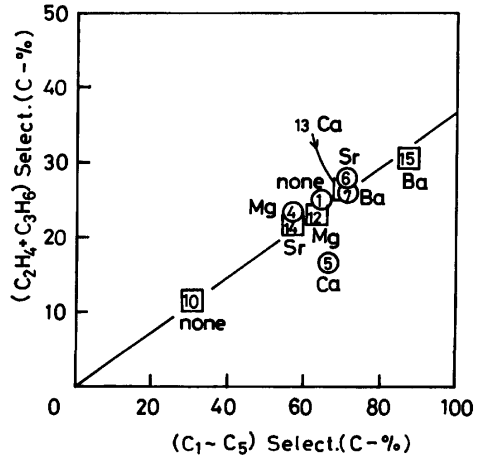

Fig. 3. Effect of alkaline earth metals on the selectivity to (C_2H_4+C_3H_6) over the iron-modified crystalline silica catalysts prepared from Fe(II) and Fe(III) compounds.
O: Prepared from Fe(III) compound, □: prepared from Fe(II) compound.
Reaction conditions: Temp=420°C, SV=1000 h^{-1}, P=10 Kg/cm^2, CO/H_2=1.
Arabic number denotes Cat. No. in Table 1.

number hydrocarbons (C_6^+) because of the lack of restrictions caused by the zeolitic structure. Therefore, to restrict this moving of iron, an alkaline earth metal (acetate) was added. Figure 3 shows the effect of alkaline earth metals on the selectivity. A remarkable increase in total gaseous hydrocarbons was observed over the alkaline earth metal-modified crystalline silica catalysts prepared from the Fe(II) compound. The selectivity to (C_2H_4+C_3H_6) also increased in the order: Sr<Mg<Ca<Ba. However, this effect was not observed for catalysts prepared from the Fe(III) compound. The activity of these catalysts were about 30 percent lower than those of catalysts containing no alkaline earth metals. Moreover, the activity and the selectivity of these catalysts hardly changed at 420°C even after 50—60 h.

This work was supported by the National Research and Development Program of the Ministry of International Trade and Industry.

References

1) V. U. S. Rao and R. J. Gormely, *Hydrocarbon Proceeding*, Nov., 139 (1980).
2) R. J. Jacobs and D. V. Wouwe, *J. Mol. Catal.*, **17**, 145 (1982).
3) G. A. Melson, J. E. Crawford, J. M. Stencel and V. U. S. Rao, "Intrazeolite Chemistry" ed by G. D. Stucky and F. G. Dwyer, ACS Sym. Ser., **218**, 397 (1983).
4) Eur. Pat. 0050525 (1982).
5) Japan Kokai 57-183316.
6) Japan Kokai 57-183317.
7) Japan Kokai 57-183320.
8) T. Sano, K. Okabe, Y. Kohtoku, Y. Shimazaki, K. Saito, H. Takaya, and K. Bando, *ZEOLITES* in press.

The Crystal Structure of the β-Form of α-Monolaurin

Midori GOTO* and Toshimichi TAKIGUCHI
National Chemical Laboratory for Industry, 1-1, Higashi, Yatabe, Ibaraki 305
(Received September 8, 1984)

Synopsis. The crystal structure of the β form of α-monolaurin has been determined. The space group is $P2_1$, with a=9.2472(3), b=74.310(2), c=4.9523(1) Å, β=97.514 (3)°, and Z=8. Two types of molecular conformations of monolaurin exist in the crystal.

The α-monoglycerides have been shown by powder X-ray diffractions to exist in four crystalline forms, 1) α-form, 2) subα-form, 3) β′-form, and 4) β-form.[1] The β-form is a stable form at room temperature. Larsson found two different forms of the β-form and named them the β_1- and β_2- forms.[2] Both were monoclinic and had the same cell dimentions, but they differed in the absent reflections. He assigned the space group of $P2_1/m$ and Am for β_1 and β_2 respectively. He described the chain packing, but did not solve the structure of the glycerol parts.[2] The present authors obtained a single crystal of the β-form (β_1-form by Larsson's nomenclature) of α-monolaurin and undertook an X-ray crystal structure analysis.

Experimental and Structure Determination

The α-monolaurin was prepared by the Nihon Glyceride Co. Ltd. The β-form crystal was obtained by crystallization in a chloroform solution. The cell dimensions and diffraction intensities were measured on a Rigaku-Denki four-circle diffractometer by using graphite monochromated Cu-$K\alpha$ radiation at room temperature. 963 independent reflections with 2θ values up to 120° ($|F_o| \geqq 3\sigma(|F_o|)$) were used for the analysis. No correction was made for absorption. The systematic absences ($k=2n+1$ for $0k0$) and intensity statistics indicated $P2_1$ as the space group. The crystal data were as follows: $C_{15}H_{30}O_4$; monoclinic, $P2_1$; Z=8; a=9.2472 (3), b=74.310 (2), c=4.9523 (1) Å, β=97.514 (3)°; D_x=1.06 gcm^{-3}; mp=63.0°C. The structure was solved by MULTAN.[3] The hydrogen atoms except for the one near the end of the carbon chains were placed at the calculated positions. The structural parameters were refined by a block-diagonal least-squares method, using the UNICS III system.[4] The final refinement led to the R value of 0.070. The other possible space group $P2_1/m$ was found to be definitely incorrect because the R value did not decrease to less than 0.3.

Results and Discussion

The asymmetric unit contains four crystallographicaly independent molecules. They will hereafter be named the A_1, A_2, B_1, and B_2 molecules. Two pairs, A_1 and A_2, and B_1 and B_2, are enantiomers to each other. The numbering of atoms in the molecules is shown in Fig. 1, while the final atomic coordinates are given in Table 1.[5]

The difference in the conformation of monolaurin between A and B exists in the glycerol parts, as illustrated in Fig. 1. The dihedral angles φ (O2–C13–C14–O3) are 177° (A_1) and 175° (A_2) for the A molecules, and 62° (B_1) and −58° (B_2) for the B molecules. The dihedral angles φ (O3–C14–C15–O4) are −66° (A_1) and 60° (A_2) for the A molecules and 165° (B_1)

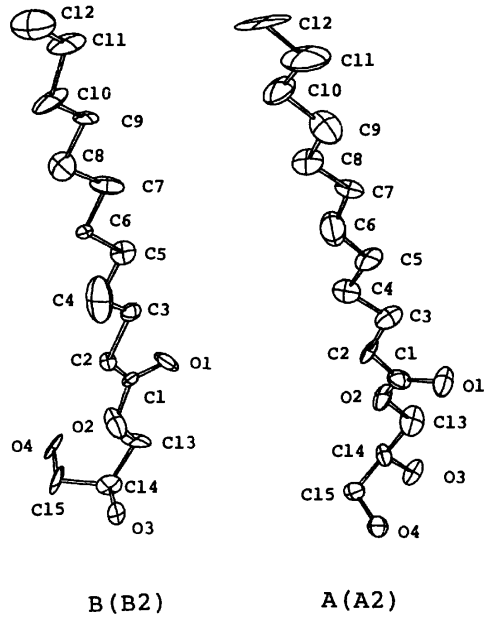

Fig. 1. ORTEP drawing along the C-direction and the numbering system of atoms.
The ellipsoids are drawn to enclose 40% probability.

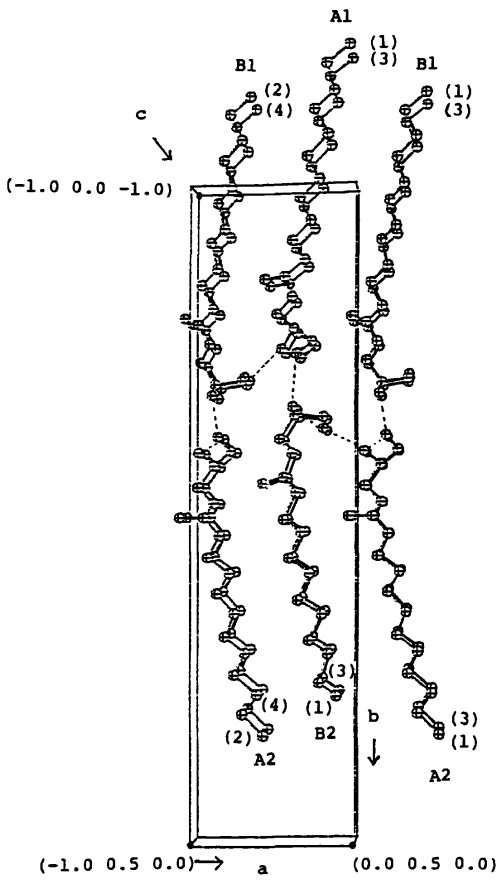

Fig. 2. Perspective view of the molecular packing (1) x,y,z (2) $x-1,y,z$ (3) $x,y,z-1$ (4) $x-1,y,z-1$.

TABLE 1. FRACTIONAL ATOMIC COORDINATES ($\times 10^4$) AND THERMAL PARAMETERS FOR NON-HYDROGEN ATOMS
$B_{eq}=4/3\sum_i\sum_j\beta_{ij}a_ia_j$

ATOM	X	Y	Z	B_{eq}/Å^2	ATOM	X	Y	Z	B_{eq}/Å^2
C12A1	42(61)	-805(8)	-23255(99)	15.0	C12A2	5074(55)	4068(5)	-19487(84)	14.7
C11A1	-1253(57)	-677(7)	-23294(112)	14.1	C11A2	3848(58)	3922(6)	-18573(120)	13.8
C10A1	-837(32)	-490(6)	-22136(61)	6.7	C10A2	4630(33)	3791(6)	-16377(69)	8.7
C 9A1	-1968(40)	-372(7)	-20976(74)	8.0	C 9A2	3280(37)	3647(6)	-16395(66)	7.9
C 8A1	-1229(36)	-202(7)	-20022(62)	7.6	C 8A2	3828(34)	3498(6)	-14104(50)	5.4
C 7A1	-2412(29)	-51(5)	-19493(51)	5.5	C 7A2	2598(27)	3381(5)	-13523(37)	3.2
C 6A1	-1793(36)	95(6)	-17194(54)	4.1	C 6A2	3114(44)	3215(8)	-12113(87)	9.5
C 5A1	-2942(28)	228(6)	-16806(47)	5.0	C 5A2	2016(34)	3073(6)	-11031(58)	5.7
C 4A1	-2357(32)	381(5)	-14959(47)	4.5	C 4A2	2714(33)	2930(6)	-9174(50)	4.6
C 3A1	-3452(26)	520(5)	-14321(50)	4.1	C 3A2	1402(31)	2811(5)	-8745(51)	4.8
C 2A1	-2756(33)	647(6)	-12261(64)	6.2	C 2A2	2024(28)	2652(5)	-6892(50)	3.3
C 1A1	-3939(45)	765(7)	-11466(70)	7.6	C 1A2	1079(35)	2518(6)	-6111(63)	4.2
C13A1	-4505(31)	1021(6)	-8273(65)	4.2	C13A2	613(36)	2294(3)	-3040(42)	5.6
C14A1	-3539(27)	1122(5)	-6306(48)	3.0	C14A2	1532(29)	2135(5)	-1740(56)	3.4
C15A1	-2427(37)	1227(5)	-8074(59)	5.1	C15A2	2577(30)	2025(5)	-3228(56)	3.6
O 1A1	-5077(28)	783(5)	-11962(52)	8.7	O 1A2	-307(22)	2516(5)	-7182(43)	6.0
O 2A1	-3546(23)	898(5)	-9337(45)	6.1	O 2A2	1578(21)	2415(5)	-4159(43)	4.7
O 3A1	-4305(21)	1270(5)	-4960(38)	6.2	O 3A2	547(19)	2032(5)	-497(29)	3.8
O 4A1	-3265(21)	1324(5)	-10231(39)	5.2	O 4A2	1886(18)	1920(4)	-5269(35)	4.0
C12B1	4263(49)	-498(8)	-17481(81)	12.4	C12B2	-725(50)	3782(7)	-21703(71)	10.0
C11B1	3024(39)	-383(6)	-16036(67)	7.9	C11B2	-1742(42)	3692(6)	-20332(69)	8.1
C10B1	3685(38)	-207(7)	-15012(81)	8.8	C10B2	-1260(41)	3485(6)	-19822(74)	7.5
C 9B1	2577(42)	-74(6)	-13826(76)	8.1	C 9B2	-2384(32)	3396(5)	-18262(50)	3.2
C 8B1	2983(30)	108(6)	-12882(60)	5.2	C 8B2	-1686(30)	3211(6)	-17293(65)	6.2
C 7B1	2094(30)	217(5)	-10958(69)	5.9	C 7B2	-3072(34)	3114(5)	-16194(57)	5.2
C 6B1	2478(32)	405(6)	-10572(58)	6.3	C 6B2	-2432(26)	2925(5)	-14861(47)	2.7
C 5B1	1596(30)	491(6)	-8442(62)	4.7	C 5B2	-3669(29)	2816(6)	-13726(64)	4.4
C 4B1	1976(34)	679(7)	-7824(68)	5.3	C 4B2	-2959(37)	2627(6)	-12700(64)	4.1
C 3B1	981(29)	790(6)	-6391(54)	3.7	C 3B2	-4029(29)	2539(5)	-10896(46)	3.1
C 2B1	1629(38)	961(7)	-5402(73)	6.1	C 2B2	-3303(33)	2343(6)	-10306(59)	3.0
C 1B1	674(29)	1072(7)	-3563(63)	4.7	C 1B2	-4096(30)	2233(6)	-8654(64)	4.5
C13B1	676(30)	1350(6)	-1084(62)	4.2	C13B2	-4371(39)	1944(6)	-6473(71)	5.0
C14B1	1574(33)	1517(6)	-1270(56)	2.9	C14B2	-3473(36)	1762(6)	-6179(58)	4.3
C15B1	3114(33)	1490(6)	0(52)	3.8	C15B2	-1809(34)	1776(6)	-5149(61)	5.5
O 1B1	-219(23)	1019(5)	-2519(46)	6.0	O 1B2	-5356(22)	2273(5)	-7570(46)	5.4
O 2B1	1328(22)	1218(5)	-3036(48)	4.9	O 2B2	-3611(23)	2054(5)	-8132(50)	6.0
O 3B1	1480(24)	1606(5)	-4036(41)	4.5	O 3B2	-3519(20)	1710(5)	-8923(32)	2.9
O 4B1	3193(27)	1449(5)	2778(43)	6.9	O 4B2	-1858(20)	1859(5)	-2472(34)	4.2

and 171° (B_2) for the B molecules. The dihedral angles φ (O2-C13-C14-C15) are 64°, −69°, −52°, and 54° for the A_1, B_1, A_2, and B_2 molecules respectively. Therefore, the A and B molecules take a *trans-gauche* and a *gauche-trans* conformation respectively. The molecules are linked by hydrogen bonds, the average hydrogen-bond distance being 2.68 Å. The packing of the molecules in the crystal is shown in Fig. 2.

We are indebted to Dr. T. Sakurai and Miss K. Kobayashi of the Institute of Physical and Chemical Research for the UNICS III programs used in this work; we are also indebted to the Nihon Glyceride Co., Ltd., for providing the compound.

References

1) R. T. O'Conner, "Fatty Acids," ed by K. S. Markley, Intersci. Pub., (1960), Part 1, p. 330.
2) K. Larsson, *Ark. Kemi*, **23**, 29 (1964).
3) P. Main, M. M. Woolfson, and G. Germain, MULTAN, "A Computer Programme for the Automatic Solution of Crystal Structures," Univ. of York, England, & Univ. de Louvain, Leuven, Belgium (1971).
4) T. Sakurai and K. Kobayashi, *Rikagaku Kenkyusho Hokoku*, **55**, 69 (1978).
5) The lists of the structure factors, the atomic parameters for the hydrogen atoms, and the anisotropic thermal parameters for the non-hydrogen atoms are deposited at the Office of the Chemical Society of Japan. (Document No. 8515).

Polarized Raman and Infrared Spectra of Tetramethyl-d_{12}-pyrazine

Masayoshi MAEHARA, Yoshinori NIBU,† Hiroko SHIMADA,* and Ryoichi SHIMADA†
Department of Chemistry, Faculty of Science, Fukuoka University, Jonan-ku, Fukuoka 814
†*Department of Chemistry, Faculty of Science, Kyushu University 33, Hakozaki, Higashi-ku, Fukuoka 812*
(Received November 12, 1984)

Synopsis. Assignments of the normal vibrations of tetramethyl-d_{12}-pyrazine were made based on the polarization behavior of the Raman and infrared bands and also on the normal coordinate calculation. The result ascertains the assignments of the normal vibrations given previously for tetramethylpyrazine.

Very recently we gave assignments of the normal vibrations for tetramethylpyrazine.[1] In order to confirm the results, tetramethyl-d_{12}-pyrazine was synthesized and the normal vibrations were studied.

Experimental

Material. Tetramethyl-d_{12}-pyrazine(TMP-d_{12}) was synthesized by the reaction of tetramethylpyrazine (TMP-d_0) and D_2O with DCl. Isotopic purity of the product was determined by the nuclear magnetic resonance measurement.

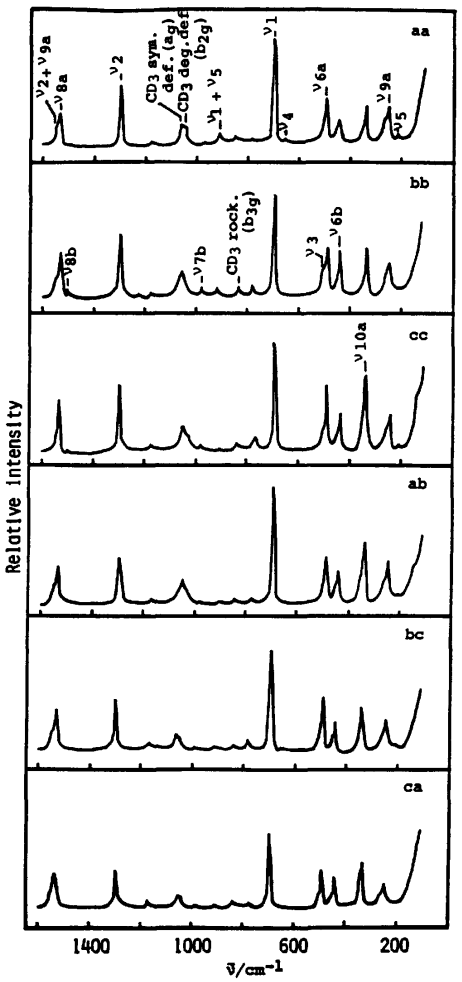

Fig. 1. Polarized Raman spectrum of tetramethyl-d_{12}-pyrazine.
The first letter in ab spectrum *etc.* refers to the direction of polarization of the excitation light and the second to that of the scattering light.

Optical Measurements. The apparatus and methods used for the measurements of the polarized Raman and infrared spectra of TMP-d_{12} single crystals were exactly the same as those described previously.[1]

Results and Discussion

The polarized Raman and infrared spectra of TMP-d_{12} single crystals are shown in Figs. 1 and 2. The polarization behavior of the Raman and infrared bands, and the rotational envelope of the infrared bands of TMP-d_{12} belonging to the same symmetry species are expected to be the same as those of TMP-d_0, because both molecules have the same molecular and crystal structures, and the nearly equal moments of inertia. The potential field and the force constants used for the normal coordinate calculation of TMP-d_{12} were taken to be exactly the same as those used in TMP-d_0 and the calculated vibrational frequencies

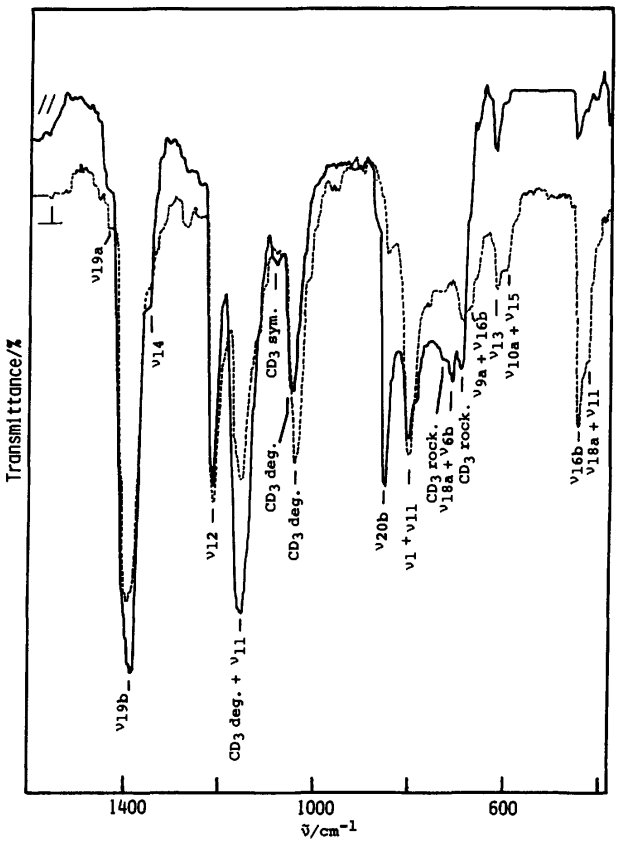

Fig. 2. Polarized infrared sectrum of tetramethyl-d_{12}-pyrazine.
// and ⊥ spectra refer to the infrared spectra measured with the incident light polarized parallel and perpendicular to the crystal growth direction. Polarization behaviors are classified into three types. The relative intensities of the // and ⊥ bands are the following; $I_{//} \approx I_{\perp}$ for type-I, $I_{//} > I_{\perp}$ for type-II, and $I_{//} < I_{\perp}$ for type-III.

TABLE 1. NORMAL VIBRATIONS OF TETRAMETHYL-d_{12}-PYRAZINE

Symmetry species	Mode	Obsd $\tilde{\nu}$/cm^{-1}	Calcd $\tilde{\nu}$/cm^{-1}
a_g	ν_{8a} Ring	1533	1534
	ν_2 ϕ-CD_3 str.	1296	1296
	ν_1 Ring	695	692
	ν_{6a} Ring	489	491
	ν_{9a} CD_3 bend.	247	235
b_{1u}	ν_{19a} Ring	1435	1440
	ν_{12} Ring	1210	1204
	ν_{13} ϕ-CD_3 str.	615	600
	ν_{18a} CD_3 bend.	270[a]	278
b_{3g}	ν_{8b} Ring	1507	1518
	ν_{7b} ϕ-CD_3 str.	970	970
	ν_3 CD_3 bend.	503	501
	ν_{6b} Ring	439	426
b_{2u}	ν_{19b} Ring	1390	1404
	ν_{14} Ring	1337	1323
	ν_{20b} ϕ-CD_3 str.	840	820
	ν_{15} CD_3 bend.	250[a]	245
b_{2g}	ν_4 Ring	667	657
	ν_5 CD_3 wag.	215	214
	ϕ-CD_3 tor.		80
b_{3u}	ν_{16b} Ring	445	454
	ν_{11} CD_3 wag.	110[a]	117
	ϕ-CD_3 tor.		138
b_{1g}	ν_{10a} CD_3 wag.	340	346
	ϕ-CD_3 tor.	160	158
a_u	ν_{16a} Ring		502
	ν_{17a} CD_3 wag.		189
	ϕ-CD_3 tor.		68
	Characteristic vibrations of CD_3 group		
a_g	Antisym. C-D str.	2155	2185
	Sym. C-D str.	2050	2020
	CD_3 sym. def.	1055	1043
b_{1u}	Antisym. C-D str.	2210	2233
	CD_3 rock.	733	737
b_{3g}	Antisym. C-D str.	2210	2233
	CD_3 rock.	840	837
b_{2u}	Antisym. C-D str.	2235	2233
	Sym. C-D str.	2040	2020
	CD_3 Sym. def.	1080	1088
	CD_3 deg. def.	1045	1040
	CD_3 rock.	690	692
b_{2g}	CD_3 deg. deg.	1040	1038
b_{3u}	CD_3 deg. def.	1040	1038

a) Frequencies were estimated from combination bands.

and modes are given in Table 1. Vibrational analyses of the Raman and infrared bands were made in the same way as that described for TMP-d_0.[1]

a_g Species: Strongly polarized Raman bands observed at 1533, 1296, 695, and 489 cm^{-1} in the depolarization measurements in liquid phase were straightforwardly assigned to the totally symmetric ν_{8a}, ν_2 (ϕ-CD_3 stretching), ν_1, and ν_{6a} vibrations, respectively. A weak and almost depolarized Raman band observed at 247 cm^{-1} in liquid does not show any polarization behavior corresponding to non-totally symmetric vibrations in single crystal, thus, this band was assigned to the ν_{9a}(CD_3 bending) vibration.

b_{3g} Species: Raman bands observed at 1507, 970, 503, and 439 cm^{-1} have stronger intensity in the bb and cc spectra than in other spectra, therefore, these were assigned to the ν_{8b}, ν_{7b} (ϕ-CD_3 stretching), ν_3(CD_3 bending), and ν_{6b} vibrations, respectively.

b_{2g} Species: Raman bands at 667 and 215 cm^{-1} were found only in the aa and cc spectra with very weak intensity, therefore, these were assigned to the ν_4 and ν_5 (CD_3 wagging) vibrations, respectively.

b_{1g} Species: A Raman band observed at 340 cm^{-1} has strong intensity in the cc and ab spectra, thus this was assigned to the ν_{10a} (CD_3 wagging) vibration.

b_{1u} Species: Infrared bands observed at 1210 and 615 cm^{-1} showed the B band-type and the type-I polarization, thus, these were assigned to the ν_{12} and ν_{13} (ϕ-CD_3 stretching) vibrations, respectively. A weak infrared band observed at 1435 cm^{-1} showing the type-I polarization was assigned to the ν_{19a} vibration. A medium intense infrared band observed at 710 cm^{-1} showed the A band-type and the type-II polarization, therefore, this could be assigned to a combination band of the ν_{6b} (b_{3g}) and ν_{18a} (b_{1u}) vibrations. This gives frequency of 270 cm^{-1} for the ν_{18a} (CD_3 bending) vibration.

b_{2u} Species: A very strong infrared band observed at 1390 cm^{-1} and a medium intense band at 840 cm^{-1} showed the A band-type and the type-II polarization. Therefore, these bands were assigned to the ν_{19b} and ν_{20b} (ϕ-CD_3 stretching) vibrations, respectively. A shoulder band observed at 1337 cm^{-1} showing the type-II polarization was assigned to the ν_{14} vibration. A weak infrared band at 595 cm^{-1} showing the type-III polarization could be assigned to a combination band of the ν_{10a} (b_{1g}) and ν_{15} (b_{2u}) vibrations. This gives frequency of 250 cm^{-1} for the ν_{15} (CD_3 bending) vibration.

b_{3u} Species: A medium intense band observed at 445 cm^{-1} showed the C band-type and the type-III polarization, thus, this was assigned to the ν_{16b} vibration. A strong infrared band observed at 1150 cm^{-1} showing the b_{2u} polarization behavior could be assigned to a combination band of the CD_3 degenerate deformation (b_{1g}) and ν_{11} (b_{3u}) vibrations, which is generally observed very strongly in the six-membered aromatics. This assignment gives frequency of 110 cm^{-1} for the ν_{11} (CD_3 wagging) vibration. The summary of assignments is given in Table 1.

The calculation indicates that the ν_4 vibration couples with the CD_3 rocking vibration in TMP-d_{12}. This was supported by our assignments, which show that the frequency of the ν_4 vibration of TMP-d_{12} is lower than those of pyrazine and TMP-d_0. The calculated frequencies and modes well coincide with the observed frequencies and polarization behavior of the Raman and infrared bands of TMP-d_{12}. This indicates that the assignments given for the normal vibrations of TMP-d_0 are quite reasonable.

References

1) Y. Ishibashi, F. Arakawa, H. Shimada, and R. Shimada, *Bull. Chem. Soc. Jpn.*, **56**, 1327 (1983).

Mössbauer Emission Spectra of ^{119m}Sn in Tin Organosol

Sumio ICHIBA* and Toshio SAKAMOTO
Department of Chemistry, Faculty of Science, Hiroshima University, Higashisenda-machi, Naka-ku, Hiroshima 730
(Received July 26, 1984)

Synopsis. The electron-scavenging effects of adding various solutes to a suspension of tin in ethanol were studied by Mössbauer emission spectroscopy. The yield of the aliovalent species of Sn^{4+} as the after-effects of the converted isomeric transition in ^{119m}Sn varied from the value of the suspension of tin in ethanol, depending on the properties of electron trapping of the solute added.

After-effects of converted isomeric transition (CIT) in ^{119m}Sn have been studied by means of Mössbauer spectroscopy.[1-3] As the after-effects, the aliovalent species of oxidized Sn^{4+} were observed in the emission spectra of ^{119m}Sn in the $SnCl_2$ adducts and rapidly frozen solutions of $SnCl_2$, and the species of reduced Sn^{2+} in the $SnBr_4$ adducts.[4-6] The mechanisms of the competing acceptors for the electrons between hot atoms and the surrounding medium for the stabilization of the oxidized Sn^{4+} and autoradiolysis of the ligands for the stabilization of reduced Sn^{2+} were elucidated by taking the properties of the ligands and solvents into consideration.

In this study, an organosol of tin in ethanol containing ^{119m}Sn was prepared and the emission spectra were measured by adding various solutes to the suspension to determine the reactivity of the solute toward the electrons produced in the Auger cascade following CIT in ^{119m}Sn.

Experimental

The sources of the tin organosol were prepared from ^{119m}Sn metal obtained from New England Nuclear Co., according to the method reported previously.[7] For each source, 0.25 mCi of ^{119m}Sn with the specific activity of 0.082 mCi mg^{-1} was suspended in 5 ml of ethanol. The concentration of the solutes added to the suspension in ethanol was 1 mol dm^{-3} except for CH_3I, the concentration of which was 3 mol dm^{-3}.

The emission spectra were measured against the ^{119}Sn enriched $CaSnO_3$ absorber (2.0 mg ^{119}Sn cm^{-2}) at room temperature by cooling the source in a liquid nitrogen cryostat. Mössbauer parameters were deduced from Lorentzian curves computer-fitted to the spectra by the least-squares method.

Results and Discussion

The concentration of tin in the suspension was 0.6 mg cm^{-3}, so that the particle size would be about 300 Å and/or less as reported previously.[7] The Mössbauer emission and absorption spectra of the organosol of tin in ethanol are shown in Fig. 1. The absorption spectrum of the organosol of tin in Fig. 1(a) showed that the tin in the suspension was purely β-Sn, but a portion of the oxidized aliovalent species of Sn^{4+} was observed at about 0 mm s^{-1} in the emission spectrum. The emission spectra on adding various solutes to

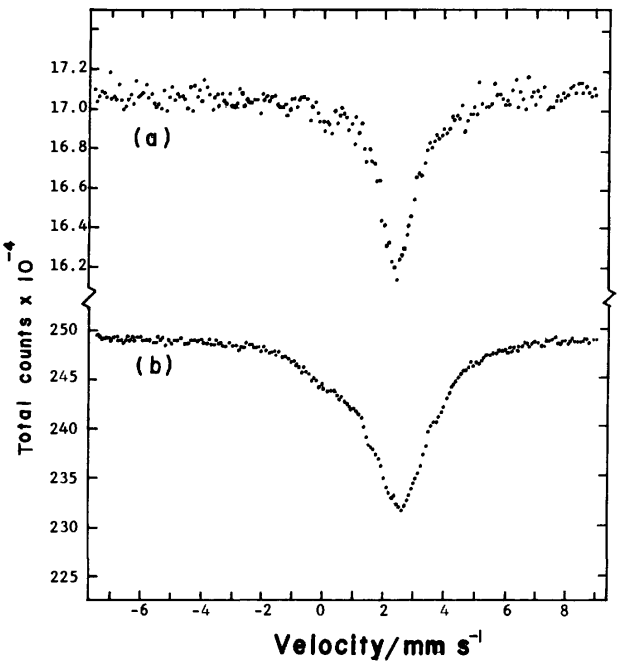

Fig. 1. Mössbauer absorption (a) and emission (b) spectra of the suspension of tin in ethanol at 93 K.

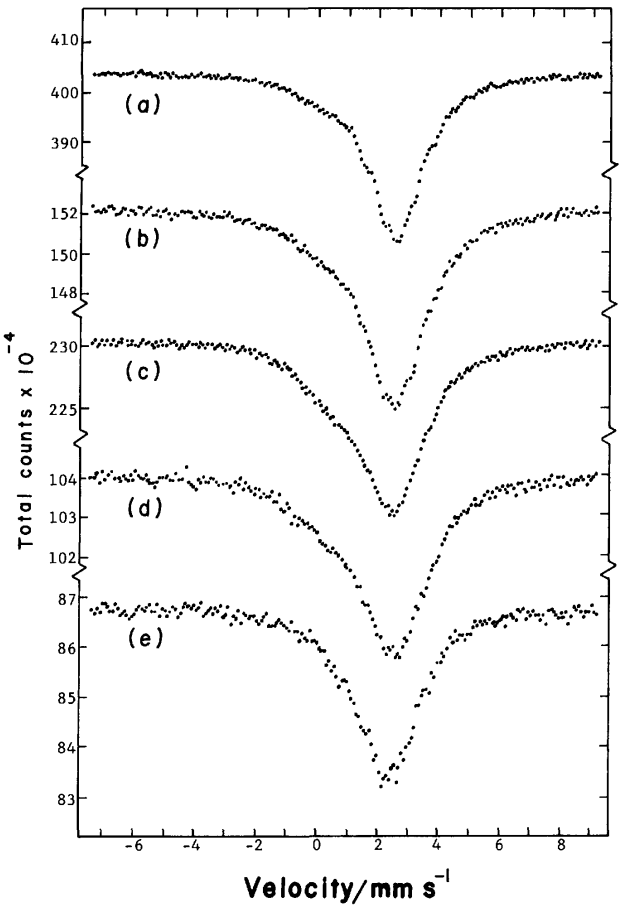

Fig. 2. Mössbauer emission spectra of adding solutes to the suspension of tin in ethanol: (a) $(CH_3)_2SO$; (b) $(C_6H_5)_2SO$; (c) C_5H_5N; (d) CCl_4; (e) CH_3I.

TABLE 1. MÖSSBAUER EMISSION PARAMETERS AND AREA RATIO OF Sn^{4+} TO TOTAL FOR THE ORGANOSOLS OF TIN IN ETHANOL SOLUTIONS AT 93 K

Solute	Sn		Sn^{4+}		$A(Sn^{4+})/A(Total)$ /%
	δ / mm s^{-1}	Γ / mm s^{-1}	δ / mm s^{-1}	Γ / mm s^{-1}	
—	2.58	2.34[a]	0.17[b]	2.34[a]	12.32
$(CH_3)_2SO$	2.58	2.05	0.17	2.05	9.03
$(C_6H_5)_2SO$	2.58	2.35	0.17	2.35	9.62
C_5H_5N	2.56	2.58	0.17	2.58	14.76
CCl_4	2.49	2.46	0.17	2.46	16.81
CH_3I	2.41	2.39	0.17	2.39	5.22

a) Equal line-width. b) Constraining to the value of the suspension in ethanol.

the suspension are shown in Fig. 2. The Mössbauer parameters deduced by constraining the line-width to be equal in both lines of β-Sn and Sn^{4+} and the isomer shift of Sn^{4+} to be 0.17 mm s^{-1} of the value of the suspension in ethanol are shown in Table 1 along with the area ratio of Sn^{4+} to the total. The suspension of tin is similar to the solution of $SnCl_2$ in that the electrons emitted by an Auger cascade enter the medium and are trapped by it, stabilizing the aliovalent species of Sn^{4+} in tin microcrystals. The recapture of electrons from the surroundings to return the atom to a normal valence state may be impeded by an insulator formed on the surface of the particle in consequence of the radiolytic effects. The yield of Sn^{4+} in the suspension, 12.32%, was naturally lower than the yield of 28% in the solution of $SnCl_2$ in ethanol reported previously.[6] However, the increased yield of Sn^{4+} is detected in the suspension by adding CCl_4 and C_5H_5N and the decreased yield by adding $(CH_3)_2SO$, $(C_6H_5)_2SO$, and CH_3I compared with the value of the suspension in ethanol, though the differences in the yield of Sn^{4+} among the emission spectra of the solutions of $SnCl_2$ in C_2H_5OH, $(CH_3)_2SO$, and C_5H_5N are not distinguished clearly.[6]

In glassy ethanol, the trapped excess electrons generated by ionization have been explained in terms of a small polaron model.[8,9] This model suggests that the generated Auger electrons following the CIT in ^{119m}Sn are assumed to be trapped by OH groups and shallower traps associated with the alkane moiety; thus the oxidized aliovalent Sn^{4+} species are stabillized. The increased yield of Sn^{4+} by adding CCl_4 can be explained in terms of the well known electron scavenging properties of CCl_4 toward the Auger electrons. Pyridine also increases the yield of Sn^{4+} so that it traps Auger electrons and acts as an electron scavenger in the ethanol solution.

The yield of Sn^{4+} decreases considerably on adding CH_3I though it is a good electron scavenger.[10] It is well known that CH_3I decomposes to methyl radical-halide anion pairs formed by dissociative electron capture.[11] The methyl radicals thus created would reduce a portion of aliovalent species of Sn^{4+} to the original state. The decreased yield of Sn^{4+} by adding $(CH_3)_2SO$ can also be explained in the same way as for CH_3I, because $(CH_3)_2SO$ also decomposes to methyl radical-methanesulfenate anion pairs by dissociative electron capture.[12]

References

1) H. Sano and M. Kanno, *Chem. Commun.*, **1969**, 601.
2) Y. Llabador and J. M. Friedt, *Chem. Phys. Lett.*, **8**, 592 (1971).
3) P. P. Seregin, F. S. Nasredinov, and L. N. Vasilev, *Phys. Status Solidi A*, **45**, 30 (1978).
4) S. Ichiba, M. Yamada, and H. Negita, *Radiochem. Radioanal. Lett.*, **35**, 31 (1978).
5) S. Ichiba, M. Yamada, and H. Negita, *Radiochem. Radioanal. Lett.*, **36**, 93 (1978).
6) S. Ichiba and M. Yamada, *Polyhedron*, **2**, 499 (1983).
7) S. Ichiba, H. Ono, S. Kawasaki. S. Nakagawa, and M. Yamada, *Bull. Chem. Soc. Jpn.*, **56**, 2837 (1983).
8) R. L. Bush and K. Funabashi, *J. Chem. Soc., Faraday Trans. 2*, **73**, 274 (1977).
9) G. V. Buxton, J. Kroh, and G. A. Salmon, *J. Phys. Chem.*, **85**, 2021 (1981).
10) G. W. Klein and R. H. Schuler, *J. Phys. Chem.*, **77**, 978 (1973).
11) M. Shioya and J. Soma, *Kagaku*, **30**, 161 (1975).
12) Y. J. Chung, K. Nishikida, and F. Williams, *J. Phys. Chem.*, **78**, 1882 (1974).

Synthesis and Swelling Properties of Fluorine Micas with Variable Layer Charges

Kunio KITAJIMA,* Fumihiko KOYAMA, and Nobuo TAKUSAGAWA
Department of Synthetic Chemistry, Faculty of Engineering, Shinshu University, Wakasato, Nagano 380
(Received September 25, 1984)

Synopsis. A series of tetrasilicic Na-micas with variable layer charges (x) between x=1 and x=0.32, $Na_xMg_{3-x}Li_x(Si_4O_{10})F_2$, was synthesized. The expansibility of the synthesized Na-micas upon swelling increased with decreasing layer charge.

Some of the synthetic fluorine micas are swellable with water.[1] However, detailed studies on the effect of the magnitude of layer charge upon the expansibility of fluorine micas have been lacking. The layer charge results generally from positive charge deficiencies in both tetrahedral and octahedral sheets. The value of layer charge, which is expressed as the net negative charge per formula unit, is an important parameter for the classification of layer silicates. Na-taeniolite[2] $NaMg_2Li(Si_4O_{10})F_2$ is a representative species of these synthetic expansible fluorine micas. In this note, the substituted analogues of Na-taeniolite with decreasing layer charge, $Na_xMg_{3-x}Li_x(Si_4O_{10})F_2$ ($1 \leqq x \leqq 0.1$), are synthesized to examine the limit of variability in layer charge and also to elucidate the correlation between the magnitude of layer charge and the swelling properties. In this series the layer charge results from charge deficiency only in octahedral sheet and its value is the same as the x-value.

Raw materials used were chemically pure NaF, MgO, MgF_2, LiF, and SiO_2. Raw materials mixed in proportions corresponding to the formula described above, were sealed in platinum tubes and heated at 1420 °C for 2 h. The temperature was then lowered at a rate of 2—3 °C per minute to 800 °C and the tube was taken out of the furnace to cool in air. The crystal aggregates thus obtained were powdered and purified by sedimentation in distilled water. The products were investigated by powder X-ray diffractometry, electron scanning microscopy, and infrared spectroscopy. The chemical analysis was done for Na and Li by a flame-emission method after the purified samples were dissolved in HF–H_2SO_4 solutions. The layer charge for micas is determined from the content of interlayer Na. The infrared spectra were measured by a KBr pellet method. Swelling of the micas was investigated by an X-ray diffraction method through the measurements of basal spacing (d_{001}) of the samples wetted with water, ethylene glycol, or glycerol.

The batches with the x-value of 1.0—0.6 were melted at 1420 °C, whereas the batches with the x-value smaller than 0.6 was not melted but sintered. The size of mica crystals decreased with decreasing x-value. X-Ray diffraction patterns indicated that only mica was formed from the batches having the x-value of 1.0—0.8. However, the traces of coexistent minerals such as fluor-richterite, α-cristobalite, and α-tridymite were observed for the batches having the x-value of 0.7—0.5, and their contents were not negligible at x= 0.4—0.1.

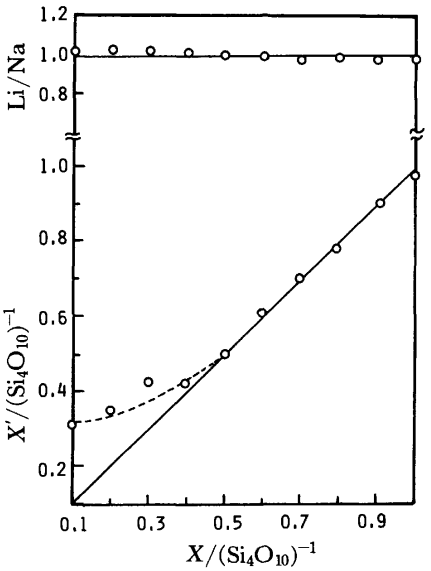

Fig. 1. The determined layer charge (x') and Li/Na mole ratio of synthesized Na-micas plotted against the ideal layer charge (x) calculated from batch composition.

The infrared spectra of the micas showed that the main absorption band at 980 cm^{-1} for x=1.0, which is assigned to e_1^1 mode of Si_2O_5 group,[3] gradually shifted towards higher frequencies with decreasing x-value although the shifting was not observed below x=0.4. On the other hand, another main band at 1110 cm^{-1}, which is assigned to a_1^1 mode of Si_2O_5 group,[3] shifted reversely to lower frequencies with decreasing x-value. The linear relationship is obtained between x-values and wavenumber ($\tilde{\nu}$) in the range x=1.0—0.5 as follows:

$$e_1^1;\ \tilde{\nu} = 980 + 28x\ (cm^{-1})$$
$$a_1^1;\ \tilde{\nu} = 1110 + 40x\ (cm^{-1})$$

This implies that the tetrahedral lattice vibrations are affected by the magnitude of layer charge and/or the changes of octahedral and interlayer compositions.

Figure 1 shows the relationship between the determined layer charge (x') of the synthesized micas and the ideal layer charge (x) calculated from batch composition. The observed mole ratio of Na and Li in mica crystals is also plotted against the x-value in Fig. 1. The ratios of Na to Li are 1.00±0.03 corresponding to the theoretical value of 1.00 throughout the series. The dotted line shows the variation of x'-values, while the full line shows that of x-values. If the synthesis was fully successful, the x'-value should be equal to the x-value. As seen in Fig. 1, the curve of x'-values almost agrees with that of x-values in the range of x=1.0—0.4. However, the x'-value deviates from the x-value below x=0.3, converging to about

Table 1. Basal spacings[a] of Na-micas upon water, ethylene glycol, and glycerol solvation

	$x/(Si_4O_{10})^{-1}$	1.0	0.9	0.8	0.7	0.6	0.5	0.4	0.3	0.2	0.1
$\frac{d_{001}}{Å}$	Water	15.1 (12.2)	15.1 (12.2)	15.1	15.1	18.4 (15.1)	18.4 (15.1)	f.s.[b] (18.4)	f.s.	f.s.	f.s.
	Ethylene glycol	12.3	12.3	12.3 (16.7)	12.3 (16.7)	16.7 (12.3)	16.7 (12.3)	16.7	16.7	16.7	16.7
	Glycerol	12.7	12.6	14.3 (12.6)	14.2 (12.6)	14.5	14.3 (17.7)	18.0 (14.3)	18.0	17.9	17.8

a) The basal spacing of minor phase is shown in parenthesis. b) f.s. shows free swelling.

x'=0.32 with decreasing x-value. Although solid state reaction was attempted repeatedly for the samples of x=0.2—0.1 at 1450°C for prolonged times in a sealed platinum tube, no x'-value lower than 0.32 was found. These results suggest that the micas having the desired compositions precipitated in the range x=1.0—0.4 and that there is a limitation in the variability of layer charge for the Na-micas. At present it is not clear whether this limitation originates from synthetic conditions or crystallochemical factors such as the weakening of the interlayer bonding in the mica structure.

Table 1 gives the basal spacings of the Na-micas which were wetted with water, ethylene glycol, and glycerol for at least 2 h. The basal spacings of minor phases simultaneously observed are also shown in parentheses. In contact with water, all the micas of the series with layer charge lower than 0.5 exhibited so-called free swelling: X-ray patterns show diffuse scattering at low angles. It is clearly seen in Table 1 that the Na-micas undergo either free swelling or limited swelling according to the magnitude of layer charge. Our study shows also that there is a critical point at the layer charge where the maximum basal spacing is limited to either 15.1 Å of double-layer hydrate or 18.4 Å of three-layer hydrate state. The coexistence of two hydrate phases can be explained by the heterogeneity of layer charge in successive layers and also by the kinetics of swelling. Accordingly, the actual layer charge obtained from chemical analysis should be considered as the mean value of the successive layers. In contact with ethylene glycol, the formed complexes gave the basal spacing ranging from 12.3 Å to 16.7 Å, suggesting that the arrangement of ethylene glycol molecules in the interlayer regions is dependent upon the magnitude of layer charge. The basal spacings of 12.3 Å and 16.7 Å correspond to a single-layer[4] and a double-layer complex,[5] respectively. The boundary between the double-layer complex and single-layer one appears at about x=0.7. In contact with glycerol, the complexes gave the basal spacing ranging from 12.7 Å (single-layer) to 18.0 Å (double-layer). The 14.2 Å phase may also correspond to a single-layer complex with a different arrangement of glycerol molecules. The boundaries between the complexes of glycerol appear at the layer charge of x=0.9 and x=0.5.

It is concluded from these results that the expansion of basal spacings in the expansible fluorine micas becomes greater as the layer charge decreases whatever the solvation is. This can be attributed to the weakening of interlayer coulombic force resulted from the decrease of layer charge and also to the increase of the density of interlayer vacancies.

References

1) H. R. Shell and K. H. Ivey, "Fluorine Mica," U. S. Bur. Mines, Bulletin 647 (1969).
2) K. Kitajima, K. Sugimori, and N. Daimon, *Nippon Kagaku Kaishi*, **1973**, 1885.
3) V. C. Farmer, " The Infrared Spectra of Minerals," Mineralogical Society Monograph, London (1974), p. 344.
4) R. C. Reynolds, *Am. Mineral.*, **50**, 990 (1965).
5) W. F. Bradley, E. J. Weiss, and R. A. Rowland, *Clays Clay Minerals*, **10**, 117 (1963).

Redox Behavior of *N,N'*-Ethylenebis(salicylideneaminato)-bis(triphenylphosphine)ruthenium(II)

Hideo DOINE,* Francis F. STEPHENS, and Roderick D. CANNON†
College of Industrial Technology, Nihon University, 2-1 Izumicho, Narashino-shi, Chiba 275
†*School of Chemical Sciences, University of East Anglia, Norwich NR4 7TJ, England*
(Received October 1, 1984)

Synopsis. Visible spectra and electrochemical behavior of the title complex [Ru{C_2H_4(N=CHC_6H_4O-*o*)$_2$}{P(C_6H_5)$_3$}$_2$] (**I**) are reported. The redox potentials of the ruthenium complex were determined at 25 °C to be E°= 0.27±0.01 V (in CH_2Cl_2) and −0.161±0.005 V (in CH_3OH), relative to $E^\circ(Fe(C_5H_5)_2)^{+/0})$=0.400 V.

In the previous electrochemical studies of binuclear complexes,[1] cyclic voltammetric data on ruthenium-(II) Schiff-base complexes were reported. In this study, the redox potentials of the title compound **I** have been first measured and the compound was found to be a convenient reference material for testing the electrochemical cell system from the following fact: the title complex is soluble enough for the electrochemical measurement in both polar and nonpolar solvents, and the oxidation states of ruthenium ion in the complex **I** have no influence on the observed redox potentials. The complex was first synthesized by Thornback and Wilkinson[2] and found to be extremely air-sensitive. When the absorption spectra of the carefully prepared solutions of the complex **I** in deaerated solvents are compared with those previously reported,[3] it appears that the latter corresponds to an oxidized ruthenium(III) species. We have reinvestigated the preparation, handling and redox properties of the complex.

Preparation

The complex $RuCl_2(PPh_3)_3$[4] (0.20 g) was added under nitrogen to a solution of *N,N'*-ethylenebis (salicylideneamine) (H_2L)[5] (0.058 g) and Et_3N (1 ml) in THF in a flask having sintered glass filter-outlet already fitted. After refluxing 2 h some white solid was filtered off under nitrogen pressure. The solvent was removed, and the product was pumped dry, washed with petroleum (40—60°), and recrystallized under nitrogen by dissolving in a little THF and adding excess petroleum. The by-product Et_3NHCl was effectively removed in this way, mp 130—140°(dec). Found: C, 69.1; H, 5.07; N, 3.16%. Calcd for $C_{52}H_{44}N_2O_2P_2Ru$, C, 70.0; H, 4.94; N, 3.14%.

Results

Oxidation State. The complex **I** is readily oxidized by iodine and $FeCl_3$ in nonaqueous solvents but attempts to verify the stoichiometry by spectrophotometric and potentiometric titrations gave irreproducible results. This problem was overcome using a two-phase method as follows. An aliquot of **I** was weighed into a dry flask. The air was displaced with oxygen-free nitrogen, and a measured volume of a freshly prepared solution of resublimed iodine in methanol was added. After the reaction was complete

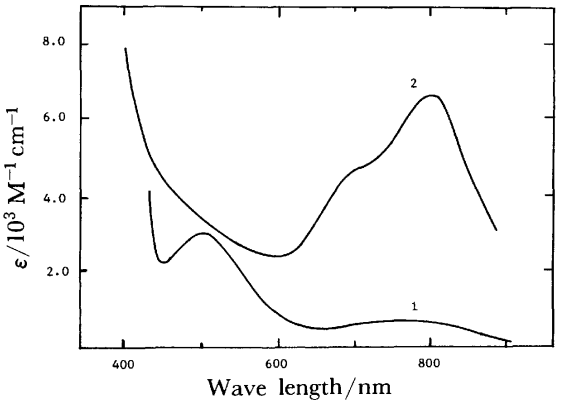

Fig. 1. Spectrum (1) of $RuL(PPh_3)_2$, and (2) of the product on air-oxidation, both in THF, where 1 M=1 mol dm^{-3}.

(5 min were allowed) 5 ml of toluene was added, then an aliquot of aqueous sodium thiosulfate. After shaking, the aqueous layer was run off, and the organic phase was washed with water. The combined extracts were back-titrated with iodine in methanol using starch indicator. The iodine solution was standardized by direct titration with the $Na_2S_2O_3$, and the experiment was repeated with various amounts of **I** and iodine. Molar ratios [Ru complex (added)]/[I_2(consumed)] were found to be 1.94±0.09 from 10 titrations.

Absorption Spectra and Electrochemical Properties. The purple-brown crystalline complex **I** is stable in air when dry, but for quantitative work it was stored under nitrogen. The solution in THF is pink-brown with λ_{max}=770 nm and 505 nm (Fig. 1). On admitting oxygen the THF solution changed rapidly to green with an increase in intensity, and the resulting absorption spectrum (2 in Fig. 1) was similar to that reported by West *et al.*[3] Similar color changes were noted in the solvents CH_2Cl_2 and MeOH, ease of oxidation increasing in the order THF<CH_2Cl_2<MeOH.

The spectra of oxidized and reduced forms have sharp isosbestic points (Fig. 2).

Cyclic voltammetry, in organic solvents under nitrogen, showed a single wave with equal anodic and cathodic peak heights, proportional to Ru concentration. The free ligand H_2L was inactive in the range studied (−0.8 to +0.9 V). The same signal was observed for both the solutions of **I** and air-oxidized form of **I**. On adding iodine, the anodic wave was supressed. In the presence of oxygen also, the anodic wave was supressed but on resuming the nitrogen flow the original peaks reappeared. The wave is assigned to the $Ru^{III/II}$ couple. In methanol, the couple is highly reversible, as judged by the peak-to-peak separations ΔE_{pp} and by the lack of dependence on scan rate. (ΔE_{pp}=60 mV, scan rate 100 to 2000 mV s^{-1}, with 0.1

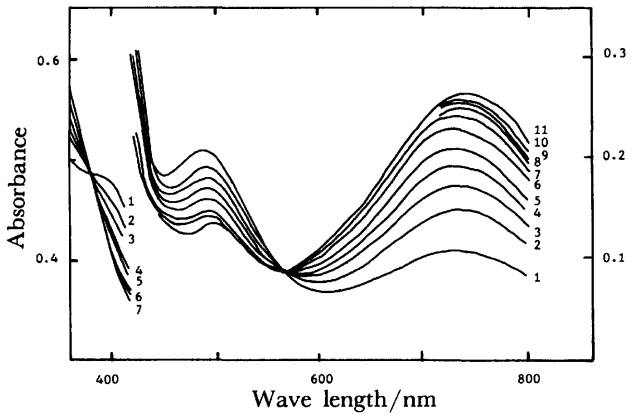

Fig. 2. Spectra (1) of $RuL(PPh_3)_2$, and (2—11) with successive addition of O_2. In methanol, $[Ru]_T = 3.34 \times 10^{-5}$ mol dm^{-3}, cell length of 1 cm.

mol dm^{-3} $NaClO_4$ supporting electrolyte. With 0.1 mol dm^{-3} [n-Bu_4N][BF_4], ΔE_{pp}=90 mV). In CH_2Cl_2, ΔE_{pp} increased from 120 mV at V=20 mV s^{-1} to 150 mV at 100 mV s^{-1}, and at 1000 mV s^{-1} another wave appeared at *ca.* −0.55 V. In THF the couple was found to be quasi-reversible, ΔE_{pp}=170 mV. Redox potentials were determined as $E_{1/2}$=0.27±0.01 V (in CH_2Cl_2); and $E_{1/2}$=−0.161±0.005 V (in MeOH, with 0.1 mol dm^{-3} n-$Bu_4N[ClO_4]$), based on $E^\ominus$ ($Fe(C_5H_5)_2^{+/0}$)=0.400 V.[6]

This work was supported by the Royal Society and the Science and Engineering Research Council (UK). HD held a Monbusho Scholarship.

References

1) H. Doine, F. F. Stephens, and R. D. Cannon, *Inorg. Chim. Acta*, **75**, 135 (1983); **82**, 149 (1984).
2) J. R. Thornback and G. Wilkinson, *J. Chem. Soc. Dalton Trans.*, 110 (1978).
3) K. S. Murray, A. M. van den Bergen, and B. O. West, *Aust. J. Chem.*, **31**, 203 (1978).
4) T. A. Stephenson and G. Wilkinson, *J. Inorg. Nucl. Chem.*, **28**, 945 (1966).
5) Gmelins Hanhbuch der anorganischen Chemie, 8th ed., "Kobalt," B, Supplement part 1 (1963), p. 206.
6) R. R. Gagné, C. A. Koval, and G. C. Lisensky, *Inorg. Chem.*, **19**, 2855 (1980).

Enantioface-differentiating Addition of Butyllithium to Acetophenone by the Use of (1*S*,2*S*,5*S*)-3-[(*S*)-2-Methoxy-1-alkylethylimino]-2-pinanols as Chiral Ligands

Yuhsuke KAWAKAMI,* Toshiki AOKI, and Yuya YAMASHITA

Department of Synthetic Chemistry, Faculty of Engineering, Nagoya University, Furo-cho, Chikusa-ku, Nagoya 464

(Received May 30, 1984)

Synopsis. Butyllithium and acetophenone gave optically active 2-phenyl-2-hexanol (33% e.e.) in good yield in the presence of (1*S*,2*S*,5*S*)-3-[(*S*)-2-methoxy-1-alkylethylimino]-2-pinanol (**1**).

Although successful asymmetric reductions of prochiral ketones to optically active secondary alcohols by chiral hydride reagents have been extensively reported,[1,2] studies on enantioface-differentiating additions by metal alkyls to yield optically active tertiary alcohols are limited.[3-6] We wish to report here an example of asymmetric addition of butyllithium (BuLi) to acetophenone in the presence of chiral ligands.

Experimental

General. The ^{1}H NMR spectra were recorded at 60 MHz with tetramethylsilane as an internal standard, and the chemical shifts are given in δ values.

Syntheses of the Schiff Bases. The Schiff bases (**1a—1d**) used in this study as chiral ligands were synthesized according to Scheme 1.

(1S,2S,5S)-3-[(S)- or (R)-2-Methoxy-1-methylethylimino]-2-pinanol ((S)- or (R)-1a): (1*S*,2*S*,5*S*)-2-Hydroxy-3-pinanone (**2**) (4.1 g, 25 mmol) was caused to react with (*S*)-1-methoxy-2-propanamine ((*S*)-**3a**) (3.3 g, 37 mmol) in dichloromethane under reflux for 4 h. After quenching with sodium carbonate, (*S*)- or (*R*)-**1a** was isolated by distillation (3.7 g, 67%). Other Schiff bases (1*S*,2*S*,5*S*)-3-[(*S*)-2-methoxy-1-isopropyl-ethylimino]-2-pinanol ((*S*)-**1b**), (1*S*,2*S*,5*S*)-3-[2-methoxyethylimino]-2-pinanol **1c**), and (1*S*,2*S*,5*S*)-3-[(*S*)-2-hydroxy-1-methylethylimino]-2-pinanol ((*S*)-**1d**) were synthesized similarly to (*S*)-**1a**. Physical constants of the schiff bases are shown in Table 1.

Typical Asymmetric Addition Reactions to Aectophenone. In situ *System*: BuLi (4.6 mmol) was subjected to react with (*S*)-**1a** (0.3 g, 1.3 mmol) for 1 h in hexane (23 ml) at room temperature. After the reaction system was cooled down to −78 °C, acetophenone (0.16 g, 1.3 mmol) was added, and the reaction was quenched with 1 M hydrochloric acid (6 ml (1 M = 1 mol dm^{-3})) after 2 h. After usual work-up, 2-phenyl-2-hexanol was isolated by column chromatography (silica gel, ethyl acetate).

Prereacted System: After the reaction of BuLi with (*S*)-**1a** in specified molar ratio for 1 h, the reaction system was evacuated under vacuum, and the solid product was washed with hexane for several times. The product was suspended in hexane and treated with newly added one equivalent BuLi for 1 h. Acetophenone was added to the reaction system and allowed to react for 2 h.

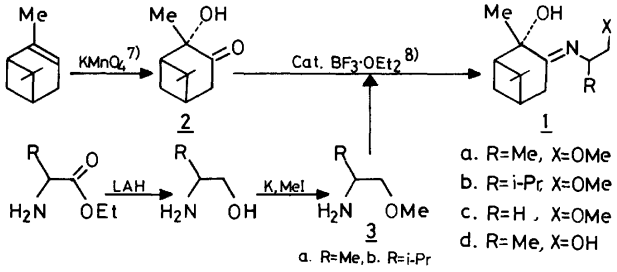

Scheme 1. Synthetic routes to the chiral ligands. Me, MeO, and *i*-Pr are methyl, methoxyl, and isopropyl groups, respectively.

TABLE 1. ANALYTICAL DATA OF SCHIFF BASE LIGANDS **1a—1d**

Compd	Bp	$[\alpha]_D$	Analysis (%)[a]			IR[b]	^{1}H NMR[c]
	(θ_m/°C)/mmHg†	°	C	H	N	ν/cm^{-1}	(δ)ppm
(*S*)-**1a**	74.5/0.22	+16.8[d]	70.29 (70.25)	10.58 (10.53)	5.67 (5.85)	3440 1640 1385 1370 1105	1.06 (3H, d, *J*=6.0Hz, C*H*$_3$CH), 0.87 and 1.33 (6H, two s, (C*H*$_3$)$_2$C), 1.43 (3H, s, C*H*$_3$C-O), 1.88—2.20 (2H, m, C*H*$_2$), 1.90—2.48 (2H, m, C*H*), 2.48—2.70 (2H, m, C*H*$_2$ C=N), 3.30 (3H, s, OC*H*$_3$), 3.30—3.42 (2H, AMX type q, J_1=6.0Hz, J_2=2.0Hz, C*H*$_2$O), 3.41—4.00 (1H, AMX type m, J_1=6.0Hz, J_2=2.0Hz, NC*H*)
(*R*)-**1a**	—	0.0[e]	—	—	—		
(*S*)-**1b**	90.0/0.36	−16.4[f]	71.66 (71.86)	10.51 (10.93)	4.83 (5.24)	3440 1640 1385 1370 1100	0.87 and 0.96 (6H, dd, *J*=5.8Hz, (C*H*$_3$)$_2$CH), 0.89 and 1.33 (6H, two s, (C*H*$_3$)$_2$CH), 1.43 (3H, s, C*H*$_3$ C-O), 1.90—2.21 (2H, m, C*H*$_2$), 1.87—2.47 (2H, m, C*H*), 2.47—2.69 (2H, m, C*H*$_2$ C=N), 3.28 (3H, s, C*H*$_3$O), 3.30—3.70 (3H, m, OC*H*$_2$C*H*N)
1c	76.0/0.40	+6.2[g]	69.10 (69.30)	10.29 (10.29)	5.86 (6.22)	3440 1640 1385 1370	0.87 and 1.33 (6H, two s, (C*H*$_3$)$_2$C), 1.45 (3H, s, C*H*$_3$C-O), 1.87—2.40 (4H, m, C*H*$_2$, C*H*), 2.40—2.67 (2H, broad s, C*H*$_2$ C=N), 3.30 (3H, s, C*H*$_3$O), 3.30—3.88 (4H, m, NC*H*$_2$C*H*$_2$O)
(*S*)-**1d**	101—103[h]	+40.6[i]	68.86 (69.30)	9.91 (10.29)	6.23 (6.22)	1110 —	0.88 and 1.31 (6H, two s, (C*H*$_3$)$_2$C), 1.08 (3H, d, *J*=6.0Hz, C*H*$_3$CH), 1.46 (3H, s, C*H*$_3$C-O), 1.80—2.12 (2H, broad, C*H*$_2$), 2.12—2.60 (2H, m, C*H*), 2.60—2.88 (2H, broad, C*H*$_2$C=N), 3.35—4.05 (3H, m, NC*H*C*H*$_2$O)

a) Values in parentheses are calculated ones. b) Measured as NaCl sandwich. c) Measured in $CDCl_3$ except (*S*)-**1d**, which was measured in CD_3OD. d) c 1.79, $CHCl_3$, 23 °C. e) c 2.56, $CHCl_3$, 21 °C. f) c 0.73, $CHCl_3$, 21 °C. g) c 1.78, $CHCl_3$, 22 °C. h) mp (θ_m/°C). i) c 3.29, $CHCl_3$, 23 °C. †1 mmHg=133.322 Pa.

The enantiomeric excess (% e.e.) was determined by the α-methyl signal splitting in ^{1}H NMR using chiral shift reagent, tris[3-(trifluoromethylhydroxymethylene)-*d*-camphorate]europium (III) (Eu(tfc)$_3$).[9]

Results and Discussion

Species Responsible for Asymmetric Induction. ^{1}H NMR and IR spectra of the reaction system of BuLi and (*S*)-**1a** indicated the structure **4** for the reaction product in 1:1 molar ratio. Peak broadening of the methylene protons of BuLi in the ^{1}H NMR of the reaction system in 2:1 molar ratio suggested that the principal product in this molar ratio was the associated species of BuLi with **4**. In the ^{1}H NMR of the product in 3.5:1 molar ratio, not only peak broadening but also further changes were observed: C-4 Methylene signal decreased and a new peak appeared around at 4.5 ppm. This signal is assignable to olefinic proton of lithioenamine.[10] Quantitative analysis of Li (5.68%) and incorporation of deuterium atom at 4-position by quenching with dilute D_2O–DCl strongly suggested the formation of lithioenamine **5** in the reaction of 3.5:1 molar ratio.

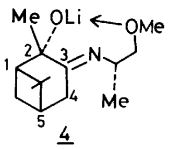

4

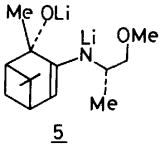

5

The results of asymmetric addition are shown in Table 2. The reaction did not proceed when less than two equimolar amounts of BuLi to (*S*)-**1a** were used. No reaction was observed either, when one equivalent BuLi was added to prereacted system **4** (run No. 9). Only small optical yield was obtained in 3:1 *in situ* system (No. 2), or when one equivalent BuLi was added to the prereacted system (2:1) (No. 10), although high chemical yield could be attained. The species of 3.5:1 systems gave reasonably high chemical and optical yields (No. 3, 11), and the highest optical yield was obtained when one equivalent BuLi was used with 3.5:1 prereacted system (No. 12). Only small asymmetric induction was observed when acetophenone was added immediately after (*S*)-**1a** was mixed with 3.5 mole equivalent BuLi at −78°C. Since formation of **5** from BuLi and **4** takes a little time, the above mentioned facts strongly indicate the importance of the formation of lithioenamine **5** in the asymmetric induction. It seems that species responsible for the asymmetric addition is formed through the interaction of BuLi with **5**, and that the contribution of the species is the highest at 3.5:1 molar ratio in *in situ* system. The optical yield decreased when the molar ratio became higher than 4:1, although chemical yield remained high. Under this condition, proportion of free BuLi which added to acetophenone without the influence of chiral ligand system **5** is high, resulting in a decrease of the optical yield.

Effects of α-Substituent on Optical Yield. The effects of the configuration, and alkyl substituent at α-carbon of imino ether component of **1** are also shown in Table 2. Bulky substituent at α-carbon seems to have higher regulating power (No. 6). (*R*)-**1a** gave opposite sign in the product (No. 4). These facts indicate that α-substituent directly influences the enantioface-selection, and that in BuLi-(*S*)-**1** systems, the regulation by α-alkyl group and pinane skeleton work to same direction, but in (*R*)-**1** to opposite direction. This speculation is supported by that in BuLi-**1c** system, where no substituent was attached to α-carbon, small positive value was observed by the influence of pinane skeleton (No. 7). Racemic **1a** gave small (−) value for the product (No. 5). Imino alcohol ligand (*S*)-**1d** showed only a weak regulating power (No. 8), which indicates the importance of methoxyl group in the ligand **1** to form species responsible for the asymmetric induction.

TABLE 2. ENANTIOFACE-DIFFERENTIATING ADDITION OF BULI TO ACETOPHENONE[a]

No.	Ligand System	[BuLi]/[Ligand]	Conv.[b] %	$[\alpha]_D^{25}$ ° $\left(\frac{\text{Conc.}}{\text{g dl}^{-1}}\right)$[c]	% e.e.
	In situ system[d]				
1	(*S*)-**1a**	1.0	0	—	—
2	(*S*)-**1a**	3.0	61	+2.9 (1.53)	11
3	(*S*)-**1a**	3.5	80	+6.3 (0.79)	23
4	(*R*)-**1a**	3.5	29	−2.4 (3.3)[e]	4
5	rac-**1a**	3.5	—	−0.5 (1.0)	2
6	(*S*)-**1b**	3.5	48	+9.0 (0.23)	33
7	**1c**	3.5	71	+2.2 (1.75)	8
8	(*S*)-**1d**	3.5	80	+0.4 (1.2)	2
	Prereacted system[d]				
9	(*S*)-**1a** (1 :1)[f]	1.0	0	—	—
10	(*S*)-**1a** (2 :1)[f,g]	1.0	70	+0.7 (4.47)	3
11	(*S*)-**1a** (3.5:1)[f,g]	0	80	+4.7 (0.60)	20
12	(*S*)-**1a** (3.5:1)[f]	1.0	8	+7.1 (0.42)	26

a) Reactions were carried out in hexane at −78°C at the concentration of acetophenone and ligand ranging 0.08—0.50 mol/l. b) Determined by disappearance of acetophenone in GLC. c) Solvent $CHCl_3$. d) See experimental. e) 28°C. f) Molar ratio of BuLi to ligand in the preparation of prereacted system. g) Prereacted system as evacuated without washing with hexane was used.

References

1) K. Soai and T. Mukaiyama, *Bull. Chem. Soc. Jpn.*, **52**, 3371 (1979).
2) E. R. Grandbois, S. J. Howard, J. D. Morrison, "Asymmetric Syntheses," ed by J. D. Morrison, Academic Press, New York (1983), Vol. 2, Part A, p. 71.
3) H. Nozaki, T. Aratani, and T. Toraya, *Tetrahedron Lett.*, **1968**, 4097.
4) N. Allentoff and G. F. Wright, *J. Org. Chem.*, **22**, 1 (1957).
5) T. D. Inch, G. J. Lewis, G. L. Sainsbury, and D. J. Sellers, *Tetrahedron Lett.*, **1969**, 3657.
6) G. Solladié, "Asymmetric Syntheses," ed by J. D. Morrison, Academic Press, New York (1983), Vol. 2, Part A, p. 157.
7) R. G. Carlson and J. K. Pierce, *J. Org. Chem.*, **36**, 2319 (1971).
8) T. Oguri, N. Kawai, T. Shioiri, and S. Yamada, *Chem. Pharm. Bull.*, **26**, 803 (1978).
9) H. L. Goering, J. N. Eikenberry, and G. S. Koemer, *J. Am. Chem. Soc.*, **93**, 5913 (1971).
10) A. I. Meyers, D. R. Williams, S. White, and G. W. Erickson, *J. Am. Chem. Soc.*, **103**, 3088 (1981).

Change of Orientation in Photoreaction by Oxygen. Effect of Oxygen on Photo-methoxylation of Dimethyl Esters of 2,4- and 3,4-Pyridinedicarboxylic Acid

Toru SUGIYAMA,* Mitsuharu KANAI, Setsuko TAKENAKA, and Akira SUGIMORI*

Department of Chemistry, Faculty of Science and Technology, Sophia University, Kioi-cho 7-1, Chiyoda-ku, Tokyo 102

(Received August 7, 1984)

Synopsis. The UV-irradiation of dimethyl 2,4- and 3,4-pyridinedicarboxylates in methanol in the presence of H_2SO_4 under O_2 brings about methoxylation at the β- position of the pyridine ring, while under N_2 methoxylation occurs at the α-position.

In a preceding paper,[1] we described a remarkable effect of oxygen on the photoreaction of methyl 4-pyridinecarboxylate in methanol: Even a small amount of oxygen causes a change of orientation in the photo-methoxylation. The role of oxygen cannot be explained by any generally accepted effect (the acceleration of intersystem crossing or charge-transfer interaction). To survey the scope of this novel types of effect, we have studied the effect of oxygen on the photoreactions of dimethyl pyridinedicarboxylates in acidic methanolic solutions.

Results and Discussion

Photoreactions in the Presence or in the Absence of O_2. Similar to the photoreaction of 4-pyridinecarboxylic ester, the photoreactions of dimethyl pyridinedicarboxylates show a remarkable oxygen effect: Oxygen causes the change of the position of methoxylation at the α-position of the pyridine ring into that at the β-position.

UV-irradiation of dimethyl 2,4-pyridinedicarboxylate (**1**) under N_2 in methanol in the presence of H_2SO_4 brings about methoxylation mainly at the 6-position of the pyridine ring (**4**), accompanied by the methylation at the 5- and 6-positions (**5**),(**6**) and hydroxymethylation at the 6-position (**7**) in low yields (Table 1).[2]

On the other hand, under O_2 these reactions are supperssed and the methoxylation at the 5-position (**3**) predominates (Table 1).

Dimethyl 3,4-pyridinedicarboxylate (**2**) undergoes photo-methoxylation at the 5-position (**8**) under O_2, while under N_2 the methoxylation occurs only at the 2-position (**9**), accompanied by methylation at the 6-position (**10**) (Table 1).

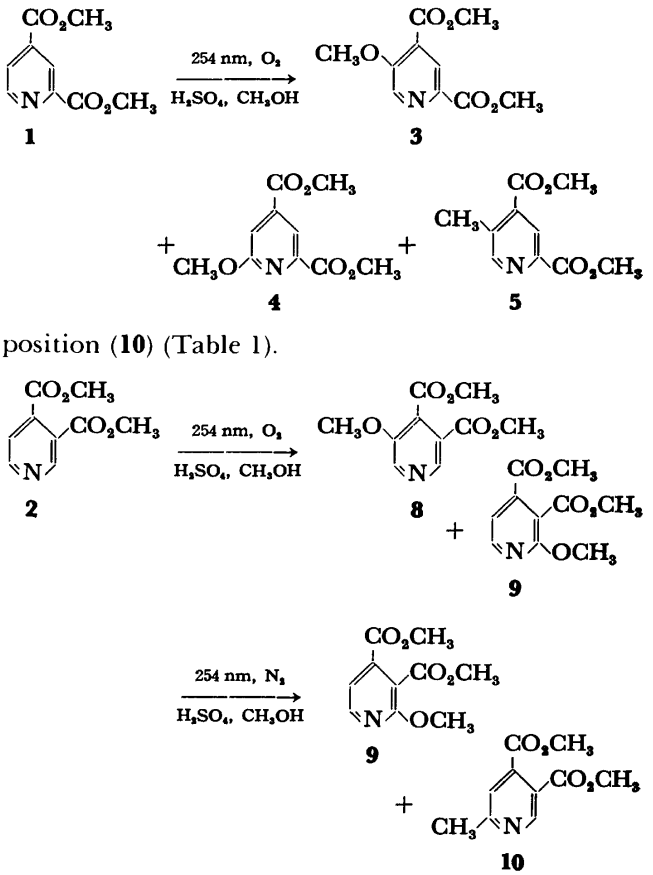

Role of Oxygen for the Methoxylation at the β-Position. Similar to the case of 4-pyridinecarboxylic ester in the photo-methoxylation at the β-position,[1] oxygen does not serve as an oxidant in the methoxylation at the β-position of pyridinedicarboxylic esters because after the irradiation of **1** under N_2 the addition of $K_3[Fe(CN)_6]$ or bubbling oxygen has no effect on the formation of the methoxylated product at the 5-position (Table 1).

TABLE 1. PHOTOREACTIONS OF **1** AND **2** IN METHANOL IN THE PRESENCE OF H_2SO_4[a]

Diester	Atmosphere	Conversion %	Additive	Yield of product/%[b] 3	4	5	6	7	8	9	10
1	O_2	16	—	9	4	0.4	0	0	—	—	—
1	N_2	20	—	0	12	4	0.7	4	—	—	—
1	N_2	20	O_2(bubbled)[c]	0	12	4	0.3	4	—	—	—
1	N_2	20	$K_3[Fe(CN)_6]$[d]	0	12	4	0.2	4	—	—	—
1	N_2	2	Ph_2CO(365 nm)[e]	0	0	0	0	0	—	—	—
2	O_2	23	—	—	—	—	—	—	3	5	0
2	N_2	24	—	—	—	—	—	—	0	11	1

a) $[\mathbf{1}]=[\mathbf{2}]=0.01\,mol\,dm^{-3}$; $[H_2SO_4]=1.0\,mol\,dm^{-3}$; Irradiation time, 1 h; Temp., 30 °C. b) Yields are based on the amount of **1** and **2** consumed. c) O_2 was bubbled after the irradiation. d) $K_3[Fe(CN)_6]$ was added after the irradiation. e) $[Ph_2CO]=0.05\,mol\,dm^{-3}$; irradiated for 2.5 h with a 100 W high pressure mercury lamp through 365 nm filter.

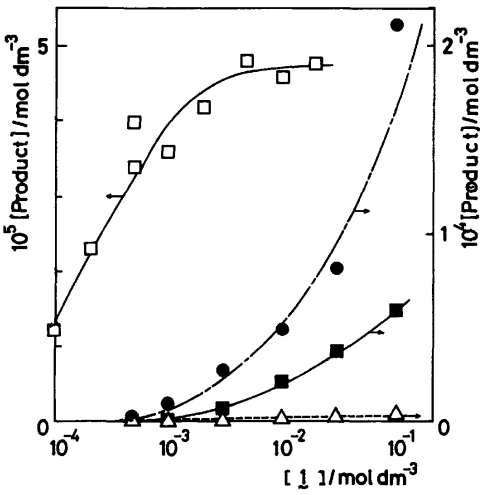

Fig. 1. Dependences of the photoreactions of **1** under O_2 and under N_2 on the concentration of **1**.
-●---: **3**; -■—: **4**; --△---: **5** (under O_2); -□—: **4** (under N_2).

When the irradiation of **1** with 365 nm light was carried out in the presence of benzophenone under N_2, the methoxylation at the 5-position was not observed as is shown in Table 1. *trans*-1,3-Pentadiene, a triplet quencher, does not quench the reaction. These facts indicate that the methoxylation at the β-position occurs from an excited singlet state of the pyridinium form of **1** and thus oxygen does not accelerate the intersystem crossing from the excited singlet state to the triplet excited state.

Because the UV-absorption spectra of **1** in acetonitrile were not markdly affected by oxygen, it is concluded that under these conditions the contribution of a ground state contact charge-transfer complex between the protonated **1** and O_2 is very improbable. Similar oxygen effects were also observed in the photomethoxylation at the β-position of 4-pyridinecarboxylic ester.[1]

Since the methoxylation at the 6-position of **1** under N_2 shows the dependence on the concentration of the substrate, the reaction may proceed *via* an excimer.[2] The methoxylation of **1** at the 6- and 5-positions under O_2 are also more dependent on the concentration of the substrate over the range of higher concentration than that under N_2 as are shown in Fig. 1. It is noteworthy that the concentration dependence curves of the methoxylations are not reduced by oxygen but are shifted to the region of higher concentrations in the presence of oxygen. These results indicate that the decrease of the methoxylation at the 6-position is not due to the quenching of the excimer by oxygen. The participation of another excited complex in the reaction can be presumed. It may be an excited terplex which consists of two molecules of protonated **1** and one molecule of oxygen.

Experimental

Materials. Dimethyl pyridinedicarboxylates (**1**, **2**) were synthesized by the esterification of pyridinedicarboxylic acids with methanol in the presence of hydrogen chloride.

UV-irradiation. Through the solutions of **1** or **2** (0.01 mol dm^{-3}) containing 1.0 mol dm^{-3} of H_2SO_4, O_2, or N_2 were bubbled for 45 min before irradiation. The solutions were irradiated with a 17 W low pressure mercury lamp at 30 °C.

Isolation and Identification of Photo-products. After the irradiation, the solutions were concentrated under reduced pressure, were neutralized with sodium carbonate, and were extracted with ethyl acetate. The products were separated by means of TLC (plate, GF_{254} (Type 60) of E. Merck Co.; developing solvent, ethyl acetate–dichloromethane 1:4) or by means of GLC (column, PEG 20 M 2%, 2 m on Celite 545 (60/80 mesh); Temp., 200 °C) with a Ohkura gas chromatograph model GC 103.

Dimethyl 5-methoxy-2,4-pyridinedicarboxylate (**3**), mp 142—144 °C; ^{1}H NMR ($CDCl_3$) δ=8.52 (1H, s, H at 6-position), 8.42 (1H, s, H at 3-position), 4.09 (3H, s, OCH_3), 3.99 and 3.94 (6H, s, CO_2CH_3); IR (KBr) 1726 and 1714 (ester C=O) and 1255 cm^{-1} (C–O–C); MS (70 eV), *m/z* (rel intensity), 225 (M^+; 11), 195 (14), 194 (18), 167 (100), and 166 (18). Found: *m/z* 225.0649. Calcd for $C_{10}H_{11}NO_5$: M, 225.0636; Found: C, 53.01; H, 5.02; N, 6.38%. Calcd for $C_{10}H_{11}NO_5$: C, 53.33; H, 4.92; N, 6.22%.

Other photo-products of **1** (**4**—**7**) see Ref. 2.

Dimethyl 5-methoxy-3,4-pyridinedicarboxylate (**8**), mp 67—68 °C (lit,[3] 78—80 °C); ^{1}H NMR ($CDCl_3$) δ=8.82 (1H, s, H at 2-position), 8.48 (1H, s, H at 6-position), 3.93 (3H, s, OCH_3), 3.90 and 3.88 (6H, s, CO_2CH_3); IR (KBr), 1750 and 1730(ester C=O) and 1245 cm (C–O–C); MS (70 eV), *m/z* (rel intensity), 225 (M^+; 37), 194 (100), 193 (21), 166 (24), and 135 (20). Found: *m/z* 225.0637.

Dimethyl 2-methoxy-3,4-pyridinedicarboxylate (**9**), mp 48—51 °C; ^{1}H NMR ($CDCl_3$) δ=8.24 (1H, d, J=5 Hz, H at 6-position), 7.32 (1H, d, J=5 Hz, H at 5-position), 3.96 (3H,s,OCH_3), 3.90 and 3.87 (6H, s, CO_2CH_3); IR (KBr), 1730 (ester C=O) and 1270 cm^{-1}(C–O–C); MS (70 eV), *m/z* (rel intensity), 225 (M^+; 43), 195 (11), 194 (100), 193 (31), 180 (39), and 135 (31). Found: *m/z* 225.0637. Calcd for $C_{10}H_{11}NO_5$: M, 225.0636; Found: C, 53.23; H, 5.04; N, 6.18%. Calcd for $C_{10}H_{11}NO_5$: C, 53.33; H, 4.92; N, 6.22%.

Dimethyl 6-methyl-3,4-pyridinedicarboxylate (**10**), mp 63—64 °C; ^{1}H NMR ($CDCl_3$) δ=8.96 (1H, s, H at 2-position), 7.30 (1H, s, H at 5-position), 3.93 and 3.90 (6H, s, CO_2CH_3), and 2.65 (3H, s, CH_3); IR (KBr), 1742 and 1720 cm^{-1} (ester C=O); MS (70 eV), *m/z* (rel intensity), 209 (M^+; 19), 208 (12), 179 (24), 178 (100), and 150 (11). Found: *m/z* 209.0691.

Qunatitative Analysis of Photo-products. The yields of the products were determined by means of HPLC (column, 4.0 mm×25 cm column of Lichrosorb RP-18, 7 μm: eluent, H_2O–CH_3CN 8:2 or 81:19 v/v) with a Shimadzu liquid chromatograph model LC 3A or with a Hitachi model 655 and/or by means of GLC (column, PEG 20 M 5%, 1 m on Celite 545 (60/80 mesh)) with a Shimadzu gas chromatograph model GC 6A.

Spectral Measurements. ^{1}H NMR spectra were recorded on a Hitachi R 22 NMR spectrometer (90 MHz) with tetramethylsilane as an internal standard and IR spectra were measured on a Hitachi 260—50 spectrometer. Mass spectra were determined with a JEOL D-300 spectrometer. UV spectra were recorded on a Hitachi 228 spectrophotometer.

References

1) T. Sugiyama, K. Yagi, Y. Ito, and A. Sugimori, *Chem. Lett.*, **1982**, 917; T. Sugiyama, K. Kusano, K. Yagi, Y. Ito, and A. Sugimori, *Bull. Chem. Soc. Jpn.*, **57**, 1882 (1984).

2) A. Sugimori and M. Kanai, *Nippon Kagaku Kaishi*, **1984**, 37.

3) W. Korytnyk and N. Angelino, *J. Med. Chem.*, **20**, 745 (1977).

Synthesis of Cylindrical Large Ring Crown Hosts

Kazuya KOBIRO,* Katsuhiro OHNISHI, Kiyomi KAKIUCHI, Yoshito TOBE, and Yoshinobu ODAIRA
Department of Applied Fine Chemistry, Faculty of Engineering, Osaka University, Suita, Osaka 565
(Received September 20, 1984)

Synopsis. New cylindrical crown hosts, tridecalino-27-crown-9, tridecalino-21-crown-7, didecalino-cyclohexano-21-crown-7, and didecalinio-21-crown-7 have been synthesized.

In resemblance to naturally occurring cyclic antibiotics, increasing interests are being shown in the large ring crown hosts such as 27-crown-9 and 21-crown-7.[1] As part of the study of a new type of cylindrical crown host (Fig. 1), we have previously revealed that didecalino-18-crown-6† exhibits an excellent complexing ability and conspicuous stoichioselectivity toward alkali metal ions due to the remarkable embedding effect of decalin moieties.[2,3] In this connection, we report herein the synthesis of novel cylindrical large ring crown hosts, *i.e.*, tridecalino-27-crown-9 (**8**), tridecalino-21-crown-7 (**9**), didecalino-cyclohexano-21-crown-7† (**10**), and didecalino-21-crown-7 (**11**), which would be expected to form complexes with organic guest cations.

Cylindrical crown host tridecalino-27-crown-9 (**8**) was synthesized as outlined in Scheme 1. Reaction of *cis*-4*a*,8*a*-decalindiol (**1**) with diethylene glycol ditosylate gave didecalinodiol **2** in 27% yield. Williamson synthesis of **2** with chloroacetic acid followed by esterification and hydride reduction produced "two-arm" alcohol **4** in 36% overall yield. Similarly, "two-arm" tosylate **7** was synthesized from **1** in 57% overall yield. According to similar synthetic routes, **9**, **10**, and **11** were also synthesized from **2** with appropriate "two-arm" tosylates (**9**: 6.5%, semisolid; **10**: 2.0%, oily; **11**: 4.9%, oily). Thus we could synthesize cylindrical crown hosts in spite of difficulties which were easily expected for the etherification of the tertiary alcohol. Moreover, it was proved that the synthetic method using chloroacetic acid was very useful for the synthesis of cylindrical crown hosts.

Studies on the complexing abilities of these cylindrical large ring crown hosts with various organic cations, such as guanidinium cation,[4] are in progress.[5]

Experimental

IR spectra were recorded using a Hitachi 260-10 spectrometer. ^1H and ^{13}C NMR spectra were obtained on a JEOL JNM-PS-100 and JEOL JNM-FX-60 spectrometer respectively, using Me_4Si as an internal standard and $CDCl_3$ as a solvent unless otherwise stated. Mass spectra were measured with a Hitachi RMU-6E spectrometer.

1,2:10,11-Didecalino-3,6,9-trioxaundecane-1,11-diol (2). A mixture of 10.0 g (59 mmol) of **1**,[2] 1.68 g (70 mmol) of NaH, and 80 ml of *N*,*N*-dimethylformamide (DMF) was stirred for 1 h at room temperature. To this mixture a solution of 12.0 g (29 mmol) of diethylene glycol ditosylate[6] in 80 ml of DMF was added dropwise and the mixture was stirred for 57 h. After addition of small amount of water, the reaction mixture was filtered through Celite. The filtrate was evaporated, and the residue was extracted with chloroform. The organic layer was washed with water, dried ($MgSO_4$), and evaporated. 5.80 g (58%) of **1** was recovered by vacuum distillation (155 °C/1.5 Torr (1 Torr=133.322 Pa)) and the residue (>160 °C/1.5 Torr) was chromatographed over silica gel to give additional 0.47 g (5%) of **1** (ether/petroleum ether=3/7) and 3.3 g (27%) of **5** (ether/petroleum ether=5/5) as a colorless oil: IR (neat) 3550, 1080 cm^{-1}; ^1H NMR δ=1.00—2.16 (m, 32H), 2.42 (br s, 2H), 3.48—3.88 (m, 8H); MS *m/z* 392 (M^+-H_2O). Found: C, 70.27; H, 10.61%. Calcd for $C_{24}H_{42}O_5$: C, 70.20; H, 10.31%.

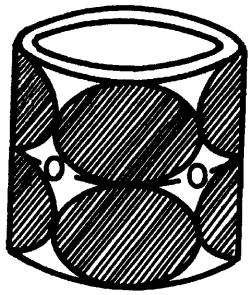

Fig. 1.

4,5:13,14-Didecalino-3,6,9,12,15-pentaoxaheptadecanedioic Acid Diethyl Ester (3). A mixture of 6.36 g (16 mmol) of **2** and 2.23 g (93 mmol) of NaH in 150 ml of tetrahydrofuran (THF) was refluxed for 1.5 h under N_2. To this suspension was added dropwise a solution of 3.66 g (39 mmol) of chloroacetic acid in 50 ml of THF. The mixture was stirred under reflux for 15 h. After addition of water (2 ml), the solvent was evaporated and 50 ml of water was added to the residue. The aqueous solution was acidified with concentrated aqueous HCl and extracted with chloroform. The organic phase was dried ($MgSO_4$) and evaporated to afford 10.1 g of oil. This crude oil was dissolved in 90 ml of 1:1 mixture of absolute ethanol and benzene, and 0.13 g of *p*-toluenesulfonic acid was added. The mixture was refluxed for 10 h, with continuous circulation of condensed vapor through anhydrous Na_2SO_4. After removal of the solvent, the residue was dissolved in dichloromethane, washed with aqueous $NaHCO_3$ and brine, and dried ($MgSO_4$). The solvent was evaporated to afford 9.27 g of oil. The crude product was chromatographed over silica gel to give 3.78 g (42%) of **3** and 1.51 g (24%) of unreacted diol **2** (ether/petroleum ether=3/7): IR (neat) 1750, 1720 cm^{-1}; ^1H NMR δ=1.00—2.60 (m, t at 1.28, 38H), 3.32—3.88 (m, 8H), 4.18 (q, 4H), 4.32 (d, 4H); MS *m/z* 582 (M^+). Found: C, 66.04; H, 9.64%. Calcd for $C_{32}H_{54}O_9$: C, 65.95; H, 9.34%.

4,5:13,14-Didecalino-3,6,9,12,15-pentaoxaheptadecane-1,17-diol (4). Ester **3** (3.65 g, 6.27 mmol) was reduced with 0.63 g (17 mmol) of lithium aluminum hydride (LAH) in 30 ml of boiling THF. Usual workup gave 2.63 g (84%) of **4** as a colorless oil: IR (neat) 3400, 1090 cm^{-1}; ^1H NMR δ=1.00—2.20 (m, 32H), 3.00—4.00 (m, 18H); MS *m/z* 498 (M^+). Found: C, 67.25; H, 10.29%. Calcd for $C_{28}H_{50}O_7$: C, 67.43; H, 10.11%.

4,5-Decalino-3,6-dioxaoctane-1,8-diol (6). Ester **5** was prepared from **1** according to the similar procedure described for **3** in 70% yield as an oil: bp 131—132 °C/0.3 Torr; IR (neat) 1750, 1730 cm^{-1}; ^1H NMR (CCl_4) δ=1.00—2.20 (m, t at 1.24, 22H), 3.92—4.24 (m, 8H); MS *m/z* 342 (M^+).

†Ortho-fused cyclic compounds are tentatively named "decalino" and "cyclohexano" for decahydronaphtho[4*a*,8*a*] and perhydrobenzo respectively.

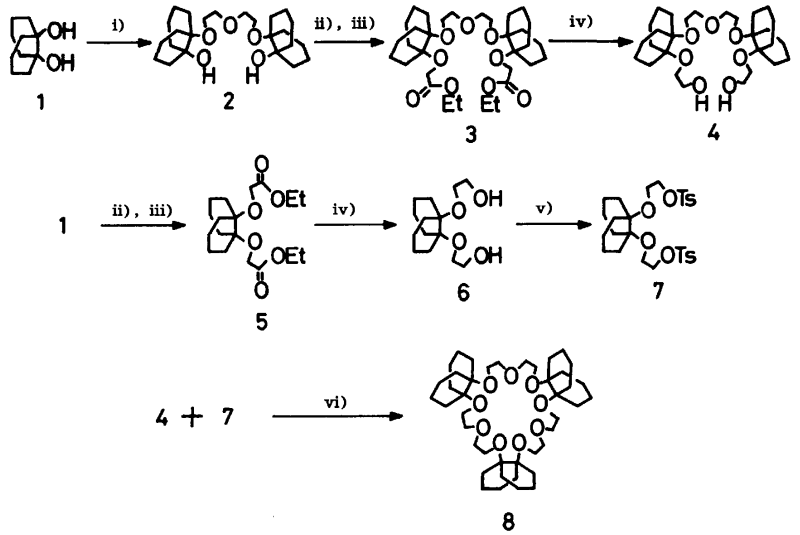

i) $TsOCH_2CH_2OCH_2CH_2OTs$, NaH, DMF; ii) $ClCH_2COOH$, NaH, THF; iii) EtOH, TsOH, C_6H_6; iv) $LiAlH_4$, THF; v) TsCl, C_5H_5N; vi) NaH, THF.

Scheme 1.

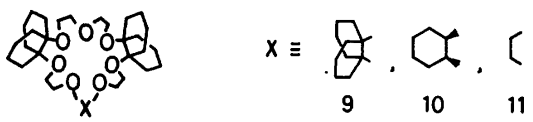

Found: C, 63.42; H, 8.93%. Calcd for $C_{18}H_{30}O_6$: C, 63.13; H, 8.83%. LAH reduction of **5** gave **6** in 85% yield after recrystallization from ligroin: mp 83—85 °C; IR (KBr) 3400, 3310, 1095, 1060 cm^{-1}; ^1H NMR (CCl_4) δ=1.00—2.40 (m, 16H), 3.00—4.12 (m, 10H); MS *m/z* 258 (M^+). Found: C, 64.96; H, 10.17%. Calcd for $C_{14}H_{26}O_4$: C, 65.08; H, 10.14%.

4,5-Decalino-3,6-dioxaoctane-1,8-diol Ditosylate (7). **7** was prepared from **6** by the method similar to that of Dale and Kristiansen[6] in 96% yield after recrystallization from ethanol: mp 97—99 °C; IR (KBr) 3050, 1595, 1350, 1170 cm^{-1}; ^1H NMR δ=1.00—2.00 (m, 16H), 2.40 (s, 6H), 3.20—3.80 (m, 4H), 3.92—4.12 (2d, 4H), 7.42 (AB q, 8H). Found: C, 59.05; H, 6.80; S, 11.25%. Calcd for $C_{28}H_{38}O_8S_2$: C, 59.34; H, 6.76; S, 11.31%.

Tridecalino-27-crown-9 (8). To a refluxing mixture of 1.99 g (4.0 mmol) of diol **4** and 0.48 g (20 mmol) of NaH in 100 ml of THF was added dropwise over 10 h a solution of 2.26 g (4.0 mmol) of **7** in 50 ml of THF. The mixture was refluxed for 36 h, and then another 2.26 g (4.0 mmol) of **7** in 50 ml of THF was added over 10 h. The mixture was refluxed for 36 h and cooled. Water (2 ml) was added and the solvent was evaporated. The residue was extracted with dichloromethane and dried ($MgSO_4$), and the solvent was removed to give 4.69 g of oil. This oil was chromatographed over silica gel (ether/petroleum ether=5/5) to afford 1.01 g (35%) of **8**, which was recrystallized from ether: mp 90—91 °C; IR (KBr) 1080 cm^{-1}; ^1H NMR δ=1.00—2.00 (m, 48H), 3.20—3.92 (m, 24H); ^{13}C NMR (57 °C) δ=22.0 (t, 12C), 30.3 (t, 12C), 60.7 (t, 6C), 71.2 (t, 6C), 77.9 (s, 6C); MS *m/z* 614 ($M^+-C_4H_{10}O_3$ (diethylene glycol)). Found: C, 69.95; H, 10.07%. Calcd for $C_{42}H_{72}O_9$: C, 69.96; H, 10.07%.

Tridecalino-21-crown-7 (9). A solution of 0.33 g (0.58 mmol) of **7** and 0.24 g (0.58 mmol) of **2** in 20 ml of DMF was added to a suspension of 0.28 g (12 mmol) of NaH in 50 ml of DMF over 3 h under N_2 at room temperature and the mixture was stirred for 7 d. Workup as described above gave 24 mg (6.5%) of **9** as a semisolid and 155 mg of recovered diol **2** (65%): IR (neat) 1080 cm^{-1}; ^1H NMR δ=1.00—2.40 (m, 48H), 3.28—4.00 (m, 16H); MS *m/z* 632 (M^+). Found: C, 72.33; H, 10.30%. Calcd for $C_{38}H_{64}O_7$: C, 72.11; H, 10.19%.

Didecalino-cyclohexano-21-crown-7 (10). Reaction of 3.86 g (9.4 mmol) of **2**, 4.82 g (9.4 mmol) of 4,5-cyclohexano-3,6-dioxaoctane-1,8-diol ditosylate prepared from *cis*-cyclohexane-1,2-diol according to the similar method described for **7**, and 4.5 g of NaH in 300 ml of DMF for 7 d gave 3.5 g (93%) of unreacted diol **2** and 11 mg (2.0%) of **10** as an oil: IR (neat) 1080 cm^{-1}, ^1H NMR δ=1.00—2.20 (m, 40H), 3.20—4.00 (m, 18H); MS *m/z* 578 (M^+). Found: C, 70.31; H, 10.21%. Calcd for $C_{34}H_{58}O_7$: C, 70.55; H, 10.10%.

Didecalino-21-crown-7 (11). Reaction of 11.4 g (27.8 mmol) of **2**, 57.6 g (126 mmol) of triethylene glycol ditosylate,[6] and 12.6 g (525 mmol) of NaH in 550 ml of DMF for 7 d gave 7.5 g (66%) of unreacted diol **2** and 72 mg (4.9%) of **11** as an oil: IR (neat) 1080 cm^{-1}; ^1H NMR δ=1.12—2.10 (m, 32H), 3.24—4.00 (m, 20H); MS *m/z* 419 ($M^+-C_4H_9O_3$ (diethylene glycol-H)). Found: C, 68.54; H, 9.95%. Calcd for $C_{30}H_{52}O_7$: C, 68.67; H, 9.99%.

References

1) B. Son, B. P. Czech, D. A. Babb, and R. A. Bartsh, *Tetrahedron Lett.*, **25**, 1647 (1984), and references cited therein.

2) K. Kobiro, Y. Tanaka, K. Okubo, Y. Hiramatsu, K. Kakiuchi, Y. Tobe, and Y. Odaira, *Chem. Lett.*, **1983**, 1507.

3) K. Kobiro, K. Kakiuchi, Y. Tobe, and Y. Odaira, *Chem. Lett.*, **1984**, 487.

4) J. A. A. de Boer, J. W. H. M. Uiterwijk, J. Geevers, S. Harkema, and D. N. Reinhoudt, *J. Org. Chem.*, **48**, 4821 (1983).

5) Preliminary experiments have revealed that the large ring crown host **8** gave 1:1 crystalline complex with an organic salt, guanidinium perchlorate, in good yield (mp 165—167 °C, 55%), though, as compared with dicyclohexano-21-crown-7, none of the crown hosts **9**—**11** showed notable alkali metal cation selectivities upon solvent extraction of aqueous alkali metal picrates.

6) J. Dale and P. O. Kristiansen, *Acta. Chem. Scand.*, **26**, 1471 (1972).

Catalytic Debromination of Vicinal Dibromides *via* Phase Transfer of Diaryltellurium Compounds

Hitomi SUZUKI,* Akiko KONDO, and Atsuhiro OSUKA†
Department of Chemistry, Faculty of Science, Ehime University, Bunkyo-cho, Matsuyama 790
(Received October 2, 1984)

Synopsis. Several vicinal dibromides were debrominated to olefins by potassium disulfite in the presence of catalytic amounts of bis(4-methoxyphenyl) telluride in a two-phase system.

In recent years, there has been remarkable interest in the development of new synthetic methods using organotellurium compounds.[1] However, there have been only a limited number of successes involving the catalytic use of organotellurium compounds and/or tellurium salts.[2,3] Now we wish to report that several vicinal dibromides have been debrominated to their corresponding olefins by potassium disulfite in the presence of catalytic amounts of diaryltellurium compounds.

First, the debromination of *erythro*-1,2-dibromo-1,2-diphenylethane (**1**) in the presence of bis(4-methoxyphenyl) telluride (**3**) was investigated. The reaction system was composed of an aqueous potassium disulfite solution (0.5 mol dm^{-3}, 20 cm^3) and benzene (30 cm^3) as an organic phase that included the dibromide (**1**) and catalytic amounts of **3**. Upon stirring the two-phase system at a benzene-refluxing temperature, dibromide **1** was reduced to *trans*-stilbene (**2**) at varying rates, depending upon the amounts of **3** (Fig. 1). In this experiment, *cis*-stilbene was not found in detectable amounts by GLPC (<1%). In a blank experiment without **3**, the formation of **2** was not observed even after 24 h. Thus, apparently the presence of the diaryl telluride **3** is necessary for the conversion of **1** into **2**. It is interesting that **1** was quantitatively reduced to **2** in the presence of only 5% mol amounts of **3** after a 24 h run (Run 3, Fig. 1). Debromination was speeded up as the concentration of **3** was increased. Thus, in the presence of 10 and 20% mol amounts of **3**, debromination was complete in 12 h and 2 h, respectively (Runs 1 and 2, Fig. 1). On the other hand, in experiments with much smaller amounts of **3**, debromination was incomplete even after prolonged heating; 63% in the presence of 2% mol amounts of **3** and 33% in the presence of 1% mol amounts of **3** (Runs 4 and 5, Fig. 1). From the latter two experiments, the maximum turnover number of the diaryl telluride **3** can be roughly estimated to be 30.

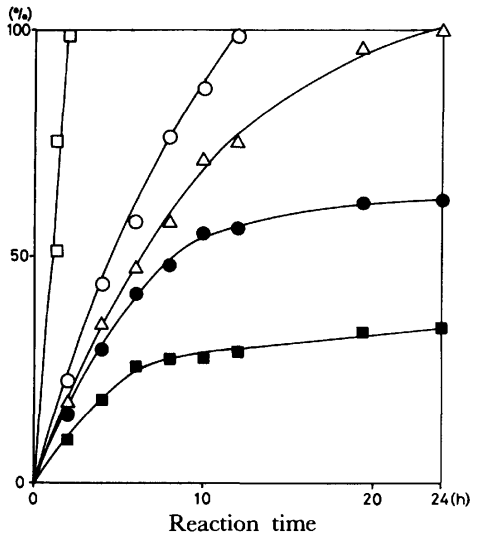

Fig. 1. Catalytic debromination of *meso*-1,2-dibromo-1,2-diphenylethane by $K_2S_2O_5$ using bis(4-methoxyphenyl) telluride (**3**).
Run 1, □: 20% mole amounts, Run 2, ○: 10% mole amounts, Run 3, △: 5% mole amounts, Run 4, ●: 2% mole amounts, Run 5, ■: 1% mole amounts.

It is widely known that a class of diaryltellurium(II) species are easily brominated to diaryltellurium(IV) dibromides with a variety of brominating reagents, including vicinal dibromide, and that the debromination of diaryltellurium(IV) dibromides can be achieved upon treatment with potassium disulfite in hot water.[4] Therefore, the catalytic cycle of the debromination of **1** can be plausibly depicted as shown in Scheme 1, where the diaryltellurium compound, itself, acts as an electron carrier. Indeed, bis(4-methoxyphenyl) tellurium dibromide (**4**) is soluble enough in water to be consistent with the mechanism in Scheme 1. Further, the addition of **4**, instead of **3**, to the reaction mixture also effected the debromination of **1** with a similar efficiency.

The debromination of other vicinal dibromides was tried under the same conditions as Run 3 in Fig. 1. The results are summarized in Table 1. Only *trans*-stilbene and *trans*-4-styrylpyridine were obtained from *erythro*-dibromides, whereas debromination from *threo*-1,2-dibromo-1,2-diphenylethane was modestly stereoselective. Chalcone and ethyl cinnamate were similarly obtained from corresponding dibromides in 61 and 57% yields, respectively. However, 1,2-dibromocyclohexadecane was not debrominated under these conditions.[6]

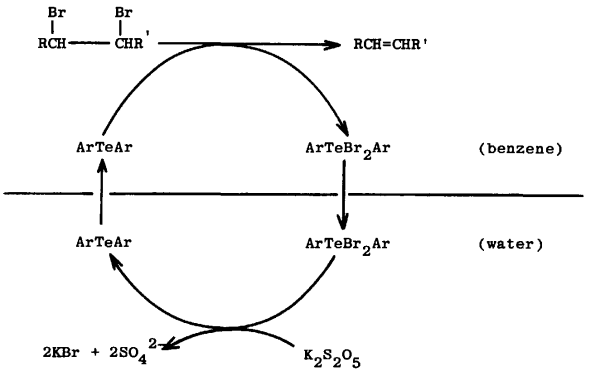

Scheme 1.

†Present address: Department of Chemistry, Faculty of Science, Kyoto University, Kitashirakawa, Sakyo-ku, Kyoto 606.

Table 1. Two-phase debromination of vicinal dibromides by potassium disulfite using bis(4-methoxyphenyl) telluride

	Dibromide $[R^1CH(Br)CH(Br)R^2]$	Olefin (*trans*/*cis*)	Yield/%[b]
1	$R^1=R^2=$Ph *erythro*	PhCH=CHPh (100/0)	100 (92)[c]
2	$R^1=R^2=$Ph *threo*	PhCH=CHPh (6/94)	100 (88)[c]
3	$R^1=$Ph, $R^2=$4-pyridyl *erythro*	PhCH=CH-4-pyridyl (100/0)	100
4	$R^1=$Ph, $R^2=$COPh	PhCH=CHCOPh (100/0)	61
5	$R^1=$Ph, $R^2=CO_2Et$	$PhCH=CHCO_2Et$ (100/0)	57
6	$R^1=$H, $R^2=C_{14}H_{29}$	$CH_2=CHC_{14}H_{29}$	0

a) All reactions were performed as described in detail in the text. b) GLPC yield. c) Isolated yield.

Experimental

Bis(4-methoxyphenyl) telluride was prepared according to the method of Bergman.[5]

General Procedure for the Catalytic Debromination of Vicinal Dibromides by Potassium Disulfite Using Bis(4-methoxyphenyl) Telluride. To a solution of vicinal dibromide (1 mmol) and bis(4-methoxyphenyl) telluride (17 mg, 0.05 mmol) in 30 cm^3 of benzene was added a solution of potassium disulfite (2.22 g, 10 mmol) in 20 cm^3 of water. The resulting mixture was refluxed with vigorous stirring for a suitable time. The progress of the reaction was followed by GLPC (a Hitachi Model 163, using a 3 mm×2 m stainless steel column packed with 10% SE 30 on Celite 545 AW). After completion of the reaction , the reaction mixture was cooled to room temperature. The organic layer was separated, washed with water, dried over Na_2SO_4, and evaporated to give the crude product, which was purified by chromatography over silica gel. The products were identified by comparison with the authentic samples.

References

1) a) S. Uemura, *J. Synth. Org. Chem. Jpn.*, **41**, 804 (1983); b) S. Uemura, *Kagaku*, **36**, 381 (1981).

2) a) S. V. Ley, C. A. Meerholz, and D. H. R. Barton, *Tetrahedron Lett.*, **1980**, 1785; b) S. V. Ley, C. A. Meerholz, and D. H. R. Barton, *Tetrahedron*, **37**, Supplement No. 1, 213 (1981).

3) a) L. Engman and M. P. Cava, *J. Org. Chem.*, **47**, 3946 (1982); b) L. Engman, *Tetrahedron Lett.*, **1982**, 3601.

4) K. J. Irgolic, "The Organic Chemistry of Tellurium," Gordon and Breach, London (1974); b) M. de M. Campos, N. Petragnani, and C. Thomé, *Tetrahedron Lett.*, **1960**, No. 15, 5; c) N. Petragnani and M. de M. Campos, *Chem. Ber.*, **94**, 1759 (1961).

5) J. Bergman, *Tetrahedron*, **28**, 3323 (1972).

6) Irradiation with high-pressure Hg lamp of benzene solution of 1,2-dibromohexadecane and equimolar amounts of bis(4-methoxyphenyl) telluride gave rise to the formation of 1-hexadecene in 70% yield. However, irradiation of two-phase system described in this paper in the presence of catalytic amounts of **3** did not give the olefin.

The Solid State Photochemistry of 2(1*H*)-Pyrazinones. Structural Revision of the Photoproduct

Takehiko NISHIO,* Naoko NAKAJIMA, Masaji KONDO, and Yoshimori OMOTE
Department of Chemistry, University of Tsukuba, Sakura-mura, Niihari-gun, Ibaraki 305
(Received October 6, 1984)

Synopsis. Irradiation of 1-methyl-5,6-diphenyl-2(1*H*)-pyrazinone (**1a**) and 1-methyl-5,6,7,8-tetrahydro-2(1*H*)-quinoxalinone (**1b**) in the solid state gave the [4+4] *syn-trans* cyclodimers (**4a—b**) in almost quantitative yields, while these pyrazinones in solution phase were inert upon irradiation. On the other hand, the 2(1*H*)-pyrazinones (**1c—e**) were inert to photolysis in both the solution and solid states.

The [2+2] and [4+4] photocyclodimerization of aromatic compounds is a well-established photoreaction; examples of both inter- and intramolecular [4+4] cycloadditions of naphthalenes and anthrathenes are known.[1] However, those of heteroaromatic compounds have received little attention. The photochemical [4+4] cyclodimerizations of 2-pyridones and 2-pyrones in the solution phase have been reported by Taylor and Kan,[2] Paquette and Slomp,[3] and de Mayo and Yip.[4] A similar photochemical [4+4] cyclodimerization of 4,6-diphenyl-2-pyrone in both solution and the solid state was reported by Rieke and Copenhafer.[5] The photocyclodimer, thus obtained, was assigned to be an *anti-trans* configuration. In a series of photochemical studies on the 2(1*H*)-pyrazinones (**1**), we have reported that the 2(1*H*)-pyrazinones (**1**) reacted with singlet oxygen to give stable *endo*-peroxides (**2**),[6,7] and irradiation of **1** in alcohol under an oxygen atmosphere yielded amide derivatives (**3**).[7] The solid state photochemistry of the 2(1*H*)-pyrazinones (**1**) was also studied. In a previous paper[8] we reported the photoreaction of 2(1*H*)-pyrazinone (**1a**) in the solid state and the structure of *anti-trans* cyclodimer (**5**) was erroneously given to the photoproduct. An X-ray crystallographic analysis,[9] which was measured by Kaftory however, clarified the photoproduct was *syn-trans* cyclodimer (**4a**). In this paper we like to revise the structure of the photoproduct.

The 2(1*H*)-pyrazinones (**1a—e**) were photochemically inert in the solution phase under an argon atmosphere.[10] Meanwhile, the irradiation of 1-methyl-5,6-diphenyl-2(1*H*)-pyrazinone (**1a**) in the solid state with a high-pressure mercury lamp at room temperature for 20 min gave the [4+4] *syn-trans* cyclodimer (**4a**) in a quantitative yield. The structure of **4a** was confirmed

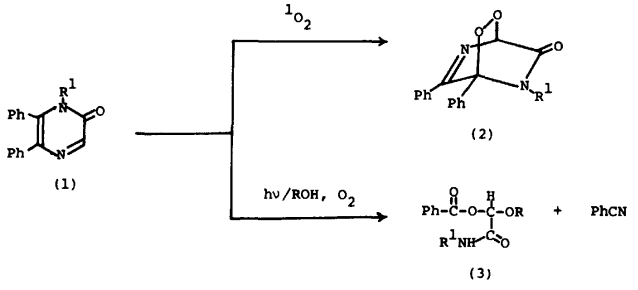

Scheme 1.

on the basis of spectroscopic properties, elemental analysis, and furthermore, X-ray crystallographic analysis.[9] The usual analytical and mass spectral data (*m/z* 524, M^+: $C_{34}H_{28}N_4O_2$, field desorption mass) of **4a** indicate the photoproduct to be dimer. The IR spectrum of **4a** showed a carbonyl stretching at 1660 cm^{-1}, versus 1640 cm^{-1} for **1a**. The ^{1}H-NMR specrum of **4a** showed two singlets at δ 2.58 and 6.35, and a multiplet at δ 6.85—7.35 in the ratio of 3:1:10 assignable to methyl, methine, and aromatic protons, respectively, while that of **1a** showed two singlets at δ 3.31 (3H) and 8.30 (1H), and the multiplet at δ 7.1—7.45 (10H) assignable to methyl, olefinic, and aromatic protons, respectively. The singlet absorption at δ 6.35, which was assigned to methine protons at the 3 and 3′ positions, was shifted further downfield than the expected value of δ (about 4.5).[11] A molecular model of **4a** showed that these hydrogens can be affected by a strong anisotropic deshielding effect from the four phenyl groups in the 5-, 5′-, 6-, and 6′-positions. Furthermore, ^{13}C-NMR spectrum of **4a** displayed peaks at 31.9 (q), 70.1 (d) 76.7 (s), 169.8 (s), and 178.5 ppm (s) due to carbons at 7-, 3-, 6-, 5-positions, and carbonyl carbon, respectively, in addition to aromatic carbon signals. One of four possible structures such as *syn-trans*, *syn-cis*, *anti-trans*, and *anti-cis* cyclodimers might be adopted for the photocyclodimer (**4a**).

The structure of **4a** was finally clarified to be *syn-trans* configuration by an X-ray crystallographic analysis.[9] Similar irradiation of the 2(1*H*)-pyrazinone (**1a**) in the solid state at 254 nm for 4 h through a quartz filter also gave the [4+4] *syn-trans* cyclodimer (**4a**) in 86% yield. The [4+4] *syn-trans* dimer (**4a**) thus obtained was stable at room temperature, however, heating of **4a** to reflux in benzene or to its melting point (148—150 °C) regenerated the starting 2(1*H*)-pyrazinone (**1a**) quantitatively. Furthermore, irradiation of a solution of [4+4] *syn-trans* dimer (**4a**) in methanol through a quartz tube at 254 nm for 30 min causes reversion to the starting 2(1*H*)-pyrazinone (**1a**) in almost quantitative yield. The [4+4] *syn-trans* dimer (**4b**) was also obtained in quantitative yield when 1-methyl-5,6,7,8-tetrahydro-2(1*H*)-quinoxalinone (**1b**) was irradiated in the solid state under the same conditions as described above. On the other hand, irradiation of 1-ethyl-5,6-diphenyl-(**1c**), 1-methyl-5,6-di-*p*-tolyl-(**1d**), and 1,3-dimethyl-5,6-diphenyl-2(1*H*)-pyrazin-one (**1e**) in the solid state did not give the corresponding cyclodimers and the starting 2(1*H*)-pyrazinones (**1c—e**) were recovered quantitatively. These results suggest that the ability of the molecules to react is highly dependent on the mutual orientation and close proximity of possible reacting centers[9] and these conditions seem to be provided by the crystal lattice and are not achieved in the solution phase.

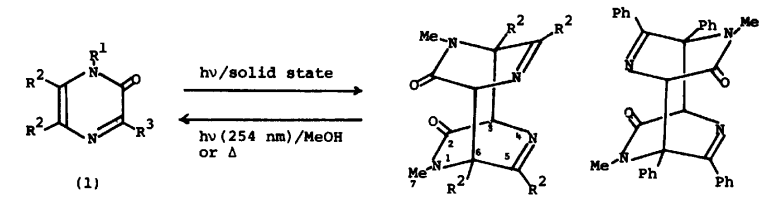

(1)

	R^1	R^2	R^3
a:	Me	Ph	H
b:	Me	$-(CH_2)_4-$	H
c:	Et	Ph	H
d:	Me	p-Tol	H
e:	Me	Ph	Me

(4)

a: R^2=Ph

b: R^2=$-(CH_2)_4-$

(5)

Scheme 2.

Experimental

Melting points are uncorrected and were measured with a Yanaco micro-melting apparatus (MP-J3). UV spectra were determined with a JASCO UVIDEC-505 spectrometer and IR spectra were recorded on a Hitachi 260-30 spectrometer. NMR spectra were run on a JEOL FX 100 spectrometer (100 MHz).

Starting Materials. The 2(1*H*)-pyrazinones (**1a** and **1c—d**) were prepared according to the method previously described.[7] The 2(1*H*)-pyrazinones (**1b** and **1e**) were prepared by modification of this method.

1-Methyl-5,6,7,8-tetrahydro-2(1H)-quinoxalinone (1b); mp 126.5—128°C; UV (EtOH) (ε) 231 (8300) and 340 nm (6900); IR (KBr) 1645 cm^{-1} (C=O); ^{1}H-NMR ($CDCl_3$) δ=1.7—1.9 (4H, m, methylene), 2.5—2.8 (4H, m, methylene), 3.48 (3H, s, NCH_3), and 8.01 (1H, s, 3-H); ^{13}C-NMR ($CDCl_3$) δ=21.7 (t), 21.8 (t), 26.1 (t), 29.6 (t), 29.5 (q, NCH_3), 131.4 (s, C-5 or C-6), 135.0 (s, C-6 or C-5), 144.2 (d, C-3), and 156.3 (s, C=O). Found: C, 65.58; H, 7.34; N, 16.96%. Calcd for $C_{19}H_{12}N_2O$: C, 65.83; H, 7.36; N, 17.06%.

1,3-Dimethyl-5,6-diphenyl-2(1H)-pyrazinone (1e); mp 169—170°C; UV (EtOH) (ε) 268 (11300) and 338 nm (8700); IR (KBr) 1645 cm^{-1} (C=O); ^{1}H-NMR ($CDCl_3$) δ=2.58 (3H, s, CH_3), 3.29 (3H, s, NCH_3), and 7.1—7.4 (10H, m, ArH); ^{13}C-NMR ($CDCl_3$) δ=21.1 (q, CH_3), 33.9 (q, NCH_3), 126.8 (d), 127.7 (d), 128.2 (d), 128.9 (d), 129.3 (d), 130.1 (d), 132.3 (s), 132.6 (s), 136.5 (s, C-5 or C-6), 137.9 (s, C-6 or C-5), 155.2 (s, C-3), and 155.9 (s, C=O). Found: C, 78.24; H, 5.78; N, 10.12%. Calcd for $C_{18}H_{16}N_2O$: C, 78.23; H, 5.83; N, 10.13%.

Photochemical Reactions of the 2(1H)-Pyrazinones (1a—e) in the Solid State. The recrystallized 2(1*H*)-pyrazinone (**1**) (100 mg) was sandwiched between a pair of Pyrex plates or quartz plates (thickness 2 mm) and this solid sample was irradiated with a high-pressure (300 W) or low-pressure mercury lamp (20 W) for 20 min—4 h at a distance *ca.* 5 cm at room temperature. After irradiation, the reaction product was purified by recrystallization from chloroform-hexane to afford the [4+4] *syn-trans* cyclodimer (**4**).

The [4+4] syn-trans *cyclodimer (4a)*; mp 148—150°C; UV (EtOH) (ε) 261 (3600) and 351 nm (450); IR (KBr) 1660 cm^{-1} (C=O); ^{1}H-NMR ($CDCl_3$) δ=2.58 (6H, s, NCH_3), 6.35 (2H, s, 3-H), and 6.85—7.35 (20H, m, ArH); ^{13}C-NMR ($CDCl_3$) δ= 31.9 (q, NCH_3), 70.1 (d, C-3), 76.7 (s, C-6), 127.1 (d), 127.4 (d), 128.4 (d), 128.6 (d), 136.5 (s), 138.4 (s), 169.8 (s, C-5), and 178.5 (s, C=O); *m/z* (Field desorption mass) 524 (M^+). Found: C, 77.84; H, 5.37; N, 10.67%. Calcd for $C_{34}H_{28}N_4O_2$: C, 77.86; H, 5.25; N, 10.62%.

The [4+4] syn-trans *cyclodimer (4b)*; mp 138.5—140°C; IR (KBr) 1660 cm^{-1} (C=O); ^{1}H-NMR ($CDCl_3$) δ=1.53—2.18 (10H, m, methylene), 2.2—2.36 (2H, m, methylene), 2.38—2.8 (4H, m, methylene), 2.75 (6H, s, NCH_3), and 4.48 (2H, s, 3-H); ^{13}C-NMR ($CDCl_3$) δ=18.6 (t), 22.1 (t), 32.4 (t), 36.2 (t), 30.5 (NCH_3), 67.3 (s, C-6), 72.2 (d, C-3), 172.0 (s, C-5), and 177.9 (s, C=O); *m/z* (Chemical ionization mass) 329 (QM^+). Found: C, 65.59; H, 7.32; N, 16.79%. Calcd for $C_{18}H_{24}N_4O_2$: C, 65.83; H, 7.36; N, 17.06%.

Tha authors thank Dr. M. Kaftory for providing the photograph of stereoscopic view of the photodimer (**4a**).

References

1) N. J. Turro, "Modern Molecular Photochemistry," Benjamin/ cummings, Melano Park, California (1978) p. 415.
2) E. C. Taylor and R. O. Kan, *J. Am. Chem. Soc.*, **85**, 776 (1963).
3) L. A. Paquette and G. Slomp, *J. Am. Chem. Soc.*, **85**, 765 (1963).
4) P. de Mayo and R. W. Yip, *Proc. Chem. Soc. London*, **1964**, 84.
5) R. D. Rieke and R. A. Copenhafer, *Tetrahedron Lett.*, **1971**, 879.
6) T. Nishio, N. Nakajima, and Y. Omote, *Tetrahedron Lett.*, **22**, 753 (1981).
7) T. Nishio, N. Nakajima, M. Kondo, Y. Omote, and M. Kaftory, *J. Chem. Soc., Perkin Trans. 1*, **1984**, 391.
8) Preliminary report: T. Nishio, N. Nakajima, and Y. Omote, *Tetrahedron Lett.*, **21**, 2529 (1980).
9) M. Kaftory, *J. Chem. Soc., Perkin Trans. 2*, **1984**, 757.
10) In the solution photochemistry, Furrer reported that 1,3,5,6-tetramethyl-2(1*H*)-pyrazinone gave the unstable photoisomer, 1,2,4,6-tetramethyl-2,5-diazabicyclo[2.2.0]hex-5-en-3-one, which could not be isolated and was identified as the reduced derivative by hydrogenation of the photoisomer: H. Furrer, *Chem. Ber.*, **105**, 2780 (1972).
11) T. J. Batterhan, "NMR Spectra of Simple Heterocycles," John Wiley & Sons, New York (1973) p. 67.

Furan Derivatives. VII. Synthesis of Cyclohepta[*cd*]benzofurans

Takaaki HORAGUCHI,* Naohiro HIRATSUKA, Shigeru TAMURA, and Tsuneo SUZUKI†
Department of Chemistry, Faculty of Science, Niigata University, Ikarashi, Niigata 950-21
†*Nippon Dental University, Niigata, Hamaura-cho, Niigata 951*
(Received October 15, 1984)

Synopsis. 7-Methoxy-3,4-dihydrocyclohepta[*cd*]benzofuran and 7-methoxycyclohepta[*cd*]benzofuran were synthesized.

Benzofurans are readily synthesized by heating (2-acylphenoxy) acetic acids with sodium acetate in acetic anhydride.[1] In the previous paper,[2] we applied the reaction to acids **1a**, **1b**, and **1c** which had a cyclic ketone (n=2, 3, and 4). The five-membered cyclic ketone **1a** gave no furan **5a**, and the six-membered cyclic ketone **1b** afforded a furan **5b** and a lactone in 1:1 ratio. However, the seven-membered cyclic ketone **1c** produced almost a furan **5c**. Royer *et al.*[3] early reported that a seven-membered cyclic ketone was more effective for furan-ring formation than a six-membered cyclic ketone. The facile furan-ring formation of **1c** is attributed to flexibility of the seven-membered cyclic ketone.[2,4] For the furan-ring formation, an anion such as **8** attacks the carbonyl carbon atom from the upper side of the carbonyl plane.[5] If the carbonyl plane is fixed in the same plane with the benzene ring, the furan-ring formation would be difficult. We introduced double bonds in the seven-membered cyclic ketone to reduce flexibility of the ring and to examine whether the furan-ring formation is possible or not. In this paper, the reaction of acids **3a** and **4a** with sodium acetate in acetic anhydride is reported. However, we abandoned synthesis of **2a** because a ketone **2b** was thermally unstable and polymerized easily. The results are summarized along with the reaction of the related acid **1c** in Table 1.

The acid **3a** produced a furan **6** in 93% yield and the corresponding lactone was not detected. The facile furan-ring formation suggests that seven-membered cyclic ketone in **3a** is still flexible and the carbonyl group can take a favorable conformation for the attack of an anion. We are particularly interested in the furan-ring formation from the acid **4a** as the seven-membered cyclic ketone is fully unsaturated and considered to be rigid. Indeed, the acid **4a** gave easily a furan **7** in 81% yield. It shows that the carbonyl group is yet flexible. The furan **7** is an interesting new class of compound because it has both structures and properties of benzofuran and benzoheptafluvene. The furan **7** is not so stable and polymerizes during storage. Thus, the furan-ring formation was very easy in spite of the additional double bonds in the seven-membered cyclic ketone.

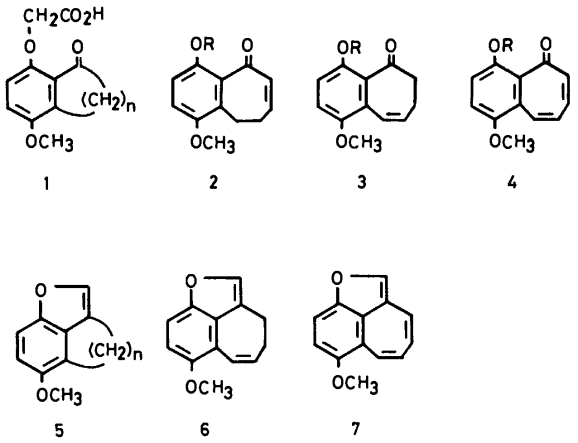

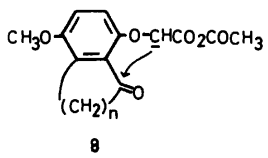

TABLE 1. REACTION OF ACIDS **1c**, **3a**, AND **4a** WITH SODIUM ACETATE IN ACETIC ANHYDRIDE[a]

Compound	Product	Yield/%
1c	**5c**	89[b]
	lactone	3[c]
3a	**6**	93[b]
	lactone	0[d]
4a	**7**	81[b]

a) Reactions were carried out at 150°C for 1 h. b) Isolated yield. c) Lactone was initially produced but it was hydrolyzed to the starting material during isolation procedure. d) Lactone was not produced.

Experimental

The column chromatography was performed on silica gel. ^{1}H and ^{13}C NMR spectra were determined at 90 MHz on a JEOL JNM-FX 90Q FT NMR spectrometer.

(1-Methoxy-5-oxo-6,7-dihydro-5H-benzocyclohepten-4-yloxy)-acetic Acid (3a). A mixture of **3b** (4.11 g; prepared from 8[2] through four steps[6]), ethyl bromoacetate (8.22 g), potassium phosphate (12.0 g), and acetone (50 ml) was refluxed for 10 h. The mixture was poured into ice-water, acidified with 6 M hydrochloric acid (1 M = 1 mol dm^{-3}), and extracted with ether. The ethereal layer was washed, dried, and evaporated. The residue was dissolved in ethanol and saponified with a 2 M potassium hydroxide solution. The alkaline solution was acidified with 6 M hydrochloric acid and the resulting acid was extracted with ether. The ethereal layer was washed, dried, and evaporated. The residue was chromatographed and eluted with benzene(9)-ether(1) to give **3a** (2.20 g, 42%), colorless needles from acetone, mp 129—130 °C. IR (KBr) ν_{max} 1770, 1750 (COOH), 1685, and 1670 cm^{-1} (CO). ^{1}H NMR (CD_3COCD_3) δ=2.34—2.56 (2H, m), 2.89—3.05 (2H, m), 3.82 (3H, s), 4.69 (2H, s), 6.17 (1H, dt, J=6 and 12 Hz), 6.73 (1H, d, J=12 Hz), and 7.05 (2H, s). ^{13}C NMR (CD_3COCD_3) δ=25.5 (t), 47.6 (t), 56.8 (q), 68.7 (t), 114.6 (d), 116.4 (d), 125.1 (s), 125.3 (d),

132.5 (s), 132.7 (d), 149.4 (s), 152.7 (s), 170.2 (s), and 204.4 (s). Found: C, 63.98; H, 5.48%. Calcd for $C_{14}H_{14}O_5$: C, 64.12; H, 5.38%.

(1-Methoxy-5-oxo-5H-benzocyclohepten-4-yloxy)acetic Acid (4a). The compound **4a** (40%) was prepared from **4b** (synthesized from **8**[2] through three steps[7]) in a manner similar to synthesis of **3a**, colorless prisms from acetone, mp 150—151 °C. IR (KBr) ν_{max} 1770 (COOH) and 1640 cm^{-1} (CO). ^1H NMR ($CDCl_3$) δ=3.95 (3H, s), 4.85 (2H, s), and 6.64—8.06 (6H, m). ^{13}C NMR ($CDCl_3$) δ=56.7 (q), 68.7 (t), 113.2 (d), 116.7 (d), 126.7 (s), 127.1 (d), 129.8 (s), 129.9 (d), 134.1 (d), 134.9 (d), 149.3 (s), 152.7 (s), 170.2 (s), and 191.5 (s). Found: C, 64.39; H, 4.68%. Calcd for $C_{14}H_{12}O_5$: C, 64.61; H, 4.65%.

7-Methoxy-3,4-dihydrocyclohepta[cd]benzofuran (6). A mixture of **3a** (1.0 g), acetic anhydride (15 ml), and sodium acetate (4.6 g) was heated at 150 °C for 1 h. The mixture was poured into ice-water (200 ml), stirred for 5 min to decompose excess acetic anhydride, and extracted with ether. The ethereal layer was washed three times with a 0.5 M potassium carbonate solution (30 ml) and then with water, dried, and evaporated. The residue was chromatographed and eluted with benzene to give **6** (0.71 g, 93%), colorless oil, bp 112—115 °C (0.7 Torr). ^1H NMR ($CDCl_3$) δ=2.40—2.60 (2H, m), 2.70—2.90 (2H, m), 3.83 (3H, s), 6.10 (1H, dt, J=7 and 12 Hz), 6.83 (1H, d, J=9 Hz), 6.95 (1H, d, J=12 Hz), 7.23 (1H, d, J=9 Hz), and 7.29 (1H, s). ^{13}C NMR ($CDCl_3$) δ=24.3 (t), 28.2 (t), 57.1 (q), 109.4 (d), 109.8 (d), 119.9 (s), 122.2 (s), 123.8 (d), 127.8 (s), 131.2 (d), 140.4 (d), 150.5 (s), and 152.2 (s). Found: C, 77.80; H, 6.10%. Calcd for $C_{13}H_{12}O_2$: C, 77.98; H, 6.04%.

7-Methoxycyclohepta[cd]benzofuran (7). The compound **7** (81%) was prepared from **4a** in a manner similar to synthesis of **6**, yellow oil, bp 128—130 °C (1 Torr (1 Torr=133.322 Pa)). ^1H NMR ($CDCl_3$) δ=3.72 (3H, s), 5.19—6.35 (4H, m), 6.56 (1H, d, J=9 Hz), 6.86 (1H, d, J=9 Hz), and 6.91 (1H, s). ^{13}C NMR ($CDCl_3$) δ=56.9 (q), 111.7 (d), 111.8 (d), 123.1 (s), 125.0 (s), 125.6 (d), 125.6 (d), 126.7 (d), 127.0 (d), 131.6 (s), 138.5 (d), 150.5 (s), and 151.6 (s). Found: C,78.78; H, 5.20%. Calcd for $C_{13}H_{10}O_2$: C, 78.77; H, 5.08%.

The authors wish to thank Mr. Yoshiaki Matsuda for the elemental analyses.

References

1) A. W. Burgstahler and L. D. Worden, *Org. Synth.*, **46**, 28 (1966); F. M. Dean, P. Halewood, S. Mongholsuk, A. Robertson, and W. B. Whalley, *J. Chem. Soc.*, **1953**, 1250; W. B. Whalley, *ibid.*, **1951**, 3229; P. C. Johnson and A. Robertson, *ibid.*, **1950**, 2381.

2) T. Horaguchi, S. Tamura, N. Hiratsuka, and T. Suzuki, *J. Chem. Soc., Perkin Trans. 1* (in press).

3) R. Royer, E. Bisagni, and G. Menichi, *Bull. Soc. Chim. France*, **1964**, 2112.

4) V. C. Farmer, F. N. Hayes, and R. H. Thomson, *J. Chem. Soc.*, 3600 (1956); E. A. Braude and F. Sondheimer, *ibid.*, 3754 (1955).

5) M. C. Roux-Shmitt and J. Seden-Penne, *Tetrahedron*, **28**, 4965 (1972); P. Cagniant and D. Cagniant, "Advances in Heterocyclic Chemistry," ed by A. R. Katritzy and A. J. Boulton, Academic Press, London (1975), Vol 18, p. 418.

6) G. R. Proctor and A. H. Renfrew, *J. Chem. Soc. C*, **1968**, 1187; M. Curphey, M. Lennin, E. Murphy, and G. R. Proctor, *J. Chem. Soc., Perkin Trans. 1*, **1979**, 2013.

7) E. W. Collington and G. Jones, *J. Chem. Soc. C*, **1969**, 2656; J. Mc Lean, V. Poesapati, and G. R. Proctor, *J. Chem. Soc., Perkin Trans. 1*, **1979**, 98.

Pressure-induced Proton NMR Chemical Shift of Some Simple Hydrocarbon Molecules in Hexane Solution. Marked Low Field Shift of Ethynyl Proton Resonance

Hiroaki YAMADA,* Shuji ONISHI, Masako YOKOYAMA, and Akira SERA
Department of Chemistry, Faculty of Science, Kobe University, Nada-ku, Kobe 657
(Received October 24, 1984)

Synopsis. Pressure dependence of the ethynyl proton chemical shift of phenylacetylene was studied in comparison with some simple hydrocarbons. The pronounced low field displacement is interpreted taking account of a geometric feature of the ethynyl group, where the terminal hydrogen atom is exposed to a closer contact with solvent molecules.

High-pressure high-resolution NMR spectroscopy represents one of the promising new area of research at high pressure.[1] Considerable efforts with use of this technique have been devoted to the investigation of high pressure effect on the rate process and chemical equilibrium. However, little is known about the pressure sensitivities of the NMR chemical shifts.

In preceding paper, we reported a notable pressure dependence of the ethynyl proton chemical shift of neat phenylacetylene.[2] The result was interpreted in terms of the increased effect in the solvent magnetic anisotropy, σ_a, which is caused by the intensified intermolecular hydrogen bonding (I) at high pressure.

$$\begin{array}{l} C_6H_5-C\equiv C-H \\ \quad\quad\quad | \\ \quad\quad H-C\equiv C-C_6H_5 \end{array} \quad (I)$$

We have now made a re-examination of phenylacetylene in a hexane solution in comparison with some simple hydrocarbons and have found a recurrence of the low field pressure shift of the ethynyl proton resonance. Since hexane behaves as a magnetically isotropic solvent, an interpretation of the low field shift can no longer be sought in the solvent magnetic anisotropy effect. The present paper attempted to offer a preliminary account of this anomalous pressure shift.

Experimental

High-pressure NMR experiment was conducted on a Jeol PS-100 spectrometer (ν_0=100 MHz) using a thermal expansion type high-pressure cell with sample spinning conditions.[3] Most measurements were carried out with 5 mol% solutions in hexane. The temperature of the sample under the NMR conditions was maintained at 35.0±0.2°C. At least ten measurements were made at a fixed pressure. The standard deviation of the chemical shift was ±0.1—0.2 Hz.

Results and Discussion

Observed relative pressure shifts $\delta\Delta(150)$[4] are presented in Table 1. The ethynyl proton resonance, as compared with the other hydrocarbon resonances, evidently exhibits a marked low field displacement by the application of hydrostatic pressure.

It might be possible that the self association of the type (I)[5] still exists in the 5 mol% solution. In this association mode, both the hydrogen-bonding shift σ_H and the magnetic anisotropy shift σ_a, caused by $\Delta\chi_{C\equiv C}$ of another molecule, contribute to down field displacement of the ethynyl proton signal. Therefore, if the association mode (I) is favored at high pressure, a negative pressure shift, $\delta\Delta(150)<0$ would be induced. In order to examine this possibility, concentration dependence of the relative pressure shift was carefully measured for phenylacetylene. As shown in Fig. 1, no significant change was observed in the pressure shift upon dilution of the solution. On this basis, we consider that the contribution of the self association effect to the pressure shift is negligibly small at 5 mol% concentration. It is also approximated that the data for the other hydrocarbons, being based on the 5 mol% solution, represent the pressure shifts which are free from self association effects.

Table 1. Relative pressure shifts,[a] 5 mol% in hexane, ν_0=100 MHz, 35.0°C

Compounds	$\delta\Delta(150)$/Hz	Compounds	$\delta\Delta(150)$/Hz
Ph_3CH[b]	+1.9	H_2CCl_2	+0.1
$(CH_2)_6$	+1.5	$CH_3(CH_2)_4CH_3$	0.0
$HCCl_3$	+1.2	$PhCH_3$	−0.7
$CH_3(CH_2)_4CH_3$	+1.0	$Ph_2C=CH_2$	−1.9
Ph_2CH_2	+0.5	$PhC\equiv CH$	−5.3

a) Relative to the hexane CH_3 pressure shift. b) Because of the poor solubility, a 1 mol% solution was used.

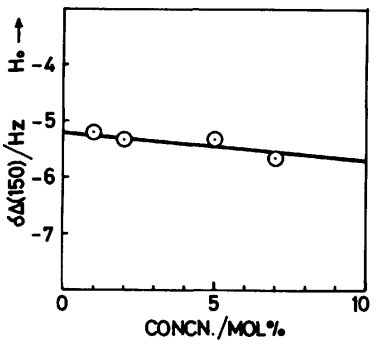

Fig. 1. Concentration dependence of the ethynyl proton relative pressure shift. For a 95 mol% solution, $\delta\Delta(150)=-7.7$ Hz.

Under the present experimental conditions, the solvent effect on the proton chemical shift can be divided into two kinds of main contribution:[6] (i) The σ_E effect which is related to the C-H bond polarization induced by so-called reaction field;[7] This should be mainly governed by the polarity of the solute molecule and the dielectric constant of the medium. (ii) The σ_w contribution arising from the weak van der Waals interaction between the resonating proton and solvent molecules;[6,8] When the resonating proton is more

strongly subject to the van der Waals contact with medium molecules, a greater σ_w contribution (*i.e.*, a pronounced low field shift) should be expected.[9] Since the pressurization produces an increase in the dielectric constant of the medium and also intensifies the intermolecular van der Waals contacts, both the effects, (i) and (ii), would be amplified at high pressure, giving rise to a possible low field contribution to the pressure shift.

In an attempt to evaluate the contribution of the effect (i), the data were examined in connection with polar properties of the solute molecule. Although the examinations are only qualitative, several interesting points arise. For example, the pressure shifts for chloroform (μ=1.2 D) and phenylacetylene (μ=0.5 D, with a negative end directing toward the ethynyl group) exhibit a trend evidently opposite to that expected from the reaction field consideration. Furthermore, toluene shows a larger negative pressure shift relative to triphenylmethane, whereas, considering acidities of these hydrocarbons (pK_a=41, 32, respectively), one would predict the opposite. On these grounds, we conclude that the effect (i) cannot be a main contributor to the pressure shift.

We may now turn to the effect (ii). In Table 1, it will be noticed that the steric environment near the resonating proton is playing a dominant role in determining the pressure shift. For instance, a regular trend toward larger negative pressure shift can be seen as the steric overcrowding is liberated in the order of triphenylmethane, diphenylmethane, and toluene. In this view, the pronounced negative pressure shift of the ethynyl proton seems to be best rationalized on the basis of the geometric feature of the ethynyl group where the proton is located at the end of a rod shaped C≡C bond and, in the absence of a geminal hydrogen, it is well exposed to the van der Waals contact with solvent molecules. Axially symmetric electronic environment around the ethynyl proton should also lead to pronounced susceptibility to the σ_w effect.[6] Present result indicates that the previously observed pressure shift, −9 Hz, for neat phenylacetylene[2] could largely be interpreted as being due to this van der Waals contact effect rather than the σ_a effect.

This study has shown that a protrusion of a C≡C bond out of the molecule plays an important role in causing the marked low field pressure shift of the ethynyl proton. It should be pointed out that this stand out in sharp contrast to the ring proton of 1,4-di-*t*-butylbenzene,[10] which, being located in a cavity in the molecule, has proved to give a considerable high field pressure shift.

The present work was supported by Grant-in-Aid for Scientific Research No. 56550572 from the Ministry of Education, Science and Culture.

References

1) J. Jonas, *Ann. Rev. Phys. Chem.*, **26**, 167 (1975); J. Jonas, *Rev. Phys. Chem. Jpn.*, **50**, 19 (1980).

2) H. Yamada, S. Nishitani, and A. Sera, *Chem. Lett.*, **1981**, 791. A low field displacement of 9.0 Hz, relative to internal cyclohexane, was observed upon pressurization up to 150 MPa.

3) H. Yamada, K. Fujino, M. Nakatsuka, and A. Sera, *Chem. Lett.*, **1979**, 217.

4) $\delta\Delta(150)=\delta(150)-\delta(0.1)$, displacement of the chemical shift relative to that of the chemical shift of internal hexane CH_3, caused by pressurization of the sample up to 150 MPa (1500 bar).

5) N. Nakagawa and S. Fujiwara, *Bull. Chem. Soc. Jpn.*, **33**, 1634 (1960).

6) A. D. Buckingham, T. Shaefer, and W. G. Schneider, *J. Chem. Phys.*, **32**, 1227 (1960).

7) A. D. Buckingham, *Can. J. Chem.*, **38**, 300 (1960).

8) F. H. A. Rummens, W. T. Raynes, and H. J. Bernstein, *J. Phys. Chem.*, **72**, 2111 (1968).

9) For the contribution of σ_w, at the ordinary pressure, about −0.2 ppm has been estimated.[8]

10) H. Yamada, C. Itani, and K. Otsuka, *J. Am. Chem. Soc.*, **99**, 3572 (1977).

Crowned Tetrathiafulvalene Derivatives

Tetsuo OTSUBO* and Fumio OGURA
Department of Applied Chemistry, Faculty of Engineering, Hiroshima University, Saijo, Higashi-Hiroshima 724
(Received October 30, 1984)

Synopsis. A new type of tetrathiafulvalene derivatives, fused with crown ethers, was prepared, which did not form a complex with sodium cation or TCNQ acceptor but readily with silver cation.

With an attempt to develop the new character of tetrathiafulvalene (TTF) by use of a functional heterocyclic ring, we have studied novel TTF derivatives **1** and **2** which are fused with crown ethers. Complexation with metal cation at the crown ligand might make some influence on the donor character of the TTF.

The metallic[1] or electrochemical[2] reduction of carbon disulfide in aprotic media provides a synthetic entry for the preparation of thio-substituted derivatives of TTF.[3] Thus, sodium 2-thioxo-1,3-dithiole-4,5-dithiolate **4**, generated in situ by reduction of carbon disulfide with sodium in dry *N,N*-dimethylformamide, was allowed to react with methyl iodide to give 4,5-bis(methylthio)-1,3-dithiole-2-thione **5** in 70% yield.[1] On the other hand, a similar treatment of the dianion **4** with tetraethylene glycol ditosylate gave crown-fused 1,3-dithiole-2-thione **6** in only 0.8% yield as well as its dimer **7** in rather higher yield (6.5%). The yield of the key compound **6** was fairly increased up to 14% by effecting the reaction under a high dilution technique. Subsequently, heating of **6** at 110°C in triethyl phosphite resulted in self-coupling to bis-crowned tetrathiafulvalene **1** in 44% yield. A cross reaction of two 1,3-dithiole-2-thiones **5** and **6** led to a mixture of **1** (31%), **2** (21%), and **3**[4] (13%), which were readily separated from one another by column chromatography. Another type of crowned tetrathiafulvalene **8** was, in addition, prepared in a very low yield (2.9%) by a similar cross reaction of **5** and **7**.

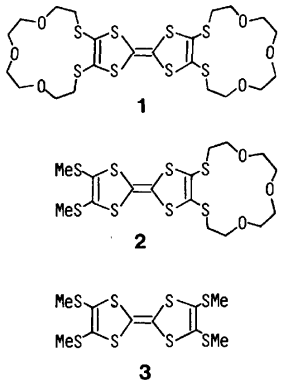

Fig. 1.

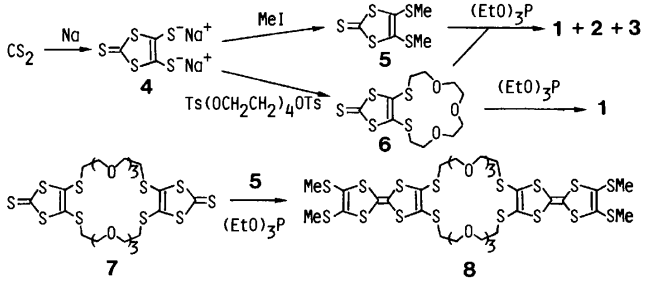

Fig. 2.

The cyclic voltammograms of TTF derivatives **1**, **2**, and **3** exhibit two reversible oxidation waves due to TTF, whose half-wave potentials are situated at 0.521 and 0.748 V for **1**, at 0.509 and 0.757 V for **2**, and at 0.498 and 0.805 V for **3** *vs.* a silver reference electrode in dichloromethane. The almost identical voltammetric behaviors indicate that their π-donor abilities are nearly equal. However, crowned TTF **1** and **2**, in contrast to **3**,[3] did not form crystalline charge-transfer complexes with tetracyanoquinodimethane (TCNQ). The steric requirement of the crown ligand seems to prevent the complexation of the TTF. In addition, the crown ligand failed to complex sodium salts such as Na^+TCNQ^- and NaSCN. However, crowned TTF **1** and **2** strongly interacted with silver nitrate, forming crystalline 1:2 and 1:1 complexes, respectively. The electrical conductivities of these complexes are relatively low; σ_{RT} (compressed pellet) 6×10^{-9} $\Omega^{-1}cm^{-1}$ for $2AgNO_3$ complex of **1** and 4×10^{-7} $\Omega^{-1}cm^{-1}$ for $AgNO_3$ complex of **2**.

This work was supported by the grant in aids of special research project on properties of molecular assemblies (No. 59112003) from the Ministry of Education, Science and Culture, Japan.

Experimental

NMR spectra were determined on a JEOL PMX-60 spectrometer (60 MHz), MS spectra on a JEOL JMS-DX 300 spectrometer at 70 eV using a direct insertion technique, and IR spectra on a Hitachi 260-30 spectrophotometer. Cyclic voltammetry was made at 100 mVsec^{-1} scan rate in 2 mV dichloromethane solution with added tetrabutylammonium perchlorate by a Hokuto Denko HA-301 potentiostat and a Hokuto Denko HB-104 functional generator using a Ag/AgCl reference electrode, a glassy carbon working electrode, and a platinum counter electrode. Electrical conductivity was measured on a compressed pellet with a two probe method.

Crowned 1,3-Dithiole-2-thione (6). Sodium (1.68 g, 73 mmol) was added into a solution of carbon disulfide (12 ml) and dry *N,N*-dimethylformamide (20 ml) under nitrogen. The mixture was gently refluxed with stirring overnight, and meanwhile sodium gradually dissolved to bring about a viscous dark red solution containing dianion **4**. It was then diluted with ethanol (55 ml, previously bubbled by nitrogen gas) and introduced into a dropping funnel through a needle bridge. A solution of tetraethylene glycol ditosylate (18.32 g, 36.5 mmol) in tetrahydrofuran (100 ml) was placed in another dropping funnel. Both the solutions were dropwise and simultaneously added into a stirred ethanol solution (250 ml) at 50°C under nitrogen. The addition took half a day, and heating was continued further overnight. After the resulting insoluble salt was removed by filtration, the filtrate

was evaporated and extracted with dichloromethane. The extract was washed, dried (Na_2SO_4), and evaporated. The residual red oil was purified by flash chromatography on silica gel with 1:2 dichloromethane–ether and then gel-permeation liquid chromatography with chloroform, giving **6** (1.79 g, 14%), yellow columns from hexane–dichloromethane, mp 70—74 °C. ^{1}H NMR ($CDCl_3$): δ=3.04 (t, J=6 Hz, 4H, CH_2S), 3.66 (s, 8H, CH_2O), 3.77 (t, J=6 Hz, 4H, CH_2O). MS: m/z 356 (M^+). IR (KBr): 1055 (C=S), 1120 (C–O) cm^{-1}. Found: C, 36.78; H, 4.51%. Calcd for $C_{11}H_{16}O_3S_5$: C, 37.05; H, 4.52%.

The same reaction without the above dilution technique gave a mixture of **6** (0.8%) and **7** (6.5%). The dimer **7** was separated from **6** by liquid chromatography, yellow fine crystals from ethanol–dichloromethane, mp 84.5—85.5 °C. ^{1}H NMR ($CDCl_3$): δ=3.08 (t, J=6 Hz, 8H, CH_2S), 3.62 (s, 16H, CH_2O), 3.73 (t, J=6 Hz, 8H, CH_2O). MS: m/z 712 (M^+). IR (KBr): 1065 (C=S), 1120 (C–O) cm^{-1}. Found: C, 36.95; H, 4.50%. Calcd for $C_{22}H_{32}O_6S_{10}$: C, 37.05; H, 4.52%.

Bis-crowned TTF (1). Compound **6** (356 mg, 1.0 mmol) was heated in triethyl phosphite (2 ml) under nitrogen. The starting material completely dissolved with a rise of temperature, and orange microcrystals precipitated at 110 °C. After 30 min at 110 °C, the product **1** was collected by filtration and washed with hexane (142 mg, 44%), orange fine crystals from acetonitrile, mp 211—212 °C. ^{1}H NMR ($CDCl_3$): δ=2.99 (t, J=6 Hz, 8H, CH_2S), 3.65 (s, 16H, CH_2O), 3.74 (t, J=6 Hz, 8H, CH_2O). MS: m/z 648 (M^+). IR (KBr): 1120 (C–O) cm^{-1}. Found: C, 40.71; H, 4.85%. Calcd for $C_{22}H_{32}O_6S_8$: C, 40.72; H, 4.97%.

Mono-crowned TTF (2). A mixture of **5** (226 mg, 1.0 mmol) and **6** (356 mg, 1.0 mmol) was heated at 110 °C in triethyl phosphite (3 ml) for 30 min under nitrogen. After evaporation, the residue was chromatographed on silica gel to give a red eluate with dichloromethane and then two red eluates with 1:20 ether–dichloromethane. The first red eluate gave **3** (25 mg, 13%), orange columns from acetonitrile, mp 93—94 °C (lit,[3] 94.5—96 °C). The second red eluate gave **2** (108 mg, 21%), orange plates from ethanol–chloroform, mp 125—126 °C. ^{1}H NMR ($CDCl_3$): δ=2.43 (s, 6H, CH_3), 2.97 (t, J=6 Hz, 4H, CH_2S), 3.64 (s, 8H, CH_2O), 3.73 (t, J=6 Hz, 4H, CH_2O). MS: m/z 518 (M^+). IR (KBr): 1115 (C–O) cm^{-1}. Found: C, 36.90; H, 4.10%. Calcd for $C_{16}H_{22}O_3S_8$: C, 37.04; H, 4.27%. The third red eluate gave **1** (100 mg, 31%).

Crowned bis-TTF (8). Compound **7** (142 mg, 0.2 mmol) was heated together with **5** (180 mg, 0.8 mmol) in triethyl phosphite (2 ml) at 110 °C under nitrogen. The reaction mixture was worked up as described for **2**, giving **8** (6 mg, 2.9%), orange fine crystals from acetonitrile, mp 109—111 °C. ^{1}H NMR ($CDCl_3$) δ=2.43 (s, 12H, CH_3), 3.02 (t, J=6 Hz, 8H, CH_2S), 3.64 (s, 16H, CH_2O), 3.69 (t, J=6 Hz, 8H, CH_2O). IR (Neat): 1115 (C–O) cm^{-1}. Found: C, 37.19; H, 4.13%. Calcd for $C_{32}H_{44}O_6S_{16}$: C, 37.04; H, 4.27%.

Complexation with Silver Nitrate. A mixture of **2** (52 mg, 0.1 mmol) and silver nitrate (17 mg, 0.1 mmol) was dissolved in hot ethanol (*ca.* 20 ml). The clear solution was cooled in a refrigerator, giving reddish orange fine crystals of mono-crowned TTF·$AgNO_3$ complex (34 mg), dec. 150 °C with melt. IR (KBr): 1385 (NO_3), 1115 (C–O) cm^{-1}. Found: C, 27.87; H, 3.20; N, 1.63%. Calcd for $C_{16}H_{22}NO_6S_8Ag$: C, 27.90; H, 3.22; N, 2.03%.

Bis-crowned TTF·$2AgNO_3$ complex was prepared in a similar manner; orange fine crystals, dec. 218 °C with melt. IR (KBr): 1380 (NO_3), 1115 (C–O) cm^{-1}. Found: C, 27.02; H, 3.28; N, 2.60%. Calcd for $C_{22}H_{32}N_2O_{12}S_8Ag_2$: C, 26.72; H, 3.26; N, 2.83%.

References

1) G. Steimecke, H. J. Sieler, R. Kirmse, and E. Hoyer, *Phosphorus Sulfur*, **7**, 49 (1979).

2) S. Wawzonek and S. M. Heilmann, *J. Org. Chem.*, **39**, 511 (1974); M. F. Hurley and J. Q. Chambers, *ibid.*, **46**, 775 (1981).

3) P. R. Moses and J. Q. Chambers, *J. Am. Chem. Soc.*, **96**, 945 (1974).

4) M. Mizuno, A. F. Garito, and M. P. Cava, *J. Chem. Soc., Chem. Commun.*, **1978**, 18.

The Ullmann Coupling Reaction of Axially Chiral (*S*)-2,2′-Bis-(1-iodo-2-naphthyloxycarbonyl)-1,1′-binaphthyl

Sotaro MIYANO,* Kunitoshi SHIMIZU, Shinya SATO, and Harukichi HASHIMOTO
Department of Applied Chemistry, Faculty of Engineering, Tohoku University, Aramaki-Aoba, Sendai 980
(Received October 31, 1984)

Synopsis. The intramolecular Ullmann coupling of the title diester proceeded in low yield but with virtually complete asymmetric induction in joining the two naphthyl units leading to the 12-membered cyclic diester of (*S,S*)-configuration, which is the same diastereomer obtained from the reaction of (*S*)-2,2′-bis(1-bromo-2-naphthoyloxy)-1,1′-binaphthyl.

In our previous paper,[1] we have reported that the intramolecular Ullmann coupling of chiral diester (*S*)-**3** derived from *chiral diol* (*S*)-**1** and *1-bromo-2-naphthoic acid* **2** proceeds with complete asymmetric induction in joining the two naphthyl units leading to the formation of only (*S,S*)-cyclic diester ((*S,S*)-**5**) without (*S,R*)-diastereomer, although accompanied by the formation of reduction product ((*S*)-**4**) and others derived by intermolecular reactions (Scheme). We reasoned that the remarkable stereoselectivity of the unimolecular coupling should be ascribed to the steric requirement in the product 12-membered cyclic diester which contains two sets of bulky, and rigid 1,1′-binaphthyl moieties; as CPK molecular models of the two possibilities indicate, severe steric compression in (*S,R*)-**5** as compared to (*S,S*)-**5** would exclude the formation of the former, irrespective of the mechanism of the coupling process.

If this is the case, the other feasible route to the cycle **5** *via* aryl coupling, namely the Ullmann reaction of another chiral bifunctional diester (*S*)-**9**, which is derived from *axially chiral binaphthyldicarboxylic acid* (*S*)-*8* and *1-halo-2-naphthol* **7**, should also give rise to exclusive formation of (*S,S*)-**5** as the unimolecularly coupled product.

To test this hypothesis, optically active (*S*)-**9a** was prepared from axially chiral (*S*)-**8** (91% e.e.) and 1-iodo-2-naphthol **7a**. The Ullmann reaction was carried out by slowly adding a DMF solution of (*S*)-**9a** to a vigorously stirred suspension of an activated copper powder in DMF heated at reflux. Although the ease of copper-promoted halogen displacement from the aromatic ring is generally I>Br, (*S*)-**9a** was much less reactive than (*S*)-**3**, suggesting the importance of the activation of the halogen by the carbonyl function in the *ortho*-position in the latter.[2] Thus, deiodination of (*S*)-**9a** was incomplete under the comparable conditions where (*S*)-**3** reacted completely.[3,4] This and concurrent occurrence of intermolecular reaction resulted in somewhat complex products, while HPLC analysis of the mixture revealed only three components, (*S,S*)-**5**, (*S*)-**10**, and (*S*)-**11**, as the unimolecular products from (*S*)-**9a**.

Unfortunately, the dominant reaction of (*S*)-**9a** with copper was reductive substitution to (*S*)-**10**.[5] However, the first eluting component on HPLC, which was recovered in a 11% yield by column chromatography followed by TLC purification, showed the IR and MS spectrum similar to those of the authentic (*S,S*)-**5** obtained in the previous work *via* path **a**.[1] As there seemed little possibility of enantiomeric concentration of the monomeric cycle during the chromatographic purification (see Experimental), the recovered sample of (*S,S*)-**5** should represent the component in the reaction mixture. The ester linkage of the sample of (*S,S*)-**5** was reductively cleaved by treatment with LAH

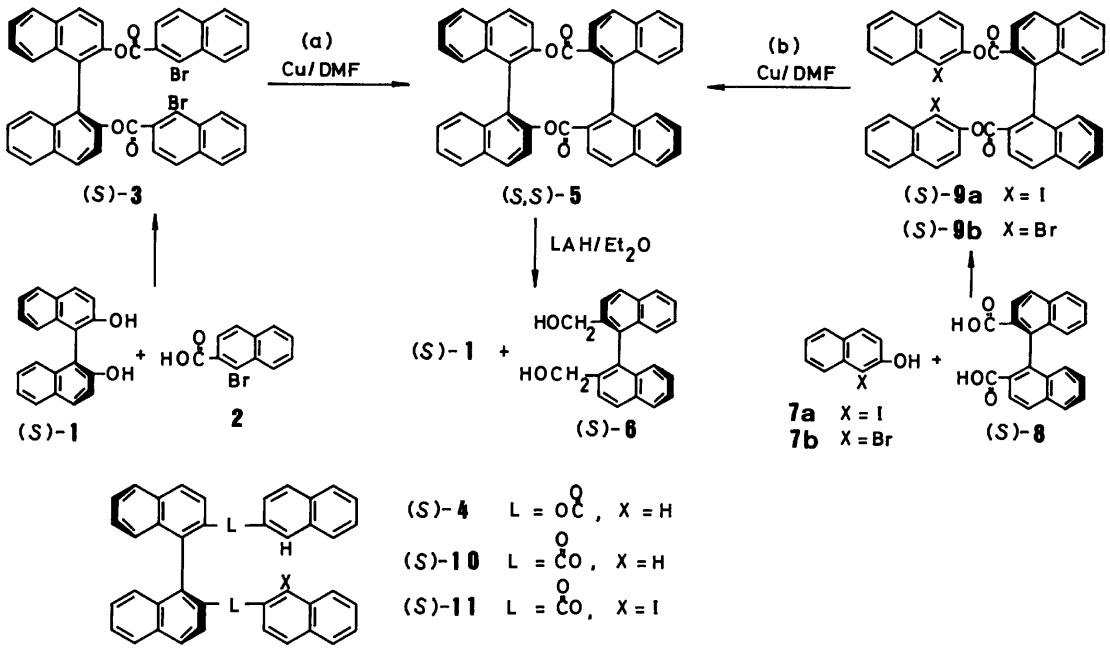

Scheme 1.

to give (*S*)-**1** and (*S*)-**6**; the optical purity of these diols was essentially identical (88—90%), as determined by comparison of the optical rotations with those of pure enantiomers.[6] This is likely to suggest that the enantiomeric purity of the recovered (*S,S*)-**5** should be close to 90%; this value is in turn in fairly good agreement with that estimated from the optical rotation of the (*S,S*)-**5** itself by comparing with that of the enantiomerically pure cycle ($[\alpha]_D^{23}$ −457.6°) obtained in the previous work.[1] Thus, as the enantiomeric purity of the recovered cycle practically coincided with that of the starting (*S*)-**8**, it follows that the unimolecular Ullmann coupling of (*S*)-**9a** (path **b**) also proceeded with virtually complete diastereoselectivity to give the (*S,S*)-cycle.

In conclusion, the stereochemistry of the intramolecular coupling of the two aryl units attached, with appropriate spacing groups, at the 2,2′-positions of 1,1′-binaphthyl skeleton is likely to be highly controlled by the axial chirality of the parent binaphthyl moiety as well as the steric requirement of the product cycle.

Experimental

Measurement and materials were similar to those described in the previous paper unless otherwise noted.[1] Melting points are uncorrected. **7a** was prepared by a literature procedure, mp 92—93 °C (lit,[7] 92 °C).

(S)-8. According to the procedure by Hall and Turner,[8] the less soluble quinine salt was recrystallized three times from EtOH to give hexagonal plates, mp 173—175 °C; $[\alpha]_D^{23}$ −85.8° (*c* 1.00, acetone). Decomposition of the salt gave the free acid, which was dried *in vacuo* at 120 °C, mp 152—154 °C; $[\alpha]_D^{24}$ −99.7° (*c* 1.08, 0.1 M NaOH (1 M = 1 mol dm^{-3})).[9] Found: C, 77.27; H, 4.06%. Calcd for $C_{22}H_{14}O_4$: C, 77.18; H, 4.12%. A sample of the (*S*)-**8** was boiled with LAH in ether to give (*S*)-**6**, $[\alpha]_{546}^{24}$ −78.8° (*c* 1.80, acetone).

(S)-9a. After (*S*)-**8** (2.80 g, 8.19 mmol) had been refluxed in $SOCl_2$ (*ca.* 30 ml) for 3 h, volatiles were removed *in vacuo*. The organic residue was dissolved in benzene (60 ml) and pyridine (10 ml), to which was added **7a** (5.30 g, 19.6 mmol). The mixture was stirred overnight at room temperature and then heated at reflux for 3 h. The reaction was worked up as usual, and the crude diester was purified by an alumina column chromatography with benzene as eluant, 5.95 g (86%); mp 144—147 °C; $[\alpha]_D^{22}$ +72.3° (*c* 1.03, PhH); IR (KBr) 1750, 1200, and 1090 cm^{-1}. Found: C, 60.08; H, 2.93; I, 29.56%. Calcd for $C_{42}H_{24}I_2O_4$: C, 59.60; H, 2.86; I, 29.98%.

Ullmann Reaction of (S)-9a. According to the procedure described before,[3] (*S*)-**9a** (2.67 g, 3.16 mmol) in 30 ml of DMF was added over a 5 h period to a vigorously stirred copper powder (5.0 g, 79 mmol) in DMF (100 ml) heated at reflux. The mixture was refluxed for another 2 h, and it was worked up as before to give 1.77 g of a pale brown residue, which contained 1.54% of iodine by combustion analysis; $[\alpha]_D^{22}$ −82.0° (*c* 1.1, PhH). HPLC analysis (JASCO SC-01 column, MeCN/H_2O (10/1)) showed the presence of, in the order of elution, (*S,S*)-**5** (1.00), (*S*)-**10** (1.63), and (*S*)-**11** (2.26), and other higher oligomeric products (in parentheses are shown retention volumes relative to (*S,S*)-**5**). The mixture (1.70 g) was subjected to a silica-gel column chromatography (Wako Gel C-200) using $CHCl_3$ (1% EtOH) as eluant to give a 245 mg of the first fraction comprised mostly of (*S,S*)-**5** and small amount of (*S*)-**10**; $[\alpha]_D^{23}$ −385° (*c* 1.03, PhH). A part of the sample (*ca.* 85 mg) was treated with LAH, and the products were purified by TLC (silica gel, $CHCl_3$/AcOEt (4/1)) to give 2-naphthol (trace), (*S*)-**1**, 25 mg, $[\alpha]_D^{23}$ −30.9° (*c* 1.15, THF) and (*S*)-**6**, 32 mg, $[\alpha]_{546}^{24}$ −77.8° (*c* 1.28, acetone). The remainder of the fraction was further purified by TLC (silica gel, PhH) to give (*S,S*)-**5** which appeared to be homogeneous by HPLC, 130 mg; $[\alpha]_D^{24}$ −409° (*c* 0.352, PhH); IR (KBr) 1750, 1250, 1220, and *ca.* 1110 cm^{-1}; MS (70 eV) *m/z* (rel intensity) 592 (M^+, 19.0), 280 (9.9), 268 (21.8), and 252 (6.9). LAH treatment of the (*S,S*)-**5** (107 mg, 0.181 mmol) gave (*S*)-**1**, 41 mg, $[\alpha]_D^{23}$ −31.4° (*c* 1.18, THF) and (*S*)-**6**, 47 mg, $[\alpha]_{546}^{24}$ −78.0° (*c* 1.31, acetone).

From the second fraction of the column effluent was recovered (*S*)-**10**, 590 mg; $[\alpha]_D^{23}$ +39.0° (*c* 1.03, PhH); 182—185 °C; IR (KBr) 1740, 1230, 1210, and 1120 cm^{-1}. Found: C, 84.57; H, 4.32%. Calcd for $C_{42}H_{26}O_4$: C, 84.83; H, 4.41%. LAH treatment of the sample (250 mg) gave 2-naphthol (85 mg) and (*S*)-**6**, 110 mg, $[\alpha]_{546}^{24}$ −77.3° (*c* 1.55, acetone). (*S*)-**11** was deduced from MS (M^+ 720) and from positive Beilstein test conducted on the third fraction of the column effluent.

We are grateful for support of this work by Takeda Science Foundation.

References

1) S. Miyano, M. Tobita, and H. Hashimoto, *Bull. Chem. Soc. Jpn.*, **54**, 3522 (1981).
2) J. Lindley, *Tetrahedron*, **40**, 1433 (1984).
3) S. Miyano, S. Handa, K. Shimizu, K. Tagami, and H. Hashimoto, *Bull. Chem. Soc. Jpn.*, **57**, 1943 (1984).
4) When (*S*)-**9b** was treated with copper under the similar conditions, only 50% of the total bromine was consumed giving (*S,S*)-**5** only in poor yield.
5) See for example, F. E. Ziegler and J. A. Schwartz, *J. Org. Chem.*, **43**, 985 (1978).
6) See Ref. 1): (*S*)-**1**: $[\alpha]_D^{22}$ −35.0° (*c* 1.18, THF). (*S*)-**6**: $[\alpha]_{546}^{23}$ −86.0° (*c* 1.43, acetone).
7) K. T. Potts, *J. Chem. Soc.*, **1953**, 3711.
8) D. M. Hall and E. E. Turner, *J. Chem. Soc.*, **1955**, 1242.
9) The maximum rotation reported, $[\alpha]_D$ −110°; A. K. Colter and L. M. Clemens, *J. Am. Chem. Soc.*, **87**, 847 (1965).

Electrogenerated Acid as an Efficient Catalyst for the Protection and Deprotection of Alcohols with Dihydropyran and Transesterification of Glyceride

Sigeru Torii,* Tsutomu Inokuchi, Kazumi Kondo, and Hiroshi Ito
Department of Industrial Chemistry, School of Engineering, Okayama University, Okayama 700
(Received October 31, 1984)

Synopsis. Protection of alcohols with 3,4-dihydro-2*H*-pyran and hydrolysis of the resulting tetrahydropyranyl ethers are cleanly performed by using an electrogenerated acid (EG acid) as a catalyst. Transesterification of glyceride was also achieved with EG acid.

The protection of hydroxyl groups with 3,4-dihydro-2*H*-pyran (DHP) and deprotection of the resulting tetrahydropyranyl (THP) ethers into hydroxyl groups are two essential procedures in modern synthetic chemistry and a variety of catalysts have been already proposed for this purpose.[1] In the course of our study on electrolyses with perchlorate salts, we recently found prominent aspects of acid-catalyzed reactions in an MeOH–$LiClO_4$–(Pt) electrolysis system, which comprise an acid-catalyzed hemiacetalization of α-hydroxy ketones with methanol and the subsequent oxidative fission of 1,2-diol groups, giving keto esters.[2] As the results of our continuing studies on electrogenerated acid,[3] we disclose here a simple procedure for the protection of alcohol **1** with DHP by using an electrochemically generated acid[4] *in situ* after passing a small amount of electricity in a CH_2Cl_2–$LiClO_4$–(and/or Et_4NClO_4)–platinum electrodes system.

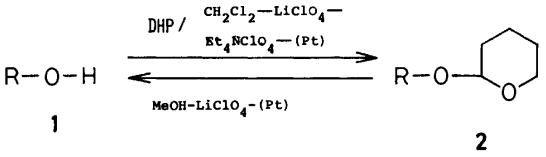

1 2

It is noted that *p*-toluenesulfonic acid is frequently used for tetrahydropyranylation of alcohols as a routine catalyst,[5] and it seems to be superior to other catalysts such as hydrochloric acid,[6] phosphoryl chloride,[7] and boron trifluoride etherate.[8] Owing to its strong acidity, however, some milder and more efficient catalysts, *i.e.*, pyridinium *p*-toluenesulfonate (PPTS),[9a] poly(2- or 4-vinylpyridinium *p*-toluenesulfonate),[9b] and bis(trimethylsilyl) sulfate [$(Me_3Si)_2SO_4$],[10] have been devised for this purpose. The present electrochemical procedure for the preparation of THP ether **2** can constitute a facile alternative to reported ones due to its high efficiency (most of the operations complete within several minutes and provide excellent yields).

The electrochemical protection of alcohol **1** (1 mmol) with DHP was carried out using platinum electrodes in a simple undivided cell. Thus, electrolysis of cinnamyl alcohol **1a** and an excess equivalent (1.2—2.0 equiv) of DHP in dichloromethane containing lithium perchlorate ($LiClO_4$, 1 mg) and/or tetraethylammonium perchlorate (Et_4NClO_4, 5 mg) gave the corresponding THP ether **2a** in more than 90% yield only by passing a catalytic quantity of electricity.

Some typical results of the electrochemical tetrahydropyranylation of alcohols are summarized in Table 1.

The acid catalyst generated in the electrolysis medium is also effective for removal of the THP group from **2**. Stirring of **2a** at 55—60 °C for 5 min in methanol containing a small amount of $LiClO_4$ after passing 0.01 F/mol of electricity in the anode compartment of a divided cell gave the parent alcohol **1a** in 95% yield. The results of deprotection experiments are also summarized in Table 1.

In addition to the above results, the electrogenerated acid can be used as a catalyst for the transesterification of glyceride **3**.[11] Heating of **3** with the pre-electrolyzed solution of $LiClO_4$ in either methanol, ethanol, or 1-propanol provided the corresponding palmitates **4a—c** in 95—98% yields.

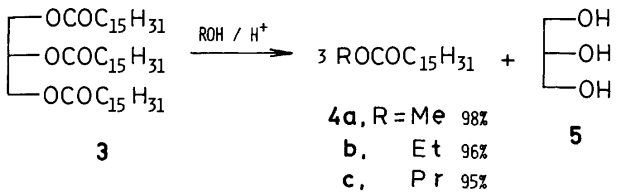

Experimental

General Procedure for Protection of Alcohol 1 with Dihydropyran. A mixture of cinnamyl alcohol (**1a**, 134 mg, 1.0 mmol), 3,4-dihydro-2*H*-pyran (101 mg, 1.2 mmol), and $LiClO_4$[12] (1 mg, 0.009 mmol) was dissolved in CH_2Cl_2[13] (5 ml) in an undivided cell. Two platinum foil electrodes were immersed in the solution and voltage of 10 V (current: 0.4 mA) was applied. TLC monitoring revealed that the reaction has terminated after passage of about 0.0002 F/mol of electricity (it took about 1 min) based on **1a**. Pyridine (45 mg, 0.57 mmol) was then added. Evaporation of volatile material and column chromatography (SiO_2, hexane–AcOEt 15:1) of the residue gave the corresponding THP ether **2a** in 92% yield (Table 1).

Spectral data along with elemental analyses of the THP ether of carbohydrates **1e**, **1g**, and **1h** are as follows. **2e**: IR (neat) 1450, 1385, 1375, 1335, 1285, 1250, 1205, 1165, 1127, 1080, 972, 915, 870, 786, 733 cm^{-1}; ^1H NMR (60 MHz) δ 1.30—1.80 (m, 6, CH_2), 1.35, 1.40 (s, 6, CH_3), 1.41 (s, 6, CH_3), 3.30—4.95 (m, 10, CH_2O, CH–O). Anal. Calcd for $C_{17}H_{28}O_7$: C, 59.29; H, 8.19. Found: C, 59.36; H, 8.20. **2g**: IR (neat) 1450, 1435, 1375, 1365, 1245, 1207, 1148, 1118, 1068, 965, 840, 760 cm^{-1}; ^1H NMR (100 MHz) δ 1.30—2.00 (m, 6, CH_2), 1.35 (s, 6, CH_3), 1.45, 1.52 (s, 6, CH_3), 3.44—4.96 (m, 9, CH_2O, CH–O), 5.96 (d, J=4 Hz, 1, CH–O). Anal. Calcd for $C_{17}H_{28}O_7$: C, 59.29; H, 8.19. Found: C, 59.27; H, 8.11. **2h**: IR (neat) 1446, 1435, 1375, 1366, 1255, 1200, 1155, 1060, 1005, 955, 845, 810 cm^{-1}; ^1H NMR δ 1.20—1.90 (m, 6, CH_2), 1.36, 1.40 (s, 6, CH_3), 1.51 (s, 6, CH_3), 3.50—5.08 (m, 9, CH_2O, CH–O), 5.80 (s, 1, CH–O). Anal. Calcd for $C_{17}H_{28}O_7$: C, 59.29; H, 8.19. Found: C, 59.25; H, 8.18.

General Procedure for Deprotection of 2. An MeOH solution (6 ml) containing $LiClO_4$ (12 mg) was placed in each compartment of the electrolysis cell. Electric current was

Table 1. Electrochemical protection and deprotection of alcohols **1**

	Alcohol **1**	Protection with DHP[a] electrolyte[c]	F/mol (min)	yield[d] of **2**/%	bp [°C/Torr][e] mp [°C][ref.lit.]	Deprotection[b] F/mol (min)	yield[d] of **1**/%
a	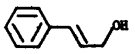	A	0.0002 (1)	92	95—96°/0.02 ([10]125—130°/1)	0.01 (5)	95
b	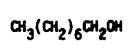	A	0.0003 (10)	98	69—72°/0.03	0.01 (5)	95
c	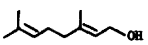	A	0.037 (5)	85	74—77°/0.016 ([10]78—85°/1)	0.01 (150)	96
d	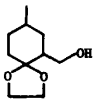	A	0.024 (12)	72	90—92°/0.02	0.01 (90)	90
e	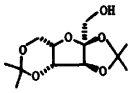	A	0.0005 (1)	94	113—116°/0.03	f)	
f	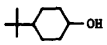	B	0.015 (12)	97	81—82°/0.022 ([10]82—89°/0.04)	0.01 (5)	98
g	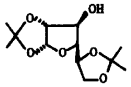	B	0.021 (10)	96	103—105°/0.019	f)	
h	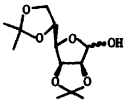	B	0.0189 (15)	87	109—114°/0.016	f)	

a) Carried out using **1** (1.0 mmol) and DHP (1.2—2.0 mmol) in CH_2Cl_2 (5 ml) at 20 °C. b) Carried out using **2** (1.0 mmol) in MeOH (6 ml)-$LiClO_4$ (12 mg) at 55 °C. c) A: $LiClO_4$ (1 mg); B: $LiClO_4$ (1 mg)-Et_4NClO_4 (5 mg). d) Isolated yield. e) Air bath temperature. f) Unsatisfactory for selective hydrolysis of tetrahydropyranyl moiety.

passed under an applied voltage of 10 V (current: 8 mA) using platinum electrodes. After the passage of 0.01 F/mol of electricity (based on the THP ether **2f**) for two minutes, the anolyte was transfered to **2f** (240 mg, 1.0 mmol) placed in another flask. The mixture was heated at 55—60 °C for 5 min while stirring and quenched with pyridine (0.2 ml). Usual workup and chromatography (SiO_2, hexane-AcOEt 10:1) gave 153 mg (98%) of 4-*t*-butylcyclohexanol (**1f**): mp 64—68 °C.

Transesterification of Tripalmitate (3). A solution of MeOH (10 ml) containing $LiClO_4$ (10 mg) was electrolyzed under a constant current of 5 mA in the anode compartment of the electrolysis cell. After the passage of 1.0 F/mol of electricity (based on **3**), the anolyte was added to **3** (204 mg, 0.25 mmol) placed in another flask. The mixture was heated to reflux for 3 h and quenched with pyridine (0.1 ml). Concentration and chromatography (SiO_2, hexane-AcOEt 20:1) gave 202 mg (98%) of **4a** (R=Me): mp 28—29 °C (lit,[14] 28 °C); bp 115—117 °C (3 mm).

Similarly, **4b** (R=Et) and **4c** (R=Pr) were obtained in 96% and 95% yields by heating for 4—7 h. **4b**:[14] bp 117—119 °C (2 mm). **4c**:[14] bp 120—123 °C (2 mm).

References

1) a) T. W. Green, "Protective Group in Organic Synthesis," John Wiley & Sons, New York (1981); b) J. F. McOmie, "Protective Groups in Organic Chemistry," Plenum Press, London (1973).

2) a) S. Torii, T. Inokuchi, and R. Oi, *J. Org. Chem.*, **47**, 47 (1982); b) S. Torii, T. Inokuchi, and R. Oi, *ibid*, **48**, 1944 (1983).

3) For another use of the electrogenerated acid as a catalyst, see a) K. Uneyama, A. Ishimura, K. Fujii, and S. Torii, *Tetrahedron Lett.*, **24**, 2853 (1983); b) K. Uneyama, N. Nishiyama, and S. Torii, *Tetrahedron Lett.*, **25**, 4137 (1984); c) K. Uneyama, Y. Masatsugu, T. Ueda, and S. Torii, *Chem. Lett.*, **1984**, 529; d) S. Torii and T. Inokuchi, *ibid.*, **1983**, 1349; e) S. Torii, T. Inokuchi, and T. Kobayashi, *ibid.*, **1984**, 897.

4) a) R. Kossai, J. Simonet, and D. Dauphin, *Tetrahedron Lett.*, **21**, 3575 (1980); b) J. Delaunay, A. Lebouc, A. Tallec, and J. Simonet, *J. Chem. Soc., Chem. Commun.*, **1982**, 387; c) J. Y. Becker and B. Zinger, *J. Am. Chem. Soc.*, **104**, 2327 (1982); d) *idem, J. Chem. Soc., Perkin Trans. 2*, **1983**, 395.

5) a) A. C. Ott, M. F. Murray, and R. L. Pederson, *J. Am. Chem. Soc.*, **74**, 1239 (1952); Ion-exchange resin containing SO_3H groups (Amberlyst H-15) can be used as a catalyst; b) A. Bongini, G. Cardillo, M. Orena, and S. Sandri, *Synthesis*, **1979**, 618.

6) R. G. Jones and M. J. Mann, *J. Am. Chem. Soc.*, **75**, 4048 (1953).

7) C. W. Creenhalgh, H. B. Henbest, and E. R. H. Jones, *J. Chem. Soc.*, **1951**, 1190.

8) H. Alper and L. Dinkes, *Synthesis*, **1973**, 81.

9) a) M. Miyashita, A. Yoshikoshi, and P. A. Grieco, *J. Org. Chem.*, **42**, 3772 (1977); b) F. M. Menger and C. H. Chu, *ibid*, **46**, 5044 (1981).

10) Y. Morizawa, I. Mori, T. Hiyama, and H. Nozaki, *Synthesis*, **1981**, 899.

11) a) C. E. Rehberg, *Org. Synth. Coll. Vol. III*, **1955**, 146. b) J. C. Sauer, B. E. Hain, and P. W. Boutwell, *ibid*, **1955**, 605.

12) Commercially available, anhydrous $LiClO_4$ was dried before use in an oven at about 110 °C for 12 h.

13) Dichloromethane was once distilled over P_2O_5.

14) H. Pyan and T. Dillon, *J. Chem. Soc., I*, **1913**, 583.

Pressure Dependence of L-Leucine-*p*-nitroanilide Hydrolysis by Leucine Aminopeptidase

Mitsuhiro FUKUDA,* Hiroshi SHIMA, and Shigeru KUNUGI†
Department of Polymer Chemistry, Kyoto University, Sakyo-ku, Kyoto 606
†*Department of Applied Chemistry, Fukui University, Bunkyo, Fukui 910*
(Received November 10, 1984)

Synopsis. The effect of pressure on the hydrolysis of L-leucine-*p*-nitroanilide catalyzed by leucine aminopeptidase from pig kidney was investigated. The activation volumes for k_{cat} process were $-8\,cm^3/mol$ and $-9\,cm^3/mol$ for the native enzyme and the modulated one by Mg^{2+}, respectively. The volume changes for the K_m process were $\simeq 0\,cm^3/mol$ for both enzymes.

Aminopeptidase is most widely distributed in the living organisms,[1] but least studied among the several types of proteinases and peptidases. Leucine aminopeptidase (LAP) from pig kidney has a molecular weight of 320000 composed of six identical subunits[2] and contains one Zn^{2+} per subunit at the active site.[3] LAP from various sources requires divalent metal ions for their activities.[4] Recently, Van Wart and Lin purified pig kidney enzyme by affinity chromatography[2] and found that one subunit has an additional metal binding site for activating metal ion such as Mg^{2+} or Mn^{2+} (regulatory site) beside the one occupied by Zn^{2+} (catalytic site).

We have investigated the pressure dependence of catalytic reactions of several proteases[5] and obtained important informations on their mechanisms. In the present study, we applied this technique to the hydrolysis of L-leucine-*p*-nitroanilide (Leu-*p*NA) catalyzed by LAP to investigate its reaction mechanism.

Experimental

LAP from porcine kidney (type III-CP, Lot 111F-8015) was purchased from Sigma Chemical Co. (St. Louis, USA) and purified by affinity chromatography over L-leucylglycyl-AH-Sepharose according to the literature.[2] For native enzyme with Zn^{2+} (represented by [(LAP)Zn_6-]) and Mg-incubated enzyme ([(LAP)Zn_6Mg_6]), metal analysis was carried out by atomic absorption spectroscopy with a Jarrel ash AA 780 instrument. The metal content was 5.6—5.9 mol per mol enzyme for Zn^{2+} and Mg^{2+} on the basis of protein absorbance ($\varepsilon_{280nm}=400000\,M^{-1}cm^{-1}$ ($1\,M=1\,mol\,dm^{-3}$)).[2] Leu-*p*NA was obtained from the Protein Research Foundation (Osaka). An ultraviolet-visible spectrophotometer with a high pressure optical cell was used as previously described.[5] The concentration of Leu-*p*NA was determined spectrophotometrically by using $\varepsilon_{320nm}=13900$ ($M^{-1}cm^{-1}$) and the initial velocities were calculated from the slope of the absorbance change by using $\varepsilon_{405nm}=9900$ ($M^{-1}cm^{-1}$). The extinction coefficient under high pressure was corrected as previously described.[5] The k_{cat} and K_m values were evaluated from Eadie plot. Tris(hydroxymethyl)aminomethane (Tris) buffer was used[1,2,6] and the pressure dependence of its pK_a was corrected.[5a]

Results and Discussion

Figure 1 shows the pH dependence of k_{cat}/K_m for [(LAP)Zn_6Mg_6] at 0.1 MPa ($\simeq$1 atm) and 100 MPa ($\simeq$1000 atm). Under 100 MPa the activity increased

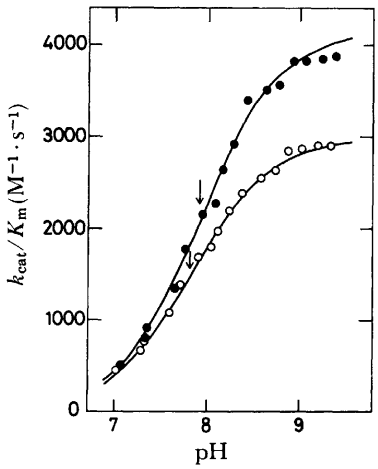

Fig. 1. The pH dependence of k_{cat}/K_m for the hydrolysis of Leu-*p*NA catalyzed by [(LAP)Zn_6Mg_6] at (○) 0.1 MPa and (●) at 100 MPa
$[S]_0<0.05$ mM, $[E]_0=0.018\,\mu M$, 25 °C. 0.02 M Tris-HCl, containing 5 mM $MgCl_2$, 0.5 M KCl and 0.8% (v/v) dimethyl sulfoxide. Arrows indicate the position of pK_a.

1.36 fold for [(LAP)Zn_6Mg_6] and 1.40 fold [(LAP)Zn_6-] at pH around 9. The logarithm of k_{cat}/K_m *vs.* pressure showed a linear correlation for both enzyme forms. The pressure effect was fully reversible in the present pressure range (0.1 MPa—100 MPa) and the observed time scale (less than one hour). These results indicate that there occurs no significant pressure-induced denaturation or dissociation of the hexamer under our experimental conditions,[7] though several oligomeric enzymes were reported to be denaturated or inactivated by medium pressure.[8] The apparent pK_a value was determined for [(LAP)Zn_6Mg_6] by nonlinear regression[5a] and it shifted toward higher pH (pK_a=7.91) under 100 MPa from atmospheric value (7.82). The moderate increase in enzyme activity and the slight pK_a shift to a higher value by pressure increase apparently resemble those of a neutral protease from *Bacillus subtilis*, another type of zinc protease.[5c]

Table 1 shows $\Delta V^{\neq}$ of k_{cat} and ΔV of K_m for [(LAP)-Zn_6Mg_6] and [(LAP)Zn_6-]. Mg^{2+} enhanced the enzyme activity more than 10 fold, which is related not to K_m but k_{cat}.[2] For both forms of the enzyme, k_{cat} increased with increasing pressure, while K_m values were rather pressure independent. Interestingly $\Delta V^{\neq}$ values of the two forms of the enzyme are practically equal. Activation by Mg^{2+} doesn't accompany drastic structural or hydrational change. The reaction mechanisms of LAP was proposed more than twenty years ago[9] and no significant interpretation has been made since then. $\Delta V^{\neq}$ values similar to the present ones were obtained in other zinc protease such as carboxypeptidase

TABLE 1. ACTIVATION VOLUMES AND VOLUME CHANGES FOR Leu-*p*NA HYDROLYSIS AT 0.1 MPa[a)]

Enzyme	k_{cat}	$\Delta V^{\neq}$ for k_{cat}	K_m	ΔV for K_m	k_{cat}/K_m	$\Delta V^{\neq}$ for k_{cat}/K_m
	s^{-1}	cm^3/mol	mM	cm^3/mol	$M^{-1}s^{-1}$	cm^3/mol
[(LAP)Zn_6Mg_6]	1.73	−8±1	0.60	−1±1	2890	−7.6±0.7
[(LAP)Zn_6^-]	0.13	−9±3	0.61	0±3	210	−8.9±1.0

a) Assays are carried out in 0.02 M Tris-HCl buffer containing 0.5 M KCl and 5.6%(v/v) dimethyl sulfoxide, pH 9.0 at 25 °C, except for the presence of 5 mM $MgCl_2$ for [(LAP)Zn_6Mg_6]. [Leu-*p*NA]=0.03—0.57 mM.

A (CPA)[5b)] where the ligating group of the substrate on the active site zinc ion is considered as carbonyl oxygen of the scissile bond. These $\Delta V^{\neq}$'s are to be interpreted by a common mechanism for these metalloproteases.[10)]

The nearly zero ΔV values for K_m show that the substrate binding process does not primarily contain the electrostatic interaction, provided that the apparent K_m value mainly reflects the properties of the substrate binding process, which is consistent with the lack of the evidence of acyl-enzyme intermediate.[11)] This result is also consistent with the facts that LAP favors more hydrophobic side chain in both the amino-terminal and the next residues and that the hydrolysis requirs free amino group.[1,6)] The volume change upon the formation of hydrophobic interaction is considered to be very small.[12)] In this context LAP reaction is in contrast with the reaction of CPA,[5b)] which also favors hydrophobic side chain but requires an ionized (carboxylate) terminal to give a large ΔV value (20—35 cm^3/mol) of K_m^{-1}, reflecting the electrostatic aspect of the substrate recognition. With respect to the pressure dependence of the catalytic process, LAP resembles CPA[5b)] but as for the substrate binding it resembles the mesophilic neutral protease,[5c)] where mostly the hydrophobic nature of the enzyme-substrate interaction was observed.

We gratefully acknowledge Professor N. Ise, Kyoto University, for his advice and encouragement throughout the study. We wish to thank Dr. E.Nakayama, Instrumental Analysis Research Center, Kyoto University for his atomic absorption measurement.

References

1) J. Delange and E. L. Smith, *Enzymes*, 3rd ed. **3**, 81 (1971).
2) H. E. Van Wart and S. H. Lin, *Biochemistry*, **20**, 5682 (1981).
3) S. R. Himmelhoch, *Arch. Biochem. Biophys.*, **134**, 597 (1969).
4) a) E. L. Smith, *J. Biol. Chem.*, **163**, 15 (1946); b) M. P. Allen, A. H. Yamada, and F. H. Carpenter, *Biochemistry*, **22**, 3778 (1983).
5) a) S. Kunugi, M. Fukuda, and N. Ise, *Biochim. Biophys. Acta*, **704**, 107 (1982); b) M. Fukuda, S. Kunugi, and N. Ise, *Bull. Chem. Soc. Jpn.*, **56**, 3308 (1983); c) M. Fukuda and S. Kunugi, *Eur. J. Biochem.*, **142**, 565 (1984); d) M. Fukuda and S. Kunugi, Abst. 24th High Pressure Conf. Japan. (Fukuoka) p. 66 (1983).
6) J. O. Baker and J. M. Prescott, *Biochemistry*, **22**, 5322 (1983).
7) This statement does not exclude the possibility that a reversible dissociation of the hexamer enzyme into protomers or oligomers without changing any catalytic activity of each subunit can occur upon the pressure application, which is not detectable by the present principle of the measurement.
8) R. Jaenicke, *Annu. Rev. Biophys. Bioeng.*, **11**, 1 (1981).
9) a) E. L. Smith and P. H. Spackman, *J. Biol. Chem.*, **212**, 271 (1955); b) G. F. Bryce and B. R. Rabin, *Biochem. J.*, **90**, 513 (1964).
10) S. Kunugi and M. Fukuda, *Polymer Preprint Japan*, **33**, 2035 (1984).
11) S. H. Lin and H. E. Van Wart, *Biochemistry*, **21**, 5528 (1982).
12) a) A. Ben-Naim, Hydrophobic Interaction, Ch. 5, Plenum Press, New York (1980); b) K. Heremans, *Annu. Rev. Biophys. Bioeng.*, **12**, 1 (1982).

Reverse Osmosis Separations of Aqueous NaCl-Organic Solute Systems

Yoshiaki Kiso and Takane Kitao
Laboratory of Sanitary Engineering, Faculty of Engineering, Toyohashi University of Technology, Tenpaku-cho, Toyohashi 440
(Received September 13, 1984)

Synopsis. Some of alcohols, amides, aromatic hydrocarbons and surfactants were used as organic solute. Addition of NaCl increased the rejections of aromatic hydrocarbons and decreased the rejections of amides. It was also found that the permeability of NaCl was influenced by organic solutes.

In reverse osmosis process, it is well known that the solute permeability in multi-component solution system is different from that in single solute system. The results of bisolute systems containing only inorganic salts indicate that univalent ions may permeate more easily by addition of multivalent ions, and that rejections of multivalent ions are increased.[1,2] However, very little are known concerning the effects of inorganic salts on the permeabilities of nonionic organic solutes. As the effective forces between membrane and organic solutes are different from the forces between membrane and ions, it is difficult to evaluate the effects of salt addition on the permeabilities of nonionic organic solutes. The object of this work is to examine the effects of NaCl addition on the rejections of organic solutes (*i.e.* alcohols, amides, aromatic hydrocarbons and surfactants).

Experimental

Cellulose acetate membranes were prepared by the previous method.[1] The membranes were anealed in a water bath at 351—357 K for 10 min followed by precompaction under 7 MPa during 24 h. The reverse osmosis cell used was batch type one reported previously.[1] The experiments were carried out at 4.0 MPa at 303 K. The concentrations of the solutions used in feed solution except aqueous aromatic hydrocarbon and surfactant solutions were 10×10^{-3} mol dm^{-3}. The concentrations of surfactant solutions were above the critical micell concentration. The organic solutes used in this work were listed in Table 1. Na^+ ion was analysed by an atomic flame spectrometer and the concentrations of organic solutes were measured by a total organic carbon (TOC) analyser and a UV-spectrometer. NaCl rejections (R_{NaCl}) and solution flux (J_v; g cm^{-2} s^{-1}) of the used membranes were as follows: Memb. 1 (R_{NaCl}=97.3%, $J_v=4.565\times10^{-4}$), Memb. 2 (R_{NaCl}=89.3%, $J_v=9.276\times10^{-4}$, and Memb. 3 (R_{NaCl}=83.9%, $J_v=7.879\times10^{-4}$).

Results and Discussion

When R^S_{org} and R^M_{org} denote the rejections of single organic solutes and of organic solutes with NaCl, respectively, the relationship between R^S_{org} and R^M_{org} is shown in Fig. 1. Although difference between R^S_{org} and R^M_{org} were not large, it was found that each group of organic solutes indicated different tendency. The addition of NaCl reduced the rejections of aromatic hydrocarbons by 1.1—10.2% and the largest depression of rejection was found in biphenyl whose rejection in a single solute system was the highest in all of this group. On the other hand, the rejections of amides were increased by NaCl addition. The results of the experiment on the effect of NaCl concentration on the rejection of amides are shown in Fig. 2. It was recognized that the rejection of amides increased as increasing NaCl concentrations and that this effect appeared clearly in formamide and acetamide whose rejections in single solute systems were lower than others. The rejections of alcohols and surfactants, however, were not affected very much by NaCl addition.

When R^S_{NaCl} and R^M_{NaCl} mean the NaCl rejection in single solute system and mixed solute system, respectively, the relationship between ΔR_{org} ($=R^M_{org}-R^S_{org}$) and ΔR_{NaCl} ($=R^M_{NaCl}-R^S_{NaCl}$) is shown in Fig. 3. Although ΔR_{NaCl} is smaller than ΔR_{org}, the sign of ΔR_{NaCl} also varies by the group of organic solute. The effects of NaCl addition on the solute rejection were summarised as follows: as to aromatic hydrocarbons and surfactants $\Delta R_{org}<0$ and $\Delta R_{NaCl}>0$, amides $\Delta R_{org}>0$ and $\Delta R_{NaCl}<0$, and alcohols $\Delta R_{NaCl}<0$.

If, even in the mixed solutes system, the diffusibities of solutes in the pore of membrane remain the same as in single solute systems, the solute permeabilities may be influenced by the partition of solute between bulk solution and membrane surface or pore of membrane.

Table 1. Organic solutes

No.	Solute	conc.[a]	memb.No.	No.	Solute	conc.[a]	memb.No.
1	Ethyl alcohol	10	1	11	Benzene	14.3	2
2	Propyl alcohol	10	1	12	Toluene	4.71	3
3	Isopropyl alcohol	10	1	13	*o*-Xylene	1.76	3
4	Isobutyl alcohol	10	1	14	1,3,5-Trimethyl-		
5	*t*-Butyl alchol	10	1		benzene	1.72	2
6	Formamide	10	1	15	Chlorobenzene	6.29	2
7	Acetamide	10	1	16	Biphenyl	0.031	2
8	Butyramide	10	1	17	SDS[b]	10	1
9	*N,N*-Dimethyl-			18	SDBS[c]	5	1
	formamide	10	1	19	Brij-35	10	1
10	*N,N*-Dibutyl-						
	formamide	10	1				

a) mmol dm^{-3}. b) Sodium dodecyl sulfate. c) Sodium dodecylbenzenesulfonate.

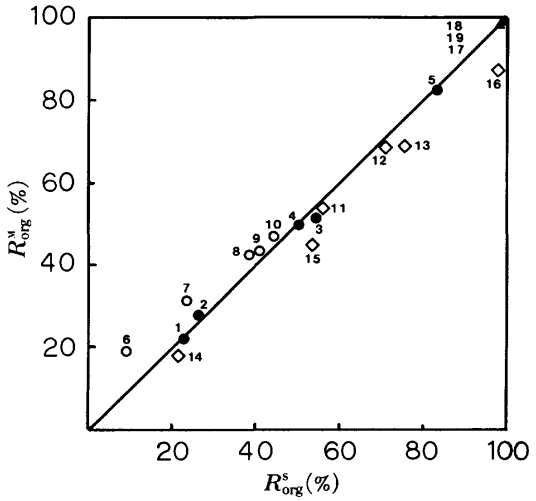

Fig. 1. R^M_{org} *vs.* R^S_{org}.
●: Alcohols, ○: Amides, ◇: Aromatic hydrocarbons, ▲: Surfactants.

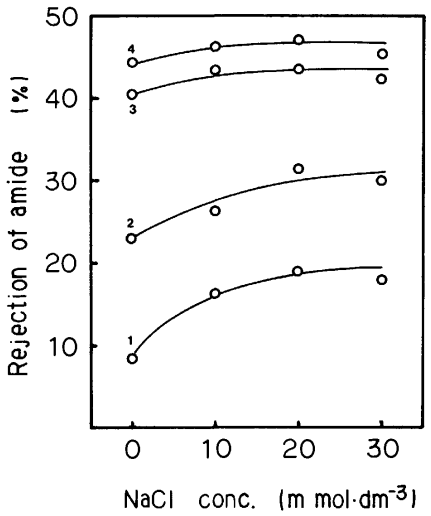

Fig. 2. The effect of NaCl concentration on the rejection of amides.

Kesting *et al.*[3] and Kamizawa and Ishizaka[4] previously indicated that surfactants are adsorbed on the surface of cellulose acetate membrane. Matsuura and Sourirajan[5] mentioned that the preferential sorption layer of aromatic hydrocarbon was formed on the membrane surface. As the solubilities of aromatic hydrocarbons decrease by NaCl addition, these solutes may be adsobed more easily on the membrane and therfore

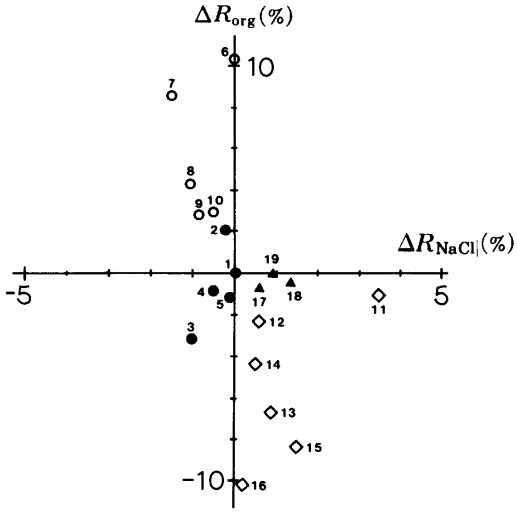

Fig. 3. ΔR_{org} *vs.* ΔR_{NaCl}.
●: Alcohols, ○: Amides, ◇: Aromatic hydrocarbons, ▲: Surfactants.

the rejection of the aromatic hydrocarnons may decrease. On the other hand, it is considered that the sorption layer of the aromatic hydrocarbons or surfactants hindered the permeation of ions through the membrane by following reasons: 1) The pore size of membrane decreases by sorption of organic solute, 2) ionic solutes are difficult to come near the membrane due to the increase of hydrophobic hydration, and 3) the sorption layer of ionic surfactant particularly acts as a kind of ionic membrane. As to amides, the mechanism of the effect of NaCl addition on solute rejection are not clear. The results, however, suggested that ionic solute might hindered the transport of amides into the pore of membrane. From the results of this work, it is concluded that the effect of NaCl addition on the rejection of organic solute depended on the permeation mechanism of the organic solute.

References

1) M. Sugahara, Y. Kiso, T. Kitao, Y. Terashima, and S. Iwai, *J. Chem. Eng. Jpn.*, **11**, 366 (1978).
2) J. P. Agrawal and S. Sourirajan, *Ind. Eng. Chem. Process Des. Dev.*, **9**, 12 (1970).
3) R. E. Kesting, W. J. Subcasky, and D. J. Paton, *J. Colloid Interface Sci.*, **28**, 156 (1968).
4) C. Kamizawa and S. Ishizaka, *Bull. Chem. Soc. Jpn.*, **45**, 2967 (1972).
5) T. Matsuura and S. Sourirajan, *J. Appl. Polym. Sci.*, **17**, 3683 (1973).

Photoelectrochemical Reduction Products of Carbon Dioxide at Metal Coated p-GaP Photocathodes in Aqueous Electrolytes

Shoichiro IKEDA,* Makoto YOSHIDA, and Kaname ITO
Department of Synthetic Chemistry, Nagoya Institute of Technology, Gokiso-cho, Showa-ku, Nagoya 466
(Received September 3, 1984)

In order to increase the current efficiency of the photoelectrochemical reduction of CO_2 in aqueous electrolytes, metals such as Pb and Zn, which have a higher overpotential for the hydrogen evolution reaction, were coated on a p-GaP photocathode by sputtering and electroplating. Au was also coated by sputtering. Then, the photoelectrolytic experiments were carried out in a gas-tight cell with a cyclic gas-flow system. The products in a gas phase were determined as well as the products in the electrolyte. Accordingly, CO in addition to HCOOH as a reduction product of CO_2 was found to be produced as well as substantial amount of H_2 as a by-product. However, other products such as HCHO and CH_3OH were not found at all. In the case of the Pb coated p-GaP electrode, the current (faradaic) efficiency, η, for HCOOH formation was increased up to 48.2%, although in the case of bare p-GaP it was only 4.8% at maximum. On the other hand, the η for CO formation at the Zn-coated p-GaP electrode went up to 16.5%. While, in the case of an Au-coated p-GaP, the η for the CO_2 reduction was not so changed as for the bare p-GaP photocathode.

In a previous paper,[1] we reported that the some organic compounds such as formic acid, formaldehyde and methanol, which had been reported as photoelectrochemical reduction products of carbon dioxide (CO_2) by a few authors,[2,3] were also produced by the photolysis of cell materials such as electrolytes and epoxy resins. Also, the real reduction product of CO_2 at the p-GaP photocathodes in aqueous electrolytes was experimentally confirmed to be only formic acid, for which the current (faradaic) efficiency, η, was 4.8% at maximum.

The photoelectrochemical reduction of CO_2 is a competitive reaction with the reduction of water, *i.e.*, the hydrogen-evolution reaction (HER). Therefore, η for a CO_2 reduction may be increased if the electrode surface is covered with a thin layer of a metal such as Zn or Pb which have higher overvoltages for HER.

In the present paper, the discussed photoelectrolytic experiments were carried out in a gas-tight cell with a cyclic gas-flow system. The products in the gas phase were determined as well as the products in the electrolytes. In order to increase η for the CO_2 reduction, coatings using such metals as Au, Zn, and Pb were placed on the surfaces of p-GaP photocathodes and the effects on the reduction products and the characteristic properties as a photocathode were investigated. In this paper, mainly an analysis of the reduction products is reported. The properties of the metal-coated electrodes will be the subject of our next paper.

Experimental

Materials. The photocathode was prepared by molding a p-GaP wafer, Sanyo Electric Co. Ltd., Zn-doped 2.8—6.0×10^{17} cm^{-3}, of 1.0 cm^2 with epoxy resin, after an ohmic contact was made with an In-Zn (2%) alloy solder. It was etched in aqua regia for 1 min before use. In order to prevent the photolysis of the epoxy resin, the epoxy region of an electrode was shaved off only to the extent as not to cause a failure of the insulation (Fig. 1).

The electrolytes used were 0.1 mol dm^{-3} aqueous solutions of $(C_2H_5)_4NClO_4$ [TEAP], $(C_2H_5)_4NBr$ [TEABr], and $(n\text{-}C_4H_9)_4NBr$ [TBABr]. TEAP was synthesized with TEABr and perchloric acid.[4] The other reagents were all commercial grade and were used without further purification except for the case of TBABr, which was twice recrystallized with distilled water because it contained detectable amounts of methanol and ethanol.

Apparatus and Procedure. A photoelectrolytic cell with a quartz glass window, (made of Teflon), was designed to separate the cathode and anode chambers with an ion-exchange membrane, Nafion-315, and to be able to operate with a small volume (*ca.* 5 ml) as a catholyte for the easy determination of products (Fig. 2). The cell was gas-tight and the gas, CO_2 or N_2, was supplied by a cyclic gas-flow system which was assembled with a mini peristaltic pump, a manometer and a gas sampler (Fig. 3). The cell and a UV-37 filter, which was used to cut off ultraviolet rays shorter than 370 nm in order to prevent the photolysis of

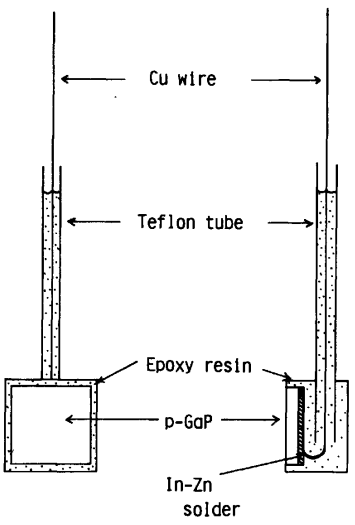

Fig. 1. Structure of p-GaP electrode.

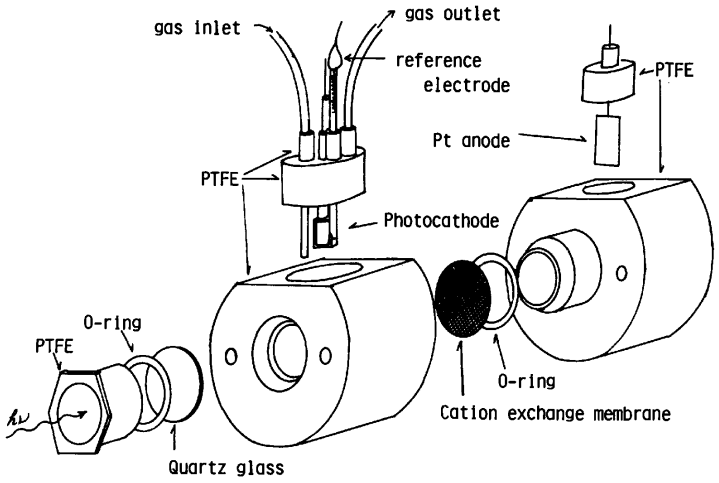

Fig. 2. Structure of photoelectrolytic cell.

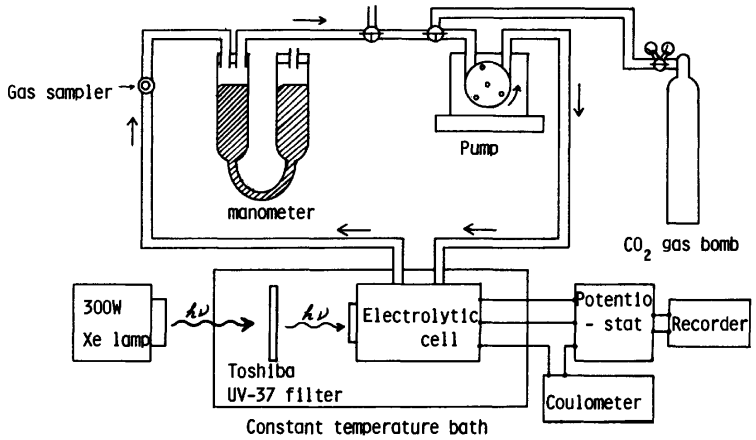

Fig. 3. Diagram of photoelectrolytic apparatus with cyclic gas flow system.

cell materials, were immersed in a water bath for the prevention of overheating due to illumination.

The photoelectrochemical reduction was carried out potentiostatically using a potentiostat and a xenon lamp, Model VIX-300; Varian Co. Ltd. The photocurrent was recorded using a conventional pen-recorder. The quantity of charge passed was monitored with an electronic coulometer, Model HF-102; Hokuto Denko Co. Ltd. After CO_2 or N_2 gas was blown into the cell from each cylinder and was exhausted through the cyclic gas-flow system for about 30 min, the line was closed to make it gas-tight. During the experiment, the gas in the system was circulated using a peristaltic pump with a rate of 1 ml/min.

Analysis. The products in the gas phase were determined qualitatively and quantitatively by gas chromatography, Model GC-3AH, Shimadzu Corp., having a TC detector on a column of activated charcoal 60/80, 3 mm×3 m, at 100 °C using He gas as a carrier with a rate of 13 ml/min. The products in the electrolyte were sampled after the line was exposed to the atmosphere and were then determined by high-performance liquid chromatography. The equipment used was a Model HSLC-022; Atto Corp., with RI and UV detectors with 225 nm on a column of Shodex HC-125S using 1% H_3PO_4 aqueous solution at 1.0 ml/min and 35 °C as an elueant. An analysis was also performed using steam chromatography, SSC-1 Model 103; Ohkura Riken, with a FID on a column of Chromosorb 101, 2 mm×3 m, at 120 °C using steam as a carrier at 8.6 ml/min (5.4 μl/min as water) for the determination of alcohols and aldehydes, although they were not detected at all in the present work.

Metal Coating. The molded p-GaP electrode was coated with a thin layer of Au, Pb, or Zn by sputtering and electroplating methods. The sputtering was carried out at DC 700 V under *ca.* 1 Pa air using an ion cleaner, Model IB-1; Eiko Co. Ltd., where the coverage was controlled by the sputtering time *i.e.*, 7, 15 or 20 min. Au of 99.99%, Pb of 99.99% and Zn of 99.9999% were used as the target metal. Typical weights of coated metals measured by weighing method were 0.06, 0.07, and 0.02 mg cm^{-2} in the cases of Au, Pb and Zn, respectively, for 10-min sputtering.

The electroplating method under photo-illumunation was also used for the coating of Pb and Zn. The electroplating was carried out potentiostatically usig an H-type Pyrex cell with a quartz window under the illumination of a xenon lamp. The amounts of the coated metals were monitored with a coulometer connected in series between the anode and the potentiostat.

In the case of Pb plating, 0.5 mol dm^{-3} of lead acetate was used as an electrolyte, and a p-GaP electrode, a Pb sheat

(99.99%) electrode and a Ag/AgCl/sat'd KCl electrode served as a cathode, an anode and a reference electrode, respectively. The electroplating was carried out at a potential of −0.4 V *vs.* Ag/AgCl/sat'd KCl, during which almost a uniformly deposited gray film of Pb was obtained.

In the case of Zn coating, the electrolyte was a solution of zinc sulfate (300 g) and ammonium chloride (20 g) dissolved into 1 dm^3 of distilled water; a zinc plate (99.9999%) served as an anode. Electroplating was carried out at −0.2 V, and a uniform film of Zn was deposited.

Under these experimental conditions, no hydrogen evolution was observed at all, so that the deposited amounts per coulomb should correspond to 1.0 mg C^{-1} and 0.33 mg C^{-1} for Pb and Zn, respectively. Therefore, the amounts of metals coated on the p-GaP electrodes were controlled by the quantities of electricity passed.

In the present paper, these metal coated p-GaP electrodes are named as Au(s)-p-GaP, Pb(s)-p-GaP, and Zn(s)-p-GaP prepared by sputtering and Pb(e)-p-GaP and Zn(e)-p-GaP by electroplating, respectively.

Results and Discussion

Photoelectrochemical Reduction Products of CO_2. The photoelectrochemical reduction products of CO_2, when metal coated p-GaP electrodes by sputtering were used as a photocathode and the photoelectrolysis was carried out at −1.2 V up to 100 C in various aqueous solutions, are summerized in Table 1. This table demonstrates that the reduction products are only formic acid in the electrolytes and hydrogen and carbon monoxide in the gas phase. No products such as other carboxilic acids, alcohols or aldehydes were observed at all, although these organic compounds had been reported as photoelectroreduction products by some authers.[2,3,5]

In the case of the metal-coated p-GaP electrodes prepared by electroplating (Table 2), the products were also formic acid, carbon monoxide and hydrogen. The current efficiency for CO production increased up to about 16.5% at the Zn(e)-P-GaP

Table 1. Photoelectrochemical reduction products of CO_2 on bare and metal coated p-GaP photocathodes, prepared by sputtering method, at −1.2 V *vs.* Ag/AgCl/sat'd KCl. Quantity of electricity; 100 C.

Electrode	Electrolyte	Time	HCOOH		CO		H_2		$\eta_1+\eta_2$	$\eta_1+\eta_2+\eta_3$
		min	n_1/μ mol	η_1/%	n_2/μ mol	η_2/%	n_3/μ mol	η_3/%	%	%
p-GaP	TEAP	560	65	12.6	17	3.3	350	68	15.9	83.9
	TEABr	805	52	10.1	30	5.8	340	66	15.9	81.9
	TBABr	345	11	2.2	5.3	1.0	480	92	3.2	95.2
Au(s)-p-GaP	TEAP	255	28	5.4	14	2.7	460	88	8.1	96.1
	TEABr	570	62	12.1	26	5.0	370	72	17.1	89.1
	TBABr	235	68	13.1	24	4.5	430	84	17.6	101.6
Zn(s)-p-GaP	TEAP	555	44	8.4	17	3.3	350	68	11.7	79.7
	TEABr	455	74	14.4	34	6.6	360	70	21.0	91.0
	TBABr	300	26	4.9	11	2.2	470	91	7.1	98.1
Pb(s)-p-GaP	TEAP	825	60	11.5	13	2.5	360	69	14.0	83.0
	TEABr	625	63	12.1	22	4.2	290	56	16.3	72.0
	TBABr	775	53	10.3	21	4.1	340	66	14.4	80.4

η_1, η_2, and η_3 are current efficiencies for HCOOH, CO, and H_2, respectively.

Table 2. Photoelectrochemical reduction products of CO_2 on metal coated p-GaP photocathodes, prepared by electroplating method, at −1.2 V *vs.* Ag/AgCl/sat'd KCl in 0.1 M† TEABr aq

Electrode	Q_e	Q	Time	HCOOH		CO		H_2		$\eta_1+\eta_2$	$\eta_1+\eta_2+\eta_3$
	C	C	min	n_1/μ mol	η_1/%	n_2/μ mol	η_2/%	n_3/μ mol	η_3/%	%	%
Zn(e)-p-GaP	0.06	20	610	14	13.2	11	10.9	64	62	24.1	86.1
	0.07	20	870	15	14.7	15	14.9	68	66	29.6	95.6
	0.08	20	655	26	25.1	17	16.5	49	47	41.6	88.6
	0.09	20	460	15	14.7	15	14.7	63	63	29.4	92.4
Pb(e)-p-GaP	0.06	100	710	87	16.7	8.2	1.6	350	67	18.3	85.3
	0.07	50	605	95	36.5	8.5	3.3	120	48	39.8	87.8
	0.08	20	310	50	48.2	5.0	4.8	33	31	53.0	84.0
	0.09	20	360	49	47.2	4.1	3.9	41	40	51.1	91.1

Q_e; quantity of electricity for electroplating. † 1 M = 1 mol dm^{-3}.

electrode and that for formic acid production increased up to 48.2% at Pb(e)-p-GaP electrode. These results suggest that formic acid is effectively produced at the Pb(e)-p-GaP photocathode, as the side reactions such as HER is depressed by coating the metal with a high overpotential for HER. These results are thought to be due to the fact that the metal is deposited preferably onto the active sites of the p-GaP electrode. Thus, the metal plays the role more effectively than that deposited by sputtering.

In the case of a Pb(s)-p-GaP photocathode, the surface changed to a silvery color upon the reduction of lead during the photoelectrolysis. Figure 4 shows the current efficiencies for HCOOH and CO production plotted with respect to the quantity of charge passed. At the point of 25 C (coulomb), where the surface was not silvery, current efficiencies for HCOOH and CO were as small as 5.6% and 1.0%, respectively, while, over the point of 50 C, they became about twice a large as before. In order to clarify this situation, the gas in the cyclic gas-flow system was progresively analysed while watching the surface state of the Pb(s)-p-GaP. The results are shown in Fig. 5. The open triangle in that figure represents the point where the surface became silvery. The formation of H_2 became smaller and, in contrast to this, that of CO became larger after this point. The content of CO_2 gradually decreased with the passage of current and air gradually penetrated into the line. Although the products in the electrolytes were not analyzed, the current efficiency for HCOOH formation may be estimated to increase after this point by the depression of HER.

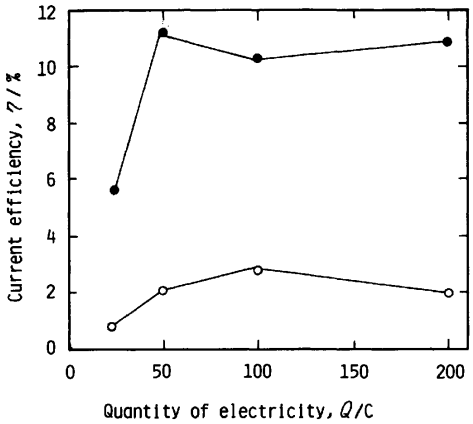

Fig. 4. Current efficiencies, η, for HCOOH (●) and CO (○) formations with respect to quantity of electricity, Q, at Pb(s)-p-GaP (7 min) electrode in 0.1 M TEABr aq.

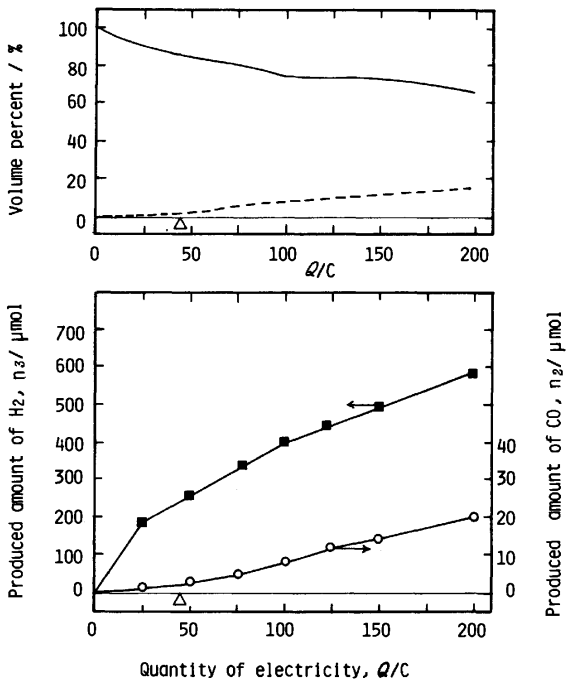

Fig. 5. Amount of products, CO (○) and H_2 (■), and contents of CO_2 (——) and air (----) in gaseous phase with respect to quantity of electricity, Q, when photoelectrochemical reduction of carbon dioxide was performed at Pb(s)-p-GaP (7 min) electrode in 0.1 M TEABr aq. Triangle represents the point where the surface of the electrode became silvery.

TABLE 3. PHOTOELECTROCHEMICAL REDUCTION PRODUCTS OF CO_2 AT -1.2 V *vs.* Ag/AgCl/sat'd KCl. QUANTITY OF ELECTRICITY FOR ELECTROPLATING Zn AND Pb ON p-GaP; 0.07 COULOMB

Electrolyte	Electrode	Q	t	HCOOH		CO		H_2		$\eta_1+\eta_2$	$\eta_1+\eta_2+\eta_3$
		C	min	n_1/μ mol	η_1/%	n_2/μ mol	η_2/%	n_3/μ mol	η_3/%	%	%
TEAP	p-GaP	100	500	65	12.6	17	3.3	350	68	15.9	83.9
	Zn(e)-p-GaP	14	640	19	26.5	6.5	8.9	48	64	35.4	99.4
	Pb(e)-p-GaP	50	645	118	45.5	10	4.0	95	37	49.4	86.5
TEABr	p-GaP	100	805	52	10.1	30	5.8	340	66	15.9	81.9
	Zn(e)-p-GaP	20	375	32	31.0	7.5	7.2	55	53	38.2	91.2
	Pb(e)-P-GaP	50	605	95	36.5	8.5	3.3	120	48	39.8	87.7
TBABr	p-GaP	100	345	11	2.2	5.4	1.0	480	92	3.2	95.2
	Zn(e)-p-GaP	20	745	19	18.6	9.0	8.7	39	37	27.3	64.3
	Pb(e)-p-GaP	40	715	42	20.0	11	5.1	110	54	25.1	79.5

In order to check the mechanism of CO formation, a blank test was carried out using a Pb(s)-p-GaP electrode in an 0.1 mol dm^{-3} TEABr aq solution previously containing 0.01 mol dm^{-3} HCOOH under N_2 atomsphere for 100 C at -1.2 V *vs.* Ag/AgCl. The product was only hydrogen and CO was not observed. Also, the concentration of formic acid did not change. Therefore, it may be concluded that the CO obtained in the above-mentioned experiments was not obtained through HCOOH from CO_2 but was produced by the direct reduction of CO_2.

Table 3 shows the effect of the supporting electrolyte on the current efficiencies for the reduction products when bare p-GaP, Zn(e)-p-GaP, or Pb(e)-p-GaP were used as photocathodes. In the cases of TEAP and TEABr, the current efficiencies, η, for HCOOH, CO and H_2 productions were not so much affected by the electrolytes, but were largely affected by the coating metals. The η for CO_2 reduction became about 50% at Pb(e)-p-GaP photocathode in TEAP aq. In the case of TBABr, however, a bare p-GaP electrode showed extremely lower η for HCOOH or CO production. The η for CO was up to the same values in the former electrolytes by coating of Pb or Zn. The η for HCOOH, however, was only recovered up to half values. These results indicate that the η for CO_2 reduction is affected not by an anion but the cation size of the supporting electrolytes. The favorable formation of nonaqueous circumstance by large cation of tetrabutylammonium salts on the electrode surface may depress the effect of a lead or zinc coating.

Reduction Mechanism. The photoelectrochemical reduction of CO_2 starts from the formation of a carbon dioxide anion radical, $\cdot CO_2^-$, by the electron acceptance of a CO_2 molecule,[6] and the anion radical is thought to be adsorbed on the electrode surface. The HER also takes place on the same electrode surface and becomes adsorbed atomic hydrogen as follows.[7]

$$CO_2 + e^- \rightarrow \cdot CO_{2\,ad}^- \quad (1)$$

$$H^+ + e^- \rightarrow H_{ad} \quad (2)$$

Now, formic acid, the main reduction product of CO_2 in aqueous electrolytes, is produced according to Reactions 3 and/or 4.

$$\cdot CO_{2\,ad}^- + H_{ad} \rightarrow HCOO^- \quad (3)$$

$$\cdot CO_{2\,ad}^- + H^+ + e^- \rightarrow HCOO^- \quad (4)$$

Hydrogen is produced by HER as follows.

$$H_{ad} + H^+ + e^- \rightarrow H_2\uparrow \quad (5)$$

$$H_{ad} + H_{ad} \rightarrow H_2\uparrow \quad (6)$$

By coating the electrode surface with metals such as Pb and Zn having a higher overpotential for the HER, the rates of Reactions 5 and 6 become slow and the HER is suppressed. Concequently, the rate of formic acid formation by Reaction 3 or 4 through Reaction 1 becomes larger.

On the other hand, carbon monoxide is produced by the disproportionation reaction of the CO_2 anion radical according to Reaction 7.[8]

$$\cdot CO_{2\,ad}^- + \cdot CO_{2\,ad}^- \rightarrow CO + CO_3^{2-} \quad (7)$$

This reaction is thought to be competitive with Reaction 3 or 4. In the case of the Pb(e)-p-GaP electrode, the rates of Reaction 3 and/or 4 are larger than that of Reaction 7. Thus, the formic acid is the predominant product from CO_2. For the case of the Zn(e)-p-GaP electrode, the rate of Reaction 7 is approximately equal to that of Reaction 3 or 4, so that substantial amounts of formic acid and CO are produced.

This work was partially supported by Grant-in-Aid for Energy Research (Nos. 57045052 and 58045068) from the Ministry of Education, Science and Culture.

References

1) K. Ito, S. Ikeda, M. Yoshida, S. Ohta, and T. Iida, *Bull. Chem. Soc. Jpn.*, **57**, 583 (1984).
2) M. Halmann, *Nature*, **275**, 115 (1978).
3) Y. Taniguchi, H. Yoneyama, and H. Tamura, *Bull. Chem. Soc. Jpn.*, **55**, 2034 (1982).
4) K. Ito, S. Ikeda, T. Iida, and H. Niwa, *Denki Kagaku*, **49**, 106 (1981).
5) D. Canfield and K. W. Frese, Jr., *J. Electrochem. Soc.*, **130**, 1772 (1983).
6) J. Jordan and P. T. Smith, *Proc. Chem. Soc.*, 246 (1960).
7) K. J. Vetter, *Electrochemical Kinetics*, p. 537 (1967). Academic Press.
8) C. Amatore and J. M. Saveant, *J. Am. Chem. Soc.*, **103**, 5021 (1981).

 © 1985 The Chemical Society of Japan Bull. Chem. Soc. Jpn., 58, 1358—1366 (1985) [Vol. 58, No. 5

Infrared Multiphoton Decomposition of 1-Chloro-1-fluoroethene

Hiroo OGURA
The Institute of Space and Astronautical Science, Komaba, Meguro-ku, Tokyo 153
(Received November 13, 1984)

Unimolecular dissociation and subsequent reactions of CH_2=CFCl subjected to the infrared multiphoton excitation were studied with a focused geometry using the P(10) line of the 10.6 μm CO_2 band at 952.9 cm^{-1}. The final products of the photolysis observed were CH≡CCl, CH≡CF, CH≡CH, CH_2≡CHF, and CH_2=CF_2. A series of diagnostic experiments shows that the primary processes of photolysis involve the molecular elimination of HF and HCl, to minor extent C-Cl bond rupture. The relative importance of the primary steps is tentatively estimated to be approximately 100:65:25, respectively. Primarily formed CH≡CCl and CH≡CF suffer from secondary photolysis, absorbing additional photons. More fraction of CH≡CF primary yield is decomposed than that of CH≡CCl, due to the accidental resonance with the laser excitation line. CH≡CH and CH_2=CHF are concluded to be formed by the H atom abstraction reactions of CH≡C· and CH_2=CF· radicals generated during the photolysis, respectively, CH_2=CF_2 being formed by the recombination reaction between CH_2=CF· radical and F atom. In the shock tube pyrolysis the formation of CH≡CF predominates over that of CH≡CCl. A mechanistic change to form CH≡CF in the shock tube pyrolysis is suggested.

Infrared multiphoton excitation (IRMPE) could be a novel method to energize polyatomic molecules on the ground electronic potential, by depositing energy into particular vibrational modes, and to study the dynamics of highly vibrationally excited polyatomic molecules such as unimolecular decomposition.[1] The study of polyatomic molecules with multiple competitive exit channels can provide information about the internal energy distribution of the excited molecules. Partially chlorofluorinated ethanes and ethenes are some of the most suitable molecules for such studies of infrared multiphoton decomposition (IRMPD), since they usually show strong absorption for CO_2 laser lines and have at least two competitive unimolecular dissociation pathways, *i.e.*, HF andHCl molecular elimination channels.[2-7] Jalenak and Nogar studied the IRMPD of CH_2=CFCl by monitoring the emission intensities from HF and HCl, and measured the branching ratio between HF and HCl elimination channels as a function of pressure and pulse energy.[4]

The elimination of molecular fragments also facilitates the IRMPD study by means of final product analysis in gas cell experiments. However, secondary photolysis in the IRMPD has been shown to occur in a very short time scale in the pulse duration, and true primary processes might be masked by such secondary photolysis to generate radicals or atoms due to radical-substrate and radical-atom interactions.[7-9] It has been recognized that the dynamics of unimolecular dissociation processes is not properly addressed by gas cell experiments with focused geometry, where total chemical transformations are observed.[10-12] The results do, however, serve as a useful basis set with which to discuss the unimolecular dissociation, subsequent reactions, and the effects of collisional processes. Several shock tube pyrolysis experiments were also carried out, since in many cases thermal excitation results are helpful to establish the photolysis mechanism.

Experimental

The experimental apparatus and analytical procedure used here are essentially the same as in a previous study,[7] and have been described fully. The pulsed beam from a Lumonics 103-2 TEA CO_2 laser was passed through an aperture with a diameter of 14-mm and focussed in an irradiation cell (46-mm diameter, 22-cm long, NaCl windows) by means of a planoconvex Ge lens with a focal length of 12.7 cm. The pulse consisted of a sharp initial spike (80—100 ns FWHM), followed by a low intensity tail of 1—2 μs.[13] The laser was tuned to the P(10) line of the 10.6 μm at 952.9 cm^{-1}, which falls within the ν_6 mode of CH_2=CFCl corresponding to a CH_2 planar rock,[14] and operated at 1 Hz repetition rate for all runs. The output pulse was attenuated by CaF_2 flats, and the incident pulse energy was measured with a calibrated pyroelectric detector, shot-to-shot fluctuation being within 5%. MKS Baratron transducers were used for the pressure measurements.

All photolysis products were identified by comparative GC retention times with known samples, in particular, with the IRMPD products of CH_2ClCHFCl,[7] identification being straightforward. For quantitative determination of the photolysis products, temperature programmed gas chromatographic analyses (flame ionization detector) were carried out using Porapak N column. The reactant CH_2=CFCl (PCR Inc.) was purified by gas chromatography, and then further distilled under vacuum at low temperature. The experimental details of single-pulse shock tube were fully described previously.[15]

Results

Upon the photolysis at 952.9 cm^{-1}, serveral products were observed. A gas chromatographic analysis of a photolyzed sample shows that major products are CH≡CCl and CH≡CF, three minor, yet important products being CH≡CH, CH_2=CHF, and CH_2=CF_2.

Dependence on Reactant Pressure. The product yields as a function of CH_2=CFCl pressure were investigated with the same number of pulse, excitation line, geometry, and constant laser energy. The results on product yields are shown in Fig. 1, the relative yields being summarized in Table 1. As can be seen from Fig. 1, all product yields increase as the reactant pressure is increased. Major product CH≡CF increases more rapidly in its yield than that of CH≡CCl at higher pressures. Minor product CH≡CH and CH_2=CHF yields increase in a similar manner with higher pressure, while the other minor product CH_2=CF_2 yield increases very gradually with increasing CH_2=CFCl pressure. The relative yields of CH≡CF, CH≡CH, and CH_2=CHF show a very rapid increase at higher pressures, on the other hand, that of CH_2=CF_2 shows a slight decrease with higher reactant pressure.

Dependence on Pulse Energy. The dependence of total yield on pulse energy at CH_2=CFCl pressure of 0.4 Torr (1 Torr=133.322 Pa) is shown in a log-log plot in Fig. 2. The plots are linear and obey the relationship: $Y(\text{yield}) \propto E_0^{1.44}$ (pulse energy). The value of the exponent obtained is very close to 3/2, of which fluence dependence has been observed in many systems with "tightly" focused geometry.[12] At the pressures and fluences where the yield-energy relationship of 3/2 power dependence is observed, a simple threshold model is applicable, in which the reaction zone can be approximated simply by a "double cone" geometry.[16] This model is based on the assumption that all molecules contained in a conical zone where the laser fluence is above some critical fluence ϕ_c, decompose with unit probability (reaction zone), any reactions outside the reaction zone being neglected. In the fluence range where a simple threshold model is applicable, it has been recognized that relative yields are insensitive to the change of pulse energy.[10,11] Actually, very small variance is observed for the relative yields.

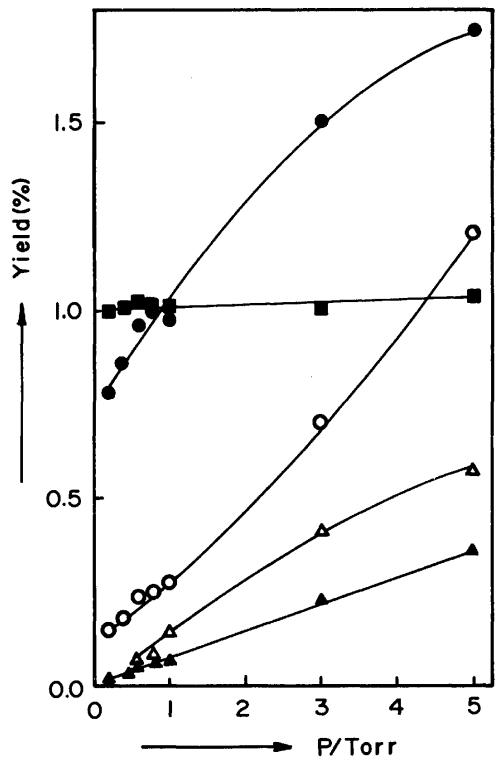

Fig. 1. Product yields as a function of reactant pressure. (Conditions: pulse energy E_0=0.255 J/pulse, pulse number n=500, excitation line ν=952.9 cm^{-1}). ●: CH≡CCl, ○: CH≡CF, ▲: CH≡CH, △: CH_2=CHF(×10), ■: CH_2=CF_2(×10).

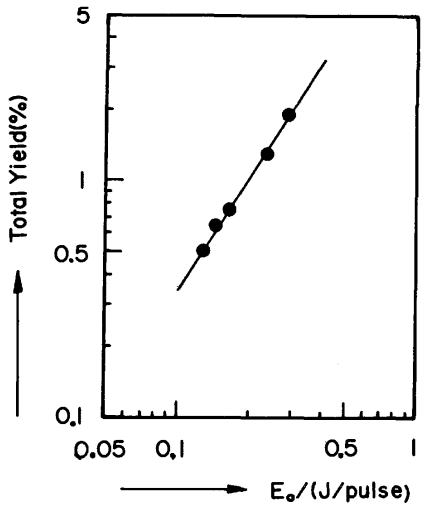

Fig. 2. Total yield as a function of laser energy. (Reactant pressure=0.40 Torr, n=500, ν=952.9 cm^{-1})

Table 1. Pressure dependence of relative yields[a]

P/Torr	0.20	0.40	0.60	0.80	1.0	3.0	5.0
CH≡CF	18.9	20.7	24.9	25.4	27.8	46.3	69.5
CH_2=CF_2	12.6	12.8	12.2	10.7	10.8	7.07	7.59
CH≡CH	2.79	4.21	5.38	5.74	6.70	15.2	20.7
CH_2=CHF	b)	0.401	0.752	0.821	1.49	2.70	3.29
CH≡CCl	100	100	100	100	100	100	100
	(0.789)	(0.857)	(0.957)	(0.998)	(0.966)	(1.50)	(1.74)

a) Relative yields at E_0=0.255 J/pulse and 500 shots. The yield of CH≡CCl in % conversion per 500 shots is in parenthesis, being taken as 100. b) The yield is too small to be determined quantitatively.

Dependence on Pulse Number. The total yield as a function of pulse number was examined at 1.0 Torr substrate pressure, the other photolysis parameters being kept the same. The results on the total yield is shown in Fig. 3. Unreacted fraction (a/a_0), where a and a_0 denote final and initial pressure, respectively, decreases exponentially with increasing pulse number n up to 1000. $(a/a_0)=\exp(-dn)$, where d corresponds to the slope and can be regarded as an apparent first-order dissociation rate constant for CH_2=CFCl. Furthermore, d corresponds to the fractional volume of the reaction zone(V_r) to the cell volume(V) in a simple threshold model ($d=V_r/V$), where the laser fluence exceeds the lowest critical fluence for the dissociation of CH_2=CFCl.

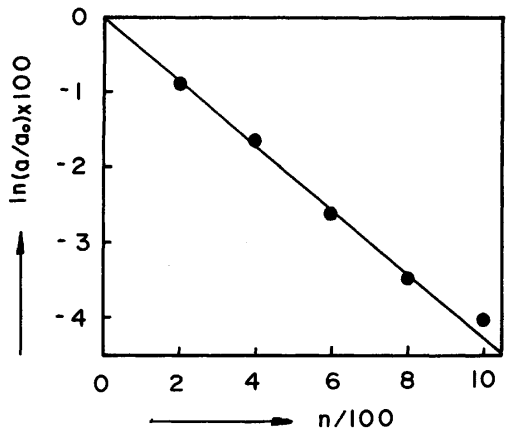

Fig. 3. Total yield as a function of pulse number. (Reactant pressure=1.0 Torr, E_0=0.257 J/pulse, ν=952.9 cm^{-1}).

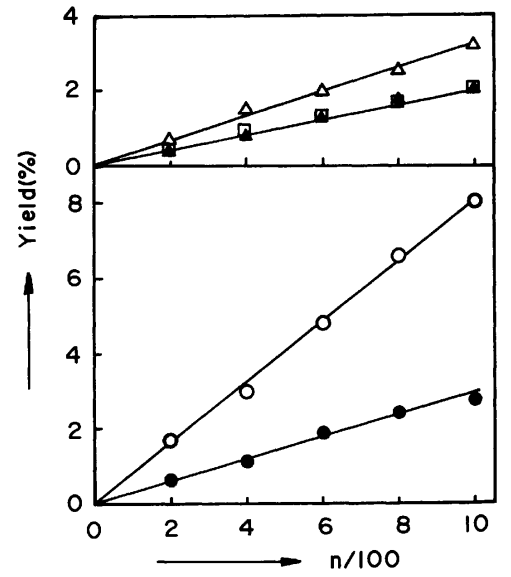

Fig. 4. Product yields as a function of pulse number. (Reactant pressure=1.0 Torr, E_0=0.257 J/pulse, ν=952.9 cm^{-1}).
●: CH≡CCl, ○: CH≡CF(×10), ▲: CH≡CH(×10), △: CH_2=CHF(×10), □: CH_2=CF_2(×10).

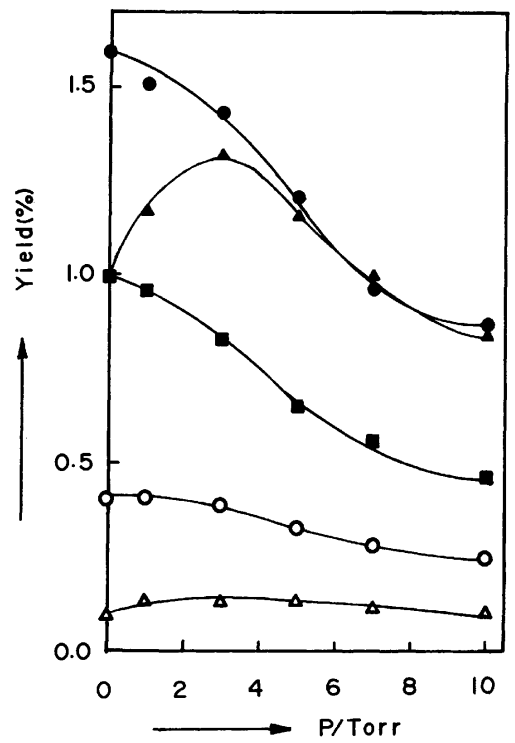

Fig. 5. Product yields as a function of N_2 pressure. (Reactant pressure=1.0 Torr, E_0=0.257 J/pulse, n=500, ν=952.9 cm^{-1}).
●: CH≡CCl, ○: CH≡CF, ▲: CH≡CH(×10), △: CH_2=CHF(×10), ■: CH_2=CF_2(×10).

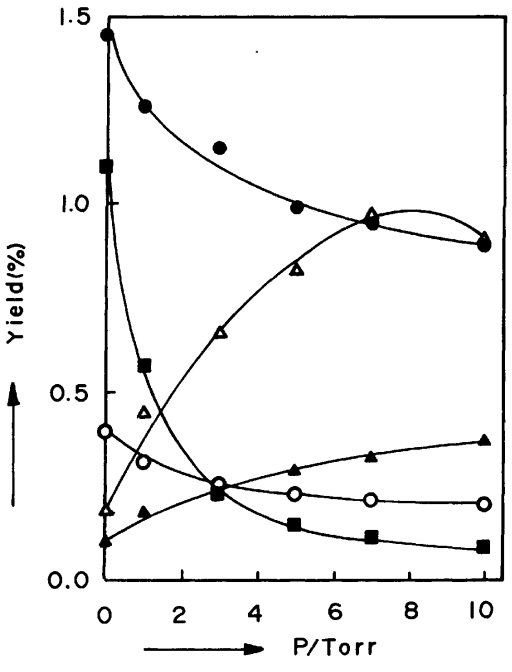

Fig. 6. Product yields as a function of H_2 pressure. (Reactant pressure=1.0 Torr, E_0=0.255 J/pulse, n=500, ν=952.9 cm^{-1}).
●: CH≡CCl, ○: CH≡CF, ▲: CH≡CH, △: CH_2=CHF(×10), ■: CH_2=CF_2(×10).

From the d value obtained (4.05×10^{-5}), the lowest critical fluence ϕ_c for CH_2=CFCl is estimated as 15.3 J/cm^2. Each product yield is plotted in Fig. 4 as a function of n. As can be seen from Fig. 4, each product yield is proportional to pulse number up to 1000, which strongly suggests that formation of each product is one shot event.

Dependence on N_2 and H_2 Pressure. Effects of buffer gas on the product yields were investigated as a function of N_2 and H_2 pressure up to 10 Torrr, the other parameters being the same and the reactant pressure kept constant at 1.0 Torr. The product yields with increasing N_2 and H_2 pressure are shown in Figs. 5 and 6, the relative yields being summarized in Table 2. Upon the addition of N_2 into the reactant, the yields of major products CH≡CCl and CH≡CF together with CH_2=CF_2 decrease in a similar manner, while the yields of CH≡CH and CH_2=CHF increase at lower N_2 pressures and then decrease at higher pressures. Rotational hole filling effect, which has been observed for small molecules,[17] is appreciable for CH≡CH and CH_2=CHF at lower pressures, but is not so clear for CH≡CCl and CH≡CF as observed in the IR emission study by Jalenak and Nogar.[4] Plausible explanation for this apparent discrepancy may be sought in the experimental arrangements: While the reported product yields in the present study represent the averages over all reaction zone corresponding to different fluence values, the observations conducted by Jalenak and Noger were near the focal point, where the fluence is considered to be rather uniform. However, the yields of CH≡CCl and CH≡CF decrease more slowly at lower pressures than those at pressures above 3.0 Torr. In the presence of H_2, the yields of CH≡CCl and CH≡CF decrease more rapidly even at lower pressures, while the yields of CH≡CH and CH_2=CHF increase significantly with increasing H_2 pressure.

In view of relative yields, those for all products show a slight increase with higher N_2 pressure, but CH_2=CF_2 yield shows a slight decrease. Upon the addition of H_2, the relative yields for CH≡CH and CH_2=CHF increase rapidly with increase in H_2 pressure, whereas that of CH_2=CF_2 decreases remarkably with higher H_2 pressure, that of CH≡CF decreasing very slightly.

Effects of Nature of Additives. Effects of collisional deactivation on the yields were examined by

Table 2. Dependence of relative yields on N_2[a] and H_2[b] pressure

	P/Torr	0.0	1.0	3.0	5.0	7.0	10.0
a)	CH≡CF	25.0	26.5	26.8	27.2	28.5	27.2
	CH_2=CF_2	6.27	6.21	5.78	5.45	5.58	5.36
	CH≡CH	6.30	7.75	9.16	9.67	9.99	9.59
	CH_2=CHF	0.86	0.85	0.90	1.16	1.07	1.23
	CH≡CCl	100	100	100	100	100	100
b)	CH≡CF	26.7	24.6	22.1	22.6	21.4	22.2
	CH_2=CF_2	7.64	4.48	2.08	1.41	1.20	0.704
	CH≡CH	6.89	14.5	21.8	29.2	33.9	40.5
	CH_2=CHF	1.25	4.27	6.51	8.37	10.2	9.90
	CH≡CCl	100	100	100	100	100	100

a) Relative yields in the presence of N_2 at E_0=0.257 J/pulse and 500 shots. Reactant pressure is 1.0 Torr for these runs. b) Relative yields in the presence of H_2 at E_0=0.255 J/pulse and 500 shots, reactant pressure being kept constant at 1.0 Torr.

Table 3. Effects of additives on product yields[a] and relative yields[b]

	Gas	He	Ar	H_2	N_2	NO	CH_4	CF_4
a)	CH≡CF	0.284	0.329	0.252	0.385	0.346	0.288	0.276
	CH_2=CF_2	0.0777	0.0817	0.0237	0.0853	0.0960	0.00500	0.0625
	CH≡CH	0.0780	0.109	0.249	0.132	0.111	0.211	0.104
	CH_2=CHF	0.0107	0.0191	0.0642	0.0151	0.0132	0.0172	0.00644
	CH≡CCl	1.08	1.21	1.14	1.41	1.77	1.23	0.909
b)	CH≡CF	26.2	27.2	22.1	27.3	19.5	23.4	30.4
	CH_2=CF_2	7.19	6.75	2.08	6.05	5.42	0.407	6.88
	CH≡CH	7.22	9.01	21.8	9.36	6.27	17.2	11.4
	CH_2=CHF	0.991	1.58	5.63	1.07	0.746	1.40	0.708
	CH≡CCl	100	100	100	100	100	100	100

a) Yields in % conversion per 500 shots at E_0=0.255 J/pulse. Reactant pressure is 1.0 Torr, those of additives being 3.0 Torr for these runs. b) Relative yields as compared to the yield of CH≡CCl.

Table 4. Product yields[a] formed by pyrolysis

CH≡CF	0.384	0.798	1.42	5.50	8.10	11.8	17.8
CH≡CCl	0.187	0.307	0.420	1.20	1.76	2.97	4.17
T_5/K[b]	1237	1273	1295	1350	1367	1385	1417
τ/μs[c]	750	825	800	815	840	800	825
P_0/Torr[d]	738	636	657	734	685	636	703
P_0°/Torr[e]	5.90	5.09	5.26	5.87	5.48	5.09	5.62

a) Product yield in % conversion. b) Temperature behind reflected shock wave. c) Dwell time. d) Total pressure behind reflected shock wave. e) Reactant gas pressure behind reflected shock wave.

adding three pairs of gases of 3.0 Torr into the parent gas of 1.0 Torr. The results are tabulated in Table 3, NO being included. On the addition of H containing molecules such as H_2 and CH_4, the increase in the yields of CH≡CH and CH_2=CHF is accompanied by significant decrease in the yield of CH_2=CF_2. Considerable decrease in the yields of CH≡CCl and CH≡CF is observed upon the addition of He and H_2 in the He–Ar and H_2–N_2 pairs.

Shock Tube Pyrolysis. Several shock tube experiments were carried out with a single-pulse shock tube. A reaction mixture of 0.8% CH_2=CFCl diluted with argon was used. Reaction temperature[13] ranged from 1237 to 1417 K, the dwell times and reactant pressures being about 810 μs and 5.5 Torr, respectively. Under these conditions, the conversions ranged from 0.57 to 23.4%. The results are summarized in Table 4. All products found in the IR photolysis of CH_2=CFCl were also obtained in the shock tube pyrolysis. Minor products CH_2=CF_2, CH≡CH, and CH_2=CHF were formed only at higher temperatures. At 1417 K, % yields of CH_2=CF_2, CH≡CH, and CH_2=CHF were 0.899, 0.434, and 0.0934, respectively, these yields being omitted from Table 4. Table 4 shows that the yield of CH≡CF, in contrast to that in the IRMPD of CH_2=CFCl, is greater than that of CH≡CCl over the temperature range examined. The branching ratio between CH≡CF and CH≡CCl formation channels increases with increasing temperature.

Discussion

Mechanism of Primary Photolysis. The elimination of molecular hydrogen halide from the parent molecule is in line with previous IRMPD studies of halogenated ethenes[18,19] together with thermal activation studies.[20,21] Other competitive dissociation channels may be available for CH_2=CFCl:[7]

$$\begin{aligned} CH_2{=}CFCl &\rightarrow CH{\equiv}CCl + HF \quad \Delta H^\circ \simeq 19.4 \pm 10 \text{ kcal/mol}, \\ &\rightarrow CH{\equiv}CF + HCl \quad \Delta H^\circ \simeq 41.3 \pm 15 \text{ kcal/mol}, \\ &\rightarrow CH_2{=}CF\cdot + Cl \quad \Delta H^\circ \simeq 80-90 \text{ kcal/mol}, \\ &\rightarrow CH{\equiv}CH + FCl \quad \Delta H^\circ \simeq 75.5 \text{ kcal/mol}. \end{aligned}$$

In the FCl elimination reaction, the vinylidenecarbene CH_2=C: very rapidly isomerizes to CH≡CH due to very low barrier for the rearrangement. Therefore, this channel can be regarded as a direct pathway to form CH≡CH. The standard enthalpy change of reactions ΔH° (1 cal_{th}=4.184 J) was estimated at 298 K.

Final product analysis shows that CH≡CCl and CH≡CF are major products in the IRMPD of CH_2=CFCl in the reactant pressure range up to 5 Torr. Coupled with the IR emission study by Jalenak and Nogar, primary photolysis processes are concluded to be direct eliminations of HF and HCl:

$$CH_2{=}CFCl + nh\nu \rightarrow CH{\equiv}CCl + HF, \quad (1)$$

$$\rightarrow CH{\equiv}CF + HCl. \quad (2)$$

Reactions 1 and 2 produce vibrationally excited HF and HCl. A significant increase in the yield of CH_2=CHF upon the addition of H_2 and CH_4 strongly suggests that C–Cl bond rupture is occurring at the same time, CH_2=CHF being formed by the H atom abstraction reaction of CH_2=CF· radical from H_2 and CH_4:

$$CH_2{=}CFCl + nh\nu \rightarrow CH_2{=}CF\cdot + Cl, \quad (3)$$

$$CH_2{=}CF\cdot + RH \rightarrow CH_2{=}CHF + R\cdot, \quad (4)$$

where RH denotes any H atom donors, CH_2=CFCl molecule itself being RH in the absence of any additives. The yield of CH≡CH as well as CH_2=CHF increases with increasing H_2 pressure, which can be attributed to the H atom abstraction reaction of CH≡C· radical from H atom donor, but not to the FCl molecular elimination.[7] The source of CH≡C· radical would be the secondary photolysis of the primary products CH≡CCl and CH≡CF:

$$\begin{aligned} CH{\equiv}CCl &\rightarrow CH{\equiv}C\cdot + Cl \quad \Delta H^\circ \simeq 100 \pm 15 \text{ kcal/mol},^{22} \\ CH{\equiv}CF &\rightarrow CH{\equiv}C\cdot + F \quad \Delta H^\circ \simeq 111 \pm 20 \text{ kcal/mol}, \\ CH{\equiv}C\cdot &+ RH \rightarrow CH{\equiv}CH + R\cdot. \quad (5) \end{aligned}$$

Effects of Pressure on Mechanism. At higher pressure where collisional effects can not be neglected, a simple threshold model is not sufficient, but the simple extended threshold model presented by Hackett *et al.*[11] is useful to discuss the photolysis mechanism in bulk experiments with focused

geometry. In the extended threshold model, collision induced dissociation by energy pooling process of excited molecules is taken into account outside the reaction zone. For multiple channel system, the relative yields from various dissociation channels are the ratios of volumes defined by the critical fluence contours which describe them.

Primary dissociation reaction induced by infrared multiphoton absorption occur inside the reaction zone. The threshold energy for C-Cl bond rupture is much greater than those of HF and HCl elimination reactions, which are estimated to be 54.7 and 56.5 kcal/mol, respectively.[4] As a result, the critical fluence for C-Cl bond scission will be also much greater than those of HF and HCl elimination. In the primary photolysis, HF and HCl elimination occurs inside the outer reaction zone, while the C-Cl bond rupture predominates inside the inner reaction zone. As the reactant pressure is increased, collision induced decomposition occurs outside the reaction zone, increasing the yields of the products generated inside the outer reaction zone, *i.e.*, CH≡CCl and CH≡CF:

$$2CH_2{=}CFCl^* \rightarrow CH_2{=}CFCl^* + CH_2{=}CFCl, \quad (6)$$

$$CH_2{=}CFCl^* \rightarrow CH{\equiv}CCl + HF, \quad (7)$$

$$\rightarrow CH{\equiv}CF + HCl, \quad (8)$$

where CH_2=CFCl* and CH_2=CFCl** denote the CH_2=CFCl molecules excited below and above the energy threshold for the unimolecular dissociation, respectively. It is not unreasonable that collision induced decomposition exits preferentially *via* the lower HF and HCl elimination channels.

The relative yield of CH≡CF increases rapidly at higher reacatant pressures (Table 1), which indicates that the yield of CH≡CF increases more rapidly than that of CH≡CCl with increasing substrate pressure. According to the simple extended threshold model, the increase in the yields of CH≡CCl and CH≡CF results from the collision induced decomposition, *viz.* Reactions 6—8. In addition, the CH≡CCl and CH≡CF bormed by the collision induced decomposition outside the reaction zone appear to remain undecomposed by the secondary photolysis, since the relative yield of CH≡CF at higher pressures is greater than that at lower pressues. On the other hand, the CH≡CCl and CH≡CF primarily formed inside the reaction zone suffer from the secondary photolysis:

$$CH{\equiv}CCl + mh\nu \rightarrow CH{\equiv}C\cdot + Cl, \quad (9)$$

$$CH{\equiv}CF + mh\nu \rightarrow CH{\equiv}C\cdot + F. \quad (10)$$

In view of the heat of reaction, C-F bond rupture would require more activation energy than that of C-Cl, indicating smaller decomposition yield for CH≡CF than that for CH≡CCl. The relative yield dependence of CH≡CF on the reactant pressure indicates, on the contrary, that more fraction of primary CH≡CF yield is decomposed than that of CH≡CCl in the secondary photolysis. If in the primary photolysis CH≡CF and CH≡CCl were formed in the vibrationally excited states of their quasicontinuum, CH≡CCl would decompose more easily than CH≡CF because of its lower energy threshold. The enhancement of CH≡CF decomposition could be attributed to the enhanced absorption of CH≡CF due to the accidental resonance with the laser excitation line at 952.9 cm^{-1}.[23] On the other hand, CH≡CCl has no absorption bands in the CO_2 laser range.

The presence of F atom in the photolysis system is supported by the formation of CH_2=CF_2. Two possible reactions are:

$$F + CH_2{=}CFCl \rightarrow \cdot CH_2CF_2Cl^* \rightarrow CH_2{=}CF_2 + Cl,$$

$$\cdot CH_2CF_2Cl^* \xrightarrow{M} \cdot CH_2CF_2Cl,$$

$$CH_2{=}CF\cdot + F \xrightarrow{M} CH_2{=}CF_2. \quad (11)$$

The addition reaction mentioned above appears to be unimportant, since CH_2=CF_2 formation *via* the addition reaction would decrease with increasing reactant pressure. On the contrary, the yield of CH_2=CF_2 increases slightly with higher substrate pressure. Another support for Reaction 11 is obtained upon the addition of H_2 and CH_4. F atom abstracts H atom very rapidly from H_2 and CH_4,[24] decreasing the yield of CH_2=CF_2 remarkably in the presence of H_2 and CH_4 (Table 3):

$$F + H_2 \rightarrow HF + H, \quad (12)$$

$$F + CH_4 \rightarrow HF + CH_3\cdot. \quad (13)$$

Furthermore, CH≡CF yield decreases significantly on the addition of H_2 as compared with that on the addition of N_2. In the presence of H_2, the recombination reaction between CH≡C· radical and F atom to regenerate CH≡CF competes with the H atom abstraction reactions of F atom and CH≡C· radical one another:

$$CH{\equiv}C\cdot + F \xrightarrow{M} CH{\equiv}CF, \quad (14)$$

$$F + H_2 \rightarrow HF + H, \quad (12)$$

$$CH{\equiv}C\cdot + H_2 \rightarrow CH{\equiv}CH + H. \quad (5')$$

In a similar manner to CH_2=CF_2, the yield of CH≡CF is decreased by the addition of H_2. Similarly, CH≡CCl yield starts decreasing more rapidly on the addition of H_2 than that upon the addition of N_2. Therefore, H atom abstraction reactions would compete with the recombination reaction between CH≡C· radical and Cl atom:

$$CH{\equiv}C\cdot + Cl \xrightarrow{M} CH{\equiv}CCl, \quad (15)$$

$$CH{\equiv}C\cdot + H_2 \rightarrow CH{\equiv}CH + H, \quad (5')$$

$$Cl + H_2 \rightarrow HCl + H. \quad (16)$$

In the He-Ar pair no chemical reactions of CH≡C· radical and the atoms with the rare gases are expected. Therefore, considerable difference in the yields of CH≡CCl and CH≡CF in the He-Ar pair could be explained in terms of the difference in the collisional quenching efficiency between He and Ar to Reactions 14 and 15. The recombination reaction between CH_2=CF· radical and Cl atom may be also occurring, but is hidden by the presence of a large amount of CH_2=CFCl parent gas:

$$CH_2{=}CF\cdot + Cl \xrightarrow{M} CH_2{=}CFCl \qquad (17)$$

The pressure behaviors of CH≡CH and CH_2≡CHF observed on the addition of N_2 (Fig. 5) can be explained qualitatively in terms of a competition between rotational hole filling and collisional deactivation. Rotational hole filling is related to the rotational relaxation of particular rotational-vibrational state depopulated by the laser pumping, while collisional deactivation is vibrational energy transfer from the laser excited species. Apparently enhanced yields of CH≡CF and CH≡CCl at lower N_2 pressures in relation to those on the addition of H_2, result from the coupled effects of rotational hole filling and the recombination reactions to regenerate CH≡CCl and CH≡CF, *viz.* Reactions 14 and 15: By the addition of N_2, the yields of CH≡CF and CH≡CCl are increased apparently by the hole filling effect. However, more fraction of the primary CH≡CF and CH≡CCl yields are decomposed by the secondary photolysis to CH≡C· radical, resulting in the increase in the yield of CH≡CH at lower N_2 pressures (Fig. 5). On the other hand, CH≡CF and CH≡CCl are regenerated to some extent by Reactions 14 and 15, resulting in an apparent increase in the yields of CH≡CF and CH≡CCl relative to that on the addition of H_2. In the case of H_2 addition, H atom abstraction reaction of CH≡C· radical, Reaction 5′ is much faster than the recombination reactions to regenerate CH≡CF and CH≡CCl, more rapid decrease in the yields of CH≡CF and CH≡CCl being observed at lower H_2 pressures than that on the addition of N_2.

Product Distribution: Summing up the above considerations of the photolysis mechanism, primary photolysis occurs *via* HF, HCl molecular eliminations, and C-Cl bond rupture, the product species being CH≡CCl, CH≡CF, and CH_2=CF· radical, respectively. Primarily formed CH≡CF and CH≡CCl are decomposed by the secondary photolysis to unknown extent, yielding CH≡C· radical. Primary product yields could be given by $[CH{\equiv}CCl]_0=[CH{\equiv}C\cdot]^{Cl}+H[CH{\equiv}CCl]$, $[CH{\equiv}CF]_0=[CH{\equiv}C\cdot]^{F}+[CH{\equiv}CF]$, and $[CH{=}CF\cdot]_0$, where $[CF{\equiv}CCl]_0$, $[CH{\equiv}C\cdot]^{Cl}$, and [CH≡CCl] denote the yield of CH≡CCl primarily formed. that of CH≡CCl decomposed, and that survived in the secondary photolysis, respectively. In the present gas chromatographic analysis of the final products, CH≡C· and CH_2=CF· radicals are converted to CH≡CH, CH_2=CHF, and CH_2=CF_2. No C_4H_2 was found in the GC analysis. The recombination reaction between two CH≡C· radicals together with that of CH_2=CF· radical would contribute to much smaller extent than the H atom abstraction reactions and the recombination reactions between the radicals and the atoms, to regenerate stable species from CH≡C· and CH_2=CF· radicals for the GC analysis. he yields of CH≡C· and CH_2=CF· could be approximated by those of CH≡CH and CH_2=CHF plus CH_2=CF_2, respectively. As can be seen from Fig. 1, the yield of CH_2=CF_2 is relatively constant in the reactant pressure range examined, indicating that the yields of CH_2=CF· radical and F atom (consequently CH≡C· radical as well) remain rather constant at these pressures. More fraction of CH≡C· and CH_2=CF· radical yields is scavenged with increasing CH_2=CFCl pressure by H atom abstraction reactions of CH≡C· and CH_2=CF· radicals from CH_2=CFCl molecules. Accordingly, the estimate of the yields of CH≡C· and CH_2=CF· radicals could be made at 5.0 Torr reactant pressure rather than at 0.2 Torr. The yields of stable species could be estimated at 0.2 Torr reactant pressure, where the contribution from the collision induced decomposition is minimized in the present substrate pressure range. In the neat IRMPD at 5.0 Torr CH_2=CFCl, the yield of CH≡CF increases by about 4 times more rapidly than that of CH≡CCl, more fraction of primarily formed CH≡CF yield being decomposed by the secondary photolysis than that of CH≡CCl inside the reaction zone. It might be fair to assume that CH≡C· radical arises from CH≡CF only. In the neat IRMPD of CH_2=CFCl, the product distribution could be estimated as $[CH{\equiv}CCl]_0:[CH{\equiv}CF]_0:[CH_2{=}CF\cdot]_0 \simeq 100:65:25$.

As is seen from Fig. 6, H_2 molecule serves to scavenge efficiently CH≡C· and CH_2=CF· radicals. The increase and decrease in the product yields become very slow at higher H_2 pressures, showing an approach to a steady product distribution. From Table 2, at 10 Torr the product distribution is obtained as $[CH{\equiv}CCl]_0:[CH{\equiv}CF]_0:[CH_2{=}CF\cdot]_0 \simeq 100:63:11$. CH_2=CFCl and H_2 as the radical scavengers give similar value for $[CH{\equiv}CF]_0$, but give considerably different value for $[CH_2{=}CF\cdot]_0$. For the present estimation of the product distribution, greater values would be preferred:

$$[CH{\equiv}CCl]_0 : [CH{\equiv}CF]_0 : [CH_2{=}CF\cdot]_0 \simeq 100 : 65 : 25 \qquad (18)$$

The C-Cl bond rupture channel would contribute significantly at high fluences, where IR emission study could not detect this channel directly, DX(X=Cl, F) emission being unobserved upon the addition of D_2CO.[4]

Comparison with Shock Tube Pyrolysis. The product distribution estimated above indicates that in the IRMPD of CH_2=CFCl, HF molecular elimination is dominant channel over that of HCl. In addition, Jalenak and Nogar have reported that the intensity ratio $I(HCl)/I(HF)=[CH{\equiv}CF]_0/[CH{\equiv}CCl]_0$ increases with increasing laser fluence (0.29—0.43 in the pulse energy range 0.2—0.9 J/pulse), showing HCl elimination might predominate at higher fluences. In the shock tube pyrolysis of CH_2=CFCl, the formation of CH≡CF is preferred channel to that of CH≡CCl, apparently showing that HCl molecular elimination, in contrast to the IRMPD, predominates over that of HF. The ratio [CH≡CF]/[CH≡CCl], however, also increases with increasing temperature (2.0—4.6 in the temperature 1237—1367 K).

In a thermal system a higher channel can predominate over the lower channel above a certain temperature, as far as some requirements for activation energy and frequency factor are satisfied, the same being true for the system subjected to uniform laser fluence. However, in a "tightly" focused geometry, according to the simple extended threshold model, branching ratio is the ratio of reaction volumes divided by the critical fluences. As a result, branching ratio of a higher channel, in general, never exceeds 1.0 in relation to the lower channel.

While in the present shock tube experiments, no direct observations of HF and HCl elimination processes were made, the IR emission study did observe the HF and HCl elimination processes, since HF and HCl emission was monitored. The Arrhenius parameters of HF and HCl elimination reactions on thermal excitations have been reported on a number of halogenated ethanes and ethenes: $\log A$=13—15 and E_a=55—85 kcal/mol for HF elimination; $\log A$=11—14 and E_a=40—70 kcal/mol for HCl elimination.[20,21,25] Generally, HCl elimination is lower channel, Ishikawa and Arai showing in their IR emission studies of CH_2ClCF_2Cl and CHFClCHFCl IRMPD that at very high fluences HF emission exceeds that of HCl.[5,6]

With the assumption that CH≡CF and CH≡CCl formation was first-order in CH_2=CFCl, the rate constants were evaluated from Table 4. Apparent activation energies and frequency factors for CH≡CCl and CH≡CF formation reactions were obtained as 64.4 and 80.0 kcal/mol, and 4.8×10^{11} and 6.4×10^{14} s^{-1}, respectively. These values seemingly fall within nomal value range quoted above, except that the values for HCl and HF elimination are exchanged each other, which would not be unreasonable, since HF elimination is the lower channel in CH_2=CFCl. The activation energy of 80.0 kcal/mol for CH≡CF formation reaction is comparable to that of the C-Cl bond rupture in CH_2=CFCl molecule. Therefore, in the present IRMPD experiments with a "tightly" focused geometry, CH≡CF would have been generated inside the inner reaction zone, where the C-Cl bond dissociation channel predominated. In reality, CH≡CF was formed by the collision induced decomposition outside the reaction zone, indicating CH≡CF formation *via* IRMPD predominated inside the outer reaction zone, but not inside the inner reaction zone. The CH≡CF formation pathway with an apparent activation energy of 80.0 kcal/mol obtained in the shock tube pyrolysis does not correspond exactly to the HCl molecular elimination which generates CH≡CF molecule at the same time, but would suggest that this channel might be closely related to the C-Cl bond rupture channel, which generates CH_2=CF· radical. As shown by the IR emission study, the HCl molecular elimination to generate CH≡CF does occur but would not predominate over HF molecular elimination at the temperatures examined in the shock tube experiments. However, the C-Cl bond rupture channel coluld predominate over those of HF and HCl elimination in the present temperature range due to its greater frequency factor and higher activation energy. Thus plausible explanation for the reversed predominance of CH≡CF formation in the shock tube pyrolysis would be that primarily formed CH_2=CF· radical undergoes secondary unimolecular decomposition:

$$CH_2{=}CFCl \rightarrow CH{\equiv}CCl + HF, \quad (19)$$

$$\rightarrow CH{\equiv}CF + HCl, \quad (20)$$

$$\rightarrow CH_2{=}CF\cdot + Cl, \quad (21)$$

$$CH_2{=}CF\cdot \rightarrow CH{\equiv}CF + H, \quad (22)$$

$$CH{\equiv}CCl \rightarrow CH{\equiv}C\cdot + Cl, \quad (23)$$

$$CH{\equiv}CF \rightarrow CH{\equiv}C\cdot + F. \quad (24)$$

Activation energy for Reaction 22 could be estimated as in the range of 40—50 kcal/mol by analogy with that for CH_2=CH· radical.[26] Due to very low activation energy for CH_2=CF· radical decomposition, sequential bond rupture might occur. The C-X(X=Cl, F) bond scissions of CH≡CCl and CH≡CF require more than 100 kcal/mol, and secondary decomposition of CH≡CCl and CH≡CF would occur to much smaller extent in the shock tube pyrolysis.

In the IRMPD of CH_2=CFCl, primarily formed CH≡CCl and CH≡CF are shown to decompose by the secondary photolysis. In a thermal system, the excitation is uniform to all species. As a result, in the shock tube pyrolysis, CH_2=CF· radical with the lowest activation energy among the primary pyrolysis products is decomposed to much greater extent. In infrared multiphoton excitation, on the other hand, the excitation depends on the vibrational states of the primarily formed species. When the primary products are in their quasicontinuum region, they can absorb any laser photons. As a result, the mechanism

in both pyrolysis and IR photolysis would become similar to each other, except for the form of excitations, *i.e.*, molecular collisions and photon absorption. In the present IRMPD experiments, CH≡CH together with CH_2=CHF shows, as noted earlier (Fig. 5), a clear bottleneck upon the addition of N_2, indicating that CH≡CCl and CH≡CF are lowerly excited below the quasicontinuum region in the primary photolysis. More enhanced decomposition of CH≡CF than that of CH≡CCl has been ascribed to the accidental resonance of the CH≡CF band with the excitation laser line. The excess energy of the dissociating parent molecule would be greater for HF and HCl molecular elimination channels with the lower energy thresholds than that for the C-Cl bond rupture channel. Since even the CH≡CCl and CH≡CF formed primarily *via* the lower channels appear to be lowerly excited, the excess energy of the dissociating parent molecule would hardly be partitioned into the vibration of the CH_2=CF· radical generated *via* the higher channel. Thus primarily formed CH_2=CF· radical would be hardly dissociated by the additional IR photon absorption, except for the accidental coincidence of CH_2=CF· absorption band with the laser excitation line.

The author would like to thank Professor Kenji Kuratani, the Institute of Space and Astronautical Science, for his encouragement and interest in this work.

References

1) J. I. Steinfeld, Ed., "Laser-Induced Chemical Processes," Plenum, New York (1981); P. A. Schultz, Aa. Sudbø, D. J. Krajnovich, H. S. Kwok, Y. R. Shen, and Y. T. Lee, *Ann. Rev. Phys. Chem.*, **30**, 379 (1979).

2) A. V. Baklnov, Yu. N. Molin, and A. K. Petrov, *Chem. Phys. Lett.*, **68**, 329 (1979).

3) T. Yano, S. Ozaki, H. Ogura, and E. Tschuikow-Roux, *J. Phys. Chem.*, submitted 1984.

4) W. A. Jalenak and N. S. Nogar, *J. Chem. Phys.*, **79**, 816 (1983).

5) Y. Ishikawa and S. Arai, *Chen. Phys. Lett.*, **103**, 68 (1983).

6) Y. Ishikawa and S. Arai, *Bull. Chem. Soc. Jpn.*, **57**, 681 (1983).

7) H. Ogura and T. Yano, *Bull. Chem. Soc. Jpn.*, submitted 1984.

8) S. Kato, Y. Makide, K. Takeuchi, and T. Tominaga, *J. Phys. Chem.*, **88**, 3977 (1984).

9) I. A. Boriev, E. B. Gordon, A. A. Nadeikin, A. I. Nikitin, V. L. Talrose, A. M. Velichko, *Chem. Phys. Lett.*, **96**, 407 (1983); *ibid.*, **105**, 555 (1984).

10) R. E. Weston, Jr., *J. Phys. Chem.*, **86**, 4864 (1982).

11) P. A. Hackett, C. Wills, M. Drouin, and E. Weinberg, *J. Phys. Chem.*, **84**, 1873 (1981).

12) K. Takeuchi, I. Inoue, R. Nakane, Y. Makide, S. Kato, and T. Tominaga, *J. Chem. Phys.*, **76**, 398 (1982).

13) Y. Makide, S. Kato, T. Tominaga, and K. Takeuchi, *Appl. phys. B*, **28**, 341 (1982); Y. Ishikawa and S. Arai, *Chem. Phys. Lett.*, **109**, 264 (1984).

14) D. C. Mann, N. Acquista, and E. K. Plyler, *J. Chem. Phys.*, **23**, 2122 (1955).

15) H. Ogura, *Bull. Chem. Soc, Jpn.*, **50**, 1044 (1977).

16) M. Gauthier, P. A. Hackett, and C. Wills, *Chem. Phys.*, **45**, 39 (1980); W. Fuss and T. P. Cotter, *Appl. Phys.*, **12**, 265 (1977).

17) I. P. Harman and J. B. Marling, *Chem. Phys. Lett.*, **64**, 75 (1979).

18) C. R. Quick. Jr. and C. Wittig, *J. Chem. Phys.*, **72**, 1694 (1980).

19) C. Reisler, F. M. Lussier, C. C. Jensen, and J. I. Steinfeld, *J. Am. Chem. Soc.*, **101**, 350 (1979).

20) J. M. Simmie, W. J. Wuiring, and E. Tschuikow-Roux, *J. Phys. Chem.*, **74**, 992 (1970); J. M. Simmie and E. Tschuikow-Roux, *ibid.*, **74**, 4075 (1970).

21) F. Zabel, *Int. J. Chem. Kinet.*, **9**, 651 (1977).

22) Heat of formation for C_2H radical used is 122±5 kcal/mol. S. W. Benson, "Thermochemical Kinetics," Wiley, New York (1968).

23) G. R. Hunt and M. K. Wilson, J. Chem. Phys., **34**, 1301 (1061).

24) M. A. A. Clyne, D. J. McKenney, and R. F. Walker, *Can. J. Chem.*, **51**, 3596 (1973).

25) P. J. Robinson and K. A. Holbrook, "Unimolecular Reactions," Wiley-Interscience, London (1972), pp. 231—233. M. V. C. Sekhar and E. Tschuikow-Roux, *J. Phys. Chem.*, **78**, 472 (1974).

26) F. P. Lossing, *Can. J. Chem.*, **49**, 357 (1971).

Vibrational Spectra of β-Lactams. I. 2-Azetidinone and Its Isotopic Compounds

Kazuhiko HANAI,* Yoshifumi MAKI, and Akio KUWAE†
Gifu Pharmaceutical University, Mitahora-higashi, Gifu 502
†*Faculty of General Education, Nagoya City University, Mizuho-ku, Nagoya 467*
(Received November 16, 1984)

The infrared and Raman spectra of 2-azetidinone and its 1-*d*, 3,3-d_2, and 1,3,3-d_3 and their ^{15}N compounds have been recorded, and the observed bands have been assigned on the basis of the isotope effects and the normal coordinate analysis. The refined force constants have reproduced the observed frequencies satisfactorily. The C–N stretching mode is strongly coupled with the N–H bending vibration to give a band near 1380 cm^{-1}. However, this coupling does not give rise to any bands corresponding to the amide II and III bands. The concentration dependence of the infrared spectrum suggests the presence of an equilibrium of monomer $\rightleftharpoons$ cyclic dimer in carbon tetrachloride solution. The solvent effects on the N–H and C=O stretching bands have also been examined.

2-Azetidinone (2-AZ) is the simplest four-membered lactam. For penicillins and cephalosporins known as β-lactam antibiotics, the relationship between their biological activities and lactam C=O stretching frequencies has been reported in the literature.[1,2] This correlation arises from the fact that the amide resonance affects both the lactam C=O stretching frequency and the ease of hydrolysis of the lactam amide bond.[1–3] Therefore, it is interesting to compare the C=O stretching force constants (or C=O frequencies) or the C–N stretching force constants with the ease of hydrolysis for simple β-lactams. The present paper deals with the vibrational analysis of 2-azetidinone and its seven isotopic compounds.

Experimental

Materials. 2-Azetidinone (2-AZ) was prepared from β-alanine by using Mukaiyama's reagent.[4] β-Alanine (0.89 g) was suspended in 1 L of acetonitrile, and 3.15 g of triphenylphosphine and 2.64 g of di-2-pyridyl disulfide were added with stirring. After the reaction mixture was refluxed for 5 h, the solvent was distilled off and the residue was subjected to sublimation under reduced pressure. The sublimate (0.44 g) was collected and recrystallized three times from hexane–chloroform; mp 77 °C. Its purity was checked by elemental analysis.

2-AZ-^{15}N was prepared from β-alanine-^{15}N, which was obtained by the same method as described in the literature[5] except that an anion exchange resin (Amberlite IRA-45) was used for the isolation of free β-alanine (an isotopic purity of starting material, ammonium-^{15}N sulfate, 99.9%, SHOKO Co., Ltd., Japan); mp 77 °C.

The α-position(to the carbonyl group)-deuterated compounds (2-AZ-3,3-d_2 and 2-AZ-3,3-d_2-^{15}N) were prepared from β-alanine-α,α-d_2 and β-alanine-α,α-d_2-^{15}N, respectively, which were obtained by the following methods. β-Alanine was dissolved in an excess of deuterium oxide, and the solvent was distilled away *in vacuo*. The β-alanine-*N*,*N*,*O*-d_3 thus obtained was dried over phosphorus pentaoxide and heated in an excess of 19.9% hydrochloric acid-*d* (CEA, France, an isotopic purity of 99.5%) under reflux for 80 h,[6] and the solution was evaporated *in vacuo* to dryness. The aqueous solution was passed through an Amberlite IRA-45 column and the water was distilled away *in vacuo*. The β-alanine-α,α-d_2 obtained was purified by recrystallization from aqueous ethanol. β-Alanine-α,α-d_2-^{15}N was obtained by hydrolysis of methyl 3-(phthalimido-^{15}N)-propionate, which was the intermediate product in the preparation of β-alanine-^{15}N, in an excess of 19.9% hydrochloric acid-*d* under reflux for 55 h, and then by treatment with Amberlite IRA-45. The crude azetidinones were recrystallized from hexane–chloroform; mp 77.5 °C for both 2-AZ-3,3-d_2 and 2-AZ-3,3-d_2-^{15}N. Their deuteration degree was checked by NMR spectroscopy and mass spectrometry and estimated to be over 95%. The N-deuterated compounds were obtained by the exchange reaction with deuterium oxide.

Spectra. The infrared spectra of the solids were recorded in KBr disks and Nujol or hexachlorobutadiene mulls on a JASCO DS-403G grating infrared spectrophotometer. The infrared spectra of carbon tetrachloride, chloroform, and benzene solutions were measured. Carbon tetrachloride and benzene were of spectrophotometric grade. Chloroform was purified by a usual method. Raman spectra in the solid state were recorded on a JEOL S-1 laser Raman spectrometer equipped with an argon ion laser (excitation line: 488.0 or 514.5 nm).

The infrared and Raman spectra are shown in Figs. 1—4, and the observed frequencies are listed in Tables 1—4 together with the calculated values.

Results and Discussion

CH_2 Group Vibrations. Assignment of some CH_2 vibrations is straightforwardly made by comparison between Figs. 1 and 2 and between Figs. 3 and 4. In Fig. 3 the two bands at 3003 and 2956 cm^{-1} are attributed to the α-CH_2 stretching vibrations, since they clearly disappear on α-C-deuteration. However, three bands of medium to strong intensity are observed in the CD_2 stretching region of the Raman spectra. The corresponding infrared absorptions are observed as weak bands at the same frequencies. The third band can be explained in terms of Fermi resonance. The highest frequency band at 2255 cm^{-1} which does not shift on N-deuteration is assigned to the CD_2 antisymmetric stretching vibration. Fermi resonance occurs probably between the CD_2 symmet-

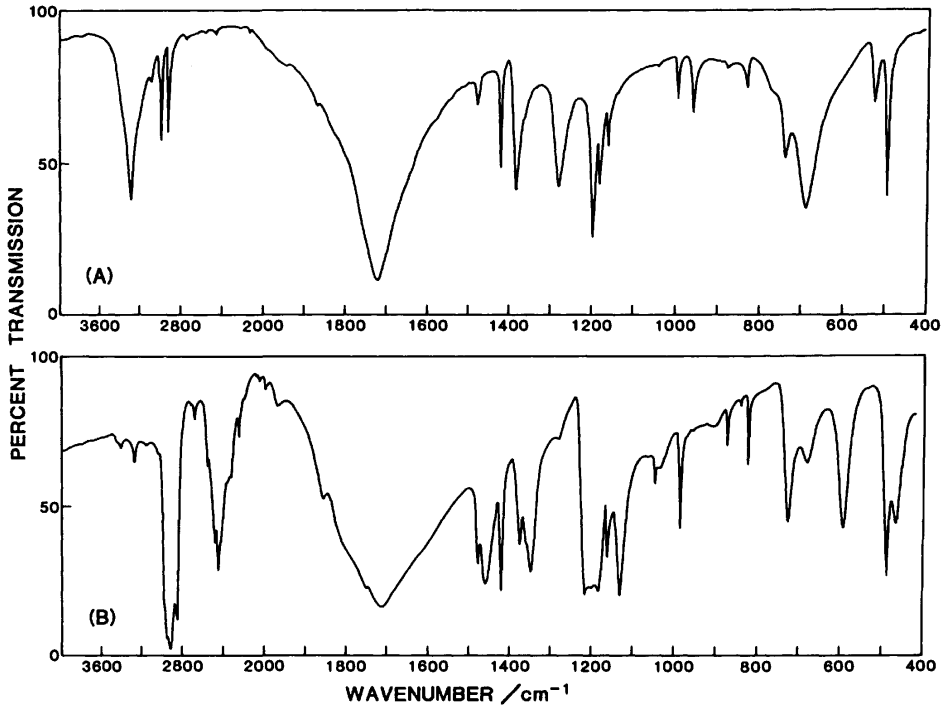

Fig. 1. (A) Infrared spectrum of 2-azetidinone (in a KBr disk); (B) infrared spectrum of 2-azetidinone-1-*d* (in a Nujol mull).

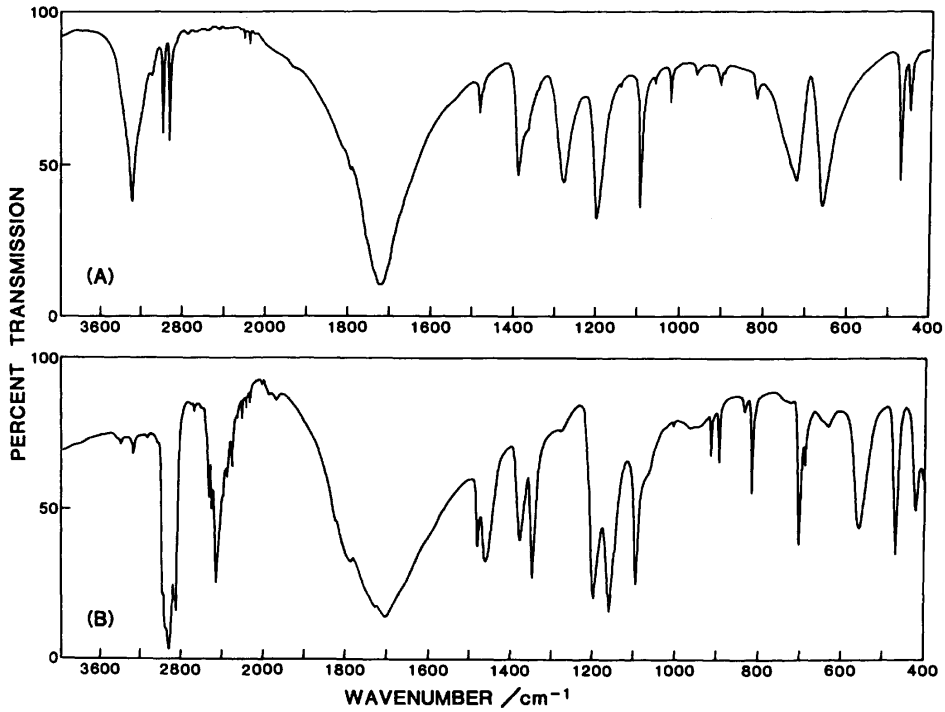

Fig. 2. (A) Infrared spectrum of 2-azetidinone-3,3-d_2 (in a KBr disk); (B) infrared spectrum of 2-azetidinone-1,3,3-d_3 (in a Nujol mull).

ric stretching vibration and the first overtone of the CD_2 bending vibration (1098 cm^{-1}) and gives rise to the two Raman bands at 2209 and 2156 cm^{-1} in 2-AZ-3,3-d_2. From the ^{15}N-isotopic shift, however, it seems that the resonance in 2-AZ-1,3,3-d_3 occurs between the CD_2 symmetric stretching and a combination of the 1350 and 815 cm^{-1} vibrations. A correction for Fermi resonance[7] has revealed that the intrinsic CD_2 symmetric stretching frequencies are 2177 cm^{-1} in 2-AZ-3,3-d_2 and 2175 cm^{-1} in 2-AZ-1,3,3-d_3.

In general a CH_2 bending vibration is the most localized mode of CH_2 deformation vibrations. The 1479 and 1422 cm^{-1} infrared bands of 2-AZ are assigned to this mode; the former is due to the β-CH_2

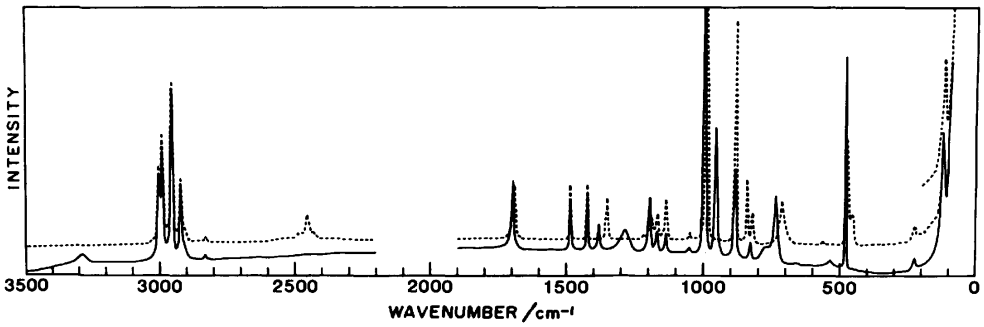

Fig. 3. Raman spectra of 2-azetidinone (solid line) and 2-azetidinone-1-*d* (broken line).

Table 1. Observed and calculated fundamental frequencies (cm^{-1}) for 2-azetidinone

	Obsd			Calcd	$\Delta\nu(^{15}N)$	P. E. D.[b]
	IR	$\Delta\nu(^{15}N)$[a]	Raman			
a'	3282 s	−9	3285 w	3306	−7	1 (100)
	2955 vw	0	2956 s	2971	0	2 (96)
	2921 m	0	2922 m	2918	0	3 (96)
	1723 vs	0	1697 m	1698	−2	4 (74), 11 (15), 13 (10)
	1479 w	0	1486 m	1484	0	7 (86)
	1422 m	0	1423 m	1426	0	6 (77), 8 (11)
	1385 ms	−14	1379 w	1381	−11	11 (28), 5 (25), 9 (19)
	1370 sh	−10	—	1368	−6	5 (62), 9 (10)
	1281 m	−7	1285 w	1246	0	9 (56), 8 (18), 10 (10), 11 (10)
	1182 m	−2	—	1158	−3	8 (58), 14 (30), 11 (14)
	999 w	−7	997 vs	1002	−8	11 (21), 14 (19), 12 (15)
	961 wm	−6	953 ms	957	−5	14 (32), 12 (28), 8 (14)
	880 vw	−7	884 m	897	−11	13 (40), 12 (28), 15 (10)
	741 m	−3	735 m	731	−1	17 (25), 12 (13), 16 (11), 15 (10)
	494 ms	−2	479 vs	477	−3	10 (81), 13 (23), 15 (16), 16 (15)
a''	3002 sh	0	3003 m	3021	0	19 (98)
	2986 m	0	2992 ms	2992	0	20 (98)
	1198 ms	−4	1193 m	1223	0	23 (45), 24 (44)
	1162 w	−1	1167 w	1173	−1	22 (27), 23 (27), 24 (20), 21 (11)
	1048 vw	−1	1051 vw	1019	−1	22 (66), 24 (16), 21 (14)
	832 w	0	828 w	836	0	21 (73), 23 (37)
	690 s	−3	—	671	−5	25 (95), 24 (37), 26 (23)
	527 wm	−1	535 vw	504	0	26 (94), 25 (22), 23 (18)
			119 m	94	0	27 (28), 28 (27), 29 (25), 30 (22)

a) ^{15}N-Isotopic shifts in the infrared spectrum. b) Potential energy distributions, 100 $F_{kk}L_{ki}^2/\lambda_i$, are given in parentheses, where contributions less than 10% have been omitted. The coordinate numbers refer to the following descriptions: 1, NH(ND) stretch; 2, α-$CH_2(CD_2)$ sym stretch; 3, β-CH_2 sym stretch; 4, CO stretch; 5, NH(ND) in-plane bend; 6, α-$CH_2(CD_2)$ bend; 7, β-CH_2 bend; 8, α-$CH_2(CD_2)$ wag; 9, β-CH_2 wag; 10, CO in-plane bend; 11, CN stretch; 12, NC^β stretch; 13, CC^α stretch; 14, $C^\alpha C^\beta$ stretch; 15, CNC^β bend; 16, NCC^α bend; 17, $CC^\alpha C^\beta$ bend; 18, $C^\alpha C^\beta N$ bend; 19, α-$CH_2(CD_2)$ antisym stretch; 20, β-CH_2 antisym stretch; 21, α-$CH_2(CD_2)$ twist; 22, β-CH_2 twist; 23, α-$CH_2(CD_2)$ rock; 24, β-CH_2 rock; 25, NH(ND) out-of-plane bend; 26, CO out-of-plane bend; 27, CN torsion; 28, NC^β torsion; 29, CC^α torsion; 30, $C^\alpha C^\beta$ torsion.

group and the latter to the α-CH_2 group as is evident from the deuteration behavior. The bands at 1281 and 1182 cm^{-1} can be assigned to the wagging vibrations of the β-CH_2 and α-CH_2 groups, respectively. The band at 1198 cm^{-1} which does not disappear on N- and C-deuteration may be ascribed to a CH_2 deformation of the *a″* species.

Amide Group Vibrations. The N-H stretching band occurs at 3282 cm^{-1} and is at a higher frequency than those of 2-pyrrolidinone (γ-butyrolactam) and 2-piperidinone (δ-valerolactam), which are observed at 3252[8,9] and 3226 cm^{-1},[9,10] respectively. The infrared C=O stretching band is observed at 1723 cm^{-1} higher in frequency than those of 2-pyrrolidinone (1690 cm^{-1})[8,9] and 2-piperidinone (1664 cm^{-1}).[9,10]

There is noncoincidence of frequencies in many bands, particularly the C=O band, between the infrared and Raman spectra. This fact suggests that the two molecules of 2-AZ form a cyclic dimer which has the center of symmetry. In this case the C=O vibration which is symmetric with respect to the center of symmetry is observed at 1697 cm^{-1} in the Raman spectrum and the asymmetric stretching mode

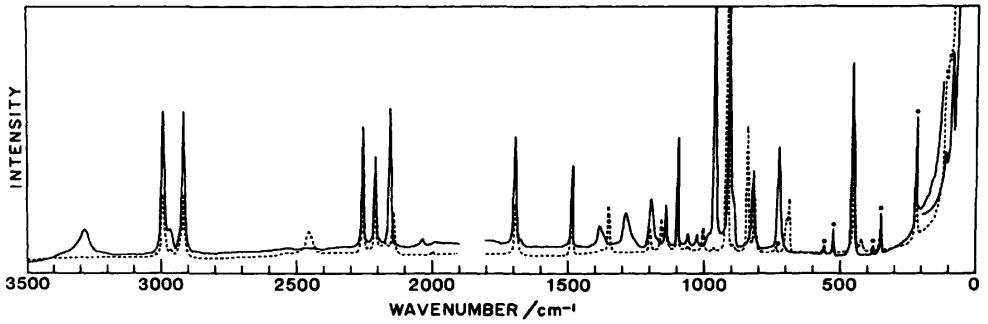

Fig. 4. Raman spectra of 2-azetidinone-3,3-d_2 (solid line) and 2-azetidinone-1,3,3-d_3 (broken line).
* The emission lines of an Ar^+ laser. At 220 cm^{-1} a weak Raman band is overlapped.

TABLE 2. OBSERVED AND CALCULATED FUNDAMENTAL FREQUENCIES (cm^{-1}) FOR 2-AZETIDINONE-1-*d*

	Obsd			Calcd	$\Delta\nu(^{15}N)$	P. E. D.[b]
	IR	$\Delta\nu(^{15}N)$[a]	Raman			
a′	2956 w	−1	2956 s	2971	0	2 (96)
	2921 m	−1	2921 m	2918	0	3 (96)
	2450 s	−17	2452 w	2416	−11	1 (100)
	1712 vs	−2	1690 m	1690	−1	4 (78), 11 (15), 13 (10)
	1481 wm	−1	1486 m	1484	0	7 (87)
	1422 m	0	1422 m	1426	0	6 (78), 8 (11)
	1350 ms	−12	1349 m	1370	−7	9 (31), 11 (29), 10 (13), 7 (10), 14 (10)
	1214 s	−4	1215 vw	1246	−1	9 (53), 8 (19), 11 (12)
	1182 s	−3	1188 w	1154	−1	5 (45), 12 (15), 4 (10)
	1129 s	−14	1134 m	1157	−20	8 (51), 11 (24), 14 (22)
	986 m	−4	987 vs	982	−1	14 (50), 8 (18)
	875 w	−6	881 vs	894	−10	12 (57), 13 (26)
	842 vw	0	839 m	857	−2	5 (31), 13 (15), 11 (11), 18 (11)
	726 ms	−1	715 m	715	−1	17 (21), 5 (13), 16 (12)
	486 s	−2	472 ms	472	−2	10 (81), 13 (22), 15 (16), 16 (15)
a″	3003 w	−1	3003 m	3021	0	19 (98)
	2987 m	−2	2990 ms	2992	0	20 (98)
	1199 s	−4	1188 w	1215	0	23 (54), 24 (37)
	1162 m	−1	1167 w	1169	−1	22 (32), 24 (27), 23 (18)
	1046 w	−1	1048 vw	1006	−1	22 (63), 24 (25), 21 (18)
	824 m	0	819 wm	832	0	21 (69), 23 (36), 24 (11)
	592 ms	−4	566 vw	601	−5	26 (65), 25 (54), 24 (13), 23 (12)
	465 ms	−3	454 w	452	−1	25 (66), 26 (51), 24 (17), 23 (10)
			117 m	90	0	27 (28), 28 (26), 29 (25), 30 (22)

a) ^{15}N-Isotopic shifts in the infrared spectrum. b) See footnote b in Table 1.

Table 3. Observed and calculated fundamental frequencies (cm^{-1}) for 2-azetidinone-3,3-d_2

	Obsd			Calcd	$\Delta\nu(^{15}N)$	P. E. D.[b]
	IR	$\Delta\nu(^{15}N)$[a]	Raman			
a'	3281 s	−9	3282 m	3306	−7	1(100)
	2918 m	0	2917 s	2920	0	3(99)
	2208 vw, 2156 vw [c] (2179)	−1, −1	2209 ms, 2156 s [c] (2177)	2153	0	2(99)
	1720 vs	0	1695 ms	1698	−3	4(74), 11(15), 13(10)
	1482 w	−1	1484 ms	1484	−1	7(88)
	1389 m	−12	1383 wm	1380	−12	5(33), 11(27), 9(18)
	1370 sh	−9	1375 sh	1367	−5	5(54), 9(14)
	1277 m	−8	1289 m	1228	−2	9(62), 11(22), 10(14)
	1095 ms	0	1098 ms	1102	−2	6(55), 14(18)
	1061 vw	0	1059 w	1069	0	14(52), 8(42)
	963 w	−7	962 vs	974	−14	12(45), 11(21), 6(10)
	906 w	−3	909 vs	866	−9	13(34), 12(25), 6(11)
	819 w	−4	821 m	798	−1	8(59), 14(13), 6(12)
	723 ms	−1	726 ms	711	−1	17(26), 6(13), 16(11)
	472 ms	−1	458 s	459	−2	10(78), 13(23), 15(15), 16(15)
a''	2985 m	0	2992 s	2993	0	20(101)
	2252 vw	0	2255 s	2237	0	19(102)
	1198 ms	−4	1193 m	1197	0	24(66), 22(15)
	1025 w	0	1024 w	1049	−2	22(74), 23(15), 24(14)
	896 vw	0	898 sh	888	0	23(63), 21(14)
	658 ms	−2	—	673	−3	25(46), 26(32), 24(31), 21(12)
	—	—	—	645	−1	25(55), 21(51), 23(14), 24(11)
	452 wm	0	453 sh	471	0	26(81), 21(33), 23(26), 25(13)
			114 w	91	−1	27(28), 28(27), 29(25), 30(22)

a) ^{15}N-Isotopic shifts in the infrared spectrum. b) See footnote b in Table 1. c) Splittings due to Fermi resonance. The values in parentheses are frequencies corrected for it.

at 1723 cm^{-1} in the infrared spectrum. 2-Pyrrolidinone and 2-piperidinone also form such dimers and show similar frequency differences[8,10] as given in Table 9.

The C-N stretching vibration is expected to be coupled with other ring stretchings or deformations to give complicated modes. However, it is possible to assign the band to which the C-N stretching vibration contributes considerably. The ^{15}N isotopic compounds are useful for this purpose. The infrared band at 1385 cm^{-1} shows a ^{15}N shift of 14 cm^{-1} to a lower frequency as given in Table 1 and can be assigned to this vibration. For 2-AZ-3,3-d_2 the corresponding band is observed at 1389 cm^{-1} with a ^{15}N shift of 12 cm^{-1}. The N-H bending bands in 2-AZ and 2-AZ-3,3-d_2 occur at 1370 cm^{-1} and show ^{15}N shifts of about 10 cm^{-1}. Although these bands are observed as poorly-characterized shoulders, the corresponding vibration of 2-AZ-3,3-d_2-^{15}N appears at 1361 cm^{-1} as a clear-cut band. 2-AZ does not show any band in the 1550 cm^{-1} region; the amide II band, which is very characteristic of *trans* secondary amides, is absent from the spectra of small ring lactams.[9] The infrared bands at 690 and 527 cm^{-1} are ascribed to the N-H and C=O out-of-plane modes, respectively, or their coupled modes.

Skeletal Vibrations. For 2-AZ the three infrared bands (999, 961, and 880 cm^{-1}), which have the strong Raman counterparts, are observed in the 1000—800 cm^{-1} region and exhibit ^{15}N-isotopic shifts of about 7 cm^{-1}. Therefore, these bands are assigned to the skeletal vibrations, although an appreciable contribution of other vibrations must be considered as can be seen from the deuteration behavior.

Combination and Overtone Bands. In addition to the bands due to the fundamentals, a number of weak bands are observed and assignable to combinations or overtones. They are listed for 2-AZ and 2-AZ-3,3-d_2 in Table 5.

The origin of a weak band around 3100 cm^{-1} was discussed for *cis* secondary amides by Miyazawa[11a,b] and explained in terms of the combination of the C=O stretching and N-H in-plane bending vibrations. In the present study this conclusion was confirmed by the ^{15}N shift; the ^{15}N substitution shifts the frequency by 16 cm^{-1} depending upon the shift of the N-H bending frequency, whereas the α-C-deuteration does not affect it.

TABLE 4. OBSERVED AND CALCULATED FUNDAMENTAL FREQUENCIES (cm^{-1}) FOR 2-AZETIDINONE-1,3,3-d_3

	Obsd			Calcd	$\Delta\nu(^{15}N)$	P. E. D.[b]
	IR	$\Delta\nu(^{15}N)$[a]	Raman			
a'	2919 m	−2	2916 m	2920	0	3(99)
	2454 s	−15	2454 wm	2416	−11	1(100)
	2207 w, 2138 w[c]	−1, −10	2209 m, 2140 m[c]	2153	0	2(99)
	(2177)		(2175)			
	1705 vs	−5	1691 m	1690	−2	4(78), 11(15), 13(11)
	1481 wm	0	1485 m	1484	−1	7(89)
	1349 m	−10	1350 m	1368	−7	9(35), 11(28), 10(12), 7(10), 13(10)
	1197 s	−6	1200 wm	1226	−2	9(59), 11(27), 10(13)
	1158 s	−15	1158 wm	1161	−17	5(47), 12(13), 4(10)
	1092 s	−1	1097 m	1094	−2	6(50), 14(34)
	1063 sh	−1	1059 vw	1060	−2	8(42), 14(36), 6(11)
	914 wm	−4	918 vs	894	−7	12(58), 5(12)
	835 w	0	842 ms	840	−4	13(29), 6(23), 5(18)
	817 m	−5	815 m	788	−1	8(46), 14(11)
	703 ms	−2	697 w	696	−1	17(22), 16(12), 6(12), 5(11)
	467 ms	−2	453 s	455	−2	10(79), 13(22), 15(15), 16(14)
a''	2987 m	0	2991 m	2993	0	20(101)
	2254 vw	0	2256 m	2237	0	19(102)
	1197 s	−6	1200 wm	1185	0	24(65), 22(20)
	1005 vw	−4	1003 wm	1039	−1	22(69), 24(22), 23(19)
	894 wm	0	896 vw	881	−1	23(59), 21(16), 22(10)
	689 wm	−1	688 m	665	−1	21(40), 26(34), 23(17), 24(10)
	556 ms	0	—	565	−4	25(64), 21(37), 26(23), 23(16) 24(12)
	420 m	0	422 w	436	−1	26(58), 25(49), 21(17), 23(16) 24(15)
			112 m	87	−1	27(28), 28(26), 29(25), 30(22)

a) ^{15}N-Isotopic shifts in the infrared spectrum. b) See footnote b in Table 1. c) Splittings due to Fermi resonance. The values in parentheses are frequencies corrected for it.

Normal Coordinate Analysis. The normal coordinate calculations were carried out according to the GF matrix method. A 2-AZ molecule was assumed to have the symmetry plane, *i.e.*, to belong to the point group C_s. This assumption seems to be reasonable from the X-ray studies on 1-substituted 2-azetidinones[12,13] and from the quantum chemical studies on 2-AZ.[14,15] The bond lengths and angles were taken from 1-(4-bromophenyl)-2-azetidinone,[12] 1-(2-bromophenyl)-2-azetidinone[13] and 5-iodomethyl-2-pyrrolidinone.[16] Table 6 gives the structural parameters used in the calculation. The internal symmetry coordinates were constructed in the usual form. A Urey-Bradley force field, to which some constants of valence force type for the *a''* species were added, was used in the calculation. In the initial calculation the force constants were transferred from *N*-acetylglycine methylamide[17] and 2-piperidinone[18] and refined by the least-squares method. The final force constants which give the best fit between the observed and calculated frequencies are given in Table 7. For the two force constants (F(HC$^{\beta}$H) and F(C$^{\alpha}$CO)), the negative values seem to be inevitable in the force field where only a small number of interaction constants are included.

The agreement between the observed and calculated frequencies is satisfactory. Although the observed frequencies of the ^{15}N compounds have not been used in the force constant refinement, the force constants in Table 7 reproduce well the ^{15}N shifts as given in Tables 1—4. It can be seen from the potential energy distributions (P. E. D.) that the vibrations below 1400 cm^{-1} are highly coupled modes as is to be expected.

In *trans* secondary amides, the N–H bending vibration is strongly coupled with the C–N stretching mode to give two bands near 1550 (amide II) and 1270 cm^{-1} (amide III). In 2-AZ the 1385 cm^{-1} band arises from mixing of the C–N stretching and N–H bending vibrations. However, this mixing does not give rise to any bands corresponding to the above characteristic frequencies for *trans* amides. The vibrational modes of *cis* *N*-methylacetamide and 2-piperidinone are interesting in connection with the

Table 5. Combination and overtone bands (cm^{-1})

	IR	Raman	Assignment
2-AZ:	3087		1723+1370=3093
	2855		1479+1385=2864
		2831	2×1422=2844
	2745		1385+1370=2755, 2×1370=2740
	2560		2×1281=2562
	2460		1281+1182=2463
	2232		1182+1048=2230
	2147		1182+961=2143
	1868		1182+690=1872
	1735		999+741=1740
	1138	1135	?
	775	775	?
2-AZ-3,3-d_2:	3086		1720+1370=3090
		2965	2×1484=2968
	2744		1720+1025=2745, 2×1370=2740
	2666		1389+1277=2666
	2559		1370+1198=2568
	2438		1482+963=2445
	2208	2209	2×1095=2190
	2156	2156	(Fermi resonance)
	2116		2×1061=2122
		2034	2×1024=2048
	1793	1794	2×896=1792, 906+896=1802
	1143	1139	?

Table 6. Bond lengths and angles used in the calculation

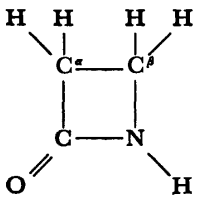

Bond length (l/Å)		Bond angle (ϕ/°)	
C=O	1.21	NCO	131.9
N-H	1.03	$C^{\alpha}CO$	135.4
C^{α}-H	1.08	$C^{\alpha}CN$	92.7
C^{β}-H	1.09	CNH	132.9
C-N	1.37	$C^{\beta}NH$	132.9
C-C^{α}	1.51	CNC^{β}	94.2
N-C^{β}	1.48	$CC^{\alpha}H$	113.5
C^{α}-C^{β}	1.55	$C^{\beta}C^{\alpha}H$	113.5
		$HC^{\alpha}H$	113.98
		$CC^{\alpha}C^{\beta}$	85.9
		$NC^{\beta}H$	112.5
		$C^{\alpha}C^{\beta}H$	119.0
		$HC^{\beta}H$	105.83
		$C^{\alpha}C^{\beta}N$	87.1

result of this calculation. Miyazawa[11a] calculated the normal vibrations of the *cis* isomer of *N*-methylacetamide and compared them with the infrared frequencies of 2,5-piperazinedione. The potential energy distributions for the former molecule show that the 1445 cm^{-1} vibration consists of the N-H bending (78%) and the C=O stretching (22%), and that the 1386 cm^{-1} vibration consists of the C-N

Table 7. Force constants[a]

K(N-H)	5.391	$F(C^{\alpha}C^{\beta}H)$	0.448
$K(C^{\alpha}$-H)	4.386	$F(NC^{\beta}H)$	0.367
$K(C^{\beta}$-H)	4.379	F(NCO)	1.586
K(C=O)	8.652	$F(C^{\alpha}CO)$	−0.0219
K(C-N)	4.786	$F(CNC^{\beta})$	0.350
$K(N$-$C^{\beta})$	1.872	$F(C^{\alpha}CN)$	0.520
K(C-C^{α})	2.578	$F(CC^{\alpha}C^{\beta})$	0.300
$K(C^{\alpha}$-$C^{\beta})$	2.561	$F(C^{\alpha}C^{\beta}N)$	0.270
H(CNH)	0.393	$\kappa(C^{\alpha})$	0.157
$H(C^{\beta}NH)$	0.0903	$\kappa(C^{\beta})$	0.0822
$H(HC^{\alpha}H)$	0.254	p(C-N, N-C^{β})	0.050
$H(C^{\beta}C^{\alpha}H)$	0.115	$p(N$-C^{β}, C^{α}-$C^{\beta})$	−0.155
$H(CC^{\alpha}H)$	0.230	$p(C^{\alpha}$-C^{β}, C-$C^{\alpha})$	−0.172
$H(HC^{\beta}H)$	0.401	p(C-C^{α}, C-N)	0.0262
$H(C^{\alpha}C^{\beta}H)$	0.179	$f_1[\gamma$(N-H)]	0.256
$H(NC^{\beta}H)$	0.367	$f_2[\gamma$(C=O)]	0.635
H(NCO)	0.759	$f_3[\tau$(C-N)]	0.030[b]
$H(C^{\alpha}CO)$	0.106	$f_4[\tau(N$-$C^{\beta})]$	0.030[b]
$H(CNC^{\beta})$	0.538	$f_5[\tau(C^{\alpha}$-$C^{\beta})]$	0.030[b]
$H(C^{\alpha}CN)$	0.170	$f_6[\tau$(C-C^{α})]	0.030[b]
$H(CC^{\alpha}C^{\beta})$	0.618	$f_{1,2}$	0.0096
$H(C^{\alpha}C^{\beta}N)$	0.169	$f_{1,3}$	0.0147
F(CNH)	0.0797	$f_{1,4}$	0.030
$F(C^{\beta}NH)$	0.848	$f_{2,3}$	−0.0554
$F(HC^{\alpha}H)$	0.0611	$f[\delta$(N-H), $\omega(C^{\beta}H_2)]$	0.0603
$F(C^{\beta}C^{\alpha}H)$	0.330	$f[\rho(C^{\alpha}H_2), \gamma$(C=O)]	0.237
$F(CC^{\alpha}H)$	0.631	$f[\rho(C^{\beta}H_2), \gamma$(N-H)]	0.195
$F(HC^{\beta}H)$	−0.0725		

a) K, H, F, p, f_i, $f_{i,j}$, and f in mdyn/Å (10^2 N/m). κ in mdyn Å (10^{-18} N m). In the constants, f_i, $f_{i,j}$, and f, γ, τ, δ, ω, and ρ denote out-of-plane bending, torsion, in-plane bending, wagging, and rocking, respectively. b) Assumed.

stretching (71%) and the C-CH_3 stretching (24%). On the other hand, in 2-piperidinone,[18] the 1425 cm^{-1} band originates in the N-H bending (56%) and the C=O stretching vibration (14%). However, the C-N stretching mode is dispersed in several vibrations, and there are no bands to which it contributes largely. From these results it seems that the *cis* CONH group does not have any characteristic bands similar to those of the *trans* CONH group except for the N-H stretching and C=O stretching bands owing to the coupling of the CONH vibrations with other modes in varying degrees.

Solution Spectra. Figure 5 shows the infrared spectra of 2-AZ in carbon tetrachloride over the concentration range from 0.06 to 0.001 M. The relative intensities of the free N-H stretching band at 3435 cm^{-1} and the hydrogen-bonded N-H band at 3236 cm^{-1} change with concentration in the expected manner, but their frequencies remain invariant within experimental deviation over the whole concentration range. Furthermore, the shape of the 3236 cm^{-1} band remains symmetric in different con-

centrations; this band does not seem to be overlapped with other bands. These findings suggest that the two species are predominantly present in carbon tetrachloride solution, namely an equilibrium of monomer $\rightleftharpoons$ dimer occurs in this solution as in 2-pyrrolidinone[8,9] and 2-piperidinone.[9,19] Possibly this associated species is the same cyclic dimer as in the crystal. The weak band at 3113 cm^{-1} is ascribed to a combination of the C=O stretching and N-H in-plane bending vibrations. The C=O stretching bands also exhibit the behavior corresponding to the above spectra. The free and hydrogen-bonded C=O stretchings occur at 1781 and 1769 cm^{-1}, respectively. The band at 1756 cm^{-1}, which is observed as a shoulder, may be ascribed to an overtone or combination.

Table 8. EFFECT OF SOLVENTS ON THE INFRARED N-H AND C=O STRETCHING FREQUENCIES (cm^{-1}) OF 2-AZETIDINONE

		Crystal (KBr disk)	CCl_4[a] (0.06 −0.001M)	$CHCl_3$[a] (0.1 −0.01M)	Benzene[a] (0.1 −0.01M)
ν_{N-H}	free	—	3435	3429	3408
	bonded	3282	3236	3260[b]	3245
$\nu_{C=O}$	free	—	1781	1767	1776
	bonded	1723	1769	—	1755[c]
			1756[c]	1753[c,d]	

a) 1 M = 1 mol dm^{-3}. b) Very weak even in 0.1 M. c) Shoulder bands. d) The intensity does not vary with concentration.

Table 8 gives the infrared N-H and C=O stretching frequencies in a few solvents. The solvent dependence of the spectra of the free molecule can be explained as follows. In chloroform solution the lactam C=O associates weakly with chloroform to give the 1767 cm^{-1} band, which is at a lower frequency by 14 cm^{-1} than the C=O band in carbon tetrachloride. On the other hand, benzene appears to interact with the lactam hydrogen to a considerable extent, since the free N-H frequency is lowest in benzene; it is observed at 3408 cm^{-1}, which is lower by 27 cm^{-1} than that in carbon tetra-

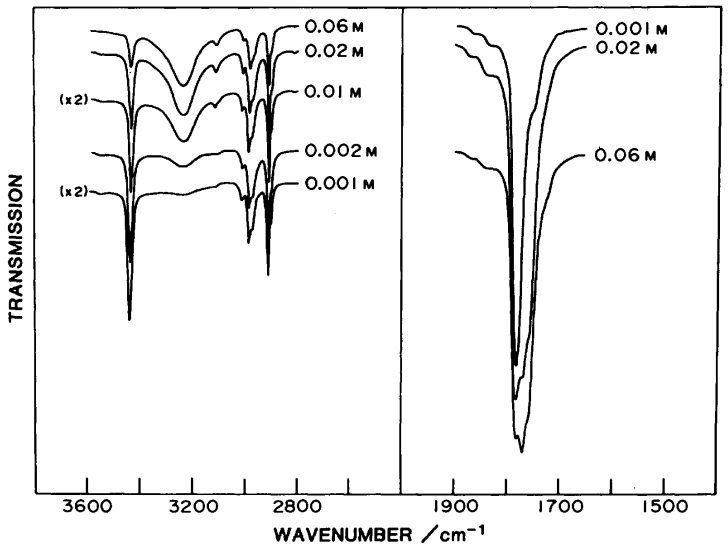

Fig. 5. Infrared spectra of 2-azetidinone in CCl_4.

Table 9. N-H AND C=O STRETCHING FREQUENCIES (cm^{-1}) OF LACTAMS[a]

	n = 4 2-Azetidinone[b]	5 2-Pyrrolidinone[c,d]	6 2-Piperidinone[d,e]	7 ε-Caprolactam[f]
Crystal(C) or Liquid(L)				
ν_{N-H}	3282(C)	3252(L)	3226(L)	3211(C)
$\nu_{C=O}$ IR	1723(C)	1690(L)	1664(L)	1664(C)
$\nu_{C=O}$ Raman	1697(C)	1658(L)	1627(L)	
CCl_4 solution				
ν_{N-H} free	3435	3453	3416	3428
ν_{N-H} bonded	3236	3204	3203	3216
$\nu_{C=O}$ free	1781	1717	1677	1676
$\nu_{C=O}$ bonded	1769	1700	1672	1672

a) Infrared frequencies unless otherwise noted. b) This work. c) Ref. 8. d) For the solution spectra, Ref. 9. e) Ref. 10. f) Ref. 9.

chloride. Other amides and lactams also exhibit this effect.[8,20,21]

Comparison with γ-, δ-, and ε-Lactams. The C=O frequencies of alicyclic ketones depend on the ring size.[22] Table 9 gives the N–H and C=O stretching frequencies of 2-AZ compared with those of five-, six-, and seven-membered lactams reported in the literature.[8,9,10] In the crystalline or liquid states, the N–H stretching and C=O stretching frequencies decrease with increase of the ring size. However, in carbon tetrachloride solution both the associated and free N–H stretching frequencies do not change regularly with the ring size, whereas the C=O stretching frequencies decrease in the expected manner. An explanation for the former behavior cannot be given, but there is a possibility that the steric effect of the CH_2 group adjacent to the N–H is responsible for it.

We wish to thank Professor Katsunosuke Machida of Kyoto University for the use of a JEOL laser Raman spectrometer. Thanks are also due to Mrs. Michiko Hosokawa and Mrs. Masako Hayashi of Gifu Pharmaceutical University for the elemental and mass spectral analyses. Throughout this work an ACOS SYSTEM 650 computer of Nagoya City University was used.

References

1) P. V. Demarco and R. Nagarajan, "Cephalosporins and Penicillins," ed by E. H. Flynn, Academic Press, New York and London (1972), Chap. 8, pp. 315—320 and references therein.

2) D. B. Boyd, "Chemistry and Biology of β-Lactam Antibiotics," ed by R. B. Morin and M. Gorman, Academic Press, New York and London (1982), Vol. 1, Chap. 5, pp. 493—498.

3) R. M. Sweet, "Cephalosporins and Penicillins," ed by E. H. Flynn, Academic Press, New York and London (1972), Chap. 7, pp. 303—308.

4) S. Kobayashi, T. Iimori, T. Izawa, and M. Ohno, *J. Am. Chem. Soc.*, **103**, 2406 (1981).

5) V. M. Rodionov and N. G. Yartseva, *Bull. Acad, Sci. U. R. S. S., Classe Sci. Chim.*, **1948**, 251 (*C. A.*, **42**, 4942a (1948)).

6) V. P. Kumarev and G. A. Almanov, *Zh. Fiz. Khim.*, **49**, 1361 (1975) (*C. A.*, **83**, 206502n (1975)).

7) A. Kuwae and K. Machida, *Spectrochim. Acta*, **35A**, 27 (1979).

8) J. A. Walmsley, E. J. Jacob, and H. B. Thompson, *J. Phys. Chem.*, **80**, 2745 (1976).

9) C. Y. S. Chen and C. A. Swenson, *J. Phys. Chem.*, **73**, 2999 (1969).

10) M. Rey-Lafon and M. T. Forel, *J. Chim. Phys., Physicochim. Biol.*, **67**, 757 (1970).

11) a) T. Miyazawa, *J. Mol. Spectrosc.*, **4**, 155 (1960); b) *ibid.*, **4**, 168 (1960).

12) G. Kartha and G. Ambady, *J. Chem. Soc., Perkin Trans. 2*, **1973**, 2042.

13) H. Fujiwara, R. L. Varley, and J. M. van der Veen, *J. Chem. Soc., Perkin Trans. 2*, **1977**, 547.

14) C. Glidewell and G. S. M. Mollison, *J. Mol. Struct.*, **72**, 203 (1981).

15) S. Vishveshwara and V. S. R. Rao, *J. Mol. Struct.*, **92**, 19 (1983).

16) J. A. Molin-Case, E. Fleischer, and D. W. Urry, *J. Am. Chem. Soc.*, **92**, 4728 (1970).

17) Y. Koyama and T. Shimanouchi, *Biopolymers*, **6**, 1037 (1968).

18) M. Rey-Lafon, M. T. Forel, and C. Garrigou-Lagrange, *Spectrochim. Acta*, **29A**, 471 (1973).

19) M. Tsuboi, *Bull. Chem. Soc. Jpn.*, **24**, 75, (1951).

20) J. A. Walmsley, *J. Phys. Chem.*, **82**, 2031 (1978).

21) I. Suzuki, M. Tsuboi, T. Shimanouchi, and S. Mizushima, *J. Chem. Phys.*, **31**, 1437 (1959).

22) B. Galabov, S. Suzuki, and W. J. Orville-Thomas, *Chem. Phys. Lett.*, **73**, 561 (1980) and references therein.

A Novel Iterative Transfer Perturbation Method and Its Application to the Extended Hückel Method

Akira IMAMURA* and Yuriko AOKI
Department of Chemistry, Faculty of Science, Hiroshima University, Higashisenda-machi, Hiroshima 730
(Received December 14, 1984)

An efficient iterative transfer perturbation method, which enabled us to take into account the contribution of the high order terms in the perturbation series without directly deriving the formulas for terms above third order, is proposed. Consequently we can calculate an infinite series of higher order terms in the perturbation expansion by applying this method iteratively until convergence in the expansion is obtained. By applying this method to methanol, the validity and applicability of our theory are shown at the level of the extended Hückel method.

Various types of perturbation methods have been developed in the field of quantum chemistry and have been applied to many interesting problems in physical chemistry. However, in many cases, the higher order terms in the perturbation expansion have been neglected past the second or the third order because of the intractability in the explicit expression of these terms. However, this truncation often leads to unreliable results.

In the present article, we propose a novel perturbation method in the Hartree-Fock-Roothaan formalism, in which the higher order terms are automatically transfered to the first and second order terms by iteration of this perturbation expansion, that is, by carrying over the perturbation terms into the next zero-order terms. This iterative procedure should be repeated until convergence in the density matrix and the total energy are achieved. For the simple test of this perturbation method, we applied this method to a simple system (methanol and its analogs) at the level of the extended Hückel method,[1] since the fundamental points in the perturbation method should be included even at the level of the extended Hückel method. In these test calculations, it is found that this novel perturbation method is able to remove completely the error caused by neglecting the terms of higher than second order.

Theoretical

The perturbation expansion is carried out with Roothaan's Hartree Fock SCF matrix equation,

$$FC = SCE \tag{1}$$

where F is the Fock matrix, C is the coefficient matrix, S is the overlap matrix and E the orbital energy matrix. These orbitals are normalized through the matrix equation

$$C^{\mathrm{T}}SC = 1. \tag{2}$$

Here, C^{T} is the transpose of the C matrix.

At the beginning, each matrix of Eq.1 is expanded in a perturbation series as follows

$$F = F^{(0)} + F^{(1)} + F^{(2)} + \cdots, \tag{3}$$

$$S = S^{(0)} + S^{(1)}, \tag{4}$$

$$C = C^{(0)} + C^{(1)} + C^{(2)} + \cdots, \tag{5}$$

$$E = E^{(0)} + E^{(1)} + E^{(2)} + \cdots, \tag{6}$$

where in the overlap matrix, all the difference between the zero order term and the perturbed terms is included in the first-order perturbed term, $S^{(1)}$. On the other hand, in the Fock matrix, the integral for the perturbed terms includes the change in the density matrix, and this density matrix should be expanded in an infinite series because of Eq. 5. Consequently, the Fock matrix given by Eq. 3 should be expanded also in an infinite series. For the zero-order terms, the following equations are satisfied.

$$F^{(0)}C^{(0)} = S^{(0)}C^{(0)}E^{(0)} \tag{7}$$

$$C^{(0)\mathrm{T}}S^{(0)}C^{(0)} = 1 \tag{8}$$

By using formulas from general perturbation theory for the extended Hückel method, which had been reported previously,[2] the matrix elements of the perturbed matrices $C^{(1)}$, $C^{(2)}$, $E^{(1)}$, and $E^{(2)}$ are given as follows:

$$\begin{aligned} C_{ti}^{(1)} = & -\sum_{\substack{j \\ (j\neq i)}}{}' C_{tj}^{(0)}/(E_j^{(0)} - E_i^{(0)}) \\ & \sum_r\sum_s (F_{rs}^{(1)} - S_{rs}^{(1)}E_i^{(0)})C_{rt}^{(0)}C_{sj}^{(0)} \\ & -\frac{1}{2}C_{ti}^{(0)}\sum_r\sum_s C_{rt}^{(0)}C_{si}^{(0)}S_{rs}^{(1)}, \end{aligned} \tag{9}$$

$$E_i^{(1)} = \sum_r\sum_s (F_{rs}^{(1)} - S_{rs}^{(1)}E_i^{(0)})C_{ri}^{(0)}C_{si}^{(0)}, \tag{10}$$

$$\begin{aligned} C_{ti}^{(2)} = & -\sum_{\substack{j \\ (j\neq i)}}{}' C_{tj}^{(0)}/(E_j^{(0)} - E_i^{(0)}) \\ & [\sum_r\sum_s \{F_{rs}^{(2)} - (S_{rs}^{(2)}E_i^{(0)} + S_{rs}^{(1)}E_i^{(1)})\}C_{ri}^{(0)}C_{sj}^{(0)} \\ & + \sum_r\sum_s \{F_{rs}^{(1)} - (S_{rs}^{(0)}E_i^{(1)} + S_{rs}^{(1)}E_i^{(0)})\} \\ & \times C_{ri}^{(1)}C_{sj}^{(0)}] \\ & -\frac{1}{2}C_{ti}^{(0)}\sum_r\sum_s \{C_{ri}^{(1)}C_{si}^{(1)}S_{rs}^{(0)} \\ & + (C_{ri}^{(1)}C_{si}^{(0)} + C_{ri}^{(0)}C_{si}^{(1)})S_{rs}^{(1)}\}, \end{aligned} \tag{11}$$

$$E_i^{(2)} = \sum_r \sum_s (F_{rs}^{(2)} - S_{rs}^{(1)} E_i^{(1)}) C_{ri}^{(0)} C_{si}^{(0)} + \sum_r \sum_s \{F_{rs}^{(1)} - (S_{rs}^{(0)} E_i^{(1)} + S_{rs}^{(1)} E_i^{(0)})\} \times C_{ri}^{(1)} C_{si}^{(0)}, \quad (12)$$

where i,j denote molecular orbitals and r,s atomic orbitals, and $\sum_j'$ means that the summation covers all levels except i. Strictly speaking, Eqs. 9—12 should be solved iteratively since the Fock matrices $F_{rs}^{(1)}$ and $F_{rs}^{(2)}$ include the perturbed density matrix that is calculated by using $C_{ri}^{(1)}$ and $C_{ri}^{(2)}$. By using Eqs. 9—12, we can obtain the first and the second order terms of C and E.

Next, we redefine the zero-order terms for C and E as follows:

$$C^{(0,1)} = C^{(0)} + C^{(1)} + C^{(2)}, \quad (13)$$

$$E^{(0,1)} = E^{(0)} + E^{(1)} + E^{(2)}, \quad (14)$$

where matrix elements of $C^{(1)}$ and $C^{(2)}$ are given by Eqs. 9 and 11 and that of $E^{(1)}$ and $E^{(2)}$ by Eqs. 10 and 12. The superscript (0,1) in $C^{(0,1)}$ and $E^{(0,1)}$ denotes the zero-order term defined by Eqs. 13 and 14 in the first iteration. In order that $C^{(0,1)}$ and $E^{(0,1)}$ are the zero-order terms, the corresponding zero-order Fock matrix $F^{(0,1)}$ and the overlap matrix $S^{(0,1)}$ must fulfill the following relations:

$$F^{(0,1)} C^{(0,1)} = S^{(0,1)} C^{(0,1)} E^{(0,1)}, \quad (15)$$

$$C^{(0,1)\mathrm{T}} S^{(0,1)} C^{(0,1)} = 1. \quad (16)$$

In other words, $F^{(0,1)}$ and $S^{(0,1)}$ are determined from the Eqs. 15 and 16. The explicit expressions for $S^{(0,1)}$ and $F^{(0,1)}$ are obtained by using $C^{(0,1)}$ and $E^{(0,1)}$ as follows. Multipling the Eq.16 on the left by $(C^{(0,1)\mathrm{T}})^{-1}$, on the right by $(C^{(0,1)})^{-1}$, the overlap matrix of the zero-order is

$$S^{(0,1)} = (C^{(0,1)\mathrm{T}})^{-1}(C^{(0,1)})^{-1} = (C^{(0,1)} C^{(0,1)\mathrm{T}})^{-1} = (P^{(1)})^{-1} \quad (17)$$

where the matrix $P^{(1)}$ has its element given by the Eq. 18.

$$P_{rs}^{(1)} = \sum_i^{\mathrm{all}} C_{ri}^{(0,1)} C_{si}^{(0,1)} \quad (18)$$

Eq. 15 is multiplied by $(C^{(0,1)})^{-1}$ on the right followed by a substitution of Eq. 17.

$$F^{(0,1)} = S^{(0,1)} C^{(0,1)} E^{(0,1)} (C^{(0,1)})^{-1} = (C^{(0,1)\mathrm{T}})^{-1}(C^{(0,1)})^{-1}(C^{(0,1)} E^{(0,1)} (C^{(0,1)})^{-1} = (C^{(0,1)\mathrm{T}})^{-1} E^{(0,1)} (C^{(0,1)})^{-1} = (P_E^{(1)})^{-1}, \quad (19)$$

where, $P_E^{(1)}$ is defined as follows:

$$P_E^{(1)} = \sum_i^{\mathrm{all}} C_{ri}^{(0,1)} C_{si}^{(0,1)} / E_i^{(0,1)}. \quad (20)$$

The perturbed terms in the first iteration are defined by using the Eqs. 3 and 4 as follows:

$$F^{(1,1)} = F - F^{(0,1)} = (F^{(0)} + F^{(1)} + F^{(2)}) - F^{(0,1)}, \quad (21)$$

$$S^{(1,1)} = S - S^{(0,1)} = (S^{(0)} + S^{(1)}) - S^{(0,1)}. \quad (22)$$

In the Eq. 21, the expansion is truncated at the second order term. $F^{(2,1)}$ should be calculated by including $C^{(1,1)}$ and $C^{(2,1)}$. In the present perturbation method, the perturbed terms change their value each iteration and the higher order terms in the perturbation expansion are incorporated automatically by iterations of the above-mentioned procedure. Therefore, for the t-th iteration, the following general expressions are obtained.

Each matrix of Eq. 1 is expanded in the perturbation series as follows:

$$F = F^{(0,t)} + F^{(1,t)} + F^{(2,t)}, \quad (23)$$

$$C = C^{(0,t)} + C^{(1,t)} + C^{(2,t)} + \cdots, \quad (24)$$

$$S = S^{(0,t)} + S^{(1,t)}, \quad (25)$$

$$E = E^{(0,t)} + E^{(1,t)} + E^{(2,t)} + \cdots, \quad (26)$$

where the subscript t denotes the iterative step. Throughout this process the zero order coefficient matrix and orbital energy matrix are obtained as follows, respectively:

$$C^{(0,t)} = C^{(0)} + C^{(1)} + C^{(2)}, \quad (27)$$

$$E^{(0,t)} = E^{(0)} + E^{(1)} + E^{(2)}. \quad (28)$$

By means of these equations perturbation calculations are iterated until convergence on $C^{(0,t)}$ and $E^{(0,t)}$ is obtained. The matrices $C^{(1)}$, $E^{(1)}$, $C^{(2)}$, and $E^{(2)}$ can be obtained for each iteration from Eps. 9—12 derived by the usual perturbation expansion up to second order.

Calculations

In the present work, the test calculations for the iterative transfer perturbation method are carried out using the extended Hückel method. The concrete procedures for this test calculation are as follows:

1. The Hamiltonian $F^{(0,0)}$, overlap integral $S^{(0,0)}$, eigenvector $C^{(0,0)}$ and energy $E^{(0,0)}$ matrices obtained by the extended Hückel method in the non-perturbed system are stored as the zero order matrix.
2. In a similar manner, the Hamiltonian matrix and overlap integrals in the perturbed system are also obtained.
3. The difference between the non-perturbed system 1 and the perturbed system 2 for the Hamiltonian matrix and the overlap integrals are taken to be the first order terms, $F^{(1,0)}$ in the Eq. 23 and $S^{(1,0)}$ in the Eq. 25, respectively.
4. From these matrix elements the first and second order terms in the eigenvector and energy, that is $C^{(1)}$, $E^{(1)}$, $C^{(2)}$, and $E^{(2)}$ in the Eqs. 9—12, are obtained by using general perturbation theory for the extended Hückel method. Theoretical details of this perturbation method have been extensively described in the previous paper.[2]
5. By using the Eqs. 13 and 14, we can obtain the next zero order terms in the eigenvector $C^{(0,1)}$ and energy $E^{(0,1)}$ equal

to the sum up to second order terms in this iterative step; then the next iteration is started.

6. Using the matrices $C^{(0,1)}$ and $E^{(0,1)}$ obtained at 5, zero-order terms in the Hamiltonian $F^{(0,1)}$ and the overlap $S^{(0,1)}$ matrices in the next iterative step are determined again from the Eqs. 17—20.

7. The first order terms of the Hamiltonian and the overlap integrals in the iterative step are defined as the difference between the zero-order terms obtained in 6 and the sum up to the initial second order term obtained in 1 and 2, that is, $F^{(1,1)}$ in an Eq. 21 and $S^{(1,1)}$ in an Eq. 22, respectively.

8. If these first order terms obtained in 7 are larger than some fixed threshold value, the succeeding iteration is restarted by returning to 4. This means that if there are relatively large contributions of the terms higher than second order, the third and fourth order terms are introduced in succession. These perturbation calculations are iterated until the first order terms converge to a negligibly small value.

Results

This iterative transfer perturbation theory was tested on methanol with bond distances of C-O=1.43 Å (Fig. 1(a)) for the zero-order terms and C-O=1.63 Å (Fig. 1(b)) for the perturbed terms. Furthermore, this procedure was also applied to the perturbed system shown in Fig. 1(c), in which N is substituted for C. The results of these perturbation calculations are

TABLE 1. THE ORBITAL ENERGIES AND THE HIGHEST OCCUPIED MOLECULAR ORBITALS FOR THE NON-PERTURBED AND THE PERTURBED SYSTEMS BY USING THE EXTENDED Hückel AND PERTURBATION CALCULATIONS

0-th order	Perturbed system			
CH_3OH	CH_3OH		$+NH_3OH$	
C-O (1.43 Å) O-H (0.96 Å)	C-O (1.63 Å) O-H (0.96 Å)	C-O (1.63 Å) O-H (0.96 Å)	N-O (1.43 Å) O-H (1.05 Å)	N-O (1.43 Å) O-H (1.05 Å)
E. H.	E. H.	I. P.	E. H.	I. P.
		Orbital energy (in eV)		
34.423	32.052	32.054	14.040	14.041
9.745	9.454	9.454	3.225	3.231
9.587	9.411	9.411	2.301	2.301
7.917	6.764	6.764	1.577	1.572
−0.671	−5.433	−5.433	−4.953	−4.953
−13.761	−14.167	−14.167	−14.281	−14.281
−14.037	−14.421	−14.422	−14.719	−14.719
−15.571	−15.433	−15.433	−16.924	−16.924
−15.788	−15.507	−15.508	−17.123	−17.124
−16.573	−16.302	−16.303	−17.479	−17.479
−23.072	−23.674	−23.675	−26.819	−26.820
−33.850	−33.472	−33.472	−34.808	−34.808
		HOMO		
H1				
0.3202 (1s)	−0.2968	0.2968	0.1675	0.1675
H2				
−0.0000 (1s)	0.0000	0.0000	0.0000	−0.0000
H3				
−0.3202 (1s)	0.2968	−0.2968	−0.1675	−0.1675
C4				
−0.0000 (2s)	−0.0000	0.0000	0.0000	0.0000
0.0000 ($2p_x$)	0.0000	0.0000	0.0000	0.0000
0.4176 ($2p_y$)	−0.4082	0.4082	0.2927	0.2927
0.0000 ($2p_z$)	0.0001	0.0000	0.0000	0.0000
O5				
0.0000 (2s)	−0.0000	0.0000	0.0000	0.0000
0.0000 ($2p_x$)	−0.0000	0.0000	−0.0000	0.0000
0.7768 ($2p_y$)	0.7773	−0.7773	−0.9465	−0.9465
0.0001 ($2p_z$)	−0.0001	0.0000	−0.0000	0.0000
H6				
0.0000 (1s)	0.0000	0.0000	−0.0000	0.0000

E. H.: Extended Hückel method. I. P.: Iterative transfer perturbation method.

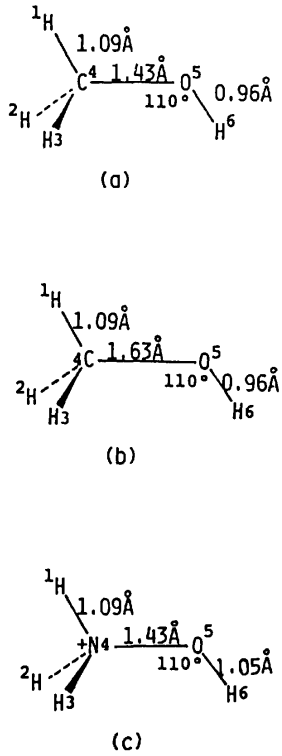

Fig. 1. (a) Structure of methanol in the non-perturbed system. (b), (c) Structures of model molecules in the perturbed systems.

listed in Table 1 compared to the direct extended Hückel calculations. The first column of Table 1 contains the orbital energies and coefficients of the highest occupied molecular orbitals for the non-perturbed system in Fig. 1(a) from the usual extended Hückel method. The second and third columns are for the perturbed system shown in Fig. 1(b) and the fourth and fifth are for the one in Fig. 1(c), showing the extended Hückel and iterative transfer perturbation methods for comparison. In Table 2 the energy of the highest occupied molecular orbitals are listed each iteration for the perturbed systems shown in Fig. 1(b) and (c). After the orbital energies have quickly converged within four iterations (Table 2), they are in good agreement with the direct method (Table 1). This shows that the approximations made within this iterative transfer perturbation method are comparable to those made in the general extended Hückel method.

Table 2. Energies of the highest occupied molecular orbitals for the perturbed systems shown in Fig. 1(b) and Fig. 1(c) each iteration

Iteration	CH_3OH	$+NH_3OH$
0	−13.761486	−13.761486
1	−14.174451	−14.312610
2	−14.167489	−14.280391
3	−14.167489	−14.280800
4	−14.167489	−14.280800

Conclusions

We could concisely show the validity and the applicability of this method that incorporates the higher order terms in the perturbation expansion in a fairly simple way. There is little advantage of this method compared to direct extended Hückel calculations in the present case using these simple molecules. But it should be mentioned further that this perturbation method can be applied also in the case that a polymer interacts with an impurity molecule at short range and the change of the charge is localized within only a part of the polymer. This approach is rather straightforward if the perturbation method for the interaction between polymers[3] is applied to the above-mentioned problem. This method may be of use to us in the interpretation of various phenomena in the electronic states of biopolymers. However, for the general use of this method it is indispensable to formulate equations, in which the divergence due to the nearly degenerate molecular orbitals is avoided, as has already been done by O'Shea and Santry.[4] Based on this, work is in progress applying this iterative transfer perturbation method to *ab initio* calculations on polymer systems.

Numerical calculations were performed on the HITAC M-200H computer system at the Information Center of Hiroshima University. The authors are grateful to Dr. D. Munch for his stimulating suggestions.

References

1) R. Hoffmann, *J. Chem. Phys.*, **39**, 1397 (1963).
2) A. Imamura, *Mol. Phys.*, **15**, 225 (1968).
3) A. Imamura, S. Suhai, and J. Ladik, *J. Chem. Phys.*, **76**, 6067 (1982).
4) S. F. O'Shea and D. P. Santry, *Theor. Chim. Acta*, **37**, 1 (1975).

Characterization of α- and β-Dodecamolybdophosphate Complexes Formed in Aqueous Solutions Including Acetonitrile, Acetone, or Dioxane

Toshitaka HORI* and Taitiro FUJINAGA†
Department of Chemistry, College of Liberal Arts and Sciences, Kyoto University, Sakyo-ku, Kyoto 606
†*Nara University of Education, Takabatake-cho, Nara 630*
(Received September 5, 1984)

On the basis of a spontaneous conversion reaction of molybdophosphate (formed in an aqueous medium including acetonitrile, acetone, or dioxane), the existence of β-modification of dodecamolybdophosphate has been substantiated. The conversion reaction was highly affected by the presence of the organic solvents. In the absence and/or the presence of the organic solvent of less than 20% by volume, the reaction proceeded instantaneously and, in consequence, β-modification practically did not exist, but α-modification existed entirely. Whereas, in the presence of the organic solvent ranging from 30 to 60%, β-modification was so stable, it could be observed for a fairly long duration. However, it was still thermodynamically unstable and finally converted to α-modification at a certain rate depending on the concentration of the organic solvent. With more of the organic solvent than 65%, the formation of β-modification and thence α-modification, were prohibited. As a result of these facts, α- and β-modifications were individually prepared in solutions consisting of 0.05 M Mo(VI)/1.2 M HCl/40% acetonitrile. On each modification thus formed, a chemical reduction (with such metals as nickel, iron, or lead) and solvent-extraction isolation (using chloroform as an auxiliary solvent) were performed. The inherent absorption spectra of the two modifications were clearly distinguished in both oxidized yellow and reduced blue forms. The utility of β-modification in a sensitive spectrophotometric determination of phosphate ion was also discussed.

It has been well known that the yellow color of molybdophosphate in aqueous solutions is markedly enhanced by the presence of certain water-miscible organic solvents such as acetone,[1,2,3] dioxane,[4] ethanol,[5] tetrahydrofuran,[6] and acetonitrile.[7] The enhanced yellow color has been widely utilized for spectrophotometric determinations of the orthophosphate ion.

Chalmers and Sinclair investigated[2] in detail the color enhancement in an aqueous acetone medium and ascribed it to the formation of β-modification of dodecamolybdophosphate (abbreviated as β-molybdophosphate, hereafter). This modification might exhibit higher absorbances in the near-ultraviolet region than the ordinary α-modification of dodecamolybdophosphate (abbreviated α-molybdophosphate). They explained that β-molybdophosphate might be stabilized to exist in an aqueous acetone medium since acetone molecules preferably replace with water molecules in the coordination sphere of the molybdate complex and suppress the hydrolytic dissociation of the complex (which dissociation would be the initial step for the spontaneous conversion of β to α). On the basis of these concepts, Chalmers and Sinclair[2] postulated a possible structure for β-molybdophosphate. The similar structure was found, in fact, by Matsumoto *et al.*[8] in β-modification of dodecatungstosilicate. Nevertheless, as for molybdophosphate, the spontaneous conversion reaction itself, which must be the most inherent property to β-molybdophosphate and is most likely to occur from the analogy with the β to α conversion in molybdosilicate,[9] has not been substantiated yet. It is only known that the two modifications of α and β would also exist in molybdophosphate and would be distinguishable from their different intensities in the yellow color.

Employing acetonitrile as an organic solvent, we[10] previously investigated the color enhancement of molybdophosphate as a function of the concentration of the solvent. As a result, it was found that the solvent had two different effects on the yellow color.

The first effect was observable at acetonitrile concentrations of around 5% by volume. It became evident with an increase of the solvent up to 20%, and finally saturated with more of the solvent. The most notable point regarding this effect was that it was a reversible reaction, that is, the yellow color of molybdophosphate was intensified up to the same extent in either case when the organic solvent was present before or was added after the formation of the molybdate complex. This effect might be attributable to the reversible formation equilibrium of α-molybdophosphate, which is favoured by the presence of the organic solvent.

The second effect of the organic solvent was only appreciated when molybdophosphate was formed in the presence of acetonitrile more than 30%. Most strikingly, it involved the irreversible reaction. Actually, the yellow color had an intensity approximately twice as strong as that due to the first effect, but faded gradually on standing and reached the same intensity as that attained by the first effect. This extraordinary intense yellow color was then estimated to be due to β-molybdophosphate and the fading of the yellow color was due to the conversion of β to α-molybdophosphate.

According to these previous observations,[10] we report in the present paper on preparation of individual α- and β-molybdophosphate using an aqueous

medium containing acetonitrile, acetone, or dioxane. Specifically, regarding β-molybdophosphate, its inherent properties were carefully investigated and distinguished from those of the well-established α-molybdophosphate. The so-called solvent effects on the color development of molybdophosphate can be thoroughly explained in terms of the charactersistic conversion reaction between α and β. Some confusions which have been hitherto experienced regarding the different intensities of the yellow color of molybdophosphate, are considered consistent.

Experimental

Reagents. A standard 0.100 M (1 M=1 mol dm^{-3}) phosphate solution and 0.5 M molybdate(VI) solution were prepared from KH_2PO_4 and $Na_2MoO_4 \cdot 2H_2O$, respectively.

A mixed molybdate reagent, with which phosphate ion was reacted to form molybdophosphate, was prepared by mixing 20 cm^3 of a 0.5 M molybdate(VI) solution, 20 cm^3 of concentrated hydrochloric acid and the desired amounts (usually 80 cm^3) of acetonitrile, and diluting to 200 cm^3 with water. The acetonitrile (Wako Pure Chemicals, GR grade) was used without further purification. The mixed reagent, otherwise indicated, was a 40%(v/v) acetonitrile solution. It was stored in a polyethylene bottle without appreciable deterioration for at least one month. Also, a mixed molybdate reagent in acetone or dioxane was similarly prepared using acetone and dioxane (Wako Pure Chemicals, GR grade) in place of acetonitrile.

Nickel metal with 99.95% purity (in a sponge type and pulverized to a size to pass through a 300-mesh filter) was used for the reduction of molybdophosphate. The metal could be used as supplied (Wako Pure Chemicals), but, if necessary, further purified by washing with 40% aqueous acetonitrile including 1.2 M hydrochloric acid. It was subsequently washed with 40% aqueous acetonitrile and dried in the open air for 2 d. Iron with 99.99% purity (in a sponge type and pulverized to pass through a 100-mesh filter), cobalt with 99% purity (in a powder form), copper with 99.85% purity (in a powder form), and lead with 95% purity (in a powder form) were also commercially available products and were used in the comparative studies with the nickel reduction. These metals were usually weighed into a 60-mg dose and wrapped in glazed paper.

As an auxiliary solvent, chloroform was used after the removal of a stabilizer ethanol, just before use, by washing three times with water and drying over anhydrous sodium sulfate.

Apparatus. A Shimadzu UV 240 automatic recording spectrophotometer equipped with a constant-temperature housing (kept at 25±0.2 °C) for the cuvettes, was used. Quartz cuvettes with path-lengths of 1 (with a glass-stopper), 0.2, and 0.1 cm were properly used according to the magnitude of the absorbances of the samples.

Results and Discussion

Formation and Conversion of β-Molybdophosphate in Aqueous Media Including Acetonitrile, Acetone, or Dioxane. At various concentrations of acetonitrile in the reaction medium, the formation of molybdophosphate was monitored by measuring the changes in absorbance at 420 nm according to the following techniques.

Into a quartz cuvette having a path-length of 1 cm, take a 4-cm^3 aliquot of mixed molybdate reagent composed of 0.05 M Mo(VI)/1.2 M HCl/ acetonitrile ranging from nil to 70% (v/v), and equilibrate it at 25 °C. Into the reagent solution, inject 40 mm^3 of 0.1 M phosphate standard solution using a calibrated micropipette. Shake it quickly. Then, set the reaction time to zero and record the absorbance change with regard to time.

The typical absorbance-time curve obtained in the 40% acetonitrile medium is shown in Fig. 1. It can be seen from the curve that the absorbance increases rapidly and reaches a higher stational level (1.600 in absorbance unit) within 2 s, and then decreases quite slowly, until it goes down to a lower constant level (0.970 in abs. unit). The higher absorbances temporarily observed at the initial period seem to be attributable to the formation of an extraordinary molybdophosphate other than the ordinary α-molybdophosphate. The extraordinary one was expected to be β-molybdophosphate. In a later paragraph, this will be further confirmed by discussion involving both the extraction isolation and the chemical reduction of the complex.

The final absorbance, on the other hand, was due to α-molybdophosphate. This was confirmed from the fact that the same absorbance could be attained with a solution which was prepared by dissolving into 40% aqueous acetonitrile a corresponding amount of synthesized crystal of molybdophosphate, *i.e.*, $24MoO_3 \cdot P_2O_5 \cdot 3H_2O$,[11] which had been well-

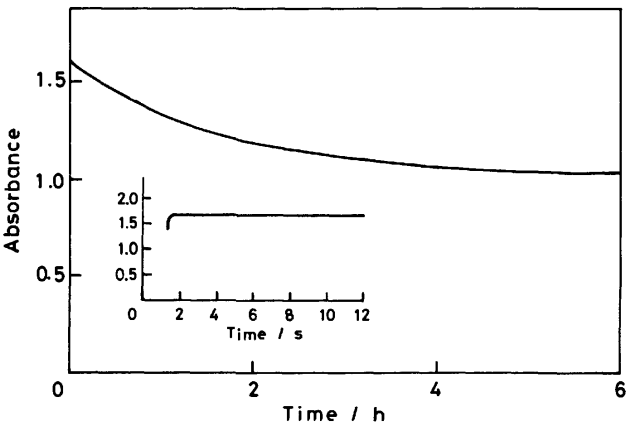

Fig. 1. Formation and conversion of β-molybdophosphate in the 40% aqueous acetonitrile medium at 25 °C.
A 40 mm^3 of 0.1 M phosphate standard solution was injected into a 4 cm^3 aliquot of the mixed molybdate reagent consisting of 0.05 M Mo(VI)/1.2 M HCl/40 % acetonitrile, and the absorbance change at 420 nm of the mixture was recorded against time.

established as Keggin structure.[12]

In consequence, it can be said that the decreasing absorbance recorded in Fig. 1 corresponds to the spontaneous conversion of β to α-molybdophosphate. By the kinetic analysis for the absorbance-time curve, it was assured that the conversion proceeded according to first-order reaction kinetics with respect to the concentration of β-molybdophosphate, and the rate constant in the 40% acetonitrile medium was observed as 1.79×10^{-4} s^{-1}.†

Although the formation and the conversion of β-molybdophosphate were similarly observed in an aqueous medium including more than 20% of acetonitrile, the reaction rate depended on the acetonitrile concentration. This dependence is featured in Fig. 2. As shown in the right-hand part of curve a in the Figure, extraordinarily higher absorbances were recorded at an early period around 2 min, indicating the formation of β-molybdophosphate. Upon standing, however, these absorbances decreased gradually through curves b—e and finally reached curve f (which was the ordinary absorbance level attributable to the formation of α-molybdophosphate).

In a 60% acetonitrile medium, for instance, it can be seen from the Figure that β-molybdophosphate takes more than 30 h to convert completely to α-molybdophosphate.

With the presence of more acetonitrile than 65% in the medium, the formation of β-molybdophosphate, thence that of α-molybdophosphate as well, was fairly prohibited. The reason, however, has not been explained yet.

In the absence and/or the presence of acetonitrile less than 20% (see the left-hand part of Fig. 2), the absorbances of molybdophosphate solutions increased rapidly and reached directly to those indicated by curve a, neither the extraordinarily higher absorbances nor the gradual decrease of the absorbance being

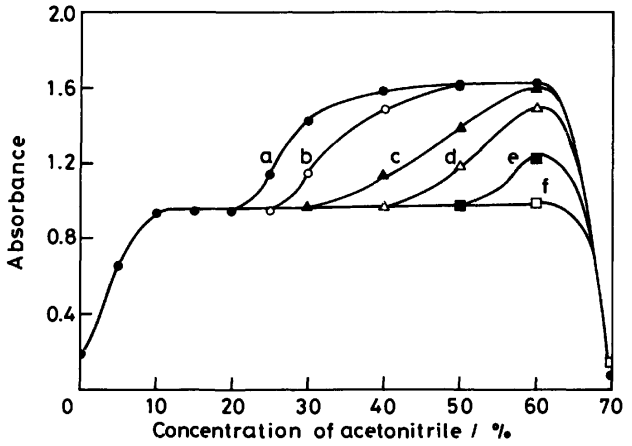

Fig. 2. Profile for the formation and survival of β-molybdophosphate in aquoeus acetonitirle media at the time: (a) 2 min, (b) 20 min, (c) 2 h, (d) 5 h, (e) 14 h, and (f) 38 h, elasped since the injection was made of a 40 mm^3 of 0.1 M phosphate solution into a 4 cm^3 of the mixed molybdate reagent consisting of 0.05 M Mo(VI)/1.2 M HCl/varing concentrations of acetonitrile.

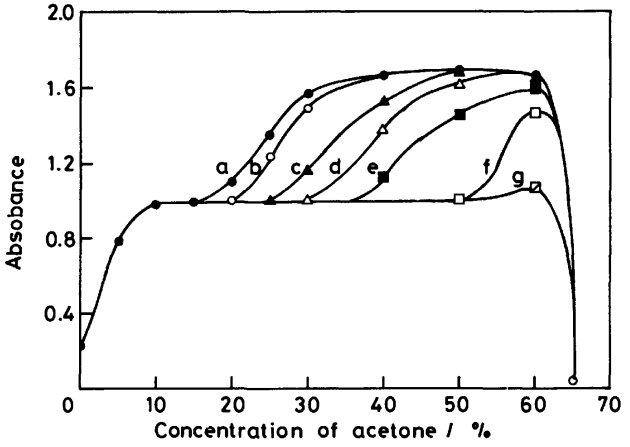

Fig. 3. Profile for the formation and survival of β-molybdophosphate in aqueous acetone media at the time: (a) 6 min, (b) 20 min, (c) 2 h, (d) 5 h, (e) 14 h, (f) 38 h, and (g) 262 h.
The same conditions as those in Fig. 2 were applied except that acetone was used.

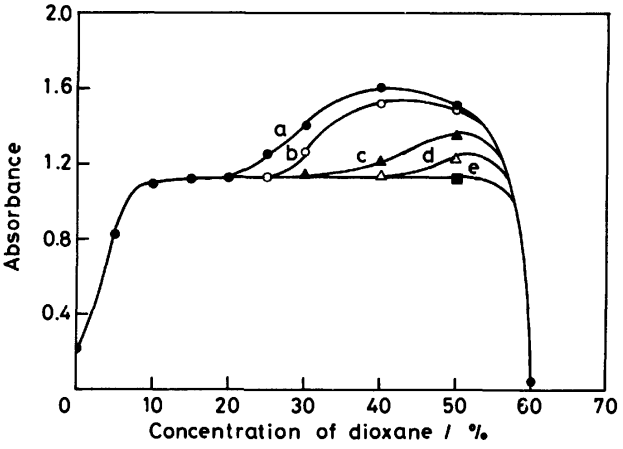

Fig. 4. Profile for the formation and survival of β-molybdophosphate in aqueous dioxane media at the time: (a) 6 min, (b) 20 min, (c) 2 h, (d) 5 h, and (e) 14 h.

† Let $C_{\alpha,t}$ and $C_{\beta,t}$ be the respective concentrations of α and β-molybdophosphate at time t during the conversion. The values of $C_{\alpha,t}$ (or those of $C_{\beta,t}$) were calculated by solving the following equations: $E_t=\varepsilon_\alpha \cdot C_{\alpha,t}+\varepsilon_\beta \cdot C_{\beta,t}$ and $C=C_{\alpha,t}+C_{\beta,t}$, where ε_α and ε_β denote the molar absorption coefficients of α- and β-molybdophosphate at 420 nm (being calculated from the final and the initial absorbances in Fig. 1 as 1.60×10^3 and 9.70×10^2 l mol^{-1} cm^{-1}, respectively), C is the total concentration of molybdophosphate and is known as 1×10^{-3} M in this experiment. The plot of log $C_{\beta,t}$ against time gave a straight line and the first-order rate constant for the conversion reaction was evaluated from the slope of the line.

observed at all. Only at elevated temperatures above 30 °C, extraordinary absorbances could be observed,[7] although they decreased to the ordinary values within several seconds. In consequence, it can be said that at these lower acetonitrile concentrations, β-molybdophosphate scarecely exists because of a rapid conversion to α-molybdophosphate.

β-Molybdophosphate can similarly be stabilized by virtue of acetone or dioxane in the reaction medium. The formation and the conversion of the complex in these media are illustrated in Figs. 3 and 4. By comparing Figs. 2—4, it is shown that any of the organic solvents employed here have essentially the same effect on the formation of β-molybdophosphate but the largest effect is attained by acetone, the complex being stabilized to exist even after 5 h in 60% acetone medium (curve d in Fig. 3, for example).

Preparation of α- and β-Molybdophosphate. As the most convenient method for preparing α-and β-molybdophosphate individually, the following procedures and conditions are recommended.

To obtain a 10-cm³ solution of either α- or β-molybdophosphate add a desired amount (should be less than 200 mm³, however) of 0.1 M phosphate standard solution into a 10-cm³ aliquot of the mixed molybdate reagent composed of 0.05 M Mo(VI)/1.2 M HCl/40% acetonitrile (being equilibrated at 25 °C) and shake the mixture well.. Thus, β-molybdophosphate will be formed instantaneously and will survive almost entirely through the following 20 min (during which, the degree of the conversion can be practically neglected). To obtain α-molybdophosphate, stand the same solution for more than 6 h. It is quite possible, of course, to prepare the complexes in an aqueous acetone medium. But, note that when acetone is used instead of acetonitrile β-molybdophosphate takes several minutes to form and takes a few days to convert to α completely. Also note, when dioxane is used, the complex forms in 2 min and converts to the other complex in *ca.* 6 h.

From the foregoing examinations, it is obvious that β-molybdophosphate should be prepared freshly for every use and exercised out within 20 min after preparation. However, α-molybdophosphate is stable enough to be stored for at least one month.

Chemical Reduction of α- and β-Molybdophosphate to the Respective Blue Species. In order to obtain a pure blue species of β-molybdophosphate by retaining a critical concentration of acetonitrile in the medium, several kinds of metals were tested as the dry reductants.

For the test, a series of 10-cm³ solutions of 5×10^{-5} M β-molybdophosphate were prepared in the 40% acetonitrile medium and shaken vigorously with a 60-mg dose of each metal such as nickel, iron, cobalt, lead, and copper. The formation of the blue species was monitored by measuring the absorbance at 788 nm. The results obtained with nickel are represented in Fig. 5A as a function of the shaking time with the metal and the standing time thenafter. As indicated by curve a in the Figure, when the reduction was initiated by shaking for several seconds, the solution slowly turned to blue and the absorbance reached a constant value on standing. Curves b and c show that the longer the shaking time is prolonged, the more rapidly the reduction proceeds. It is also shown by d and e, however, that the longer-shaking exceeding over 1 min is not profitable for the reduction, since other unstable blue species are produced (which give more deeply blue color but decay slowly on standing). The absorption spectrum of the most stable blue species of β-molybdophosphate is shown in Fig. 6 as curve a.

Quite similarly, α-molybdophosphate was reduced

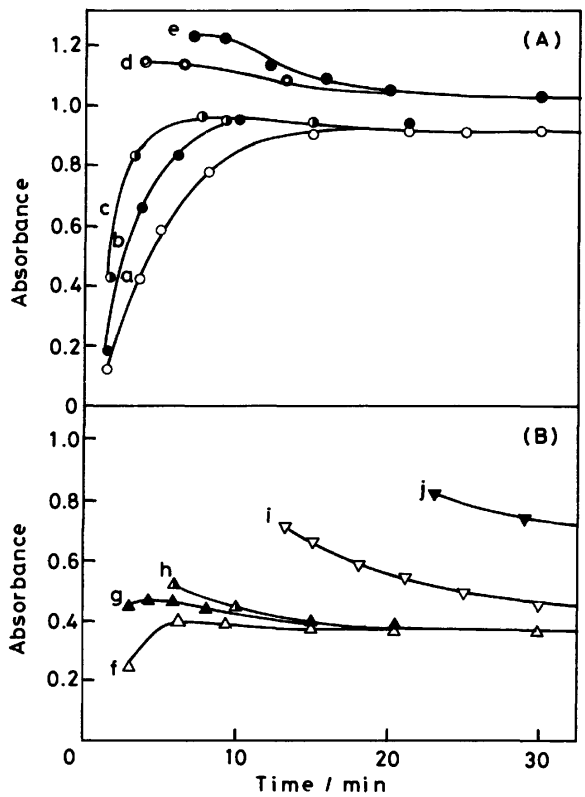

Fig. 5. The shaking time with nickel reductant and the standing time needed for the reduction of α- or/and β-molybdophosphate to the respective blue species. A 10 cm³ of 5×10^{-5} M solution of either α- or/and β-molybdophosphate prepared in the 40 % aqueous acetonitrile medium, was shaken with a 60 mg dose of nickel. For β (in the upper part of the Figure), the shaking time was varied as: (a) 6 s, (b) 10 s, (c) 30 s, (d) 1 min, and (e) 15 min and the formation of the blue species was monitored as a function of the standing time thenafter. For α (in the lower part of the Figure), the shaking time was as: (f) 30 s, (g) 1 min, (h) 4 min, (i) 10 min, and (j) 20 min.

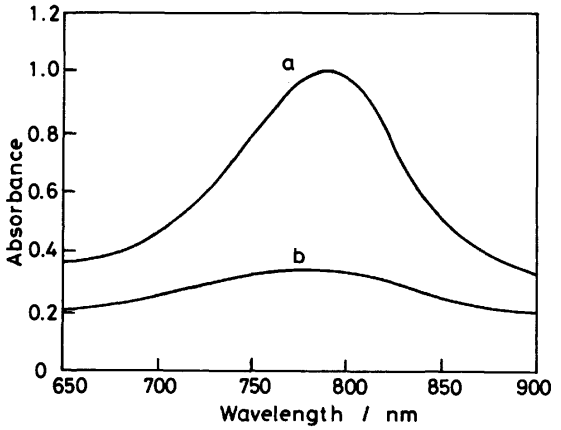

Fig. 6. Absorption spectra of the blue species of α- or/and β-molybdophosphate in the 40 % aqueous acetonitrile medium.
Curve a is for 5×10^{-5} M β-molybdophosphate, reduced with a 60 mg dose of nickel by shaking for several seconds and standing it for 15 min, and curve b for 5×10^{-5} M α-molybdophosphate reduced by shaking for 30 s and standing for 15 min.

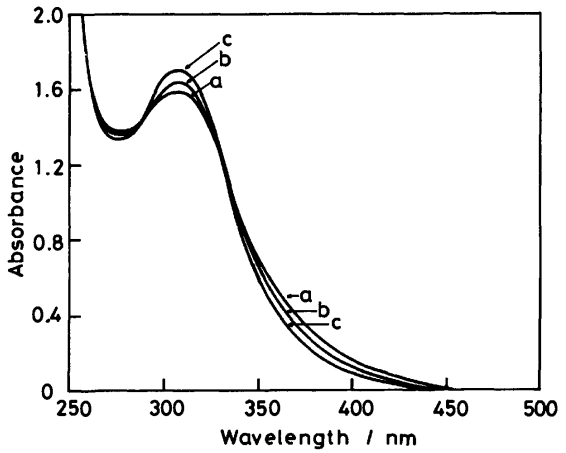

Fig. 7. Absorption spectra inherent to the respective α- or/and β-molybdophosphate.
Curve a is for β extracted at $t=10$ min and curve c is for α at $t=8$ h, during the conversion of β to α(see the text for the detailed extraction procedure). Thence, curve b for the mixture of α and β extracted at $t=1$ h. The initial concentration of the complexes in the 40 % aqueous acetonitrile medium, 4.5×10^{-5} M, was finally concentrated up to 7.5×10^{-5} M through this extraction.

to the corresponding blue species by using nickel. The shaking time and the standing time required for the reduction are shown in Fig. 5B. As shown by curve f, one of the most stable blue species was attained by shaking for 30 s and standing for 15 min. The absorption spectrum is given in Fig. 6 as curve b and compared with that of the reduced β-molybdophosphate (curve a). α- and β-molybdophosphate can be characterized even in their reduced forms; the former showing an absorption maximum at 770 nm with $\varepsilon=(6.43\pm0.15)\times10^3$ and the latter at 788 nm with $\varepsilon=(1.99\pm0.06)\times10^4$ l mol^{-1} cm^{-1}, respectively.

Similar to nickel, iron and lead also reduced the complexes although, the reduction with these metals proceeded rather faster than with nickel. Moreover, with these metals it was seen by visual observation that the solutions of the molybdophosphate complexes turned to a greenish blue. This was solely because the background color (reddish yellow) due to the reduction of the reagent molybdate covered the blue color of the reduced complexes. In fact, in the absorption spectrum being measured using a spectrophotometer, the inherent absorption maxima of the blue species were clearly revealed since the background color only occurred in a spectral region shorter than 500 nm.

Copper was less reactive compared with the three metals mentioned above and the reduction remained incomplete. Cobalt was even less reactive, the molybdophosphate complexes being slightly blue.

Extraction Isolation of α- and β-Molybdophosphate. For either α- or/and β-molybdophosphate formed in the 40% acetonitrile medium, an addition of the proper amount of chloroform was quite effective to extract the complex. Such an extra addition of chloroform served to extract a sufficient amount of acetonitrile from the medium into an organic phase, to which molybdophosphate was quantitatively extracted, the reagent molybdate being left in the aqueous phase. As to our examination performed here, chloroform was one of the unique solvents and the most excellent for such extraction isolation.

In practice, at appropriate intervals during the conversion of β to α, 3.0-cm^3 of chloroform was added to a 10-cm^3 solution of 4.5×10^{-5} M molybdophosphate, and either α- or/and β-molybdophosphate or their mixture was extracted. At every extraction an approximate 6 cm^3 of organic phase was recovered at the lower layer. The absorption spectra of these organic extracts were measured as superimposed in Fig. 7: Curve a was for β-molybdophosphate (which was attained by the extraction at $t=10$ min), curve b for the mixture of α and β (at $t=1$ h), and curve c for α (at $t=8$ h). According to the conversion reaction, the absorption spectrum changed from that of β to that of α, keeping isosbestic points at around 285 nm and 335 nm.

In paralell to these spectral measurements, the organic extracts were analyzed with respect to the contents of molybdenum and phosphorus, and the Mo/P ratios were determined. As the result, it was confirmed that, irrespective of the differences among the absorption spectra of a, b, and c in Fig. 7, the Mo/P ratios in the organic extracts remained unchanged and equally fell into a value of 12.1±0.3. That is, α- and β-molybdophosphate are quite identi-

cal in their compositions but possibly different in their structures. The detailed structure of β-molybdophosphate has not been analyzed yet because of the difficulty in crystallization, but it would be successfully deduced by Chalmers[2] from the Keggin structure.

It was also possible to extract the blue species of α- and β-molybdophosphate by the similar addition of chloroform. It is recommended to add 0.3 cm^3 of the solvent into a 10-cm^3 solution where the molybdophosphate complex is in a reduced form. Usually, an approximate 1.56 cm^3 of the organic phase is recovered at the upper layer, and the reduced complexes are effectively concentrated into the phase.[††] Although the blue color was highly increased in the organic phase, the characteristic absorption maxima of α- and β-molybdophosphate were retained unchanged even after the extraction.

Extraction isolation of the molybdophosphate complexes was unsuccessful in aqueous acetone and aqueous dioxane media because suitable solvents were not yet found for the phase separations of the mixed solvents.

Analytical Consideration. A variety of sensitive methods for phosphate determination have been reported by using water-miscible organic solvents such as acetone. Among these methods, however, the recommended procedures or the optimum conditions are widely different or even contradictory to each other. Now, it can be obviously said that in these methods two different effects by the organic solvent are involved, and either one of the effects has been overlooked. As confirmed in this paper, one of the solvent effect is due to the stabilization of α-molybdophosphate, where the organic solvent serves to shift the *reversible* formation equilibrium of the complex to the completion, and the other is due to the kinetic stabilization of β-molybdophosphate, where the *irreversible* conversion of the complex is retarded by the solvent.

For the same reason as above, one could not obtain β-molybdophosphate even by treating with organic solvents the crystallized molybdophosphate, *e.g.*, $24MoO_3 \cdot P_2O_5 \cdot 3H_2O$, or by extracting molybdophosphate from its aqueous solutions into various organic solvents. In either case, the conversion of β to α had already been completed. In consequence, an aqueous medium (including certain organic solvents) is indispensably needed for preparing β-molybdophosphate.

It was made evident that β-molybdophosphate shows higher absorbances than α-molybdophosphate in both forms of the reduced blue (Fig. 6) and the oxidized yellow (Fig. 7). This spectroscopic nature is capable of more sensitive determination of phosphate ion by utilizing the formation of β-molybdophosphate rather than that of α-molybdophosphate, especially in its reduced blue form. In addition to this, the extraction of the blue complex may further sensitize the phosphate determination by concentrating it into a small volume of the organic phase by the aid of auxiliary solvent of chloroform.

[††] At this extraction using a relatively small amount of chloroform (0.3 cm^3), approximately 1.4% of reagent molybdate is extracted along with the molybdophosphate complexes. However, the reagent molybdate is colorless and causes no practical interference with the spectral measurements in the visible region of the reduced blue complexes.

References

1) D. N. Bernhart and A. R. Wreath, *Anal. Chem.*, **27**, 440 (1955).
2) R. A. Chalmers and A. G. Sinclair, *Anal. Chim. Acta*, **33**, 384 (1965); *Anal. Chim. Acta*, **34**, 412 (1966).
3) A. Halász, E. Pungor, and K. Polyák, *Talanta*, **18**, 577 (1971).
4) J-M. Fruchart and P. Souchay, *Compt. Rend.* **C266**, 1571 (1968).
5) T. Fujinaga, S. Okazaki, and T. Hori, *Bunseki Kagaku*, **29**, 367 (1980).
6) T. Fujinaga, M. Koyama, and T. Hori, *Talanta*, **18**, 960 (1971).
7) T. Hori and T. Fujinaga, *Talanta*, **30**, 925 (1983).
8) K. Y. Matsumoto, A. Kobayashi, and Y. Sasaki, *Bull. Chem. Soc. Jpn.*, **48**, 3146 (1975).
9) J. D. H. Strickland, *J. Amer. Chem. Soc.*, **74**, 862, 868, 872 (1952).
10) T. Hori and T. Fujinaga, *Chem. Lett.*, **1983**, 687.
11) H. Wu, *J. Biol. Chem.*, **43**, 189 (1920).
12) J. F. Keggin, *Proc. Royal Soc.*, **A144**, 75 (1934)

 © 1985 The Chemical Society of Japan Bull. Chem. Soc. Jpn., 58, 1386—1391 (1985) [Vol. 58, No. 5

Kinetics of the Ligand-exchange Reactions in Th(tta)$_4$ and Th(tta)$_4$dmso in Organic Solvents

Naoshi FUJIWARA, Hiroshi TOMIYASU, and Hiroshi FUKUTOMI*
Research Laboratory for Nuclear Reactors, Tokyo Institute of Technology, O-okayama, Meguro-ku, Tokyo 152
(Received October 16, 1984)

The exchange reactions of 2-thenoyltrifluoroacetonate (tta) in Th(tta)$_4$ and of dimethyl sulfoxide (dmso) in Th(tta)$_4$dmso have been studied by the NMR method. It was found that the first-order rate constant of tta exchange in acetonitrile-d_3 depended linearly on the concentrations of Htta in the enol form, Htta$_{enol}$, and that the rate was retarded markedly by the addition of DMSO. The activation parameters ΔH^* (kJ mol^{-1}) and ΔS^* (JK^{-1} mol^{-1}) were determined to be 43.9±0.5 and −58.4±1.5, respectively and the mechanism including the formation of a nine-coordinate intermediate was proposed. For Th(tta)$_4$dmso, the rate of dmso exchange in acetone-d_6 was much faster than that of β-diketonate exchange, and an interchange mechanism was proposed on the basis of a nonlinear dependency of the first-order rate constant on the free DMSO concentration.

In previous papers,[1,2] we reported the kinetics of the ligand exchange reaction in tetrakis(acetylacetonato)thorium(IV), Th(acac)$_4$, and proposed that the reaction proceeded *via* a nine-coordinate intermediate for the acac exchange. It has been known that thorium(IV) forms an eight-coordinate complex[3] with 4,4,4-trifluoro-1-(2-thienyl)-1,3-butanedione, whose common name is 2-thenoyltrifluoroacetone (Htta). On extraction of Th(IV) by Htta, a marked synergic effect was observed in the presence of unidentate donor bases, *e.g.* tributyl phosphate and trioctylphosphine oxide.[4,5,6] This synergic effect suggests that Th(tta)$_4$ may form nine-coordinate complexes with unidentate bases. In fact, several nine-coordinate adducts between Th(tta)$_4$ and bases were isolated.[7,8] From these facts, it is expected that some nine-coordinate intermediate probably plays an important role in the ligand-exchange reaction between Th(tta)$_4$ and Htta. In this paper, we report the formation of nine-coordinate Th(tta)$_4$L(L: unidentate ligand), and the kinetic results of the exchange reaction of tta and dmso in Th(tta)$_4$ and Th(tta)$_4$dmso, respectively.

Experimental

Materials. The Th(tta)$_4$ complex was prepared as follows. An aqueous solution (40 cm^3) containing thorium tetrachloride (0.01 mol) was stirred with the same volume of a benzene solution which contained a large excess amount of Htta. Aqueous ammonia was added to the mixture until the pH of the solution became 5. The brownish yellow benzene phase was separated and a yellow precipitate was obtained by evaporation of benzene under reduced pressure. The precipitate was washed with hexane and recrystallized from hot benzene, and then from 1,2-dichloroethane. Found: C, 34.5; H, 1.4%. Calcd for $C_{32}H_{16}O_8F_{12}S_4Th$: C, 34.4, H, 1.1%.

Purification of 2-thenoyltrifluoroacetone was carried out by recrystallization from hexane. Dimethyl sulfoxide and hexamethyl phosphoric triamide (HMPT) were distilled under reduced pressure. Acetonitrile was dried over phosphorus pentaoxide and distilled. Acetone-d_6 and acetonitrile-d_3 were dried over molecular sieve 4A.

Measurements of UV and NMR Spectra. UV spectra were measured by using Shimadzu 210A and UV-365 spectrophotometers with 0.1 mm and 1.0 mm quartz cells. A JEOL JNM-FX 100 FT-NMR equipped with a JNM-VT-3B temperature controller was used for NMR measurements.

Determination of the Fraction of Keto- and Enol-forms in Htta. The concentration ratio, [enol]/[keto], was determined by area measurements of methine and methylene proton signals for enol- and keto-isomers, respectively. In order to obtain the temperature dependence of the ratio, the area measurements were performed in the temperature range from 30 to 70 °C. The values of enthalpy and entropy were ΔH=−15.5±0.8 kJ mol^{-1} and ΔS=−24.3±2.4 J K^{-1} mol^{-1} in CD_3CN. The fractions of the enol isomer at each temperature were calculated by using these values.

Rate Analysis. The first-order rate constants of ligand-exchange reactions were determined from the line shape analysis of NMR signals by using the two-site model.[2,9] A Sord M-232 microcomputer system was used for the calculation.

Results

Ligand-exchange between Th(tta)$_4$ and Htta. The absorption spectrum of Th(tta)$_4$ shows a peak at 350 nm with the molar extinction coefficient of 8.3×10^4 M^{-1} cm^{-1} (1 M=1 mol dm^{-3}) in acetonitrile. The spectrum of the mixture of Th(tta)$_4$ and Htta coincided with the sum of those of each component in acetonitrile, and remained unchanged for several hours. As is shown in Fig. 1, the ^{1}H NMR spectra of the mixture of Th(tta)$_4$ and Htta in CD_3CN and CD_3COCD_3 gave two methine proton signals at room temperature, and the signal in the higher magnetic field was assigned to coordinated tta and that in the lower field to free Htta in the enol-form. The ^{19}F NMR spectra of the reaction mixture in CD_3CN showed also two ^{19}F signals of trifluoromethyl at room temperature, where the one in the higher field was assigned to Htta and the other to Th(tta)$_4$. In both the ^{1}H and ^{19}F spectra

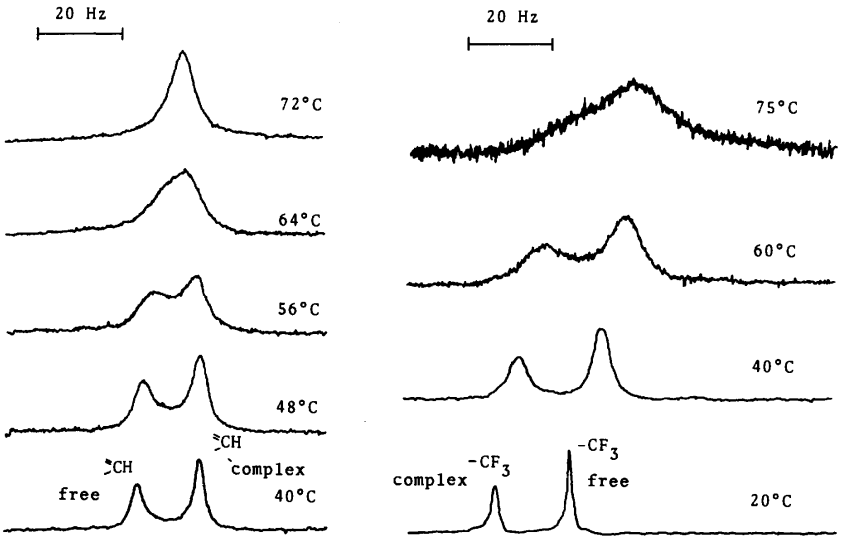

Fig. 1. Changes in methine proton signals (left) and trifluoromethyl ^{19}F signals of the mixture of Th(tta)$_4$ and Htta in CD_3CN with temperature.

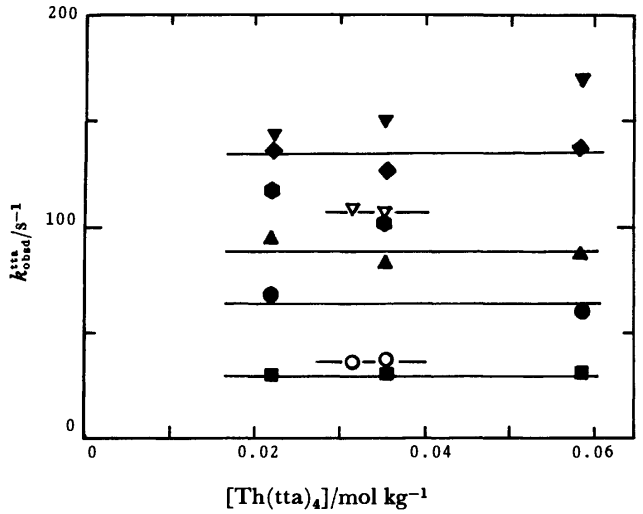

Fig. 2. Dependence of k^{tta}_{obsd} on the concentration of Th(tta)$_4$ in CD_3CN at various temperatures. ■: 30, ●: 40, ▲: 48, ⬢: 52, ◆: 56, ▼: 60 °C.
Open marks: [Htta]$_{total}$=0.130−0.133 mol kg^{-1},
Closed marks: [Htta]$_{total}$=0.192−0.193 mol kg^{-1}.

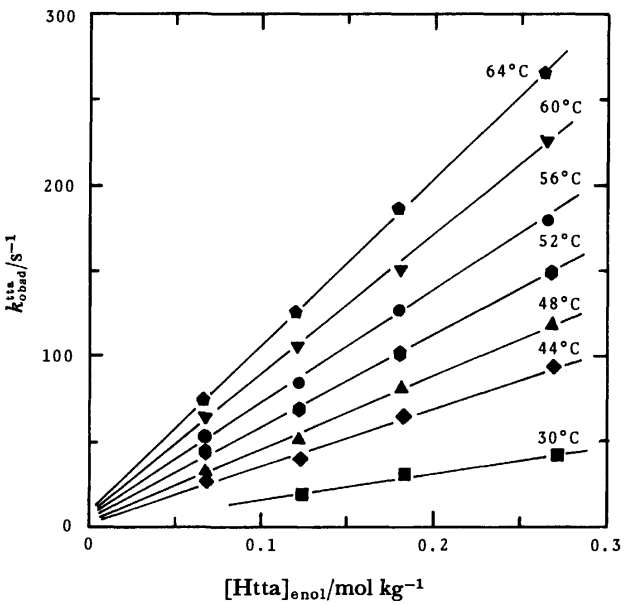

Fig. 3. Dependence of k^{tta}_{obsd} on the concentration of Htta in the enol form in CD_3CN.
[Th(tta)$_4$]=0.0357−0.0363 mol kg^{-1}.

in CD_3CN, the ≥CH and -CF_3 signals coalesced as the temperature was raised (Fig. 1). These changes in NMR spectra can be attributed to the ligand exchange between Th(tta)$_4$ and Htta in the enol-form. No change was observed in methylene proton signals of Htta in the keto-form. Therefore, the ligand-exchange reaction between Th(tta)$_4$ and Htta in the enol-form can be described as follows.

$$Th(tta)_4 + Htta^*_{enol} \rightleftharpoons Th(tta)_3tta^* + Htta_{enol}, \quad (1)$$

where the asterisk denotes the exchanging species.

The observed first-order rate constant, k^{tta}_{obsd}, for the tta exchange reaction is given by

$$k^{tta}_{obsd} = 4\tau_c^{-1}, \quad (2)$$

where τ_c is the life time of tta in the coordination site. Plots of k^{tta}_{obsd} against the concentrations of Th(tta)$_4$ and Htta$_{enol}$ are shown in Figs. 2 and 3, respectively. The first-order rate constant was independent of [Th(tta)$_4$] though the data at 52 and 60 °C deviated from straight lines and linearly depended on [Htta]$_{enol}$. The intercepts in Fig. 3 might be regarded to be zero within experimental errors. These results lead to the following relationship between k^{tta}_{obsd} and [Htta]$_{enol}$,

$$k^{tta}_{obsd} = k[Htta]_{enol} \quad (3)$$

where k refers to the second order rate constant, and the values of k are listed in Table 1. The rate of tta

Table 1. Kinetic parameters of the tta exchange of $Th(tta)_4$ in CD_3CN

T / °C	k / $s^{-1}\,mol^{-1}\,kg$
30	153±29
44	337±26
48	432±29
52	517±20
56	647±16
60	814±21
64	981±14
ΔH^* (kJ mol^{-1})	43.9±0.5
ΔS^* ($JK^{-1}\,mol^{-1}$)	−58.4±1.5

Table 2. Change in absorbance of $Th(tta)_4$[a] by addition of DMSO in acetonitrile

[DMSO] 10^{-5} mol dm^{-3}	Absorbance (350 nm)
0	0.382
2.0	0.377
4.0	0.374
6.0	0.372
8.0	0.368
10	0.366
12	0.366
14	0.366

a) $[Th(tta)_4]=4.58\times10^{-5}$ mol dm^{-3}.

exchange was retarded in the presence of free DMSO. Under the conditions that $[Th(tta)_4]$=0.0443 mol kg^{-1}, $[Htta]_{total}$=0.181 mol kg^{-1} and [DMSO]=0.197 mol kg^{-1} in CD_3CN, the methine proton signals of $Th(tta)_4$ and $Htta_{enol}$ were separated even at 70 °C, and their line widths were slightly broader than those at 20 °C.

Formation of $Th(tta)_4L$ Complexes and the dmso Exchange in $Th(tta)_4$dmso. The molar extinction coefficient of $Th(tta)_4$ in acetonitrile was measured in the presence of DMSO or HMPT. Slight changes in absorption spectra with an isosbestic point at 340 nm were observed by the addition of DMSO, and the results are shown in Table 2. Similar spectral changes were also observed in the presence of HMPT. These changes in spectra suggest the formation of adduct complexes between $Th(tta)_4$ and DMSO or HMPT. In addition, the ^1H NMR spectra of mixtures of $Th(tta)_4$ and DMSO or HMPT in acetone-d_6 may give additional evidence for 1:1 adduct complex formation. As seen in Fig. 4, the ^1H NMR spectra of the solution containing $Th(tta)_4$ and DMSO gave a sharp signal of methyl protons at −20 °C. As the temperature of the solution was lowered, this signal broadened and then split into two peaks, in which the peak in the higher field was assigned to the methyl protons of free DMSO, while the solution containing $Th(tta)_4$ (0.0662 mol kg^{-1})

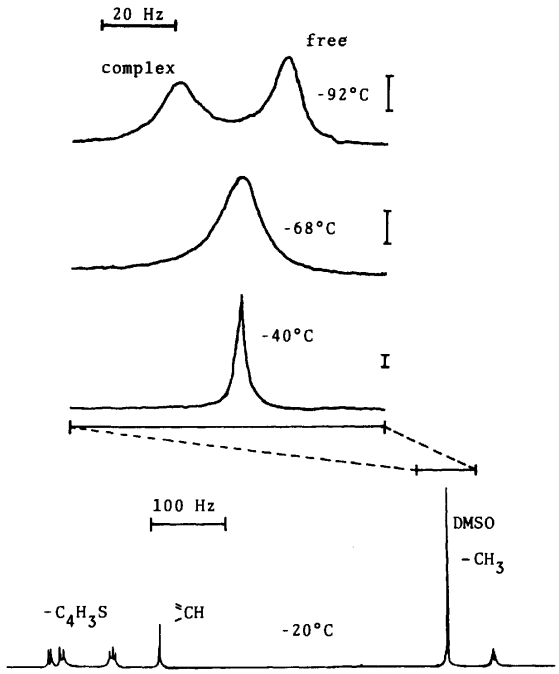

Fig. 4. ^1H NMR spectrum of the mixture of $Th(tta)_4$ and DMSO, and a change in methyl proton signals in CD_3COCD_3 with temperature.
$[Th(tta)_4]=0.0508$ mol kg^{-1}, [DMSO]=0.103 mol kg^{-1}.

and DMSO (0.0270 mol kg^{-1}) whose concentration was less than equivalent showed a single methyl proton signal, and no methyl proton signal of free DMSO was observed at any temperature. The chemical shift of this single methyl proton signal coincided with that of the peak in the lower field in Fig. 4. This fact also suggests that DMSO in the mixture forms a 1:1 adduct complex with $Th(tta)_4$, and the left-hand peak in Fig. 4 can be assigned to the methyl protons of the adduct complex, $Th(tta)_4$dmso. Similar changes in NMR spectra were observed for the mixture of $Th(tta)_4$ and HMPT as is shown in Fig. 5, in which two signals of methyl protons of HMPT were observed at 10 °C and each signal split into two peaks at −40 °C. Left-hand peaks (C) of each signal can be assigned to the methyl protons of the complex, $Th(tta)_4$hmpt. Attempts to determine accurate values of formation constants of 1:1 adduct complexes between $Th(tta)_4$ and DMSO or HMPT in acetonitrile and acetone were unsuccessful because of very large values of molar extinction coefficients for complexes and of rather small changes in absorbance on adduct formation. The value for $Th(tta)_4$dmso is estimated to be some value between 10^4 and 10^5 $mol^{-1}\,kg$. A simulated line shape of NMR spectrum, which is obtained from the two-site model by assuming that the left-hand peak in Fig. 4 is the methyl protons of $Th(tta)_4$dmso, and that the dmso exchange reaction takes place between $Th(tta)_4$dmso and free DMSO, shows satisfactory agreement with the observed

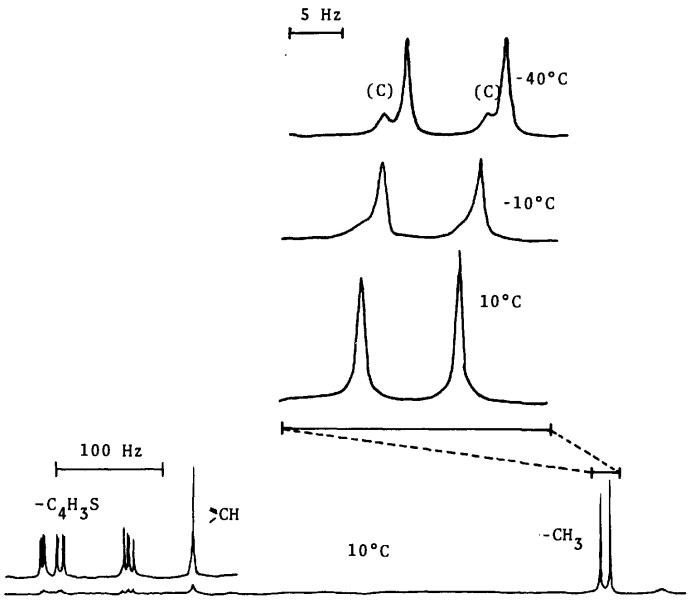

Fig. 5. ^{1}H NMR spectrum of the mixture of Th(tta)$_4$ and HMPT, and a change in methyl proton signals in CD_3COCD_3 with temperature.
[Th(tta)$_4$] = 0.048 mol kg^{-1}, [HMPT] = 0.210 mol kg^{-1}.

signals.

All these results indicate that Th(tta)$_4$ and L (L=dmso or hmpt) form the nine-coordinate complex, Th(tta)$_4$L, and the change in ^{1}H NMR spectra in Fig. 4 can be attributed to the dmso exchange reaction in Th(tta)$_4$dmso as written by Eq. 4.[10]

$$\text{Th(tta)}_4\text{dmso} + \text{DMSO}^* \rightleftharpoons \text{Th(tta)}_4\text{dmso}^* + \text{DMSO} \quad (4)$$

The observed first-order rate constant of the dmso exchange in Th(tta)$_4$dmso, k_{obsd}^{dmso}, does not depend linearly on the concentration of DMSO as shown in Fig. 6. Plots of $k_{obsd}^{dmso^{-1}}$ *vs.* [DMSO]$^{-1}$ give straight lines with intercepts and yield

$$k_{obsd}^{dmso^{-1}} = p + q[\text{DMSO}]^{-1}, \quad (5)$$

where p and q are constants.

Discussion

A pathway which is similar to the mechanism proposed for the acac exchange in Th(acac)$_4$[2] is proposed for the mechanism of the tta exchange reaction in Th(tta)$_4$. As shown in Fig. 7, Th(tta)$_4$ forms a nine-coordinate intermediate, Th(tta)$_4$Htta*, with Htta$^*_{enol}$, and the proton of Htta$^*_{enol}$, is transferred to one of the coordinated tta (II→II′), followed by rapid dissociation of Htta$_{enol}$ from the coordination sphere (II′→I′). If complexes I and II are in fast equilibrium, and [II] is much smaller than [I], the first-order rate constant, k_{ex}, can be written by

$$k_{ex} = k_2K_1[\text{Htta}]_{enol}, \quad (6)$$

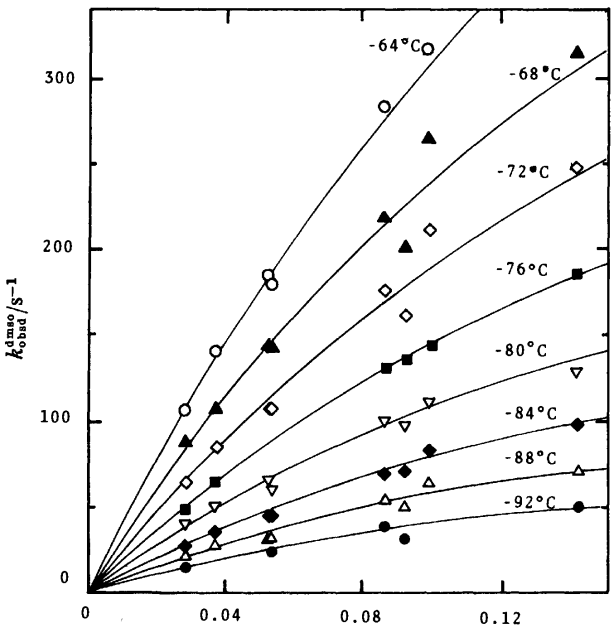

Fig. 6. Plots of k_{obsd}^{dmso} *vs.* [DMSO] in CD_3COCD_3.
[Th(tta)$_4$dmso] = 0.0227 − 0.0672 mol kg^{-1}.

where K_1 is the formation constant of complex II, and k_2 is the rate constant for the proton transfer reaction. Equation 6 is the same as Eq. 3 obtained experimentally, where k corresponds to k_2K_1.

The retardation effect by the addition of DMSO can be interpreted by the formation of nine-coordinate adduct complex (III). It seems reasonable to assume that the formation of Th(tta)$_4$Htta is hindered by DMSO. The rate of the tta exchange reaction in

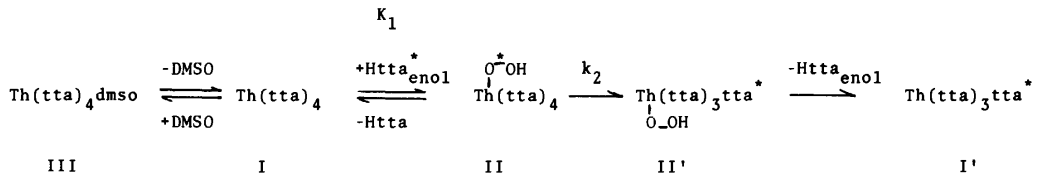

Fig. 7. Mechanism of the tta exchange in $Th(tta)_4$ in CD_3CN.

TABLE 3. ACTIVATION PARAMETERS FOR THE SECOND-ORDER RATE CONSTANTS OF LIGAND EXCHANGE REACTIONS IN β-DIKETONATO COMPLEXES

Complex	Solvent	ΔH^* / kJ mol^{-1}	ΔS^* / JK^{-1} mol^{-1}	Ref
$VO(acac)_2$	DCE[a]	46.7	−61.9	13
$Zr(tfac)_4$[b]	C_6H_6	46.4	−63	12
$Hf(tfac)_4$	C_6H_6	49.8	−54	12
$U(fod)_4$[c]	CCl_4	21.8	−109	11
$Th(acac)_4$	AN[d]	29.4	−98	2
$Th(tta)_4$	AN	43.9	−58	This work
$V(acac)_3$	AN	73	−90.7	14
$Ga(acac)_3$	THF[e]	79	−84	15
$Zr(acac)_4$	C_6H_6	76.9	37	12
$Hf(acac)_4$	C_6H_6	74.0	26	12

a) 1,2-Dichloroethane. b) 1,1,1-Trifluoroacetylacetonate. c) 6,6,7,7,8,8,8-Heptafluoro-2,2-dimethyl-3,5-octanedionate. d) Acetonitrile. e) Tetrahydrofuran.

$Th(tta)_4$ was slower than that of the acac exchange reaction in $Th(acac)_4$. According to the proposed mechanism (Fig. 7), the difference in reaction rate might be ascribed to the following causes: (1) The formation constant of $Th(tta)_4Htta$ is smaller than that of $Th(acac)_4Hacac$. (2) Replacement of coordinated tta by incoming $Htta_{enol}$ is slower than the acac replacement in $Th(acac)_4Hacac$. However, it is difficult at present to determine which causes to be predominant.

The values of activation parameters for the second-order rate constant of ligand-exchange reactions in β-diketonato complexes are listed in Table 3. In spite of a variety of ligands and solvents, it seems that there is a linear relationship between the values of ΔH^* and ΔS^* for the ligand-exchange reactions in $Th(acac)_4$, $Th(tta)_4$, $U(fod)_4$, $Zr(tfac)_4$, $Hf(tfac)_4$, and $VO(acac)_2$.[2,11-13] Although it is hardly discernible whether this relationship is held by accident or implies a mechanistic similarlity, almost the same mechanism has been proposed for the ligand-exchange reactions in $Th(acac)_4$, $Th(tta)_4$ and $U(fod)_4$, while different reaction mechanisms are proposed for $V(acac)_3$[14] and $Ga(acac)_3$.[15]

As described above, k_{obsd}^{dmso} does not follow the linear relationship with respect to free DMSO concentration. This fact suggests that neither the dissociative mechanism (D) nor the associative mechanism (A) fits the dmso exchange mechanism in $Th(tta)_4dmso$. On

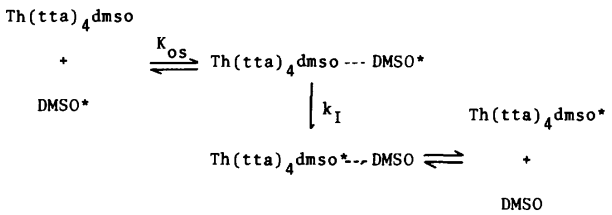

Fig. 8. Mechanism of the dmso exchange in $Th(tta)_4dmso$ in CD_3COCD_3.

the other hand, the interchange mechanism (I)[16] seems to be probable as seen in Fig. 8, where free DMSO and $Th(tta)_4dmso$ form an outer-sphere complex, and the interchange process between the coordinated dmso and DMSO in the outer-sphere is the rate-determining step. On the basis of the I mechanism, the first-order rate constant of dmso exchange, k_{ex}^{dmso}, is expressed by

$$k_{ex}^{dmso} = \frac{k_I K_{os}[DMSO]}{1+K_{os}[DMSO]}, \quad (7a)$$

or

$$k_{ex}^{dmso^{-1}} = \frac{1}{k_I} + \frac{1}{k_I K_{os}}[DMSO]^{-1}, \quad (7b)$$

where k_I is the rate constant of the interchange process and K_{os} is the formation constant of the outer-sphere complex. Equation 7b is identical with Eq. 5, which was determined experimentally. Hence, the proposed I mechanism can interprete well the dmso exchange reaction in $Th(tta)_4dmso$ in acetone-d_6. Values of k_I and K_{os}, which were obtained from $k_I=1/p$ and $K_{os}=1/qk_I$, are listed in Table 4. The rate of the dmso exchange in $Th(tta)_4dmso$ is much faster than that of the tta exchange in $Th(tta)_4$. This fact supports the assumption that $Th(tta)_4$ and $Th(tta)_4Htta$ are in a fast equilibrium as shown in Fig. 7.

The *N,N*-dimethylformamide (dmf) exchange in eight-coordinate complexes, $[Tb(dmf)_8]^{3+}$, $[Er(dmf)_8]^{3+}$, and $[Tm(dmf)_8]^{3+}$, were studied by Merbach *et al.*[17-18] and they reported that the smaller the size of the central metal ion was, the more dissociative the character of the exchange mechanism was. In spite of the large negative value of ΔS^*, the I_d mechanism was proposed for $[Tb(dmf)_8]^{3+}$, where Tb(III) has a large ionic radius, and the D mechanism was proposed for $[Tm(dmf)_8]^{3+}$. Based on these facts, we

Table 4. Kinetic parameters of dmso exchange in $Th(tta)_4dmso$ in CD_3COCD_3

T / °C	k_I / $10^2\ s^{-1}$	K_{os} / $mol^{-1}\ kg$
−64	11.8±4.1	3.5
−68	7.4±1.9	4.7
−72	7.9±3.1	3.2
−76	5.8±0.2	3.3
−80	3.0±1.6	5.3
−84	3.2±1.2	3.2
−88	1.6±0.8	4.9
−92	1.0±0.3	6.1
	$\Delta H^* = 25.1 \pm 2.5$ kJ mol^{-1}	
	$\Delta S^* = -65 \pm 13$ J K^{-1} mol^{-1}	

can not rule out the possibility of the I_d mechanism in the dmso exchange in $Th(tta)_4dmso$, though the I_a mechanism seems to be more likely by considering a large ionic radius of Th(IV) and the negative ΔS^* value.

The authors wish to thank Professor James H. Espenson of Iowa State University for helpful discussions. The present work was partly supported by a Grant-in-Aid for Scientific Research No. 57470035 from the Ministry of Education, Science and Culture.

References

1) N. Fujiwara, H. Tomiyasu, and H. Fukutomi, *Chem. Lett.*, **1983**, 377.
2) N. Fujiwara, H. Tomiyasu, and H. Fukutomi, *Bull. Chem. Soc. Jpn.*, **57**, 1576 (1984).
3) M. Lenner and O. Lindqvist, *Acta Crystallogr., Sec. B* **35**, 600 (1979).
4) T. V. Healy, *Nucl. Sci. Eng.*, **16**, 413 (1963).
5) T. V. Healy, *J. Inorg. Nucl. Chem.*, **19**, 314 (1961).
6) T. V. Healy, *J. Inorg. Nucl. Chem.*, **19**, 328 (1961).
7) L. D. C. Bok, G. F. S. Wessels, and J. G. Leipoldt, *Z. Anorg. Allg. Chem.*, **404**, 76 (1974).
8) J. G. Leipoldt, G. F. S. Wessels, and L. D. C. Bok, *J. Inorg. Nucl. Chem.*, **37**, 2487 (1975).
9) Y. Ikeda, H. Tomiyasu, and H. Fukutomi, *Bull. Chem. Soc. Jpn.*, **56**, 1060 (1983).
10) The two-site exchange model is not applicable to hmpt exchange in $Th(tta)_4hmpt$.
11) G. Folcher, N. Keller, C. Kiener, and J. Paris, *Can. J. Chem.*, **55**, 3559 (1977).
12) A. C. Adams and E. M. Larsen, *Inorg. Chem.*, **5**, 814 (1966).
13) M. Nishizawa and K. Saito, *Bull. Chem. Soc. Jpn.*, **51**, 483 (1978).
14) A. Watanabe, H. Kido, and K. Saito, *Inorg. Chem.*, **20**, 1107 (1981).
15) C. Chatterjee, K. Matsuzawa, H. Kido, and K. Saito, *Bull. Chem. Soc. Jpn.*, **47**, 2809 (1974).
16) C. H. Langford and H. B. Gray, "Ligand Substitution Processes," Benjamin, London (1974).
17) D. L. Pisaniello and A. E. Merbach, *Helv. Chim. Acta*, **65**, 573 (1982).
18) D. L. Pisaniello, L. Helm, D. Zbinden, and A. E. Merbach, *Helv. Chim. Acta*, **66**, 1872 (1983).
19) D. L. Pisaniello, L. Helm, P. Meier, and A. E. Merbach, *J. Am. Chem. Soc.*, **105**, 4528 (1983).

 © 1985 The Chemical Society of Japan Bull. Chem. Soc. Jpn., 58, 1392—1400 (1985) [Vol. 58, No. 5

Preparation and Characterization of Some Co(III) Complexes Containing (1*R*,2*R*)-Dimethyl-1,2-cyclohexanediamine. Crystal Structure of (+)$_{435}$-*trans*-[$CoCl_2$(*R*,*R*-dmchxn)$_2$]-Cl·HCl·$2H_2O$

Mitsunobu SATO,† Yasuhiko YOKOO, Morio YASHIRO, Shigenobu YANO,* Sadao YOSHIKAWA,* Kimiko KOBAYASHI,†† and Tosio SAKURAI††

Department of Synthetic Chemistry, Faculty of Engineering, The University of Tokyo, Hongo, Bunkyo-ku, Tokyo 113

††*The Institute of Physical and Chemical Research (Rikagaku Kenkyusho), Wako-shi 351*

(Received November 13, 1984)

(−)$_{546}$-*trans*-[$Co(NO_2)_2$(*R*,*R*-dmchxn)$_2$]$^+$ and (+)$_{546}$-*Λ*-[$Co(CO_3)$(*R*,*R*-dmchxn)$_2$]$^+$, which had been newly prepared, reacted with concentrated HCl to give, respectively, (−)$_{435}$-*trans*-(*SSSS*)-[$CoCl_2$(*R*,*R*-dmchxn)$_2$]$^+$ and (+)$_{435}$-*trans*-(*SRRS*)-[$CoCl_2$(*R*,*R*-dmchxn)$_2$]$^+$ stereospecifically, where *R*,*R*-dmchxn=(1*R*,2*R*)-*N*,*N*′-dimethyl-1,2-cyclohexanediamine. The stereospecific formation of (+)$_{546}$-*Λ*-[$Co(CO_3)$(*R*,*R*-dmchxn)$_2$]$^+$ has been observed. The *trans*-dichloro complexes and their precursors have been characterized by elemental analysis and by electronic absorption, circular dichroism, ^{1}H NMR, and ^{13}C NMR spectroscopies. An X-ray crystal-structure determination was undertaken on one of the *trans*-dichloro isomers, (+)$_{435}$-[$CoCl_2$(*R*,*R*-dmchxn)$_2$]Cl·HCl·$2H_2O$, whose structure could not be characterized by usual spectroscopies. This complex forms triclinic crystals with a=11.395(10) Å, b=11.674(8) Å, c=11.031(8) Å, α=98.62(6)°, β=102.48(8)°, γ=118.24(5)°, and Z=2, in the space group P1. Least-squares refinements converged at an R value of 0.041 for 4870 independent reflections with $F_o > 3[\sigma(F_o)]$. The complex cation has an approximately twofold symmetry. The conformations of the two five-membered chelate rings are both *λ*. The arrangements of the groups around the two secondary nitrogen atoms are *R* and *S* in each diamine. The isomerization from the (+)$_{435}$-*trans*-dichloro complex to the (−)$_{435}$ isomer has been observed under mild basic conditions.

It is an interesting subject to design ligands suitable for metal-assisted asymmetric synthesis where the orientation of the donor substituents can play a major role in the diastereotopic discrimination of the substrate. To examine the coordination behavior of the *N*-substituted polyamine from this point of view is an interesting subject, since the *N*-alkyl groups in the polyamines or diamines significantly affect the structures of metal complexes.[1,2]

As a part of a study to develop useful optical-active ligands for asymmetric synthesis, we have been investigated cobalt(III) complexes of the *N*-alkylated diamines. During this investigation, we have obtained two isomers of the *trans*-dichlorobis(diamine)cobalt(III) complex, where the diamine is (1*R*,2*R*)-*N*,*N*′-dimethyl-1,2-cyclohexanediamine (*R*,*R*-dmchxn), whose chelate ring would be fixed in the *λ* gauche conformation with its rigid cyclohexane-ring skeleton. These *trans*-dichloro isomers, which are important precursors of the corresponding amino acidato complexes, (−)$_{435}$-*trans*-[$CoCl_2$(*R*,*R*-dmchxn)$_2$]$^+$ and (+)$_{435}$-*trans*-[$CoCl_2$(*R*,*R*-dmchxn)$_2$]$^+$, were derived from (−)$_{546}$-*trans*-[$Co(NO_2)_2$(*R*,*R*-dmchxn)$_2$]$^+$ and (+)$_{546}$-[$Co(CO_3)$(*R*,*R*-dmchxn)$_2$]$^+$ respectively.

In this paper we wish to report the syntheses and characterization of these four cobalt(III) complexes containing *R*,*R*-dmchxn, including an X-ray crystal-strauctured determination of one of the *trans*-dichloro isomers, (+)$_{435}$-*trans*-[$CoCl_2$(*R*,*R*-dmchxn)$_2$]Cl·HCl·$2H_2O$, whose structure could not be characterized by usual spectroscopies. In addition, the conversion reaction between the two *trans*-dichloro complexes has been investigated in order to elucidate the relationship between the two isomers.

† Present address: Department of Engineering, National Science Museum, Ueno Park, Taito-ku, Tokyo 110.

Experimental

Measurement. The visible absorption spectra were recorded on a Shimadzu UV-210 spectrophotometer. The circular dichroism spectra were measured with a JASCO J-500A recording spectropolarimeter. The spectra were obtained in methanol for the *trans*-dichloro complexes and in water for the dinitro and carbonato complexes. The ^{1}H NMR spectra were measured on a HITACHI R-40 (90 MHz) spectrometer, with tetramethylsilane or sodium 3-trimethylsilyl-1-propanesulfonate as an internal standard. The ^{13}C NMR spectra were obtained on a JEOL PS-100 (100 MHz) spectrometer, with tetramethylsilane as the external standard. Elemental analyses were performed by Shounan Bunseki Center Co., Ltd.

Materials. All the reagents were of the best commercial grade and were used without further purification. (1*R*,2*R*)-*N*,*N*′-Dimethyl-1,2-clohexanediamine (*R*,*R*-dmchxn) was prepared by the method of Kashiwabara *et al.*[3]

Preparation of (−)$_{546}$-trans-[Co(NO$_2$)$_2$(R,R-dmchxn)$_2$]ClO$_4$·H$_2$O (1a). A solution of *R*,*R*-dmchxn (4.4 g) in water (30 mL) was added, drop by drop, to an aqueous solution containing sodium hexanitrocobaltate(III) (7.7 g), after which the solution was heated at 70 °C for 1 h while being stirred. After cooling to room temperature, a solution of sodium perchlorate (2.5 g) in water (10 mL) was added to the reacted solution with stirring, and the solution was left to stand overnight at room temperature. The resulting yellow crystals were filtered, washed with

ice-cold water, and air-dried. Recrystallization was performed from a minimum amount of water at 55 °C; yield, 6.5 g. Anal. Calcd for $C_{16}H_{38}N_6O_9ClCo$: C, 34.76; H, 6.93; N, 15.20. Found: C, 34.55; H, 6.87; N, 15.15. ^1H NMR (D_2O) δ=2.10 (*s*, N-CH_3). ^{13}C NMR (D_2O) δ= 25.5, 31.2, 38.2, and 69.3.

Preparation of $(-)_{435}$-trans-*[$CoCl_2$(R,R-dmchxn)$_2$]Cl·HCl·$2H_2O$ (**1b**).* Slightly soluble perchlorate salt, $(-)_{546}$-*trans* $[Co(NO_2)_2(R,R\text{-dmchxn})_2]ClO_4\cdot H_2O$ (**1a**) (3.5 g) was converted to more soluble chloride salt by the vigorous stirring of the perchlorate salt with an anion-exchange resin (QAE-Sephadex, 100—200 mesh, 2 g) in the Cl^- form for 6 h. Concentrated hydrochloric acid (50 mL) was then poured onto the chloride salt of the *trans*-$[Co(NO_2)_2(R,R\text{-dmchxn})_2]^+$, which had been obtained by the evaporation of the aqueous solution after the removal of the resin. The solution was heated on a water bath at 90 °C and concentrated at that temperature continuously. The original violet color turned to green, and green crystals gradually formed in the solution. Then the solution was cooled to room temperature and allowed to stand overnight. The resulting green crystals were filtered, washed with a small amount of hydrochloric acid (1 M (1 M=1 mol dm^{-3})), and air-dried; yield, 2.1 g. Anal. Calcd for $C_{16}H_{41}N_4O_2Cl_4Co$: C, 36.84; H, 8.60; N, 10.62. Found: C, 37.18; H, 8.68; N, 10.38. ^1H NMR (CD_3OD) δ=2.43 (*d*, N-CH_3). ^{13}C NMR (D_2O-DCl) δ=24.4, 29.8, 37.8, and 69.5.

Preparation of $(+)_{546}$-*[$Co(CO_3)$(R,R-dmchxn)$_2$]Cl·$2H_2O$ (**2a**).* *R,R*-Dmchxn (2.8 g) was added to a fresh solution (30 mL) containing sodium tricarbonatocobaltate(III) trihydrate (3.6 g). The solution was warmed on a water bath for 1 h at 50 °C. The original green color gradually turned to a reddish purple. After cooling to room temperature, an aqueous solution (30 mL) of sodium chloride (2.5 g) was stirred into the solution. Then, the solution was allowed to stand overnight. The resulting crystals were recrystallized from water at 60 °C. The reddish purple crystals which separated were filtered, washed with ethanol and ether, and air-dried; yield, 4.0 g. The formation of only one isomer has been observed. Anal. Calcd for $C_{17}H_{40}N_4O_5ClCo$: C, 42.99; H, 8.48; N, 11.80. Found: C, 43.01; H, 8.73; N, 11.89. ^1H NMR (D_2O) δ=2.02 and 2.05 (*s*, N-CH_3). ^{13}C NMR (D_2O) δ=24.6, 25.2, 29.2, 30.8, 31.4, 32.7, 63.3, 65.9, and 168.6.

Preparation of $(+)_{435}$-trans-*[$CoCl_2$(R,R-dmchxn)$_2$]Cl·HCl·$2H_2O$ (**2b**).* 2.0 g of the $(+)_{546}$-$[Co(CO_3)(R,R\text{-dmchxn})_2]$-$Cl\cdot 2H_2O$ (**2a**) obtained above was dissolved in a minimum volume of water. The solution was acidified with concentrated hydrochloric acid (50 mL), followed by foaming. The solution was heated on a water bath at 90 °C and then concentrated. The green crystals which separated were filtered, washed with ice-cold hydrochloric acid (1 M), and air-dried. Recrystallization was performed from 6 M hydrochloric acid; yield, 2.0 g. Anal. Calcd for $C_{16}H_{41}N_4O_2Cl_4Co$: C, 36.84; H, 8.60; N,10.62. Found: C, 36.80; H, 8.91; N, 10.73. ^1H NMR (CD_3OD) δ=2.25 and 2.34 (*d*, N-CH_3). ^{13}C NMR (D_2O-DCl) δ=25.1, 25.6, 29.6, 37.8, 38.2, 64.7, 65.2, and 68.0.

Conversion Reaction from $(+)_{435}$-trans-*[$CoCl_2$(R,R-dmchxn)$_2$]$^+$ Ion to* $(-)_{435}$-trans *Isomer.* A sample (100 mg) of either the $(+)_{435}$-*trans* or $(-)_{435}$-*trans* isomer was dissolved in methanol (60 mL). To the solutions we then added 1 mL of a methanol solution containing 2,6-lutidine (40 mg), after which the solutions were stored at 45 °C. The CD spectra were recorded every 30 min. After 1 d, the CD spectra of the $(+)_{435}$-*trans* isomer became identical with that of the $(-)_{435}$-*trans* isomer, which did not change under the same conditions. The same reaction was also followed by ^1H NMR measurements. The results obtained by these two ways agreed with each other.

X-Ray Analysis. The crystal used in the data collection was a green prism with the approximate dimensions of 0.51×0.24×0.43 mm^3. The diffraction data were measured on a Rigaku AFC-5 diffractometer with graphite monochromatized Mo $K\alpha$ radiation. Within the range of $2\theta<65°$, 4870 independent reflections with $F_o>3[\sigma(F_o)]$ were obtained. The intensities were corrected for Lorentz and polarization factors and for absorption (μ=11.7 cm^{-1}).

Crystal data are: Triclinic, P1, a=11.395(10), b=11.674 (8), c=11.031(8) Å, α=98.62(6), β=102.48(8), γ=118.24(5)°, Z=2, D_m=1.435, D_x=1.438 gcm^{-3}.

The structure was solved by the heavy-atom method and refined by a block-diagonal least-squares method. A unit-weight weighting scheme was employed. All the hydrogen atoms except for those of the water and hydrochloride of crystallization were located by assuming a tetrahedral coordination; they are all included in the final refinement with the isotropic temperature factors. The atomic-scattering factors and values of f' and f'' for Co, Cl, O, and C were taken from Ref 4. The final indicies were R=0.041 and R'=0.044.

All the calculations were performed on a FACOM M-380 computer at the Institute of Physical and Chemical Research with Universal Program System UNICS III.[5]

Results and Discussion

Preparations. Two types of procedures were used for the preparation of *trans*-$[CoCl_2(R,R\text{-dmchxn})_2]^+$-type complexes. In the methods, the resulting *trans*-dichloro complexes, **1b** and **2b**, were obtained from **1a** and **2a** respectively by treatment with concentrated hydrochloric acid.

Method 1. The $(-)_{546}$-*trans*-$[CoCl_2(R,R\text{-dmchxn})_2]^+$ complex (**1b**) was obtained by the usual substitution reaction, using hexanitrocobaltate(III) as the starting material.[6] The reaction scheme is:

$$[Co(NO_2)_6]^{3-} + 2R,R\text{-dmchxn} \longrightarrow trans\text{-}[Co(NO_2)_2(R,R\text{-dmchxn})_2]^+ \quad (\mathbf{1a}).$$

$$(\mathbf{1a}) + \text{concd HCl} \longrightarrow trans\text{-}[CoCl_2(R,R\text{-dmchxn})_2]^+ \quad (\mathbf{1b}).$$

Method 2. The $(+)_{435}$-*trans*-$[CoCl_2(R,R\text{-dmchxn})_2]^+$ complex (**2b**) was also obtained by the usual substitution reaction, using tricarbonatocobaltate(III) as the starting material.[7] The reaction scheme is:

$$[Co(CO_3)_3]^{3-} + 2R,R\text{-dmchxn} \longrightarrow \Lambda\text{-}[Co(CO_3)(R,R\text{-dmchxn})_2]^+ \quad (\mathbf{2a}).$$

$$(\mathbf{2a}) + \text{concd HCl} \longrightarrow trans\text{-}[CoCl_2(R,R\text{-dmchxn})_2]^+ \quad (\mathbf{2b}).$$

For each complex, **1a**, **1b**, **2a**, or **2b**, only one isomer was obtained stereospecifically. The structural assignments of the geometries of the present complexes are based on (a) the ^{1}H NMR signals of the *N*-methyl groups, (b) the ^{13}C NMR signals of the complexes, and (c) the electronic absorption and the circular dichroism spectra. The data on the electronic spectra and circular dichroism curves for the dinitro, carbonato, and the dichloro complexes are given in Fig. 1 and Table 1. The results of the ^{1}H and ^{13}C NMR spectra of the four complexes are presented in the Experimental section.

Structures of Two trans*-Dichloro Complexes.* The dichloro complexes **1b** and **2b** obtained are green, which is characteristic of the *trans*-$[CoCl_2N_4]^+$ type. The visible absorption spectra of **1b** and **2b** are very similar to each other and give typical *trans*-$[CoCl_2N_4]^+$ absorptions (Fig. 1b). On the other hand, the CD spectra of **1b** and **2b** are significantly different from each other. The changes in the CD spectrum of $(+)_{435}$-*trans*-$[CoCl_2(R,R\text{-dmchxn})_2]^+$ during the conversion reaction are shown in Fig. 2. In the CD spectra of the $(-)_{435}$-*trans*-dichloro complex **1b**, no change has been observed during the same treatment. The reaction scheme is:

$$(+)_{435}\text{-}trans\text{-}[CoCl_2(R,R\text{-dmchxn})_2]^+ \ (\mathbf{2b}) \xrightarrow{\text{2,6-lutidine}} (-)_{435}\text{-}trans\text{-}[CoCl_2(R,R\text{-dmchxn})_2]^+ \ (\mathbf{1b}).$$

It is generally accepted that the absolute configuration of the asymmetric nitrogen atoms coor-

Table 1. Numerical data of absorption (AB) and circular dichroism (CD)

	AB$\bar{\nu}$, 10^3 cm^{-1} (log ε)	CD$\bar{\nu}$, 10^3 cm^{-1} ($\varepsilon_l-\varepsilon_r$)
$(-)_{546}$-*trans*-$[Co(NO_2)_2$-$(R,R\text{-dmchxn})_2]^+$ (**1a**)	21.6(2.45) 28.5(3.40)	21.7(−4.60)
$(+)_{546}$-$[Co(CO_3)$-$(R,R\text{-dmchxn})_2]^+$ (**2a**)	18.7(2.21) 26.5(2.16)	18.4(+4.26) 24.5(+0.46) 27.8(+0.19)
$(-)_{435}$-*trans*-$[CoCl_2$-$(R,R\text{-dmchxn})_2]^+$ (**1b**)	15.3(1.67) 19.8(1.52) 24.1(1.90)	16.3(+0.41) 19.4(+1.57) 24.8(−0.97)
$(+)_{435}$-*trans*-$[CoCl_2$-$(R,R\text{-dmchxn})_2]^+$ (**2b**)	15.2(1.79) 19.8(1.58) 24.1(1.98)	16.1(+0.87) 22.5(+0.06) 25.0(−0.62)
trans-$[CoCl_2$-$(R,R\text{-chxn})_2]^+$ a)	16.3(1.62) 21.7(1.47) 25.8(1.70)	16.1(+1.05) 21.3(−0.10)

a) Ref. 27).

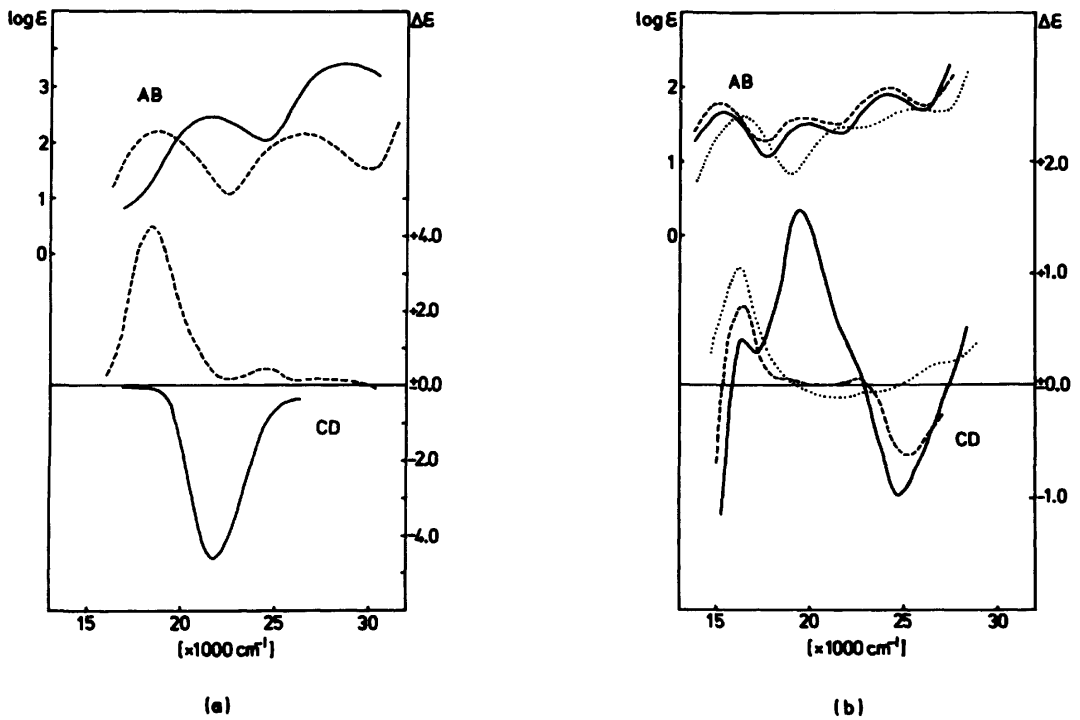

Fig. 1. (a) The AB and CD spectra of $(-)_{546}$-*trans*-$[Co(NO_2)_2(R,R\text{-dmchxn})_2]^+$ (**1a**) and $(+)_{546}$-Λ-$[Co(CO_3)(R,R\text{-dmchxn})_2]^+$ (**2a**) complexes. The solid line indicates the former complex ion. (b) The AB and CD spectra of *trans*-$[CoCl_2(R,R\text{-dmchxn})_2]^+$ complexes in methanol. The solid line and the broken line indicate the $(-)_{435}$-isomer (**1b**) and the $(+)_{435}$-isomer (**2b**), respectively. The AB and CD spectra of *trans*-$[CoCl_2(R,R\text{-chxn})_2]^+$ in methanol is presented by the dotted line.

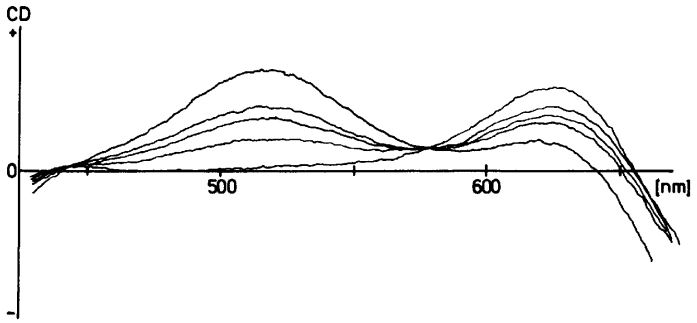

Fig. 2. The changes in the CD spectrum of $(-)_{435}$-*trans*-$[CoCl_2(R,R\text{-dmchxn})_2]^+$ during the conversion reaction.

dinated to a Co(III) can be changed under mild basic conditions without any change in the absorption spectrum, which is generally sensitive to any change in the structure of the complex.[8] The present conversion reaction using 2,6-lutidine proceeded from **2b** to **1b** without any color change, and the CD curves of **2b** during the reaction passed through the isodichroic points (439 and 578 nm, Fig. 2). Accordingly, these results indicate that the two dichloro complexes obtained differ in the absolute configurations of the coordinated secondary nitrogen centers, and that the isomeric mixtures produced during the reaction are composed of **2b** and **1b**.

The ^1H NMR spectrum of **1b** shows and *N*-methyl doublet at δ 2.43. The ^{13}C NMR spectrum of **1b** gives only four signals, though this complex contains 16 carbon atoms as its components. These NMR results prove that the four methyl groups on the nitrogen atoms are in the same chemical environment.

The X-ray structure analysis and circular dichroism studies of *trans*-[$CoCl_2$(*N*-methyl-substituted diamine)$_2$]$^+$ suggest the following empirical rule: the sign of the CD band near 22000 cm^{-1} ($A_{1g} \rightarrow A_{2g}$-($D_{4h}$) CD band) can be closely related to the configuration of the asymmetric nitrogen centers, as has been shown for *trans*-dichlorobis(diamine)-cobalt(III) complexes of *N*-methyl and *C*-methylethylenediamine.[9-11] When a complex involving five-membered chelate rings of λ-gauche conformations gives a positive Cotton effect in this region, it should be assigned to the *S* configuration around the asymmetric nitrogen center. According to this rule and the NMR results of **1b**, the absolute configurations around the four asymmetric nitrogen centers of the $(-)_{435}$-*trans*-dichloro complex **1b** might be concluded to be all *S*, since a large positive Cotton effect has been observed in the corresponding region (Fig. 1b) and since (1*R*,2*R*)-1,2-cyclohexanediamine adopts the λ-gauche conformation toward the Co(III) ion. Consequently, the structure of the $(-)_{435}$-isomer **1b** can be identified as the

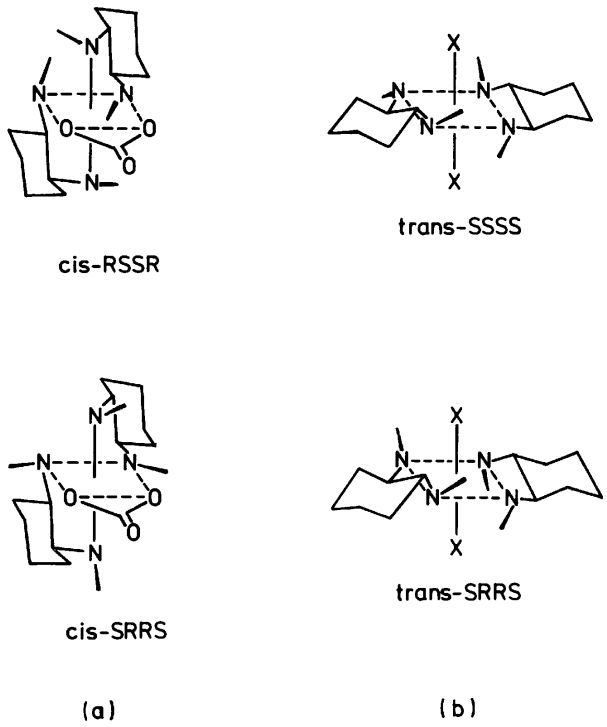

Fig. 3. (a) Two possible isomers of Λ-$[Co(CO_3)(R,R\text{-dmchxn})_2]^+$, and (b) structures of *trans*-type complexes, *trans*-$[CoX_2(R,R\text{-dmchxn})_2]^+$ ($X=NO_2^-$ or Cl^-).

trans-SSSS structure (Fig. 3b, $X=Cl^-$), which is thought to be most stable of the combinations of asymmetric nitrogen atoms.

On the other hand, the ^1H NMR spectrum of **2b** gives two kinds of *N*-methyl doublets, showing the presence of two pairs of *N*-methyl groups in different chemical environments. The ^{13}C NMR spectrum of **2b**, moreover, suggests that one twofold axis through the Co(III) ion exists, as eight signals were observed. The CD spectrum of the complex **2b** is very similar to that of the complex *trans*-$[CoCl_2(1R,2R)\text{-chxn})_2]^+$[12], which has four coordinated primary nitrogen atoms and no asymmetric center except for the asymmetric carbon atoms belonging to the (1*R*,2*R*)-1,2-cyclohexanediamine. Since no contribution from the asymmetric nitrogen centers appears in the CD spectrum,

Table 2. Atomic parameters for non-hydrogen atoms, with their standard deviations in parentheses[a)]

Atom	x	y	z	B_{eqv}
Co(1)	1(1)	0(1)	−1(1)	1.7
Co(2)	−204(1)	4864(1)	4945(1)	1.5
Cl(1)	611(2)	−106(2)	−1814(2)	2.7
Cl(2)	−647(2)	112(2)	1749(2)	2.8
Cl(3)	−246(2)	5149(2)	6983(2)	2.4
Cl(4)	−160(2)	4537(2)	2884(2)	2.4
Cl(5)	2496(2)	9072(2)	3686(2)	3.8
Cl(6)	7060(3)	10527(3)	5977(3)	4.9
Cl(7)	−5716(3)	7838(2)	8635(2)	4.8
Cl(8)	−4784(2)	2001(2)	1076(2)	4.0
O(1)	−5209(7)	964(7)	6306(7)	4.7
O(2)	−5134(8)	8758(8)	3237(7)	5.1
O(3)	−4583(7)	9584(7)	1395(6)	4.8
O(4)	−5699(8)	356(8)	8243(7)	5.5
N(1)	−538(6)	1309(5)	−486(5)	2.0
N(2)	1970(6)	1619(5)	868(5)	2.2
N(3)	−1884(6)	−1665(6)	−1004(5)	2.1
N(4)	582(5)	−1258(5)	570(5)	1.9
N(5)	−2212(5)	4350(5)	4335(5)	1.8
N(6)	280(6)	6737(5)	4905(5)	2.0
N(7)	−632(5)	2977(5)	4800(5)	1.8
N(8)	1835(6)	5446(5)	5690(5)	2.0
C(1)	697(7)	2740(6)	245(7)	2.2
C(2)	2016(7)	2732(6)	316(7)	2.1
C(3)	3346(8)	4142(7)	1027(8)	3.0
C(4)	3286(9)	5173(7)	350(8)	3.2
C(5)	1964(9)	5206(8)	253(9)	3.6
C(6)	628(9)	3779(8)	−420(9)	3.3
C(7)	−1880(8)	1173(8)	−374(8)	3.2
C(8)	2547(9)	2025(8)	2292(8)	3.2
C(9)	−1774(7)	−2883(6)	−970(7)	2.2
C(10)	−766(6)	−2596(6)	327(6)	1.9
C(11)	−609(7)	−3786(7)	474(7)	2.4
C(12)	−2046(8)	−5040(7)	241(8)	3.0
C(13)	−3045(8)	−5368(8)	−1083(8)	3.4
C(14)	−3190(8)	−4182(8)	−1276(9)	3.5
C(15)	−2655(9)	−1790(8)	−2331(7)	3.3
C(16)	1615(7)	−1452(7)	86(8)	2.6
C(17)	−2230(7)	5636(6)	4543(6)	2.0
C(18)	−1029(7)	6645(6)	4159(6)	2.0
C(19)	−996(8)	7978(7)	4252(8)	2.8
C(20)	−2411(9)	7724(8)	3461(8)	3.2
C(21)	−3589(8)	6765(8)	3893(8)	2.9
C(22)	−3641(7)	5437(7)	3815(8)	2.7
C(23)	−3252(8)	3354(8)	4832(8)	3.0
C(24)	1092(8)	7832(7)	6144(7)	2.8
C(25)	694(7)	2963(6)	5029(6)	1.9
C(26)	1858(7)	4272(6)	6071(6)	2.1
C(27)	3256(8)	4351(8)	6365(8)	3.1
C(28)	3154(8)	3111(8)	6750(9)	3.4
C(29)	1994(9)	1807(8)	5727(8)	3.1
C(30)	600(7)	1734(7)	5410(7)	2.6
C(31)	−1740(7)	1874(7)	3606(7)	2.5
C(32)	2829(8)	6112(8)	4993(8)	3.3

a) Positional parameters are multiplied by 10^4.

the complex **2b** may have the same numbers of secondary nitrogen centers in opposite configurations, two *R* and two *S*. From these spectral results, three geometrical isomers (*trans-SRRS*, *trans-RSSR*, and *trans-SSRR*) are possible for the *trans*-dichloro complex with one C_2 symmetry. Accordingly, it is difficult to assign the geometry of **2b** by means of the AB, CD, and NMR spectroscopies. The following section will deal with the detailed structural results concerning the **2b** complex obtained from X-ray diffraction.

Crystal and Molecular Structure of 2b. The final atomic coordinates of non-hydrogen atoms are listed in Table 2. The thermal parameters, the parameters for the hydrogen atoms, and the lists of structure factor amplitudes are available as supplementary material.[13)] Selected bond lengths and angles are presented in Tables 3 and 4. Perspective drawings of the complex cations showing ellipsoids of thermal

Table 3. Bond distances (l/Å)[a)]

Co(1)-Cl(1)	2.260(3)	Co(2)-Cl(3)	2.237(2)
Co(1)-Cl(2)	2.218(3)	Co(2)-Cl(4)	2.263(3)
Co(1)-N(1)	1.998(7)	Co(2)-N(5)	1.990(6)
Co(1)-N(2)	2.010(7)	Co(2)-N(6)	1.996(7)
Co(1)-N(3)	1.998(7)	Co(2)-N(7)	1.996(7)
Co(1)-N(4)	2.002(6)	Co(2)-N(8)	2.013(6)
N(1)-C(1)	1.517(10)	N(5)-C(17)	1.495(10)
N(2)-C(2)	1.500(10)	N(6)-C(18)	1.486(10)
N(3)-C(9)	1.491(10)	N(7)-C(25)	1.486(10)
N(4)-C(10)	1.516(10)	N(8)-C(26)	1.501(10)
N(1)-C(7)	1.495(11)	N(5)-C(23)	1.491(11)
N(2)-C(8)	1.469(12)	N(6)-C(24)	1.473(11)
N(3)-C(15)	1.482(12)	N(7)-C(31)	1.490(10)
N(4)-C(16)	1.486(11)	N(8)-C(32)	1.484(12)
C(1)-C(2)	1.492(11)	C(17)-C(18)	1.521(11)
C(9)-C(10)	1.503(11)	C(25)-C(26)	1.521(11)

a) Estimated standard deviations in parentheses.

Table 4. Bond angles (degree ϕ/°)[a)]

Cl(1)-Co(1)-Cl(2)	178.4(1)	Cl(3)-Co(2)-Cl(4)	178.8(1)
N(1)-Co(1)-N(2)	86.5(3)	N(5)-Co(2)-N(6)	86.3(3)
N(3)-Co(2)-N(4)	86.5(3)	N(7)-Co(2)-N(8)	86.1(3)
Co(1)-N(1)-C(1)	108.1(5)	Co(2)-N(5)-C(17)	107.5(5)
Co(1)-N(2)-C(2)	106.0(5)	Co(2)-N(6)-C(18)	107.7(5)
Co(1)-N(3)-C(9)	108.5(5)	Co(2)-N(7)-C(25)	109.6(5)
Co(1)-N(4)-C(10)	106.6(4)	Co(2)-N(8)-C(26)	107.0(5)
Co(1)-N(1)-C(7)	119.9(5)	Co(2)-N(5)-C(23)	119.8(5)
Co(1)-N(2)-C(8)	118.4(4)	Co(2)-N(6)-C(24)	117.6(5)
Co(1)-N(3)-C(15)	120.3(5)	Co(2)-N(7)-C(31)	118.2(5)
Co(1)-N(4)-C(16)	119.9(5)	Co(2)-N(8)-C(32)	119.6(5)
C(1)-N(1)-C(7)	110.3(6)	C(17)-N(5)-C(23)	110.6(6)
C(2)-N(2)-C(8)	114.6(7)	C(18)-N(6)-C(24)	114.5(6)
C(9)-N(3)-C(15)	111.3(6)	C(25)-N(7)-C(31)	110.2(6)
C(10)-N(4)-C(16)	112.2(6)	C(26)-N(8)-C(32)	115.0(6)

a) Estimated standard deviations in parentheses.

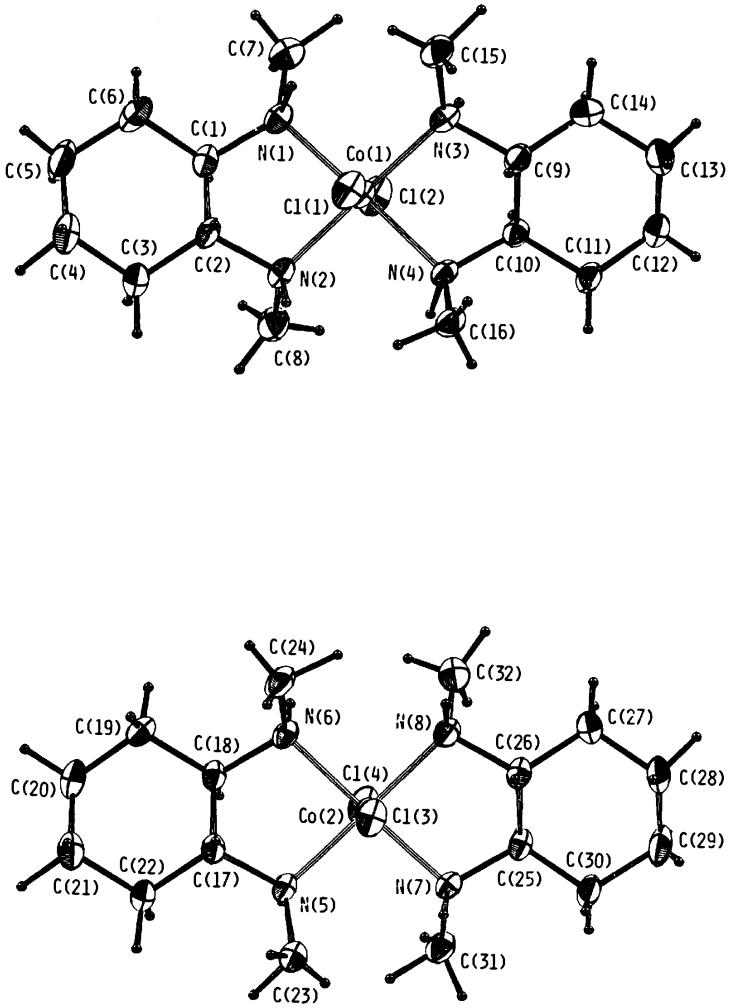

Fig. 4. Perspective drawings of the complex cations $(-)_{435}$-*trans*-$[CoCl_2(R,R\text{-dmchxn})_2]^+$ and the numbering scheme for the atoms.

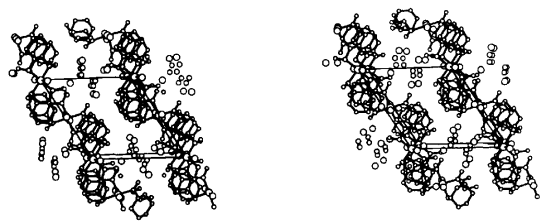

Fig. 5. A stereoscopic illustration of one unit cell, viewed down the c axis with the a axis vertical.

motion are given in Fig. 4. A stereoview of the contents of one unit cell and each conformation of the diamine-chelate rings are shown in Fig. 5 and 6 respectively.

The unit cell consists of 2 complex cations, chloride counterions, hydrochloride molecules, and the 4 waters of crystallization. The two complex cations in one unit cell have almost identical structures. The complex cations have an approximately C_2 symmetry. Each cobalt atom is surrounded by four nitrogen atoms and two chlorine atoms at the apices of a slightly distorted octahedron. The chloro groups are in the trans positions. The absolute configurations around the asymmetric carbon centers are both *R* for each cyclohexanediamine. The conformations of the two five-membered chelate rings are both λ in each complex ion. The four cyclohexane rings adopt the chair conformation, and all the *C*-methylene groups have equatorial orientation with respect to the chelate rings. The structure of (1*R*,2*R*)-1,2-cyclohexanediamine, used in the syntheses, agrees with the known absolute configurations.[14,15] The arrangements around the secondary nitrogen atoms are the pair of the *R* and *S* configurations in the notation of Cahn, Ingold, and Prelog.[16] In each complex ion, two *N*-methyl groups have equatorial orientations, while the other groups have axial orientations, with respect to the chelate rings. The *N*-methyl group bonded to the nitrogen atom of the *R* or *S* configuration in each diamine is neighboring with the group linked to that of the same configuration of the other respective diamine. This findings as to the structure around the asymmetric nitrogen centers, which involves the asymmetric nitrogen atoms of two *R* and two *S* configurations in each complex ion, agrees with the spectral assignment of **2b** (*vide supra*).

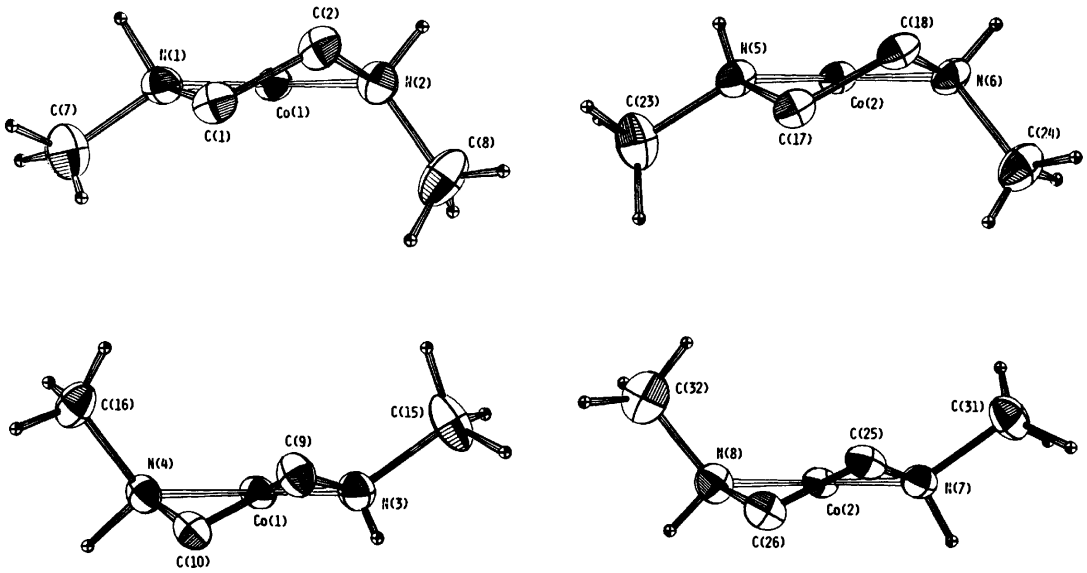

Fig. 6. Each conformation of the four diamine-chelate rings.

The average Co–N bond distance is 1.998(6) Å, slightly longer than the recent values reported for *trans*-$[CoCl_2(en)_2]^+$; the average Co–N(ethylenediamine) lengths are 1.960(5), 1.960(10), and 1.950(3) Å.[17] Moreover, the present Co–N value is slightly long as compared with the average distances reported for the Co–N bond in *tris*-type complexes involving *trans*-1,2-cyclohexanediamine, 1.972(5) and 1.984(4) Å for $(-)_{589}$-$[Co((+)\text{-chxn})_2((-)\text{-chxn})]^{3+}$ and $(-)_{589}$-$[Co((-)\text{-chxn})_3]^{3+}$ respectively.[14,15] Such as elongation of the chelate bond Co–N is also occasionally observed in the complexes involving *N*-alkylated diamines, for example, $(-)_{546}$-*trans*-$[Co(NO_2)_2((-)_{589}\text{-}2,2'\text{-bpp})_2]^+$,[18] *trans*-$[Co(pip)_2(tpp)]^+$,[19] and $(-)_{589}$-*cis*-$[Co(NO_2)_2(N^1\text{-me-}(S)\text{-pn})_2]^+$,[20] where 2,2′-bpp, pip, tpp, and N^1-me-(*S*)-pn represent 2,2′-bipiperidine, piperidine, the 5,10,15,20-tetraphenylporphinate anion, and (2*S*)-N^1-methyl-1,2-propanediamine respectively, the average Co–N(2,2′-bpp), Co–N(pip), and Co–N(N^1-me-(*S*)-pn) distances being 2.004(5), 2.060(3), and 2.015(5) Å respectively. The ring angles at the cobalt atom for the five-membered chelate rings, N(1)–Co(1)–N(2), N(3)–Co(1)–N(4), N(5)–Co(2)–N(6), and N(7)–Co(2)–N(8), are 86.3(2), 86.2(2), 86.7(2), and 86.4(2)° respectively, the average being 86.4(2)°. These angles appear normal for Co(III) five-membered chelate rings, which are usually less than 90°, though the angles of the present complex are slightly larger than those observed in the complexes coordinating the bidentate ligands *trans*-1,2-cyclohexanediamine and 2,2′-bipiperidine described above, which range from 84.1(2) to 84.7(2)°. The Co–Cl bond lengths of Co(1)–Cl(1) and Co(2)–Cl(4) are 2.261(3) and 2.264(3) Å, which can be compared with the mean values of 2.253(2), 2.254(3), 2.244(1), and 2.26 Å in *trans*-$[CoCl_2(en)_2]^+$,[17] 2.26 Å in *trans*-$[CoCl_2(1,3\text{-propanediamine}_2]^+$,[21] and 2.257(2) Å in *trans*-$[CoCl_2((-)\text{-}1,2\text{-cyclopentanediamine})_2]^+$,[22] where as the bond lengths of Co(1)–Cl(2) and Co(2)–Cl(3) are 2.217(3) and 2.236(3) Å respectively, slightly shorter than the other values. The average N–C and C–C distances, 1.491(11) and 1.518(12) Å respectively, are comparable with the reported values in $(-)_{589}$-$[Co((+)\text{-chxn})_2((-)\text{-chxn})]^{3+}$ (1.486(7) and 1.498(8) Å) and $(-)_{589}$-$[Co((-)\text{-chxn})_3]^{3+}$ (1.494(7) and 1.516(8) Å), for the mean N–C and C–C distances respectively of the cyclohexanediamine. The average C–C bond distance of the chelate-ring carbon atoms is 1.509(11) Å, which is quite normal for Co(III) five-membered chelate rings. The average bond angle at the carbon and nitrogen atoms for the (1*R*,2*R*)-*N*,*N*′-dimethyl-1,2-cyclohexanediamine is 111.6°, which is slightly large as compared with the idealized tetrahedral values of 109.5°. This enlargement of the average bond angle of the ligand is mainly due to the larger angles at the carbon and nitrogen atoms belonging to the asymmetric nitrogen atoms whose absolute configurations are *R* around them; for example, the bond angles of N(2)–C(2)–C(3), N(4)–C(10)–C(11), N(6)–C(18)–C(19), and N(8)–C(26)–C(27) are 114.5(7), 116.5(6), 116.9(7), and 115.8(5)° respectively.

Thus, the exact structure of the $(+)_{435}$-*trans*-dichloro complex **2b**, which could not be determined by usual spectroscopy, has been elucidated as the isomer *trans*-*SRRS* (Fig. 3b, X=Cl^-). On the basis of the spectral evidence and the crystal structure of these two *trans*-dichloro complexes **1b** and **2b**, the structures of their precursors, **1a** and **2a**, will be discussed in the following section.

Structural Assignment of the Precursors. It is generally acknowledged that the AB spectral patterns of Co(III) diacidobis(diamine) complexes are characteristic of their geometry.[23] It is recognized that *cis*- and *trans*-dinitro complexes of Co(III) show

λ_{max} at ≈330 nm and ≈350 nm respectively. The present dinitro complex **1a** shows λ_{max} at 351 nm (Fig. 1a), showing that it has the *trans* configuration with respect to the two nitro groups. The ^1H NMR spectrum of Ia shows an *N*-methyl signal at δ 2.10, indicating that the four methyl groups in the complex ion are in the same chemical environment. In the ^{13}C NMR spectrum of **1a**, moreover, four signals were observed when irradiating all of the hydrogen nuclei. Because the dinitro complex **1a** contains 16 carbon atoms, this result means that **1a** has a triple twofold symmetry, like the derived dichloro complex **1b**. Generally, the absolute configuration of the coordinated asymmetric nitrogen centers can be effected to fit in with *S* arrangements when the five-membered chelates adopt the λ-gauche conformations, as has been indicated in the case of the Co(III) complex containing *N*-methylethylenediamine.[24] The absolute configurations around the four asymmetric nitrogen atoms of **1a**, therefore, can be concluded to all be *S*, and the four methyl groups can be concluded to have an equatorial orientation with respect to the chelate rings (Fig. 3b, *trans-SSSS*, X=NO_2^-).

The visible absorption spectrum of **2a** is very similar to that of *cis*-$[Co(CO_3)(en)_2]^+$,[25] and it gives the typical *cis*-$[CoN_4O_2]^+$ absorption (Fig. 1a). In the CD spectrum of **2a**, a large positive Cotton effect has been observed in the first absorption region, comparable with that of Λ-$[Co(CO_3)((2R)\text{-1,2-propanediamine})_2]^+$.[26] The absolute configuration around Co(III) can be assigned to Λ on the basis of this observaton. The ^1H NMR spectrum of **2a** shows two kinds of *N*-methyl signals, like the derived dichloro complex **2b**. Moreover, nine signals were observed in the ^{13}C NMR spectrum of **2a**, though the carbonato complex contains 17 carbon atoms. It has been elucidated by the present X-ray study that the *trans*-dichloro complex **2b** derived from this carbonato complex **2a** has two secondary nitrogen atoms of the *R* configuration and two of those of the *S* arrangement in each diamine. It can be expected that the carbonato complex reacts with hydrochloric acid to yield the *trans*-dichloro complex, with a retention of the absolute configuration of the asymmetric nitrogen centers. From these considerations, the structure of the carbonato complex **2a** may be restricted to either the *cis-SRRS* or *cis-RSSR* isomer (Fig. 3a), though ten structures are theoretically possible. According to the molecular model study, the *cis-SRRS* isomer seems to be more stable than the latter, since the *N*-methyl groups bonded to the asymmetric nitrogen atom of the *R* configuration in the isomer is distant from the neighboring diamine chelate ring, while those of the *S* configuration in the *cis-RSSR* are close to the corresponding chelate ring. Thus, the present carbonato complex **2a** can be tentatively assigned to the *cis-SRRS* isomer.

Thus, the new complexes, $(-)_{546}$-*trans*-(*SSSS*)-$[Co(NO_2)_2(R,R\text{-dmchxn})_2]^+$, $(+)_{546}$-Λ-$[Co(CO_3)(R,R\text{-dmchxn})_2]^+$, $(-)_{435}$-*trans*-(*SSSS*)-$[CoCl_2(R,R\text{-dmchxn})_2]^+$, and $(+)_{435}$-*trans*-(*SRRS*)-$[CoCl_2(R,R\text{-dmchxn})_2]^+$, were prepared and characterized. It is evident that $(+)_{546}$-Λ-$[Co(CO_3)(R,R\text{-dmchxn})_2]^+$ was converted by concentrated HCl to $(+)_{435}$-*trans*-(*SRRS*)-$[CoCl_2(R,R\text{-dmchxn})_2]^+$, with a retention of the configuration of the secondary nitrogen atoms. This observation will be very important in discussing the mechanism of the *cis-trans* conversion reaction when the exact structure of the starting carbonato complex can be determined by means of X-ray crystallography.

For all four complexes investigated in this study, the stereospecific formation has been observed. For the $[Co(CO_3)(R,R\text{-dmchxn})_2]^+$ complex, only the Λ isomer has been detected. This result indicates that suitably designed diamines could govern the overall geometry of the complexes and afford useful coordination sites for the asymmetric reactions, as is observed in the case of the linear tetradentate tetraamines.[1,2,27]

Studies are now in progress to establish the stereochemistry of this system in hoping to clarify the mechanism for the *cis-trans* conversion reaction and to develop suitable ligands for metal-assisted asymmetric reactions.

This work was partially supported by a Grant-in-Aid for Scientific Research (No. 364209) from the Ministry of Education, Science, and Culture.

References

1) M. Ajioka, K. Matsuda, S. Yano, and S. Yoshikawa, *J. Am. Chem. Soc.*, **103**, 2459 (1981).
2) M. Yamaguchi, S. Yamamatsu, T. Furusawa, S. Yano, M. Saburi, and S. Yoshikawa, *Inorg. Chem.*, **19**, 2010 (1980).
3) K. Kashiwabara, K. Hanaki, and J. Fujita, *Bull. Chem. Soc. Jpn.*, **53**, 2275 (1980).
4) "International Tables for X-ray Crystallography," Kynoch Press: Birmingham, England, Vol. IV (1974).
5) T. Sakurai and K. Kobayashi, *Rikagaku Kenkyusho Hokoku*, **55**, 69 (1979).
6) a) "Inorg. Synth.," Vol. IV, p. 176; b) F. Mizukami, H. Ito, J. Fujita, and K. Saito, *Bull. Chem. Soc. Jpn.*, **44**, 3051 (1971).
7) a) M. Shibata, *Nippon Kagaku Zasshi*, **87**, 771 (1966); b) "Inorg. Synth.," Vol. XIV, p. 68.
8) M. Ajioka, S. Yano, M. Saburi, and S. Yoshikawa, *Inorg. Chem.*, **20**, 884 (1981).
9) C. J. Hawkins, *J. Chem. Soc., Dalton Trans.*, **1969**, 777.
10) M. Saburi, Y. Tsujito, and S. Yoshikawa, *Inorg. Chem.*, **9**, 1476 (1970).
11) J. A. Tiethof and D. M. Cooke, *Inorg. Chem.*, **11**, 315 (1972).

12) R. S. Treptow, *Inorg. Chem.*, **5**, 1593 (1966).
13) These numerical data are deposited as Document No. 8518 at the Office of the Editor of Bull. Chem. Soc. Jpn.
14) S. Sato and Y. Saito, *Acta Crystallogr. Sect. B*, **33**, 860 (1977).
15) A. Kobayashi, F. Marumo, and Y. Saito, *Acta Crystallogr. Sect. B*, **28**, 2709 (1972).
16) R. S. Cahn, C. K. Ingold, and V. Prelog, *Experientia*, **12**, 81 (1956).
17) A. S. Foust, V. Janickis, and K. Maroy, *Inorg. Chem.*, **19**, 1044 (1980).
18) M. Sato, Y. Sato, S. Yano, S. Yoshikawa, K. Toriumi, H. Itoh, and T. Itoh, *Inorg. Chem.*, **21**, 2360 (1982).
19) W. R. Scheidt, J. A. Cunningham, and J. L. Hoard, *J. Am. Chem. Soc.*, **95**, 8289 (1973).
20) T. Makino, S. Yano, and S. Yoshikawa, *Inorg. Chem.*, **18**, 1048 (1979).
21) K. Matsumoto, S. Ooi, and H. Kuroya, *Bull. Chem. Soc. Jpn.*, **43**, 1903 (1970).
22) M. Goto, K. Ohta, K. Toriumi, and T. Ito, *Acta Crystallogr. Sect. B*, **37**, 1189 (1981).
23) a) H. Kuroya and R. Tsuchida, *Bull. Chem. Soc. Jpn.*, **15**, 427 (1940); b) M. Linhard and M. Wiegel, *Z. Anorg. Allg. Chem.*, **266**, 49 (1951); c) *ibid.*, **267**, 113 (1951); d) *ibid*, **271**, 101 (1952).
24) D. A. Buckingham, L. G. Marzilli, and A. M. Sargeson, *J. Am. Chem. Soc.*, **89**, 3428 (1967).
25) A. J. MaCaffery, S. F. Mason, and B. J. Norman, *J. Chem. Soc., Dalton Trans.*, 5094 (1965).
26) S. M. Martinette and J. C. Bailar, Jr., *J. Am. Chem. Soc.*, **74**, 1054 (1952).
27) P. J. Toscano and L. G. Marzilli, *Inorg. Chem.*, **22**, 3342 (1983).

 © 1985 The Chemical Society of Japan Bull. Chem. Soc. Jpn., 58, 1401—1406 (1985)

New Type of Aldol Condensations Catalyzed by Metal(II) Complexes of α-Amino Acid Esters and that with Cyclodextrin System

Ken-ichi WATANABE,* Yoichi YAMADA, and Katsuhisa GOTO
Department of Chemistry, Faculty of Science, Tokyo Metropolitan University, Fukazawa, Setagayaku, Tokyo 158
(Received May 18, 1984)

The aldol condensations of *p*-nitrobenzaldehyde with acetone catalyzed by metal complexes of α-amino acid esters proceeded under mild and neutral conditions to afford an enantiomeric excess aldol-type product, 4-hydroxy-4-(4-nitrophenyl)-2-butanone, along with some dehydrated products without any by-product. The most effective catalyst system was a zinc(II) complex of the tyrosine ethyl ester, Zn^{II}–$(TyrOEt)_2$ in MeOH. Complexes of the second-row transition metals were inadequate for the reactions. Reactions at 30—40 °C for 24 h were favorable regarding the asymmetric induction. An H_2O solvent was the best for aldol-type product formations without asymmetric induction. An assistant effect of cyclodextrins(especially, β-CD) on the catalysis of the Zn^{II}–TyrOEt complex were thought to be observed.

Aldol-condensation reactions are generally catalyzed using bases and acids. Accordingly, some side reactions are apt to occur, and it is not always easy to get only cross-aldol-reaction products. Recently, we found that the reactions are generelly catalyzed under neutral conditions by 2,2′-bipyridine complexes of the first-row transition metals[1] and also by cobalt(II) complexes of pyridine-containing copolymers.[2] The reactions of various aldehydes with ketones in the presence of these metal complex catalysts afford liberated condensation products in satisfactory yields without any by-products. However, the reaction products are always α,β-unsaturated ketones(2) derived through the dehydration of the aldol-type products, β-hydroxy ketones(1).

$$\mathrm{RCH(=O) + CH_3C(=O)R' \xrightarrow[\text{DMF., 80 °C}]{\text{M(II)-L}_n} \underset{\text{aldol-type product (1)}}{\mathrm{RCH(OH)CH_2C(=O)R'}}}$$

$$\xrightarrow{-H_2O} \underset{\text{dehydrated product (2)}}{\mathrm{RCH{=}CHC(=O)R'}}$$

We have developed a new investigative technique for the following three objectives regarding these complex-catalyzed aldol reactions:

1) To produce the aldol-type product(1) without the dehydrated product(2), or to depress any dehydration if it occurs.

2) To get an optically active aldol-type product(1) by use of a chiral metal-complex catalysts with optically active ligands.

3) To apply the inclusion effects of cyclodextrins to enhance the catalytic activity of the metal-complex system.

In order to realize these objectives, reactions of *p*-nitrobenzaldehyde with acetone were adopted as the standards due to their high reactivity and of a relative difficulty regarding the dehydration of the aldol-type product. Metal species of the employed complexes were the first- and second-row transition metal salts. The first-row efficiencies were investigated in one of our previous studies[1,2] and it was of interest to examine the second-row for the first time. As a result of various examinations involving chiral ligands of the complexes, we have found that esters of α-amino acids are fairly effective for the purpose of obtaining the aldol reactions with asymmetric induction. Among esters of the α-amino acids easily prepared, L-tyrosine ethyl ester (L-TyrOEt, mp 108 °C) and L-histidine methyl ester (L-HisOMe, mp 61 °C) were used, since they are crystals and can be easily handled and purified. Quinine and quinidine as ligands were also examined because pyridine and bipyridine *etc.* were the most effective ligands of the complex catalysts for the aldol condensations.[1,2]

Since the 1970's, many studies have been reported in regard to the aldol reactions utilizing organometallic compounds as an auxiliary reagent for diasteroselective additions through metal enolate intermediates.[3] Our studies since 1978 have been essentially different in that metal complexes were used as catalysts. Such studies as the asymmetric aldol reactions catalyzed by chiral metal complexes of an α-amino acid system under neutral conditions have not been reported yet.

Cyclodextrins(CD) possess hydrophobic cavities in which hydrophobic molecules are able to be selectively included. For this reason, many studies on the effect of the inclusion behavior on catalytic, regioselective, and enantioselective reactions by use of CDs have been reported.[4] Such inclusion effects are sometimes used to simulate an enzyme action. We have investigated assistant effects of CDs on complex-catalyzed aldol reactions. In this paper, the scope and limitations of these complex-catalyzed aldol reactions are reported in detail.

Results and Discussion

Effects of Metal Species and Ligands of the Complex Catalysts. Effects of metal species and ligands of

TABLE 1. ALDOL CONDENSATIONS OF *p*-NITROBENZALDEHYDE WITH ACETONE (1) (EFFECTS OF CHIRAL LIGANDS OF $Zn(NO_3)_2$ COMPLEXES[a])

Ligand	M : L	Yield of (1)/%[b] (isolated)	$[\alpha]_D$ (in EtOH)	Yield of (2)/%[c] (NMR)
L-TyrOEt	1 : 1	35	−6.4	13
L-TyrOEt	1 : 2	40	−11.2	42
D-TyrOEt	1 : 2	41	+11.9	
DL-TyrOEt	1 : 2	20	0	26
L-TyrOMe	1 : 2	39	−8.3	30
L-HisOMe[d]	1 : 2	14	−5.3	
L-HisOMe[e]	1 : 2	47	−1.9	Trace
L-AlaOEt	1 : 2	30	−2	4
Q[f]	1 : 1	40	+1	Trace
Q	1 : 1/2	54	0	
Q'[g]	1 : 2	13	0	0
Q+bpy[h]	1 : 1 : 1	72[i]	0	Trace
Q'+bpy[h]	1 : 1 : 1	75[i]	0	Trace
Q+L-TyrOEt	1 : 1 : 1	61	−1.3	10
L-TyrOEt+bpy	1 : 1 : 1	26.4	−8.8	+
L-TyrOEt+Im[j]	1 : 1 : 1	34.6	−1.6	+

a) Reaction conditions: aldehyde 0.66 mmol, acetone 2 ml(excess), catalyst 16 mol% of the aldehyde, solvent MeOH 7 ml, at 40 °C for 24 h. b) Aldol-type product. c) Dehydrated product, by NMR. d) Reaction for 48 h. e) $Zn(OAc)_2$ complex was used for 48 h. f) Quinine. g) Quinidine. h) Reaction at 30 °C. i) 100% by NMR. j) Imidazol.

complex catalysts on the reactions of *p*-nitrobenzaldehyde with acetone were examined for the first time. Tables 1 and 2 show that among the metal ions and ligands examined, an Zn^{2+}–L-TyrOEt system was the most adequate catalyst.

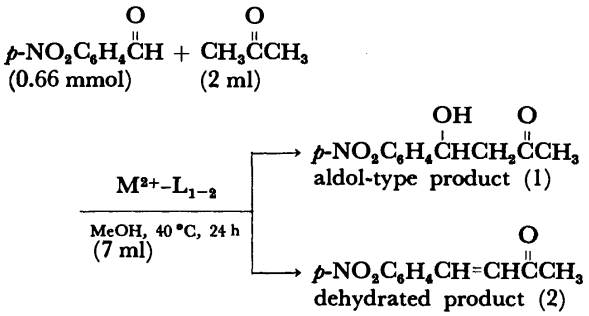

In order to prepare the complex catalysts, the metal salt and the ligand compound were mixed with dry methanol and stirred for a while; and, the complex solution was subsequently used without the isolation of the complex in its crystal form. The homogeneous reaction proceeded smoothly at 40 °C for 24 h and the aldol-type product(1), 4-hydroxy-4-(4-nitrophenyl)-2-butanone, was obtained from the reaction mixture by means of column chromatography with silica-gel. The reaction did not proceed without the catalyst and was extremely slow when only the metal salts were used without the ligand. As was expected, the reactions with an L-TyrOEt complex afforded an enantiomeric excess product(1) having a minus sign $[\alpha]_D$. A plus sign in the reaction with the D-TyrOEt complex, indicated that an asymmetric regulation occurred (Table 1). The Zn^{II}–$(TyrOEt)_2$ (1:2) complex was superior to the 1:1 complex with respect to the product yield and the asymmetric induction.

TABLE 2. ALDOL CONDENSATIONS OF *p*-NITROBENZALDEHYDE WITH ACETONE (2) (EFFECTS OF METAL SPECIES OF L-TyrOEt COMPLEXES(M : L = 1 : 2)[a])

Metal salts	Yield of (1)/%[b] (isolated)	$[\alpha]_D$ (in EtOH)	Yield of (2)/%[c] (NMR)
$Co(OAc)_2 \cdot 4H_2O$	33	−5.7	13
$Ni(OAc)_2 \cdot 4H_2O$	26	−8.2	11
$Ni(NO_3)_2 \cdot 6H_2O$[d]	63	−3.0	+
$Cu(OAc)_2 \cdot H_2O$	9	−2.7	4
$Zn(OAc)_2 \cdot 2H_2O$	22	−6.2	30
$Zn(NO_3)_2 \cdot 6H_2O$	40	−11.2	42
$ZnCl_2$	19	−4.9	48
$RuCl_3 \cdot 3H_2O$[e]	0		0
$RuCl_3 \cdot 3H_2O$[f]	14	+2.5	8
$Pd(OAc)_2$[g]	0		0
$RhCl_3 \cdot 3H_2O$	0		0

a) Reaction conditions were similar to those shown in Table 1. b) Aldol-type product. c) Dehydrated product. d) Reaction for 48 h. e) Formation of acetal (62%) with MeOH without any aldol condensation products. f) Reaction in 9 ml. acetone without MeOH. g) Deposition of Pd° during the reaction.

The reactions with quinine(Q) and quinidine(Q') complexes showed no asymmetric induction at all. Examinations with other Q-complexes were further

carried out using Co, Ni, and $Cu(OAc)_2$, $RuCl_3$, and $Pd(OAc, NO_3$, and $Cl)_2$ *etc.*; but, almost no reaction took place. It was found that mixed ligand complexes of Zn^{II}–Q (or Q′)-bpy (1:1:1) showed a high catalytic activity to give only product(1) quantitatively even at 30 °C (100%, by NMR) but without any asymmetric induction. The reaction with a $Zn(NO_3)_2$–bpy_2 complex gave product(1) (40 °C, 24 h, racemate) in a 60% yield (by NMR).

From the results in Table 2, it is evident that $Zn(NO_3)_2$ is a very effective metal species. On the contrary, the second-row transition metal salts were all inadequate for the reactions. Besides $Pd(OAc)_2$, $Pd(NO_3)_2$, and $PdCl_2$ were also examined but none of them showed any catalytic activity at all. In the presence of the $RuCl_3$–(L-TyrOEt)$_2$ complex, an acetal of the aldehyde with a MeOH solvent was formed in a 62% yield(NMR) and no aldol reaction took place at all (see experimental). Then, the reaction was carried out in acetone without MeOH, no notable result was obtained (product(1), 14%).

Now, the optical purity of the aldol-type product obtained in the reactions is still unknown since the specific rotation of the pure enantiomer is unknown. We tried to determine the enantiomeric excess of the aldol-type product(1) by means of ^{1}H-NMR spectroscopy with shift reagents (Eu(tbc)$_3$ and Eu(tfc)$_3$) or by some other methods. However, definite values were not obtained.

Examination of the Complex Formation. When the metal salts and the ligand compounds were added together in methanol, a color change was observed, indicating a complex formation. In order to further understand this formation, UV spectra of $Ni(OAc)_2 \cdot 4H_2O$, L-TyrOEt, and $Ni(OAc)_2$–(L-TyrOEt)$_{1-2}$ complexes were measured. Also, the pH of the solution (MeOH+H_2O) and their optical rotation (in EtOH) were measured (Table 3). The absorption maximum of the Ni^{2+} (670 nm) showed a blue shift after the addition of L-TyrOEt. The hyperchromic effect was observed, indicating a change of the electronic state of the Ni^{2+} ion by the coordination of the ligand. On the other hand, the pH of a TyrOEt solution itself (7.8) turned almost neutral (7.0—7.2) in a Ni^{II}–TyrOEt complex solution (M:L=1:1, 1:2) which was similar in pH to a $Ni(OAc)_2$ solution. This means that the NH_2 group of the ligand was masked by the coordination. With regard to the specific rotation, $[\alpha]_D$=+19.8° of the TyrOEt turned into −2.5°—−3.3°, indicating a chiral complex formation.

Examination of Catalysis of $Zn(NO_3)_2$-(L-TyrOEt)$_2$ Complex System. On the basis of the above examinations, the effects of the solvent, temperature, reaction time, and the amount of the catalyst were widly studied with regard to catalysis of the $Zn(NO_3)_2$–(TyrOEt)$_2$ complex. The results of reactions in various solvents are shown in Table 4. DMF, THF, and HMPA as solvents were also examined, but the reactions did not proceed well and isolation of the products was difficult. According to Table 4, a H_2O solvent was the best in view of the aldol-type product formation (100%, by NMR). However, almost no asymmetric induction was observed. On the other hand, MeOH was the best regarding asymmetric induction. Acetone might represent a special case, as it is the substrate for the reactions and the reactions were completed within 8 h.

It may be presumed that the aldol-type(1) and the dehydrated-type(2) were in equilibrium; hence, the reaction in pure H_2O did not afford (2) at all. The

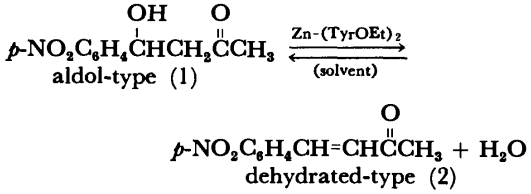

Table 3. Physical properties of Ni^{II}-L-TyrOEt complexes and the components

Compound[a]	pH	$[\alpha]_D$ (in EtOH)	UV λ_{max}	UV A
$Ni(OAc)_2 \cdot 4H_2O$	7.1	0	670	0.18
L-TyrOEt	7.8	+19.8		
Ni^{II}-L-TyrOEt	7.2	−3.3	656	0.29
Ni^{II}-(L-TyrOEt)$_2$	7.0	−2.5	644	0.39

a) 0.11 mmol each(except for Ni^{II}-(L-TyrOEt)$_2$) in MeOH(5 ml) + H_2O(2 ml) solvent.

Table 4. Aldol condensations with $Zn(NO_3)_2$-(L-TyrOEt)$_2$ complex (1)[a] (Effects of solvent)

Solvent (7 ml)	Yield of (1)/%[b] (isolated)	$[\alpha]_D$ (in EtOH)	Yield of (2)/%[c] (NMR)
MeOH	40	−11.2	42
EtOH	33	−8.0	53
Dioxane	32	−5.7	40
Acetone[d]	52	−11.3	40
H_2O[e]	83[f]	−1.4	0
MeOH + H_2O (ml)			
6 1	42	−12.2	9
5 2	45	−9.7	+
3 4	77	−3.2	+
1 6	81	−2.2	0

a) Reactions and the reaction conditions are similar to those shown in Table 2(40 °C, 24 h, catalyst: 16 mol% of the aldehyde). b) Aldol-type product. c) Dehydrated product. d) Acetone 9 ml. e) pH 7. f) 100% by ^{1}H-NMR, the reaction was completed within 20 h.

results of the reactions in MeOH–H_2O mixed solvents at various ratios support the above equilibrization. The low $[\alpha]_D$ value of the product(1) may be due to the reversible dehydration-hydration reactions which cause the racemization of (1). In order to ascertain this assumption, the aldol-type(1) showing $[\alpha]_D=-12°$ was treated with a catalyst in H_2O or MeOH under similar conditions to those shown in Table 4. Treating in H_2O (addition of a small amount of MeOH to make the system homogeneous), the racemization occurred ($[\alpha]_D$ decreased to $-5°$), but no racemization occurred in the MeOH solvent (Eq. 1).

$$\text{(1) } ([\alpha]_D=-12°) \xrightarrow{\text{cat}} \begin{cases} \xrightarrow{H_2O} \text{(2) } 11\%\cdots[\alpha]_D \rightarrow -5° \\ \xrightarrow{\text{MeOH}} \text{(2) } 38\%\cdots[\alpha]_D \rightarrow -12° \end{cases} \quad (1)$$

$$\text{(2)} \xrightarrow{\text{cat., } H_2O} \text{(1) } 18\% \quad (2)$$

On the other hand, the hydration of (2) in H_2O occurred in a 18% yield (Eq. 2). Thus, an equilibrium between (1) and (2) in connection with the racemization was confirmed.

The effects of the reaction temperature, time, and the amount of the catalyst are summarized in Table 5. Comparing Entries 1(20 °C), 2(30 °C), 6(40 °C), and 8(50 °C) with each other, the elevation of the temperature seems to affect the dehydration and racemization. In Entry 3(48 h), $[\alpha]_D$ value of (1) is low compared with 2(24 h) and the prolonged reaction time seems to unfavorably affect the results accompanying racemization and dehydration, even in the MeOH solvent.

When twice the amount of the catalyst was employed (Entry 4, 32 mol% of the aldehyde), the reaction proceeded quickly (conversion 100%, by NMR, 24 h), but the dehydration increased up to 52% (NMR). On the contrary, when half the amount of catalyst was used (Entry 5, 8 mol% of the aldehyde), the reaction was very slow (conversion 30%, by NMR, 24 h) and gave a small amount of (2). Thus, an amount of the catalyst affected both the reaction velocity and the dehydration rate, but not to the degree of the racemization in the MeOH solvent. Benzaldehyde and *p*-chlorobenzaldehyde were also reactive with this catalyst system, but a high degree of the dehydration was notable under these conditions. As a general conclusion, the factors controlling the reactions are solvent, reaction temperature, time, and the amount of the catalyst. The effect of the reaction temperature seems to be most serious for asymmetric induction.

Assistant Effects of Cyclodextrins on the Catalysis of Zn^{II}-L-TyrOEt Complex. It has been known that aromatic aldehydes such as *p*-nitrobenzaldehyde are included well in the cavity of the CD.[4,5] In this system, the coordination of the *sec.* hydroxyl group located on the edge of the CD to the Zn^{2+} ion of the complex coexisted will occur. Then, the coordination of the formyl group to the Zn^{2+} ion may be accelerated. As a result, an increase in the reactivity may be expected. Since the CDs were soluble in H_2O but not in MeOH, reactions with a CD–Zn^{II}–TyrOEt system (1:1:1) were carried out in H_2O (pH 6 and 7). The pH of the reaction mixture with CD–Zn^{II}–TyrOEt was 6, and a buffer KH_2PO_4/NaOH was employed to adjust the pH to 7. The results of the experiments are shown in Table 6.

The sole α- or β-CD did not show any catalytic activity under these conditions. Entry 1 gave the aldol-type product in not very high yield in contrast with the reaction with the 1:2 complex (Table 4, 83%[f]). Whereas, in Entry 2, the catalytic activity increased much (100% yield, by NMR) without any

TABLE 5. ALDOL CONDENSATIONS WITH $Zn(NO_3)_2$-(L-TyrOEt)$_2$ COMPLEX (2)[a]
(EFFECTS OF TEMPERATURE, TIME, AND CATALYST)

No.	Temp/°C	Time/h	Yield of (1)/%[b] (isolated)	$[\alpha]_D$ (in EtOH)	Yield of (2)/%[c] (NMR)
1	20	48	52	−15	+
2[d]	30	24	35	−19	20
3	30	48	34	−9.7	43
4[e]	30	24	40	−17	52
5[f]	30	24	21	−19.5	4
6	40	24	40	−11.2	42
7	40	16	34	−12.8	30
8	50	24	62	−4.4	+
9[g]	40	24	16[i]		76[j]
10[h]	40	24	22[i]		53

a) Reaction conditions are similar to those shown in Table 2. Reactions Nos. 1—8, *p*-nitrobenzaldehyde with acetone, No. 9, benzaldehyde with acetone, No. 10, *p*-chlorobenzaldehyde with acetone. b) Aldol-type product. c) Dehydrated product. d) In the case with Zn^{II}-TyrOEt(1 : 1) complex, the yield of (1) was 16%, $[\alpha]_D=-16.4°$. e) Catalyst: ×2(32 mol%). f) Catalyst: ×1/2(8 mol%). g) Reaction of benzaldehyde. h) Reaction of *p*-chlorobenzaldehyde. i) Yield by ^{1}H-NMR. j) Contaminated with acetal.

Table 6. Formation of the aldol-type product(1) with CD-$Zn(NO_3)_2$-L-TyrOEt catalyst systems[a] (Effects of cyclodextrins)

No.	Catalyst (1 : 1 : 1)	Yield of (1)/%[b]		Remarks
		pH 6	pH 7[c]	
1	Zn^{II}+TyrOEt (1 : 1)	53	68	No dehydration
2	α-CD+Zn^{II}+TyrOEt	58	100	
3	β-CD+Zn^{II}+TyrOEt	100	100	
4	β-CD+Zn^{II}+TyrOEt	67		For 16 h reaction
5	β-CD+Zn^{II}+TyrOEt	56		At 30 °C
6	α-CD+Zn^{II}+TyrOEt		55	(3 : 1 : 1) system
7	β-CD+$Zn(OAc)_2$+TyrOEt	69		Dehydration 19%
8	β-CD+Zn^{II}+TyrOEt	49		With C_6H_5CHO (dehydration 18%)
9	β-CD+Zn^{II}+TyrOEt	18		With p-ClC_6H_4CHO

a) Reactions of p-nitrobenzaldehyde with acetone, conditions: catalyst, 16 mol% of the aldehyde, 40 °C, 24 h in H_2O. b) By ^1H-NMR. c) Buffer, KH_2PO_4/NaOH, was used.

dehydration. The assistant effect of the CD was more remarkable with the β-CD, as shown in Entry 3. The yield of (1) increased up to 100% even in the pH 6 solution.

The retio of the added CD seemed to be adequate in CD-Zn^{II}-TyrOEt=1:1:1. When three times the amount of α-CD was used (Entry 6, 3:1:1), the yield of (1) decreased to 55%, even in the pH 7 solution (unreacted aldehyde 45%). This was lower than that for a reaction without the CD (Entry 1). In Entry 7, the yield of (1) was lower than that for reactions with the $Zn(NO_3)_2$ complex system. All the reactions in Table 6 were carried out in an H_2O solvent; therefore, it could be infered that almost no asymmetric induction was observed in the reactions. When mixed solvents were used (MeOH 4 ml+H_2O 3 ml) under similar conditions to those in Entry 2(pH 7), the yield of (1) was only 20% in contrast with 100% in Entry 2. Accordingly, it may be necessary to find an adequate solvent system or some other reaction methods for asymmetric induction.

Conclusion. An original and preliminary survey on the aldol reactions catalyzed by metal complexes bearing ligands of the α-amino acid ester have been achieved. The most adequate catalytic system to afford an enantiomeric excess of the aldol-type product was the $Zn(NO_3)_2$-(L-TyrOEt)$_2$ in MeOH. The assistant effects of α- and β-cyclodextrins, especially of the β-CD, on the catalysis of the Zn^{II}-TyrOEt complex in the aldol reactions were observed evidently.

Aldol reactions in biological systems have been known to be catalyzed by aldolase enzymes, Class-I and -II.[6] The latter is a metalloenzyme containing a Zn^{2+} ion at the active sites. However, the catalysis of the Class-II aldolase has not been sufficiently elucidated. Therefore, our reaction systems with Zn^{II}-L-TyrOEt and CD-Zn^{II}-L-TyrOEt may present novel possibilities for understanding a Zn^{2+} ion catalysis from the point of view of organic catalytic reactions.

Experimental

Instruments. The ^1H-NMR spectra were taken with a Hitachi Perkin-Elmer R-20A spectrophotometer (60 MHz). The UV and IR spectra were taken with a Hitachi 220A double-beam spectrophotometer and a Hitachi 260-10 Infrared spectrophotometer, respectively. The optical rotations were measured with a JASCO DIP-140 digital polarimeter (Nippon Bunko).

Materials. L-, D-, and DL-Tyrosine ethyl esters and the L-tyrosine methyl ester were prepared from their original amino acids with alcohols in the presence of small quantities of concd sulfuric acid, L-TyrOEt: mp 105 °C, $[\alpha]_D$=+19.5° (EtOH), (lit,[7] 108 °C, +20°), DL-TyrOEt: mp 99—102 °, L-TyrOMe: mp 128—131 °C, $[\alpha]_D$=+28.0° (EtOH) (lit,[8] 135 °C, +25.7°). L-Histidine methyl ester was obtained from L-HisOMe·2HCl, mp 60—61 °C, $[\alpha]_D$=+11.2° (MeOH), Anal ($C_7H_{11}O_2N_3$) C,H,N. Other ligand compounds were commercially available, quinine: mp 177 °C, $[\alpha]_D$=−117° (in $CHCl_3$), qunidine: mp 175 °C, $[\alpha]_D$=−230° (in $CHCl_3$), 2,2′-bipyridine: mp 69.7 °C (recrystallyzed from EtOH-H_2O). The solvents used were distilled before use, and the dry methanol was preserved with molecular sieves. α- and β-cyclodextrins were commercially available, α-CD: $[\alpha]_D$=+133°, β-CD: $[\alpha]_D$=+154° (in H_2O).

The Aldol Reactions with Chiral Metal Complexes. As a representative example, the reaction of p-nitrobenzaldehyde with acetone in the presence of $Zn(NO_3)_2$-(TyrOEt)$_2$ in MeOH is described. To a solution of $Zn(NO_3)_2 \cdot 6H_2O$ (33 mg, 0.11 mmol) in MeOH (3.5 ml), L-TyrOEt (46.mg, 0.22 mmol) in MeOH (3.5 ml) was added and the mixed solution was well stirred (M:L=1:2). A solution of the complex catalyst was added to a solution of p-nitrobenzaldehyde (100 mg, 0.66 mmol) in 2 ml of acetone in a 20-ml flask. The flask was plugged and the reaction mixture was stirred with a magnetic stirrer for 24 h at 40 °C. After the reaction, the reaction mixture was diluted with water and extracted with ethyl acetate. The organic layer separated was dried over anhydrous magnesium sulfate and then evaporated under a reduced pressure at room temperature to give an oily mixture of unreacted aldehyde, aldol

type product, and its dehydrated product. The oily mixture was submitted to column chromatography on silica-gel (eluent: hexane and ethyl acetate, 1:1) to give the aldol-type product which was monitored by TLC on silica gel (R_f value: aldol-type 0.32, dehydrated-type 0.53, aldehyde 0.67). In the case of the determination of the ratio of these components, the ^{1}H-MNR spectra of the oily mixture was measured ($CDCl_3$, TMS 1%) before the chromatographic separation, and each percentage was calculated. The fractions of the aldol-type product were collected together and evaporated under reduced pressure. Thus, the aldol-type product, 4-hydroxy-4-(4-nitrophenyl)-2-butanone, was obtained. The enantimeric excess one was oily but the racemate was light-yellowish crystals of mp 63 °C.[9] Its optical rotation was measured in EtOH with D-line and the specific rotation was calculated.

The Aldol Reactions with Cyclodextrin(CD)-Zn^{II}-L-TyrOEt System. $Zn(NO_3)_2 \cdot 6H_2O$ (33 mg, 0.11 mmol) and β-CD (124 mg, 0.11 mmol) were dissolved together in H_2O (7 ml). To this solution, a solution of L-TyrOEt (23 mg, 0.11 mmol) in acetone (1 ml) was added and stirred. This was a water solution of the CD-Zn^{II}-L-TyrOEt (1:1:1) catalyst system. Then, a solution of *p*-nitrobenzaldehyde (100 mg, 0.66 mmol) in acetone (1 ml) was added to the catalyst solution and the pH of the reaction mixture was adjusted to 6 or 7. The amount of the catalyst system was 16 mol% of the aldehyde used. The flask was plugged and kept at 40 °C for 24 h (magnetic stirring). The procedures after the reaction were similar to that of the reactions without the CD. An extraction with ethyl acetate was also carried out.

The Acetal Formation with $RuCl_3$ Complexes. In a reaction with $RuCl_3$-$(TyrOEt)_2$ in MeOH (Table 2), only the *p*-nitrobenzaldehyde dimethyl acetal was obtained in a 62% yield without any aldol reaction product at all. The acetal was isolated by means of column chromatography as well as the aldol-type product. Thereupon, it was prepared separately from the aldehyde and methanol by the conventional method (HCl catalyst) for further identification. R_f value: 0.54 by silica-gel TLC, bp 64.7 °C ^{1}H-NMR ($CDCl_3$): δ=3.39 (3H, s, CH_3), 5.51 (1H, s, CH), 7.59—8.34 (q, aromatic proton). It was found that acetals were also formed with the $RuCl_3$-$(bpy)_2$ complex as follows.

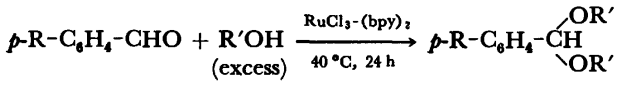

R	R'OH	Catalyst (mol% of CHO)	Yield/% (NMR)
NO_2	MeOH	16	100
		1	100
	EtOH	1	80
	i-PrOH	1	41
H	MeOH	2	100
OMe		2	54

Reaction Products. 4-Hydroxy-4-(4-nitrophenyl)-2-butanone (racemate),[9] mp 63 °C, Found: C, 57.44; H, 5.30; N, 6.61%. Calcd for $C_{10}H_{11}O_4N$: C, 57.41; H, 5.30; N, 6.70%. IR (cm^{-1}): 3400 (OH), 1710 (C=O), 1510, 1440 (NO_2). ^{1}H-NMR ($CDCl_3$): δ=2.19 (s, 3H), 2.88 (d, 2H), 4.10 (br.s, OH), 5.18 (t, 1H), 7.56—8.15 (q, aromatic proton). 4-(4-nitrophenyl)-3-buten-2-one(dehydrated product),[9] mp 114—116 °C, ^{1}H-NMR ($CDCl_3$): δ=2.42 (s, 3H), 6.68—6.96 (d, 1H), 7.30—7.46 (d, 1H), 7.64—8.37 (q, aromatic proton). 4-hydroxy-4-phenyl-2-butanone, oil, ^{1}H-NMR ($CDCl_3$): δ=2.14 (s, 3H), 2.73 (d, 2H), 5.19 (t, 1H), 7.36-8.03 (m, aromatic proton). 4-hydroxy-4-(4-chlorophenyl)-2-butanone, oil, ^{1}H-NMR ($CDCl_3$): δ=2.14 (s, 3H), 2.73 (d, 2H), 5.10 (t, 1H), 7.32—7.82 (q, aromatic proton).

References

1) K. Irie and K. Watanabe, *Bull. Chem. Soc. Jpn.*, **54**, 1195 (1981); **53**, 1366 (1980); *Chem. Lett.*, **1978**, 539.

2) K. Watanabe and A. Imazawa, *Bull. Chem. Soc. Jpn.*, **55**, 3208 (1982).

3) C. H. Heathcock,"Asymmetric Synthesis," ed by J. D. Morrison, Academic Press (1984), Vol. **3B**, p. 111; H. O. House, "Modern Synthetic Reactions," W. A. Benjamin Inc. (1972), p. 629.

4) M. L. Bender and M. Komiyama,"Cyclodextrin Chemistry," Springer (1978); H. Dugas and C. Penny,"Bioorganic Chemistry," Springer (1981), p. 290; I. Tabushi, *Acc. Chem. Res.*, **15**, 66 (1982).

5) F. Cramer, *Chem. Ber.*, **84**, 851 (1951); F. Cramer, W. Saenger, and H. Ch-Spatz, *J. Am. Chem. Soc.*, **89**, 14 (1967); R. L. VanEtten, J. F. Sebastian, G. A. Clowes, and M. L. Bender, *ibid.* **89**, 3243 (1967).

6) D. E. Morse and B. L. Horecker, *Adv. Enzymolo.*, **31**, 125 (1968); B. L. Horecker, O. Tasles, and C. Y. Lai, "The Enzymes," 3rd ed. Ed. by P. D. Boyer, Academic Press (1972), Vol. **7**, p. 213.

7) E. Fischer, *Ber.*, **34**, 451 (1901).

8) E. Fischer, *Ber.*, **41**, 855 (1908).

9) D. S. Noyce and W. L. Reed, *J. Am. Chem. Soc.*, **80**, 5539 (1958); R. E. Corbett and C. L. Davey, *J. Chem. Soc.*, **1955**, 296.

 © 1985 The Chemical Society of Japan Bull. Chem. Soc. Jpn., 58, 1407—1412 (1985)

Preparation and Chiroptical Properties of Optically Active Tetracyclic Cage-shaped Hydrocarbons; [*m*.0]Triblattanes and [*m*.1]Triblattanes

Koichiro NAEMURA,* Tohru KATOH, Rinkō FUKUNAGA, Hiroaki CHIKAMATSU, and Masao NAKAZAKI

Department of Chemistry, Faculty of Engineering Science, Osaka University, Toyonaka, Osaka 560

(Received November 13, 1984)

Horse liver alcohol dehydrogenase mediated reduction of tetracyclo[4.3.0.$0^{2,5}$.$0^{3,8}$]nonan-9-one ([1.0]triblattan-9-one) (**17**) gave (+)-**17** and (−)-tetracyclo[4.3.0.$0^{2,5}$.$0^{3,8}$]nonan-9-ol (**18**). Hydrogenolysis of (+)-**17** with 5% rhodium-alumina to (+)-(1*R*,3*R*,6R8*R*)-twist-brendan-9-ol with known absolute rotation allowed us to assign the 1*S*,2*S*,3*R*,5*R*,6*R*,8*R* absolute configuration to (+)-**17** and to calculate the absolute rotation of (+)**17**. Wolff-Kishner reduction of (+)-**17** gave (+)-[1.0]triblattane. BF_3-Catalyzed diazomethane ring expansion of (+)-**17** was followed by Wolff-Kishner reduction to afford optically active [*m*.0]triblattanes. (+)-Tetracyclo-[5.2.1^{2,6}.$0^{4,8}$]decan-5-one ([1.1]triblattan-5-one) with known absolute configuration and absolute rotation was transformed to optically active [*m*.1]triblattanes by diazomethane ring expansion with BF_3 etherate followed by Wolff-Kishner reduction. The known optical purities of our starting materials permitted calculation of the absolute molecular rotations of [*m*.0]triblattanes and [*m*.1]triblattanes. The chiroptical properties of triblattanes are discussed.

The C2–C8 diagonal bridging of D_3-twisted bicyclo[2.2.2]octane (**1**) with a polymethylene bridge provides a tricyclic cage-shaped hydrocarbon **2**, and further C3–C6 diagonal bridging of the chiral molecule with a polymethylene bridge gives a tetracyclic hydrocarbon **3**. Final C5–C7 diagonal bridging furnishes a pentacyclic hydrocarbon **4**.

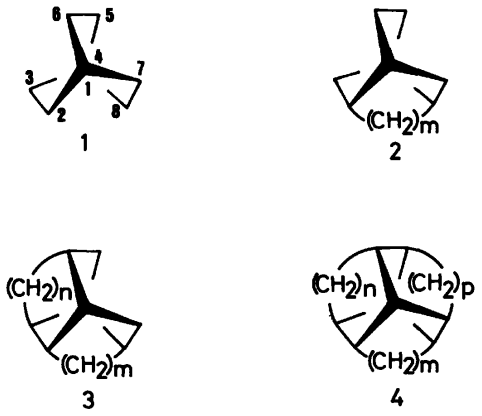

Chart 1.

We have coined for these hydrocarbons **2**, **3**, and **4** the generic names [*m*], [*m*.*n*], and [*m*.*n*.*p*]triblattane, respectively. Since our first preparation of twistane ([2]triblattane) in an optically active form,[1] we have been interested in the preparation, stereochemistry, and biological transformation of triblattanes.

Figure 1 shows the correlation between bridge span (*m*) and absolute molecular rotation ($[M]_{D\ abs.}$) in triblattanes[2,3] which have been prepared in optically active modification in our laboratory, except for [0]triblattane.[4] Inspection of the Fig. 1 reveals the interesting chiroptical features, (a) all dextrorotatory enantiomers possess a central core, D_3-twisted bicyclo[2.2.2]octane framework, fixed in a P-helical conformation, (b) however, triblattanes having two long diagonal bridges are levorotatory in spite of possessing the central core with P-helicity as shown in a se-

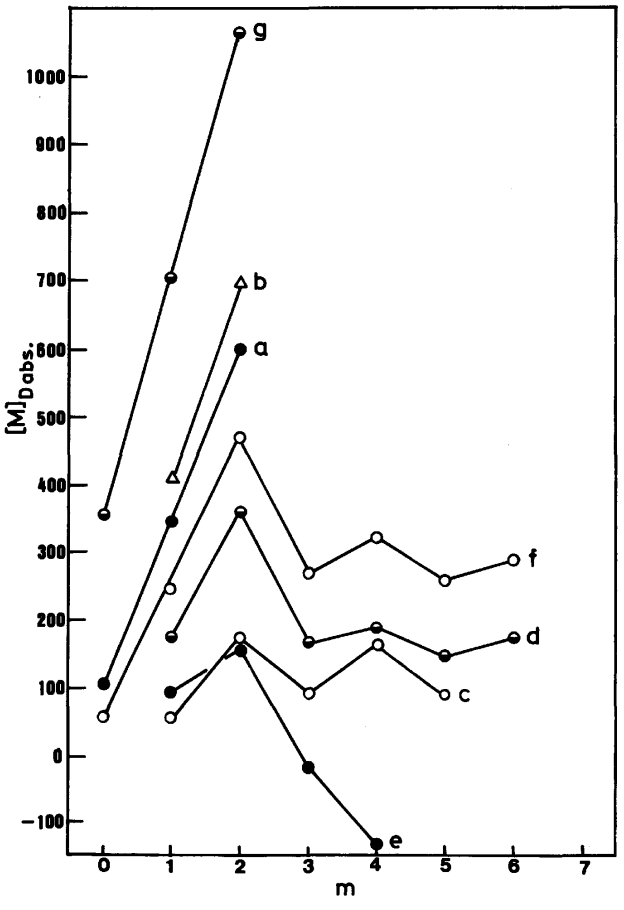

Fig. 1. Correlation between bridge span (*m*) and absolute molecular rotation ($[M]_{D\ abs.}$); a: [*m*]triblattane (**2**), b: [*m*.1]triblattane (**3**, $n=1$), c: [*m*.1.0]triblattane (**4**, $n=1$ $p=0$), d: [*m*.2.0]triblattane (**4**, $n=2$ $p=0$), e: [*m*.3.0]triblattane (**4**, $n=3$ $p=0$), f: [*m*.1.1]triblattane (**4**, $n=p=1$), g: [*m*.2.2]triblattane (**4**, $n=p=2$).

ries of [*m*.3.0]triblattanes ($m \geqq 3$), (c) for all series of triblattanes, the values of molecular rotations increase linearly with bridge span (*m*) to $m=2$, (d) the values drop abruptly on going from $m=2$ to $m=3$ and then remain almost constant.

Natural extension of these studies led us to investigate chiroptical properties of series of tetracyclic triblattanes. In this paper, we wish to report the preparation of series of optically active [*m*.0]triblattanes (**5**—**8**) and [*m*.1]triblattanes (**9**—**15**) with known absolute configuration and discuss their chiroptical properties.

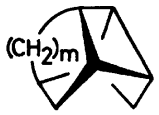

(+)-5 m=1
(+)-6 m=2
(+)-7 m=3
(−)-8 m=4

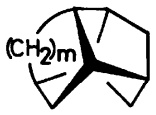

(+)-9 m=1 (+)-13 m=5
(+)-10 m=2 (+)-14 m=6
(+)-11 m=3 (+)-15 m=7
(+)-12 m=4

Chart 2.

Results and Discussion

Optical Resolution of [1.0]Triblattan-9-one. The diagonal bridging between C3 and C6 positions of [0]triblattane (**2**, $m=0$), being the smallest triblattane, furnishes a series of [*m*.0]triblattanes (**3**, $n=0$). The first task is optical resolution of (±)-[1.0]triblattan-9-one (**17**), being the starting material for the preparation of [*m*.0]triblattanes. Acid hydrolysis of 9,9-ethylenedioxytetracyclo[4.3.0.$0^{2,5}$.$0^{3,8}$]nonane (**16**), prepared according to Toyne's procedure,[5] gave (±)-**17** which was resolved by horse liver alcohol dehydrogenase (HLADH) mediated reduction. The ketone (±)-**17** was incubated for 5 min at 25 °C with NAD^+ and HLADH in 1/15 M (1 M=1 mol dm^{-3}) Sørensen phosphate buffer solution (pH 7.0). GLC analysis of the ether-extracted metabolite revealed the presence of the recovered ketone **17** (51%) and a 4:

16 X=<O O>
(+)-17 X=O

(−)-18

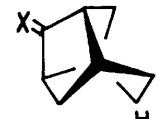

(+)-19 X=<H OH>
20 X=<O O>

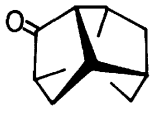

(+)-21

Chart 3.

1 mixture of diastereomeric alcohols (49%). Column chromatography of the metabolite on alumina furnished (+)-**17**, mp 96—98 °C (in a sealed tube) $[\alpha]_D$ +46.3°, and the major alcohol (−)-**18**, mp 118—120 °C (in a sealed tube) $[\alpha]_D$ −67.7°, but attempts to purify the minor alcohol were unsuccessful. The mixture of metabolite alcohols was oxidized with chromium trioxide in acetone gave (−)-**17**, $[\alpha]_D$ −33.0°, as a sole product.

Our next task is determination of the absolute configuration of (+)-**17** and (−)-**18**. Circular dichroism (CD) spectra of cage-shaped ketones,[2] prepared from intermediates of known absolute configuration, indicate that the sign of CD curve due to n-π^* transition can be predicted by applying the octant rule to the "outer ring"[6] in the projection formula which holds the carbonyl group at the "point of twist".[7] Applying this generalization to the projection formula **22** of the ketone (+)-**17** with negative Cotton effect, we obtain the 1*S*,2*S*,3*R*,5*R*,6*S*,8*R* absolute configuration for (+)-**17**. In other words, (+)-**17** possess the D_3-twisted bicyclo[2.2.2]octane framework fixed in a P-helical conformation.

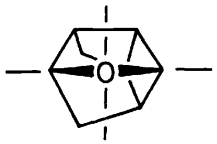

22

Chart 4.

This conclusion was unambiguously confirmed by the chemical conversion of (+)-**17** to (+)-twistbrendan-9-ol (**19**), whose absolute configuration and absolute rotation have been determined in our laboratory.[8] Hydrogenolysis of 9,9-ethylenedioxytetracyclo[4.3.0.$0^{2,5}$.$0^{3,8}$]nonane (**16**) with 5% rhodium-alumina to 9,9-ethylenedioxytwistbrendane (**20**) has been reported by Toyne.[5] The ketone (+)-**17**, $[\alpha]_D$ +46.3°, was hydrogenolyzed with 5% rhodium-alumina in cyclohexane to yield (+)-(1*R*,3*R*,6*R*,8*R*)-twistbrendan-9-ol (**19**), $[\alpha]_D$ +122° (46.5% optical purity).[8] The result permitted us to confirm the absolute configuration and calculate the absolute rotation of (+)-**17** ($[\alpha]_{D\,abs.}$ +99.6°). Jones oxidation of the major alcohol (−)-**18**, $[\alpha]_D$ −67.7°, to (−)-**17**, $[\alpha]_D$ −55.7° (55.9% o.p.), possessing the central core of M-helicity, allowed us to calculate the optical purity of the metabolite alcohol (−)-**18** and to prove the central core of (−)-**18** to be fixed in a M-helical conformation. However, the configuration of the hydroxyl group is unknown.

Preparation of [m.0]Triblattanes. The ketone (+)-**17**, $[\alpha]_D$ +46.3°, was reduced by Wolff-Kishner reduction and the product was chromatographed on alumina to give [1.0]triblattane (**5**), mp 103—105 °C (in a sealed tube) $[\alpha]_D$ +48.9°. In a previous paper,[3,9]

we reported our successful preparation of series of pentacyclic triblattanes by diazomethane ring expansion of cage-shaped ketones. Our preliminary experiment utilizing (±)-**17** indicated that when kept at 0 °C for 6 d an ethereal solution of (±)-**17** containing 10 equiv of diazomethane gave a mixture of [1.0]triblattanone and [2.0]triblattanones with unknown location of the carbonyl group in the expanded bridge. The mixture was directly reduced by Wolff-Kishner reduction to yield a 6:4 mixture of [1.0]triblattane (**5**) and [2.0]triblattane (**6**).

Addition of boron trifluoride was found to push the ring expansion further furnishing a product consisting of higher homologs. An ethereal solution of (+)-**17** containing diazomethane and 1 equiv of BF_3 etherate was kept at 0 °C for 30 min. To reveal composition of the ring-expanded product, the product was directly converted to a mixture of hydrocarbons by Wolff-Kishner reduction and the product was analyzed by GLC. The results are given in Table 1.

After these preliminary experiments utilizing (±)-**17**, we carried out the preparative experiment with (+)-**17**. An ethereal solution of (+)-**17**, $[\alpha]_D$ +46.3°, containing of 4 equiv of diazomethane and 1 equiv of BF_3 etherate was kept at 0 °C for 1 h. The mixture of ring-expanded ketones was directly transformed to a mixture of [*m*.0]triblattanes by Wolff-Kishner reduction. After being analyzed by GLC, the product was separated by preparative GLC to furnish (+)-**6**, (+)-**7**, and (−)-**8**. The structures of these hydrocarbons were confirmed on the basis of their mass spectra and elemental analyses.

*Preparation of [*m.1*]Triblattanes.* The synthesis of a series of [*m*.1]triblattanes (**3**, n=1) began with tetracyclo[5.2.1.$0^{2,6}$.$0^{4,8}$]decan-5-one ([1.1]triblattan-5-one) (**21**) which has been prepared in an optically active form with known absolute configuration and absolute rotation in our laboratory.[10] Diazomethane ring expansion of (±)-**21** without catalyst gave no ring-expanded product. Treatment of (±)-**21** with excess of diazomethane and 1 equiv of BF_3 etherate followed by Wolff-Kishner reduction yielded a mixture of ring-expanded hydrocarbons. The results are given in Table 2.

We carried out the preparative experiment with (+)-**21**, $[\alpha]_D$ +145° (59.6% o.p.), which was dissolved in an ethereal solution containing of 15 equiv of diazomethane and 1 equiv of BF_3 etherate. After the mixture was kept at 0 °C for 1 h, the resulting mixture of ring-expanded ketones was reduced by Wolff-Kishner reduction to yield a mixture of [*m*.1]triblattanes which was analyzed by GLC. Preparative GLC separated and purified these hydrocarbons **9**—**15**.

Table 1. Reaction of (±)-**17** and diazomethane with BF_3 etherate

CH_2N_2 (equiv)	Product ratio				
	5	**6**	**7**	**8**	Higher homologs
1	65	25	5	4	1
2	35	41	10	11	3
3	13	46	14	20	7
4	7	34	12	26	21

Table 2. Reaction of (±)-**21** and diazomethane with BF_3 etherate

CH_2N_2 (equiv)	Temp °C	Product ratio					
		9	**10**	**11**	**12**	**13**	Higher homologs
2	0	79	17	2	1	1	0
5	0	49	25	8	13	5	0
10	0	36	23	11	20	6	4
10	−78	4	2	4	16	13	61
15	0	9	15	12	27	6	31

*Chiroptical Properties of [*m.0*]Triblattanes and [*m.1*]-Triblattanes.* The known optical purities of our starting materials (+)-**17** and (+)-**21** permitted us to calculate the absolute molecular rotations of these new triblattanes (Table 3).

These values are plotted in Fig. 2 together with that of [2.2]-triblattane.[11] A few conspicuous features are worth noting, (a) all [*m*.1]triblattanes having the central core of P-helicity are dextrorotatory, (b) [*m*.0]triblattanes possessing a short diagonal bridge (m<4) as well as the central core of P-helicity are dextrorotatory, but [4.0]triblattane, like [*m*.3.0]triblattanes (m=3,4), is levorotatory in spite of having the central core fixed in a P-helical conformation, (c) the presence of a zero bridge in [*m*.0]triblattanes is reflected in a markedly decreased molecular rotation relative to [*m*.1]triblattanes and [*m*.2]triblattanes.

Experimental

Infrared spectral data were obtained from a Hitachi 260-10 spectrophotometer. Optical rotations were measured with a JASCO-DIP-140 automatic polarimeter. Circular dichroism data were collected with a JASCO J-40 spectropolarimeter. Mass spectra were taken with a Hitachi RMS-4 spectrometer. Elemental analyses were performed on a

Table 3. Absolute molecular rotations ($[M]_{D\ abs.}$) of [*m*.0]triblattanes and [*m*.1]triblattanes

5	**6**	**7**	**8**	**9**	**10**	**11**	**12**	**13**	**14**	**15**
+74.0°	+129°	+4.9°	−39.0°	+407°	+692°	+376°	+382°	+295°	+382°	+293°

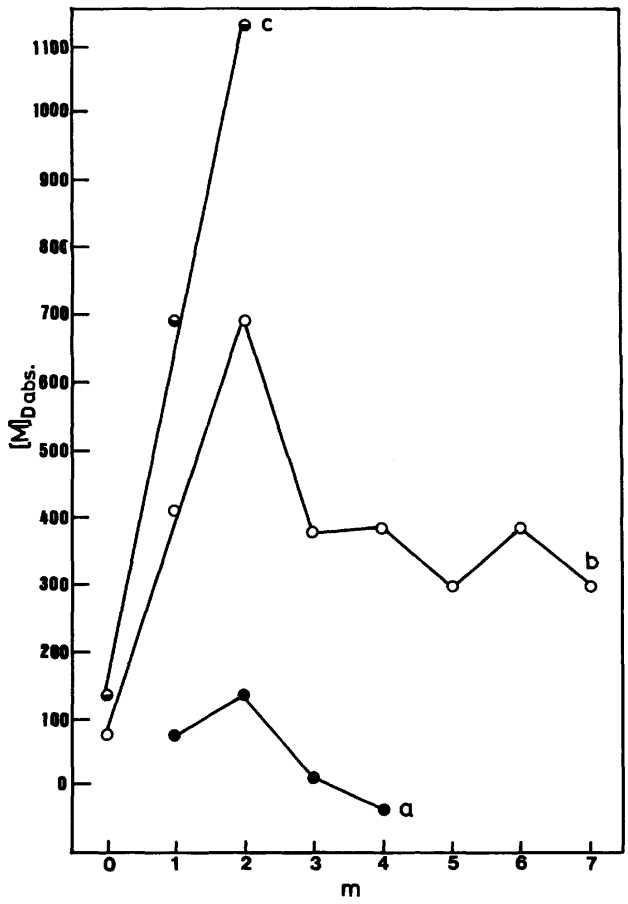

Fig. 2. Correlation between bridge span (m) and absolute molecular rotation ($[M]_{D\ abs.}$) in three series of tetracyclic triblattane; a: [m.0]triblattane, b: [m.1]-triblattane, c: [m.2]triblattane.

Yanagimoto CHN-Corder, Type II. GLC analyses were performed on a JGC-20 K equipped with a FID and using a 1 m×3 mm column of 10% PEG 20 M on UniportHP. Preparative GLC were done on a JGC-20 K equipped with a TCD and using a 2 m×3 mm column of 10% PEG 20 M on UniportHP. HLADH was purchased from Boehringer (Mannheim) as a crystalline suspension in phosphate buffer containing 10% ethanol.

(±)-Tetracyclo[4.3.0.0^{2,5}.0^{3,8}]nonan-9-one (17). 9,9-Ethylenedioxytetracyclo[4.3.0.0^{2,5}.0^{3,8}]nonane (**16**) (670 mg, 3.76 mmol), prepared according to Toyne's procedure,[5] was mixed with 5% sulfuric acid (20 mL) and the mixture was stirred for 2 d at room temperature. After the reaction mixture was extracted with ether, the extract was worked up as usual. The product was chromatographed on alumina and elution with pentane gave a solid which was sublimed at 50—60 °C (20 mmHg (1 mmHg=133.322 Pa)) to yield 216 mg of **17** (43% yield); mp 100—101 °C (in a sealed tube); IR (KBr) 1760 cm^{-1}; Found: C, 80.41; H, 7.53%. Calcd for $C_9H_{10}O$: C, 80.56; H, 7.51%.

HLADH-mediated Reduction of (±)-Tetracyclo[4.3.0.0^{2,5}.0^{3,8}]nonan-9-one (17). The ketone (±)-**17** (92.3 mg, 0.690 mmol) was dissolved in 1 L of 1/15 M Sφrensen phosphate buffer solution (pH 7.0) and then to the solution was added NAD^+ (42.6 mg, 0.0594 mmol), ethanol (1 mL), and HLADH (4 mg). After being incubated at 25 °C for 5 min, the mixture was extracted with ether. The extract was washed with water, dried ($MgSO_4$), and concentrated to give a metabolite mixture (81 mg). GLC analysis of the metabolite revealed the presence of **17** (51%) and a 4:1 mixture of diastereomeric alcohols (49%). The product was chromatographed on alumina, and elution with pentane afforded 37 mg of **17**; mp 98—100 °C (in a sealed tube); $[\alpha]_D^{22}$ +46.3° (*c* 0.220, $CHCl_3$); C.D. (*c* 4.43×10^{-2} mol dm^{-3}, 2,2,4-trimethylpentane) $[\theta]_{291}$ −3.92×10^2 (sh), $[\theta]_{296}$ −5.59×10^2 (sh), $[\theta]_{300}$ −6.35×10^2, $[\theta]_{303}$ −6.18×10^2 (sh); Found: C, 80.43; H, 7.52%. Calcd for $C_9H_{10}O$: C, 80.56; H, 7.51%. Elution with pentane–ether (95:5. v:v) gave 22 mg of **18**; 118—120 °C (in a sealed tube); $[\alpha]_D^{24}$ −67.7° (*c* 0.200, $CHCl_3$); Found: C, 79.18; H, 8.85%. Calcd for $C_9H_{12}O$: C, 79.37; H, 8.88%. Further elution with the same solvent gave 13 mg of a mixture of diastereomeric alcohols.

Oxidation of the Mixture of Diastereomeric Alcohols. To a solution of the 4:1 mixture of alcohols (140 mg, 1.03 mmol) in acetone (2 mL) was added excess of 8 N Jones' reagent.[14] After being stirred for 3 h at room temperature, the reaction mixture was diluted with water (10 mL) and extracted with ether. After a usual workup, the extract was concentrated to give a solid which was chromatographed on alumina (pentane eluent) to furnish 119 mg of (−)-**17** (86% yield); mp 99—101 °C (in a sealed tube); $[\alpha]_D^{23}$ −33.0° (*c* 0.372, $CHCl_3$); Found: C, 80.39; H, 7.51%. Calcd for $C_9H_{10}O$: C, 80.56; H, 7.51%.

Oxidation of the Major Alcohol 18. Oxidation of (−)-**18** (50 mg, 0.37 mmol), $[\alpha]_D$ −67.7°, which 8N Jones' reagent in acetone was carried out by the same procedure described above. Chromatography of the product on alumina followed by sublimation furnished 42 mg of (−)-**17** (85% yield); mp 98—99 °C (in a sealed tube); $[\alpha]_D^{22}$ −55.7° (*c* 0.250, $CHCl_3$); Found: C, 80.44; H, 7.53%. Calcd for $C_6H_{10}O$: C, 80.56; H, 7.51%.

Hydrogenolysis of (+)-Tetracyclo[4.3.0.0^{2,5}.0^{3,8}]nonan-9-one (17). A mixture of (+)-**17** (79 mg, 0.59 mmol), $[\alpha]_D$ +46.3°, rhodium–alumina (50 mg), and cyclohexane (20 mL) was shaken at room temperature in a hydrogenation flask at 1 atm of hydrogen. After the hydrogen absorption had ceased, the catalyst was filtered off. The filtrate was concentrated to give a solid which was purified by preparative GLC to furnish 42 mg of (+)-**19**; mp 162—164 °C (in a sealed tube) (lit,[8] mp 162—165 °C); $[\alpha]_D^{24}$ +122° (*c* 0.115, MeOH) (lit,[8] $[\alpha]_D^{23}$ +164° (MeOH)). Spectral comparison with an authentic specimen confirmed its identity.

(+)-Tetracyclo[4.3.0.0^{2,5}.0^{3,8}]nonane (5). A mixture of (+)-**17** (80 mg, 0.60 mmol), $[\alpha]_D$ +46.3°, 100% hydrazine hydrate (0.1 mL), potassium hydroxide (53 mg), and triethylene glycol (2 mL) was heated for 1 h at 110—120 °C and then for an additional 3 h at 190—200 °C. After cooling to room temperature, the reaction mixture was diluted with water and extracted with pentane. The extract was washed with water, dried ($MgSO_4$), and concentrated. The product was chromatographed on alumina (pentane eluent) to give a solid which was sublimed at 50—60 °C (760 mmHg) to yield 27 mg of (+)-**5** (38% yield); mp 103—105 °C (in a sealed tube); $[\alpha]_D^{25}$ +48.9° (*c* 0.180, $CHCl_3$); MS, *m/z* 120 (M^+); Found: C, 89.84; H, 10.01%. Calcd for C_9H_{12}: C,

89.94; H, 10.06%.

Product Distribution in the Diazomethane Ring Expansion of (±)-Tetracyclo[4.3.0.0^{2,5}.0^{3,8}]nonan-9-one (17). Without Catalyst: An ethereal solution of diazomethane (630 mg, 14.9 mmol) was added to an ice cooled solution of (±)-**17** (200 mg, 1.49 mmol) in dry ether (20 mL). The reaction mixture was allowed to stand at 0 °C for 6 d. The product was analyzed by GLC.

With BF_3 etherate Catalyst: The following experimental procedure is typical. An ethereal solution of diazomethane (63 mg, 1.5 mmol) was added to a stirred and chilled (0 °C) solution of (±)-**17** (200 mg, 1.49 mmol) and BF_3 etherate (0.19 mL, 1.5 mmol) in dry ether (20 mL). After the mixture was kept at 0 °C for 30 min, a deposited solid was removed by filtration and the filtrate was washed with aq $NaHCO_3$ solution and water, dried ($MgSO_4$), and concentrated to give an oily product (190 mg). The product was mixed with 100% hydrazine hydrate (0.24 mL), potassium hydroxide (130 mg), and triethylene glycol (2 mL) and then the mixture was heated for 1 h at 110—120 °C and for an additional 4 h at 190—200 °C. After a workup described for the preparation of (+)-**5**, the product (110 mg) was analyzed by GLC.

Preparation of (+)-[2.0]Triblattane (6), (+)-[3.0]Triblattane (7), and (−)-[4.0]Triblattane (8). An ethereal solution of diazomethane (188 mg, 4.47 mmol) was added to a stirred solution of (+)-**17** (150 mg, 1.12 mmol), $[\alpha]_D$ +46.3°, and BF_3 etherate (0.14 mL, 1.1 mmol) in dry ether (15 mL) with ice-cooling. After being stirred for 1 h at 0 °C, the reaction mixture was worked up as described for the reaction of (±)-**17** to yield 145 mg of a mixture of ring expanded ketones, which was without purification used in the next reaction. Wolff-Kishner reduction of the crude product with 100% hydrazine hydrate (0.18 mL), potassium hydroxide (95 mg), and triethylene glycol (2 mL) was carried out by the same procedure as described for the preparation of (+)-**5**. GLC analysis of the product (120 mg) revealed the presence of **5** (3%), **6** (57%), **7** (25%), and **8** (15%). Preparative GLC (at 120 °C) provided specimens of **6** (42 mg); R_t. 2′48″, **7** (18 mg); R_t. 5′48″, and **8** (13 mg); R_t. 11′54″. (+)-[2.0]Triblattane (**6**); mp 123—124 °C (in a sealed tube); $[\alpha]_D^{22}$ +76.1° (*c* 0.325, $CHCl_3$); MS *m/z* 134 (M^+); Found: C, 89.42; H, 10.47%. Calcd for $C_{10}H_{14}$: C, 89.49; H, 10.51%. (+)-[3.0]Triblattane (**7**); semisolid; $[\alpha]_D^{22}$ +2.60° (*c* 0.153, $CHCl_3$); MS *m/z* 148 (M^+); Found: C, 89.17; H, 10.81%. Calcd for $C_{11}H_{16}$: C, 89.12; H, 10.88%. (−)-[4.0]Triblattane (**8**); oil; $[\alpha]_D^{22}$ −19.3° (*c* 0.127, $CHCl_3$); MS *m/z* 162 (M^+); Found: C, 88.78; H, 11.15%. Calcd for $C_{12}H_{18}$: C, 88.82; H, 11.18%.

Product Distribution in the Diazomethane Ring-expansion of (±)-Tetracyclo [5.2.1.0^{2,6}.0^{4,8}]decan-5-one (21). The following experimental procedure is typical. To a chilled (0 °C) solution of (±)-**21** (100 mg, 0.675 mmol) in dry ether (10 mL) was added BF_3 etherate (0.085 mL, 0.68 mmol) and then to the mixture was added an ethereal solution of diazomethane (28 mg, 0.68 mmol). After being stirred for 1 h at 0 °C, the mixture was worked up as described for the reaction of (±)-**17**. Wolff-Kishner reduction of the crude mixture of ring-expanded ketones was carried out by the same procedure as described for the preparation of (+)-**5** and the product was analyzed by GLC.

Preparation of Optically Active [m.1]Triblattanes (9—15). A solution of (+)-**21** (500 mg, 3.37 mmol), $[\alpha]_D^{23}$ +145° ($CHCl_3$) (59.6% o.p.)[10], in dry ether (50 mL) was cooled in an ice bath. To the chilled solution was successively added BF_3 etherate (0.425 mL, 3.37 mmol) and an ethereal solution of diazomethane (2.10 g, 50.0 mmol). After being stirred for 30 min at 0 °C, the reaction mixture was worked up as described for the reaction of (±)-**17** to give 480 mg of a mixture of ketones, which was without purification used in the next reaction. Wolff-Kishner reduction of the crude product was carried out with 100% hydrazine hydrate (0.55 mL), potassium hydroxide (300 mg), and triethylene glycol (10 mL) by the same manner described for the preparation of (+)-**5**. GLC analysis of the product (450 mg) revealed the presence of **9** (9%), **10** (15%), **11** (14%), **12** (25%), **13** (4%), **14** (19%), and **15** (14%). Preparative GLC (at 150 °C) provided specimens of **9** (40 mg); *R*. 2′10″, **10** 56 mg); R_t. 2′55″, **11** (55 mg); R_t. 3′48″, **12** (85 mg); R_t. 8′36″, **13** (20 mg); R_t. 17′00″, **14** (50 mg), R_t. 29′06″, and **15** (25 mg), R_t. 42′06″. (+)-[1.1]Triblattane (**9**); mp 163—164 °C (in a sealed tube) (lit,[10] mp 164.5—165.5 °C); $[\alpha]_D^{23}$ +234° (*c* 0.360, $CHCl_3$); the identity was established by the comparison of its GLC retention time with that of an authentic sample. (+)-[2.1]Triblattane (**10**); mp 138—140 °C (in a sealed tube) (lit,[11] mp 140—141 °C); $[\alpha]_D^{23}$ +276° (*c* 0.330, $CHCl_3$); the identity was established by the comparison of its GLC retention time with that of an authentic sample. (+)-[3.1]Triblattane (**11**); oil; $[\alpha]_D^{23}$ +138° (*c* 0.532, $CHCl_3$); MS *m/z* 162 (M^+); Found: C, 88.58; H, 11.28%. Calcd for $C_{12}H_{18}$: C, 88.82; H, 11.18%. (+)-[4.1]Triblattane (**12**); oil; $[\alpha]_D^{24}$ +129° (*c* 0.833, $CHCl_3$); MS *m/z* 176 (M^+); Found: C, 88.31; H, 11.46%. Calcd for $C_{13}H_{20}$: C, 88.56, H, 11.44%. (+)-[5.1]Triblattane (**13**); oil; $[\alpha]_D^{24}$ +92.4° (*c* 0.208, $CHCl_3$); MS *m/z* 190 (M^+); Found: C, 88.55; H, 11.54%. Calcd for $C_{14}H_{22}$: C, 88.35; H, 11.65%. (+)-[6.1]Triblattane (**14**); oil; $[\alpha]_D^{25}$ +111° (*c* 0.485, $CHCl_3$); MS *m/z* 204 (M^+); Found: C, 87.93; H, 11.80%. Calcd for $C_{15}H_{24}$: C, 88.16; H, 11.84%. (+)-[7.1]-Triblattane (**15**); oil; $[\alpha]_D^{25}$ +80.0° (*c* 0.254, $CHCl_3$); MS *m/z* 218 (M^+); Found: C, 87.84; H, 11.88%. Calcd for $C_{16}H_{26}$: C, 88.00; H, 12.00%.

This research was partially supported by the Ministry of Education, Science and Culture (Grant-in-Aid No. 58340029).

References

1) K. Adachi, K. Naemura, and M. Nakazaki, *Tetrahedron Lett.*, **1968**, 5467.

2) M. Nakazaki and K. Naemura, *Yuki Gosei Kagaku Kyokai Shi*, **40**, 1128 (1982).

3) K. Naemura, T. Katoh, H. Chikamatsu, and M. Nakazaki, *Chem. Lett.*, **1984**, 1371.

4) J. A. Jenkins, R. E. Doehner, Jr., and L. A. Paquette, *J. Am. Chem. Soc.*, **102**, 2131 (1980).

5) K. J. Toyne, *J. Chem. Soc., Perkin Trans. 1*, **1976**, 1346.

6) G. Snatzke and F. Werner-Zamojska, *Tetrahedron Lett.*, **1972**, 4275.

7) C. Djerassi and W. Klyne, *Proc. Natl. Acad. Sci. U.S.A.*, **48**, 1093 (1962).

8) M. Nakazaki, K. Naemura, and S. Harita, *Bull. Chem. Soc. Jpn.*, **48**, 1907 (1975).

9) M. Nakazaki, K. Naemura, and M. Hashimoto, *Bull. Chem. Soc. Jpn.*, **56**, 2543 (1983).

10) M. Nakazaki, K. Naemura, and N. Arashiba, *J. Org.*

Chem., **43**, 689 (1978).
11) M. Nakazaki, K. Naemura, Y. Kondo, S. Nakahara, and M. Hashimoto, *J. Org. Chem.*, **45**, 4440 (1980).
12) M. Nakazaki, K. Naemura, and S. Nakahara, *J. Org. Chem.*, **43**, 4745 (1978).
13) M. Nakazaki, K. Naemura, H. Chikamatsu, M. Iwasaki, and M. Hashimoto, *J. Org. Chem.*, **46**, 2300 (1981).
14) J. Meinwald, J. Crandall, and W. E. Hymans, *Org. Synth.*, Coll. Vol. V, 866 (1973).

Oxidative Removal of *N*-(4-Methoxybenzyl) Group on 2,5-Piperazinediones with Cerium(IV) Diammonium Nitrate

Masanori YAMAURA, Tsuneji SUZUKI, Hironobu HASHIMOTO, Juji YOSHIMURA,* Thoru OKAMOTO,† and Chung-gi SHIN†

Laboratory of Chemistry for Natural Products, Faculty of Science, Tokyo Institute of Technology, Nagatsuta, Midori-ku, Yokohama 227

†*Laboratory of Organic Chemistry, Faculty of Technology, Kanagawa University, Rokkakubashi, Kanagawa-ku, Yokohama 221*

(Received November 15, 1984)

It was shown that *N*-(4-methoxybenzyl) group on 2,5-piperazinediones can be oxidatively removed with cerium(IV) diammonium nitrate under mild conditions, and the oxidative removal was performed in some model compounds which have several functional groups.

For syntheses of biologically active 2,5-piperazinediones (PDO) having complicated structures such as bicyclomycin,[1] antibiotic 593A,[2] sirodesmin,[3] aspirochlorine[4] *etc.*, the selection of a suitable *N*-protecting group is an important problem. The protecting group should be easily introducible, improvable the solubility of this class of polar compounds, stable under various reaction conditions for conversions, and selectively removable under mild conditions. Up to the present, methylthiomethyl,[5] methoxymethyl,[5,6] and acyl[5,7] groups have been used, but, there are still remaining some problems in stability or conditions for deprotection. In a previous communication,[8] we reported that *N*-(4-methoxybenzyl) group on PDO can be removed by cerium(IV) diammonium nitrate (CAN), and satisfied the aforementioned conditions. This paper describes detailed data of the communication.

The oxidative removal of *O*-benzyl and *O*-(4-methoxybenzyl) groups has been done by the use of DDQ,[9] triphenylmethyl tetrafluoroborate,[10] chromium trioxide[11] and electrolytic oxidation[12] *etc.* For *N*-protecting group of β-lactams, oxidative removal of 2,4-dimethoxybenzyl[13] and 3,4-dimethoxybenzyl[14] groups with potassium peroxodisulfate and of 4-(methoxymethyloxy)phenyl[15] and 4-methoxyphenyl groups[16] with CAN have been reported, but, the introduction of these protecting groups is more or less tedious. Autoxidative removal of *N*-benzyl group in an amino sugar with potassium *t*-butoxide–dimethyl sulfoxide[17] is known, but the strongly alkaline conditions are unsuitable for PDO derivatives. Recently, 4-methoxybenzyl group was actually utilized for the synthesis of bicyclomycin.[18]

Results and Discussion

Model compounds (**1i**, **3e—i**, **5a—c**, **6a**) for the examination of oxidative deprotection were synthesized as follows. Condensation of *N*,*N*′-diacetylanhydroglycine with *p*-tolualdehyde in the presence of potassium *t*-butoxide[19] gave the corresponding (*Z*)-1-acetyl-3-(4-methylbenzylidene)-PDO (**1a**) in 87% yield. *N*-Benzylation of the corresponding 3-isobutylidene derivative[19] in *N*,*N*-dimethylformamide (DMF) with sodium hydride and benzyl bromide gave the *N*-benzyl derivative (**1b**) in 73% yield. When benzyl chloride instead of the bromide was used, a 1:1 mixture of **1b** and the corresponding *O*-benzyl derivative (**2**) of the enolate was produced, but the formation of **2** was generally less than 5% in the reaction with the bromide. In a similar way, 3-benzylidene (**1c**) and 3-(4-methylbenzylidene) (**1d**) derivatives were obtained. The formation of **2** may be attributed to the steric hindrance and conjugation of 3-alkylidene group, and also to the soft-hard interrelation between reagents and atoms of the reaction center. A similar reaction of (*Z*)-1-acetyl-3-isobutylidene-PDO[19] with 4-methoxybenzyl bromide gave **1e** in 93% yield. Treatment of **1b—d** with hydrazine gave quantitatively the corresponding *N*-deacetylated derivatives (**1f—h**). Hydrogenation of **1f,g** and the corresponding 6-benzylidene-1-methyl-[20] and 1-benzyl-6-[(ethoxycarbonyl)ethylidene]-PDO[21] in the presence of 10% palladium–carbon gave the corresponding saturated compounds (**3a—d**) in good yields, respectively. *N*-(4-Methoxybenzyl)ation in nonhindered site of **3a—c** proceeded smoothly with sodium hydride and the chloride to give the corresponding 4-(4-methoxybenzyl)-PDO (**3e—g**) in good yields. A similar reaction of **1f—h** and **3d** gave also **1i—k** and **3h**, respectively. Treatment of **1i—k** in methanol with *N*-bromosuccinimide gave the corresponding 6-(1-bromoalkyl)-6-methoxy-PDO (**4a—c**) in good yields. Hydrogenation of **4a—c** in the presence of palladium–carbon gave the corresponding debrominated PDO (**5a—c**) in 47—60% yields.

While, catalytic hydrogenation of **1e** gave 1-acetyl-3-isobutyl-4-(4-methoxybenzyl)-PDO (**3i**) in 94% yield, and a successive treatment of **3e** in tetrahydrofuran with lithium 2,2,6,6-tetramethylpiperidide and allyl bromide at −78 °C gave crystalline 3-allyl-1-benzyl-

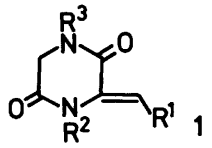

1

	R^1	R^2	R^3
a	Tol	H	Ac
b	i-Pr	Bn	Ac
c	Ph	Bn	Ac
d	Tol	Bn	Ac
e	i-Pr	MBn	Ac
f	i-Pr	Bn	H
g	Ph	Bn	H
h	Tol	Bn	H
i	i-Pr	Bn	MBn
j	Ph	Bn	MBn
k	Tol	Bn	MBn

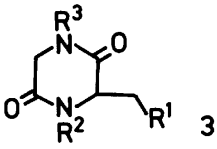

3

	R^1	R^2	R^3
a	i-Pr	Bn	H
b	Ph	Bn	H
c	Ph	Me	H
d	CH_2CO_2Et	H	Bn
e	i-Pr	Bn	MBn
f	Ph	Bn	MBn
g	Ph	Me	MBn
h	CH_2CO_2Et	MBn	Bn
i	i-Pr	MBn	Ac
j	i-Pr	H	Ac

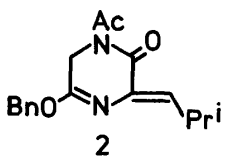

2

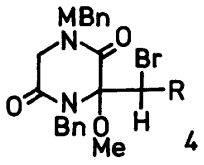

4

	R
a	i-Pr
b	Ph
c	Tol

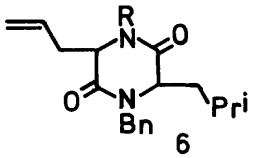

6

	R
a	MBn
b	H

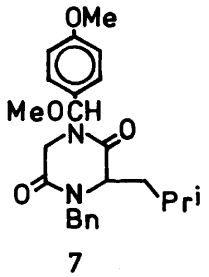

7

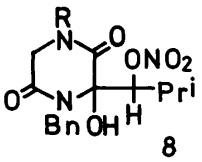

8

	R
a	H
b	MBn

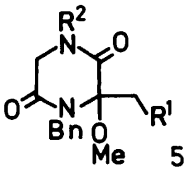

5

	R^1	R^2
a	i-Pr	MBn
b	Ph	MBn
c	Tol	MBn
d	i-Pr	H
e	Ph	H
f	Tol	H

6-isobutyl-4-(4-methoxybenzyl)-PDO (**6a**) of *cis*-configuration in 46% yield. Thus, various PDO having different *N*-protecting groups and unsaturated bonds were synthesized.

An attempted oxidation of **3e** with DDQ under various conditions did not proceed, and oxidation with 5 equiv of 0.1 M (1 M=1 mol dm^{-3}) chromium trioxide in acetic acid at room temperature for 1 day gave *N*-de(4-methoxybenzyl)ated product, **3a**, in 41% yield. The results in the similar oxidation with CAN are summarized in Table 1.

The oxidation of **3e** in aqueous acetonitrile with a low concentration of CAN (Run 1) did not proceed even for a longer reaction time, but with 0.17 M solution (Run 2) gave **3a** in 55% yield, indicating the existence of concentration-dependency in this reaction. Thus, the reaction with 0.25 M CAN (Run 3) gave **3e** in quantitative yield. The reaction proceeded smoothly, even in the presence of only small amount of water (Run 4) and also at a lower temperature (Runs 5—6), if a proper concentration of excess CAN is maintained. Methanol can also be used as a solvent (Runs 7—8), but, 1-benzyl-6-isobutyl-4-(α,4-dimethoxybenzyl)-PDO (**7**) was produced as the major product, when absolute methanol was used (Run 9). The formation of **7** indicates that methoxide anion attacks the intermediate iminium cation [$>\overset{+}{N}=$CH-C_6H_4-OMe], which was produced by the direct electron transfer from alkylbenzene moiety to cerium(IV) ion or *via* a benzylic hydrogen abstraction by the metal ligands,[22] in methanol solution. In the presence of water, the attack of hydroxide anion gave the *N*-free PDO and *p*-anisaldehyde, and the latter was actually isolated in the corresponding yield.

As shown in Table 2, a similar oxidation of **3f—h** (Runs 1—3) gave **3b—d**, respectively. No oxidation of *N*-benzyl and terminal alkylbenzene moiety was observed, and an ester function was not affected under the reaction conditions. A lower yield of **3c** may be attributed to its low solubility in ethyl acetate for extraction. Oxidation of **5a—c** and **3i** (Runs 4—7) proceeded smoothly to give **5d—f** and **3j**, respectively. In these cases, 6-*O*-methoxyl and *N*-acetyl groups were not affected. The oxidation of **1i** with 0.5 M CAN (Run 8) was unexpectedly accompanied with an oxidative addition reaction to give 1-benzyl-

Table 1. Oxidative removal of 4-methoxybenzyl group of **3e** with CAN

Run	CAN		Solvent	Temp	Time	Product	Yield
	Molar equivalent	Concentration / mol dm^{-3}	H_2O-CH_3CN(A) H_2O-MeOH(B)	°C	h		%
1	2.0	0.0	(A) 1:9	r.t.	42	—	—
2	2.0	0.17	(A) 1:90	r.t.	12	**3a**	55
3	4.0	0.25	(A) 1:3	r.t.	1	**3a**	96
4	5.0	1.32	(A) 1:100	r.t.	2	**3a**	98
5	2.5	0.33	(A) 1:2	0	12	**3a**	94
6	5.0	0.45	(A) 5:6	0	10	**3a**	95
7	3.8	0.25	(B) 1:1	0	2	**3a**	92
8	3.8	0.25	(B) 1:11	0	2	**3a**	86
9[a)]	3.8	0.25	MeOH	r.t.	3	**3a**	18
						7	67

a) **3e** was recovered in 15% yield.

Table 2. Oxidative removal of 4-methoxybenzyl group of various PDO with CAN

Run	Substrate	CAN		H_2O-CH_3CN	Temp	Time	Product	Yield
		Molar equivalent	Concentration / mol dm^{-3}		°C	h		%
1	**3f**	4.0	0.25	1:3	r.t.	0.5	**3b**	93
2	**3g**	4.0	0.25	1:3	r.t.	1.0	**3c**	48
3	**3h**	2.5	0.33	1:2	r.t.	0.5	**3d**	71
4	**5a**	5.0	0.45	5:6	0	10	**5d**	92
5	**5b**	4.0	0.25	1:3	r.t.	0.5	**5e**	80
6	**5c**	4.0	0.25	1.3	r.t.	0.5	**5f**	83
7	**3i**	3.8	0.29	1:2	r.t.	1.0	**3j**	62
8	**1i**	7.6	0.50	1:1	r.t.	1.0	**8a**	50
9	**1i**	3.8	0.05	1:19	r.t.	3	**8b**	66
10	**6a**	2.5	0.33	1:2	0	12	**6b**	85

6-hydroxy-6-[2-methyl-1-(nitrooxy)propyl]-PDO (**8a**), whereas only oxidative addition product (**8b**) was obtained by the reaction with 0.05 M CAN (Run 9). These results indicate that CAN can not be applied for the selective removal of *N*-(4-methoxybenzyl) group in alkylidene-PDO. However, oxidation of **6a** having an isolated methylene function (Run 10) gave successfully the expected product (**6b**), without accompanying with the addition reaction.

Structures of new compounds were ascertained by ^{1}H NMR spectra (see Experimental). It is characteristic that the H-6 protons of (*Z*)-alkylidene-PDO commonly appeared as a singlet, whereas those of alkyl-PDO as nonequivalent multiplets. The lower chemical shift of methylene protons (δ=5.29s) of *O*-benzyl group of **2** compared with those (δ=4.63s—4.96s) of *N*-benzyl groups of alkylidene-PDO supported its enol ether structure. The α-methoxyl signals of **7** indicated that it is composed of two epimers at the benzylic position. In addition, the chemical shift of H-1′ of **8a** (δ=5.05d) and **8b** (δ=5.00d) supported the assignment of the position of nitrate. This assignment was further confirmed from the δ value of C-1″ of **8b** in ^{13}C NMR (Table 3). Comparison of data for **6a** and **6b** proved the lack of *N*-(4-methoxybenzyl) group in **6b** and its effect was observed in the chemical shifts of C-3, C-6, C-1′, C-2′, and may be C-5.

In conclusion, it was shown that 4-methoxybenzyl group can be easily introduced to PDO skeleton as a suitable *N*-protecting group and also smoothly removed by CAN oxidation under mild conditions, except for alkylidene-PDO.

Experimental

General. Melting points were determined with a Mel-temp apparatus or with a Yanagimoto micro melting-point apparatus, and were not corrected. IR spectra were recorded with a Hitachi EPI-G2 grating spectrometer. ^{1}H and ^{13}C NMR spectra were recorded with a JEOL JMN PS-100 and a JEOL FX-90Q spectrometers, respectively, in $CDCl_3$ solution with tetramethylsilane as the internal standard. Column chromatography was performed on Wakogel C-200 or C-300 (Wako Pure Chemical Industries. Ltd.).

TABLE 3. ^{13}C NMR DATA (δ) OF **6a,b**, AND **8b**

Carbon	6a	6b	8b
C-2	*{ 167.0 s	*{ 169.1 s	*{ 164.2 s
C-5	{ 166.0 s	{ 166.4 s	{ 163.5 s
C-3	56.8 d	52.6 d	49.8 t
C-6	56.8 d	58.2 d	83.6 s
C-1′	34.6 t	36.2 t	—
C-2′	131.1 d	132.6 d	—
C-3′	120.1 t	120.2 t	—
C-1″	40.4 t	40.4 t	87.7 d
C-2″	24.4 d	24.5 d	27.4 d
C-3″	23.4 q	23.2 q	21.5 q
	22.4 q	21.9 q	16.5 q
CH_2 in Bn	46.8 t	47.8 t	49.8 t
CH_2 in MBn	45.4 t	—	44.4 t
C-Aromatic	159.4 s	—	159.3 s
	135.5 s	135.8 s	135.0 s
	127.4 s	—	125.4 s
	129.7 d	—	129.0 d
	128.7 d	128.7 d	127.9 d
	128.5 d	128.1 d	127.8 d
	128.0 d	128.0 d	126.8 d
	114.3 d	—	114.0 d
OMe	55.3 q	—	54.8 q

* The assignment may be reversed.

*(Z)-1-Acetyl-3-(4-methylbenzylidene)-2,5-piperazinedione (**1a**).* To a solution of *N,N′*-diacetylanhydroglycine (4.00 g, 20.6 mmol) and *p*-tolualdehyde (3.71 g, 30.9 mmol) in *N,N*-dimethylformamide (DMF, 54 cm^3) was added dropwise 0.5 M potassium *t*-butoxide in *t*-butyl alcohol (43.3 cm^3, 21.6 mmol) with stirring at 0 °C. The resulting solution was kept for 1 h at 0 °C and then overnight at room temperature, neutralized with acetic acid, and poured into ice-water. The precipitate formed was filtered, and recrystallized from methanol to give **1a** (4.63 g) as colorless needles in 87% yield. Mp 153—154 °C, ν_{max}^{KBr} (cm^{-1}): 3260 (NH), 1700 (C=O), ^1H NMR δ=8.0 (bs, 1H, NH), 7.28 (s, 4H, Ph), 7.16 (s, 1H, H-1′), 4.49 (s, 2H, H-6), 2.64 (s, 3H, Me), 2.40 (s, 3H, NAc).

Found: C, 65.03; H, 5.51; N, 10.62%. Calcd for $C_{14}H_{14}N_2O_3$: C, 65.10; H, 5.46; N, 10.85%.

N-Benzylation of (Z)-1-Acetyl-3-alkylidene-2,5-piperazinediones. (*Z*)-1-Acetyl-4-benzyl-3-isobutylidene-2,5-piperazinedione (**1b**) was typically prepared as follows. To a suspension of 50% sodium hydride (2.52 g, 52.5 mmol) in dry DMF (250 cm^3) was added a solution of (*Z*)-1-acetyl-3-isobutylidene-2,5-piperazinedione (10.5 g, 50.0 mmol) in dry DMF (50 cm^3) with stirring at 0 °C, and after keeping the conditions for 30 min benzyl bromide (9.0 g, 52.5 mmol) was further added dropwise, and stirred for 2 h at 0 °C. The resulting solution was kept at room temperature overnight, neutralized with acetic acid, poured into ice-water, and then extracted with ether. The usual work-up of the extract gave a crude syrup, which was purified on a column of silica gel (hexane–ethyl acetate 7:3) to give colorless syrupy **1b** (10.9 g, 73%) and syrupy (*Z*)-1-acetyl-5-benzyloxy-3-isobutylidene-3,6-dihydro-2(1*H*)-pyrazinone (**2**: 0.75 g, 5.0%).

1b: ^1H NMR δ=7.4—7.1 (m, 5H, Ph), 6.15 (d, 1H, $J_{1',2'}$= 9.0 Hz, H-1′), 4.89 (s, 2H, CH_2 in Bn), 4.42 (s, 2H, H-6), 2.77 (dqq, 1H, H-2′), 2.25 (s, 3H, NAc), 1.04 (d, 6H, $J_{2',3'}$=6.0 Hz, H-3′).

Found: C, 67.86; H, 6.68; N, 9.21%. Calcd for $C_{17}H_{20}N_2O_3$: C, 67.98; H, 6.71; N, 9.33%.

2: ^1H NMR δ=7.5—7.1 (m, 5H, Ph), 6.47 (d, 1H, $J_{1',2'}$= 10.0 Hz, H-1′), 5.29 (s, 2H, CH_2 in Bn), 4.20 (s, 2H, H-6), 3.20 (dsep, 1H, H-2′), 2.61 (s, 3H, NAc), 1.07 (d, 6H, $J_{2',3'}$=6.0 Hz, H-3′).

Found: C, 67.78; H, 6.66; N, 9.32%. Calcd for $C_{17}H_{20}N_2O_3$: C, 67.98; H, 6.71; N, 9.33%.

(*Z*)-1-Acetyl-4-benzyl-3-benzylidene-2,5-piperazinedione (**1c**): yield 65% from (*Z*)-1-acetyl-3-benzylidene-2,5-piperazinedione,[19] mp 132 °C (prisms from carbon tetrachloride), ν_{max}^{KBr} (cm^{-1}): 1700 (C=O), 1640 (C=C), ^1H NMR δ=7.3—6.8 (m, 6H, Ph and H-1′), 7.44 (s, 5H, Ph), 4.70 (s, 2H, CH_2 in Bn), 4.56 (s, 2H, H-6), 2.54 (s, 3H, NAc).

Found: C, 71.89; H, 5.61; N, 8.21%. Calcd for $C_{20}H_{18}N_2O_3$: C, 71.84; H, 5.43; N, 8.38%.

(*Z*)-1-Acetyl-4-benzyl-3-(4-methylbenzylidene)-2,5-piperazinedione (**1d**): yield 93% from **1a**, mp 173—174 °C (prisms from carbon tetrachloride), ν_{max}^{KBr} (cm^{-1}): 1710 (C=O), 1630 (C=C), ^1H NMR δ=7.3—6.8 (m, 5 H, Ph and H-1′), 7.30 (s, 5H, Ph), 4.70 (s, 2H, CH_2 in Bn), 4.53 (s, 2H, H-6), 2.53 (s, 3H, Me), 2.43 (s, 3H, NAc).

Found: C, 72.41; H, 5.88; N, 8.01%. Calcd for $C_{21}H_{20}N_2O_3$: C, 72.39; H, 5.79; N, 8.04%.

*Deacetylation of **1b—d**.* (*Z*)-1-Benzyl-6-isobutylidene-2,5-piperazinedione (**1f**) was typically prepared as follows. To an ice-cooled solution of **1b** (10.0 g, 35.5 mmol) in DMF (50 cm^3) was added 70% hydrazine (3.30 g, 66.6 mmol) with stirring at 0 °C. The resulting solution was kept at 0 °C for 3 h, poured into ice-water, and extracted with ethyl acetate. The usual processing of the extract gave the product which was recrystallized from ether–hexane to give **1f** quantitatively as colorless prisms. Mp 124—126 °C, ν_{max}^{KBr} (cm^{-1}): 3180 (NH), 1695 and 1690 (C=O), 1665 (C=C), ^1H NMR δ=7.48 (bd, 1H, NH), 7.4—7.1 (m, 5H, Ph), 6.05 (d, 1H, $J_{1',2'}$=11.0 Hz, H-1′), 4.96 (s, 2H, CH_2 in Bn), 4.02 (d, 2H, $J_{3,NH}$= 2.5 Hz, H-3), 2.69 (dq, 1H, H-2′), 1.00 (d, 6H, $J_{2',3'}$= 6.0 Hz, H-3′).

Found: C, 69.87; H, 6.98; N, 10.79%. Calcd for $C_{15}H_{18}N_2O_2$: C, 69.74; H, 7.02; H, 10.83%.

(*Z*)-1-Benzyl-6-benzylidene-2,5-piperazinedione (**1g**): yield 99% from **1c**, mp 183 °C (prisms from ethanol), ν_{max}^{KBr} (cm^{-1}): 3180 (NH), 1700 (C=O), 1630 (C=C), ^1H NMR δ= 7.88 (bd, 1H, NH), 7.3—6.8 (m, 6H, Ph and H-1′), 7.40 (s, 5H, Ph), 4.71 (s, 2H, CH_2 in Bn), 4.10 (d, 2H, $J_{3,NH}$=2.0 Hz, H-3).

Found: C, 73.92; H, 5.56; N, 9.55%. Calcd for $C_{18}H_{16}N_2O_2$: C, 73.95; H, 5.52; N, 9.58%.

(*Z*)-1-Benzyl-6-(4-methylbenzylidene)-2,5-piperazinedione (**1h**): yield 92% from **1d**, mp 195 °C (prisms from ethanol), ν_{max}^{KBr} (cm^{-1}): 3160 (NH), 1680 (C=O), 1630 (C=C), ^1H NMR δ=7.3—6.8 (m, 5H, Ph and H-1′), 7.27 (s, 5H, Ph), 6.82 (bd, NH), 4.73 (s, 2H, CH_2 in Bn), 4.14 (d, 2H, $J_{3,NH}$=2.0 Hz, H-3), 2.43 (s, 3H, Me).

Found: C, 74.38; H, 5.96; N, 9.09%. Calcd for $C_{19}H_{18}N_2O_2$: C, 74.49; H, 5.92; N, 9.15%.

Catalytic Reduction of Alkylidene-2,5-piperazinediones. The procedure is exemplified by the preparation of 1-benzyl-6-isobutyl-2,5-piperazinedione (**3a**). A solution of **1f** (2.00 g, 7.74 mmol) in ethanol (200 cm^3) was catalytically hydrogenated with 10% palladium-carbon (200 mg) at room temperature for 2 h. The usual processing of the reaction mixture gave the product which was recrystallized from ether–hexane to give **3a** (1.88 g, 93%). Mp 98 °C, ν_{max}^{KBr} (cm^{-1}): 3220 (NH), 1690 (C=O), ^1H NMR δ=7.59 (bd, 1H, NH), 7.45—7.15 (m, 5H, Ph), 5.30 and 3.99 (ABq, 2H, J= 15.0 Hz, CH_2 in Bn), 3.89 (dd, 1H, $J_{6,1'a}$=6.0, $J_{6,1'b}$=8.0 Hz, H-6), 3.02 (d, 2H, $J_{3,NH}$=3.0 Hz, H-3), 1.9—1.45 (m, 3H, H-2′ and 1′), 0.91 (d, 6H, $J_{2',3'}$=6.0 Hz, H-3′).

Found: C, 69.35; H, 8.10; N, 10.84%. Calcd for $C_{15}H_{20}N_2O_2$: C, 69.20 H, 7.74; N, 10.76%.

1,6-Dibenzyl-2,5-piperazinedione (**3b**): yield 96% from **1g**, mp 183—184 °C (prisms from ethanol), ν_{max}^{KBr} (cm^{-1}): 3250 (NH), 1650 (C=O), ^1H NMR δ=7.5—7.1 (m, 11H, 2×Ph and NH), 5.45 and 3.89 (ABq, 2H, J=15.0 Hz, NCH_2 in Bn), 4.09 (t, 2H, $J_{6,1'}$=4.0 Hz, H-1′), 3.53 (dd, 1H, $J_{3a,NH}$=3.0, $J_{3a,3b}$= 17.5 Hz, H-3a), 2.55 (d, 1H, H-3b).

Found: C, 77.08; H, 5.45; N, 8.04%. Calcd for $C_{22}H_{18}N_2O_2$: C, 77.17; H, 5.30; N, 8.18%.

6-Benzyl-1-methyl-2,5-piperazinedione (**3c**): yield 93% from (*Z*)-6-benzylidene-1-methyl-2,5-piperazinedione,[20] mp 169 °C (prisms from ethanol), ν_{max}^{KBr} (cm^{-1}): 3460 (NH), 1650 (C=O), ^1H NMR δ=7.4—7.0 (m, 5H, Ph), 6.80 (bd, 1H, NH), 4.15 (dd, 1H, $J_{6,1'a}$=3.0, $J_{6,1'b}$=2.5 Hz, H-6), 3.45 (dd, 1H, $J_{3a,NH}$=3.5 Hz, H-3a), 3.26 and 3.16 (dABq, 2H, J=14.0 Hz, H-1′), 3.07 (s, 3H, NMe), 2.48 (d, 1H, $J_{3a,3b}$= 14.0 Hz, H-3b).

Found: C, 65.98; H, 6.52; N, 12.79%. Calcd for $C_{12}H_{14}N_2O_2$: C, 66.03; H, 6.47; N, 12.84%.

1-Benzyl-3-[2-(ethoxycarbonyl)ethyl]-2,5-piperazinedione (**3d**): yield 93% from (*Z*)-1-benzyl-3-[2-(ethoxycarbonyl)ethylidene]-2,5-piperazinedione,[21] mp 104 °C (prisms from carbon tetrachloride); ν_{max}^{KBr} (cm^{-1}): 3240 (NH), 1740 (ester), 1690 (C=O), 1660 (C=C), ^1H NMR δ=7.55 (bs, 1H, NH), 7.29 (s, 5H, Ph), 4.60 (s, 2H, CH_2 in Bn), 4.3—4.0 (m, 3H, H-3 and CH_2 in Et), 3.85 (s, 2H, H-6), 2.6—2.0 (m, 4H, H-1′ and 2′), 1.24 (t, 3H, Me in Et).

Found: C, 63.09; H, 6.70; N, 9.19%. Calcd for $C_{16}H_{20}N_2O_4$: C, 63.14; H, 6.62 N, 9.21%.

1-Acetyl-3-isobutyl-4-(4-methoxybenzyl)-2,5-piperazinedione (**3i**): yield 94% from **1e**; mp 114 °C (prisms from diisopropyl ether), ν_{max}^{KBr} (cm^{-1}): 1670 (C=O), ^1H NMR δ= 7.16 and 6.85 (each d, 4H, J_{ortho}=8.5 Hz, MBn), 5.08 and 4.01 (ABq, 2H, J=14.5 Hz, CH_2 in MBn), 4.92 and 3.97 (ABq, 2H, J=17.5 Hz, H-6), 3.90 (dd, 1H, $J_{3,1'a}$=5.5, $J_{3,1'b}$= 9.0 Hz, H-3), 3.77 (s, 3H, OMe), 2.51 (s, 3H, NAc), 1.9—1.4 (m, 3H, H-1′ and 2′), 0.93 (d, 6H, $J_{2',3'}$=6.0 Hz, H-3′).

Found: C, 64.96; H, 7.33; N, 8.31%. Calcd for $C_{18}H_{24}N_2O_4$: C, 65.04; H, 7.28; N, 8.43%.

N-(4-Methoxybenzyl)ation of 2,5-Piperazinediones. 4-Methoxybenzyl bromide was prepared by an improved method of that for 4-methoxybenzyl chloride[23] as follows. A mixture of 4-methoxybenzyl alcohol (1.00 g, 7.25 mmol) and conc hydrobromic acid (2.0 cm^3) was vigorously stirred at room temperature for 15 min and then extracted with ether (50 cm^3). The extract was washed with saturated sodium hydrogencarbonate and then water, dried over calcium chloride, and then evaporated to give unstable 4-methoxybenzyl bromide (1.45 g) quantitatively as a liquid, which can be used for the next reaction without purification.

The reaction procedure is exemplified by the preparation of (*Z*)-1-benzyl-6-isobutylidene-4-(4-methoxybenzyl)-2,5-piperazinedione (**1i**). To a suspension of 50% sodium hydride (337 mg, 7.01 mmol) in dry DMF (35 cm^3) was added with stirring a solution of **1f** (1.73 g, 6.68 mmol) in dry DMF (5 cm^3) at 0 °C. After keeping the conditions for 30 min, 4-methoxybenzyl bromide (1.61 g, 8.02 mmol) was further added dropwise at 0 °C. The resulting solution was kept at 0 °C for 2 h and then overnight at room temperature, neutralized with acetic acid, poured into ice-water, and then extracted with ethyl acetate. The usual processing of the extract gave a crude syrup which was purified on a column of silica gel (hexane–ethyl acetate 7:3) to give colorless syrup. The syrup was crystallized from ethanol–ether to give **1i** (2.01 g) as colorless prisms in 80% yield. Mp 98.5 °C, ν_{max}^{KBr} (cm^{-1}): 1695, 1675 sh (C=O), 1635 (C=C), ^1H NMR δ=7.4—7.05 (m, 5H, Ph), 7.15 and 6.83 (each d, 4H, J_{ortho}=8.0 Hz, MBn), 6.11 (d, 1H, $J_{1',2'}$=11.0 Hz, H-1′), 4.91 (s, 2H, CH_2 in Bn), 4.56 (s, 2H, CH_2 in MBn), 3.88 (s, 2H, H-3), 3.80 (s, 3H, OMe), 2.67 (dq, 1H, H-2′), 1.02 (d, 6H, $J_{2',3'}$=6.0 Hz, H-3′).

Found: C, 72.68; H, 6.69; N, 7.19%. Calcd for $C_{23}H_{26}N_2O_3$: C, 72.98; H, 6.93; N, 7.40%.

(*Z*)-1-Benzyl-6-benzylidene-4-(4-methoxybenzyl)-2,5-piperazinedione (**1j**): syrup, yield 89% from **1g**, ν_{max}^{KBr} (cm^{-1}): 1690 (C=O), 1630 (C=C), ^1H NMR δ=7.5—6.7 (m, 15H, 2×Ph, MBn and H-1′), 4.66 (s, 2H, CH_2 in Bn), 4.55 (s, 2H, CH_2 in MBn), 3.94 (s, 2H, H-3), 3.72 (s, 3H, OMe).

Found: C, 74.69; H, 6.21; N, 6.81%. Calcd for $C_{26}H_{24}N_2O_3$: C, 74.98; H, 6.04; N, 7.00%.

(*Z*)-1-Benzyl-4-(4-methoxybenzyl)-6-(4-methylbenzylidene)-2,5-piperazinedione (**1k**): syrup, yield 85% from **1h**, ν_{max}^{KBr} (cm^{-1}): 1700 (C=O), 1630 (C=C), ^1H NMR δ=7.4—6.7 (m, 14H, 2×Ph, MBn and H-1′), 4.63 (s, 2H, CH_2 in Bn), 4.50 (s, 2H, CH_2 in MBn), 3.88 (s, 2H, H-3), 3.67 (s, 3H, OMe), 2.31 (s, 3H, Me).

Found: C, 75.88; H, 6.21; N, 6.41%. Calcd for $C_{27}H_{26}N_2O_3$: C, 76.03; H, 6.15; N, 6.57%.

(*Z*)-1-Acetyl-3-isobutylidene-4-(4-methoxybenzyl)-2,5-piperazinedione (**1e**): yield 94% from (*Z*)-1-acetyl-3-isobutylidene-2,5-piperazinedione,[19] mp 93—94 °C (prisms from ether–hexane), ^1H NMR δ=7.05 and 6.78 (each d, 4H, J_{ortho}=8.5 Hz, Bn), 6.13 (d, 1H, $J_{1',2'}$=11.0 Hz, H-1′), 4.80 (s, 2H, CH_2 in MBn), 4.37 (s, 2H, H-6), 3.75 (s, 3H, OMe), 2.72 (dq, 1H, H-2′), 2.49 (s, 3H, NAc), 1.08 (d, 6H, $J_{2',3'}$=6.0 Hz, H-3′).

Found: C, 65.46; H, 6.86; N, 8.39%. Calcd for $C_{18}H_{22}N_2O_4$: C, 65.44; H, 6.71; N, 8.48%. For the preparation of **3e—g**, 4-methoxybenzyl chloride instead of the bromide was used.

1-benzyl-6-isobutyl-4-(4-methoxybenzyl)-2,5-piperazinedione (**3e**): yield 90% from **3a**, mp 104—105 °C (needles from cyclohexane), ν_{max}^{KBr} (cm^{-1}): 1675, 1665 (C=O), ^1H NMR δ=7.4—7.1 (m, 5H, Ph), 7.12 and 6.82 (each d, 4H, J_{ortho}=8.0 Hz, MBn), 5.22 and 3.94 (ABq, 2H, J= 15.0 Hz, CH_2 in MBn), 4.0—3.7 (m, 1H, H-6), 3.87 (s, 2H, H-3), 3.78 (s, 3H, OMe), 1.95—1.4 (m, 3H, H-2′ and 1′), 0.91 (d, 6H, $J_{2',3'}$=6.0 Hz, H-3′).

Found: C, 72.33; H, 7.34; N, 7.27%. Calcd for $C_{23}H_{28}N_2O_3$: C, 72.60; H, 7.42; N, 7.36%.

1,6-Dibenzyl-4-(4-methoxybenzyl)-2,5-piperazinedione (**3f**): yield 90% from **3b**, mp 137 °C (needles from ether–hexane), ν_{max}^{KBr} (cm^{-1}): 1660, 1650 (C=O), ^{1}H NMR δ= 7.25—6.9 (m, 12H, 2×Ph and 1/2×MBn), 6.81 (d, 2H, J_{ortho}=8.0 Hz, 1/2×MBn), 5.44 and 3.92 (ABq, 2H, J=14.5 Hz, CH_2 in Bn), 4.30 and 4.24 (ABq, 2H, J=14.0 Hz, CH_2 in MBn), 4.22 (dd, 1H, $J_{6,1'a}$=4.0, $J_{6,1'b}$=4.5 Hz, H-6), 3.79 (s, 3H, OMe), 3.39 and 2.36 (ABq, 2H, J=17.5 Hz, H-3), 3.20 and 3.14 (dABq, 2H, J=14.0 Hz, H-1').

Found: C, 75.26; H, 6.44; N, 6.63%. Calcd for $C_{26}H_{26}O_3N_2$: C, 75.34; H, 6.32; N, 6.76%.

3-Benzyl-1-(4-methoxybenzyl)-4-methyl-2,5-piperazinedione (**3g**): yield 92% from **3c**; mp 154—155 °C (needles from ether–hexane), ν_{max}^{KBr} (cm^{-1}): 1675, 1665 (C=O), ^{1}H NMR δ=7.3—6.9 (m, 7H, Ph and 1/2×MBn), 6.79 (d, 2H, J_{ortho}=8.0 Hz, 1/2×MBn), 4.34 and 4.22 (ABq, 2H, J=14.0 Hz, CH_2 in MBn), 4.22 (t, 1H, $J_{3,1'}$=4.5 Hz, H-3), 3.77 (s, 3H, OMe), 3.30 and 3.27 (dABq, 2H, J=14.0 Hz, H-1'), 3.01 (s, 3H, NMe), 3.00 and 2.28 (ABq, 2H, J= 17.0 Hz, H-6).

Found: C, 70.81; H, 6.48; N, 8.03%. Calcd for $C_{20}H_{22}N_2O_3$: C, 70.98; H, 6.55; N, 8.28%.

1-Benzyl-3-[2-(ethoxycarbonyl)ethyl]-4-(4-methoxybenzyl)-2,5-piperazinedione (**3h**): syrup, yield 84% from **3d**, ν_{max}^{KBr} (cm^{-1}): 1730 (COOEt), 1660 (C=O), ^{1}H NMR δ=7.3—7.1 (m, 5H, Ph), 7.10 and 6.73 (each d, 4H, J_{ortho}= 8.0 Hz, MBn), 5.10 and 4.31 (ABq, 2H, J=15.0 Hz, CH_2 in Bn), 4.63 (d, 1H, J=14.0 Hz, 1/2×CH_2 in MBn), 4.3—3.7 (m, 4H, H-6, 3 and 1/2×CH_2 in MBn), 4.05 (q, 2H, CH_2 in Et), 3.67 (s, 3H, OMe), 2.5—1.9 (m, 4H, H-1' and 2'), 1.17 (t, 3H, J=6.0 Hz, Me in Et).

Found: C, 67.87; H, 6.71; N, 6.34%. Calcd for $C_{24}H_{28}N_2O_5$: C, 67.90; H, 6.65; N, 6.60%.

*6-Alkyl-1-benzyl-6-methoxy-4-(4-methoxybenzyl)-2,5-piperazinediones (**5a—c**).* Compounds **5a—c** were obtained from **1i—k** by successive reactions of NBS and reduction. The procedure is exemplified by the conversion of **1i** into **5a** as follows. To a solution of **1i** (1.90 g, 5.02 mmol) in methanol (80 cm^3) was added NBS (938 mg, 5.27 mmol), and the mixture was stirred at room temperature for 30 min, evaporated, and the residue was extracted with ethyl acetate. The usual processing of the extract gave a crude syrup which was purified on a column of silica gel (hexane–ethyl acetate 7:3) to give 1-benzyl-6-(1-bromo-2-methylpropyl)-6-methoxy-4-(4-methoxybenzyl)-2,5-piperazinedione (**4a**: 2.48 g, 98%) as a colorless syrup. ^{1}H NMR δ=7.5—7.1 (m, 7H, Ph and 1/2×MBn), 6.82 (d, 2H, J_{ortho}=8.0 Hz, 1/2×MBn), 4.65 (s, 2H, CH_2 in Bn), 4.59 (s, 2H, CH_2 in MBn), 4.17 and 3.88 (ABq, 2H, J=16.0 Hz, H-3), 4.08 (d, 1H, $J_{1',2'}$=3.0 Hz, H-1'), 3.79 (s, 3H, OMe), 3.05 (s, 3H, 3-OMe), 2.58 (dqq, 1H, H-2'), 1.01 (d, 6H, $J_{2',3'}$=7.0 Hz, H-3').

Found: C, 56.88; H, 5.66; N, 5.53; Br, 15.60%. Calcd for $C_{24}H_{29}N_2O_5Br$: C, 57.03; H, 5.78; N, 5.54; Br, 15.81%.

The same compound was obtained in 96% yield by treatment of **1i** with a mixture of equimolar bromine and excess methanol.

A solution of **4a** (450 mg, 0.890 mmol) in methanol (50 cm^3) was catalytically hydrogenolyzed in the presence of 10% palladium–carbon (200 mg) and ammonium acetate (343 mg, 4.45 mmol) at room temperature for 24 h. The usual processing of the reaction mixture gave the crude product which was purified on a silica gel column (hexane–ethyl acetate 7:3) to give 1-benzyl-6-methoxy-4-(4-methoxybenzyl)-6-(2-methylpropyl)-2,5-piperazinedione (**5a**: 237 mg, 62%) as a colorless syrup. ^{1}H NMR δ=7.5—7.1 (m, 7H, Ph and 1/2×MBn), 6.83 (d, 2H, J_{ortho}=8.0 Hz, 1/2×MBn), 4.77 and 4.33 (ABq, 2H, J=14.0 Hz, CH_2 in Bn), 4.73 and 4.53 (ABq, 2H, J=14.5 Hz, CH_2 in MBn), 3.99 (s, 2H, H-3), 3.79 (s, 3H, OMe), 2.87 (s, 3H, 3-OMe), 2.13 and 1.86 (dABq, 2H, $J_{1',2'}$=8.0 and 4.5, $J_{A,B}$=15.0 Hz, H-1').

Found: C, 67.38; H, 7.21; N, 6.46%. Calcd for $C_{24}H_{30}N_2O_5$: C, 67.58; H, 7.09; N, 6.57%.

Compounds **5b,c** were obtained without characterization of the intermediates, **4b,c**.

1,6-Dibenzyl-6-methoxy-4-(4-methoxybenzyl)-2,5-piperazinedione (**5b**): yield 48% from **1j**, mp 115 °C (prisms from cyclohexane), ^{1}H NMR δ=7.6—6.7 (m, 14H, 2×Ph and MBn), 5.13 and 4.08 (ABq, 2H, J=13.5 Hz, CH_2 in Bn), 4.52 and 4.42 (ABq, 2H, J=14.0 Hz, CH_2 in MBn), 3.74 (s, 3H, OMe), 3.37 and 3.27 (ABq, 2H, J=13.5 Hz, H-1'), 3.28 and 2.36 (ABq, 2H, J=17.5 Hz, H-3), 2.84 (s, 3H, 3-OMe).

Found: C, 72.92; H, 6.29; N, 6.31%. Calcd for $C_{27}H_{28}N_2O_4$: C, 72.95; H, 6.35; N, 6.30%.

1-Benzyl-6-methoxy-4-(4-methoxybenzyl)-6-(4-methylbenzyl)-2,5-piperazinedione (**5c**): yield 56% from **1k**, syrup, ^{1}H NMR δ=7.5—6.6 (m, 13H, Ph, Tol and MBn), 5.10 and 5.37 (ABq, 2H, J=14.0 Hz, CH_2 in Bn), 4.42 and 4.13 (ABq, 2H, J=14.0 Hz, CH_2 in MBn), 3.70 (s, 3H, OMe), 3.42 and 2.41 (ABq, 2H, J=13.5 Hz, H-1'), 2.79 (s, 3H, 3-OMe), 2.19 (s, 3H, Me).

Found: C, 73.26; H, 6.61; N, 6.03%. Calcd for $C_{28}H_{30}N_2O_4$: C, 73.34; H, 6.59; N, 6.11%.

*3-Allyl-1-benzyl-6-isobutyl-4-(4-methoxybenzyl)-2,5-piperazinedione (**6a**).* To a solution of 2,2,6,6-tetramethylpiperazine (508 mg, 3.60 mmol) in tetrahydrofuran (12 cm^3) was successively added dropwise with stirring butyllithium (1.6 M hexane solution, 604 cm^{-3}, 3.60 mmol) and a solution of **3e** (1.14 g, 3.00 mmol) in tetrahydrofuran (7 cm^3) at −78 °C. After keeping the conditions for 15 min, allyl bromide (436 mg, 3.60 mmol) was further added and stirred for 1 h at −78 °C. The temperature of the reaction mixture was raised slowly to room temperature, poured into saturated ammonium chloride solution, and extracted with dichloromethane. The usual processing of the extract gave a crude syrup which was purified on a column of silica gel (hexane–ethyl acetate 7:3) to give a colorless syrup. The syrup was crystallized from ethanol–ether to give **6a** (695 mg, 46%). Mp 123—124 °C, ν_{max}^{KBr} (cm^{-1}): 1650 (C=O), ^{1}H NMR δ=7.22 (s, 5H, Ph), 7.13 and 6.81 (each d, 4H, J_{ortho}=9.0 Hz, MBn), 5.8—5.25 (m, 1H, H-2'), 5.47 and 3.83 (ABq, 2H, J=15.0 Hz, CH_2 in Bn), 5.47 and 3.79 (ABq, 2H, J=15.0 Hz, CH_2 in MBn), 5.40 (dd, 1H, $J_{3'a,3'b}$=2.0, $J_{3'a,2'}$=1.5 Hz, H-3'a), 5.17 (dd, 1H, $J_{3'b,2'}$=8.0 Hz, H-3'b), 4.05—3.6 (m, 2H, H-3 and 6), 3.80 (s, 3H, OMe), 3.1—2.5 (m, 2H, H-1'), 1.9—1.45 (m, 3H, H-1'' and 2''), 0.95 and 0.87 (each d, 6H, $J_{2',3'}$=5.5 Hz, H-3'').

Found: C, 73.96; H, 7.72; N, 6.48%. Calcd for $C_{26}H_{32}N_2O_5$: C, 74.25; H, 7.67; N, 6.66%.

*Oxidation of **3e** with Chromium Trioxide.* A mixture of a solution of **3e** (200 mg, 0.526 mmol) and chromium trioxide (263 mg, 1.58 mmol) in glacial acetic acid (25 cm^3) was stirred for 24 h at room temperature, poured into ice-water, and extracted with ethyl acetate. The usual process-

ing of the extract gave a crude syrup which was purified on a column of silica gel to give **3a** (56 mg) in 41% yield.

Oxidative Removal of N-(4-Methoxybenzyl) Group of 3e—i,1i,5a—c, and 6a with Cerium(IV) Diammonium Nitrate. The general procedure is exemplified by the conversion of **3e** into **3a**. A solution of **3e** (95.1 mg, 0.25 mmol) and CAN (548 mg, 1.00 mmol) in acetonitrile (3.0 cm^3) and water (1.0 cm^3) was stirred at room temperature for 2 h, poured into water, and then extracted with ethyl acetate. The extract was successively washed with saturated sodium hydrogencarbonate and water, dried over anhydrous magnesium sulfate, and then evaporated to give crude product, which was purified on a flash column of silica gel (hexane–ethyl acetate 7:3) to give **3a** (62.7 mg) in 96% yield.

A similar oxidation of **3f—h** gave **3b—d**, respectively. Compounds **5a—c**, **3i**, and **6a** were also successfully converted into **5d—f**, **3j**, and **6b**, respectively.

1-Benzyl-6-isobutyl-6-methoxy-2,5-piperazinedione (**5d**): syrup, ν_{max}^{KBr} (cm^{-1}): 3250 (NH), 1680, 1660 (C=O), ^1H NMR δ=8.24 (bs, 1H, NH), 7.5—7.1 (m, 5H, Ph), 4.66 (s, 2H, CH_2 in Bn), 4.24 and 4.08 (ABq, 2H, J=17.5 Hz, H-3), 2.92 (s, 3H, 3-OMe), 2.1—1.5 (m, 3H, H-1′ and 2′), 0.81 and 0.53 (each d, 6H, $J_{2',3'}$=7.0 Hz, H-3′).

Found: C, 66.03; H, 7.47; N, 9.51%. Calcd for $C_{16}H_{22}N_2O_3$: C, 66.18; H, 7.64; N, 9.65%.

1,6-Dibenzyl-6-methoxy-2,5-piperazinedione (**5e**): mp 157 °C (prisms from ethanol–ether), ν_{max}^{KBr} (cm^{-1}): 3320 (NH), 1710 (C=O), ^1H NMR δ=7.72 (bd, 1H, NH), 7.6—6.9 (m, 10H, 2×Ph), 5.18 and 4.35 (ABq, 2H, J=14.0 Hz, CH_2 in Bn), 3.62 (dd, 1H, $J_{3a,NH}$=2.5 Hz, H-3a), 3.29 (s, 2H, H-1′), 2.81 (s, 3H, 3-OMe), 2.48 (d, 1H, $J_{3a,3b}$=17.0 Hz, H-3b).

Found: C, 70.17; H, 6.08; N, 8.41%. Calcd for $C_{19}H_{20}N_2O_3$: C, 70.35; H, 6.22; N, 8.64%.

1-Benzyl-6-methoxy-6-(4-methylbenzyl)-2,5-piperazinedione (**5f**): mp 190 °C (prisms from ethanol–ether), ν_{max}^{KBr} (cm^{-1}): 3290 (NH), 1700 (C=O), ^1H NMR δ=7.80 (bd, 1H, NH), 7.6—6.9 (m, 9H, Ph and Tol), 5.18 and 4.46 (ABq, 2H, J=15.0 Hz, CH_2 in Bn), 3.68 (dd, 1H, $J_{3a,NH}$=5 Hz, H-3a), 3.26 (s, 2H, H-1′), 2.83 (s, 3H, 3-OMe), 2.51 (d, 1H, $J_{3a,3b}$=17.5 Hz, H-3b), 2.26 (s, 3H, Me).

Found: C, 70.81; H, 6.61; N, 8.16%. Calcd for $C_{20}H_{22}N_2O_3$: C, 70.98; H, 6.55; N, 8.28%.

1-Acetyl-3-isobutyl-2,5-piperazinedione (**3j**): mp 136 °C (prisms from ethanol–ether), ν_{max}^{KBr} (cm^{-1}): 3180 (NH), 1710 (C=O), ^1H NMR δ=6.90 (bd, 1H, NH), 4.47 and 4.30 (ABq, 2H, J=17.8 Hz, H-6), 4.04 (dt, 1H, $J_{3,1'}$=7.9, $J_{3,NH}$=2.6 Hz, H-3), 2.58 (s, 3H, NAc), 1.9—1.5 (m, 3H, H-2′ and 3′), 1.01 and 0.98 (each d, 6H, $J_{2',3'}$=5.7 Hz, H-3′).

Found: C, 56.41; H, 7.55; N, 13.01%. Calcd for $C_{10}H_{16}N_2O_3$: C, 56.59; H, 7.60; N, 13.20%.

3-Allyl-1-benzyl-6-isobutyl-2,5-piperazinedione (**6b**): mp 109 °C (prisms from ethanol–ether), ν_{max}^{KBr} (cm^{-1}): 3210 (NH), 1685 (C=O), 1655 (C=C), ^1H NMR δ=7.45—7.1 (m, 5H, Ph), 6.89 (d, 1H, NH), 6.0—5.5 (m, 1H, H-2′), 5.32 and 3.92 (ABq, 2H, J=14.5 Hz, CH_2 in Bn), 5.24 (d, 1H, $J_{3'a,2'}$=12.0 Hz, H-3′a), 5.12 (d, 1H, $J_{3'b,2'}$=1.0 Hz, H-3′b), 4.10 (dd, 1H, $J_{6,1''a}$=4.0, $J_{6,1''b}$=8.0 Hz, H-6), 3.77 (ddd, 1H, $J_{3,1'a}$=4.0, $J_{3,1'b}$=8.0, $J_{3,NH}$=0.5 Hz, H-3), 3.05—2.4 (m, 2H, H-1′), 1.9—1.45 (m, 3H, H-1″ and 2″), 0.96 (d, 6H, $J_{2'',3''}$= 6.0 Hz, H-3″).

Found: C, 71.99; H, 8.00; N, 9.31%. Calcd for $C_{18}H_{24}N_2O_2$: C, 71.97; H, 8.05; N, 9.33%.

A similar oxidation of **1i** was accompanied with an oxidative addition reaction to give **8a** or **8b**, depending on the concentration of oxidant.

1-Benzyl-6-hydroxy-6-(2-methyl-1-nitrooxypropyl)-2,5-piperazinedione (**8a**): mp 137 °C (prisms from ethyl acetate–hexane), ν_{max}^{KBr} (cm^{-1}): 3380 (OH), 3320 (NH), 1700, and 1665 (C=O), 1645, 1275, 840 (ONO_2), ^1H NMR δ=7.68 (d, 1H, NH), 7.5—7.2 (m, 5H, Ph), 5.43 (bs, 1H, OH), 5.05 (d, 1H, $J_{1',2'}$=4.5 Hz, H-1′), 4.78 and 4.48 (ABq, 2H, J=14.0 Hz, CH_2 in Bn), 4.26 (d, 1H, $J_{3a,3b}$=18.0 Hz, H-3a), 3.90 (dd, 1H, $J_{3b,NH}$=6.0 Hz, H-3b), 2.5—2.0 (m, 1H, H-2′), 1.12 and 0.92 (each d, 6H, $J_{2',3'}$=6.5 Hz, H-3′).

Found: C, 53.30; H, 5.68; N, 12.51%. Calcd for $C_{15}H_{19}N_3O_6$: C, 53.40; H, 5.68; N, 12.46%.

1-Benzyl-6-hydroxy-4-(4-methoxybenzyl)-6-(2-methyl-1-nitrooxypropyl)-2,5-piperazinedione (**8b**): syrup, ν_{max}^{KBr} (cm^{-1}): 3380 (OH), 1660 (C=O, ONO_2), 1275, 830 (ONO_2), ^1H NMR δ=7.55—7.05 (m, 7H, Ph and 1/2×MBn), 6.73 (d, 2H, J_{ortho}=8.0 Hz, 1/2×MBn), 5.26 (s, 1H, OH), 5.00 (d, 1H, $J_{1',2'}$=4.0 Hz, H-1′), 4.73 and 4.44 (ABq, 2H, J=15.0 Hz, CH_2 in Bn), 4.60 and 4.49 (ABq, 2H, J=15.0 Hz, CH_2 in MBn), 4.22 and 3.78 (ABq, 2H, J=17.5 Hz, H-3), 3.79 (s, 3H, OMe), 2.5—2.05 (m, 1H, H-2′), 1.11 and 0.88 (each d, 6H, $J_{2',3'}$=7.0 Hz, H-3′).

Found: C, 60.62; H, 5.67; N, 8.98%. Calcd for $C_{23}H_{27}N_3O_7$: C, 60.38; H, 5.95; N, 9.19%.

Oxidation of **3e** with CAN in methanol gave, 1-benzyl-3-isobutyl-4-(α,4-dimethoxybenzyl)-2,5-piperazinedione (**7**); syrup, ν_{max}^{KBr} (cm^{-1}): 1670 (C=O), ^1H NMR δ=7.4—7.05 (m, 7H, Ph and 1/2×MBn), 6.88 (d, 2H, J_{ortho}=8.0 Hz, MBn), 6.59 (s, 1H, CH in MBn), 5.23 and 3.97, 5.22 and 3.99 (each ABq, 2H, each J=15.0 Hz, CH_2 in Bn), 4.0—3.7 (m, 3H, H-3 and 6), 3.83 (s, 3H, OMe), 3.43 and 3.40 (each s, 3H, 3-OMe), 2.0—1.4 (m, 3H, H-2′ and 1′), 0.94 (m, 6H, H-3′).

Found: C, 70.13; H, 7.33; N, 6.65%. Calcd for $C_{24}H_{30}N_2O_4$: C, 70.22; H, 7.37; N, 6.82%.

References

1) T. Miyoshi, N, Miyairi, H. Aoki, M. Kohsaka, H. Sakai, and H. Imanaka, *J. Antibiot.*, **25**, 569 (1972); S. Miyamura, N. Ogasawara, H. Otsuka, S. Miwayama, H. Tanaka, T. Take, T. Uchiyama, H. Ochiai, K. Abe, K. Koizumi, K. Asao, K. Matsuki, and T. Hoshino, *ibid.*, **25**, 610 (1972).

2) C. O. Gitterman, E. L. Rickes, D. E. Wolf, J. Madas, S. B. Zimmerman, T. H. Stoudt, and T. C. Demny, *J. Antibiot.*, **23**, 305 (1970); B. H. Arison and J. L. Beck, *Tetrahedron*, **29**, 2743 (1973).

3) P. J. Curtis, D, Greatbanks, B. Hesp, A. F. Cameron, and A. A. Freer, *J. Chem. Soc., Perkin Trans. 1*, **1977**, 180; J. P. Férézou, C. Riche, A. Quesneau-Thierry, C. Pascard-Billy, M. Barbier, J. F. Bousquet, and G. Boudart, *Nouv. J. Chem.*, **1**, 327 (1977); J. P. Férézou, A. Quesneau-Thierry, M. Barbier, A. Kollmann, and J. F. Bousquet, *J. Chem. Soc., Perkin Trans. 1*, **1980**, 113.

4) K. Sakata, H. Masago, A. Sakurai, and N. Takahashi, *Tetrahedron Lett.*, **23**, 2095 (1982).

5) Y. Kishi, S. Nakatsuka, T. Fukuyama, and M. Mavel, *J. Am. Chem. Soc.*, **95**, 6493 (1973); T. Fukuyama, S. Nakatsuka, and Y. Kishi, *Tetrahedron*, **37**, 2045 (1981).

6) S. Nakatsuka, H. Miyazaki, and T. Goto, *Tetrahedron*

Lett., **21**, 2817 (1980).
7) H. Maag, J. F. Blount, D. L. Coffen, T. V. Steepe, and F. Wong, *J. Am. Chem. Soc.*, **100**, 6786 (1978).
8) J. Yoshimura, M. Yamaura, T. Suzuki, and H. Hashimoto, *Chem. Lett.*, **1983**, 1001.
9) Y. Oikawa, T. Yoshioka, and O. Yonemitsu, *Tetrahedron Lett.*, **23**, 885 (1982).
10) H. Takaku and K. Kamaike, *Chem. Lett.*, **1982**, 189.
11) M. Bertolini and C. P. J. Glaudemans, *Carbohydr. Res.*, **15**, 263 (1970).
12) W. Schmidt and E. Steckhan, *Angew. Chem.*, **90**, 717 (1978); **91**, 851 (1979).
13) J. B. Gleason, D. B. Bryan, R. F. Hall, K. G. Holden, W. F. Huffman, *J. Am. Chem. Soc.*, **99**, 2353 (1977).
14) A. K. Bose, M. S. Manhas, J. M. Van der Veen, S. G. Amin, I. F. Fernandez, K. Gala, R. Gruska, J. C. Kapur, M. S. Khajavi, J. Kreder, L. Mukkarilli, B. Ram, M. Sugiura, and S. E. Vincent, *Tetrahedron*, **37**, 2321 (1981).
15) T. Fukuyama, R. K. Frank, C. F. Jewell Jr., *J. Am. Chem. Soc.*, **102**, 2122 (1980).
16) D. R. Kronenthal, C. Y. Han, and M. K. Taylor, *J. Org. Chem.*, **47**, 2765 (1982).
17) R. Gigg and R. Conant, *J. Chem. Soc., Chem. Commun.*, **1983**, 465.
18) R. M. Williams, R. W. Armstrong, and J.-S. Dung, *J. Am. Chem. Soc.*, **106**, 5748 (1984); J. Yoshimura, M. Yamaura, T. Suzuki, and H. Hashimoto, *Chem. Lett.*, **1984**, 2157.
19) C. Gallina and A. Liberatori, *Tetrahedron Lett.*, **1973**, 1135; *Tetrahedron*, **30**, 667 (1974).
20) C. Shin, Y. Sato, M. Hayakawa, and M. Kondo, *Heterocycles*, **16**, 1573 (1981).
21) C. Shin, Y. Sato, S. Honda, and J. Yoshimura, *Bull. Chem. Soc. Jpn.*, **56**, 2652 (1983).
22) S. Torii, H. Tanaka, T. Inokuchi, S. Nakane, M. Akada, N. Saito, and T. Sirakawa, *J. Org. Chem.*, **47**, 1647 (1982), and references cited therein.
23) K. Rorig, J. D. Johnston, R. W. Hamilton, T. J. Telinski, W. S. Johnson, S. Seltzer, and P. Yates, *Org. Synth.*, Coll. Vol. **4**, 576.

N-Hydroxy Amides. III.[1] Active Esters of Polystyrene-bound 1-Hydroxy-2-pyrrolidinone and Their Use in Peptide Synthesis

Masayasu AKIYAMA,* Kazuyuki SHIMIZU, Seiichi AIBA, and Hiroaki KATOH
Department of Applied Chemistry for Resources, Tokyo University of Agriculture and Technology, Koganei, Tokyo 184
(Received November 20, 1984)

A polymer-bond cyclic *N*-hydroxy amide has been prepared by reaction of aminomethylated copoly(styrene–2% divinylbenzene) with 1-hydroxy-5-oxo-3-pyrrolidinecarboxylic acid using dicyclohexylcarbodiimide (DCC) as a condensing agent. Several *N*-blocked α-amino acids have been loaded on this resin by use of DCC. The amino acid resin can be utilized for peptide synthesis. Repetitive usage of the resin in the form of esters and facile synthesis of a biologically active pentapeptide, Leu[5]-enkephalin, show the usefulness of the polymer-bound 1-hydroxy-2-pyrrolidinone.

It is well documented that polymer-bound reagents are useful and economical in syntheses where repetitive procedures are required.[2–5] Thus a number of polymeric active esters have been prepared, including recent examples, and used in peptide synthesis.[6–11] *N*-Hydroxy ester-type polymers are prefered to a phenolic ester type to suppress racemization.[12] For recycling, however, *N*-hydroxysuccinimide polymers[7] are of limited utility because of a side reaction between *N*-hydroxysuccinimide (HOSu) and dicyclohexylcarbodiimide (DCC).[13] Polymers of highly active 1-hydroxybenzotriazole esters[8] are recognized to be sensitive to moisture and alcohols.[10]

In the course of our study,[14] it was found that 1-hydroxy-5-oxo-3-pyrrolidinecarboxylic acid (**4**) is readily obtainable from 2-methylenesuccinic acid. A pyrrolidinone ring is more stable than a HOSu ring due to the lack of one of the two carbonyl groups; yet esters of the *N*-hydroxypyrrolidinone are expected to retain a high reactivity, as many hydroxamate esters have been used as an acylating agent.[15,16] It is necessary to explore various functional groups in order to provide practical polymers. No polymer having a cyclic hydroxamic moiety has been tested so far. This paper describes the preparation and use of polymer-bound 1-hydroxy-2-pyrrolidinone as a recyclable polymeric hydroxy component together with synthesis of a biologically active peptide, Leu[5]-enkephalin[17].

Results and Discussion

1-Hydroxy-2-pyrrolidinone Derivatives. Mild heating of *N*-hydroxy-3-carboxy-3-butenamide (**2**) gave 1-hydrpxy-5-oxo-3-pyrrolidinecarboxylic acid (**4**). The compound was also obtained *via* a reaction of 2-methylenesuccinic acid with *O*-benzylhydroxylamine. Scheme 1 shows these transformations. Reaction of **4** with aniline or benzylamine in the presence of DCC yielded the corresponding amides **5a** and **5b**. Acetic anhydride converted the amide **5a** to the acetoxy pyrrolidinone **6a** whose characteristic ester absorption is observed at 1800 cm^{-1}. The acetoxy amide **6a** reacted with cyclohexylamine to give *N*-cyclohexylacetamide. An amino acid ester **6b** can be obtained and used as an active ester. However, compound **4** is more suitable as a polymeric ligand, since problems such as solubility and crystallinity encountered with monomeric derivatives can be avoided through attachment to a polymer.

Polymer-bound 1-Hydroxy-2-pyrrolidinone and Its

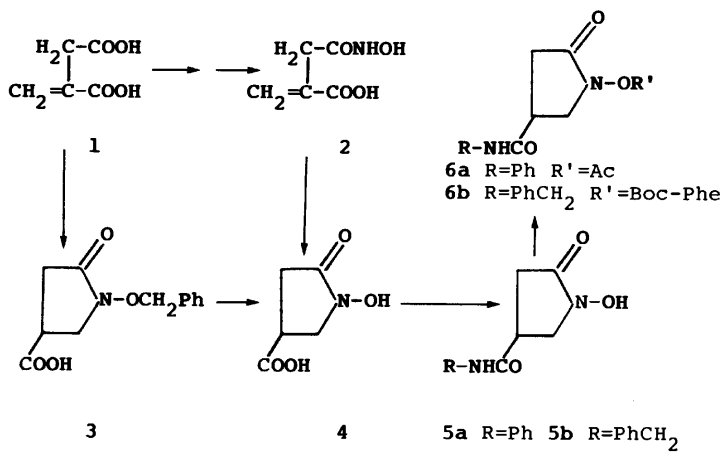

Scheme 1.

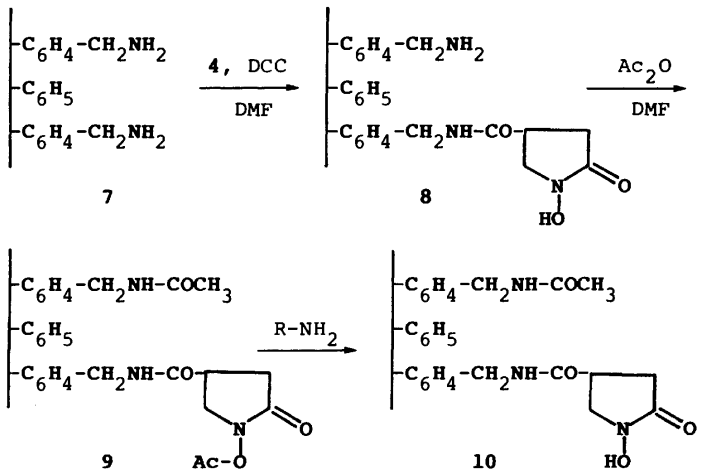

Scheme 2.

Amino Acid Esters. Commercial beads of styrene–2% divinylbenzene (DVB) copolymer were used as the starting material. A 2% content of DVB is adequate for a base polymer in several respects.[5] Aminomethyl resin **7** (1.41—3.73 mmol/g) was prepared by phthalimidomethylation of the starting polymer beads.[18] The key step in the resin preparation was introduction of the hydroxy pyrrolidinone unit to the polymer **7** (Scheme 2). The aminomethyl resin **7** reacted with **4** in *N,N*-dimethylformamide (DMF) in the presence of DCC, without any protection of the hydroxamic acid moiety. The extent of the reaction was in the range of 60—80%, and complete removal of unchanged **4** was difficult at this stage. Exhaustive acetylation of the resin blocked the *N*-hydroxy group and any remaining free amino groups of polymer **8**. The *O*-acetyl group of polymer **9** is readily removed by aminolysis, affording the desired *N*-hydroxypyrrolidinone resin **10** (0.85—3.17 mmol/g). The resin **7** similarly reacted with 1-benzyloxy-5-oxo-3-pyrrolidinecarboxylic acid (**3**), but subsequent debenzylation was difficult to perform. The content of the *N*-hydroxypyrrolidinone unit was estimated by aminolysis of the *O*-acetyl group.[8,19]

The pyrrolidinone resin has the good mechanical property of the starting beads and swells well in DMF, THF, $CHCl_3$, CH_2Cl_2, and benzene. The bead-type resin can be easily filtered and washed with these and alcoholic solvents.

Molecular models suggest that the *N*-hydroxy amide moiety of the pyrrolidinone ring extends from the polymer backbone due to the trans configuration of the linking amide linkage.

Preparation of polymer-bound active esters was performed by reaction of appropriate *N*-protected amino acids with resin **10** in DMF in the presence of DCC. The esterified resin showed a characteristic peak at 1800 cm^{-1}. The amino acid content was determined by titration.[8,19] Figure 1 shows the progress of a loading reaction of Boc-Phe-OH, chosen as an example. It takes 40 h with DCC alone, but addition of 1-hydroxybenzotriazole accelerates the reaction. The symmetric anhydride technique is effective in shortening the reaction time. Table 1 shows typical results obtained with DCC alone. The polymers are stable for months when stored in a desiccator.

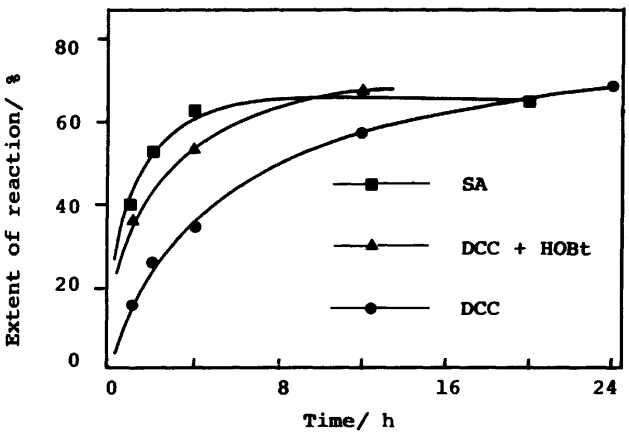

Fig. 1. Progress of the loading reaction of Boc-Phe-OH on the *N*-OH resin (**10**); 2 mol reagents were used for 1 mol *N*-OH unit, in DMF at room temperature; SA, symmetric anhydride method; HOBt, 1-hydroxybenzotriazole. The extent of the reaction was followed by aminolysis.

Peptide Synthesis by Use of Polymer Reagents. The coupling procedure to form a peptide bond is simple; addition of an amino component to an appropriate resin suspension and removal of a wasted polymer after a suitable reaction time. The usual work-up gives a peptide. In a coupling between Boc-Phe resin and H-Leu-OBzl, a rather prolonged time (48 h) for completion was observed in contrast to

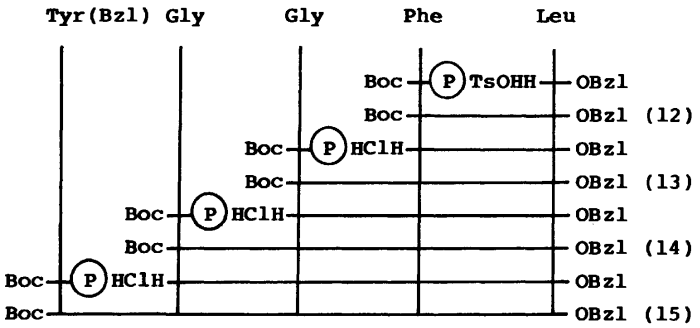

Scheme 3.

the case of HOSu esters, where the coupling usually completes within 20 h at room temperature.[7] Nevertheless, a routine coupling was carried out in DMF at 35 °C for 24 h to give a practical yield.

Repetitive usage is an important factor for polymer reagents. This was examined using the same resin repeatedly. Good reproducible results in the peptide formation are notable (Table 2). Further use was not attempted since some of the polymer beads became powdered.

Table 1. Polymer-bound active esters of *N*-blocked amino acids[a]

N-Blocked amino acid bound to polymer	Content of ester mmol/g
Boc-Ala	0.93
Boc-Gly	1.05
Boc-Phe	0.88
Boc-Pro	0.56
Boc-Val	0.64
Cbz-Ala[b]	0.70
Cbz-Gly[b]	0.55
Cbz-Leu[b]	0.65
Cbz-Tyr(Bzl)	0.97

a) Polymer-bound 1-hydroxy-2-pyrrolidinone having an *N*-OH content = 1.27 mmol/g was used; the content of ester was assayed by the titration method. b) Polymer of an *N*-OH content = 1.04 mmol/g was used; the ester content was estimated from weight gain.

Table 2. Results of repetitive use of a single polymer

Peptide formed	Recycle run[a]	Yield/%
Boc-Phe-Leu-OBzl[b]	1	94
	2	87
	3	94
Boc-Gly-Phe-Leu-OBzl[c]	4	69
	5	71
	6	68

a) Boc-Phe resin (*ca.* 4 g) was used as a starting polymer. b) Reaction of the Boc-Phe resin with H-Leu-OBzl gave *ca.* 1.5 g of the peptide. c) After complete detachment of Boc-Phe residue with cyclohexylamine, the resin was loaded with Boc-Gly and subjected to aminolysis with H-Phe-Leu-OBzl to give *ca.* 1.0 g of the peptide.

Leu^5*-Enkephalin.* In an extension of these couplings, synthesis of the protected peptide of Leu^5-enkephalin was carried out as depicted in Scheme 3. This coupling order of amino acids is rather few, since the Gly^2-Gly^3 sequence is usually prepared separately.[17] Removal of the protective groups, followed by column chromatography, gave the free petide (**16**), Leu^5-enkephalin. The peptide was digested almost completely by an aminopeptidase and was physiologically effective.

The present results show that the 1-hydroxy-2-pyrrolidinone unit is a useful functional moiety when utilized as a polymeric ligand, although aminolysis of its esters is rather slow.

Experimental

All the melting points are uncorrected. IR spectra were obtained with a JASCO 403G spectrophotometer and ^{1}H NMR spectra were recorded on a JEOL C-60HL spectrometer with TMS as internal standard. Optical rotations were measured with a JASCO ORD/UV-5 spectrometer. HPLC was carried out with a JASCO model twincle apparatus using a column packed with Finepak SIL C_{18}. Microanalysis was performed by the Analytical Section, Institute of Physical and Chemical Research, Saitama. TLC was carried out using Merck precoated silica gel $60F_{254}$ plates: R_f^1, EtOAc; R_f^2, $CHCl_3$-MeOH-C_6H_6 (6:1:3); R_f^3, THF-hexane (1:1); R_f^4, $CHCl_3$-MeOH-AcOH-H_2O (30:20:4:6). Aminopeptidase M (Sigma) was used as received. 1 M = 1 mol dm^{-3}.

1-Benzyloxy-5-oxo-3-pyrrolidinecarboxylic Acid (3). A mixture of 2-methylenesuccinic acid (30 g, 0.24 mol), *O*-benzylhydroxylamine (25.6 g, 0.24 mol) and water (240 mL) was refluxed for 1 h, and the hot, aqueous layer removed by decantation. The residue was recrystallized from water to give 43 g (78%) of **3**, 151—152 °C; IR, 1725 (-CO_2H) and 1635 (-CO-N-) cm^{-1}. Found: C, 61.19; H, 5.55; N, 5.94%. Calcd for $C_{12}H_{13}NO_4$: C, 61.27; H, 5.57; N, 5.96%.

1-Hydroxy-5-oxo-3-pyrrolidinecarboxylic Acid (4). (A): *N*-Hydroxy-3-carboxy-3-butenamide (**2**)[14] (0.50 g, 3.4 mmol) in 1-butanol (30 mL) was refluxed for 0.5 h and evaporated

to give an oil which crystallized on cooling (0.30 g, 60%). Recrystallization from acetone–hexane gave a sample, mp 145—146 °C; IR, 1700 (-CO_2H) and 1630 (-CO-N) cm^{-1}; ^1H NMR (DMSO-d_6) δ=3.62 (2H, m, -CH_2-N), 3.20 (1H, m, -CH-COO) and 2.44 (2H, d, -CH_2-CO-N, J=7.2 Hz). Found: C, 40.99; H, 4.84; N, 9.60%. Calcd for $C_5H_7NO_4$: C, 41.38; H, 4.84; N, 9.60%.

(*B*): A solution of **3** (6.0 g, 25 mmol) in MeOH (160 mL) was hydrogenated with H_2 in the presence of 10% Pd/C (0.20 g) under the atmospheric pressure for 2 d to give, after recrystallization, 2.8 g (88%) of **4**, mp 150—151 °C.

*1-Hydroxy-4-phenylcarbamoyl-2-pyrrolidinone (**5a**).* To a chilled solution of **4** (1.00 g, 6.9 mmol) and aniline (0.96 g, 10 mmol) in DMF (20 mL) was added a solution of dicyclohexylcarbodiimide (DCC) (1.42 g, 7 mmol) in DMF (3 mL); the mixture was stirred overnight at room temperature. *N,N'*-Dicyclohexylurea (DCU) was filtered off and the solvent evaporated. The residue was recrystallized from acetone–hexane to yield 1.06 g (70%) of **5a**, mp 183—184 °C (decomp); IR, 1685 (-CO-N(OH)-) and 1665 (-CONH-) cm^{-1}. Found: C, 59.93; H, 5.69; N, 12.92%. Calcd for $C_{11}H_{12}N_2O_3$: C, 59.99; H, 5.49; N, 12.72%.

*1-Hydroxy-4-benzylcarbamoyl-2-pyrrolidinone (**5b**).* *N*-Ethyl-*N'*-(3-dimethylaminopropyl)carbodiimide (WSC) (1.60 g, 8.5 mmol) was added to a solution containing **4** (1.0 g, 6.9 mmol) and benzylamine (0.84 g, 7.8 mmol) in DMF (15 mL), and the mixture stirred for 24 h at room temperature. The usual work-up gave 0.25 g (15%) of **5b**, mp 185—186 °C. Found: C, 61.78; H, 6.10; N, 11.75%. Calcd for $C_{12}H_{14}N_2O_3$: C,61.52; H, 6.02; N, 11.96%.

*1-Acetoxy-4-phenylcarbamoyl-2-pyrrolidinone (**6a**).* A suspension mixture of **4** (0.50 g, 2.3 mmol) and acetic anhydride (0.35 g, 3.4 mmol) in THF (7 mL) was stirred for 5 h at room temperature, the mixture evaporated. The residue was recrystallized from THF–hexane to give 0.38 g (68%) of **6a**, mp 111—112 °C; IR, 1795 (CH_3CO), 1715 (-CO-N) and 1665 (-CONH-) cm^{-1}. Found: C, 59.59; H, 5.41; N, 10.69%. Calcd for $C_{13}H_{14}N_2O_4$: C, 59.53; H, 5.38; N, 10.68%.

*Acetylation with **6a**:* A mixture of **6a** (0.26 g, 1 mmol) and cyclohexylamine (0.10 g, 1 mmol) in THF (3 mL) was stirred for 2 h at room temperature to give *N*-cyclohexylacetamide (0.70 g, 50%), mp 99—100 °C (104 °C for a pure sample).

*1-[N-(t-Butoxycarbonyl)phenylalanyloxy]-4-benzylcarbamoyl-2-pyrrolidinone (**6b**).* To a chilled solution containing **5b** (0.18 g, 0.75 mmol) and Boc-Phe-OH (0.20 g, 0.76 mmol) in DMF (9 mL) was added WSC (0.20 g, 1.0 mmol). The mixture was stirred for 18 h at room temperature and evaporated. Work-up and recrystallization from THF–hexane gave 0.18 g (45%) of **6b**, mp 103—106 °C. Found: C, 64.69; H, 6.40; N, 8.65%. Calcd for $C_{26}H_{31}N_3O_6$: C, 64.85; H, 6.49; N. 8.73%.

*Aminomethylated Polystyrene (**7**).* Commercial copoly(styrene-2% divinylbenzene) beads (100—200 mesh) were washed and subjected to phthalimidomethylation.[18] The following is as example: Resin beads (15.6 g) and *N*-(chloromethyl)phthalimide (15.3 g, 78 mmol) in CH_2Cl_2 (140 mL) containing $SnCl_4$ (9.45 g, 36 mmol) were stirred for 15 h at room temperature. The resin was washed with CH_2Cl_2, EtOH, MeOH, and Et_2O, and dried, yielding 27.2 g. The content of phthalimido group (IR 1775 and 1715 cm^{-1}) was 2.51 mmol/g from microanalysis; 2.66 mmol/g from weight gain.

The resulting phthalimidomethyl resin (26.9 g) was hydrolyzed in aqueous methylamine solution (60 mL; 40%) at first for 100 h and additionally for 20 h at room temperature, to give 19.6 g of **7** (aminomethyl content, 3.73 mmol/g; no peak at 1775 and 1715 cm^{-1}). By a similar procedure polymers (**7**) having different aminomethyl contents (1.41—3.73 mmol/g) were obtained.

*Preparation of Polymer-bound 1-Hydroxy-2-pyrrolidinone (**10**).* A mixture of aminomethyl polystyrene (**7**) (5.00 g; 3.73 mmol/g) and the pyrrolidinone **4** (3.00 g, 21 mmol) in DMF (50 mL) was kept for 2 h at room temperature with stirring and chilled. To this was added DCC (4.25 g, 21 mmol) in DMF (20 mL), and the suspension kept at 0 °C for 2 h and at room temperature for 18 h. The resin was filtered off, washed with DMF and hot MeOH alternatively 3 times, then with ether, and dried under vacuum.

The dried resin was allowed to react with acetic anhydride (16.3 g, 160 mmol) in DMF (50 mL) for 40 h at room temperature. The resin was filtered, washed with CH_2Cl_2 and MeOH alternatively 4 times, then with ether, and dried under vacuum.

The dried acetylated resin (**9**) was swollen in AcOEt–CH_2Cl_2 solution (60 mL; 5:7 v/v). To this was added cyclohexylamine (2.60, 26 mmol) and stirred for 45 h at room temperature. The resin was filtered off, washed with DMF, MeOH, CH_2Cl_2, and ether, and dried under vacuum, affording the *N*-hydroxypyrrolidinone resin (**10**) (6.67 g; 3.17 mmol/g).

The Acyl Group Content of the Polymers. Titration: *O*-Acyl resin (*ca.* 35 mg) was heated with benzylamine in toluene (1 mL; 0.30 M) at 80 °C for 1 h. After cooling the mixture was titrated with $HClO_4$ in AcOH (0.01 M) using Methylene Blue as an indicator.

HPLC Procedure: Excess benzylamine unconsumed in the aminolysis was analyzed by HPLC. The column was eluted with MeOH–0.1% phosphate buffer (65:35 v/v).

*Preparation of Polymer-bound Amino Acid Esters (**11**).* A mixture of polymer-bound pyrrolidinone (**10**) (3.47 g; 1.27 mmol/g) and an *N*-protected amino acid (8.81 mmol) in DMF (30 mL) was stirred for 2 h at room temperature and chilled. To this was added DCC (8.8 mmol) in DMF (10 mL) at 0 °C; the suspension was stirred for 2 h at 0 °C and for 22 h at room temperature. The resin was filtered off and washed with DMF (2×20 mL), MeOH–$CHCl_3$ (2×20 mL, 1:1 v/v), and Et_2O, and then dried under vacuum. The content of the resin was determined by titration using a part of the resin. Typical data were summarized in Table 1. 1-Hydroxybenzotriazole-DCC procedure was similarly carried out as above. In a symmetric anhydride procedure, an anhydride derived from Boc-Phe-OH (2 equiv) and DCC (1 equiv) in DMF was added *in situ* to a resin suspension at room temperature.

Synthesis of Protected Peptides with Polymer-bound Reagents. General Procedure: Boc-amino acid resin (3.6 mmol) was swollen in DMF (30 mL) for 1 h. A mixture of a hydrochloride or tosylate of an amino component (3.0 mmol) and Et_3N (0.303 g, 3.0 mmol) in DMF (10 mL) was added to the swollen suspension and stirred for 30 h at 35 °C. The resin was filtered off and washed with DMF (3×20 mL). The combined filtrate and washings were evaporated to give a residue which was diluted with EtOAc (60 mL). The EtOAc layer was washed with 5% $NaHCO_3$

(3×20 mL), water, 5% citric acid (3×20 mL) and water, and dried (Na_2SO_4). Evaporation of the solvent gave a product.

Boc-Phe resin and TsOH·H-Leu-OBzl gave *Boc-Phe-Leu-OBzl* (**12**), 1.32 g (94%); mp 84—85 °C. Recrystallization from Et_2O-petroleum ether, mp 85—86 °C (lit, [17a] 85.5—86.5 °C); $[\alpha]_D$ −16.3° (THF); R_f^1=0.86, R_f^2=0.91, R_f^3=0.90.

Boc-Gly resin (3.15 g; 1.17 mmol/g) and HCl·H-Phe-Leu-OBzl (1.34 g, 3.31 mmol) produced *Boc-Gly-Phe-Leu-OBzl* (**13**) as an oil; 1.16 g (68%); R_f^1=0.80, R_f^2=0.67, R_f^3=0.75. The peptide **13** gave HCl·H-Gly-Phe-Leu-OBzl by treatment with HCl-dioxane. Neutralization of the hydrochloride and recrystallization from Et_2O gave the free peptide, mp 103—104 °C; $[\alpha]_D$ −16° (THF). Found: C, 67.68; H, 7.38; N, 9.85%. Calcd for $C_{24}H_{31}N_3O_4$: C, 67.74; H, 7.34; N, 9.88%.

Boc-Gly resin (4.82 g; 1.10 mmol/g) and HCl·H-Gly-Phe-Leu-OBzl (2.20 g, 4.76 mmol) gave *Boc-Gly-Gly-Phe-Leu-OBzl* (**14**), 2.20 g (79%). Recrystallization from THF-petroleum ether gave mp 160—161.5 °C (lit,[17d] mp 162.5—163.5 °C); $[\alpha]_D$ −16.7° (THF); R_f^1=0.27, R_f^2=0.56, R_f^3=0.41.

Boc-Try(Bzl)-Gly-Gly-Phe-Leu-OBzl (**15**) was produced from Boc-Tyr(Bzl) resin (2.26 g; 0.62 mmol/g) and HCl·H-Gly-Gly-Phe-Leu-OBzl (0.648 g, 1.25 mmol); 0.853 g (81%), mp 181—182 °C. Recrystallization from MeOH-petroleum ether gave a sample of mp 187—188 °C; $[\alpha]_D$ −17.4° (DMF); R_f^2=0.52, R_f^3=0.17. Found: C, 66.87; H, 6.83; N, 8.26%. Calcd for $C_{47}H_{57}N_5O_9 \cdot 1/2H_2O$: C, 66.80; H, 6.92; N, 8.29%.

Leu^5-Enkephalin. The protective groups of **15** were removed by hydrogenation and then by treatment with HCl-dioxane, followed by column chromatography,[17b] to give H-Tyr-Gly-Gly-Phe-Leu-OH (**16**); 0.29 g (42%) from 0.76 g of **15**, mp 200—201 °C (lit,[17b-d] mp 206—208 °C); $[\alpha]_D$ −22.5° (DMF) (lit, [17b,d] $[\alpha]_D$ −23.4°); R_f^4=0.76.

Biological Assay: The peptide (**16**) (3 mg) was incubated with aminopeptidase M (0.016 mg) in phospate buffer (1 mL; pH=7.2) at 36 °C; 8 μL aliquots of the mixture were analyzed for the peptide using HPLC at appropriate time intervals. The peptide was virtually digested with the pseudo-first-oder rate within 1.5 h. *In vivo* analgesic activity was observed for 5-week-old male mice with the peptide in dimethyl sulfoxide solution (16.7 mg/mL). 10 μL (300 nmol) of the solution was injected intracerebroventricularly and, in a few minutes, the analgesic state was carefully watched for the mouse. The state lasted for *ca.* 15 min.

We thank Messrs. Masashi Maruyama, Masahisa Yoshimi, and Toshikazu Nagura for performing some of the experiments.

References

1) Part II: K. Shimizu, K. Nakayama, and M. Akiyama, *Bull. Chem. Soc. Jpn.*, **57**, 2456 (1984).
2) C. C. Leznoff, *Chem. Soc. Rev.*, **3**, 65 (1974); *Acc. Chem. Res.*, **11**, 327 (1978).
3) D. C. Neckers, *J. Chem. Educ.*, **52**, 695 (1975).
4) J. I. Crowley and H. Rapoport, *Acc. Chem. Res.*, **9**, 135 (1976).
5) A. Akelah and D. C. Sherrington, *Chem. Rev.*, **81**, 557 (1981).
6) M. Fridkin, A. Patchornik, and E. Katchalski, *J. Am. Chem. Soc.*, **88**, 3164 (1966); T. Wieland and C. Birr, *Angew. Chem.*, **78**, 303 (1966).
7) M. Fridkin, "The Peptides," ed by E. Gross and J. Meienhofer, Academic Press, New York, (1980), Vol. 2, p. 333.
8) a) R. Kalir, A. Warshawsky, M. Fridkin, and A. Patchornik, *Eur. J. Biochem.*, **59**, 55 (1975); b) R. Kalir, M. Fridkin, and A. Patchornik, *ibid.*, **42**, 151, (1974).
9) S. Hase Nakagawa and E. T. Kaiser, *J. Org. Chem.*, **48**, 678 (1983).
10) B. J. Cohen, H. Karoly-Hafeli, and A. Patchornik, *J. Org. Chem.*, **49**, 922 (1984).
11) M. Akiyama, K. Shimizu, and M. Narita, *Tetrahedron Lett.*, **1976**, 1015.
12) G. W. Anderson, F. M. Callahan, and J. E. Zimmerman, *J. Am. Chem. Soc.*, **89**, 178 (1967).
13) H. Gross and L. Bilk, *Tetrahedron*, **24**, 6935 (1968).
14) M. Akiyama, K. Shimizu, S. Aiba, and F. Banba, *J. Chem. Soc., Perkin Trans. 1*, **1980**, 2122.
15) T. R. Govindachari, K. Nagarajan, S. Rajappa, A. S. Akerkar, and V. S. Iyer, *Tetrahedron*, **22**, 3367 (1966); S. Rajappa, K. Nagarajan, and V. S. Iyer, *ibid.*, **23**, 4805 (1967).
16) L. Lubiewska-Nakonieczna, B. Rzeszotarka, and E. Taschner, *Liebigs Ann. Chem.*, **741**, 157 (1970).
17) a) J. Hughes, T. W. Smith, H. W. Kosterlitz, L. A. Fothergill, B. A. Morgan, and H. R. Morris, *Nature*, **258**, 577 (1975); b) J. D. Bower, K. P. Guest, B. A. Morgan, *J. Chem. Soc., Perkin Trans. 1*, **1976**, 2488; c) W. Voeltre, E. Pietrzik, and H. Kalbacher, *Tetrahedron Lett.*, **1976**, 2119; d) E. R. Stimson, Y. C. Meinwald, and H. A. Scheraga, *Biochemistry*, **18**, 1661 (1979); e) W. A. Klis, E. Nawracka, I. Z. Siemion, A. Plech, Z. Stachura, and Z. S. Herman, *Bioorg. Chem.*, **8**, 255 (1979).
18) A. R. Mitchell, S. B. H. Rent, B. W. Erickson, and R. B. Merrifield, *Tetrahedron Lett.*, **1976**, 3795.
19) J. S. Fritz and N. M. Liskicki, *Anal. Chem.*, **23**, 589 (1951).

 © 1985 The Chemical Society of Japan Bull. Chem. Soc. Jpn., 58, 1426—1431 (1985) [Vol. 58, No. 5

Bilirubin in Aqueous Solution. Absorption Spectrum, Aqueous Solubility, and Dissociation Constants

Yoshikiyo MOROI,* Ryohei MATUURA, and Tetsuo HISADOME†

Department of Chemistry, Faculty of Science, Kyushu University 33, Higashi-ku, Fukuoka 812

†*Department of Surgery 1, Faculty of Medicine, Kyushu University 60, Higashi-ku, Fukuoka 812*

(Received November 28, 1984)

This report analyzes the change of both spectrum and solubility of bilirubin with pH in buffer solutions. Bilirubin (AH_2) is a dibasic acid which dissociates by two steps ($AH_2 \overset{K_1}{\rightleftharpoons} AH_1 \overset{K_2}{\rightleftharpoons} A$) with increasing pH; the wavelengths at the resulting three isosbestic points are 457 nm (AH_2 and AH_1), 485 nm (AH_1 and A), and 472 nm (A and AH_2). The solubility increases with increasing pH, where the total concentration ($[AH_2]+[AH_1]+[A]$) changes subject to a second-order curve of $1/a_{H^+}$. From the spectral change and the three coefficients of the solubility curve, K_1 and K_2 values were estimated to be $(6.7\pm2.6)\times10^{-7}$ and $(3.4\pm1.0)\times10^{-8}$, respectively. These dissociation constants are much smaller than those of aliphatic carboxylic groups, and the reason for it was discussed together with the values already reported and their reliability.

Bilirubin is one of the major components of gallstone[1,2] and is solubilized together with cholesterol in the mixed micelle of bile salts and lecithin in human bile.[3-6] Indeed, gallstone formation has been much investigated for twenty years from the view point of solubilization,[4-7] but the mechanism of the formation has not been made clear yet. Through these studies, the aqueous solubility of free bilirubin has been found to play a very important role in an elucidation of gallstone formation, and hence the two dissociation constants of bilirubin which are closely related to its solubility have been tried to be speculated or determined by several investigators.[8,9] Nevertheless, the correct values have not been determined yet because of the extremely small solubility of bilirubin even at neutral pH.

Bilirubin decomposes easily under oxygen, and its photooxidation has been extensively studied.[10-12] So, its purification is an important requirement to have reliable experimental results, and several purification methods have been proposed.[13-15] In this report, the authors have examined the solution properties of purified bilirubin in buffer solutions from the spectrum and solubility changes with pH. In the preceding paper,[16] the solubility change with pH was found to be very useful to determine acidity constants of acids which are sparingly soluble in aqueous solution. The solubility method is a modification of the isoextraction method for determination of dissociation constants.[17]

Accordingly, the main attention has been paid only to the determination of the two dissociation constants of bilirubin using two methods, a spectrophotometric and a solubility method. In this paper, therefore, the authors do not relate the constants to bilirubin metabolism or other biochemical events but make clear the physicochemical properties of aqueous bilirubin in solution.

The constants obtained independently by the two methods were in reasonable agreement. In any event, it is the first time that the two constants have been determined reliably. Therefore, they will become invaluable for future study on gallstone formation and on the pathological influence of bilirubin upon the human body.

Experimental

Materials. Chloroform of guaranteed reagent grade was further purified by alternate washing with dilute acid and alkali three times each followed by distilled water several times and then stored under distrilled water in the dark. Bilirubin from Sigma Chem. Corp. was purified as described previously[13] in the most respects. The different repect is the following; the bilirubin was dissolved first in the chloroform which had been beforehand passed through the column of anhydrous sodium sulfate heated at 300 °C for three hours, and then the chloroform solution of bilirubin was run down the column again shielded from light. Other reagents were of analytical reagent grade and used without further purification. Water used was distilled twice from alkaline permanganate.

Rate of Decomposition. Immediately after dissolution of bilirubin in 0.05 mol dm^{-3} NaOH solution, an aliquot of the solution was transfered into a photometric cell containing buffer solution whose ionic strength was 0.05, and then the change of the optical density of the solution with time was followed for more than two hours by spectrophotometer (Hitachi 100-50), where the bilirubin concentration is 2.5×10^{-6} mol dm^{-3} and the temperature is at 25 °C.

Spectrum. The absorption spectra of bilirubin in buffer solution (H_3PO_4-NaH_2PO_4-Na_2HPO_4 for pH≤8 and H_3BO_3-NaH_2BO_3 for pH>8) whose ionic strength(I) is 0.05 were obtained at 25 °C; immediately after the bilirubin had dissolved in alkaline solution (I=0.05), an aliquot of the solution was introduced into the buffer solutions, where the bilirubin concentration was 1.39×10^{-6} mol dm^{-3}. It took less than five minutes to finish recording the absorption spectra after the bilirubin dissolution. Almost no change in pH of the solutions were observed before and after the spectrum measurement.

Solubility. The apparatus and procedure are the same as those in the previous paper.[16] In preparing buffer solutions, ionic strength and temperature were made to resemble human bile (I=0.15 and 37 °C) and the reagents

used were the same as in the spectrum section. As bilirubin is not only chemically unstable but also photosensitive, the solubility measurement was carried out in a dark room and under the conditions of short dissolution time. First of all, the amount of bilirubin powder to be suspended in the buffer solution (3 ml) which is necessary to reach dissolution equilibrium within one hour was first examined and was found to be about 30 mg. Then, the solubility was determined spectrophotometrically at 37 °C against $1/a_{H^+}$ of each buffer solution under the above conditions.

Results and Discussion

Purity. Elemental analysis of purified bilirubin was 67.71 (67.79)% for C, 6.28 (6.21)% for H, and 9.49 (9.58)% for N, where the values in parentheses are calculated ones. The absorption spectra of original and purified bilirubin in chloroform are shown in Fig. 1. Impurities absorbing below 350 nm in chloroform solution were almost completely removed by the above purification process. The molar absorption coefficients in chloroform and in aqueous alkali solution are 5.67×10^4 mol^{-1} dm^3 cm^{-1} at 455 nm and 5.45×10^4 mol^{-1} dm^3 cm^{-1} at 438 nm,

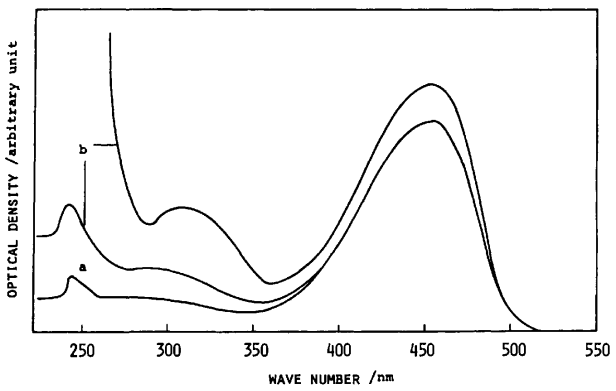

Fig. 1. Absorption spectra of purified(a) and unpurified bilirubin(b) in chloroform solution.

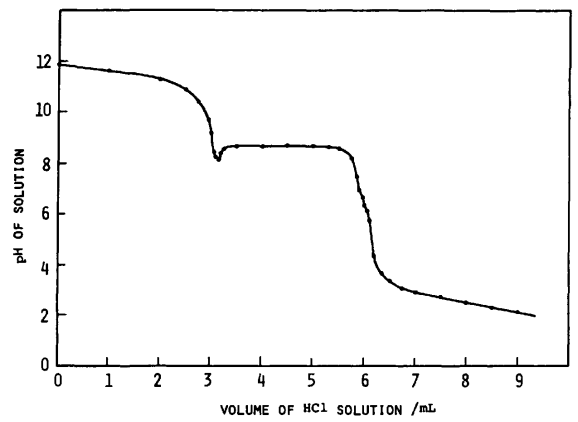

Fig. 2. Back-titration curve of bilirubin in alkali solution by HCl solution; 42.25 mg bilirubin dissolved in 10 ml of 3.018×10^{-2} mol dm^{-3} NaOH solution was titrated with 4.994×10^{-2} mol dm^{-3} HCl solution.

respectively. The former value can be compared with the literature value 6.07×10^4.[13] The titration curve is illustrated in Fig. 2. The result is appreciably different from that reported before.[9] The purity was found to go up to 99.8% with respect to two carboxyl groups from 90.4% of unpurified bilirubin. It is quite clear from this titration curve that bilirubin is dibasic acid in the pH region below 10 and that there exist two steps on pH decrease around the endpoint of titration due to different dissociation constants. The titration curve is quite similar to that of bile acids[18] which start micelle formation above their cmc,[19] but their physicochemical meaning is much different as will be clear later. The almost flat initial part of the curve represents the titration of excess NaOH. After neutralization of excess NaOH, the pH continues to decrease steeply with a small amount of HCl and then rises sharply again. With each successive addition of HCl, an almost equivalent amount of bilirubin is precipitated, where the pH of titration solution with bilirubin solid suspension hardly decreases keeping the value of 8.5 to the endpoint of the neutralization. The sharp rise of pH is accompanied by the precipitation of bilirubin. This indicates that supersaturation of bilirubin is broken at pH 8.15. The extent of the supersaturation can be estimated to be more than 10^{-4} mol dm^{-3} from the titration curve. Other acidic groups with $pK>10$ are out of the present discussion.[20]

Decomposition of Bilirubin in Buffer Solutions. Biomolecules are very easy to decompose, once they are taken out from their mother tissue. Thus, it is very important for the present investigation to know how easily bilirubin degrades in buffer solutions. As the decay kinetics of bilirubin is not the main purpose, very simple first-order kinetics is adopted, neglecting the effect of H^+ or OH^- ions;

$$OD = OD_0 \exp(-k^{app}t). \quad (1)$$

where an optical density(OD) is used in place of concentration, k^{app} is an apparent first-order rate constant, and t is time in unit of hour. The decay curves turned out to be approximately expressed by Eq. 1. The k^{app} values and the wavelength pursued are given in Table 1. From the results, more than 90% of birirubin can remain unchanged for one hour.

Spectrum Change with pH. It has become clear from the titration curve that bilirubin is a dibasic acid. Therefore, it dissociates stepwise from acidic to basic form with increasing pH;

$$\underset{1}{AH_2} \overset{K_1}{\rightleftharpoons} \underset{2}{AH_1^-} \overset{K_2}{\rightleftharpoons} \underset{3}{A^{2-}}. \quad (2)$$

Figure 3 shows the absorption spectra in several buffer solutions. As is expected, the spectrum

Table 1. Apparent rate constant (k^{app}) of decomposition of bilirubin in buffer solutions of different pH at 25 °C

pH	λ^{obsd}/nm	$10^2\,k^{app}/k^{-1}$
12.68	438	18.0
8.84	438	4.5
8.15	438	2.7
7.96	440	7.3
7.37	450	9.0
7.07	450	11.5
6.38	453	10.1
6.09	440	5.1
4.41	440	7.8

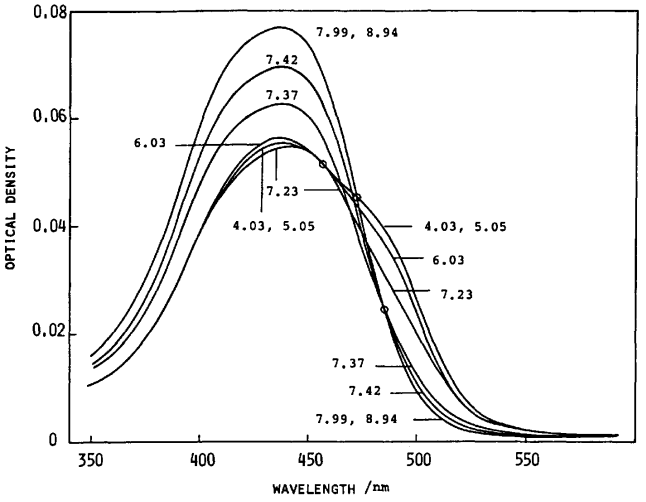

Fig. 3. Absorption spectra of bilirubin in buffer solutions with different pH and three isosbestic points(o): the number in the figure is pH of buffer solution and the bilirubin concentration is 1.39×10^{-6} mol dm^{-3}.

changes with pH of the solution. The concentration of each solution is 1.39×10^{-6} mol dm^{-3} which is higher than the solubility at pH 8, 1.0×10^{-6} mol dm^{-3} (Fig. 4). However, any precipitation has not been observed, because the concentration is so small that the supersaturation is easy to stand far up to 10^{-4} mol dm^{-3} as can be seen from the titration curve. The spectra of A^{2-} above pH 8 remain the same and has the absorption maximum at 438 nm with the molar absorption coefficient of 5.45×10^4 mol^{-1} dm^3 cm^{-1}. On the other hand, the spectra of AH_2 below pH 5 also remain unchanged, where the wavelength of the absorption maximum is 437 nm with the molar absorption coefficient of 3.92×10^4 mol^{-1} dm^3 cm^{-1}. The wavelength of three isosbestic points obtained from many spectra of different pH are 457 nm for AH_2 and AH_1^-, 485 nm for AH_1^- and A^{2-}, and 472 nm for A^{2-} and AH_2.

Solubility. The solubilities determined spectrophotometrically at 37 °C against $1/a_{H^+}$ of each buffer solution are shown in Fig. 4. Bilirubin which

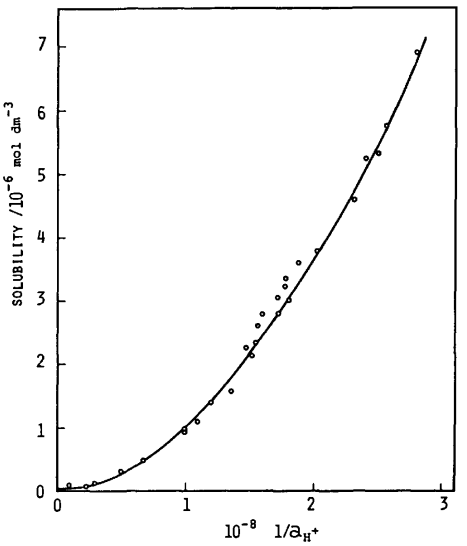

Fig. 4. Solubility of bilirubin in buffer solution as a function of $1/a_{H^+}$: ionic strength=0.15 and temperature=37 °C.

is a dibasic acid dissociates by two steps, and the total analytical concentration then becomes[16]

$$C_t = [AH_2] + [AH_1] + [A] = [AH_2]\left\{1+\frac{K_1}{\gamma_2}\frac{1}{a_{H^+}}+\frac{K_1K_2}{\gamma_3}\left(\frac{1}{a_{H^+}}\right)^2\right\}. \quad (3)$$

The concentration $[AH_2]$ should remain constant at constant temperature and ionic strength as far as AH_2 solid coexists in the solution, because AH_2 in the solution is in chemical equilibrium with solid AH_2. Since every parameter except $1/a_{H^+}$ of the right side of Eq. 3 is constant based on the above reasons, the total concentration C_t changes with the second-power curve of $1/a_{H^+}$. Three coefficients of the curve $(A+B(1/a_{H^+})+C(1/a_{H^+})^2)$ were estimated by applying the second-power curve to the solubility data where the method of least square was employed for the best fit between them, and they were found to be

$$A = 1.132\times10^{-9},\ B = 1.728\times10^{-15},$$

and

$$C = 8.176\times10^{-23}\ \text{mol dm}^{-3}.$$

Now it became clear that the total analytical concentration increases with increasing pH by being subject to the second-power curve of $1/a_{H^+}$ in this case, too. This means that dimerization or polymerization of bilirubin does not take place in these buffer solutions. It is incorrect that the logarithm of the solubility varies linearly with pH.[21]

Evaluation of Dissociation Constants

Spectrophotometric Method. Spectrum of bilirubin depends on the pH of its solution as seen

above. At any wavelength except that of the isosbestic point, the optical density can be expressed as

$$OD = \varepsilon_1 C_1 + \varepsilon_2 C_2 + \varepsilon_3 C_3 \quad (4)$$

where ε_i is molar absorption coefficient and C_i is molar concentration of species i. On the other hand, the total concentration is

$$C_t = C_1 + C_2 + C_3 \quad (5)$$

and they can be related with one another by the dissociation constants as

$$K_1 = \frac{C_2 \gamma_2 a_{H^+}}{C_1 \gamma_1} \quad (6)$$

and

$$K_2 = \frac{C_3 \gamma_3 a_{H^+}}{C_2 \gamma_2}, \quad (7)$$

where γ_i is the activity coefficient of i. By combining the above four equations, there results

$$\frac{\gamma_3 a_{H^+}^2}{K_1 K_2}\varepsilon_1 + \frac{\gamma_3 a_{H^+}}{\gamma_2 K_2}\varepsilon_2 + \varepsilon_3 = \frac{OD}{C_t}\left(\frac{\gamma_3 a_{H^+}^2}{K_1 K_2} + \frac{\gamma_3 a_{H^+}}{\gamma_2 K_2} + 1\right) \quad (8)$$

where γ_1 is assumed to be unity because of uncharged species of **1**. ε_1 and ε_3 are easily determined from the spectrum of low and high pH solutions of bilirubin, respectively, and their activity coefficients can be estimated at the ionic strength(I) of 0.05 and 25 °C from the equation suggested by Bates[22]

$$\log \gamma_i = -\frac{0.5|z_i|^2\sqrt{I}}{1+1.5\sqrt{I}} \quad (9)$$

where z_i is a valency of i. Now, it is theoretically possible to determine K_1, K_2, and ε_2 values from three different OD values of different pH solution at fixed wavelength and at known total concentration. Practically, however, the spectrum whose variation with pH is large can be used for the present purpose; only K_i which brings about larger spectrum change with small pH change can be determined with high accuracy. Two wavelengths, 490 and 438 nm, were used for the determination of K_1 and K_2 values, respectively. The molar absorption coefficients used are

$$\varepsilon_1 = 2.46 \times 10^4,$$
$$\varepsilon_3 = 1.24 \times 10^4 \text{ mol}^{-1}\text{ dm}^3\text{ cm}^{-1} \text{ at } 490 \text{ nm}$$

and

$$\varepsilon_1 = 3.88 \times 10^4,$$
$$\varepsilon_3 = 5.45 \times 10^4 \text{ mol}^{-1}\text{ dm}^3\text{ cm}^{-1} \text{ at } 438 \text{ nm}.$$

The K_i values thus obtained are

$$K_1 = (3.1\text{—}8.7) \times 10^{-7},$$
$$K_2 = (2.5\text{—}5.1) \times 10^{-8} \text{ at } 25\,^\circ\text{C}.$$

Solubility Method. As is clear from Eq. 3, the values of K_1 and K_2 can be obtained from the three coefficients of the second-power curve $(A+B(1/a_{H^+})+C(1/a_{H^+})^2)$ as

$$K_1 = \gamma_2 B/A, \quad (10)$$
$$K_2 = \gamma_3 C/\gamma_2 B, \quad (11)$$

From the three coefficients given above, K_1 and K_2 values become

$$K_1 = 9.7 \times 10^{-7} \text{ and } K_2 = 2.4 \times 10^{-8} \text{ at } 37\,^\circ\text{C}.$$

Although the A value cannot be precisely determined for a scarcely soluble acid like the present, B and C values are rather easy and more accurate to determine. Therefore, K_2 value is more reliable than K_1 value. In our preceding paper[16] the authors reported the method to determine K_1 value of dibasic acid by employing $[AH_2]$ as a parameter. However, this method can be used only when the two coefficients, B and C, are very accurate. In the present case, on the other hand, bilirubin is not so stable and these coefficients cannot be accurately determined, as is obvious from the plots in Fig. 4.[23] The feasible concentration range of AH_2 based on the range of K_1 values obtained above is shown in Fig. 5, supposing B value to be fairly accurate. Indeed there results some difference in value between the two dissociation constants depending on the methods employed, but the diminution of the difference is quite difficult in this case judging from the instability of bilirubin as is obvious in the section of its decomposition.

Now it can be said that K_1 value ranges from 3×10^{-7} to 1×10^{-6}, while K_2 value is between 2×10^{-8} and 5×10^{-8}, although the values obtained from the two methods are not coincident each other. The dissociation constants of aliphatic monocarboxylic acids as in bilirubin usually range from 10^{-5} to 10^{-3} and the second dissociation constants of corresponding dicarboxylic acids are between 10^{-8} and 10^{-5}.[24] The

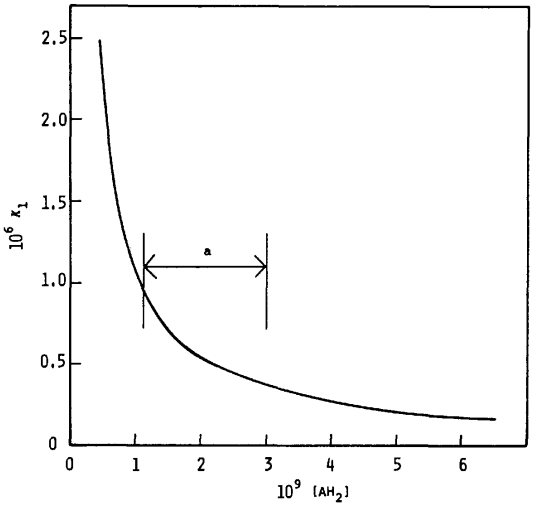

Fig. 5. Variation of K_1 value as a function of concentration of AH_2 and its feasible concentration range(a).

extreme small second dissociation constant of bilirubin can be ascribed partly to a free energy increase by electrostatic repulsion between two carboxylato groups[25] when the second dissociation takes place, as has been done in most cases. The distance between the two groups can range from 0 to 10 Å by CPK molecular model. This range can become the factor somehow to explain the difference between the obtained K_1 and K_2 values. The K_1 value of 10^{-6} at maximum also seems too small for the carboxyl group judging from dissociation constants of most aliphatic monocarboxylic acids. It is then highly possible that the smaller values of K_1 and K_2 are due to stabilization of the carboxyl groups by intramolecular hydrogen bond formation.

Finally, a few remarks on previous works by other investigators on the solubility, the absorption spectra, and the dissociation constants will be made. Overbeek *et al.* expected the dissociation constants for the two carboxyl groups, $K_1=4\times10^{-5}$ and $K_2=1\times10^{-5}$, and estimated the total solubility of 2×10^{-4} mol dm^{-3} at pH=8.[8] It is two hundred times higher than that of present case at the same pH, which indicates that their expected dissociation constants might be totally incorrect. On the other hand, the solubility determined by Brodersen, 9×10^{-8} mol dm^{-3} at pH=8,[21] is one tenth of the solubility determined by us because of extremely scanty solubility of solid bilirubin; 2.5 mg of solid bilirubin in 25 ml buffer solution was too small to reach the solubility equilibrium within one hour in our preliminary experiment. In addition, they attributed the spectrum change with time to bilirubin aggregation.[21] Even if it were true that the bilirubin aggregation took place during the process of spectral measurement in lower pH buffer solutions, the spectrum in Fig. 3 would be trustworthy with more than 98% confidence judging from k^{app} values in Table 1 obtained from higher bilirubin concentration than that for spectral measurement and from the time required for the measurement. Hansen *et al.* insisted that the dissociation constants(pK) of the two carboxyl groups should be well below 7 and obtained the calculated value of pK=4.4.[20] As mentioned above, the pH value with pH titration for the suspended neutralized precipitate bilirubin is around 8.5. If pK=4.4 is correct, $[A^{2-}]/[AH^-]$ must be larger than 10^4 at pH=8.5 and the total solubility becomes more than 10^{-1} mol dm^{-3}, $[AH_2]$ being assumed to be 10^{-9} mol dm^{-3}. Such a high solubility should not bring about the bilirubin precipitation during the back titration. On the other hand, Krasner and Yaffe concluded that both carboxyls have pK=7.55 at 26 °C from the titration curve.[9] The values are almost equal to the present K_2 value.

The strong dependence of the solubility of bilirubin on solution pH must have great importance for gallstone formation. The rapid decrease of solubility of bilirubin below pH 8 suggests that gallstone formation might be due to a lowering of pH in gall bladder. The solubility of bilirubin in buffer solutions has been extensively measured by several investigators. Nevertheless, the reported values have shown a wide variety depending on methods and conditions employed. However, the solubilities obtained here are rather accurate, and therefore we believe that they will become very useful for future study of the pathological function of bilirubin in the human body.

We wish to thank Dr. T. Furusawa of Koga surgery hospital for discussion of bilirubin properties in aqueous solutions from the viewpoint of gallstone formation. Thanks are also due to the Ito Science Foundation for financial support. Technical help of Mr. H. Noma is greatly acknowledged.

References

1) H. Bogren and K. Larsson, *Scand. J. Clin. Lab. Invest.*, **15**, 457 **15**, 569 (1963).
2) W. H. Admirand and D. M. Small, *J. Clin. Invest.*, **47**, 1043 (1968).
3) A. A. Arianoff, *Acta Gastroenterol. Belg.*, **29**, 733 (1966).
4) T. Furusawa, *Fukuoka Acta Medica*, **53**, 710 (1962).
5) T. Nakama, *Fukuoka Acta Medica*, **67**, 413 (1976).
6) T. Furusawa, T. Nakama, H. Itoh, and T. Hisadome, *Gastroenterol. Jpn.*, **12**, 253 (1977).
7) U. Wosiewits and S. Schroebler, *Experientia*, **35**, 717 (1979).
8) J. T. G. Overbeek, C. L. J. Vink, and H. Deenstra, *Rec. Trav. Chim. Pays-Bas*, **74**, 81 (1955).
9) J. Krasner and S. J. Yaffe, *Biochem. Med.*, **7**, 128 (1973).
10) R. Bonnett and J. C. M. Stewart, *J. Chem. Soc., Chem. Commum.*, 596 (1972).
11) C. S. Foote and T.-Y. Ching, *J. Am. Chem. Soc.*, **97**, 6209 (1975).
12) R. Bonnett, *Biochem. Soc. Trans.*, **4**, 222 (1976).
13) J. Fog, *Scand. J. Clin. Lab. Invest.*, **16**, 49 (1964).
14) R. Brodersen, *Acta Chem. Scand.*, **20**, 2895 (1964).
15) A. F. McDonald and F. Assisi, *Biochem. J.*, **129**, 797 (1972).
16) Y. Moroi and R. Matuura, *Anal. Chim. Acta*, **152**, 239 (1983).
17) P. Mukerjee and Y. Moroi, *Anal. Chem.*, **50**, 1589 (1978).
18) P. P. Nair and D. Kritchevsky, "The Bile Acids; Chemistry, Physiology, and Metabolism," Vol. 1, Plenum Press, New York-London (1971), p. 288.
19) K. Shinoda, "Colloidal Surfactants," Academic Press (1963), Chap. 1.
20) P. E. Hansen, H. Thiessen, and R. Brodersen, *Acta Chem. Scand. B* **33**, 281 (1979).
21) R. Brodersen, *J. Biol. Chem.*, **254**, 2364 (1979).
22) R. G. Bates, "Determination of pH; Theory and

Practice," 2nd ed, John Wiley, New York, N.Y. (1973).
23) The results ($[AH_2]=2.3\times10^{-8}$ mol dm^{-3} and $K_1=4.8\times10^{-8}$) obtained from the parameter method clearly oppose the results by the above two methods, which arises mainly from an exaggeration of inaccuracy of B value, 1.728×10^{-15}, in this methods.
24) G. Kortum, W. Vogel, and K. Andrussow, "Dissociation Constants of Organic Acids in Aqueous Solution," Butterworths, London (1961).
25) R. A. Robinson and R. H. Stokes, "Electrolyte Solutions," 2nd ed, Butterworths, London (1959), p. 346.

Preparation of New Nitrogen-bridged Heterocycles. 11.[1] A New Synthetic Method of Pyrazolo[1,5-*a*]pyridines from the Alkaline Treatment of 1-[(Acylmethylthio)-methyleneamino]pyridinium Salts

Akikazu KAKEHI,* Suketaka ITO, Masayoshi ITO, Toshiaki YOTSUYA, and Kenji NAGATA
Department of Industrial Chemistry, Faculty of Engineering, Shinshu University, Wakasato, Nagano 380
(Received November 29, 1984)

Alkaline treatment of 1-[(acylmethylthio)methyleneamino]pyridinium halides gave unexpectedly 3-acyl- or 3-(acylthio)pyrazolo[1,5-*a*]pyridine derivatives in 35—87% yields. Some 4,4a-dihydropyrido[1,2-*d*][1,3,4]thiadiazine intermediates involved in these reactions could be detected by their nmr follows and three related 4a,8-dimethyl derivatives were isolated. Substituent effect and possible mechanisms are also discussed.

In our previous communication[2] we have reported abnormal syntheses of 2-alkylthio-3-acyl- and 2-alkylthio3-(acylthio)pyrazolo[1,5-*a*]pyridine derivatives by the reactions of 1-[(acylmethlthio)methyleneamino]pyridinium salts with base, and assumed that these reactions must proceed *via* the desulfurization and the rearrangement of transient pyrido[1,2-*d*][1,3,4]-thiadiazine intermediates. Recently, Schmidt[3] has descrirbed that the 1,3,4-thiadiazinyl anions generated from the deprotonation of 6*H*-thiadiazines are thermally labile and are converted smoothly to desulfurized pyrazoles and the rearranged 4-mercaptopyrazoles. Our intermediates stated above are isoelectronic with such anions and are very intriguing molecules which have an antiaromatic (or a nonaromatic) 12-pi electron system. In this paper we wish to report a new synthetic method for 2-alkylthio-3-acyl- and 3-(acylthio)pyrazolo[1,5-*a*]pyridine derivatives and our attemps to detect the intermediates involved in the synthetic reactions of these compounds.

Result and Discussion

Reactions of Pyridinium Salts with Base. Treatment of 1-[(ethoxycarbonylmethylthio)methyleneamino]pyridinium bromides **11—19**. Obtainable by the alkylations of the corresponding pyridinium *N*-ylides **1—9** with ethyl bromoacetate **10** in quantitatively yields, with excess potassium carbonate in chloroform at room temperature afforded ethyl pyrazolo-[1,5-*a*]pyridine-3-carboxylate **20—28** in 35—82% yields along with the release of sulfur. (Scheme 1) The same pyrazolopyridines **20—22** could be aslo obtained from similar reactions of pyridinium iodides **30—32** which were prepared from the *N*-ylides **7—9** and methyl iodide **29**. The reaction of unsymmetrically substituted 3-methylpyridinium salt **34** with base gave a *ca.* 2:1 mixure of the corresponding 4-methyl- **35** and 6-methylpyrazolopyridine derivative **36** in 83% yield. (Scheme 2) On the other hand, the alkaline treatment of 1-[(phenacylthio)methyleneamino]pyridinium bromides **42—62** prepared from *N*-ylides **1—6** and phenacyl bromides **37—41** did not yield the initially expected 3-aroylpyrazolo[1,5-*a*]pyridines such as **63** at all, but, instead of them, afforded 3-(aroylthio)pyrazolo[1,5-*a*]pyridine derivatives in good yields, respectively. (Scheme 3) Similarly, unsymmetrical 3-methylpyridinium bromides **85** and **86** provided the corresponding isomeric mixtures **87** and **88** (its ratio was *ca.* 9:7), and **89** and **90** (its ratio was *ca.*

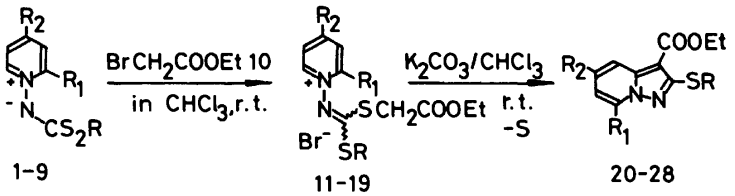

	R_1	R_2	R
1	H	H	Me
2	Me	H	Me
3	H	Me	Me
4	H	H	Et
5	Me	H	Et
6	H	Me	Et
7	H	H	CH_2COOEt
8	Me	H	CH_2COOEt
9	H	Me	CH_2COOEt

Prod.	Salt	R_1	R_2	R
20	11	H	H	Me
21	12	Me	H	Me
22	13	H	Me	Me
23	14	H	H	Et
24	15	Me	H	Et
25	16	H	Me	Et
26	17	H	H	CH_2COOEt
27	18	Me	H	CH_2COOEt
28	19	H	Me	CH_2COOEt

Scheme 1.

4:3) in 69 and 86% yields. (Scheme 4)

In order to investigate further the substituent effect in these reactions, we examined the reactions of pyridinium salts having an acetyl and a cyano group. The reactions of salts **93** and **95** synthesized from *N*-ylides **1** and **3** and bromoacetone **91** with base afforded only 3-(acetylthio)pyrazolopyridines **99** and **101**, but similar reactions of iodides **96** and **98** prepared from the same *N*-ylides and chloroacetone **92** in the presence of sodium iodide gave 3-acetyl derivatives **102** and **104** as major products together with the formation of a small amount of 3-acetylthio compound **101**. However, no 7-methylpyrazolopyridine derivatives such as **100** and **103** could be obtained from the reactions of 2-methylpyridinium bromide **94** and iodide **97**. (Scheme 5) On the other

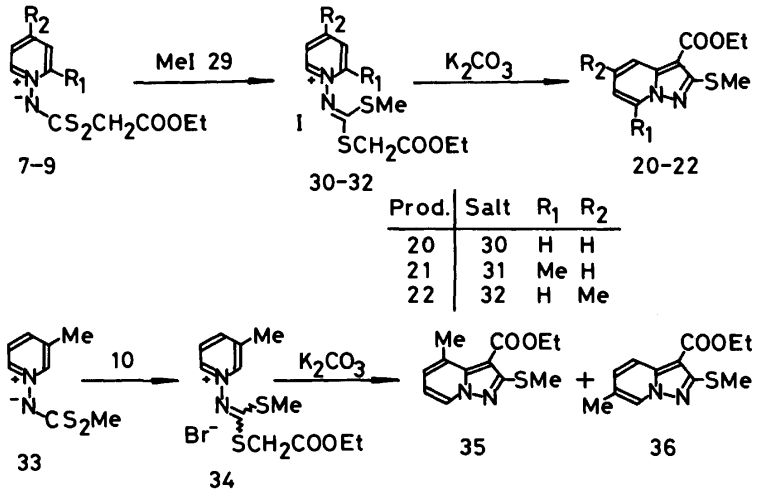

Prod.	Salt	R_1	R_2
20	30	H	H
21	31	Me	H
22	32	H	Me

Scheme 2.

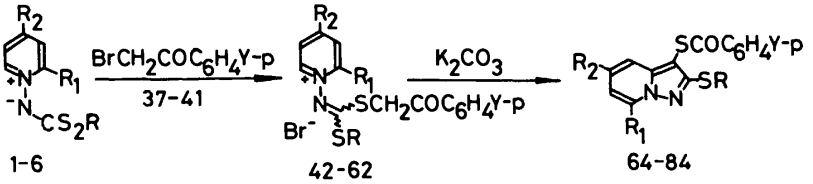

	Y
37	H
38	Cl
39	Br
40	Me
41	Ph

Prod.	Salt	R_1	R_2	R	Y
64	42	H	H	Me	H
65	43	H	H	Me	Cl
66	44	H	H	Me	Br
67	45	H	H	Me	Me
68	46	H	H	Me	Ph
69	47	Me	H	Me	H
70	48	Me	H	Me	Cl
71	49	Me	H	Me	Br
72	50	Me	H	Me	Me
73	51	Me	H	Me	Ph
74	52	H	Me	Me	H

Prod.	Salt	R_1	R_2	R	Y
75	53	H	Me	Me	Cl
76	54	H	Me	Me	Br
77	55	H	Me	Me	Me
78	56	H	Me	Me	Ph
79	57	H	H	Et	H
80	58	H	H	Et	Cl
81	59	Me	H	Et	H
82	60	Me	H	Et	Cl
83	61	H	Me	Et	H
84	62	H	Me	Et	Cl

Scheme 3.

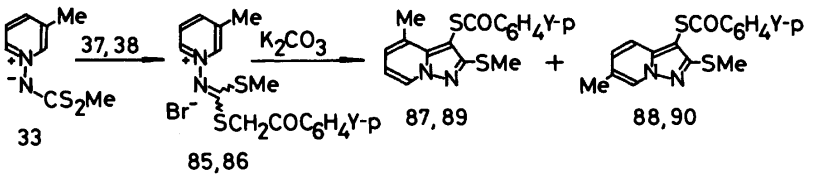

Prod.	Salt	Y
87+88	85	H
89+90	86	Cl

Scheme 4.

hand, the reactions of 1-[(cyanomethylthio)methyleneamino]pyridinium salts **107—112** with base gave only 3-cyano derivatives **113—115** in 32—55% yield but not 3-(thiocyanato)pyrazolopyridines at all. (Scheme 6)

The structures of 3-ethoxycarbonyl- **20—28**, **35**, and **36**, 3-acetyl- **102** and **104**, and 3-cyanopyrazolo[1,5-*a*]-pyridines **113—115** were decided by their physical and spectral inspections and partly by the comparisons of **20—22** with authentic samples prepared independently.[4] In particular, the chemical shifts and the signal patterns attributable to the skeletal protons in their NMR spectra (See Table 1) were quite similar to those of known pyrazolo[1,5-*a*]-pyridine-3-carboxylate[5] and 3-vinylpyrazolo[1,5-*a*]-pyridines.[6] Their microanalyses and mass spectra were in good accord with the molecular compositions involving only one sulfur atom, and the detection of the sulfur from the reaction mixtures also supported our proposed structures. On the other hand, their analyses and some mass spectra of products **64—84** and **87—90** obtained from 1-[(phenacylthio)methyleneamino]pyridinium bromides **42—62**, **85** and **86**, showed results different apparently from those of 3-aroylpyrazolo[1,5-*a*]pyridine derivatives such as **63** expected initially, that is, they suggested the molecular compositions having two sulfur atoms. In order to obtain further information about these structures, we attempted the syntheses of some 3-benzoylpyrazolopyridines and the comparisons of the resulting products with 3-aroylthio derivatives. As might be expected, 3-benzoyl-2-(methylthio)pyrazolo-[1,5-*a*]pyridines **120—122** were synthesized in very good yields by the reactions of 1-aminopyridinium iodides **116—118** with 2-benzoyl-1,1-bis(methylthio)-ethylene **119** in the presence of excess potassium carbonate in chloroform. (Scheme 7) There was little difference between both NMR spectra (See Table 1) of these 3-benzoylthio-3-(methylthio)pyrazolopyridines **64**, **69**, and **74** and 3-benzoyl compounds **120—122**, but, in their IR spectra, the large differences between their carbonyl absorptions were observed: Each band of **64**, **69**, and **74** appeared at much

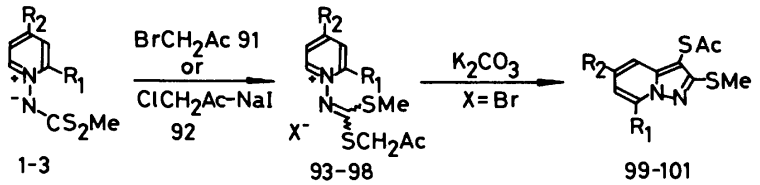

Salt	R_1	R_2	X
93	H	H	Br
94	Me	H	Br
95	H	Me	Br
96	H	H	I
97	Me	H	I
98	H	Me	I

Prod.	Salt	R_1	R_2
99	93	H	H
(100)	94	Me	H
101	95	H	Me

Prod.	Salt	R_1	R_2
102	96	H	H
(103)	97	Me	H
104	98	H	Me

Scheme 5.

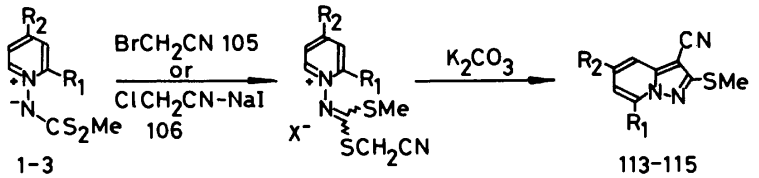

Salt	R_1	R_2	X
107	H	H	Br
108	Me	H	Br
109	H	Me	Br
110	H	H	I
111	Me	H	I
112	H	Me	I

Prod.	Salt	R_1	R_2
113	107,110	H	H
114	108,111	Me	H
115	109,112	H	Me

Scheme 6.

higher region (1665—1675 cm^{-1}) than those (1600—1610 cm^{-1}) of **120—122**, indicative of the absence of the conjugation between the benzoyl and the aromatic pyrazolopyridine ring. Further structural support for compounds **64—84**, **87—90**, **99**, and **101** was provided by their acid hydrolyses. Disulfides **123—125** could be obtained easily by heating 3-(benzoylthio)pyrazolopyridines **64**, **69**, and **74** with concentrated hydrochloric acid. (scheme 8) Compound **123** was also obtained by only heating 3-(acetylthio)pyrazolopyridine **99** with ethanol. The structures of **123—125** were assigned to be bis[2-(methylthio)pyrazolo-[1,5-*a*]pyridine-3-yl] disulfides, because their NMR spectra showed both presences of a methylthio group and a pyrazolopyridine skeleton and their Mass spectra exhibited the molecular weights bearing four sulfur atoms in each molecule.

The X-ray analysis of 3-(*p*-chlorobenzoylthio)-7-methyl-2-(methylthio)pyrazolo[1,5-*a*]pyridine **70** was carried out (See Fig. 1), and the structures of other rearranged products **64—69**, **71—84**, **87—90**, **99**, and **101** were finally concluded by the physical and spectral analogies with **70**.

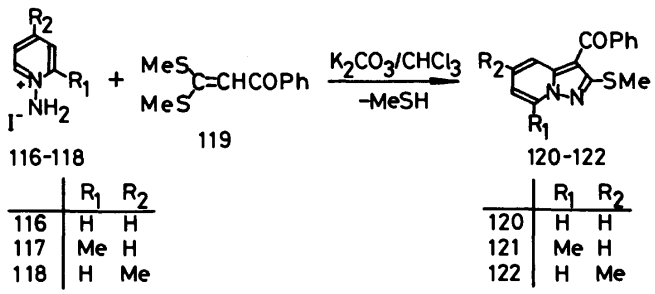

	R_1	R_2
116	H	H
117	Me	H
118	H	Me

	R_1	R_2
120	H	H
121	Me	H
122	H	Me

Scheme 7.

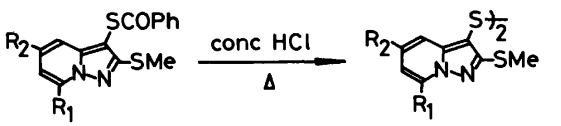

Prod.	R_1	R_2
123	H	H
124	Me	H
125	H	Me

Scheme 8.

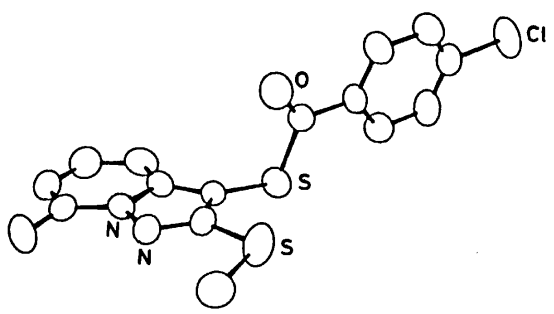

Fig. 1. ORTEP drawing of 3-(*p*-chlorobenzoylthio)-7-methyl-2-(methylthio)pyrazolo[1,5-*a*]pyridine Hydrogen atoms are not shown.

Detection and Isolation of Pyrido[1,2-d][1,3,4]thiadiazine Derivatives. On the TLC of the mixtures at the early reaction stage, we often observed certain significant spots different clearly from those of products described above. Our attempts to isolate these substances were unuccessful because of their thermal instability, but some of them could be detected by the NMR follows of the reactions of pyridinium salts with base. For example, treatment of pyridinium bromides **11—13** with DBN in deuteriochloroform in a NMR tube caused instantly the disappearance of the salts and the generations of new nonaromatic compounds **126—131**. The same products **126—131** were also observed in the reactions of pyridinium iodides **30—32** with DBN. In the NMR spectra of **126—131** (See Table 2), the signals due to all skeletal protons appeared in an olefinic region of δ 3.4—6.5 and not in an aromatic region as shown in those of pyrazolo[1,5-*a*]pyridine derivatives (Table 1). These values of **126—131** were considerably similar to those of 3,3a-dihydropyrazolo-[1,5-*a*]pyridines[7] and 1,9a-dihydropyrido[1,2-*b*][1,2,4]-triazines,[8] and this fact suggested strongly the presence of a 1,2-dihydropyridine moiety in these molecules. We next examined the syntheses of isolable pyridothiadiazines possessing a methyl group at the 4a-position, since the instability of these molecules might be caused by the susceptibility to the oxidation of the 4- and 4a-protons. The treatment of 2,6-dimethylpyridinium bromides **133—135** with DBU in chloroform gave considerably stable 4a,8-dimethyl-4,4a-dihydropyrido[1,2-*d*][1,3,4]thiadiazines **136—138** in 81, 43, and 78% yields, respectively. (Scheme 9) In contrast with the above reactions of **11—13** and **30—32**, compounds **136—138** were not *cis-trans* mixtures (See Table 2) but their configurations could not be decided because of the absence of the coupling constants between the 4- and the 4a-substituents.

Reaction Mechanisms. Possible mechanisms for these reactions are shown in Scheme 10. The reactions must be initiated by the dehydrohalogenation of pyridinium salts, and undergo the 1,6-cyclization of the resulting ionic intermediates **139** to give 4,4a-dihydropyridothiadiazines **140** as detected partly by their NMR spectrometry. The oxidation of **140** may afford antiaromatic (or nonaromatic) 12-pi pyridothiadiazines **141**, and their symmetry-allowed disrotatory cyclizations may give rise to tricyclic thiiranes **142**. The desulfurization of the reactive species **142** should provide 3-acyl- **20—28**, **35**, **36**, and **102—104** and 3-cyanopyrazolopyridines **113—115**, while the opening of the thiirane ring with the acyl migration

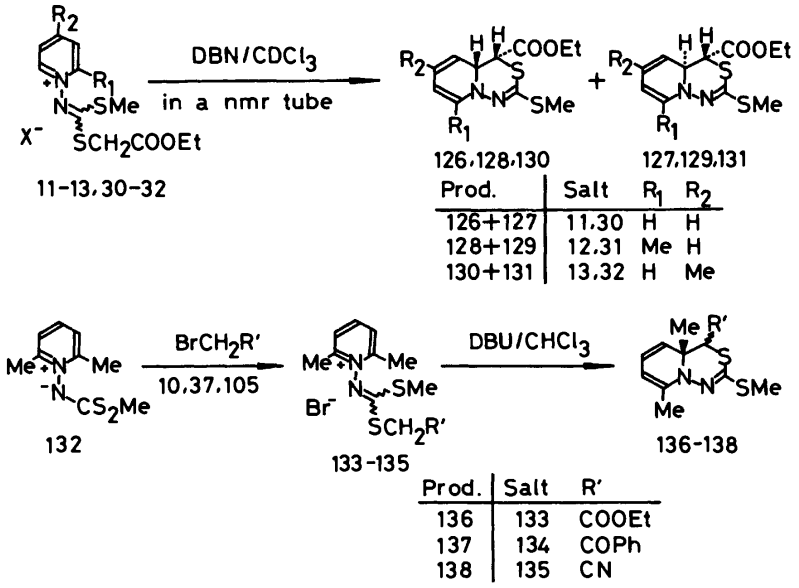

Scheme 9.

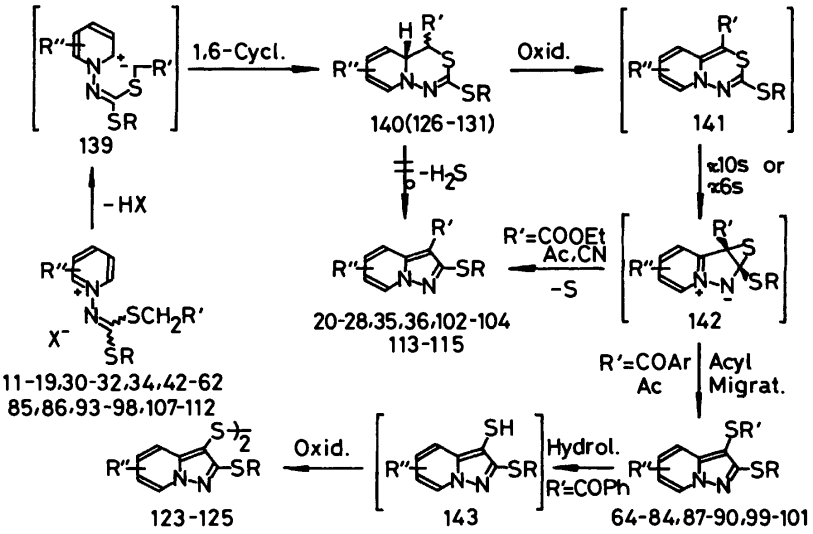

Scheme 10.

should lead to 3-(acylthio)pyrazolopyridines **64—84**, **87—90**, and **99—101**. An alternative route from dihydropyridothiadiazines **140** to 3-acyl- or 3-cyanopyrazolopyridines *via* the elimination of hydrogen sulfide is negligible, since no evolution of gaseous hydrogen sulfide could be observed. Of the reaction sequence the routes from pyridothiadiazines **141** to two types of pyrazolopyridines are the same with those described for the thiadiazinyl anion-pyrazoles transformation by Schmidt,[3] except the acyl migration in place of the proton transfer. The substituent effect which influences the desulfurization and the rearrangement in these reactions is still uncertain, but it may be related to the migrating or eliminating ability of these substituents. The formation of disulfides **123—125** can be interpreted reasonably by the acid hydrolyses of 3-(benzoylthio)pyrazolo[1,5-*a*]-pyridines **64**, **69**, and **74** followed by the air oxidation of the resulting thiols **143** to the disulfides.

Experimental

Melting points were measured with a Yanagimoto micromelting point apparatus and are uncorrected. Microanalyses were carried out on a perkin-Elmer 240 Elemental Analyzer. The NMR spectra were determined with a Varian EM360A Spectrometer in deuteriochloroform with tetramethylsilane as an internal standard. The chemical shifts are expressed in δ values. The IR spectra were taken with a Hitachi 260-10 Infrared Spectrophotometer. The Mass spectra were obtained with a JEOL JMS-01SG-2 Mass Spectrometer attached with a JEC-6 Spectrocomputer.

Preparations of Pyridinium N-Ylides. These pyridinium *N*-ylides **1—9**, **33**, and **132** were synthesized ac-

TABLE 1. NMR DATA OF PYRAZOLO[1,5-*a*]PYRIDINE DERIVATIVES

Compd[a)]	C-4	C-5	C-6	C-7	SR			R′	
20	8.05	7.37	6.84	8.45	2.65			1.43	4.41
	br d	br t	dt	d	s			t	q
21	7.93	7.29	6.68	2.73	2.67			1.43	4.39
	dd	q	br d	s	s			t	q
22	7.80	2.43	6.68	8.31	2.63			1.42	4.39
	br s	s	dd	d	s			t	q
23	8.11	7.42	6.90	8.50	1.46	3.29		1.48	4.44
	br d	br t	dt	d	t	q		t	q
24	8.01	7.35	6.77	2.77	1.47	3.33		1.51	4.45
	br d	q	br d	s	t	q		t	q
25	7.87	2.47	6.72	8.36	1.44	3.27		1.47	4.43
	br s	s	dd	d	t	q		t	q
26	8.13	7.42	6.91	8.46	4.05	1.30	4.28	1.44	4.43
	br d	br t	dt	br d	s	t	q	t	q
27	7.98	7.32	6.75	2.72	4.03	1.29	4.26	1.43	4.41
	dd	q	br d	s	s	t	q	t	q
28	7.80	2.43	6.68	8.25	3.99	1.28	4.23	1.42	4.38
	br s	s	dd	d	s	t	q	t	q
35	2.73	7.09	6.73	8.30	2.62			1.43	4.39
	s	br d	t	dd	s			t	q
36	7.93	7.09	2.37	8.25	2.63			1.43	4.39
	d	d	s	br s	s			t	q
64	b)	b)	6.76	8.47	2.67			7.0—8.3	
			dt	d	s			m	
65	b)	b)	6.78	8.46	2.68			7.0—8.2	
			dt	d	s			m	
66	7.39	7.20	6.79	8.48	2.68			7.5—8.1	
	br d	br t	dt	d	s			m	
67	b)	b)	6.75	8.45	2.67			7.0—8.1	2.43
			dt	d	s			m	s
68	b)	b)	6.77	8.46	2.68			7.0—8.3	
			dt	d	s			m	
69	b)	b)	6.63	2.77	2.69			7.0—8.3	
			br d	s	s			m	
70	b)	b)	6.67	2.78	2.69			7.0—8.3	
			br d	s	s			m	
71	b)	b)	6.63	2.77	2.68			7.0—8.1	
			br d	s	s			m	
72	b)	b)	6.63	2.77	2.69			7.0—8.1	2.44
			br d	s	s			m	s
73	b)	b)	6.63	2.77	2.70			7.0—8.4	
			br d	s	s			m	
74	7.12	2.36	6.60	8.33	2.65			7.3—8.3	
	br s	s	dd	d	s			m	
75	7.10	2.36	6.60	8.33	2.64			7.3—8.2	
	br s	s	dd	d	s			m	
76	7.11	2.38	6.62	8.34	2.67			7.4—8.1	
	br s	s	dd	d	s			m	
77	7.10	2.37	6.59	8.32	2.64			7.1—8.1	2.43
	br s	s	dd	d	s			m	s
78	7.13	2.36	6.60	8.33	2.64			7.3—8.3	
	br s	s	dd	d	s			m	
79	b)	b)	6.83	8.53	1.41	3.25		7.0—8.3	
			dt	d	t	q		m	
80	b)	b)	6.87	8.53	1.42	3.25		7.0—8.3	
			dt	d	t	q		m	

TABLE 1. Continued

Compd[a]	C-4	C-5	C-6	C-7	SR		R'
81	b)	b)	6.64 br d	2.76 s	1.42 t	3.25 q	7.0—8.3 m
82	b)	b)	6.67 br d	2.77 s	1.41 t	3.24 q	7.0—8.3 m
83	7.19 br s	2.38 s	6.67 dd	8.40 d	1.40 t	3.22 q	7.4—8.3 m
84	7.18 br s	2.41 s	6.68 dd	8.41 d	1.42 t	3.23 q	7.3—8.3 m
87	2.56 s	6.97 br d	6.69 t	8.38 dd	2.67 s		7.1—8.3 m
88	b)	6.97 d	2.34 s	8.32 br s	2.67 s		7.1—8.3 m
89	2.56 s	7.00 br d	6.70 t	8.41 br d	2.66 s		7.1—8.3 m
90	b)	7.01 d	2.34 s	8.34 br s	2.66 s		7.1—8.3 m
99	7.41 br d	7.28 br t	6.78 dt	8.47 d	2.67 s		2.43 s
101	7.12 br s	2.39 s	6.61 dd	8.32 d	2.64 s		2.42 s
102	8.18 br d	7.43 br t	6.90 dt	8.44 d	2.68 s		2.59 s
104	7.97 br s	2.47 s	6.73 dd	8.31 d	2.68 s		2.59 s
113	7.64 br d	7.45 br t	6.95 dt	8.49 d	2.72 s		—
114	7.60 br d	7.38 q	6.85 br d	2.79 s	2.77 s		—
115	7.39 br s	2.48 s	6.78 dd	8.37 d	2.71 s		—
120	b)	b)	6.83 dt	8.47 d	2.61 s		7.0—7.9 m
121	b)	b)	6.73 br	2.78 s	2.65 s		7.0—7.9 m
122	7.20 br s	2.31 s	6.68 dd	8.32 d	2.59 s		7.3—7.8 m
123	——6.5—7.0—— m			8.31 br d	2.58 s		—
124	6.6—7.0 m		6.48 br	2.68 s	2.61 s		—
125	6.53 br s	2.37 s	6.47 dd	8.21 d	2.59 s		—

a) The coupling constants are as follows: $J_{4,5}=9.0$, $J_{5,6}=J_{6,7}=J_{Et}=7.0$, $J_{4,6}=2.0$, and $J_{5,7}=1.0$ Hz. b) Overlapped with the phenyl proton signals.

cording to the procedure reported by us[6c] and by Yoshida *et al.*[9] Some data of new *N*-ylides are as follows: **3**, 87%, colorles needles, mp 126—127 °C. Found: C, 48.33; H, 5.10; N, 14.24%. Calcd for $C_8H_{10}N_2S_2$: C, 48.45; H, 5.08; N, 14.13%. **4**, 74%, colorless needles, mp 107—108 °C. Found: C, 48.61; H, 5.03; N, 14.03%. Calcd for $C_8H_{10}N_2S_2$: C, 48.45; H, 5.08; N, 14.13%. **6**, 75%, Colorless needles, mp 117—118 °C. Found: C, 50.93; H, 5.63; N, 13.24%. Calcd for $C_9H_{12}N_2S_2$: C 50.91; H 5.70; N, 13.19%. **7**, 47%, pale yellow needles, mp 94—95 ° C. Found: C, 46.62; H, 4.63; N, 10.85%. Calcd for $C_{10}H_{12}N_2O_2S_2$: C, 46.85; H,4.72; N, 10.93%. **8**, 82%, pale yellow needles, mp 105—107 °C. Found: C, 48.96; H, 5.09; N,10.40%. Calcd for $C_{11}H_{14}N_2O_2S_2$: C, 48.87; H, 5.22: N, 10.36%. **9**, 97%, pale yellow needles, mp 127—128 °C. Found: C, 48.58; H, 5.13: N, 10.17%. Calcd for $C_{11}H_{14}N_2O_2S_2$: C, 48.87; H 5.22; N, 10.36%. **33**, 84%, colorless needles, mp 117—118 °C. Found: C, 48.23; H, 5.08; N, 14.19%. Calcd for $C_8H_{10}N_2S_2$: C, 48.45; H, 5.08; N, 14.13%.

Preparations of Pyrazolo[1,5-a]pyridine Derivatives. *General Method A*: A chloroform solution (20 ml) of pyridinium *N*-ylide (2 mmol) was allowed to react overnight with a small excess of an alkylating agent (2.4 mmol) at room temperature. The resulting solution was then concentrated at reduced pressure and the residue was washed three times with ether to remove the remaining alkylating agent. The

almost pure pyridinium salt was dissolved again in chloroform (30 ml) and treated with potassium carbonate (5 g) at room temperature until the salt was completely consumed. (about 1 or 2 d) The reaction mixture was filtered to remove insoluble inorganic substances and the filtrate was concentrated at reduced pressure. The residue was separated by column chromatography on alumina using hexane, ether, and chloroform as eluents. Evaporation of the chloroform layer and recrystallzation of the resulting crude product from ethanol afforded pure pyrazolopyridine derivative.

B: Pyridinium iodides **96—98** and **110—112** were prepared by the reactions of pyridinium *N*-ylides **1—3** (4 mmol) with a large excess of chloride **92** or **106** (5 g) in the presence of sodium iodide (5 g) in acetone (60 ml) at room temperature for 2 d. After the evaporation of acetone and the removal of excess chloride by repeated washings with ether, the resulting salts were dissolved in chloroform (60 ml) and allowed to react with potassium carbonate (10 g) at room temperature for 3 d. Similar work-ups of the reaction mixtures provided the corresponding pyrazolopyridine derivatives.

In the reactions of pyridinium salts **11—19**, **30—32**, and **34** with base the elimination of sulfur was observed, though its quantity could not be decided because of the heterogeneous reactions. On the other hand, no evolution of hydrogen sulfide from these reaction systems could be detected. Compound **99** was converted easily to disulfide **120** by the recrystallization from ethanol. The Mass spectra of **20—22**, **26—28**, **64—68**, and **113—115** gave satisfactory values 236, 250, 250, 308, 322, 322, 300, 336, 380, 314, 376, 189, 203, and 203, for each molecular ion, respectively. These results and some properties are listed in Tables 1 and 3.

Preparations of 3-Benzoylpyrazolo[1,5-a]pyridines 120—122. General Method: A mixture of 1-aminopyridinium iodide (2 mmol) and 2-benzoyl-1,1-bis(methylthio)ethylene **119** (2 mmol) was stirred with potassium carbonate (5 g) in chloroform (30 ml) at room temperature for 2 d. The reaction mixture was then filtered to remove inorganic substances and the filtrate was concentrated at reduced pressure. The residue was separated by column chromatography (alumina) using hexane, ether, and chloroform as eluents. After the evaporation of the solvent, recrystallization of the residue from ethanol afforded 3-benzoyl-2-(methylthio)-pyrazolo[1,5-*a*]pyridine derivative. Some data except their NMR spectra (see Table 1) of these products are as follows: **120**, 93%, colorless needles, mp 104—105 °C, ν (KBr) 1605 cm^{-1} (CO). Found: C, 67.22; H, 4.48; N, 10.43%. Calcd for $C_{15}H_{12}N_2OS$: C, 67.14; H, 4.51; N, 10.44%. **121**, 91%, colorless needles, mp 126—128 °C, ν (KBr) 1605 cm^{-1} (CO). Found: C, 68.01: H, 4.90; N, 10.09%. Calcd for $C_{16}H_{14}N_2OS$: C, 68.06; H, 5.00 N, 10.09%. **122**, 93%, colorless needles, mp 161—162 °C, ν (KBr) 1601 cm^{-1} (CO). Found: C, 67.98; H, 4.98; N, 9.85%. Calcd for $C_{16}H_{14}N_2OS$: C, 68.06; H, 5.00; N,9.92%.

Acid Hydrolyses of 3-(Benzoylthio)pyrazolo[1,5-a]pyridines 64, 69, and 74. General Method: A mixture of 3-benzoylthio derivative (1 mmol) and a concentrated hydrochloric acid (10 ml) was heated at 60—80 °C in a water bath for 30 min. After cooling to room temperature, the reaction mixture was neutralized carefully with an aqueous potassium carbonate and then extracted twice with 100 ml portion of chloroform. The combined extracts were filtered through phase-separating filter paper and the resulting solution was then concentrated at reduced pressure. The residue was separated by column chromatography on alumina using hexane and ether as eluents. The evaporation of the ether layer and recrystallization of the crude crystals from a mixture of ether—hexane gave the disulfide.

These disulfides **123—125** were also formed by refluxing

Table 2. NMR data of 4,4a-dihydropyrido[1,2-*d*][1,3,4]thiadiazines

Compd[a,b]	SMe	C-4	C-4a	C-5	C-6	C-7	C-8	R′	
126 or **127** (Major)	2.45 s	c)	c)	5.15 br d	5.80 m	4.56 br t	6.48 d	1.25 t	4.22 q
127 or **126** (Minor)	2.41 s	c)	c)	a)	5.80 m	4.64 br t	6.48 d	1.33 t	4.25 q
128 or **129** (Major)	2.50 s	c)	c)	5.16 br d	5.90 m	4.51 br d	2.01 s	1.25 t	4.23 q
129 or **128** (Minor)	2.48 s	c)	c)	c)	5.90 m	4.62 br d	2.01 s	1.33 t	4.28 q
130 or **131** (Major)	2.48 s	c)	c)	4.94 br s	1.70 s	4.46 dd	6.51 d	1.24 t	4.22 q
131 or **130** (Minor)	2.46 s	c)	c)	c)	1.70 s	4.56 dd	6.47 d	1.32 t	4.28 q
136	2.47 s	3.48 s	1.39 s	5.00 d	5.81 q	4.58 br d	2.02 s	1.20 t	4.15 q
137	2.43 s	4.58 s	1.57 s	4.87 d	5.70 q	4.60 br d	2.08 s	7.1—8.2 m	
138	2.49 s	3.44 s	1.41 s	5.10 d	6.02 q	4.78 br d	2.07 s	—	

a) $J_{6,7}=J_{7,8}=7.0$, $J_{5,6}=9.0$, $J_{5,7}=1.5$, $J_{Et}=7.0$ Hz. b) The ratios of major and minor isomers could not be decided because of the absence of the signals separated clearly. c) These signals could not be assigned by their overlapping with those of DBN(and its salt) and the ethoxycarbonyl group.

TABLE 3. RESULTS AND SOME PROPERTIES OF PYRAZOLO[1,5-*a*]PYRIDINES

Compd No.	Reactants: Ylide	Reactants: Halide	Reactants: (Salt)	Yield %	Mp θ_m/°C	$\nu_{C=O}^{KBr}$(CN)/cm^{-1}	Formula	Calcd (%): C	Calcd (%): H	Calcd (%): N	Found (%): C	Found (%): H	Found (%): N
20	**1**	**10**	(**11**)	75	102—103	1671	$C_{11}H_{12}N_2O_2S$	55.91	5.12	11.86	56.04	5.13	11.73
	1	**29**	(**30**)	83	102—103								
21	**2**	**10**	(**12**)	82	120—122	1666	$C_{12}H_{14}N_2O_2S$	57.58	5.64	11.19	57.71	5.67	11.03
	2	**29**	(**31**)	89	120—122								
22	**3**	**10**	(**13**)	79	139—140	1675	$C_{12}H_{14}N_2O_2S$	57.58	5.64	11.19	57.36	5.68	11.18
	3	**29**	(**32**)	87	139—140								
23	**4**	**10**	(**14**)	82	71—73	1690	$C_{12}H_{14}N_2O_2S$	57.58	5.64	11.19	57.41	5.64	11.14
24	**5**	**10**	(**15**)	76	64—66	1689	$C_{13}H_{16}N_2O_2S$	59.07	6.10	10.60	59.16	6.13	10.60
25	**6**	**10**	(**16**)	80	83—85	1682	$C_{13}H_{16}N_2O_2S$	59.07	6.10	10.60	58.90	6.09	10.53
26	**7**	**10**	(**17**)	72	90—91	1719 1691	$C_{14}H_{16}N_2O_4S$	54.53	5.23	9.08	54.59	5.29	8.97
27	**8**	**10**	(**18**)	48	125—126	1720 1680	$C_{15}H_{18}N_2O_4S$	55.89	5.63	8.69	55.92	5.56	8.72
28	**9**	**10**	(**19**)	35	110—111	1728 1672	$C_{15}H_{18}N_2O_4S$	55.89	5.63	8.69	55.99	5.57	8.64
35+**36**[a]	**33**	**10**	(**34**)	83	d)	1706	$C_{12}H_{14}N_2O_2S$	57.58	5.64	11.19	57.54	5.74	11.13
64	**1**	**37**	(**42**)	77	136—138	1668	$C_{15}H_{12}N_2OS_2$	59.97	4.03	9.33	60.10	4.10	9.44
65	**1**	**38**	(**43**)	87	158—160	1672	$C_{15}H_{11}N_2OS_2Cl$	53.81	3.31	8.37	53.66	3.34	8.65
66	**1**	**39**	(**44**)	80	177—179	1668	$C_{15}H_{11}N_2OS_2Br$	47.50	2.92	7.39	47.39	2.92	7.48
67	**1**	**40**	(**45**)	83	125—126	1670	$C_{16}H_{14}N_2OS_2$	61.12	4.49	8.91	60.89	4.50	9.22
68	**1**	**41**	(**46**)	73	138—141	1675	$C_{21}H_{16}N_2OS_2$	66.99	4.28	7.44	67.27	4.31	7.14
69	**2**	**37**	(**47**)	72	94—95	1667	$C_{16}H_{14}N_2OS_2$	61.12	4.49	8.91	61.00	4.41	8.82
70	**2**	**38**	(**48**)	64	136—138	1671	$C_{16}H_{13}N_2OS_2Cl$	55.08	3.76	8.03	54.91	3.72	7.95
71	**2**	**39**	(**49**)	69	154—156	1669	$C_{16}H_{13}N_2OS_2Br$	48.86	3.33	7.12	48.72	3.32	7.12
72	**2**	**40**	(**50**)	86	109—110	1663	$C_{17}H_{16}N_2OS_2$	62.17	4.91	8.53	61.94	4.93	8.45
73	**2**	**41**	(**51**)	66	148—149	1670	$C_{22}H_{18}N_2OS_2$	67.66	4.65	7.12	67.84	4.59	7.05
74	**3**	**37**	(**52**)	68	126—128	1672	$C_{16}H_{14}N_2OS_2$	61.12	4.49	8.91	61.17	4.53	9.19
75	**3**	**38**	(**53**)	66	162—164	1673	$C_{16}H_{13}N_2OS_2Cl$	55.08	3.76	8.03	54.93	3.73	7.98
76	**3**	**39**	(**54**)	79	167—170	1671	$C_{16}H_{13}N_2OS_2Br$	48.86	3.33	7.12	48.74	3.43	7.15
77	**3**	**40**	(**55**)	87	157—159	1669	$C_{17}H_{16}N_2OS_2$	62.17	4.91	8.53	61.90	5.00	8.81
78	**3**	**41**	(**56**)	58	196—197	1672	$C_{22}H_{18}N_2OS_2$	67.66	4.65	7.12	67.81	4.70	7.27
79	**4**	**37**	(**57**)	83	95—96	1673	$C_{16}H_{14}N_2OS_2$	61.12	4.49	8.91	61.30	4.56	8.85
80	**4**	**38**	(**58**)	81	117—120	1676	$C_{16}H_{13}N_2OS_2Cl$	55.08	3.76	8.03	55.24	3.87	7.76
81	**5**	**37**	(**59**)	66	115—116	1684	$C_{17}H_{16}N_2OS_2$	62.17	4.91	8.53	61.93	4.94	8.40
82	**5**	**38**	(**60**)	69	93—95	1671	$C_{17}H_{15}N_2OS_2Cl$	56.27	4.17	7.72	56.13	4.17	7.52
83	**6**	**37**	(**61**)	83	107—109	1676	$C_{17}H_{16}N_2OS_2$	62.17	4.91	8.53	62.16	4.99	8.45
84	**6**	**38**	(**62**)	83	119—121	1677	$C_{17}H_{15}N_2OS_2Cl$	56.27	4.17	7.72	56.14	4.12	7.51

87+**88**[c]	**33**	**37**	(**85**)	69	b)	1675	$C_{16}H_{14}N_2OS_2$	61.12	4.49	8.91	60.94	4.51	8.97
89+**90**[d]	**33**	**38**	(**86**)	86	b)	1670	$C_{16}H_{13}N_2OS_2Cl$	55.08	3.76	8.03	54.99	3.74	8.26
99[e]	**1**	**91**	(**93**)	62	92—94	1698	$C_{10}H_{10}N_2OS_2$	50.40	4.23	11.75	50.38	4.30	11.70
100	**2**	**91**	(**94**)	0									
101	**3**	**91**	(**95**)	76	104—105	1703	$C_{11}H_{12}N_2OS_2$	52.35	4.79	11.10	52.26	5.02	10.96
102	**1**	**92**	(**96**)	12	131—132	1639	$C_{10}H_{10}N_2OS$	58.23	4.89	13.58	58.53	4.57	13.60
103	**2**	**92**	(**97**)	0									
101+**104**[f]	**3**	**92**	(**98**)	*ca.* 25	124—126[g]	1640[g]	$C_{11}H_{12}N_2OS^{g)}$	59.97	5.49	12.72	60.13	5.56	12.49
113	**1**	**105**	(**107**)	32	136—137	(2218)	$C_9H_7N_3S$	57.12	3.73	22.21	57.05	3.63	22.38
	1	**106**	(**110**)	55	136—137								
114	**2**	**105**	(**108**)	38	128—129	(2215)	$C_{10}H_9N_3S$	59.09	4.46	20.67	58.93	4.36	20.93
	2	**106**	(**111**)	43	128—129								
115	**3**	**105**	(**109**)	47	134—135	(2200)	$C_{10}H_9N_3S$	59.09	4.46	20.67	58.98	4.38	20.87
	3	**106**	(**112**)	49	134—135								

a) The ratio of **35** to **36** was *ca.* 2 : 1. b) Mixture. c) The ratio of **87** to **88** was *ca.* 9 : 7. d) The ratio of **89** to **90** was *ca.* 4 : 3. e) This compound was recrystallized from chloroform–hexane at low temperature. f) The ratio of **101** to **104** was *ca.* 1 : 5. g) These physical data were those of pure 3-acetylpyrazolo[1,5-*a*]-pyridine **104**.

3-(benzoylthio)pyrazolopyridines **64**, **69**,and **74** in ethanol in the presence of an amine such as piperidine or DBU, but the reaction rate was generally slow and the separation of the disulfide from the unreacted starting material was difficult. Some data of **123**—**125** are as follows: **123**, 38%, pale yellow needles, mp 176—178 °C, ν (KBr) 757, 1362, and 1630 cm^{-1}. Found: C, 49.64; H,3.61; N, 14.31%; M$^+$, 390. Calcd for $C_{16}H_{14}N_4S_4$: C, 49.90; H, 3.61; N, 14.35%. **124**, 31%, pale yellow needles, mp 146—148 °C, ν (KBr) 771, 1342, and 1625 cm^{-1}. Found: C, 51.56; H, 4.21; N, 13.46%; M$^+$, 418. Calcd for $C_{18}H_{18}N_4S_4$: C, 51.64; H, 4.33; N, 13.38%. **125**, 45%, pale yellow needles, mp 177—178 °C, ν (KBr) 783, 1356, and 1639 cm^{-1}, Found: C, 51.82; H, 4.39; N, 13.14%; M$^+$, 418. Calcd for $C_{18}H_{18}N_4S_4$: C, 51.64; H, 4.33; N, 13.38%.

X-Ray Crystallography. The crystal of 3-(*p*-chlorobenzoylthio)-7-methyl-2-(methylthio)pyrazolo[1,5-*a*]pyridine **70** was grown from ethanol. A suitable crystal was mounted on a Rigaku AFC-6B diffractometer and the intensity data of $|F_o|>3\sigma|F_o|$ were colleted using Mo($K\alpha$) radiation of 0.71070 Å wave length within the range of $2\theta<55°$. Total reflections usd for the analysis were 1617. The structure was solved by the MULTAN method and the final R values was 9.1%.

The crystal data are as follows (see Fig. 2 for the bond lengths and the bond angles of this molecule): **70**, $C_{16}H_{13}N_2OS_2Cl$, F.W.=348.9, monoclinic, space group $P2_1/C$, a=16.816(6) Å, b=6.331(1) Å, c=17.026(5) Å, β=116.21(2)°, z=4, Dc=1.42 g/cm^3.

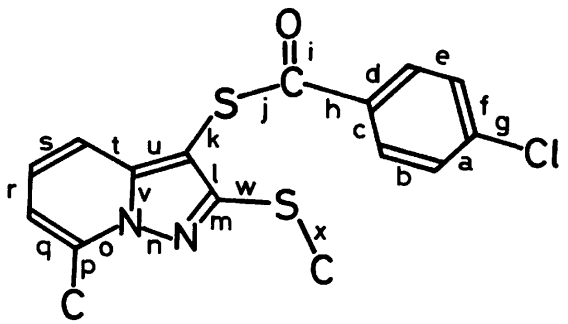

Fig. 2.

Bond lengths (Å): a=1.364(20), b=1.410(21), c=1.381(15), d=1.410(20), e=1.421(22), f=1.365(19), g=1.750(23), h=1.482(20), i=1.205(13), j=1.784(19), k=1.741(17), l=1.369(16), m=1.337(19), n=1.374(13), o=1.373(21), p=1.489(16), q=1.360(17), r=1.424(17), s=1.384(23), t=1.412(17), u=1.414(19), v=1.385(13). w=1.747(13), x=1.824(14).

Bond angles (°): ab=117.7(13), af=124.0(10), ag=117.8(12), bc=120.2(10), cd=121.3(10), ch=122.8(9), de=117.6(14), dh=115.9(13), ef=19.2(11), fg=118.2(9), hi=124.0(9), hj=114.0(11), ij=122.0(8), jk=102.9(10), kl=129.2(8), ku=124.0(10), lm=113.7(9), lu=106.1(10), lw=124.7(10), mn=103.3(9), mw=121.6(10), no=123.5(8), nv=113.0(11), op=118.0(11), oq=116.3(9), ov=123.4(11), pq=125.7(11), qr=123.2(12), rs=119.5(13) st=117.5(10), tu=136.0(9), tv=120.1(11), uv=103.9(12), wx=101.9(11).

Detections of 4,4a-Dihydropyrido[1,2-d][1,3,4]thiadiazines ***126—131.*** *General Method*: A deuteriochloroform solution (0.5 ml) of pyridinium halide (0.1 mmol) which was placed in a NMR tube was treated with two drops of DBN (about 40 mg, 0.26 mmol). The NMR spec-

trum of resulting solution which was turned instantly red was measured. However, our attempts to isolate these intermediates **126—131** from the reaction mixtures were unsuccessful because their column separations did not afford them at all but gave always only ethyl 2-(methylthio)pyrazolo[1,5-*a*]pyridine-3-carboxylates **20—22**. In addition, compounds **126—131** were completely decomposed by heating them at **50—60** °C for only a few minutes. The NMR spectral data of **126—131** are shown in Table 2.

Isolations of 4a,8-Dimethyl-4,4a-dihydropyrido[1,2-d][1,3,4]-thiadiazines 136—138. General Method: 2,6-Dimethylpyrildinium *N*-ylide **132** (424 mg, 2 mmol) was treated with bromide (3 mmol) in chloroform (20 ml) at room temperature for 1 d. The reaction mixture was then concentrated at reduced pressure and the residue was washed three times with ether to remove excess alkylating agent. The pyridinium salt was again dissolved in chloroform (15 ml) and the resulting solution was cooled to 0 °C in an ice bath. DBU (453 mg,3 mmol) was added dropwise into the solution under stirring at 0 °C and the reddish solution was immediately separated by column chromatography (two times) on alumina using chloroform as an eluent. The removal of chloroform at reduced pressure at below 40 °C afforded oils of **136—138**. However, the preparations of pure samples for the analyses were unsuccessful because of their thermal instability and the failure to their crystallization. These compounds **136—138** could be stored for about a week in the freezer but decomposed completely at room temperature for about 1 d. Some data except their NMR spectra (see Table 2) are as follow: **136**, 81%, orange oil, ν (Neat) 1738 (CO), 1630, 1368, 1150, 711 cm^{-1}. **137**, 43%, yellow oil, ν (Neat) 1681 (CO), 1491, 1370, 1210, 981 cm^{-1}. **138**, 78%, Orenge oil, ν (Neat) 2245 (CN),1648,1586,1370,1138,715 cm^{-1}.

The authors wish to thank Dr. Yoshinori Tominaga (Nagasaki University) for the offer of authentic samples of pyrazolo[1,5-*a*]pyridines and Mr. Toshihiko Hori (Rigaku Denki Co. Ltd) for the X-ray analysis of 3-(*p*-chlorobenzoylthio)pyrazolo-[1,5-*a*]pyridine.

Refernces

1) For part 10 of this series, see A. Kakehi, S. Ito, S. Yonezu, K. Maruta, and K. Yuito, *Heterocycles*, **23**, 33 (1985).

2) A Kakehi, S. Ito, M. Ito, T. Yotsuya, *Heterocycles*, **22**, 2237 (1984).

3) R. Schmidt, *Angew. Chem. Internat. Edd.*, **14**, 581 (1975).

4) These Pyrazolopyridines **20—22** were synthesized by the reactions of 1-aminopyridinium iodides **116—118** with 1-[1-ethoxycarbonyl-2,2-bis(methylthio)vinyl]pyridinium iodide in the presence of base. Our private communication from Dr. Y. Tominaga, Nagasaki University.

5) a) V. Boekelheide and N. A. Fedoruk, *J. Org. Chem.*, **33**, 2062 (1968); b) Y. Tamura, A. Yamakami, and M. Ikeda, *Yakugaku Zasshi*, **91**, 1154 (1971).

6) a) A. Kakehi, S. Ito, K. Uchiyama, and K. Kondo, *J. Org. Chem.*, **43**, 2896 (1978); b) A. Kakehi, S. Ito, K. Watanabe, T. Ono, and T. Miyajima, *J. Chem. Res. (S)*, **1980**, 18, *(M)*, **1981**,401—425 (1980); c) A. Kakehi, S. Ito, and K. Watanabe, *Bull. Chem. Soc. Jpn.*, **53**, 1775 (1980).

7) T. Sasaki, K. Kanematsu, and A. Kakehi, *J. Org. Chem.*, **37**, 3106 (1972).

8) a) A. Kakehi and S. Ito, *J. Org. Chem.*, **39**, 1542 (1974); b) A. Kakehi, S. Ito, T. Manabe, H. Amano, and Y. Shimaoka, *ibid.*, **41**, 2739 (1976); c) A. Kakehi, S. Ito, T. Manabe, T. Maeda, and K. Imai, *ibid*, **42**, 2514 (1977).

9) H. Yoshida, K. Urushibata, and T. Ogata, *Bull. Chem. Soc, Jpn.*, **56**, 1561 (1983).

Preparation and Some Reactions of Diarylgermylenedialkali Metals

Kunio MOCHIDA,* Naoki MATSUSHIGE, and Mari HAMASHIMA
Department of Chemistry, Faculty of Sciences, Gakushuin University, 1-5-1 Mejiro, Toshima-ku, Tokyo 171
(Received November 7, 1984)

The reactions of diarylgermanes with alkali metals in HMPA/THF or THF were found to give the corresponding diarylgermylenedialkali metals in high yields. Diphenylgermylenedipotassium reacted with aryl halides or carbonyl compounds to give reduction products predominantly. With alkyl halides, diphenylgermylenedipotassium gave mainly substitution products.

The reactions of organogermylalkali metals with organic halides or carbonyl compounds are useful for the formation of carbon-germanium bonds.[1-10] Because of its importance, the study of organogermylalkali metals has been reviewed.[1] Among them, however, there are only a few reports regarding organogermylenedialkali metals (probably due to the lack of a useful preparative method). For example, Krause and Carney examined the reaction of germane (GeH_4) with sodium in liquid ammonia but only suggested the probable existence of germylenedisodium (GeH_2Na_2).[11] Cross and Glockling found the reaction of tetrabenzylgermane with lithium in ethylene glycol dimethyl ether or butyllithium to yield dibenzylgermylenedilithium in 7.8% or 2% yields, respectively.[12] Recently, Bulten and Noltes have reported briefly on the reaction of dibutyldichlorogermane with potassium in HMPA to give dibutylgermylenedipotassium in 22% yield.[13] Yields of organogermylenedialkali metals reported are low and the reactions of organogermylenedialkali metals with organic substrates remain to be disclosed.

In this paper, we present the preparation of diarylgermylenedialkali metals from diarylgermanes and alkali metals in HMPA/THF or THF in high yields and then the reactions of diphenylgermylenedipotassium with organic halides and carbonyl compounds.

Results and Discussion

Preparation of Diarylgermylenedialkali Metals. Diarylgermylenedialkali metals (Ar_2GeM_2, **1**, Ar= C_6H_5, p-$CH_3C_6H_4$, M=Li, Na, K) were prepared from the corresponding diarylgermanes (Ar_2GeH_2) and alkali metals in HMPA/THF or THF. The color of **1** was reddish brown (λ_{max} 320 nm in case of diphenylgermylenedipotassium).

I, thus prepared, was characterized by the following experiments: (1) ^1H and ^{13}C NMR of **1**, and (2) the formation of diarylgermanes-d_2 by hydrolysis of **1** with D_2O.

$$Ar_2GeH_2 + 4M \xrightarrow[\text{or THF}]{\text{HMPA/THF}} Ar_2GeM_2 + 2MH \quad (1)$$
$$Ar = C_6H_5,\ p\text{-}CH_3C_6H_4,\ M = Li,\ Na,\ K$$

$$Ar_2GeM_2 \xrightarrow{D_2O} Ar_2GeD_2 \quad (2)$$

(1) ^1H and ^{13}C NMR parameters of diphenylgermylenedipotassium (Ph_2GeK_2, **1a**) and di (p-tolyl)germylenedipotassium ((p-$CH_3C_6H_4)_2GeK_2$, **1b**) are summarized in Table 1, together with those of the starting materials. The chemical shifts of aromatic protons in **1a** and **1b** in comparison with those of the corresponding diarylgermanes are shifted slightly to a higher field, while those of C-1 carbon drastically to a lower field. The observed shifts may be due to the unusual charge distribution; $Ar_2Ge^{\delta-}K_2^{\delta+}$ in comparison with $Ar_2Ge^{\delta+}H_2^{\delta-}$. Thus, negative charge on the aromatic ring may produce an upfield shift of aromatic protons and downfield shift of C-1 carbon. Such phenomena for NMR spectra of organometallic compounds have been reported.[14-18]

(2) It is well known that organogermanium hydrides are formed quantitatively by hydrolysis of

Table 1. ^1H and ^{13}C NMR data of diarylgermylenedipotassium and diarylgermanes in THF-d_8

Compound	^1H NMR			^{13}C NMR				
	Ge-Ph	Ge-H	Me	C-1	C-2	C-3	C-4	Me
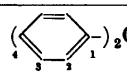 -)$_2$GeK$_2$	6.48—7.79 (*m*)			164.0	138.3	127.6	124.3	
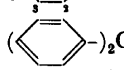 -)$_2$GeH$_2$	7.15—7.64 (m, 5H)	4.99 (s, 1H)		135.7	137.7	130.2	130.9	
(Me- 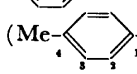 -)$_2$GeK$_2$	6.51—7.48 (dd, 4H)		2.11 (s, 3H)	160.0	138.7	128.8	133.0	22.7
(Me- 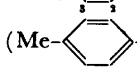 -)$_2$GeH$_2$	6.99—7.50 (dd, 4H)	4.91 (s, 1H)	2.25 (s, 3H)	140.7	137.0	131.0	132.4	22.6

organogermylalkali metals.[1] Therefore, the formation and yield of organogermanium hydrides after hydrolysis can be regarded as those of organogermylalkali metals. The yields of **1** were estimated to be 83—96% on the basis of those of diarylgermanes-d_2 formed by hydrolysis of **1** with D_2O.

Reactions of Diphenylgermylenedipotassium, 1a. Reactions of **1a** with organic halides and carbonyl compounds were examined at room temperature for 30 min. Hydrolysis of the reaction mixtures led to reduction products, substitution products, digermanes, and polymers containing germanium. Products were isolated by preparative GLC and TLC, and identified by comparing their IR, NMR, and retention times on GLC with those authentic samples.

Reactions of **1a** with halotoluenes (halogen=Br, Cl, and F) were examined. Reactions of **1a** with bromotoluene gave toluene in 127.7% yield. Digermanes and polymers were also formed. However, no substitution products, diphenylditolylgermane or diphenyltolylgermane, were detected. Reaction of **1a** with chlorotoluene gave toluene in 3.6% yield. No tolylgermanes were formed. Diphenylgermane obtained by hydrolysis of **1a** was recovered in 45.9% yield, and digermanes and polymers were observed. With fluorotoluene, **1a** gave neither toluene nor tolylgermanes. Diphenylgermane was found in 47.1% yield. Digermanes and polymers were formed. The yield of toluene in the reactions of **1a** with halotoluenes increased in the order Br>Cl>F.

In contrast, reactions of **1a** with alkyl halides or benzyl chloride gave predominantly substitution products. Reduction products were also formed as minor products. Reactions of **1a** with alkyl bromides or iodides gave predominantly dialkyldiphenylgermanes. Alkyldiphenylgermanes were minor products. Similarly, dibenzyldiphenylgermane was formed in the reaction of **1a** with benzyl chloride mainly. On the other hand, **1a** reacted with alkyl chlorides to give alkyldiphenylgermanes predominantly. However, **1a** reacted with *t*-butyl chloride to give no *t*-butylgermanes. No diphenylgermane was recovered. Digermanes and polymers were formed. Furthermore, **1a** reacted with 1,4-dibromobutane or 1,5-dibromopentane to give 1,1-diphenylgermacyclopentane or 1,1-diphenylgermacyclohexane, respectively. These results are summarized in Table 2. In a separate experiment, reactions of KH which can be produced in the preparation of **1a** from diphenylgermane and potassium with organic halides were also examined under similar conditions. KH reacted with bromotoluene to give toluene in 10—15% yield. With chlorotoluene, benzyl chloride, or alkyl halides, no reduction products were formed.

With carbonyl compounds, **1a** gave reduction products and aldol condensation products as the main products. Unidentified substitution products were also formed as minor products. Digermanes and polymers were again observed. In a separate experiment, KH was found to react with carbonyl compounds to give aldol condensation products under similar conditions, but no reduction products. There-

Table 2. Reactions of diphenylgermylenedipotassium with organic halides[a]

Reactant (mmol)		Products,[c] Yield/%			
Ph_2GeK_2[b]	RX	R-H	$Ph_2Ge(H)R$	Ph_2GeR_2	Ph_2GeH_2
0.535	Me- -F (7.35)	0	0	0	47.1
0.535	Me- -Cl (7.41)	3.6	0	0	45.9
0.535	Me- -Br (7.39)	127.7	0	0	0
0.534	EtCl (excess)	d)	60.1	33.3	0
0.534	EtBr (7.40)	d)	24.9	65.4	0
0.534	EtI (2.70)	d)	32.7	51.5	0
0.507	*i*-PrCl (6.30)	d)	82.8	0	0
0.534	*n*-BuBr (7.50)	d)	25.6	58.1	0
0.712	*t*-BuCl (8.20)	d)	0	0	0
0.507	n-$C_6H_{17}Br$ (6.30)	8.4	38.0	61.4	0
0.813	-CH_2Cl (4.88)	2.4	0	60.3	0
0.709	$Br(CH_2)_4Br$ (7.64)	0	0	$GePh_2$ 23.6	0
0.709	$Br(CH_2)_5Br$ (7.47)	0	0	$GePh_2$ 13.5	0

a) The reactions were carried out at room temperature for 30 min. The yields of products were based on the concentrations of consumed Ph_2GeK_2. b) The concentration of Ph_2GeK_2 was determined by that of Ph_2GeD_2 by hydrolysis with D_2O. c) Digermanes and polymers contained germanium were also formed. d) The yields of products could not be determined by GLC.

TABLE 3. REACTIONS OF DIPHENYLGERMYLENEDIPOTASSIUM AND KH WITH CARBONYL COMPOUNDS[a]

Reactants (mmol)	Products (Yield/%)[b]
Ph_2GeK_2 (0.527)[c], $(CH_3)_2CO$ (2.11)	$(CH_3)_2CHOH$ (trace), 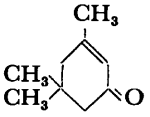 (76.0)
KH (24.9), $(CH_3)_2CO$ (86.1)	$(CH_3)_2CHOH$ (0) 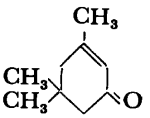 (41.0)
Ph_2GeK_2 (0.527), $PhCOCH_3$ (2.11)	$PhCH(OH)CH_3$ (54.0), $PhCOCH_2PhCHCH_3$ (57.0)
KH (49.9), $PhCOCH_3$ (200.0)	$PhCH(OH)CH_3$ (0) $PhCOCH_2PhCHCH_3$ (2.1)
Ph_2GeK_2 (0.527), Ph_2CO (2.11)	Ph_2CHOH (30.5)
KH (49.9), Ph_2CO (86.1)	No products
Ph_2GeK_2 (0.527), =O (2.11)	-OH (12.8) 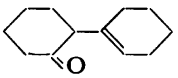 (32.0)
KH (27.4), =O (50.9)	-OH (0) 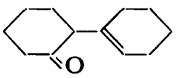 (12.4)

a) The reactions were carried out at room temperature for 30 min. The yields of products were based on the concentrations of consumed Ph_2GeK_2 and KH. b) Digermanes, polymers, and other unidentified products were also formed. c) The concentration of Ph_2GeK_2 was determined by that of Ph_2GeD_2 by hydrolysis with D_2O.

fore, the reduction products should have arisen from the reaction of **1a** with carbonyl compounds. The results in the reactions of **1a** with carbonyl compounds and KH with carbonyl compounds are summarized in Table 3. The yields of reduction products shown in Table 3 increased in the order benzophenone>acetophenone>acetone.

The results of the reactions of **1a** with organic halides and carbonyl compounds shown in Tables 2 and 3 are different from those of organogermylalkali metals.[1] It has been reported that organogermylalkali metals react with halotoluenes or carbonyl compounds to give tolylgermanes or organogermylcarbinols as main products, respectively.

The mechanism for the reactions of **1a** with organic halides or carbonyl compounds are not clear. However, taking the formation of reduction products shown in Tables 2 and 3 into consideration, electron transfer between **1a** and organic substrates might be important.

Experimental

Materials. Ph_2GeH_2,[19] Ph_2GeD_2,[20] bp 140—143 °C/0.7 mmHg (1 mmHg≈133.322 Pa), Ph_2GeBr_2, bp 115—120 °C/0.15 mmHg,[21] Ph_2GeEt_2, bp 100—108 °C/0.3 mmHg,[22] $Ph_2Ge(H)Et$, bp 110—115 °C/0.8 mmHg,[23] Ph_2GeBu_2, bp 125 °C/0.4 mmHg,[22] $Ph_2Ge(H)Bu$, bp 107—109 °C/0.08 mmHg,[23] $Ph_2Ge(C_8H_{17})_2$, bp 195—198 °C/0.3 mmHg,[24] $(p\text{-}CH_3C_6H_4)_2GeBr_2$, bp 230—233 °C/13 mmHg,[25] $Ph_3Ge(C_8H_{17})$, mp 72—73 °C,[26] 1,1-diphenylgermacyclopentane, bp 118—122 °C/0.15 mmHg,[27] and 1,1-diphenylgermacyclohexane, bp 118 °C/0.16 mmHg[27] were prepared as described in the cited references. KH is commercially available.

Preparation of Di(p-tolyl)germane. A mixture of di(*p*-tolyl)dibromogermane (4.1 g, 0.01 mol) and lithium aluminum hydride (1.0 g, 0.025 mol) in ether (100 cm³) was stirred with reflux for 3 h. After hydrolysis, the organic layer was dried over calcium chloride. The solvent was removed and then fractional distillation gave di(*p*-tolyl)germane (1.9 g, 7.5 mmol, 75.0%), bp 115 °C/2.0 mmHg; n^{20} 1.5839; IR (neat, cm^{-1}) 2050 (Ge-H). Found: C, 65.72: H, 6.46%, Calcd. for $C_{14}H_{16}Ge$: C, 65.46: H, 6.28%.

Preparation of Diphenyloctylbromogermane. Diphenyloctylbromogermane was prepared by bromination of triphenyloctylgermane (8.3 g, 0.02 mol) with an equivalent of bromine (3.2 g, 0.02 mol) in refluxing 1,2-dibromoethane (50 cm³) for 2 h. The solvent was removed under reduced pressure, leaving about 10 cm³ of residue. Fractional distillation gave crude diphenyloctylbromogermane (5.8 g, 14 mmol, 69.1%), bp 136—150 °C/0.05 mmHg; NMR (δ in $CDCl_3$) 0.52—1.88 (m, 17H), 6.88—7.78 (m, 10H).

Preparation of Diphenyloctylgermane. A mixture of diphenyloctylbromogermane (5.8 g, 14 mmol) and lithium aluminum hydride (1.0 g, 25 mmol) in ether (100 cm³) was stirred with reflux for 3h. After hydrolysis, the organic layer was dried over calcium chloride. The solvent was removed and then fractional distillation gave diphenyloctylgermane (1.3 g, 3.8 mmol, 38.1%), bp 150—158 °C/0.7 mmHg; n^{20} 1.5429; IR (neat, cm^{-1}) 2030 (Ge-H); NMR (δ in $CDCl_3$) 0.35—1.95 (m, 17H), 4.90—5.10 (m, 1H), 6.85—7.95 (m, 10H). Found: C, 70.39; H, 8.35%, Calcd. for $C_{20}H_{28}Ge$: C, 70.44: H, 8.26%.

Preparation of Isopropyldiphenylgermane. Isopropylmagnesium chloride was prepared from isopropyl chloride (9.0 g, 0.12 mol) and magnesium (4.0 g, 0.12 g atom) in ether (50 cm³) and benzene (20 cm³). To this Grignard reagent, diphenyldibromogermane (3.9 g, 0.01 mol) dis-

solved in ether (2 cm^3) was added. Toluene (50 cm^3) was added dropwise to this reaction mixture, and the ether was replaced immediately by toluene through distillation. The reaction mixture was stirred with reflux for 7 h. After hydrolysis, the organic layer was dried over calcium chloride. The solvent was removed and then fractional distillation gave isopropyldiphenylgermane (1.1 g, 4.06 mmol, 40.6%), bp 100—104 °C/0.4 mmHg; n^{20} 1.5718; IR (neat, cm^{-1}) 2025 (Ge-H); NMR (δ in $CDCl_3$) 0.91—1.40 (d, J=6.8 Hz, 6H), 0.65—2.10 (m, 1H), 4.80—5.00 (d, J=4.0 Hz, 1H), 6.85—7.75 (m, 10H). Found: C, 66.64: H, 6.79%, Calcd. for $C_{15}H_{18}Ge$: C, 66.51: H, 6.70%.

Preparation of Dibenzyldiphenylgermane. Benzylmagnesium chloride was prepared from benzyl chloride (12.7 g, 0.10 mol) and magnesium (2.3 g, 0.1 g atom) in ether (100 cm^3). To this Grignard reagent, diphenyldibromogermane (3.9 g, 0.01 mol) dissolved in ether (5 cm^3) was added. The reaction mixture was stirred with reflux for 5 h. After hydrolysis, the organic layer was dried over calcium chloride. The solvent was removed and then fractional distillation gave dibenzyldiphenylgermane (0.8 g, 2.0 mmol, 19.6%), bp 156 °C/0.08 mmHg; n^{20} 1.6321; NMR (δ in $CDCl_3$) 2.61 (s, 1H), 6.54—7.33 (m, 5H). Found: C, 76.46: H, 6.02%, Calcd. for $C_{26}H_{24}Ge$: C, 76.34: H, 5.91%.

Preparation of Diphenylgermylenedipotassium. Potassium (1.8 g, 0.046 g atom) was cut into small pieces and placed in the reaction vessel containing anhydrous HMPA (7.5 cm^3, 0.045 mol) and THF (11.0 cm^3) under argon. The vessel (50 cm^3 two-necked flask) was fitted with a condenser, drying tube argon inlet, and pressure equalizing dropping funnel. Diphenylgermane (1.20 g, 5.0 mmol) dissolved in THF (1.0 cm^3) was placed in the dropping funnel. The reaction vessel was blanketed with argon and K/HMPA/THF was stirred vigorously. The color of the solution changed to blue. The diphenylgermane solution was added dropwise and the change from blue to reddish brown usually appeared after about 40 min. The yield of diphenylgermylenedipotassium was determined from the concentration of diphenylgermane-d_2 after hydrolysis with D_2O (84—96%).

Preparation of Diphenylgermylenedilithium or Diphenylgermylenedisodium. Diphenylgermylenedilithium or diphenylgermylenedisodium was prepared as described above diphenylgermylenedipotassium.

*Reaction of Diphenylgermylenedipotassium, **1a**, with Ethyl Bromide.* A typical example for the reactions of **1a** with organic halides was described. A solution of **1a** (0.534 mmol) in HMPA/THF was added to ethyl bromide (7.40 mmol) dissolved in THF (1.0 cm^3) and stirred for 30 min. The reaction vessel was cooled with water bath. After hydrolysis, the reaction mixture was extracted with ether. The organic layer was dried over anhydrous sodium sulfate.

*Reaction of **1a** with Acetophenone.* A typical example for the reactions of **1a** with carbonyl compounds was described. A solution of **1a** (0.527 mmol) in HMPA/THF was added to acetophenone (2.11 mmol) dissolved in THF (1.0 cm^3) and stirred for 30 min. The reaction vessel was cooled with water bath. After hydrolysis, the reaction mixture was extracted with ether. The organic layer was dried over anhydrous sodium sulfate.

Reaction of KH with p-Bromotoluene. A typical example for the reactions of KH with organic halides was described. KH(1.0 g, 24.9 mmol) was placed in the reaction vessel containing anhydrous HMPA (8.0 cm^3) and THF (16.0 cm^3) under argon. To this solution, *p*-bromotoluene (1.7 g, 10.0 mmol) was added and stirred for 30 min. The reaction vessel was cooled with water bath. After hydrolysis, the reaction mixture was extracted with ether. The organic layer was dried over anhydrous sodium sulfate.

Reaction of KH with Acetone. A typical example for the reactions of KH with carbonyl compounds was described. KH (1.0 g, 24.9 mmol) was placed in the reaction vessel containing anhydrous HMPA (8 cm^3) and THF (16 cm^3) under argon. To this solution, acetone (5.8 g, 0.10 mol) was added and stirred for 30 min. The reaction vessel was cooled with water bath. After hydrolysis, the organic layer was dried over anhydrous sodium sulfate.

The authors are grateful to Professor Hideki Sakurai and Dr. Mitsuo Kira of Tohoku University for elementary analysis and GC-Mass measurements. We also thank Mr. Takeyoshi Kondo of Tohoku University for ^{13}C NMR measurements.

References

1) D. D. Davies, *Organomet. Chem. Rev., Sect. A*, **6**, 283 (1970).

2) E. J. Bulten and J. G. Noltes, *J. Organomet. Chem.*, **29**, 397 (1971).

3) E. J. Bulten and J. G. Noltes, *J. Organomet. Chem.*, **29**, 409 (1971).

4) C. Eaborn, R. E. E. Hill, and P. Simpson, *J. Organomet. Chem.*, **37**, 275 (1972).

5) W. Kitching, H. Olszowy, and J. Waugh, *J. Org. Chem.*, **43**, 898 (1978).

6) J. -P. Quintaed, S. Hauvette-Frey, M. Peryre, C. Couret, and J. Sátge, *Compt. Rend. Acad. Sci. Paris*, **287**, 247 (1981).

7) W. Kitching, H. Olszowy, and K. Harvey, *J. Org. Chem.*, **46**, 2423 (1981).

8) W. Kitching, H. Olszowy, and K. Harvey, *J. Org. Chem.*, **47**, 1893 (1982).

9) K. Mochida and N. Matsushige, *J. Organomet. Chem.*, **229**, 11 (1982).

10) D. A. Bravo-Zhivotovshi, S. D. Pigarev, I. D. Kalikhman, O. A. Vyazankina, and N. S. Vyazankin, *J. Organomet. Chem.*, **248**, 51 (1983).

11) C. A. Kraus and E. S. Carney, *J. Am. Chem. Soc.*, **56**, 765 (1934).

12) R. J. Cross and F. Glockling, *J. Chem. Soc.*, **1964**, 4125.

13) E. J. Bulten and J. G. Noltes, *Tetrahedron Lett.*, **1967**, 1443.

14) G. Fraenkel, D. G. Adams, and R. R. Dean, *J. Phys. Chem.*, **72**, 944 (1968).

15) A. L. Jones, D. M. Grant, J. G. Russell, and G. Fraenkel, *J. Phys. Chem.*, **73**, 1624 (1969).

16) R. H. Cox, E. G. Janzen, and W. B. Harrison, *J. Magn. Reson.*, **4**, 274 (1971).

17) G. A. Olah and R. J. Hunadi, *J. Am. Chem. Soc.*, **102**, 6989 (1980).
18) R. J. Batchelor and T. Birchall, *J. Am. Chem. Soc.*, **105**, 3848 (1983).
19) O. H. Johnson, W. H. Nebergall, and D. H. Harris, *Inorg. Synth.*, **5**, 76 (1957).
20) J. R. Duig, J. B. Turner, B. M. Gibson, and C. W. Sink, *J. Mol. Struct.*, **4**, 79 (1969).
21) W. Metlesis and H. Zeiss, *J. Am. Chem. Soc.*, **82**, 3321 (1960).
22) R. J. Cross and F. Glockling, *J. Organomet. Chem.*, **3**, 146 (1965).
23) C. Eaborn and B. Singh, *J. Organomet. Chem.*, **177**, 333 (1979).
24) S. A. Sarankina, Z. M. Mannulkin, and A. B. Kuchkarov, *Dokl. Akad. Hauk. USSR.*, **22**, 35 (1965).
25) R. Schwarz and M. Lewinsohn, *Chem. Ber.*, **64**, 2352 (1931).
26) R. Fuchs and H. Gilman, *J. Org. Chem.*, **22**, 1009 (1957).
27) P. Mazerolles, J. Dubac, and M. Lesbre, *J. Organomet. Chem.*, **5**, 35 (1966).
28) P. Mazerolles, *Bull. Soc. Chim. Fr.*, **1962**, 1907.

 © 1985 The Chemical Society of Japan Bull. Chem. Soc. Jpn., 58, 1448—1451 (1985) [Vol. 58, No. 5

Synthesis Utilizing Reducing Ability of Carbon Monoxide. New Methods for Synthesis of *N*-Substituted Selenoamides

Akiya OGAWA, Jun-ichi MIYAKE, Nobuaki KAMBE, Shinji MURAI, and Noboru SONODA*
Department of Applied Chemistry, Faculty of Engineering, Osaka University, Suita, Osaka 565
(Received November 12, 1984)

Convenient one-pot syntheses of *N*-substituted selenoamides (**2**) from nitriles, metallic selenium, carbon monoxide, water, and amines have been developed on the basis of an amino-group-exchange reaction of *in situ* formed *N*-unsubstituted selenoamides (**1**) with primary or secondary amines. The reactions consist of two processes, *i.e.*, the formation of selenoamides **1** by the reaction of nitriles and H_2Se formed from selenium, carbon monoxide and water, and the subsequent amino-group-exchange reaction of **1** with aliphatic amines. The obtained **2** are generally stable enough to be kept for several weeks under the atmosphere of nitrogen at 0 °C without any appreciable degradation. In the cases of primary amines, the corresponding selenoamides were also obtained from nitriles, selenium, carbon monoxide, and primary amines by a single-step mixing at the beginning of the reaction.

The development of new synthetic reactions using carbon monoxide has been the subject of continuing interest.[1] One of the fascinating applications of carbon monoxide to organic synthesis is as reducing agent.[2] Recently, we reported that elemental selenium is readily reduced to hydrogen selenide by carbon monoxide and water under mild conditions,[3] and that a variety of *N*-unsubstituted selenoamides (**1**) can be synthesized in high yields from the corresponding nitriles by use of this reaction system (Eq. 1).[4]

$$RCN + Se + CO + H_2O \xrightarrow{base} \underset{\mathbf{1}}{R\text{-}\overset{\overset{Se}{\|}}{C}\text{-}NH_2} + CO_2 \qquad (1)$$

Selenoamides are not only useful for the synthesis of selenium–nitrogen heterocycles such as 1,3-selenazoles,[5] but also synthetically promising because they can be expected to react with various organic or inorganic reagents owing to the high reactivity of their carbon–selenium double bond. But the development of their chemistry has been greatly restricted by the lack of general procedures for the formation of selenoamides. The hitherto known procedures for synthesis of *N*-substituted selenoamides (**2**) were limited to the following three methods: (i) The reaction of amides with phosphorus selenide,[6] (ii) the substitution reaction of selenoesters with amines,[7] and (iii) the addition of secondary amines to alkyneselenols.[8] However, these methods are not general, and in some cases the yields are very low.

Now we wish to describe new efficient methods for the synthesis of selenoamides **2**, which were developed by the modification of the reaction system of Eq. 1.

Results and Discussion

Our strategy for the synthesis of **2** is the amino-group-exchange reaction of **1** formed *in situ* from the reaction of Eq. 1 with primary or secondary amines (Eq. 2).

$$RCN + Se + CO + H_2O \xrightarrow[-CO_2]{base} [\mathbf{1}] \xrightarrow[-NH_3]{R^1NH_2} \underset{\mathbf{2}}{R\text{-}\overset{\overset{Se}{\|}}{C}\text{-}NHR^1} \qquad (2)$$

The reaction of benzonitrile with selenium, carbon monoxide, and water in the presence of triethylamine in THF at 100 °C for 5 h, followed by treatment of the resulting mixture with butylamine at 100 °C for 3 h successfully afforded *N*-butylbenzenecarboselenoamide (**2b**) (81%) [Method A].

The representative results are shown in Table 1. The reaction appears general with respect to the substituents of selenoamides: Both aromatic and aliphatic, and both *N*-mono- and *N*,*N*-disubstituted selenoamides were all easily synthesized in moderate to high yields. But the yields of aromatic selenoamides (**2a—2g**) differed depending on the bulkiness of the alkyl groups of amines (R=primary alkyl group: >80%; secondary: 30—50%; tertiary: 0%). In the cases of *N*-(*s*-alkyl) derivatives (**2a**, **2c**, and **2f**), better yields were obtained when the amino-group-exchange reaction was conducted for a longer reaction time (20h). On the other hand, the amino-group-exchange reaction with aromatic amines did not take place under these reaction conditions.

Structural assignments of selenoamides were based on spectral analyses (IR, ^{1}H-NMR, and Mass spectrum: see Table 1) and elemental analyses after purification of the products by column chromatography on silica gel.

N-Substituted selenoamides are yellow crystalline or red oil, and are generally stable enough to be kept for several weeks under an atmosphere of nitrogen at about 0 °C without degradation. Upon exposure to air, however, they gradually decomposed along with the deposition of elemental selenium.

In addition to Method A, a more facile procedure (Method B) became available for the preparation of

Table 1. Synthesis of *N*-substituted Selenoamides[a)]

Entry	Selenoamide		Yield/%[b,c)] Method A	Yield/%[b,c)] Method B	IR cm^{-1}	^{1}H-NMR, δ (CCl_4)	Mass (M^+)	Mp θ_m/°C
1	Ph-C(=Se)-NHC$_3$H$_7^t$	**2a**	41 (74)	36 (77)	3180 1525	1.42(d, 6H), 4.85(m, 1H), 7.00—7.70(m, 5H), 8.20 (brs, 1H)	227	68
2	Ph-C(=Se)-NHC$_4$H$_9^n$	**2b**	81	93	3180 1530	0.84(t, 3H), 1.00—1.90(m, 4H), 3.53(m, 2H), 6.70—7.70 (m, 5H), 8.40(brs, 1H)	241	Oil
3	Ph-C(=Se)-NHC$_4$H$_9^s$	**2c**	34 (77)	27 (61)	3180 1530	0.98(t, 3H), 1.28(d, 3H), 1.70 (m, 2H), 4.64(m, 1H), 6.80—7.85(m, 5H), 8.00(brs, 1H)	241	Oil
4	Ph-C(=Se)-NHC$_4$H$_9^t$	**2d**	(0)	(0)	—	—	—	—
5	Ph-C(=Se)-NHCH$_2$Ph	**2e**	87	94	3155 1520	4.84(d, 2H), 7.00—7.80 (m, 10H), 8.20(brs, 1H)	275	76—78
6	Ph-C(=Se)-NH-	**2f**	47 (75)	42 (82)	3135 1530	0.50—2.50(m, 10H), 4.52 (m, 1H), 7.00—7.80(m, 5H), 7.95(brs, 1H)	267	95
7	Ph-C(=Se)-NHC$_8$H$_{17}^n$	**2g**	88	95	3180 1530	0.60—2.00(m, 15H), 3.57 (m, 2H), 6.80—7.70(m, 5H), 8.50(brs, 1H)	297	Oil
8	Ph-C(=Se)-NMe$_2$	**2h**	46	0	1525	2.98(s, 3H), 3.52(s, 3H) 7.14(s, 5H)	213	46—46.5
9	Ph-C(=Se)-N	**2i**	45	0 (0)	1500	1.74(m, 6H), 3.46(m, 2H), 4.38(m, 2H), 7.18(m, 5H)	253	89—89.5
10	*n*-C$_3$H$_7$-C(=Se)-NHC$_4$H$_9^n$	**2j**	54	18	3200 1540	0.87—1.17(m, 6H), 1.17—2.09(m, 6H), 2.66(t, 2H), 3.62(q, 2H), 8.70(brs, 1H)	207	Oil
11	*n*-C$_3$H$_7$-C(=Se)-NHCH$_2$Ph	**2k**	74	31	3125 1530	0.93(t, 3H), 1.80(t-q, 2H), 2.62(t, 2H), 4.75(d, 2H), 7.26(s, 5H), 8.10(brs, 1H)	241	53.5—54
12	CH$_3$-C(=Se)-NHCH$_2$Ph	**2l**	48	30	3155 1550	2.59(s, 3H), 4.80(d, 2H), 7.33(s, 5H), 8.00(brs, 1H)	213	88—89
13	PHCH$_2$-C(=Se)-NHCH$_2$Ph	**2m**	71	74	3145 1545	4.13(s, 2H), 4.81(m, 2H), 7.20(s, 5H), 7.25(s, 5H), 7.70(brs, 1H)	289	94.5—95.5

a) All reactions were performed on 5 mmol scale according to the procedures described in the text. b) Isolated yield. c) The yields in the parentheses refer to that obtained by the reaction conducted for prolonged reaction periods in the amino-group-exchange reaction (20 h).

N-monosubstituted selenoamides (Eq. 3). For example, *N*-benzylbenzenecarboselenoamide (**2e**) was obtained in 94% yield by heating the mixture of benzonitrile, selenium, and benzylamine under CO pressure in THF.

$$RCN + Se + CO + 3R^1NH_2 \longrightarrow \mathbf{2} + (R^1NH)_2C{=}O + NH_3 \quad (3)$$

As shown in Eq. 3, Method B affords the corresponding urea derivative as a by-product concomitantly, which is easily separable from **2**. A suggested reaction path is illustrated in Eq. 4.

$$2R^1NH_2 + Se + CO \xrightarrow[-(R^1NH)_2C{=}O]{} H_2Se \xrightarrow{RCN} \mathbf{1} \xrightarrow[-NH_3]{R^1NH_2} \mathbf{2} \quad (4)$$

This method is inapplicable to synthesis of *N,N*-disubstituted selenoamides probably because the reaction of secondary amines with carbon monoxide and selenium does not give hydrogen selenide but the ammonium salts of selenocarbamic *Se*-acids.[9)]

In summary, general and convenient methods for the synthesis of selenoamides using carbon monoxide and selenium have been developed. The present

methods offer several advantages against hitherto known methods: (i) A wide range of applicability to a variety of selenoamides (aromatic and aliphatic; *N*-monosubstituted, and *N,N*-disubstituted); (ii) satisfactory yields of a variety of selenoamides; (iii) one-pot syntheses with simple operations without troublesome handling of hydrogen selenide.

Experimental

General. The instruments used were as follows: Melting points, Yanagimoto micro melting point apparatus; ^{1}H-NMR, Hitachi R-24B; IR, Shimadzu IR-400; MS, Hitachi RMU-6A.

All reactions were carried out using a 50-mL stainless-steel autoclave (SUS-304) purchased from Taiatsu Scientific Glass Co., Ltd.

Metallic selenium (99.99%) from Nakarai Chem. Co., Ltd. and carbon monoxide (99.99%) from Neriki Gas Co. Ltd. were used as purchased. Nitriles (benzonitrile, butyronitrile, acetonitrile, and phenylacetonitrile), amines (isopropylamine, butylamine, *s*-butylamine, *t*-butylamine, benzylamine, cyclohexylamine, octylamine, dimethylamine, piperidine, and triethylamine), and solvent (tetrahydrofuran) were all purchased from commercial sources, and purified by distillation or recrystallization. CO pressures mentioned in the paper refer to those at 25 °C.

General Experimental Procedure for Synthesis of 2 (Method A). In an autoclave were placed benzonitrile (0.52 g, 5 mmol), selenium (0.43 g, 5.5 mmol), water (1 mL, 56 mmol), triethylamine (1 mL), THF (5 mL), and a magnetic stirring bar. The autoclave was flushed with carbon monoxide three times, charged at 5 kg/cm^2, and set in an oil bath maintained at 100 °C. The reaction was carried out for 5 h with magnetic stirring. Then the autoclave was cooled to room temperature, and the carbon monoxide was purged in a well-ventilated hood. Butylamine (1.0 mL, 10 mmol) was immediately added to the reaction mixture under an atmosphere of nitrogen, and the reaction was continued at 100 °C for 3 h under nitrogen. After the reaction was complete, the resulting mixture was transferred to a 100 mL flask, dried overnight ($MgSO_4$), and then filtered. Evaporation of the filtrate, followed by purification by the column chromatography on silica gel (hexane–Et_2O) gave 0.97 g (4.0 mmol, 81%) of **2b**: Found: C, 55.39; H, 6.58; N, 5.85. Calcd for $C_{11}H_{15}NSe$: C, 55.00; H, 6.29; N, 5.83.

Similarly prepared were the followings.

2a: Found: C, 53.38; H, 5.85; N, 6.18%. Calcd for $C_{10}H_{13}NSe$: C, 53.10; H, 5.79; N, 6.19.

2c: Found: C, 55.38; H, 6.51; N, 5.72. Calcd for $C_{11}H_{15}NSe$: C, 55.00; H, 6.29; N, 5.83.

2e: Found: C, 61.36; H, 4.76; N, 5.01. Calcd for $C_{14}H_{13}NSe$: C, 61.32; H, 4.78; N, 5.11.

2f: Found: C, 58.66; H, 6.29; N, 5.15. Calcd for $C_{13}H_{17}NSe$: C, 58.65; H, 6.44; N, 5.26.

2g: Found: C, 60.97; H, 8.05; N, 4.87. Calcd for $C_{15}H_{23}NSe$: C, 60.80; H, 7.82; N, 4.73.

2h: Found: C, 50.98; H, 5.34; N, 6.57. Calcd for $C_9H_{11}NSe$: C, 50.95; H, 5.23; N, 6.60.

2i: Found: C, 57.21; H, 6.08; N, 5.50. Calcd for $C_{12}H_{15}NSe$: C, 57.15; H, 5.99; N, 5.55.

2j: Found: C, 47.09; H, 8.71; N, 6.81. Calcd for $C_8H_{17}NSe$: C, 46.60; H, 8.31; N, 6.79.

2k: Found: C, 55.13; H, 6.34; N, 5.72. Calcd for $C_{11}H_{15}NSe$: C, 55.00; H, 6.29; N, 5.83.

2l: Found: C, 51.18; H, 5.18; N, 6.55. Calcd for $C_9H_{11}NSe$: C, 50.95; H, 5.23; N, 6.60.

2m: Found: C, 62.60; H, 5.24; N, 4.82. Calcd for $C_{15}H_{15}NSe$: C, 62.50; H, 5.25; N, 4.86.

(Method B). Benzonitrile (0.52 g, 5 mmol), selenium (0.43 g, 5.5 mmol), butylamine (2.0 mL, 20 mmol), and THF (5 mL) were placed in an autoclave with a magnetic stirring bar. The reaction was carried out under the pressure of CO (5 kg/cm^2) at 80 °C for 5 h in a similar manner to that described in Method A. After the reaction was complete, the autoclave was cooled to room temperature and the carbon monoxide was purged. The reaction mixture was trasferred to a 100 mL flask and left overnight under the atmosphere of air in order to decompose benzenecarboselenoamide (**1**) and the remaining hydrogen selenide. The depositing metallic selenium was filtered off, and the solvent was removed from the filtrate under reduced pressure. The resulting residue was chromatographed on silica gel to give 1.12 g (4.7 mmol, 93%) of **2b** and 0.86 g (5.0 mmol) of *N,N'*-dibutylurea.

This work was supported in part by a Grant-in-Aid for Scientific Research No. 57470061 from the Ministry of Education, Science, and Culture of Japan.

References

1) For recent reviews on the use of carbon monoxide in organic synthesis, see: J. Farbe, "New Syntheses with Carbon Monoxide," Springer-Verlag, New York (1980); I. Wender and P. Pino, "Organic Syntheses via Metal Carbonyls," Wiley, New York (1977), Vol. 2; H. Siegel and W. Himmele, *Angew. Chem. Int. Ed. Engl.*, **19**, 178 (1980); "Catalytic Activation of Carbon Monoxide," ed by P. C. Ford, *ACS Symposium Ser.*, **152** (1981); I. Tkatchenko, in "Comprehensive Organometallic Chemistry," ed by G. Wilkinson, F. G. A. Stone, and E. W. Abel, Pergamon Press (1982), Vol. 8, Chapter 50.3, p. 101; G. Consiglio and P. Pino, in "Topics in Current Chemistry," ed by F. L. Boschke, Springer-Verlag (1982), **105**, 77.

2) See for example: P. C. Ford, *Acc. Chem. Res.*, **14**, 31 (1981); A. D. King, Jr., R. B. King, and D. B. Yang, *J. Am. Chem. Soc.*, **102**, 1028 (1980); J. C. Bricker, C. C. Nagel, and S. G. Shore, *J. Am. Chem. Soc.*, **104**, 1444 (1982); H. W. Walker, R. G. Pearson, and P. C. Ford, *ibid.*, **105**, 1179 (1983); D. Choudhury and D. J. Cole-Hamilton, *J. Chem. Soc., Dalton Trans.*, **1982**, 1885; J. M. Kelly and J. G. Vos, *Angew. Chem. Int. Ed. Engl.*, **21**, 628 (1982); K. Murata and A. Matsuda, *Bull. Chem. Soc. Jpn.*, **54**, 2089 (1981); Y. Watanabe, N. Suzuki, and Y. Tsuji, *ibid.*, **55**, 2445 (1982).

3) N. Sonoda, K. Kondo, K. Nagano, N. Kambe, and F. Morimoto, *Angew. Chem. Int. Ed. Engl.*, **19**, 308 (1980).

4) A. Ogawa, J. Miyake, Y. Karasaki, S. Murai, and N. Sonoda, *J. Org. Chem.*, **50**, 384 (1985).

5) E. Bulka, *Chemica Scripta*, **8A**, 39 (1975).
6) K. A. Jensen and P. H. Nielsen, *Acta Chem. Scand.*, **20**, 597 (1966); J. Voss and F. -R. Bruhn, *Justus Liebigs Ann. Chem.*, **1979**, 1931; C. Collard-Charon and M. Renson, *Bull. Soc. Chim. Belges.*, **72**, 304 (1963).
7) V. I. Cohen, *J. Org. Chem.*, **42**, 2645 (1977).
8) F. Malek-Yazdi and M. Yalpani, *Synthesis*, **1977**, 328; R. S. Sukhai, R. de Jong, and L. Brandsma, *ibid.*, **1977**, 888.
9) K. Kondo, N. Sonoda, K. Yoshida, M. Koishi, and S. Tsutsumi, *Chem. Lett.*, **1972**, 401.

Stereochemical Control in Electron-transfer Induced Reactions. Cyclic Voltammetry and Cathodic Reduction of Epimeric 3-Halogeno-6-nitro-5-cholestenes[1)]

Takeo SATO,* Takahiro WADA, Yoshihisa KOMEICHI, and Masatsune KAINOSHO
Department of Chemistry, Tokyo Metropolitan University, Setagaya-ku, Tokyo 158
(Received November 21, 1984)

The cathodic electrolyses and cyclic voltammetric measurements were carried out for epimeric 3-halogeno-6-nitro-5-cholestenes. The stability and the fate of anion radicals were found to be highly dependent on the stereochemistry of homoallylic halogen groups. Half-lives of the anion radical from 3α-chloro- and 3α-bromo derivatives were found to be 12.5 and 1.6 s, respectively, while those of 3β-halogeno derivatives were much shorter. On cathodic reduction 3β-derivatives gave a cyclosteroid, 6β-nitro-3α,5α-cyclo-5α-cholestane in a two-electron process, whereas 3α-derivatives gave a dimer, 6β,6′β-dinitro-3α,3′α-cholesta-4,4′-diene, as the major product *via* a one-electron process. Detailed CV studies were carried out for 6-nitro-5-cholestene as a model. The stereochemistry of 3,3′-dimer was established by the ^{1}H NMR measurements.

In a previous paper of this series[2)] we have shown that the cathodic reduction of nitro olefinic esters **1** in *N,N*-dimethylformamide (DMF) gives two types of products, namely, a 3,3′-dimer, 6β,6′β-dinitro-3α,3′α-cholesta-4,4′-diene (**2**), and a cyclosteroid, 6β-nitro-3α,5α-cyclo-5α-cholestane (**3**), depending on a leaving-group ability of an equatorial ester group at C-3. For example, tosylate **1a** gave **3** as the major product while acetate **1b** gave only the dimer **2**. Trifluoroacetate **1c** showed an intermediate behavior and gave equimolar amounts of **2** and **3**. In these reactions a nitro olefinic moiety served as an electron inlet and no reduction of the nitro group itself occurred.

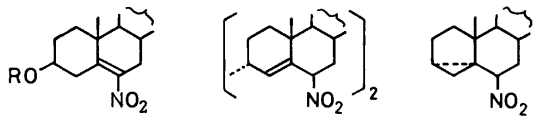

R
1a p-Ts
1b CH_3CO
1c CF_3CO

2 3

Recently, Yates and coworker[3)] reported that the reaction of **1b** with lithium dimethylcuprate(I) in ether gave 3α,5α-cyclooxime but no dimeric product. The reaction was assumed to occur *via* a one-electron reduction mechanism.

We have shown[1,2)] that the cyclic voltammogram (CV) is highly dependent on the C-3 ester groups. Indeed the CV method has been shown to be used effectively to predict the reaction course which was dependent on the stability of an initially-formed anion radicals.

In this paper we describe further substituent effects on the CV behavior and cathodic reactions using epimeric 3α- and 3β-halogeno-6-nitro-5-cholestenes (**4a**), (**4b**), (**5a**), and (**5b**). We also describe the stereochemistry of dimer **2** studied by using proton NMR.

Preparation. 3β-Chloro- and 3β-bromo-6-nitro-5-cholestenes (**4a**) and (**4b**) were prepared from

4a X=Cl
4b X=Br

5a X=Cl
5b X=Br

cholesterol by halogenation followed by nitration according to the literature.[4a,b)] We found 3α derivatives **5a** and **5b** could be prepared simply by reversing the reaction order. Namely, **5a** and **5b** were obtained by the halogenation of 6-nitrocholesterol with phosphorus pentachloride or phosphorus tribromide which gave the corresponding halogeno products with inversion of stereochemistry at C-3 in 38 and 20% yields respectively. Low yields were outweighed by shorter reaction steps. The conventional route for 3α derivatives required lengthy steps involving halogenation with inversion at C-3 of 3β-hydroxy-5α-cholestan-6-one followed by lithium aluminum hydride reduction, dehydration, and nitration.

The stereochemistry of substitution at C-3 has been known to be controlled by the π electron density at C-5.[4c)] In the present case, low-electron density at C-5 in nitro-olefinic group directed the reaction course toward inversion which was common both for halogenation of cholestanol[4c)] and also for acetoxylation of 3-chlorocholest-5-en-7-one.[5)]

Cyclic Voltammetry. The CV measurements were carried out in DMF containing 0.1 mol dm^{-3} of tetrabutylammonium perchlorate (TBAP) for solutions with concn 10^{-3}—10^{-4} mol dm^{-3}. For a reversible wave $E=E_{pc}-(E_{pc}-E_{pa})/2$ was calculated. When no anodic peak was recorded E was approximated by the potential at which $i=0.85\ i_{pc}$.[6)] The results are summarized in Tables 1 and 2. Table 1 shows data for compound **6** in detail together with those for **1a**, **1b**, and **1c** for comparison purpose.[2)] Table 2 summarizes the data for **4a**, **4b**, **5a**, and **5b**. With compounds **6**, **4b**, and **5b** a series of measurements

TABLE 1. THE CYCLIC VOLTAMMETRY DATA FOR THE NITRO STEROIDS **1a**—**c** AND **6**[a]

Compound	Scan rate / mV s^{-1}	Peak potetial/-V E_{pc}	E_{pa}	Peak pot. diff. $E_{pa}-E_{pc}$/mV	E/-V	Current ratio i_{pa}/i_{pc}	Peak current $i_{pc}/\mu A$
1a[b]	50	1.49			1.44[c]		
	100	1.55			1.48[c]		
	250	1.69			1.58[c]		
	500	1.74			1.55[c]		
1b[b]	50	1.47	1.23	240	1.35	0.84	
	100	1.55	1.18	370	1.36	0.82	
	250	1.63	1.10	530	1.37	0.72	
	500	1.70	1.01	690	1.36	0.55	
1c[b]	500	1.61	1.10	510	1.36	0.55	
6[d]	5	1.52	1.45	70	1.49	0.93	7.5
	10	1.53	1.44	90	1.49	0.94	9.5
	15	1.54	1.43	110	1.49	0.94	11.2
	25	1.55	1.42	130	1.49	0.89	14.0
	50	1.56	1.41	150	1.49	0.89	19.0
	100	1.58	1.40	180	1.49	0.90	25.0
	150	1.59	1.39	200	1.49	0.91	29.8
	250	1.62	1.37	250	1.50	0.89	36.0
	500	1.67	1.34	330	1.51	0.84	47.8
	750	1.72	1.33	390	1.53	0.78	57.8
	1000	1.74	1.32	420	1.53	0.79	66.5
	2500	1.85	1.25	600	1.55	0.70	105.7
	5000	1.92	1.20	720	1.56	0.56	139.3
	7000	2.00	1.16	840	1.58	0.65	168.0

a) The cyclic voltammetry was carried out in DMF-TBAP (0.1 mol dm^{-3}) using a platinum inlay electrode (Beckman No. 39273) and platinum wire as cathode and reference electrodes, respectively. An SCE was used as reference. b) Data from Ref. 2. c) The potential at which $i=0.85\ i_{pc}$ is shown. d) The concentration of solution, 1.0×10^{3} mol dm^{-3}.

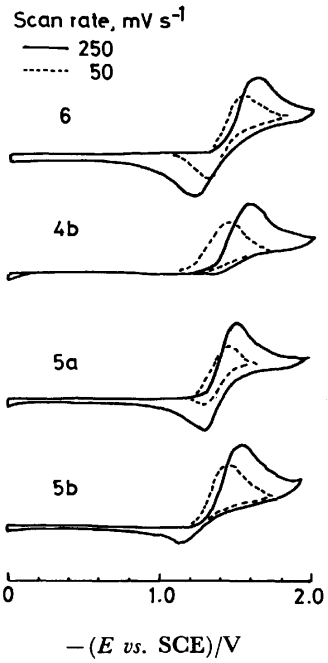

Fig. 1. The cyclic voltammograms for compounds **4b**, **5a**, **5b**, and **6** determined in DMF-TBAP; Scan rates, 50 and 250 mV s^{-1}.

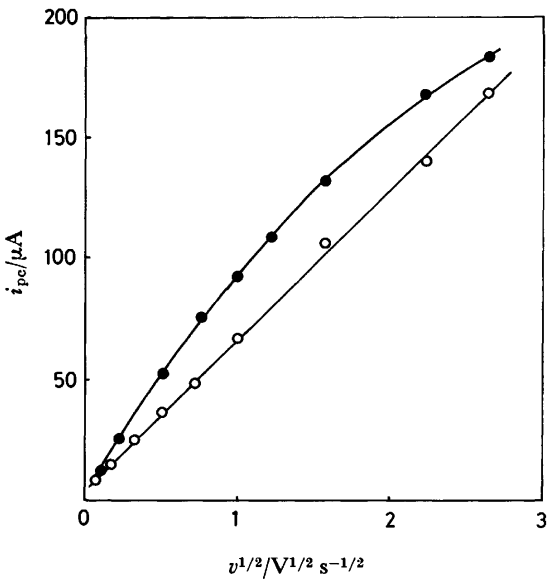

Fig. 2. The plot of square root of scan rate, $v^{1/2}$, *vs.* peak current, i_{pc}, for compounds **5b** (—●—) and **6** (—○—). The slope for compound **6**, $i_{pc}\ v^{-1/2}=61.7/\mu A\ s^{1/2}\ V^{-1/2}$.

TABLE 2. THE CYCLIC VOLTAMMETRY DATA FOR THE NITRO STEROIDS **4a**, **4b**, **5a**, AND **5b**[a]

Compound	Scan rate / mV s^{-1}	Peak potential/-V		Peak pot. diff. $E_{pa}-E_{pc}$/mV	E/-V	Current ratio i_{pa}/i_{pc}	Peak current i_{pc}/μA
		E_{pc}	E_{pa}				
4a	50	1.48			1.43[b]		
	100	1.52			1.56[b]		
	150	1.54			1.48[b]		
	250	1.56			1.49[b]		
	500	1.58			1.50[b]		
4b	10	1.42			1.36[b]		11.0[c]
	25	1.43			1.37[b]		16.9[c]
	50	1.47			1.40[b]		23.7[c]
	100	1.50			1.43[b]		32.8[c]
	150	1.52			1.45[b]		39.7[c]
	250	1.55			1.49[b]		49.8[c]
	500	1.59			1.52[b]		67.8[c]
	750	1.61			1.53[b]		83.2[c]
	1000	1.64			1.55[b]		93.8[c]
	2500	1.72			1.61[b]		134.4[c]
	5000	1.80			1.69[b]		182.0[c]
	7000	1.89			1.73[b]		210.0[c]
	10000	1.93			1.76[b]		259.0[c]
5a	50	1.47	1.34	130	1.41	0.48	
	100	1.50	1.33	170	1.42	0.49	
	150	1.51	1.31	200	1.41	0.58	
	250	1.52	1.30	220	1.41	0.63	
	500	1.56	1.25	310	1.41	0.81	
5b	10	1.50			1.42[b]		11.9[c]
	25	1.56			1.49[b]		17.7[c]
	50	1.61			1.54[b]		25.1[c]
	75	1.63	1.19	440	1.41	0.37	30.4[c]
	100	1.65	1.17	480	1.41	0.37	35.1[c]
	150	1.67	1.15	520	1.41	0.38	42.0[c]
	250	1.70	1.13	570	1.42	0.42	52.0[c]
	500	1.74	1.09	650	1.42	0.46	71.0[c]
	600	1.76	1.07	690	1.42	0.49	76.4[c]
	700	1.77	1.06	710	1.42	0.50	82.0[c]
	750	1.78	1.05	730	1.42	0.51	83.6[c]
	1000	1.83	1.00	830	1.42	0.56	92.4[c]
	1500	1.86	0.96	900	1.41	0.61	108.0[c]
	2500	1.90	0.94	960	1.42	0.81	132.0[c]
	5000	1.95	0.90	1050	1.43	0.76	168.0[c]
	7000	1.98	0.87	1110	1.43	0.74	184.0[c]

a) The measurements were carried out similarly as those in Table 1. b) The potential at which $i=0.85\ i_{pc}$ is shown. c) The concentration of solution, 6.7×10^{-4} mol dm^{-3}.

were conducted using a single solution and the peak current data are tabulated together with the other parameters.

In order to examine the effect of C-3 substituents and its stereochemistry on the electron-transfer process we first investigated the CV of 6-nitro-5-cholestene (**6**) in detail as the model (Table 1, Figs. 1 and 2).

Compound **6** showed a reversible wave for varied scan rates indicating reversible electron-transfer between **6** and its anion radical **7**. The CV curves for 50 and 250 mV s^{-1} are shown in Fig. 1. The cathodic potential E was found to be −1.5 V. The anion radical is fairly stable and assumed to be composed of a resonance hybrid between **8** and **9**. At lower scan rates the current ratio i_{pa}/i_{pc} became almost unity. The peak potential difference, $E_{pa}-E_{pc}$, was 70 mV at the scan rate of 5 mV s^{-1}, the value of which was close to 56 mV required for an ideal one-electron transfer process.[6]

When higher scan rates were used, however, the peak potential difference showed a steady increase, reflecting limited electron-transfer rate. At the scan rate of 7V s^{-1} recorded using a wave-memory technique, the peak potential difference reached 840 mV, while the peak current ratio decreased to 0.65.

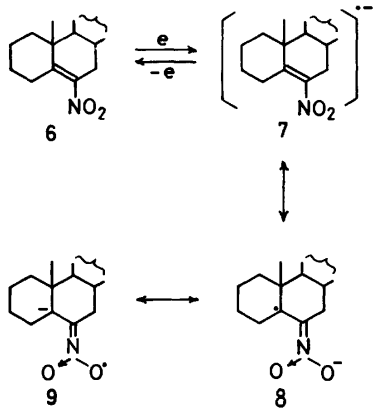

Figure 2 shows the dependence of the cathodic current i_{pc} on the square root of the scan rate. A good linear relation was obtained as expected from the Randles-Sevcik equation,[6]

$$i_p = 2.687\times10^5 n^{3/2} A D^{1/2} C v^{1/2}$$

The effect of a homoallylic substituent at C-3 was then investigated using substrates **4** and **5** (Table 2, Fig. 1). The CV curves for 3-axial halogeno derivatives **5a** and **5b** recorded in two speeds, 50 and 250 mV s^{-1}, are shown in Fig. 1. 3-Axial chloro derivative **5a** showed a reversible wave for both scan rates. The corresponding bromo derivative **5b**, however, showed no anodic peak at the scan rate of 50 mV s^{-1} but it appeared as a small peak at −1.42 V on increasing the scan rate fivefold indicating the presence of coupled chemical reactions. Reversibility was increased markedly by employing higher scan rates. The plot between i_{pc} and $v^{1/2}$ for 3α-bromo derivative **5b** results in a nonlinear correlation unlike the case of compound **6** (Fig. 2).

In 3α-derivatives a reversible electron-transfer process is assumed to be coupled with chemical reactions with the rate of k_1. The CV behavior indicated that k_1 was larger for bromo derivative than for chloro derivative. These results indicate the anion radical formed from **5a** and **5b** have a limited stability.

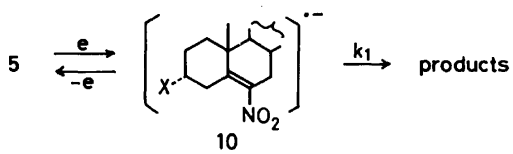

For 3β-chloro and 3β-bromo derivatives, **4a** and **4b**, no anodic peak was recorded even when high speed CV determination was carried out. This indicates a higher reactivity of the 3β-halogeno anion radical **11** compared with the 3α-halogeno anion radical **10** ($k_2 > k_1$). The CV behavior of **4** resembles to that of 3β-tosylate **1a**.[2] Figure 1 shows voltammograms at two speeds of **4b**. Compound **4a** also showed similar voltammograms.

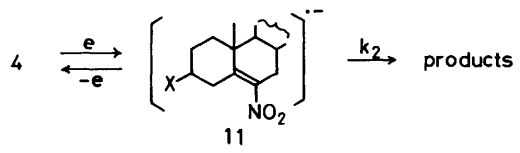

Whereas halogeno substituents at C-3 and its stereochemistry were found to affect the voltammograms in various ways, the cathodic potentials for these compounds were found to fall within a narrow range of −1.4—−1.5 V.

Half lives for these anion radical can be estimated by using the House method.[7] One assumes a simple EC reaction composed of a reversible electron transfer coupled with an irreversible chemical reaction. By carrying out the CV determination at various speeds one can obtain a voltammogram with i_{pa} just half of i_{pc}. The half-life of an anion radical can be regarded as the elapsed time between the cathodic peak and the anodic peak on potential reversal.

Compound **6** showed a good reversible wave throughout the scan ranges used even when a very slow sweep rate was employed. By contrast, equatorial halogeno derivatives **4a** and **4b** showed no anodic peak even when higher scan rates were employed, the situation is similar to tosylate **1a**, indicative of short life of the corresponding anion radicals. Axial isomers **5a** and **5b** showed an intermediate behavior and half-lives for anion radicals **10** were estimated to be 12.5 s for chloro derivative **5a** and 1.6 s for bromo derivative **5b**. Thus the stability of the anion radicals from the following compounds decreases in the order;

6>5a>5b>4a, 4b, 1a

Cathodic Reaction. The cathodic reduction was carried out in DMF containing 0.1 mol dm^{-3} of tetrabutylammonium perchlorate (TBAP) as a supporting electrolyte using a divided cell under nitrogen. Constant current conditions (0.45 mA cm^{-2}) were employed to compare with the results for esters **1** which were electrolyzed similarly. The results are summarized in Table 3.

When 1 F mol^{-1} of electricity had been consumed the reaction was stopped: Both equatorial compounds **4a** and **4b** gave cyclosteroid **3** in 40 and 43% yields, respectively. On further electrolysis **4a** gave 61% yield of **3** when 1.8 F mol^{-1} of electricity was passed. The yield of **3** from **4b** reached 70% when 1.9 F mol^{-1} was consumed. Apparently the reaction proceeds in a two-electron scheme involving an anion radical **12** to give **13** followed by further electron transfer and protonation as proposed before.[2]

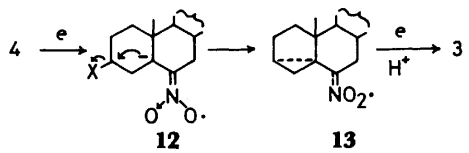

TABLE 3. CONTROLLED-CURRENT ELECTROLYSES OF NITRO ESTERS **4a**,**4b**,**5a**, AND **5b**[a)]

Compound	Concn/mmol dm^{-3}	Electricity / F mol^{-1}	Yield/%		Recovery/%
			2	**3**	
4a	22.2	1.0	5	40	45
	22.2	1.8	8	61	0
	25.6[b)]	1.3	4	52	0
4b	20.2	1.0	Trace	43	49
	20.2	1.9	Trace	70	Trace
5a	20.0	1.0	37	0	0
5b	20.2	1.0	35	0	0

a) The electrolysis reactions were carried out at constant-current conditions in DMF–TBAP (0.1 mol dm^{-3}) using platinum electrodes. SCE was used as a reference. Current density was 0.45 mA cm^{-2} except for b) for which 0.85 mA cm^{-2} was used.

Similarly, axial isomers **5a** and **5b** were electrolyzed cathodically under conditions shown in Table 3. These gave dimer **2** in 37 and 35% yields, respectively possibly *via* a radical species as depicted in a previous paper.[2)]

Epimeric compounds were found to behave differently and the two competing reactions leading to **2** and **3** were dependent not only on the leaving group ability but also on the stereochemistry. The equatorial chloro and bromo derivatives behaved similarly to tosylate **1a** indicating the importance of leaving group ability on cyclosteroid formation. By contrast, the axial halogeno derivatives underwent dimerization reaction typical to acetate **1b**. The results can be rationalized by assuming that a favorite geometry for concerted elimination to form the cyclosteroid is possible only for an equatorial leaving group as in **12**.

The CV results again were found to be instructive: Those with reversible wave tend to give the dimer whereas those with irreversible wave the cyclosteroid. In other words those compounds forming short-lived anion radicals such as tosylate **1a** and equatorial halogeno derivatives **4a** and **4b** were lost rapidly in an intramolecular cyclosteroid formation, whereas those with long-lived anion radicals such as acetate **1b**, **5a**, and **5b** underwent an intermolecular coupling.

The Stereochemistry of 6β,6′β-Dinitro-3α,3′α-cholesta-4,4′-diene (2). Although the orientation of the 6-nitro group in compound **2** was established to be axial based on the NMR evidence the stereochemistry of ring junction between C-3 and C-3′ has remained unsettled.[2)]

There are several reports on the formation of dimeric steroids. Fried and Abraham[8)] reported the formation of a pinacol by the modified Birch reduction of estrone methyl ether. The stereochmistry at the ring juncture was deduced to be 3α,3′α by comparing the NMR spectra with those of monomeric compounds. Other examples of reductive coupling in steroidal ketones include dehydroepiandrosterone[9)] and some α,β-unsaturated ketones.[10)]

TABLE 4. THE 360 MHz ^{1}H NMR SPECTRAL DATA FOR DIMER **2**

Proton	Chemical shift/δ	Coupling constant/Hz	
C-2H$_{eq}$	2.020		
		$J_{2a,3e}$	3
C-3H$_{eq}$	2.175		
		$J_{3e,4}$	3
C-4H	5.905		
C-6H$_{eq}$	4.678		
		$J_{6e,7a}$	5.3
C-7H$_{eq}$	2.635		

Grignard reaction of 3-chlorocholestane[11)] or 3-chloro-5-cholestene[12)] produced a dimeric product, which was structually closely related to our dimer **2**, in a low yield but the configuration at C-3 and C-3′ remained unsettled.

The cathodic reaction of nitro olefin **1b** produced[2)] dimer **2** in a 54% yield, which separated out from the solution during the electrolysis. The examination of crude material by using NMR spectroscopy revealed that the material was a single compound although three stereoisomers, 3α,3′α-, 3α,3′β-, and 3β,3′β-types, were possible.

The proton NMR spectra of **2** were determined in $CDCl_3$ at the frequency of 360 MHz where nearly all proton signals in rings A and B were observed as separate signals. Five one-proton signals, C-2, 3, 4, 6, and 7H, were assigned by the first order analysis as shown in Table 4. The absorption due to C-3H appeared as a narrow peak at δ 2.175. The expanded spectrum clearly showed that it consisted of a double-doublet with J=3 Hz. The configuration of C-3H was deduced to be equatorial since $J_{2a,3e}=J^3_{e,4}=3$ Hz. Accordingly the stereochemistry of bonding between C-3 and C-3′ was established as α,α′-type.

Experimental

3β-Halogeno-6-nitro-5-cholestene (4a and 4b). 3β-Chloro-6-nitro-5-cholestene (**4a**) was prepared by the

nitration of 3β-chloro-5-cholestene,[4a] recrystallized from acetone, colorless needles, mp 153.5—154.5 °C. Similarly, 3β-bromo-6-nitro-5-cholestene (**4b**) was prepared,[4b] colorless needles from acetone, mp 158—159 °C.

3α-Chloro-6-nitro-5-cholestene (5a). To a stirred chloroform suspension (750 cm^3) containing 6-nitrocholestrol (20 g, 46 mmol) and barium carbonate (40 g), phosphorus pentachloride (37 g, 0.18 mol) was added under cooling in an ice bath. After 1.5 h stirring, water (400 cm^3) was added and the chloroform layer was washed with water, aq sodium carbonate, and water. Evaporation of chloroform, after being dried over calcium chloride, gave a solid which was purified by passing through a silica-gel column using hexane-benzene (4:1) as an eluent. Recrystallization from acetone gave **5a** (7.9 g, 38% yield) as colorless plates, mp 163—164 °C; IR (nujol) 1660 (C=C) and 1515 cm^{-1} (conj NO_2); ^1H NMR ($CDCl_3$) δ=0.72 (3H, s, C-18H), 1.15 (3H, s, C-19H), and 4.51 (1H, m, $w_{1/2}$=8.0 Hz, C-3H_{eq}).

Found: C, 72.13; H, 9.83; N, 3.20%. Calcd for $C_{27}H_{44}NO_2Cl$: C, 72.05; H, 9.85; N, 3.11%.

3α-Bromo-6-nitro-5-cholestene (5b). To a refluxing benzene solution (70 cm^3) of 6-nitrocholesterol (25 g, 58 mmol) was added phosphorus tribromide (7.5 cm^3, 79 mmol) in benzene (10 cm^3). After 2 h refluxing benzene was removed by evaporation and the residue was taken up in ether. The ethereal layer was washed with aq sodium hydroxide and water, and dried over magnesium sulfate. The product was purified by passing through a silica-gel column using hexane-benzene (2:1) as an eluent to give **5b** (5.7 g, 20%) after recrystallization from acetone, mp 154—155 °C; IR (nujol) 1660 (C=C) and 1515 cm^{-1} (conj NO_2); ^1H NMR ($CDCl_3$) δ=0.72 (3H, s, C-18H), 1.14 (3H, s, C-19H), and 4.65 (1H, m, $w_{1/2}$=8.0 Hz, C-3H_{eq})

Found: C, 65.53; H, 8.83; N, 2.85%. Calcd for $C_{27}H_{44}NO_2Br$: C, 65.57; H, 8.97; N, 2.83%.

Electrolyses. The controlled current electrolysis, using either 0.45 mA/cm^2 or 0.85 mA/cm^2, was carried out for **4a**, **4b**, **5a**, and **5b**. A Hokuto potentiostat/galvanostat HA-101 apparatus with max. output 30 V (1 A) was used. The cylindrical cell used previously[2] was equipped with a side arm for connecting the reference electrode, SCE, with the aid of two junction bridges, filled with satd KCl and DMF-TBAP (0.1 mol dm^{-3}) solutions. A ceramic thimble was used as a divider and was placed over a glass spacer to allow efficient stirring by a magnetic stirrer. A punched platinum electrode with an area of 118 cm^2 was used as the cathode together with a platinum wire anode placed in the above thimble. Representative examples are summarised in Table 3.

As an example the cathodic reduction of 3β-chloro-6-nitro-5-cholestene (**4a**) is described.

a) Electricity; 1 F mol^{-1}. After passing purified nitrogen for 20 m, a solution of **4a** (0.5 g, 1.1 mmol) in DMF (50 cm^3) containing 0.1 mol dm^{-3} of TBAP was electrolyzed at the current density of 0.42 mA cm^{-2} until 1 F mol^{-1} of electricity was consumed. DMF was evaporated *in vacuo* and the residue was extracted with ether. When the etherial solution was washed with water a part of TBAP was separated out, which was filtered off. The ethereal solution was washed with water again and dried. The ether extract contained **4a** (R_f=0.38) and a cyclosteroid **3** (R_f=0.35) together with dimer **6** as a slow moving fraction on examination by TLC. The mixture **4a** and **3** was separated on a Merck Lobar column using hexane-benzene (4:1) as an eluent. Recovery of **4a** was 45% while compounds **2**[2] and **3**[2] were obtained in 5 and 40% yields respectively.

b) Electricity; 1.8 F mol^{-1}. When the electrolysis was further continued, the voltage between the working and the reference electrodes was raised steadily. The electrolysis was switched to a controlled potential mode when the voltage reached −1.55 V. Current stopped essentially when 1.8F mol^{-1} of electricity had been consumed. The reaction mixture contained **2** (8%) and **3** (61%), no starting material being left.

Cyclic Voltammetry. The cyclic voltammetry measurements were carried out using the combination of a function generator, Hokuto HB-107A, and a potantiostat, Hokuto HA-101. For high-speed record, the output was stored in a wave-memory device, NF Circuit Block WM-812A. A modified H-type cell, separated by a sintered glass divider, is equipped with two side arms for connecting a nitrogen bubbler and a reference electrode, SCE, which is connected using two junction bridges filled with KCl and DMF-TBAP solutions. Molecular sieve 1A (Wako chemicals) was added to the bridge directly immersed in the cell to avoid contamination by water. Results are summarized in Tables 1 and 2. Representative CV curves are shown in Figure 1.

NMR Spectra. The ^1H NMR spectra were recorded with a Bruker WM-360 spectrometer.

We thank Professor Y. Kyogoku, The Protein Research Institute of Osaka University, for the NMR measurements.

References

1) Electron-organic Chemistry IX. For part VIII; See T. Sato, Y. Komeichi, and T. Wada, *Nippon Kagaku Kaishi*, **1984**, 1815.

2) T. Sato, Y. Komeichi, S. Kobayashi, and A. Omura, *Bull. Chem. Soc. Jpn.*, **55**, 520 (1982).

3) S. Stiner and P. Yates, *J. Chem. Soc., Chem. Commun.*, **1983**, 50.

4) a) K. F. Blau and C. G. Stuckwisch, *J. Org. Chem.*, **27**, 370 (1962); C. W. Shoppee and G. H. R. Summers, *J. Chem. Soc.*, **1952**, 3361; c) C. W. Shoppee, *ibid.*, **1946**, 1147.

5) R. E. Marker, *J. Am. Chem. Soc.*, **59**, 619 (1937).

6) A. J. Fry, "Synthetic Organic Electrochemistry," Harper and Row Publishers (1972), Chap. 3, pp. 79—95.

7) K. W. Bowers, R. W. Giese, J. Grimshaw, H. O. House, N. H. Kolodny, K. Kronberger, and D. K. Eoe, *J. Am. Chem. Soc.*, **92**, 2783 (1970).

8) J. Fried and N. A. Abraham, *Tetrahedron Lett.*, **1964**, 1879.

9) P. G. Marshall, "Rodd's Chemistry of Carbon Compounds", Second ed, ed by S. Coffey, Elsevier Scientific Publishing Co. (1970), Vol. II, Part D, Chap. 17, p. 336.

10) P. Bladon, J. Cornforth, and R. H. Jaeger, *J. Chem. Soc.*, **1958**, 863.

11) E. N. Squire, *J. Am. Chem. Soc.*, **73**, 2586 (1951).

12) R. H. Baker and E. N. Squire, *J. Am. Chem. Soc.*, **70**, 1487 (1948).

Amide Ion Formation and *N*-Alkylation of Aminoanthraquinones in the Presence of Potassium Hydroxide in Dimethyl Sulfoxide[1)]

Sadao Arai, Seijiro Kato, and Mitsuhiko Hida*
Department of Industrial Chemistry, Faculty of Technology, Tokyo Metropolitan University, Fukazawa, Setagaya-ku, Tokyo 158
(Recieved November 21, 1984)

Amide ions were formed by the deprotonation of the amino group of amino- and (monoalkylamino)-anthraquinones in the presence of powdered potassium hydroxide in dimethyl sulfoxide (DMSO). Under a nitrogen atmosphere these amide ions changed to their radical anions. The amide ions of 1-amino-anthraquinones reacted with excess alkyl halides to yield 1-alkylaminoanthraquinones, while the *N*-alkylation of 2-aminoanthraquinones afforded 2-dialkylaminoanthraquinones in good yields. 2-Aminobenzophenone underwent mono-*N*-alkylation, while 4-aminoazobenzene and p-nitroaniline underwent di-*N*-alkylation. It was also found that the carbanion of DMSO easily attacked the carbonyl group of the (dialkylamino)-anthraquinones.

During the course of our studies on the photonucleophilic reactions[2)] we examined a reaction between an hydroxide ion and aminoanthraquinones. We found that the color of the aminoanthraquinones rapidly changed from red or orange to green upon being mixed with powdered potassium hydroxide (KOH) in dipolar aprotic solvents such as dimethyl sulfoxide (DMSO), *N*,*N*-dimethylformamide (DMF), and pyridine. The color changes of aminoanthraquinones caused by the action of alkali hydroxide have attracted attention for a long time in relation to the mechanism of indanthrone formation by the fusion of 2-aminoanthraquinone with KOH.[3-5)] However, no decisive evidence regarding the mechanism of the color reactions has been presented, and the behavior of aminoanthraquinones in an alkaline media still remains obscure.

In this paper we describe in detail the behavior of aminoanthraquinones in an KOH–DMSO system under air and nitrogen atmosphere. It also describes how aminoanthraquinones and some aromatic amines having an electron-withdrawing group are easily *N*-alkylated by alkyl halides *via* their amide ions in the presence of powdered KOH in DMSO.

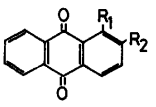

	1	2	3	4	5	6	7	8
R_1	NH_2	$NHCH_3$	$N(CH_3)_2$	N⟨ ⟩	H	H	H	H
R_2	H	H	H	H	NH_2	NHC_4H_9	$N(C_4H_9)_2$	N⟨ ⟩

Results and Discussion

The Formation of Amide Ion. When 1-aminoanthraquinone(**1**) was mixed with powdered KOH[6)] in DMSO at room temperature, the solution turned from orange to green. The visible absorption spectra of a **1**–KOH–DMSO system are shown in Fig. 1. Although a green solution also formed in dipolar aprotic solvents such as DMF and pyridine, DMSO was the most effective solvent among them, because of the good solubility of KOH. The color of the solution immediately turned from green to orange, the original color, after the addition of water, and **1** was nearly quantitatively recovered (Table 3, Entry 1). Although Shah reported the formation of indanthrone from **1** and KOH in DMSO at 60 °C[4,5)], no

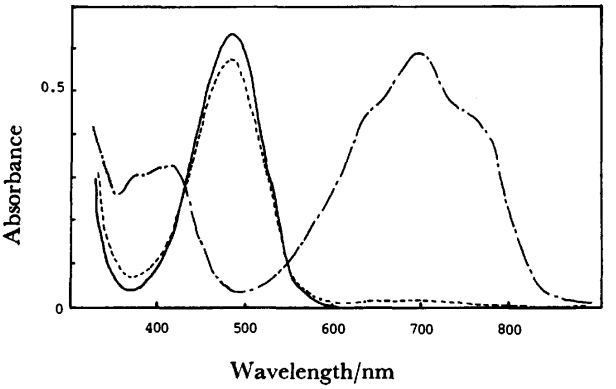

Fig. 1. Absorption spectra of **1** in DMSO.
[**1**]=*ca.* 1×10^{-4} mol·dm^{-3}. KOH free (——), in the presence of KOH(– – –), addition of H_2O into KOH–DMSO system(----).

indanthrone was observed in our system. In the green solution no paramagnetic species was detected by an ESR measurement. These results ruled out Brunner and Deffner's proposal[7] that the color change was caused by the formation of a charge-transfer complex between **1** and the carbanion of DMSO ($CH_3SO\overset{\ominus}{C}H_2$). Further, after the addition of alkyl halide to the green solution, it became red and an *N*-alkylated product was obtained in good yield at room temperature (*vide infra*). Consequently, we concluded that the color change of **1** in an KOH-DMSO solution was undoubtedly caused by the loss of a proton from the amino group to afford the amide ion:

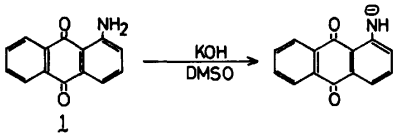

(1)

1

Similar results were also obtained in the case of 2-aminoanthraquinone(**5**); that is, the new absorption band appeared in the region of 550—850 nm (Table 1) and disappeared after the addition of water. The resulting green solution also afforded an *N*-alkylated product after the addition of an alkyl halide. Although Bradley reported that **5** exhibited no alkali color reaction in a pyridine containing methanolic KOH,[8] our results indicated that the amino group of **5** was easily deprotonated in an KOH-DMSO solution to give the amide ion.

Monoalkylaminoanthraquinones(**2** and **6**) also gave green solution on being mixed with powdered KOH in DMSO. Although the color returned to the original one after the addition of water, a TLC examination showed both the recovered one and the dealkylated product(**1** or **5**). These results show that the dealkylation occurs under basic conditions, although (monoalkylamino)anthraquinones have been known to give the dealkylated products under acidic conditions.[9]

The color of 1-dimethylaminoanthraquinone(**3**), having no N-H bond, was little affected by the addition of powdered KOH in DMSO. This result also supports the idea that the color changes of aminoanthraquinones were caused by the loss of a proton from the amino group to afford the amide ion.

Table 1. Absorption spectra of aminoanthraquinones in the presence of powdered KOH in DMSO

AQs	λ_{max}/nm		
	in DMSO	in KOH-DMSO	
		under air	under N_2
AQ	326	—	552, 515(sh), 410(sh), 393
1-NH_2AQ (**1**)	482	695	568, 510
1-CH_3NHAQ (**2**)	509	695	560, 510
2-NH_2AQ (**5**)	456	670	545, 432, 408
2-C_4H_9NHAQ (**6**)	474	706	545, 471

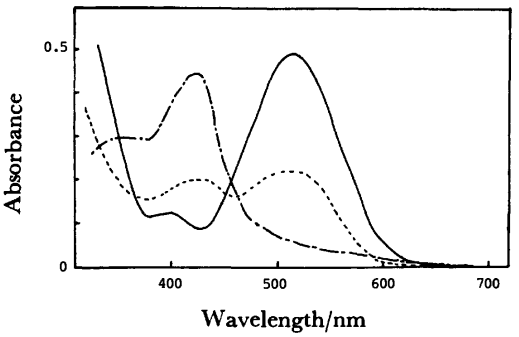

Fig. 2. Absorption spectra of **3** in DMSO. [**3**]=*ca.* 1×10^{-4} mol·dm^{-3}. KOH free(——), in the presence of KOH pretreated with methanol(———), addition of H_2O into KOH-DMSO system(----).

The Reaction of (Dialkylamino)anthraquinones with DMSO. In order to prepare a fine KOH powder, KOH was dissolved in anhydrous methanol and then methanol was evaporated *in vacuo*. When **3** was mixed with the resulting fine, white KOH powder in DMSO, the color immediately changed from red to yellow. Figure 2 shows that the absorption band (510 nm) of **3** disappeared and a new band appeared at 420 nm. The color change was hypsochromic, contrary to the formation of amide ion. Since no radicals were detected in the yellow solution during ESR measurements, the yellow species could not be the radical anion.

After the addition of D_2O to the yellow solution of **3**, the absorption spectra did not return to the original state and a TLC examination indicated two spots, red and yellow. It was found that the mass spectrum of the red component was identical with that of **3** and no deuteration took place. This result showed that the hypsochromic change was not attributed to the formation of the carbanion of aminomethyl group of **3**:

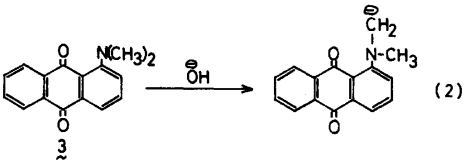

(2)

3

These color changes were not observed in a DMF solution. This result indicated that DMSO was responsible for the hypsochromic changes. The mass spectra[*m/z* 329(M+), 251, 78] clearly indicated that the yellow hygroscopic compound was an 1:1 adduct of **3** and DMSO. Actually, sulfur atoms were detected using the standard method with lead acetate. The IR spectrum showed the appearances of a hydroxyl group (3250 cm^{-1}) and a sulfinyl group (1015 cm^{-1}). ^{1}H NMR analysis also supported the idea that the new yellow compound was a DMSO addition com-

pound(**9**). However, the definitive evidences whether the addition occurred at 9- or 10-carbonyl group of **3** could not be obtained. These results indicated that potassium methylsulfinylmethanide (CH_3SOCH_2K) was formed by the reaction of DMSO with KOH pretreated with methanol (probably potassium methoxide[10]) and reacted with **3** to yield DMSO addition compound(**9**) as shown in Eq. 3.

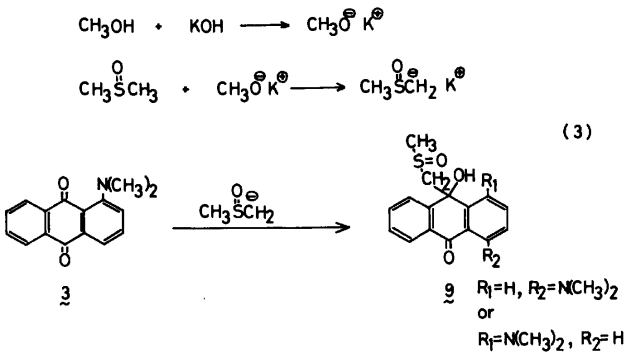

It has been reported that methylsulfinylmethanide, formed by the reaction of DMSO with potassium *t*-butoxide or sodium hydride, reacted quantitatively with benzophenone to yield the β-hydroxy sulfoxide.[11]

A similar hypsochromic change was also observed in the case of (dialkylamino)anthraquinones(**4**, **7**, and **8**)(Table 2). However, the color changes of aminoanthraquinones(**1**, **2**, **5**, and **6**), which were caused by the KOH pretreated with methanol, were the same as those treated with powdered KOH. These results indicate that methylsulfinylmethanide does not attack the amide ions.

The Formation of Radical Species under a Nitrogen Atmosphere. When anthraquinone was mixed with powdered KOH in DMSO under a nitrogen atmosphere, a red solution immediately resulted. The red solution showed a well-resolved ESR spectrum: The hyperfine coupling constants were a_{H_1}=0.94 G(1 G=10^{-4} T) and a_{H_2}=0.29 G. These values almost agreed with those of anthraquinone radical anion generated by electrochemical reduction.[12] These results suggest that aminoanthraquinones may be reduced to the radical anion in KOH–DMSO solution under a nitrogen atmosphere.

Under a N_2 atmosphere the color of **1** rapidly changed from orange to green similar to a system under air when mixed with powdered KOH in DMSO. This green solution, however, slowly turned to violet. The spectral changes are shown in Fig. 3. The violet solution was paramagnetic(g=2.003) and showed well-resolved ESR spectrum (Fig. 4). When air was bubbled through the violet solution, it became green and no radical species were detected. Further the addition of water caused this aerated solution to change from green to orange. These results revealed that the radical species was not a radical anion of **1**, but one of the amide ions:

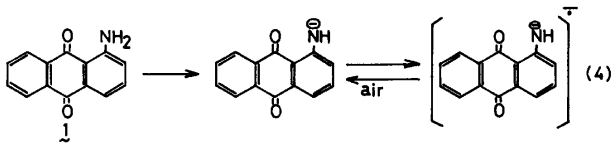

A radical anion would be formed by an electron transfer from a naked hydroxide ion to the amide ion.

The (monoalkylamino)anthraquinones(**2** and **6**)

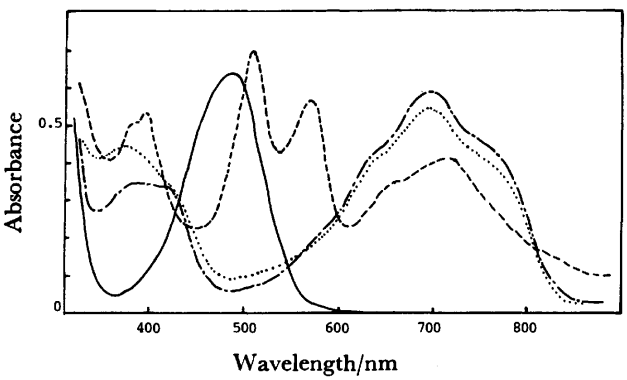

Fig. 3. Absorption spectra of **1** in DMSO under nitrogen atmosphere.
[**1**]=*ca.* 1×10^{-4} mol·dm^{-3}. KOH free(——), in the presence of KOH after 9 min(— — —), after 20 h(----), air was bubbled into the solution after 20 h(……).

Table 2. Absorption spectra of dialkylamino-anthraquinones in the presence of powdered KOH pretreated with methanol in DMSO

AQs	λ_{max}/nm		
	in DMSO	in KOH-DMSO	
		under air	under N_2
1-$(CH_3)_2$NAQ (**3**)	510	420	568, 535(sh), 402
1- NAQ (**4**)	520	405	569, 535(sh), 401, 387
2-$(C_4H_9)_2$NAQ (**7**)	491	372	542, 506(sh), 338
2- NAQ (**8**)	477	386	549, 510(sh), 397

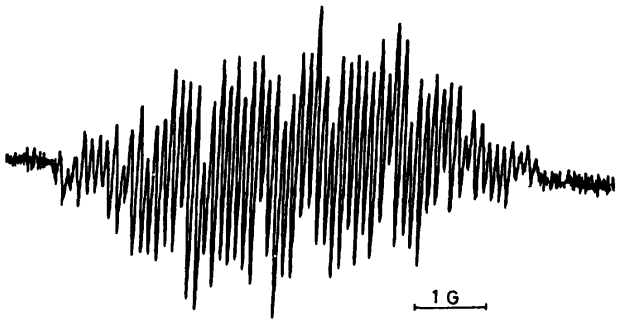

Fig. 4. ESR spectrum of the radical species of **1** in KOH–DMSO system under nitrogen atmosphere.

changed to the radical anions of their amide ions more rapidly than **1** and **5**. The spectral data are shown in Table 1. The colors of (dialkylamino)anthraquinones(**3**, **4**, **7**, and **8**) did not change in powdered KOH–DMSO system, while those in the presence of KOH pretreated with methanol in DMSO rapidly changed from red to yellow and then to violet. By the introduction of air into violet solution, a yellow solution was reproduced. The radical species would be the radical anion of the yellow DMSO addition compound.

The N-Alkylation of Aminoanthraquinones via their Amide Ions. The amide ions formed in an KOH–DMSO system would be easily *N*-alkylated by alkyl halides. The compound(**1** or **5**) was first converted to its amide ion by treating it with powdered KOH in DMSO under air. Then, excess alkyl halide was added at 30 °C. Table 3 lists the results of *N*-alkylation. In KOH-free systems the yields were negligibly small. However, the yields dramatically increased after the addition of powdered KOH. This result confirmed that the amino group of **1** and **5** was deprotonated in the KOH–DMSO system.

Table 3 shows that **1** was converted to its monoalkylamino derivatives while **5** gave the (dialkylamino)anthraquinones in high yields. The different reactivities between **1** and **5** toward alkyl halides may be explained as follows. 1-Alkylaminoanthraquinone was also deprotonated to give its amide ion, but the attack of alkyl halide to the amide ion may be

Table 3. *N*-Alkylation of aminoanthraquinones in KOH–DMSO system[a)]

Entry	AQ	RX	*t*/min	Recovered NH_2AQ/%	Product	Yield/%
1	1-NH_2AQ (**1**)	—	90	92	—	—
2[b)]	1-NH_2AQ (**1**)	*n*-C_4H_9I	60	96	1-C_4H_9NHAQ (**16**)	3
3	1-NH_2AQ (**1**)	*n*-C_4H_9I	5	0	1-C_4H_9NHAQ (**16**)	75
4	1-NH_2AQ (**1**)	*n*-C_4H_9I	60	0	1-C_4H_9NHAQ (**16**)	52
5	1-NH_2AQ (**1**)	*n*-$C_{16}H_{33}Br$	60	0	1-$C_{16}H_{33}$NHAQ (**17**)	51
6	1-NH_2AQ (**1**)	*n*-$C_{16}H_{33}Br$	450	0	1-$C_{16}H_{33}$NHAQ (**17**)	34
7	2-NH_2AQ (**5**)	—	90	95	—	—
8[b)]	2-NH_2AQ (**5**)	*n*-C_4H_9I	60	90	2-C_4H_9NHAQ (**18**)	7
9	2-NH_2AQ (**5**)	*n*-C_4H_9I	5	0	2-C_4H_9NHAQ (**18**)+ 2-$(C_4H_9)_2$NAQ (**19**)	8 87
10	2-NH_2AQ (**5**)	*n*-C_4H_9I	60	0	2-$(C_4H_9)_2$NAQ (**19**)	93
11	2-NH_2AQ (**5**)	*n*-$C_{16}H_{33}Br$	60	0	2-$(C_{16}H_{33})_2$NAQ (**20**)	70
12	2-NH_2AQ (**5**)	*n*-$C_{16}H_{33}Br$	450	0	2-$(C_{16}H_{33})_2$NAQ (**20**)	88

a) AQ=1 mmol, RX=10 mmol, KOH=10 mmol, DMSO=30 ml, temp 30 °C. b) KOH-free system.

Table 4. *N*-Alkylation with *n*-butyl iodide in KOH–DMSO system[a)]

Substrate	*t*/min	Product: Yield/%
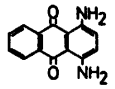 (**10**)	30	—[b)]
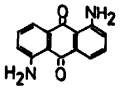 (**11**)	30	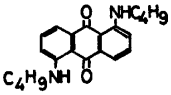 (**21**): 77 + 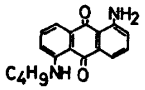 (**22**): 8
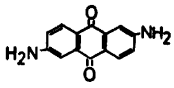 (**12**)	30	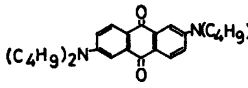 (**23**): 69 + 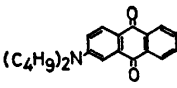 (**24**): 14
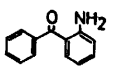 (**13**)	60	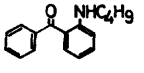 (**25**): 84
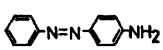 (**14**)	60	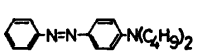 (**26**): 79
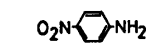 (**15**)	60	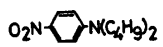 (**27**): 81

a) Substrate=1 mmol, *n*-C_4H_9I=10 mmol, KOH=10 mmol, DMSO=30 ml, at 30 °C. b) Several unidentified products were obtained.

sterically hindered by the adjacent carbonyl group. On the other hand, the alkylation of the amide ion of **5** is insensitive to such a steric factor. Consequently, **5** was easily converted into its dialkylamino derivatives, while the *N*-alkylation of **1** stopped at the stage of monoalkylation. When the reaction of **5** with butyl iodide was quenched with water after 5 min, 2-butylaminoanthraquinone was also obtained together with 2-dibutylaminoanthraquinone (Table 3, Entry 9). Table 3 also shows that the yield of *N*-alkylation of **1** decreased with the increase of the reaction time, contrary to the reaction of **5**.

The *N*-alkylation of diaminoanthraquinones also took place under similar conditions. 1,4-Diaminoanthraquinone(**10**) changed from violet to marine blue, 1,5-diaminoanthraquinone(**11**) from red to cobalt blue, and 2,6-diaminoanthraquinone(**12**) from orange to dark green in KOH–DMSO solution. By the addition of butyl iodide, **11** and **12** were easily *N*-alkylated, but in the reaction of **10** several unidentified products were formed. Table 4 shows that 1-amino group suffered monoalkylation and 2-amino group suffered dialkylation in analogy with monoaminoanthraquinone(**1** and **5**).

N-Alkylation of Aromatic Amines with Electron-withdrawing Group. The *N*-alkylation of aromatic amines activated by the electron-withdrawing group would also be expected by using an KOH–DMSO system. The color of 2-aminobenzophenone(**13**) was changed from yellow to red, *p*-aminoazobenzene(**14**) from orange to deep red, and *p*-nitroaniline(**15**) from yellow to orange when treated with powdered KOH in DMSO. The results of *N*-alkylation of these amines are shown in Table 4. Table 4 shows the very similar results to the case of aminoanthraquinones, that is, **13** underwent mono-*N*-alkylation, while **14** and **15** underwent di-*N*-alkylation.

Table 5. Physical properties and analytical data of alkylaminoanthraquinones and alkylaminoaromatics

Compound	^{1}H NMR (δ) in $CDCl_3$	Formula	MS $m/z(M^+)$		Calcd (%)	Found (%)
16[a]	0.8—1.9(7H, m, $CH_2C_3\underline{H}_7$), 3.0—3.4(2H, m, $NC\underline{H}_2$), 6.7—8.3(7H, m, aromatic), 9.64(1H, br s, N<u>H</u>)	$C_{18}H_{17}NO_2$	279	C:	77.39	77.56
				H:	6.14	6.20
				N:	5.02	4.91
17[a]	0.6—1.9(31H, m, $CH_2C_{15}\underline{H}_{31}$), 3.0—3.4(2H, m, $NC\underline{H}_2$) 6.7—8.8(7H, m, aromatic), 9.6(1H, br s, N<u>H</u>)	$C_{30}H_{41}NO_2$	447	C:	80.49	80.21
				H:	9.23	9.52
				N:	3.13	3.10
18[b]	——	$C_{18}H_{17}NO_2$	279	C:	77.39	77.00
				H:	6.14	6.01
				N:	5.02	4.83
19[a]	0.7—2.0(14H, m, $CH_2C_3\underline{H}_7$), 3.33(4H, t, $NC\underline{H}_2$) 6.6—8.3(7H, m, aromatic)	$C_{22}H_{25}NO_2$	335	C:	78.77	78.90
				H:	7.51	7.39
				N:	4.18	4.07
20[a]	0.7—2.1(62H, m, $CH_2C_{15}\underline{H}_{31}$), 3.40(4H, t, $NC\underline{H}_2$) 6.6—8.3(7H, m, aromatic)	$C_{46}H_{73}NO_2$	672	C:	82.21	81.98
				H:	10.95	11.38
				N:	2.08	2.03
21	0.8—2.0(14H, m, $CH_2C_3\underline{H}_7$), 3.1—3.5(4H, m, $NC\underline{H}_2$) 7.0—7.8(7<u>H</u>, m, atomic), 9.88(1H, br s, NH)	$C_{22}H_{26}N_2O_2$	350	C:	75.40	75.42
				H:	7.48	7.40
				N:	7.99	7.87
22	0.8—2.1(7H, m, $CH_2C_3\underline{H}_7$), 3.1—3.6(2H, m, $NC\underline{H}_2$) 6.6—7.9(8H, m, aromatic), 9.9(1H, br s, NH)	$C_{18}H_{18}N_2O_2$	294	C:	73.45	73.61
				H:	6.16	6.32
				N:	9.52	9.27
23	0.8—1.9(21H, m, $CH_2C_3\underline{H}_7$), 3.50(8H, t, $NC\underline{H}_2$) 6.8—8.3(6H, m, aromatic)	$C_{30}H_{42}N_2O_2$	462	C:	77.88	77.60
				H:	9.15	8.99
				N:	6.05	5.85
24	0.8—1.9(21H, m, $CH_2C_3\underline{H}_7$), 3.1—3.7(6H, m, $NC\underline{H}_2$) 4.60(1H, br s, NH), 6.8—8.3(6H, m, aromatic)	$C_{26}H_{34}N_2O_2$	406	C:	76.81	76.65
				H:	8.43	8.24
				N:	6.88	6.71
25	0.7—2.1(7H, m, $CH_2C_3\underline{H}_7$), 3.25(2H, t, $NC\underline{H}_2$) 6.4—8.1(9H, m, aromatic), 8.69(1H, br s, NH)	$C_{17}H_{19}NO$	253		——	
26	0.7—2.0(14H, m, $CH_2C_3\underline{H}_7$), 3.34(2H, t, $NC\underline{H}_2$) 6.6—8.1(9H, m, aromatic)	$C_{20}H_{27}N_3$	309		——	
27	0.7—1.9(14H, m, $CH_2C_3\underline{H}_7$), 3.34(4H, t, $NC\underline{H}_2$) 6.53(2H, d, aromatic), 8.01(2H, d, aromatic)	$C_{14}H_{22}N_2O_2$	250		——	

a) NMR data in CCl_4. b) The NMR spectra could not be measured because of low solubility.

Although the *N*-alkylation of nitrogen heterocyclic compounds and aromatic amines by the use of various bases has been reported,[13] these results indicate that the reaction using an KOH–DMSO system affords a rapid, simple, and mild method of *N*-alkylation of aromatic amines.

Experimental

Materials. Commercial reagent-grade chemicals were used without further purification. Dimethyl sulfoxide was distilled twice under reduced pressure and stored under a nitrogen atmosphere. Aminoanthraquinones (Sumitomo Chemical Co.) were purified as follows: **1** and **2** were purified by alumina column chromatography and recrystallized from benzene. The compounds **10** and **11** were purified by recrystallization from toluene. The purification of **5** and **12** were performed by Maki's method.[14] Compound **3** was prepared by the condensation of 1-chloroanthraquinone and dimethylamine in ethanol and purified by column chromatography on silica gel with benzene as eluent and recrystallized from ethanol (Found: C, 76.53; H, 5.16; N, 5.50%). The Preparation of **4** and **8** were performed by the reaction of 1- and 2-chloroanthraquinone with piperidine and purified by column chromatography on silica gel and recrystallized from ethanol (Found: **4**; C, 78.24; H, 5.88; N, 4.86%. **8**; C, 78.13; H, 5.71; N, 4.63%). The compound **13** was prepared according to the literature[15].

Instruments. Visible spectra were recorded with a Shimadzu UV-210 spectrometer. ^{1}H NMR spectra were measured with a Hitachi R-24 spectrometer in $CDCl_3$ and CCl_4 with tetramethylsilane and in D_2O with sodium 3-trimethylsilyl-1-propanesulfonate as an internal standard. IR spectra were recorded on a JASCO IRA-1 spectrophotometer. Mass spectra were recorded with a JEOL JMS-D 100 mass spectrometer by direct insertion. The ESR spectra were taken on a JEOL-PE-3X instrument, equipped with a 100 KHz field modulation unit. Elementary analyses were performed on a Yanaco MT2 CHN corder.

Reaction of 1-Dimethylaminoanthraquinone. Powdered KOH 560 mg (10 mmol) was dissolved in anhydrous methanol (20 ml) and then solvent was evaporated under reduced pressure. The fine, powdered KOH was dissolved in 100 ml of DMSO. 251 mg (1 mmol) of **3** was added to the solution and stirred for 10 min at room temperature. The resulting orange mixture was poured into water (700 ml), followed by extraction with benzene several times. After the benzene was evaporated, the residue was chromatographed on a silica gel by employing first benzene and then benzene–ethanol(20+1) as eluents. The early red fractions contained 28 mg of the starting material **3** (11%). The later yellow fractions contained 279 mg of DMSO addition compound(**9**)(85%). The spectral properties of **9** are as follows: ^{1}H NMR(D_2O) 2.34 (s, 3H), 2.84 (s, 6H), 3.36 (s, 2H), 6.9—8.1 (m, 7H). IR(KBr) 3250, 1640, 1268, 1015, 785, 695 cm^{-1}. MS(*m/z*) 329(M+), 312, 251, 248, 78. UV(C_2H_5OH) 424 nm.

Procedure for N-Alkylation. A typical procedure is described for the reaction of **1** with butyl iodide. The compound **1** (1 mmol) was stirred with powdered KOH (10 mmol) in DMSO (30 ml) for 30 min at 30 °C. The color of the mixture changed rapidly from red to green. Then, butyl iodide (10 mmol) was added to the mixture and the solution was stirred for 5 min at 30 °C. By the addition of butyl iodide, the color of the solution turned to dark red and the reaction was quenched with water (700 ml). The mixture was then extracted with benzene several times, washed with water and evaporated. Then the residue was submitted to column chromatography on silica gel using benzene as the eluent. The physical properties and analytical data for the *N*-alkylated products are given in Table 5.

We wish to express their thanks to Dr. Kinji Anda and his colleagues of Tokyo Metropolitan Industrial Technology Center for mass spectral measurements.

References

1) A part of this work has been reported in a preliminary form: S. Arai, T. Yamagishi, and M. Hida, *Chem. Lett.*, **1981**, 1789.

2) S. Kato, H. Inoue, and M. Hida, *Nippon Kagaku Kaishi*, **1978**, 1411.

3) W. Bradley and H. E. Nursten, *J. Chem. Soc.*, **1951**, 2170.

4) M. K. Shah and K. H. Shah, *Indian J. Technol.*, **13**, 312 (1975).

5) D. C. Mansharamani, M. K. Shah, and K. H. Shah, *J. Indian Chem. Soc.*, **53**, 1671 (1976).

6) Powdered KOH was prepared by grounding a commercial KOH (Tokyokasei GR) with an ordinary mortar and pestle, followed by vacuum drying.

7) E. Brunner and U. Deffner, *Melliand Textilber. Int.*, **50**, 437 (1969).

8) W. Bradley, *J. Soc. Dyers Colour.*, **58**, 2 (1951); W. Bradley and E. Leete, *J. Chem. Soc.*, **1951**, 2129.

9) W. Bradley and R. F. Maisey, *J. Chem. Soc.*, **1954**, 247.

10) J. C. R. Kelly and P. E. Snyder, *J. Am. Chem. Soc.*, **73**, 4114 (1951).

11) E. J. Corey and M. Chaykovsky, *J. Am. Chem. Soc.*, **84**, 867 (1962); A. Ledwith and N. McFarlane, *Proc. R. Soc. London, Ser. A.*, **1964**, 108.

12) E. W. Stone and A. H. Maki, *J. Chem. Phys.*, **36**, 1944 (1962).

13) K. Sukata, *Bull. Chem. Soc. Jpn.*, **56**, 280 (1983), and references therein.

14) T. Maki, *Kogyo Kagaku Zasshi*, **36**, 174 (1933).

15) *Org. Synth.*, Col. Vol. **IV**, 34.

Pentoside Synthesis by Dehydrative Glycosylation. Synthesis of *O*-α-L-Arabinofuranosyl-(1→3)-*O*-β-D-xylopyranosyl-(1→4)-D-xylopyranose

Shinkiti KOTO,* Naohiko MORISHIMA, Kazuhiro TAKENAKA, Chisa UCHIDA, and Shonosuke ZEN
School of Pharmaceutical Sciences, Kitasato University, Shirokane, Minato-ku, Tokyo 108
(Received December 5, 1984)

O-α-L-Arabinofuranosyl-(1→3)-*O*-β-D-xylopyranosyl-(1→4)-D-xylopyranose isolated from the hydrolyzate of corncobs arabinoxylan was synthesized by way of dehydrative glycosylation.

Dehydrative glycosylation has been used in the synthesis of several trisaccharides.[1] This report deals with the synthesis of the trisaccharide, *O*-α-D-arabinofuranosyl-(1→3)-*O*-β-D-xylopyranosyl-(1→4)-D-xylopyranose (**25**), isolated from the hydrolytic products of corncobs arabinoxylan by a xylanase from *Streptomyces* sp. E-86[2], using dehydrative glycosylation.[3]

Direct benzylation of methyl β-D-xylopyranoside (**1**) in benzyl chloride in the presence of lithium hydroxide and dimethyl sulfoxide afforded the 2,4-dibenzyl ether **2** in a practical yield. Benzylation of the acetate **5** in benzyl chloride with potassium hydroxide gave mainly the 2,4-dibenzyl ether **6**. On the other hand, cyclohexylidenation of benzyl α-D-xylopyranoside (**4**) gave the 2,3-acetal **7** preferentially. This was derived into the 2,3-dibenzyl ether **9** *via* a sequence of reactions: allylation, decyclohexylidenation, benzylation and deallylation. The location of the unprotected hydroxyl group of these partially benzylated xylosides was determined by observing H-1 NMR spectra of their acetates (Table 1).

Methyl 2,4-di-*O*-benzyl-α-D-xylopyranoside (**10**)[4] was allylated and then hydrolyzed into the protected xylose **11**. The 2,4-dibenzyl ether **6** was acetylated and then treated with titanium tetrachloride, followed by hydrolysis on moist silica gel, to furnish the protected xylose **12**.[5] The corresponding benzoate **13** was also obtained similarly from **6** *via* benzoylation.

Using these donors and acceptors, a stepwise synthesis of **25** was then attempted as shown in Fig. 1. The first β-xylosylation was carried out using only the allylated donor **11** for the acceptor **9** and the NSD mixture composed of *p*-nitrobenzenesulfonyl chloride (NsCl), silver trifluoromethanesulfonate (AgOTf), and 1,8-diazabicyclo [5.4.0] undec-7-ene (DBU). The

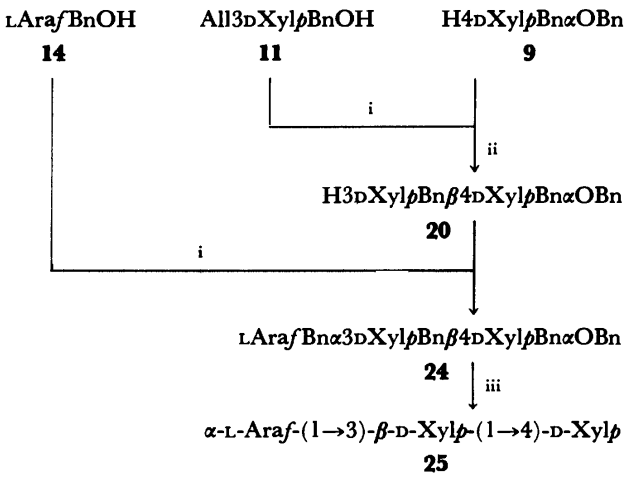

i *p*-$NO_2C_6H_4SO_2Cl + CF_3SO_3Ag$ + DBU
ii Deallylation (*t*-BuOK/DMSO and then $HCl/Me_2CO + H_2O$)
iii Debenzylation (H_2/Pd-C/AcOH)

Fig. 1. Synthetic diagram of α-L-Araf-(1→3)-β-D-Xylp-(1→4)-D-Xylp.

Table 1. Data of H-1 NMR of the acetate of the partially protected D-xylopyranosides (at 90 MHz in $CDCl_3$ with TMS)

Compound	H-1	H-2	H-3	H-4	H-5e	H-5a	Me	Ac
	$J_{1,2}$	$J_{2,3}$	$J_{3,4}$	$J_{4,5e}$	$J_{4,5a}$	$J_{5e,5a}$		
2	4.29	3.27	5.13	—	3.95	—	3.51	1.91
	7.5	9.3	9.3	4.2	—	10.2		
6	4.41	3.27	5.12	—	—	—	3.34	1.93
	7.5	9.0	9.0	—	—	—		
7	5.05	3.38	3.20	4.88	3.78	4.01	—	1.97
	3.0	9.8	9.8	5.2	9.8	9.8		
8	5.11	4.81	3.99	3.49	3.93	3.79	—	2.06
	3.6	10.5	8.4	5.1	9.8	9.8		
9	4.80	3.50	3.97	4.95	3.73	3.51	—	1.93
	3.6	9.3	9.3	6.3	10.8	10.8		

reaction proceeded with a poor selectivity. Similar xylosylation using the acylated donors, **12** and **13**, gave the α-anomer selectively. The acyloxyl group at the C-3 position appears to effect for the formation of the α-anomer in this dehydrative xylosylation. The second glycosylation of the xylobiose derivarive **20** was performed using the arabinofuranosyl donor **14**

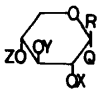

All=-$CH_2CH=CH_2$
Bn=-CH_2Ph
ME=-CH_2CH_2OMe

	Q	R	X	Y	Z
1	H	OMe	H	H	H
2	H	OMe	Bn	H	Bn
3	OH,	H	H	H	H
4	OBn	H	H	H	H
5	H	OME	Ac	Ac	Ac
6	H	OME	Bn	H	Bn
7	OBn	H			H
8	OBn	H	H		
9	OBn	H	Bn	Bn	H
10	OMe	H	Bn	H	Bn
11	OH,	H	Bn	All	Bn
12	OH,	H	Bn	Ac	Bn
13	OH,	H	Bn	Bz	Bn

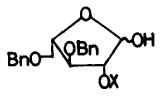

14

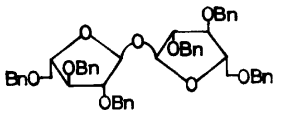

16

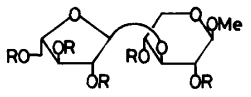

15 R=Bn
17 R=H

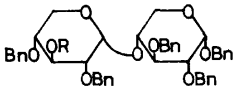

18 R=All
21 R=H
22 R=Ac
23 R=Bz

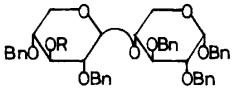

19 R=All
20 R=H

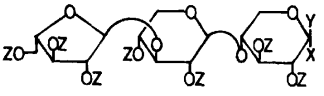

24 X=OBn; Y=H; Z=Bn
25 X, Y=OH, H; Z=H

and the NSD mixture. The condensation gave the desired α-anomer selectively. The acceptor **2** was also α-arabinosylated. Deprotection of the fully benzylated trisaccharide **24** gave the trisaccharide **25**, of which C-13 NMR spectrum was consistent with the proposed structure as shown in Table 3. The optical rotation value of **25** agreed well with the expected value based on the data of the relevant compounds (Table 4). Therefore, these results indicate that the trisaccharide from corncobs arabinoxylan has the structure that has been proposed.[2]

Experimental

The instruments used for determining the physical characters of the compounds and chromatography have been described in previous reports.[1] The evaporation of the solvent was carried out under reduced pressure at 35—45 °C unless otherwise stated. Data regarding the chemical shifts of the anomeric carbon are in Table 2. Analytical and physical data of the compounds are summarized in Table 5.

Methyl 2,4-Di-O-benzyl-β-D-xylopyranoside (2). A mixture of methyl β-D-xylopyranoside (**1**, Pfanstiehl, 100 mg, 0.61 mmol), lithium hydroxide (88 mg)[6], dimethyl sulfoxide (0.35 ml) and benzyl chloride (2.0 ml) was vigorously stirred at 130 °C for 0.5 h. After the usual work-up, the mixture was chromatographed (gradient, toluene 2-butanone=100/1→1/1) to give the tribenzyl ether (33 mg, 2%. Found: C, 74.56; H, 6.97%), **2** (111 mg, 53%) and then a mixture of the 2,3- and the 3,4-dibenzyl ethers (78 mg, 37%. Found: C, 69,82; H, 6.95%).

Benzyl α-D-xylopyranoside (4). A mixture of D-xylose **3**, Wako, 15 g, 100 mmol), benzyl alcohol (15 ml) and *p*-toluenesulfonic acid monohydrate (4.4 g) was stirred at 75 °C for 1.5 h. After the addition of chloroform (30 ml) and triethylamine (3.6 ml), the mixture was directly chromatographed (chloroform/methanol=100/1→1/1). The obtained crude solid (6.2 g) was recrystallyzed from ethyl acetate containing 2-butanone to give pure **4** (4.5 g, 19%).

2-Methoxylethyl 2,3,4-tri-O-benzyl-β-D-xylopyranoside (5). Acetic acid (4.0 ml) was added into a stirred suspension of **3** (3.0 g, 20 mmol) in acetyl bromide (7.0 m) at 0 °C.[7]

Table 2. Chemical shifts of the anomeric carbon of the protected glycosides (at 25.1 MHz in $CDCl_3$ with TMS)

Compound	$C_{xyl}-1$ α	$C_{xyl}-1$ β	$C_{xyl}-1'$ α	$C_{xyl}-1'$ β	$C_{ara}-1''$ α
2		104.9			
9	96.1				
15		105.4			106.7
18	95.6		99.0		
19	95.8			102.8	
20	95.9			102.4	
21	95.5		98.3		
22	95.5		98.6		
23	95.5		98.5		
24	95.8			102.7	106.7

Table 3. C-13 NMR data of methyl 3-*O*-(α-L-arabinofuranosyl)-β-D-xylopyranoside and *O*-α-L-arabinofuranosyl-(1→3)-*O*-β-D-xylopyranosyl-(1→4)-D-xylopyranose (at 25.1 MHz in D_2O with ext. TMS)

C	XX[8]	MXX[9]	17	25
1α	92.8			93.4
1β	97.8	105.1		97.9
2α	72.3			72.7
2β	74.9	74.0		75.3
3α	71.9			72.3
3β	74.9	75.0		75.3
4α	77.5			77.9
4β	77.3	77.7		77.9
5α	59.8			60.2
5β	63.9	64.1		64.3
1′	102.9	103.1	105.2	103.1
2′	73.7	74.0	74.2	74.1
3′	76.5	76.9	83.3	83.0
4′	70.1	70.4	69.2	69.2
5′	66.1	66.5	66.3	66.3
1″			109.6	109.5
2″			82.6	82.6
3″			77.9	77.9
4″			85.4	85.4
5″			62.6	62.6

XX=4-*O*-(β-D-xylopyranosyl)-D-xylose, MXX=methyl 4-*O*-(β-D-xylopyranosyl)-β-D-xylopyranoside.

After being stirred at room temperature for 2 h, evaporation and co-evaporation with toluene gave a syrup. This was stirred in nitromethane (9 ml) containing 2-methoxyethanol (4.6 ml) and mercury(II) cyanide (8.6 mg). After the usual processing, the chromatography (toluene/2-butanone= 100/1→1/1) of the mixture gave crude solid (5.1 g), which was crystallized with hexane containing diisopropyl ether to give **5** (1.7 g, 26%).

2-Methoxyethyl 2,4-Di-O-benzyl-β-D-xylopyranoside (6). A mixture of **5** (1.0 g, 3.0 mmol), potassium hydroxide

Table 4. Optical rotation value of *O*-α-L-arabinofuranosyl-(1→3)-*O*-β-D-xylopyranosyl-(1→4)-D-xylopyranose and related substances in water

Compound	$[\alpha]_D$(deg)	$[M]_D$(obsd)	$[M]_D$(calcd)
X	+19[10]	+29	
MX	−66[11]	−108	
MA	−135[12]	−221	
XX	−25[13]	−71	−79(X+MX)
AX	−77[2]	−217	−192(X+MA)
17	−113	−334	−329(MX+MA)
25	−17[14]	−70	−305(X+**17**)
	−88[2]	−364	−292(MA+XX)
	−72	−298	

X=D-xylose, MX=methyl β-D-xylopyranoside, MA=methyl α-L-arabinofuranoside, XX=4-*O*-(β-D-xylopyranosyl)-D-xylose, AX=3-*O*-(α-L-arabinofuranosyl)-D-xylose.

Table 5. Analytical and physical data of the compounds

Cpd.	Mp (θ_m/°C)	$[\alpha]_D^{20}$ (*c*, solv)[a]	Mol Form	Calcd(%)		Found(%)		Lit.
				C	H	C	H	
2		+2° (0.5, C)	$C_{20}H_{24}O_5$	69.75	7.02	69.71	6.89	b)
4	128—129	+140° (0.7, W)	$C_{12}H_{16}O_5$	59.99	6.71	59.55	6.67	c)
5	84—86	−49° (0.6, C)	$C_{14}H_{22}O_9$	50.30	6.63	50.26	6.61	d)
6		+8° (0.8, C)	$C_{22}H_{28}O_6$	68.02	7.27	68.16	7.21	
7		+109° (3.1, C)	$C_{18}H_{24}O_5$	67.48	7.55	67.24	7.59	
8		+118° (5.8, C)				67.18	7.59	
9	82—83	+90° (0.2, C)	$C_{26}H_{28}O_5$	74.26	6.71	74.53	6.68	e)
11	88—90	+17° (0.7, C)	$C_{22}H_{26}O_5$	71.33	7.07	70.94	6.97	
12		+19° (1.2, C)	$C_{21}H_{24}O_6$	67.73	6.50	67.22	6.42	
13	68—71	+46° (1.9, C)	$C_{26}H_{26}O_6$	71.87	6.03	71.27	5.93	
15		−7° (1.1, C)	$C_{46}H_{50}O_9$	73.97	6.75	74.27	6.66	
16		−65° (0.1, C)	$C_{52}H_{54}O_9$	75.88	6.61	75.48	6.59	
17		−113° (1.2, W)	$C_{11}H_{20}O_9 \cdot 1.5H_2O$	40.87	7.17	40.53	6.86	
18		+78° (1.4, C)	$C_{48}H_{52}O_9$	74.59	6.78	74.36	6.71	
19		+36° (1.4, C)				74.26	6.67	
20		+39° (2.2, C)	$C_{45}H_{48}O_9$	73.75	6.60	73.55	6.61	
21		+92° (2.5, C)				73.29	6.70	
22		+86° (1.8, C)	$C_{47}H_{50}O_{10}$	72.85	6.50	72.98	6.45	
23		+82° (2.5, C)	$C_{52}H_{52}O_{10}$	74.62	6.26	74.85	6.21	
24		+14° (1.5, C)	$C_{71}H_{74}O_{13}$	75.11	6.57	74.76	6.59	
25		−72° (0.5, W)	$C_{15}H_{26}O_{13} \cdot 0.5H_2O$	42.26	6.43	42.15	6.58	f)

a) C=$CHCl_3$, W=H_2O. b) Ref. 15. $[\alpha]_D^{23}$ +3° (*c* 1, $CHCl_3$). c) Ref. 16. mp 127—128.5 °C, $[\alpha]_D^{25}$ +139.2° (*c* 4, H_2O). d) Ref. 17. mp 92 °C, $[\alpha]_D^{23}$ −59.8° (*c* 2, $CHCl_3$). e) Ref. 18. $[\alpha]_D^{28}$ +15° (*c* 2, $CHCl_3$). f) Ref. 2. $[\alpha]_D^{22}$ −88° (*c* 2.5, H_2O), Ref. 14. $[\alpha]_D^{25}$ −17.3° (*c* 0.34, H_2O).

(1.5 g), and benzyl chloride (20 ml) was vigorously stirred at 120 °C for 16 h, followed by chromatography (toluene/2-butanone=100/1→1/1), to afford the tribenzyl ether (0.26 g, 18%), **6** (0.64 g, 55%), and then a mixture of the other dibenzyl ethers (0.32 g, 28%).

Benzyl 2,3- and 3,4-O-Cyclohexylidene-α-D-xylopyranosides (7 and 8). A mixture of **4** (800 mg, 3.3 mmol), 1,1-dimethoxycyclohexane (2 ml), *p*-toluenesulfonic acid monohydrate (10 mg), and *N,N*-dimethylformamide (5 ml) was heated at 120 °C for 4 h. After the addition of triethylamine (0.1 ml), the solution was evaporated at 70 °C and the obtained residue was chromatographed (toluene/2-butanone=100/1→1/1) to give **8** (117 mg, 11%) and then **7** (451 mg, 42%).

Benzyl 2,3-Di-O-benzyl-α-D-xylopyranoside (9). A mixture of **7** (0.41 g, 1.3 mmol), sodium hydride (≈60%, 0.2 g) and allyl bromide (4 ml) was stirred at 80 °C for 1 h. The mixture was filtered and the filtrate was concentrated to give a syrup which was dissolved in aq acetic acid (80%, 6 ml) containing acetone (1 ml). After kept standing for 1 h at room temperature, the solution was evaporated and co-evaporated with toluene. The obtained syrup was heated in benzyl chloride (4.5 ml) containing crushed potassium hydroxide (1.5 g) at 120 °C for 2 h. After the usual work-up, the mixture was chromatographed (toluene/2-butanone=100/1→1/1). The fully benzylated derivative thus obtained (0.54 g, 92% from **7**) was heated in dimethyl sulfoxide (2 ml) containing potassium *t*-butoxide (0.4 g) under a stream of nitrogen at 115 °C for 1 h. After dilution with toluene, the solution was washed with water and evaporated. The obtained residue was treated with acetone (10 ml) containing aq hydrochloric acid (2 M†, 0.5 ml) at room temperature for 0.5 h. After the addition of sodium hydrogencarbonate, the mixture was evaporated and chromatographed (toluene/2-butanone=100/1→1/1) to afford **9** (204 mg, 48% from **7**).

3-O-Allyl-2,4-di-O-benzyl-D-xylopyranose (11). Methyl 2,4-di-*O*-benzyl-α-D-xylopyranoside (**10**) (680 mg, 2.0 mmol) was heated in allyl bromide (7 ml) containing sodium hydride (≈60%, 168 mg) at 80 °C for 0.5 h. After filtration and evaporation, the residue was heated in aq acetic acid (80%, 5 ml) containing aq sulfuric acid (3 M, 0.8 ml) at 90 °C for 0.5 h. After the addition of sodium hydrogencarbonate (0.6 g), evaporation and chromatography (toluene/2-butanone=100/1→1/1), gave **11** (380 mg, 52%).

3-O-Acetyl-2,4-di-O-benzyl-D-xylopyranose (12). Compound **6** (245.9 mg, 0.63 mmol) was treated with acetic anhydride (2 ml) and pyridine (2 ml) overnight. The pure acetate (278.2 mg, $[\alpha]_D^{20}$ +5° (*c* 0.8, $CHCl_3$). Found: C, 67.67; H, 6.94%) obtained after a brief chromatography (toluene/2-butanone=10/1) was dissolved in dichloromethane (4.5 ml) and then treated with titanium tetrachloride (41 μl) for 15 min at room temperature. After the usual work-up, the mixture was adsorbed on a silica-gel column and chromatographed (toluene/2-butanone=100/1→1/1) to afford **12** (164.1 mg, 67%).

3-O-Benzoyl-2,4-di-O-benzyl-D-xylopyranose (13). Compound **6** (317.7 mg, 0.82 mmol) was benzoylated with benzoyl chloride (0.2 ml) and pyridine (2 ml) overnight. After the usual processing the mixture was chromatographed (toluene/2-butanone=20/1) to give pure benzoate ($[\alpha]_D^{20}$ +24° (*c* 0.8, $CHCl_3$). Found: C, 70.26, H; 6.46%). This was treated with titanium tetrachloride (57 μl) in dichloromethane (7.2 ml), followed by work-up as described for **12**, to afford **13** (234.2 mg, 73%).

Methyl 3-O-(2,3,4-Tri-O-benzyl-α-L-arabinofuranosyl)-β-D-xylopyranoside (15). DBU (45.5 μl) was added into a stirred mixture of 2,3,4-tri-*O*-benzyl-L-arabinofuranose (**14**, Pfanstiehl, 57.3 mg, 0.14 mmol), **2** (36.1 mg, 0.10 mmol), NsCl (67.5 mg), and AgOTf (78.3 mg) in dichloromethane (0.96 ml) at −55 °C. The bath temperature was rised to 0 °C at which temperature the mixture was stirred overnight. The mixture was chromatographed (toluene/2-butanone=100/1→1/1) to give the self-condensation product **16** (15.8 mg, 14%; δ_C ($CDCl_3$, TMS) 102.5 (C-1), 88.3, 84.1, 81.5, 73.6, 72.4, 72.1, 70.1) and **15** (57 mg, 73%).

Methyl 3-O-(α-L-Arabinofuranosyl)-β-D-xylopyranoside (17). The hydrogenolysis of **15** (50 mg, 0.067 mmol) over palladium on carbon (10%, 40 mg) in acetic acid (6 ml) under 340 kPa of hydrogen at room temperature overnight, followed by chromatography (chloroform/methanol=10/1=1/1), affofded **17** (15.9 mg, 80%).

Benzyl 4-O-(3-O-Allyl-2,4-di-O-benzyl-α- and -β-D-xylopyranosyl)-2,3-di-O-benzyl-α-D-xylopyranoside (18 and 19). DBU (53 μl) was added into a stirred mixture of **11** (100 mg, 0.27 mmol), **9** (87.3 mg, 0.21 mmol), NsCl (78.2 mg), and AgOTf (90.9 mg) in dichloromethane (1.0 ml) at −55 °C. The bath temperature was rised to 0 °C and then the mixture was stirred overnight. The chromatography of the reaction mixture (toluene/2-butanone=100/1→1/1) furnished **18** (27.6 mg, 17%) and then **19** (76.2 mg, 47%).

Benzyl 4-O-(2,4-Di-O-benzyl-β-D-xylopyranosyl)-2,3-di-O-benzyl-α-D-xylopyranoside (20). A mixture of **19** (93.1 mg, 0.12 mmol) and potassium *t*-butoxide (77 mg) in dimethylsulfoxide (0.4 ml) was heated at 120 °C for 6 h under a stream of nitrogen. Toluene and water were added to the solution and the organic layer was evaporated and then hydrolyzed in acetone (4 ml) containing aq hydrochloric acid (2 M, 0.1 ml) at room temperature. After addition of sodium hydrogencarbonate and concentration, chromatography (toluene/2-butanone=100/1→1/1) of the residue gave **20** (20.7 mg, 53%).

Benzyl 4-O-(2,4-Di-O-benzyl-α-D-xylopyranosyl)-2,3-di-O-benzyl-β-D-xylopyranoside (21). A mixture of **18** (27.6 mg, 0.036 mmol), tris(triphenylphosphine)rhodium(I) chloride (10 mg), ethanol (0.7 ml), benzene (0.3 ml) and water (0.1 ml) was refluxed for 5.5 h. Evaporation and treatment with aq hydrochloric acid (1 M, 0.04 ml) in acetone (1.5 ml), followed by chromatography (toluene/2-butanone=10/1), gave **21** (20.7 mg, 79%).

Benzyl 4-O-(3-O-Acetyl-2,4-di-O-benzyl-α-D-xylopyranosyl)-2,3-di-O-benzyl-α-D-xylopyranoside (22). The condensation of **12** (129.4 mg, 0.35 mmol) and **9** (112.4 mg, 0.27 mmol) was carried out using NsCl (101 mg), AgOTf (117 mg), and DBU (63.5 μl) in dichloromethane (1.42 ml) in the manner described for the synthesis of **18** and **19**. Chromatography gave **22** (45 mg, 22%). This was deacetylated in methanolic sodium methoxide (0.075 M, 2 ml) containing acetone (0.5 ml) at room temperature, followed by chromatography, to give **21**.

Benzyl 4-O-(3-O-Benzoyl-2,4-di-O-benzyl-α-D-xylopyranosyl)-2,3-di-O-benzyl-α-D-xylopyranoside (23). A similar condensation of **13** (146.6 mg, 0.34 mmol) and **9** (108.4 mg,

† 1 M=1 mol dm^{-3}.

0.26 mmol) by use of NsCl (97.3 mg), AgOTf (112.8 mg), and DBU (61.2 μl) in dichloromethane (1.39 ml) gave **23** (49.2 mg, 23%). This was treated with methanolic sodium methoxide (0.15 M, 2 ml) containing acetone (0.5 ml) at room temperature, followed by chromatography, gave **21**.

Benzyl O-(2,3,4-Tri-O-benzyl-α-L-arabinofuranosyl)-(1→3)-O-(2,4-di-O-benzyl-β-D-xylopyranosyl)-(1→4)-2,3-di-O-benzyl-α-D-xylopyranoside (24). Condensation of **14** (34.7 mg, 0.083 mmol) and **19** (46.5 mg, 0.064 mmol) was carried out using NsCl (40.9 mg), AgOTf (47.4 mg), and DBU (27.5 μl) in dichloromethane (0.58 ml) in the same manner as described above. Chromatography (toluene/2-butanone=100/1→1/1) gave **24** (54.8 mg, 76%).

O-α-L-Arabinofuranosyl-(1→3)-O-β-D-xylopyranosyl-(1→4)-D-xylopyranose (25). Hydrogenolysis of **24** (30 mg, 0.026 mmol) over palladium on carbon (10%, 30 mg) in acetic acid (6 ml) under 340 kPa of hydrogen at 25 °C overnight. Chromatography (chloroform/methanol=10/1→1/1) gave **25** (5.6 mg, 51%).

References

1) S. Koto, S. Inada, T. Yoshida, M. Toyama, and S. Zen, *Can. J. Chem.*, **59**, 255 (1981); S. Koto, N. Morishima, Y. Kihara, H. Suzuki, S. Kosugi, and S. Zen, *Bull. Chem. Soc. Jpn.*, **56**, 188 (1983); S. Koto, N. Morishima, H. Sato, Y. Sato, and S. Zen, *ibid.*, **58**, 120 (1985); S. Koto, N. Morishima, M. Owa, and Z. Zen, *Carbohydr. Res.*, **130**, 73 (1984).

2) I. Kusakabe, T. Yasui, and T. Kobayashi, *J. Agr. Chem. Soc. Jpn.*, **51**, 669 (1977).

3) Partly presented at the 47th National Meeting of the Chem. Soc. Jpn., Tokyo, Apr. 1984.

4) N. Morishima, S. Koto, C. Kusuhara, and S. Zen, *Bull. Chem. Soc. Jpn.*, **55**, 631 (1982).

5) N. Morishima, S. Koto, K. Kanamitsu, and S. Zen., *Chem. Lett.*, **1983**, 1189.

6) N. Morishima, S. Koto, M. Oshima, A. Sugimoto, and S. Zen, *Bull. Chem. Soc. Jpn.*, **56**, 2849 (1983), S. Koto, K. Takenaka, N. Morishima, and S. Zen, *ibid.*, **57**, 3603 (1984).

7) S. Koto, T. Yoshida, K. Takenaka, and S. Zen, *ibid.*, 55, 3667 (1982).

8) J. C. Gast, R. H. Atalla, R. D. McKelxey, *Carbohydr. Res.*, **84**, 137 (1980).

9) P. Kovác and J. Hirsch, *ibid.*, **100**, 177 (1982).

10) C. S. Hudson and E. Yanowsky, *J. Am. Chem. Soc.*, **39**, 1013 (1917).

11) C. S. Hudson, *J. Am. Chem. Soc.*, **47**, 265 (1925).

12) I. Augestad and E. Berner, *Acta Chem. Scand.*, **8**, 251 (1954).

13) R. J. Beveridge and G. N. Richards, *Carbohydr. Res.*, **29**, 79 (1973).

14) R. F. H. Dekker and G. N. Richards, *Carbohydr. Res.*, **43**, 335 (1975).

15) E. Petráková and P. Kovác, *Carbohydr. Res.*, **101**, 141 (1982).

16) C. E. Ballow, S. Roseman, and K. P. Link, *J. Am. Chem. Soc.*, **73**, 1140 (1951).

17) C. K. de Bruyne and G. van der Groen, *Carbohydr. Res.*, **5**, 95 (1967).

18) D. V. Myhre and F. Smith, *J. Org. Chem.*, **26**, 4609 (1961).

Synthesis and Properties of Gramicidin S Analogs Containing Pro-D-Phe Sequence in Place of D-Phe-Pro Sequence in the β-Turn Part of the Antibiotic

Makoto TAMAKI,* Michiaki TAKIMOTO, and Ichiro MURAMATSU†
Department of Chemistry, Faculty of Science, Toho University, Miyama, Funabashi-shi, Chiba 274
†*Department of Chemistry, College of Science, Rikkyo University, Nishi-ikebukuro, Tokyo 171*
(Received December 10, 1984)

Two analogs of gramicidin S, [L-Pro⁴, D-Phe⁵]-gramicidin S and [L-Pro⁴·⁴′, D-Phe⁵·⁵′]-gramicidin S, were synthesized in order to investigate the relationships among positions of Pro residues, antibiotic activity and CD spectra. [L-Pro⁴·⁴′, D-Phe⁵·⁵′]-gramicidin S showed little activity. On the other hand, the activity of [L-Pro⁴, D-Phe⁵]-gramicidin S against *Bacillus subtilis* and *Micrococcus flavus* was the same as that of gramicidin S, and its activity toward other microorganisms tested was 1/2 that of gramicidin S. The CD spectra of these analogs and gramicidin S in an aqueous solution differ from each other, indicating that these peptides have different conformations in aqueous solutions. The CD spectrum of [L-Pro⁴, D-Phe⁵]-gramicidin S resembles a graphical average of the CD spectra of gramicidin S and [L-Pro⁴·⁴′, D-Phe⁵·⁵′]-gramicidin S.

The secondary structure of gramicidin S (GS)[1] (Fig. 1) is established as an antiparallel β-sheet conformation containing two type-II′ β-turns derived from a D-Phe-Pro sequence.[2] In studies regarding the structure-activity relationship of GS, it has been proposed that a specific conformation is necessary in order to exhibit any antibiotic activity.[3,4] Recently, we synthesized two GS analogs containing D-Phe-Pro-D-Val or Phe-Pro-D-Val sequences in place of the D-Phe-Pro-Val sequence in the β-turn part of this antibiotic and discussed the role of the D-Phe-Pro-Val sequence for exhibiting the activity.[5] We also reported that during studies of an antibiotic cyclododecapeptide, gratisin, *cyclo*(-Val[1]-Orn[2]-Leu[3]-D-Phe[4]-Pro[5]-D-Tyr[6]-)₂, *cyclo*(-Val-Orn-Leu-D-Phe-D-Tyr-Pro-)₂ and *cyclo*(-Val-Orn-Leu-Pro-D-Phe-D-Phe-)₂ (in which the Pro residues ocuppy positions different from each other) possessed a strong activity.[6] In connection with these results, it is of interest to study the relationship among positions of Pro residues, secondary structures, and the antibiotic activity of GS.

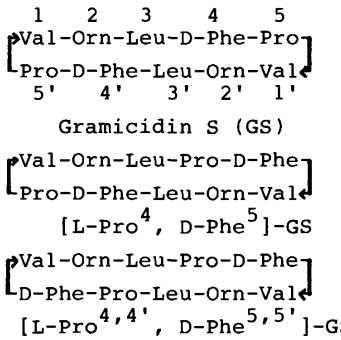

Fig. 1. Primary structure of gramicidin S and its analogs.

In the present paper, we wish to describe the synthesis, antibiotic activity and CD spectra of [L-Pro⁴, D-Phe⁵]- and [L-Pro⁴·⁴′, D-Phe⁵·⁵′]-GS (Fig. 1), in which one or two of D-Phe-Pro sequences in GS is replaced with a Pro-D-Phe sequence.

The synthetic routes of [L-Pro⁴, D-Phe⁵]- and [L-Pro⁴·⁴′, D-Phe⁵·⁵′]-GS are shown in Schemes 1 and 2. The synthetic methods are similar to those discussed in a previous paper of this series.[5] The yields, physical properties and analytical data of the intermediary products are summerized in Table 1. The homoge-

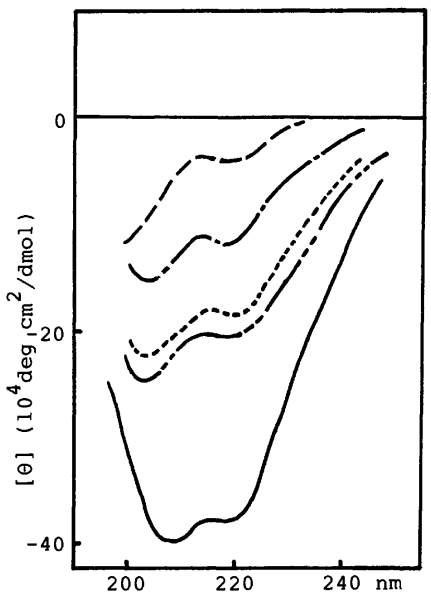

Fig. 2. CD spectra of GS and its analogs in aqueous solution.
——, GS: – – –, [L-Pro⁴, D-Phe⁵]-GS: ———, [L-Pro⁴·⁴′, D-Phe⁵·⁵′]-GS: – – –, equimolar mixture of GS and [L-Pro⁴·⁴′, D-Phe⁵·⁵′]-GS: ———, graphical average of the CD spectra of GS and [L-Pro⁴·⁴′, D-Phe⁵·⁵′]-GS.

neity of the analogs was confirmed by thin-layer chromatography, cellulose plate electrophoresis, elemental analysis, amino acid analysis and fast-atom-bomberdment (FAB) mass spectrometry (Table 2).

The CD spectra of [L-Pro^{4}, D-Phe^{5}]-GS, [L-Pro$^{4,4'}$, D-Phe$^{5,5'}$]-GS and GS in aqueous solutions are shown in Fig. 2. The shapes of [L-Pro$^{4,4'}$, D-Phe$^{5,5'}$]-GS and GS differ from each other, indicating that these peptides have different conformations in aqueous solutions. On the other hand, the feature of the CD spectrum of

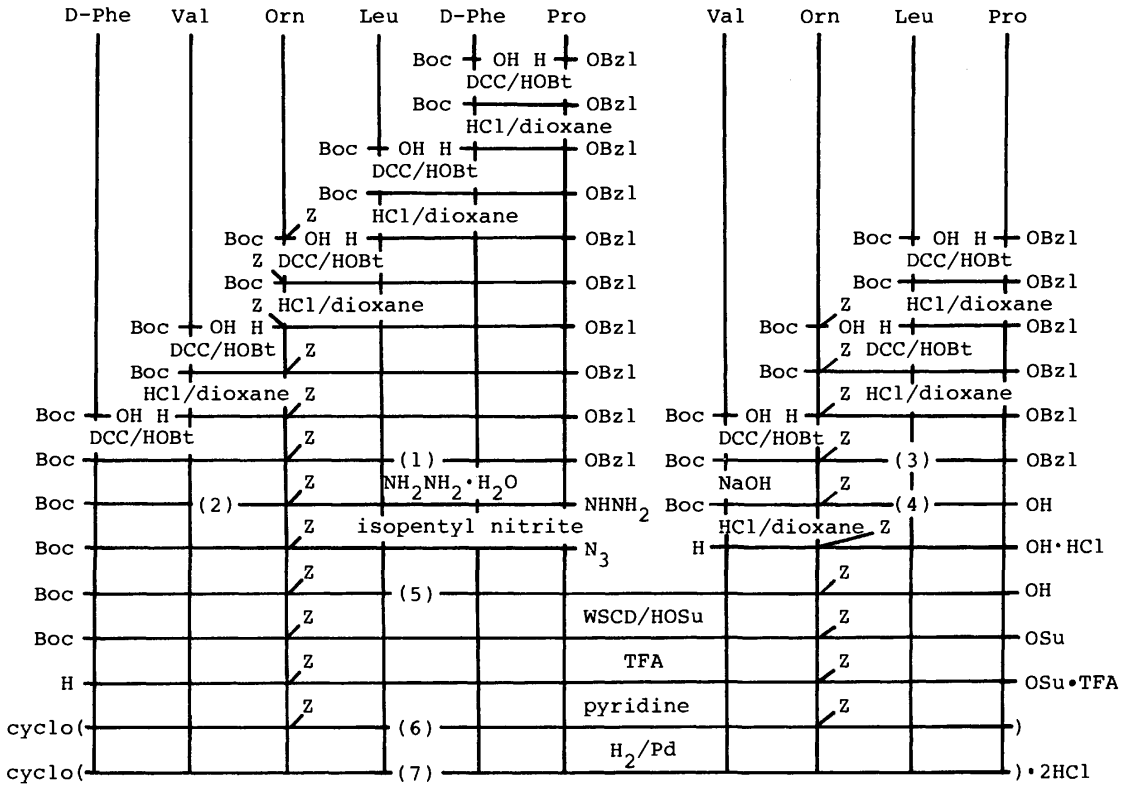

Scheme 1. Synthesis of [L-Pro^{4}, D-Phe^{5}]-GS.

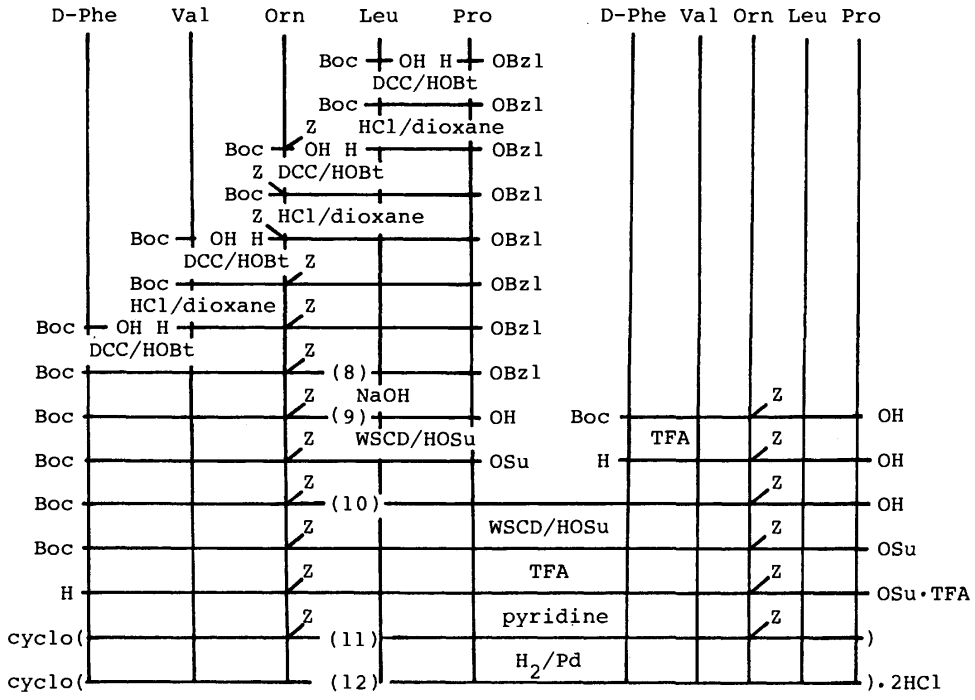

Scheme 2. Synthesis of [L-Pro$^{4,4'}$, D-Phe$^{5,5'}$]-GS.

[L-Pro⁴, D-Phe⁵]-GS resembles the graphical average of the spectra of GS and [L-Pro⁴,⁴′, D-Phe⁵,⁵′]-GS. The latter was also very similar to the spectrum of an equimolar mixture of both peptides. The difference found in the ellipticities of these compounds seems to reflect the difference of the stability of their structures in aqueous solutions. The existence of the additivity in a CD spectra of these analogs and GS suggests that D-Phe–Pro and Pro–D-Phe sequences of each β-turn part contribute separately to their spectra of these peptides.

The antibiotic activity of GS and these two analogs

Table 1. Yields, physical properties and analytical data of intermediary products of GS analogs[a]

		Yield %	Mp (θ_m/°C)	$[\alpha]_D^{25}$ (°) (c 1, DMF)		Elemental analysis (%)			R_f^1	R_f^3
						C	H	N		
3	Boc-Val-Orn(Z)-Leu-Pro-OBzl	73	101—102	−55.0	$C_{41}H_{59}O_9N_5$	C: 64.29 F: 64.19	7.76 7.85	9.15 8.88	0.66	0.60
4	Boc-Val-Orn(Z)-Leu-Pro-OH[b]	62	105—109	−45.6	$C_{34}H_{53}O_9N_5 \cdot 1/2H_2O$	C: 59.63 F: 59.38	7.95 7.75	10.23 10.36	0.45	0.48
5	Boc-D-Phe-Val-Orn(Z)-Leu-D-Phe-Pro-Val-Orn(Z)-Leu-Pro-OH	56	161—165	−55.8	$C_{81}H_{114}O_{17}N_{12}$	C: 63.68 F: 63.23	7.52 7.60	11.00 11.01	0.49	0.56
6	*cyclo*[-D-Phe-Val-Orn(Z)-Leu-D-Phe-Pro-Val-Orn(Z)-Leu-Pro-]	46	250—253	−90.3 (c 0.5)	$C_{76}H_{104}O_{14}N_{12}$	C: 64.75 F: 64.43	7.44 7.49	11.92 11.95	0.64	0.58
8	Boc-D-Phe-Val-Orn(Z)-Leu-Pro-OBzl	54	158—160	−25.5	$C_{50}H_{68}O_{10}N_6$	C: 65.77 F: 65.43	7.51 7.55	9.20 9.09	0.65	0.50
9	Boc-D-Phe-Val-Orn(Z)-Leu-Pro-OH	86	192—193	−18.3	$C_{43}H_{62}O_{10}N_6 \cdot 1/2H_2O$	C: 62.08 F: 62.14	7.63 7.63	10.10 10.10	0.38	0.42
10	Boc-[D-Phe-Val-Orn(Z)-Leu-Pro-]$_2$-OH	49	143—147	−18.4	$C_{81}H_{114}O_{17}N_{12} \cdot 2H_2O$	C: 62.21 F: 62.28	7.60 7.49	10.75 10.58	0.46	0.45
11	*cyclo*[-D-Phe-Val-Orn(Z)-Leu-Pro-]$_2$	61	289—290	−12.2 (c 0.5)	$C_{76}H_{104}O_{14}N_{12} \cdot 2H_2O$	C: 63.14 F: 63.38	7.53 7.47	11.63 11.46	0.65	0.53

a) Compounds **1** and **2** have been reported in the literature.[6] b) Mp 158—160 °C; $[\alpha]_D^{22}$ −62.2° (c 1, MeOH) in the literature.[8]

Table 2. Yields, physical properties and analytical data of GS analogs

7 *cyclo*(-Val-Orn-Leu-D-Phe-Pro-Val-Orn-Leu-Pro-D-Phe-)·2HCl

Yield, 56%; mp 262—265 °C (dec); $[\alpha]_D^{28}$ −140.0° (c 0.2, EtOH) R_f^3 0.55, R_f^4 0.75. Amino acid ratios: Val, 1.01; Orn, 0.95; Leu, 1.01; Phe, 1.04; Pro, 1.00. MS (FAB), *m/z* 1141 ($C_{60}H_{93}O_{10}N_{12}$, MH⁺). Fonnd: C, 55.97; H, 7.98; N, 12.96%. Calcd for $C_{60}H_{92}O_{10}N_{12} \cdot 2HCl \cdot 4H_2O$: C, 56.01; H, 7.99; N, 13.06%.

12 *cyclo*(-Val-Orn-Leu-Pro-D-Phe-)$_2$·2HCl

Yield, 61%.; mp 262—265 °C (dec); $[\alpha]_D^{28}$ −43.4° (c 0.2, EtOH) R_f^3 0.50, R_f^4 0.77. Amino acid ratios: Val, 1.00; Orn, 0.95; Leu, 1.01; Phe, 1.02; Pro, 1.03. MS (FAB), *m/z* 1141 ($C_{60}H_{93}O_{10}N_{12}$, MH⁺). Found: C, 55.16; H, 8.07; N, 12.80%. Calcd for $C_{60}H_{92}O_{10}N_{12} \cdot 2HCl \cdot 5H_2O$: C, 55.25; H, 8.04; N, 12.89%.

Table 3. Antibiotic activity of GS and its analogs[a]

Test organisms	GS	[L-Pro⁴, D-Phe⁵]-GS	[L-Pro⁴,⁴′, D-Phe⁵,⁵′]-GS
Staph. aureus ATCC 6538 P	1.6	3.1	50
Strept. pyogenes N.Y. 5	1.6	3.1	25
Micrococcus flavus ATCC 10240	0.8	0.8	25
Corynebact. diphtheriae P.W. 8	0.8	1.6	50
Bac. subtilis ATCC 6633	3.1	3.1	25
E. coli NIHJ-JC2	>100	>100	>100
Proteus vulgaris OX 19	>100	>100	>100

a) Minimum inhibitory concentration in μg/ml: The minimum amount of the compounds necessary for the complete inhibition of growth was determined by a agar dilution method with 10^6 organisms per milliter.

toward several microorganisms are summerized in Table 3. [L-Pro$^{4,4'}$, D-Phe$^{5,5'}$]-GS showed little activity. This indicates that the positions of the two Pro residues of GS can not be transposed without a loss of activity. Several gratisin isomers, in which Pro residues occupy positions different from esch other, showed strong activity.[6] The significant difference in this regard may result from the distinction of their rings.

The activity of [L-Pro^4, D-Phe^5]-GS against *Bacillus subtilis* and *Micrococcus flavus* was the same as that of GS, and the activity toward other organisms tested was a little less compared to GS. This shows that a single D-Phe-Pro sequence in the β-turn part of GS can be inverted without affecting the activity. Similar results have been reported by Sofuku *et al.* for [δ-Ava$^{4-5}$]- and [δ-Ava$^{4-5,4'-5'}$]-GS, in which D-Phe-Pro sequences of GS are replaced, singly or together, with a δ-Ava residue.[7] That is, [δ-Ava$^{4-5}$]-GS showed antibiotic activity, but [δ-Ava$^{4-5,4'-5'}$]-GS not active. Recently, in studies on [L-Pro$^{4,4'}$, D-Ala$^{5,5'}$]-GS, in which D-Phe-Pro sequences in GS were replaced with Pro-D-Ala sequence, it was reported that this analog showed no activity,[8] and that it could take a GS-like conformation in an aqueous solution, but its population decreased in a less-polar environment.[9] In the present studies, it is likely that when the synthetic analogs interact with a cell membrane of target microorganisms, the presence of a D-Phe-Pro sequence in [L-Pro^4, D-Phe^5]-GS makes this analog feasible to adopt the GS-like conformation, while [L-Pro$^{4,4'}$, D-Phe$^{5,5'}$]-GS cannot take the GS-like conformation.

Experimental

The synthetic manners of the analogs are similar to those reported in a previous paper of this series.[5] The yields, physical properties and analytical data of the intermediary and final products are summerized in Tables 1 and 2. All melting points are uncorrected. The molecular weights of GS analogs were determined by fast-atom-bomberdment (FAB) mass spectrometry using a JMS D-300 mass spectrometer. Amino acid analyses were carried out using a Hitachi 835 amino acid analyzer, after the hydrolysis of peptides in 6 M† HCl at 110 °C for 24 h. Thin-layer chromatography was performed on Merck silica-gel F_{254} plates with the following solvent systems (v/v): R_f^1, $CHCl_3$-MeOH (9:1); R_f^2, $CHCl_3$-MeOH-AcOH (95:5:3); R_f^3, *n*-BuOH-AcOH-H_2O (4:1:1); R_f^4, *n*-BuOH-pyridine-AcOH-H_2O (4:1:1:2). The yields of peptides **3** and **8** were calculated on the basis of the amount of Pro-OBzl as a starting material. The CD spectra shown in Fig. 2 were obtained using a JASCO spectropolarimeter (model J-500). The CD spectroscopy of GS and the analogs was carried out with an aqueous solution of their dihydrochlorides. Cellulose plate electrophoresis was carried out with a cellulose (Avicel) plate and with a solvent system of HCOOH-AcOH-MeOH-H_2O (1:3:6:10 v/v, PH 1.4) for 2 h at 500 V/20 cm. Each of the analogs revealed a single spot, the mobility being the same as that of GS.

† 1 M=1 mol dm^{-3}.

We are grateful to the staff of the Research Laboratories of Toyo Jozo Co. for elemental analyses, microbiological assays and the measurements of FAB Mass.

References

1) Recently, it was reported that natural GS is a mixture of several homologs. The GS signified in the present paper corresponds to gramicidin S-1 in the report: S. Nozaki and I. Muramatsu, *J. Antibiotics.*, **37**, 689 (1984).

2) D. C. Hodgkin and B. M. Oughton, *Biochem. J.*, **65**, 752 (1957).

3) N. Izumiya, T. Kato, H. Aoyagi, M. Waki and M. Kondo, "Synthetic Aspects of Biologically Active Cyclic peptide-Gramicidin S and Tyrocidines" Kodansha, Tokyo, and Halsted Press, New York (1979), pp. 49—97.

4) Amino acid residues with no plefix are of L-configuration. The abbreviations for amino acids and peptides are in accordance with the rules of IUPAC-IBU Commission of Biological Nomencalture. Abbreviations used are as follows: Boc, *t*-butoxycarbonyl; Z, benzyloxycarbonyl; OBzl, benzyloxy; WSCD, 1-ethyl-3-(3-dimethylaminopropyl)-carbodiimide; HOBt, 1-hydroxybenzotriazole; HOSu, *N*-hydroxysuccinimide; TFA, trifluoroacetic acid.

5) M. Tamaki, T. Okitsu, M. Araki, H. Sakamoto, M. Takimoto, and I. Muramatsu, *Bull. Chem. Soc. Jpn.*, **58**, 531 (1985).

6) M. Tamaki, *Bull. Chem. Soc. Jpn.*, **57**, 3210 (1984).

7) a) I. Muramatsu, S. Sofuku, and A. Hagitani, *J. Antibiotices.*, **25**, 189 (1972). b) S. Sofuku, I. Muramatsu, K. Okada, and A. Hagitani, *Bull. Chem. Soc. Jpn.*, **48**, 2888 (1975).

8) K. Sato and U. Nagai, *Bull. Chem. Soc. Jpn.*, **56**, 3329 (1983).

9) T. Higashijima, K. Sato, U. Nagai and T. Miyazawa, "Peptide Chemistry 1981" T. Shioiri (Ed.), Protein Research Foundation, Osaka (1982), pp. 177.

Syntheses and Properties of Oligo-L-leucines Containing α-Aminoisobutyric Acid Residues. The Novel Strategy for Solubility Improvement in Helical Oligopeptides Based on the Restriction of the Values of the Backbone Dihedral Angles φ and ψ of α-Aminoisobutyric Acid Residues[1]

Mitsuaki NARITA,* Masamitsu DOI, Hiroki SUGASAWA, and Kazunori ISHIKAWA
Department of Industrial Chemistry, Faculty of Technology, Tokyo University of Agriculture and Technology, Koganei, Tokyo 184
(Received December 12, 1984)

In order to provide a succinct demonstration of the usefulness of a new strategy for solubility improvement in protected peptide fragments included in α-helical regions of proteins, model oligo(Leu)s containing Aib or Ala residues were prepared by stepwise elongation and fragment condensation methods. The peptides prepared were the following: Boc-(Leu$_3$-Aib)$_n$-OBzl, Boc-(Leu$_4$-Aib)$_n$-OBzl, and Boc-(leu$_3$-Ala)$_n$OBzl (n=1—3). Carboxyl component peptides having Aib residues at the C-terminals smoothly reacted with amino component peptides in high yields with no care of racemization due to the absence of chiral centers in Aib residues. As expected, peptides containing Aib residues have high solubility in moderate- and high-polar organic solvents and are easily purified by recrystallization from aqueous ethanol. This is in remarkable contrast with the result that the octa- and dodecapeptides containing Ala residues are barely soluble or insoluble in these solvents. Conformational analyses by IR spectroscopies indicated that Boc-(Leu$_3$-Aib)$_n$-OBzl and Boc-(Leu$_4$-Aib)$_n$-OBzl (n=2 and 3) had helical conformations (3_{10}- or α-helices) in dichloromethane, whereas Boc-(Leu$_3$-Ala)$_n$-OBzl (n=2 and 3) had fully developed β-sheet structures in the solid state. The high solubility of the peptides containing Aib residues is explained by the observation that replacement of C$^\alpha$ hydrogen atoms with methyl groups greatly disturbs β-sheet structures, promoting helical folding in peptides. The implications of the new findings for the chemistry of peptides and proteins containing α,α-disubstituted α-amino acid residues is also discussed by building up a CPK model of an α-helical structure.

In our recent papers,[2-8] we have demonstrated that a β-sheet aggregation plays an important role in the insolubility of oligopeptides larger than octa- or nonapeptide levels, and that the temporary protection of a NH peptide bond in a central position of a peptide chain helps improve solubility to a remarkable extent. The solubility improvement is attributed to the existence of tertiary peptide bonds of X-(Z)Y bonds, where X and Y are arbitrary amino acid residues and Z is a temporary protecting group for the X-Y peptide bond. The tertiary peptide bond causes disturbance of the β-sheet structure by the rotation of the tertiary peptide bond plane, and we called this segmentation of structures the "peptide segment separation."[2] On the basis of these results, solubility prediction of protected polypeptides was also successfully performed by making use of both the randomness of peptide structures in the solid state and the existence of tertiary peptide bonds.[6]

At this juncture, we would like to propose a novel strategy for improving solubility of protected oligo- and polypeptide fragments included in α-helical regions of proteins. The protected peptide fragments ranging from octa- to around pentadecapeptides have, in general, β-sheet structures and are less soluble in organic solvents.[2,6,9,10] Insolubility of protected peptide fragments is one of serious problems in the efforts of protein syntheses, and it has been found very difficult to achieve further elongation of these peptide chains.[11-16] Thus, solubility improvement in the peptides is one of the upmost important problems to be solved in protein syntheses. The strategy for solubility improvement as proposed in this paper is based on the restriction of the values around the helical regions of the backbone dihedral angles φ and ψ of Aib residues in partial replacement of Ala residues with Aib residues. The conformational space of an Aib residue is sterically severely restricted, and, φ,ψ torsional angles of the Aib residue in a linear polypeptide are mainly found in the region of conformational map which includes both the α-helix (φ=±57°, ψ=±47°) and 3_{10}-helix (φ=±60°, ψ=±30°).[17] The conformational preferences of linear peptides containing α,α-disubstituted α-amino acids have recently been reviewed, and the ability of Aib residues to promote helical folding in peptides is well documented in the conformational analyses of membrane-channel-forming polypeptides like alamethicin and suzukacillin.[18] Thus, partial replacement of Ala residues with Aib residues in protected polypeptide fragments included in α-helical regions of proteins is expected to disturb β-sheet structures, which are general conformations of the protected polypeptide fragments ranging from octa- to around pentadecapeptides included in α-helical regions of proteins, and to promote helical folding in peptides, providing solubility improvement in the peptide fragments (Fig. 1). In this connection, it is well recognized that the β→helical conformational transformation results in remarkable solubil-

ity improvement. Furthermore, CPK models of α-helical structures suggest to us that the replacement takes place without difficulty keeping the nature of proteins intact. Therefore, replacement of a few Ala residues with Aib residues in proteins offers the prospect for creating novel proteins not found in nature.

In this paper, we report syntheses of oligo(Leu)s containing Aib or Ala residues and demonstrate the effect of the replacement of Ala residues with Aib residues on solubility and conformations of the oligo(Leu)s.

Results

Syntheses and Solubilities of Oligo(Leu)s Containing Aib or Ala Residues. In order to demonstrate the usefulness of the strategy for solubility improvement in helical oligopeptides, model oligo(Leu)s containing Aib or Ala residues were prepared by stepwise elongation and fragment condensation methods. The synthetic scheme is shown below. Boc-Leu_3-Aib-OBzl (**1**), Boc-Leu_4-Aib-OBzl (**4**), and Boc-Leu_3-Ala-OBzl (**7**) were prepared by a stepwise elongation, starting with H-Aib-OBzl and H-Ala-OBzl as amino components. The stepwise elongation was performed in dichloromethane using DCC activation. The liberation of the amino group from Boc-peptide Bzl esters in the stepwise elongation was carried out by treatment with 3 M HCl/AcOEt (1 M=1 mol dm^{-3}) followed by treatment with NMM. Removal of the

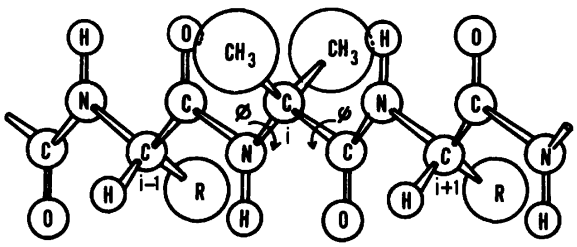

Fig. 1. Disturbance of a β-sheet structure by the restriction of the values of the backbone dihedral angles ϕ and Ψ of an Aib residue.

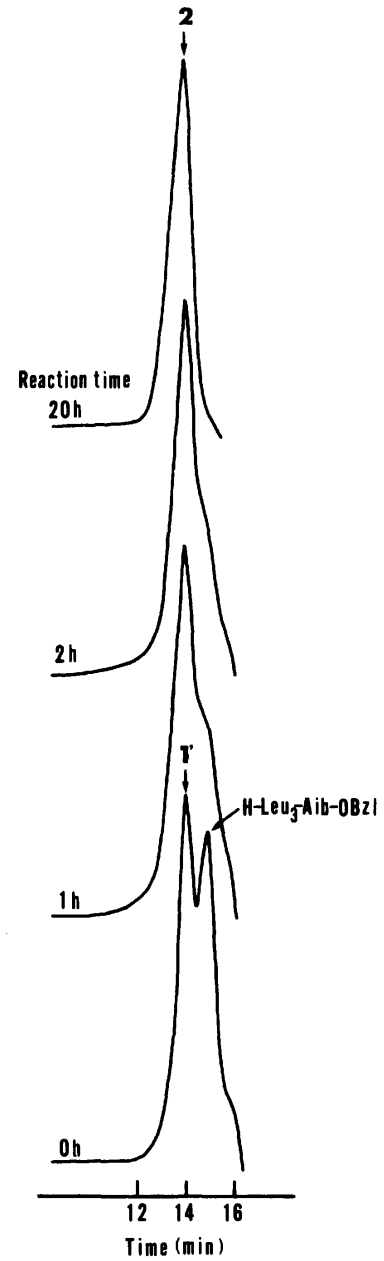

Fig. 2. Monitoring of a fragment condensation of Boc-Leu_3-Aib-OH with H-Leu_3-Aib-OBzl by HPLC.

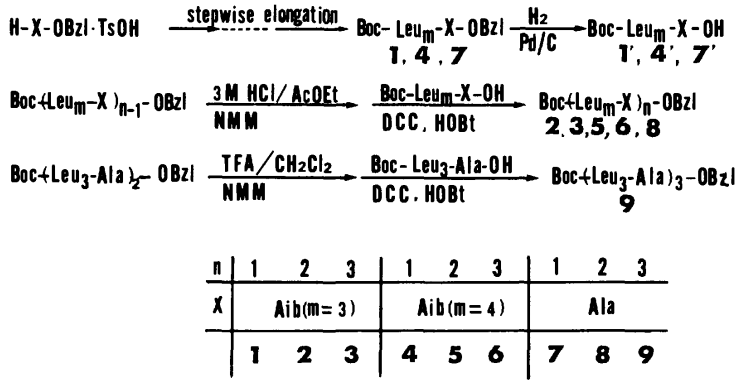

n	1 2 3	1 2 3	1 2 3
X	Aib(m=3)	Aib(m=4)	Ala
	1 2 3	4 5 6	7 8 9

Scheme

Bzl group from the peptides **1**, **4**, and **7** was performed by hydrogenolysis using Pd/C as a catalyst and the products **1'**, **4'**, and **7'** were used as carboxyl components in a subsequent fragment condensation. Boc-(Leu$_3$-Aib)$_n$-OBzl (n=2, **2**; n=3, **3**), Boc-(Leu$_4$-Aib)$_n$-OBzl (n=2, **5**; n=3, **6**), and Boc-(Leu$_3$-Ala)$_n$-OBzl (n=2, **8**; n=3, **9**) were prepared in dichloromethane, DMF, or HMPA by a fragment condensation method using DCC activation in the presence of HOBt. Removal of the Boc group from the peptides **1**, **2**, **4**, **5**, **7**, and **8** was carried out by treatment with 3 M HCl/AcOEt or TFA/CH_2Cl_2 (1/2, v/v). The coupling reactions were monitored by HPLC on a gel filtration column and a representative result was shown in Fig. 2. Boc-Leu$_3$-Aib-OH and Boc-Leu$_4$-Aib-OH were easily coupled with H-(Leu$_3$-Aib)$_n$-OBzl and H-(Leu$_4$-Aib)$_n$-OBzl (n= 1 and 2) in high yields, respectively, and the reactions could be performed with no care of racemization since Aib residues had no asymmetric carbon.

All the peptides containing Aib residues have high solubility in moderate- and high-polar organic solvents such as dichloromethane, chloroform, acetone, EtOH, MeOH, DMF, DMA, NMP, and HMPA (Table 1), and are easily purified by recrystallizations from aqueous ethanol. This is in remarkable contrast with the result that the peptides **8** and **9** are barely soluble or insoluble in these solvents except HMPA and are purified by washing with hot methanol. Homogeneity of the peptides except **8** and **9** was easily ascertained as the peptides had a single peak on HPLC. The synthetic results and physical properties of the peptides are assembled in Table 2. Elemental and amino acid analyses of the peptides shown in Table 3 are in good agreement with the calculated values.

IR Absorption Studies of Oligo(Leu)s Containing Aib or Ala Residues. Conformational analyses of the peptides **1**—**6** by IR absorption measurements were first carried out in dichloromethane. Figure 3 shows the most significant spectral regions for the conformational assignments (3600—3200 cm^{-1}, amide A; 1750—1600 cm^{-1}, amide I; 500—400 cm^{-1}, far-IR). As expected from solubility data and the nature of Aib residues, no band at around 3280 cm^{-1} and 1630 cm^{-1} is observed in all of the peptides **1**—**6**, indicating

Table 1. Solubility properties[a] of the peptides **1**—**9** (c=1.0 g/dl)

Compound	Solvent[b]												
	HMPA	NMP	DMA	DMF	DMSO	MeOH	EtOH	AC	CF	DCM	CT	BE	AcOEt
1	A	A	A	A	A	A	A	A	A	A	A	A	A
2	A	A	A	A	A	A	A	A	A	A	A	A	B
3	A	A	A	A	B	A	A	A	A	A	A	A	B
4	A	A	A	A	A	A	A	A	A	A	B	B	B
5	A	A	A	A	B	A	A	B	A	A	B	B	C
6	A	A	A	A	B	A	A	B	A	A	B	B	C
7	A	A	A	A	A	A	B	B	A	A	D	C	B
8	A	C	D	D	C	D	D	D	D	D	D	D	D
9	B	C	D	D	C	D	D	D	D	D	D	D	D

a) Solubility: A, soluble at room temperature; B, soluble at 80 °C or refluxing temperature; C, partially soluble at the same temperature; D, nearly insoluble at the same temperature. b) Abbreviations: AC, acetone; CF, chloroform; DCM, dichloromethane; CT, carbon tetrachloride; BE, benzene. Others, see text.

Table 2. Synthetic results and physical properties of the peptides **1**—**9**

Compound	Yield/%	Recrystallization solvent	Mp θ_m/°C	$[\alpha]_D^{20}$ (c=1.0, MeOH)	Retention time/min
1	92[a]	EtOH/H_2O (6/5)	121—123	−63.0	14.0
1'	96	EtOH/H_2O (6/5)	91— 92	−70.5	13.8
2	89	EtOH/H_2O (3/2)	199—203	−52.5	13.6
3	84	EtOH/H_2O (3/2)	227—228	−28.5	13.5
4	94[a]	EtOH/H_2O (6/5)	231—232	−58.5	13.7
4'	95	EtOH/H_2O (6/5)	198—199	−70.5	13.7
5	74	EtOH/H_2O (3/2)	227—228	−31.5	13.4
6	81	EtOH/H_2O (3/2)	236—239	−15.0	13.3
7	89[a]	EtOH	201—203	−85.5	13.9
8	90	b)	over 250	—	—
9	82	b)	over 250	—	—

a) Final coupling step. b) Washing with hot methanol.

that the restricted torsional angles of ϕ and ψ of the Aib residues efficiently hinder development of a β-sheet structure. The IR spectrum of the peptide **1** has two strong bands at 3430 cm^{-1} and 3340 cm^{-1} in the amide A region, indicating the existence of both the nonhydrogen bonding NH and hydrogen bonding NH bonds.[19] The IR spectrum of the peptide **1** has also a medium-intensity shoulder band at 1700 cm^{-1} and a strong band at 1675 cm^{-1} in the amide I region, assigned to the hydrogen-bonded urethane and free amide carbonyl groups, respectively.[20] Due to a strong preference of the Aib residues to form a helical

TABLE 3. ELEMENTAL AND AMINO ACID ANALYSES OF THE PEPTIDES **1**—**9**

Compound	Formula	Found (Calcd)			Found (Calcd)
		C/%	H/%	N/%	Leu/Aib
1	$C_{34}H_{56}N_4O_7$	64.37 (64.53)	9.28 (8.92)	8.82 (8.85)	2.91 (3)
1'	$C_{27}H_{50}N_4O_7$	59.80 (59.76)	9.50 (9.29)	10.10 (10.32)	3.13 (3)
2	$C_{56}H_{96}N_8O_{11}0.5H_2O$	63.18 (63.07)	9.47 (9.17)	10.45 (10.51)	3.11 (3)
3	$C_{78}H_{136}N_{12}O_{15}H_2O$	62.79 (62.45)	9.64 (9.27)	11.02 (11.21)	3.04 (3)
4	$C_{40}H_{67}N_5O_8$	64.65 (64.40)	9.51 (9.05)	9.35 (9.39)	3.99 (4)
4'	$C_{33}H_{61}N_5O_8$	60.59 (60.43)	9.57 (9.05)	10.24 (10.68)	4.19 (4)
5	$C_{68}H_{118}N_{10}O_{13}H_2O$	62.90 (62.74)	9.51 (9.29)	10.76 (10.76)	4.06 (4)
6	$C_{96}H_{169}N_{15}O_{18}1.5H_2O$	62.41 (62.38)	9.30 (9.38)	10.95 (11.37)	4.00 (4)
7	$C_{33}H_{54}N_4O_7H_2O$	64.13 (63.84)	9.03 (9.09)	9.00 (9.02)	3.13 (3)[a]
8	$C_{54}H_{92}N_8O_{11}H_2O$	62.78 (62.87)	9.15 (9.19)	10.82 (10.86)	3.06 (3)[a]
9	$C_{75}H_{130}N_{12}O_{14}1.5H_2O$	61.97 (62.09)	9.12 (9.24)	11.61 (11.58)	3.04 (3)[a]

a) Leu/Ala.

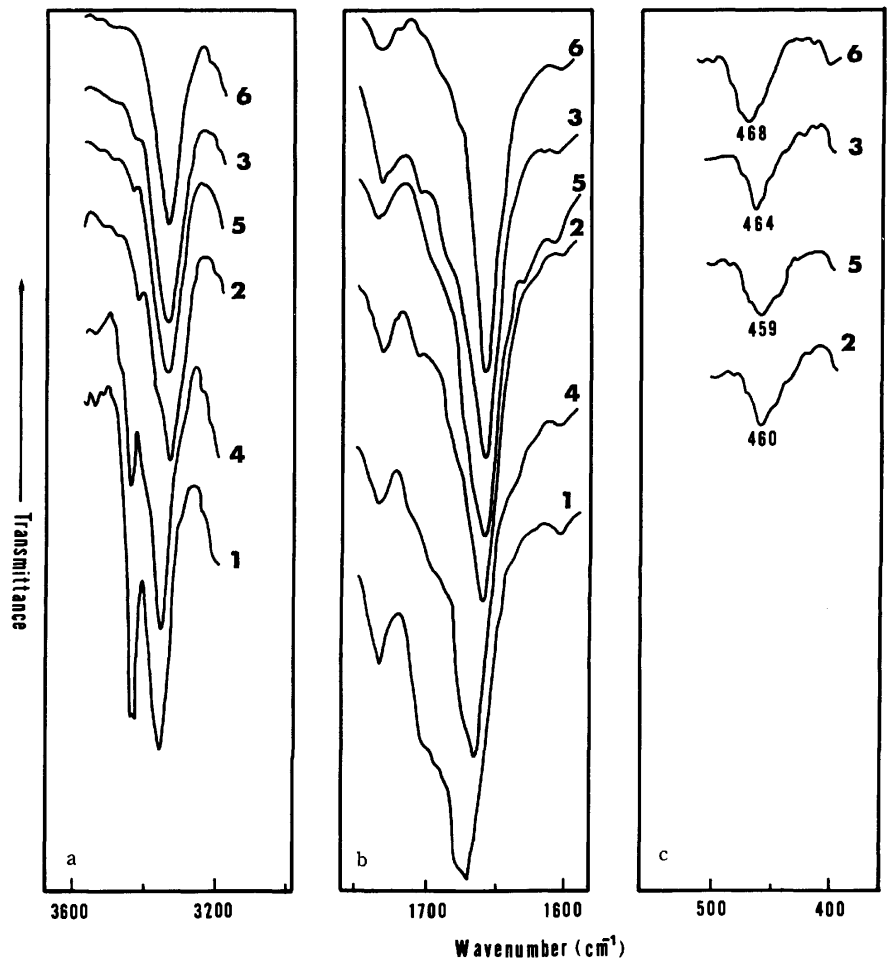

Fig. 3. IR absorption spectra of the peptides **1**—**6**. a: The amide A region, in methylene chloride; b: the amide I region, in methylene chloride; c: the far-IR, in a solid state.

conformation (3_{10}- or α-helix), the peptides **2**—**6** show strong intensity bands at 3340—3320 cm^{-1} and 1665—1659 cm^{-1}, indicating a helical structure (3_{10}- or α-helix), although the frequencies of the amide I region are rather high.[21] Weak or medium-intensity bands at 3430—3420 cm^{-1} of the peptides **2**—**6** are also assigned to the nonhydrogen bonding NH bonds, which are attributed to the NH bonds of two or three Leu residues at the N-terminal portions. The helical structure in the solid state also seems to be evidenced by a far-IR band at 468-459 cm^{-1} (Fig. 3c), which is characteristic of Leu residues with an α-helical conformation.[22] Figure 4 shows IR spectra of the peptides **8** and **9** in the solid state. Both peptides are barely soluble or insoluble in dichloromethane, and their IR measurement can not be performed in dichloromethane. In contrast with the peptides containing Aib residues, the peptides containing Ala residues (**8** and **9**) show strong bands at 3270 cm^{-1} and 1628 cm^{-1} and a weak band at 1693 cm^{-1}, assigned to antiparallel β-sheet structures.[21]

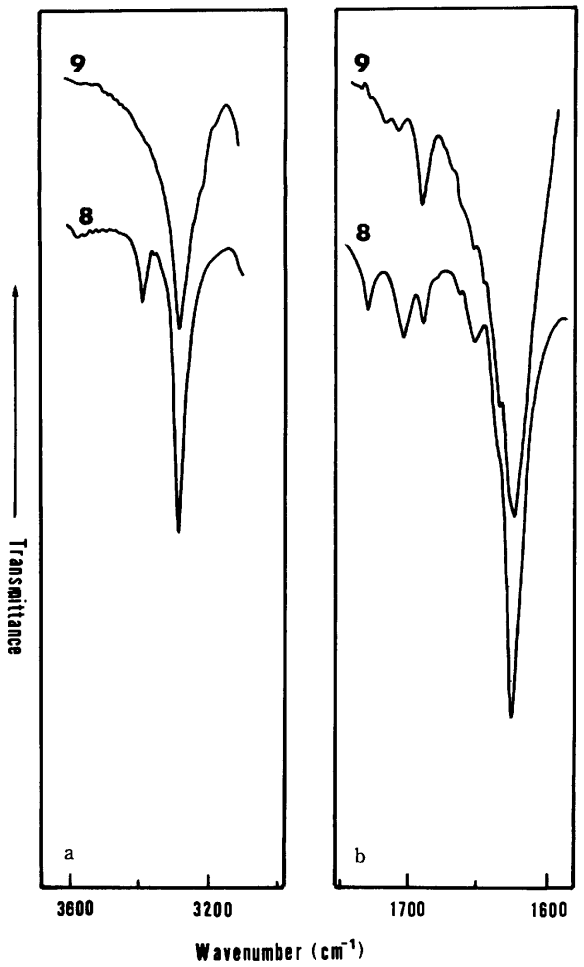

Fig. 4. IR absorption spectra of the peptides **8** and **9** in a solid state. a: The amide A region; b: the amide I region.

Discussion

As shown in Fig. 2, the carboxyl component peptides having Aib residues at the C-terminals react smoothly with amino component peptides in high yields, although the C-terminal Aib residues are sterically hindered.[23] The reaction of H-Aib-OBzl with Boc-Leu-OH is also performed by the usual stepwise method. Extreme difference in solubility between the peptides containing Ala residues and those containing Aib residues is readily explained by the conformational transformation of the peptides from β-sheet to helical structures. The ability of Aib residues to promote helical folding in peptides is outstanding in this study. The replacement of two Ala residues in the peptide **8** with two Aib residues constrains helical folding in the peptide **2**, and dramatic change takes place in solubility. Helical folding in the peptide **4** having the only one Aib residue at the C-terminal is also remarkable. Details of IR absorption conformational analyses of the peptides **1** and **4** will be presented in the following paper.[20] In the relation with this structure, the structures of the pentapeptides of Boc-Leu-Aib-Pro-Val-Aib-OMe and Boc-Ala-Aib-Ala-Aib-Aib-OMe, which were fragments of alamethicin and suzukacillin, were determined in the solid state, by X-ray diffraction analyses, to be a 3_{10}-helix.[24,25] The conformational-energy calculations for an Aib residue have demonstrated that only two small regions of the Ramachandran map are available.[26,27] The regions correspond to less than 1.0% of the total surface, where the right- and left-handed α-helices ($\phi=\pm57°$, $\psi=\pm47°$) and 3_{10}-helices ($\phi=\pm60°$, $\psi=\pm30°$) are found. 3_{10}- and α-helical conformations, however, could not be distinguished by the present IR analyses. Therefore, ^1H NMR analyses of the peptides are necessary to characterize their intramolecular hydrogen bonding patterns (3_{10}-helix, 4→1; α-helix, 5→1).[28]

In order to evaluate the influence on the nature of proteins of the replacement of a few Ala residues with Aib residues, a CPK model of the α-helical structure of Boc-$(Leu_3$-Aib$)_3$-OBzl is shown in Fig. 5. Figure 5 indicates that the replacement of C^α hydrogen atoms of Ala residues with methyl groups would have no or a little influence on the total feature of the α-helical regions of proteins and that the nature of proteins would be kept intact. The C^β_D methyl groups are identified by arrows in the model, where the C^β_D carbon atom that substitutes for the C^α hydrogen atom in Ala is designated as C^β_D. Figure 5 also indicates that the replacement of C^α hydrogen atoms of Leu residues with methyl groups is sterically permitted. The C^α hydrogen atoms are also identified by H^α in the model.

Based on the above discussion,[29] the perspective in

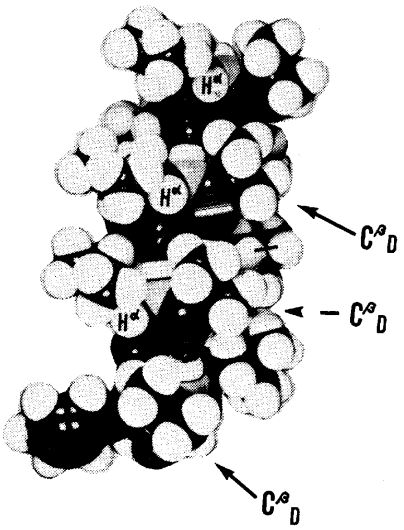

Fig. 5. The CPK model of the α-helical structure of the peptide 3. The arrows in the model indicate C^{β}_{D} methyl groups of Aib residues. The H^{α} atoms in the model indicate C hydrogen atoms of Leu residues.

the chemistry of peptides and proteins containing α,α-disubstituted α-amino acid residues gets into shape as follows: (1) Carboxyl component peptides having Aib residues at the C-terminals react with amino component peptides with no care of racemization due to the absence of chiral centers in Aib residues, and the reaction is carried out in high yields in common organic solvents using usual coupling reagents, (2) partial replacement of C^{α} hydrogen atoms with methyl groups remarkably helps improve solubility of intermediate peptide fragments included in α-helical regions of natural proteins and make further chain elongation easy in the modified protein syntheses, and (3) the replacement in α-helical regions of natural proteins keeps the nature of proteins intact.

Conclusion

The novel strategy for solubility improvement based on the restricted values of the backbone dihedral angles ϕ and ψ of Aib residues was successfully applied to model oligo(Leu)s. Partial replacement of C^{α} hydrogen atoms with methyl groups in α-helical regions of proteins is estimated, by building up the CPK model of the α-helical structure, to give no or a little influence on the nature of proteins. Thus, this strategy opens up a new breakthrough in creating proteins with novel properties which can not be achieved by genetic engineering technology.

Experimental

General. The uncorrected capillary melting points were reported. The optical rotations were taken in a 1 cm cell on a JASCO model ORD/UV-5 optical rotatory dispersion recorder. The amino acid compositions of acid hydrolysates were determined with a Shimadzu HPLC LC-3A all amino acid analysis system. The acid hydrolyses of the peptides were carried out with propionic acid/12 M HCl (2/1, v/v) for 2 d at 115 °C in sealed tubes. Analytical HPLC of the peptides was performed on a column packed with an acrylonitrile-divinylbenzene-styrene copolymer (7.5×500 mm)[30] using a mini micro pump NSP-800-5DX (Nihon Seimitsu Kagaku) and a refractive index detector model RI-3H (Japan Analytical Industry). The operating conditions of HPLC were the following: Column with exclusion limit of 5000; solvent, DMF; flow rate, 1 ml/min; chart speed, 0.5 cm/min; temperature, room temperature. The IR spectra in the solid state were recorded for nujor mulls with a JASCO model DS-701G spectrometer. Those in solution were recorded employing 0.025 mm pathlength cells with potassium bromide windows. The concentration of the solution was kept near 3.0 g/dl.

Preparation of the Peptides 1 and 4. DCC (11.3 g, 1.0 equiv) was added to an ice-chilled, stirred mixture of Boc-Leu-OH·H_2O (13.7 g, 1.0 equiv), H-Aib-OBzl·TsOH (20.0 g, 54.8 mmol), and NMM (5.6 g, 1.0 equiv) in dichloromethane (500 ml). The reaction mixture was stirred in an ice-chilled bath for 3 h, at room temperature overnight, and then filtered. The filtrate was washed with water, 10% citric acid, and 5% sodium hydrogencarbonate, dried over sodium sulfate, using charcol for decolorization, filtered, and concentrated *in vacuo*. The residue was used for the subsequent coupling reaction as an amino component after removal of the Boc group by treatment with 3 M HCl/AcOEt. The preparative procedure of Boc-Leu_2-Aib-OBzl, Boc-Leu_3-Aib-OBzl, and Boc-Leu_4-Aib-OBzl were essentially the same with that of Boc-Leu-Aib-OBzl. The peptides **1** and **4** were purified by recrystallization from aqueous ethanol.

Preparation of the Peptide 7. Preparation of the peptide **7** was carried out in dichloromethane (200 ml) in the same manner described above, using Boc-Leu-OH·H_2O (6.4 g, 1.1 equiv), H-Leu_2-Ala_2-OBzl·HCl (11.7 g, 23 mmol), and NMM (2.3 g, 1.0 equiv). The peptide **7** was purified by recrystallization from AcOEt.

General Procedure for Hydrogenolyses of the Peptides 1, 4, and 7. Hydrogenolyses of the peptides **1**, **4**, and **7** were performed in a mixture of acetic acid and methanol (1/5, v/v) at atmospheric pressure overnight using 10% Pd/C (10 wt.%) as a catalyst. After removal of Pd/C by filtration, the filtrate was concentrated *in vacuo*, and the residue was triturated with water. After filtration and drying, the products were purified by recrystallization from aqueous ethanol.

General Procedure for Removal of the Boc Group from the Peptides 1, 2, 4, 5, and 7. Each peptide (5 mmol) in 3 M HCl/AcOEt (30 ml) was stirred in an ice-chilled bath for 1.5 h. The mixture was concentrated *in vacuo*, followed by repetition of addition and removal, *in vacuo*, of dichloromethane. The residue was used with NMM (5 mmol) as an amino component for the subsequent coupling.

Removal of the Boc Group from the Peptide 8. The peptide **8** (5 mmol) in TFA/dichloromethane (1/2, v/v) (70 ml) was stirred at room temperature for 1 h. The solution was concentrated *in vacuo*, and the residue was dis-

solved in methanol containing an excess of NMM. The solution was poured into water to precipitate crystalline materials, which were used as an amino component for the subsequent coupling reaction.

Preparation of the Peptides 2, 3, 5, 6, 8, and 9. DCC (1.1 equiv) and HOBt (1.1 equiv) were added to an ice-chilled, stirred mixture of a carboxyl component (1.1 equiv), NMM (1.0 equiv), and an amino component. In the preparation of the peptides **2**, **3**, **5**, and **6**, the coupling reactions were carried out in dichloromethane. The reaction mixture was stirred in an ice-chilled bath for 3 h, at room temperature overnight, and then filtered. The filtrate was subjected to the same work-up procedure described above. The products were purified by recrystallization from aqueous ethanol. In the preparation of the peptides **8** and **9**, the coupling reaction was carried out in DMF and HMPA, respectively. The reaction mixture was stirred in an ice-chilled bath for 3 h, at room temperature for 2 d, and filtered. The filtrate was concentrated *in vacuo*, and the crystalline residue was purified by washing with hot methanol. The synthetic results and analytical data were shown in Tables 2 and 3.

References

1) Part I of "Peptides and Proteins Containing α,α-Disubstituted α-Amino Acid Residues." The abbreviations for amino acids are those recommended by the IUPAC-IUB Commission on Biochemical Nomenclature *J. Biol. Chem.*, **247**, 977 (1972). Amino acid symbols denote the L-configuration. Additional abbreviations used are the following: Aib, α-aminoisobutyric acid residue; Boc, *t*-butoxycarbonyl; OBzl, benzyl ester; TsOH, *p*-toluenesulfonic acid; AcOEt, ethyl acetate; NMM, *N*-methylmorpholine; DCC, dicyclohexylcarbodiimide; HOBt, 1-hydroxy-1*H*-benzotriazole; DMF, *N*,*N*-dimethylformamide; HMPA, hexamethylphosphoric triamide; TFA, trifluoroacetic acid; DMA, *N*,*N*-dimethylacetamide; NMP, *N*-methylpyrrolidone; DMSO, dimethyl sulfoxide.

2) M. Narita, T. Fukunaga, A. Wakabayashi, K. Ishikawa, and H. Nakano, *Int. J. Peptide Protein Res.*, **23**, 306 (1984).

3) M. Narita, S. Nagasawa, J.-Y. Chen, H. Sato, and Y. Tanaka, *Makromol. Chem.*, **185**, 1069 (1984).

4) M. Narita, K. Ishikawa, H. Nakano, and S. Isokawa, *Int. J. Peptide Protein Res.*, **24**, 14 (1984).

5) M. Narita, N. Ohkawa, S. Nagasawa, and S. Isokawa, *Int. J. Peptide Protein Res.*, **24**, 129 (1984).

6) M. Narita, K. Ishikawa, J.-Y. Chen, and Y. Kim, *Int. J. Peptide Protein Res.*, **24**, 580 (1984).

7) S. Isokawa, T. Asakura, and M. Narita, *Macromolecules*, in press.

8) S. Isokawa, I. Tominaga, T. Asakura, and M. Narita, *Macromolecules*, in press.

9) R. Katakai, H. Shida, and T. Takada, *Biopolymers*, **23**, 1397 (1984).

10) R. Katakai and Y. Iizuka, *Biopolymers*, **23**, 1411 (1984) and references cited therein.

11) R. G. Strachan, W. J. Paleveda, Jr., R. F. Nutt, R. A. Vitali, D. F. Veber, M. J. Dickinson, V. Garsky, J. E. Deak, E. Walton, S. R. Jenkins, F. W. Holly, and R. Hirschmann, *J. Am. Chem. Soc.*, **91**, 503 (1969).

12) S. R. Jenkins, R. F. Nutt, R. S. Dewey, D. F. Veber, F. W. Holly, W. J. Paleveda, Jr., T. Lanza, Jr., R. G. Strachan, E. F. Schoenewaldt, H. Barkemeyer, M. J. Dickinson, J. Sondey, R. Hirschmann, and E. Walton, *J. Am. Chem. Soc.*, **91**, 505 (1969).

13) H. Yajima and Y. Kiso, *Chem. Pharm. Bull.*, **22**, 1087 (1974).

14) M. Fujino, S. Shinagawa, T. Fukuda, M. Takaoki, H. Kawaji, and Y. Sugino, *Chem. Pharm. Bull.*, **25**, 1486 (1977).

15) H. Romovacek, S. R. Dowd, K. Kawasaki, N. Nishi, and K. Hofmann, *J. Am. Chem. Soc.*, **101**, 6081 (1979).

16) T. Kimura, Y. Takai, Y. Masui, T. Morikawa, and S. Sakakibara, *Biopolymers*, **20**, 1823 (1981).

17) Y. Paterson, S. M. Rumsey, E. Benedetti, G. Nemethy, and H. A. Scheraga, *J. Am. Chem. Soc.*, **103**, 2947 (1981) and references cited therein.

18) C. Toniolo, G. M. Bonora, A. Bavoso, E. Benedetti, B. Di Blasio, V. Pavone, and C. Pedone, *Biopolymers*, **22**, 205 (1983).

19) a) M. Palumbo, S. D. Rin, G. M. Bonora, and C. Toniolo, *Makromol. Chem.*, **177**, 1477 (1976); b) E. Benedett, A. Bavoso, B. D. Blasio, V. Pavone, C. Pedone, C. Toniolo, G. M. Bonora, and M. Crisma, *Int. J. Peptide Protein Res.*, **22**, 385 (1983).

20) M. Narita, K. Ishikawa, H. Sugasawa, and M. Doi, *Bull. Chem. Soc. Jpn.*, in press.

21) T. Miyazawa and E. J. Blout, *J. Am. Chem. Soc.*, **83**, 712 (1961).

22) K. Itoh and H. Katabuchi, *Biopolymers*, **12**, 921 (1973).

23) M. T. Leplawy, D. S. Jones, G. W. Kenner, and R. C. Sheppard, *Tetrahedron*, **11**, 39 (1960).

24) C. P. Rao and P. Balaram, *Biopolymers*, **21**, 2461 (1982).

25) A. K. Francis, M. Iqbal, P. Balaram, and M. Vijayan, *Biopolymers*, **22**, 1499 (1983).

26) G. R. Marshall, in "Intra-Science Chemistry Report," vol. 5, ed by N. Kharasch, Gordon and Breach, New York, pp. 305—316 (1971).

27) A. W. Burgess and S. J. Leach, *Biopolymers*, **12**, 2599 (1973).

28) E. K. S. Vijayakuman and P. Balaram, *Biopolymers*, **22**, 2133 (1983).

29) The idea of the partial replacement of Ala residues with Aib residues in synthetic analogs of proteins has previously proposed by A. W. Burgess and S. J. Leach [*Biopolymers*, **12**, 2599 (1973)], but no progress has been made.

30 We thank Professor Yasuyuki Tanaka and Dr. Hisaya Sato, Department of material systems Engineering, Faculty of Technology, Tokyo University of Agriculture and Technology, for their gift of the column.

 © 1985 The Chemical Society of Japan Bull. Chem. Soc. Jpn., 58, 1480—1483 (1985) [Vol. 58, No. 5

Retentive Stereospecificity in Deoxygenation of Epoxides with Sn-Al or Si-Al Reagents

Seijiro MATSUBARA, Tsuyoshi NONAKA, Yasuhiro OKUDA, Shigekazu KANEMOTO, Koichiro OSHIMA,* and Hitosi NOZAKI

Department of Industrial Chemistry, Faculty of Engineering, Kyoto University, Yoshida, Kyoto 606

(Received December 24, 1984)

Reaction of epoxides with [*n*-$Bu_3SnAlMe_3$]$^-Li^+$ affords β-oxido stannanes which collapse to alkene with overall retention of stereochemistry. The S_N2 type ring opening of epoxides by tributylstannyl anion followed by anti elimination of Bu_3Sn and OAl^-Me_3 groups explains the stereochemical results. The method can be successfully applied to hydroxy epoxides derived from (*E*)-2-nonen-1-ol. The deoxygenation of epoxides with $PhMe_2SiAlEt_2$ also provides olefins of the same geometry as epoxides.

Reagents believed to contain Si–Mg, Si–Al, Sn–Mg, and Sn–Al linkage are obviously reductants in which a Lewis acid center is incorporated. The single bond is weak and the previously reported reaction[1,2] with an acetylenic linkage affords simple and general access to the cis-addition products of the component atoms. In order to examine the nature of these reagents more precisely, we have studied the deoxygenation of epoxides by means of Sn–Al or Si–Al reagents.

The deoxygenation of epoxides to olefins has been widely studied and numerous reagents have been developed. The reduction with strongly reductive metals or metal salts such as chromium(II) ion,[3] tungsten complexes,[4] $TiCl_3/LiAlH_4$,[5] $NbCl_5/NaAlH_4$,[6] and $FeCl_3/n$-BuLi[7] produces olefins non-stereospecifically through a radical intermediate. For instance, treatment of *cis*- or *trans*-5,6-epoxydecane with $TiCl_3/LiAlH_4$ has provided a mixture of (*Z*)- and (*E*)-5-decene in a 21/79 or 18/82 ratio,[5] respectively. In contrast, the reaction with Me_3SiK[8] or $PhMe_2SiLi$[9] has proceeded stereospecifically to give the olefin of geometry opposite to that of the starting epoxide.[10] Here we wish to report that [*n*-$Bu_3SnAlMe_3$]$^-Li^+$ (**1**) is effective for the deoxygenation of epoxides to provide olefins of the same geometry as epoxides (Scheme 1).[11]

Treatment of (*E*)-5-decene oxide with the reagent **1** derived from *n*-Bu_3SnLi[12] and Me_3Al at 25 °C gave (*E*)-5-decene exclusively, while (*Z*)-5-decene oxide provided (*Z*)-5-decene as a single product. The results are summarized in Table 1. With some exceptions,[13] the deoxygenation reactions proceeded mostly with high stereospecificities. The deoxygenated product of (*Z*)-stilbene oxide, (*Z*)-stilbene, proved to isomerize partially under the reaction conditions, since treatment of (*Z*)-stilbene with the reagent **1** at 25 °C for 24 h gave a mixture of (*E*)-stilbene and (*Z*)-isomer (*E*/*Z*=40/60).

A priori, the overall retention of configuration can

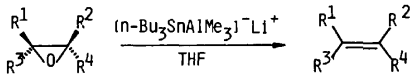

Scheme 1.

Table 1. Deoxygenation of epoxides with [*n*-$Bu_3SnAlMe_3$]$^-Li^+$ [a]

Run	Epoxide	Reaction Time (h)	Olefin Y/%	Olefin *E*/*Z*
1	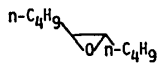	18	80	99% *E*
2	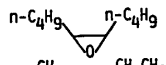	24	67	99% *Z*
3	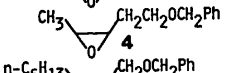	16	63	99% *Z*
4	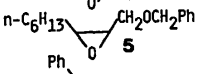	40	70	99% *Z*
5	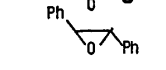	3	98	99% *E*
6		24[b]	100	99% *E*
7	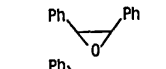	6	88	34/66
8	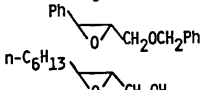	17	88	99% *E*
9		18	75	99% *E*
10	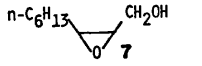	40	65	99% *Z*

a) The reactions were performed in THF at 25 °C. b) [*n*-$Bu_3SnAlEt_3$]$^-Li^+$ was used instead of [*n*-$Bu_3SnAlMe_3$]$^-Li^+$.

be explained by two ways: (1) S_N2 attack of *n*-Bu_3Sn anion followed by anti-elimination of Bu_3Sn and OAl^-Me_3 groups, or alternatively (2) retentive C–Sn bond formation under the epoxide ring opening and successive syn elimination of above groups. The stereochemistry of the elimination reaction was studied on the reaction of *erythro*- and *threo*-6-(tributylstannyl)-5-decanols (**2** and **3**) with organoaluminum reagent. Reaction of (*E*)- or (*Z*)-5-decene oxide with tributyltin sodium[14] in 1,2-dimethoxyethane gave the desired erythro- or threo isomer (**2** or **3**), respectively. Exposure of *erythro*-6-(tributylstannyl)-5-decanol **2** to [Me_4Al]$^-Li^+$ derived from Me_3Al and MeLi, yielded (*E*)-5-decene exclusively, whereas the threo isomer **3** gave (*Z*)-5-decene with high stereoselectivity (Scheme 2).[15] These results proved that the elimination proceeded in anti fashion[16] and therefore

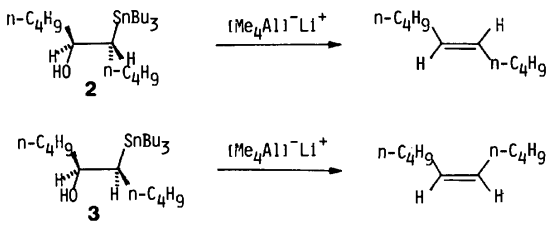

Scheme 2.

the epoxide ring opening must have proceeded with inversion of its stereochemistry at the carbon bearing oxygen. Moreover, both processes are stereospecific.

The intermediate alkoxy stannanes have not been characterized in the deoxygenation reaction with the reagent **1** and we assume that two positional isomers are present, derived from either mode of S_N2 epoxide opening in the case of unsymmetrical epoxides such as **4**, **5**, **6**, and **7**. This complication in no way impairs conversion to olefins in the case of **4** and **5**, since elimination of *n*-Bu_3Sn and oxide group from each pair of intermediates provides the same (*Z*)-alkene **8** (Scheme 3). Situation is more complicated in the case of epoxides **6** and **7** derived from (*E*)- and (*Z*)-2-nonen-1-ol. The S_N2 type ring opening of the (*E*)-epoxide **6** could afford two isomeric β-oxido stannanes **9** and **10**. The former β-oxido stannane **9** would provide (*E*)-2-nonen-1-ol **11** by anti elimination, whereas the latter isomer **10** would produce 1-nonen-3-ol (**12**) in addition to starting allylic alcohol **11**. The absence of the compound **12** in the reaction mixture implies that a single isomer **9** is produced by epoxide ring opening. We are tempted to assume the following reaction scheme. The hydroxyl group is converted into aluminum alkoxide with the first stannyl reagent. The epoxide-oxygen coordinates to the aluminum and this coordination plays the important role in the product determining ring opening step. The epoxide carbon

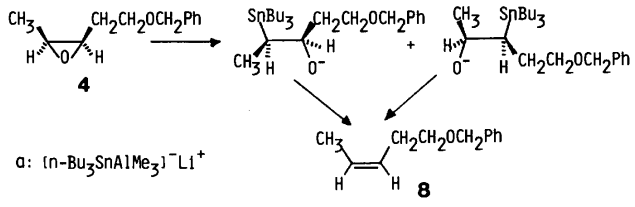

Scheme 3.

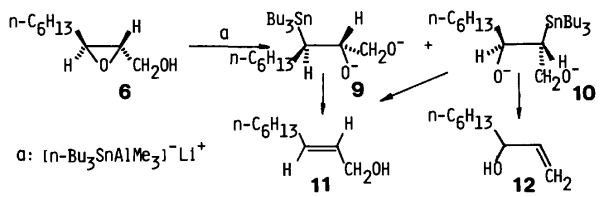

Scheme 4.

Table 2. Deoxygenation of epoxides with Si-Al reagents

Epoxide	Reagent	Conditions Temp °C	Conditions Time h	Olefin Y/%	Olefin *E*/*Z*
	A[a]	25	4	71	*E* only
	A	25	5	75	7/3
	A[b]	25	3	40	*E* only
	A	25	4	54	—
	B[c]	25	18	72	*Z* only

a) $PhMe_2SiAlEt_2$ in hexane. b) $PhMe_2SiAlEt_2$ in $ClCH_2CH_2Cl$. c) $[PhMe_2SiAlMe_3]^-Li^+$ in THF.

(C_3)-oxygen bond is cleaved by the attack of the stannyl anion liberated from the second molecule **1** (Scheme 4)[17]

Another stannylalanate reagent, [*n*-$Bu_3SnAlEt_3$]$^-$-Li^+ derived from *n*-Bu_3SnLi and Et_3Al was as effective as the reagent **1** for the reduction of epoxides, although the prolonged reaction time was needed for the completion (run 5 and 6 in Table 1). A stannylaluminum, *n*-$Bu_3SnAlEt_2$ prepared from *n*-Bu_3SnLi and Et_2AlCl was not effective for the transformation. The starting epoxides were recovered unchanged after heating the reaction mixture in CH_2ClCH_2Cl or THF. High nucleophilicity of tributylstannyl anion of the ate complex **1** could explain the facile epoxide ring opening in S_N2 fashion.

Finally, the reaction of epoxides with silyl-metal reagents such as $[PhMe_2SiAlMe_3]^-Li^+$ and $PhMe_2SiAlEt_2$ were examined. These reagents have proven to be less reactive for the deoxygenation of epoxides than the above mentioned stannyl reagents. Highly reactive epoxides bearing a phenyl substituent only gave the corresponding olefins in moderate yields (Table 2). Other purely aliphatic epoxides such as 5-decene oxide and 1-dodecene oxide gave the complex mixture containing the desired olefins as a minor component (<20%) after prolonged heating in CH_2ClCH_2Cl or benzene.

Experimental

The IR spectra were determined on a Shimadzu IR-27-G spectrometer, the mass spectra on a Hitachi M-80 machine, and the proton NMR spectra on a Varian EM-390 spectrometer, and the ^{119}Sn NMR spectra on a JEOL JNM-FX 90Q spectrometer. The chemical shifts of the proton NMR are given in δ with TMS as an internal standard, and those of the ^{119}Sn NMR are given in δ with tetramethylstannane as an internal standard. The analyses were carried out by the

staff at the Elemental Analyses Center of Kyoto University. Tetrahydrofuran was freshly distilled from sodium benzophenone ketyl. Purificaton of products was performed by column chromatography on silica-gel (Wakogel C-100) or preparative thin-layer chromatography (TLC). Analytical GLPC was performed with a Yanagimoto GCG-550-F and a Shimadzu GC-4CPT.

General Procedure for the Deoxygenation of Epoxide with [n-Bu$_3$SnAlMe$_3$]$^-$Li$^+$. Transformation of (*E*)-5-decene oxide into (*E*)-5-decene is representative. Butyllithium (1.7 M* hexane solution, 3.5 ml, 6.0 mmol) was added dropwise to a suspension of anhydrous $SnCl_2$ (0.38 g, 2.0 mmol) in THF (5.0 ml) at 0 °C under an argon atmosphere. The solution turned to reddish brown immediately. After stirring for 10 min, a hexane solution of Me_3Al (1.0 M, 2.0 ml, 2.0 mmol) was added. The resulting mixture was stirred for another 10 min, then a solution of epoxide (0.16 g, 1.0 mmol) in THF (2.0 ml) was added. The whole was stirred for 24 h at 25 °C and the reaction mixture was poured into 1 M HCl and extracted with ether. The organic layer was dried (Na_2SO_4) and concentrated *in vacuo* to give 5-decene which was purified by silica-gel column chromatography. In order to check the *cis:trans* ratio of the product, the olefin was transformed into epoxide upon treatment with 86% *m*-chloroperbenzoic acid (0.60 g, 3.0 mmol) in CH_2Cl_2. Workup and purification by silica-gel column chromatography gave (*E*)-5-decene oxide exclusively (0.12 g, 80% overall yield): bp 95 °C/15 Torr** (bath temp); NMR (CCl_4) δ=1.83 (t, J=6 Hz, 6H), 1.16—1.46 (m, 12H), 2.30—2.55 (m, 2H). GLPC examination of the epoxide showed only one peak at t_r=4.0 min (Silicone OV-17 3% on Uniport HP, 2 m, 100 °C). The peak at t_r=4.6 min corresponding to (*Z*)-5-decene oxide (NMR (CCl_4) δ 1.83 (t, J=6 Hz, 6H), 1.10—1.46 (m, 12H), 2.30—2.55 (m, 2H)) was not observed.

erythro-*6-(Tributylstannyl)-5-decanol (2).* The title compound was obtained according to the reported procedure[14] using *n*-Bu_3SnCl instead of Ph_3SnCl. A solution of tributyltin chloride (4.1 g, 12.5 mmol) in DME (4.0 ml) was added slowly to a DME solution (10 ml) of sodium naphthalene prepared from sodium metal (0.58 g, 0.025 g-atom) and naphthalene (0.26 g, 21 mmol) to maintain a green color at all times. After complete addition, the solution was stirred for 2 h and then cooled in an ice bath and a solution of *trans*-5-decene epoxide (0.78 g, 5.0 mmol) in DME (2.0 ml) was added dropwise. The resulting solution was stirred for another 1.5 h. Workup and purification by silica-gel column chromatography gave stannyl compound **2** as a colorless oil: bp 140 °C (dec. 0.1 Torr, bath temp); IR (neat) 3350, 2900, 1460, 1385, 1060, 1000 cm^{-1}; ^{1}H-NMR ($CDCl_3$) δ=0.71—1.05 (m, 21H), 1.10—1.75 (m, 26H), 3.73—3.95 (m, 1H), ^{119}Sn-NMR ($CDCl_3$) δ=−15.7. Found: *m/z* 389.2045. $C_{18}H_{39}O^{119}Sn$: M−C_4H_9 389.2019.

threo-*6-(Tributylstannyl)-5-decanol (3)*: Bp 140 °C (dec. 0.1 Torr, bath temp); IR (neat) 3400, 2900, 1460, 1378, 1070, 1000 cm^{-1}; ^{1}H-NMR ($CDCl_3$) 0.75—1.10 (m, 21H), 1.15—1.75 (m, 26H), 3.70—3.95 (m, 1H), ^{119}Sn-NMR ($CDCl_3$) δ=−19.3. Found: *m/z* 389.1997. Calcd for $C_{18}H_{39}O^{119}Sn$: M−C_4H_9 389.2019.

Elimination of erythro- *and* threo-*6-(Tributylstannyl)-5-decanol to (E)- and (Z)-5-decene.* A solution of *erythro* β-hydroxy stannane **2** (0.67 g, 1.5 mmol) in THF (3.0 ml) was added to a solution of [Me_4Al]$^-$Li$^+$ derived from Me_3Al (1.0 M hexane solution, 3.0 ml, 3.0 mmol) and MeLi (1.5 M ether solution, 2.0 ml, 3.0 mmol) at 0 °C. The mixture was stirred for 40 h at 25 °C. Workup (1 M HCl, ether) and purification by silica-gel column chromatography gave (*E*)-5-decene (0.14 g, 65% yield) which was oxidized into 5-decene oxide upon treatment with *m*CPBA. The purity of the resulting epoxide was found to be >99% (*E*) by the GLPC examination. Starting from *threo* isomer **3** (0.67 g, 1.5 mmol), (*Z*)-5-decene (0.12 g, 57% yield) was obtained as a single isomer (>99% (*Z*)).

Conversion of trans-*2,3-epoxy-1-nonanol (6) into (E)-2-nonen-1-ol.* A solution of [*n*-Bu$_3$SnAlMe$_3$]$^-$Li$^+$ (5.08 mmol) was prepared from *n*-Bu_3SnLi[18] and Me_3Al according to the procedure described above. A THF solution of epoxide **6** (0.20 g, 1.27 mmol) was added and the whole was stirred for 18 h at 25 °C. Extractive workup (1 M HCl, ether) and purification by preparative thin-layer chromatography on silica-gel gave (*E*)-allylic alcohol (0.11 g, 75% yield) as a colorless oil. The alcohol was treated with *m*CPBA to give epoxy alcohol whose purity (>99% (*E*)) was determined by GLPC (t_r=6.0 min, Silicone OV-17 3% on Uniport HP, 2 m, 120 °C). The epoxy alcohol derived from (*Z*)-2-nonen-1-ol had a longer retention time (t_r=7.0 min).

General Procedure for the Deoxygenation of Epoxides by Means of PhMe$_2$SiAlEt$_2$. Reduction of (*E*)-stilbene oxide to (*E*)-stilbene is representative. A THF solution of $PhMe_2SiLi$[19] (0.65 M, 3.0 ml, 2.0 mmol) was added to a hexane solution of diethylaluminium chloride (1.0 M, 2.0 ml, 2.0 mmol) at 0 °C under an argon atmosphere. After stirring for 20 min at 25 °C, the solvent was evaporated *in vacuo* and hexane (8 ml) was introduced to the residue. Then a hexane solution of (*E*)-stilbene oxide (0.20 g, 1.0 mmol) was added and the resulting mixture was stirred at 25 °C for 4 h. The mixture was diluted with AcOEt and poured into 1 M HCl. Organic layer was dried (Na_2SO_4) and concentrated *in vacuo*. The remaining semisolid was submitted to preparative thin-layer chromatography on silica-gel to give (*E*)-stilbene (0.13 g, 71% yield) as crystals which was identical with an authentic sample. The purity of the compound was checked by NMR and GLPC (t_r=8.0 min, Silicone OV-17 3% on Uniport HP, 2 m, 140 °C). (*Z*)-stilbene had a longer retention time (t_r=11.0 min).

Deoxygenation of Epoxide derived from Cinnamyl Alcohol Benzyl Ether by Means of [PhMe$_2$SiAlMe$_3$]$^-$Li$^+$. A hexane solution of Me_3Al (1.0 M, 2.0 ml, 2.0 mmol) was added dropwise to a THF solution of $PhMe_2SiLi$ (0.3 M, 6.5 ml, 2.0 mmol) at 0 °C. After stirring for 10 min, a THF solution of epoxide (0.24 g, 1.0 mmol) was added and the reaction mixture was warmed to room temperature, the whole was stirred for 18 h. The mixture was poured into water and extracted with ether. Purification by silica-gel column chromatography gave cinnamyl alcohol as a colorless oil. GLPC analysis proved that the purity of the alcohol was >97% (*Z*) (t_r=11.5 min, Silicone OV-17 3% on Uniport HP, 2 m, 180 °C). Retention time of (*E*)-isomer was 18.0 min.

Financial support by the Ministry of Education, Science, and Culture (Grant-in-Aid for Special Project Research #59104005) is acknowledged.

* 1 M=1 mol dm^{-3}.

** 1 Torr=133.322 Pa.

References

1) H. Hayami, M. Sato, S. Kanemoto, Y. Morizawa, K. Oshima, and H. Nozaki, *J. Am. Chem. Soc.*, **105**, 4491 (1983); J. Hibino, S. Matsubara, Y. Morizawa, K. Oshima, and H. Nozaki, *Tetrahedron Lett.*, **25**, 2151 (1984).

2) *n*-$Bu_3SnAlEt_2$ reagent has been found to be effective for Reformatsky type reaction. N. Tsuboniwa, S. Matsubara, Y. Morizawa, K. Oshima, and H. Nozaki, *Tetrahedron Lett.*, **25**, 2569 (1984); *idem, Bull. Chem. Soc. Jpn.*, **57**, 3242 (1984).

3) J. K. Kochi, D. M. Singleton, and L. J. Andrews, *Tetrahedron*, **24**, 3503 (1968).

4) K. B. Sharpless, M. A. Umbreit, M. T. Nieh, and T. C. Flood, *J. Am. Chem. Soc.*, **94**, 6538 (1972).

5) J. E. McMurry, M. G. Silverstri, M. P. Fleming, T. Hoz, and M. W. Grayston, *J. Org. Chem.*, **43**, 3249 (1978).

6) M. Sato and K. Oshima, *Chem. Lett.*, **1982**, 157.

7) T. Fujisawa, K. Sugimoto, and H. Ohta, *Chem. Lett.*, **1974**, 883.

8) P. B. Dervan and M. A. Shippey, *J. Am. Chem. Soc.*, **98**, 1265 (1976).

9) M. T. Reetz and M. Plachky, *Synthesis*, **1976**, 199.

10) Olefin inversion by phosphorus betaine method has been reported. E. Vedejs and P. L. Fuchs, *J. Am. Chem. Soc.*, **95**, 822 (1973). Control of olefin stereochemistry has been also achieved by concerted fragmentation of heterocyclic olefin precursors *via vic*-diols. (1) 1,3-dioxolane-2-thiones: E. J. Corey, F. A. Carey, and R. A. E. Winter, *J. Am. Chem. Soc.*, **87**, 934 (1965); E. J. Corey and J. I. Shulman, *Tetrahedron Lett.*, **1968**, 3655. (2) 2-acyloxy-1,3-dioxolanes: J. S. Josan and F. W. Eastwood, *Aust. J. Chem.*, **21**, 2013 (1968); T. Hiyama and H. Nozaki, *Bull. Chem. Soc. Jpn.*, **46**, 2248 (1973). (3) 2-phenyl-1,3-dioxolanes: T. Aratani, Y. Nakanishi, and H. Nozaki, *Tetrahedron*, **26**, 4339 (1970); G. H. Whittam and M. Wright, *J. Chem. Soc. C.*, **1971**, 883, 886, 891. Review for the olefin inversion, see P. E. Sonnet, *Tetrahedron*, **36**, 557 (1980).

11) Several other methods for the transformation of epoxides to the starting olefins with retention of stereochemistry have been reported. These methods are based on the sequence of S_N2 opening of epoxide by iodide and trans elimination of iodohydrin derivatives. P. E. Sonnet, *J. Org. Chem.*, **43**, 1841 (1978); *idem, Synthesis*, **1980**, 828; R. Caputo, L. Mangoni, O. Neri, G. Palumbo, *Tetrahedron Lett.*, **22**, 3551 (1981).

12) C. Tamborski, F. E. Ford, and E. J. Soloski, *J. Org. Chem.*, **28**, 237 (1963); W. C. Still, *J. Am. Chem. Soc.*, **99**, 4836 (1977) and **100**, 1481 (1978); W. Kitching, H. A. Olszowy, and K. Harvey, *J. Org. Chem.*, **47**, 1893 (1982).

13) The reaction of cyclododecene oxides also proceeded with less stereospecificity. *cis*-Epoxide provided a mixture of (*E*)-cyclododecene: (*E*)-isomer=75:25, while *trans*-epoxide gave a mixture of *E*:*Z*=61:39.

14) D. D. Davis and C. E. Gray, *J. Org. Chem.*, **35**, 1303 (1970).

15) In order to see the fate of the stannyl group, the crude products were carefully examined to find methyltributylstannane (10% yield) contaminated with polymeric stannyl residue.

16) Davis *et al.* reported that perchloric acid-catalyzed elimination of β-hydroxy stannane proceeded in anti fashion. In our new method, organoaluminium acts as a Lewis acid and the coordination of oxygen of hydroxyl group facilitates the elimination. D. D. Davis and C. E. Cray, *J. Organomet. Chem.*, **18**, Pl (1969); T. Kauffmann, R. Konig, R. Kriegesmann, M. Wensing, *Tetrahedron Lett.*, **25**, 641 (1984).

17) T. Suzuki, H. Saimoto, H. Tomioka, K. Oshima, and H. Nozaki, *Tetrahedron Lett.*, **23**, 3597 (1982); A. Pfaltz and A. Mattenberger, *Angew. Chem. Suppl.* **1982**, 161; W. R. Roush, M. A. Adam, S. M. Peseckis, *Tetrahedron Lett.*, **24**, 1377 (1983).

18) C. Tamborski, F. E. Ford, and E. J. Soloski, *J. Org. Chem.*, **28**, 237 (1963); W. C. Still, *J. Am. Chem. Soc.*, **99**, 4836 (1977) and **100**, 1481 (1978); W. Kitching, H. A. Olszowy, and K. Harvey, *J. Org. Chem.*, **47**, 1893 (1982).

19) H. Gilman and G. D. Lichtemwalter, *J. Am. Chem. Soc.*, **80**, 607 (1958).

 © 1985 The Chemical Society of Japan Bull. Chem. Soc. Jpn., 58, 1484—1489 (1985) [Vol. 58, No. 5

Brillouin Scattering of Supercooled Liquids. I. *Tri-o*-tolyl Phosphate

Shinobu KODA, Hiroyasu NOMURA,* Masayuki NAKAMURA, and Yutaka MIYAHARA
Department of Chemical Engineering, School of Engineering, Nagoya University, Chikusa-ku, Nagoya 464
(Received August 6, 1984)

The sound velocities of *tri-o*-tolyl phosphate in the GHz region were measured by means of the Brillouin scattering method over a wide range of temperatures. In the temperature range from 283 to 313 K, the sound velocity dispersion was observed directly. The relaxation curves of the longitudinal modulus could be analyzed using a B.E.L. model with a parameter of K=0.5. With a rising temperature, a deviation from the B.E.L. model appeared. We considered that the deviation was attributed to the rotational molecular motion of *tri-o*-tolyl phosphate.

Supercooled liquids or glassy materials have abnormally large viscosities compared with those of ordinary liquids. The relaxation times of dynamic shear and bulk viscosities of supercooled liquids are so long that they are within the measurable frequency range. Therefore, the supercooled liquids have been accepted as to be pertinent in clarifying the structure and dynamic properties of liquids.

Earlier investigations of the viscoelastic properties of supercooled liquids have been surveyed by Harrison.[1] Most investigations described were those carried out in the MHz region using ultrasonic and dielectric methods.

Barlow, Lamb and their coworkers[2-6] have extensively studied the viscoelastic properties of many supercooled liquids by means of transverse and longitudinal ultrasonic methods. They showed that the shear modulus of supercooled liquids displays a relaxation phenomena and the distribution of the relaxation times was considerably broader than that predicted from the single Maxwellian relaxation model. It was concluded that the relaxation behavior observed in most supercooled liquids can be described in terms of the generalized B. E. L. (Barlow-Erginsav-Lamb) model.[3]

On the other hand, Litovitz and his coworkers[7-11] have given another description of the relaxation phenomena of supercooled liquids. They indicated that the relaxation behavior of supercooled liquids can be explained by taking account of the distribution of the relaxation times of the cooperative motion of the molecules.[11] Moreover, they measured the relaxation times of the shear and bulk moduli of molten salt, B_2O_3, from 650 to 1000 °C and showed that the shear relaxation process can be represented by a single relaxation time in the temperature range above 800 °C where the shear viscosity is of the Arrhenius type. On the other hand, the shear and bulk relaxation processes exhibit an increasingly broad distribution of relaxation times in the non-Arrhenius region of the lower temperatures.[11] They also found that the master curve of the reduced longitudinal modulus of glycerol in the GHz region is not consitent with the corresponding master curve in the MHz region.[9]

In studying the relaxation phenomena of supercooled liquids, it is necessary to perform experiments over wider temperature and frequency ranges. In order to obtain the longitudinal modulus in the GHz region, the Brillouin scattering method is very useful. Recently, several experimental results regarding supercooled liquids investigated by the Brillouin scattering method have been reported.[12-18] In these works, much attention was given to the Rayleigh dip due to the shear mode of the thermal motion of the molecules in liquids. Scant attention was attracted to the longitudinal mode.

The purpose of this study was to obtain the longitudinal sound velocity in the GHz region for *tri-o*-tolyl phosphate using the Brillouin scattering method as a function of temperature and scattering angle. The sample, *tri-o*-tolyl phosphate, was chosen since its longitudinal and shear moduli in the MHz region have been well investigated by the present authors[19] and Barlow *et al.*[2-6] The longitudinal modulus of *tri-o*-tolyl phosphate in the GHz region is compared with those in the MHz region and a discussion is given regarding the basis of the B. E. L. model. The molecular dynamical investigations of the sample were carried out by means of Raman and depolarized Rayleigh scattering methods.

Experimental

Sample. *Tri-o*-tolyl Phosphate, *tris*(2-methylphenyl) phosphate (practical grade) was obtained from Eastman Organic Chemicals. *Tri-o*-tolyl Phosphate is hereafter abbreviated as TOTP. The sample was purified by fractional distillation under reduced pressure and was checked by Raman spectroscopy.

Brillouin Spectra. The Brillouin spectra were measured using a pressure-scanning Fabry-Perot interferometer. The light source was a He-Ne laser (NEC, GLG 5800) with an output of 50 mw. A detailed description of the apparatus and procedure is found in a previous paper.[20]

In order to obtain the Brillouin spectra over wider temperature ranges, a sample cell (as shown in Fig. 1) was used. This cell was made of Pyrex glass and the diameter of

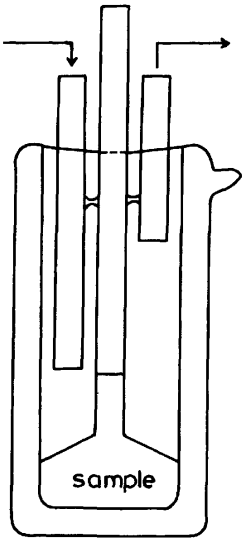

Fig. 1. Brillouin cell. The temperature is regulated by flowing the heated air or cooled air by liquid nitrogen.

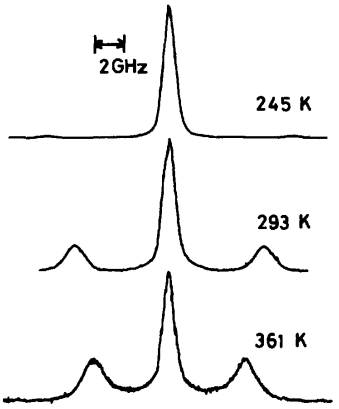

Fig. 2. Representative Brillouin spectra. ($\theta=90°$)

the inner cylinder containing the samle was 5 cm and that of the outer cylinder was 7 cm. The temperature of the sample was regulated by flowing heated and/or cooled air with liquid nitrogen around the inner glass cylinder. The attainable temperature ranges within this cell are from 210 to 350 K with an accuracy of ±1 K. The measured scattering angles were from 20 to 160° for each temerature. The Brillouin spectrum was recorded using an X-Y recorder. At the same time, the spectral intensity and the pressure were punched out on tape as digital data. These data were analyzed to determined the Brillouin frequency shift using a computer.[20] For illustration, the typical Brillouin spectra of TOTP are shown in Fig. 2.

The refractive indexes necessary for the analysis of a sample were measured by means of an Abbe refractometer (Atago) in the temperature range 278 to 337 K.

Raman Spectra. The Raman spectra were measured using a laser Raman Spectrometer JEOL-Ul (Japan Electron Optical Laboratory Co., Ltd.) and an argon ion laser (Coherent Radiation Co., Ltd.), operating at 488 nm (800 mw). The temperature dependence of the Raman spectra was measured with a variable-temperature Raman cell of the Harney-Miller type. The 1047 cm^{-1} band, P-O stretching vibrational mode, of TOTP was measured by using polarizing scattered beam parallel, $I_{\parallel}(\omega)$ and perpendicular, $I_{\perp}(\omega)$ to the electric field vector $\vec{E}$ of the incident light.

Deplorarized Rayleigh Scattering Spectra. The light scattering spectrometer used was consisted of a He-Ne laser (NEC, GLG 5800, 50 mw) and a piezoelectrically driven Fabry Perot interferometer (Burleigh RC 11) with a stabilization system (Burleigh DAS 10, RC 43). The laser beam was irradiated on a sample cell made of quartz. The scattered light at 90° was collimated by a lens through a Glan Thomson prism and the observed spectra were stored in a multichannel analyzer (Anberra Series 30). These spectra could be transfered in a digital form to a microcomputer (Sharp Mz-80c) for further processing. The exeprimental procedures and the correction of instrumental width have been reported elsewhere in details.[21,22] The measuring temperature ranged from 263 to 373 K with an accuracy of±0.5 K.

Results

The sound velocity, V, was calculated from the equation[23]

$$V=\left(\frac{\Delta\omega}{\omega_0}\right)\frac{c}{2n\sin(\theta/2)}, \quad (1)$$

where $\Delta\omega$ is the Brillouin frequency shift, ω_0 the frequency of the incident light, c the velocity of light, n the refractive index of a liquid sample, and θ the scattering angle. The temperature dependence of sound velocities measured at various scattering angles are shown in Fig. 3. It is noted that the constancy of the scattering angle does not always correspond to the constancy of the frequency, because of the temperature dependence of refractive index of a sample. However, as is shown in Fig. 3, at larger scattering angles and lower temperatures, the sound velocity was independent of the scattering angle. This sound velocity can be treated as the sound velocity at the high frequency limit for each temperature. Upon increasing the temperature, the dispersion of sound

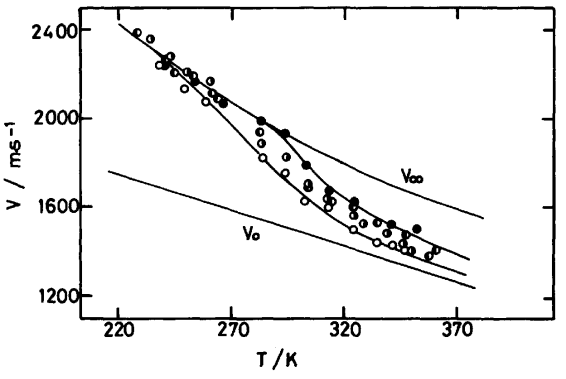

Fig. 3. Temperature dependence of the sound velocity. (●); $\theta=133°$, (◐); $\theta=90°$, (◑); $\theta=60°$, (○); $\theta=35°$.

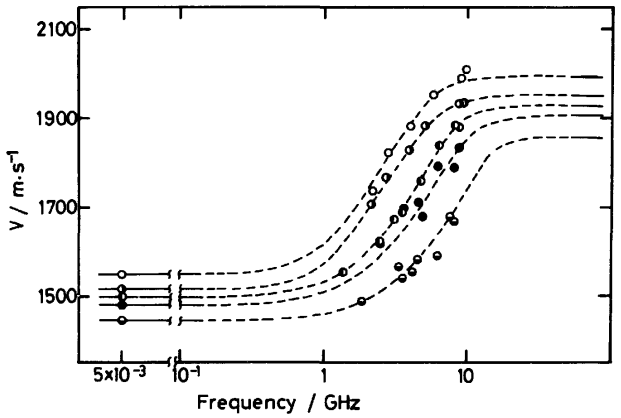

Fig. 4. Frequency dependence of the sound velocity. (○); $T=283$ K, (◑); $T=293$ K, (◐); $T=298$ K, (●); $T=303$ K, (◒); $T=313$ K.

velocity was observed as shown in Fig. 3. On the other hand, Fig. 4 shows the frequency dependence of sound velocity at a constant temperature between 283 and 313 K. The curves clearly show the sound velocity dispersion and the dispersion strength decreases with increasing temperature. In Figs. 3 and 4, the sound velocity at the high frequency limit, V_∞ for each temperature was estimated by extrapolating the V_∞ below 270 K, which were observed directly as shown in Fig. 3. The sound velocity at low frequency limit, V_0, was sometimes measured using by an ultrasonic interferometer working at 4.0 MHz. In wider temperature ranges, the empirical equation proposed by Barlow *et al.*[6] was used.

The Brillouin scattering data also give the Landau-Placzek ratio, $I_R/2I_B$, where I_R and I_B are the intensities of the Rayleigh and Brillouin lines, respectively. However, in this experiment, the accurate intensities of the Rayleigh and Brillouin lines could not be obtained because of the following factors; the diffuse reflection of the cell, a correction of instrumental broadening, the extremely low intensity of Brillouin lines at low temperatures (see Fig. 2) and so on. Therefore, our attention was concentrated upon the Brillouin frequency shift, that is, the sound velocity.

Information regarding the reorientational motion of TOTP can be obtained from an analysis of the Raman line shape[24-26] and/or the depolarized Rayleigh line shape.[27] The half-width refers to the reorientational motion of a molecule, ω_{or}, and can be estimated from the difference between the half-widths of the anisotropic and isotropic Raman lines, $\omega_{anis}(1/2)$ and ω_{isot} (1/2). Details regarding data analysis are presented elsewhere.[28] Figure 5 shows the temperature dependences of $\omega_{isot}(1/2)$ and $\omega_{anis}(1/2)$ after a correction for the broadening effect due to the slit width. As shown in Fig. 5, ω_{or}-

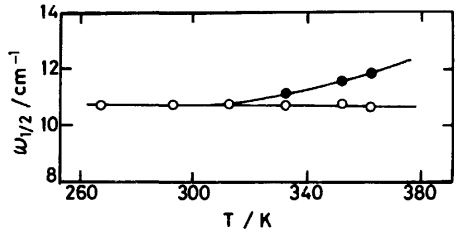

Fig. 5. Temperature dependences of $\omega_{isot}(1/2)$ (○) and $\omega_{anis}(1/2)$ (●).

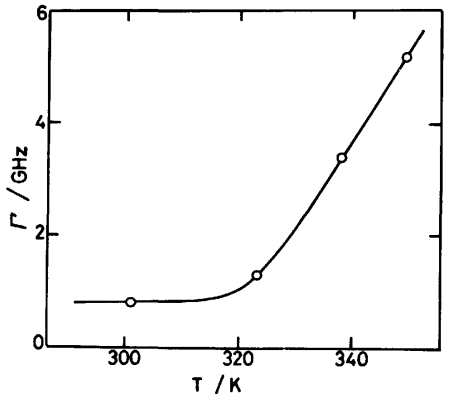

Fig. 6. Temperature dependence of the half-width, Γ, obtained from the depolarized Rayleigh spectrum.

$(=\omega_{anis}(1/2)-\omega_{isot}(1/2))$ was nearly equal to zero at lower temperatures within experimental error, but at a temperature above about 310 K, ω_{or} increased with increasing temperature.

The reorientational correlation times of TOTP can also be obtained from the half-width, Γ, at the half-peak height of the depolarized Rayleigh spectrum.[27] The temperature dependence of Γ after the correction of the instrumental slit width is shown in Fig. 6. In the lower temperature region, the values of Γ do not depend on temperature but at a temperature above 310 K, they increase with increasing temperature.

In the case of a simple molecule, such as a symmetric top, the reorientational correlation time of molecules at a particular molecular axis can be estimated from data of ω_{or} of Raman lines and/or Γ of depolarized Rayleigh lines. However, the molecules such as TOTP are not so simple as to give well defined reorientational correlation times. Therefore, we can not estimate the reorientational correlation time of TOTP from the data of ω_{or} and/or Γ. At least in our opinion, however, ω_{or} and/or Γ can be a measure of the reorientational motion of a molecule in liquids.

Discussion

Generally, there are two mechanisms which give rise to the dispersion of the sound velocity in the GHz region; one is vibrational relaxation due

to an energy transfer from the vibrational mode to the translational motion and the other is the structural relaxation.

The relaxation strength, ε, defined as[29]

$$\varepsilon = \frac{(V_\infty^2 - V_0^2)}{V_0^2}, \tag{2}$$

is shown in Fig. 7 as a function of temperature. The ε, ranging from 220 to 280 K, decreases with increasing temperature. This result indicates that the observed relaxation in this temperature range is not the vibrational relaxation, since the relaxation strength of the vibrational one should increase with temperature.[30] Besides, the value of ε which was estimated theoretically by Planck-Einstein relation was one order of magnitude smaller than those obtained experimentally.[31]

Barlow *et al.* indicated that the relaxation process observed for TOTP in the MHz region can be interpreted as the structural relaxation.[2-6] Figure 8 shows a plot of the longitudinal modulus ($M=1/\rho V^2$) reduced by the shear modulus of the high-frequency limit against the normalized freguency, $\eta\omega/G_\infty$, where η is the viscosity. The values of G_∞ at each temperaure used were those reported previously.[19] The reduced longitudinal moduli result in a master curve within experimental errors. The same quantity

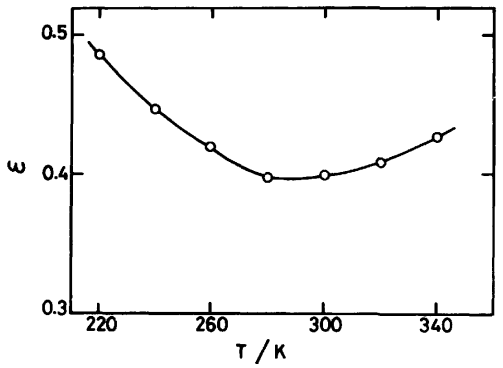

Fig. 7. Temperature dependence of the relaxation strength, ε.

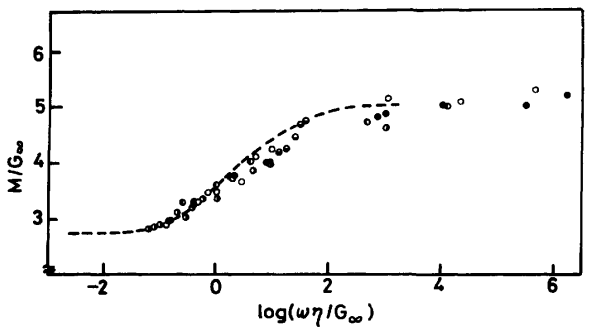

Fig. 8. Values of the reduced longitudinal modulus, M/G_∞, plotted as a function of $\log(\omega\eta/G_\infty)$. The broken line represents the data obtained by Barlow *et al.*[6]

in the MHz region, which was obtained by Barlow *et al.*[6], was compared as in Fig. 8. It seems that the values of M/G_∞ in the GHz region deviate slightly from those in the MHz region.

Various expressions have been used to describe the structural relaxation of supercooled liquids.[1] Such expressions can be classified into two types; one refers to the distribution of the relaxation and the other to the phenomenological parameters. At this stage, it is difficult to determine the distribution function of the relaxation times explicitly and sometimes, a distribution function is assumed. On the other hand, the relaxation behavior of a supercooled liquid in the MHz region is reduced to the normalized curve which is represented by the B. E. L. equation.[3] Moreover, the B. E. L. equation has also been described by a defect-diffusion model at the molecular level.,[32,33] It is worth comparing the applicability of the B. E. L. model to the experimental result in the GHz region.

According to the generalized B. E. L. model,[1,3] the complex compliance $J^*(i\omega)$, is represented by

$$\frac{J^*(i\omega)}{J_\infty^*} = 1 + \frac{G_\infty}{i\eta\omega} + 2K\left(\frac{G_\infty}{i\eta\omega}\right)^{1/2} \tag{3}$$

where J_∞^* is the compliance of the high-frequency limit and K the parameter where $K=0$ corresponds to the single relaxation process of the Mexwellian. Starting from Eq.3, the real parts of the shear, bulk and longitudinal moduli can be estimated. In Figs. 9 and 10, the normalized longitudinal modulus obtained in this experiment is compared with the value estimated from the generalized B. E. L. model. As is seen in Fig. 9, the experimental results are fitted to the generalized B. E. L. model equation, with the value of K being between 0.5 and 1.0. In Fig. 10, the experimental results above $\log(\eta\omega/G_\infty)\geqq 0$ are also reproduced with the generalized B. E. L. equation within experimental errors. The temperature corres-

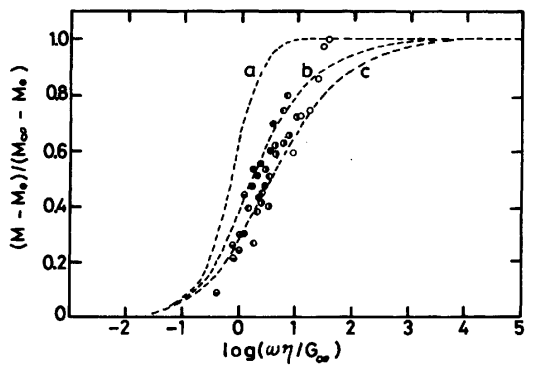

Fig. 9. Values of the normalized longitudinal modulus, $(M-M_0)/(M_\infty-M_0)$ plotted as a function of $\log(\omega\eta/G_\infty)$. The broken lines are calculated for $K=$ 0 (a), 0.5 (b) and 1.0 (c). The symbols are the same in Fig. 4.

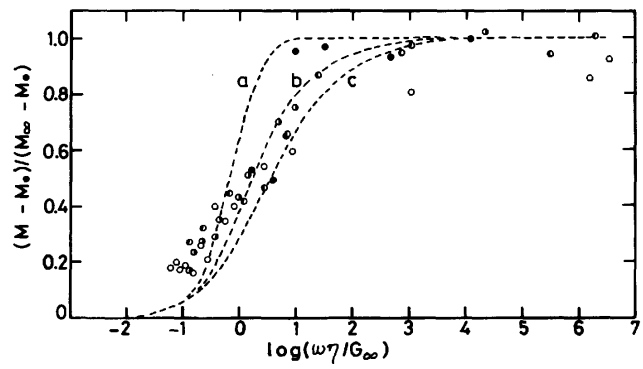

Fig. 10. Values of the normalized longitudinal modulus, $(M-M_0)/(M_\infty-M_0)$ plotted as a function of log $(\omega\eta/G_\infty)$. The broken lines are calculated for K = 0 (a), 0.5 (b) and 1.0 (c). The symbols are the same in Fig. 3.

ponding to $\log(\eta\omega/G_\infty)\simeq 0$ in the GHz region is about 310 K. Therefore,the relaxation of the longitudinal modulus below 310 K is described by the B. E. L. model. Above 310 K, the deviation from the B. E. L. model is appreciable, as can be seen in Fig. 10.

The deviation may be attributed to the following; above 310 K, the dynamic state of TOTP changes and this affects the structural relaxation due to the collective motion of the TOTP molecules. This consideration is supported by the molecular dynamical results of the Raman and depolarized Rayleigh scattering.

The ω_{or} and Γ give information about the molecular motion as described in the previous section. As can be seen in Figs. 6 and 7, the values of ω_{or} and Γ increase with temperature above 310 K. Below that temperature, the value of ω_{or} is nearly equal to zero and that of Γ levels off. These facts indicate that the reorientational motion of TOTP below 310 K is very slow or is almost frozen. Above this temperature, however, reorientational motion will occur. At the same temperature, the temperature dependence of the relaxation strength of sound dispersion of TOTP changed to positive. This asserts that at higher temperatures, the relaxation process may involve the rotational motion of TOTP molecules.

It is a very interesting point how the distribution of relaxation times of the longitudinal modulus relate to the liquid structure and molecular motion. This distribution of relaxation times somewhat depends on the temperature, that is measured frequency ranges (see Fig. 8). At least, we conclude that the deviation from the B. E. L. model at higher temperatures is attributed to the changes of liquid structure of TOTP, especially the changes regarding its dynamical state.

The authors would like to express their appreciation to Dr. T. Kato of Institute of Molecular Science for permission to use the light-scattering spectrometer of depolarized Rayleigh scattering spectra, and also to Mr. T. Watanabe, Glass-technician of Work Shop for Experimentation and Practice, School of Engineering, Nagoya University for making the low temperature cell (see Fig. 1). This work was supported in part by a Grant-in-Aid for Scientific Research from the Ministry of Education, Japan (No. 58540255).

References

1) G. Harrison, "The Dynamic Properties of Supercooled Liquids," Academic Press, London, (1976).
2) A. J. Barlow, J. Lamb, A. J. Matheson, P. R. K. L. Padmini, and J. J. Richter, *Proc. Roy. Soc.*, **A298**, 467 (1967).
3) A. J. Barlow, A. Erginsav, and J. Lamb, *Proc. Roy. Soc.*, **A298**, 481 (1967).
4) A. J. Barlow, A. Erginsav, and J. Lamb, *Proc. Roy. Soc.*, **A301**, 473 (1969).
5) A.J.Barlow and A. Erginsav, *Proc. Roy. Soc.*, **A327**, 175 (1972).
6) A. J. Barlow and R. P. Singth, *J. Chem. Soc., Faraday Trans. 2*, **68**, 1404 (1972).
7) R. Meister, C. J. Marhoeffer, R. Sciamanda, L. Cotter, and T. A. Litovitz, *J. Appl. Phys.*, **31**, 854 (1960).
8) C. J. Montrose, V. A. Solovyev, and T. A. Litovitz, *J. Acoust. Soc. Amer.*, **43**, 117 (1968).
9) D. A. Pinnodw, S. J. Candau, J. T. LaMacchla, and T. A. Litovitz, *J. Acoust. Soc. Amer.*, **43**, 132 (1968).
10) C. J. Montrose and T. A. Litovitz, *J. Acoust. Soc. Amer.*, **47**, 1250 (1970).
11) J. Tauke, T. A. Litovitz, and P. B. Macedo, *J. Amer. Ceram. Soc.*, **51**, 158 (1968)
12) G. D. Enright and B. P. Stoicheff, *J. Chem. Phys.*, **64**, 3658 (1976).
13) Y. Higashigaki and C. H. Wang, *J. Chem. Phys.*, **74**, 3175 (1981).
14) P. J. Chappell, M. P. Allen, R. L. Hallen, and D. Kivelson, *J. Chem. Phys.*, **74**, 5929 (1981).
15) P. Bezot, C. Hess-Bezot, N. Ostrowsky, and B. Ouentrec, *Mol. Phys.*, **39**, 549 (1980)
16) C. H. Wang, *Mol. Phys.*, **41**, 541 (1980).
17) G. Fytas, C. H. Wang, D. Lilge, and Th. Dorfmuller, *J. Chem. Phys.*, **75**, 4247 (1981).
18) C. H. Wang and Quan-L. Liu, *J. Chem. Phys.*, **78**, 4263 (1983).
19) H. Nomura, H. Shimizu, M. Kato, and Y. Miyahara, *Rept. Prog. Polym. Phys. Jpn*, **21**, 109 (1978).
20) H. Nomura, H. Shimizu, Y. Tanaka, S. Koda, T. Okunishi, S. Kato, and Y. Miyahara, *Bull. Chem. Soc. Jpn.*, **55**, 3899 (1982).
21) T. Kato, M. Yudasaka, and T. Fujiyama, *Bull. Chem. Soc. Jpn.*, **54**, 1632 (1981).
22) N. Itoh and T. Kato, *J. Phys. Chem.*, **88**, 801 (1984).
23) I. L. Fabelinskii, "Molecular Scattering of Light," Plenum Press, New York, (1968) p 86.
24) W. G. Rothschild, "Dynamics of Molecular Liquids," John Wiley & Sons, New York, (1984).
25) F. J. Baltoli and T. A. Litovitz, *J. Chem. Phys.*, **56**, 404, 413 (1972).

26) J. E. Griffiths, M. Clerc, and P. M. Rentzepis, *J. Chem. Phys.*, **60**, 3824 (1974).
27) B. J. Berne and R. Pecora, "Dynamic Light Scattering," John Wiley & Sons, New York, (1976).
28) S. Koda, H. Nomura, and Y. Miyahara, *Bull. Chem. Soc. Jpn.*, **52**, 1828 (1981).
29) K. F. Herzfeld and T.A.Litovitz, "Absorption and Dispersion of Ultrasonic Waves," Academic Press, New Yowk, (1959).
30) For example, K. Takagi, and K.Negishi, *J. J. Appl. Phys.*, **16**, 1319 (1977).
31) In calculation, the vibrational frequencies of TOTP are 167, 180, 270, 452, 525, 560, 592, 608, 702, 726, 769, 800, 992, 1048, 1157, 1243, 1383, and 1589 cm^{-1}, whose values are obtained from the Raman spectrum of TOTP. The vibrational frequencies of the infrared active modes are not taken into account, but the corrected value may not be beyond twice.
32) S. Glarum, *J. Chem. Phys.*, **33**, 639 (1960).
33) M. C. Phillips, A. J.Barlow, and J. Lamb, *Proc. Roy. Soc.*, **A329**, 193 (1972).

Effects of Addition of Vanadium to Alumina-supported Ruthenium Catalyst on Adsorption and Hydrogenation of Carbon Monoxide

Toshiyuki ENOMOTO, Toshio OKUHARA,* and Makoto MISONO
Department of Synthetic Chemistry, Faculty of Engineering, The University of Tokyo, Hongo, Bunkyo-ku, Tokyo 113
(Recieved September 29, 1984)

The hydrogenation of carbon monoxide to hydrocarbons (Fischer-Tropsch synthesis) was studied over Ru/Al_2O_3 catalysts to which transition metals such as V, Cr, Mn, and Ag were added. Among these additives, V was most effective for the suppression of methane formation, without changing the olefin/paraffin ratio and the propagation probability. The catalytic activity decreased and the infrared band of adsorbed carbon monoxide shifted only slightly upon the V addition, showing little change in the electronic state of Ru. The particle size of the Ru remained almost unchanged, although the degree of hydrogen adsorption decreased to half. This indicates that Ru particles were partially covered by V (or an oxide of V). The effect on the turnover frequency of hydrogenation of CO was compared with those for the hydrogenation of benzene, and the hydrogenolysis of ethane. These effects were found to be very similar to an ensemble effect reported for $Ru-Cu/SiO_2$ catalysts. On the basis of these results, it is concluded that the addition of V brought about an effect similar to the ensemble effect.

In Fischer-Tropsch synthesis, it has been reported that the addition of some transition metal elements sharply changed the activity and selectivity. A Co catalyst containing a Mn oxide showed a high selectivity to ethylene.[1] Mn and V oxides were also important components for producing lower olefins in composite catalysts based on Fe.[2] In the synthesis of C_2-oxygenated compounds over Rh catalysts, transition-metal elements such as Mn, Fe, Zr, and Ti were also effective additives.[3-5] Although little is known about the structure of these catalysts, bimetallic catalysts composed of group-VIII metals and early transition metals are becoming important in CO hydrogenation.[4]

Ru is the most active catalyst among group-VIII metals for Fischer-Tropsch synthesis,[6] but there is now only a little basic research being conducted regarding the role of additives to it.[7] Mori *et al.* reported that the addition of V or Mo to Ru/Al_2O_3 increased the rate of CO dissociation.[8] We observed that the addition of V to Ru/Al_2O_3 suppressed the formation of methane.[9] In addition, Kikuchi *et al.* have reported that V_2O_3 was an effective support for Ru in the formation of lower olefins.[10]

In the present work, the effects of transition metals added to Ru/Al_2O_3 on both the hydrogenation and the adsorption of CO were studied concurrently. Catalysts were characterized by hydrogen adsorption and electron microscopy (EM), and by comparing the effect of these additives on other reactions.

Experimental

Catalysts. A Ru/Al_2O_3 catalyst was prepared by incipient-wetness impregnation of γ-Al_2O_3 with an aqueous solution of $RuCl_3$.[11] The catalysts containing other transition metals were prepared by the co-impregnation of mixed aqueous solutions of $RuCl_3$ and VCl_3, $Co(OCOCH_3)_2$, $Cr(OCOCH_3)_3$, or $Mn(OCOCH_3)_2$ onto Al_2O_3. The catalyst containing Ag was prepared by the impregnation of an aqueous solution of $AgNO_3$ with the Ru/Al_2O_3 dried at 100 °C. After the impregnation, these catalysts were dried at 100 °C for 10 h. They contained 1.6% Ru, and the atomic ratio of additive-metals to Ru was 1. In the case of V and Cr, the amounts added were varied while keeping the amount of Ru constant. Hereafter, these catalysts will be designated *e.g.*, as $Ru-V(1:5)/Al_2O_3$ and $Ru-Cr(1:1)/Al_2O_3$, where the ratio is the atomic ratio of Ru to the additive metals.

Procedure. The hydrogenation of CO was examined in a closed circulation system (200 cm^3) at 220 °C using a 1:2 mixture of CO and H_2 under a total pressure of 500 Torr (1 Torr=133.3 Pa) with a trap kept at liquid-nitrogen temperature in order to suppress any secondary reactions of products. The activities and selectivities were determined in the second run in which the reaction proceeded at a steady rate.[11] The reaction was also performed in a conventional flow reactor at 260 °C under an atmospheric pressure ($H_2/CO=2$) using 0.6—1.2 g of catalysts.[12] The products were analyzed using gas chromatography. CO and methane were analyzed using a Molecular Sieve 5A column at 25 °C. C_1-C_{12} hydrocarbons were analyzed using an FID gas chromatograph (Yanagimoto GC 2800) equipped with a VZ-10 column and a Silicone SE-30 column. The formation of methanol, ethanol, and acetaldehyde was checked using a Porapak R column and was found to be negligible.

The hydrogenolysis of ethane was carried out in the circulation system at 150 °C under 150 Torr of a 1:2 mixture of ethane and H_2. The hydrogenation of benzene was performed using a pulse method at 120 °C. 50 mg of the catalyst was loaded in a glass tubular reactor (8 mm diameter) and benzene (1 μl) was injected into H_2 stream (25 ml/min) at the inlet of the reactor. All these reactions were carried out after the catalysts were pretreated with H_2 at 450 °C for 2 h.

Other Measurements. The adsorption of CO and H_2 was measured at room temperature with a high-vacuum static system after a reduction by H_2 at 450 °C for 2 h.[11] The infrared spectra of the adsorbed CO were recorded

using an FT-IR (JEOL IR-10) after the same procedure as described previously.[11] Transmission electron micrographs were obtained with a JEOL JEM 1250 electron microscope (1000 keV, final magnification: ×150000). Particles of the catalysts reduced at 450 °C were suspended in water and collected on a microgrid. More than ten micrographs of each catalyst were taken and the particle-size distributions were estimated from a total of 60—90 particles of Ru.

Results

Hydrogenation of CO. Table 1 summarizes the effects of the addition of various metals to Ru/Al_2O_3 regarding the hydrogenation of CO which was carried out in the closed-circulation system. As for the catalytic activity, no remarkable change was observed, except for the Ag which appreciably lowered the activity. The addition of V suppressed the formation of methane and enhanced the selectivity to C_2–C_4 olefins (suppression of methane formation was also found for Mn to some extent). Then, the effect of the content of V was examined in the same system, and compared with the effect of Cr. When the atomic ratio of Cr to Ru increased from 0.1 to 2, both the activity and selectivity remained almost unchanged. On the other hand, upon the addition of V (V/Ru=5 in atomic ratio), the activity decreased to about 1/5 and the selectivity of C_2–C_4 olefins increased from 42 to 64%, and methane decreased from 28 to 22% in weight. To examine the effect of the addition of V in greater detail, the reaction was carried out in the flow system at 260 °C.

Table 1. Effect of the addition of transition metals to Ru/Al_2O_3 on the hydrogenation of CO[a]

Additives[b]	none	V	Ag	Co	Cr	Mn
Catalytic activity[c]	8.9	5.0	2.1	8.1	7.5	11.4
Selectivity[d]						
C_1	28	23	37	27	27	23
C_2–C_4 olefins	42	52	46	45	41	38
C_2–C_4 paraffins	7	7	6	11	11	12
$C_{5(+)}$	23	18	11	17	21	27

a) Circulation system, 220 °C, 500 Torr ($H_2/CO=2$). b) Ru : additives = 1 : 1 in atomic ratio. c) 10^2 ml (STP)g-Ru^{-1} h^{-1}. d) Weight percentage.

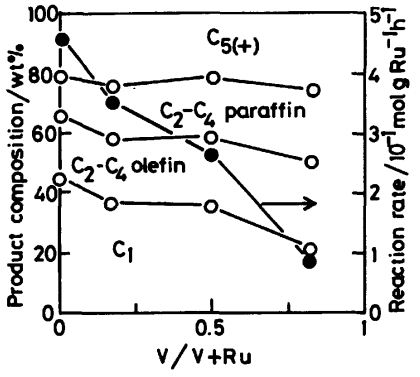

Fig. 1. Effects of the content of V in Ru–V/Al_2O_3 on catalytic activity and selectivity in the CO hydrogenation (flow system, $T=260$ °C, $P=1$ atm, $H_2/CO=2$). The conversion (based on CO) was adjusted in the range of 5—11%.

Figure 1 shows the changes of the reaction rate and selectivity as a function of the V content. The rate decreased monotonously as the V/(V+Ru) ratio increased from 0 to 0.83 (from 0 to 5 in V/Ru ratio). As for the selectivity, the fraction of methane decreased with the increase of the V content; methane was 25% in weight at V/(V+Ru)=0.83, while it was 45% over Ru/Al_2O_3. Due to the difference of the reaction conditions, the selectivity change observed here did not agree quantitatively with that obtained in the circulation system. However, the trend was similar.

The distributions of product hydrocarbons followed the Schultz-Flory plot, as shown in Fig. 2. The propagation probabilities (α) obtained from the slopes were 0.53, 0.53, and 0.57 for Ru/Al_2O_3, Ru–V(1:1)/Al_2O_3 and Ru–V(1:5)/Al_2O_3, respectively. The α values obtained from the intercepts were nearly equal to the α values from the slopes.

Figure 3 shows plots of the distribution of carbon number *vs.* the conversion for Ru/Al_2O_3 and Ru–V(1:5)/Al_2O_3. Over both catalysts, the product distribution was almost independent of the conversion up to about 30%. That is, the lower selectivity to methane observed over Ru–V(1:5)/Al_2O_3 was retained at high conversions.

In Fig. 4, the propene/propane ratio in the product is plotted against the conversion. For comparison, the results for Ru/Al_2O_3 treated with K or P are included in the figure.[9,12] Over these catalysts

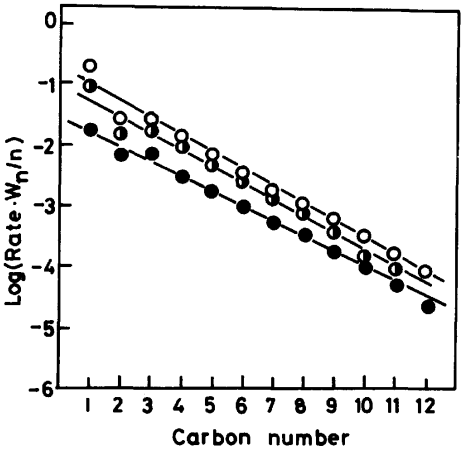

Fig. 2. Schultz-Flory plot (logarithm of $(Rate \cdot W_n/n)$, where W_n is weight percentage, and n is carbon number). The conversion was adjusted in the range of 5—11 %.
○: Ru/Al_2O_3, ◑: Ru–V (1 : 1)/Al_2O_3, ●: Ru–V (1 : 5)/Al_2O_3.

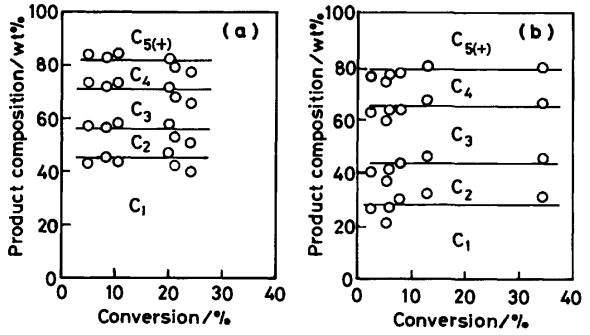

Fig. 3. Product distribution *vs.* conversion for the CO hydrogenation over Ru catalysts at 260 °C under 1 atm ($H_2/CO=2$).
(a): Ru/Al_2O_3, (b): $Ru-V(1:5)/Al_2O_3$

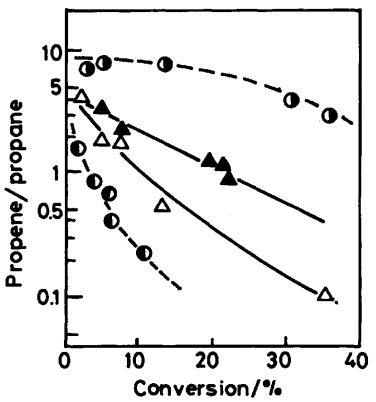

Fig. 4. Effect of conversion on the propene/propane ratio in the CO hydrogenation of CO over various Ru catalysts at 260 °C under 1 atm ($H_2/CO=2$).
▲: Ru/Al_2O_3, △: $Ru-V(1:5)/Al_2O_3$, ◑: Ru/Al_2O_3 treated with K (K; 1 wt%), ◐: Ru/Al_2O_3 treated with P (P; 0.9 wt%).

except for Ru/Al_2O_3 treated with K, the ratio greatly decreased as the conversion increased. The change in the ratio over $Ru-V(1:5)Al_2O_3$ was not very different from that over Ru/Al_2O_3, while the addition of K and P had great effects on the change in the ratio.[12]

Chemisorption of H_2 and CO. Chemisorption data of H_2 and CO are summarized in Table 2, where H/Ru and CO/Ru are respectively the number of hydrogen atoms or CO molecules adsorbed divided by the number of Ru atoms in the catalysts. The H/Ru decreased monotonously from 0.2 to 0.1 as the ratio of V/Ru increased from 0 to 5. Hereafter, the dispersion will be defined as H/Ru, by assuming that a hydrogen atom is adsorbed on a surface Ru atom at 1:1 stoichiometry.[13] The CO/Ru ratio was always greater than H/Ru, and also decreased as the amount of V increased.

Figure 5 shows the infrared spectra of CO adsorbed on Ru/Al_2O_3 and $Ru-V(1:5)/Al_2O_3$. The spectra were recorded at 25 °C after evacuation at several temperatures. In addition to the high frequency band at 2144 cm^{-1}, broad bands at about 1900—2100 cm^{-1}

Table 2. Adsorption of CO and H_2 on $Ru-V/Al_2O_3$

V/Ru[a]	0	0.2	1.0	5.0
CO/Ru[b]	0.63	0.54	0.59	0.34
H/Ru[c]	0.20	0.16	0.16	0.10

a) Atomic ratio. b) Irreversible adsorption at 25 °C. c) Total adsorption at 25 °C.

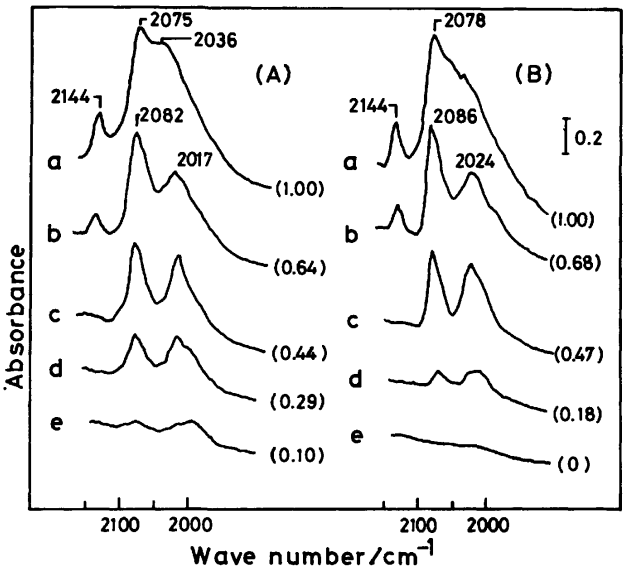

Fig. 5. Infrared spectral changes of adsorbed CO during stepwise thermal desorption on (A) Ru/Al_2O_3 and (B) $Ru-V(1:5)/Al_2O_3$. The spectra of CO were taken at 25 °C after evacuation at (a) 25 °C, (b) 100 °C, (c) 200 °C, (d) 250 °C, and (e) 300 °C. The figures in parentheses are the integrated absorbance relative to that obtained after the evacuation at 25 °C.

were observed over both catalysts. After an evacuation at above 100 °C, three resolved bands appeared at 2144, 2082, and 2017 cm^{-1} over Ru/Al_2O_3, and were quite similar to that on $Ru-V(1:5)/Al_2O_3$. The difference in the band position was less than about 8 cm^{-1}. The figures in parentheses indicate the integrated intensity of the infrared bands of adsorbed CO. The CO bands of the two catalysts decreased very similarly when the evacuation temperature was raised.

Figure 6 shows the particle size distributions of Ru measured by EM after the catalysts were reduced. The distribution pattern on $Ru-V(1:5)/Al_2O_3$ was almost similar to that of Ru/Al_2O_3. The average particle sizes were estimated to be 106 and 104 Å for Ru/Al_2O_3 and $Ru-V(1:5)/Al_2O_3$, respectively.

Effect of V Content on Turnover Frequency. Figure 7 shows the changes in the turnover frequencies (designated as TOF; relative to those over Ru/Al_2O_3) of hydrogenation of CO and benzene, and of hydrogenolysis of ethane as a function of the V content. The TOF values of these reactions all decreased, but the extent of the decrease was greatly

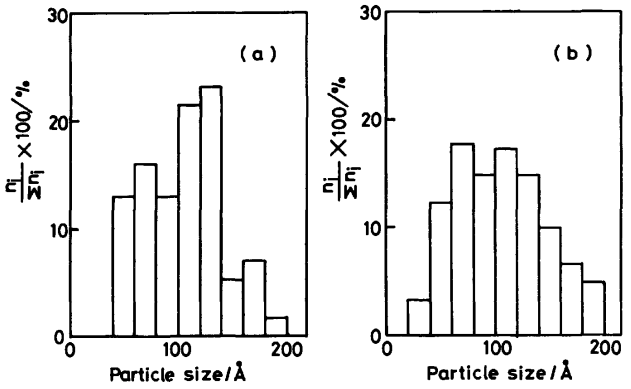

Fig. 6. Distribution of particle size of Ru on (a) Ru/Al_2O_3 and (b) $Ru–V(1:5)/Al_2O_3$. n_i is number of particles having i Å of diameter.

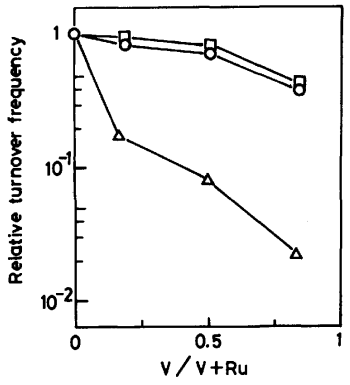

Fig. 7. Changes in TOF of various reactions over $Ru–V/Al_2O_3$ as a function of V content.
○: Hydrogenation of CO (260 °C, 1 atm, $H_2/CO=2$). □: Hydrogenation of benzene (120 °C, 1 atm, in a flowing H_2). △: Hydrogenolysis of ethane (150 °C, ethane; 50 Torr, H_2; 100 Torr).

different depending on the kind of reaction. When V/(Ru+V) was 0.83, the TOF for the hydrogenolysis of ethane lowered to 1/50, while the TOF of the other two reactions decreased only to 1/2.5. It was observed that the addition of Cr (Cr/(Cr+Ru)= 0—0.5) decreased only slightly the TOF for the hydrogenolysis of ethane.

Discussion

Effects of Dispersion caused by the V-addition. As shown in Fig. 6, the particle-size distribution of Ru changed only slightly upon the addition of V, while H/Ru decreased considerably (Table 2). Therefore, the reason for the decrease in H/Ru is probably that the surfaces of Ru particles (≈100 Å) were partially covered with V, and H or CO could not be adsorbed on the V-covered surface. The chemical state of V is not clear at present, but the V is probably present in a form of an oxide.

Several reports[11,14,15] have shown that the dispersion of Ru on Ru/Al_2O_3 greatly affects the TOF of the hydrogenation of CO. When the dispersion of Ru was controlled by altering the amount of loaded Ru, the TOF of the CO hydrogenation increased monotonously from 28×10^{-3} s^{-1} to 117×10^{-3} s^{-1} at 250 °C as the dispersion decreased from 0.60 to 0.23.[14] However, in the present case, when the dispersion (H/Ru) was lowered by the addition of V (V/Ru = 5) from 0.2 to 0.1, the TOF of the CO hydrogenation decreased (Fig. 7). Thus, the decrease in the TOF after the addition of V cannot be explained by any changes in the dispersion. As for the selectivity *vs.* conversion, it was reported that the product distribution was almost independent of the dispersion of Ru in this dispersion range.[11,14,15] Therefore, a considerable decrease in the fraction of methane caused by V (Fig. 1) also indicates that the effects of V are different from the dispersion effect reported.

Table 3. Effects of additives on the hydrogenation and adsorption of CO over Ru/Al_2O_3

Additives	P	K	V
Activity	+	−	−
Selectivity			
C_1	+	−	−
O/P[a]	−	+	(−)
α[b]	−	+	no
CO Adsorption			
Strength	−	+	no
Amount	−	−	−
Frequency of ir band	+	−	no

+: Increase, −: Decrease, (−): Slight decrease, no: No effect. a) Olefin/paraffin ratio. b) Propagation probability.

Electronic Effects. It is known that the addition of electron-donating additives like alkali metals and electron-withdrawing additives like P changed the electronic state of catalytically active metals. By this effect, the activity and selectivity varied greatly,[16–18] and those changes in the electronic state are reflected in the shift of the infrared bands of adsorbed CO.[12] The effects are summarized in Table 3, in which the effects of V found in the present work are also included. Since no significant shift of the infrared band of adsorbed CO was observed upon the addition of V (Fig. 5), it may be concluded that the change in the electronic state of Ru was small in the case of V-addition.[19] Mori *et al.* also reported that the infrared band position of CO was unchanged upon the addition of V to Ru/Al_2O_3.[20] Furthermore, in contrast to K and P-addition (electronic effect), the olefin/paraffin ratio and the propagation probability little varied upon the addition of V, supporting a small electronic effect for V.

It was reported by Kikuchi *et al.* that when V_2O_3 was used as a suppurt for Ru, the activity was

enhanced and the products shifted to higher hydrocarbons.[10] They assumed that the effect of V_2O_3-support was ascribed to an electron transfer from V_2O_3 to Ru (SMSI effect). This effect of V_2O_3-support on both the activity and selectivity is quite different from that of the addition of V to Ru/Al_2O_3 observed in the present study. Although the details are not clear, the difference in the from of V is a possible reason; for example, Ru is partially covered by V in the present study, while it is not covered in the case of V_2O_3-support.

Ensemble Effects. Considering a model of $Ru-V(1:5)/Al_2O_3$, in which part of Ru surface is covered by V, the changes in the surface structure of Ru seem to have affected the catalytic reactions. It is well known that the addition of an inert group-IB metal to group-VIII metals greatly changes the catalytic activities for hydrogenolysis of hydrocarbons and hydrogenation of CO.[21-23] These changes have usually been ascribed to a geometric effect due to the changes in the size of the surface metal ensemble (ensemble effect), and these reactions are regarded as structure-sensitive reactions.[21,22,23] In the case of bimetallic $Ru-Cu/SiO_2$, the addition of Cu to Ru at 1:1 atomic ratio decreased the amount of hydrogen adsorption to about half and decreased the catalytic activity.[23] But the structure-sensitivity varied depending upon the kind of reactions. The TOF of the hydrogenolysis of ethane decreased to about 1/1000, while that of the hydrogenation of CO decreased 1/50, when Cu was added to Ru at 1:1 atomic ratio, though both were reported to be structure-sensitive.[22,23] This difference in the extent of the decrease of the TOF between the two reactions was quite similar to that observed in the present work (Fig. 7). The TOF decreased to about 1/50 and 1/2.5 for the hydrogenolysis of ethane and the hydrogenation of CO by the addition of V (V/Ru= 5). Therefore, the changes of the activity and selectivity with the addition of V is presumably due to an effect similar to the ensemble effect. As shown in Fig. 2, there was no effect due to the addition of V on the propagation probability. This is in contrast to the case of K and P[12] and is consistent with the fact that the propagation probability is almost independent of the particle size of Ru.[11,14]

A notable change in the selectivity caused by V was a decrease in methane formation (Fig. 1). There is a possibility that methane was produced mainly by the hydrogenolysis of higher hydrocarbons and the addition of V suppressed the hydrogenolysis, since the rate of hydrogenolysis of ethane was greatly decreased by the addition of V, as shown in Fig. 7. However, most of methane was not a secondary product, since the fraction of methane was independent of the conversion (Fig. 3). The suppression of methane formation by the addition of V is probably due to the ensemble effect, since a decrease in the methane selectivity due to the effect has also been observed for Ru-Cu/zeolite.[24] The lower methane formation reported for Fe and Co catalysts containing V or Mn,[1,2] also seems to be brought about by an effect similar to the ensemble effect.

The present work was supported in part by a Grant-in-Aid for Scientific Research No. 58045027 from the Ministry of Education, Science and Culture. We gratefully acknowledge Mr. Hideo Tsunakawa, Engineering Research Institute, for measurement of electron micrograph.

References

1) A. L. Dent and M. Lin, *Adv. Chem. Ser.*, **178**, 47 (1979).
2) B. Bussemeier (Ruhrchemie), Ger. Offen. 2518964 (1976); Ger. Offen. 2536488 (1976).
3) P. C. Ellgen, W. J. Bartley, M. M. Bhasin, and T. P. Wilson, *Adv. Chem. Ser.*, **178**, 147 (1979).
4) M. M. Bhasin, W. J. Bartley, P. C. Ellgen, and T. P. Wilson, *J. Catal.*, **54**, 120 (1978).
5) M. Ichikawa, K. Sekizawa, and K. Shikakura, *J. Mol. Catal.*, **11**, 167 (1981).
6) M. A. Vannice, *J. Catal.*, **37**, 449 (1975).
7) J. Barrault, "Metal-Support and Metal-Additive Effects in Catalysis," ed by B. Imelik *et al.* p. 225 Elsevier, Amsterdam, 1982.
8) T. Mori, A. Miyamoto, N. Takahashi, M. Fukagaya, H. Niizuma,T. Hattori, and Y. Murakami, *J. Chem. Soc., Chem. Commun.*, **1984**, 678.
9) T. Enomoto, T. Okuhara, and M. Misono, Meeting of the Catalysis Society of Japan, Sapporo, Aug. 1983, 3D02.
10) E. Kikuchi, H. Nomura, M. Matsumoto, and Y. Morita, *Appl.Catal.*, **7**, 1 (1983).
11) T. Okuhara, T. Kimura, K. Kobayashi, M. Misono, and Y.Yoneda, *Bull. Chem. Soc. Jpn.*, **57**, 938 (1984).
12) T. Okuhara, T. Enomoto, H. Tamura, and M. Misono, *Chem. Lett.*, **1984**, 1491.
13) R. A. Della Betta, *J. Catal.*, **34**, 57 (1974).
14) D. L. King, *J. Catal.*, **51**, 386 (1978).
15) C. S. Kellner and A. T. Bell, *J. Catal.*, **75**, 251 (1982).
16) G. B. McVicker and M. A. Vannice, *J. Catal.*, **63**, 25 (1980).
17) R. D. Gonzalez and H. Miura, *J. Catal.*, **77**, 338 (1982).
18) T. Okuhara, K. Kobayashi, T. Kimura, M. Misono, and Y.Yoneda, *J. Chem. Soc., Chem. Commun.*, **1981**, 1114.
19) T. Okuhara, T. Enomoto, H. Tamura, and M. Misono, *Shokubai*, **26**, 291 (1984).
20) T. Mori, H. Masuda, H. Imai, A. Miyamoto, H. Niizuma, M. Fukagaya, N. Takahashi, T. Hattori, and Y. Murakami, *Shokubai*, **26**, 85 (1984).
21) J. H. Sinfelt, J. L. Carter, and D. J. C. Yates, *J. Catal.*,**24**, 283 (1972).
22) G. C. Bond and B. D. Turnham, *J. Catal.*, **45**, 128 (1976).
23) J. H. Sinfelt, *J. Catal.*, **29**, 308 (1973).
24) D. J. Elliot and J. H. Lunsford, *J. Catal.*, **57**, 11 (1979).

 © 1985 The Chemical Society of Japan Bull. Chem. Soc. Jpn., 58, 1495—1499 (1985)

Raman Spectra of Compounds under Inversion Motions. IV. *N*-Methyl-2-pyrrolidone

Kunio FUKUSHIMA* and Masahiro YAMAJI
Department of Chemistry, Faculty of Science, Shizuoka University, 836, Oya, Shizuoka 422
(Received December 8, 1984)

The Raman spectra of *N*-methyl-2-pyrrolidone in various states were measured. Remarkable changes in the spectrum of CH_2 bending vibrations were found besides a spectrum change of the skeletal vibrations. Normal vibration calculations and measurements regarding band-intensity changes associated with temperature changes suggest that a change of the ring conformation takes place in this molecule by hydrogen bonding to a nitrogen atom.

Former studies[1] made it clear that hydrogen bonding to some kind of nitrogen atom causes the frequencies of the Raman bands of the skeltal-deformation vibrations to change remarkably, and the phenomenon was interpreted to be associated with an inversion at the nitrogen. In the present study, *N*-methyl-2-pyrrolidone was investigated from the point of view that the molecule may have a lower potential barrier for inversion at the nitrogen because of a tendency of the CONCC skeleton to form a plane by resonance and, therefore, might show a specific spectrum change due to hydrogen bonding to the nitrogen.

Experimental

Sample *N*-methyl-2-pyrrolidone was a commercial product from Tokyo Kasei Co. (grade GR). The Raman spectra were recorded on a Model R-800T Raman spectrometer (Japan Spectroscopic Co.) with an excitation effected by a Spectra Physics argon ion laser (Model 165) at 514.5 nm (300 mW). The depolarization ratio was measured with a system consisting of a half-wave plate, a lens, and a polarizer. Liquid samples at room temperature were measured with 0.3 ml Raman cells, while crystals, solutions, and pure liquids at lower temperatures were measured with an Oxford-type cryostat and liquid nitrogen. Experimental results are shown in Tables 1 and 2 and Figs. 1—3.

Normal Coordinate Treatment

Normal vibration calculations regarding the axial and equatorial conformers of *N*-methyl-2-pyrrolidone were carried out according to Wilson's GF matrix method[2] by use of the Computation Center, University of Tokyo and the library programs BGLZ and LSMB. The molecular parameters used are: bond

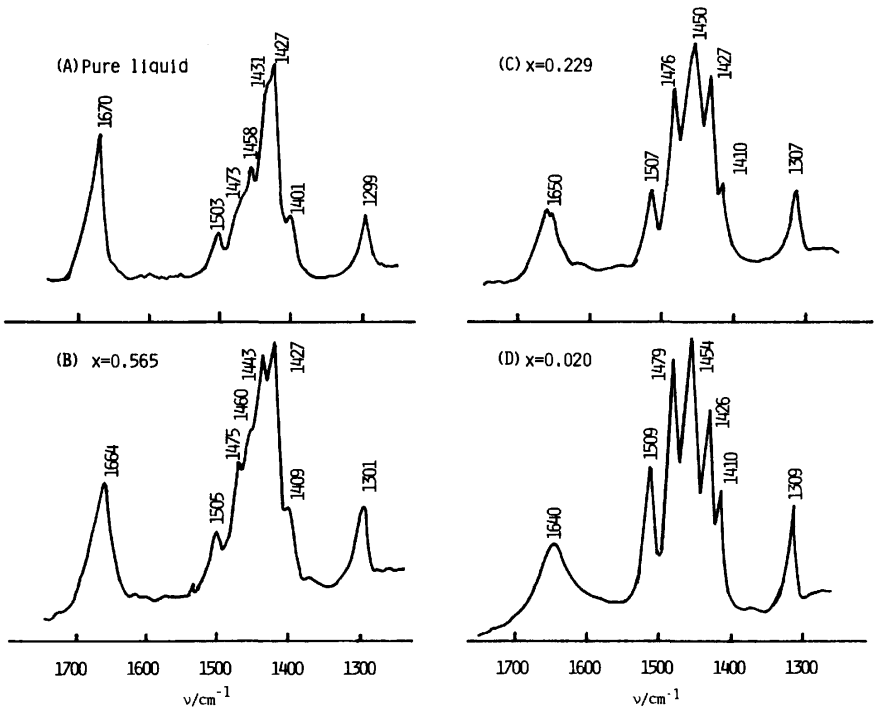

Fig. 1. Concentration dependence of spectra of *N*-methyl-2-pyrrolidone in aqueous solutions (x: mol fraction of *N*-methyl-2-pyrrolidone).

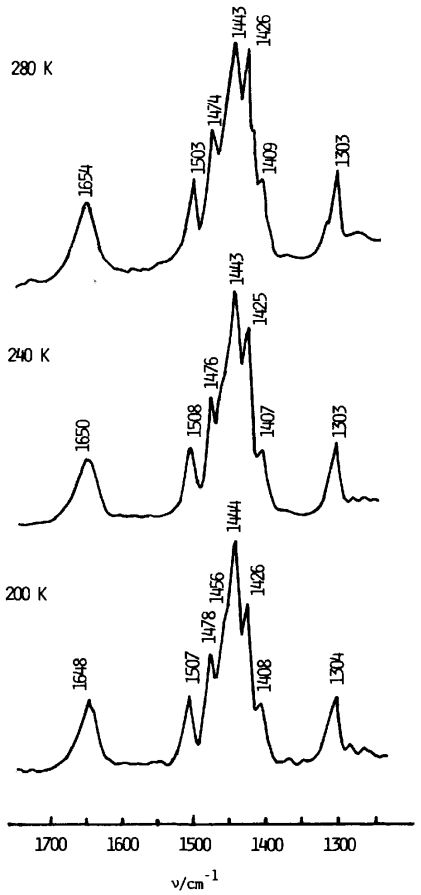

Fig. 2. Temperature dependence of spectra of *N*-methyl-2-pyrrolidone in an aqueous solution (mol fraction of *N*-methyl-2-pyrrolidone : 0.406).

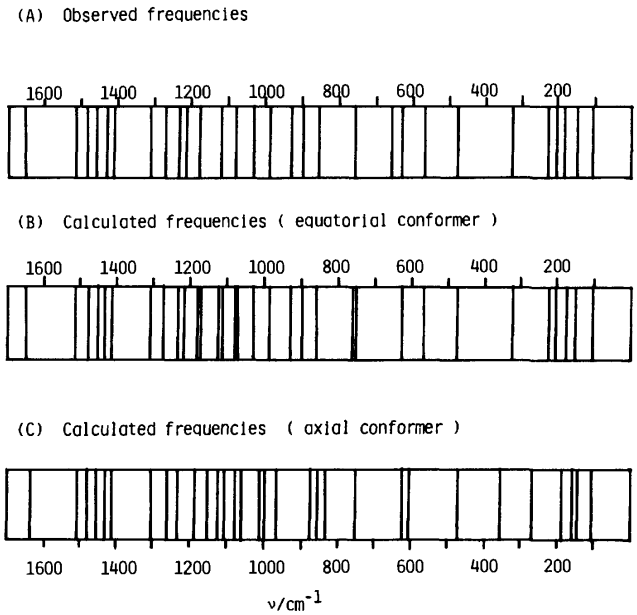

Fig. 3. Calculated frequencies of conformers of *N*-methyl-2-pyrrolidone compared with observed frequencies of pure liquid.

lengths, r(N-CO)=1.48 Å, r(CH_2-CO)=1.53 Å, r(CH_2-CH_2)=1.54 Å, r(CH_2-CN)=1.53 Å, r(CH_2-N)=1.48 Å, r(C=O)=1.24 Å, r(N-CH_3)=1.49 Å, r(C-H)=1.09 Å; bond angles, (CH_2-N-CO)=100.8°, (CH_3-N-CO)=(CH_2-N-CH_3)=111.6°, (CH_2-CO-N)=(CH_2-CH_2-N)=105°, (CH_2-CH_2-CO)=(CH_2-CH_2-CH_2)=104°, (N-C=O)=(CH_2-C=O)=127.5°, and bond angles of CH_3 group=tetrahedral angles.[3,4] For the molecular models, an envelope structure for the five membered ring was used as in the case of *N*-methylpyrrolidine.[5] Most of the force constants used are those of *N*-methylpyrrolidine.[5] The result of the calculation is shown in Fig. 3.

Results and Discussion

Spectrum Change Associated with the State Change from Liquid to Solid. As shown in Table 1, no appreciable spectrum change was observed except for the change in the region, 100 cm^{-1}—250 cm^{-1} where several new bands of lattice vibrations appear in the spectrum of the solid, and also the appearance of some bands in the spectra of the solid, which were not clearly observed in the spectra of the pure liquid because of weakness and broadness. This shows that one kind of conformer exists both in the solid and liquid states.

Spectra of Solutions for Non Hydrogen Bonding Solvents. The spectra of *N*-methyl-2-pyrrolidone in benzene, carbon tetrachloride, acetone, acetonitrile, and pyridine are almost the same as that of a pure liquid. Therefore, the conformer in these solutions is the same as that of a pure liquid. In Table 2, as a representative, the Raman bands of benzene solution are shown.

Spectrum Change Associated with Solution into Hydrogen Bonding Solvents. Change of Raman bands of skeletal deformation vibrations: The Raman bands at 310 cm^{-1} and 170 cm^{-1} in the spectra of a pure liquid shift to 325 cm^{-1} and 225 cm^{-1}, respectively, in spectra of solutions (refer to Table 1). A normal vibration calculation shows that these frequency shifts are not caused by a conformational change, equatorial conformer to axial conformer (refer to Fig. 3) and also that the former band is due to the vibrational mode of the C-N-C skeleton. These shifts, along with temperature dependence of intensities of these bands, suggest that the same kind of change of valence state of nitrogen atom (as described in former studies[1]) also takes place in this molecule. Corresponding frequencies for solutions of formic acid, acetic acid or aqueous hydrochloric acid (refer to Table 2) confirm that the frequency change in aqueous solutions is due to conformational change arising from the change of valence state of nitrogen atom.

The band of pure liquid at 170 cm^{-1}, which is

TABLE 1. RAMAN SPECTRA OF *N*-METHYL-2-PYRROLIDONE

Pure liquid			Solid		H_2O soln						CH_3OH soln		
					$x=0.565$			$x=0.033$					
ν	I	ρ	ν	I	ν	I	ρ	ν	I	ρ	ν	I	ρ
			105	7									
			150	13									
170	sh		178	25	190	sh							
			203	15	210	sh		225	sh				
			247	2									
310	48	0.53	308	100	313	40	0.56	325	32	0.44	319	28	0.49
			359	3									
			378	4									
472	11	0.55	473	17	472	9	0.66	475	8	0.62	475	7	0.59
			500	2									
564	6	0.47	567	11	563	6	0.67	569	6	0.44	561	7	0.39
617	60	0.36	619	89	618	62	0.40	623	57	0.36	617	63	0.32
657	8	0.63	649	14	656	8	0.75	660	8	0.70	660	8	0.68
746	100	0.09	748	58	746	100	0.11	753	86	0.10	744	94	0.09
			822	4									
850	28	0.10	842	31	851	32	0.17	856	39	0.18	850	35	0.13
895	5	0.40	894	7	895	6	0.53	896	8	0.47	895	6	0.25
925	97	0.10	923	83	925	99	0.10	932	100	0.07	925	6	0.25
			959	2									
938	9	0.33	983	11	983	12	0.34	988	17	0.38	985	16	0.38
1022	17	0.62	1027	34	1024	19	0.65	1029	21	0.55			
1070	2	0.64	1065	7	1070	2	0.72	1073	3	0.73	1034*		
			1095	4									
1113	4	0.73	1111	14	1113	5	0.57	1118	6	0.73			
			1135	5									
			1145	3									
1174	1	0.67	1172	4	1175	2	0.61	1176	2	0.75	1107*		
											1152*		
1205	7	0.67	1206	13	1206	9	0.63						
								1214	11	0.48	1211	6	0.75
1224	15	0.75	1226	17	1225	18	0.69	1229	24	0.69	1224	13	0.75
1263	vw				1266	2	0.48						
1277	vw		1278	3									
1299	12	0.19	1298	8	1301	16	0.21						
								1308	21	0.23	1304	12	0.17
1316	1	0.20	1313	3							1316	5	0.15
					1321	3	0.40	1325	8	0.18			
			1328	4									
			1356	3									
			1369	3									
			1394										
1401	13	0.45	1404	14	1409	16	0.55						
								1412	23	0.32			
1427	43	0.56	1423	39	1427	48	0.60	1428	41	0.52	1427	45	0.56
1431	39	0.51											
			1442	37	1443	46	0.53				1448	97	0.45
1458	22	0.60	1458	14	1460	31	0.63	1456	56	0.45	1455	80	0.56
			1468	13									
1473	12	0.54	1476	16	1475	25	0.43	1480	52	0.34	1472	65	0.59
1503	8	0.58	1507	19	1505	12	0.37	1510	29	0.13	1501	23	0.61
			1659	23									
1670	30	0.13	1673	7	1664	24	0.27	1647	13	0.25	1665	13	0.31

ν: Raman shift frequency. I: Relative intensity. ρ: Depolarization ratio. *: Solvent band. x: Mol fraction of *N*-methyl-2-pyrrolidone.

TABLE 2. RAMAN SPECTRA OF *N*-METHYL-2-PYRROLIDONE IN SOLUTIONS

Pure liquid			C_6H_6 soln			CH_3COOH soln			HCl soln		
ν	I	ρ	ν	I	ρ	ν	I	ρ	ν	I	ρ
170	sh										
			228	sh							
						277	sh		275	sh	
310	48	0.53	310	52	0.48						
						325	31	0.60	330	16	0.76
									356	7	0.50
									419	4	0.67
									458	6	0.73
472	11	0.55	473	12	0.60	480	7	0.73	475	6	0.67
									506	5	0.25
564	6	0.47	565	8	0.69	565	7	0.75	558	9	0.64
617	60	0.36	*			*			618	71	0.48
657	8	0.63	658	10	0.74	662	11	0.75	642	27	0.70
746	100	0.09	746	92	0.09	749	97	0.09	746	59	0.09
850	28	0.10	853	63	0.41	855	sh		852	64	0.12
895	5	0.40	893	3	0.65	*			890	21	0.40
925	97	0.10	925	100	0.07	926	100	0.09	928	100	0.10
983	9	0.33		sh		985	17	0.41	982	41	0.56
1022	17	0.62	1024	30	0.39	1024	24	0.64	1023	31	0.69
1070	2	0.64	1074	4	0.42	1070	4	0.75	1066	6	0.50
1113	4	0.73	1108	3	0.48	1118	6	0.71	1113	8	0.76
1174	1	0.67	*			1170	3	0.44	1182	6	0.67
1205	7	0.60				1206	10	0.62	1207	7	0.61
1224	15	0.75	1221	19	0.65	1225	22	0.75	1228	30	0.75
1263	vw										
1277	vw					*			1276	6	0.50
1299	12	0.19	1298	12	0.20	1304	15	0.27			
1316	1	0.20				1315	6	0.42	1313	38	0.26
									1325	30	0.13
1401	17	0.42	1406	31	0.31						
						*			1415	77	0.48
1427	43	0.56	1426	52	0.58	*					
1431	39	0.51									
1458	22	0.60	1459	22	0.75				1453	48	0.69
1473	12	0.54	1474	20	0.57	1476	43	0.45	1474	57	0.56
1503	8	0.58	1502	9	0.61	1506	27	0.18			
						1637	26	0.20			
1670	30	0.13	1685	33	0.34						
									1702	42	0.29

ν: Raman shift frequency. I: relative intensity. ρ: depolarization ratio. *: solvent band.

assigned to C-C, C-N torsional modes by normal vibration calculation and, therefore, is caused by ring vibration, shifts by 55 cm^{-1} on hydrogen bond formation to nitrogen atom. This change of ring vibration associated with hydrogen bond formation is a discovery in the present study along with the following remarkable change of CH_2 bending vibrations.

Remarkable Change of Raman Bands of CH_2 Bending Vibration: As shown in Table 1 and Fig. 1, a remarkable spectrum change was observed for aqueous solutions in the region of 1400—1550 cm^{-1}. With a decreasing concentration of *N*-methyl-2-pyrrolidone, intensities of the bands at 1401 cm^{-1}, 1431 cm^{-1}, 1503 cm^{-1} decrease, while those of the newly observed bands at 1410 cm^{-1}, 1450 cm^{-1}, 1510 cm^{-1} increase, The band at 1458 cm^{-1}, 1473 cm^{-1} also increase their intensities. These bands are clearly assigned to the CH_2 bending vibrations. Usually, the CH_2 bending vibrations do not show any great changes, and such a change has not been reported so far. It is amazing that the CH_2 bending bands of the

molecule change so much. The band at 1426 cm^{-1} decreases in intensity as the temperature decrease, while the band at 1443 cm^{-1} increases its intensity (refer to Fig. 2).

From the measurement of the intensity change, an enthalpy change of −2.0 kJ/mol was obtained, showing that the latter band is assigned to the conformer having a smaller enthalpy value and therefore, it is due to the hydrogen-bonded conformer. Considering the change of the band at 170 cm^{-1}, which shows a change in ring conformation by hydrogen bonding, the above change of the CH_2 vibration bands suggests that the shape of the ring in the molecule changes by hydrogen bonding to a nitrogen atom, and the electronic state of the carbon atom of the CH_2 groups changes to cause a remarkable change in the CH_2 vibrations. As the skeleton of 2-pyrrolidone was reported to take a planar conformation,[3] the real molecular ring of *N*-methyl-2-pyrrolidone might be also an almost planar ring a little different from the envelope model, which is commonly approved for five-membered ring and used in the present calculation, and nitrogen atom might be nearly in sp^2 state. The above spectrum change may be caused by the change of the sp^2 state of nitrogen into an sp^3 state by hydrogen bond formation.

For solutions for formic acid, acetic acid, aqueous hydrochloric acid, where a proton is attached to the nitrogen atom to form an sp^3 state nitrogen atom, only three bands appear at ≈1415 cm^{-1}, ≈1453 cm^{-1} and ≈1474 cm^{-1}, which correspond to the bands at ≈1410 cm^{-1}, ≈1450 cm^{-1}, and ≈1477 cm^{-1} increasing intensities in aqueous solutions. This is more evidence that the change in aqueous solutions may be a state change of the nitrogen atom from sp^2 to sp^3.

References

1) K. Fukushima, *Bull. Chem. Soc. Jpn.*, **52**, 287 (1979); K. Fukushima and H. Takahashi, *ibid.*, **54**, 2603 (1981).

2) E. B. Wilson, *J. Chem. Phys.*, **7**, 1047 (1939); **9**, 76 (1941).

3) R. L. Kayushina and B. K. Vainshtein, *Kristallografija*, **10**, 833 (1965).

4) Y. Onishi and K. Kojima, *Bull. Chem. Soc. Jpn.*, **41**, 1323 (1968).

5) K. Fukushima and H. Sasaki, *Bull. Chem. Soc. Jpn.*, **56**, 1740 (1983).

Role of the Intermediate Layer and Factors Determining Chemical Composition of the Film in the Electroless Ferrite-plating

Yutaka TAMAURA,* Yukitoshi TANNO,† and Masanori ABE†

Department of Chemistry, Tokyo Institute of Technology, Ookayama, Meguro-ku, Tokyo 152

†*Department of Physical Electronics, Tokyo Institute of Technology, Ookayama, Meguro-ku, Tokyo 152*

(Received August 21, 1984)

This paper describes electroless ferrite-plating on a Cu substrate whose surface is oxidized (the Cu-oxide layer works as an intermediate layer for the plating). Electron-diffraction and cathodic-reduction analyses showed that a Fe_3O_4 thin layer is formed on the intermediate layer during the initial reaction of the plating. This thin layer grows by the repetition of the adsorption of metal ions to the surface of the layer and the oxidation of the adsorbed Fe^{II} ions. Based on the adsorption-equilibrium of the metal ions on the surface of the film, the relationship between the composition of the metal ions adsorbed and that of the metal ions incorporated into the Co-ferrite film was formulated in terms of the concentrations of the metal ions in the reaction solution and the reaction pH. The analysis of the experimental data with this equation showed that the Co^{II} ions are more readily incorporated into the ferrite layer, as the mol ratio of the adsorbed Co^{II} ions to adsorbed iron ions ($R_{ads.}$) increases, but that a higher $R_{ads.}$ becomes unfavorable for the incorporation.

Recently, we reported a new method which enables the formation of crystalline-spinel film in an aqueous solution at low temperatures (below 80 °C).[1,2] Ferrite films are formed on the substrates by the oxidation of a mixed suspension of Fe^{II} and other metal ions (M^{n+}) in which the substrates are soaked. We can use various oxidizing agents such as air ("the air-bubbling method"), nitrate ion, hydrogen peroxide *etc.*, and anodic current. Thus, our method is a kind of electroless (chemical) plating or electro-plating. In the electroless ferrite plating on the poly(ethylene terephthalate)(PET) and stainless-steel substrates, an intermediate layer (an oxide layer of chemically plated copper or electro-plated Fe_3O_4) is required.[1,2]

The purposes of the present paper are 1) to clarify the initial reaction occurring on the intermediate layer of copper oxide in the electroless ferrite plating, and 2) to study the relationship between the adsorption behavior of the metal ions and the composition of the ferrite films formed during the electroless plating. For the performance of the study on the latter subject, we have devised a specially designed apparatus. We call the method using this apparatus, "the rotating-disc method."

Experimental

Chemicals and Substrates. Chemical reagents of analytical grade were used. NaOH solutions were prepared by dissolving NaOH in distilled water free from CO_2 and O_2. Copper sheets (30 μm×10×20 mm) whose surface had been oxidized in air at 160 °C for 30 min, were used as substrates.

Experiment of the Initial Reaction. After passing nitrogen gas into the solution containing Fe^{II} ions (17 mmol dm^{-3}, pH 7.0, T=70 °C) for 2 h, the Cu-substrate was dipped in the solution for 30 s—2h under a nitrogen atmosphere. The electron-diffraction pattern and cathodic-reduction curves of the oxides formed on the substrate were taken. The cathodic-reduction curves were taken using a Beckman Electroscan Model 30, applying a DC current at 10 A cm^{-1} in a stagnant borate buffer solution (pH 8.4, consisting of equal volumes of 0.075 mol dm^{-3} $Na_2B_4O_7 \cdot 10H_2O$ and 0.075 mol dm^{-3} H_3BO_3 solutions) at 25 °C under a slow nitrogen gas stream. The borate buffer solution was deaerated before the measurement by passing nitrogen gas for several hours.

The Rotating-disc Method. A specially designed

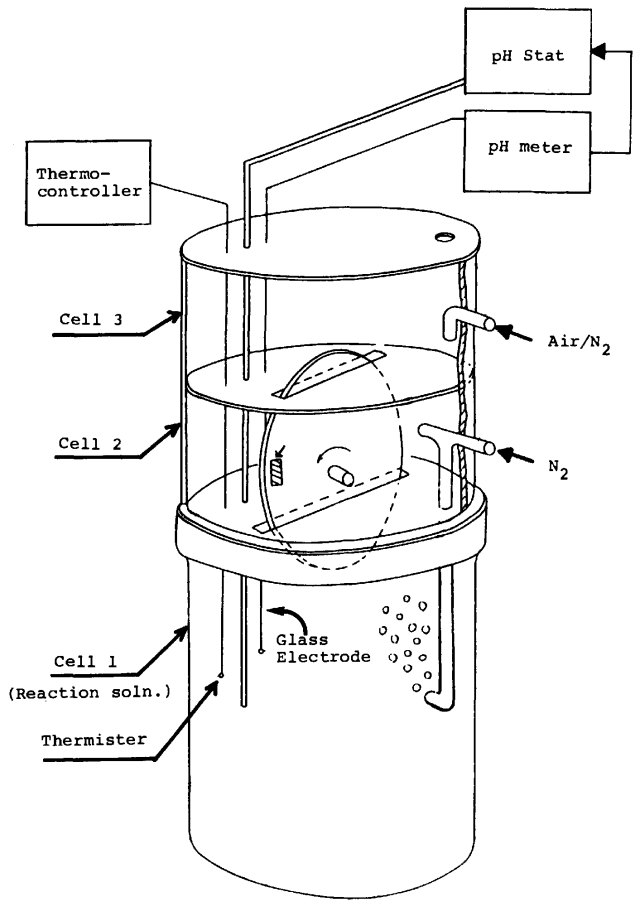

Fig. 1. The improved apparatus used for the chemical ferrite-plating.

apparatus (as illustrated in Fig. 1) was used. It is composed of three separated cells of a reaction solution (cell-1), an N_2 ambient to screen the reaction solution from oxygen (cell-2), and an air/N_2 (1:50) ambient (cell-3).

The Cu-substrates were mounted on the disc, and Cell number 1 was filled with about 1 dm^3 of distilled water through which nitrogen gas had been passed for 1 h to remove any dissolved oxygen. Nitrogen gas was passed through all the cells. After raising the temperature of the water in cell 1 to 70 °C, $FeCl_2 \cdot 3.5H_2O$ and $CoCl_2 \cdot 6H_2O$ were dissolved (Fe^{II}; 5.2 mmol dm^{-3}, Co^{II}; 0—15 mmol dm^{-3}). The pH was adjusted to a desired value (6.0—7.5) by adding an NaOH solution, and then the disc was rotated at 50—60 min^{-1}. After 5 min, the air/N_2 gas (1:50) was passed through cell 3 in place of nitrogen gas. After 2 h, the rotation of the disc was stopped, and the substrates were removed from the disc. The phase of the film was examined by electron and X-ray diffraction methods.

In "the rotating-disc method", the oxidation reaction takes place only on the surface of the substrate in cell 3, and a little amount of the metal ions are consumed during the formation of the ferrite film. Therefore, the concentrations of the metal ions in the reaction solution can be kept constant during the reaction. The thickness of the film was estimated by the chemical analysis of the film, assuming the chemical formula of $(Fe, Co)_{3.00}O_{4.00}$ and the density equal to that for $CoFe_2O_4$.

Chemical Anaylsis. Iron and cobalt contents in the ferrite films were determined by the atomic absorption method after dissolving the films in an HCl solution (1:1).

Results and Discussion

Formation of a Thin Fe_3O_4 Layer on the Cu-substrate in the Initial Reaction. The electron-diffraction

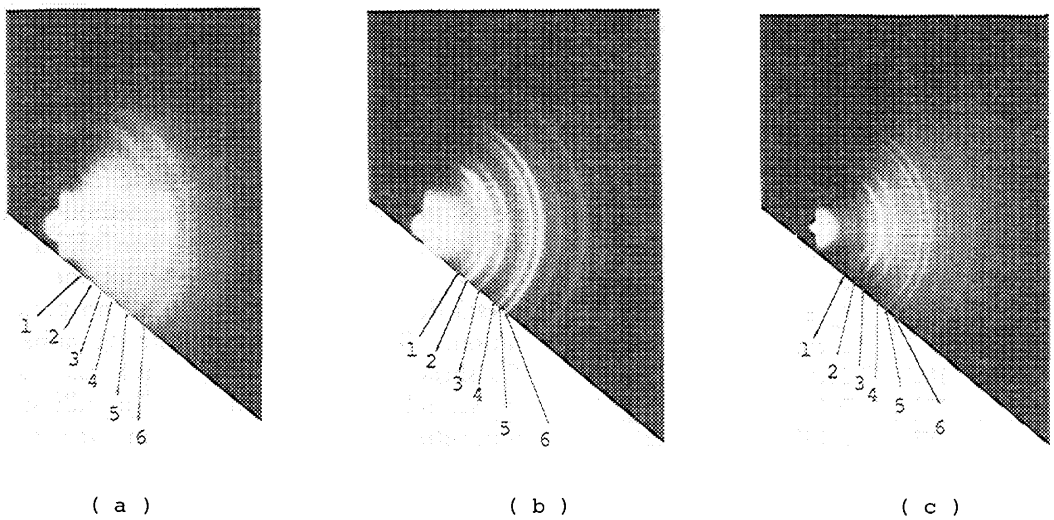

Fig. 2. Electron diffraction photographs for (a) the surface coating as formed on the Cu-sheet, (b) the Fe_3O_4 layer top coating formed on the Cu-oxide coating, and (c) a Co-ferrite film ($Co_{0.3}Fe_{2.7}O_4$) prepared by the rotating-disc method.

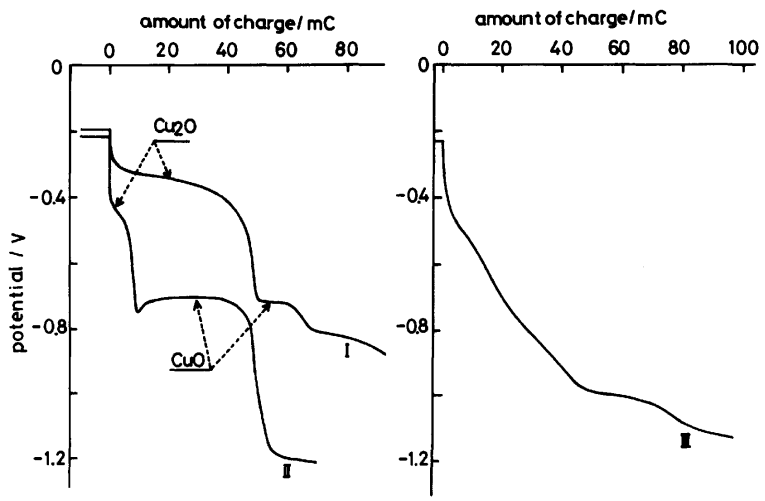

Fig. 3. Cathodic reduction curves for (a) the surface coating as formed on the Cu-sheet by heating in air at 160 °C for 10 min.(curve I) and 30 min.(curveII), and (b) the Fe_3O_4 top coating formed on the Cu-oxide coating.

pattern (Fig. 2a) and the *d* values (Table 1a) showed that the surface of the Cu-substrate was covered with oxide layers of Cu_2O and CuO. Curves I and II in Fig. 3a show the cathodic-reduction curves of the coatings formed on the Cu-substrate by heating in air at 160 °C for 10 and 30 min, respectively. They show two plateaus at the potential characteristic of CuO and Cu_2O, respectively. The ratio of CuO/Cu_2O increases as the heating time increases from 10 to 30 min. When the Cu-substrate with the Cu-oxide coating (30 min oxidation) was soaked in the reaction solution containing Fe^{II} ion (17 mmol dm^{-3}) at pH 7.0 and 70 °C under a nitrogen atmosphere for 30 s, a thin Fe_3O_4 layer was formed on the Cu-sheet substrate, as shown by the electron diffraction data and the cathodic-reduction measurement of Fig. 2b, Table 1b, and Fig. 3b. The layer was very thin; strong metallic copper color appeared through the film (its thickness could not be measured). This reaction was completed almost instantly; the thin Fe_3O_4 layer did not grow any more, even though the dipping time was extended to 2 h. It is assumed that the Fe^{II} ions are oxidized on the surface of the Cu-oxide layer, and that the thin Fe_3O_4 layer is deposited on its surface. This reaction will stop when the surface of the Cu-sheet substrate is completely covered with the thin Fe_3O_4 layer. This would be the cause for the formation of the thin layer. The formation of ferrite films (or particles) in the aqueous solution proceeds in two stages;[1-4] 1) the adsorption of the metal ions to the solid surface, and 2) the ferrite-formation with the oxidation of Fe^{II} ions to Fe^{III}. The Cu-oxide coating on the Cu-sheet substrate exhibits the activity of not only adsorbing the ions but also oxidizing Fe^{II} into Fe^{III}, thus forming the thin Fe_3O_4 layer.

Table 1. The "*d*"-values observed in the electron diffraction patterns of Figs. 1(a), (b), and (c), which are compared to literature values obtained by X-ray diffractometry for Cu-oxides, Fe_3O_4, and $CoFe_2O_4$, respectively

(a) No. in Fig. 2(a)	d observed / nm	Cu_2O[a] and CuO[b] nm		(*hkl*)
1	0.300	0.3020	Cu_2O	(110)
2	0.254	0.2530	CuO	(002)
		0.2523	CuO	($\bar{1}11$)
		0.2465	Cu_2O	(111)
3	0.186	0.1866	CuO	($\bar{2}02$)
4	0.159	0.1581	CuO	(202)
5	0.137	0.1375	CuO	(220, 113)
6	0.127	0.1287	Cu_2O	(311)

(b) No. in Fig. 2(b)	d observed / nm	Fe_3O_4[c] nm	(*hkl*)
1	0.301	0.2967	(220)
2	0.254	0.2532	(311)
3	0.211	0.2099	(400)
4	0.171	0.1715	(422)
5	0.162	0.1616	(511, 333)
6	0.149	0.1485	(440)

(c) No. in Fig. 2(c)	d observed / nm	$CoFe_2O_4$[d] nm	(*hkl*)
1	0.309	0.296	(220)
2	0.261	0.2531	(311)
3	0.216	0.2099	(400)
4	0.173	0.1713	(422)
5	0.163	0.1615	(511, 333)
6	0.150	0.1483	(440)

a) ASTM X-ray Data Card 5-667, b) 5-661, c) 19-629, d) 22-1086.

Formation of Co-ferrite Films on the Cu-substrate by "the Rotating-disc Method." Figure 2c and Table 1c show the results of the electron diffractometry on the Co-ferrite film ($Co_{0.3}Fe_{2.7}O_4$, 370 nm thickness) deposited by "the rotating-disc method" (the mol ratio of $Co^{II}/Fe^{II}=0.50$ in the reaction solution, pH 7.0). X-ray diffractometry showed that the film has the crystallized spinel structure with no preferred orientation. This film showed strong adhesion to the Cu-sheet substrate, and could not be detached by scratching with a nail. The adhesion and the magnetic property of the film will be published elsewhere.[5] Co-ferrite films with various compositions ($Co_xFe_{3-x}O_4$, $x=0.10$—0.52; the oxidation state of the Co-ferrite film is not unequivocal) were plated on the Cu-substrate in the pH range of 6.5—7.5 and at the mol ratios of $[Co^{II}]/[Fe^{II}]=0.5$—3.0 in the reaction solution. At pH 5.5, where little amount of the metal ions of Fe^{II} and Co^{II} are adsorbed,[3] no Co-ferrite films were deposited, although we used the substrate whose surface had been oxidized.

The reaction mechanism of the formation of the Co-ferrite film is considered as follows: When the substrate is dipped into the reaction solution (pH 7.0), Fe^{II} and Co^{II} ions are adsorbed on the surface of the Cu-oxide coating. When some of the adsorbed Fe^{II} ions are oxidized by Cu-oxide, the metal ions (Fe^{II}, Fe^{III}, Co^{II}) on the surface are transformed into a Co-ferrite, forming a thin ferrite layer on the surface. The ferrite layer, thus formed, can adsorb the Co^{II} and Fe^{II} ions. Some of the adsorbed Fe^{II} ions are oxidized by oxygen in cell 3, and a new Co-ferrite layer is formed. These adsorption-oxidation reactions are repeated by rotating the disc, which results in the growth of the ferrite layer.

The adsorption reaction occurs at a higher rate than

that of the ferrite-formation reaction;[3] the adsorption reaction is the rate-determining step. Furthermore, in "the rotating-disc method", the concentrations of the metal ions in the reaction solution (cell-1) are kept constant. This means that, in "the rotating-disc method", the chemical composition of the ferrite film can be discussed based on the adsorption-equilibrium of the metal ions in terms of the concentrations of the metal ions and the reaction pH.

Effect of Concentrations of Metal ions in the Reaction Solution and the Reaction pH on the Composition of the Co-ferrite Films. We assume here that a layer of ferrite, say Fe_3O_4, has been already formed on the oxide coating of the substrate. The OH group at the solid/liquid interface exhibits an amphoteric property, as

$$\begin{matrix} Fe^{3+} \\ >O^- \\ Fe^{2+} \end{matrix} \overset{H^+}{\rightleftharpoons} \begin{matrix} Fe^{3+} \\ >OH \\ Fe^{2+} \end{matrix} \overset{H^+}{\rightleftharpoons} \begin{matrix} Fe^{3+} \\ >OH^{2+}. \\ Fe^{2+} \end{matrix} \quad (1)$$

The OH group works as the adsorption site for the metal ions. In general, there are two types of adsorption, *i.e.*, those unaccompanied and accompanied by hydrolysis: For the Fe^{2+} ions

$$\begin{matrix} Fe^{3+} \\ >OH \\ Fe^{2+} \end{matrix} + Fe^{2+} \overset{K_1^{Fe}}{\rightleftharpoons} \begin{matrix} Fe^{3+} \\ >O^-\text{-}Fe^{2} \\ Fe^{2+} \end{matrix} + H^+ \quad (2a)$$

and

$$\begin{matrix} Fe^{3+} \\ >OH \\ Fe^{2+} \end{matrix} + Fe^{2+} + H_2O \overset{K_2^{Fe}}{\rightleftharpoons} \begin{matrix} Fe^{3+} \\ >O^-\text{-}Fe^{2+}\text{-}OH^- \\ Fe^{2+} \end{matrix} + 2H^+, \quad (2b)$$

and for the Co^{2+} ions,

$$\begin{matrix} Fe^{3+} \\ >OH \\ Fe^{2+} \end{matrix} + Co^{2+} \overset{K_1^{Co}}{\rightleftharpoons} \begin{matrix} Fe^{3+} \\ >O^-\text{-}Co^{2+} \\ Fe^{2+} \end{matrix} + H^+, \quad (2a')$$

and,

$$\begin{matrix} Fe^{3+} \\ >OH \\ Fe^{2+} \end{matrix} + Co^{2+} + H_2O \overset{K_2^{Co}}{\rightleftharpoons} \begin{matrix} Fe^{3+} \\ >O^-\text{-}Co^{2+}\text{-}OH^- \\ Fe^{2+} \end{matrix} + 2H^+. \quad (2b')$$

Here, K_1^{Fe} and K_2^{Fe} (K_1^{Co} and K_2^{Co}) are the equilibrium constants for the adsorption of the Fe^{2+} (Co^{2+}) ions. The adsorption unaccompanied by the hydrolysis (Eqs. 2a and 2a') dominates when the pH of the solution is low, while that accompanied by the hydrolysis (Eqs. 2b and 2b') dominates when the pH is high.[6] When some of the Fe^{II} ions [adsorbed following Eqs. 2a and 2b] are oxidized, the ions on the surface (Fe^{II}, Fe^{III}, and Co^{II}), both hydrolyzed and unhydrolyzed, are transformed into spinel ferrite.

In the rotating-disc method, the concentrations of the Fe^{II} and Co^{II} ions in the solution are kept constant. In the pH range studied here (6—7.5), almost all of the Fe^{II} and Co^{II} ions in the solution are Fe^{2+} and Co^{2+}. Therefore, the equilibrium constants for the adsorption of the ions are expressed in terms of the concentrations in the reaction solution of cell-1 (Fig. 1) as follows:

For Eqs. 2a and 2b,

$$K_1^{Fe} = [>O^-\text{-}Fe^{2+}][H^+]/([Fe^{2+}][>OH]), \quad (3a)$$

$$K_2^{Fe} = [>O^-\text{-}Fe^{2+}\text{-}OH^-][H^+]^2/([Fe^{2+}][>OH]), \quad (3b)$$

and for Eqs. 2a′ and 2b′,

$$K_1^{Co} = [>O^-\text{-}Co^{2+}][H^+]/([Co^{2+}][>OH]), \quad (3a')$$

$$K_2^{Co} = [>O^-\text{-}Co^{2+}\text{-}OH^-][H^+]^2/([Co^{2+}][>OH]). \quad (3b')$$

Here, $[H^+]$, $[Fe^{2+}]$, and $[Co^{2+}]$ are the concentrations of the respective ions in the solution, [>OH] is that of the adsorption site, and $[>O^-\text{-}Fe^{2+}]$,$[>O^-\text{-}Fe^{2+}\text{-}OH^-]$, $[>O^-\text{-}Co^{2+}]$, and $[>O^-\text{-}Co^{2+}\text{-}OH^-]$ are those of the Fe^{II} and Co^{II} ions adsorbed without and with the hydrolysis*, respectively.

The ratio of the adsorbed Co^{II} ions to the adsorbed Fe^{II} ions is given by

$$\begin{aligned} R_{ads.} &= (Co/Fe)_{ads.} \\ &= ([>O^-\text{-}Co^{2+}] + [>O^-\text{-}Co^{2+}\text{-}OH^-])/ \\ &\quad ([>O^-\text{-}Fe^{2+}] + [>O^-\text{-}Fe^{2+}\text{-}OH^-]) \end{aligned} \quad (4)$$

Using Eqs. 3a—3b′, we can substitute the adsorbed-ion concentrations in Eq. 4 with the ion concentrations in the reaction solution as

$$R_{ads.} = ([Co^{2+}]/[Fe^{2+}])(K_1^{Co}[H^+] + K_2^{Co})/(K_1^{Fe}[H^+] + K_2^{Fe}). \quad (5)$$

Now, we introduce a ratio, t, as

$$t = R_{film}/R_{ads.}, \quad (6)$$

where R_{film} is the mol ratio of Co^{II} to Fe_{total} in the ferrite film. From Eqs. 5 and 6, we obtain

$$\log R_{film} = \log \frac{[Co^{2+}]}{[Fe^{2+}]} + \log\left(t\frac{K_1^{Co}[H^+] + K_2^{Co}}{K_1^{Fe}[H^+] + K_2^{Fe}}\right) \quad (7)$$

which expresses R_{film} as a function of $[Co^{2+}]/[Fe^{2+}]$, t, and the pH. Figure 4 shows the relationship between log R_{film} and pH at $[Co^{2+}]/[Fe^{2+}]$=0.50, 0.75, and 3.0. The composition of the ferrite film (R_{film}) increases linearly with an increase in the reaction pH at a given mol ratio of $[Co^{2+}]/[Fe^{2+}]$. Thus, the second term of the right side in Eq. 7 varies linearly with the reaction pH (the 1st term is constant for each curve.)

Here, we discuss the ratio t. Assuming that t at $[Co^{2+}]/[Fe^{2+}]$=3.0 (Curve A in Fig. 4) as t_o, and those for 0.75 and 0.5 (Curves B and C in Fig. 4) as t_n, we can calculate t_n/t_o for various pH values

* The concentrations of the ions, *i.e.*, $[H^+]$, $[Fe^{2+}]$, and $[Co^{2+}]$, are expressed in the unit of mol/volume, while those of the adsorption sites and the adsorbed ions, *i.e.*, [>OH], $[>O^-\text{-}Fe^{2+}\text{-}OH^-]$, $[>O^-\text{-}Co^{2+}]$, *etc.*, are in number/area.

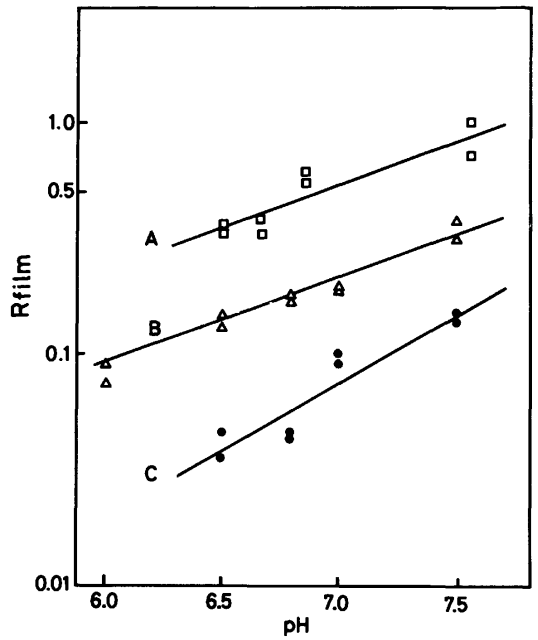

Fig. 4. The pH dependence of the atomic ratio (R_{film} =Co/Fe) of the films prepared by the rotaing-disc method using the solutions with the ion ratios of [Co^{II}]/[Fe^{II}]=3.0 (Curve A), 0.75 (B), and 0.50 (C).

using Eq. 7. When the t_n/t_o is k_n, Eq. 6 is rewritten as

$$\log R_{film}/k_n = \log R_{ads.} + \log t_0. \quad (8)$$

Since t_o is constant for a given pH value, Eq. 8 shows that the change in the value of log R_{film}/k_n at constant pH value is that in the value of $R_{ads.}$ Thus, for a given reaction pH, the relationship between k_n and R_{film}/k_n will give how the $R_{ads.}$ affects the incorporatation of the Co^{II} ions into the ferrite layer. This is given by Fig. 5. As can be seen here, the Co^{II} ions are more readily incorporated into the ferrite layer, as the mol ratio of the adsorbed Co^{II} ions to the adsorbed iron ions ($R_{ads.}$) increases. However, a higher $R_{ads.}$ becomes unfavorable for the incorporation.

Conclusion

(1) In the initial reaction of the electroless ferrite-plating, the intermediate layer of the Cu-oxide adsorbs the metal ions and oxidizes the adsorbed Fe^{II} ions, and a thin ferrite-layer is formed on the surface.

(2) Co-ferrite films ($Co_xFe_{3-x}O_4$, x=0.10—0.52) were plated on the Cu-substrate with the intermediate layer of the Cu-oxides by "the rotating-disc method" in the pH range 6.5—7.5 and at the mol ratios of [Co^{II}]/[Fe^{II}]=0.5—3.0 in the reaction solution (T=70 °C).

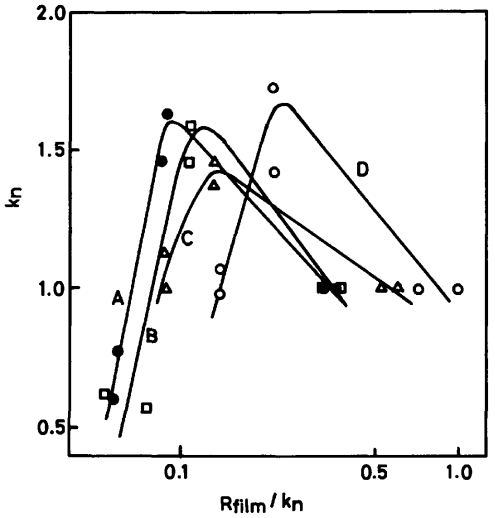

Fig. 5. The relationship between k_n and R_{film}/k_n at pH 6.5 (Curve A), 6.8(B), 7.0(C), and 7.5(D).

(3) Based on the adsorption-equilibrium of the metal ions on the surface of the film, the relationship between the composition of the metal ions adsorbed and that of the metal ions incorporated into the Co-ferrite film was formulated in terms of the concentrations of the metal ions in the reaction solution and the reaction pH. The analysis of the experimental data with this equation showed that the Co^{II} ions are more readily incorporated into the ferrite layer, as the mol ratio of the adsorbed Co^{II} ions to adsorbed iron ions ($R_{ads.}$) increases, but that a higher $R_{ads.}$ becomes unfavorable for the incorporation.

References

1) M. Abe and Y. Tamaura, *JJAP Lett.*, **22**, 511 (1983).
2) M. Abe and Y. Tamaura, *J. Appl. Phys.*, **55**, 2614 (1984).
3) Y. Tamaura, K. Ito, and T. Katsura, *J. Chem. Soc., Dalton Trans.*, **1983**, 189.
4) Y. Tamaura, Yukiko Kobori, and T. Katsura, *Nippon Kaggaku Kaishi*, **1983**, 1433.
5) M. Abe, Y. Tanno, and Y. Tamaura, to be publised in J. Appl. Phys.
6) M. M. Benjamin and J. O. Leckie, *J. Colloid Interface Sci.*, **79**, 209 (1981).

Solubility of Tris(acetylacetonato)chromium(III) in Aqueous Alcohol Mixtures

Manabu YAMAMOTO
Department of Chemistry, Faculty of Science, Hiroshima University, Higashisenda, Nakaku, Hiroshima, 730
(Received December 10, 1984)

From the temperature dependence of the solubility of tris(acetylacetonato)chromium(III) in aqueous *t*-butyl alcohol mixtures and in aqueous methanol mixtures, thermodynamic parameters of the solution were calculated. The solubility and these parameters in aqueous *t*-butyl alcohol mixtures could be explained qualitatively by the cavity formation terms of the scaled particle theory. It was suggested that tris(acetylacetonato)chromium(III) is in water microphases at $X_{BuOH} \leqq 0.04$ and in *t*-butyl alcohol microphases over this region.

2,4-Pentanedione(acetylacetone) is one of the most useful reagents in analytical chemistry to separate a particular metal ion from various matrixes. Besides the analytical purpose, acetylacetonato complexes such as tris(acetylacetonato)chromium(III) ($Cr(acac)_3$), and tris(acetylacetonato)cobalt(III) ($Co(acac)_3$) seem to be useful model compounds in solution chemistry to clarify solute-solvent interactions of metal chelates as they are stable, large, spherical and rigid solutes.[1,2]

In a previous study,[1] the solubility of $Cr(acac)_3$ was measured from 5 to 75 °C in water, which shows a characteristic feature of a hydrophobic solute with a solubility minimum at 45 °C. With a hard sphere diameter of 8.97 Å for $Cr(acac)_3$, a cavity formation term was calculated by the scaled particle theory (SPT),[3,4] and it was shown that the aqueous solubility of $Cr(acac)_3$ could be explained qualitatively by the cavity formation term.

In the present study, the solubility of $Cr(acac)_3$ was measured in aqueous *t*-butyl alcohol and a few of aqueous methanol mixtures, and the dependences of the solubility on the temperature and concentrations of alcohols were examined in connection with the structural properties of the solvents.

Experimental

A preparation of $Cr(acac)_3$ was given in the previous paper.[1] *t*-Butyl alcohol (*t*-BuOH) was a special grade and methanol (MeOH) was a liquid chromatography grade. The procedure for the solubility measurement followed that of the previous study.[1] Solubility measurements were performed from 5 to 60 °C for X_{BuOH} of 0.005 to 0.015 and X_{MeOH} of 0.025 to 0.05, and from 5 to 45 °C for the other mixtures. The solubility was determined spectrophotometrically by the following equation,

$$\varepsilon = am + bm^2, \tag{1}$$

where ε is the absorbance at 380 nm at 25±1 °C, m is the concentration in mol/kg. Parameters a and b for each solvent were given in Table 1. Solubility measurements were repeated at appropriate intervals until the concentrations agreed within ±1%.

Table 1. Parameters of Eq. 1 for aqueous alcohol mixtures

X_{ROH}	a	b
	t-Butyl alcohol	
0	429	−441
0.005−0.02	423	0
0.03, 0.04	414	0
0.075	411	0
0.1	406	0
	Methanol	
0.025	425	−8328
0.05	422	−4483
0.11	422	−7718
0.2	411	−5926

Results and Discussion

Solubility curves of $Cr(acac)_3$ in aqueous *t*-butyl alcohol are shown in Fig. 1. For the region $X_{BuOH} < 0.04$, the solubility minimum is observed as in water, but when X_{BuOH} becomes higher than 0.04, the solubility increases monotonically with increasing temperature. A similar trend was observed for the solubility in aqueous methanol, where the solubility curves are like that in water at $X_{MeOH} \leqq 0.11$.

On the calculation of the thermodynamic parameters of the solution from the temperature dependence of solubility, several equations were examined to represent the solubility curves and equations with three or four parameters were confirmed to be sufficient as found in the previous study for water.[1] In this study the simplest of the following equations were used,

$$\Delta C_p = A, \tag{2}$$

$$\Delta H_{soln} = \Delta H_0 + AT, \tag{3}$$

$$\ln m = -\Delta H_0/RT + (A/R) \ln T + B/R. \tag{4}$$

The parameters of these equations are given in Table 2. Solubilities calculated by Eq. 4 agreed with experimental ones within the error of less than ±1%. Thermodynamic parameters at 25 °C are

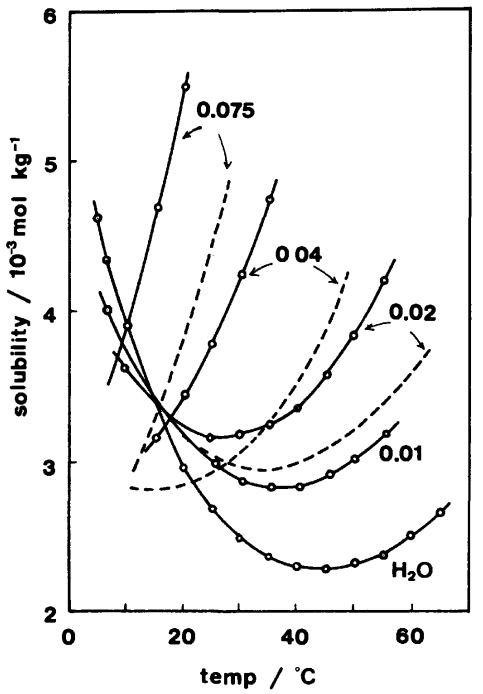

Fig. 1. Solubility of $Cr(acac)_3$ in aqueous *t*-butyl alcohol mixtures.
----: Calculated by SPT.

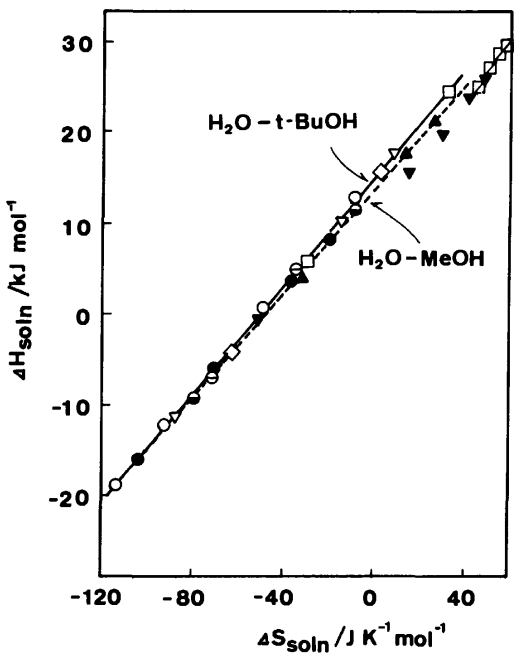

Fig. 2. $\Delta H-\Delta S$ Compensation plots.
X_{BuOH}: ○, 0.0: ⊖, 0.01; ▽, 0.02; ◇, 0.03; □, 0.04; ⊡, 0.075. X_{MeOH}: ●, 0.025; ◒, 0.05; ▲, 0.11; ▼, 0.2.

TABLE 2. PARAMETERS FOR SOLUBILITY EQUATIONS

X_{ROH}	$A(=\Delta C_p)$ / J K⁻¹ mol⁻¹	$-B/R$ / —	$-\Delta H_0{}^*10^{-5}$ / J mol⁻¹
	t-Butyl alcohol		
0	638.1	524.89	2.0253
0.005	620.5	509.67	1.9484
0.01	605.0	496.12	1.8767
0.015	545.0	446.41	1.6640
0.02	556.3	454.18	1.6663
0.03	562.5	456.12	1.6104
0.04	471.8	379.55	1.2552
0.075	85.28	62.688	−0.018289
0.1	47.47	31.552	−0.14025
	Methanol		
0.025	495.4	407.45	1.5417
0.05	437.0	358.17	1.3142
0.11	355.5	287.53	0.95280
0.2	206.3	162.92	0.41424

TABLE 3. THERMODYNAMIC PARAMETERS FOR THE SOLUTION OF $Cr(acac)_3$ IN AQUEOUS ALCOHOL MIXTURES AT 25 °C

X_{ROH}	ΔG_{soln} / kJ mol⁻¹	ΔH_{soln} / kJ mol⁻¹	ΔS_{soln} / J K⁻¹ mol⁻¹
	t-Butyl alcohol		
0	14.68	−12.30	−92.1
0.01	14.38	−7.28	−71.1
0.02	14.25	−0.79	−50.2
0.03	14.07	6.65	−25.1
0.04	13.82	15.15	4.18
0.075	12.35	27.24	50.21
0.1	11.59	28.20	54.4
	Methanol		
0.05	14.10	−1.13	−50.2
0.11	13.59	10.71	−8.37
0.2	11.92	20.08	29.3

given in Table 3. ΔH_{soln} changes from exothermic to endothermic with increasing the mole fraction of alcohols, which was accompanied by the change of ΔS_{soln} from negative to positive values.

$\Delta H-\Delta S$ compensation plots for these two aqueous alcohol mixtures seems to consist of nearly the same line as shown in Fig. 2. The compensation temperature is almost the same, that is, 291±1 *K* for $0 \leq X_{BuOH} \leq 0.04$, and 286±1 *K* for $0 \leq X_{MeOH} \leq 0.11$. Compensation temperatures become higher for both of the mixtures over these regions.

These facts show that the solution process in highly aqueous regions is strongly dependent on the water structure, and then the structural change of water around $Cr(acac)_3$ is reflected on the thermodynamic parameters of the solution of $Cr(acac)_3$ in these solvents.

The deviation of plots from this compensation line with increasing the concentration of alcohols is due to the fact that the structure of the medium changes from water like to organic, and $Cr(acac)_3$ may become to be solvated selectively by alcohols.

In an SPT flame, the free energy of solvation of a gaseous solute (ΔG_{solv}) can be separated into a cavity

formation term (G_{cav}) and an interaction term (ΔG_{int}) as Eq. 5,[4]

$$\Delta G_{solv} = G_{cav} + \Delta G_{int} + RT\ln(RT/V), \quad (5)$$

where V is the apparent molar volume of the mixed solvent. The free energy of the solution of a solid solute (ΔG_{soln}) used in the present study could be obtained after a correction of the sublimation energy.[1] The free energy of transfer from water to an aqueous mixture (shown in Fig. 3) does not necessitate such a correction. G_{cav} of Cr(acac)3 in aqueous t-butyl alcohol mixtures were calculated by Eq. 6,[4-6]

$$G_{cav} = -RT\ln(1-y_3) + RT[3y_2/(1-y_3)]a_2 + RT[3y_1/(1-y_3) + 4.5y_2^2/(1-y_3)^2]a_2^2 - (1/6)\pi NPa_2^3, \quad (6)$$

where a_2 is the diameter of the solute molecule, $y_i=(\pi/6)\sum_j \rho_j \sigma_j^i$, $i=1-3$, ρ_j and σ_j are the number density and the hard-sphere diameter of the jth component, and P is the pressure. In the following calculation, 9.87 Å,[1] 2.77 Å,[4] and 5.29 Å[6] were used as hard sphere diameters of Cr(acac)3, water and t-butyl alcohol, respectively. Densities of aqueous t-butyl alcohol mixtures were from Desnoyers *et al.*[7]

A free energy of transfer (ΔG_{tr}) and a free enrgy of transfer of cavity formation ($\Delta G_{cav,tr}$) are given in Fig. 3. Corresponding to the ΔH-ΔS compensation, ΔG_{tr} is only a little negative or positive in a highly aqueous region. Upon increasing the temperature, and upon increasing X_{BuOH}, ΔG_{tr} becomes negatively large.

As an example of the dependences of G_{cav} on the hard sphere diameter of t-butyl alcohol, $\Delta G_{cav,tr}$ at 25 °C were calculated with different hard sphere diameters of t-butyl alcohol. As shown in Fig. 3, the hard sphere diameter of t-butyl alcohol is a very important parameter for estimating G_{cav} quantitatively. But these curves indicate that the trend of the transfer function, and therefore the dependence of solubility on the solvent compositions can be represented only by the G_{cav} terms qualitatively.

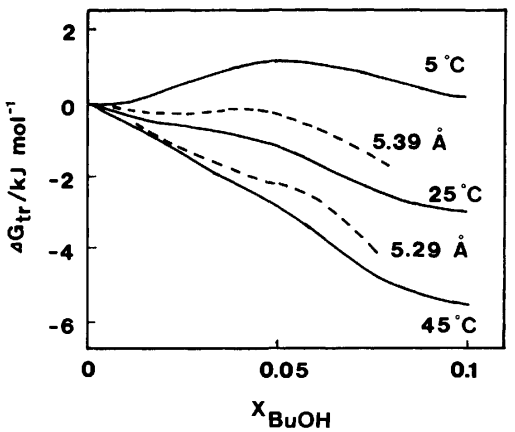

Fig. 3. Free energy of transfer of Cr(acac)3 from water to aqueous t-butyl alcohol mixtures.
----: $\Delta G_{cav,tr}$ calculated by SPT for the hard sphere diameter of t-butyl alcohol as 5.39 Å and 5.29 Å at 25 °C.

Assuming an interaction term of ΔG_{int} to be constant in the present range and estimating ΔG_{int} from ΔG_{soln} an G_{cav} in water, ΔG_{soln} in aqueous t-butyl alcohol mixtures were calculated and solubilities corresponding to these ΔG_{soln} are plotted in Fig. 1. The calculated solubilities for aqueous t-butyl alcohol mixtures were lower than the observed ones, though these solubility curves reproduce the presence of the temperature at which solubilities are approximately equal at $X_{BuOH} \leq 0.04$ as observed in the experimental solubility curves. That the cavity formation terms can reproduce such a phenomena means that G_{cav} changes in a similar way. Such a change of G_{cav} may be due to a change in the solvent structure, caused by an equilibrium of the two phases in these solvent mixtures.

For the structure of the aqueous t-butyl alcohol mixture, it was proposed that when $X_{BuOH} \leq 0.045$, a clathrate-like species of t-BuOH$(H_2O)_{21}$ is dispersed in the water and at $X_{BuOH} > 0.045$, (t-BuOH$(H_2O)_{21})_5$ is dispersed in t-butyl alcohol.[8] Therefore a fraction of free water available for the hydration of Cr(acac)3 decreases with an increase in the mole fraction of t-butyl alcohol at $X_{BuOH} \leq 0.045$. If Cr(acac)3 is considered to dissolve in the aqueous microphase at $X_{BuOH} \leq 0.045$, it is reasonable that the solubility curves in this mole fraction range are like that in water. In this case, it is also expected that the solubility decreases with increasing the concentration of t-butyl alcohol at lower temperatures, where the clathrate hydrate is stable. On the other hand, by assuming that Cr(acac)3 dissolves mainly in microphase of t-butyl alcohol at $X_{BuOH} > 0.045$, the solubility is also expected to increase monotonically with increasing temperature, observed usually on the solubility in organic solvents. The breakdown of the clathrate hydrate-like structure with increasing temperature at $X_{BuOH} > 0.045$[8] brings about an increase of the t-butyl alcohol available for Cr(acac)3 and then the solubility begins to increase steeply with temperature.

The fact that the ΔH-ΔS compensation curves for propanol mixture was explained in a similar way, that is, benzene is in an aqueous medium when $X_{PrOH} \leq 0.1$, but beyond this region dissolves in the 2-propanol microphases and benzene enhances the formation of 2-propanol microphases.[9]

The fact that the ΔH-ΔS compensation curves for aqueous t-butyl alcohol mixtures and aqueous methanol mixtures almost coincide in the highly aqueous region means that regarding the solubility of Cr(acac)3, the difference of chemical interactions of methanol and t-butyl alcohol with Cr(acac)3 is only a

minor importance compared with the difference of hydrophobicities, or the difference of abilities of these two alcohols to modify the water structure.

The large negative entropy in water, most of which is evaluated as S_{cav},[1] changes from a large negative value to a positive value at $X_{BuOH}=0.04$ at 25 °C. Corresponding to this entropy change, a large ΔC_p in water, most of which is also due to the large C_{cav},[1] decreases only a little in the mole fraction range of 0 to 0.04, and after that it changes suddenly to a very small value (Table 2). Values of ΔC_p include ambiguity when they were obtained as second delivatives of solubility curves. Though it was claimed that ΔC_p is rather independent of temperature for a process where $\Delta H-\Delta S$ compensation occurs due to the structural change of water.[10] Therefore ΔC_p obtained by Eq. 2 (assuming ΔC_p=constant) may be reliable as a measure of the change of the local structure on the solution of $Cr(acac)_3$ for the highly aqueous region. The dependences of ΔS_{soln} and ΔC_p on the mole fraction of *t*-butyl alcohol also suggest a change in the solvation of $Cr(acac)_3$ from the hydrophobic hydration in a highly aqueous region to selective solvation by *t*-butyl alcohol at $X_{BuOH}>0.04$, by dissolving in *t*-butyl alcohol microphase. The stabilization of $Cr(acac)_3$ observed in ΔG_{tr} at temperatures higher than 25 °C at $X_{BuOH}>0.04$ can also be understood by assuming such a change of solvation.

The difference in the solubilities between the observed and the calculated values may be mainly due to the ambiguity of cavity formation terms by SPT, and also due to the uncertainly of the hard sphere diameter of *t*-butyl alcohol. The solvation schema discussed above tends to change the solubility of $Cr(acac)_3$ in a similar way as expected from the cavity formation terms by SPT. Therefore, the overlap of these two factors, especially selective solvation by *t*-butyl alcohol in the alcohol rich region, may be relevant to the higher solubility compared to the calculated one.

The author is grateful to Professor Yuroku Yamamoto of Hiroshima University for his valuable discussion throughout the work. He also express his thanks to Mr. Hiroshi Tamai for assistance with the experiments.

References

1) M. Yamamoto, *J. Phys. Chem.*, **88**, 3356 (1984).
2) T. Tominaga, K. Tanabe, and J. Takanaka, *J. Solution Chem.*, **13**, 563 (1984).
3) H. Reiss, *Adv. Chem. Phys.*, **9**, 1 (1966).
4) R. A. Pierotti, *Chem. Rev.*, **76**, 717 (1976).
5) J. L. Lebowitz, E. Helfand, and E. Paestgaard, *J. Chem. Phys.*, **43**, 774 (1965).
6) M. Lucas, R. W. Cargill, *J. Phys. Chem.*, **81**, 703 (1977).
7) C. deVisser, G. Perron, and J. E. Desnoyers, *Can. J. Chem.*, **55**, 856 (1977).
8) K. Iwasaki and T. Fujiyama, *J. Phys. Chem.*, **81**, 1907 (1977); **83**, 463 (1979).
9) J. Lara, L. Avedikian, G. Perron, and J. E. Desnoyers, *J. Solution Chem.*, **10**, 301 (1981).
10) R. Lumry and S. Rajender, *Biopolymers*, **9**, 1125 (1970).

 © 1985 The Chemical Society of Japan Bull. Chem. Soc. Jpn., 58, 1509—1515 (1985)

Cobalt(III) Complexes with [N6−nXn]-type Ligands. V.[1] The Preparation and Properties of *N,N'*-Disalicylidene-substituted Quadridentate Amine Cobalt(III) Complexes

Yoshihisa YAMAMOTO* and Shoko TSUKUDA
Faculty of Pharmaceutical Sciences, Higashi Nippon Gakuen University, Ishikari-Tobetsu, Hokkaido 061-02
(Received August 4, 1984)

(1,8-*N*-Disalicylidene-3,6-diazaoctane-1,8-diamine)cobalt(III) chloride hydrate (**1a**; *x,y,z*: 2,2,2),

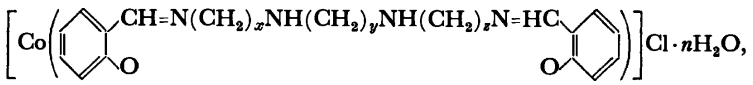

(1,9-*N*-disalicylidene-3,7-diazanonane-1,9-diamine)cobalt(III) chloride (**2a**; *x,y,z*: 2,3,2), (1,10-*N*-disalicylidene-4,7-diazadecane-1,10-diamine)cobalt(III) chloride (**3a**; *x,y,z*: 3,2,3), and (1,11-*N*-disalicylidene-4,8-diazaundecane-1,11-diamine)cobalt(III) chloride hydrate (**4a**; *x,y,z*: 3,3,3) have been isolated from a reaction mixture of $[CoCl_2L]Cl\cdot nH_2O$ (L: quadridentate amine), AgOH, and salicylaldehyde or from one of quadridentate amine, salicylaldehyde, $CoCl_2\cdot 6H_2O$ and air, and characterized. The ^1H and ^{13}C chemical shifts of their amine protons, methylene protons, and methylene carbons have been assigned. The configurations of **1a** and **2a** are the *trans,cis(mf2m)* configuration for the two CH=N− and two phenoxyl groups of the coordinated *N,N'*-disalicylidene-substituted quadridentate amine ligands. On the other hand, complexes **3a** and **4a** have the *cis,trans(fm2f)* configuration.

Previously, we have been concerned with the preparation and properties of isomers of the mixed ligand complexes of the $[CoN_{6-n}O_n]$ type, *e.g.*, the diamminebis(salicylideneaminato)cobalt(III) complexes,[1]

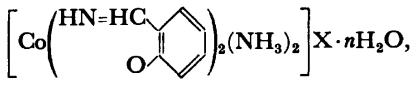

and salicylato(quadridentate amine)cobalt(III) complexes,[2-5] $[Co(sal\text{-}R)L]X\cdot nH_2O$ (R: H, Me; L: 2,2,2-tet, 2,3,2-tet, 3,2,3-tet, and 3,3,3-tet). Three isomers of the former complexes have been isolated; their configurations are the *trans,trans,trans-*, *trans,cis,cis-*, and *cis,trans,cis*-positions for the two ammine ligands, two CH=NH, and two phenoxyl groups of the coordinated salicylideneaminato ligands respectively. In the latter complexes, the *cis*-β_1 and β_2 isomers have been isolated, and the ^1H and ^{13}C chemical shifts of their amine protons,[3] center methylene, and NH_2- and NH-side methylene protons and carbons[5] have previously been assigned. The assignments of the =N-side methylene protons and carbons have, however, so far remained unsolved.

Many investigations of metal complexes (metal: Cu^{II}, Co^{II}, Ni^{II}, Al^{III}, Ga^{III}, Mn^{III}, Fe^{III}, Co^{III}) with the *N,N'*-disalicylidene-substituted quadridentate amine ligand,

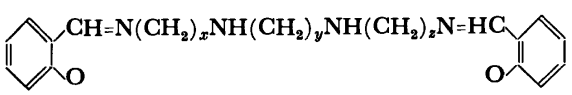

(*x,y,z*: 2,2,2), have been reported, especially with regard to their preparation,[6-8] IR spectra,[6-8] magnetic susceptibility,[8,9] and geometrical isomerism,[9] but the NMR spectra have never been reported. These metal complexes have a *trans,cis(mf2m)*[10,11] configuration for the two CH=N and two phenoxyl groups, but complexes with a *trans,cis(f4)*, *cis,trans(fm2f)* or *cis,cis-(f2mf* or *fmf2)*[10,11] configuration have never been described except for iron complexes[12] with the *N,N'*-disalicylidene-substituted quadridentate amine ligand (*x,y,z*: 3,2,3 and 3,3,3), which has the *cis,-trans(fm2f)* configuration. Even now, the metal complexes with the *N,N'*-disalicylidene-substituted quadridentate amine ligand (*x,y,z*: 2,3,2) have not yet been reported. In addition, very little is known of the properties and general chemistry of the metal complexes with the ligands of *x,y,z*: 2,3,2; 3,2,3 and 3,3,3, in contrast with the large amount of information available on the complexes with the ligand of *x,y,z*: 2,2,2. The present paper deals with the preparation and properties of the cobalt(III) complexes with the *N,N'*-disalicylidene-substituted quadridentate amine ligand (*x,y,z*: 2,2,2; 2,3,2; 3,2,3 and 3,3,3); it also deals with the assignments of the configurations of the isomers and of the ^1H and ^{13}C chemical shifts of the =N-side methylene protons and carbons.

Results and Discussion

The (*N,N'*-disalicylidene-substituted quadridentate amine)cobalt(III) chloride hydrates, **1a**, **2a**, **3a**, and **4a** (Scheme 1), have been isolated from a reaction mixture of $[CoCl_2L]Cl\cdot nH_2O$ (L: quadridentate amine),

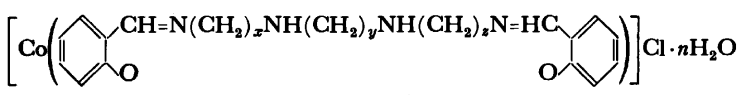

	x, y, z			x, y, z	
1a	2	2	2	**3a**	3	2	3
2a	2	3	2	**4a**	3	3	3

Scheme 1.

AgOH, and salicylaldehyde or from one of quadridentate amine, salicylaldehyde, $CoCl_2 \cdot 6H_2O$, and air. The corresponding nitrates (**1b**, **2b**, **3b**, **4b**) and picrates (**1c**, **2c**, **3c**, **4c**) have been prepared from a reaction mixture of silver nitrate or picric acid and **1a**, **2a**, **3a**, or **4a**, respectively.

The electric conductivities of **1a**, **2a**, **3a**, and **4a** in aqueous solutions were 97—103 S cm^2 equiv^{-1}. The IR spectra of these complexes showed a strong peak for CH=N stretching[6,7] at *ca.* 1620 or *ca.* 1640 cm^{-1} and three strong peaks for C-N stretching[6,7] in the 1126—1208 cm^{-1} region. The absorption spectra of **1a** and **3a** are closely similar to those of **2a** and **4a** respectively, as is shown in Fig. 1 and Table 1. The absorption bands at 388—403 nm and at about 590 nm or 628 nm are assigned to the charge-transfer band[13-15] and the first absorption band ($^1T_{1g} \leftarrow {}^1A_{1g}$ in an O_h approximation) respectively.

The ^{1}H NMR spectra of all the complexes were measured in dimethyl sulfoxide (DMSO-d_6) or MeOH-d_4, while the ^{13}C NMR spectra of **1a**, **2a**, **3a**, and **4a** were measured in D_2O. Their spectra suggested a C_2 symmetry, as is shown in Fig. 2. The ^{1}H NMR spectra of **1c** and **3c** are similar to those of **2c** and **4c** respectively. The signals at δ 1.3—4.3 are assigned to the methylene protons of the coordinated *N,N'*-disalicylidene-substituted quadridentate amine ligand (abbreviation: sexidentate ligand). The signals at δ 4.6—6.0 are assigned to the NH protons. The multiplet signals at δ 6.2—7.4 are assigned to the ring protons. The signals at δ 7.6—8.4 are assigned to the CH=N protons. The lowest signals are assigned to the picrate protons. The methylene-proton signals of **1c** and **2c** can be divided into three or four groups at the δ 1.7—2.1, 2.2—2.8, 2.8—3.1, and 4.2—4.3 regions. The signal at δ 1.7—2.1 of **2c** is assigned to the center methylene protons ($NHCH_2C\underline{H}_2CH_2NH$), while the signals at δ 2.2—2.8 and 2.8—3.1 of **1c** and **2c** are assigned to the NH-side methylene protons ($=NCH_2C\underline{H}_2NHC\underline{H}_2-$) of the coordinated sexidentate ligands by comparison with those of salicylato(quadridentate amine)cobalt(III) chloride hydrate, $[Co(sal)L]Cl \cdot nH_2O$ (**5**), (L: 2,2,2-tet; 2,3,2-tet; 3,2,3-tet and 3,3,3-tet), previously reported.[5] Thus, the signals at δ 4.2—4.3 of **1c** and **2c** have been assigned to the =N-side methylene protons ($=NC\underline{H}_2CH_2NH$) of the coordinated sexidentate ligands. In the NH-side methylene-proton signals of **2c**, the intensity ratio of two methylene-proton signals at δ 2.35 and 2.86 is 6:2; *i.e.*, the two methylene protons at δ 2.86 are overlapped with those at δ 2.35 because of the influence of C-5 center methylene. Therefore, the signals at δ 2.35 and 2.86 of **2c** can be assigned to the C-3, C-7 methylene protons (*cf.* Table 2) and the C-4, C-6 methylene protons respectively. The signals at δ 2.3—3.6 of **3c** and 1.4—3.9 of **4c** are difficult to assign to the individual methylene protons. The ^{13}C NMR spectra of **1a**, **2a**, **3a**, and **4a** showed 3—5 signals for the quadridentate amine carbons at δ 20—60 and 7 signals at δ 117—170 for the salicylidene carbons, as is shown in Fig. 2. The chemical shifts of the center methylene carbons at δ 20—31, the NH-side methylene carbons at 45—54, and the ring

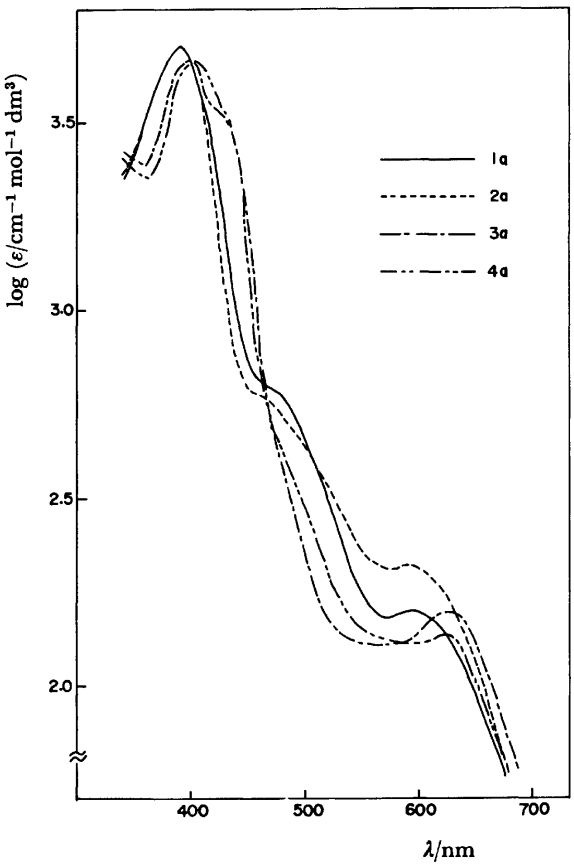

Fig. 1. The electronic absorption spectra of **1a**, **2a**, **3a**, and **4a** complexes in methanol.
1a: $[Co(sal_2{-}2,2,2\text{-tet})]Cl \cdot H_2O$, **2a**: $[Co(sal_2{-}2,3,2\text{-tet})]Cl$, **3a**: $[Co(sal_2{-}3,2,3\text{-tet})]Cl$, **4a**: $[Co(sal_2{-}3,3,3\text{-tet})]Cl \cdot H_2O$.

TABLE 1. SOME PHYSICAL PROPERTIES OF COMPLEXES

Complex No.	IR spectra cm^{-1}				Absorption bands in methanol			Decomp θ_m/°C	Electric conductivity of aqueous solutions S cm^2 $equiv^{-1}$
	C=$N_{str.}$	C-$N_{str.}$			λ/nm (ε/cm^{-1} mol^{-1} dm^3)				
1a	1642	1204	1150	1129	388(5200)	470 sh(615)	590(155)	236—238	97
1b	1642	1198	1150	1128	388(4900)	470 sh(580)	590(145)	230—233	
1c	1640	1202	1152	1128			590(158)	284—285	
2a	1642	1199	1146	1128	388(5200)	470 sh(566)	590(208)	241—242	103
2b	1644	1200	1149	1129	388(5000)	470 sh(546)	590(200)	236—238	
2c	1644	1198	1148	1128			590(209)	226—228	
3a	1621	1206	1146	1130	398(4610)	430 sh(3270)	628(159)	289—291	103
3b	1620	1206	1144	1128	398(4590)	428 sh(3230)	628(157)	303—305	
3c	1621	1210	1148	1130			628(160)	265—268	
4a	1620	1208	1148	1126	403(4600)	427 sh(3200)	627(135)	256—258	100
4b	1620	1208	1148	1125	403(4550)	427 sh(3160)	628(132)	275—277	
4c	1620	1205	1142	1121			628(136)	236—238	

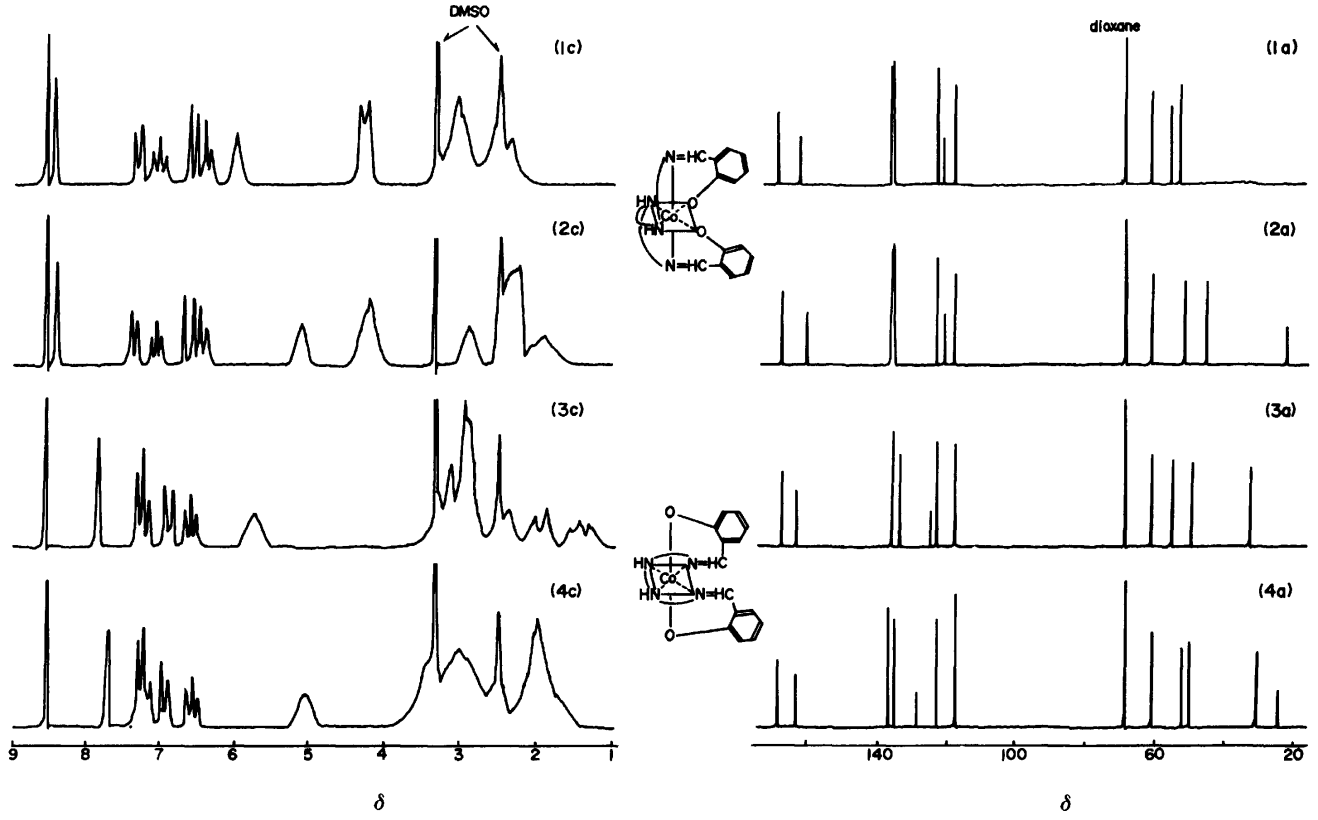

Fig. 2. The ^1H and ^{13}C NMR spectra of complexes.
1a: [Co($sal_2$2,2,2-tet)]Cl·H_2O, **1c**: [Co($sal_2$2,2,2-tet)]pic, **2a**: [Co($sal_2$2,3,2-tet)]Cl **2c**: [Co($sal_2$2,3,2-tet)]pic, **3a**: [Co($sal_2$3,2,3-tet)]Cl, **3c**: [Co($sal_2$3,2,3-tet)]pic, **4a**: [Co($sal_2$3,3,3-tet)]Cl·H_2O, **4c**: [Co($sal_2$3,3,3-tet)]pic.

carbons were assigned on the basis of the results of **5**[5] and salicylato(tetraammine)cobalt(III) chloride monohydrate,[16] [Co(sal)(NH_3)$_4$]Cl·H_2O (**6**), as is shown in Table 2. Thus, the signals at *ca.* δ 60 have been assigned to the =N-side methylene carbons of the coordinated sexidentate ligands. The chemical shifts of the =N-side methylene protons and carbons are lower than those of the NH-side methylene protons and carbons respectively. Therefore, the order of the ^1H and ^{13}C chemical shifts of the center, NH_2–,[5] NH–, and =N-side methylene protons or carbons is as is shown in Scheme 2;

TABLE 2. ^1H AND ^{13}C NMR SPECTRA OF COMPLEXES

^1H

Complex No.	Methylene protons δ			NH proton δ	-N=HC, -O (δ)					Picrate δ
	Center methylene C-2, C-5, C-8	NH-side methylene C-3, C-7	=N-side methylene C-4, C-6	C-1, C-9		H-5	H-3	H-4	H-6	CH=N	
1a		2.58(4H)	3.07(4H)	4.26(4H)	6.04(2H)	6.28—6.65(m,4H)		6.97(t,2H)	7.30(d,2H)	8.42(2H)[1]	
1b		2.58(4H)	3.07(4H)	4.25(4H)	5.97(2H)	6.28—6.65(m,4H)		6.97(t,2H)	7.28(d,2H)	8·41(2H)[1]	
1c		2.2—2.8(4H)	3.15(4H)	4.32(4H)	5.98(2H)	6.30—6.65(m,4H)		6.99(t,2H)	7.28(d,2H)	8.40(2H)	8.52(2H)[1]
2a	1.87(2H)	2.29(6H)	2.80(2H)	4.20(4H)	5.18(2H)	6.35—6.70(m,4H)		7.02(t,2H)	7.35(d,2H)	8.45(2H)[1]	
2b	1.90(2H)	2.28(6H)	2.80(2H)	4.20(4H)	5.14(2H)	6.38—6.70(m,4H)		7.03(t,2H)	7.35(d,2H)	8.40(2H)[1]	
2c	1.7—2.1(2H)	2.35(6H)	2.86(2H)	4.22(4H)	5.18(2H)	6.35—6.70(m,4H)		7.03(t,2H)	7.32(d,2H)	8.40(2H)	8.52(2H)[1]
3a	1.3—2.1(4H)	2.4—3.8(12H)[a]			5.30(2H)	6.56(t,2H)	6.90(d,2H)	7.02—7.30(m,4H)		7.65(2H)[2]	
3b	1.2—2.1(4H)	2.3—3.7(12H)[a]			5.72(2H)	6·55(t,2H)	6.85(d,2H)	7.05—7.33(m,4H)		7.80(2H)[1]	
3c	1.2—2.2(4H)	2.3—3.6(12H)[a]			5.75(2H)	6.54(t,2H)	6.84(d,2H)	7.05—7.32(m,4H)		7.80(2H)	8.50(2H)[1]
4a		1.4—3.9(18H)[b]			4.60[c]	6.65(t,2H)	6.95(d,2H)	7.05—7.30(m,4H)		7.57(2H)[2]	
4b		1.5—3.9(18H)[b]			5.02(2H)	6.55(t,2H)	6.91(d,2H)	7.07—7.31(m,4H)		7.68(2H)[1]	
4c		1.4—3.9(18H)[b]			5.00(2H)	6.53(t,2H)	6.90(d,2H)	7.05—7.34(m,4H)		7.70(2H)	8.50(2H)[1]

^{13}C

	Center methylene carbon δ		NH-side methylene carbon δ		=N-side methylene carbon δ	-N=HC, -O (δ)						
	C-5	C-2 C-8	C-3, C-4 C-6 and C-7		C-1 C-9	C-1	C-2	C-3	C-4	C-5	C-6	C-7
1a			51.9	54.2	59.5	120.5	163.2	117.3	136.2	122.3	136.0	169.5[3]
2a	20.5		45.4	50.5	60.0	120.7	162.2	117.7	136.4	122.9	136.0	168.7[3]
3a		31.1	49.0	53.7	59.7	125.1	164.3	117.7	136.1	123.5	134.4	169.0[3]
4a	23.3	28.8	49.2	50.7	59.8	129.0	165.4	117.3	136.4	123.0	135.0	169.6[3]

Solvents and Standard: 1) DMSO-d_6, internal TMS; 2) MeOH-d_4, internal TMS; 3) D_2O, internal dioxane ($\delta=0$). a) This signal contains the NH-side and =N-side methylene proton signals. b) This signal contains the center methylene, NH-side methylene, and =N-side methylene proton signals. c) This signal overlaps with the signal of the solvent.

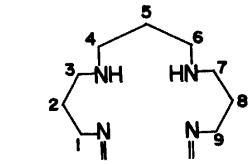

Positions of the methylene protons or carbon in complexes.

$$=N\underline{CH_2}(CH_2)_nCH_2NH < NH_m\underline{CH_2}(CH_2)_n\underline{CH_2}NH < NH_2\underline{CH_2}CH_2NH < NH_2\underline{CH_2}CH_2CH_2NH$$

=N-side methylene protons (or carbon); NH-side methylene protons (or carbon); NH_2-side methylene protons (or carbon)

$$< {=}NCH_2\underline{CH_2}CH_2NH < NHCH_2\underline{CH_2}CH_2NH < NH_2CH_2\underline{CH_2}CH_2NH \quad \begin{pmatrix} m: 0, 1 \text{ or } 2 \\ n: 0 \text{ or } 1 \end{pmatrix}$$

center methylene protons (or carbon)

Scheme 2.

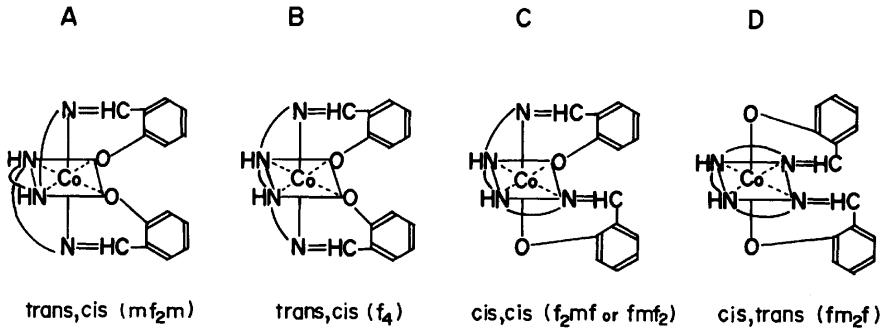

Fig. 3. The configurations of (*N,N'*-disalicylidene-substituted quadridentate amine)cobalt(III) complexes.

Complexes **1a**, **2a**, **3a**, and **4a** have four isomers of **A**, **B**, **C**, and **D**, as is shown in Fig. 3. The configurations of **A**, **B**, and **D** have a C_2 symmetry, while the configuration of **C** has a C_1 symmetry. The IR, ^1H, and ^{13}C NMR spectra of Complexes **1a**, **2a**, **3a**, and **4a** are suggestive of a C_2 symmetry;[13,15,17,18] *i.e.*, the isomers of these complexes can be assigned to the **A**, **B**, or **D** configurations. A clear distinction between one group of **1a**, **2a** complexes and the other group of **3a**, **4a** complexes was found in the color, solubility, IR, electronic absorption, NMR spectra, and the Dreiding stereo model. **1a** and **2a** are brown, while **3a** and **4a** are green. Complexes **1a** and **2a** are very soluble in DMSO, though **3a** and **4a** are only slightly soluble. The C=N stretching signals (at 1642 cm^{-1} for **1a** and at 1620 cm^{-1} for **3a**) in the IR spectra, the electronic absorption bands (at 388, 470, and 590 nm for **1a** and at 398, 430, and 628 nm for **3a**), and the methylene-proton signals, the CH=N proton signals (at δ 8.4 for **1a** and at δ 7.6 for **3a**), and the ring-proton signals (multiplet, triplet, and doublet signals for **1a** and triplet, doublet, and multiplet signals for **3a**) of the ^1H NMR spectra of **1a** and **3a** are closely similar to those of **2a** and **4a** respectively, as is shown in Tables 1 and 2. In the Dreiding stereo model, the methylene-loop rings of the coordinated sexidentate ligands of former complexes show that the **A** isomer[6] is not strained, though the other isomers, **B** and **D**, are greatly strained. Thus, the complexes of the former group are assigned to the **A** isomer, which has a *trans,cis*(mf_2m)[10,11] configuration[6] for the two CH=N and two phenoxyl groups. On the other hand, in the methylene-loop rings of the latter complexes, the **A**, **B**, and **D** isomers are not strained, though the methylene protons of the methylene-loop ring of the **A** and **B** isomers have a steric repulsion because of the non-planar structure. It has been established that, in iron[8,9,12] and cobalt[19] complexes of [$Fe^{III}Sal_2$3,2,3-tet]$^+$, and [$Fe^{III}Sal_2$2,2,2-tet]$^+$ and of [$Co^{III}Cl_2$3,2,3-tet]$^+$, [$Co^{III}Cl_2$2,2,2-tet]$^+$, the 3,2,3-tet ligand takes a structure with four nitrogens in plane, while the 2,2,2-tet ligand usually adopts a non-planar structure. Thus, the complexes of the latter group are assigned to the **D** isomer, which has a *cis,trans* (fm_2f)[10,11] configuration for the two CH=N and two phenoxyl groups. The color, solubility, IR, electronic absorption, and NMR spectra of the latter complexes are very different from those of the former complexes. These differences are due to the configuration of the complexes.

Experimental

Measurements. The NMR spectra were recorded with an FX-60 spectrometer (JEOL) for ^{13}C NMR and with an R-40 apparatus (Hitachi) for ^1H NMR. The IR spectra were recorded over potassium bromide disks with an IR-27G spectrophotometer (Shimadzu). The visible absorption spectra were recorded with a Shimadzu MPS-5000 recording spectrophotometer. The electric conductivities of the aqueous solution were determined by the use of a conductometric meter, CM-30 (Shimadzu), at room temperature.

Preparation of Complexes. (1,8-N-Disalicylidene-3,6-diazaoctane-1,8-diamine)cobalt(III) Chloride (1a): *Method A*: *cis*-α or β-Dichloro(3,6-diazaoctane-1,8-diamine(trien))cobalt(III) chloride[20,21] (3.0 g, 9.63 mmol) was added to moistened fresh AgOH, which has been made from silver nitrate (3.27 g, 19.25 mmol) and potassium hydroxide (1.08 g, 19.25

mmol). The mixture was stirred for several minutes at room temperature and then stirred for about 40 min at 60 °C. The silver chloride thus precipitated was filtered off. A methanol solution (20 cm^3) of salicylaldehyde (2.36 g, 19.33 mmol) was then added, drop by drop, to the reddish violet filtrate. The solution was stirred at 50 °C for 24 h. The solution was concentrated on a rotary evaporator, and the reaction mixture was dried over silica gel. Complex **1a** was extracted with dry methanol or dry ethanol from the dried reaction mixture. The purification of the complexes was achieved by column chromatography on alumina. When the solvent was then eluted with methanol or ethanol, the effluent of the first brown band of Complex **1a** was collected and the solution was concentrated. Then, the precipitated complex was recrystallized twice from ethanol–ether (3:2). Yield: 2.41 g (53.8%).

No other isomer was isolated from the second red band and third pink bands, which perhaps $[CoCl(OH)trien]^+$ or $[Co(OH)_2trien]^+$.[22]

Method B: A methanol solution (10 cm^3) of trien (1.46 g, 9.98 mmol) was added to a methanol solution (40 cm^3) of salicylaldehyde (2.44 g, 19.98 mmol), and the mixture was stirred 10 min at room temperature. Then, the solution was added to a methanol solution (50 cm^3) of $CoCl_2 \cdot 6H_2O$ (2.38 g, 10.0 mmol). Air was bubbled into the solution for 7 h, and the solution was concentrated on a rotary evaporator. The complex thus precipitated was recrystallized twice from water–acetone or ethanol–ether. Yield: 2.34 g (50.4%). Found: C, 51.41; H, 6.00; N, 12.04; Cl, 8.02%. Calcd for $CoC_{20}H_{26}N_4O_3Cl$ (MW 464.84) C, 51.68; H, 5.64; N, 12.05; Cl, 7.63%. Color: brownish black.

*(1,8-*N*-Disalicylidene-3,6-diazaoctane-1,8-diamine)cobalt(III) Nitrate Hydrate (**1b**)*: An aqueous solution of silver nitrate (0.18 g, 1.06 mmol) was added to an aqueous solution of **1a** (0.48 g, 1.03 mmol). The mixture was stirred, and the silver chloride thus precipitated was filtered. The filtrate was concentrated on a rotary evaporator. Then, the precipitated complex was recrystallized twice from methanol–ether. Yield: 0.22 g (43.4%). Found: C, 48.56; H, 5.69; N, 14.22%. Calcd for $CoC_{20}H_{26}N_5O_6$ (MW 491.39) C, 48.89; H, 5.33; N, 14.25%. Color: brown.

*(1,8-*N*-Disalicylidene-3,6-diazaoctane-1,8-diamine)cobalt(III) Picrate (**1c**)*: An aqueous solution of picric acid (0.10 g, 0.436 mmol) was added to an aqueous solution of **1a** (0.20 g, 0.430 mmol). The mixture was stirred, and then the precipitated complex was filtered, washed with water, and dried. Yield: 0.26 g (94.5%). Found: C, 48.80; H, 4.28; N, 15.89%. Calcd for $CoC_{26}H_{26}N_7O_9$ (MW 639.47) C, 48.84; H, 4.10; N, 15.33%. Color: yellowish brown.

*(1,9-*N*-Disalicylidene-3,7-diazanonane-1,9-diamine)cobalt(III) Chloride (**2a**)*: A methanol solution (10 cm^3) of 3,7-diazanonane-1,9-diamine (2,3,2-tet) (1.60 g, 9.98 mmol) was added to a methanol solution (40 cm^3) of salicylaldehyde (2.44 g, 19.98 mmol), after which the mixture was stirred 10 min at room temperature. Then the solution was added to a methanol solution (50 cm^3) of $CoCl_2 \cdot 6H_2O$ (2.38 g, 10.0 mmol). Air was bubbled into the solution for 7 h, the solution was concentrated in a rotary evaporator, and the reaction mixture was dried over silica gel. Complex **2a** was extracted with dry methanol from the dried mixture. The purification of the complexes was achieved by column chromatography on alumina. When the solvent was eluted with methanol, the effluent of the first brown band of Complex **2a** was collected and the solution was concentrated. Then, the precipitated complex was recrystallized twice from methanol–acetone–ether. Yield: 1.20 g (26.1%). Found: C, 54.51; H, 6.01; N, 12.07; Cl, 7.93%. Calcd for $CoC_{21}H_{26}N_4O_2Cl$ (MW 460.85) C, 54.73; H, 5.69; N, 12.16; Cl, 7.69%. Color: brownish black.

*(1,9-*N*-Disalicylidene-3,7-diazanonane-1,9-diamine)cobalt(III) Nitrate (**2b**)*: Complex **2b** has been prepared from the reaction mixture of silver nitrate (0.18 g, 1.06 mmol) and Complex **2a** (0.46 g, 0.998 mmol) according to the method used for **1b**. Yield: 0.16 g (32.9%). Found: C, 51.11; H, 5.08; N, 14.60%. Calcd for $CoC_{21}H_{26}N_5O_5$ (MW 487.40) C, 51.75; H, 5.38; N, 14.37%. Color: brown.

*(1,9-*N*-Disalicylidene-3,7-diazanonane-1,9-diamine)cobalt(III) Picrate (**2c**)*: Complex **2c** has been prepared from the reaction mixture of **2a** (0.2 g, 0.434 mmol) and picric acid (0.1 g, 0.436 mmol) according to the method used for **1c**. Yield: 0.16 g (56.4%). Found: C, 49.28; H, 4.49; N, 15.04%. Calcd for $CoC_{27}H_{28}N_7O_9$ (MW 653.49) C, 49.62; H, 4.32; N, 15.00%. Color: yellowish brown.

*(1,10-*N*-Disalicylidene-4,7-diazadecane-1,10-diamine)cobalt(III) Chloride (**3a**)*: Complex **3a** has been prepared from a reaction mixture of *trans*-dichloro(4,7-diazadecane-1,10-diamine)cobalt(III) chloride hydrate[23] (3.0 g, 8.39 mmol), AgOH (2.09 g, 16.74 mmol) which had been obtained from silver nitrate, and potassium hydroxide and salicylaldehyde (2.05 g, 16.79 mmol) according to the method used for **A** of **1a**. The green complex of **3a** was recrystallized twice from methanol–ether. Yield: 0.75 g (18.8%). Found: C, 55.49; H, 5.72; N, 12.09; Cl, 8.02%. Calcd for $CoC_{22}H_{28}N_4O_2Cl$ (MW 474.88) C, 55.64; H, 5.94; N, 11.80; Cl, 7.47%. Color: green.

*(1,10-*N*-Disalicylidene-4,7-diazadecane-1,10-diamine)cobalt(III) Nitrate (**3b**)*: Complex **3b** was prepared from the reaction mixture of Complex **3a** (0.47 g, 0.99 mmol) and silver nitrate (0.17 g, 1.00 mmol) according to the method used for **1b**. Yield: 0.22 g (44.3%). Found: C, 52.70; H, 5.78; N, 14.01%. Calcd for $CoC_{22}H_{28}N_5O_5$ (MW 501.43) C, 52.70; H, 5.63; N, 13.97%. Color: green.

*(1,10-*N*-Disalicylidene-4,7-diazadecane-1,10-diamine)cobalt(III) Picrate (**3c**)*: This complex was prepared from the reaction mixture of Complex **3a** (0.16 g, 0.337 mmol) and picric acid (0.08 g, 0.349 mmol) according to the method used for **1c**. Yield: 0.18 g (80.0%). Found: C, 50.64; H, 4.51; N, 15.09%. Calcd for $CoC_{28}H_{30}N_7O_9$ (MW 667.52) C, 50.38; H, 4.53; N, 14.69%. Color: yellowish green.

*(1,11-*N*-Disalicylidene-4,8-diazaundecane-1,11-diamine)cobalt(III) Chloride Hydrate (**4a**)*: A methanol solution (10 cm^3) of 4,8-diazaundecane-1,11-diamine (3,3,3-tet) (1.88 g, 9.98 mmol) was added to a methanol solution (40 cm^3) of salicylaldehyde (2.44 g, 19.98 mmol), and the mixture was stirred 10 min at room temperature. Then, the solution was added to a methanol solution (50 cm^3) of $CoCl_2 \cdot 6H_2O$ (2.38 g, 10.0 mmol). Air was bubbled into the solution for 7 h, and the solution was concentrated on a rotary evaporator. The concentrated solution was submitted to a column chromatography on alumina. On eluting the solvent with methanol, the eluent of the first brown band was collected and concentrated. The purification of the complex was achieved by the use of a column of ion-exchange resin (SP-Sephadex C-25 Na^+ form). After the mixture had been

eluted with 0.2 mol dm^{-3} of NaCl the fourth green band of Complex **4a** was collected and concentrated on a rotary evaporator, and the precipitated NaCl was removed by filtration. The green complex was recrystallized twice from methanol–ether. Yield: 0.43 g (8.5%). Found: C, 54.92; H, 6.55; N, 10.72; Cl, 7.31%. Calcd for $CoC_{23}H_{32}N_4O_3Cl$ (MW 506.92) C, 54.50; H, 6.36; N, 11.05; Cl, 6.99%. Color: green.

Attempts to isolate another isomer from this reaction mixture were unsuccessful, because the other bands in the column of the ion-exchange resin were small.

*(1,11-*N*-Disalicylidene-4,8-diazaundecane-1,11-diamine)cobalt(III) Nitrate (4b)*: This complex was prepared from the reaction mixture of Complex **4a** (0.50 g, 0.986 mmol) and silver nitrate (0.17 g, 1.00 mmol) according to the method used for **1b**. Yield: 0.26 g (51.1%). Found: C, 53.51; H, 5.59; N, 13.28%. Calcd for $CoC_{23}H_{30}N_5O_5$ (MW 515.45) C, 53.59; H, 5.87; N, 13.59%. Color: green.

*(1,11-*N*-Disalicylidene-4,8-diazaundecane-1,11-diamine)cobalt(III) Picrate (4c)*: This complex was prepared from the reaction mixture of Complex **4a** (0.19 g, 0.375 mmol) and picric acid (0.09 g, 0.393 mmol) according to the method used for **1c**. Yield: 0.23 g (90.0%). Found: C, 51.29; H, 5.04; N, 14.24%. Calcd for $CoC_{29}H_{32}N_7O_9$ (MW 681.55) C, 51.11; H, 4.73; N, 14.39%. Color: yellowish green.

Solubility: Complexes **1a—c** and **2a—c** are very soluble in DMSO, DMF, and methanol and are soluble in ethanol. Complexes **1a—b** and **2a—b** are very soluble in water, though **1c** and **2c** are insoluble in water. Complexes **3a** and **4a** are soluble in methanol, though they are only slightly soluble in water, DMSO, and DMF. Complexes **3b—c** and **4b—c** are soluble in DMSO, DMF and methanol, though they are insoluble in water.

References

1) Part IV. Y. Yamamoto and E. Toyota, *Bull. Chem. Soc. Jpn.*, **57**, 2650 (1984).

2) Y. Yamamoto and E. Toyota, *Chem. Pharm. Bull.*, **26**, 2275 (1978).

3) Y. Yamamoto and E. Toyota, *Bull. Chem. Soc. Jpn.*, **52**, 2540 (1979).

4) Y. Yamamoto, E. Toyota, and N. Mitsudera, *Bull. Chem. Soc. Jpn.*, **53**, 3517 (1980).

5) Y. Yamamoto, H. Kudo, and E. Toyota, *Bull. Chem. Soc. Jpn.*, **56**, 1051 (1983).

6) B. D. Sarma and J. C. Bailar, Jr., *J. Am. Chem. Soc.*, **77**, 5476 (1955).

7) B. D. Sarma, K. R. Ray, R. E. Sievers, and J. C. Bailar, Jr., *J. Am. Chem. Soc.*, **86**, 14 (1964).

8) M. F. Tweedle and L. J. Wilson, *J. Am. Chem. Soc.*, **98**, 4824 (1976).

9) E. Sinn, G. Sim, E. V. Dose, M. F. Tweedle, and L. J. Wilson, *J. Am. Chem. Soc.*, **100**, 3375 (1978).

10) Y. Yoshikawa, *Bull. Chem. Soc. Jpn.*, **49**, 159 (1976).

11) IUPAC Nomenclature of Inorganic Chemistry, Definitive Rules 1970, Butterworths, London (1971).

12) T. Ito, M. Sugimoto. H. Ito, K. Toriumi, H. Nakayama, W. Mori, and M. Sekizaki, *Chem. Lett.*, **1983**, 121.

13) Y. Yamamoto, *Chem. Lett.*, **1980**, 1555.

14) Y. Yamamoto, R. Kataoka, S. Imahara, and T. Amano, *Bull. Chem. Soc. Jpn.*, **54**, 2972 (1981).

15) Y. Yamamoto and E. Toyota, *Bull. Chem. Soc. Jpn.*, **57**, 47 (1984).

16) Y. Yamamoto, *Bull. Chem. Soc. Jpn.*, **51**, 2894 (1978).

17) S. Utsuno, A. Hayashi, S. Kondo, and M. Utsumi, *Chem. Lett.*, **1979**, 351.

18) S. Utsuno and M. Sekizaki, *Inorg. Nucl. Chem. Lett.*, **15**, 259 (1979).

19) M. D. Alexander and H. G. Hamilton, Jr., *Inorg. Chem.*, **8**, 2131 (1969).

20) A. M. Sargeson and G. H. Searle, *Inorg. Chem.*, **6**, 787 (1967).

21) "Shin Jikken Kagaku Koza," ed by the Chemical Society of Japan, Maruzen, Tokyo (1977), Vol. 8, Chap. 3, p. 1445.

22) E. Kyuno, L. J. Boucher, and J. C. Bailar, Jr., *J. Am. Chem. Soc.*, **87**, 4458 (1965).

23) B. Bosnich, J. M. Harrowfield, and H. Boucher, *Inorg. Chem.*, **14**, 815 (1975).

The Identification of the Compositions of the Compounds Formed in an Addition Reaction Involving Insoluble Substances

Goro HIHARA,* Tadashi SHIMIZU,† Hiroshi MIYAMAE, and Miharu NAGATA
Department of Chemistry, Faculty of Science, Josai University, Sakado, Saitama 350-02
(Received August 7, 1984)

A method has been developed for the identification of the compositions of all the insoluble compounds which are formed in the reaction of an insoluble substance (A) with a soluble one (B). It consists of allowing a fixed amount of A to react with various amounts of B in a fixed volume of a solution, determining the concentrations of B(=[B]) remaining unreacted after the equilibrium is reached, and then finding the number of the formed compounds and their compositions from the variations in [B] on the basis of the phase rule. This method was applied to the reactions of PbI_2 with diethylenetriamine (dien) and with 1,3-propanediamine (pren); the presence of the following addition compounds was found: $PbI_2 \cdot Y$(dien) (Y=1/2 and 1) and $PbI_2 \cdot Y$(pren) (Y=4/5, 1, and 2).

In studying coordination compounds, the first step is to determine the compositions of the complexes formed in the reaction. When all of the species involved are soluble in a common solvent, there have already been developed several useful methods, such as the continuous variation[1-3] and the mole ratio methods.[4] However, they can not be used when some of the species concerned are insoluble. A method which is applicable to such a case was reported in a previous paper.[5] It consists, essentially, in pursuing the variations in the concentrations of a soluble substance [B] in equilibrium with the insoluble ones.

In the present study, this method was applied to the reactions of PbI_2 with diethylenetriamine and with 1, 3-propanediamine; it will be pointed out that the examination of the powder X-ray diffraction patterns of the insoluble compounds is very helpful in confirming the presence of complexes formed in the reaction, especially when such complexes are otherwise apt to be overlooked.

Theoretical

Let us assume that an insoluble substance, A, reacts with a soluble one, B, in a solution according to Eqs. 1 and 2 to yield two insoluble addition compounds;

$$\text{A(solid)} + m\text{B(soln.)} = \text{A}\cdot m\text{B(solid)} \quad (1)$$

$$\text{A}\cdot m\text{B(solid)} + n\text{B(soln.)} = \text{A}\cdot(m+n)\text{B(solid)}. \quad (2)$$

The degree of freedom of this system, f, is given on the basis of the phase rule by:

$$f = c + 2 - p, \quad (3)$$

in which c is the number of the components, and p, the number of phases. Since the system is composed of A, B, and a solvent, c equals 3. Therefore,

$$f = 5 - p. \quad (4)$$

Under a constant temperature and pressure, f becomes $(3-p)$:

$$f = 3 - p. \quad (5)$$

When the equilibrium is established between the solution and one of three solid phases, A, A·mB, or A·$(m+n)$B, the system becomes univariant and the concentration of B in the solution is capable of variation within a definite range. On the other hand, when two solid phases and the solution are in equilibrium, there appears an invariant state and the concentrations of B remain fixed, as long as either A and A·mB or A·mB and A·$(m+n)$B coexist in the solid.

When a fixed amount of A is put in a fixed volume of a solution containing various quantities of B and each mixture is allowed to stand until an equilibrium is established, the concentration of B remaining in each solution is determined in some way. The relations between the amounts of B taken at the beginning and the concentrations of B remaining at the end of the reaction are depicted by the solid curve in Fig. 1, which is tentatively termed a "concentration curve."

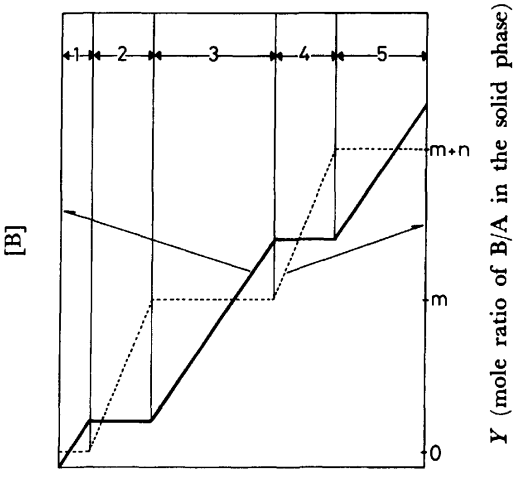

Fig. 1. A typical phase diagram for a ternary system where two insoluble addition compounds, A·mB and A·$(m+n)$B form.

† Present address: Colcoat Co., Ltd.,Gyoda, Saitama 361.

The two plateaus on the concentration curve represent two invariant states, one of which corresponds to the coexistence of A and A·mB, and the other, A·mB and A·$(m+n)$B. Each incline on the curve is related to each univariant state.

The composition of each sediment which is equilibrated with the solution can be calculated from Eq. 6;

$$Y = (X - V[\mathrm{B}])/Z, \quad (6)$$

where Y is the mole ratio of B/A in the sediment; X, the amount of B in mol taken at the beginning; [B], the concentration of B in mol/dm^3 in the final solution; V, the volume of the solution in dm^3, and Z, the total amount of A in mol taken at the beginning. The composition of each sediment calculated is also plotted by the dashed curve in Fig. 1, which is tentatively termed a "composition curve." The curve should reveal three plateaus, which correspond to the compositions of A, A·mB, and A·$(m+n)$B in the solid phase.

Experimental

Apparatus. A Toa Denpa HM-5H pH meter was used to determine the concentration of amines in the solution and the content of amines in the sediments. When it was necessary to characterize the sediments, use was made of powder X-ray diffractometry with a Rigaku Denki Geigerflex Diffractometer.

Reagents. PbI_2 was prepared by mixing a solution of KI with that of $Pb(NO_3)_2$ in a stoichiometric ratio. The diethylenetriamine (dien) (99.0% pure) was obtained from Wako Pure Chemical Industries, Ltd. The 1, 3-propanediamine (pren) (99.0% pure) was obtained from Tokyo Kasei Co., Ltd. These amines were used without any further purification. The ethanol was dehydrated with molecular sieves (4Al/16) and then distilled.

The Addition Reaction of PbI_2 with dien. One g (2.17 mmol) of finely powdered PbI_2 was suspended in an ampoule with 10.0 ml of an ethanol solution containing the desired amount of dien. The mole ratio of dien/PbI_2 was varied in the range of 0.3—3.0. Then each ampoule was sealed and kept at 20.0±0.2 °C for about two months. For the smooth progress of the reaction, each ampoule was shaken violently for 10 min twice 1 d. The sediments were separated from the solutions and then subjected to chemical analysis and powder X-ray diffractometry. The concentration of dien in each solution was also determined. A similar treatment was done in the case of the reaction of PbI_2 with pren.

Analysis of the Solutions and the Sediments. Five ml of each solution separated from the sediment was diluted with about 35 ml of water, and the amine was potentiometrically titrated with 0.1 M (1 M=1 mol dm^{-3}) HCl. The content of Pb^{2+} in the solution was determined by titrating with 0.01 M EDTA, using xyrenol orange as an indicator.[6] For the determination of the amine content in the sediments, about 10—20 mg of the sediment was dissolved in 10.00 ml of 0.1 M HCl. After 30 ml of water had been added, the excess of HCl back-titrated potentiometrically by 0.1 M NaOH. The Pb content of the sediments was determined by the complexometric titration described above after about 10—20 mg of each sediment had been dissolved into 40 ml of water containing 0.5 ml of 1 M HNO_3.

Results and Discussion

Preliminary experiments confirmed that PbI_2 does not react with ethanol and is scarcely soluble in it, even in the presence of pren or dien. The direct reactions of PbI_2 with dien were made in various mole ratios of dien/PbI_2, 0.5, 1, 2, and 3. The unreacted dien was removed by pressing the products with a filter paper. The diffraction patterns of the products were similar to those of the products formed in the ethanolic solution containing the amine. These facts show that the net reactions in the ethanolic solutions are the addition reactions of PbI_2 with the amines and that ethanol acts merely as a diluent.

The findings on the reaction of PbI_2 with pren are shown in Fig.2 in the same manner as in Fig. 1. The concentration curve ascends from about 0.8 of X/Z(=pren/PbI_2) on the abscissa, and the composition curve becomes flat at Y=0.8 in the range of about 0.75—1.35 of X/Z. This shows the presence of an addition compound, PbI_2·4/5(pren). The occurrence of two other compounds, PbI_2·pren and PbI_2·2pren, can be pointed out in a similar way.

Figure 3 represents the findings on the reaction of

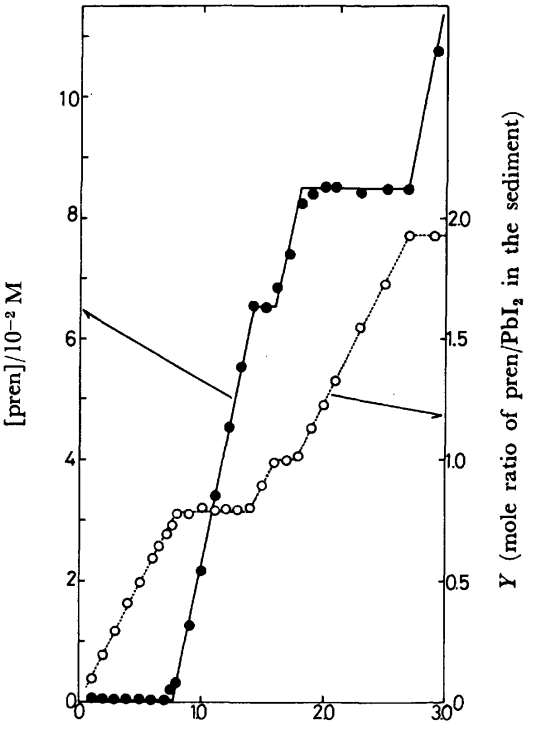

Fig. 2. The relation between the concentration of 1,3-propanediamine (pren) remaining in the solution and the composition of the sediments at 20 °C.

PbI_2 with dien. The concentration curve ascends from 0.5 and becomes flat at 0.55 of X/Z (=dien/PbI_2). The value of Y in the region of 0.5—0.55 of X/Z can be read as 0.5 from the composition curve, although it does not seem to have the corresponding plateau because of the narrow range. This is considered to imply the presence of $PbI_2 \cdot 1/2$(dien) according to the phase rule. The presence of $PbI_2 \cdot 1/2$(dien) can be confirmed from the powder X-ray diffraction patterns of the sediments, which are shown in Fig. 4. When the patterns are examined, it can be seen that the characteristic peak of 9.4°(=2θ) has a maximum intensity at Y=0.5 and that it disappears at Y=0.0 and 1.0. This fact indicates the presence of $PbI_2 \cdot 1/2$(dien). The presence of one more compound, PbI_2·dien, can be pointed out, since the concentration curve ascends from about 1.1 of X/Z(=dien/PbI_2) and the composition curve becomes flat at Y=1.0 in the range of 1.1—2.3 of X/Z in Fig. 3. Table 1 lists the data on the compositions of some sediments found by chemical analysis. The values of Y of $PbI_2 \cdot Y$(dien) obtained by substituting the equilibrated concentrations of dien for [B] in Eq. 6 agree very closely with those found by chemical analysis.

If a compound forms over a wide range of X/Z (=B/A), its presence can be confirmed on the basis of the resulting slope of the concentration curve and the corresponding plateau of the composition curve. This is the case with such compounds as $PbI_2 \cdot 4/5$ (pren) and $[Ag(thiopyrine)_3]ClO_4$.[8] However, if a compound forms in a narrow range of X/Z, its presence is liable to be overlooked because the corre-

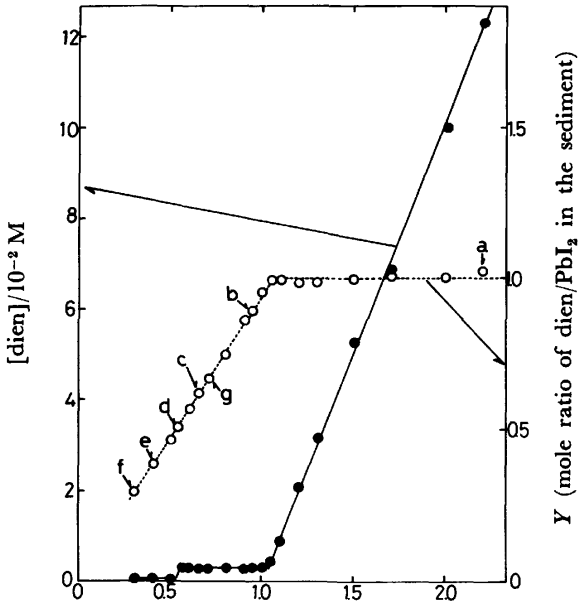

Fig. 3. The relation between the concentration of dien remaining in the solution and the composition of the sediments at 20 °C. The range of the mole ratio over 2.3 was omitted since the concentrations increased monotonously and the mole ratio of the sediments was equal to nearly 1.

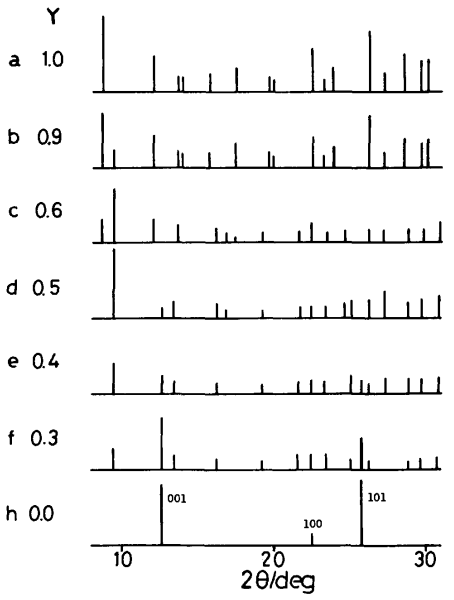

Fig. 4. The powder X-ray diffraction patterns of $PbI_2 \cdot Y$ (dien) where Y represents the mole ratio of dien/PbI_2 found by chemical analysis. The marks a—f are shown in Fig. 3 and h is the pattern of the sediment obtained by immersing PbI_2 in ethanol. Its peaks are the same as those of PbI_2 and are indexed.[9]

Table 1. The composition of some sediments grown in the PbI_2-dien-ethanol system

Sediment[a]	Found by chemical analysis				Determined from dien concn.[c]	
	Pb %	PbI_2[b] %	dien %	Recovery %	Y(mole ratio of dien/PbI_2)	
a	37.3	83.0	18.7	102	1.01	1.03
f	42.9	95.5	6.7	102	0.31	0.30
g	39.0	86.8	14.2	101	0.73	0.67

a) The sediments analyzed are shown in Fig. 3. b) The weight percentage of PbI_2 was calculated from the content of lead. c) These mole ratios were evaluated from Eq. 6, using the concentration of dien in the solution after the equilibration.

sponding plateau does not always appear in the composition curve, even though the concentration curve ascends. This is the case with such compounds as $PbI_2 \cdot 1/2$(dien) and $PbI_2 \cdot 2/3$(en) (en=ethylenediamine). In a previous paper[5] on the reaction of PbI_2 with en, spectrophotometry[7] could follow the minute variations in the concentrations of en in the vicinity of the range where $PbI_2 \cdot 2/3$(en) formed, and its presence was pointed out clearly, although the plateau did not appear in the composition curve. Since the minute variations in the concentrations of dien could not be followed accurately in the range where $PbI_2 \cdot 1/2$(dien) formed, X-ray powder diffractometry was used instead of spectrophotometry in order to confirm its presence. X-Ray powder diffractometry as well as spectrophotometry was found to be helpful in confirming the presence of the compounds which formed in a narrow range of X/Z.

When the present method is compared with the mole ratio and continuous variation methods, it is found to be more similar to the former than to the latter, since a fixed amount of one of two substances is allowed to react with various amounts of the other. The present method is applied to a heterogeneous system, while the mole ratio method is applied to a homogeneous system. Therefore, the method described here may be taken as a substitute for the mole ratio method in a heterogeneous system.

The method for the identification of the insoluble addition compounds was found to be applicable to the reactions of PbI_2 with pren and dien. The following addition compounds were confirmed: $PbI_2 \cdot Y$(pren) (Y=4/5, 1, and 2) and $PbI_2 \cdot Y$(dien) (Y=1/2 and 1). Many compounds have been reported of PbI_2 with Lewis bases, such as aniline,[10] thiourea,[11] and *N*,*N*-dimethylformamide.[12] Since most of them have the composition of 1:1 or 1:2 (=PbI_2:base), $PbI_2 \cdot 4/5$(pren) and $PbI_2 \cdot 1/2$(dien) have unusual compositions. On the other hand, there have been few reports on crystal structures of compounds of PbI_2 with Lewis bases: $PbI_2 \cdot 2$(dimethylsuloxide),[13] $PbI_2 \cdot 2$(pyridine),[14] and $PbI_2 \cdot 2$(en).[15] An X-ray study of $PbI_2 \cdot 2$(pren) and $PbI_2 \cdot$dien is now in progress in our laboratory.

We are grateful to Professor Hiroshi Suguro of this University for his helpful discussions.

References

1) Y. Shibata, T. Inoue, and Y. Nakatsuka, *Nippon Kagaku Kaishi*, **42**, 983 (1921) ; *Chem. Abstr.*, **16**, 2075 (1922).
2) P. Job, *Ann. Chim.*, **9**, 113 (1928).
3) W. C. Vosburgh and G. R. Cooper, *J. Am. Chem. Soc.*, **63**, 437 (1941).
4) J. A. Yoe and A. L. Jones, *Ind. Eng. Chem., Anal. Ed.*, **16**, 11 (1944).
5) G. Hihara, H. Miyamae, and M. Nagata, *Chem. Lett.*, **1982**, 647.
6) J. Körbl and R. Pribil, *Chemist-Analyst* **45**, 102 (1956).
7) G. Hihara, H. Miyamae, and M. Nagata, *Bull. Chem. Soc. Jpn.*, **54**, 2668 (1981).
8) T. Tanaka, *Yakugaku Zasshi*, **92**, 1252 (1972).
9) R. W. G. Wyckoff, "Crystal Structures," 2nd ed., Interscience Publishers, New York(1960), Vol. 1, P. 269.
10) V. M. Koshkin, V. V. Kukol', A. P. Mil'ner, Yu. R. Zabrodskiĭ, and K. A. Katrunov, *Sov. Phys. Solid State*, **19**, 939 (1971).
11) M. Glavas, *Therm. Anal., Proc. Int. Conf.*, 3rd **1971** (Pub. 1972), 2, 341.
12) I. Wharf, T. Gramstad, R. Makhija, and M. Onyszchuk, *Can. J. Chem.*, **54**, 3430 (1976).
13) H. Miyamae, Y. Numahata, and M. Nagata, *Chem. Lett.*, **1980**, 663.
14) H. Miyamae, H. Toriyama, T. Abe, G. Hihara, and M. Nagata, *Acta Crystallogr.*, **1984**, C40, 1559.
15) G. Hihara, H. Miyamae, and M. Nagata, 45th National Meeting of the Chemical Society of Japan, Tokyo, April 1982, Abstr., No. 2B17.

 © 1985 The Chemical Society of Japan Bull. Chem. Soc. Jpn., 58, 1520—1523 (1985)

Bivalent Cobalt Complexes with 1-(2-Pyridylazo)-2-naphthol and Analogous Ligands

Katsura MOCHIZUKI* and Masatoshi FUJIMOTO*,†
Department of Chemistry, Yokohama City University, Yokohama 236
†*Department of Chemistry, Faculty of Science, Hokkaido University, Sapporo 060*
(Received September 25, 1984)

Bivalent cobalt complexes with the title ligands were synthesized, isolated, and characterized by absorption spectra and magnetic moments. It has been suggested that the cobalt(II) complexes have more flexible structures than the corresponding cobalt(III) complexes. The cobalt(II) complexes were found to be oxidized to the cobalt(III) complexes in DMSO in the presence of copper(II) ions. Cyclic voltammetry elucidated the reversible Co^{II}/Co^{III} couples of the cobalt complexes in acetonitrile. The values of $E_{1/2}$ for the Co^{II}/Co^{III} couples were found to depend on the coordinating ligands. The relation between $E_{1/2}$ and pK_a of the *ortho*-hydroxyl group in the ligands was discussed.

Some *o*-hydroxy azo compounds in the following structural formula[1] are well known to behave as terdentate ligands,[2,3] which form colored chelates with many metal ions.[4] They have been used as sensitive analytical reagents for the spectrophotometric determination of cobalt,[5,6] because they form very stable cobalt(III) complexes.[7]

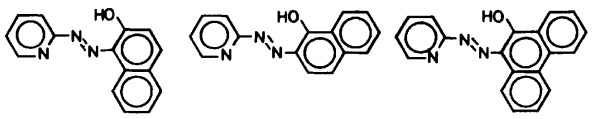

In the reactions between cobalt(II) ion and the title ligands in aqueous media, the cobalt(II) complexes formed are immediately oxidized by dissolved oxygen to the corresponding cobalt(III) complexes.[7] Therefore it is difficult to isolate the cobalt(II) complexes and to investigate their characters, whereas the formation[7] and the structures[8,9] of the cobalt(III) complexes have been well characterized. In addition, some information about redox behavior of such cobalt complexes has been obtained: (1) The cobalt(II) complexes are easily oxidized in aqueous solution, but they are considerably stable in organic solvents,[5,10] and (2) the cobalt(III) complex with β-PAN are reduced to the cobalt(II) complex by hyperoxide in dimethyl sulfoxide, DMSO,[11] though details of the electrochemical data about the Co^{II}/Co^{III} couples, which enable us to predict what complex prefers the cobalt(III) state, have not been reported so far.

In the present paper,[10] we report the synthesis, isolation, and characterization of the cobalt(II) complexes with the title ligands, as well as the electrochemical study of their cobalt complexes in acetonitrile solution by cyclic voltammetry.

Experimental

Measurements. Absorption spectra were recorded on Hitachi EPS-3T and 340 spectrophotometers. Magnetic susceptibilities were measured by Gouy method. The pH was measured with a TOA HM-20E pH-meter equipped with a composite electrode, type GST-155C.

Cyclic voltammograms were recorded at 25±0.3 °C with a Yanagimoto Polarographic Analyzer P-1100. The three-electrode system, consisting of a glassy carbon indicator electrode, GCE, (surface area: 7.1×10^{-2} cm^2), a platinum-wire auxiliary electrode, and a reference electrode, was employed. The reference electrode systems were as follows: (A) sample || salt bridge with saturated Et_4NClO_4 || saturated KCl || agar bridge of saturated KCl || SCE, and (B) sample || CH_3CN salt bridge containing 0.1 mol dm^{-3} Et_4NClO_4 || Ag–Ag^+(0.01 mol dm^{-3} $AgNO_3$) in acetonitrile. G4-sintered glasses were set between bridges and samples or reference electrodes. The difference in potentials observed for the above two systems, $E(Ag/Ag^+)-E(SCE)$, was always constant, −0.315 V, in all our measurements.[12] The potentials measured in (A) are listed in the text and tables. A glassy carbon electrode was polished up with diamond powder (Royal Diamond Compound 1-W-47) until the surface became a mirror before each run, so that sufficient reproducibilities could be obtained. Et_4NClO_4 was used as a supporting electrolyte.

Materials. Commercial grade acetonitrile dried over CaH_2 was twice distilled under nitrogen atmosphere. The purified solvent was stored under nitrogen atmosphere.

The cobalt complexes, $[Co^{III}(\beta\text{-pan})_2]Cl$[11] and $[Co^{III}(\beta\text{-pan})(dien)](ClO_4)_2$,[9] were reported previously.

The bivalent cobalt complex, $[Co^{II}(\beta\text{-tan})_2]$ was prepared from the stoichiometric amount of $Co(ClO_4)_2\cdot6H_2O$ and β-TAN in a similar way to $[Co^{III}(\beta\text{-pan})_2]Cl$, and easily isolated. The composition (metal to ligand ratio=1:2) and the oxidation state of the cobalt were confirmed by UV spectra[15] and elemental analysis. On the other hand, the bivalent cobalt complexes with β-PAN, α-PAN, and PAPhen could not be obtained by mixing the components. The syntheses of the cobalt(II) complexes were as follows:

1) Free acid form of β-PAN (1.0 g) and ascorbic acid (1.0 g) were completely dissolved in ethanol (500 cm^3) by heating under nitrogen atmosphere. To the solution, $CoCl_2$ (0.26 g) dissolved in a small amount of ethanol was added. The mixture was stirred and kept at 50 °C for 1.5 h. The green product formed was filtered, washed with ethanol, and dried *in vacuo* (yield 1.25 g). The green complex of a definite composition was always obtained

under the above conditions. Found: C, 54.51; H, 3.74; N, 10.86; Cl, 6.62%. Calcd for $C_{30}H_{20}N_6O_2Co \cdot C_6H_8O_6 \cdot (3/2)HCl$: C, 54.99; H, 3.78; N, 10.69, Cl, 6.76%. An analogous product was obtained for α-PAN. IR spectrum of the green complex shows the bands corresponding to ascorbic acid at around 1753 and 1650—1680 cm^{-1}. The magnetic moment μ_{eff} at 300 K is 1.94 BM. ESR spectra show no signals of organic radicals. Above data suggest that the green complex is a bivalent cobalt complex, though the state of ascorbic acid in the green complex and the structure of the green complex are not clear. A similar product was obtained for PAPhen by the analogous method. Found: C, 58.78; H, 3.87; N, 9.77%. Calcd for $C_{38}H_{24}N_6O_2Co \cdot C_6H_8O_6 \cdot 2HCl$: C, 57.29; H, 3.89; N, 9.54%.

2) To an ethanol solution (500 cm^3) of the green complex (1.0 g) with β-PAN, sodium metal (0.1 g) dissolved in ethanol (5 cm^3) was added. The solution turned red immediately. The red complex precipitated by evaporation was filtered, washed with ethanol thoroughly, recrystallized from ethanol-chloroform (1:1 v/v) several times, and dried *in vacuo* (yield *ca.* 60%). The red complex is more soluble in nonpolar solvents such as chloroform than in ethanol and insoluble in water, indicating itself acting as a noncharged complex. ESR spectra at 77 K showed the signal of cobalt(II) ion for the red complex, whereas no signal appeared for $[Co^{III}(\beta\text{-pan})_2]Cl$. The red complexes, $[Co^{II}(\alpha\text{-pan})_2]$ and $[Co^{II}(paphen)_2]$, were also synthesized by the analogous method. $[Co^{II}(\beta\text{-pan})_2]$: Color: deep reddish purple. Crystal form: too fine to be identified. Found: C, 63.52; H, 3.65; N, 14.39; Cl, 1.27%. Calcd for $C_{30}H_{20}N_6O_2Co \cdot (1/4)NaCl$: C, 63.21; H, 3.54; N, 14.74; Cl, 1.55%. $[Co^{II}(\alpha\text{-pan})_2]$: Color: dark purple. Tabular crystals. Found: C, 63.17; H, 3.65; N, 14.83%. Calcd for $C_{30}H_{20}N_6O_2Co \cdot (1/4)NaCl$: C, 63.21; H, 3.54; N, 14.74%. $[Co^{II}(paphen)_2]$: Color: deep red purple. Tabular crystals. Found: C, 68.04; H, 3.59; N, 12.87%. Calcd for $C_{38}H_{24}N_6O_2Co$: C, 69.62; H, 3.69; N, 12.82%.

Results and Discussion

Characterization of the Red Cobalt(II) Complexes. The data of absorption spectra in $CHCl_3$ and magnetic moments (solid) at room temperature for the red complexes are listed in Table 1. The absorption spectrum of $[Co^{II}(\beta\text{-pan})_2]$ is the same as that of the cobalt(II) complex observed in the rapid-scan spectral study of the reaction between Co^{2+} ion and β-PAN[7] and in the reduction product of $[Co^{III}(\beta\text{-pan})_2]Cl$ by O_2^- ion.[11] The data of elemental analysis and the absence of absorption bands assignable to cobalt(III) in the spectra measured in $CHCl_3$ indicate that the complexes do not contain cobalt(III) complexes. Though the absorption spectra of these complexes did not change in an aprotic solvent, DMSO, even bubbled with O_2 for *ca.* 30 min, the absorption spectra changed immediately to those corresponding to the cobalt(III) complexes, when a small amount of water (0.5 cm^3 H_2O to 3.5 cm^3 DMSO) was added.

Table 1. Data of absorption spectra and magnetic moments

Complex	λ_{max}/nm	$\varepsilon/10^4$ mol^{-1} dm^3 cm^{-1}	μ_{eff}/BM at 297 K
$[Co^{II}(\beta\text{-pan})_2]$	522	2.83	2.31
$[Co^{II}(\alpha\text{-pan})_2]$	322	2.80	2.16
	545	3.44	
$[Co^{II}(paphen)_2]$	310	3.38	2.52
	520	3.74	

Magnetic moments of the red complexes also show that these complexes are not cobalt(III) complexes but cobalt(II) complexes with more than one spin. It is well known that μ_{eff} of a cobalt(II) complex is variable depending on its spin-state, coordination number and geometry.[16] For example, the μ_{eff} values are expected to be 5.0—5.8, 1.80—1.85, and 2.2—2.9 BM, for octahedral high-spin, octahedral low-spin, and four-coordinated low-spin cobalt(II) complexes, respectively.[16] The μ_{eff} values listed in Table 1 are smaller than those for octahedral high-spin complexes and larger than those for octahedral low-spin complexes. The reason for this anomalous magnetic moment is interpreted as follows: 1) A mixture of high-spin cobalt(II) complexes and diamagnetic cobalt(III) complexes, 2) four-coordinated low-spin complexes, or 3) spin-state equilibrium between ^2E_g and $^4T_{1g}$ states. The possibility for 1) is excluded from results of absorption spectra and elemental analyses as mentioned above. From the results of temperature-dependence of the magnetic moment for $Co^{II}(paphen)_2 \cdot 4EtOH \cdot (1/3)CHCl_3$ (pink complex), Pandeya *et al.* took the spin-state equilibrium between ^2E_g and $^4T_{1g}$ into account.[17] Though the composition of their complex is different from that synthesized in the present study, the similarity of our data to theirs suggests that the case 3) is more probable for the other red complexes, $[Co^{II}(\beta\text{-pan})_2]$ and $[Co^{II}(\alpha\text{-pan})_2]$. Therefore, the structures of the cobalt(II) complexes are expected to be considerably flexible, whereas cobalt(III) complexes have rigid structures.[9]

These cobalt(II) complexes were found to react with copper(II) ions in DMSO. The red solutions of the cobalt(II) complexes in DMSO changed to green by the addition of copper(II) perchlorate; the same changes were observed for other copper(II) salts as well. The spectra of the final products corresponded to those for the cobalt(III) complexes. The effect of perchlorate ions was neglected, since no changes in the spectra of the cobalt(II) complexes were observed by the addition of perchlorates of other metals such as zinc(II). The oxidation by copper(II) ions should form copper(I) ions. The difference between the spectra of the final products with and without addition of 2,2′-biquinoline gave the spectrum of

copper(I)-2,2′-biquinoline complex, indicating the presence of copper(I) ions in the solutions of final products. These observations reveal the oxidation of the cobalt(II) complexes to the corresponding cobalt(III) complexes by copper(II) ions in DMSO.

Cyclic Voltammetry on the Cobalt Complexes. Cyclic voltammetry was carried out between −0.5 and +0.7 V *vs.* SCE in the scan-speed range from 10 to 500 m V s^{-1}. $[Co^{III}(\beta\text{-pan})_2]Cl$ showed one peak in both cathodic and anodic runs in this potential range. The other cobalt complexes with analogous ligands also showed similar cyclic voltammograms in the same potential range. Figure 1 shows the typical cyclic voltammogram of $[Co^{III}(\beta\text{-pan})_2]Cl$ in acetonitrile.[18] The cyclic voltammograms observed on $[Co^{II}(\beta\text{-pan})_2]$ and $[Co^{III}(\beta\text{-pan})_2]ClO_4$ were essentially the same to that of $[Co^{III}(\beta\text{-pan})_2]Cl$. The data for $[Co^{III}(\beta\text{-pan})_2]^+$ are listed in Table 2. It was found that (1) the cathodic and anodic peak currents of the observed wave, $(i_p)_c$ and $(i_p)_a$, measured at various sweep rates, v, were propotional to $v^{1/2}$, (2) the difference between cathodic ($(E_p)_c$) and anodic ($(E_p)_a$) peak potentials, $\Delta E=(E_p)_c-(E_p)_a$ was always *ca.* 60 mV, (3) the values of $(E_p)_c$ and $(E_p)_a$ were independent of v, (4) $(i_p)_a/(i_p)_c=1$ for all v, and (5) the peak potentials were independent of the kinds of indicator electrodes: A very similar wave was obtained when a GCE was changed to a Pt-electrode. On the basis of these results, the wave observed can be regarded as a simple one-electron transfer reversible system, $A+e \rightleftharpoons B$.[19]

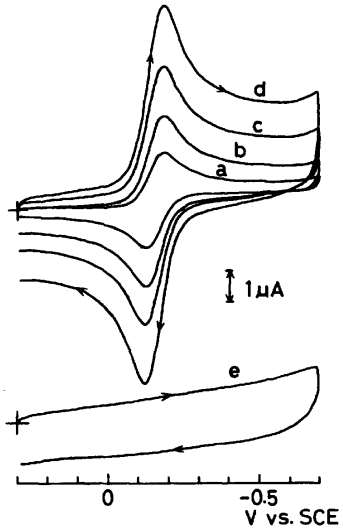

Fig. 1. Cyclic voltamograms of 2.0×10^{-4} mol dm^{-3} $[Co^{III}(\beta\text{-pan})_2]^+$ in acetonitrile solution cotaining 0.1 mol dm^{-3} Et_4NClO_4 at 25 °C. Sweep rate: **a**, 20; **b**, 50; **c**, 100; **d**, 200 mV s^{-1}. **e** is blank at sweep rate = 100 mV s^{-1}.

In order to elucidate the products of one-electron reduction of $[Co^{III}(\beta\text{-pan})_2]^+$, the constant potential electrolysis of the cobalt(III) complex at −1.0 V *vs.* Ag/Ag^+ (−0.68 V *vs.* SCE) was performed under the same conditions as in the measurement of the cyclic voltammogram. The absorption spectrum of the solution was observed during the electrolysis. As the absorption at 600 nm due to the cobalt(III) complex decreased gradually, a new band at about 520 nm due to the cobalt(II) complex appeared. Finally, the absorption spectrum almost coincided with that of $[Co^{II}(\beta\text{-pan})_2]$. Therefore, the above mentioned one-electron reversible process can be assigned

Table 2. Data of cyclic voltammetry on $[Co^{III}(\beta\text{-pan})_2]^+$ in acetonitrile[a]

v/mV s^{-1}	$(i_p)_c/\mu A$	$(i_p)_a/\mu A$	$(i_p)_c/(i_p)_a$	$(E_p)_c$/V[b]	$(E_p)_a$/V[b]	ΔE_p/mV
10	1.3_2	1.2_3	1.0_7			
20	1.8_0	1.7_0	1.0_6			
50	2.8_6	2.7_5	1.0_4	-0.18_0	-0.12_0	~60
100	4.0_7	3.7_5	1.0_9			
200	5.7_1	5.2_8	1.0_8			
500	9.0_4	8.1_0	1.1_2			

a) $[Co^{III}(\beta\text{-pan})_2]^+$: 2.0×10^{-4} mol dm^{-3}. $I=0.1$ (Et_4NClO_4). $T=25$ °C. b) *vs.* SCE.

Table 3. Data of the waves assigned to the Co^{II}/Co^{III} couple[a]

Complex	$(E_p)_c$/V	$(E_p)_a$/V	ΔE_p/V	$E_{1/2}$/V[b]	pK_a[c]
$[Co^{III}(\beta\text{-pan})_2]^+$ [d]	-0.18_0	-0.12_0	0.06_0	-0.15_0	12.7
$[Co^{II}(\beta\text{-pan})_2]$[e]	-0.18_0	-0.12_0	0.06_0	-0.15_0	
$[Co^{III}(\beta\text{-pan})(dien)]^{2+}$ [d]	-0.32_6	-0.26_5	0.06_1	-0.29_6	
$[Co^{II}(\alpha\text{-pan})_2]$[e]	-0.07_5	-0.01_0	0.06_5	-0.04_3	10.7
$[Co^{II}(paphen)_2]$[e]	-0.20_0	-0.14_0	0.06_0	-0.17_0	13.5
$[Co^{II}(\beta\text{-tan})_2]$[e]	$+0.02_0$	$+0.08_0$	0.06_0	$+0.05_0$	9.5

a) In acetonitrile. *vs.* SCE. $I=0.1$ (Et_4NClO_4). $T=25$ °C. b) $E_{1/2}=((E_p)_c+(E_p)_a)/2$. c) 50%(v/v) dioxane-water media. $I=0.1$ (KCl). $T=25$ °C. d) The forward scan is to negative direction and the backward to positive. e) The forward scan is to positive direction and the backward to negative.

to the electron transfer, $[Co^{III}(\beta\text{-pan})_2]^+ + e \rightleftharpoons [Co^{II}(\beta\text{-pan})_2]$. The waves observed for the other cobalt complexes were also assignable to that for the Co^{II}/Co^{III} couples.

The data for the cobalt complexes with β-PAN and analogous ligands in acetonitrile are listed in Table 3 with the values of pK_a for the *ortho*-hydroxyl groups in the ligands. It is obvious that $E_{1/2}$ of the Co^{II}/Co^{III} couple is dependent on the coordinating ligands. Some features are as follows: $E_{1/2}$ of the Co^{II}/Co^{III} couple shifts to the more negative side in $[Co^{III}(\beta\text{-pan})(dien)]^{2+}$ which has one β-PAN, than in $[Co^{III}(\beta\text{-pan})_2]^+$. The value of $E_{1/2}$ of $[Co^{II}(\beta\text{-pan})_2]$ is more negative than that of $[Co^{II}(\alpha\text{-pan})_2]$ where α-PAN is different from β-PAN in the position of the azo and *ortho*-hydroxyl groups attached to the naphthol moiety. From the comparison between $[Co^{II}(\beta\text{-pan})_2]$ and $[Co^{II}(\beta\text{-tan})_2]$, in which the ligands have the same moieties, 2-naphthols, $E_{1/2}$ of the complex with thiazolyl group is more positive than that of the complex with pyridyl group. Therefore, $[Co^{II}(\beta\text{-tan})_2]$ is expected to be more stable than $[Co^{II}(\beta\text{-pan})_2]$ against the oxidation by dissolved oxygen in aqueous solution (the half-wave potential for $O_2 \rightarrow O_2^-$, $E_{1/2} = -0.05$ V *vs.* SCE in aqueous neutral solution[20]). Indeed, the observations such as, the easy extraction of $[Co^{II}(\beta\text{-tan})_2]$ into organic phase[15] and the considerably easy isolation of the complex, support the above idea. For the cobalt complexes with these analogous ligands, there is a remarkable feature of the relation between $E_{1/2}$ and pK_a of the ligands. It can be seen that as the pK_a value of the *ortho*-hydroxyl group in the coordinating ligand increases, $E_{1/2}$ shifts to the more negative direction. This suggests that cobalt(III) state is more stabilized as the basicity of the coordinating ligand increases, *i.e.*, as the ligand can coordinate strongly to the cobalt ion.

The authors thank Professor Akira Yamada, Yokohama City University for the kind advices in the measurements of cyclic voltammograms and Professor Yoshio Matsunaga, Hokkaido University for the kindness in the measurements of magnetic susceptibilities.

References

1) Ligand abbreviations: α-PAN=2-(2-pyridylazo)-1-naphthol; β-PAN=1-(2-pyridylazo)-2-naphthol: PAPhen=10-(2-pyridylazo)-9-phenanthrol; β-TAN=1-(2-thiazolylazo)-2-naphthol; dien=diethylenetriamine.

2) S. Ooi, D. Cater, and Q. Fernando, J. Chem. Soc., *Chem. Commun.*, **1967**, 1301.

3) M. Kurahashi, *Chem. Lett.*, **1974**, 1271; *Bull. Chem. Soc. Jpn.*, **49**, 127, 872, 1419, 2927, 3053 (1976).

4) S. Shibata, "2-Pyridylazo Compounds in Analytical Chemistry," in "Chelates in Analytical Chemistry," ed by H. A. Flaschka and A. J. Barnard, Jr., Vol. 4, Marcel Dekker, Inc., New York, (1972), p. 1; R. G. Anderson and Nickless, *Analyst*, **92**, 207 (1967); **93**, 13, 20 (1968); S. Shibata, *Bunseki Kagaku*, **21**, 551 (1972); H. Wada, *ibid.*, **21**, 543 (1972); H. R. Hovind, *Analyst*, **100**, 769 (1975).

5) K. L. Cheng and R. H. Bray, *Anal. Chim. Acta*, **27**, 782 (1955); G. Goldstein, D. L. Manning, and O. Menis, *ibid.*, **31**, 192 (1959); T. Yotsuyanagi, R. Yamashita, and K. Aomura, *ibid.*, **44**, 1091 (1972).

6) R. Yamashita, T. Yotsuyanagi, and K. Aomura, *Bunseki Kagaku*, **20**, 1282 (1971) and the literatures cited therein.

7) K. Mochizuki, T. Imamura, T. Ito, and M. Fujimoto, *Chem. Lett.*, **1976**, 1207; *Bull. Chem. Soc. Jpn.*, **51**, 1743 (1978).

8) K. Mochizuki, T. Ito, and M. Fujimoto, *Bull. Chem. Soc. Jpn.*, **52**, 441 (1979).

9) K. Mochizuki and M. Fujimoto, *Bull. Chem. Soc. Jpn.*, **53**, 2531 (1980).

10) A preliminary report: K. Mochizuki and M. Fujimoto, *Chem. Lett.*, **1980**, 1541.

11) K. Mochizuki, T. Imamura, and M. Fujimoto, *Bull. Chem. Soc. Jpn.*, **53**, 1757 (1980).

12) Similar results have been reported for the reduction of $Co(ClO_4)_2 \cdot 6H_2O$ in acetonitrile, $E_{1/2} = -0.96$ V (DME, 0.1 mol dm^{-3} TBAP, Ag/0.01 mol dm^{-3} $AgNO_3$, at 25 °C)[13] and −0.65 V (DME, 0.1 mol dm^{-3} $NaClO_4$, SCE, at 25 °C).[14]

13) I. M. Kolthoff and J. F. Coetzee, *J. Am. Chem. Soc.*, **79**, 1852 (1957).

14) A. I. Popov and D. H. Geske, *J. Am. Chem. Soc.*, **72**, 2074 (1957).

15) A. Kawase, *Japan Analyst*, **12**, 817 (1963).

16) B. N. Figgis and J. Lewis, "Progress in Inorganic Chemistry," Interscience Publishers, New York, N.Y. (1964). Vol 6, p. 37.

17) K. B. Pandeya, R. P. Singh, and Y. K. Bhoon, *J. Coord. Chem.*, **6**, 71 (1976); Y. K. Bhoon, R. P. Singh and A. K. Gregson, *ibid.*, **9**, 251 (1979).

18) The wave with $(E_p)_c = -0.82$ and $(E_p)_a = -0.77$ V was observed by more negative sweep. This is assumed to be due to the reduction of the azo group or of the cobalt(II) ion.

19) A. M. Bond, "Modern Polarographic Methods in Analytical Chemistry," Marcel Dekker, Inc, 1980, Chapter 5.

20) I. M. Kolthoff and C. S. Miller, *J. Am. Chem. Soc.*, **63**, 1013 (1941).

 © 1985 The Chemical Society of Japan Bull. Chem. Soc. Jpn., 58, 1524—1528 (1985) [Vol. 58, No. 5

Recovery of Heavy Metals with Calcium Silicon Alloy. IV. Stoichiometric Discussion of the Reduction of Lead(II), Nickel(II), Iron(III), and Mercury(II) Ions

Shuzo TOKUNAGA
National Chemical Laboratory for Industry, Yatabe, Ibaraki 305
(Received September 25, 1984)

The reduction of Pb^{2+} and Ni^{2+} ions to the metallic state with the Ca–Si alloy powder can be stoichiometrically interpreted by the following elementary reactions 1—4 including the decomposition of water, a side reaction:

$$Ca^0 + Me^{z+} = Ca^{2+} + Me^0 \quad (1)$$

$$(Ca^0 + 2Me^{z+} = Ca^{2+} + 2Me^{z-1}) \quad (1')$$

$$Si^0 + 2Me^{z+} + 3H_2O = H_2SiO_3 + 2Me^0 + 4H^+ \quad (2)$$

$$(Si^0 + 4Me^{z+} + 3H_2O = H_2SiO_3 + 4Me^{z-1} + 4H^+) \quad (2')$$

$$Ca^0 + 2H_2O = Ca^{2+} + H_2 + 2OH^- \quad (3)$$

$$Si^0 + 3H_2O = H_2SiO_3 + 2H_2 \quad (4)$$

The occurrence of a reaction other than the above ones was suggested for the reduction of Fe^{3+} to Fe^{2+} ion under strongly acidic conditions. The reduction of Pb^{2+} and Ni^{2+} ions proceeded very slowly. On viewing the equivalents oxidized, the contribution of Ca in the alloy to the overall reaction was greater than that of Si; Si scarcely participated at all in the reduction of Fe^{3+} ion. Based on the above elementary reactions, the reduction of Hg^{2+} ion was discussed stoichiometrically. Almost the same equivalents of Hg^0 and Hg^I species formed in a 20-matom dm^{-3} Hg^{2+} solution, with an initial pH of 4.0. The contribution of Si to the reaction was greater than that of Ca.

Cu^{2+}, Hg^{2+}, Fe^{3+}, Pb^{2+}, Cr^{6+}, Cd^{2+}, and Zn^{2+} ions can be effectively removed from aqueous solutions with some silicon alloy powders containing Ca or Mg.[1-4] It has been considered that the removal of these metal ions is mainly due to their reduction to the insoluble species in the lower oxidation states and to their hydrolysis by OH^- ion formed by the decomposition of water, a side reaction. However, the mechanisms of these reactions have not been well elucidated. Of these reactions, the reduction of Cu^{2+} ion with the Ca–Si alloy was, in Part III, investigated stoichiometrically under weakly acidic conditions in order to prevent the hydrolysis of metal ions.[5] It has proved that the overall reaction can be substantially represented by the following four elementary reactions:

$$Ca^0 + Cu^{2+} = Ca^{2+} + Cu^0 \quad (5)$$

$$Si^0 + 2Cu^{2+} + 3H_2O = H_2SiO_3 + 2Cu^0 + 4H^+ \quad (6)$$

$$Ca^0 + 2H_2O = Ca^{2+} + H_2 + 2OH^- \quad (7)$$

$$Si^0 + 3H_2O = H_2SiO_3 + 2H_2 \quad (8)$$

The reduction of metal ions had been thought to take place mainly by Ca in the alloy, which, in the elementary state, has an extremely low standard-electrode potential, E^0=−2.866 V.[6] However, the above mechanism has shown that Si (E^0=−0.857 V)[6] in the alloy, a practically nonreactive element in aqueous solutions, mainly because of the effect of passivation, also exhibits great reducing power. Especially in solutions with Cu^{2+} concentrations higher than *ca.* 10 matom dm^{-3}, the equivalents of Si oxidized were greater than those of Ca.

The objectives of the present study are to elucidate the reaction mechanism of the reduction of metal ions other than Cu^{2+} ion with the Ca–Si alloy powder and to investigate the behavior of the reaction products, which has been obscure in the previous studies. By applying the method used for the reduction of Cu^{2+} ion, stoichiometric discussions will be made of all the reaction products of the reduction of Pb^{2+}, Ni^{2+}, Fe^{3+}, and Hg^{2+} ions, which differ in standard electrode potential and in the variation of the pH and the oxidation state. In Part I, the reducing effects of the alloy on various metal ions were examined by determining the dissolved components after a 24-h reaction period under the reaction conditions of *ca.* 0.2- to 18-matom dm^{-3} metal-ion concentrations and acidities of pH *ca.* 4 to 1-mol dm^{-3} HCl.[3] Subsequent studies by the author have revealed the following facts: The reducing effects on Ni^{2+} and Co^{2+} ions become appreciable only at neutral conditions, oxidation products of Si exist in the solid phase as well as in the solution, and the reaction rates greatly vary with the metal ions, resulting in different degrees of the side reaction. Therefore, in the present study, reactions were carried out under conditions agreeing with the respective metal ions. Concentration changes of the reaction products with the passage of time were determined in order to discuss their behavior and the relation between the metal-ion reduction and the side reaction.

Experimental

Metal-ion Solutions. Sample solutions were prepared by dissolving lead(II), nickel(II), iron(III), and mercury(II) chlorides of a reagent grade in distilled water.

Experimental Procedure. The procedure used was that reported in Part III.[5]

Results and Discussion

Outline of the Overall Reaction. In weakly acidic aqueous solutions, Cu^{2+}, Pb^{2+}, and Ni^{2+} ions are reduced by the Ca-Si alloy to form Cu^0, Pb^0, and Ni^0, respectively, in the solid phase. In the reduction of Hg^{2+} ion, insoluble Hg^0 and Hg^I species form simultaneously. A decrease in the pH is observed in these metal-ion solutions at high concentrations. Fe^{3+} ion is reduced to Fe^{2+} ion, and no solid product of iron, except hydroxide, forms. At that time, the pH tends to increase independently of the Fe^{3+} concentration.

The alloy, on the other hand, is oxidized concurrently with the metal-ion reduction to form Ca^{II} and Si^{IV} species. In addition to these reactions, there occurs a decomposition of water by the alloy as a side reaction. As has been reported previously, the alloy is practically stable and scarcely causes decomposition of water in metal-ion-free aqueous solutions above pH *ca.* 3.[3] It can, therefore, be said that the reaction with metal ions increases the active surface of the alloy, consequently causing such an appreciable side reaction.

Method of Stoichiometric Discussion. From the phenomena accompanying the reduction of metal ions by the alloy, the overall reaction is considered to be composed of the following elementary reactions, similarly to the case of the Cu^{2+} reduction:

$$Ca^0 + Me^{z+} = Ca^{2+} + Me^0 \quad (1)$$

$$(Ca^0 + 2Me^{z+} = Ca^{2+} + 2Me^{z-1}) \quad (1')$$

$$Si^0 + 2Me^{z+} + 3H_2O = H_2SiO_3 + 2Me^0 + 4H^+ \quad (2)$$

$$(Si^0 + 4Me^{z+} + 3H_2O = H_2SiO_3 + 4Me^{z-1} + 4H^+) \quad (2')$$

$$Ca^0 + 2H_2O = Ca^{2+} + H_2 + 2OH^- \quad (3)$$

$$Si^0 + 3H_2O = H_2SiO_3 + 2H_2 \quad (4)$$

Reactions 1 and 2 are for a reduction of divalent metal ions to the metallic state, such as those of Pb^{2+} and Ni^{2+} ions. Reactions 1′ and 2′ are for a one-electron reduction, such as those of Fe^{3+} and Hg^{2+} ions. Whether or not the above reactions are valid can be decided by ascertaining the equality between the total equivalents of the reduction and the oxidation products. The total-reduction equivalent is expressed by the sum of the equivalents of metal ions reduced and hydrogen produced. Both of them can be determined except in the reaction of Hg^{2+} ion, where Hg^0 and Hg^I species form in the solid phase and where, consequently, their separate determination is difficult. On the other hand, the total-oxidation equivalent is expressed by the sum of the equivalents of Ca^{II} and Si^{IV} species. Ca^{II} species is considered to be present in acidic solutions entirely in the form of Ca^{2+} ion, consequently it can readily be determined. However, the determination of Si^{IV} species is very difficult, since they exist not only in the dissolved form, but also in amorphous silica in the solid phase, together with the unreacted alloy. If the above elementary reactions are valid, the amounts of Si^{IV} species must be equal to either $(H_2+\Delta H^+)$ in equivalent when the pH decreases in the course of the reaction or to $(H_2-\Delta OH^-)$ when the pH increases. Therefore, the validity of the above reactions was evaluated by using the values of Si^{IV} calculated in such a way, while those of the other products were determined directly. For this purpose, stoichiometric discussions were made of the reactions of Pb^{2+}, Ni^{2+}, and Fe^{3+} ions, where only a single species of the metal product forms, and where, consequently, the equivalents of the metal ion reduced can readily be determined.

Reduction of Pb^{2+} Ion. The equality of the total equivalents between the oxidation products $(Ca^{2+}+Si^{IV})$ and the reduction products (Pb^0+H_2) was examined with 10.0-, 20.0-, and 30.0-matom dm^{-3} Pb^{2+} solutions, all with an initial pH of 4.0. The standard electrode potential for the reduction of Pb^{2+} ion to Pb^0 is not very high: $E^0=-0.126$ V.[6] The reaction proceeded slowly, and only 61, 52, and 44% of the Pb^{2+} ions were reduced in 60 min in the 10.0-, 20.0-, and 30.0-matom dm^{-3} solutions, respectively. All the Pb^{2+} ions was not reduced even in 3 h. However, separate experiments showed that all the Pb^{2+} ions was reduced at Pb^{2+} concentrations lower than *ca.* 1 matom dm^{-3} in 1 h. The pH decreased to *ca.* 3.6, 3.0, and 2.7 after 60 min in the 10.0-, 20.0-, and 30.0-matom dm^{-3} solutions, respectively, because of the formation of H^+ ion in the reduction of Pb^{2+} ion by Si. Equivalents of the reaction products in a 60-min reaction period for each sample solution are collectively illustrated in Fig. 1.

The total-oxidation equivalents $(Ca^{2+}+Si^{IV})$ showed good agreement with the total-reduction equivalents (Pb^0+H_2) through the 60-min reaction period in each solution. This fact indicates that the above elementary reactions 1—4, just as in the reduction of Cu^{2+} ion, are also valid for the reduction of Pb^{2+} ions. Consequently, the estimation of the equivalents of Si^{IV} oxidized is also appropriate.

In each solution, the equivalents of Ca oxidized showed a small increase in the vicinity of 60 min. On the other hand, that of Si showed a tendency to increase. This seemed related to the relative amounts

of Ca and Si remaining unreacted. The equivalents of Ca oxidized were greater than those of Si, indicating the greater contribution of Ca to the reaction. It was more significant at higher Pb^{2+} concentrations. The proportion of the equivalents of H_2 to the total-reduction values became smaller at higher Pb^{2+} concentrations. Thus, the alloy acted more effectively on the reduction of Pb^{2+} ion.

Reduction of Ni^{2+} Ion. The results regarding a 5.0-matom dm^{-3} Ni^{2+} solution are shown in Fig. 2. The initial pH was adjusted at *ca.* 6 since, at pH's lower than *ca.* 5, Ni^0 forming in the reaction readily dissolves and does not deposit in the solid phase. The reaction rate was very small since the reaction was carried out at pH's around neutrality and since, in addition, the standard electrode potential for the reduction of Ni^{2+} to Ni^0 is very low: $E^0=-0.250$ V.[6] About 17% of the Ni^{2+} ions were reduced in *ca.* 1 h; thereafter, the reaction became inappreciable. The pH rose to 7.2 after 5 min, but thereafter tended to decrease slowly, indicating the reduction of Ni^{2+} ion by Si. A satisfactory equivalence was established between the total equivalents of the reduction products and those of the oxidation products. Therefore, the redution of Ni^{2+} ion with a low standard-electrode potential can also be interpreted by the same elementary reactions as those for Cu^{2+} and Pb^{2+} ions. The reaction under neutral conditions (pH 6—7) is one of the causes of the slight extent of water decomposition. The equivalents of Ca oxidized were about twice those of Si, indicating that Ca contributes more greatly to the overall reaction, such as in the case of the Pb^{2+}-ion reduction.

Reduction of Fe^{3+} Ion. Fe^{3+} ion can readily be hydrolyzed and so become little subject to reduction by the alloy. The initial pH of the sample solution was adjusted at 2.0 to prevent the hydrolysis. It proved improper to use Fe^{3+} solutions of concentrations lower than *ca.* 10 matom dm^{-3} under such strongly acidic conditions, since the decomposition of water was dominant over the metal-ion reduction. Then a stoichiometric discussion was made of a 20-matom dm^{-3} Fe^{3+} solution where the reduction of Fe^{3+} ion was predominant. The results are shown

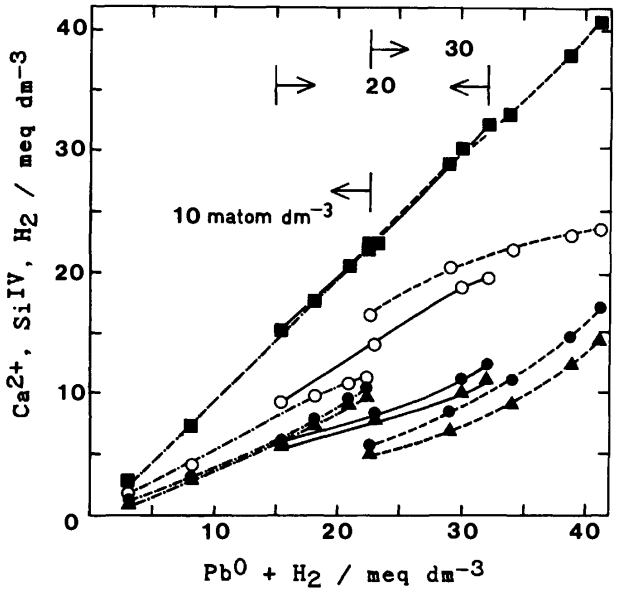

Fig. 1. Relation between equivalents of reduction products (Pb^0 and H_2) and oxidation products (Ca^{2+} and Si^{IV}).
○: Ca^{2+}, ●: Si^{IV}, ■: $Ca^{2+}+Si^{IV}$, ▲: H_2.

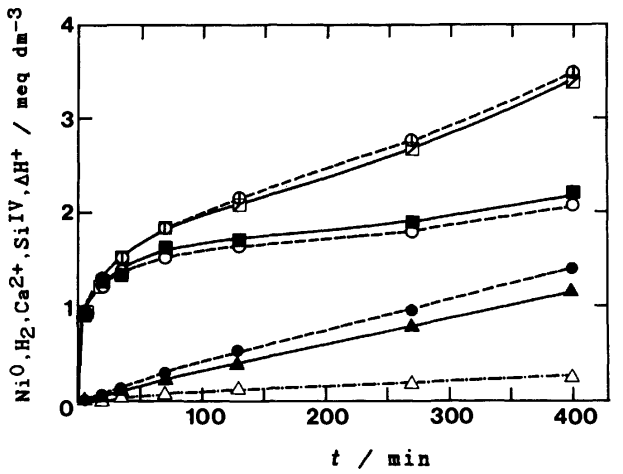

Fig. 2. Behavior of the reaction products in the reduction of 5.0-matom dm^{-3} Ni^{2+} solution and the relation between equivalents of reduction products and oxidation products.
■: Ni^0, ▲: H_2, ○: Ca^{2+}, ●: Si^{IV}, △: ΔH^+, ⊠: Ni^0+H_2, ⊕: $Ca^{2+}+Si^{IV}$.

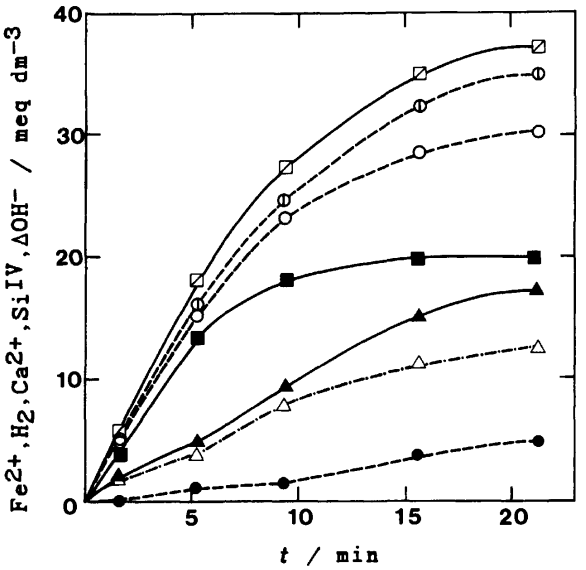

Fig. 3. Behavior of the reaction products in the reduction of 20.0-matom dm^{-3} Fe^{3+} solution and the relation between equivalents of reduction products and oxidation products.
■: Fe^{2+}, ▲: H_2, ○: Ca^{2+}, ●: Si^{IV}, △: ΔOH^-, ⊠: $Fe^{2+}+H_2$, ⊕: $Ca^{2+}+Si^{IV}$.

in Fig. 3. The standard electrode potential for the reduction of Fe^{3+} ion to Fe^{2+} ion is very high: E^0=0.771 V.[6] Fe^{3+} ion was entirely reduced in 15 min. Equivalence was not established between the total-oxidation equivalents and the total-reduction equivalents, the former being *ca.* 0.8—0.9 times the latter. Such a disagreement in equivalent has also been observed in the reduction of Cu^{2+} ion at an initial pH of 2.0, though the runs at an initial pH of 4.0 show complete agreement. This disagreement can principally be attributed to the existence of elementary reactions other than 1′, 2′, 3, and 4, for example, the formation of insoluble Ca^{II} species in the solid phase under such strongly acidic conditions.

The equivalents of Ca oxidized were much greater than those of Si. No decrease in pH at all was observed in the Fe^{3+} reduction, but a pH decrease was noticed in the Cu^{2+} run, even at an initial pH of 2.0. These facts indicate that Fe^{3+} ion is reduced mainly by Ca and that Si is consumed in the decomposition of water. It is a remarkable feature of the Fe^{3+} reduction that Si scarcely participates in the reduction reaction of a high standard-electrode potential. The cause of this has not yet been ascertained.

Reduction of Hg^{2+} Ion. Hg^{2+} ion is reduced by the alloy to form Hg^0 and Hg^I species (Hg_2Cl_2 in the present case, where chloride ion solely exists as an anion) simultaneously in the solid phase. Because of the difficulty of the separate determination of the two solid mercury species, different in the oxidation state, no detailed stoichiometric discussions have been made.[7] The above results in the present study indicate that the elementary reactions 1—4, 1′, and 2′ can also be applied as the reaction mechanism to the reduction of Hg^{2+} ion in weakly acidic solutions.

Based on these elementary reactions, the following two equations hold in equivalent: $Hg^0+Hg^I+H_2=Ca^{2+}+Si^{IV}$ and $Si^{IV}=H_2+\Delta H^+$. The amounts of Hg^0 and Hg^I can be estimated as follows:
Let x and y be the numbers of Hg^0 and Hg^I atoms formed, respectively, and let a and b be those of the removed Hg^{2+} and the total equivalent of the reduced Hg^{2+}, respectively. Then we obtain:

$$a = x + y \quad \text{and}$$
$$b = 2x + y.$$

By solving these equations, we get:

$$x = b - a \quad \text{and}$$
$$y = 2a - b.$$

In this way, the behavior of the reaction products in a 20-matom dm^{-3} Hg^{2+} solution with an initial pH of 4.0 was discussed. The results are shown in Fig. 4. Almost all the Hg^{2+} ions were removed in *ca.* 5 min. At that time, nearly equal equivalents of Hg^0 and Hg_2Cl_2 were formed in the solid phase,

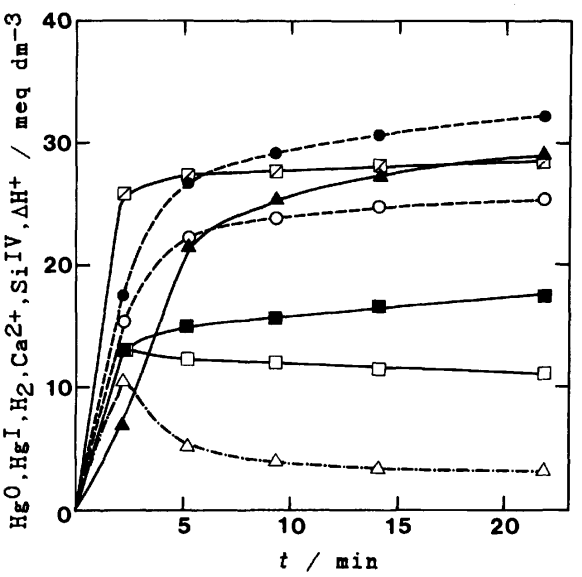

Fig. 4. Behavior of the reaction products in the reduction of 20.0-matom dm^{-3} Hg^{2+} solution.
▨: Hg^0+Hg^I, ■: Hg^0, □: Hg^I, ▲: H_2, ○: Ca^{2+}, ●: Si^{IV}, △: ΔH^+.

indicating that only one-third the initial amounts of Hg^{2+} ions were reduced to Hg^0, since the equivalent of Hg^0 is twice that of Hg^I. The standard electrode potentials for the reduction of Hg^{2+} to Hg^I and that of Hg^I to Hg^0 are 0.920 and 0.788 V, respectively.[8] These values are much higher than that of Cu^{2+} ion (E^0=0.337 V), which proceeds very efficiently to form the metallic species. In this system, the presence of Cl^- ion resulted in the formation of very stable Hg_2Cl_2, which made the reduction of Hg^{2+} ion incomplete. From *ca.* 5 min, Hg_2Cl_2 tended to decrease, while, in turn, Hg^0 increased. The rate of the reduction was small because of the very low solubility of Hg_2Cl_2. The covering of the alloy particles by the reaction products was not significant, just as in the other metal-ion runs.

The equivalents of Si oxidized were greater than those of Ca, indicating the greater contribution of Si to the overall reaction, such as in the case of the Cu^{2+} reduction. At the initial stage of the reaction, the pH decreased to *ca.* 2 because of the formation of H^+ ion in the reduction of Hg^{2+} ion by Si. In Hg^{2+} solutions of 5 matom dm^{-3} or lower, the equivalents of Si oxidized were smaller than those of Ca. The decomposition of water occurred subsequently to the Hg^{2+} reduction and exceeded the latter after *ca.* 20 min. After the greater part of the Hg^{2+} ions had been removed, the values of ΔH^+ decreased because of the formation of OH^- ion in the decomposition of water by Ca.

Regarding the contribution of Ca and Si in the alloy to the reaction, the following conclusions can generally be reached. The reduction of metal ions with low standard-electrode potentials, such as those

of Ni^{2+} and Pb^{2+} ions, proceeds mainly by Ca. Ca in the alloy seems to have a still lower electrode potential than Si. In the reduction of high electrode potentials, such as those of Cu^{2+} and Hg^{2+} ions, the reduction of metal ions by Si becomes significant, as does that by Ca. The oxidation rates of Ca and Si increase as the electrode potential of the reduction of a metal ion and the metal-ion concentration increase. At the beginning of the reaction, the oxidation rate of Ca seems greater than that of Si because of its higher electrode potential. However, the oxidation rate of Ca tends to decrease greatly when the reaction has proceeded to some extent and, consequently, the amount of unreacted Ca has become relatively small. On the other hand, the oxidation rate of Si does not decrease so much because of its large equivalent, twice that of Ca, and its large content in the alloy.

References

1) J. P. McKaveney, W. P. Fassinger, and D. A. Stivers, *Environ. Sci. Technol.*, **6**, 1109 (1972).
2) O. P. Case, PB Report 233 143, U. S. Department of Commerce, Springfield Va., Jan. 1974.
3) S. Tokunaga, K. Uematsu, and Y. Nagawa, *Bull. Chem. Soc. Jpn.*, **54**, 733 (1981).
4) S. Tokunaga, *Bull. Chem. Soc. Jpn.*, **55**, 95 (1982).
5) S. Tokunaga, *Bull. Chem. Soc. Jpn.*, **57**, 2832 (1984).
6) "Kagaku Binran Kiso-hen II," Maruzen, Tokyo (1977), pp. 1204—1205.
7) S. Tokunaga and K. Uematsu, *Nippon Kagaku Kaishi*, **1978**, 619.

Chromatographic Study of Optical Resolution. XII. Optical Resolution of Bis(oxalato)(1,10-phenanthroline)cobaltate(III) and Its Related Anion Complexes with Cinchona Alkaloid Cations as Eluent

Katsuhiko MIYOSHI, Masahiko NATSUBORI, Naoko DOHMOTO, Shinji IZUMOTO, and Hayami YONEDA*

Department of Chemistry, Faculty of Science, Hiroshima University, Higashi-senda-machi, Naka-ku, Hiroshima 730

(Received November 29, 1984)

Ion-exchange chromatography was applied to the optical resolution of three anion complexes, $[Co(ox)_2(phen)]^-$, $[Co(ox)_2(bpy)]^-$, and $[Co(ox)_2(en)]^-$ (ox=oxalate anion, phen=1,10-phenanthroline, bpy=2,2′-bipyridine, and en=ethylenediamine) using as a chiral eluent aqueous solutions of various cinchona alkaloid cations, *i.e.*, cinchoninium, cinchonidinium, quinidinium, and quininium ions, and their 9-acetoxy and N^1-methyl derivatives. Fairly good resolution was achieved for the first two complexes with the 9-acetoxy derivatives as eluent, but no practical resolution was attained for $[Co(ox)_2(en)]^-$. Retention volumes V_R determined and separation factors α estimated from V_R revealed that both of the HO-C(9) and H-N(1)$^+$ groups of each alkaloid participate in the interaction with the complex, and that the α value is increased upon acetylation of the OH group with the elution order reversed. These observations were interpreted in terms of two concomitant interaction modes in which the HO-C(9) and H-N(1)$^+$ groups are hydrogen-bonded to the ox ligand(s) and the quinoline ring is stacked with the phen or bpy ligand of the anion complex.

Many examples of successful optical resolution by chromatography have been reported for cationic metal complexes, and the mechanism by which chiral discrimination is effected there have been discussed in detail.[1,2] On the other hand, only few anionic metal complexes have been subjected to chromatographic resolution simply because suitable cationic resolving agents are not available. Cinchona alkaloids, *i.e.*, (8*R*,9*S*)-cinchonine, (8*S*,9*R*)-cinchonidine, (8*R*,9*S*)-quinidine, and (8*S*,9*R*)-quinine, have long been used as resolving agents in optical resolution of several anionic complexes *via* diastereomer formation. Thus, these chiral alkaloid cations may potentially serve as eluent in chromatographic resolution of anionic complexes. In fact, Yamazaki[3] succeeded in complete resolution of $[Co(edta)]^-$ and *cis*-$[Co(ida)_2]^-$ (edta and ida=ethylenediaminetetraacetate and iminodiacetate anions, respectively) using quininium ion as an ion-pairing reagent in reversed-phase chromatography, and Izumoto *et al.*[4] extended this technique to the optical resolution of several anion complexes of the type *cis*-$[Co(O)_4(N)_2]^-$. However, these anion complexes are not easily resolved by normal-phase ion-exchange chromatography even with cinchona alkaloid cations used as eluent. This is probably because these alkaloids exhibit no strong tendency to associate with common anionic complexes unless they are introduced into some special environment, *e.g.*, hydrophobic environment as in reversed-phase chromatography.

In our previous paper,[5] it was reported that monoprotonated species of cinchona alkaloids bear a strong ability to displace the chiral equilibrium between two enantiomers of a labile metal complex, $[Cr(ox)_2(phen)]^-$ (ox=oxalate anion and phen=1,10-phenanthroline) in aqueous solution. This observation suggests that cinchona alkaloid cations associate appreciably with $[Cr(ox)_2(phen)]^-$ and impose their spacial demands on the two enantiomers differently. Therefore, the corresponding inert cobalt(III) complex is expected to be resolved by usual ion-exchange chromatography if these alkaloids are used as eluent. With this expectation in mind, an attempt was made to resolve the three anion complexes, $[Co(ox)_2(phen)]^-$, $[Co(ox)_2(bpy)]^-$, and $[Co(ox)_2(en)]^-$, (bpy=bipyridine and en=ethylenediamine) with various cinchona alkaloid cations employed as a chiral eluent, and their stereoselective interactions are discussed in detail.

Experimental

Materials. $Na[Co(ox)_2(en)]\cdot H_2O$[6] and $K[Co(ox)_2(bpy)]\cdot 3H_2O$[7] were prepared as described in the literature. $K[Co(ox)_2(phen)]\cdot 4H_2O$ was derived from $[Co(ox)(phen)_2]\cdot[Co(ox)_2(phen)]\cdot 3H_2O$[7] at room temperature according to the procedures applied to the corresponding bpy complex.[7,8] Absolute configurations of these complexes were assigned previously. 9-Acetoxy and N^1-methyl derivatives of various cinchona alkaloids used as eluent were obtained as monohydrochlorides and monochlorides, respectively, according to the procedures presented earlier.[4,8] They were found to be satisfactorily pure by elemental analysis. Unmodified cinchona alkaloids commercially available were also converted to monohydrochlorides to prepare their aqueous solutions. The anion-exchange resin used was IEX-520 QAE-SIL (Toyo Soda Manufacturing Co. Ltd.), which carries quaternary ammonium groups covalently bonded to the surface of silica gel.

Chromatography. Columns (4×150 mm) were packed with IEX-520 QAE-SIL and each was equilibrated with an aqueous eluent containing one of various cinchona alkaloids as monohydrochloride or monochloride salt at a concentration of 0.01 mol/dm^3. Each eluent with pH adjusted to 4.0 with acetic acid, was degassed by an

aspirator before use. An aqueous solution (20 μl) of a racemic complex (0.1 mol/dm³) containing bis(ethylenediamine)copper(II) chloride (0.05 mol/dm³) as a marker for void volume measurement, was injected by a syringe on the top of the column and was eluted at an elution rate of 1.0 cm³/min. The eluate was guided to a flow cell to detect the complex at 535 nm with a Shimadzu UV-140 spectrophotometer. The adjusted retention volumes V_R of both enantiomers were estimated from the elution curves thus recorded and were found to be reproducible to within at least ±0.2 cm³ for $[Co(ox)_2(phen)]^-$ and $[Co(ox)_2(bpy)]^-$ and ±0.1 cm³ for $[Co(ox)_2(en)]^-$. The elution order was determined by the CD spectra of fractionally collected eluates. Each complex was also eluted with an aqueous NaCl solution (0.01 mol/dm³) to estimate its intrinsic affinity for the resin. The chromatographic apparatus used in this study was the same as in our previous works[9] except that a Jasco BIP-1 pump for HPLC was newly employed. The CD spectra were recorded on a Jasco J-40CS spectropolarimeter at ambient temperature.

Results and Discussion

Elution Curves. Figure 1 shows the structures of the cinchona alkaloids used as eluents in the present study. In addition to these naturally occurring alkaloids, their 9-acetoxy (9-AcO) and N^1-methyl (N^1-Me) derivatives were used. The three racemic complexes $[Co(ox)_2(phen)]^-$, $[Co(ox)_2(bpy)]^-$, and $[Co(ox)_2(en)]^-$ were at first eluted with a neutral eluent in which each alkaloid exists predominantly as a monoprotonated species. The adjusted retention volumes V_R, however, showed no satisfactory reproducibility. This implies that protonation and deprotonation take place on the N(1) and N(1′) atoms of the alkaloid as well as on the incompletely alkylated amine groups present in the resin. On the other hand, the separation factor α, the ratio of V_R for the late-eluted enantiomer to V_R for the other, was found to be higher than that obtained with a slightly acidified eluent (pH=4.0 with acetic acid) used in the later runs. For example, α values of 1.10 and 1.05 were derived for the phen and bpy complexes, respectively, with a neutral (8*S*,9*R*)-9-acetoxycinchonidinium (9-AcO-CD) chloride solution, whereas 1.08 and 1.03 were obtained respectively with an acidified 9-AcO-CD chloride solution. The present study was undertaken to elucidate the mechanisms of chromatographic resolution of the anion complexes rather than to search for the optimum conditions for the resolution. Accordingly, acidified eluents were used throughout the following chromatographic runs at the expense of discrimination efficiency. Under these conditions, each alkaloid exists predominantly as a diprotonated species, and protonation is complete on the incompletely alkylated amine groups partly present in the resin.

In Figs. 2 and 3 are shown typical elution curves of the three anion complexes recorded with (8*R*,9*S*)-quinidinium (QD) chloride and (8*R*,9*S*)-9-acetoxyquinidinium (9-AcO-QD) chloride as eluent, respectively. Fairly good resolution is achieved for $[Co(ox)_2(phen)]^-$ with QD (separation factor α=1.09) and for $[Co(ox)_2(bpy)]^-$ and $[Co(ox)_2(phen)]^-$ with 9-AcO-QD (α=1.10 and 1.16, respectively), but no practical resolution is accomplished for $[Co(ox)_2$-

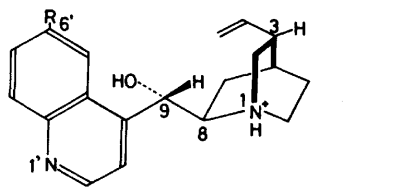

R=H
(8R,9S)-Cinchoninium(CN)
(8S,9R)-Cinchonidinium(CD)
R=MeO
(8R,9S)-Quinidinium(QD)
(8S,9R)-Quininium(QN)

Fig. 1. Structures of cinchona alkaloids used as an eluent.

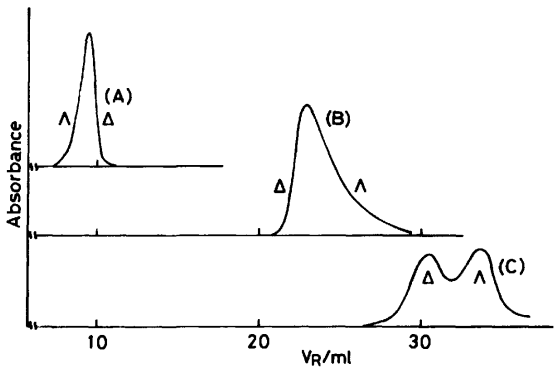

Fig. 2. Elution curves of $[Co(ox)_2(en)]^-$ (A), $[Co(ox)_2(bpy)]^-$ (B), and $[Co(ox)_2(phen)]^-$ (C) obtained with (8*R*,9*S*)-quinidinium (QD) chloride as an eluent.

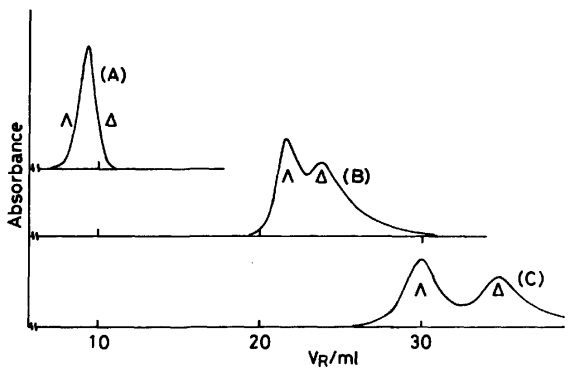

Fig. 3. Elution curves of $[Co(ox)_2(en)]^-$ (A), $[Co(ox)_2(bpy)]^-$ (B), and $[Co(ox)_2(phen)]^-$ (C) obtained with (8*R*,9*S*)-9-acetoxyquinidinium (9-AcO-QD) chloride as an eluent.

(en)]$^-$ with any of the two eluents, as seen in Figs. 2 and 3. It is also notable that the elution order is reversed for the phen and bpy complexes when the HO-C(9) group of QD is acetylated. The reversal in the elution order is also observed for the two complexes with other alkaloids, as seen later (Table 1).

Retention Volumes V_R *and Separation Factors* α. In Table 1 are summarized the fast-eluted enantiomers (Λ or Δ), average retention volumes V_R, and separation factors α obtained for the three complexes with various cinchona alkaloid cations as eluents. Several important observations are noted here. (1) Better resolution is attained for the phen complex with a particular eluent than for the bpy complex, while no practical resolution is possible for $[Co(ox)_2(en)]^-$ with any of the eluents examined. (2) Except for $[Co(ox)_2(en)]^-$, the Δ enantiomer is generally eluted faster with the unmodified and N^1-methylated alkaloids having an (8*R*,9*S*) configuration, and the Λ enantiomer is eluted faster with those having an (8*S*,9*R*) configuration. The elution order is completely reversed upon acetylation of the HO-C(9) group on each alkaloid. (3) The elution ability of each alkaloid is diminished upon acetylation of the HO-C(9) group and N^1-methylation for all three complexes, while the former modification leads not only to the reversal in the elution order but also to the increased separation factor α for the phen and bpy complexes. (4) The alkaloids with an (8*R*,9*S*) configuration bear a stronger elution ability for each complex than those with an (8*S*,9*R*) configuration. (5) For the unmodified and N^1-methylated alkaloids, the (8*S*,9*R*) isomers afford higher α values than the (8*R*,9*S*) isomers, whereas higher α values are obtained with the (8*R*,9*S*) isomers for the 9-AcO derivatives. It is not obvious from the data in Table 1 whether α values of the en complex also depend on the configurations of the C(8) and C(9) atoms of the eluent alkaloids. (6) The alkaloids carrying a methoxy (MeO) group at the 6′ position on the quinoline ring, *i.e.*, quinidine (QD) and quinine (QN) and their derivatives afford lower V_R values for each complex, *i.e.*, they bear a greater elution ability for it, than cinchonine (CN) and cinchonidine (CD) and their derivatives, respectively. This does not hold for the en complex.

The first observation suggests that the aromatic phen or bpy ligand plays an essential role in the interaction with the eluent cation. In fact, the pmr measurements reported previously[8] indicate that the quinoline ring of QN or 9-AcO-QN is stacked with the phen ligand of $[Co(ox)_2(phen)]^-$ in D_2O. Since the stacking is expected to be more extensive with the phen ligand, observation (1) is consistent with the pmr measurements. If the MeO group on the quinoline ring works to strengthen the stacking between the two aromatic rings, for example by its π electron-releasing effect,[10] observation (6) also supports the view that the stacking leads to an appreciable association between the eluent cation and the phen or bpy complex in water. For the en complex, no such stacking is possible, so that no practical resolution is achieved with any of the cinchona alkaloids and the presence of the MeO group should have no effect on the elution ability of any alkaloid for this complex, as is actually the case.

Observation (3) is interpreted to mean that both of

Table 1. Fast-eluted enantiomers, averaged retention volumes V_R, and separation factors α

Eluent (chloride salt)	$[Co(ox)_2(phen)]^-$			$[Co(ox)_2(bpy)]^-$			$[Co(ox)_2(en)]^-$		
		V_R/ml	α		V_R/ml	α		V_R/ml	α
(8*R*, 9*S*)-CN	Δ	40.3[a]	—[c]	Λ[e]	23.5	—[c]	Λ	9.5	—[c]
(8*S*, 9*R*)-CD	Λ	40.1	1.05	Λ	24.6	—	Δ	9.6	—
(8*R*, 9*S*)-QD	Δ	32.0	1.09	Δ	22.8	—	Λ	9.4	—
(8*S*, 9*R*)-QN	Λ	36.2	1.11	Λ	23.4	—	Δ	9.6	—
(8*R*, 9*S*)-N^1-Me-CN	Λ[e]	41.4[b]	—[c]	Λ[e]	25.1	—[c]	—[d]	10.1	1.00
(8*S*, 9*R*)-N^1-Me-CD	Λ	45.3	1.03	Λ	26.1	—	—	10.4	1.00
(8R, 9*S*)-N^1-Me-QD	Δ	36.2	1.07	Δ	23.9	—	—	9.4	1.00
(8*S*, 9*R*)-N^1-Me-QN	Λ	40.8	1.10	Λ	25.3	—	—	10.6	1.00
(8*R*, 9*S*)-9-AcO-CN	Λ	41.1	1.11	Λ	26.1	1.04	Λ	10.6	—[c]
(8*S*, 9*R*)-9-AcO-CD	Δ	44.6	1.08	Δ	27.8	1.03	Δ	11.2	—
(8*R*, 9*S*)-9-AcO-QD	Λ	32.3	1.16	Λ	22.8	1.10	Λ	9.3	—
(8*S*, 9*R*)-9-AcO-QN	Δ	38.4	1.14	Δ	25.7	1.06	Δ	10.4	—
(8*R*, 9*S*)-9-AcO-N^1-Me-CN	Λ	42.4	1.13	Λ	26.6	1.07	—[d]	10.8	1.00
(8*S*, 9*R*)-9-AcO-N^1-Me-QN	Δ	45.8	1.18	Δ	30.3	1.08	—	12.5	1.00
NaCl	—[d]	90.6	1.00	—[d]	46.3	1.00	—[d]	16.8	1.00

a) V_R for the late-eluted enantiomer. b) V_R for the fast-eluted enantiomer. c) Partial resolution. d) No practical resolution. e) Type 2 mode predominates over the type 1 mode (see the text).

the HO-C(9) and H-N(1)$^+$ groups of each alkaloid participate in the interaction with the anion complexes. These acidic groups are likely to form hydrogen bonds to the basic ox ligand(s) of the complex. Then, acetylation and N^1-methylation of each alkaloid naturally prohibit these hydrogen-bonding interaction, its elution ability being thereby lowered. It is also probable from observation (3) that acetylation of each alkaloid leads to a drastic change in the interaction mode with the phen and bpy complexes. On the other hand, N^1-methylation leads only to diminished elution ability of each alkaloid for the respective complexes. The elution ability is similarly lowered for the 9-AcO derivatives upon N^1-methylation with the elution order unaltered.

Observation (4) implies that each complex interacts with the eluents by responding differently to their (8*R*,9*S*) and (8*S*,9*R*) isomers. Since these isomers are not enantiomeric owing to the presence of other two asymmetric carbon atoms (3*R*,4*S*) in common, the vinyl group at the C(3) atom must have some influence on the interaction with the complex.

Association Models. All the implications drawn from the experimental data given in Table 1 are interpreted reasonably within the framework of the association models advanced previously to account for the stereochemical aspects of the Pfeiffer effect of [Cr(ox)$_2$(phen)]$^-$.[8] The model called the type 1 is reproduced in Figs. 4 and 5 for the phen complex with (8*S*,9*R*)-QN and (8*R*,9*S*)-QD, respectively. In this model, two interaction modes are involved; the stacking between the phen and quinoline rings, and the hydrogen bonds of the H-N(1)$^+$ and HO-C(9) groups to the ox ligand(s). The simultaneous hydrogen bonds of the two groups to the complex are possible only when the complex approaches the alkaloid from above, as seen in Figs. 4 and 5. That is, type 1 model is valid only for the alkaloids having the OH group available for the hydrogen-bonding interaction.

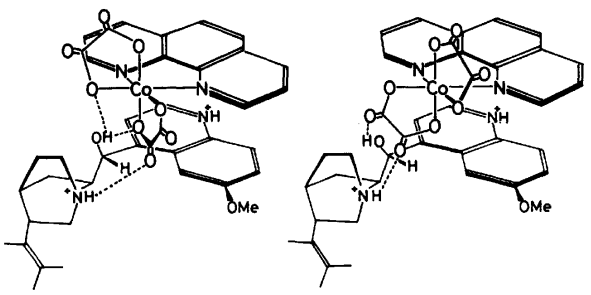

Fig. 4. Type 1 association models for (8*S*,9*R*)-quininium (QN) ion with *Λ*-[Co(ox)$_2$(phen)]$^-$ (left) and with *Δ*-[Co(ox)$_2$(phen)]$^-$ (right).

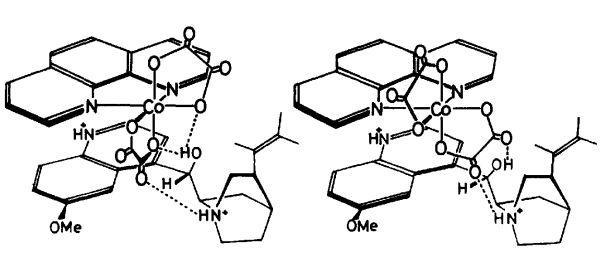

Fig. 5. Type 1 association models for (8*R*,9*S*)-quinidinium (QD) ion with *Δ*-[Co(ox)$_2$(phen)]$^-$ (left) and with *Λ*-[Co(ox)$_2$(phen)]$^-$ (right).

When the complex has a *Λ* configuration, the HO-C(9) group of (8*S*,9*R*)-QN can be nicely located to form hydrogen bonds to both ox ligands, and the H-N(1)$^+$ group is also hydrogen-bonded to the carbonyl group on one of the ox ligands (left model in Fig. 4). On the other hand, when the complex has a *Δ* configuration, only one ox ligand can participate in the hydrogen-bonding interaction with (8*S*,9*R*)-QN (right model in Fig. 4). In this way, chiral discrimination between the two enantiomers is effected for [Co(ox)$_2$(phen)]$^-$, and [Co(ox)$_2$(bpy)]$^-$ is similarly discriminated, though to a lesser extent owing to the reduced aromaticity of the ligand.

With (8*R*,9*S*)-QD, the *Δ* complex can interact more favorably, as seen in Fig. 5, in keeping with the elution orders listed in Table 1. When a comparison is made between (8*S*,9*R*)-QN and (8*R*,9*S*)-QD with respect to type 1 interaction, they behave evidently in an enantiomeric fashion; no definite difference is discernible between them. Then, it follows that the dependence of V_R and α on the configurations around the C(8) and C(9) atoms is not accounted for by the type 1 model alone. Further discussions are needed to interpret observations (4) and (5) reasonably (see later).

If the H-N(1)$^+$ group of each alkaloid is methylated, it ceases to hydrogen bond to the C=O group on the ox ligand. Then, it is natural for the elution ability to be lowered upon N^1-methylation in the type 1 model. Since the elution ability is similarly lowered for the en complex, the hydrogen-bonding interaction of the H-N(1)$^+$ group certainly prevails also for the en complex.

The chromatographic behavior exhibited by the 9-AcO derivatives is now examined in detail. It is evident that the 9-AcO-derivatives cannot adopt the type 1 mode in which the hydrogen-bonding interaction of the HO-C(9) group is indispensable. Then, an alternative association model (called type 2) is proposed in which the complex approaches the alkaloid from below to gain the stacking between the phen and quinoline rings as before (Figs. 6 and 7). In this model, the AcO group is not involved in the interaction with the complex, but it blocks access of the complex from above. Hence, the *Δ* complex can associate more favorably through dual hydrogen bonds with (8*S*,9*R*)-9-AcO-QN (left model in Fig. 6), the parent alkaloid of which (*i.e.*, (8*S*,9*R*)-QN) favors

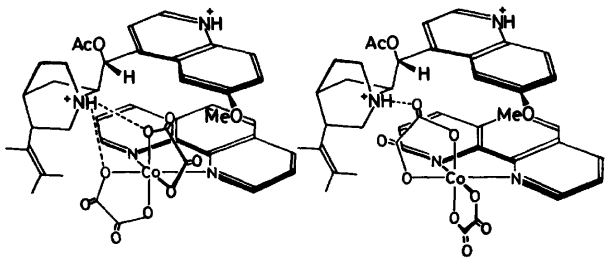

Fig. 6. Type 2 association models for (8*S*,9*R*)-9-acetoxyquininium (9-AcO-QN) ion with *Δ*-$[Co(ox)_2(phen)]^-$ (left) and with *Λ*-$[Co(ox)_2(phen)]^-$ (right).

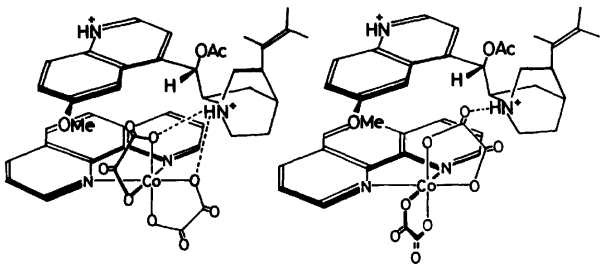

Fig. 7. Type 2 association models for (8*R*,9*S*)-9-acetoxyquinidinium (9-AcO-QD) ion with *Λ*-$[Co(ox)_2(phen)]^-$ (left) and with *Δ*-$[Co(ox)_2(phen)]^-$ (right).

the opposite enantiomer in the type 1 model (Fig. 4). By contrast, the *Λ* complex interacts with (8*S*,9*R*)-9-AcO-QN only through a single hydrogen bond (right model in Fig. 6). The reversal in the elution order upon acetylation is rationalized in this way. Furthermore, it is to be expected from a consideration of Figs. 6 and 7 that the elution ability of each alkaloid will be lowered upon acetylation, because only the H–N(1)$^+$ group is involved in the hydrogen bond to the complex in the type 2 mode, and that N^1-methylation of the 9-AcO derivatives will lead to their further diminished elution ability.

Figure 7 shows how (8*R*,9*S*)-9-AcO-QD interacts more favorably with the *Λ* complex than with the *Δ* complex *via* the type 2 mode, in accordance with the elution orders of the phen and bpy complexes. However, a close comparison between (8*R*,9*S*)-9-AcO-QD and (8*S*,9*R*)-9-AcO-QN with respect to the type 2 interaction reveals that steric hindrance is anticipated between the vinyl group at the C(3) atom and one ox ligand when the interacting alkaloid has an (8*S*,9*R*) configuration like QN and CD (Fig. 6). On the contrary, the vinyl group is far from any part of the complex when the alkaloid has an (8*R*,9*S*) configuration like QD and CN (Fig. 7). In other words, the type 2 model predicts that (8*R*,9*S*)-CN and (8*R*,9*S*)-QD associate with the complex more smoothly than (8*S*,9*R*)-CD and (8*S*,9*R*)-QN, respectively, in the type 2 mode. This prediction is fulfilled by the V_R and α values obtained with their 9-AcO derivatives which adopt the type 2 mode exclusively; (8*R*,9*S*)-9-AcO-CN and (8*R*,9*S*)-9-AcO-QD afford smaller V_R values and higher α values than (8*S*,9*R*)-9-AcO-CD and (8*S*,9*R*)-9-AcO-QN, respectively, for both phen and bpy complexes.

It is easily accepted that the unmodified and N^1-methylated alkaloids having the HO–C(9) group can also adopt the type 2 mode in which the OH group is not involved. Then, it follows that the (8*R*,9*S*)-alkaloids, for example, favor the *Δ* complex in the type 1 mode, but they favor the *Λ* complex in the type 2 mode. The overall elution order is of course governed by the type 1 mode, since the type 1 mode predominates over the type 2 mode (with three exceptions, see below.) owing to the presence of the hydrogen-bonding interaction of the HO–C(9) group in the former mode. Then, lower α values are naturally obtained with the unmodified and N^1-methylated alkaloids which adopt the two modes simultaneously than with their 9-AcO derivatives which are forced to adopt the type 2 mode only. Furthermore, the unmodified and N^1-methylated alkaloids with an (8*R*,9*S*) configuration should exhibit much lower α values and stronger elution ability, since they interact with the complex more intimately in the type 2 mode than do those with an (8*S*,9*R*) configuration. In this way, the dependence of V_R and α values on the configurations around the C(8) and C(9) atoms is explained for these unmodified and N^1-methylated alkaloids in terms of the two concomitant interaction modes (type 1 and type 2) which favor opposite enantiomers of each complex with a particular alkaloid.

It is evident from Table 1 that (8*R*,9*S*)-CN and (8*R*,9*S*)-N^1-Me-CN afford very low α values, as expected, while α values obtained with (8*R*,9*S*)-QD and (8*R*,9*S*)-N^1-Me-QD carrying a MeO group are not so low as compared with those obtained with (8*S*,9*R*)-QN and (8*S*,9*R*)-N^1-Me-QN. This suggests that the MeO group works to strengthen the stacking in the type 1 mode to a greater extent than in the type 2 mode. In fact, if the (8*R*,9*S*)-alkaloids having no MeO group like CN and N^1-Me-CN are used as eluent, the resulting elution order is reverse to that predicted by the type 1 model. Thus, it is fairly likely that the type 2 mode predominates over the type 1 mode for these alkaloids. In this way, the three exceptional elution orders are rationalized. The above discussions lead us to conclude that the 9-AcO derivatives, particularly those with an (8*R*,9*S*) configuration, are effective as eluents in the chromatographic resolution of $[Co(ox)_2(phen)]^-$ and $[Co(ox)_2(bpy)]^-$, since these eluents adopt the type 2 mode exclusively and interact with the complex smoothly in the type 2 mode. N^1-Methylation of these 9-AcO derivatives tends to give rise to further improved discrimination efficiency.

Resolution of $[Co(ox)_2(en)]^-$. The above discussions apply to the phen and bpy complexes only. For the en complex, no practical resolution is achieved by usual ion-exchange chromatography with any alkaloids as eluent probably owing to the absence of the stacking interaction mentioned earlier. Izumoto *et al.*,[4] on the other hand, resolved this complex successfully by reversed-phase chromatography using (8*S*,9*R*)-QN as an ion-pairing reagent (α=1.14 at pH=4.9), and they proposed a mode of chiral discrimination in which the hydrogen bond of the H-N(1)$^+$ group to the ox ligands served as a dominant interaction, but the HO-C(9) group was not involved at all. The discrimination mechanism they proposed, however, fails to accommodate our present experimental results that V_R of the en complex also depends on the configurations around the C(8) and C(9) atoms of the eluent alkaloid and it is increased upon acetylation. As judged from the elution orders of the en complex obtained in the present study, this complex is likely to interact with each alkaloid dominantly *via* the type 2 mode. If the type 1 and 2 modes are compared from the electrostatic point of view, the negative charge on the ox ligands is more effectively neutralized in the latter mode by the positively charged H-N(1)$^+$ group. Since the en complex has no aromatic ligand leading to an appreciable association with the eluent alkaloid, electrostatic and hydrogen-bonding interactions are expected to serve as the main driving forces for the en complex to interact with the eluent. As a result, it is not unreasonable to suppose that the en complex adopts the type 2 mode predominantly in which the electrostatic interaction prevails to a greater extent than in the type 1 mode. Then, it is exactly what is predicted in the type 2 mode that the (8*R*,9*S*)-alkaloids elute this complex faster than the (8*S*,9*R*)-alkaloids. In addition, the elution order of the en complex is naturally unaltered upon acetylation. The contribution of the type 1 mode is, of course, not ruled out, since the lowered elution ability for this complex upon acetylation of each eluent could not otherwise be explained.

The present work was partially supported by a Grant-in-Aid for Scientific Research (No. 59540392) from the Ministry of Education, Science and Culture.

References

1) H. Yoneda, *J. Liq. Chromatogr.*, **2**, 1157 (1979); *J. Chromatogr.*, **313**, 59 (1984).
2) Y. Yoshikawa and K. Yamasaki, *Coord. Chem. Rev.*, **28**, 205 (1979).
3) S. Yamazaki, Ph. D. Thesis, Hiroshima Univ., 1982.
4) S. Izumoto, U. Sakaguchi, and H. Yoneda, *Bull. Chem. Soc. Jpn.*, **56**, 1646 (1983).
5) K. Miyoshi, Y. Matsumoto, and H. Yoneda, *Chem. Lett.*, **1980**, 1319.
6) F. P. Dwyer, I. K. Reid, and F. L. Garvan, *J. Am. Chem. Soc.*, **83**, 1285 (1961).
7) A. J. Broomhead, M. Dwyer, and N. Kane-Maguire, *Inorg. Chem.*, **7**, 1388 (1968).
8) K. Miyoshi, N. Dohmoto, and H. Yoneda, *Inorg. Chem.*, **24**, 210 (1985).
9) Part XI of this series, H. Yoneda, K. Nakatani, and S. Yamazaki, *J. Chromatogr.*, *319*, 35 (1985).
10) H. G. Brittain, *J. Chem. Soc., Dalton Trans.*, 2369 (1980).

Hexaamminecobalt(III)-Hydrogen Ion Exchange in α- and θ-Zirconium Phosphates with Various Particle-size Distribution[1)]

Yoshitsugu HASEGAWA* and Kunio FUJITA
Department of Industrial Chemistry, Faculty of Technology, Tokyo University of Agriculture and Technology, Nakamachi, Koganei, Tokyo 184
(Received December 17, 1984)

The hexaamminecobalt(III)-hydrogen ion exchange in zirconium phosphates was studied by means of the batch method, mainly with regard to the particle-size distribution of zirconium phosphates. α-Zirconium phosphates were prepared by the direct-precipitation method. The degree of ion exchange increased with the fineness of the zirconium phosphates used. The ion exchange proceeded to a lesser extent in highly crystalline α-zirconium phosphate. θ-Zirconium phosphate with the interlayer distance of 10.4 Å took up the complex cation selectively and easily. Fifty percent of the protons in the θ-zirconium phosphate were thus replaced with hexaamminecobalt(III), and the interlayer distance was expanded to 11.2 Å.

An inorganic ion exchanger, α-zirconium phosphate, $Zr(HPO_4)_2 \cdot H_2O$, has been investigated by many workers. Its crystal structure is known precisely, and the ion-exchange behavior toward many cations has been discussed with regard to the structure.[2,3)] α-Zirconium phosphate acts as an ion-sieve due to its structural restriction. However, α-zirconium phosphate can also be used as an ion-exchanger with large cations, such as cobaltcene, hexaamminecobalt(III), and tetraammineplatinum(II) ions, in spite of probable steric hindrance.[4—6)]

The ion-exchange properties of α-zirconium phosphate have been influenced by the method of preparation, since the method has much effect on the crystallinity and particle-size distribution.[7)] Although the effect of crystallinity has been studied extensively, that of particle size has been investigated only for the potassium-hydrogen ion exchange by means of α-zirconium phosphate, which has the same crystallinity.[8)]

α-Zirconium phosphate also has a possibility of use as a catalyst or catalytic support.[3)] When α-zirconium phosphate is applied to a catalytic support, a complex cation which has an ionic radius larger than 1.3 Å may be used. Hexaamminecobalt(III) was selected as a model of the complex cation, and the ion exchange was studied previously. In this case, not all the protons in α-zirconium phosphate involved in the ion exchange, and the unreacted α-zirconium phosphate coexisted with the hexaamminecobalt(III) form of α-zirconium phosphate.[5)] During the course of these experiments, our attention was called to a subtle difference in the ion-exchange behavior among α-zirconium phosphates toward the complex cation.

According to Haynes, Jr., the particle-size distribution should be considered in some cases in estimating catalytic effectiveness in a heterogeneous catalyst.[9)] Synthetic zeolite catalysts are typical examples of this case. Hence, it is of interest to study the hexaamminecobalt(III)-hydrogen ion exchange with regard to the particle-size distribution of α-zirconium phosphate.

Alberti *et al.* pointed out that a highly hydrated zirconium phosphate, for example, θ-zirconium phosphate, can easily exchange several cations with large ionic radii.[10)] However, their method of preparation was complex in procedure, and severe conditions were required for the starting material. Since Kijima recently reported a simple method of preparation,[11)] the same ion exchange has now been studied with θ-zirconium phosphate.

Experimental

Preparation of α- and θ-Zirconium Phosphates and Hexaamminecobalt(III) Trichloride. α-Zirconium phosphates were prepared by two direct-precipitation methods. One of the methods was previously reported, and Samples A and B were obtained.[12)] When Sample A was prepared, the zirconium dichloride oxide octahydrate used as a starting material was purified to remove the free hydrochloric acid; Sample B was prepared without the purification. The Inoue and Yamada method was modified to prepare Sample C.[13)] The following conditions were employed: $ZrOCl_2 \cdot 8H_2O$ 0.26 mol dm^{-3}, HF 1.7 mol dm^{-3}, H_3PO_4 6.2 mol dm^{-3}; reaction temperature, 50 °C, and reaction time, 120 h. Since large crystallites were obtained, the products were sieved and the fraction under 400-mesh was used. Sample D was prepared from the large crystallites obtained in the preparation of Sample C. They were ground and sieved under a 400 mesh.

θ-Zirconium phosphate, $Zr(HPO_4)_2 \cdot 6H_2O$, was prepared according to the literature.[11)] The exchanger thus obtained will herein be referred to as Sample E. Identification was made by means of X-ray diffractometry.

Hexaamminecobalt(III) trichloride, $[Co(NH_3)_6]Cl_3$, was prepared according to the literature.[14)]

Ion Exchange. The ion exchange was carried out by the batch method. In view of the rate of the reaction and the stability of hexaamminecobalt(III) ions in the solution, the experimental conditions were determined as follows; the concentration of the complex cation, 0.02 mol dm^{-3}, reaction temperature, 90 °C, and reaction time, 30 min. After the end of the reaction, the exchanger was separated by centrifugation. The

pH value of the supernatant was determined with a pH meter. The exchanger was again added to a new complex solution, and the ion exchange was carried out. This procedure was repeated until the pH value of the supernatant was over 5.

Particle-size Distribution and Structural Study. The particle-size distribution was measured with a Shimadzu centrifugal particle-size analyzer SA-CP2 for Samples A, B, and C and with a Seishin Kogyo microphotosizer SKA-5000 for Sample D. Distilled water or a sucrose solution was used as the dispersion medium.

The crystallite size of zirconium phosphates was estimated from the Scherrer equation: $D=K\lambda/\beta\cos\theta$, where K=constant(0.9), β=corrected breadth at half-height, λ=wave length(1.542 Å), and θ=Bragg angle.[15]

The change in the interlayer distance was observed by means of X-ray diffractometry. The powder patterns were recorded with a Rigaku Denki Geigerflex diffractometer, using Ni-filtered Cu $K\alpha$ radiation(λ=1.542 Å).

Results and Discussion

Particle-size Distribution. Since α-zirconium phosphate has a layered structure and has been obtained as thin hexagonal or triangular platelets,[2] the apparent Stokes radius should be considered as an approximate index. The particle-size distribution curves are shown in Fig.1. Sample A had the $D50$ of 3 μm, where $D50$ means 50% diameter(median size); most of the fraction of the particles was present under 2 μm. The $D50$ of Sample B was 2 μm, and 32% of the particles were present between 2—1 μm. The particles of Sample C were coarse. The $D50$ was equal to 30 μm, and 50% of the sample had a diameter of 20—30 μm. Two percent of the sample were present under 5 μm. Sample D was more coarse than Sample C and had a $D50$ of 50 μm. Both Samples C and D had much the same high crystallinity.

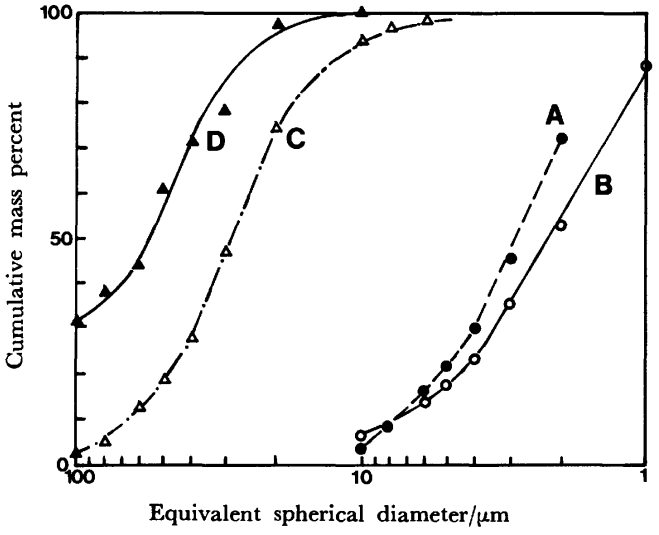

Fig. 1. Particle size distribution of Samples A,B,C, and D.

Since Sample E (θ-zirconium phosphate) was very fine, the crystallite size was measured by means of X-ray diffractometry. Sample E had an average thickness of 0.06 μm in the direction of (002). Another sample of α-zirconium phosphate (Sample F) was obtained by drying θ-zirconium phosphate in air at room temperature. The particle size of Sample F in the direction of (002) was almost equal to 0.04 μm. The estimated size is compatible with the predicted value of 0.043 μm. Since the interlayer distance of θ-zirconium phosphate decreases upon drying from 10.4 to 7.6 Å, it is possible to predict the crystallite size of Sample F. The crystallinities of Sample E and F can be considered to be much the same. The order of particle sizes was as follows: Sample F<Sample E<Sample B<Sample A<Sample C<Sample D.

Ion Exchange. The pH value of the supernatant solution was employed as an index to estimate the degree of the ion-exchange reaction.

Figure 2 shows the pH change in the supernatant. Sample A and B behaved similarly. Here, the reaction proceeded considerably at the early runs of the ion exchange. The pH change was moderate through the whole ion-exchange runs in Sample C. The degree of ion exchange per run was smaller in Sample C than in Samples A and B. In contrast to Sample C, the pH values increased rapidly in Sample D.

The above fact indicate that the particle-size distribution of the exchanger was related to the ion-exchange behavior and the degree of ion exchange. The smaller the particles were, the more easily could the reaction take place. When the pH change in Sample C is compared with that of Sample D, it can be stated that, even though the exchangers have the same crystallinity, the ion-exchange behavior differs significantly. The difference between Samples

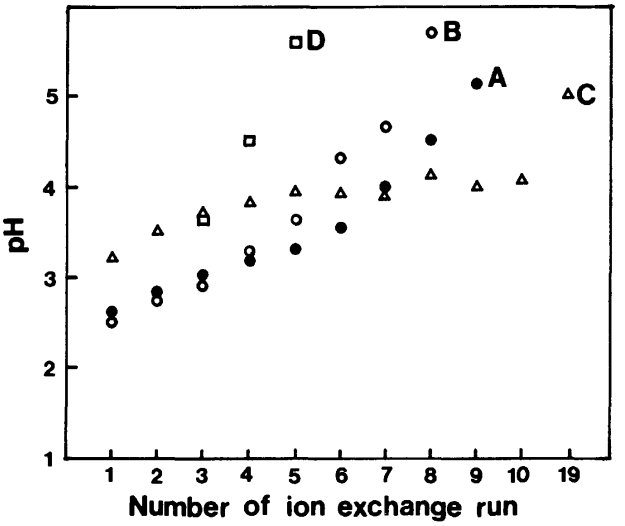

Fig. 2. pH change in the supernatant with the ion-exchange run for Samples A,B,C, and D.
In Sample C pH values of the first two runs overlapped with those of Sample A.

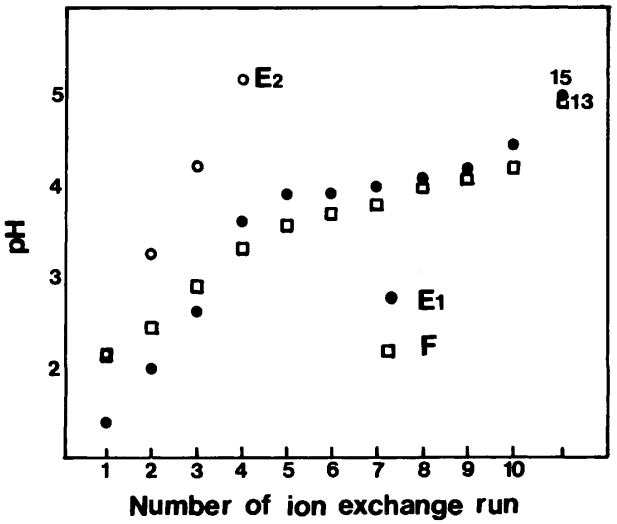

Fig. 3. pH change in the supernatant with the ion-exchange run for Samples E and F.

A and B and Sample D is probably caused by the nature of the surfaces. Since the cleavage of α-zirconium phosphate by grinding will take place mainly at the (002) plane, it is probable that the ratio of the protons on the surface to those in the crystallite increases and that the ion exchange accelerates at early runs.

The pH change in Samples E and F is shown in Fig. 3. Since θ-zirconium phosphate easily lost hydrated waters and changed to α-form in air, it must be stored in distilled water. Therefore, it is unable to weigh the exchanger to be used. In this figure, two typical pH changes are shown. The ratio of the amounts of exchanger to the volume of the complex solution was larger for E1 than for E2. The two curves appear quite different. The curves show that the pH value of the supernatant was lower for E1 than for E2 and that E1 needed more ion-exchange runs to the end of the reaction. For this difference, there are two possible explanations. One is that more complex cations must be used to replace more protons. Another is that, because the complex cation is more stable in an acidic solution than in a neutral or alkaline solution, the ion-exchange reaction proceeded more for E1.

The ion-exchange reaction proceeded extensively, especially when the ratio was high. When the complex solution was added to Sample E, the color of the exchanger surface turned orange, the same as the complex cation. These facts indicate that the ion exchange occurred fast, even at room temperature. The pH value of the supernatant for E1 was significantly low in the first run. This means that θ-zirconium phosphate took up selectively the complex cation and that the degree of the reaction was high.

In Sample F the ion exchange proceeded similarly to Samples A and B, though the pH values were lower in the first two ion-exchange runs. This is probably because the particle size of Sample F was smaller than that of Samples A and B.

Table 1. Content of nitrogen, hydrogen, and ignition loss

Sample	N(%)	H(%)	Ig. loss (%)	(H/N) molar ratio
Sample A	5.48	2.45	19.99	6.19
Sample B	6.93	2.75	21.51	5.57
Sample C	3.03	1.97	16.81	9.02
Sample D	3.02	1.95	17.14	8.98
Sample E	7.25	2.81	24.46	5.38
Sample F	4.70	2.26	19.12	6.69

Table 1 shows the contents of nitrogen and hydrogen and the ignition loss of the sample. It is possible for the molecular formula of the exchanger at the final ion-exchange run to be represented as $Zr[Co(NH_3)_6]_x(H)_{2-3x}(PO_4)_2 \cdot 2H_2O (x=0—2/3)$ (see below for Sample E (θ-zirconium phosphate)).[5,16] The amount of nitrogen is $6x$, and that of hydrogen, $18x+(2-3x)+4=15x+6$. Thus, the following relationship is derived: molar ratio of hydrogen to nitrogen, $r=H/N=(15x+6)/6x=2.5+1/x$. When x is equal to 1/3, r becomes 5.5. This is the case for Sample E. Consequently, the larger the ratio r, the lower the degree of the ion-exchange. The degree almost corresponded to that predicted from Figs. 2 and 3 and to the order of particle size except for Sample F. For this anomalous behavior of Sample F, no adequate explanation can be given.

For θ-zirconium phosphate the compound obtained on the final ion-exchange run, referred to as θ-ZPCo, was analyzed chemically. Found; Zr, 23.9 (1.00): PO_4, 48.9 (2.02): Co, 5.15 (0.33): N, 7.25 (1.98): H, 2.81% (10.6). In parentheses are given the molar ratio of each element to zirconium. Calcd for $Zr[Co(NH_3)_6]_{0.33}H(PO_4)_2 \cdot 2H_2O$; Zr, 24.5: PO_4, 51.5: Co, 5.28: N, 7.53: H, 2.99%. It should be noted that the ratio of nitrogen to cobalt was equal to 5.9. It can be stated that fifty percent of the protons in θ-zirconium phosphate were exchanged with the hexaamminecobalt(III) ion.

Structural Study. It is well known that the interlayer distance of zirconium phosphate is dependent on an existing cation between layers. In general, two peaks due to the original zirconium phosphate and its salt form appear in the lowest-angle region of an X-ray diffractogram.[5,6] Hence, the approximate degree of the ion exchange can be estimated by comparing the intensity of the two peaks. After the final ion-exchange run, an X-ray diffractogram of each sample was recorded. As is shown in Figs. 4 and 5, the interlayer distance of α-zirconium phosphates expanded from 7.6 Å(2θ=11.7°) to 11.2 Å(2θ=7.7°).

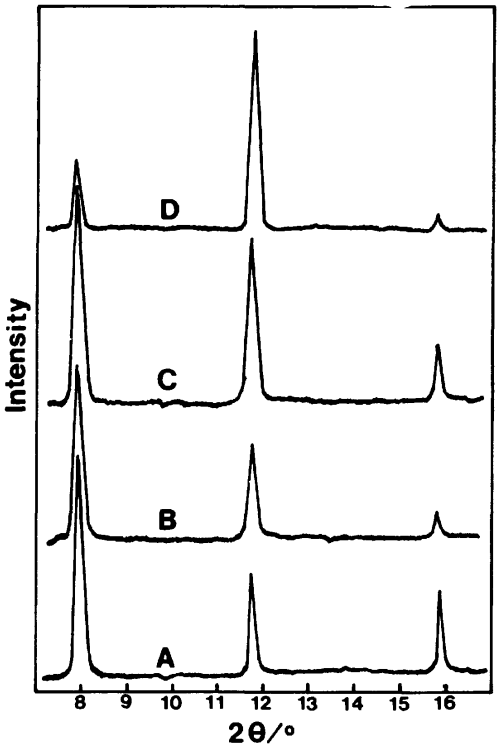

Fig. 4. Schematic diagram of X-ray powder diffraction at the lowest angle region for Samples A,B,C, and D.

The X-ray diffractograms of Samples A and B were similar, but that of Sample C was different. The diffractogram of Sample D showed that most of the α-zirconium phosphates were present unreacted. These facts agreed with what would be expected from Table 1.

An interlayer distance of 11.2 Å was observed, and the peak of 10.4 Å corresponding to the interlayer distance of θ-zirconium phosphate disappeared in the first ion exchange of Sample El. Since the difference between the two distances was small, and since θ-zirconium phosphate took up considerable amounts of the complex cation, the interlayer distance could expand easily.

In the case of Sample F, only the peak of 11.2 Å was present in the diffractogram. This differed distinctly from the cases of other α-zirconium phosphates and suggests that hydrogen-hexaamminecobalt(III) ion-exchange can be affected by factors other than those discussed in this work.

We are grateful to Mr. Seiichiro Iwafune for his measurements of the particle-size distribution.

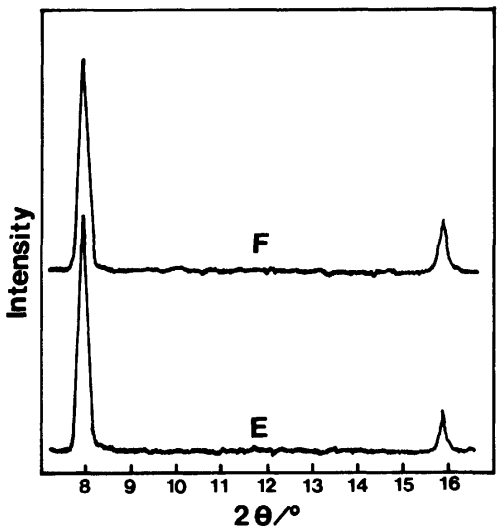

Fig. 5. Schematic diagram of X-ray powder diffraction at the lowest angle region for Samples E and F.

References

1) A part of this work was presented at the 47th National Meeting of the Chemical Society of Japan, Kyoto, April, 1983, Abstr. No. 1V04.

2) a) A. Clearfield and G. D. Smith, *Inorg. Chem.*, **8**, 431 (1969); b) J. M. Troup and A. Clearfield, *Inorg. Chem.*, **16**, 3311 (1977).

3) G. Alberti, *Acc. Chem. Res.*, **11**, 163 (1978).

4) L. W. Johnson, *J. Chem. Soc., Chem. Commun.*, **1980**, 263.

5) Y. Hasegawa, S. Kizaki, and H. Amekura, *Bull. Chem. Soc. Jpn.*, **56**, 734 (1983).

6) Y. Hasegawa and G. Yamamine, *Bull. Chem. Soc. Jpn.*, **56**, 3765 (1983).

7) G. Alberti, U. Costantino, S. Allulli, M. A. Massucci, and M. Pelliccioni, *J. Inorg. Nucl. Chem.*, **35**, 1347 (1973).

8) M. G. Bernasconi, M. Casciola, and U. Costantino, *J. Inorg. Nucl. Chem.*, **41**, 1047 (1979).

9) H. W. Haynes, Jr., *J. Catal.*, **79**, 479 (1983).

10) G. Alberti, U. Costantino, and J. S. Gill, *J. Inorg. Nucl. Chem.*, **38**, 1733 (1976).

11) T. Kijima, *Bull, Chem. Soc. Jpn.*, **55**, 3031 (1982).

12) Y. Hasegawa and M. Kuwayama, *Bull. Chem. Soc. Jpn.*, **51**, 3485 (1978).

13) Y. Inoue and Y. Yamada, *Bull. Chem. Soc. Jpn.*, **52**, 3528 (1979).

14) "Inorganic Synthesis," ed by W. C. Fernelius, McGraw-Hill, New York (1946), Vol II, pp. 216—217.

15) A. Clearfield, A. Oskarsson, and C. Oskarsonn, *Ion Exch. Membr.*, **1**, 91 (1972).

16) Y. Hasegawa and S. Kizaki, *Chem. Lett.*, **1980**, 241.

The Polarographic Behavior of Tl(I) and Na(I) Ions and Bis(*o*-phenylenediamine)nickel(II) in *N,N*-Dimethylformamide-Dimethyl Sulfoxide Mixtures

Shigeo SAWADA
Department of Chemistry, Faculty of Science and Technology, Kinki University, Kowakae, Higashi-Osaka 577
(Received July 24, 1984)

The polarographic behavior of Tl(I) and Na(I) ions and the bis(*o*-phenylenediamine)nickel(II) [Ni(opd)$_2$] complex were studied using *N,N*-dimethylformamide (DMF)–dimethyl sulfoxide (DMSO) mixed solvents of various compositions. The diffusion currents of the Tl(I) and Na(I) ions and [Ni(opd)$_2$] complex decreased linearly with an increase in the concentration of the supporting electrolyte in DMF–DMSO solvent mixtures. The ratio of the slope to the intercept is related to the D coefficient in the revised Jones-Dole equation of viscosity. Ion-solvent interaction was considered from the Stokes radius, calculated from the diffusion current at an infinite dilution of the supporting electrolyte. The half-wave potentials of both the Tl(I) ion and the [Ni(opd)$_2$] complex shifted to a negative direction with an increase in the concentration of the supporting electrolyte. Although the half-wave potential of the [Ni(opd)$_2$] complex shifted to a slightly positive potential, that of the Tl(I) ion shifted to a negative potential with an increase in the content of DMSO.

It has been reported that, in water-organic mixed solvent systems, the observed diffusion current (i_d) becomes lower than that calculated from the solution viscosity (η) by means of this equation: $i_d = i_{d,aq}\,\eta_{aq}^{1/2}/\eta^{1/2}$ (aq=aqueous solution) with an increase in the organic solvent contents for metal ions and ionic organic compounds, but the reverse tendency is found for neutral organic compounds.[1] In such systems, the phenomena may be due to the characteristics of water as a solvent, that is, its strong capacities of hydrogen-bonding and dissociation. DMF–DMSO mixed solvents in which both components have similar dielectric constants and dipole moments, but different viscosities, were chosen in order to clarify the above points. The present paper aims to examine the change in polarographic behavior between ionic and neutral depolarizers with the change in the composition of DMF–DMSO mixed solvents by using the Tl(I) ion and the [Ni(opd)$_2$] complex.

Experimental

DMF and DMSO were used as the solvents. The solvents were purified by distillation under reduced pressure, adding Wako 5A molecular sieves. The water contents, as determined by the Karl-Fischer method, were less than 0.01%. The mixed solvents were represented in volume %. The $TlClO_4$ was recrystallized once from distilled water. The tetraethylammonium perchlorate (TEAP), after having been prepared in the usual manner, was recrystallized at least eight times from distilled water.[2] The tetrapropylammonium perchlorate (TPAP) was prepared in the usual manner and recrystallized from distilled water. The tetrabutylammonium perchlorate (TBAP) was prepared by ion-exchange methods[3] and purified by recrystallization from acetone–water and ethanol–water. These crystals were dried under reduced pressure at 60 °C. The [Ni(opd)$_2$] was prepared by air-oxidizing, for over 24 h, nickel(II) chloride hexahydrate and *o*-phenylenediamine; it was purified by using Soxlet's extractor with acetone.[4]

The polarographic diffusion current was measured by means of a Yanagimoto Type P-8 polarograph. An aqueous saturated calomel electrode was used as the reference electrode. The characteristics of the dropping mercury electrode used were m=1.710 mg s^{-1} and t=4.1 s at h=50 cm. The counter electrode was 0.5 mm ϕ platinum wire. The electrolytic cell was an H-shaped cell separated by a diaphragm; contact between the electrolytic cell and the reference electrode was made by means of an agar bridge containing saturated NaCl and a 1500-cps methylcellulose bridge containing 1 M (1 M=1 mol dm^{-3}) $NaClO_4$ in the same solvent composition as the test solution.[5] These bridge were renewed for each experiment. The viscosity and density were measured with, respectively, an Ostwald viscometer and a Weld-type picnometer at 25 °C.

Results and Discussion

The wave heights of the Tl(I) ion at various concentrations of TBAP were measured in DMF–DMSO mixed solvents. The results are shown in Fig. 1. Since the concentration (c) of the supporting electrolyte is

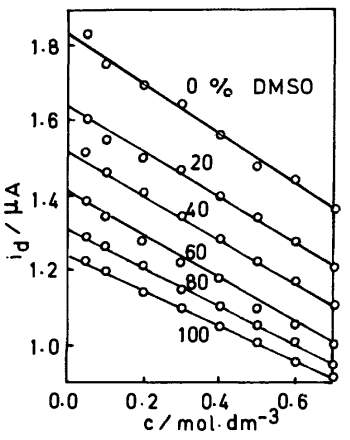

Fig. 1. Variation of i_d of Tl(I) with concentration of TBAP in DMF–DMSO.

sufficiently higher relative to the depolarizer, there was no influence of the migration current. The diffusion current of the Tl(I) ion varies little with the c of the supporting electrolyte in an aqueous solution, but it varies significantly in DMF–DMSO mixed solvents. According to the tracer-diffusion theory, the diffusion coefficient, D, decreases linearly with the $c^{1/2}$ of the supporting electrolyte; also, the diffusion current must decrease linearly with the $c^{1/2}$ of the supporting electrolyte. In the present work, however, the diffusion current decreased linearly with the c of the supporting electrolyte at higher concentrations of the supporting electrolyte. This might be attributed to a depreciation of solvent activity due to the solvation of the ion. The measurements were also carried out by exchanging the supporting electrolyte with $NaClO_4$, TEAP, and TPAP. Furthermore, the measurements were also carried out on the Na(I) ion and $[Ni(opd)_2]$, depolarizers other than the Tl(I) ion. In order to facilitate the comparison of the slope of the plot of i_d *vs.* the c of the supporting electrolyte, the following equation was used:

$$i_{d,r} = i_d/i_{d,0} = 1 - \alpha c \qquad (1)$$

where i_d is the diffusion current at the c of the supporting electrolyte; $i_{d,0}$, that at an infinite dilution of the supporting electrolyte, and α, the slope. Table 1 represents the α values for Tl(I) and Na(I) ions and for $[Ni(opd)_2]$ in DMF–DMSO mixed solvents containing each supporting electrolyte. It may be seen from Table 1 that the α values become larger in this order: TEAP, $NaClO_4$, and TBAP. However, since the effect of the c of the supporting electrolyte on the viscosity of the solution is contained in the magnitude of the value of α, the concentration dependence of the viscosity must also be examined.

The viscosity of the solution at various concentra-

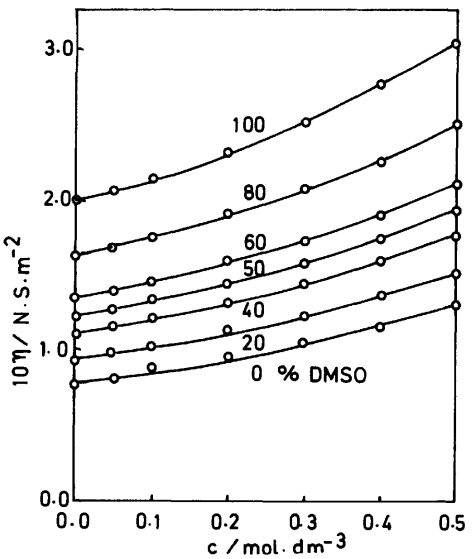

Fig. 2. Plots of η *vs.* concentration of TBAP in DMF–DMSO.

TABLE 1. α VALUES IN DMF–DMSO MIXED SOLVENTS FOR $NaClO_4$, TEAP, AND TBAP AS SUPPORTING ELECTROLYTES

DMSO%	α/l·mol^{-1}						
	Tl(I)			Na(I)		$[Ni(opd)_2]$	
	$NaClO_4$	TEAP	TBAP	TEAP	TBAP	TEAP	TBAP
0	0.32	0.19	0.37	0.12	0.39	0.15	0.31
20	0.31	0.16	0.35	0.17	0.36	0.24	0.32
40	0.30	0.20	0.40	0.17	0.34	0.15	0.36
50	0.30	0.20	0.41	0.20	0.33	—	—
60	0.25	0.23	0.41	0.26	0.33	0.29	0.38
80	0.22	0.22	0.39	0.20	0.33	0.27	0.42
100	0.32	0.30	0.38	0.27	0.34	0.23	0.38

TABLE 2. A, B, AND D COEFFICIENTS OF THE Jones-Dole EQUATION FOR $NaClO_4$, TEAP, TPAP, AND TBAP

DMSO%	A/l$^{1/2}$·mol$^{-1/2}$				B/l·mol^{-1}				D/l^2·mol^{-2}			
	$NaClO_4$	TEAP	TPAP	TBAP	$NaClO_4$	TEAP	TPAP	TBAP	$NaClO_4$	TEAP	TPAP	TBAP
0	−0.088	0.021	0.042	0.022	0.70	0.61	0.60	0.75	1.10	0.24	0.71	0.84
20	0.009	0.010	−0.023	0.011	0.35	0.60	0.59	0.70	0.66	0.26	0.62	0.94
40	0.038	0.039	−0.003	0.067	0.56	0.46	0.66	0.58	0.52	0.30	0.42	0.98
50	0.070	0.104	—	0.068	0.46	0.49	—	0.56	0.69	0.34	—	1.05
60	0.054	0.054	0.021	0.021	0.56	0.52	0.62	0.68	0.36	0.28	0.45	0.81
80	−0.008	0.030	−0.009	0.017	0.71	0.49	0.58	0.68	0.47	0.29	0.52	0.87
100	−0.046	0.010	−0.026	0.018	0.79	0.47	0.50	0.58	0.47	0.29	0.67	0.87

Table 3. K values in DMF-DMSO mixed solvents for $NaClO_4$, TEAP, and TBAP as supporting electrolytes

DMSO%	K/l·mol^{-1}						
	Tl(I)			Na(I)		[Ni(opd)$_2$]	
	$NaClO_4$	TEAP	TBAP	TEAP	TBAP	TEAP	TBAP
0	0.163	0.133	0.069	0.214	0.028	0.141	0.136
20	0.057	0.162	0.078	0.148	0.083	0.058	0.128
40	0.049	0.107	0.009	0.151	0.086	0.160	0.073
50	0.062	0.072	−0.002	0.076	0.117	—	—
60	0.096	0.063	−0.017	0.024	0.117	−0.019	0.060
80	0.175	0.049	−0.005	0.077	0.105	−0.016	−0.012
100	0.125	−0.072	0.004	−0.012	0.079	−0.005	0.055

tions of TBAP were measured in DMF–DMSO mixed solvents. Fig. 2 shows the results. The viscosity of the solution increased quadratically with the concentration of the electrolyte, and the relative viscosity obeyed the following revised Jones-Dole equation[6]:

$$\eta_r = \eta/\eta_0 = 1 + Ac^{1/2} + Bc + Dc^2 \quad (2)$$

where η is the viscosity at the c of the electrolyte, where η_0 is that at zero of c, and where A, B, and D are constants. The experiment was carried out by exchanging the electrolyte with $NaClO_4$, TEAP, and TBAP. The values of the constants were evaluated by the least-squares method. Table 2 shows the results. It may be seen from Table 2 that the magnitudes of both A and B for the four electrolytes are nearly equal, but that of D becomes larger in this order: TEAP, $NaClO_4$, and TBAP, as in the case of the α values. Hence, the D coefficient and the α values may have the same cause.

If the cause of the i_d depression with the increase in the concentration of the supporting electrolyte were only the increase in the viscosity, then $i_{d,r}\eta_r^{1/2}$ would remain at unity. However, as influences other than the viscosity act on it, $i_{d,r}\eta_r^{1/2}$ varies from unity with the c of the supporting electrolyte as follows:

$$i_{d,r}\eta_r^{1/2} = 1 + Kc \quad (3)$$

where K is the coefficient representing the deviation from the Stokes equation. The above equation holds within about 0.5 M only. The values of K was evaluated in each case. Table 3 shows the results. In the cases in which the supporting electrolyte is TEAP or TBAP without the Na(I) ion, the value of K gradually decreases with the increase in the DMSO content. In the cases in which the depolarizer is the Tl(I) ion, the value of K for TBAP as the supporting electrolyte is smaller than TEAP. On the other hand, in the cases in which the depolarizer is [Ni(opd)$_2$], there is no difference between the values of K for TEAP and TBAP. The results show that the extent of the solvation of the depolarizer varies with the c of the electrolyte and that tendency differs with the kind of electrolyte and the kind of depolarizer[7].

The interaction between the supporting electrolyte and the solvent or the interaction between the solvents appears in the supporting-electrolyte-concentration-dependence of the polarographic diffusion current, but the interaction between the depolarizer and the solvent appears in the diffusion current at an infinite

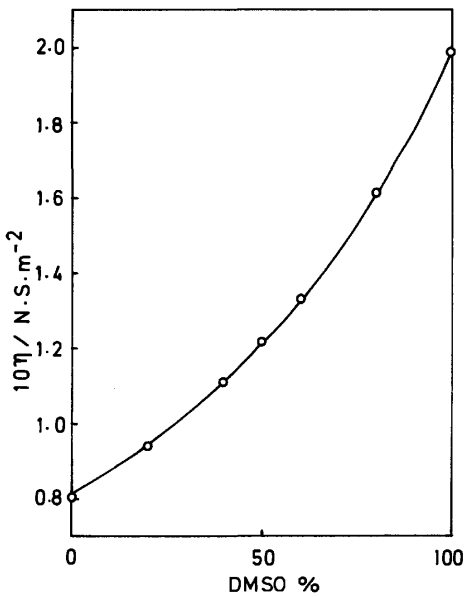

Fig. 3. Plots of η *vs.* DMSO % in DMF-DMSO.

Table 4. Stokes radii in DMF-DMSO

DMSO%	r_s/Å		
	Tl(I)	Na(I)	[Ni(opd)$_2$]
0	2.5	3.2	3.0
20	2.5	3.2	2.9
40	2.3	3.1	2.8
50	2.4	3.1	—
60	2.3	3.1	2.8
80	2.3	3.0	2.7
100	2.0	2.9	2.7

TABLE 5. $E_{1/2}$ OF Tl(I) AND [Ni(opd)$_2$] IN DMF-DMSO MIXED SOLVENTS CONTAINING 0.1 OR 0.7 M TETRAALKYLAMMONIUM PERCHLORATE

Concn.	DMSO%	TEAP			TBAP		
		Tl(I)	[Ni(opd)$_2$]		Tl(I)	[Ni(opd)$_2$]	
			1st	2nd		1st	2nd
0.1 M	0	−0.42	−0.93	−1.63	−0.49	−0.96	−1.65
	20	−0.47	−0.93	−1.62	−0.54	−0.95	−1.63
	40	−0.50	−0.92	−1.62	−0.57	−0.92	−1.62
	60	−0.51	−0.91	−1.60	−0.58	−0.92	−1.60
	80	−0.52	−0.91	−1.59	−0.58	−0.91	−1.60
	100	−0.53	−0.90	−1.56	−0.58	−0.91	−1.59
0.7 M	0	−0.41	−0.91	−1.59	−0.47	−0.91	−1.59
	20	−0.44	−0.90	−1.57	−0.52	−0.90	−1.56
	40	−0.47	−0.90	−1.56	−0.53	−0.90	−1.55
	60	−0.50	−0.89	−1.56	−0.54	−0.89	−1.54
	80	−0.50	−0.88	−1.54	−0.55	−0.89	−1.53
	100	−0.52	−0.88	−1.51	−0.55	−0.88	−1.54

dilution of the supporting electrolyte. The diffusion current extrapolated to the concentration zero of the supporting electrolyte is independent of the kind of supporting electrolyte and is the same if the depolarizer and the solvent are the same. The diffusion coefficient D was evaluated from the diffusion current at an infinite dilution by means of the Ilkovic equation. The viscosity of the solvent in DMF-DMSO mixtures varied, as Fig. 3 shows. The Stokes radius was calculated by means of the following Stokes-Einstein equation:

$$r_s = kT/(6\pi\eta_0 D) \quad (4)$$

where k is the Boltzmann constant and η_0, the viscosity of the solvent. Table 4 shows the results. It may be seen that the Stokes radius becomes smaller with an increase in the DMSO content. Since DMSO is easier to solvate than DMF, the size of the diffusing particle in DMSO should become larger. However, the greater the DMSO content, the smaller the size of the observed Stokes radius. This might be ascribed to the presence of the association of DMSO.[8]

Table 5 shows the half-wave potentials of the Tl(I) ion and the [Ni(opd)$_2$] complex in DMF-DMSO mixed solvents containing 0.1 or 0.7 M TPAP and TBAP. The half-wave potentials of the Tl(I) ion and the [Ni(opd)$_2$] complex shifted to positive potentials with an increase in the concentrations of TPAP and TBAP in every solvent composition. This is attributable to the shift to the positive potential of the liquid-junction potential with an increase in the concentration of the supporting electrolyte. The half-wave potentials shifted to slightly negative potentials with an increase in the numbers of carbon atoms in the alkyl group of the tetraalkylammonium ion. While the half-wave potential of [Ni (opd)$_2$] shifted by about 0.03 V to a positive potential with an increase in the content of DMSO, the half-wave potential of the Tl(I) ion shifted by about 0.10 V to a negative potential. This is attributable to the stronger solvation of the Tl(I) ion by DMSO than by DMF, while [Ni(opd)$_2$], having a large size and a zero charge, is solvated only weakly in both solvents.

References

1) M. Suzuki and S. Sawada, *Rev. Polarography (Kyoto)*, **17**, 69 (1971).
2) C. K. Mann, *Electroanal. Chem.*, **3**, 133 (1969).
3) S. Yamaguchi, Y. Yamakawa, and T. Tsukamoto, *Rew. Polarography (Kyoto)*, **17**, 145 (1971).
4) A. L. Balch and R. H. Holm, *J. Amer. Chem. Soc.*, **88**, 5201 (1966).
5) M. Suzuki and T. Shimizu, *Denki Kagaku*, **45**, 361 (1977).
6) D. Feakins and K. G. Lawrence, *J. Chem. Soc. (A)*, 1966 212.
7) J. O' M. Bockris and P. P. S. Saluja, *J. Phys. Chem.*, **76**, 2140 (1972).
8) N. Yao and D. N. Bennion, *J. Phys. Chem*, **75**, 1727 (1971).

Fe K-Edge XANES and EXAFS of the X-Ray Absorption Spectra of $FeCl_3$ Aqueous Solutions. A Structural Study of the Solute, Iron(III) Chloro Complexes

Kiyotaka ASAKURA, Masaharu NOMURA,† and Haruo KURODA*

Department of Chemistry and Research Center for Spectrochemistry, Faculty of Science, The University of Tokyo, Hongo, Bunkyo-ku, Tokyo 113

(Received September 3, 1984)

The Fe K-edge spectra were measured on $FeCl_3$ aqueous solutions by use of synchrotron radiation to reveal the solute structure from the analysis of Fe K-edge EXAFS and XANES. It is concluded that the solute exists mainly as $[Fe(H_2O)_6]^{3+}$ but partially as $[FeCl(H_2O)_5]^{3+}$ at $FeCl_3$ concentration of 0.1—1 mol dm^{-3}, and it exsits mainly as $[FeCl_2(H_2O)_4]^+$ at the concentration of 3—4 mol dm^{-3}. In the diliquescent product of $FeCl_3$, about a half of the solute is in the state of $[FeCl_4]^-$ and the remaining half is likely to be in the state of $[FeCl_2(H_2O)_4]^+$. No indication was found for the dimer formation of $FeCl_3$ even in the deliquescent product.

The structures of the iron(III) chloro complexes which are formed in the aqueous solution of $FeCl_3$, have been extensively investigated by means of X-ray diffraction.[1—10] But the conclusions given by different authors are still mutually conflicting in several respects. Recently, Magini *et al.* concluded that the dominant solute species existing in an aqueous solution of $FeCl_3$ at the concentration of about 4 mol dm^{-3} was octahedral chloro complexes.[5,10] On the other hand, Wertz *et al.* reported that the octahedral aqua complex $[Fe(H_2O)_6]^{3+}$ was dominant in the solution of the same concentration, which was freshly prepared from $FeCl_3 \cdot 6H_2O$, but octahedral chloro complexes $[FeCl_x(H_2O)_{6-x}]$ were gradually formed to have an average composition $[FeCl_{1.4}(H_2O)_{4.6}]$ after aging the solution for 14 months, whereas the tetrahedral chloro complexes were dominant when the solution was prepared from anhydrous $FeCl_3$.[7,8] From the examination of the X-ray diffraction pattern of the melt of $FeCl_3 \cdot 6H_2O$, Magini *et al.* claimed that the dimer of $FeCl_3$ was partially formed in this melt.[6] Wertz *et al.* also assumed without any direct experimental evidence, that the dimeric species Fe_2Cl_6 should exist also in a concentrated aqueous solution of about 4 mol dm^{-3} prepared from anhydrous $FeCl_3$.[7]

There could be several different kinds of the chloro complex coexisting in the $FeCl_3$ solution and the dominant species should vary depending on the solute concentration, but little is known about their equilibrium.[5] It is desirable to study over a wide range of the solute concentration from this point of view. But the X-ray diffraction studies hitherto reported were done only on the $FeCl_3$ solutions of a relatively high concentration, mostly above 1 mol dm^{-3}, because X-ray diffraction data inevitably contain a large contribution of the diffraction by the solvent. In this respect, it is of great interest to use extended X-ray absorption fine structure (EXAFS) and X-ray absorption near edge structure (XANES), since one can obtain from the analysis of EXAFS and XANES of Fe K-edge spectrum the information on the local structure surrounding Fe atom without being greatly disturbed by the presence of solvent even in the case of a considerably dilute solution.[11] We have already used this technique successfully in the structural studies on the systems involving Fe–Cl bond such as anhydrous $FeCl_3$[12] and $FeCl_3$-doped polyacetylene.[13]

In the present study, we measured Fe K-edge EXAFS and XANES in the X-ray absorption spectra of $FeCl_3$ aqueous solutions to derive the structural information on the solute.

Experimental

Preliminary experiments of X-ray absorption spectra (XAS) were carried out by use of the in-laboratory EXAFS spectrometer which was described elsewhere,[14] but final XAS data were obtained by use of synchrotron radiation employing the EXAFS facilities at BL-10B of the Photon Factory in the National Laboratory for High-Energy Physics (KEK-PF). The details of this experimental setup have been described elsewhere.[15] In the present study, a Si(311) channel-cut crystal was used to monochromatize X-rays from 2.5 GeV electron storage ring. The sample cell used in the XAS measurement of a liquid sample had two hard polypropylene windows to pass X-rays. The separation between the two windows was variable by changing the spacer between the windows. We set the sample thickness so as to keep the absolute absorbance at Fe K-edge below 3.0 in all cases. All XAS measurements were carried out at room temperature.

The sample solutions investigated in the present study are listed in Table 1, together with their abbreviated symbols, where the number stands for the concentration in mol dm^{-3} and the characters N and A stand for the neutral and acidified cases, respectively. Each solution was prepared by dissolving an appropriate amount of $FeCl_3 \cdot 6H_2O$ (reagent grade) into distilled water. We used nitric acid to acidify the solution except in the sample which is

† Present address: Photon Factory, Natinal Laboratory for High Energy Physics, Oho-machi, Tsukuba-gun, Ibaraki 305.

Table 1. Compositions of the solutions

Symbols of Samples	Fe^{3+} / mol dm^{-3}	$[HNO_3]$ / $[Fe^{3+}]$	$[HCl]$ / $[Fe^{3+}]$
4N	4.3		
3N	3.0		
0.7N	0.74		
0.1N	0.14		
3A	3.0	1	
0.5A	0.50	1	
Cl3A	3.1		1
DP	Deliquescent product of anhydrous $FeCl_3$		

denoted as Cl3A where HCl was used to see the effect of Cl^- ion, the ratio [acid]/[$FeCl_3$] being unity in all acidified samples. The deliquescent product of anhydrous $FeCl_3$(DP in Table 1) was taken up as the most concentrated non-acidified solution of $FeCl_3$.

We also measured the UV-visible absorption spectra of the sample solutions in order to characterize the solute state by comparing them with the reported data.[16-18] In the measurement of UV-visible absorption spectrum, perchloric acid was used to acidify the solutions instead of nitric acid, because NO_3^- has a strong absorption band at 220 nm.

Results

UV-visible absorption spectrum is known to be useful to characterize the coordination state of iron(III) complex. The absorption spectrum of a nitromethane solution of $[N(C_2H_5)_4][FeCl_4]$ and that of an aqueous solution of $Fe(ClO_4)_3 \cdot 6H_2O$ are shown in Fig. 1. The former is a typical case where the solute exists exclusively in the form of $[FeCl_4]^-$. The strong peaks at 317 and 365 nm and the weak peaks at 446, 532, 606, 685, and 728 nm in its absorption spectrum are the ones characteristic of $[FeCl_4]^-$.[19] In the aqueous solution of $Fe(ClO_4)_3 \cdot 6H_2O$, the peaks at 240 and 330 nm and the shoulder at 440 nm are the structure characteristic of $[Fe(H_2O)_6]^{3+}$ and its hydrolysis products.[20] We denote the species existing in this case as $[Fe(H_2O)_6]^{3+}$ for convenience, although it could be partially in the state of the hydrolysis product. The UV-visible absorption spectra of non-acidified aqueous solutions of $FeCl_3$ are shown in Fig. 2. According to the general features of the observed spectra, we can classify the solutions into the following three groups; the solutions where $FeCl_3$ concentration is less than 1 mol dm^{-3} (Group 1), the solutions with the concentration of 3—4 mol dm^{-3} (Group 2) and the very concentrated solutions such as DP (Group 3). The absorption spectra of the solutions of Group 1 exhibit strong peaks at 220 and 335 nm, and resemble the spectrum of $[Fe(H_2O)_6]^{3+}$ except for a small difference as regards the positions and relative intensities of absorption maxima. This type of spectrum has been attributed to the octahedral chloro complexes such as $[FeCl(H_2O)_5]^{2+}$ and/or $[FeCl_2(H_2O)_4]^+$.[16-18] On the other hand, the absorption spectrum of DP (a solution of Group 3) exhibits the features characteristic of $[FeCl_4]^-$, suggesting that $[FeCl_4]^-$ is the dominant species in this case. The spectra of

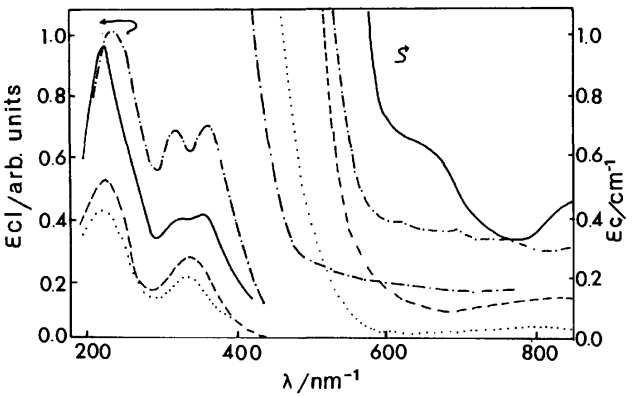

Fig. 2. UV-visible absorption spectra of non-acidified aqueous solutions of $FeCl_3$. —·—: DP, ——: 4N, — —: 1N, ·····: 0.2N.

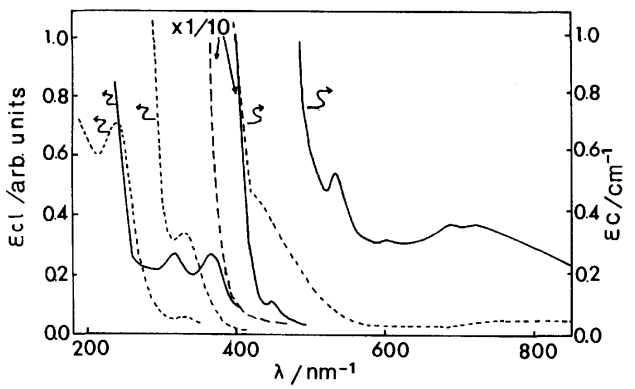

Fig. 1. UV-visible absorption spectra of the nitromethane solution of $[N(C_2H_5)_4][FeCl_4]$ (solid line) and the aqueous solution of $Fe(ClO_4)_3 \cdot 6H_2O$ (broken line).

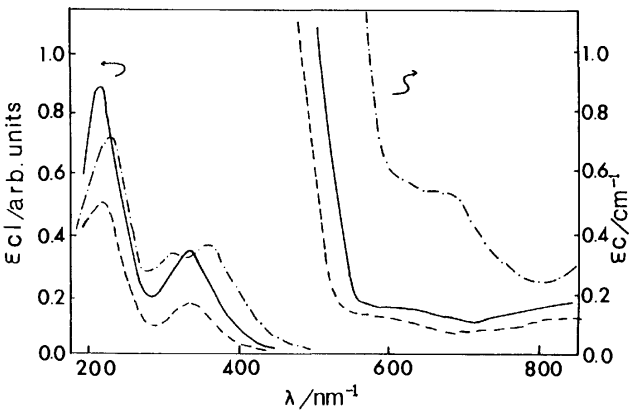

Fig. 3. UV-visible absorption spectra of acidified aqueous solutions of $FeCl_3$. —·—: 3A, ——: 1A, — —: 0.5A.

the solutions of Group 2 show the features in-between the above-mentioned two cases. This seems to be due to the co-existence of the octahedral and tetrahedral complexes. Figure 3 shows the spectra of the solutions acidified with perchloric acid. No remarkable change can be found in the spectrum on acidifying the solution.

Figure 4 shows the Fe K-edge region of the X-ray absorption spectra of the crystalline powders of $Fe(NO_3)_3 \cdot 9H_2O$, $FeCl_3 \cdot 6H_2O$, and $[N(C_2H_5)_4][FeCl_4]$. In these compounds, the local structure around Fe atom can be described as $[Fe(H_2O)_6]^{3+}$, *trans*-$[FeCl_2(H_2O)_4]^+$, and $[FeCl_4]^-$, respectively. Since XANES is determined by the local structure surrounding the X-ray absorbing atom, the spectra shown here can be taken respectively as those characteristic of the above-mentioned three kinds of iron(III) complex. All three spectra show a pre-edge structure which is attributable to the 1s-3d transition, but its shape and intensity are different between octahedral complexes and a tetrahedral one. In the cases of $[Fe(H_2O)_6]^{3+}$ and $[FeCl_2(H_2O)_4]^+$, both of which are octahedral complexes, the 1s-3d transition splits into two weak peaks, whereas it gives a relatively strong sharp peak in the case of the tetrahedral complex $[FeCl_4]^-$. Difference can be found also in the region above the absorption edge. The spectrum of $[Fe(H_2O)_6]^{3+}$ exhibits a considerably sharp peak just above the absorption edge, which is accompanied by a weak shoulder structure, the spectrum of $[FeCl_2(H_2O)_4]^+$ shows two broad absorption maxima around the absorption edge, and the spectrum of $[FeCl_4]^-$ exhibits three relatively sharp peaks followed by a broad structure.

XANES regions of the X-ray absorption spectra of the non-acidified solutions are shown in Fig. 5. The spectra shown here can be classified into three types. The first is the case observed for relatively dilute solutions where $FeCl_3$ concentration is less than 1 mol dm^{-3}. In this case, the spectrum exhibits weak 1s-3d double peaks in the pre-edge region and a relatively sharp peak just above the absorption edge. The second is the case observed for the solutions of the concentration range of 3—4 mol dm^{-3}, where the spectra again show weak double pre-edge peaks like in the first case, but the maximum just above the absorption edge splits into two peaks. The third is the case observed for a very concentrated solution like DP. In this case, the spectrum shows a sharp pre-edge 1s-3d peak and a shoulder structure and two peaks around the absorption edge. This classification of non-acidified solutions from XANES corresponds to the one which we have done from UV-visible absorption spectroscopy. The appearance of weak double pre-edge peaks associated with 1s-3d transition is characteristic of iron(III) octahedral complex as we have mentioned. The spectrum of the first type,observed for the relatively dilute solutions (the solutions of Group 1), resembles the spectrum of $[Fe(H_2O)_6]^{3+}$, but the spectral shape above the absorption edge is a little different from the latter. Seemingly the difference is due to the coexistence of the octahedral chloro complex. The general shape of the

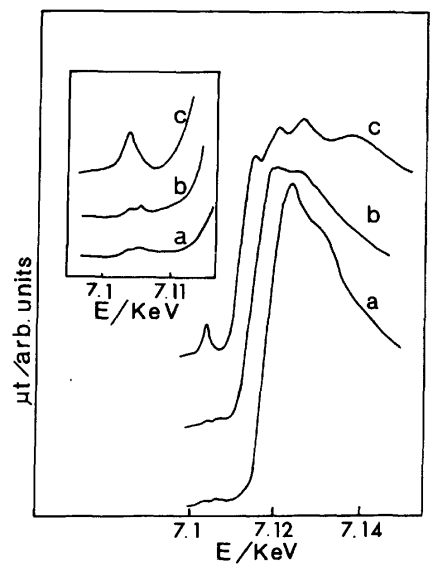

Fig. 4. Fe K-edge XANES spectra of reference compounds. (a): $Fe(NO_3)_3 \cdot 9H_2O$, (b): $FeCl_3 \cdot 6H_2O$, (c): $[N(C_2H_5)_4][FeCl_4]$. The pre-edge region is shown in the inset with an expanded scale.

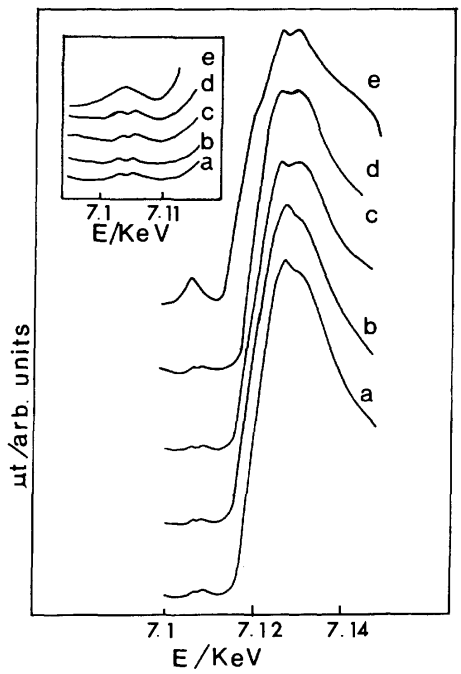

Fig. 5. Fe K-edge XANES spectra of non-acidified solutions of $FeCl_3$. (a): 0.1N, (b): 0.7N, (c): 3N, (d): 4N, (e): DP. The pre-edge region is shown in the inset with an expanded scale.

spectrum of the second type, observed for the 3—4 mol dm^{-3} solutions (the solutions of Group 2), corresponds to the spectrum of $[FeCl_2(H_2O)_4]^+$, indicating that the solute exists predominantly in the state of the octahedral chloro complex, but there are relatively sharp structrures above the absorption edge, which look like the structures due to $[FeCl_4]^-$ coexisting in the solution. The spectrum of DP exhibits a sharp single pre-edge 1s–3d peak and relatively sharp structures above the absorption edge, both of which are characteristic of the tetrahedral complex $[FeCl_4]^-$. However, the intensity of the pre-edge peak relative to the Fe K-edge jump is significantly smaller as compared with the spectrum of $[N(C_2H_5)_4]$ $[FeCl_4]$. This fact indicates that the solution contains not only $[FeCl_4]^-$, but also octahedral complexes. The above-mentioned conclusions derived from XANES are consistent with those from UV-visible absorption spectroscopy. From the intensity of the pre-edge peak relative to the edge-jump, we approximately estimate the fraction of $[FeCl_4]^-$ ion among the total amount of the solute to be about 50%.[21]

Figure 6 shows the XANES spectra of the acidified solutions. Their spectral shapes are almost the same as those of the non-acidified solutions. Wertz *et al.* suggested that $[FeCl_4]^-$ comes to be the prominent species when the solution is acidified with hydrochloric acid.[9] However, little difference was observed among the spectra of C13A, 3A, and 3N. This means that the main species are not significantly different among these solutions and that $[FeCl_4]^-$ is not predominant in C13A.

The EXAFS oscillation $\chi(k)$ was extracted from an observed XAS spectrum by the following way. The smoothly varying component $\mu_s(\lambda)$ was estimated by fitting the observed spectrum using the cubic spline technique.[11] We estimated the absorbance for the free atom, $\mu_o(\lambda)$, in the region of 50—60eV from the edge by subtracting the background μ_b from μ_s. The background μ_b was determined by a smooth extrapolation from the pre-edge region by use of Victoreen's equation.

$$\mu_b(\lambda) = C\lambda^3 + D\lambda^4 \quad (1)$$

The μ_o value in other region was estimated by assuming that its wavelength dependence was describable with the Victreen's equation, the parameters of which were taken from the literature.[22] The photon energy E was converted to the photoelectron wave number k by Eq. 2.

$$k = \sqrt{2m(E-E_0)}/\hbar \quad (2)$$

where E_o is the ionization threshold. Then the EXAFS oscillation $\chi(k)$ was calculated by using Eq. 3.

$$\chi(k) = (\mu-\mu_s)/\mu_0 \quad (3)$$

The Fourier transforms of $k^3\cdot\chi(k)$ over the region of k=4.0—12.0 Å^{-1} are shown in Figs. 7—9. Both for non-acidified and acidified cases, the main peak of Fourier transform is at 1.60—1.61 Å when the solute concentration is less than 1 mol dm^{-3} (the

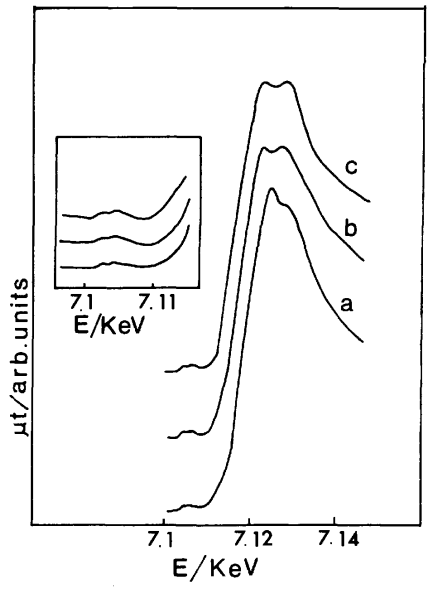

Fig. 6. Fe K-edge XANES spectra of acidified solutions of $FeCl_3$. (a): 0.5A, (b): 3A, (c): C13A. The pre-edge region is shown in the inset with an expanded scale.

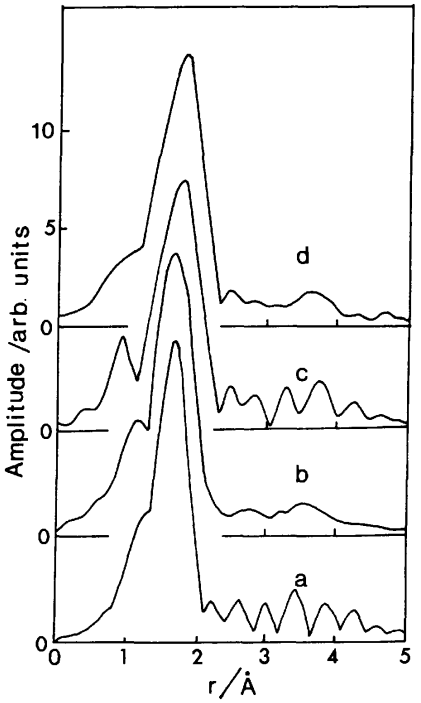

Fig. 7. Fourier transfeorms of $k^3\cdot\chi(k)$ for non-acidified aqueous solutions of $FeCl_3$. (a): 0.1N, (b): 0.7N, (c): 3N, (d): 4N.

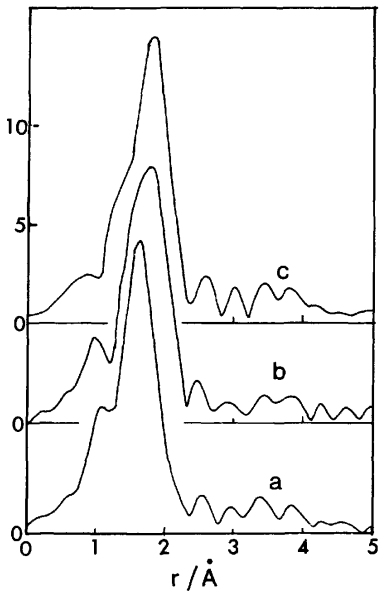

Fig. 8. Fourier transforms of $k^3 \cdot \chi(k)$ for acidified aqueous solutions of $FeCl_3$. (a): 0.5A, (b): 3A, (c): Cl3A.

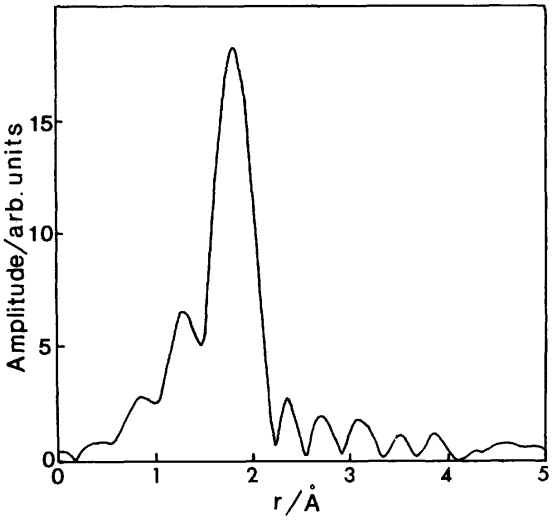

Fig. 9. Fourier transform of $k^3 \cdot \chi(k)$ for DP.

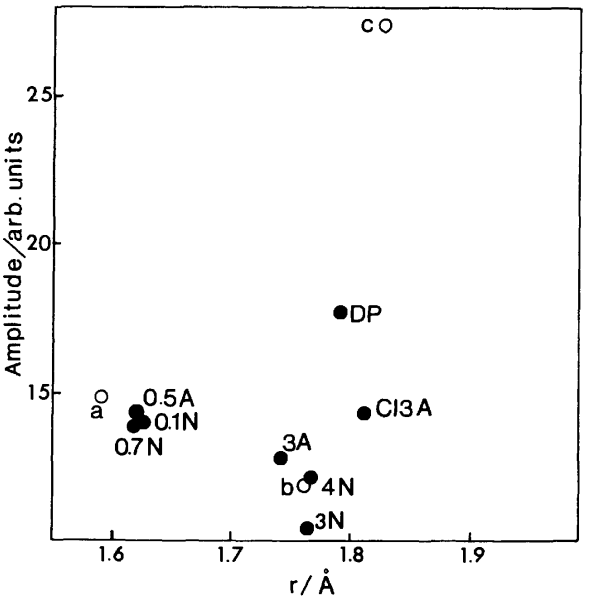

Fig. 10. Plots of the amplitude of the main peak of Fourier transform against the peak position. (a): $Fe(NO_3)_3 \cdot 9H_2O$, (b): $FeCl_3 \cdot 6H_2O$, (c): $[N(C_2H_5)_4][FeCl_4]$. Refer to Table 1 for abbreviated symbols of the solutions.

solutions of Group 1), but the corresponding peak shifts to 1.76 Å in the case of DP. The solutions of the Group 2 show the corresponding peak at a position in-between these two cases. The above-mentioned main peak of Fourier transform is attributable to Fe-Cl and/or Fe-O(H_2O). Since Fe-Cl distance is longer than Fe-O distance, the shift of the main peak is associated with the increase of the number of Cl atoms coordinating to Fe atom. The peak amplitude should be also dependent on the Cl/O ratio surrounding Fe atom. In Fig.10, we plotted the amplitude of the main peak of Fourier transform against the peak position. The position of the point in this plot could be a good criterion of the average state of the solute.[23] Note that the points for the solutions 0.1N, 0.7N, and 0.5A (Group 1) are nearly at the same position, whereas the points for much concentrated solutions fall in a quite different area. We have also shown the points obtained for the reference materials in which the local structures surrounding Fe atom are $[Fe(H_2O)_6]^{3+}$, $[FeCl_2(H_2O)_4]^+$ and $[FeCl_4]^-$, respectively. We can see that the point for $[Fe(H_2O)_6]^{3+}$ is located at the position shifted a little to the left from the points for the $FeCl_3$ solutions of Group 1, and the point for $[FeCl_2(H_2O)_4]^+$ is in the area where the points for much concentrated $FeCl_3$ solutions are located. This fact again indicates that the solute is in the state of $[Fe(H_2O)_6]^{3+}$ along with chloro complexes in the solutions of Group 1, while it is mainly in the states of $[FeCl_2(H_2O)_4]^+$ and other chloro complexes in much concentrated solutions. Note that the point for DP is significantly separated from the point for $[FeCl_4]^-$. This fact again indicates that the solute is not entirely in the state of $[FeCl_4]^-$ in DP as we have concluded from XANES.

Performing the inverse Fourier transformation over the region of the main peak (r=1.0–2.2 Å) of each Fourier transform, we carried out further analysis of EXAFS oscillation by means of the nonlinear least square curve-fitting method, using the Eq.4.

$$k^3 \cdot \chi(k) = \sum_j k^2 S_j(k)(N_j/r_j^2)F_j(k) \times \exp(-2\sigma_j^2 k^2) \sin(2kr_j + \phi_j(k)) \quad (4)$$

TABLE 2. RESULTS OF THE CURVE-FITTING ANALYSIS OF THE EXAFS DATA OF THE REFERENCE COMPOUNDS

Sample	Coordination number		Distance (r/Å)*		S**
	Cl	O	Fe-Cl	Fe-O	
$Fe(NO_3)_3 \cdot 9H_2O$	0	6		1.90 (2) [1.99][a]	0.43
$FeCl_3 \cdot 6H_2O$	2	4	2.30 (3) [2.30][b]	2.06 (3) [2.07][b]	0.40
$[N(C_2H_5)_4][FeCl_4]$	4	0	2.19 (2) [2.19][c]		0.53
$(NH_4)_2[FeCl_5(H_2O)]$	5	1	2.34 (3) [2.38][d]	2.05 (3) [2.08][d]	0.43
$[Co(NH_3)_6][FeCl_6]$	6	0	2.37 (2) [2.39][e]		0.50

* The interatomic distances determined by crystal structure analysis are given in brackets; (a) from Ref. 30, (b) from Ref. 31, (c) from Ref. 32, (d) from Ref. 33, (e) from Ref. 34. ** The inaccuracy of these S values was found to be 20—30%.

where N_j is the coordination number of the j-th shell at the distance r_j from the X-ray absorbing atom, $F_j(k)$ the back-scattering amplitude for the photoelectron wave number k, $\phi_j(k)$ the phase shift, σ_j the Debye-Waller factor of the atoms in the j-th shell. $S_j(k)$ is the amplitude reduction factor, which was assumed to be independent of k in the present study.[24]

The theoretical functions given in the literature were used for $F_j(k)$ and $\phi_j(k)$ in Eq. 4.[25] The validity of the assumed back-scattering amplitude and phase shift founctions were checked by carrying out the analysis of the EXAFS of the reference samples. As shown in Table 2, the results from EXAFS showed a satisfactory agreement with the crystallographic data.

In general, the amplitude reduction factor S_j should be different for different kinds of atom. But we assumed it to be the same value for the nearest neighbor Cl and O atoms.[26] We took this approximation in order to avoid the nonlinear least square analysis converging to the odd minimum points.

In the final refinement stage, we assumed the sum of the coordination numbers of Cl and O to be 6 for all solutions except for DP, where the best fit between the observed and calculated EXAFS oscillations was attained when the coordination numbers of Cl and O were assumed to be 3 and 2, respectively. The above-mentioned assumption is based on the conclusions derived from XANES and UV-visible absorption spectra, which show that the main species are octahedral complexes in all solutions except DP. The final results of curve-fitting analysis are summarized in Table 3. The average Fe-O distance obtained in the present study was 2.0 Å, which is close to the value reported by Magini *et al.*[6] The Fe-Cl distances were found to be 2.26—2.35 Å for the solutions of Group 1 and Group 2. This value corresponds to the distance which is usually found for the octahedral chloro complexes in the crystals of iron(III) compounds: The distance is known to be 2.30 Å in $FeCl_3 \cdot 6H_2O$,[27] 2.36 Å in $FeSbCl_8 \cdot 8H_2O$[28] and 2.368 Å in FeOCl.[29] In the solutions of Group 1, the best result in the curve-fitting analysis was attained only when the contribution of Cl atoms was taken into account. Probably this means that a fraction of the solute is in the form of octahedral chloro complexes even in the relatively dilute solutions. The coordination numbers obtained for the solutions of Group 2, well correspond to $[FeCl_2(H_2O)_4]^+$. Possibly this is the main solute species in these solutions. The Fe-Cl distance found for DP is 2.22 Å, which is shorter than the Fe-Cl distances found for more dilute solutions. This Fe-Cl distance is close to the value expected for the tetrahedral complex $[FeCl_4]^-$, but the best fit was not attainable between the calculated and observed EXAFS oscillations when the contribution of O atoms was neglected. As we have already mentioned, the coordination numbers for the best fit are 3 and 2 for Cl and O, respectively. These average coordination numbers imply that the octahedral chloro complexes of the type $[FeCl_x(H_2O)_{6-x}]$ are coexisting with $[FeCl_4]^-$ in DP. Another point that we noted in the analysis of the Fe K-edge EXAFS of DP, is that no peak attributable to Fe-Fe could be found in the Fourier transform (see Fig. 9). Thus the dimeric species Fe_2Cl_6 is unlikely to exist, at least as one of the main solute species, in DP and in a concentrated solution of $FeCl_3$.

TABLE 3. RESULTS OF THE CURVE-FITTING ANALYSIS OF THE EXAFS DATA OF $FeCl_3$ SOLUTIONS

Solution	Coordination number		Distance (r/Å)		S*
	Cl	O	Fe-Cl	Fe-O	
0.1N	0.8	5.2	2.35 (4)	1.99 (2)	0.50
0.7N	0.8	5.2	2.28 (3)	2.00 (2)	0.40
3N	2.0	4.0	2.30 (3)	2.02 (2)	0.42
4N	1.8	4.2	2.30 (3)	2.02 (2)	0.60
0.5A	0.8	5.2	2.26 (3)	1.98 (2)	0.52
3A	2.0	4.0	2.30 (3)	2.01 (2)	0.60
Cl3A	2.0	4.0	2.30 (3)	2.04 (2)	0.50
DP	3.0	2.0	2.22 (2)	1.93 (4)	0.40

* The inaccuracy of these S values was found to be 20—30%.

Discussion

Summarizing the experimental results concerned with Fe K-edge EXAFS and XANES together with those of UV-visible absorption spectroscopy, we can derive the following conclusion for the solute state in the $FeCl_3$ aqueous solution. In the solutions of $FeCl_3$ concentration of 0.1—1 mol dm^{-3}, the solute is mainly in the state of $[Fe(H_2O)_6]^{3+}$ but partially in the state of other complexes, such as $[FeCl(H_2O)_5]^{2+}$. The average Cl coordination number increases with the increase of $FeCl_3$ concentration, and $[FeCl_2(H_2O)_4]^+$ becomes the main solute species in the solutions of the concentration of 3—4 mol dm^{-3}. Although the coexistence of $[FeCl_4]^-$ is expected from the results of UV-visible absorption spectroscopy, its amount is likely to be very small as far as we judge from the results of X-ray absorption spectroscopy. In the discussion given in the present paper, we have not explicitly taken up the hydrolysis products of the type $[FeCl_x(H_2O)_{6-x-y}(OH)_y]$ derivable from $[FeCl_x(H_2O)_{6-x}]$, which are reported to be formed in a non-acidified solution. Unfortunately, it is hard to distinguish the formers from the latters in the analysis of the EXAFS data. Therefore, whenever we say $[FeCl_x(H_2O)_{6-x}]$, it should be taken to include also the corresponding hydrolysis products.

Magini and Radnai considered that the main species in the solution of $FeCl_3$ concentration of about 4 mol dm^{-3} is $[FeCl_3(H_2O)_3]$.[5] But this kind of octahedral chloro complex has never been found among the crystals of iron(III) compounds, and the results of the present study have shown that the solute mainly exists in the state of $[FeCl_2(H_2O)_4]^+$ in the solution of the $FeCl_3$ concentration of 3—4 mol dm^{-3}, in disagreement with the conclusion by Magini and Radnai. There seems to be no indication for the existence of $[FeCl_3(H_2O)_3]$. Seemingly in an aqueous solution of $FeCl_3$, an octahedral complex becomes less stable than a tetrahedral complex as the Cl coordination number exceeds 2 probably because of the increase of the repulsive cis-cis interaction between Cl^- ions.

In the case of DP, the EXAFS data indicate that the solute is partly in the state of $[FeCl_4]^-$ and partly in the state of the octahedral chloro complexes. We estimated the fraction of $[FeCl_4]^-$ to be about 50% from the height of the pre-edge peak associated with 1s-3d transition. The remaining part is most likely to be in the state of $[FeCl_2(H_2O)_4]^+$. The Cl/Fe ratio derived from the analysis of the EXAFS data can be satisfactorily understood with this model. From the present study of XANES and UV-visible absorption spectra we can conclude that $[FeCl_4]^-$ starts to be formed at the $FeCl_3$ concentration of about 4 mol dm^{-3}, though the amount may not be so large at this concentration. Inoue *et al.* reported that the physical properties of the $FeCl_3$ aqueous solution abruptly change at the $FeCl_3$ concentration of about 4 mol dm^{-3}, and attributed this behavior to the formation of $[FeCl_4]^-$.[30] This is consistent with our conclusions.

It has been often assumed that the $FeCl_3$ dimer, Fe_2Cl_6, is formed in a concentrated $FeCl_3$ solution.[5,6,8] However, no peak corresponding to Fe-Fe distance of Fe_2Cl_6, which is reported to be 2.75—2.80 Å by Magini,[6] can be found in the Fourier transform of the EXAFS data of DP. Thus we conclude that Fe_2Cl_6 is unlikely to exist, at least as one of the dominant species, in a concentrated $FeCl_3$ solution.

The authours are grateful to Dr. T. Matsushita and Dr. H. Oyanagi for their helpful advice for the XAS measurement at the Photon Factory. The authors also thank to Dr. I. Ikemoto and Dr. N. Kosugi for their discussions and helps in the XAS experiments.

References

1) G. W. Brady, *J. Chem. Phys.*, **29**, 1371 (1958).
2) G. L. Standley and R. F. Kruh, *J. Chem. Phys.*, **34**, 1450 (1961).
3) G. W. Brady, M. B. Robin, and J. Varimbi, *Inorg. Chem.*, **3**, 1168 (1964).
4) M. D. Lind, *J. Chem. Phys.*, **46**, 2010 (1967).
5) M. Magini and T. Radnai, *J. Chem. Phys.*, **71**, 4255 (1979).
6) M. Magini, *J. Chem. Phys.*, **76**, 1111 (1982).
7) D. L. Wertz and M. L. Steele, *Inorg. Chem.*, **19**, 1652 (1980).
8) D. L. Wertz and M. D. Luter, *Inorg. Chem.*, **20**, 3118 (1981).
9) M. D. Luter and D. L. Wertz, *J. Phys. Chem.*, **85**, 3542 (1981).
10) G. Giubilo, M. Magini, G. Lichen, G. Pashina, G. Piccaluga, and G. Pinna, *Inorg. Chem.*, **22**, 1001 (1983).
11) "EXAFS Spectroscopy," ed by B. K. Teo and J. C. Joy, Plenum Press (1981).
12) M. Nomura, K. Asakura, U. Kaminaga, T.Mastushita, K. Kohra, and H. Kuroda, *Bull. Chem. Soc. Jpn.*, **55**, 3911 (1982).
13) H. Kuroda, I. Ikemoto, K. Asakura, H. Ishii, H. Shirakawa, T. Kobayashi, H. Oyanagi, and T. Mastushita, *Solid. State. Commun.*, **46**, 235 (1983).
14) M. Nomura, D. Sci. Thesis, The University of Tokyo, Tokyo, Japan, 1982.
15) H. Oyanagi, T. Matsushita, M. Ito, and H. Kuroda, *KEK Report* 83/30 (1984).
16) E. Rabinowitch and W. H. Stockmayer, *J. Am. Chem. Soc.*, **64**, 335 (1942).
17) H. L. Friedman, *J. Am. Chem. Soc.*, **74**, 5 (1952).
18) G. A. Gamlem and D. O. Jordan, *J. Chem Soc.*, **1953**, 1435.
19) S. Balt, *Mol. Phys.*, **14**, 233 (1968).
20) L. N. Mulay and P. W. Selwood, *J. Am. Chem. Soc.*, **76**, 6207 (1954).

21) The height of the pre-edge peak observed in the spectra of $[FeCl_4]^-$ and $[FeCl_2(H_2O)_4]^+$ were used for the evaluation of the amount of $[FeCl_4]^-$ from the spectrum of DP.

22) "International Tables for X-ray Crystallography," ed by C. H. Macgillavry, G. D. Rieck, and K. Lonsdale, Kynoch Press (1962).

23) The relative positions of the points in this plot were not affected by changing the E_0 value or by extending the k range of the EXAFS data used in Fourier transformation. No essential change was resulted even if we took the Fourier transform of $k \cdot \chi(k)$ instead of that of $k^3 \cdot \chi(k)$.

24) B. K. Teo, M. R. Antonio, and B. A. Averill, *J. Am. Chem. Soc.*, **105**, 3751 (1983).

25) B. K. Teo, P. A. Lee, A. L. Simons, P. Eisenberger, and B. M. Kincaid, *J. Am. Chem. Soc.*, **99**, 3854 (1977); P. A. Lee, B. K. Teo, and A. L. Simons, *ibid*, **99**, 3856 (1977).

26) From the study of the reference samples, the S value was concluded to be about 0.5 both for Cl and O.

27) M. D. Lind, *J. Chem. Phys.*, **47**, 990 (1967).

28) A. Ferrari, L. Cavalca, and M. Tani, *Gazz. Chim. Ital.*, **87**, 22 (1957).

29) M. D. Lind, *Acta. Crystallogr., Sect. B*, **26**, 1058 (1970).

30) Y. Inoue, S. Seki, M. Yokoyama, N. Masaie, and Y. Kanaji, *Nippon Kagaku Kaishi*, **1974**, 2297.

31) N. J. Hair and J. K. Beattie, *Inorg. Chem.*, **16**, 245 (1977).

32) B. Zaslow and R. E. Rundle, *J. Phys. Chem.*, **61**, 490 (1957).

33) B. N. Figgis, C. L. Taston, R. P. Sharme, and A. H. White, *Aust. J. Chem.*, **31**, 2717 (1976).

34) J. K. Bearrje and C. J. Moore, *Inorg. Chem.*, **21**, 1292 (1982).

The Co-amination of Phenol and Cyclohexanol with Palladium-on-carbon Catalyst in the Liquid Phase. An Application of a Hydrogen-transfer Reaction

Hideaki HAMADA, Makoto YAMAMOTO,† Yasushi KUWAHARA, Takehiko MATSUZAKI, and Katsuhiko WAKABAYASHI*

National Chemical Laboratory for Industry, Yatabe, Tsukuba, Ibaraki 305
†Tokyo Metropolitan Industrial Technic Institute, Nishigaoka, Kita-ku, Tokyo 115
(Received September 19, 1984)

Phenol and Cyclohexanol are simultaneously aminated to aniline and cyclohexylamine by ammonolysis with the palladium-on-carbon catalyst in the liquid phase, although the amination of either phenol or cyclohexanol hardly occurs without the other. In contrast, carbon-supported ruthenium, rhodium, and platinum catalysts are ineffective for this co-amination; they are active only for the amination of cyclohexanol to cyclohexylamine. These results are explained by the specific activity of palladium for hydrogen transfer between phenol and cyclohexanol.

It is well known that the amination of phenol to aniline by ammonolysis catalyzed by acidic catalysts, such as silica-alumina,[1,2] zeolites,[3] and metal chlorides.[4] Supported metal catalysts are known to be effective for the amination of cyclohexanol to cyclohexylamine, the hydroamination of phenol to cyclohexylamine, and the dehydroamination of cyclohexanol to aniline. For example, Richardson and Lu[5] reported that the vapor-phase dehydroamination of cyclohexanol to aniline took place over supported platinum catalysts. Recently, it has been found that these supported metal catalysts, in cooperation with hydrogen or hydrogen-transfer agents, are also effective for the amination of phenol to aniline. Ono and Ishida[6] reported that phenol was successfully aminated to aniline with ammonia and hydrogen over palladium-on-alumina in the vapor phase. We previously reported[7] that phenol was aminated with ammonia with palladium-on-carbon in the presence of cyclohexanone, which is a hydrogen-transfer agent.

The following reaction pathway has been proposed for the amination of phenol over supported metal catalysts:[7]

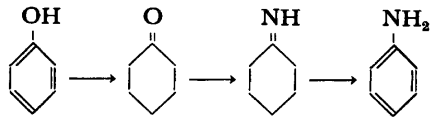

(1)

The first step of this scheme is the formation of cyclohexanone due to the hydrogenation of phenol, which means that hydrogen or hydrogen-transfer agents are needed.

On the other hand, the amination of cyclohexanol to cyclohexylamine with ammonia over supported metal catalysts has been considered to proceed through the pathway indicated below.[8] In this case, the first step is the dehydrogenation of cyclohexanol to cyclohexanone.

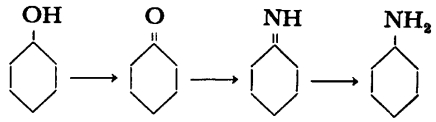

(2)

Taking these two reaction schemes into consideration, we investigated the possibility of the liquid-phase co-ammonolysis of phenol and cyclohexanol; we have found that phenol and cyclohexanol can be simultaneously aminated with the palladium-on-carbon catalyst.

We have already reported a part of our results in a letter.[9] This paper is a detailed report of this co-amination reaction. The specific catalytic activity of palladium and the reaction scheme are also discussed.

Experimental

Catalysts and Reagents. The 5 wt% metal-on-carbon catalysts were of commercial origin (Nippon Engelhard Co.). The reagents were of a guaranteed reagent grade and were used without further purification except in the case of *N*-cyclohexylaniline, which was prepared by the reaction of phenol and cyclohexylamine using palladium-on-carbon. The ammonia and hydrogen were supplied from gas cylinders.

Procedures. Each experiment was run in a 100-cm^3 stainless-steel autoclave. Unless otherwise specified, phenol, cyclohexanol, and the catalyst were put into the autoclave. The autoclave was sealed, purged with hydrogen, and evacuated successively, and then ammonia was introduced into the autoclave from a pressure-resistant gas-collecting tube. The autoclave thus prepared was set in an electric furnace and heated for the reaction. At the end of each reaction, the autoclave was cooled and the excess ammonia was released. The contents were filtered to remove the catalyst. 2-Propanol was used as a solvent to assist in removing the reaction mixture from the autoclave and in washing the filter cake. The filtered reaction mixture was analyzed by means of gas chromatography. A 5-m column of Silicon DC-550 (20 wt%) on Chromosorb W AW-DMCS, operating at 145 °C, was used to analyze phenol, aniline,

cyclohexylamine, and cyclohexanone. A 3-m column of PEG-20 M (20 wt%) on Chromosorb W AW-DMCS, operating from 130 °C to 220 °C, was used to analyze cyclohexanol, dicyclohexylamine, *N*-cyclohecylaniline, and diphenylamine.

Results and Discussion

Need of Coexistence of Phenol and Cyclohexanol for Co-amination. Mixtures of phenol and cyclohexanol in various compositions were allowed to react with ammonia in the presence of palladium-on-carbon at 250 °C for 3 h. Figure 1 shows the effect of the mixture composition. Aniline and cyclohexylamine were obtained in high yields when nearly equal amounts of phenol and cyclohexanol were used, but the amination of phenol or cyclohexanol alone hardly took place at all. The maximum aniline yield was obtained at a 50% phenol content, while the cyclohexylamine yield reached its maximum value at a 20% phenol content. From these results, it is concluded that the amination of phenol and cyclohexanol with the palladium-on-carbon catalyst is promoted by the coexistence of the two components. *N*-cyclohexylaniline and dicyclohexylamine were also obtained as by-products. These by-products are considered to be formed by means of condensation reactions.

Effect of Reaction Temperature. The effect of the reaction temperature of the co-ammonolysis of equal amounts of phenol and cyclohexanol was examined in the temperature range of 200—270 °C with the palladium-on-carbon catalyst. As is shown in Fig. 2, the product yields increased with the reaction temperature. It should be noted thet the aniline yield was always higher than the cyclohexylamine yield, and that a considerable amount of *N*-cyclohexylaniline was formed at higher temperatures.

Effect of Ammonia Amount. Figure 3 shows the effect of the amount of ammonia. As can be seen in this figure, the product distribution changed greatly with the amount of ammonia. When phenol and cyclohexanol were allowed to react in the absence of ammonia, cyclohexanone was formed as the only product because of the hydrogen-transfer from cyclohexanol to phenol.

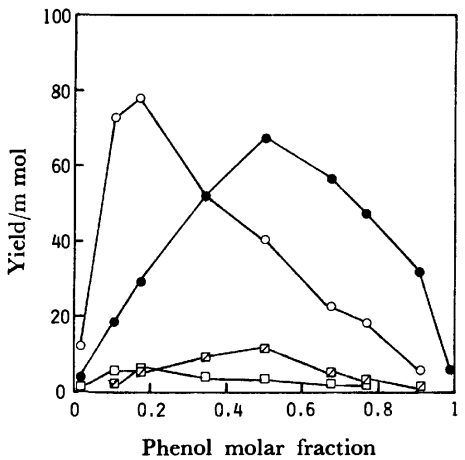

Fig. 1. Ammonolysis of phenol and cyclohexanol with various composition. Phenol and cyclohexanol (total 0.2 mol) are allowed to react with ammonia (1 mol) at 250 °C for 3 h over Pd/C (1 g).
●: Aniline yield, ○: cyclohexylamine yield, ⊠: *N*-cyclohexylaniline yield ×2, □: dicyclohexylamine yield ×2.

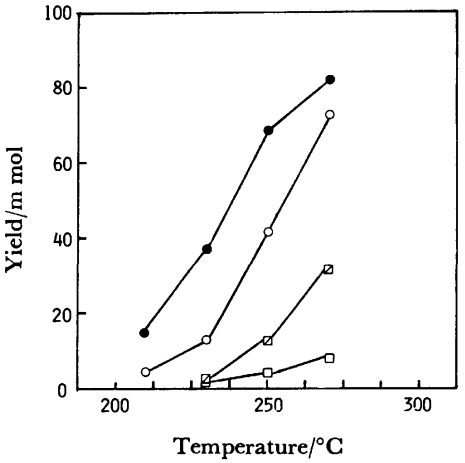

Fig. 2. Effect of reaction temperature on the co-amination. Phenol (0.1 mol) and cyclohexanol (0.1 mol) are allowed to react with ammonia (1 mol) for 3 h over Pd/C (1 g).
●: Aniline yield, ○: cyclohexylamine yield, ⊠: *N*-cyclohexylaniline yield ×2, □: dicyclohexylamine yield ×2.

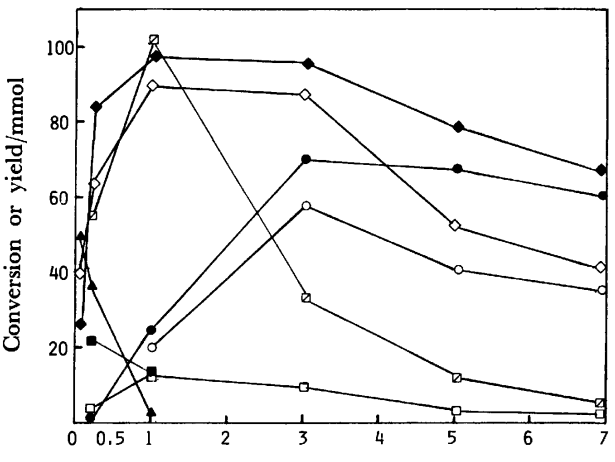

Fig. 3. Effect of ammonia amount on the co-amination. Phenol (0.1 mol) and cyclohexanol (0.1 mol) are allowed to react with ammonia at 250 °C for 3 h over Pd/C (1 g).
◆: Phenol conversion, ◇: cyclohexanol conversion, ●: aniline yield, ○: cyclohexylamine yield, ▲: cyclohexanone yield, ■: diphenylamine yield ×2, ⊠: *N*-cyclohexylaniline yield ×2, □: dicyclohexylamine yield ×2.

When the amount of ammonia increased to 0.2 mol, which was equivalent to the molar quantities of phenol plus cyclohexanol, the cyclohexanone yield decreased rapidly, while amination products composed mainly of *N*-cyclohexylaniline were observed to increase in yield. In this case, there was also a little formation of dicyclohexylamine, diphenylamine, aniline, and cyclohexylamine.

When the amount of ammonia increased in the ranges beyond 0.2 mol, the conversions of phenol and cyclohexanol gradually decreased again; the yields of *N*-cyclohexylaniline and dicyclohexylamine also decreased. Therefore, the selectivities to aniline and cyclohexylamine increased. In the presence of excess ammonia, the main products shifted to aniline and cyclohexylamine.

Effect of Reaction Time. The effect of the reaction time is shown in Fig. 4. The conversions and yields increased with the reaction time. It is noteworthy that the formation of aniline from phenol prevailed over that of cyclohexylamine from cyclohexanol at the initial stage of reaction.

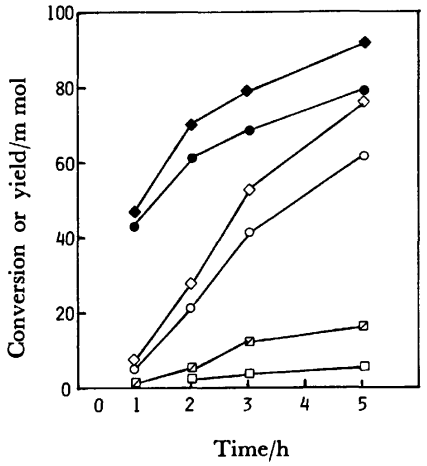

Fig. 4. Effect of reaction time on the co-amination. Phenol (0.1 mol) and cyclohexanol (0.1 mol) are allowed to react with ammonia (1 mol) at 250 °C over Pd/C (1 g).
◆: Phenol conversion, ◇: cyclohexanol conversion, ●: aniline yield, ○: cyclohexylamine yield, ⊠: *N*-cyclohexylaniline yield ×2, □: dicyclohexylamine yield ×2.

Cataltic Activities of Carbon-supported Platinum-group Metals. The catalytic activities of various carbon-supported platinum-group metals are compared in Table 1. As may be seen in this table, palladium was the only effective catalyst for the co-amination. Ruthenium, rhodium, and platinum were ineffective for the co-amination, and aniline was not formed from phenol, though the amination of cyclohexanol to cyclohexylamine did occur.

Reaction Scheme of Co-amination. The co-amination of phenol and cyclohexanol with the palladium-on-carbon catalyst is considered to proceed through the following reaction steps:

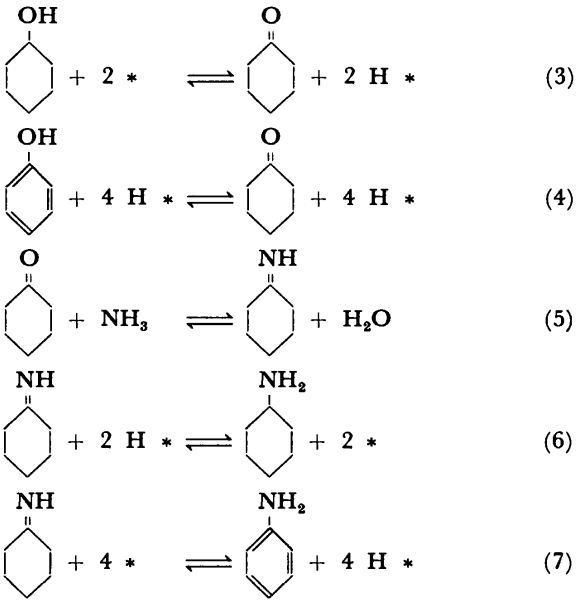

In these equations, * and H* represent an empty catalytic site and an adsorbed hydrogen atom respectively.

In the absence of cyclohexanol, the amination of phenol cannot occur because there is no adsorbed hydrogen, which is necessary for Eq. 4. Howerver, in the co-existence of phenol and cyclohexanol, they are effectively converted into cyclohexanone through hydrogen-transfer by Eqs. 3 and 4. In fact, the formation of a large amount of cyclohexanone by the reaction of phenol and cyclohexanol was observed in the absence of ammonia (Fig. 3). The resulting cyclohexanone reacts easily with ammonia to be converted into cyclohexanimin (Eq. 5), which is either hydrogenated

Table 1. Activities of carbon-supported platinum-group metal catalysts

Catalyst	Product (Yield/m mol)			
	Aniline	Cyclohexylamine	*N*-Cyclohexylaniline	Dicyclohexylamine
Pd/C	68	41	6.0	1.9
Ru/C	0	71	0	0
Rh/C	4.0	44	0	0
Pt/C	1.9	74	0	0

Phenol (0.1 mol) and cyclohexanol (0.1 mol) are allowed to react with ammonia (1 mol) in the presence of a catalyst (1 g) at 250 °C for 3 h.

TABLE 2. AMMONOLYSIS OF PHENOL-CYCLOHEXYLAMINE OR ANILINE-CYCLOHEXANOL MIXTURES

Reactant	Product (Yield/m mol)					
	Phenol	Cyclohexanol	Aniline	Cyclohexylamine	*N*-Cyclohexylaniline	Dicyclohexylamine
Phenol-cyclohexylamine	9.3	0.7	68	77	18	3.8
Aniline-cyclohexanol	0	63	98	32	3.2	1.4

The reactant mixtures (0.1 mol+0.1 mol) are allowed to react with ammonia (1 mol) in the presence of Pd/C (1 g) at 250 °C for 3 h.

to cyclohexylamine (Eq. 6) or dehydrogenated to aniline (Eq. 7).

Figures 2 and 4 suggest that the amination of phenol to aniline (Steps 4, 5, and 7) prevails over that of cyclohexanol to cyclohexylamine (Steps 3, 5, and 6) in the early stages of the reaction. The factor which determines the ratio of these two reaction rates is not clear, but the concentration of adsorbed hydrogen may play an important role.

Taking the above reaction schemes into consideration,it is conceivable that the amination rate of phenol to aniline is accelerated in the presence of cyclohexylamine, because hydrogen-transfer can take place between phenol and cyclohexylamine. Also, the amination rate of cyclohexanol to cyclohexylamine may be accelerated in the presence of aniline. In order to examine the probable validity of these assumptions, phenol–cyclohexylamine and cyclohexanol–aniline mixtures were allowed to react with ammonia in the presence of the palladium-on-carbon catalyst. The results, shown in Table 2, support these assumptions.

Specificity of Palladium. As has been mentioned above, palladium-on-carbon was the only effective catalyst for the co-amination of phenol and cyclohexanol among the carbon-supported platinum-group metal catalysts. This specificity could be interpreted in terms of its specific catalytic activity for hydrogen-transfer reactions.

To get further insights into the specificity of palladium, the hydroamination of phenol was studied. Figure 5 shows the effect of the initial hydrogen pressure on the hydroamination of phenol with carbon-supported palladium. The yields of cyclohexylamine and dicyclohexylamine as well as the phenol conversion increased with an increase in the hydrogen pressure. It should be noted that considerable amounts of aniline were formed, along with *N*-cyclohexylaniline, at low hydrogen pressures. Figure 6 shows the effect of the reaction time. It is also worth noting that cyclohexylamine and dicyclohexylamine were formed at an early stage of the reaction, and that aniline and *N*-cyclohexylaniline increased in their yields with the reaction time. The latter result is consistent with the results in Table 2.

In order to compare the ruthenium catalyst with palladium, the hydroamination of phenol with

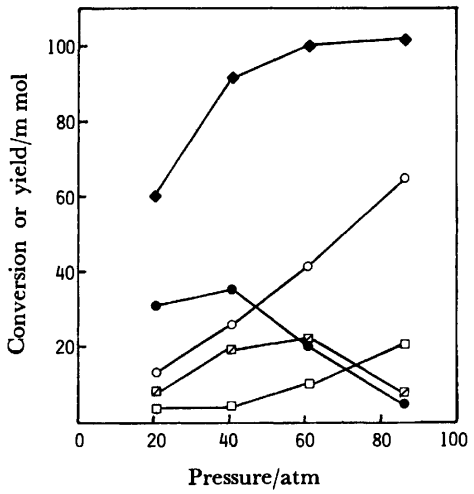

Fig. 5. Effect of initial hydrogen pressure on the hydroamination of phenol over Pd/C. Phenol (0.1 mol) is allowed to react with ammonia (0.6 mol) and hydrogen at 250 °C for 3 h over Pd/C (0.5 g).
◆: Phenol conversion, ●: aniline yield, ○: cyclohexylamine yield, ⊠: *N*-cyclohexylaniline yield ×2, □: dicyclohexylamine yield ×2.

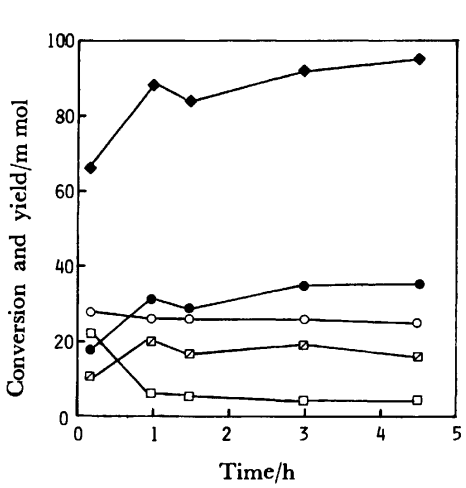

Fig. 6. Effect of reaction time on the hydroamination of phenol over Pd/C. Phenol (0.1 mol) is allowed to react with ammonia (0.6 mol) and hydrogen (40 atm) at 250 °C over Pd/C (0.5 g).
◆: Phenol conversion, ●: aniline yield, ○: cyclohexylamine yield, ⊠: *N*-cyclohexylaniline yield ×2, □: dicyclohexylamine yield ×2.

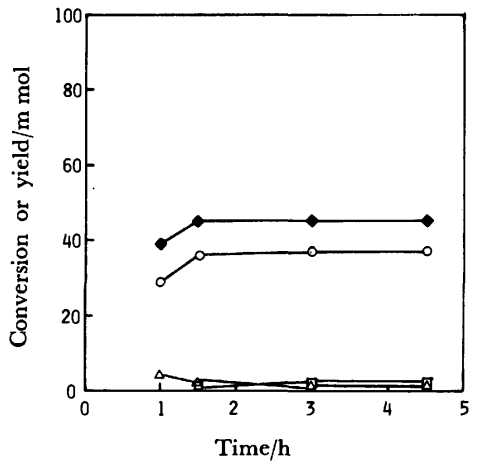

Fig. 7. Effect of reaction time on the hydroamination of phenol over Ru/C. Phenol (0.1 mol) is allowed to react with ammonia (0.6 mol) and hydrogen (40 atm) at 250 °C over Ru/C (0.5 g).
◆: Phenol conversion, ○: cyclohexylamine yield, △: cyclohexanol yield, □: dicyclohexylamine yield ×2.

ruthenium-on-carbon was studied. The effect of the reaction time is shown in Fig. 7. In this case, aniline was not formed, although the hydroamination of phenol to cyclohexylamine did take place. Therefore, it is concluded that ruthenium cannot catalyze hydrogen-transfer reactions. This conclusion might also apply to the cases of rhodium and platinum.

From these results, it is clear that the specificity of palladium is due to its unique catalytic activity for hydrogen-transfer reactions. Further work is necessary to elucidate the reason for this specificity of palladium.

References

1) R. S. Barker, U. S. Patent 3272865 (1966).
2) I. Mckechnie, F. Bayer, and J. Drennan, *Chem. Eng.*, Dec. 29, p. 26 (1980).
3) M. Yamamoto, N. Takamiya, and S. Murai, *Nippon Kagaku Kaishi*, **1974**, 2135.
4) H. Hamada, T. Matsuzaki, and K. Wakabayashi, *Nippon Kagaku Kaishi*, **1980**, 613.
5) J. T. Richardson and W. -C. Lu, *J. Catal.*, **42**, 275 (1976).
6) Y. Ono and H. Ishida, *J. Catal.*, **72**, 121 (1981).
7) H. Hamada, T. Matsuzaki, and K. Wakabayashi, *Nippon Kagaku Kaishi*, **1979**, 248.
8) A. Guyot and M. Fournier, *Bull. Soc. Chim.*, **47**, 203 (1930).
9) H. Hamada, M. Yamamoto, T. Matsuzaki, and K. Wakabayashi, *Chem. Lett.*, **1980**, 239.

 © 1985 The Chemical Society of Japan Bull. Chem. Soc. Jpn., 58, 1556—1559 (1985) [Vol. 58, No. 5

Lumiflavin-sensitized Photooxygenation Accelerated by Adenine. III. Flash Photolytic Studies

Akio YOSHIMURA* and Shunji KATO†
Chemistry Department, College of General Education, Osaka University, Toyonaka, Osaka 560
(Received November 20, 1984)

Flash photolytic studies have been made of aqueous systems of lumiflavin-adenine-tryptophan, where the accelerating effect of adenine is observed on the lumiflavin-sensitized photooxygenation of tryptophan. The electron transfer occurs first from adenine to the triplet state of lumiflavin. When a little tryptophan is present in the aerated solutions, the tryptophan is oxidized by the successive electron-transfer reactions and the tryptophan decomposes instead of adenine. The rate parameter for each process has been determined.

The present authors showed previously that the lumiflavin-sensitized photooxygenation of tryptophan is accelerated by the addition of adenine when the concentration of tryptophan is low.[1] The singlet oxygen can be excluded from the intermediates on the basis of the following results: This effect is specific for flavin dyes (containing FAD), and the quantum yield using flavin dyes, which is higher than that using other dyes, increases with the oxygen concentration at very low oxygen concentrations, but decreases at higher concentrations. The addition of adenine accelerates the flavin-sensitized photooxygenation not only of tryptophan, but also of many reactants (indole, 3-indoleacetic acid, histidine, methionine, guanine, *etc.*),[1,2] and it does not affect the reaction products.[2]

To make clear this accelerating effect of adenine, flash photolytic studies have been made of these systems. Several papers have been published on the flash photolysis of flavin dyes.[3-5] In the present study, the electron transfer from adenine to the triplet state of lumiflavin and the succeeding reactions, especially in the presence of oxygen, were investigated. On irradiation, riboflavin loses its 440 nm absorption (photofading), but in the case of lumiflavin which does not have a ribityl side-chain, photofading does not occur at all in air.

Experimental

Materials. The lumiflavin was synthesized by the method of Hemmerich *et al.*[7] The adenine was recrystalized from water. The other reagents used were of a G. R. Grade.

Apparatus and Procedure. The flash photolysis was carried out in a 10-cm cylindrical quartz cell thermostated (25±0.1 °C) with circulated water, with exciting light from two xenon flash lamps connected in series to a 0.3 μF condensor charged to a potential of 18 kV (FWHM: 2 μs) through blue glass filters (Toshiba V-42). The monitoring light from a xenon short-arc lamp (Canrad-Hanovia L5122) was passed through the reaction cell and a Nalumi RM-23 monochromator and was detected with a Hamamatsu R928 photomultiplier. The transient signals were stored in a transient memory (Kawasaki Electronica M-500T; 0.5 μs; 10 bits×1 k words) and then transferred to a 16-bit minicomputer made by Dr. Tatebe[8] (34 k-word memory; 32 commands; cycle time: 0.4 μs). The subtraction of the signal due to the scatter light or the fluorescence, the calculation of the transient-absorbance change (Δabsorbance)(which was accumulated several times in the case of a weak signal), and the first- and second-order decay analysis plotting ln(Δabsorbance) and 1/(Δabsorbance) were carried out by the use of the computer.

The photolysis by a steady light of 436 nm was performed as previously described[1] at 25±0.1 °C.

Unless otherwise noted, all the experiments were carried out in a 0.05 M†† phosphate buffer at pH 7.2. The solution with a reduced concentration of oxygen was prepared by bubbling it with a mixture of oxygen and nitrogen of a known composition.

Results and Discussion

The fluorescence of lumiflavin was little quenched by adenine, tryptophan, oxygen, and iodide ions at the concentrations studied in this paper; therefore, the reactions of irradiated lumiflavin with these substances can be restricted to the reactions through the triplet state of lumiflavin. The degree of the conversion of lumiflavin to the triplet state by a single flash excitation was estimated from the difference in transient fluorescence intensities with and without sufficient triplet quenchers; iodide ions.[9] By the use of a 50 J flash excitation of 5 μM lumiflavin in the deaerated solution, 56% of lumiflavin was accumulated in the triplet state during the flash pulse. Using this ratio, the molar (decadic) absorption coefficient of the triplet state of lumiflavin was estimated to be 4400±300 M^{-1} cm^{-1} at 700 nm.

It has been reported that the lumiflavin triplet state is reduced to its semiquinone radical by some reductants; the molar absorption coefficient of the radical at pH 7.2 was estimated to be 3400±200 M^{-1} cm^{-1} at 600 nm.[4] The reactions of the lumiflavin triplet state were followed in the solutions

† Present address: Kobegakuin University, Nishi-ku, Kobe, 673.

†† 1 M=1 mol dm^{-3}.

containing 5 μM lumiflavin and 20—60 μM of each reactant, such as the tryptophan, adenine, oxygen, and iodide ions, at 700 nm. The electron transfer to lumiflavin occurred in the quenching reactions of the lumiflavin triplet state by the tryptophan and adenine (the observed efficiencies were 70%), while the semiquinone of lumiflavin was not observed in the quenching by the oxygen and iodide ions. The quenching-rate parameters measured were as follows:

$$^3LF + Trp \xrightarrow{k_1} LF^{\cdot-} + Trp^{+} \quad (LF + Trp) \quad (3.7\pm0.2)\times10^9\ M^{-1}\ s^{-1}, \quad (1)$$

$$^3LF + Ade \xrightarrow{k_2} LF^{\cdot-} + Ade^{+} \quad (LF + Ade) \quad (1.6\pm0.2)\times10^9\ M^{-1}\ s^{-1}, \quad (2)$$

$$^3LF + O_2 \xrightarrow{k_3} LF + O_2 \quad (1.2\pm0.1)\times10^9\ M^{-1}\ s^{-1}, \quad (3)$$

$$^3LF + I^- \xrightarrow{k_4} LF + I^- \quad (5.8\pm0.3)\times10^9\ M^{-1}\ s^{-1}, \quad (4)$$

$$^3LF \xrightarrow{k_5} LF \quad (1.5\pm0.1)\times10^3\ s^{-1}, \quad (5)$$

$$^3LF + LF \xrightarrow{k_6} 2LF \quad (7\pm0.5)\times10^8\ M^{-1}\ s^{-1}, \quad (6)$$

where LF, ^{3}LF, $LF^{\cdot-}$, Trp^{+}, and Ade^{+} denote the ground state, the triplet state, and the semiquinone radical of lumiflavin, the half-oxidized tryptophan radical, and the half-oxidized adenine radical respectively. The triplet state of lumiflavin is also quenched by the triplet state of lumiflavin, but the triplet-triplet quenching is negligible under weak light. It is not necessary to distinguish between Reactions 5 and 6 in this work, and the sum total of k_5+k_6[LF] ($5000\pm300\ s^{-1}$ at 5 μM lumiflavin) was used for the analysis.

The lumiflavin semiquinone decayed by the second-order because of the back-electron-transfer reactions. In the flash photolysis of deaerated solutions of lumiflavin with adenine or tryptophan, the lumiflavin was almost completely recovered, with little permanent photobleaching. The disproportionation reaction of the lumiflavin semiquinone was negligible when the lumiflavin was reduced by tryptophan or adenine.

In the flash photolysis of aerated solutions of lumiflavin, the lumiflavin semiquinone was also observed in the presence of sufficient tryptophan or adenine, as is shown in Fig. 1. The decay of the semiquinone was apparently first- order and was faster than that in the deaerated solutions. It has been reported that the semiquinone reacts with oxygen in the anionic form, but not in the neutral form.[6] The pK_a value of the lumiflavin semiquinone has been reported to be 8.36 from this reactivity with oxygen. In the aerated conditions, the electron-transfer reaction from lumiflavin semiquinone to oxygen preceded the back-electron-transfer reactions, as has been described above. The

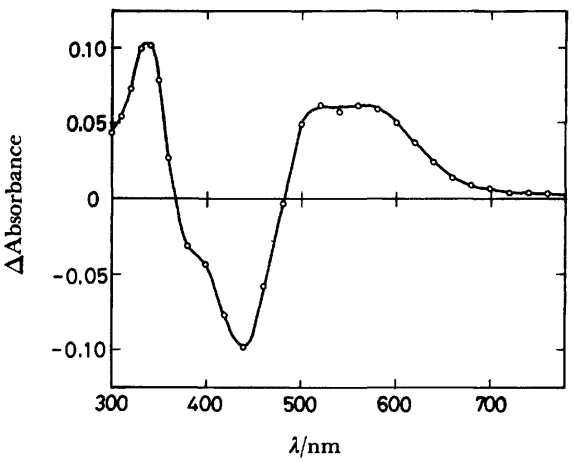

Fig. 1. The transient absorption spectrum at 40 μs after the flash excitation of 5 μM lumiflavin with 0.3 mM adenine in the aerated solutions at pH 7.2. (10-cm cell)

pseudo-first-order reaction of lumiflavin semiquinone with oxygen and the second-order recombination reactions are observed as follows:

$$LF^{\cdot-}(LFH\cdot) + O_2 \xrightarrow{k_7} LF + O_2^{\cdot-} \quad (3.7\pm0.2)\times10^7\ M^{-1}\ s^{-1}, \quad (7)$$

$$LF^{\cdot-}(LFH\cdot) + Trp^{+} \xrightarrow{k_8} LF + Trp \quad (2\pm0.4)\times10^9\ M^{-1}\ s^{-1}, \quad (8)$$

$$LF^{\cdot-}(LFH\cdot) + Ade^{+} \xrightarrow{k_9} LF + Ade \quad (2\pm0.4)\times10^9\ M^{-1}\ s^{-1}. \quad (9)$$

The rate parameter, k_7, is the apparent value at pH 7.2; it increases with the pH because of the increment in the ratio of $LF^{\cdot-}$/LFH·. Reaction 7 is the main reaction of the lumiflavin semiquinone in the steady-light photolysis of aerated solutions when the concentration of the intermediate is much lower than the concentration of oxygen.

When lumiflavin was irradiated in the presence of adenine and oxygen, a transient absorption was observed after the disappearance of semiquinone. This transient absorption at pH 7.2 was not appreciable enough for a quantitative analysis to be done because of the overlap of the absorbance change of lumiflavin semiquinone. On the other hand, at pH 8.5, the semiquinone disappeared very fast, reacting with oxygen, and a clear absorption spectrum of the long-lived species was obtained. The transient absorption spectrum after the lumiflavin semiquinone was completely disappeared is shown in Fig. 2-a. This species with a long lifetime was safely assigned to the half-oxidized adenine radical, because the addition of 10 μM tryptophan hastened the decay. This result is in accord with the previously reported results that the lumiflavin-sensitized photooxygena-

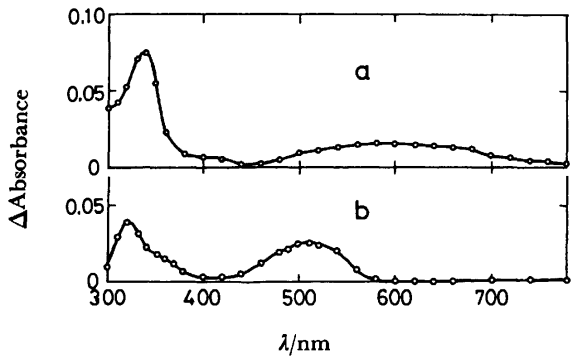

Fig. 2. The transient absorption spectra at 100 μs after the flash excitation of 5 μM lumiflavin with 0.3 mM adenine (a) and with 0.2 mM tryptophan (b) in the aerated solutions at pH 8.5. (10-cm cell)

tion of dilute tryptophan in a steady-light photolysis was accelerated by the addition of adenine.[1] The decomposition of tryptophan was observed also in this flash photolysis. The half-oxidized adenine radical decayed faster in the deaerated solutions than in the aerated solutions as a result of the electron-transfer reaction between Ade^{+} and LF^{-} in the deaerated solutions. The absorption coefficient of this half-oxidized adenine radical was estimated to be $5100\pm300\ M^{-1}\ cm^{-1}$ at 340 nm, assuming that the initial production of lumiflavin semiquinone is equal to that of the half-oxidized adenine radical in this aerated solution with sufficient adenine.

In the presence of tryptophan instead of adenine, the transient absorption spectrum obtained after the disappearance of lumiflavin semiquinone is shown in Fig. 2-b. This spectrum was assigned to the half-oxidized neutral radical of tryptophan (the pK_a of the radical is 4.3), as is shown in Ref. 10. The molar absorption coefficient at 510 nm was estimated in the above-mentioned manner to be $1700\pm100\ M^{-1}\ cm^{-1}$, which was in agreement with the reported value ($1800\pm50\ M^{-1}\ cm^{-1}$).[10] A similar transient spectrum was obtained with indole instead of tryptophan.

The transient absorption of the half-oxidized tryptophan radical was observed also by means of the flash-excitation lumiflavin with 0.3 mM adenine and 10 μM tryptophan, it was not observed without adenine because little redox reaction occurred in the aerated solution with such a little tryptophan.

The decay-rate parameter of the half-oxidized tryptophan radical in the aerated solutions (pH 8.5) was measured at 510 nm as follows:

$$Trp^{+} + O_2^{-} \xrightarrow{k_{10}} \text{Products} \qquad (1.5\pm0.3)\times10^{9}\ M^{-1}\ s^{-1}, \quad (10)$$

while those of the half-oxidized adenine radical (pH 8.5) were observed at 340 nm as:

$$Ade^{+} + O_2^{-} \xrightarrow{k_{11}} Ade + O_2 \qquad (1.2\pm0.3)\times10^{9}\ M^{-1}\ s^{-1}, \quad (11)$$

$$Ade^{+} + Trp \xrightarrow{k_{12}} Ade + Trp^{+} \qquad (1.6\pm0.3)\times10^{8}\ M^{-1}\ s^{-1}. \quad (12)$$

A little decomposition of adenine was observed upon successive flashing on lumiflavin in the presence of oxygen (0.1 μM/flash), but the addition of a little tryptophan suppressed the decomposition of adenine (10 μM tryptophan is sufficient to suppress the adenine decomposition completely) and tryptophan decomposed as has been described above. This effect was continued after the complete decomposition of tryptophan; the photooxygenation products of tryptophan also suppressed the decomposition of adenine. The half-oxidized adenine radical with a long lifetime takes an electron from the substrates, and so the indirect sensitized photooxygenation of the substrates occurs. Now, the accelerating effect of adenine on the lumiflavin-sensitized photooxygenation at a low concentration of reactants can be clarified from the flash photolysis, shown schematically as follows:

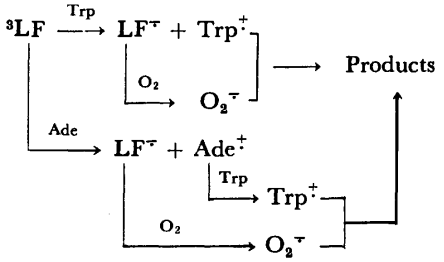

It had been reported in the previous paper[1] that the effect of the addition of the iodide ion as a triplet-quencher for the lumiflavin-sensitized photooxygenation was independent of the presence or absence of adenine; this was regarded as the result of no direct reactivity of adenine with the triplet state of lumiflavin. However, the flash photolysis now shows that adenine reacts with the triplet state of lumiflavin. To resolve this conflict, the steady-light photolysis of the lumiflavin-sensitized photooxygenation of tryptophan has been reexamined over a wide range of concentrations of adenine and iodide ions.

The Stern-Volmer equation for the inhibition by iodide ions as against the lumiflavin-sensitized photooxygenation of tryptophan is written as:

$$\frac{\Phi_0}{\Phi_I} = 1 + \frac{k_4[I^-]}{k_1[Trp]+k_3[O_2]+k_5+k_6[LF]}, \quad (13)$$

where Φ_I and Φ_0 denote the quantum yield of the photooxygenation with and without iodide ions. The inverse of the slope of the Stern-Volmer plots, which were measured at various concentrations of tryptophan, were plotted against the concentration of tryp-

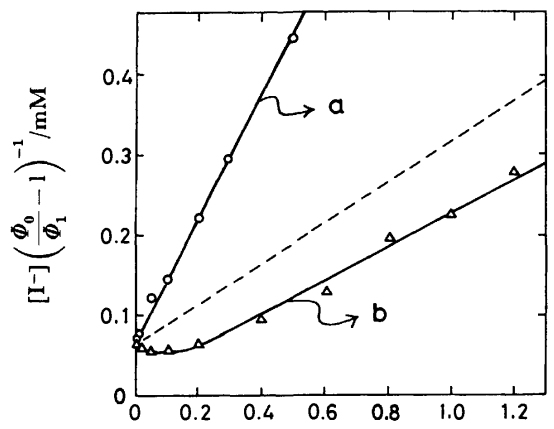

Fig. 3. The inhibition of iodide ion on the lumiflavin-sensitized photooxygenation of tryptophan in the presence and absence of adenine. Variation of the inverse of Stern-Volmer plots with the concentration of tryptophan (a) and adenine with 0.5 μM tryptophan (b).

tophan, as is shown in Fig. 3-a; the obtained linear relationship is written as:

$$[I^-]/\left(\frac{\Phi_0}{\Phi_I}-1\right)=\frac{k_1[\mathrm{Trp}]+k_3[O_2]+k_5+k_6[\mathrm{LF}]}{k_4}. \quad (14)$$

In the presence of adenine in various concentrations and a small amount of tryptophan (5 μM), the inhibiting effect of the iodide ion against the lumiflavin-sensitized photooxygenation of tryptophan was examined in the same manner. A linear relationship was also observed in the Stern-Volmer plot at every adenine concentration. In the presence of a large excess of adenine, the direct reaction between tryptophan and the triplet state of lumiflavin can be neglected; hence, the following simple relation between the inverse of the slope of the Stern-Volmer plots and the concentration of adenine can be expected by replacing the k_1[Trp] in Eq 14 with k_2[Ade]:

$$[I^-]/\left(\frac{\Phi_0}{\Phi_I}-1\right)=\frac{k_2[\mathrm{Ade}]+k_3[O_2]+k_5+k_6[\mathrm{LF}]}{k_4}. \quad (15)$$

The observed values are shown in Fig. 3-b; they deviate below from the broken line, which shows the values calculated from Eq. 15 using the rate parameter mentioned above. The inhibiting effect of the iodide ion is larger than that simply expected; the iodide ion quenches not only the triplet state of lumiflavin, but also any other intermediate. The slope of the Stern-Volmer plots in the presence of 0.2 mM adenine is, by chance, equal to that with dilute tryptophan and without adenine. In the previous work,[1] from this accidental coincidence of the effect of iodide ions, it was incorrectly inferred that adenine does not directly attack the triplet state of lumiflavin.

This additional inhibiting effect by iodide ions was also examined by means of flash photolysis. The decay of the half-oxidized adenine radical was examined in the presence of 0.05—0.2 mM of iodide ions at pH 8.5; the following reaction was thus observed:

$$\mathrm{Ade}^+ + I^- \longrightarrow \mathrm{Ade} + I\cdot \quad (4\pm1)\times10^7\ M^{-1}\ s^{-1}. \quad (16)$$

Although this rate parameter is small, the contribution was large even at low concentrations of iodide ions in the steady-light photolysis, because the rate of Reaction 10, in contrast with that of Reaction 16, depends on the light intensity. The slight decomposition of adenine by lumiflavin-sensitized steady-light photolysis in the aerated solutions was also suppressed by the addition of a small amount of iodide ions (50% by 5 μM iodide ions). The permanent oxidation of iodide ions was not observed in such a system by the starch-iodine complex method; the generated iodine should be reduced by O_2^-.

Now the conflict between the steady-light and flash photolyses is resolved. The previous explanation in Ref. 1 should be corrected.

References

1) A. Yoshimura and S. Kato, *Bull. Chem. Soc. Jpn.*, **46**, 1141 (1973).

2) A. Yoshimura and S. Kato, *Bull. Chem. Soc. Jpn.*, **49**, 813 (1976).

3) B. Hormström, *Arkiv Kemi*, **22**, 329 (1964); A. Terenin, V. Tachin, and P. Shakhverdov, *Photochem. Photobiol.*, **4**, 505 (1965); A. Knowles, *ibid.*, **13**, 225 (1971); D. B. McCormick, M. C. Falk, F. Rizzuto, and G. Tollin, *ibid.*, **22**, 175 (1975).

4) A. Knowles and E. M. Roe, *Photochem. Photobiol.*, **7**, 421 (1968); E. J. Land and A. J. Swallow, *Biochemistry*, **8**, 2120 (1969).

5) S. P. Vaish and G. Tollin, *J. Bioenerg.*, **1**, 181 (1970).

6) S. P. Vaish and G. Tollin, *J. Bioenerg.*, **2**, 61 (1971).

7) P. Hemmerich, S. Fallab, and H. Erlenmeyer, *Helv. Chim. Acta*, **39**, 1242 (1956).

8) N. Tatebe, Ph. D. Thesis, Osaka University, Osaka, Japan, 1976.

9) S. Kato, "Zikken Kagaku Koza, Zoku 11, Denshisupekutoru," ed by S. Nagakura, Maruzen Tokyo (1956), p.5323.

10) J. F. Baugher and L. I. Grossweiner, *J. Phys. Chem.*, **81**, 1349 (1977).

 © 1985 The Chemical Society of Japan Bull. Chem. Soc. Jpn., 58, 1560—1569 (1985) [Vol. 58, No. 5

Synthesis of Naphthalenoferrocenophanes

Akira KASAHARA,* Taeko IZUMI, Iwao SHIMIZU, Tadashi OIKAWA, Hiroshi UMEZAWA, Manabu MURAKAMI, and Osamu WATANABE

Department of Applied Chemistry, Faculty of Engineering, Yamagata University, Yonezawa 992

(Received November 10, 1984)

Several naphthalenoferrocenophanes, in which the two cyclopentadienyl rings are linked by two naphthalene rings, were synthesized *via* intramolecular reductive coupling of the corresponding formyl compounds with a low valent titanium reagent. Their structures are deduced from IR, NMR, and UV spectra. Transannular π-electronic interaction between the two naphthalene rings is discussed on the basis of electronic spectra.

Recently a wide variety of cyclophanes with stacked aromatic nuclei have widely been studied as pertinent model compounds for π-electronic interactions.[1] From this point of view, we have previously reported of a synthesis of several ferrocenophanes containing aromatic nuclei: benzene[2] and biphenyl.[3] If one or two benzene rings are replaced by naphthalene ring, which has a larger molecular surface and a lower ionization potential than benzene, it is expected that such ferrocenophanes will show stronger transannular interactions. In this report, as a part of our studies on the metallocenophane chemistry, we describe of synthesis and properties of naphthalenoferrocenophanes **1a—d**, in which the two cyclopentadienyl rings are linked by one or two naphthalene rings.

Results and Discussion

Synthesis. Previous successful use of a reductive coupling reaction on appropriate carbonyl compounds for synthesis of [2.2.2] paracycloferrocenophanes[2] and biphenyloferrocenophanes[3] promoted us to attempt the synthesis of **1a—d** by this method. In connection with the synthesis of **1a—d**, it was desirable to synthesize in quantity intermediary compounds: 1,1′-bis(5-formyl-1-naphthyl)ferrocene (**2a**), 1,1′-bis(6-formyl-1-naphthyl)ferrocene (**2b**), 1,1′-bis(7-formyl-1-naphthyl)ferrocene (**2c**), and 1-(*p*-formylphenyl)-1′-(4-formyl-1-naphthyl)ferrocene (**2d**). The synthesis of intermediates **2a—c** was carried out by Gomberg's arylation of ferrocene with diazonium salts **3a—c** derived from 5-amino-naphthoic acid (**4a**), 5-amino-2-naphthoic acid (**4b**), and 8-amino-2-naphthoic acid (**4c**), followed by esterification, reduction with $LiAlH_4$, and oxidation with active MnO_2 in chloroform. On the other hand, the synthesis of the intermediate **2d** was carried out by Gomberg's arylation of (*p*-ethoxycarbonyl)ferrocene (**6**) with diazonium salts derived from 4-ethoxycarbonyl-1-naphthylamine (**7**), followed by reduction with $LiAlH_4$, and oxidation with active MnO_2 in chloroform.

The reductive coupling reactions of dialdehydes **2a—c** with low valent titanium reagents ($TiCl_4$–Zn[4]) using the high dilution method led to the formation of unsaturated naphthalenoferrocenophanes, [2](1,5)naphthaleno[0](1,1′)ferroceno[0](1,5)-naphthalenophan-1-ene (**5a**), [2](2,5)naphthaleno-[0](1,1′)ferroceno[0](1,6)naphthalenophan-1-ene (**5b**), and [2](2,8)naphthaleno[0](1,1′)ferroceno[0](1,7)-naphthalenophan-1-ene (**5c**), accompanied by the formation of reduction products of dialdehydes **2a—c**, respectively. The catalytic hydrogenation of the unsaturated ferrocenophane **5a—c** afforded the saturated naphthalenoferrocenophanes, [2](1,5)-naphthaleno[0](1,1′)ferroceno[0](1,5)naphthalenophane (**1a**), [2](2,5)naphthaleno[0](1,1′)ferroceno[0](1,6)-naphthalenophane (**1b**), and [2](2,8)naphthaleno-[0](1,1′)ferroceno[0](1,7)naphthalenophane (**1c**), respectively. However, the intramolecular reductive coupling of **2d**, for preparing the unsaturated ferrocenophane **5d**, was unsuccessful and led to the formation of reduction products of **9d**. Therefore, the saturated ferrocenophane, [2]paracyclo[0](1,1′)-ferroceno[0](1,4)naphthalenophane (**1d**), was prepared by ring closure of 1-[*p*-(bromomethyl)phenyl]-1′-[4-(bromomethyl)-1-naphthyl]ferrocene (**8**) with butyllithium.

Structures. The structures of the ferrocenophanes **1a—d** and **5a—d** were determined on the basis of IR, NMR, and mass spectra and elementary analyses. The ^1H NMR and IR spectral data of all the ferrocenophanes and the reference compounds are summarized in Tables 1 and 2, respectively. For the unsaturated ferrocenophane **5a**, the configuration of the olefinic bond has been confirmed to be cis because the IR spectrum of **5a** exhibits a band at 720 cm^{-1} chracteristic of *cis*-vinylene linkage and because the characteristic C–H out of deformation modes of *trans*-vinylene linkage around 960 cm^{-1} are absent. With the ^1H NMR spectrum of **5a**, it is noteworthy that the downfield shift of vinylene protons(δ=7.56) is observed, as with the case of [2.2.2](1,3,5)cyclophane-1,9,17-triene(vinylene protons, δ=7.37).[5] For both **1a** and **5a**, two possible conformations are considered from their ^1H NMR spectra, syn or skew. In addition, **1a** and **5a** have the same conformation so that **1a** could be synthesized from **5a** by catalytic hydrogenation, in which the

TABLE 1. ^{1}H NMR SPECTRA OF THE FERROCENOPHANES **1a—d** AND **5a—c** AND THE REFERENCE COMPOUNDS **9a—d** (δ FROM TMS, IN $CDCl_3$)

Compound	Aromatic ring protons	Ferrocene ring protons	Other protons
1a	6.57—7.01 (m, 8H, Ha—c, e) 7.42 (m, 2H, Hd) 7.64 (m, 2H, Hf)	4.32 (m, 4H, H_β) 4.56 (m, 4H, H_α)	2.74 (m, 4H, $-CH_2-$)
5a	6.49—6.95 (m, 8H, Ha—c, e) 7.52 (m, 2H, Hd) 7.85 (m, 2H, Hf)	4.39 (m, 4H, H_β) 4.54 (m, 2H, H_α) 4.70 (m, 2H, H_α)	7.56 (s, 2H, -CH=CH-)
9a	7.19—7.66 (m, 8H, Ha—c, e) 7.90 (m, 2H, Hd) 8.32 (m, 2H, Hf)	4.38 (m, 4H, H_β) 4.58 (m, 4H, H_α)	2.62 (s, 6H, $-CH_3$)
1b	6.02 (m, 2H, He) 6.64—7.41 (m, 10H, Ha—d, f)	4.27 (m, 2H, $H_{\alpha'}$) 4.40 (m, 4H, H_β) 4.84 (m, 2H, H_α)	3.44 (m, 4H, $-CH_2-$)
5b	6.21 (m, 2H, He) 6.88—7.78 (m, 10H, Ha—d, f)	3.48 (m, 2H, $H_{\alpha'}$) 4.31 (m, 4H, H_β) 4.78 (m, 2H, H_α)	7.28 (s, 2H, -CH=CH-)
9b	6.68—7.48 (m, 10H, Ha—e) 7.85 (m, 2H, Hf)	4.27 (t, 4H, H_β) 4.58 (t, 4H, H_α)	2.31 (s, 6H, $-CH_3$)
1c	7.18—7.75 (m, 10H, Ha—e) 7.82 (m, 2H, Hf)	4.36 (m, 4H, H_β) 4.75 (m, 4H, H_α)	3.46 (s, 4H, $-CH_2-$)
5c	7.18—7.68 (m, 10H, Ha—e) 7.78 (m, 2H, Hf)	4.32 (m, 4H, H_β) 4.98 (m, 4H, H_α)	6.49 (s, 2H, -CH=CH-)
9c	7.11—7.44 (m, 6H, Ha, b, e) 7.56—7.78 (m, 4H, Hc, d) 8.28 (m, 2H, Hf)	4.38 (m, 4H, H_β) 4.63 (m, 4H, H_α)	2.33 (s, 6H, $-CH_3$)
1d	5.41 (d, J=8 Hz, 1H, Ha') 6.26 (d, J=8 Hz, 1H, Hb') 6.52 (d, J=8 Hz, 1H, Ha) 6.89 (d, J=7 Hz, 1H, Hc) 7.00 (d, J=8 Hz, 1H, Hb) 7.21 (d, J=7 Hz, 1H, Hd) 7.41 (m, 2H, Hf+Hg) 7.98 (m, 1H, Hh) 8.25 (m, 1H, He)	4.26 (m, 2H, H_β) 4.36 (m, 2H, H_δ) 4.52 (m, 1H, H_α) 4.68 (m, 1H, H_γ) 4.80 (m, 1H, H_α) 4.92 (m, 1H, $H_{\gamma'}$)	3.13 (m, $-CH_2-+H_{exo}$) 4.00 (m, 1H, H_{endo})
6d	7.06 (d, J=8 Hz, 2H, Ha) 7.30 (m, 2H, Hf+Hg) 7.42 (d, J=7 Hz, 1H, Hc) 7.47 (d, J=8 Hz, 2H, Hb) 7.70 (d, J=7 Hz, 1H, Hd) 8.02 (m, 1H, Hh) 8.49 (m, 1H, He)	4.22 (t, 2H, H_β) 4.30 (t, 2H, H_δ) 4.50 (t, 2H, H_α) 4.61 (t, 2H, H_γ)	2.29 (s, 3H, $-C_6H_4-CH_3$) 2.69 (s, 3H, $-C_{10}H_6-CH_3$)

rotation of syn to skew at the 5-position of naphthalene ring is made impossible by bridging. The smaller upfield shift of protons Ha and Hd relative to protons Hb, Hc, He, and Hf in the naphthalene ring would be expected if **5a** had a skew form as with[2.2](1,5)naphthalenophane.[6] In the ^{1}H NMR spectra of **5a**, however, all the protons of naphthalene rings appear at higher fields than the corresponding protons of the reference compound, 1,1′-bis(5-methyl-1-naphthyl)ferrocene (**9a**), showing a shielding effect by the opposite naphthalene ring. This phenomenon suggests a *syn*-conformation for both **1a** and **5a** rather than a skewed one (**10**). In **1a** and **5a**, the molecule probably exists in such a conformation that the naphthalene rings approximately parallel to one another and approximately coplanar to the cyclopentadienyl ring. In ferrocene, the distance between the two cyclopentadienyl rings is 3.32 Å,[7] while the Van der Waals separation between parallel π-systems is 3.345 Å.[8] Thus, in **1a** and **5a**, a substantial repulsive interaction must exist between the two naphthalene rings which are bound together by ethylene or vinylene bridges at both the 5-positions. In the ^{1}H NMR spectra of both **1b** and **5b**, the aromatic protons He and Hf are shifted to higher field by about 0.9 ppm, compared with those of the reference compound, 1,1′-bis(6-methyl-1-naphthyl)ferrocene (**9b**). However, the signals of protons Ha, Hb, Hc, and Hd are observed at nearly the same positions as those of **9b**. These data support

TABLE 2. IR SPECTRA OF FERROCENOPHANE AND REFERENCE COMPOUNDS

Compound	KBr, $\tilde{\nu}$/cm^{-1}
1a	3100, 805 (1,1′-disubstituted ferrocene ring), 1600, 1580, 780, 770 (naphthalene ring), 715, and 685 (distorted naphthalene ring).
5a	3100, 805 (1,1′-disubstituted ferrocene ring), 1600, 1580, 785, 775 (naphthalene ring), 1620, 720 (cis -CH=CH-), 710, and 685 (distorted naphthalene ring).
9a	3100, 805 (1,1′-disubstituted ferrocene ring), 1590, and 770 (naphthalene ring).
1b	3100, 805 (1,1′-disubstituted ferrocene ring), 1590, 780, and 765 (naphthalene ring).
5b	3100, 805 (1,1′-disubstituted ferrocene ring), 1600, 1580, 775 (naphthalene ring), 1625, and 720 (cis -CH=CH-).
9b	3100, 810 (1,1′-disubstituted ferrocene ring), 1590, 785, and 770 (naphthalene ring).
1c	3100, 810 (1,1′-disubstituted ferrocene ring), 1600, and 830 (naphthalene ring).
5c	3100, 810 (1,1′-disubstituted ferrocene ring), 1590, 830 (naphthalene ring), 1620, and 735 (cis -CH=CH-).
9c	3100, 810 (1,1′-disubstituted ferrocene ring), 1600, and 830 (naphthalene ring).
1d	3100, 810 (1,1′-disubstituted ferrocene ring), 1600, 1580, 840, 820, 765 (naphthalene ring+*p*-disubstituted benzene ring), 725, and 695 (distorted aromatic ring).
9d	3100, 800 (1,1′-disubstituted ferrocene ring), 1600, 1580, 820, and 760 (naphthalene ring+*p*-disubstituted benzene ring).

the view that both **1b** and **5b** exist exclusively in the *anti*-conformation rather than in the *syn*-conformation owing to a π-π repulsive instabilization in the latter conformation. Furthermore, in **1b** and **5b**, the cyclopentadienyl protons Hα' are shifted to higher field by about 0.5 and 1.0 ppm, respectively, compared with those of **9b**. The remarkable upfield shifts of protons Hα' in **1b** and **5b** are probably due to a diamagnetic shielding effect on the opposed naphthalene ring and clearly indicate the *anti*-conformation rather than the vertically stacked conformation (**1b′**). In the ^{1}H NMR spectra of both **1c** and **5c**, the aromatic proton signals, except for Hf, are observed at nearly the same positions as those of the reference compound, 1,1′-bis(7-methyl-1-naphthyl)-ferrocene (**9c**). On the other hand, the aromatic protons Hf are shifted to higher fields by about 0.45 ppm, compared with those of the reference compound **9b**. These data suggest that, in both **1c** and **5c**, the two naphthalene rings are held not in a face to face conformation but in an *anti*-conformation. On the other hand, the ferrocenophane **1d** shows its signals of the bridge ethylene protons to be roughly divided into two groups of multiplets. Of these, the lower field multiplet is associated with the endo proton of methylenes attached to the condensed aromatic ring for the 1,4-bridged systems. The downfield shift of the proton is explained in terms of the large deshielding effect of the neighboring condensed aromatic ring. The phenyl protons show upfield shifts compared with those of the reference compound, 1-(*p*-tolyl)-1′-(4-methyl-1-naphthyl)-ferrocene (**9d**), and may reasonably be assigned by considering the diamagnetic anisotropy of the opposite aromatic ring. In the ferrocenophane **1d**, the upfield shifts (1.21 and 1.65 ppm) of the phenyl protons Ha′ and Hb′ are drastic as compared with those of protons Ha (0.47 ppm) and Hb (0.54 ppm), suggesting that protons Ha′ and Hb′ are situated above the center of the opposite naphthalene ring. The naphthalene protons Hc and Hd show reasonable upfield shifts. However, protons Hf and Hg show absorptions at a rather lower field and shifts of protons He and Hh are negligible. These data are best accounted for on the basis of the conformation **1d**, in which the benzene and naphthalene rings are approximately parallel to each other and are held face to face in close proximity by the ethylene bridges at both the 4-positions.

Electronic Spectra. Toluene and 1-methylnaphthalene show no absorption in the long wavelength region above 300 nm.[9] Figures 1,2,3, and 4 show the electronic spectra of naphthalenoferrocenophanes

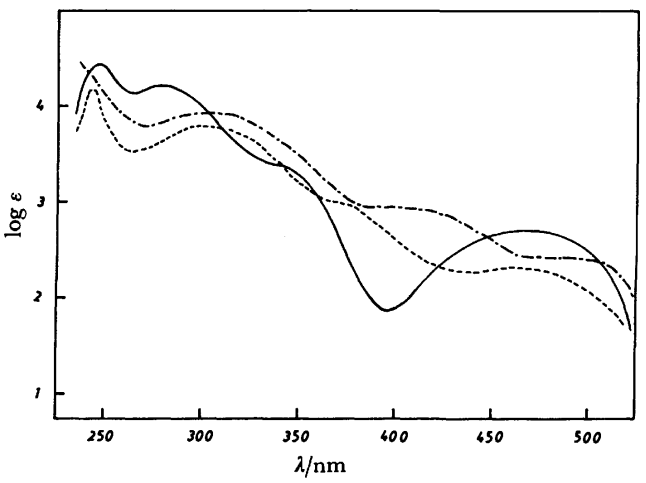

Fig. 1. Electronic spectra of **1a**, **5a**, and **9a** in dioxane.
——: **1a**, — — —: **5a**, - - - -: **9a**.

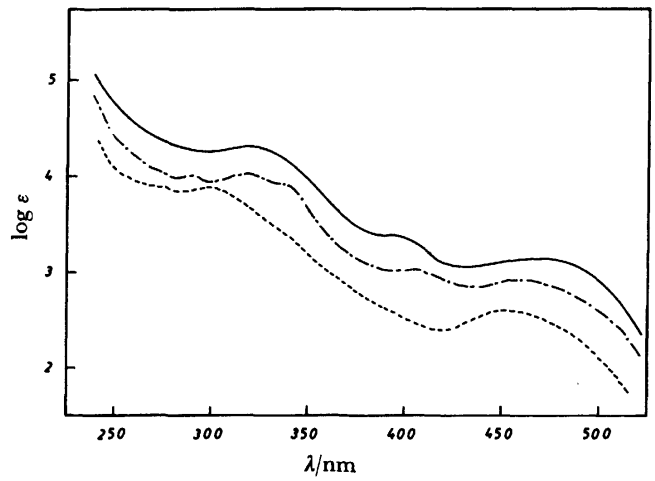

Fig. 2. Electronic spectra of **1b**, **5b**, and **9b** in dioxane.
——: **1b**, – – –: **5b**, ----: **9b**.

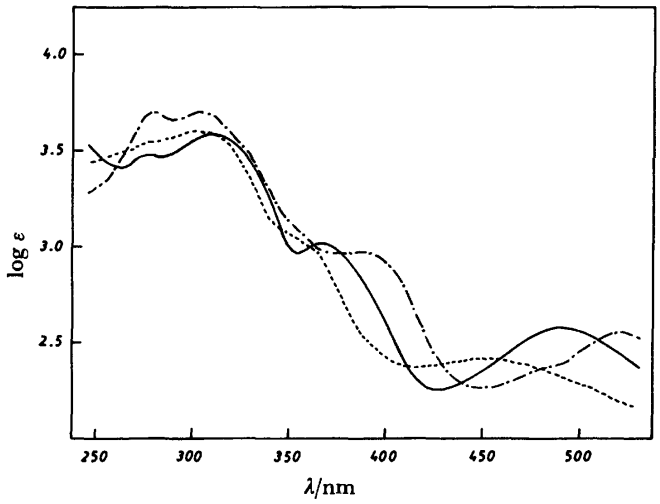

Fig. 3. Electronic spectra of **1c**, **5c**, and **9c** in dioxane.
——: **1c**, – – –: **5c**, ----: **9c**.

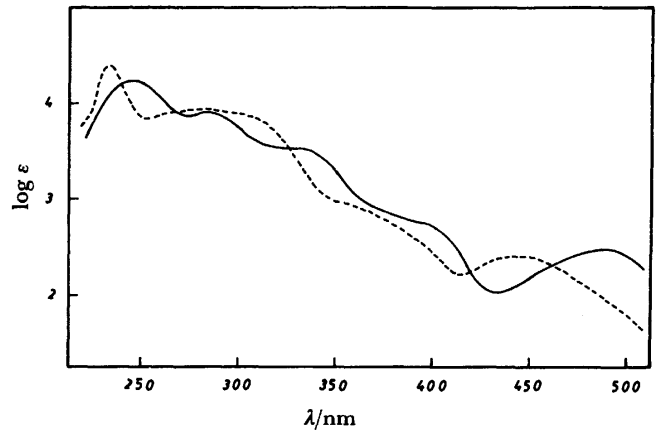

Fig. 4. Electronic spectra of **1d** and **9d** in dioxane.
——: **1d**, ----: **9d**.

1a—d and **5a—c** together with those of the reference compounds **9a—d**. The electronic spectra of **1a**, **1b**, **5a**, and **5b** show somewhat bathochromic and hyperchromic shifts in the range 220—320 nm, compared with those of the reference compounds **9a** and **9b**, respectively. This may be due to transannular π-electronic interactions between the two naphthalene chromophores in **1a**, **1b**, **5a**, and **5b**. Furthermore, in **1a**, **1b**, **5a**, and **5b**, the bathochromic shifts of the unsaturated series are more significant than those of the saturated series, suggesting that the two naphthalene rings in the unsaturated ferrocenophanes **5a** and **5b** are closer in orientation to vertical stacking than those of the saturated ferrocenophanes **1a** and **1b**. On the other hand, in the 220—320 nm region, the electronic spectra of **1c** and **5c** are similar to the spectra of the reference compound 9c. This phenomenon and the small shielding effects on all the aromatic protons but proton Hf in the NMR spectra, indicate that the interactions between the two naphthalene rings in **1c** and **5c** are relatively weak. The electronic spectrum of ferrocene has two main absorptions at 325 and 440 nm. It has been shown that both the position and intensity of the 440 nm band are particularly sensitive to ferrocene ring-tilt distortion.[10] In the 330—500 nm region, the electronic spectra of the ferrocenophanes **1a—d** and **5a—c** show an increased intensity and a bathochromic shift to longer wavelengths, compared with those of the reference compounds **9a—d** bearing an untilted ferrocene ring. These phenomena suggest that, in all ferrocenophanes, ferrocene ring-tilt distortion will occur. In compounds **1a**, **5a**, and **1d**, the ferrocene ring-tilt distortion may be caused by the strong π-π repulsions between the two faced naphthalene rings or between the benzene and naphthalene rings. In **1b** and **5b**, the planes of the cyclopentadienyl and naphthalene rings probably have a nonplanar orientation owing to the short length of the side chain which is bridging at the 6-position of the naphthalene ring, and the ferrocene ring-tilt distortions may be caused by the repulsions between the B rings in the two naphthalene rings. On the other hand, in compounds **1c** and **5c**, the interactions between the two naphthalene rings are relatively weak, and accordingly the ferrocene ring-tilt distortions may be caused by the strain due to the short length of the side chain which is bridging at the 7-position in naphthalene rings.

Infrared Spectra. IR spectra of the [2.2]paracyclophane system are known to reveal obvious features. One is the increase in the intensity of a band in the 1580—1600 cm^{-1} region, which is related to the increased double-bond character due to the distortion of the benzene ring.[11] The other is the appearance of a strong new maximum in the 710 cm^{-1} region. Longone and Warren[11b] reported that the strong

maxima at 725 cm^{-1} in [2.2]paracyclophane and 710 cm^{-1} in 4,7,12,15-tetramethyl[2.2]paracyclophane might be characteristic bands associated with the distorted benzene ring in the [2.2]paracyclophane system. We also reported of the same phenomenon in the [2]paracyclo[0](1,1')ferroceno[0]paracyclophane bearing the distorted benzene ring.[2] The naphthalenophanes **1a**, **5a**, and **1d** exhibit characteristic bands

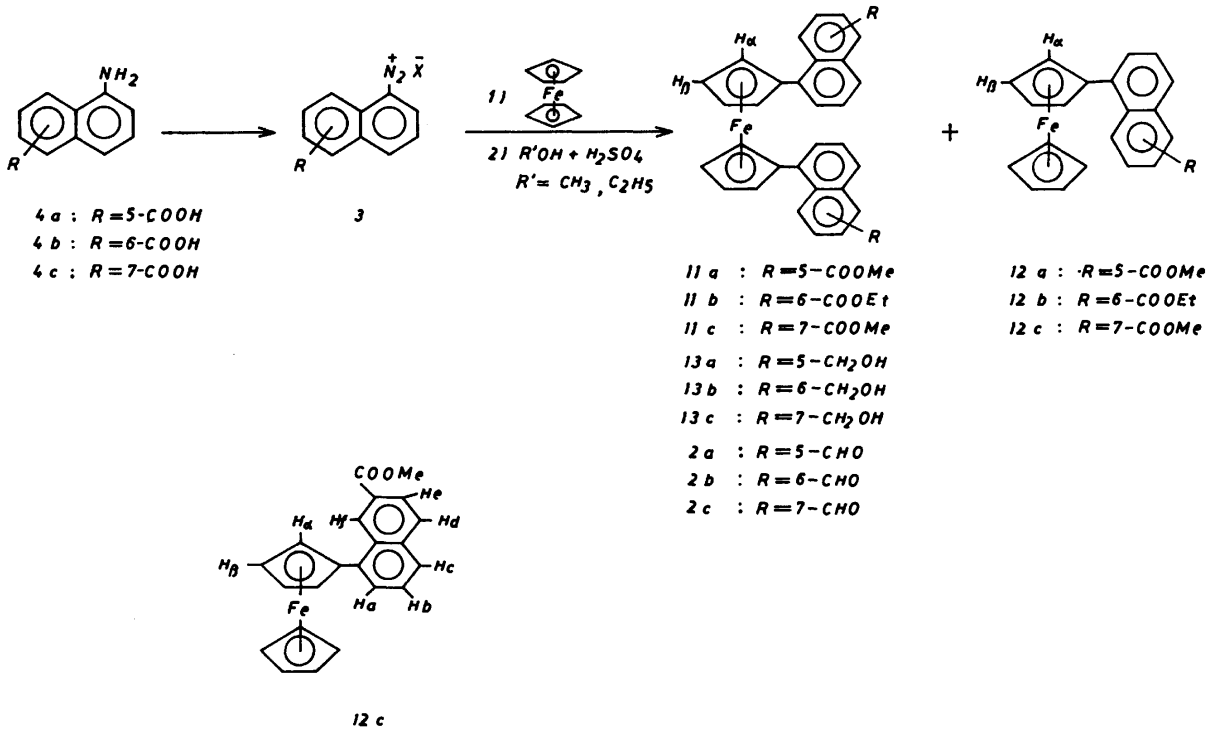

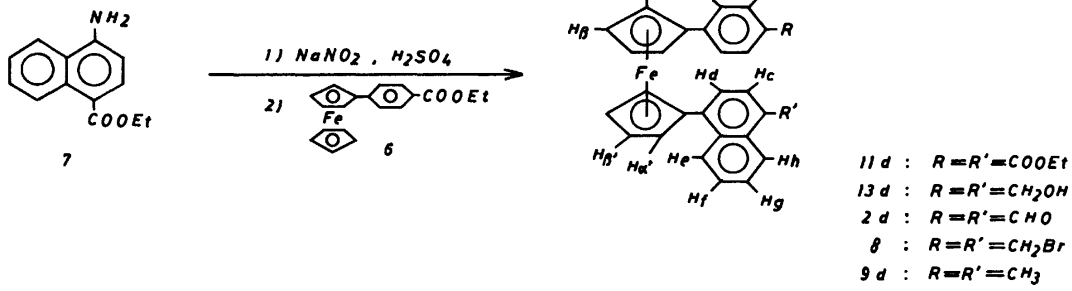

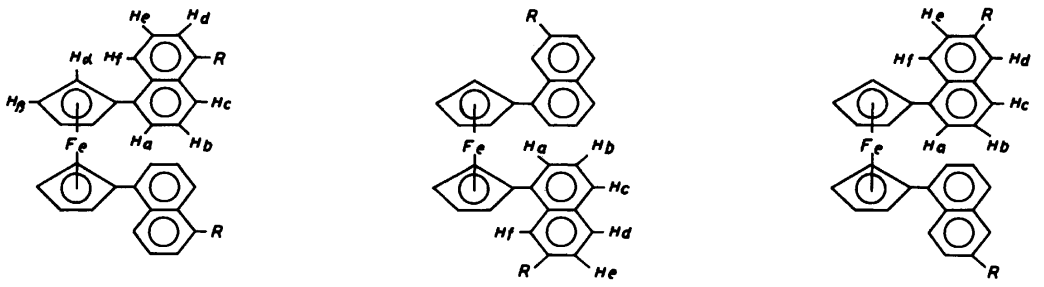

Scheme 1.

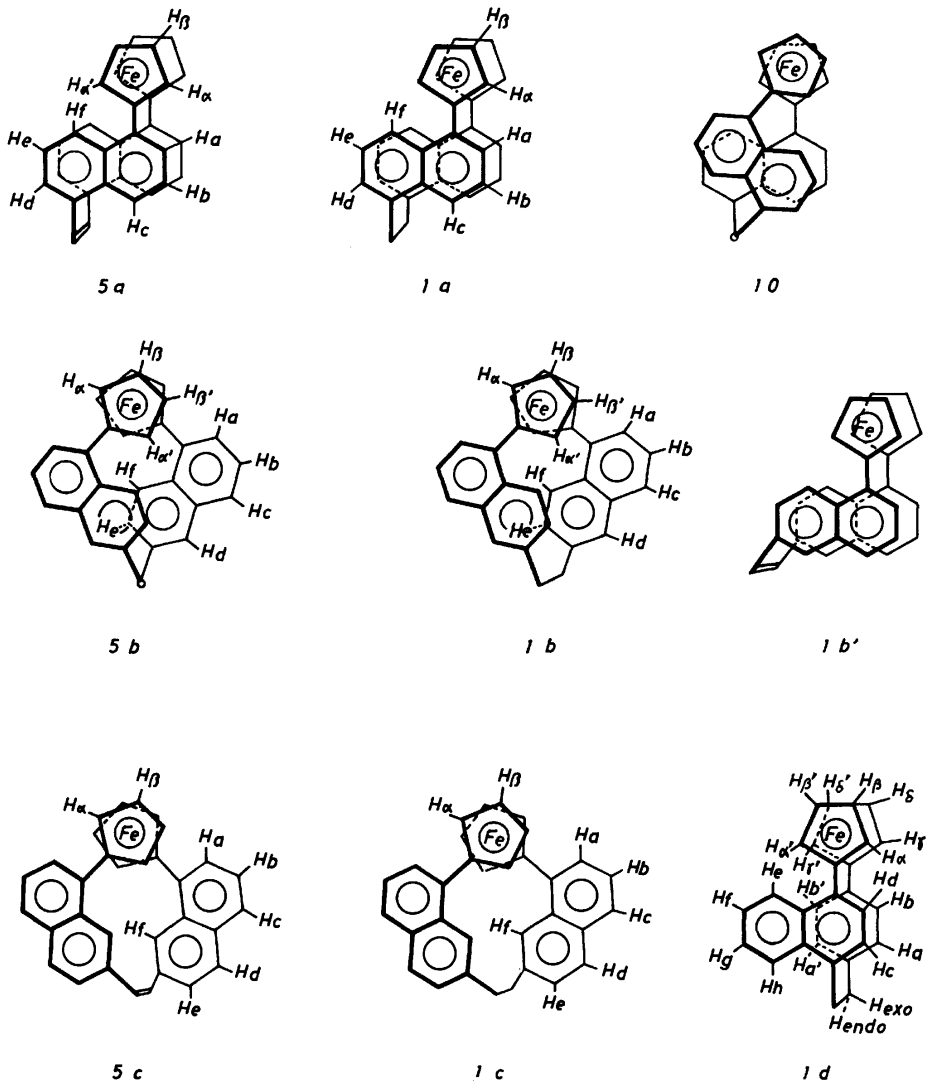

Scheme 2.

around 700 cm^{-1}, whereas the reference compounds **9a** and **9d** bearing strain-free aromatic rings exhibit no bands in this region. This phenomenon may be due to the distortion of the aromatic rings in **1a**, **5a**, and **1d**. On the other hand, near 700 cm^{-1}, the IR spectra of **1b**, **5b**, **1c**, and **5c** are similar to those of the open-chain models **9b** and **9c**. This may be due to the lack of distortion of the aromatic rings in **1b**, **5b**, **1c**, and **5c** (see Table 2).

Experimental

Materials and Measurements. All melting points are uncorrected. 5-Amino-1-naphthoic acid (**4a**),[12] 5-amino-2-naphthoic acid (**4b**),[13] 8-amino-2-naphthoic acid (**4c**),[13] (*p*-ethoxycarbonylphenyl)ferrocene (**6**),[14] and 4-ethoxycarbonyl--1-naphthylamine (**7**)[15] were prepared by the methods described in the literature. IR, ^1H NMR, mass, and electronic spectra were recorded with Hitachi 260-10, Hitachi R-22, Hitachi RMU-6M, and Hitachi 200-10 spectrometers, respectively.

*1,1'-Bis[5-(methoxycarbonyl)-1-naphthyl]ferrocene (**11a**).* The amine **4a** (9.36 g, 50 mmol) was diazotized in 10% sulfuric acid at 0—5 °C with sodium nitrite (3.45 g, 50 mmol). After the diazotization the solution was added dropwise to a solution of ferrocene (3.72 g, 20 mmol) in acetic acid (150 cm^3) under a nitrogen atmosphere. The resulting dark brown solution was stirred overnight at room temperature and then poured into water. The precipitates formed were filtered off, washed with water, dried at room temperature, and then esterified in refluxing methanol (300 cm^3) containing 5 cm^3 of concd H_2SO_4 under a nitrogen atmosphere. After removal of the solvents *in vacuo*, the residue was extracted with chloroform and the chloroform extracts were washed with 5% sodium hydrogencarbonate solution and brine, dried over anhyd $MgSO_4$, filtered, and concentrated. The residue was purified by column chromatography (silica gel).

The first elution with benzene gave the starting material ferrocene (1.12 g, 30%), mp 173 °C.

The second elution with benzene afforded 1.17 g (15.9%

yield based on ferrocene) of (5-methoxycarbonyl-1-naphthyl)-ferrocene (**12a**): orange yellow crystal; mp 114—115 °C; IR (KBr) 3100, 1100, 1000, 805 (monosubstituted ferrocene ring), 1710 (-$COOCH_3$), 1600, 1500, 810, 790, and 770 cm^{-1} (naphthalene ring); ^1H NMR ($CDCl_3$) δ=3.96 (s, 3H, -CH_3), 4.13 (s, 5H, H_γ), 4.36 (t, 2H, H_β), 4.57 (t, 2H, H_α), and 7.31—8.80 (m, 6H, Ar-H). Found: C, 71.13; H, 4.81; M^+, 370. Calcd for $C_{22}H_{18}FeO_2$: C, 71.27; H, 4.89; M, 370.

The third elution with benzene gave 1.58 g (14.2% yield based on ferrocene) of reddish crystals, mp 156—158 °C, which were determined to be 1,1'-bis(5-methoxycarbonyl-1-naphthyl)ferrocene (**11a**): IR (KBr) 3100,805 (1,1'-disubstituted ferrocene ring), 1720 (-$COOCH_3$), 1600, 1500, 820, 790, and 770 cm^{-1} (naphthalene ring); ^1H NMR ($CDCl_3$) δ=3.91 (s, 6H, -CH_3), 4.42 (m, 4H, H_β), 4.58 (m, 4H, H_α), and 7.32—8.50 (m, 12H, Ar-H). Found: C, 73.53; H, 4.56; M^+, 554. Calcd for $C_{34}H_{26}FeO_4$: C, 73.65; H, 4.72; M, 554.

1,1'-Bis[6-(ethoxycarbonyl)-1-naphthyl]ferrocene (11b). Gomberg's arylation of ferrocene with diazonium salts derived from **4b**, followed by esterification in ethanol, was carried out in the same way as described above, and (6-ethoxycarbonyl-1-naphthyl)ferrocene (**12b**) (orange yellow crystals, mp 98—99 °C) and **11b** (reddish crystals, mp 130—132 °C) were obtained in 14 and 8% yields, respectively.

11b: IR (KBr) 3100, 810 (1,1'-disubstituted ferrocene ring), 1720 (-COOEt), 1600, 1500, 780, and 770 cm^{-1} (naphthalene ring); ^1H NMR ($CDCl_3$) δ=1.38 (t, 6H, -CH_3), 4.40 (t, 4H, H_β), 4.44 (q, 4H, -CH_2-), 4.61 (t, 4H, H_α), and 7.20—8.49 (m, 12H, naphthalene ring protons). Found: C, 74.39; H, 5.26; M^+, 582. Calcd for $C_{36}H_{30}FeO_4$: C, 74.23; H, 5.19; M, 582.

12b: IR (KBr) 3100, 1100, 1000, 805 (monosubstituted ferrocene ring), 1720 (-COOEt), 1600, 1500, 780, and 770 cm^{-1} (naphthalene ring); ^1H NMR ($CDCl_3$) δ=1.38 (t, 3H, -CH_3), 4.12 (s, 5H, H_γ), 4.37 (t, 2H, H_β), 4.41 (q, 2H, -CH_2), 4.60 (t, 2H, H_α), and 7.34—8.60 (m, 6H, naphthalene ring protons). Found: C, 71.75; H, 5.17; M^+, 384. Calcd for $C_{23}H_{20}FeO_2$: C, 71.88; H, 5.24; M, 384.

1,1'-Bis[7-(methoxycarbonyl)-1-naphthyl]ferrocene (11c). Gomberg's arylation of ferrocene with diazonium salts derived from **4c**, followed by esterification in methanol, was carried out in the same way as described for **11a**, and (7-methoxycarbonyl-1-naphthyl)ferrocene (**12c**) (orange yellow crystals, mp 90—92 °C) and **11c** (reddish orange crystals, mp 152—153 °C) were obtained in 12.5 and 6.2% yields, respectively.

11c: IR (KBr) 3100, 800 (1,1'-disubstituted ferrocene ring), 1720 (-$COOCH_3$), 1600, 1500, 835, and 740 cm^{-1} (naphthalene ring); ^1H NMR ($CDCl_3$) δ=3.96 (s, 6H, -CH_3), 4.50 (t, 4H, H_β), 4.90 (t, 4H, H_α), 7.11—7.93 (m, 10H, H_{a-e}), and 9.57 (br-s, 2H H_f). Found: C, 73.51; H, 4.58; M^+, 554. Calcd for $C_{34}H_{26}FeO_4$: C, 73.65; H, 4.72; M, 554.

12c: IR (KBr) 3100, 1100, 1000, 805 (monosubstituted ferrocene ring), 1720 (-$COOCH_3$), 1600, 1500, 835, and 740 cm^{-1} (naphthalene ring); ^1H NMR ($CDCl_3$) δ=3.92 (s, 3H, -CH_3), 4.19(s, 5H, H_γ), 4.42 (t, 2H, H_β), 4.66 (t, 2H, H_α), 7.29—8.11 (m, 5H, H_{a-e}), and 8.56 (br-s, 1H, H_f). Found: C, 71.22; H, 4.74; M^+, 370. Calcd for $C_{22}H_{18}FeO_2$: C, 71.37; H, 4.90; M, 370.

1-(p-Ethoxycarbonylphenyl)-1'-(4-ethoxycarbonyl-1-naphthyl)-ferrocene (11d). The amine **7** (3.01 g, 14 mmol) was diazotized in 5% sulfuric acid (830 cm^3) at 0—5 °C with sodium nitrite (1.0 g, 14.4 mmol). After the diazotization the diazotized salt solution was added rapidly to a solution of compound **6** (4.01 g, 12 mmol) in acetic acid (600 cm^3) in an atmosphere of nitrogen. The resulting dark brown solution was stirred overnight at room temperature and then poured into water. The reaction mixture was extracted with chloroform and the chloroform extracts were washed with 5% aqueous sodium hydrogencarbonate solution and with brine, dried over anhyd $MgSO_4$, filtered, and concentrated. The residue was purified by column chromatography with silica gel.

The first elution with hexane-diethyl ether (4:1) afforded the starting material **6** (0.78 g, 19.4%), mp 87—88 °C.

The second elution with hexane-diethyl ether (4:1) afforded 0.98 g (15.3% yield based on **6**) of **11d** in reddish oil: IR ($CHCl_3$) 3100, 805 (1,1'-disubstituted ferrocene ring), 1720 (-COOEt), 1600, 1500, 780, and 730 cm^{-1} (aromatic ring); 1H NMR ($CDCl_3$) δ=1.37 (t, 3H, -CH_3), 1.44 (t, 3H, -CH_3), 4.31(t, 2H, H_β), 4.38(t, 2H, $H_{\beta'}$), 4.41 (m, 4H, -CH_2-), 4.57 (t, 2H, H_α), 4.69 (t, 2H, $H_{\alpha'}$), and 7.34—8.94 (m, 10H, aromatic protons). Found: C, 72.06; H, 5.18; M^+, 532. Calcd for $C_{32}H_{28}FeO_4$: C, 72.18; H, 5.30; M, 532.

1,1'-Bis[5-(hydroxymethyl)-1-naphthyl]ferrocene (13a). To a suspension of $LiAlH_4$ (0.42 g, 11 mmol) in anhyd diethyl ether (50 cm^3) was added dropwise a solution of **11a** (2.21 g 4 mmol) in dry benzene (50 cm^3) at room temperature over 1 h, and the reaction mixture was then heated under reflux for an additional 4 h. After the mixture was decomposed with a amall amount of cold water, the organic layer was washed successively with 5% hydrochloric acid, 5% sodium hydrogencarbonate solution, and brine, and dried over anhyd $MgSO_4$. After removal of the solvents, the residue was purified by column chromatography on silica gel (benzene-diethyl ether, 1:1) to afford **13a** as orange yellow crystals, which were recrystallized from ethanol, mp 168—169 °C, in 72% yield: IR (KBr) 3100, 805 (1,1'-disubstituted ferrocene ring), 3400, 1020 (-OH), 1600, 820, 780, and 770 cm^{-1} (naphthalene ring); ^1H NMR ($CDCl_3$) δ=1.72 (br-s, 2H, -OH), 4.42 (t, 4H, H_β), 4.62 (t, 4H, H_α), 5.08 (s, 4H, -CH_2-), and 7.12—8.48 (m, 12H, naphthalene ring protons). Found: C, 77.28; H, 5.21; M^+, 498. Calcd for $C_{32}H_{26}FeO_2$: C, 77.12; H, 5.26; M, 498.

1,1'-Bis[6-(hydroxymethyl)-1-naphthyl]ferrocene (13b). A reduction of **11b** with $LiAlH_4$ was carried out in the same way as described above, and **13b** (orange yellow crystals, mp 163—164 °C) was obtained in 66% yield: IR (KBr) 3100, 805 (1,1'-disubstituted ferrocene ring), 3350, 1020 (-OH), 1590, 825, 780, and 760 cm^{-1} (naphthalene ring); ^1H NMR ($CDCl_3$) δ=1.72 (br-s 2H, -OH), 4.42 (t, 4H, H_β), 4.58 (t, 4H, H_α), 4.74 (s, 4H, -CH_2-), and 6.91—8.39 (m, 12H, naphthalene ring protons). Found: C, 77.21; H, 5.35; M^+ 498. Calcd for $C_{32}H_{26}FeO_2$: C, 77.12; H, 5.26; M, 498.

1,1'-Bis[7-(hydroxymethyl)-1-naphthyl]ferrocene (13c). A reduction of **11c** with $LiAlH_4$ was carried out in the same way as described for the ruduction of **11a** with $LiAlH_4$ and the product **13c** (orange yellow crystals, mp 136—137 °C) was obtained in 51% yield: IR (KBr) 3100, 810 (1,1'-disubstituted ferrocene ring), 3450, 1020 (-OH), 1590, 835, and 740 cm^{-1} (naphthalene ring); ^1H NMR ($CDCl_3$) δ=1.80 (br-s, 2H, -OH), 4.39 (t, 4H, H_β), 4.66 (s, 4H, -CH_2-), 4.78 (t, 4H, H_α), and 7.11—8.70 (m, 12H, naphthalene ring protons). Found: C, 69.96; H, 5.13; M^+, 498. Calcd for

$C_{32}H_{26}FeO_2$: C, 77.11; H, 5.25; M, 498.

1-[p-(Hydroxymethyl)phenyl]-1'-[4-(hydroxymethyl)-1-naphthyl]-ferrocene (13d). A reduction of **11d** with $LiAlH_4$ was carried out in the same way as described for the reduction of **11a** with $LiAlH_4$, and the product **13d** (orange yellow crystals, mp 60—62 °C) was obtained in 90% yield: IR (KBr) 3100,805 (1,1'-disubstited ferrocene ring), 3300, 1000 (-OH), 1600, 820, and 760 cm^{-1} (naphthalene ring); ^1H NMR ($CDCl_3$) δ=1.89 (s, 2H, -OH), 4.30 (t, 2H, Hβ), 4.34 (t, 2H, Hβ'), 4.57 (m, 4H, $-CH_2-$+Hα), 4.63 (t, 2H, Hα), 5.09 (s, 2H, $-CH_2-$), 7.06 (d, J=8 Hz, 2H, Ha), and 7.23—8.48 (m, 8H, Hb+naphthalene ring protons). Found: C, 76.46; H, 5.50; M^+, 448. Calcd for $C_{28}H_{24}FeO_2$: C, 76.37; H, 5.40; M, 448.

1,1'-Bis(5-formyl-1-naphthyl)ferrocene (2a). At room temperature, active manganese(IV) oxide (49 g) was added to a solution of **13a** (2.59 g, 5.2 mmol) in chloroform (150 cm^3) and the mixture was stirred in the dark for 12 h. After filtration to remove MnO_2, the reddish chloroform solution was evaporated to dryness and the residue was chromatographed by elution of chloroform on silica gel to afford reddish crystals **2a** (1.80 g, 70% yield): mp 175—176 °C; IR (KBr) 3100, 805 (1,1'-disubstituted ferrocene ring), 1680 (-CHO), 1590, 780, and 770 cm^{-1} (naphthalene ring); ^1H NMR ($CDCl_3$) δ=4.50 (t, 4H, Hβ), 4.59 (t, 4H, Hα), 7.24—8.73 (m, 10H, Ha, b, d, e, f), 9.14 (d, 2H, Hc), and 10.33 (s, 2H, -CHO). Found: C, 77.86; H, 4.55; M^+, 494. Calcd for $C_{32}H_{22}FeO_2$: C, 77.75; H, 4.49; M, 494.

1,1'-Bis(6-formyl-1-naphthyl)ferrocene (2b). An oxidation of **13b** with active manganese(IV) oxide was carried out in the same way as described above, and reddish crystals **2b** (mp 191—193 °C) were obtained in 81% yield: IR (KBr) 3100, 800 (1,1'-disubstituted ferrocene ring), 1690 (-CHO), 1590, 830, and 790 cm^{-1} (naphthalene ring); ^1H NMR ($CDCl_3$) δ=4.46 (t, 4H, Hβ), 4.63 (t, 4H, Hα), 7.20—8.52 (m, 12H, naphthalene ring protons), and 10.02 (s, 2H, -CHO). Found: C, 77.91; H, 4.58; M^+, 494. Calcd for $C_{32}H_{22}FeO_2$: C, 77.74; H, 4.48; M, 494.

1,1'-Bis(7-formyl-1-naphthyl)ferrocene (2c). An oxidation of **13c** with active manganese(IV) oxide was carried out in the same way as described for the oxidation of **13a** with active MnO_2, and reddish crystals **2c** (mp 204—205 °C) were obtained in 66% yield: IR (KBr) 3100, 800 (1,1'-disubstituted ferrocene ring), 1690 (-CHO), 1590, 830, and 760 cm^{-1} (naphthalene ring); ^1H NMR ($CDCl_3$) δ=4.51 (t, 4H, Hβ), 4.78 (t, 4H, Hα), 7.13—7.74 (m, 10H, Ha, b, c, d, e), 9.02 (s, 2H, Hf), and 9.81 (s, 2H, -CHO). Found: C, 77.62; H, 4.35; M^+, 494. Calcd for $C_{32}H_{22}FeO_2$: C, 77.75; H, 4.49; M, 494.

1-(p-Formylphenryl)-1'-(4-formyl-1-naphthyl)ferrocene (2d). An oxidation of **13d** with active manganese(IV) oxide was carried out in the same way as described for the oxidation of **13d** with active MnO_2, and reddish crystals **2d** (mp 168—170 °C) were obtained in 64% yield: IR (KBr) 3100, 805 (1,1'-disubstituted ferrocene ring), 1690 (-CHO), 1590, 830, 760, and 730 cm^{-1} (aromatic ring); ^1H NMR ($CDCl_3$) δ=4.46 (t, 2H, Hβ), 4.50 (t, 2H, Hβ'), 4.72 (T, 2H, Hα), 4.76 (t, 2H, Hα'), 7.23—8.92 (m, 10H, aromatic ring), 10.06 (s, 1H, -CHO), and 10.21 (s, 1H, -CHO). Found: C, 75.81; H, 4.59; M^+, 444. Calcd for $C_{28}H_{20}FeO_2$: C, 75.69; H, 4.54; M, 444.

1-[p-(Bromomethyl)phenyl]-1'-[4-(bromomethyl)-1-naphthyl]-ferrocene (8). In an atmosphere of nitrogen, chlorotrimethylsilane (8.47 g, 78 mmol) was added to a solution of anhyd lithium bromide (5.82 g, 67 mmol) in dry acetonitrile (210 cm) with stirring at room temperature. The alcohol **13d** (8.06 g, 18 mmol) was then added and the reaction mixture was heated under reflux for 0.5 h. After cooling, the mixture was extracted with diethyl ether (500 cm^3), and the extract was washed successively with water, 5% sodium hydrogencarbonate solution, and brine, and dried over anhyd $MgSO_4$. After removal of the solvents, the residue was purified by column chromatography on silica gel (dichloromethane) to afford **8** in reddish oil in 56% yield: IR ($CHCl_3$) 3100, 805 (1,1'-disubstituted ferrocene ring), 1600, 1500, 840, and 760 cm^{-1} (aromatic ring); ^1H NMR ($CDCl_3$) δ=4.28 (t, 2H, Hβ), 4.31 (t, 2H, Hβ), 4.38 (s, 4H, $-CH_2-$), 4.48 (t, 2H, Hα), 4.54 (t, 2H, Hα'), 7.18 (d, 2H, Ha), and 7.24—8.54 (m, 8H, Hb+naphthalene ring protons). Found: C, 58.46; H, 3.77; M^+ 574. Calcd for $C_{28}H_{22}Br_2Fe$: C, 58.57; H, 3.86; M, 574.

Intramolecular Reductive Coupling of 2a with $TiCl_4$-Zn. In an atmosphere of nitrogen, zinc dust (1.17 g, 18 mmol) was added in small portions to a stirred solution of $TiCl_4$ (1.80 g, 9 mmol) in dry THF (50 cm^3) at 0—5 °C. After the mixture was refluxed for 1.5 h, a solution of **2a** (0.89 g, 1.8 mmol) and dry pyridine (0.10 g) in dry THF (200 cm^3) was added over 14 h under reflux and the mixture was allowed to reflux for an additional 10 h and then quenched by addition of 50 cm^3 of saturated potassium carbonate solution. The mixture was stirred for 0.5 h, diluted with chloroform, and filtered through Celite. The chloroform layers were washed with brine and dried over anhyd $MgSO_4$. After removal of the solvents, the residue was dissolved in hexane and chromatographed on silica gel.

The first fraction, eluted with hexane–ether (5:1) and subjected to evaporation and recrystallization from ethanol, gave yellow orange crystals (0.09 g, 10.7%), mp 135—137 °C, which were determined to be 1,1'-bis(5-methyl-1-naphthyl)ferrocene(**9a**). Found: C, 82.56; H, 5.69; M^+, 466. Calcd for $C_{32}H_{26}Fe$: C, 82.41; H, 5.62; M, 466.

The second fraction, eluted with hexane–diethyl ether (5:1) and subjected to evaporation and recrystallization from benzene, gave reddish crystals (0.15 g, 18.0%), mp 241—242 °C, which were determined to be *syn*-[0](1,5)-naphthaleno[2](1,5)naphthaleno[0](1,1')ferrocenophan-9-ene (**5a**). Found: C, 83.21; H, 4.96; M^+, 462. Calcd for $C_{32}H_{22}Fe$: C, 83.13; H, 4.80; M, 462.

The third fraction, eluted with chloroform and subjected to evaporation and recrystallization from ethanol, gave orange yellow crystals (0.21 g, 23% yield), mp 168—169 °C, which were identified with 1,1'-bis(5-hydroxymethyl-1-naphthyl)ferrocene (**4a**) by comparison of IR, NMR, and mass spectra and a mixed-melting-point value with those of the authentic sample **4a**.

Reaction of 2b with $TiCl_4$-Zn. The reductive coupling of **2b** with $TiCl_4$–Zn was carried out in the same way as has been described above, and the products were separated by chromatography on silica gel.

The first fraction, eluted with benzene–hexane (1:1) and subjected to evaporation and recrystallization from ethanol, gave orange yellow crystals, mp 175—177 °C (8% yield), which were determined to be 1,1'-bis(6-methyl-1-naphthyl)-ferrocene (**9b**). Found: C, 82.55; H, 5.72; M^+, 466. Calcd for $C_{32}H_{26}Fe$: C, 82.41; H, 5.62; M, 466.

The second fraction, eluted with benzene and subjected

to evaporation and recrystallization from ethanol, gave deep reddish crystals, mp 224—226 °C (37.5% yield), which were determined to be *anti*-[0](1,6)naphthaleno[2](2,5)naphthaleno[0](1,1′)ferrocenophan-9-ene (**5b**). Found: C, 83.25; H, 4.93; M+, 462. Calcd for $C_{32}H_{22}Fe$: C, 83.13; H, 4.80; M, 462.

The third fraction, eluted with chloroform and subjected to evaporation and recrystallization from ethanol, gave yellowish crystals (mp 163—164 °C, 26% yield), which were identified with **4b** by comparison of IR, NMR, and mass spectra and a mixed-melting-point value with those of the authentic sample **4b**.

Reaction of 2c with $TiCl_4$–Zn. The reductive coupling of **2c** with $TiCl_4$–Zn was carried out in the same way as has been described for the reductive coupling of **2a** with $TiCl_4$–Zn, and the products were separated by chromatography on silica gel. The first fraction, eluted with hexane and subjected to recrystallization from ethanol, gave orange yellow crystals (mp 60—62 °C, 4.3% yield), which were determined to be 1,1′-bis(7-methyl-1-naphthyl)ferrocene (**9c**). Found: C, 82.28; H, 5.56; M+ 466. Calcd for $C_{32}H_{26}Fe$: C, 82.40; H, 5.61; M, 466.

The second fraction, eluted with hexane–THF (5:1) and subjected to evaporation and recrystallization from ethanol, gave deep reddish crystals (mp 246—247 °C, 20% yield), which were determined to be *anti*-[0](1,7)-naphthaleno[2](2,8)naphthaleno[0](1,1′)ferrocenophan-9-ene (**5c**). Found: C, 83.02; H, 4.67; M+, 462. Calcd for $C_{32}H_{22}Fe$: C, 83.13; H, 4.80; M, 462.

The third fraction, eluted with chloroform and subjected to evaporation and recrystallization from ethanol, gave yellowish crystals (mp 136—137 °C, 14% yield), which were identified with **4c** by comparison of IR, NMR, and mass spectra and a mixed-melting-point value with those of the authentic sample **4c**.

Reaction of 2d with $TiCl_4$–Zn. The reaction of **2d** with $TiCl_4$–Zn was carried out in the same way described for the reductive coupling of **2a** with $TiCl_4$–Zn, and the products were separated by chromatography on silica gel. The first fraction, eluted with hexane and subjected to evaporation and recrystallization from ethanol, gave reddish orange crystals (mp 51—52 °C, 32% yield), which were determined to be 1-(*p*-tolyl)-1′-(4-methyl-1-naphthyl)-ferrocene(**9d**). Found: C, 80.85; H, 5.94; M+, 416. Calcd for $C_{28}H_{24}Fe$: C, 80.78; H, 5.81; M, 416.

Catalytic Hydrogenation of 5a. In a mixture of dioxane (100 cm³) and ethanol (100 cm³), compound **5a** (0.50 g) was hydrogenated with PtO_2 (0.01 g) at room temperature under the ordinary pressure. The reaction mixture was filtered to remove the catalyst and the filtrate was evaporated to dryness *in vacuo*. The residue was chromatographed on silica gel with hexane to give reddish orange crystals (mp 182—184 °C, 82% yield), which were determined to be [0](1,5)naphthaleno[2](1,5)naphthaleno-[0](1,1′)ferrocenophane (**1a**). Found: C, 82.90; H, 5.35; M+, 464. Calcd for $C_{32}H_{24}Fe$: C, 82.77; H, 5.21; M, 464.

Catalytic Hydrogenation of 5b. The catalytic hydrogenation of **5b** was carried out in the same way as described above, and the product was purified by column chromatography on silica gel with benzene to give reddish orange crystals (mp 233—235 °C (dec), 80% yield), which were determined to be [0](1,6)naphthaleno[2](2,5)-naphthaleno[0](1,1′)ferrocenophane(**1b**). Found: C, 82.90; H, 5.35; M+, 464. Calcd for $C_{32}H_{24}Fe$: C, 82.77; H, 5.21; M, 464.

Catalytic Hydrogenation of 5c. The catalytic hydrogenation of **5c** was carried out in the same way as described for the catalytic hydrogenation of **5a**, and the product was purified by column chromatography on silica gel with benzene to give reddish crystals (mp 237—238 °C, 85% yield), which were determined to be [0](1,7)-naphthaleno[2](2,8)naphthaleno[0](1,1′)ferrocenophane(**1c**). Found: C, 82.70; H, 5.08 ; M+ 464. Calcd for $C_{32}H_{24}Fe$: C, 82.76; H, 5.20; M, 464.

Intramolecular Coupling of 8 with Butyllithium. In an atmosphere of nitrogen, a 15% solution of butyllithium in hexane (16 cm³) was added dropwise to a solution of **8** (4.50 g, 7.84 mmol) in dry THF (450 cm³) at −50 °C, and stirred at the same temperature for 2 h and then at 0 °C for 4 h. After a successive addition of water (50 cm³) and 1 M hydrochloric acid (70 cm³) (1 M=1 mol dm^{-3}), the mixture was extracted with chloroform. The chloroform extracts were washed successively with 1 M hydrochloric acid, brine, 5% sodium hydrogencarbonate solution, and brine, and dried over anhyd $MgSO_4$. After removal of the solvents, the residue was chromatographed on silica gel with hexane–diethyl ether (4:1) to give reddish crystals (mp 220 °C (dec), 20.5% yield), which were determined to be [2]paracyclo[0](1,1′)ferroceno[0](1,4)naphthalenophane(**1d**). Found: C, 81.25; H, 5.46; M+, 414. Calcd for $C_{28}H_{22}Fe$: C, 81.17; H, 5.35; M, 414.

This work was supported by a Grant-in-Aid for Science Research No. 58540296 from the Ministry of Education, Science and Culture.

References

1) S. Misumi, *Kagaku No Ryoiki*, **28**, 927 (1974); **32**, 651 (1978); Y. Sakata, *ibid.*, **28**, 947 (1974); *Yuki Gosei Kagaku Kyokai Shi*,**38**, 164 (1980); S. Misumi and T. Otsubo, *Acc. Chem. Res.*, **11**, 251 (1978).

2) I. Shimizu, H. Umezawa, T. Kanno, T. Izumi, and A. Kasahara, *Bull. Chem. Soc. Jpn.*, **56**, 2023 (1983); A. Kasahara, T. Izumi, I. Shimizu, T. Oikawa, H. Umezawa, and I. Hoshino, *ibid.*, **56**, 1143 (1983).

3) I. Shimizu, Y. Kamei, T. Tezuka, T. Izumi, and A. Kasahara, *Bull. Chem. Soc. Jpn.*, **56**, 192 (1983).

4) T. Mukaiyama, T. Sato, and J. Hanna, *Chem. Lett.*, **1973**, 1041.

5) V. Boekelheide and R. A. Hollins, *J. Am. Chem. Soc.*, **92**, 3512 (1970).

6) M. W. Haenel, *Chem. Ber.*, **111**, 1789 (1978).

7) J. D. Dunitz, L. E. Orgel, and A. Rich, *Acta Crystallogr.*, **9**, 373 (1956).

8) G. E. Bacon, *Acta Crystallogr.*, **4**, 558 (1951).

9) R. A. Friedel and M. Orchin, "Ultraviolet spectra of aromatic compounds," John Wiley & Sons, Inc., New York (1951).

10) T. H. Barr and W. E. Watts, *J. Organomet. Chem.*, **15**, 177 (1968).

11) a) D. J. Cram and H. Steinberg, *J. Am. Chem. Soc.*, **73**, 5691 (1951); b) D. T. Longone and C. L. Warren, *ibid.*,

84, 1507 (1962).
12) F. Bell and W. H. D. Morgan, *J. Chem. Soc.*, **1954**, 1716.
13) C. C. Price and R. H. Michel, *J. Am. Chem. Soc.*, **74**, 3652 (1952).
14) A. N. Nesmeyanov, *Proc. R. Soc. London, Ser. A*, **246**, 495 (1958).
15) S. I. Sergievskaya and V. V. Nesvad'ba, *J. Gen. Chem. (USSR)*, **8**, 924 (1938); *Chem. Abstr.*, **3**, 1307 (1939).

 © 1985 The Chemical Society of Japan Bull. Chem. Soc. Jpn., 58, 1570—1573 (1985) [Vol. 58, No. 5

Generation of Nonstabilized Thiazolium and 2-Methylthiazolium Methylides

Otohiko TSUGE,* Shuji KANEMASA, and Satoru KURAOKA
Research Institute of Industrial Science, and Department of Molecular Science and Technology, Interdisciplinary Graduate School of Engineering Science, Kyushu University, Kasugakoen, Kasuga 816
(Received December 24, 1984)

Desilylation of 3-(trimethylsilylmethyl)thiazolium triflates including 2-methyl derivatives with CsF generates the corresponding thiazolium methylides which are trapped with acetylenic and olefinic dipolarophiles. This paper presents the first example for the generation of nonstabilized thiazolium methylides including 2-methyl derivatives.

Thiazolium salts are versatile reagents in the filed of heterocyclic synthesis as their deprotonation leads to two sorts of reactive species. The deprotonation at the α-position of a highly acidic alkyl moiety on the nitrogen generates thiazolium methylides as 1,3-dipoles[1] and at the 2-alkyl substituent 2-methylenethiazolines as nucleophilic ketene acetals.[2] As shown with an example of 2-methyl-3-phenacylbenzothiazolium bromide,[3] however, even in the case of 2-methylthiazolium salts bearing a highly acidic alkyl moiety such as a phenacyl group on the nitrogen, the deprotonation occurs at the 2-methyl group leading to 2-methylenethiazolines. Thus, thiazolium methylides having 2-methyl group have not been reported up to date. In addition, nonstabilized methylides in thiazolium series, which carry no stabilizing substituents on the ylide carbon, have not been investigated, although increasing interest is recently being shown in nonstabilized nitrogen ylides.[4]

We have recently demonstrated that pyridinium triflates having a trimethylsilylmethyl group on the nitrogen generate nonstabilized pyridinium methylides when desilylated with a silylophile.[5] This method will be effectively applied to the generation of nonstabilized thiazolium methylides.

In the present paper we wish to report the generation of nonstabilized thiazolium methylides including 2-methyl derivatives from 3-(trimethylsilylmethyl)-thiazolium triflates.

When 3-(trimethylsilylmethyl)benzothiazolium triflate (**1**) and its 2-methyl derivative **2**, which were easily prepared from the corresponding thiazole and trimethylsilylmethyl triflate, were allowed to react with dimethyl acetylenedicarboxylate (DMAD, 2 equivalents) in the presence of cesium fluoride (1 equivalent) under reflux in 1,2-dimethoxyethane (DME) for 24 h, oily products **5** and **6** were obtained in 69 and 88% yields, respectively. On the basis of spectral data, the products **5** and **6**, in which two molecules of DMAD were incorporated, were assigned as a mixture of *N*-arylpyrrole compounds whose alkenylthio moieties on the phenyl group are in *E* and *Z* configurations. The NMR spectra were helpful for the structural determination since those

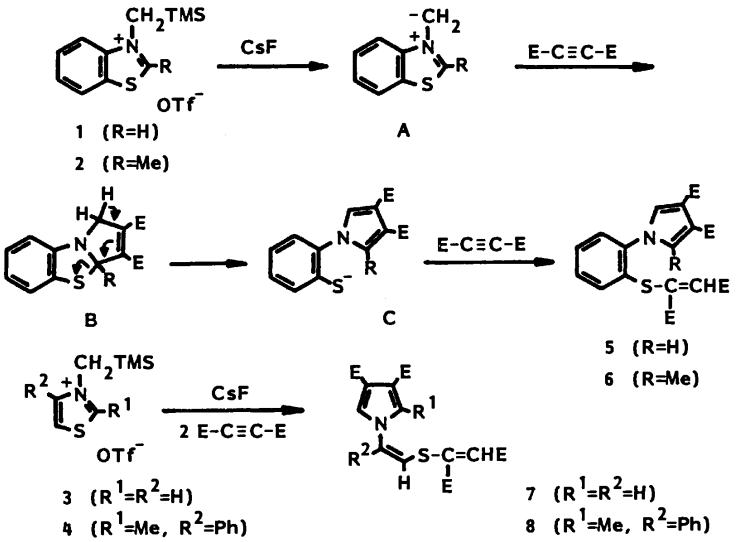

Scheme 1.

for the aryl moieties on the nitrogen were readily assigned by comparison with those of a model compound, a mixture of dimethyl phenylthiofumarate and -maleate obtainable from thiophenol and DMAD.[6]

As shown in Scheme 1, the formation of **5** and **6** strongly supports the intervention of a nonstabilized benzothiazolium methylide **A**. The methylide **A** is generated by the desilylation of the triflate **1** or **2**, and then **A** adds to DMAD forming a [3+2] cycloadduct **B**. The proton elimination in **B** opens the thiazoline ring to yield an anionic intermediate **C**, which is trapped with the second molecule of DMAD to give the final product **5** or **6**. The process from **B** to **C** is closely similar to that of rearrangement of intermediary [3+2] cycloadducts formed from stabilized thiazolium[1a,c] and imidazolium methylides[1a] and DMAD.

Even when an equivalent of DMAD was used in the above reaction a 1:1 adduct was not formed but instead **5** and **6** were obtained in low yields.

Under the same reaction conditions, the reaction of 3-(trimethylsilylmethyl)thiazolium triflate (**3**) and its 2-methyl-4-phenyl derivative **4** with DMAD in the presence of cesium fluoride proceeded through the same course to give the *N*-alkenylpyrroles **7** and **8** in 33 and 36% yields, respectively. In the compounds **7** and **8** the alkenylthio moieties originated from the second addition of DMAD are in *E* and *Z* forms.

Although stabilized thiazolium methylides reacted with DMAD to give rearranged products,[1a,c] they gave stable [3+2] cycloadducts in the reactions with olefinc dipolarophiles.[1d,f,h] Thus, we investigated the reaction with cyclic olefins, maleimides, in order to obtain the direct evidence for the generation of a nonstabilized thiazolium methylide through isolation of a [3+2] cycloadduct.

In fact, a nonstabilized thiazolium methylide such as **A** in the reaction with a maleimide was trapped as an isolabe [3+2] cycloadduct.

The reaction of the triflate **1** with *N*-(*p*-tolyl)maleimide or *N*-methylmaleimide (1 equivalent) in the presence of cesium fluoride (1 equivalent) in DME at room temperature for 24 h afforded a mixture of the corresponding *exo*-**9a** or **9b** and *endo*-cycloadduct **10a** or **10b**, together with recovery of the maleimide.

Under the same conditions, the triflate **2** reacted with *N*-(*p*-tolyl)maleimide in the presence of cesium fluoride to give a mixture of the *exo*- **9c** and *endo*-cycloadduct **10c** (Scheme 2). Owing to polymerization of the imide, however, [3+2] cycloadducts were not obtained in the reactions of triflates **3** and **4** under the same reaction conditions.

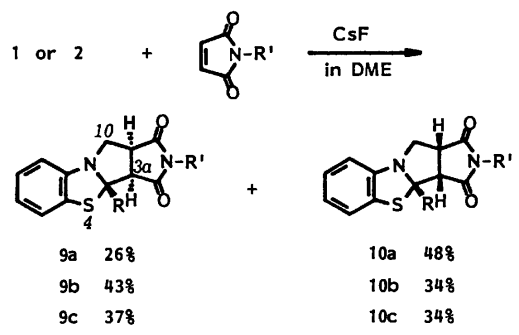

Scheme 2.

Structural elucidation of cycloadducts **9** and **10** was accomplished on the basis of spectral data. In the ^{1}H NMR spectra the 3a-H and 3b-H or 3b-Me in *exo*-cycloadducts **9** appeared downfield of those in *endo*-cycloadducts **10** owing to the anisotropy of 4-sulfur atom and 3-carbonyl group, respectively.

It should be emphasized that these cycloadducts are stable enough to be isolated,[7] and that these nonstereoselective cycloadditions are in contrast with the highly *endo*-selective cycloadditions of stabilized thiazolium methylides.[1d,f-h]

The present results provide the first example for the generation of nonstabilized thiazolium methylides as well as 2-methylthiazolium methylides.[8]

Experimental

General. IR spectra were obtained on a JASCO A-702 spectrometer. ^{1}H NMR spectra were recorded on a Hitachi R-40 or a JEOL FX-100 instrument, and ^{13}C NMR spectra were measured on a JEOL FX-100 spectrometer at 25.05 MHz. Chemical shifts are expressed in parts per million downfield from tetramethylsilane. Mass spectra were taken with a JEOL JMS-01SG-2 spectrometer at 75 eV ionization energy. Elemental analyses were performed on a Hitachi O26 CHN micro analyzer. All reactions were carried out under dry nitrogen.

Materials. Trimethylsilylmethyl triflate was prepared according to the reported method.[9] The following reagents were commercially available: benzothiazole, 2-methylbenzothiazole, thiazole, 2-methyl-4-phenylthiazole, dimethyl acetylenedicarboxylate and *N*-(*p*-tolyl)maleimide, and *N*-methylmaleimide.

General Procedure for the Preparation of Thiazolium Triflate. A solution of a thiazole (12.7 mmol) in dry CH_2Cl_2 (20 mL) was added dropwise to a solution of trimethylsilylmethyl triflate (3.0 g, 12.7 mmol) in dry CH_2Cl_2 (20 mL) at 0 °C. The reaction mixture was then allowed to warm to room temperature with stirring. After the mixture was stirred at room temperature for 1 h, the solvent was removed in vacuo to leave pure thiazolium triflate in good yield.

3-(Trimethylsilylmethyl)benzothiazolium Triflate (1): yield 100%; mp 110—111 °C; colorless needles; IR (KBr) 1250, 1150, 1030, 850 cm^{-1}; ^{1}H NMR (DMSO-d_6) δ=0.07 (s, 9H, $(CH_3)_3Si$), 4.64 (s, 2H, CH_2), 7.75—7.98 (m, 2H, 5- and 6-**H**), 8.34—8.54 (m, 2H, 4- and 7-**H**), 10.33 (s, 1H, 2-**H**); MS *m/z* 222 (M^+), 135 (M^+-CH_2TMS, base peak). Found:

C, 38.66; H, 4.48; N, 4.06%. Calcd for $C_{12}H_{16}NO_3S_2SiF_3$: C, 38.80; H, 4.34; N, 3.77%.

2-Methyl-3-(trimethylsilylmethyl)benzothiazolium Triflate (2): yield 100%; mp 119—120 °C; colorless prisms; IR (KBr) 1250, 1150, 1025, 850 cm^{-1}; ^1H NMR (DMSO-d_6) δ=0.13 (s, 9H, $(CH_3)_3Si$), 3.31 (s, 3H, 2-CH_3), 4.53 (s, 2H, CH_2), 7.68—7.95 (m, 2H, 5- and 6-**H**), 8.24—8.45 (m, 2H, 4- and 7-**H**); MS *m/z* 236 (M^+, base peak). Found: C, 40.29; H, 4.68; N, 3.84%. Calcd for $C_{13}H_{18}NO_3S_2SiF_3$: C, 40.50; H, 4.71; N, 3.63%.

3-(Trimethylsilylmethyl)thiazolium Triflate (3): yield 94%; mp 119—120 °C; colorless prisms; IR (KBr) 1250, 1140; 1020, 845 cm^{-1}; ^1H NMR (DMSO-d_6) δ=0.08 (s, 9H, $(CH_3)_3Si$), 4.19 (s, 2H, CH_2), 8.34 (t, 2H, *J*=1.0 Hz, 4- and 5-**H**), 9.92 (t, 1H, *J*=1.0 Hz, 2-**H**); MS *m/z* 172 (M^+, base peak). Found: C, 29.94; H, 4.35; N, 4.63%. Calcd for $C_8H_{14}NO_3S_2SiF_3$: C, 29.90; H, 4.39; N, 4.36%.

2-Methyl-4-phenyl-3-(trimethylsilylmethyl)thiazolium Triflate (4): Yield 83%; mp 130—132 °C; pale yellow prisms; IR (KBr) 1250, 1145, 1025, 850 cm^{-1}; ^1H NMR (DMSO-d_6) δ=−0.14 (s, 9H, $(CH_3)_3Si$), 2.95 (s, 3H, 2-CH_3), 4.23 (s, 2H, CH_2), 7.69 (s. 5H, Ar**H**), 8.18 (s, 1H, 5-**H**); MS *m/z* 262 (M^+), 135 (base peak). Found: C, 43.51; H, 4.70; N, 3.65%. Calcd for $C_{15}H_{20}NO_3S_2SiF_3$: C, 43.78; H, 4.90; N, 3.40%.

Reaction of Triflate 1 with DMAD in the Presence of Cesium Fluoride. A mixture of **1** (371 mg, 1 mmol), DMAD (284 mg, 2 mmol) and CsF (152 mg, 1 mmol) in dry DME (3 mL) was refluxed for 24 h. To the reaction mixture was added water (30 mL), and the resultant mixture was extracted with $CHCl_3$ (50 mL×2). The $CHCl_3$ extract was dried over $MgSO_4$, and concentrated *in vacuo*. The residue was chromatographed on silica gel using $CHCl_3$–Et_2O (9/1) as an eluent to give 300 mg (69%) of a mixture of *E* and *Z* forms of *N*-arylpyrrole **5** as brownish yellow viscous oil, which was thermally unstable: IR (neat) 1720 cm^{-1}; ^1H NMR ($CDCl_3$) δ=3.48, 3.75 (each s, 3H×5/6, OCH_3 in *Z* form), 3.58, 3.68 (each s, 3H×1/6, OCH_3 in *E* form), 3.83 (s, 6H×5/6, OCH_3 in *Z* form), 3.85 (s, 6H×1/6, OCH_3 in *E* form), 5.75 (s, 1H×1/6, =C**H** in *E* form), 6.55 (s, 1H×5/6, =C**H** in *Z* form), 7.34—7.50 (m, 6H, Ar**H** and α-**H** of pyrrole ring); ^{13}C NMR ($CDCl_3$) of *Z* form δ=51.49, 52.02, 52.96 (each q), 116.48 (s, β-**C** of pyrrole ring), 123.17 (d, =**C**H), 127.28 (s), 129.40 (d, α-**C** of pyrrole ring), 129.75, 130.22, 134.68 (each d), 140.37 (s), 145.72 (s, =**C**^{S–}), 163.56, 163.85, 164.86 (each s, **C**=O); HRMS *m/z* 433.0841 ($C_{20}H_{19}NO_8S$ requires 433.0830).

Similarly, triflates **2**—**4** reacted with DMAD (2 equivalents) under the influence of CsF (1 equivalent) in dry DME under reflux for 24 h to give a mixture of *E* and *Z* forms of the corresponding pyrrole compounds **6**—**8**, respectively.

6: Yield 88%; red-colored viscous oil; IR (neat) 1720 cm^{-1}; ^1H NMR ($CDCl_3$) δ=2.15 (s, 3H×1/11, C-CH_3 in *E* form), 2.20 (s, 3H×10/11, C-CH_3 in *Z* form), 3.48, 3.61, 3.68, 3.72 (each s, 3H×1/11, OCH_3 in *E* form), 3.52, 3.76, 3.80, 3.85 (each s, 3H×10/11, OCH_3 in *Z* form), 5.79 (s, 1H×1/11, =C**H** in *E* form), 6.65 (s, 1H×10/11, =C**H** in *Z* form), 7.17—7.50 (m, 5H, Ar**H**); MS *m/z* 447 (M^+), 356 (base peak). Found: C, 56.48; H, 4.85; N, 2.91%. Calcd for $C_{21}H_{21}NO_8S$: C, 56.37; H, 4.73; N, 3.13%.

7: Yield 33%; brownish yellow viscous oil; IR (neat) 1720 cm^{-1}; ^1H NMR ($CDCl_3$) δ=3.75 (s, 3H×2/5, OCH_3 in *Z* form), 3.79 (s, 3H×3/5, OCH_3 in *E* form), 3.83 (s, 6H, OCH_3 in *E* and *Z* forms), 3.85 (s, 3H×3/5, OCH_3 in *E* form), 3.89 (s, 3H×2/5, OCH_3 in *Z* form), 5.95 (d, 1H×3/5, *J*=3.8 Hz, =C^{S–}**H** in *E* form), 6.04 (s, 1H×3/5, =C**H**E in *E* form), 6.05 (d, 1H×3/5, *J*=3.8 Hz, =C^{N<}**H** in *E* form), 6.69 (s, 1H×2/5, =C**H**E in *Z* form), 6.79 (d, 1H×2/5, *J*=8.6 Hz, =C^{S–}**H** in *Z* form) 6.95 (d, 1H×2/5, *J*=8.6 Hz, =C^{N<}**H** in *Z* form), 7.55 (s, 2H×2/5, α-**H** of pyrrole ring in *Z* form), 7.59 (s, 2H×3/5, α-H of pyrrole ring in *E* form); ^{13}C NMR ($CDCl_3$) of a mixture of *E* and *Z* forms δ=51.65, 52.19, 53.36, 53.51 (each q), 106.72, 111.54 (each d, =C**H**E), 116.81, 117.20 (each s, β-**C** of pyrrole ring), 117.23, 123.72 (each d, =**C**^{N<}**H**), 126.80, 129.52 (each d, =**C**^{S–}**H**), 127.87, 128.01 (each d, α-**C** of pyrrole ring), 143.31, 144.68 (each s, =**C**^{S–}**H**), 163.15, 163.29, 163.63, 163.83, 164.76 (each s, **C**=O); MS *m/z* 383 (M^+), 292 (base peak). Found: C, 49.88; H, 4.48; N, 3.79%. Calcd for $C_{16}H_{17}NO_8S$: C, 50.12; H, 4.47; N, 3.65%.

8: Yield 36%; brownish yellow viscous oil; IR (neat) 1715 cm^{-1}; ^1H NMR ($CDCl_3$) δ=2.16 (s, 3H×8/9, C-CH_3 in *E* form), 2.21 (s, 3H×1/9, C-CH_3 in *Z* form), 3.74 (s, 3H×8/9, OCH_3 in *E* form), 3.76 (s, 3H×1/9, OCH_3 in *Z* form), 3.81 (s, 3H, OCH_3 in *E* and *Z* forms), 3.86 (s, 3H×8/9, OCH_3 in *E* form), 3.89 (s, 3H×1/9, OCH_3 in *Z* form), 3.91 (s, 3H, OCH_3 in *E* and *Z* forms), 6.05 (s, 1H×8/9, =C**H**E in *E* form), 6.74 (s, 1H×1/9, =C**H**E in *Z* form), 7.00—7.37 (m, 7H, Ar**H** and α-**H** of pyrrole ring); MS *m/z* 473 (M^+), 382 (base peak). Found: C, 58.34; H, 4.99; N, 3.08%. Calcd for $C_{23}H_{23}NO_8S$: C, 58.34; H, 4.86; N, 2.96%.

Reaction of Triflate 1 with Maleimide in the Presence of Cesium Fluoride. A mixture of **1** (742 mg, 2 mmol), *N*-(*p*-tolyl)maleimide (374 mg, 2 mmol) and CsF (304 mg, 2 mmol) in dry DME (6 mL) was stirred at room temperature for 24 h. To the reaction mixture was added water (30 mL), and the resultant mixture was extracted with $CHCl_3$ (50 mL×2). The extract was dried over $MgSO_4$ and concentrated *in vacuo* to leave a residue. The residue was chromatographed on silica gel to give 177 mg (26%) of the *exo*-cycloadduct **9a** (from $CHCl_3$ elution) and 323 mg (48%) of the *endo*-cycloadduct **10a** (from $CHCl_3$–Et_2O (9/1) elution), together with recovery of 90 mg (24%) of the maleimide (from $CHCl_3$ elution).

9a: Pale yellow prisms; mp 153—154 °C; IR (KBr) 1765, 1695 cm^{-1}; ^1H NMR (benzene-d_6) δ=1.99 (s, 3H, CH_3), 2.66 (ddd, 1H, *J*=8.7, 8.0, 3.9 Hz, 10a-**H**), 3.03 (dd, 1H, *J*=8.7, 2.7 Hz, 3a-**H**), 3.13 (dd, 1H, *J*=10.1, 8.0 Hz, 10-**H**), 3.38 (dd, 1H, *J*=10.1, 3.9 Hz, 10-**H**), 5.52 (d, 1H, *J*=2.7 Hz, 3b-**H**), 6.44—7.23 (m, 8H, Ar**H**); MS *m/z* 336 (M^+), 150 (base peak). Found: C, 68.12; H, 4.75; N, 8.17%. Calcd for $C_{19}H_{16}N_2O_2S$: C, 67.84; H, 4.79; N, 8.33%.

10a: Colorless solid; mp 69—71 °C;[10] IR (KBr) 1770, 1690 cm^{-1}; ^1H NMR (benzene-d_6) δ=1.94 (s, 3H, CH_3), 2.44 (t, 1H, *J*=7.8 Hz, 10a-**H**), 2.61 (t, 1H, *J*=7.8 Hz, 3a-**H**), 2.67 (dd, 1H, *J*=12.0, 7.8 Hz, 3b-**H**), 6.38—7.50 (m, 8H, Ar**H**); MS *m/z* 336 (M^+), 107 (base peak).

Similarly, **1** reacted with *N*-methylmaleimide (1 equivalent) in the presence of CsF (1 equivalent) in dry DME at

room temperature for 24 h to give the *exo*-cycloadduct **9b** and *endo*-cycloadduct **10b** in 43 and 34% yields respectively, besides recovery of the maleimide (20%).

9b: Colorless needles; mp 134—135 °C; IR (KBr) 1775, 1700 cm^{-1}; ^1H NMR (benzene-d_6) δ=2.47 (s, 3H, NCH_3), 2.52 (dt, 1H, J=3.9, 7.8 Hz, 10a-**H**), 2.92 (dd, 1H, J=7.8, 2.6 Hz, 3a-**H**), 3.08 (dd, 1H, J=10.5, 7.8 Hz, 10-**H**), 3.28 (dd, 1H, J=10.5, 5.3 Hz, 10-**H**), 5.43 (d, 1H, J=2.6 Hz, 3b-**H**) 6.45—6.94 (m, 4H, Ar**H**); MS m/z 260 (M^+), 150 (base peak). Found: C, 59.80; H, 4.61; N, 10.63%. Calcd for $C_{13}H_{12}N_2O_2S$: C, 59.98; H, 4.65; N, 10.76%.

10b: Colorless solid; mp 116—120 °C;[10] IR (KBr) 1775, 1700 cm^{-1}; ^1H NMR (benzene-d_6) δ=2.25 (s, 3H, NCH_3), 2.32—2.62 (m, 3H, 3a-**H**, 10-**H**, and 10a-**H**), 3.87 (dd, 1H, J=12.7, 1.2 Hz, 10-**H**), 4.70 (d, 1H, J=7.7 Hz, 3b-**H**), 6.32—6.95 (m, 4H, Ar**H**); MS m/z 260 (M^+), 150 (base peak).

Reaction of Triflate **2** *with* N-(p-*Tolyl*)*maleimide in the Presence of Cesium Fluoride.* After the reaction of **2** (1.155 g, 3 mmol) with the maleimide (561 mg, 3 mmol) in the presence of CsF (456 mg, 3 mmol) in dry DME (9 mL) was performed at room temperature for 24 h, purification of the reaction mixture by chromatography (SiO_2) afforded the *exo*-cycloadduct **9c** (385 mg, 37%) and *endo*-cycloadduct **10c** (361 mg, 34%), together with recovery of the maleimide (60 mg, 11%).

9c: Colorless prisms; mp 140—141 °C; IR (KBr) 1770, 1695 cm^{-1}; ^1H NMR ($CDCl_3$) δ=1.76 (s, 3H, 3b-CH_3), 2.39 (s, 3H, CH_3), 3.41 (dd, 1H, J=9.4, 7.9 Hz, 10-**H**), 3.64 (ddd, 1H, J=8.7, 7.9, 1.9 Hz, 10a-**H**), 3.87 (dd, 1H, J=7.9, 1.9 Hz, 10-**H**), 3.89 (d, 1H, J=8.7 Hz, 3a-**H**), 8.00—8.33 (m, 8H, Ar**H**); MS m/z 350 (M^+), 163 (base peak). Found: C, 68.30; H, 5.21; N, 7.81%. Calcd for $C_{20}H_{18}N_2O_2S$: C, 68.53; H, 5.18; N, 8.00%.

10c: Colorless solid; mp 67—70 °C;[10] IR (KBr) 1770, 1700 cm^{-1}; ^1H NMR ($CDCl_3$) δ=1.88 (s, 3H, 3b-CH_3), 2.29 (s, 3H, CH_3), 3.31—3.76 (m, 3H, 3a-**H**, 10-**H**, and 10a-**H**), 4.25 (d, 1H, J=10.7 Hz, 10-**H**), 6.49—7.17 (m, 8H, Ar**H**); MS m/z 350 (M^+), 163 (base peak).

References

1) a) V. Boekelheide and N. A. Fedoruk, *J. Am. Chem. Soc.*, **90**, 3830 (1968); b) J. Fröhlich, U. Habermalz, and F. Kröhnke, *Tetrahedron Lett.*, **1970**, 271; c) K. T. Potts, D. R. Choudhury, and T. R. Westby, *J. Org. Chem.*, **41**, 187 (1976); d) O. Tsuge, H. Shimoharada, and M. Noguchi, *Heterocycles*, **15**, 807 (1981); e) G. A. Kraus and J. O. Nagy, *Tetrahedron Lett.*, **22**, 2727 (1981); f) O. Tsuge, H. Shimoharada, M. Noguchi, and S. Kanemasa, *Chem. Lett.*, **1982**, 711; g) O. Tsuge and H. Shimoharada, *Chem. Pharm. Bull.*, **30**, 1903 (1982); h) O. Tsuge, S. Kanemasa, and S. Takenaka, *Heterocycles*, **20**, 1907 (1983); i) G. A. Kraus and J. O. Nagy, *Tetrahedron Lett.*, **24**, 3427 (1983).

2) a) F. Kröhnke and W. Friedrich, *Chem. Ber.*, **96**, 1195 (1963); b) J. Metzger, H. Larive, E. Vincent, and R. Dennilauler, *J. Chem. Phys.*, **60**, 944 (1963); c) D.-B. Reuschling and F. Kröhnke, *Chem. Ber.*, **104**, 2110 (1971); d) O. Tsuge, M. Tanaka, H. Shimoharada, and S. Kanemasa, *Bull. Chem. Soc. Jpn.*, **56**, 1688 (1983).

3) O. Tsuge, M. Tanaka, H. Shimoharada, and M. Noguchi, *Heterocycles*, **16**, 1705 (1981).

4) a) E. Vedejs and G. R. Martinez, *J. Am. Chem. Soc.*, **101**, 1753 (1979); b)E. Vedejs and G. R. Martinez, *ibid.*, **102**, 7993 (1980); c) K. Achiwa and M. Sekiya, *Chem. Lett.*, **1981**, 1213; d) A. Achiwa and M. Sekiya, *Tetrahedron Lett.*, **23**, 2589 (1982); e) Y. Terao, N. Imai, K. Achiwa, and M. Sekiya, *Chem. Pharm. Bull.*, **30**, 3167 (1982); f) A. Padwa and Y.-Y. Chen, *Tetrahedron Lett.*, **24**, 3447 (1983); g) A. Padwa, G. Hoffmann, and M. Tomas, *ibid.*, **24**, 4303 (1983); h) T. Livinghous and R. Smith, *J. Chem. Soc., Chem. Commun.*, **1983**, 210; i) R. Smith and T. Livinghous, *J. Org. Chem.*, **48**, 1554 (1983); j) E. Vedejs and F. G. West, *ibid.*, **48**, 4773 (1983); k) S.-F. Chen, J. W. Ullrich, and P. S. Mariano, *J. Am. Chem. Soc.*, **105**, 6160 (1983); l) O. Tsuge, S. Kanemasa, A. Hatada, and K. Matsuda, *Chem. Lett.*, **1984**, 801; m) A. Hosomi, Y. Sakata, and H. Sakurai, *ibid.*, **1984**, 1117; n) K. Achiwa, N. Imai, T. Motoyama, and M. Sekiya, *ibid.*, **1984**, 2041.

5) O. Tsuge, S. Kanemasa, S. Kuraoka, and S. Takenaka, *Chem. Lett.*, **1984**, 279; O. Tsuge, S. Kanemasa, S. Kuraoka, and S. Takenaka, *ibid.*, **1984**, 281.

6) The reaction of thiophenol with DMAD (1 equivalent) in the presence of catalytic amount of NaOMe in refluxing THF for 20 h gave a mixture of dimethyl phenylthiofumarate and -maleate (1/1) in 93% yield: yellow viscous oil; ^1H NMR ($CDCl_3$) δ=3.32, 3.64, 3.70, 3.77 (each s, 3H×1/2, OCH_3), 5.48, 6.38 (each s, 1H×1/2, =**CH**), 7.24—7.60 (m, 5H, Ar**H**); ^{13}C NMR ($CDCl_3$) δ=51.61, 52.43, 52.66 (each q), 113.90, 118.77 (each d, =**CH**), 149.71, 151.18 (each s, $\overset{O}{\underset{S}{}}C=$**C**=), 163.69, 164.39, 164.92, 165.09 (each s, **C**=O).

7) The cycloadducts between nonstabilized pyridinium methylides and olefinic dipolarophiles are too labile to be isolated (see Ref. 5).

8) When treated with triethylamine (1 equivalent) in DME at room temperature, the triflates **2** and **4** generated the corresponding 2-methylenethiazolines **D** and **E** which were trapped as benzoylated products, respectively.

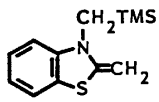

D

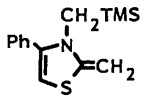

E

9) S. Ambusht, S. K. Chiu, P. E. Peterson, and J. Queen, *Synthesis*, **1980**, 318.

10) Purification of *endo*-cycloadducts, **10a—10c**, was difficult owing to their thermal instability.

Synthetic Photochemistry. XXIX.[1] A Convenient Preparation of 1,2,3-Substituted Cyclopentenes from the Photoadducts of Methyl 2,4-Dioxopentanoate-Isoprene

Nobuo KATO and Hitoshi TAKESHITA*
Research Institute of Industrial Science, 86, Kyushu University, Kasuga-koen, Kasuga, Fukuoka 816
(Received November 30, 1984)

Photoadducts obtained by cycloaddition of isoprene with methyl 2,4-dioxopentanoate were converted to cyclopentene derivatives. The stereochemistry of the intermediate glycols was estabilished by chemical correlations to each other; only the *cis*-glycols were convertible to the cyclopentenes under the conditions employed, suggesting a fore-going acetylation of the hindered glycol functions.

Previously, we have obtained two photocycloadducts (**1** and **2**) from isoprene (**3**) and methyl 2,4-dioxopentanoate (**4**),[2] and have utilized them for mono- and sesquiterpenoid syntheses; *i.e.*, **1** to geijerone and γ-elemene,[2] and **2** to dehydroiridodial and chrysomelidial.[3] It is noteworthy that the easy access of cyclopentane derivatives from **2** in the latter case provided a new method of C_5-homologation leading to the higher terpenic cyclopentanes having correct head-to-tail arrangement.[4] Since the photochemical addition proceeds in a highly regioselective manner,[5] and is effective even with the conjugated olefins,[1,6] fundamental understanding of this cyclopentane formation is important. We wish herein to present experimental details of the formation of 1,2,3-substituted cyclopentane derivatives from the photoadducts, **1** and **2**, by the Mukaiyama-McMurry reaction.[7]

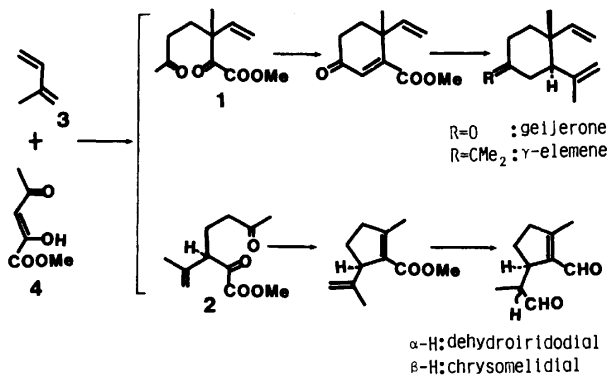

Scheme 1.

The Reductive Cyclization of Methyl 3-Methyl-3-vinyl-2,6-dioxoheptanoate (1). When methyl 3-methyl-3-vinyl-2,6-dioxoheptanoate (**1**) was treated with titanium(II) chloride in tetrahydrofuran (THF), prepared *in situ* from titanium(IV) chloride and zinc, four isomeric reductive cyclisates, 1,2-dihydroxy-2-methoxycarbonyl-1,3-dimethyl-3-vinylcyclopentanes, **5** (45%), **6** (1%), **7** (2%), and **8** (37%), were obtained. Two major products (**5** and **8**) afforded 2,2-dimethyl-1,3-dioxolane derivatives (**9** and **10**) by treatment with 2,2-dimethoxypropane (DMP) and pyridinium *p*-toluenesulfonate (PPTS) in benzene, while the other two (**6** and **7**) were recovered unchanged. Based on these facts, **5** and **8** are deduced to be *cis*-glycol derivatives, and **6** and **7** are thus *trans*-glycols.

Consecutive treatments of **10** with sodium hydroxide in dimethyl sulfoxide (DMSO), and with iodine and sodium hydrogencarbonate in acetonitrile afforded, *via* the carboxylic acid (**11**), iodo γ-lactone derivatives (**12** and **13**), in 92 and 6% yields. Therefore, the ester and vinyl groups of **8** and **10** are in a *cis* relationship, and the full stereochemistry of **5** and **8** must be depicted as shown.

Moreover, the lithium aluminum hydride (LAH)-reduction of **5**, **7**, and **8** yielded the triol derivatives (**14**, **15**, and **16**) in good yields. Upon treatment of **14** with PPTS and DMP, the single dioxolane derivative (**17**) was obtained in 94% yield. Treatment of **17** with thionyl chloride in pyridine gave a 5:2-mixture of the unsaturated, anhydro 1,3-dioxolane derivatives (**18** and **19**), in 81% yield. On the other hand, the same treatment of **16** gave, *via* the 1,3-dioxolane (**20**), a 2:1-mixture of the unsaturated 1,3-dioxolane derivatives (**21** and **22**).

In the case of **15** (the triol derived from **7**), one of the *trans*-glycols, the DMP treatment afforded two acetals; one was the 1,3-dioxolane (**23**), and the other, a 1,3-dioxane (**24**). Treatment of **23** with thionyl chloride caused a facile dehydration to a mixture of unsaturated 1,3-dioxolanes, which consisted of **18** and **19** on the basis of NMR and gas-liquid chromatographic analyses. Therefore, the remaining products, **6** and **7**, must also have the configurations indicated.

Interestingly, the glycols, **5** and **8**, were reduced to the same cyclopentene derivative (**25**) by zinc in acetic acid and acetic anhydride, while the trans-isomers, **6** and **7**, merely formed monoacetates (**26** and **27**) under comparative conditions.

The Reductive Cyclization of Methyl 3-Isopropenyl-2,6-dioxoheptanoate (2). Methyl 3-isopropenyl-2,6-dioxoheptanoate (**2**) was treated with titanium(II) chloride to obtain three cyclopentanediols (**28**, **29**, and **30**) in a ratio of 1:1.5:9. By further reduction

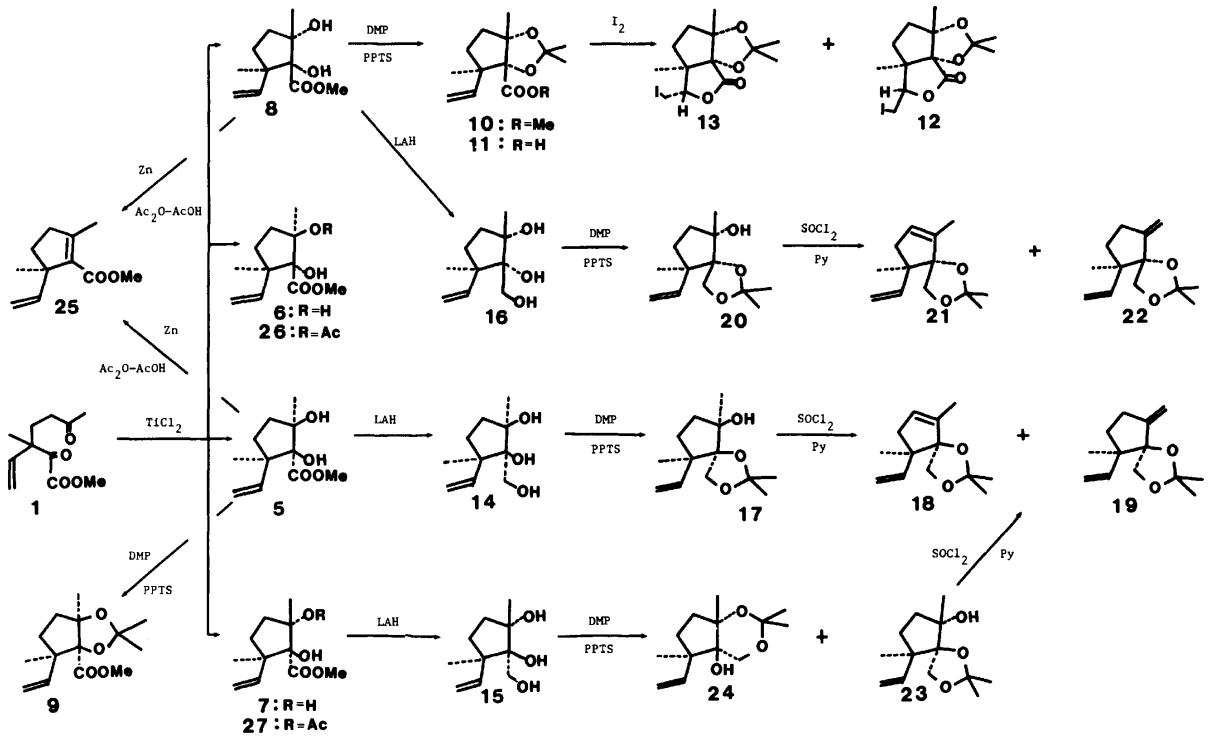

Scheme 2.

with zinc in acetic acid and acetic anhydride,[3] **28** and **30** yielded the same cyclopentene (**31**),[8] while the remaining **29** resulted in a monoacetylation to **32**, but not to **31**. By analogy with **6** and **7**, this might indicate the *trans* relationship for the glycol function of **29**. Indeed, **28** and **30** afforded the 2,2-dimethyl-1,3-dioxolane derivatives (**33** and **34**). The iodolactonization reaction of the acid (**35**) derived from **34** produced two iodo γ-lactones (**36** and **37**); the major product, **36**, colorless needles, showed an IR absorption due to $\nu_{C=O}$ at 1780 cm^{-1}. These two observations clarified the stereochemistry of **28** and **30** as depicted.

The stereochemistry of the minor product, **29**, was unambiguously elucidated by the following chemical correlations; the LAH-reduction of **28**, **29**, and **30** respectively afforded the triol derivatives (**38**, **39**, and **40**) in good yields. Treatment of **38** with DMP and PPTS in THF gave the 1,3-dioxolane (**41**), which upon treatment with thionyl chloride in pyridine afforded an isomeric pair of unsaturated 1,3-dioxolanes (**42** and **43**). Similarly, the DMP-treatment of **40** with PPTS afforded another 1,3-dioxolane (**44**), which was converted to a mixture of unsaturated 1,3-dioxolanes (**45** and **46**).

Subsequently, the DMP-treatment of the remaining triol (**39**) with PPTS was carried out to obtain two products, **47**, 40%, and **48**, 49%; the NMR analysis indicated that **47** was the expected 1,3-dioxolane, while **48** was the 1,3-dioxane. The similar dehydration of **47** as in the cases of **41** and **44**, afforded a mixture of the unsaturated 1,3-dioxolanes. This mixture was indeed identical with **45** and **46** in respect of NMR spectral and gas-liquid chromatographic analyses. Therefore, **39** and **40** mutually differ in the stereochemistry of the methyl and hydroxyl groups at C-1; the structure of **29** should be as shown.

In conclusion, it is particularly noteworthy that, for both series, the major cyclopentanediols were *cis*-derivatives. And the highly specific conversion to cyclopentene derivatives from only *cis*-glycols has supported the correctness of the orthoacetate mechanism already proposed.[9] Namely, the difference between the *cis*- and *trans*-glycols can be explained in of the structural difference of "diacetates"; it is well known that even hindered *cis*-glycols form diacetates by acetyl migration *via* bridged intermediates, while the *trans*-glycols can not make such an intermediate. It is true that in this case no *cis*-diacetate could be detected, and probably, they should have been rapidly reduced to olefins under the reaction conditions. On the other hand, the *trans*-diacetate, whose formation was in fact identified,[10] must suffer a severe steric hindrance. Should the reduction proceed *via* the *trans* elimination like ordinary debromination, the *trans*-isomers must be more favorable than the *cis*-isomers. But, this was not the case. Therefore, the reduction should occur from the orthoester acetates, 2-acetoxy-2-methyl-1,3-dioxolanes, which should be formed from the immediate precursors by the acid-catalyzed solvolysis.[11] Furthermore, this cyclopentene formation is to be expectable only with the photoadducts of **4** but not with those of acetylacetone, due to their readiness to give the cyclohexenones.[12] The relative unreactivity of the pho-

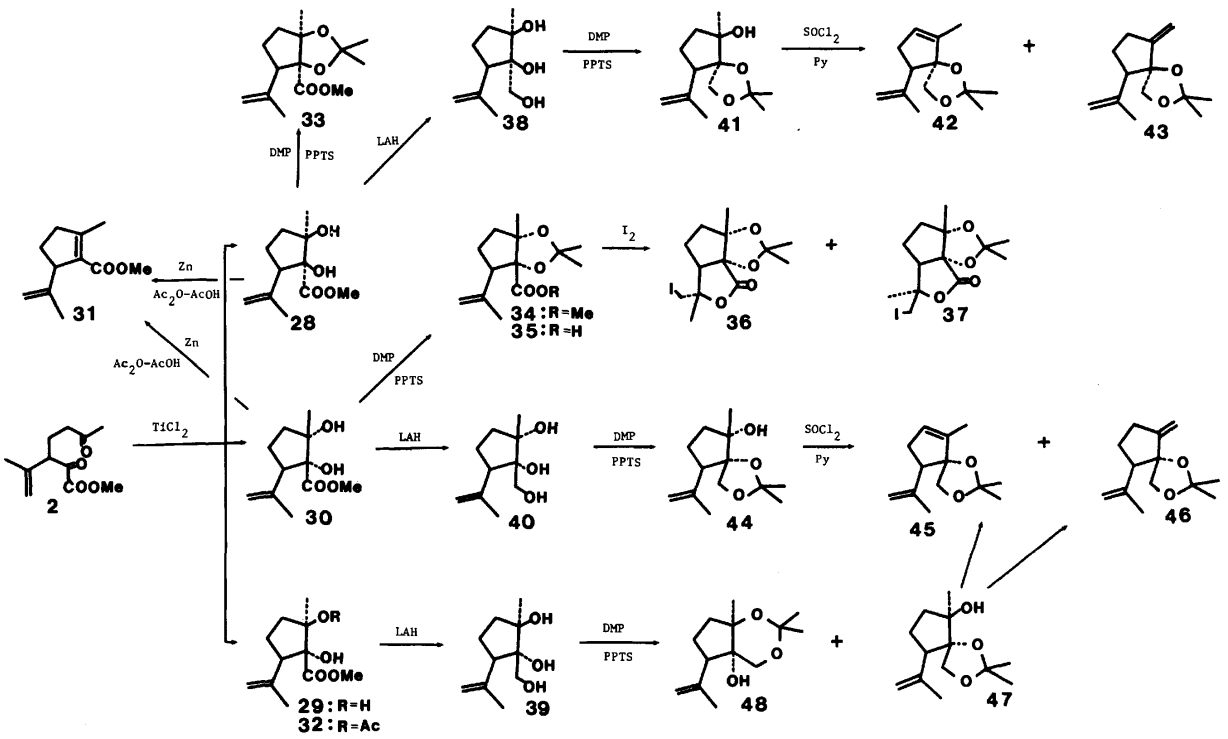

Scheme 3.

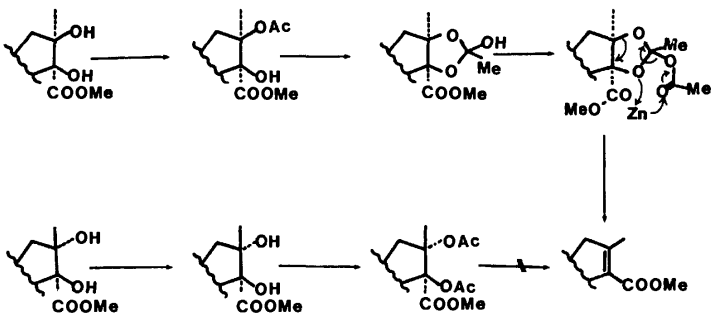

Scheme 4.

toadducts of **4** towards acid and base should have become favorable for this reductive cyclization.

Experimental

The mps were measured with Yanagimoto Micro-mp apparatus, and not corrected. The elemental analyses were performed by Miss S. Hirashima of this Institute. All the NMR spectra were taken on a JEOL FX 100 Model spectrometer in $CDCl_3$ solutions, and the chemical shifts expressed in δ unit were from the internal Me_4Si. Mass spectra were measured on a JEOL 01SG-2 Model apparatus. The IR spectra were measured on a Jasco IRA 102 Model spectrophotometer. The gas-liquid chromatographic analyses were performed on a JEOL JGC 20 K Model apparatus with a 200 cm column of 20% DOP on Uniport B (temperatures of column and injection chamber were 140 °C and 160 °C, and carrier gas (N_2) flow was 32 cm³/min), and the retention times measured under those conditions were designated by the term, *RT*.

$TiCl_2$-reduction of 1. To a THF-complex of $TiCl_4$ (prepared from 1.65 cm³) in anhydrous THF (200 cm³), Zn (2.0 g) was added at 0 °C under stirring. After a yellow coloration of the complex faded out completely, pyridine (1.2 cm³) was added. Then, into the resultant suspension, **1** (2.12 g) was added dropwise over a period of 30 min. After additional stirring for 1 h at 15—25 °C, the mixture was quenched with aqueous 30%-K_2CO_3, and fractionated with ether. After removing the precipitates through a short Celite column, the filtrate was evaporated, and chromatographed on a silica-gel (Wakogel C 300) column. From the least polar fractions from hexane–EtOAc (6:1), colorless granules, mp 59.5—60.5 °C, 960 mg (45%), **5** [Found: C, 61.47; H, 8.51%. Calcd for $C_{11}H_{18}O_4$: C, 61.66; H, 8.47%. ^{1}H-NMR δ=1.10 (3H, s), 1.28 (3H, s), 1.6—2.3 (4H, m), 2.90 (1H, br. s, OH), 3.71 (3H, s), 3.84 (1H, s, OH), 4.92 (1H, dd, J=10.3, 1.6 Hz), 4.98 (1H, dd, J=17.8, 1.6 Hz), and 5.78 (1H, dd, J=17.8, 10.3 Hz). ^{13}C-NMR δ=24.2, 24.9, 33.3, 35.7, 50.5, 52.4, 80.6, 88.8, 112.6, 144.0, and 175.3. ν: 3475, 3400, 2955, 1730, 1637, 1438, 1248, 1154, 1132, 1006, and 901 cm^{-1}. *m/z*: 214 (M^+)], was obtained. Subsequently, colorless

prisms, mp 66—66.5 °C, **6** [Found: C, 61.93; H, 8.50%. ^{1}H-NMR δ=1.26 (3H, s), 1.33 (3H, s), 1.7—2.1 (4H, m), 2.70 (1H, s, OH), 3.78 (3H, s), 3.94 (1H, br. s, OH), 5.17 (1H, dd, J=17.3, 1.6 Hz), 5.25 (1H, dd, J=10.9, 1.6 Hz), and 5.94 (1H, dd, J=17.3, 10.9 Hz). ^{13}C-NMR δ=23.5, 26.0, 34.2, 37.2, 51.7, 52.1, 84.0, 86.0, 115.8, 142.3, and 174.3. ν: 3500, 3400, 2965, 1706, 1640, 1451, 1383, 1252, 1198, 1042, 1029, and 906 cm^{-1}. m/z: 214 (M^+)], 19 mg (1%), and colorless needles, mp 105.5—106 °C, **7** [Found: C, 61.65; H, 8.52%. ^{1}H-NMR δ=1.20 (3H, s), 1.34 (3H, s), 1.4—2.3 (4H, m), 2.98 (1H, s, OH), 3.58 (1H, br. s, OH), 3.71 (3H, s), 4.87 (1H, dd, J=11, 1.4 Hz), 4.91 (1H, dd, J=17.4, 1.4 Hz), and 6.17 (1H, dd, J=17.4, 11 Hz). ^{13}C-NMR δ=20.5, 23.5, 36.8, 37.3, 51.2, 52.2, 83.9, 88.5, 111.3, 145.9, and 174.0. ν: 3470, 3340, 2975, 1712, 1634, 1390, 1251, 1068, 1036, 907, and 865 cm^{-1}. m/z: 214 (M^+)], 45 mg (2%), were obtained. The most polar fractions eluted with hexane-EtOAc (4:1) were colorless plates, mp 25 °C, **8** [Found: M^+, 214.1196. Calcd for $C_{11}H_{18}O_4$: 214.1204. ^{1}H-NMR δ=1.03 (3H, s), 1.13 (3H, s), 1.7—2.2 (4H, m), 2.64 (1H, br. s, OH), 3.64 (1H, s, OH), 3.80 (3H, s), 5.02 (1H, dd, J=11.1, 1.4 Hz), 5.04 (1H, dd, J=17.4, 1.4 Hz), and 6.33 (1H, dd, J=17.4, 11.1 Hz). ^{13}C-NMR δ=21.9, 24.2, 33.4, 36.2, 50.2, 52.4, 81.0, 89.2, 111.5, 144.3, and 174.5. ν: 3470, 3410, 2950, 1724, 1633, 1244, and 1138 cm^{-1}], 790 mg (37%).

DMP-acetalization of 5 to 9. A mixture of **5** (86 mg), DMP (1 cm^3), and PPTS (15 mg) in benzene (2 cm^3) was refluxed on an oil bath for 15 h. The mixture was then poured into $NaHCO_3$ solution, extracted with ether, and chromatographed on a silica-gel column with hexane-EtOAc (15:1) to give a colorless oil, 92 mg (90%), **9** [Found: M^+, 254.1512. Calcd for $C_{14}H_{22}O_4$: 254.1517. ^{1}H-NMR δ=1.21 (3H, s), 1.32 (3H, br. s), 1.50 (3H, br. s), 1.58 (3H, s), 1.6—2.0 (4H, m), 3.70 (3H, s), 5.00 (1H, dd, J=10.1, 1.3 Hz), 5.02 (1H, dd, J=18.0, 1.3 Hz), and 5.91 (1H, dd, J=18.0, 10.1 Hz). ν: 2990, 1738, 1637, 1460, 1380, 1267, 1086, 1058, 1043, 998, and 914 cm^{-1}].

DMP-acetalization of 8 to 10. Similarly, a benzene solution of **8** (67 mg) was refluxed for 15 h with DMP (1 cm^3) and PPTS (15 mg). Chromatographic purification of the product afforded a colorless oil, 77 mg (98%), **10** [Found: M^+, 254.1506. ^{1}H-NMR δ=1.01 (3H, br. s), 1.28 (3H, br. s), 1.47 (3H, br. s), 1.61 (3H, s), 1.7—2.4 (4H, m), 3.73 (3H, s), 4.99 (1H, dd, J=17.4, 1.4 Hz), 5.07 (1H, dd, J=10.9, 1.4 Hz), and 6.08 (1H, dd, J=17.4, 10.9 Hz). ν: 2990, 1738, 1637, 1454, 1380, 1265, 1088, 1046, 913, and 848 cm^{-1}].

Saponification and Iodolactonization of 10 to 12 and 13 via 11. To a DMSO solution (1 cm^3) of **10** (47 mg), an aqueous 20%-NaOH (0.6 cm^3) was added and refluxed for 2 h. The mixture was acidified with dil HCl, and extracted with ether to give colorless needles, mp 60.5—61.5 °C, **11**, 44 mg (100%) [Found: C, 64.78; H, 8.40%. Calcd for $C_{13}H_{20}O_4$: C, 64.98; H, 8.39%. ^{1}H-NMR δ=1.09 (3H, br. s), 1.37 (3H, br. s), 1.49 (3H, br. s), 1.60 (3H, s), 1.7—2.4 (4H, m), 5.06 (1H, dd, J=17.3, 1.3 Hz), 5.11 (1H, dd, J=11.0, 1.3 Hz), and 5.98 (1H, dd, J=17.3, 11.0 Hz). ν: 3500—2500, 2990, 1705, 1638, 1450, 1378, 1272, 1090, 1073, 1030, and 910 cm^{-1}. m/z: 240 (M^+)].

This acid, **11**, was then treated with I_2 (100 mg) in MeCN (2 cm^3) in the presence of $NaHCO_3$ (100 mg). After being stirred at 15—25 °C for 15 h, excess I_2 was decomposed with aqueous $NaHSO_3$, and extracted with ether. Silica-gel column chromatography (hexane-EtOAc=6:1) gave two epimeric iodo lactones, the major isomer, 62 mg (92%), colorless prisms, mp 84.5—85 °C, **12** [Found: C, 42.85; H, 5.34%. Calcd for $C_{13}H_{19}O_4I$: C, 42.64; H, 5.23%. ^{1}H-NMR δ=1.11 (3H, br. s), 1.41 (3H, br. s), 1.45 (3H, br. s), 1.62 (1H, m), 1.63 (3H, s), 2.1—2.3 (3H, m), 3.06 (1H, dd, J=11, 10 Hz), 3.38 (1H, dd, J=10, 5.5 Hz), and 5.01 (1H, dd, J=11, 5.5 Hz). ν: 2975, 1790, 1380, 1332, 1164, 1045, 1026, 915, 875, and 846 cm^{-1}. m/z: 366 (M^+)], and the minor, 4 mg (6%), a colorless oil, **13** [^{1}H-NMR δ=1.33 (3H, s), 1.42 (3H, br. s), 1.51 (3H, br. s), 1.61 (3H, s), 2.2—2.5 (4H, m), 3.59 (1H, dd, J=10, 6.5 Hz), 3.78 (1H, dd, J=10, 8.5 Hz), and 4.45 (1H, dd, J=8.5, 6.5 Hz)].

The LAH-reduction of 5 to 14. An anhydrous THF solution of **5** (214 mg) was treated with LAH (150 mg) at 15—25 °C for 1 h. The mixture was treated with EtOAc, diluted with aqueous NH_4Cl, and extracted with ether. Silica-gel column chromatography (hexane-EtOAc=1:1) of the extract gave colorless needles, mp 123—123.5 °C, 170 mg (91%), **14** [Found: C, 64.68; H, 9.57%. Calcd for $C_{10}H_{18}O_3$: C, 64.49; H, 9.74%. ^{1}H-NMR δ=1.15 (3H, s), 1.39 (3H, s), 1.6—2.0 (4H, m), 2.21 (1H, dd, J=7.3, 6.2 Hz, OH), 2.60 (1H, s, OH), 3.61 (1H, dd, J=11.8, 6.2 Hz), 3.66 (1H, dd, J=11.8, 7.3 Hz), 3.77 (1H, s, OH), 5.01 (1H, dd, J=10.1, 1.3 Hz), 5.05 (1H, dd, J=17.8, 1.3 Hz), and 5.84 (1H, dd, J=17.8, 10.1 Hz). ν: 3440, 3380, 2980, 1657, 1373, 1042, 1004, and 927 cm^{-1}. m/z: 186 (M^+)].

The LAH-reduction of 7 to 15. An anhydrous THF solution (5 cm^3) of **7** (74 mg) was reduced similarly with LAH (60 mg) to give colorless prisms, mp 69—70 °C, 53 mg (82%) **15** [Found: C, 64.51; H, 9.70%. ^{1}H-NMR δ=1.12 (3H, s), 1.36 (3H, s), 1.6—2.1 (4H, m), 2.14 (1H, br. s, OH), 2.43 (1H, br. m, OH), 2.78 (1H, s, OH), 3.57 (1H, dd, J=11.5, 5 Hz), 3.88 (1H, dd, J=11.5, 4 Hz), 5.01 (1H, dd, J=10.5, 1.4 Hz), 5.07 (1H, dd, J=17.7, 1.4 Hz), and 6.13 (1H, dd, J=17.7, 10.5 Hz). ν: 3545, 3390, 2970, 2950, 1630, 1467, 1058, 1006, 994, and 902 cm^{-1}. m/z: 168 (M^+−18)].

The LAH-reduction of 8 to 16. Similarly, **8** (214 mg) was reduced with LAH (150 mg) to give colorless needles, mp 90—91 °C, 148 mg (80%) **16** [Found: C, 64.23; H, 9.69%. ^{1}H-NMR δ=1.08 (3H, s), 1.33 (1H, m), 1.44 (3H, s), 1.7—2.1 (3H, m), 2.10 (1H, dd, J=7.6, 5.5 Hz, OH), 2.82 (1H, s,, OH), 3.43 (1H, s, OH), 3.63 (1H, dd, J=11.0, 5.5 Hz), 3.69 (1H, dd, J=11.0, 7.6 Hz), 5.05 (1H, dd, J=17.3, 1.4 Hz), 5.11 (1H, dd, J=11.0, 1.4 Hz), and 6.15 (1H, dd, J=17.3, 11.0 Hz). ν: 3430, 3370, 2970, 1636, 1379, 1121, 1009, and 975 cm^{-1}. m/z: 168 (M^+−18)].

Reaction of 14 with DMP and PPTS. An anhydrous THF solution (5 cm^3) of **14** (170 mg) was treated with DMP (0.5 cm^3) and PPTS (30 mg), and kept at 15—25 °C for 3 h. The mixture was diluted with aqueous K_2CO_3 and extracted with ether. Silica-gel column chromatography (hexane-EtOAc=8:1) gave a colorless oil, **17**, 195 mg (94%) [Found: M^+, 226.1558. Calcd for $C_{13}H_{22}O_3$: 226.1568. ^{1}H-NMR δ=1.16 (3H, s), 1.25 (3H, s), 1.42 (3H, br. s), 1.46 (3H, br. s), 1.5—1.9 (4H, m), 3.13 (1H, br. s, OH), 3.88 (2H, s), 5.01 (1H, dd, J=10.6, 1.3 Hz), 5.03 (1H, dd, J=17.5, 1.3 Hz), and 5.83 (1H, dd, J=17.5, 10.6 Hz). ν: 3530, 2990, 1635, 1460, 1382, 1372, 1243, 1215, 1048, 914, 875, and 852 cm^{-1}].

Dehydration of 17 to 18 and 19. A pyridine solution (1 cm^3) of **17** (35 mg) was treated with $SOCl_2$ (30 mg) at 0 °C for 1 h. Then the mixture was poured into $NaHCO_3$ solu-

tion, and extracted with ether. The extract was rapidly passed through a silica-gel column with hexane-ether (15:1) to give a colorless oil, 26 mg (81%), whose gas-liquid chromatogram showed the presence of two compounds, **18** [Found: M^+, 208.1482. Calcd for $C_{13}H_{20}O_2$: 208.1462. *RT*=23.4 min], and **19** [Found: M^+, 208.1478. *RT*=23.9 min], in a ratio of 5:2. This was further confirmed by the ^{1}H-NMR spectral analysis of the mixture [δ=1.15 (3H, s), 1.42 (6H, s), 1.73 (3H, q, *J*=2 Hz), 2.0—2.4 (2H, m), 3.62 (1H, d, *J*=9 Hz), 3.87 (1H, d, *J*=9 Hz), 5.02 (1H, dd, *J*=11.0, 1.5 Hz), 5.05 (1H, dd, *J*=17.3, 1.5 Hz), 5.49 (1H, m), and 5.98 (1H, dd, *J*=17.3, 11.0 Hz) for **18**; δ=1.03 (3H, s), 1.44 (6H, s), 1.5—1.7 (2H, m), 2.3—2.5 (2H, m), 3.66 (1H, d, *J*=8.5 Hz), 3.96 (1H, d, *J*=8.5 Hz), 5.01 (1H, td, *J*=2.5, 0.8 Hz), 5.02 (1H, dd, *J*=17.2, 1.6 Hz), 5.05 (1H, dd, *J*=11.0, 1.6 Hz), 5.25 (1H, br. t, *J*=2.5 Hz), and 5.97 (1H, dd, *J*=17.2, 11.0 Hz) for **19**].

Acetal Formation of 16 with DMP. An anhydrous THF solution (5 cm^3) of **16** (148 mg) was treated with DMP (0.5 cm^3) and PPTS (30 mg) at 15—25 °C for 4 h. The extraction and silica-gel column chromatography of the mixture afforded a colorless oil, **20**, 166 mg (92%) [Found: M^+, 226.1578. ^{1}H-NMR δ=1.02 (3H, s), 1.33 (3H, s), 1.37 (3H, br. s), 1.44 (3H, br. s), 1.7—2.1 (4H, m), 3.41 (1H, s, OH), 3.85 (1H, d, *J*=9.5 Hz), 3.98 (1H, d, *J*=9.5 Hz), 4.97 (1H, dd, *J*=17.1, 1.4 Hz), 5.03 (1H, dd, *J*=11.2, 1.4 Hz), and 6.10 (1H, dd, *J*=17.1, 11.2 Hz). ν: 3510, 2990, 1638, 1460, 1382, 1372, 1243, 1050, 878, and 854 cm^{-1}].

Dehydration of 20 to 21 and 22. A pyridine solution (1 cm^3) of **20** (30 mg) was treated with $SOCl_2$ (30 mg) at 0 °C for 1 h. The mixture was poured into $NaHCO_3$ solution, extracted with ether, and passed through a silica-gel column to give colorless oils, **21**, 13 mg (46%) [Found: M^+, 208.1445. Calcd for $C_{13}H_{20}O_2$: 208.1462. *RT*=25.6 min. δ=1.08 (3H, s), 1.32 (3H, br. s), 1.43 (3H, br. s), 1.75 (3H, q, *J*=2 Hz), 1.93 (1H, d of quint, *J*=16, 2 Hz), 2.48 (1H, d of quint, *J*=16, 2 Hz), 3.78 (1H, d, *J*=9 Hz), 3.90 (1H, d, *J*=9 Hz), 5.03 (1H, dd, *J*=17.6, 1.6 Hz), 5.03 (1H, dd, *J*=10.7, 1.6 Hz), 5.52 (1H, m), and 6.18 (1H, dd, *J*=17.6, 10.7 Hz)], and **22**, 7 mg (24%) [Found: M^+, 208.1483. *RT*=22.5 min. δ=0.92 (3H, s), 1.35 (3H, br. s), 1.40 (3H, br. s), 1.40 (1H, m), 1.96 (1H, ddd, *J*=13, 10, 7 Hz), 2.2—2.7 (2H, m), 3.86 (1H, d, *J*=9 Hz), 3.90 (1H, d, *J*=9 Hz), 5.00 (1H, td, *J*=2.5, 0.8 Hz), 5.02 (1H, dd, *J*=17.2, 1.6 Hz), 5.09 (1H, dd, *J*=11.1, 1.6 Hz), 5.27 (1H, br. t, *J*=2.5 Hz), and 6.09 (1H, dd, *J*=17.2, 11.1 Hz)].

Acetal Formation of 15 with DMP. An anhydrous THF solution (2 cm^3) of **15** (49 mg) was treated with DMP (0.2 cm^3) and PPTS (20 mg) at 15—25 °C for 1 h. The mixture was diluted with aqueous $NaHCO_3$, ether extracted, and chromatographed on a silica-gel column to give a colorless oil, **24**, 17 mg (29%) [Found: M^+, 226.1557. ^{1}H-NMR δ=1.05 (3H, s), 1.25 (3H, br. s), 1.39 (3H, s), 1.43 (3H, br. s), 1.6—2.0 (4H, m), 2.28 (1H, br. s, OH), 3.18 (1H, d, *J*=12 Hz), 3.61 (1H, d, *J*=12 Hz), 5.01 (1H, dd, *J*=17.6, 1.4 Hz), 5.02 (1H, dd, *J*=10.5, 1.4 Hz), and 5.89 (1H, dd, *J*=17.6, 10.5 Hz). ν: 3485, 2980, 2950, 1640, 1467, 1448, 1376, 1225, 1052, 913, and 834 cm^{-1}], and a colorless oil, **23**, 35 mg (59%) [Found: M^+, 226.1557. ^{1}H-NMR δ=1.12 (3H, s), 1.31 (3H, s), 1.37 (3H, br. s), 1.44 (3H, br. s), 1.6—2.0 (4H, m), 1.80 (1H, s, OH), 3.86 (1H, d, *J*=10 Hz), 4.19 (1H, d, *J*=10 Hz), 5.01 (1H, dd, *J*=10.5, 1.4 Hz), 5.10 (1H, dd, *J*=17.7, 1.4 Hz), and 6.04 (1H, dd, *J*=17.7, 10.5 Hz). ν: 3500, 2990, 1634, 1454, 1381, 1372, 1209, 1049, 1021, 913, and 857 cm^{-1}].

Dehydration of 23 to 18 and 19. A pyridine solution of **23** (33 mg) was treated with $SOCl_2$ (30 mg) at 0 °C for 1 h. The mixture was washed with aqueous $NaHCO_3$, and extracted with ether to give a colorless oil, 25 mg (82%), whose NMR was identical with that of the products, a mixture of **18** and **19**, obtained from **17**, and the gas-liquid chromatograms from the both sources were mutually indistinguishable other than for a small difference in the ratio of **18** and **19**.

Reduction of 5 with Zn to 25. A mixed solution of AcOH (2 cm^3) and Ac_2O (1 cm^3) of **5** (21 mg) was refluxed with powdered Zn (300 mg) for 8 h. Zn was removed by filtration and the filtrate was poured into $NaHCO_3$, and extracted with benzene. The extract was rapidly passed through a silica-gel column to give a colorless liquid, 17 mg (95%), **25** [Found: M^+, 180.1155. Calcd for $C_{11}H_{16}O_2$: 180.1149. ^{1}H-NMR δ=1.31 (3H, s), 1.6—2.0 (2H, m), 2.05 (3H, br. s), 2.39 (2H, br. t, *J*=7 Hz), 3.67 (3H, s), 4.88 (1H, dd, *J*=10.8, 1.6 Hz), 4.90 (1H, dd, *J*=17.0, 1.6 Hz), and 5.96 (1H, dd, *J*=17.0, 10.8 Hz). ^{13}C-NMR δ=16.9, 24.4, 37.3, 38.0, 50.6, 52.4, 110.3, 133.6, 145.2, 155.0, and 166.4. ν: 2955, 1710, 1637, 1435, 1340, 1263, 1220, 1062, 908, and 788 cm^{-1}].

Reduction of 8 to 25. Similarly, **8** (21 mg) gave **25**, 16 mg (90%).

Attempted Reduction of 6 or 7. Mixed solutions of AcOH (1.3 cm^3) and Ac_2O (0.7 cm^3) respectively containing **6** (20 mg) and **7** (16 mg) were refluxed for 7 h with powdered Zn (200 mg); only the products isolated after the ordinary work-up and silica-gel column chromatography (hexane-EtOAc=8:1) were colorless oily monoacetates, **26**, 18 mg (77%) [Found: M^+, 256.1313. Calcd for $C_{13}H_{20}O_5$: 256.1310. ^{1}H-NMR δ=1.00 (3H, s), 1.49 (3H, s), 1.92 (3H, s), 2.0—2.5 (4H, m), 3.76 (3H, s), 4.01 (1H, s, OH), 5.05 (1H, dd, *J*=10.9, 1.2 Hz), 5.05 (1H, dd, *J*=17.7, 1.2 Hz), and 6.07 (1H, dd, *J*=17.7, 10.9 Hz). ν: 3500, 2955, 1740, 1730, 1638, 1439, 1371, 1256, 1212, 1143, 1020, and 908 cm^{-1}],[10] and **27**, 15 mg (78%) [Found: M^+, 256.1317. ^{1}H-NMR δ=1.16 (3H, s), 1.60 (3H, s), 1.91 (3H, s), 2.0—2.6 (4H, m), 3.67 (3H, s), 3.90 (1H, s, OH), 4.94 (1H, dd, *J*=10.3, 1.2 Hz), 4.98 (1H, dd, *J*=17.8, 1.2 Hz), and 5.83 (1H, dd, *J*=17.8, 10.3 Hz). ν: 3500, 2990, 2955, 1741, 1730, 1640, 1438, 1376, 1370, 1258, 1242, 1143, 1019, and 916 cm^{-1}].

$TiCl_2$-reduction of 2 to 28, 29, and 30. To an anhydrous THF suspension (300 cm^3) of pyridine complex of $TiCl_2$, prepared from $TiCl_4$ (3.3 cm^3), Zn (4 g), and pyridine (2.4 cm^3), a THF solution (20 cm^3) of **2** (4.25 g) was added dropwise over a period of 1 h under cooling with water. After continued stirring for 30 min at 15—25 °C, the mixture was treated with 30%-aqueous K_2CO_3 (300 cm^3), to which ether was added, and the precipitates were filtered off. The filtrate was extracted with ether and chromatographed on a silica-gel column. A colorless oil, 320 mg (8%), **28** [Found: C, 61.52; H, 8.51%. Calcd for $C_{11}H_{18}O_4$: C, 61.66; H, 8.47%. ^{1}H-NMR δ=1.08 (3H, s), 1.74 (3H, br. s), 1.9—2.0 (4H, m), 2.88 (1H, br. s, OH), 3.10 (1H, br. m), 3.75 (3H, s), 3.79 (1H, s, OH), and 4.79 (2H, m). ^{13}C-NMR δ=22.8, 23.1, 23.6, 34.9, 51.7, 52.3, 80.9, 88.5, 110.7, 143.9, and 174.5. ν: 3510, 2955, 1728, 1646, 1442, 1245, 1227, 1123,

1089, 951, and 890 cm^{-1}. *m/z*: 214 (M^+)], was eluted at first.

Subsequently, colorless needles, mp 57.5—58 °C, 470 mg (11%), **29** [Found: C, 61.54; H, 8.31%. ^{1}H-NMR δ=1.28 (3H, s), 1.69 (3H, br. s), 1.7—2.2 (4H, m), 2.83 (1H, s, OH), 3.28 (1H, br. s, OH), 3.43 (1H, m), 3.80 (3H, s), 4.89 (1H, br. s), and 5.00 (1H, m). ^{13}C-NMR δ=21.8, 23.5, 25.7, 37.5, 52.0, 52.6, 84.3, 85.1, 113.2, 140.9, and 175.4. *ν*: 3470, 3340, 2950, 1700, 1645, 1400, 1292, 1254, 1142, 1110, 1040, 928, and 893 cm^{-1}. *m/z*: 214 (M^+)], and a colorless oil, 2.91 g (68%), **30** [Found: C, 61.53; H, 8.50%. ^{1}H-NMR δ=1.26 (3H, s), 1.72 (3H, br. s), 1.7—2.1 (4H, m), 3.07 (1H, br. s, OH), 3.18 (1H, br. m), 3.61 (1H, s, OH), 3.80 (3H, s), 4.80 (1H, br. s), and 4.89 (1H, br. s). ^{13}C-NMR δ=22.5, 25.0, 25.1, 38.9, 51.0, 52.3, 81.6, 85.2, 112.9, 143.4, and 174.7. *ν*: 3490, 2950, 1725, 1641, 1440, 1376, 1257, 1121, 1047, and 892 cm^{-1}. *m/z*: 214 (M^+)], were obtained from the elutions with hexane–EtOAc (3:1).

*Reduction of **28** with Zn to **31**.* A mixture of AcOH (4 cm^3), Ac_2O (2 cm^3), and **28** (60 mg) was refluxed with powdered Zn (600 mg) for 8 h. The mixture was filtered to remove Zn, washed with $NaHCO_3$, and extracted with ether. Silica-gel column chromatography of the extract gave a colorless oil, **31**,[8] 22 mg (44%) [^{1}H-NMR δ=1.65 (1H, m), 1.68 (3H, dd, *J*=1.3, 1.0 Hz), 2.10 (1H, m), 2.11 (3H, q, *J*=1.2 Hz), 2.3—2.6 (2H, m), 3.56 (1H, br. m), 3.66 (3H, s), 4.61 (1H, m), and 4.64 (1H, m). ^{13}C-NMR δ=16.3, 20.6, 28.7, 39.2, 50.8, 53.2, 109.1, 129.5, 148.0, 156.4, and 166.5. *ν*: 2950, 1714, 1648, 1435, 1218, 1117, 1062, and 885 cm^{-1}].

*Reduction of **30** with Zn to **31**.* Similarly, **30** (150 mg) was reduced with Zn to **31**, 68 mg (54%), identical with the sample prepared from **28**.

*Attempted Reduction of **29**.* To a mixed solution of AcOH (1.3 cm^3) and Ac_2O (0.7 cm^3) of **29** (19 mg) was similarly refluxed with powdered Zn (200 mg) for 7 h. After the work-up the product isolated was **32**, 19 mg (83%) [Found: M^+, 256.1316. Calcd for $C_{13}H_{20}O_5$: 256.1310. ^{1}H-NMR δ=1.55 (3H, s), 1.74 (3H, br. s), 1.96 (3H, s), 1.8—2.4 (4H, m), 3.27 (1H, br. s, OH), 3.37 (1H, br. t, *J*=9 Hz), 3.79 (3H, s), 4.82 (1H, br. s), and 4.91 (1H, m). *ν*: 3510, 2955, 1742, 1730, 1642, 1439, 1370, 1246, 1116, 1022, and 892 cm^{-1}].

*DMP-treatment of **28**.* A mixture of **28** (45 mg), DMP (1 cm^3), and PPTS (10 mg) in benzene (1 cm^3) was refluxed for 25 h. The mixture was distilled *in vacuo*, and the residue was passed through a silica-gel column to give a colorless oil, **33**, 46 mg (86%) [Found: M^+ 254.1502. Calcd for $C_{14}H_{22}O_4$: 254.1517. ^{1}H-NMR δ=1.40 (3H, s), 1.45 (3H, br. s), 1.55 (3H, br. s), 1.75 (3H, br. s), 1.7—2.3 (4H, m), 2.90 (1H, br. m), 3.68 (3H, s), 5.71 (1H, br. s), and 5.79 (1H, m). *ν*: 2990, 1755, 1738, 1649, 1447, 1436, 1376, 1228, 1125, 1089, 1002, 887, and 870 cm^{-1}].

*DMP-treatment of **30**.* Similarly, a benzene solution (5 cm^3) of **30** (160 mg), DMP (2 cm^3), and PPTS (25 mg) was refluxed for 14 h to afford a colorless oil, **34**, 171 mg (90%) [Found: M^+, 254.1529. ^{1}H-NMR δ=1.38 (3H, s), 1.45 (6H, br. s), 1.71 (3H, br. s), 1.5—2.1 (4H, m), 3.03 (1H, br. m), 3.77 (3H, s), 4.72 (1H, br. s), and 4.82 (1H, m). *ν*: 2990, 1757, 1732, 1648, 1456, 1438, 1378, 1265, 1127, 1055, 1022, and 887 cm^{-1}].

*Saponification and Iodolactonization of **34** to **36** and **37** via **35**.* Into a DMSO solution (1 cm^3) of **34** (53 mg), 20%-NaOH solution (0.6 cm^3) was added and refluxed for 2 h. The mixture was then acidified with dil HCl, and extracted with ether to give 50 mg (100%), **35**, colorless granules, mp 86.5—87.5 °C [Found: C, 64.78; H, 8.37%. Calcd for $C_{13}H_{20}O_4$: C, 64.98; H, 8.39%. ^{1}H-NMR δ=1.48 (6H, s), 1.51 (3H, br. s), 1.73 (3H, br. s), 1.6—2.1 (4H, m), 3.06 (1H, br. m), 4.77 (1H, br. s), and 4.87 (1H, m). *ν*: 3400—2500, 2980, 1713, 1692, 1648, 1377, 1278, 1259, 1122, 1009, and 886 cm^{-1}. *m/z*: 240 (M^+)].

Then, **35** was treated with excess of I_2 (100 mg) in MeCN (2 cm^3) in the presence of $NaHCO_3$ (100 mg). After stirring at 15—25 °C for 15 h, I_2 was decomposed by $NaHSO_3$ solution, and extracted with ether. From the aqueous layer, starting **35** (25 mg) was recovered. Silica-gel column chromatography of the neutral extract afforded two isomeric iodo lactones, **36**, colorless prisms, mp 117.5—188 °C, 19 mg (50%) [Found: C, 42.76; H, 5.24%. Calcd for $C_{13}H_{19}O_4I$: C, 42.64; H, 5.23%. ^{1}H-NMR δ=1.48 (6H, s), 1.52 (3H, s), 1.77 (3H, s), 1.8—2.4 (5H, m), and 3.35 (2H, br. s). *ν*: 2990, 1780, 1371, 1285, 1185, and 1012 cm^{-1}. *m/z*: 366 (M^+)], and **37**, a colorless oil, 7 mg (18%) [^{1}H-NMR δ=1.48 (6H, s), 1.51 (3H, s), 1.69 (3H, s), 1.7—2.4 (5H, m), 3.63 (1H, d, *J*=11 Hz), and 3.76 (1H, d, *J*=11 Hz). *ν*: 2990, 1787, 1382, and 1000 cm^{-1}].

*LAH-reduction of **28** to **38**.* An anhydrous THF solution (7.5 cm^3) of **28** (118 mg) was treated with LAH (100 mg) at 15—25 °C for 1 h. Purification of the products by silica-gel column chromatography gave a colorless oil, 94 mg (92%) **38** [Found: C, 64.26; H, 9.78%. Calcd for $C_{10}H_{18}O_3$: C, 64.49; H, 9.74%. ^{1}H-NMR δ=1.25 (3H, s), 1.6—1.9 (4H, m), 1.88 (3H, br. s), 2.41 (1H, br. m, OH), 2.79 (1H, br. s, OH), 2.90 (1H, br. t, *J*=9 Hz), 3.44 (1H, s, OH), 3.46 (1H, dd, *J*=12, 7 Hz), 3.64 (1H, dd, *J*=12, 5 Hz), 4.84 (1H, br. s), and 4.93 (1H, m). *ν*: 3400, 2790, 1642, 1450, 1380, 1120, 1045, 928, and 892 cm^{-1}. *m/z*: 168 (M^+−18)].

*LAH-reduction of **29** to **39**.* An anhydrous THF solution (5 cm^3) of **29** (70 mg) was treated with LAH (60 mg) at 15—25 °C for 1 h. From the mixture, a colorless oil, 47 mg (77%), **39** [Found: C, 64.27; H, 9.68%. ^{1}H-NMR δ=1.37 (3H, s), 1.5—2.1 (4H, m), 1.88 (3H, br. s), 1.99 (1H, s, OH), 2.15 (1H, br. s, OH), 2.83 (1H, dd, *J*=9, 3 Hz, OH), 3.09 (1H, br. t, *J*=9 Hz), 3.49 (1H, dd, *J*=11, 9 Hz), 3.74 (1H, dd, *J*=11, 3 Hz), 4.89 (1H, br. s), and 5.07 (1H, m). *ν*: 3400, 2975, 1638, 1375, 1106, 1032, 926, and 895 cm^{-1}. *m/z*: 168 (M^+−18)], was obtained.

*LAH-reduction of **30** to **40**.* Similarly, **30** (210 mg) in THF (10 cm^3) was reduced by LAH (150 mg) to colorless needles, mp 106.5—107 °C, 157 mg (86%), **40** [Found: C, 64.37; H, 9.95%. ^{1}H-NMR δ=1.35 (3H, s), 1.83 (3H, br. s), 1.5—2.1 (4H, m), 2.40 (1H, br. m, OH), 2.48 (1H, m), 2.75 (1H, br. s, OH), 3.17 (1H, br. s, OH), 3.65 (2H, br. d, *J*=4 Hz), 4.81 (1H, br. s), and 4.93 (1H, m). *ν*: 3445, 3400, 2955, 1633, 1377, 1343, 1120, 1097, 934, and 899 cm^{-1}. *m/z*: 168 (M^+−18)].

*DMP-treatment of **38** to **41**.* An anhydrous THF solution (2 cm^3) of **38** (53 mg) was treated with DMP (0.2 cm^3) and PPTS (20 mg) at 15—25 °C for 3 h. Extraction and silica-gel chromatographic purification afforded a colorless oil, 63 mg (98%), **41** [Found: M^+, 226.1569. Calcd for $C_{13}H_{22}O_3$: 226.1568. ^{1}H-NMR δ=1.23 (3H, s), 1.36 (3H, br. s), 1.46 (3H, br, s), 1.4—1.9 (4H, m), 1.82 (3H, br. s), 2.56 (1H, br. s, OH), 3.12 (1H, br. m), 3.76 (1H, d, *J*=9.5 Hz),

3.88 (1H, d, J=9.5 Hz), 4.77 (1H, br. s), and 5.03 (1H, m). ν: 3550, 2990, 1645, 1454, 1382, 1372, 1211, 1146, 1068, 888, 877, and 853 cm^{-1}].

*Dehydration of **41** to **42** and **43**.* A pyridine solution (1 cm^3) of **41** (27 mg) was treated with $SOCl_2$ (30 mg) at 0 °C for 1 h. The mixture was then quenched with $NaHCO_3$ solution and extracted with a 1:1-mixture of hexane–ether to give a colorless oil, 21 mg (85%), a 3:1-mixture of **42** [Found: M^+, 208.1465. Calcd for $C_{13}H_{20}O_2$: 208.1462. ^{1}H-NMR δ=1.37 (3H, br. s), 1.44 (3H, br. s), 1.55 (3H, dd, J=1.5, 0.8 Hz), 1.72 (3H, q, J=2 Hz), 2.08 (1H, dm, J=17 Hz), 2.64 (1H, dd of quint, J=17, 8, 2 Hz), 3.09 (1H, dd, J=8, 3.5 Hz), 3.81 (1H, d, J=9 Hz), 4.01 (1H, d, J=9 Hz), 4.81 (2H, m), and 5.57 (1H, m). RT= 30.4 min], and **43** [Found: M^+, 208.1477. ^{1}H-NMR δ= 1.40 (3H, br. s), 1.47 (3H, br. s), 1.78 (3H, dd, J= 1.5, 0.8 Hz), 1.5—2.1 (2H, m), 2.3—2.6 (2H, m), 2.69 (1H, dd, J=9.5, 7 Hz), 3.79 (1H, d, J=9 Hz), 4.06 (1H, d, J=9 Hz), 4.77 (1H, br. s), 4.91 (1H, m), 4.97 (1H, td, J=2.5, 0.8 Hz), and 5.22 (1H, br. t, J=2.5 Hz). RT=29.7 min].

*DMP-treatment of **40** to **44**.* An anhydrous THF solution (3 cm^3) of **40** (90 mg) was treated with DMP (0.3 cm^3) and PPTS (30 mg) at 15—25 °C for 3 h. The work-up gave a colorless oil, 105 mg (96%), **44** [Found: M^+, 226.1573. ^{1}H-NMR δ=1.24 (3H, s), 1.35 (3H, br. s), 1.4—2.1 (4H, m), 1.43 (3H, br. s), 1.82 (3H, br. s), 2.43 (1H, m), 2.87 (1H, br. s, OH), 3.84 (1H, d, J=9 Hz), 4.04 (1H, d, J=9 Hz), 4.76 (1H, br. s), and 4.87 (1H, m). ν: 3520, 2980, 1642, 1453, 1382, 1372, 1217, 1068, 890, and 860 cm^{-1}].

*Dehydration of **44** to **45** and **46**.* A pyridine solution (1.5 cm^3) of **44** (47 mg) was treated with $SOCl_2$ (45 mg) at 0 °C for 1 h. The reaction mixture was poured into aqueous $NaHCO_3$ and extracted with a 1:1-mixture of hexane–ether. The extract was passed through a silica-gel column with hexane–ether (15:1) to give a colorless oil, 36 mg (83%), a 3:1-mixture of **45** [Found: M^+, 208.1445. RT=23.9 min. ^{1}H-NMR δ=1.33 (3H, br. s), 1.42 (3H, br. s), 1.73 (3H, q, J=2 Hz), 1.75 (1H, dd, J=1.5, 0.8 Hz), 2.2—2.4 (2H, m), 2.74 (1H, dd, J=7.5, 5.5 Hz), 3.87 (2H, s), 4.78 (2H, m), and 5.52 (1H, m)] and **46** [Found: M^+, 208.1471. RT=26.9 min. ^{1}H-NMR δ=1.36 (3H, br. s), 1.45 (3H, br. s), 1.80 (3H, dd, J=1.5, 0.8 Hz), 1.6—2.0 (2H, m), 2.2—2.4 (3H, m), 3.85 (1H, d, J=8.5 Hz), 3.96 (1H, d, J=8.5 Hz), 4.71 (1H, br. s), 4.85 (1H, m), 5.01 (1H, td, J=2.5, 0.8 Hz), and 5.26 (1H, br. t, J=2.5 Hz)].

*DMP-treatment of **39** to **47** and **48**.* An anhydrous THF solution (1.5 cm^3) of **39** (37 mg) was treated with DMP (0.15 cm^3) and PPTS (15 mg^3) at 15—25 °C for 1 h, after which, the mixture was diluted with aqueous $NaHCO_3$, extracted with ether, and chromatographed on a silica-gel column. The fractions eluted from hexane–ether (4:1) were a colorless oil, 22 mg (49%), **48** [Found: C, 68.96; H, 9.88%. Calcd for $C_{13}H_{22}O_3$: C, 68.99; H, 9.80%. ^{1}H-NMR δ=1.37 (3H, br. s), 1.41 (3H, s), 1.48 (3H, br. s), 1.84 (3H, br. s), 1.6—2.0 (5H, m), 3.18 (1H, br. m), 3.52 (1H, d, J=12 Hz), 3.73 (1H, d, J=12 Hz), 4.89 (1H, br. s), and 5.08 (1H, m). ν: 3530, 2995, 2950, 1638, 1453, 1379, 1191, 1075, and 891 cm^{-1}. m/z: 211 (M^+−15)]. Subsequently, a colorless oil, 18 mg (40%), **47** [Found: M^+, 226.1564. ^{1}H-NMR δ=1.28 (3H, br. s), 1.33 (3H, s), 1.41 (3H, br. s), 1.84 (3H, br. s), 1.5—2.1 (5H, m), 2.84 (1H, br. m), 3.88 (1H, d, J=9 Hz), 4.21 (1H, d, J=9 Hz), 4.78 (1H, br. s), and 4.93 (1H, m). ν: 3495, 2960, 1638, 1455, 1381, 1371, 1207, 1060, 880, and 851 cm^{-1}], was obtained.

*Dehydration of **47** to **45** and **46**.* A pyridine solution (0.5 cm^3) of **47** (16 mg) was treated with $SOCl_2$ (15 mg) at 0 °C for 1 h. The mixture was diluted with aqueous $NaHCO_3$, extracted with ether, and chromatographed on a silica-gel column to give a colorless oil, 12 mg (81%), which proved to be a 6:1-mixture of **45** and **46** from the NMR spectral and gas-liquid chromatographic analyses.

The authors thank The Ministry of Education, Science and Culture for the financial support by the Grant in Aids for Scientific Reasearch to H. T. (No. 57218019 and No. 591040006) and to N. K. (No. 58740246 and No. 59740260).

References

1) Part XXVIII. H. Takeshita, A. Mori, and S. Nakamura, *Bull. Chem. Soc. Jpn.*, **57**, 3152 (1984).

2) H. Takeshita, T. Hatsui, and T. Masuda, *Kyushu Daigaku Sogo Rikogaku Kenkyuka Hokoku*, **1**, 35 (1979).

3) H. Takeshita, T. Hatsui, N. Kato, T. Masuda, and H. Tagoshi, *Chem. Lett.*, **1982**, 1153.

4) H. Takeshita, N. Kato, K. Nakanishi, H. Tagoshi, and T. Hatsui, *Chem. Lett.*, **1984**, 1495.

5) H. Takeshita, S. Hatta, and T. Hatsui, *Bull. Chem. Soc. Jpn.*, **57**, 619 (1984).

6) H. Takeshita, A. Mori, and S. Itô, *Bull. Chem. Soc. Jpn.*, **47**, 1767 (1974); H. Takeshita, A. Mori, and Y. Toyonaga, *ibid.*, **48**, 307 (1975); *Idem.*, *Kyushu Daigaku Seisan Kagaku Kenkyusho Hokoku*, **64**, 25 (1976).

7) T. Mukaiyama, T. Sato, and J. Hanna, *Chem. Lett.*, **1973**, 1041; J. E. McMurry and M. P. Fleming, *J. Am. Chem. Soc.*, **96**, 4708 (1974).

8) T. Sakan, S. Isoe, S. B. Hyeon, R. Katsumura, T. Maeda, J. Wolinsky, D. Dickerson, M. Slabaugh, and D. Nelson, *Tetrahedron Lett.*, **1965**, 4097; J. Wolinsky and D. Nelson, *Tetrahedron*, **25**, 3767 (1969).

9) G. Goto, *Bull. Chem. Soc. Jpn.*, **50**, 186 (1977), and the references cited therein.

10) Formation of diacetates from the *trans*-glycols might gradually occur under the conditions; indeed as the by-product of **26** from **6**, a colorless oily diacetate [δ=1.44 (3H, s), 1.70 (3H, s), 1.95 (3H, s), 2.00 (3H, s), 2.0—2.6 (4H, m), 3.71 (3H, s), 4.95 (1H, dd, J=11, 1.5 Hz), 4.96 (1H, dd, J=17.5, 1.5 Hz), and 6.07 (1H, dd, J=17.5, 11 Hz)] was isolated in 8% yield.

11) This formation of these orthoester derivatives by solvolysis was employed for optical resolution of these iridoids. This will be reported in the near future.

12) P. de Mayo and H. Takeshita, *Can. J. Chem.*, **40**, 440 (1963).

Synthetic Photochemistry. XXX.[1] The Addition Reactions of Cycloheptatriene with Some Aromatic *p*-Quinones[2]

Akira MORI and Hitoshi TAKESHITA*
Research Institute of Industrial Science, 86, Kyushu University, Kasuga-koen, Kasuga, Fukuoka 816
(Received January 16, 1985)

The photochemical reactions of cycloheptatriene with *p*-benzoquinone and 1,4-naphthoquinone yielded the spirocyclic ethers, which had 7-oxabicyclo[4.2.1]nona-2,4-diene structures, by the characteristic (6+2)π cycloaddition process. The latter quinone further produced the carbocyclic (2+2)π and (6+2)π cycloadducts.

Previously, we have investigated the photoaddition reactions of cycloheptatriene (**1**) with methyl 2,4-dioxopentanoate, an enolized β-diketone,[3] and benzil and methyl pyruvate, α-dicarbonyl compounds,[4] to give the ene-reaction products in the major process; in the cases of the β-diketone, the (4+2)π and (6+2)π cycloadducts were also produced. From cyclic α-dicarbonyl compounds such as acenaphthenequinone and 1,2-naphthoquinone,[5] various kinds of cycloadducts were formed; the former gave the (2+2)π and (6+2)π cycloadducts along with the ene-reaction products, and the latter, the (6+2)π, (4+2)π, and (4+4)π cycloadducts. Thus, since **1** is remarkable in giving various *peri*-cycloadducts in the photoinduced reactions, we have been interested in *p*-quinones, the conjugated dicarbonyl compounds. Although the photochemical reactions of aromatic quinones with olefins have been widely studied,[6] studies of the reactions of **1** with *p*-quinones have been limited to those of 1,4-naphthoquinone (NQ) in benzene to give the so-called "1:1-spirooxetane adduct" (**2**),[7] which does, however, seem to lack a sound rationale for its structure deduction. Other than this, the recent photo-induced cycloaddition of duroquinone has been reported to form cage compounds (**3** and **4**).[8]

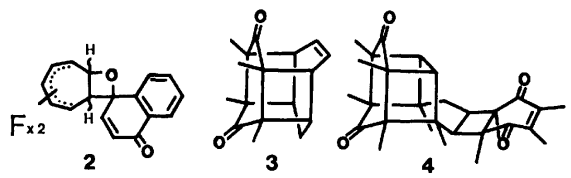

Chart 1.

Results and Discussion

Upon the irradiation of a benzene solution of *p*-benzoquinone (BQ) and **1**, an oily 1:1-adduct (**5**) was obtained in 50—70% yields. Its structure was determined by the following spectroscopic data: the appearance of eight olefinic protons and four aliphatic protons in the ^{1}H NMR and only one carbonyl carbon at the ^{13}C NMR spectra indicated it to be a 1:1-adduct between the carbonyl part of BQ and the olefinic part of **1**. In order to determine the pericyclic mode of the addition, the decoupling experiments by double irradiation (NMDR) were performed in the presence of a lanthanoide-shift reagent. The irradiation of the doublet (J=13 Hz) at δ=3.21 (H-a) caused the doublet of triplets (J=13, 6.5 Hz) at 3.64 (H-b) to collapse to a triplet (J=6.5). The irradiation of H-b caused both the doublet of H-a and the triplet (J=6.5 Hz) at 5.48 (H-d), which was assigned to the proton at the ethereal carbon, to collapse to a singlet and a doublet (J=6.5 Hz) respectively. The irradiation of the triplet (J=6.5 Hz) at 4.00 (H-c) caused H-b to collapse to a doublet of doublets (J=13, 6.5 Hz). Therefore, the two allylic protons (H-d and H-c) did not spin-couple in each other. The observed magnitude (J=13 Hz) of the gem-coupling constant for the non-allylic methylene protons should be appropriate for that of a tetrahydrofuran. Consequently, **5** must be the (6+2)π cycloadduct.

The treatment of the adduct **5** with hydrogen chloride in ethanol resulted in its conversion to a phenol derivative (**6**) and its ethyl ether (**7**) *via* the dienone-phenol rearrangement.

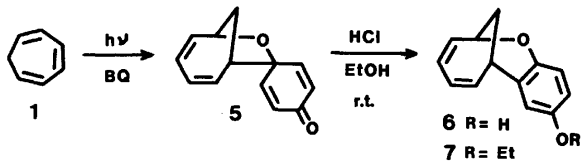

Scheme 1.

Subsequently, the photoreaction of **1** with 1,4-naphthoquinone (NQ) was investigated. In the literature,[7] the formation of an oxetane derivative (**2**), as orange crystals, has been described, but this mode of the reaction was quite different from that in our present study. This might be also worth reinvestigating. Thus, when a benzene solution of NQ and **1** was exposed to a 400-W high-pressure mercury lamp, four 1:1-adducts (**8**, **9**, **10**, and **11**) were formed in a ratio of 58:4:17:21, in addition to a dehydro derivative (**12**) of **11**. The structures of these compounds were confirmed by the chemical and spectroscopic evidence. The ^{1}H NMR spectra of **8** and **9** closely resemble each other; when we compare

Table 1. The NMR data of 5 and the NMDR data of 5(31.4 mg) and $Eu(dpm)_3$(60.7 mg) in $CDCl_3$

	5	5+$Eu(dpm)_3$					
Ha		3.21, d(13)	irr	s	x	x	x
Hb	2.75, m	3.64, dt(13, 6.5)	t(6.5)	irr	dd(13, 6.5)	dd(13, 6.5)	x
Hc		4.00, t(6.5)	x	—	irr	x	d(6.5)
Hd	4.70, t(6.5)	5.48, t(6.5)	x	d(6.5)	x	irr	d(6.5)
He							
)		6.40, m	x	x	o	o	irr
Hh	5.90, m						
Hi		10.64, d(9.5)					
Hj		10.76, d(9.5)					
Hk	6.71, dd(9.5, 3)	8.22, dd(9.5, 3)					
Hl	7.01, dd(9.5, 3)	8.58, dd(9.5, 3)					

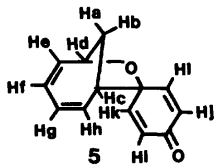

The symbols used here are defined as follows: o, changed; x, unchanged; —, unobserved. The values shown in parentheses are the coupling constants (J)/Hz.

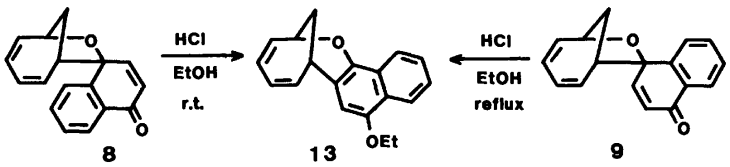

Scheme 2.

the chemical shifts of the corresponding pairs of hydrogens, one of the methylene protons of **9**, at 2.40, appeared in a higher field than that of **8**, at 2.68, and one of the four vinyl protons of **8**, at 5.10, caused a marked up-field shift, while all four vinyl protons of **9**, from 5.7 to 6.7, behaved normally. Therefore, the stereochemistries of **8** and **9** were deduced to be as depicted in Scheme 2. It is interesting that the sterically more crowded isomer, **8**, was predominant over the less crowded isomer, **9**.

The addition of hydrogen chloride in ethanol at room temperature also caused the dienone-phenol rearrangement of **8** to an aromatized ethyl ether (**13**), while it was necessary to reflux **9** to get the same product (**13**).

The third photoproduct (**10**) showed a rather poorly resolved ^1H NMR spectrum. However, since the methylene protons at 2.49 and 2.74 were proven to be allylic carbon by NMDR experiments, **10** can not be a (6+2)π cycloadduct. The catalytic reduction of **10** with platinum(IV) oxide gave an octahydro derivative (**14**), which was identical with the reduction product, a tetrahydro derivative, of one of the photoproducts (**15**) of NQ with cycloheptene. Therefore, **10** is a (2+2)π cycloadduct.

Next, the fourth product, **11**, was deduced from the NMDR experiments to be a symmetrical *exo*-(6+2)π cycloadduct. The irradiation of olefinic protons caused the broad doublet of doublets (J=7.5, 6 Hz) at 3.25 (H-c) to collapse to a broad doublet (J=6 Hz), but it did not affect the broad doublet signal (J=13 Hz) at 1.87 (H-a) or the doublet of triplets

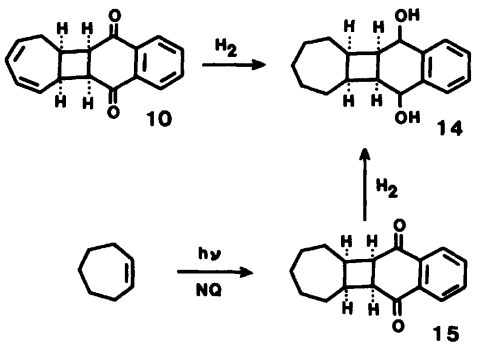

Scheme 3.

(J=13, 6 Hz) at 2.04 (H-b). The coupling constant between H-c and H-d, being nearly zero, led us to conclude that the geometry of the ring juncture was that of the *exo*-adduct.

The remaining product, **12**, also exhibited a symmetrical ^1H NMR spectrum; the results of the elemental analysis suggested that it was a dehydrogenation product of **11**. Indeed, the DDQ (2,3-dichloro-5,6-dicyano-*p*-benzoquinone)-treatment of **11** afforded **12**.

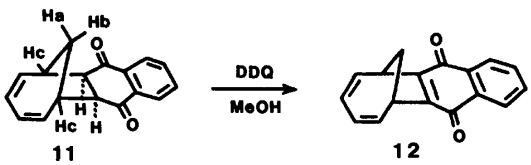

Scheme 4.

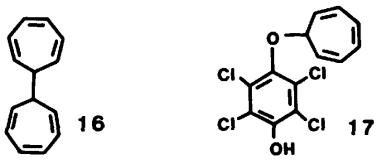

Chart 2.

The attempted photoreaction of **1** with 2,3,5,6-tetrachloro-*p*-benzoquinone (CB) gave no cycloadduct; the only products identified were the hydroquinone of CB and 1,1′-bicycloheptatrienyl (1,1′-bitropyl, **16**),[5,9] not the formerly reported monotropyl ether of tetrachlorohydroquinone (**17**).[10] Thus, CB behaved as an oxidizing agent rather than as a photocycloaddend toward **1**.

In conclusion, the photoreaction of **1** with BQ gave the single (6+2)π photoproduct, which coupled at the carbonyl group and the triene function of **1**, while the photoproducts of **1** with NQ, (6+2)π and (2+2)π cycloadducts, were derived from both the C=O group and the C=C group. This can be explained in terms of the nature of the excited species; that is, the lowest triplet of BQ is an n,π^* excited state, while that of NQ is thought to be considerably mixed with the n,π^* and π,π^* excited states.[11] The absence of any (4+2)π adduct in the photoproducts is consistent with the prediction based on the Woodward-Hoffmann rule,[12] but is in contrast to the reaction with a unique photocycloaddend, methyl 2,4-dioxopentanoate.[3]

Experimental

All the mps, which were measured by means of a Yanagimoto Micro-mp Apparatus, are uncorrected. The irradiations were performed by means of a 400-W high-pressure mercury lamp through a Pyrex glass filter, with running water-cooling under a nitrogen atmosphere. Elemental analyses were performed either at the Research Institute of Industrial Science or at the Analyses Center, Faculty of Science, Kyushu University. The NMR spectra were measured by the use of a JEOL FX 100 Spectrometer in a $CDCl_3$ solution, unless otherwise specified; the chemical shifts were expressed in δ unit from the internal Me_4Si. The mass spectra were measured by means of a JEOL 01SG-2 Spectrometer. The IR spectra were taken in either as KBr disks or as inserted liquid film between NaCl plates using a Jasco IR-A 102 spectrometer. All the UV spectra were taken by means of a Hitachi 124 Spectrophotometer in methanol.

Photoaddition of 1 with BQ. An anhydrous benzene solution (5 cm^3) of **1** (916 mg) and BQ (541 mg) was irradiated for 8.5 h. The mixture was filtered to remove the polymeric solid, and then, the filtrate was evaporated *in vacuo* to a give viscous syrup (1.2 g), which was chromatographed on a silica-gel column with benzene to yield a pale yellow oil; bp 115—118 °C (bath temp)/2 mm Hg, 681 mg (68%), **5** [Found: C, 77.72; H, 6.12%. Calcd for $C_{13}H_{12}O_2$: C, 77.98; H, 6.04%. ^{13}C NMR δ=31.1, 47.3, 75.0, 89.1, 125.0, 126.8, 127.4, 127.8, 133.1, 133.6, 148.1, 149.9, and 184.6. λ_{max}: 228 nm (ε=15500), 264.5 (4400). *m/z*: 200 (M$^+$)].

Acid-catalyzed Rearrangement of 5. The photoadduct **5** (36.8 mg) was dissolved in EtOH (3 cm^3) containing concd HCl (0.03 cm^3), after which the mixture was kept at room temperature for 80 min with stirring. The mixture was then poured into water and extracted with ether. The extract was dried on $MgSO_4$ and chromatographed on a silica-gel column with benzene to yield a colorless oil; 23.2 mg (55%), **7** [Found: C, 79.07; H, 7.11%. Calcd for $C_{15}H_{16}O_2$: C, 78.92; H, 7.06%. ^{1}H NMR δ=1.33 (3H, t, *J*=7 Hz), 1.96 (1H, ddd, *J*=14, 2.5, 1 Hz), 2.58 (1H, ddd, *J*=14, 6, 4.5 Hz), 3.68 (1H, br. t, *J*=6 Hz), 3.93 (2H, q, *J*=7 Hz), 4.93 (1H, m), and 5.75—6.9 (7H, m). ^{13}C NMR δ=14.9, 28.9, 29.7, 33.5, 63.7, 114.0, 115.4, 117.9, 124.1, 125.0, 128.5, 131.9, 137.8, 146.2, and 152.6. λ_{max}: 222 nm (ε=12500), 249 (5000), 292 (2900). *m/z*: 228 (M$^+$)], and colorless crystals; mp 85—87 °C; 8.3 mg (23%); **6** [Found: 78.08; H, 6.02%. Calcd for $C_{13}H_{12}O_2$: C, 77.98; H, 6.04%. ^{1}H NMR δ=1.98 (1H, ddd, *J*=14, 2, 1 Hz), 2.56 (1H, ddd, *J*=14, 6.5, 4 Hz), 3.68 (1H, dd, *J*=8.5, 6.5 Hz), 4.94 (1H, m), and 5.7—6.1 (3H, m). ^{13}C NMR δ=28.9, 33.3, 70.7, 114.8, 116.2, 118.1, 124.4, 125.1, 128.7, 131.8, 137.7, 146.1, and 149.0. ν: 3460, 3360 cm^{-1}. *m/z*: 200 (M$^+$)].

Photoaddition of 1 to NQ. An anhydrous benzene solution (10 cm^3) of **1** (920 mg) and NQ (790 mg) was irradiated for 1.5 h. The resultant mixture was chromatographed on a silica-gel column with hexane-benzene to afford a colorless oil; 292 mg (35%); **8** [Found: C, 81.37; H, 5.85%. Calcd for $C_{17}H_{14}O_2$: C, 81.58, H, 5.64%. ^{1}H NMR δ=2.68 (1H, d, *J*=12.5 Hz), 2.73 (1H, t, *J*=7 Hz), 3.00 (1H, td, *J*=12.5, 7 Hz), 4.76 (1H, t, *J*=7 Hz), 5.10 (1H, dd, *J*=11, 7 Hz), 5.6—6.2 (3H, m), 6.05 (1H, d, *J*=10.5 Hz), 7.18 (1H, d, *J*=10.5 Hz), and 7.2—8.0 (4H, m). ^{13}C NMR δ=32.4, 52.3, 74.6, 95.3, 125.8, 125.9, 127.2, 127.6, 128.2, 128.9, 130.9, 131.3, 133.0, 134.9, 141.0, 152.2, and 184.4. λ_{max}: 224 nm (ε=12500), 242.5 (9500), 253 (10200), 270 (sh., 7600). *m/z*: 250 (M$^+$)], a colorless oil; 20.5 mg (2.4%); **9** [Found: C, 81.49; H, 5.72%. ^{1}H NMR δ=2.40 (1H, d, *J*=12 Hz), 2.5—3.2 (2H, m), 4.85 (1H, br. t, *J*=6 Hz), 5.7—6.7 (4H, m), 6.17 (1H, d, *J*=10.5 Hz), 7.28 (1H, d, *J*=10.5 Hz), and 7.2—8.2 (4H, m). ν: 1680, 1607 cm^{-1}], colorless crystals; mp 103—104 °C; 108 mg (13%); **10** [Found: C, 81.37; H, 5.72%. ^{1}H NMR δ=2.49 (1H, ddd, *J*=13, 6.5, 4.5 Hz), 2.74 (1H, ddd, *J*=13, 9, 4 Hz), 3.0—3.6 (3H, m), 3.80 (1H, dd, *J*=9, 7.5 Hz), 5.95 (4H, m), and 7.6—8.2 (4H, m). ν: 1680, 1600 cm^{-1}], colorless crystals; mp 87—88 °C; 81.2 mg (10%); **11** [Found: C, 81.48; H, 5.67%. ^{1}H NMR δ=1.87 (1H, br. d, *J*=13 Hz), 2.04 (1H, dtm, *J*=13, 6 Hz), 3.25 (2H, dd, *J*=7.5, 6 Hz), 3.74 (2H, br. s), 5.84 (2H, dt, *J*=12, 3.5 Hz), 6.0—6.2 (2H, m), 7.6—7.9 (2H, m), and 8.0—8.2 (2H, m). ^{13}C NMR δ=31.3, 44.0, 62.1, 125.1, 126.7, 133.9, 134.9, 136.8, and 195.8. ν: 1673, 1588 cm^{-1}], and yellow crystals; mp 160—162 °C; 35 mg (8%); **12** [Found: C, 82.14; H, 4.83%. Calcd for $C_{17}H_{12}O_2$: C, 82.24; H, 4.87%. ^{1}H NMR δ=1.69 (1H, d, *J*=12 Hz), 2.36 (1H, dtt, *J*=12, 7, 1.5 Hz), 3.98 (1H, t, *J*=7 Hz), 5.8—6.3 (4H, m), 7.6 (2H, m), and 8.2 (2H, m). ν: 1645, 1590, 1583 cm^{-1}], and recovered NQ, 260 mg.

Acid-catalyzed Rearrangement of 8. The photoadduct **8** (65.7 mg) was dissolved in EtOH (5 cm^3) containing concd

HCl (0.03 cm^3), after which the mixture was kept at room temperature for 22 h. Then, the mixture was poured into water and extracted with ether. After drying on $MgSO_4$, the extract was chromatographed on a silica-gel column with benzene to yield colorless plates; mp 129—130 °C; 15.4 mg (21%); **13** [Found: C, 81.79; H, 6.52%. Calcd for $C_{19}H_{18}O_2$: C, 81.98; H, 6.52%. ^1H NMR δ=1.47 (3H, t, J=7 Hz), 2.04 (1H, ddd, J=14, 2.5, 1 Hz), 2.68 (1H, ddd, J=14, 5.5, 4 Hz), 3.68 (1H, dddd, J=8.5, 5.5, 2, 1 Hz), 4.08 (2H, q, J=7 Hz), 5.14 (1H, m), 5.7—6.5 (4H, m), 6.40 (1H, s), and 7.2—8.2 (4H, m). ν: 1628, 1595 cm^{-1}].

Acid-catalyzed Rearrangement of 9. Similarly, an EtOH solution (5 cm^3) of **9** (36.1 mg) and concd HCl (0.03 mg) was refluxed to yield colorless crystals (mp 129—130 °C; 17 mg (42%)), which were identical in every respect with the sample of **13** obtained from **8**.

Photoreaction of Cycloheptene with NQ. An anhydrous benzene solution (10 cm^3) of cycloheptene (1.95 g) and NQ (1.58 g) was irradiated for 22.5 h. Silica-gel column chromatography of the reaction mixture afforded colorless crystals; mp 71.5—72 °C; 140 mg (11%); **15** [Found: C, 80.08; H, 7.08%. Calcd for $C_{17}H_{18}O_2$: C, 80.28; H, 7.13%. ^1H NMR δ=1.0—2.2 (10H, m), 2.4—2.9 (2H, m), 3.0—3.2 (2H, m), and 7.6—8.1 (4H, m). ν: 1680, 1595, 1295, 1280 cm^{-1}], and recovered NQ, 786 mg (50%).

Catalytic Reduction of 10. An MeOH solution (4 cm^3) of **10** (46.1 mg) was hydrogenated with PtO_2. The subsequent removal of the solvent left the octahydro derivative (**14**) of **10**; 46.8 mg (100%); colorless crystals; mp 248—250 °C [Found: C, 78.69; H, 8.67%. Calcd for $C_{17}H_{22}O_2$: C, 79.03, H, 8.58%. ν: 3420, 2940, 1460, 1325, 1040, 750 cm^{-1}].

Catalytic Reduction of 15. An MeOH solution (2 cm^3) of **15** (23 mg) was similarly hydrogenated with PtO_2. The product isolated consisted of colorless crystals (mp 248—250 °C, 22.1 mg (95%)), which were identical in every respect with the authentic **14**.

Dehydrogenation of 11 with DDQ. An MeOH solution (2 cm^3) of **11** (51.7 mg) was refluxed with DDQ (50.2 mg) for 2 h. After the solvent had been removed *in vacuo*, the residue was chromatographed on a silica-gel column to give colorless crystals (mp 158—160 °C; 40.1 mg (78%)), which were identical in every respect with **12**.

Photoreaction of 1 with CB. An anhydrous benzene solution of **1** (2 g) and CB (1.22 g) was irradiated for 3 h. The reaction mixture was then filtered to remove an insoluble solid, which consisted of recovered CB and its hydroquinone (1.04 g (85%)); the filtrate was then chromatographed on a silica-gel column to give **16** (33 mg; colorless plates; mp 62.5—63.5 °C), whose identity with an authentic sample (lit,[5] mp 64—67 °) was confirmed by direct comparisons.

References

1) Part XXIX: N. Kato and H. Takeshita, *Bull. Chem. Soc. Jpn.*, **58**, 1574 (1985).

2) A part of this study has previously been reported: A. Mori and H. Takeshita, *Chem. Lett.*, **1975**, 599. The delayed publication of this paper is mainly due to a loss of samples which were burned in a fire.

3) H. Takeshita, A. Mori, and S. Itô, *Bull. Chem. Soc. Jpn.*, **47**, 1767 (1974).

4) H. Takeshita, A. Mori, N. Yamamoto, and T. Fujita, *Kyushu Daigaku Seisan Kagaku Kenkyusho Hokoku*, **66**, 9 (1977).

5) H. Takeshita, A. Mori, M. Funakura, and H. Mametsuka, *Bull. Chem. Soc. Jpn.*, **50**, 315 (1977).

6) J. M. Bruce, "Photochemistry of Quinones," in "The Chemistry of the Quinonoid Compounds," in the Series of S. Patai (ed.), "The Chemistry of Functional Groups," Wiley-Interscience, New York (1974), p 465.

7) R. P. Gandhi, S. N. Dhawan, and S. M. Mukherji, *Indian J. Chem.*, **9**, 283 (1971).

8) K. Ogino, T. Minami, S. Kozuka, and T. Kinoshita, *J. Org. Chem.*, **45**, 4694 (1980).

9) W. von E. Doering and L. H. Knox, *J. Am. Chem. Soc.*, **79**, 352 (1957).

10) G. O. Schenck, E. K. von Gustorf, B. Kim, G. v. Bünau, and G. Pfundt, *Angew. Chem., Intern. Edi.*, **1**, 516 (1962).

11) K. Maruyama, Y. Naruta, and T. Otsuki, *Bull. Chem. Soc. Jpn.*, **48**, 1553 (1975).

12) R. B. Woodward and R. Hoffmann, "The Conservation of Orbital Symmetry," Verlag Chemie GmbH, Weinheim/Bergstr., 1970.

Photovoltaic Properties of Coumarin Dye Films

Sei-ichiro IIJIMA,* Fumio MIZUTANI, and Yoshio TANAKA
Research Institute for Polymers and Textiles, 1-1-4 Yatabe-Higashi, Tsukuba, Ibaraki 305
(Received August 24, 1984)

Synopsis. Al/vacuum-deposited dye/Ag(or Au) photocells prepared by using four kinds of coumarin dyes indicate that a Schottky barrier formed at an Al/dye interface is the origin of their photovoltaic effects. Quantum yields of the short-circuit photocurrent of 0.05—0.77% and the photovoltages of 0.30—0.95 V were obtained under 0.1 mW/cm² light.

Highly fluorescent coumarin dyes have been frequently used in the studies of the electronic-energy transfer between organic molecules.[1,2] In photoelectric energy-conversion systems, interesting applications can be expected for such coumarin dyes as "antenna pigments" by utilizing their high-emission intensities. For example, Fromherz and Arden have reported[3] a pH-modulated "molecular device" consistig of coumarin monolayer/cyanine monolayer/indium-tin oxide. The photoelectric properties of coumarin dyes themselves, however, have not been investigated so far, although studies of the properties are necessary for further applications of the dyes in photoenergy conversion. We wish to report in this article that some of the coumarin derivatives used in dye lasers act as p-type semiconductors in the photocells of the Al/dye/Ag(or Au) configuration.

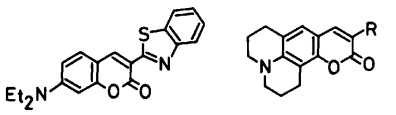

1

R=COOH 2
$COOC_2H_5$ 3
$COCH_3$ 4

The coumarin dyes **1**—**4** were purchased from Eastman Kodak and were used without further purification. The photocells were formed in the sandwich-type configuration: Al/dye film/Ag(or Au). First, the semitransparent electrode of Al was vacuum-deposited onto a glass substrate, and then the dye was evaporated onto the Al-coated substrate in a vacuum below 5×10^{-4} Pa by heating up to 200 °C. Finally, Ag(or Au) was deposited onto the organic layer to form an effective area of 0.5 cm². A 300-W xenon arc lamp equipped with an interference filter was used as the monochromatic light source. The cells were usually illuminated from the Al side except in the illuminating-direction experiment on the Al/dye **1**/Au cell. The photovoltaic parameters were determined for the photocells with dye-layer thicknesses of 0.1—0.3 μm. Reproducible results, little affected by the film thickness, were obtained in this thickness range.

The current-voltage curves of Al/3-(2-benzothiazolyl)-7-diethylaminocoumarin (**1**)/Ag are shown in Fig. 1 as typical examples. For all the photocells in the present work, the Al electrode always became negative against the Ag (or Au) electrode on illumination, and the dark current-voltage curves showed rectification in such a way that negative bias of Al was in a forward direction. This behavior indicates that the coumarin dyes are char-

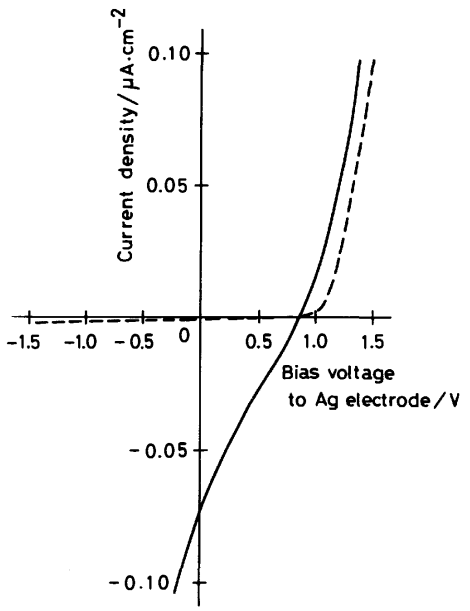

Fig. 1. Current-voltage curves for an Al/dye **1**/Ag cell: The dark state (----) and the illuminated state with 460 nm light of 0.1 mW/cm² (——).

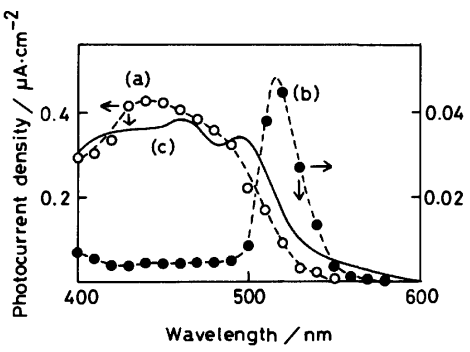

Fig. 2. Action spectra of short-circuit photocurrent for an Al/dye **1**/Ag cell and optical absorption spectrum of a dye **1** film. The values of photocurrent are corrected to the incident photon flux of 1×10^{15} photons/cm²·s.
(a) Action spectrum under the illumination from the Al side. (b) Action spectrum under the illumination from the Au side. (c) Absorption spectrum of a dye **1** film in an arbitrary unit.

acterized as p-type semiconductors forming a Schottky junction at the Al interface and an ohmic contact at the Ag(or Au) electrode. The existence of a photoactive region at the Al/dye interface was confirmed by an illuminating-direction experiment on an Al/dye **1**/Au cell (Fig. 2). The action spectrum of the short-circuit photocurrent obtained on illumination from the Al side resembled the optical-absorption spectrum of a vacuum-deposited **1** film (Fig. 2-(a)). On illumination from the Au side, on the other hand, an optical filtering effect of the dye phase[4] was observed (Fig. 2-(b)), indicating that the photons absorbed near the Al interface contribute mainly to the current generation.

The values of the open-circuit photovoltage (V_{oc}), the quantum yield of the short-circuit photocurrent (Φ_{sc}), and the photoenergy conversion efficiency (η) were determined under a monochromatic light at the peak-absorption wavelength of the dye film (Table 1). When measured, the fill factors were found to be around 0.25, almost independent of the dye structures. Among the four photocells of the Al/dye/Ag configuration, the cell using dye **2**, which has a carboxyl group at the 3-position of the coumarin ring, gave the best values of Φ_{sc} and η. This result is in accordance with the suggestion by Piechowski *et al.*[5] for merocyanine-based photocells that the strong adsorption of the electron-rich end of the dye molecule to Al_2O_3 layer forming over the Al surface is efficient in the cell performance. The comparison of the data for Al/dye **1**/Au with those for Al/dye **1**/Ag in Table 1, on the other hand, demonstrates that the cell performance is fairly much improved by the use of Au in place of Ag as the contact electrode. A tendency for a dye showing a higher fluorescence efficiency in solution to give a higher Φ_{sc} value has been pointed out for merocyanine-based photocells.[5] However, no such tendency was observed for the coumarin dyes.

Table 1. Photovoltaic parameters[a]

Photocell	V_{oc}/V	Φ_{sc}/%	η/%
Al/dye **1**/Ag	0.84	0.19	0.015
Al/dye **1**/Au	0.95	0.25	0.022
Al/dye **2**/Ag	0.49	0.77	0.033
Al/dye **3**/Ag	0.30	0.046	0.0012
Al/dye **4**/Ag	0.43	0.16	0.0058

a) Under a monochromatic light with an input intensity of 0.1 mW/cm^2. The wavelength of the light is 460 nm for Al/dye **1**/Ag and Al/dye **1**/Au, and 430 nm for the other photocells.

Studies of pH-modulated photoelectrodes utilizing the semiconductor characteristics of coumarin dyes themselves will be published elsewhere.[6]

References

1) G. Jones, II, S. F. Griffin, C. Choi, and W. R. Bergmark, *J. Org. Chem.*, **49**, 2705 (1984).
2) T. L. Penner and D. Möbius, *J. Am. Chem. Soc.*, **101**, 7407 (1982).
3) P. Fromherz and W. Arden, *J. Am. Chem. Soc.*, **102**, 6211 (1980).
4) J. F. McCann, S. Hinkley, and D. Haneman, *J. Electroanal. Chem.*, **137**, 17 (1982).
5) A. P. Piechowski, G. R. Bird, D. L. Morel, and E. L. Stogryn, *J. Phys. Chem.*, **88**, 934 (1984).
6) F. Mizutani, S. Iijima, Y. Tanaka, and K. Tsuda, 5th International Conference on Photochemical Conversion and Strage of Solar Energy, Osaka, August 1984, Abstr. No. B44(5).

The C-13 NMR Spectra of Thiophenes. II. 2-Substituted Thiophenes

Kunimi FUJIEDA, Kensuke TAKAHASHI,*† and Tyo SONE††

Instrument Division, Hitachi, Ltd., New Marunouchi Bldg., 5-1, Marunouchi 1-Chome, Chiyoda-ku, Tokyo 100
†*Department of Industrial Chemistry, Nagoya Institute of Technology, Gokiso-cho, Showa-ku, Nagoya 466*
††*Department of Applied Chemistry, Faculty of Engineering, Yamagata University, Jonan, Yonezawa 992*

(Received September 20, 1984)

Synopsis. Carbon-13 NMR data of 14 2-substituted thiophenes were obtained in $CDCl_3$. The correlation between the carbon chemical shifts and the Hammet constants was poor. The charge densities of typical compounds were calculated by the CNDO/2 method and they discussed in connection with the observed C-13 chemical shifts.

As an extension of our NMR studies of substituted thiophenes,[1-3] we have measured the C-13 NMR spectra of 14 2-substituted thiophenes and compared the data with those of the corresponding benzene derivatives.

Experimental

The C-13 NMR spectra were measured in a moderately concentrated solution (50 mg/0.8 ml) in $CDCl_3$ using a Varian XL-200 spectrometer with a frequency of 50.3 MHz. The chemical shifts were referred to an internal TMS signal. The compounds examined were prepared according to the methods previously reported in the literature. The chemical shifts and the coupling constants were obtained by the first-order analyses.

Results and Discussion

The C-13 chemical shifts and the one-bond carbon-proton coupling constants observed are tabulated in Tables 1 and 2, in which the values for monosubstituted benzenes, measured at a similar concentration (50 mg/0.8 ml) in $CDCl_3$, are also included for the sake of comparison. The values in Table 1 are almost entirely consistent with previously reported values in a pure liquid[1,2] and in an acetone solution.[4]

As may be seen in Table 1, the C_2 chemical-shift range (94 ppm) is rather wide as compared with those of the C_3 (34 ppm), the C_4 (5), and the C_5 (24). This indicates that, besides the inductive effect, the magnetic anisotropy effect of the substituent considerably affects the C_2 chemical shift, as has been pointed out previously for the monosubstituted benzenes.[5] The C_2, C_3, C_4, and C_5 shifts show parallel correlations with those of the C_{ipso}, C_o, C_m, and C_p of the corresponding monosubstituted benzenes respectively. The relation can be expressed by a simple equation as follows:

$$\delta(\mathrm{T}) = a \cdot \delta(\mathrm{B}) + b,$$

where δ(T) is a C-13 chemical shift of a thiophene derivative and δ(B) is that of the corresponding benzene. The correlation coefficients are 0.981, 0.871, and 0.935, and the proportional coefficients (a) are about 1.40, 1.62, and 1.42 for the C_2, C_3, and C_5 shifts respectively. Among the three, the C_3 shifts have the lowest correlation coefficient, because they suffer the so-called ortho-effect from their substituents. The C_5 shifts have a better correlation with the C_p shifts, for which the change was interpreted by the resonance effect of the substituents.[5] The C_4 shifts change little with the substituents and have no linear relation with the corresponding C_m shifts.

The electron densities of the carbons in the thiophenes have been calculated by the CNDO/2 method with or without d-orbitals.[6] The geometry of the thiophene skeleton was taken from a microwave geometry,[7] while those of the substituents were assumed to be the standard ones described previously.[8] Two planar geometries are considered in such

TABLE 1. ^{13}C NMR CHEMICAL SHIFTS OF 2-SUBSTITUTED THIOPHENES AND MONOSUBSTITUTED BENZENES IN ppm RELATIVE TO TETRAMETHYLSILANE IN $CDCl_3$ AT 50.3 MHz[a]

No.	Substituent	Thiophenes					Benzenes				
		C_2	C_3	C_4	C_5	Others	C_{ipso}	C_{ortho}	C_{meta}	C_{para}	Others
1	CHO	144.06	136.28	128.33	135.09	182.95	136.42	129.76	129.00	134.47	192.44
2	CH_3CO	144.60	132.46	128.11	133.75	26.91 190.68	137.16	128.57	128.30	133.09	26.58 198.09
3	I	73.06	136.86	128.83	131.45		94.35	134.46	130.21	127.42	
4	CO_2CH_3	133.62	133.46	127.73	132.33	52.13 162.68	130.22	129.59	128.37	132.90	52.07 167.11
5	CN	109.91	137.41	127.67	132.60	114.22	112.47	132.14	129.13	132.78	118.83
6	NO_2	152.51[b]	128.58	127.02	132.56		148.24	123.48	129.31	134.58	
7	Br	112.14	129.81	127.61	126.95		122.51	131.53	130.01	126.85	
8	H	125.10	126.85	126.85	125.10		128.33	128.33	128.33	128.33	
9	Cl	130.05	126.05	126.60	124.07		134.28	128.62	129.70	126.42	
10	CH_3	139.59	125.11	126.87	123.02	15.04	137.86	129.05	128.25	125.32	21.44
11	C_2H_5	147.38	123.24	126.66	122.63	16.05 23.27	144.25	128.29	127.85	125.57	15.61 28.88
12	OCH_3	166.71	103.75	124.71	111.74	60.37	159.56	113.90	129.43	120.64	55.09
13	$NHCOCH_3$	138.96	111.94	123.87	118.04	23.24 166.72	138.08	120.19	128.89	124.28	24.37 169.01
14	SO_2Cl	144.03	135.83	127.78	134.91		144.44	126.99	129.71	135.25	

a) Errors are estimated to be ±0.03 ppm. b) The value was obtained in a more concentrated solution (172 mg/0.8 ml).

Table 3. CNDO/2 Calculated total charge densities on the carbons of 2-substituted thiophenes ($\times 10^3$)[a)]

No.	Without d orbitals				With d orbitals			
	C_2	C_3	C_4	C_5	C_2	C_3	C_4	C_5
1	−11 (−8)	+14 (+24)	−18 (−21)	+17 (+23)	−43 (−40)	+51 (+62)	+31 (+28)	−27 (−21)
2	−16 (−13)	+10 (+22)	−18 (−20)	+16 (+22)	−46 (−46)	+48 (+60)	+31 (+28)	−29 (−21)
5	+38	+0	−12	+10	+9	+42	+37	−34
6	+8 (+23)	+33 (+12)	−15 (−4)	+26 (+13)	−19 (−5)	+67 (+52)	+36 (+45)	−19 (−29)
8	+5	−9	−9	+5	−36	+38	+38	−36
9	+20	−36	+1	−2	+41	+48	+37	−32
10	+55	−36	−4	−3	+18	+9	+44	−45
12	+193 (+197)	−97 (−85)	+13 (+10)	−19 (−14)	+156 (+156)	−50 (−41)	+64 (+59)	−60 (−55)

a) The value in parentheses is that calculated in another planar geometry (see text) except in the case of **6**, in which the plane of the substituent group is taken as perpendicular to the molecular plane. The values are given in units of the absolute value of the charge of an electron.

Table 2. The coupling constants between carbon-13 and directly bonded protons in thiophenes in Hz[a)]

No.	$^1J(C_3H_3)$	$^1J(C_4H_4)$	$^1J(C_5H_5)$
1	168	171	186
2	168	170	185
3	172	169	187
4	171	169	183
5	173	172	187
6	176	173	187
7	173	171	188
8	168	168	186
9	172	170	189
10	165	167	185
11	165	166	186
12	167	168	189
14	176	174	187

a) Errors are estimated to be ±1.3 Hz.

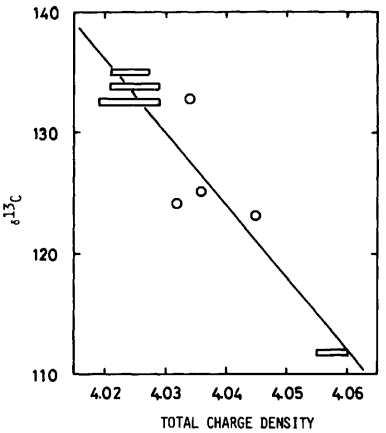

Fig. 1. Plot of C-13 chemical shifts in ppm (ordinate) *vs.* total charge densities (abscissa) for the C_5 of 2-substituted thiophenes.

cases as **2** where the orientation of the conjugated substituent can be in two ways on a molecular plane. Therefore, the results are shown by several sticks in Fig. 1 and are given in Table 3. The two ends of the stick in Fig. 1 correspond to the charge densities of the C_5 with two substituent orientations. Thus, the length of the stick shows the variation in the charge density dependent upon the conformation of the substituent. The proportionality coefficient of the C_5 shifts *vs.* their total charge densities is deduced to be −604 ppm/electron from Fig. 1 (r=0.93). As can be seen in Table 3, our calculation shows that the total charge densities increase at the C_α carbons and decrease at the C_β carbons when the d-orbitals are included in the calculation. Recently Osamura *et al.* pointed out the importance of the vacant d-orbitals of the sulfur atom.[9)]

As we have described before,[1)] the correlation between the C_5 shifts and the Hammet constants σ_p is not very good (r=0.85). The correlation with σ_p^+ seems to be better (r=0.90) than that with σ_p.[10)]

References

1) K. Takahashi, T. Sone, and K. Fujieda, *J. Phys. Chem.*, **74**, 2765 (1970).
2) K. Fujieda, K. Takahashi, and T. Sone, Preprint presented at the 9th Symposium on NMR Spectroscopy of the Chemical Society of Japan, Kanazawa, Oct. 1970, p. 193.
3) T. Sone, K. Fujieda, and K. Takahashi, *Org. Magn. Reson.*,**7**, 572 (1975).
4) S. Gronowitz, I. Johnson, and A.-B. Hornfeldt, *Chemica Scripta*,**7**, 76 (1975).
5) H. Spiesecke and W. G. Schneider, *J. Chem. Phys.*, **35**, 731 (1961).
6) The CNDO/2 MO calculations were carried out by using the HITAC-8450 or HITAC-M160-II computer system installed at the Nagoya Institute of Technology or by using the HITAC M-200H computer system installed at the Computer Center, Institute for Molecular Science at Okazaki.
7) B. Bak, D. Christensen, L. H-Nygaard, and J. R. Andersen, *J. Mol. Spectr.*, **7**, 58 (1961).
8) J. A. Pople and D. L. Beveridge, "Approximate Molecular Orbital Theory," McGraw-Hill Book Company, New York (1970).
9) Y. Osamura, O. Sayanagi, and K. Nishimoto, *Bull. Chem. Soc. Jpn.*, **41**, 845 (1976).
10) C. G. Swain and E. C. Lupton, Jr., *J. Am. Chem. Soc.*, **90**, 4328 (1968).

Influences of Supporting Silica Gel on the Catalytic Activity of B-18 Crown Ether-KCl Complex for the Selective Dehydrochlorination of 1,1,2-Trichloroethane

Hiroshi FUJITSU,* Takeshi TAKAGI,† and Isao MOCHIDA
Research Institute of Industrial Science
†*Department of Molecular Engineering, Graduate School of Engineering Sciences, Kyushu University, 86, Kasuga 816*
(Received November 10, 1984)

Synopsis. Catalytic dehydrochlorination of 1,1,2-trichloroethane into 1,1-dichloroethylene proceeded selectively around 200 °C over dibenzo-18-crown-6-KCl complex supported on silica gels. The reaction rate depended very much on the kinds of silica gel and impregnation levels of the complex, suggesting some roles of surface hydroxyl groups in this catalysis.

It has been established that basic substances promote the selective dehydrochlorination of 1,1,2-trichloroethane (TCE) into 1,1-dichloroethylene (1,1-DCE), whereas acidic ones promotes the formation of 1,2-dichloroethylene (1,2-DCE).[1] The selective synthesis of 1,1-DCE from TCE with recovery of dry hydrogen chloride is the most desirable process for the practical purpose; however, basic substances such as KOH react with hydrogen chloride eliminated to form the corresponding salts, proceeding the reaction stoichiometrically.

ICI patent claims the catalysis by CsCl on silica gel.[2] We reported previously some acid-proof basic catalysts,[3-5] such as hydrochlorinated 2-methylimidazole immobilized on silica gel. These catalysts exhibited high selectivity but low activity.

Naso and Ronzini,[6] and Viout[7] have reported the activity of crown ether-alkali halide complexes for the elimination and substitution reaction of alkyl and alkenyl halides. Mizuno *et al.*[8] reported the reactivity of alkyl halides over a complex (KCl-B18) supported on silica gel.

We report here the catalytic activity of the crown ether-potassium chloride complex supported on some silica gels. The liberation of hydrogen chloride can be expected rapid when a crown ether and a halide are properly selected. Nevertheless the elimination efficiency of the complex may also depend on the surface properties of silica gel, since hydrogen chloride produced inevitably interacts which the functional groups of the surface.

Experimental

Crown ether (dibenzo-18-crown-6:B-18) were purchased from Nippon Soda Co. Used silica gels were C-200 (650 m^2/g, Wako Junyaku Co.), MB-3A and MB-4A (500 and 260 m^2/g, respectively, Fuji-Davison Inc.). The catalyst was prepared by repeated impregnation (three times) of crown ether-KCl complex on to the silica gel from its methanol solution.

The dehydrochlorination of TCE was studied with a micro-catalytic gas chromatographic pulse technique.[9] The catalyst (1 g) was packed in a glass U tube and 2 μl of TCE was injected with a microsyringe after the hydrogen gas flow for 2 h at the reaction temperature.

Results

Catalytic activity of KCl-B18 supported on MB-3A (KCl-B18/MB-3A) in the successive pulses at several reaction temperatures is shown in Fig. 1. A very high conversion (94%) was observed in the first pulse at 250 °C, however the conversion decreased sharply with repeated pulses, reaching a constant value of conversion (25%) after the 7th pulse. Injection of 100 μl methanol after the 7th pulse recovered the conversion of 8th pulse to the level of 5th pulse, and its another injection maintained the conversion in the successive pulse. Lower reaction temperatures (200 or 220 °C) decreased the conversion in the first pulse (20 and 40%, respectively) as well as the extent of activity decrease with the repeated pulse. Remarkably high selectivities for 1,1-DCE formation over 90% were obtained at all reaction temperatures examined. Under the present reaction conditions, KCl supported alone on the silica gel (KCl 10%, 1 g) showed a very low activity (conversion in the first pulse: 9%), suggesting that KCl-B18 is the catalytic active species.

Catalytic activity of KCl-B18/MB-3A depended markedly on the loading levels of KCl-B18. The conversion in the first pulse increased considerably until

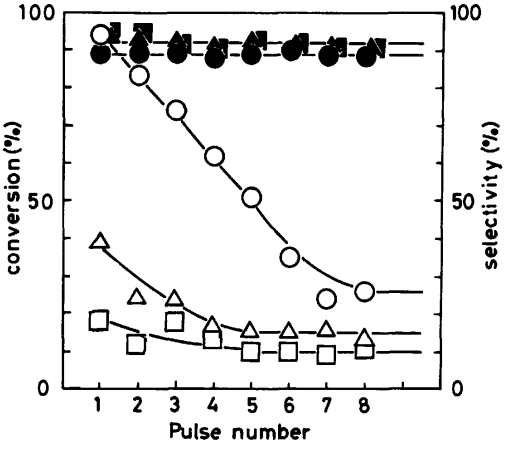

Fig. 1. Dehydrochlorination of TCE over KCl-B18/MB-3A cat. (loading level 19 wt%): 1 g, pulse size: 2 μl
○,●: React. temp: 250 °C, △,▲: react. temp: 220 °C, □,■: react. temp: 200 °C.
Open: conversion, closed: selectivity for 1,1-DCE formation, pulse interval was 1 h.

Table 1. Dehydrochlorination of TCE in the first pulse over KCl-B18 supported on several silica gels[a)]

Support	Conv./%	Selectivity/%	
		1,1-DCE	1,2-DCE
C-200	17	92	8
MB-3A	94	90	10
MB-4B	56	91	9

a) Catalyst (19 wt%): 1 g, react temp: 250 °C, pulse size: 2 μl.

the loading level reached 19 wt%, where the maximum value (94% conversion) was observed. More loading decreased the conversion which was as low as 43% at 37% loading. In contrast, the selectivity for 1,1-DCE formation was independent of the loading level.

Catalytic activities and selectivities of KCl-B18 supported on some silica gels in the first pulse are summarized in Table 1. Catalytic activity depended remarkably on the kind of supports, whereas selectivities were independently high. The activity order was as follows: MB-3A>MB-4B>C-200. The activity of MB-3A supporting catalyst was almost 5 times that of C-200 supporting one. Such a difference is much larger than that expected from their surface areas, suggesting positive roles of silica gels in this catalysis.

The amount of B-18 remaining on the gel after the 9th pulse determined by extracting the complex with methanol was 40% of originally supported one. Thermogravimetric measurements revealed that 78% of KCl-B18 remained on the silica surface at 250 °C without the dehydrochlorination reaction. These results suggest that the sublimation of B-18 accelerated by hydrogen chloride as well as the slow rate of hydrogen chloride release from the catalyst surface cause the significant decrease of activity in the repeated pulses.

Catalytic activity of KCl-B18/MB-3A was examined using a flow reactor (TCE: 3.5 kPa, catalysts (loading: 10%): 1 g, H_2 carrier: 60 $cm^3 \cdot min^{-1}$). The conversion of TCE was 13% at 250 °C in initial few minutes and then decreased very slowly to *ca.* 5% within 10 h. The total turnover number (reacted TCE/KCl-B18 in moles) reached more than 20 within 10 h at 250 °C. The selectivity for 1.1-DCE was constant to be *ca.* 90% throughout the reaction.

Discussion

Active species of KCl-crown ether complex supported on SiO_2 is assumed to its naked Cl^- ion,[6,8] which can abstract first the most acidic proton from TCE to be liberated as hydrogen chloride. The intermediate trichloroethanide anion is selectively converted into 1,1-DCE and may regenerate the active species by providing Cl^-.

According to the mechanism described, the stable activity may be expected, when no sublimation of the crown ether takes place. However, the activity decreased by the repeated pulses. Its recovery by methanol injection or lower activity in the flow reactor may suggest that the desorption of produced hydrogen chloride from the catalyst surface influences the activity. Marked variation of the activity in the first pulse due to silica gel supports also may indicate their significant roles in the elimination of hydrogen chloride as well as the better dispersion of KCl-crown ether complex on their surface. Such roles of silica gel support have been scarecely discussed.[10] The surface hydroxyl groups which can interact the chloride at the elimination stage may be the origin for these roles.

References

1) I. Mochida, J. Take, Y. Saito, and Y. Yoneda, *J. Org. Chem.*, **32**, 3894 (1967), **33**, 2161, 2163 (1968). I. Mochida, Y. Anju, A. Kato, and T. Seiyama, *Bull. Chem. Soc. Jpn.*, **44**, 3305 (1971); *idem.*, *J. Org. Chem.*, **39**, 3785 (1974).

2) British Patent 59, 007 (1971).

3) I. Mochida, H. Watanabe, H. Fujitsu, and K. Takeshita, *J. Chem. Soc., Chem. Commun.*, **1980**, 793.

4) I. Mochida, H. Watanabe, H. Fujitsu, and K. Takeshita, *Ind. Eng. Chem. Prod. Res. Dev.*, **22**, 38 (1983).

5) I. Mochida, H. Watanabe, A. Uchino, H. Fujitsu, K. Takeshita, M. Furuno, T. Sakura, and H. Nakajima, *J. Mol. Catal.*, **12**, 359 (1981).

6) F. Naso and L. Ronzini, *J. Chem. Soc., Perkin Trans. 1*, **1974**, 340.

7) P. Viout, *J. Mol. Catal.*, **10**, 231 (1981).

8) H. Mizuno, H. Watanabe, M. Misono, J. Take, and Y. Yoneda, *Chem. Lett.*, **1977**, 731.

9) R. J. Kokes, H. Tobin, and P. H. Emmett, *J. Am. Chem. Soc.*, **77**, 5860 (1955).

10) K. Tanabe, T. Seiyama, and K. Hueki Ed., "Metal Oxides and Complex Oxides" Kodansha Scientific, Tokyo, 1978, p113.

The Structure of Dichlorobis(L-proline)zinc(II)

Yasuhiko YUKAWA,* Noriko YASUKAWA, Yoshie INOMATA, and Toshio TAKEUCHI
Department of Chemistry, Faculty of Science and Technology, Sophia University, 7-1, Kioi-cho, Chiyoda-ku, Tokyo 102
(Received July 31, 1984)

Synopsis. The title complex was prepared at pH 4.0. The crystal and molecular structures have been determined by X-ray diffraction. The crystals of $ZnCl_2(C_5H_9NO_2)_2$, F.W.=366.55, were orthorhombic: space group $P2_12_12_1$, a=13.527(3), b=16.263(3), c=6.598(1) Å, U=1451.4(5) Å^3, Z=4, D_m=1.67 g cm^{-3}, D_x=1.68 g cm^{-3}, and μ(Mo $K\alpha$)=21.2 cm^{-1}. The zinc atom is coordinated in a tetrahedral geometry to two chlorine atoms and the two carboxyl oxygen atoms of two L-proline ligands. Each L-proline is coordinated as a monodentate ligand.

The various coordination types of amino acid complexes are important for the discussion of the different metal-binding site models on proteins. Many complexes should be prepared under different conditions. However, most of the complexes with amino acids have been prepared under neutral or basic conditions. Therefore, we tried to prepare amino acid complexes at low pH, in order to study different coordination types from ones under neutral or basic conditions. In this work, as part of the program, a zinc complex of L-proline (Hpro) was prepared at low pH and the structure was determined in order to compare it with the cadmium complexes having analogous amino acid ligands.[1,2]

Experimental

Preparation of Dichlorobis(L-proline)zinc(II). To an aqueous solution of 4.61 g (0.04 mol) of Hpro, 2.73 g (0.02 mol) of $ZnCl_2$ was added. Then the solution (pH 4.0) was stirred for several hours on a water bath at 50—60 °C. Clear colorless prisms were obtained by standing at room temperature; they were air-dried. Found: C, 32.50; H, 4.90; N, 7.50; Zn, 17.7%. Calcd for $ZnCl_2(C_5H_9NO_2)_2$: C, 32.76; H, 4.96; N, 7.74; Zn, 17.84%. An almost quantitative yield of the complex was obtained.

X-Ray Measurements. The reflection intensities were collected by the θ—2θ scan technique ($2\theta \leqq 60°$) on a Philips PW1100 automated four-circle diffractometer. The intensities ($|F_o| \geqq 3\sigma(|F_o|)$) were corrected for Lorentz and polarization factors, but not for absorption, because of the low magnitude of μr (=0.25). All calculations were carried out on a HITAC M-280H computer at the Computer Center of The University of Tokyo, using the local version of UNICS.[3] The scattering factors were taken from tables.[4]

Structure Determination. The structure was solved by a heavy-atom method and refined by a block-diagonal least-squares method. The weighting scheme was $W=1/[\{\sigma(|F_o|)\}^2+(0.045\times|F_o|)^2)$. The final R value[5] was 0.035, with anisotropic temperature factors for all the non-hydrogen atoms.

Results and Discussion

The final atomic coordinates and the equivalent isotropic temperature factors, except for those of calculated hydrogen atoms, are shown in Table 1. The bond lengths and bond angles are in Table 2.[6]

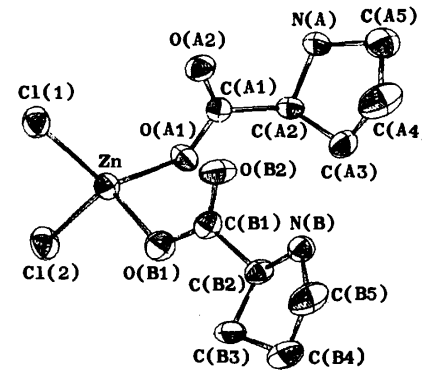

Fig. 1. The perspective drawing of the complex and the numbering scheme.

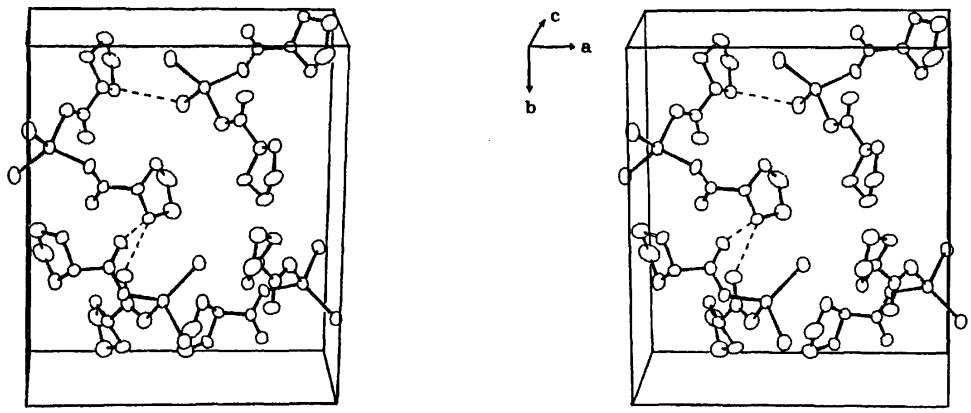

Fig. 2. The crystal packing diagram of $ZnCl_2(Hpro)_2$.
(----: Hydrogen bonding)

Table 1. Final atomic coordinates ($\times 10^4$) and equivalent isotropic temperature factors, with estimated standard deviations in parentheses

Atom	x	y	z	B_{eq}/Å^2 a)
Zn	690.4(3)	1822.9(3)	1475.5(7)	2.46
Cl(1)	−450.1(7)	920.1(7)	444(2)	3.55
Cl(2)	56.3(8)	2569.5(8)	4087(2)	3.72
O(A1)	1965(2)	1460(2)	2664(5)	2.84
O(A2)	2049(2)	236(2)	1148(5)	3.13
N(A)	3888(3)	−58(2)	2296(7)	2.84
C(A1)	2411(3)	806(2)	2075(6)	2.15
C(A2)	3516(3)	806(2)	2600(7)	2.37
C(A3)	4112(3)	1322(3)	1112(9)	3.76
C(A4)	4489(5)	740(4)	−438(8)	4.97
C(A5)	4664(4)	−49(3)	664(8)	4.19
O(B1)	1230(2)	2646(2)	−405(5)	3.47
O(B2)	1879(3)	1661(2)	−2338(6)	3.75
N(B)	2788(2)	2733(2)	−4826(6)	2.78
C(B1)	1772(3)	2377(3)	−4826(6)	2.69
C(B2)	2396(3)	3034(2)	−2825(7)	2.58
C(B3)	1895(4)	3842(2)	−3334(9)	3.75
C(B4)	2496(4)	4165(3)	−5103(11)	4.93
C(B5)	2703(4)	3415(3)	−6360(8)	4.40

a) The equivalent isotropic temperature factors were computed using the following expression: $B_{eq}=4/3(B_{11}a^2+B_{22}b^2+B_{33}c^2)$. The B_{ij}'s are defined by: $\exp[-(h^2B_{11}+k^2B_{22}+l^2B_{33}+2klB_{23}+2hlB_{13}+2hkB_{12})]$.

A perspective drawing of the complex, with the numbering scheme, is shown in Fig. 1 and the crystal packing diagram in Fig. 2.

As shown in Fig. 1, the zinc atom is coordinated in a tetrahedral geometry to two chlorine atoms and two carboxyl oxygen atoms of two L-proline ligands: each of them is a zwitter ion. The angles around the zinc atom are not exactly tetrahedral angles, as shown in Table 2.

The nitrogen atom, N(A), is associated with two intermolecular hydrogen bonds, N(A)···O(A2)^{I} (2.856(6) Å) and N(A)···O(B2)^{I} (2.815(5) Å), as shown in Fig. 2. On the other hand, N(B) seems to connect only with Cl(2)^{II} *via* a hydrogen bond (N(B)···Cl(2)^{II}; 3.145(5) Å).[7] The difference of the intermolecular hydrogen bonds reflects the difference of the shapes of the two pyrrolidine rings. By these intermolecular hydrogen bonds, the complex molecules are connected to each other in three dimensions.

The system is different from those of $CdCl_2$(Hhpro) and $CdCl_2$(Hpro)·H_2O.[1,2] Both consist of one-dimensional polymers bridged by chlorine atoms and a carboxyl group, and the ligand 4-hydroxy-L-proline (Hhpro) or Hpro is coordinated to the metal with only carboxyl oxygen atoms as a zwitter ion. The polymers are aligned in parallel by hydrogen bonds or van der Waals' contacts in the crystals.

Table 2. Bond lengths and bond angles, with estimated standard deviations in parentheses

Bond length	l/Å	Bond length	l/Å
Zn-Cl(1)	2.234(2)	Zn-Cl(2)	2.275(1)
Zn-O(A1)	1.984(3)	Zn-O(B1)	1.967(3)
O(A1)-C(A1)	1.282(5)	O(B1)-C(B1)	1.265(5)
O(A2)-C(A1)	1.213(5)	O(B2)-C(B1)	1.223(5)
C(A1)-C(A2)	1.535(5)	C(B1)-C(B2)	1.515(6)
C(A2)-C(A3)	1.523(7)	C(B2)-C(B3)	1.516(6)
C(A3)-C(A4)	1.484(8)	C(B3)-C(B4)	1.518(9)
C(A4)-C(A5)	1.494(8)	C(B4)-C(B5)	1.501(8)
C(A5)-N(A)	1.505(7)	C(B5)-N(B)	1.507(6)
N(A)-C(A2)	1.505(5)	N(B)-C(B2)	1.505(6)
Bond angle	ϕ/°	**Bond angle**	ϕ/°
Cl(1)-Zn-Cl(2)	108.65(5)	O(A1)-Zn-O(B1)	97.47(13)
Cl(1)-Zn-O(A1)	121.61(9)	Cl(1)-Zn-O(B1)	120.76(11)
Cl(2)-Zn-O(A1)	100.81(9)	Cl(2)-Zn-O(B1)	104.76(11)
O(A1)-C(A1)-O(A2)	126.6(4)	O(B1)-C(B1)-O(B2)	127.1(4)
O(A1)-C(A1)-C(A2)	113.0(3)	O(B1)-C(B1)-C(B2)	113.8(4)
O(A2)-C(A1)-C(A2)	120.3(3)	O(B2)-C(B1)-C(B2)	119.0(4)
C(A1)-C(A2)-C(A3)	111.7(4)	C(B1)-C(B2)-C(B3)	117.4(3)
C(A1)-C(A2)-N(A)	107.2(3)	C(B1)-C(B2)-N(B)	110.6(3)
C(A3)-C(A2)-N(A)	104.6(3)	C(B3)-C(B2)-N(B)	104.2(3)
C(A2)-C(A3)-C(A4)	106.0(4)	C(B2)-C(B3)-C(B4)	103.4(4)
C(A3)-C(A4)-C(A5)	105.5(5)	C(B3)-C(B4)-C(B5)	104.1(4)
C(A4)-C(A5)-N(A)	104.3(4)	C(B4)-C(B5)-N(B)	104.0(4)

The difference of the crystal structures results from the halogeno zinc or cadmium complexes retaining the traces of the zinc or cadmium halide: zinc and cadmium chlorides consist of $ZnCl_4$ tetrahedra and $CdCl_6$ octahedra, respectively. In aqueous solutions of cadmium halides, there are significant amounts of the undissociated halides and polymeric species, as is well known.

The authors wish to express their thanks to Professor Yoichi Iitaka of The University of Tokyo for the collection of the intensity data. They would also like to thank Dr. F. S. Howell of Sophia University for correcting this manuscript.

References

1) Y. Yukawa, Y. Inomata, T. Takeuchi, M. Shimoi, and A. Ouchi, *Bull. Chem. Soc. Jpn.*, **55**, 3135 (1982).

2) Y. Yukawa, Y. Inomata, and T. Takeuchi, *Bull. Chem. Soc. Jpn.*, **56**, 2125 (1983).

3) "The Universal Crystallographic Computation Program System (UNICS)," ed by T. Sakurai, Crystallographic Society of Japan, Tokyo (1967).

4) "International Tables for X-Ray Crystallography," Kynoch Press, Birmingham, U. K. (1974), Vol. IV.

5) $R=\Sigma||F_o|-|F_c||/\Sigma|F_o|$

6) The final atomic parameters containing calculated hydrogen atoms, the final F_o—F_c values, and some additional data are deposited as Document No. 8522 at the Office of the Editor of the Bulletin of the Chemical Society of Japan.

7) Key to symmetry operations: I. 0.5−x, −y, 0.5+z; II. 0.5+x, 0.5−y, −z.

The Synthesis and the Crystal and Molecular Structure of [Tris(dibutyl sulfoxide)bis(*O,O'*-diisopropyl dithiophosphato)neodymium(III)] [Tetrakis(*O,O'*-diisopropyl dithiophosphato)neodymium(III)] $[Nd\{(C_3H_7O)_2PS_2\}_2\{(C_4H_9)_2SO\}_3][Nd\{(C_3H_7O)_2PS_2\}_4]$

Yoshiyuki OHKI,† Masao NAKAMURA, Yasuo SUZUKI,† Kiyofumi NAGAI, Mamoru SHIMOI, and Akira OUCHI*

Department of Chemistry, College of Arts and Sciences, The University of Tokyo, Komaba, Meguro-ku, Tokyo 153

†*Department of Industrial Chemistry, Faculty of Engineering, Meiji University, Higashi-Mita, Tama-ku, Kawasaki, Kanagawa 214*

(Received November 7, 1984)

Synopsis. The title complex has been synthesized, and its crystals and molecular structure has been determined by the use of the single-crystal X-ray-diffraction method. The crystal of $Nd_2C_{60}H_{138}O_{15}P_6S_{15}$, F. W.=2055.03, was monoclinic, with a space group of An; a=23.696(4), b=23.466(4), c=20.208(4) Å, β=111.22(2)°, Z=4, V=10475(4) Å^3, D_m=1.30(3), D_x=1.30 Mg m^{-3}, and μ(Mo $K\alpha$)=1.41 mm^{-1}. The complex consists of cationic and anionic species, as is shown in the title. The metal atom of the cationic complex is hepta-coordinated and is in a pentagonal-bipyramidal geometry, while the anionic one is octa-coordinated and is in a dodecahedral geometry.

In previous papers, we reported the syntheses and the structure determination of several *O,O'*-diisopropyl dithiophosphate (iPr_2dtp)—Lewis base mixed complexes.[1-4] One of them, $[Eu(iPr_2dtp)_2(dmso)_3][Eu(iPr_2dtp)_4]$ (**1**) (where dmso=dimethyl sulfoxide),[4] consists of a cationic complex and an anionic complex. We tried to obtain the same types of complexes from some other ligands, and found from its elemental analysis, that the title one could be expected to have that structure. However, as the ligand size of the title complex is much larger than that of **1**, it might have a structure different from that of **1**. Therefore, we determined its structure by the single-crystal X-ray-diffraction method.

Experimental

Synthesis of $[Nd(iPr_2dtp)_2(dbso)_3][Nd(iPr_2dtp)_4]$ (where dbso=Dibutyl Sulfoxide). Neodymium(III) chloride hexahydrate (0.59 g, 1.6 mmol) and $Na(iPr_2dtp)$ (1.7 g, 7.1 mmol) were added to 35 cm^3 of 2-propanol, and the mixture was refluxed for 20 min. After cooling, the residue was filtered off, and to the filtrate dbso (0.76 g, 5.0 mmol) was added. The solution was then refluxed for 10 min at about 65 °C and concentrated to about 7 cm^3 by the use of a vacuum rotary evaporator at about 60 °C, after which the solution was left standing in a refrigerator (about 5 °C) several days. Pure crystals appeared. Yield, 0.29 g (17%). The isomorphous europium(III) complex, $[Eu(iPr_2dtp)_2(dbso)_3][Eu(iPr_2dtp)_4]$ (**2**), was also obtained in the same way. Anal. ($M_2C_{60}H_{138}O_{15}P_6S_{15}$) M, C, H, S. (where M=Nd or Eu)

From lanthanum(III) chloride another type of complex, one with the formula of $La(iPr_2dtp)_3(dbso)_2$, was obtained. Anal. ($LaC_{34}H_{78}O_8P_3S_8$) La, C, H.

Single-crystal X-Ray Analysis. A crystal 0.3×0.3×0.25 mm^3 in size (all the edges were cut off, and it was shaped almost into a sphere) was used. The reflections within the range of 3°<2θ<55° were collected on a Rigaku AFC-6A four-circle automated X-ray diffractometer, with graphite-monochromated Mo $K\alpha$ radiation (scan speed, 4° min^{-1}) by means of the ω-scan technique. Of the 9536 reflections measured, 4674 reflections with $|F_o|>3\sigma(|F_o|)$ were used for the refinement. The intensities were corrected for the Lorentz and polarization factors, but no correction was made for the absorption and extinction. All the calculations were carried out on a HITAC M-280H computer at the Computer Center of The University of Tokyo, using the local version of the UNICS.[5] The scattering factors were taken from the tables.[6]

The structure was solved by the heavy-atom method. Although those of the central metal atoms and the neighboring atoms were exactly determined, those of the butyl and isopropyl carbon atoms were found to have relatively large standard deviations, even after repeated refinements, probably because they are not fixed tightly in the crystal, as in cases of the other adducts of the lanthanoid *O,O'*-dialkyl dithiophosphates.[1-4,7] The positions of six carbon atoms, C(9), C(11), C(103), C(123), C(124), and C(128), were fixed to the respective most probable positions. The position of a dbso sulfur atom, S(10), was divided into two; the occupancy factors of S(10A) and S(10B) are 53 and 47% respectively. The final R value was 0.055[8] reached by applying anisotropic temperature factors for all the atoms except the fixed ones.

The Measurement of the Visible Absorption Spectra. The visible absorption spectra were measured with a Hitachi 124 spectrophotometer, using an acetonitrile solution of the complexes (1.0×10^{-3}—10^{-2} mol dm^{-3} in concentration).

Results and Discussion

Selected bond lengths and bond angles are given in Table 1.[9] Perspective drawings of the cationic (**3**) and the anionic (**4**) complexes, along with the num-

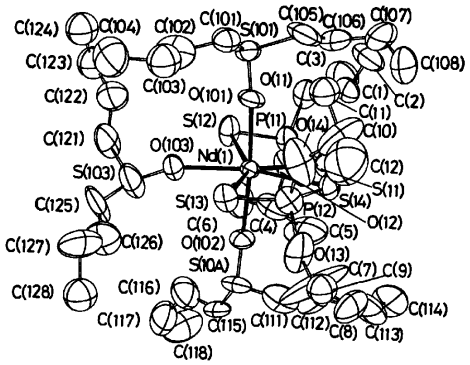

Fig. 1. A perspective drawing of $[Nd(iPr_2dtp)_2(dbso)_3]^+$ and the numbering scheme. (S(10B) is not shown in the figure)

Table 1. Selected bond lengths and bond angles of the complex, with estimated standard deviations in parentheses

Bond length	l/Å	Bond length	l/Å	Bond length	l/Å
Nd(1)-S(11)	2.889(8)	Nd(1)-S(12)	2.895(7)	Nd(1)-S(13)	2.916(8)
Nd(1)-S(14)	2.908(6)	Nd(1)-O(101)	2.284(18)	Nd(1)-O(102)	2.317(16)
Nd(1)-O(103)	2.356(17)	Nd(2)-S(21)	2.938(7)	Nd(2)-S(22)	2.911(8)
Nd(2)-S(23)	2.904(9)	Nd(2)-S(24)	2.939(6)	Nd(2)-S(25)	2.928(5)
Nd(2)-S(26)	2.933(5)	Nd(2)-S(27)	2.882(5)	Nd(2)-S(28)	2.950(5)
Bond angle	**ϕ/°**	**Bond angle**	**ϕ/°**	**Bond angle**	**ϕ/°**
O(101)-Nd(1)-O(103)	89.2(6)	O(102)-Nd(1)-O(103)	85.6(6)	O(101)-Nd(1)-S(11)	98.9(5)
O(102)-Nd(1)-S(11)	86.7(4)	O(101)-Nd(1)-S(12)	84.9(5)	O(102)-Nd(1)-S(12)	96.2(4)
O(101)-Nd(1)-S(13)	88.1(5)	O(102)-Nd(1)-S(13)	88.3(4)	O(101)-Nd(1)-S(14)	88.8(5)
O(102)-Nd(1)-S(14)	94.0(4)	O(103)-Nd(1)-S(11)	142.5(4)	O(103)-Nd(1)-S(12)	76.0(4)
O(103)-Nd(1)-S(13)	76.0(4)	O(103)-Nd(1)-S(14)	144.6(4)	S(11)-Nd(1)-S(12)	68.5(2)
S(13)-Nd(1)-S(14)	68.6(2)	S(11)-Nd(1)-S(14)	72.6(2)	O(101)-Nd(1)-O(102)	174.3(6)
S(21)-Nd(2)-S(22)	68.0(2)	S(23)-Nd(2)-S(24)	67.7(2)	S(25)-Nd(2)-S(26)	67.49(14)
S(27)-Nd(2)-S(28)	68.50(15)	S(21)-Nd(2)-S(24)	68.53(18)	S(25)-Nd(2)-S(28)	68.63(15)
S(22)-Nd(2)-S(23)	155.7(2)	S(26)-Nd(2)-S(27)	155.25(15)		

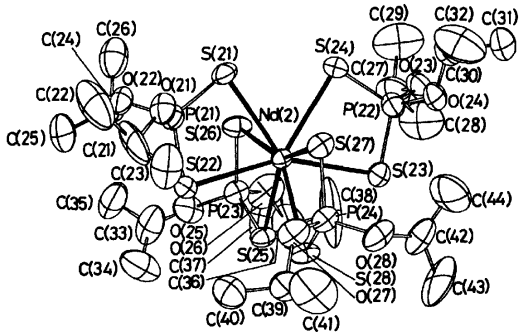

Fig. 2. A perspective drawing of $[Nd(iPr_2dtp)_4]^-$ and the numbering scheme.

bering scheme, are shown in Figs. 1 (for **3**) and 2 (for **4**),[9]

In **3**, $[Nd(iPr_2dtp)_2(dbso)_3]^+$, the neodymium(III) atom is hepta-coordinated and is in a pentagonal-bipyramidal configuration. Four sulfur atoms of two iPr_2dtp ligands, as well as one oxygen atom of a dbso ligand, bond equatorially, and two oxygen atoms of the dbso ligands are coordinated from the two ends of the axis. The average positional deviation of the central metal and the ligating four sulfur and one oxygen atoms from the average pentagon plane is 0.156 Å (the maximum deviation is 0.283 Å for S(14)). The angles between the average pentagon plane and the axis, O(101)-Nd(1) and O(102)-Nd(1), are 84.5 and 87.3 ° respectively.

In **4**, $[Nd(iPr_2dtp)_4]^-$, the central metal atom is octa-coordinated and is in a dodecahedral geometry. Each iPr_2dtp ligand spans an *m*-edge coordinated through both sulfur atoms.[9] The atomic positional deviations of the central metal and ligated sulfur atoms from their average trapezium plane are 0.055 Å on the average (0.097 Å at the maximum for S(28)). The dihedral angle between the two trapezia is 88.0 °.

Therefore, both **3** and **4** are in about the same type of configuration as those of **1**, although **3** and **4** are a little more deviated from the ideal forms than the respective ions of **1**.

The acetonitrile solution of **2** shows a charge-transfer band. The wavelength and the absorption coefficient of the absorption maximum are 410 nm and 1.8×10^2 dm^3 mol(Eu)$^{-1}$ cm^{-1}. These values are almost the same as those of **1**; the absorption coefficient is about one-half of the value of a neutral complex such as $Eu(iPr_2dtp)_3(bza)_2$ (bza=benzamide, $\varepsilon_{max}=4.2\times10^2$ dm^3 mol(Eu)$^{-1}$ cm^{-1}.[1])

The authors are greatly obliged to the Shin-Etsu Chemical Ind. Co., Ltd., for aiding this study by presenting highly pure lanthanoid oxides. The present work was supported partially by a Grant-in-Aid for Scientific Research (No. 57430011) from the Ministry of Education, Science, and Culture.

References

1) R. Nakamura, K. Nagai, M. Shimoi, and A. Ouchi, *Bull. Chem. Soc. Jpn.*, **57**, 2919 (1984).

2) K. Nagai, R. Nakamura, M. Shimoi, and A. Ouchi, *Bull. Chem. Soc. Jpn.*, **57**, 2725 (1984).

3) K. Nagai, Y. Sato, S. Kondo, and A. Ouchi, *Bull. Chem. Soc. Jpn.*, **56**, 2605 (1983).

4) Unpublished data; to be published elsewhere.

5) "Universal Crystallographic Computation Program System (UNICS)," ed by T. Sakurai, Crystallographic Society of Japan, Tokyo (1967).

6) "International Tables for X-ray Crystallography," Kynoch Press, Birmingham (1974), Vol. IV. pp. 72, 150.

7) A. A. Pinkerton and D. Schwarzenbach, *J. Chem. Soc., Dalton Trans.*, **1976**, 2464, 2466.

8) $R=\Sigma||F_o|-|F_c||/\Sigma|F_o|$.

9) The final atomic coordinates and thermal parameters, the final F_o—F_c table, and some additional data about the bond lengths and bond angles, as well as the crystal packing diagram and a schematic drawing of **3** and **4**, are deposited as Document No. 8521 at the Office of the Editor of *Bull. Chem. Soc. Jpn.*

Cobalt(III) Complexes with Quadridentate Ligands. VI.[1] The Preparation and Properties of "*cis*-β_1 and β_2"-Isomers of the Salicylaldehydato(triethylenetetramine)-cobalt(III) Complex

Yoshihisa YAMAMOTO,* Eiko TOYOTA, and Shoko TSUKUDA
Faculty of Pharmaceutical Sciences, Higashi Nippon Gakuen University, Ishikari-Tobetsu, Hokkaido 061-02
(Received November 13, 1984)

Synopsis *cis*-β_1 and β_2-Salicylaldehydato(triethylenetetramine)cobalt(III) chloride dihydrate have been isolated from a reaction mixture of salicylaldehyde, *cis*-α or β-dichloro(triethylenetetramine)cobalt(III) chloride and Ag_2O. The IR spectra of the complexes showed four strong absorption peaks in the 990—1100 cm^{-1} region. The complexes were assigned to the β-form. Their *cis*-β_1 and *cis*-β_2 configurations have been established by their ^1H NMR spectra.

Previously, we have been concerned with the preparation and properties of isomers of the mixed-ligand complexes of *cis*-β_1, β_2-salicylato(quadridentate amine)cobalt(III) chloride hydrates,[2,3] [Co(sal)L]Cl·$n$$H_2O$ (L: 2,2,2-tet; 2,3,2-tet; 3,2,3-tet; 3,3,3-tet. The abbreviation, tet, means tetramin; *e.g.*, triethylenetetramine is abbreviated to 2,2,2-tet). The preparation of the mixed-ligand metal complexes with salicylaldehydato and amine ligands had been very difficult, because the metal complexes with Schiff base ligands[4] had been obtained, such as (*N,N'*-disalicylidene-substituted triethylenetetramine)metal complexes in an octahedral configuration and (*N,N'*-disalicylidenepolymethylenediamine)metal complexes in a planar configuration. Thus, very little was known regarding the preparation and properties of aldehydato metal complexes with amine ligands in contrast with the large amount of information regarding salicylato metal complexes[1-3,5] with amine ligands. The present paper deals with the preparation and properties of the mixed-ligand cobalt(III) complexes with salicylaldehydato and triethylenetetramine ligands and deals with the assignments of the configuration of *cis*-β_1 and β_2 isomers.

Results and Discussion

A mixture of *cis*-β_1 and β_2-salicylaldehydato(triethylenetetramine)cobalt(III) chloride dihydrate has been isolated from a reaction mixture of *cis*-α or β-[$CoCl_2$trien]Cl, Ag_2O, and salicylaldehyde. The separation of the *cis*-β_1 isomer (complex **1**) and the *cis*-β_2 isomer (complex **2**, Fig. 1) was attempted using an ion-exchange resin. The *cis*-α isomer could not be obtained.

The electric conductivities of **1** and **2** in aqueous solutions were about 210 S cm^2 $equiv^{-1}$. The IR spectra of **1** and **2** showed four strong peaks in the 990—1100 cm^{-1} region (*cf.* Experimental section) and five peaks in the 3000—3300 cm^{-1} region. Thus, complexes **1** and **2** were assigned to the *cis*-β configuration.[6] The electronic absorption spectrum of **1** is very similar to that of **2**. The absorption bands at 420 and 510 nm were assigned to the charge-transfer band and the first d-d absorption band ($^1T_{1g} \leftarrow {}^1A_{1g}$), respectively. In the ^1H NMR spectra, the lowest field signals at δ 8.5—8.6 were assigned to the aldehyde group protons,[7] and the signals at δ 2.3—3.6 and 4.3—6.7 were assigned to the methylene protons[2] and the amine protons[2] of the coordinated triethylenetetramine ligand (abbreviation: trien ligand), respectively. The methylene proton signals at δ 2.4—2.8 and 2.8—3.6 of **2** were assigned to the NH_2-side and NH-side methylene protons,[3] respectively. The color, solubility, IR, ^{13}C and electronic absorption spectra of **1** were similar to those of **2**.

A clear distinction between **1** and **2** complexes was found in the ^1H NMR spectra. The chemical shift (δ=4.30) of the proton signal of the N(1)H_2 group of the coordinated trien of **2** was at a higher field than that (δ=4.40) of **1** as shown in Table 1.

Therefore, the N(1)H_2 group of **2** is considered to be at a position *trans*[2] to the phenoxyl oxygen of the salicylaldehydato ligand, which is more electronegative than the aldehyde group oxygen.

In addition, the methylene proton signal of **2** was separated to two group signals at δ 2.3—2.7 and 2.7—3.6, and their intensity ratio was 2:10, *i.e.*, two protons of the NH_2-side methylene protons at δ 2.4—

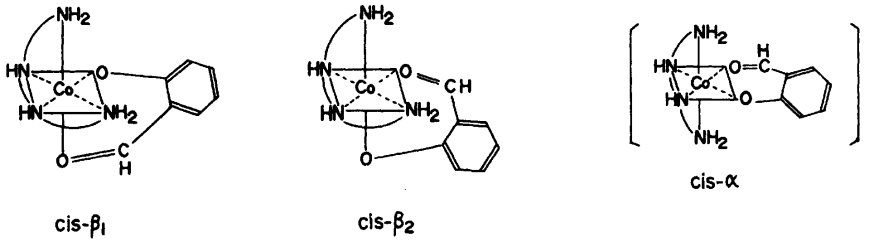

Fig. 1. The α, β_1, and β_2 configurations of salicylaldehydato(triethylenetetramine)cobalt(III) complex.

Table 1. ^1H, ^{13}C NMR and absorption spectra of complexes **1** and **2**.

^1H	$NH_2CH_2CH_2NHCH_2CH_2NHCH_2CH_2NH_2$ δ					Salicylaldehydato δ		Absorption bands in methanol
Complex No.	NH_2-side methylene protons	NH-side methylene protons	N(1)H_2	N(4)H_2	N(3)H	[N(2)H+ ring protons]	CHO	λ/nm (ε/cm^{-1} mol^{-1} dm^3)
1	2.42—3.64(12H)		4.40(2H)	4.98(2H)	6.20(1H)	[6.5—7.6 (5H)]	8.48(1H)[a]	418(2000) 500(292)
2	2.35—2.75(2H)	2.75—3.57(10H)	4.30(1H)	4.43—4.92(2H)	5.08(1H) 6.15(1H)	[6.5—7.6 (5H)]	8.59(1H)[a]	418(1830) 500(270)

^{13}C	NH_2-side methylene carbons δ		NH-side methylene carbons δ				δ						
							c-1	c-2	c-3	c-4	c-5	c-6	CHO
1[c]	42.7	47.6	48.6	50.2	51.7	52.9	120.2	170.2	118.1	141.6	124.2	137.7	196.7[b]
2[c]	42.4	47.6	48.7	50.2	52.2	53.0	120.1	170.0	118.1	141.2	124.4	137.4	196.2[b]

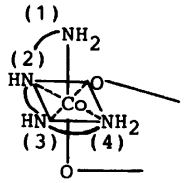

Solvent and Standard: a) 1.8 mol dm^{-3} D_2SO_4, internal DSS (δ=0), b) D_2O, internal dioxane (δ=67.4). c) *cf.* Ref. 3, 8 and 9.

2.8 overlap to the NH-side methylene protons at δ 2.8—3.6. While, the methylene proton signal of **1** was not separated to the two group signals. These properties are similar to those of the *cis*-β_2-salicylato-(quadridentate amine)cobalt(III) chloride hydrate,[2,3] *cis*-β_2-[Co(sal)L]Cl·nH_2O. Thus, the configurations of complexes **2** and **1** have been assigned to *cis*-β_2 and β_1, respectively.

Experimental

Measurements. The NMR spectra were recorded with an FX-60 spectrometer (JEOL) for ^{13}C NMR and with an R-40 apparatus (Hitachi) for ^1H NMR. The IR spectra were recorded over potassium bromide disks with a 270—30 spectrophotometer (Hitachi). The visible absorption spectra were recorded with a Shimadzu UV-210 recording spectrophotometer. The electric conductivities of an aqueous solution were determined by the use of a conductometric meter, CM-30 (Shimadzu), at room temperature.

Preparation of Complexes. Mixture of cis-β-*Salicylaldehydato(triethylenetetramine)cobalt(III) Chloride Dihydrate (1 and 2) and* cis-β-*Salicylato(triethylenetetramine)cobalt(III) Chloride Hydrate (3)*: *cis*-α or β-Dichloro(trien)cobalt(III) chloride (6.0 g, 19.26 mmol) was added to moistend fresh Ag_2O, which was made from silver nitrate (6.54 g, 38.50 mmol) and potassium hydroxide (2.16 g, 38.5 mmol). The mixture was stirred for several minutes at room temperature and then for about 40 min at 60 °C. The precipitated silver chloride was filtered off. The methanol solution (20 cm^3) of salicylaldehyde (2.36 g, 19.32 mmol) was added, drop by drop, to the reddish-violet filtrate. The solution was stirred at room temperature for 50 h and was then concentrated on a rotary evaporator. Then the concentrated solution was injected into a column chromatograph on alumina. On elution of methanol or ethanol, the eluent of the first red band was collected and concentrated. The purification was achieved by a column of ion-exchange resin (SP-Sephadex C-25, Na^+ form, 2.5×60 cm). On elution with 0.2 mol dm^{-3} NaCl, the first russet band was assigned to the *cis*-β-salicylato(trien)cobalt(III) chloride hydrate (**3**), and the second orange band (of complexes **1** and **2**) was collected and concentrated on a rotary evaporator. The precipitated NaCl was removed by filtration. Yields: Orange complexes **1** and **2**: 3.2 g (38.4%); russet complex **3**: 1.4 g (18.4%).

Separation of cis-β_1-*Salicylaldehydato(triethylenetetramine)-cobalt(III) Chloride Dihydrate (1) and* cis-β_2-*Salicylaldehydato-(triethylenetetramine)cobalt(III) Chloride Dihydrate (2)*: The separation of complexes **1** and **2** from the orange complex of 0.5 g was achieved by a column of ion-exchange resin (SP-Sephadex C-25, Na^+ form, 2.5×100 cm). On elution with 0.1 mol dm^{-3} NaCl, the effluent of the first orange band (complex **2**) and the second orange band (complex **1**) was collected and concentrated on a rotary evaporator, and the precipitated NaCl was removed by filtration. Yields: 0.13 g for **1**, 0.14 g for **2**. Found **1**: C, 35.90; H, 5.95; N, 12.68; Cl, 15.91%. **2**: C, 36.26; H, 6.52; N, 12.85; Cl, 16.01%. Calcd for $CoC_{13}H_{27}N_4O_4Cl_2$ (MW 433.22) C, 36.04; H, 6.28; N, 12.93; Cl, 16.37%. Dp: 187—189 °C for **1**; 184—185 °C for **2**. Λ=222 for **1**, 213 S cm^2 $equiv^{-1}$ for **2** in water. IR spectra **1**: 1002, 1032, 1059, and 1083 cm^{-1}; 3058, 3100, 3120, 3180, and 3210 cm^{-1}. **2**: 1002, 1035, 1059, and 1080 cm^{-1}; 3082, 3100, 3120, 3190, and 3200 cm^{-1}. Complexes **1** and **2** are very soluble in alcohols, dimethyl sulfoxide, and water, but insoluble in acetone and ether. Both complexes are highly hygroscopic.

The present work was partially supported by a Grant-in-Aid for Scientific Research No. 58740285 from the Ministry of Education, Science and Culture.

References

1) Part V: Y. Yamamoto and H. Kudo, *Bull. Chem. Soc. Jpn.*, **57**, 287 (1984).
2) Y. Yamamoto and E. Toyota, *Bull. Chem. Soc. Jpn.*, **52**, 2540 (1979).
3) Y. Yamamoto, H. Kudo, and E. Toyota, *Bull. Chem. Soc. Jpn.*, **56**, 1051 (1983).
4) "Progress in Inorganic Chemistry" ed by F. A. Cotton, Interscience Publishers, New York (1966), Vol. 7, p. 83.
5) Y. Yamamoto, E. Toyota, and N. Mitsudera, *Bull. Chem. Soc. Jpn.*, **53**, 3517 (1980).
6) L. G. Marzilli and D. A. Buckingam, *Inorg. Chem.*, **6**, 1042 (1967).
7) C. J. Pouchert and J. R. Campbell, "The Aldrich Library of NMR Spectra," Aldrich Chemical Compary INC., Milwaukee, Wisconsin (1974), Vol. 6, p. 80 D.
8) L. F. Johnson and W. C. Jankowski, "Carbon-13 NMR Spectra, A Collection of Assigned, Coded, and Indexed Spectra," Wiley-Interscience, New York (1972), No. 231, 292.
9) Y. Yamamoto, *Bull. Chem. Soc. Jpn.*, **51**, 2894 (1978).

Biaryl Formation in the Copper(I) Mediated Arylation of Stable Enolate Anions with *o*-Halogenonitrobenzenes

Singanallore V. THIRUVIKRAMAN and Hitomi SUZUKI*
Department of Chemistry, Faculty of Science, Ehime University, Bunkyo-cho, Matsuyama 790
(Received July 16, 1984)

Synopsis. *o*-Bromo- and *o*-iodonitrobenzenes react with stable enolate anions in hot DMF in the presence of copper(I) iodide, to afford not the expected arylation products but the coupling products, 2,2′-dinitrobiphenyls.

When heated in aprotic dipolar solvents such as DMF and HMPA in the presence of copper(I) iodide, nonactivated aromatic halides are activated to such an extent as to react with a variety of heteronucleophiles[1-7] and enolate anions,[8-11] giving the corresponding arylation products in good to moderate yields. However, moderately activated aryl halides such as halogenonitrobenzenes (**1**) behave differently from nonactivated ones to afford, in addition to the normal substitution product (**2**), significant amounts of *N*,*N*-dimethylanilines (**3**) and/or nitrobenzenes (**4**). Aryl-aryl coupling to form dinitrobiphenyls (**6**) is yet another unexpected pathway in the reaction of halogenonitrobenzenes, and is described herein.

Our attempts to prepare 2-(2-nitrophenyl)-3-oxobutanoate esters (**7**) as intermediates for the synthesis of heterocycles, by reacting *o*-bromo- or *o*-iodonitrobenzenes (**5**) with 3-oxobutanoate (acetoacetate) anion in the presence of copper(I) iodide in DMF at 100—120 °C, gave instead 2,2′-dinitrobiphenyls (**6a—6h**) as products. Table 1 lists several biphenyls obtained; in majority of cases their formation was achieved in good yields. The structures of all biphenyls were established by their elemental analyses, IR and ^{1}H NMR spectra, and agreement of their mps with those reported in literature. The effect of various enolate anions on the formation of dinitrobiphenyls is shown in Table 2. Also the role of enolate anion and copper(I) iodide is illustrated in Table 3.

Unlike the above cases, *m*-iodo- and *o*-chloronitrobenzenes suffered extensive reductive dehalogenation under similar conditions to give nitrobenzene as major product. Also *p*-iodonitrobenzene gave a mixture of ethyl 2-(4-nitrophenyl)-3-oxobutanoate and nitrobenzene accompained by a small amount of 4,4′-dinitrobiphenyl. Highly activated aromatic halides such as 2,4-dinitrochlorobenzene and 2,6- dinitroiodobenzene underwent normal S_NAr reaction without yielding any biphenyls.

As regards the mechanism which operates in the biphenyl formation, we withhold any comment at present, although it bears many features suggesting the involvement of electron transfer process.[12]

Experimental

*Reaction of o-Iodonitrobenzene (**5a**).* Sodium hydride (0.04 g, 1 mmol; 60% suspension in paraffin oil) was placed in a 25 ml flask and triturated with dry hexane. The oil-free grey solid was then covered with DMF (0.73 g, 10 mmol), and ethyl 3-oxobutanoate (0.065 g, 0.5 mmol) was added with stirring. After several minutes when hydrogen evolution ceased, copper(I) iodide (0.18 g, 1 mmol) was added to the resultant yellow solution. The solution

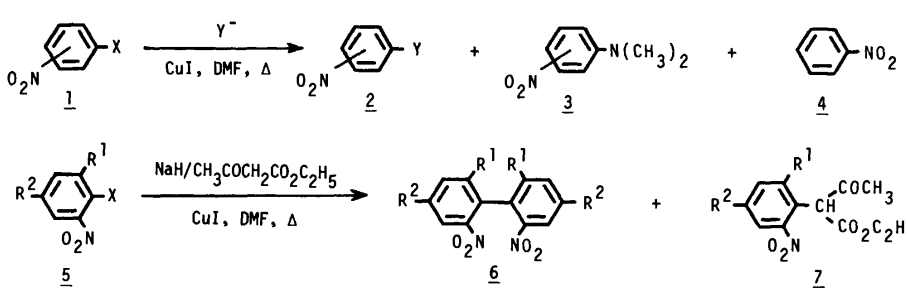

TABLE 1. 2,2′-DINITROBIPHENYLS **6** FROM THE COPPER(I) MEDIATED REACTION OF *o*-HALOGENONITROBENZENES **5** WITH 3-OXOBUTANOATE ANION

	Starting halide **5**			Reaction time	Temperature	Dinitrobiphenyl **6**[a]	
	R^1	R^2	X	*t*/h	θ_m/°C	Mp θ_m/°C	Yield/%
a[18]	H	H	I	4	100	123—124[13]	75
b[18]	H	H	Br	6	140	123—124	55
c[19]	CH_3	H	I	5	100	108[25]	55
d[20]	H	CH_3	I	5	100	140[26]	65
e[21]	H	CH_3	Br	7	140	140	40
f[22]	H	CH_3O	I	4	100	131[b]	70
g[22]	H	CH_3O	Br	7	140	131[27]	52
h[24]	CO_2H	H	I	5	120	263—266[28]	74

a) Melting points were uncorrected. Yields refer to the isolated compounds. b) Found: C, 55.53; H, 3.85; N, 9.09%. Calcd for $C_{14}H_{12}N_2O_6$: C, 55.27; H, 3.98; N, 9.21%.

Table 2. Influence of enolate nucleophiles on the yield of 2,2'-dinitrobiphenyl **6a**[a]

Enolate nucleophile	Reaction time t/h	Temperature θ_m/°C	Product yield/%
Ethyl 3-oxobutanoate	4	100	75
2,4-Pentadione	3	80	71
1-Phenyl-1,3-butadione	3	60	83
Diethyl 3-oxopentadioate	3	70	74
Ethyl 3-phenyl-3-oxopropanoate	3	60	78
Diethyl malonate	5	110	50
Acetone	6	80	10
Ethyl 2-cyanoethanoate	6	80	—

a) Reaction conditions: Substrate **5a** 1.0 mmol, NaH 1.0 mmol, enolate 0.5 mmol, CuI 1 mmol, and DMF 10 mmol. Yields refer to the isolated ones.

Table 3. Influence of the amounts of enolate and catalyst, and temperature on the yield of 2,2'-dinitrobiphenyl **6a**[a]

3-Oxobutanoate enolate/mmol	CuI/mmol	Temperature θ_m/°C	Product yield/%
0	1.0	100	~5
0.1			55
0.3			67
0.5			75
1.0			73
2.0			75
0.5	0	100	0
	0.15		54
	0.3		60
	0.5		65
	1.0		75
	2.0		74
0.5	1.0	140—150	60
		120	70
		100	75
		80	63
		30	—

a) Reaction conditions: Substrate **5a** 1.0 mmol, NaH 1.0 mmol, and DMF 10 mmol; reaction time 5—6 h. Yields refer to the isolated ones.

changed to orange color, and later to brown when *o*-iodonitrobenzene (0.249 g, 1 mmol) was added. The mixture was heated gradually to 100 °C and the progress of reaction was monitored by TLC. After 4 h the mixture was allowed to cool, poured into water (10 ml), and acidified to pH 5—6, and extracted twice with ether (2×15 ml). The combined extracts were washed with water, dried, and evaporated to yield crude 2,2'-dinitrobiphenyl (**6a**) as a pasty solid. It was purified by column chromatography over silica gel, followed by recrystallization from benzene/hexane to give yellow crystals of the product. Yield, 0.09 g (75%). Mp 123—124 °C (lit,[13] mp 123.5—124.5 °C).

Reaction of p-*Iodonitrobenzene.* The reaction was carried out at 140 °C using the same ratio of substrate, nucleophile, catalyst and solvent, as described above. After 4 h, when the reaction was over, the mixture was worked up as usual. The oily product obtained after removal of solvent consisted of three components as revealed by TLC. They were separated by column chromatography over silica gel to give nitrobenzene (0.037 g, 30%); 4,4'-dinitrobiphenyl (0.005 g, 4%), white solid melting at 238 °C (lit,[14] 237 °C); and ethyl 2-(4-nitrophenyl)-3-oxobutanoate[15] (0.10 g, 40%), yellow oil.

Reaction of 2, 4-Dinitrochlorobenzene. The reaction was carried out by stirring a mixture of halide (0.20 g, 1 mmol), sodium hydride (0.04 g, 1 mmol), keto ester (0.13 g, 1 mmol), copper(I) iodide (0.19 g, 1 mmol), and DMF (0.73 g, 10 mmol) at 60 °C for 3 h, and the reaction mixture was worked up as usual. The crude product obtained was further purified by column chromatography over silica gel to give ethyl 2-(2,4-dinitrophenyl)-3-oxobutanoate as pale yellow crystals. Yield, 0.266 g (90%). Mp 93—94 °C (lit,[16] mp 93—94 °C).

References

1) H. Suzuki, H. Abe, and A. Osuka, *Chem. Lett.*, **1980**, 1365.
2) H. Suzuki, H. Abe, N. Ohmasa, and A. Osuka, *Nippon Kagaku Kaishi*, **1980**, 445.
3) H. Suzuki, H. Abe, and A. Osuka, *Chem. Lett.*, **1981**, 151.
4) H. Suzuki, H. Abe, N. Ohmasa, and A. Osuka, *Chem. Lett.*, **1981**, 1115.
5) H. Suzuki and M. Shinoda, *Synthesis*, **1977**, 640.
6) H. Suzuki, K. Miyoshi, and M. Shinoda, *Bull. Chem. Soc. Jpn.*, **53**, 1765 (1980).
7) A. Osuka, N. Ohmasa, Y. Yoshida, and H. Suzuki, *Synthesis*, **1983**, 69.
8) A. Osuka, Y. Mori, and H. Suzuki, *Chem. Lett.*, **1982**, 2031.
9) H. Suzuki, T. Kobayashi, Y. Yoshida, and A. Osuka, *Chem. Lett.*, **1983**, 193.
10) A. Osuka, T. Kobayashi, and H. Suzuki, *Synthesis*, **1983**, 67.
11) H. Suzuki, S. V. Thiruvikraman, and A. Osuka, *Synthesis*, **1984**, 616.
12) R. A. Rossi and R. H. de Rossi, "Aromatic Substitution by the $S_{RN}1$ Mechanism," ACS Monograph 178 (1983).
13) R. C. Fuson and E. A. Cleveland, *Org. Synth.*, Coll. Vol. **III**, 339 (1965).
14) F. Ullmann and K. Fernaro, *Chem. Ber.*, **34**, 2177 (1901).
15) Z. Bankowska, D. Stopa, and I. Zadrozna, *Pol. J. Chem.*, **53**, 1563 (1979).
16) G. E. Hall, D. Hughes, D. Roe, and A. P. Rhodes, *Tetrahedron Lett.*, **1967**, 241.
17) M. A. F. Holleman, *Recl. Trav. Chim. Pays-Bas*, **32**, 136 (1913).
18) M. Schopft, *Chem. Ber.*, **23**, 1840 (1890).
19) M. T. Bogert and R. W. Allen, *J. Am. Chem. Soc.*, **49**, 1318 (1927).
20) St. von Niementowski, *Chem. Ber.*, **34**, 3325 (1901).
21) C. S. Gibson and J. D. A. Johnson, *J. Chem. Soc.*, **1929**, 1229.
22) H. Hahle, *J. Prakt. Chem.*, **43**, 62 (1891).
23) R. V. Henley and E. E. Turner, *J. Chem. Soc.*, **1930**, 928.
24) P. J. Culhane, *Org. Synth.*, Coll. Vol. 1, 125 (1967).
25) F. Ullmann and L. Frentzel, *Chem. Ber.*, **38**, 725 (1905).
26) F. Ullmann and W. R. Forgan, *Chem. Ber.*, **34**, 3802 (1901); R. B. Carlin and G. E. Flotz, *J. Am. Chem. Soc.*, **78**, 1997 (1956).
27) J. Gerald, Ger. Offen., 2939259 (1980); *Chem. Abstr.*, **94**, 22884j (1981).
28) R. Kuhn and O. Albrecht, *Justus Liebigs Ann. Chem.*, **455**, 272 (1927).

Utilization of "2-Pyrrolidone Hydrotribromide" in the Synthesis of Flavones

Noboru TAKENO, Tohoru FUKUSHIMA, Shin-ichi TAKEDA,* and Kazuyasu KISHIMOTO†
Department of Industrial Chemistry, Muroran Institute of Technology, Muroran, Hokkaido 050
(Received October 13, 1984)

Synopsis. The reaction of flavanone with "2-pyrrolidone hydrotribromide" in tetrahydrofuran gave 3-bromoflavanone in a good yield. On the other hand, flavone was obtained in 97% yield when this reaction was carried out in dimethyl sulfoxide at 80 °C. Under the same conditions, most flavones were obtained from the corresponding flavanones in high purity and good yields.

The most commonly used methods for the synthesis of flavones are the acid-catalyzed cyclodehydration of 1-(*o*-hydroxyphenyl)-1,3-diketone derivatives[1] and the dehydrogenation of flavanones by selenium dioxide,[2] phosphorus pentachloride,[3] and 2,3-dichloro-5,6-dicyano-1,4-benzoquinone.[4] Flavanones also can be converted into the corresponding flavones by bromination at the C_3 position, followed by the base-catalyzed dehydrobromination.[5]

We now report that flavones can be easily obtained from the corresponding flavanones and "2-pyrrolidone hydrotribromide" (2-pyrrolidone-hydrogen bromide–bromine complex $(C_4H_7NO)_3 \cdot HBr \cdot Br_2$,[6] abbreviated to PHT) by a one-pot procedure.

The results obtained are summarized in Table 1. The reaction was followed by TLC and the reaction time was determined by the disappearance of the flavanones. The reaction of flavanone(**1**) with PHT in tetrahydrofuran(THF) gave 3-bromoflavanone(**2**) in excellent yield, although the product was a mixture of *cis*- and *trans*-isomers: The ratio of the former to the latter was determined on the basis of the ^1H NMR spectrum,[7] since the isomers cannot be separated. The ratio of the *cis*-isomer to the *trans*-isomer strongly depends on the reaction temperature used. An attempt to prepare flavone(**3**) by the above method was unsuccessful, although **2** was obtained in a good yield.

The reaction of **1** with PHT in dimethyl sulfoxide (DMSO) at room temperature gave a mixture of **2** and **3**: the ratio of the former to the latter was also determined on the basis of ^1H NMR spectrum, as shown in Table 1. On the other hand, when the reaction was caried out at 80 °C, **1** gave exclusively **3**, which was easily isolated from the reaction mixture (97%). Similarly, the other flavones were also obtained by this procedure in excellent yields except for 4′-methoxyflavanone(**4**) and 4′,7-dimethoxyflavanone(**5**) (see below). The key for direct formation of flavones from the corresponding flavanones involves the use of DMSO as a solvent. Since DMSO is an effective dehydrobromination agent,[8] the results indicates that the conversion of flavanones to the corresponding flavones proceed *via* 3-bromoflavanones. **4** and **5** gave the corresponding flavones in somewhat decreased yields, for it gave the corresponding 3-bromoflavones as by-product. The decreased yields of flavones may be due to the presence of an electron-releasing methoxyl group at the *p*-position in the phenyl group. In this case, it

TABLE 1. THE REACTIONS OF FLAVANONES WITH "2-PYRROLIDONE HYDROTRIBROMIDE"

Entry	Starting material	Reaction conditions			Product(s)	Yield/%
		Solvent	Temp/°C	Time/h		
1	Flavanone	THF	Room	10.0	3-Bromoflavanone (*cis*:*trans*=4:6)[a]	98
2	Flavanone	THF	Reflux	1.5	3-Bromoflavanone (*cis*:*trans*=6:4)[a]	91
3	Flavanone	DMSO	Room	20.0	3-Bromoflavanone (*cis*:*trans*=1:9)[a]	34
					Flavone	60
4	Flavanone	DMSO	80	2.0	Flavone	97
5	7-Methoxyflavanone	DMSO	80	2.5	7-Methoxyflavone	98
6	3′-Methoxyflavanone	DMSO	80	2.0	3′-Methoxyflavone	98
7	3′,7-Dimethoxyflavanone	DMSO	80	2.5	3′,7-Dimethoxyflavone	97
8	4′-Methoxyflavanone	DMSO	80	2.0	4′,-Methoxyflavone	72
					3-Bromo-4′-methoxyflavone	25
9	4′,7-Dimethoxyflavanone	DMSO	80	2.5	4′,7-Dimethoxyflavone	67
					3-Bromo-4′,7-dimethoxyflavone	21

a) The ratio of *cis*-isomer to *trans*-isomer was determined on the basis of ^1H NMR spectrum.

† Present adress: Tomakomai Clinical Laboratory Co. Ltd., Hiyoshi, Tomakomai, Hokkaido 053.

is natural to suppose that 2,3-dibromoflavanones, obtained by the addition of Br_2 to the previously produced flavones, underwent dehydrobromination by DMSO to give the corresponding 3-bromoflavones.

In conclusion, most flavones were easily obtained from the corresponding flavanones and PHT in high purity and good yields.

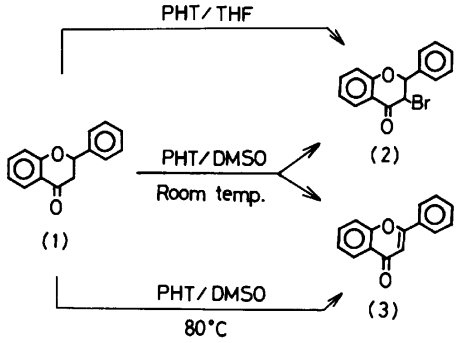

Exprimental

^1H NMR spectra were obtained on a Hitachi R-22 with tetramethylsilane as internal reference. Mass spectra were measured with a JMS-D300 double-focusing mass spectrometer.

Materials. Flavanones were prepared according to a reported procedure.[9] Flavanones except for the new materials were identified by comparison with reported data.[10] *3'-Methoxyflavanone*: mp 76—77 °C. ^1H NMR (CCl_4) δ=2.62—3.10 (2H, m, C_3-H_{ax}, H_{eq}), 3.77 (3H, s, 3'-OCH_3), 5.34 (1H, dd, $J_{ax,ax}$=12.5 Hz, $J_{ax,eq}$=5.5 Hz, C_2-H_{ax}), 6.72—7.49 (7H, m, Aromatic), 7.86 (1H, dd, J_{ortho}=6.5 Hz, J_{meta}=1.5 Hz, C_5-H). Found: C, 75.78; H, 5.56. Calcd for $C_{16}H_{14}O_3$: C, 75.57; H, 5.55. *3',7-Dimethoxyflavanone*: mp 101—102 °C. ^1H NMR ($CDCl_3$) δ=2.66—3.20 (2H, m, C_3-H), 3.83 (6H, s, 2×OCH_3), 5.43 (1H, dd, $J_{ax,ax}$=11 Hz, $J_{ax,eq}$=4 Hz, C_2-H), 6.49—7.42 (6H, m, Aromatic), 7.86 (1H, d, J_{ortho}=8 Hz, C_5-H). MS, Found: M^+=284. Calcd for $C_{17}H_{16}O_4$: M=284. *4'-Methoxyflavanone*: mp 87—88 °C [lit,[11] 96—97]. Though its melting point is different from the value in literature, we identified this material with 4'-methoxyflavanone from the following data. ^1H NMR (CCl_4) δ=2.58—3.13 (2H, m, C_3-H_{ax}, H_{eq}), 3.78 (3H, s, 4'-OCH_3), 5.33 (1H, dd, $J_{ax,ax}$=12 Hz, $J_{ax,eq}$=4.5 Hz, C_2-H_{ax}), 6.78—7.50 (7H, m, Aromatic), 7.83 (1H, dd, J_{ortho}=9 Hz, J_{meta}=2 Hz, C_5-H). Found: C, 75.60; H, 5.49. Calcd for $C_{16}H_{14}O_3$: C, 75.57; H, 5.55.

Reaction Procedure. To a solution of flavanone (4.46 mmol) in the solvent (50 ml) was added a solution of PHT (4.84 mmol) in the solvent (50 ml). The mixture was stirred for a suitable time and temperature as indicated in Table 1. The reaction was followed by TLC (silica gel: benzene as sovent). Water was added to the cooled reaction mixture. The mixture was extracted with benzene and the organic extract was washed with brine, dried and evaporated.

Products of Reaction in THF. The residue was recrystallized from EtOH-H_2O: mp 85—105 °C. The product was a mixture of *cis*- and *trans*-3-bromoflavanone, indicated by integration of the ^1H NMR spectrum (see Table 1). ^1H NMR ($CDCl_3$) δ (ppm); *cis*-form: 4.54 (1H, d, J=2 Hz, β-H) [lit,[7] 4.53], 5.42 (1H, d, J=2 Hz, α-H) [lit,[7] 5.38], *trans*-form; 4.98(1H, d, J=8 Hz, β-H) [lit,[7] 4.98], 5.56 (1H, d, J=8 Hz, α-H) [lit,[7] 5.53].

Products of Reaction in DMSO. The product of reaction at room temperature was a mixture of 3-bromoflavanone and flavone as indicated by integration of ^1H NMR spectrum (see Table 1). Flavone: ^1H NMR ($CDCl_3$), δ=6.82 (1H, s, C_3-H), 7.31—7.99 (8H, m, Aromatic), 8.24 (1H, dd, J_{ortho}=8 Hz, J_{meta}=2 Hz, C_5-H). The residue of reaction at 80 °C was purified by silica-gel column chromatography (dichloromethane-diethyl ether, 5:1). Flavones and 3-bromo-4'-methoxyflavone, except for the new product, were identified by comparison with the reported data.[12] Satisfactory analysis was obtained for the new product, 3-bromo-4',7-dimethoxyflavone: mp 150—151 °C; ^1H NMR ($CDCl_3$) δ=3.91 (6H, s, 2×OCH_3), 6.85—7.90 (6H, m, Aromatic), 8.14 (1H, d, J_{ortho}=8 Hz, C_5-H); MS, Found: M^+=360, 362. Calcd for $C_{17}H_{13}O_4Br$: M=360, 362.

The authors wish to thank Dr. Tadashi Yoshida of Government Industrial Development Laboratory, Hokkaido, for his assistances in obtaining the mass spectra.

References

1) V. V. Virkor and T. S. Wheeler, *J. Chem. Soc.*, **1939**, 1681.
2) S. Matsuura and T. Kunii, *Yakugaku Zasshi*, **94**, 645 (1974).
3) F. Cramer and G. H. Elshnig, *Chem. Ber.*, **89**, 1 (1956).
4) S. Matsuura, M. Iinuma, and K. Ishikawa, *Chem. Pharm. Bull.*, **26**, 305 (1978).
5) K. Nakazawa and S. Matsuura, *Yakugaku Zasshi*, **75**, 467 (1955).
6) D. V. C. Awang and S. Wolfe, *Can. J. Chem*, **47**, 706 (1969).
7) S. K. David, L. Main, and K. B. Old, *J. Chem. Soc., Perkin Trans. 2*, **1981**, 1367.
8) J. Grimshaw, J. T. Grimshar, and H. R. Juneja, *J. Chem. Soc., Perkin Trans. 1*, **1972**, 50.
9) T. A. Geissman and R. O. Clinton, *J. Am. Chem. Soc.*, **68**, 697 (1946).
10) A. Lowenbin, *Chem. Ber.*, **57**, 1515 (1924); S. v. Kostanecki and M. L. Stoppani, *Chem. Ber.*, **37**, 1180 (1904); K. Juppen and S. v. Kostanecki, *ibid.*, **37**, 4161 (1904).
11) T. Koyamada, *Nippon Kagaku Kaishi*, **64**, 864 (1943).
12) T. S. Wheeler, *Org. Synth.*, **32**, 72 (1952); N. Narasimachari and T. R. Seshadri, *Proc. Ind. Acad. Sci., A*, **30**, 151 (1949); Y. Hoshino, S. Takeda, H. Hamada, and N. Takeno, *Nippon Kagaku Kaishi*, **1982**, 1564; B. L. Shaw and T. H. Simpson, *J. Chem. Soc.*, **1952**, 5027; K. v. Auwers and L. Aushutz, *Chem. Ber.*, **54**, 1543 (1921); H. K. Pendse and S. D. Limaye, *Rasayanam*, **2**, 107 (1956); J. Tambor, *Chem. Ber.*, **49**, 1704 (1916).

Stereoselectivity in the Reduction of Cyclic Ketones with Sodium Borohydride. Effect of the Ratio of the Components of a Mixed Solvent of Tetrahydrofuran and Methanol

Kenso Soai* and Kazumi Ohi
Department of Applied Chemistry, Faculty of Science, Science University of Tokyo, Kagurazaka, Shinjuku-ku, Tokyo, 162
(Received November 19, 1984)

Synopsis. Reduction of relatively conformationally rigid cyclic ketones with sodium borohydride was examined in a mixed solvent of tetrahydrofuran(THF) and methanol(MeOH) with varying the ratio of the components. The highest stereoselectivities of the reductions were observed in the *mixed solvent*, and not in each *individual solvent*.

Sodium borohydride($NaBH_4$, **1**) has been used widely,[1] and its chemoselectivity is affected by the solvent.[2] Several reports have appeared on the stereoselectivity of the reduction of cyclic ketones with **1**.[3] However, nearly all the reductions have been carried out in a *single solvent*. To the best of our knowledge, the effect of *mixed solvents* on the stereoselectivity of **1** has not been closely examined.[4]

During our continuing study on asymmetric synthesis,[5] we reported that diastereoselectivity is higher in the reduction with **1** of chiral α-keto-amides in a mixed solvent of THF and MeOH than in either individual solvent.[6]

In the present paper, we describe the reduction of relatively conformationally rigid cyclic ketones with **1** in a mixed solvent of THF and MeOH. Cyclic ketones (**2**—**4**) were reduced with **1** at 0 °C in the mixed solvent of THF and MeOH with varying ratio of the components. Stereoselectivities were determined by GLC analyses of the isomeric alcohols formed. Predominant isomers from the reductions of 2-methylcyclohexanone(**2**), 4-*t*-butylcyclohexanone(**3**), and camphor(**4**) were *trans*-2-methylcyclohexanol (**5a**), *trans*-4-*t*-butylcyclohexanol(**6a**), and isoborneol (**7a**) respectively (Eq. 1—3. Only one enantiomer is shown in Eqs. 1 and 3. The actual products were racemic mixtures).

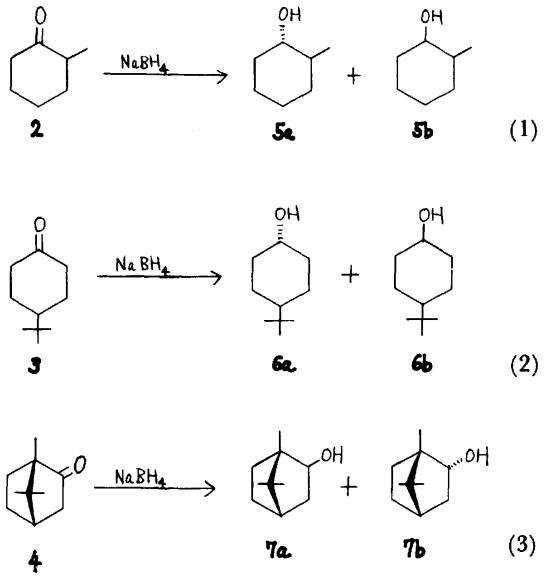

As shown in Figs. 1—3, in each case, stereoselectivities {shown as diastereomeric excesses (% d.e.)} of the product alcohols depended upon the volumetric ratio of THF and MeOH. The highest stereoselectivities in the reduction of cyclic ketones (**2**—**4**) were observed *in mixed solvent of THF and MeOH, and not in each individual solvent.* Diastereomeric excesses in the above mixed solvent of the appropriate ratio of components were higher than in the single solvent

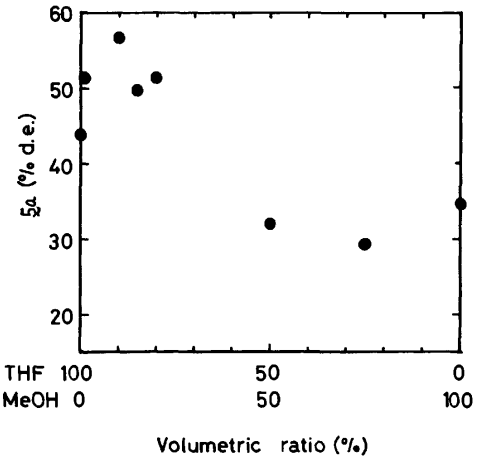

Fig. 1. Relation between Stereoselectivity of the Reduction of **2** and the Ratio of the Components of Mixed Solvent.

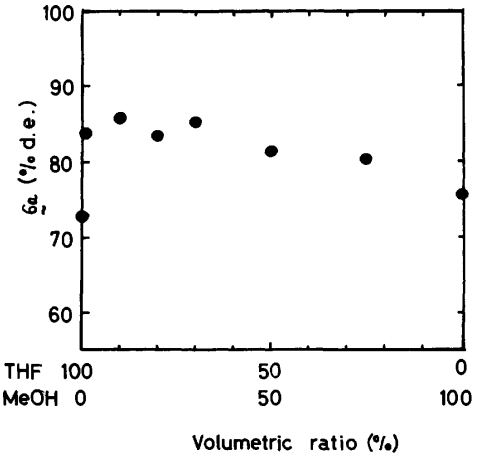

Fig. 2. Relation between Stereoselectivity of the Reduction of **3** and the Ratio of the Components of Mixed Solvent.

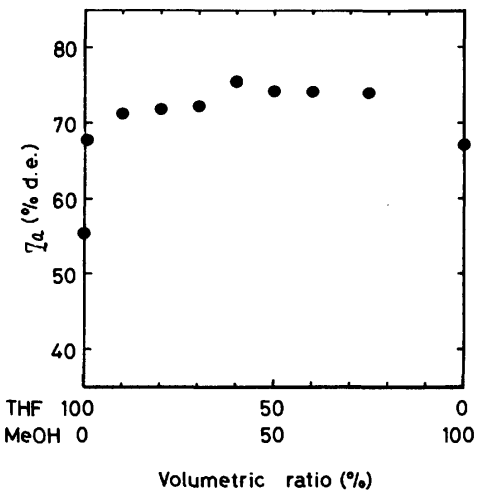

Fig. 3. Relation between Stereoselectivity of the Reduction of **4** and the Ratio of the Components of Mixed Solvent.

2-propanol. In the present mixed solvent of THF-MeOH, diastereomeric excesses of **5a**, **6a**, and **7a** reached 57, 86, and 75% d. e. respectively. On the other hand, reductions of **2**, **3**, and **4** with **1** in 2-propanol give **5a**, **6a**, and **7a** of 38, 66, and 72% d. e. respectively.[7,8] Therefore this mixed solvent may achieve higher stereoselectivities in the reduction of complicated cyclic ketones. Ketones **3** and **4** are conformationally rigid regardless of the ratio of the components of the mixed solvent.[9] Therefore the higher stereoselectivities in mixed solvent may be attributed, at least partly, to other than the ketones themselves, *i.e.* nature of the reducing species or mechanism of the reduction.

As described, mixed solvent of THF–MeOH is an influential factor on the stereoselective reduction of cyclic ketones with **1**.

Experimental

General Procedure for the Reduction of Ketones. Mixed solvent (1ml, THF–MeOH) was added to 1mmol of **1** with cooling in ice-bath, and was stirred for 5min. Ketone (1mmol) in 3ml of the above mixed solvent was added over a period of 15min. The mixture was stirred for 7—10h (ketones except camphor disappeared by TLC analysis). For the reduction of camphor, 3 molar amounts of **1** was used (reaction time 10 h). 1MHCl (1 M=1 mol dm^{-3}) was added to quench the reaction. Aqueous layers were extracted with ether and chloroform. The extracts were condensed, and were subjected to GLC analyses. In GLC analyses, all the products were identical with authentic samples purchased. GLC [poly(ethylene glycol)(PEG)-20 M or silicone SE-30, 25 m capillary column, flame ionization detector]. Column temp for 2-methylcyclohexanol; 65 °C, retention time, *cis*-**5b**; 21.1 min., *trans*-**5a**; 23.6 min., 4-*t*-butylcyclohexanol; 120 °C, *cis*-**6b**; 8.0 min., *trans*-**6a**; 9.2 min., isoborneol(**7a**); 5.9 min., borneol(**7b**); 6.1 min. 120 °C.

References

1) For a review, E. R. H. Walker, *Chem. Soc. Rev.*, **5**, 23 (1976).

2) K. Soai, H. Oyamada, and A. Ookawa, *Synth. Commun.*, **12**, 463 (1982); K. Soai, H. Oyamada, M. Takase, and A. Ookawa, *Bull. Chem. Soc. Jpn.*, **57**, 1948 (1984); K. Soai, H. Oyamada, and M. Takase, *ibid.*, **57**, 2327 (1984); K. Soai and H. Oyamada, *Synthesis*, **1984**, 605; K. Soai, H. Oyamada, and M. Takase, "Peptide Chemistry 1983," ed by E. Munekata, Protein Research Foundation, Osaka (1984), pp. 85—88; K. Soai, A. Ookawa, H. Oyamada, and M. Takase, *Heterocycles*, **19**, 1371 (1982).

3) For a review, D. C. Wigfield, *Tetrahedron*, **35**, 449 (1979).

4) H. Haubenstock and E. L. Eliel, *J. Am. Chem. Soc.*, **84**, 2368 (1962).

5) K. Soai, T. Yamanoi, and H. Oyamada, *Chem. Lett.*, **1984**, 251; K. Soai, H. Oyamada, and T. Yamanoi, *J. Chem. Soc., Chem. Commun.*, **1984**, 413; K. Soai, A. Ookawa, and Y. Nohara, *Synth. Commun.*, **13**, 27 (1983).

6) K. Soai, K. Komiya, Y. Shigematsu, H. Hasegawa, and A. Ookawa, *J. Chem. Soc., Chem. Commun.*, **1982**, 1282; K. Soai and H. Hasegawa, *J. Chem. Soc., Perkin Trans. 1*, **1985**, 769.

7) H. C. Brown and J. Muzzio, *J. Am. Chem. Soc.*, **88**, 2811 (1966).

8) E. L. Eliel and Y. Senda, *Tetrahedron*, **26**, 2411 (1970).

9) E. L. Eliel, "Stereochemistry of Carbon Compounds," McGraw-Hill, New York (1962), Chap. 8.

Synthesis of Dicyclopropylideneethane and Its Reaction with Some Dienophiles

Takashi Tsuji,* Ryo Kikuchi, and Shinya Nishida
Department of Chemistry, Faculty of Science, Hokkaido University, Sapporo 060
(Received November 22, 1984)

Synopsis. Preparation of dicyclopropylideneethane in three steps from 3-dimethylaminosulfolane and its reaction with some dienophiles are reported.

Dicyclopropylideneethane, **1**, a conjugated diene constituted of two highly strained, reactive methylenecyclopropanes, is of considerable interest in its physical as well as chemical properties. In particular, [4+2] cycloaddition products of **1** with acetylenic dienophiles, namely dispiro[2.2.2.2]deca-4,9-diene derivatives, **2**, will serve as the valuable substrate to synthesize variously-substituted [8]-paracycloph-4-enes and [4.2]paracyclophanes, as demonstrated previously in our laboratory.[1]

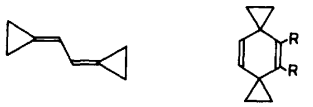

1 **2**

In 1972, Heinrich and Lüttke[2] have reported the formation of **1** as a minor component in the reaction of biallenyl with diazomethane. Since this approach will hold no preparative potential, it is desirable to explore proper synthetic routes for **1**. Paquette *et al.* have recently reported the synthesis of **1** from 1-trimethylsilylcyclopropanecarbaldehyde in several steps.[3] We independently prepared **1** from readily accessible 3-dimethylaminosulfolane[4] in three steps. By our hands, **1** reacted smoothly with some representative dienophiles and the yields of the adducts were substantially better than those reported by Paquette *et al.*[3]

Results and Discussion

3-Dimethylaminosulfolane, **3**, was dicyclopropanated in one pot. Thus, the successive treatment of **3** in the presence of 2 equiv of oxirane with 2 equiv of *n*-BuLi, 2 equiv of benzenesulfonyl chloride, and 2 equiv of lithium diisopropylamide (LDA) afforded **4** in 40% yield. Oxidation of the amine, **4**, with 30% H_2O_2 followed by the thermal decomposition of the resulting *N*-oxide gave **5** in 80% yield.[5] Reduction of **5** with $LiAlH_4$ in refluxing THF afforded **1**[6] (50% yield by GLC; 28% yield by the isolation). The dicyclopropanated sulfolene, **5**, was thermally fairly stable and the attempted thermolysis (up to 250°C) failed to give appreciable amount of **1**.[7] Dicyclopropylideneethane, **1**, could be isolated as colorless crystals by preparative GLC, though **1** was liable to polymerize readily at room temperature.

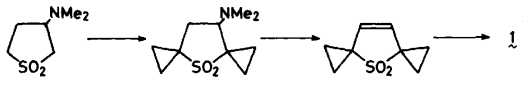

3 **4** **5**

1,1,4,4-Tetrasubstituted butadienes are generally reluctant to undergo [4+2] cycloaddition because of the difficulty to attain *s-cis* conformation requisite for the reaction.[8] The diene, **1**, however, proved to be a fairly reactive one. Relief of the strain appears to contribute to the enhanced reactivity of **1**. The reaction of **1** with 4-phenyl-3*H*-1,2,4-triazole-3,5(4*H*)-dione (PTAD) was instantaneous at room temperature in benzene and the adduct, **6**, was obtained in 90% yield. The reaction with dimethyl acetylenedicarboxylate (DMAD) was much slower and required heating of a mixture of **1** and DMAD for 2 h at 80°C. Chromatographic purification of the product afforded **7** as colorless crystals in 35% yield. The addition of tetracyanoethylene (TCNE) to **1** smoothly proceeded at room temperature in dichloromethane. Chromatographic separation of the product mixture afforded **8** in 43% yield together with a 25% yield of **9**. It has recently been shown that some [2+2] adducts of TCNE to 1,3-butadienes relatively readily rearrange to the corresponding cyclohexene derivatives.[9] The latter product, **9**, however, showed no tendency to isomerize to **8** under the reaction conditions.

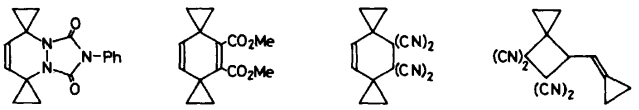

6 **7** **8** **9**

Therefore, the observed product distribution is a kinetically controlled result. The formation of [2+2] adduct, **9**, is at variance with the result of Paquette *et al.*, who carried out the reaction in carbon tetrachloride and isolated **8** in 27% yield, but none of **9**.[3] [2+2] Cycloaddition of TCNE to unsaturated compounds is generally accepted as a two-step process by way of zwitterion[9,10] and hence accelerated in polar solvents. The observed difference in the product compositions may be accounted for at least partly by the solvent polarity effect.

The preparation of **1** described above is simple and the reaction of **1** with dienophiles provides a convenient route to variously-substituted dispiro-[2.2.2.2]decene and -decadiene derivatives. The present methodology may also be extended to the preparation of related tetrasubstituted butadienes.

Experimental

Melting points are uncorrected. NMR spectra were

obtained at 100 MHz. Mass spectra were recorded at an ionizing voltage of 70 eV; ions of each spectrum were normalized to the spectrum's most intense ion set equal to 100.

Dicyclopropanation of 3. A solution of 3-dimethylaminosulfolane[4] (2.0 g, 12 mmol) and oxirane (1.5 ml, *ca.* 30 mmol) in 30 ml of THF was treated with 10 ml of 2.5 mol dm^{-3} hexane solution of *n*-BuLi (25 mmol) at 0—−10°C. After 20 min, a solution of benzenesulfonyl chloride (4.4 g, 24 mmol) in 10 ml of THF was added at −20—−30°C. The resulting mixture was stirred for 20 min at the above temperature, then treated with 25 mmol of LDA in 30 ml of THF below −40°C, and slowly warmed up to room temperature. After removal of solvent *in vacuo*, 9 ml of water was added and the product was extracted with five 50 ml portions of ether. The extracts were combined, dried with $MgSO_4$, and concentrated. The residual oil was distilled *in vacuo* to give 1.1 g of **4** (40%), bp 115—125 °C/10^{-3} mmHg (1 mmHg = 133.3 Pa), which solidified on standing and when crystallized from hexane had mp 71—72°C. NMR($CDCl_3$): δ=0.8—1.1 (m, 3H), 1.2—1.6 (m, 5H), 1.94 (dd, J=7.5 and 13.5 Hz, 1H), 2.29 (s, 6H), 2.48 (dd, J=7.5 and 13.5 Hz, 1H), 3.44 (t, J=7.5 Hz, 1H). IR (KBr): 1290, 1150, 1110, 1060, 1045, 1040, 690 cm^{-1}. MS *m/z*: 215 (M^+, 4), 136 (19), 110 (23), 96 (100), 82 (33), 71 (28), 44 (28), 42 (26). Found: C, 55.70; H, 7.99; N, 6.47; S, 14.95%. Calcd for $C_{10}H_{17}O_2NS$: C, 55.78; H, 7.96; N, 6.61 S, 14.89%.

Preparaion of 5. To a solution of 4 (4.35 g, 20.2 mmol) in 2.6 ml of methanol was added 2.2 ml of 30% aq H_2O_2. After 2 d at room temperature, a small amount of platinum black was added to destroy excess H_2O_2 and the mixture was stirred until evolution of gas had almost ceased. After removal of the catalyst, the solution was concentrated *in vacuo* and the residual oil was heated at 110°C/0.1 mmHg. Pungent gas evolution which ceased after 5 min was observed. The product sublimed and crystallized on the upper cold glass wall of the apparatus. The crude product was collected and sublimated at 110—120°C/14 mmHg giving 2.77 g of **5** (80%). Crystallization from methanol gave **5** melting at 123.5—124.5°C. NMR ($CDCl_3$): δ=1.1—1.8 (AA'XX' m, 8H), 5.67 (s, 2H). IR (KBr): 1290, 1135, 955, 730 cm^{-1}. UV(EtOH) max: 206.5 nm (ε, 10,600). Found: C, 56.45; H, 5.88; S, 18.93%. Calcd for $C_8H_{10}O_2S$: C, 56.45; H, 5.92; S, 18.83%.

Reductive Elimination of SO_2 from 5. To a suspension of 150 mg of $LiAlH_4$ (3.9 mmol) in 15 ml of THF was added 150 mg of **5** (0.88 mmol) and the mixture was refluxed. After 2 h, the sulfone had been consumed. The reaction mixture was cooled in an ice bath and treated successively with 150 µl of water, 150 µl of 15% NaOH, and 450 µl of water.[11] The resulting suspension to which a small amount of hydroquinone was added was filtered and the precipitate was washed well with pentane. The solvent was removed through a 15 cm packed column and the residue was subjected to preparative GLC (Apiezone Grease L 20% on Celite 545, 4 mm×2 m, 100 °C) giving 26 mg of **1** (28%) as colorless crystals melting at 39.5—42 °C. The yield of **1** determined by GLC with internal standard was 50%. The physical property of **1** agreed with that reported.[2,3]

Reaction of 1 with PTAD. To a solution of **1** (32 mg, 0.30 mmol) in 0.5 ml of benzene was added 50 mg of PTAD (0.29 mmol) in 0.5 ml of benzene under argon. The reaction was almost instantaneous and colorless crystals soon precipitated giving 72 mg of **6** (90%). Crystallization from benzene–hexane (1:1) gave analytically pure **6** melting at 149.5—150 °C. NMR($CDCl_3$): δ=0.7—1.3 (m, 4H), 1.9—2.5 (m, 4H), 5.25 (s, 2H), 7.47 (s, 5H). IR(KBr): 1760, 1695, 1505, 1420, 1330, 1150 cm^{-1}. MS *m/z*: 281 (M^+, 100), 254 (32), 147 (51), 135 (48), 134 (66), 119 (49), 126 (32), 91 (89), 79 (35). UV(EtOH) max: 220 (ε, 19,000), 250 nm (1200). Found: C, 68.43; H, 5.37; N, 15.02%. Calcd for $C_{16}H_{15}O_2N_3$: C, 68.31; H, 5.38; N, 14.94%.

Reaction of 1 with DMAD. A solution of **1** (24 mg, 0.23 mmol) in 150 µl of DMAD was heated at 80 °C for 2 h and then subjected to chromatography on SiO_2 with benzene elution. The fraction containing the product (R_f=0.22) was concentrated and the residue was crystallized from hexane to give 20 mg of **7** (35%) melting at 92—93 °C (lit,[3] 92.5—93 °C). UV(EtOH) max: 290 nm (ε, 6000). The NMR, IR, and MS spectra of **7** agreed with those reported.[3] Found: C, 67.92; H, 6.57%. Calcd for $C_{14}H_{16}O_4$: C, 67.73; H, 6.50%.

Reaction of 1 with TCNE. A solution of 96 mg of **1** (0.87 mmol) and 145 mg of TCNE (1.13 mmol) in 30 ml of CH_2Cl_2 was stirred at room temperature for 4 d. Chromatography of the product mixture on SiO_2 with benzene elution afforded first 85 mg of **8** (43%, R_f=0.32), which showed a decomposition point of *ca.* 190 °C (lit,[3] 182 °C). Further elution with benzene produced 50 mg of **9** (25%, R_f=0.24) melting at 151.5—152.5 °C. The NMR and MS spectra of **8** agreed with those reported.[3] **8**: IR(KBr): 1640, 1440, 1410, 1270, 1035, 980, 955, 890, 760 cm^{-1}. Found: C, 71.70; H, 4.22; N, 23.89%. Calcd for $C_{14}H_{10}N_4$: C, 71.78; H, 4.30; N, 23.92%. **9**: ^{1}H-NMR($CDCl_3$): δ=0.8—1.7 (m, 8H), 4.32 (d, J=9 Hz, 1H), 5.9 (dm, J=9 Hz, 1H). ^{13}C-NMR($CDCl_3$): δ=2.7(t), 3.9(t), 9.5(t), 10.4(t), 33.1(s), 41.0(s), 42.3(s), 50.9(d), 108.3(d), 108.8(s), 109.1(s), 110.1(s), 137.8(s). IR(KBr): 2255, 1420, 1280, 1045, 1030, 965, 935, 855, 800 cm^{-1} MS *m/z*: 234 (M^+, 4), 233 (22), 206 (28), 91 (100), 78 (27), 51 (29), 39 (53). Found: C, 71.83; H, 4.34; N, 23.73%. Calcd for $C_{14}H_{10}N_4$: C, 71.78; H, 4.30; N, 23.92%.

References

1) T. Tsuji and S. Nishida, *Acc. Chem. Res.*, **17**, 56 (1984) and references cited therein.

2) F. Heinrich and W. Lüttke, *Angew. Chem., Int. Ed. Engl.*, **11**, 234 (1972).

3) L. A. Paquette, G. J. Wells, and G. Wickham, *J. Org. Chem.*, **49**, 3618 (1984).

4) G. Loev, *J. Org. Chem.*, **26**, 4394 (1961).

5) *Cf.* A. C. Cope and E. Ciganek, *Org. Synth.*, Coll. Vol. IV, 612 (1963).

6) Y. Gaoni, *Tetrahedron Lett.*, **1977**. 947.

7) E. Block,"Reactions of Organosulfur Compounds," Academic Press, New York (1978), p. 252.

8) C. A. Stewart, Jr., *J. Am. Chem. Soc.*, **84**, 117 (1962); P. D. Bartlett, *Q. Rev. Chem. Soc.*, **24**, 473 (1973).

9) F. Kataoka, N. Shimizu, and S. Nishida, *J. Am. Chem. Soc.*, **102**, 711 (1980).

10) R. Huisgen, *Acc. Chem. Res.*, **10**, 117, 199 (1977).

11) L. F. Fieser and M. Fieser, "Reagents for Organic Synthesis," Wiley, New York (1967), Vol. 3, p 584.

The Reaction of Cyclopentanone with Carbon Disulfide and Glycine Esters

Naoaki FUKADA* and Kayoko YAMAMOTO
Department of Chemistry, Faculty of Science, Chiba University, Yayoicho, Chiba 260
(Received December 5, 1984)

Synopsis. 2-(Methoxy- and ethoxycarbonylmethylimino)cyclopentanecarbodithioic acids were synthesized from cyclopentanone, carbon disulfide, and glycine esters. In the presence of sulfur, glycine, alanine, and phenylalanine esters reacted to give the corresponding oxidatively coupled products of dithiocarboxylic acid.

In the previous paper,[1] we have reported a convenient, one-step synthesis of 2-(alkylimino)-cyclopentanecarbodithioic acids by reaction of cyclopentanone with carbon disulfide in an aqueous amine medium. Earlier reports described the preparation of 2-imino-[2,3] and 2-(alkylimino)cycloalkanecarbodithioic acids.[4-6]

In this note, we wish to report the reaction of cyclopentanone with carbon disulfide in an aqueous solution of glycine esters. While the reaction of alkylamine was carried out below 10 °C for 0.5—2 h,[1] the present reaction required 6—8 h at room temperature. Although the yields were inferior, 2-(methoxy- and ethoxycarbonylmethylimino)cyclopentanecarbodithioic acids **1a** and **1b** were obtained from the corresponding glycine methyl and ethyl esters, respectively. In the case of alanine or phenylalanine ethyl ester, the reaction proceeded to give a crude unstable product in lower yield. However, it was difficult to isolate the corresponding pure dithiocarboxylic acid. The oxidatively coupled products **2a—d** were also directly obtained by the above reaction involving addition of sulfur to the starting materials.

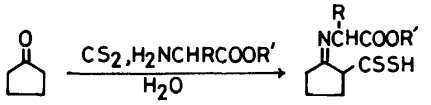

1

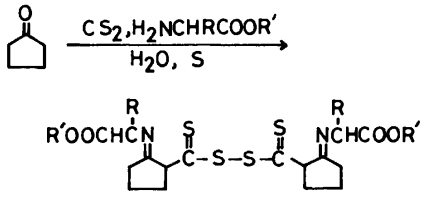

2

The UV spectra of **1** and **2** as shown in Table 1 were similar to those of 2-(alkylimino)cyclopentanecarbodithioic acids (λ_{max} 304—306 and 393—398 nm in ethanol) and their oxidative dimers (λ_{max} 312—315 and 407—416 nm in chloroform).[1] Both the dithiocarboxylic acids **1a** and **1b** were exceedingly sensitive to Ni(II) ion, giving a pink red precipitate.[2,7]

Experimental

2-(Methoxycarbonylmethylimino)cyclopentanecarbodithioic Acid (1a). To a cooled mixture of cyclopentanone (5.7 g, 0.068 mol) and carbon disulfide (7.3 g, 0.096 mol) were added a solution of glycine methyl ester hydrochloride (9 g, 0.072 mol) in water (15 ml) and then a solution of sodium hydroxide (3 g, 0.075 mol) in water (15 ml). The mixture was shaken under nitrogen at room temperature for 6 h and allowed to stand overnight. The oily product was collected and washed with a small amount of ethanol. The yellow solid was purified by reprecipitation with acetone— a 2M HCl aqueous (1M=1 mol dm^{-3}) solution, IR (KBr), 2435 s (SH) 1740 *vs.* (C=O), and 1595 *vs.* cm^{-1} (C=N). Found: C, 46.87; H, 5.75; N, 6.00; S, 27.25%. Calcd for $C_9H_{13}NO_2S_2$: C, 46.73; H, 5.66; N, 6.05; S, 27.72%.

2-(Ethoxycarbonylmethylimino)cyclopentanecarbodithioic Acid (1b): Reprecipitated with acetone— a 2M HCl aqueous solution. IR (KBr), 2435 s (SH), 1740 *vs.* (C=O), and 1600 *vs.* cm^{-1} (C=N). Found: C, 48.99; H, 6.07; N, 5.74; S, 25.48%. Calcd for $C_{10}H_{15}NO_2S_2$: C, 48.95; H, 6.16; N, 5.71; S, 26.14%.

The Oxidatively Coupled Products of Dithiocarboxylic Acid (2). General Procedure. To a cooled mixture of cyclopentanone (1.5 g, 0.018 mol), carbon disulfide (2 g, 0.026 mol), and sulfur (0.1 g, 0.0031 mol) were added a solution of amino acid (glycine, alanine, or phenylalanine) ester hydrochloride (0.018 mol) in water (5 ml) and then a solution of sodium hydroxide (0.75 g, 0.019 mol) in water (4 ml). The mixture was shaken at room temperature for

Table 1. Yield and UV spectra

Compd	R	R'	Yield %	Mp θ_m/°C	UV nm (log ε)
1a	H	CH_3	32	142—144	308 (3.89), 398 (4.34)[a]
1b	H	C_2H_5	29	113—114	307 (4.01), 397 (4.34)[a]
2a	H	CH_3	31	173—174 (decomp)	317 (4.02), 414 (4.68)[b]
2b	H	C_2H_5	45	163—164 (decomp)	318 (4.06), 415 (4.68)[b]
2c	CH_3	C_2H_5	43	133—134 (decomp)	316 (4.03), 412 (4.67)[b]
2d	$CH_2C_6H_5$	C_2H_5	13	140—141 (decomp)	317 (3.98), 416 (4.66)[b]

a) In EtOH. b) In $CHCl_3$.

7—11 h and kept for 2 days at 4—18 °C. The oily product was collected, washed with ethanol and then carbon disulfide, and recrystallized or reprecipitated.

*Bis[2-(methoxycarbonylmethylimino)cyclopentyl(thiocarbonyl)] Disulfide (**2a**)*: Recrystallized with aniline–ethanol. IR (KBr), 1743 *vs.* (C=O) and 1580 *vs.* cm^{-1} (C=N). Found: C, 47.00; H, 5.25; N, 6.06; S, 27.40%. Calcd for $C_{18}H_{24}N_2O_4S_4$: C, 46.93; H, 5.25; N, 6.08; S, 27.84%.

*Bis[2-(ethoxycarbonylmethylimino)cyclopentyl(thiocarbonyl)] Disulfide (**2b**)*: Recrystallized with ethanol. IR (KBr), 1740 *vs.* (C=O) and 1582 *vs.* cm^{-1} (C=N). Found: C, 48.99; H, 5.80; N, 5.48; S, 25.99%. Calcd for $C_{20}H_{28}N_2O_4S_4$: C, 49.15; H, 5.78; N, 5.73; S, 26.24%.

*Bis[2-[ethoxycarbonyl(methyl)methylimino]cyclopentyl(thiocarbonyl)] Disulfide (**2c**)*: Reprecipitated with chloroform–hexane. IR (KBr), 1739 *vs.* (C=O) and 1578 *vs.* cm^{-1} (C=N). Found: C, 51.10; H, 6.21; N, 5.30; S, 24.45%. Calcd for $C_{22}H_{32}N_2O_4S_4$: C, 51.13; H, 6.24; N, 5.42; S, 24.82%.

*Bis[2-[benzyl(ethoxycarbonyl)methylimino]cyclopentyl(thiocarbonyl)] Disulfide (**2d**)*: To the resulting reaction mixture was added a 2M HCl aqueous solution (15 ml) and the mixture was extracted with chloroform. After the solvent was evaporated, ether (15 ml) was added to the orange red oil and a small amount of light yellow solid was removed by filtration. From the filtrate yellow solid **2d** was obtained and reprecipitated with chloroform–hexane. IR (KBr), 1740 *vs.* (C=O) and 1580 *vs.* cm^{-1} (C=N). Found: C, 60.85; H, 6.02; N, 4.14; S, 18.96%. Calcd for $C_{34}H_{40}N_2O_4S_4$: C, 61.05; H, 6.03; N, 4.19; S, 19.17%.

The authors wish to thank Dr. Tatsuo Takeshima for his helpful suggestion and warm encouragement.

References

1) N. Fukada, K. Arai, and T. Takeshima, *Synthesis*, **1980**, 566.

2) T. Takeshima, M. Yokoyama, T. Imamoto, M. Akano, and H. Asaba, *J. Org. Chem.*, **34**, 730 (1969). For the improved preparative method, see: T. Takeshima, M. Muraoka, N. Fukada, A. Takayama, and T. Yamamoto, *J. Org. Chem.*, **42**, 3383 (1977).

3) T. Takeshima, A. Yano, N. Fukada, Y. Hirose, and M. Muraoka, *J. Chem. Res. (S)*, **1979**, 140; *J. Chem. Res. (M)*, **1979**, 1732.

4) R. Mayer and J. Jentzsch, *J. Prakt. Chem.*, **23**, 83 (1964).

5) B. Bordás, P. Sohár, G. Matolcsy, and P. Berencsi, *J. Org. Chem.*, **37**, 1727 (1972).

6) T. Takeshima, N. Fukada, T. Miyauchi, M. Muraoka, T. Yamamoto, and T. Hayashi, *J. Chem. Soc., Perkin Trans. 1*, **1974**, 914.

7) N. K. Dutt and T. Seshadri, *Anal. Chim. Acta*, **47**, 571 (1969); P. Thomas and A. Poveda, *Z. Chem.*, **11**, 153 (1971).

Transition-metal-catalyzed Grignard Reaction of Isoprene Bromohydrin

Shuki ARAKI, Masayuki OHMURA, and Yasuo BUTSUGAN*
Department of Synthetic Chemistry, Nagoya Institute of Technology, Gokiso-cho, Showa-ku, Nagoya 466
(Received December 10, 1984)

Synopsis. The coupling reaction of isoprene bromohydrin with aryl and alkyl Grignard reagents catalyzed by tetrakis(triphenylphosphine)palladium(0) selectively gave the vinyl-group-migrated products.

Isoprene bromohydrin (1-bromo-2-methyl-3-buten-2-ol) (**1**), easily obtainable from the reaction of *N*-bromosuccinimide and isoprene in tetrahydrofuran–water, is an interesting compound because of the unique behavior toward organometallic reagents. The reaction of **1** with allylic Grignard reagents in the presence of copper(I) iodide selectively gave vinyl-group-migrated products.[1] The copper(I)-catalyzed reaction of **1** with alkyllithium which has β-hydrogen yielded 2-alkyl-4-penten-2-ol, whereas with methyl-, phenyl-, or benzyllithium, 4-substituted 2-methyl-2-buten-1-ol was formed exclusively.[2] In order to examine further the transition-metal-catalyzed Grignard reaction of **1**, we tested various transition metal compounds and found that a palladium(0) complex was the most effective for the migration of the vinyl group of **1**.

Using phenylmagnesium bromide as a representative Grignard reagent, the product distribution under various catalysts was examined. The reactions were carried out in tetrahydrofuran using 5-fold excess of the Grignard reagent. In the absence of catalysts, a mixture of 2-methyl-4-phenyl-2-buten-1-ol (**4a**) and 2-methyl-1-phenyl-3-buten-1-ol (**5a**) was formed in the ratio of 37:63, together with trace amounts of 2-phenyl-4-penten-2-ol (**2a**) and 2-methyl-1-phenyl-3-buten-2-ol (**3a**). The alcohols (**4a** and **5a**) are considered to be produced *via* isoprene oxide.[2] Eight kinds of transition metal complexes, which are known as effective catalysts for the cross-coupling between Grignard reagents and organic halides,[3] were examined. Results are summarized in Table 1. Titanocene dichloride and cobalt(II) chloride did not show a significant catalytic effect. The reaction yields were poor in the cases of tris(1,3-diketonato)-iron(III) complexes and palladium(II) chloride. As reported,[1] copper(I) iodide-catalyzed reaction gave a 56:44 mixture of **2a** and **3a**. The selectivity (**2a** *vs.* **3a**) was improved by the use of bis(triphenylphosphine)-

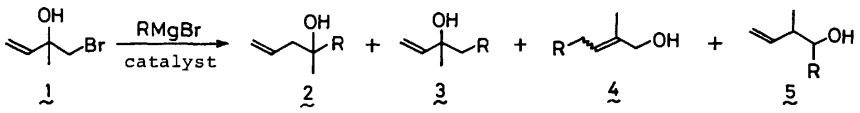

1 **2** **3** **4** **5**

a: R = Ph
b: p-$CH_3C_6H_4$
c: n-C_4H_9
d: n-C_6H_{13}

TABLE 1. YIELD AND PRODUCT DISTRIBUTION OF THE TRANSITION-METAL-CATALYZED GRIGNARD REACTION OF **1**

RMgBr	Catalyst	(mol%)[a]	Total Yield/%	Product Distribution			
				2	**3**	**4**(*E*/*Z*)	**5**
PhMgBr	none	—	62	tr	tr	37(3/2)	63
PhMgBr	Cp_2TiCl_2	(5)	82	tr	tr	52(4/1)	48
PhMgBr	$CoCl_2$	(5)	96	34	2	40(8/1)	24
PhMgBr	$Fe(DBM)_3$[b]	(5)	21	90	10	—	—
PhMgBr	$Fe(acac)_3$	(5)	19	89	11	—	—
PhMgBr	$PdCl_2$	(5)	7	100	tr	—	—
PhMgBr	CuI	(50)	78	56	44	—	—
PhMgBr	$Ni(PPh_3)_2Cl_2$	(5)	82	95	5	—	—
PhMgBr	$Pd(PPh_3)_4$	(0.5)	85	100	—	—	—
p-$CH_3C_6H_4MgBr$	$Pd(PPh_3)_4$	(0.5)	75	100	—	—	—
n-C_4H_9MgBr	$Pd(PPh_3)_4$	(0.5)	53	100	—	—	—
n-$C_6H_{13}MgBr$	$Pd(PPh_3)_4$	(0.5)	89	100	—	—	—

a) Of the bromohydrin used. b) Tris(dibenzoylmethanato)iron(III).

nickel(II) chloride. Of the eight catalysts which are examined, tetrakis(triphenylphosphine)palladium(0) was found to be the most effective, leading exclusive formation of the vinyl-group-migrated product (**2a**) in 85% yield. *p*-Tolylmagnesium bromide also gave the migration product (**2b**) with high selectivity in the presence of a catalytic amount (0.5 mol%) of the palladium(0) complex. This catalyst is also effective for the reaction with alkyl Grignard reagents. Coupling reactions with butyl- and hexylmagnesium bromides exclusively gave the respective homoallylic alcohols (**2c** and **2d**) in 53 and 89% yields. However, the reactions of **1** with allyl and benzylmagnesium chlorides gave complex reaction mixtures even in the presence of the palladium(0) complex.

Experimental

General. Infrared spectra were recorded on a JASCO IRA-1 spectrophotometer. ^{1}H NMR spectra were recorded on a Hitachi R-24A spectrometer (60 MHz) or on a Varian XL-200 spectrometer (200 MHz) with Me_4Si as internal standard. Mass spectra were determined using a Hitachi M-52 instrument at 20 eV. Glc analyses and preparative glc were performed on a Yanaco G1800 gas chromatograph equipped with a column packed with 20% polyethylene glycol (PEG) 20M on Celite 545 (1 m×3 mm). Elemental analyses were performed at the Elemental Analysis Center of Kyoto University. For Kugelrohr distillation, a Shibata GTO-250R glass tube oven was used.

Preparation of 1. To a suspension of *N*-bromosuccinimide (12.3 g, 69 mmol) in a mixture of tetrahydrofuran (THF)–water (3:2) (120 cm^3) was added a solution of isoprene (7.0 g, 103 mmol) in THF (50 cm^3) at 0 °C. The reaction mixture was left at 0 °C for 3 h and then overnight at room temperature. The reaction mixture was poured into a saturated aqueous sodium chloride solution and the organic layer was separated. The aqueous layer was extracted with ether and the combined organic extracts were washed with brine and dried (Na_2SO_4). The solvent was evaporated and the residue was distilled under reduced pressure to give **1** as a colorless oil (6.9 g, 61%). **1**:[4] bp 69—70 °C/46 Torr (1 Torr≈133.322 Pa); IR (neat) 3430, 2990, 1412, 1372, 1239, 1056, and 930 cm^{-1}; ^{1}H NMR (CCl_4) 5.85 (dd, *J*=17, 10 Hz, 1H, olefin), 5.25 (dd, *J*=17, 2 Hz, 1H, olefin), 5.08 (dd, *J*=10, 2 Hz, 1H, olefin), 3.37 (s, 2H, CH_2), 2.02 (bs, 1H, OH), 1.33 (s, 3H, CH_3).

Transition-metal-catalyzed Grignard Reaction of Isoprene Bromohydrin (1). The following example represents the general procedure. To a solution of phenylmagnesium bromide, prepared from magnesium turnings (600 mg, 25 mg-atom) and bromobenzene (2.12 cm^3, 25 mmol) in THF (20 cm^3), was added tetrakis(triphenylphosphine)-palladium (29 mg, 0.025 mmol) and the mixture was stirred at 0 °C for 10 min. A solution of **1** (825 mg, 5 mmol) in THF (5 cm^3) was then added at 0 °C and the mixture was left overnight at room temperature. The reaction was quenched by the addition of water and the product was extracted with ether. The extracts were dried (Na_2SO_4) and the solvent was evaporated. In order to remove less polar impurities such as biphenyl, the residue was adsorbed on a silica-gel column and eluted first with benzene (50 cm^3) and then with ether (100 cm^3). The ether eluate was concentrated and distilled (Kugelrohr) (bp 100 °C/3 Torr) to produce a colorless oil (689 mg, 85%). Glc analysis revealed that this oil was pure **2a**.

In other experiments, the reaction mixture was treated in a similar manner and the product distribution was analyzed by glc. Results are summarized in Table 1. Pure samples of the products were obtained by preparative glc and the structures were deduced by their spectral and analytical data.

*2-Phenyl-4-penten-2-ol (**2a**)*: IR (neat) 3430, 1642, 1498, 1448, 917, 768, and 702 cm^{-1}; ^{1}H NMR ($CDCl_3$) 7.50—7.20 (m, 5H, Ph), 5.66 (m, 1H, olefin), 5.16 (m, 2H, olefin), 2.63 (m, 2H, CH_2), 1.60 (bs, 1H, OH), 1.58 (s, 3H, CH_3); Mass *m/z* 162 (M^+); Found: C, 81.19; H, 8.55%. Calcd for $C_{11}H_{14}O$: C, 81.44; H, 8.70%.

*2-Methyl-1-phenyl-3-buten-2-ol (**3a**)*: IR (neat) 3420, 1646, 1608, 1498, 1454, 1103, 928, and 706 cm^{-1}; ^{1}H NMR (CCl_4) 7.00 (m, 5H, Ph), 5.78 (dd, *J*=17, 10 Hz, 1H, olefin), 4.95 (dd, *J*=17, 2 Hz, 1H, olefin), 4.81 (dd, *J*=10, 2 Hz, 1H, olefin), 2.68 (s, 2H, CH_2), 1.60 (bs, 1H, OH), 1.17 (s, 3H, CH_3); Mass *m/z* 162 (M^+); Found: C, 81.43; H, 8.56%. Cacld for $C_{11}H_{14}O$: C, 81.44; H, 8.70%.

*2-Methyl-4-phenyl-2-buten-1-ol (**4a**)* (a 3:2 mixture of *E*- and *Z*-isomers):[5] IR (neat) 3350, 2924, 1602, 1498, 1456, 1016, and 996 cm^{-1}; ^{1}H NMR (CCl_4) 7.03 (m, 5H, Ph), 5.43 (t, *J*=7 Hz, 1H, olefin), 4.03 (s, 0.8H, *Z*-$C\underline{H}_2OH$), 3.83 (s, 1.2H, *E*-$C\underline{H}_2OH$), 3.27 (d, *J*=7 Hz, 2H, $C\underline{H}_2Ph$), 2.03 (bs, 1H, OH), 1.72 (m, 1.2H, *Z*-CH_3), 1.67 (s, 1.8H, *E*-CH_3); Mass *m/z* 162 (M^+).

*2-Methyl-1-phenyl-3-buten-1-ol (**5a**)* (a 5:4 mixture of diastereomers): IR (neat) 3430, 1644, 1498, 1454, 1022, 916, 765, and 702 cm^{-1}; ^{1}H NMR ($CDCl_3$) 7.35 (m, 5H, Ph), 5.80 (m, 1H, olefin), 5.30—5.00 (m, 2H, olefin), 4.63 (d, *J*=5 Hz, 0.56H, C$\underline{H}$OH), 4.38 (d, *J*=8 Hz 0.44H, C$\underline{H}$OH), 2.56 (m, 1H, C$\underline{H}$CH$_3$), 1.97 (bs, 1H, OH), 1.01 (d, *J*=7 Hz, 1.67H, CH_3), 0.87 (d, *J*=7 Hz, 1.33H, CH_3); Mass *m/z* 162 (M^+); Found: C, 81.39; H, 8.94%. Calcd for $C_{11}H_{14}O$: C, 81.44; H, 8.70%.

*2-(p-Tolyl)-4-penten-2-ol (**2b**)*: IR (neat) 3430, 1644, 1521, 1374, 920, and 822 cm^{-1}; ^{1}H NMR ($CDCl_3$) 7.21 (AA'BB', 4H, Ph), 5.60 (m, 1H, olefin), 5.06 (m, 2H, olefin), 2.50 (m, 3H, CH_2+OH), 2.30 (s, 3H, CH_3), 1.49 (s, 3H, CH_3); Mass *m/z* 176 (M^+); Found: C, 81.50; H, 8.97%. Calcd for $C_{12}H_{16}O$: C, 81.77; H, 9.15%.

*4-Methyl-1-octen-4-ol (**2c**)*:[2] IR (neat) 3400, 1646, 1472, 1380, 1160, and 914 cm^{-1}; ^{1}H NMR (CCl_4) 6.10—4.60 (m, 3H, olefin), 2.10 (d, *J*=7 Hz, 2H, allyl CH_2), 1.70 (bs, 1H, OH), 1.30 (m, 6H, CH_2×3), 1.03 (s, 3H, CH_3), 0.88 (bt, 3H, CH_3); Mass *m/z* 124 ($M-H_2O$).

*4-Methyl-1-decen-4-ol (**2d**)*:[6] IR (neat) 3400, 1645, 1472, 1382, 1159, and 916 cm^{-1}; ^{1}H NMR (CCl_4) 6.20—4.80 (m, 3H, olefin), 2.15 (d, *J*=7 Hz, 2H, allyl CH_2), 1.65 (bs, 1H, OH), 1.30 (m, 10H, CH_2×5), 1.08 (s, 3H, CH_3), 0.89 (bt, 3H, CH_3), Mass *m/z* 152 ($M-H_2O$).

References

1) Y. Butsugan, I. Kadosaka, and S. Araki, *Chem. Lett.*, **1979**, 527.

2) S. Araki and Y. Butsugan, *Chem. Lett.*, **1980**, 185.

3) R. Noyori, "Transition Metal Organometallics in Organic Synthesis," ed by H. Alper, Academic Press, New York (1976), Vol. 1, pp. 83—187.

4) D. R. Dalton and R. M. Davis, *Tetrahedron Lett.*, **1972**, 1057.

5) G. C. M. Aithie and J. A. Miller, *Tetrahedron Lett.*, **1975**, 4419.

6) G. P. Boldrini, D. Savoia, E. Tagliavini, C. Trombini, and A. Umani-Ronchi, *J. Org. Chem.*, **48**, 4108 (1983).

Oxidation of Anthracenols and Anthrone to Anthraquinones with Oxygen Mediated by Copper(II) Ion and Imidazole

Masaaki IWATA* and Hiroyoshi KUZUHARA
Riken (The Institute of Physical and Chemical Research), Wako, Saitama 351-01
(Received December 11, 1984)

Synopsis. The copper(II) chloride-imidazole-ethanol system turned out to oxidize 2-anthracenols to 1,2-anthraquinones and 2-methoxy-9-anthrone to 2-methoxy-9,10-anthraquinone in practical synthetic yield.

In the preliminary report,[1] copper(II) chloride and imidazole in the presence of oxygen in ethanol was found to be a tyrosinase mimic, which was exemplified by specific and enhanced oxidation of 2-anthracenol (**1**) to 1,2-anthraquinone (**2**) identified as the corresponding phenazine derivative (**3**). Simplicity and effectiveness of the method suggested that this could be applied for general practical synthesis of quinones.

To start with, 9-(2-*p*-cymenyl)-2-anthracenol (**4**) was stirred at ambient temperature with copper(II) chloride dihydrate and imidazole in ethanol for 22 h, resulting in 9-(2-*p*-cymenyl)-1,2-anthraquinone (**5**) in 86% yield. ^{1}H NMR spectrum of **5** supported the structure by appearance of doublet signals at δ 6.48 (C_3–H) and 7.60 (C_4–H), and a singlet signal at 7.81 (C_{10}–H).

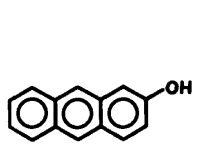

1

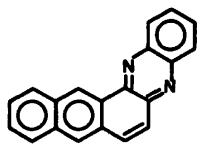

3

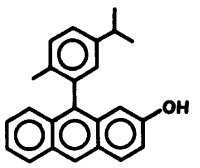

4

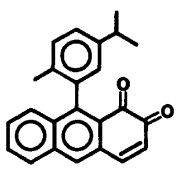

5

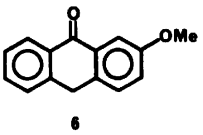

6

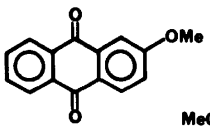

7

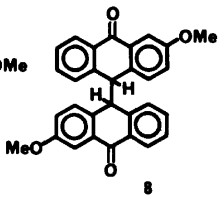

8

Secondary, 2-methoxy-9-anthrone (**6**)[2] was treated at ambient temperature in the presence of copper(II) chloride dihydrate and imidazole in ethanol for 25 h, resulting in 2-methoxy-9,10-anthraquinone (**7**) in 81% yield, accompanied by 2,2′-dimethoxy-10,10′-bianthrone (**8**) in 6% yield. When an amount of imidazole was decreased, the reaction was retarded markedly.

These experiments imply that (a) in the presence of air, the mixture of copper(II) chloride and imidazole in ethanol works as effective oxidation catalysis for anthracenols and anthrone and (b) imidazole is indispensable for the oxidation reaction.

The practical synthetic method of 1,2-anthraquinones has been limited hitherto.[3] Fremy's salt is known to be only practical oxidant for the purpose.[4] The other methods[4] such as iron(III) chloride and chromium trioxide for 2-amino-1-anthracenol and chromium trioxide for 1,2-diacetoxyanthracene suffer from the moderate yields and the difficulty of the synthesis of the precursors. As for the synthesis of *o*-quinones, the morpholinocopper(II)–ethanol system[5] is unique and the first tyrosinase mimic. However, the system is far from the practical synthesis of *o*-quinones because it is only applicable to naphthols and phenols of the benzene series and always gives morpholine-substituted *o*-quinones.

9,10-Anthraquinones are of great importance for manufacture of dyes. The classical synthetic route through the cyclization of *o*-benzoylbenzoic acids is not always convenient because the position at which cyclization should take place is deactivated by the electron-withdrawing group at the ortho-position. Improvement has been made by the finding of the path through the cyclization of *o*-benzylbenzoic acids.[6] The resulting anthrones are, then, oxidized by chromium trioxide in refluxed acetic acid in "good" yield. The present system seems to afford advantage over the chromium trioxide method because of easy work-up and mild reaction conditions preventing from the formation of undesirable by-products.

The reaction mechanism of the present system is attractive especially in relation to copper-bound tyrosinase. The mechanism will be discussed elsewhere.

Experimental

The ^{1}H NMR spectra were recorded on JEOL JNM GX-400 instrument with Me_4Si as the internal standard. Electronic absorption spectra (UV) were recorded on a Hitachi 124 spectrophotometer. Infrared spectra (IR) were obtained on a Shimadzu IR-27 apparatus. Mass spectra (MS) were obtained with a Hitachi RMU 6-MG spectrometer by using a direct-inlet method, an ionizing potential at 20 eV. Merck silica gel 60 (Art 7734, 0.063—0.20) was used for column chromatography. Thin layer chromatography (tlc) was performed with precoated plates (Merck, Art. 5715, silica gel 60 F_{254}).

2-Anthracenol was prepared by demethylation of 2-methoxyanthracene by the method exemplified by that of 9-(2-*p*-cymenyl)-2-methoxyanthracene (*vide infra*), which was prepared by the Grignard reaction of 2-methoxy-9-

anthrone with 2-bromo-*p*-cymene.[2]

Oxidation of 2-Anthracenol (1). The mixture of **1** (0.516 mmol), copper(II) chloride dihydrate (0.347 mmol), and imidazole (0.347 mmol) in 20 ml of ethanol was shaken in oxygen atmosphere at ambient temperature. After the calculated amount of oxygen was uptaken, the mixture was filtered through Celite (No. 545) and washed several times with chloroform. The combined filtrate was evaporated. The residue was dissolved into acetic acid (5 ml) and 0.516 mmol of *o*-phenylenediamine was added. Dark red precipitate was collected in one day, and recrystallized from benzene to give the phenazine derivative of 1,2-anthraquinone (**3**): mp 220 °C (221—222 °C[7]; 185—190 °C[8]).

Demethylation of 9-(2-p-Cymenyl)-2-methoxyanthracene. According to the previous method,[9] the mixture of 1.43 g of 9-(2-*p*-cymenyl)-2-methoxyanthracene,[2] 20 ml of acetic acid, and 20 ml of 47% hydrobromic acid was refluxed for 3.5 h. Cooled reaction mixture was extracted with benzene and chromatographed on a silica-gel column eluted with benzene to give 0.85 g (62% yield) of 9-(2-*p*-cymenyl)-2-anthracenol (**4**) as viscous liquid; Calcd for $C_{24}H_{22}O$: C, 88.31; H, 6.79%. Found: C, 87.93; H, 6.51%. IR (neat): ν_{OH} 3500 and 3400 cm^{-1}.

Oxidation of 9-(2-p-Cymenyl)-2-anthracenol (4). **4** (0.613 mmol) was mixed in 20 ml of ethanol with copper(II) chloride dihydrate (0.3 mmol) and imidazole (0.3 mmol), and stirred at ambient temperature for 22 h. The reaction mixture was filtered through Celite (No. 545) and washed twice with chloroform. The filtrate was evaporated to dryness and the residue was chromatographed on a silica-gel column eluted with benzene–ethyl acetate (9:1 v/v) to give 9-(2-*p*-cymenyl)-1,2-anthraquinone (**5**) in 86% yield, which was recrystallized from benzene–petroleum ether; yellow red crystals, mp 170—172 °C. Calcd for $C_{24}H_{20}O_2$: C, 84.68; H, 5.92%. Found: C, 84.43; H, 5.92%. IR (KBr disk) $\nu_{C=O}$ 1660 cm^{-1}. UV (ethanol) λ_{max} 236.5, 298.5 and 444.5 nm. MS, a parent peak at *m/z* 340. ^1H NMR (CCl_4) δ=1.26 (6H, d, J=7.0, $-CH(C\underline{H}_3)_2$), 2.89 (1H, quin, J=7.0, $-C\underline{H}(CH_3)_2$), 1.86 (3H, s, Ar-$C\underline{H}_3$), 6.48 (1H, d, J=10.0, C_3-$\underline{H}$), 7.60 (1H, d, J=10.0, C_4-$\underline{H}$), and 7.81 (1H, s, C_{10}-$\underline{H}$).

Oxidation of 2-Methoxy-9-anthrone (6). The mixture of **6**[2] (1.12 g; 4.99 mmol), copper(II) chloride dihydrate (0.568 g; 3.33 mmol), and imidazole (0.573 g; 8.42 mmol) in 100 ml of ethanol was stirred at ambient temperature for 25 h. The reaction mixture was filtered through Celite (No. 545) and washed well with chloroform. The combined filtrate was evaporated and chromatographed on a silica-gel column eluted with benzene to give 0.96 g (81% yield) of 2-methoxy-9.10-anthraquinone (**7**) and 0.277 g (6% yield) of 2,2′-dimethoxy-10,10′-bianthrone (**8**).

7: IR (KBr) $\nu_{C=O}$ 1673 cm^{-1}; $\nu_{=C-O-C}$ 1305, 1290 cm^{-1}. ^1H NMR ($CDCl_3$) δ=3.99 (3H, s, O-$C\underline{H}_3$), 7.27 (1H, q, $J_{1,3}$=2.69, $J_{3,4}$=8.79, C_3-$\underline{H}$), 7.73 (1H, d, $J_{1,3}$=2.69, C_1-$\underline{H}$), and 8.26 (1H, d, $J_{3,4}$=8.79, C_4-$\underline{H}$).

8: IR (KBr) $\nu_{C=O}$ 1662 cm^{-1}; $\nu_{=C-O-C}$ 1320 cm^{-1}. ^1H NMR δ=3.85 (3H, s, O-$C\underline{H}_3$), 3.87 (3H, s, O-$C\underline{H}_3$), and 4.71 (2H, s, C_{10}- and $C_{10'}$-$\underline{H}$).

References

1) M. Iwata and S. Emoto, *Chem. Lett.*, **1974**, 759.
2) M. Iwata and S. Emoto, *Bull. Chem. Soc. Jpn.*, **47**, 1687 (1974).
3) "Rodd's Chemistry of Carbon Compounds," 2nd ed. ed by S. Coffey, Elsevier Scientific Publishing Company, Amsterdam, Vol. III H, 1979, pp 41-2.
4) L. F. Fieser and M. Fieser, "Reagents for Organic Synthesis," John Wiley and Sons Inc., New York, Vol. I (1967), pp 940.
5) W. Brackman and E. Havinga, *Recl. Trav. Chim. Pays-Bas*, **74**, 937, 1021, 1070, 1100, 1107 (1955).
6) M. G. Sarngadharan and T. R. Seshadri, *Indian J. Chem.*, **4**, 503 (1966).
7) K. Lagodzinski, *Ann.*, **342**, 59 (1905).
8) H. Joachim and N. Goetz, *Chem. Ber.*, **87**, 1236 (1954).
9) L. Long, Jr. and A. Burger, *J. Org. Chem.*, **6**, 852 (1941).

Iodination of Benzene with Iodine and Metal Salts in Acidic Solvents

Atsushi SHIMIZU,* Kazunori YAMATAKA,* and Toshiro ISOYA
Technical Development Department of Petrochemical Intermediates, Asahi Chemical Ind. Co., Ltd.
Nagahama-cho 4-3401, Nobeoka, Miyazaki 882
(Received December 12, 1984)

Synopsis. Iodobenzene was obtained by a reaction of benzene with molecular iodine in trifluoromethanesulfonic acid in oxygen atmosphere in the presence of vanadium salt as a catalyst. The method affords a new aromatic iodination process in which benzene is iodinated directly with molecular iodine.

Aromatic compounds can be brominated or chlorinated with bromine or chlorine in the presence of a catalyst, most often iron. On the other hand, iodine is the least reactive of the halogens in aromatic halogenation reactions where an oxidizing agent is normally required to oxidize iodine to a better electrophile, as opposed to the case of active substrates. Generally, iodination of benzene can be accomplished by iodine in the presence of nitric acid.[1] Recently several synthetic methods of iodoarens have been reported, which include (1) iodination of aromatics with molecular iodine in the presence of oxidizing agents,[2-4] (2) iodination of aromatics with a potent iodine donor[5,6] (3) decomposition of arylthallium compounds with potassium iodide or iodine,[7,8] and (4) electrochemical iodination of aromatics.[9,10] These procedures have some deficiencies. Metal salts are required as stoichiometric agents, iodine donors are hard to be prepared, or iodine is lost from the reaction as hydrogen iodide or metallic iodide.

Recently fluorine containing compounds such as trifluoromethanesulfonic acid or trifluoroacetic acid have been used as catalysts or solvents in various reactions to show remarkable effects. We have found that iodination of benzene with molecular iodine occurs in trifluoromethanesulfonic acid in the presence of sodium vanadate(V) and oxygen gas. The present paper will describe a new catalytic iodination of benzene.

Experimental

The Typical Procedures. In a 200-ml three-necked glass autoclave were placed 5.08 g (65.1 mmol) of benzene, 2.03 g (8.00 mmol) of iodine, 0.33 g (2.7 mmol) of sodium vanadate(V), and 12.5 g of trifluoromethanesulfonic acid. The mixture was magnetically stirred at 100 °C under 10 atm of air. When the colour of iodine was discharged and the solution became black after 1.5 h, the mixture was poured into 300 ml of ice-water containing 10% of sodium thiosulfate, and the products were extracted with 100 ml of hexane. Removal of hexane left 3.13 g of an oil which contained 2.99 g (14.7 mmol) of iodobenzene, 0.13 g (0.39 mmol) of *p*-diiodobenzene, and 0.01 g (0.04 mmol) of *o*-diiodobenzene. The yields based on iodine were 91.9, 2.5, and 0.2% respectively. All the products were characterized by comparison of NMR spectra, mass spectra, and GC retention times with those of authentic samples.

Results and Discussion

The results of the iodination in trifluoromethanesulfonic acid are shown in Table 1.

The reaction was performed as a two-layer system. The upper layer was benzene and the lower layer was trifluoromethanesulfonic acid. An increase in the quantity of trifluoromethanesulfonic acid was accompanied by an increase in the yield of iodobenzene. The presence of oxygen was essential in the reaction because iodobenzene was not obtainable without oxygen. Iodinations were examined in various combinations of solvents and metal salts, and the use of vanadium salt and trifluoromethanesulfonic acid gave an excellent yield of iodobenzene. The molar ratio of the iodobenzene to the metal salt reveals that the metal salt acts as a catalyst. Since the molar ratio

TABLE 1. IODINATION OF BENZENE IN CF_3SO_3H

Run	Benzene mmol	Iodine mmol	Metal Salt mmol	CF_3SO_3H g	Press kg/cm²	Temp °C	Time h
1	65.1	8.00	$NaVO_3$ 2.71	12.5	air 10	100	1.5
2	67.2	15.1	V_2O_5 1.37	12.5	O_2 2	100	5.5
3	129	15.1	V_2O_5 8.25	1.19	O_2 5	100	9.0
4	64.1	15.0	V_2O_5 1.38	12.5	N_2 5	100	8.0

Run	IB/M[a]	C_6H_5I mmol	Select.[b] of C_6H_5I %	Select.[b] of *p*-$C_6H_4I_2$ %	Select.[b] of *o*-$C_6H_4I_2$ %	Conv. of Benzene %
1	5.4	14.7	91.9	2.5	0.2	27.6
2	17.9	24.5	81.1	6.7	1.0	44.7
3	0.21	1.74				
4		trace				

a) IB/M is a molar ratio of the iodobenzene to the metal salt. b) Selectivity was based on iodine.

Table 2. Iodobenzene/catalyst molar ratio in CH_3SO_3H (100 °C, 8 h)

Cat.	C_6H_5I/Cat.	Cat.	C_6H_5I/Cat.	Cat.	C_6H_5I/Cat.
$FeCl_2 \cdot 4H_2O$	1.0	VCl_3	3.7	$ZnCl_2$	0.0
$FeCl_3$	1.0	$TiCl_4$	2.7	$CdCl_2 5/2H_2O$	0.0
Fe_2O_3	0.5	$ZrCl_4$	trace	Ag_2O	0.65
$Fe(OH)_3$	1.0	Co_3O_4	0.51	TlCl	trace
$Fe(AcAc)_3$	0.0	NiO	0.0	MnO_2	1.3
$CuCl_2$	3.0	$PdCl_2$	trace	$SbCl_3$	trace
CuO	1.0	CrO_4	1.6	V_2O_5	1.8
MoO_3	trace	$NaVO_3$	1.6	WO_3	0.0

Other reaction conditions are as follows: Ag_2O, Fe_2O_3, V_2O_5=1.35 mmol; Co_3O_4=0.9 mmol; others=2.7 mmol; C_6H_6=5 g; CH_3SO_3H=12.5 g; O_2=5 kg/cm^2.

Table 3. Iodination of benzene in CF_3COOH

Run	C_6H_6	Iodine	Cat.		CF_3COOH	Press.		Temp	Time	C_6H_5I
	mmol	mmol	mmol		g	kg/cm^2		°C	h	mmol
1	65.3	15.2	V_2O_5	1.37	12.5	air	10	100	5.5	2.60
2	128.0	23.6	$FeCl_2 \cdot 4H_2O$	0.352	10.5	O_2	2	100	48.0	2.56

of consumed benzene to iodine was about 2:1, the overall reaction can be shown as follows:

$$2C_6H_6 + I_2 + 1/2O_2 \longrightarrow 2C_6H_5I + H_2O$$

The iodobenzene also gave diiodobenzene by a reaction with iodine.

Activities of various metal salts in the iodination were examined in methanesulfonic acid. All the results are summarized in Table 2.

Cu, Ti, Fe, and Mn salts were comparatively effective. Since the sorts of counter ions of metal ions do not seem to be important, we may describe that the metal salts were oxidizing catalysts, and not Lewis acids.

Trifluoroacetic acid could also be used as the solvent. Table 3 gives the results.

The iodination rate was dependent on the acidity of the solvent because the iodination rate decreased in the order $CF_3SO_3H > CH_3SO_3H > CF_3COOH$ and was nearly zero in CH_3COOH. The combination of acidic solvent, oxygen gas, and oxidizing catalyst are indispensable in the iodination reaction. We may describe the reaction pathways as follows:

$$CF_3SO_3H + I_2 \longrightarrow CF_3SO_3^- + HI_2^+$$

$$HI_2^+ \longrightarrow HI + I^+$$

$$I^+ + C_6H_6 \longrightarrow C_6H_5I + H^+$$

$$HI \longrightarrow H^+ + I^-$$

$$I^- + V^{5+} \longrightarrow 1/2I_2 + V^{4+}$$

$$V^{4+} + H^+ + 1/4O_2 \longrightarrow V^{5+} + 1/2H_2O$$

Although the reactive intermediate is represented as iodine ion in the pathways, possible intermediates other than iodine ion are HIO, CF_3SO_3I, CH_3SO_3I, or CF_3COOI.[3,4] It is not clear which is the true active intermediate.

References

1) F. B. Dains and R. Q. Brewster, *Org. Synth.*, Coll. Vol. I, 323 (1941).

2) S. Uemura, A. Onoe, and M. Okano, *Bull. Chem. Soc. Jpn.*, **47**,147 (1974).

3) Y. Ogata and K. Nakajima, *Tetrahedron*, **20**, 43 (1964).

4) Y. Ogata and K. Nakajima, *Tetrahedron*, **20**, 2751 (1964).

5) W. C. Baird, Jr. and J. H. Surridge, *J. Org. Chem.*, **35**, 3436 (1970).

6) T. Sugita, M. Idei, Y. Ishibashi, and Y. Takegami, *Chem.Lett.* **1982**, 1481.

7) A. McKillop, J. D. Hunt, M. J. Zelesko, J. S. Fowler, E. C. Taylor, G. McGillivray, and F. Kienzle, *J. Am. Chem. Soc.*, **93**, 4841 (1971).

8) N. Ishikawa and A. Sekiya, *Bull. Chem. Soc. Jpn.*, **47**, 1680 (1974).

9) L. L. Miller, E. P. Kujawa, and C. B. Campbell, *J. Am. Chem. Soc.*, **92**, 2821 (1970).

10) R. Lines and V. D. Parker, *Acta Chem. Scand., Ser. B*, **34**, 47 (1980).

Synthesis of *cis-transoid-cis-* and *cis-cisoid-cis-* Tricyclo[6.3.0.0^{2,6}]undecan-1-ols

Kiyomi KAKIUCHI,* Hideyuki TAKEUCHI, Yoshito TOBE, and Yoshinobu ODAIRA
Department of Applied Fine Chemistry, Faculty of Engineering, Osaka University, Suita, Osaka 565
(Received December 19, 1984)

Synopsis. Two isomeric linear triquinanes, *cis-transoid-cis-* and *cis-cisoid-cis*-tricyclo[6.3.0.0^{2,6}]undecan-1-ols, were effectively synthesized by means of the modified Barbier cyclization.

Recently, much attention has been focused on linearly fused triquinanes (tricyclo[6.3.0.0^{2,6}]undecanes), since a lot of natural products which possess this ring system have been found out and some of them, such as hirsutic acid and coriolin, display significant levels of biological activities.[1] In this connection, we wish to report here the facile synthesis of two isomeric linear triquinanes, *cis-transoid-cis-* and *cis-cisoid-cis*-tricyclo[6.3.0.0^{2,6}]undecan-1-ols (**1a**) and (**1b**) by means of a new cyclopentane annelation, that is, the modified Barbier cyclization.[2]

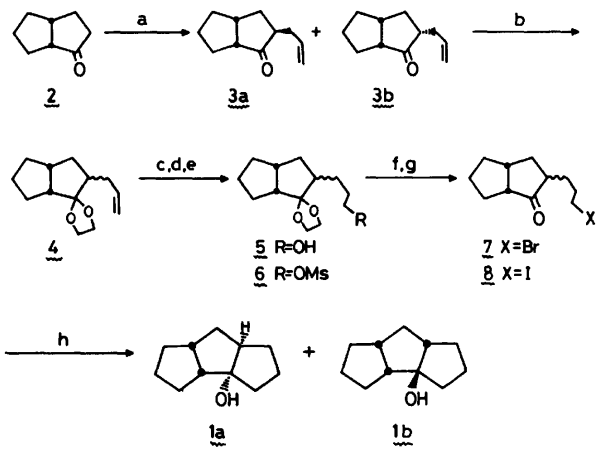

Scheme 1.

a) CH_2=$CHCH_2OH$, $CH_3C(OCH_3)_2CH_3$, TsOH, △; b) $HO(CH_2)_2OH$, TsOH; c) B_2H_6; d) H_2O_2; e) CH_3SO_2Cl (MsCl), Et_3N; f) LiBr; g) NaI; h) Mg, $HgCl_2$.

An ingenious adaptation of the Claisen rearrangement[3] of a diquinane, *cis*-bicyclo[3.3.0]octan-2-one (**2**),[4] gave the 3-allyl derivatives **3a** and **3b** (an approximate 1:1 ratio) in 73% yield. The mixture **3a** and **3b** was readily transformed to the 3-iodopropyl derivatives **8** as follows: i) acetalization, ii) hydroboration-oxidation of the acetals **4**, iii) mesylation of the alcohols **5**, iv) reaction of the mesylates **6** with lithium bromide,[5] and v) treatment of the bromides **7** with sodium iodide. Finally, reaction of **8** with magnesium activated by $HgCl_2$ afforded the desired alcohols **1a** and **1b** in 17% and 11% isolated yields from **3a** and **3b**, which were readily separated by column chromatography on silica gel.

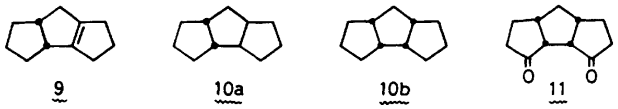

Their structures were elucidated on the basis of spectroscopic data and the following chemical transformations. Elimination of the mesylates of **1a** and **1b** with $LiAlH_4$[6] gave the same olefin, *cis*-tricyclo[6.3.0.0^{2,6}]undec-1(8)-ene (**9**), in 65% and 67% yields, respectively. Hydrogenation of **9** with Pd on charcoal gave two hydrocarbons, tricyclo[6.3.0.0^{2,6}]-undecanes (**10a**) and (**10b**), in 43% and 35% yields. The hydrocarbon **10b** was also obtained in 45% yield by reductive deoxygenation[7] of the diethyl phosphate of **1b** with lithium in diethylamine. The *cis-cisoid-cis* stereochemistry of **10b** was determined by comparison with the authentic sample derived from *cis-cisoid-cis*-tricyclo[6.3.0.0^{2,6}]undecane-3,11-dione (**11**)[8] by Wolff-Kishner reduction. Consequently, **1b** was established to be the *cis-cisoid-cis*-isomer, and **1a** and **10a** were characterized to be *cis-transoid-cis*-isomers.

Experimental

All boiling points are uncorrected. Measurements of IR, MS, ^{1}H NMR, and ^{13}C NMR as well as analytical and preparative GLC were done on the same instruments as in the previous work.[6] Column chromatography was carried out with silica gel (Wakogel C-200). Yields were calculated from the isolated products based on the consumed starting materials.

exo- *and* endo-*3-(2-Propenyl)-*cis*-bicyclo[3.3.0]octan-2-ones (3a) and (3b).* A solution composed of **2** (10.0 g, 80.6 mmol), allyl alcohol (11.2 g, 193 mmol), 2,2-dimethoxypropane (10.0 g, 96.2 mmol), and *p*-toluenesulfonic acid monohydrate (TsOH·H_2O) (10 mg) and benzene (44 ml) was distilled through a spinning band column and operated at a reflux ratio of 10. After 19 ml of distillate had been collected at 55—60 °C, the distillation was continued with a reflux ratio of 3 until the overhead temperature reached 95 °C. Yellow residue was distilled *in vacuo* to give the recovered **2** (3.59 g; bp 51 °C/2 mmHg (mmHg=133.322 Pa)) and the allyl ketones **3a** and **3b** (6.21 g, 73%; bp 70 °C/1 mmHg) which were purified by column chromatography. Since **3a** and **3b** could not be separated by GLC or column chromatography, they were characterized as a mixture (an approximate 1:1 ratio calculated from ^{13}C NMR spectrum). **3a** and **3b**: IR 3080, 1740, 1640, 915 cm^{-1}; MS *m/z* 164 (M$^+$), 68 (base); ^{13}C NMR ($CDCl_3$) δ=223.4 (s), 220.9 (s), 136.1 (d), 135.9 (d), 116.2 (t), 115.9 (t), 52.2 (d), 51.3 (d), 49.8 (d), 46.6 (d), 38.5 (d), 37.8 (d), and ten triplets. Found: C, 80.56; H, 10.05%. Calcd for $C_{11}H_{16}O$: C, 80.44; H, 9.83%.

cis-transoid-cis- *and* cis-cisoid-cis-*Tricyclo[6.3.0.0^{2,6}]undecan-1-ols (1a) and (1b).* Reaction[9] of **3a** and **3b** (6.39 g, 39 mmol), ethylene glycol (12.2 g, 194 mmol), and TsOH·H_2O (194 mg) in toluene (220 ml) gave the acetals **4**: IR 3070, 1040, 915 cm^{-1}. Hydroboration[6] of the crude acetals **4** with diborane generated from $NaBH_4$ (2.94 g, 26.0 mmol) and BF_3·Et_2O (4.24 g, 31.2 mmol) in THF (170 ml), and the subsequent oxidation with H_2O_2 gave the alcohols **5**: IR 3400, 1040 cm^{-1}. Mesylation[9] of the crude alcohols **5** with methanesulfonyl chloride (9.1 ml, 116 mmol) and triethylamine (27.2 ml, 194 mmol) in dry ether (300 ml) gave the mesylates **6**: IR 1345, 1170 cm^{-1}. Reaction[9] of the crude mesylates **6** with lithium bromide (12.5 g, 119 mmol) in acetone (320 ml) gave the bromides **7**: 6.24 g, 65% from **3a** and **3b**; bp 120—122 °C/1.5 mmHg; IR 1735 cm^{-1}.

A suspension of **7** (25.5 mmol) and sodium iodide (7.65 g, 51.0 mmol) in acetone (93 ml) was stirred at room temperature for 2 h. The reaction mixture was concentrated *in vacuo* and ether was added. The organic layer was washed with 10% $NaHSO_3$ solution, water, and dried ($MgSO_4$). The solvent was removed *in vacuo* to give the crude iodides **8**: IR 1735 cm^{-1}.

A mixture of magnesium (1.7 g, 70.0 mmol) and $HgCl_2$ (0.4 g) in THF (90 ml) was heated to 45 °C. A solution of the above iodides **8** in THF (55 ml) was added over a period of *ca.* 30 min. During addition the temperature of the reaction mixture was maintained at 45—50 °C. After refluxing for 24 h, the mixture was hydrolyzed with water and decanted from the excess magnesium. The solution was extracted with ether and the organic layer was washed with water, dried ($MgSO_4$), and concentrated *in vacuo*. The residue was chromatographed to give the alcohols **1a** and **1b**. **1a**: 1.08 g, 26% from **8**; IR 3350 cm^{-1}; MS *m/z* 166 (M^+), 84 (base); ^1H NMR (CCl_4) δ=1.3—2.6 (m); ^{13}C NMR ($CDCl_3$) δ=92.0 (s), 53.1 (d), 50.4 (d), 42.9 (d), 41.5 (t), 37.7 (t), 34.1 (t), 30.8 (t), 28.1 (t), 26.6 (t), 23.7 (t). Found: C, 79.33; H, 11.21%. Calcd for $C_{11}H_{18}O$: C, 79.46; H, 10.92%. **1b**: 0.65 g, 17% from **8**; IR 3350 cm^{-1}; MS *m/z* 166 (M^+) 119 (base); ^1H NMR (CCl_4) δ=0.78 (q, 1H), 1.2—3.0 (m, 17H); ^{13}C NMR ($CDCl_3$) δ=93.6 (s), 55.4 (d), 55.0 (d), 44.8 (d), 39.6 (t), 35.9 (t), 31.8 (t), 29.6 (t), 28.0 (t), 26.6 (t), 25.4 (t). Found: C, 79.16; H, 11.19%. Calcd for $C_{11}H_{18}O$: C, 79.46; H, 10.92%.

cis-*Tricyclo[6.3.0.0^{2,6}]undec-1(8)-ene (9).* Mesylation of **1a** (50 mg, 0.30 mmol) as described above followed by treatment[6] of the crude mesylate with $LiAlH_4$ (23 mg, 0.60 mmol) gave the olefin **9**: 29 mg, 65% from **1a**; MS *m/z* 148 (M^+), 119 (base); ^1H NMR (CCl_4) δ=1.2—2.4 (m, 14H), 2.6—3.2 (m, 2H); ^{13}C NMR ($CDCl_3$) δ=148.2 (s), 144.4 (s), 47.6 (d), 46.8 (d), 37.4 (t), 35.7 (t), 30.3 (t), 29.4 (t), 28.2 (t), 27.9 (t), 26.0 (t). Found: C, 88.89; H, 11.14%. Calcd for $C_{11}H_{16}$: C, 89.12; H, 10.88%. The isomeric alcohol **1b** (50 mg, 0.30 mmol) was dehydrated as described for **1a** to give **9** (30 mg, 67%).

cis-transoid-cis- *and* cis-cisoid-cis-*Tricyclo[6.3.0.0^{2,6}]undecanes (10a) and (10b).* The olefin **9** (217 mg, 1.46 mmol) was hydrogenated as described previously[6] to give the two hydrocarbons **10a** and **10b**. **10a**: 95 mg, 43%; MS *m/z* 150 (M^+), 67 (base); ^{13}C NMR ($CDCl_3$) δ=52.3 (d, 2C), 44.8 (d, 2C), 40.1 (t), 33.9 (t, 2C), 32.9 (t, 2C), 26.1 (t, 2C). Found: C, 87.76; H, 12.32%. Calcd for $C_{11}H_{18}$: C, 87.92; H, 12.08%. **10b**: 78 mg, 35%; MS *m/z* 150 (M^+), 67 (base); ^{13}C NMR ($CDCl_3$) δ=47.3 (d, 2C), 47.2 (d, 2C), 40.2 (t), 31.5 (t, 2C), 28.4 (t, 2C), 27.2 (t, 2C). Found: C, 87.78; H, 12.36%. Calcd for $C_{11}H_{18}$: C, 87.92; H, 12.08%.

Synthesis of 10b by Reductive Deoxygenation from 1b. The reaction of the lithium alkoxide [derived from **1b** (486 mg, 2.93 mmol) and butyllithium (1.56 M hexane solution (1 M=1 mol dm^{-3}), 3.9 ml, 5.96 mmol)] with diethyl phosphorochloridate (506 mg, 2.93 mmol) gave the diethyl phosphate: IR 1250, 1010 cm^{-1}. Treatment of the crude phosphate with lithium (200 mg) in dry diethylamine (140 ml) followed by *t*-BuOH (1.5 ml) and THF (40 ml) gave 199 mg (45% from **1b**) of **10b** after usual workup.[7]

Synthesis of an Authentic Sample of 10b. Wolff-Kishner reduction of the diketone **11**[8] (500 mg, 2.81 mmol) as described previously[6] gave the hydrocarbon (165 mg, 39%) whose Mass and ^{13}C NMR spectra were identical with those of **10b**.

References

1) L. A. Paquette, *Top. Curr. Chem.*, **79**, 41 (1979); **119**, 1 (1984).
2) J. K. Crandall and H. S. Magaha, *J. Org. Chem.*, **47**, 5638 (1982).
3) N. B. Lorette and W. L. Howard, *J. Org. Chem.*, **26**, 3112 (1961).
4) Y. Fujikura, N. Takaishi, and Y. Inamoto, *Tetrahedron*, **37**, 4465 (1981).
5) This lithium bromide process also brought about deacetalization; for example, see Ref. 9.
6) K. Kakiuchi, T. Tsugaru, M. Takeda, I. Wakaki, Y. Tobe, and Y. Odaira, *J. Org. Chem.*, **50**, 488 (1985).
7) R. E. Ireland, D. C. Muchmore, and U. Hengartner, *J. Am. Chem. Soc.*, **94**, 5098 (1972).
8) G. Mehta, A. Srikrishna, A. V. Peddy, and M. S. Nair, *Tetrahedron*, **37**, 4543 (1981).
9) S. Danishefsky, K. Vaughan, R. C. Gadwood, and K. Tsuzuki, *J. Am. Chem. Soc.*, **103**, 4136 (1981).

Syntheses of Diferrocenyl Trithiocarbonate and a Tetrathio-substituted Ethylene Derivatives of Ferrocene

Masaru SATO* and Sadatoshi AKABORI†
Chemical Analysis Center, Saitama University, Urawa, Saitama 338
†*Department of Chemistry, Faculty of Science, Toho University, Funabashi, Chiba 274*
(Received December 14, 1984)

Synopsis. Diferrocenyl trithiocarbonate, 1,3-dithia-[3]ferrocenophane-2-thione, and 2,2′-bi(1,3-dithia[3]-ferrocenophan-2-ylidene) were prepared.

Electron-rich olefins,[1] in which all substituents are electron-donating groups, are interesting from the viewpoints of both their chemical reactivities and their physical properties. Tetrathio-substituted ethylene derivatives attract much attention in connection with tetrathiafulvalene which forms high-conducting complexes with DDQ,[2] but only a few derivatives have been prepared.[3] We now report the synthesis of tetrathio-substituted ethylene derivatives of ferrocene through 1,1′-ferrocenediyl trithiocarbonate.

Ferrocenethiol (**1**) reacted with 1,1′-thiocarbonyldiimidazole (**2**) in tetrahydrofuran (THF) at room temperature to give diferrocenyl trithiocarbonate (**3**) in good yield. Similarly, the reaction of 1,1′-ferrocenedithiol (**4**) with **2** gave 1,3-dithia[3]ferrocenophane-2-thione (**5**) in a 78% yield. The structure of these compounds was confirmed by elemental analysis, mass- and ^{1}H-NMR spectra. For example, ^{1}H-NMR spectrum ($CDCl_3$) of **2** showed only two signals at δ 4.21 (s, 10H) and 4.43 (m, 8H), due to the cyclopentadienyl ring protons of a ferrocene nucleus. The comparison of the IR and electronic spectra of **5** and **3** is interesting. The stretching frequency of the thiocarbonyl group in **5** (975 cm^{-1}) appeared at lower frequency than that of **3** (1043 cm^{-1}). In the electronic spectrum, the absorption band of **5** (424 nm) showed a large bathochromic shift compared with that of **3** (406 nm). These results suggest that there is some interaction between the nonbonding d (e_{2g}) orbital of the ferrocene nucleus and the antibonding orbital of the thiocarbonyl double bond.

The compound **5** was refluxed for 24 h with triphenylphosphine to give 2,2′-bi(1,3-dithia[3]ferrocenophan-2-ylidene) (**6**) in good yield. A similar reaction of **5** with trimethyl phosphite gave **6** in a 44% yield. However, the reaction of **3** with triphenylphosphine or trimethyl phosphite affords no ethylenic compound. The compound **6** was insoluble in almost all common organic solvents, but slightly soluble in chloroform. The structure of **6** was determined by elemental analysis, mass (M^+ m/z 520) and ^{1}H-NMR spectra [δ 4.36 (t, 8H) and 4.19 (t, 8H)]. Attempt to prepare the charge-transfer complex with tetracyanoquinodimethane or tetracyanoethylene and oxidation with silver tetrafluoroborate in chloroform were unsuccessful.

Experimental

Materials. Ferrocenethiol,[4] 1,1′-ferrocenedithiol,[5] and 1,1′-thiocarbonyldiimidazole[6] were prepared according to the literature.

Diferrocenyl Trithiocarbonate (3). To a solution of ferrocenethiol (**1**) (0.40 g, 1.8 mmol) in N_2-saturated THF (10 cm^3) was added 1,1′-thiocarbonyldiimidazole (**2**) (0.19 g, 1.08 mmol). The solution was stirred for 2 h at room temperature. After evaporation, the residue was chromatographed on silica gel by elution with toluene to give diferrocenyl trithiocarbonate (**3**) (0.35 g, 81%) as orange crystals. Recrystallization from benzene–hexane gave an analytically pure sample as orange leaflets, mp 193—194 °C. Found: C, 52.90; H, 3.91%. Calcd for $C_{21}H_{18}S_3Fe_2$:

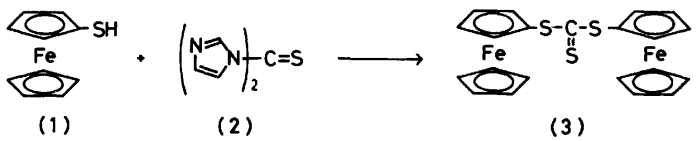

(1) (2) (3)

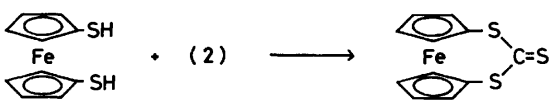

(4) (5)

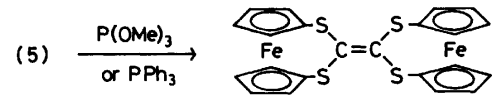

(6)

C, 52.74; H, 3.79%. MS (75 eV): *m/z* 476 (M^+, 100%). IR (KBr): 1043 cm^{-1}. UV-VIS (EtOH): λ_{max} 406 nm (log ε 3.09). ^{1}H-NMR ($CDCl_3$): δ=4.43 (m, 8H) and 4.21 (s, 10H).

1,3-Dithia[3]ferrocenophane-2-thione (5). To a solution of 1,1′-ferrocenedithiol (**4**) (1.74 g, 7 mmol) in N_2-saturated THF (100 cm^3) was added **2** (1.46 g, 8.2 mmol). The solution was stirred for 1 h at room temperature. After evaporation, the residue was chromatographed on silica gel; elution with dichloromethane gave the title compound **5** (1.59 g, 78%) as red orange crystals. Recrystallization from benzene gave an analytically pure sample as red plates, mp 195 °C (dec). Found: C, 45.18; H, 2.79%. Calcd for $C_{11}H_8S_3Fe$: C, 45.21; H, 2.76%. MS (75 eV): *m/z* 292 (M^+, 100%). IR (KBr): 975 cm^{-1}. UV-VIS (EtOH): λ_{max} 424 nm (log ε 3.18). ^{1}H-NMR ($CDCl_3$): δ=4.54 (t, 4H, J=1.8 Hz) and 4.36 (t, 4HJ=1.8 Hz).

2,2′-bi(1,3-dithia[3]ferrocenophan-2-ylidene) (6). A solution of 1,3-dithia[3]ferrocenophane-2-thione (**5**) (0.20 g, 0.7 mmol) and triphenylphosphine (0.23 g, 0.88 mmol) in anhydrous toluene (5 cm^3) was refluxed for 24 h under nitrogen. After keeping at room temperature overnight, the resulting crystals (123 mg, 68%) were filtered. The yellow crystals were recrystallized from a large volume of chloroform. mp 250 °C. Found: C, 50.97; H, 3.28%. Calcd for $C_{22}H_{16}S_4Fe_2$: C, 50,79; H, 3.10%. IR (KBr): 3070, 1410, 1164, 1025, 895, and 815 cm^{-1}. ^{1}H-NMR ($CDCl_3$): δ=4.36 (t, 8H, J=1.8 Hz) and 4.19 (t, 8H, J=1.8 Hz).

A solution of **5** (0.20 g, 0.7 mmol) and trimethyl phosphite (0.1 cm^3, 0.85 mmol) in anhydrous benzene (5 cm^3) was refluxed for 2 h. After a similar work-up described above, yellow crystals (80 mg, 44%) of **6** were obtained.

References

1) R. W. Hoffmann, *Angew. Chem., Int. Ed. Engl.*, **7**, 754 (1968).

2) J. H. Perlstein, *Angew. Chem., Int. Ed. Engl.*, **16**, 519 (1977).

3) D. L. Coffen, J. Q. Chambers, D. R. Williams, P. E. Garrett, and N. D. Canfield, *J. Am. Chem. Soc.*, **93**, 2258 (1971) and references therein.

4) G. P. Knox and P. L. Pauson, *J. Chem. Soc.*, **1958**, 692.

5) G. P. Knox, I. G. Morrison, and P. L. Pauson, *J. Chem. Soc. (C)*, **1967**, 1842.

6) H. A. Staab and G. Walther, *Liebigs Ann. Chem.*, **675**, 98 (1962): T. J. Pullukat and G. Urry, *Tetrahedron Lett.*, **1967**, 1953.

Response of Copper(II) and Cadmium(II) Ion-selective Electrodes in Some Nonaqueous Solvents

Makoto AIHARA,* Sachiko KANETAKE, and Yuka FUKUDA
Laboratory of Inorganic Chemistry, Faculty of Home Life Science, Fukuoka Women's University, Higashi-ku, Fukuoka 813
(Received October 2, 1984)

Synopsis. The response of cadmium(II) and copper(II) ion-selective electrodes was evaluated in methanol, ethanol, acetonitrile solutions and their mixtures with water. The electrodes showed an almost Nernstian behavior in nonaqueous solutions and their mixtures with water except in acetonitrile.

Application of ion-selective electrodes to nonaqueous solutions has been expanded by using solid membrane ion-selective electrode. Properties of the electrodes, *e.g.* their sensitivity, selectivity and response time are expected to be solvent dependent. Several authors reported the response of solid membrane electrode in a variety of organic solvents and their mixtures with water.[1-5] The response of solid membrane electrodes in different solvents is interesting but little is known about such solvent dependence.

This paper is concerned with the response of cadmium(II) and copper(II) ion-selective electrodes at direct potentiometry and potentiometric titrations in methanol, ethanol, acetonitrile and their mixtures with water.

Experimental

For the study, Ag_2S/MS (M=Cu or Cd) membrane disks were supplied by Denki Kagaku Keiki Co. LTD (Tokyo). A cross-section of the ion selective electrode made is shown in Fig. 1. Other apparatus were the same as in the previous report.[6]

Direct potentiometry and potentiometric titration in solution containing 0.1 M (1 M=1 mol dm^{-3}) sodium perchlorate were performed by the usual method. In every case, the electrode system was allowed to attain equilibrium (±0.1 mV) . Potentials at each titration became stable after a period of 5—30 min. All measurements were made at 25.0±0.1 °C.

Results and Discussion

Response of Cadmium(II) Ion-selective Electrode in Direct Potentiometry. Measurements by direct potentiometry of Cd (II) in methanol-water mixtures and pure methanol are shown in Fig. 2. Nernstian response in pure methanol was observed to 2×10^{-6} M at constant ionic strength of 0.1 M. The response becomes more ideal when some water is added.

In ethanol-water mixtures, the electrode responds similarly to the behavior in water-methanol mixtures.

In acetonitrile-water mixtures, the behavior of the electrode was different from the former cases. Approximate Nernstian response to cadmium concentration at constant ionic strength was observed from 10^{-3} M to 10^{-5} M at a solvent mixture containing 40 vol % acetonitrile and 60 vol % water (abbreviated as 40% acetonitrile solution). But intereference of an unknown nature gave very low readings in 80% acetonitrile solution.

Response of Copper(II) Ion-selective Electrode in Direct Potentiometry. In methanol-water mixture, the copper(II) electrode responds very well to copper concentration of 6×10^{-6} M and the Nernstian response was observed in the 80% methanol solution. But the electrode indicated the large shifts of the potential at the low concentration of copper(II) in 100% ethanol solution as shown in Fig. 3.

In ethanol-water mixtures, responses are linear in 20 and 40% ethanol solutions, but indicated the large

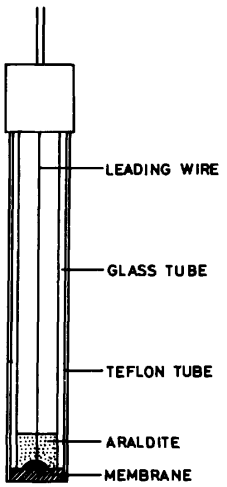

Fig. 1. Cross-section of metal sulfide membrane ion-selective electrode.

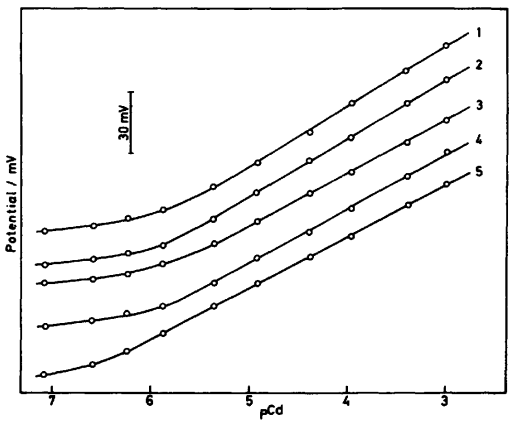

Fig. 2. Calibration curves for cadmium(II) ions in methanol-water mixtures
1; 100 % methanol, 2, 80 % methanol, 3; 40 % methanol, 4; 20 % methanol, 5; water

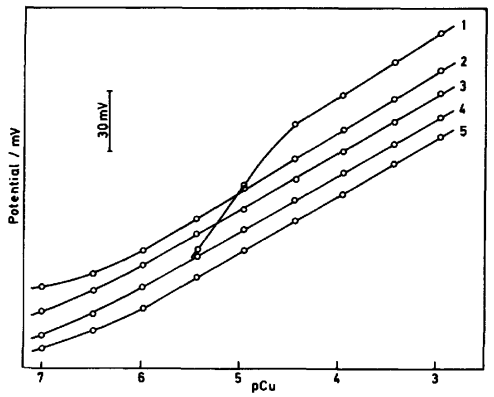

Fig. 3. Calibration curves for copper(II) ions in ethanol–water mixtures.
1; 100 % ethanol, 2; 80 % ethanol, 3; 40 % ethanol, 4; 20 % ethanol, 5; water

TABLE 1. RESPONSE OF COPPER(II) AND CADMIUM(II) ION-SELECTIVE ELECTRODES IN VARIOUS SOLVENTS

Solvent		Cu(II) electrode		Cd(II) electrode	
		Slope[a]	Lower limit of usable range[b]	Slope[a]	Lower limit of usable range[b]
		−mV/decade	pC_{Cu}	−mV/decade	pC_{Cd}
Water		31	6.2	29	6.5
Methanol	20%	30	6.2	29	5.8
	40%	30	6.2	28	5.8
	80%	31	6.2	30	5.7
	100%	28	4.4	31	5.7
Ethanol	20%	32	6.4	29	5.9
	40%	32	6.4	29	5.9
	80%	32	4.8	31	5.6
	100%	32	4.8	35	5.7
Acetonitrile	20%			26	4.6
	40%			26	4.6

a) Extending over the range $3<pC<5$. b) Evaluated as the point of intersection of the approximately linear segments of the curve in the regions $3<pC<5$ and $6<pC<7$.

TABLE 2. SELECTIVITY COEFFICIENTS FOR SEVERAL CATIONS

Solvent		Cu(II)-electrode	Cd(II)-electrode
		$\log K_{Cu,Fe}$	$\log K_{Cd,Zn}$
Water		0.8	5.0
Methanol	20%	0.8	5.3
	40%	0.4	5.2
	80%	1.5	5.4
Ethanol	20%	1.1	5.3
	40%	1.5	5.4
	80%	1.8	5.5
Acetonitrile	20%		5.3

shifts of potential at 80% ethanol and 100% ethanol concentration.

The results of these electrode responses are present in Table 1.

Evaluation of Selectivity Coefficients. The selectivity coefficients of these electrodes were determined by the mixed solution method. The values of the selectivity constants of the electrodes for two metals are given in Table 2. The selectivity coefficients in methanol-water and ethanol-water mixtures were somewhat larger than those in water.

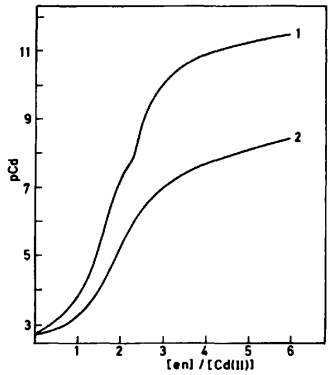

Fig. 4. Titration curves of 2×10^{-3} M $Cd(ClO_4)_2$ with 0.1 M en in 100 % methanol and ethanol solutions.
1; 100 % ethanol, 2; 100 % methanol.

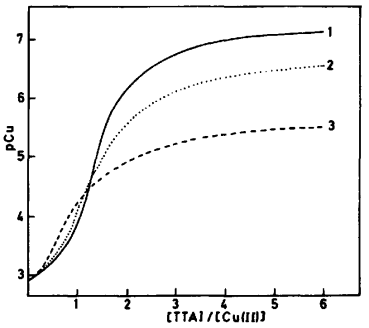

Fig. 5. Titration curves of 2×10^{-3} M $Cu(ClO_4)_2$ with 0.1 M TTA in 80 % ethanol solution.
1; pH=6.9, 2; pH=5.1, 3; pH=4.1.

Complex Formation Studies. In Figs. 4 and 5 are shown the potentiometric titration curves of cadmium(II) solution with ethylenediamine(en) in 100% methanol and ethanol solutions and copper(II) solution with thenoyltrifluoroacetone(TTA) in 80% ethanol solution. None of the titration curves showed any distinct break. The successive formation of complexes is proposed and more detail discussion is required for the determination of successive formation constants.

The authors wish to thank Denki Kagaku Keiki Co., LTD (Tokyo) for partial support of this work. We are grateful to Mr. Toru Ito for many helpful suggestions.

References

1) G. A. Rechnitz and N. C. Kenny, *Anal. Lett.*, **2**, 395 (1969).
2) L. A. Heerman and G. A. Rechnitz, *Anal. Chem.*, **44**, 1655 (1972).
3) J. F. Coetzee and M. W. Martin, *Anal. Chem.*, **52**, 2412 (1980).
4) J. F. Coetzee and W. K. Istone, *Anal. Chem.*, **52**, 53 (1980).
5) J. F. Coetzee , W. K. Istone, and M. Carralho, *Anal. Chem.*, **52**, 2353 (1980).
6) M. Aihara and Y. Oho, *Sci. Human Life, Fukuoka Women's Univ.*, **12**, 95 (1979).

Effects of Uniaxial Pressure and Shear on the Electrical Conductivity of Solid. II. Electrical Conductivity in Some Amorphous Coordination Polymers[1)]

Seiichi KANDA,* Kuwako OHKAWA,† Kenichi YAMASHITA,††
Nobuo ODA,††† and Hideaki CHIHARA**
Department of Applied Chemistry, Faculty of Engineering, The University of Tokushima, Minamijosanjima, Tokushima 770
**Department of Chemistry, Faculty of Science, Osaka University, Toyonaka 560*
(Received April 27, 1984)

Three amorphous coordination polymers, R_2dtoaCu, where R=CH_3, $C_6H_5CH_2$, or cyclohexyl and dtoa= (*N,N'*-disubstituted dithiooxamidato), were prepared and the effect of uniaxial pressure on their electrical resistivities in the direction of the external pressure was measured. Application of the pressure up to 6×10^8 Pa caused an increase in the resistivity but, before reaching the equilibrium state, the resistivity exhibited a complicated time variation, which was not completely reversible upon pressure release as far as the measurement could trace. The results were explained on the basis of a model in which at least two competing processes occur. One of the processes is assumed to be reorientation of the two-dimensional network of molecules perpendicular to the applied pressure, which is a slow process and takes as long as hundreds of hours to reach the equilibrium. Activation energies of various processes were derived.

The three coordination polymers (R_2dtoaCu; R= CH_3, $C_6H_5CH_2$, and *cyclo*-C_6H_{11}) treated in this study are representatives of several *catena*-μ- (*N,N'*-disubstituted dithiooxamidato)-copper(II) coordination polymers, the resistivities of which range from 10^5 to 10^{10} Ωcm at 30°C.[2)] Although the technique of X-ray structural analysis[4)] is not applicable due to the amorphous structures, a two-dimensional network structure has been proposed on the basis of some evidence.[3)] An example of such a network model (Fig. 1) will be discussed later.

While numerous studies have been reported on the electrical properties of semiconductive polymers, there have been a few that dealt with the effect of pressure on the electrical properties, *e.g.* resistivity,[5-8)] dielectric constant,[5)] activation energy for conduction,[6)] electronic mobility,[7)] and superconducting transition;[8)] there have been no studies on the kinetic aspect of the pressure effect. Generally, the electrical resistivity of powder samples has been measured on compressed pellets or under pressure.[9)] The resistivity of semiconductive organic crystals usually decreases reversibly by several orders of magnitude with an increase of pressure up to 10^{10} Pa. Beyond 10^{10} Pa, irreversible chemical changes occur in some compounds, which result in irreversible changes in their resistivity.[10)] One exception was reported in the case of poly(phenylacetylene), where a large reversible increase in resistivity upon increasing the pressure was attributed to a large positive volume of activation.[11)]

In contrast to these cases, application of a uniaxial pressure less than 10^9 Pa on R_2dtoaCu coordination polymers results in an increase in resistivity and complicated hysteresis.[1)] Enhancement of this tendency with an application of shear stress substantiates the idea that the anomaly is attributed to the anisotropic structure of the macromolecule and its response to an external pressure.[12)] In the last report[1)] a semiquantitative study was presented on the hysteresis effect in the resistivity-pressure-temperature relationship. A model was then proposed which assumes molecular motions that depend on the temperature, the pressure, and the history of treatment. In this paper the phenomenon will be more quantitatively examined from standpoints of rate process and equilibrium properties.

Experimental

Materials. *N,N'*-dimethyldithiooxamide ($(CH_3)_2$dtoa-H_2), *N,N'*-dibenzyldithiooxamide ($(C_6H_5CH_2)_2$dtoaH_2), and *N,N'*-dicyclohexyldithiooxamide ($(C_6H_{11})_2$dtoaH_2), were kindly donated by Mallinckrodt Chemical Works, and were recrystallized from ethanol. The copper coordination polymers were prepared by mixing an aqueous solution of copper sulfate and a water-ethanol solution of the equivalent amounts of the ligands according to the reaction of the type:

$$Cu^{2+} + \begin{matrix} RHN & & S \\ \diagdown & & \diagup \\ & C-C & \\ \diagup & & \diagdown \\ S & & NHR \end{matrix} \longrightarrow 2H^+ + \text{the coordination polymer}$$

The structural model of the polymers is depicted in the Fig. 1. The amorphous precipitates were centrifuged and washed repeatedly with water and ethanol, successively.

Analyses of the Three Coordination Polymers. $(CH_3)_2$dtoa-Cu, Found: H, 2.83; C, 20.72; N, 11.22; Cu, 29.22%. Calcd for $C_4H_6N_2S_2Cu$: H, 2.89; C, 22.90; N, 13.35; Cu, 30.29%. $(C_6H_5CH_2)_2$dtoaCu, Found: H, 3.97; C, 53.27; N, 7.60; Cu, 16.70%. Calcd for $C_{16}H_{14}N_2S_2Cu$: H, 3.90; C, 53.10; N, 7.74; Cu, 17.47%. $(C_6H_{11})_2$dtoaCu, Found: H, 6.54; C, 48.4; N, 7.97; Cu, 18.41%. Calcd for $C_{14}H_{22}N_2S_2Cu$: H, 6.40; C, 48.6; N, 8.10; Cu, 18.36%. The slightly low values of nitrogen are frequently observed in coordination polymers containing copper(II) directly coordinated by nitrogen.[13)] The atomic ratios of the elements in the polymers were calculated from the analytical values by fixing the number of carbon atoms at the limiting value for infinite degree of polymerization.

†Present address: Training Institute for Environmental pollution Control, 3-3 Namiki, Tokorozawa, Saitama 359.
††Present address: Osaka Titanium Co., Ltd., Amagasaki, Hyogo 660.
†††Present address: Matsumura Oil Research Corp., Ashiharacho, Nishinomiya, Hyogo 662.

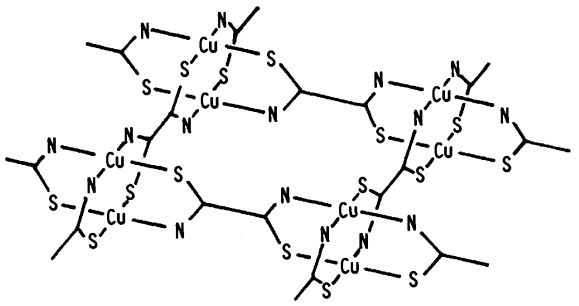

Fig. 1. The non-stereospecific two-dimensional network model with dimer structure of copper acetate type. For simplicity, substituents on nitrogen atoms are not shown.

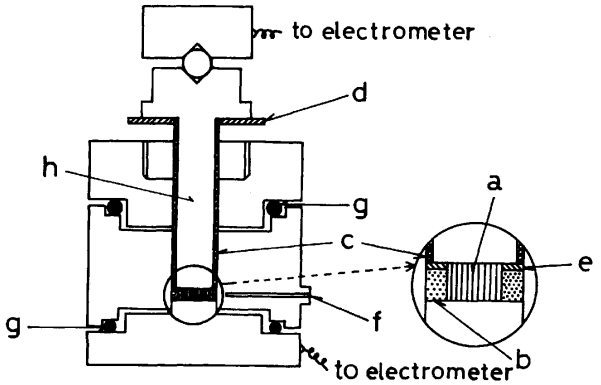

Fig. 2. High pressure cell remodeled from a pellet press.
a): Pellet of sample, b): pyrophyllite gasket, c): Teflon film for electrical insulation, d): polyethylene sheet, e): Teflon sheet, f): re-entrant well for thermocouple, g): O-ring for sealing, h): piston serving both as an electrode and a pressure transducer.

The reasonable agreements between the calculated and observed atomic ratios show that the polymers obtained have nearly stoichiometric composition, $(RNSC)_2Cu^{II}$. In fact, the polymers assume a two-dimensional network structure in which some vacancies of Cu sites are, in principle, possible. If it occurs, electroneutrality requires two additional hydrogen atoms to replace a copper atom. This is reflected in the low values of copper and the correspondingly high values of hydrogen in the elemental analyses.

Electrical Measurements. As a high pressure cell for the resistivity measurements, a pellet press was used with a steel piston having a diameter of 11.5 mm. The piston was used as an electrode with insulating Teflon film (0.2 mm thick) around it as shown in Fig. 2. By use of an oil pump and the above-mentioned cell, a maximum pressure of 9.0×10^8 Pa can be applied to the specimen. The temperature was controlled by a ribbon heater wound around the outside can, which is not shown in Fig. 2. A thermocouple for temperature measurements was inserted into the re-entrant well at the lower end. The vessel was not evacuated, but was sealed from the atmosphere with O-rings. The powder specimen was first premolded in 5 mm diameter at 1.8×10^8 Pa; the small pellet was mounted at the center of a pyrophyllite gasket which had been pretreated at 700 °C for 30 min; the assembly shown in Fig. 2 with a piece of thin Teflon ring, was pressed.

Electrical data under pressure were taken *in situ* a few minutes after the electrical field was applied. The electrical resistance was measured by means of a valve voltmeter with an applied electric field of 15 V cm^{-1}. The pellet assembly was replaced for each run at one temperature, which usually took as long as several hundred hours because of the long equilibration time under applied pressure. When, however, we measured the temperature dependence of the equilibrium resistivity values as shown later in Figs. 8 and 9, a single loading of the specimen was used. The effects of pressure were examined by using a uniaxial pressure of 6.0×10^8 Pa throughout this study. The same pressure value was used for determining the resistivity values of the specimens of the pellet form, which was applied only instantaneously and intermittently during the runs in which relaxation after pressure release was studied. Such instantaneous application of pressure would not affect the long-time response of the specimen. For the polymers under investigation there is a fast process which occurs upon compression or pressure release and which is followed by a very slow process as we will discuss in detail.

Results and Discussion

The Rate Process under a Uniaxial Pressure (6.0×10^8 Pa). Changes in the resistivity of $(CH_3)_2$dtoaCu, $(C_6H_5CH_2)_2$-dtoaCu, and $(C_6H_{11})_2$dtoaCu under a constant external pressure as the function of time are shown in Figs. 3, 4, and 5. The resistivities begin to change immediately after the external pressure was applied or released. These changes occur in a very short time and were not traced. However, such an initial stage of change was followed by a very gradual drift of the resistivity values extending up to several hundred hours. It is such a long-time behavior that we are interested in. In Figs. 3—5, $\rho_0^{\pm}$ is the initial resistivity value determined immediately after the fast process has been completed, the superscript $\pm$ meaning the compression or the pressure release operation.

The general feature of the time dependence as exemplified in Fig. 3a is that it is a kind of relaxation phenomenon. Ordinarily, such a relaxation process is characterized by a time constant which governs the first order rate process. In other words, the rate of change of resistivity, $d\rho^{\pm}/dt$, can be described by

$$d\rho^{\pm}/dt = -k^{\pm}(P, T)(\rho^{\pm} - \rho_{eq}^{\pm}) \quad (1)$$

Here, $\rho_{eq}^{\pm}$ is the asymptotic (equilibrium) value of the resistivity, k is the rate constant and equal to the reciprocal of the relaxation time.

The experimental values of resistivity were fitted to Eq. 1 in the integrated form and it was found that the equations can reproduce the observed results in certain ranges of time. The values of k thus derived are listed in Table 1 together with the activation energies derived from the Arrhenius equation

$$k^{\pm} = k_0^{\pm} \exp(-\Delta H_{\pm}^{\pm}/RT). \quad (2)$$

The plots of $k^{\pm}$ *vs.* T^{-1} are shown in Fig. 6.

The results of Figs. 3a and 3b fit Eq. 1 over the almost

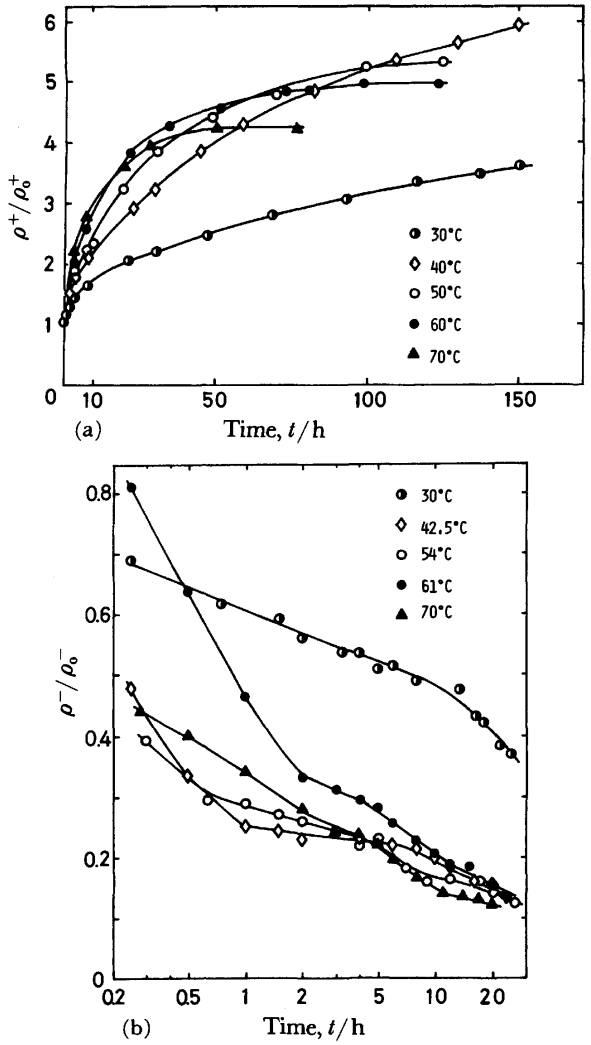

Fig. 3. Resistivity changes of $(CH_3)_2$dtoaCu.
a): Under uniaxial pressure, b): under ambient pressure after the operation of a).
For definition of ρ_0, see in the text.

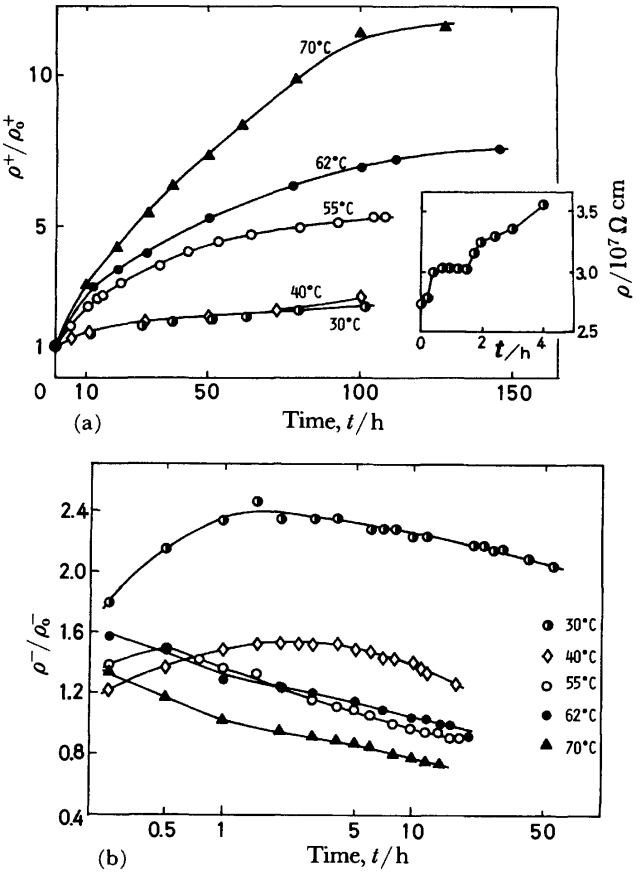

Fig. 4. Resistivity changes of $(C_6H_5CH_2)_2$dtoaCu.
a): Under uniaxial pressure, b): under ambient pressure after the operation of a).

entire range of time, whereas for the dibenzyl complex (Fig. 4b) and the dicyclohexyl complex (Fig. 5a), Eq. 1 can be applied only in the ranges in which $d\rho/dt<0$ in Fig. 4b and $d\rho/dt>0$ in Fig. 5a.

As shown by the insert of Fig. 4a, the resistivity of the dibenzyl complex does not show a monotonous change but has a small plateau. In the case of the dicyclohexyl complex (Fig. 5a), the initial change of the resistivity is opposite to the cases of the other two polymers, *i.e.* the resistivity decreases with time under a constant external pressure. After this initial process, the behavior (after 10 h. at 110°C) can be described by Eq. 1.

These additional features for which Eq. 1 does not apply strongly suggest that the time dependence of the resistivities, or the relaxation process, is not a simple process but there must be two or more mechanisms having different rate constants (or relaxation times) that proceed competitively.

A Structural Model. Application of uniaxial pressure usually decreases the resistivity of polycrystalline semiconductors parallel to the external stress. It is interpreted as due to improved contact between grains and decreased intermolecular distances. All the three substances examined in the present study, on the contrary, showed an increase in the resistivity under uniaxial pressure. However, the conditions of time and/or temperature were different from substance to substance, under which such an anomalous behavior was observed. This means that there must be some special cause that operates in these substances and opposes the ordinary compaction effects mentioned above. The special cause, which we will try to identify, will give rise to a complex overall behavior as seen in Fig. 5a in the case of the cyclohexyl complex.

Similarly, the release of the uniaxial pressure results in a decrease in the resistivity although here again there are differences in the overall behavior among the coordination polymers.

In order to find a mechanism by which such anomalous pressure dependence occurs, let us first consider about the structure of these polymers. The model of Fig. 1 is based on some evidence obtained from the composition, the X-ray diffraction pattern, and the magnetic data.[3] In this model, the polymer complex forms a two-dimensional network with the substituent, methyl, benzyl, or cyclohexyl group, attached at every N atom. The substituents will therefore protrude above and below the network plane but it is not easy to

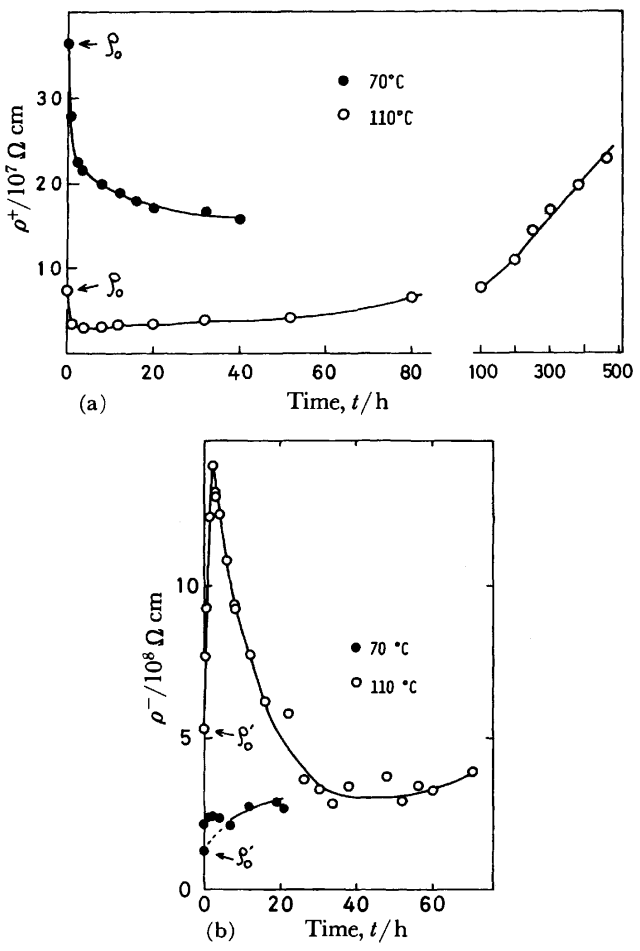

Fig. 5. Resistivity change of $(C_6H_{11})_2$dtoaCu.
a): Under uniaxial pressure, b): under ambient pressure after the operation of a).

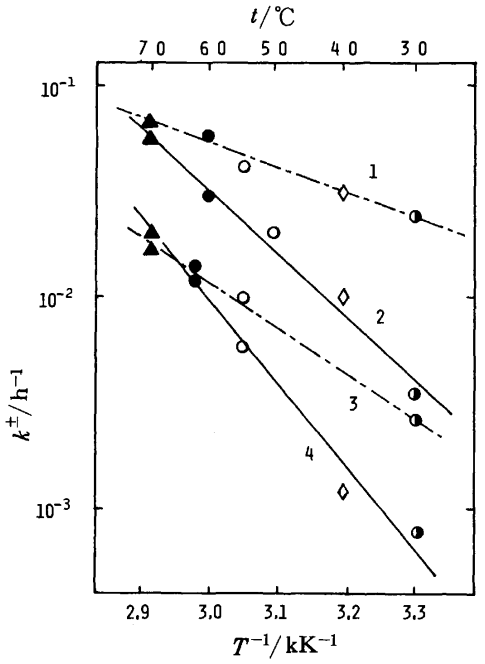

Fig. 6. Arrehnius plots of the rate constants for R_2dtoaCu.
(1): CH_3, $k^-(P=0)$, (2): CH_3, $k^+(P=6.0\times10^8$ Pa), (3): $C_6H_5CH_2$, $k^-(P=0)$, (4): $C_6H_5CH_2$, $k^+(P=6.0\times10^8$ Pa).

speculate about the conformation of the substituents. It is interesting in this connection to note that the measured bulk densities of the complexes under ordinary pressures were 1.55, 1.659, 1.76 g cm^{-3} for the methyl, benzyl, and cyclohexyl complexes, respectively; *i.e.* the methyl complex has the largest void space fraction and the cyclohexyl complex the smallest. In other words, the bulky substituents may lie more or less flat in parallel to the network plane. The electronic conduction will be very anisotropic because the electrons are likely to be delocalized whithin a network plane and only van der Waals interaction exists between the planes.

Now, the plausible explanation for the anomalous positive pressure coefficient of the electrical resistivity seems to be that there occurs some rearrangement of molecules as a result of compression. The increase in the resistivity in the direction of applied pressure will mean an increased contribution of the resistivity component perpendicular to the molecular plane. The polymer specimens as prepared have little preferred orientation but, as the uniaxial pressure is applied, the molecular plane will be gradually reoriented so that the plane tends to become perpendicular to the stress, thus increasing the resistivity in the direction of the stress. Such reorientation effect will, of course, be accompanied by deformation of grains. In quite general terms, the uniaxial stress causes randomly oriented molecular planes to be more or less ordered.

Change of Resistance with Time–An Interpretation. It should be noted that the pressure effects are not completely reversible. After a cycle of compression and pressure release, the resistivity does not completely return to its original value. This indicates that there are plastic parts in the deformation as well as elastic parts. Furthermore, if one compares Fig. 4a with Fig. 4b, the benzyl complex shows a smooth change of the resistivity upon compression, but, when the pressure is released, it shows a maximum in the resistance below 55 °C. Therefore, there are at least two competitive processes which give rise to a maximum in the resistivity; one is faster than the other. The faster process is not seen at or above 62 °C in Fig. 4b because the process becomes too rapid at higher temperature in the case of the benzyl complex. The fast process is the process by which the resistivity increases upon pressure release; this is the normal behavior in semiconductors and will be called the process N hereafter. The second process will be called the process A which shows an anomalous effect of decreasing resistivity upon pressure release (we assume that the processes N and A occur upon compression as well as upon pressure release).

The case of the cyclohexyl complex may be interpreted in an analogous way. Upon pressure release (Fig. 5b), there is a maximum in the resistivity which is seen at 110 °C. It is again the competitive effect of the processes N and A, only the process N being observed at 70 °C in a short time (less than 20 h). Upon

TABLE 1. PARAMETERS FOR THE RATE PROCESSES UPON COMPRESSION AND RELEASE

Under uniaxial pressure of 6.0×10^8 Pa

$(CH_3)_2$dtoaCu			$(C_6H_5CH_2)_2$dtoaCu			$(C_6H_{11})_2$dtoaCu	
t	k^+	$\Delta H_+^{\neq}$	t	k^+	$\Delta H_+^{\neq}$	t	k^+
°C	10^{-3} h^{-1}	kJ mol^{-1}	°C	10^{-3} h^{-1}	kJ mol^{-1}	°C	10^{-4} h^{-1}
30	3.5		30	0.7		90	3.6
40	10.1		40	1.2		110	3.8
50	20	57.2	55	5.6	75.5	(time>10 h)	
60	$30._8$	±3.2	62	12	±3.6		
70	55		70	20			
Under ambient pressure							
t	k^-	$\Delta H_-^{\neq}$	t	k^-	$\Delta H_-^{\neq}$	t	k^-
°C	10^{-2} h^{-1}	kJ mol^{-1}	°C	10^{-2} h^{-1}	kJ mol^{-1}	°C	10^{-3} h^{-1}
30	2.4		30	0.2_7		110	$11._8$
$42._5$	3.0		40	1.4[a]		(20>time>4 h)	
54	4.1	23.0	55	1.0	40.8		
61	5.8	±1.7	62	1.4	±1.6		
70	6.6		70	1.7			

a) Omitted for the calculation of $\Delta H_-^{\neq}$.

compression (Fig. 5a), only the process N is seen in a short time particularly at a lower temperature. For this complex, the change of the resistivity was measured to 500 h (Fig. 5a) and the process A is seen to proceed slowly.

The case of the methyl complex looks simple, but it is probably because the process N finishes in a very short time. With regard to the process A, the value of $k^{\pm}$ (Table 1) is generally much larger for the methyl complex than for the other two complexes. This suggests a quicker response of the methyl complex with regard to the process N. The rate of the two processes depends strongly on temperature; at lower temperatures the process N can be so slow (as slow as the process A) that the two processes are not separable, causing a maximum in the resistivity to appear at a certain time as in the case of the dibenzyl and the dicyclohexyl complexes.

To rationalize the relationship between experimental observations on the processes N and A and the usual dynamics of the viscoelastic body, let us consider the Voigt model.[14]

Strain γ of polymer solids due to an external load is analyzed by use of a spring for elasticity and a dash-pot for plasticity. The two elements, the spring and the dash-pot, can be combined in parallel to build the Voigt element, which represents anelasticity *i.e.* time-dependent elastic deformation. The three macroscopic deformations (elastic, plastic and relaxationally elastic), γ_e, γ_p, and γ_r, are expressed schematically as a function of time in Fig. 7a. The elastic after-effect of anelasticity is given by

$$\gamma_r = \gamma_\infty[1 - \exp(-t/\tau)]. \quad (3)$$

The reciprocal of the relaxation time τ corresponds to $k^{\pm}$ in Eq. 1. The change in time of the resistivity of the three coordination polymers, $\Delta\rho$, generally have components, $(\Delta\rho)_e$, $(\Delta\rho)_p$, and $(\Delta\rho)_r$, in a manner similar to the case of the macroscopic deformation. While the sign of all the components of γ is the same, the sign of the $(\Delta\rho)_e$ is opposite to the sign of $(\Delta\rho)_r$ or $(\Delta\rho)_p$ in the compound studied (Fig. 7b). Typical examples of combination of these components are shown in Fig. 7c. It should be noticed that the apparent τ's (*i.e.* $1/k$) can be different during the compression and during release because of the relaxational components in the Voigt model.

If we associate the $(\Delta\rho)_e$ components mainly with the process N and $(\Delta\rho)_r$ and $(\Delta\rho)_p$ mainly with the process A, we obtain good correspondence between the behavior of the Voigt model and the time-dependence of the resistivities. Thus the elastic portion or the process N has a very fast response to external stimulations, whereas the process A is slower and causes an apparent hysteresis even if the molecular processes involved are the same upon compression and upon release.

What happens when the specimen is compressed will be viewed in the following way. The initial process will be deformation or collapse of grains to fill the void space between the grains (improved contact between grains), which is followed by a simple compression (time-dependent elastic deformation) which changes the intermolecular distances. This corresponds to the process N. The instantaneous elastic deformation will bring the molecular arrangement into an energetically unstable configuration which will then be relaxed by the time dependent elastic process and by the slow plastic deformation process (the process A). If we pursue our picture a little further, this relaxation will occur in such a way as to reorient the network planes so that the planes will become perpendicular to the direction of the stress. As the molecular arrangement is gradually relaxed, further elastic deformation will become possible at successively new molecular configuration and such secondary elastic deformation

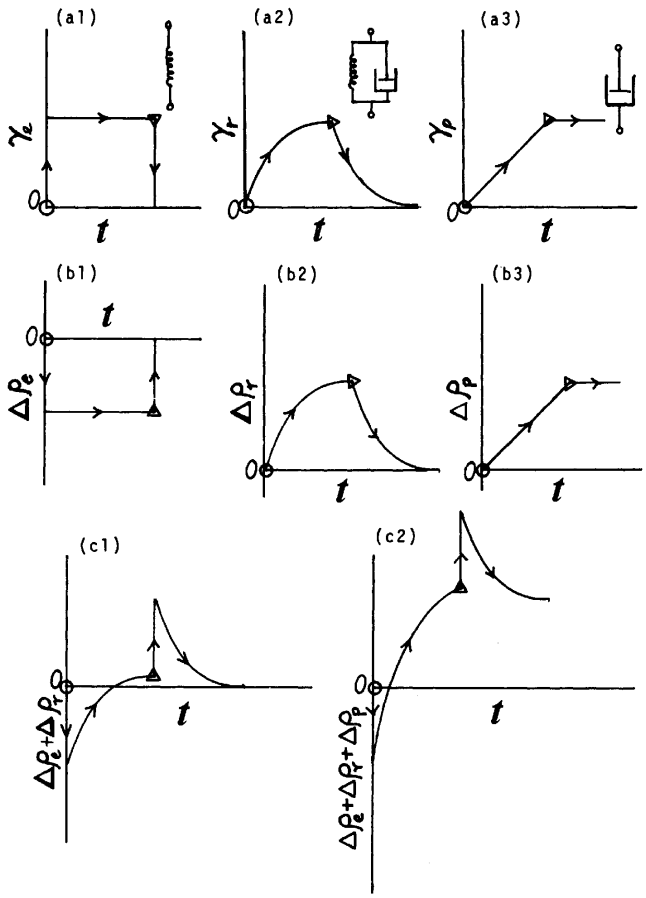

Fig. 7. Schematic representation of time evolution of the strain γ, and the electrical resistivity $\Delta\rho$ for elastic, Voigt, and plastic models: a1—a3 for the three models of γ respectively, b1—b3 for the three models of $\Delta\rho$, c1—c2 for combinations of the models of $\Delta\rho$.
See in the text.
○: Starting-point of stress application, ▷: starting-point of stress release.

will cause further relaxation due to plastic deformation. Therefore, the elastic and plastic processes mutually affect each other and so do the processes N and A. The values of $k^{\pm}$ in Table 1, in this vein, should be considered to correspond not to a well-defined single process but to a composite process.

Activation Energies for The Mechanical Process. From the plots of Fig. 6, the apparent activation energies of the relaxation process (the process A) were derived for the methyl and benzyl complexes as listed in Table 1. In both substances, the activation energy is larger upon compression than upon pressure release. The differences between the values for the two directions are almost the same in the two substances, 34 kJ mol^{-1} (57.2—23.0) and 35 kJ mol^{-1} (75.5—40.8) for the methyl and the benzyl complex, respectively. If the same activated state can be assumed in the two directions, the equality shows that the difference in energy between the initial state (random molecular arrangement) and the final state (oriented molecular arrangement) does not depend on whether the substituent is methyl or benzyl; the difference between the two substances lies in the height of the potential barrier hindering the relaxation.

Temperature Dependence of Equilibrium Resistivity. Because the long-time behavior was an extremely slow process, it was not easy to obtain the reliable equilibrium values of resistivity $\rho^{\pm}_{eq}(P,T)$ at a given temperature. The criterion for equilibrium and the method for determining the equilibrium values were as follows: (1) An attempt was first made to wait until a steady value was obtained under a constant external pressure at a temperature. (2) The temperature was then lowered under the same pressure and the specimen was brought to a state of equilibrium at that temperature. After a certain length of time, usually a few hours, the specimen was heated back to the original temperature where the resistivity approached the equilibrium value from the opposite side to the case (1). If the final value agreed with the value obtained in (1), it was taken as the equilibrium value. If it did not, the average value was adopted. This procedure was employed only at 70 °C.

Figures 8 and 9 will illustrate such sequence of changes. In Fig. 8, the point on the line 1 corresponds to the equilibrium state at the ambient pressure, which we call the random state. Suppose that the specimen (the dimethyl complex) which had been brought to equilibrium at 70 °C under the ambient pressure was pressed for 77 h; the final steady value was assumed to be the equilibrium state. The specimen was then cooled under pressure to a lower temperature where a new equilibrium was waited. Such a cooling was done usually in a short time and the change in the resistivity that occurred in this time is indicated by the broken lines in Figs. 8 and 9. After the equilibrium at 40 °C was obtained for the dimethyl complex (Fig. 8), it was heated back to 70 °C. This heating was done also in a short time and the change in resistivity followed the broken line. At 70 °C, the equilibrium state was approached from the opposite side this time, as explained in (2). Figure 9 shows similar results for the dibenzyl complex. It is interesting to note that the broken lines are more nearly parallel to the line 1 in Figs. 8 and 9 in comparison with the line 2 which connects the equilibrium values under pressure and has a larger slope than the line 1.

Now let us examine the activation energy for electronic conduction in the same direction as that of the external stress as obtained from Figs. 8 and 9. Under no uniaxial stress it was 0.34 eV (33 kJ mol^{-1}) and 0.29 eV (28 kJ mol^{-1}) for the methyl and benzyl complex, respectively. Under the stress of 6.0×10^8 Pa, the values are 0.45 eV (44 kJ mol^{-1}) and 0.43 eV (41 kJ mol^{-1}) corresponding to the state of oriented molecular arrangement. On the other hand, the non-equilibrium resistivity under the pressure gave the same activation energy as the equilibrium resistivity at the ambient pressure (dashed line and line 1 of Fig. 8). This fact

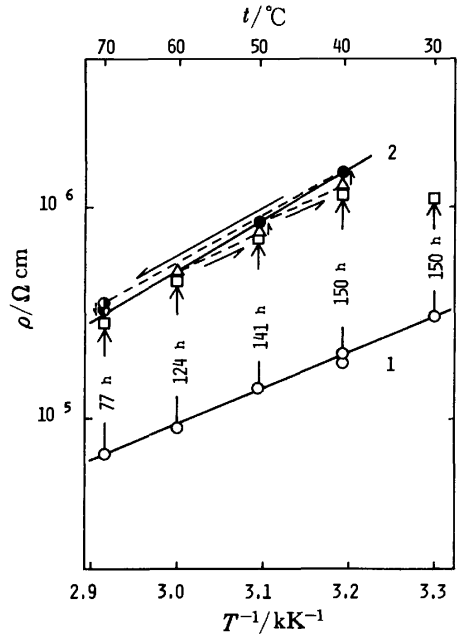

Fig. 8. Resistivity-temperature relation in the transient and the equilibrium states of $(CH_3)_2$dtoaCu. 1 and ○ correspond to the initial random state; 2 and ● the oriented equilibrium state, △ is the cooled state where a new equilibrium state ● is waited, ◑ is the heated-back state where the equilibrium is approached through ◐. □ is the values after the indicated elapse of time. See in the text.

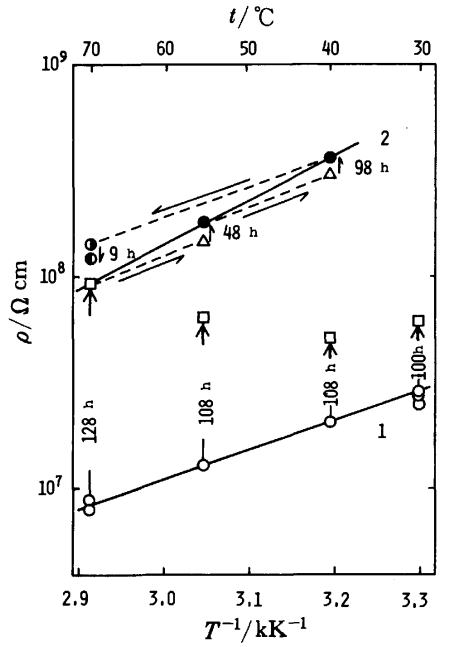

Fig. 9. Resistivity-temperature relation in the transient and the equilibrium states of $(C_6H_5CH_2)_2$dtoaCu. △, ●, ◑, ◐, and □ are essentially the same as in Fig. 8.

justifies our interpretation that the initial process that occurs when the specimen is compressed is the process N involving the improved contact between grains and the elastic deformation. The process A which follows brings the specimens to a state (the oriented state corresponding to the line 2) which requires higher activation energy of conduction (0.45 eV and 0.43 eV). The fact that the difference in the activation energy with or without the external stress is small indicates that reorientation of network planes is not complete under the stress of 6.0×10^8 Pa; the solid would become almost an insulator if the molecular reorientation were complete. Nevertheless the activation energy does increase rather than decrease upon compression and such an effect is also consistent with our picture about the nature of the process A by which the resistivity component increases in the direction perpendicular to the network plane.

Finally, it is very interesting to note that despite the close similarity in the response to uniaxial stress, the methyl and the benzyl complexes show very different equilibrium resistivity values, by a factor of about 10^2 both in the random and the oriented state. The methyl and benzyl complexes have very similar activation energy in their oriented state. Bulkiness and steric hindrance of the substituents are probably related to such a large difference in the resistivity through the deformation of the network structure.

The authors wish to express their thanks to Mr. Satoru Morinishi and Mr. Hideo Minami for their assistance in the measurment and the instrumentation. The present work was partially supported by Grant-in-Aid for Scientific Research No. 754123 from the Ministry of Education, Science and Culture.

References

1) Part I of this study was published in S. Kanda, *Kogyo Kagaku Zasshi*, **71**, 1426 (1968); Part of this study was presented at the 14th High Pressure Conference of Japan, Osaka, October 1972, Abstr., No. 23A12, and at the 29th National Meeting of the Chemical Society of Japan, Hiroshima, October 1973, Abstr., No. 4S09.

2) S. Kanda, *Nippon Kagaku Zasshi*, **83**, 560 (1962).

3) S. Kanda, A. Suzuki, and K. Ohkawa, *Ind. Eng. Chem., Prod. Res. Dev.*, **12**, 88 (1973).

4) R. Hasegawa, Y. Tanabe, M. Kobayashi, and H. Tadokoro, *J. Polym. Sci., A-2*, **8**, 1073 (1970).

5) V. A. Zhorin, S. I. Beshenko, Yu. A. Berlin, and N. S. Enikolopyan, *J. Appl. Polym. Sci.*, **28**. 2467 (1983).

6) J. P. Crine, *Phys. Status Solidi A*, **72**, 789 (1982).

7) H. A. Phol and J. R. Wyhof, *J. Polym. Sci., A1*, **10**, 387 (1972).

8) K. J. Dunn, F. P. Bundy, and L. V. Interrante, *Condens. Matter*, **23**, 106 (1981).

9) One of the earliest examples: H. Inokuchi, *Bull. Chem. Soc. Jpn.*, **28**, 570 (1955).

10) W. H. Bentley and H. G. Drickamer, *J. Chem. Phys.*, **42**, 1573 (1965).

11) G. M. Holob and P. Ehrlich, *J. Polym. Sci., Polym. Phys. Ed.*, **15**, 627 (1977).

12) H. A. Pohl and D. A. Opp, *J. Phys. Chem.*, **66**, 2121 (1962).

13) S. Kanda, K. Yamashita, and K. Ohkawa, *Bull. Chem. Soc. Jpn.*, **52**, 3296 (1979).

14) T. Alfrey, "Mechanical Behavior of High Polymers," Interscience, N. Y. (1948).

Structural and Compositional Changes of Blue Orthorhombic Hydrogen Molybdenum Bronze, $H_{0.30}MoO_3$, by Vacuum Heating and Catalytic Activity for 1-Butene Isomerization

Noriyuki SOTANI,* Noritetsu YOSHIDA,† Yukio YOSHIOKA,† and Shozo KISHIMOTO†

College of Liberal Arts, Kobe University, Tsurukabuto, Nada, Kobe 657

†*Department of Chemistry, Faculty of Science, Kobe University, Rokkodai, Nada, Kobe 657*

(Received August 8, 1984)

Orthorhombic bronze, $H_{0.30}MoO_3$, was decomposed by vacuum heating to $MoO_{2.86}$ with a rhombic MoO_3 structure. The surface area increased slightly with the increase in the rhombic structure in which vacancies were produced. An approximate linear relationship was found between the catalytic activity of 1-butene isomerization and the hydrogen content(x) in the samples which were treated in air at 65 °C or *in vacuo* below 220 °C. On the other hand, the activity above 220 °C increased with the formation of vacancies.

Molybdenum bronzes (formulated as H_xMoO_3) are obtained from the reduction of MoO_3 by atomic hydrogen.[1-5] Four distinct phases are found in the range $0<x\leqq2.0$[4] and the homogenieties of these phases are as follows; (i) blue orthorhombic; $0.23<x<0.4$, (ii) blue monoclinic; $0.85<x<1.04$, (iii) monoclinic; $1.55<x<1.72$, and (iv) green monoclinic; $x=2.0$.

These bronzes were expected to be hydrogen reservoirs and interest, therefore, was centered on their catalytic properties. Sermon and Bond[6] have reported that hydrogen in 1% $Pt/H_{1.6}MoO_3$ was useful for 1-pentene hydrogenation. Marcq *et al.*[7] studied the catalytic hydrogenation reaction of ethylene on the red monoclinic bronze, $H_{1.6}MoO_3$, obtained from Pt-supported MoO_3 by hydrogen spillover and confirmed that the atomic hydrogen in the bronze was active for the catalytic hydrogenation of ethylene.

The authors studied the behavior of hydrogen in the blue orthorhombic bronze, $H_{0.30}MoO_3$, by thermogravimetry[8] and by the TPD method.[9] They confirmed that the bronze decomposed to $MoO_{2.86}$, a nonstoichiometric compound with the rhombic MoO_3 structure, in three steps when the bronze was heated under a vacuum of 10^{-4} Torr† and in a helium atomosphere.

Using proton NMR studies,[10] the authors found no difference in the behavior of the protons in the untreated and treated samples and indicated that the environments surrounding the protons did not change throught heat treatment.

In the present work, the catalytic activity for 1-butene isomerization over the bronzes was studied. The structural and compositional changes of the bronzes after these treatments were also studied. The authors tried to reveal the relationship between the catalytic activity and the hydrogen content(x) or between that and the structural and compositional changes of the samples.

Experimental

The preparation and identification of $H_{0.30}MoO_3$ used in the present experiments were described previously.[8-10] Samples, having various hydrogen contents, were prepared by heating the bronze *in vacuo* or in air. The structural and compositional changes of the samples were studied by X-ray powder diffractometry and infrared spectrophotometry.

1-Butene from Takachiho Kagaku Co. Ltd. was purified by repeated distillation *in vacuo*. The purity was confirmed by gaschromatography to be higher than 99%. A closed circulating system connected to a conventional vacuum line was used for isomerization of the 1-butene. The reaction mixtures were analyzed for each fixed time using the gaschromatograph with a coloum of 2,5-dimethylsulforan (DMS).

The surface area was determined by the BET method.

† 1 Torr≈133.322 Pa.

Results and Discussion

Structural and Compositional Changes of $H_{0.30}MoO_3$. Figure 1 shows the X-ray diffraction pattern of the samples heated at various temperatures *in vacuo* for 60 min. The sample heated at 238 °C showed an X-ray diffraction pattern due to the original orthorhombic structure. However, the pattern due to the rhombic structure appeared on samples treated at 297 and 349 °C. This result means that these samples consist of a mixture of the orthorhombic and rhombic structures. While the sample heated *in vacuo* at 398 °C showed only the X-ray patterns due to the rhombic structure,

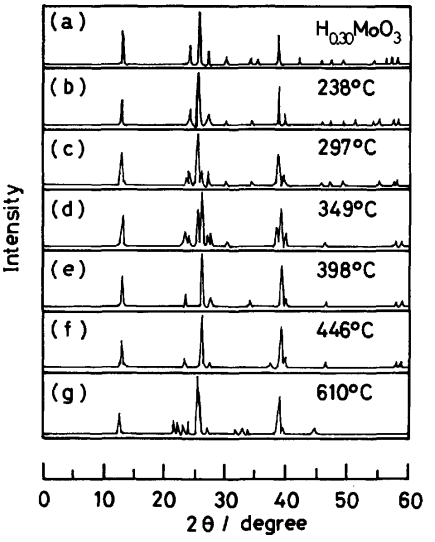

Fig. 1. X-ray diffraction patterns of the blue orthorhombic bronze, $H_{0.30}MoO_3$(a), and the samples treated at 238 °C(b), 297 °C(c), 349 °C(d), 398 °C(e), 446 °C(f), and 610 °C(g).

and the sample heated at 610 °C showed patterns due to mixture of the rhombic MoO_3 and Mo_4O_{11} structures.

As mentioned above, the samples treated at 297 and 349 °C were mixtures of orthorhombic and rhombic structures. The ratio of the orthorhombic to rhombic components was obtained to be 0.76/0.24 (297 °C) and 0.38/0.62 (349 °C), respectively. As the minimum phase limit of the orthorhombic structure was x=0.21 in the present work, the ratio can also be calculated from thermogravimetric data. The ratio was 0.80/0.20 (297 °C) and 0.35/0.65 (349 °C), respectively. These values are in very good agreement with each other. This suggests that the ratio obtained from the thermogravimetric data is easier to use than that obtained from the X-ray results. The sample in which the hydrogen content was x=0.06 showed only a pattern due to the rhombic structure. During vacuum heating, the only gas liberated from the sample was H_2O. No other gas was detected using a quadrupole gas analyzer. This result suggests that the hydrogen atoms in the samples reacted with lattice oxygen to produce H_2O. The bronze with the lowest hydrogen content (x=0.21) transformed to a compound with a hydrogen content of x= 0.06 and finally to a nonstoichiometric compound with a rhombic MoO_3 structure, which contains no hydrogen atoms. These results lead to the conclusion that vacancies should be produced in the samples during the evolution of H_2O under vacuum heating. These changes are formulated as follows;

$$H_{0.30}MoO_3 \xrightarrow{\approx 287^\circ C} H_{0.21}MoO_{2.95}{}^{*} \xrightarrow{\approx 390^\circ C} H_{0.06}MoO_{2.88}{}^{**} \xrightarrow{\approx 446^\circ C} MoO_{2.86}{}^{***} \xrightarrow{\approx 610^\circ C} MoO_3 + Mo_4O_{11}$$

*; Orthorhombic bronze with the lowest hydrogen content.

**; Isomorphous with rhombic MoO_3.

***; Nonstoichiometric compound with the rhombic MoO_3 structure.

Figure 2 shows the IR spectra of a sample treated at various temperatures for 60 min under a vacuum of 10^{-4} Torr. The orthorhombic bronze showed bands at 1004, 626, 569, and 355 cm^{-1}. These bands agree well with those reported by Schroder and Weizel.[3] The intensities of the bands at 1004, 626, and 428 cm^{-1} gradually decreased during vacuum heating. On the other hand, the bands at 986, 853, 819, 569, and 368 cm^{-1} appeared after heating at 297 °C and the intensities of these bands gradually increased by further heating. According to the X-ray results mentioned above, the samples treated at 297 and 398 °C were mixtures of orthorhombic and rhombic structures and the sample treated at 398 °C was a nonstoichiometric compound with a rhombic MoO_3 structure. These facts suggest

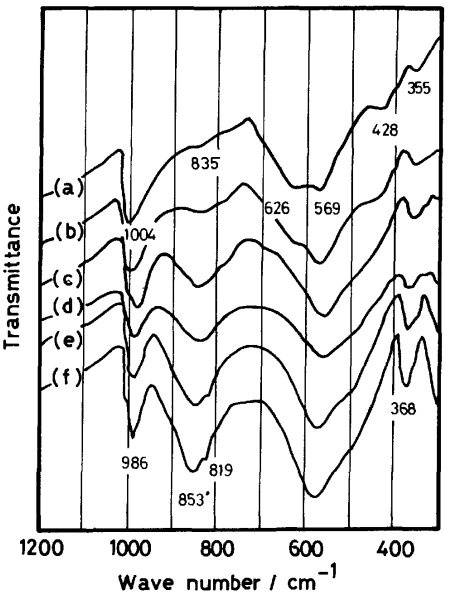

Fig. 2. IR spectra of the blue orthorhombic bronze, $H_{0.30}MoO_3$(a), and the samples treated at 238 °C(b), 297 °C(c), 349 °C(d), 398 °C(e) and 446 °C(f).

that a compound with a rhombic MoO_3 structure shows bands at 986, 853, and 819 cm^{-1}. These bands are a little lower than those at 998, 878, and 820 cm^{-1} in literatures.[11-13] This difference may be considered as a result of nonstoichometry. According to Nakamoto[12] and Feraro,[13] as shown in Fig. 3 (A1 and A2), the bands at 986, 853, and 819 cm^{-1} can be assigned to Mo=O(1), Mo-O(3,3')-Mo, and Mo-O(2,2')-Mo, respectively. Figure 3 also shows the coordination of the oxygen atoms arround the molybdenum atom in MoO_3 (B) and in the orthorhombic bronze(C). In MoO_3, the bond lengths of Mo-O(2'), Mo-O(3), and Mo-O(3') are 1.95, 2.25, and 1.73 Å, respectively. On the other hand, in orthorhombic bronze, that of Mo-O(2'), Mo-O(3), and Mo-O(3') is 1.96 Å. That is, by an insertion of atomic hydrogen into MoO_3, the bond length of Mo-O(3) in MoO_3 is shortened to 1.96 Å in the orthorhombic bronze and that of Mo-O(3'), longthened to 1.96 Å. However, that of Mo=O(1) showed no difference between the MoO_3 and the orthorhombic bronze. The band at 1004 cm^{-1} of the orthorhombic bronze is assumed to correspond to that at 998 cm^{-1} of the rhombic MoO_3. On the other hand, any band corresponding to the bands at 878 and 820 cm^{-1} due to MoO_3 was not observed in orthorhombic bronze. However, as atomic hydrogen was removed by vacuum heating, the bands at 986 and 819 cm^{-1} appeared and the intensities increased. These results suggest that, though small bands due to Mo-O(3,3')-Mo and Mo-O(2,2')-Mo in the orthorhombic bronze should be expected, they were not observed.

Changes in Surface Area. The changes in the surface areas of the samples treated under vacuum

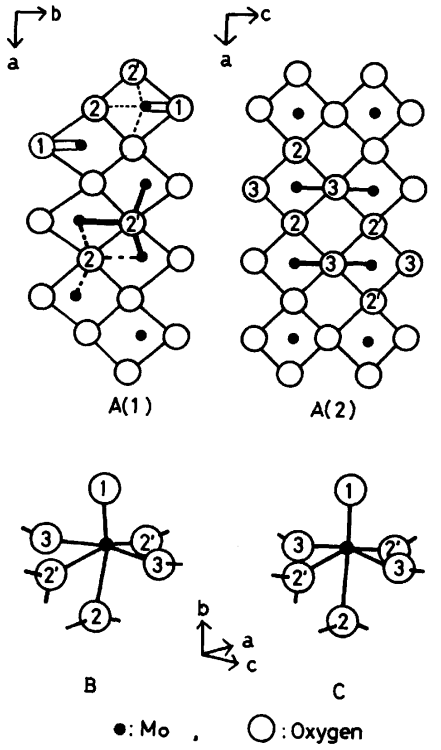

Fig. 3. Schematic model of MoO_3(A1,A2) and coordination of oxygen atoms around the molybdenum atoms in MoO_3(B) and in the bronze(C).

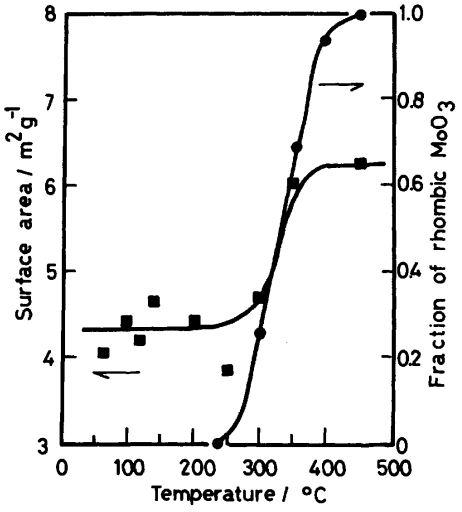

Fig. 4. Changes of the surface area and the fraction of the rhombic MoO_3 structure in the samples after vacuum heating.

heating at various temperatures are shown in Fig. 4. No large change was observed below 300°C, but the area increased slightly to a constant value at 360°C. The fraction of the rhombic structures in the samples is also shown in Fig. 4. The change in the fraction agrees well with that for the surface area. As mentioned above, isomorphous and nonstoichiometric compounds with rhombic structures have many vacancies produced by the reaction of lattice oxygen with hydrogen. Therefore, the increase in the surface area may be caused by an increase in the rhombic structure which has

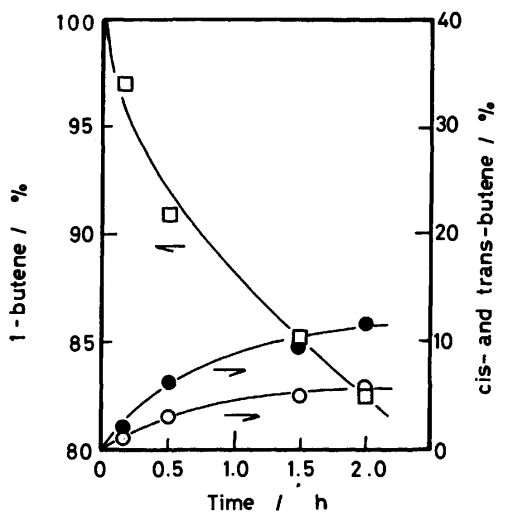

Fig. 5. Isomerization of 1-butene over $H_{0.24}MoO_3$ at 65°C.
□: 1-Butene, ●: *cis*-2-butene, and ○: *trans*-2-butene.

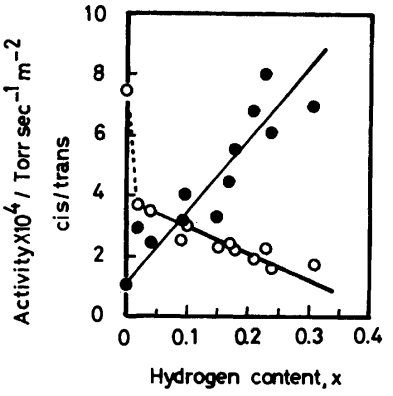

Fig. 6. Activity and the cis/trans ratio of 1-butene isomerization over the samples with various hydrogen contents, x. ●: Activity and ○: cis/trans ratio.

vacancies.

Isomerization of 1-Butene. Catalytic isomerization of 1-butene was studied at 65°C over the bronzes treated at various temperatures in air and *in vacuo*. The activity was determined from the initial rate of decrease of 1-butene, which was divided by the surface area of the catalyst. The skeletal isomerization could not be observed. No other gasous hydrocarbons other than butenes were detected in the reaction mixtures under the present experimental conditions. Figure 5 shows typical changes of butenes with time over $H_{0.24}MoO_3$ at 65°C. The *cis*-2-butene is predominantly formed.

The samples with various hydrogen contents were obtained by heating the bronze in air at 65°C for various heating times. The activities of 1-butene isomerization were plotted against x, as shown in Fig. 6. A linear relationship exists between the activity and x. The activity of commercial MoO_3 was about 1/500 of the MoO_3 obtained from a bronze of which hydrogen was completely removed by heating in an oxygen

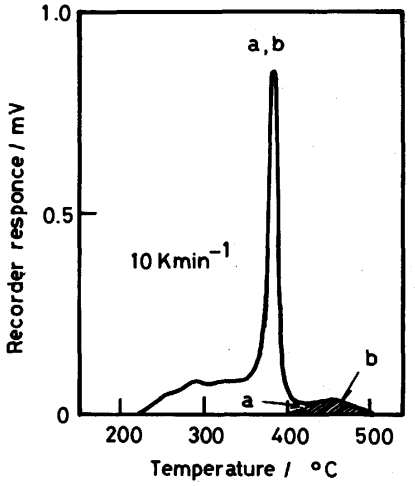

Fig. 7. TPD spectra of $H_{0.24}MoO_3$(a) and the sample after exposure to 1-butene.

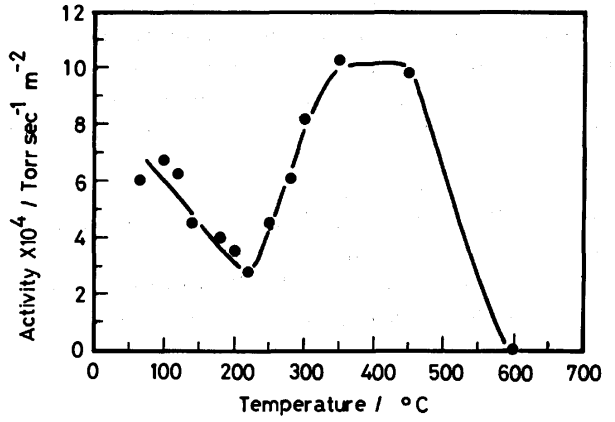

Fig. 8. Effect of evacuation temperature on catalytic activity of 1-butene isomerization.

atomosphere. Further, when the atomic hydrogen of the bronze was replaced by alkali metal ions, such as potassium ions, the activities of the alkali metal bronzes decreased markedly. As in the case of the hydrogenation of 1-pentene and ethylene over $H_{1.6}MoO_3$, the above results lead to the conclusion that hydrogen atoms in orthorhombic bronze, $H_{0.30}MoO_3$, are effective for the catalytic isomerization of 1-butene.

Figure 7 shows the TPD spectra of the orthorhombic bronze, $H_{0.24}MoO_3$(a), and the sample(b) after use as a catalyst for 1-butene isomerization. The shaded part is observed only in the spectrum of a used sample. The gas liberated as H_2O was trapped at −60—−63 °C. The value of the trapped gas obtained from the used sample was the same as that from the unused sample. This suggested that the area was equal to that of the unused sample. These results suggest that the bronze did not change at all throught the 1-butene isomerization. This leads to the conclusion that the hydrogen atoms in the bronze were effective for the catalytic isomerization of 1-butene. The shaded part is difficult to identify, but may be a strongly adsorbed species of hydrocarbons.

The cis/trans ratios of 1-butene isomerization over the samples were also plotted against x. As shown in Fig. 6, the ratio over MoO_3 obtained from the bronze is high. However, when small amounts of hydrogen is introduced, the ratio decreases steeply at first. Then, it decreased gradually to 1.6—1.7 with an increase in x. The cis/trans ratio at an equilibrium composition of butenes at 65 °C, as calculated from the thermodynamical data,[14] was 0.4. In the present work, therefore, the *cis*-2-butene was predominantly formed. It is well known[15] that when a solid acid catalyst is used for 1-butene isomerization, the cis/trans ratio is 1—2, while in the case of the solid base catalyst the ratio is more than 2. Considering the facts that the cis/trans ratios linearly decreased to 1.6—1.7 over the samples for which x increased, the bronze with small amounts of hydrogens was assumed to act as the solid acid catalyst. As hydrogen is involved with the bronze as atoms, it is reasonable that this atomic hydrogen acts as a solid acid catalyst.

Figure 8 shows the change in the activity of the samples which were treated *in vacuo* at various temperatures. The activity decreased linearly up to 220 °C, increased monotonously to a maximum value at 350 °C, and decreased sharply to nearly zero from 450 to 600 °C. The activity below 220 °C decreases linearly with a decrease in the hydrogen content of the samples without any structural change. In addition to the results mentioned above, this result suggests that the activity depends on the hydrogen atoms.

The activity increased from 220 to 350 °C and reached a constant value. In these temperature ranges, $H_{0.21}MoO_{2.95}$ decomposed rather rapidly to $H_{0.06}MoO_{2.88}$ with the rhombic MoO_3 structure with the formation of vacancies, which caused an increase in the surface area. The change from $H_{0.06}MoO_{2.88}$ to $MoO_{2.86}$ showed no significant change in the structure and in the surface area. Considering the above results, it is reasonable to conclude that the catalytic activity at this temperature range(220—350 °C) is attributed to the vacancies produced in the samples.

In this case, the cis/trans ratio on the samples treated below 220 °C varied with x, while the ratio above 220 °C was nearly constant at 1.4—1.7. As reported previously,[15] these ratios fell just in those ranges on the solid acid catalysts. As mentioned above, the activity for the isomerization of 1-butene above 220 °C is due to the vacancies produced in the bronze which show a reduced state. Considering the above results, it can be said that the activity above 220 °C results from the vacancies formed during treatment and that these vacancies act as a solid acid-like catalyst. A precise investigation is in progress.

The activity decreased markedly from 450 to 600 °C. From the X-ray and thermogravimetric results, the sample was confirmed to be a mixture of MoO_3 and Mo_4O_{11}. $MoO_{2.86}$, the nonstoichiometric compound with a rhombic structure, is converted to the stoichio-

metric MoO_3 and Mo_4O_{11}. The catalytic activity of 1-butene isomerization on MoO_3 and Mo_4O_{11} is very small. Therefore, these results lead to the conclusion that the decrease in the activity can be attributed to the existence of the stoichiometric MoO_3 and Mo_4O_{11}.

This work was supported by a Grant-in-Aid for Scientific Research No. 58550502, from the Ministry of Education, Science and Culture, and by a Hyogo Prefecture Foundation for the Promotion of Science and Technology, for which the authors' thanks are due.

References

1) O. Glemser and G. Lutz, *Z. Anorg. Allg. Chem.*, **264**, 17 (1951); **269**, 93 (1952); **285**, 173 (1956).
2) K. A. Wilhelm, *Acta Chem. Scand.*, **23**, 419 (1969).
3) F. A. Schroder and H. Weitzel, *Z. Anorg. Allg. Chem.*, **435**, 247 (1977).
4) J. J. Birtill and P. C. Dickens, *Mater Res. Bull.*, **13**, 311 (1978).
5) R. C. Slader, T. K. Halstead, and P. G. Dickens, *J. Solid State Chem.*, **34**, 183 (1980).
6) P. A. Sermon and G. C. Bond, *J. Chem. Soc., Faraday Trans. 1*, **76**, 889 (1980).
7) J. P. Marcq, X. Wispenninckx, G. Poncelet, D. Krevis, and J. J. Fripiat, *J. Catal.*, **73**, 309 (1982).
8) N. Sotani, Y. Kawamoto, and M. Inui, *Mater Res. Bull.*, **18**, 797 (1983).
9) N. Sotani, N. Yoshida, Y. Kawamoto, S. Kishimoto, and M. Hasegawa, *Bull. Chem. Soc. Jpn.*, **57**, 3032 (1984).
10) N. Sotani, M. Kunitomo, and M. Hasegawa, *Chem. Lett.*, **1983**, 647.
11) N. Sotani, Y. Saito, M. Oita, and M. Hasegawa, *Nippon Kagaku Kaishi*, **1974**, 673.
12) K. Nakamoto, "Infrared Spectra of Inorganic and Coordination Compound," John Willey and Sons, New York (1970), p. 166.
13) J. R. Feraro, "Low Frequency Vibration of Inorganic and Coordination Compounds," Plenum Press, New York (1971), p. 75.
14) "Kagaku Binran, I," ed by the Chemical Society of Japan, Maruzen, Tokyo (1980), p. 971.
15) T. Okuhara and M. Misono, *Shokubai*, **25**, 279 (1983).

The Crystal and Molecular Structure of Anhydrous Zinc 8-Quinolinolate Complex, $[Zn(C_9H_6NO)_2]_4$†

Yasushi KAI, Masahiro MORITA,†† Noritake YASUOKA,††† and Nobutami KASAI*
Department of Applied Chemistry, Faculty of Engineering, Osaka University, Yamadaoka, Suita, Osaka 565
(Received October 25, 1984)

The molecular structure of an anhydrous zinc 8-quinolinolate obtained by sublimation has been determined by means of X-ray diffraction. The complex forms triclinic crystals; $a=11.858(1)$, $b=13.019(2)$, $c=10.834(1)$ Å, $\alpha=106.56(1)$, $\beta=109.00(1)$, and $\gamma=74.14(1)°$, space group $P\bar{1}$ (No. 2) with one $[Zn(C_9H_6NO)_2]_4$ molecule. The structure was solved by the heavy atom method and refined by the block-diagonal least-squares procedure to $R=0.043$ for 3320 non-zero reflections. The molecule is centrosymmetric and tetrameric; four $[Zn(C_9H_6NO)_2]$ units being connected by oxygen atoms of 8-quinolinolate ligands. Two types of bridging oxygen atoms were found. Two crystallographically independent zinc atoms take different geometries, hexa-, and penta-coordinations.

Many investigations have been carried out on the crystal structures of metal 8-quinolinolate complexes hitherto. Interesting weak intermolecular interactions have been found between metal and oxygen atoms of ligands in crystal structures of anhydrous copper 8-quinolinolates.[1-4]

The crystal structure of zinc 8-quinolinolate dihydrate has been determined by Merritt, Cady and Mundy,[5] redetermination of which has been carried out by Palenik.[6] Ogawa[7] reported a preliminary result of the X-ray studies on the solution-grown crystals of anhydrous zinc 8-quinolinolate; triclinic, $a=11.1$, $b=9.20$, $c=11.1$ Å, $\alpha=114.9$, $\beta=75.1$, $\gamma=90.8°$, and $Z=2$. This paper will deal with the crystal and molecular structure of an anhydrous zinc 8-quinolinolate recrystallized directly from the gas phase. Interestingly, 8-quinolinolate complexes of zinc were obtained by S. Ikeda and co-worker by the direct reaction of 8-quinolinol with zinc metal,[8] the study of which closely related to the dissolution of zinc and this fact promoted the present study.

Experimental

Anhydrous zinc 8-quinolinolate was prepared by drying the zinc 8-quinolinolate dihydrate above 130°C under vacuum. The complex was sublimed at about 400°C and recrystallized directly from the gas phase. Only few crystals with pale yellow color and small polyhedral shape were available for the X-ray experiment.

Crystal Data: $C_{72}H_{48}N_8O_8Zn_4$, M 1414.7, triclinic, space group $P\bar{1}$(No. 2), $a=11.858(1)$, $b=13.019(2)$, $c=10.834(1)$ Å, $\alpha=106.56(1)$, $\beta=109.00(1)$, and $\gamma=74.14(1)°$, $V=1485.3(3)$ Å^3, $D_c=1.581$ g cm^{-3} for $Z=1$.

Unit-cell dimensions were determined by the least-squares fit of 2θ values of higher order reflections using Mo $K\alpha$ radiation ($\lambda=0.71069$ Å). The unit-cell was first taken as a base-centered lattice, $A\bar{1}$ and later transformed to the reduced standard cell, $P\bar{1}$. The measurement of the crystal density was omitted because no extra crystal was available but for the X-ray experiment.

A Rigaku automated, four-circle diffractometer was used for the intensity data collection. The integrated intensities were measured by the $\theta-2\theta$ scan technique using zirconium-filtered Mo $K\alpha$ radiation. The peak scan of each reflection was started at an angle of $(2\theta-1.0)°$ with the scan width of $(2.0+0.7\tan\theta)°$ and the scan rate in 2θ was 2° min^{-1}. Backgrounds were measured for 10 s at both ends of a scan. During the X-ray experiment the intensity fluctuations of four standard reflections measured after every 50 reflections were within the error of counting statistics. A total of 3659 independent reflections were measured. The intensities were corrected for usual Lorentz and polarization effects but not for the absorption [μ(Mo $K\alpha$)=17.1 cm^{-1}]. The crystal used had approximate dimensions of 0.1×0.1×0.2 mm.

Structure Solution and Refinement

The structure was solved by the heavy atom method. The initial coordinates of two crystallographically independent zinc atoms in an asymmetric unit were easily determined from the three-dimensional Patterson map. Non-hydrogen atoms could be located by the subsequent Fourier synthesis. The structure was refined by the block-diagonal least-squares procedure (*HBLS* V),[9] the function minimized being $\sum w(\Delta F)^2$. At the initial stage of the refinement, the intensity data used were limited within a sphere of $(\sin\theta)/\lambda \leqq 0.481$ (2743 out of 3659 total reflections) and $w=1$. Four cycles of isotropic refinement gave the R value of 0.076. Further refinement with anisotropic temperature factor for zinc atoms gave the R of 0.062. Anisotropic temperature factors were then introduced for the other non-hydrogen atoms. Hydrogen atoms were located on the calculated positions, almost all of which were confirmed by the difference Fourier synthesis, and they were also included in the structure factor calculation but their atomic coordinates were fixed with equal temperature factors ($B=3.0$ Å^2). Four cycles of the refinement improved the R to 0.051. At this stage, all of the reflection data were included in the least-squares calculation and the positional and thermal parameters of hydrogen atoms were also refined using small damping factors (one-tenth of those of the heavy atoms). After several cycles of the refinements the R index converged to 0.043 for non-zero (0.052 for all)

†Read at the 26th Annual Meeting of the Chemical Society of Japan, Tokyo, April (1972).

††Present address: Rubber & Plastics Division, Sumitomo Electric Industries Ltd., Konohana-ku, Osaka 554.

†††Present address: Institute for Protein Research, Osaka University, Yamadaoka, Suita, Osaka 565.

TABLE 1. FINAL ATOMIC COORDINATES[a] WITH ESTIMATED STANDARD DEVIATIONS IN PARENTHESES

Atom	x	y	z	B_{eq}/Å^2
Zn(1)	0.09937(5)	0.39703(5)	−0.04956(6)	3.01
Zn(2)	0.28152(6)	0.20180(5)	0.09065(6)	3.02
O(1)	0.2787(3)	0.3157(3)	0.0029(4)	3.7
O(2)	−0.0760(3)	0.4829(3)	−0.1157(4)	3.7
O(3)	0.0874(3)	0.2698(3)	0.0349(4)	3.0
O(4)	0.4573(4)	0.1269(4)	0.1497(4)	4.2
N(1)	0.1911(4)	0.4750(4)	−0.1296(5)	3.7
N(2)	0.0333(4)	0.2996(4)	−0.2482(5)	3.5
N(3)	0.2146(4)	0.0662(4)	−0.0266(4)	3.1
N(4)	0.2953(4)	0.2321(4)	0.2913(5)	3.7
C(11)	0.1453(6)	0.5520(5)	−0.1991(7)	4.5
C(12)	0.2121(7)	0.5825(5)	−0.2638(7)	5.4
C(13)	0.3320(7)	0.5348(5)	−0.2500(7)	5.4
C(14)	0.5090(6)	0.3990(6)	−0.1548(7)	4.9
C(15)	0.5506(5)	0.3196(6)	−0.0824(7)	4.9
C(16)	0.4766(5)	0.2883(5)	−0.0280(6)	4.0
C(17)	0.3560(5)	0.3401(5)	−0.0444(6)	3.4
C(18)	0.3107(5)	0.4247(4)	−0.1171(5)	3.2
C(19)	0.3862(6)	0.4537(5)	−0.1741(6)	4.1
C(21)	0.0907(6)	0.2061(5)	−0.3093(6)	4.1
C(22)	0.0291(7)	0.1451(5)	−0.4293(7)	5.4
C(23)	−0.0919(7)	0.1799(5)	−0.4850(6)	5.0
C(24)	−0.2783(6)	0.3198(6)	−0.4725(7)	5.2
C(25)	−0.3312(6)	0.4162(6)	−0.4028(7)	5.2
C(26)	−0.2647(5)	0.4749(5)	−0.2827(6)	4.1
C(27)	−0.1438(5)	0.4360(5)	−0.2298(6)	3.5
C(28)	−0.0865(5)	0.3359(5)	−0.3030(5)	3.3
C(29)	−0.1539(6)	0.2785(5)	−0.4225(6)	4.2
C(31)	0.2814(5)	−0.0324(5)	−0.0556(6)	3.9
C(32)	0.2267(6)	−0.1218(5)	−0.1305(6)	4.2
C(33)	0.1037(5)	−0.1084(5)	−0.1758(6)	3.9
C(34)	−0.0966(5)	0.0194(5)	−0.1947(6)	4.2
C(35)	−0.1588(5)	0.1244(5)	−0.1633(6)	4.1
C(36)	−0.0991(5)	0.2106(5)	−0.0851(6)	3.8
C(37)	0.0254(5)	0.1919(4)	−0.0366(5)	3.0
C(38)	0.0910(5)	0.0835(4)	−0.0710(5)	3.0
C(39)	0.0310(5)	−0.0033(5)	−0.1474(5)	3.2
C(41)	0.2129(6)	0.2837(5)	0.3584(6)	4.3
C(42)	0.2358(7)	0.2876(6)	0.4959(7)	5.6
C(43)	0.3446(6)	0.2347(6)	0.5606(7)	5.3
C(44)	0.5493(6)	0.1202(6)	0.5531(6)	5.2
C(45)	0.6269(6)	0.0646(6)	0.4771(7)	5.3
C(46)	0.5995(5)	0.0650(5)	0.3425(6)	4.4
C(47)	0.4892(5)	0.1216(5)	0.2756(6)	3.9
C(48)	0.4045(5)	0.1795(5)	0.3549(5)	3.5
C(49)	0.4348(6)	0.1771(5)	0.4934(6)	4.2

a) Only those of non-hydrogen atoms with equivalent isotropic temperature factors, B_{eq}[12] are given. Those of hydrogen atoms are kept at the Chemical Society of Japan, Document No. 8525.

reflections (R_W=0.049). The weighting schemes used were $w=F_{wt}$ for $|F_o|=0$, $w=1.0$ for $|F_o| \leqq F_{max}$, and $w=(F_{max}/|F_o|)^{-2}$ for $F_{max}<|F_o|$, where F_{max}=70.0 and F_{wt}=0.2, respectively. Neutral atomic scattering factors used for non-hydrogen atoms were taken from International Tables for X-Ray Crystallography[10] and for hydrogen atoms from Stewart, Davidson, and Simpson.[11] The final atomic coordinates and thermal parameters of atoms in an asymmetric unit are listed in Table 1.††††

††††A list of observed and calculated structure facotrs and anisotropic thermal parameters are kept at the Chemical Society of Japan, Document No. 8525.

TABLE 2. BOND LENGTHS AND BOND ANGLES AROUND THE ZINC ATOMS[a] WITH ESTIMATED STANDARD DEVIATIONS IN PARENTHESES

Bond lengths[l/Å]			
Zn(1)–O(1)	2.072(4)	Zn(2)–O(1)	1.965(4)
Zn(1)–O(2)	2.075(4)	Zn(2)–O(3)	2.176(4)
Zn(1)–O(2′)	2.053(4)	Zn(2)–O(4)	2.020(4)
Zn(1)–O(3)	2.163(4)		
Zn(1)–N(1)	2.165(5)	Zn(2)–N(3)	2.047(4)
Zn(1)–N(2)	2.178(5)	Zn(2)–N(4)	2.055(5)
Bond angles[ϕ/°]			
O(1)–Zn(1)–O(2)	174.5(2)	O(1)–Zn(2)–O(3)	79.2(2)
O(1)–Zn(1)–O(3)	77.3(2)	O(1)–Zn(2)–O(4)	106.9(2)
O(1)–Zn(1)–O(2′)	105.5(2)	O(3)–Zn(2)–O(4)	173.9(2)
O(2)–Zn(1)–O(3)	107.6(2)		
O(2)–Zn(1)–O(2′)	77.0(2)		
O(1)–Zn(1)–N(1)	77.2(2)	O(1)–Zn(2)–N(3)	118.0(2)
O(1)–Zn(1)–N(2)	101.1(2)	O(1)–Zn(2)–N(4)	122.4(2)
O(2)–Zn(1)–N(1)	97.7(2)	O(3)–Zn(2)–N(3)	78.9(2)
O(2)–Zn(1)–N(2)	76.9(2)	O(3)–Zn(2)–N(4)	94.7(2)
O(3)–Zn(1)–N(2)	88.8(2)	O(4)–Zn(2)–N(3)	97.6(2)
O(3)–Zn(1)–O(2′)	93.1(2)	O(4)–Zn(2)–N(4)	82.4(3)
N(1)–Zn(1)–N(2)	90.2(2)	N(3)–Zn(2)–N(4)	116.6(2)
N(1)–Zn(1)–O(2′)	99.4(2)		
N(1)–Zn(1)–O(3)	153.8(2)		
N(2)–Zn(1)–O(2′)	153.1(2)		
Zn(1)–O(1)–Zn(2)	106.7(2)	Zn(1)–O(2)–Zn(1′)	103.1(2)
Zn(1)–O(1)–C(17)	116.4(4)	Zn(1)–O(2)–C(27)	116.5(4)
Zn(2)–O(1)–C(17)	136.1(4)	Zn(1′)–O(2)–C(27)	138.4(4)
Zn(1)–O(3)–Zn(2)	96.6(2)	Zn(2)–O(4)–C(47)	111.7(4)
Zn(1)–O(3)–C(37)	122.3(4)		
Zn(2)–O(3)–C(37)	110.7(4)		

a) List of those in quinolinolate ligands is kept at the Chemical Society of Japan, Document No. 8525.

Results and Discussion

Molecular Structure. The molecular structure is shown in Fig. 1 with the numbering scheme of atoms in an asymmetric unit. The bond lengths and bond angles are listed in Table 2.

As seen in Fig. 1, two [$Zn(C_9H_6NO)_2$] units connected by two bridging oxygen atoms form an asymmetric unit. Two asymmetric units (x, y, z and $-x$, $1-y$, $-z$) related by a center of symmetry, connected by two bridging oxygen atoms, make the whole molecule tetrameric.

Geometry Around the Zinc Atoms. Two crystallographically independent zinc atoms have different coordination geometries. The Zn(1) atom takes a hexacoordination whereas the Zn(2) a penta-coordination.

The coordination geometry of the Zn(1) atom is octahedral but largely distorted. Bond lengths from the Zn(1) atom to the O(1), O(2), and O(2′) are equal [2.072(4), 2.075(4) and 2.053(4)Å]. These values are equal to the Zn–O bond length [2.066(15)Å] observed with the octahedrally coordinated zinc atom in the zinc 8-quinolinolate dihydrate.[6] But they are significantly shorter than the Zn(1)–O(3) length [2.163(4)Å]. Two Zn(1)–N bonds are equal in length [2.165(5) and 2.178(5) Å]. The O(1)–Zn(1)–O(2) angle is 174.5(2)°, which is close to 180°. But, the other two bond angles, N(1)–

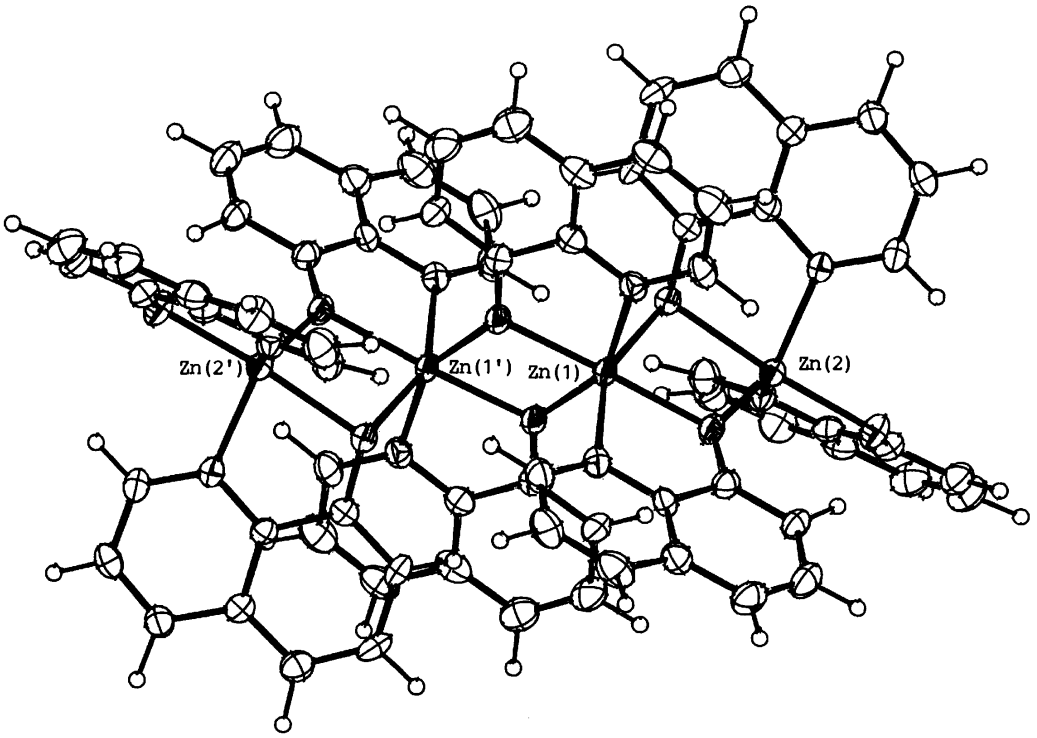

(a)

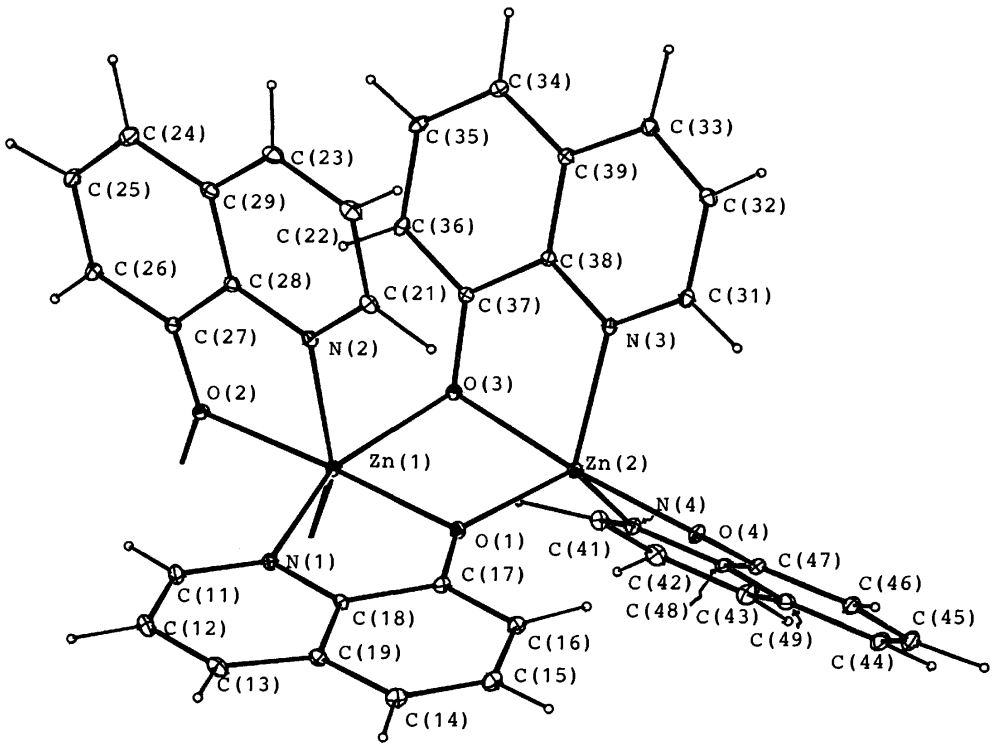

(b)

Fig. 1. Molecular structure[13] of $[Zn(C_9H_6NO)_2]_4$.
(a) A perspective view.
Non-hydrogen atoms are drawn as thermal ellipsoids with 30% probability level and hydrogen atoms with $B=1.0$ Å^2.
(b) Numbering scheme of atoms in an asymmetric unit.

Zn(1)–O(3) [153.8(2)°] and N(2)–Zn(1)–O(2') [153.1(2)°] show large deviations from 180°. All of the other bond angles around the Zn(1) atom [between 77.0(2) and 107.6(2)°] deviate from 90°.

The geometry around the Zn(2) atom is distorted trigonal bipyramidal. The Zn(2) atom deviated by 0.20

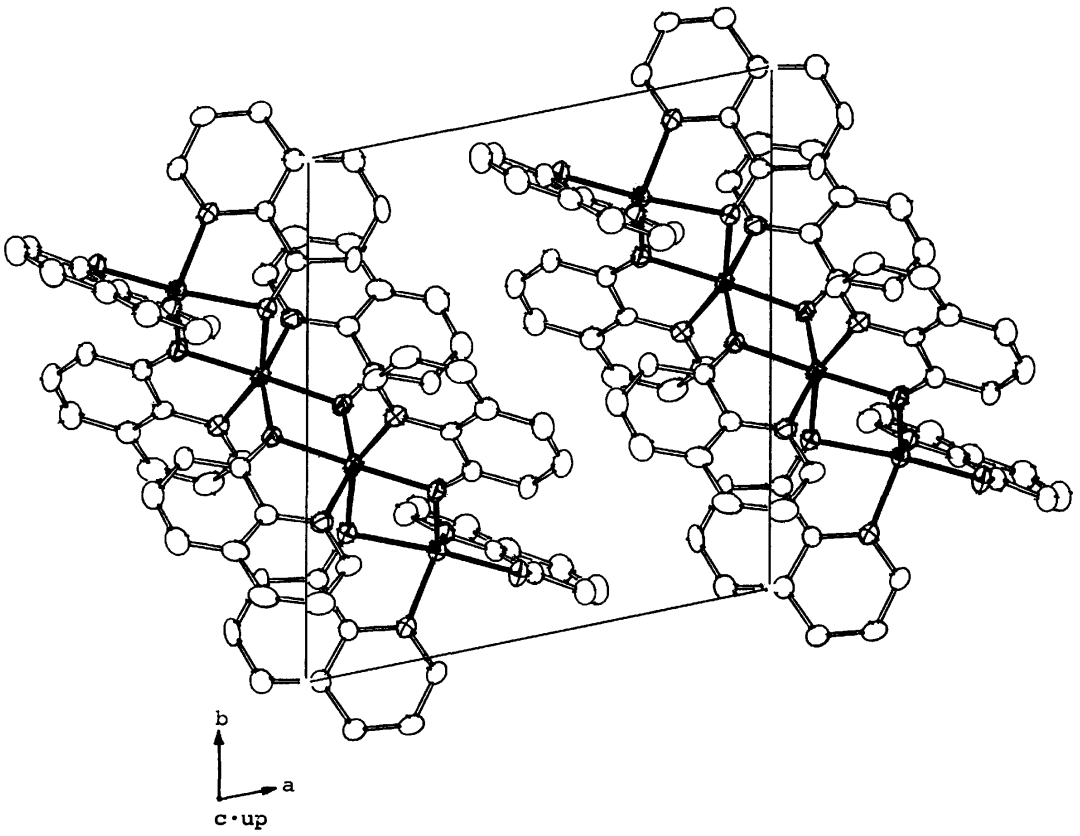

Fig. 2. Crystal structure[13] of $[Zn(C_9H_6NO)_2]_4$.
Non-hydrogen atoms are drawn as thermal ellipsoids with 30% probability level. Hydrogen atoms are omitted for clarity.

Å from the base plane defined by the O(1), N(3), and N(4) atoms. The O(3)-Zn(2)-O(4) angle is 173.9(2)°, three bond angles in the base plane are 116.6(2), 118.0(2), and 122.4(2)°, and the other angles are between 78.9(2) and 106.9(2)°. The Zn(2)-O(1) bond [1.965(4)Å] is the shortest among three Zn(2)-O bonds, and this is also the shortest Zn-O bond in the present complex. The Zn(2)-O(3) bond length [2.176(4)Å] is equal to the Zn(1)-O(3). These two are the longest Zn-O bonds and both involved with the O(3) atom. The sum of the three bond angles about the O(3) atom [329.6°] is largely deviated from 360°, whereas those about the O(1) [359.2°] and O(2) [358.0°] atoms are all equal to 360°. The Zn(2)-O(4) bond length is 2.020(4)Å, which is comparable to those of three Zn(1)-O bonds except the Zn(1)-O(3). The O(4) atom is the non-bridging oxygen atom at the apical position of the distorted trigonal bipyramid. Two Zn(2)-N bonds in the base plane [2.047(4) and 2.055(5)Å] are significantly shorter than the Zn(1)-N bonds which appeared in the geometry of the octahedrally coordinated Zn(1) atom.

Structure of the Quinolinolate Moieties. All of the corresponding bond lengths and bond angles in four quinolinolate moieties are equal within the limits of error.†††† The planarity of four quinolinolate moieties are slightly poor, they are planar within 0.08Å. These dimensions are similar to those of zinc 8-quinolinolate dihydrate[6] and β-copper 8-quinolinolate anhydride.[2]

†††† Bond lengths and bond angles in the quinolinolate moieties are also deposited at the Chemical Society of Japan, Document No. 8525.

TABLE 3. SHORT INTERMOLECULAR ATOMIC CONTACTS [*l*/Å] LESS THAN 3.6 Å WITH ESTIMATED STANDARD DEVIATIONS IN PARENTHESES

C(33)·····C(36)[a]	3.472(8)	key:	a,	$-x$,	$-y$,	$-z$
C(34)·····C(38)[a]	3.479(8)		b,	x,	y,	$-1+z$
C(39)·····C(39)[a]	3.477(11)		c,	$1-x$,	$-y$,	$1-z$
C(19)·····C(43)[b]	3.436(9)		d,	$1-x$,	$-y$,	$-z$
C(44)·····C(44)[c]	3.399(14)					
C(44)·····C(45)[c]	3.480(10)					
C(45)·····C(49)[c]	3.538(10)					
O(4)·····C(31)[d]	3.378(7)					

Crystal Structure. Crystal structure projected along the c axis is depicted in Fig. 2. Several short interatomic contacts (less than 3.6Å) are observed (Table 3). Almost all of them are involved between carbon atoms of quinolinolate groups in adjacent molecules. The closest contact is observed between the O(4)(x, y, z) atom and C(31)($1-x$, $-y$, $-z$) [3.378(7)Å].

Calculations were mostly done on a NEAC 2200-700 computer at the Computation Center, Osaka University and at the final stage on an ACOS 850 computer at the Crystallographic Research Center, Institute for Protein Research, Osaka University.

The authors wish to express their deep thanks to

Professor Shigero Ikeda, Faculty of Science, Osaka University for supply of crystals.

References

1) F. Kanamaru, K. Ogawa, and I. Nitta, *Bull. Chem. Soc. Jpn.*, **36**, 422 (1963).
2) G. J. Palenik, *Acta Crystallogr.*, **17**, 687 (1964).
3) J. A. Bevan, D. P. Graddon, and J. F. McConell, *Nature*, **199**, 373 (1963).
4) R. C. Hoy and R. H. Morriss, *Acta Crystallogr.*, **22**, 476 (1967).
5) L. L. Merrit, Jr., R. T. Cady, and B. W. Mundy, *Acta Crystallogr.*, **7**, 473 (1954).
6) G. J. Palenik, *Acta Crystallogr.*, **17**, 696 (1964).
7) K. Ogawa, private communication.
8) S. Ikeda and M. Arimura, Abst. 22nd Annual Meeting *Chem. Soc. Jpn.*, 12629 (1969).
9) T. Ashida, *HBLS* V, "The Universal Crystallographic Computing System-Osaka," The Computation Center, Osaka Univ., 1973, p. 55.
10) International Tables for X-Ray Crystallography, Vol. IV, Kynoch Press, Birmingham (1974), p. 71.
11) R. F. Stewart, E. R. Davidson and W. T. Simpson, *J. Chem. Phys.*, **42**, 3175 (1965).
12) W. C. Hamilton, *Acta Crystallogr.*, **12**, 609 (1959).
13) C. K. Johnson, *ORTEP* II, Report ORNL-5138, Oak Ridge National Laboratory, Tennessee (1976).

Tetraalkylammonium Ion-selective Electrodes with Supporting Electrolytes. An Experimental Test of the Theory of Liquid Ion-exchange Membrane Ion-selective Electrodes Based on the Concept of the Mixed Ion-transfer Potential

Takashi KAKIUCHI, Ichiro OBI, and Mitsugi SENDA*

Department of Agricultural Chemistry and Research Center for Cell and Tissue Culture, Faculty of Agriculture, Kyoto University, Sakyo-ku, Kyoto 606

(Received November 19, 1984)

Selectivity characteristics of liquid-membrane ion-selective electrodes for tetraethylammonium and triethylmethylammonium ion-selective electrodes in the presence of homologous tetraalkylammonium ions as interfering ions were studied with supporting electrolytes both in the liquid membrane and in the sample solution. The emf *vs.* logarithm of the concentration of the primary ion curves in the presence of interfering ion were well described by the theory of liquid-membrane ion-selective electrodes which is based on the concept of the mixed ion-transfer potential at the liquid-membrane/sample solution interface. The dependence of the selectivity coefficients on the concentrations of the primary ion in the liquid membrane and of the interfering ion in the sample solution agreed well with the theoretical prediction.

This paper reports a systematic study of the response of tetraethylammonium and triethylmethylammonium ion-selective liquid-membrane electrodes to the primary ion in the presence of interfering ions (a series of homologous tetraalkylammonium ions) in the sample solution and of the primary ion in the liquid membrane; the liquid membrane and the sample solution contained tetrapentylammonium tetraphenylborate (TPnATPB) and lithium sulfate, respectively, as the supporting electrolyte. In a previous paper,[1] we derived the theoretical equations for the response of ion-selective electrodes of liquid ion-exchange membrane type and presented the theory of the selectivity coefficient based on the concept of the mixed ion-transfer potential at the liquid-membrane/sample solution interface. The theory expresses the potential and the selectivity coefficient of the electrodes as functions of three factors: difference in the standard ion-transfer potential between the primary and interfering ions, the concentration ratios of the primary and interfering ions, and the mass-transfer coefficient ratios of these ions. The aim of this study is to verify experimentally these theoretical predictions by using the ion-selective electrodes which meet with the assumptions underlying the theory. The theory has assumed the presence of sufficient amounts of supporting electrolytes in both the liquid membrane and sample solution to ensure the absence of the migration of the relevant ions. This assumption is to simplify the treatment and to sculpture the fundamental characteristics of the ion-selective electrodes which are primarily determined by the ion-transfer processes at the liquid-membrane/sample solution interface. Such ion-transfer processes should also be essential in the liquid membrane ion-selective electrodes without having supporting electrolytes, like most of the ion-selective electrodes with liquid ion-exchangers hitherto studied.

Experimental

The electrochemical cells used in the present study are generally represented by:

I	II	III	IV	V	VI	VII	VIII
Ag	AgCl	2 mmol dm^{-3} R_1Cl (water)	*a* mmol dm^{-3} R_1TPB, 0.1 mol dm^{-3} TPnATPB (nitrobenzene)	*b* mmol dm^{-3} R_2Cl, *x* mmol dm^{-3} R_1Cl, 0.1 mol dm^{-3} Li_2SO_4 (water)	satd. KCl	AgCl	Ag

(I)

where phase III is the internal reference solution, phase IV is the liquid membrane, and phase V is the sample solution. R_1^+ and R_2^+ are the primary and the interfering ions, respectively, and TPB^- is tetraphenylborate ion. We used tetraethylammonium ion (TEA^+) for R_1^+ and trimethylethylammonium ion (Me_3EtN^+), trimethylpropylammonium ion (Me_3PrN^+), trimethylbutylammonium ion (Me_3BuN^+), and triethylmethylammonium ion (Et_3MeN^+) for R_2^+ in a series of experiments, and also Et_3MeN^+ for R_1^+ with TEA^+ for R_2^+ in the other series of experiments. Nitrobenzene was used as a solvent of the liquid membrane. In nitrobenzene, the tetraphenylborate salts of these alkylammonium ions are virtually completely dissociated as judged from the conductivity measurements.[2] The values of the standard ion-transfer potentials $\Delta^{W}_{NB}\varphi^{0}$ for the nitrobenzene–water system and of the diffusion coefficients of the relevant ions are given in Table 1, which shows that both $\Delta^{W}_{NB}\varphi^{0}_{R_1^+}$ and $\Delta^{W}_{NB}\varphi^{0}_{R_2^+}$ are much more negative than either of $\Delta^{W}_{NB}\varphi^{0}_{Li^+}$ and $\Delta^{W}_{NB}\varphi^{0}_{TPB^-}$ and, simultaneously, much more positive than either of $\Delta^{W}_{NB}\varphi^{0}_{TPnA^+}$ and $\Delta^{W}_{NB}\varphi^{0}_{SO_4^{2-}}$. Thus, the participation of the supporting electrolytes (TPnATPB in the liquid membrane and Li_2SO_4 in the sample solution) in the ion-transfer processes across the liquid-membrane/sample solution interface is very small[3] in the concentration ranges of R_1^+ and R_2^+ studied. The interference caused by supporting electrolytes becomes appreciable only when the ratio of the concentration of R_1^+ in the liquid membrane to that in the sample solution is very small.[1] In the following, the emf *vs.* logarithm of the concentration curves are analyzed in the lower concentration range of the primary ion in sample solution, where

TABLE 1. STANDARD POTENTIALS OF ION TRANSFER FROM WATER TO NITROBENZENE AND DIFFUSION COEFFICIENTS OF THE IONS IN WATER

ion	$\Delta^{W}_{NB}\phi°$/V	D/cm^2 s^{-1} [5]
Li^+	0.395[1]	—
Me_3EtN^+	0.040[2]	11.0×10^{-6}
Me_3PrN^+	0.006[2]	9.9×10^{-6}
Et_3MeN^+	−0.007[2]	8.2×10^{-6}
Me_3BuN^+	−0.025[2]	8.8×10^{-6}
TEA^+	−0.028[2]	8.3×10^{-6}
$TPnA^+$	−0.343[3]	—
Cl^-	−0.324[1]	—
SO_4^{2-}	≪−0.4[4]	—
TPB^-	0.372[1]	—

1) Ref. 3. 2) Calculated from the data in Ref. 4. 3) Extrapolated from the data in Ref. 3. 4) Ref. 5. 5) Ref. 6.

the interference of the supporting electrolyte becomes negligible. $\Delta^{W}_{NB}\varphi^{0}_{Cl^-}$ is also much more negative than either of $\Delta^{W}_{NB}\varphi^{0}_{R_1^+}$ and $\Delta^{W}_{NB}\varphi^{0}_{R_2^+}$. Accordingly, R_1^+ and R_2^+ are practically the only ionic species which pertain to the ion-transfer processes across the interface in the concentration ranges we are concerned with. The potential difference between phases III and IV is solely determined by the distribution potential of a R_1^+ ion for the ions used in this study.[3] It is also unaffected by the composition of phase V, because the liquid membrane is sufficiently thick.[1] The change of the liquid junction potential between phases V and VI with the change of the electrolyte concentration in phase V is negligibly small because of the presence of supporting electrolytes. Therefore, the change of the electromotive force of the cell with the electrolyte concentration in phase V can be ascribed to the change of the potential difference between phases IV and V.

The electrochemical cell(I) was formed in a U-shaped poly(tetrafluoroethylene) tube 9 mm in inner diameter and 10 cm tall. About 8 ml of a nitrobenzene solution was first poured in the cell and then a reference solution and a sample solution were added to the nitrobenzene solution, one in each leg of the cell. A saturated potassium chloride solution saturated with silver chloride made contact with a sample solution *via* a glass frit. The cell was immersed into a water bath kept at 25.0±0.2 °C. The electromotive force (emf) of cell(I) was measured with a Keithley 616 electrometer. The emf was usually stable within 5 min after the formation of the liquid-membrane/sample solution contact, except at the lowest concentration of R_1^+, 0.1 mmol dm^{-3}, at which the emf values were less reproducible, probably due to impurities in the nitrobenzene solution.

Iodide salts of Me_3EtN^+, Me_3PrN^+, Me_3BuN^+, and Et_3MeN^+ were synthesized from trialkylamines and alkyl iodides[7] and then converted to the chloride salts.[8] These alkylammonium chloride and TEACl(Wako Pure Chem. Ind., Japan) were dried over P_2O_5 and used to prepare the stock solutions using thrice distilled water. The stock solutions were treated with silver chloride powder to remove trace iodide ions. TEATPB, Et_3MeTPB, and TPnATPB were prepared by precipitation from aqueous solution (for TEA^+ and Et_3MeN^+) or ethanol solution (for $TPnA^+$) of the iodide salts by adding an equimolar quantity of aqueous or ethanol solution of sodium tetraphenylborate (Dojin Lab., Japan) and were twice recrystallized from acetone. Reagent grade nitrobenzene was treated with active alumina and then equilibrated with thrice-distilled water. All other chemicals were of reagent grade.

Results

Tetraethylammonium Ion-selective Electrode. The electromotive force of the cell(I) was measured at a fixed concentration of TEATPB(R_1TPB) in the liquid membrane and of R_2Cl in the sample solution by varying the concentration of TEACl(R_1Cl) between 0.1 mmol dm^{-3} and 0.5 mol dm^{-3} in the sample solution. The interfering ions R_2^+ studied were Me_3EtN^+, Me_3PrN^+, Me_3BuN^+, and Et_3MeN^+, whose $\Delta^{W}_{NB}\varphi^{0}$'s are all more positive than that of TEA^+ ion. The measured sets of a and b values in the cell(I) are summarized in Table 2. The results for a=2 mmol dm^{-3} are shown in Figs. 1—4. In the absence of R_2^+ ion the emf showed a linear Nernstian response over the concentration range of TEACl studied, except at the highest concentrations (a=0.2 and 0.5 mol dm^{-3}) where interference by the supporting electrolyte occurs. The solid lines in these figures are the theoretical ones calculated from Eqs. 16—21 in Ref. 1 using the values in Table 1 for

TABLE 2. CONCENTRATIONS OF THE ELECTROLYTES IN CELL (I) FOR THE EMF MEASUREMENTS OF TEA^+ ION-SELECTIVE ELECTRODES

a/mmol dm^{-3}	b/mmol dm^{-3}	x/mmol dm^{-3}
0.5	1, 10, 50	0.1—500
1	0.2, 1, 2, 5, 10, 50	0.1—500
2	0.2, 1, 2, 5, 10, 50	0.1—500
5	1, 10, 50	0.1—500

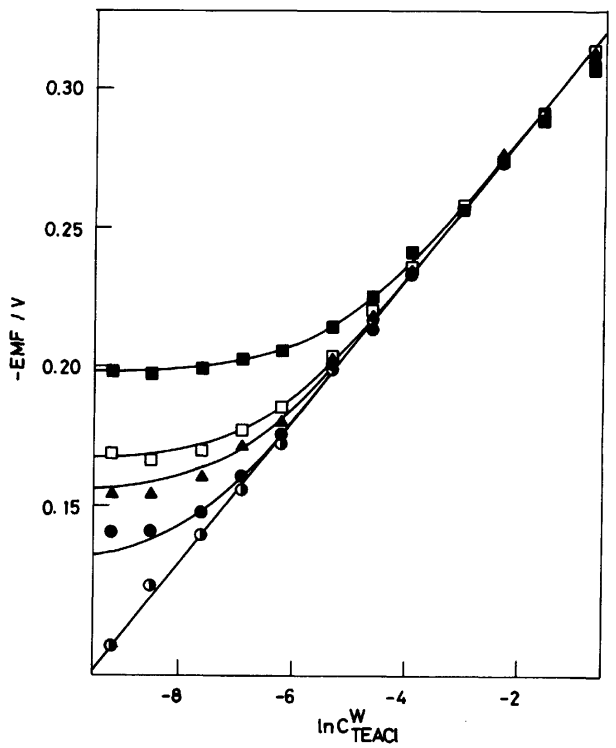

Fig. 1. Response of the TEA^+ ion-selective electrode in the presence of Me_3EtN^+ ion at a=2 mmol dm^{-3} and b=0(◑), 1(●), 5(▲), 10(□), and 50(■) mmol dm^{-3}.

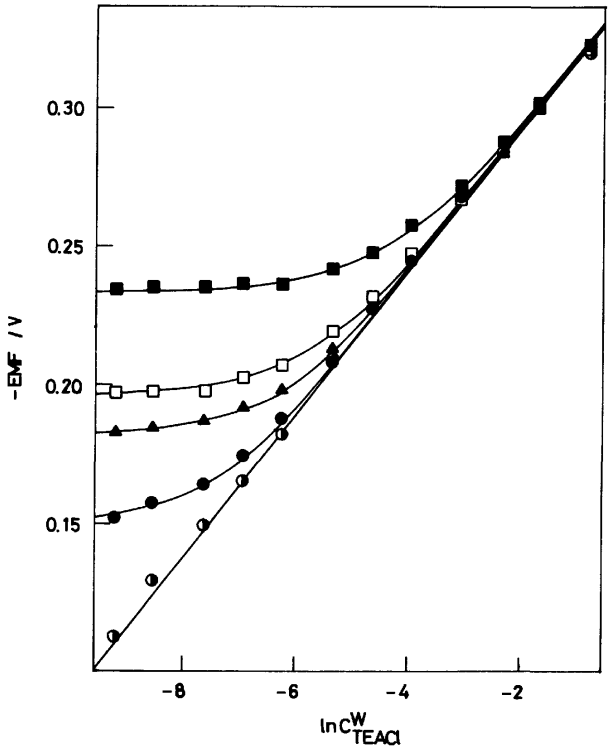

Fig. 2. Response of the TEA^+ ion-selective electrode in the presence of Me_3PrN^+ ion at $a=2$ mmol dm^{-3} and $b=0$(◑), 1(●), 5(▲), 10(□), and 50(■) mmol dm^{-3}.

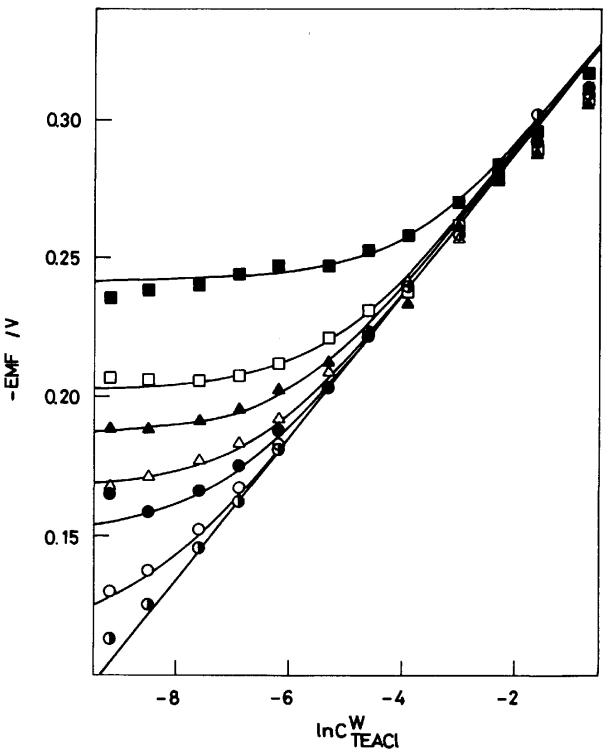

Fig. 3. Response of the TEA^+ ion-selective electrode in the presence of Et_3MeN^+ ion at $a=2$ mmol dm^{-3} and $b=0$(◑), 0.2(○), 1(●), 2(△), 5(▲), 10(□), and 50(■) mmol dm^{-3}.

the standard ion-transfer potentials and diffusion coefficients of these ions. The values for the diffusion

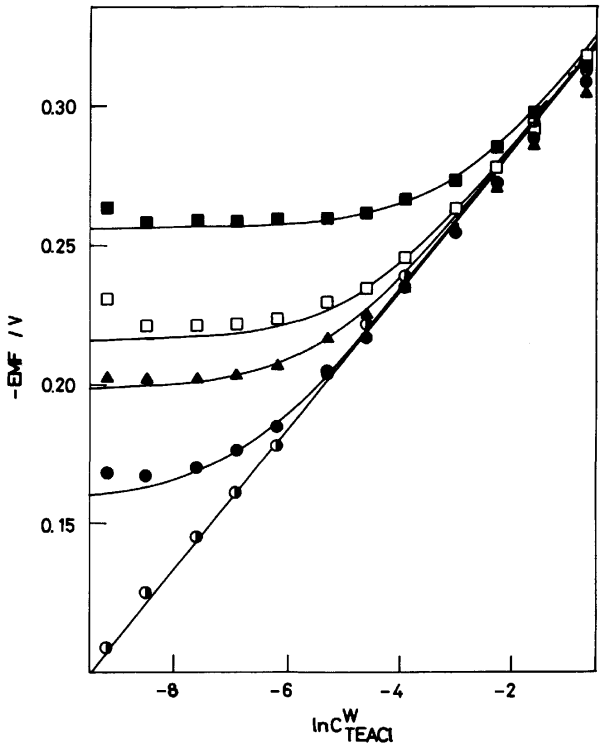

Fig. 4. Response of the TEA^+ ion-selective electrode in the presence of Me_3BuN^+ ion at $a=2$ mmol dm^{-3} and $b=0$(◑), 1(●), 5(▲), 10(□), and 50(■) mmol dm^{-3}.

coefficients in the liquid-membrane were taken as halves of those in the aqueous solution.[9] The ratios of the mass-transfer coefficients of the two ions were equated with the square root of the ratio of their diffusion coefficients; the mass-transfer was considered to occur primarily through diffusion in the present system.

Triethylmethylammonium Ion-selective Electrode. When the standard ion-transfer potential of an interfering ion is negative than that of the primary ion, the theory predicts that the degree of interference becomes more significant and the selectivity coefficient decreases with the decrease of the interfering ion concentration, in contrast to the cases where the standard ion transfer potential of an interfering ion is more positive than that of the primary ion. As an example of such a case, we studied the response of the Et_3MeN^+ ion-selective electrode in the presence of TEA^+ ion at $a=2$ mmol dm^{-3} and $b=0.2$, 1, 2, 5, 10, and 50 mmol dm^{-3}. The results are shown in Fig. 5. The solid lines are the theoretical curves calculated as described above.

Discussion

Figures 1—5 clearly show that for all the combinations of the primary and interfering ions studied the calculated curves agree well with the experimental points over wide ranges of the concentrations of the primary and interfering ions. This confirms that the theory of liquid ion-exchange membrane ion-selective electrodes previously derived by Kakiuchi and

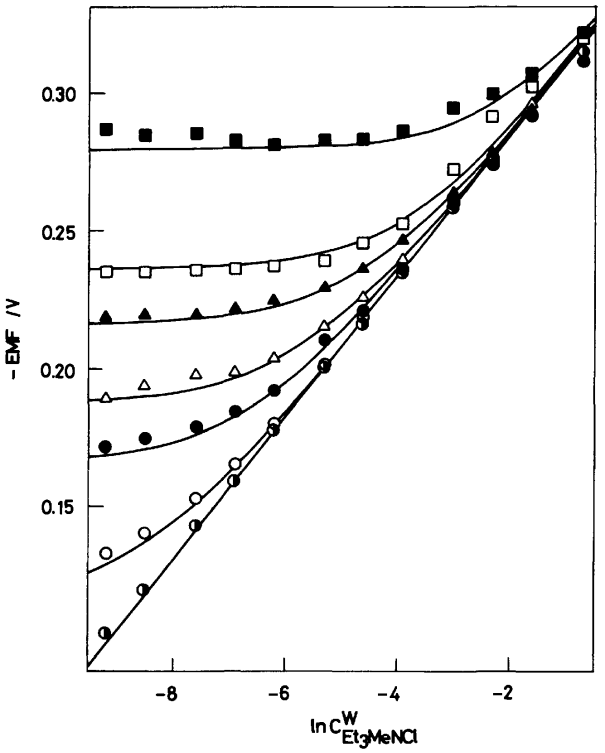

Fig. 5. Response of the Et_3MeN^+ ion-selective electrode in the presence of TEA^+ ion at $a=2$ mmol dm^{-3} and $b=0$(◑), 0.2(○), 1(●), 2(△), 5(▲), 10(□), and 50(■) mmol dm^{-3}.

Senda[1] satisfactorily describes the emf response of the ion-selective electrodes of the type represented by cell(I).

The selectivity characteristics of ion selective electrodes are usually evaluated by using the selectivity coefficient, $k_{i,j}^{pot}$, defined by the Nicolsky equation.[10] Although $k_{i,j}^{pot}$ is not a physical constant intrinsic to a given electrode system but depends on experimental conditions such as the concentrations of the relevant ions,[11] it has been widely used as a convenient measure of the selectivity of ion-selective electrodes.[12] Moreover, the manner of change of $k_{i,j}^{pot}$ with the concentration of primary ion has been sometimes used as a criterion for the validity of a theory of ion-selective electrodes.[13] We evaluated the selectivity coefficient of the ion-selective electrode(I) defined by a Nicolsky-type equation:[1]

$$E = E_{R_1}^0 - \frac{RT}{F} \ln \frac{c_{R_1}^W + k_{i,j}^{pot} c_{R_2}^W}{c_{R_1}^0} \qquad (1)$$

where E is the emf, $E_{R_1}^0$ is $\Delta_{NB}^W \varphi_{R_1}^0 + \Delta E_{ref}$, being the potential difference associated with the reference electrodes in the cell(I), and $c_{R_1}^W$, $c_{R_2}^W$, and $c_{R_1}^0$ are the concentrations of R_1^+ and R_2^+ ions in the sample solution and of R_1^+ ion in the liquid membrane, respectively. We used two methods to determine the $k_{i,j}^{pot}$ values: Method I using the intersection point of the two linear portions of the emf *vs.* $\log c_{R_1}^W$ curve and Method II using the concentration of a primary ion at which the emf *vs.* $\log c_{R_1}^W$ curve in the presence of an interfering ion deviates by $(RT/F)\ln 2 = 18$ mV from the curve without interfering ion. The former method gives the $k_{i,j}^{pot}$ value at the infinitely small $c_{R_1}^W$,[1] whereas the latter gives the one at the $c_{R_1}^W$ at which the curve deviates by 18 mV from the linear Nernstian response. Method I seems less sensitive to the scattering of the experimental emf values than Method II, since Method I necessarily averages out the scattering by using several points to draw a horizontal line at the lower values of $c_{R_1}^W$. However, Method I is not applicable to cases where such a horizontal part of the emf *vs.* $c_{R_1}^W$ curve is not attainable experimentally. The results are given in Tables 3—5 together with the theoretical values based on Eq. 24 in Ref. 1. For both methods, the calculated values of $k_{i,j}^{pot}$ agree well with the observed ones. Taking account of the fact that the observed $k_{i,j}^{pot}$ value is very sensitive to small scattering of emf values, this general agreement seems enough evidence of the validity of the theory for predicting the response of the ion-selective electrode of the type represented by the cell(I).

Table 3 shows that the $k_{i,j}^{pot}$ values decrease with the increase of the concentration of the interfering ions. This is what is theoretically expected for the case when the standard ion-transfer potential of the primary ion (TEA^+) is more negative than that of the interfering ion (Me_3EtN^+, Me_3PrN^+, Me_3BuN^+, and Et_3MeN^+). In the case of TEA^+ ion interference with respect to Et_3MeN^+ ion, the standard ion-transfer potential of the primary ion (Et_3MeN^+) is more positive than that of the interfering ion(TEA^+). The theory predicts in this case that the $k_{i,j}^{pot}$ value increases with increasing concentration of the interfering ion, which was confirmed experimentally as shown in Table 4. Such an inversion in the concentration dependence of $k_{i,j}^{pot}$ has been found also for a nitrate ion-selective electrode of liquid ion-exchange membrane type without supporting electrolytes.[15]

According to the theory, $k_{i,j}^{pot}$ depends not only on the concentration of the ions in sample solution but also on the concentration of the primary ion in liquid membrane. The $k_{i,j}^{pot}$ values for the TEA^+ ion-selective electrode at $a=0.5$, 1, 2, and 5 mmol dm^{-3} in the presence of Et_3MeN^+ in the sample solution at $b=10$ mmol dm^{-3} in cell(I) are given in Table 5. The $k_{i,j}^{pot}$ values determined by Method I clearly show the increasing tendency of $k_{i,j}^{pot}$ with the increase of the concentration of TEA^+ ion in the liquid membrane. Such a change of $k_{i,j}^{pot}$ was less conspicuous for the $k_{i,j}^{pot}$ estimated by Method II, probably because of the larger error inherent to this method.

The selectivity coefficients for a series of interfering ions for a given primary ion are usually discussed in terms of the difference in single ion partition coefficient defined by $K_i = c_i^W / c_i^O$ for i ion. By definition the difference in the single ion partition coefficient between two ions, i and j, is related to the difference in the standard ion-transfer potential between the two ions by

TABLE 3. SELECTIVITY COEFFICIENTS OF TEA^+ ION-SELECTIVE ELECTRODE[1)]

Interfering ion	$c^W(R_2Cl)$ / mmol dm^{-3}	Method I k^{pot}_{exptl}	Method I k^{pot}_{calcd}	Method II k^{pot}_{exptl}	Method II k^{pot}_{calcd}
Me_3EtN^+	1	—	0.33	0.28	0.26
	5	—	0.19	0.15	0.15
	10	0.14	0.15	0.11	0.13
	50	0.10	0.10	0.09	0.09
Me_3PrN^+	1	—	0.60	0.43	0.51
	5	—	0.41	0.35	0.37
	10	0.36	0.37	0.30	0.33
	50	0.32	0.31	0.37	0.30
Et_3MeN^+	0.2	—	0.88	0.88	0.81
	1	—	0.70	0.64	0.63
	2	—	0.63	0.62	0.56
	5	0.55	0.55	0.50	0.50
	10	0.54	0.50	0.45	0.48
	50	0.41	0.46	0.41	0.45
Me_3BuN^+	1	—	0.70	0.64	0.63
	5	0.55	0.55	0.50	0.50
	10	0.54	0.50	0.45	0.48
	50	0.41	0.46	0.41	0.45

1) The concentration of TEATPB in the liquid membrane was 2 mmol dm^{-3}.

TABLE 4. SELECTIVITY COEFFICIENTS OF Et_3MeN^+ ION-SELECTIVE ELECTRODE IN THE PRESENCE OF TEA^+ ION[1)]

c^W(TEACl) / mmol dm^{-3}	Method I k^{pot}_{exptl}	Method I k^{pot}_{calcd}	Method II k^{pot}_{exptl}	Method II k^{pot}_{calcd}
0.2	—	1.08	1.37	1.16
1	—	1.38	1.70	1.64
2	1.78	1.64	1.94	1.89
5	—	1.95	2.03	2.10
10	2.02	2.10	1.87	2.18
50	2.79	2.23	2.63	2.25

1) The concentration of Et_3MeN^+ ion in the liquid membrane was 2 mmol dm^{-3}.

TABLE 5. CHANGE OF THE SELECTIVITY COEFFICIENT OF THE TEA^+ ION-SELECTIVE ELECTRODE WITH THE CHANGE OF THE CONCENTRATION OF TEA^+ ION IN THE LIQUID MEMBRANE[1)]

c^{NB}(TEATPB) / mmol dm^{-3}	Method I k^{pot}_{exptl}	Method I k^{pot}_{calcd}	Method II k^{pot}_{exptl}	Method II k^{pot}_{calcd}
0.5	0.45	0.46	0.60	0.45
1	0.51	0.48	0.46	0.46
2	0.54	0.50	0.45	0.48
5	0.64	0.56	0.50	0.52

1) The concentration of Et_3MeN^+ ion in the sample solution was 10 mmol dm^{-3}.

$$\ln(K_i/K_j) = \frac{F}{RT}(z_j\Delta^W_0\varphi^0_j - z_i\Delta^W_0\varphi^0_i) \qquad (2)$$

where K_i and K_j are the single ion partition coefficients for the ions i and j, and z_k is the electric charge of the ion k(k=i or j). When the liquid-membrane contains lipophilic ligands, X, (usually belonging to the family of ionophores) which form complexes MX_n (n=1, 2, ···) with the ion M (M=i or j) transferred across the liquid-membrane/sample solution interface, the standard ion-transfer potential $\Delta^W_0\varphi^0_M$ (M=i or j) in Eq. 2 should be replaced by the apparent standard ion-transfer potential $\Delta^W_0\varphi^0_{M,app}$[16)] defined by

$$\Delta^W_0\varphi^0_{M,app} = \Delta^W_0\varphi^0_M - \frac{RT}{z_MF}\ln(\sum_n \beta_n c_X^n) \qquad (3)$$

where β_n is the over-all stability constant (β_0=1) of the complexes MX_n (n=0, 1, 2, ···), and c_X is the bulk concentration of X in the liquid membrane.

The experimental linear correlation between the logarithm of the selectivity coefficient and the logarithm of the single ion-partition coefficient have long been recognized for the liquid ion-exchange membrane ion-selective electrodes.[17)] The linear correlation is one of the important conclusions of Sandblom *et al.*'s theory[18)] for membrane electrode potential and hence the experimental linear correlation has been considered as demonstrating the essential validity of their theory. In our previous paper we have shown that the dependence of the logarithm of selectivity coefficient on the difference in the standard ion-transfer potential between the primary and interfering ions is approximately linear under certain conditions, but can be remarkably non-linear, depending on the mass-transfer coefficients of the ions. (See Fig. 4 in Ref. 1). Figure 6 shows a plot of the logarithm of the k^{pot}_{ij} by method I at a=2 mmol dm^{-3} and b=10 mmol dm^{-3} against the difference between the standard ion-transfer potentials of the primary and interfering ions. The upper four circles in Fig. 6 are for the TEA^+ ion-selective electrode with the interfering ions Me_3EtN^+, Me_3PrN^+, Et_3MeN^+, and Me_3BuN^+ and the lowest circle is for the Et_3MeN^+ ion-selective electrode with the interfering ion TEA^+. The selectivity coefficient increased with the increase

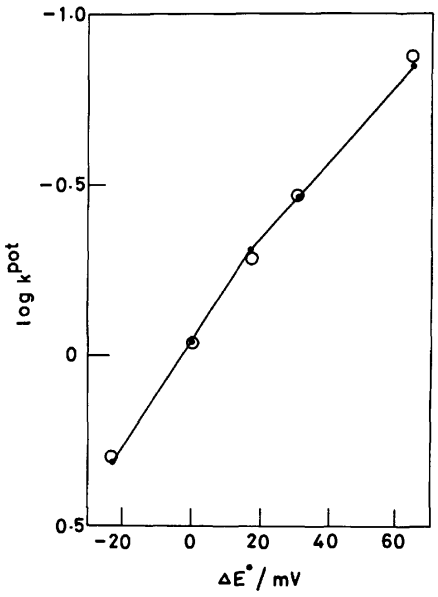

Fig. 6. Change of the logarithm of selectivity coefficient with the change of the difference between the standard ion-transfer potentials of the primary and interfering ions, ΔE. Upper four points are for the TEA^+ ion-selective electrode and the lowest point for the Et_3MeN^+ ion-selective electrode.

of the hydrophobicity of the interfering ions, *i.e.*, with the decrease of the standard ion-transfer potential. The solid line in Fig. 6 connects the theoretical points of $k_{i,j}^{pot}$ indicating a good agreement between the theory and the experimental results. The nonlinearity of the plot in Fig. 6 clearly demonstrates the validity of the theory in which the effect of the mass transfer coefficients of the ions is taken into account.

As demonstrated by this study, the emf response of the liquid ion exchange membrane ion-selective electrodes of the type represented by cell(I) is described well by the theory based on the concept of the mixed ion-transfer potential at the liquid-membrane/sample solution interface. This indicates that the ion-transfer processes at the interface between the liquid membrane and the sample solution has a general importance for the understanding of the basic properties of liquid ion-exchange membrane ion-selective electrodes.

The authors thank Mitsuru Shiomi for his assistance in emf measurements.

References

1) T. Kakiuchi and M. Senda, *Bull. Chem. Soc. Jpn.*, **57**, 1801 (1984).
2) T. Kakiuchi and M. Senda, Unpublished results.
3) L. Q. Hung, *J. Electroanal. Chem. Interfacial Electrochem.*, **115**, 159 (1980).
4) T. Osakai, T. Kakutani, Y. Nishiwaki, and M. Senda, *Bunseki Kagaku*, **32**, E18, (1983).
5) T. Kakiuchi and M. Senda, unpublished results.
6) T. Osakai, T. Kakutani, Y. Nishiwaki, and M. Senda, unpublished results.
7) A. Simon and U. Uhlig, *Chem. Ber.*, **85**, 977 (1952).
8) A. P. Phillips and R. Baltzly, *J. Am. Chem. Soc.*, **74**, 5231 (1952).
9) Z. Samec. V. Marecek, J. Koryta, and M. W. Khail, *J. Electroanal. Chem. Interfacial Electrochem.*, **83**, 393 (1977).
10) B. P. Nicolsky, *Zh. Fiz. Khin.*, **10**, 495 (1937).
11) W. E. Morf, "The Principles of Ion-selective Electrodes and of Membrane Transport," Elsevier, Amsterdam (1981).
12) E. Pungor, K. Toth, and A. Hrabeczy-Pall, *Pure Appl. Chem.*, **59**, 1915 (1979).
13) Ref. 10, Chap. 11.
14) J. Koryta, "Ion-selective Electrode," Cambridge Univ. Press, Cambridge, 1975.
15) K. Srinivasan and G. A. Rechnitz, *Anal. Chem.*, **41**, 1203 (1969).
16) For a review, see J. Koryta, *Ion-selective Electrode Rev.*, **5**, 131 (1983).
17) R. Scholer and W. Simon, *Helv. Chim. Acta*, **55**, 1801 (1972).
18) J. Sandblom, G. Eisenman, and J. L. Walker, Jr., *J. Phys. Chem.*, **71** 3862 (1967).

The Reaction of [CoL_2] or [$CoL_2(NO)$] (L=4-Methyl-8-quinolinolate Ion) with Nitrogen Monoxide

Eiichi Miki,* Mikio Tanaka,† Katsunori Saito, Toshiaki Maejima, Kunihiko Mizumachi, and Tatsujiro Ishimori

Department of Chemistry, College of Science, Rikkyo University, Nishi-Ikebukuro, Toshima-ku, Tokyo 171

†*Laboratory of Chemistry, Nippon Medical School, Kosugi, Nakahara-ku, Kawasaki 211*

(Received November 30, 1984)

[$Co(4mqn)_2$]·$2H_2O$ (4mqn=4-methyl-8-quinolinolate ion) reacted with nitrogen monoxide in CH_2Cl_2 or in DMF at room temperature to give [$Co(4mqn)_2(NO)$] (**1**). [$Co(4mqn)_2$]·$2H_2O$ and **1** reacted with nitrogen monoxide in 10 vol% pyridine–DMF and in pyridine at *ca.* 283—288 K to precipitate [$Co(4mqn)_2(NO)(py)$] (**2**). When the reaction was carried out at *ca.* 293—303 K, [$Co(4mqn)_2(NO_2)(py)$] (**3**) instead of **2** was precipitated. From the filtrates, [$Co(4mqn)_2(NO_3)(py)$]·py·$2H_2O$ (**4**) was obtained. The gaseous product of the reactions giving **2** and **4**, and **3** and **4**, was dinitrogen oxide. The stoichiometries of the reactions in the pyridine–DMF and in pyridine were confirmed by mass analyses for the residual nitrogen monoxide and the produced dinitrogen oxide.

A number of studies of the reactions of transition-metal or transition-metal nitrosyl complexes with nitrogen monoxide, NO, have been reported.[1] However, there have been no careful examinations of the effects of the solvents used or those of the substituents of the ligands used on the reactions.

Bis(8-quinolinolato)cobalt(II) reacted with NO in CH_2Cl_2, which has a poor coordination ability, to give [$Co^{III}(qn)_2(NO)$] (qn=8-quinolinolate ion) with the NO^- group, and the nitrosyl reacted further with NO in CH_2Cl_2 to give [NO][$Co^{III}(qn)_2(NO_3)(NO_2)$], with the liberation of N_2O.[2] In this reaction, the nitrosyl group forms the NO_2^- with a retention of the original Co–NO bond. On the other hand, bis(2-methyl-8-quinolinolato)cobalt(II) reacted with NO in CH_2Cl_2 to give $[NO]_3[Co^I(2mqn)_2(NO_3)(NO_2)]$ and [$Co^0(2mqn)_2$-$(NO)_2$] (2mqn=2-methyl-8-quinolinolate ion), with the liberation of N_2O.[3] The difference in the reactions of NO with the corresponding cobalt ions seems to be due to the electron-donative power of the CH_3 group in the 2mqn.

In a solvent possessing a strong coordinating ability, such as pyridine, [$CoL_2(NO)$] with the NO^- group (L=5-chloro- or 5-nitro-8-quinolinolate ion) reacted with NO to give the nitrato complex, [$CoL_2(NO_3)(py)$], involving scrambling between the NO^- group and the NO.[4]

The present paper will describe the reactions of [$Co(4mqn)_2$]·$2H_2O$ or [$Co(4mqn)_2(NO)$] (4mqn=4-methyl-8-quinolinolate ion) with NO in CH_2Cl_2, DMF, 10 vol% pyridine–DMF, or pyridine; the effects of the solvents and the substituents in the quinoline ring on the reactions are also discussed. The stoichiometries of the reactions are also examined on the basis of the determination of the relative molar ratio of the residual NO to the N_2O produced.

Experimental

The JIS-GR CH_2Cl_2, DMF, and pyridine were dried over Zeorum A-4, stored under argon, and carefully degassed by three cycles of freeze-pump-thaw prior to use. The JIS-GR diethyl ether used as a precipitation reagent was deaerated with dinitrogen before use. The ^{15}NO was prepared by the reaction of $K^{15}NO_3$ (^{15}N atom%=99) with concd H_2SO_4 and mercury. The 4-methyl-8-quinolinol was prepared from *o*-aminophenol and methyl vinyl ketone.[5] The [$Co(4mqn)_2$]·$2H_2O$ was prepared by the ordinary method. Anal. ($CoC_{20}H_{20}O_4N_2$) Co, C, H, N.

The IR spectra of the solid products were measured on JASCO A-202 (400—4000 cm^{-1}) and JASCO IR-F (200—650 cm^{-1}) spectrometers. The isotopic shifts upon ^{15}N-substitution were carefully measured at 80 K. For identifying the gaseous products and examining the stoichiometry of the reaction in 10 vol% pyridine–DMF or in pyridine, a Hitachi M-80 double-focusing mass spectrometer equipped with a Hitachi data-processing system (M-003) was used; the IR bands of the gaseous materials and the ^{15}N-isotopic shifts[6] in the 1000—4000 cm^{-1} region were also measured. The magnetic susceptibilities of the solid products were measured by the Gouy method at room temperature.

All the reactions were treated in a vacuum line. The representative scale and the procedure were as follows: NO (5.0 mmol) was trapped in a reaction vessel (*ca.* 150 cm^3) containing [$Co(4mqn)_2$]·$2H_2O$ (0.5 mmol) suspended or dissolved in the organic solvents (10 cm^3) with the aid of liquid nitrogen. The reaction vessel was shaken under running water until the frozen solution thawed, and then the contents were stirred for 1—3 d to obtain the precipitate. By dropping the filtrate into deoxygenated diethyl ether, another product was precipitated. These products were washed with diethyl ether and dried under a vacuum. When [$Co(4mqn)_2(NO)$] was used as the starting material, the degassed pyridine–DMF or pyridine was poured into the reaction vessel containing the nitrosyl complex, which had been kept at the temperature of liquid nitrogen, and then NO was trapped. The contents were stirred after having been thawed under running water.

Results and Discussion

The elementary analyses, the chemical formulae, and the yields of the solid products are shown in Table 1. All the compounds were diamagnetic, indicating that they are low-spin type cobalt(III) compounds, since the formal oxidation number of the coordinating NO in the nitrosyl compounds is −I, as will be discussed later. The compounds are stable in the solid state under air, but the nitrosyl compounds are unstable in the

TABLE 1. ELEMENTARY ANALYSES AND YIELDS OF THE SOLID PRODUCTS

Complex (Color)	Yield/%		Elementary analysis Co(%)	C(%)	H(%)	N(%)	Reactant[a]	Temperature	Solvent
1 $[Co(4mqn)_2(NO)]$	60—90	Found	14.4	58.9	3.9	10.4	A		CH_2Cl_2
(dark green)		Found	14.0	59.2	3.9	10.3	A		DMF
		Calcd	14.6	59.3	4.0	10.4			
2 $[Co(4mqn)_2(NO)(py)]$	40—60	Found	11.9	60.9	4.5	11.4	A	b)	10vol%py-DMF
(yellowish khaki)	60	Found		60.9	4.4	11.7	A		py
		Found	11.9	61.7	4.4	11.6	1		10vol%py-DMF
	20	Found		60.3	4.3	11.6	1		py
		Calcd	12.2	62.0	4.4	11.6			
3 $[Co(4mqn)_2(NO_2)(py)]$	40	Found		60.2	4.4	11.5	A	c)	10vol%py-DMF
(yellowish khaki)	30—50	Found		59.4	4.3	11.4	1		10vol%py-DMF
		Calcd		60.0	4.2	11.2			
4 $[Co(4mqn)_2(NO_3)(py)]$	30—40	Found	9.4	56.8	4.5	11.3	A	b)	10vol%py-DMF
$\cdot py \cdot 2H_2O$	30	Found		57.6	4.5	11.0	A		py
(brownish khaki)	40—50	Found	9.2	56.4	4.4	11.1	1	c)	10vol%py-DMF
		Calcd	9.4	57.1	4.8 (4.4)[d]	11.1			

a) **A**, $[Co(4mqn)_2]\cdot 2H_2O$. b) At *ca.* 283—288 K. c) At *ca.* 293—303 K. d) The hydrogen content on the assumption that the $2H_2O$ of **4** leaves during the preliminary treatment of the elementary analysis. 4mqn=4-methyl-8-quinolinolate ion.

dissolved state.

Reaction of $[Co(4mqn)_2]\cdot 2H_2O$ with NO in CH_2Cl_2 or in DMF. $[Co(4mqn)_2]\cdot 2H_2O$ reacted with NO to precipitate $[Co(4mqn)_2(NO)]$ (**1**). No further reaction proceeded in CH_2Cl_2; however, in DMF **1** reacted further with NO to give a clear, reddish-brown solution, with the liberation of N_2O. However, the precipitate obtained by adding the solution to diethyl ether could not be characterized.

The IR bands at 1658(vs), 551(s), and 537(s) cm^{-1} for **1** shifted down by 31, 6, and 7 cm^{-1} respectively upon ^{15}N-substitution. The 1658 cm^{-1} band was assigned to the N-O stretching vibration, and the 551 and 537 cm^{-1} bands, to the skeletal vibrations between the cobalt and the NO group.[7] The wave numbers of the N-O stretching band and the electrophilic attack of NO on the NO group, as will be mentioned later, suggest that **1** is an NO^- complex.[4,7] The reaction giving **1** can be regarded as an oxidative addition of NO to cobalt(II).

Reaction of $[Co(4mqn)_2]\cdot 2H_2O$ or $[Co(4mqn)_2(NO)]$ with NO in 10vol% Pyridine-DMF or in Pyridine. The gaseous product was always only N_2O.

Reaction at ca. *283—288 K*: $[Co(4mqn)_2]\cdot 2H_2O$ reacted with NO to precipitate $[Co(4mqn)_2(NO)(py)]$ (**2**). The N-O stretching and the skeletal vibrations between the cobalt and the NO group were observed at 1616, 558, and 431 cm^{-1}. The wave numbers of the N-O stretching vibration for **1**, 1658 cm^{-1}, shifted down to 1616 cm^{-1} by the coordination of pyridine to the cobalt ion. The 321(s) cm^{-1} band of **2** could be assigned to the Co-N(pyridine) stretching vibration by a careful comparison of the IR spectrum for **2** with that for **1**.[8]

By adding the filtrate to deaerated diethyl ether, a brownish khaki product, **4**, was precipitated. This product was not clearly characterized. The IR band at 823(w) cm^{-1} shifted to 810 cm^{-1} upon ^{15}N-substitution, but no isotopic shifts for any other bands could be observed.[9]

The stoichiometries of the reactions to be discussed later can be reasonably explained on the assumption that **4** contains a nitrate ion. If so, the 823 cm^{-1} band can be assigned to the out-of-plane bending of NO_3^-.[4] The 321 cm^{-1} (s) band was assigned to the Co-N (pyridine) stretching vibration, as had been **2**. By the reactions of $[CoL_2]$ (L=5-chloro- or 5-nitro-8-quinolinolate ion) with NO in the same solvents, $[CoL_2(NO_3)(py)]$ was isolated.[4] **4** seems to be $[Co(4mqn)_2(NO_3)(py)]\cdot py\cdot 2H_2O$ considering the similarities of the reactions, the elementary analysis, the IR spectrum, and the stoichiometry of the reaction. The bands characteristic of a coordinating nitrate ion, with the exception of the 823 cm^{-1} band, seem to be hidden under the strong absorptions due to the 4mqn and pyridine. The water of crystallization in **4** may come from a small quantity of water contained in diethyl ether.

The reaction of $[Co(4mqn)_2]\cdot 2H_2O$ with NO consists of a nitrosylation reaction ($Co^{2+}+NO \rightarrow Co^{3+}+NO^-$) and the disproportionation of NO to NO_3^- and N_2O ($Co^{2+}+5NO \rightarrow Co^{3+}+NO_3^-+2N_2O$).

$[Co(4mqn)_2(NO)]$ reacted with NO to give the same products, **2** and **4**. The reaction can be described as $Co^{3+}+NO^-+4NO \rightarrow Co^{3+}+NO_3^-+2N_2O$.

Reaction at ca. *293—303 K*: Both $[Co(4mqn)_2]\cdot 2H_2O$ and **1** reacted with NO to precipitate $[Co(4mqn)_2(NO_2)(py)]$ (**3**). The terminal N-O stretching band of the nitrosyl complex could not be observed. The 1402(s) and 1314(s) cm^{-1} bands shifted to 1383 and 1291 cm^{-1} respectively upon ^{15}N-substitution (see Fig. 1). These bands can be assigned to the N-O stretching bands characteristic of the coordinating nitro ion.[4] The strong band at 320 cm^{-1} is the Co-N(pyridine) stretch-

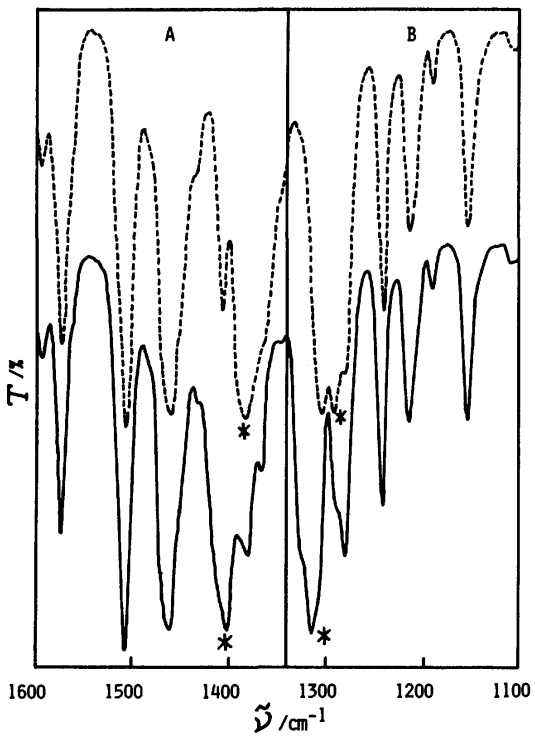

Fig. 1. IR spectra of $[Co(4mqn)_2(NO_2)(py)]$ (4mqn= 4-methyl-8-quinolinolate ion).
——: $^{14}NO_2$ complex, -----: $^{15}NO_2$ complex (^{15}N atom%=99).
* indicates the N–O stretching band characteristic of the coordinating nitro ion. The bands due to the nitro ion, and the bands due to the coordinating 4mqn and pyridine partially overlapped.
A region: poly(chlorotrifluoroethylene) oil mull, B region: Nujol mull.

ing vibration. The precipitate from the filtrate was **4**, like that prepared at a low temperature. The stoichiometry of the reaction reasonably explains that **3** and **4** contain a NO_2^- and a NO_3^- respectively, as will be discussed later.

The reaction of $[Co(4mqn)_2]\cdot 2H_2O$ with NO can be regarded as the disproportionations of NO to NO_2^- and N_2O ($Co^{2+}+3NO \rightarrow Co^{3+}+NO_2^-+N_2O$) and to NO_3^- and N_2O ($Co^{2+}+5NO \rightarrow Co^{3+}+NO_3^-+2N_2O$), involving the oxidation of Co^{2+} to Co^{3+}.

On the reaction of **1** with NO, the coordinating NO^- group was electrophilically attacked by NO to give NO_2^- and NO_3^-, with the liberation of N_2O: $Co^{3+}+NO^-+2NO \rightarrow Co^{3+}+NO_2^-+N_2O$ and $Co^{3+}+NO^-+4NO \rightarrow Co^{3+}+NO_3^-+2N_2O$.

Characterization of Reactions. The stoichiometries of the reactions in the pyridine-DMF and in pyridine were also examined. The relative molar ratios of the residual NO to the gaseous product, N_2O, were calculated from the reaction formulae, based on the yields of the solid products. The reaction formulae are shown in the last item. The observed ratios agreed with the calculated ones, shown in Table 2, indicating that the reactions shown in the last item proceed.

For examining the mechanism of the reaction of **1** with NO in the pyridine-DMF at *ca.* 288 K, the following isotopic combinations were used; *A*, (the ^{14}NO complex)-(^{15}NO gas) and *B*, (the ^{15}NO complex)-(^{14}NO gas). In the case of *A*, the molar ratio of ^{14}NO to ^{15}NO observed in the residual NO gas was almost equal to that of ^{14}NO to ^{15}NO contained in the reaction system. The same phenomenon was also observed for the case of *B*. Moreover, $[Co(4mqn)_2(^{14}NO)]$ reacted with ^{15}NO to give $[Co(4mqn)_2(^{14,15}NO)(py)]$, showing the ^{14}N–O and ^{15}N–O stretching bands. On a reaction at a higher temperature (*ca.* 298 K), the same ^{14}N–^{15}N scrambling as that at a lower temperature was observed.

These facts suggest that **1** decomposes perfectly to the cobalt(II) complex, $[Co(4mqn)_2]$, and NO, and that the resulting NO gas, together with NO gas, an original reactant, reacts again with $[Co(4mqn)_2]$ to give **1**. A part of the **1** is precipitated as **2** at a low temperature. On the other hand, at a high temperature, **1** reacts further with NO to give **3**. This reaction seems to proceed with a cleavage of the Co–NO bond, because the coordination of pyridine unstabilizes the Co–NO bond in the dissolved state.[4] The remaining part of **1** in the dissolved state reacts with NO to give **4**.

When a smaller amount of **1**, for example, 0.2 mmol, was used without changing the amounts of NO and the pyridine-DMF, only **4** was obtained. **2** reacted with NO in the pyridine-DMF on the same scale as has

Table 2. Stoichiometry of the reaction

Reactants		Solid products		NO/N_2O[c] Found	Calcd	Solvent
At a low temperature[a]						
A(0.50)[d]	NO(5.0)	**2**(0.18)	**4**(0.20)	9.4	9.6	10vol%py-DMF
A(0.50)	NO(5.0)	**2**(0.31)	**4**(0.17)	11	11	py
1(0.75)	NO(5.0)	**2**(0.54)	**4**(0.20)	9.2	10	py
1(0.33)	NO(5.0)	**2**(0.07)	**4**(0.22)	11	9.4	py
At a high temperature[b]						
A(0.50)	NO(5.0)	**3**(0.21)	**4**(0.17)	6.8	6.4	10vol%py-DMF
1(0.50)	NO(5.0)	**3**(0.24)	**4**(0.19)	6.1	6.1	10vol%py-DMF

a) At *ca.* 283—288K. b) At *ca.* 293—303K. c) Relative molar ratio of the residual NO to the produced N_2O. d) mmol unit. **A**, $[Co(4mqn)_2]\cdot 2H_2O$. **1**, $[Co(4mqn)_2(NO)]$. **2**, $[Co(4mqn)_2(NO)(py)]$. **3**, $[Co(4mqn)_2(NO_2)(py)]$. **4**, $[Co(4mqn)_2(NO_3)(py)]\cdot py\cdot 2H_2O$. 4mqn=4-methyl-8-quinolinolate ion.

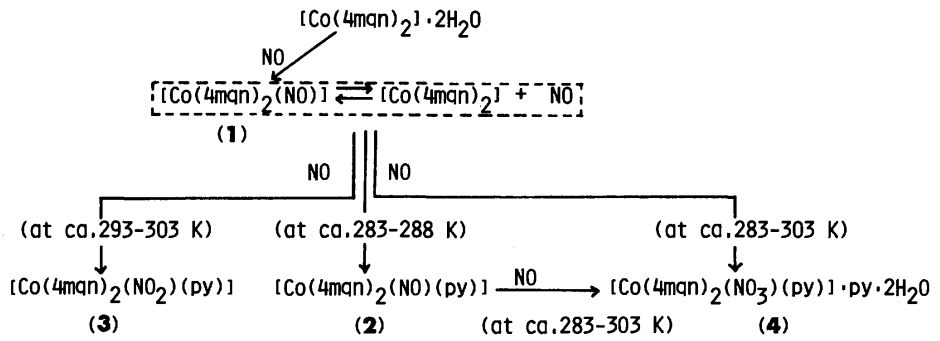

Scheme 1. Reaction of $[Co(4mqn)_2]\cdot 2H_2O$ or $[Co(4mqn)_2(NO)]$ with NO in 10 vol% py-DMF or in py.
(4mqn = 4-methyl-8-quinolinolate ion).

been described in the Experimental section to give only **4**, but to leave the unreacted **2** behind at both low and high temperatures. These facts suggest that **2** in the dissolved state reacts with NO to produce **4**, while **3** does not come from **2**. **3** hardly dissolved at all in the pyridine–DMF or in pyridine; hence, it did not react with NO to be recovered quantitatively. This indicates that **4** does not come from **3**. The reactions of $[Co(4mqn)_2]\cdot 2H_2O$ and $[Co(4mqn)_2(NO)]$ with NO are summarized in Scheme 1.

The critical temperature in the preparation of **2** or **3** was ambiguous. At 288—293 K, **2**, **3**, or their mixture was precipitated in subtly different conditions on that occasion.

In CH_2Cl_2, the reaction of $[Co(4mqn)_2]\cdot 2H_2O$ with NO was expected to be similar to that of $[Co(2mqn)_2]\cdot H_2O$ with NO because of the electron-donative power of the CH_3 group in the ligands.[3] However, the reaction gave only $[Co(4mqn)_2(NO)]$, and no further reaction with NO could be found such as was observed for the reactions of $[CoL_2]$ (L=5-chloro- or 5-nitro-8-quinolinolate ion) with NO.[4]

As for the reactions of $[Co(4mqn)_2]\cdot 2H_2O$ or $[Co(4mqn)_2(NO)]$ with NO in 10 vol% pyridine–DMF and in pyridine, $[Co(4mqn)_2(NO)(py)]$ and $[Co(4mqn)_2(NO_2)(py)]$ were prepared with $[Co(4mqn)_2(NO_3)(py)]\cdot py\cdot 2H_2O$ at low and high temperatures respectively, although $[CoL_2]$ and $[CoL_2(NO)]$ (L=8-quinolinolate, 5-chloro-, or 5-nitro-8-quinolinolate ion) reacted with NO in the same solvents to produce $[CoL_2(NO_3)(py)]$. No remarkable effects of the substituent in the quinoline ring on the reactions could be found except for the solubilities of the obtained compounds. The nitro complex, $[Co(4mqn)_2(NO_2)(py)]$, in the present study may be isolated because of its sparing solubility, since it is generally expected that, after $[CoL_2]$ has been nitrosylated, the NO^- group reacts with NO to give NO_3^- by way of NO_2^-.[4]

The present reaction in DMF could not be elucidated as observed for the reactions of $[CoL_2]$ (L=2-methyl- or 5-chloro-8-quinolinolate ion) with NO because the coordinating ability of DMF is not stronger than that of pyridine, and so complicated reactions may occur.

In the present study, the stoichiometries of the reactions in the pyridine–DMF and in pyridine were confirmed because all the products could be identified. It is very interesting that NO^- or NO_2^- is formed, together with NO_3^-, by the disproportionation of NO with a difference in the reaction temperature.

References

1) J. H. Enemark and R. D. Feltham, *Coord. Chem. Rev.*, **13**, 339 (1974); K. G. Caulton, *ibid.*, **14**, 317 (1975); J. A. McCleverty, *Chem. Rev.*, **79**, 53 (1979); K. K. Pandey, *Coord. Chem. Rev.*, **51**, 69 (1983).

2) E. Miki, *Chem. Lett.*, **1980**, 835.

3) E. Miki, K. Saito, K. Mizumachi, and T. Ishimori, *Bull. Chem. Soc. Jpn.*, **56**, 3515 (1983).

4) E. Miki, K. Ishimaru, K. Mizumachi, T. Ishimori, and M. Tanaka, *Bull. Chem. Soc. Jpn.*, **58**, 962 (1985).

5) J. P. Phillips, R. L. Elbinger, and L. L. Merritt, Jr., *J. Am. Chem. Soc.*, **71**, 3986 (1949).

6) J. Laane and J. R. Ohlsen, "Characterization of Nitrogen Oxides by Vibrational Spectroscopy," in "Progress in Inorganic Chemistry," ed by S. J. Lippard, An Interscience Publication by John Wiley & Sons, New York (1980), Vol. 27, pp. 465—513.

7) E. Miki, H. Okamura, K. Mizumachi, and T. Ishimori, *Bull. Chem. Soc. Jpn.*, **51**, 1768 (1978), and the references cited therein.

8) R. J. H. Clark and C. S. Williams, *Inorg. Chem.*, **4**, 350 (1965).

9) The carbon-13 and nitrogen-15 NMR measurements for **4** in DMSO-d_6 were performed at *ca.* 333 K to increase its low solubility to DMSO and decrease the high viscosity of the solution at room temperature, but **4** decomposed in DMSO to precipitate an uncharacterized product. The experimental conditions were the same as those described in Ref. 4.

Partial Molal Volumes and Volume Changes for the Complex Formation of Metal Chelate Electrolytes, $Na_2[M(edta)]$ and $K[M(hedta)(H_2O)]$

Kouzou YOSHITANI
Faculty of General Education, Gifu University, Yanagido, Gifu 501-11
(Received December 1, 1984)

The partial molal volumes, V^∞, of $[M(edta)]^{2-}$ and $[M(hedta)(H_2O)]^-$ (M=Mn(II), Co(II), Ni(II), Cu(II), and Zn(II) and H_3hedta=*N*-(2-hydroxyethyl)ethylenediamine-*N*,*N*′,*N*′-triacetic acid) and two free ligands, $edta^{4-}$ and $hedta^{3-}$, have been determined from density measurements at 25 °C. From the results for V^∞, the volume changes for the complex formation of $[M(edta)]^{2-}$ and $[M(hedta)(H_2O)]^-$, ΔV^∞, were estimated. The values of ΔV^∞ for $[M(edta)]^{2-}$ (32.8 to 45.8 $cm^3 mol^{-1}$) and for $[M(hedta)(H_2O)]^-$ (25.2 to 36.5 $cm^3 mol^{-1}$) were large, positive ones, and a linear relationship between ΔV^∞ and ΔS was observed for these metal chelate ions.

The ethylenediaminetetraacetate ion, $edta^{4-}$, is well known as a chelating reagent and is capable of acting as a sexidentate ligand. The stereochemistries of various edta metal chelates have been established in the solid state by means of X-ray studies.[1] However, the structures of the edta chelates in aqueous solutions remain ambiguous, though they have been investigated by a variety of methods.[2-10] A previous study has shown that the partial molal volumes, V^∞, and volume changes for the complex formation, ΔV^∞, are useful in studying the solute-solvent interactions and complex-formation reactions of the metal chelate electrolytes.[11] The volume changes on complexation must be interpreted not only in terms of the simple electrostatic theory, but also by paying attention to the complex structural and solvation changes. Therefore, it seems of interest to compare the ΔV^∞ of $[M(edta)]^{2-}$ with that of $[M(phen)_3]^{2+}$.[11] The former has anionic and hydrophilic ligands, but the latter has neutral and hydrophobic ones.

However, the V^∞ and ΔV^∞ for the edta chelates have not been reported except for $[Ni(edta)]^{2-}$.[12] In this study, the partial molal volumes of $[M(edta)]^{2-}$ and $[M(hedta)(H_2O)]^-$ are determined, and the volume changes of complex formation are estimated.

Experimental

Materials. The edta chelates, $Na_2[Mn(edta)]\cdot 4H_2O$, $Na_2[Co(edta)]\cdot 3.5H_2O$, $Na_2[Ni(edta)]\cdot 3H_2O$, $Na_2[Cu(edta)]\cdot 3H_2O$, and $Na_2[Zn(edta)]\cdot 3.5H_2O$, were obtained from Nakarai Chemicals, Ltd., and were recrystallized twice from an water–ethanol mixture according to the literature method.[13] The hedta chelate electrolytes, $K[Mn(hedta)(H_2O)]\cdot 3H_2O$, $K[Co(hedta)(H_2O)]\cdot 1.5H_2O$, $K[Ni(hedta)(H_2O)]\cdot 1.5H_2O$, $K[Cu(hedta)(H_2O)]\cdot 1.5H_2O$, and $K[Zn(hedta)(H_2O)]\cdot 1.5H_2O$, were prepared by the following manner, similar to that used for the edta chelates.[13]

N-(2-Hydroxyethyl)ethylenediamine-*N*,*N*′,*N*′-triacetic acid (27.8 g, 0.1 mol) was slowly stirred into a mixture of a calculated amount of basic metal carbonate or cobalt acetate and water (50 ml). The slurry was warmed to 90 °C, after which stirring was continued for 30 min. Then, $KHCO_3$ (10 g or 30 g for the Co-chelate) was added slowly to the reaction mixture, and stirring was continued for a further 10 min at 90 °C. Absolute ethanol was vigorous stirred into the resulting solution, after which it was warmed almost to the boiling point, until the precipitate began to form. The solution was then cooled in an ice bath. The resulting precipitate was filtered and washed with ethanol and ether. The crude product was recrystallized twice from the water–ethanol mixture. The recrystallized metal chelate was placed in a desiccator over silica gel.

The purities of all the products obtained here were checked by analysis.

The metal chelate electrolytes were dried *in vacuo* for one week at 90 °C before use. The tetra sodium salt of edta and the tri sodium salt of hedta (Nakarai Chemicals, Ltd.) were used without further purification and were dehydrated *in vacuo* to a constant weight at 110 °C. All the solutions were prepared by weight with deionized and distilled water.

Apparatus. The densities were measured at 25 °C with a digital density meter (Shibayama Scientific Co., Ltd., Model SSD-200) described in a previous paper.[11] The temperature of the thermostated bath was set at ±0.03 °C and regulated to ±0.002 °C.

Results

The apparent molal volumes, ϕ_v, of the metal chelate electrolytes were calculated from the density data using this equation:

$$\phi_v = \frac{M}{d} + \frac{1000(d^\circ - d)}{m\, d\, d^\circ}, \quad (1)$$

where M is the molecular weight of the metal chelate, m is the the molality, and d° and d are the densities of the solvent and the solution respectively. The partial molal volumes at infinite dilution, V^∞, were obtained by means of the Redlich-Mayer equation:[14]

$$\phi_v - S_v C^{1/2} = V^\infty + b_v C, \quad (2)$$

where S_v is the theoretical Debye-Hückel limiting slope (1.868 and 9.706 $cm^3 dm^{3/2} mol^{-3/2}$ for 1:1 and 1:2 electrolytes respectively), C is the molar concentration, and b_v is the empirical constant. In Figs. 1 and 2, the plots of the $\phi_v - S_v C^{1/2}$ of the edta and hedta chelates against C are shown. The V^∞ and b_v values obtained by the least-squares method are shown in Table 1. The standard deviations of the fits are mostly less than 0.1 $cm^3 mol^{-1}$.

The ϕ_v of sodium salts of edta and hedta can not be directly determined from the densities of their aque-

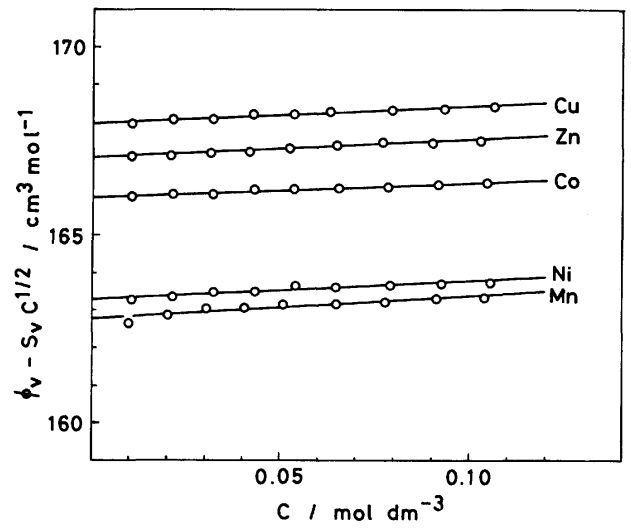

Fig. 1. Apparent Molal Volumes of $Na_2[M(edta)]$ at 25 °C.
$S_v = 1.868\,cm^3\,dm^{3/2}\,mol^{-3/2}$.

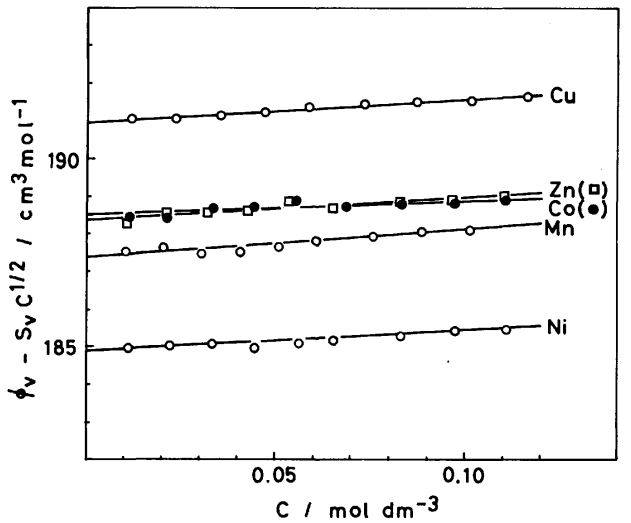

Fig. 2. Apparent Molal Volumes of $K[M(hedta)(H_2O)]$ at 25 °C.
$S_v = 9.706\,cm^3\,dm^{3/2}\,mol^{-3/2}$.

ous solutions because of the partial hydrolysis. Therefore, the stock solutions of the hypothetical solutes, $Na_4edta \cdot NaOH$ and $Na_3hedta \cdot NaOH$, were made up by mixing the anhydrous salts, stoichiometric amounts of the standard aqueous NaOH solution (0.3 mol dm^{-3}), and pure water. In this case, the pH values of the mixed solutions were around 12, and $edta^{4-}$ or $hedta^{3-}$ was assumed to be predominantly present from the pK_a values. The ϕ_v values, which were caluculated by introducing the molecular weight of the hypothetical solutes, fit the equation well over the present range of concentrations (0.01—0.1 mol dm^{-3}):

$$\phi_v = V^\infty + A_v C^{1/2} + B_v C, \quad (3)$$

where A_v and B_v are the fitting parameters. The parameters of Eq. 3, as determined by the least-squares method, are given in Table 1. The standard deviations of the fits are 0.2 $cm^3\,mol^{-1}$. The V^∞ values for Na_4 edta and Na_3 hedta are obtained by the subtraction of the V^∞ value for NaOH according to additivity rule.

The volume changes at infinite dilution, ΔV^∞, on the complex formation of:

$$[M(H_2O)_6]^{2+} + edta^{4-} \longrightarrow [M(edta)]^{2-} + 6H_2O, \quad (4)$$

$$[M(H_2O)_6]^{2+} + hedta^{3-} \longrightarrow [M(hedta)(H_2O)]^- + 5H_2O, \quad (5)$$

may be estimated from the V^∞ values of the reactants and the products according to the relationships for the edta chelates:

$$\Delta V^\infty = V^\infty([M(edta)]^{2-}) + 6V^*(H_2O) - V^\infty([M(H_2O)_6]^{2+}) - V^\infty(edta^{4-}), \quad (6)$$

and for the hedta chelates:

$$\Delta V^\infty = V^\infty([M(hedta)(H_2O)]^-) + 5V^*(H_2O) - V^\infty([M(H_2O)_6]^{2+}) - V^\infty(hedta^{3-}), \quad (7)$$

where $V^\infty([M(edta)]^{2-})$, $V^\infty([M(hedta)(H_2O)]^-)$, $V^\infty([M(H_2O)_6]^{2+})$, $V^\infty(edta^{4-})$, and $V^\infty(hedta^{3-})$ are the partial molal volumes of the species described in parentheses and $V^*(H_2O)$ is that of pure water. The V^∞ values of the hexaaqua-metal ions can be estimated by means

Table 1. Standard partial molal volumes at 25 °C

Solute	V^∞	b_v [a]	A_v [b]	B_v [b]
	$cm^3\,mol^{-1}$	$cm^3\,dm^3\,mol^{-2}$	$cm^3\,dm^{3/2}\,mol^{-3/2}$	$cm^3\,dm^3\,mol^{-2}$
$Na_2[Mn(edta)]$	162.7	6.22		
$Na_2[Co(edta)]$	166.0	3.94		
$Na_2[Ni(edta)]$	163.3	4.88		
$Na_2[Cu(edta)]$	168.0	4.56		
$Na_2[Zn(edta)]$	167.0	4.91		
$K[Mn(hedta)(H_2O)]$	187.3	7.37		
$K[Co(hedta)(H_2O)]$	188.5	2.46		
$K[Ni(hedta)(H_2O)]$	184.8	5.37		
$K[Cu(hedta)(H_2O)]$	190.9	6.46		
$K[Zn(hedta)(H_2O)]$	188.4	5.78		
$Na_4edta \cdot NaOH$	139.7		81.5	−85.0
$Na_3hedta \cdot NaOH$	143.6		87.2	−83.7

a) An adjustable parameter of Eq. 2. b) Parameters of Eq. 3.

of this relation:[11,15]

$$V^{\infty}([M(H_2O)_6]^{2+}) = V^{\infty}(M^{2+}) + 6V^{*}(H_2O), \quad (8)$$

where $V^{\infty}(M^{2+})$ is the partial molal volume of the transition metal cation, which is generally obtained in the literature. The $V^{\infty}(M^{2+})$ values were estimated from the literature values for $Mn(ClO_4)_2$, $Co(ClO_4)_2$, $Ni(ClO_4)_2$, $Cu(ClO_4)_2$, and $Zn(ClO_4)_2$ using the additivity principle with $V^{\infty}(ClO_4^-)=49.5\,cm^3\,mol^{-1}$.[16,17] The ionic partial molal volumes of $[M(edta)]^{2-}$, $[M(hedta)(H_2O)]^-$ and the free ligands are given in Table 2; they were obtained using $V^{\infty}(Na^+)=-6.6$, $V^{\infty}(K^+)=3.6$, and $V^{\infty}(OH^-)=1.4\,cm^3\,mol^{-1}$.[17]

Discussion

The values of V^{∞} found for the bivalent metal edta chelates vary from 175.9 $cm^3\,mol^{-1}$ for $[Mn(edta)]^{2-}$ to 181.2 $cm^3\,mol^{-1}$ for $[Cu(edta)]^{2-}$; therefore, they do not significantly differ from each other. The same phenomenon is found in the case of the V^{∞} values of the hedta chelate ions, which vary from 181.2 $cm^3\,mol^{-1}$ for $[Ni(hedta)(H_2O)]^-$ to 187.3 $cm^3\,mol^{-1}$ for $[Cu(hedta)(H_2O)]^-$. These V^{∞} values are almost the same as those of the free ligands. The same facts were found for $[M(phen)_3]^{2+}$, which were about 4 to 6% smaller than three times the V^{∞} values of the free 1,10-phenanthroline.[11]

The estimated ΔV^{∞} values for the complex formation of $[M(edta)]^{2-}$ are in this order:

$$[Mn(edta)]^{2-} < [Co(edta)]^{2-} < [Ni(edta)]^{2-} < [Cu(edta)]^{2-} > [Zn(edta)]^{2-}.$$

This order is the same as in the Irving-Wiliams series. The ΔV^{∞} values for $[M(hedta)(H_2O)]^-$ are in a sequence similar to that of the edta chelates. In any case, the ΔV^{∞} values for $[M(edta)]^{2-}$ and $[M(hedta)(H_2O)]^-$ are $\Delta V^{\infty}([M(edta)]^{2-}) > \Delta V^{\infty}([(M(hedta)(H_2O)]^-]$, where M^{2+} is the same central metal ion. Furthermore, the formation of Mn(II) chelate ions of edta and hedta is accompanied by a markedly small ΔV^{∞} value in comparison with those of the other metal chelate ions. This can be attributed to the larger V^{∞} value of the high-spin d^5 Mn(II) aqua ion. For the other aqua ions, the V^{∞} are not so different and the ΔV^{∞} values of these edta and hedta chelates are almost the same.

The resultant ΔV^{∞} values for the edta and hedta chelates have markedly large positive values in comparison with the ΔV^{∞} values of the other complex formation reactions and ion-pair formation reactions. These large positive ΔV^{∞} values may be due to the large amount of water molecules released from the electrostricted solvation spheres of the reactants by the partial neutralization of the charges.

The volume changes in the ion-pair formation may serve as a reference for the volume change in the neutralization of the charges. For the inner-sphere ion-pair formation of $CaSO_4$, the ΔV^{∞} value has been reported to be 25.2 $cm^3\,mol^{-1}$,[18] which is similar in magnitude to the ΔV^{∞} values of the hedta chelates. However, the ΔV^{∞} values for the transition metal sulfate ion-pairs are fairly smaller, varying from 7.4 $cm^3\,mol^{-1}$ for $MnSO_4$ to 11.4 $cm^3\,mol^{-1}$ for $CuSO_4$.[19] For these ion-pairs, the amount of the inner-sphere ion-pair is estimated to be about 20%; therefore, the electrostricted solvation spheres of the constituent ions are not completely lost upon these ion-pairing processes.[19]

A positive contribution to the ΔV^{∞} values of edta and hedta can also be expected from the delocalization of the charge on the large metal chelate ion. This contribution becomes large when the ligand is a large hydrophobic one such as 1,10-phenanthroline. Previously, the formation of $[M(phen)_3]^{2+}$ has been reported.[11] In this system, the neutralization of the charge is not included, though the ΔV^{∞} values (*ca.* 20 $cm^3\,mol^{-1}$) except for $[Fe(phen)_3]^{2+}$ are comparable to that of an inner-

Table 2. Ionic partial molal volumes at 25 °C

Ion	V^{∞}(ion) / $cm^3\,mol^{-1}$
$[Mn(edta)]^{2-}$	175.9
$[Co(edta)]^{2-}$	179.2
$[Ni(edta)]^{2-}$	176.5 (170.3)[a]
$[Cu(edta)]^{2-}$	181.2
$[Zn(edta)]^{2-}$	180.2
$[Mn(hedta)(H_2O)]^-$	183.7
$[Co(hedta)(H_2O)]^-$	184.9
$[Ni(hedta)(H_2O)]^-$	181.2
$[Cu(hedta)(H_2O)]^-$	187.3
$[Zn(hedta)(H_2O)]^-$	184.8
$edta^{4-}$	171.3 (174.4)[a]
$hedta^{3-}$	168.6

a) Ref. 12.

Table 3. Ionic partial molal volumes of M^{2+} and volume changes for the formation of $[M(edta)]^{2-}$ and $[M(hedta)(H_2O)]^-$ at 25 °C

M(II)	$V^{\infty}(M^{2+})$ / $cm^3\,mol^{-1}$	$\Delta V^{\infty}([M(edta)]^{2-})$ / $cm^3\,mol^{-1}$	$\Delta V^{\infty}([M(hedta)(H_2O)]^-)$ / $cm^3\,mol^{-1}$
Mn(II)	−28.2	32.8	25.2
Co(II)	−36.2	44.1	34.4
Ni(II)	−39.2	44.4 (25.5)[a]	33.7
Cu(II)	−35.9	45.8	36.5
Zn(II)	−35.5	44.4	33.6

a) Ref. 12.

sphere ion pairing such as $CaSO_4$.[11]

A comparison of the ΔV^∞ values of the edta and hedta chelates with those of the bivalent metal carboxylato-complex formation reactions would be more instructive. For the 1:1 complex formation of Cu^{2+} with the unidentate carboxylate anions, acetate and propionate, the volume changes in the dilute solutions, ΔV, have been reported to be 13 $cm^3 mol^{-1}$ at 30 °C.[20] Furthermore, the ΔV values for the 1:1 complex of Cu^{2+} with the bidentate dicarboxylates, malonate, tartrate and maleate, are rather larger (27, 29, and 28 $cm^3 mol^{-1}$ respectively at 30 °C); these values are twice the ΔV values produced by the formation of Cu(II)-monocarboxylato complexes.[20] Therefore, it is of interest to compare the ΔV value for the edta chelate with that of the hedta chelate of the same central metal cation. The ΔV^∞ value for the latter is about three fourths that of the former; the ΔV^∞ values of these chelates are also in proportion to the number of carboxylate groups in the ligands. This means that the great part of the large positive ΔV^∞ values for the edta and the hedta chelates is responsible for the coordination of the carboxylate groups to the metal ions, even though the contributions of the nitrogen donor atoms to the ΔV^∞ can not be estimated. However, they are assumed to be smaller than those of the carboxylate groups. For example, the ΔV for Cu(II)-glycinato and Cu(II)-alaninato complexes are reported to be 14 and 15 $cm^3 mol^{-1}$ respectively at 30 °C, and for these systems the volume changes responsible for the coordinated nitrogen donor atoms are estimated to be 1—3 $cm^3 mol^{-1}$.[20]

The complex formation reactions of edta and hedta with the bivalent transition metal cations are characterized by large positive volume and entropy changes. As is shown in Fig. 3, a linear relationship between the ΔS value at an ionic strength of 0.1 mol dm^{-3} and ΔV^∞ value for the complexation of edta and hedta is observed within the limits of experimental error. Such large values for ΔS and ΔV^∞ are related, in large part, to the electrostriction effects: *i.e.*, the neutralization effect by the coordination of the acetate groups to the metal ions and the reduction of the electrostriction by the delocalization of the residual charges on the large metal chelate ions.[12] The lower ΔS and ΔV^∞ values for the hedta chelates than for the edta chelates suggest that the 2-hydroxyethyl group is not bonded to the metal ion and that fewer molecules of water are released on the complexation of the hedta chelates.

Smaller ΔS values for the edta and hedta chelates of Mn(II) than those of the analogous chelates are also found in the same manner as with ΔV^∞. The edta chelate of Mn(II) has been shown to have a seven-coordinated structure, with one water molecule.[6,9] This may be one of the reasons why the formation of the Mn(II)-edta chelate ion is accompanied by smaller ΔS and ΔV^∞ values, for at least one water molecule remains in the electronic field of the central metal cation. Therefore, it may be considered that the smaller ΔS and

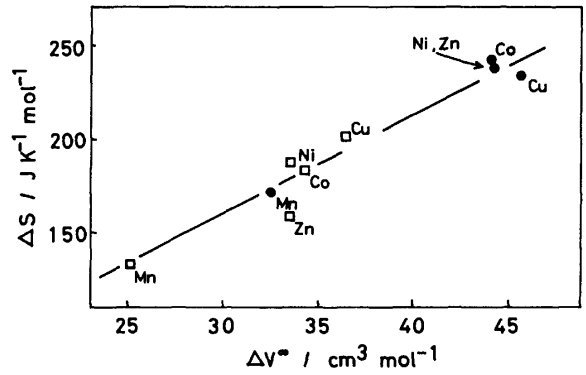

Fig. 3. Relationship between ΔV^∞ and ΔS at 25 °C.
●: $[M(edta)]^{2-}$, □: $[M(hedta)(H_2O)]^-$.

ΔV^∞ values of the Mn(II)-edta chelate than those of the other edta chelates are due to the different coordination geometry and the larger ionic size of the Mn(II) aqua ion. In the case of Mn(II)-hedta, its structure is not known; however, the present result may be supposed to indicate that the Mn(II)-hedta chelate has the same seven-coordinated structure as the Mn(II)-edta chelate, except for the two coordinated water molecules.

Many authors have concluded, on the basis of various methods of studies, that the edta chelates of Co(II), Ni(II), Cu(II), and Zn(II) in aqueous solutions are dynamic equilibrium mixtures between the dominant sexidentate form and the quinquedentate form, which contains one water molecule and a free carboxylate group.[2-10] If that is the case, the V^∞ values of the edta chelates may be written as:

$$V^\infty = \alpha V^\infty_{\mathrm{I}} + (1-\alpha)V^\infty_{\mathrm{II}} - (1-\alpha)V^*(H_2O), \quad (9)$$

where the V^∞_{I} and α are the partial molal volume and the fraction of the edta chelate in the sexidentate form and where V^∞_{II} is the partial molal volume in the quinquedentate form or the seven-coordinated form for the Mn(II)-edta chelate respectively. Therefore, the ΔV^∞ values for the edta chelates are expressed as:

$$\Delta V^\infty = V^\infty_{\mathrm{I}} + (1-\alpha)V^\infty_{\mathrm{II}} + (5+\alpha)V^*(H_2O) - V^\infty([M(H_2O)_6]^{2+}) - V^\infty(edta^{4-}). \quad (10)$$

The substitution of Eq. 9 into Eq. 10 leads to the same result as Eq. 6. The α's were estimated in the range from 60 to 80% for the edta complexes of Co(II), Ni(II), Cu(II), and Zn(II),[3,9,10] and the volume change between the quinquedentate form and the sexidentate form ($\Delta V^\infty_{\mathrm{II}\to\mathrm{I}} = V^\infty_{\mathrm{I}} + V^*(H_2O) - V^\infty_{\mathrm{II}}$) is calculated to be 4.9 $cm^3 mol^{-1}$ for the Co(II)-edta chelate.[10] When one substitutes these values into Eq. 10, the V^∞_{I} and V^∞_{II} values can be estimated separately. Such a treatment indicates that the dynamic equilibrium between the sexidentate form and the quinquedentate form of the edta chelate should have only a small effect on ΔV^∞, which is estimated to be 1—2 $cm^3 mol^{-1}$. The ΔV^∞ values for the edta chelates, except for Mn(II)-edta, are, unfortunately, not so effective in determining the structures of the edta chelates in aqueous solutions.

However, the large differences between the ΔV^{∞} values for the edta and the hedta chelate and the rather small volume change between the quinquedentate form and the sexidentate form of the edta chelate may be ascribed to the fact that the uncoordinated carboxylate group of the edta chelate in the quinquedentate form has already been situated in the second coordination sphere of the central metal cation and weakly interacts with it. This figure, except for the case of the Mn(II)–edta chelate, does not conflict with the results of the recent work on the structures of the edta chelates in aqueous solutions.

The author wishes to thank Professor Yuroku Yamamoto of Hiroshima University for his kind advice and encouragement throughout the present work. The author is also grateful to Dr. Manabu Yamamoto for his useful discussions. The present work was partially supported by a Grant-in-Aid for Scientific Research No. 59740294 from the Ministry of Education, Science and Culture.

References

1) R. H. Nuttall and D. M. Stalker, *Talanta*, **24**, 355 (1977).
2) C. K. Jorgensen, *Acta Chem. Scand.*, **9**, 1362 (1955).
3) W. C. E. Higginson and B. Samuel, *J. Chem. Soc. (A)*, **1970**, 1579.
4) T. R. Bhat and M. Krishnamurthy, *J. Inorg. Nucl. Chem.*, **25**, 1147 (1963).
5) K. Krishnan and R. A. Plane, *J. Am. Chem. Soc.*, **90**, 3195 (1968).
6) A. A. McConnell, R. H. Nuttall, and D. M. Stalker, *Talanta*, **25**, 425 (1978).
7) M. W. Grant, H. W. Dodgen, and J. P. Hunt, *J. Am. Chem. Soc.*, **93**, 6828 (1971).
8) M. S. Zetter, M. W. Grant, E. J. Wood, H. W. Dodgen, and J. P. Hunt, *Inorg. Chem.*, **11**, 2701 (1972).
9) J. Oakes and E. G. Smith, *J. Chem. Soc., Faraday Trans. 2*, **77**, 299 (1981); J. Oakes and E. G. Smith, *J. Chem. Soc., Faraday Trans. 1*, **79**, 543 (1983).
10) S. Harada, Y. Funaki, and T. Yasunaga, *J. Am. Chem. Soc.*, **102**, 136 (1980); Y. Funaki, S. Harada, K. Okumiya, and T. Yasunaga, *J. Am. Chem. Soc.*, **104**, 5325 (1982).
11) K. Yoshitani, M. Yamamoto, and Y. Yamamoto, *Bull. Chem. Soc. Jpn.*, **56**, 1978 (1983).
12) Y. K. Sze and W. A. E. McBryde, *Can. J. Chem.*, **58**, 1795 (1980).
13) D. T. Sawyer and P. J. Paulsen, *J. Am. Chem. Soc.*, **81**, 816 (1959).
14) O. Redlich and D. M. Mayer, *Chem. Rev.*, **64**, 221 (1964).
15) K. Kurotaki and S. Kawamura, *J. Chem. Soc., Faraday Trans. 1*, **77**, 217 (1981).
16) J. J. Spitzer, P. P. Singh, K. G. McCurdy, and L. G. Hepler, *J. Solution Chem.*, **7**, 81 (1978); J. J. Spitzer, P. P. Singh, I. V. Olofsson, and L. G. Hepler, *ibid.*, **7**, 623 (1978).
17) F. J. Millero, "Water and Aqueous Solutions, Structure, Thermodynamics and Transport Processes," ed by R. A. Horn, Wiley-Interscience, New York (1972), Chap. 13.
18) F. J. Millero, F. Gombar, and J. Oster, *J. Solution Chem.*, **6**, 269 (1977).
19) A. Lo Surdo and F. J. Millero, *J. Solution Chem.*, **9**, 163 (1980).
20) S. Katz, M. P. Donovan, and L. C. Roberson, *J. Phys. Chem.*, **79**, 1930 (1975).
21) D. L. Wright, J. H. Holloway, and C. N. Reilley, *Anal. Chem.*, **37**, 884 (1965).

An X-Ray Diffraction Study on the Structures of Mono(glycinato)zinc(II) and Tris(glycinato)zincate(II) Complexes in Aqueous Solution

Kazuhiko Ozutsumi and Hitoshi Ohtaki*
Department of Electronic Chemistry, Tokyo Institute of Technology at Nagatsuta, 4259, Nagatsuta-cho, Midori-ku, Yokohama 227
(Received January 5, 1985)

The structure of zinc(II) complexes with glycinate ion in solution was investigated by the X-ray diffraction method. The measurements were performed at 20 °C for the solutions with the C_{gly}/C_{Zn} mole ratios of 1.49 (solution A) and 5.09 (solution B), where C_i denotes the total concentration of species i. From the analysis of the radial distribution curve of solution A, in which comparable amounts of the hexaaqua- and mono(glycinato)-zinc(II) complexes existed, it was found that the mono(glycinato)zinc(II) complex combined with four water molecules at the distance of (2.12±0.01) Å. The Zn-OH_2 bond length within the complex was longer than that within the hexaaquazinc(II) ion (2.08 Å). The Zn-O and Zn-N distances, where O and N denote oxygen and nitrogen atoms within the glycinate ion in the $[Zn(gly)(OH_2)_4]^+$ complex, were both (2.12±0.02) Å. Thus the mono(glycinato)zinc(II) complex had a regular octahedral structure. The nonbonding Zn···C distance was found to be (2.84±0.02) Å. The X-ray diffraction data of solution B, which contained the $[Zn(gly)_3]^-$ ion as a predominant species, showed that the tris(glycinato)zincate(II) complex had a regular octahedral structure with the both Zn-O and Zn-N bond distances of (2.12±0.01) Å. The nonbonding Zn···C(COO), Zn···C(CH_2), and Zn···O(O=C) lengths were (2.87±0.03) Å, (2.93±0.03) Å, and (4.10±0.04) Å, respectively. The solubility of the bis(glycinato)zinc(II) complex was so low that the structural determination of the complex by the present X-ray diffraction method was not possible.

Zinc(II) ion often changes the structure in the course of ligand substitution reactions. The hexaaquazinc-(II) ion has been reported to be regular octahedral in perchlorate, sulfate and nitrate solutions.[1,2] The Zn-OH_2 bond distance was found to be 2.08 Å in the former two solutions[1] and 2.093 Å in the latter.[2]

Yamaguchi and Ohtaki[3] found that the tetraamminezinc(II) complex has no water molecules in the first coordination shell and thus the tetraamminezinc(II) complex has a regular tetrahedral structure with the Zn-N bond length of 2.03 Å. The triamminemonochlorozinc(II) complex found in a dilute ammoniacal solution has a distorted tetrahedral structure. The Zn-N and Zn-Cl bond distances were determined to be 2.00 Å and 2.30 Å, respectively.

The structure of the bis(ethylenediamine)zinc(II) ion is a regular tetrahedron with the Zn-N bond length of 2.131 Å, although the structure of the tris(ethylenediamine)zinc(II) complex is a regular octahedron with a longer Zn-N bond distance of 2.276 Å.[4] Thus the coordination number of zinc(II) ion changed from 6 to 4 in the course of the formation of the ammine complexes, while the coordination number of zinc(II) ion within the ethylenediamine complexes varied from 6 within the hexaaquazinc(II) ion to 4 within the bis-(ethylenediamine)zinc(II) and then again to 6 within the tris(ethylenediamine)zinc(II) complex.

Structural changes in complex formation reactions with increasing number of ligands coordinated were found in Zn(II)-chloro[5] and Zn(II)-bromo complexes[6] in solution.

In previous studies[7,8] we determined the structures of the mono- and tris(glycinato) complexes of nickel-(II) and copper(II) ions in aqueous solutions by the X-ray diffraction method. In the present work we have attempted to determine the structure of glycinato-zinc-(II) complexes in a series of structural study of chelate complexes of transition metals in solution.

Many crystallographic data are available for amino carboxylato complexes. Though zinc(II) ion plays an important role in biochemical reactions as copper(II) ion does, less structural information on the zinc(II)-amino carboxylato complexes has been presented than that on the copper(II) complexes. The structure of the bis(glycinato)zinc(II) complex has been determined to be octahedral with two more carbonyl oxygen atoms within glycinate ions coordinated to adjacent zinc(II) ion in crystal.[9] However, structures of other complexes of zinc(II) ion with glycine have not been known even in crystal due to difficulty in preparation of stable single crystals of the mono- and tris(glycinato) complexes of zinc(II) ion. Therefore, we studied the structure of the mono(glycinato)zinc(II) and tris(glycinato)-zincate(II) complexes in aqueous solution. To find a structural change, if it occurs, of the complexes with changing number of the ligand is another aim of this investigation. The structure of the bis(glycinato)zinc-(II) complex in solution was not determinable by the X-ray diffraction method due to its low solubility in water.

Raman spectroscopic measurements have been carried out as a supplement to the structural determination of the complexes.

Experimental

Preparation and Analysis of Sample Solutions. All chemicals used were of reagent grade. Two test solutions were prepared in the similar way to that reported in previous papers.[7,8] *Solution A*, which contained the mono(glycinato)-zinc(II) complex as a predominant species, was prepared by dissolving crystals of the bis(glycinato)zinc(II) to a zinc(II) nitrate solution. In order to prevent hydrolysis of zinc(II) ion, a small amount of glycine was added to this solution. *Solution B*, in which the tris(glycinato)zincate(II) com-

Table 1. The composition (mol dm^{-3}) and stoichiometric volume V per zinc atom in the solutions

	A	B
Zn	2.031	1.245
Na	—	3.843
O	57.09	50.03
N	5.085	6.333
C	6.070	12.67
H	102.9	100.1
V/Å^3	817.6	1334
C_{gly}/C_{Zn}	1.49	5.09
density/g cm^{-3}	1.294	1.312

plex was formed as a main species, was prepared by mixing the bis(glycinato)zinc(II) and sodium glycinate in water.

Bis(glycinato)zinc(II) was prepared by mixing powder of zinc(II) oxide and glycine in boiling water and then recrystallized from a sodium glycinate solution. Sodium glycinate was obtained by the same manner previously reported.[7] Zinc(II) nitrate and glycine were recrystallized from water.

The total concentration of zinc(II) ions (C_{Zn}) in the sample solutions was determined by EDTA titration and gravimetry as $ZnNH_4PO_4$. The results of the two independent methods agreed each other within 0.2%. The total glycine concentration (C_{gly}) was determined by the Kjeldahl method. The concentrations of nitrate ions in solution A and sodium ions in solution B were evaluated by the material balance of ions in the solutions. Densities of the test solutions were measured pycnometrically. The composition of the solutions is listed in Table 1.

X-Ray Scattering Measurements. X-Ray scattering measurements were performed with a JEOL θ—θ diffractometer by using Mo $K\alpha$ radiation (λ=0.7107 Å). The observed range of scattering angle (2θ) was from 2° to 140°. Times required to acummulate 120000 counts at each angle were recorded. The method of measurements and data treatments were described in previous papers.[1,8,10] Calculations were carried out by using KURVLR[11] and NLPLSQ[12] programs with the computer at the Tokyo Institute of Technology and partly with the computer at the Institute for Molecular Science in Okazaki.

Raman Spectroscopic Measurements. Raman spectra for the sample solutions were measured with a JEOL laser Raman spectrophotometer JRS-SI with the use of the 5145 Å excited line of Ar^+ laser.

Results and Discussion

According to the stability constants of zinc(II)–glycine complexes,[13] solution A contains comparable amounts of the hexaaqua- and mono(glycinato)zinc(II) complexes and a small amount of the bis(glycinato)zinc(II) complex. However, the concentration of the bis(glycinato)zinc(II) is so small that the formation of the complex was neglected in the course of the analysis of the X-ray scattering data. In solution B almost all of the zinc(II) ions are expected to form the tris(glycinato)zincate(II) complex, since the C_{gly}/C_{Zn} mole ratio is 5.09.

The observed $s \cdot i(s)$ and $D(r)$ curves for solutions A and B are shown in Figs. 1 and 2, respectively.

The parameter values for the intramolecular structure within glycinate ion, as well as those within water molecule and nitrate ion, used for the computation of the X-ray scattering data are the same as those described in a previous paper.[7] Numbering of the atoms within the glycinate ion coordinated to the

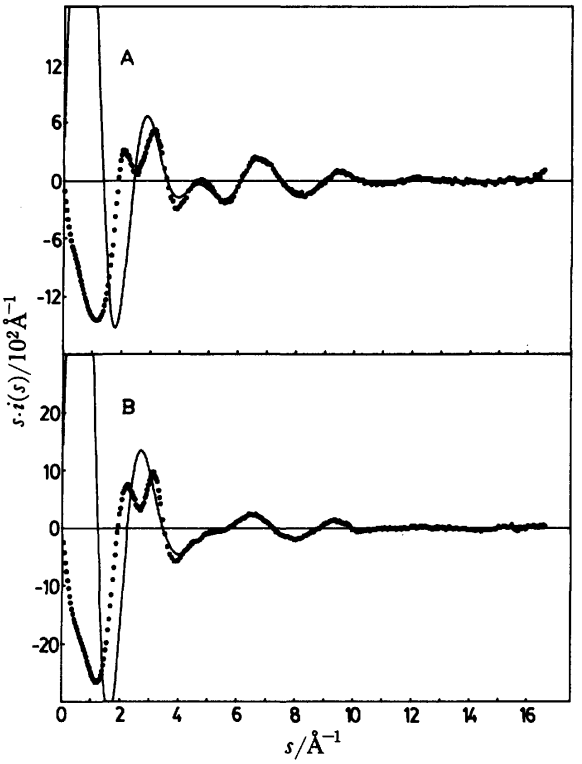

Fig. 1. The reduced intensities multiplied by s for solutions A and B. The observed $s \cdot i(s)$ values are shown by dotted lines and calculated ones by solid lines.

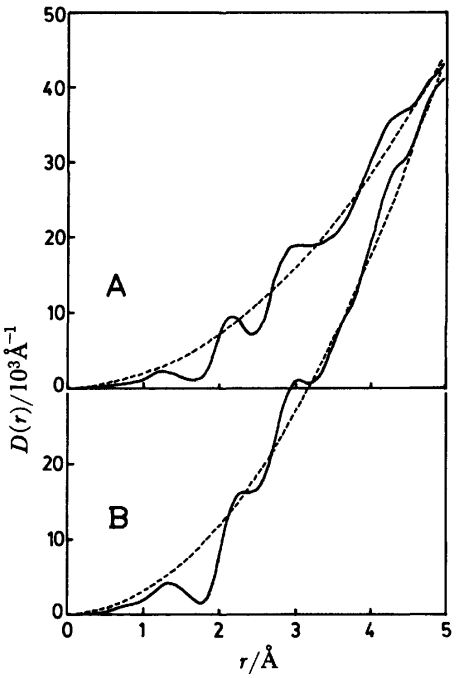

Fig. 2. The $D(r)$ curves for solutions A and B. The dashed lines indicate the curve of $4\pi r^2\rho_o$.

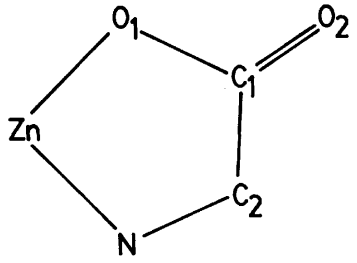

Fig. 3. The numbering of the atoms within the glycinate ion coordinated to the zinc(II) ion.

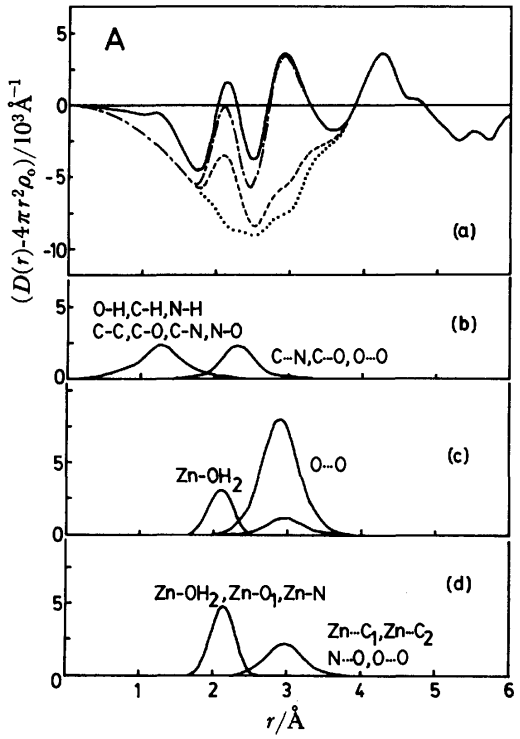

Fig. 4. (a) The $(D(r)-4\pi r^2\rho_0)$ curve for solution A. (b) The theoretical peaks for the O–H bonds within water molecule, intramolecular interactions within glycinate ion and N–O and O···O pairs within nitrate ion. (c) The theoretical peak shapes calculated for Zn–OH_2 and O···O pairs within the hexaaquazinc(II) ion and O···O contacts of water molecules in the bulk. (d) The theoretical peaks for Zn–OH_2, Zn–O_1, Zn–N, Zn···$C_{1,2}$, N···O, and O···O pairs within the mono-complex. The chain, dashed and dotted lines indicate the residual curves after subtracting the theoretical peaks in (b), (c), and (d), respectively.

zinc(II) ion is given in Fig. 3.

Solution A. In the $D(r)$ (Fig. 2A) and $D(r)-4\pi r^2\rho_0$ (Fig. 4a) curves, where ρ_0 represents the average scattering density in the stoichiometric volume V per zinc atom of the solution, we see four peaks at about 1.3, 2.2, 2.9, and 4.2 Å. The small and broad peak around 1.3 Å is owing to the O–H bonds within water molecules, the C–H, N–H, C_1–C_2, C_2–N, C_1⋍O_1, and C_1⋍O_2 bonds within glycinate ions and the N–O bonds within nitrate ions. The second peak appearing at 2.2 Å is mainly ascribed to the Zn–OH_2 bonds within the hexaaquazinc(II) ion and the Zn–OH_2, Zn–O_1, and Zn–N bonds within the mono(glycinato)zinc(II) complex. Nonbonding C_2···O_1, C_2···O_2, C_1···N, and O_1···O_2 interactions within glycinate ions and O···O contacts within nitrate ions also contribute, in part, to the peak. The third peak at about 2.9 Å is composed of peaks owing to nonbonding Zn···C_1 and Zn···C_2 interactions within the mono(glycinato)zinc(II) ion and interactions between ligand atoms in the first coordination sphere within the complexes, as well as the O···O contacts of the bulk water. In the fourth peak at 4.2 Å various longer range interactions, which will not be taken into account in the present analysis, may be included.

In order to evaluate the structure parameters of the mono(glycinato)zinc(II) complex, we firstly subtracted the theoretical peaks of the known interactions within water molecules, glycinate and nitrate ions from the observed radial distribution curve. The residual curve obtained (chain line in Fig. 4a) showed the peak at about 2.1 Å and the peak was well interpreted in terms of the octahedral configuration of six oxygen and nitrogen atoms around all zinc atoms in the solution, independent of the concentration ratio of the $[Zn(OH_2)_6]^{2+}$ to $[Zn(gly)]^+$ complexes. Since the Zn–O and Zn–N bonds were practically indistinguishable by the X-ray analysis, the result indicated that the mono(glycinato)zinc(II) complex should have six ligand atoms in the first coordination shell. Thus, we concluded that the $[Zn(gly)]^+$ complex has an octahedral structure combined with one glycinate ion and additional four water molecules.

The structure parameters of the mono(glycinato)zinc(II) complex were refined by using a least-squares method for the $s\cdot i(s)$ data over the range $s>5$ Å^{-1}. In order to avoid the introduction of errors by neglecting long-range interactions, the lower limit of the s-value was changed from 5.0 to 7.0 Å^{-1}. The concentration ratio of the $[Zn(OH_2)_6]^{2+}$ to $[Zn(gly)(OH_2)_4]^+$ complexes was assumed to be 40:60 in the present stage of the calculation. The parameter values first guessed from the analysis of the radial distribution curve of the mono(glycinato)zinc(II) ion were refined by the least-squares procedure at the fixed composition of the solution. The structural parameters of the hexaaquazinc(II) ion and the O···O contacts of bulk water were taken from the works by Ohtaki *et al.*[1] and by Narten[14] and were fixed at the literature values during the calculation. Since the lengths of the Zn–O_1 and Zn–N bonds were not determinable separately with a reasonable accuracy, we assumed that the Zn–O_1 and Zn–N bonds had the same structure parameters. The results obtained were listed in Table 2. We also tested another assumption for initial values inserted in the least-squares calculation. A tetrahedral coordination around the Zn(II) ion within the mono(glycinato)zinc(II) complex was assumed and the number of the Zn–OH_2 bond was set to be 2. When the refinement was carried out by floating the number of the Zn–OH_2

Table 2. Results of the least-squares refinements of solution A. Parameter values refined were bond distances (r/Å), temperature factors (b/Å^2) and frequency factors (n). The values in parentheses represent standard deviation

Interaction	Parameter	A-I (s>5.0 Å^{-1})	A-II (s>6.0 Å^{-1})	A-III (s>7.0 Å^{-1})
$Zn-OH_2$	r	2.12(1)	2.12(1)	2.12(1)
	b	0.003(1)	0.003(1)	0.003(1)
	n	3.9(1)	4.0(1)	4.0(1)
$OH_2\cdots OH_2$	r	3.0(1)	3.0(1)	3.0(2)
	b	0.010[a]	0.010[a]	0.010[a]
$Zn-O_1$, $Zn-N$	r	2.12(2)	2.13(2)	2.12(2)
	b	0.003(1)	0.003(1)	0.003(1)
	n	1.9(1)	2.0(2)	1.9(2)
$OH_2\cdots O_1$, $OH_2\cdots N$	r	3.0[a]	3.0[a]	3.0[a]
	b	0.010[a]	0.010[a]	0.010[a]
$N\cdots O_1$	r	2.8[a]	2.8[a]	2.8[a]
	b	0.010[a]	0.010[a]	0.010[a]
$Zn\cdots C_1$, $Zn\cdots C_2$	r	2.84(2)	2.87(2)	2.79(2)
	b	0.010(2)	0.009(2)	0.007(2)

a) The values were kept constant during the calculation.

bonds at fixed frequency factor of the $Zn-O_1$ and Zn–N bonds, the number of the $Zn-OH_2$ bonds reached nearly 4 in the course of the calculation. Thus the octahedral structure of the mono(glycinato)zinc(II) complex was confirmed by the least-squares calculation. The $Zn-OH_2$ bond length was determined to be 2.12 Å and the distance of the $Zn-O_1$ and Zn–N bonds was also evaluated to be 2.12 Å.

Since we assumed that the $Zn-O_1$ and Zn–N bonds had the same structure parameters in the least-squares calculation described above, a possibility of the different lengths of the $Zn-O_1$ and Zn–N bonds was not well excluded. At the next step of calculation we examined assumptions of various lengths of the $Zn-O_1$ and Zn–N bonds. The residual radial distribution curve ascribed to the Zn–O and Zn–N bonds was extracted from the second peak of the distribution curve in Fig. 2A by subtracting intramolecular interactions of water molecules, glycinate and nitrate ions (Fig. 5). The curve consisted of peaks attributed to the interactions between Zn(II) ion and donor atoms within the complex around 2.1 Å and longer-range interatomic interactions at r>2.5 Å. The peak at 2.1 Å was drawn by assuming that it was a symmetrical Gaussian curve.

Calculations were carried out in order to minimize the error-square sum defined by Eq. 1 for various sets of the temperature factors of the $Zn-OH_2$ bond, lengths of the $Zn-O_1$ and Zn–N bonds and the concentration ratio of $[Zn(OH_2)_6]^{2+}$ to $[Zn(gly)(OH_2)_4]^+$.

$$U = \sum w\{D(r)^{2nd}_{calcd} - D(r)^{2nd}_{obsd}\}^2 \quad (1)$$

In Eq. 1, $D(r)^{2nd}$ represents the second peak extracted from the original radial distribution curve by the procedure described above. w is given as $\exp(-\alpha\cdot\Delta l^2)$, where $\Delta l = r_o - r$ and r_o denotes the r-value at the center of the peak. In this case we assumed that the r_o value was 2.11 Å and the value α was evaluated from the half-width of the second peak. In the course of the calculation the lengths of the $Zn-O_1$ and Zn–N bonds as well as

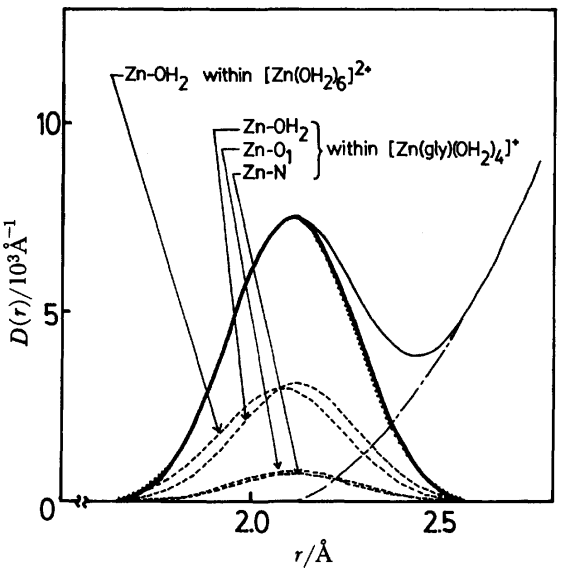

Fig. 5. The second peak of the radial distribution curve for solution A. The thin and thick solid lines show the experimental and extracted $D(r)$ curves, respectively, and the chain line indicates the residual curve after extraction. The theoretical peak shapes owing to the $Zn-OH_2$ bonds within the $[Zn(OH_2)_6]^{2+}$ ion, and the $Zn-OH_2$, $Zn-O_1$, and Zn–N bonds within the $[Zn(gly)(OH_2)_4]^+$ complex are shown by dashed lines. The dotted line represents the peak by summing peak shapes shown by dashed lines.

the concentration ratio of $[Zn(OH_2)_6]^{2+}$ to $[Zn(gly)(OH_2)_4]^+$, were stepwise changed. In addition, the temperature factor of the $Zn-OH_2$ bond within the mono(glycinato)zinc(II) complex was varied from 0.003 Å^2 to 0.005 Å^2. On the other hand, we fixed the values of the structure parameters of the $[Zn(OH_2)_6]^{2+}$ complex at the literature values,[1] as well as the length of the $Zn-OH_2$ bond within the mono(glycinato)zinc(II) complex at 2.12 Å and the temperature factor of the $Zn-O_1$ and Zn–N bonds at 0.003 Å^2.

At the temperature factor of 0.003 Å^2 for the $Zn-OH_2$ bond within the mono(glycinato)zinc(II) complex, a

TABLE 3. RESULTS OF THE ANALYSIS OF THE SECOND PEAK IN THE $D(r)$ CURVE OF SOLUTION A. ERROR-SQUARE SUMS ($U\times10^{-4}$/Å^{-2}) WERE CALCULATED ACCORDING TO Eq. 1. THE Zn–OH_2 BOND DISTANCE AND ALL TEMPERATURE FACTORS WITHIN THE MONO-COMPLEX WERE KEPT CONSTANT AT 2.12 Å AND 0.003 Å^2, RESPECTIVELY, IN THE COURSE OF THE CALCULATION

		mole fraction			
	Zn^{2+} :	0.3	0.4	0.5	0.6
	$Zn(gly)^+$:	0.7	0.6	0.5	0.4
Bond distance r/Å		$U\times10^{-4}$/Å^{-2}			
Zn–O_1	2.08	11.2	8.9	17.2	36.2
Zn–N	2.16				
Zn–O_1	2.10	10.8	6.7	14.3	33.0
Zn–N	2.14				
Zn–O_1	2.12	10.3	*6.2*	13.0	31.2
Zn–N	2.12				

minimum error-square sum was obtained at each set of the lengths of Zn–O_1 and Zn–N bonds. When we changed the length of the Zn–O_1 and Zn–N bonds and the concentration ratio of $[Zn(OH_2)_6]^{2+}$ to $[Zn(gly)(OH_2)_4]^+$ at the value of 0.003Å^2 for the temperature factor of the Zn–OH_2 bond, the minimum error-square sum was obtained when we assumed that the Zn–O_1 and Zn–N bonds have the same distance of 2.12Å and the concentration ratio of the $[Zn(OH_2)_6]^{2+}$ to $[Zn(gly)(OH_2)_4]^+$ was approximately 40:60 in the test solution (Table 3). Figure 5 represents the shape of the calculated curve from the Zn–OH_2 bonds within the $[Zn(OH_2)_6]^{2+}$ ion and the Zn–OH_2, Zn–O_1, and Zn–N bonds within the $[Zn(gly)(OH_2)_4]^+$ complex. The curve fitted well the extracted peak shape. Thus we concluded that the $[Zn(gly)(OH_2)_4]^+$ complex is regular octahedral.

Solution B. The $(D(r)-4\pi r^2\rho_o)$ curve given in Fig. 6a shows four peaks around 1.3, 2.3, 2.9, and 4.2Å and a small hump at 3.4Å. The peak at 1.3Å was attributed to the O–H bonds within water molecules and the C–H, N–H, C_1–C_2, C_2–N, C_1⋯O_1, and C_1⋯O_2 bonds within glycinate ions. The second peak appearing at 2.3Å mainly consisted of the Zn–O_1 and Zn–N interactions within the tris(glycinato)zincate(II) complex. Nonbonding C_2⋯$O_{1,2}$, C_1⋯N, and O_1⋯O_2 interactions within glycinate ions and Na–O pairs within hydrated sodium ions were also included in the peak. The peak around 2.9Å was composed of peaks owing to the nonbonding Zn⋯$C_{1,2}$ pairs and the interactions between ligand atoms in the first coordination sphere within the tris(glycinato)zincate(II) complex. The O⋯O contacts of water molecules in the bulk also contributed to the peak. In the fourth peak at about 4.2Å nonbonding Zn⋯O_2 and other long range interactions were contained.

In order to estimate the structural parameters of the $[Zn(gly)_3]^-$ complex, the peak shapes owing to interactions among water molecules, glycinate and sodium ions should be subtracted from the radial distribution function. We assumed an octahedral hydration of a

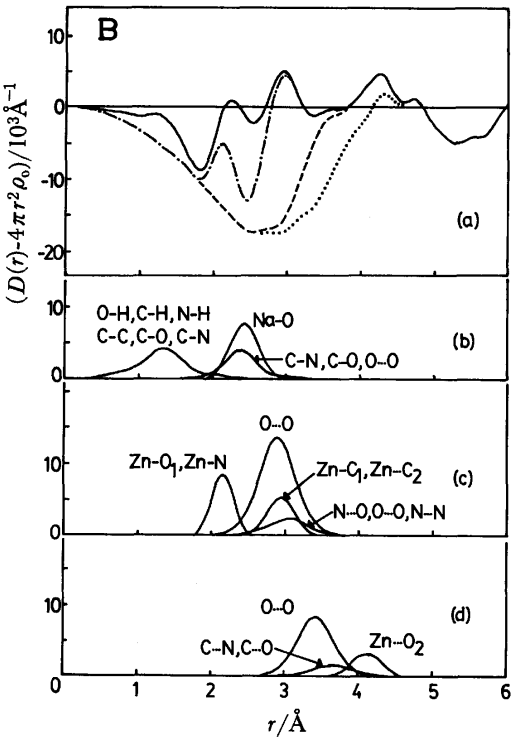

Fig. 6. (a) The $(D(r)-4\pi r^2\rho_o)$ curve for solution B. (b) The theoretical peak shapes calculated for the O–H bonds within water molecule, intramolecular interactions within glycinate ion and Na–O pairs within hydrated sodium ion. (c) The theoretical peaks for Zn–O_1, Zn–N, Zn⋯$C_{1,2}$, N⋯O, N⋯N, and O⋯O pairs within the tris-complex and O⋯O contacts of water molecules in the bulk. (d) The theoretical peaks for O⋯O contacts within hydrated sodium ion and Zn⋯O_2, $C_{1,2}$⋯N, $C_{1,2}$⋯O_1 pairs within the tris-complex. The chain, dashed and dotted lines show the residual curves after subtracting the theoretical peaks in (b), (c), and (d), respectively.

sodium ion since there was a small hump at 3.4Å which might be ascribable to the O⋯O contacts within a hydrated sodium ion as was previously pointed out.[7] The peak remained at 2.12Å (chain line in Fig. 6a) must be attributed to the Zn–O_1 and Zn–N interactions within the tris(glycinato)zincate(II) complex. From the analysis of the peak shape the Zn–O_1 and Zn–N bonds were found to have the same length of 2.12Å and the temperature factor of the bonds was evaluated to be about 0.003Å^2. The peak area corresponded to the sum of the peak areas of six bonds of Zn–O_1 and Zn–N. Thus the structure of the tris(glycinato)zincate(II) complex was concluded to be regular octahedral. The distance of longer range interactions within the tris(glycinato)-zincate(II) complex were estimated by using a suitable structure model of chelating glycinate ions. Subtraction of the above peaks from the radial distribution curve led to a smooth background curve (dotted line in Fig. 6a) having no appreciable peak over the range $r<4$Å.

The structure parameters of the tris(glycinato)zin-

Table 4. Results of the least-squares refinements of solution B. Parameter values refined were bond distances (r/Å), temperature factors (b/Å^2) and frequency factors (n). Standard deviations are given in parentheses

Interaction	Parameter	B-I	B-II	B-III
$Zn-O_1$	r	2.12(1)	2.12(1)	2.12(1)
	b	0.0031(6)	0.0029(7)	0.0028(9)
	n	3.0(1)	3.0(1)	3.0[b]
Zn–N	r	2.12(1)	2.12(1)	2.12(1)
	b	0.0029(6)	0.0026(8)	0.0025(9)
	n	3.0(1)	3.0(1)	3.0[b]
$N\cdots O_1$[a]	r	2.7(2)	2.8[b]	2.8[b]
$O\cdots O$[a]	r	3.1(2)	3.1[b]	3.1[b]
$N\cdots O$[a]	r	3.1(2)	3.0[b]	3.0[b]
$N\cdots N$[a]	r	3.1(2)	3.2[b]	3.2[b]
$Zn\cdots C_1$	r	2.87(2)	2.86(2)	2.87(3)
	b	0.008(2)	0.010(3)	0.009(3)
	n	3.1(1)	3.2(2)	3.0[b]
$Zn\cdots C_2$	r	2.93(2)	2.93(2)	2.93(3)
	b	0.009(2)	0.010(3)	0.008(3)
	n	3.1(1)	3.3(2)	3.0[b]
$Zn\cdots O_2$	r	4.08(4)	4.07(4)	4.10(4)
	b	0.010(2)	0.011(3)	0.011(3)
	n	3.1(1)	3.2(2)	3.0[b]

a) Temperature factors of these interactions were fixed at 0.006 Å^2. b) The values were kept constant during the calculation.

cate(II) complex were finally determined by a least-squares calculation for the $s\cdot i(s)$ curve over the range $s>4$Å^{-1}. The calculations were performed by inserting the values for each interatomic interaction evaluated by the analysis of the radial distribution function. Three types of calculations were carried out on slightly different assumptions. In the B-I type calculation all the parameter values listed in Table 4 were floated as independent variables. In the B-II treatment some interatomic distances were allowed to remain unchanged. On the B-III assumption, similar to the B-II treatment, the frequency factors of all atom pairs in the table were fixed at the given values. No significant difference was found in the bond lengths in the three calculations.

In the course of the calculation the existence of the *fac-* and *mer*-isomers of the tris(glycinato)zincate(II) complex was taken into consideration. However, the structural difference between the isomers was too small to improve the result by the introduction of the existence of the isomers.

Raman Spectra of Solutions A and B. Krishnan and Plane[15] reported Raman spectra for aqueous zinc(II) nitrate–glycine solutions in the pH range 2.0—7.0. From a Job plot with the total concentration of zinc(II) ion plus glycinate ion keeping approximately constant, the Zn–N stretching frequencies for the mono(glycinato)zinc(II), bis(glycinato)zinc(II) and tris(glycinato)zincate(II) complexes were assigned to be *ca.* 445, 430, and 425 cm^{-1}, respectively. In solution A of the present work (Fig. 7) the line at 441 cm^{-1} was assignable to the Zn–N stretching vibration for the mono(glycinato)zinc(II) complex. Other lines at 520, 580, and 920 cm^{-1} were attributable to the CO_2^- rocking, CO_2^- wagging and C–C stretching vibrations, respectively, within glycinate ion. The $\tilde{\nu}_4$-band of the

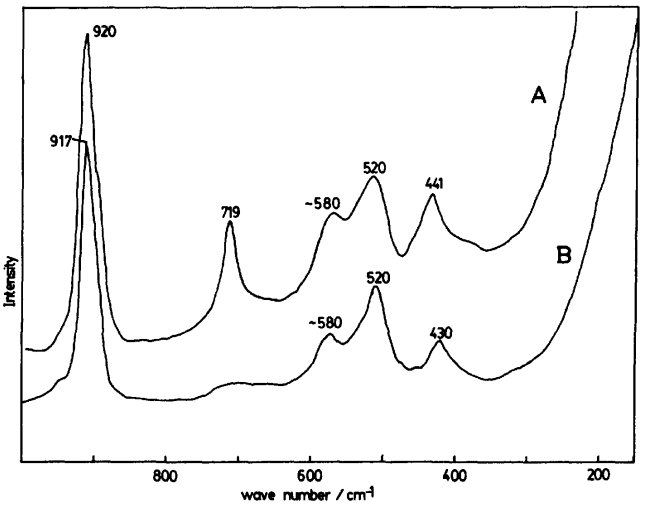

Fig. 7. Raman spectra of solutions A and B.

nitrate ion appeared at 720 cm^{-1}. In solution B we found a band ascribed to the Zn–N stretching for the tris(glycinato)zincate(II) complex at 430 cm^{-1}. Since solution B contained the tris(glycinato)zincate(II) complex as a main species, our result of the Zn–N frequency for the tris(glycinato)zincate(II) complex may be more reliable than that observed by Krishnan and Plane, because the concentration of the complex is sufficiently high in our solution. On the other hand the concentration of the tris-complex may be low under their experimental conditions where they kept the total concentration of zinc(II) and glycinate ions almost constant. The Raman spectra measured in the present work showed that the Zn–N stretching frequency was higher in the mono(glycinato)zinc(II) complex than in the tris(glycinato)zincate(II) ion, although the length of the Zn–N bond within the both complexes was practically

the same. The Zn–O and Zn–N bond lengths determined in the former complex may contain larger uncertainties than those in the latter do, because in the course of the structural analysis of the $[Zn(gly)(OH_2)_4]^+$ complex we have to evaluate lengths of three different kinds of bonds whilst the $[Zn(gly)_3]^-$ complex has bonds of two different kinds.

The mono(glycinato)zinc(II) and tris(glycinato)zincate(II) complexes in solution have a regular octahedral structure with the lengths between zinc(II) and ligand atoms of 2.12 Å. In crystal of the $[Zn(gly)_2]\cdot H_2O$[9] the equatorial square plane around the zinc(II) ion was occupied by chelating two glycinate ions and two apices of the distorted octahedron were filled with carbonyl oxygen atoms of glycinate ions combined with adjacent zinc(II) ions, though the bond distances between the Zn(II) ion and donor atoms were not determined. All the structures of the zinc(II)–glycinato complexes were octahedral and the metal-ligand bond lengths were practically indifferent in the complexes with varying numbers of the ligand coordinated, in contrast to the case of zinc(II)–ammine[3] and zinc(II)–ethylenediamine complexes.[4]

The work has been financially supported, in part, by the Grant-in-Aid for Scientific Research No. 57470054 from the Ministry of Education, Science and Culture. The financial aid by the Asahi Glass Foundation for Industrial Technology and the Japan Society for Promotion of Science is also acknowledged. A part of the computer calculations carried out in the present study has been performed at the Institute for Molecular Science in Okazaki.

References

1) H. Ohtaki, T. Yamaguchi, and M. Maeda, *Bull. Chem. Soc. Jpn.*, **49**, 701 (1976).
2) W. Bol, G. J. A. Gerrits, and C. L. van Panthaleon van Eck, *J. Appl. Crystallogr.*, **3**, 486 (1970).
3) T. Yamaguchi and H. Ohtaki, *Bull. Chem. Soc. Jpn.*, **51**, 3227 (1978).
4) T. Fujita, T. Yamaguchi, and H. Ohtaki, *Bull. Chem. Soc. Jpn.*, **52**, 3539 (1979).
5) D. L. Wertz and J. R. Bell, *J. Inorg. Nucl. Chem.*, **35**, 137 (1973).
6) D. L. Wertz, R. M. Lawrence, and R. F. Kruh, *J. Chem. Phys.*, **43**, 2163 (1965); E. Kálmán, I. Serke, G. Pálinkás, G. Johansson, G. Kabisch, M. Maeda, and H. Ohtaki, *Z. Naturforsch., A*, **38**, 225 (1983).
7) K. Ozutsumi and H. Ohtaki, *Bull. Chem. Soc. Jpn.*, **56**, 3635 (1983).
8) K. Ozutsumi and H. Ohtaki, *Bull. Chem. Soc. Jpn.*, **57**, 2605 (1984).
9) B. W. Low, F. L. Hirshfeld, and F. M. Richards, *J. Am. Chem. Soc.*, **81**, 4412 (1959).
10) H. Ohtaki, M. Maeda, and S. Ito, *Bull. Chem. Soc. Jpn.*, **47**, 2217 (1974).
11) G. Johansson and M. Sandström, *Chem. Scr.*, **4**, 195 (1973).
12) T. Yamaguchi, Doctor Thesis, Tokyo Institute of Technology, March (1978).
13) L. G. Sillén and A. E. Martell, "Stability Constants," Special Publication No. 17 (1964), The Chemical Society, London; A. E. Martell and R. M. Smith, "Critical Stability Constants," Plenum, New York (1974), Vol. 1.
14) A. H. Narten, *ORNL*-**4578** (1970).
15) K. Krishnan and R. A. Plane, *Inorg. Chem.*, **6**, 55 (1967).

The Stereoselective Retardation of the Alkaline Hydrolysis of Organic Esters by Binuclear Cu(II) Complexes with Cyclodextrins

Yoshihisa MATSUI* and Daisuke SUEMITSU
Department of Agricultural Chemistry, Shimane University, Nishikawatsu, Matsue 690
(Received November 21, 1984)

The alkaline hydrolysis of *p*-nitrophenyl acetate (*p*-NPA) in 1.0 mol dm^{-3} NaOH at 25 °C was almost completely retarded by the addition of a binuclear Cu(II) complex with α-cyclodextrin (Cu_2α-CD). The dissociation constant for an inclusion complex of Cu_2α-CD with *p*-NPA was determined to be 0.059 mmol dm^{-3}, which is about one 200th that for an inclusion complex of α-CD with *p*-NPA. The alkaline hydrolysis of *o*- and *m*-nitrophenyl acetates was also retarded by Cu_2α-CD, though the extent of retardation was much less than that for *p*-NPA. A binuclear Cu(II) complex with β-cyclodextrin (Cu_2β-CD) also caused a stereoselective deceleration of the alkaline hydrolysis of the esters. However, the stereoselectivity of Cu_2 β-CD was not so remarkable as that of Cu_2α-CD. Dissociation constants for inclusion complexes of Cu_2α-CD with several alcohols and other organic substrates were determined by the kinetic examination of the competitive inhibition effect of the substrates on the association of Cu_2α-CD with *p*-NPA. Cu_2α-CD formed stable inclusion complexes with such disk-like molecules as cyclohexanol, cycloheptanol, and *p*-nitrobenzyl alcohol. The geometry of a Cu_2α-CD-*p*-NPA inclusion complex was presumed on the basis of these results.

Copper(II) forms a binuclear complex (Cu_2CD) with cyclodextrin (CD) in an alkaline solution.[1] Although the structure of the complex has not been fully elucidated, it has been suggested that the two pairs of C2 and C3′ secondary hydroxyl groups of contiguous glucose units of CD are cross-linked by the $Cu(OH^-)_2$-Cu or $Cu(OH^-)(O^{2-})$Cu ion bridge (Fig. 1).[2]

The present work was undertaken to examine the binding and catalytic actions of this complex on organic substrates. The complex holds the CD cavity within which an organic molecule is included. The Cu(II) ions or the alkoxide ions of the complex may catalyze some reaction of an included molecule. Thus, it could be anticipated that the complex becomes a good model of metalloenzymes. The alkaline hydrolysis of nitrophenyl acetates (NPA) and the related esters was chosen as a test reaction in the present work, since the reaction has widely been used to examine the catalytic effects of CD itself[3-7] and modified CD's.[8-15] The catalytic property of the Cu_2CD complex has been reported only on the alkaline hydrolysis of a few organic phosphates[16] and monothiophosphates.[17]

Experimental

Materials. The α- and β-CD's commercially available were purified according to the directions of Cramer and Henglein.[18] Methyl α-D-glucopyranoside(MGP) of a reagent grade was used without further purification. $CuSO_4 \cdot 5H_2O$ of a reagent grade was recrystallized from water. The acetates (*o*-, *m*-, and *p*-NPA and 4-NNA) of *o*-, *m*-, and *p*-nitrophenols and 4-nitro-1-naphthol (*o*-, *m*-, and *p*-NP and 4-NN) were prepared by the reactions of the phenols and naphthol with acetic anhydride in pyridine at room temperature. The 4-NN (mp 164—166°, lit,[19] mp 164°) was prepared by the method of Hodgson and Kilner.[20] *p*-Nitrophenyl propionate (*p*-NPP) was prepared by the reaction of *p*-NP with propionyl chloride in pyridine. Mp 61—62°C. Alcohols such as 1-butanol, 1-pentanol, 2-methyl-2-propanol, 2,2-dimethyl-1-propanol, cyclohexanol, cycloheptanol, benzyl alcohol, and *p*-nitrobenzyl alcohol were commercially available and were used without further purification. *p*-Nitrobenzoic acid and methyl acetate commercially available were also used without further purification.

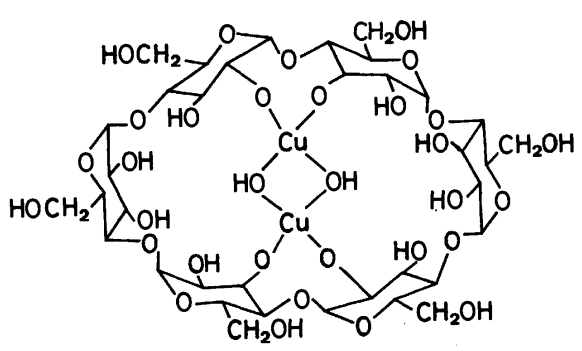

Fig. 1. A suggested structure of a Cu_2α-CD complex.

Kinetics. The rates of the alkaline hydrolyses of the esters were measured by following the appearance of the absorptions of the corresponding phenolate and naphtholate anions with an Union Giken stopped-flow reaction analyzer, Model RA-1100. A typical run is as follows. An alkaline CD solution was mixed with an aqueous $CuSO_4$ solution in such a way that the molar quantity of Cu in a resulting mixture was twice that of CD. The mixture was turbid and was shaken till it became clear, giving a Cu_2CD solution. The solution was rapidly mixed with an equal volume of an aqueous solution containing an organic ester at 25°C. The initial concentration of the ester in a reaction mixture and the wavelength at which the hydrolysis was followed are listed in Table 1. The change of absorbance with

TABLE 1. INITIAL CONCENTRATION OF ESTER AND WAVELENGTH AT WHICH THE HYDROLYSIS WAS FOLLOWED

Ester	[Ester] / mmol dm^{-3}	Wavelength / nm
o-NPA	0.12	410
m-NPA	0.20	400
p-NPA	0.030	410
p-NPP	0.031	410
4-NNA	0.020	457

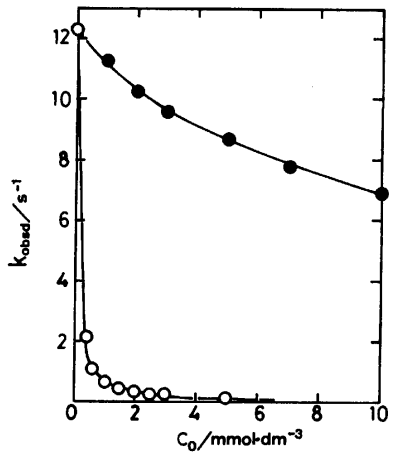

Fig. 2. Plots of k_{obsd} *vs.* c_0 for a Cu_2CD–*p*-NPA system in 1.0 mol dm^{-3} NaOH at 25 °C.
○: $Cu_2\alpha$-CD, ●: $Cu_2\beta$-CD.

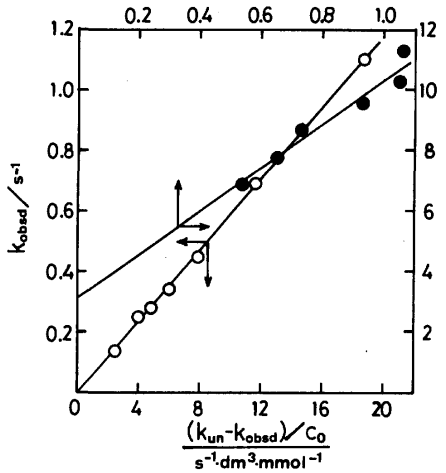

Fig. 3. Plots of k_{obsd} *vs.* $(k_{un}-k_{obsd})/c_0$ for a Cu_2CD–*p*-NPA system.
○: $Cu_2\alpha$-CD, ●: $Cu_2\beta$-CD.

time was treated according to the ordinary pseudo-first-order rate equation. The rate constants were calculated by the least-squares curve-fitting method with a microcomputer. All the reactions examined obeyed good first-order kinetics with regard to substrates irrespective of the absence or the presence of Cu_2CD in solution.

Determination of the Dissociation Constants and Rate Constants of Cu_2CD–Ester Complexes. As is illustrated in Fig. 2 for an example, the observed first-order rate constant (k_{obsd}) for each substrate approached a minimum value as the Cu_2CD concentration (c_0) increased. This saturation behavior suggests that the rate process involves the prior formation of an inclusion complex of Cu_2CD with a substrate. Upon the assumption of the formation of a 1:1 Cu_2CD–substrate complex, k_{obsd} is represented by the following equation if c_0 is much higher than the concentration of a substrate:[3]

$$k_{obsd} = \frac{K_d(k_{un}-k_{obsd})}{c_0} + k_c. \quad (1)$$

In this equation, K_d is the dissociation constant of an inclusion complex, and k_{un} and k_c, the rate constants for free and complexed substrates, respectively. The plot of k_{obsd} *vs.* $(k_{un}-k_{obsd})/c_0$ was virtually linear for each Cu_2CD–substrate system as is shown in Fig. 3. The values of K_d and k_c were calculated from the slope and intercept, respectively, of the straight line obtained by the use of the least-squares method.

Kinetic Determination of Dissociation Constants for Inclusion Complexes of $Cu_2\alpha$-CD with Alcohols and Other Organic Substrates. Dissociation constants (K_i) for inclusion complexes of $Cu_2\alpha$-CD with several alcohols and other organic substrates were determined by the kinetic examination of the competitive inhibition effect of the substrates on the association of $Cu_2\alpha$-CD with *p*-NPA in 1.0 mol dm^{-3} NaOH at 25 °C. An aqueous solution containing 0.06 mmol dm^{-3} *p*-NPA and varying amounts of an organic substrate was rapidly mixed with an equal volume of 2.0 mol dm^{-3} NaOH solution containing 3.0—5.0 mmol dm^{-3} $Cu_2\alpha$-CD at 25 °C. The k_{obsd} value for the alkaline hydrolysis of *p*-NPA in the presence of $Cu_2\alpha$-CD increased with increasing concentration (c_i) of the organic substrate. Relationships between k_{obsd} and c_i were analyzed by an equation derived by VanEtten, *et al.*:[3]

$$c_i = \frac{c_0 \cdot K_i}{K_d} \times \frac{k_{obsd}-k_c}{k_{un}-k_{obsd}} - K_i \quad (2)$$

Polarimetric Determination of Dissociation Constants for the Inclusion Complexes of CD or Cu_2CD with the p-*Nitrophenolate Ion.* The dissociation constant for the inclusion complex of CD or Cu_2CD with the *p*-NP anion was determined by a polarimetric examination of the effect of *p*-NP on the optical rotation of a CD or Cu_2CD solution at 25 °C. A Union Giken Model PM-101 polarimeter was used for the measurement. The optical rotation of the solution at λ=589 nm increased with the addition of *p*-NP. The K_d value was estimated using an ordinary Hildebrand-Benesi plot.

Results and Discussion

The effect of CD itself on the hydrolysis rates of *m*- and *p*-NPA had been examined in aqueous solutions (pH 10.0—10.6).[3] The present investigation was carried out in 1.0 mol dm^{-3} NaOH, since Cu(II) forms a stable 2:1 complex with CD in such a concentrated alkaline solution.[2] Table 2 shows the effects of CD and its Cu(II) complex on the hydrolysis rate of *p*-NPA at 25 °C. Although the hydrolysis was only slightly decelerated by the addition of α- or β-CD, the addition of $Cu_2\alpha$-CD or $Cu_2\beta$-CD markedly retarded the reaction. Among them, $Cu_2\alpha$-CD depressed the hydrolysis rate below one tenth the original rate. On the other hand, the

Table 2. Effects of CD and its Cu(II) complex on the hydrolysis rate of *p*-NPA in 1.0 mol dm^{-3} NaOH at 25 °C

CD	[CD] / mmol dm^{-3}	[Cu] / mmol dm^{-3}	k_{obsd}/s^{-1}
None	0.00	0.00	12.3±0.1
α-CD	5.00	0.00	11.2±0.1
α-CD	5.00	10.00	0.12±0.01
β-CD	5.00	0.00	12.2±0.4
β-CD	5.00	10.00	8.7±0.2
MGP[a]	5.00	2.50	12.8±0.1

a) MGP: Methyl α-D-glucopyranoside.

TABLE 3. K_d AND k_c VALUES FOR Cu_2CD-ORGANIC ESTER SYSTEMS IN 1.0 mol dm^{-3} NaOH AT 25 °C (1mM=1 mmol dm^{-3})

Ester		$Cu_2\alpha$-CD			$Cu_2\beta$-CD		
	k_{un}/s^{-1}	k_c/s^{-1}	k_c/k_{un}	K_d/mM	k_c/s^{-1}	k_c/k_{un}	K_d/mM
o-NPA	10.5	2.8	0.27	12	2.0	0.19	4
m-NPA	8.5	5.5	0.65	6	2.9	0.34	2
p-NPA	12.3	0.00	0.000	0.059	3.1	0.25	7
p-NPP	11.9	0.00	0.000	0.028	—	—	—
4-NNA	12.7	11.2	0.88	3	8.4	0.66	3
1a[a]	42.0[b]	5.8[b]	0.14	7	0.0[b]	0.00	9
1b[a]	11.0[b]	1.5[b]	0.14	17	0.0[b]	0.00	4
1c[a]	26.7[b]	17.2[b]	0.64	9	0.0[b]	0.00	18
2a[a]	3.68[b]	0.68[b]	0.19	2.7	0.07[b]	0.02	1.3
2b[a]	0.65[b]	0.27[b]	0.41	5.1	0.10[b]	0.15	2.4
2c[a]	2.23[b]	2.7[b]	1.2	0.9	0.25[b]	0.11	0.54

a)

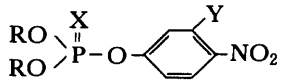

1a: R=Me, X=O, Y=H (Ref. 16)
1b: R=Et, X=O, Y=H (Ref. 16)
1c: R=Me, X=O, Y=Me (Ref. 16)
2a: R=Me, X=S, Y=H (Ref. 17)
2b: R=Et, X=S, Y=H (Ref. 17)
2c: R=Me, X=S, Y=Me (Ref. 17).

b) These values are $10^3 \cdot k_{un}$/s^{-1} or $10^3 \cdot k_c$/s^{-1}.

addition of a Cu(II) complex with MGP resulted in a slight acceleration of the hydrolysis. MGP forms a 1:1 complex with Cu(II) in an alkaline solution.[1] Thus, it is obvious that the marked retardation of the *p*-NPA cleavage by $Cu_2\alpha$-CD is not simply related to the direct action of the Cu(II) ion. The hydrolyses of *m*- and *o*-NPA and 4-NNA were also retarded by $Cu_2\alpha$-CD or $Cu_2\beta$-CD, though the extents of the retardation were not so large as that for a $Cu_2\alpha$-CD-*p*-NPA system. Interestingly, the hydrolysis of *p*-NPP was greatly retarded by $Cu_2\alpha$-CD to an extent similar to that of *p*-NPA.

The K_d and k_c values for these Cu_2CD-organic carboxylate systems were determined by the analysis of the relationships between k_{obsd} and the concentration (c_0) of Cu_2CD (Fig. 3). Table 3 gives the values obtained, together with those for Cu_2CD-organic phosphate and monothiophosphate systems reported previously.[16,17] These results indicate that $Cu_2\alpha$-CD causes a markedly stereoselective deceleration of the alkaline hydrolysis of organic carboxylates such as *o*-, *m*-, and *p*-NPA, *p*-NPP, and 4-NNA: The k_c/k_{un} value is virtually equal to zero for *p*-NPA and *p*-NPP, whereas it is 0.27 for *o*-NPA, 0.65 for *m*-NPA, and 0.88 for 4-NNA. Another remarkable stereoselectivity was observed for the binding of the esters to $Cu_2\alpha$-CD: The K_d value was determined to be 0.028 mmol dm^{-3} for *p*-NPP and 0.059 mmol dm^{-3} for *p*-NPA, these values being much smaller than those for *o*- and *m*-NPA and 4-NNA. According to VanEtten, *et al.*,[3] the K_d value for an α-CD-*p*-NPA system is equal to 12 mmol dm^{-3}, which is about 200 times that for a $Cu_2\alpha$-CD-*p*-NPA system. The K_d value for an α-CD-*m*-NPA system is 19 mmol dm^{-3} which is only 3 times that (6.3 mmol dm^{-3}) for a $Cu_2\alpha$-CD-*m*-NPA system. The binding site of $Cu_2\alpha$-CD may be significantly different in structure from that of uncomplexed α-CD.

$Cu_2\beta$-CD also caused a stereoselective deceleration of

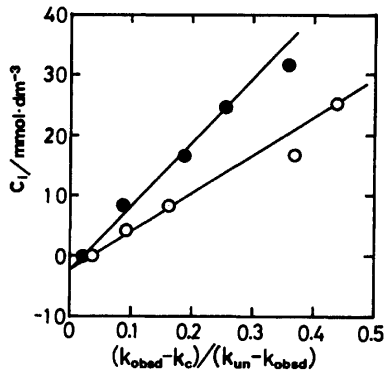

Fig. 4. Plots of c_i *vs.* $(k_{obsd}-k_c)/(k_{un}-k_{obsd})$ for a $Cu_2\alpha$-CD-*p*-NPA-cyclohexanol system in 1.0 mol dm^{-3} NaOH at 25 °C.
○: [$Cu_2\alpha$-CD]=1.5 mmol dm^{-3}, ●: [$Cu_2\alpha$-CD]=2.5 mmol dm^{-3}.

the alkaline hydrolysis of the carboxylates. However, the stereoselectivity of $Cu_2\beta$-CD is not so remarkable as that of $Cu_2\alpha$-CD with regard to both k_c/k_{un} and K_d. Furthermore, the retardation effect of $Cu_2\beta$-CD was less prominent in the carboxylates than in the phosphates and monothiophosphates. On the other hand, the binding and catalytic actions of $Cu_2\alpha$-CD on the phosphates and monothiophosphates are less stereoselective than those on the carboxylates. These results suggest that the binding and catalytic properties of Cu_2CD depend not only on the structures of the phenyl and acid moieties of the phenyl esters but also on the size of the CD ring.

In order to characterize the structure of the binding site of $Cu_2\alpha$-CD, dissociation constants (K_i) for inclusion complexes of $Cu_2\alpha$-CD with several alcohols and other organic molecules were determined by a kinetic examination of the competitive inhibition effect of the molecules on the association of $Cu_2\alpha$-CD with *p*-NPA in 1.0 mol dm^{-3} NaOH at 25 °C. Figure 4 shows the plots of c_i *vs.* $(k_{obsd}-k_c)/(k_{un}-k_{obsd})$, based on Eq. 2,

TABLE 4. K_i VALUES FOR $Cu_2\alpha$-CD COMPLEXES

Substrate	K_i/mM[a] ($Cu_2\alpha$-CD)	K_d/mM[b] (α-CD)	K_i/K_d
	(Normal Alkanol)		
1-Butanol	10.3	11.1	0.93
1-Pentanol	3.3	3.1	1.1
	(Branched Alkanol)		
2-Me-2-Propanol	220	230	1.0
2,2-DiMe-1-Propanol	10	34	0.30
	(Cyclic Alkanol)		
Cyclopentanol	25	22	1.1
Cyclohexanol	2.2	15	0.15
Cycloheptanol	1.5	13	0.12
	(Aromatic Alcohol)		
Benzyl Alcohol	26	46	0.6
p-Nitrobenzyl Alcohol	0.47	—	—
	(Others)		
Methyl Acetate	40	—	—
p-Nitrophenolate ion	6.5	5.8[a]	1.1
p-Nitrobenzoate ion	250	—	—

a) In 1.0 mol dm^{-3} NaOH at 25 °C. b) In 0.10 mol dm^{-3} H_2SO_4 at 25 °C (Ref.21).

for a $Cu_2\alpha$-CD–cyclohexanol system at c_0=1.5 and 2.5 mmol dm^{-3}. The plots were virtually linear in both cases. The extrapolation of the straight lines to $(k_{obsd}-k_c)/(k_{un}-k_{obsd})=0$ gave virtually the same K_i value of 2.2 mmol dm^{-3}. As Eq. 2 suggests, the slopes of the straight lines are equal to $c_0 \cdot K_i/K_d$. The K_d values, thus estimated, were 0.052 mmol dm^{-3} in both cases. The value is very close to that directly determined (K_d=0.059 mmol dm^{-3}). Table 4 shows the K_i values obtained, together with the K_d value for a $Cu_2\alpha$-CD complex with the *p*-NP anion estimated by the polarimetric method. The K_d values for inclusion complexes of α-CD itself with these substances are also shown in the table for the sake of comparison.[21]

Although the K_d values for inclusion complexes of $Cu_2\alpha$-CD with *p*-NPA and *p*-NPP were very small, the K_i value for a $Cu_2\alpha$-CD complex with methyl acetate, as well as the K_d values for $Cu_2\alpha$-CD complexes with *o*- and *m*-NPA, was significantly large. It is obvious that the *p*-nitrophenyl moiety of *p*-NPA or *p*-NPP is essential for the strong binding of *p*-NPA or *p*-NPP to $Cu_2\alpha$-CD. This presumption is supported by the fact that the K_i value for a $Cu_2\alpha$-CD–*p*-nitrobenzyl alcohol system is considerably small (0.47 mmol dm^{-3}). However, the K_d or K_i values for a $Cu_2\alpha$-CD complex with the *p*-nitrophenolate or *p*-nitrobenzoate anion was not so small as the K_d value for a $Cu_2\alpha$-CD complex with *p*-NPA or *p*-NPP. $Cu_2\alpha$-CD holds two negative charges, and the inclusion of the *p*-nitrophenolate or *p*-nitrobenzoate anion within the $Cu_2\alpha$-CD cavity may be retarded by the electrostatic repulsive force. The K_i values for $Cu_2\alpha$-CD complexes with normal and branched alkanols such as 1-butanol, 1-pentanol, and 2-methyl-2-propanol were comparable to the corresponding K_d values for α-CD complexes with the alkanols. On the other hand, the K_i values for $Cu_2\alpha$-CD complexes with cycloalkanols such as cyclohexanol and cycloheptanol were considerably smaller than the corresponding K_d values for α-CD complexes with the cycloalkanols. It has been suggested that the macrocyclic ring of α-CD is distorted to the ellipsoidal form by the formation of a $Cu_2\alpha$-CD complex (Fig. 1),[2] whereas the ring is virtually regular hexagonal in α-CD inclusion complexes.[22,23] The ellipsoidal cavity of $Cu_2\alpha$-CD may be favorable for the inclusion of such disk-like molecules as cycloalkanols, *p*-nitrobenzyl alcohol, *p*-NPA, and *p*-NPP.

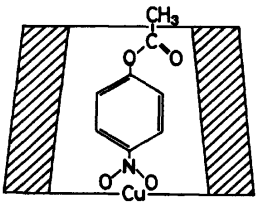

Fig. 5. The proposed geometry of *p*-NPA within the cavity of $Cu_2\alpha$-CD.

The geometry of the $Cu_2\alpha$-CD–*p*-NPA inclusion complex was presumed to be as is shown in Fig. 5 on the basis of the results described above. The substrate, *p*-NPA, may penetrate into the ellipsoidal cavity of $Cu_2\alpha$-CD so deeply that the maximum van der Waals contact with the cavity is attained. The coordination of the Cu(II) ion of $Cu_2\alpha$-CD to the nitro group of *p*-NPA may be possible to occur, resulting in the additional force for the strong binding of the substrate to $Cu_2\alpha$-CD. The carbonyl moiety of *p*-NPA may aloso be included within the cavity, so that the nucleophilic attack of the hydroxide ion on the carbonyl carbon is almost completely retarded by the steric hindrance of the α-CD macrocycle. In the cases of the organic phosphates and monothiophosphates, two methoxyl or two ethoxyl groups attached to the phosphorus atom may be too large to be included deeply within the cavity of $Cu_2\alpha$-CD. Then, the phosphorus atom is subject to the nucleophilic attack of the hydroxide ion from bulk solution. The *o*- and *m*-isomers of NPA may also be impossible to be deeply included within the $Cu_2\alpha$-CD cavity, owing to the steric hindrance of the substituents. $Cu_2\beta$-CD has a larger cavity in size than $Cu_2\alpha$-CD. Thus, *p*-NPA cannot fit the $Cu_2\beta$-CD cavity so closely as it fits the $Cu_2\alpha$-CD cavity, and the K_d and k_c/k_{un} values for a $Cu_2\beta$-CD–*p*-NPA system is much larger than those for a $Cu_2\alpha$-CD–*p*-NPA system. On the contrary, *o*- and *m*-NPA and 4-NNA as well as the organic phosphates and monothiophosphates may be more deeply included within the $Cu_2\beta$-CD cavity than within the $Cu_2\alpha$-CD cavity. Then, the k_c/k_{un} values for $Cu_2\beta$-CD complexes with these substrates are smaller than those for the corresponding $Cu_2\alpha$-CD complexes.

In conclusion, complex formation between Cu(II) and α-CD causes a large conformational change in the macrocycle of α-CD, which is responsible both for the markedly stereoselective binding of *p*-NPA and for the stereoselective retardation of the alkaline hydrolysis of

p-NPA by $Cu_2\alpha$-CD. Similar effects of metal ions on the conformation and binding and catalytic properties of enzymes have often been reported on metalloenzymes.[24,25] Thus, we can refer to the Cu_2CD complex as a good model of metalloenzymes.

References

1) Y. Matsui, T. Kurita, and Y. Date, *Bull. Chem. Soc. Jpn.*, **45**, 3229 (1972).

2) Y. Matsui, T. Kurita, M. Yagi, T. Okayama, K. Mochida, and Y. Date, *Bull. Chem Soc. Jpn.*, **48**, 2187 (1975).

3) R. L. VanEtten, J. F. Sebastian, G. A. Clowes, and M. L. Bender, *J. Am. Chem. Soc.*, **89**, 3242 (1967).

4) H. Kitano and T. Okubo, *J. Chem. Soc., Perkin Trans., 2*, **1977**, 432.

5) M. Komiyama and M. L. Bender, *J. Am. Chem. Soc.*, **100**, 4576 (1978).

6) M. Komiyama and M. L. Bender, *Bull. Chem. Soc. Jpn.*, **53**, 1073 (1980).

7) M. Komiyama and H. Hirai, *Chem. Lett.*, **1980**, 1471.

8) F. Cramer and G. Mackensen, *Chem. Ber.*, **103**, 2138 (1970).

9) R. Breslow and L. E. Overman, *J. Am. Chem. Soc.*, **92**, 1075 (1970).

10) W. B. Gruhn and M. L. Bender, *Bioorg. Chem.*, **3**, 324 (1974).

11) Y. Kitaura and M. L. Bender, *Bioorg. Chem.*, **4**, 237 (1975).

12) Y. Iwakura, K. Uno, F. Toda, S. Onozuka, K. Hattori, and M. L. Bender, *J. Am. Chem. Soc.*, **97**, 4432 (1975).

13) R. Breslow, M. F. Czarniecki, J. Emert, and H. Hamaguchi, *J. Am. Chem. Soc.*, **102**, 762 (1980).

14) K. Fujita, A. Shinoda, and T. Imoto, *J. Am. Chem. Soc.*, **102**, 1161 (1980).

15) K. Fujita, A. Shinoda, and T. Imoto, *Tetrahedron Lett.*, **21**, 1541 (1980).

16) K. Mochida, Y. Ozoe, H. Miyazaki, and Y. Matsui, *Bull. Fac. Agric., Shimane Univ.*, **14**, 158 (1980).

17) K. Mochida, Y. Ozoe, H. Iwasaki, and Y. Matsui, *Bull. Fac. Agric., Shimane Univ.*, **13**, 190 (1979).

18) F. Cramer and F. M. Henglein, *Chem. Ber.*, **91**, 308 (1958).

19) I. Heilbron and H. M. Bunbury, "Dictionary of Organic Compounds," Oxford Univ., New York (1953), Vol. 3, p. 746.

20) H. H. Hodgson and E. Kilner, *J. Chem. Soc.*, **127**, 807 (1924).

21) Y. Matsui and K. Mochida, *Bull. Chem. Soc. Jpn.*, **52**, 2808 (1979).

22) W. Saenger, "Environmental Effects on Molecular Structure and Properties," ed by B. Pullman, D. Reidel, Dordorecht-Holland (1976), p. 265.

23) K. Harata, *Bull. Chem. Soc. Jpn.*, **50**, 1416 (1977).

24) F. R. N. Gurd and G. F. Bryce, "The Biochemistry of Copper," ed by J. Peisach, P. Aisen, and W. E. Blumberg, Academic Press, New York (1966), p. 115.

25) J. E. Coleman and J. F. Chlebowski, *Adv. Inorg. Biochem.*, **1**, 1 (1979).

 © 1985 The Chemical Society of Japan Bull. Chem. Soc. Jpn., 58, 1663—1668 (1985)

Reactions of Tropone Tosylhydrazone Sodium Salt with Anthracene, 1,3-Diphenylisobenzofuran, and Phenylacetylene: [2+2] and [4+2] Type Cycloaddition Reactions of Cycloheptatrienylidene or 1,2,4,6-Cycloheptatetraene

Katsuhiro SAITO,* Yoichi OMURA, and Toshio MUKAI†

Department of Chemistry, Nagoya Institute of Technology, Gokiso-cho, Showa-ku, Nagoya 466

†*Department of Chemistry, Faculty of Science, Tohoku University, Aoba, Aramaki, Sendai 980*

(Received December 3, 1984)

The reaction of tropone tosylhydrazone sodium salt (**1**) with anthracene gave a [4+2]-type adduct and the reaction of **1** with 1,3-diphenylisobenzofuran afforded *endo*- and *exo*-[4+2]-type adducts as well as a heptafulvene derivative. The reaction of **1** with phenylacetylene yielded a [2+2]-type adduct, which rearranged into 2-phenylindene upon heating. The addition reactions are thought to proceed *via* the allene intermediate, 1,2,4,6-cycloheptatetraene, which is a valence-bond isomer of the carbene intermediate, cycloheptatrienylidene, initially generated by the pyrolysis of **1**. The photoreaction of adduct **3** with a high-pressure mercury lamp afforded a ring-closure product *via* the photobicyclization reaction of the cycloheptatriene moiety of the adduct. Thermal interconversions between the three products of the reaction of **1** with 1,3-diphenylisobenzofuran were investigated.

It is known that tropone tosylhydrazone sodium salt (**1**) generates the carbene, cycloheptatrienylidene (**3a**) accompanied by nitrogen gas and sodium *p*-toluenesulfinate (**2**) by pyrolysis or photolysis.[1] Cycloheptatrienylidene is recognized to be a nucleophilic singlet carbene, due to the contribution of a canonical formula (**3b**), which is stabilized by the 6 π-electrons aromatic system.[2] Actually, **3a** preferentially reacts with electron-deficient double bonds.[2] Recently, Jones *et al.* suggested the possibility of a valence-bond isomerization between the carbene **3a** and an allene, 1,2,4,6-cycloheptatetraene (**3c**), and proved experimentally that **3c** rearranged into **3a**.[3] However, the reverse isomerization, **3a** to **3c**, has never been found. We have pyrolyzed **1** in the presence of various olefins and we have evidence which suggests the isomerization of **3a** to **3c**. Here, we wish to report our findings.

Results

When **1** was allowed to react with anthracene (**4**) in anhydrous diglyme at 120 °C for 15 min, the [4+2]-type adduct **5** was afforded in a yield of 21%. The reaction of **1** with 1,3-diphenylisobenzofuran (**6**) under the identical conditions gave two [4+2]-type adducts, **7** and **8**, accompanied by the heptafulvene derivative **9**, in yields of 28, 3, and 4%, respectively. The analogous reaction of **1** with phenylacetylene (**10**) afforded a [2+2]-type adduct **11** and 2-phenyl-1*H*-indene (**12**)[4] in yields of 8 and 5%, respectively.

Compound **5** was thermally stable and was recovered quantitatively after heating at 150 °C for 40 h, but turned to polymeric materials upon heating at 180 °C for 20 h. No change was observed when **7** and **8** were kept at 120 °C for 15 min (the conditions of the pyrolysis of **1**), but upon heating at 130 °C for 25 h, **7** gave **8** and **9** in yields of 6 and 42%, respectively, as well as a 30% yield of recovered **7**. Under conditions analogous to the above, **8** afforded **7**, **9**, and recovered **8** in yields of 2, 20, and 68%, respectively. Upon heating at 120 °C for 1 h, **11** rearranged into **12** in a 55% yield. The red oil **9** was unstable and readily decomposed to a resinous material, but catalytic hydrogenation of **9** over palladium–charcoal resulted in the formation of a colorless oil **13** in 96% yield by absorbing 4 molar equivalents of hydrogen.

The irradiation of a methanol solution of **5** using a high-pressure mercury lamp afforded the ring-closure product **14** in a yield of 88%.

The structures of **5**, **7**, and **8** were deduced on the basis of their physical properties and confirmed by a comparison of these properties with those of analogous compounds.[5] The stereochemistries of **7** (*endo*-adduct) and **8** (*exo*-adduct) were deduced on the basis of the following arguments. According to Dreiding models, H_a of **8** (δ 2.60) and H_b of **7** (δ 4.75) are expected to appear in a higher field in the NMR spectra compared to H_a of **7** (δ 3.68) and H_b of **8** (δ 5.15), because of the diamagnetic anisotropic effects from the *o*-disubstituted benzene moiety. Furthermore, the chemical shifts of H_a of **7** (δ 3.68) and **8** (δ 2.60) are

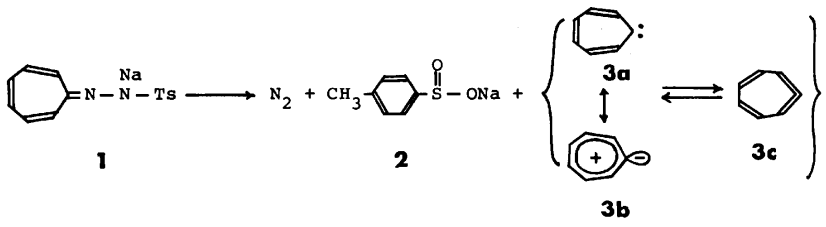

Fig. 1.

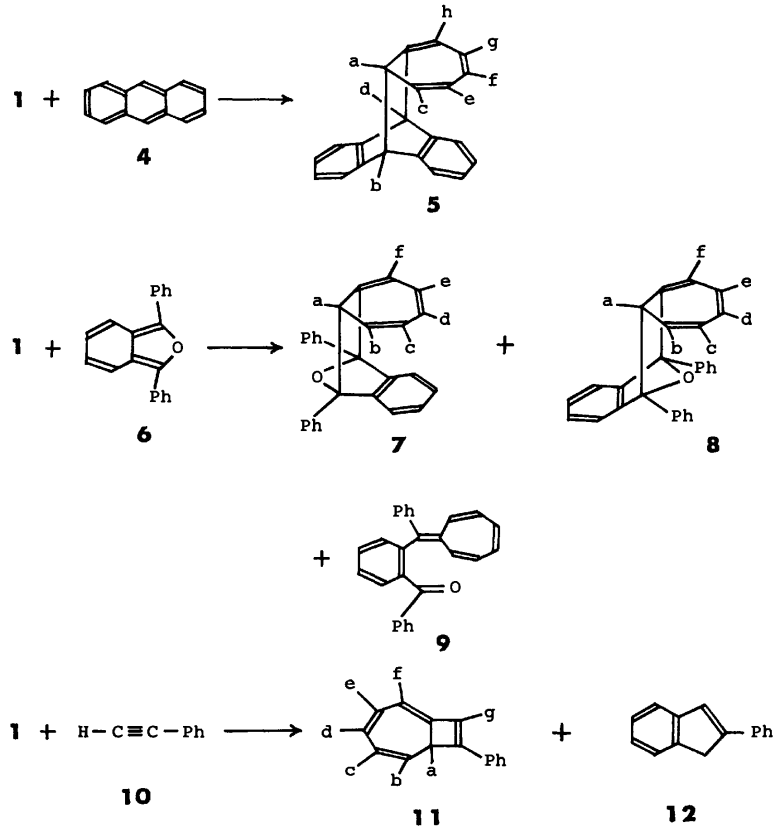

Fig. 2.

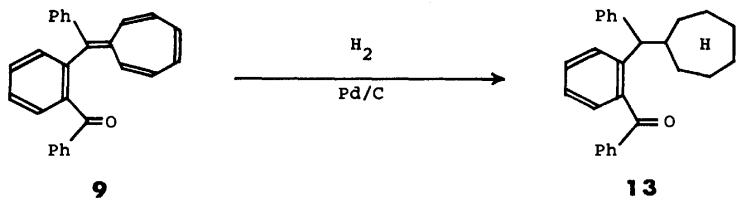

Fig. 3.

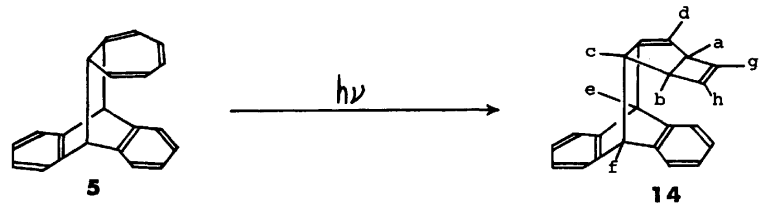

Fig. 4.

consistent with that of the bridge-head proton of the endo-adduct of **6** with cycloheptatriene (δ 3.88)[5d] and that of H_a of **5** (δ 2.46), respectively, indicating that each pair of protons is located in nearly the same chemical environment.

The structure of **9** was deduced mainly from its UV spectrum, which is characteristic of heptafulvene derivatives,[6] and its IR spectrum, which shows a carbonyl band in the same region as that of benzophenone. The absorbing of 4 molar equivalents of hydrogen by **9** to give a stable colorless oil **13** seems to support the structure of **9**.[6d]

The structure of the photoproduct **14** was deduced on the basis of the physical properties and confirmed by a comparison of the physical properties with those of the analogous compounds.[7]

Discussion

The mechanism for the formation of **9** from **7** and **8** initially involves the cleavage of the bond at 7-position of the cycloheptatriene moiety of **7** and **8** to give a tropylium cation (**15a**) or a tropylium radical intermediate (**15b**), which in turn affords **9** *via* an ether bond cleavage as shown in Fig. 5. The stability of the tropylium cation and/or the tropylium radical[8] and

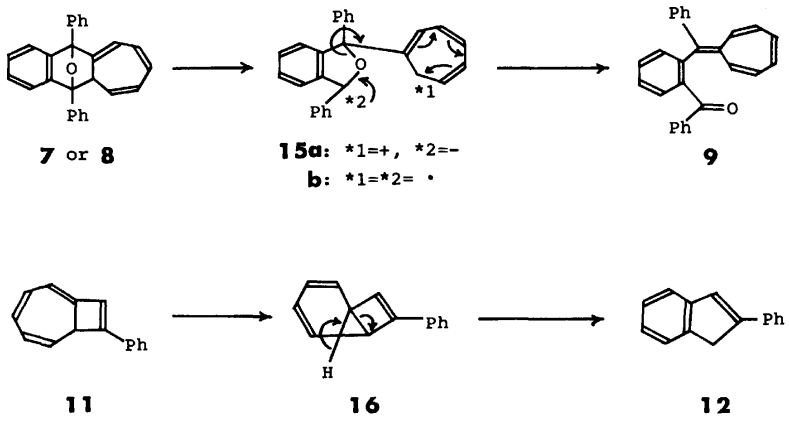

Fig. 5.

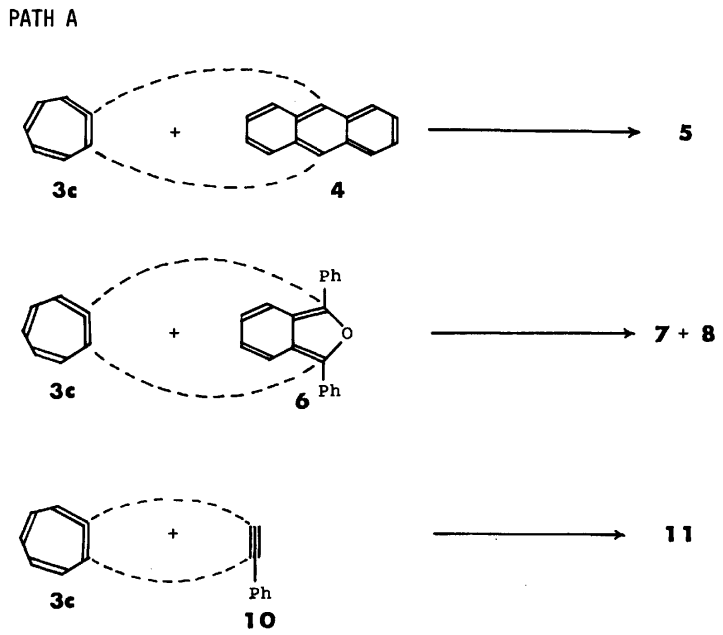

Fig. 6.

the formation of the stable benzophenone moiety can be regarded as the driving force for this reaction.

The isomerization mechanism of **11** to **12** may be explained as follows. The valence-bond isomerization of the cycloheptatriene moiety of **11** gives rise to the norcaradiene structure (**16**),[9] which rearranges to **12** *via* a hydrogen shift. The analogous reaction mechanism has been proposed for the formation of indane derivatives in the thermal reactions of spiro[2.6]nona-4,6,8-triene derivatives.[1b,7c,10] The photochemical formation of **14** proceeds *via* the well known 4 π-electrons photo-allowed disrotatory cyclization process.[7,11]

Two possible mechanisms may be considered for the reaction of **1** with **4**, **6**, and **10**. Pathway A involves an allene intermediate **3c** followed by a [4+2] or [2+2] addition reaction of the allenic double bond of **3c** with the appropriate moieties of **4**, **6**, and **10** to give the corresponding adducts. Pathway B involves the carbene intermediate **3a**, which reacts with **4**, **6**, and **10** to afford the tropylium cation intermediates **17a**, **15a**, and **18a**, respectively, or the tropylium radical intermediates **17b**, **15b**, and **18b**, respectively. Subsequent cyclization reactions of these intermediates lead to the formation of the corresponding products.

A closer examination into pathway B reveals two facts which do not adequately explain the observed products. First, intermediate **3a** is a nucleophilic carbene; therefore, the addition of this carbene to **4**, **6**, and **10** is not favored since these compounds do not contain any electron-defficient double bonds. Second, the yield of the *endo*-adduct **7** is higher than that of the *exo*-adduct **8**. According to Dreiding model, there is no obvious difference between the steric repulsions in the formation of **7** and **8** from**15**. On this basis, **7** and **8** are expected to be formed in an equal yield from **15**. The fairly large difference between the yield of **7** and **8** would suggest that the reaction does not proceed *via* **15**. On the other hand, several advantages are envisioned regarding pathway A. Compounds **4** and **6** are known to react readily as 4π-components

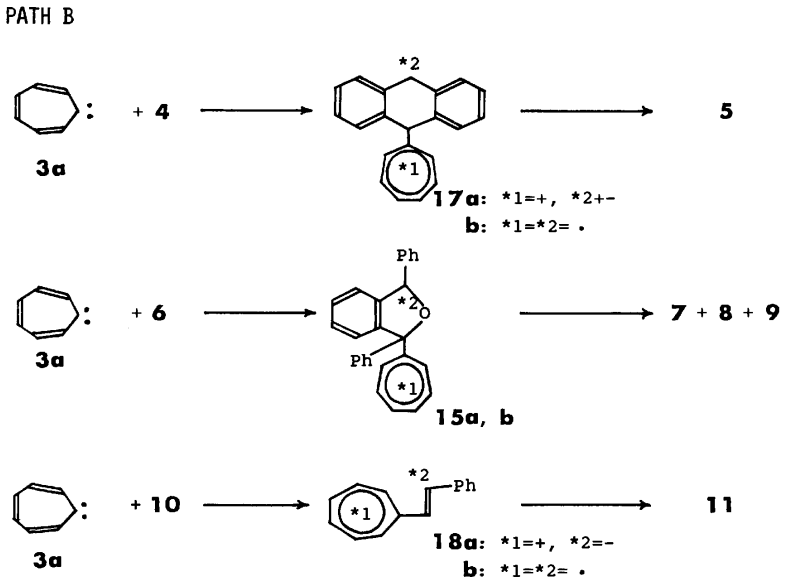

Fig. 7.

in [4+2]-type addition reactions.[12] Oda has reported that a cyclic conjugated allene derivative has been allowed to react with **6** to give *endo* and *exo* [4+2]-type adducts in a yield ratio of 5:1, without defining the stereochemistry of the adducts.[13] The major formation of the *endo*-adduct **7** can be explained as the result of the secondary orbital interaction in the transition state.[11]

As discussed above, it is difficult to decide whether the carbene intermediate **3a** or the allene intermediate **3c** is involved in the addition reactions, but a plausible pathway for the reaction would involve the allene intermediate **3c**. As for the reaction with **10**, pathway B seems to have still some possibility, because pathway A may involve a thermally forbidden [π2s+π2s] addition process.[14]

Experimental

The photoreactions were performed with a 400-W high-pressure mercury lamp, UVL-400P of Riko Kagaku Sangyo Ltd. under a nitrogen stream at room temperature. Thermal isomerizations were carried out in sealed ampoules. All melting points are uncorrected. UV and IR spectra were measured with the Hitachi 220A and DS-701G spectrometers, respectively. Mass spectra were measured with the Hitachi M-52 and JMS-DX300 spectrometers, and the NMR spectra were measured with a Hitachi R-20B or a Varian XL 200 spectrometer with tetramethylsilane as an internal standard. Wako Gel C-200 and activated alumina of Wako Pure Chemical Industries Ltd. were used for column chromatography. Wako Gel B5F was used for thin-layer chromatography.

Reaction of 1 with 4. A mixture of **1** (13.50 g, 46 mmol), **4** (25.00 g, 140 mmol) and anhydrous diglyme (120 ml) was heated at 120 °C for 15 min. After evolution of nitrogen gas had ceased (11, 97%), the gray powder of **2** (7.70 g, 95%) was removed by filtration. The filtrate was extracted with benzene, washed with water, and dried over anhydrous sodium sulfate. After filtration, the solvent was removed on a rotary evaporator to yield black crystals, which were recrystallized from benzene to give crystals of recovered **4** (21.29 g). The filtrate was chromatographed on silica gel to yield recovered **4** (0.85 g) by pet ether–benzene 9:1 and colorless crystals of **5** (2.57 g, 21%) by pet ether–benzene 8:2. The crystals of **5** were purified by recrystallization from benzene–ethanol. **5**: Mp 135—136 °C. Found: C, 93.80; H, 6.03%. Calcd for $C_{21}H_{16}$: C, 93.99; H, 6.01%. Mass *m/z* (rel intensity): 268 (M^+, 95), 191 (23), 178 (100). UV (EtOH): 276 nm (log ε, 3.53). IR (KBr): 3030, 1600, 1480 cm^{-1}. NMR ($CDCl_3$) δ=2.46 (m, H_a), 4.47 (d, H_b), 4.63 (dd, H_c), 4.78 (s, H_d), 5.86 (m, H_e), 6.20 (m, H_f, H_g, H_h), 7.0—7.5 (m, 8H, Ph). Coupling constants in Hz: J_{ab}=3, J_{ac}=5, J_{ce}=10, J_{ea}=2, J_{ef}=5.

Reaction of 1 with 6. A mixture of **1** (24.00 g, 80 mmol), **6** (43.00 g, 160 mmol) and anhydrous diglyme (200 ml) was heated at 120 °C for 15 min to evolve nitrogen gas (1.7 l, 96%). After separation of the gray powder of **2** (13.86 g, 96%) by filtration, the filtrate was treated, as usual, to yield a mixture of crystals and an oil. The crystals of recovered **6** (23.60 g) were separated by filtration and the filtrate was chromatographed on alumina to yield colorless crystals **7** (6.20 g) and mixed crystals of **7** and **8** (3.03 g) by pet ether–benzene 3:1 and a red oil **9** (1.15 g, 4%) by ether. The NMR spectrum of the mixed crystals showed that this mixture contained **7** and **8** in a ratio of 2:1. Thus, the yields of **7** and **8** were 8.22 g (28%) and 1.01 g (3%), respectively. Repeated recrystallization from benzene gave pure crystals of **7** and **8**. The red oil of **9** was further purified with thin-layer chromatography on silica gel using benzene as a developing solvent (R_f=0.60). **7**: Mp 189—190 °C. Found: C, 90.23; H, 5.43%. Calcd for $C_{27}H_{20}O$: C, 89.97; H, 5.59%. Mass *m/z* (rel intensity): 360 (M^+, 100), 255 (87), 105 (82). UV (EtOH): 278 nm (log ε, 3.44). IR (KBr): 3030, 1600, 1450 cm^{-1}. NMR ($CDCl_3$) δ=3.68 (m, H_a), 4.75 (dd, H_b), 5.85 (m, H_c), 6.13 (m, H_d), 6.20 (m, H_e, H_f), 7.0—7.8 (m, 14H, Ph). Coupling constants in Hz: J_{ab}=4, J_{ac}=2, J_{bc}=10, J_{cd}=5, J_{de}=11. **8**: Mp 177—178 °C. Found: C, 89.62; H, 5.59%. Calcd for $C_{27}H_{20}O$: C, 89.97; H, 5.59%. Mass *m/z* (rel intensity): 360 (M^+, 45), 255 (100), 105 (55). UV (EtOH): 278 nm (log ε, 3.67). IR (KBr): 3030, 1600, 1450 cm^{-1}. NMR ($CDCl_3$) δ=2.60 (m, H_a), 5.15 (dd, H_b), 6.05 (m, H_c), 6.32 (m, H_d), 6.43 (m, H_e, H_f), 7.0—7.8 (m, 14H, Ph).

Coupling constants in Hz: J_{ab}=4, J_{ac}=2, J_{bc}=10, J_{cd}=5, J_{de}=11. **9**: Found: C, 90.22; H, 5.61%. Calcd for $C_{27}H_{20}O$: C, 89.97; H, 5.59%. Mass *m/z* (rel intensity): 360 (M^+, 38), 209 (44), 152 (34), 105 (100). UV (EtOH): 248 nm (log ε, 4.32), 332 (3.93). IR (neat): 3030, 1670, 1600 cm^{-1}. NMR ($CDCl_3$) δ=5.3—6.5 (m, 6H), 7.0—7.4 (m, 14H, Ph).

Reaction of 1 with 10. A mixture of **1** (5.92 g, 20 mmol), **10** (10.20 g, 100 mmol), and anhydrous diglyme (50 ml) was heated at 120 °C for 15 min to evolve nitrogen gas (450 ml, 100%). After separation of the gray powder **2** (3.56 g, 100%), by filtration, the usual workup gave a black oil, which gave recovered **10** (7.69 g) by distillation under a reduced pressure (0.5 Torr†, bath temperature 75 °C). The residue was chromatographed on silica gel to give a tarry material (680 mg) by pet ether, which was thin layer chromatographed on silica gel using pet ether as a developing solvent to give crystals of **12** (207 mg, 5%, R_f=0.45, mp 167—168 °C, lit,[4] 166—167 °C) and a colorless oil of **11** (320 mg, 8%, R_f=0.40). **11**: Found *m/z* 192.0967. Calcd for $C_{15}H_{12}$: 192.0964. Mass *m/z* (rel intensity): 192 (100), 179 (11), 165 (20), 115 (14). UV (EtOH): 270 nm (log ε, 4.23). IR (neat): 3050, 2960, 1660 cm^{-1}. NMR ($CDCl_3$) δ=4.71 (m, H_a), 5.21 (m, H_b), 5.75 (m, H_c), 5.8—6.7 (m, H_d, H_e, H_f), 6.37 (d, H_g), 7.1—7.5 (m, 5H, Ph). Coupling constants in Hz: J_{ab}=4, J_{bc}=10, J_{ce}=5, J_{gf}=2.

Hydrogenation of 9. A solution of **9** (150 mg, 0.42 mmol) in benzene (15 ml) was hydrogenated with palladium-charcoal (30 mg) to absorb hydrogen gas (38 ml, 17 mmol). After filtration, the solvent was removed on a rotary evaporator to yield a colorless oil, which was thin-layer chromatographed on silica gel using benzene as a developing solvent to yield a colorless oil of **13** (146 mg, 96%, R_f=0.70). **13**: Found: C, 87.97; H, 7.43%. Calcd for $C_{27}H_{28}O$: C, 88.00; H, 7.66%. Mass *m/z* (rel intensity): 368 (M^+, 100), 309 (57), 270 (44), 165 (24). UV (EtOH): 250 nm (log ε, 4.31). IR (neat): 3030, 2950, 1673, 1600 cm^{-1}. NMR ($CDCl_3$) δ=1.3—2.4 (two broad peaks, 14H), 7.0—7.4 (m, 14H, Ph).

Thermal Isomerization of 7. A solution of **7** (80 mg) in benzene (0.3 ml) was kept at 130 °C for 25 h in a sealed ampoule. Thin-layer chromatography of the reaction mixture on silica gel using benzene as a developing solvent gave mixed crystals of **7** and **8** (30 mg, R_f=0.85) and a red oil of **9** (34 mg, 42%, R_f=0.60). The NMR spectrum of the mixed crystals showed that the crystals contained **7** and **8** in a ratio of 5:1; thus,the yields of **7** and **8** were 25 mg (30%) and 5 mg (6%), respectively.

Thermal Isomerization of 8. A solution of **8** (80 mg) in benzene (0.3 ml) was kept at 130 °C for 25 h. Thin-layer chromatography of the reaction mixture under the same conditions as above gave mixed crystals of **7** and **8** (56 mg) and a red oil of **9** (16 mg, 20%). The NMR spectrum showed that the mixed crystals contained the recovered **7** (54 mg, 68%) and **8** (2 mg, 2%).

Thermal Isomerization of 11. A solution of **11** (40 mg) in benzene (5 ml) was kept at 120 °C for 1 h. After evaporation of the solvent, the reaction mixture was thin-layer chromatographed on silica gel using pet ether as a developing solvent to yield crystals of **12** (22 mg, 55%, R_f=0.45).

Photoreaction of 5. A solution of **5** (100 mg) in methanol (200 ml) was irradiated with a high-presssure mercury lamp for 2 h. After evaporation of the solvent on a rotary evaporator, the residue was thin-layer chromatographed on silica gel using pet ether-benzene 8:2 as a developing solvent to yield a colorless oil of **14** (88 mg, 88%, R_f=0.80). **14**: Found: *m/z* 268.1227. Calcd for $C_{21}H_{16}$: *m/z* 268.1251. Mass *m/z* (rel intensity): 268 (14), 178 (100), 151 (7). UV (EtOH) 212 nm (sh, log ε, 4.45). IR (neat): 3030, 2980, 1460 cm^{-1}. NMR ($CDCl_3$) δ=2.76 (m, H_a), 3.10 (m, H_b), 4.19 (s, H_c), 4.35 (d, H_d), 5.54 (bs, H_e, H_f), 6.02 (d, H_g), 6.28 (d, H_h), 7.0—7.3 (m, 8H, Ph). Coupling constants in Hz: J_{ab}=4, J_{ad}=3, J_{gh}=3.

The authors are indebted to Professor Tadashi Sasaki of Nagoya University for his fruitful suggestions. This work was supported by a Scientific Research Grant from the Ministry of Education, Science, and Culture.

References

1) a) W. M. Jones and C. L. Ennis, *J. Am. Chem. Soc.*, **89**, 3069 (1967); b) T. Mukai, T. Nakazawa, and K. Isobe, *Tetrahedron Lett.*, **1968**, 565.

2) W. M. Jones, B. N. Hammon, R. C. Joines, and C. L. Ennis, *Tetrahedron Lett.*, **1969**, 3909; W. M. Jones and C. L. Ennis, *J. Am. Chem. Soc.*, **91**, 6391 (1969); T. Mitsuhashi and W. M. Jones, *J. Chem. Soc., Chem. Commun.*, **1974**, 103; W. M. Jones, R. A. Labar, U. H. Brinker, and P. H. Gebert, *J. Am. Chem. Soc.*, **99**, 6379 (1977).

3) K. G. Untch, G. Mattheus, and T. Hylton, International Symposium on the Chemistry of Non-Benzenoid Aromatic Compounds, Sendai, Japan, 1970; C. Mayor and W. M. Jones, *Tetrahedron Lett.*, **1977**, 3855; K. Saito, Y. Omura, and T. Mukai, *Chem. Lett.*, **1980**, 349.

4) W. E. Parham and C. D. Wright, *J. Org. Chem.*, **22**, 1473 (1957); B. B. Corson, W. J. Heintzelman, H. Moe, and C. R. Rousseau, *ibid.*, **27**, 1636 (1962).

5) a) C. H. Jutz, I. Rommel, I. Lengyel, and J. Feeney, *Tetrahedron*, **22**, 1809 (1966); b) A. S. Kende, *Tetrahedron Lett.*, **1967**, 2661; c) T. Toda, K. Saito, and T. Mukai, *ibid.*, **1972**, 1981; d) T. Sasaki, K. Kanematsu, H. Hayakawa, and M. Sugiura, *J. Am. Chem. Soc.*, **97**, 355 (1975).

6) a) W. von E. Doering and D. W. Wiley, *Tetrahedron*, **11**, 183 (1960); b) T. Nozoe, T. Mukai, K. Osaka, and N. Shishido, *Bull. Chem. Soc. Jpn.*, **34**, 1384 (1961); c) Y. Kitahara, K. Doi, and T. Kato, *ibid.*, **37**, 1747 (1964); d) T. Toda, K. Saito, and T. Mukai, *ibid.*, **52**, 151 (1979).

7) a) R. Srinivasan, *J. Am. Chem. Soc.*, **84**, 3432 (1962); b) L. B. Jones and V. K. Jones, *ibid.*, **89**, 1880 (1967); c) K. Saito, T. Toda, and T. Mukai, *Bull. Chem. Soc. Jpn.*, **47**, 331 (1974).

8) G. Vincow, H. D. Dauben, Jr., F. R. Hunter, and W. V. Volland, *J. Am. Chem. Soc.*, **91**, 2823 (1969); K. Okamoto, K. Komatsu, O. Murai, O. Sakaguchi, and Y. Matsui, *Bull. Chem. Soc. Jpn.*, **46**, 1785 (1973); M. Pomerantz, G. L. Combs, Jr., and R. Fink, *J. Org. Chem.*, **45**, 143 (1980).

9) E. Ciganeck, *J. Am. Chem. Soc.*, **87**, 1149 (1965); R. Hoffmann, *Tetrahedron Lett.*, **1970**, 2907, and the thesis cited therein.

10) T. Toda, K. Saito, and T. Mukai, *Chem. Lett.*, **1973**, 1123.

11) R. B. Woodward and R. Hoffmann, *Angew. Chem., Int. Ed. Engl.*, **8**, 781 (1969).

12) M. Oda, N. Fukazawa, and Y. Kitahara, *Tetrahedron Lett.*, **1977**, 3277; K. Saito, Y. Omura, E. Maekawa, and P. G. Gassman, *ibid.*, **25**, 2573 (1984).

13) M. Oda, Y. Ito, and Y. Kitahara, *Tetrahedron Lett.*,

† 1 Torr ≈ 133.322 Pa.

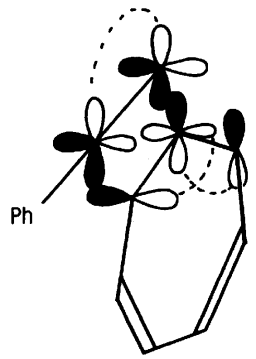

Fig. 8.

1975, 2587.

14) It is known that ketenes proceed [2+2]-type concerted addition reactions under thermal conditions, in which ketenes actually react as 4π components, forming thermally allowed [π4s+π2s] addition process.[15] The pathway A for the reaction of **3c** with **10** may be considered to be actually a thermally allowed [π4s+π2s] addition process, in which **3c** plays as a 4π component in the seemingly [2+2] type addition reaction as shown in Fig. 8.

15) V. J. Brady, *Synthesis*, **1971**, 415, and the thesis cited therein.

Chemoselective Reduction of Phenyl Ketones with Amino Alcohol-Borane Complexes

Shinichi ITSUNO,* Takashi WAKASUGI, Koichi ITO, Akira HIRAO,† and Seiichi NAKAHAMA†
School of Materials Science, Toyohashi University of Technology, Tempaku-cho, Toyohashi 440
†*Department of Polymer Science, Tokyo Institute of Technology, Ohokayama, Meguro-ku, Tokyo 152*
(Received December 6, 1984)

A new reducing agent was prepared from borane and amino alcohols. The reagent is very effective for chemoselective reduction of ketones in the presence of esters, oxime ethers, tertiary amides, nitriles, halides, and acyl chlorides. The polymeric reagent prepared from borane and polymer-supported amino alcohol was also prepared easily. Aldehydes are highly selectively reduced to primary alcohols in the presence of ketone with the polymeric reagent. Simple filtration separated cleanly the unchanged ketone from the polymeric reagent which gave, after hydrolysis, only primary alcohol as the product. The polymeric reagent was regenerated by treatment with borane and could be reused.

Borane reagents such as diborane, borane-tetrahydrofuran (THF), borane-dimethyl sulfide, alkylboranes, and amine-boranes are known to be effective reducing agents for a number of organic compounds.[1] Many attempts for the chemoselective reductions have been made using borane and its derivatives to get significant selectivities.[2-6] In previous papers,[7-9] we have shown that the borane complexes with chiral amino alcohols reduced prochiral ketones highly enantioselectively to give optically active alcohols with quantitative yields. In order to apply these novel borane-amino alcohol complexes to chemoselective reductions their reducing properties were investigated. Indeed a high chemoselectivity was realized in the reduction of ketones in the presence of many other functional groups by use of the reducing agents, easily prepared from commercially available amino alcohols and borane in THF. Polymer-supported amino alcohol-borane complexes were also examined to show an excellent selectivity in the reduction of aldehyde in the presence of ketone. Easy separation of the polymer-supported species from unreacted species present in the reaction mixture was performed by simple filtration. Easy recovery of the polymer-supported amino alcohol makes it possible to regenerate and reuse the reagent.

Results and Discussion

In the first place, the reducing agent prepared from 2-aminoethanol and borane was used to investigate its reducing properties. The molar ratio of borane to the amino alcohol affected the reactivity of the complex in the reduction of ketones. Acetophenone was reduced rapidly by the reagent prepared from 2:1 ratio of borane and 2-aminoethanol, whereas the reagent from 1:1 reacted slowly under the experimental conditions. Isopropylamine-borane and ethoxyborane did not also show so high reactivity. Surprisingly, the rate of ketone reduction by the reagent from 2:1 of borane and the amino alcohol was faster than borane itself as shown in Fig. 1. After treatment of 2-aminoethanol with two equimolar borane in THF, the excess of borane and solvent was evaporated off to give a white pasty solid which could also reduce acetophenone as rapidly as the non-evaporated reagent. In order to avoid the reduction by free borane, this highly-reactive, evaporated 2:1 complex was used for the selected organic compounds containing various functional groups. Results are summarized in Table 1. Carbonyl groups of aldehydes and ketones are rapidly and quantitatively reduced at room temperature in THF to give the primary and secondary alcohols, respectively. Epoxide ring of styrene oxide was cleaved with the complex at the more substituted position (anti-Markovnikov opening as a consequence of electrophilic attack). This high regioselectivity is the same as found for the conventional borane reduction. Unlike the ketone reductions, hydroboration of styrene with this complex was not so fast as with borane itself. The

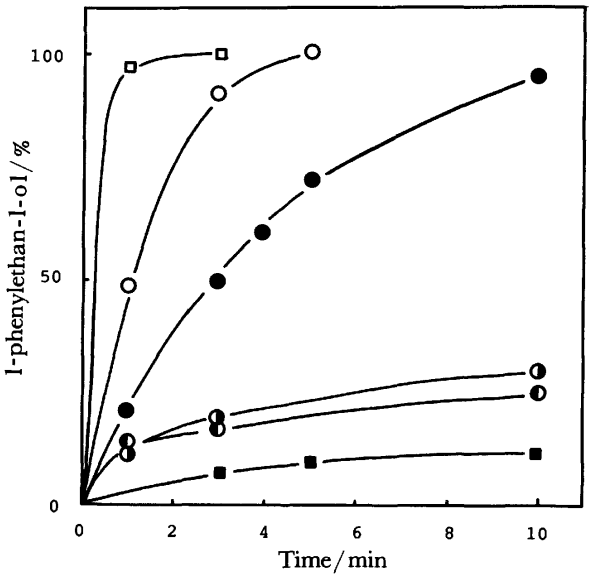

Fig. 1. Time-Conversion Curves for the Reduction of Acetophenone with Amino Alcohol-Borane Complexes.
□: 2-Aminoethanol-borane (1:2) complex; [2-aminoethanol]:[borane]:[acetophenone]=1:2:1, ○: [borane]:[acetophenone]=2:1, ●: [borane]:[acetophenone]=1:1, ■: 2-Aminoethanol-borane (1:1) complex; [2-aminoethanol]:[borane]:[acetophenone]=1:1:1, ◑: ethoxyborane; [ethanol]:[borane]:[acetophenone]=1:1:1, ◐: isopropylamine-borane; [isopropylamine]:[borane]:[acetophenone]=1:1:1.

Table 1. Reactivity of the reagent prepared from 2-aminoethanol and borane in THF at 30 °C

Substrate	Product	Reaction time[a]/h
$C_6H_5-\overset{O}{\overset{\|\|}{C}}-H$	$C_6H_5-CH_2OH$	1 min
$C_6H_5-\overset{O}{\overset{\|\|}{C}}-CH_3$	$C_6H_5-\overset{OH}{\overset{\|}{C}}H-CH_3$	5 min
$C_6H_5CH\overset{O}{\diagup\diagdown}CH_2$	$C_6H_5CH_2CH_2OH$	2
$C_6H_5-CH=CH_2$	$C_6H_5CH_2CH_2OH + C_6H_5-\overset{OH}{\overset{\|}{C}}H-CH_3$	3
$C_6H_5-\overset{N-OCH_2C_6H_5}{\overset{\|\|}{C}}-CH_3$	$C_6H_5-\overset{NH_2}{\overset{\|}{C}}H-CH_3$	20
$C_6H_5-\overset{O}{\overset{\|\|}{C}}N(CH_3)_2$	$C_6H_5CH_2N(CH_3)_2$	48
$C_6H_5-\overset{O}{\overset{\|\|}{C}}OH$	Unreactive	—
C_6H_5-CN	Unreactive	—
$C_6H_5CH_2Cl$	Unreactive	—
$C_6H_5-\overset{O}{\overset{\|\|}{C}}Cl$	Unreactive	—

a) Reaction time required for quantitative reduction.

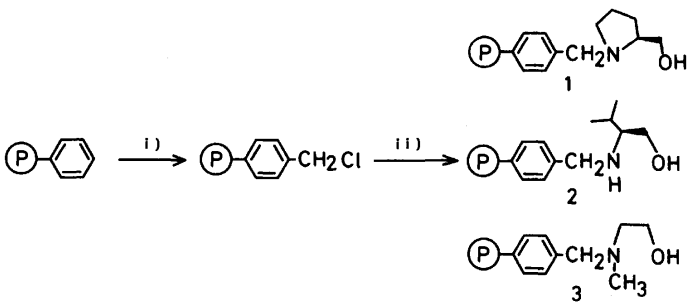

Scheme. Reagents: i) CH_3OCH_2Cl, $SnCl_4$; ii) amino alcohol, K_2CO_3, toluene.

regioselectivity was the same as borane, producing mainly 2-phenylethanol after oxidative treatment with alkaline hydrogen peroxide. The reduction of oxime ethers and tertiary amides proceeded slowly and smoothly to give the corresponding primary and tertiary amine respectively. Although this complex reacts with carboxylic acid to generate hydrogen, reduction did not occur under the experimental conditions. The use of more than two fold excess of the reagent allowed to reduce carboxylic acid to primary alcohol in good yield. It was observed that ester, nitrile, chloride, and acyl chloride are all inert toward the reagent. H. C. Brown *et al.*[10] already reported that the reactivity of borane with various functional groups decreases in the order; carboxylic acids>olefins>ketones>nitriles>epoxides>esters>acyl chlorides. Therefore, the amino alcohol-borane complex is quite different in the order of reactivity.

In view of the considerable attention focused in recent years on the use of polymer-supports to modify the reactivity and selectivity of various reagents,[11] we prepared polymer-supported amino alcohols (Scheme) which were treated with borane to give polymeric reducing agents. Polymer-supported amino alcohol-borane complex could also reduce ketones. Heterogeneous reactions by the use of cross-linked poly(styrene-divinylbenzene) copolymer as a polymer-support took place more slowly than those with the corresponding monomeric reagents. Complete reduction of acetophenone with a 2% cross-linked polymer-supported reagent required 50 h. The higher the degree of cross-linking, the slower is the reaction rate.

Chemoselective Reduction. By taking advantage of a high reactivity of this complex toward ketones, chemoselective reduction of ketones in the presence of ester was examined in THF at room temperature. 2-Aminoethanol-borane complex reduced acetophenone exclusively to give 1-phenylethanol within 30 min. No reduction of ethyl benzoate occured under these conditions. After usual work-up GLPC analysis showed only

Table 2. Chemoselective reduction of 1 : 1 molar mixture of acetophenone and ethyl benzoate with amino alcohol–borane complex in THF

Run	Amino alcohol	Reaction time/h	Product distribution[a]/%			
			$PhCCH_3$ (O)	$PhCHCH_3$ (OH)	$PhCOEt$ (O)	$PhCH_2OH$
1	$H_2NCH_2CH_2OH$	0.5	0	100	100	0
2[b]	**2**	2.4	0	100	100	0
3[c]	**1**	55	0	100	100	0

a) Determined by GLPC. b)Ⓟ: 2% cross-linked polystyrene resin. Degree of ring substitution is 61%. c) P: 1% cross-linked polystyrene resin. Degree of ring substitution is 60%.

Table 3. Chemoselective reduction of 1 : 1 molar mixture of acetophenone and oxime ether with amino alcohol–borane complex

Amino alcohol	Reaction time/h	Product distribution/%			
		$PhCCH_3$ (O)	$PhCHCH_3$ (OH)	$PhCCH_3$ (N-OBz)	$PhCHCH_3$ (NH_2)
$H_2NCH_2CH_2OH$	0.5	0	100	100	0
1[a]	50	0	100	100	0

a)Ⓟ: 2% Cross-linked polystyrene resin. Degree of ring substitution is 67%.

Table 4. Chemoselective reduction of 1 : 1 molar mixture of acetophenone and N,N-dimethylbenzamide with amino alcohol–borane complex

Amino alcohol	Reaction time/h	Product distribution/%			
		$PhCCH_3$ (O)	$PhCHCH_3$ (OH)	$PhCNMe_2$ (O)	$PhCH_2NMe_2$
$H_2NCH_2CH_2OH$	0.5	20	80	83	17
1[a]	50	0	100	100	0

a)Ⓟ: 2% Cross-linked polystyrene resin. Degree of ring substitution is 67%.

two peaks of unreacted ethyl benzoate and 1-phenylethanol (Table 2). Polymer-supported amino alcohol–borane complexes (run 2,3) also gave the same result. As we expected from our previous results[12] the polymer-supported complex containing tertiary amine such as **1** required a longer reaction time to attain a quantitative reduction of ketone than the complex of secondary amine **2**. In addition to the successful chemoselective reduction, polymer-supported complex could be advantageously used to separate the reacted ketones from the unreactive esters by simple filtration. In other words, the ketone was selectively taken out of the mixture containing esters. This useful separation was realized only when the polymer-supported complex was used. We also examined the selective reduction of keto esters. Methyl acetoacetate and methyl benzoylformate were reduced chemoselectively to give only hydroxy esters. No diols were detected by ^{1}H-NMR or GLPC. Similarly, the inertness of organic halides toward the reagent allows the selective reduction of ketones in the presence of halo groups. Thus, chloroacetophenone and bromoacetophenone were selectively reduced to halohydrins which could be transformed to the synthetically useful epoxides. In the mixture of acetophenone and its oxime ether 2-aminoethanol–borane or polymer-supported complex reduced the ketone selectively (Table 3). Although a clear discrimination between acetophenone and *N*,*N*-dimethylbenzamide was difficult by 2-aminoethanol–borane complex because of its powerful reducing ability, polymer-supported complex from **1** and borane could reduce only acetophenone in the presence of *N*,*N*-dimethylbenzamide in 50 h (Table 4). The chemoselective reduction of aldehydes to primary alcohols in the presence of ketones was then examined with the complex. The chemoselectivity in the competitive reductions of benzaldehyde and acetophenone with several amino alcohol–borane complexes is illustrated in Table 5. In the case of the soluble amino alcohol–borane complexes (run 1, 2), its powerful reducing ability to the ketone carbonyl groups could not discriminate between aldehyde and ketone. On the other hand, the polymer-supported reagents could clearly discriminate between them. Degree of cross-linking of the polymer-support affects not only chemoselectivity but also reaction rate. Both reactivity and selectivity increased with decreasing degree of cross-linking (run 3—5). Separation of the aldehyde, reacted with polymer-supported complex, from the unreacted ketone was performed easily also in this case by simple filtration. Benzyl alcohol was obtained quantitatively after hydrolysis. The recovered polymer-supported amino alcohol could be reused for the reduction after the treatment with borane. In conclusion, the present study confirms the versatility of

Table 5. Chemoselective reduction of 1:1 molar mixture of benzaldehyde and acetophenone with amino alcohol–borane complex

Run	Amino alcohol	Degree of cross-linking/%	Degree of ring substitution/%	Reaction time/h	Product distribution/%			
					$PhCH\overset{O}{\overset{\|\|}{}}$	: $PhCH_2OH$	: $PhC\overset{O}{\overset{\|\|}{C}}H_3$	: $PhCH\overset{OH}{\overset{\|}{C}}H_3$
1	$H_2NCH_2CH_2OH$	—	—	0.5	0	100	0	100
2	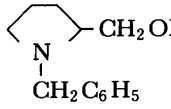	—	—	0.5	0	100	0	100
3	**1**	1	61	1	0	100	100	0
4	**1**	2	43	3	2	98	98	2
5	**1**	5	48	20	20	80	80	20
6	**2**	1	60	1	0	100	100	0
7	**3**	2	54	3.5	0	100	100	0
8	**3**	2	54	5	0	100	80	20

the reagent has the unique reducing properties different from borane itself and the other hydrides. The complex showed an exceptionally powerful reducing ability toward the ketone carbonyl groups. This enabled the chemoselective reduction of ketone in the presence of other functional compounds such as esters, oximes, amides, nitriles; and halides. Its relatively easy availability should make this complex valuable for a variety of selective reductions. Furthermore, water-soluble amino alcohol made separation and isolation of organic products easy. Polymer-supported amino alcohol–borane complex also reduced ketones selectively. Aldehydes were distinguishable from ketones only when the polymer-supported complex was used as reducing agent. In addition to this highly chemoselective property, there are several advantages that polymer-supported complex makes the separation of the reacted substrate from the unreacted one easy by simple filtration and that it was easily recovered and reused.

Experimental

General. GLPC analyses were performed on a Yanaco G180 instrument with a stainless steel analytical column (3 m×3 mm) packed with PEG 20 M on Diasolid L. The products distributions were determined by their peak areas. ^{1}H-NMR spectra were measured on a JEOL JNM-PMX60 (60 MHz) spectrometer. IR spectra were measured on a JASCO A-3 instrument for nujol mulls. TLC was run on silica gel 60 F-254 pre-coated plates with chloroform as the mobile phase.

Materials. All reactions were carried out under an atmosphere of nitrogen. Tetrahydrofuran (THF) was heated under reflux over sodium metal and distilled from lithium aluminium hydride in a nitrogen atmosphere. Benzaldehyde, acetophenone, styrene oxide, ethyl benzoate, benzonitrile, benzyl chloride, methyl acetoacetate, methyl benzoylformate, and *N,N*-dimethylbenzamide were dried and distilled over calcium hydride. Benzoyl chloride, 2-aminoethanol, and 2-(methylamino)ethanol were purified by fractional distillation. α-Chloroacetophenone and α-bromoacetophenone were recrystallized from carbon tetrachloride and methanol, respectively. Acetophenone oxime O-benzyl ether was prepared by the methods of French and Harrison[13] and Karabatsos and Hsi[14] and purified by fractional distillation. Bp 145 °C/667 Pa. ^{1}H-NMR($CDCl_3$) δ=2.16 (3H, s), 5.16 (2H, s), 7.00—7.80 (10H, m). Borane–THF was prepared by the reaction of sodium borohydride with boron trifluoride–diethyl ether complex according to the procedure of Brown.[15] Ethoxyborane was prepared by the reaction of borane–THF with 1 equiv of ethanol. Isopropylamine–borane was prepared by the reaction of borane–THF with 1 equiv of isopropylamine. The purities of all reagents were checked by GLPC and ^{1}H-NMR spectroscopy. All materials described were stored under a nitrogen atmosphere prior to use. (*S*)-*N*-Benzylprolinol was prepared by the reaction of (*S*)-prolinol, which was obtained by the reaction of (*S*)-proline with $LiAlH_4$ in refluxing THF, with benzyl chloride in the presence of K_2CO_3 in refluxing toluene according to the method developed by Govindachari *et al.*[16] Bp 90—92 °C/27 Pa. $[\alpha]_D^{25}$ −59.9 °(*c* 1.0, $CHCl_3$). Polymer-supported (*S*)-prolinol (**1**) was prepared from 1,2, or 5% cross-linked chloromethylated polystyrene resin and (*S*)-prolinol according to the method previously reported.[12,17] Polymer-supported (*S*)-valinol (**2**) and polymer-supported 2-(methylamino)ethanol (**3**) were similarly prepared from chloromethylated polystyrene resin and (*S*)-valinol or 2-(aminomethyl)ethanol, respectively. The degree of ring substitution of polymer-supported amino alcohols is 40—70%.

Reduction of Acetophenone with the Reagent Prepared from 2-Aminoethanol and Borane in THF. To a solution of 2-aminoethanol (3 ml, 5 mmol) in dry THF was added borane–THF (5 ml, 10 mmol), initially at −78 °C and the mixture was warmed and kept at 30 °C overnight, followed by evaporation of the unchanged borane under reduced pressure (13 Pa) for 5 h. The reagent thus formed was allowed to desolve in THF (10 ml) under nitrogen. To this solution was added acetophenone (0.6 g, 5 mmol) with stirring, and the resulting mixture was stirred for 30 min at room temperature. After hydrolysis with 1 M† HCl, ether extract was washed with water, and then analyzed by GLPC (100% conversion). The crude product was distilled by bulb-to-bulb distillation to give 1-phenylethanol (0.56 g, 92% of isolated materials); it was characterized by IR and ^{1}H-NMR spectroscopies. Other

† 1 M=1 mol dm^{-3}.

substrates were reduced and analyzed by a similar procedure.

Chemoselective Reduction of Acetophenone in the Presence of Ethyl Benzoate. To a solution of the reagent prepared from aminoalcohol (5 mmol) and borane (10 mmol) in THF was added a mixture of acetophenone (0.6 g, 5 mmol) and ethyl benzoate (0.72 ml, 5 mmol) at 30 °C. After 30 min the reaction mixture was quenched with 1 M HCl. The ether extract of the organic layer was washed with water, and then analyzed by GLPC and ^{1}H-NMR which indicated the mixture to contain only 1-phenylethanol and unreacted ethyl benzoate.

Chemoselective Reduction of Acetophenone in the Presence of Benzonitrile. To a solution of the reagent prepared from 2-aminoethanol (5 mmol) and borane (10 mmol) in THF was added a mixture of acetophenone (0.6 g, 5 mmol) and benzonitrile (0.51 ml, 5 mmol) at 30 °C. After 30 min the reaction mixture was quenched with 1M HCl. The ether extract of the organic layer was washed with water, and then analyzed by GLPC and ^{1}H-NMR which indicated the mixture to contain only 1-phenylethanol and unreacted benzonitrile.

Chemoselective Reduction of Acetophenone in the Presence of Benzyl Chloride. To a solution of the reagent prepared from 2-aminoethanol (5 mmol) and borane (10 mmol) in THF was added a mixture of acetophenone (0.6 g, 5 mmol) and benzyl chloride (0.58 ml, 5 mmol) at 30 °C. After 30 min the reaction mixture was quenched with 1 M HCl. The ether extract of the organic layer was washed with water, and then analyzed by GLPC and ^{1}H-NMR which indicated the mixture to contain only 1-phenylethanol and unreacted benzyl chloride.

Chemoselective Reduction of Acetophenone in the Presence of Benzoyl Chloride. To a solution of the reagent prepared from 2-aminoethanol (5 mmol) and borane (10 mmol) in THF was added a mixture of acetophenone (0.6 g, 5 mmol) and benzoyl chloride (0.58 ml, 5 mmol) at 30 °C. After 30 min no acetophenone was detected by TLC (R_f=0.46) and benzoyl chloride was confirmed to remain by TLC (R_f=0.80). The reaction mixture was then hydrolyzed with 1 M HCl. The ether extract of organic layer was shaken with 1 M NaOH, washed with water, and then analyzed by GLPC which indicated 1-phenylethanol.

Chemoselective Reduction of α-Chloroacetophenone to Styrenechlorohydrin. To a solution of the reagent prepared from 2-aminoethanol (5 mmol) and borane (10 mmol) in THF was added α-chloroacetophenone (0.77 g, 5 mmol) in THF (5 ml) at 30 °C. After 30 min the reaction mixture was quenched with 1 M HCl. The ether extract of the organic layer was washed with water, dried ($MgSO_4$), and distilled (bulb-to-bulb) to give 2-chloro-1-phenylethan-1-ol (0.7 g, 90% of isolated material), it was characterized by ^{1}H-NMR spectroscopy. ^{1}H-NMR($CDCl_3$) δ=3.53 (2H, d), 4.40 (1H, s), 4.75 (1H, t), 7.18 (5H, m).

α-Bromoacetophenone was reduced to styrenebromohydrin in 88% yield by a similar procedure mentioned above.

Chemoselective Reduction of Methyl Acetoacetate to Methyl 3-Hydroxybutyrate. Methyl acetoacetate was converted to methyl 3-hydroxybutyrate (92% yield) by a similar procedure as mentioned above. It was characterized by ^{1}H-NMR spectroscopy. ^{1}H-NMR ($CDCl_3$) δ=1.24 (3H, d), 2.46 (2H, d), 3.70 (3H, s), 4.20 (1H, s).

Methyl benzoylformate was also converted to methyl mandelate in 85% yield, which was characterized by ^{1}H-NMR spectroscopy.

Chemoselective Reduction of Benzaldehyde in the Presence of Acetophenone with Polymer-supported Reagent. Polymer-supported reagent was prepared from polymer-bound (*S*)-prolinol (1% cross-linking, 60.8% ring substitution, 3.67 mmol/g, 2.72 g, 10 mmol) and borane (20 mmol) by the same method as monomeric one. To a THF suspension of the reagent was added a mixture of benzaldehyde (5 mmol) and acetophenone (5 mmol) at 30 °C. Reaction was checked by TLC. After 1 h the suspension was filtered carefully under a nitrogen atmosphere. Obtained polymer was hydrolyzed with 1 M HCl to give benzylalcohol alone, determined by GLPC and ^{1}H-NMR analyses. From the filtrate unreduced acetophenone was completely recovered.

References

1) A. Hajos, "Complex Hydrides and Related Reducing Agents in Organic Synthesis," Elsevier Scientific Publishing Company, Amsterdam, Oxford, New York (1979), pp. 24—35.

2) E. R. H. Walker, *Chem. Soc. Rev.*, **5**, 23 (1976).

3) J. H. Babler and S. J. Sarussi, *J. Org. Chem.*, **48**, 4416 (1983).

4) G. C. Andrews and T. C. Crawford, *Tetrahedron Lett.*, **21**, 693 (1980).

5) G. C. Andrews, *Tetrahedron Lett.*, **21**, 697 (1980).

6) S. Kim, H. J. Kang, and S. Yang, *Tetrahedron Lett.*, **25**, 2985 (1984).

7) S. Itsuno, A. Hirao, S. Nakahama, and N. Yamazaki, *J. Chem. Soc., Perkin Trans. 1*, **21**, 1697 (1983).

8) S. Itsuno, K. Ito, A. Hirao, and S. Nakahama, *J. Chem. Soc., Chem. Commun.*, **1983**, 469.

9) S. Itsuno, K. Ito, A. Hirao, and S. Nakahama, *J. Org. Chem.*, **49**, 555 (1984).

10) H. C. Brown and W. Korytnyk, *J. Am. Chem. Soc.*, **82**, 3866 (1960).

11) A. MacKillop and D. W. Young, *Synthesis*, **1979**, 401, 481.

12) S. Itsuno, K. Ito, A. Hirao, and S. Nakahama, *J. Chem. Soc., Perkin Trans. 1*, in the press.

13) C. M. French and D. Harrison, *J. Chem. Soc.*, **1955**, 3513.

14) H. C. Karabatsos and N. Hsi, *Tetrahedron*, **23**, 1079 (1967).

15) H. C. Brown, "Organic Syntheses *via* Boranes," John Wiley and Sons, New York (1975).

16) T. R. Govindachari, T. G. Rajagopalan, and N. Viswanathan, *J. Chem. Soc., Perkin Trans. 1*, **1974**, 1161.

17) S. Itsuno, A. Hirao, S. Nakahama, and N. Yamazaki, *Makromol. Chem., Rapid Commun.*, **3**, 673 (1982).

Conformational Aspect of Indazole Adenine Dinucleotides in Aqueous Solution

Shuichi TONO-OKA,* Ichiro AZUMA, and Isao SEKIKAWA
Section of Chemistry, Institute of Immunological Science, Hokkaido University, Kita-ku, Sapporo 060
(Received December 18, 1984)

Conformational properties of various title compounds in aqueous solution were examined with the aid of 500 MHz ^{1}H-NMR spectroscopy. In particular, the signals of aromatic protons on both the indazole and adenine rings were shifted to higher fields without exception, compared with the corresponding signals in indazole and adenine mononucleotides. These observations, which can be explained as resulting from diamagnetic shielding effect of the indazole and adenine rings, indicate that the base pairs in the dinucleotides are closely stacked in parallel planes. On the other hand, the average conformation of riboses were deduced from $J_{1',2'}$-values as a proportion of $N \rightleftharpoons S$ equilibrium composition. Indazole riboses showed a roughly 50/50 equilibrium, whereas adenine riboses showed a small preference for the *N*-type conformer. Such a conformational state may be indispensable for taking up the strongly folded conformation between the base pairs in the dinucleotides, as judged by a somewhat favored *S*-type conformation of both riboses in the indazole- and adenine mononucleotides.

In studies of nucleoside and nucleotide compounds, the conformational analysis of the furanose rings is an important subject, because the difference in conformation of the compounds influences the biological activity. For that reason, nucleic acid-ribonucleosides components (adenosine, cytidine, uridine, *etc.*)[1,2] and some related compounds (alkylated, halogenated, aza, deaza analogs, *etc.*)[3-5] have been examined for molecular conformation with the aid of NMR spectroscopy. On the other hand, the stereochemistry in aqueous solution of pyridine dinucleotides has so far been studied in connection with coenzyme function. The conformational properties of two riboses, as well as the relative conformations of both the pyridine and adenine bases, were investigated with NAD and its alkylated analogs or the like.[6-9] Recently we have reported the synthesis and biochemical activity of some novel 2*H*-indazole dinucleotides.[10] The indazole dinucleotides, which contain a bicyclic base instead of pyridine one, are expected to adopt a different conformation in comparison with that of pyridine dinucleotides. This paper describes the conformational aspects of the indazole nucleotides in aqueous solution, comparing them with those of pyridine nucleotides, on the basis of the information obtained by high-frequency ^{1}H-NMR spectroscopy.

Experimental

Materials. The indazole adenine dinucleotides, indazole mononucleotides, and adenine mononucleotide (AMP) used for this study were prepared by an enzymic method in our laboratory.[10] Deuterium oxide (D_2O, 99.8%) and sodium 3-trimethylsilyl-1-propanesulfonate (DSS) were obtained from E. Merck, Darmstadt.

NMR Spectroscopy. ^{1}H-NMR measurements were performed in D_2O (pH 7) at a *ca.* 0.01 M (1 M=1 mol dm^{-3}) concentration of each sample, which was once lyophilized beforehand from D_2O, on a 500 MHz JEOL FX-500 spectrometer operating in a pulse Fourier-transform mode with quadrature detection. All spectra were obtained from accumulation of 64—128 free induction decays after each 45° pulse (5 μs) repeated every 4 s and were observed over a range of 5×10^3 Hz, corresponding to 32 K data points. Chemical shifts (δ-values) were measured in parts per million (ppm) downfield from DSS as an internal standard and estimated with an accuracy within ±0.001 ppm. Coupling constants were determined as an average value based on two measurements under the same conditions, and the precision was ±0.2 Hz. The residual HDO signal was suppressed by the gated decoupling method.[11]

Results and Discussion

Conformation between Indazole and Adenine Bases. NMR studies by Sarma *et al.*[7,8] have strongly indicated that both the oxidized and reduced pyridine dinucleotides exist in a folded conformation, in which the pyridine and adenine rings are stacked in parallel planes, rather than in an unfolded conformation. This conclusion has been derived from interpretation based on the following NMR spectral observations: All aromatic protons on both the pyridine and adenine rings, and anomeric protons are shifted to higher fields as compared with those in the NAD-constituting nicotinamide mononucleotide (NMN) and adenine

Table 1. Chemical shift difference (Δδ) of adenine protons between indazole adenine dinucleotide and AMP[a]

Entry	R^1/R^2	Δδ/ppm[b] Adenine		
		H_2	H_8	$C_1'H$
1	H/H	0.267	0.264	0.133
2	NH_2/H	0.291	0.407	0.188
3	H/NH_2	0.262	0.344	0.216
4	NHAc/H	0.335	0.390	0.150
5	H/NHAc	0.341	0.444	0.148
6	OH/H	0.277	0.431	0.179
7	H/OH	0.259	0.380	0.201
8	OCH_3/H	0.294	0.387	0.136
9	H/OCH_3	0.248	0.380	0.175
10	Cl/H	0.257	0.369	0.122
11	H/Cl	0.252	0.414	0.123

a) All spectra were measured in D_2O (pH 7) at a 0.01 M concn of each sample at 25°C. b) The precision was within ±0.001 ppm.

TABLE 2. CHEMICAL SHIFT DIFFERENCE ($\Delta\delta$) OF INDAZOLE PROTONS BETWEEN INDAZOLE DINUCLEOTIDE AND INDAZOLE MONONUCLEOTIDE[a]

Entry	$\Delta\delta$/ppm[b] Indazole					
	H_3	H_4	H_5	H_6	H_7	$C_1'H$
1	0.350	0.292	0.240	0.248	0.283	0.250
2	0.219	n.o.[c]	—	0.175	0.253	0.174
3	0.261	0.244	0.171	—	n.o.[c]	0.130
4	0.399	0.315	—	0.336	0.369	0.288
5	0.361	0.401	0.420	—	0.284	0.298
6	0.324	0.368	—	0.342	0.353	0.222
7	0.369	0.356	0.323	—	n.o.[c]	0.195
8	0.296	0.376	—	0.360	0.320	0.213
9	0.275	0.323	0.354	—	0.373	0.193
10	0.381	0.450	—	0.381	0.361	0.253
11	0.306	0.330	0.329	—	0.420	0.261

a,b) See the footnote in Table 1. c) The signals were not observed.[10]

mononucleotide (AMP). The upfield resonances in the dinucleotide could be explained as resulting from diamagnetic shielding due to the mutual "ring-current effect" of the pyridine and adenine bases. Thus, the base pairs were found to be stacked in parallel planes. In connection with these studies based on the difference in chemical shifts, Freyne *et al.*[9] have also investigated 3-acetyl-5-alkylpyridine analogs of NAD and shown the occurrence of significant intramolecular interaction between the base pairs.

Various 2*H*-indazole adenine dinucleotides (**1**—**11**) which we have recently prepared[10] were examined for their chemical shifts of aromatic protons at pH 7 by 500 MHz ^{1}H-NMR spectroscopy. The chemical shift difference ($\Delta\delta$) of adenine and anomeric protons between each indazole dinucleotide and AMP are summarized in Table 1. All the resonances of H_2 ($\Delta\delta$ 0.25—0.34), H_8 ($\Delta\delta$ 0.26—0.44), and $C_1'H$ ($\Delta\delta$ 0.12—0.22) were shifted to higher fields compared with those in AMP. As for NAD, $\Delta\delta$-values of H_2, H_8, and $C_1'H$ in the adenine moiety have been estimated to be 0.15, 0.14, and 0.13 ppm, respectively.[6] These values are less than in indazole dinucleotides. On the other hand, the $\Delta\delta$-values of indazole protons between each indazole dinucleotide and the corresponding mononucleotide were also evaluated by a third order approximation (Table 2). It is apparent that, in the dinucleotide, all the aromatic signals are shifted remarkably to higher fields ($\Delta\delta$ 0.17—0.45) as observed for adenine protons. Furthermore, the substituent *O*-methyl and *N*-acetyl protons showed a slight upfield shift ($\approx$0.10 and $\approx$ 0.02 ppm, respectively). Previously Jardetzky and Wade-Jardetzky[6] have reported the $\Delta\delta$-values of pyridine signals between NAD and NMN (Table 3). One can see from Tables 2 and 3 that $\Delta\delta$-values between the indazole nucleotides are, on the whole, greater than those between the pyridine nucleotides. Thus, it was found that, in the indazole dinucleotides, the indazole and adenine rings suffer more diamagnetic shielding effect of each other than the pyridine and adenine base pairs in NAD. The enhancement of the anisotropic effect

TABLE 3. CHEMICAL SHIFT DIFFERENCE ($\Delta\delta$) OF PYRIDINE PROTONS BETWEEN NAD AND NMN

Compd	$\Delta\delta$/ppm[a] Pyridine				
	H_2	H_4	H_5	H_6	$C_1'H$
NAD	0.286	0.198	0.105	0.213	0.070

a) Calculated from the chemical shifts previously reported by Jardetzky and Wade-Jardetzky.[6]

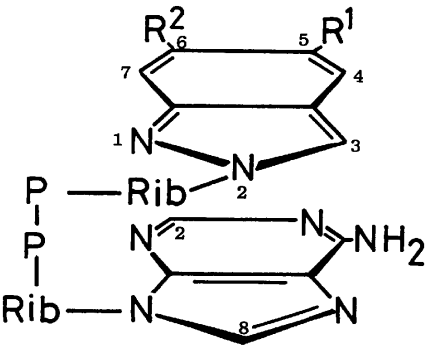

Fig. 1. Closely folded conformation for indazole dinucleotides.

seems to arise from the two-aromatic-ring system of indazole base, which may provide a wide shielding zone in the direction perpendicular to the ring plane.

These observations indicate that the base pairs in the indazole dinucleotide are more closely stacked in parallel planes as compared to those in the pyridine dinucleotide (Fig. 1).

Ribose Conformations. Altona and Sundaralingam[12] have introduced a comprehensible notation of furanose ring conformations based on the concept of pseudorotation: *N*-type conformers include the classical C(2')-*exo* and C(3')-*endo* conformations; *S*-type conformers include the classical C(2')-*endo* and C(3')-*exo* forms (Fig. 2). They have also shown that both conformers in dinucleotides as well as in mononucleotides in solution are present in a dynamic equilibrium. An equilibrium shift should bring about a change of average torsion angle between vicinal C–H bonds, and a coupling con-

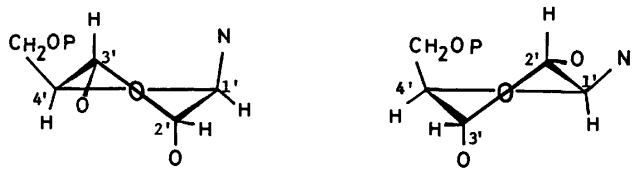

Type N Type S

Fig. 2. Perspective views of the *N*- and *S*-type ribose rings.[12]

Table 4. The $J_{1',2'}$-values of indazole dinucleotides and mononucleotides

Entry	$J_{1',2'}$/Hz[a]		
	Dinucleotide		Mononucleotide[b]
	Adenine	Indazole	Indazole
1	3.9	5.4	5.8
2	4.4	4.9	5.4
3	4.4	4.9	
4	4.4	4.4	
5	4.0	4.2	5.2
6	4.2	4.9	5.4
7	4.2	4.9	
8	4.2	5.1	
9	4.3	4.9	
10	4.3	4.9	5.3
11	4.4	4.9	

a) Average value of two measurements: the precision was ±0.2 Hz. b) Obtained from the dinucleotide of the corresponding entry number.

stant for the vicinal protons can be expressed in terms of the dihedral torsion angle.[13] From a Dreiding model, one can see that the adoption of either of *N*- and *S*-type conformers induces no significant change of the vicinal torsion angle between C_2'–H and C_3'–H bonds. Thus, a practical and simple equation was proposed to deduce the conformational aspect of a ribose ring from the vicinal coupling constant, $J_{1',2'}$ or $J_{3',4'}$: $S(\%)=10\times J_{1',2'}$ or $10\times(10.1-J_{3',4'})$.[12]

Even in the 500 MHz NMR spectra of indazole dinucleotides, the signals of an indazole C_3'H and adenine C_3'H were overlapped each other to such an extent that a reasonable estimate of each $J_{3',4'}$ is impossible. As to the anomeric protons, which appeared as two clearly separate doublets, the two $J_{1',2'}$'s could be accurately determined. We, therefore, use the value of $J_{1',2'}$ to estimate equilibrium compositions of *N*- and *S*-type conformers. $J_{1',2'}$-values observed with indazole nucleotides are summarized in Table 4. In the dinucleotides, all indazole riboses show a greater $J_{1',2'}$-value, compared with adenine riboses, by 0.3—1.5 Hz. Upon conversion of the dinucleotides into mononucleotides, the coupling constant came to increase by 0.3—1.0 Hz in the indazole ribose and by 1.3—2.0 Hz in the adenine ribose, indicating a small change in conformation of respective ribose rings. Concerning pyridine dinucleotides, it has previously been reported[9] that pyridine $J_{1',2'}$-values were less than adenine ones by ≈0.5 Hz.

Table 5. Equilibrium composition of *N*-type conformers in indazole nucleotides[a]

Entry	*N*-type conformation/%[b]		
	Dinucleotide		Mononucleotide[c]
	Adenine	Indazole	Indazole
1	61	47	42
2	56	51	46
3	56	51	
4	56	56	
5	60	58	48
6	58	51	46
7	58	51	
8	58	49	
9	57	51	
10	57	51	47
11	56	51	

a) Calculated from the equation of Altona and Sundaralingam:[12] $S(\%)=10\times J_{1',2'}$. b) $N(\%)=100-S(\%)$. c) See the footnote b in Table 4.

The percentages of *N*-type conformer (100—*S*%) in the indazole nucleotides were calculated by taking the aforementioned equation (Table 5). In the dinucleotides, the adenine ribose showed a small preference for the *N*-type conformer, whereas the indazole ribose was observed to exist in a roughly 50/50 equilibrium between both conformers with a few exceptions. In the indazole mononucleotides, a slightly increased proportion of *S*-type form occurs in all cases. In the AMP ribose ($J_{1',2'}$=6.0 Hz), the percentage of *N*-type form (40%) decreased in favor of *S*-type form (60%). Such difference in ribose conformation of the dinucleotides compared with the mononucleotides may be closely correlated with the folded conformation between the indazole and adenine base pairs. The conformational deviation of ribose rings are probably necessary for the occurrence of enhanced intramolecular interaction between the base pairs, which would contribute to the stable conformation with a lower energy level for the whole molecule.

In a part of the previous paper of Freyne *et al.*[9] regarding the ribose conformation in pyridine dinucleotides, the percentage of *S*-type conformers has been based on $J_{3',4'}$-value. However, the method using $J_{3',4'}$ should be restricted to the case where $J_{1',2'}+J_{3',4'}=10.1$.[12] In their report, $J_{1',2'}$'s and $J_{3',4'}$'s for the pyridine ribose have been estimated to be 5.2—5.4 and 2.4—2.8 Hz, respectively. The sum of the two terms (*ca.* 8 Hz) may be too little to fit the equation. It can, therefore, be said that the *S* percentages (more than 70%) they have estimated are much greater than those actually to be expected.

The authors wish to thank Mr. M. Ikura (High-Resolution NMR Laboratory, Faculty of Science) for skillful measurement of ^{1}H-NMR spectra.

References

1) E. Westhof, O. Röder, I. Croneiss, and H.-D. Lüdemann,

Z. Naturforsch., C, **30**, 131 (1975).
2) J. L. Alderfer, R. E. Loomis, and T. J. Zielinski, *Biochemistry*, **21**, 2738 (1982).
3) F. E. Evans and J. M. Wright, *Biochemistry*, **19**, 2113 (1980).
4) H.-D. Lüdemann, E. Westhof, and I. Cuno, *Z. Naturforsch., C*, **31**, 135 (1976).
5) L. S. Kan, D. M. Cheng, P. S. Miller, J. Yano, and P. O. P. Ts'o, *Biochemistry*, **19**, 2122 (1980).
6) O. Jardetzky and N. G. Wade-Jardetzky, *J. Biol. Chem.*, **241**, 85 (1966).
7) R. H. Sarma, V. Ross, and N. O. Kaplan, *Biochemistry*, **7**, 3052 (1968).
8) R. H. Sarma and N. O. Kaplan, *Biochemistry*, **9**, 557 (1970).
9) E. J. Freyne, E. L. Esmans, J. A. Lepoivre, and F. C. Alderweireldt, *J. Carbohyd. Nucleos. Nucleot.*, **8**, 481 (1981).
10) S. Tono-oka, Y. Tone, V. E. Marquez, D. A. Cooney, I. Sekikawa, and I. Azuma, *Bull. Chem. Soc. Jpn.*, **58**, 309 (1985).
11) D. I. Hoult and R. E. Richards, *Proc. R. Soc. London, Ser., A*, **344**, 311 (1975).
12) C. Altona and M. Sundaralingam, *J. Am. Chem. Soc.*, **95**, 2333 (1973).
13) M. Karplus, *J. Am. Chem. Soc.*, **85**, 2870 (1963).

An Improved Preparation of the *p*-Tropoquinone Mono- and Diacetals by Thallium(III) Nitrate Oxidation of 2-Alkoxy-5-hydroxytropones

Hitoshi TAKESHITA,* Akira MORI, and Yasutoshi ISAYAMA†
Research Institute of Industrial Science, 86, Kyushu University, Kasuga-koen, Kasuga, Fukuoka 816
†*Graduate School of Engineering Sciences, 39, Kyushu University, Kasuga-koen, Kasuga, Fukuoka 816*
(Received December 27, 1984)

The thallium(III) nitrate-oxidation of 2-alkoxy-5-hydroxytropones gave, in good yields, the mono- and diacetals of tropoquinones, which can be used for the introduction of oxygen functions to the seven-membered nucleus and preparation of the substituted tropoquinones. An improved synthesis of 4-methyl-*p*-tropoquinone or 4-methoxy-*p*-tropoquinone was accomplished.

We have previously synthesized a tropoquinone monoacetal, 7,7-ethylenedioxycyclohepta-2,5-diene-1,4-dione (**1**) by triethylamine-treatment and further manganese(IV) oxide oxidation of the endoperoxide of ethylenedioxytropone acetal (**2**) which can be prepared either by the dye-sensitized photooxidation of the corresponding tropone acetal (**3**) or by *p*-toluenesulfonic acid-catalyzed acetalization of the tropone endoperoxide (**4**).[1] Since **1** and its derivatives may behave as typical unsaturated ketones and are useful for the synthesis of various seven-membered derivatives, it is important and desirable to develop more effective routes to obtain the acetal derivatives.

The oxidation of 5-hydroxytropolone (**5**) with silver acetate,[2] which is a one-electron oxidizing agent, was already shown to form the derivatives of either *p*-tropoquinone (**6**) or 2,10-dihydroxydicyclohepta[*b*,*d*]-furan-3,9-dione (**7**) depending on the amounts of the oxidizing agent. Since the formation of **6** and **7** involved a common intermediate, the semiquinone radical, the yields of the derivatives of **7** should be improved by use of 5-hydroxy-2-methoxytropone (**8**) or its derivatives; unlike those from free 5-hydroxytropolones, the semiquinone radical derived from **8** is not convertible to **6**.[3] Taking these two points into account, it is predictable that the oxidation of **8** with an appropriate two-electron oxidizing agent in methanol may produce the acetal, 7,7-dimethoxy-2,5-cycloheptadiene-1,4-dione (**9**) but not **7**. Indeed, DDQ (2,3-dichloro-5,6-dicyano-*p*-benzoquinone) was effective for the purpose; as a preliminary study, we have employed it to obtain 4-methyl-*p*-tropoquinone (**10**).[4] Even more, thallium(III) nitrate (TTN)[5] seems to be a favorable choice, and **8** was accordingly oxidized in

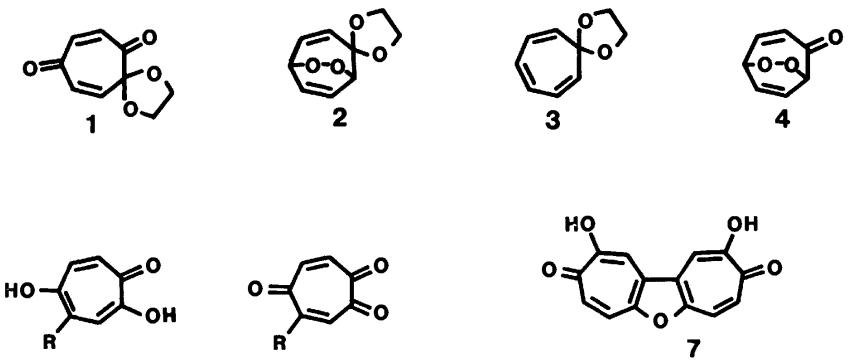

Chart 1.

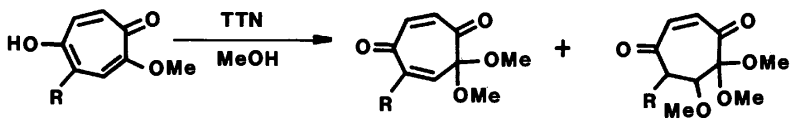

Scheme 1.

methanol at 15—25 °C for 4 h; the products obtained after brief work up were indeed **9**, a colorless oil, 90% yield, and its Michael type adduct, 5,5,6-trimethoxy-2-cycloheptene-1,4-dione (**11**), a colorless oil, 8% yield. On the other hand, prolonged treatment of **9** with TTN in methanol gave **11** in 77% yield. The position of the newly introduced methoxyl group was established by an aid of deuterio derivative of **8** (**8d**). Thus, heating of **8** in deuterium oxide yielded 5-hydroxy-2-methoxytropone-4-*d* (**8d**), whose ^{1}H NMR spectrum showed a disappearance of C-4 proton, δ=6.74.[6] The treatment of **8d** with TTN gave corresponding deuterio derivatives of **9** and **11** (**9d** and **11d**), 8% and 40% yields, respectively. The ^{1}H NMR spectrum of **11d** showed a diminishment of the signal at δ=2.87, together with change of splitting patterns of the proton signal (to d, J=4 Hz) at 3.95, ascribable to the proton on the carbon bearing the methoxyl group. Consequently, the position of the methoxyl group is C-6.

In parallel to this facile Michael reaction, the acetals smoothly underwent the Thiele-type addition reaction; *e.g.*, the brief treatment of **9** with a 1:1-mixture of acetic acid and acetic anhydride with a catalytic amount of sulfuric acid at 15—25 °C gave 4,5-diacetoxy-2-methoxytropone (**12**) in nearly quantitative yield.

The structure of **12** was obtained on the basis of the NMR spectral analysis as well as chemical derivations; thus, the further treatment of **12** with trifluoroacetic anhydride (TFAA) and acetic anhydride in acetic acid gave colorless crystalline triacetoxytropone (**13**). A mild hydrolysis of **12** with aqueous acetic acid afforded 2-acetoxy-5-hydroxy-4-methoxytropone (**14**) and 5-hydroxy-4-methoxytropolone (**15**), the latter of which was oxidized with DDQ to a derivative which must be 4-methoxy-*p*-tropoquinone (**16**): *i.e.*, the ^{1}H NMR spectrum of **16** revealed a 1H-singlet at δ=6.22, and a lack of the long-range coupling with other aromatic protons at 6.80 and 6.94, appearing as an AB pair (J=13 Hz), ruled out the possibility of the methoxyl group at C-3, whose singlet appeared at 3.90. Previously, the Thiele reaction of **6** itself was carried out by Hirama and Itô to form 2,4,7-triacetoxytropone in 7% yield by acetic anhydride and sulfuric acid;[7] the improvement of the yield of the present results was thus satisfactory and the site of the attack indicated the reaction should have been started by the protonation on the acetal oxygen.

Other than this, the attempted hydrolysis of **9** under modified conditions tends to cause a ring contraction to the benzenoid derivative; thus, the reaction of **9** or

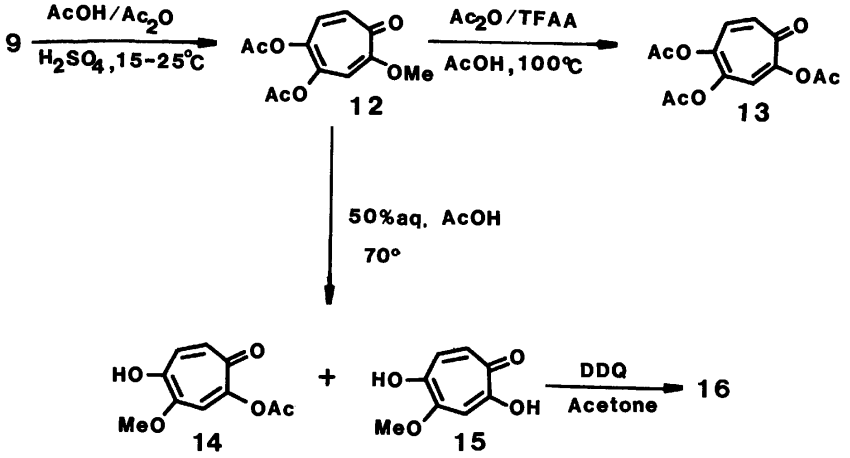

Scheme 2.

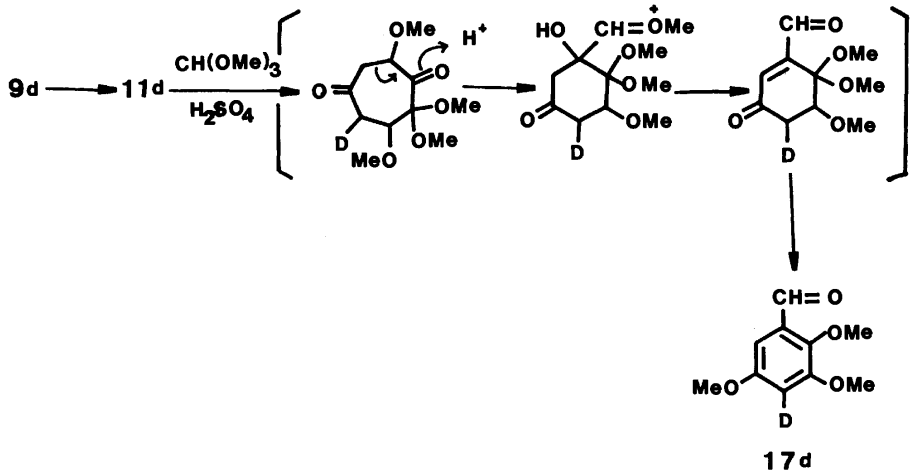

Scheme 3.

11 with trimethoxymethane and sulfuric acid gave 2,3,5-trimethoxybenzaldehyde (**17**),[8] as the only identifiable product in 51 and 76% yields, respectively. Its formation mechanism, shown in Scheme 3, was verified by an aid of **9d**; the deuterium in **17d** was determined to be at C-4.

In general, a conversion of **5** to **6** has been achieved by the DDQ oxidation, however, sometimes there were experimental difficulties, *e.g.*, in order to prepare **10**, we have prepared 5-hydroxy-2-methoxy-4-methyltropone (**18**) by sequential reactions from **8**,[4] but every attempt to hydrolyze **18** to 5-hydroxy-4-methyltropolone (**19**) was unsuccessful. Alternatively, **18** was oxidized with DDQ in methanol to 7,7-dimethoxy-5-methyl-2,5-cycloheptadiene-1,4-dione (**20**), whose mild hydrolysis is known to afford the desired **10**.[4] For the formation of **20** from **18**, TTN was much superior than DDQ; the yield was 98%.

Furthermore, the TTN-oxidation of 5-hydroxy-2-(2-hydroxyethoxy)tropone (**21**) in methanol gave a crystalline diacetal, 4,5-dimethoxy-4,5-(ethylenedioxy)-2,6-cycloheptadien-1-one (**22**), 28%, and its monohemiacetal, the crystalline 4-hydroxy-5-methoxy derivative (**23**), 57%. The stereochemistry of **22** was shown to be trans on the basis of NMR observations of its dihydro derivative (**24**); *i.e.*, in the ^{1}H NMR spectrum, two methyl signals appeared separately, and the ^{13}C NMR spectrum exhibited all non-overlapped eleven signals. The **22** and **23** were also acetoxylated with acetic anhydride and sulfuric acid in acetic acid at room temperature for 3 h to 6-acetoxy-2,3-(ethylenedioxy)tropone (**25**)[9] through a rearrangement.

In conclusion, the present method provided a convenient entry to *p*-tropoquinone acetals, which are versatile intermediates for various functionalized troponoids. However, this method was not applicable to the free tropolone derivatives like 5-methoxytropolone; by the addition of TTN, the substrates precipitated out by salt formation, and prevented the oxidation to be taken place.

Some new aspects of the tropoquinone chemistry developed therefrom will be reported in future.

Experimental

Elemental analyses were performed by Miss S. Hirashima at this Institute. The mps were measured by a Yanagimoto Micro-mp Apparatus and were uncorrected. The IR spectra were taken as KBr disks with a Jasco Model A 102 Spectrometer. The NMR spectra were measured in $CDCl_3$ solution, unless otherwise specified, by a JEOL FX 100 Model Spectrometer, and the chemical shifts were expressed in the δ unit from the internal Me_4Si. The mass spectra were measured on a JEOL 01SG-2 Model Spectrometer.

TTN-Oxidation of 5-Hydroxy-2-methoxytropone (8). a) An anhydrous MeOH solution (12 cm^3) of **8** (400 mg) was treated with TTN (1.17 g) at −20 °C, and the mixture was kept with stirring at 15—25 °C for 0.5 h. Silica-gel column chromatography of the mixture afforded a colorless oil, **9**, 430 mg (90%) [Found: M$^+$, 182.0574. Calcd for $C_9H_{10}O_4$: M$^+$, 182.0577. ^{1}H NMR δ=3.36 (6H, s), 6.25 (1H, dt, J=12, 1 Hz), 6.43 (1H, d, J=12 Hz), and 6.49 (2H, d, J=1 Hz). ^{13}C NMR δ= 50.7 (2C), 103.0, 133.5, 133.8, 136.7, 138.9, 190.8, and 192.7], and a colorless oil, **11**, 45 mg (8%) [Found: C, 55.77; H, 6.55%. Calcd for $C_{10}H_{14}O_5$: C, 56.07; H, 6.59%. ^{1}H NMR δ=2.87 (1H, dd, J=17, 3.8 Hz), 3.18 (1H, dd, J=17, 3.8 Hz), 3.18 (3H, s), 3.37 (3H, s), 3.40 (3H, s), 3.94 (1H, t, J=3.8 Hz), 6.34 (1H, d, J=13 Hz), and 6.54 (1H, d, J=13 Hz). ^{13}C NMR δ=43.4, 49.6, 50.9, 58.6, 75.5, 103.6, 133.4, 138.1, 193.4, and 197.3. $\lambda_{max}^{CHCl_3}$: 243 nm (ε=6900), 348 (1400). *m/z*: 182 (M$^+$−32), 75 (base peak)].

b) Prolonged treatment of the mixture of **8** (30 mg) and TTN (88 mg) in MeOH (0.5 cm^3) at 15—25 °C for 10 h and then at 50 °C for 2 h resulted in the formation of **11**, 33 mg (77%).

Preparation of Deuterio Derivative of 8 (8d). A mixture of **8** (1 g) and D_2O (10 cm^3) containing AcOH (50 mg) was heated at 90 °C for 23 h in a sealed tube. After cooling the mixture, yellow crystals (850 mg) [*m/z*, 152, 153, 154 (11:86:3). ^{1}H NMR (CD_3OD) δ=3.83 (3H, s), 6.5—6.8 (0.1H), 7.08 (1H, s), and 7.10 (2H, s)] obtained by filtration was identified to be **8d**.

TTN-Oxidation of 8d to 9d and 11d. An anhydrous MeOH solution (1 cm^3) of **8d** (50 mg) was treated with TTN (150 mg) under the same conditions to those of deuterium-free **8**. Silica-gel chromatography of the mixture afforded **9d**, 5 mg (8.5%) [*m/z*, 182, 183, 184 (18:76:6). ^{1}H NMR δ=3.30 (6H, s), 6.42 (1.2H, m), and 6.50 (1.8H, s)], and **11d**, 28 mg

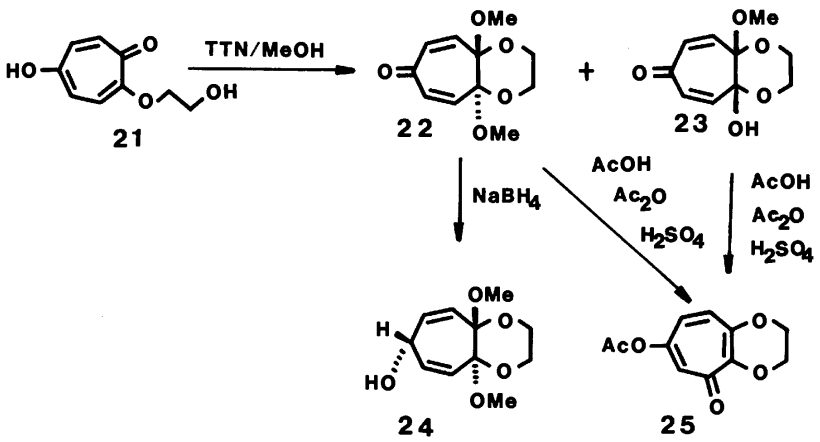

Scheme 4.

(40%) [*m/z*, 183 (M^+-32), 182 (M^+-33), 75 (base peak). ^{1}H NMR δ=2.8—3.1 (1.2H, m), 3.18 (3H, s), 3.37 (3H, s), 3.41 (3H, s), 3.95 (1H, d, J=4 Hz), 6.34 (1H, d, J=13 Hz), and 6.51 (1H, dm, J=13 Hz)].

Reaction of **9** *with* Ac_2O *and* H_2SO_4. A mixture of **9** (50 mg), Ac_2O (0.3 cm^3), AcOH (0.3 cm^3), and H_2SO_4 (20 mg) was stirred at 15—25 °C for 0.5 h. Silica-gel column chromatography of the mixture afforded colorless needles, mp 116—117 °C, 46 mg (98%), **12** [Found: C, 57.14; H, 4.80%. Calcd for $C_{12}H_{12}O_6$: C, 57.03; H, 4.67%. ^{1}H NMR δ=2.28 (3H, s), 2.32 (3H, s), 3.80 (3H, s), 6.65 (1H, d, J=10.5 Hz), 6.70 (1H, s), and 6.91 (1H, d, J=10.5 Hz). ^{13}C NMR δ=20.4, 20.6, 56.5, 116.7, 121.0, 122.1, 148.2, 159.1, 168.2, 168.5, and 176.2. $\lambda_{max}^{CHCl_3}$: 247 nm (ε=38000), 257 (26000), 308 (5300)], and the recovered **9**, 16 mg.

Conversion of **9** *to 2,4,5-Triacetoxytropone (***13***).* A mixture of **9** (120 mg), Ac_2O (5 cm^3), TFAA (0.3 cm^3), and AcOH (60 mg) was heated at 100 °C for 4.5 h. The mixture was heated *in vacuo* to remove the solvents, and the residue chromatographed on a silica-gel column to give colorless needles, mp 121.5—123 °C, 23 mg (17%),[10] **13** [Found: C, 55.69; H, 4.31%. Calcd for $C_{13}H_{12}O_7$: C, 55.72; H, 4.32%. ^{1}H NMR δ=2.26 (6H, s), 2.32 (3H, s), 6.89 (1H, d, J=11.5 Hz), 7.06 (1H, s), and 7.11 (1H, d, J=11.5 Hz). ^{13}C NMR δ=20.4, 20.6, 20.8, 121.9, 123.5, 129.9, 146.5, 153.6, 153.8, 166.1, 167.2, 167.5, and 167.8].

Controlled Hydrolysis of **12** *to* **14** *and* **15**. A 50%-aqueous AcOH solution (3 cm^3) of **12** (1.2 g) was heated at 70 °C for 2 d. The mixture was heated *in vacuo* to remove the solvent, the residual mass was chromatographed on a silica-gel column to give colorless needles, mp 127—128 °C, 420 mg (42%), **14** [Found: C, 57.04; H, 4.83%. Calcd for $C_{10}H_{10}O_5$: C, 57.14; H, 4.80%. ^{1}H NMR δ=2.28 (3H, s), 3.86 (3H, s), 6.83 (1H, d, J=11 Hz), 6.93 (1H, s), and 6.96 (1H, d, J=11 Hz). ^{13}C NMR δ=20.3, 56.6, 109.1, 110.8, 126.6, 142.7, 161.1, 162.4, 168.9, and 175.6. $\lambda_{max}^{CHCl_3}$: 250 nm (ε=31500), 267 (15000), 325 (6400), 340 (4800), 355 (3600)], and pale yellow crystals, mp 209 °C, 250 mg (31%), **15** [Found: M^+, 168.0423. Calcd for $C_8H_8O_4$: 168.0423. ^{1}H NMR δ(CD_3OD)=4.14 (3H, s), 7.52 (1H, d, J=12 Hz), 7.64 (1H, d, J=12 Hz), and 7.67 (1H, s). ^{13}C NMR δ=58.2, 115.0, 125.5, 126.6, 158.1, 158.9, 161.6, and 165.3. λ_{max}^{MeOH}: 248 nm (ε=29600), 344 (11400). ν: 3100—2500, 1600, 1520, 1450—1400 cm^{-1}].

*Synthesis of 4-Methoxy-*p*-tropoquinone (***16***) from* **15**. An MeOH solution (2 cm^3) of **15** (50 mg) was mixed with DDQ (68 mg) and kept at 15—25 °C for 30 min. Silica-gel column chromatography of the mixture gave a yellow oil, 30 mg (61%), **16** [Found: M^+, 166.0267. Calcd for $C_8H_6O_4$ 166.0267. ^{13}C NMR δ=57.3, 108.8, 134.3, 137.6, 160.8, 181.5, 183.5, and 184.7].

The Reaction of **9** *with Trimethoxymethane and* H_2SO_4. A mixture of **9** (55 mg), $CH(OMe)_3$ (0.1 cm^3), MeOH (0.5 cm^3), and H_2SO_4 (30 mg) was kept at 15—25 °C for 1 h. Colorless crystals obtained, **17**, mp 62 °C, 30 mg (52%), was identified to be 2,3,5-trimethoxybenzaldehyde (lit,[8] mp 67 °C) [^{1}H NMR δ=3.80 (3H, s), 3.83 (3H, s), 3.85 (3H, s), 6.73 (1H, d, J=3 Hz), 6.83 (1H, d, J=3 Hz), and 10.38 (1H, s)].

The Reaction of **9d** *with Trimethoxymethane and* H_2SO_4. Similar to above, **9d** (75 mg) was treated in MeOH (1.5 cm^3) with $CH(OMe)_3$ (0.15 cm^3) and H_2SO_4 (50 mg) to give **17d**, 58 mg (72%) [^{1}H NMR δ=3.78 (3H, s), 3.85 (3H, s), 3.90 (3H, s), 6.72 (0.65H, d, J=3 Hz), 6.81 (0.65H, d, J=3 Hz), 6.81 (0.35H, s), and 10.32 (1H, s). *m/z*: 196, 197, 198 (68:29:3)].

The Reaction of **11** *with Trimethoxymethane and* H_2SO_4. Similarly, a mixture of **11** (40 mg), $CH(OMe)_3$ (0.1 cm^3), MeOH (2 cm^3), and H_2SO_4 (30 mg) was kept at 50 °C for 2 h. The product isolated was **17**, 28 mg (76%), identical in every respect to the sample prepared from **9**.

TTN-Oxidatin of **18** *in MeOH to 7,7-Dimethoxy-5-methyl-2,5-cycloheptadiene-1,4-dione (***20***).* An anhydrous MeOH solution (1.5 cm^3) of **18** (45 mg), prepared as previously,[4] was treated with TTN (120 mg) at −20 °C, and gradually raised the temperature to 20 °C within 1 h. The silica-gel chromatography of the mixture afforded **20**, 50 mg (93%).[4]

*TTN-Oxidation of 5-Hydroxy-2-(2-hydroxyethoxy)tropone (***21***) in MeOH.* To an anhydrous MeOH suspension (1.5 cm^3) of **21** (30 mg) which was prepared as previously,[1] TTN (73 mg) was added at −20 °C. After standing at 20 °C for 1 h, the mixture was chromatographed on a silica-gel column to give colorless crystals, mp 108—109 °C, 10.4 mg (28%), **22** [Found: C, 58.60; H, 6.22%. Calcd for $C_{11}H_{14}O_5$: C, 58.40; H, 6.24%. ^{1}H NMR δ=3.27 (6H, s), 3.8 (4H, m), 6.09 (2H, d, J=12.5 Hz), and 6.28 (2H, d, J=12.5 Hz). ^{13}C NMR δ=50.1 (2C), 58.8 (2C), 96.8 (2C), 131.3 (2C), 141.9 (2C), and 189.8], and colorless crystals, mp 123—124 °C, 20 mg (57%), **23** [Found: C, 56.46; H, 5.67%. Calcd for $C_{10}H_{12}O_5$: C, 56.60; H, 5.70%. ^{1}H NMR δ=3.29 (3H, s), 3.5—3.7 (2H, m), 3.9—4.5 (2H, m), 6.02 (1H, d, J=13 Hz), 6.14 (1H, d, J=13 Hz), 6.32 (1H, d, J=13 Hz), and 6.37 (1H, d, J=13 Hz). ^{13}C NMR δ=50.1, 58.6, 58.9, 93.5, 97.0, 129.9, 131.6, 142.2, 144.0, and 190.3].

NaBH$_4$*-Reduction of* **22** *to Dihydro Derivative (***24***).* An MeOH solution (2 cm^3) of **22** (30 mg) was mixed with $NaBH_4$ (12 mg) at 0 °C, and kept **1d** at 15—25 °C. Silica-gel column chromatography of the mixture afforded colorless needles, mp 105—107 °C, 17 mg (56%), **24**, [Found: M^+, 228.0991. Calcd for $C_{11}H_{16}O_5$: 228.0996. ^{1}H NMR δ=3.26 (3H, s), 3.30 (3H, s), 3.4—4.1 (4H, m), 4.90 (1H, qd, J=2.5, 2 Hz), 5.49 (1H, dd, J=11.5, 2.5 Hz), 5.50 (1H, dd, J=12.5, 2 Hz), 5.86 (1H, ddd, J=12.5, 2.5, 1.7 Hz), and 5.98 (1H, ddd, J=11.5, 2.5, 1.7 Hz). ^{13}C NMR δ=49.2, 49.3, 58.4, 58.6, 68.7, 95.3, 97.8, 127.3, 128.6, 134.1, and 136.8. ν: 3520 cm^{-1}].

Modified Thiele Reaction of **22** *to* **25**. A mixture of **22** (16 mg), Ac_2O (0.5 cm^3), AcOH (0.5 cm^3), and H_2SO_4 (30 mg) was kept at 15—25 °C for 3 h. After dilution with water, the mixture was extracted with ether. Silica-gel column chromatography of the extract gave a colorless oil, 10 mg (64%), **25** [Found: C, 59.31: H, 4.57%. Calcd for $C_{11}H_{10}O_5$: C, 59.46; H, 4.54%. ^{1}H NMR δ=2.26 (3H, s), 4.2—4.5 (4H, m), 6.53 (1H, dd, J=12.5, 2.8 Hz), 6.90 (1H, dd, J=12.5, 0.5 Hz), and 6.93 (1H, dd, J=2.8, 0.5 Hz), whose *ABC* system was deduced by simulation. ^{13}C NMR δ=21.0, 63.8, 64.0, 124.4, 129.3, 129.9, 147.5, 148.7, 154.6, 168.6, and 176.6].

References

1) A. Mori and H. Takeshita, *Kyushu Daigaku Sogo Rikogaku Kenkyuka Hokoku*, **3**, 125 (1982).

2) H. Takeshita, T. Kusaba, and A. Mori, *Bull. Chem. Soc. Jpn.*, **55**, 1659 (1982).

3) H. Takeshita, T. Kusaba, and A. Mori, *Chem. Lett.*, **1982**, 701.

4) A. Mori, Y. Isayama, T. Kusaba, and H. Takeshita, *Kyushu Daigaku Sogo Rikogaku Kenkyuka Hokoku*, **6**, 171 (1985).

5) A. McKillop, D. H. Perry, M. Edwards, S. Antus, L. Farkas, M. Mogradi, and E. C. Taylor, *J. Org. Chem.*, **41**, 282

(1976).

6) T. Kusaba, A. Mori, and H. Takeshita, *Bull. Chem. Soc. Jpn.*, **58**, 515 (1985).

7) M. Hirama and S. Itô, *Chem. Lett.*, **1977**, 627.

8) K. K. Purushothaman and S. Vansanth, *J. Chem. Soc., Perkin Trans. 1*, **1976**, 2594.

9) The structure of **25** was deduced on the NMR and UV spectral evidence, *i.e.*, i) δ=176.6 in the ^{13}C NMR is attributable to the carbonyl carbon of a 2-alkoxytropone, ii) J_{vic}= 12.5 Hz of δ=6.53 (H-4) and 6.90 (H-5) indicates the retention of the tropone system [λ_{max}^{MeOH} = 225 nm (log ε=4.11), 254 (4.42), 261 (4.35), 298 (3.53), 307 (3.66), 319 (3.51), 357 (3.56), 370 (3.51)], which constituted an *ABC* system with one more proton at δ=6.93 (H-7), and iii) $\Delta\delta$=0.40 between H-4 and H-5 must be explained in terms of the upfield shift due to the acetoxyl group on C-6. These observations are compatible with only the structure depicted.

10) Improved procedure of this acetolysis will be a subject of an independent paper.

The Synthesis of Internal Conjugated (*E*)-Enynyldialkylboranes and Their Applications to the Syntheses of Conjugated Alkynones, Conjugated (*E*)-Enynes, and Conjugated Enynes Bearing an Unsaturated Group on the Double Bond

Masayuki Hoshi, Yuzuru Masuda, and Akira Arase*
Department of Industrial Chemistry, Kitami Institute of Technology, Kitami 090
(Received December 27, 1984)

Internal conjugated (*E*)-enynyldialkylboranes were synthesized by successive reactions of 1-iodo-1-alkynes with dialkylboranes and 1-alkynyllithiums in 31—79% yields. (*E*)-Enynyldialkylboranes, thus obtained, gave regio- and/or stereospecifically defined corresponding conjugated alkynones by alkaline hydrogen peroxide oxidation, conjugated (*E*)-enynes by protonolysis with acetic acid, and conjugated enynes bearing an unsaturated group on the internal alkenyl carbon atom by bis(acetylacetonato)copper-catalyzed cross-coupling reaction with allyl bromide or 1-bromo-1-hexyne respectively.

The authors recently investigated a cross-coupling reaction of 1-halo-1-alkenyldialkylboranes with alkylmagnesium halides. Regio- and stereospecifically designed internal (*E*)-alkenyldialkylboranes, thus obtained, could be utilized for regio- and stereospecific syntheses of ketones,[1] (*E*)-alkenes[1] and trisubstituted ethylenes[2] (Scheme 1).

An introduction of an alkynyl group to the α-carbon atom of alkenyldialkylboranes by a similar cross-coupling reaction was highly attractive because organoboranes which had an enyne structure on boron atom were expected to have a wide variety of applications as intermediates.

Zweifel *et al.* have previously reported a formation of internal (*Z*)-enynyldialkylboranes by a controlled hydroboration of conjugated diynes with dialkylborane.[3] However, in view of regioselectivity, this

$$R^1C{\equiv}C\text{-}C{\equiv}CR^2 \xrightarrow{R_2BH} R^1CH{=}C(BR_2)\text{-}C{\equiv}CR^2 + R^1C{\equiv}C\text{-}C(BR_2){=}CHR^2$$

reaction is applicable only to such diynes in which two alkyl groups are of the same structure with each other because of ambiguity of the site of hydroboration.

On the contrary, in internal enynyldialkylboranes, which might be obtained by our cross-coupling reaction, the situation of boron–carbon bond was clearly defined and both alkyl groups on the unsaturated bond could be chosen arbitrarily to a certain extent. In addition, the configuration of the alkenyl moiety was expected to be *E*.

Results and Discussion

To find an appropriate procedure for the cross-coupling reaction, 1-bromo- or 1-iodo-1-hexyne was chosen as a starting material. It was hydroborated with dialkylborane and then treated with 1-hexynyl metal compound. As the hydroborating agent, dicyclohexylborane, bis(1,2-dimethylpropyl)borane and 9-borabicyclo[3.3.1]nonane (9-BBN) were examined, and as the 1-hexynyl metal compound, 1-hexynylmagnesium bromide and 1-hexynyllithium were examined respectively.

At the moment, we have no appropriate means to estimate the yield of the enynyldialkylborane (**2**), coupling product in Scheme 2, directly. However, it has been shown that alkenylboranes react readily with alkaline hydrogen peroxide to afford corresponding carbonyl derivatives.[4,5] Thus the yield of **2** was estimated from the amount of 7-dodecyn-6-one (**4a**) formed by alkaline hydrogen peroxide oxidation of the reaction mixture (Scheme 2).

In all cases examined, **4a** was formed in the yields ranging from 13% to 66%, based on the starting 1-halo-1-alkyne, indicating that **2** was formed at least in these yields. On the other hand, appreciable amount of cyclohexyl pentyl ketone or 2,3-dimethyl-4-nonanone (**5**) was formed in most cases, except for the case of 9-BBN, indicating that internal alkenyldialkylborane (**3**), whose one of the alkyl groups on the double bond was transfered from boron atom, (transfer product, in

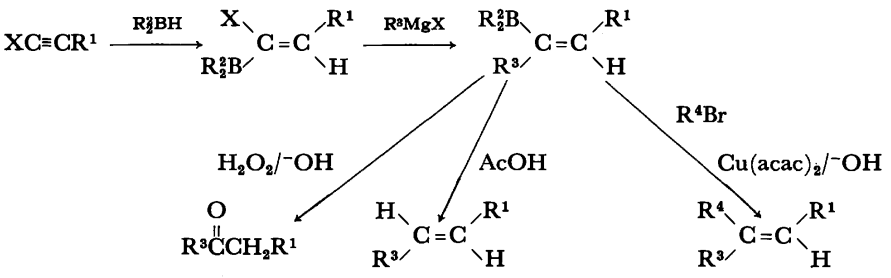

Scheme 1.

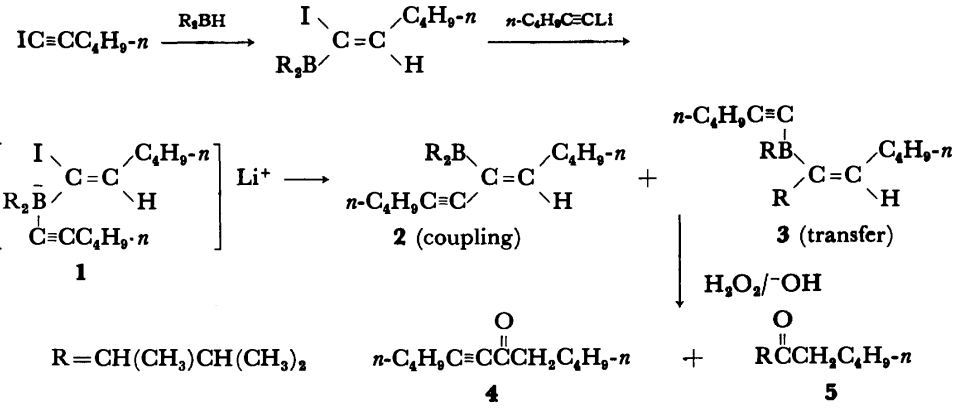

Scheme 2.

Table 1. Yields of organoboranes obtained by the reactions of 1-halo-1-hexenyldialkylboranes with alkynyllithiums[a]

R^2[d]	X	$R^3C{\equiv}CLi$ (10 mmol) R^3	Solvent	Products and yields/%[c] $R^2_2B(R^3C{\equiv}C)C{=}C(C_4H_9\text{-}n)H$ ($R^3C{\equiv}CCOC_5H_{11}\text{-}n$)	$R^2B(C{\equiv}CR^3)(R^2)C{=}C(C_4H_9\text{-}n)H$ ($R^2COC_5H_{11}\text{-}n$)[e]
c-C_6H_{11}	I	*n*-C_6H_{13}	THF	13	76
C_5H_{11}	I	*n*-C_6H_{13}	THF	60	14
C_5H_{11}	Br	*n*-C_4H_9	THF	43	33
C_5H_{11}	I	*n*-C_4H_9	THF	66	20
C_5H_{11}	I	*n*-C_4H_9	THF (30 ml) HMPT (5 ml)	79	7

a) The reactions were carried out in THF at −78 °C for 1 h. b) Prepared from 10 mmol of 1-halo-1-alkyne and 10 mmol of dialkylborane. c) Estimated from the amounts of ketones obtained by the alkaline hydrogen peroxide oxidation of the reaction mixture. d) C_5H_{11} is 1,2-dimethylpropyl. e) See Ref. 6.

Table 2. Yields of organoboranes obtained by the reactions of 1-iodo-1-alkenyl-bis(1,2-dimethylpropyl)boranes with alkynyllithiums[a]

R^1	$R^3C{\equiv}CLi$ (10 mmol) R^3	Products and yields/%[c] $R^2_2B(R^3C{\equiv}C)C{=}C(R^1)H$ ($R^3C{\equiv}CCOCH_2R^1$)	$R^3C{\equiv}CB(R^2)(R^2)C{=}C(R^1)H$ ($R^2COCH_2R^1$)[d]
n-C_4H_9	*n*-C_4H_9	(**4a**), 79	7
n-C_4H_9	*t*-C_4H_9	(**4b**), 70	5
n-C_4H_9	*n*-C_6H_{13}	(**4c**), 75	5
n-C_4H_9	C_6H_5	(**4d**), 31	14
n-C_6H_{13}	*n*-C_4H_9	(**4e**), 72	4

a) The reactions were carried out in 30 ml of THF and 5 ml of HMPT at −78 °C for 1 h. b) Prepared from 10 mmol of 1-iodo-1-alkyne and 10 mmol of bis(1,2-dimethylpropyl)borane. c) Estimated from the amounts of ketones (in the parentheses) obtained by the alkaline hydrogen peroxide oxidation of the reaction mixture. d) See Ref. 6.

Scheme 2), was also formed in the reaction.[6]

The best result was obtained when 1-iodo-1-hexyne was hydroborated with equimolar amount of bis(1,2-dimethylpropyl)borane in THF, and then treated with equimolar amount of 1-hexynyllithium in a mixture of hexane and THF, giving 66% yield of **4a** and 20% yield of **5** after the hydrogen peroxide oxidation. An addition of hexamethylphosphoric triamide (HMPT), as a co-solvent, showed a remarkable effect on the distribution of the products, increasing the amount of **4a** to 79% and decreasing the amount of **5** to 7%. Some of these results are shown in Table 1.

Coupling reactions of 1-iodo-1-alkenylbis(1,2-dimethylpropyl)boranes with some 1-alkynyllithiums

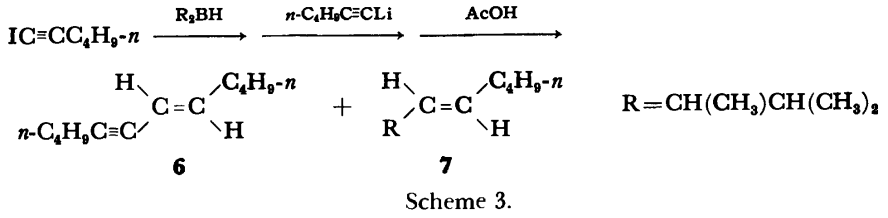

Scheme 3.

TABLE 3. YIELDS OF ALKENYNES AND ALKENES OBTAINED BY THE PROTONOLYSES OF THE INTERNAL ENYNYLBIS(1,2-DIMETHYLPROPYL)BORANES[a]

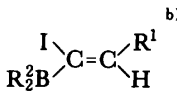 [b]	$R^3C{\equiv}CLi$ (10 mmol)	Products and yields/%[c]	
		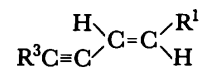	[d]
R^1	R^3		
n-C_4H_9	n-C_4H_9	**6a**, 76	7
n-C_4H_9	t-C_4H_9	**6b**, 69	5
n-C_4H_9	n-C_6H_{13}	**6c**, 70	5
n-C_4H_9	C_6H_5	**6d**, 50	19
n-C_6H_{13}	n-C_4H_9	**6e**, 68	5

a) The protonolyses were carried out using 10 ml of acetic acid at room temperature for 5 h. b) Prepared from 10 mmol of 1-iodo-1-alkyne and 10 mmol of bis(1,2-dimethylpropyl)borane. c) Determined by GLC. d) See Ref. 8.

were examined in the same manner as described above. These results are shown in Table 2.

Not only in the case of unbranched alkynyllithiums but also in the case of a branched one, 3,3-dimethyl-1-butynyllithium, desired enynyldialkylboranes were formed in fairly good yields. These results suggest that the present reaction is generally applicable to the introduction of alkynyl group on the α-alkenyl carbon atom of the alkenyldialkylboranes. (Phenylethynyl)-lithium also gave the desired product, though the yield was somewhat poor.

It has been shown that protonolysis of alkenylboranes with carboxylic acid provided corresponding alkenes in retention of configuration.[7] Accordingly, protonolysis of the internal enynyldialkylboranes should provide corresponding enynes, and thus examinations of the structure of these enynes should reveal the configuration of the alkenyl moiety of the internal enynyldialkylboranes.

As expected, conjugated enynes were obtained by the protonolysis of the reaction mixtures. For example, the reaction mixture, obtained by the successive reactions of 1-iodo-1-hexyne with bis(1,2-dimethylpropyl)borane and 1-hexynyllithium, was protonolyzed with acetic acid giving 76% yield of (*E*)-5-dodecen-7-yne (**6a**) and 7% yield of (*E*)-2,3-dimethyl-4-nonene (**7**) respectively (Scheme 3).

Examinations of these enynes by GLC using a glass capillary column and by ^1H NMR spectra revealed that they were isomerically pure. The *E* configuration was assigned for all of them by their absorptions of the alkenyl proton in IR spectra, near 965 cm^{-1}, and in ^1H NMR spectra, coupling constant, about 16 Hz. Thus, it was revealed that the coupling reaction occured in a complete inversion of configuration giving internal (*E*)-enynyldialkylboranes (Scheme 2). In the protonolysis reactions, a small amount of (*E*)-alkenes,[8] in which one of alkyl groups was transfered from the boron atom, was formed in nearly comparative yield to that of the corresponding alkanones appeared in Table 2. These results are shown in Table 3.

From the results shown in Tables 2 and 3, it is suggested that two reactions are involved in the present reaction. For example, both the coupling product **2** and the transfere product **3** are formed from borate complex (**1**) in a competitive manner.

The reactions, described above, are of interest as synthetic methods for conjugated alkynones and conjugated (*E*)-enynes using organoboranes. However, during the progress of our work, Brown *et al.* reported a synthesis of internal conjugated enynylborinic ester and its application to the synthesis of conjugated alkynones (61—63% yield).[9]

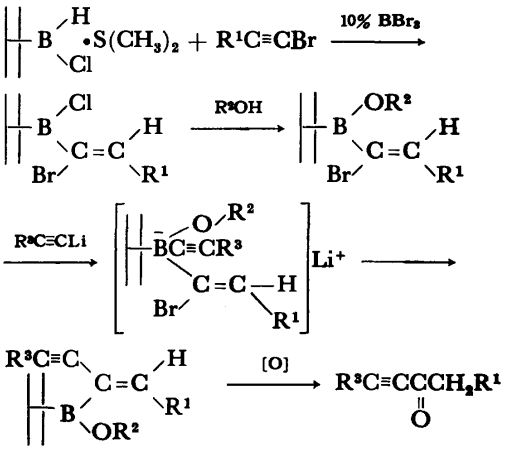

However, the internal (*E*)-enynyldialkylboranes obtained by our reaction seemed to be potential inter-

mediates in organic synthesis. Thus, we continued our program to find new applications using these internal enynyldialkylboranes.

The authors previously found that a cross-coupling reactions of internal (*E*)-alkenyldialkylboranes, prepared by the reaction of 1-halo-1-alkenyldialkylboranes with alkylmagnesium halides, with allyl bromide or 1-bromo-1-alkynes was effectively catalyzed by bis(acetylacetonato)copper, giving (*E*)-1,4-dienes or conjugated (*E*)-enynes.[2] An application of this reaction to the present internal (*E*)-enynyldialkylboranes was expected to provide conjugated enynes having a third unsaturated carbon–carbon bond.

As expected, such triply unsaturated hydrocarbons were obtained in the reactions and some of these results have been communicated briefly.[10] However the authors wish to report more detailed experimental results of the reactions. Because the reactions were carried out by relatively simple procedure and *in situ*, giving dienynes or endiynes in highly regio- and/or stereospecific manner, and, thus, they seemed synthetically interesting.

Preliminary experiments using the reaction mixture of **2** and **3**, obtained as described above, with allyl bromide revealed that this cross-coupling reaction was affected appreciably by the reaction conditions, such as the reaction temperature, the amount of catalyst, and the kind and the amount of alkali metal hydroxide added as the aqueous solution. The best result was obtained when the reaction mixture was treated with equimolar amount of allyl bromide at −15 °C in the presence of 5 mole% of bis(acetylacetonato)copper and equimolar amount of aqueous potassium hydroxide (Scheme 4).

6-Allyl-5-dodecen-7-yne (**8a**) was isolated from the worked-up reaction mixture by column chromatography in 70% yield, based on starting 1-iodo-1-hexyne. A comparison of δ value (5.82) of the conjugated alkenyl proton of **8** in ^{1}H NMR with that (5.55) of (*E*)-6-allyl-5-dodecen-7-yne (**10**) obtained by our previous work,[2] revealed that the reaction proceeded in retention of configuration. Thus, **8a** has *Z* configuration.

Similar results were also obtained with such (*E*)-enynyldialkylboranes, substituted by *t*-butyl or phenyl group at the triple bond, giving corresponding regio- and stereospecifically substituted enynes in fairly good yields.

A cross-coupling reaction of **2** with 1-bromo-1-hexyne was also carried out in similar reaction conditions (Scheme 5). In this case, aqueous sodium hydroxide was preferable to aqueous potassium hydroxide. 7-Pentylidene-5,8-tridecadiyne (**11a**) was formed almost uncontaminated by **12**. **11a** was isolated from the worked-up reaction mixture by column chromatography. Similar enediynes were obtained in the reactions of other internal (*E*)-enynyldialkylboranes with 1-bromo-1-alkynes.

At present, we cannot reveal configurations of these enediynes from their spectral data or by direct comparisons with authentic samples. However, in bis(acetylacetonato)copper-catalyzed cross-coupling reactions of alkenyldialkylboranes with 1-halo-1-alkynes, 1-alkynyl groups were exclusively introduced to the α-carbon atom in retention of configuration.[2,11] Thus, these enediynes seem to be formed in retention of configuration.

These results are shown in Table 4.

Examinations of these triply unsaturated hydrocarbons by ^{1}H NMR and by GLC using a glass capillary column revealed that they were isomerically pure, indicating that the reaction proceeded in a stereospecific manner.

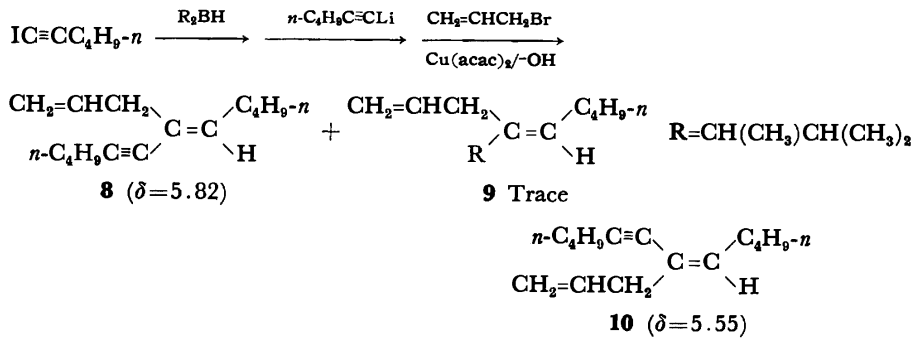

Scheme 4.

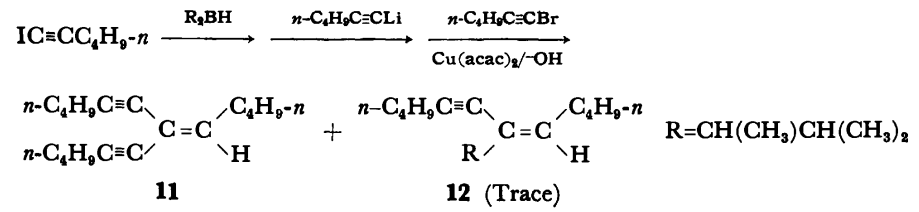

Scheme 5.

TABLE 4. YIELDS OF THE SUBSTITUTED ENYNES OBTAINED BY THE CROSS-COUPLING REACTIONS OF THE ENYNYL-BIS(1,2-DIMETHYLPROPYL)BORANES WITH ALLYL BROMIDE OR 1-BROMO-1-HEXYNE[a)]

R^2_2B / $R^3C{\equiv}C$ C=C R^1 / H [b)]		Bromides	Products and yields/%[c)]	
			$CH_2{=}CHCH_2$ / $R^3C{\equiv}C$ C=C R^1 / H	n-$C_4H_9C{\equiv}C$ / $R^3C{\equiv}C$ C=C R^1 / H
R^1	R^3	(10 mmol)		
n-C_4H_9	n-C_4H_9	$CH_2{=}CHCH_2$	**8a**, 70	
n-C_4H_9	t-C_4H_9	$CH_2{=}CHCH_2$	**8b**, 71	
n-C_4H_9	n-C_6H_{13}	$CH_2{=}CHCH_2$	**8c**, 66	
n-C_4H_9	C_6H_5	$CH_2{=}CHCH_2$	**8d**, 61	
n-C_6H_{13}	n-C_4H_9	$CH_2{=}CHCH_2$	**8e**, 66	
n-C_4H_9	n-C_4H_9	n-$C_4H_9C{\equiv}C$		**11a**, 45
n-C_4H_9	t-C_4H_9	n-$C_4H_9C{\equiv}C$		**11b**, 40
n-C_4H_9	n-C_6H_{13}	n-$C_4H_9C{\equiv}C$		**11c**, 30
n-C_4H_9	C_6H_5	n-$C_4H_9C{\equiv}C$		**11d**, 35
n-C_6H_{13}	n-C_4H_9	n-$C_4H_9C{\equiv}C$		**11e**, 42

a) The reactions were carried out in the presence of alkaline $Cu(acac)_2$. b) Prepared by the successive reactions of 10 mmol of 1-iodo-1-alkyne with 10 mmol of bis(1,2-dimethylpropyl)borane and 10 mmol of 1-alkynyllithium. c) Isolated by column chromatography using silica gel and based on starting 1-iodo-1-alkyne.

As appeared in Table 2, the internal (*E*)-enynyldialkylboranes, obtained in the present reaction, were always contaminated by a certain amount of corresponding internal (*E*)-alkenyldialkylboranes, (transfer product). In the cross-coupling reactions with allyl bromide or 1-bromo-1-hexyne, these contaminants should also provide corresponding coupling products, because in our previous work, the internal (*E*)-alkenyldialkylboranes provided corresponding enynes under similar reaction conditions.[2] However, fortunately, there have been detected only trace amount of such enynes in the present coupling reactions. For example, a mixture of about 7.9 mmol of **2** and 0.7 mmol of **3** provided 7 mmol of **8a** in the reaction with allyl bromide, and 4.9 mmol of **11a** in the reaction with 1-bromo-1-hexyne, almost uncontaminated by **9** and **12** respectively (Scheme 4 and Scheme 5).

These results may be attributed to the electronic character of the alkenyl moiety of organoboranes. That is, it is specurated that bis(acetylacetonato)copper can coordinate preferentially with the conjugated enynyl group on **2** to the enyl group on **3**, giving only the substituted enynes derived from **2**.

Some works, in which the alkenyl group of organoboranes were combined with the allyl or 1-alkynyl group giving doubly unsaturated hydrocarbons, have been reported.[2,11,13-15] However, in the present reaction, two unsaturated groups, one 1-alkynyl and one allyl groups or two 1-alkynyl groups, were introduced successively to the α-carbon atom of the alkenyl group of organoboranes in regio- and stereospecific manners. Thus, triply unsaturated hydrocarbons, which cannot easily be obtained by other methods, are synthesized in the present reaction.

Experimental

Instruments. IR spectra (film) were recorded by using a Hitachi 285 spectrometer. ^1H and ^{13}C sectra ($CDCl_3$, TMS) were run on a JNM-FX200S spectrometer. Mass spectra were recorded by using a Hitachi M-52 mass spectrometer.

Reagents. 2-Methyl-2-butene and cyclohexene were dried over lithium aluminium hydride and distilled under argon stream. Commercial 1-hexyne, 1-octyne and phenylacetylene were dried over Molecular Sieve 4A. 3,3-dimethyl-1-butyne was prepared by the method described in the literature,[16] and dried over Molecular Sieve 4A. 1-Iodo-1-hexyne,[17] 1-iodo-1-octyne,[17] and 1-bromo-1-hexyne[18] were prepared by the method described in the literatures, and they were dried over Molecular Sieve 4A. Bis(1,2-dimethylpropyl)borane and dicyclohexylborane in THF were prepared as described in the literature.[19] HMPT was distilled under argon stream after drying over calcium hydride and stored over Molecular Sieve 4A.

Representative Procedures. The Synthesis of 2 and Its Hydrogen Peroxide Oxidation. A 100-ml round-bottomed flask, equipped with a gas inlet for argon, a sample inlet with a serum cap and a magetic stirring bar, was flushed with argon. In the flask, 1-iodo-1-hexenylbis(1,2-dimethylpropyl)borane was prepared by the addition of 1.40 g of 2-methyl-2-butene (20 mmol) to BH_3 (10 mmol) in THF at −10 °C and the solution was stirred at 0 °C for 2 h. 2.08 g of 1-iodo-1-hexyne (10 mmol) was added slowly to the solution at −10 °C and the solution was stirred at 0 °C for 1 h, and then allowed to stand for additional 1 h to complete the reaction. Then 5 ml of anhydrous HMPT was added as the co-solvent and the solution was cooled to −78 °C immediately. To this solution, 1-hexynyllithium, prepared by the reaction of 0.82 g of 1-hexyne (10 mmol) in THF with butyllithium (10 mmol) in hexane, was added and the reaction mixture was maintained at −78 °C for 1 h. Then the solution was allowed to warm to room temperature and oxidized with alkaline hydrogen peroxide. The reaction mixture was extracted three times with diethyl ether, and the combined extracts were washed twice with NaCl-saturated water. Then it was dried over anhydrous magnesium sulfate. The solution was analyzed by GLC (5% FFAP, Diasolid M) using the internal standard method.

In the preparative reaction, the solvent was evaporated

off after the work-up and the residue was put on a column packed with silica gel (Wako gel Q-50). 1.3 g (72% yield) of 7-dodecyn-6-one, **4a**, was eluted with benzene. ^{1}H NMR δ=0.93 (t, J=7 Hz, 6H), 1.25—1.75 (m, 10H), 2.37 (t, J=7 Hz, 2H), and 2.52 (t, J=7 Hz, 2H);[20] ^{13}C NMR δ=13.50, 13.89, 18.63, 21.97, 22.40, 23.86, 29.75, 31.16, 45.51, 80.90 (C≡C), 94.21 (C≡C), and 188.62 (C=O); IR 2200 (C≡C) and 1680 (C=O) cm^{-1};[18] MS m/z 180 (M$^+$).

The Protonolysis of **2**. To the reaction mixture, obtained as described above, 10 ml of acetic acid was added at 0 °C, and the solution was stirred at room temperature for 5 h. 10 ml of water was added to the solution and the solution was extracted three times with hexane. The combined extracts were neutralized with aqueous sodium carbonate, washed twice with NaCl-saturated water and dried over anhydrous magnesium sulfate. The solution was analyzed by GLC (5% FFAP, Diasolid M) using the internal standard method. In the preparative reaction, the solvent was evaporated off after work-up and the residue was put on a column packed with silica gel (Wako gel Q-50). 1.1 g (76% yield) of (*E*)-5-dodecen-7-yne, **6a**, was isolated by elution with *n*-hexane. ^{1}H NMR δ=0.91 (m, 6H), 1.25—1.60 (m, 8H), 2.00—2.14 (m, 2H), 2.23—2.34 (m, 2H), 5.45 (dt, J=16 and 1.5 Hz, 1H), and 6.04 (dt, J=16 and 7 Hz, 1H);[21] ^{13}C NMR δ=13.65, 13.39, 19.07, 22.01, 22.18, 30.97 (2C), 32.67, 79.18 (C≡C), 88.64 (C≡C), 109.80 (-CH=) and 143.32 (-CH=); IR 2200 (C≡C) and 960 (⟋C=C⟍) cm^{-1};[19] MS m/z 164 (M$^+$).

The Cross-Coupling Reaction of **2** *with Allyl Bromide.* From the reaction mixture containing **2**, and **3**, obtained as described above, the solvents (THF and *n*-hexane) were removed under reduced pressure, and 10 ml of new THF was added. Then, 5 ml of aqueous 2 mol dm^{-3} solution of KOH was added at 0 °C and stirring was continued for 0.5 h at room temperature. The solution was cooled again to −15 °C, and 0.13 g of Cu(acac)$_2$ (0.5 mmol) was added under weak argon flow. Then the reaction mixture was warmed to room temperature, and stirring was maintained for 20 h. The solution was oxidized with alkaline hydrogen peroxide to decompose the residual organoboranes. The solution was extracted three times with diethyl ether. The combined extracts were washed twice with NaCl-saturated water and dried over anhydrous magnesium sulfate. The solvent was evaporated off and the residue was put on a column packed with silica gel (Wako gel Q-50). 1.43 g (70% yield) of (*Z*)-6-allyl-5-dodecen-7-yne, **8a**, was isolated by elution with *n*-hexane. ^{1}H NMR δ=0.91 (m, 6H), 1.25—1.55 (m, 8H), 1.95—2.15 (m,2H), 2.29 (t, J=6 Hz, 2H), 2.87 (d, J=6 Hz, 2H), 4.95—5.15 (m, 2H), 5.81 (t, J=7 Hz, 1H), and 5.75—5.90 (m, 1H); ^{13}C NMR δ=13.65, 13.94, 18.97, 21.97, 22.38, 27.92, 31.04, 31.45, 35.76, 82.39 (C≡C), 87.42 (C≡C), 115.42 (CH_2=), 120.87 (>C=), 135.51 (-CH=), and 137.27 (-CH=); IR 910 (CH_2=) cm^{-1}; MS m/z 204 (M$^+$).

The Cross-Coupling Reaction of **2** *with 1-Bromo-1-hexyne.* The reaction and the work-up procedures were the same as described above. 1.21 g (45% yield) of 7-pentylidene-5,8-tridecadiyne, **11a**, was isolated by elution with *n*-hexane. ^{1}H NMR δ=0.81—1.00 (m, 9H), 1.18—1.75 (m, 12H), 2.20—2.40 (m, 6H), and 6.14 (t, J=7 Hz, 1H); ^{13}C NMR δ=13.62, 13.87, 13.96, 19.00, 19.19, 21.97, 22.01, 22.33, 30.21, 30.33, 30.77 (2C), 76.72 (C≡C), 79.27 (C≡C), 86.84 (C≡C), 93.50 (C≡C), 105.81 (>C=), and 146.70 (-CH=); IR 2220 (C≡C) cm^{-1}; MS m/z 244 (M$^+$).

Analytical data of the other products are as follows.

*2,2-Dimethyl-3-decyn-5-one (**4b**)*: ^{1}H NMR δ=0.90 (t, J=7 Hz, 3H), 1.28 (s, 9H), 1.30—1.40 (m, 4H), 1.60—1.75 (m, 2H) and 2.51 (t, J=7 Hz, 2H); IR (film) 2210 (C≡C) and 1680 (C=O) cm^{-1}; MS m/z 180 (M$^+$).

*7-Tetradecyn-6-one (**4c**)*: ^{1}H NMR δ=0.90 (t, J=7 Hz, 6H), 1.25—1.75 (m, 14H), 2.36 (t, J=7 Hz, 2H), and 2.51 (t, J=7 Hz, 2H); IR 2200 (C≡C) and 1680 (C=O) cm^{-1}; MS m/z 208 (M$^+$).

*1-Phenyl-1-octyn-3-one (**4d**)*: ^{1}H NMR δ=0.91 (m, 3H), 1.25—1.40 (m, 4H), 1.65—1.80 (m, 2H), 2.64 (t, J=7 Hz, 2H), 7.35—7.45 (m, 3H), and 7.50—7.60 (m, 2H); IR 2190 (C≡C) and 1670 (C=O) cm^{-1}; MS m/z 200 (M$^+$).

*5-Tetradecyn-7-one (**4e**)*: ^{1}H NMR δ=0.93 (m, 6H), 1.25—1.75 (m, 14H), 2.37 (t, J=7 Hz, 2H), and 2.52 (t, J=7 Hz, 2H); IR 2210 (C≡C) and 1680 (C=O) cm^{-1}; MS m/z 208 (M$^+$).

*(E)-2,2-Dimethyl-5-decen-3-yne (**6b**)*: ^{1}H NMR δ=0.89 (t, J=7 Hz, 3H), 1.23 (s, 9H), 1.25—1.40 (m, 4H), 2.00—2.12 (m, 2H), 5.44 (dt, J=16 and 1.5 Hz, 1H), and 6.02 (dt, J=16 and 7 Hz, 1H); IR 2200 (C≡C) and 960 (⟋C=C⟍) cm^{-1}; MS m/z 164 (M$^+$).

*(E)-5-Tetradecen-7-yne (**6c**)*: ^{1}H NMR δ=0.89 (m, 6H), 1.25—1.60 (m, 12H), 2.00—2.15 (m, 2H), 2.20—2.35 (m, 2H), 5.44 (dt, J=16 and 1.5 Hz, 1H), and 6.03 (dt, J=16 and 7 Hz, 1H); IR 2220 (C≡C) and 960 (⟋C=C⟍) cm^{-1}; MS m/z 192 (M$^+$).

*(E)-1-Phenyl-3-octen-1-yne (**6d**)*: ^{1}H NMR δ=0.89 (t, J=7 Hz, 3H), 1.25—1.45 (m, 6H), 2.05—2.20 (m, 2H), 5.67 (dt, J=16 and 1.5 Hz, 1H), 6.22 (dt, J=16 and 7 Hz, 1H), 7.20—7.30 (m, 3H), and 7.35—7.45 (m, 2H); IR 2200 (C≡C) and 960 (⟋C=C⟍) cm^{-1}; MS m/z 184 (M$^+$).

*(E)-7-Tetradecen-5-yne (**6e**)*: ^{1}H NMR δ=0.91 (m, 6H), 1.20—1.60 (m, 12H), 2.00—2.10 (m, 2H), 2.20—2.35 (m, 2H), 5.44 (dt, J=16 and 1.5 Hz, 1H), and 6.03 (dt, J=16 and 7 Hz, 1H); IR 2210 (C≡C) and 960 (⟋C=C⟍) cm^{-1}; MS m/z 192 (M$^+$).

*(Z)-2,2-Dimethyl-5-allyl-5-dodecen-3-yne (**8a**)*: ^{1}H NMR δ=0.89 (m, 3H), 1.23 (s, 9H), 1.20—1.60 (m, 4H), 2.00—2.20 (m, 2H), 2.86 (d, J=6 Hz, 2H), 4.95—5.15 (m, 2H), 5.79 (t, J=7 Hz, 1H), and 5.70—5.95 (m, 1H); ^{13}C NMR δ=13.91, 22.38, 27.90, 30.87 (-C-), 31.21 (CH_3-, 3C), 31.45, 35.93, 80.71 (C≡C), 95.91 (C≡C), 115.32 (CH_2=), 120.92 (>C=), 135.56 (-CH=), and 136.75 (-CH=); IR 2220 (C≡C) and 910 (CH_2=) cm^{-1}; MS m/z 204 (M$^+$).

*(Z)-6-Allyl-5-tetradecen-7-yne (**8c**)*: ^{1}H NMR δ=0.89 (m, 6H), 1.20—1.60 (m, 12H), 2.00—2.15 (m, 2H), 2.28 (t, J=6 Hz, 2H), 2.87 (d, J=6 Hz, 2H), 4.95—5.20 (m, 2H), 5.81 (t, J=7 Hz, 1H), and 5.75—5.95 (m, 1H); ^{13}C NMR δ=13.94, 14.06, 19.31, 22.38, 22.60, 27.92, 28.56, 28.95, 31.40, 31.48, 35.76, 82.44 (C≡C), 87.50 (C≡C), 115.40 (CH_2=), 120.94 (>C=), 135.54 (-CH=), and 137.22 (-CH=); IR 910 (CH_2=) cm^{-1}; MS m/z 232 (M$^+$).

*(Z)-1-Phenyl-3-allyl-3-octen-1-yne (**8d**)*: ^{1}H NMR δ=0.91 (m, 3H), 1.20—1.60 (m, 4H), 2.05—2.25 (m, 2H), 2.98 (d, J=6 Hz, 2H), 4.95—5.25 (m, 2H), 5.75—6.15 (m, 1H), 6.03 (t, J=7 Hz, 1H), and 7.15—7.60 (m, 5H); ^{13}C NMR δ=13.94, 22.38, 28.14, 31.35, 35,47, 86.86 (C≡C), 91.56 (C≡C), 115.76 (CH_2=), 120.55 (>C=), 123.77 (>C=), 127.71 (-CH=), 128.19 (-CH=, 2C), 131.45 (-CH=, 2C), 135.22 (-CH=), and 139.30 (-CH=); IR 910 (CH_2=) cm^{-1}; MS m/z 224 (M$^+$).

*(Z)-7-Allyl-7-tetradecen-5-yne (**8e**)*: ^{1}H NMR δ=0.91 (m, 6H), 1.15—1.60 (m, 12H), 1.95—2.15 (m, 2H), 2.29 (t, J=6 Hz, 2H), 2.89 (d, J=6 Hz, 2H), 4.95—5.15 (m, 2H), 5.81 (t, J=7 Hz, 1H), and 5.70—5.95 (m, 1H); ^{13}C NMR δ=13.62, 14.08, 19.00, 21.97, 22.62, 28.22, 29.02, 29.29, 31.06, 31.72, 35.76, 82.41 (C≡C), 87.40 (C≡C), 115.37 (CH_2=), 120.89 (>C=), 135.51

(-CH=), and 137.27 (-CH=); IR 910 (CH_2=) cm^{-1}; MS *m/z* 232 (M^+).

(E)-6-(3,3-Dimethyl-1-butynyl)-5-tetradecen-7-yne (11b): ^1H NMR δ=0.90 (m, 6H), 1.23 (s, 9H), 1.20—1.55 (m, 8H), 2.20—2.40 (m, 4H), and 6.14 (t, *J*=7 Hz, 1H); IR 2220 (C≡C) cm^{-1}; MS *m/z* 244 (M^+).

(E)-6-(1-Hexynyl)-5-tetradecen-7-yne (11c): ^1H NMR δ=0.90 (m, 9H), 1.15—1.70 (m, 16H), 2.25—2.40 (m, 6H), and 6.14 (t, *J*=7 Hz, 1H); ^{13}C NMR δ=13.62, 13.89, 14.06, 19.00, 19.19, 19.31, 19.51, 21.97, 22.33, 22.57, 28.65, 30.21, 30.77, 31.38, 76.72 (C≡C), 79.27 (C≡C), 86.91 (C≡C), 93.48 (C≡C), 105.84 (>C=), and 146.68 (-CH=); IR 2220 (C≡C) cm^{-1}; MS *m/z* 272 (M^+).

(E)-6-(2-Phenylethynyl)-5-dodecen-7-yne (11d): ^1H NMR δ= 0.94 (m, 6H), 1.20—1.70 (m, 8H), 2.30—2.50 (m, 4H), 6.33 (t, *J*=7 Hz, 1H), and 7.20—7.55 (m, 5H); ^{13}C NMR δ=13.60, 13.87, 19.22, 21.97, 22.35, 30.41, 30.75 (2C), 76.09 (C≡C), 85.820 (C≡C), 88.25 (C≡C), 94.23 (C≡C), 105.79 (>C=), 123.25 (>C=), 128.02 (-CH=), 128.17 (-CH=, 2C), 131.57 (-CH=, 2C), and 148.26 (-CH=); IR 2200 (C≡C) cm^{-1}; MS *m/z* 264 (M^+).

7-Heptylidene-5,8-tridecadiyne (11e): ^1H NMR δ=0.91 (m, 9H), 1.10—1.65 (m, 16H), 2.10—2.55 (m, 6H), and 6.14 (t, *J*= 7 Hz, 1H); ^{13}C NMR δ=13.65 (2C), 14.11, 19.00, 19.22, 21.97, 22.01, 22.62, 28.65, 28.95, 30.53, 30.77 (2C), 31.67, 76.72 (C≡C), 79.25 (C≡C), 86.86 (C≡C), 93.50 (C≡C), 105.74 (>C=), and 146.83 (-CH=); IR 2220 (C≡C) cm^{-1}; MS *m/z* 272 (M^+).

References

1) A. Arase, M. Hoshi, and Y. Masuda, *Bull. Chem. Soc. Jpn.*, **57**, 209 (1984).

2) M. Hoshi, Y. Masuda, and A. Arase, *Chem. Lett.*, **1984**, 1029.

3) G. Zweifel and N. L. Polston, *J. Am. Chem. Soc.*, **92**, 4068 (1970).

4) H. C. Brown and S. K. Gupta, *J. Am. Chem. Soc.*, **94**, 4370 (1972).

5) S. U. Kulkarni, H. D. Lee, and H. C. Brown, *Synthesis*, **1982**, 193.

6) Mass spectra of minor products appeared in Table 1 and 2 coincided with those of corresponding ketones obtained by the method described in the following literature: G. Zweifel and H. Arzoumanian, *J. Am. Chem. Soc.*, **89**, 5086 (1967).

7) H. C. Brown and G. Zweifel, *J. Am. Chem. Soc.*, **83**, 3834 (1961).

8) Mass spectra of minor products appeared in Table 3 coincided with those of corresponding alkenes obtained by the method described in the literature of reference 6.

9) H. C. Brown, N. G. Bhat, and D. Basavaiah, *Synthesis*, **1983**, 885.

10) A. Arase, M. Hoshi, and Y. Masuda, *Chem. Lett.*, **1984**, 2093.

11) M. Hoshi, Y. Masuda, and A. Arase, *Bull. Chem. Soc. Jpn.*, **56**, 2855 (1983).

12) E. Negishi, G. Lew, and T. Yoshida, *J. Chem. Soc., Chem. Commun.*, **1973**, 874.

13) Y. Yamamoto, H. Yatagai, and I. Moritani, *J. Am. Chem. Soc.*, **97**, 5606 (1975); Y. Yamamoto, H. Yatagai, H. Sonoda, and S. Murahashi, *J. Chem. Soc., Chem. Commun.*, **1976**, 452.

14) N. Miyaura, K. Yamada, and A. Suzuki, *Tetrhedron Lett.*, **1979**, 3437; N. Miyaura, T. Yano, and A. Suzuki, *ibid.*, **1980**, 2865.

15) J. B. Campbell Jr. and H. C. Brown, *J. Org. Chem.*, **45**, 550 (1980); H. C. Brown and G. A. Molander, *ibid.*, **46**, 645 (1981).

16) W. L. Collier, R. S. Macomber, *J. Org. Chem.*, **38**, 1367 (1973).

17) P. L. Southwick and J. R. Kirchiner, *J. Org. Chem.*, **27**, 3305 (1962).

18) K. E. Schulte and M. Goes, *Arch. Pharm.*, **290**, 118 (1959).

19) H. C. Brown and A. W. Moerikofer, *J. Am. Chem. Soc.*, **83**, 3471 (1961).

20) Some of these values are coincided with those described in reference 3.

21) Some of these values are coincided with those described in reference 12.

 © 1985 The Chemical Society of Japan Bull. Chem. Soc. Jpn., 58, 1690—1695 (1985) [Vol. 58, No. 6

Restricted Rotation Involving the Tetrahedral Carbon. LVI. NMR and Molecular Mechanics Studies on the Stereodynamics of 8,13-Dichloro-9-methoxy-1,4-dimethyltriptycene[1]

Gaku YAMAMOTO* and Michinori ŌKI
Department of Chemistry, Faculty of Science, The University of Tokyo, Bunkyo-ku, Tokyo 113
(Received January 8, 1985)

The 400 MHz ^{1}H NMR spectrum of the title compound at −100 °C in dichloromethane revealed the presence of two isomers in a ratio of 88:12, which results from restricted rotation about the triptycyl-oxygen single bond. The major isomer was assigned to the *ap* rotamer on the basis of the low temperature ^{13}C NMR spectrum. Dynamic NMR studies gave the activation parameters for the $ap \rightarrow \pm sc$ conversion: $\Delta H^{\ddagger}=11.9\pm0.5$ kcal/mol (1 $cal_{th}=4.184$ J), $\Delta S^{\ddagger}=2.6\pm2.5$ eu, $\Delta G^{\ddagger}_{200K}=11.4$ kcal/mol. Results of molecular mechanics calculations on the compound are discussed.

Abundant reports have appeared on dynamic NMR studies of restricted rotation about carbon–carbon single bonds including sp^3-sp^3, sp^3-sp^2, and sp^2-sp^2 combinations.[2] On the other hand, only a few examples have been reported on restricted rotation of carbon–oxygen bonds studied by NMR spectroscopy. In most cases, the bond in question is the one between an oxygen and an sp^2-hybridized carbon atoms, as in aryl esters,[3] diaryl ethers,[4] and most recently in chromium complexes of substituted anisoles.[5] While our interest is focused on rotational barriers which mainly originate from the differential steric effects in the ground and the transition states, several examples are known for another type of C(sp^2)–O rotational barriers which are mainly caused by destruction of conjugative stabilization.[6]

As for NMR studies on restricted rotation about sp^3-carbon-to-oxygen bonds, few reports have appeared. As far as we know, temperature dependence of ^{1}H NMR spectra of a quinone acetal, 4-ethoxy-2,3,5,6-tetramethylphenoxy dimer,[7] and more recently that of bis(9-anthrylmethyl) ether derivatives[8] have been reported. In both reports, mechanistic details of the dynamic process are not discussed, only the possible structure of the stable conformation being speculated.

We recently reported the preliminary results of dynamic NMR studies on the stereodynamics of 9-(2-alkylphenoxy)triptycenes (**1**).[9] Molecules of compounds **1** constitute a bevel gear system with a two-toothed and a three-toothed wheels in both static and dynamic sense: Correlated disrotation of the triptycyl–oxygen and aryl–oxygen bonds is observed by dynamic NMR spectroscopy. In this system, ground state conformations and the dynamic processes occurring are well defined.

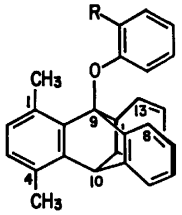

1a: R = CH_3
1b: R = $CH(CH_3)_2$

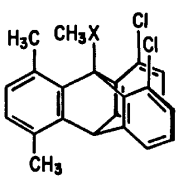

2: X = O
3: X = CH_2

We felt it essential to study a simpler and more fundamental system, 9-methoxytriptycenes, in order to get deeper insight into the general nature of rotational barriers of C–O bonds in comparison with those of C–C bonds. As a methyl group is considerably smaller than the aryl group in **1**, it seemed necessary to introduce substituents at three *peri*-positions (1, 8, and 13 positions) to obtain a sufficient steric congestion in the transition state for rotation so that the restricted rotation is observed by NMR spectroscopy. We therefore chose 8,13-dichloro-9-methoxy-1,4-dimethyltriptycene (**2**) as the target, taking also the synthetic ease into account.

In this article, we report on the dynamic NMR and molecular mechanics studies of **2** and discuss the results in comparison with those of the corresponding 9-ethyl derivative (**3**)[1] and of related compounds.

Results and Discussion

Synthesis. 1,8-Dichloroanthrone was methylated with dimethyl sulfate and alkali to give 1,8-dichloro-9-methoxyanthracene (**4**). Reaction of **4** with 3,6-dimethylbenzyne afforded **2** as colorless crystals with low solubility in common solvents.

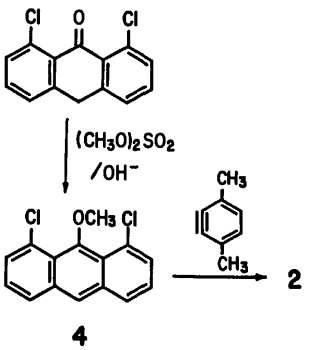

4

NMR Spectra and Rotamer Equilibria. In the ^{1}H NMR spectrum of **2** at ambient temperature, three singlets are observed for the methyl groups reflecting fast internal rotation about the C_9–OCH_3 bond (Table 1). Of the two singlets ascribed to the aromatic methyl groups, the high-field one at δ 2.31 is unambiguously assigned to 4-methyl on the basis of nuclear Overhauser

Table 1. ^{1}H NMR data of **2** in CD_2Cl_2 at 400 MHz[a)]

Temp °C	Pop %	1-CH_3	4-CH_3	OCH_3	10-H	Rotamer assigned
25		2.71_0	2.31_4	3.98_4	5.44_0	
−100	88	2.69_2	2.30_2	3.95_0	5.54_2	*ap*
	12	2.73_5	2.53_8	3.85_4	5.51_3	±*sc*
		(-0.04_3)	(-0.23_6)	(0.09_6)	(0.02_9)	

a) Data for aromatic protons are omitted; see Experimental. Chemical shifts are given in δ. In parentheses are chemical shift differences in ppm between the rotamers at −100 °C.

effect (NOE) experiments: Irradiation of this signal causes the intensity enhancement by *ca.* 20% of the signal at δ 5.44 ascribed to the bridgehead proton (10-H), while irradiation of the low-field methyl signal at δ 2.71 leaves the 10-H signal intact.

On lowering the temperature, each of the singlets broadens and splits into two unequally intense peaks. At −100 °C in dichloromethane-d_2, two sets of signals are observed indicating the presence of two isomers in a ratio of 88:12. It may be quite reasonable to assume that these isomers are rotamers about the C_9–OCH_3 bond, *ap* and ±*sc* (an equimolar mixture of +*sc* and −*sc*), but the rotamer assignment is not so straightforward from the ^{1}H NMR spectra, because the compound does not contain a prochiral group (*e.g.* $-CX_2Y$), which would definitely identify the chiral nature of the ±*sc* rotamer. The aromatic proton signals of the major rotamer appear rather simple, however, implying that it is *ap*.

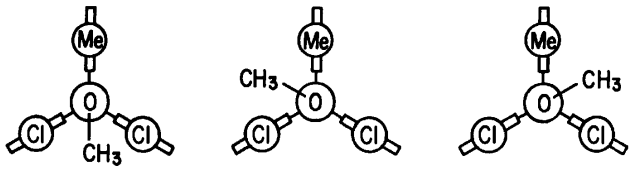

ap +*sc* −*sc*

We expected that the unambiguous assignment of the rotamers could be made from the ^{13}C NMR spectrum at low temperature: The ±*sc* rotamer should give rise to eighteen different signals in the aromatic carbon region while the *ap* rotamer twelve peaks according to the molecular symmetry. Therefore we measured a 100 MHz ^{13}C NMR spectrum of **2** at −82 °C. Actually twelve large peaks assignable to the major isomer were observed in the region of δ 120—150 together with more than twelve small peaks derived from the minor isomer. This strongly suggests that the major isomer is *ap*, although all of the eighteen peaks are not detected for the minor isomer because of the overlap with the major peaks and the interference by noise peaks. The ^{13}C NMR data are given in Table 2 together with tentative assignments of the major peaks.

Predominance of the *ap* rotamer is reasonable on the basis of the generally accepted order of bulkiness of the *peri*-substituents, CH_3>Cl:[10] The methoxyl methyl group should be more comfortable when it is flanked by two Cl's than by CH_3 and Cl. Similar rotamer distribution was observed in the corresponding 9-ethyl compound (**3**), where the population of *ap* is 57% in chloroform-*d* at 35 °C.[1]

Table 2. ^{13}C NMR data of **2**[a)]

at 25 °C	at −82 °C major	at −82 °C minor	Tentative assignment
18.39 q	18.20	17.93	4-CH_3
20.24 q	20.05	19.15	1-CH_3
51.20 d	49.72	≈49.9[b)]	10
57.18 q	56.69	55.86	OCH_3
92.17 s	91.00	c)	9
122.35 d	121.92		5,16
126.80 d	125.70		2
127.43 d	126.89		7,14
129.27 d	128.38		6,15
129.47 s	129.15		1
129.52 d	128.47		3
130.20 s	129.25		8,13
131.73 s	130.17		4
141.34 s	140.06		4a
141.56 s	140.18		10a,11
145.03 s	145.35		9a
146.49 s	144.69		8a,12

a) Obtained at 100.5 MHz in CD_2Cl_2. Chemical shifts of the aromatic carbons of the minor rotamer are not read. b) Shoulder. c) Not identified.

Inspection of Table 1 reveals an intriguing feature. The signals at −100 °C due to the 4-methyl group, which is remoter from the site of restricted rotation than 1-methyl, show a larger chemical shift difference (0.24 ppm) between the rotamers than those due to the latter (0.04 ppm). This seems quite unusual but the reason is not certain.

Dynamic NMR Studies and Rotational Barriers. Pairs of signals at low temperatures which are ascribed to the 1-methyl, 4-methyl, and methoxyl groups coalesce to single peaks at about −71, −62, and −50 °C, respectively, upon raising the temperature. While rigorous determination of the coalescence temperatures was not made, rate constants for the *ap*⇌±*sc* interconversion were obtained by simulating the three sets of signals at six temperatures between −81 and −56 °C. The data are given in Table 3 together with the activation parameters therefrom.

Comparison of the data with those of the carbon analog **3** reveals some interesting points. Generally, rotational barriers about C–O bonds are lower than those about the corresponding C–C bonds as typically illustrated by methanol *vs.* ethane (1.07 *vs.* 2.88 kcal/mol), and dimethyl ether *vs.* propane (2.7 *vs.* 3.4

TABLE 3. DYNAMIC NMR DATA OF **2** IN CD_2Cl_2 AT 400 MHz[a)]

$$ap \underset{k_{-1}}{\overset{2k_1}{\rightleftharpoons}} \pm sc \qquad K = 2k_1/k_{-1}$$

Temp	K	k_1	ΔG^*	ΔH^*	ΔS^*
°C		s^{-1}	kcal/mol	kcal/mol	eu
−81.0	0.143	0.45	11.39	11.9±0.5	2.6±2.5
−76.0	0.156	1.0	11.38		
−70.9	0.156	2.0	11.40		
−65.9	0.163	4.6	11.35		
−60.8	0.176	9.7	11.33		
−55.7	0.176	18.5	11.33		

a) The parameters refer to the $ap \rightarrow \pm sc$ process.

kcal/mol).[11] This seems to be principally resulted from the fact that there are three eclipsing interactions in the transition state for C–C rotation, while only one for C–O rotation. As the lone pair electrons on oxygen are much smaller in their effective size than hydrogen or alkyl groups and highly polarizable, steric interaction

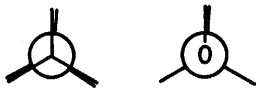

involving the lone pair electrons are considered to be negligible.

In this sense, the lower barrier in **2** than in **3** (ΔG^*=20.2 kcal/mol at 94 °C)[1] may be quite reasonable. However the larger barrier difference of about 9 kcal/mol is in striking contrast to the rather small difference found between **1a** and its carbon analog (**5**):[9,12] The gearing process in which the aryl group passes over the *peri*-methyl group has ΔG^* of 18.1 kcal/mol in **1a** and 20.0 kcal/mol in **5**.

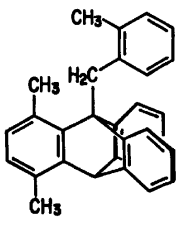

5

In order to understand this apparent discrepancy, secondary factors affecting the barrier difference should be considered. Among them, the difference in bond length between C–C and C–O would be the most important. In the following discussion, the effects of bond lengths in the transition states are considered, the other secondary factors being neglected. Effects of these factors as well as the bond lengths in the ground states are assumed to be smaller than in the transition states.

The probable transition states for the $ap \rightleftharpoons \pm sc$ interconversion in **2** and **3** are shown by **6** and **7**, respectively. Local steric interaction due to eclipsing of the β-methyl group in the 9-substituent and the *peri*-chloro group will not differ largely between **6** and **7**, because not only the C_9–O bond but also the O–CH_3 bond in **6** are shorter than the corresponding C–C bonds in **7**. Therefore the presence or absence of

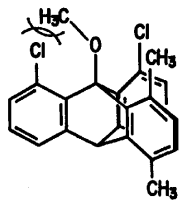

6

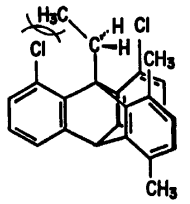

7

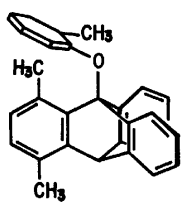

8

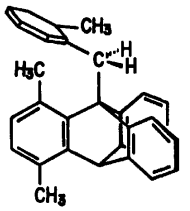

9

the eclipsing interaction between the α-hydrogen in the 9-substituent and the *peri*-chloro or *peri*-methyl group most effectively affects the transition state energy, resulting in the large barrier difference between **2** and **3**.

On the other hand, in the probable transition states (**8** and **9**) for the $ap \rightleftharpoons \pm sc$ gearing process in **1a** and **5**, respectively, the repulsive interaction between the *peri*-methyl and the aryl groups will be far severer in **8** than in **9**, because the C_9–O bond in **8** is shorter than the C_9–CH_2 bond in **9** while the difference between the Ar–O and Ar–CH_2 bond lengths does not seem to significantly affect this situation. Therefore the small barrier difference between **1a** and **5** may be understood by assuming that the sum of the eclipsing interactions between the aryl group and the *peri*-methyl group and those between the α-hydrogens and the *peri*-hydrogens in **9** do not largely exceed the eclipsing interaction between the aryl group and the *peri*-methyl group in **8**.

One may pose a possibility that the interconversion between the isomers might occur by configurational inversion at the oxygen atom by way of a transition state with a linear C–O–C arrangement, which is often called

a lateral shift, rather than internal rotation about the C–O bond. Although we do not have experimental evidence at hand for or against the hypothesis, there seems an indication against it. Kawada and Iwamura reported that the energy barrier to interconversion between the "phase isomers" in bis(9-triptycyl) ether derivatives (**10**) are 42—44 kcal/mol.[13] They rejected the lateral shift as the mechanism of the interconversion, and thus the inversion barrier at oxygen should be higher than these values in **10**, and there

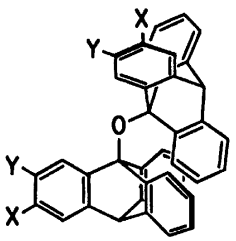

10 X or Y = Cl

is no reason to assume that the inversion barrier in **2** is largely different from those in **10**.[14]

Molecular Mechanics Calculations. In order to confirm the rotamer assignment mentioned above by evaluating the relative energies of the rotamers and to have some insights into the molecular geometries of the rotamers, we performed molecular mechanics calculations on **2** and also on **3** for comparison, using the MM2 force field.[15] Several parameters were newly inputted in addition to those originally included in the program, which are given in the experimental section. Calculated total steric energies of the rotamers of **2** and **3** and their components are compiled in Table 4.

In both **2** and **3**, the *ap* rotamer is calculated to be more stable than ±*sc*, reproducing qualitatively the observation. The steric energy difference between the rotamers is fortuitously the same between **2** and **3**, but the component analysis shows that the contributing factors are different. In the oxygen compound **2**, the bending and torsion terms most contribute to the energy difference, both favoring the *ap* rotamer. In the methylene analog **3**, the torsion term strongly favors *ap*, while the van der Waals terms favor ±*sc*, partially compensating the contribution by torsion.

As the accurate values for the enthalpy and entropy differences between the rotamers could not be determined experimentally by the ^{1}H NMR studies, quantitative comparison between the experiment and the calculation is not straightforward. If it is assumed that the statistical factor of 2 for ±*sc* is the only contributor to the entropy difference, the populations of the *ap* rotamer are calculated from the steric energy difference of 1.18 kcal/mol to be 94% at −100 °C and 71% at 35 °C, which are compared with the observed values of 88% at −100 °C for **2** and 57% at 35 °C for **3**. Agreement seems fairly good.

The optimized geometries of *ap*-**2** and +*sc*-**2** are shown in Fig. 1. In both rotamers, the benzo bridge antiperiplanar to the *O*-methyl group is completely in a single plane together with the substituent(s) attached to it, and the benzo bridges flanking the *O*-methyl group and the *peri*-substituents attached to them bend away from the *O*-methyl group so as to relieve the steric congestion. No extraordinary bond lengths are found. The bonds connecting the benzo bridges to 9-C are somewhat longer (1.53—1.55 Å) than the normal sp^3-sp^2 carbon bond of 1.49 Å, and this feature is generally found in 9-substituted triptycene derivatives studied by X-ray crystallography.[16] The C_9–O–CH_3 angles are 113.7 and 113.4° in *ap*-**2** and ±*sc*-**2**, respectively, increasing by *ca.* 7° from the standard value of 106.8°.

In order to obtain the energy barrier to rotation about the C_9–OCH_3 bond in **2** by molecular mechanics calculations, dependence of the steric energy upon the dihedral angle C_{9a}–C_9–O–CH_3 was calculated by the "one-bond drive" technique. The transition state for the *ap*⇌±*sc* interconversion, in which the *O*-methyl group eclipses a *peri*-chlorine, was calculated to be 15.7 kcal/mol higher than the *ap* state. The calculated energy barrier is somewhat higher than the experimentally obtained one (11.9 kcal/mol). We must allow for the fact that highly strained transition states are usually difficult to be reproduced by using the parameters which are empirically determined so as to reproduce the energy and geometry of molecules in the ground state.

Table 4. Steric energies and their components by MM2[a]

	2			**3**		
	ap	±*sc*	Δ*E*	*ap*	±*sc*	Δ*E*
Total steric energy	30.87	32.05	−1.18	33.02	34.20	−1.18
Compression	3.44	3.46	−0.02	4.98	4.92	0.06
Bending	15.27	15.58	−0.31	17.14	17.18	−0.04
Stretch-bend	−0.27	−0.27	0.00	−0.26	−0.27	0.01
van der Waals						
1,4-	20.18	20.23	−0.05	19.63	19.52	0.11
other	−2.29	−2.33	0.04	1.28	0.83	0.45
Torsion	−7.41	−6.67	−0.74	−9.38	−7.66	−1.72
Dipole	1.95	2.05	−0.10	−0.37	−0.32	−0.05

a) in kcal/mol.

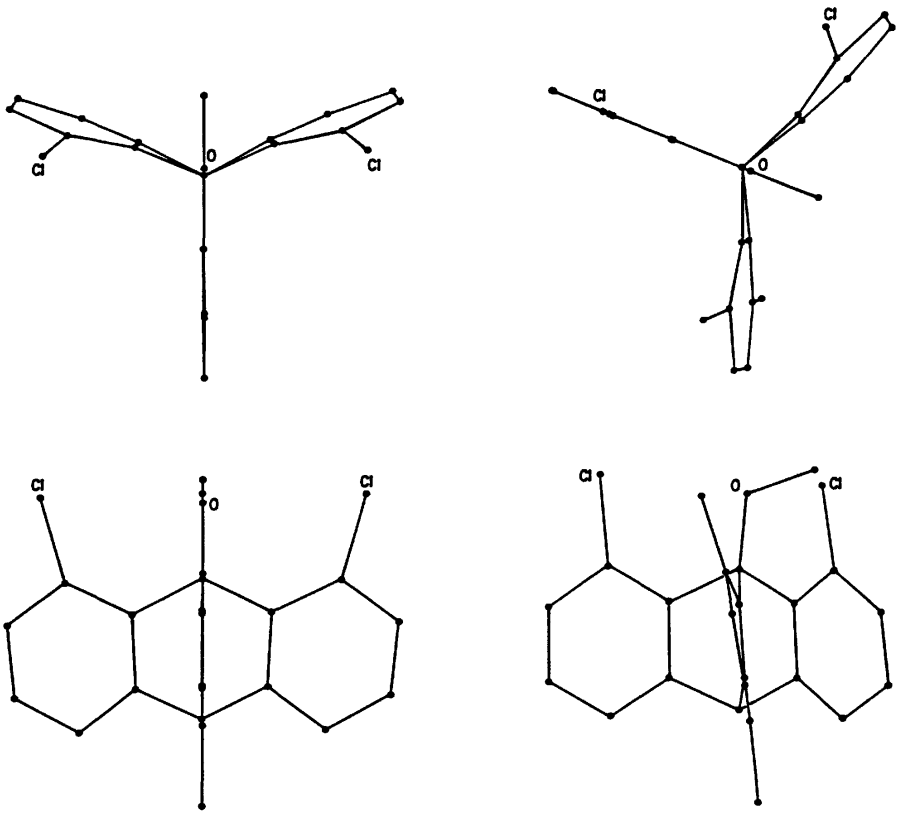

Fig. 1. The optimized geometries of *ap*-**2** and *+sc*-**2**. In each molecule, 9-C and 10-C are placed on the *z*-axis and 9a-C in the *xz* plane, and projections onto the *xy* (upper) and *yz* (lower) planes are shown. Hydrogens are not indicated.

The energy barrier to the direct $+sc \rightleftharpoons -sc$ interconversion, which is not experimentally obtained, was calculated to be 18.3 kcal/mol. As the *O*-methyl group eclipses the *peri*-methyl in the transition state, the higher barrier to this process than that to the $ap \rightleftharpoons \pm sc$ process may be reasonable.

More detailed and sophisticated molecular mechanics calculations on the potential surface of **2** are in progress and the results will be reported separately.

Experimental

1,8-Dichloro-9-methoxyanthracene (4). To a stirred solution of 2.63 g (10.0 mmol) of 1,8-dichloroanthrone[17] in 200 mL of ethanol was added alternately in small portions a solution of 3.0 g of sodium hydroxide in 15 mL of water, and 6.0 mL of dimethyl sulfate. The solid formed was collected by filtration, washed with water and then with methanol, and dried in air, affording 2.30 g (83%) of **4**, mp 170—172 °C (from tetrahydrofuran). Found: C, 64.72; H, 3.36; Cl, 25.57%. Calcd for $C_{15}H_{10}Cl_2O$: C, 65.01; H, 3.64; Cl, 25.58%. ^{1}H NMR ($CDCl_3$): δ=3.38 (3H, s), 7.2—8.2 (6H, m), 8.19 (1H, s).

8,13-Dichloro-9-methoxy-1,4-dimethyltriptycene (2). A solution of 3.30 g (20 mmol) of 3,6-dimethylanthranilic acid[18] in 30 mL of 1,2-dimethoxyethane was added dropwise in the course of 1 h to a boiling solution of 2.62 g (9.44 mmol) of **4** and 2 mL of isopentyl nitrite in 50 mL of dichloromethane. The mixture was heated under reflux for another 30 min and concentrated. The residue was chromatographed through an alumina column with benzene as the eluent. Recrystallization of the eluate from benzene gave 1.34 g (37%) of **2**, mp 279—281 °C. Found: C, 72.19; H, 4.59; Cl, 18.60%. Calcd for $C_{23}H_{18}Cl_2O$: C, 72.45; H, 4.76; Cl, 18.60%. The 400 MHz ^{1}H NMR spectrum of **2** at 25 °C in CD_2Cl_2 allows analysis of the aromatic proton signals: δ=6.635 and 6.669 (AB-q, J=7.8 Hz, 2,3-H_2), 7.061 (dd, J=7.1 and 7.9 Hz, 6,15-H_2), 7.081 (dd, J=1.2 and 7.9 Hz, 7,14-H_2), 7.312 (dd, J=1.2 and 7.1 Hz, 5,16-H_2).

Spectral Measurements. ^{1}H NMR spectra at ambient temperature were recorded on a Varian EM-390 spectrometer operating at 90.0 MHz. Variable temperature ^{1}H and ^{13}C NMR spectra were obtained on a JEOL GX-400 spectrometer operating at 399.65 and 100.53 MHz, respectively. Temperatures were read as digital outputs from the variable temperature accesory and are not corrected.

Computer Simulation. Theoretical spectra were obtained on a HITAC M-280H computer system at the Computer Center of the University of Tokyo (CCUT) using a modified version of the DNMR3 program by Binsch.[19] Three pairs of signals due to the 1-, 4-, and *O*-methyl groups were simulated at each temperature and the most consistent value of rate constant was chosen.

Molecular Mechanics Calculations. The calculations were performed on the HITAC M-280H system using the MM2 program in the CCUT Program Library (code name: Y4/TC/MM2). The force field in the program has been modified by Professor E. Ōsawa from the original program[15] in order that the four-fold torsional potential term (V_4) is considered. Any necessary modification of the calculation procedure accompanying the incorporation of the V_4 terms has been properly taken into account in the program. As

the force field does not contain the parameters concerning C_{arom}–Cl bonds, several parameters were newly added. For the compression and bending force constants, those obtained for tetrachloroethylene were used.[20] For the torsional parameters involving the aromatic chlorine, the corresponding hydrogen parameters in the program were diverted. New parameters are shown below together with modifications for C_{arom}–C_{arom} bonds. The atom type numbers represent as follows; 1: sp^3-carbon, 2: aromatic carbon, 5: hydrogen, 12: chlorine.

Compression	K_s/mdyn†/Å	l_0/Å
2 — 2	8.067	1.3937
2 —12	2.66	1.715

Bending	K_b/mdyn Å/rad^2	t_0/deg
2—2—12	0.400	120.0

Torsion	V_1	V_2	V_3	V_4/kcal/mol
1—2—2—12	0.0	16.4	0.0	−2.3
2—2—2—12	0.0	16.4	−1.06	−2.3
5—2—2—12	0.0	16.4	0.0	−2.3

The authors are grateful to Professor E. Ōsawa for helpful discussion on the molecular mechanics calculations, and to Dr. G. Izumi of Nippon Kayaku Co., Ltd. for the measurements of 400 MHz ^{1}H and 100 MHz ^{13}C NMR spectra.

† 1 dyn = 10^{-5} N.

References

1) Part LV: G. Yamamoto and M. Ōki, *Bull. Chem. Soc. Jpn.*, **57**, 2219 (1984).

2) S. Sternhell, in "Dynamic Nuclear Magnetic Resonance Spectroscopy," ed by L. M. Jackman and F. A. Cotton, Academic Press, New York (1975), pp. 163—201; M. Ōki, *Angew. Chem., Int. Ed. Engl.*, **15**, 87 (1976).

3) T. H. Siddall, III, W. E. Stewart, and M. L. Good, *Can. J. Chem.*, **45**, 1290 (1967).

4) D. A. Bolon, *J. Am. Chem. Soc.*, **88**, 3148 (1966); H. Kessler, A. Rieker, and W. Rundel, *Chem. Commun.*, **1968**, 475; J. J. Bergman and W. D. Chandler, *Can. J. Chem.*, **50**, 353 (1972).

5) E. M. Campi, B. M. K. Gatehouse, W. R. Jackson, I. D. Rae, and M. G. Wong, *J. Chem. Soc., Chem. Commun.*, **1984**, 175.

6) For example: M. Ōki and H. Nakanishi, *Bull. Chem. Soc. Jpn.*, **43**, 2558 (1970); T. B. Grindley, *Tetrahedron Lett.*, **23**, 1757 (1982).

7) W. G. B. Huysmans, W. J. Mijs, J. G. Westra, W. J. van den Hoek, H. A. Gaur, and J. Smidt, *Tetrahedron*, **25**, 2249 (1969).

8) H.-D. Becker and K. Andersson, *J. Org. Chem.*, **47**, 354 (1982).

9) G. Yamamoto and M. Ōki, *Chem. Lett.*, **1984**, 97.

10) G. Bott, L. D. Field, and S. Sternhell, *J. Am. Chem. Soc.*, **102**, 5618 (1980). See also: W. D. Hounshell, L. D. Iroff, D. J. Iverson, R. J. Wrozynski, and K. Mislow, *Isr. J. Chem.*, **20**, 65 (1980).

11) J. P. Lowe, *Prog. Phys. Org. Chem.*, **6**, 1 (1968).

12) G. Yamamoto and M. Ōki, *Bull. Chem. Soc. Jpn.*, **54**, 481 (1981).

13) Y. Kawada and H. Iwamura, *J. Am. Chem. Soc.*, **105**, 1449 (1983).

14) Gordon and Gallagher reported a dynamic process with a barrier of 20 kcal/mol in a diaryl ether derivative which might involve the inversion of a divalent oxygen, but the mechanism seems controversial: A. J. Gordon and J. P. Gallagher, *Tetrahedron Lett.*, **1970**, 2541.

15) N. L. Allinger, *J. Am. Chem. Soc.*, **99**, 8127 (1977); N. L. Allinger and Y. H. Yuh, *QCPE*, No. 395.

16) For example: M. Mikami, K. Toriumi, M. Konno, and Y. Saito, *Acta Crystallogr.*, **B31**, 2474 (1975); N. Nogami, M. Ōki, S. Sato, and Y. Saito, *Bull. Chem. Soc. Jpn.*, **55**, 3580 (1980).

17) E. de B. Barnett and M. A. Mathews, *J. Chem. Soc.*, **123**, 2549 (1923).

18) S. Gronowitz and G. Hansen, *Arkiv Kemi*, **27**, 145 (1967); M. S. Newman and J. A. Cella, *J. Org. Chem.*, **38**, 3482 (1973).

19) G. Binsch, *Top. Stereochem.*, **3**, 97 (1968); D. A. Kleier and G. Binsch, *QCPE*, No. 165.

20) D. E. Mann, L. Fano, J. H. Meal, and T. Shimanouchi, *J. Chem. Phys.*, **27**, 51 (1957).

Efficient Additions of an Electronically Stabilized Persistent Aminyl Radical to Conjugated Alkenes[1)]

Yozo Miura,* Teruo Kunishi, and Masayoshi Kinoshita
Department of Applied Chemistry, Faculty of Engineering, Osaka City University, Sumiyoshi-ku, Osaka 558
(Received January 9, 1985)

It has been found that an electronically stabilized persistent *N*-(4-chlorophenylthio)-3,5-di-*t*-butylphenylaminyl radical (**1**) adds to conjugated alkenes to afford 1:2 adducts of the alkenes and **1** in fair to excellent yields, along with small amounts of 1:1 adducts of the alkenes and **1**.

In contrast to the very large number of studies of the additions of carbon-centered free radicals to alkenes, reports in the literature concerning the additions of nitrogen-centered free radicals to alkenes are rare.[2-10)] Therefore, there is much less information regarding the additions of nitrogen-centered free radicals to alkenes, and the addition reactions are not yet well enough understood.

It has been reported that some aminyl radicals, including $\dot{N}H_2$ and dialkylamino radicals, add to alkenes to give 1:1 and 1:2 adducts of the alkenes and the radicals in low yields. For instance, the photolysis of a solution of tetramethyltetrazene and isopropenylbenzene in cyclohexane affords a 1:2 adduct of the alkene and the dimethylamino radical in a 10% yield, along with a minor formation of 1:1 adducts.[9)]

We have recently found that *N*-(4-chlorophenylthio)-3,5-di-*t*-butylphenylaminyl radical (**1**) adds to some conjugated alkenes to give 1:2 adducts of the alkenes and **1** in fair to excellent yields. Radical **1** is quite persistent, even in the presence of air, and can be isolated as the hydrazine-type dimer **2**, which, upon dissolution into ordinary solvents, dissociates into **1** with a relatively large dissociation constant.[11)] The efficient additions of such an electronically stabilized aminyl radical to conjugated alkenes are rather surprising and considerably interesting. We wish to report herein the products derived from the additions of **1** to conjugated alkenes; the mechanism of the formation of the adducts are also briefly described.

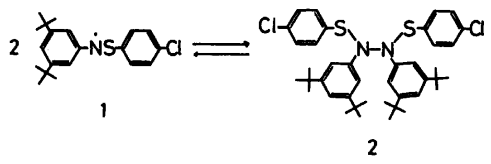

1 2

Results and Discussion

The reactions of **1** with alkenes were carried out in degassed benzene at 50 °C. When mixtures of **1** and alkenes (excess) were heated to 50 °C for 0.3—60 h, the dark blue color attributable to **1** disappeared almost completely, and the mixture became orange or red. The mixtures, after column chromatography, afforded 1:2 adducts of the alkenes and **1** in fair to excellent yields, along with small amounts of 1:1 adducts of alkenes and **1**. The results of the reactions are summarized in Table 1; the yields in the Table are averaged over at least three runs in most cases.

The reaction with styrene yielded, after heating for 14 h, two products (**3a** and **4a**) derived from styrene, along with **5** (11%) and **6** (41%), which do not contain the styrene moiety. Since the latter two products have been found to be formed *via* the self-decomposition of **1** (and **2**),[12)] considerable parts of the products seem to be generated by this reaction. In the former two products, **3a**, which is a 1:2 adduct of styrene and **1**, is the major product (31%), while the minor product, **4a**, which is a 1:1 adduct of styrene and **1**, is formed in a 12% yield. It is almost certain that these products are formed by the routes shown in Scheme 1. Furthermore, the predominant formation of **3a** shows that the intermediate radical, which is derived from the addition of **1** to styrene, is predominantly captured by another molecule of **1** to give **3a**, while hydrogen-atom abstraction from the intermediate radical, probably by **1**, is less important. Therefore, we believe that **1** is not highly active in hydrogen-atom abstraction.

The reaction with isopropenylbenzene afforded three products (**3b**, **4b**, and **7**) derived from the alkene, along with **5** (8.1%) and **6** (27%). The major product **3b**, which is formed in a 40% yield, is a 1:2 adduct of the alkene and **1**, much as in the case of styrene. On the other hand, two minor products, **4b** and **7**, are formed in 3.9 and 6.6% yields respectively. For the formation of **4b**, hydrogen-atom abstraction from the intermediate radical **8** is most likely. On the other hand, for the formation of **7** there are two possible routes: one is hydrogen-atom abstraction from the methyl group of **8**, and the second is first hydrogen-atom abstraction from

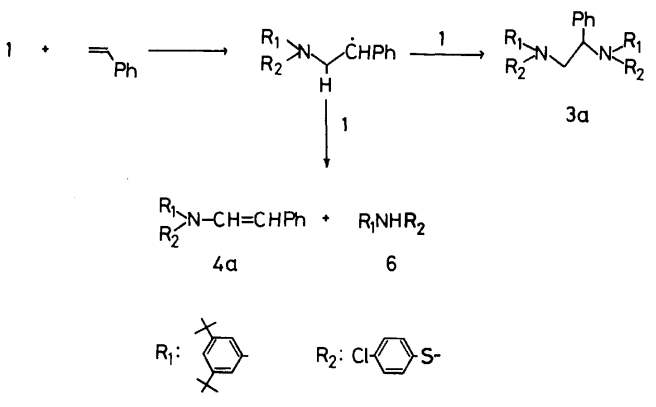

Scheme 1.

the methyl group of isopropenylbenzene, followed by the combination of the resultant intermediate radical with **1**. Although we can not determine unequivocally which route is predominant, we favor the former route, since **1** does not seem to be so active as to abstract a hydrogen atom from the methyl group of isopropenylbenzene.

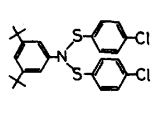

5

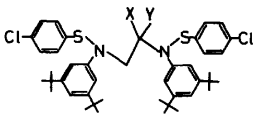

3b: X=Me, Y=Ph
3c: X=Y=Ph

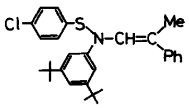

4b

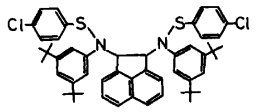

3d

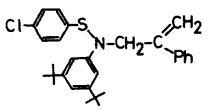

7

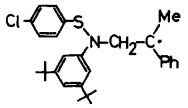

8

The reaction with 1,1-diphenylethylene afforded **3c** in an 88% yield, while the reaction with acenaphthylene gave **3d** in a 38% yield. In neither case could a 1:1 adduct corresponding to **4a** or **4b** be isolated from the reaction mixtures.

The reactions with 1-octene and (*E*)-1,2-diphenylethylene gave neither 1:2 nor 1:1 adducts; even when the mixture of **1** and the alkenes were heated at 50 °C for 60 h, the only products isolated were **5** and **6**.

The reaction with indene was complete within only 0.3 h and gave **9** in a 37% yield, instead of the corresponding 1:2 adduct. Although the TLC of the reaction mixture showed a spot suggesting the formation of trace amounts of the 1:2 adduct, it could not be isolated because they were only trace amounts. It is

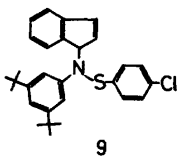

9

most likely that this product is formed by the first abstraction of the allylic hydrogen of indene, probably by **1**, followed by combination of the resultant intermediate radical with **1**. Therefore, the hydrogen-atom abstraction is predominant over the addition of **1** to the double bond of indene; this is in accord with the highly reactive allylic hydrogens of indene.

As can be seen from Table 1, the total yields of the 1:1 and 1:2 adducts increase in the following order: 1-octene ≈(*E*)-1,2-diphenylethylene<acenaphthylene< styrene<isopropenylbenzene<1,1-diphenylethylene.

Table 1. Results of the reactions of **1** with alkenes[a—c]

Alkene[d]	Time[e] h	Products (%)[f]
1-Octene	60	g)
Styrene	14	**3a** (31), **4a** (12)
Isopropenylbenzene	11	**3b** (40), **4b** (3.9), **7** (6.6)
1,1-Diphenylethylene	7	**3c** (88)
(*E*)-1,2-Diphenylethylene	60	g)
Acenaphthylene	5	**3d** (38)
Indene	0.3	**9** (37)

a) Dimer **2**: 0.577 mmol. b) Temperature: 50 °C. c) Solvent: benzene 10 cm^3. d) Alkene: 7.7 mmol. e) Time required for the complete reaction of **1**. f) Isolated yield based on **1**. g) No formation of adducts was revealed by a TLC inspection of the reaction mixture.

This order is parallel to the stabilities of the intermediate radicals resulting from the addition of **1** to the alkenes. The only exception is (*E*)-1,2-diphenylethylene. In this case no formation of adducts can be reasonably explained in terms of the steric inhibition in the addition reaction.

Experimental

The melting point were taken on a Yanagimoto micro-melting point apparatus and are uncorrected. The IR spectra were run on a JASCO A-200 spectrometer as KBr pellets. The ^{1}H NMR spectra were measured with a JEOL PS-100 spectrometer, using TMS as the internal standard.

Styrene, isopropenylbenzene, 1,1-diphenylethylene, and indene were, after column chromatography on alumina (Merck art 1097; column size, 3×10 cm; eluant, hexane), distilled under reduced pressure prior to use, while acenaphthylene was purified by recrystallization (ethanol) and sublimation. *N,N'*-Bis(4-chlorophenylthio)-*N,N'*-bis(3,5-di-*t*-butylphenyl)hydrazine (**2**) was prepared by our previously reported method.[11]

General Procedure for Reactions of 1 with Alkenes. Dimer **2** (400 mg, 0.577 mmol), alkene (7.7 mmol), and benzene (10 cm^3) were placed in a glass tube, the content was degassed by three freeze-pump-thaw cycles, and the tube was sealed off from the vacuum system. The tube was then immersed in a water-bath heated to 50 °C, and the precipitate, **2**, in the solution was dissolved with occasional shaking. When the blue color of the reaction mixture had been changed to orange or red, the tube was broken and the mixture was evaporated under reduced pressure. Column chromatography of the residue on silica gel (Wako gel C-200, column size, 3×45 cm) at 3—5 °C gave products, **3**—**7** and **9**.

Reaction with Styrene. After being heated for 14 h, the reaction mixture (orange) was evaporated; subsequent column chromatography of the residue, with 1:7 benzene–hexane as the eluant, gave the following products: **5**, 30 mg (0.061 mmol), which was identified by its melting point [118—119 °C (from methanol) (lit,[12] 119—121 °C)] and by comparing its IR spectrum with that of an authentic sample. **4a**: 60 mg (0.13 mmol, 12%); colorless needles; mp 131—132 °C (from methanol); IR 2950—2850 (C–H of *t*-Bu) and 1640 cm^{-1} (vinyl); NMR ($CDCl_3$) δ=1.30 (s, *t*-Bu, 18H), 6.37 (d, J=15 Hz, vinylic, 1H), and 7.20—7.38 (m, aromatic, 12H, and vinylic, 1H). Found: C, 74.93; H, 7.05; N, 2.90%. Calcd

for $C_{28}H_{32}ClNS$: C, 74.72; H, 7.17; N, 3.11%. **3a**: 141 mg (0.177 mmol, 31%); colorless prisms; mp 179.5—180.5 °C (from methanol-benzene); NMR ($CDCl_3$) δ=1.13 and 1.23 (each s, *t*-Bu, 36H), 4.24 (dd, *J*=5 and 15 Hz, CHH-N, 1H), 4.52 (dd, *J*=7 and 15 Hz, CHH-N, 1H), 5.68 (dd, *J*=5 and 7 Hz, CH-N, 1H), and 6.76—7.29 (m, aromatic, 19H). Found: C, 72.16; H, 7.59; N, 3.64%. Calcd for $C_{48}H_{58}Cl_2N_2S_2$: C, 72.24; H, 7.33; N, 3.51%. **6**: 163 mg (0.468 mmol), which was identified by its melting point [151—152 °C (from hexane) (lit,[11] 150—151 °C)] and by comparing its IR spectrum with that of an authentic sample.

Reaction with Isopropenylbenzene. After being heated for 11 h, the reaction mixture (orange) was evaporated; subsequent column chromatography of the residue, with 1:7 benzene-hexane as the eluant, gave the following five products: **5**, 23 mg (0.047 mmol), which was identified by its melting point [118—119 °C (from methanol)(lit,[12] 119—121 °C] and by comparing its IR spectrum with that of an authentic sample. **4b**: 21 mg (0.045 mmol, 3.9%); colorless prisms; mp 96—97 °C (from methanol); IR 2950—2850 (C-H of *t*-Bu) and 1620 cm^{-1} (vinyl); NMR ($CDCl_3$) δ=1.28 (s, *t*-Bu, 18H), 1.97 (d, *J*=1.2 Hz, CH_3, 3H), 6.59 (q, *J*=1.2 Hz, vinylic, 1H), and 7.01—7.18 (m, aromatic, 12H). Found: C, 75.33; H, 7.29; N, 3.10%. Calcd for $C_{29}H_{34}ClNS$: C, 75.05; H, 7.38; N, 3.02%. **7**: 36 mg (0.078 mmol, 6.6%); colorless needles; mp 119—120 °C (from methanol); IR 2950—2850 (C-H of *t*-Bu) and 1630 cm^{-1} (vinyl); NMR ($CDCl_3$) δ=1.26 (s, *t*-Bu, 18H), 4.72 (s, CH_2, 2H), 5.22 (s, vinylic, 1H), 5.46 (s, vinylic, 1H), and 6.97—7.37 (m, aromatic, 12H). Found: C, 75.64; H, 7.51; N, 2.64%. Calcd for $C_{29}H_{34}ClNS$: C, 75.05; H, 7.38; N, 3.02%. **3b**: 186 mg (0.229 mmol, 40%); colorless prisms; mp 159—161 °C (from methanol-benzene); NMR (CCl_4) δ=1.12 and 1.20 (each s, *t*-Bu, 36H), 1.80 (s, CH_3, 3H), 4.31 (d, *J*=15 Hz, CHH-N, 1H), 4.56 (d, *J*=15 Hz, CHH-N, 1H), and 6.63—7.28 (m, aromatic, 19H). Found: C, 72.37; H, 7.37; N, 3.45%. Calcd for $C_{49}H_{60}Cl_2N_2S_2$: C, 72.47; H, 7.45; N, 3.45%. **6**: 108 mg (0.310 mmol), which was identified by its melting point [151—152 °C (from hexane) (lit,[11] 150—151 °C)] and by comparing its IR spectrum with that of an authentic sample.

Reaction with 1,1-Diphenylethylene. After being heated for 7 h, the reaction mixture (orange) was evaporated; subsequent column chromatography of the residue, with 1:5 benzene-hexane as the eluant, gave 445 mg (0.509 mmol, 88%) of **3c**: colorless needles; mp 116—117 °C (from methanol-benzene); NMR (CCl_4) δ=1.18 and 1.20 (each s, *t*-Bu, 36H), 4.62 (s, CH_2, 2H), and 6.46—7.50 (m, aromatic, 24H). Found: C, 74.05; H, 7.14; N, 3.31%. Calcd for $C_{54}H_{62}Cl_2N_2S_2$: C, 74.20; H, 7.15; N, 3.21%.

Reaction with Acenaphthylene. Afer being heated for 5 h, the reaction mixture (red) was evaporated; subsequent column chromatography of the residue, with 1:5 benzene-hexane as the eluant, gave 184 mg (0.217 mmol, 38%) of **3d**: colorless needles; mp 206—209 °C (decomp) (from methanol-benzene); NMR (CCl_4) δ=1.15 (s, *t*-Bu, 36H), 6.25 (s, CH, 2H), and 6.75—7.73 (m, aromatic, 20H). Found: C, 74.11; H, 6.88; N, 3.36%. Calcd for $C_{52}H_{58}Cl_2N_2S_2$: C, 73.82; H, 6.91; N, 3.31%.

Reaction with Indene. After being heated for 0.3 h, the reaction mixture (light orange) was evaporated; subsequent column chromatography of the residue, with 1:7 benzene-hexane as the eluant, gave 147 mg (0.423 mmol, 37%) of **9**: colorless needles; mp 149.5—150.5 °C (from methanol); NMR (CCl_4) δ=1.19 (s, *t*-Bu, 18H), 5.52 (dd, *J*=1.8 and 2.2 Hz, CH, 1H), 6.38 (dd, *J*=1.8 and 5.7 Hz, olefinic, 1H), 6.78 (dd, *J*=2.2 and 5.7 Hz, olefinic, 1H), and 6.84—7.40 (m, aromatic, 11H). Found: C, 75.13; H, 7.11; N, 3.27%. Calcd for $C_{29}H_{32}ClNS$: C, 75.37; H, 6.98; N, 3.03%..

References

1) ESR Studies of Nitrogen Centered Free Radicals 25. For Part 24 see: Y. Miura, T. Kunishi, M. Isogai, and M. Kinoshita, *J. Org. Chem.*, in press.
2) R. S. Neale, *Synthesis*, **1971**, 1.
3) Y. Ogata, Y. Izawa, and H. Tomioka, *Tetrahedron*, **23**, 1509 (1967).
4) S. Shih, R. J. Buenker, S. D. Peyerimhoff, and C. J. Michejda, *J. Am. Chem. Soc.*, **94**, 7620 (1972).
5) P. V. Khe and R. Lesclaux, *J. Phys. Chem.*, **83**, 1119 (1979).
6) B. R. Cowley and W. A. Waters, *J. Chem. Soc.*, **1961**, 1228.
7) A. Good and J. C. J. Thynne, *J. Chem. Soc., B*, **1967**, 684.
8) K. Sugiyama, T. Nakaya, and M. Imoto, *Makromol. Chem.*, **175**, 1497 (1974).
9) C. J. Michejda and D. H. Campbell, *Tetrahedron Lett.*, **1977**, 577; *J. Am. Chem. Soc.*, **101**, 7687 (1979).
10) D. F. Church and W. A. Pryor, *J. Org. Chem.*, **45**, 2866 (1980).
11) Y. Miura, A. Yamamoto, Y. Katsura, and M. Kinoshita, *J. Org. Chem.*, **45**, 3875 (1980).
12) Y. Miura, A. Yamamoto, and M. Kinoshita, *Bull. Chem. Soc. Jpn.*, **54**, 3215 (1981).

Enantiodivergent Total Syntheses of Nanaomycins and Their Enantiomers, Kalafungins

Kuniaki TATSUTA,* Kohji AKIMOTO, Masahiko ANNAKA,
Yutaka OHNO, and Mitsuhiro KINOSHITA
Department of Applied Chemistry, Faculty of Science and Technology, Keio University, Hiyoshi, Kohoku-ku, Yokohama 223
(Received January 10, 1985)

The first, enantiospecific total syntheses of pyranonaphthoquinone antibiotics, nanaomycins D and A, and their enantiomers, kalafungin and 4-deoxykalafunginic acid are described by an "enantiodivergent" strategy from a common optically active intermediate, (1*S*,3*RS*,4*S*)-3,4-dihydro-5,9,10-trimethoxy-1-methyl-1*H*-naphtho[2,3-*c*]pyran-3,4-diol, which has been derived from L-rhamnose *via* condensation of 4-methoxy-3-(phenylsulfonyl)-1(3*H*)-isobenzofuranone and methyl 3,4,6-trideoxy-α-L-*glycero*-hex-3-enopyranosid-2-ulose.

Nanaomycin D[1] (**1**), kalafungin[2] (**2**), granaticin[3] (**3**), medermycin[4] (**4**), and nanaomycin A[5] (**5**) are members of a growing family of pyranonaphthoquinone (benzoisochromanquinone) antibiotics (Chart 1), which have been shown to possess significant antimicrobial activities and potential antitumor activities.[6] Remarkably, nanaomycin D (**1**) and kalafungin (**2**) are enantiomers with each other, and both antipode systems have been found as major constituents of many kinds of pyranonaphthoquinone antibiotics such as **3** and

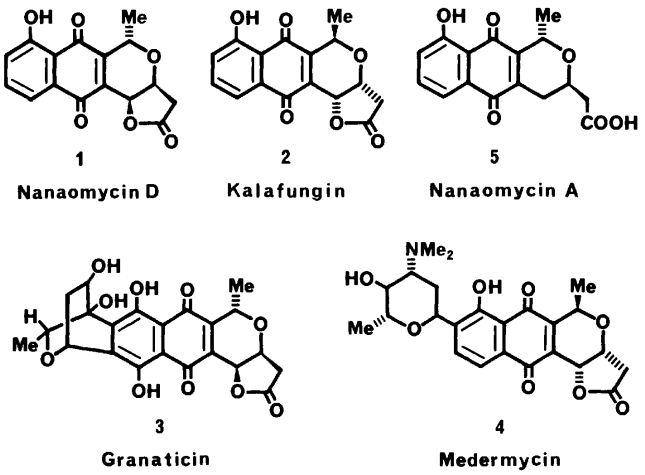

Chart 1.

4. These unique structural features as well as the opportunities to develop synthetic strategies for the construction of more diverse analogs of these interesting antibiotics prompted the immense investigations of their syntheses.[7] No fewer than ten syntheses of racemic nanaomycin A (**5**), in particular, have been described with various strategies,[8] however, stereospecific syntheses of these kinds of optically active antibiotics have not been reported to date. Very recently, the first, total syntheses of natural nanaomycin D (**1**) and kalafungin (**2**) were disclosed in our laboratories.[9]

Described herein with full details are the first, enantiospecific total syntheses of nanaomycins D (**1**) and A (**5**), and their enantiomers, kalafungin (**2**) and 4-deoxykalafunginic acid (**5'**) from a common optically active intermediate **7** by the "enantiodivergent" strategy.[10]

The antithetic strategy relating both antipodes **1** and **2** to the starting material, L-rhamnose (**11**) is put forth in Scheme 1. The alcoholysis of the lactone moiety of **1** leads to the hydroxy ester **6**, which in turn leads to the hemiacetal **7** upon application of the indicated retro Michael cyclization and retro Wittig reaction at the C-3 position. On the other hand, the alcoholysis of **2** with the fascinating epimerization at the C-1 and C-4 positions leads to the other hydroxy ester **8**, which returns similarly to the key intermediate **7**. The common intermediate is expected to be derived from condensation of **9**[11] with **10**.

In the synthetic sense (Scheme 2), conversion of L-rhamnose (**11**) to methyl 3,4,6-trideoxy-α-L-*glycero*-hex-3-enopyranosid-2-ulose[12] (**10**) was initially achieved by the following practical procedure. Methyl α-L-rhamnoside, which was prepared from L-rhamnose (**11**), was converted into methyl 2,3-di-*O*-carbonyl-6-

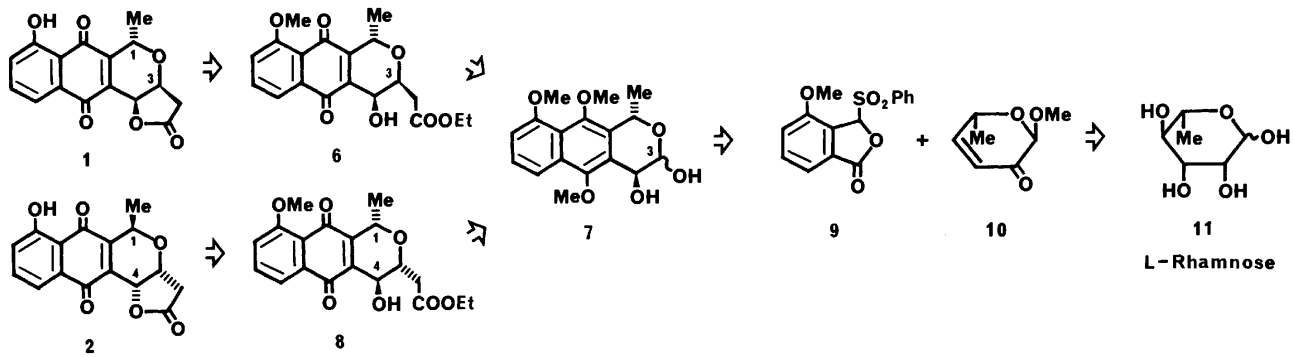

Scheme 1.

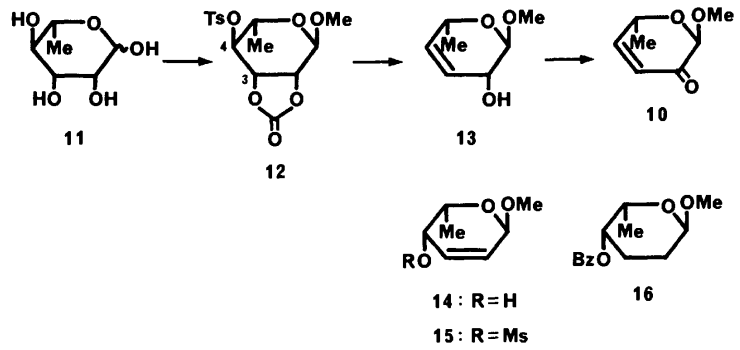

Scheme 2.

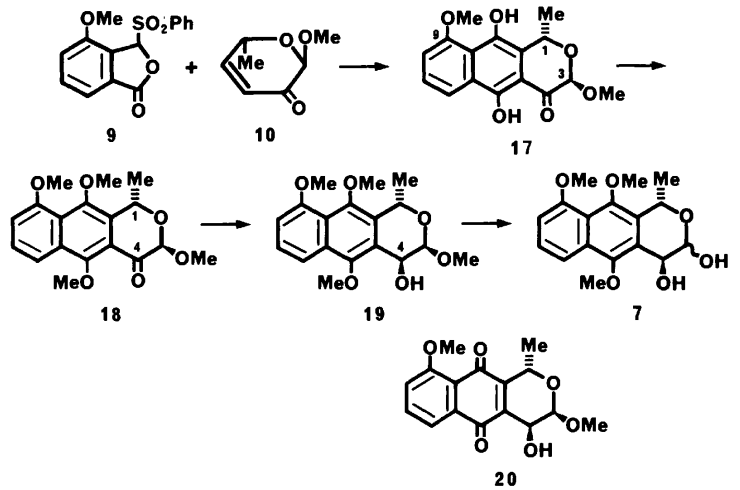

Scheme 3.

deoxy-4-*O*-tosyl-α-L-mannoside (**12**) in an 80% overall yield by a one-pot reaction with trichloromethyl chloroformate and then tosyl chloride in pyridine. Treatment of **12** with zinc powder and sodium iodide in refluxing aqueous acetonitrile gave, presumably through the corresponding 3,4-epoxide[13] with removal of the carbonate-protecting group, a mixture of the desired unsaturated alcohol, methyl 3,4,6-trideoxy-α-L-*threo*-hex-3-enopyranoside[12] (**13**) and its migrated alcohol, methyl 2,3,6-trideoxy-α-L-*threo*-hex-2-enopyranoside (**14**) in 60 and 28% yields. Oxidation of **13** with pyridinium chlorochromate afforded the stable α,β-unsaturated ketone (**10**) in an 86% yield. The migrated alcohol **14** was efficiently recycled to **13** along with its C-2 epimeric alcohol in an 85% yield by mesylation to give methyl 2,3,6-trideoxy-4-*O*-mesyl-α-L-*threo*-hex-2-enopyranoside (**15**) followed by exposure to potassium carbonate in aqueous tetrahydrofuran to result in the S_N2' type solvolysis. The mixture thus obtained could be similarly converted into the desired ketone **10**. The stereochemistry of **14** was clarified by the ^{1}H NMR study of the corresponding benzoylated compound, methyl 4-*O*-benzoyl-2,3,6-trideoxy-α-L-*threo*-hexopyranoside (**16**), which existed in the $^1C_4$ conformation.

The other starting material, 4-methoxy-3-(phenylsulfonyl)-1(3*H*)-isobenzofuranone (**9**) was synthesized according to the Hauser's conditions.[11]

As shown in Scheme 3, condensation of **10** with the lithium *t*-butoxide generated anion of **9** gave, in an 80% yield, the hydroquinone, (1*S*,3*R*)-5,10-dihydroxy-3,9-dimethoxy-1-methyl-1*H*-naphtho[2,3-*c*]-pyran-4(3*H*)-one (**17**), which was treated with dimethyl sulfate to produce quantitatively (1*S*,3*R*)-3,5,9,10-tetramethoxy-1-methyl-1*H*-naphtho[2,3-*c*]pyran-4(3*H*)-one (**18**). Reduction of **18** with sodium borohydride afforded exclusively (1*S*,3*R*,4*S*)-3,4-dihydro-3,5,9,10-tetramethoxy-1-methyl-1*H*-naphtho[2,3-*c*]pyran-4-ol (**19**) in a 90% yield. The stereoselective hydride delivery is assisted in the desired sense by the *syn* stereodirecting influence of the pyrano oxygen atom[14] as partly depicted in Chart 2, where the C-3 *O*-methyl group would be oriented to be in axial by the anomeric effect[15] as commonly seen in carbohydrates. The (*S*)-con-

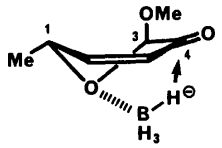

Chart 2.

figuration at the C-4 of **19** was confirmed by the ^{1}H NMR study of the following derivatives **21** ($J_{3,4}$= 3.0 Hz) and **22** ($J_{3,4}$=9.5 Hz), and the reasonable trans-

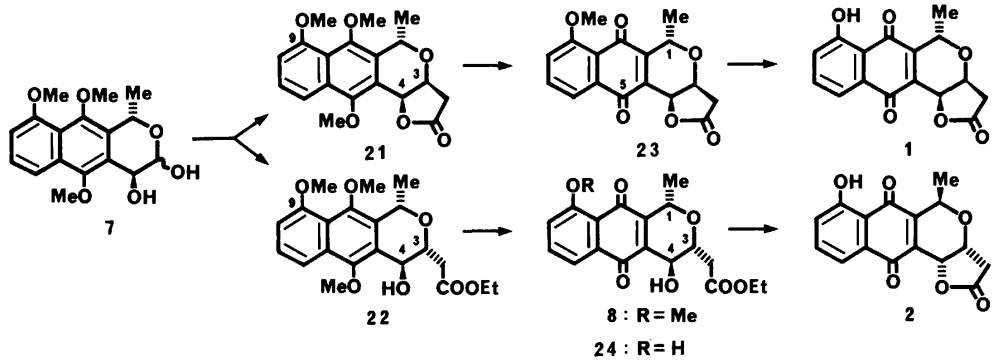

Scheme 4.

Table 1. Minimal inhibitory concentration (mcg/ml) of **1**, **2**, **5**, **5'**, **21**, **22**, **23**, and **24**

	1	**2**	**5**	**5'**	**21**	**22**	**23**	**24**
Staphylococcus aureus FDA209P	<0.2	<0.2	<0.2	<0.2	6.25	100	1.56	12.5
Staphylococcus aureus Smith	<0.2	<0.2	<0.2	<0.2	6.25	>100	1.56	3.12
Micrococcus flavus FDA16	<0.2	0.39	0.39	0.78	25	>100	3.12	12.5
Bacillus subtilis PCI219	0.39	<0.2	0.78	0.78	12.5	>100	3.12	6.25
Escherichia coli NIHJ	3.12	6.25	12.5	25	>100	>100	25	100
Shigella dysenteriae JS11910	3.12	1.56	6.25	6.25	100	>100	12.5	25
Mycobacterium smegmatis ATCC607	12.5	6.25	25	25	50	100	>100	12.5

formation from **21** to **1**. Reaction of **19** with ammonium cerium(IV) nitrate[8b] gave the quinone, (1*S*,3*R*,4*S*)-3,4-dihydro-4-hydroxy-3,9-dimethoxy-1-methyl-1*H*-naphtho[2,3-*c*]pyran-5,10-dione (**20**), which was also derived directly from **17** by reduction with sodium borohydride followed by air oxidation. Acid hydrolysis of **20** gave the corresponding hemiacetal, which, however, was not a useful intermediate for the following Wittig reaction, because the reaction afforded several products in low yields. Then, **19** was hydrolyzed with dil. hydrochloric acid, giving quantitatively the key intermediate, (1*S*,3*RS*,4*S*)-3,4-dihydro-5,9,10-trimethoxy-1-methyl-1*H*-naphtho[2,3-*c*]pyran-3,4-diol (**7**) without epimerization at the C-1 and C-4. The hemiacetal **7** was submitted to Wittig reaction with ethoxycarbonylmethylenetriphenylphosphorane in refluxing toluene to give two products as expected:[8b,16] (1*S*,3*S*,4*S*)-3,4,11,12-tetrahydro-5,9,10-trimethoxy-1-methyl-1*H*-furo[3,2-*b*]-naphtho[2,3-*d*]pyran-12-one (**21**) and ethyl (1*S*,3*R*,4*S*)-3,4-dihydro-4-hydroxy-5,9,10-trimethoxy-1-methyl-1*H*-naphtho[2,3-*c*]pyran-3-acetate (**22**) in 53 and 41% yields, respectively (Scheme 4). The lactone **21** results from a two-step sequence including the intramolecular Michael cyclization of the intermediary Wittig α,β-unsaturated ester and concomitant lactonization of the resultant 3,4-*cis* hydroxy ester such as **6**. The other 3,4-*trans* hydroxy ester **22** results from the Michael cyclization without lactonization. The lactone **21** was treated with ammonium cerium(IV) nitrate[8b] to give, in a 92% yield, 9-*O*-methylnanaomycin D (**23**), which was equivalent to the structure **6**. The ^{1}H NMR spectrum of **23** has already been superimposable on that of nanaomycin D (**1**) except in the phenyl- and *O*-methyl-signals region. De-*O*-methylation of **23** was attempted with two known reagents, boron tribromide[8c] and aluminium chloride.[8b] Reaction with boron tribromide, however, furnished a mixture of nanaomycin D (**1**) and its brominated product, which were detected by thin-layer chromatography only with a solvent system of dichloromethane–chloroform. De-*O*-methylation with aluminium chloride provided (−)-nanaomycin D (**1**) in a 95% yield as a single product identical in all respects including antibacterial activity (Table 1) with an authentic sample of the natural antibiotic, thereby confirming the absolute structure.

On the other hand, the ester **22** was converted by the aforesaid cerium(IV) oxidative demethylation into ethyl (1*S*,3*R*,4*S*)-3,4,5,10-tetrahydro-4-hydroxy-9-methoxy-1-methyl-5,10-dioxo-1*H*-naphtho[2,3-*c*]pyran-3-acetate (**8**), which was treated with aluminium chloride to give ethyl (1*S*,3*R*,4*S*)-3,4,5,10-tetrahydro-4,9-dihydroxy-1-methyl-5,10-dioxo-1*H*-naphtho[2,3-*c*]-pyran-3-acetate (**24**) in an 84% overall yield. On the final stage, the favored epimerization of the C-1 and C-4 positions was realized by exposure to sulfuric acid[7a] in benzene along with some lactonization, followed by refluxing in toluene to complete the lactonization, affording, in a 92% yield, (+)-kalafungin (**2**) identical with an authentic sample of the natural antibiotic in all respects including antibacterial activity (Table 1). This stereocontrolled epimerization indicated that the C-3 stereochemistry was so vital for the subsequent development of the correct chirality at the C-1 and C-4 positions.

Hydrogenolysis of **1** and **2** furnished quantitatively nanaomycin A (**5**) and its enantiomer, 4-deoxykalafunginic acid (**5'**), respectively, the former of

which was identical with the natural antibiotic. Both compounds **5** and **5'** were readily recycled to **1** and **2**, respectively, by air oxidation.[1] Since compound **5'** has not been in the natural sources yet, these results suggest that, also in the biosynthesis, nanaomycin A (**5**) would be derived from nanaomycin D (**1**) by the appropriate reductase.[17]

The antibacterial activities (Table 1) of **1**, **2**, **5**, **5'**, **21**, **22**, **23**, and **24** revealed that the naphthoquinone and lactone portions were positively required for the appearance of stronger activities.

Thus, both antipodes of antibiotics, (−)-nanaomycins (**1** and **5**) and (+)-kalafungins (**2** and **5'**) have been synthesized from L-rhamnose (**11**) through a common key intermediate **7** in overall yields of approximately 18 and 13%, respectively, by the "enantiodivergent" strategy, which is promising for application to the syntheses of both optical antipodes of the other members of this important class of antibiotics.

Experimental

Melting points were determined on a micro hot-stage Yanaco MP-S3 and were uncorrected. IR spectra were recorded on a Hitachi Perkin-Elmer 225 spectrometer, UV spectra on JAS-CO UVIDEC-1 spectrometer, and ^{1}H-NMR spectra with TMS as internal standard on a Varian EM-390 (90 MHz) or a JEOL GX-400 (400 MHz) spectrometer. Optical rotations were measured on a JAS-CO DIP-360 photoelectric polarimeter. Silica gel TLC and column chromatography were performed on Merck TLC 60F-254 and Kieselgel 60, respectively. In general, organic solvents were purified and dried by the appropriate procedures, and evaporation and concentration were carried out under reduced pressure below 30 °C, unless otherwise noted.

The starting material, 4-methoxy-3-(phenylsulfonyl)-1(3*H*)-isobenzofuranone (**9**) was prepared according to the published procedure[11] and recrystallized from ethyl acetate–hexane to give needles: mp 189—191 °C.

Methyl 2,3-Di-O-carbonyl-6-deoxy-4-O-tosyl-α-L-mannoside (12). A) Through the Isolated 2,3-Carbonate: A solution of L-rhamnose monohydrate (**11**; 33.7 g) in methanol (169 ml) with 10% methanolic hydrogen chloride solution (2 ml) was refluxed for 72 h. After neutralization with $NaHCO_3$, the precipitated salt was filtered off and the filtrate was evaporated to a residue, which was dissolved in acetone (170 ml). After filtration, the filtrate was evaporated to give a crude solid of methyl α-L-rhamnoside (33 g).

To a stirred and ice-cooled solution of the crude solid (33 g) in pyridine (330 ml) was added dropwise trichloromethyl chloroformate (22.0 ml), and stirring was continued at room temperature for 1 h. After addition of water (7.3 ml), the mixture was evaporated and co-evaporated with toluene to give a residue, which was partitioned between ethyl acetate and a saturated aqueous $NaHCO_3$ solution. The combined organic layers were washed with a saturated aqueous NaCl solution, dried (Na_2SO_4), and evaporated to give a crude solid of the 2,3-carbonate (38 g). A part of the solid was recrystallized from ethyl acetate to afford plates of the 2,3-carbonate: mp 169—171 °C; $[\alpha]_D^{24}$ −59° (*c* 1.0, $CHCl_3$); IR (KBr) 1810 cm^{-1} (carbonate).

A solution of the crude solid (37.8 g) in pyridine (378 ml) was stirred with tosyl chloride (52.9 g) at 60 °C for 36 h. After addition of ethanol (16 ml), the mixture was evaporated to a residue, which was partitioned between ethyl acetate and a saturated aqueous $NaHCO_3$ solution. The combined organic layers were washed with a saturated aqueous NaCl solution, dried and evaporated to a residue, which was chromatographed on silica gel (1330 g) with 6:1 benzene–ethyl acetate to give a solid. Recrystallization from ethyl acetate–ether gave needles of **12** (53.0 g, 80% from **11**): R_f 0.72 (4:1 benzene–ethyl acetate); mp 99.5—101 °C; $[\alpha]_D^{24}$ +23° (*c* 1.0, $CHCl_3$); IR (KBr): 1816, 1792, and 1179 cm^{-1}; ^{1}H-NMR (90 MHz, $CDCl_3$): δ=1.38 (3H, d, Me, $J_{5,Me}$=6 Hz), 2.48 (3H, s, Me of Ts), 3.40 (3H, s, OMe), 3.86 (1H, dq, H-5, $J_{4,5}$=9.0 Hz), 4.23—4.72 (3H, m, H-2, 3, and 4), 4.93 (1H, s, H-1), 7.40 (2H, d, Ts, J_{AB}=9 Hz), 7.87 (2H, d, Ts).

Found: C, 50.02; H, 5.09; S, 8.90%. Calcd for $C_{15}H_{18}O_8S$: C, 50.27; H, 5.06; S, 8.95%.

B) Without Isolation of the 2,3-Carbonate: The crude methyl α-L-rhamnoside (49.9 g), which was prepared from L-rhamnose monohydrate (**11**; 50 g) as described above, was dissolved in pyridine (500 ml), and trichloromethyl chloroformate (32.1 ml) was added with cooling. After stirring at room temperature for 2 h, to the reaction mixture was added tosyl chloride (103 g), and stirring was continued at 80 °C for another 24 h. The resulting mixture was worked up as described above to give a solid of **12** (79.6 g, 81%), which was used for the next step.

Methyl 3,4,6-Trideoxy-α-L-threo-hex-3-enopyranoside (13) and Methyl 2,3,6-Trideoxy-α-L-threo-hex-2-enopyranoside (14). To a solution of **12** (70.1 g) in 95% aqueous acetonitrile (700 ml) were added NaI (235 g) and Zn powder (102 g), and the suspension was stirred under argon at 75 °C for 36 h and then cooled to room temperature. The suspension was filtered and the insoluble mass was washed with ethyl acetate. The filtrates and washings were combined, washed with 5% aqueous $Na_2S_2O_3$ solution, dried and evaporated at 85 °C under atmospheric pressure to give a residue. This was chromatographed on silica gel (1400 g) with 7:4 carbon tetrachloride–ethyl acetate to give **13** (16.9 g, 60%) and **14** (7.89 g, 28%) having the R_f-values of 0.26 and 0.20 (2:1 benzene–ethyl acetate), respectively.

13: Oil; bp 90 °C (933 Pa); $[\alpha]_D^{24}$ −206° (*c* 1.0, $CHCl_3$) [lit,[12] $[\alpha]_D^{20}$ −74° (*c* 1, $CHCl_3$)]; IR ($CHCl_3$): 1447, 1402, 1371, and 1345 cm^{-1}; ^{1}H-NMR (90 MHz, $CDCl_3$+D_2O): δ=1.29 (3H, d, Me, $J_{5,Me}$=6.5 Hz), 3.49 (3H, s, OMe), 3.76 (1H, broad s, H-2), 4.30 (1H, dq, H-5, $J_{4,5}$=1.5 Hz), 4.71 (1H, s, H-1), 5.90 (2H, apparently s, H-3 and 4, $J_{3,4}$=10.5 Hz).

Found: C, 58.05; H, 8.17%. Calcd for $C_7H_{12}O_3$: C, 58.32; H, 8.39%.

14: Oil [bp 75 °C (400 Pa)], which, after distillation under reduced pressure, was changed to cottony crystals (mp 45—47 °C); $[\alpha]_D^{24}$ +123° (*c* 1.0, $CHCl_3$); IR (KBr): ≈1620, 1441, 1405, 1393, and 1386 cm^{-1}; ^{1}H-NMR (90 MHz, $CDCl_3$+D_2O): δ=1.30 (3H, d, Me, $J_{5,Me}$=6.5 Hz), 3.45 (3H, s, OMe), 3.55 (1H, sharp m, H-4, half-width of 10.5 Hz), 4.12 (1H, dq, H-5, $J_{4,5}$=2.2 Hz), 4.85 (1H, d, H-1, $J_{1,2}$=3 Hz), 5.88 (1H, dd, H-2, $J_{2,3}$=10.5 Hz), 6.20 (1H, dd, H-3, $J_{3,4}$=6 Hz).

Found: C, 58.06; H, 8.46%. Calcd for $C_7H_{12}O_3$: C, 58.32; H, 8.39%.

Methyl 2,3,6-Trideoxy-4-O-mesyl-α-L-threo-hex-2-enopyranoside (15). A solution of **14** (152 mg) in pyridine (3.0 ml) was stirred with mesyl chloride (0.10 ml) at room temperature for 30 min. After addition of ethanol (0.076 ml), the

mixture was evaporated to a residue, which was partitioned between ethyl acetate and water. The combined organic layers were evaporated to a residue, which was chromatographed on silica gel (10 g) with 5:1 benzene–ethyl acetate followed by recrystallization from ethyl acetate–hexane to give labile needles of **15** (222 mg, 95%): R_f 0.49 (2:1 benzene–ethyl acetate); mp 97—98 °C; $[\alpha]_D^{24}$ +168° (*c* 1.0, $CHCl_3$); IR (KBr): ≈1630 (olefin), and 1179 cm^{-1} (SO_2); ^{1}H-NMR (90 MHz, $CDCl_3$): δ=1.37 (3H, d, Me-5, $J_{5,Me}$=6.5 Hz), 3.06 (3H, s, Ms), 3.45 (3H, s, OMe), 4.26 (1H, dq, H-5, $J_{4,5}$=2.5 Hz), 4.65—4.80 (1H, sharp m, H-4, half-width of 8.0 Hz), 4.92 (1H, d, H-1, $J_{1,2}$=2.0 Hz), 5.95—6.32 (2H, m, H-2 and 3).

Found: C, 43.60; H, 6.08%. Calcd for $C_8H_{13}O_5S$: C, 43.43; H, 5.92%.

*Methyl 4-O-Benzoyl-2,3,6-trideoxy-α-*L*-*threo*-hexopyranoside (16).* A solution of **14** (1.10 g) in pyridine (22.2 ml) was stirred with benzoyl chloride (1.8 ml) at room temperature for 45 min. After addition of ethanol (1 ml), the mixture was evaporated to a residue, which was partitioned between ethyl acetate and a saturated aqueous NaCl solution. The combined organic layers were evaporated to a residue, which was chromatographed on silica gel (95 g) with 10:1 hexane–ethyl acetate to give a syrup of the benzoate (1.73 g, 90.8%): R_f 0.33 (10:1 hexane–ethyl acetate).

A solution of the syrup (235 mg) in ethanol (2.4 ml) was shaken with 5% palladium–carbon and 3-atm hydrogen at room temperature for 12 h, filtered and evaporated to a residue. This was chromatographed on silica gel (23 g) with 10:1 hexane–ethyl acetate to give a syrup of **16** (188 mg, 80%): R_f 0.35 (10:1 hexane–ethyl acetate); $[\alpha]_D^{24}$ −65° (*c* 1.0, $CHCl_3$); IR (neat): 1721, 1605, 1588, 1493, and 1455 cm^{-1}; ^{1}H-NMR (400 MHz, $CDCl_3$): δ=1.195 (3H, d, Me-5, $J_{5,Me}$=6.5 Hz), 1.61 (1H, dddd, H-2eq, $J_{1,2eq}$=2 Hz, $J_{2ax,2eq}$=13.5 Hz, $J_{2eq,3ax}$=4.5 Hz, $J_{2eq,3eq}$=2.5 Hz), 1.92 (1H, ddt, H-3eq, $J_{2ax,3eq}$=4 Hz, $J_{3ax,3eq}$= 13.5 Hz, $J_{2eq,3eq}$=$J_{3eq,4}$=2.5 Hz), 2.02 (1H, tt, H-2ax, $J_{1,2ax}$=4 Hz, $J_{2ax,3ax}$=13.5 Hz), 2.155 (1H, ddt, H-3ax, $J_{3ax,4}$=2.5 Hz), 3.41 (3H, s, OMe), 4.11 (1H, dq, H-5, $J_{4,5}$=1.5 Hz), 4.81 (1H, dd, H-1), 5.06 (1H, sharp m, H-4), 7.46 (2H, t, Bz, *J*=6.85 Hz), 7.57 (1H, t, Bz), and 8.12 (2H, d, Bz).

Found: C, 67.15; H, 7.18%. Calcd for $C_{14}H_{18}O_4$: C, 67.18; H, 7.25%.

*Methyl 3,4,6-Trideoxy-α-*L*-*glycero*-hex-3-enopyranosid-2-ulose (10).* *A) From 13*: To a stirred and ice-cooled solution of **13** (487 mg) in dry dichloromethane (9.75 ml) were added Molecular Sieves 3A powder (1.02 g) and pyridinium chlorochromate (1.46 g), and stirring was continued at room temperature for 30 min. The mixture was diluted with ether and passed through a silica-gel column (12 g) with 1:1 chloroform–ether to give eluates containing **10**. The eluates were evaporated at 75 °C under atmospheric pressure, leaving a pale yellow syrup of **10** (0.41 g, 86%), which was used for the next step: R_f 0.72 (2:1 benzene–ethyl acetate).

An analytically pure sample was obtained by distillation under reduced pressure: bp 74 °C (666 Pa); $[\alpha]_D^{24}$ −58° (*c* 1.0, $CHCl_3$)[lit,[12] $[\alpha]_D^{20}$ −93° (*c* 1, MeOH)]; IR (neat) 1762, 1705, 1618, 1450 1390, and 1378 cm^{-1}; ^{1}H-NMR (90 MHz, $CDCl_3$) δ=1.40 (3H, d, Me, $J_{5,Me}$=7.5 Hz), 3.55 (3H, s, OMe), 4.69 (1H, ddq, H-5, $J_{3,5}$=2.5 Hz, $J_{4,5}$=1.5 Hz), 4.73 (1H, s, H-1), 6.06 (1H, dd, H-3, $J_{3,4}$=10.5 Hz), 6.91 (1H, dd, H-4).

Found: C, 58.84; H, 7.26%. Calcd for $C_7H_{10}O_3$: C, 59.15; H, 7.09%.

B) From 15: A solution of **15** (83.3 mg) in 50% aqueous tetrahydrofuran (0.83 ml) was stirred with K_2CO_3 (156 mg) at 50 °C for 9 h. The mixture was partitioned between ethyl acetate and a saturated aqueous NaCl solution, and the combined organic layers were dried and evaporated at 80 °C under atmospheric pressure to give a residue. This was chromatographed on silica gel (3 g) with 2:1 benzene–ethyl acetate to give, after removal of the solvent under atmospheric pressure, a syrup (48.8 mg) containing **13** and its C-2 epimer.

The syrup was oxidized by the procedure described in the preparation (A) to give a syrup of **10** (40 mg, 72% from **15**).

*(1S,3R)-5,10-Dihydroxy-3,9-dimethoxy-1-methyl-1*H*-naphtho-[2,3-c]pyran-4(3*H*)-one (17).* A solution of lithium *t*-butoxide (7.23 mmol) was initially prepared by adding butyllithium (4.50 ml of 1.6 M† solution, 7.23 mmol) to *t*-butyl alcohol (0.75 ml, 7.93 mmol) in tetrahydrofuran (6.85 ml) at 0 °C under argon. This solution was cooled to −78 °C, and **9** (805 mg, 2.65 mmol) was added in one portion with stirring to generate a slurry of the anion. After 15 min, to the stirred slurry was added a solution of **10** (341 mg, 2.40 mmol) in tetrahydrofuran (1.40 ml) at −78 °C, and stirring was continued at this temperature for 15 min and then at room temperature for 3 h under argon. The reaction mixture was partitioned between ethyl acetate and a saturated aqueous NH_4Cl solution, and the combined organic layers were dried and evaporated to a residue. This was chromatographed on silica gel (14 g) with 5:1 hexane–ethyl acetate followed by recrystallization from ethyl acetate to give yellow needles of **17** (580 mg, 80%): R_f 0.34 (4:1 hexane–acetone); mp 123—125 °C; $[\alpha]_D^{24}$ −304° (*c* 1.0, $CHCl_3$); IR (KBr): 1647, 1631, 1610, and 1588 cm^{-1}; UV (MeOH) λ (ε) 221 (24400), 265 (22800), 268 (23400), 321 (2800), 329 (3210), 386 (2440), and 431 nm (5420); ^{1}H-NMR (90 MHz, $CDCl_3$): δ=1.73 (3H, d, Me-1, $J_{1,Me}$=6.5 Hz), 3.60 (3H, s, OMe-3), 4.09 (3H, s, OMe-9), 5.08 (1H, s, H-3), 5.40 (1H, q, H-1), 7.02 and 8.07 (each 1H, dd, H-6 and 8, *J*=8 and 1.5 Hz), 7.40 (1H, t, H-7, *J*=8 Hz), 9.20 and 12.32 (each 1H, s, OH-5 and 10, *vice versa*).

Found: C, 63.44; H, 5.55%. Calcd for $C_{16}H_{16}O_6$: C, 63.15; H, 5.30%.

*(1S,3R)-3,5,9,10-Tetramethoxy-1-methyl-1*H*-naphtho[2,3-c]-pyran-4(3*H*)-one (18).* A solution of **17** (1.10 g) in acetone (22 ml) was stirred with dimethyl sulfate (1.20 ml) and K_2CO_3 (1.75 g) at 40 °C for 12 h. After further addition of dimethyl sulfate (0.60 ml) and K_2CO_3 (874 mg), stirring was continued at 40 °C for another 12 h. The reaction mixture was partitioned between ethyl acetate and a saturated aqueous $NaHCO_3$ solution, and the combined organic layers were washed with a saturated aqueous NaCl solution, dried and evaporated to give a yellow syrup of **18** (1.2 g), which was used for the next step.

An analytically pure sample was obtained by a silica-gel column chromatography with 9:1 benzene–ethyl acetate to give a yellow syrup: R_f 0.32 (4:1 hexane–acetone); $[\alpha]_D^{24}$ −154° (*c* 1.0, $CHCl_3$); IR ($CHCl_3$): 1701, 1603, 1578, 1569, and 1449 cm^{-1}; UV (MeOH) λ (ε) 221 (24500), 262 (26100), 295 (3860), 305 (4030), 320 (3540), 379 (3190), and 385 nm (Infl., 3450); ^{1}H-NMR (90 MHz, $CDCl_3$): δ=1.69 (3H, d, Me-1, $J_{1,Me}$=6.5 Hz), 3.55 (3H, s, OMe-3), 3.84 (3H, s, OMe), 4.04 (6H, s, OMe ×2), 4.94 (1H, s, H-3), 5.41 (1H, q, H-1), 7.02 and 7.98 (each 1H, d, H-6 and 8, *J*=8 Hz), 7.46 (1H, t, H-7).

Found: C, 64.80; H, 6.15%. Calcd for $C_{18}H_{20}O_6$: C, 65.05; H, 6.07%.

*(1S,3R,4S)-3,4-Dihydro-3,5,9,10-tetramethoxy-1-methyl-1*H-

† 1 M=1 mol dm^{-3}.

naphtho[2,3-c]pyran-4-ol (19). A crude sample of **18** (1.20 g) was stirred with $NaBH_4$ (164 mg) in methanol (36 ml) at room temperature for 5 min. The reaction mixture was neutralized with Amberlite CG-50 (H type), filtered and then evaporated to a residue, which was chromatographed on silica gel (50 g) with 1:1 hexane–ethyl acetate followed by recrystallization from ethyl acetate–hexane to afford pale yellow cubics of **19** (1.06 g, 88% from **17**): R_f 0.48 (4:1 benzene–acetone); mp 176—177.5 °C (changed at 168 °C); $[\alpha]_D^{24}$ −97° (*c* 1.0, $CHCl_3$); IR (KBr): 1596, 1572, 1500, 1462, 1448, 1368, and 1266 cm^{-1}; UV (MeOH) λ (ε) 235 (53800), 293 (5620), 307 (7180), 322 (6000), and 337 nm (4740); ^{1}H-NMR (400 MHz, $CDCl_3$): δ=1.67 (3H, d, Me-1, $J_{1,Me}$=7.0 Hz), 3.28 (1H, d, OH-4, $J_{4,OH}$=4.0 Hz), 3.62 (3H, s, OMe-3), 3.82, 4.01 and 4.04 (each 3H, s, OMe×3), 4.95 (1H, d, H-3, $J_{3,4}$= 2.0 Hz), 5.07 (1H, dd, H-4), 5.44 (1H, q, H-1), 6.88 and 7.70 (each 1H, d, H-6 and 8, J=8 Hz), and 7.40 (1H, t, H-7).

Found: C, 64.43; H, 6.52%. Cacd for $C_{18}H_{22}O_6$: C, 64.66; H, 6.63%.

(1S,3R,4S)-3,4-Dihydro-4-hydroxy-3,9-dimethoxy-1-methyl-1H-naphtho[2,3-c]pyran-5,10-dione (20). A) From 19: A solution of **19** (33.5 mg) in acetonitrile (1 ml) was stirred with an aqueous solution (0.48 ml) of ammonium cerium(IV) nitrate (120 mg) at room temperature for 10 min. The reaction mixture was partitioned between ethyl acetate and water, and the combined organic layers were washed with a saturated aqueous NaCl solution, dried and evaporated to a residue. This was chromatographed on silica gel (1.5 g) with 1:1 hexane–ethyl acetate to give a yellow syrup of **20** (28 mg, 91%): R_f 0.19 (2:1 benzen–ethyl acetate); $[\alpha]_D^{24}$−248° (*c* 0.95, $CHCl_3$); IR ($CHCl_3$): 1665, 1660, 1656, 1590, and 1579 cm^{-1}; UV (MeOH) λ (ε) 211 (24500), 248 (14600), 261 (13900), 265 (Infl., 12900), 331 (2480), 385 (Infl., 3830), and 407 nm (4070); ^{1}H-NMR (90 MHz, $CDCl_3$+D_2O): δ=1.50 (3H, d, Me-1, $J_{1,Me}$= 6.5 Hz), 3.53 (3H, s, OMe-3), 3.97 (3H, s, OMe-9), 4.80—5.05 (3H, m, H-1, 3 and 4), 7.20—7.80 (3H, m, H-6,7 and 8).

Found: C, 63.42; H, 5.44%. Calcd for $C_{16}H_{16}O_6$: C, 63.15; H, 5.30%.

B) From 17: An ice-cooled solution of **17** (28 mg) in methanol (0.56 ml) was stirred with $NaBH_4$ (4.2 mg) for 3 min and then neutralized with Amberlite CG-50 (H type). After filtration, the filtrate was vigorously stirred under atmosphere at room temperature for 12 h and evaporated to a residue, which showed two spots having R_f-values of 0.19 and 0.30 on TLC with 2:1 benzene–ethyl acetate. The R_f 0.19-substance was identical with the aforesaid product **20**. Although the R_f 0.30-substance seemed to be the C-4 epimeric alcohol, it was not further investigated.

(1S,3RS,4S)-3,4-Dihydro-5,9,10-trimethoxy-1-methyl-1H-naphtho[2,3-c]pyran-3,4-diol (7). A sample of **19** (516 mg) was dissolved in a mixture of 0.5 M HCl (20.6 ml) and acetic acid (4.1 ml), and the solution was kept at 75 °C for 2 h. After neutralization with a saturated aqueous $NaHCO_3$ solution, the resulting mixture was extracted with ethyl acetate. The extracts were washed with a saturated aqueous NaCl solution, dried and evaporated to a residue, which was chromatographed on silica gel (20 g) with 3:1 benzene–acetone to give a yellow syrup of **7** (477 mg, 97%): R_f 0.22 (4:1 benzene–acetone); $[\alpha]_D^{24}$ −34° (*c* 1.0, $CHCl_3$); IR ($CHCl_3$); 1597, 1573, 1496, 1450, 1372, and 1339 cm^{-1}; UV (MeOH) λ (ε) 235 (61100), 265 (Infl., 940), 297 (6410), 307 (7920), 322 (6640), 337 (5190), 385 nm (Infl., 313); ^{1}H-NMR (90 MHz, $CDCl_3$+D_2O) δ=1.67 (3H, d, Me-1, $J_{1,Me}$=6.5 Hz), 3.81, 4.02 and 4.05 (each 3H, s, OMe ×3), 4.90 (1H, sharp d, H-4, $J_{3,4}\cong$1 Hz), 5.30 (1H, sharp d, H-3), 5.48 (1H, q, H-1), 6.90 and 7.72 (each 1H, d, H-6 and 8, J=7.5 Hz), 7.41 (1H, t, H-7).

Found: C, 63.44; H, 6.56%. Calcd for $C_{17}H_{20}O_6$: C, 63.74; H, 6.29%.

(1S,3S,4S)-3,4,11,12-Tetrahydro-5,9,10-trimethoxy-1-methyl-1H-furo[3,2-b]naphtho[2,3-d]pyran-12-one (21) and Ethyl (1S,3R,4S)-3,4-dihydro-4-hydroxy-5,9,10-trimethoxy-1-methyl-1H-naphtho-[2,3-c]pyran-3-acetate (22). To a solution of **7** (160 mg) in toluene (4.83 ml) was added ethoxycarbonylmethylenetriphenylphosphorane (526 mg), and the mixture was refluxed at 105 °C for 30 h and then evaporated to a residue. This was chromatographed on silica gel (10 g) with 7:1 benzene–ethyl acetate to give **21** (91.6 mg, 53%) and **22** (80.0 mg, 41%) having the R_f-values of 0.44 and 0.57 (3:1 benzene–ethyl acetate), respectively.

21: Pale yellow cubics from ethyl acetate–benzene; mp 232—234 °C (changed at 214 °C); $[\alpha]_D^{24}$ −279° (*c* 1.0, $CHCl_3$); IR (KBr): ≈1790, 1591, 1571, 1448, and 1338 cm^{-1}; UV (MeOH) λ (ε) 215 (22300), 235 (45500), 264 (Infl., 2570), 293 (4570), 309 (5860), 324 (4510), and 340 nm (4060); ^{1}H-NMR (400 MHz, $CDCl_3$): δ=1.57 (3H, d, Me-1, $J_{1,Me}$=7.0 Hz), 2.71 (1H, d, H-11, $J_{11,11'}$=17.5 Hz, $J_{3,11}$=0 Hz), 2.99 (1H, dd, H-11′, $J_{3,11'}$=5.0 Hz), 3.85, 4.03 and 4.07 (each 3H, s, OMe ×3), 4.75 (1H, dd, H-3, $J_{3,4}$=3.0 Hz), 5.37 (1H, q, H-1), 5.58 (1H, d, H-4), 6.93 and 7.72 (each 1H, d, H-6 and 8, J=8.0 Hz), 7.43 (1H, t, H-7).

Found: C, 66.20; H, 5.87%. Calcd for $C_{19}H_{20}O_6$: C, 66.27; H, 5.85%.

22: Yellow syrup; $[\alpha]_D^{24}$ −25° (*c* 1.0, $CHCl_3$); IR ($CHCl_3$): ≈1726, 1591, 1567, 1366, and 1335 cm^{-1}; UV (MeOH) λ (ε) 236 (57400), 265 (Infl., 1550), 296 (6130), 308 (7540), 322 (6220), and 337 nm (4670); ^{1}H-NMR (400 MHz, $CDCl_3$): δ=1.30 (3H, t, Me of Et, J=7.0 Hz), 1.64 (3H, d, Me-1, $J_{1,Me}$=6.5 Hz), 2.63 (1H, dd, H-11, $J_{11,11'}$=15.5 Hz, $J_{3,11}$=9.5 Hz), 3.07 (1H, dd, H-11′, $J_{3,11'}$= 3.5 Hz), 3.78 (3H, s, OMe), 3.92 (1H, dt, H-3, $J_{3,4}$=9.5 Hz), 4.00 and 4.01 (each 3H, s, OMe ×2), 4.221 and 4.224 (each 1H, q, CH_2 of Et), 4.77 (1H, d, OH-4, $J_{4,OH}$=1.0 Hz), 4.86 (1H, broad d, H-4), 5.19 (1H, q, H-1), 6.88 and 7.64 (each 1H, d, H-6 and 8, J=8.0 Hz), and 7.40 (1H, t, H-7).

Found: C, 64.31; H, 6.66%. Calcd for $C_{21}H_{26}O_7$: C, 64.60; H, 6.71%.

9-O-Methylnanaomycin D (23). A solution of **21** (205 mg) in acetonitrile (4.1 ml) was stirred with an aqueous solution (2.6 ml) of ammonium cerium(IV) nitrate (653 mg) at room temperature for 15 min. The reaction mixture was partitioned between ethyl acetate and water, and the combined organic layers were washed with a saturated aqueous NaCl solution, dried and evaporated to a residue. This was chromatographed on silica gel (15 g) with 3:1 benzene–ethyl acetate followed by recrystallization from ethyl acetate–petr. ether to give orange needles of **23** (171 mg, 92%): R_f 0.21 (3:1 benzene–ethyl acetate); mp 214—216 °C (dec.); $[\alpha]_D^{24}$ −65° (*c* 0.5, $CHCl_3$); IR (KBr): ≈1786, ≈1658, and 1585 cm^{-1}; UV (MeOH) λ (ε) 212 (21700), 252 (12400), 265 (Infl., 9600), 386 (3390), and 403 nm (3560); ^{1}H-NMR (90 MHz, $CDCl_3$): δ= 1.56 (3H, d, Me-1, $J_{1,Me}$=6.5 Hz), 2.65 (1H, d, H-11, $J_{11,11'}$= 18 Hz, $J_{3,11}$=0 Hz), 2.96 (1H, dd, H-11′, $J_{3,11'}$=5.0 Hz), 4.05 (3H, s, OMe), 4.69 (1H, dd, H-3, $J_{3,4}$=3 Hz), 5.08 (1H, q, H-1), 5.27 (1H, d, H-4), 7.3—7.9 (3H, m, H-6, 7 and 8).

Found: C, 65.12; H, 4.55%. Calcd for $C_{17}H_{14}O_6$: C, 64.97; H, 4.49%.

Nanaomycin D (1). To a stirred and ice-cooled solution

of **23** (19 mg) in dichloromethane (0.95 ml) was added $AlCl_3$ (190 mg), and stirring was continued at room temperature for 30 min. The reaction mixture was partitioned between chloroform and water, and the combined organic layers were washed with a saturated aqueous NaCl solution, dried and evaporated to a solid, which was recrystallized from ethyl acetate–petr. ether to give dark red rods and/or needles of **1** (17.2 mg, 95%).

An analytically pure sample was obtained by purification on PLC with 3:1 dichloromethane–chloroform followed by recrystallization from ethyl acetate–petr. ether to afford red rods of **1**, which changed into orange needles after a day: R_f 0.41 (3:1 benzene–ethyl acetate); R_f 0.55 (12:4:1 CH_2Cl_2–$CHCl_3$–acetone); red rods: mp 171—173 °C (lit,[1] mp 170—173 °C); orange needles: mp 196—203 °C; $[\alpha]_D^{24}$ −163° (*c* 0.44, $CHCl_3$); IR (KBr): ≈1778, 1766, 1760, 1668, 1651, 1629, and 1452 cm^{-1}; UV (MeOH) λ (ε) 212 (36400), 258 (11200), 265 (Infl., 10200), 385 (Infl., 2890), and 427 nm (4420); ^{1}H-NMR (400 MHz, $CDCl_3$): δ=1.57 (3H, d, Me-1, $J_{1,Me}$=7.0 Hz), 2.71 (1H, d, H-11, $J_{11,11'}$=18 Hz, $J_{3,11}$=0 Hz), 2.97 (1H, dd, H-11′, $J_{3,11'}$=5.0 Hz), 4.69 (1H, dd, H-3, $J_{3,4}$=3.0 Hz), 5.09 (1H, q, H-1), 5.26 (1H, d, H-4), 7.31 and 7.71 (each 1H, dd, H-6 and 8, *J*=8.0 and 2.0 Hz), 7.68 (1H, t, H-7, *J*=8.0 Hz), 11.84 (1H, s, OH-9).

Its IR, UV, and ^{1}H-NMR spectra, and antibacterial activity (Table 1) were identical with those of an authentic sample of the natural antibiotic.

Found: C, 64.14; H, 4.02%. Calcd for $C_{16}H_{12}O_6$: C, 64.00; H, 4.03%.

Ethyl (1S,3R,4S)-3,4,5,10-Tetrahydro-4-hydroxy-9-methoxy-1-methyl-5,10-dioxo-1H-naphtho[2,3-c]pyran-3-acetate (8). A sample of **22** (271 mg) was treated by the procedure described in the preparation of **23** and then worked up to give an orange syrup of **8** (220 mg, 88%): R_f 0.34 (3:1 benzene–ethyl acetate); $[\alpha]_D^{24}$ −269° (*c* 0.5, $CHCl_3$); IR ($CHCl_3$): 1730, 1656, 1626, 1590, 1471, and 1450 cm^{-1}; UV (MeOH) λ (ε) 211 (22000), 247 (13000), 267 (Infl., 11500), 332 (2150), 385 (Infl., 3670), and 396 nm (3520); ^{1}H-NMR (400 Hz, $CDCl_3$): δ=1.28 (3H, t, Me of Et, *J*=7.0 Hz), 1.49 (3H, d, Me-1, $J_{1,Me}$=6.5 Hz), 2.57 (1H, dd, H-11, $J_{3,11}$=9.0 Hz, $J_{11,11'}$=16 Hz), 2.98 (1H, dd, H-11′, $J_{3,11'}$=3.0 Hz), 3.85 (1H, dt, H-3, $J_{3,4}$=9.0 Hz), 4.01 (3H, s, OMe), 4.12 (1H, d, OH-4, $J_{4,OH}$=1.0 Hz), 4.196 and 4.204 (each 1H, q, CH_2 of Et), 4.61 (1H, ddd, H-4, $J_{1,4}$=2.0 Hz), 4.89 (1H, dq, H-1), 7.31 and 7.73 (each 1H, d, H-6 and 8, *J*=8 Hz), and 7.67 (1H, t, H-7).

Found: C, 63.06; H, 5.65%. Calcd for $C_{19}H_{20}O_7$: C, 63.33; H, 5.59%.

Ethyl (1S,3R,4S)-3,4,5,10-Tetrahydro-4,9-dihydroxy-1-methyl-5,10-dioxo-1H-naphtho[2,3-c]pyran-3-acetate (24). A sample of **8** (22.9 mg) was treated by the procedure described in the preparation of **1** and then worked up to give orange crystals of **24** (20.9 mg, 95%): R_f 0.65 (3:1 benzene–ethyl acetate); mp 100—102 °C; $[\alpha]_D^{24}$ −433° (*c* 0.5, $CHCl_3$); IR (KBr): 1728, 1634, 1612, 1572, and 1460 cm^{-1}; UV (MeOH) λ (ε) 213 (28000), 250 (8550), 257 (8640), 264 (Infl., 8250), 272 (9280), 385 (Infl., 2860), and 420 nm (3800); ^{1}H-NMR (90 MHz, $CDCl_3$): δ=1.29 (3H, t, Me of Et, *J*=7.0 Hz), 1.52 (3H, d, Me-1, $J_{1,Me}$=6.5 Hz), 2.54 (1H, dd, H-11, $J_{3,11}$=9.0 Hz, $J_{11,11'}$=16 Hz), 2.98 (1H, dd, H-11′, $J_{3,11'}$=3.0 Hz), 3.85 (1H, dt, H-3, $J_{3,4}$= 9.0 Hz), 3.99 (1H, d, OH-4, $J_{4,OH}$=1 Hz), 4.20 (2H, q, CH_2 of Et, *J*=7.0 Hz), 4.64 (1H, dull d, H-4), 4.87 (1H, dq, H-1, $J_{1,4}$=2.5 Hz), 7.2—7.7 (3H, m, H-6, 7 and 8).

Found: C, 62.21; H, 5.04%. Calcd for $C_{18}H_{18}O_7$: C, 62.42; H, 5.24%.

Kalafungin (2). To a stirred and ice-cooled solution of **24** (16.5 mg) in benzene (0.34 ml) was added conc. H_2SO_4 (0.11 ml), and stirring was continued at room temperature for 30 min. After cooling to 5 °C, the reaction mixture was partitioned between ice-cooled ethyl acetate and water. The combined organic layers were washed sequentially with saturated aqueous $NaHCO_3$ and NaCl solutions under ice-cooling, dried and evaporated to a residue, which showed two spots having R_f-values of 0.55 and 0.32 on TLC (12:4:1 CH_2Cl_2–$CHCl_3$–acetone; **24** R_f 0.70). Their R_f-values were identical with those of kalafungin (**2**) and ethyl kalafunginate, the latter of which was derived from kalafungin according to the published procedure.[2b]

The residue was dissolved in toluene (0.4 ml), and the resulting solution refluxed at 105 °C for 7 h and then evaporated to a solid, which was recrystallized from ethyl acetate–petr. ether to give red rods of **2** (13.1 mg, 92%).

An analytically pure sample was obtained by purification on PLC with 3:1 dichloromethane–chloroform followed by recrystallization from ethyl acetate–petr. ether to afford red rods of **2**: R_f 0.41 (3:1 benzene–ethyl acetate); R_f 0.55 (12:4:1 CH_2Cl_2–$CHCl_3$–acetone); mp 171—173 °C; $[\alpha]_D^{24}$ +160° (*c* 0.30, $CHCl_3$)[lit,[2] mp 163—166 °C; $[\alpha]_D^{25}$+159° (*c* 1, $CHCl_3$)].

Its IR, UV, and ^{1}H-NMR spectra, and TLC-behavior were identical with those of the aforesaid nanaomycin D (**1**), and also with those of an authentic sample of the natural kalafungin (**2**). The antibacterial activity was also identical with those of the natural antibiotic as shown in Table 1.

Found: C, 64.19; H, 4.06%. Calcd for $C_{16}H_{12}O_6$: C, 64.00; H, 4.03%.

Nanaomycin A (5). A solution of **1** (16 mg) in ethanol (3 ml) was shaken with platinum oxide and 3-atm hydrogen at room temperature for 1 h, filtered and evaporated to give orange crystals of **5** (15.7 mg, 98%).

An analytically pure sample was obtained by purification on PLC with 3:2 benzene–acetone followed by recrystallization from ethanol to give orange needles of **5**: R_f 0.20 (3:1 benzene–acetone; **1**: R_f 0.68); mp 179—181 °C (lit,[5] mp 178—180 °C); $[\alpha]_D^{20}$ −21° (*c* 0.4, $CHCl_3$); IR ($CHCl_3$): 1714, 1663, 1645, 1620, and 1576 cm^{-1}; UV (MeOH) λ (ε) 248 (11800), 273 (14400), 385 (Infl., 3760), and 420 nm (5450); ^{1}H-NMR (90 MHz, $CDCl_3$): δ=1.58 (3H, Me, $J_{1,Me}$=7 Hz), 2.33 (1H, ddd, H-4, $J_{1,4}$=2 Hz, $J_{3,4}$=10 Hz, $J_{4,4'}$=19 Hz), 2.72 (2H, d, CH_2-11, *J*=6.5 Hz), 2.87 (1H, dd, H-4′, $J_{3,4'}$=3 Hz), 4.34 (1H, m, H-3), 5.04 (1H, dq, H-1), 7.2—7.7 (3H, m, H-6,7, and 8), 8.8 (1H, broad signal, COOH), 12.03 (1H, s, OH-9).

Its IR, UV and ^{1}H-NMR spectra were identical with the published data of the natural antibiotic.[5]

Found: C, 63.54; H, 4.56%. Calcd for $C_{16}H_{14}O_6$: C, 63.57; H, 4.66%.

4-Deoxykalafunginic Acid (Enantiomer of Nanaomycin A) (5′). A sample of **2** (15 mg) was hydrogenated by the procedure described in the preparation of **5** to give orange crystals of **5′** (14.5 mg, 97%), which was purified to afford needles: R_f 0.20 (3:1 benzene–acetone); mp 179—181 °C; $[\alpha]_D^{20}$ +21° (*c* 0.4, $CHCl_3$).

Its IR, UV, and ^{1}H-NMR spectra and TLC-behavior were identical with those of nanaomycin A (**5**).

Found: C, 63.44; H, 4.49%. Calcd for $C_{16}H_{14}O_6$: C, 63.57; H, 4.66%.

We are grateful to Prof. Sumio Umezawa, Institute of

Bioorganic Chemistry, and Prof. Hamao Umezawa, Institute of Microbial Chemistry, for their generous support of our program. We also thank Prof. Satoshi Ōmura, Kitasato University and the Kitasato Institute, and Dr. Hiroshi Naganawa, Institute of Microbial Chemistry, for their generous gifts of natural nanaomycin D and kalafungin, and indebted to Mr. Saburo Nakada for elemental analyses.

References

1) S. Ōmura, H. Tanaka, Y. Okada, and H. Marumo, *J. Chem. Soc., Chem. Commun.*, **1976**, 320.

2) a) M. E. Bergy, *J. Antibiot.*, **21**, 454 (1968); b) H. Hoeksema and W. C. Krueger, *J. Antibiot.*, **29**, 704 (1976).

3) W. Keller-Schlierlein, M, Brufani, and S. Barcza, *Helv. Chim. Acta.*, **51**, 1257 (1968).

4) H. Ogura and K. Furuhata, 9 th International Congress of Heterocyclic Chemistry, Tokyo, August 1983, Abst., No. S-IV-6 (p. 114).

5) S. Ōmura, H. Tanaka, Y. Koyama, R. Ōiwa, M. Katagiri, J. Awaya, T. Nagai, and T. Hata, *J. Antibiot.*, **27**, 363 (1974); H. Tanaka, Y. Koyama, T. Nagai, H. Marumo, and S. Ōmura, *ibid.*, **28**, 868 (1975).

6) H. W. Moore, *Science*, **197**, 527 (1977).

7) a) Total synthesis of racemic kalafungin: T.-t. Li and R. H. Ellison, *J. Am. Chem. Soc.*, **100**, 6263 (1978); b) Review: Y. Naruta and K. Maruyama, *J. Synth. Org. Chem. Japan*, **42**, 415 (1984).

8) a) For recent synthesis, see: M. S. South and L. S. Liebeskind, *J. Am. Chem. Soc.*, **106**, 4181 (1984) and references cited therein; b) T. Kometani, Y. Takeuchi, and E. Yoshii, *J. Chem. Soc., Perkin Trans. 1*, **1981**, 1197; c) M. F. Semmelhack, L, Keller, T. Sato, and E. Spiess, *J. Org. Chem.*, **47**, 4382 (1982); M. F. Semmelhack, J. J. Bozell, T. Sato, W. Wulff, E. Spiess, and A. Zask, *J. Am. Chem. Soc.*, **104**, 5850 (1982); M. F. Semmelhack and A. Zask, *J. Am. Chem. Soc.*, **105**, 2034 (1983).

9) K. Tatsuta, K. Akimoto, M. Annaka, Y. Ohno, and M. Kinoshita, *J. Antibiot.*, **38**, in press.

10) P. A. Bartlett, J. D. Meadows, and E. Ottow, *J. Am. Chem. Soc.*, **106**, 5304 (1984).

11) F. M. Hauser and D. Mal, *J. Am. Chem. Soc.*, **106**, 1098, (1984); F. M. Hauser and D. Mal, *ibid.*, **106**, 1862 (1984).

12) H. Paulsen and W. Koebernick, *Chem. Ber.*, **110**, 2127 (1977).

13) K. Tatsuta, K. Akimoto, and M. Kinoshita, *J. Am. Chem. Soc.*, **101**, 6116 (1979); K. Tatsuta, K. Akimoto, and M. Kinoshita, *J. Antibiot.*, **33**, 100 (1980); K. Tatsuta, K. Akimoto, and M. Kinoshita, *Tetrahedron*, **37**, 4365 (1981).

14) M. Nakata, Y. Ikeyama, H. Takao, and M. Kinoshita, *Bull. Chem. Soc. Jpn.*, **53**, 3252 (1980).

15) R. U. Lemieux, "Molecular Rearrangement Part II," ed by P. de Mayo, Interscience, New York (1963), p. 709.

16) a) K. Tatsuta, *Yuki Gosei Kagaku Kyokai Shi* **42**, 497 (1984); b) R. D. Dawe and B. Fraser-Reid, *J. Org. Chem.*, **49**, 522 (1984).

17) C. Kitao, H. Tanaka, S. Minami, and S. Ōmura, *J. Antibiot.*, **33**, 711 (1980).

 © 1985 The Chemical Society of Japan Bull. Chem. Soc. Jpn., 58, 1707—1710 (1985)

Dechlorination of Polychlorobenzenes over Triiron Tetraoxide in the Presence of Hydrogen Donating Solvents

Cui Xiang Hao,† Masahiro Nakada,* Tatsuaki Yamaguchi, Sachio Fukushi, and Minoru Hirota††

Chemical Laboratory, Chiba Institute of Technology, Narashino 275

††Department of Applied Chemistry, Faculty of Engineering, Yokohama National University, Hodogaya-ku, Yokohama 240

(Received November 19, 1984)

Dechlorination of polychlorobenzenes over Fe_3O_4 was investigated by a pulse micro-reactor technique. Dechlorinations of various polychlorobenzenes in hexane and cyclohexane were carried out in the gas phase at the temperatures ranging from 498 to 623 K. In the presence of such hydrogen donating solvents, dechlorination was shown to proceed almost exclusively. The relative rates of dechlorination were measured by gas chromatography. It was found that the solvents used to dissolve polychlorobenzenes plays a role of a hydrogen donor in this reaction. The different rates among unequivalent chlorine atoms in a molecule were interpreted by the effect of steric acceleration caused by the neighboring chlorine atom(s). The reaction will probably proceed *via* hydrogenolytic cleavage of C-Cl bonds.

Recently, environmental contamination with polyhalogenated aromatic compounds has been a serious problem in many countries. For the first time, poisoning caused by polychlorinated biphenyls attracted the public attention, which stimulated the investigations on physical and biological properties, as well as chemical reactions, of other polyhalogenated aromatics.[1] Considerably large number of researches concerning their occurrence in environment, hazard, toxicity, and metabolism were reported.[2] And dehalogenation of polyhalogenated aromatic compounds have been investigated rather extensively in the view point of their detoxication. In this respect, several photochemical dehalogenation procedures have been reported in this decade.[3,4] However, the chemical behaviors of polyhalobenzenes have not been studied so extensively as polychlorobiphenyls.

In our previous reports, thermal decomposition of tribromobenzenes[5] and photochemical dehalogenation of polyhalobenzenes in hexane solution[6] were surveyed and their mechanism was discussed. From these experiments, the reactivities of halogen (Cl or Br) atoms occupying different positions were interpreted in terms of steric acceleration. In this paper, the authors wish to report an efficient method for the dechlorination of polychlorobenzenes by Fe_3O_4 in the presence of hexane or cyclohexane.

Experimental

Materials. Triiron tetraoxide (Fe_3O_4) was prepared by hydrolyzing a 1:1 (molar ratio) mixture of iron(II) and iron(III) chlorides with urea in aqueous solution. Under these conditions, fine particles of Fe_3O_4 were produced, their average size being determined to be 8.0 nm in diameter from the line broadening of the powder X-ray diffraction lines.

Some of polychlorobenzenes used in this investigation were prepared by a combination of direct halogenation and nitration followed by reduction and the Sandmeyer reaction (replacement by Cl) of appropriately halogenated benzenes and anilines. Commercially available materials were used after purification by distillation or by chromatography. All of polychlorobenzenes were identified by their melting and/or boiling points and by spectral properties.

Reactions. Dechlorination of polychlorobenzenes over Fe_3O_4 was carried out in a stream of helium as a carrier gas by use of a pulse micro-reactor technique in combination with gas chromatography for analysis.[7] The products and the residual reactant were determined quantitatively by means of gas chromatography. Gas chromatographic analyses were carried out on a Shimadzu GC-4B PFT apparatus equipped with a PEG 20 M column (glass, 3 mm×2 m). Details of the apparatus for the reactions were described in our previous paper.[8] The hexane or cyclohexane solution of polychlorobenzene was injected in portions (each 1.0 μl) to the reaction chamber containing 550 mg of Fe_3O_4.

Results and Discussion

Dehalogenation Activity and Activation of Fe_3O_4 by Hydrogen Donating Solvents. Newly prepared Fe_3O_4 is inactive towards dechlorination of polychlorobenzenes. For this reason, a pretreatment procedure was contrived in order to activate the new Fe_3O_4. While we are investigating the dechlorination in hexane solution, the treatment by hexane was shown to be effective for the activation of Fe_3O_4 by chance. And the dechlorination proceeded smoothly when a hexane solution of polychlorobenzene was injected to the reaction column containing pretreated Fe_3O_4. By the further examination with various solvents, Fe_3O_4 was shown to be activated by the pretreatment with hydrogen donating solvents, such as hexane, cyclohexane, and tetraline. Reactivity of Fe_3O_4 towards dehalogenation was influenced considerably by the nature and the amount of the hydrogen donor used for the pretreatment.[9]

Figure 1 shows the reactivity of Fe_3O_4 as a function of the amount of hexane used for the pretreatment. In this figure, the ordinate is scaled by an arbitrary unit proportional to the amount of the dechlorination product of 1,2,3-trichlorobenzene used as a probe for the reactivity towards dechlorination. In the process of the pretreatment, hydrogen was thought to be supplied to the surface of Fe_3O_4 from the hydrogen donating solvent. The hydrogen uptake of Fe_3O_4 was proven by the fact that a small amount of benzene was detected

†On leave from Department of Chemistry, Jilin University, Chanchun, People's Republic of China.

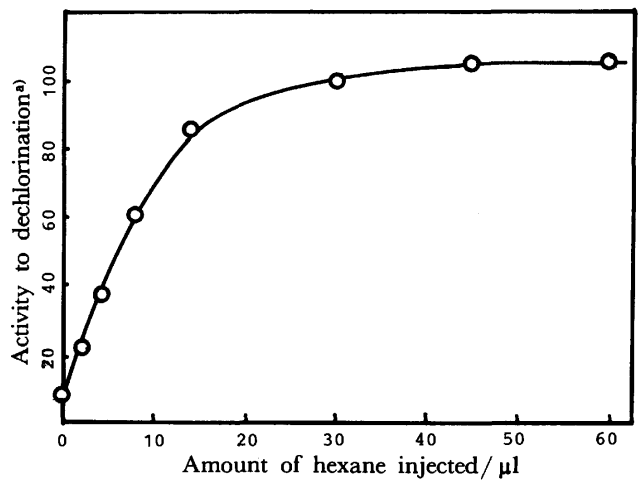

Fig. 1. Effect of the amount of hexane used for the pretreatment on the activity of Fe_3O_4 at 623 K (Amount of Fe_3O_4; 13.8 mg.

during the pretreatment of Fe_3O_4 by cyclohexane at 623 K. Since gaseous hydrogen reduces Fe_3O_4 to metallic iron under similar conditions,[10] the surface of Fe_3O_4 might be partly be reduced to Fe(0) during the pretreatment. In the case shown in Fig. 1, the Fe_3O_4 system seemed to have reached to an equilibrium after the pretreatment by 60 μl of hexane (as can be deduced from the plateau of the reactivity *vs.* the amount of hydrogen donor curve in this figure). The pretreated Fe_3O_4 showed the diffraction lines of original Fe_3O_4 in its powder X-ray spectrum, however.

Fe_3O_4 could be activated more effectively by use of a hydrogen donor stronger than hexane. Thus, Fe_3O_4 activated by 1,2,3,4-tetrahydronaphthalene (tetraline) is more reactive towards dechlorination. Naphthalene was detected as a product on passing tetraline over Fe_3O_4, rendering another support for the dehydrogenation on the surface of Fe_3O_4. On the other hand, benzene is little effective for the activation, and Fe_3O_4 shows no activity even after passing a considerable amount of benzene over the newly prepared Fe_3O_4. During the process of pretreatment by hydrogen donor, the color of Fe_3O_4 powder changed from dark brown to dark grey getting still darker after used for dechlorination.

Dechlorination of Polychlorobenzenes over Fe_3O_4. The dechlorination was carried out at first with the hexane solution of polychlorobenzene at 623 K, where the vaporized solvent played a part of hydrogen donor in the reaction, by use of the fine powder of Fe_3O_4 (550 mg) prepared as described in the experimental section and pretreated by 500 μl of hexane. Further pretreatment did not improve the activity to a measurable extent. The results are summarized in Table 1.

We have already correlated the migrating ability of the halogen atoms of polyhalobenzenes with the steric and the electronic factors during the Jacobsen type rearrangement[11] and also during the photo-dehalo-

Table 1. Dechlorination of various polychlorobenzenes over Fe_3O_4 in the presence of hydrogen donating substance[a)]

Substrate[b)]	Solvent[d)]	Conversion	Produced (poly)chlorobenzenes/%										
		%	none	mono	ortho	meta	para	1,2,3	1,2,4	1,3,5	1,2,3,4	1,2,3,5	1,2,4,5
C_6H_5Cl	h	59.2	59.2	40.8									
	ch	58.3	58.3	41.7									
o-$C_6H_4Cl_2$	h	80.6	47.0	33.6	19.4								
	ch	78.9	46.0	32.9	21.1								
m-$C_6H_4Cl_2$	h	19.7	11.5	8.2		80.3							
	ch	13.8	8.1	5.8		86.1							
p-$C_6H_4Cl_2$	h	19.7	11.5	8.2			80.3						
	ch	13.1	7.7	5.4			86.9						
$C_6H_3Cl_3$	h	88.2	28.2	20.3	16.3	23.4		11.8					
(1,2,3)	ch	90.2	30.4	21.7	16.2	22.0		9.8					
$C_6H_3Cl_3$	h	70.6	6.9	15.5	0.9	29.5	27.8		29.4				
(1,2,4)	ch	74.2	11.4	8.1	2.3	27.1	25.3		25.8				
$C_6H_3Cl_3$	h	13.6	0.8	0.6		12.2				86.4			
(1,3,5)	ch	13.8	trace	trace		13.8				86.2			
$C_6H_2Cl_4$	h	96.2	12.0	8.4	9.8	24.5	14.1	6.4	21.0		3.8		
(1,2,3,4)	ch	94.7	14.9	10.7	8.2	20.6	11.4	6.3	22.6		5.3		
$C_6H_2Cl_4$	h	80.0	3.4	3.0	trace	12.5	6.0	0.4	21.7	33.0		20.0	
(1,2,3,5)	ch	87.1	5.0	3.6	0.8	16.6	11.9		18.9	30.3		12.9	
$C_6H_2Cl_4$[c)]	h	79.3	3.5	2.4		19.1	18.5		35.8				20.7
(1,2,4,5)	ch	81.5	4.0	2.8		20.4	19.9		34.4				18.5
C_6HCl_5[c)]	h	98.0	4.8	3.0	trace	18.2	14.9		28.4	12.7			18.0
	ch	97.2	5.6	4.3	trace	18.8	14.7		27.3	12.1			17.2
C_6Cl_6[c)]	ch	100.0				13.8	15.1	2.8	48.0	20.3			

a) 550 mg of Fe_3O_4 was used after pretreatment with 500 μl of hexane or cyclohexane. b) A 1.0 μl portion of the hexane or the cylohexane solution of the substrate (concn., 1.0 mol/l) was injected at a time. c) Saturated solution. d) h and ch refer hexane and cyclohexane, respectively.

genation.[6] In connection with these previous studies, we have paid much attention on the effect of the number and the positions of chlorine atoms on their reactivities, *i. e.*, the ease of removal. In this series of experiments with Fe_3O_4, the polychlorobenzene tends to be more reactive in the following order: 1,3,5-trichloro<1,4-dichloro<1,3-dichloro<monochloro<1,2,4-trichloro<1,2-dichloro<1,2,3,5-tetrachloro<1,2,3-trichloro<1,2,3,4-tetrachloro<pentachloro<hexachloro derivative. In general, the dechlorination becomes easy with the increase in the steric hindrance caused by the neighboring chlorine atoms and also by the buttressing effect[12] of the next neighbor chlorine atoms. Additional isolated halogen atom(s) on the ring tend to deactivate the dechlorination reaction as evidenced by the first four compounds of the above sequence. In other words, hexachlorobenzene is the most reactive, and the reactivity decreases in the following order: Polychlorobenzene having five adjacent Cl atoms> that having four adjacent Cl atoms>those having three adjacent Cl atoms>those having two adjacent Cl atoms>those having isolated Cl atom(s) only. For example, 1,2,3-trichlorobenzene is the most reactive and 1,3,5-trichloro derivative the least reactive among isomeric trichlorobenzenes. When compared intramolecularly, the most crowded chlorine atom tends to be eliminated most easily. Thus the dechlorination of 1,2,3-trichlorobenzene gives *m*-dichlorobenzene most predominantly by the elimination of the most hindered 2-chlorine atom. Similarly, 1,2,4-trichlorobenzene is the most predominant product by the dechlorination of 1,2,3,4-tetrachlorobenzene. The results are very similar to the photochemical dechlorination of polychlorobenzenes in hexane.[6] Hydrogen chloride was not detected as a gaseous product in any runs carried out over the newly pretreated Fe_3O_4.[9] When cyclohexane was used as a solvent, nearly the same results as in hexane were obtained.

Dechlorinations of trichlorobenzene isomers dissolved in hexane and cyclohexane were carried out over Fe_3O_4 in the temperature range of 498—623 K in order to examine the dependence on temperature. The temperature affected the products of the reaction in a very similar way when hexane and cyclohexane solutions were dechlorinated. Thus, only the results on their hexane solutions are illustrated in Fig. 2 as a typical example. In these runs, Fe_3O_4 was again pretreated by 500 μl of cyclohexane. The difference in the reactivity among the positional isomers is mainly determined by the circumstances of chlorine atoms in the molecule. At higher temperatures, chlorobenzene was also formed. Although in a low yield, 1,2,3-trichlorobenzene was found as a product of the reaction over Fe_3O_4 of 1,2,4-trichlorobenzene carried out at lower temperatures (Fig, 2(b)). Formation of the more crowded isomer is especially interesting. It can be a product of intramolecular rearrangement on which we have discussed previously with tribromobenzenes.[11] However,

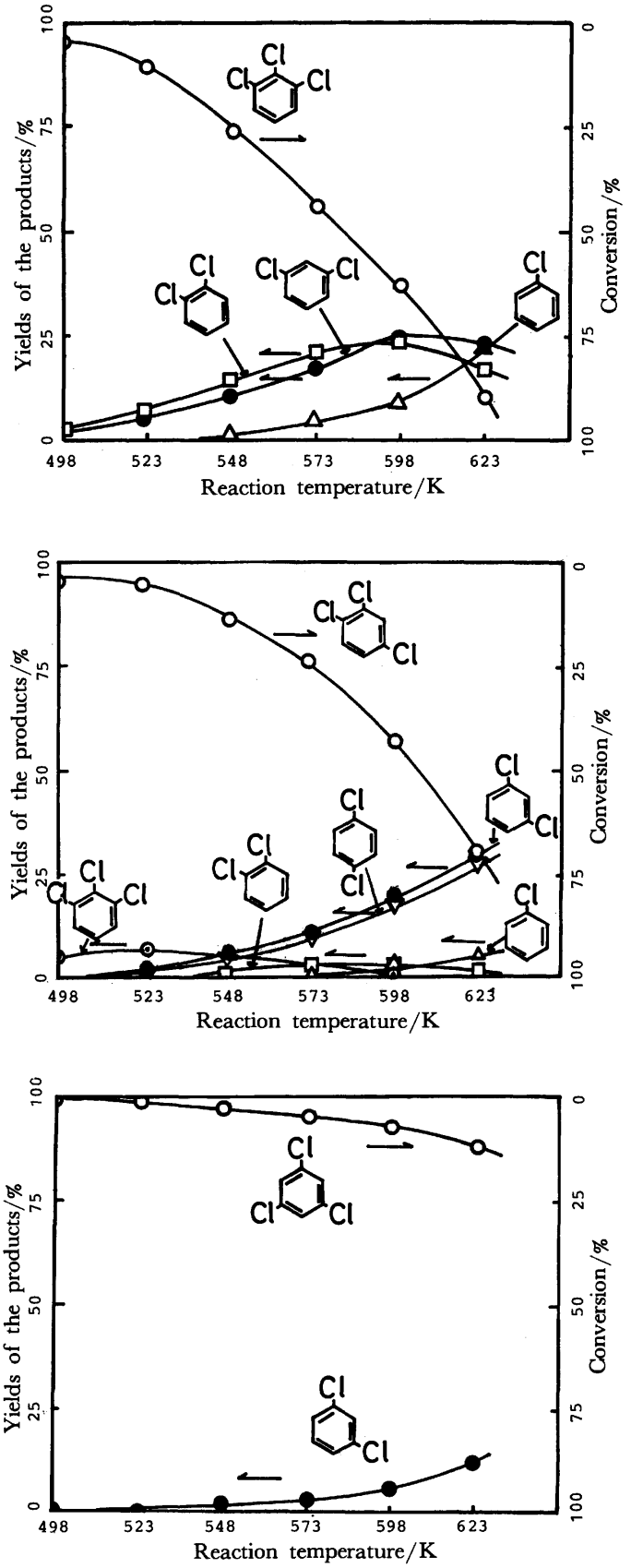

Fig. 2. Temperature dependence of the dechlorination products of isomeric trichlorobenzenes (on 550 mg of Fe_3O_4 pretreated with 500 μl of hexane). (a) 1,2,3-Trichlorobenzene, (b) 1,2,4-trichlorobenzene, and (c) 1,3,5-trichlorobenzene.

Table 2. Reactions of some neat chlorobenzenes over Fe_3O_4 at 623 K[a)]

Substrate	Conversion	Produced (poly)chlorobenzenes/%									
	%	none	mono	ortho	meta	para	1,2,3	1,2,4	1,3,5	1,2,3,4	1,2,3,5&1,2,4,5
C_6H_5Cl	22.1	14.8	77.9	5.7	0.6	0.8	0.2				
o-$C_6H_4Cl_2$	27.6	19.5	0.4	72.4			6.5	1.2			
m-$C_6H_4Cl_2$	30.9	17.0	0.3	0.9	69.1		3.2	8.8	0.7		
$C_6H_3Cl_3$[b)]	19.3	6.7	trace	0.1	0.4	0.4	5.0	80.7	trace	2.1	4.6
		(1)	(2)	(5)	(3)	(4)	(8)	(7)	(6)	(10)	(9)

a) 550 mg of Fe_3O_4 was used for the reaction. b) Numbers in paretheses correspond to the peaks in Fig. 3.

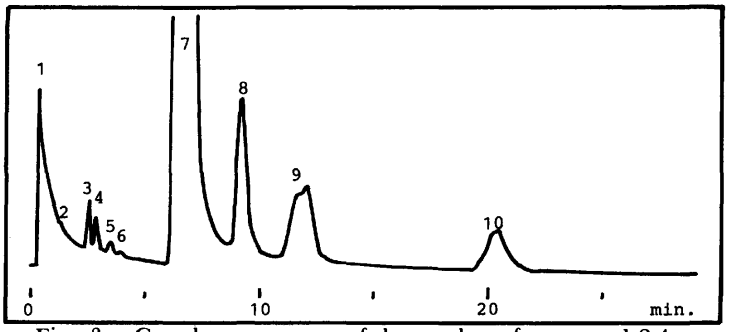

Fig. 3. Gas chromatogram of the products from neat 1,2,4-trichlorobenzene passed over Fe_3O_4 without pretreatment at 623 K. The numbers in this figure correspond to those of the products in Table 2.

further investigation is necessary to conclude the mechanism of its formation.

The dechlorination did not proceed when the benzene solution was injected, probably because benzene is a poor hydrogen donor in this reaction.

Dechlorination carried out by injecting neat polychorobenzene (chlorobenzene, *o*-dichlorobenzene, *m*-dichlorobenzene, and 1,2,4-trichlorobenzene) over pretreated Fe_3O_4 gave dechlorination products only in extremely low yields (Table 2). Alternatively, isomerized and highly substituted polychlorobenzenes were also detected as products. As an example, the gas chromatogram of the products from 1,2,4-trichlorobenzene is shown in Fig. 3. They might be formed secondarily by the substitution reactions by free chlorine atom (free radical) which is generated primarily by the cleavage of C–Cl bond, because the pattern of the substitution is rather random and suggestive of free radical reactions. The results resemble to those of the thermal decomposition of polybromobenzenes.[5)]

In conclution, the following scheme can explain the overall reactions: (i) Hydrogen is supplied from hydrogen donor (solvent) prior to the dechlorination. (ii) Cleavage of C–Cl bond proceeds by the catalysis of Fe_3O_4 forming polychlorophenyl free radical. (iii) Generated free radical receives hydrogen very promptly from a hydrogen donor molecule or from the surface of partly hydrogenated Fe_3O_4. Another path alternative to (ii) and (iii) is also possible, in which (ii′) C–Cl bond is hydrogenolytically cleaved on the surface of the partly reduced Fe_3O_4 containing hydrogen. Chlorine atom formed in the second stage ((ii) or (ii′)) might be bound rather tightly on the surface. Formation of iron chloride is probable but not detected by any means (powder X-ray, surface IR, *etc.*). At present there is no decessive evidence to differentiate the two alternative mechanism.

The authors are grateful to Miss Harue Okada for her assistance to this investigation.

References

1) a) D. B. Pealal, *CRC Crit. Rev. Environ. Control*, **5**, 469 (1975); b) A. K. Ahmed, *Environment*, **18**, 6 (1976); c) W. Klein and I. Weisgerber, *Environ. Qual. Saf.*, **5**, 237 (1976).

2) H. H. Vogt, *Chem. Labor. Betr.*, **29**, 136, 139 (1978).

3) L. Vollner, H. Rohlender, W. Klein, and F. korte, *GSF-Ber.*, **205**, 71 (1975).

4) L. J. Bailin, B. L. Hertzler, and D. A. Oberacker, *Environ. Sci. Technol.*, **12**, 673 (1978).

5) M. Nakada, S. Fukushi, H. Tomita, Y. Mashiko, and M. Hirota, *Nippon Kagaku Kaishi*, **1972**, 1680.

6) M. Nakada, S. Fukushi, H. Nishiyama, K. Okubo, K. Kume, M. Hirota, and T. Ishii, *Bull. Chem. Soc. Jpn.*, **56**, 2447 (1983).

7) C. J. Thompson, H. J. Coleman, R. L. Hopkins, and H. T. Rall, *Anal. Chem.*, **37**, 1042 (1965).

8) M. Nakada, A. Uzawa, S. Fukushi, H. Tomita, and M. Hirota, *Nippon Kagaku Kaishi*, **1984**, 728.

9) Repeated injection of the sample causes a gradual decrease in the dechlorination activity of Fe_3O_4. The activity tends to be constant after several (5 to 7) times of injection. Fe_3O_4 in this state still retains about 60% of initial activity. The decreased activity could be regained partly (60 to 70%) by injecting sufficient hexane as a hydrogen donor, some chlorinated hydrocarbons being released from the Fe_3O_4 powder during the process.

10) S. Hamada, M. Eto, and Y. Kudo, *Nippon Kagaku Kaishi*, **1984**, 843.

11) M. Nakada, K. Ishibashi, S. Fukushi, and M. Hirota, *Bull. Chem. Soc. Jpn.*, **52**, 3671 (1979).

Substituent Effects on Azomethine Proton Chemical Shifts and ^{13}C-H Coupling Constants in *N*-Benzylideneanilines. Generality of Inverse Substituent Effects on the Azomethine Proton Chemical Shifts

Ryoichi AKABA, Hirochika SAKURAGI, and Katsumi TOKUMARU*
Department of Chemistry, University of Tsukuba, Sakura-mura, Ibaraki 305
(Received November 22, 1984)

Azomethine proton chemical shifts were measured for series of *N*-benzylideneanilines; $C_6H_5CH{=}NC_6H_4X$-4, 4-$YC_6H_4CH{=}NC_6H_5$, 4-$NMe_2C_6H_4CH{=}NC_6H_4X$-4, 4-$YC_6H_4CH{=}NC_6H_4NMe_2$-4, 4-$NO_2C_6H_4CH{=}NC_6H_4X$-4, 4-$YC_6H_4CH{=}NC_6H_4NO_2$-4, and 4-$YC_6H_4CH{=}NC_6H_3(CH_3)_2$-2,6. It was found that for *N*-benzylideneanilines carrying the variable substituents X on the anilino benzene ring the azomethine protons undergo upfield shifts with increasing electron-withdrawing property of X, whereas those for *N*-benzylideneanilines carrying the variable substituents Y on the benzylidene benzene ring exhibited expected lowfield shifts with increasing electron-withdrawing property of Y. ^{13}C-H coupling constants for azomethine carbon-hydrogen bonds ($J(^{13}C$-H)) were also measured for several derivatives of 4-$NO_2C_6H_4CH{=}NC_6H_4X$-4, 4-$YC_6H_4CH{=}NC_6H_4NO_2$-4, and 4-$YC_6H_4CH{=}NC_6H_3(CH_3)_2$-2,6. In contrast with the substituent effects on the azomethine proton chemical shifts, the coupling constant increases with increasing electron-withdrawing property of the substituent X or Y, regardless of the position of the substituents, indicating that a through-bond electronic effect of the substituent is a predominant factor to determine the magnitude of the coupling constant. These results show that the anomalous substituent effects on the azomethine proton chemical shifts are a general phenomenon in *N*-benzylideneanilines which carry variable substituents on the anilino benzene ring, and support our previous proposition that the anomaly is likely to originate primarily from the change of molecular conformation of these *N*-benzylideneanilines in solution.

Although inverse substituent effects on the azomethine proton chemical shifts in *N*-benzylideneanilines (for example, 4-NO_2 substitution on the anilino benzene ring (ring A) causes an upfield shift of the azomethine proton) have been reported by several groups,[1] only a few systematic studies have been made to elucidate the anomalos substituent effects.[1e,1f,2] In a previous paper, we have suggested that the anomalous effect of the 4-NO_2 group is likely to originate primarily from the change of molecular conformation (twist angle θ_N) induced by the 4-NO_2 substitution.[3] We have also reported the ^{13}C-NMR spectra of a wide variety of *N*-benzylideneanilines, and demonstrated, on the basis of nonadditivity of the multiple substituent effects on the azomethine carbon chemical shifts, that in disubstituted derivatives such as 4-$NO_2C_6H_4$-$CH{=}NC_6H_4X$-4, and 4-$YC_6H_4CH{=}NC_6H_4NMe_2$-4 the twist angle θ_N may be a function of electronic properties of the substituents X and Y.[4] It is therefore of interest to investigate the substituent effects on the azomethine proton chemical shifts for *N*-benzylideneanilines with a variety of substituents.

In the present study, the azomethine proton chemical shifts have been measured for six series of *N*-benzylideneanilines, **1**—**6**. (Scheme 2). In order to assist understanding the nature of the substituent effects on the azomethine proton chemical shifts, ^{13}C-H coupling constants for the azomethine carbon-hydrogen bonds

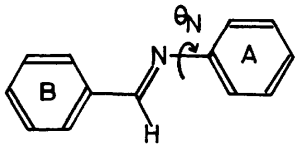

Scheme 1.

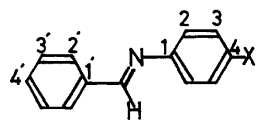

1a, X = NMe_2; **1b**, OCH_3; **1c**, CH_3; **1d**, H; **1f**, Cl; **1j**, NO_2.

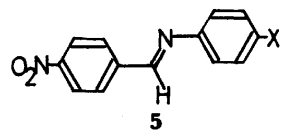

5

5a, X = NMe_2; **5b**, OCH_3; **5c**, CH_3; **5d**, H; **5e**, F; **5f**, Cl; **5h**, CO_2Et; **5i**, CN; **5j**, NO_2.

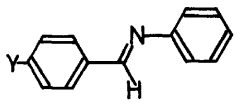

2

2a, Y = NMe_2, **2b**, OCH_3; **2c**, CH_3; **2d**, H; **2f**, Cl; **2i**, CN; **2j**, NO_2.

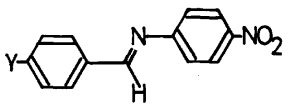

6

6a, Y = NMe_2, **6b**, OCH_3; **6c**, CH_3; **6d**, H; **6f**, Cl; **6j**, NO_2.

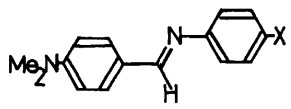

3

3a, X = NMe_2; **3b**, OCH_3; **3c**, CH_3; **3d**, H; **3j**, NO_2.

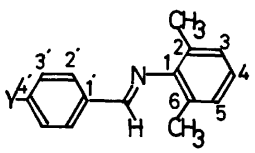

7

7a, Y = NMe_2, **7b**, OCH_3; **7c**, CH_3; **7d**, H; **7f**, Cl.

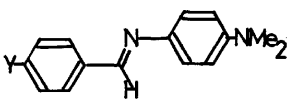

4

4a, Y = NMe_2; **4b**, OCH_3; **4c**, CH_3; **4d**, H; **4i**, CN; **4j**, NO_2.

Scheme 2.

($J^{13}C$-H)) have also been measured for the series of **5** and **6**. The coupling constants were also recorded

Table 1. Azomethine proton chemical shifts (δ) and ^{13}C-H coupling constants ($J(^{13}C$-H) of *N*-benzylideneanilines in $CDCl_3$

Compound	Substituent Y	Substituent X	δ/(ppm/TMS)	$J(^{13}C$-H)/Hz	Compound	Substituent Y	Substituent X	δ/(ppm/TMS)	$J(^{13}C$-H)/Hz
1a	H	NMe_2	8.54		**4i**	CN	NMe_2	8.58	
1b	H	OCH_3	8.50	156.6[a]	**4j**	NO_2	NMe_2	8.64	158.8
1c	H	CH_3	8.48	156.5[a]	**5a**	NO_2	NMe_2	8.64	158.8
1d	H	H	8.49	157.3[a]	**5b**	NO_2	OCH_3	8.58	160.7
1f	H	Cl	8.51		**5c**	NO_2	CH_3	8.57	161.0
1j	H	NO_2	8.46	158.6[a]	**5d**	NO_2	H	8.56	161.0[a]
2a	NMe_2	H	8.35	154.1[a]	**5e**	NO_2	F	8.56	
2b	OCH_3	H	8.40	156.1[a]	**5f**	NO_2	Cl	8.54	
2c	CH_3	H	8.50	156.5[a]	**5h**	NO_2	CO_2Et	8.54	161.4
2d	H	H	8.49	157.3[a]	**5i**	NO_2	CN	8.54	
2f	Cl	H	8.50	158.1[a]	**5j**	NO_2	NO_2	8.55	161.8
2i	CN	H	8.58		**6a**	NMe_2	NO_2	8.31	155.9
2j	NO_2	H	8.56	161.0[a]	**6b**	OCH_3	NO_2	8.35	157.7
3a	NMe_2	NMe_2	8.40		**6c**	CH_3	NO_2	8.38	158.1
3b	NMe_2	OCH_3	8.37		**6d**	H	NO_2	8.46	158.6
3c	NMe_2	CH_3	8.34		**6f**	Cl	NO_2	8.39	159.9
3d	NMe_2	H	8.35	154.1[a]	**6i**	CN	NO_2	8.49	161.4
3j	NMe_2	NO_2	8.31	155.9	**6j**	NO_2	NO_2	8.55	161.8
4a	NMe_2	NMe_2	8.40		**7a**	NMe_2	H		153.7
4b	OCH_3	NMe_2	8.47		**7b**	CH_3	H		158.7
4c	CH_3	NMe_2	8.51		**7d**	H	H		159.6
4d	H	NMe_2	8.54		**7f**	Cl	H		160.3

a) Ref. 1d.

for some of the derivatives of **7**, which may be regarded as model compounds taking considerably twisted conformations.[5,6]

First, the results on the anomalous substituent effects on the azomethine proton chemical shifts are presented and the origin of the anomaly will be discussed. Second, efficiency of transmission of the substituent effects will also be briefly discussed on the basis of the results of the coupling constants. The present results support our previous proposition that coformational changes with substituents will be an important factor to cause the anomalous substituent effects on the azomethine proton chemical shifts in *N*-benzylideneanilines.

Results

Azomethine Proton Chemical Shifts. *N*-Benzylideneanilines, **1**—**4**, were prepared and their azomethine proton chemical shifts were measured under the conditions corresponding to infinite dilution using $CDCl_3$ as a solvent. The results are summarized in Table 1.

Examination of Table 1 indicates that for *N*-benzylideneanilines, **2**, **4**, and **6**, which carry the variable substituents Y on the benzylidene benzene ring (ring B), their azomethine proton chemical shifts tend to undergo downfield shifts with increasing the electron-withdrawing property of substituents Y to give normal substituent effects. In a striking contrast, those of **1**, **3**, and **5**, in which the variable substituents X are on the anilino benzene ring (ring A), exhibit anomalous upfield shifts with increasing electron-withdrawing property of the substituents X (inverse substituent effects). Careful inspection of Table 1 also reveals that the azomethine proton chemical shifts in **5** remain roughly constant independent of the electron-withdrawing groups such as CO_2Et, CN, and NO_2. These trends can well be seen in Figs. 1—3 in which the chemical shifts are plotted against Hammett σ constants.[7] The ρ values and correlation coefficients are shown in Table 2 in which a positive sign in the ρ values refers to the inverse substituent effect and a negative sign refers to the normal substituent effett. Table 3 depicts 4-NO_2 and 4-NMe_2 group-induced shifts of the azomethine proton chemical shifts in going from **2** to **6**, and to **4**, respectively.

^{13}C-H Coupling Constants. The $J(^{13}C$-H) values were also measured for the series of **5**, **6**, and **7**, and are also shown in Table 1 together with those of **1** and

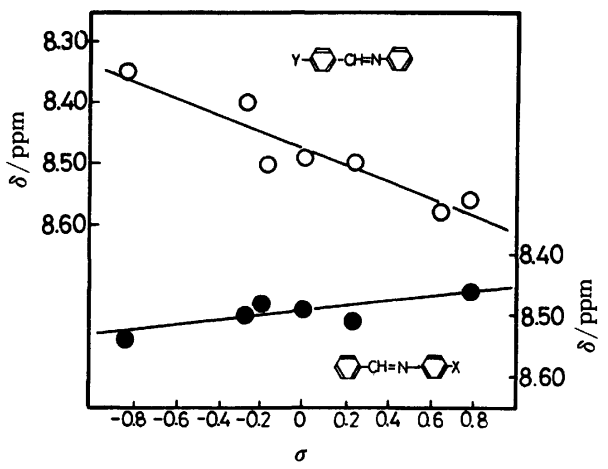

Fig. 1. Hammett Correlations of Azomethine Proton Chemical Shifts in **1** and **2**.

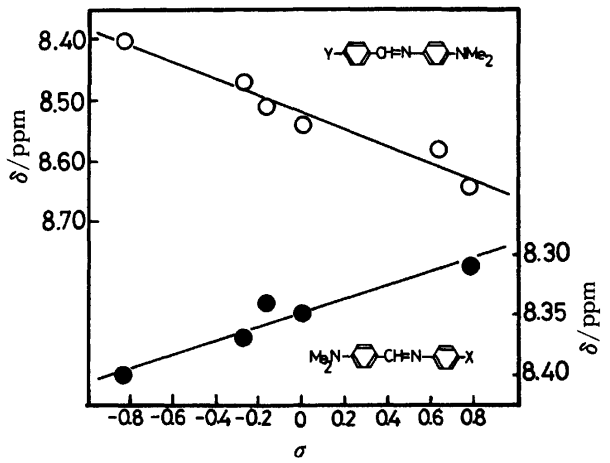

Fig. 2. Hammett Correlations of Azomethine Proton Chemical Shifts in **3** and **4**.

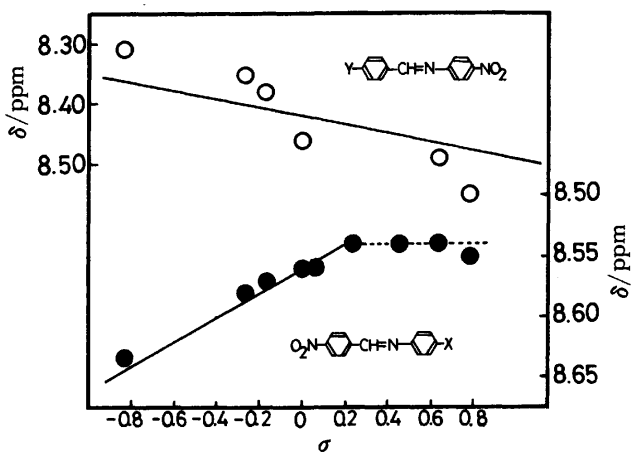

Fig. 3. Hammett Correlations of Azomethine Proton Chemical Shifts in **5** and **6**.

TABLE 2. HAMMETT CORRELATIONS OF THE AZOMETHINE PROTON CHEMICAL SHIFTS[a)]

Series	ρ Value	Correlation coefficient
1	+0.04	0.812
2	−0.14	0.937
3	+0.06	0.952
4	−0.13	0.976
5	+0.06	0.886
5[b)]	+0.09	0.991
6[c)]	−0.15	0.956

a) Regression analyses were carried out with relative values ($\delta_H-\delta_X$ or $\delta_H-\delta_Y$) of the chemical shifts. b) The chemical shifts of **5h**, **5i**, and **5j** were omitted in the regression analysis. c) The chemical shift of **6f** was omitted in the regression analysis.

2 reported by Inamoto *et al.*[1d)] As shown in Table 1, the $J(^{13}C-H)$ values for all the series studied increase with increasing electron-withdrawing property of the substituents X or Y regardless of the positions of the substituents, which is in sharp contrast with the results of the azomethine proton chemical shifts. It is also clear that the $J(^{13}C-H)$ values of the disubstituted derivatives

TABLE 3. 4-NO_2 AND 4-NMe_2 GROUP-INDUCED SHIFTS OF THE AZOMETHINE PROTON CHEMICAL SHIFTS (ppm)[a)]

Y	NO_2-induced shift	NMe_2-induced shift
NMe_2	+0.04	−0.05
OCH_3	+0.05	−0.07
CH_3	+0.12	−0.01
H	+0.03	−0.05
CN	+0.09	0.00
NO_2	+0.01	−0.08

a) Positive values denote upfield shifts.

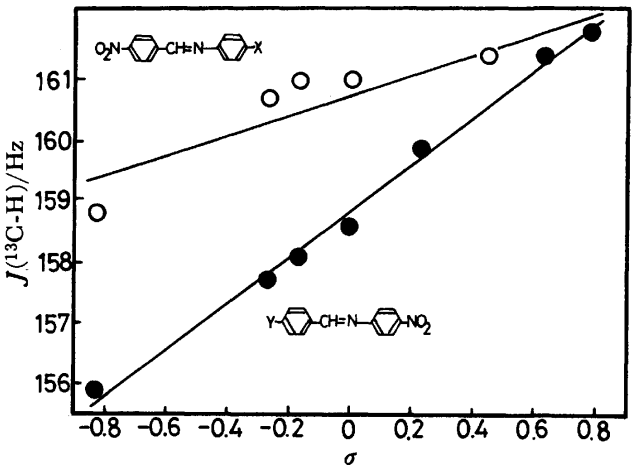

Fig. 4. Plot of $J(^{13}C-H)$ *vs.* Hammett σ Constants in **5** and **6**.

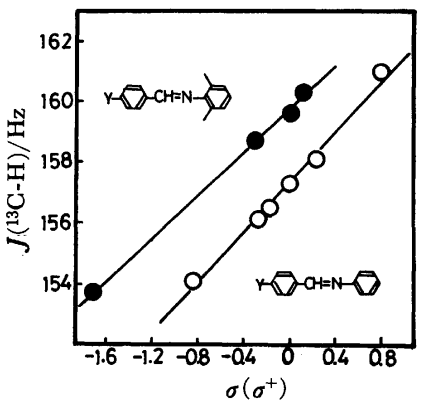

Fig. 5. Plot of $J(^{13}C-H)$ *vs.* Hammett σ^+ and σ Constants in **7** and **2**, respectively.

5 and **6** are greater than those of the monosubstituted derivatives **1** and **2**, respectively. Comparison of the $J(^{13}C-H)$ values between **2** and **7** indicates that replacement of two hydrogen atoms by the 2,6-dimethyl groups on the ring A usually increases the $J(^{13}C-H)$ values. Plots of the $J(^{13}C-H)$ values of **5**, **6**, and **7** against Hammett σ or σ^+ constants result in linear relationships as shown in Figs. 4 and 5. In Fig. 5, the Hammett plot is also shown for **2** for the sake of comparison. The ρ values and correlation coefficients are listed in Table 4.

Discussion

Inverse Substituent Effects on the Azomethine Proton

Chemical Shifts. As previously found by other workers,[1] the inverse substituent effect on the azomethine proton chemical shifts in **1** was also observed in the present study. Furthermore, the anomalous effects of the 4-substituents were shown to be a general phenomenon since the inverse substituent effects were also found for **3** and **5** which respectively carry 4′-NMe_2 and 4′-NO_2. The anomalous substituent effects in **1**, **3**, and **5** become more clear when we compare them with the substituent effects on the $J(^{13}C-H)$ values and the azomethine carbon chemical shifts. The comparison reveals that a principal controlling factor of the azomethine proton chemical shifts is different from that of the $J(^{13}C-H)$ values and the azomethine carbon chemical shifts. For example, the azomethine carbon chemical shifts of **5a**, **5d**,and **5j** are reported 151.46 (ppm/TMS in $CDCl_3$), 157.38, and 159.89, respectively, indicating that the azomethine carbon chemical shifts suffer substituent electronic effects.[4] The $J(^{13}C-H)$ values for the same series are, as shown in Table 1, 158.8 (Hz), 161.0, and 161.8, respectively. It is well known that the $^{13}C-H$ coupling constant is a function of *s* character of the C–H bond.[8] The above trend clearly indicates that the *s* character of the azomethine carbon–hydrogen bonds increases with increasing electron-withdrawing properties of the substituents X in **5**. These expected changes of the azomethine carbon chemical shifts and the $J(^{13}C-H)$ values indicate that through-bond electronic effects of the substituents X are important to determine the mode of the substituent effects on the $J(^{13}C-H)$ values and the azomethine carbon chemical shifts, whereas the azomethine proton chemical shifts will be governed by some other effects induced by the substituents. This does not mean that the through-bond electronic effect is absent as a controlling factor of the azomethine proton chemical shifts; it is hidden under the other effects. It has been once suggested[9] that the anomalous substituent effect of 4-NMe_2 group, for example, could be ascribed to dominance of the inductive effect over the resonance effect because it was then thought that *N*-benzylideneanilines take generally twisted conformations in solution regardless of the substituents on them. However, the present study clearly indicates that this view is not sufficient to explain the inverse substituent effects since the azomethine carbon chemical shifts and the $J(^{13}C-H)$ values suffer the normal substituent electronic effects, which indicates that the azomethine protons must also suffer (though not observed) similar substituent effects.

The present findings are consistent with our previous proposition that the inverse substituent effect may arise primarily from the change of the twist angle θ_N which subsequently changes the contribution of the paramagnetic deshielding effect of the ring A exerted on the azomethine proton. Actually, it is strongly suggested by Zollinger[10] and Kubota[11] that **5a** will take a nearly planar confromation in solution. Our previous NMR study also supports the view,[4] and furthermore, implies that the twist angle θ_N may decrease in going from X=NO_2 to NMe_2 in **5**. Under these circumstances, the paramagnetic deshielding effect of the ring A will greatly increase to result in the anomalous lowfield shift in **5a**, compared with, for example, **5j**. Since the azomethine carbon chemical shift as well as the $J(^{13}C-H)$ undergoes, as described above, the expected change upon the introduction of the electron-releasing groups, the electron density on the azomethine carbon must increase and the *s* character of the azomethine carbon–hydrogen bond must decrease in going from **5j** to **5a**. This should lead to upfield shift of the azomethine proton in going from **5j** to **5a**. The observed low field shift with increasing electron-donating property of the substituents X strongly suggests that change of the chemical shift caused by the paramagnetic deshielding effect (caused by the change of the twist angle θ_N) is larger than that by the through-bond electronic effect of the substituent X.

Comments should also be made on the findings that a better correlation of the azomethine proton chemical shifts with Hammett σ constants (correlation coefficient 0.991) was found when the electron-withdrawing groups (4-CO_2Et, 4-CN, and 4-NO_2) were excluded in the regression analysis, and that the chemical shifts almost remain constant for the derivatives bearing these substituents. In a previous paper,[4] we reported that the correlation coefficients for the azomethine carbon chemical shifts *vs.* Hammett σ and σ^+ constants in **5** are 0.978 and 0.999, respectively. As shown in Table 4, that for the $J(^{13}C-H)$ *vs.* Hammett σ constants is 0.928. Based on these values, the linearity of the azomethine proton chemical shifts with Hammett σ constants should also be similarly good with a *negative* ρ value if they suffer only the substituent electronic effects. The good correlation with a *positive* ρ value could imply that the paramagnetic deshielding effect (and hence the twist angle θ_N) is linearly changed with the substituent electronic effects.

The small variations of the chemical shifts in **5h**, **5j**, and **5i** could be interpreted in terms of combined effects of 4′-NO_2 group and minor conformational changes among these derivatives. Thus, the 4′-NO_2 group decreases electron density on the C–H bond so that the second electron-withdrawing group such as 4-CN and 4-NO_2 is not very effective to cause significant change of the chemical shift. Also if the twist angles θ_N among these derivatives are similar to each other, the ring current effects exerted on the azomethine proton may also be similar to each other to give roughly the same chemical shifts. It is not unreasonable to assume that the twist angles θ_N among **5h**, **5j**, and **5i** do not differ as much as they do among the derivatives bearing the electron-releasing groups such as 4-NMe_2 and 4-OCH_3, since through-conjugative interaction between the 4′-NO_2 and the 4-substituent, which is important to determine the twist angle θ_N for **5a** and **5b**,[4,10,11] is absent in **5h**, **5j**,

and **5i**. Probably, small changes of the chemical shifts caused by the 4′-NO_2 and those by the minor conformational changes will be cancelled by each other to give the observed chemical shifts.

The anomalous substituent effects in **1** and **3** can also be explained similarly. As shown in the previous paper,[4] azomethine carbon chemical shift in **3** suffers normal substituent effect. Although the $J(^{13}C\text{–}H)$ values are not available for all the compounds of **3**, those of **3d** and **3i** are 151.4 (Hz) and 155.9, respectively. These trends indicate, as discussed above, that the through-bond electronic effect of the substituents X is of primary importance for both NMR constants. On taking into account that 4-NMe_2[10] and 4-NO_2[3–6] substitutions tend to decrease and increase the twist angle θ_N, respectively, it is not unreasonable to consider that the inverse substituent effects in **3** may also arise primarily from the change of molecular conformation (twist angle θ_N) induced by the substituents.

The anomaly dicussed above may also be ascertained by comparison of the azomethine proton chemical shifts between **2** and **6**, and **2** and **4**. The comparison makes it clear that the 4-NO_2 and 4-NMe_2 substitution almost always generate the anomalous up- and low-field shifts, respectively, regardless of the nature of the substituents on the ring B.

Finally, it is worth noting that the anomalous substituent effect on the azomethine proton chemical shifts should not be simply ascribed to the twisted conformations of *N*-benzylideneanilines. Difference in conformation among the substituted *N*-benzylideneanilines should be taken into account to get a deeper understanding on it.[2]

J(¹³C–H) and Transmission of the Substituent Effects. We used in the previous section the results on the $J(^{13}C\text{–}H)$ values to get a deeper understanding on the origin of the anomalous substituent effects on the azomethine proton chemical shifts. It is also of interest to discuss the $J(^{13}C\text{–}H)$ values of **7**, and the efficiency of transmission of the substituent effects on the basis of the $J(^{13}C\text{–}H)$ values of **5**, **6**, and **7**.

Comparison of the $J(^{13}C\text{–}H)$ values between **2** and **7** is of particular interest. Since a methyl group is moderately electron-donating, the *s* character of the azomethine carbon–hydrogen bond would decrease from **2** to **7** to give rise to a larger $J(^{13}C\text{–}H)$ in **2** than in **7**. However, the reverse situation was found except Y=NMe_2. These results can well be explained in terms of considerably twisted conformations of **7**; introduction of the 2,6-dimethyl groups on the ring A forces the aromatic ring to be highly twisted, and the twisting is accompanied by enhancement of *N*-lone pair delocalization to the ring A, as shown in Scheme 3. Contribution of the canonical structure A must cause an increased *s* character of the azomethine carbon-hydrogen bond giving rise to the larger coupling constants in **7** than in **2**. The pronounced effect of the dimethylamino group to decrease the coupling

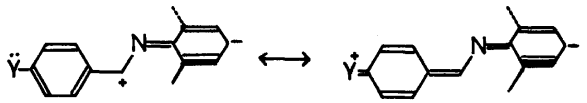

A B

Scheme 3.

Table 4. Hammett correlations of the coupling constants.

Series	ρ Value/(Hz/σ)	Correlation Coefficient	Substituent Constant
1[a]	1.99	0.980	σ
2[a]	4.45	0.995	σ
5	1.72	0.928	σ
6	3.80	0.997	σ
7	6.48	0.988	σ
7	3.57	0.999	σ^+

a) Ref. 1d.

constant indicates the efficient electron donation as shown in the canonical structure B. This finding is an alternative support for the enhanced *N*-lone pair delocalization in **7**, as shown earlier by Kobayashi.[12] The scheme is also consistent with a more enhanced transmission of the substituent effects in **7** than in **2** (see below).

The efficiency of transmission of substituent effects can be evaluated by the ρ values. As shown in Table 4, the ρ value for **7** (6.48) is larger than that for **2** (4.45). This shows that substituent effect is better transmitted in **7** than in **2**, and can be explained in terms of the development of positive charge on the azomethine carbons in **7**, as shown in the Scheme 3. Better correlation of the $J(^{13}C\text{–}H)$ values with Hammett σ^+ constants than with σ constants in **7** is also consistent with the scheme.

Concerning **5** and **6**, the ρ value was found to be larger in **6** than in **5**. This can be interpreted in terms of the through-bond substituent effect on the coupling constants as discussed in the previous section; the azomethine carbon–hydrogen bond in **6** is one bond closer to the substituent Y than to X in **5**.[1d]

Conclusion

Substituent effects on the azomethine proton chemical shifts for several series of mono- and disubstituted *N*-benzylideneanilines were examined. The inverse substituent effects were found to be a general phenomenon for *N*-benzylideneanilines carrying variable substituents at the 4-position of the anilino benzene ring regardless of the nature of the 4-substituents on the benzylidene benzene ring. On the basis of the results on similar substituent effects on the azomethine carbon chemical shifts and the $^{13}C\text{–}H$ coupling constants for the azomethinecarbon–hydrogen bonds together with available data on the molecular conformations of *N*-

benzylideneanilines, a concept of conformational change with substituents was invoked to account for the anomalous substituent effects.

Experimental

Materials. Most of the derivatives of **1**—**7** are available from a previous work.[4] Other compounds were similarly prepared, and identified by comparison of the physical and spectroscopic data with those of authentic samples.

Measurements of the Azomethine Proton Chemical Shifts. All measurements were run on a JEOL MH-100 spectrometer at room temperature (probe temperature was *ca.* 27°C). The solvent was spectral grade $CDCl_3$. Each solution was prepared by dissolving each sample in $CDCl_3$ containing 1% tetramethylsilane as an internal reference. An aliquot of each solution was taken for further dilution. In most cases, we have examined the chemical shifts in two or three concentrations; however, no appreciable dilution shifts were observed at the concentrations below 0.07 mol dm^{-3}. The chemical shifts were obtained at each concentration as the mean of at least three scans, in most cases, four scans. Sample concentrations were *ca.* 0.03—0.07 mol dm^{-3}.

Measurements of the ^{13}C-H Coupling Constants. The ^{13}C-H coupling constants were taken from a JEOL FX-60 spectrometer in $CDCl_3$ by the gated decoupling technique. Because of low solubility, the measurements of **5b**—**5j** and **6b**—**6j** were run at 40°C of the probe temperature. Other measurements were run at room temperature.[13]

References

1) a) K. Tabei and E. Saitou, *Bull. Chem. Soc. Jpn.*, **42**, 440 (1969); b) A. van Putten and J. W. Pavlik, *Tetrahedron*, **27**, 3007 (1971); c) V. M. S. Gil and M. E. L. Saravia, *ibid.*, **27**, 1309 (1971); d) N. Inamoto, K. Kushida, S. Masuda, H. Ohta, S. Satoh, Y. Tamura, K. Tokumaru, K. Tori, and M. Yoshida, *Tetrahedron Lett.*, **1974**, 3617; e) N. Inamoto, S. Masuda, K. Tokumaru, M. Yoshida, Y. Tamura, and K. Tori, *ibid.*, **1975**, 3797; f) N. Inamoto, S. Masuda, K. Tokumaru, K. Tori, and M. Yoshida, *ibid.*, **1975**, 3701; g) J. S. Sandhu, D. Mago, and B. J. Wakefield, *ibid.*, **1975**, 1091; h) D. Mago, J. S. Sandhu, and B. J. Wakefield, *J. Chem. Soc., Perkin Trans. 2*, **1977**, 715; i) A. S. Al-Tai, D. M. Hall, and A. R. Mears, *ibid.*, **1973**, 133.

2) M. Holík, J. Běluša, and J. Břicháček, *Collect. Czech. Chem. Commun.*, **43**, 610 (1978).

3) R. Akaba, H. Sakuragi, and K. Tokumaru, *Bull. Chem. Soc. Jpn.*, **58**, 301 (1985).

4) R. Akaba, H. Sakuragi, and K. Tokumaru, *Bull. Chem. Soc. Jpn.*, **58**, 1186 (1985).

5) R. Akaba, K. Tokumaru, and T. Kobayashi, *Bull. Chem. Soc. Jpn.*, **53**, 1993 (1980).

6) R. Akaba, K. Tokumaru, T. Kobayashi, and C. Utsunomiya, *Bull. Chem. Soc. Jpn.*, **53**, 2002 (1980).

7) O. Exner, "Advences in Linear Free Energy Relationship," ed by N. B. Chapman and J. Shorter, Plenum Press, London (1972), Chapter 1.

8) a) C. H. Yoder, R. H. Tuck, and R. E. Hess, *J. Am. Chem. Soc.*, **91**, 539 (1969); b) C. H. Yoder, C. D. Schaeffer, Jr., and R. E. Hess, *J. Chem. Eng. Data*, **17**, 385 (1972); c) N. Inamoto, S. Masuda, A. Terui, and K. Tori, *Chem. Lett.*, **1972**, 107.

9) A. S. Al-Tai, D. M. Hall, and A. R. Mears, *J. Chem. Soc., Perkin Trans. 2*, **1976**, 133.

10) P. Skrabal, J. Steiger, and H. Zollinger, *Helv. Chim. Acta*, **58**, 800 (1975).

11) K. Ezumi, H. Nakai, S. Sakata, K. Nishikida, M. Shiro, and T. Kubota, *Chem. Lett.*, **1974**, 1393.

12) M. Yoshida, H. Minato, and M. Kobayashi, *Chem. Lett.*, **1976**, 1097.

13) The authors express their sincere thanks to Mr. T. Hinomoto of JEOL for measuring the ^{13}C-H coupling constants.

 © 1985 The Chemical Society of Japan Bull. Chem. Soc. Jpn., 58, 1717—1722 (1985)

Anodic Oxidation of Cyclohexanone on Lead Dioxide Electrode in Aqueous Sulfuric Acid Solution

Atsutaka KUNAI,* Kazuhito HATOH, Yoshinobu HIRANO, Junji HARADA, and Kazuo SASAKI
Department of Applied Chemistry, Faculty of Engineering, Hiroshima University, Shitami, Saijo-cho, Higashi-Hiroshima 724
(Received December 3, 1984)

The electrolytic behavior of cyclohexanone was examined by potentiometry with rotating disk electrode as well as by product analyses. The reaction was activation controlled and the reaction orders were first with respect to cyclohexanone and zero for proton. Cyclohexanone reacted by approximately 6 electrons to give adipic acid mainly which accumulated proportionally to the electricity consumed. Changes in temperature, proton concentration, and current density resulted in only minor effects on the reaction. In neutral solution, however, the oxidation was suppressed and oxygen evolution dominated. Other electrode materials such as Pt, graphite, RuO_2, and PtO_2 were inactive. The chemical oxidation with PbO_2 itself did not occur. From these facts, reaction mechanism was discussed.

It is well known that lead dioxide electrode is effective to the anodic oxidation of certain organic compounds. Especially, the oxidation of aromatic compounds, such as benzene, toluene, or phenol, with lead dioxide electrode leads to the formation of *p*-benzoquinone in good yields, and therefore, this reaction has been investigated by many workers from the industrial and mechanistic points of view.[1-13] The reason is, however, still left uncertain why PbO_2 electrode is actually effective to the oxidation of aromatic compounds.

This electrode is known to be active also to the oxidation of a certain alicyclic ketone such as cyclohexanone, but the formation of different products has been reported by Yokoyama,[14] Pyrrone,[15] and Sugawara and Sato.[16] At present time, no quantitative information is shown yet about the electrochemical behavior of PbO_2 electrode toward aliphatic ketones, in views of the special reactivity of this electrode, the product selectivity, or the reaction mechanism.

In this study, we should like to discuss in detail the basic behavior of PbO_2 in the presence of aliphatic ketones. For this purpose, cyclohexanone was chosen as the representative of the ketones and its oxidation behavior was compared with that of benzene. The main object was placed on studying the effectiveness of this particular electrode and evaluating the active species on PbO_2 as well as clarifying product selectivity.

Experimental

Cyclohexanone was reagent grade which was distilled and checked by GLC before use. All the other chemicals were analytical grade and were used as purchased.

All the electrochemical measurements were made using a Nichia Keiki NPG 1070E potentiostat. For preparative electrolysis, a Kikusui Denki PAD 110-1.5L regulated DC power supply was used. Proton concentration of the solutions was determined by a Toa Dempa MH-7B pH meter. All the potential values cited in this paper were those referred to Hg/Hg_2SO_4 electrode in 0.5 M† sulfuric acid. The reaction products were analyzed by Hitachi 665 high pressure liquid and 163 gas chromatographs.

The rotating disk electrode was prepared by filling a Pb rod of 5 mm in diameter into the center of a teflon holder, and the surface of the electrode was shaved planarly with a lathe and polished with cellulose fiber paper. The PbO_2 film was coated on the cleaned Pb surface by first stepping the electrode potential to 1.70 V for 25 min and to 1.10 V for another 20 min. The PbO_2 film was freshly prepared before each series of the experiments and the current values were determined after ten min of polarization.

For macro-scale electrolysis, a Pb plate of 5×6 cm in size was used as the anode which was pretreated before use in a similar manner as described above. An anolyte of 150 cm^3 in volume containing 0.34 M cyclohexanone was polarized under controlled current conditions in a divided cell. A small quantity of the sample was taken up in each interval and analyzed by HPLC using Merck Lichrosorb RP-18 (particle size 10 μm, 4×125 mm) as the column and a mixed solvent of acetonitrile (20%) and phosphate buffer solution of pH 3.5 (80%) as the eluent. The amounts were determined at 220 nm for adipic acid and at 280 nm for both cyclohexanone and 2-cyclohexenone.

For analysis of lactones, the electrolyzed solution was continuously extracted with ether and the concentrated extract was subjected to GLC analysis using PEG 20 M and KG 2 as columns and diethyl phthalate as the internal standard material. In some experiments, carboxylic acids were analyzed after the treatment with methanolic BF_3 solution. The products, 5-hexanolide, 4-hexanolide, and methyl esters of adipic, 5-oxohexanoic, glutaric, and succinic acids were isolated by preparative GLC and their spectrometric properties were compared with those of authentic samples.

Electrolyses were made also using other electrode materials, platinum, graphite, PtO_2, and RuO_2. The latter two electrodes were prepared by thermally depositing the metal oxide layer on Ti plates in the usual way.[17,18]

Results and Discussion

1. Current-potential Curves. Typical polarization curves obtained with the rotating disk electrode at 1500 rpm†† are shown in Fig. 1. In 0.5 M sulfuric acid solution, an apparent Tafel slope of 125 mV was observed and the current was independent of rotating velocity. On addition of cyclohexanone, the anodic current increased in the wide range of the potential

† M=mol dm^{-3}.

†† rpm=120 π rad s^{-1}.

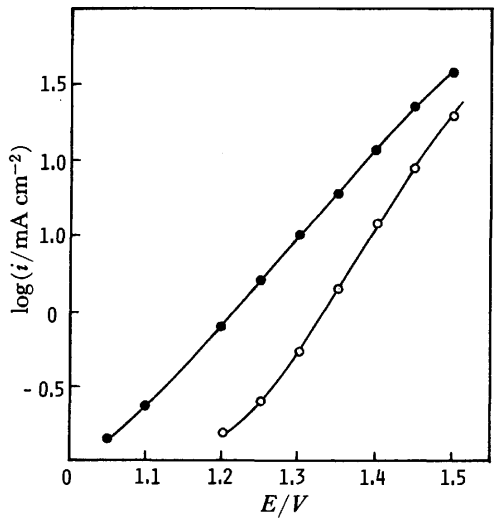

Fig. 1. Polarization curve for rotating PbO_2 electrode in 0.5 M H_2SO_4 (ω=1500 rpm), (O) in the absence and (●) in the presence of cyclohexanone (100 mM).

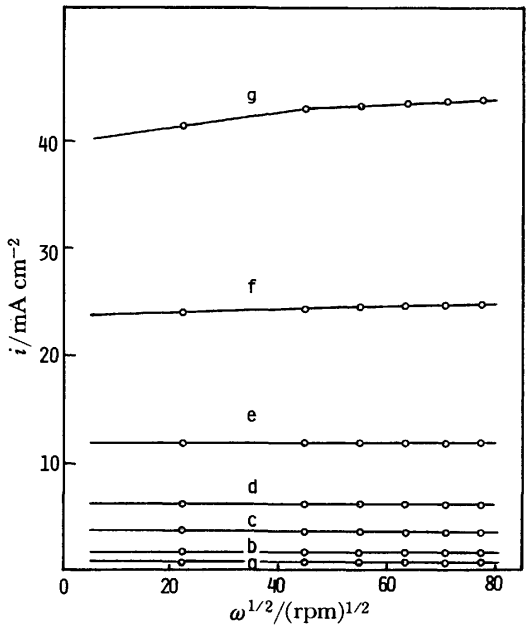

Fig. 2. Variation of total oxidation current as a function of $\omega^{1/2}$ at potentials of (a) 1.20, (b) 1.25, (c) 1.30, (d) 1.35, (e) 1.40, (f) 1.45, and (g) 1.50 V.

studied, and the Tafel region was observed in the potential range between 1.15 and 1.40 V.

The effect of rotating velocity on the current in the cyclohexanone solution is shown in Fig. 2. At the potential lower than 1.4 V, the anodic current was completely independent of rotating velocity. Although a slight influence of diffusion controlled process was observed at higher potential than 1.45 V, the oxidation of cyclohexanone on this electrode seemed to be essentially reaction controlled.

Figure 3 shows the effect of the concentration of cyclohexanone on the current at a rate of 1500 rpm. The plot of the currents against the concentrations within 200 mM exhibited a good linearity at each po-

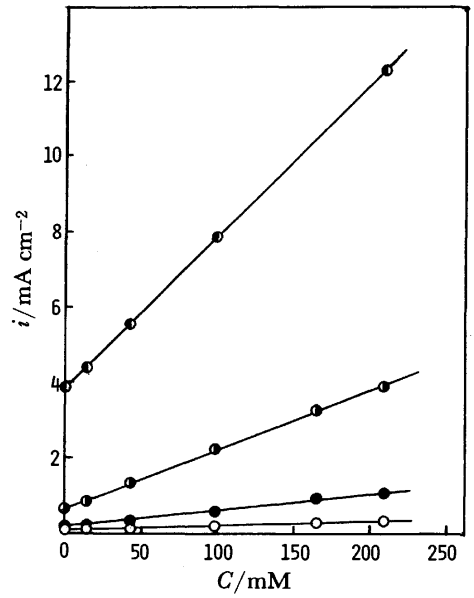

Fig. 3. Variation of total oxidation current as a function of cyclohexanone concentration, at potentials of (O) 1.10, (●) 1.20, (◑) 1.30, and (◐) 1.40 V (ω= 1500 rpm).

tential applied, 1.1, 1.2, 1.3, and 1.4 V, respectively. The extrapolated intercept of each line coincided with the value of the back ground current of the base solution. This indicates that there is no appreciable change in residual current even in the presence of high concentration of cyclohexanone. This is a marked difference from the case of benzene solution reported by Clarke *et al.*,[9] where oxygen evolution was substantially suppressed.

2. Reaction Order. The mass transport study (Fig. 2) and product analysis (section 3) clearly demonstrate that both diffusion and electrode potential little affect the reaction. The main reaction is the formation of adipic acid:

$$C_6H_{10}O + 3H_2O \longrightarrow C_6H_{10}O_4 + 6H^+ + 6e.$$

In general, activation controlled process can be expressed by the form of Eq. 1 for the anodic reaction:

$$i = nFk[C]^p\,[H^+]^q \exp(\alpha nFE/RT), \qquad (1)$$

where [C] is the concentration of cyclohexanone, E the electrode potential applied, and i the current. In this case, the current i should be the net oxidation current i_{net}, which is the difference between observed and residual currents. The reaction orders p with respect to cyclohexanone and q for proton should be, therefore, conveniently obtained from Eq. 2.

$$\log i_{net} = p\log[C] + q\log[H^+] + (\alpha nF/RT)E + \text{constant}. \qquad (2)$$

For the determination of p, i_{net} at 1500 rpm was plotted against log[C] in 0.5 M sulfuric acid solutions, where the concentration of proton was assumed to be constant (Fig. 4). The slopes of the log i_{net} *vs.* log[C] satis-

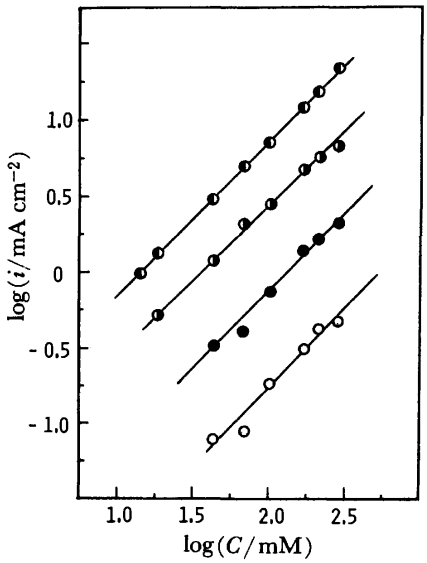

Fig. 4. Logarithmic plots of net oxidation current *vs.* cyclohexanone concentration obtained at potentials of (○) 1.10, (●) 1.20, (◑) 1.30, and (◐) 1.40 V (ω=1500 rpm).

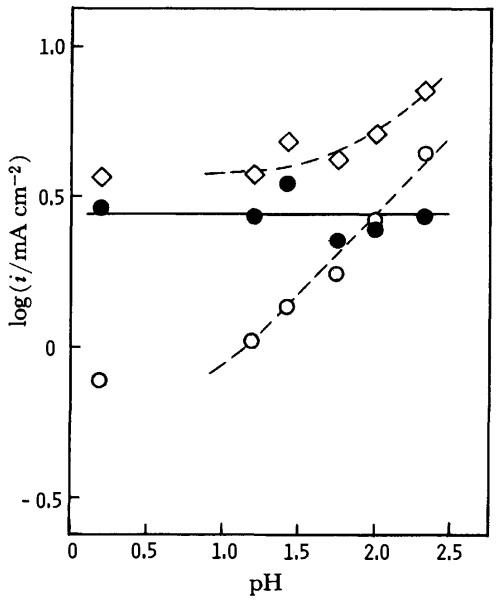

Fig. 5. Plot of oxidation currents *vs.* pH obtained in sulfate solutions (1.30 V, ω=1500 rpm). Symbols stand for (○) residual current in base solution, (◇) total current of cyclohexanone solution (200 mM), and (●) net oxidation current.

fied good linearities and were exactly 1.0 at each potential applied, 1.1, 1.2, 1.3, and 1.4 V, respectively. This means that the oxidation of cyclohexanone is first order with respect to cyclohexanone.

For evaluating the participation of proton to the anodic process, we prepared a series of sulfate solutions within the pH range of 1 to 2.5, where the total concentration of the sulfate was adjusted to be 0.5 M.

We examined the relation of pH and logarithmic current of i_{net} under constant potential conditions, 1.3 V, where the concentration of cyclohexanone and the potential were kept unchanged. As shown in Fig. 5, the net oxidation current was unaffected by pH and the reaction order for proton was concluded to be zero.

3. Product Analysis. As a typical run, a solution of 0.34 M cyclohexanone in 0.5 M sulfuric acid was electrolyzed on PbO_2 anode under the constant current conditions (2 A dm^{-2}, 10 °C).

Product Isolation: The electrolyzed solution was extracted with ether. The concentrated extract was distilled *in vacuo*. The initial fraction consisted of mostly cyclohexanone recovered and the second fraction contained two products, 5-hexanolide (δ-lactone) and 4-hexanolide (γ-lactone), which were isolated by preparative GLC.

The nonvolatile residue showed strong IR absorption bands of carboxyl groups. Isolation of carboxylic acids was first tried by preparative LC (reverse phase), but complete identification was failed because of poor separation. The acids were, therefore, isolated as their methyl esters after the treatment with methanolic BF_3 solution. By preparative GLC, the esters of adipic, 5-oxohexanoic, glutaric, and succinic acids were isolated.

GLC Analysis: After passing 1.2 F mol^{-1} of the electricity,[†††] products were extracted with ether and analyzed by GLC. Taking an average over nine individual experiments, we estimated that the conversion rate of cyclohexanone was 155 mmol F^{-1} where approximately 6.5 electrons were necessary for a molecule that disappeared (Table 1). The chemical selectivity of δ- and γ-lactones were 25 and 4%, respectively. Traces of 2-cyclohexenone were detected.

In another run, the extract was esterified and analyzed by GLC (Table 2). The main product, adipic acid, was detected only in 7—8% of selectivity by this method because of, presumably, poor extraction efficiency of the dicarboxylic acids.

HPLC Analysis: The changes in concentration of cyclohexanone and carboxylic acids were monitored by reverse phase HPLC in the time course of the electrolysis. Cyclohexanone disappeared linearly at a rate of 150 mmol F^{-1} and, instead, a distinctive peak corresponding to adipic acid increased. The accumulation of this material was proportional to the quantities of electricity consumed. Supposing that this peak consisted of solely adipic acid, we obtained the accumulation rate to be 80.8 mmol F^{-1}. If this is the case, the chemical selectivity and the current efficiency for adipic acid reach to 54 and 49%, respectively. Other acids identified before seemed to be rather minor by HPLC analysis. The linear accumulation of adipic acid clearly shows that adipic acid is not formed by reoxidation of some solution phase products, such as lactones, but formed directly from cyclohexanone on the electrode.

These results were little affected by temperature, concentration of sulfuric acid, or current density which

[†††] F=96480C.

Table 1. GLC analysis of lactones

Electricity consumed	Cyclohexanone reacted		δ-Lactone		γ-Lactone		Total	
	Amount	Conv.	Amount	Select.	Amount	Select.	Amount	Select.
F mol^{-1}	mmol F,$^{-1}$	%	mmol F,$^{-1}$	%	mmol F,$^{-1}$	%	mmol F,$^{-1}$	%
1.20	155	19	33.1	21	6.4	4	39.5	25

Solutions of 0.34 M cyclohexanone in 0.5 M sulfuric acid (100, 120, or 150 cm^3) were electrolyzed on the pretreated PbO_2 electrode. Average values over nine individual runs are shown in the Table.

Table 2. GLC analysis of carboxylic acids after esterification

Methyl ester[a)] of acid	Method A		Method B	
	Amount/mmol F,$^{-1}$	Select./%	Amount/mmol F,$^{-1}$	Select./%
Adipic	10.3	6.9	11.3	7.6
Glutaric	6.6	4.4	6.1	4.1
Succinic	2.9	2.0	2.3	1.5
5-Oxohexanoic	9.2	6.2	7.6	4.9
Total	29.0	19.5	27.3	18.1

Solutions of 0.34 M cyclohexanone in aqueous sulfuric acid (150 cm^3) were electrolyzed until 1.5 F mol^{-1} of the electricity was consumed under the conditions of 10 °C in temp., 2.0 A dm^{-2} in current density, and 0.5 M in H_2SO_4 concentration.
a) Method A: Treated with methanolic BF_3 solution; Method B: Heated in methanol in the presence of H_2SO_4.

Table 3. Effects of electrolytic conditions on the formation of adipic acid

Run	Changes in conditions	Cyclohexanone reacted			Adipic acid		
		Amount	Conv.	n	Amount	Select.	Current efficiency
		mmol,	%,		mmol,	%,	%
1	Unchanged[a)]	11.5	23	6.7	6.18	54	49
2	Temp 0 °C	12.0	24	6.4	6.24	52	49
3	Temp 20 °C	14.8	29	5.2	6.36	43	50
4	Acid 3 M	13.8	27	5.5	8.42	61	66
5	Acid 6 M	14.6	29	5.2	7.29	50	57
6	C.D. 1 A dm^{-2}	14.4	28	5.3	7.96	55	62
7	C.D. 4 A dm^{-2}	12.3	24	6.2	6.01	49	47
8	MeCN 2 v/v%	11.0	22	7.0	6.92	63	54
9	MeCN 50 v/v%	10.3	20	7.4	7.38	72	58

a) The standard conditions were the same as those described in Table 2.

Table 4. Effect of pH on the oxidation of cyclohexanone

Base solution	pH (final)	Cyclohexanone reacted/mmol	Adipic acid mmol	δ-Lactone mmol	γ-Lactone mmol	Cyclohexenone mmol
0.5 M H_2SO_4	0.3	11.5	6.18	1.71	0.45	0.18
0.5 M NaH_2PO_4[a)]	1.6	5.75	1.33	0.74	0.37	0.07
1.0 M NaH_2PO_4[a)]	2.2	4.87	0.63	0.65	0.21	0.04
1.0 M NaH_2PO_4 −1.0 M K_2HPO_4[a)]	5.3	1.45	Trace	Trace	Trace	Trace

Electrolytic conditions were the same as those described in Table 2.
a) The solution contains 0.1 M Na_2SO_4.

were changed in the range of 0—20 °C, 0.5—6.0 M, or 0.5—4.0 A dm^{-2}, respectively (Table 3).

Effect of pH: When the electrolyses were done in phosphate buffer solutions containing 0.1 M sodium sulfate, the oxidation of cyclohexanone also occurred. Its reactivity, however, markedly decreased with the increase of pH (Table 4). At higher pH's, the chemical selectivity and the current efficiency of adipic acid were considerably suppressed, but the chemical selectivity of lactones did not much changed.

Comparison of Electrode Materials: In order to evaluate the effectiveness of PbO_2 as the electrode material for the oxidation of cyclohexanone, we studied the behaviors of other electrode materials. The polarization curves obtained with the stationary Pt and graphite electrodes were compared in the absence and presence of cyclohexanone. On addition of cyclohexanone, the total currents were rather suppressed over the potential range measured.

The macro-scale electrolyses with these electrodes

TABLE 5. COMPARISON OF ELECTRODE MATERIALS

Electrode	Cyclohexanone reacted/mmol F^{-1}	Adipic acid mmol F^{-1}	δ-Lactone mmol F^{-1}	γ-Lactone mmol F^{-1}	Cyclohexenone mmol F^{-1}
PbO_2	150	81	22	5.9	2.4
Bare Pt	17.3	—	Trace	Trace	0.4
Graphite	40	8.9	Trace	Trace	1.2
PtO_2/Ti	10.7	—	—	—	0.4
RuO_2/Ti	17.4	—	—	—	—

Electrolytic conditions were the same as those described in Table 2.

were carried out under similar conditions as described before. The reactivity of cyclohexanone was, as expected by the polarization curves, extremely small and substantial oxygen evolution occurred. We also tried to use PtO_2 and RuO_2 electrodes, but cyclohexanone was not oxidized on these electrodes (Table 5).

4. Reaction Mechanism. First, we briefly summarize the results for the oxidation of cyclohexanone on PbO_2 elcctrode. As discussed in *product analysis* study, PbO_2 shows particularly high oxidation ability toward cyclohexanone, but other electrode materials, such as Pt, graphite, RuO_2, and PtO_2, are almost inactive. At lower pH's, cyclohexanone consumes *ca.* 6 electrons on PbO_2 to afford adipic acid with 50—65% of the current efficiencies. Other products, such as lower carboxylic acids and lactones, are minor. Such results are almost unchanged with the increase of the acid concentrations. Furthermore, adipic acid is formed as the primary electrode product on PbO_2 surface, where ε-lactone is not the intermediate. All of these facts have not been clarified in earlier reports.[14-16]

By examination of *current-potential curves*, it is also confirmed that the velocity of the reaction is affected only by the cyclohexanone concentrations obeying first order law, but not by mass transport and proton concentrations.

The effect of pH on the reaction seems, however, drastic at higher pH's. In neutral solutions, only the oxygen evolution occurs. These phenomena are undoubtedly due to the properties of PbO_2 itself and independent of organic substrates, because similar observations have been reported in the cases of benzene[9] and thiophen.[21] This means that the reaction is governed only by the active state of PbO_2, *i.e.* β-PbO_2 in acidic media, [19] but not by acid-catalyzed enol formation. We now consider the relation of the reaction and β-PbO_2 in detail.

Many reports have been published for β-PbO_2 in views of preparation, structure, and chemical properties. Beta-lead dioxide is formed in acidic media by either oxidation of Pb(II) ion or, more conveniently, anodization of Pb itself. This material is thermodynamically an unstable form of Pb(IV) and therefore highly active, which oxidizes even water slowly to leave Pb(II) and oxygen.[19,20]

Here it should be worth noting the work reported by Clarke *et al.*[9] who discussed the oxidation of benzene on PbO_2 electrode in detail. They excluded the possibilities of the direct electron transfer to the electrode[8] and the hydroxylation reaction with adsorbed atomic oxygen[2,3] because of, mainly, highly selective formation of *p*-benzoquinone at low electrode potentials as well as completely unsimilar reactivity of other electrode materials such as Pt and graphite. Instead, they proposed the homogeneous phase reaction between benzene and PbO_2 followed by the electrochemical regeneration of PbO_2, where the former step was rate determining and the concentration of PbO_2 was a potential dependent term. The evidence for this mechanism was the fact that *p*-benzoquinone and maleic acid were formed chemically by shaking the benzene emulsion in the presence of PbO_2 powder for 24 h.

Their assumption should be understood in the following aspects. Namely, PbO_2 is practically insoluble in moderately acidic solutions such as 0.5 M sulfuric acid. The solubility is reported as $\log[Pb^{4+}]=-8.26-4pH$, if free from complexing agents.[20] Such a situation seems unfavorable to the homogeneous reaction proposed. Suppose that the homogeneous reaction with PbO_2 occurs, probably as a form of Pb^{4+} in the bulk solution, it might be expected that the subsequently formed low valent Pb, *i.e.*, hardly soluble $PbSO_4$, deposits into the solution in the course of the electrolysis. Such phenomena were, however, not found in our cases, the oxidation of cyclohexanone.

Another thinkable possibility is that the oxidation with Pb(IV) occurs only in the limited region of diffusion double layer and the low valent Pb does not diffuse away into the bulk solution. If this is the case, the surface of the electrode will be covered finally with the low valent Pb salt resulting in the marked decrease in the electrode potential unless the electrode is externally anodized.

Taking these mechanisms into consideration, we carried out additional experiments. A very thin layer of β-PbO_2 was electro-deposited on Pt surface (0.34 μmol cm^{-2}) and the chemical durability of this electrode was examined by measuring the change in the open circuit potentials both in the presence and absence of cyclohexanone. In typical runs, the potential of this electrode, *ca.* 900 mV, was unchanged in the base solution for 60 min and then felt down rapidly. When some depolarizing materials such as form-

aldehyde or phenol were present in the solution, the duration time of this electrode was definitely shortened. On addition of cyclohexanone, however, the duration time was not changed at all. These facts may indicate that the chemical oxidation in the above manner is, even if occurs, extremely slow compared to the oxidation of the solvent water itself, in the case of cyclohexanone.

From all of the experimental results, one should deduce a clear conclusion that cyclohexanone is oxidized directly on the electrode but not oxidized chemically in the manner of the mediation with the lead(IV)/lead(II) couple. The simplest explanation is, of course, the occurrence of the direct electron transfer to the electrode inducing the subsequent chemical and electrochemical reactions, in which the rate determining step is activation controlled. As a result, adipic acid is formed directly on the electrode surface. This mechanism seems to satisfy most experimental results except for the particular effectiveness of PbO_2 compared to other electrode materials.

Alternative explanation is the participation of a particular surface species formed on the PbO_2 electrode. Lead dioxide has a large oxygen overvoltage, which may cause the accumulation of precursors of O_2 evolution in high concentration. The probable candidate for the reactive species is adsorbed hydroxyl radical.[10,21] Hydroxyl radical is highly reactive and electrophilic species. For example, it adds to benzene ($k=3.5\times10^9$ $M^{-1}s^{-1}$) to give hydroxycyclohexadienyl radical or abstracts α-hydrogen from acetone ($k=6\times10^7$ $M^{-1}s^{-1}$).[22] If this is applicable to our case, the abstraction of hydrogen from cyclohexanone should be rate determining step. Once organic radicals are formed on the electrode surface, they are trapped immediately with another oxygen species and/or oxidized electrodically to give other organic species in turn, leading to the final formation of stable products, such as adipic acid.

In summary, we should point out again at the present time that the anodic oxidation of cyclohexanone on PbO_2 may be accounted for by direct electron-transfer mechanism or, alternatively, by the reaction of hydroxyl radical formed on the electrode surface.

References

1) A. Renard, *Compt. Rend.*, **91**, 175 (1880).
2) F. Fichter and R. Stocker, *Ber.*, **47**, 2012 (1914).
3) G. Miodon and A. Seyewitz, *Bull. Soc. Chim. Fr., Ser. 4*, **33**, 449 (1923).
4) H. Inoue and M. Shikata, *Kogyo Kagaku Zasshi*, **24**, 567 (1921).
5) Y. Isomura, *Nippon Kagaku Kaishi*, **62**, 1167 (1941).
6) K. S. Udupa, G. S. Subramanian, and H. V. K. Udupa, *Bull. Acad. Pol. Sci., Ser. Sci. Chim.*, **9**, 45 (1961).
7) S. Itoh, K. Sasaki, Y. Murakami, and H. Shiba, *Denki Kagaku*, **40**, 733 (1972).
8) M. Fremery, H. Höver, and G. Schwarzlose, *Chem.-Ing.-Tech.*, **46**, 635 (1974).
9) J. S. Clarke, R. E. Ehigamusoe, and A. T. Kuhn, *J. Electroanal. Chem.*, **70**, 333 (1976).
10) J. G. Sunderland, *Electr. Counc. Res. Cent.*, [Memo], ECRC/M 1065 (1977); *Chem. Abstr.*, **87**, 124470u (1977).
11) G. C. Jones and D. A. Payne, U. S. Patent 3994788; *Chem. Abstr.*, **86**, 35759g (1977).
12) G. C. Jones and H. R. Meer, U. S. Patent 4035253; *Chem. Abstr.*, **87**, 75732v (1977).
13) C. Oleman, *AIChE Symp. Ser.*, **77**, [204] 264 (1981).
14) M. Yokoyama, *Bull. Chem. Soc. Jpn.*, **8**, 71 (1933).
15) F. Pirrone, *Gazz. Chim. Ital.*, **66**, 244 (1936).
16) M. Sugawara and M. Sato, *Denki Kagaku*, **43**, 407 (1975).
17) C. Iwakura, K. Fukuda, and H, Tamura, *Electrochim. Acta*, **21**, 501 (1976).
18) C. Iwakura, F. Goto, and H. Tamura, *Denki Kagaku*, **48**, 20 (1980).
19) P. Delahey, M. Pourbaix, and P. V. Rysselberghe, *J. Electrochem. Soc.*, **98**, 57 (1951).
20) M. Pourvaix, "Atlas of Electrochemical Equilibria in Aqueous Solutions," Pergamon Press, Oxford (1966), p. 485.
21) I. Izumi and I. Yamamoto, *Denki Kagaku*, **51**, 333 (1983).
22) K. U. Ingold, "Free Radicals," ed by J. K. Kochi, Weiley-Interscience, New York (1973), p. 37.

 © 1985 The Chemical Society of Japan Bull. Chem. Soc. Jpn., 58, 1723—1726 (1985)

Syntheses of Benzilic Acids through Electrochemical Reductive Carboxylation of Benzophenones in the Presence of Carbon Dioxide

Yoshikazu IKEDA* and Eiichiro MANDA
National Chemical Laboratory for Industry, Tsukuba 305
(Received December 14, 1984)

Reaction conditions for the electrochemical synthesis of benzilic acid (**2a**) under the atmosphere of carbon dioxide was investigated from the preparative points of view. The highest yield of **2a** (86%) was obtained under the following conditions; cathode: mercury, electricity passed: 2.3 F/mol, constant current density: 2.5 mA/cm^2, benzophenone (**1a**) (8.2×10^{-3}mol), electrolyte(KI, 1.7×10^{-2}mol) in DMF (50 ml). This method and conditions were applied to the syntheses of twelve benzilic acids (**2b—2m**) and yielded acids in the range of 10—92%. The yields were strongly depended on the electronic effect of substituents and benzilic acids were not obtained when the ring substituent was NO_2, OH, or Br group.

There are many reports on the production of carboxylic acids by bubbling CO_2 during reduction processes through catholytes containing organic materials. Among these, Wawzoneck *et al.*[1] have shown that benzophenone(**1a**) and acetophenone could be carboxylated to form benzilic acid (**2a**) and 2-hydroxy-2-phenylpropionic acid, respectively, during the course of mechanistic investigation on the reduction process of aromatic ketones. The yields of these acids were 54 and 6%, but the synthetic aspects of this reaction were not investigated.

We recently reported[2] that the electrochemical carboxylation reaction of 4-isobutylacetophenone in *N,N*-dimethylformamide (DMF) gave significant amounts of 2-hydroxy-2-(4-isobutylphenyl)propionic acid by a modification of the method of Wawzoneck for the synthetic application of organic electrochemistry. As an extension of this work, we report here a preparative electrochemical syntheses of benzilic acids from benzophenones in high yields under controlled conditions.

Experimental

All the melting points were measured on a Yanagimoto micromelting point apparatus and were uncorrected. IR spectra were recorded on a JASCO A-302 grating spectrometer in KBr. NMR spectra were measured on a Hitachi R-24 high resolution spectrometer (90 MHz) in $CDCl_3$ using TMS as an internal standard. Elemental analyses were performed by Microanalysis Laboratory of the Physical and Chemical Research Institute.

Materials. DMF was dried over anhydrous potassium carbonate for several days and distilled prior to use. Acetonitrile was refluxed and distilled from phosphorus pentaoxide and calcium hydride. Reagent grade lithium, sodium, potassium, rubidium, cesium and tetrabutylammonium iodide were used as supporting electrolytes without further purification. Benzophenones used were also reagent grade and were recrystallized from ethanol. Carbon dioxide used was 99.99% pure.

Electrolysis Apparatus. Preparative electrolysis experiments were carried out by using a Hokuto Denko HA-105 potentio-galvanostat equipped with a Hokuto Denko HF-201 coulometer. The electrolysis cell was a 200 ml H type vessel divided (3.6 cm dia.) with a sintered glass diaphragm. The cathode compartment was fitted with a glass bubbler tube placed very close to the cathode surface for introduction of CO_2.

General Electrolysis Procedure. All compounds listed in Table 2 were synthesized and isolated by using the procedures described in detail for the typical example below. A typical electrolysis procedure is as follows.

Preparative Scale Electroreduction of Benzophenones in the Presence of CO_2, the Synthesis of **2a**. A mercury pool (surface area 10.2 cm^2) was used as the cathode and the anode was a platinum plate (4.0 cm^2). 50 ml of DMF containing 14.2 g of KI was placed in each compartment. **1a** (1.5 g, 8.2×10^{-3} mol) was then added to the cathode compartment and CO_2 was passed through the catholyte for 60 min before the beginning of electrolysis. Catholyte was stirred magnetically and electrolysis was carried out under a fine stream of CO_2. The catholyte slowly turned opaque pale grayish with the progress of the electrolysis. After 2.3 F/mol of electricity was passed with a constant current of 2.5 mA/cm^2, the contents of the catholyte was poured into a separatory funnel. The mercury was taken off and DMF was removed under reduced pressure by a rotary evaporator. The residue was taken up in 150 ml of ether and the residue remaining after removal of the ether was dissolved in 100 ml of water and filtered. The filtrate was acidified with concentrated hydrochloric acid to yield white precipitates, which were collected by filtration, washed thoroughly with water, and dried *in vacuo*. Recrystallization from ethanol gave a pure compound of **2a**. Yield and physical properties are listed in Table 2.

Results and Discussion

At first, the synthesis of **2a** by electrochemical reduction of **1a** in the presence of CO_2 was investigated. Mercury pool cathode in DMF containing 8.6×10^{-3} mol of KI was used in a divided cell. Electricity passed was 2.0 F/mol of **1a** at a constant current of 2.5 mA/cm^2. The products and yields obtained in this system were essentially identical with those obtained previously.[1] **2a** was not obtained under the same conditions using undivided cell.

In order to optimize the yield of **2a**, the following experiments were carried out to investigate the influence of supporting electrolyte, solvent, concentrations of substrate and supporting electrolyte, amount of

TABLE 1. EFFECT OF SUPPORTING ELECTROLYTES AND SOLVENTS ON THE ELECTROCHEMICAL CARBOXYLATION OF **1a**[a]

Entry	Supporting electrolyte	Solvent	Yield of **2a**[b] %
1	LiI	DMF	4
2		CH_3CN	c)
3	NaI	DMF	29
4		CH_3CN	8
5	KI	DMF	49
6		CH_3CN	9
7	RbI	DMF	34
8		CH_3CN	c)
9	CsI	DMF	46
10		CH_3CN	c)
11	Bu_4NI	DMF	33
12		CH_3CN	30

a) Catholyte: **1a**(4.7 mmol) in 50 ml of DMF containing of 16 mmol of supporting electrolyte. Mercury pool was used as a cathode. Constant current density, 2.5 mA/cm². Electricity, 2.0 F/mol. Temperature, *ca.* 20°C. b) Isolated yield, based on **1a**. c) It can not be determined, because supporting electrolyte did not solved entirely in CH_3CN.

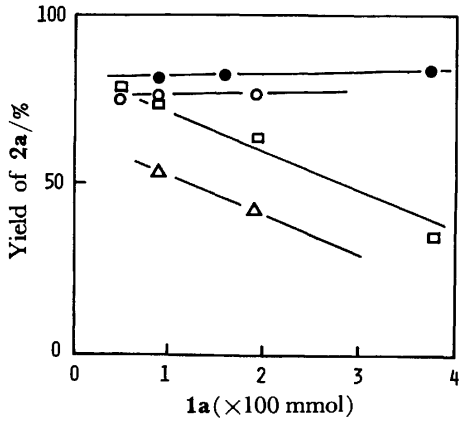

Fig. 1. The influence of the concentration of **1a** on the yield of **2a** under various concentration of KI as a supporting electrolyte.
Concentration of KI: -●-: 85.5 mmol, -○-: 47.0 mmol, -□-: 16.0 mmol, -△-: 8.0 mmol.
Divided cell, mercury cathode, 2.0 F/mol, constant current density (2.5 mA/cm²), solvent dry DMF (50 ml).

electricity, and cathode material. The influence of supporting electrolyte and solvent is shown in Table 1. Under similar experimental conditions, the maximum yield was obtained with KI-DMF system and effect of solvent was larger for alkali metal supporting electrolyte than for tetraalkylanmonium salt such as *n*-Bu_4NI, but remarkable improvement of the yield was not realized under these conditions.

The most significant effect was observed with the concentration of KI and the molar ratio of substrate to KI in KI-DMF system as shown in Fig. 1. The best yield (80%) was obtained when 10 moles of KI per mole of **1a** was used at high concentration of electrolyte, but further increase of the molar ratio showed no effect. In addition, the amount of electricity affected the yield of **2a**. The yield rose upon increasing the amount of electricity up to about 2.5 F/mol and then gradually decreased with excess faraday per mole of **1a**. However, an increase of the amount of polymeric materials as by-products, which were reported in earlier studies,[1] was not observed in the reaction products from the electrolysis of the excess faraday. These observations seem to suggest that good yields are attained by the inhibition of the migration *via* diffusion of a substrate caused by a high potential gradient at low concentration of supporting electrolyte (KI) and prolonged reaction time during the passage of larger amount of electricity.

The influence of cathode materials was found to be none under the same conditions. The employment of graphite plate cathode instead of mercury decreased the yield of **2a** to 14%. In the case of cadmium, platinum, nickel, copper and zinc cathode, a similar electrolysis of **1a** resulted in the formation of tarry materials predominantly and **2a** could not be isolated. On the basis of these experimental results, the current density of 2.5 mA/cm², 2.3 F/mol of electricity, DMF as solvent, KI as supporting electrolyte and highly concentrated solution of KI which KI is 10 times or more to the concentration of **1a** were selected as the most suitable synthetic conditions for the electrochemical carboxylation of **1a**. The carboxylic acid, **2a**, could be isolated in 86% yield under the above conditions.

On the other hand, **2a** has been synthesized *via* the reductive carboxylation of **1a** by using alkali metal[3] or radical anion of arylpyridine sodium,[4] benzilic acid rearrangement,[5] solvolytic reaction of diphenylketene,[6] and the reaction of benzoyl cyanide and imines.[7] The reported yields are in the range from 55 to 88% and these methods are very tedious compared with the present method.

This method is proved to be useful by the syntheses of substituted benzilic acids which cannot be easily synthesized by conventional methods.[8-11] The synthesis of twelve benzilic acids (**2b—2m**), affording relatively high yield, were carried out under the optimum conditions for the preparative synthesis of **2a**. The application to the syntheses of 4-bromo-, 4-nitro-, 4-hydroxy- and 4-(dimethylamino)benzilic acids were unsuccessful in the reaction system under the conditions employed by us. Resulting benzilic acids are summarized in Table 2 together with some previously reported data for comparison. Present method also indicates superiority in isolated yield over the previously reported one on the synthesis of substituted benzilic acids, as shown in the case of **2i**. All the methylated compounds (**2b—2g**) showed high yields in the range of 81—83% yield except the case of **2g**. Methoxy compounds (**2h—2i**) were obtained in the range of 64—75% yield. In a series of halogen compounds (**2j—2l**), **2k** was obtained in the yield of 92%. It is noteworthy that C-Cl bond cleavage[12] which resulted in a normal

Table 2. Yield, elemental analyses and physical data[b] of substituted benzilic acid[a]

Entry	Substituted benzilic acid[c]	Isolated yield[d] %	Found (Calcd) % C	H	X	IR (KBr) ν/cm^{-1}	Mp(θ_m/°C) Obsd (lit)
13	(**2a**) Unsubstituted	86 (55,60,67,88)	73.21 (73.67)	5.23 (5.30)		3420, 1720	151—152 (150)[g]
14	(**2b**) 2-Methyl	83 [f]	74.48 (74.36)	5.79 (5.82)		3530, 1710	116—117 (114—115.4)[h]
15	(**2c**) 3-Methyl	83 [f]	74.49 (74.36)	5.79 (5.82)		3460, 1730	115—118 (118—119)[h]
16	(**2d**) 4-Methyl	83 (35,70)	74.58 (74.36)	5.82 (5.82)		3440, 1725	132 (132—133.2)[i]
17	(**2e**) 2,4-Dimethyl	81 [f]	74.85 (74.98)	6.24 (6.29)		3590, 1700	131—131.5 (129.5—131.5)[h]
18	(**2f**) 4,4′-Dimethyl	81 [f]	75.14 (74.98)	6.29 (6.29)		3440, 1720	126 (132—133.8)[h]
19	(**2g**) 2,4′,5-Trimethyl	10 [f]	75.67 (75.53)	6.73 (6.71)		3450, 1725	155—156
20	(**2h**) 4-Methoxy	75 (6,48)	69.57 (69.76)	5.40 (5.46)		3410, 1723	142—144 (147—147.5)[j]
21	(**2i**) 4,4′-Dimethoxy	64 (0)	66.84 (66.66)	5.57 (5.60)		3240, 1742	161—163 (165—167)[k]
22	(**2j**) 4-Fluoro	88 [f]	68.50 (68.29)	4.46 (4.50)		3490, 1725	117—117.5
23	(**2k**) 4-Chloro	92 [f]	64.11 (64.01)	4.18 (4.22)	13.47 (13.50)	3460, 1732	129—130 (131)[l]
24	(**2l**) 4,4′-Dichloro	73[e] [f]	56.62 (56.59)	3.26 (3.39)	23.81 (23.86)	3400, 1710	115—117 (114—115)
25	(**2m**) 4-Phenyl	92 (53, 91)	78.98 (78.93)	5.35 (5.30)		3420, 1725	164—167 (167.2—168.6)[m]

a) Catholyte: benzophenones(8.2 mmol) in 50 ml of DMF containing 85.5 mmol of KI, Hg pool cathode, A constant current(2.5 mA/cm^2, 2.3 F/mol) was applied. b) Although NMR signals of OH and COOH in benzilic acids were not ascertained clearly, other signals of phenyl and alkyl displayed proper assignment. The proportions of integration of protons were consistent with the structure of benzilic acids when were integrated as involving two protons of OH and COOH in the phenyl signal. c) The products obtained were identified by a comparison of their physical and IR-spectral data with the literature data. d) Value in parentheses refers to yield of literature data. e) Electrolyzed were carried out with 2.4 mmol of 4,4′-dichlorobenzophenone and 85.5 mmol of KI in 50 ml of DMF. f) Yield has not been described. g) In Ref. 3, 4, 6, and 7. h) In Ref. 8. i) In Ref. 3 and 8. j) In Ref. 3 and 9. k) In Ref. 3, 8, and 10. l) In Ref. 10. m) In Ref. 4, 8, and 11.

electrochemical reduction of 4-chlorobenzophenone in DMF did not occur in our reaction system. In contrast, 4-bromobenzophenone gave **2a** in 30% yield, which resulted from the reductive cleavage of C–Br bond.[12] Also, **2j** was obtained in 88% yield. A syntheticaly useful intermediate for tick insecticide, **21**, was obtained in the yield of 73% when the reaction was carried out at low concentration of 4,4′-dichlorobenzophenone becauce of its low solubility in DMF. Likewise, **2m** was obtained in 92% yield. These results show that the yields are generally affected by electric effects of substituents. Steric effect is not observed for **2b—2d** in a series of methylated compounds. In the case of 4-nitrobenzophenone, the reduction of nitro group took place and the isolated product was 4,4′-dibenzoylazobenzene[13] (60%). 4-Dimethylamino- and 4-hydroxybenzophenone mainly provided tarry products.

The reduction potentials of the first reduction wave of methoxy-, unsubstituted and 4,4′-dichlorobenzophenones were −1.68, −1.63, and −1.52 V *vs.* Ag/AgCl by polarographic measurements in the presence of CO_2. The relationship between Hammett's substituent con-

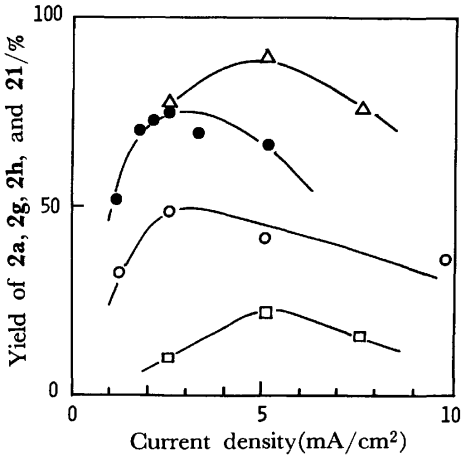

Fig. 2. The relation of the yields of benzilic acids with the current density in the electrochemical carboxylation of substituted benzophenones containing KI (85.5 mmol) in 50 ml DMF using a Hg pool cathode.
-○-: **2a**; **1a** (9.3 mmol), 2.0 F/mol, KI (16.0 mol), -△-: **2h**; 4-methoxybenzophenone (8.2 mmol), 2.3 F/mol, -●-: **21**; 4,4′-dichlorobenzophenone (2.4 mmol), 2.3 F/mol, -□-: **2g**; 2,4′,5-trimethylbenzophenone (8.2 mmol), 2.3 F/mol.

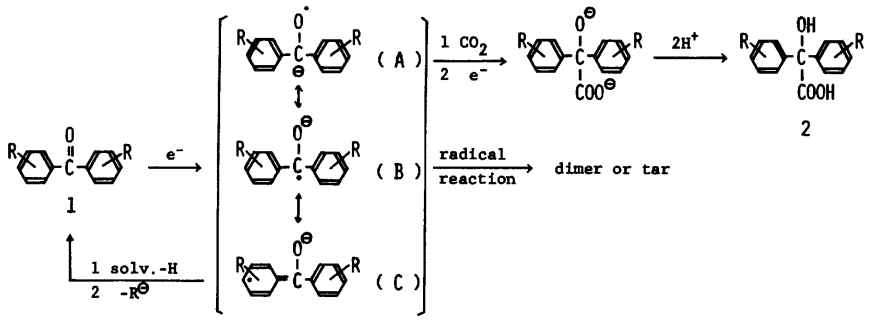

Fig. 3. Reaction scheme.

stants and the reduction potentials is in accord with the result reported with benzophenones.[14] On the assumption that the reduction potentials correspond to the current density, we tried to improve the yield of **2h**, **2g**, and **2l** by changing the current density as shown in Fig. 2. The yield of **2h** increased from 73% to 95% by increasing a current density from 2.5 mA/cm² to 5.0 mA/cm². In a similar manner the yield of **2g** also increased to 25% but, this value was not so good as expected. The yield of **2l**, which is expected to increase at lower current density, could not be improved by changing the current density above or even below 2.5 mA/cm². In addition, similar treatment for the syntheses of 4-bromo- and 4-hydroxybenzilic acid could not produce benzilic acids. Thus it became evident that the influence of the working reduction potential on the product yields is relatively small compared to that of the electronic effect of substituents.

Although it is not completely understood as yet whether the mechanism of the electrochemical carboxylation of aromatic carbonyl compounds proceed through ECEC or EECC path such as successive electrochemical(E) and chemical(C) reaction, it is obvious that the reaction begins with the formation of a ketyl radical by one-electron reduction of a substrate.[15] The electron distributions of a ketyl radical are shown in Fig. 3, and structure A may be predominant when R is electron-withdrawing and structure B may be predominant when R is electron-donating. Thus, benzilic acid may be obtained easily from the substrate having electron-withdrawing substituents *via* successive carboxylation, electrochemical reduction and protonation. In contrast, the substrates having electron-donating substituents have the possibility of radical reactions such as coupling or polymerization, and the yield of benzilic acids may go down. When the substituent moiety is more reactive than carbonyl moiety in the reaction system, the obtained products are not corresponding benzilic acids but some other products as are shown in 4-bromo, 4-nitro, 4-hydroxy, and 4-dimethylamino derivatives.

In conclusion, we found suitable reaction conditions for the synthesis of **2a** through the electrochemical reduction of **1a** in the presence of CO_2 in view of preparative points. This method and conditions were successfully applied to the syntheses of some substituted benzilic acids. The results also showed that the electrochemical carboxylation is easily affected by the electronic effects of substituent together with the reduction potential of substrate.

We wish to thank Dr. Chizuko Nishihara of our institute for the measurement of polarography.

References

1) S. Wawzoneck and A. Gundersen, *J. Electrochem. Soc.*, **107**, 537 (1960).
2) Y. Ikeda and E. Manda, *Chem. Lett.*, **1984**, 453.
3) S. Selman and T. F. Eastham, *J. Org. Chem.*, **30**, 3804 (1965).
4) B. Angelo, *Bull. Chem. Soc. Fr.*, **1969**, 1710.
5) D. A. Ballard and W. M. Dehn, *Org. Synth.*, Coll. Vol. I, 29 (1921).
6) I. Lillien, *J. Org. Chem.*, **29**, 1631 (1964).
7) A. Dornow and D. Lupfert, *Chem. Ber.*, **89**, 2718 (1956).
8) C. D. Shacklett and H. A. Smith, *J. Am. Chem. Soc.*, **75**, 2654 (1953).
9) E. R. Bockstahler and D. L. Wright, *J. Am. Chem. Soc.*, **71**, 3760 (1949).
10) A. H. Ford-Moore, *J. Chem. Soc.*, **1947**, 952.
11) F. F. Blicke and N. Grier, *J. Am. Chem. Soc.*, **65**, 1725 (1943).
12) L. Nadio and J. M. Saveant, *J. Electroanal. Chem.*, **30**, 41 (1971).
13) T. Posner, *Chem. Ber.*, **35**, 2343 (1902).
14) P. Zuman, O. Exner, R. F. Pekker, and W. Th. Nauta, *Collect. Czech. Chem. Commun.*, **33**, 3213 (1968).
15) P. H. Given, M. E. Peover, and J. Schoen, *J. Chem. Soc.*, **1958**, 2674; D. E. G. Austen, P. H. Given, D. J. E. Ingram, and M. E. Peover, *Nature*, **182**, 1784 (1958).

Structure-Taste Relationships of Aspartyl Tetrapeptide Esters

Yasuo ARIYOSHI
Central Research Laboratories, Ajinomoto Co., Inc., Suzuki-cho, Kawasaki-ku, Kawasaki 210
(Received January 10, 1985)

A series of fourteen analogues of L-α-Asp-Gly-Gly-Gly-OMe has been synthesized in relation to structural features of sweet peptides. The rule in the structure-taste relationships of tripeptides barely applies to the aspartyl tetrapeptide esters. In order for the aspartyl tetrapeptide esters to be sweet, the second amino acid must have a D-configuration and a small, compact alkyl side chain. However, the sweetness was accompanied by a bitter or astringent taste. Moreover, some of the tetrapeptides were not sweet but bitter, though they satisfied the requirements for sweet peptides. With increasing length of a peptide, it becomes difficult to fit the deep receptor pocket.

It has been suggested that sweet compounds have the AH-B-X[1](γ)[2] system in a molecule as a glucophore. In an attempt to elucidate structure-taste relationships, a large number of analogues of L-α-Asp-L-Phe-OMe[3] have been synthesized by several groups.[4-15] In previous papers,[16-18] the tastes of aspartyl dipeptides have been rationalized through projection formulas. In the structures (Ia and II), a small alkyl group (S or R^2) has been considered to participate in binding with the receptor through a hydrophobic interaction. The carboxyl and amino groups serve as a proton acceptor and a proton donor, respectively, in the hydrogen bonding with the receptor. The hydrophilic-hydrophobic balance in a molecule is another important factor. Space-filling properties are also important, since the receptor site seems to be in the shape of a deep pocket.[17] As described above, peptides with limited structures have shown sweetness, whereas various hydrophobic peptides are bitter. It has been known that peptides can be classified as bitter or nonbitter depending upon the magnitude of the hydrophobicity of their side chains.[19]

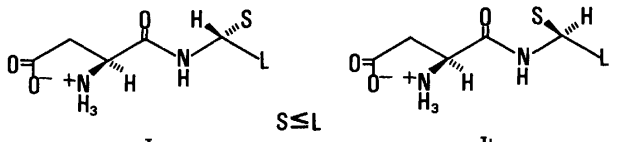

Ia Sweet Ib Nonsweet

Fig. 1. General structure for sweet aspartyl dipeptide esters: S=small hydrophobic group (1—4 atoms): L=larger hydrophobic group (3—6 atoms).[16,18]

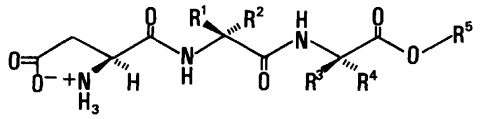

II

Fig. 2. L-α-Aspartyl tripeptide esters.

In an attempt to extend the general structure for sweet tripeptides to tetrapeptides, various aspartyl tetrapeptides were synthesized in the present study.

TABLE 1. PROTECTED TRIPEPTIDES

No.	Compound[a]	Yield %	TLC R_f[b]	Mp (θ_m/°C)	Recrys. solvent[c]	Appearance[d]	$[\alpha]_D^{25}$ Degree[e]	Formula[f]
1	Boc-Gly-Gly-Gly-OMe[g]	74.4	0.37	136—137	E	P		$C_{12}H_{21}O_6N_3$
2	Boc-D-Ala-L-Ala-L-Ala-OMe	76.1	0.67	108—110 (95)[h]	E-H	A	−37.4	$C_{15}H_{27}O_6N_3$
3	Boc-D-Ala-L-Ala-L-Val-OMe	83.7	0.76	152—153	E-H	N	−25.0	$C_{17}H_{31}O_6N_3$
4	Boc-D-Ala-L-Ala-L-Leu-OMe	84.6	0.70	117—118	E	N	−38.0	$C_{18}H_{33}O_6N_3$
5	Boc-D-Ala-L-Val-L-Ala-OMe	84.6	0.76	130—131	E-H	N	−27.3	$C_{17}H_{31}O_6N_3$
6	Boc-D-Ala-L-Val-L-Val-OMe	79.5	0.83	156—157	E-H	N	−16.2	$C_{19}H_{35}O_6N_3$
7	Boc-D-Val-L-Ala-L-Ala-OMe	54.6	0.80	163—164	E	A	−40.1	$C_{17}H_{31}O_6N_3$
8	Boc-D-Val-L-Ala-L-Val-OMe	79.6	0.82	155—156	E-H	N	−30.0	$C_{19}H_{35}O_6N_3$
9	Boc-D-Val-L-Val-L-Ala-OMe	79.0	0.83	146—148	E	A	−27.7	$C_{19}H_{35}O_6N_3$
10	Boc-D-Val-L-Val-L-Val-OMe	71.8	0.88	185—186	E	N	−18.9	$C_{21}H_{39}O_6N_3$
11	Boc-L-Ala-L-Ala-L-Ala-OMe[i]	74.0	0.68	186—188	E	N	−79.4	$C_{15}H_{27}O_6N_3$
12	Boc-L-Ala-L-Val-L-Ala-OMe[j]	84.5	0.71	177—178	E-H	N	−82.1	$C_{17}H_{31}O_6N_3$
13	Boc-L-Val-L-Ala-L-Ala-OMe	78.2	0.73	146—147	E-H	N	−75.4	$C_{17}H_{31}O_6N_3$
14	Boc-L-Val-L-Val-L-Ala-OMe	80.0	0.78	176.5—177.5	E-H	N	−79.8	$C_{19}H_{35}O_6N_3$

a) Abbreviations follow the recommendations of the IUPAC-IUB Commission on Biochemical Nomenclature in *J. Biol. Chem.*, **247**, 977(1972). b) TLC: $CHCl_3$:MeOH:AcOH=45:4:1 (v/v), detected with I_2 vapor. c) Recrystallization solvent: E, Ethyl Acetate; H, Hexane. d) Appearance: P, Prisms; A, Amorphous powder; N, Needles. e) In methanol, c=1.0%. f) All compounds were analyzed for C, H, and N, and the results were within ±0.3% of the theoretical values. Complete analytical data for all compounds have been deposited at the office of the Chemical Society of Japan (Document No. 8524). g) G.M. Bonora, C. Toniolo, V.N.R. Pillai, and M.Mutter, *Gazz. Chim. Ital.*, **110**, 503 (1980); mp 130—131 °C. h) Softened. i) D. Le Nguyen, J.-R. Dormoy, B. Castro, and D. Prevot, *Tetrahedron*, **37**, 4229 (1981); mp 190 °C, $[\alpha]_D^{20}$ −69.3° (c 1, EtOH). j) See reference i); mp 173 °C; $[\alpha]_D^{20}$ −56.8° (c 1, EtOH).

Table 2. Protected tetrapeptides, Z-L-Asp(OBzl)-X

Compd No.	X	Yield %	TLC R_f[a]	Mp (θ_m/°C)	Recrys. solvent[b]	Appearance[c]	$[\alpha]_D^{25}$ Degree[d]	Formula[e]
15	Gly-Gly-Gly-OMe	80.0	0.52	133—135	E-H	A	−4.6	$C_{26}H_{30}O_9N_4$
16	D-Ala-L-Ala-L-Ala-OMe	76.7	0.71	174—176	E	A	−21.4	$C_{29}H_{36}O_9N_4$
17	D-Ala-L-Ala-L-Val-OMe	72.2	0.78	156—158	E	N	−15.2	$C_{31}H_{40}O_9N_4$
18	D-Ala-L-Ala-L-Leu-OMe	88.6	0.73	124—126	E-H	A	−24.2	$C_{32}H_{42}O_9N_4$
19	D-Ala-L-Val-L-Ala-OMe	91.4	0.76	200—201 (180)[f]	D-E	N	−25.0	$C_{31}H_{40}O_9N_4$
20	D-Ala-L-Val-L-Val-OMe	80.9	0.80	186—187	E	N	−19.8	$C_{33}H_{44}O_9N_4$
21	D-Val-L-Ala-L-Ala-OMe	90.2	0.77	198.5—199.5	E	A	−17.9	$C_{31}H_{40}O_9N_4$
22	D-Val-L-Ala-L-Val-OMe	74.5	0.85	194.5—195.5	E	N	−9.9	$C_{33}H_{44}O_9N_4$
23	D-Val-L-Val-L-Ala-OMe	77.0	0.83	213.5—214.5	D-E	A	−22.4[g]	$C_{33}H_{44}O_9N_4$
24	D-Val-L-Val-L-Val-OMe	81.7	0.85	207—208	E	N	−13.4	$C_{35}H_{48}O_9N_4$
25	L-Ala-L-Ala-L-Ala-OMe	80.7	0.80	201—203.5	D-E-H	A	−38.5	$C_{29}H_{36}O_9N_4$
26	L-Ala-L-Val-L-Ala-OMe	73.4	0.88	227—228	D-E-H	A	−39.4	$C_{31}H_{40}O_9N_4$
27	L-Val-L-Ala-L-Ala-OMe	74.9	0.87	182—184	D-E-H	A	−37.1	$C_{31}H_{40}O_9N_4$
28	L-Val-L-Val-L-Ala-OMe	89.2	0.91	224—226	E-A	A	−44.1	$C_{33}H_{44}O_9N_4$

a) TLC: $CHCl_3$:MeOH:AcOH=45:4:1 (v/v), detected with I_2 vapor. b) Recrystallization solvent: E, Ethyl Acetate; H, Hexane; D, *N*,*N*-Dimethylformamide. c) Appearance: A, Amorphous powder; N, Needles. d) In acetic acid, c=1.0%. e) All compounds were analyzed for C, H, and N, and the results were within ±0.3% of the theoretical values. Complete analytical data for all compounds have been deposited at the office of the Chemical Society of Japan (Document No. 8524). f) Softened. g) c=0.5%.

Table 3. Tetrapeptide esters, L-α-Asp-X

Compd No.	X	Yield %	TLC R_f[a]	Mp (θ_m/°C(dec))	Recrys. solvent[b]	Appearance[c]	$[\alpha]_D^{25}$ Degree[e]	Formula[e]
29	Gly-Gly-Gly-OMe	72.4	0.06	156.5—157.5	W-A	N	+28.9	$C_{11}H_{18}O_7N_4\cdot 2H_2O$
30	D-Ala-L-Ala-L-Ala-OMe	62.5	0.23	200—201	W	N	−25.6	$C_{14}H_{24}O_7N_4\cdot 1.5H_2O$
31	D-Ala-L-Ala-L-Val-OMe	70.5	0.32	201.5—202.5	W-A	A	−14.5	$C_{16}H_{28}O_7N_4\cdot 0.5H_2O$
32	D-Ala-L-Ala-L-Leu-OMe	57.8	0.31	187—188	W-A	N	−22.5	$C_{17}H_{30}O_7N_4\cdot 0.75H_2O$
33	D-Ala-L-Val-L-Ala-OMe	65.1	0.36	213—214	W	N	−22.3	$C_{16}H_{28}O_7N_4\cdot 2H_2O$
34	D-Ala-L-Val-L-Val-OMe	67.8	0.43	205—206	W	N	−11.8	$C_{18}H_{32}O_7N_4\cdot 3H_2O$
35	D-Val-L-Ala-L-Ala-OMe	80.2	0.34	210—211	W	N	−22.3	$C_{16}H_{28}O_7N_4\cdot 3.5H_2O$
36	D-Val-L-Ala-L-Val-OMe	76.0	0.39	227—228	W	N	−13.2	$C_{18}H_{32}O_7N_4\cdot 0.5H_2O$
37	D-Val-L-Val-L-Ala-OMe	69.9	0.45	>240	W	N	−21.8[f]	$C_{18}H_{32}O_7N_4\cdot H_2O$
38	D-Val-L-Val-L-Val-OMe	71.4	0.50	>240	W	N	−1.6[g]	$C_{20}H_{36}O_7N_4\cdot H_2O$
39	L-Ala-L-Ala-L-Ala-OMe[h]		0.16	paste				
40	L-Ala-L-Val-L-Ala-OMe	70.2	0.38[i]	227—228	W	A	−57.6[g]	$C_{16}H_{28}O_7N_4\cdot H_2O$
41	L-Val-L-Ala-L-Ala-OMe	69.5	0.34	212—214	W	N	−94.6	$C_{16}H_{28}O_7N_4\cdot 1.5H_2O$
42	L-Val-L-Val-L-Ala-OMe	61.3	0.49[f]	>240	W	A	−50.0[g]	$C_{18}H_{32}O_7N_4\cdot H_2O$

a) TLC: $CHCl_3$:MeOH:AcOH:H_2O=32:15:1:3 (v/v), detected with ninhydrin. b) Recrystallization solvent: W, Water; A, Acetone. c) Appearance: A, Amorphous powder; N, Needles. d) In water, c=1.0%. e) All compounds were analyzed for C, H, and N, and the results were within ±0.3% of the theoretical values. Complete analytical data for all compounds have been deposited at the office of the Chemical Society of Japan (Document No. 8524). f) c=0.5. g) In acetic acid, c=0.5%. h) Not analyzed. i) *n*-BuOH:AcOH:H_2O=4:1:1 (V/V).

Another interesting problem is to examine whether the above rule for bitter peptides can be applied to tetrapeptides with a possible sweet structure in their molecules.

Synthesis

Synthesis of Boc-dipeptide esters and the removal of the Boc group were carried out according to the method described in a previous paper.[18] The protected tripeptides in Table 1 were prepared by condensation of the appropriate dipeptide ester with a Boc-amino acid *N*-hydroxysuccinimide ester. The Boc group of the tripeptide esters was removed with *p*-toluenesulfonic acid (TosOH) in methanol.[20] The protected tetrapeptides in Table 2 were prepared by condensation of *N*-benzyloxycarbonyl-L-aspartic acid β-benzyl α-succinimido ester (Z-L-Asp(OBzl)-ONSu[18]) with the appropriate tetrapeptide ester. The desired tetrapeptide esters in Table 3 were obtained by deprotection of the benzyloxycarbonyl and benzyl groups from the protected tetrapeptides in Table 2 by hydrogenation over Pd/C.

Results and Discussion

In order to evaluate the contributions of the side chains of each amino acid, the substituents R^1—R^6 of III (Fig. 3) were systematically modified. The results are summarized in Table 4. In order for aspartyl tripeptides to be sweet, the second amino acid must

Table 4. Taste of tetrapeptides (L-α-Asp-X)[a]

Compd No.	X	R^1	R^2	R^3	R^4	R^5	R^6	Taste[b]
29	Gly-Gly-Gly-OMe	H	H	H	H	H	H	0
30	D-Ala-L-Ala-L-Ala-OMe	H	Me	H	Me	Me	H	0.5
31	D-Ala-L-Ala-L-Val-OMe	H	Me	H	Me	*i*-Pr	H	−
32	D-Ala-L-Ala-L-Leu-OMe	H	Me	H	Me	*i*-Bu	H	−
33	D-Ala-L-Val-L-Ala-OMe	H	Me	H	*i*-Pr	Me	H	2
34	D-Ala-L-Val-L-Val-OMe	H	Me	H	*i*-Pr	*i*-Pr	H	−
35	D-Val-L-Ala-L-Ala-OMe	H	*i*-Pr	H	Me	Me	H	+
36	D-Val-L-Ala-L-Val-OMe	H	*i*-Pr	H	Me	*i*-Pr	H	−
37	D-Val-L-Val-L-Ala-OMe	H	*i*-Pr	H	*i*-Pr	Me	H	5(−)
38	D-Val-L-Val-L-Val-OMe	H	*i*-Pr	H	*i*-Pr	*i*-Pr	H	−
39	L-Ala-L-Ala-L-Ala-OMe	Me	H	H	Me	Me	H	−
40	L-Ala-L-Val-L-Ala-OMe	Me	H	H	*i*-Pr	Me	H	0
41	L-Val-L-Ala-L-Ala-OMe	*i*-Pr	H	H	Me	Me	H	0
42	L-Val-L-Val-L-Ala-OMe	*i*-Pr	H	H	*i*-Pr	Me	H	0

a) For structures, see Fig. 3. b) Times sucrose (weight basis, sucrose=1). 0=tasteless: −=bitter; +=faintly sweet; (−)=sweet-bitter.

have a D-configuration and a small alkyl side chain.[18] Therefore, in systematic structural variation of the tetrapeptides (III), a small alkyl group was introduced at R^2 so as to meet the sweet structure (II). An L-antipode was introduced for the third amino acid, because the modification of tripeptides showed that an L-configuration of the third amino acid was required for a potent sweet taste.

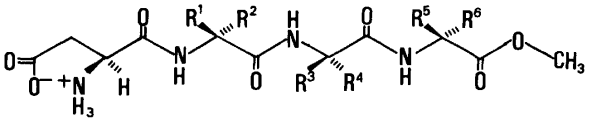

III

Fig. 3. L-α-Aspartyl tetrapeptide esters.

As the first step, L-α-Asp-Gly-Gly-Gly-OMe (**29**) was synthesized. The peptide (**29**) was tasteless. The first candidate for sweet tetrapeptides was L-α-Asp-D-Ala-L-Ala-L-Ala-OMe (**30**). As expected, it was slightly sweet, 0.5 times as sweet as sucrose (Table 4). Replacement of a methyl group at R^5 of **30** by an isopropyl or isobutyl group gave L-α-Asp-D-Ala-L-Ala-L-Val-OMe (**31**) and L-α-Asp-D-Ala-L-Ala-L-Leu-OMe (**32**), respectively, which were weakly bitter. Replacement of a methyl group at R^4 of **30** by an isopropyl group gave a sweet peptide, L-α-Asp-D-Ala-L-Val-L-Ala-OMe (**33**). When a methyl group at R^5 of **33** was replaced by an isopropyl group, the resulting peptide, L-α-Asp-D-Ala-L-Val-L-Val-OMe (**34**), was bitter

Next, the second D-Ala was replaced by D-Val. The resulting peptides were faintly sweet (**35**), weakly bitter (**36** and **38**), and sweet-bitter (**37**).

Finally, the required configuration (R^1=H; R^2= small alkyl group) at the second amino acid was confirmed by synthesizing several tetrapeptides having an opposite configuration at this chiral center (**39**—**42**). All of them were devoid of sweetness. Thus, the requirement was confirmed.

In conclusion, the rule in the structure-taste relationships of tripeptides barely applies to the sweet tetrapeptides. However, the sweetness was accompanied by a bitter or astringent taste. Moreover, some of the tetrapeptides were not sweet but bitter, though they satisfied the requirements for the sweet peptides. The taste of aspartyl tetrapeptide esters tends to follow Ney's rule for bitter peptides. With increasing length of a peptide, it becomes difficult to fit the narrow receptor pocket. This may be a major reason that some of the tetrapeptides were not sweet but bitter, though they satisfied the requirements for sweet peptides. A similar result has been obtained in the modification of tripeptides,[18] in which the sweetness potencies significantly fell off when sweet dipeptides have been lengthen to tripeptides. Accordingly, the results obtained for the tetrapeptides, in conjunction with the results of di-[16] and tripeptides,[18] support that the receptor site is in the shape of a deep pocket with the binding site inside it.[17]

Experimental

All melting points were taken on a Yanagimoto capillary melting point apparatus Model MP-21 and are uncorrected. Optical rotations were measured on a JASCO DIP-140 digital polarimeter with a 10-cm water-jacketed cell at 25 °C and a 1% concentration. TLC was performed on precoated silica gel $60F_{254}$ plates (E. Merck) and spots were detected with ninhydrin or I_2 vapor. All compounds were essentially homogeneous on TLC. Sweetness potency was not evaluated by the panel method due to the small quantities available. In general, a panel evaluation needs a large quantity of sample. The yield, after purification, of each peptide (Table 3) was less than 0.8 g. The quantity of tetrapeptides obtained here was insufficient for the panel evaluation. Therefore, sweetness evaluation was carried out by the author by matching a threshold concentration of each compound with that of sucrose. Test solutions of the tetrapeptides were prepared at several concentrations. A series of the solutions was tasted up and down. Thus, it was possible to reproducibly determine the concentration which matched a 0.6% aqueous solution of sucrose. Therefore, it has been considered that the sweetness potencies in Table 4 are reproducible and reliable

enough to discuss the functions of a small hydrophobic group.

Materials. Boc-amino acids were purchased from Peptide Institute Inc. Esters of Gly and L-Val were synthesized in our laboratory. Z-L-Asp(OBzl)-OH and esters of L-Ala and L-Leu were purchased from Kokusan Chemical Works Ltd.

Protected Tripeptide Esters (1—14). A typical run (**6** in Table 1) was as follows: To a solution of Boc-L-Val-L-Val-OMe[21] (2.31 g, 7 mmol) in 20 ml of methanol was added TosOH·H_2O (1.60 g, 8.4 mmol). The mixture was stirred at 30°C for 5 h. The solvent was evaporated under reduced pressure at a bath temperature of 50°C to give H-L-Val-L-Val-OMe·TosOH as an oily residue. The oil was dissolved in 40 ml of chloroform and cooled in an ice-bath. To this solution was added triethylamine (Et_3N, 0.85 g, 8.4 mmol), followed by Boc-D-Ala-ONSu (1.72 g, 7 mmol) with stirring. The mixture was stirred at room temperature for 3 h and then kept standing overnight. The reaction mixture was washed successively with water, a 10% citric acid solution, a 5% sodium hydrogencarbonate solution and water, and then concentrated under reduced pressure to leave an oily product. The oil was crystallized from ethyl acetate–hexane to give Boc-D-Ala-L-Val-L-Val-OMe (**6**) as needles. Recrystallization was carried out from the same solvent. The data are given in Table 1.

Protected Tetrapeptide Esters (15—28). A typical run (**20** in Table 2) was as follows: To a solution of Boc-D-Ala-L-Val-L-Val-OMe (**6**, 1.73 g, 4.3 mmol) in 20 ml of methanol was added TosOH·H_2O (1.00 g, 5.3 mmol). The mixture was stirred at 30°C for 5 h. The solvent was evaporated under reduced pressure at a bath temperature of 50°C to give H-D-Ala-L-Val-L-Val-OMe·TosOH as a solid residue. The residue was dissolved in 30 ml of chloroform and cooled in an ice-bath. To this solution was added Et_3N (0.53 g, 5.3 mmol), followed by Z-L-Asp(OBzl)-ONSu[18] (1.82 g, 4 mmol) with stirring. The mxiture was stirred for 3 h and then kept standing overnight. The reaction mixture was washed successively with water, 1 M HCl (1 M=1 mol dm^{-3}), a 5% sodium hydrogencarbonate solution and water, and then concentrated under reduced pressure to leave an oily product. The oil was crystallized from ethyl acetate–hexane to give Z-L-Asp(OBzl)-D-Ala-L-Val-L-Val-OMe (**20**) as needles. Recrystallization was carried out from the same solvent. The data are given in Table 2.

Tetrapeptide Esters (29—42). A typical run (**34** in Table 3) was as follows: Z-L-Asp(OBzl)-D-Ala-L-Val-L-Val-OMe (**20**, 1.60 g) was dissolved in a mixture of acetic acid (40 ml) and water (10 ml), and hydrogenated in the presence of 5% Pd/C (0.45 g) with stirring at atmospheric pressure and room temperature for 5 h. The reaction mixture was filtered and the filtrate was concentrated to dryness under reduced pressure. The residue was dissolved in water and the solvent was evaporated under reduced pressure to remove the trace amount of remaining acetic acid. The procedure was repeated four times. The crystalline residue thus obtained was recrystallized from water to give 0.80 g (67.8%) of L-α-Asp-D-Ala-L-Val-L-Val-OMe·$3H_2O$ (**34**) as needles. The data are given in Table 3.

References

1) L. B. Kier, *J. Pharm. Sci.*, **61**, 1394 (1972).
2) R. S. Shallenberger and M. G. Lindley, *Food Chem.*, **2**, 145 (1977).
3) R. H. Mazur, J. M. Schlatter, and A. H. Goldkamp, *J. Am. Chem. Soc.*, **91**, 2684 (1969).
4) R. H. Mazur, A. H. Goldkamp, P. A. James, and J. M. Schlatter, *J. Med. Chem.*, **13**, 1217 (1970).
5) M. T. Briggs and J. S. Murley, Brit. Patent, 1299265 (1972); *Chem. Abstr.* **78**, 111760c (1973).
6) M. Fujino, M. Wakimasu, K. Tanaka, H. Aoki, and N. Nakajima, *Naturwissenschaften*, **60**, 351 (1973).
7) R. H. Mazur, J. A. Reuter, K. A. Swiatek, and J. M. Schlatter, *J. Med. Chem.*, **16**, 1284 (1973).
8) Y. Ariyoshi, N. Yasuda, and T. Yamatani, *Bull. Chem. Soc. Jpn.*, **47**, 326 (1974).
9) M. Fujino, M. Wakimasu, M. Mano, K. Tanaka, N. Nakajima, and H. Aoki, *Chem. Pharm. Bull.*, **24**, 2112 (1976).
10) M. Miyoshi, K. Nunami, H. Sugano, and T. Fujii, *Bull. Chem. Soc. Jpn.*, **51**, 1433 (1978).
11) S. A. MacDonald, C. G. Willson, M. Chorev, F. S. Vernacchia, and M. Goodman, *J. Med. Chem.*, **23**, 413 (1980).
12) S. W. King and C. H. Stammer, *J. Org. Chem.*, **46**, 4780 (1981).
13) J. M. Tinti, C. Nofre, and D. Durozard, *Naturwissenschaften*, **68**, 143 (1981).
14) M. Kawai, R. Nyfeler, J. M. Berman, and M. Goodman, *J. Med. Chem.*, **25**, 397 (1982).
15) T. M. Brennan and M. E. Hendrick, Eur. Pat. Appl. EP 34876 (1982); *Chem. Abstr.*, **96**, 104780c (1982).
16) Y. Ariyoshi, *Agric. Biol. Chem.*, **40**, 983 (1976).
17) Y. Ariyoshi, *Agric. Biol. Chem.*, **44**, 943 (1980).
18) Y. Ariyoshi, *Bull. Chem. Soc. Jpn.*, **57**, 3197 (1984).
19) K. H. Ney, *Z. Lebensm., Unters. Forsch.*, **147**, 64 (1971).
20) J. Goodacre, R. J. Ponsford, and I. Stirling, *Tetrahedron Lett.*, **1975**, 3609.
21) D. J. Shafer, *J. Chem. Soc., Perkin Trans. 1*, **1972**, 1452.

 © 1985 The Chemical Society of Japan Bull. Chem. Soc. Jpn., 58, 1731—1737 (1985)

The Ability of an α-Aminoisobutyric Acid Residue to Promote Helical Folding in Oligopeptides[1)]

Mitsuaki NARITA,* Kazunori ISHIKAWA, Hiroki SUGASAWA, and Masamitsu DOI
Department of Industrial Chemistry, Faculty of Technology, Tokyo University of Agriculture and Technology, Koganei 184
(Received January 11, 1985)

In order to investigate the ability of an Aib residue to promote helical folding in oligopeptides, oligo(Leu)s containing an Aib residue were prepared by stepwise elongation and fragment condensation methods. The peptides prepared were the following: Boc-Aib-Leu$_n$-OBzl (n=3—6 and 9), Boc-Leu$_n$-Aib-OBzl (n=3—6 and 9), Boc-Leu$_3$-Aib-Leu$_3$-OBzl, Boc-Leu$_4$-Aib-Leu$_4$-OBzl, Boc-Leu$_8$-Aib-Leu$_4$-OBzl, Boc-Leu$_4$-Aib-Leu$_8$-OBzl, and Boc-Leu$_8$-Aib-Leu$_8$-OBzl. The IR absorption conformational analyses of Boc-Aib-Leu$_n$-OBzl (n=3—6) in dichloromethane have shown the occurrence of incipient helical structures (α- or 3_{10}-helixes) formed by one, two, three, and so forth $i \rightarrow i$—4 or $i \rightarrow i$—3 hydrogen-bonding patterns. All the peptides except Boc-Aib-Leu$_9$-OBzl and Boc-Leu$_n$-Aib-OBzl (n=6 and 9) have also shown helical structures (α- or 3_{10}-helixes), indicating the great ability of an Aib residue to promote helical folding in peptides. This is in remarkable contrast with the fact that homologous oligo(Leu) counterparts have β-sheet structures. The solubility properties of the peptides were in good agreement with those speculated from their conformations. The initiation and stabilization mechanism of helical folding in peptides has been illustrated schematically and attributed to the restriction of the values of the backbone dihedral angles ϕ and ψ of an Aib residue due to steric hindrance, followed by the restriction of the values of ϕ and ψ of other amino acid residues due to hydrogen bonds initiated by the Aib residue. The great ability of an Aib residue to promote helical folding in peptides also suggests that the restriction of the values of the backbone dihedral angles ϕ and ψ (right-handed α-helix: ϕ=−57°, ψ=−47°) of an amino acid residue in peptide chains is one of important initiation mechanisms of α-helical folding in natural proteins. The implication of the new findings for the study of proteins containing Aib residues is presented on the basis of the stabilizing efficacy of Aib residues on helical regions of proteins.

Aib-rich peptide fragments are often found in membrane-channel-forming polypeptides like alamethicin[2—4)] and suzukacillin,[5)] and are well recognized to have 3_{10}- and α-helical structures.[6)] The wide occurrence of Aib residues in microbial, particularly in the peptaibophols, has been attributed to their role in constraining the peptide backbones. In a previous paper,[7)] we have demonstrated the usefulness of a novel strategy for solubility improvement in helical oligopeptides based on the restriction of the values of the backbone dihedral angles ϕ and ψ of Aib residues, and the results have been attributed to the ability of the Aib residue to promote helical folding in the peptide. We have also shown that the properties described there for an Aib residue have important implications for the study of proteins and that the introduction of a few Aib residues in place of Ala residues in helical regions of proteins offers the prospect for creating novel proteins not found in nature. In this relation, it is very interesting to investigate how many Leu residues in model oligo(Leu)s are constrained in helical folding by the introduction of an Aib residue at N- or C-terminal or at a central portion.

On the other hand, the investigation on the initiation mechanism of α-helical folding in proteins is one of the upmost interesting problems for understanding the mechanism of protein folding and the prediction of folding from amino acid sequence. Helical folding in Boc-Leu$_n$-Aib-OBzl (n=3 and 4) in the previous study[7)] apparently suggests that the restriction of the values of ϕ and ψ of an amino acid residue is one of the important mechanisms for the initiation of helical folding in proteins.

In this paper, we report syntheses and conformations of model oligo(Leu)s containing an Aib residue and the ability of Aib residues to promote helical folding in oligopeptides.

Experimental

General. The uncorrected capillary melting points will be reported. Analytical instruments and conditions were described in the previous paper.[7)]

General Procedure for the Stepwise Elongation Using DCC Activation. The preparation of Boc-Leu$_n$-OBzl (n=3—6) was described in a previous paper.[8)] The preparation of Boc-Aib-Leu$_n$-OBzl and Boc-Leu$_n$-Aib-OBzl (n=3—6) is essentially the same with that of Boc-Leu$_n$-OBzl. The preparation of Boc-Leu$_n$-Aib-OBzl (n=3 and 4) was actually described in the previous paper.[7)]

General Procedure for Removal of the Boc Group. A Boc-peptide Bzl ester (10 mmol) in 3 M[†] HCl/AcOEt (70 ml) was stirred in an ice-chilled bath for 1.5 h, and the mixture was concentrated *in vacuo*. The residue was used for a subsequent coupling reaction without further purification.

General Procedure for Removal of the Bzl Group. A Boc-peptide Bzl ester (7 mmol) was hydrogenated overnight at atmospheric pressure in a mixture of acetic acid and methanol (1/4, v/v) (100 ml) using 10% Pd/C (10 wt%) as a catalyst. After removal of Pd/C by filtration, the filtrate was concentrated *in vacuo*. The residue was triturated with water and purified by recrystallization from appropriate solvents (mainly aqueous ethanol).

General Procedure for Fragment Condensation Using DCC Activation in the Presence of HOBt. DCC (1.1 equiv) was added to an ice-chilled stirred mixture of a carboxyl component (1.1 equiv), HOBt (1.2 equiv), and an amino component (5 mmol) (obtained by treatment of the HCl salt with an equivalent NMM) in dichloromethane (100 ml). The reaction mixture was stirred in an ice-chilled bath for

[†] 1 M=1 mol dm^{-3}.

3 h, at room temperature overnight, and then filtered. The filtrate was washed with 10% citric acid, 5% sodium hydrogencarbonate, and water, dried over sodium sulfate, and concentrated *in vacuo*. The residue was purified by recrystallization from appropriate solvents shown in Table 1. The coupling reaction for the peptide **12** was performed in a mixture of dichloromethane and DMF (3/2, v/v) in an ice-chilled bath for 3 h and then at room temperature for 2 d, and that for the peptide **10**, in NMP on the same reaction conditions.

Results

Syntheses of Oligo(Leu)s Containing an Aib Residue. Oligo(Leu)s containing an Aib residue were prepared by stepwise elongation and fragment condensation methods. The synthetic scheme is shown below. Boc-Aib-Leu$_n$-OBzl (n=3—6: **1—4**) and Boc-Leu$_n$-Aib-OBzl (n=3—6: **6—9**) were prepared by a stepwise elongation, starting with H-Leu-OBzl and H-Aib-OBzl as amino components, respectively. The synthetic procedure was essentially the same with that described before.[7,8] Removal of the Bzl group from the peptides **6** and **7** was performed by hydrogenolyses using Pd/C as a catalyst and the products **6'** and **7'** were used as carboxyl components in subsequent fragment condensations for the preparation of Boc-Leu$_3$-Aib-Leu$_3$-OBzl (**11**) and Boc-Leu$_4$-Aib-Leu$_4$-OBzl (**12**), respectively. Boc-Aib-Leu$_9$-OBzl (**5**) and Boc-Leu$_9$-Aib-OBzl (**10**) were similarly prepared by fragment condensations of Boc-Aib-Leu$_6$-OH with H-Leu$_3$-OBzl, and of Boc-Leu$_3$-OH with H-Leu$_6$-Aib-OBzl, respectively. Boc-Leu$_8$-Aib-Leu$_4$-OBzl (**13**), Boc-Leu$_4$-Aib-Leu$_8$-OBzl (**14**), and Boc-Leu$_8$-Aib-Leu$_8$-OBzl (**15**) were also prepared by fragment condensations of Boc-Leu$_4$-OH with H-Leu$_4$-Aib-Leu$_4$-OBzl, of Boc-Leu$_4$-Aib-Leu$_4$-OH with H-Leu$_4$-OBzl, and of Boc-Leu$_4$-OH with H-Leu$_4$-Aib-Leu$_8$-OBzl, respectively. Through the preparation in the scheme, the fragment condensations were performed in high yields using DCC activation in the presence of HOBt, and were monitored by HPLC on a gel filtration column. Liberation of the amino groups from Boc-peptide Bzl esters was carried out by treatment with 3 M HCl/AcOEt followed by treatment with NMM. Removal of the Bzl groups from

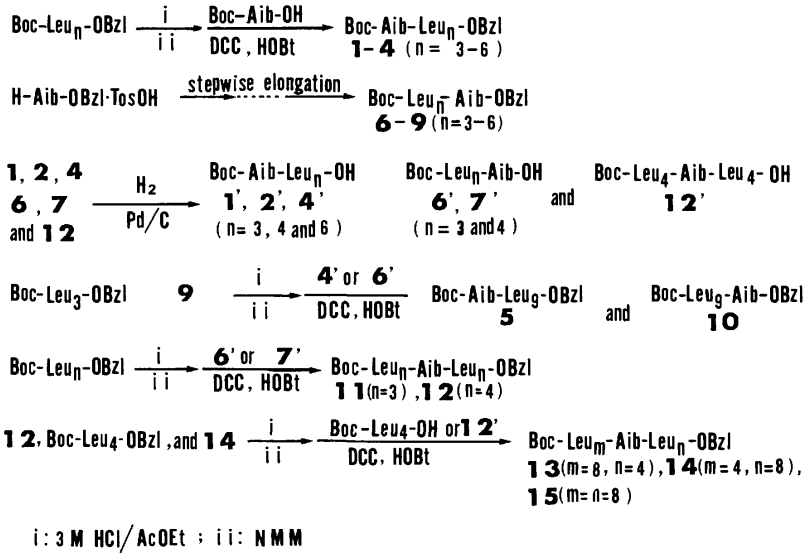

TABLE 1. SYNTHETIC RESULTS AND PHYSICAL PROPERTIES OF THE PEPTIDES **1—15**

Compound	Yield/%[a]	Recrystallization solvent	Mp(θ_m/°C)	$[\alpha]_D^{20}$ (c=1.0, MeOH)	Retention time/min
1	53	Ether/hexane (1/1)	145—147	−52.5	14.1
2	96	Ethanol/water (2/3)	188—193	−46.5	14.0
3	96	Ethanol/water (1/1)	218—222	−40.5	13.8
4	73	Ethanol/water (4/1)	over 250	−45.0	13.8
5	69	b)	over 250	—	—
6	92	Ethanol/water (6/5)	121—123	−63.0	14.0
7	94	Ethanol/water (2/1)	230—232	−58.5	13.8
8	65	Ethanol/water (1/1)	over 250	−55.5	13.7
9	70	Ethanol/water (4/1)	over 250	—	—
10	57	b)	over 250	—	—
11	84	Ethanol/water (7/3)	73—77	−49.5	13.8
12	85	Ethanol/water (7/3)	147—155	−33.0	13.8
13	83	Ethanol/water (2/1)	163—168	−47.3	13.8
14	75	Ethanol/water (2/1)	over 250	−34.5	13.8
15	67	Ethanol	over 250	—	—

a) Final coupling yield. b) Washing with hot methanol.

Table 2. Elemental and Amino Acid Analyses of the Peptides **1**—**15**

Compound	Formula	Found (Calcd)			Found (Calcd)
		C(%)	H(%)	N(%)	Leu/Aib
1	$C_{34}H_{56}N_4O_7$	64.87 (64.53)	9.29 (8.92)	8.91 (8.85)	3.20 (3.00)
2	$C_{40}H_{67}N_5O_8 \cdot 0.5H_2O$	63.60 (63.63)	9.54 (9.08)	9.32 (9.28)	4.04 (4.00)
3	$C_{46}H_{78}N_6O_9$	64.35 (64.31)	9.59 (9.15)	10.20 (9.78)	4.56 (5.00)
4	$C_{52}H_{89}N_7O_{10} \cdot 2H_2O$	62.29 (61.94)	9.21 (9.30)	9.65 (9.81)	6.09 (6.00)
5	$C_{70}H_{122}N_{10}O_{13} \cdot 2H_2O$	62.32 (62.38)	9.57 (9.42)	10.20 (10.39)	9.01 (9.00)
6	$C_{34}H_{56}N_4O_7$	64.37 (64.53)	9.28 (8.92)	8.82 (8.85)	2.98 (3.00)
7	$C_{40}H_{67}N_5O_8$	64.65 (64.40)	9.51 (9.05)	9.35 (9.39)	4.19 (4.00)
8	$C_{46}H_{78}N_6O_9$	64.26 (64.31)	9.65 (9.15)	9.98 (9.78)	4.60 (5.00)
9	$C_{52}H_{89}N_7O_{10} \cdot 0.5H_2O$	63.21 (63.65)	9.69 (9.24)	10.21 (9.99)	6.13 (6.00)
10	$C_{70}H_{122}N_{10}O_{13} \cdot H_2O$	63.03 (63.23)	9.67 (9.40)	10.66 (10.53)	8.78 (9.00)
11	$C_{52}H_{89}N_7O_{10} \cdot H_2O$	63.06 (63.07)	9.48 (9.26)	9.93 (9.90)	5.73 (6.00)
12	$C_{64}H_{111}N_9O_{12}$	63.99 (64.13)	9.69 (9.33)	10.55 (10.55)	7.70 (8.00)
13	$C_{88}H_{155}N_{13}O_{16} \cdot 1.5H_2O$	63.07 (62.97)	9.66 (9.49)	10.51 (10.85)	12.26 (12.00)
14	$C_{88}H_{155}N_{13}O_{16} \cdot H_2O$	63.18 (63.32)	9.72 (9.48)	10.86 (10.91)	11.88 (12.00)
15	$C_{112}H_{199}N_{17}O_{20} \cdot 2H_2O$	62.95 (62.86)	9.74 (9.56)	11.32 (11.03)	15.99 (16.00)

Table 3. IR Absorption Frequencies (Wave Numbers in cm^{-1}) of the Peptides **1**—**15** in Dichloromethane[a)]

Compound	Amide A		Amide I		
	3600—3200		1700—1600		
1	3425 (m)	3340 (s)	1700 (w)	1672 (s)	
2	3430 (m)	3340 (s)	1700 (w)	1665 (s)	
3	3430 (w)	3330 (s)	1690 (w)	1662 (s)	
4	3430 (w)	3320 (s)	1698 (w)	1662 (s)	
5[b)]		3265 (s)	1693 (m)	1660—1640 (m, sh)	1627 (s)
6	3430 (s)	3340 (s)	1700 (m, sh)	1673 (s)	
7	3430 (m)	3340 (s)	1695 (m, sh)	1665 (s)	
8	3420 (w)	3330 (s)	1690 (m, sh)	1663 (s)	
9[b)]		3280 (s)	1692 (m)	1660—1640 (m, sh)	1630 (s)
10[b)]		3270 (s)	1693 (m)	1660—1640 (m, sh)	1630 (s)
11	3425 (w)	3320 (s)	1690 (m, sh)	1659 (s)	
12	3425 (w)	3320 (s)	1690 (m, sh)	1659 (s)	
13	3430 (w)	3330 (s)		1659 (s)	
14	3420 (w, sh)	3330 (s)		1659 (s)	
15		3320 (s)		1659 (s)	

a) The following symbols are used: s, strong; m, medium; w, weak; sh, shoulder. b) The IR spectra were recorded in a solid state for nujor mulls.

other peptides was also performed by hydrogenolyses using Pd/C as a catalyst. Homogeneity of the peptides except the peptides **5** and **10** was easily ascertained as the peptides had a single peak on HPLC. The synthetic results and physical properties of the peptides are assembled in Table 1, and data of elemental and amino acid analyses of the peptides, in Table 2. The analytical data are in good agreement with the calculated values.

IR Absorption Conformational Analyses of the Peptides 1—15 in Dichloromethane. As a method of phase transformation of peptides from solution to a solid state greatly influences their solid-state conformational properties at critical size for development of helical structures,[9] the ability of an Aib residue to promote helical folding in oligo(Leu)s was examined in dichloromethane using IR absorption spectroscopies. Due to low solubility of the peptides **5**, **9**, and **10** in dichloromethane, these IR spectra were measured in the solid state for nujor mulls. The results in the most important spectral regions for the conformational assignments (3600—3200 cm^{-1}, amide A; 1700—1600 cm^{-1}, amide I) are listed in Table 3. As representative examples, the IR spectra of the peptides **1**—**4** are presented in Fig. 1. Those of the peptides **11**, **12**, and **15** are also shown in Fig. 2. All the peptides in solution show strong bands at 3340—3320 cm^{-1} in the amide A region and strong bands at 1673—1659 cm^{-1} in the amide I region, indicating helical structures.[10] Weak or medium-intensity bands at 3430—3420 cm^{-1} of the peptides are assigned to the free urethane and amide NH groups,[11] while the strong bands at 3340—3320 cm^{-1} to the intramolecular hydrogen-bonded NH groups (α-helix: $i \rightarrow i$—4, C_{13} or 3_{10}-helix: $i \rightarrow i$—3, C_{10}).[11] The latter absorption shifts to lower frequencies with increasing peptide chain length. In addition, the ratio of the intensity of the band of the hydrogen-bonded NH group to free NH group (A_H/A_F) increases regularly with increasing peptide chain length. The same tendency has been observed in the study of IR absorption spectra in deuteriochloroform in the 3480—3300 cm^{-1} frequency range of Z-(Aib)$_n$-O-*t*-Bu (n=3—5).[11b)]

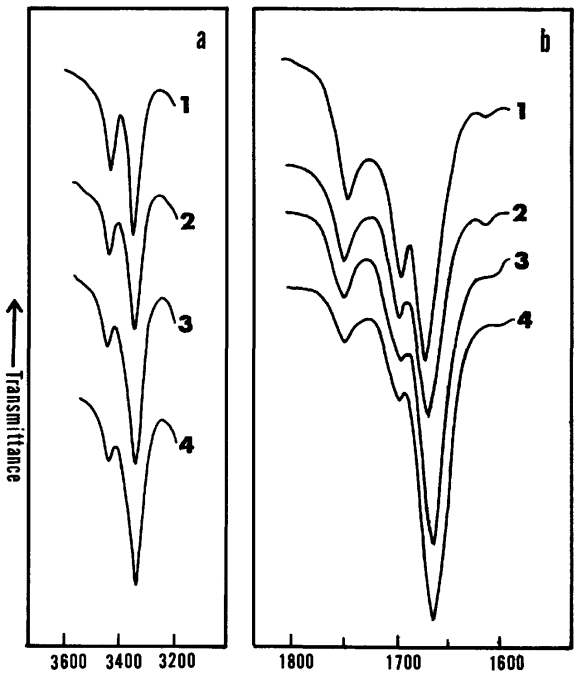

Fig. 1. IR absorption spectra of the peptides **1**—**4**. a: The amide A region; b: the amide I region.

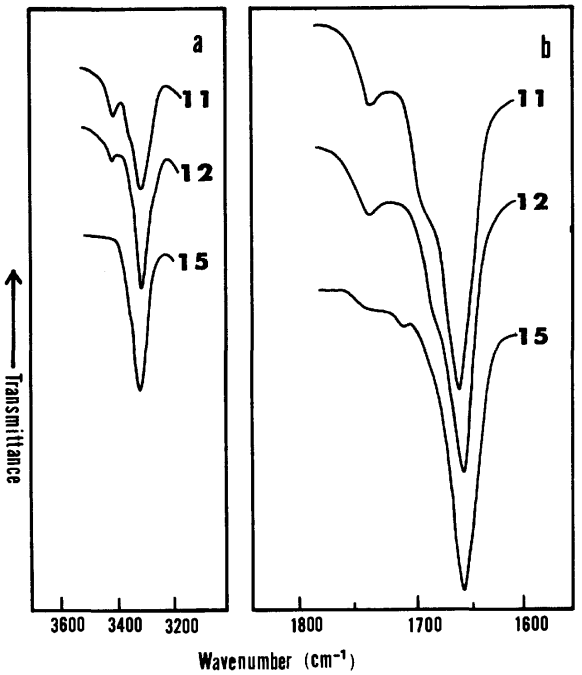

Fig. 2. IR absorption spectra of the peptides **11**, **12**, and **15**. a: The amide A region; b: the amide I region.

On the other hand, the solid-state conformations of the insoluble peptides **5**, **9**, and **10** are predominantly antiparallel β-sheet structures, judging from strong bands at 3280—3265 cm^{-1} in the amide A region and medium-intensity bands at 1692—1693 cm^{-1} and strong bands at 1630—1627 cm^{-1} in the amide I region,[10] accompanied with medium-intensity shoulders at 1660—1640 cm^{-1}, which was assigned to helical or coiled conformations.[10]

Solubility Properties. The relationship between solubilities and conformations of protected peptides has well documented and the severe insolubility of protected peptides in organic solvents results from their β-sheet aggregation.[7,8,12-14] The solubility data of the peptides **1**—**15** in various organic solvents are assembled in Table 4. The results are in agreement with those speculated from the conformations.

Discussion

The great ability of an Aib residue to promote helical folding in model oligo(Leu)s is clearly demonstrated by the IR absorption conformational analyses of the peptides **1**—**15**. The helical conformations of the peptides **1**—**4**, **6**—**8**, and **11**—**14** in dichloromethane are in remarkable contrast with the β-sheet

Table 4. Solubility properties[a] of the peptides **1**—**15** (c=1.0 g/dl)

Compound	Solvent[b]												
	HMPA	NMP	DMA	DMF	DMSO	MeOH	EtOH	AC	CF	DCM	CT	BE	AcOEt
1	A	A	A	A	A	A	A	A	A	A	A	A	A
2	A	A	A	A	A	A	A	A	A	A	B	B	A
3	A	A	A	A	B	A	A	A	A	A	C	B	B
4	A	A	A	A	D	A	A	A	A	A	C	C	C
5	B	B	C	C	D	D	D	D	C	C	D	D	D
6	A	A	A	A	A	A	A	A	A	A	A	A	A
7	A	A	A	A	A	A	A	A	A	A	B	B	B
8	A	A	A	A	B	A	B	B	A	A	C	C	D
9	A	B	B	B	C	B	C	D	B	C	D	D	D
10	B	C	C	C	D	D	D	D	D	D	D	D	D
11	A	A	A	A	A	A	A	A	A	A	A	A	A
12	A	A	A	A	C	A	A	A	A	A	A	A	A
13	A	A	A	A	C	A	A	B	A	A	A	A	B
14	A	A	A	A	B	A	A	B	A	A	A	A	B
15	A	A	B	B	C	B	C	B	B	B	B	B	D

a) Solubility: A, soluble at room temperature; B, soluble at 80 °C or refluxing temperature; C, partially soluble at the same temperature; D, nearly insoluble at the same temperature. b) Abbreviations: HMPA, hexamethylphosphoric triamide; DMA, *N*,*N*-dimethylacetamide; DMSO; dimethyl sulfoxide; MeOH, methanol; EtOH, ethanol; AC, acetone; CF, chloroform; DCM, dichloromethane; CT, carbon tetrachloride; BE, benzene. Others, see text.

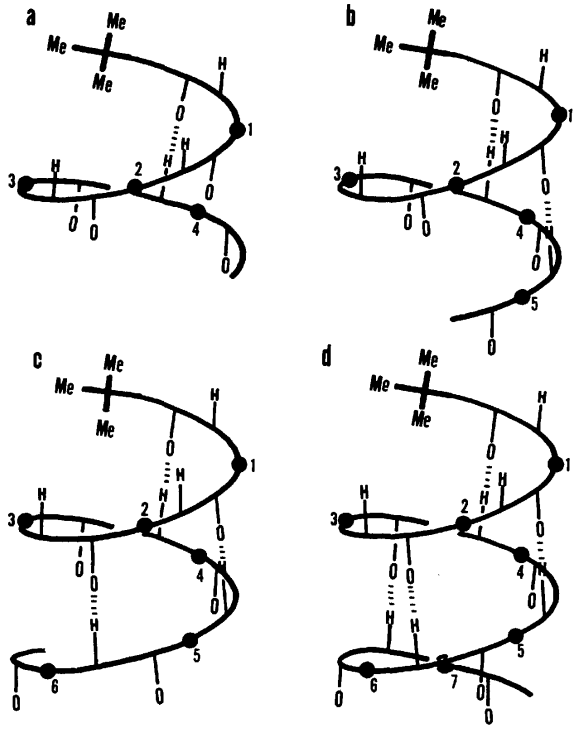

Fig. 3. Initiation and propagation of α-helical structures of the peptides **1**—**4**. a: **1**; b: **2**; c: **3**; d: **4**.

structures of the homologous oligo(Leu) counterparts.[7,15-17] Each Aib residue of these peptides apparently stabilizes helical folding in the peptides to great extent. For example, in Fig. 2, the ratio of the intensity of the amide A bands of the hydrogen-bonded NH groups to free NH groups increases regularly from the tetrapeptide **1** to the heptapeptide **4**, indicating helical propagation together with increasing peptide chain length. This is illustrated schematically in Fig. 3, where α-helical structures ($i \rightarrow i$—4 hydrogen-bonding patterns) are adopted as an example.[18] The initiation and propagation of helical structures of the peptides **1**—**4** is apparently attributed to the restriction of the Aib residue to conformations in the helical region ($\phi = \pm 60 \pm 20$, $\psi = \pm 30 \pm 20$) due to its steric hindrance,[19,20] followed by the restriction of the values of ϕ and ψ of other Leu residues due to hydrogen bonds initiated by the Aib residue. It is suggested that the restriction of the values of ϕ and ψ of an amino acid residue is one of the important mechanisms for the initiation of helical folding in proteins. Thus, we characterize this route for helical formation in protein folding as an initiation mechanism by the restriction of the values of the ϕ and ψ of an amino acid residue. The analogous idea of helix initiation was proposed by Blagdon and Goodman,[21] and characterized as terminal initiation mechanism by polar groups and by turns.

In Fig. 3, the urethane carbonyl groups of the peptides **1**—**4** participate in the 5→1 hydrogen-bonding. A shift of the frequencies of the urethane carbonyl groups to 1700—1690 cm^{-1} (Table 3) apparently supports the involvement of the carbonyl groups in the hydrogen bond.[22] In Fig. 3a, the amide carbonyl groups of the peptide **1** do not participate in a hydrogen bond, and this is supported by the observation that the peptide **1** has a strong band at 1672 cm^{-1} in the amide I region (Table 3). The α-helical structure of the peptide **1** in Fig. 3a, however, implies the restriction of the values of ϕ and ψ of the three Leu residues. The carbonyl absorption in the peptides **1**—**4** shifts to lower frequencies together with the NH absorption of the intramolecular hydrogen-bonding NH groups (Table 3), indicating propagation of helical structures with increasing peptide chain length as shown in Fig. 3. This observation is very close to the results that the X-ray diffraction and IR absorption conformational analyses of Z-$(Aib)_n$-OH (n=3—5) in the solid state have shown the occurrence of incipient 3_{10}-helixes, formed by one, two, and three type III (or type III′) β turns, respectively.[11b] In solvents of low polarity, the IR absorption data of Z-$(Aib)_n$-OH (n=3—5) were also in favor of the same intramolecular hydrogen-bonded forms as found in the solid state.[11b] The peptides **1**—**4**, however, could not be obtained as crystalline materials having helical structures, because α-helical→β conformational transformation took place during phase transformation of the peptides from solution to the solid state. Figure 4 presents the α- and 3_{10}-helical structures of the peptide **12** as an example. The α-helix in Fig. 4a appears to be more stable than the 3_{10}-helix in Fig. 4b, judging from the angles of hydrogen bonds, although it is well recognized that Aib-rich peptides favor 3_{10}-helixes.[2-6] The peptide **5** is soluble in a reaction mixture of dichloromethane during the coupling reaction, but it becomes less soluble as shown in Table 4 after obtaining as a crystalline material. The solubility data of the peptide **5** are in good agreement with the ones speculated from the β-sheet conformation.

The IR data of the peptides **6**—**8** in Table 3 also indicate that the helical structures correspond to those of the peptides **1**—**3** (Fig. 3a—c), respectively. In the peptides **6**—**10**, however, only the value of the backbone dihedral angle of ϕ of the Aib residues is restricted. Difference in helical stability between the peptides **4** and **9** appears to be illustrated by no participation of the ester group of the Aib residue of the peptide **9** in helical folding, while the Boc group bound to the Aib residue of the peptide **4** participates in helical folding. Thus, the peptides **9** and **10** are predominantly in favor of antiparallel β-sheet structures, and are less soluble in organic solvents (Table 4).

The peptides **9**—**15** are regarded to be produced by the hybridization, through an Aib residue, of the peptides having an Aib residue at C-terminal ends with those at N-terminal ends. The IR data in Table 3 clearly indicate that helical structures of the peptides **11**—**15** are efficiently stabilized by the hybridization of the

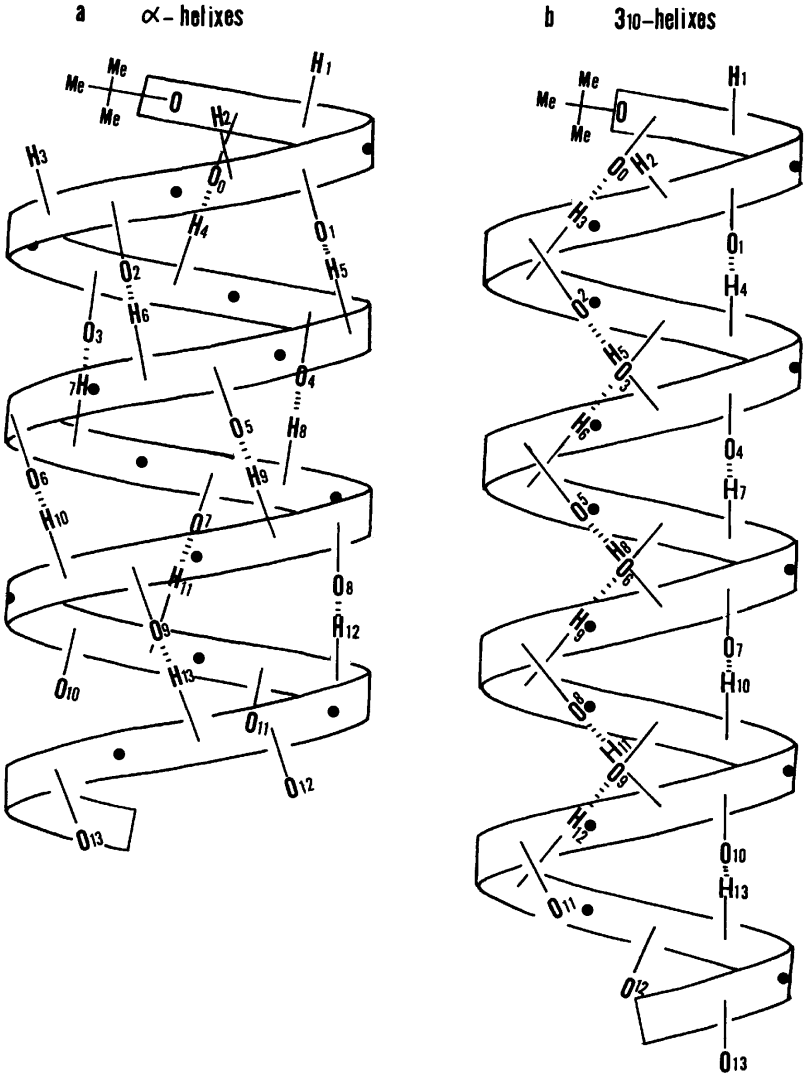

Fig. 4. α- and 3_{10}-helical structures of the peptide **12**.

corresponding two peptides. For example, the hybridization, through the Aib residue, of the peptide **1** with the peptide **6** and of the peptide **2** with the peptide **7** produces three additional hydrogen bonds in the peptides **11** and **12**, and strongly stabilizes the helical structure. This is illustrated schematically in Fig. 5, where α-helical structures are also postulated as an example. Difference in helical stability among the peptides **5**, **10**, and **13**—**15** is apparently resulted from the additional hydrogen bonds in the peptides **13**—**15**.

In this study the strategy for solubility improvement in protected peptides based on the restricted values of the backbone dihedral angles ϕ and ψ of an Aib residue[7] was also successfully applied to the model oligo(Leu)s. The solubility data of the peptides **1**—**15** directly reflect their conformations (Tables 3 and 4). The high solubility of the peptides **4** and **11**—**14** is in remarkable contrast with the observation that their homologous oligo(Leu) counterparts are barely soluble or insoluble in various organic solvents.[7,8]

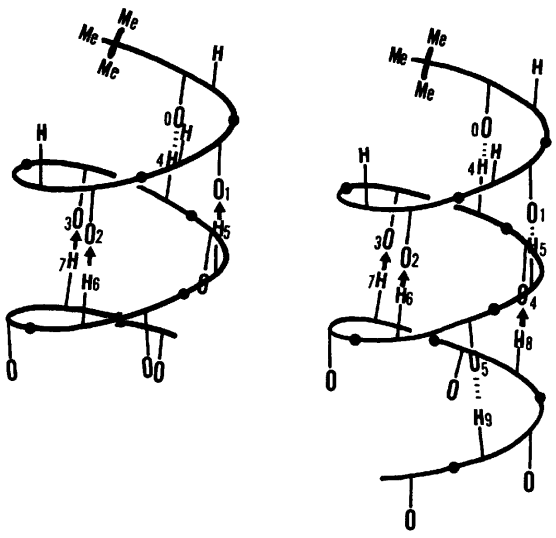

Fig. 5. Stabilization of α-helical structures of the peptides **11** and **12**. Three additional hydrogen bonds are shown by the arrow (→).

Conclusions

The great ability of an Aib residue to promote helical folding in peptides is clearly demonstrated using model oligo(Leu)s. The results make clear that the restriction of the values of the backbone dihedral angles ϕ and ψ of an amino acid residue is one of initiation mechanisms of helical folding in peptides, suggesting it to be one of important initiation mechanisms of α-helical folding in natural proteins. The stabilizing efficacy of an Aib residue on helical structures is also attributed to the restriction of the values of the backbone dihedral angles ϕ and ψ of the Aib residue, followed by the restriction of the values of those of other amino acid residues through hydrogen bonds initiated by the Aib residue. The properties of an Aib residue for stabilizing helical structures have innovative implications for the study of proteins. For example, replacement of a few Ala residue with Aib residue in helical regions of enzymes offers the prospect for creating novel enzymes, having thermostable properties and a wide range of pH optimum. The techniques offer the potential for altering protein function in ways not possible by any other method, just as mentioned in protein engineering pioneered by genetic technology.[24]

References

1) Part II of "Peptides and Proteins Containing α,α-disubstituted α-Amino Acid Residues" series; for part I, M. Narita, M. Doi, H. Sugasawa, and K. Ishikawa, *Bull. Chem. Soc. Jpn.*, in press. Abbreviations used are the following: Leu, L-leucine residue; Aib, α-aminoisobutyric acid residue; Boc, *t*-butoxycarbonyl; OBzl, benzyl ester; AcOEt, ethyl acetate; DCC, dicyclohexylcarbodiimide; HOBt, 1-hydroxy-1*H*-benzotriazole; NMM, *N*-methylmorpholine; DMF, *N*,*N*-dimethylformamide; NMP, *N*-methylpyrrolidone; TosOH, *p*-toluenesulfonic acid; Z, benzyloxy; *t*-Bu, *t*-butyl.

2) P. Mueller and D. O. Rudin, *Nature*, **217**, 713 (1968).

3) R. C. Pandey, J. C. Cook, Jr., and K. L. Rinehart, Jr., *J. Am. Chem. Soc.*, **99**, 8469 (1977).

4) R. Nagaraj and P. Balaram, *Acc. Chem. Res.*, **14**, 356 (1981).

5) G. Jung, W. A. Konig, D. Liebfritz, T. Ooka, and G. Boheim, *Biochim. Biophys. Acta*, **433**, 164 (1976).

6) C. P. Rao and P. Balaram, *Biopolymers*, **21**, 2461 (1982) and references cited therein.

7) M. Narita, M. Doi, H. Sugasawa, and K. Ishikawa, *Bull. Chem. Soc. Jpn.*, in press.

8) M. Narita, T. Fukunaga, A. Wakabayashi, K. Ishikawa, and H. Nakano, *Int. J. Pept. Protein Res.*, **23**, 306 (1984).

9) R. Katakai and Y. Iizuka, *Biopolymers*, **23**, 1411 (1984).

10) T. Miyazawa and E. J. Blout, *J. Am. Chem. Soc.*, **83**, 712 (1961).

11) a) M. Palumbo, S. D. Rin, G. M. Bonora, and C. Toniolo, *Makromol. Chem.*, **177**, 1477 (1976); b) E. Benedetti, A. Bavoso, B. D. Blasio, V. Pavone, C. Pedone, M. Crisma, G. M. Bonora, and C. Toniolo, *J. Am. Chem. Soc.*, **104**, 2437 (1982).

12) M. Narita, K. Ishikawa, J.-Y. Chen, and Y. Kim, *Int. J. Pept. Protein Res.*, **24**, 580 (1984).

13) S. A. E. Rhaman, H. Anzinger, and M. Mutter, *Biopolymers*, **19**, 173 (1980).

14) V. N. R. Pillai and M. Mutter, *Acc. Chem. Res.*, **14**, 122 (1981).

15) G. M. Bonora, A. Maglione, and C. Toniolo, *Polymer*, **15**, 767 (1974).

16) M. Narita, S. Isokawa, Y. Tomotake, and S. Nagasawa, *Polymer J.*, **15**, 25 (1983).

17) M. Narita, Y. Tomotake, S. Isokawa, T. Matsuzawa, and T. Miyauchi, *Macromolecules*, **17**, 1903 (1984).

18) It is difficult to determine by the IR absorption conformational analyses whether Aib residues favor 3_{10}- or α-helical conformations in the peptide series. An NMR study on the peptides **1**—**4** is attempted for determinating their intramolecular hydrogen-bonding patterns.

19) a) G. R. Marshall, in "Intra-Science Chemistry Report," Vol. 5, N. Kharasch, Ed., Gordon and Breach, New York, pp. 305—316 (1971); b) A. W. Burgess and S. J. Leach, *Biopolymers*, **12**, 2599 (1973).

20) Y. Paterson, S. M. Rumsey, E. Benedetti, G. Nemethy, and H. A. Scheraga, *J. Am. Chem. Soc.*, **103**, 2947 (1981).

21) D. E. Blagdon and M. Goodman, *Biopolymers*, **14**, 241 (1975).

22) M. Branik and H. Kessler, *Chem. Ber.*, **108**, 2176 (1975).

23) E. Benedetti, A. Bavoso, B. D. Blasio, V. Parone, C. Pedone, M. Crisma, G. M. Bonora, and C. Toniolo *J. Am. Chem. Soc.*, **104**, 2437 (1982).

24) K. M. Ulmer, *Science*, **219**, 666 (1983).

Effective Cleavage of 7-Alkoxytricyclo[6.4.0.0^{2,7}]dodecan-3-one System

Tsutomu KOJIMA, Yoshinobu INOUYE, and Hiroshi KAKISAWA*
Department of Chemistry, University of Tsukuba, Sakura-mura, Niihari-gun, Ibaraki 305
(Received January 14, 1985)

Several effective methods for the cleavage of the cyclobutane ring in 7-alkoxytricyclo[6.4.0.0^{2,7}]dodecan-3-one system are described. These involve reactions with hydriodic acid, with trimethylsilyl trifluoromethanesulfonate, and with KOH in H_2O–DMSO *via* a lactone derivative.

Among various naturally occuring materials, taxane (**1**)[1] and ophiobolane (**2**)[2] are interesting from a synthetic view point, for they have a unique carbon skeleton, that of an 8-membered ring condensed with a 6- or 5-membered ring.

In the course of our synthetic study to the taxane skeleton, the combination of regio- and stereo-controlled intramolecular enone-olefin cycloaddition with subsequent cyclobutane cleavage[3] has been employed as a key reaction. We described previously that the irradiation of 5,5-dimethyl-3-(3-methyl-2-cyclohexenylmethoxy)-2-cyclohexenone afforded a cyclobutane derivative **3**.[4] The remaining problem was how to cleave the cyclobutane ring to a bicyclo[6.4.0]dodecane derivative. In the present study, we will report several effective methods for the cleavage of the cyclobutane system.

The starting cyclobutane **6** was prepared from **3** *via* reaction sequences in Scheme 1. Allylation of the photocycloadduct **3** afforded a mixture of 2-allyl ketones **5** and an enol ether **4**; the mixture on heating underwent a Claisen rearrangement, providing a stereoisomeric mixture of **5a** (73%) and **5b** (9%). The stereochemistry of the allyl group in **5a** was confirmed by the pseudocontact shifts on the addition of Eu-FOD to the alcohol **7a** (see Experimental). The allyl group of **5a** was hydrogenated over PtO_2 to afford the 2-propyl ketone **6**.

In 1973, Tamura and co-workers reported that the photoadduct **8** could be cleaved into a cyclooctane derivative **9** in 53% yield by refluxing **8** in water.[5]

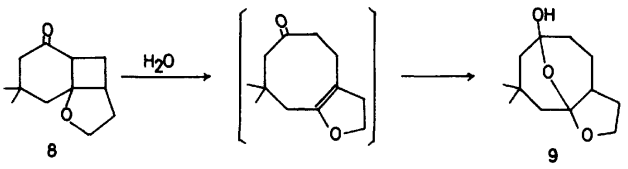

8 9

Scheme 2.

However, a similar attempt with **6** was unsuccessful. A more drastic conditions such as refluxing with aqueous hydriodic acid was required and, in this case, a fused 8-membered ring derivative **10** was obtained in 70% yield. The structure of **10** was confirmed by spectroscopic evidence. Besides the carbonyl group (1705 cm^{-1} in IR and δ 214.5 in ^{13}CNMR), an enol ether group is recognized in ^{13}CNMR spectrum at δ 115.6 and 145.4. The disappearance of eight-carbon signals in ^{13}CNMR spectrum suggests the conforma-

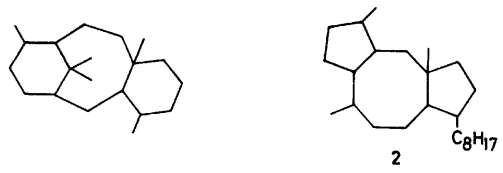

2

Fig. 1.

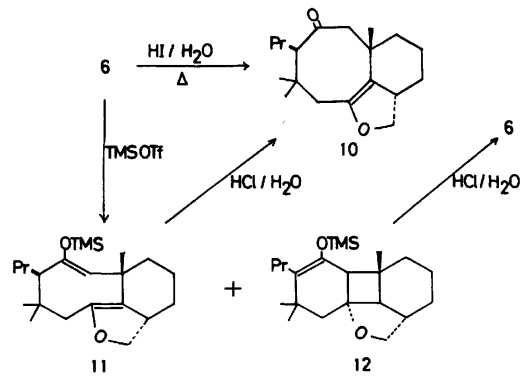

11 12

Scheme 3.

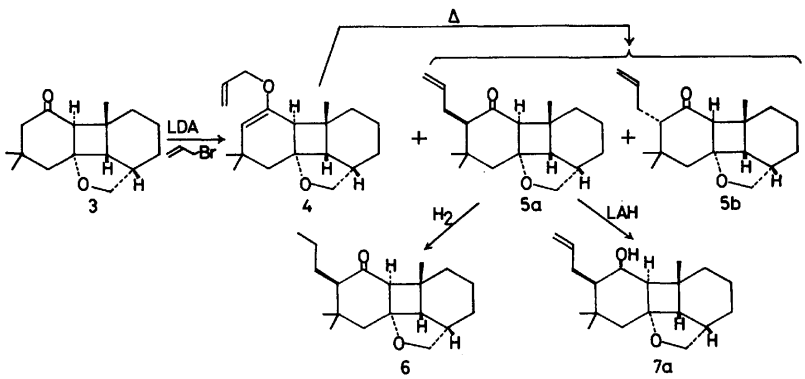

Scheme 1.

tional mobility of the cyclooctane ring.

In searching for milder conditions, we found that trimethylsilyl trifluoromethanesulfonate (TMSOTf)[6] would be effectively employed for the cleavage of the cyclobutane system under neutral conditions. Treatment of the ketone **6** with freshly prepared TMSOTf in purified carbon tetrachloride under an argon atmosphere gave a ring-opened compound **11** in 84% yield, accompanied by a small amount of a simple enol silyl ether **12** (11%) and recovered starting material **6** (5%). In ^{1}H NMR spectrum of **11**, the methylene protons attached to oxygen appear at δ 3.80 (1H, dd, J=9 and 3 Hz) and 4.23 (1H, t, J=9 Hz), and a vinyl proton at 4.53 (1H, s); four vinylic carbons are recognized in ^{13}C NMR spectrum at δ 115.2 (d), 115.9 (s), 145.1 (s), and 152.2 (s). The enol silyl ether **11** was quantitatively converted into the ketone **10** on aqueous hydrochloric acid in THF. This is the first example of the cleavage of the cyclobutane ring by means of TMSOTf.

An alternative procedure for the preparation of an 8-membered ring system *via* a lactone **13** is as follows.

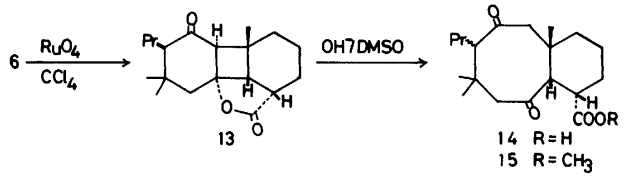

Scheme 4.

The oxidation of **6** was successful by using a stoichiometric amount of RuO_4[7] in purified carbon tetrachloride for only several minutes at room temperature. The γ-lactone **13** (1765 cm^{-1} in IR) was obtained in 86% yield. Saponification of **13** in DMSO gave a diketo acid **14** in 80% yield. The ^{13}C NMR spectrum of the methyl ester **15** (214.2, C=O; 213.6, C=O; 176.0, ester) and mass spectrum [m/z 336 (M^+), 321 (M^+—CH_3), and 305 (M^+—OCH_3)] indicate that the cyclobutane ring is cleaved to an cyclooctane ring system.

In summary, the preparation of the fused 8-membered ring system can now be achieved not only under acidic or basic but also under neutral conditions.

Experimental

All the melting points are uncorrected. IR spectra were recorded on a Hitachi 215 grating spectrophotometer. ^{1}H NMR spectra were measured on JEOL MH-100 and LMN-FX90Q spectrometers and ^{13}C NMR on a JEOL LMN-FX90Q, using TMS as the internal standard. Mass spectra were obtained on a Hitachi RMU-6MG analyzer. High resolution mass spectra were performed at Nippon Roche Research Center, Kamakura.

4-Allyl-1,5,5-trimethyl-8-oxatetracyclo[8.3.1.0^{2,7}.0^{7,14}]tetradecan-3-one (5). To 5 ml of a dry THF solution of lithium diisopropylamide (LDA, 8.75 mmol), were added 5 ml of hexamethylphosphoric triamide (HMPA) at −78 °C and then 424 mg (1.71 mmol) of 1,5,5-trimethyl-8-oxatetracyclo-[8.3.1.0^{2,7}.0^{7,14}]tetradecan-3-one (**3**)[4] in 3 ml of dry THF. The mixture was stirred for 30 min, then allyl bromide was added at a once and the whole allowed to warm to room temperature. After 3 h, the mixture was poured into a saturated ammonium chloride solution, and extracted with ether. The ether layer was washed with water and brine, and dried over anhyd Na_2SO_4. Evaporation of the solvent gave an oil. Flash-chromatography on silica gel (elution with hexane-ethyl acetate=30:1—20:1) afforded 432 mg of an enol ether **4** and 88 mg of a mixture of **5a** and **5b**.

4: IR (CCl_4) 1650, 1145, 1050, 990, and 920 cm^{-1}; ^{1}H NMR ($CDCl_3$) δ=1.06 (3H, s), 1.08 (6H, s), 1.78 (2H, s), 2.75 (1H, br s), 3.75 (1H, t, J=9 Hz), 4.04 (1H, t, J=9 Hz), 4.13 (2H, m), 4.55 (1H, s), and 5.0—6.3 (3H, m); MS m/z 288 (M^+).

The enol ether **4** was heated in a sealed tube at 195 °C for 2 h. The combined mixture of **5a** and **5b** was flash-chromatographed on silica gel (elution with hexane-ethyl acetate=100:1—20:1) to give 359 mg of **5a** (73%) as crystals and 44 mg of **5b** (9%) as an oil.

5a: mp 70—71 °C (pentane); IR (CCl_4) 1685, 1635, 1170, 1040, 990, and 905 cm^{-1}; ^{1}H NMR (CCl_4) δ=0.82 (3H, s), 1.05 (3H, s), 1.08 (3H, s), 1.94 (2H, AB center, J=16 Hz), 2.4 (2H, m), 2.74 (1H, s), 3.63 (1H, dd, J=10 and 9 Hz), 3.93 (1H, t, J=9 Hz), 4.7—4.9 (2H, m), and 5.6—6.1 (1H, m); MS m/z 288 (M^+, 2%) and 109 (100%).

Found: C, 79.09; H, 9.83%. Calcd for $C_{19}H_{28}O_2$: C, 79.12; H, 9.78%.

5b: oil; IR (CCl_4) 1710, 1045, 995, and 915 cm^{-1}; ^{1}H NMR (CCl_4) δ=0.83 (3H, s), 1.17 (3H, s), 1.20 (3H, s), 2.74 (1H, br s), 3.76 (1H, t, J=9 Hz), 4.09 (1H, t, J=9 Hz), and 4.8—6.0 (3H, m); MS m/z 288 (M^+, 4%) and 109 (100%).

4-Allyl-1,5,5-trimethyl-8-oxatetracyclo[8.3.1.0^{2,7}.0^{7,14}]tetradecan-3-ol (7a). To a suspension of 20 mg of lithium aluminum hydride in 1 ml of dry THF, was added 21 mg of **5a** in 0.5 ml of dry THF at 0 °C. The mixture was stirred at that temperature for 15 min and then at room temperature for 30 min. Work up as usual and flash chromatography on silica gel with hexane-ethyl acetate (10:1) gave **7a** (71%) and **7b** (28%).

7a: mp 93—94 °C (hexane, 0 °C); IR (CCl_4) 3600, 1045, 980, and 920 cm^{-1}; ^{1}H NMR (CCl_4) δ (the Δ values show the pseudocontact shift upon the addition of 0.23 equiv of Eu-FOD)=0.76 (3H, s, Δ0.44), 0.95 (3H, s, Δ0.44), 1.27 (3H, s, Δ0.98), 2.65 (1H, br d, J=9 Hz, Δ2.57), 3.60 (1H, t, J=9 Hz, Δ0.30), 3.80 (1H, t, J=9 Hz, Δ2.34), 3.89 (1H, t, J=9 Hz, Δ0.29), and 4.8—6.2 (3H, m).

Found: C, 78.60; H, 10.41%. Calcd for $C_{19}H_{30}O_2$: C, 78.57; H, 10.42%.

7b (an epimeric alcohol of **7a**): oil; IR (CCl_4) 3300br, 1050, 1000, and 920 cm^{-1}; ^{1}H NMR (CCl_4) δ=0.91 (3H, s), 0.92 (3H, s), 1.02 (3H, s), 3.62 (1H, br d, J=5 Hz), 3.70 (1H, t, J=9 Hz), 3.93 (1H, t, J=9 Hz), and 4.8—6.0 (3H, m).

4-Propyl-1,5,5-trimethyl-8-oxatetracyclo[8.3.1.0^{2,7}.0^{7,14}]tetradecan-3-one (6). An ethanolic solution (5 ml) of **5a** (25 mg) was hydrogenated over PtO_2 under hydrogen at ordinary pressure. After 2 h, the catalysts were removed by filtration and the filtrate was evaporated to give an oil. Chromatography on silica gel with chloroform afforded 22 mg (88%) of **6**.

6: mp 63—64 °C (methanol, −20 °C); IR ($CHCl_3$) 1690 sh and 1685 cm^{-1}; ^{1}H NMR ($CDCl_3$) δ=0.75 (3H, s), 0.83 (3H, t, J=6.5 Hz), 0.98 (3H, s), 1.05 (3H, s), 1.94 (1H, d, J=15 Hz), 2.00 (1H, d, J=10 Hz), 2.06 (1H, d, J=15 Hz), 2.46 (1H, m), 2.79 (1H, br s), 3.65 (1H, t, J=9 Hz), and 3.98 (1H, t, J=9 Hz); ^{13}C NMR ($CDCl_3$) δ=14.3 (q), 16.2 (t), 22.4 (t), 22.9 (t),24.1

(t), 26.3 (q), 26.7 (q), 29.6 (q), 32.0 (s), 33.7(d), 35.8 (t), 36.4 (s), 49.2 (t), 50.6 (d), 51.6 (d), 61.4(d), 71.1 (t), 82.0 (s), and 212.9 (s); MS *m/z* 290 (M^+, 4%) and 109 (100%).

Found: C, 78.55; H, 10.44%. Calcd for $C_{19}H_{30}O_2$: C, 78.57; H, 10.42%.

11-Propyl-8,12,12-trimethyl-2-oxatricyclo[6.5.1.0^{4,14}]tetradec-1(14)-en-10-one (10). *Procedure A*: To a vigorously stirred suspension of **6** (10 mg) in 5 ml of water, 5 drops of hydriodic acid were added, and the mixture was refluxed for 4 h. The products were extracted in ether and chromatographed on silica gel with chloroform–hexane (2:1—3:1) to give a ketone **10** (7 mg, 70%) as crystals.

10: mp 68—70°C; IR (CCl_4) 1705, 1685, 1460, 1365, and 1206 cm^{-1}; ^1H NMR ($CDCl_3$) δ=0.76 (6H, s), 1.00 (3H, s), 2.0—4.0 (several broad signals), and 4.27 (1H, t, J=9 Hz); ^{13}C NMR ($CDCl_3$) δ (sharp signals only at)=14.6, 21.6, 22.2, 28.6, 36.8, 41.0, 42.7, 73.3, 115.6, 145.4, and 214.5.

Found: *m/z* 290.2245. Calcd for $C_{19}H_{30}O_2$: M 290.2247.

Procedure B: To a solution of **11** (7 mg, see below) in 5 ml of THF, were added 2 drops of a 10% hydrochloric acid. The solution was stirred for 2 h at room temperature. The whole was poured into water, extracted with ether, and the ether extract was dried over anhyd $MgSO_4$. Evaporation of the solvent gave the ketone **10** (6 mg, 100%).

11-Propyl-8,12,12-trimethyl-10-trimethylsiloxy-2-oxatricyclo-[6.5.1.0^{4,14}]tetradeca-1(14),9-diene (11). In a 5 ml flask, containing a solution of the ketone **6** (20 mg, 7×10^{-2} mmol) in 0.5 ml of dry CCl_4 (washed with concd H_2SO_4, dil KOH, H_2O, dried over P_2O_5; fractionally distilled) and a spinning bar, was added 27 mg (2.4×10^{-1} mmol) of triethylamine. After stirring for 5 min, was added drop by drop 47 mg (2.1×10^{-1} mmol) of TMSOTf at 0°C, under a dry argon atmosphere. The whole was allowed to warm to room temperature and stirred for 24 h. If some of the starting ketone **6** still remained 1 mol equivalents of Et_3N and TMSOTf were added to the solution, and the whole was again stirred over night. The resulting solution was passed through a short silica-gel column with CH_2Cl_2 to remove triethylammonium triflate. The crude products, obtained by evaporation of the solvent, were chromatographed on silica gel (with hexane–benzene=5:1) to give an 8-membered enol trimethylsilyl ether **11** (22 mg, 84%) as crystals, a simple enol trimethylsilyl ether **12** (3 mg, 11%), and **6** (1 mg, 5%).

11: IR (CCl_4) 1670, 1635, 1365, 1245, 1200, and 1120 cm^{-1}; ^1H NMR ($CDCl_3$) δ=0.19 (9H, s), 0.83 (3H, s), 0.88 (3H, s), 1.23 (3H, s), 3.80 (1H, dd, J=9 and 3 Hz), 4.23 (1H, t, J=9 Hz), and 4.53 (1H, s); ^{13}C NMR ($CDCl_3$) δ=0.4 (q, ×3), 14.9 (q), 21.9 (t, ×2), 24.3 (q), 25.4 (q), 26.3 (q), 27.5 (t), 34.8 (s, ×2), 40.8 (t), 43.3 (d), 44.0 (t), 48.1 (d), 72.3 (t), 115.7 (d), 115.9 (s), 145.1 (s), and 152.7 (s); MS *m/z* 362 (M^+, 8%) and 347 ($M^+ - CH_3$, 100%).

12: oil; IR (CCl_4) 1665 cm^{-1}; ^1H NMR ($CDCl_3$) δ=0.15 (9H, s), 0.89 (3H, t, J=7 Hz), 1.05 (6H, s), 1.55 (3H, s), 2.57 (1H, br s), 3.90 (1H, t, J=9 Hz), and 4.20 (1H, t, J=9 Hz); MS *m/z* 362 (M^+, 15%) and 347 ($M^+ - CH_3$, 100%).

4-Propyl-1,5,5-trimethyl-8-oxatetracyclo[8.3.1.0^{2,7}.0^{7,14}]tetradecane-3,9-dione (13). To a solution of the ketone **6** (40 mg) in 10 ml of purified CCl_4 (see above), was added drop by drop a solution of RuO_4 (Mitsuwa Kagaku Yakuhin Co. Ltd., Osaka, Japan; 61% activity, 38 mg) in 5 ml of pure CCl_4. The whole was stirred for 10 min. The remained RuO_4 was reduced to RuO_2 by addition of several drops of 2-propanol. RuO_2 was removed through a silica-gel column by elution with CH_2Cl_2 and the eluates were evaporated to give a crude γ-lactone **13** (36 mg, 86%) as crystals. This material was decomposed during recrystallization and, therefore, an analytical sample was obtained by sublimation (110°C, 400 pa).

13: mp 152—153°C; IR($CHCl_3$) 1765, 1695, and 1185 cm^{-1}; ^1H NMR($CDCl_3$) δ=0.87 (3H, s), 0.91 (3H, t, J=6.6 Hz), 1.08 (3H, s), 1.14 (3H, s), 2.12 (2H, AB center), 2.42 (1H, dd, J=12 and 1 Hz), 2.80 (1H, br s), and 2.92 (1H, dm, J=12 Hz); ^{13}C NMR ($CDCl_3$) δ=79.6 (C-O), 180.5 (-COO-), and 211.1 (-CO-).

Found: C, 74.92; H, 9.27%. Calcd for $C_{19}H_{28}O_3$: C, 74.96; H, 9.27%.

Methyl 4-propyl-1,5,5-trimethyl-3,7-dioxobicyclo[6.4.0]dodecane-9-carboxylate (15). The γ-lactone **13** (7 mg) was dissolved in 2 ml of DMSO and 2 ml of a 10% KOH solution was added at room temperature under an argon atmosphere. After gently refluxed for 3 h, the mixture was allowed to cool to room temperature. The whole was poured into 10 ml of ice-water, washed with benzene and then acidified with 1 M† HCl. The solution was extracted with ether. Evaporation of the solvent gave crude carboxylic acid **14** (7 mg) as crystals. A pure sample was obtained by chromatography on silica gel (with CH_2Cl_2–acetone=100:1—20:1).

14: mp 190.5—191°C; IR ($CHCl_3$) 3500—2500br and 1695 cm^{-1}; ^1H NMR($CDCl_3$) δ=0.92 (3H, s), 0.98 (9H, s), and 1.97—3.12 (7H, m).

To a solution of the crude acid **14** in 20 ml of ether, was added drop by drop an ethereal solution of diazomethane at 0°C. The whole was stirred for 30 min at that temperature, and evaporated to give a crude oil. Chromatography of the oil on silica gel (CH_2Cl_2) gave a pure methyl ester **15** (5 mg, 92%; 72% overall yield from **13**).

15: oil; IR ($CHCl_3$) 1715 and 1695 cm^{-1}; ^1H NMR ($CDCl_3$) δ=0.95 (s, 3H), 1.01 (s, 6H), 2.10 and 2.78 (AB, J=12.1 Hz), 2.23 and 3.10 (AB, J=12.7 Hz), 1.9—3.3 (3H, m), and 3.58 (3H, s); ^{13}C NMR ($CDCl_3$) δ=14.3 (q), 17.3 (q), 20.1 (q), 20.6 (t), 21.6 (t), 29.5 (t), 30.7 (t), 31.9 (q), 39.4 (s), 39.5 (s), 41.5 (t), 43.1 (d), 51.9 (q), 59.2 (t, ×2), 61.8 (d), 64.6 (d), 176.0 (s), 213.6 (s), and 214.2 (s).

Found: *m/z* 336.2295. Calcd for $C_{20}H_{32}O_4$: M 336.2302.

References

1) As for taxane derivative, see review: R. W. Miller, *J. Nat. Prod. (Lloydia)*, **43**, 425 (1980).

2) S. Nozoe, M. Morisaki, K. Tsuda, Y. Iitaka, N. Takahashi, S. Tamura, K. Ishibashi, and M. Shirasaka, *J. Am. Chem. Soc.*, **87**, 4968 (1965).

3) W. Oppolzer, *Acc. Chem. Res.*, **15**, 135 (1982).

4) T. Umehara, Y. Inouye, and H. Kakisawa, *Bull. Chem. Soc. Jpn*, **54**, 3492 (1981).

5) Y. Tamura, H. Ishibashi, Y. Kita, and M. Ikeda, *J. Chem. Soc., Chem. Commun.*, **1973**, 101.

6) H. Emde, D. Domsch, H. Feger, U. Frick, A. Götz, H. H. Hergott, K. Hofmann, K. Kober, K. Krägeloh, T. Oesterle, W. Steppan, W. West, G. Simchen, *Synthesis*, **1982**, 1 and references cited therein.

7) A. B. Smith, III, R. M. Sarborough, Jr., *Synth. Commun.*, **10**, 205 (1980) and references cited therein.

† 1 M=1 mol dm^{-3}.

The Solution Chemistry of Organotin Compounds. III. A Thermodynamic Study of the Molecular Interaction of Me_2SnCl_2 with Lewis Bases by Means of Nuclear Magnetic Resonance Spectroscopy

Hideaki FUJIWARA,* Fumihiko SAKAI, Yoshihiro MIKAWA, and Yoshio SASAKI
Faculty of Pharmaceutical Sciences, Osaka University, 1-6 Yamada-Oka, Suita, Osaka 565
(Received December 14, 1984)

Molecular interaction of Me_2SnCl_2 with Lewis bases has been investigated by measuring the concentration and temperature dependence of NMR coupling constant $^2J(^{119}Sn,H)$. It is found that 1:1 and 1(acid):2(base) complexes are formed concurrently in solution. Association constants and coupling constants in these complexes are determined at different temperatures, leading to the enthalpies ΔH° and entropies ΔS° for the relevant molecular interaction. The coupling constants are temperature independent and a merit of using this constant as a diagnostic tool has been proven. The E and C parameter treatment of ΔH°_{AB} has given reasonable E_A and C_A values for Me_2SnCl_2. Entropies ΔS° are also estimated in gas phase on the basis of molecular theory for the third-law entropy, and the contribution from solvation is shown important in the solution of $CHCl_2CHCl_2$.

Thermodynamic parameters are essential for the discussion of molecular interactions, being independent on the method of investigation and measuring conditions such as concentration and temperature unless there is a special reason to the contrary. Under this idea much effort has been devoted to determine these parameters as accurately as possible, and quite a lot of data have been collected for different interacting systems.[1] Hitherto, several useful equations have been established empirically from these data, especially from the enthalpies. That is, the E and C parameter treatment has been proposed by Drago[2] stating that $-\Delta H^\circ_{AB}=E_AE_B+C_AC_B$, while Gutman[3] proposed the donor number which is equal to $-\Delta H^\circ$ for the complex formation of bases with $SbCl_5$ in CH_2ClCH_2Cl. Such studies are important not only for the understanding of solution-chemical behavior of each compound treated but also for that of the nature of molecular interactions generally.

In this series of our study, organotin compounds which are of wide industrial and agricultural use are taken up as a model compound, and the molecular interaction is studied from the stand point of solution equilibria and thermodynamics. The authors have investigated the substituent effect in the complex formation of $MeSnCl_3$ with substituted pyridines, and derived and discussed the thermodynamic parameters in relation to the position of substituent in the Me_2SnCl_2 plus picoline systems.[4,5] In the present study acidic character of Me_2SnCl_2 is examined on the complex formation with typical Lewis bases, *N,N*-dimethylformamide (DMF), dimethyl sulfoxide (DMSO), hexamethylphosphoric triamide (HMPA), and γ-picoline *N*-oxide (PINO).[6] NMR coupling constant $^2J(^{119}Sn, H)$ is measured in an inert solvent $CHCl_2CHCl_2$, and enthalpies and entropies of the molecular interaction are determined from variable temperature experiments. The results are discussed in relation to the empirical treatment of the enthalpies and to the molecular theory of the third-law entropies.

Experimental

NMR coupling constant was measured with a Hitachi R-22 NMR spectrometer at 90 MHz. Variable temperature experiments were carried out in the conventional way. The sample temperature was measured by a copper-constantan thermocouple immersed in the solvent in a separate sample tube. Temperature variation was less than ±0.3 °C during the measurement of all samples at a given temperature. ^{119}Sn satellite position was measured by a YHP5315A frequency counter within an error of 0.05 Hz under internal mode of NMR lock.

All distillations and sample handling were done in dry boxes in order to prevent moisture contamination. $CHCl_2$-$CHCl_2$ and DMSO were dried over CaH_2, and DMF, HMPA, and PINO were over BaO, and then they were distilled under reduced pressure after decantation. Me_2SnCl_2 (Tokyo Kasei Co.) was sublimed at about 60 °C. In the Job experiment, total concentration of acid and base was held constant at about 0.15 mol dm^{-3} and the molar ratio was varied. In the concentration and temperature dependence study, molarity of Me_2SnCl_2 was held constant at a value as low as possible, *ca.* 0.025 mol dm^{-3}.

Calculations were done on a NEAC S-900 and S-1000 computers at the Computer Center in Osaka University. The program CONDEP[5,7] was used for the equilibrium analysis. Linear equations were solved by a least squares method to obtain E_A and C_A parameters of Me_2SnCl_2, making use of a Library Program TLELSD transferred from the Computer Center in Tohoku University. ΔH° and ΔS° were obtained by a linear regression analysis of van't Hoff plot, together with their error limits.

Results

Stoichiometry of the complexes formed in solution was first tested by the Job plot. An example is shown in Fig. 1 for the PINO system typically. The curve reaches its maximum at a molar ratio larger than 0.5 and contribution of an 1(acid):2(base) complex is suggested besides the 1:1 complex. In the other systems the plots show maximum at the molar ratio 0.5, and only the 1:1 is supported from this experiment. The NMR parameter $^2J(^{119}Sn, H)$ reflects well the order and degree of coordination around Sn atom and is less subject to the other subsidiary solvent effect. An example of the concentration and temperature dependence is shown in Fig. 2 for the system of DMSO. In the Me_2SnCl_2 plus DMSO system, concentration dependence of $^2J(^{119}Sn,$

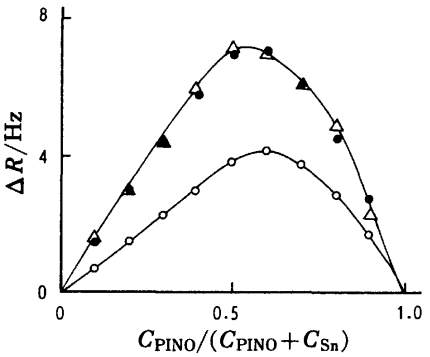

Fig. 1. Job plots for the system of Me_2SnCl_2 plus PINO at 34.1 °C. In the abscissa plotted are the molar ratio times variation in the NMR parameter, *e.g.*, $R_{acid}\cdot\Delta J$ for $^2J(^{119}Sn,H)$ where $\Delta J=J_{obsd}-J_{free}$. $\delta_H(SnCH_3)$ decreases on addition of the base and $R_{acid}\cdot(-\Delta\delta)$ is plotted.
R_{acid}=molar ratio of the acid. NMR parameters observed are: ●; $^2J(^{119}Sn,H)$, ○; $\delta_H(SnCH_3)$, △; $\delta_H(PINO,CH_3)$.
Total molarity of the acid and base is 0.18 mol dm^{-3} in $CHCl_2CHCl_2$.

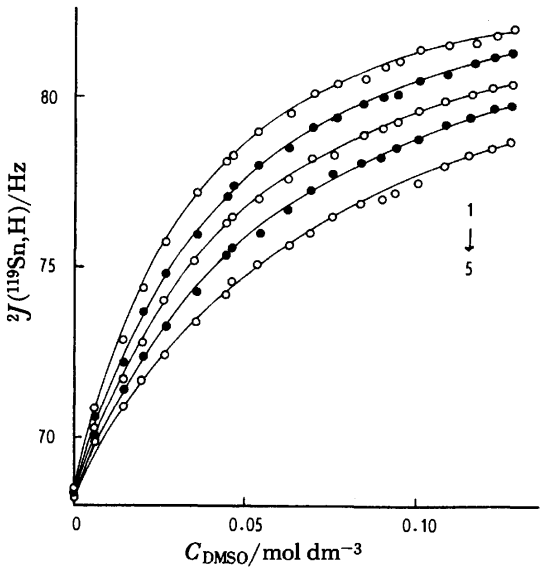

Fig. 2. Concentration and temperature dependence of $^2J(^{119}Sn,H)$ in the Me_2SnCl_2 plus DMSO system in $CHCl_2CHCl_2$.
Molarity of Me_2SnCl_2=0.025 mol dm^{-3}. Measurement temperatures are 34.1, 43.3, 51.4, 59.4, and 68.7 °C for curves 1 to 5.

H) is reproduced well within the experimental error by assuming only the 1:1 complex. This fact, together with the result of Job plot, indicates negligible contribution from 1:2 complex in solution treated here. In Table 1 analysis of the concentration dependence assuming only the 1:1 complex is compared with that assuming both 1:1 and 1:2 complexes. Standard deviation σ between the observed and the simulated coupling constants decreases only very slightly even if 1:2 complex is incorporated and one more adjustable parameter K_2 is introduced. K_2 is, if incorporated, very

Table 1. Analysis of concentration dependence of $^2J(^{119}Sn,H)$ in the system of Me_2SnCl_2 plus DMSO in $CHCl_2CHCl_2$ at 34 °C

	Model	K/dm^3 mol^{-1}	J_{AB}/Hz	σ/Hz
I[a]	A+B=AB	K_1=64±2	83.5±0.1	0.083
	AB+B=AB_2	K_2=0.14±0.02		
II	A+B=AB	58.5±1.8	84.0±0.1	0.089
III[b]	A+B=AB	64.9±1.8	83.6±0.1	0.087

a) J_{AB_2} is set to 112.4 Hz. b) Lower half of the concentration range of DMSO is used for calculation.

small and its temperature dependence is scattered, indicating negligible contribution of the 1:2 complex. Calculations are also compared for the 1:1 complex formation in Table 1 using the total and the lower half of the concentration range of DMSO. The parameters are almost unchanged in these two calculations, supporting the model assumed. The results from the lower half of the concentration range are adopted below, because ten data points are usually sufficient for the simulation of two parameters, K_1 and J_{AB}, and because contribution of the 1:2 complex becomes much smaller with lowering the concentration of DMSO if it presents at all. Calculation of this DMSO system is summarized in Table 2. The error in each parameter is an estimation from the program or reproducibility in repeated experiments whichever is larger. When dissolved in neat DMSO, Me_2SnCl_2 is expected to form the 1:2 complex predominantly as evidenced by the J value of 112.4 Hz which is much larger than those of the free tin compound (68 Hz) and of the 1:1 complex (84 Hz). However, experiments with higher concentration of DMSO complex in $CHCl_2CHCl_2$ were prevented by the insufficient solubility.

Method of analysis of the Me_2SnCl_2 plus DMF system is similar to that of the DMSO system. When 1:2 complex was taken into account, K_2 value estimated was very small, sometimes even negative at higher temperatures. Therefore, only 1:1 complex is assumed. Calculation is also summarized in Table 2. It is worth noting that J_{AB} calculated is constant throughout the temperature range studied in common with above DMSO system. It is usual that chemical shift of complex exhibits quite large temperature dependence: this value needs be determined at each temperature and is not easily compared when derived at different temperatures or by different investigators. The temperature independency found in this study for the coupling constant indicates an intrinsic merit of using this constant as an observable.

Although 1:2 complex is not suggested from the Job plot in the Me_2SnCl_2 plus HMPA system, its formation is inevitable for the interpretation of the concentration dependence. Systematic errors appear between the observed and the recalculated J values, varying systematically with the concentration of HMPA. These errors are improved satisfactorily by incorporating the 1:2 complex, and the K_2 values change consistently

TABLE 2. ANALYSIS OF CONCENTRATION AND TEMPERATURE DEPENDENCE OF $^2J(^{119}Sn,H)$ FOR THE Me_2SnCl_2 PLUS BASE SYSTEMS IN $CHCl_2CHCl_2$

Base	t/°C	K_1/dm³ mol⁻¹	K_2/dm³ mol⁻¹	J_{AB}[a]/Hz	σ/Hz
DMF	34.1	30.9±1.5		83.7±0.2	0.17
	45.2	21.6±0.7		83.2±0.2	0.11
	51.8	17.9±0.7		83.1±0.2	0.14
	60.8	11.3±0.5		83.8±0.3	0.17
	69.5	10.1±0.3		82.4±0.2	0.10
DMSO	34.1	64.9±1.8		83.6±0.1	0.09
	43.3	50.5±1.7		83.1±0.2	0.11
	51.4	34.7±1.1		83.5±0.2	0.11
	59.4	27.3±0.9		83.1±0.2	0.11
	68.7	20.4±0.7		82.8±0.2	0.11
HMPA	34.1	2450±188	0.64±0.03	86.7±0.1	0.11
	43.1	1590±58	0.53±0.02	86.8±0.1	0.10
	53.1	1058±123	0.40±0.01	86.8±0.1	0.08
	61.0	762±2	0.23±0.01	87.0±0.1	0.07
PINO	34.1	1526±700	11.5±0.4	82.4±0.2	0.17
	43.2	503±77	7.3±0.3	83.5±0.2	0.14
	51.3	501±124	5.6±0.3	83.2±0.3	0.22
	59.8	287±41	3.7±0.3	83.9±0.2	0.20
	69.5	168±13	2.1±0.2	84.5±0.2	0.16

a) J_{AB2} is set equal to the J value in neat base: 104.5(DMF), 112.4(DMSO), 121.6(HMPA), and 106.2(PINO) Hz.

with the measurement temperature. The 4-parameter calculation including J_{AB_2} in adjustable parameters, however, proved unreliable because reproducibility of the two parameters K_2 and J_{AB_2} breaks down on repeated experiments. A small amount of 1:2 complex formed in solution seems responsible for this difficulty. This resembles to the Me_2SnCl_2 plus pyridine system,[7] but differs from the case in reference[4] where four parameters are simulated successfully in calculation. For this reason, calculation was done with the three adjustable parameters, fixing J_{AB_2} at a value in neat base.

It is clear from the Job plot that 1:2 complex is formed in solution for the Me_2SnCl_2 plus PINO system (Fig. 1). The 4-parameter calculation including J_{AB_2} was tested, but it gave rather scattered value of J_{AB_2}(104.6—108.3 Hz) at different temperatures and the van't Hoff plot of K_1 and K_2 deviated much from a linear line. Therefore, 3-parameter calculation was adopted for this case.

Discussion

Thermodynamic parameters of the complex formation are derived from van't Hoff plot of K_1 and K_2 obtained above (Fig. 3 and Table 3). Enthalpy-entropy compensation relation holds approximately (Fig. 4). A linear relation is also seen between ΔH°_{AB} and ΔJ_{AB} except for PINO (Fig. 5), as is often observed in a similar case.[8] This line will go through the origin in the Figure because ΔH° should be zero when ΔJ=0. NMR coupling constants are usually interrelated with the s-character of chemical bonds. Under this concept the break down of the ΔH—ΔJ proportionality for PINO will be interpreted as due to the different type of the complex suggested from IR study.[9] The E and C parameter treatment of ΔH°_{AB} proposed by Drago and Wayland[2] gives values of E_A=13.30 and C_A=5.48

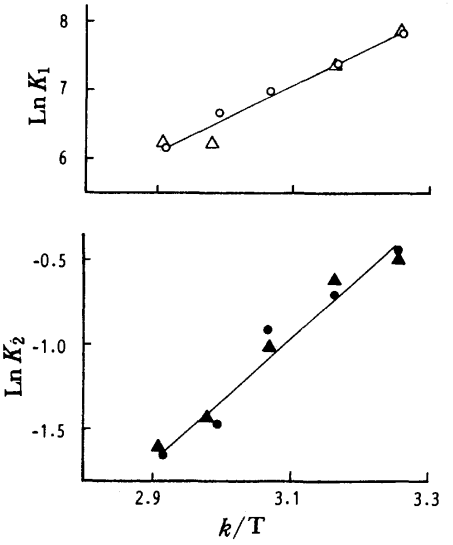

Fig. 3. van't Hoff plots for the Me_2SnCl_2 plus HMPA system from duplicate experiments. ○ and ●; run 1. △ and ▲; run 2.

TABLE 3. ENTHALPIES AND ENTROPIES FOR THE COMPLEX FORMATION OF Me_2SnCl_2 WITH BASES IN $CHCl_2CHCl_2$

Base	$-\Delta H^\circ_{AB}$	$-\Delta S^\circ_{AB}$	$-\Delta H^\circ_{AB_2}$[a]	$-\Delta S^\circ_{AB_2}$[a]
	kJ mol⁻¹	J K⁻¹ mol⁻¹	kJ mol⁻¹	J K⁻¹ mol⁻¹
DMF	30.5±1.5	70.4±4.3		
DMSO	31.8±2.6	69.3±8.1		
HMPA	40.8±1.7	67.8±5.2	70.2±3.2	166.9±9.7
PINO	45.3±5.2	87.7±15.8	85.0±6.9	195.8±20.9

a) $\Delta H^\circ_{AB_2}$ and $\Delta S^\circ_{AB_2}$ for the complex formation of AB_2 from A and 2B.

for Me_2SnCl_2 with the $r.m.s.$ deviation of 1.0 kJ mol⁻¹. These values are comparable to those for Me_3Al(E_A=12.9, C_A=1.43) and for Me_3Ga(E_A=13.3, C_A=0.881), but definitely larger than those for Me_3SnCl(E_A=5.76, C_A=

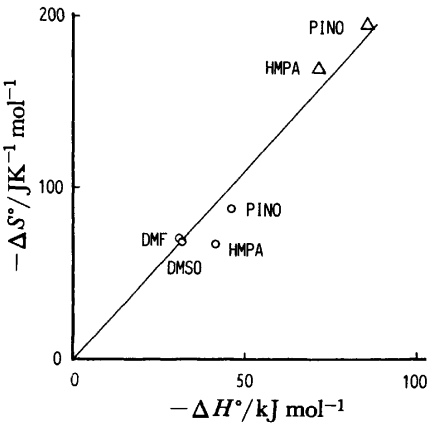

Fig. 4. Plots for enthalpy-entropy compensation relation.
O denotes data point for 1:1 complex and Δ that for 1:2 complex.

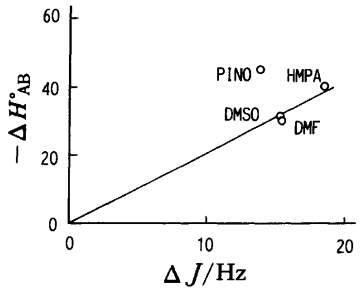

Fig. 5. Plots of ΔH-ΔJ proportionality relation for the 1:1 complex formation. $\Delta J=J_{AB}-J_A$, J_A=68.3 Hz for the free acid molecule.

0.0296[2] or E_A=6.25, C_A=0.60[10]), indicating enhanced acidity of Me_2SnCl_2.

On the contrary to enthalpies, entropy data have been overlooked frequently in the discussion of thermodynamic aspects of interacting systems. However, important informations are included in entropies, especially concerning the molecular (internal) motions and solvation of molecules. The entropy change on complex formation of A+B=AB can be equalized to the difference in the thermodynamic third-law entropies of the components, *i.e.*, $\Delta S^\circ_{AB,calcd}=S^\circ_{AB}-(S^\circ_A+S^\circ_B)$, the latters being calculated from molecular theory of thermodynamic functions.[11] This $\Delta S^\circ_{AB,calcd}$ is considered to correspond to the gas-phase value of ΔS°. Experimental entropies are compared with thus calculated ones in Table 4 where translational and rotational parts of entropy are used for calculation and the vibrational one is not included considering almost similar contributions from the starting compounds and the product.

The observed entropies are seen to be about 1/3 of the expected (calculated) values. Where does such a discrepancy come from? Some new chemical bonds are formed on complex formation, but contributions to the vibrational entropy from such bonds are very small (in the order of a few JK^{-1}mol^{-1}). Some internal motion will become restricted on complex formation, but such contribution is also small. In contrast, solvation by $CHCl_2CHCl_2$ is expected nontrivial. Its protons are known to have an acidic character, forming weak hydrogen bonding with base, and also it possesses polarity to solvate by means of electrostatic attraction. If, as a model calculation, $CHCl_2CHCl_2$ is assumed to solvate to a base molecule and the reaction proceeds in such a way as A+BS→AB+S, $\Delta S^\circ_{AB,calcd}$ is reduced in great deal in absolute value and −16 JK^{-1}mol^{-1} is obtained for the DMSO system. That is, the experimental value may be said correspond to the solvation number of 0.7. Similar number of 0.6—0.7 are reached for other systems studied here. Such calculation is only a model calculation, but it may be said soundly that the solvation as above contribute more (twice, roughly) to the entropy changes in $CHCl_2CHCl_2$ than the net entropy change in gas phase. It is well known that entropy changes in aqueous solutions become positive for ionic reactions such as protonation of bases, metal complex formation, or ion-pair formation, because of the release of water molecules on reaction. In the present case solvation does not take such a drastic role and the entropies remain negative, although the solvation takes a major part of the entropies observed.

Table 4. Comparison of the calculated entropies (in gas phase) with the experimental ones (in solution)[a]

Base	Reaction: A+B=AB		AB+B=AB$_2$	
	$-\Delta S^\circ_{calcd}$	$-\Delta S^\circ_{obsd}$	$-\Delta S^\circ_{calcd}$	$-\Delta S^\circ_{obsd}$
DMF	238	70.4		
DMSO	242	69.3		
HMPA	257	67.8	283	99.1
PINO	244	87.7	324	108.1

a) In units of J K^{-1}mol^{-1}.

References

1) M. D Joesten and L. J. Schaad, "Hydrogen Bonding," Marcel Dekker, New York, (1974).
2) R. S. Drago, *J. Chem. Educ.*, **51**, 300 (1974).
3) V. Gutmann, "Coordination Chemistry in Non-Aqueous Solutions," Springer-Verlag, Berlin (1968).
4) H. Fujiwara, F. Sakai, M. Takeyama, and Y. Sasaki, *Bull. Chem. Soc. Jpn.*, **54**, 1380 (1981).
5) H. Fujiwara, F. Sakai, and Y. Sasaki, *J. Chem. Soc., Perkin Trans. 2*, **1983**, 11.
6) PINO is taken up instead of pyridine *N*-Oxide because of the higher solubility of its complex.
7) H. Fujiwara, F. Sakai, and Y. Sasaki, *J. Phys. Chem.*, **83**, 2400 (1979).
8) E. N. Guryanova, I. P. Goldshtein, and I. P. Romm, "Donor-Acceptor Bond," John Wiley, New York, (1975) p. 124.
9) B. V. Liengme, R. S. Randall, and J. R. Sams, *Can. J. Chem.*, **50**, 3212 (1972).
10) T. F. Bolles and R. S. Drago, *J. Am. Chem. Soc.*, **88**, 3921 (1965).
11) G. Herzberg, "Infrared and Raman Spectra," Chap. 5, Van Nostrand, New Jersey (1945).

Structural Study of Germanate Glasses Irradiated with γ-Rays and Thermal Neutrons

Tetsuaki NISHIDA,* Motomi KATADA,† and Yoshimasa TAKASHIMA
Department of Chemistry, Faculty of Science, Kyushu University
33, Hakozaki, Higashiku, Fukuoka 812
†*Department of Chemistry, Faculty of Science, Tokyo Metropolitan University,*
Fukasawa, Setagaya-ku, Tokyo 158
(Received December 27, 1984)

^{119}Sn Mössbauer study of ^{60}Co-γ ray and thermal neutron irradiated potassium germanate glasses containing a small amount of SnO_2 has been performed to investigate the structural change of the glasses. The γ- and the thermal neutron-irradiation results in a disappearance of the distinct composition dependence of the Mössbauer parameters (quadrupole splitting and linewidth) observed before the irradiation. DTA measurement of the irradiated glasses also reveals drastic decreases in glass transition temperature (T_g) amounting to 20—120 °C and a simultaneous disappearance of the distinct composition dependence of T_g observed before the irradiation. This suggests a disruption of the chemical bond between germanium and oxygen atoms constituting GeO_6 units. On the other hand, Mössbauer measurement at lower temperatures reveals that a parameter of intermolecular force constant (θ^2M) obtained from the temperature dependence of the absorption area undergoes little change by the irradiations. This suggests that the irradiations bring about little changes in the ionic bond and the interatomic distance between tin and oxygen atoms, and that the irradiated germanate glasses can still be regarded as polymers from the lattice vibrational point of view.

Abnormal composition dependence of the physical properties of germanate glasses, *i.e.*, germanate anomaly has so far been found on density and refractive index,[1-3] viscosity,[4] and glass transition temperature (T_g).[4,5] Viscosity- and T_g-composition curves show maxima at the compositions of 17[4] and 15—16[5] mol% alkali oxides, respectively. The decrease in these physical properties in the higher alkali oxide content region was tentatively attributed to the formation of nonbridging oxygen (NBO) atoms, because it was expected that viscosity and T_g are well correlated with the cohesiveness and depolymerization of the glasses, respectively. The presence of NBO in germanate glasses was confirmed by Verweij and Buster[6] by means of Raman spectroscopy, and furthermore the fraction of NBO was obtained by Smets and Lommen[7] by means of X-ray photoelectron spectroscopy (XPS). In the Raman and XPS studies, the formation of NBO was concluded to start at an alkali oxide concentration of 18 mol%.

Mössbauer spectroscopy of ^{57}Fe has also been utilized for the structural studies of several kinds of glasses such as borate,[8-10] borosilicate,[11,12] phosphate,[13,14] and borophosphate[15] glasses. In ^{119}Sn Mössbauer study of germanate glasses[16] by the authors, the formation of NBO was concluded to start when the alkali oxide (K_2O) content is higher than about 16 mol%. The result was also supported by distinct composition dependences of T_g and parameter of intermolecular force constant (θ^2M) obtained from the temperature dependence of the Mössbauer absorption area. Structural studies of glasses by means of ^{119}Sn Mössbauer spectroscopy have also been performed on borate[17-20] and silicate[17,21,22] glasses, in which most Sn^{4+} species proved to be present in octahedral environment.

The present study was performed to elucidate the effects of γ- and thermal neutron-irradiation on germanate glasses by means of ^{119}Sn Mössbauer spectroscopy and DTA, because it was expected that the irradiation effects, if present, should depend upon the local structural change of the glasses based on the change in composition.

Experimental

Experimental procedures for the preparation of glass samples and for the Mössbauer and DTA measurements are already reported in our previous paper.[16] Gamma-ray irradiation of the germanate glasses denoted by $xK_2O\cdot(100-x)GeO_2\cdot 2SnO_2$ was performed in the ^{60}Co-γ ray irradiation facility of Kyushu University, with a dose rate of 5.9×10^5 R h^{-1} for 170 h at the ambient temperature (*ca.* 40 °C). Thermal neutron irradiation was carried out in the reactor of Atomic Energy Research Institute of Rikkyo University, with a flux of 5×10^{11} n cm^{-2} s^{-1} for 6 h at the ambient temperature. The γ-ray dose rate in the reactor is estimated to be 1×10^6 R h^{-1}. During the irradiation, each glass sample was kept in a sealed polyethylene bag filled with dry nitrogen gas, and the bag was placed in a glass tube or polyethylene capsule filled with dry nitrogen gas and silica gel to protect the sample from the atmospheric moisture.

Results and Discussion

Mössbauer spectra for the potassium germanate glasses irradiated with γ-rays of 10^8 R or thermal neutrons of 10^{16} n cm^{-2} consist apparently of a single absorption peak, which can be analyzed into a quadrupole doublet just like in the case of germanate glasses before the irradiation.[16] Change in the isomer shift of ^{119}Sn with K_2O content of the glasses is shown in Fig. 1, in which a broken line refers to the result obtained before the irradiation.[16] These isomer shift values correspond to the tetravalent ionic species (Sn^{4+}) with octahedral symmetry,[23] and the Sn^{4+} ion is considered to be present as a network modifier at an interstitial site of the network composed of GeO_4 and GeO_6 units.[16] It is seen from Fig. 1 that the isomer

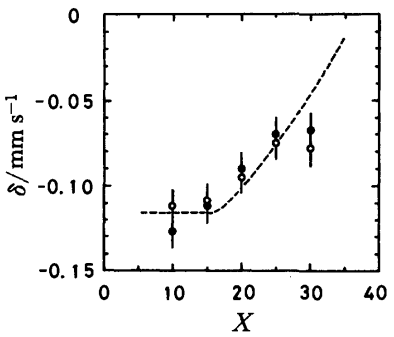

Fig. 1. Variation of the isomer shift of ^{119}Sn with K_2O content. (○): γ-Ray irrad., (●): thermal neutron irrad. The broken line refers to that of unirradiated glasses.

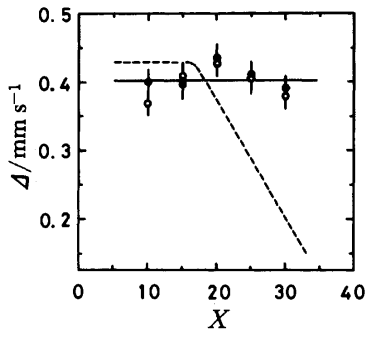

Fig. 2. Variation of the quadrupole splitting of Sn^{4+} with K_2O content. (○): γ-Ray irrad., (●): thermal neutron irrad. The broken line refers to that of unirradiated glasses.

shifts show little change by the γ- and the thermal neutron-irradiation, although only a small decrease is observed in the germanate glass with the alkali oxide content of x=30. The result shown in Fig. 1 is similar to the results of phosphate[14] and borophosphate[15] glasses in which both the isomer shift and quadrupole splitting show little change by the ^{60}Co-γ ray irradiations of 10^6 and 10^8 R. These results may be correlated with the structural role of Mössbauer nucleus, *i.e.*, both the iron (Fe^{2+} and Fe^{3+}) and tin (Sn^{4+}) play a role of network modifier which is present at an interstitial site of three-dimensional network in the case of phosphate,[13,14] borophosphate,[15] and germanate[16] glasses. On the other hand, the role of tin in borate and borosilicate glasses is reported to be a network former which is present at a substitutional site of tetrahedral boron or silicon atoms.[8,11] Irradiations of borate[9,24-26] and borosilicate[27] glasses with ^{60}Co-γ rays and thermal neutrons are reported to result in a decrease in isomer shift or an increase in the fraction of Fe^{2+} produced by the irradiation.

Change in the quadrupole splitting of Sn^{4+} in the germanate glasses irradiated with γ-rays and thermal neutrons is shown in Fig. 2, in which a broken line refers to the result obtained before the irradiation.[16] It is surprising that a drastic change in the quadrupole splitting observed before the irradiation disappears almost completely by the γ-ray (10^8 R) and thermal neutron (10^{16} n cm^{-2}) irradiations. This is very interesting and also quite different from the results of phosphate[14] and borophosphate[15] glasses in which little change in quadrupole splitting and linewidth was observed by ^{60}Co-γ ray irradiation. Irradiation of borate[9,24-26] and borosilicate[27] glasses with γ-rays or thermal neutrons is also reported to produce little change in the quadrupole splitting. The result of Fig. 2 therefore suggests that the irradiation brings about a structural change which has not been observed in the oxide glasses such as borate, borosilicate, and phosphate glasses. It is noteworthy that the quadrupole splitting values for the irradiated glasses are identical with those for the unirradiated germanate glasses with the alkali oxide content lower than 16 mol%. This means a disappearance of the structural role of NBO which has been concluded to be present only in GeO_4 units and causes an increase in the symmetry around Sn^{4+} ions.[16] Two possible explanations are given to the disappearance of the structural role of NBO in the irradiated glasses of which alkali oxide content is higher than 16 mol%, *i.e.*, one is a displacement of NBO from the neighboring site of Sn^{4+} to other site, and the other is a generation of a positive hole on an NBO atom. The former explanation, however, seems to be improbable because a displacement of NBO will bring about a change in the coordination number of tin (IV) and because such a change will be somewhat reflected in isomer shift. (Change in the coordination number of Sn^{4+} from 6 to 5 or 4 will result in an increase in the isomer shift of ^{119}Sn.) The latter explanation, *i.e.*, a generation of a positive hole on an electronegative NBO atom ($-O^-$) seems to be probable because the resultant oxygen atom is equivalent to a bridging oxygen from the electronical point of view. Therefore, the decreased symmetry around Sn^{4+} caused by the γ- and the thermal neutron-irradiaion is ascribed to a disappeared anionic character of NBO. This will result in a decreased Coulombic attraction between Sn^{4+} and NBO, and then a decrease in the symmetry around tin will be observed.

As is shown with a broken line in Fig. 3, a gradual and drastic increase in the linewidth (FWHM) has been observed for the unirradiated glasses with the alkali oxide content higher than 17 or 18 mol%. The increase in the linewidth has been attributed to the increased disorder brought about by NBO which is present at the neighboring site of Sn^{4+}.[19] It is obvious from Fig. 3 that γ- and thermal neutron-irradiation also results in a disappearance of the drastic increase in the linewidth caused by NBO. The disappearance of the drastic increase in the linewidth in the alkali oxide content region higher than 17—18 mol% is also concluded to be due to the disappeared structural role of NBO, because the magnitude of linewidth observed for the irradiated glasses is identical with that for the unirradiated glasses with the alkali oxide content lower than 17 mol%, just like the case of quadrupole splitting described above.

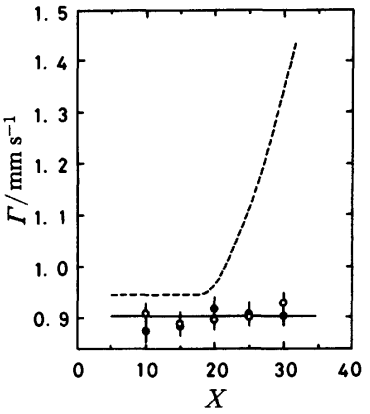

Fig. 3. Variation of the linewidth of Sn^{4+} with K_2O content.
(○): γ-Ray irrad., (●): thermal neutron irrad.
The broken line refers to that of unirradiated glasses.

The decrease in the linewidth is therefore explained by a rearrangement of oxygen atoms around Sn^{4+} as a result of the generation of a positive hole on an NBO atom, although no other experimental proof to support this idea has been obtained in the present study.

It is expected that some structural change, if present, will affect the physical properties such as T_g and viscosity. DTA measurement of the γ-ray irradiated germanate glasses was then carried out. This is shown in Fig. 4. It is noted that the irradiation gives rise to the decreases in T_g amounting to 20—120°C and a simultaneous disappearance of the distinct composition dependence of T_g observed before the irradiation. The composition dependence of T_g observed in the unirradiated glasses reflects, as described in our previous paper,[16] the formations of GeO_6 units and NBO in GeO_4 units in the alkali oxide content region lower than 16 mol% and in the range of 16—30 mol%, respectively. The decrease in the T_g brought about by the irradiation is ascribed to the disruption of the chemical bond between germanium and oxygen atoms constituting GeO_6 units, because the increase in T_g in the unirradiated glasses has been attributed to the formation of GeO_6 units.[16] This irradiation-effect seems not to affect the Mössbauer parameters such as isomer shift, quadrupole splitting, and linewidth, probably because the germanium or oxygen atoms in a GeO_6 unit of which chemical bond is disrupted by the irradiation are not present in the first or second coordination sphere of Mössbauer nucleus (^{119}Sn). (It is considered that a tin atom is interposed between two GeO_4 units to take an octahedral symmetry, and that a GeO_6 unit may be located at a site farther than the GeO_4 units.)

Mössbauer measurements at lower temperatures were also carried out to elucidate the extent of the irradiation-induced disruption of the chemical bond between germanium and oxygen constituting GeO_6 units, because a parameter of intermolecular force constant (θ^2M) obtained from the temperature dependence

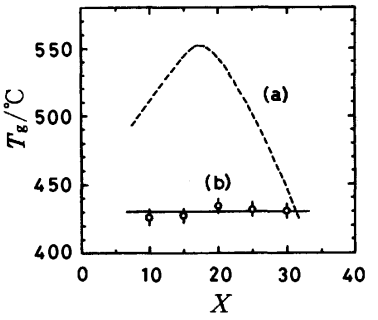

Fig. 4. Variation of the glass transition temperature (T_g) with K_2O content. (a): Unirrad., (b): γ-Ray irrad.

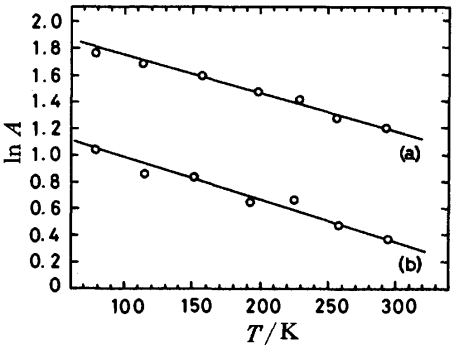

Fig. 5. Plots of the absorption area of $20K_2O \cdot 80GeO_2 \cdot 2SnO_2$ glass against temperature. (a): γ-Ray irrad., (b): thermal neutron irrad.

of the Mössbauer absorption area is known to give much information on the degree of polymerization and molecular association.[16,28] In the θ^2M value, M is the mass of Mössbauer nucleus and θ indicates Debye temperature. The correlation between θ and the maximum lattice vibration frequency ν_{max} for overall the glass matrix is expressed as $k\theta=h\nu_{max}$ where k is Boltzmann constant and h is Planck constant. The θ^2M value can be correlated with the Mössbauer recoil-free fraction f by using a Debye approximation,[23,29] and is expressed as

$$\theta^2M = \frac{3E^2}{kc^2}\left(\frac{-\mathrm{d}\ln f}{\mathrm{d}T}\right)^{-1}, \quad (1)$$

where E is Mössbauer transition energy and c is the velocity of light. Figure 5 shows the results of the Mössbauer measurements of $20K_2O \cdot 80GeO_2 \cdot 2SnO_2$ glass at lower temperatures, in which natural logarithm of the absorption area ($\ln A$) is plotted against measuring temperature T because $\ln f$ can be approximated by $\ln A$ when a very thin sample is used and the absorption is not saturated. It is seen from Fig. 5 that the absorption area for the thermal neutron irradiated germanate glass is more than one order smaller than that for the γ-ray irradiated glass. This means, as is generally known, that the thermal neutron irradiation results in a more drastic structural change in the network structure than the γ-ray irradiation. The decreased absorption area also suggests that the irradiations result in a disruption of the chemical bonds

in the germanate glass, because the recoil-free fraction is closely concerned with the rigidity of the matrix in which Mössbauer nucleus is incorporated. The disruption of the chemical bonds caused by the irradiations, if present, may also affect the θ^2M value for the germanate glass. These values being estimated from Eq.1 by dividing the value of $3E^2/kc^2$, *i.e.*, 2.13×10^4 in the case of 23.9 keV ^{119}Sn, with the slope of the individual straight line are 7.3×10^6 and 6.7×10^6 for the γ-ray and the thermal neutron irradiated germanate glasses, respectively. It is noted that the θ^2M value is 7.0×10^6 in the case of the $20K_2O\cdot80GeO_2\cdot2SnO_2$ glass before the irradiation.[16] Considering the magnitude of the error of θ^2M, *i.e.*, ±0.1—0.2, these results suggest that the γ- and the thermal neutron-irradiation results in little effect on the intermolecular force between two independent GeO_4 units which are connected with each other with the aid of a network modifier such as K^+ and Sn^{4+}. The irradiations are therefore concluded to bring about little change in the ionic bond between tin and the neighboring oxygen atoms constituting GeO_4 units, as is also concluded from the result of isomer shift shown in Fig. 1. The interatomic distance between tin and the neighboring oxygen atoms is also concluded to be unchanged, because the change in the isomer shift is reported to be closely correlated with the interatomic distance between Mössbauer atom and the neighboring atom.[30] This is well consistent with the unchanged θ^2M values observed for the irradiated glasses, because θ^2M value is also known to be closely affected by the degree of packing around Mössbauer nucleus besides the degree of polymerization. In the irradiated germanate glasses, recoil energy and the recoil momentum of Mössbauer γ-rays will therefore be transferred in almost the same way as do those in the unirradiated glasses. In other words, the irradiated germanate glasses studied in the present paper can still be regarded as polymers from the lattice vibrational point of view, although the chemical bond between germanium and oxygen constituting GeO_6 units is considered to be fairly disrupted.

The authors are indebted to Prof. Sumio Sakka of Kyoto University for his useful suggestion on the structure of germanate glasses. They are also indebted to Prof. Hirotoshi Sano of Tokyo Metropolitan University for his useful discussion. The authors are grateful to Profs. Teruaki Nagahara and Tatsuo Matsuura of Rikkyo University for their kind help in the thermal neutron irradiations, and also to Mr. Kiyoshi Matsumoto of Kyushu University for his kind help in the ^{60}Co-γ ray irradiations.

References

1) A. O. Ivanov and K. S. Yestropovb, *Dokl. Akad. Nauk SSSR*, **145**, 797 (1962).
2) M. K. Murthy and J. Ip, *Nature*, **201**, 285 (1964).
3) M. K. Murthy and B. Scroggie, *Phys. Chem. Glasses*, **6**, 162 (1965).
4) J. E. Shelby, *J. Am. Ceram. Soc.*, **57**, 436 (1974).
5) J. E. Shelby, *J. Appl. Phys.*, **46**, 193 (1975).
6) H. Verweij and J. H. J. M. Buster, *J. Non-Cryst. Solids*, **34**, 81 (1979).
7) B. M. J. Smets and T. P. A. Lommen, *J. Non-Cryst. Solids*, **46**, 21 (1981).
8) T. Nishida and Y. Takashima, *J. Non-Cryst. Solids*, **37**, 37 (1980).
9) T. Nishida, T. Shiotsuki, and Y. Takashima, *J. Non-Cryst. Solids*, **41**, 161 (1980).
10) T. Nishida, T. Hirai, and Y. Takashima, *J. Non-Cryst. Solids*, **43**, 221 (1981).
11) T. Nishida, T. Hirai, and Y. Takashima, *Phys. Chem. Glasses*, **22**, 94 (1981).
12) T. Nishida, T. Hirai, and Y. Takashima, *Bull. Chem. Soc. Jpn.*, **54**, 3735 (1981).
13) T. Nishida, T. Shiotsuki, and Y. Takashima, *J. Non-Cryst. Solids*, **43**, 115 (1981).
14) T. Nishida, T. Shiotsuki, and Y. Takashima, *J. Non-Cryst. Solids*, **43**, 123 (1981).
15) T. Nishida, Y. Miyamoto, and Y. Takashima, *Bull. Chem. Soc. Jpn.*, **56**, 439 (1983).
16) T. Nishida, M. Katada, and Y. Takashima, *Bull. Chem. Soc. Jpn.*, **57**, 3566 (1984).
17) K. P. Mitrofanov and T. A. Sidorov, *Sov. Phys. -Solid State*, **9**, 693 (1967).
18) N. A. Eissa, E. E. Shaisha, and A. L. Hussiun, *J. Non-Cryst. Solids*, **16**, 206 (1974).
19) A. Paul, J. D. Donaldson, M. T. Donoghue, and M. J. K. Thomas, *Phys. Chem. Glasses*, **18**, 125 (1977).
20) A. Lechtenbohmer, B. D. Mosel, W. Müller-Warmuth, and H. Dutz, *Glastechn. Ber.*, **55**, 161 (1982).
21) G. M. Bartenev, S. M. Brekhovskikh, A. Z. Varisov, L. M. Landa, and A. D. Tsyganov, *Sov. Phys. -Solid State*, **12**, 972 (1970).
22) H. Dannheim, H. J. Oel, and G. Tomandl, *Glastechn. Ber.*, **49**, 170 (1976).
23) P. A. Flinn, "Tin Isomer Shifts," in "Mössbauer Isomer Shift," ed by G. K. Shenoy and F. E. Wagner, North-Holland Publ. Co., Amsterdam, New York (1978), Chap. 9a.
24) T. Nishida, Y. Takashima, and Y. Nakayama, *J. Solid State Chem.*, **33**, 141 (1980).
25) T. Nishida, T. Hirai, and Y. Takashima, *Radiochem. Radioanal. Lett.*, **42**, 189 (1980).
26) T. Nishida, T. Hirai, and Y. Takashima, *Radiochem. Radioanal. Lett.*, **53**, 153 (1982).
27) T. Nishida, T. Hirai, and Y. Takashima, *Radiochem. Radioanal. Lett.*, **49**, 307 (1981).
28) S. Matsubara, M. Katada, K. Sato, I. Motoyama, and H. Sano, *J. Phys. (Paris), Colloq. C2*, **40**, 363 (1979).
29) N. N. Greenwood and T. C. Gibb, "Mössbauer Spectroscopy," Chapman and Hall Ltd., London (1971), Chaps. 1 and 3.
30) R. Ingalls, F. Van der Woude, and G. A. Sawatzky, "Iron and Nickel," in "Mössbauer Isomer Shift," ed by G. K. Shenoy and F. E. Wagner, North-Holland Publ. Co., Amsterdam, New York (1978), Chap. 7.

 © 1985 The Chemical Society of Japan Bull. Chem. Soc. Jpn., 58, 1749—1754 (1985)

Complex Formation and Solvation of $[CuCl_n]^{(2-n)+}$ in Acetonitrile and in *N,N*-Dimethylformamide

Shin-ichi ISHIGURO, Bojana G. JELIAZKOVA,† and Hitoshi OHTAKI*

Department of Electronic Chemistry, Tokyo Institute of Technology at Nagatsuta, 4259, Nagatsuta-cho, Midori-ku, Yokohama 227

†*Department of Analytical Chemistry, Sofia University, Anton Ivanov 1, Sofia, Bulgaria*

(Received January 21, 1985)

Complex formation equilibria between copper(II) and chloride ions have been studied by calorimetry and spectrophotometry in acetonitrile(AN) containing 0.1 mol dm^{-3} $(C_2H_5)_4NClO_4$ as a constant ionic medium at 25°C. Both calorimetric and spectrophotometric titration curves could be well explained in terms of formation of a series of four mononuclear complexes, $[CuCl_n]^{(2-n)+}$ (n=1—4), and formation constants, enthalpies and entropies of formation of the complexes were determined. Stepwise enthalpies ΔH_n° (n=1—4) were all negative, the ΔH_4° value being especially largely negative. On the other hand, the stepwise entropy ΔS_n° was largely positive for n=1—3, but largely negative for n=4. The result suggested that solvation of the $[CuCl_3]^-$ complex was extremely weak in AN and that release of solvent molecules from $[CuCl_3]^-$ was not so significant that the enthalpy and entropy of formation of $[CuCl_4]^{2-}$ were mainly attributable to those of desolvation of Cl^- followed by a bond formation between the $[CuCl_3]^-$ complex and the chloride ion. The $[CuCl_4]^{2-}$ complex might have no solvent molecules in the primary coordination sphere of the metal ion within the complex in AN. Enthalpies of solution of anhydrous $CuCl_2$ crystals were measured in AN and *N,N*-dimethylformamide(DMF) in order to evaluate enthalpies of transfer ΔH_t° of Cu^{2+} from water to the aprotic solvents. The ΔH_t° values well correlated with Gutmann's donor number of the solvents. The enthalpies of transfer ΔH_t° of $[CuCl_n]^{(2-n)+}$ (n=0—4) from AN to DMF were evaluated, and the enthalpy values monotonously increased with n. The $\Delta H_t^\circ(CuCl_4^{2-})$ value was only slightly positive as well as $\Delta H_t^\circ(Cl^-)$, and the result also suggested that the metal ion within the complex was not primarily solvated with solvent molecules in both AN and DMF. Electronic spectra of individual copper(II) chloride complexes were determined in AN.

In a previous paper,[1] we discussed about complex formation equilibria between copper(II) and chloride ions in *N,N*-dimethylformamide (DMF) studied by calorimetry and spectrophotometry.

It has already been pointed out that the formation of copper(II) chloride complexes is enhanced in aprotic solvents with either weaker (acetonitrile[2] and propylene carbonate[3]) or stronger (dimethyl sulfoxide[3] and DMF[4]) donicity than water.[5] According to Ahrland,[6] it can be explained in terms of difference in solvation of chloride ion between aprotic solvents and water. Solvation of chloride ion is more favorable in water owing to hydrogen-bonding with water molecules than in aprotic solvents.

Formation constants of copper(II) chloride complexes are largely different among aprotic solvents. Since the acceptor property of acetonitrile (AN) (the acceptor number (A_N)=19.3) is not largely different from that of DMF (A_N=16.0),[7] more favorable formation of copper(II) chloride complexes in AN than in DMF may be ascribed to weaker solvation of copper(II) ion with the former solvent (the donor number (D_N)=14.1) than with the latter (D_N=26.6).[7] Although the formation constants of copper(II) chloride complexes have been determined in AN,[2] no values of enthalpies and entropies of formation of the complexes have been reported.

In the present work, we investigated complex formation equilibria between copper(II) and chloride ions in acetonitrile by means of calorimetry and spectrophotometry as employed in a previous study[1] and determined formation constants, enthalpies and entropies of formation of the complexes. Enthalpies of solution of anhydrous $CuCl_2$ crystals were measured in AN and DMF in order to elucidate solvation phenomena of each complex species. Enthalpies of transfer of Cu^{2+} from water to the aprotic solvents were first evaluated, and then, enthalpies of transfer of individual copper(II) chloride complexes from AN to DMF were evaluated from the enthalpies of formation of the copper(II) chloride complexes obtained in both AN and DMF[1] and the enthalpies of transfer of Cu^{2+} and Cl^- from AN to DMF.

Electronic spectra of individual copper(II) chloride complexes were determined in AN and were compared with those determined in DMF, which suggested the difference in structures of the solvated neutral $[CuCl_2]$ complex in AN and DMF.

Experimental

Reagents. *Copper(II) perchlorate acetonitrile solution* was prepared according to Hathaway and Underhill[8] by the reaction of metallic copper with nitrosyl perchlorate, $Cu+2NOClO_4=Cu(ClO_4)_2+2NO$, in acetonitrile under a reduced pressure. Nitrosyl perchlorate was prepared by passing nitrogen oxides, which was obtained by dropwise adding concentrated nitric acid to sodium nitrate crystals, into 70% perchloric acid, and nitrosyl perchlorate thus obtained were filtered and then sucked under a dry atmosphere. About 10 g of nitrosyl perchlorate thus prepared was repeatedly washed with acetonitrile on a glass filter with a P_2O_5 guard-tube and finally a free-flowing powder was obtained. The dry nitrosyl perchlorate was reacted with metallic copper in *ca.* 100 cm^3 of dry acetonitrile within a round-bottle flask, which was evacuated through a P_2O_5 guard-tube with a

water pump. The reaction was continued for several hours and then the solution was filtered under a nitrogen atmosphere through a G4 glass filter to remove residual nitrosyl perchlorate and copper metals. The concentration of copper(II) perchlorate in the stock solution was determined electrogravimetrically.

Tetraethylammonium perchlorate and *tetraethylammonium chloride* of reagent grade were used without further purification and dried at 100 °C in a vacuum oven. Impurities of halide ions in the tetraethylammonium perchlorate was negligibly small because no precipitate of silver halide was found by titrating the aqueous solution of the salt with a silver nitrate solution.

Acetonitrile was dried with calcium hydride, and then distilled under an atmospheric pressure and stored over 4A 1/16 molecular sieves in a bottle closed with a P_2O_5 guard-tube. The residual water determined by a Karl-Fisher test was less than 50 ppm.

All test solutions were prepared in a dry box over P_2O_5 under an atmosphere of dried nitrogen gas.

Measurements. All calorimetric and spectrophotometric titrations were carried out in acetonitrile containing 0.1 mol dm^{-3} $(C_2H_5)_4NClO_4$ as a constant ionic medium.

Calorimetric measurements were carried out in a thermostated bath controlled at (25.000±0.007) °C placed in a room thermostated at (25.0±0.2) °C. A 100 cm^3 of copper(II) perchlorate solution was first placed in a Dewar vessel, which was filled with nitrogen gas and prevented from moisture with a P_2O_5 guard-tube, and then titrated with a 0.1 mol dm^{-3} $(C_2H_5)_4NCl$ solution. The heat of dilution of chloride ions was separately determined by titrating a 0.1 mol dm^{-3} $(C_2H_5)_4NClO_4$ solution without copper(II) perchlorate with the $(C_2H_5)_4NCl$ solution, and was 0.065 J cm^{-3} per the addition of a unit volume of the titrant. A heat of reaction evolved at each point of titration was ranged 0—5 J with certainty ±0.05 J. Calorimetric measurements were carried out by using a fully automatic on-line system as described elsewhere.[9]

Enthalpies of solution of anhydrous $CuCl_2$ crystals in a solvent were measured by using an MPS-11 calorimeter (Tokyo Riko, Tokyo) equipped with a PC-8801 computer (NEC, Tokyo) by breaking an ampoule containing a given amount of the salt in 50 cm^3 of the solvent without any ionic medium in a tefron vessel. Detailed procedure of measurement and analysis of heat evolved were described previously.[10]

Spectrophotometric measurements were carried out in acetonitrile solutions with a flow cell of a light-pass length of 0.5 cm which was connected with a titration vessel through tefron and glass tubes. A 15 cm^3 of $Cu(ClO_4)_2$ acetonitrile solution was placed in a vessel under a nitrogen atmosphere and then titrated with a 0.1 mol dm^{-3} $(C_2H_5)_4NCl$ solution. Electronic spectra were measured with a HITACHI 340 spectrophotometer (Hitachi, Tokyo) equipped with a JEC 6 electronic computer (JEOL) which recorded data at selected wavelengths at every 2 nm in the range 240—520 nm. The formation constants of copper(II) chloride complexes were determined spectrophotometrically by using absorbances obtained at 10 different wavelengths, 254, 278, 294, 304, 310, 330, 406, 420, 460, and 480 nm.

Analysis of Calorimetric and Spectrophotometric Data. A heat q_i evolved at a titration point i is represented by using formation constants β_n and overall enthalpies $\Delta H^\circ_{\beta n}$ of formation of $[CuCl_n]^{(2-n)+}$ complexes as follows:

$$q_i = -(V_i\sum_n \beta_n \Delta H^\circ_{\beta n} m_i x_i^n - V_{i-1}\sum_n \beta_n \Delta H^\circ_{\beta n} m_{i-1} x_{i-1}^n), \quad (1)$$

where V denotes the volume of the test solution, and m and x stand for concentrations of free copper(II) and chloride ions, respectively, which are related to their total concentrations C_M and C_X according to the mass-balance Eqs. 2 and 3:

$$C_M = m_i + \sum_n \beta_n m_i x_i^n, \quad (2)$$

$$C_X = x_i + \sum_n n\beta_n m_i x_i^n. \quad (3)$$

The formation constants and enthalpies were determined by minimizing the error-square sum, $U=\sum_i (q_{i,obsd} - q_{i,calcd})^2$ by using the program KALORI.[11]

Absorbance A_{ij} at a titration point i and a selected wavelength λ_j is represented by Eq. 4 by using formation constants and molar extinction coefficients $\varepsilon_n(\lambda_i)$ of the $[CuCl_n]^{(2-n)+}$ complexes.

$$A_{ij} = \sum_n \varepsilon_n(\lambda_j)\beta_n m_i x_i^n \quad (\beta_0 = 1). \quad (4)$$

The formation constants and molar extinction coefficients were determined by minimizing the error-square sum, $U=\sum_i\sum_j (A_{ij,obsd} - A_{ij,calcd})^2$, by using the program SPEC.

Results and Discussion

Calorimetric titration curves obtained in acetonitrile (AN) are depicted in Fig. 1. The enthalpy ΔH/kJ mol^{-1} of reaction per a unit mole addition of chloride ions at each titration point was plotted against the ratio C_X/C_M, where C_X and C_M denote the total cocentrations of chloride and copper(II) ions, respectively, in a solution. As seen in Fig. 1, remarkable changes in ΔH were observed at C_X/C_M=1 and 3, which indicate the formation of a series of four copper(II) chloride complexes having significantly different enthalpies of formation between $[CuCl]^+$ and $[CuCl_2]$ and between $[CuCl_3]^-$ and $[CuCl_4]^{2-}$, but inappreciable different ones between $[CuCl_2]$ and $[CuCl_3]^-$. Therefore, calorimetric data obtained were analyzed by assuming the formation of $[CuCl_n]^{(2-n)+}$ (n=1—4) by the least-squares method

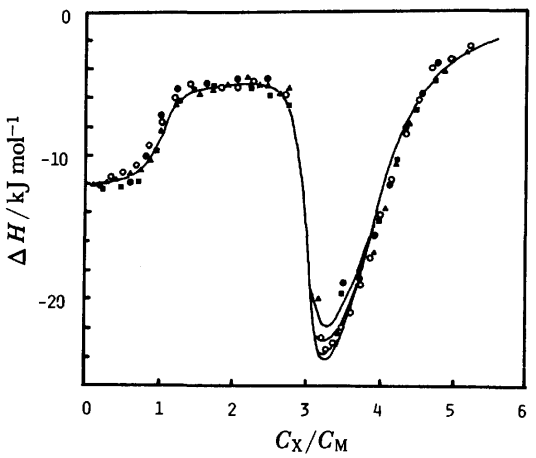

Fig. 1. Calorimetric titration curves of copper(II) chloride acetonitrile solutions containing 0.1 mol dm^{-2} $(C_2H_5)_4NClO_4$. Initial concentrations of copper(II) perchlorate (C_M/mmol dm^{-3}): 16.06 (○), 11.66 (▲), 9.67 (●), and 6.282 (■). The solid lines were calculated by using the constants in Table 1.

Table 1. Overall formation constants, $\beta_n/mol^{-n}dm^{3n}$ and enthalpies, $\Delta H^\circ_{\beta n}/kJ\,mol^{-1}$, for the reaction, $Cu^{2+}+nCl^-=CuCl_n^{(2-n)+}$ (n=1—4), in acetonitrile containing 0.1 mol dm^{-3} $(C_2H_5)_4NClO_4$ as a constant ionic medium at 25 °C

	Calorimetry	Spectrophotometry
log β_1	9.69	9.76
log β_2	17.64	17.36
log β_3	22.58	22.50
log β_4	25.43	25.44
$\Delta H^\circ_{\beta 1}$	−11.66	−12.61 (0.2)
$\Delta H^\circ_{\beta 2}$	−16.66	−16.62 (0.2)
$\Delta H^\circ_{\beta 3}$	−21.09	−21.10 (0.3)
$\Delta H^\circ_{\beta 4}$	−55.39	−54.54 (0.4)
U[a)]	2.91	0.374
NP[b)]	129	250

a) Least-squares sum, b) The number of data points. The values in parentheses refer to standard deviations.

to determine both formation constants and enthalpies of formation of the complexes. The theoretical curves calculated by using the constants thus optimized are illustrated by the solid lines in Fig. 1, and they well reproduced the experimental curves over the whole range of C_X/C_M examined. The formation constants and enthalpies of formation of the copper(II) chloride complexes finally obtained are summarized in Table 1. The formation constants determined by spectrophotometry are also listed in Table 1. $\Delta H^\circ_{\beta n}$ values given in the column of "Spectrophotometry" in Table 1 were those estimated by inserting the formation constants thus evaluated from the spectrophotometric data to the calorimetric data in Fig. 1. A reasonable agreement was obtained between the formation constants and enthalpies of formation determined by calorimetry and spectrophotometry, although standard deviations for each constant determined by calorimetry were not well evaluated.

Formation of Copper(II) Chloride Complexes in AN. Thermodynamic quantities, $\log(K_n/mol^{-1}dm^3)$, ΔG°_n/kJ mol^{-1}, ΔH°_n/kJ mol^{-1} and ΔS°_n/J $K^{-1}mol^{-1}$, for the stepwise reaction, $CuCl_{n-1}^{(3-n)+}+Cl^-=CuCl_n^{(2-n)+}$ (n=1—4), in the 0.1 mol dm^{-3} $(C_2H_5)_4NClO_4$ AN solution are summarized in Table 2, together with those in the 0.2 mol dm^{-3} $(C_2H_5)_4NClO_4$ DMF solution.[1)]

Formation of the copper(II) chloride complexes was more favorable in AN than in DMF, as visualized in Fig. 2 by the distribution curves of the complexes in the solvents. The more enhanced formation of the complexes in AN than in DMF was mainly owing to the more negative enthalpy values in the former solvent than in the latter, since the entropy values of formation of the complexes were not largely different at each consecutive step n=1—3 in these solvents, and the formation of the $[CuCl_4]^{2-}$ complex was entropically less favorable in the former solvent than in the latter. The favorable enthalpies of formation of copper(II) chloride complexes in AN than in DMF may be ascribed to weaker solvation of the metal ion in the former

Table 2. Thermodynamic quantities, $\log(K_n/mol^{-1}dm^3)$, $\Delta G^\circ_n/kJ\,mol^{-1}$, $\Delta H^\circ_n/kJ\,mol^{-1}$ and $\Delta S^\circ_n/J\,K^{-1}mol^{-1}$, for stepwise reaction, $CuCl_{n-1}^{(3-n)+}+Cl^-=CuCl_n^{(2-n)+}$ (n=1—4), in acetonitrile and in N,N-dimethylformamide at 25 °C

	AN	DMF[a)]
log K_1	9.69	6.79
log K_2	7.95	4.54
log K_3	4.94	4.00
log K_4	2.85	1.52
ΔG°_1	−55.3	−38.8
ΔG°_2	−45.4	−25.9
ΔG°_3	−28.2	−22.8
ΔG°_4	−16.3	−8.7
ΔH°_1	−11.7	10.3
ΔH°_2	−5.0	9.7
ΔH°_3	−4.4	7.3
ΔH°_4	−34.3	−8.1
ΔS°_1	147	165
ΔS°_2	135	120
ΔS°_3	80	101
ΔS°_4	−61	2

a) Ref. 1.

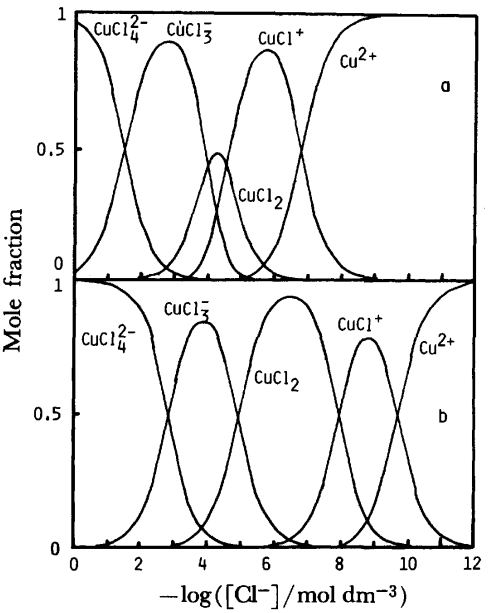

Fig. 2. Distribution curves of the copper(II) chloride complexes in the 0.1 mol dm^{-3} $(C_2H_5)_4NClO_4$ (a) N,N-dimethylformamide and (b) acetonitrile solutions.

solvent, as is expected from the smaller donor number of AN.[7)] The difference in solvation of copper(II) ions in AN and DMF will be discussed in the following section.

The ΔH°_4 value was much more negative than other ΔH°_n (n=1—3) values in AN, the trend being more significant in AN than in DMF. Formation of a complex in a solution is accompanied by desolvation of both metal ion and ligand. Since the desolvation reactions are endothermic, the stronger the solvation of metal ion, the less negative enthalpy of formation of a complex would result. Therefore, the largely negative

ΔH_4° value than the ΔH_n° (n=1—3) values should be ascribed to the difference in solvation between $[CuCl_3]^-$ and $[CuCl_n]^{(2-n)+}$ (n=0—2) in AN, because the metal-ligand bond within a complex is usually weaker in a complex formed at a higher consecutive step. The metal-solvent interactions within $[CuCl_3]^-$ may be much weaker than those within $[CuCl_n]^{(2-n)+}$ (n=0—2) in AN, and thus, a relatively less energy for removing solvent molecules from the coordination sphere of the $[CuCl_3]^-$ complex might be needed in the course of formation of $[CuCl_4]^{2-}$.

As described in a previous paper,[1] a largely positive ΔS_n° (n=1—3) value indicated that desolvation of solvent molecules also played an important role in the course of the formation of $[CuCl_n]^{(2-n)+}$ in AN. On the other hand, a negative ΔS_4° value suggested that desolvation of the $[CuCl_3]^-$ complex did not play an essential role, and thus, the complex might not be strongly solvated. Thus, we concluded that the $[CuCl_4]^{2-}$ complex may practically have no solvent molecules in the primary coordination sphere of the metal ion within the complex in AN.

Enthalpies of Transfer of Cu^{2+}. Enthalpies of transfer of Cu^{2+} from water to AN and to DMF were determined by measuring enthalpies of solution of anhydrous $CuCl_2$ crystals in the solvents. Copper(II) chloride dissolved was expected to be completely dissociated into copper(II) and chloride ions in water,[5,10] but it was mostly associated in AN and in DMF.

Enthalpies of solution of $CuCl_2$ crystals for the following processes were determined in AN and DMF:

$$CuCl_2(c) = Cu^{2+}(s) + 2Cl^-(s);\ \Delta H_s^\circ(Cu^{2+}, 2Cl^-), \quad (5)$$

$$CuCl_2(c) = CuCl_2(s);\ \Delta H_s^\circ(CuCl_2), \quad (6)$$

by measuring the enthalpy of solution $\Delta H_{s,obsd}^\circ$ and by using Eqs. 7 and 8:

$$\Delta H_s^\circ(Cu^{2+}, 2Cl^-) = \Delta H_{s,obsd}^\circ - \sum_n \alpha_n \Delta H_{\beta n}^\circ, \quad (7)$$

$$\Delta H_s^\circ(CuCl_2) = \Delta H_s^\circ(Cu^{2+}, 2Cl^-) - \Delta H_{\beta 2}^\circ, \quad (8)$$

where c and s stand for crystalline and solution states, respectively, and α_n denotes the mole fraction of the $[CuCl_n]^{(2-n)+}$ complex. The α_n values were calculated in each measurement by knowing the formation constants of the copper(II) chloride complexes and the total concentration of $CuCl_2$ in a solvent. The results are listed in Table 3.

The enthalpy of transfer $\Delta H_t^\circ(Cu^{2+}, 2Cl^-)$ from water to another solvent (S) was represented as the sum of enthalpies of transfer of each ionic component as follows:

$$\Delta H_t^\circ(Cu^{2+}, 2Cl^-) = \Delta H_{s,S}^\circ(Cu^{2+}, 2Cl^-) - \Delta H_{s,W}^\circ(Cu^{2+}, 2Cl^-), \quad (9)$$

$$= \Delta H_t^\circ(Cu^{2+}) + 2\Delta H_t^\circ(Cl^-). \quad (10)$$

The $\Delta H_t^\circ(Cl^-)$ values from water to AN and to DMF have been reported by Cox *et al.*[12] on the basis of the extrathermodynamic assumption, $\Delta H_t^\circ(Ph_4As^+) = \Delta H_t^\circ(BPh_4^-)$, and thus, the $\Delta H_t^\circ(Cu^{2+})$ values from water to the aprotic solvents were calculated by subtracting the contribution of Cl^- ions from $\Delta H_t^\circ(Cu^{2+}, 2Cl^-)$. The results are also given in Table 3. The $\Delta H_t^\circ(Cu^{2+})$ values thus obtained were plotted against the donor number[7] of the solvents in Fig. 3, which showed a very good linear relationship. Figure 3 indicates that copper(II) ion is more strongly solvated in DMF than in water, and much more than in AN.

The $\Delta H_t^\circ(Cu^{2+})$ value from water to AN obtained was 18.9 kJ mol^{-1}, which was more positive than the value (11.5 kJ mol^{-1}) obtained by Libuś *et al.*[13] by employing a thermodynamic cycle different from that employed in the present work.

Enthalpies of Transfer of $[CuCl_n]^{(2-n)+}$ from AN to DMF. The differences in overall enthalpies of formation of the copper(II) chloride complexes in AN and in DMF are related to enthalpies of transfer of species pertaining to the complex formation reactions as follows:

$$\Delta H_{\beta n}^\circ(DMF) - \Delta H_{\beta n}^\circ(AN) = \Delta H_t^\circ(CuCl_n^{(2-n)+}) - \Delta H_t^\circ(Cu^{2+}) - n\Delta H_t^\circ(Cl^-). \quad (11)$$

TABLE 3. ENTHALPIES OF SOLUTION ΔH_s° OF ANHYDROUS $CuCl_2$ AND ENTHALPIES OF TRANSFER ΔH_t° OF COPPER(II) AND CHLORIDE IONS FROM WATER TO ACETONITRILE AND TO *N,N*-DIMETHYLFORMAMIDE AT 25 °C

	ΔH°/kJ mol^{-1}		
	Water[a]	AN	DMF
$\Delta H_{s,obsd}^\circ$	−56.3	−15.9	−55.3
$\Delta H_s^\circ(CuCl_2)$	—	−15.9	−54.7
$\Delta H_s^\circ(Cu^{2+}, 2Cl^-)$	−56.3	0.6	−74.5
$\Delta H_t^\circ(Cl^-)$	—	19.0[b]	21.3[b]
$\Delta H_t^\circ(Cu^{2+})$	—	18.9	−60.8

a) Ref. 10, b) Ref. 12.

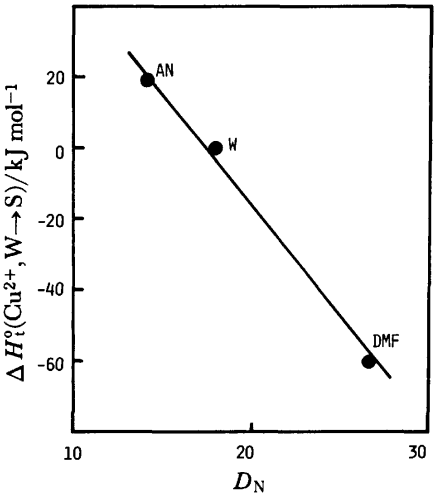

Fig. 3. Enthalpies of transfer of Cu^{2+} from water to AN and to DMF plotted against the donor number D_N of the solvents.

TABLE 4. THERMODYNAMIC QUANTITIES OF TRANSFER, ΔG_t°/kJ mol^{-1}, ΔH_t°/kJ mol^{-1} AND ΔS_t°/J K^{-1} mol^{-1}, OF COPPER(II) CHLORIDE COMPLEXES FROM ACETONITRILE TO *N,N*-DIMETHYLFORMAMIDE AT 25 °C

Species	ΔG_t°	ΔH_t°	ΔS_t°	$\Delta\Delta G_n^{\circ a)}$	$\Delta\Delta H_n^{\circ a)}$	$\Delta\Delta S_n^{\circ a)}$
Cu^{2+}	−77.4[b]	−79.7	−8			
Cl^-	3.7[c]	2.3[c]	−5[c]			
$[CuCl]^+$	−57.2	−55.4	6	16.5	22.0	18
$[CuCl_2]$	−34.0	−38.4	−15	19.5	14.7	−15
$[CuCl_3]^-$	−25.3	−24.4	3	5.0	11.7	21
$[CuCl_4]^{2-}$	−14.0	4.1	61	7.6	26.2	63

a) $\Delta\Delta G_n^\circ=\Delta G_n^\circ(DMF)-\Delta G_n^\circ(AN)$, $\Delta\Delta H_n^\circ=\Delta H_n^\circ(DMF)-\Delta H_n^\circ(AN)$, $\Delta\Delta S_n^\circ=\Delta S_n^\circ(DMF)-\Delta S_n^\circ(AN)$, for the reaction, $CuCl_{n-1}^{(3-n)+}+Cl^-=CuCl_n^{(2-n)+}$ (n=1—4). b) Ref. 15. c) Ref. 12.

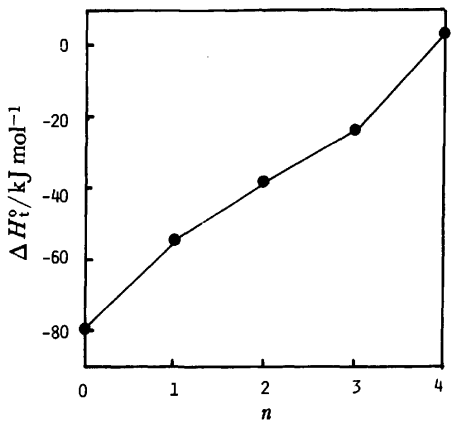

Fig. 4. Enthalpies of transfer of the $[CuCl_n]^{(2-n)+}$ (n=0—4) complexes plotted against n, the number of chloride ions bound per metal ion within a complex.

The $\Delta H_t^\circ(CuCl_n^{(2-n)+})$ value can be calculated, since all the values in Eq. 11 except for $\Delta H_t^\circ(CuCl_n^{(2-n)+})$ have been determined. The $\Delta H_t^\circ(CuCl_n^{(2-n)+})$ (n=1—4) values thus calculated are summarized in Table 4, and are also plotted against n in Fig. 4.

Although the absolute values of formal charges of the $[CuCl_n]^{(2-n)+}$ (n=0—4) complexes vary with n from 2 (n=0) to 0 (n=2) and then again 2 (n=4), the $\Delta H_t^\circ(CuCl_n^{(2-n)+})$ values monotonously changed with n from the $\Delta H_t^\circ(Cu^{2+})$ value of −79.7 kJ mol^{-1} to the $\Delta H_t^\circ(CuCl_4^{2-})$ value of 4.1 kJ mol^{-1}. Since the relative dielectric constant of AN (36.0) is not different from that of DMF (36.7), it is obvious that simple electrostatic theories (such as Born's equation and its derivatives with respect to temperature) are not applicable to explain the change in enthalpies of transfer of the complexes between the solvents. Such a monotonous variation of ΔH_t° values has also been observed for enthalpies of transfer of mercury(II) halide complexes $[HgX_n]^{(2-n)+}$ (n=1—4) from dimethyl sulfoxide to pyridine,[14] the solvents having largely different dielectric constants.

Accordingly, the enthalpy of transfer of $[CuCl_n]^{(2-n)+}$ from AN to DMF should be ascribed to different solvation of the both metal and ligand ions within the complex between the solvents. It is expected that solvation of Cl^- ion within $[CuCl_n]^{(2-n)+}$ may not be significantly different between AN and DMF, since the $\Delta H_t^\circ(Cl^-)$ value from AN to DMF is only slightly positive. The enthalpy of transfer of $[CuCl_n]^{(2-n)+}$ should thus be mainly attributed to the difference in solvation of the metal ion within the complex in the solvents.

The $\Delta H_t^\circ(CuCl_n^{(2-n)+})$ (n=1—3) values from AN to DMF were negative as well as $\Delta H_t^\circ(Cu^{2+})$, indicating that the metal ion within $[CuCl_n]^{(2-n)+}$ (n=1—3) was more strongly solvated with DMF than with AN. The ΔH_t° values increased in the sequence $[CuCl]^+<[CuCl_2]<[CuCl_3]^-$, which may be due, probably, to the decrease in the solvation number of the complexes with an increase in the number of chloride ions within the complexes, although the numbers of solvent molecules coordinating to the metal ion within the complexes have not been known.

The $\Delta H_t^\circ(CuCl_4^{2-})$ value was only slightly positive as well as $\Delta H_t^\circ(Cl^-)$, indicating that the metal ion within the complex was probably not primarily solvated with solvent molecules in both AN and DMF, and thus, the enthalpy of transfer of the $[CuCl_4]^{2-}$ complex was mainly determined by the change in solvation of chloride ions within the complex between the solvents.

Gibbs Energies and Entropies of Transfer of $[CuCl_n]^{(2-n)+}$ from AN to DMF. The Gibbs energy of transfer ΔG_t° of Cu^{2+} has been reported by Coetzee and Istone[15] to be 59.4 and −18.0 kJ mol^{-1} from water to AN and to DMF, respectively, and thus, the $\Delta G_t^\circ(Cu^{2+})$ value from AN to DMF is −77.4 kJ mol^{-1}. The $\Delta G_t^\circ(Cl^-)$ value has also been reported to be 3.7 kJ mol^{-1} from AN to DMF.[12]

By using the ΔG_t° values of copper(II) and chloride ions from AN to DMF, we calculated the Gibbs energies of transfer of $[CuCl_n]^{(2-n)+}$ (n=1—4) by the same procedure as used for evaluation of ΔH_t° of the complexes in a previous section.

The entropies of transfer ΔS_t° of $[CuCl_n]^{(2-n)+}$ (n=1—4) from AN to DMF could thus be calculated from the Gibbs energies and enthalpies of transfer of the complexes. The results are summarized in Table 4.

All the $[CuCl_n]^{(2-n)+}$ (n=1—4) complexes were more stable in DMF than in AN, as indicated by negative ΔG_t° values of the complexes, which were predominantly contributed by the enthalpy term except for the $[CuCl_4]^{2-}$ complex. As to the $[CuCl_4]^{2-}$ complex, the largely positive ΔS_t° value led to the negative ΔG_t° value, the ΔH_t° value being even slightly positive.

However, the reason why the $\Delta S_t^\circ(CuCl_4^{2-})$ value was so largely positive compared with the $\Delta S_t^\circ(CuCl_n^{(2-n)+})$ (n=1—3) values still remained unknown.

Electronic Spectra of Copper(II) Chloride Complexes. Electronic spectra of copper(II) chloride solutions at various concentrations of chloride ions were measured in the 0.1 mol dm^{-3} $(C_2H_5)_4NClO_4$ AN solution. Each spectrum obtained was resolved into spectra of individual copper(II) chloride complexes by knowing the formation constants of the copper(II) chloride complexes in the solution. Molar extinction coefficients of individual copper(II) chloride complexes at various wavelengths thus obtained in the 0.1 mol dm^{-3} $(C_2H_5)_4NClO_4$ AN solution are depicted in Fig. 5.

The absorption maxima of the individual copper(II) chloride complexes obtained in AN are given in Table 5, together with those obtained in DMF.[1] An absorption maximum of $[CuCl]^+$ was found at slightly longer wavelength by *ca.* 35 nm in AN than in DMF. Remarkably different spectra were observed for the $[CuCl_2]$ complex between AN and DMF. Three absorption maxima of the complex were found at *ca.* 255, 308, and 406 nm in AN, while only one absorption maximum was found at *ca.* 265 nm in DMF. The $[CuCl_3]^-$ complex showed three absorption maxima at almost the same wavelengths as those of $[CuCl_2]$ in AN, but only two maxima were found in DMF within the wavelength region examined here. The absorption spectrum of the $[CuCl_4]^{2-}$ complex with two absorption maxima at *ca.* 290 and 405 nm in AN was very similar to that in DMF.

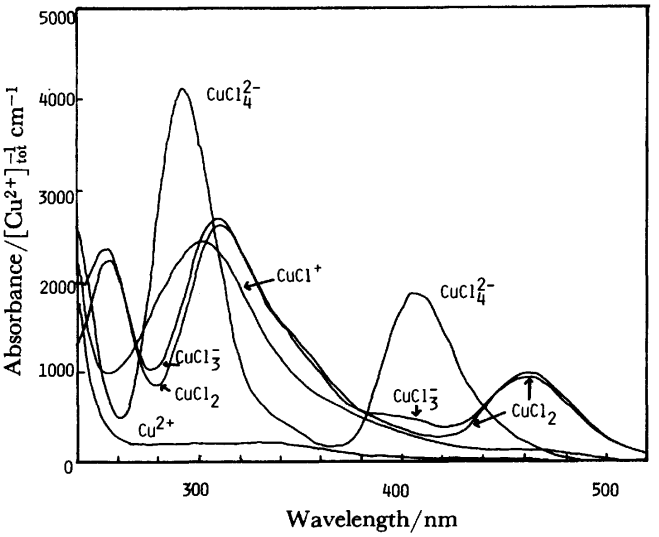

Fig. 5. Molar extinction coefficients of individual copper(II) chloride complexes at various wavelengths in the 0.1 mol dm^{-3} $(C_2H_5)_4NClO_4$ AN solution.

TABLE 5. ABSORPTION MAXIMA, λ_{max}/nm, OF ELECTRONIC SPECTRA OF COPPER(II) CHLORIDE COMPLEXES IN ACETONITRILE AND IN *N*,*N*-DIMETHYLFORMAMIDE

	AN	DMF[a]
$[CuCl]^+$	300	265
$[CuCl_2]$	255	265
	308	
	460	
$[CuCl_3]^-$	255	
	308	300
	460	440
$[CuCl_4]^{2-}$	290	296
	405	410

a) Ref. 1 in the 0.2 mol dm^{-3} $(C_2H_5)_4NClO_4$ DMF solution.

It has been indicated from thermodynamic quantities of formation and of transfer of $[CuCl_4]^{2-}$ in previous sections that the complex may have no solvent molecules in the primary coordination sphere of the metal ion within the complex. The structure of the $[CuCl_4]^{2-}$ complex in AN should be the same as that in DMF,[1] as indicated by the similar absorption spectra in both the solvents.

According to Fergusson,[16] as mentioned in a previous paper,[1] the presence of an absorption maximum between 435 and 455 nm of a copper(II) chloride complex was indicative of the D_{2d} form of the complex. Therefore, it is plausible that the $[CuCl_2]$ and $[CuCl_3]^-$ complexes have the D_{2d} form in AN, since their spectra have an absorption maximum at *ca.* 460 nm. On the other hand, the $[CuCl_2]$ complex in DMF has no maximum in the wavelength region 400—500 nm, and thus, the different solvate structures of the $[CuCl_2]$ complex in AN and in DMF were expected.

The work has been supported by the Grant-in-Aid for Scientific Research No. 59540386 from the Ministry of Education, Science and Culture.

References

1) S. Ishiguro, B. G. Jeliazkova and H. Ohtaki, *Bull. Chem. Soc. Jpn.*, **58**, 1144 (1985).
2) S. E. Manahan and R. T. Iwamoto, *Inorg. Chem.*, **4**, 1409 (1965).
3) M. Ellev, J. Meullemeestre, M. J. Schwing-Weill, and F. Vierling, *Inorg. Chem.*, **21**, 1477 (1982).
4) M. Ellev, J. Meullemeestre, M. J. Schwing-Weill, and F. Vierling, *Inorg. Chem.*, **19**, 2699 (1980).
5) M. A. Khan and M. J. Schwing-Weill, *Inorg. Chem.*, **15**, 2202 (1976).
6) S. Ahrland, *Pure & Appl. Chem.*, **55**, 977 (1983).
7) V. Gutmann, "*The Donor-Acceptor Approach to Molecular Interactions*," Prenum, New York (1978).
8) B. J. Hathaway and A. E. Underhill, *J. Chem. Soc.*, **1960**, 3705.
9) S. Ishiguro, Y. Oka, and H. Ohtaki, *Bull. Chem. Soc. Jpn.*, **56**, 2426 (1983).
10) S. Ishiguro and H. Ohtaki, *Bull. Chem. Soc. Jpn.*, **57**, 2622 (1984).
11) R. Karlsson and L. Kullberg, *Chem. Scr.*, **9**, 54 (1976).
12) B. G. Cox, G. R. Hedwig, A. J. Parker, and D. W. Watts, *Aust. J. Chem.*, **27**, 477 (1974).
13) W. Libuś, M, Meçik, and H. Strzelecki, *J. Solution Chem.*, **9**, 723 (1980).
14) S. Ahrland and S. Ishiguro, unpublished data.
15) J. F. Coetzee and W. K. Istone, *Anal. Chem.*, **52**, 53 (1980).
16) J. Fergusson, *J. Chem. Phys.*, **40**, 3406 (1964).

 © 1985 The Chemical Society of Japan Bull. Chem. Soc. Jpn., 58, 1755—1760 (1985)

Dialkylcarbamato Complexes of Ni(II), Zn(II), and Cd(II)-Tetraazacycloalkanes Obtained from CO_2-Uptake, and X-Ray Structure of (Diethylcarbamato)((7*RS*,14*RS*)-5,5,7,12,12,14-hexamethyl-1,4,8,11-tetraazacyclotetradecane)nickel(II) Perchlorate

Haruko Ito† and Tasuku Ito*

Department of Applied Molecular Science, Institute for Molecular Science, Okazaki National Research Institutes, Okazaki 444

(Received January 23, 1985)

Nickel(II), zinc(II), and cadmium(II) complexes of certain tetraazacycloalkanes (L), $[M(L)](ClO_4)_2$, take up CO_2 as $R_2NCO_2^-$ to give carbamato complexes, $[M(O_2CNR_2)(L)]^+$, where L=(7*RS*,14*RS*)-5,5,7,12,12,14-hexamethyl-1,4,8,11-tetraazacyclotetradecane (L^1) for $M=Ni^{2+}$, and L=1,4,8,11-tetramethyl-1,4,8,11-tetraazacyclotetradecane (L^2) for $M=Ni^{2+}$, Zn^{2+}, and Cd^{2+}. The resulting complexes have been characterized by means of IR, and NMR or electronic spectroscopy. X-Ray analysis of $[Ni(O_2CN(C_2H_5)_2)(L^1)]ClO_4$ (monoclinic C2/c, a=15.842(3), b=13.675(3), c=13.753(2) Å, β=109.94(1)°) shows that it is a discrete six-coordinate complex with *cis*-NiO_2N_4 geometry, and the carbamato ligand is bidentate. Desired carbamato complexes were hardly obtained with $[M(L)]^{2+}$ containing tetraaza macrocyclic ligand which favors square-planar coordination. All the data indicate that carbamate ions chelate the metals, and thus use of tetraazacycloalkanes which fold readily is essential for this type of CO_2 uptake.

Considerable attention has been paid to the reaction of CO_2 with transition metal complexes in connection with the fixation and utilization of CO_2. We found that zinc(II)[1] and nickel(II)[2] complexes having certain tetraazacycloalkanes (L) take up CO_2 in basic alcohol solution as monoalkyl carbonate to give $[M(O_2COR)(L)]^+$. The reaction increases the coordination number of metal ion from four to five or six, as described below,

$$[M(L)]^{2+} + CO_2 + ROH + B \longrightarrow [M(O_2COR)(L)]^+ + HB^+$$

where B is base such as triethylamine or alkoxide. The starting complex, $[M(L)]^{2+}$, is of the square-planar type. In case of coordination of $ROCO_2^-$, geometry of $[M(L)]^{2+}$ changes to an octahedral or a trigonal bipyramidal type, giving rise to reactive vacant sites. Such a coordinately unsaturated nature of the $[M(L)]^{2+}$ complex is an important factor for the facile up-take reaction of the $ROCO_2^-$ ligand.

In the present study, similar reactions of certain nickel(II), zinc(II), and cadmium(II)-tetraazacycloalkane, in which CO_2 is taken up as carbamate ligand, $R_2NCO_2^-$, have been studied. The formation of free carbamate ion by the reaction of CO_2 with dialkylamine has been well characterized.[3] The tetraazacycloalkane ligand (L) used are (7*RS*,14*RS*)-5,5,7,12,12,14-hexamethyl-1,4,8,11-tetraazacyclotetradecane (L^1) or 1,4,8,11-tetramethyl-1,4,8,11-tetraazacyclotetradecane (L^2). They are known to fold readily to afford five or six-coordinate complexes.

Carbamato complexes reported so far are obtained either by CO_2 insertion to metal-imido bond[3-5] or by ligand-exchange reaction with the carbamato ligand which has been produced in solution.[6-11] In this sence, the present reactions are of a unique type.

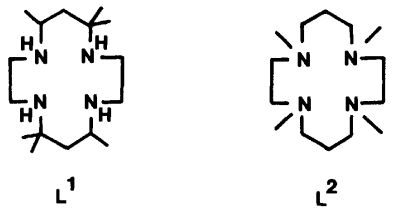

L^1 L^2

Experimental

Materials. α-$[Ni(L^1)](ClO_4)_2$,[12] $[Ni(O_2COCH_3)(L^2)](ClO_4)$,[2] $[Zn(O_2COH)(L^2)](ClO_4)$,[13] $[Zn(O_2COCH_3)(L^2)](ClO_4)$,[1] $[Cd(O_2COH)(L^2)](ClO_4)$,[13] and $[Cd(O_2COCH_3)(L^2)](ClO_4)$[13] were prepared according to the literature. The macrocyclic ligand L^2 was purchased from Strem Chemicals, Inc.

$[Ni(O_2CN(C_2H_5)_2)(L^1)](ClO_4)$ (1). CO_2 was bubbled through a suspended mixture of acetonitrile (10 cm^3) and 1.08 g (2 mmol) of α-$[Ni(L^1)](ClO_4)_2$ for a few minutes. The violet solids of α-$[Ni(L^1)(CH_3CN)_2](ClO_4)_2$ were immediately dissolved upon addition of 0.29 g (4 mmol) of diethylamine to give blue violet solution. Continuous bubbling of CO_2 resulted in the formation of violet crystals. The mixture was kept in a freezer (−10 °C) overnight. Violet crystals (0.85 g) were recrystallized from acetonitrile. Yield: 76%.

$[Ni(O_2CNR_2)(L^1)](ClO_4)$, R=$CH_3$ (2), n-C_3H_7 *(3), and* n-C_4H_9 *(4).* These complexes were prepared in a similar way, except that chloroform was used as solvent in the case of dimethylamine.

$[Ni(O_2CN(C_2H_5)_2)(L^2)](ClO_4)$ (5). CO_2 was bubbled through chloroform solution containing 0.48 g (1 mmol) of $[Ni(O_2COCH_3)(L^2)](ClO_4)$ and 0.15 g (2 m mol) of diethylamine. The color of the solution changed from green to emerald green. CO_2 was bubbled for a minute, and diethyl ether (5 cm^3) was added. Keeping the solution at −10 °C overnight, emerald green solids (0.47 g) were obtained and recrystallized from $CHCl_3$-ether. Yield 88%.

$[Ni(O_2CN(CH_3)_2)(L^2)](ClO_4)$ (6). This compound was prepared in the same way as **5** with use of dimethylamine.

$[Zn(O_2CNR_2)(L^2)](ClO_4)$, R=$CH_3$ (7), and C_2H_5 (8).

† Present address: Department of Chemistry, Aichi Kyoiku University, Kariya 448.

These were obtained either from $[Zn(O_2COCH_3)(L^2)](ClO_4)$ or $[Zn(O_2COH)(L^2)](ClO_4)$ in a similar way. To 3 cm^3 of chloroform solution containing 0.50 g of $[Zn(O_2COCH_3)(L^2)](ClO_4)$ (1 mmol), 0.073 g (1 m mol) of diethylamine was added. After 15 min, 10 cm^3 of diethylether was added and a white precipitate (0.38 g) of $[Zn(O_2CN(C_2H_5)_2)(L^2)](ClO_4)$ was obtained. Yield 70%.

$[Cd(O_2CNR_2)(L^2)](ClO_4)$, R=$CH_3$ (9), and C_2H_5 (10). These complexes were also prepared either from $[Cd(O_2COCH_3)(L^2)](ClO_4)$ or $[Cd(O_2COH)(L^2)](ClO_4)$ in a way similar to those for the corresponding zinc(II) complexes.

Elemental analyses of all the complexes prepared in this study were consistent with $[M(O_2CNR_2)(L)](ClO_4)$.

Measurements. The electronic and infrared spectra were recorded on a Hitachi 340 spectrophotometer and on a Jasco IR-810 infrared spectrophotometer, respectively. ^1H and ^{13}C NMR spectra were obtained on a Jeol FX-100 at 100 MHz and a Jeol GX-400 at 100 MHz, respectively. About 0.1 mmole of the sample was dissolved in 0.7 cm^{-3} of $CDCl_3$ for each NMR measurement.

X-Ray Analysis. A single crystal of $[Ni(O_2CN(C_2H_5)_2)(L^1)](ClO_4)$ with approximate dimensions 0.34×0.20×0.20 mm was used for X-ray study. Diffraction data were obtained on a Rigaku AFC-5 diffractometer with graphite monochromatized Mo $K\alpha$ radiation. Intensities were corrected for Lorentz and polarization factors. Crystal data are: monoclinic, C2/c, a=15.842(3), b=13.675(3), c=13.753(2) Å, β=109.94(1)°, V=2800.7(9) $Å^3$, Z=4, D_m=1.33, D_x=1.33 g cm^{-3}, μ(Mo $K\alpha$)=0.83 mm^{-1}. The structure was solved by the heavy atom method and refined by block-diagonal least-squares method. The weighting scheme, $w=[\sigma_{count}^2+(0.015|F_o|)^2]^{-1}$, was employed. All the hydrogen atoms except for methyl hydrogens of carbamate ion were located by the difference Fourier syntheses. Hydrogens for the methyl groups were located at calculated positions. In the final refinement, all the hydrogen atoms were included with the isotropic temperature factors. The final R indicies were R=0.048 and R_w=0.055 for 2193 independent reflections with $|F_o|>3\sigma(F_o)$.[14]

Calculations were carried out on the HITAC M-200H computer at the Computer Center of the Institute for Molecular Science with the Universal Crystallographic Computation Program System, UNICS III.[15]

Results and Discussion

Synthesis. There are two routes, (A) and (B) for the preparation of the carbamato complexes, $[M(O_2CNR_2)(L)]^+$.

$$(A)\quad [M(L)]^{2+} + CO_2 + 2R_2NH \longrightarrow [M(O_2CNR_2)(L)]^+ + NH_2R_2^+,$$

$$(B)\quad [M(O_2CX)(L)]^+ + R_2NH \longrightarrow [M(O_2CNR_2)(L)]^+ + HX,$$

where $X=CH_3O^-$ or OH^-. The complexes, $[Ni(O_2CNR_2)(L^1)](ClO_4)$, were obtained easily through route (A). The reaction proceeds *via* the following mechanism.

$$2NHR_2 + CO_2 \rightleftharpoons (NH_2R_2)(O_2CNR_2),$$

$$\alpha\text{-}[Ni(L^1)](ClO_4)_2 + (NH_2R_2)(O_2CNR_2) \longrightarrow [Ni(O_2CNR_2)(L^1)](ClO_4) + NH_2R_2ClO_4.$$

In the case of L^2 complexes, carbamato complexes were obtained easily and cleanly *via* route (B) from corresponding hydrogencarbonato or monomethyl carbonato complexes. The formation may occur *via* the following scheme.

$$[M(O_2CX)(L^2)]^+ \rightleftharpoons [M(L^2)]^{2+} + CO_2 + X^-,$$

$$[M(L^2)]^{2+} + CO_2 + X^- + NHR_2 \longrightarrow [M(O_2CNR_2)(L^2)]^+ + HX.$$

As to the preparation of $[Ni(O_2CNR_2)(L^1)]^+$, it may be worthwhile to point out the following facts. The complex, $[Ni(L^1)]^{2+}$, is known to exist as three isomeric α-, β-, and γ-forms.[12,16] Of these three isomers, only the α-isomer reacts readily with a bidentate ligand such as oxalate,[12] acetylacetonate,[16] acetate,[17] or tartrate[18] to form *cis*-type six-coordinate complexes with the macrocyclic ligand folded. Thermodynamically most stable isomer is of the β-type, and the α-isomer isomerizes in neutral or at much faster rate in basic media to the β-isomer. Therefore, it is necessary to add dialkylamine after CO_2 is bubbled thoroughly into the solution containing α-$[Ni(L^1)](ClO_4)_2$, when the carbamato complex is synthesized through route (A). Desired carbamato complexes were hardly obtained in the case of β-$[Ni(L^1)](ClO_4)_2$, $[Ni(meso\text{-}Me_6[14]aneN_4)](ClO_4)_2$, or $[Ni([14]aneN_4)](ClO_4)_2$, where the macrocyclic ligands take the conformation that can not fold (*meso*-$Me_6[14]aneN_4$=(7*SR*,14*RS*)-form of L^1 and $[14]aneN_4$=1,4,8,11-tetraazacyclotetradecane).

Infrared Spectra. Infrared spectra of nickel(II) and cadmium(II) complexes show strong ν_{CN} bands in the range of 1500—1520 cm^{-1}, while the corresponding absorptions of the zinc(II) complexes appear around 1580—1585 cm^{-1} (Tables 1 and 2). These frequency values of nickel(II) and cadmium(II) complexes are similar to the value of structurally determined compound **1**. Therefore, the carbamato ligands coordinate to the metals in bidente fashion. However, the values of zinc(II) complexes are somewhat higher than those of nickel(II) and cadmium(II) complexes, although they are in the normal range of bidentate carbamato ligands.[4] Rather high frequency values of zinc(II) complexes might be indicative of unsymmetric chelation of carbamate ion, since the frequency values are close to the value (ν_{CO}=1592 cm^{-1}) of $[Cd(O_2COH)(L^2)](ClO_4)$ in which two Cd-O bonds are nonequivalent and bond lengths differ by 0.152 Å.[13] Nonequivalent Zn-O bonds have also been found in six-coordinate $[Zn(O_2NC(CH_3)_2)(L^2)](ClO_4)$.[19]

Electronic Spectra of Nickel(II) Complexes. The electronic absorption spectra of nickel(II) complexes consist of three d-d bands corresponding to six-coordinate nickel(II) (Table 1). The absorption peaks of $[Ni(O_2CNR_2)(L^1)](ClO_4)$ are very close to those observed for NiL^1 complexes with *cis*-NiN_4O_2 chromophore, $[\{Ni(L^1)\}_2(d\text{-tart})(H_2O)](ClO_4)_2$,[18] and $[Ni(H_2O)_2(L^1)]Cl_2$.[20] The absorption spectra of $[Ni(O_2CNR_2)(L^2)](ClO_4)$ are quite similar to that of structurally

TABLE 1. INFRARED (IR) AND ELECTRONIC ABSORPTION (AB) SPECTRAL DATA OF $[Ni(O_2NR_2)(L)](ClO_4)$

Compounds	IR[a] $\nu_{CN,CO}/cm^{-1}$		AB[b] $\nu_{max}(\varepsilon)$		
$[Ni(O_2CN(CH_3)_2)L^1](ClO_4)$	1540[m]	1520	10.4(16)	17.4(20)	27.3(28)
$[Ni(O_2CN(C_2H_5)_2)L^1](ClO_4)$	1540[m]	1520	10.4(17)	17.4(20)	27.3(29)
$[Ni(O_2CN(n\text{-}C_3H_7)_2)L^1](ClO_4)$	1525	1510	10.4(17)	17.4(20)	27.3(29)
$[Ni(O_2CN(n\text{-}C_4H_9)_2)L^1](ClO_4)$	1530[sh]	1510	10.4(16)	17.4(28)	27.3(28)
$[Ni(O_2CN(CH_3)_2)L^2](ClO_4)$	1550	1515	9.52(15)	15.7(27)	25.7(52)
$[Ni(O_2CN(C_2H_5)_2)L^2](ClO_4)$	1530[m]	1520	9.39(13)	15.8(34)	25.7(48)

a) Symbols m, and sh stand for medium absorption and shoulder band, respectively. b) in $CHCl_3$. ν_{max} and ε are given in $10^3\,cm^{-1}$ and in $M^{-1}cm^{-1}$, respectively (1 M=1 mol dm^{-3}).

TABLE 2. INFRARED,[a] ^1H AND ^{13}C NMR DATA[b] OF $[Zn(O_2CNR_2)(L^2)](ClO_4)$ AND $[Cd(O_2CNR_2)(L^2)](ClO_4)$.

Compounds	ν_{CN}/cm^{-1}[c]		^1H NMR[d] -CH$_3$	-CH$_2$-	^{13}C NMR[e] -CH$_3$	-CH$_2$-	C-C-C	N-CH$_3$	N-CH$_2$-	N-CH$_2$-
$[Zn(O_2CN(CH_3)_2)L^2](ClO_4)$	1608[m]	1583	2.89[s]		37.0		21.5	44.8	56.8	60.3[b]
$[Zn(O_2CN(C_2H_5)_2)L^2](ClO_4)$	1610[m]	1585	1.08[t]	3.28[q]	14.5	41.5	21.5	44.9	56.9	60.4[b]
$[Cd(O_2CN(CH_3)_2)L^2](ClO_4)$	1525[sh]	1515	2.90[s]		37.5		22.3	44.5	57.0	61.2[b]
$[Cd(O_2CN(C_2H_5)_2)L^2](ClO_4)$	1515[sh]	1510	1.07[t]	3.27[q]	14.3	42.2	22.3	44.5	57.0	61.2[b]

a) Nujol mull. b) In $CDCl_3$, TMS internal standard. c) Symbols m, and sh stand for medium absorption, and shoulder band, respectively. d) Alkyl groups in the carbamato ligand. e) b: broad.

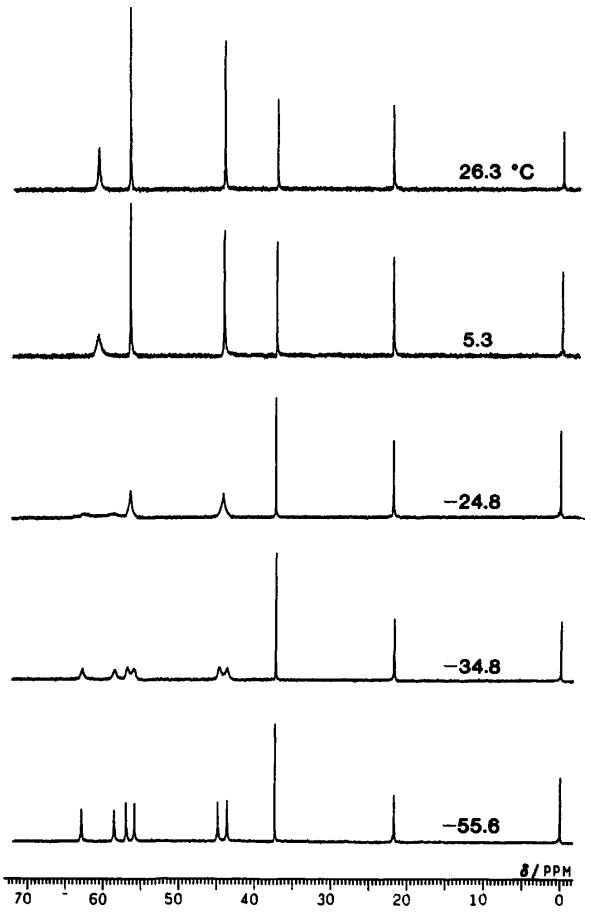

Fig. 1. The temperature dependence of ^{13}C NMR spectra of $[Cd(O_2CN(CH_3)_2)(L^2)](ClO_4)$ in $CDCl_3$. TMS is used as an internal standard.

characterized $[Ni(O_2NCH(CH_3))(L^2)](ClO_4)$, the coordination geometry of which is of the *cis*-NiN_4O_2 type.[19] The X-ray analysis of the latter complex revealed that the *N*-methyl orientation is of the three-up-one-down type in terms of Bosnich's notation.[21] The same *N*-methyl orientation may be assigned to the present $[Ni(O_2CNR_2)(L^2)]^+$ complexes from the following observations as well as the absorption data. Both $[Ni(O_2CNR_2)(L^2)](ClO_4)$ and $[Ni(O_2NCH(CH_3))(L^2)](ClO_4)$ show a single ligand field band at 502 nm in dilute perchloric acid solution, where they decompose to square-planar four coordinate species, $[Ni(L^2)]^{2+}$. On the other hand, the ligand field absorption of the complex, $[Ni(L^2)](ClO_4)_2$, prepared from nickel(II) perchlorate and L^2 (the four-up form),[22] and of the complex prepared from *N*-methylation of the two-up-two-down form of $[Ni([14]aneN_4)]^{2+}$,[23] occurs at 514 and 493 nm, respectively, in the same solvent.

NMR Spectra. ^1H and ^{13}C NMR spectral data for $[Zn(O_2CNR_2)(L^2)](ClO_4)$ and $[Cd(O_2CNR_2)(L^2)](ClO_4)$ are given in Table 2. Spectral patterns, chemical shifts, and relative intensity relations are consistent, in all respects, with $[M(O_2CNR_2)(L^2)]^+$. In all the compounds studied, two alkyl groups of the carbamato ligand are pairwise equivalent. Interestingly, the ligand L^2 shows only four sharp signals in ^{13}C NMR spectra at room temperature, that is, one-forth of the ligand is magnetically independent on ^{13}C NMR time scale. When the temperature is lowered, a sharp singlet due to the central carbon of the six-membered chelate ring and signals of the carbamato ligand remained unchanged even at 217 K but the remaining three absorptions of L^2 broaden and finally each splits into two signals. Figure 1 shows such an example for $[Cd(O_2CN(CH_3)_2)(L^2)](ClO_4)$. The spectral pattern at 217

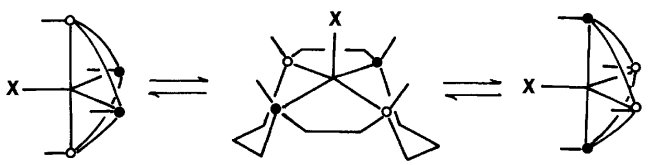

trigonal bipyramidal square pyramidal trigonal bipyramidal

K indicates that the complex adopts C_2 symmetry. A very similar temperature dependence was also observed for $[Zn(O_2CN(CH_3)_2)(L^2)](ClO_4)$ in $CDCl_3$. This observation can be interpreted by the dynamic process shown above, as characterized well for $[ZnX(L^2)]^+$, where X is Cl^- or NCS^-,[24] and $[Cd(L^2)](NO_3)_2$.[25] The activation parameters of the dynamic processes were obtained by full line-shape analyses with use of DNMR3 program.[26] The results were $\Delta H^*=34\pm3$ and 33 ± 4 kJ mol^{-1}, and $\Delta S^*=-63\pm13$ and -61 ± 20 J deg^{-1} mol^{-1}, for zinc(II) and cadmium(II) complex respectively. The similarity of the activation parameters of both zinc(II) and cadmium(II) supports the same dynamic process.[25]

Although the infrared data indicate the formation of six-coordinate complex with the chelated carbamato ligand, the occurrence of the dynamic process suggests that the coordination geometry about the metal can be taken as the trigonal bipyramidal type. The two donor oxygens of the carbamato ligand occupy an apex of the trigonal bipyramid as shown below. In

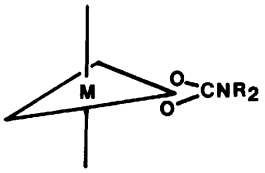

fact, X-ray structural analyses of $[Zn(O_2NC(CH_3)_2)(L^2)](ClO_4)$,[19] $[Cd(O_2COH)(L^2)](ClO_4)$,[13] and $[Cd(NO_3)(L^3)]_2[Cd(NO_3)_4]$,[27] where L^3 denotes 1,5,9,13-tetramethyl-1,5,9,13-tetraazacyclohexadecane, revealed that their coordination geometries are very similar to the structure shown above and are described better as pseudo trigonal bipyramidal. At the low temperature, the dynamic process is frozen and the complex is considered to have the trigonal bipyramidal geometry with C_2 symmetry, where the carbamato ligand chelates the metal symmetrically through two oxygen atoms.[28] In the NMR studies of the L^2 complexes of zinc(II) and cadmium(II), there were no indications for the presence of the three-up-one-down form found for the

Table 3. Atomic coordinates ($\times10^4$) and thier standard deviations

Atom	x	y	z
Ni†1	0	2288(0)	2500
Cl†1	0	−1302(1)	2500
N(L)†1	0	5067(3)	2500
C(L)†1	0	4080(3)	2500
O(L)	517(2)	3612(2)	3279(2)
Cl(L)	563(3)	5606(3)	3380(4)
C2(L)	139(7)	5914(7)	4110(5)
N(1)	−901(2)	1340(2)	1447(2)
N(4)	748(2)	2205(2)	1487(2)
C(2)	−682(3)	1439(3)	493(3)
C(3)	322(3)	1397(4)	761(3)
C(5)	1756(3)	2204(4)	1898(3)
C(6)	2075(3)	1412(3)	2730(3)
C(7)	1870(3)	1515(3)	3730(3)
Cl(M)	2076(3)	3197(4)	2318(4)
C2(M)	2139(4)	1992(5)	1031(5)
C3(M)	2489(3)	825(4)	4542(4)
OP(1)†1,3	−744(6)	−998(7)	1672(7)
OP(2)†1,3	375(8)	−2078(6)	2088(7)
OP(3)†1,3	−548(7)	−678(8)	2929(8)
OP(4)†2,3	−68(12)	−601(10)	3239(10)
OP(5)†2,3	−679(11)	−1818(11)	1814(12)

†1 Occupancy factor is 0.5. †2 Occupancy factor is 0.25. †3 Perchlorate oxgens (OP) were found to be in disorder, and were located at five major positions. The occupancy factors were tentatively determined so that their thermal parameters became nealy equal.

Table 4. Bond lengths (l/Å) and bond angles (ϕ/°) within the complex cation and their estimated standard deviations

Ni	-O(L)	2.121(2)	
Ni	-N(1)	2.099(3)	
Ni	-N(4)	2.117(3)	
O(L)	-C(L)	1.276(3)	
C(L)	-N(L)	1.351(6)	
N(L)	-Cl(L)	1.438(5)	
Cl(L)	-C2(L)	1.449(11)	
N(1)	-C(2)	1.472(6)	
N(1)	-C(7′)	1.489(5)	
N(4)	-C(3)	1.488(5)	
N(4)	-C(5)	1.501(5)	
C(2)	-C(3)	1.507(7)	
C(5)	-C(6)	1.530(6)	
C(6)	-C(7)	1.523(7)	
C(5)	-Cl(M)	1.495(7)	
C(5)	-C2(M)	1.539(9)	
C(7)	-C3(M)	1.534(6)	

O(L)	-Ni	-O(L′)	62.8(1)	C(2)	-N(1)	-C(7′)	112.5(3)
O(L)	-Ni	-N(1)	158.5(1)	Ni	-N(4)	-C(3)	104.7(3)
O(L)	-Ni	-N(4)	99.9(1)	Ni	-N(4)	-C(5)	120.9(2)
O(L)	-Ni	-N(1′)	97.1(1)	C(3)	-N(4)	-C(5)	115.7(3)
O(L)	-Ni	-N(4′)	85.4(1)	N(1)	-C(2)	-C(3)	109.2(3)
N(1)	-Ni	-N(1′)	103.7(1)	N(4)	-C(3)	-C(2)	109.6(4)
N(1)	-Ni	-N(4)	85.1(1)	N(4)	-C(5)	-C(6)	108.7(4)
N(1)	-Ni	-N(4′)	91.1(1)	N(4)	-C(5)	-Cl(M)	108.8(4)
N(4)	-Ni	-N(4′)	173.9(1)	N(4)	-C(5)	-C2(M)	111.0(3)
Ni	-O(L)	-C(L)	88.7(2)	C(6)	-C(5)	-Cl(M)	111.8(3)
O(L)	-C(L)	-O(L′)	119.9(4)	C(6)	-C(5)	-C2(M)	109.2(4)
O(L)	-C(L)	-N(L)	120.1(2)	Cl(M)	-C(5)	-C2(M)	107.4(4)
C(L)	-N(L)	-Cl(L)	120.8(2)	C(5)	-C(6)	-C(7)	119.4(4)
Cl(L)	-N(L)	-Cl(L′)	118.4(4)	C(6)	-C(7)	-C3(M)	108.7(4)
N(L)	-Cl(L)	-C2(L)	115.6(5)	C(6)	-C(7)	-N(1′)	111.3(3)
Ni	-N(1)	-C(2)	104.3(2)	C3(M)	-C(7)	-N(1′)	112.8(4)
Ni	-N(1)	-C(7′)	115.7(2)				

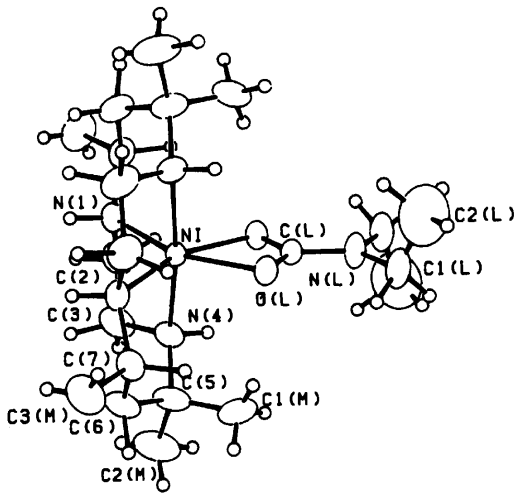

Fig. 2. ORTEP view of $[Ni(O_2CN(C_2H_5)_2)L^1]^+$ along with the atom numbering scheme.

corresponding nickel(II) complexes.

X-Ray Structure. The crystal structure of $[Ni(O_2CN(C_2H_5)_2)(L^1)](ClO_4)$ has been determined by X-ray analysis. Atomic parameters and relevant bond lengths and angles are given in Tables 3 and 4, respectively. Figure 2 shows an ORTEP view of the complex cation along with the atom numbering scheme.

Three types of coordination bonding modes are known for carbamato ligand:[4-11] (1) unidentate, (2) bidentate chelate, and (3) bridging. The present X-ray analysis revealed that the carbamato ligand adopts the type (2) structure.

The complex has crystallographic C_2 symmetry, the C_2-axis passing through Ni, C(L) and N(L) atoms. The metal-donor atom set, NiN_4O_2, is a distorted octahedron as is seen from the bond angles about Ni (Table 4). The Ni–N distances within NiN_2O_2 plane are slightly shorter than those of the axial Ni–N bonds. The C(L)–N(L) bond is shortened to 1.351(6)Å evidently through the influence of the $-CO_2^-$ group and has partial double bond character. The bond angles around C(L) and N(L) are approximately 120°, and the NiO_2CNC_2 moiety is planar within experimental error.

As has often been found for other carbamato complexes, methyl groups of the carbamato ligand have large thermal parameters due to the disordered orientation of the ethyl groups.[8] Short distances, N(L)–Cl(L)= 1.44(1) and Cl(L)–C2(L)=1.45(1)Å arise likely from such a situation.

All the present results including IR, NMR, electronic spectral and X-ray data indicate that the carbamato complexes obtained in this study have coordination geometry of *cis*-MO_2N_4 type. The desired carbamato complexes $[M(O_2CNR_2)(L)]^+$ were obtained with the tetraazacycloalkanes such as L^1 and L^2 which are known to fold readily, whereas tetraaza macrocyclic ligands which favor square-planar coordination did not work nicely. From these results, it is concluded that use of macrocyclic ligands of the former type is essential for the $R_2NCO_2^-$ uptake reaction by $[M(L)]^{2+}$ complexes. It is in contrast to the case of monoalkyl carbonato complex, $[M(O_2COR)(L)]^+$, formed similarly upon CO_2 uptake in basic alcohol.[1,2]

For the formation of $[M(O_2CNR_2)(L)]^+$ as well as $[M(O_2COR)(L)]^+$ unsaturated coordination of the starting complex $[M(L)]^{2+}$ is very important. Nickel(II), zinc(II) and cadmium(II) fulfill the required coordination behavior and work nicely.

The present study was supported by Grant-in-Aid for Scientific Research No. 58470039 from the Ministry of Education, Science and Culture.

References

1) M. Kato and T. Ito, *Inorg. Chem.*, **24**, 504 (1985).
2) M. Kato and T. Ito, Presented at 34th Meeting on Coordination Chemistry, Nagaoka, Oct. 1984, 3A05.
3) For example, A. Jensen, M. B. Jensen, and C. Faurholt, *Acta Chem. Scand.*, **8**, 1129 (1954); G. Astarita, G. Marrucci, and F. Gioia, *Chem. Eng. Sci.*, **19**, 95 (1964).
4) M. H. Chisholm and M. W. Extine, *J. Am. Chem. Soc.*, **99**, 782 (1977).
5) M. H. Chisholm and M. W. Extine, *J. Am. Chem. Soc.*, **99**, 792 (1977).
6) M. H. Chisholm, F. A. Cotton, M. W. Extine, and D. C. Rideout, *Inorg. Chem.*, **17**, 3536 (1978).
7) T. V. Ashworth, M. Nolte, and E. Singleton, *J. Organomet. Chem.*, **121**, C57 (1976).
8) F. Calderazzo, G. Dell'Amico, R. Netti, and M. Pasquali, *Inorg. Chem.*, **17**, 471 (1978); F. Calderazzo, G. Dell' Amico, M. Pasquali, and G. Perego, *ibid.*, **17**, 474 (1978).
9) F. Ozawa, T. Ito, and A. Yamamoto, *Chem. Lett.*, **1979**, 735.
10) T. Yamamoto, M. Kubota, and A. Yamamoto, *Bull. Chem. Soc. Jpn.*, **53**, 680 (1980).
11) D. B. Dell'Amico and F. Calderazzo, *J. Chem. Soc., Dalton Trans.*, **1984**, 647.
12) L. G. Warner and D. H. Busch, *J. Am. Chem. Soc.*, **91**, 4092 (1969).
13) H. Ito and T. Ito, to be published elsewhere.
14) Tables of hydrogen atomic coordinates, anisotropic thermal parameters, and observed and calculated structure factors are kept in the office of the Chemical Society of Japan (Document No. 8527).
15) T. Sakurai and K. Kobayashi, *Rikagaku Kenkyusho Hokoku*, **55**, 69 (1979).
16) N. F. Curtis, D. A. Swann, and T. N. Waters, *J. Chem. Soc., Dalton Trans.*, **1973**, 1963.
17) P. O. Whimp, M. F. Bailey, and N. F. Curtis, *J. Chem. Soc., A*, **1970**, 1956.
18) H. Ito, J. Fujita, K. Toriumi, and T. Ito, *Bull. Chem. Soc. Jpn.*, **54**, 2988 (1981).
19) H. Ito and T. Ito, presented at 34th Meeting on Coordination Chemistry, Nagaoka, Oct. 1984, 1PA10.
20) H. Ito, M. Sugimono, and T. Ito, *Bull. Chem. Soc. Jpn.*, **55**, 1971 (1982).
21) B. Bosnich, M. L. Tobe, and G. A. Webb, *Inorg. Chem.*, **4**, 1100 (1965).
22) E. K. Barefield and F. Wagner, *Inorg. Chem.*, **12**, 2435

(1973).
23) F. Wagner, M. T. Mocella, M. J. D'Aniello, Jr., A. H. J. Wang, and E. K. Barefield, *J. Am. Chem. Soc.*, **96**, 2625 (1974).
24) N. W. Alcock, N. Herron, and P. Moore, *J. Chem. Soc. Dalton, Trans.*, **1978**, 1282.
25) N. W. Alcock, E. H. Curson, N. Herron, and P. Moore, *J. Chem. Soc. Dalton Trans.*, **1979**, 1987.
26) B. Binsch, *Top. Stereochem.*, **3**, 97 (1968).
27) E. Farkas, I. Sovago, T. Kiss, and A. Gergely, *J. Chem. Soc. Dalton Trans.*, **1984**, 611.
28) Even at the low temperature, there is a possibility such that the carbamato ligand is coordinated in a unidentate fashion through one oxygen atom and bonded and non-bonded oxygen atoms exchange rapidly.[4]

 © 1985 The Chemical Society of Japan Bull. Chem. Soc. Jpn., 58, 1761—1766 (1985)

Formation of Blocking Contacts at *p*-Type Porphyrin/ITO or Electrolyte Junctions

Kazuo YAMASHITA,* Yutaka HARIMA, and Yuhei MATSUMURA
Department of Environmental Science, Faculty of Integrated Arts and Sciences, Hiroshima University, Hiroshima 730
(Received December 25, 1984)

Energetics of ITO/*p*-type porphyrin/electrolyte interfaces are discussed on the basis of photoelectrochemical and photovoltaic measurements. When sensitized by a layer of 5,10,15,20-tetraphenylporphyrinatomagnesium(II)(MgTPP), the indium-tin oxide (ITO) electrode acts as only a photocathode in an aqueous electrolyte solution. However, the ITO electrode modified with a film of ZnTPP, CuTPP or H_2TPP having oxidation potential more positive than that of MgTPP acts as not only a photocathode but also a photoanode, depending on the electrode potential and the direction of irradiation on the ITO/porphyrin electrode. The cathodic component in the photocurrents is attributed to the downward band-bending in a space charge layer at the porphyrin/electrolyte (blocking) contact and the anodic component to that at the ITO/porphyrin (blocking) contact. The upward band-bending, on the contrary, is found inefficient in producing charge carriers, because the accumulation layer is conducting (ohmic) for majority carriers (holes). The porphyrin/electrolyte junction shows certain similarities to an ITO or metal/porphyrin (semiconductor) junction. However, it should be noted that a Helmholtz double layer exists at the porphyrin/electrolyte interface. The results are rationalized from the energy levels of the porphyrin films, ITO and the redox couple solutions with due regard to the orientation of water dipoles at the porphyrin surface.

A recent interest in the dye sensitization research has centered on modelling the primary energy conversion processes in photosynthesis and on the application to conversion of solar energy into electrical and/or chemical energy.[1] The organization of dye and substrate can be varied over a wide range and can therefore be optimized with respect to the quantum efficiency of the sensitization effect. Hence, organic materials such as phthalocyanines,[2-6] merocyanines[7-10] and porphyrins[11-19] have received much attention as the promising sensitizers.

Previously we have demonstrated that the most efficient photoelectrochemical cells based on synthetic *p*-type porphyrin films on Al reach power conversion efficiencies of 1% and generate photovoltages greater than 1 V.[11,20] The dark- and photo-electrochemical properties of the cells are attributed to the MIS Schottky barrier consisting of Al-Al_xO_y-porphyrin, where conduction and valence band (CB and VB) edges of the porphyrin bend downwards under short-circuit conditions. Furthermore we have noted that a blocking contact is not formed at a *p*-type porphyrin/Ag or Pt junction. Some workers, however, have shown different views from ours.[14-16] For instance, they have attributed the cathodic photocurrents at the irradiated Pt/*p*-type porphyrin electrodes to the formation of blocking contacts at the Pt/porphyrin junctions and described that the upward band-bending in a space charge layer at the porphyrin/Pt interface is effective in producing charge carriers.

In order to build more efficient devices using porphyrin films as sensitizers it is necessary and important to solve the inconsistency and to obtain a consensus. This paper represents the energetics of ITO/*p*-type porphyrin/electrolyte interfaces and clarifies the conditions under which a blocking or an ohmic contact is formed at the junction.

Experimental

Metal-free porphyrin [5,10,15,20-tetraphenylporphyrin (H_2TPP)] and its metal derivatives (MgTPP, ZnTPP, and CuTPP) were purchased from Strem Chemicals and were purified by chromatography (Woelm alumina grade I) followed by recrystallization. These porphyrins have been characterized as *p*-type organic semiconductors.[11,14,19] *p*-Benzoquinone (BQ) from Katayama Chemicals was used after sublimation. Other chemicals used were of reagent grade. An indium-tin oxide (ITO) film was used as substrate for the porphyrin electrode because of the superiority of light-transparency and the metallic property.[21,22] An ITO film was produced on a piece of cleaned slide glass (Matsunami No. 0) by means of a Tokuda CFS-8EP closed field sputtering apparatus. O_2 partial pressure of 1.3×10^{-2} Pa and Ar partial pressure of 6.7×10^{-1} Pa were employed for fabrication of the ITO electrode. The thickness of ITO films was about 100 nm. The electric resistance was about a few hundreds ohm/square and the transparency larger than 80% in the visible region of the solar spectrum. Films of the porphyrins (100—300 nm thick) and metals (Au, Ag, and Al, *ca.* 10 nm thick) were prepared by sublimation and evaporation at pressure 10^{-4} Pa, respectively. The porphyrin-coated ITO or metal electrode was insulated from the electrolyte with epoxy resin except for the portion to be exposed to light. The photoelectrochemical measurements of the porphyrin electrodes were carried out using a two or three electrode system. For potentiostatic steady-state measurements a coiled platinum wire was used as the auxiliary electrode and a saturated calomel electrode (SCE) served as the reference. Unless otherwise stated, dissolved oxygen in solution was removed by bubbling Ar gas. A custom-built potentiostat was used to obtain the steady-state current-potential curves. Voltages and currents produced by the cells were measured with a Takeda TR 8651 electrometer. Applied voltages were provided by a Takeda TR 6141 voltage supply and monitored with a Takeda TR 6855 digital multimeter. The light source consisted of a 45 W tungsten-halogen lamp and a Baush-Lomb Cat. No. 33-86-76 monochromator. An Ushio

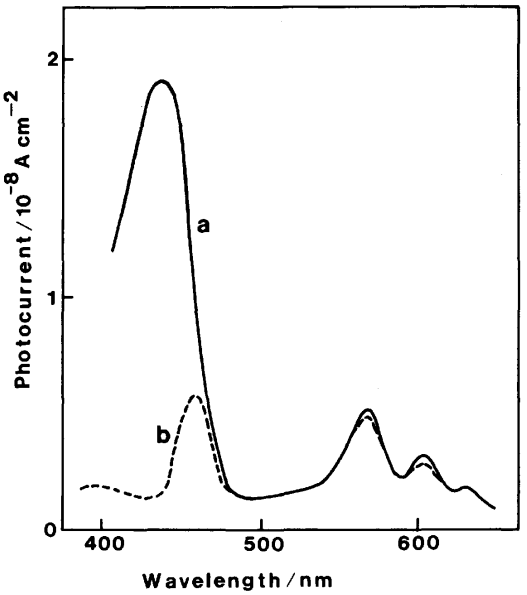

Fig. 1. Action spectra of short-circuit photocurrents of the ITO/MgTPP (*ca.* 200 nm thick)/HQ-BQ, phosphate buffer/Pt cell. (a) and (b) are obtained by irradiation of the MgTPP/electrolyte and ITO/MgTPP junctions.

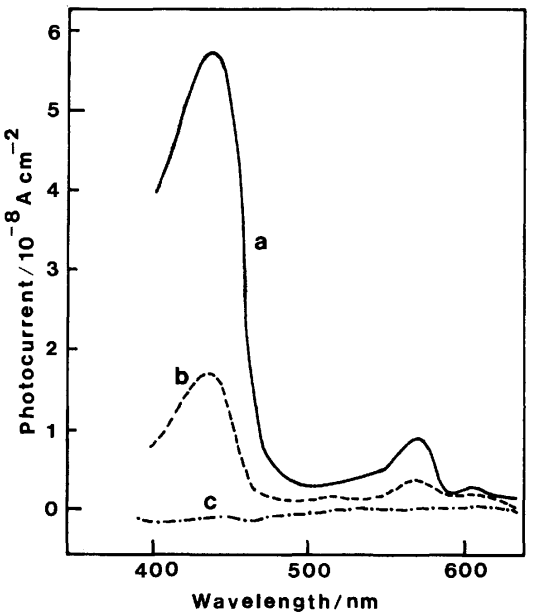

Fig. 2. Voltage dependence of the photocurrent action spectrum for the ITO/MgTPP/HQ-BQ/Pt cell. (a), (b), and (c) are obtained by irradiation of the MgTPP/electrolyte junction at voltages of −0.21 V, 0 V and +0.2 V, being applied to the ITO electrode.

500 W xenon lamp was also used as light source with a Toshiba KL-43 interference filter. Light intensity was measured with a calibrated Eppley thermopile of 16 junctions. Optical absorption spectra were recorded on a Shimadzu UV-240 spectrometer. All measurements were carried out at room temperature.

Results and Discussion

Figure 1 shows action spectra of short-circuit photocurrents for the ITO/MgTPP/electrolyte/Pt cell. The electrolyte was a phosphate buffer [0.025 M (1 M=1 mol dm^{-3}) KH_2PO_4, 0.025 M Na_2HPO_4 and 0.1 M KCl: pH 6.87], containing 1 mM hydroquinone (HQ) and 1 mM BQ. Curves (a) and (b) were obtained by irradiation of the MgTPP/electrolyte and ITO/MgTPP interfaces, respectively. The photocurrents have been normalized in such a way that the intensity of the incident light on the interface between MgTPP and ITO or electrolyte is constant (about 30 μW cm^{-2}) in consideration of the absorption of light with ITO or the electrolyte and the reflection at the glass/ITO or electrolyte interface. The photocurrents flowed from Pt to ITO through the MgTPP/electrolyte interface regardless of the wavelength and the direction of irradiation. Taking account of this and the finding that the action spectrum (a) resembles the optical absorption spectrum of a MgTPP film, the difference in shape between the action spectra (a) and (b) is attributable to an optical filtering effect of the MgTPP phase.[8] Namely it shows that the photocurrent is generated *via* the excited states of the porphyrin and that only the light absorbed near the blocking (electrolyte) contact is effective in producing charge carriers.[23,24] This was confirmed by the voltage dependence of the photocurrent action spectrum obtained under irradiation of the MgTPP/electrolyte interface (Fig. 2). When a negative bias voltage was applied to the ITO electrode, the cathodic photocurrent was strikingly enhanced. On the contrary, when a positive voltage was applied the photocurrent was reduced to zero.

In case of the ITO electrode modified with ZnTPP, which is uneasily oxidized in comparison with MgTPP, there was a wavelength region of around the peak of a Soret band (440 nm) of the ZnTPP film, where small anodic photocurrents were observed by irradiation of the ITO/ZnTPP interface under short-circuit conditions (Table 1). This shows the existence of a small Schottky barrier (blocking contact) at the ITO/ZnTPP junction and coincides with the dark current-voltage characteristics of the ITO/ZnTPP/Ag cell (Fig. 3). The observed rectification effect is due to the blocking contact at the ITO/ZnTPP junction, since the ZnTPP/Ag junction has been found an ohmic contact.[11,12]

For ITO electrodes modified with films of CuTPP and H_2TPP with oxidation potentials more positive than those of MgTPP and ZnTPP, both cathodic and anodic photocurrents were clearly observed, depending on the direction of irradiation on the ITO/porphyrin electrodes (Table 1). This indicates that blocking contacts are formed at both junctions of the porphyrin with ITO and the electrolyte and thus the ITO/porphyrin electrodes act as photocathodes and also as photoanodes. The observation of the anodic photocurrents seemingly depends on the oxidation potentials of the porphyrins.

Figure 4 illustrates energy levels of ITO, redox agents and porphyrin films studied. The free energy

TABLE 1. SUMMARY OF THE PHOTORESPONSE OF THE PORPHYRIN FILMS ON ITO IN THE ITO/PORPHYRIN/HQ–BQ, PHOSPHATE BUFFER/Pt CELL

Porphyrin	λ_{max}[a]/nm	$h\nu$→ITO/porphyrin	porphyrin/electrolyte←$h\nu$	$E_{1/2}$[b]/V *vs.* SCE
MgTPP	445	~	—[c]	0.61
Zn TPP	440	+[c]	—	0.78
Cu TPP	430	++	—	0.96
H_2 TPP	445	++	—	1.04

a) Peak of a Soret band of a porphyrin solid film, at which irradiation is carried out. b) Oxidation at Pt in CH_2Cl_2 with 0.1 M tetrabutylammonium perchlorate. c) Plus and minus signs denote anodic and cathodic photocurrents, respectively. Double plus and minus signs mean stronger photoresponse.

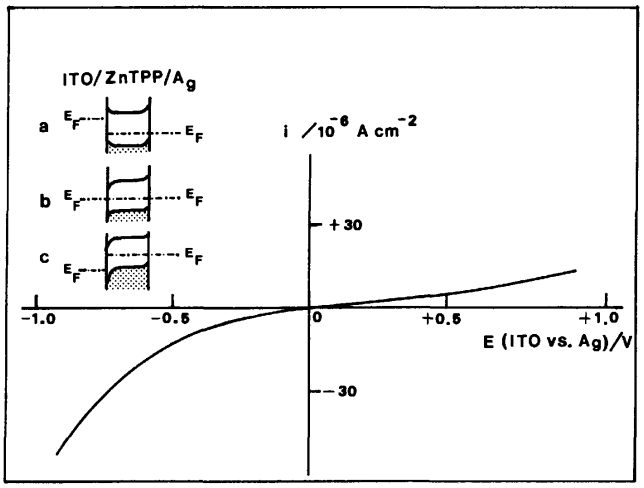

Fig. 3. Dark current-voltage curve for the ITO/ZnTPP/Ag cell. The inset shows the band-bending at the ITO/ZnTPP/Ag contact at (a) negative, (b) zero and (c) positive bias voltages.

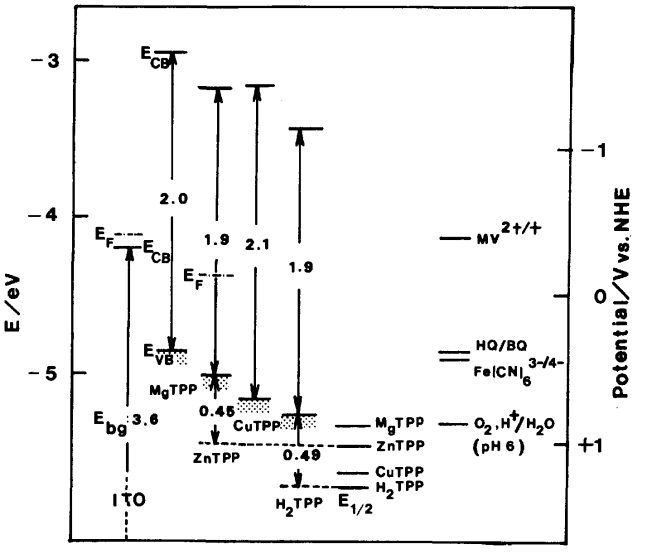

Fig. 4. Energy levels of ITO, porphyrin films and redox systems.

of electrons in a semiconductor or a metal is characterized by the Fermi level (E_F). The Fermi level in ITO lies just above the CB edge because of degeneracy of the *n*-type semiconductor. Hence, the electric behavior of ITO is similar to that of a metal. The E_F in a ZnTPP film has been found slightly closer to the VB, *viz.* E_{VB}=−5.0 eV, E_F=−4.3 eV and E_{CB}=−3.0 eV from the vacuum level.[14] The E_{VB} for a H_2TPP film is located at 5.2 eV below the vacuum level.[25] The values of E_{VB} of MgTPP and CuTPP films were estimated from the first ring oxidation potentials ($E_{1/2}$) obtained for the porphyrins in nonaqueous solutions assuming that the VB edges were situated at potentials 0.47 V higher than the oxidation potentials.[6] The energy difference of 0.47 eV was the average for experimental results (0.45 eV for ZnTPP and 0.49 eV for H_2TPP). The Fermi levels for MgTPP, CuTPP, and H_2TPP films might be about 0.7 eV higher than their respective VB edges as observed for ZnTPP film. The values of optical band gaps for the porphyrins were estimated from the spectral properties of the porphyrin films.

If a porphyrin film, whose Fermi level lies below that for ITO, is brought into contact with ITO, the Fermi levels will be equilibrated by electron transfer from the ITO to the porphyrin. This results in the formation of a space charge layer in the porphyrin, while counter charge remains very close to the interface in the ITO layer. Thus a blocking contact is formed at the ITO/porphyrin junction, where the CB and VB edges bend downwards, and leads to the production of anodic photocurrents. The anodic photocurrent at the irradiated ITO/porphyrin electrode depended upon the relative position of the Fermi levels of ITO and the porphyrin. For example, no distinct anodic photocurrent is observed by irradiation of the ITO/MgTPP electrode (Table 1), because the Fermi levels of ITO and MgTPP are almost the same. For a film of ZnTPP, CuTPP or H_2TPP having oxidation potential more positive than that of MgTPP, the Fermi level lies below that of ITO and the blocking contact must be formed at the ITO/porphyrin junction. In effect, the anodic photocurrents were observed. An upward band-bending, in principle, may be produced at a contact of ITO with a *p*-type porphyrin, of which Fermi level lies above that of ITO. However, such a contact should be ohmic for majority carriers (holes), unless surface states exist. This may be inferred from the finding that no obvious cathodic photocurrent is observed for the ITO/ZnTPP/Ag cell at negative bias voltages applied to the ITO electrode, where the upward band-bending is formed as shown in the inset of Fig. 3.

The Fermi level in an electrolyte solution corresponds to the redox potential of a redox couple in-

volved in the electrolyte.[26] Apparently, judging from the positions of the Fermi levels for the porphyrin films studied and the redox potential of the HQ/BQ couple (Fig. 4), the porphyrin/electrolyte contacts are supposed to be ohmic because the Fermi levels of the porphyrins lie above the redox potential of the HQ/BQ couple and at equilibrium upward band-bendings are produced at the porphyrin/electrolyte junctions. However, actually the cathodic photocurrents are observed by irradiation of the porphyrin/electrolyte interfaces. In view of the fact the photoelectric behaviors of the ITO/porphyrin contacts can reasonably be explained in terms of the energy diagram of Fig. 4, the inconsistency between the prediction and the experimental result reminds us of two plausible reasons. One is an existence of surface states at the porphyrin/electrolyte interface, which causes Fermi level pinning[27] and the other is that the energy levels of the porphyrin films in aqueous solution might be different from those *in vacuo*.

At first, we consider a few points about the possibility of the Fermi level pinning at the porphyrin/electrolyte interface. The positions of the Fermi level and band edges at the surface of the porphyrin contacting the electrolyte can be estimated from measurement of the flat-band potential (E_{fb}). Figure 5 illustrates the steady-state photocurrent-potential curves for the ITO/ZnTPP electrode in aqueous electrolyte solutions. Without oxdizing agents, only small photocurrents were observed over the potential range of −0.5 V to +1.0 V *vs.* SCE under irradiation of the ZnTPP/electrolyte interface at 430 nm [curve (a)]. In this case, the ZnTPP film used was so thick (*ca.* 200 nm) that the light hardly reached the ITO/ZnTPP interface through the porphyrin phase. The cathodic photocurrents obtained by irradiation of the ZnTPP/electrolyte interface were enhanced by the addition of oxidizing agents such as O_2, $[Fe(CN)_6]^{3-}$, BQ, methylviologen (MV^{2+}), 2,3-dichloro-5,6-dicyano-*p*-benzoquinone and $Cr_2O_7^{2-}$. The onset potential (E_{op}) of about +0.5 V *vs.* SCE was almost independent of the oxidizing species except for MV^{2+} and of pH in the range 5.5—9.0. It is well known that the surface states formed at inorganic semiconductors sometimes bring about the Fermi level pinning, which results in an output photovoltage independent of the redox potential of an electrolyte.[27] However, this may be not the case for the porphyrin electrode since the E_{op} of the ZnTPP electrode is found independent of the kind of the oxidizing species ranging in potential from +0.2 V to +0.7 V *vs.* NHE as described above. In other words, the band edges of the porphyrin films are fixed at the porphyrin/electrolyte interfaces.[28]

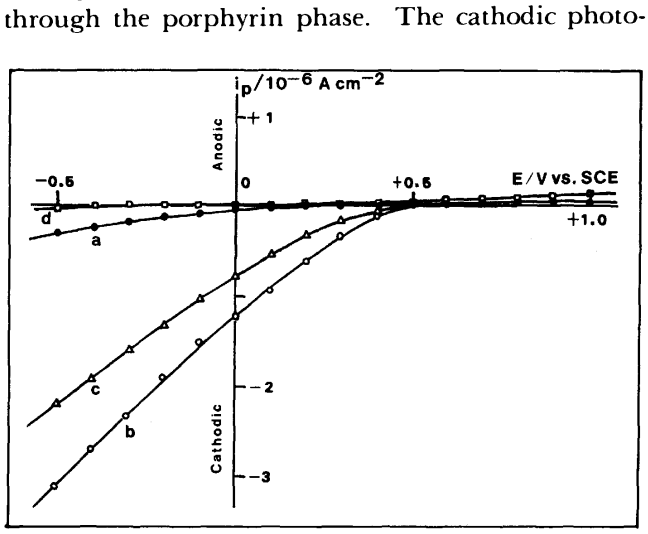

Fig. 5. Potential dependence of the steady-state photocurrent for the ITO/ZnTPP electrode. (a), (b) and (c) are obtained by irradiation of the ZnTPP/electrolyte junction, and (d) obtained by irradiation of the ITO/ZnTPP junction. (a): acetate buffer (1 M CH_3COOH and 1 M CH_3COONa, pH 4.7); (b): in (a) +0.2 mM O_2; (c) and (d): 0.1 M KCl+0.2 mM O_2.

Secondly, we discuss the difference in energy levels of the porphyrin films *in vacuo* and in aqueous electrolyte solution. The E_{op} of about +0.5 V is probably near the flat-band potential at the ZnTPP/electrolyte interface, from which the Fermi level of the ZnTPP film in the aqueous electrolyte solution is estimated to be about 0.9 eV lower than that (−4.3 eV) *in vacuo*. The contribution of the Helmholtz double layer, especially an inner Helmholtz layer, should be taken into consideration to account for the energy difference. In view of similarity between the E_{fb} for a semiconductor and the zero charge potential (E_{pzc}) for a metal, surface potential due to orientaion of water dipoles at the porphyrin is one of the plausible factors responsible for the energy difference. According to Trasatti,[29] the relationship between E_{pzc} and work function (ϕ) for a metal is written in the following form, $E_{pzc}=\phi-4.61-0.40\ \alpha$, where α is defined as the degree of orientation of water at the metal. The maximum surface potential of −0.40 V indicates that the dipole of water points the negative end (oxygen) towards the metal and forms an angle of about 34° with the metal surface. A surface potential of about 0.75 V corresponds to the perpendicular dipoles. On these bases, it may be possible to ascribe a part of the potential difference of +0.9 V to the surface potential due to the orientation of water dipoles at the porphyrin electrode. We note that in this case a water molecule must be oriented with the positive end (hydrogen) toward the porphyrin.

When the ITO/ZnTPP interface was irradiated in solution containing oxidizing agents, no evident photocurrent was observed [curve (d) in Fig. 5]. However, in the presence of reducing agents such as HQ and $[Fe(CN)_6]^{4-}$ instead of the oxidizing agents the ITO/ZnTPP electrode exhibited anodic photocurrents at potentials more positive than about −0.1 V *vs.* SCE (Fig. 6).

On these bases, the energy diagram of the ITO/ZnTPP/electrolyte interfaces is represented as shown in Fig. 7. At this time we should note the fact that the band edges are fixed at the porphyrin surfaces. It is

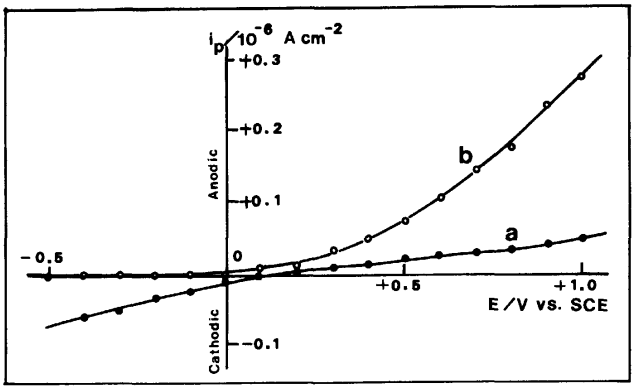

Fig. 6. Potential dependence of the steady-state photocurrent for the ITO/ZnTPP electrode in 0.5 mM $[Fe(CN)_6]^{4-}$ and 0.1 M KCl. (a) and (b) are obtained by irradiation of the ZnTPP/electrolyte and ITO/ZnTPP junctions, respectively.

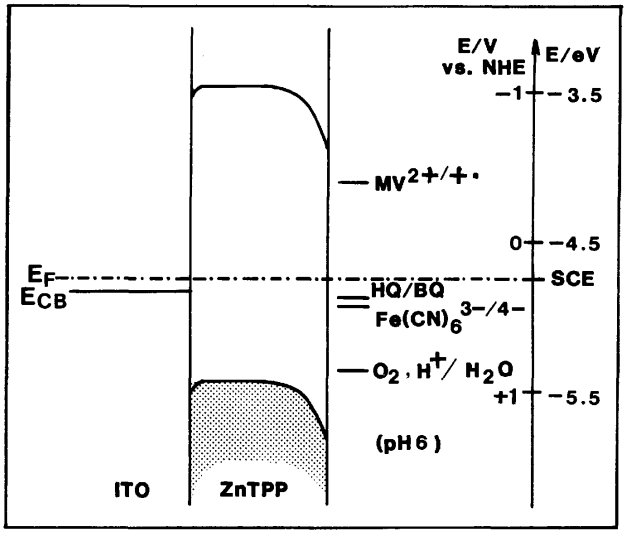

Fig. 7. Band model for the ITO/ZnTPP/electrolyte contacts at 0 V *vs.* SCE.

of great interest that photoelectrochemical reduction of methylviologen (MV^{2+}) occurs even near the flat-band potential, because such a *p*-type porphyrin electrode can be used as a photocathode for reduction of H_2O to produce H_2. The redox potential of HQ/BQ is negative so that at equilibrium the downward band-bending is produced at the ZnTPP/electrolyte interface, which brings about the cathodic photocurrent under short-circuit conditions (Fig. 8). This is in good agreement with the result for the photoelectrochemical cell with ZnTPP (Table 1). Similarly the steady-state photocurrent-potential curves of the ITO/H_2TPP electrode are understood (Fig. 9). The E_{op} for the cathodic photocurrent was negative a little more than that for the ZnTPP electrode. By all accounts it is deduced that the cathodic photocurrents observed at the Pt/ZnTPP electrode[14-16] might be due to the ZnTPP/electrolyte (blocking) contact and not to the Pt/ZnTPP contact.

This work was supported in part by the Grant-in-Aid for Energy Research (No. 59040051) from the Ministry of Education, Science and Culture.

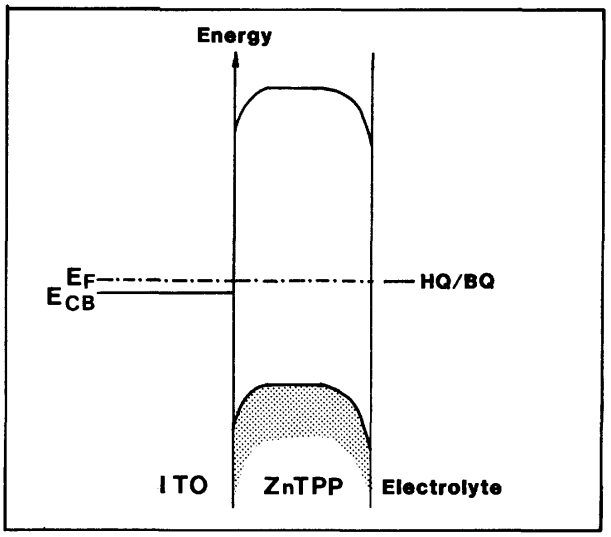

Fig. 8. Equilibrium electron energies for the ITO/ZnTPP electrode in contact with the HQ/BQ couple.

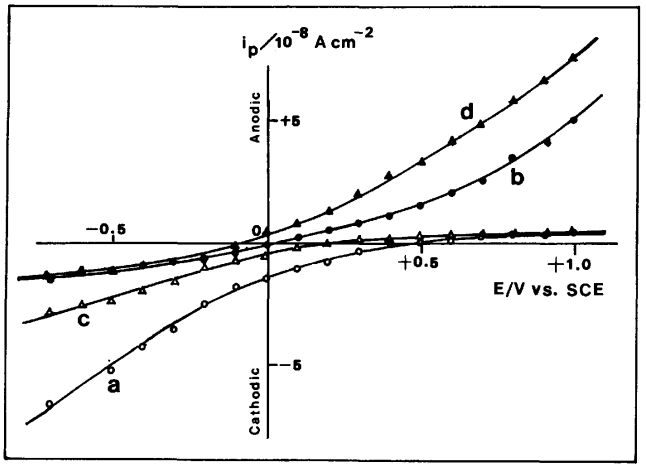

Fig. 9. Potential dependence of the steady-state photocurrent for the ITO/H_2TPP electrode in the presence of about 0.2 mM O_2 [(a) and (b)] and 0.5 mM $[Fe(CN)_6]^{4-}$ [(c) and (d)]. (a) and (c) are obtained by irradiation of the H_2TPP/electrolyte junction, and (b) and (d) obtained by irradiation of the ITO/H_2TPP junction.

References

1) D. Mobius, "Light-Induced Charge Separation in Biology and Chemistry," ed by H. Gerischer and J. J. Katz, Verlag Chemie, Weinheim, New York (1979), p. 171.

2) R. O. Loutfy and E. R. Menzel, *J. Am. Chem. Soc.*, **102**, 4967 (1980).

3) F.-R. Fan and L. Faulkner, *J. Chem. Phys.*, **69**, 3341 (1978).

4) F.-R. Fan and L. Faulkner, *J. Am. Chem. Soc.*, **101**, 4779 (1979).

5) C. D. Jaeger, F.-R. Fan, and A. J. Bard, *J. Am. Chem. Soc.*, **102**, 2592 (1980).

6) A. Giraudeau, F.-R. Fan, and A. J. Bard, *J. Am. Chem. Soc.*, **102**, 5137 (1980).
7) D. L. Morel, A. K. Ghosh, T. Feng, E. L. Stogryn, P. E. Purwin, R. F. Shaw, and C. Fishman, *Appl. Phys. Lett.*, **32**, 495 (1978).
8) A. K. Ghosh and T. Feng, *J. Appl. Phys.*, **49**, 5982 (1978).
9) T. Morizumi and K. Kudo, *Appl. Phys. Lett.*, **38**, 85 (1981).
10) K. Iriyama and M. Yoshiura, *Appl. Phys. Lett.*, **42**, 206 (1983).
11) F. J. Kampas, K. Yamashita, and J. Fajer, *Nature*, **284**, 40 (1980).
12) K. Yamashita, K. Maenobe, and J. Fajer, *Chem. Lett.*, **1982**, 307.
13) K. Yamashita, N. Kihara, H. Shimidzu, and H. Suzuki, *Photochem. Photobiol.*, **35**, 1 (1982).
14) T. Kawai, K. Tanimura, and T. Sakata, *Chem. Phys. Lett.*, **56**, 541 (1978).
15) T. Katsu, K. Tamagake, and Y. Fujita, *Chem. Lett.*, **1980**, 289.
16) H. Jimbo, H. Yoneyama, and H. Tamura, *Photochem. Photobiol.*, **32**, 319 (1980).
17) Y. Umezawa and T. Yamamura, *J. Chem. Soc., Chem. Commun.*, **1978**, 1106.
18) H. T. Tien and J. Higgins, *J. Electrochem. Soc.*, **127**, 1475 (1980).
19) K. Yamashita and N. Kihara, *Chem. Lett.*, **1981**, 467.
20) K. Yamashita, *Chem. Lett.*, **1982**, 1085.
21) M. Buchanan, J. B. Webb, and D. F. Williams, *Appl. Phys. Lett.*, **37**, 213 (1980).
22) J. Shewchun, J. Dubow, A. Myszkowsky, and R. Singh, *J. Appl. Phys.*, **49**, 855 (1978).
23) K. Yamashita and Y. Matsumura, *Denki Kagaku*, **51**, 73 (1983).
24) K. Yamashita, Y. Matsumura, Y. Harima, S. Miura, and H. Suzuki, *Chem. Lett.*, **1984**, 489.
25) A. D. Adler, F. R. Longo, and F. J. Kampas, "The Porphyrins," ed by D. Dolphin, Academic Press, New York (1978), Vol. V, p. 483.
26) H. Gerischer and W. Ekardt, *Appl. Phys. Lett.*, **43**, 393 (1983).
27) A. J. Bard, A. B. Bocarsly, F.-R. Fan, E. G. Walton, and M. S. Wrighton, *J. Am. Chem. Soc.*, **102**, 3671 (1980).
28) A. J. Nozik, "Photochemical Conversion and Storage of Solar Energy," ed by J. S. Connolly, Academic Press, Inc., New York (1981), p. 271.
29) S. Trasatti, *J. Electroanal. Chem. Interfacial Electrochem.*, **33**, 351 (1971).

 © 1985 The Chemical Society of Japan Bull. Chem. Soc. Jpn., 58, 1767—1771 (1985)

Intermolecular Hydrogen Bonding of Enantiomers of Pantolactone Studied by Infrared and ^{1}H-NMR Spectroscopy

Yoshihiko NAKAO, Hiromu SUGETA,* and Yoshimasa KYOGOKU
Institute for Protein Research, Osaka University, Suita, Osaka 565
(Received December 6, 1984)

Intermolecular associations of the enantiomers of pantolactone in carbon tetrachloride solution have been studied by infrared and ^{1}H-NMR spectroscopic methods. The spectroscopic data have been analyzed by the least squares method to obtain the association constants and thermodynamic parameters. It was found that pantolactone takes a cyclic dimer structure by dint of hydrogen bonding. The association constant for homochiral dimerization was obtained to be 8.9 mol^{-1} dm^3 at 26°C and the enthalpy and entropy changes were −35 kJ mol^{-1} and −97 J K^{-1} mol^{-1}, respectively. The association constant for heterochiral dimerization is just twice as large as that for homochiral dimerization, that is, no selective association exists between enantiomers.

In a previous study a general method for analyzing spectrophotometric data of a multicomponent equilibrium system has been developed.[1] The method was applied to the analysis of intermolecular hydrogen bond system of pantolactone **1** in carbon tetrachloride solution. Some spectroscopic measurements of pantolactone have been made, infrared spectra by Kuhnert-Brandstätter and Friedl[2] and Raman and ^{1}H-NMR spectra by Johnson *et al*,[3] but no quantitative analysis on intermolecular hydrogen bonding has yet been worked out. In the present work the infrared and ^{1}H-NMR studies of pantolactone were undertaken for elucidating the association mode and obtaining the association constants and thermodynamic parameters of the intermolecular hydrogen bonding. Pantolactone is an optically active molecule and a stereoselective association between enantiomers is possible. In order to elucidate this problem the quantitative analysis of the concentration dependence of the OH proton chemical shift was made on the solutions of the pure enantiomer (L-pantolactone), racemic mixture (DL-pantolactone), and the mixture of the enantiomers (D- and L-pantolactones) at different ratios.

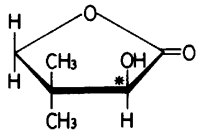

1

Experimental

Materials and Methods. Enantiomers of pantolactone (dihydro-3-hydroxy-4,4-dimethyl-2(3*H*)-furanone) were purchased from Tokyo Kasei Co. and purified by sublimation *in vacuo*. Spectroscopic grade carbon tetrachloride was dried over molecular sieves of 3A and was used as the solvent.

Infrared spectra were measured on a JASCO A-3 infrared spectrophotometer interfaced to a personal computer (NEC PC-9801). The concentration dependences of the absorption intensities in the O–H and C=O stretching regions were measured in the concentration range from 0.08 to 0.003 M (1 M=1 mol dm^{-3}) at 26°C. The temperature dependence of the absorption intensities of the O–H stretching vibrations was measured at several temperatures from 20 to 58°C. The Raman spectra of L-pantolactone in CCl_4 solution (0.08 M) were measured on a JEOL-400D Raman spectrometer.

^{1}H-NMR spectra were measured mainly on a JEOL FX-200 spectrometer operated at 200 MHz and in part on a JEOL GX-500 spectrometer at 500 MHz locked on deuterium of 5 vol% cyclohexane-d_{12} in CCl_4 solvent at 30°C. Chemical shifts were measured relative to the ^{1}H resonance of internal tetramethylsilane. Solutions were prepared in the concentration range from 0.07 to 0.0005 M for pure L-enantiomer, and from 0.2 to 0.01 M for racemic mixture (DL-pantolactone). The measurements for the solutions of different mole ratio of D- and L-enantiomers were performed at the total concentration of 0.07 M.

Procedure for Analysis. The self association of pure enantiomer (D- or L-pantolactone) is expressed for n merization by

$$nX \rightleftharpoons X_n, \quad K_n = [X_n]/[X]^n, \tag{1}$$

where X stands for D or L, [X] and [X_n] are the concentrations of monomer and n-mer, respectively, and K_n is the association constant for n merization of pure enantiomer.

In the solution of mixture of D- and L-enantiomers the following equilibrium was assumed,

$$\begin{aligned} &2D \rightleftharpoons D_2, \quad 2L \rightleftharpoons L_2, \\ &\quad K_2 = K_{DD} = K_{LL} = [D_2]/[D]^2 = [L_2]/[L]^2, \\ &D + L \rightleftharpoons DL, \\ &\quad K_{DL} = [DL]/[D][L], \end{aligned} \tag{2}$$

where $K_2(=K_{DD}=K_{LL})$ and K_{DL} are the association constants for dimerization of pure enantiomer and for hetero-association of D- and L-enantiomers, respectively. [D] and [D_2] ([L] and [L_2]) are concentrations of monomer and dimer of the D- (L-) enantiomer and [DL] is the concentration of heteroassociate DL between D- and L-enantiomers.

The absorbances A for the solution containing n absorbing components are expressed by the sum of absorptions of n components,

$$A_\nu = l \sum_{i=1}^{n} E_{\nu i} C_i(K), \tag{3}$$

where A_ν is the absorbance at the wave number ν, l is the path length, $E_{\nu i}$ is the molar absorption coefficient at the wave number ν of the i-th absorbing component, and C_i is the concentration of the i-th component which is a function of the association constant K. The association constants and molar absorption coefficients were determined from the observed absorbance data by the method of least squares as

described previously.[1]

The chemical shifts (Δ) of the OH proton of pantolactone in the chemical equilibrium system (2) are expressed by

$$\Delta_D = \delta_D P_D + \delta_{DD} P_{DD} + \delta_{DL} P_{DL}(D),$$
$$\Delta_L = \delta_L P_L + \delta_{LL} P_{LL} + \delta_{DL} P_{DL}(L), \quad (4)$$

where Δ_D and Δ_L are observed chemical shifts for the D- and L-enantiomers, $\delta_D(=\delta_L)$, $\delta_{DD}(=\delta_{LL})$ and δ_{DL} are the intrinsic chemical shifts for the D- (or L-) monomer, homo-dimer D_2 (or L_2) and hetero-associate DL, respectively. P_i is the fraction of the i species given by

$$P_D = [D]/([D] + 2[D_2] + [DL]),$$
$$P_{DD} = 2[D_2]/([D] + 2[D_2] + [DL]),$$
$$P_{DL}(D) = [DL]/([D] + 2[D_2] + [DL]), \quad (5)$$

and P_L, P_{LL} and $P_{DL}(L)$ are given similarly. The association constants K_2 and K_{DL} and limiting shifts δ_D, δ_{DD}, and δ_{DL} were determined by the least squares method[1] with reference to the observed chemical shifts.

Results and Discussion

Infrared Spectra. The concentration dependences of absorption bands of the O-H and C=O stretching vibrations of L-pantolactone in CCl_4 solutions at 26°C are shown in Figs. 1 and 2, respectively. The broad band at 3460 cm^{-1} which is enhanced with concentration can readily be assigned to the intermolecularly hydrogen-bonded O-H stretching vibration, while the band at 3570 cm^{-1} enhanced with dilution can be assigned to the O-H stretching vibration of the monomer species. The observation of an isosbestic point at 3550 cm^{-1} suggests that the chemical equilibrium between two components would be predominant in this system. The temperature dependence of absorption intensities in the O-H stretching region was measured (data are not shown). No absorption band above 3600 cm^{-1} was recognized even at high temperature of 70 °C in the dilute solution. It is known that the hydrogen bond free O-H stretching band appears at the wave number above 3600 cm^{-1}.[4] Therefore it suggests that pantolactone exists exclusively in intra- and/or intermolecular hydrogen bonded forms. In the C=O stretching region the main peak at 1795 cm^{-1} is enhanced while the shoulders at 1780 and 1765 cm^{-1} diminish with dilution. Then the band at 1795 cm^{-1} is assigned to the C=O stretching vibration of the monomer species, while the shoulders at 1780 and 1765 cm^{-1} are assigned to the bands of intermolecularly hydrogen-bonded species.

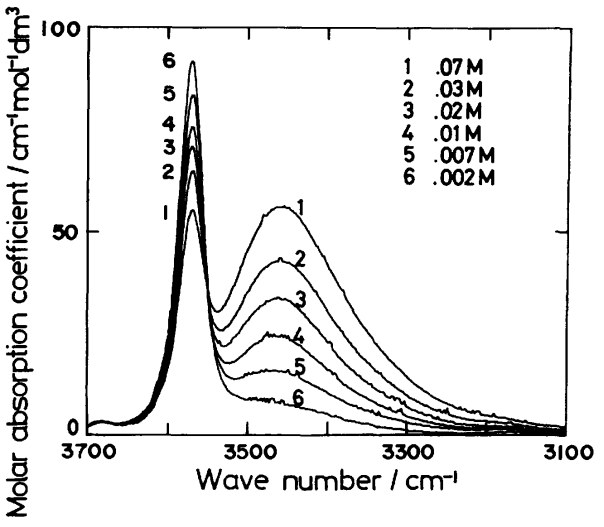

Fig. 1. Concentration dependence of the infrared spectra in the O-H stretching region of L-pantolactone in CCl_4 solutions at 26°C.

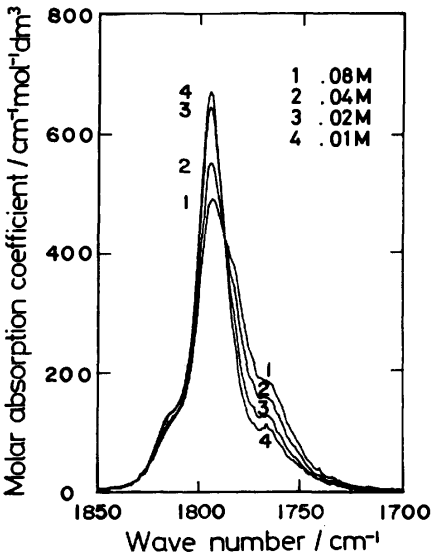

Fig. 2. Concentration dependence of the infrared spectra in the C=O stretching region of L-pantolactone in CCl_4 solutions at 26°C.

^{1}H-NMR Spectra. In ^{1}H-NMR spectrum of L-pantolactone two methyl groups give rise to the separate signals at δ 1.0 and 1.2 and methylene protons give rise to the AB quartet at δ 3.9 because of the existence of an asymmetric carbon atom. These methyl and methylene chemical shifts are independent of the concentration. The resonance lines of hydroxyl and methine protons are spin-spin coupled with each other and exhibit concentration dependence. Their chemical shifts vary from δ 3.5 to 2.2 and from δ 4.03 to 3.92, respectively, and the spin-spin coupling constant $^3J_{HCOH}$ changes from 3.7 to 2.3 Hz with the change in concentration from 0.07 to 0.0005 M.

In Fig. 3 is shown the mole ratio dependence of ^{1}H-NMR spectra for the solutions of the total concentration 0.07 M of the mixture of D- and L-enantiomers. The hydroxyl and methine proton signals are observed at δ 3.48 and 4.03 for the pure L-enantiomer solution of 0.07 M (Fig. 3(a)), but at δ 3.40 and 4.01 for the racemic solution (L:D=1:1) (Fig. 3(f)). At the mole ratios of $0<D/L<1$, the chemical shifts monotonously change between the extreme values (Fig. 4) and the peak areas are proportional to the mole ratio of enantiomers.[5-9]

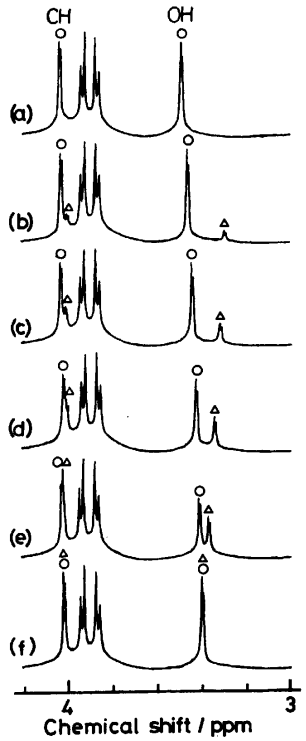

Fig. 3. 500 MHz proton magnetic resonance spectra of CCl_4 solutions of the total concentration 0.07 M of D- and L-pantolactone at 30 °C. The resonance lines of L- and D-enantiomers are denoted with the circles (O) and triangles (Δ), respectively. Enantiomeric compositions *D*:*L* are: (a) 0:1; (b) 1:9; (c) 2:8; (d) 3:7; (e) 4:6; (f) 5:5.

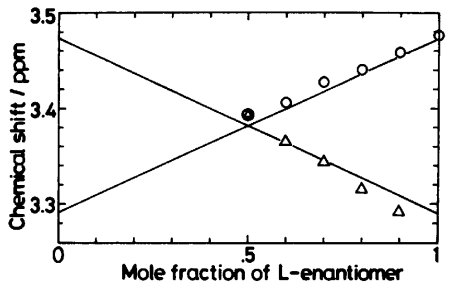

Fig. 4. The observed and calculated chemical shifts of the OH proton resonance against the mole fraction of L-enantiomer in the solutions of the total concentration 0.07 M of D- and L-pantolactone. The solid lines (—) are calculated, and the circles (O) and triangles (Δ) are observed for L- and D-enantiomers, respectively.

Homochiral Association. The concentration dependences of infrared absorption intensities in the O–H and C=O stretching regions of L-pantolactone were analyzed on the basis of the monomer-dimer equilibrium model by the method of the least squares.[1] The association constants for homochiral association were obtained as K_{LL}=8.9±0.6 and 9.8±0.8 M^{-1} at 26 °C from the spectral analyses in the O–H and C=O stretching regions, respectively. The calculated molar absorption coefficients of monomer and dimer species are shown in Figs. 5 and 6, in which those of dimer species

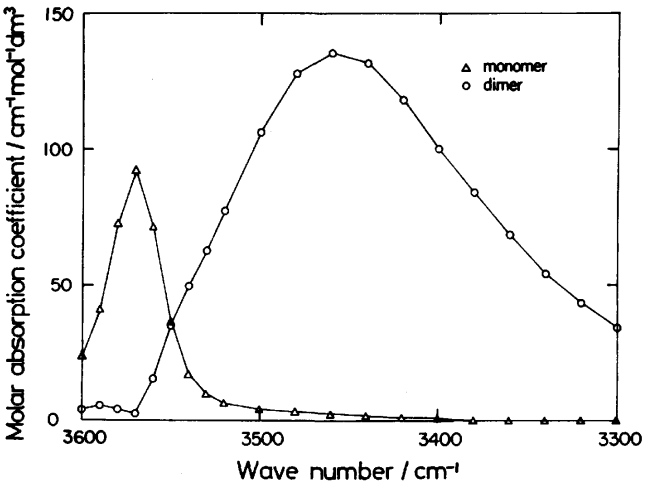

Fig. 5. Molar absorption coefficients for monomer (Δ) and dimer (O) species of L-pantolactone in the O–H stretching region at 26 °C.

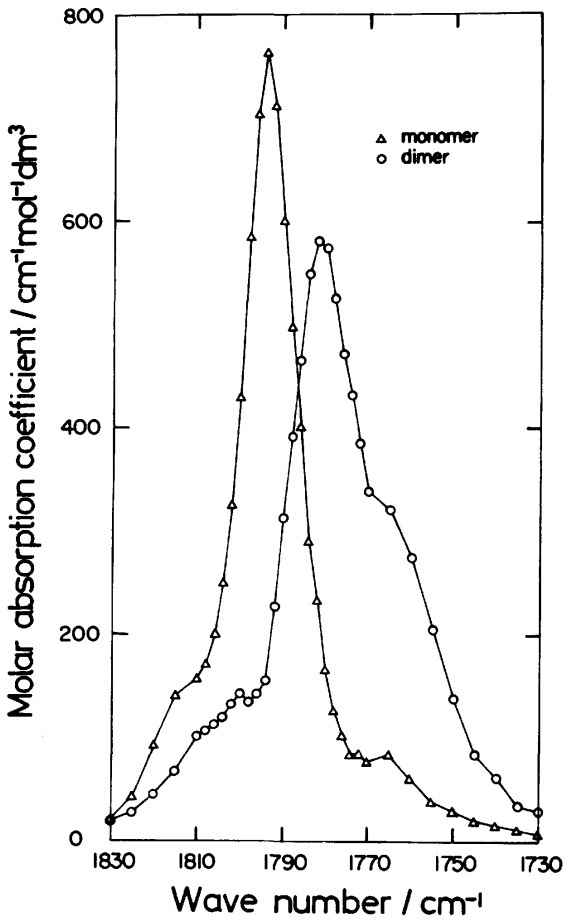

Fig. 6. Molar absorption coefficients for monomer (Δ) and dimer (O) species of L-pantolactone in the C=O stretching region at 26 °C.

are given in values per monomer unit. The observed spectra could be reproduced by using the coefficients with root-mean-squares deviations of 0.66 and 4.2 molar absorption units in the O–H and C=O stretching regions, respectively. The monomer-trimer model

was also applied to the analysis but the agreement between the observed and calculated spectra was poor as compared with the monomer-dimer model. The least squares treatment on the monomer-dimer-trimer model could not give convergence. Therefore the dimerization would be predominant in the concentration range employed.

In the C=O stretching region the band at 1780 cm^{-1} can be observed, at most, as a shoulder even in the saturated solution as shown in Fig. 2. However, the quantitative analysis employed in this study clearly indicates that dimer species has a main peak at 1780 cm^{-1} and a shoulder at 1765 cm^{-1} as seen in Fig. 6. All the bands in the C=O stretching region were polarized in Raman scattering. Accordingly, the band at 1780 cm^{-1} could be assigned to the C=O stretching vibration of the dimer species and the shoulder at 1765 cm^{-1} might be an overtone or a combination band enhanced by a Fermi (anharmonic) resonance. The low frequency shift from 1795 to 1780 cm^{-1} of the C=O stretching suggests that the C=O groups are the proton acceptor sites of the intermolecular hydrogen bond.[10,11] In the calculated molar absorption spectra in Fig. 5, the dimer species exhibits only a broad band centered at 3460 cm^{-1} due to the intermolecular hydrogen bond but does not show any O-H stretching band free from hydrogen bonding. Therefore all the OH groups in the dimer species are responsible for intermolecular hydrogen bonding. It is consequently concluded that pantolactone takes a cyclic dimer structure as shown in **2**.

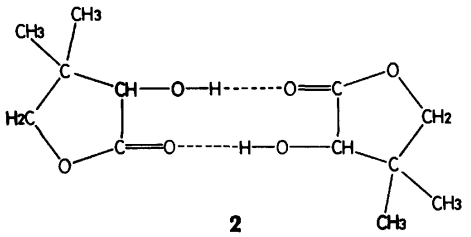

2

The dimer model is further supported by the analysis of the concentration dependence of the OH proton chemical shift in ^{1}H-NMR. The calculations of the least squares fitting[1] were carried out on the basis of several association models. The monomer-dimer model gives a better fit between the observed and calculated data as shown in Fig. 7.

The concentration dependence of the absorption intensities in the O-H stretching region was examined at various temperatures. The results were summarized in Table 1. The dimer model was not inferior to the other models as well. From the van't Hoff plot the enthalpy and entropy changes for dimerization were obtained as ΔH=−35±2 kJ mol^{-1} (−18±2 kJ mol^{-1} per hydrogen bond) and ΔS=−97±4 J K^{-1} mol^{-1}, respectively. The thermodynamic parameters obtained in the present study may be compared with those for the cyclic dimerization of carboxylic acids in CCl_4 solutions which

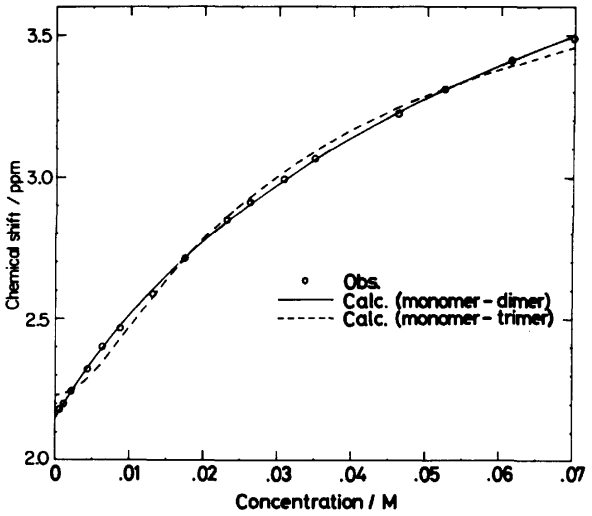

Fig. 7. Concentration dependence of the observed (O) and calculated OH proton chemical shifts of L-pantolactone in CCl_4 solutions at 30 °C. The solid (—) and broken (---) lines are calculated curves on the basis of the monomer-dimer and monomer-trimer models, respectively.

Table 1. Association constants of L-pantolactone at various temperatures

Temperature T/°C	Association constants K_2/M^{-1} O-H stretching	C=O stretching
20	11.6±0.7	
26	8.9±0.6	9.8±0.8
30	7.6±0.5	
40	5.3±0.5	
49	3.3±0.4	
58	2.3±0.3	

have been reported as ΔH=−12 to −23 kJ mol^{-1} and ΔS=−30 to −66 J K^{-1} mol^{-1} per hydrogen bond.[12] No absorption band of hydrogen-bond free O-H stretching above 3600 cm^{-1} could be observed even at 70 °C in the dilute solution (0.003 M). Therefore the monomer species would be stabilized at least by 6 kJ mol^{-1} by dint of an intramolecular hydrogen bond.

Heterochiral Association. Figure 8 shows the concentration dependences of the OH proton chemical shifts for the solutions of L-pantolactone (pure enantiomer) and DL-pantolactone (L:D=1:1). One can clearly recognize the differences between the chemical shifts for the pure enantiomer and racemic solutions in the high concentrations. It suggests that the association constant and/or limiting chemical shift for the heterochiral dimer would be different from those for the homochiral dimer.

In the pure enantiomer solution (*e.g.* L-pantolactone) of the stoichiometrical concentration, C=[L]+2[L_2], the concentration of dimer is given from Eq. 2 by

$$[\text{dimer}] = [L_2] = K_{LL}[L]^2 = K_2[\text{monomer}]^2. \quad (6)$$

In the racemic solution (DL-pantolactone) the total concentration of D- and L-pantolactone, C', is given by

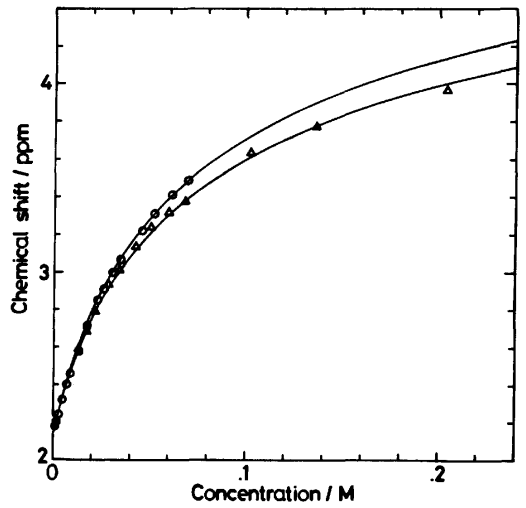

Fig. 8. Concentration dependence of the observed and calculated (solid line) OH proton chemical shifts of pantolactone in CCl_4 solutions at 30°C. The observed shifts are denoted with O and Δ for L- and DL-pantolactone, respectively.

$$C' = [D] + [L] + 2[D_2] + 2[L_2] + 2[DL] = 2[L] + 4[L_2] + 2[DL], \quad (7)$$

and the concentration of dimer species in the racemic solution is given as

$$\begin{aligned}[\text{dimer}] &= [D_2] + [L_2] + [DL] \\ &= K_2([D]^2 + [L]^2) + K_{DL}[D][L] \\ &= \frac{1}{4}(2K_2 + K_{DL})([D] + [L])^2 \\ &\quad + \frac{1}{4}(2K_2 - K_{DL})([D] - [L])^2 \\ &= \frac{1}{4}(2K_2 + K_{DL})[\text{monomer}]^2, \end{aligned} \quad (8)$$

where the relations in the racemic solution, [D]=[L] and [monomer]=[D]+[L], were employed. From the comparison of Eqs. 6 and 8, if the relation of $K_{DL}=2K_2$ ($=2K_{LL}$) holds, the degree of dimer formation in the racemic solution may be regarded to be the same as that in the solution of the pure enantiomer.

In order to elucidate the difference between the homo- and hetero-chiral associations in pantolactone the simultaneous analysis of the concentration dependence of the OH proton chemical shifts was undertaken for the solutions of pure enantiomer (L-pantolactone), racemic mixture (DL-pantolactone), and different mole ratios of D- and L-enantiomers with the total concentration of 0.07 M. The results were summarized in Table 2. The calculated chemical shifts are in good agreement with the observed data as shown in Figs. 4 and 8. It turns out that the association constant for heterochiral dimerization, K_{DL}, is just twice as large as that for homochiral dimerization, K_2 ($=K_{LL}$), that is, no selective association exists between enantiomers. It is consequently concluded that the difference between the chemical shifts of the solutions of pure enantiomer and racemic mixture can be ascribed to the dissimilarity between the limiting chemical shifts of homo- and hetero-chiral dimers.

Table 2. Association constants and limiting chemical shifts at 30°C

K_{LL}	6.9±0.4 M^{-1}
K_{DL}	13.8±0.4 M^{-1}
δ_L	2.132±0.008
δ_{LL}	5.74±0.08
δ_{DL}	5.25±0.05

References

1) H. Sugeta, *Bull. Chem. Soc. Jpn.*, **54**, 3706 (1981).
2) M. Kuhnert-Brandstätter and L. Friedl, *Mikrochim. Acta*, **2**, 97 (1979).
3) J. H. Johnson, E. A. Grula, K. D. Berlin, and B. M. Fung, Biomol. Struct. Funct., [Symp.] 1977 (Pub. 1978), 115. ed by P. F. Agris, Academic, New York; N. Y.
4) M. St. C. Flett, *Spectrochim. Acta*, **10**, 21 (1957).
5) T. Williams, R. G. Pitcher, P. Bommer, J. Gutzwiller, and M. Uskoković, *J. Am. Chem. Soc.*, **91**, 1871 (1969).
6) M. I. Kabachnik, T. A. Mastryukova, E. I. Fedin, M. S. Vaisberg, L. L. Morozov, P. V. Petrovsky, and A. E. Shipov, *Tetrahedron*, **32**, 1719 (1976).
7) M. J. P. Harger, *J. Chem. Soc., Chem. Commun.*, **1976**, 555.
8) M. T. Cung, M. Marraud, and J. Neel, *Biopolymers*, **16**, 715 (1977).
9) M. T. Cung, M. Marraud, and J. Neel, *Biopolymers*, **17**, 1149 (1978).
10) R. N. Jones, P. Humphries, F. Herling, and K. Dobriner, *J. Am. Chem. Soc.*, **74**, 2820 (1952).
11) S. Searles, M. Tamres, and G. M. Barrow, *J. Am. Chem. Soc.*, **75**, 71 (1953).
12) G. C. Pimentel and A. L. McClellan, "The Hydrogen Bond," ed by L. Pauling, W. H. Freeman and Company, San Francisco and London (1960), Chap. 7.

Infrared Spectrum of Dichloroborane Produced by CO_2 Laser Enhanced Reaction

Kuk-Haeng LEE,† Harutoshi TAKEO, Shigeo KONDO,* and Chi MATSUMURA
National Chemical Laboratory for Industry, Tsukuba
Research Center, Yatabe, Ibaraki 305
(Received February 7, 1985)

Infrared spectra of $HBCl_2$ and $DBCl_2$ produced by a TEA CO_2 laser enhanced reaction of BCl_3 and H_2/D_2 have been observed by an FT-IR spectrometer at a resolution of 0.12 cm^{-1}. A detailed analysis has been carried out for the ν_1 band of $HBCl_2$ to obtain the precise molecular parameters, and they are compared with the microwave data. The fundamental frequencies other than the ν_3 band have all been determined. These frequency data combined with the results of an *ab initio* MO calculation have yielded the general symmetry force field through a least squares method. Some characteristic features on the CO_2 laser reaction of BCl_3 and H_2 are also discussed.

Infrared spectra of dichloroborane have been observed by several investigators.[1-7] However, very few analyses of the vibration-rotation bands of this molecule have been reported. Lynds and Bass[6,7] observed the ν_1 and ν_6 bands of dichloroborane with a low resolution using a conventional grating spectrometer, and determined the molecular structure from the observed values of the rotational constants $(A-\bar{B})$.[6] These authors and Dewames[8] calculated the fundamental frequencies of $HBCl_2$ assuming a force field which is similar to that of BCl_3. This was done only to make assignments of the observed bands. Mandirola and Westerkamp also calculated the fundamental frequencies of this molecule assuming appropriate values of the force constants.[9] However, there have been no attempts to determine the force field of this molecule. Quite recently Sugie *et al.*[10] studied the microwave spectra of this molecule. They obtained the rotational constants of $H^{11}B^{35}Cl_2$, $H^{10}B^{35}Cl_2$, $H^{11}B^{35}Cl^{37}Cl$, and $D^{11}B^{35}Cl_2$, and determined the precise structural parameters.

In Ref. 1—7, $HBCl_2$ was produced by heating a mixture of BCl_3 and H_2 in the presence of catalysts, where various compounds such as B_2H_6, B_2H_5Cl, *etc.* besides $HBCl_2$ and HCl were produced. Recently this reaction has been investigated by the use of CO_2 laser photolysis since the strong degenerate stretching band of BCl_3 coincides with a laser band of CO_2.[11-16] Rockwood and Hudson[16] found that the reaction of BCl_3 with H_2 by the irradiation of pulsed CO_2 laser yields only $HBCl_2$ and HCl as final products, the fact being in contrast with the case of thermal reaction. They also found that the efficiency of the reaction is as high as 122 (10.6 μ) photons per $HBCl_2$ molecule.

The purpose of the present study is to observe the vibration-rotation bands of $HBCl_2$ and $DBCl_2$ with relatively high resolution to determine the spectroscopic constants. The study also aims to determine the molecular force field from the observed frequency data. An *ab initio* MO method was used to calculate the force constants, which compensated the insufficient observed data. In connection with the preparation of sample, a CO_2 laser enhanced reaction between BCl_3 and H_2 was investigated.

Experimental

H_2 and D_2 gases were purchased from Showa Denko Co. and BCl_3 gas from Takachiho Chemical Co. These samples were used without further purification. The BCl_3/H_2 and BCl_3/D_2 gas mixtures were irradiated with a CO_2 laser beam in a glass reaction vessel of 13 cm in length and 3.2 cm in diameter fitted with KBr windows. Grease was not used in the vacuum sampling system to avoid contamination. A Pirani vacuum gauge and an MKS Baratron capacitance manometer were used to measure the pressures. A Lumonics model TEA-101-2 pulsed CO_2 laser was used to irradiate the sample. Burn patterns were made in thermal paper to check the distribution of the laser radiation. The laser power was measured with a Lumonics model 20D pyroelectric detector. The laser power was changed by placing an infrared absorption cell filled with an appropriate amount of BCl_3 gas before the reaction cell. The reaction was monitored by the absorbance of infrared spectrum taken after the irradiation with the laser shots.

The vibration-rotation spectra were measured with a Nicolet 7199 FT-IR spectrometer equipped with a Ge coated KBr beam splitter and a water cooled Glober source. All the spectra were observed at a resolution of 0.12 cm^{-1}. Since no attempt was made to separate and purify the sample of $HBCl_2$, absorption bands of BCl_3 and HCl/DCl were also observed.

Results and Discussion

Observed Spectra. Since the ν_1, ν_2, and ν_3 modes belong to A_1 species, they should give B-type bands. The ν_1 band which is associated with the B–H stretching mode showed a symmetrical band contour as shown in Fig. 1. In a prolate symmetric top approximation, the frequencies of the Q branch peaks are given by

$$\nu_0^{sub} = \nu_0 + (1\pm 2K)(A'-\bar{B}') + \{(A'-A'')-(\bar{B}'-\bar{B}'')\}K^2 \mp D_k(2K^2\mp 2K+1)(2K+1), \quad (1)$$

where the single and double primes refer to the upper and lower states, respectively. D_k is a centrifugal distortion constant. $\bar{B}$ is an average of B and C rotational constants. The observed frequencies of $H^{11}BCl_2$ were

†Present address: Department of Chemistry, College of Education, Jeonbug National University, Jeonju, Republic of Korea.

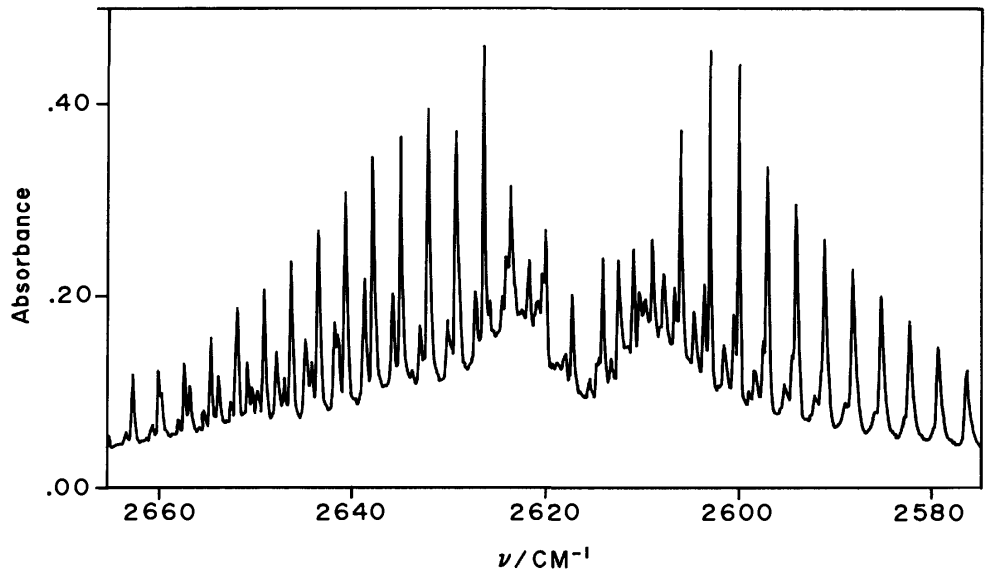

Fig. 1. Spectrum of ν_1 band of $H^{11}BCl_2$.

used for a least squares method by using Eq. 1 leading to the following;

$$\nu_1^{sub} = 2616.25 + 1.4580(1\pm 2K) - 0.00352(K^2) \mp 0.0000479(2K^2\mp 2K+1)(2K+1). \quad (2)$$

Since the band center area is overlapped by the hot bands as well as by the absorption of various isotopic species, the lines of small K values were not included in the calculation. Thus, the band center of ν_1 was determined as 2616.25 cm^{-1} for ^{11}B species. For ^{10}B species, the assignment was made so that the resulting values of the rotational constants agree well with the microwave values,[10] and the band center was determined as 2628.00 cm^{-1}. No assignment was made for the hot bands. The resulting values of the spectroscopic constants for this band are summarized in Table 1. The rotational constants are in good agreement with the microwave values shown in Table 2.[10] This fact con-

Table 1. Analysis of the ν_1 band of $HBCl_2$. (cm^{-1})

K[a]	$H^{11}B^{35}Cl_2$		$H^{10}B^{35}Cl_2$	
	Obsd	O-C	Obsd	O-C
3	2626.421	−0.003		
4	2629.312	0.006	2641.780	0.003
5	2632.165	−0.001	2644.791	−0.002
6	2635.038	0.005	2647.788	−0.003
7	2637.878	0.003	2650.778	0.006
8	2640.701	0.000	2653.729	−0.004
9	2643.500	−0.010	2656.675	0.001
10	2646.299	−0.003		
11	2649.068	−0.007		
12	2651.851	0.024		
13	2654.559	0.001		
14	2657.258	−0.009		
15	2659.949	−0.001		
−5	2603.094	0.025		
−6	2600.115	−0.016	2610.960	−0.001
−7	2597.191	−0.001	2607.865	0.012
−8	2594.245	−0.010	2604.728	−0.006
−9	2591.319	0.000	2601.624	0.011
−10	2588.392	0.006	2598.487	−0.007
−11	2585.456	−0.002		
−12	2582.536	0.001		
ν_0	2616.258(21)		2628.003(12)	
$A'-\bar{B}'$	1.4580(15)		1.5382(16)	
$(A'-A'')-(\bar{B}'-\bar{B}'')$	−0.00352(25)		−0.00506(30)	
D_K	0.0000479(57)		0.000051(11)	
$A''-\bar{B}''$	1.46152		1.54326	
$A''-\bar{B}''$[b]	1.46194		1.54155	

a) Negative K numbers are for P-branch transitions. b) Ref. 10.

Table 2. The rotational constants of $HBCl_2$ in the ground vibrational state[a] (cm^{-1})

	$H^{11}B^{35}Cl_2$	$H^{10}B^{35}Cl_2$	$D^{11}B^{35}Cl_2$
A''	1.5647846(23)	1.6445345(27)	1.1725796(23)
B''	0.1062708(3)	0.1062568(3)	0.1062738(3)
C''	0.0994171(3)	0.0997143(13)	0.0973419(3)
$A''-\bar{B}''$	1.461940(2)	1.541549(4)	1.070772(2)

a) Ref. 10.

firms that the observed ν_1 spectrum is definitely due to $HBCl_2$ molecule.

The ν_2 band is due to the symmetric BCl stretching mode. The band center was determined as 734.62 cm^{-1} for $H^{11}B^{35}Cl_2$ species from the analysis of the vibration-rotation band, while for $H^{10}BCl_2$ species, assignment was not made, because the band center area was disturbed by the ν_4 band in addition to the hot bands. The ν_3 band, which is expected to be in the far-ir region, could not be detected.

The out-of-plane bending mode of this molecule gives a C-type band ν_4. For this band each rotational fine structure was observed as a doublet due to isotopic species of $HB^{35}Cl^{37}Cl$ whose abundance is *ca.* two thirds of $HB^{35}Cl_2$. The band centers were determined as 785.92 and 785.73 cm^{-1} for $H^{11}B^{35}Cl_2$ and $H^{11}B^{35}Cl^{37}Cl$, respectively. For ^{10}B species, the band center was determined only for $H^{10}B^{35}Cl_2$ species as 798.70 cm^{-1}.

The B_2 vibrational modes give A-type bands, which have a similar appearance to that of a parallel band of symmetric top molecule. The ν_5 B–Cl asymmetric stretching band was found at 1091.1 cm^{-1} for $H^{11}BCl_2$ and 1108.0 cm^{-1} for $H^{10}BCl_2$. The B–H in-plane deformation band, ν_6, was observed at 895.4 cm^{-1} for $H^{11}BCl_2$ and 916.5 cm^{-1} for $H^{10}BCl_2$. The ν_5 and ν_6 bands have conspicuously strong intensities compared with the other bands. The ν_6 band center area of $H^{11}BCl_2$ was slightly different in its shape from that of ν_5. From this fact, a large difference of the rotational constant A between the upper and lower states of ν_6 is expected. The observed frequency data for $HBCl_2$ are summarized in Table 3.

For $DBCl_2$ molecule, two bands were observed with about equal intensities in the BD streching band region. This is because the ν_1 and $2\nu_5$ bands are in Fermi resonance with each other. A slightly stronger one was tentatively assigned to the ν_1 band. Thus, the ν_1 band center for $D^{11}BCl_2$ was determined as 1979.94 cm^{-1}. This band is strongly disturbed also by the DCl rotation-vibration lines and by the hot bands. The ν_2 band center of $D^{11}BCl_2$ is completely obscured by the ν_6 band. The ν_3 band which is expected to be in the far-ir region could not be detected for $DBCl_2$, either.

The band center of the out-of-plane mode, ν_4, was found to be 647.21 cm^{-1} for $D^{11}BCl_2$ and 662.60 cm^{-1} for $D^{10}BCl_2$. As shown in Fig. 2, the splittings due to $DB^{35}Cl^{37}Cl$ species were also observed and its band center was determined as 646.99 cm^{-1}.

The B–Cl asymmetric stretching band, ν_5, was found at 975.20 cm^{-1} for $D^{11}BCl_2$. However, the band region for $D^{10}BCl_2$ was heavily overlapped by the ν_3 band of BCl_3, and we could not observe the band shape clearly. The B–D in-plane deformation band, ν_6, of $D^{11}BCl_2$ located at about 723 cm^{-1} is disturbed by the ν_2 band. Therefore, it was difficult to determine the band center precisely; the value given above is an approximate one. The observed date of $DBCl_2$ are also summarized in Table 3.

Force Constants. A normal coordiate calculation was carried out by the convensional GF method developed by Wilson *et al.*[17] In Fig. 3, the internal coordinates of $HBCl_2$ are illustrated. The out-of-plane coordinate, γ, is the angle between the BH bond and the ClBCl plane. The symmetry coordinates are given in terms of the internal coordinates as listed in Table 4. The adjustment of force constants was

Table 3. The observed and calculated fundamental frequencies of dichloroborane (cm^{-1})

Mode			$H^{11}B^{35}Cl_2$	$H^{10}B^{35}Cl_2$	$D^{11}B^{35}Cl_2$	$D^{10}B^{35}Cl_2$
A_1	ν_1	Obsd.[a]	2616.25	2628.00	1979.94	—
		Fitted[b]	2622.6	2634.0	1938.4	1955.5
		Calcd.[c]	2866.1	2878.4	2117.2	2135.6
	ν_2	Obsd.	734.62	—	—	—
		Fitted	735.0	757.4	712.4	731.1
		Calcd.	777.2	801.2	753.9	773.9
	ν_3	Obsd.	—	—	—	—
		Fitted	285.8	287.7	283.9	285.8
		Calcd.	316.8	318.9	314.7	316.8
B_1	ν_4	Obsd.	785.92	798.70	647.21	662.60
		Fitted	786.0	799.0	646.7	662.5
		Calcd.	863.6	877.9	710.1	727.3
B_2	ν_5	Obsd.	1091.11	1107.96	975.20	—
		Fitted	1091.4	1108.6	974.1	1012.4
		Calcd.	1234.1	1248.8	1057.8	1097.4
	ν_6	Obsd.	895.35	916.50	723.0	—
		Fitted	895.5	917.5	721.5	722.6
		Calcd.	960.7	988.0	805.8	808.5

a) Observed value. b) Calculated with the determined force constants listed in Table 5. c) *Ab initio* value.

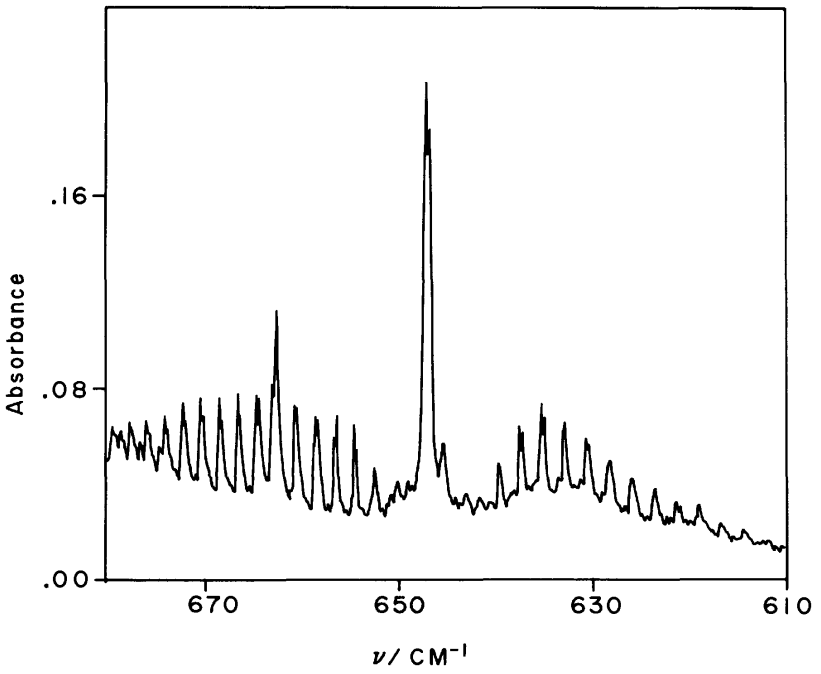

Fig. 2. Spectrum of ν_4 band of $D^{11}BCl_2$.

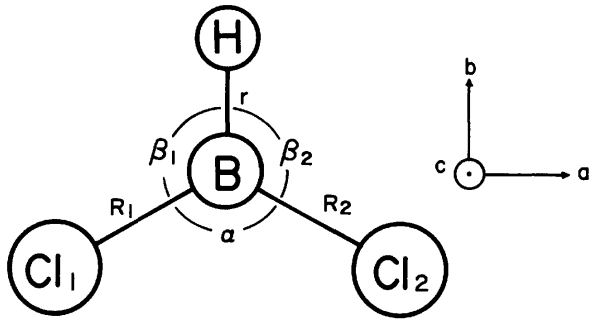

Fig. 3. Internal coordinates of $HBCl_2$ molecule.

Table 4. Symmetry coordinates for $HBCl_2$ molecule

Species	Band type	Symmetry coordinate	Mode
A_1	B	$S_1=\Delta r$	B-H str
		$S_2=(\Delta R_1+\Delta R_2)/\sqrt{2}$	B-Cl sym-str
		$S_3=(2\Delta\alpha-\Delta\beta_1-\Delta\beta_2)/\sqrt{6}$	B-Cl sym-def
B_1	C	$S_4=\Delta\gamma$	out-of-plane
B_2	A	$S_5=(\Delta R_1-\Delta R_2)/\sqrt{2}$	B-Cl antisym-str
		$S_6=(\Delta\beta_1-\Delta\beta_2)/\sqrt{2}$	B-H def

made by using a standard least squares method such as developed by Shimanouchi *et al.*,[18] where, in each repeating cycle of the refinement procedure, the corrections to the force constants, $\Delta\boldsymbol{P}$, were made by solving the following normal equation;

$$\boldsymbol{J}'\boldsymbol{W}\boldsymbol{J}\Delta\boldsymbol{P}=\boldsymbol{J}'\boldsymbol{W}\Delta\boldsymbol{\nu} \quad (3)$$

where $\boldsymbol{J}$ denotes the Jacobian matrix, $\boldsymbol{W}$ the weight vector for the observed frequencies, and $\Delta\boldsymbol{\nu}$ the frequency error vector.

For B_1 and B_2 species, the number of the data was enough to determine all force constants uniquely and the results of the least-squares calculation are shown in Table 5. However, for A_1 species the number of the data was not enough to determine all six force constants uniquely. Then, in order to make predictions of the harmonic force field, an *ab initio* MO calculation was carried out. The calculation was made with the Pople's 4-31G* basis set by using the HONDOG computer program.[19] After geometry optimization was carried out by the gradient method,[20] the harmonic force field $\boldsymbol{F}_x$ was calculated. The $\boldsymbol{F}_x$ was transformed to a symmetry coordinates expression to give the $\boldsymbol{F}_s$ matrix. The harmonc force field of $HBCl_2$ thus obtained is shown in the second column of Table 5. These force constants were found to reproduce the observed fundamental frequencies fairly well as is clearly seen in Table 3. The agreement is markedly improved if the calculated frequencies are multiplied by an arbitrary factor of 0.9. This means that a factor of 0.81 should be used for the calculated force constants to fit them to the observed. Therefore, in order to determine the force constants for A_1 block from the

Table 5. Quadratic force constants of $HBCl_2$ (mdyne/Å or rad)

	Determined	*ab initio*
F_{11}	3.747(42)	4.518
F_{12}	0.084[a]	0.104
F_{13}	−0.076[a]	−0.094
F_{22}	4.214(172)	4.665
F_{23}	0.160[a]	0.197
F_{33}	0.647[a]	0.799
F_{44}	0.448(8)	0.538
F_{55}	3.265(71)	3.721
F_{56}	0.256(21)	0.312
F_{66}	0.428(11)	0.553

a) Constrained.

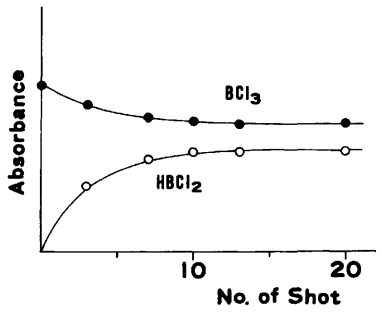

Fig. 4. Relation between the spectral intensities and number of laser shots for BCl_3 and $HBCl_2$.

observed frequencies, the values of F_{12}, F_{13}, F_{23}, and F_{33} were constrained to the *ab initio* values multiplied by a factor of 0.81. The resulting values of the force constants are listed in Table 5. The calculated values of the fundamental frequencies from these force constants are also compared with the observed in Table 3.

CO_2 Laser Reaction of BCl_3 with H_2. As to the laser induced reaction used in the present study, a few characteristic features were noticed. For example, when the partial pressure of BCl_3 was less than 1 Torr†, we did not observe any appreciable changes in the infrared spectrum of the sample even after the 1000 shots of laser irradiation with fluence of 1.27 J/cm²/pulse, *i.e.* neither any absorption due to $HBCl_2$ nor any appreciable intensity change in BCl_3 bands was observed. However, the reaction did take place when the laser power density was increased by focusing the beam with an optical lens. When the sample pressures were raised to 5 Torr of BCl_3 and 5 Torr of H_2, the reaction became very rapid and it reached equilibrium after only 10 laser shots as shown in Fig. 4. This means that the threshold laser fluence for the reaction of BCl_3 with H_2 strongly depends on the pressure of BCl_3. It is concluded from this experiment that the average number of photons absorbed per molecule per pulse also depends on the pressure of the sample. This conclusion is demonstrated in Fig. 5, where non-linear dependence of the laser absorption on the BCl_3 sample pressure is clearly shown. The plotted data were obtained by taking the ratios of the laser power measured before and after the laser beam passes through the sample cell. In Fig. 5, the result of similar measurements for SiF_4 gas by P(42) CO_2 laser line is also shown for comparison. In both cases, non-linearity of the relationship between the absorbance and gas pressure is clearly demonstrated. Since almost the same absorption coefficients are obtained for the different laser fluences, the non-linearity may not be caused by the largeness of laser power. The most likely explanation of this phenomenon is that the pressure broadening of the BCl_3 absorption line is necessary to absorb the CO_2 laser efficiently. The very low absorption coefficient of the laser at low pressure probably causes the existence

† 1 Torr≈133.322 Pa.

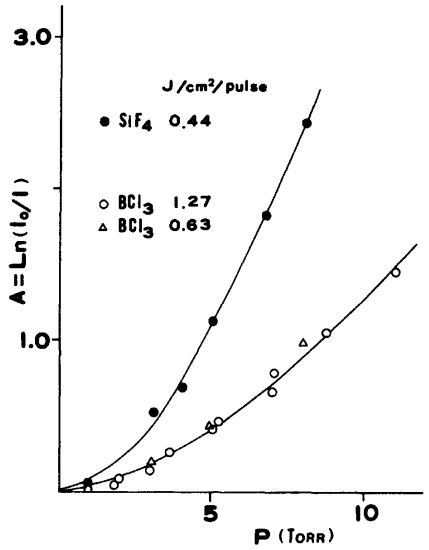

Fig. 5. Non-linear relationship between the absorbance and partial pressure for laser beam absorption by BCl_3 and SiF_4.

of the power threshold for the laser induced reaction between BCl_3 and H_2. The fact that the equilibrium mixture of BCl_3 and $BHCl_2$ is obtained as shown in Fig. 4 suggests that this reaction is almost thermal.

As described previously, the laser induced reaction between BCl_3 and H_2 does not produce B_2H_5Cl, although the external heating does. One reason may be that the catalyst is not used in the laser reaction and, therefore, the reaction occurs purely in the gas phase. Another possible reason is that the reaction products are cooled very rapidly in the pulsed laser reaction. This frozens the high temperature state so that the by-product such as B_2H_5Cl which is not stable at elevated temperatures cannot be produced.

One of the authors (KHL) wishes to express his gratitude to Japan International Cooperation Agency for providing the opportunity to carry out the present study.

References

1) T. Onak, H. Landesman, and I. Shapiro, *J. Phys. Chem.*, **62**, 1605 (1958).
2) L. Lynds and D. R. Stern, *J. Am. Chem. Soc.*, **81**, 5006 (1959).
3) H. G. Nadeau and D. M. Oaks, *Anal. Chem.*, **32**, 1480 (1960).
4) H. W. Myers and R. F. Putnam, *Inorg. Chem.*, **2**, 655 (1963).
5) C. D. Bass, L. Lynds, T. Wolfram, and R. E. Dewames, *Inorg. Chem.*, **3**, 1063 (1964).
6) L. Lynds and C. D. Bass, *J. Chem. Phys.*, **40**, 1590 (1964).
7) L. Lynds, *J. Chem. Phys.*, **44**, 1721 (1966).
8) C. D. Bass, L. Lynds, and R. E. Dewames, *J. Chem. Phys.*, **40**, 3611 (1964).
9) O. B. Mandirola and J. F. Westerkamp, *Spectrochim. Acta*, **20**, 1633 (1964).
10) M. Sugie, H. Takeo, and C. Matsumura, to be pub-

lished.

11) R. V. Ambartzumian, N. V. Chekaline, V. S. Doljikov, V. S. Letokhov, and E. A. Ryabov, *Chem. Phys. Lett.*, **25**, 515 (1974).

12) S. M. Freund and J. J. Ritter, *Chem. Phys. Lett.*, **32**, 255 (1975).

13) R. V. Ambartzumian, N. V. Chekaline, V. S. Letokhov and E. A. Ryabov, *Chem. Phys. Lett.*, **36**, 301 (1975).

14) J. H. Lyman and S. D. Rockwood, *J. Appl. Phys.*, **47**, 595 (1976).

15) V. N. Bourimov, V. S. Letokhov, and E. A. Ryabov, *J. Photochem.*, **5**, 49 (1976).

16) S. D. Rockwood and J. W. Hudson, *Chem. Phys. Lett.*, **34**, 542 (1975).

17) See, E. B. Wilson, J. C. Decius, and P. C. Cross, "Molecular vibrations," McGraw-Hill Book Co., (1955).

18) See, T. Shimanouchi and I. Suzuki, *J. Chem. Phys.*, **42**, 296 (1965).

19) H. F. King and M. Dupuis, *J. Comp. Phys.*, **21**, 144 (1976).

20) P. Pulay, "Applications in Electronic Structure Theory," Ed. H. F. Schaefer, Plenum, New York (1977) p. 153.

Topological Index and Thermodynamic Properties. III.† Classification of Various Topological Aspects of Properties of Acyclic Saturated Hydrocarbons

Hideyuki NARUMI and Haruo HOSOYA*††
Department of Chemistry, Hokkaido University, Sapporo 060
††*Department of Chemistry, Ochanomizu University, Bunkyo-ku, Tokyo 112*
(Received February 12, 1985)

To elucidate the physical meaning of the structure-activity relationship of alkanes, correlation coefficients between 24 thermodynamic properties of hexane, heptane, octane, and nonane isomers and four different topological indices were calculated. These properties were classified into five different types depending on the signs and magnitudes of their correlation coefficients with the two indices, Z and p_3. It is interpreted that Z and p_3, respectively, represent the dynamical and static features of the topological properties of molecules. The merit of correlation pattern recognition is demonstrated.

There have been proposed a number of empirical formulas relating various properties of chemical substances with their structural parameters, such as the topological index.[1-18] Although the term topological index was proposed first by one of the present authors for the Z-index defined below,[7,19] recently it is used as a common name given to a group of indices for characterizing certain aspects of the topological skeleton of a molecule obtained according to the specified algorithm.[8,10,20-24] Given a good structure-activity relationship for a certain property or a set of properties, two different directions are open for further studies, namely, predictable (or practical) and interpretable (or conceptual) ones.[13] A majority of QSAR (quantitative structure-activity relationship) studies aim the former goal by using as many parameters as possible for attaining accurate predictions.[1,8,9] On the other hand, toward the latter goal, continuing attempts have been undertaken to unveil the physical or microscopic meaning of various magic parameters, the topological indices.[4,7] Thermodynamic properties of saturated hydrocarbons seem to be the best probe for this study, since their isomeric differences seem to be governed mainly by the topological structure of the carbon atom skeleton, and a number of experimental data of good quality are available.[25]

The present authors have shown that the boiling point and entropy of saturated hydrocarbons are correlated fairly well with the Z index and many empirical rules on these properties can be derived by assuming linear relationships between Z and these properties.[7,14-16]

The pioneering works by Wiener[2] and Platt[3] established that almost all the thermodynamic properties can be correlated well with the combination of two different topological indices, *e.g.*, Wiener's path number w and polarity number p or p_3. Randić and Wilkins[13,17] chose another set of parameters, p_2 and p_3, for graph-theoretical ordering of the hydrocarbon isomers to analyze the molecular property correlation, where p_2 is the number of paths of length two, or the so-called Gordon-Scantlebury index, N_2.[18] It is interesting to note that similar two-parameter dependency of thermodynamic properties is observed in a systematic factor analysis by Cramer[12] for a larger group of substances of considerable diversity from helium to anthracene and from alkanes to amides. He claims that his two parameters B and C respectively represent molecular cohesiveness and molecular bulkiness.

What is then the best set of two parameters representing the different topological aspects of branching and cyclization? They should also be as orthogonal as possible to each other, and their physical meaning should be clear or at least interpretable. For this purpose those simple, say, interger topological indices, Z, w, p_2, and p_3, which have been introduced above are desirable. In this paper we have studied the correlation between the twenty four thermodynamic properties of saturated hydrocarbons and the individual and various combinations of these topological indices. The properties studied were found to be well classified into several types depending on the mixing-phase of the correlation coefficients with respect to the two parameters, Z and p_3. Attempts to get the physical interpretation of the two-parameter dependency of these properties are being under way.

I. Topological Indices

Definitions. The carbon atom skeleton of a (saturated) hydrocarbon molecule can be expressed as a non-directed graph G composed of lines (C–C bonds) and N points (C atoms), whose adjacency relation is to be expressed by an $N\times N$ adjacency matrix $\boldsymbol{A}$ with elements $a_{ij}=1$ and 0, respectively, for the bonding and non-bonding ij pairs of points. The distance matrix $\boldsymbol{D}$ is defined as the $N\times N$ matrix with elements d_{ij} as the number of shortest path from point i to j. The half sum of the off-diagonal matrix elements of $\boldsymbol{D}$ is defined as w.[2,7] One half of the number of $d_{ij}=2$ elements in $\boldsymbol{D}$ is defined as p_2 or N_2 (Gordon-Scantlebury index),[18] while that of $d_{ij}=3$ as p_3 or p.[2] The non-adjacent number $p(G,k)$ for G is defined as the number of ways for choosing k disjoint lines from G.[7] The total number of $p(G,k)$ is defined as Z_G (topological index or Z-index).[7] As shown in Fig. 1 we can

†Part II. *Bull. Chem. Soc. Jpn.*, **53**, 1228 (1980).

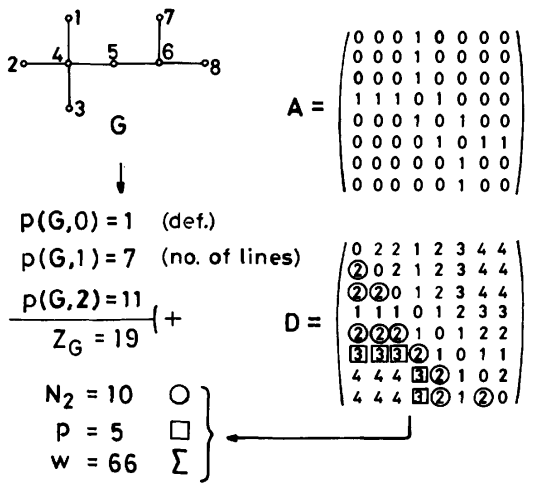

Fig. 1 Enumeration of various topological indices for 2,2,4-trimethylpentane. G: graph, A: adjacency matrix, and D: distance matrix.

Table 1. Various topological indices of hexane, heptane, and octane isomers

No.[a]	Name[b]	Z[c]	w	p_3	p_2
6-1	6	13	35	3	4
2	3m-5	12	31	4	5
3	2m-5	11	32	3	5
4	23m-4	10	29	4	6
5	22m-4	9	28	3	7
7-1	7	21	56	4	5
2	3e-5	20	48	6	6
3	3m-6	19	50	5	6
4	2m-6	18	52	4	6
5	23m-5	17	46	6	7
6	33m-5	16	44	6	8
7	24m-5	15	48	4	7
8	22m-5	14	46	4	8
9	223m-4	13	42	6	9
8-1	8	34	84	5	6
2	3e-6	32	72	7	7
3	3m-7	31	76	6	7
4	4m-7	30	75	6	7
5	2m-7	29	79	5	7
6	34m-6	29	68	8	8
7	3m3e-5	28	64	9	9
8	2m3e-5	28	67	8	8
9	23m-6	27	70	7	8
10	24m-6	26	71	6	8
11	33m-6	25	67	7	9
12	25m-6	25	74	5	8
13	234m-5	24	65	8	9
14	22m-6	23	71	5	9
15	233m-5	23	62	9	10
16	223m-5	22	63	8	10
17	224m-5	19	66	5	10
18	2233m-4	17	58	9	12

a) These numbers are used in Figs. 3—8. b) Platt's nomenclature.[3] c) The definitions of these indices are given in the text.

easily enumerate these topological indices with 2,2,4-trimethylpentane as an example. In Table 1 are tabulated the Z, w, p_2, and p_3 values for all the haxane, heptane, and octane isomers.[26,27]

Correlation among Z, w, p_2, and p_3. In Table 2 the correlation coefficients among the four different topological indices for eighteen octane isomers are given. It is evident that p_3 is the least correlated with other three indices. Among them w has rather large $|\rho|$ value of 0.79 with p_3. They are far from being orthogonal to each other. The index p_2 also has relatively large $|\rho|$ values both with Z and w, and is not a good candidate for an element of an orthogonal pair of indices.

Table 2. Correlation coefficients among the various topological indices for the eighteen octane isomers

	Z	w	p_3	p_2
Z	1			
w	0.761	1		
p_3	−0.257	−0.787	1	
p_2	−0.936	−0.903	0.543	1

On the other hand, the pair of Z and p_3 is found to be the most orthogonal to each other, whereas the $|\rho|$ value for the pair of Z and p_2 is the largest, though negative. As shown in Table 3 correlations among these indices were also calculated for other isomer sets with N=6, 7, and 9, and also for their cumulative sets (given in parentheses). Correlation patterns are found to be all the same for each isomer set.

Some of the above correlation patterns can be explained by the graph-theoretical properties of these indices. By definition w includes both p_2 and p_3 as its components. As seen in Table 2 the $|\rho|$ values among these three parameters are very large and thus one cannot choose any two of them as a good orthogonal pair of indices, although Randić and Wilkins classified the thermodynamic and some other physical properties according to their correlation patterns with respect to p_2 and p_3.[13] The value of p_2 increases by 1 and 2, respectively, for each tertiary and quarternary branching, just in the opposite direction for the case of the components of Z. Namely, p(G,2), an element of Z, decreases by 1 and 3, respectively, for each tertiary and quarternary branching.[7] On the other hand, the values of Z and p_3 forming a good orthogonal pair are derived from different countings, *i.e.*, Z from disjoint line selection and p_3 from distant point-pair selection.

It is to be noted that even for the orthogonal pair of Z and p_3, their correlation coefficients get dramatically large if more than two isomer sets with different carbon numbers are combined as shown in the parentheses in Table 3. Also for the pair of Z and w the correlation coefficient gets as large as 0.94 even in the cumulative set up to octanes. One can expect ρ=1 for the correlation between many different molecular quantities such as heat of formation and just the number of carbon atoms if an infinitely large number of hydrocarbons are taken! It is not necessarily true for the structure-activity correlation study that the larger the better.

Then in the following discussion we will mainly be

Table 3. Correlation coefficients among the various topological indices for hexane to nonane isomers

No. of Carbon	No. of Isomer	$Z-p_3$	$w-p_3$	$Z-w$	p_3-p_2
6	5	0.000	−0.333	0.924	0.080
7	9	−0.091	−0.648	0.796	0.394
	(14)[a]	(0.507)	(0.457)	(0.923)	(0.566)
8	18	−0.257	−0.787	0.761	0.543
	(32)	(0.543)	(0.512)	(0.940)	(0.727)
9	35	−0.142	−0.782	0.665	0.461
	(67)	(0.587)	(0.511)	(0.938)	(0.739)

a) The numbers in parentheses are obtained for the set of hydrocarbons cumulated from the hexane isomers.

Table 4. Correlation coefficients between thermodynamic properties and the topological index and polarity number

Type number	Property	$\rho(Z)$			$\rho(p_3)$			$\bar{\rho}(Z)$	$\bar{\rho}(p_3)$
		N[a]=6	7	8	6	7	8		
A1	Heat of vaporization	0.983	0.985	0.955	0.015	−0.147	−0.262	0.97	−0.19
A2	Entropy	0.961	0.919	0.930	−0.132	−0.233	−0.485	0.93	−0.36
A3,5	Heat of formation[b,c]	0.979	0.981	0.896	0.078	−0.079	0.059	0.93	0.02
A4	Boiling point	0.977	0.966	0.888	0.082	0.038	0.088	0.92	0.07
A'6	Entropy of vaporization	0.979	0.931	0.836	−0.077	−0.385	−0.595	0.88	−0.46
A'7	Entropy of fusion[d]	0.943	0.911	0.764	−0.538	−0.356	−0.600	0.83	−0.52
A'8	Cryoscopic constant[d]	0.830	0.826	0.726	−0.549	−0.283	−0.589	0.77	−0.50
A'9	Heat of fusion[d]	0.974	0.937	0.672	−0.496	−0.393	−0.508	0.79	−0.47
B1	Density of liquid	0.590	0.306	0.104	0.798	0.914	0.974	0.23	0.93
B2	Critical pressure	−0.383	−0.284	−0.465	0.871	0.970	0.966	−0.40	0.95
B3	Refractive index	0.696	0.375	0.133	0.705	0.877	0.963	0.28	0.90
B4	Pressure coefficient of vaporization	0.803	0.335	0.026	0.493	0.766	0.864	0.23	0.78
C1,4	Molal refraction[e]	−0.119	−0.124	−0.037	−0.982	−0.975	−0.990	−0.07	−0.98
C2	Molal volume	−0.592	−0.308	−0.112	−0.793	−0.912	−0.973	−0.24	−0.93
C3	Refractivity intercept	0.802	0.317	0.151	−0.519	−0.930	−0.933	0.29	−0.87
W1	Specific dispersion	−0.773	−0.552	−0.387	−0.614	−0.723	−0.864	−0.49	−0.79
W2	Critical temperature	0.919	0.712	0.322	0.332	0.558	0.764	0.52	0.64
W3	Critical volume	0.915	0.434	0.293	−0.290	−0.682	−0.725	0.42	−0.65
W4	Critical density	−0.905	−0.432	−0.292	0.312	0.677	0.716	−0.42	0.65
X1	Melting point[d]	0.131	−0.295	−0.402	−0.226	0.290	0.333	−0.30	0.24
X2	Critical pV/RT	−0.516	−0.325	−0.597	0.493	0.151	0.321	−0.51	0.30
X3	Free energy of formation	0.922	0.686	−0.075	0.295	0.143	0.826	0.28	0.56

a) Number of carbon atoms. b) Only this property is correlated with $-Z$. c) A5 is heat of combustion, which has the same correlation coefficients as heat of formation. d) Data are not available for several isomers. e) C4 is specific refraction, which has the same correlation coefficients as molal refraction.

concerned with the correlation between the thermodynamic properties of isomeric hydrocarbons and the two topological indices Z and p ($=p_3$).

II. Structure-Activity Correlation

Thermodynamic Properties. From the American Petroleum Institute (API) Research Project 44[25] twenty four thermodynamic properties were chosen for five hexane, nine heptane, and eighteen octane isomers as listed in Table 4. For some of the selected cases the values of thirty five nonane isomers were also analyzed. The type symbol, such as A or B, is tentatively assigned to each property according to the discussion in the later part of this paper.[28] The correlation coefficients between these quantities and Z and p_3 were calculated as shown in Table 4. For some of the properties the data of a few isomers are missing, but no serious problem arose in comparing and discussing all the correlation coefficients given in Table 4 without further statistical correction.

Classification of Thermodynamic Properties. By looking at the patterns of the numbers in each row of Table 4, one may notice that they can roughly be grouped into four. Namely, the nine type A properties have large (0.7—1.0) positive $\rho(Z)$. However, as for $\rho(p_3)$ some of them have an appreciably large value as large as −0.6 and are assigned as type A', while the rest of them have very small $|\rho(p_3)|$ values. Type B properties have large (0.8—1.0) positive $\rho(p_3)$ values, while type C large (−0.9—−1.0) negative $\rho(p_3)$'s. The $\rho(Z)$ values of both type B and C properties are very small. For other properties in Table 4 , both the $\rho(Z)$ and $\rho(p_3)$ values are medium to small. However, if one looks at these figures more carefully, they may be grouped into two. To make these groupings more clear the ρ values of N=6, 7, and 8 isomers for each property were tentatively averaged with weights of 1, 2, and 4, respectively, to give $\bar{\rho}(Z)$ and $\bar{\rho}(p_3)$ in Table 4. Then

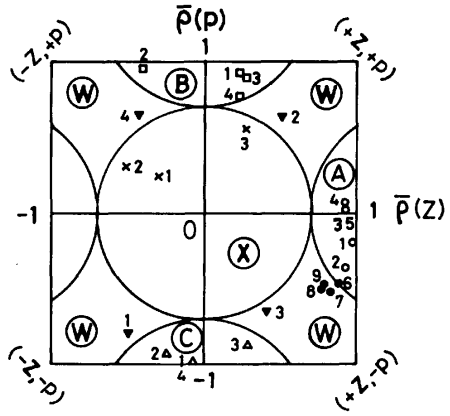

Fig. 2. Plot of $(\bar{\rho}(Z),\bar{\rho}(p_3))$ for the various thermodynamic properties averaged over hexane, heptane, and octane isomers.
○: type A, ●: type A′, □: type B, △: type C, ▼: type W, ×: type X.
The numbers near the points refer to the property numbers given in Table 4, where the $\bar{\rho}(Z)$ and $\bar{\rho}(p_3)$ values are also given.

it was found that for the entries other than types A, B, and C the correlation coefficients of $|\bar{\rho}(Z)|$ and $|\bar{\rho}(p_3)|$ are smaller than 0.5 and 0.8, respectively. Again they are divided into types W and X depending that the $|\rho(p_3)|$ value is larger or smaller than 0.6. Both the $|\rho(Z)|$ and $\rho(p_3)$ values for type X properties are smaller than 0.6.

Next the $\bar{\rho}(Z)$ and $\bar{\rho}(p_3)$ values for the twenty four properties were plotted in the rectangular coordinate plane as in Fig. 2. A pair of $(\bar{\rho}(Z), \bar{\rho}(p_3))$ is then found to be a good index for characterizing the nature of the topological factors on which the specified property depends. Namely, all the five entries of type A (boiling point, entropy, and heats of vaporization, formation, and combustion) fall into the far right arc in Fig. 2, whereas the four entries of type B (density of liquid, critical pressure, refractive index, and pressure coefficient of vaporization) and three of type C (molal refraction, specific refraction, molal volume, and refractivity intercept), are, respectively, encircled in the top and bottom arcs. Notice that by this plot all the four entries of type A′ (cryoscopic constant, heat of fusion, entropies of vaporization and fusion) get close to each other and are clearly distinct from W3 (critical volume). This supports our tentative grouping of the thermodynamic properties. Although the distance between the four A′ entries and A2 (entropy) is rather small, the latter discussion will differentiate them. It is interesting to note that all the four entries of type W (specific dispersion, critical temperature, critical volume, and cirtical density) find their respective places at the four corners showing all the possible different combinations of the modes of $\bar{\rho}(Z)$ and $\bar{\rho}(p_3)$ but are clearly distinct from the three properties of type X (melting point, critical pV/RT, and free energy of formation). It is interesting to note that these four entries are distinctively classified by Randić and Wilkins by the different combinations of the signs of the correlation with p_2 and p_3.[13] Their argument is based on the relative trends of the correlation patterns, while our criterion is based on the quantitative features of the correlation.[29]

Thus we can affirmatively classify the thermodynamic properties of alkanes into the following groups and select their typical entries as follows:

Type A: Heat of vaporization:
large $\rho(Z)$ and small $|\rho(p_3)|$

Type B: Density of liquid:
large $\rho(p_3)$ and small $|\rho(Z)|$

Type C: Molal refraction:
large $-\rho(p_3)$ and small $|\rho(Z)|$

Type W: Specific dispersion:
medium $|\rho(Z)|$ and $|\rho(p_3)|$

Type X: Melting point:
small $|\rho(Z)|$ and $|\rho(p_3)|$

However, there still remains a question if the pair of Z and p_3 parameters are the best combination for this sort of classification. To check this point the correlation coefficients of the above-mentioned five typical properties for the other parameters, w and p_2, were calculated and compared with the results for Z and p_3 in Table 5, where the $|\rho|$ values larger than 0.9 is printed in bold face. From this Table it is difficult to select such a useful pair of indices other than the pair of Z and p_3 that is capable of characterizing each type of properties. No $|\rho|$ value except for that of p_2 for Type A exceeds 0.9 suggesting inappropriateness of parameter p_2 for this purpose.

This conclusion is different from the criterion taken by Randić and Wilkins, who claim the effectiveness of the classification of the physical properties by the combination of p_2 and p_3.[30]

In Table 5 are also given important data for the $\rho(Z)$ and $\rho(p_3)$ values of thirty five nonane isomers, whose features on the ρ values are essentially the same, revealing that our tentative classification would be valid for relatively large saturated hydrocarbons.

Pattern Recognition of Correlation. Having established the classification of the thermodynamic properties into five types, let us see the similarity of the correlation pattern among each type. Figures 3 and 4 give the plots of four of type A properties (A1—A4) of the heptane and octane isomers against Z. The isomers are arranged in the increasing order of Z. The Wiener's path number w is also plotted against Z. While for heptane isomers correlation is fairly good, it gets worse for octane giving zigzag patterns.

It is worthy of notice that the zigzag patterns in the left half region of octanes of boiling point (bp) and heat of formation $(-\Delta H_f)$ in Fig. 4 have an opposite trend to w but coincide with the corresponding patterns of type B plots in Fig. 6, where all the four curves of B1—B4 amazingly run in parallel with p_3 (See

Table 5. Correlation coefficients of the five typical thermodynamic properties for four different topological indices

Type	Typical property	Parameter	Number of C atoms 7[a]	8[b]	9[c]	Parameter	C atoms 7[a]	8[b]
A	Heat of vaporization	Z	**0.985**[d]	**0.955**	**0.938**	w	0.872	0.787
		p_3	−0.147	−0.262	0.007	p_2	**−0.928**	**−0.911**
B	Density of liquid	Z	0.306	0.104	−0.104	w	−0.296	−0.597
		p_3	**0.914**	**0.974**	**0.980**	p_2	0.019	0.264
C	Molal refraction	Z	−0.124	−0.037	0.069	w	0.479	0.669
		p_3	**−0.975**	**−0.990**	**−0.982**	p_2	−0.194	−0.325
W	Specific dispersion	Z	−0.552	−0.387	−0.329	w	0.030	0.349
		p_3	−0.723	−0.864	−0.870	p_2	0.305	0.006
		$-Z-5p_3$	**0.936**	**0.981**	**0.963**			
X	Melting point	Z	−0.295	−0.402	0.120	w	−0.246	−0.322
		p_3	0.290	0.333	0.255	p_2	0.347	0.498
		$-Z+2p_3$	0.387	0.454	0.021			

a) Data taken from nine heptane isomers but seven for melting point. b) Data taken from eighteen octane isomers but fourteen for melting point. c) Data taken from thirty five nonane isomers but nineteen for melting point. d) Those figures whose absolute magnitudes exceed 0.9 are underlined.

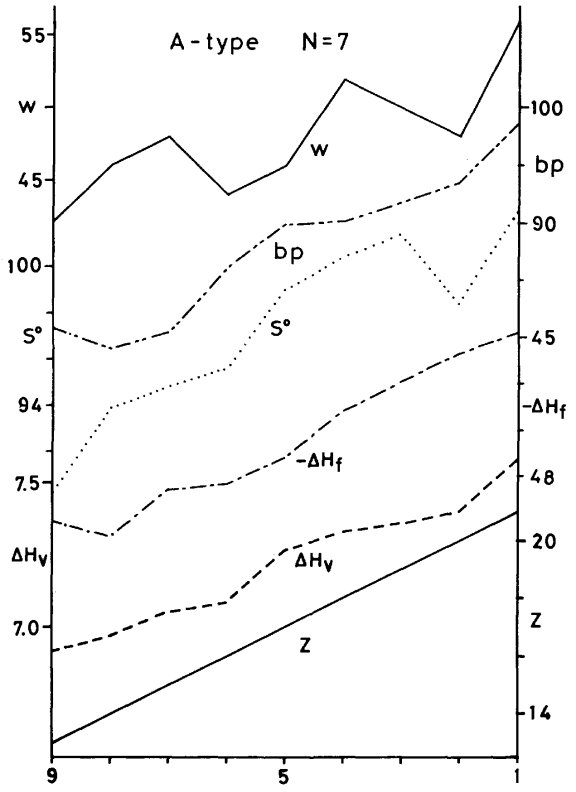

Fig. 3. Thermodynamic properties of heptanes. Type A. The numbers in the abscissa refer to the isomer numbers given in Table 1. The properties and their units are: A1, heat of vaporization (ΔH_v) in kcal·mol^{-1}; A2, entropy ($S°$) in cal·deg^{-1} mol^{-1}; A3, heat of formation ($-\Delta H_f$) in kcal·mol^{-1}; A4, boiling point (bp) in °C. (1 cal$_{th}$=4.184 J)

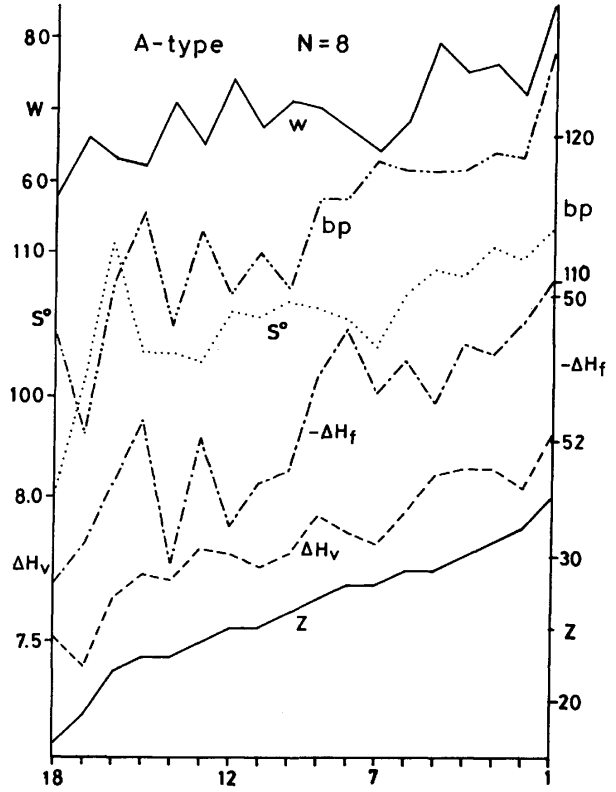

Fig. 4. Thermodynamic properties of octanes. Type A. See the footnotes of Fig. 3.

also Fig. 5 for type B properties of heptanes). Quite similarly type C properties show a good correlation with $1/p$ as demonstrated for C1—C3 in Figs. 7 and 8.

As have been shown in the above discussion the merits of drawing the correlation patterns like Figs. 3—8 lie not only in making certain of the classification of the structure-activity relationship but also in digging out the second variable hidden under the main correlation pattern. Further, if a good set of complementary indices like Z and p_3 are available, another correlation plot as Fig. 2 is found to be powerful for the analysis of structure-activity relationship.

Two-parameter Correlation. As has been inferred above, the p_3 character seems to be mixed in the correlation pattern of the boiling point against Z for octane isomers in Fig. 4. Then correlation coefficients were calculated between the A4 values of octane isomers and various in-phase linear combinations of Z and p_3. The optimum value was obtained to be $\rho(Z+p_3)=0.947$, which is to be compared with $\rho(Z)=0.888$ in Table 4.

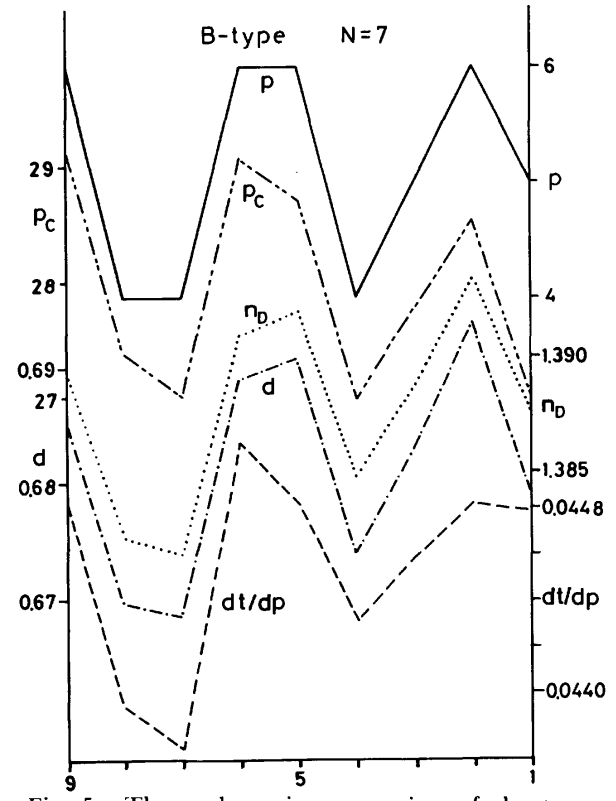

Fig. 5. Thermodynamic properties of heptanes. Type B. The numbers in the abscissa refer to the isomer numbers given in Table 1. The properties and their units are: B1, density of liquid (d^{25}) in g·ml^{-1}; B2, critical pressure (p_c) in atm.; B3, refractivity index (n_D); B4, pressure coefficient of vaporization (dt/dp) in °C·mmHg^{-1}. (1 mmHg= 133.322 Pa)

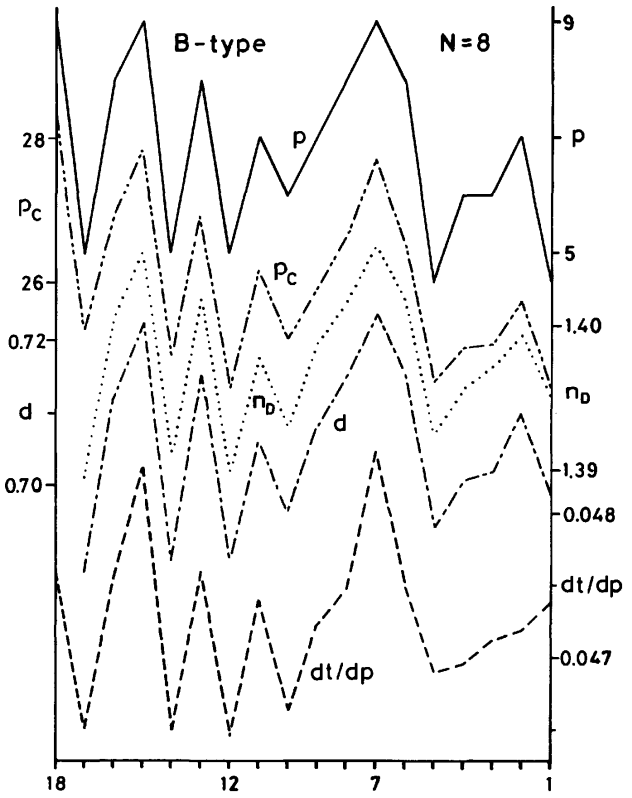

Fig. 6. Thermodynamic properties of octanes. Type B. See the footnotes of Fig. 5.

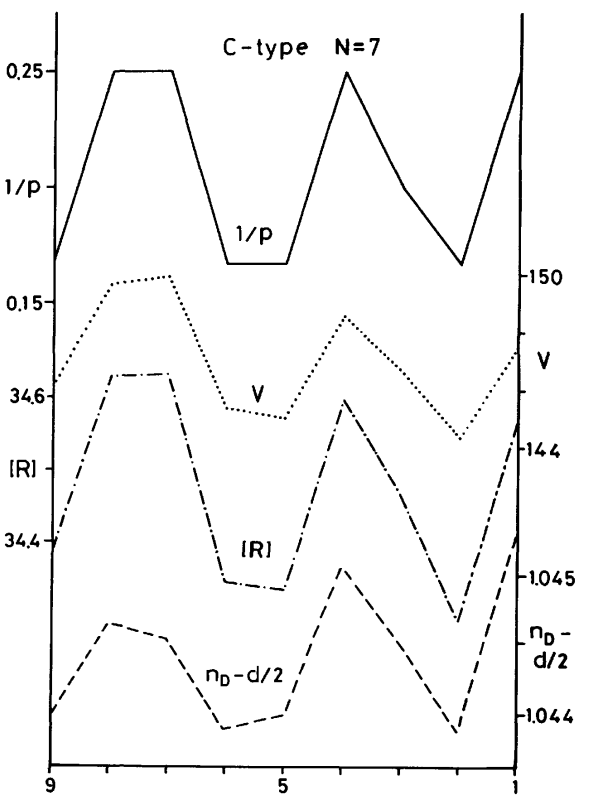

Fig. 7. Thermodynamic properties of heptanes. Type C. The numbers in the abscissa refer to the isomer numbers given in Table 1. The properties and their units are: C1, Molal refraction ([R]) in ml·mol^{-1}; C2, Molal volume (V) in ml·mol^{-1}; C3, Refractivity intercept ($n_D - d/2$).

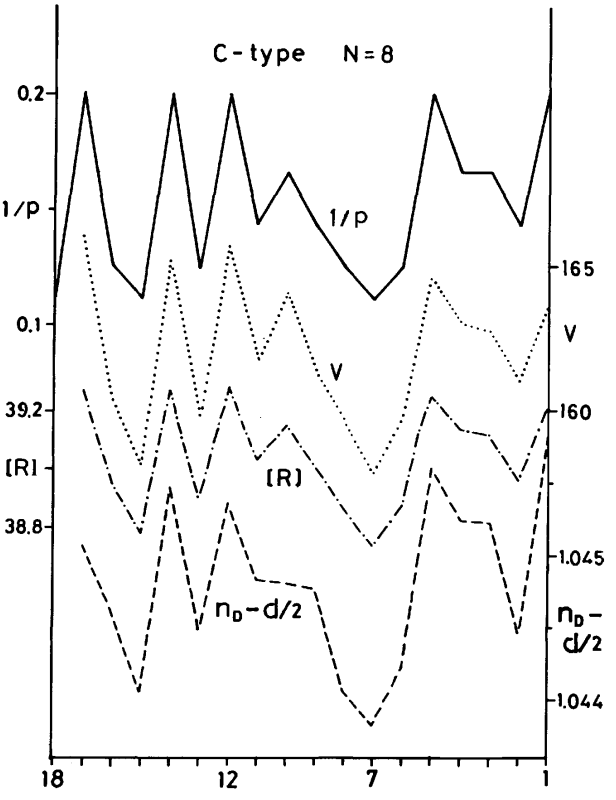

Fig. 8. Thermodynamic properties of octanes. Type C. See the footnotes of Fig. 7.

TABLE 6. EFFECT OF MIXING OF PARAMETERS Z AND p_3 ON THE CORRELATION COEFFICIENTS FOR SEVERAL THERMODYNAMIC PROPERTIES OF OCTANE ISOMERS

Property[a]	ρ (Z)[b]	ρ (p_3)[b]	$(\rho^2(Z)+\rho^2(p_3))^{1/2}$	Best ρ Value	Best ρ Combination
A1	+	−	0.990	0.990	Z
A2	+	−	1.049	0.963	$Z-p_3$
A3,5	+	+	0.898	0.981	$Z+5p_3$
A4	+	+	0.892	0.947	$Z+p_3$
A'6	+	−	1.026	0.922	$Z-2p_3$
A'7	+	−	0.971	0.846	$Z-2p_3$
A'8	+	−	0.935	0.813	$Z-2p_3$
A'9	+	−	0.842	0.735	$Z-2p_3$
W1	−	−	0.947	0.981	$-Z-5p_3$
W2	+	+	0.829	0.938	$Z+5p_3$
W3	+	−	0.782	0.732	$Z-12p_3$
W4	−	+	0.773	0.724	$-Z+12p_3$
X1	−	+	0.522	0.454	$-Z+2p_3$
X2	−	+	0.678	0.622	$-Z+p_3$
X3	−	+	0.829	0.826	p_3

a) See Table 4. b) Numerical values are given in Table 4.

Similar calculations were performed for the properties of types A', W, and X of octane isomers by varying the relative values of a and b for $\rho(aZ+bp_3)$. The results are given in Table 6, where the values of $|\rho|=(\rho^2(Z)+\rho^2(p_3))^{1/2}$ are also given. This quantity was found to be a good indicator for estimating the magnitude of the optimum value to be obtained with a mixing parameter $aZ+bp_3$. The value of $|\rho|$ itself does not have a definite meaning and thus sometimes may exceed unity. However, within each series of properties of types A, A', W, and X, good parallelism is observed between $|\rho|$ and the optimum $\rho(aZ+bp_3)$ value.

The fact that the four properties of type A' have the same optimum combination of Z and p_3 as $Z-2p_3$ corresponds to the clustering of the points for these properties in the $\rho(Z)-\rho(p_3)$ plot of Fig. 2.[31]

Note also that the signs of a and b giving the optimum value are correctly predicted by the corresponding signs of $\rho(Z)$ and $\rho(p_3)$. This is dramatically shown in the four properties of type W. All these entries are found in the four different quadrants in the $\rho(Z)-\rho(p_3)$ plot of Fig. 2. The above discussions support our tentative assignment of type W and A' properties. Among the four entries in type W, two of them (W1 and W2) achieved fair improvement in the ρ values, while the rest of them (W3 and W4) got only a little improvement. The optimum ρ values for the latter, however, are still larger than those for X1 and X2. If one looks at the data of octane isomers in Table 6, only X3 may be regrouped into type W having fairly large optimum ρ value. However, as evident in Table 4, for property X3, as well as X1, the fluctuation of the $\rho(Z)$ and $\rho(p_3)$ values is very large compared to other properties even to type W properties.

In this study only the optimum ρ value was sought for the mixing parameters of $aZ+bp_3$. Although there is a possibility to get a better result with $aZ+b/p_3$ or other combination of Z and p_3, the analysis has clarified the essential features of the two-parameter topological properties of saturated hydrocarbons.

Interpretation of Topological Factors. Then what do the two-parameter features in the structure-activity relationship mean? Among the four entries in type B properties, density of liquid d (B1) and refractive index n_D (B3) of alkanes are doubtlessly determined by the bulkiness of molecules. The fact that molal refraction $[R]$ (C1) and molal volume V (C2) of type C have large negative correlation with p_3 can also be explained by the bulkiness of molecules, since they are reciprocally related to density, respectively, as $[R]=M(n_D^2-1)/(n_D^2+2)d$ and $V=M/d$, where M is the molar mass. Since the specific refraction is expressed as $(n_D^2-1)/(n_D^2+2)d$, it should have quite the same correlation coefficients as molal refraction, and we did not include its values in Table 4. Refractive intercept $n_D-d/2$ (C3) belongs to type C but its physical meaning is left unclear.

Critical pressure (B2) is expressed as $p_c=a/27b^2$, where a and b are the constants in the van der Waals equation of state.[32] The parameters a and b are interpreted respectively to reflect intermolecular interaction and molecular size. If we assume that a is almost constant among the isomeric hydrocarbons, the critical pressure is inversely proportional to the square of b, or molecular size. Then the higher the density, the smaller the b value, leading to a parallelism between d and p_3. Similarly critical volume V_c (W3) and critical temperature T_c (W2) are related to a and b as $V_c=3b$ and $T_c=8a/27Rb$, leading to negative and positive correlation with p_3, respectively. Of course, critical density d_c (W4) is inversely proportional to V_c. Although T_c, V_c, and d_c belong to type W, the results of Table 6 show that all of them get larger ρ value if small amount of out-of-phase Z character is introduced into $\rho(aZ+bp_3)$. Thus no matter what mechanism is responsible for the good correlation between the path number p_3 and these p-related properties, the parameter p_3 surely can take account of the topological bulkiness factor. One may well call p_3 as the static

topological parameter, while the Z index as the dynamical topological parameter. The reason for the latter naming will be explained as follows.

We have shown in the previous paper[15] that the entropy $S°$ (A2) of alkanes is well correlated with the Z index except for sterically crowded and highly symmetrical molecules. The main factor in the parallelism between Z and $S°$ is due to the fact that the branching of alkanes decreases the Z value and also the freedom of rotation which eventually lowers $S°$.[33-35] Further, through the following relation

$$S° = \int_0^T C_p/T' \, dT'$$

and the Trouton's law, *i. e.*, bp (A4) is proportional to ΔH_v (A1), three of type A properties except heat of formation (A3) can be related to each other. All these properties are determined by the dynamical balance between the vigorous motion of molecules and intermolecular force. This picture is a little different from what the term cohesiveness means. Moreover, as the term molecular cohesiveness proposed by Cramer[12,17] seems to involve molecular packing and bulkiness to some extent, we prefer to say that the Z index takes account of the dynamical topological factor such as the rotational motion of molecules, and we may call Z as the dynamical topological parameter.

Deviation of the boiling point data from the Z-correlation as shown in Fig. 4 can be explained by the onset of stacking or bulkiness effect in the highly branched alkanes. A systematic study has not been done for viscosity, since a good set of data was not available. However, a preliminary study reveals that viscosity surely belongs to type W.

Now it is established that most of the thermodynamic properties, except type X properties as melting point (X1), are linear functions of two orthogonal topological parameters, namely, dynamical Z relating to the rotational degree of freedom and static p_3 governing the bulkiness of molecules. It is then deduced that the form of the linear function of a given property of hydrocarbons reflects how the two topological factors are competing in the molecular level. More detailed study, such as physical modelling and molecular dynamics type simulation calculation, can be proceeded further along the topological understanding obtained in this paper.

References

1) W. J. Taylor, J. M. Pignocco, and F. D. Rossini, *J. Res. Natl. Bur. Stand.*, **34**, 413 (1945).

2) H. Wiener, *J. Am. Chem. Soc.*, **69**, 17, 2636 (1947); *J. Phys. Chem.*, **52**, 425, 1082 (1948).

3) J. R. Platt, *J. Phys. Chem.*, **56**, 328 (1952).

4) K. Altenburg, *Kolloid Z.*, **178**, 112 (1961); *Brennstoff Chem.*, **47**, 100, 331 (1966) and other papers.

5) G. R. Somayajulu and B. J. Zwolinski, *Trans. Faraday Soc.*, **62**, 2327 (1966); *J. Chem. Soc., Faraday Trans. 2*, **68**, 1971 (1972).

6) G. Mann, *Tetrahedron*, **23**, 3375 (1967); G. Mann, M. Mühlstädt, J. Braband, and E. Döring, *ibid.*, 3393 (1967).

7) H. Hosoya, *Bull. Chem. Soc. Jpn.*, **44**, 2332 (1971).

8) L. B. Kier and L. H. Hall, "Molecular Connectivity in Chemistry and Drug Design," Academic Press, New York, 1976.

9) C. Hansch and A. Leo, "Substitutent Constants for Correlation Analysis in Chemistry and Biology," Wiley, New York, 1979.

10) A. T. Balaban, A. Chiriac, I. Motoc, and Z. Simon, "Steric Fits in Quantitative Structure-Activity Relations," Lecture Notes in Chemistry, No. 15, Springer, Berlin, 1980, p. 22.

11) O. Mekenyan, D. Bonchev, and N. Trinajstić, *Int. J. Quant. Chem.*, **18**, 369 (1980).

12) R. Cramer, III., *J. Am. Chem. Soc.*, **102**, 1837, 1849 (1980).

13) M. Randić and C. L. Wilkins, *J. Phys. Chem.*, **83**, 1525 (1979).

14) H. Hosoya, K. Kawasaki, and K. Mizutani, *Bull. Chem. Soc. Jpn.*, **45**, 3415 (1972).

15) H. Narumi and H. Hosoya, *Bull. Chem. Soc. Jpn.*, **53**, 1228 (1980).

16) H. Narumi, H. Hosoya, and M. Katayama, *Bull. Fac. Eng. Hokkaido Univ.*, No. 103, 19 (1981) (in Japanese).

17) J. T. Edward, *Can. J. Chem.*, **58**, 1897 (1980); **60**, 2573 (1982).

18) M. Gordon and G. R. Scantlebury, *Trans. Faraday Soc.*, **60**, 604 (1964).

19) D. M. Cvetković, M. Doob, and H. Sachs, "Spectra of Graphs," Academic Press, New York, 1980, p. 270.

20) D. H. Rouvray in "Chemical Application of Graph Theory," A. T. Balaban, Ed., Academic Press, London, 1976, p. 175.

21) N. Trinajstić, "Chemical Graph Theory," CRC Press, Boca Raton, Florida, 1983, Vol. II., p. 105.

22) A. T. Balaban, I. Motoc, C. Bonchev, and O. Mekenyan, *Topics in Current Chemistry*, **114**, 21 (1983).

23) A. T. Balaban, *Theor. Chim. Acta*, **53**, 355 (1979).

24) D. Bonchev and N. Trinajstić, *J. Chem. Phys.*, **67**, 4517 (1977).

25) American Petroleum Institute Research Project 44 at the National Bureau of Standards, "Selected Values of Physical and Thermodynamic Properties of Hydrocarbons," Texas A & M Univ., 1945.

26) K. Mizutani, K. Kawasaki, and H. Hosoya, *Natural Sci. Rept. Ochanomizu Univ.*, **22**, 39 (1971).

27) K. Kawasaki, K. Mizutani, and H. Hosoya, *Natural Sci. Rept. Ochanomizu Univ.*, **22**, 181 (1971).

28) Preliminary account is given in H. Hosoya, and Y. Maruyama, "Structure and Properties," (in Japanese), Asakura, Tokyo, 1975, p. 88.

29) They actually did not obtain the correlation coefficients but observed the relative tendency of the physical properties against the increase of the parameters concerned.

30) According to Randić and Wilkins our W4 and B2 belong to the same (+,+) group. Their similar character can be shown as the proximity of their points in Fig. 2. This is also the case with the (+,−) group of W1 and C2, and (−,+) group of W2 and A5. This fact suggests the different criteria of the classification of the properties taken by us and by Randić and Wilkins.

31) Actually in Fig. 2, the plot is made for the $\bar{\rho}$ averaged over N=6—8, but as seen in Table 4, the corresponding signs of ρ values within types A′ and W are all the same for different N.

32) See the reference cited in 28.

33) K. S. Pitzer, *J. Chem. Phys.*, **8**, 711 (1940).

34) W. B. Person and G. C. Pimentel, *J. Am. Chem. Soc.*, **75**, 532 (1953).

35) D. W. Scott, *J. Chem. Phys.*, **60**, 3144 (1974).

 © 1985 The Chemical Society of Japan Bull. Chem. Soc. Jpn., 58, 1787—1792 (1985)

Formation and Reaction of Carbonyl Ylides. 1,3-Dipolar Cycloaddition of 2-Benzopyrylium-4-olates with Carbonyl Compounds

Toshikazu IBATA* and Jiro TOYODA
Institute of Chemistry, College of General Education, Osaka University, Toyonaka 560
(Received January 28, 1985)

Cyclic orthoester type 1,3-dipolar cycloadducts of 1-methoxy-2-benzopyrylium-4-olate with carbonyl compounds were obtained in high yields in the copper(II) acetylacetonate-catalyzed decomposition of *o*-methoxycarbonyl-α-diazoacetophenone in the presence of carbonyl compounds such as substituted benzaldehydes, acetaldehyde, propionaldehyde, isobutyraldehyde, pivalaldehyde, acetone, methyl ethyl ketone, methyl isopropyl ketone, 1,3-dichloroacetone, substituted acetophenones, benzoyl cyanides, cyclopentanone, cyclohexanone, 1-indanone, 9-fluorenone, anthrone, and anthraquinone. However, methyl *t*-butyl ketone, benzophenone, and xthanthone gave no adduct. Aldehydes and asymmetric ketones gave endo- and exo-adducts. The regiochemistry and stereochemistry of the adducts of aldehydes were determined on the basis of their coupling constants of methine protons. The reactions of *p*-methoxyphenyl *o*-diazoacetylbenzoate also gave similar 1,3-dipolar adducts. When carbonyl compounds of medium reactivity were used as a substrate, 2:1-adduct was obtained together with the 1:1-adduct. The formation of the 2:1-adduct was attributed to the competitive reaction of the corrsponding benzopyrylium-4-olate intermediate toward the carbonyl compounds and 1:1-adduct. The regiospecificity of the 1:1-cycloaddition was explained according to the frontier orbitals calculated by STO-3G method.

The initial work of the 1,3-dipolar cycloaddition of carbonyl ylide with carbonyl compounds was reported by Ullman and Milks in the photolysis of 2,3-epoxy-2,3-diphenyl-1-indenone.[1] However, only a few examples of the cycloaddition were reported in the literature.[2] The present authors have found the novel formation of carbonyl ylides of the type of 2-benzopyrylium-4-olate (**3**) by the intramolecular carbene–carbonyl reaction[3] and studied its 1,3-dipolar cycloaddition with acetylenic[4] and ethylenic compounds.[5] As an extension of this 1,3-dipolar cycloaddition, the authors have preliminarily reported the 1,3-dipolar cycloaddition of 1-methoxy-2-benzopyrylium-4-olate (**3a**:R=OCH_3) with benzaldehydes, propionaldehyde, acetophenones and fluorenone.[6] This paper deals with the application of the cycloaddition of (**3**) with various kinds of carbonyl compounds to understand the scope and limitation of the reaction for the synthesis of cyclic orthoesters. The regiochemistry and stereochemistry was also studied.

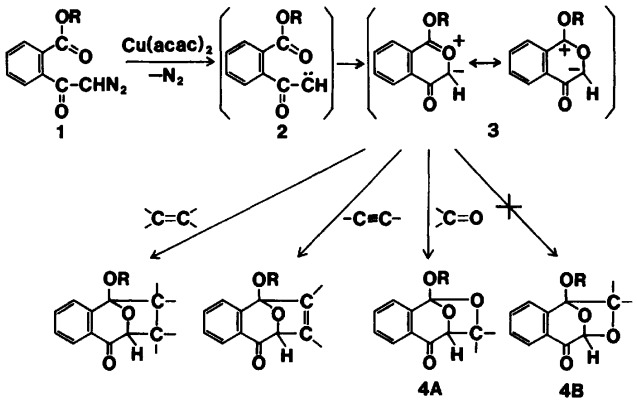

Results and Discussion

Reactions with Aldehydes. The $Cu(acac)_2$-catalyzed decomposition of *o*-methoxycarbonyl-α-diazoacetophenone (**1a**: R=OCH_3) in the presence of two molar equivalents of aromatic aldehydes gave each pair of isomeric adducts. For example, *p*-chlorobenzaldehyde gave two products of melting points at 135—137°C and 126—128°C. Results of elemental analysis and IR spectra showed that these are the isomeric adducts of **3a** and *p*-chlorobenzaldehyde having the same regiochemistry but different in configuration. The ^1H NMR coupling patterns of two methine protons of both adducts indicate that the cycloadducts have structures of orthoester as shown in formula **4A**. The higher melting product has doublet signals of methine protons at δ 5.08 and 5.53 with coupling constant J=6.0 Hz, which indicates the cis stereochemistry of two methine protons. Therefore, the substituent (**R′**) has *endo*-configuration as shown in formula **5**. The lower melting adduct has doublet siganls of methine protons at δ 4.78 and 4.86 with small coupling constant (J=1.3 Hz), which suggests the *exo*-structure (**6**) with trans configuration of two methine protons. The methine protons on C_5 (**Ha**) and C_6 (**Hb**) of the exo-adduct (**6c**) show its ^1H NMR signals at

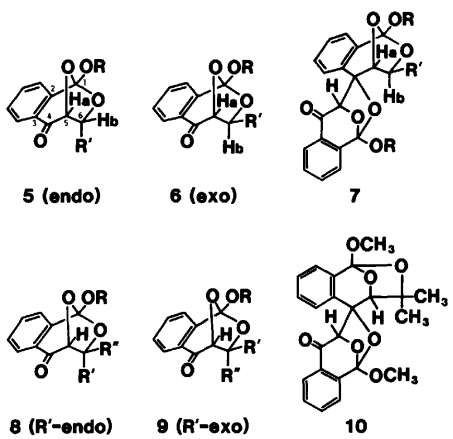

TABLE 1. YIELDS, IR, AND NMR DATA OF THE CYCLOADDUCTS OF **3** WITH ALDEHYDES

Run	R	R′	Adduct	Yield %	IR/cm^{-1}	NMR/ppm OCH$_3$[a]	Ha	Hb	Jab	Others[b]
Reactions with Aromatic Aldehydes										
a	CH_3	*p*-$CH_3OC_6H_4$	**5a**	33	c)	3.53,3.68	5.53(d)	5.09(d)	5.6	
			6a	42	1705	3.72,3.77	4.89(d)	4.78(d)	1.4	
b		C_6H_5	**5b**	38	1706	3.75	5.57(d)	5.27(d)	5.8	
			6b	44	1691	3.75	4.91(d)	4.81(d)	1.4	
c		*p*-ClC_6H_4	**5c**	42	1715	3.73,	5.53(d)	5.08(d)	6.0	
			6c	43	1708	3.72	4.86(d)	4.78(d)	1.3	
d		2,4-$Cl_2C_6H_3$	**5d**	75	1705	3.76	5.72(d)	5.38(d)	5.9	
			6d	12	c)	3.77	5.08(d)	4.83(d)	1.8	
e		2,6-$Cl_2C_6H_3$	**5e**	62	1690	3.75	5.93(d)	5.42(d)	5.4	
			6e	6	1703	3.80	5.53(d)	5.27(d)	2.3	
f		*p*-$NO_2C_6H_4$	**5f**	53	1702	3.77	5.65(d)	5.17(d)	6.0	
			6f	33	1698	3.77	4.92(s) 2H		—	
g		*m*-$NO_2C_6H_4$	**5g**	61	1690	3.78	5.72(d)	5.23(d)	5.7	
			6g	35	c)	3.78	4.93(s) 2H		—	
h	*p*-$CH_3OC_6H_4$	*p*-$CH_3OC_6H_4$	**5h**	35[d]	1705	3.68,3.80	5.27(d)	4.98(d)	5.6	
			6h	21	1711	3.69,3.79	4.70(d)	4.63(d)	1.3	
i		C_6H_5	**5i**	52[d]	1710	3.77	5.30(d)	5.01(d)	5.8	
			6i	43	1705	3.82	4.77(d)	4.69(d)	2.7	
j		*p*-$NO_2C_6H_4$	**5j**	47	1700	3.81	5.39(d)	5.11(d)	5.9	
			6j	45	1701	3.84	4.86(d)	4.71(d)	1.2	
Reactions with Aliphatic Aldehydes										
k	CH_3	CH_3	**5k**	39	1702	3.63	4.84(d)	4.54(dq)	5.5	1.05(d, CH_3)[f]
			6k	25	1710	3.68	4.52(d)	4.06(dq)	1.1	1.50(d, CH_3)[g]
l		CH_3CH_2	**5l**	e)	c)	3.95	4.86(d)	4.28(dt)	5.5	h)
			6l	e)	c)	3.63	4.56(s)	3.75(t)	—	i)
m		$(CH_3)_2CH$	**5m**	30	1708	3.63	4.90(d)	3.95(dd)	5.3	j)
			6m	47	1705	3.66	4.64(d)	3.41(dd)	1.3	k)
n		$(CH_3)_3C$	**5n**	11	1708	3.62	4.84(d)	4.13(d)	4.9	0.82(s, CH_3)
			6n	57	1710	3.43	4.64(d)	3.43(d)	1.8	1.04(s, CH_3)

a) Singlet signals. b) Signals of aromatic protons were omitted. c) The IR spectrum was not measured. d) The 2:1-adduct was obtained. e) Decomposed during column chromatography. f) J=6.5 Hz. g) J=6.5 Hz. h) δ=1.29 (dq, CH_2, J=6.9 and 7.2 Hz), 0.96 (t, CH_3, J=7.2 Hz). i) δ=1.76 (dq, CH_2, J=7.7 and 7.5 Hz), 1.07 (t, CH_3, J=7.5 Hz). j) δ=1.26 (d sep, CH, J=6.0 and 10.4 Hz), 0.90, 0.96 (d, CH_3, J=6.0 Hz). k) δ=1.95 (d sep, CH, J=6.5 and 10.4 Hz), 0.99, 1.06 (d, CH_3, J=6.5 Hz).

higher field than those of endo-adduct (**5c**). This may be attributed to shielding effect due to aryl (**R′**) and carbonyl groups located *syn* to each methine proton in the exo-adduct.

The assignment of the signals of methine protons (**Ha** and **Hb**) of the adducts (**5c** and **6c**) was determined on the basis of chemical shifts comparing with those of the adducts of aliphatic aldehydes. For example, endo-adduct of acetaldehyde has a doublet signal at δ 4.84 and a double quartet at δ 4.54 which were characterized to **Ha** and **Hb**, respectively. The exo-adduct also shows similar coupling pattern of methine protons (Table 1, Run k). The adducts of propionaldehyde and isobutyraldehyde were also identified similarly. In all of these adducts **Ha** showed a signal at lower field than that of **Hb**. The same tendency was observed in the adducts of aromatic aldehydes, and signals at δ 5.53 and 5.08 of the endo-adduct (**5c**) of *p*-chlorobenzaldehyde were assigned to **Ha** and **Hb**, respectively.

Other substituted benzaldehydes also gave similar results (Table 1, Run a—g). No adduct of the different regiochemistry as is shown by **4B** was obtained despite the detail inspection of the reaction mixture by column chromatography. The electron-attracting substituents on benzaldehyde such as *p*-NO_2 group tend to increase the yields of adducts in comparison with electron-releasing substituents (*p*-CH_3O). This means that the aldehydes with electron-attracting groups have high reactivity in this reaction system. However, these substituents do not show obvious effect on the stereoselectivity of the cycloaddition. Pivalaldehyde gave both endo- (**5n**) and exo-adduct (**6n**) in 11 and 57% respectively, reflecting the bulkyness of *t*-butyl group.

1-Methoxyphenyl *o*-diazoacetylbenzoate (**1b**:R=*p*-$CH_3OC_6H_4$) also gave similar results in the reaction with benzaldehydes. When *p*-anisaldehyde was used as a substrate, a 2:1-adduct (**7h**:R=R′=*p*-$CH_3OC_6H_4$) of **3b** and the aldehyde was obtained together with usual endo- and exo-1:1-adducts in the yields of 25, 35, and 21%, respectively. The 2:1-adduct has two singlet signals of methoxyl group at δ 3.47 (6H) and 3.73 (3H) and two doublets (δ 4.04, 4.65, J=1.5 Hz) and one singlet (δ 5.26) of methine protons besides multiplet signals of aromatic protons. The signals of the methine protons indicate the presence of two adjacent and one isolated methine protons. The coupling pattern of two dou-

TABLE 2. YIELDS, IR, AND NMR DATA OF THE CYCLOADDUCTS OF **3** WITH KETONES

Run	R	R′	R″	Adduct	Yield %	IR/cm^{-1}	NMR/ppm OCH$_3$[a]	NMR/ppm Ha[a]	NMR/ppm Others[b]
Reactions with Aliphatic Ketones									
a	CH_3	CH_3	CH_3	**8a**	75[c]	1707	3.67	4.88	1.11, 1.55(s, CH_3)
b			CH_3CH_2	**8b**	38	1705	3.65	4.50	1.05 (s, CH_3)[d]
				9b	20	1707	3.65	4.50	1.53 (s, CH_3)[e]
c			$(CH_3)_2CH$	**8c**	35	1710	3.67	4.63	0.95 (s, CH_3), f)
				9c	15	1700	3.67	4.53	1.44 (s, CH_3), g)
d		$ClCH_2$	$ClCH_2$	**8d**	96	1709	3.68	4.87	h)
Reactions with Aromatic Ketones									
e	CH_3	CH_3	*p*-$CH_3OC_6H_4$	**8e**	7	1709	3.55, 3.82	5.14	1.31 (s CH_3)
				9e	6	1707	3.50, 3.77	4.78	1.85 (s, CH_3)
f			C_6H_5	**8f**	15	1707	3.53	5.18	1.31 (s, CH_3)
				9f	18	1708	3.80	4.83	1.90 (s, CH_3)
g			*p*-$NO_2C_6H_4$	**8g**	29	1705	3.53	5.15	1.32 (s, CH_3)
				9g	46	1707	3.80	4.90	1.91 (s, CH_3)
h		CN	*p*-$CH_3OC_6H_4$	**8h**	64	1709	3.70, 3.85	5.25	
				9h	3	i)	3.64, 3.80	5.18	
i			*p*-$NO_2C_6H_4$	**8i**	86	1708	3.91	5.27	
				9i	7	i)	3.69	5.18	
j	*p*-$CH_3OC_6H_4$	CH_3	*p*-$CH_3OC_6H_4$	**8j**	—[c]				
				9j	4	1706	3.67, 3.81	4.69	1.32 (s, CH_3)
k			C_6H_5	**8k**	8[c]	i)	3.76	4.98	1.30 (s, CH_3)
				9k	13	1709	3.76	4.73	1.34 (s, CH_3)
l			*p*-$NO_2C_6H_4$	**8l**	54[c]	1710	3.80	5.00	1.33 (s, CH_3)
				9l	29	1708	3.83	4.81	1.37 (s, CH_3)

a) Singlet signal. b) Signals of aromatic protons were omitted. c) The 2:1-adduct was obtained. d) δ=1.04 (t, CH_3, J=7.3 Hz), 1.86 and 1.90 (q, CH_2, J=7.3 Hz). e) δ=0.88 (t, CH_3, J=6.7 Hz), 1.37 and 1.39 (q, CH_2, J=6.7 Hz). f) δ=1.01 (d, CH_3, J=6.8 Hz), 1.12 (d, CH_3, J=6.8 Hz), 2.19 (sep, CH, J=6.8 Hz). g) δ=0.90 (d, CH_3), 1.45 (sep, CH). h) δ=3.30 (d, CH_3, J=12.0 Hz), 3.56 (d, 1H, J=12.0 Hz), 3.87 (d, 1H, J=11.7 Hz), 4.12 (d, 1H, J=11.7 Hz). i) The IR spectrum was not measured.

TABLE 3. YIELDS, IR AND NMR DATA OF THE CYCLOADDUCTS (**8** AND **9**) OF **3** WITH CYCLIC KETONES

R	Ketone	Adduct	Yield %	IR	NMR/ppm OCH$_3$	NMR/ppm Ha	NMR/ppm Others[a]
CH_3	Cyclopentanone	**8m**	78	1706	3.63	4.61	1.2—2.3 (m, 8H, CH_2)
	Cyclohexanone	**8n**	87	1707	3.98	4.56	1.2—2.0 (m, 10H, CH_2)
	1-Indanone	**8o**	1.3[b]	1706	3.73	4.71	1.7—2.3 and 2.8—3.1 (m, 4H, CH_2)
		9o	6.8[c]	1701	3.62	5.01	1.6—2.3 and 2.8—3.1 (m, 4H, CH_2)
	9-Fluorenone	**8p**	75	1705	3.91	4.92	
	Anthraquinone	**8q**	17	1703	4.03	5.82	
	Anthrone	**8r**	21	1710	4.10	4.71	3.91 and 4.03 (d, CH, J=17.4 Hz)
p-$CH_3OC_6H_4$	9-Fluorenone	**8s**	53	1710	3.76	4.73	

a) Signals of aromatic protons were omitted. b) Isomer having phenyl moiety in endo. c) Isomer having phenyl moiety in exo.

blets is quite similar to that of exo-1:1-adduct (**6h**). Therefore, it is suggested that in the 2:1-adduct the *p*-methoxyphenyl group of the aldehyde origin has *exo* configuration, and that the 2:1-adduct is formed by the secondary cycloaddition of **3b** on exo-1:1-adduct (**6h**).

Reaction with Ketones. The decomposition of **1a** in acetone gave a similar adduct (**8a**) in 75% yield together with a 2:1-adduct (**10**: 12%) of **3a** and acetone. The adduct (**8a**) showed two singlet signals in its NMR spectrum at δ 1.55 and 1.11 which corresponded to the signals of the exo- (**6k**:δ 1.50) and endo-adduct (**5k**: δ 1.05) of acetaldehyde. Therefore, signals at δ 1.55 and 1.11 of **8a** were assigned to exo- and endo-methyl groups, respectively. Similar assignment was applied to the characterization of other methyl ketone adducts.

The NMR spectrum of the 2:1-adduct is quite similar to that of **8a** (Table 2). The spectroscopic data of the 2:1-adduct and the behavior of **3a** in the cycloaddition to carbonyl group noted above indicate that the 2:1-adduct is the secondary reaction product obtained by the cycloaddition of **3a** toward the carbonyl group of 1:1-adduct (**8a**), and is indicated by the structural formula **10**. The stereochemistry of the 2:1-adduct is not determined yet. Each of methyl ethyl ketone, methyl isopropyl ketone, substituted acetophenones and substituted benzoyl cyanides gave a pair of adducts different in the stereochemistry at C_6 (Table 2).

However, methyl *t*-butyl ketone and benzophenone did not give any adduct because of their low reactivity attributable to the steric hindrance or aromatic stabi-

lization. Cyclic ketones such as cyclopentanone, cyclohexanone, 1-indanone, 9-fluorenone, anthraquinone, and anthrone gave adducts of type **4A** (Table 3). Except 1-indanone, cyclic ketones gave single adducts because they were symmetric. 1-Indanone afforded two adducts in 1.3 and 6.8% yields which were identified as **Ph**-endo- and **Ph**-exo-adducts respectively on the basis of NMR data. The **Ph**-endo-adduct shows a signal of an aromatic proton of indanone moiety at δ 6.24 which may caused by the shielding effect of benzene ring of **3a** moiety. In the cyclic ketones used, aliphatic ketones were shown to have reactivities higher than those of aromatic ketones such as indanone, anthraquinone, and anthrone which were resonance stabilized. The exception was fluorenone, which gave an adduct in good yield in the reaction with **3a**. The adduct was confirmed to have the same structure with **4A** as the adducts of aldehydes and other ketones described above on the basis of ^{13}C NMR spectrum which showed a signal of nonaromatic quartanary carbon (C_1) at quite low field (δ 119.1). Another type of regioisomer (**4B**) may not give a signal of quarternary carbon in this region.

When the dipolarophilicity of the carbonyl compound was not so high, 2:1-adducts of the benzopyrylium-4-olates (**3**) with the dipolarophiles were also obtained along with 1:1-adducts as described above in the reaction with acetone. The details of the 2:1-adducts will be published elsewhere.

Frontier Orbital Explanation of the Regiospecificity and Reactivity of the Cycloaddition. The stereo-

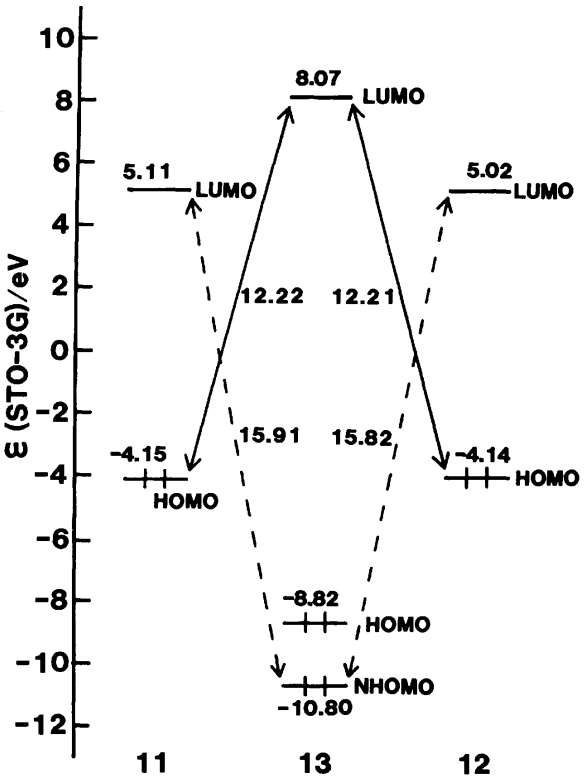

Fig. 1. HOMO and LUMO energy levels of carbonyl ylides (**11**, **12**) and acetone (**13**).

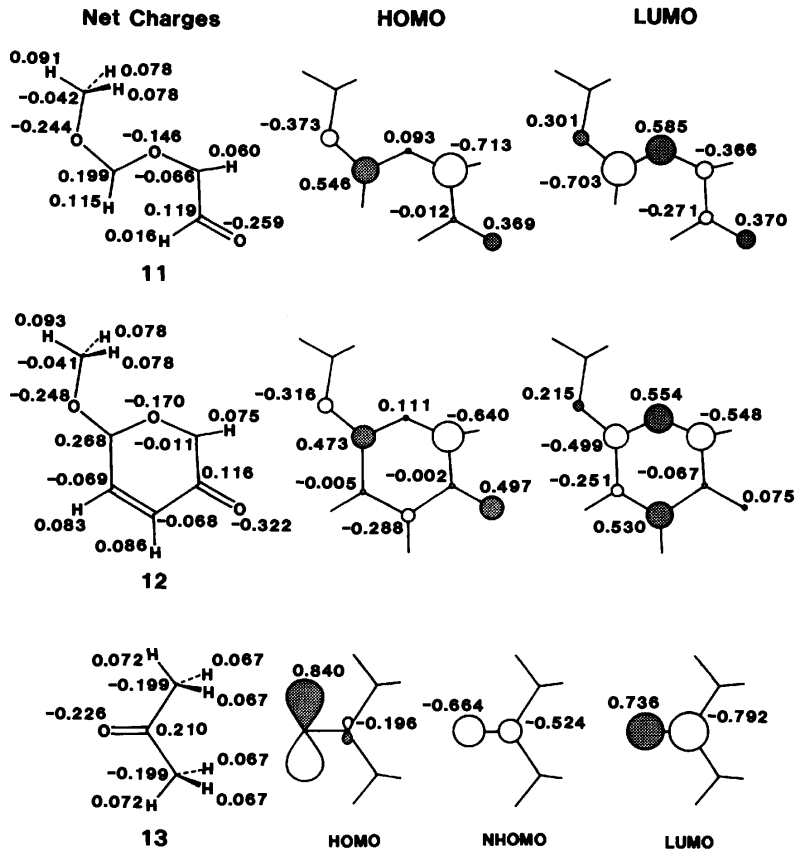

Fig. 2. Orbital coefficients of HOMO and LUMO of carbonyl ylide (**11**, **12**) and acetone (**13**).

specificity observed in the 1,3-dipolar cycloaddition of 2-benzopyrylium-4-olate (**3**) with cis- and trans-ethylenic dipolarophiles indicates that the reaction proceeds in the concerted process.[5] The regioselectivity and reactivity of the 1,3-dipolar cycloaddition has been explained by second-order perturbation expression.[7] Orbital energies and atomic orbital coefficients of carbonyl ylides and acetone were calculated by STO-3G level.[8] Instead of the complex carbonyl ylide like 1-methoxy-2-benzopyrylium-4-olate (**3a**) which has an electron-releasing methoxyl group on a carbonyl ylide carbon and an electron-attracting carbonyl group on another side, we chose 1-methoxy-3-formyl-carbonyl ylide (**11**) and 6-methoxypyrylium-3-olate (**12**) as model compounds. Energy levels of the two model carbonyl ylides (**11** and **12**) calculated are quite similar in their frontier orbitals. Frontier orbital energy levels of **11**, **12**, and acetone indicate that the cycloaddition is controled by the interaction of carbonyl ylide HOMO with carbonyl compound LUMO (Fig. 1).[9]

Atomic orbital coefficients of the frontier orbitals of carbonyl ylides (**11** and **12**) and acetone are shown in Fig. 2. The preferred orientation of the cycloaddition is that in which the atoms having larger terminal atomic coefficients of the interacting frontier orbitals are bonded. Therefore, oxygen atom of carbonyl compound bonded to carbon atom of carbonyl ylide attached by an electron-releasing group (OCH_3), to give an orthoester type adduct (**4A**), because these atoms have larger coefficients in carbonyl compound LUMO and carbonyl ylide HOMO, respectively. Dipole–dipole interaction between the carbonyl ylides, (methoxymethyleneoxonio)formylmethanide (**11**) and 6-methoxypyrylium-3-olate (**12**), and acetone shown in electron-density formula (Fig. 2) also supports the regiospecificity of the cycloaddition cited above.

Strong electron-attracting groups exert considerable

Table 4. Melting points and analitical data of adducts

Adduct	Mp (θ_m/°C)	Found(%)			Calcd(%)			Molecular Formula
		C	H	N	C	H	N	
6a	116.0—118.5	69.01	5.17	—	69.22	5.16	—	$C_{18}H_{16}O_5$
5b	87.5— 89.5	72.22	5.06	—	72.33	5.00	—	$C_{17}H_{14}O_4$
6b	110.0—110.8	72.41	5.00	—				
6c	126.5—127.5	64.41	4.14	—	64.47	4.14	—	$C_{17}H_{13}O_4Cl$
5d	136.5—138.0	58.08	3.45	—	58.14	3.44	—	$C_{17}H_{12}O_4Cl_2$
5e	148.0—150.0	57.87	3.28	—				
6e	158.0—161.0	58.08	3.44	—				
5f	152.0—154.0	62.29	4.04	4.42	62.39	4.00	4.28	$C_{17}H_{13}O_6N$
6f	147.5—148.8	62.35	4.00	4.27				
5g	115.0—117.0	62.36	4.01	4.40				
5h	118.0—119.5	71.48	5.02	—	71.28	4.98	—	$C_{24}H_{20}O_6$
5i	194.0—194.7	74.00	4.91	—	73.79	4.85	—	$C_{23}H_{18}O_5$
6i	163.0—165.0	73.85	4.89	—				
5j	236.7—239.0	65.91	4.16	3.37	65.87	4.09	3.34	$C_{23}H_{17}O_7N$
6j	199.8—201.0	65.81	4.10	3.37				
5k	78.0— 79.0	65.31	5.49	—	65.45	5.49	—	$C_{12}H_{12}O_4$
6k	76.5— 77.3	65.36	5.69	—				
5m	Liquid	67.79	6.60	—	67.73	6.50	—	$C_{14}H_{16}O_4$
6m	Liquid	67.52	6.52					
8a	117.0—112.3	66.65	6.07	—	66.66	6.02	—	$C_{13}H_{14}O_4$
8b	91.0— 94.0	67.90	6.50	—	67.73	6.50	—	$C_{14}H_{16}O_4$
9b	94.5— 95.8	67.73	6.40	—				
8c	Liquid	68.75	6.83	—	68.69	6.92	—	$C_{15}H_{18}O_4$
9c	78.5— 79.5	68.59	6.93	—				
8d	78.3— 79.5	51.57	4.03	—	51.51	3.99	—	$C_{13}H_{12}O_4Cl_2$
8e	103.0—103.5	69.66	5.56	—	69.93	5.56	—	$C_{19}H_{18}O_5$
9e	126.0—128.0	69.86	5.59	—				
8f	175.0—176.5	73.02	5.53	—	72.96	5.44	—	$C_{18}H_{16}O_4$
9f	112.0—112.6	72.51	5.47	—				
8g	208.5—209.0	63.63	4.43	4.10	63.34	4.43	4.10	$C_{18}H_{15}O_6N$
9g	120.0—122.3	63.57	4.40	4.09				
8h	171.5—173.0	67.65	4.51	4.17	67.65	4.48	4.15	$C_{19}H_{15}O_5N$
8i	169.4—171.4	61.60	3.00	7.89	61.37	3.43	7.95	$C_{18}H_{12}O_6N_2$
9j	210.0—212.0	72.06	5.40	—	71.76	5.30	—	$C_{25}H_{22}O_6$
9k	202.5—203.7	74.11	5.25	—	74.21	5.19	—	$C_{24}H_{20}O_5$
8m	Liquid	69.87	6.64	—	70.06	6.61	—	$C_{16}H_{18}O_4$
8n	Liquid	68.75	6.19	—	69.22	6.20	—	$C_{15}H_{16}O_4$
8o	143.0—143.5	73.74	5.32	—	74.01	5.23	—	$C_{19}H_{16}O_4$
9o	123.0—124.0	73.96	5.24	—				
8p	218.0—219.0	77.33	4.56	—	77.51	4.53	—	$C_{23}H_{16}O_4$
8q	208.5—210.5	74.89	4.34	—	74.99	4.20	—	$C_{24}H_{16}O_5$

lowering effect on the LUMO of the carbonyl compounds, resulting in a small energy separation between the carbonyl ylide HOMO and carbonyl compound LUMO. This explains the high reactivity of carbonyl compounds having electron-attracting substituents such as *p*-nitroacetophenone, *p*-nitrobenzoyl cyanide and 1,3-dichloroacetone.

Experimental

All melting points were measured on a Yanagimoto Melting Point Apparatus and were not corrected. The IR spectra were taken on a Hitachi Spectrometer, model 260-10 and Perkin Elmer, model 983 in KBr mull. The ^{1}H NMR spectra were recorded on a Varian EM-390 Spectrometer in a $CDCl_3$ solution using TMS as an internal standard; ^{13}C NMR spectra were recorded on a Bruker AM-360. The chemical shifts were described in ppm downfield from TMS.

Materials. *o*-Methoxycarbonyl-α-diazoacetophenone (**1a**) was prepared by the procedure described in the previous paper.[4,5] *p*-Methoxyphenyl *o*-diazoacetylbenzoate (**1b**) was synthesized in 84% yield by the reaction of excess diazomethane with corresponding acid chloride: mp 67.5—68.8°C; IR (KBr) 3080 (CH), 2100 (diazo), 1730 (ester C=O), and 1610 cm^{-1} (diazoketone C=O); NMR ($CDCl_3$) δ=3.79 (s, OCH_3), 5.60 (s, CH), 6.88, 7.14 (ABq, arom), and 7.52—7.95 (m, arom). Found. C, 64.83; H, 4.07; N, 9.42%. Calcd for $C_{16}H_{12}O_4N_2$: C, 64.86; H, 4.08; N, 9.45%.

Aldehydes and ketones used were purified just before use by distillation or recrystallization of the commercial reagents.

General Procedure of the Decomposition of 1 in the Presence of Carbonyl Compounds. The Cu(acac)$_2$-catalyzed decomposition of **1** was carried out according to the procedure described in the previous paper:[4,5] a benzene solution of **1** was added drop by drop into a benzene solution of 2—10 molar equivalents of carbonyl compounds and catalytic amount of Cu(acac)$_2$ under reflux of benzene at 80°C. The reaction mixture was heated until no more N_2 was evolved (about one hour) and then separated by silica-gel column chromatography using benzene as the eluent.

The 2:1-adduct (**7h**) between **3b** and *p*-anisaldehyde: mp 245.5—247.0°C; IR (KBr) 1711 cm^{-1} (C=O); NMR ($CDCl_3$) δ=3.47 (s, OCH_3), 3.73 (s, OCH_3), 4.04 (d, CH, *J*=1.5 Hz), 4.65 (d, CH, *J*=1.5 Hz), 5.25 (s, CH), and 6.20—8.00 (m, 16H, Ar). Found: C, 71.85; H, 4.88%. Calcd for $C_{40}H_{32}O_{10}$: C, 71.42; H, 4.79%.

The 2:1-adduct (**10**) between **3a** and acetone: mp 184.2—185.0°C; IR(KBr) 1714 cm^{-1} (C=O); NMR ($CDCl_3$) δ=1.26 (s, CH_3), 1.51 (s, CH_3), 3.63 (s, OCH_3), 3.71 (s, OCH_3), 4.38 (s, CH), 5.26 (s, CH), and 6.19 (d, 1H, arom, *J*=8.1 Hz), 6.80—7.93 (m, 7H, arom). Found: C, 67.71; H, 5.47%. Calcd for $C_{23}H_{22}O_7$: C, 67.31; H, 5.40%.

The authors express their sincere thanks to Dr. Masami Sawada and Mr. Yoshio Takai of ISIR of Osaka University for measurements of ^{13}C NMR spectra and helpful discussions on the structural investigation of the adducts, and to Dr. Kizashi Yamaguchi of Faculty of Engineering Science, Osaka University for the MO calculations and fruitful discussions.

References

1) E. F. Ullman and J. E. Milks, *J. Am. Chem. Soc.*, **86**, 3814 (1964).

2) a) R. Huisgen, *Angew. Chem., Int. Ed. Engl.*, **16**, 572 (1970); b) M. Bekhazi and J. Warkentin, *J. Am. Chem. Soc.*, **105**, 1289 (1983); and references cited therein.

3) K. Ueda, T. Ibata, and M. Takebayashi, *Bull. Chem. Soc. Jpn.*, **45**, 2779 (1972).

4) T. Ibata and K. Jitsuhiro, *Bull. Chem. Soc. Jpn.*, **52**, 3582 (1979).

5) T. Ibata, K. Jitsuhiro, and Y. Tsubokura, *Bull. Chem. Soc. Jpn.*, **54**, 240 (1981).

6) T. Ibata and J. Toyoda, *Chem. Lett.*, **1983**, 1453.

7) K. N. Houk, J. Sims, C. R. Watts, and L. J. Luskus, *J. Am. Chem. Soc.*, **95**, 7301 (1973).

8) Details on the MO calculation will be published elsewhere.

9) As the HOMO orbital of acetone has no π-component, the interaction of its NHOMO orbital was taken into account.

New Quassinoid Glucosides, Picrasinoside-A, -B, -C, -D, -E, -F, and -G and New Hemiacetals, Picrasinol-A and -B, from the Stem Bark of *Picrasma ailanthoides* PLANCHON[1)]

Masayoshi Okano,* Tomoyuki Fujita, Narihiko Fukamiya, and Takaaki Aratani
Interdisciplinary Studies of Natural Environment, Faculty of Integrated Arts and Sciences, Hiroshima University, Higashisenda-machi, Naka-ku, Hiroshima 730
(Received January 31, 1985)

New quassinoid glucosides, picrasinoside-A, -B, -C, -D, -E, -F, and -G and new quassinoid hemiacetals, picrasinol-A and -B, were isolated from the stem bark of *Picrasma ailanthoides* PLANCHON, and their structures were established by spectral analyses and chemical transformations.

Since bruceantin[2)] isolated from the Ethiopian *Brucea antidysenterica* has been shown to have antitumor activity,[3)] quassinoids[4,5)] have been noted for their biological activity.[6–8)] Quassinoids of the Japanese *Picrasma ailanthoides* PLANCHON (=*P. quassioides BENNETT*) have been investigated in detail by Murae *et al.*[9–14)] and Hikino *et al.*[15)] and more than twenty quassinoides have been obtained. However, very few reports for quassinoid glycosides[16–18)] have been found. We were interested in quassinoid glycosides of *P. ailanthoides* and tried to isolate the glycosides from the stem bark of the plant. We wish to report on the isolation and structures of seven new quassinoid glycosides and two new quassinoid hemiacetals.

The half-dried stem bark of *P. ailanthoides* was continuously extracted with methanol and the extract was defatted by partition between hexane and water containing small amounts of methanol. The aqueous layer was further extracted with chloroform. The organic layer was evaporated to give a residue which was subjected to separation by silica-gel column chromatography, thin-layer chromatography (TLC), and high-performance liquid chromatography (HPLC) to afford seven new quassinoid glucosides, picrasinoside-A (**1**, 0.0024%), -B [**5**, 0.0042%), -C (**6**, 0.0062%), -D (**7**, 0.0011%), -E (**8**, 0.0022%), -F (**9**, 0.0006%), and -G (**10**, 0.0009%) and two new quassinoid hemiacetals, picrasinol-A (**11**, 0.032%) and -B (**12**, 0.029%), together with a known neoquassin (0.026%).[10)] Structures of new compounds and their derivatives are shown in Fig. 1. Physical (mp and specific rotation) and spectral (UV and IR) data of new compounds are shown in Table 1 and the ^{1}H NMR spectra of these compounds and their derivatives are shown in Table 2.

Picrasinoside-A (**1**) takes the form of colorless plates and has a bitter taste. A spectral examination (Tables 1 and 2) showed the presence of hydroxyl (IR 3350 cm^{-1}), lactone (IR 1735 (sh) and 1230 cm^{-1}), ketone (IR 1720 cm^{-1}), α,β-unsaturated ketone (IR 1680 cm^{-1}; UV 252 nm), a proton at the lactone terminus (^{1}H

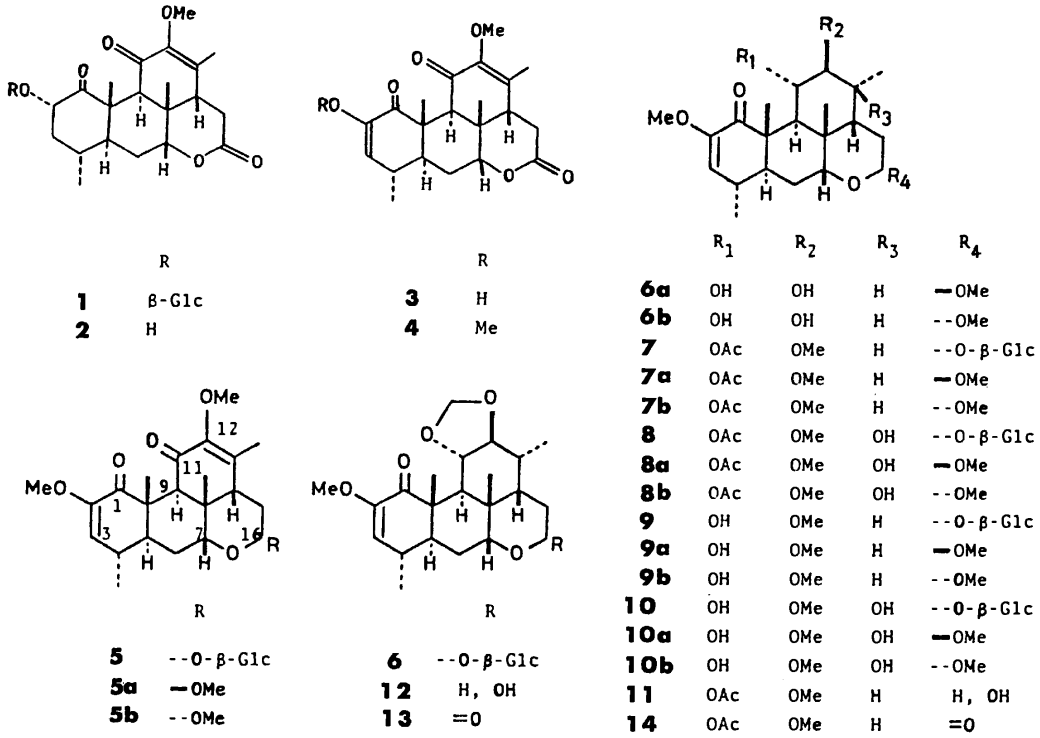

Fig. 1. Structures of quassinoid glucosides, hemiacetals, and their derivatives.

Table 1. Physical and Spectral Data of Quassinoid Glucosides and Hemiacetals

Compound	Mp(°C)	$[\alpha]_D$	$\lambda_{max}^{EtOH}(\varepsilon)$	ν_{max}/cm^{-1}
1	167.5—168.5	−32.5°	252 (8000)	3350, 1735, 1720, 1680, 1640, 1230, 1080, 1030
5	153—153.5	−15.1°	255 (11300)	3400, 1690, 1675(sh), 1640, 1085, 1040
6	163.5—164	−41.1°	261 (4400)	3400, 2740(sh), 1700, 1640, 1090, 1035
7	144—144.5	+3.3°	262 (3800)	3400, 1735, 1705, 1640, 1245, 1075, 1030
8	163—164	−14.7°	262 (3500)	3400, 1730, 1705, 1640, 1250, 1070, 1030
9	153—154	−8.2°	271 (4400)	3400, 1670, 1640, 1070, 1040
10	162—163	+24.2°	271 (6100)	3400, 1670, 1645, 1070, 1040
11	122—124	+49.6°	261 (3800)	3450, 1730, 1710, 1700, 1640, 1245
12	205—206	+12.1°	262 (4600)	3450, 2740, 1710, 1700, 1640

Table 2. ^{1}H NMR Spectra of Quassinoid Glucosides, Hemiacetals, and Their Derivatives

Compound	t-Me	s-Me	-OMe	H-9	H-11	H-12	H-7	H-3	H-16	H-1′	Others
1	1.15s 1.42s 1.89s	0.91d (J=5)	3.61s	3.24s	—	—	4.27m	a)	a)	4.6m	
5	1.06s 1.52s 1.85s	1.09d (*J*=6)	3.56s 3.63s	3.18s	—	—	3.82m	5.31d (*J*=2)	4.83dd (*J*=2.5,6)	4.65d (*J*=7)	
5a	1.06s 1.52s 1.82s	1.11d (*J*=6)	3.57s 3.62s	3.18s	—	—	a)	5.27d (*J*=2.5)	4.78dd (*J*=3,3)	—	16β-OMe 3.35s
5b	1.04s 1.53s 1.83s	1.11d (*J*=7)	3.56s 3.63s	3.18s	—	—	a)	5.27d (*J*=2.5)	4.36dd (*J*=2.5,9)	—	16α-OMe 3.46s
6	1.15s 1.38s	1.10d (*J*=6.5) 1.12d (*J*=6)	3.54s	2.74d (*J*=11)	a)	a)	3.82m	5.24d (*J*=2)	4.73dd (2.5,5)	4.61d (*J*=7)	-O-CH$_2$-O- 4.96d(*J*=1) 5.13d(*J*=1)
12	1.14s 1.20s[b] 1.38s	1.07d (*J*=6.5) 1.04d(*J*=6.5)[b] 1.08d (*J*=7)	3.55s	2.76d (*J*=11) 2.51d(*J*=11)[b]	a)	a)	3.94m	5.21d (*J*=2.5)	4.69m 5.35m[b]	—	-O-CH$_2$-O- 4.97d(*J*=1) 5.15d(*J*=1)
6a	1.14s 1.40s	1.03d (*J*=7) 1.12d (*J*=7)	3.59s	2.51d (*J*=11)	a)	a)	a)	5.44d (*J*=2.5)	4.73m	—	16β-OMe 3.31s
6d	1.12s 1.40s	1.02d (*J*=7) 1.12d (*J*=7)	3.58s	2.51d (*J*=11)	a)	a)	a)	5.43d (*J*=2.5)	4.28dd (*J*=2,8)	—	16α-OMe 3.44s
7	1.15s 1.23s	0.99d (*J*=7) 1.06d (*J*=6.5)	3.39s 3.54s	2.86d (*J*=11)	5.17dd (*J*=9,11)	3.18dd (*J*=9,11)	3.85m	5.12d (*J*=2.5)	4.73bm (12)[c]	4.60d (*J*=7)	-OAc 1.94s
11	1.14s 1.18s[b] 1.25s	0.99d (*J*=6) 1.06d (*J*=7)	3.40s 3.54s	2.87d (*J*=11)	5.18dd (*J*=9,11)	3.14dd (*J*=9,11)	3.86m	5.10d (*J*=2.5)	4.70bm 5.34m[b]	—	-OAc 1.94s
8	1.21s 1.23s 1.39s	1.07d (*J*=6.5)	3.50s 3.56s	2.83d (*J*=11)	5.49dd (*J*=9,11)	3.36d (*J*=9)	3.87m	5.13d (*J*=2.5)	4.72bm (12)[c]	4.60d (*J*=8)	-OAc 1.96s
9	1.10s 1.42s	0.98d (*J*=7) 1.10d (*J*=6)	3.57s 3.58s	2.46d (*J*=11)	a)	a)	3.83m	5.43d (*J*=2.5)	4.71dd (*J*=2.5,6)	4.60d (*J*=7)	
10	1.19s 1.34s 1.44s	1.11d (*J*=7)	3.58s 3.67s	2.48d (*J*=11)	a)	2.98d (*J*=9)	3.83m	5.42d (*J*=2)	4.71bm (12)[c]	4.60d (*J*=7)	

a) Not assigned. b) Signals due to the other isomer at C-16. c) Half width in Hz.

NMR δ 4.27, m), an anomeric proton at the glucose moiety (^{1}H NMR δ 4.6, m) two tertiary methyl groups, a secondary methyl group, and a methoxyl group (^{1}H NMR δ 1.15, s, δ 1.15, s, δ 0.91, d, and δ 3.61, s,

respectively). The FD mass spectrum of **1** ($C_{27}H_{38}O_{11}$, MW 538) showed a molecular ion at *m/z* 538 and a pseudo molecular ion at *m/z* 551 (M^++Na).

An acid hydrolysis of picrasinoside-A (**1**) gave picrasin B[15] (**2**,=nigakilactone I)[10] which was further converted to dehydropicrasin B (**3**)[15] and finally to quassin (**4**).[9] The sugar moiety was identified as D-glucose by a gas-chromatographic comparison of trimethylsilyl derivatives of the hydrolyzed product and authentic D-glucose. An enzyme hydrolysis of picrasinoside-A (**1**) using β-glucosidase also gave picrasin B (**2**) and D-glucose. From the above results, picrasinoside-A (**1**) was confirmed as 2α-*O*-β-glucopyranosylpicrasin B (=2α-*O*-β-glucopyranosylnigakilactone I).

Picrasinoside-B (**5**) takes also the form of colorless plates and has a bitter taste. The spectral data (Tables 1 and 2) showed the presence of hydroxyl (IR 3400 cm^{-1}), α,β-unsaturated ketones (IR 1690 and 1675 (sh) cm^{-1}; UV 255 nm), a proton at the hemiacetal terminus (^1H NMR δ 3.82, m), a proton at C-3 (^1H NMR δ 5.31, d), a proton at C-16 (^1H NMR δ 4.83, dd), an anomeric proton at the glucose moiety (^1H NMR δ 4.65, d), three tertiary methyl groups, a secondary methyl group, and two methoxyl groups (^1H NMR δ 1.06, s, δ 1.52, s, δ 1.85, s, δ 1.09, d, δ 3.56, s, and δ 3.63, s, respectively). The FAB mass spectrum of picrasinoside-B (**5**, $C_{18}H_{40}O_{11}$, MW 522) showed the pseudo molecular ion to be *m/z* 553 (M^++1).

An acid hydrolysis of picrasinoside-B (**5**) in methanol gave two compounds (**5a** and **5b**) and each compound (11:5) was isolated as a colorless amorphous powder by HPLC. Both compounds were characterized by the molecular formula $C_{23}H_{32}O_6$ (mass), a disappearance of the hydroxyl group (IR), and an appearance of a methoxyl group to the original compound (^1H NMR). These facts suggest that they are methanolysis products of picrasinoside-B (**5**). They were also obtained by heating neoquassin and methanol using sulfuric acid as a catalyst. ^1H NMR spectra reveal that the compound **5a** is 16β-*O*-methylneoquassin from an 16α-proton signal at δ 4.78 (dd, *J*=3,3) and the compound **5b** is 16α-*O*-methylneoquassin from an 16β-proton signal at δ 4.36 (dd, *J*=2.5, 9). Thus, picrasinoside-B (**5**) is confirmed as 16α-*O*-β-glucopyranosylneoquassin from an 16β-proton signal at δ 4.83 (dd, *J*=2.5, 6) and an 1′α-proton signal at δ 4.65 (d, *J*=7).

Picrasinol-B (**12**) forms as colorless needles and has a bitter taste. The spectral data showed the presence of hydroxyl (IR 3450 cm^{-1}), methylenedioxy (IR 2740 cm^{-1}; ^1H NMR δ 4.97, d and δ 5.15, d), α,β-unsaturated ketone IR 1710 cm^{-1}; UV 262 nm), a proton at the hemiacetal terminus (^1H NMR δ 3.94, m), a proton at C-3 (^1H NMR δ 5.21, d), a proton at C-16 (^1H NMR δ 4.69, bm and/or δ 5.35, m, tautomers), two tertiary methyl groups, two secondary methyl groups, and a methoxyl group (^1H NMR δ 1.14, s and/or δ 1.20, s, δ 1.38, s, δ 1.07, d and/or δ 1.04, d, δ 1.08, d and δ 3.55, s, respectively). The high-mass spectrum of **12** (M^+, *m/z* 392.21926) revealed the molecular to be $C_{22}H_{32}O_6$.

Picrasinol-B showed two peaks in HPLC and GC and it was positive against the silver mirror test. When each compound was isolated using a preparative HPLC and subjected to analytical HPLC, each sample showed the same chromatogram as the original one. This phenomenon shows that they are tautomers of hemiacetal. The reducing power of this substance depends upon the aldehyde as an intermediate. A Jones oxidation[19] of picrasinol-B (**12**) gave picrasin D (**13**)[15] as a colorless amorphous powder. From these results, the structure of picrasinol-B (**12**) was confirmed as shown in Fig. 1.

Picrasinoside-C (**6**) takes the form of colorless plates and exhibits a bitter taste. The spectral data indicated the presence of hydroxyl (IR 3400 cm^{-1}), a methylenedioxy group (IR 2740 (sh) cm^{-1}; ^1H NMR δ 4.96, d, and δ 5.13, d), an α,β-unsaturated ketone (IR 1700 cm^{-1}; UV 261 nm), a proton at the hemiacetal terminus (^1H NMR δ 3.82, m) a proton at C-3 (^1H NMR δ 5.24, d, a proton at C-16 (^1H NMR δ 4.73, dd), an anomeric proton at the glucose moiety (^1H NMR δ 4.61, d), two tertiary methyl groups, two secondary methyl groups, and a methoxyl group (^1H NMR δ 1.15, s, δ 1.38, s, δ 1.10, d, δ 1.12, d, δ 3.54, s, respectively). The FAB mass showed pseudo molecular ion at *m/z* 555 (M^++1).

An acid hydrolysis of picrasinoside-C (**6**) also gave two compounds (**6a** and **6b**); each compound (74:26) was isolated as a colorless amorphous powder by preparative HPLC. Both compounds were characterized by the molecular formula $C_{22}H_{34}O_6$ (mass), a disappearance of a methylenedioxy group (IR and ^1H NMR), and the appearance of a methoxyl group (^1H NMR). The disappearance of the methylenedioxy group depends upon the heating in sulfuric acid. Since picrasinol-B (**12**) and picrasin D (**13**)[15] also lost their methylenedioxy groups upon heating at 60 °C in dilute sulfuric acid to give nigakihemiacetal C[10] and nigakilactone A,[9] respectively. Hydrolyzed products (**6a** and **6b**) were obtained by heating picrasin B (**12**) in a mixture of dilute sulfuric acid and methanol at 60 °C. From these chemical transformations and chemical shifts at C-16, the hydrolyzed products (**6a** and **6b**) were revealed to be 16β-*O*-methylnigakihemiacetal C (=nigakihemiacetal F)[14] and 16α-*O*-methylnigakihemiacetal C, respectively. The sugar moiety was identified as D-glucose by a gas-chromatographic comparison of the trimethylsilyl derivative of the hydrolyzed product and authentic D-glucose. Thus, picrasinoside-C (**6**) was confirmed as 16α-*O*-β-glucopyranosylpicrasinol-B from an 16β-proton signal at δ 4.73 (dd, *J*=2.5, 5), an 1′α-proton signal at δ 4.61 (d, *J*=7), and the above results. Furthermore, an acid hydrolysis of picrasinoside-C in ethanol and 1-butanol gave, respectively, ethanolysis products and butanolysis products. The ^{13}C NMR spectrum of picrasinoside-C[20] also supports the structure as shown in Fig. 1.

Picrasinol-A (**11**) is a colorless amorphous powder and has a bitter taste. The spectral data showed the presence of hydroxyl (IR 3450 cm^{-1}), acetoxyl (IR 1730 and 1245 cm^{-1}; ^1H NMR δ 1.94, s), α,β-unsaturated ketone IR 1710 cm^{-1}; UV 261 nm), a proton at the hemiacetal terminus (^1H NMR δ 3.86, m), a proton at C-3 (^1H NMR δ 5.10, d), a proton at tertiary methyl groups, two secondary methyl groups, and two methoxyl groups (^1H NMR δ 1.14, s and/or δ 1.18, s, δ 1.21, s, δ 0.99, d, δ 1.06, d, δ 3.40, s, and δ 3.54, s, respectively. Picrasinol-A (**11**) showed the same behavior in the HPLC and silver-mirror test as those of picrasinol-B. A Jones oxidation[19] of picrasinol-A (**11**) gave nigakilactone-C (**14**)[9] as a colorless amorphous powder. From the above results, the structure of picrasinol-A (**11**) was confirmed as shown in Fig. 1.

Picrasinoside-D (**7**) takes the form of colorless plates and exhibits bitter taste. The spectral data reveal the presence of hydroxyl (IR 3400 cm^{-1}), acetoxyl (IR 1735 and 1245 cm^{-1}; ^1H NMR δ 1.94, s), α,β-unsaturated ketone (IR 1705 cm^{-1}; UV 262 nm), a proton at the hemiacetal terminus (^1H NMR δ 3.85, m), a proton at C-3 (^1H NMR δ 5.12, d), a proton at C-16 (^1H NMR δ 4.73, bm), an anomeric proton at the glucose moiety (^1H NMR δ 4.60, d), two tertiary methyl groups, two secondary methyl groups, and two methoxyl groups (^1H NMR δ 1.15, s, δ 1.23, s, δ 0.99, d, δ 1.06, d, δ 3.39, s, and δ 3.54, s, respectively). The spectral data was similar to that of picrasinol-A (**11**). The FD mass spectrum of picrasinoside-D (**7**) showed the molecular ion ($C_{30}H_{46}O_{12}$) at m/z 598.

An acid hydrolysis of picrasinoside-D (**7**) gave two compounds (**7a** and **7b**); each compound (8:3) was isolated as a colorless amorphous powder using a preparative HPLC. The two compounds (**7a** and **7b**) were also obtained by heating a mixture of picrasinol-A (**11**) and methanol using sulfuric acid as a catalyst. Therefore, they are considered as acetals of picrasinol-A (**11**). 16β-*O*-methyl derivatives (**5a** and **6a**) showed larger molecular ion intensity (90 and 54%) than that (21% and 26%) of 16α-isomers (**5a** and **6b**). Therefore, the products **7a** and **7b** should be 16β-*O*-methyl picrasinol-A (M^+, 1.9%) and 16α-*O*-methylpicrasinol-A (M^+, 0.8%), respectively. The sugar moiety was identified as D-glucose by the same method mentioned before. Picrasinoside-D (**7**) is thus confirmed as 16α-*O*-β-glucopyranosylpicrasinol-A from the above results and ^1H NMR signals of 16β-proton at δ 4.73 (half width 12 Hz) and 1′α-proton at δ 4.60 (d, J=7).

Picrasinoside-E (**8**) takes the form of colorless plates and has a bitter taste. The spectral data showed the presence of hydroxyl (IR 3400 cm^{-1}), acetoxyl (IR 1730 and 1250 cm^{-1}; ^1H NMR δ 1.96, s), an α,β-unsaturated ketone (IR 1705 cm^{-1}; UV 262 nm), a proton at the hemiacetal terminus (^1H NMR δ 3.87, m), a proton at C-3 (^1H NMR δ 5.13, d), a proton at C-16 (^1H NMR δ 4.72, bm), an anomeric proton at the glucose moiety (^1H NMR δ 4.60, d), three tertiary methyl groups, a secondary methyl group, and two methoxyl groups (^1H NMR δ 1.21, s, δ 1.23, s, δ 1.39, s, δ 1.07, d, δ 3.50, s, and δ 3.56, s, respectively). The spectral data were similar to that of nigakihemiacetal D.[12] The FD mass spectrum of picrasinoside-E (**8**, $C_{30}H_{46}O_{13}$, MW 614) showed the molecular ion at m/z 614.

An acid hydrolysis of picrasinoside-E (**8**) also gave two compounds (**8a** and **8b**); each compound (2:1) was isolated as a colorless amorphous powder using a preparative HPLC. Their mass spectra suggested that **8a** and **8b** are 16β-*O*-methylnigakihemiacetal D (M^+, 3.2%) and 16α-*O*-methylnigakihemiacetal D (M^+, 2.9%), respectively. **8a** and **8b** were converted into nigakihemiacetal D[12] by acid hydrolysis, which was identified by comparing its IR and MS spectra with those of the authentic one. The sugar moiety was identified as D-glucose in the same manner as described before. Picrasinoside-E (**8**) is, thus, confirmed as 16α-*O*-β-glucopyranosylnigakihemiacetal D from the above results and ^1H NMR signals of an 16β-proton at δ 4.72 (half width 12 Hz) and an 1′α-proton at δ 4.60 (d, J=8).

Picrasinoside-F (**9**) is also in the form of colorless plates and has a bitter taste. The spectral data showed the presence of hydroxyl (IR 3400 cm^{-1}), an α,β-unsaturated ketone (IR 1670 cm^{-1}; UV 271 nm), a proton at the hemiacetal terminus (^1H NMR δ 3.83, m), a proton at C-3 (^1H NMR δ 5.43, d), a proton at C-16 (^1H NMR δ 4.71, dd), an anomeric proton at the glucose moiety (^1H NMR δ 4.60, d), two tertiary methyl groups, two secondary methyl groups, and two methoxyl groups (^1H NMR δ 1.10, s, δ 1.42, s, δ 0.98, d, δ 1.10, d, δ 3.57, s, and δ 3.58, s, respectively). The FD mass spectrum of picrasinoside-F (**9**, $C_{28}H_{44}O_{11}$, MW 556) showed the molecular ion at m/z 556.

An acid hydrolysis of picrasinoside-F (**9**) gave two compounds (**9a** and **9b**); each one (7:3) was isolated as a colorless amorphous powder using a preparative HPLC. They were also obtained by deacetylation (alkaline hydrolysis) from **7a** and **7b**. Therefore, **9a** and **9b** should be 11-deacetoxyl-16β-*O*-methylpicrasinol-A and 11-deacetoxyl-16α-*O*-methylpicrasinol-A, respectively. The sugar moiety was identified as D-glucose in the same manner as described above. Thus, picrasinoside-F (**9**) is confirmed as 11-deacetyl-16α-*O*-β-glucopyranosylpicrasinol-A from the above results and ^1H NMR signals of an 16β-proton at δ 4.71 (dd, J=2.5, 6) and an 1′α-proton at δ 4.60 (d, J=7).

Picrasinoside-G (**10**) also takes the form of colorless plates and has a bitter taste. The spectral data showed the presence of hydroxyl (IR 3400 cm^{-1}), an α,β-unsaturated ketone (IR 1670 cm^{-1}; UV 271 nm), a proton at the hemiacetal terminus (^1H NMR δ 3.83, m), a proton at C-3 (^1H NMR δ 5.42, d), a proton at C-16 (^1H NMR δ 4.71, bm), an anomeric proton at the glucose moiety (^1H NMR δ 4.60, d), three tertiary methyl groups, a secondary methyl group, and two methoxyl groups (^1H NMR δ 1.19, s, δ 1.34, s, δ 1.44, s, δ 1.11, d,

δ 3.58, s, and δ 3.67, s, respectively). The spectral data was similar to that of nigakihemiacetal A.[10] The FD mass spectrum of picrasinoside-G (**10**, $C_{28}H_{44}O_{12}$, MW 572) showed the pseudo molecular ion at *m/z* 573 (M^++1).

An acid hydrolysis of picrasinoside-G (**10**) also gave two compounds (**10a** and **10b**) and each one (7:3) was isolated as a colorless amorphous powder using a preparative HPLC. They were also obtained by the deacetylation (alkaline hydrolysis) of **8a** and **8b**. Therefore, **10a** and **10b** were confirmed as 16β-*O*-methylnigakihemiacetal A and 16α-*O*-methylnigakihemiacetal A, respectively. This fact was supported by their mass spectra. The sugar moiety was identified as D-glucose by the same method as mentioned above. Thus, picrasinoside-G (**10**) is confirmed as 16α-*O*-β-glucopyranosylnigakihemiacetal A from the above results and the ^{1}H NMR signals of an 16β-proton at δ 4.71 (half width 12 Hz) and an 1′α-proton at δ 4.60 (d, J=7).

Thus, seven quassinoid glucosides, picrasinoside-A (**1**), -B (**5**), -C (**6**), -D (**7**), -E (**8**), -F (**9**), and -G (**10**) and two quassinoid hemiacetals, picrasinol-A (**11**) and -B (**12**) were newly isolated from the stem bark of *P. ailanthoides*, although Murae *et al.*[9-14] and Hikino *et al.*[15] had obtained eighteen quassinoids with a lactone moiety and six quassinoid hemiacetals from the stem of the plant. Among them, picrasinoside-A (**1**) and -B (**5**) were subjected to testing regarding the mean survival time (T/C%) in mice suffering from P 388 lymphocytic leukemia (test system: 3PS31); both compounds were inactive.[21] Cytotoxic and antileukemic activities in P 388 screen *in vitro* were also tested for picrasinoside-A (**1**), picrasin B (**2**), picrasinoside -B (**5**), and related compounds. The results will be reported elsewhere.[22]

Experimental

General Procedure. Melting points were determined on a MRK air-bath-type melting-point apparatus and were uncorrected. Specific rotations were obtained on a Yanagimoto OR-50 polarimeter (l=0.5 dm). Infrared (IR) and ultraviolet (UV) spectra were recorded, respectively, on a Hitachi 215 grating IR spectrometer and a Shimadzu 200-S UV spectrometer. Proton nuclear magnetic resonance (^{1}H NMR) spectra were determined on JEOL JNM-MH-60 II (60 MHz) and Hitachi R-22 (90 MHz) NMR spectrometers using tetramethylsilane as an internal standard in chloroform-*d* or pyridine-d_5. Chemical shifts and coupling constants were, respectively, shown in ppm and Hz. Mass spectra were determined on JEOL JMS-D100 (EI) and JEOL JMS-DX300 (EI and FD) instruments. Gas chromatography (GC) was performed on a Shimadzu GC-mini II gas chromatograph (2% OV-1). High-performance liquid chromatography (HPLC) was performed on a Waters ALC/GPC 206 liquid chromatograph using Radial PAK C_{18} and CN columns, and 441 UV and R401 RI detectors. Silica-gel (Merck, type 60), precoated silica-gel plates (Merck, 60 F-254, 0.25 mm), and silica gel (Merck, 60 HF-254+366) were used, respectively, for column chromatography, thin-layer chromatography (TLC), and the preparation of preparative TLC plates. The detection of components was accomplished either by the use of a UV lamp or by spraying 10% sulfuric acid solution, follwed by heating.

Plant Material and Extraction. Half-dried stem bark (3.1 kg) of *P. ailanthoides*, collected at Iwate prefecture in June of 1982, was extracted 3 times with methanol (30 l) at room temperature for 3 d. The methanol solutions were combined and the solvent was removed by evaporation until precipitates were found. The concentrated suspension was defatted with hexane (500 ml×5 times) and then extracted with chloroform (500 ml×5 times). The chloroform solutions were combined and concentrated to give a residue (40.5 g).

Separation. The residue (40.5 g) obtained by the chloroform extraction was subjected to column chromatographic separation (silica gel 1.7 kg), and eluted with chloroform–methanol (35:1, v/v, 17 l and then 8:1, v/v, 21 l); 27 fractions were collected. Each fraction was checked by TLC using two mixed solvents, ethyl acetate–ether (1:1, v/v) and chloroform–methanol–water (50:14:3, v/v, lower layer) to look for quassinoids and their glycosides which show UV absorption. As a result, fractions 19 (1.28 g) and 20 (1.14 g) were assumed to contain quassinoid glycosides, and fraction 7 (2.49 g) was considered to include their aglycons.

Isolation of Quassinoid Glycosides. Preparative TLC of fractions 19 and 20 using a mixed solvent of chloroform–methanol–water (50:14:3, v/v, lower layer) gave pale-yellow amorphous substances (715 and 642 mg, respectively), which showed strong UV absorption. The former (715 mg) showed three peaks with a shoulder in HPLC using Radial PAK C_{18} and a mixed solvent of water–methanol (3:2, v/v) and were subjected to preparative HPLC to afford picrasinoside-A (**1**, 74 mg), picrasinoside-G (**10**, 28 mg), picrasinoside-E (**8**, 68 mg), and picrasinoside-B (**5**, 111 mg), respectively. The latter (642 mg) showed four peaks with a shoulder in HPLC using Radial PAK C_{18} and a mixed solvent of water–methanol (11:9 v/v) and were subjected to preparative HPLC to give picrasinoside-F (**9**, 19 mg), picrasinoside-B (**5**, 19 mg), picrasinoside-D (**7**, 34 mg), and picrasinoside-C (**6**, 192 mg).

Acid Hydrolysis of Glycosides. Each glycoside (10—20 mg) was dissolved in methanol (4 ml) and then 1.5 M† sulfuric acid (2 ml) was added to the solution. The mixture was stirred at 60 °C (80 °C in case of picrasinoside-A) and the termination of hydrolysis was checked by TLC. After cooling, water (5 ml) was added to the reaction mixture, and the product (aglycon) was extracted with chloroform (5 ml×3 times). The extract was subjected to HPLC (radial PAK C_{18} or CN) to give pure aglycon. The water layer was neutralyzed with anion-exchange resins (Amberlite IRA-410), evaporated, and dried on P_2O_5 in a desiccator to give a residue (sugar). The residue was treated with 1-(trimethylsilyl)-imidazole at 90 °C for 1 h and then water was added to the reaction mixture to decompose the excess reagent. The reaction product was extracted with hexane (1 ml×3 times) and the hexane layer was washed with water (1 ml×3 times). The hexane solution was subjected to GC for an identification of the sugar moiety.

Enzyme Hydrolysis of Glycosides. Sixty mg of β-glucosidase (Boehringer Mannheim) was dissolved in a tris-(hydroxymethyl)methanamine–hydrochloric acid buffer solution (20 mM, pH 3.4, 3 ml) under cooling with ice-water. Each glycoside (3 mg) was suspended in a sodium acetate buffer solution (0.1 M, pH 5.0, 2 ml) and then a enzyme

† 1 M=1 mol dm^{-3}.

solution (0.1 ml) was added to the suspension. The mixture was stirred in a thermostat (25 °C). The termination of hydrolysis was checked by TLC. Aglycon and sugar were identified using the method as described above.

Isolation of Quassinoid Hemiacetals. A preparative TLC of fraction 7 using an ethyl acetate–diethyl ether (1:1, v/v) gave a pale-yellow amorphous substance (788 mg) which showed strong UV absorption. The substance showed six peaks in HPLC using Radial PAK CN and a mixed solvent of hexane–ethyl acetate (4:1, v/v), and was subjected to preparative HPLC to afford picrasinol-A (**11**, 152 mg) (corresponding to the first and the second peaks), picrasinol-B (**12**, 137 mg) (corresponding to the third and the fifth peaks), and neoquassin (123 mg) (corresponding to the fourth and the sixth peaks).

Methylation of Quassinoid Hemiacetals. A 1.5 M sulfuric acid–methanol (1:2, v/v) solution of each hemiacetal was stirred at 60 °C for 5 h and the methylated products were extracted with chloroform. The chloroform layer was washed with water and then the two products, methoxy isomers at C-16, were obtained by preparative HPLC (Radial PAK CN and a mixed solvent of hexane–ethyl acetate).

Jones Oxidation. A Jones reagent[19] (0.3 ml) was diluted with acetone (3 ml). The diluted oxidant was added to an acetone solution (1 ml) of a sample under cooling with ice-water. After the addition, the reaction mixture was stirred for 5 h and then a small amount of ethanol was added to the mixture to decompose the excess oxidant. Water (10 ml) was added to the mixture and the product was extracted with chloroform and purified by preparative HPLC (Radial PAK C_{18} and a mixed solvent of water–methanol).

Acid Hydrolysis of Picrasinoside-A (1). Picrasinoside-A (1, 19 mg) and 1.5 M sulfuric acid–methanol (1:2, v/v, 6 ml) was stirred at 80 °C for 24 h. Chloroform extraction and HPLC purification (Radial PAK C_{18}, water–methanol, 9:11, v/v) of the hydrolyzed product gave picrasin B[15] (**2**, nigakilactone I,[10] 10 mg): a colorless amorphous powder; mp 227—230 °C (lit,[15] 255—257 °C); Mass *m/z* 376 (M^+, $C_{21}H_{28}O_6$); IR ($CHCl_3$) 3500, 1735, 1720, 1680, 1640, and 1230 cm^{-1}; ^1H NMR (60 MHz, $CDCl_3$) δ 0.90 (3H, d, J=6; $C_{(4)}$-CH_3), δ 1.16 and δ 1.42 (each 3H, s; $C_{(8)}$-CH_3 and $C_{(10)}$-CH_3), δ 1.89 (3H, s; $C_{(13)}$-CH_3), δ 3.27 (1H, s; $C_{(9)}$-H), δ 3.62 (3H, s; OCH_3), and δ 4.22 (1H, m; $C_{(7)}$-H). The water layer was treated to give a TMS derivative of the sugar. The derivative was analyzed by GC (OV-17, 2%, ID 2.6 mm, length 1.4 m, 140 °C, N_2 40 ml/min) which showed two peaks (t_R 12.5 and 21.2 min) and identified as the derivatives of α- and β-D-glucose by a comparison of the retention times with those of the authentic one.

Enzyme Hydrolysis of Picrasinoside-A (1). Picrasinoside-A (**1**, 3 mg) was suspended in a sodium acetate buffer solution (0.1 M, pH 5.0, 2 ml) and then the enzyme solution was added to the suspension. The mixture was stirred in a thermostat (25 °C) for 14 d. The aglycon was extracted with chloroform and identified as picrasin B by TLC, HPLC, GC, and GC-MS comparisons with those of the authentic one. Salts in the water layer were removed by treating with cation-exchange resins (Amberlite IR-120) and anion-exchange resins (Amberlite IRA-410). The water layer was dried and an obtained residue was converted into TMS derivatives of α- and β-D-glucose (identified by GC as described above).

Conversion of Picrasin B (2) into Quassin (4). Picrasin B (**2**, 9 mg) was oxidized with the Jones reagent as described above. A chloroform extraction of the reaction mixture and a purification by HPLC (C_{18}, water–methanol, 9:11, v/v) gave a colorless amorphous powder (**3**, dehydropicrasin B,[15] 5.8 mg): IR ($CHCl_3$) 3450, 1735, 1700, 1680, 1640, and 1230 cm^{-1}; Mass *m/z* 374 (M^+, $C_{21}H_{26}O_6$). Dehydropicrasin B (**3**, 5.3 mg) was further treated with a diazomethane–diethyl ether solution and the product was purified by HPLC (Radial PAK C_{18}, water–methanol, 9:11, v/v) to give colorless amorphous powder (**4**, quassin,[9] 1.7 mg): IR ($CHCl_3$) 1730, 1700, 1680, 1645, and 1640 cm^{-1}; Mass *m/z* 388 (M^+, $C_{22}H_{28}O_6$).

Conversion of Neoquassin into Quassin (4). Neoquassin (10 mg) isolated from *P. ailanthoides* was oxidized with the Jones reagent. A chloroform extraction of the reaction mixture and the purification by HPLC (Radial PAK C_{18}, water–methanol, 1:1, v/v) gave a colorless amorphous powder (**4**, quassin,[9] 8 mg): IR ($CHCl_3$) 1730, 1700, 1685, 1645, and 1640 cm^{-1}; ^1H NMR ($CDCl_3$) δ 1.09 (3H, d, J=7; $C_{(4)}$-CH_3), δ 1.17 (3H, s; $C_{(8)}$-CH_3), δ 1.54 (3H, s; $C_{(10)}$-CH_3), δ 1.85 (3H, s; $C_{(13)}$-CH_3), δ 2.99 (1H, s; $C_{(9)}$-H), δ 3.57 and δ 3.65 (each 3H, s; OCH_3), δ 4.32 (1H, m; $C_{(7)}$-H), δ 5.33 (1H, d, J=2; $C_{(3)}$-H); Mass *m/z* 388 (M^+, $C_{22}H_{28}O_6$).

Acid Hydrolysis of Picrasinoside-B (5). Picrasinoside-B (**2**, 35 mg) and 1.5 M sulfuric acid–methanol (1:2, v/v, 6 ml) were stirred at 60 °C for 5 h. The reaction product was extracted with chloroform and subjected to preparative HPLC (Radial PAK CN, hexane–ethyl acetate, 4:1, v/v) to give two compounds as amorphous powders: 16β-*O*-methyl neoquassin (**5a**, 11 mg): IR ($CHCl_3$) 1690, 1680, and 1640 cm^{-1};. ^1H NMR (Table 2); Mass *m/z* (%) 404 (M^+, $C_{23}H_{32}O_6$; 90), 389(31), 372 (M^+—MeOH; 19), 357(13), 343(8), 329(29), 313(30), 302(33), 165(31), 154(7), 153(24), 152(100), 151(27), and 121(18) and 16α-*O*-methylneoquassin (**5b**, 5 mg): IR ($CHCl_3$) 1690, 1680, and 1640 cm^{-1}; ^1H NMR (Table 2); Mass *m/z* (%) 404 (M^+, $C_{23}H_{32}O_6$; 21), 389(4), 372 (M^+—MeOH; 79), 357(30), 343 (11), 329(42), 313(15), 302(100), 165(19), 154(4), 153(11), 152(39), 151(15), and 121(10). The water layer was treated in the same manner as described above and α- and β-D-glucose were identified.

Acid Hydrolysis of Picrasinoside-C (6). A mixture of picrasinoside-C (**6**, 20 mg) and 1.5 M sulfuric acid–methanol (1:2, v/v, 6 ml) was stirred at 60 °C for 5 h. The reaction product was extracted with chloroform and subjected to preparative HPLC (Radial PAK CN, hexane–ethyl acetate, 7:3, v/v) to give two compounds as colorless amorphous powders: 16β-*O*-methylnigakihemiacetal C (=nigakihemiacetal F,[14] **6a**, 6.4 mg): IR ($CHCl_3$) 3420, 1680, and 1640 cm^{-1}; ^1H NMR (Table 2); Mass *m/z* (%) 394 (M^+, $C_{22}H_{34}O_6$; 54), 376 (M^+—H_2O; 86), 362 (M^+—MeOH; 18), 361(45), 344 (M^+—H_2O—MeOH; 36), 329(15), 316(48), 301(100), 257(46), 165(41), 154(27), 153(48), 152(52), 151(39), and 121(47) and 16α-*O*-methylnigakihemiacetal C (**6b**, 3.9 mg): IR ($CHCl_3$) 3410, 1680, and 1640 cm^{-1}; ^1H NMR (Table 2); Mass *m/z* (%) 394 (M^+, $C_{22}H_{34}O_6$; 26), 376 (M^+—H_2O; 11), 362 (M^+—MeOH; 35), 344 (M^+—H_2O—MeOH; 100), 329(39), 316(57), 301(83), 257(41), 165(45), 154(24), 153(46), 152(49), 151(25), and 121(46). The water layer was analyzed in the same manner as described above and α- and β-D-glucose were identified.

A mixture of picrasinoside-C (**6**, 5 mg) and 1.5 M sulfuric acid–ethanol (1:2, v/v, 3 ml) was stirred at 60 °C for 5 h. The reaction product was extracted with chloroform and subjected to preparative HPLC (Radial PAK CN, hexane–ethyl acetate, 7:3, v/v) to give two compounds as colorless amorphous powders: 16β-*O*-ethyl nigakihemiacetal C (1.1 mg): Mass

m/z (%) 408 (M^+, $C_{23}H_{36}O_6$; 30), 390 (M^+-H_2O, 100), 375(69), 362(16), 344 ($M^+-H_2O-EtOH$; 47), 329(24), 316(25), 301(38), 251(30), 165(72), 154(52), 153(91), 152(100), 151(43), and 121(62) and 16α-*O*-ethylnigakihemiacetal C (0.5 mg): Mass *m/z* (%) 408 (M^+, $C_{23}H_{36}O_6$; 5), 390 (M^+-H_2O; 6), 375(4), 362(37), 344 ($M^+-H_2O-EtOH$; 100), 329(46), 316(30), 301(30), 251 (42), 165(49), 154(68), 152(63), 151(30), and 121(42).

A mixture of picrasinoside-C (**6**, 10 mg) and 1.5 M sulfuric acid-1-butanol (1:6, v/v, 3.5 ml) was stirred at 60 °C for 5 h. The reaction product was extracted with chloroform and subjected to preparative HPLC (Radial PAK CN, hexane–ethyl acetate, 7:3, v/v) to give two compounds as colorless amorphous powders: 16β-*O*-butylnigakihemiacetal C (2.5 mg): Mass *m/z* (%) 436 (M^+, $C_{25}H_{40}O_6$; 20), 418 (M^+-H_2O; 84), 403(61), 363(48), 344 ($M^+-H_2O-BuOH$; 57), 329(26), 316(39), 301(48), 251(32), 165(73), 154(61), 153(100), 152(98), 151(47), and 121(62) and 16α-*O*-butylnigakihemiacetal C (1.8 mg): Mass *m/z* (%) 436 (M^+, $C_{25}H_{40}O_6$; 6), 418 (M^+-H_2O; 6), 403(5), 362(44), 344 ($M^+-H_2O-BuOH$; 100), 329(48), 316(43), 301(43), 251(55), 165(69), 154(44), 153(84), 152 (78), 151(35), and 121(57).

*Conversion of Picrasinol-B (**12**) into Picrasin D.* Picrasinol-B (**12**, 20 mg) was oxidized with the Jones reagent in the same manner as described above. The reaction product was extracted with chloroform and subjected to preparative HPLC (Radial PAK CN, water–methanol, 1:1, v/v) to give colorless amorphous powders: (**13**, picrasin D,[15] 13 mg): IR ($CHCl_3$) 2740, 1725, 1705, 1640, and 1240 cm^{-1}; UV (EtOH) 262 nm (ε 3300); ^1H NMR (60 MHz, $CDCl_3$) δ 1.10 (6H, d, *J*= 7; $C_{(4)}$-CH_3 and $C_{(13)}$-CH_3), δ 1.27 and δ 1.42 (each 3H, s; $C_{(8)}$-CH_3 and $C_{(10)}$-CH_3), δ 3.57 (3H, s; OCH_3), δ 4.23 (1H, m; $C_{(7)}$-H), δ 5.04 and δ 5.20 (each 1H, d, *J*=1; -O-CH_2-O-), δ 5.27 (1H, d, *J*=2; $C_{(3)}$-H; Mass *m/z* 390 (M^+, $C_{22}H_{30}O_6$).

*Conversion of Picrasinol-B (**12**) into 16β-O-Methylnigakihemiacetal C (=nigakihemiacetal F, **6a**) and 16α-O-Methylnigakihemiacetal C (**6b**).* A mixture of picrasinol-B (**12**, 15 mg) and 1.5 M sulfuric acid–methanol (1:2, v/v, 6 ml) was stirred at 60 °C for 5 h. The reaction product was extracted with chloroform and subjected to preparative HPLC (Radial PAK CN, hexane–ethyl acetate, 7:3, v/v) to give two compounds as colorless amorphous powders: 16β-*O*-methylnigakihemiacetal C (=nigakihemiacetal F,[14] **6a**) and 16α-*O*-methylnigakihemiacetal C (**6b**) whose spectral data coincided with those of the authentic one.

*Conversion of Picrasinoside-B (**12**) into Nigakihemiacetal C.* A mixture of picrasinol-B (**12**, 11 mg), acetone (0.1 ml), and 1.5 M sulfuric acid (2 ml) was stirred at 60 °C for 3 h. The reaction product was extracted with chloroform and subjected to preparative HPLC (Radial PAK C_{18}, water–methanol, 1:1, v/v) to give a colorless amorphous powder (nigakihemiacetal C,[10] 7 mg): IR ($CHCl_3$) 3400, 1680, and 1640 cm^{-1}; Mass *m/z* 380 (M^+, $C_{21}H_{32}O_6$).

*Conversion of Picrasin D (**13**) into Nigakilactone A.* A mixture of picrasin D (**13**, 7 mg), which was obtained by the Jones oxidation of picrasinol-B (**12**), and 1.5 M sulfuric acid (2 ml) was stirred at 60 °C for 3 h. The reaction product was extracted with chloroform and subjected to preparative HPLC (Radial PAK C_{18}, water–methanol, 1:1, v/v) to give a colorless amorphous powder (nigakilactone A,[9] 4 mg): IR ($CHCl_3$) 3400, 1680, and 1640 cm^{-1}; Mass *m/z* 378 (M^+, $C_{21}H_{30}O_6$).

*Acid Hydrolysis of Picrasinoside-D (**7**).* A mixture of picrasinoside-D (**7**, 9 mg) and 1.5 M sulfuric acid–methanol (1:2, v/v, 6 ml) was stirred at 60 °C for 5 h. The reaction product was extracted with chloroform and subjected to preparative HPLC (Radial PAK CN, hexane–ethyl acetate, 9:1, v/v) to give two compounds as colorless amorphous powders: 16β-*O*-methylpicrasinol-A (**7a**, 4 mg): IR ($CHCl_3$) 1730, 1705, 1640, and 1245 cm^{-1}; Mass *m/z* (%) 450 (M^+, $C_{25}H_{38}O_7$; 1.9), 418 (M^+-MeOH; 15), 390 (M^+-AcOH; 20), 375(100), 372(18), 358 ($M^+-AcOH-MeOH$; 27), 344(18), 343 (43), 315(18), 299(27), 165(24), 154(14), 153(19), 152(17), 151 (16), and 121(18) and 16α-*O*-methylpicrasinol-A (**7b**, 1.5 mg): IR ($CHCl_3$) 1730, 1705, 1640, and 1245 cm^{-1}; Mass *m/z* (%) 450 (M^+, $C_{25}H_{38}O_7$; 0.8), 418 (M^+-MeOH; 2.4), 390(2.6), 386(56), 375(30), 372(3), 358 ($M^+-AcOH-MeOH$; 80), 344(100), 343 (73), 315(29), 299(52), 165(16), 154(9), 153(16), 152(15), 151 (12), and 121(16). The water layer was analyzed in the same manner as described above and α- and β-D-glucose were identified.

*Methylation of Picrasinol-A (**11**).* A mixture of picrasinol-A (**11**, 13 mg) and 1.5 M sulfuric acid–methanol (1:2, v/v, 6 ml) was stirred at 60 °C for 5 h. The reaction product was extracted with chloroform and subjected to preparative HPLC (Radial PAK CN, hexane–ethyl acetate, 9:1, v/v) to give two compounds as colorless amorphous powders: 16β-*O*-methyl picrasinol-A (**7a**) and 16α-*O*-methylpicrasinol-A (**7b**). They were identified by spectral comparisons with those of the authentic one.

*Conversion of Picrasinol-A (**11**) into Nigakilactone C.*[9] Picrasinol-A (**11**, 14 mg) was oxidized with the Jones reagent in the same manner as described above. The reaction product was extracted with chloroform and subjected to preparative HPLC (Radial PAK C_{18}, water–methanol, 1:1, v/v) to give a colorless amorphous powder (nigakilactone C,[9] 10 mg): mp 231—233 °C (lit,[9] 252.5—253 °C); IR ($CHCl_3$) 1735, 1730, 1705, 1640, and 1240 cm^{-1}; ^1H NMR (60 MHz, $CDCl_3$)δ 1.01 (3H, d, *J*=7; $C_{(13)}$-CH_3), δ 1.05 (3H, d, *J*=6; $C_{(4)}$-CH_3), δ 1.26 (6H, s, $C_{(8)}$-CH_3 and $C_{(10)}$-CH_3, δ 1.95 (3H, s, $OCOCH_3$), δ 3.41 and δ 3.54 (each 3H, s; OCH_3), δ 4.13 (1H, m; $C_{(7)}$-H, δ 5.10 (1H, d, *J*=2; $C_{(3)}$-H), and δ 5.18 (1H, dd, *J*=9, 11; $C_{(11)}$-H; Mass *m/z* 434 (M^+, $C_{24}H_{34}O_7$).

*Acid Hydrolysis of Picrasinoside-E (**8**).* A mixture of picrasinoside-E (**8**, 16 mg) and 1.5 M sulfuric acid–methanol (1:2, v/v, 6 ml) was stirred at 60 °C for 5 h. The reaction product was extracted with chloroform and subjected to preparative HPLC (Radial PAK CN, hexane–ethyl acetate, 4:1, v/v) to give two compounds as amorphous powders: 16β-*O*-methylnigakihemiacetal D (**8a**, 3.6 mg: IR ($CHCl_3$) 3450, 1730, 1705, 1640, and 1245 cm^{-1}; Mass *m/z* (%) 466 (M^+, $C_{25}H_{38}O_8$; 3.2), 434 (M^+-MeOH; 22), 406 (M^+-AcOH; 43), 391(42), 375(48), 374 ($M^+-AcOH-MeOH$; 38), 359(100), 331(46), 313(30), 299(35), 165(51), 154(24), 153(53), 152(51), 151(36), and 121(34) and 16α-*O*-methylnigakihemiacetal D (**8b**, 3.2 mg): IR ($CHCl_3$) 3450, 1730, 1705, 1640, and 1245 cm^{-1}; Mass *m/z* (%) 466 (M^+, $C_{25}H_{38}O_8$; 2.9), 434 (M^+-MeOH; 26), 406 (M^+-AcOH; 37), 391(30), 375(51), 374 ($M^+-AcOH-MeOH$; 77), 359(89), 331(100), 313(48), 299(47), 165(67), 154(32), 153(69), 152(66), 151(45), and 121(47).

*Conversion of Compounds **8a** and **8b** into Nigakihemiacetal D.* A mixture of **8a** and **8b** (4 mg) and 1.5 M sulfuric acid (2 ml) was stirred at 60 °C for 3 h. The reaction product was extracted with chloroform and subjected to preparative HPLC (Radial PAK CN, hexane–ethyl acetate, 4:1, v/v) to give a colorless amorphous powder (nigakihemiacetal D,[8] 2 mg): IR ($CHCl_3$) 3450, 1730, 1705, 1640, and 1245 cm^{-1}; Mass

m/z 452 (M^+, $C_{24}H_{36}O_8$).

Acid Hydrolysis of Picrasinoside-F (9). A mixture of picrasinoside-F (**9**, 4.2 mg) and 1.5 M sulfuric acid–methanol (1:2, v/v, 6 ml) was stirred at 60 °C for 5 h. The reaction product was extracted with chloroform and subjected to preparative HPLC (Radial PAK CN, hexane–ethyl acetate, 4:1, v/v) to give two compounds as colorless amorphous powders: 11-deacetyl-16β-*O*-methylpicrasinol-A (**9a**, 1.1 mg): IR ($CHCl_3$) 3470, 1680, and 1645 cm^{-1}; Mass *m/z* (%) 408 (M^+, $C_{23}H_{36}O_6$; 7), 390 (M^+-H_2O; 2), 376 (M^+—MeOH; 78), 361(63), 358 (M^+-H_2O—MeOH; 13), 342 (100), 328(30), 313(27), 285(16), 217(51), 165(39), 154(25), 153(63), 152(47), 151(31), and 121(55) and 11-deacetyl-16α-*O*-methylpicrasinol-A (**9b**, 0.9 mg): IR ($CHCl_3$) 3470, 1680, and 1645 cm^{-1}; Mass *m/z* (%) 408 (M^+, $C_{23}H_{36}O_6$; 3), 390 (M^+-H_2O; 0.7), 376 (M^+—MeOH; 12), 361(5), 358 (M^+-H_2O—MeOH; 9), 344(52), 328 (100), 313(72), 285(25), 217(43), 165(24), 154(21), 153(41), 152 (32), 151(19), and 121(45). The water layer was analyzed in the same manner as described before and α- and β-D-glucose were identified.

Conversion of Compounds 7a and 7b into Compounds 9a and 9b. A mixture of **7a** and **7b** (*ca.* 4 mg) and 2% potassium hydroxide–ethanol (10 ml) was stirred at 80 °C for 2 h. The solvent was removed by distillation under reduced pressure from the reaction mixture to give a residue to which water (15 ml) was added and saturated with carbon dioxide gas for about 10 h. The reaction product was extracted with chloroform and subjected to preparative HPLC (Radial PAK CN, hexane–ethyl acetate, 4:1, v/v) to give **9a** and **9b**. These were identified by spectral comparisons with authentic samples.

Acid Hydrolysis of Picrasinoside-G (10). A mixture of picrasinoside-G (**10**, 7 mg) and 1.5 M sulfuric acid–methanol (1:2, v/v, 6 ml) was stirred at 60 °C for 5 h. The reaction product was extracted with chloroform and subjected to preparative HPLC (Radial PAK CN, hexane–ethyl acetate, 17:3, v/v) to give two compounds as colorless amorphous powders: 16β-*O*-methylnigakihemiacetal A (**10a**, 3.1 mg): IR ($CHCl_3$) 3470, 1680, and 1645 cm^{-1}; Mass *m/z* (%) 424 (M^+, $C_{23}H_{36}O_7$; 9), 406 (M^+-H_2O; 45), 392 (M^+—MeOH; 22), 377 (32), 374 (M^+-H_2O—MeOH; 31), 359(17), 331(25), 304(37), 165(61), 154(50), 153(63), 152(77), 151(44), 127(100), and 121 (55) and 16α-*O*-methylnigakihemiacetal A (**10b**, 1.7 mg): IR ($CHCl_3$) 3470, 1680, and 1645 cm^{-1}; Mass *m/z* (%) 424 (M^+, $C_{23}H_{36}O_7$; 4.5), 406 (M^+-H_2O; 23), 392 (M^+—MeOH; 42), 377 (25), 374 (M^+-H_2O—MeOH; 71),359(25), 331(27), 304(26), 165(62), 154(41), 153(55), 152(74), 151(38), 127(100), and 121 (51). The water layer was analyzed in the same manner as described before and α- and β-D-glucose were identified.

Conversion of Compounds 8a and 8b into Compounds 10a and 10b. A mixture of **8a** and **8b** (*ca.* 2 mg) and 2% potassium hydroxide–ethanol (10 ml) was stirred at 80 °C for 2 h. The reaction mixture was treated in the same manner as described above and gave compounds **10a** and **10b**. These were identified by spectral comparisons with authentic samples.

Biological Activities of Picrasinoside-A (1) and -B (5). The mean survival time (*T/C*%) in mice suffering from P 388 lymphocytic leukemia (test system: 3PS31) was investigated by NCI (U.S.A.) for picrasinoside-A (**1**) and -B (**5**). The *T/C* values for picrasinoside-A (**1**) were 103, 107, and 103 at doses of 20.00, 10.00, and 5.00 mg/kg and those of picrasinoside-B (**5**) were 103, 94, and 96 at doses of 16.00, 8.00, and 4.00 mg/kg, respectively.[21]

The authors wish to thank Drs. Takashi Matsumoto and Sachihiko Imai of Hiroshima University for the ^1H NMR (90 MHz), Mr. Tomonaga Fujiwara of JEOL Co. Ltd. for the ^{13}C NMR (22.5 MHz), Dr. Tomei Oguri of Mitsubishiyuka Pharmaceutical Co. Ltd. for the FAB mass, and Miss Shigeko Miki of Meijiseika Kaisha Ltd. for the FD mass spectra.

References

1) A part of this work was preliminary reported: M. Okano, N. Fukamiya, K. Kondo, T. Fujita, and T. Aratani, *Chem. Lett.*, **1982**, 1425; M. Okano, T. Fujita, N. Fukamiya, and T. Aratani, *Chem. Lett.*, **1984**, 221.

2) S. M. Kupchan, R. W. Britton, J. A. Lacadie, M. F. Ziegler, and C. W. Sigel, *J. Org. Chem.*, **40**, 648 (1975).

3) P. D. Gillin, D. S. Reiner, and M. Suffness, *Antimicrob. Agents Chemother.*, **22**, 342 (1982).

4) J. Polonsky, *Fortschr. Chem. Org. Naturst.*, **30**, 101 (1973).

5) J. Polonsky, *Recent Advan. Phytochem.*, **6**, 31 (1973).

6) J. Polonsky, Z. Varon, and C. Moretti, *J. Nat. Prod.*, **43**, 503 (1980).

7) A. Pierre, M. Robert-Gero, C. Tempete, and J. Polonsky, *Biochem. Biophys. Res. Commun.*, **93**, 675 (1980).

8) M. Van Tri and J. Polonsky, *J. Nat. Prod.*, **44**, 279 (1981).

9) T. Murae, T. Tsuyuki, T. Ikeda, T. Nishihama, S. Masuda, and T. Takahashi, *Tetrahedron*, **27**, 1545 (1971).

10) T. Murae, T. Tsuyuki, T. Ikeda, T. Nishihama, S. Masuda, and T. Takahashi, *Tetrahedron*, **27**, 5147 (1971).

11) T. Murae, A. Sugie, T. Tsuyuki, S. Masuda, and T. Takahashi, *Tetrahedron*, **29**, 1515 (1973).

12) T. Murae, T. Ikeda, A. Sugie, T. Nishihama, T. Tsuyuki, and T. Takahashi, *Bull. Chem. Soc. Jpn.*, **46**, 3621 (1973).

13) T. Murae, A. Sugie, Y. Moriyama, T. Tsuyuki, and T. Takahashi, *Org. Mass Spectrom.*, **8**, 297 (1974).

14) T. Murae, A. Sugie, T. Tsuyuki, and T. Takahashi, *Chem. Pharm. Bull.*, **23**, 2188 (1975).

15) H. Hikino, T. Ohta, and T. Takemoto, *Phytochemistry*, **14**, 2473 (1974). And the references cited therein.

16) M. Okano, K. H. Lee, and I. H. Hall, *J. Nat. Prod.*, **44**, 470 (1981).

17) K. H. Lee, Y. Imakura, Y. Sumida, R. Y. Wu, and I. H. Hall, *J. Org. Chem.*, **44**, 2180 (1979).

18) S. Bhatnagar, J. Polonsky, T. Prange, and C. Pascard, *Tetrahedron Lett.*, **1984**, 299.

19) L. F. Fieser and M. Fieser, "Reagents for Organic Synthesis," ed by John Willey and Sons, Inc. New York (1967), p. 142.

20) ^{13}C NMR (22.5 MHz, $CDCl_3$) δ=13.1 q, 14.8 q, 19.2 q, 22.1 q, 26.1 t, 28.8 t, 32.1 d, 33.3 d, 37.1 d, 39.1 s, 44.2 d, 47.2 s, 48.1 d, 54.7 q, 62.8 t, 71.5 d, 74.9 d, 78.1 d, 78.4 d, 78.6 d, 79.0 d, 83.1 d, 95.4 t, 100.1 d, 100.8 d, 115.3 d, 148.9 s, and 198.7 s.

21) These data are the results of screening performed under the auspices of the Developmental Therapeutics Program, Division of Cancer Treatment, National Cancer Institute, Bethesda, Maryland.

22) S. Nadamitsu, M. Segawa, M. Okano, K. Kondo, and T. Aratani, *La Kromosomo* (in press).

 © 1985 The Chemical Society of Japan Bull. Chem. Soc. Jpn., 58, 1801—1806 (1985)

Synthetic Studies of Rifamycins. VII.[1] A Facile Synthesis of the Aromatic Chromophore of Rifamycin S through a Rifamycin W Aromatic Segment

Masaya NAKATA, Shigeru WADA, Kuniaki TATSUTA, and Mitsuhiro KINOSHITA*
Department of Applied Chemistry, Faculty of Science and Technology, Keio University, Hiyoshi, Kohoku-ku, Yokohama 223
(Received March 3, 1985)

The intact aromatic chromophore of rifamycin S, 7-amino-2,5-dihydroxy-2,4-dimethyl-naphtho[2,1-*b*]furan-1,6,9(2*H*)-trione, was synthesized through the rifamycin W aromatic segment, 1-[5,8-dimethoxy-2,4-bis-(methoxymethoxy)-3-methyl-6-nitro-1-naphthyl]-1-propanone which was prepared in 9 steps and 29.6% overall yield from 2,6-bis(benzyloxy)-3,5-dibromotoluene and furan.

In the preceding paper[1] of this series, we described a simple and convenient preparation of the nitronaphthalene derivative **1** which was demonstrated to be a promising aromatic segment for the total synthesis of rifamycin W (**2**)[2] by the successful aldol coupling with the aliphatic segment[3] of **2**. Although the methoxyl groups at C-2 and C-4 of **1** were quite stable during the elaboration[1] of **1** toward the total synthesis of **2**, the effective ether bond cleavage (de-*O*-methylation) on these methoxyl groups, that is indispensable at the final stage of the conquest of **2**, should naturally become the crucial problem. In this respect, we found that the new nitronaphthalene derivative **3**, which was expected to be a more promising aromatic segment for the rifamycin W synthesis,[4] was a synthetic intermediate suitable for the intact aromatic chromophore

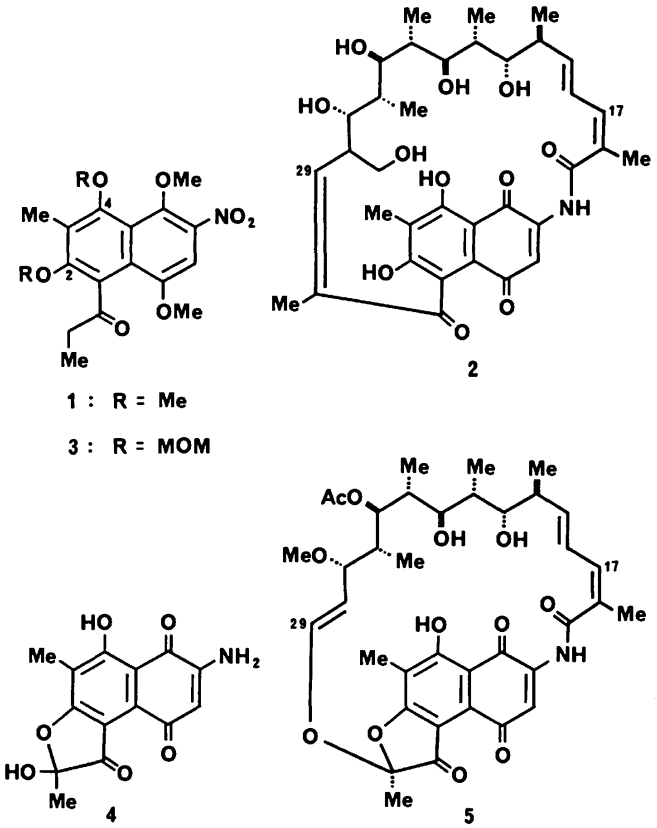

Fig. 1.

4[5] of rifamycin S (**5**). A synthesis of the aromatic segment of **5** has been reported by Kishi *et al.*[6] and an elegant and shorter synthesis of **4** has recently been reported by Kelly *et al.*[7] We now describe a facile synthesis of **4** through the new aromatic segment **3**.

The starting material, 2,6-bis(benzyloxy)-3,5-dibromotoluene (**7**), obtained in a 95% yield by benzylation of 3,5-dibromo-2,6-toluenediol (**6**),[8] was treated with 3.5 equimolar amounts of sodium amide and 30 equimolar amounts of furan in THF at 57 °C for 10 h to give the bromoepoxide **8** in a 97% yield. Lithiation of **8** with 1.2 equimolar amounts of butyllithium in

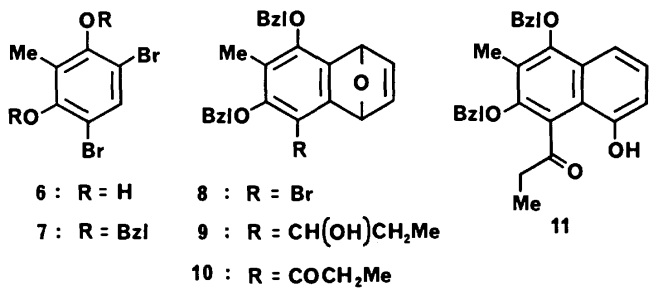

Fig. 2.

THF at −105 °C followed by treatment with 5 equimolar amounts of propanal afforded **9** in an 87% yield as an epimeric mixture. Oxidation of **9** with pyridinium chlorochromate (PCC) and subsequent treatment of the resulting epoxy ketone **10** with perchloric acid in THF at room temperature afforded the naphthol **11** in a 79% yield from **9** as a sole product. The structure shown for **11** was established by the following manner. The aforesaid lithiation of **8** followed by carboxylation afforded the naphthoic acid **12**. The ring-opening reaction of this epoxy acid by treatment with perchloric acid in THF proceeded very slowly at room temperature and was accompanied by de-

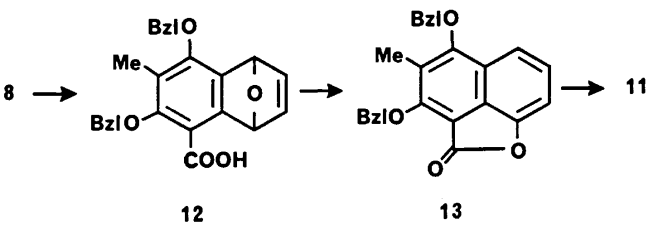

Fig. 3.

composition at elevated temperature. After many other unsuccessful results, the lactone **13** could be obtained in a 65% yield by treatment of **12** with 0.1 equimolar amounts of sulfuric acid in acetic anhydride. The reaction of **13** with equimolar amount of ethyllithium in ether afforded **11**. This sample of **11** proved to be identical with the specimen of **11** derived from **10** in all respects. To introduce a hydroxyl function at C-5 of **11**, **11** was subjected to oxidation using *N*-bromosuccinimide in aqueous acetic acid,[1,9] but only decomposition took place. Among various conditions studied, the oxidation of **11** using three equimolar amounts of thallium(III) nitrate[10] in methanol at 0°C proceeded smoothly to give the naphthoquinone **14** in an 82% yield. Catalytic hydrogena-

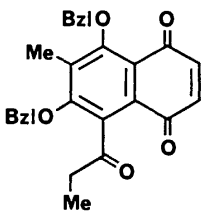

14

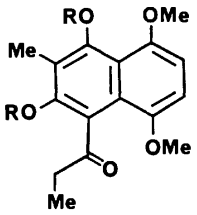

15 : R = Bzl
16 : R = H
17 : R = MOM

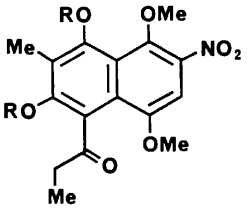

3 : R = MOM
18 : R = H
1 : R = Me

Fig. 4.

tion of **14** with hydrogen in the presence of Lindlar catalyst and pyridine in acetone afforded the air sensitive hydronaphthoquinone, which was immediately methylated with dimethyl sulfate and potassium carbonate to give **15** in a 74% yield. Conversion of the benzyl ether into the methoxymethyl ether was carried out by debenzylation of **15** followed by methoxymethylation of the resulting diol **16** to afford **17** in a 95% yield. Nitration of **17** with copper(II) nitrate[1,11] in acetic anhydride at −40°C afforded regiospecifically the nitronaphthalene **3** in a 77% yield. The structural elucidation of **3** was carried out as follows: cleavage of the methoxymethyl ether of **3** by treatment with 1 M† HCl in THF gave the diol **18**, which was methylated to give the tetramethoxynaphthalene proved to be identical with **1**[1] in all respects.

Conversion of **3** into the target chromophore **4** was achieved by the following procedure. Thus, reduction of **3** with hydrogen in the presence of 5% palladium on charcoal led to the amine **19**. To protect the amino group of **19**, the acid-labile protecting group was select-

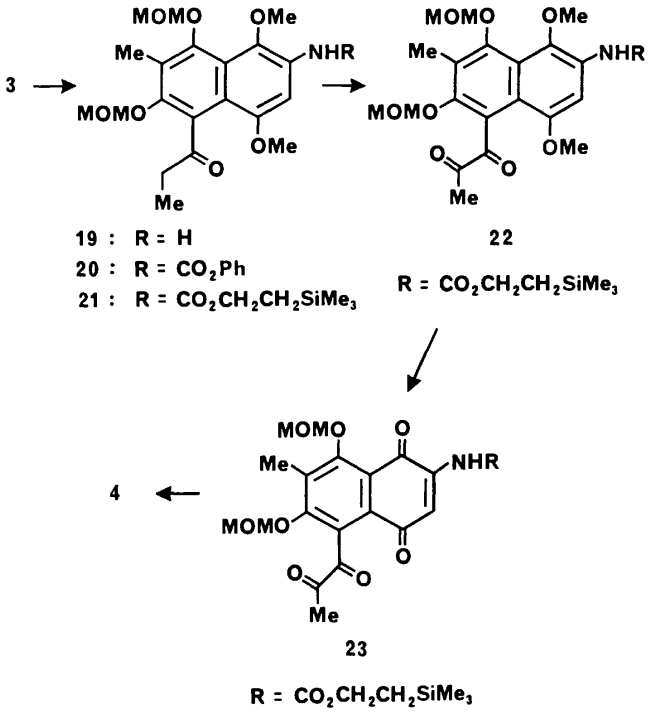

Fig. 5.

ed because acidic conditions were necessary for the formation of the furanone ring along with the removal of both the amino and the phenol protecting groups at the last stage in the synthesis of **4**. *t*-Buthoxycarbonyl group was first chosen but the corresponding carbamate was not obtained in a satisfactory yield. 2-(Trimethylsilyl)ethoxycarbonyl group afforded a good result, namely, the amine **19** was transformed by the Meyers' procedure[12] into the 2-(trimethylsilyl)ethyl carbamate **21** *via* the phenyl carbamate **20** in an 89% yield. Oxidation of **21** with oxygen[6,13] in the presence of 15 equimolar amounts of potassium *t*-butoxide in a mixture of *t*-butyl alcohol, dimethyl sulfoxide (DMSO), and 1,2-dimethoxyethane (DME) gave the α-diketone **22** in an 88% yield. In this reaction, only the starting material was recovered when DMSO was absent. Oxidative demethylation of **22** with ammonium cerium(IV) nitrate[14] in aqueous acetonitrile provided the naphthoquinone **23** in an 86% yield. Exposure of **23** to 100% trifluoroacetic acid[15] (TFA) at 0°C for 1.5 h gave the target aminonaphthoquinone **4** in a 93% yield. The spectral data (IR, UV, ^{1}H-NMR) of **4** were indistinguishable from those of naturally occurring **4**.[5]

Experimental

Melting points were determined on a micro hot-stage Yanaco MP-S3 and were uncorrected. IR spectra were recorded on a Hitachi Perkin-Elmer 225 spectrometer, UV spectra on JAS·CO UVIDEC-1 spectrometer, and ^{1}H-NMR

† 1 M=1 mol dm^{-3}.

spectra on Varian EM-390 spectrometer in $CDCl_3$ using TMS as internal standard. Silica gel TLC and column chromatography were performed on Merck TLC 60F-254 and Wakogel C-200, respectively. In general, evaporation of solvents was carried out under reduced pressure below 30°C.

2,6-Bis(benzyloxy)-3,5-dibromotoluene (7). To an ice-cold stirred suspension of **6** (1.00 g, 3.55 mmol) and potassium carbonate (1.23 g, 8.90 mmol) in dry acetone (10 ml), benzyl bromide (1.05 ml, 8.83 mmol) was added dropwise. After the addition was complete, the mixture was stirred at 60°C for 4 h and filtered with celite. The filter cake was washed with acetone and the combined filtrate and washings were evaporated. The residue was chromatographed on silica gel (82 g) with 25:1 hexane-ethyl acetate to afford **7** (1.56 g, 95%) as colorless crystals: mp 91.5—92.5°C (needles from ethyl acetate-methanol); R_f=0.34 (25:1 hexane-ethyl acetate); UV (EtOH) λ 214 nm (log ε 4.63); ^{1}H-NMR δ= 2.22 (3H, s, ArMe), 4.96 (4H, s, 2×OC<u>H</u>$_2$Ph), and 7.30—7.75 (11H, m, H-4 and 2×Ph).

Found: C, 54.32; H, 4.04; Br, 34.27%. Calcd for $C_{21}H_{18}O_2Br_2$: C, 54.57; H, 3.93; Br, 34.58%.

5,7-Bis(benzyloxy)-8-bromo-1,4-dihydro-6-methyl-1,4-epoxynaphthalene (8). To a solution of **7** (10.0 g, 21.6 mmol) in dry THF (70 ml) were added furan (47.0 ml, 646 mmol) and sodium amide (2.95 g, 75.6 mmol). After the mixture was stirred at 57°C for 10 h, the insoluble matter was filtered with celite and the filter cake was washed with ether. The combined filtrate and washings were evaporated and the residue was chromatographed on silica gel (240 g) with 50:1 toluene-ethyl acetate to give **8** (9.61 g, 99%) as a brown syrup. This syrup was treated with activated carbon in ether to afford a yollow-brown syrup (9.41 g, 97%) of **8**. An analytical sample (colorless syrup) was obtained after the additional column chromatography with 5:1 hexane-ethyl acetate: R_f= 0.13 (20:1 hexane-ethyl acetate); UV (EtOH) λ 218 nm (log ε 4.57); ^{1}H-NMR δ=2.14 (3H, s, ArMe), 4.88 and 5.05 (each 2H, each s, 2×OC<u>H</u>$_2$Ph), 5.79 and 5.93 (each 1H, each dd, H-1 and 4, J=1.0 and 2.0 Hz), 6.75 and 7.04 (each 1H, each dd, H-2 and 3, J=5.3 and 2.0 Hz), and 7.42 (10H, s, 2×Ph).

Found: C, 66.90; H, 4.82; Br, 18.02%. Calcd for $C_{25}H_{21}O_3Br$: C, 66.83; H, 4.71; Br, 17.78%.

1-[2,4-Bis(benzyloxy)-5,8-dihydro-3-methyl-5,8-epoxy-1-naphthyl]-1-propanol (9). To a stirred solution of **8** (9.41 g, 20.9 mmol) in dry THF (84 ml) at −105°C under argon was added 1.42 M butyllithium in hexane (17.7 ml, 25.1 mmol) over a period of 4 min. After being stirred at the same temperature for 6 min, propanal (7.55 ml, 105 mmol) was added to the mixture as soon as possible. The reaction mixture was stirred at the same temperature for 30 min and treated with a saturated aqueous NH_4Cl solution (80 ml). After being allowed to warm to room temperature, the resulting mixture was extracted with ether (100 ml×2), and the extract was washed with a saturated aqueous NaCl solution (70 ml), dried, and evaporated. The residue was chromatographed on silica gel (450 g) with 4:1 toluene-ethyl acetate to give **9** (7.80 g, 87%) as pale yellow-brown crystals. This sample showed two spots (R_f 0.32 and 0.21) on TLC with 15:1 chloroform-ethyl acetate. A part of this was separated by silica gel column chromatography with 15:1 chloroform-ethyl acetate to give colorless crystals of **9a** and **9b** with a ratio of 1.2:1:

9a, R_f=0.32 (15:1 chloroform-ethyl acetate), mp 107—108 °C (needles from chloroform-hexane); IR (KBr) 3410 cm^{-1}; UV (EtOH) λ (log ε) 222(4.51), 260 (sh, 3.34), and 295 nm (sh, 2.86); ^{1}H-NMR δ=0.95 (3H, t, CH$_2$<u>Me</u>, J=7.5 Hz), 1.60—2.00 (3H, m, OH and C<u>H</u>$_2$Me), 2.18 (3H, s, ArMe), 4.79 and 5.06 (each 2H, each s, 2×OC<u>H</u>$_2$Ph), 4.80—5.00 (1H, m, C<u>H</u>OH), 5.88 and 6.08 (each 1H, each dd, H-5 and 8, J=1.0 and 1.8 Hz), 6.74 and 6.98 (each 1H, each dd, H-6 and 7, J=1.8 and 5.6 Hz), and 7.44 (10H, s, 2×Ph).

Found: C, 78.35; H, 6.67%. Calcd for $C_{28}H_{28}O_4$: C, 78.48; H, 6.59%.

9b, R_f=0.21 (15:1 chloroform-ethyl acetate), mp 107—108 °C (needles from chloroform-hexane); IR (KBr) 3430 cm^{-1}; UV (EtOH) λ (log ε) 222(4.51), 260 (sh, 3.29), and 295 nm (sh, 2.81); ^{1}H-NMR δ=0.86 (3H, t, CH$_2$<u>Me</u>, J=7.5 Hz), 1.40—1.85 (3H, m, OH and C<u>H</u>$_2$Me), 2.18 (3H, s, ArMe), 4.79 and 5.06 (each 2H, each s, 2×OC<u>H</u>$_2$Ph), 4.80—5.00 (1H, m, C<u>H</u>OH), 5.88 and 6.25 (each 1H, each dd, H-5 and 8, J=1.0 and 1.8 Hz), 6.79 and 6.99 (each 1H, each dd, H-6 and 7, J=1.8 and 5.6 Hz), and 7.44 (10H, s, 2×Ph).

Found: C, 78.60; H, 6.70%. Calcd for $C_{28}H_{28}O_4$: C, 78.48; H, 6.59%.

1-[2,4-Bis(benzyloxy)-5,8-dihydro-3-methyl-5,8-epoxy-1-naphthyl]-1-propanone (10). To a stirred mixture of PCC (10.3 g, 47.8 mmol), molecular sieves 3A powder (15.9 g), and dry dichloromethane (40 ml) was added a solution of **9** (6.80 g, 15.9 mmol) in dry dichloromethane (34 ml) at room temperature. After being stirred at room temperature for 0.5 h, the reaction mixture was diluted with ether (75 ml) and the resulting suspension was transferred to a column filled with silica gel (130 g). The column was eluted with ether and the eluant was evaporated to give practically pure sample of **10** (6.70 g, 98%) as pale yellow crystals. An analytical sample was obtained after recrystallization from ethyl acetate-hexane: mp 112—114°C (colorless plates); R_f=0.45 (3:1 hexane-ethyl acetate) ; IR (KBr) 1663 cm^{-1}; UV (EtOH) λ (log ε) 212(4.39), and 247 nm (4.23) ; ^{1}H-NMR δ=1.08 (3H, t, CH$_2$-<u>Me</u>, J=7.0 Hz), 2.15 (3H, s, ArMe), 2.70—3.20 (2H, m, C<u>H</u>$_2$Me), 4.70 and 4.73 (each 1H, ABq, OC<u>H</u>$_2$Ph, J_{gem}=12.0 Hz), 5.11 and 5.21 (each 1H, ABq, OC<u>H</u>$_2$Ph, J_{gem}=12.0 Hz), 5.85 and 5.95 (each 1H, each br, H-5 and 8), 6.77 and 7.10 (each 1H, each dd, H-6 and 7, J=1.8 and 5.3 Hz), and 7.42 and 7.45 (each 5H, each s, 2×Ph).

Found: C, 78.58 ; H, 6.30%. Calcd for $C_{28}H_{26}O_4$; C, 78.85 ; H, 6.14%.

2,4-Bis(benzyloxy)-5,8-dihydro-3-methyl-5,8-epoxy-1-naphthalenecarboxylic Acid (12). To a stirred solution of **8** (960 mg, 2.14 mmol) in dry THF (8.55 ml) at −100°C under argon was added 1.39 M butyllithium in hexane (1.84 ml, 2.56 mmol). After being stirred at the same temperature for 30 min, CO_2 gas was bubbled through the reaction mixture for 20 min. The mixture was allowed to warm to 0°C and then acidified with 1 M HCl (30 ml). The mixture was extracted with ether and the extract was washed with a saturated aqueous NaCl solution, dried, and evaporated. The residue was chromatographed on silica gel (48 g) with 4:1:0.05 toluene-ethyl acetate-acetic acid to afford **12** (689 mg, 78%) as a brown syrup. This slightly impure syrup was crystallized from 1:4 acetone-hexane to afford colorless needles: mp 144—145 °C ; R_f=0.21 (4:1:0.05 toluene-ethyl acetate-acetic acid); IR (KBr) 1688 cm^{-1}; UV (EtOH) λ (log ε) 212(4.49), 233(4.47), and 297 nm (3.09); ^{1}H-NMR δ=2.21 (3H, s, ArMe), 4.91 (2H, s, OC<u>H</u>$_2$Ph), 5.15 and 5.30 (each 1H, ABq, OC<u>H</u>$_2$Ph, J_{gem}= 12.0 Hz), 6.02 and 6.53 (each 1H, each dd, H-5 and 8, J= 1.2 and 1.8 Hz), 6.78 and 7.12 (each 1H, each dd, H-6 and 7, $J_{6,7}$=5.7 Hz, J=1.8 Hz), and 7.45 (10H, s, 2×Ph).

Found: C, 75.48 ; H, 5.57%. Calcd for $C_{26}H_{22}O_5$: C, 75.35 ; H, 5.35%.

3,5-Bis(benzyloxy)-4-methyl-2H-naphtho[1,8-bc]furan-2-one (13). A 1.0 ml solution of 0.012 M concd H_2SO_4 in acetic anhydride was added to **12** (49.4 mg, 0.119 mmol) at 21 °C. The resulting white suspension was stirred for 10 min, and diluted with ether. The ether layer was washed with water (3 times) and a saturated aqueous NaCl solution, dried, and evaporated. The residue was chromatographed on silica gel (4.8 g) with 10:1 hexane-acetone to give **13** (30.5 mg, 65%) as colorless crystals. An analytical sample was obtained after recrystallization from chloroform-hexane: mp 136—137 °C (cottony crystals); R_f=0.23 (10:1 hexane-acetone); IR (KBr) 1754 cm^{-1}; UV (EtOH) λ (log ε) 220(4.50), 260(4.55), and 333 nm (4.04); ^{1}H-NMR δ=2.30 (3H, s, ArMe), 5.18 (2H, s, $OC\underline{H}_2Ph$), 6.00 (2H, s, $OC\underline{H}_2Ph$), 7.11 and 7.65 (each 1H, each d, H-6 and 8, J=7.2 Hz), and 7.30—7.60 (11H, m, 2×Ph and H-7).

Found: C, 78.50; H, 5.15%. Calcd for $C_{26}H_{20}O_4$: C, 78.77 ; H, 5.08%.

1-[2,4-Bis(benzyloxy)-8-hydroxy-3-methyl-1-naphthyl]-1-propanone (11). (a) To a solution of **10** (8.30 g, 19.5 mmol) in THF (140 ml), 60% $HClO_4$ (1.26 ml) was added. After being stirred at 25 °C for 35 h, the reaction mixture was diluted with ether (140 ml), washed with water (100 ml×3) and a saturated aqueous NaCl solution (100 ml×1), dried, and evaporated. The residue was recrystallized from THF (28 ml) and hexane (55 ml) at −25 °C overnight to afford **11** (3.21 g) as pale yellow-brown crystals. The mother liquor was evaporated and the residue was chromatographed on silica gel (250 g) with 8:1 toluene-ethyl acetate to afford additional **11** (3.53 g). The total amount was 6.74 g (81%). An analytical sample (colorless mossy crystals) was obtained after recrystallization (two times) from a mixture of chloroform and hexane: mp 188—190 °C (decomp); R_f=0.31 (8:1 toluene-ethyl acetate); IR (KBr) 3390 and 1675 cm^{-1} ;UV (0.01 M HCl-EtOH) λ (log ε) 221(4.77), 242(4.76), and 306 nm (4.00); ^{1}H-NMR δ=1.18 (3H, t, $CH_2\underline{Me}$, J=7.0 Hz), 2.39 (3H, s, ArMe), 2.94 (2H, q, $C\underline{H}_2Me$, J=7.0 Hz), 4.90 and 5.02 (each 2H, each s, 2× $OC\underline{H}_2Ph$), 6.28 (1H, s, OH), 6.81 and 7.71 (each 1H, each d, H-5 and 7, J=7.5 Hz), and 7.15—7.65 (11H, m, H-6 and 2× Ph).

Found: C, 78.60; H, 6.20%. Calcd for $C_{28}H_{26}O_4$; C, 78.85; H, 6.14%.

(b) To an ice-cold stirred suspension of **13** (30.4 mg, 0.0767 mmol) in dry ether (1.67 ml), 1.60 M ethyllithium in ether (0.0478 ml, 0.0765 mmol) was added dropwise. After being stirred at 0 °C for 1 h, a saturated aqueous NH_4Cl solution was added to the mixture. The mixture was extractred with ether and the extracts were washed with a saturated aqueous NaCl solution, dried, and evaporated. The residue was chromatographed on silica gel (3.2 g) with 8:1 toluene-ethyl acetate to give 8.5 mg (26%) of pale yellow-brown crystals and the unchanged starting lactone **13** (19.5 mg, 64% recovered). Recrystallization from chloroform-hexane gave slightly brown mossy crystals. This material was identical with **11** prepared from **10** in all respects (TLC, ^{1}H-NMR, IR, UV, mp).

5,7-Bis(benzyloxy)-6-methyl-8-propionyl-1,4-naphthalenedione (14). To an ice-cold stirred suspension of **11** (9.29 g, 21.8 mmol) in methanol (186 ml) a solution of thallium(III) nitrate trihydrate (29.0 g, 65.3 mmol) in methanol (145 ml) was added dropwise. The resulting mixture was stirred at 0 °C for 3 h and treated with ice-cold water (330 ml). The mixture was extrated with ethyl acetate (650 ml) and the extract was washed with a saturated aqueous $NaHCO_3$ solution, water, and a saturated aqueous NaCl solution successively, dried and evaporated. The residue was chromatographed on silica gel (480 g) with 13:1 toluene-ethyl acetate to afford **14** (7.90 g, 82%) as yellow crystals. An analytical sample was obtained after recrystallization (three times) from ethanol: mp 144.5—146 °C (yellow needles); R_f=0.54 (8:1 toluene-ethyl acetate); IR (KBr) 1698, 1665, and 1615 cm^{-1}; UV (EtOH) λ (log ε) 231(4.57), 253(4.35), and 363 nm (3.57); ^{1}H-NMR δ=1.25 (3H, t, $CH_2\underline{Me}$, J=7.2 Hz), 2.22 (3H, s, ArMe), 2.55—2.95 (2H, m, $C\underline{H}_2Me$), 4.83 and 4.97 (each 2H, br s and s, 2×$OC\underline{H}_2Ph$), 6.89 (2H, s, H-2 and 3), and 7.42 (10H, s, 2× Ph).

Found: C, 76.60 ; H, 5.66%. Calcd for $C_{28}H_{24}O_5$: C, 76.35 ; H, 5.49%.

1-[2,4-Bis(benzyloxy)-5,8-dimethoxy-3-methyl-1-naphthyl]-1-propanone (15). A mixture of **14** (5.00 g, 11.4 mmol), pyridine (6.89 ml, 85.2 mmol), Lindlar catalyst (1.50 g), and acetone (200 ml) was vigorously stirred at room temperature for 10 min under bulbling with H_2. The suspension was filtered with celite and the filter cake was washed with acetone under an argon atomosphere. To the combined filtrate and washings, dimethyl sulfate (10.7 ml, 113 mmol) and K_2CO_3 (7.84 g, 56.7 mmol) were added and vigorously stirred at room temperature for 41 h. To the resulting mixture dimethyl sulfate (10.7 ml, 113 mmol) and K_2CO_3 (7.84 g, 56.7 mmol) were added and stirring was continued for additional 52 h. The insoluble matter was filtered with celite and the filter cake was washed with acetone. The combined filtrate and washings were evaporatred and the residue was dissolved in ethyl acetate (300 ml). The solution was washed with water (100 ml) and a saturated aqueous NaCl solution (100 ml), dried, and evaporated. The residue was chromatographed on silica gel (300 g) with 17:1 toluene-ethyl acetate to give **15** (3.97 g, 74%) as pale green crystals. An analytical sample was obtained after recrystallization from chloroform-hexane: mp 118.7—119.5 °C (colorless needles); R_f= 0.35 (17:1 toluene-ethyl acetate); IR (KBr) 1708 cm^{-1}; UV (EtOH) λ (log ε) 222 (4.72), 249 (4.46), 327 (3.90), and 340 nm (3.86); ^{1}H-NMR δ=1.19 (3H, t, $CH_2\underline{Me}$, J=7.0 Hz), 2.36 (3H, s, ArMe), 2.83 (2H, dq, $C\underline{H}_2Me$, J_{gem}=7.0 Hz), 3.85 (6H, s, 2×OMe), 4.85 and 4.86 (each 1H, ABq, $OC\underline{H}_2Ph$, J_{gem}= 10.5 Hz), 4.92 (2H, s, $OC\underline{H}_2Ph$), 6.77 (2H, s, H-6 and 7), and 7.20—7.65 (10H, m, 2×Ph).

Found: C, 76.74; H, 6.52%. Calcd for $C_{30}H_{30}O_5$: C, 76.57; H, 6.43%.

1-(2,4-Dihydroxy-5,8-dimethoxy-3-methyl-1-naphthyl)-1-propanone (16). A solution of **15** (1.53 g, 3.25 mmol) in ethyl acetate (30 ml) was stirred with palladium black (in methanol) at 25 °C for 20 min under bubbling with H_2. The filtered solution was then evaporated to afford the crude **16** (944 mg, 100%) as yellow-brown crystals. This sample was pure enough for the next steps without further purification. A part of this was recrystallized from 1:3 ethyl acetate-hexane to give an analytical sample as yellow-green needles: mp 111—112 °C; R_f=0.40 (3:1 hexane-acetone); IR (KBr) 3305 and 1630 cm^{-1}; UV (0.01 M HCl-EtOH) λ (log ε) 232 (4.40), 272 (3.76), 315 (3.61), 347 (3.57), and 370 nm (3.41); ^{1}H-NMR δ=1.12 (3H, t, $CH_2\underline{Me}$, J=7.5 Hz), 2.21 (3H, s, ArMe), 2.35—2.80 (2H, m, $C\underline{H}_2Me$), 3.81 and 4.03 (each 3H, each s, 2×OMe), 6.67 and 6.73 (each 1H, ABq, H-6 and 7, J=9.0 Hz), and 10.26 and 10.73 (each 1H, s and br s, 2×OH).

Found: C, 65.95; H, 6.20%. Calcd for $C_{16}H_{18}O_5$: C, 66.19; H, 6.25%.

1-[5,8-Dimethoxy-2,4-bis(methoxymethoxy)-3-methyl-1-naphthyl]-1-propanone (17). To an ice-cold stirred solution of **16** (841 ml, 2.90 mmol) in dry THF (16.8 ml) was added sodium hydride (209 mg, 8.71 mmol) and the mixture was stirred at 20°C for 15 min, then cooled to 0°C. To this was added chloromethyl methyl ether (0.660 ml, 8.69 mmol) and the mixture was stirred at 20°C for 1 h. The resulting reaction mixture was poured into ice-water and the mixture was extracted with ether. The extract was washed with a saturated aqueous NaCl solution, dried and evaporated. The residue was chromatographed on silica gel (55 g) with 4:1 toluene–ethyl acetate to afford **17** (1.04 g, 95%) as a yellow-brown syrup. An analytical sample was obtained after recolumn chromatography with 3:1 hexane–acetone as a pale yellow syrup: R_f=0.23 (3:1 hexane–acetone); IR ($CHCl_3$) 1697 cm^{-1}; UV (EtOH) λ (log ε) 222 (4.62), 249 (4.40), 327 (3.88), and 340 nm (3.84); ^{1}H-NMR δ=1.20 (3H, t, $CH_2\underline{Me}$, J=7.5 Hz), 2.45 (3H, s, ArMe), 2.79 (2H, dq, $C\underline{H}_2Me$, J=7.5 and 9.0 Hz), 3.57, 3.63, 3.79, and 3.89 (each 3H, each s, 4×OMe), 4.96 and 5.05 (each 2H, *ca.* s and s, 2×OCH_2Ph), and 6.73 (2H, s, H-6 and 7).

Found: C, 63.20; H, 6.97%. Calcd for $C_{20}H_{26}O_7$: C, 63.48; H, 6.92%.

1-[5,8-Dimethoxy-2,4-bis(methoxymethoxy)-3-methyl-6-nitro-1-naphthyl]-1-propanone (3). To 10.0 ml of acetic anhydride, copper(II) nitrate trihydrate (1.00 g, 4.14 mmol) was added portionwise. The mixture was stirred at 30°C for 10 min and cooled to −40°C. To this mixture, a solution of **17** (1.43 g, 3.78 mmol) in acetic anhydride (14.3 ml) was added dropwise. After being stirred at −40°C for 1 h, ether (30 ml) and water (20 ml) were added to the mixture and the mixture was allowed to warm to room temperature. The organic layer was separated and the aqueous layer was extracted with ether (20 ml×2). The combined extracts were washed with a saturated aqueous NaCl solution (20 ml×3), dried, and evaporated. The residue was chromatographed on silica gel (80 g) with 10:1 toluene–ethyl acetate to afford **3** (1.26 g, 79%) as green crystals. This sample was treated with charcoal in ether to afford pure **3** (1.23 g, 77%) as yellow prisms: mp 89.5—90.5°C (hexane); R_f=0.30 (10:1 toluene–ethyl acetate); IR (KBr) 1715 cm^{-1}; UV (EtOH) λ (log ε) 233 (4.55), and 378 nm (3.58); ^{1}H-NMR δ=1.22 (3H, t, $CH_2\underline{Me}$, J=7.0 Hz), 2.49 (3H, s, ArMe), 2.79 (2H, dq, $C\underline{H}_2Me$, J_{gem}=7.0 Hz), 3.58 and 3.62 (each 3H, each s, 2×$CH_2O\underline{Me}$), 3.90 and 3.92 (each 3H, each s, 2×OMe), 4.97 and 5.03 (each 2H, each s, 2×OCH_2O), and 7.07 (1H, s, ArH).

Found: C, 56.45; H, 5.91; N, 3.18%. Calcd for $C_{20}H_{25}NO_9$: C, 56.73; H, 5.95; N, 3.31%.

Transformation of 3 into 1. A solution of **3** (13.9 mg, 0.0328 mmol) in THF (0.28 ml) and 1 M HCl (0.14 ml) was stirred at 23°C for 3 d. The reaction mixture was diluted with ethyl acetate, washed with water and a saturated aqueous NaCl solution, dried, and evaporated. The residual orange-yellow crystals of **18** [11.0 mg, 100%; R_f=0.49 (10:1 toluene–ethyl acetate); ^{1}H-NMR δ=1.14 (3H, t, $CH_2\underline{Me}$, J=7.5 Hz), 2.25 (3H, s, ArMe), 2.40—2.75 (2H, m, $C\underline{H}_2Me$), 3.95 and 4.11 (each 3H, each s, 2×OMe), 7.37 (1H, s, ArH), 10.30 and 10.58 (each 1H, each s, 2×OH)] was suspended in 0.22 ml of acetone and cooled to 0°C. To this were added dimethyl sulfate (0.0124 ml, 0.131 mmol) and K_2CO_3 (18.1 mg, 0.131 mmol). After being stirred at 20°C for 5 h, the mixture was filtered with celite and the filter cake was washed with acetone. The combined filtrate and washings were evaporated and the residue was chromatographed on silica gel (1.5 g) with 15:1 toluene–ethyl acetate to give yellow crystals (11.2 mg, 94% from **3**). This sample was identical with **1**[1] in all respects (^{1}H-NMR, IR, TLC, mp).

[1,4-Dimethoxy-6,8-bis(methoxymethoxy)-7-methyl-5-propionyl-2-naphthyl]carbamic Acid Phenyl Ester (20). A solution of **3** (500 mg, 1.18 mmol) in methanol (20 ml) was stirred with 5% Pd–C at 25°C for 20 min under bubbling with H_2. The filtered solution was then evaporated to afford the crude **19** (465 mg, 100%) as a yellow-brown syrup. To the ice-cold stirred solution of this syrup and dry pyridine (0.115 ml, 1.42 mmol) in dichloromethane (4.7 ml), phenyl chloroformate (0.178 ml, 1.42 mmol) was added dropwise and the mixture was stirred at 0°C for 1 h. Then the reaction was quenched by adding water, and the mixture was extracted with dichloromethane. The extract was washed with a saturated aqueous NaCl solution, dried, and evaporated. The residue was chromatographed on silica gel (61 g) with 6:1 toluene–ethyl acetate to give **20** (606 mg, 100%) as a pale yellow syrup. An analytical sample (colorless foam) was obtained after treatment with charcoal in ether and chromatographed again on silica gel with 20:1 chloroform–ethyl acetate: R_f=0.32 (6:1 toluene–ethyl acetate); IR ($CHCl_3$) 3412, 1745, and 1702 cm^{-1}; UV (EtOH) λ (log ε) 256 (4.84) and 318 nm (4.00); ^{1}H-NMR δ=1.20 (3H, t, $CH_2\underline{Me}$, J= 7.2 Hz), 2.46 (3H, s, ArMe), 2.78 (2H, dq, $C\underline{H}_2Me$, J_{gem}=7.2 Hz), 3.56, 3.61, 3.80, and 3.83 (each 3H, each s, 4×OMe), 4.92 and 4.98 (each 1H, ABq, OCH_2O, J_{gem}=7.5 Hz), 5.02 (2H, s, OCH_2O), 7.15—7.50 (5H, m, Ph), 7.80—8.00 (1H, br, NH), and 7.91 (1H, s, H-3).

Found: C, 62.80; H, 6.11; N, 2.61%. Calcd for $C_{27}H_{31}NO_9$: C, 63.15; H, 6.08; N, 2.73%.

[1,4-Dimethoxy-6,8-bis(methoxymethoxy)-7-methyl-5-propionyl-2-naphthyl]carbamic Acid 2-(Trimethylsilyl)ethyl Ester (21). To an ice-cold stirred solution of **20** (611 mg, 1.19 mmol) and 2-(trimethylsilyl)ethanol (0.511 ml, 3.57 mmol) in dry THF (7.9 ml) was added *t*-BuOK (334 mg, 2.98 mmol) under argon. The mixture was stirred at 0°C for 15 min and then partitioned between ether and water. The organic layer was washed with a saturated aqueous NaCl solution, dried, and evaporated. The residue was chromatographed on silica gel (34 g) with 8:1 toluene–ethyl acetate to afford **21** (569 mg, 89%) as a pale yellow-brown syrup. An analytical sample (colorless syrup) was obtained after the additional silica gel column chromatography with 6:1 hexane–acetone: R_f=0.35 (8:1 toluene–ethyl acetate); IR ($CHCl_3$) 3410, 1717, and 1710 cm^{-1}; UV (EtOH) λ (log ε), 255 (4.83) and 318 nm (3.97); ^{1}H-NMR δ=1.07 (2H, AA′XX′, $SiCH_2$), 1.19 (3H, t, $CH_2\underline{Me}$, J=7.4 Hz), 2.44 (3H, s, ArMe), 2.77 (2H, dq, $C\underline{H}_2Me$, J_{gem}=7.4 Hz), 3.57, 3.60, 3.73, and 3.87 (each 3H, each s, 4×OMe), 4.30 (2H, AA′XX′ $OC\underline{H}_2CH_2Si$), 4.93 and 4.95 (each 1H, each s, OCH_2O), 5.00 (2H, s, OCH_2O), 7.48 (1H, br s, NH), and 7.90 (1H, s, H-3).

Found: C, 57.81; H, 7.14; N, 2.45%. Calcd for $C_{26}H_{39}NO_9Si$: C, 58.08; H, 7.31; N, 2.61%.

[1,4-Dimethoxy-6,8-bis(methoxymethoxy)-7-methyl-5-pyruvoyl-2-naphthyl]carbamic Acid 2-(Trimethylsilyl)ethyl Ester (22). A solution of **21** (46.2 mg, 0.0859 mmol) in dry DME (0.46 ml) was added during a period of two min to a mixture of a 1.43 M *t*-BuOK in *t*-BuOH (0.90 ml, 1.29 mmol) and dry DMSO (0.39 ml) under bubbling with O_2. After the red-brown reac-

tion mixture was vigorously stirred for 30 min under bubbling with O_2, the resulting viscous red-brown mixture was added to an ice-cold stirred saturated aqueous NH_4Cl solution. The mixture was extracted with ethyl acetate and the extract was washed with a saturated aqueous NaCl solution, dried, and evaporated. The residue was chromatographed on silica gel (4.9 g) with 3:1 hexane–acetone to afford **22** (41.6 mg, 88%) as a yellow syrup. An analytical sample was obtained after an additional silica gel column chromatography with 3:1 hexane–acetone as a yellow syrup: R_f=0.25 (3:1 hexane–acetone); IR ($CHCl_3$) 3419, 1720, and 1705 cm^{-1}; UV (EtOH) λ (log ε) 253 (4.81) and 315 (3.94); ^{1}H-NMR δ= 0.08 (9H, s, $SiMe_3$), 1.01 (2H, AA'XX', $SiCH_2$), 2.37 and 2.42 (each 3H, each s, ArMe and COCOMe), 3.43 and 3.56 (each 3H, each s, 2×OCH_2OMe,), 3.70 and 3.77 (each 3H, each s, 2×OMe), 4.26 (2H, AA'XX', OCH_2CH_2Si), 4.90 and 4.98 (each 2H, each s, 2×OCH_2O), 7.47 (1H, brs, NH), and 7.91 (1H, s, ArH).

Found: C, 56.33; H, 6.65; N, 2.62%. Calcd for $C_{26}H_{37}NO_{10}Si$; C, 56.61; H, 6.76; N, 2.54%.

*[1,4-Dihydro-6,8-bis(methoxymethoxy)-7-methyl-5-pyruvoyl-1,4-dioxo-2-naphthyl]carbamic Acid 2-(Trimethysilyl)ethyl Ester (**23**).* To a cold (−20°C) solution of **22** (98.8 mg, 0.179 mmol) in acetonitrile (3.0 ml), a solution of ammonium cerium(IV) nitrate (247 mg, 0.451 mmol) in water (0.74 ml) was added dropwise. After being stirred at −20°C for 5 min, the reaction mixture was diluted with ethyl acetate (5 ml) and water (3 ml), and warmed to room temperature. The organic layer was separated and the aqueous layer was extracted with ethyl acetate. The combined extracts were washed with a saturated aqueous NaCl solution, dried, and evaporated. The residue was chromatographed on silica gel (4.9 g) with 10:1 toluene–ethyl acetate to afford **23** (80.5 mg, 86%) as yellow crystals. An analytical sample was obtained after recrystallization (three times) from acetone–pentane: mp 140—142°C (yellow needles); R_f=0.37 (10:1 toluene–ethyl acetate); IR (KBr) 3210, 1742, 1706, and 1675 cm^{-1}; UV (EtOH) λ (log ε) 222 (4.37), 259 (4.47), 309 (4.09), and 364 nm (3.51); ^{1}H-NMR δ=0.06 (9H, s, $SiMe_3$), 1.06 (2H, AA'XX', $SiCH_2$), 2.37 and 2.59 (each 3H, each s, ArMe and COCOMe), 3.47 and 3.64 (each 3H, each s, 2×OMe), 4.30 (2H, AA'XX', OCH_2CH_2Si), 4.98 and 5.11 (each 2H, each s, 2×OCH_2O), 7.34 (1H, s, ArH) and 7.91 (1H, br s, NH).

Found: C, 55.41; H, 5.95; N, 2.84%. Calcd for $C_{24}H_{31}NO_{10}Si$: C, 55.27; H, 5.99; N, 2.69%.

*7-Amino-2,5-dihydroxy-2,4-dimethyl-naphtho[2,1-b]furan-1,6,9-(2H)-trione (**4**).* A sample of **23** (254 mg, 0.487 mmol) was treated with ice-cold TFA (2.54 ml) at 0°C for 1.5 h. The reaction mixture was diluted with ice-cold water (5 ml) and the precipitated red-brown crystals was collected and washed thoroughly with water. The red-brown crystals consisted almost of **4** (131 mg, 93%): mp >200°C dec.; R_f=0.43 (10:1 chroloform–methanol); IR (nujor) 3317, 1725, 1655, 1611, and 1593 cm^{-1}; UV (EtOH) λ (log ε) 228(4.38), 273(4.25), 307(4.05), and 350 nm (4.03); UV (0.01 M HCl in EtOH) λ (log ε) 226 (4.41), 272 (4.26), 312 (4.03), and 348 nm (4.03); ^{1}H-NMR δ (TFA, TMS)=1.91 (3H, s, 2-Me), 2.34 (3H, s, ArMe), and 6.56 (1H, s, H-8).

Lit,[5a] IR (nujor) 3320, 1725, 1660, 1610, and 1598 cm^{-1}. UV (EtOH) λ (log ε) 228 (4.42), 273 (4.26), 311 (4.04), and 350 nm (4.05). ^{1}H-NMR δ (TFA, TMS)=1.93 (3H, s), 2.37 (3H, s), and 6.55 (1H, s).

Lit,[5b] IR (nujor) 3490, 3250, 1735, 1665, 1620, and 1605 cm^{-1}. UV (0.01M HCl in EtOH) λ (log ε) 225(4.43), 270 (4.30), 313(4.03), 347(4.08), and 410 nm (shoulder).

We are grateful to the Institute of Microbial Chemistry for the generous sopport of our program. We also are indebted to Mr. Saburo Nakada, Keio University, for elemental analyses.

References

1) Part VI: M. Nakata, M. Kinoshita, S. Ohba, and Y. Saito, *Tetrahedron Lett.*, **25**, 1373 (1984).

2) R. J. White, E. Martinelli, and G. Lancini, *Proc. Nat. Acad. Sci. U.S.A.*, **71**, 3260 (1974); E. Martinelli, G. G. Gallo, P. Antonini, and R. J. White, *Tetrahedron*, **30**, 3087 (1974); R. J. White, E. Martinelli, G. G. Gallo, G. Lancini, and P. Beynon, *Nature*, **243**, 273 (1973).

3) M. Nakata, H. Enari, and M. Kinoshita, *Bull. Chem. Soc. Jpn.*, **55**, 3283 (1982).

4) The synthesis of rifamycin W using **3** is now under way.

5) a) W. Oppolzer and V. Prelog, *Helv. Chim. Acta*, **56**, 2287 (1973); b) W. Kump and H. Bickel, *Helv. Chim. Acta*, **56**, 2323 (1973). See also, T. Kishi, M. Asai, M. Muroi, S. Harada, E. Mizuta, S. Terao, T. Miki, and K. Mizuno, *Tetrahedron Lett.*, **1969**, 91.

6) H. Nagaoka, G. Schmid, H. Iio, and Y. Kishi, *Tetrahedron Lett.*, **1981**, 899.

7) T. Ross Kelly, M. Behforouz, A. Echavarren, and J. Vaya, *Tetrahedron Lett.*, **1983**, 2331.

8) J. E. Lightowler and H. J. Rylance, *Brit. J. Pharmacol.*, **22**, 221 (1964).

9) S. W. Heinzman and J. R. Grunwell, *Tetrahedron Lett.*, **1980**, 4305.

10) D. J. Crouse, M. M. Wheeler, M. Goemann, P. S. Tobin, S. K. Basu, and D. M. S. Wheeler, *J. Org. Chem.*, **46**, 1814 (1981).

11) K. I. H. Williams, S. E. Cremer, F. W. Kent, E. J. Sehm, and D. S. Tarbell, *J. Am. Chem. Soc.*, **82**, 3982 (1960).

12) A. I. Meyers, K. A. Babiak, A. L. Campbell, D. L. Comins, M. P. Fleming, R. Henning, M. Heuschmann, J. P. Hudspeth, J. M. Kane, P. J. Reider, D. M. Roland, K. Shimizu, K. Tomioka, and R. D. Walkup, *J. Am. Chem. Soc.*, **105**, 5015 (1983).

13) G. A. Russell and A. G. Bemis, *J. Am. Chem. Soc.* **88**, 5491 (1966).

14) P. Jacob, III., P. S. Callery, A. T. Shulgin, and N. Castagnoli, Jr., *J. Org. Chem.*, **41**, 3627 (1976).

15) L. A. Carpino and J.-H. Tsao, *J. Chem. Soc., Chem. Commun.*, **1978**, 358.

Preparation and CD Spectra of Cobalt(III) Complexes with *S*-(Carboxymethyl)-L-cysteinate and Its Analogues

Ken-ichi Okamoto,* Masutaro Suzuki, Hisahiko Einaga,† and Jinsai Hidaka
Department of Chemistry, University of Tsukuba, Sakura, Ibaraki 305
†*Institute of Materials Science, University of Tsukuba, Sakura, Ibaraki 305*
(Received November 29, 1984)

Four cobalt(III) complexes of the [Co(L-quadridentate-*N,S,O*$_2$)(en)]$^+$ type were prepared; where L-quadridentate-*N,S,O*$_2$ denotes *S*-(carboxymethyl)-L-cysteinate(L-cmc), *S*-(2-carboxyethyl)-L-cysteinate(L-cec), *S*-(carboxymethyl)-L-homocysteinate(L-cmhc), or *S*-(2-carboxyethyl)-L-homocysteinate(L-cehc). Each complex was chromatographically separated into the quasi-enantiomeric isomers; *Λ*L-*trans*(*O*)-*S*(*S*) and *Λ*L-*cis*(*O*)-*R*(*S*) for the L-cmc, L-cmhc, and L-cehc complexes, and *Λ*L-*trans*(*O*)-*R*(*S*) and *Λ*L-*cis*(*O*)-*S*(*S*) for the L-cec one. These isomers were characterized from their absorption and ^{13}C NMR spectra. The sterically strained *Λ*L-*cis*(*O*) isomers exhibited some significant CD spectral behavior in the first d-d absorption band region. The CD spectra are discussed in relation to the sizes of the S-N and S-O chelate rings joining the chiral sulfur atom in the L-quadridentate-*N,S,O*$_2$ ligand.

In the previous papers,[1-3] we reported the stereochemical and spectrochemical properties of the cobalt(III) complexes with an L-quadridentate-*N*$_2$,*S,O* ligand, *S*-(2-aminoethyl)-L-homocysteinate (L-aehc), in which the sulfur atom is fixed by a five-membered terminal S-N and a six-membered medial S-N chelate rings. The L-quadridentate-*N,S,O*$_2$ ligand used in the present work is *S*-(carboxymethyl)-L-cysteinate (L-cmc), *S*-(2-carboxyethyl)-L-cysteinate (L-cec), *S*-(carboxymethyl)-L-homocysteinate (L-cmhc), and *S*-(2-carboxyethyl)-L-homocysteinate (L-cehc), and they are similar to L-aehc in the structure (Fig. 1). However, the L-quadridentate-*N,S,O*$_2$ ligand is different from L-aehc in the sizes of the chelate rings formed. Namely, when the L-quadridentate-*N,S,O*$_2$ ligand coordinates to the cobalt(III) ion, its terminal S-O (**A** ring in Fig. 1) and medial S-N (**B** ring) chelate rings joining the sulfur atom take the ring sizes as summarized in Table 1.

In this work, the [Co(L-quadridentate-*N,S, O*$_2$)(en)]$^+$-type complexes were prepared and chromatographically separated into two geometrical isomers, *Λ*L-*trans*(*O*) and *Λ*L-*cis*(*O*). All isomers were characterized from their absorption spectra. Of these isomers the coordinated sulfur atom of *Λ*L-*cis*(*O*)-[Co(L-cmhc or L-cehc)(en)]$^+$ is possible to take either configuration of *R*(*S*) and *S*(*S*), and these configurations were suggested on the basis of the ^{13}C NMR spectra. The CD spectral behaviors due to the difference in ring sizes of the chelates, S-N and S-O, were discussed in comparison with those of the L-aehc complexes.[1-3]

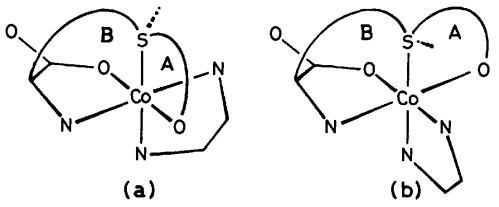

Fig. 1. Possible isomers of [Co(L-quadridentate-*N,S,O*$_2$)(en)]$^+$: (a) *Λ*L-*trans*(*O*) and (b) *Λ*L-*cis*(*O*).

TABLE 1. CHELATE RING SIZES OF **A** AND **B** RINGS IN Fig. 1

Ligand	**A** ring[a]	**B** ring[a]
L-cmc	5	5
L-cec	6	5
L-cmhc	5	6
L-cehc	6	6

a) **A** and **B** rings correspond to terminal S-O and medial S-N rings, respectively.

Experimental

Preparation of Ligands. 1) S-(Carboxymethyl)-L-homocysteine and S-(2-Carboxyethyl)-L-homocysteine: L-H$_2$*cmhc and L-H*$_2$*cehc.* These ligands were prepared by the method of Armstrong and Lewis.[4] Anal. for L-H$_2$cmhc ($C_6H_{11}NO_4S$) C, H, N. Anal. for L-H$_2$cehc ($C_7H_{13}NO_4S$) C, H, N. $[\alpha]_D^{24}$= +34.9° for L-H$_2$cmhc and $[\alpha]_D^{24}$=+44.4° for L-H$_2$cehc (*c* 1.0, 1 mol dm^{-3} HCl).

2) S-(2-Carboxyethyl)-L-cysteine: L-H$_2$*cec.* This ligand was prepared by a procedure similar to that used for (*R*)-2-(carboxymethylthio)propionic acid.[5] Anal. ($C_6H_{11}NO_4S$) C, H, N. $[\alpha]_D^{24}$=−14.8° (*c* 1.0, 1 mol dm^{-3} HCl).

3) S-(Carboxymethyl)-L-cysteine: L-H$_2$*cmc.* This ligand was supplied by the Aldrich Chemical Co. Ltd., and used without purification.

Preparation and Separation of Complexes. 4) {S-(Carboxymethyl)-L-homocysteinato}(ethylenediamine)cobalt(III) Chlolide: [Co(L-cmhc)(en)]Cl. A solution containing 2.0 g of L-H$_2$cmhc in 40 cm^3 of water was adjusted to pH 7 with a 1 mol dm^{-3} aqueous solution of sodium hydroxide. To this solution were added a solution containing 2.0 g of *trans*-[Co(Cl)$_2$(en)$_2$]Cl[6] in 10 cm^3 of water and 0.5 g of activated charcoal. The mixture was stirred at *ca.* 75 °C for 15 min, while the color of the solution changed from green to purple. After the solution had been cooled to room temperature, it was filtered and the filtrate was poured onto a column of Dowex 50W-X8 (200—400 mesh, Na^+ form, 2.0 cm×50 cm). After the column had been swept with water, the adsorbed band was eluted with a 0.05 mol dm^{-3} aqueous solution of NaCl. Two colored bands, red-violet (A-1) and red (A-2), were eluted in this order. It was found, from the absorption spectral measurements, that eluates A-1 and A-2 contained *trans*(*O*)- and *cis*(*O*)-[Co(L-cmhc)(en)]$^+$, respectively. Each eluate was concentrated to a small volume with a rotary evaporator below 25 °C and the deposited NaCl was filtered off. The filtrate was passed through a column of Sephadex G-10

(2.0 cm×150 cm) by elution with water and the eluate was concentrated again. After adding a small amount of ethanol, the solution was kept in a refrigerator. The crystals appeared were collected by filtration, and washed with ethanol and then ether. Isomer A-1 was obtained as flaky red-violet crystals and isomer A-2 as red needle ones. Found for A-1: C, 27.54; H, 5.07; N, 12.13%. Calcd for [Co(L-cmhc)(en)]Cl·0.25H_2O=$CoC_8H_{17}N_3O_4SCl$·0.25H_2O: C, 27.44; H, 5.04; N, 12.00%. Found for A-2: C, 26.54; H, 5.27; N, 11.68%. Calcd for [Co(L-cmhc)(en)]Cl·H_2O: C, 26.42; H, 5.27; N, 11.55%.

5) {S-(2-Carboxyethyl)-L-homocysteinato}(ethylenediamine)cobalt(III) Chloride: [Co(L-cehc)(en)]Cl. This complex was prepared and the isomers were chromatographically separated by the same procedure as for *4)*, using L-H_2cehc instead of L-H_2cmhc. Two colored bands, red-violet (B-1) and red (B-2), were eluted in this order, and eluates B-1 and B-2 contained *trans(O)*- and *cis(O)*-[Co(L-cehc)(en)]$^+$, respectively. Isomers B-1 and B-2 were obtained as red-violet flaky and red needle crystals, respectively. Found for B-1: C, 28.80; H, 5.47; N, 11.44%. Calcd for [Co(L-cehc)(en)]Cl·0.5H_2O=$CoC_9H_{19}N_3O_4SCl$·0.5H_2O: C, 29.31; H, 5.47; N, 11.48%. Found for B-2: C, 28.78; H, 5.65; N, 11.43%. Calcd for [Co(L-cehc)(en)]Cl·H_2O: C, 28.61; H, 5.61; N, 11.13%.

6) {S-(2-Carboxyethyl)-L-cysteinato}(ethylenediamine)cobalt(III) Chloride: [Co(L-cec)(en)]Cl. This complex was prepared and the isomers were chromatographically separated by the same procedure as for *4)*, using L-H_2cec instead of L-H_2cmhc. Two colored bands, red-violet (C-1) and red (C-2), were eluted in this order, and eluates C-1 and C-2 contained *trans(O)*- and *cis(O)*-[Co(L-cec)(en)]$^+$, respectively. Isomers C-1 and C-2 were also obtained as red-violet flaky and red needle crystals, respectively. Found for C-1: C, 26.50; H, 5.18; N, 11.75%. Calcd for [Co(L-cec)(en)]Cl·0.75H_2O=$CoC_8H_{17}N_3O_4$-SCl·0.75H_2O: C, 26.75; H, 5.19; N, 11.70%. Found for C-2: C, 25.08; H, 5.48; N, 11.21%. Calcd for [Co(L-cec)(en)]-Cl·1.75H_2O: C, 25.47; H, 5.48; N, 11.14%.

7) {S-(Carboxymethyl)-L-cysteinato}(ethylenediamine)cobalt(III) Chloride: [Co(L-cmc)(en)]Cl. This complex was also prepared and the isomers were chromatographically separated by the same procedure as for *4)*, using L-H_2cmc instead of L-H_2cmhc, except for adding activated charcoal. Two colored bands, red-violet (D-1) and red (D-2), were eluted in this order, and eluates D-1 and D-2 contained *trans(O)*- and *cis(O)*-[Co(L-cmc)(en)]$^+$, respectively. The yield of the slower eluted isomer (D-2) was very poor and this was obtained by repeating the preparation several times. Isomers D-1 and D-2 were also obtained as red-violet flaky and red needle crystals, respectively. Found for D-1: C, 24.07; H, 4.77; N, 12.24%. Calcd for [Co(L-cmc)(en)]Cl·0.75H_2O=$CoC_7H_{15}N_3O_4SCl$·0.75H_2O: C, 24.36; H, 4.82; N, 12.17%. Found for D-2: C, 24.83; H, 4.71; N, 12.52%. Calcd for [Co(L-cmc)(en)]Cl·0.25H_2O: C, 25.01; H, 4.65; N, 12.50%.

Measurements. The electronic absorption spectra were recorded with JASCO UVIDEC-1 and UVIDEC-610 spectrophotometers, and the CD spectra with a JASCO J-20 spectropolarimeter. All the measurements were carried out at room temperature.

The ^{13}C NMR spectra were recorded with a JEOL JNM-FX-100 NMR spectrometer at the probe temperature. Sodium 2,2-dimethyl-2-silapentane-5-sulfonate (DSS) was used as an internal reference.

Results and Discussion

Two quasi-enantiomeric geometrical isomers, ΛL-*trans(O)* and ΛL-*cis(O)*, are possible for the present [Co(L-quadridentate-*N,S,O*$_2$)(en)]$^+$-type complexes with L-cmc, L-cec, L-cmhc, and L-cehc (Fig. 1).[7] The ΛL-*trans(O)* isomers take the facial coordination with respect to the terminal S–O and medial S–N chelate rings joining the sulfur atom, while the ΛL-*cis(O)* isomers take the meridional one, where the terminal S–O and medial S–N chelate rings correspond to rings **A** and **B** in Fig. 1, respectively. The representative absorption spectra of [Co(L-quadridentate-*N,S,O*$_2$)(en)]$^+$ are shown in Fig. 2, and the data are summarized in Table 2. The eight isomers are classified into two groups based on the splittings of their first d-d absorption bands. One exhibits an explicit shoulder on the higher energy side of the major peak at 18.2—18.5×10^3 cm^{-1}, and the other a sharp band at 19.3—19.6×10^{3}cm^{-1}. Referring to the splitting of the first d-d absorption band of the [Co(N)$_3$(S)(O)$_2$]-type complexes,[1-3,8] the former group can be assigned as ΛL-*trans(O)* and the latter as ΛL-*cis(O)*. This assignment is consistent with that based on their ^{13}C NMR and CD spectra (*vide infra*). The terminal S–O and medial S–N chelate rings in [Co(L-quadridentate-*N,S,O*$_2$)(en)]$^+$ take the ring sizes as summarized in Table 1. As the ring size increases, the sulfur to metal charge transfer band at *ca.* 36×10^3 cm^{-1} for each of the ΛL-*trans(O)* and ΛL-*cis(O)* isomers shifts to lower energy in the following order: L-cmc>L-cmhc>L-cec>L-cehc (Table 2).

As shown in Fig. 3, the ^{13}C NMR spectra for [Co(L-quadridentate-*N,S,O*$_2$)(en)]$^+$ exhibit the resonance lines less than or equal to the numbers of the carbon

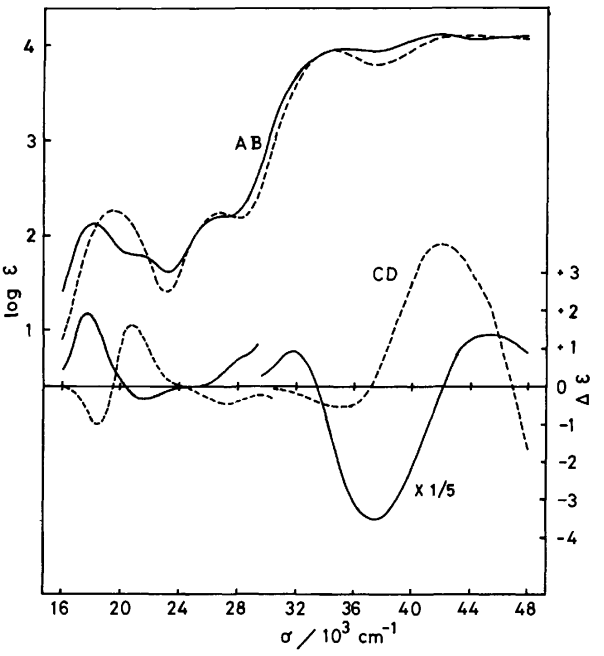

Fig. 2. Absorption and CD spectra of [Co(L-cehc)(en)]$^+$: ΛL-*trans(O)* (——) and ΛL-*cis(O)* (----).

TABLE 2. ABSORPTION AND CD SPECTRAL DATA OF [Co(quadridentate-N,S,O_2)(en)]$^+$

Complex	Absorption $\sigma/10^3\,cm^{-1}$ ($\varepsilon/mol^{-1}\,dm^3\,cm^{-1}$)	CD $\sigma/10^3\,cm^{-1}$ ($\Delta\varepsilon/mol^{-1}\,dm^3\,cm^{-1}$)
Δ_L-*trans(O)*-[Co(L-cmc)(en)]$^+$	18.51 (2.10)	17.68 (+5.88)
	20.65 (1.86sh)[a]	21.04 (−3.24)
	27.66 (2.28)	26.05 (+0.50)
	36.82 (3.87)	28.64 (+2.40)
	42.73 (4.13)	33.92 (+2.50)
	47.84 (4.10)	41.30 (−18.2)
		50.07 (−11.1)
Δ_L-*cis(O)*-[Co(L-cmc)(en)]$^+$	19.31 (2.20)	17.52 (−0.14)
	27.03 (2.31)	19.13 (+0.33)
	36.80 (3.87)	21.37 (−0.12)
	44.42 (4.14)	25.55 (+0.10)
		28.80 (−0.43)
		35.71 (−17.1)
		44.39 (+25.2)
Δ_L-*trans(O)*-[Co(L-cmhc)(en)]$^+$	18.52 (2.14)	17.66 (+4.05)
	21.05 (1.82sh)	20.74 (−1.36)
	27.12 (2.28)	28.45 (+1.32)
	36.46 (3.88)	33.07 (+4.65)
	43.17 (4.09)	39.25 (−2.09)
Δ_L-*cis(O)*-[Co(L-cmhc)(en)]$^+$	19.63 (2.16)	18.80 (−1.75)
	27.24 (2.24)	21.18 (+0.92)
	35.66 (4.00)	28.63 (−0.55)
	44.10 (4.21)	36.45 (+3.70)
		43.79 (+3.41)
Δ_L-*trans(O)*-[Co(L-cec)(en)]$^+$	18.34 (2.13)	17.65 (+2.92)
	20.75 (1.87sh)	21.46 (−1.65)
	26.71 (2.17)	28.18 (+1.07)
	36.08 (3.86)	31.90 (+0.15)
	42.90 (4.06)	35.73 (−0.75)
	48.35 (4.01)	41.87 (−14.0)
Δ_L-*cis(O)*-[Co(L-cec)(en)]$^+$	19.50 (2.32)	17.14 (−0.06)
	26.83 (2.26)	19.87 (+0.54)
	35.74 (3.93)	25.74 (+0.32)
	43.18 (3.98sh)	35.10 (−14.0)
	47.24 (4.11)	42.01 (+18.4)
		44.79 (+16.8)
Δ_L-*trans(O)*-[Co(L-cehc)(en)]$^+$	18.19 (2.13)	17.78 (+1.99)
	21.18 (1.79sh)	21.40 (−0.34)
	26.84 (2.21)	28.25 (+0.72)
	35.36 (3.95)	31.89 (+4.76)
	42.01 (4.10)	37.23 (−17.2)
		45.38 (+6.96)
Δ_L-*cis(O)*-[Co(L-cehc)(en)]$^+$	19.42 (2.28)	18.47 (−1.04)
	26.85 (2.25)	20.79 (+1.68)
	34.49 (3.94)	27.14 (−0.43)
	43.56 (4.11)	35.23 (+2.69)
		42.02 (+18.5)

a) Sh denotes a shoulder.

atoms in the L-quadridentate-N,S,O_2 and en ligands. When the complexes take only *R(S)* or *S(S)* configuration[7] with respect to the chiral sulfur atom, the ^{13}CNMR spectra can be expected to show seven resonance lines for the L-cmc complex, eight ones for the L-cec and L-cmhc complexes, and nine ones for the L-cehc complex. While, when the complexes are a mixture of the *R(S)* and *S(S)* isomers and/or the other species such as [Co(L-cmc)(en)(H_2O)]$^+$ more multiple peaks can be expected for their ^{13}CNMR spectra. The present result suggests that each of the complexes takes either *R(S)* or *S(S)* configuration. According to the model constructions, the coordinated sulfur atoms of Δ_L-*cis(O)*-[Co(L-cmc)(en)]$^+$ and Δ_L-*trans(O)*-[Co(L-cec)(en)]$^+$ are limited to *R(S)* configuration, whereas those of Δ_L-*trans(O)*-[Co(L-cmc)(en)]$^+$, Δ_L-*cis(O)*-[Co(L-cec)(en)]$^+$, Δ_L-*trans(O)*-[Co(L-cmhc)(en)]$^+$, and Δ_L-*trans(O)*-[Co(L-cehc)(en)]$^+$ to *S(S)* configuration. In contrast to the above isomers, the coordinated sulfur atom of Δ_L-*cis(O)*-[Co(L-cmhc or L-cehc)(en)]$^+$ can take either configuration of *R(S)* and *S(S)*, depending on the conformation of the medial S–N chelate ring,[9] as in the case of the L-aehc complexes.[1-3] The Δ_L-*S(S)*- and Δ_L-*R(S)*-[Co(L-aehc)(en)]$^{2+}$ isomers exhibited a well defined

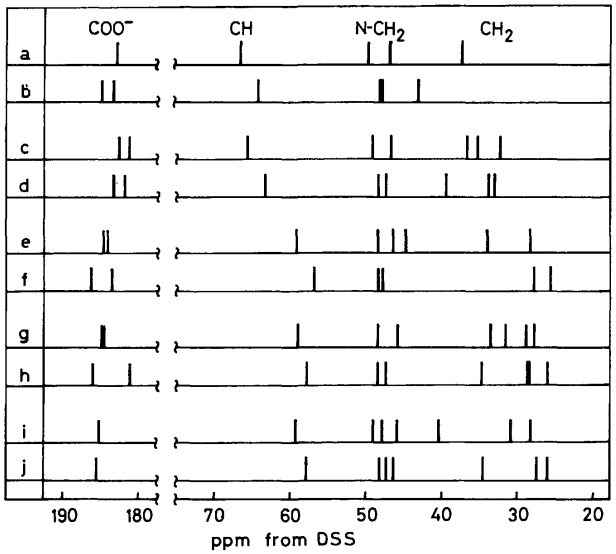

Fig. 3. The distribution of ^{13}C NMR chemical shifts of [Co(L)(en)]: L=L-cmc, a and b; L=L-cec, c and d; L=L-cmhc, e and f; L=L-cehc, g and h; and L=L-aehc, i and j. a, c, e, and g are Δ_L-*cis(O)* isomers, b, d, f, and h are Δ_L-*trans(O)* isomers, i is Δ_L isomer, and j is Λ_L isomer.

^{13}C NMR spectral relationship with regard to their β-methylene and the other carbon atom regions.[3] A similar relationship is also observed for the ^{13}C NMR spectra of the Λ_L-*trans(O)* and Δ_L-*cis(O)* isomers of each complex in the present work, especially in the methine carbon atom region (Fig. 3); namely, Λ_L-*trans(O)-S(S)* and Δ_L-*cis(O)-R(S)* for the L-cmc complex, Λ_L-*trans(O)-R(S)* and Δ_L-*cis(O)-S(S)* for the L-cec one, and Λ_L-*trans(O)-S(S)* and Δ_L-*cis(O)-R(S)* or -*S(S)* for the L-cmhc and L-cehc ones. Taking account of the shielding effect due to the two carboxyl groups[10,11] and the steric effect due to the interaction between the terminal S–O and medial S–N chelate rings, as in the L-aehc complexes,[3] the distribution of the chemical shifts for each of the methine, *N*-methylene, and carboxylate carbons in the L-quadridentate-*N,S,O*$_2$ and en ligands seems to depend on the direction of the terminal S–O chelate ring regardless of its chelate ring size. Thus, it is assumed that the Δ_L-*cis(O)* isomers of the L-cmhc and L-cehc complexes may take *R(S)* configuration.

Figure 2 shows the representative CD curves for [Co(L-quadridentate-*N,S,O*$_2$)(en)]$^+$, and the CD data are summarized in Table 2. The overall CD patterns for the L-cehc isomers are almost enantiomeric, although some deviations are observed in the region of 30—48×10^3 cm^{-1} (Fig. 2). A similar trend was also observed for the CD spectra of the isomers of each of the L-cmc, L-cec, and L-cmhc complexes (Table 2). In the first d-d absorption band region, the *trans(O)* and *cis(O)* isomers of the present complexes exhibit similar CD patterns to those of the Λ_L-*S(S)* and Δ_L-*R(S)* isomers of [Co(L-aehc)(L)] (L; ox, gly, en, and $(NH_3)_2$), respectively, whose CD patterns depend mainly on the coordination mode of the L-quadridentate-*N*$_2$*,S,O* ligand, L-aehc, regardless of the kind of ligand coordinating to the two remaining coordination sites.[1-3] These facts indicate that the *trans(O)* isomers take Λ_L coordination with respect to the configurational chirality of the coordinated L-quadridentate-*N,S,O*$_2$ ligand and the *cis(O)* isomers take Δ_L one, namely, Λ_L-*trans(O)* and Δ_L-*cis(O)*.

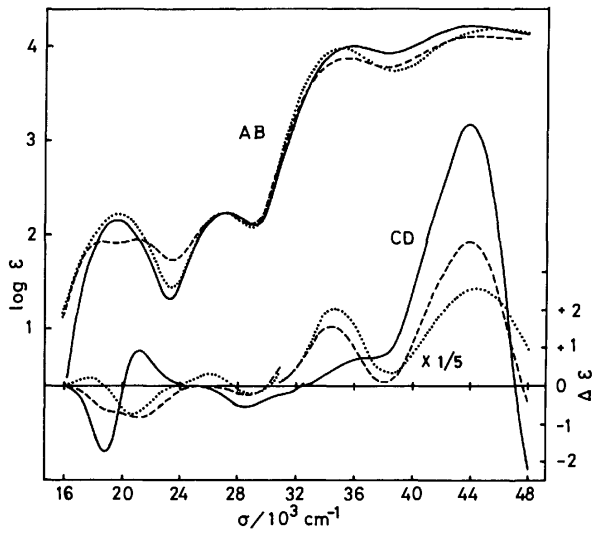

Fig. 4. Absorption and CD spectra of Δ_L-*cis(O)*-[Co(L-cmhc)(en)]$^+$ (——), Δ_L-*cis(O)*·*mer(N)*-[Co(L-aehc)(gly)]$^+$ (·····), and Δ_L-*trans(O)*·*mer(N)*-[Co(L-aehc)(gly)]$^+$ (----).

The absorption and CD spectra of Δ_L-*cis(O)-R(S)*-[Co(L-cmhc)(en)]$^+$, which has a quite similar framework and steric environment to the L-aehc complexes, are shown in Fig. 4, together with those of Δ_L-*cis(O)*·*mer(N)-R(S)*- and Δ_L-*trans(O)*·*mer(N)-R(S)*-[Co(L-aehc)(gly)]$^+$.[3] The Δ_L-*cis(O)-R(S)* L-cmhc isomer exhibits a more sharp first d-d absorption band than Δ_L-*cis(O)*·*mer(N)-R(S)*-[Co(L-aehc)(gly)]$^+$, indicating the *fac(N)* form (Fig. 4).[3] The Δ_L-*cis(O)-R(S)* L-cmhc isomer exhibits a different CD pattern in the first d-d absorption band region from Δ_L-*cis(O)*·*mer(N)-R(S)*- and Δ_L-*trans(O)*·*mer(N)-R(S)*-[Co(L-aehc)(gly)]$^+$, while Λ_L-*trans(O)-S(S)*-[Co(L-cmhc](en)]$^+$ and Λ_L-*cis(O)*·*mer(N)-S(S)*- and Λ_L-*cis(O)*·*fac(N)-S(S)*-[Co(L-aehc)(gly)]$^+$ exhibit similar CD patterns, (+) and (−) CD bands from lower energy.[1-3] These indicate that the CD pattern of the Δ_L-*cis(O)-R(S)*-[Co(L-cmhc)(en)]$^+$ isomer depends remarkably on the geometrical configuration with respect to the coordinated atom as in the case of the L-aehc complexes.[3] In the region of 32—48×10^3 cm^{-1}, it should be noted that the Δ_L-*R(S)* isomers commonly exhibit positive CD bands, suggesting that the configurational chirality due to the L-quadridentate ligand, Δ_L-*R(S)*, is mainly responsible for the CD pattern in this region, as in Δ_L-*R(S)*-[Co(L-aehc)(L)] (L; ox, gly, en, and $(NH_3)_2$).

The four Λ_L-*trans(O)* isomers of [Co(L-quadridentate-*N,S,O*$_2$)(en)]$^+$ exhibit some notable differences in CD intensity in the first d-d absorption band region. As shown in Fig. 5, the order of their CD intensities is L-

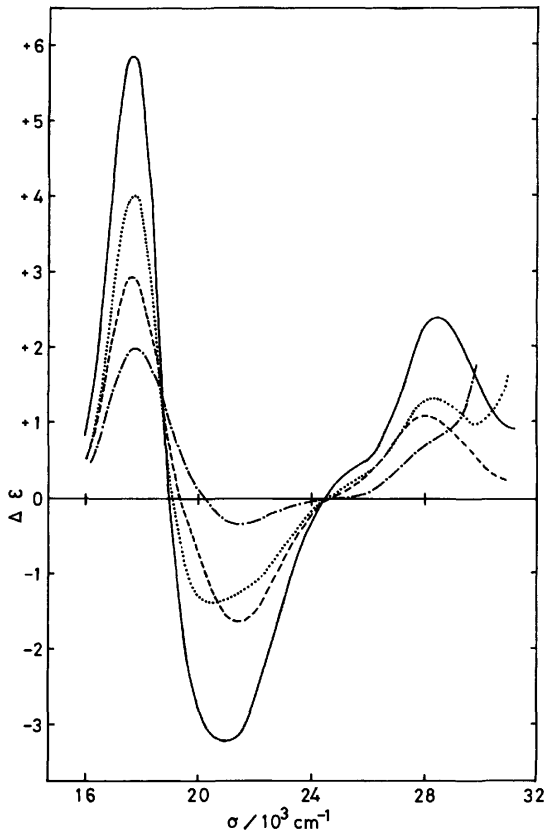

Fig. 5. CD spectra of Δ_L-*trans(O)*-[Co(L)(en)]$^+$: L=L-cmc (——), L-cmhc (·····), L-cec (----), and L-cehc (-·-·-·-).

cmc>L-cmhc>L-cec>L-cehc. This seems to be related to the ring sizes of the terminal S–O and medial S–N chelates. Namely, the L-cec and L-cehc isomers with the six-membered S–O chelate ring exhibit much weaker CD bands than the L-cmc and L-cmhc isomers with the five-membered one (Table 1). The L-cehc isomer taking the six-membered S–N chelate ring also exhibits more weak CD bands than the L-cec isomer taking the five-membered one (Table 1). A similar relationship was also observed for the L-cmc and L-cmhc isomers. The CD spectral change in intensity will be attributable to the rigidity of the chelate rings joining the chiral sulfur atom. In contrast to the Δ_L-*trans(O)* isomers, two types of the CD patterns are observed for the Δ_L-*cis(O)* isomers in the first d-d absorption band region (Fig. 6), namely, one is Δ_L-*cis(O)*-[Co(L-cmc or L-cec)(en)]$^+$ taking the medial five-membered S–N chelate ring and the other Δ_L-*cis(O)*-[Co(L-cmhc or L-cehc)(en)]$^+$ taking the six-membered one. The Δ_L-*cis(O)* isomer of [Co(L-cmhc or L-cehc)(en)]$^+$ exhibits an almost enantiomeric CD pattern to that of the corresponding Δ_L-*trans(O)* one, while the CD pattern for the Δ_L-*cis(O)* isomer of [Co(L-cmc or L-cec)(en)]$^+$ deviates significantly from that for the corresponding Δ_L-*trans(O)* one, as seen in Fig. 6. Of the four Δ_L-*cis(O)* isomers, the L-cmhc and L-cehc isomers are possible to take either configuration of *R(S)* or *S(S)* depending on the conformations

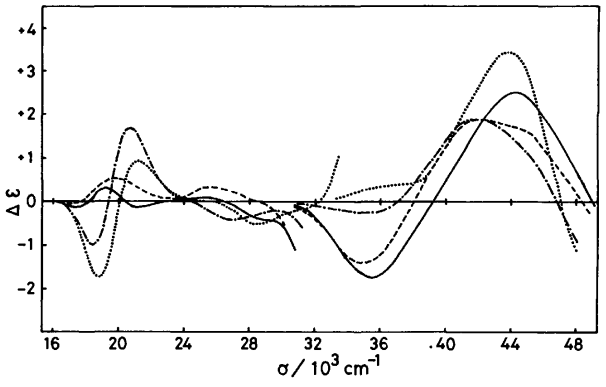

Fig. 6. CD spectra of Δ_L-*cis(O)*-[Co(L)(en)]$^+$: L=L-cmc (——), L-cmhc (·····), L-cec (----), and L-cehc (-·-·-·-).

(chair and skew-boat)[9] of the medial six-membered S–N chelate ring because of the flexible methioninate moiety.[1–3] From the good enantiomeric correspondence of the CD patterns of the two Δ_L-*cis(O)* isomers to the common CD pattern for the four Δ_L-*trans(O)*-[Co(L-quadridentate-N,S,O_2)(en)]$^+$ isomers, it is tentatively assigned that the Δ_L-*cis(O)* isomer of [Co(L-cmhc or L-cehc)(en)]$^+$ takes *R(S)* configuration in accordance with the assignment based on their ^{13}C NMR spectra. In the Δ_L-*cis(O)* isomer of [Co(L-cmc or L-cec)(en)]$^+$, on the other hand, the terminal S–O chelate ring is strongly strained because of the rigid cysteinate moiety. From this viewpoint, it may be assumed that the deviation in the CD pattern in the first d-d absorption band region is related to the flexibility around the chiral sulfur atom in the L-quadridentate-N,S,O_2 ligand.

References

1) K. Okamoto, M. Suzuki, H. Einaga, and J. Hidaka, *Bull. Chem. Soc. Jpn.*, **56**, 3513 (1983).

2) K. Okamoto, M. Suzuki, and J. Hidaka, *Chem. Lett.*, **1983**, 401.

3) M. Suzuki, O. Arisato, K. Okamoto, H. Einaga, and J. Hidaka, *Bull. Chem. Soc. Jpn.*, **57**, 2751 (1984).

4) M. D. Armstrong and J. D. Lewis, *J. Org. Chem.*, **16**, 749 (1951).

5) M. Suzuki, K. Okamoto, H. Einaga, and J. Hidaka, *Bull. Chem. Soc. Jpn.*, **55**, 3929 (1982).

6) J. C. Bailar, Jr., *Inorg. Synth.*, **2**, 222 (1946).

7) The symbols, Δ_L and Δ_L, are denoted on the basis of the configurational chirality due to the skew pair of the chelate rings of the L-quadridentate (Fig. 1). The symbols, *R(S)* and *S(S)*, denote the absolute configuration of the chiral sulfur atom (Ref. 1—3, 5, and 8).

8) K. Okamoto, H. Maki, and J. Hidaka, *Bull. Chem. Soc. Jpn.*, **57**, 595 (1984).

9) The conformation of the medial six-membered S–N chelate ring takes the chair form for the *R(S)* configuration and the skew boat form for the *S(S)* one (Ref. 1—3).

10) L. R. Froebe, S. Yamada, J. Hidaka, and B. E. Douglas, *J. Coord. Chem.*, **1**, 183 (1971).

11) M. Okabayashi, K. Okamoto, H. Einaga, and J. Hidaka, *Bull. Chem. Soc. Jpn.*, **56**, 157 (1983).

 © 1985 The Chemical Society of Japan Bull. Chem. Soc. Jpn., 58, 1812—1815 (1985) [Vol. 58, No. 6

Synthetic Inorganic Ion-exchange Materials. XXXX. Ion Exchange Properties of Tin(IV) Antimonate for Alkaline Earth and Transition Metal Ions and Its Application to Metal Separations

Mitsuo ABE* and Noboru FURUKI†

Department of Chemistry, Faculty of Science, Tokyo Institute of Technology, 2-12-1, Ookayama, Meguro-ku, Tokyo 152

(Received December 14, 1984)

Ion-exchange selectivities of alkaline earth and transition metal ions on tin(IV) antimonate cation exchanger were investigated in nitric acid media. The selectivity sequences were found to be; $Mg^{2+}<Ca^{2+}<Sr^{2+}<Ba^{2+}$ for alkaline earth metal ions and $Ni^{2+}<Mn^{2+}<Cd^{2+}<Co^{2+}<Cu^{2+}<Zn^{2+}$ for transition metal ions. The separation factors for neighboring pairs on the exchanger gave larger values than those on the ion-exchange resin of a strong acid type. The effective separations of Mg^{2+}-Ca^{2+}, Sr^{2+}-Ba^{2+}, and Na^{+}-Cs^{+}, Sr^{2+} have been achieved with a small column (5cm×0.5 cm i.d.).

The synthesis and ion-exchange properties of inorganic materials have been studied extensively by many workers.[1-4] Some inorganic ion-exchangers showed an excellent selectivity for a certain element or group of elements in the presence of large amounts of other components.

Phosphates of quadrivalent metals, such as zirconium and titanium, have been studied extensively by several workers.[5] Quadrivalent metal antimonate ion-exchangers were studied by Abe and Ito.[6] Tin(IV) and titanium(IV) antimonates (SnSbA and TiSbA) behaved as cation exchangers with relatively high capacities, and showed unusual selectivities for alkali metal ions in the order: $Na^{+}<K^{+}<Rb^{+}<Cs^{+}\ll Li^{+}$ on SnSbA,[7] and $Na^{+}<K^{+}<Rb^{+}<Li^{+}<Cs^{+}$ on TiSbA,[8] which are not included in Eisenman's selectivity series.[9] Thermal and chemical stabilities, and the selectivities of various metal antimonates for a number of metal ions have also been reported by Qureshi and co-workers.[10] The ion-exchange behavior of tin(IV) antimonate prepared by metathesis of $SnCl_4$ and $H[Sb(OH)_6]$, has been studied by Mathew and Tandon.[11] It has been known that the ion-exchange properties including the selectivities of inorganic ion-exchangers depend much on their preparative conditions. Especially, SnSbA with relatively high molar ratio of Sb/Sn up to 2.0 showed an excellent selectivity for lithium ions and could be applied to the removal of lithium ions from a large amount of sodium ions in solutions, such as seawater and hydrothermal water.[12]

This paper describes the ion-exchange properties of SnSbA for alkaline earth metal ions and its applications to chromatographic separations.

Experimental

Preparation of SnSbA. Suitable conditions were chosen so that the highest selectivity for lithium ions may be obtained.[7] The preparation procedure is as follows. A 62 cm^3 of liquid antimony(V) chloride was prehydrolyzed with an equal amount of demineralized water in order to prevent fractional precipitation of antimonic acid during the further procedures. The resultant 4 M (M=mol/dm^3) antimony (V) chloride solution was mixed with a 4 M tin(IV) chloride solution of 80 cm^3 at 80 °C. The mixed solution was hydrolyzed immediately in a 50-fold volume of demineralized water at 60 °C. The white precipitate obtained was kept in the mother solution at 60 °C overnight, then filtered and washed with water using a centrifuge (10000 min^{-1}) until the pH value of the supernatant solution was higher than 1.5. After drying at 60 °C, the product was ground and sieved to 100—200 mesh size. The collected samples were rewashed with water to remove adherent fine particle of SnSbA, and finally dried at 60 °C.

The characterization and identification of the SnSbA were carried out by powdered X-ray diffraction analysis with Ni-filtered Cu-$K\alpha$ radiation with a JEOL Model JDX-7, by IR spectra using a KBr technique with a Nihon Bunko Model 701G spectrometer, and by thermal analysis with a Rigaku Denki Thermoflex Model 8001.

Chemical Composition of the SnSbA. The composition was determined as reported previously.[7]

pH Titration Curves. The pH titration curve of the ion exchanger is one of its important characteristic properties. The character of the ion exchanging groups can be estimated from the pH titration curve as well as the ion-exchange capacity. A weighed amount (0.10 g) of the sample was immersed in 10.0 cm^3 of a mixed solution of varying ratio of $\{M(NO_3)_n+KOH\}$ or $\{M(NO_3)_n+HNO_3\}$ adjusted to an ionic strength of 0.1 with intermittent shaking at 30±0.5 °C. After the attainment of equilibrium, the pH of the supernatant solution was measured with a Toa model HM-5B pH meter. The amounts of the uptake of the metal ions were calculated from the difference in the metal ion concentration relative to the initial concentration in the solution.

Distribution Coefficient, K_d. The equilibrium K_d values of the metal ions were determined by a batch technique. The SnSbA was immersed in 10.0 cm^3 of a solution containing the metal ions of 10^{-4} M and nitric acid of different concentrations. The concentration of the metal ions in the exchanger and solution was deduced from the concentration relative to the initial concentration in the solution. The concentrations of metal ions were determined by flame photometry or atomic absorption spectrometry with a Varian Techtron 1100. The K_d values were calculated as follows:

$$K_d = \frac{\text{amount of metal ions in exchanger}}{\text{amount of metal ions in solution}} \times \frac{\text{cm}^3 \text{ of solution}}{\text{g of exchanger}}$$

†Present address: Mitsubishi Chem. Co. Ltd., Kurosaki, Yahata, Kita-kyushu 806.

Reagents. Antimony(V) chloride (>99.9% as metal, Yotsuhata Chemical Co. Ltd.) and tin(IV) chloride (Wako Chemical Co. Ltd.) were used without purification. The solutions of transition metal ions were prepared by dissolving the pure metals (>99.99%) in a nitric acid solution at a suitable concentration. Other reagents used were all of analytical grade.

Results and Discussion

Preparation of the SnSbA. The SnSbA obtained was identified by X-ray diffraction analysis, thermal analysis and IR spectra. The results showed a good agreement with those of our previous work.[7] The crystallite size of the SnSbA was found to be 41 Å by using the Scherrer's equation from a plane (110).[13]

Chemical Composition of the SnSbA. The Sb/Sn molar ratio in the SnSbA was found to be 1.88, which is similar to the previous results.[7]

The water content was determined from the weight loss of the heated sample at 950 °C, by assuming that the sample is finaly transformed to a mixture of α- and β-Sb_2O_4, and SnO_2 (cassiterite).[14]

The empirical formula of SnSbA can be given as;

$$SnO_2\ 0.94Sb_2O_5\ 4.95H_2O.$$

pH Titration Curves. A typical example of the pH titration curves is illustrated in Fig. 1. The pH titration curve of the SnSbA showed weak dibasic acid behavior, which is almost the same as reported in the previous work for alkali metal ions.[7] The uptake of strontium ions increased on increasing the pH of the solution, and is higher than that of lithium or potassium ions in the entire range studied. The ion-exchange sites in the SnSbA may be overlapping with different strength of the acidic sites. The uptakes of

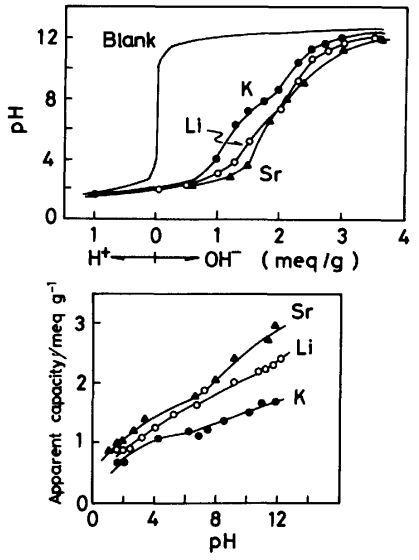

Fig. 1. pH Titration curves and apparent capacities of SnSbA.
Soln; $\{M(NO_3)_n+HNO_3\}$ or $\{M(NO_3)_n+M(OH)_n\}$ with ionic strength of 0.1, total voume; 10.0 cm³, ion-exchanger; 0.10 g, temp; 30±0.5 °C.

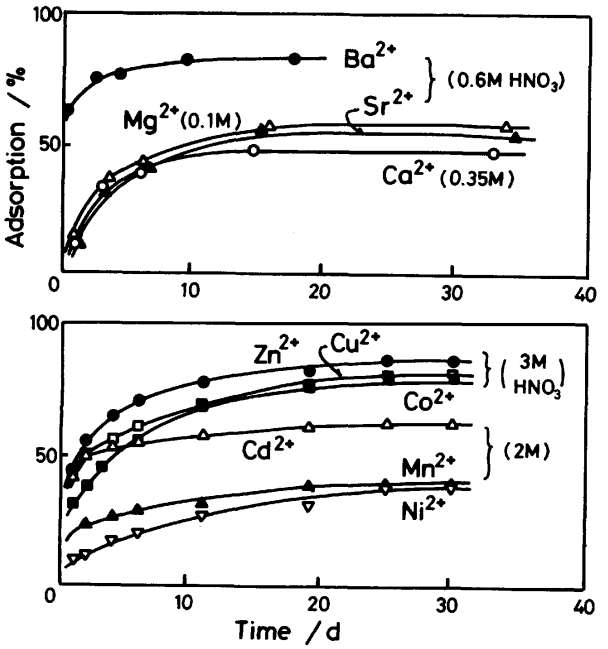

Fig. 2. Time dependence of adsorption of different metal ions on SnSbA.
Initial concn. of metal ions; 10^{-4} M, ion-exchanger; 0.10 g, total volume; 10.0 cm³, temp; 30±0.5 °C.

lithium and potassium ions on the exchangers were consistent to the amount of hydrogen ions liberated from the exchangers (Fig. 1), indicating that the dissolution of the exchangers was negligible within experimental error.

Distribution Coefficient, K_d. The time dependence on adsorption of the different metal ions was studied in order to determine the equilibrium distribution coefficient (Fig. 2). The ion-exchange equilibrium of alkali metal ions-H^+ (except Li^+-H^+) on SnSbA was attained within 24 h, while that of Li^+-H^+ was about 10 d as reported previously. The reaction with alkaline

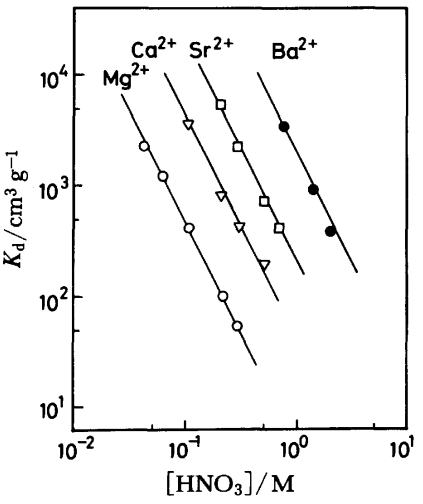

Fig. 3-a. Log-log plots K_d values of alkaline earth metal ions on SnSbA and the concentrations of nitric acid.
Initial concn. of metal ions; 10^{-4} M, ion-exchanger; 0.250 g, total volume; 25.0 cm³, temp; 30±0.5 °C.

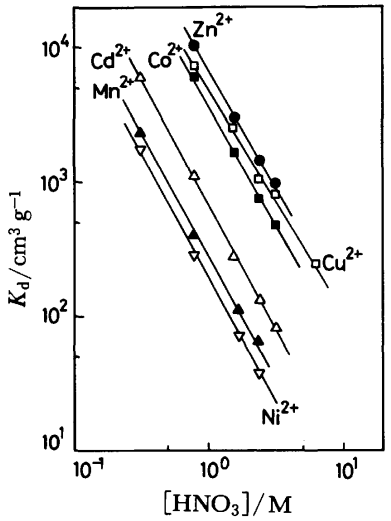

Fig. 3-b. Log-log plots of K_d values of transition metal ions on SnSbA *vs.* concentration of nitric acid. Initial concn. of metal ions; 10^{-4} M, exchanger; 0.250 g, total volume; 25.0 cm^3, temp; 30±0.5 °C.

earth or transition metal ion /H^+ was extremely slow, about 20—30 d being required for equilibrium.

The K_d values of alkali metal ions on the SnSbA showed almost the same values (except Li^+) as those on the sample (Sb/Sn ratio of 1.6) hydrolyzed at 100 °C, while the K_d values (2.2×10^4 in 0.1 M HCl) of Li^+ was lower than that (6.6×10^4) reported previously.[7] However, the selectivity sequence of alkali metal ions, $Na^+<K^+<Rb^+<Cs^+\ll Li^+$, agreed with the previous results.[7] The K_d values of alkaline earth and transition metal ions on a SnSbA are given in Figs. 3-a and 3-b, as log-log plots of K_d *vs.* $[HNO_3]$. The slope, d log K_d/d log $[HNO_3]$, was about −2, indicating ideal "1:2" ion-exchange reaction. The selectivity sequence showed: $Mg^{2+}<Ca^{2+}<Sr^{2+}<Ba^{2+}$, giving the same sequence of increasing crystal ionic radii of alkaline earth metals, as is obtained on organic ion-exchange resins of strong acid type. The K_d values and separation factors ($\alpha=K_{dB}/K_{dA}$), for a neigboring pair, are summarized in Table 1, where values from other ion-exchangers are shown for comparison. The sequence on the SnSbA is the same as that reported by Qureshi *et al.*[10] However, the separation factors for neigboring pairs of alkaline earth metal on the SnSbA are much larger than those obtained on strong acid type resins or the tin antimonate obtained by Qureshi *et al.*[10] The sequence, $Mg^{2+}<Ba^{2+}<Ca^{2+}<Sr^{2+}$, on tin antimonate prepared by Mathew and Tandon.[11] is the same as that obtained on the crystalline antimonic(V) acid which shows extremely high K_d values for Ca^{2+}, Sr^{2+} and Cd^{2+}.[14] The selectivity sequence for transition metal ions on the SnSbA, $Ni^{2+}<Mn^{2+}<Cd^{2+}<Co^{2+}<Cu^{2+}<Zn^{2+}$, is different from those on the tin antimontate prepared by Qureshi *et al.*[10] From data reported by Qureshi *et al.*, the slopes of d log K_d/d pH for transition metal ions, calculated by this author, do not show 2, even in a range of pH 0—1. In general, the K_d values also depend on the metal ion loading on the exchanger. The difference in the selectivity may be due to the difference of the loading and preparation of two exchangers. From data reported by Mathew and Tandon[11] and Qureshi *et al.*,[10] the extrapolated K_d values of bivalent metal ions to 1.0 M HNO_3 concentration were smaller

Table 1. K_d Values and separation factors(α) of alkaline earth and transition metal ions on different exchangers

Exchanger	ions											
SnSbA	K_d	Mg		Ca		Sr		Ba				
		1.9×10^1		1.9×10^2		7.0×10^2		2.1×10^4				
(1M HNO_3)	α		10		3.7		30					
AG 50W-X8[a]	K_d	7.1×10^1		1.13×10^2		1.46×10^2		2.71×10^2				
(1M HNO_3)	α		1.6		1.3		1.9					
Tin antimonate[b]	K_d	2.43×10^2		4.76×10^2		5.8×10^2		1.42×10^3				
(pH=2)	α		2.0		1.2		2.4					
		Ni		Mn		Cd		Co		Cu		Zn
SnSbA	K_d	2.0×10^2		3.0×10^2		7.0×10^2		3.7×10^3		5.0×10^3		7.0×10^3
(1M HNO_3)	α		1.5		2.3		5.3		1.4		1.4	
		Zn		Cu		Ni		Mn		Co		Cd
AG 50W-X8[a]	K_d	25.2		26.8		28.1		28.4		28.8		32.8
(1M HNO_3)	α		1.1		1.0		1.0		1.0		1.1	
		Mn		Zn		Ni		Co		Cd		Cu
Tin antimonate[b]	K_d	5.9×10^2		1.1×10^3		1.5×10^3		2.9×10^3		3.2×10^3		7.5×10^4
(pH=2)	α		1.9		1.3		2.0		1.1		2.3	

a) F. W. E. Strelow *et al.*, *Anal. Chem.*, **37**, 106 (1965). b) M. Qureshi *et al.*, *J. Chromatogr.*, **67**, 351 (1972).

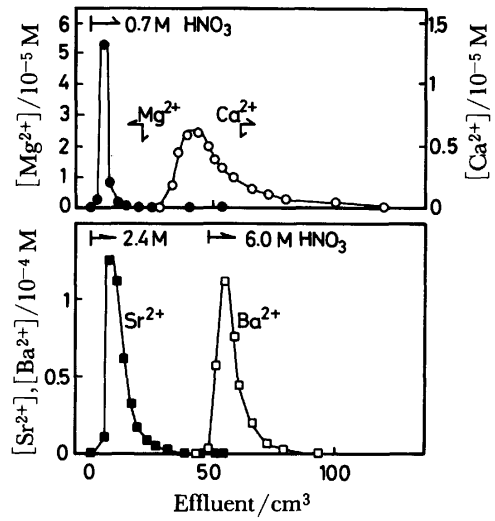

Fig. 4. Separation of alkaline earth metal ions with SnSbA column.
Column; 5.0 cm×0.5 cm i.d. (2.0 g of SnSbA), metal ion loading; 0.2 μmol for Mg^{2+} and Ca^{2+}, and 1.0 μmol for Sr^{2+} and Ba^{2+}, flow rate; 0.2 $cm^3 min^{-1}$.

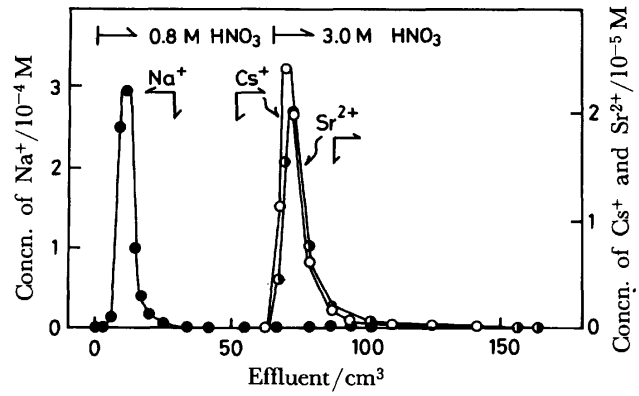

Fig. 5. Separation of Sr^{2+} and Cs^+ from Na^+ with SnSbA column.
Column; 5.0 cm×0.5 cm i.d. (2.0 g of SnSbA), metal ion loading; 2.0 μmol for Na^+, and 0.2 μmol each for Sr^{2+} and Cs^+, flow rate; 0.2 $cm^3 min^{-1}$.

than those obtained on the SnSbA. This indicates that the number of the strongly acid sites in the SnSbA are larger than those in the tin antimonate prepared by Mathew and Tandon,[11] or Qureshi *et al.*[10]

Ion Exchange Separation. It is evident from studies of the separation factors on the SnSbA that some selective separation is feasible for various metal ions including alkali metal ions. Separations of Mg^{2+}–Ca^{2+} and Sr^{2+}–Ba^{2+} have been achieved by using a small column (5.0 cm×0.5 cm i.d.) containing 2.0 g of SnSbA with nitric acid solutions of different concentrations as eluents. The quantitative separations of Mg^{2+} from Ca^{2+} and of Sr^{2+} from Ba^{2+} were performed with 99—100% recovery with relatively short time (Fig. 4). From studies of the K_d values of alkali metal ions and bivalent metal ions, small amounts of Cs^+ and Sr^{2+} can be separated effectively from a relatively large amount of sodium. A satisfactory separation of Cs^+ and Sr^{2+} was performed from 10 fold (in mmol) of Na^+ with 98% recovery (Fig. 5).

The use of SnSbA is promising for the separation of radioactive ^{90}Sr and ^{137}Cs from natural water and seawater.

References

1) C. B. Amphlett, Inorganic Ion Exchangers, Elsevier Publishing Co., Amsterdam, 1964.
2) M. J. Fuller, *Chromatogr. Rev.*, **14**, 45 (1971).
3) M. Abe, *Bunseki Kagaku*, **23**, 1245, 1561 (1974).
4) A. Clearfield, Inorganic Ion Exchange Materials, CRC press, Boca Raton, Fl., 1982.
5) G. Alberti, *Acc. Chem. Rev.*, **11**, 163 (1978).
6) M. Abe and T. Ito, *Kogyo Kagaku Zasshi*, **70**, 440 (1967).
7) M. Abe and K. Hayashi, *Sol. Extr. Ion Exch.*, **1**, 97 (1983).
8) M. Abe and M. Tsuji, *Chem. Lett.*, **1983**, 1561.
9) G. Eisenman, *Biophys. J.*, **2**, 259 (1962).
10) M. Qureshi, V. Kumer, and N. Zehara, *J. Chromatogr.*, **67**, 351 (1972).
11) J. Mathew and S. N. Tandon, *Acta Chim. Acad. Sci,*, **92**, 1, (1977).
12) M. Abe and K. Hayashi, *Hydrometallurgy*, **12**, 83 (1984).
13) B. D. Cullity, Elements of X-Ray Diffraction, Japanese Translation by G. Matsumura, AGNE, Tokyo, 1972, p. 263.
14) ASTM Card, 21-1250.

 © 1985 The Chemical Society of Japan Bull. Chem. Soc. Jpn., 58, 1816—1820 (1985) [Vol. 58, No. 6

Syntheses and Properties of Oxomolybdenum(VI), -(V), and -(IV) Complexes with Ferrocenecarbodithioate

Masami NAKAMOTO, Koji TANAKA,† and Toshio TANAKA†*

Osaka Municipal Technical Research Institute, Morinomiya, Joto-ku, Osaka 536

†*Department of Applied Chemistry, Faculty of Engineering, Osaka University, Yamada-oka, Suita, Osaka 565*

(Received December 19, 1984)

A series of ferrocenecarbodithioato-oxomolybdenum(VI), -(V), and -(IV) complexes, $Mo^{VI}O_2(S_2CC_5H_4Fe^{II}C_5H_5)_2$ (**1**), $Mo^{V}_2O_3(S_2CC_5H_4Fe^{II}C_5H_5)_4$ (**2**), and $Mo^{IV}O(S_2CC_5H_4Fe^{II}C_5H_5)_2$ (**3**) have been prepared. Complex **2** undergoes a disproportionation reaction in solution and exists as an equilibrium mixture with **1** and **3**. Cyclic voltammograms of **1** and **3** display two and three sets of quasi-reversible couples, respectively, arising from stepwise redox reactions of the molybdenum and iron sites. Electronic spectra revealed that the oxidized species $[Mo^{VI}O_2(S_2CC_5H_4Fe^{III}C_5H_5)_2]^{2+}$, $[Mo^{V}O(S_2CC_5H_4Fe^{II}C_5H_5)_2]^{+}$, and $[Mo^{V}O(S_2CC_5H_4Fe^{III}C_5H_5)_2]^{3+}$ generated electrochemically are considerably stable owing to the electron-donating ability of the ferrocenecarbodithioate ligand.

Molybdenum in high oxidation states is known to be an essential component in six well-characterized enzymes; nitrogenase, nitrate reductase, xanthine oxidase, aldehyde oxidase, and sulfite oxidase.[1] There exists a structural similarlity among the molybdenum sites of these enzymes except for nitrogenase.[2-4] Recent EXAFS studies on sulfite oxidase[3] and xanthine oxidase[4] suggest that molybdenum in those enzymes has one or two oxo ligands in sulfide-rich environments. These results have further stimulated the syntheses of a variety of oxomolybdenum complexes with sulfur-containing ligand as possible model compounds to molybdoenzymes.[5-8] Of the oxomolybdenum complexes with sulfur-containing ligands, which have been prepared so far, only the dithiocarbamate complexes have fully been characterized as a series of oxomolybdenum(VI), -(V), and -(IV) complexes.[9] Thus, the stabilization of oxomolybdenum complexes in the three oxidation states, (VI), (V), and (IV), may be resulted from the electron-donating ability of the dithiocarbamate ligand. Recently, we have briefly reported the syntheses of oxomolybdenum(VI) and -(V) complexes with ferrocenecarbodithioate,[10] which can stabilize the high oxidation states of molybdenum atoms. The present work reports the syntheses of a series of oxomolybdenum (VI), -(V), and -(IV) complexes with ferrocenecarbodithiocate, $Mo^{VI}O_2(S_2CC_5H_4Fe^{II}C_5H_5)_2$ (**1**), $Mo^{V}_2O_3(S_2CC_5H_4Fe^{II}C_5H_5)_4$ (**2**), and $Mo^{IV}O(S_2CC_5H_4Fe^{II}C_5H_5)_2$ (**3**), and their electrochemical properties.

Experimental

Materials and Methods. Dichlorodioxomolybdenum, $Mo^{VI}O_2Cl_2$,[11] and diethylammonium ferrocenecarbodithioate, $[Et_2NH_2][S_2CC_5H_4Fe^{II}C_5H_5]$[12] were prepared according to the literatures. All reactions and manipurations were carried out under nitrogen atmosphere and the solvents used for preparations and physical measurements were degassed by bubbling dry nitrogen for *ca.* 1 h or by distillation under nitrogen atmosphere prior to use.

Preparation of Complexes. Bis(ferrocenecarbodithioato)-dioxomolybdenum(VI), $Mo^{VI}O_2(S_2CC_5H_4Fe^{II}C_5H_5)_2$ (1). A methanol solution (20 cm³) of $Mo^{VI}O_2Cl_2$ (0.5 g, 2.5 mmol) was added dropwise to a stirred suspension of $[Et_2NH_2][S_2CC_5H_4Fe^{II}C_5H_5]$ (1.7 g, 5.0 mmol) in the same solvent (50 cm³) at −60 °C. The reaction mixture was stirred for further 2 h at the same temperature, followed by warming to 0 °C, which gave greenish blue precipitate. The precipitate was collected by filtration at 0 °C, washed with methanol (10 cm³×2 times), and dried *in vacuo*, 80% yield, mp>120 °C (dec). Anal. Calcd for $C_{22}H_{18}Fe_2MoO_2S_4$: C, 40.63; H, 2.79%. Found: C, 40.80; H, 2.99%. Molecular weight (MW) was measured in benzene cryoscopically: 628 (Calcd 650).

μ-Oxobis[bis(ferrocenecarbodithioato)oxomolybdenum(V)], $Mo^{V}_2O_3(S_2CC_5H_4Fe^{II}C_5H_5)_4$ (2). To a stirred aqueous solution (50 cm³) containing $Na_2Mo^{VI}O_4\cdot H_2O$ (1.2 g, 5.0 mmol) and $[Et_2NH_2][S_2CC_5H_4Fe^{II}C_5H_5]$ (3.4 g, 10 mmol) was added dropwise a 2 mol dm⁻³-HCl to adjust the pH of the solution to 5.5. The resulting dark blue precipitate was collected by filtration, washed with water and then diethyl ether, and dried *in vacuo*, 20% yield, mp>115 °C (dec). Anal. Calcd for $C_{44}H_{36}Fe_4Mo_2O_3S_8$: C, 41.14; H, 2.82%. Found: C, 41.49; H, 2.92%.

Bis(ferrocenecarbodithioato)oxomolybdenum(IV), $Mo^{IV}O(S_2CC_5H_4Fe^{II}C_5H_5)_2$ (3). A benzene solution (50 cm³) containing **1** (1.1 g, 1.7 mmol) and PPh_3 (0.47 g, 1.8 mmol) was refluxed for 2 h. After cooled to room temperature, the solution was evaporated to dryness under reduced pressures. The resulting solid was triturated with ethanol (20 cm³×2 times), collected by filtration, washed with diethyl ether (20 cm³×2 times), and dried *in vacuo*, which gave dark blue microcrystals, 88% yield, mp>180 °C (dec.). Anal. Calcd for $C_{22}H_{18}Fe_2MoOS_4$: C, 41.66; H, 2.86%. Found: C, 41.36; H, 3.03%. MW in benzene 620 (Calcd 634).

Physical Measurements. Infrared and electronic spectra were recorded on a Shimadzu IR-400 and a MPS-5000 spectrophotometer, respectively. ESR spectra were measured at 9.52 GHz with a JEOL ME-1X spectrometer. Electrochemical experiments were performed by using a Hokuto-Denko Model HA-501 potentiostat/galvanostat, a HB-104 function generater, and a HF-201 coulomb/amperehour meter. Cyclic voltammograms were recorded on a National VP-6422A X-Y recorder. Tetrabutylammonium perchlorate, $[n\text{-}Bu_4N][ClO_4]$, was used as a supporting electrolyte, and a saturated calomel electrode (SCE) was employed as a reference electrode. A platinum disk (0.20 cm²) and a platinum plate (1×1 cm²) were employed as working electrodes for the cyclic voltammetry and the controlled-potential electrolysis, respectively. The controlled-potential electrolysis was

Table 1. Infrared spectra of the oxomolybdenum complexes with ferrocenecarbodithioate

Complex	ν(Mo=O), cm^{-1} in Nujol	in CH_2Br_2
$Mo^{VI}O_2(S_2CC_5H_4Fe^{II}C_5H_5)_2$ (**1**)	922	920
	889	885
$Mo^{V}_2O_3(S_2CC_5H_4Fe^{II}C_5H_5)_4$ (**2**)	940	955 br
		920
		885
$Mo^{IV}O(S_2CC_5H_4Fe^{II}C_5H_5)_2$ (**3**)	960	962

performed at 110—180 mV more negative potentials than the cathodic peaks or more positive potentials than the anodic peaks of the complexes. Spectroelectrochemistry was accomplished by the use of an optically transparent thin-layer electrode (OTTLE) cell.[13]

Results and Discussion

Infrared Spectra in the Solid State and in Solution. The infrared spectrum of **1** in Nujol mull shows two strong ν(Mo=O) bands at 922 and 889 cm^{-1} (Table 1), which are compared with those of the corresponding dithiocarbamate complexes, $Mo^{VI}O_2(S_2CNR_2)_2$ (R=Me, Et, n-Pr, n-Bu; 912—905 and 877—875 cm^{-1}) with the two oxo ligands in *cis*-positions to each other in the octahedral configuration.[14] Complexes **2** and **3** in Nujol mulls exhibit the ν(Mo=O) bands at 940 and 960 cm^{-1}, respectively (Table 1); the former and the latter fall in the same region as the ν(Mo=O) frequencies of $Mo^{V}_2O_3(S_2CNR_2)_4$ (R=Me, Et, *i*-Pr; 943—938 cm^{-1})[15] and $Mo^{IV}O(S_2CNEt_2)_2$ (962 cm^{-1}), respectively, as well.[16] These results indicate that the ferrocenecarbodithioate ligand is coordinated to molybdenum in a bidentate manner and the present oxomolybdenum complexes **1**, **2**, and **3** may assume the geometries **A**, **B**, and **C**, respectively, which are similar to those of the corresponding dithiocarbamate complexes which have been revealed by the X-ray crystallographic analysis.[17]

The infrared spectrum of **2** in CH_2Br_2, however, displayed three ν(Mo=O) bands at 955, 920, and 885 cm^{-1}, the latter two of which are nearly the same frequencies as those of **1** in the same solvent. This is suggestive of the occurrence of the disproportionation reaction of **2** into **1** and **3** in solution (Eq. 1). Thus, the ν(Mo=O) bands arising from **2** and **3** may

$$Mo^{V}_2O_3(S_2CC_5H_4Fe^{II}C_5H_5)_4 \rightleftharpoons Mo^{VI}O_2(S_2CC_5H_4Fe^{II}C_5H_5)_2 + Mo^{IV}O(S_2CC_5H_4Fe^{II}C_5H_5)_2 \quad (1)$$

be overlapped with each other to appear as a broad one at 955 cm^{-1}. This is consistent with the fact that an equimolar mixture of **1** and **3** in CH_2Br_2 exhibited an infrared spectrum quite similar to **2** in the same solvent. Disproportionation equilibria of Eq. 1 have been reported for some μ-oxodimolybdenum complexes of the $Mo^{V}_2O_3L_4$ type (L=S_2CNR_2, S_2CSR, and S_2PPh_2) in solution[18,19] though only the dithiocarbamate complexes have so far been fully characterized throughout three different oxidation states of molybdenum, (VI), (V), and (IV).[16]

Electrochemistry. Figure 1 illustrates the cyclic voltammograms of **1**, **2**, and **3** in CH_2Cl_2. As shown in Fig. 1a, the cyclic voltammogram of **1** in CH_2Cl_2 shows two well resolved quasi-reversible waves ($E_{1/2}$=−0.89 and +0.77 V *vs.* SCE) and no wave associated with liberated ligands[20] has been observed within the potential range −2.0 to +2.0 V (*vs.* SCE). The controlled-potential electrolysis of **1** in CH_2Cl_2 at −1.05 and +0.95 V (*vs.* SCE, a little more negative or positive potential than $E_{1/2}$) have consumed 0.94 and 1.89 electrons, respectively, per one mole of **1**. This result indicates that **1** undergoes one electron reduction at $E_{1/2}$=−0.89 V (*vs.* SCE) to produce the $[Mo^{V}O_2(S_2CC_5H_4Fe^{II}C_5H_5)_2]^-$ species, and two ferrocenecarbodithioate ligands are both oxidized at the potential $E_{1/2}$=+0.77 V (*vs.* SCE) to give $[Mo^{VI}O_2(S_2CC_5H_4Fe^{III}C_5H_5)_2]^{2+}$. Thus, the redox processes of **1** can formally be expressed as Scheme 1.

A CH_2Cl_2 solution of **3** displays three discrete redox couples ($E_{1/2}$=−0.87, +0.60, and +0.98 *vs.* SCE) without any peaks due to liberated ligands, as depicted in Fig. 1c. The controlled-potential electrolysis at a little more negative or positive potential (−1.10, +0.80, and +1.25 V *vs.* SCE) than $E_{1/2}$ has consumed 1.02, 0.94, and 1.93 electrons, respectively, confirming that the cathodic peak at −0.92 V (*vs.* SCE) and the anodic one at +0.67 V (*vs.* SCE) are both one-electron processes, whereas the anodic peak at +1.12 V (*vs.* SCE) is a two-electron process. Thus, the redox couple at $E_{1/2}$=−0.87, +0.60, and +0.98 V (*vs.* SCE) may be assigned to the Mo(IV)/Mo(III), Mo(IV)/Mo(V), and Fe(II)/Fe(III) processes, respectively. The assignment for the redox couple at +0.60 V (*vs.* SCE) is consistent with the fact that an oxidized species generated by the electrolysis of **3** at +0.70 V (*vs.* SCE) in CH_2Cl_2 gives an ESR signal with g=2.007 at room temperature, as shown in Fig. 2. This g-value is quite normal for molybdenum(V) com-

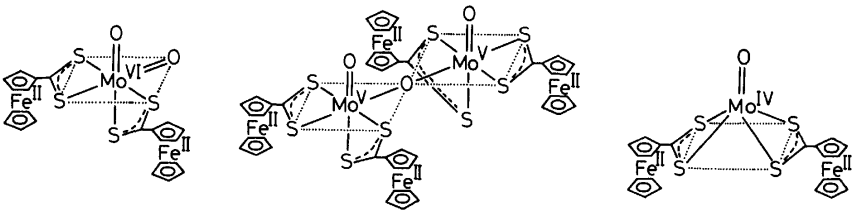

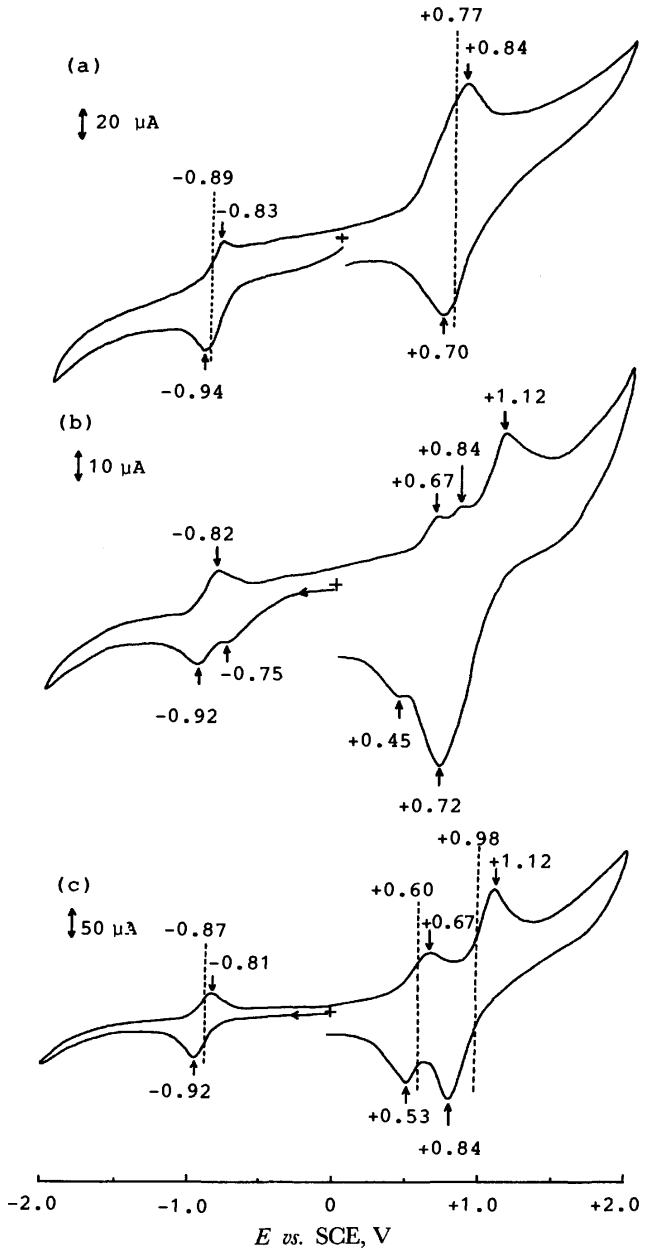

Fig. 1. Cyclic voltammograms of (a) $Mo^{VI}O_2(S_2CC_5H_4Fe^{II}C_5H_5)_2$ (**1**)(1.0×10^{-3} mol dm^{-3}), (b) $Mo^{V}_2O_3(S_2CC_5H_4Fe^{II}C_5H_5)_4$ (**2**)(4.2×10^{-4} mol dm^{-3}), and (c) $Mo^{IV}O(S_2CC_5H_4Fe^{II}C_5H_5)_2$ (**3**) (1.0×10^{-3} mol dm^{-3}) in CH_2Cl_2 containing 0.1 mol dm^{-3} [*n*-Bu_4N][ClO_4]; the scan rate 0.4 V s^{-1}.

$$[Mo^{V}O_2(S_2CC_5H_4Fe^{II}C_5H_5)_2]^- \underset{+e^-}{\overset{-e^-}{\rightleftharpoons}}$$

$$Mo^{VI}O_2(S_2CC_5H_4Fe^{II}C_5H_5)_2 \underset{+2e^-}{\overset{-2e^-}{\rightleftharpoons}}$$

1

$$[Mo^{VI}O_2(S_2CC_5H_4Fe^{III}C_5H_5)_2]^{2+}$$

Scheme 1.

plexes which exhibit a signal in the range g=1.905 (K_2MoOF_5)[21] to 2.011 ([$Mo(S_2C_2Ph_2)_3$]$^-$),[22] whereas the ferricenium radical cations display quite different g-values from 2.0 ($g_{\parallel}$=4.35—3.62 and $g_{\perp}$=1.62—1.77)[23,24]

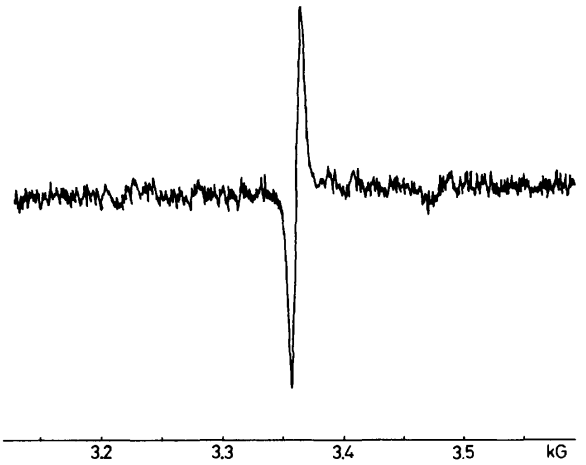

Fig. 2. Room temperature ESR spectrum of electrochemically generated $[Mo^{V}O(S_2CC_5H_4Fe^{II}C_5H_5)_2]^+$ in CH_2Cl_2 at 9.52 GHz.

at low temperatures; no ESR signal of the radical cations has been detected above 78 K[25] owing to very short relaxation times T_1.[26] In addition, the assignment of the redox process Fe(II)/Fe(III) for the couple at $E_{1/2}$=+0.98 V (*vs.* SCE) is consistent with a two-electron process of the anodic peak at +1.12 V (*vs.* SCE), where the two iron atoms of both ferrocenecarbodithioate ligands undergo simultaneous one-electron oxidation at the same potential, as in the case of **1**. The redox reactions of **3** can, therefore, be expressed as Scheme 2. Thus, complex **1** and **3** are considerably stable toward the electrochemical redox reactions, probably because of a large polarizability of the ferrocenecarbodithioate ligand with π-electron systems. This is in marked contrast to the corresponding dithiocarbamate and trithiocarbonate complexes, $M^{VI}O_2L_2$ and $Mo^{IV}OL_2$ (L=S_2CNR_2, S_2CSR), whose electrochemical redox reactions are followed by rapid irreversible chemical reactions resulting from the dissociation of the dithio ligands.[9,27]

As described above, **2** partly disproportionates into **1** and **3** in solution. The cyclic voltammogram of **2** in CH_2Cl_2, therefore, is rather complicated, as seen in Fig. 1b. A pair of cathodic and anodic waves at E_c=−0.92 V and E_a=−0.82 V (*vs.* SCE) may be an overlap of the redox couples of both **1** and **3**, since these potentials are almost the same as that of either **1** or **3** existing alone (See Fig. 1a and 1c). Thus, the cathodic peak at E_c=−0.75 V (*vs.* SCE, Fig. 1b) may be assigned to the reduction of **2**, whereas the corresponding anodic peak is not observed. The anodic wave at +0.84 V (*vs.* SCE) (Fig. 1b) is assigned to the oxidation of **1**, and those at +0.67 and +1.12 V (*vs.* SCE) (Fig. 1b) to the oxidation of the molybdenum and ferrocenyl moieties of **3**, respectively, both of which are resulted from the disproportionation of **2** (Eq. 1). The broad cathodic wave at +0.72 V (*vs.* SCE) may, therefore, be assigned to the reduction of the both Fe^{3+} ions of $[Mo^{VI}O_2(S_2CC_5H_4Fe^{III}C_5H_5)_2]^{2+}$ and $[Mo^{V}O(S_2CC_5H_4Fe^{III}C_5H_5)_2]^{3+}$. The

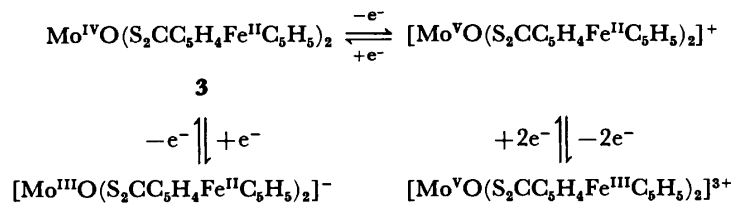

Scheme 2.

remaining cathodic wave at +0.45 V (*vs.* SCE) may constitute a redox couple, Mo(IV)/Mo(V) of **3**, with the anodic wave at +0.67 V (*vs.* SCE). These assignments may be supported from the fact that the cyclic voltammogram of **2** obtained upon an anodic scan from 0 V to +2.0 V (*vs.* SCE) followed by a reverse one to 0 V (*vs.* SCE) gave three anodic and two cathodic waves with the same potentials as Fig. 1b.

Electronic Spectra. It has been reported that both dioxomolybdenum(VI) and oxomolybdenum(IV) complexes with dithio chelate ligands exhibit the absorption band due to a molybdenum-oxygen transition around 380 nm[16] and μ-oxodimolybdenum(V) complexes with the dithio chelates display another characteristic absorption band around 510 nm as well as the 380 nm band.[16] The electronic spectra of **1—3**, however, show two absorption bands around 350 and 600 nm and their appearances resemble one another, irrespective of the oxidation state of the molybdenum atom. On the other hand, the ferrocenecarbodithioate anion exhibits two strong absorptions due to π-π^* (308 nm) and n-π^* (525 nm) transitions of the thiocarbonyl group, both of which are known to shift to higher wavelengths on coordination to metal atoms.[12] Thus, the bands due to transitions resulting from Mo=O and Mo-O-Mo bonds in the present complexes may be concealed by the strong absorptions of the ferrocenyl chromophore.

Table 2 lists the absorption maxima and the extinction coefficients in the electronic spectra of **1—3**, together with those of the electrochemical oxidized species of **1** and **3**, obtained by using a OTTLE cell. The absorption bands at 350 and 600 nm of **1** were shifted to 330 and 540 nm, respectively, on the electrochemical reduction at −1.05 V (*vs.* SCE) in CH_2Cl_2. Similarly, the reduction of **3** at −1.10 V (*vs.* SCE) in CH_2Cl_2 caused the movement of the 355 and 605 nm bands to 320 and 530 nm, respectively. Upon reoxidation of the both resulting solutions at −0.70 V (*vs.* SCE), however, neither original spectrum of **1** nor that of **3** has been recovered, suggesting that $[Mo^{V}O_2(S_2CC_5H_4Fe^{II}C_5H_5)_2]^-$ and $[Mo^{III}O(S_2CC_5H_4Fe^{II}C_5H_5)_2]^-$ decompose on the coulometric electrolysis time scale. In accordance with this, several attempts to detect the ESR signals of these reduced species generated under the controlled-potential electrolysis at −1.10 V (*vs.* SCE) of **1** and **3** in CH_2Cl_2 have been unsuccessful.

On the other hand, the two absorption bands of **1** and **3** are shifted to higher wavelengths upon electrochemical oxidations (Compare Entries 1 with 2, and 4 with 5 and 6 in Table 2). This is consistent with the bathochromic shift of ferrocenyl derivatives with electron-attracting groups in the electronic spectra.[28] The oxidation of **1** at +0.95 V (*vs.* SCE) and the subsequent reduction at +0.60 V (*vs.* SCE) afforded the original electronic spectrum, suggesting that the oxidized species, $[Mo^{VI}O_2(S_2CC_5H_4Fe^{III}C_5H_5)_2]^{2+}$, is stable. Similarly, $[Mo^{V}O(S_2CC_5H_4Fe^{II}C_5H_5)_2]^+$ and $[Mo^{V}O(S_2CC_5H_4Fe^{III}C_5H_5)_2]^{3+}$ generated by the electrochemical oxidation of **3** at +0.80 and +1.25 V (*vs.* SCE), respectively, are stable, as confirmed from the fact that the electronic spectrum of **3** was recovered completely upon oxidation-reduction cycles. In contrast to the instability of the reduced species, the stability of electrochemically oxidized species of **1** and **3** may result from an electron-donating property of the ferrocenecarbodithioate ligand.

Table 2. Electronic spectra of the oxomolybdenum complexes and their electrochemical oxidized species in CH_2Cl_2

Entry	Complex	λ_{max}/nm	ε/cm^{-1} M^{-1}
1	$Mo^{VI}O_2(S_2CC_5H_4Fe^{II}C_5H_5)_2$ (**1**)	350	24800
		600	8280
2	$[Mo^{VI}O_2(S_2CC_5H_4Fe^{III}C_5H_5)_2]^{2+}$	374	24200
		652	5000
3	$Mo^{V}_2O_3(S_2CC_5H_4Fe^{II}C_5H_5)_4$ (**2**)	350	42600
		600	14800
4	$Mo^{IV}O(S_2CC_5H_4Fe^{II}C_5H_5)_2$ (**3**)	355	25300
		605	5860
5	$[Mo^{V}O(S_2CC_5H_4Fe^{II}C_5H_5)_2]^+$	360	24100
		645	6900
6	$[Mo^{V}O(S_2CC_5H_4Fe^{III}C_5H_5)_2]^{3+}$	368	19000
		660	5170
7	$[Et_2NH_2][S_2CC_5H_4Fe^{II}C_5H_5]$	308	12700
		525	2220

References

1) a) E. I. Stiefel, *Prog. Inorg. Chem.*, **22**, 1 (1977); b) "Molybdenum Chemistry of Biological Significance," ed by W. E. Newton and S. Otsuka, Plenum Press, New York, 1980.

2) "Molybdenum and Molybdenum-Containing Enzymes," ed by M. P. Coughlan, Pergamon Press, Oxford, New York, 1981.

3) a) S. P. Cramer, H. B. Gray, and K. V. Rajagopalan, *J. Am. Chem. Soc.*, **101**, 2772 (1979). b) S. P. Cramer, R. Wahl, and K. V. Rajagopalan, *J. Am. Chem. Soc.*, **103**, 7721 (1981).

4) T. D. Tullius, D. M. Kurtz, Jr., S. D. Conradson, K. O. Hodgson, *J. Am. Chem. Soc.*, **100**, 2776 (1979).

5) K. F. Miller, A. E. Bruce, J. L. Corbin, S. Wherland,

and E. I. Stiefel, *J. Am. Chem. Soc.*, **102**, 5102 (1980).
6) J. T. Spence, M. Minelli, P. Kroneck, *J. Am. Chem. Soc.*, **102**, 4538 (1980).
7) J. R. Bradbury, A. F. Masters, A. C. McDonell, A. A. Brunette, A. M. Bond, and A. G. Wedd, *J. Am. Chem. Soc.*, **103**, 1959 (1981).
8) D. A. Smith and F. A. Schultz, *Inorg. Chem.*, **21**, 3035 (1982).
9) L. J. De Hydes, H. C. Faulkner, W. E. Doub, Jr., and D. T. Sawyer, *Inorg. Chem.*, **14**, 2110 (1975).
10) M. Nakamoto, K. Shimizu, K. Tanaka, and T. Tanaka, *Inorg. Chim. Acta*, **53**, L51 (1981).
11) F. Zado, *J. Inorg. Nucl. Chem.*, **25**, 1115 (1963).
12) S. Kato, M. Wakamatsu, and M. Mizuta, *J. Organomet. Chem.*, **78**, 405 (1974).
13) D. Lexa, J. M. Saveant, and J. Zickler, *J. Am. Chem. Soc.*, **99**, 2786 (1977).
14) F. W. Moore and R. E. Rice, *Inorg. Chem.*, **7**, 2510 (1968).
15) W. E. Newton, J. L. Corbin, D. C. Bravard, J. E. Searles, and J. McDonald, *Inorg. Chem.*, **13**, 1100 (1974).
16) R. N. Jowitt and P. C. H. Mitchell, *J. Chem. Soc. (A)*, 2632 (**1969**).
17) L. Fischer, A. Mitschler, and R. Weiss, *J. Coord. Chem.*, **3**, 277 (1974).
18) T. Matsuda, K. Tanaka, and T. Tanaka, *Inorg. Chem.*, **18**, 454 (1979).
19) T. Tanaka, K. Tanaka, T. Matsuda, and K. Hashi, "Molybdenum Chemistry of Biological Significance," ed by W. E. Newton and S. Otsuka, Plenum Press, New York, p. 361 (1980).
20) The cyclic voltammogram of the ferrocenecarbodithioate ligand in CH_2Cl_2 showed the $[S_2CC_5H_4Fe^{II}C_5H_5]_2/[S_2CC_5H_4Fe^{II}C_5H_5]^-$ couple at $E_a=+0.26$ V, $E_c=-1.43$ V (*vs.* SCE), the $[S_2CC_5H_4Fe^{III}C_5H_5]_2/[S_2CC_5H_4Fe^{II}C_5H_5]_2$ couple at $E_a=+0.88$, $E_c=+0.66$ V (*vs.* SCE), and the $[S_2CC_5H_4Fe^{II}C_5H_5]^-/[S_2CC_5H_4Fe^{II}C_5H_5]^{2-}$ couple at $E_c=-1.73$, $E_a=-1.56$ V (*vs.* SCE).
21) P. T. Manoharan and M. T. Rogers, *J. Chem. Phys.*, **49**, 5510 (1968).
22) A. Davison, N. Edelstein, R. H. Holm, and A. H. Maki, *J. Am. Chem. Soc.*, **86**, 2799 (1964).
23) R. Prins and A. R. Korswagen, *J. Organomet. Chem.*, **25**, C74 (1970).
24) D. M. Duggen and D. N. Hendrickson, *Inorg. Chem.*, **14**, 955 (1975).
25) R. Prins and F. J. Reinders, *J. Am. Chem. Soc.*, **91**, 4929 (1969).
26) H. P. Fritz, H. J. Keller, and K. E. Schwarzhans, *J. Organomet. Chem.*, **6**, 652 (1966).
27) J. Hyde, K. Venkatasubramanian, and J. Zubieta, *Inorg. Chem.*, **17**, 414 (1978).
28) C. U. Pitman, Jr., and G. O. Evans, *J. Organomet. Chem.*, **43**, 361 (1972).

 © 1985 The Chemical Society of Japan Bull. Chem. Soc. Jpn., 58, 1821—1824 (1985)

Liquid Crystal Materials with Sulfur Atoms Incorporated in the Principal Structure. IV. New Liquid Crystal Compounds; 2-(*p*-Substituted phenyl)-5-alkyl-1,3-oxathianes

Yuichiro HARAMOTO* and Hiroyoshi KAMOGAWA
Department of Applied Chemistry, Yamanashi University, Takeda 4, Kofu 400
(Received January 25, 1985)

2-(*p*-Substituted phenyl)-5-alkyl-1,3-oxathianes, new liquid crystal compounds, were synthesized by the acetal-formation reaction of the corresponding aldehydes and 2-alkyl-3-mercapto-1-propanols. The mesomorphic behaviors of these 1,3-oxathiane compounds were compared with those of the corresponding 1,3-dithianes and 1,3-dioxanes. Some of 2-(*p*-cyanophenyl)-5-alkyl-1,3-oxathianes exhibit monotropic nematic liquid crystal phase at room temperature, whereas 2-(*p*-alkoxyphenyl)-5-alkyl-1,3-oxathianes tend hardly to exhibit liquid-crystal phase. These mesomorphic characters seem to originate in the molecular width and bending at the 1,3-oxathiane ring.

In recent years, 2,5-disubstituted 1,3-dithianes and several 2,5-disubstituted 1,3-oxathianes, new types of liquid-crystalline compounds, have been reported.[1-5] The present study relates to the synthesis and mesomorphic behavior of 2-(*p*-substituted phenyl)-5-alkyl-1,3-oxathianes having the systematically changed chain length of alkyl groups. The features concerning about appearance of mesophase of these 1,3-oxathianes were compared with those of the corresponding 1,3-dithianes and 1,3-dioxanes.

Results and Discussion

2-(*p*-Substituted phenyl)-5-alkyl-1,3-oxathianes were synthesized *via* the following route.

In step **1**→**2**, the reaction temperature must be kept between 70 and 75°C. At a temperature between 90 and 95°C, the main product was the disubstituted bromide contrary to the purpose. As compounds **3** were susceptible to oxidation, step **2**→**3** required nitrogen atmosphere. In **3**→**5**, both trans and cis isomers differing at C-5 position of the 1,3-oxathiane ring were produced.

Repeated recrystallizations were required to obtain the purified trans isomers. As trans and cis isomers

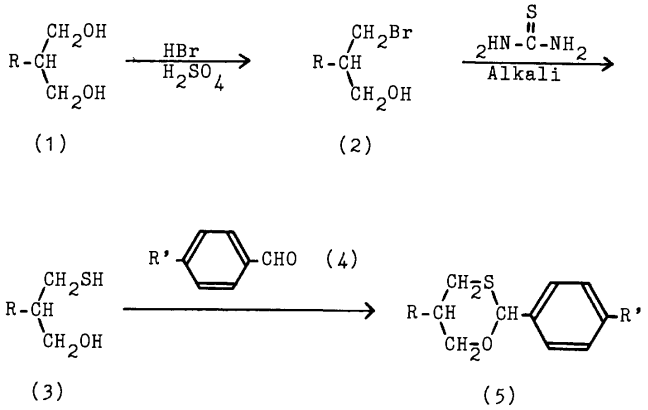

R: *n*-C_3H_7, *n*-C_4H_9, *n*-C_5H_{11}, *n*-C_6H_{13}, *n*-C_7H_{15}, *n*-C_8H_{17}.

R': OCH_3, OC_2H_5, $OC_3H_7^n$, $OC_4H_9^n$, $OC_5H_{11}^n$, CN.

Fig. 1.

exhibit C-2 proton signals of the 1,3-oxathiane ring in ^{1}H-NMR at δ 5.75 and 5.80 (R'=CN), respectively, the contamination of cis isomer can be detected by the examination of proton signals at δ 5.80.

The presence of 1,3-dithianes and 1,3-dioxanes can also be detected by the examination of C-2 proton signals at δ 5.10, and 5.30, respectively.

Absorptions of C2, C4, and C6 carbons of the 1,3-oxathiane ring in ^{13}C-NMR spectra, as determined by ^{1}H-complete decoupling (COM), ^{1}H-off resonance decoupling (OFR), and ^{1}H-selective decoupling (SEL) procedures, are located at δ 83.22, 34.84, and 75.55, respectively (R=C_8H_{17}, R'=CN). In ^{1}H-NMR, C4 proton signals are located at δ 3.4 (t), and 4.3 (m). The attribution of these two proton signals to the two protons attaching to C4 carbon of the 1,3-oxathiane ring derives from the fact that, in ^{1}H-selective decoupling of ^{13}C-NMR spectra, the peak of C2 carbon becomes more intense with irradiation of δ (3.4+4.3)/2, but indicates little change in both cases of irradiation of δ 3.4 and 4.3.

Measurements of mesomorphic ranges and assignments of the mesophases were carried out by means of a micro melting point apparatus equipped with polarizers. Mesomorphic ranges of the synthesized 2-(*p*-substituted phenyl)-5-alkyl-1,3 oxathianes and the corresponding 1,3-dithianes and 1,3-dioxanes are given in Table 1.

Transition temperatures of isotropic to nematic (T_{N-I}) for 2-(*p*-cyanophenyl)-5-alkyl-1,3-oxathianes were lower than those for the corresponding 1,3-dioxanes by about 20°C. It is known generally that the larger the molecular width, the lower the T_{N-I} is.[6] The width of 2-(*p*-cyanophenyl)-5-alkyl- 1,3-oxathianes is larger than that of the corresponding 1,3-dioxanes because of the presence of a large sulfur atom.

2-(*p*-Cyanophenyl)-5-alkyl-1,3-dithianes did not exhibit any liquid crystal phases. As molecular width of 2-(*p*-cyanophenyl)-5-alkyl-1,3-dithianes having two sulfur atoms are larger than those of 1,3-dioxane and 1,3-oxathiane compounds, they seem to be unable to exhibit a nematic phase.

As regards compounds having 2-(*p*-alkoxyphenyl)

TABLE 1. TRANSITION TEMPERATURE OF COMPOUNDS 5 AND THE CORRESPONDING 1,3-DITHIANES AND 1,3-DIOXANES

	R	R'	Transition Temp/°C[a)]
5-1	n-C_3H_7	OCH_3	C 55 I; 30
5-2	n-C_3H_7	OC_2H_5	C 54 I; 25
5-3	n-C_3H_7	n-OC_4H_9	C 57 I; 13 N 17
5-4	n-C_4H_9	OC_2H_5	C 76 I; 34
5-5	n-C_4H_9	n-OC_3H_7	C 54 I; 20
5-6	n-C_5H_{11}	OCH_3	C 75 I; 19
5-7	n-C_5H_{11}	OC_2H_5	C 85 I; 53
5-8	n-C_5H_{11}	n-OC_3H_7	C 66 I; 40
5-9	n-C_6H_{13}	OC_2H_5	C 58 I; 29 N 32
5-10	n-C_6H_{13}	n-OC_3H_7	C 58 I; 35
5-11	n-C_6H_{13}	n-OC_4H_9	C 55 I; 33
5-12	n-C_6H_{13}	n-OC_5H_{11}	C 56 I; 28 N 32
5-13	n-C_7H_{15}	OC_2H_5	C 67 I; 37 N 43
5-14	n-C_7H_{15}	n-OC_3H_7	C 64 I; 46
5-15	n-C_7H_{15}	n-OC_4H_9	C 70 I; 55 N 56
5-16	n-C_7H_{15}	n-OC_5H_{11}	C 66 I; 32 N 33
5-17	n-C_8H_{17}	OCH_3	C 54 I; 28
5-18	n-C_8H_{17}	OC_2H_5	C 68 I; 55
5-19	n-C_8H_{17}	n-OC_3H_7	C 60 I; 33 N 35
5-20	n-C_8H_{17}	n-OC_4H_9	C 61 I; 42 N 45
5-21	n-C_3H_7	CN	C 97 I; 21
5-22	n-C_4H_9	CN	C 92 I; 12
5-23	n-C_5H_{11}	CN	C 74 I; 11 N 19
5-24	n-C_6H_{13}	CN	C 73 I; 6 N 17
5-25	n-C_7H_{15}	CN	C 78 I; 15 N 30
5-26	n-C_8H_{17}	CN	C 70 I; 15 N 26

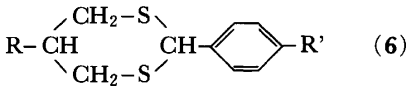

(6)

	R	R'	Transition Temp/°C[a)]
6-1	n-C_3H_7	OCH_3	C 97 I; 34
6-2	n-C_3H_7	n-OC_4H_9	C 46 I; 25
6-3	n-C_4H_9	OC_2H_5	C 75 I; 35
6-4	n-C_4H_9	n-OC_3H_7	C 65 I; 32
6-5	n-C_5H_{11}	OC_2H_5	C 57 I; 35
6-6	n-C_5H_{11}	n-OC_3H_7	C 55 I; 40
6-7	n-C_6H_{13}	OC_2H_5	C 61 I; 32 N 43
6-8	n-C_6H_{13}	n-OC_3H_7	C 75 I; 38
6-9	n-C_6H_{13}	n-OC_4H_9	C 55 I; 34 N 44
6-10	n-C_6H_{13}	n-OC_5H_{11}	C 60 I; 38 N 47
6-11	n-C_7H_{15}	OC_2H_5	C 70 I; 48 N 57
6-12	n-C_7H_{15}	n-OC_3H_7	C 60 I; 35 N 50
6-13	n-C_7H_{15}	n-OC_4H_9	C 59 I; 42 N 56
6-14	n-C_7H_{15}	n-OC_5H_{11}	C 67 I; 52 N 58
6-15	n-C_8H_{17}	n-OC_3H_7	C 56 I; 31 S_A 57
6-16	n-C_8H_{17}	n-OC_4H_9	C 57 I; 26 S_A 133
6-17	n-C_3H_7	CN	C 78 I
6-18	n-C_4H_9	CN	C 88 I; 30
6-19	n-C_5H_{11}	CN	C 98 I; 28
6-20	n-C_6H_{13}	CN	C 90 I; 36
6-21	n-C_7H_{15}	CN	C 98 I; 43
6-22	n-C_8H_{17}	CN	C 93 I; 39

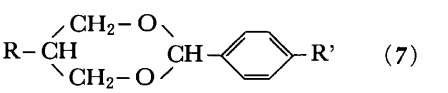

(7)

	R	R'	Transition Temp/°C[a)]
7-1	n-C_4H_9	n-OC_3H_7	C 43 I; N 25

TABLE 1. CONTINUED

	R	R'	Transition Temp/°C[a]		R	R'	Transition Temp/°C[a]
7-2	*n*-C_6H_{13}	*n*-OC_4H_9	C 35.5 S_A 44 N 50 I	**7-6**	*n*-C_6H_{13}	CN	C 47 I, N 40.5
7-3	*n*-C_7H_{15}	*n*-OC_4H_9	C 49 S_A 59.5 I	**7-7**	*n*-C_7H_{15}	CN	C 54 I, N 52
7-4	*n*-C_4H_9	CN	C 42 I, N 35.5	**7-8**	*n*-C_8H_{17}	CN	C 60 I, N 51
7-5	*n*-C_5H_{11}	CN	C 55 I, N 48				

a) C=crystal; N=nematic; I=isotropic. b) Cited from Ref. 2. c) Cited from Ref. 7.

group, compounds **5** seem hardly to exhibit liquid-crystal phases. Namely, the nematic phase is too unstable to exist over a wide range of temperature. Even with a long alkyl chain (R=C_8H_{17}), they did not exhibit smectic phase. The molecular widths in hetero rings increase in the order: 1,3-dioxane, 1,3-oxathiane, and 1,3-dithiane. Therefore, lateral molecular interactions of 1,3-oxathianes are larger than those of 1,3-dithianes from this point of view. 1,3-Oxathiane compounds, however, are bent at the 1,3-oxathiane ring due to the difference of atomic size between sulfur and oxygen.

2-(*p*-Cyanophenyl)-5-alkyl-1,3-oxathianes having an alkyl chain with odd carbon numbers tend to have somewhat higher values of T_{N-I} (R=C_5H_{11}, 19°C; R=C_7H_{15}, 30°C), whereas those having an alkyl chain of even carbon numbers tend to have somewhat lower values (R=C_6H_{13}, 17°C; R=C_8H_{17}, 26°C).

The principal features of the mesomorphic behavior of compounds **5** are (1), in *p*-cyanophenyl compounds, monotropic nematic liquid crystal phase is exhibited around ordinary room temperature, and (2), in *p*-alkoxyphenyl compounds, mesomorphic phases are hardly recognized, and even for the compounds having a long alkyl chain (C_8H_{17}), any smectic phases could not be observed.

Experimental

IR, ^{1}H-NHR, ^{13}C-NMR, and mass spectra were obtained with a Hitachi 215 spectrophotometer, a JNM-PMX 60 spectrometer, a JNM-FX 90 Q FT-NMR spectrometer, and a Hitachi RMU-6MG spectrometer, respectively. Elemental analyses were carried out with a Perkin-Elmer 250 instrument. Mesomorphic phases and the transition temperatures were determined by means of both a Mitamura Riken micro melting-point apparatus equipped with polarizers and a Rigaku Denki D.S.C. CN8059L1, CN8208A2. The rate of cooling was fixed to 1°C/min.

2-Alkyl-3-bromo-1-propanol (2). To a solution of 48% HBr (50 g) and concd H_2SO_4 (15 g) cooled in an ice bath were added successively compound **1** (0.1 mol) and concd H_2SO_4 (25 g). The solution was kept at 70—75°C, for 18 h. The reaction mixture was then poured into ice water (200 g). The mixture was stirred and extracted twice with ether (each 400 ml). The extract was washed with cold 10% aq $NaHCO_3$ (100 ml), dried over anhyd. Na_2SO_4, and concentrated on a rotary evaporator at 30°C. The residue was distilled *in vacuo* to afford transparent liquid in a 40—50% yields.

Bp: 71—74°C/1—2 mmHg† (R=C_3H_7), 85—88°C/1—2 mmHg (R=C_4H_9), 93—95°C/1—2 mmHg (R=C_5H_{11}), 118—122°C/3—5 mmHg (R=C_6H_{13}), 104—107°C/1—2 mmHg (R=C_7H_{15}), 111—113°C/1—2 mmHg (R=C_8H_{17}). IR ($CHCl_3$) 3600 (OH), 2800—3000 (Alkyl) cm^{-1}. ^{1}H-NMR ($CDCl_3$) δ= 0.6—2.1 (m, R-CH), 2.3 (s, 1H, OH), 3.4—3.8 (m, 4H, CH_2-Br, CH_2-O).

2-Alkyl-3-mercapto-1-propanol (3). To a solution of thiourea (0.064 mol, 4.9 g) in triethylene glycol (8 ml) kept at 75°C was added compound **2** (0.016 mol) in a nitrogen atmosphere, followed by stirring at 75°C for 18 h. Tetraethylenepentamine (0.016 mol, 3.03 g) was then added, and the mixture was stirred at 75°C for 2 h under a nitrogen atomosphere. The reaction mixture was distilled *in vacuo* to afford transparent liquid in a 60—70% yields.

Bp: 90—92°C/1—2 mmHg (R=C_3H_7), 105—108°C/1—2 mmHg (R=C_4H_9), 128—135°C/1—2 mmHg (R=C_5H_{11}), 136—138°C/1—2 mmHg (R=C_6H_{13}), 138—140°C/1—2 mmHg (R=C_7H_{15}), 142—146°C/1—2 mmHg (R=C_8H_{17}). IR ($CHCl_3$) 3600 (OH), 2800—3000 (Alkyl) cm^{-1}. ^{1}H-NMR ($CDCl_3$) δ= 0.6—2.0 (m, R-CH, 2SH), 2.5—2.8 (m, 2H, -CH_2S), 3.3—3.9 (m, 3H, CH_2-OH).

2-(p-Substituted phenyl)-5-alkyl-1,3-oxathiane (5). To a solution of compound **3** (0.004 mol) and *p*-substituted benzaldehyde **4** (0.004 mol) in anhyd. $CHCl_3$ (200 ml) cooled in an ice bath were added $BF_3 \rightarrow (C_2HH_5)_2O$ (0.5 g) and molecular sieves (3A, 1/15; 3 g). The mixture was stirred at 0—5°C for 8 h and then at 20—25°C for 18 h. The solution was washed with 10% aq $NaHCO_3$ (400 ml), dried over anhyd. Na_2SO_4, and evaporated *in vacuo* at 40°C. The crude product was purified by recrystallizations from hexane, then if necessary, by centrifugal liquid chromatography.

2-(p-Alkoxyphenyl)-5-alkyl-1,3-oxathianes. IR ($CHCl_3$) 2800—3000 (Alkyl), 1600 (Ar), 1300 (Ether) cm^{-1}.

^{1}H-NMR ($CDCl_3$) Compounds **5-1**, **5-6**, and **5-17**: δ= 0.7—2.1 (m, R-CH), 2.7—3.0 (d, 2H, CH_2S), 3.4, 4.3 (t; 3.4, m; 4.3, 2H, CH_2O), 3.8 (s, 3H, OCH_3), 5.7 (s, 1H, $\overset{S}{\underset{O}{\rangle}}$CH), 6.8—7.6 (q, 4H, ArH). Compounds **5-2**, **5-4**, **5-7**, **5-9**, **5-13**, and **5-18**: δ=0.7—2.1 (m, R-CH, O-CH_2-CH_3), 2.7—3.0 (d, 2H, CH_2-S), 3.4, 4.3 (t; 3.4, m; 4.3, 2H, CH_2-O), 4.05 (q, 2H, O-CH_2-CH_3), 5.7 (s, 1H, $\overset{S}{\underset{O}{\rangle}}$CH), 6.7—7.6 (q, 4H, ArH). Others: δ=0.7—2.1 (m, R-CH, OCH_2-C_nH_{2n+1}), 2.7—3.0 (d, 2H, CH_2-S), 3.4, 4.3 (t; 3.4, m; 4.3, 2H, CH_2-O) 3.95 (t, 2H, -O-CH_2-C_nH_{2n+1}), 5.7 (s, 1H, $\overset{S}{\underset{O}{\rangle}}$CH-). 6.8—7.6 (q, 4H,

†1 mmHg=133.322 Pa.

ArH).

5-1: Yield, 60%. Found: C, 66.51; H, 8.00. Calcd for $C_{14}H_{20}O_2S_1$: C, 66.63; H, 7.99. MS (*m/z*) 252 (M^+).

5-2: Yield, 56%. Found: C, 67.69; H, 8.35. Calcd for $C_{15}H_{22}O_2S_1$: C, 67.69; H, 8.35. MS (*m/z*) 266 (M^+).

5-3: Yield, 53%. Found: C, 69.41; H, 8.97. Calcd for $C_{17}H_{26}O_2S_1$: C, 69.34; H, 8.97. MS(*m/z*) 294 (M^+).

5-4: Yield, 45%. Found: C, 68.54; H, 8.61. Calcd for $C_{16}H_{24}O_2S_1$: C, 68.53; H, 8.63. MS (*m/z*) 280 (M^+).

5-5: Yield, 55%. Found: C, 69.31; H, 8.99. Calcd for $C_{17}H_{26}O_2S_1$: C, 69.34; H, 8.90. MS (*m/z*) 294 (M^+).

5-6: Yield, 45%. Found: C, 68.27; H, 8.65. Calcd for $C_{16}H_{24}O_2S_1$: C, 68.53; H, 8.63. MS (*m/z*) 280 (M^+).

5-7: Yield, 55%. Found: C, 69.34; H, 8.80. Calcd for $C_{17}H_{26}O_2S_1$: C, 69.34; H, 8.80. MS (*m/z*) 294 (M^+).

5-8: Yield, 59%. Found: C, 70.20; H, 9.12. Calcd for $C_{18}H_{28}O_2S_1$: C, 70.08; H, 9.15. MS (*m/z*) 308 (M^+).

5-9: Yield, 56%. Found: C, 70.14; H, 9.14. Calcd for $C_{18}H_{28}O_2S_1$: C, 70.08; H, 9.15. MS (*m/z*) 308 (M^+).

5-10: Yield, 64%. Found: C, 70.44, H, 9.42. Calcd for $C_{19}H_{30}O_2S_1$: C, 70.76; H, 9.38. MS (*m/z*) 322 (M^+).

5-11: Yield, 63%. Found: C, 71.42; H, 9.59. Calcd for $C_{20}H_{32}O_2S_1$: C, 71.38; H, 9.59. MS (*m/z*) 336 (M^+).

5-12: Yield, 68%. Found: C, 71.59; H, 9.82. Calcd for $C_{21}H_{34}O_2S_1$: C, 71.95; H, 9.78. MS (*m/z*) 350 (M^+).

5-13: Yield, 63%. Found: C, 70.72; H, 9.39. Calcd for $C_{19}H_{30}O_2S_1$: C, 70.76; H, 9.38. MS (*m/z*) 322 (M^+).

5-14: Yield, 59%. Found: C, 71.53; H, 9.57. Calcd for $C_{20}H_{32}O_2S_1$: C, 71.38; H, 9.59. MS (*m/z*) 336 (M^+).

5-15: Yield, 62%. Found: C, 72.15; H, 9.75. Calcd for $C_{21}H_{34}O_2S_1$: C, 71.95; H, 9.78. MS (*m/z*) 350 (M^+).

5-16: Yield, 66%. Found: C, 72.49; H, 9.95. Calcd for $C_{22}H_{36}O_2S_1$: C, 72.47; H, 9.95. MS (*m/z*) 364 (M^+).

5-17: Yield, 40%. Found: C, 71.01; H, 9.38. Calcd for $C_{19}H_{30}O_2S_1$: C, 70.76; H, 9.38. MS(*m/z*) 322 (M^+).

5-18: Yield, 44%. Found: C, 71.28; H, 9.60. Calcd for $C_{20}H_{32}O_2S_1$: C, 71.38; H, 9.59. MS(*m/z*) 336 (M^+).

5-19: Yield, 54%. Found: C, 71.90; H, 9.79. Calcd for $C_{21}H_{34}O_2S_1$: C, 71.95; H, 9.78. MS (*m/z*) 350 (M^+).

5-20: Yield, 51%. Found: C, 72.22; H, 10.01. Calcd for $C_{22}H_{36}O_2S_1$: C, 72.22; H, 9.95. MS (*m/z*) 364 (M^+).

2-(p-Cyanophenyl)-5-alkyl-1,3-oxathianes. IR ($CHCl_3$) 2800—3000 (Alkyl), 2230 (CN), 1600 (Ar) cm^{-1}. ^{1}H-NMR ($CDCl_3$) δ=0.7—2.1 (m, R-CH), 2.7—3.0 (d, 2H, CH_2-S), 3.4, 4.3 (t; 3.4, m; 4.3, 2H, CH_2O), 5.8 (s, 1H, $\overset{S}{O}$>CH), 7.65 (s, 4H, ArH).

5-21: Yield, 52% Found: C, 68.08; H, 6.92; N, 5.66. Calcd for $C_{14}H_{17}N_1O_1S_1$: C, 67.98; H, 6.93; N, 5.66. MS (*m/z*) 247 (M^+). ^{13}C-NMR ($CDCl_3$) δ=83.11 (C2 of the 1,3-oxathiane ring), 34.62 (C4), 75.42 (C6).

5-22: Yield, 36%. Found: C, 68.79; H, 7.33; N, 5.37. Calcd for $C_{15}H_{19}N_1O_1S_1$: C, 68.93; H, 7.33; N, 5.36. MS (*m/z*) 261 (M^+). ^{13}C-NMR ($CDCl_3$) δ=83.22 (C2), 34.84 (C4), 75.53 (C6).

5-23: Yield, 36%. Found: C, 69.45; H, 7.55; N, 4.99. Calcd for $C_{16}H_{21}N_1O_1S_1$: C, 69.78; H, 7.69; N, 5.09. MS (*m/z*) 275 (M^+). ^{13}C-NMR ($CDCl_3$) δ=83.11 (C2), 34.78 (C4), 75.47 (C6).

5-24: Yield, 41%. Fond: C, 70.76; H, 8.03; N, 4.81. Calcd for $C_{17}H_{23}N_1O_1S_1$: C, 70.54; H, 8.01; N, 4.84. MS (*m/z*) 289 (M^+). ^{13}C-NMR ($CDCl_3$) δ=83.22 (C2), 34.78 (C4), 75.58 (C6).

5-25: Yield, 45%. Found: C, 71.34; H, 8.31; N, 4.61. Calcd for $C_{18}H_{25}N_1O_1S_1$: C, 71.24; H, 8.30; N, 4.62. MS (*m/z*) 303 (M^+). ^{13}C-NMR ($CDCl_3$) δ=83.22 (C2), 34.78 (C4), 75.53 (C6).

5-26: Yield, 55%. Found: C, 71.76; H, 8.65; N, 4.13. Calcd for $C_{19}H_{27}N_1O_1S_1$: C, 71.88; H, 8.57; N, 4.41. MS (*m/z*) 317 (M^+). ^{13}C-NMR ($CDCl_3$) δ=83.22 (C2), 34.84 (C4), 75.55 (C6).

References

1) Y. Haramoto, and H. Kamogawa, *J. Chem. Soc., Chem. Commun.*, **1983**, 75.

2) Y. Haramoto, A. Nobe, and H. Kamogawa, *Bull. Chem. Soc. Jpn.*, **57**, 1966 (1984).

3) Y. Haramoto, K. Akazawa, and H. Kamogawa, *Bull. Chem. Soc. Jpn.*, **57**, 3173 (1984).

4) Y. Haramoto, and H. Kamogawa, *Bull. Chem. Soc. Jpn.*, **58**, 477 (1985).

5) Y. Haramoto, and H. Kamogawa, *Chem. Lett.*, **1985**, 79.

6) G. W. Gray and B. W. Worrall, *J. Chem. Soc.*, **1959**, 1545.

7) D. Demus and H. Zaschke (to V. E. W. Kombinat Mikroelectronik), Japan Pat. Appl. No 54-160916, Dec. (1979).

Determination of the Acid Strength Distribution of Manganese Dioxide by the Modified Indicator Method

Kazuo SUGIYAMA,* Yasushi NAKANO, Hiroshi MIURA, and Tsuneo MATSUDA
Department of Applied Chemistry, Faculty of Engineering, Saitama University, Shimo-ohkubo, Urawa 338
(Received October 30, 1984)

Synopsis. A new procedure for determining the distribution of acid and base centers of dark colored solids by the indicator method has been proposed. By this method weak acidic sites were found to be present on a manganese dioxide surface.

As a method for measuring the acidity of white colored solid samples such as silica-alumina, the fundamental titration procedure based on Johnson's method[1] is generally used. The acidity of colored solid samples, however, can not be measured by this method. In this case a modified procedure[2] such as the titration of the mixture of the sample and a white standard sample with known acidity is usually applied. By this modified method it is impossible to measure the acidity of black colored solids such as electrolyte manganese dioxide (EMD), because the color change of the Hammett indicator is difficult to observe.

On the EMD surface the presence of acidic sites should be predictable from the cation-exchange ability of its surface OH groups.[3,4] The understanding of the acidic properties on the EMD surface can help to improve the life of dry batteries.[5]

Recently we succeeded in determining the amounts of acid and basic areas on black colored solid samples by our modification of the indicator method. This paper describes this procedure and the distribution of the acidic sites on the EMD surface.

Experimental

Samples. EMD (type FM-H) was supplied by Toyo Soda Manufacturing Co. Ltd., and its particle size was 100—200 mesh (149—79 μ). Before the measurements it was preheated at 110—500 °C for 1 h in air. MnO was obtained by thermal decomposition of manganese carbonate at 500 °C in a stream of nitrogen. Silica-alumina (Catalysts & Chemicals Ind. Co. Ltd.; SiO_2 87%) dried at 110 °C and magnesium oxide (Wako Pure Chem. Co. Ltd.) calcined at 700 °C in air were used as a white standard probe with known acidity and basicity, respectively.

As shown in Fig. 1, a vessel developed by us is composed of a commercially available separate ground-glass Gooch crucible equipped with a cover on the head and a receiver (content volume 15 ml) on the bottom. The pore size of the glass filter is 20—30 μ (3G type).

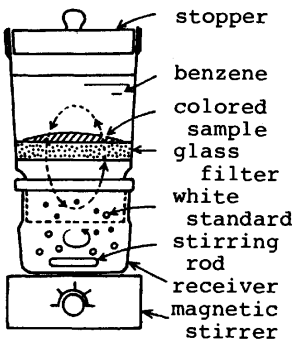

Fig. 1. The vessel to measure the acidic and basic properties of the dark colored solid samples.

Procedure. The standard probe of silica-alumina and a magnetic stirring rod are put into the receiver, to which the paired ground-glass Gooch crucible is attached. Dry benzene is poured into the crucible. When the inner pressure of the crucible is reduced by use of an aspirator, the vessel can be then degassed. The inner part of the vessel can then be easily filled with dry benzene. The known amount of preheated EMD is rapidly placed into the crucible in a stream of dry nitrogen. The weight of the EMD is about three times that of the silica-alumina. A few drops of Hammett indicator with the known pK_a is introduced into the EMD-benzene solution and stirred for 3 h, followed by standing for 12 h. At first 0.1 M† butylamine benzene solution equivalent to the amount of the acid in the silica-alumina is added to the crucible. Butylamine benzene solution is then added at 3-h intervals until the acidic color of the Hammett indicator on the silica-alumina is no longer observed. Stirring is continued all through the titration. A drop of 0.05 M trichloroacetic acid in benzene is added to ensure whether there is appreciable excess of butylamine at the end point or not.

Using benzoic acid instead of butylamine the basicity of dark colored samples can be determined in the same manner as described above.

Results and Discussion

In order to verify our method, the acidity of the white standard solid, silica-alumina, instead of black colored sample was first measured. The same results for the acidity were obtained by our method as for fundamental Johnson's method (Table 1). The silica-alumina, which has an acid strength distribution for the weak acidic sites, is suitable for the white standard probe to measure the acid amount of the EMD.

Our method showed a considerable amount of weak acidic sites were present on the EMD surface. The acid strength distribution of the EMD preheated at the various temperature were given in Table 1. A large amount of acid sites at $+6.8 \leqq H_o < +1.5$ was observed on the EMD surface preheated at 110 °C. When phenolphthalein ($pK_a = +9.3$) was used as a Hammett indicator, the basic sites could not be detected on the EMD surface. While the amount of basic sites at $H_o = +9.3$ on the MnO surface was 0.297 mmol/g.

Many OH groups are known to be present on the EMD surface.[5,6] The relation between the amount of surface OH groups determined by the KI method in *N,N*-dimethylformamide solvent[7] and the total acid amount on the EMD heat-treated at various temperature were shown in Fig. 2. Both the amounts of the surface OH groups and of the total acidic sites

† 1 M = 1 mol dm^{-3}.

Table 1. Acidic properties of electrolytic MnO_2

Sample	Calcinating temperature (°C)	Surface area (m^2/g)	Acid amount(mmol/g)			Total acid amount (mmol/g)
			$+1.5>H_o\geqq+3.3$	$+3.3>H_o\geqq+4.8$	$+4.8>H_o\geqq+6.8$	
MnO_2	110	33.2	0.006	0.072	0.023	0.101
MnO_2	200	28.5	0.005	0.046	0.037	0.088
MnO_2	300	16.3	0	0.019	0.064	0.083
MnO_2	500	12.9	0	0.015	0.025	0.040
SiO_2-Al_2O_3[a)]	110	302	0.142	0.339	0.384	0.865
SiO_2-Al_2O_3[b)]	110	302	0.144	0.333	0.381	0.858

a) By our modified method. b) By Johnson's method.

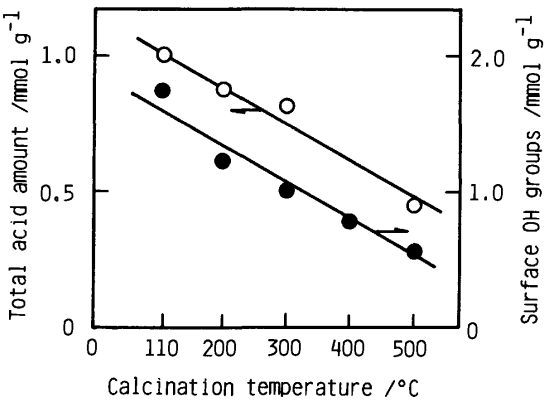

Fig. 2. Relation between both the amount of total acid and of surface OH groups on the electrolytic MnO_2 heat-treated at various temperatures.

decreased in nearly the same ratio as the pretreatment temperature was raised. These results suggest that the surface OH groups are the important factor associated with the acidic property of the EMD. The difference between the surface OH groups and the total acid amount should be expected to be either weak acid OH groups below the acid strength at H_o=+6.3 or the oxidation sites on the EMD. We propose to investigate the surface characterization for the acidic properties on the EMD in further detail.

Thus both the acidity and basicity of the dark colored solid samples can be measured satisfactorily by our method provided one selects suitable standard probes and indicators.

References

1) O. Johnson, *J. Phys. Chem.*, **59**, 827 (1955).
2) S. E. Voltz, A. E. Hirshler, A. Smith, *J. Phys. Chem.*, **64**, 1594 (1960).
3) A. Kozawa, *J. Electrochem. Soc.*, **106**, 553 (1959).
4) A. K. Covington, T. Cressey, B. G. Lever, and H. R. Thirsk, *Trans. Faraday Soc.*, **58**, 1975 (1962).
5) A. Kozawa, R. A. Powers, *J. Electrochem. Soc.*, **113**, 870 (1966).
6) K. Sugiyama, Y. Nakano, S. Sano, H. Miura, T. Mitamura, and T. Matsuda, *Denki Kagaku*, **51**, 179 (1983).
7) J. J. Laragne, J. Brenet, *Bull. Soc. Chim. (France)*, **9**, 3499 (1968).

The Promotion Effect of Surface Hydroxyl on the Oxygen Adsorption over NiO, Fe_2O_3, and CuO

Yusaku TAKITA,* Yumie SAITO, Tetsuro TASHIRO, and Fumiaki HORI
Department of Environmental Chemistry and Engineering, Faculty of Engineering, Oita University, Dannoharu, Oita 870-11
(Received Nobember 9, 1984)

Synopsis. Oxygen TPD revealed that the adsorption of water vapor at 278 K promoted the desorption of the preadsorbed oxygen at 793→278 K over NiO and Fe_2O_3. Preadsorption of water vapor at 473 K brought about a marked enhancement over Fe_2O_3 and a slight increase over CuO in the adsorption of oxygen at 473→278 K.

It has been known that the addition of water vapor promoted the catalytic oxidations of methanol,[1] propene,[2] butene,[3] 2-butanone,[4] 2-methyl propenal (methacrolein),[5] toluene,[6] and the ammoxidation of propene.[7] It was proved that water or surface hydroxyl served as a reactant in the formation of alcoholic intermediate in several catalytic oxidations.[2,3,5] The promotion mechanism for other oxidations, however, is still not elucidated.

Water vapor is formed as by-product in almost all of catalytic oxidations of organic compounds and it will more or less affect the adsorption of reactants, products, and/or intermediates, so that it is of importance to know the behavior of oxygen adsorbate in the presence of water vapor for understanding of catalytic oxidations.

Recently, it has been reported that coadsorption of water vapor affected adsorption energy of oxygen on the metal oxide surfaces. Co_3O_4 gave a temperature programmed desorption (TPD) chromatogram of oxygen which composed of three kinds of oxygen adsorbate. The desorption peak with peak maximum temperature (T_m) at 365 K shifted to higher temperature by 50 K without loss of its amount when water vapor and oxygen were coadsorbed at 473→278 K.[8] Over Ag^+–SnO_2, a broad prateau above 610 K in oxygen TPD chromatogram was transformed into a sharp peak at 570 K by the coadsorption of water vapor.[9]

However it is still not known for other metal oxides. This paper deals with the behavior of oxygen adsorption in the presence of the adsorbate derived from water over the metal oxides.

The oxygen TPD chromatograms from NiO are shown in Fig. 1. The NiO sample after the treatment A (see Table 1) gave a chromatogram which consisted of a desorption peak with T_m=695 K and a shoulder peak at around 600 K (curve 1). This well agreed with that reported by Iwamoto *et al.*[10] Water adsorption at 294 K onto the NiO sample with oxygen adsorbate by the treatment A brought about drastic changes in its chromatogram of oxygen (curve 2): by the adsorption of 5.0 μmol/g water, a small α peak appeared at around 420 K and β peak became larger but γ peak decreased without shift of T_m. The amount of oxygen desorbed up to 793 K slightly increased from 7.92 to 8.89 μmol/g by the water coadsorption. Curve 3 is a chromatogram of water desorbed simultaneously with oxygen, which is composed of two peaks with T_m=490 K and >793 K. These peaks may arise from surface hydroxyl since the desorption temperatures are higher than the normal boiling point of water.

Fe_2O_3 showed two desorption peaks with T_m=620 K and 710 K (curve 1 in Fig. 2). Both α and β peaks shifted to lower temperatures and the latter peak was much enlarged by the adsorption of water at 278 K onto the sample preadsorbed with oxygen. The total amount of desorbed oxygen increased to about 1.4 times of that of dry surface. Curve 3 in Fig. 2 revealed that all of the water vapor was chemisorbed onto Fe_2O_3. In these experiments, no oxygen was supplied from gas phase during the adsorption of water vapor at 294 K. Therefore the increment of desorbed oxygen probably came from the oxygen which should be desorbed at >793 K from the dry surface.

Figure 3 shows the results of oxygen chemisorption onto the Fe_2O_3 surface preadsorbed with water vapor.

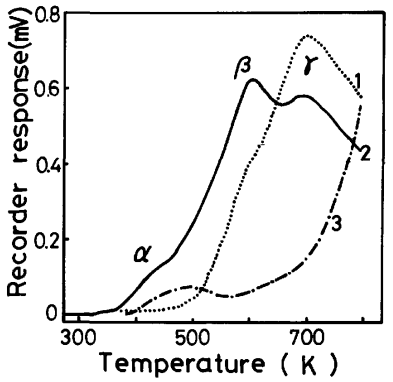

Fig. 1. TPD chromatograms from NiO.
1: Oxygen, treatment A, 2: oxygen, treatment B, 3: water, treatment B.

Table 1. Treatment of oxides

A:	Adsorption of oxygen (100 Torr*, 793 K, 30 min)	→	Cooling to r.t. (10 K/min)	→	Evacuation (r.t., 15 min)
B:	Treatment A	→	Adsorption of water vapor (2 Torr, 293 K, 30 min)	→	Evacuation (r.t., 15 min)
C:	Adsorption of oxygen (100 Torr, 473 K, 30 min)	→	Cooling to r.t. (10 K/min)	→	Evacuation (r.t., 15 min)
D:	Adsorption of water vapor (2 Torr, 473 K, 30 min)	→	Evacuation (473 K, 15 min)	→	Treatment C

* 1 Torr=133.322 Pa.

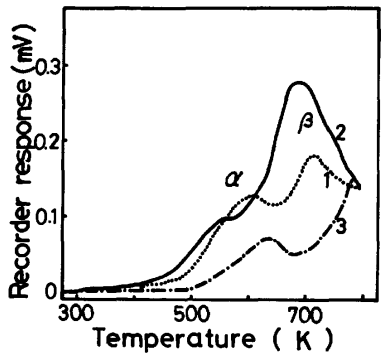

Fig. 2. TPD chromatograms from Fe_2O_3.
1: Oxygen, treatment A, 2: oxygen, treatment B, 3: water, treatment B.

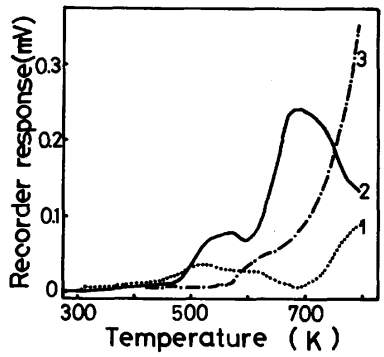

Fig. 3. TPD chromatograms from Fe_2O_3.
1: Oxygen, treatment C, 2: oxygen, treatment D, 3: water, treatment D.

In the oxygen adsorption on the dry surface at 473 K (the treatment C), only a small amount of oxygen could be chemisorbed and the chromatogram was composed of three desorption peaks with T_m=430 K, 610 K, and >793 K. The second peak (T_m=610 K) well coincided with that of α peak in curve 1 in Fig. 2. However, preadsorption of water at 473 K much promoted the adsorption of oxygen. The shape of curve 2 in Fig. 3 was much similar to that of curve 2 in Fig. 2, despite the differences in the adsorption temperature and procedure for water adsorption. The amount of desorbed oxygen was determined to be 2.35 μmol/g, which was 3.5 times larger than that of curve 1. It is noteworthy that this value exceeded the 2.06 μmol/g of oxygen adsorption at 793 K.

Assuming that surface concentration of iron(III) ion was about 10^{19} atom/m^2, surface coverages of adsorbed water and oxygen (tentatively presumed as dissociative adsorption) on the Fe_2O_3 sample after the treatment D were calculated to be 3.5 and 6.0%, respectively. Similarly, those for the NiO sample after the treatment B were 1.4 and 5.0%. Provided that all of the adsorbates are dispersed uniformly on the oxide surface, these values are too small for each adsorbate to interact with a neighboring another kind of adsorbate. So that it seems more likely that both species are adsorbed together onto some surface defects.

In the case of CuO, chromatogram of oxygen changed slightly by the preadsorption of water vapor with broadning of peak and shift of T_m to higher temperature by 25 K (curve 2 in Fig. 4).

Although most of surface hydroxyl may be desorbed

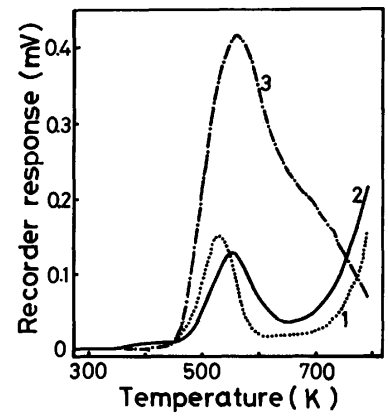

Fig. 4. TPD chromatograms from CuO.
1: Oxygen, treatment C, 2: oxygen, treatment D, 3: water, treatment D.

at higher reaction temperatures, a significant amount of surface hydroxyl may remain on the surface and modify the activity of oxygen adsorbate in the catalytic oxidation performed at moderate reaction temperatures. These phenomena may partly explain the promotion effect of water vapor in the catalytic oxidation of organic compounds.

Experimental

NiO, Fe_2O_3, and CuO were prepared by the thermal decomposition of $NiCO_3 \cdot 2Ni(OH)_2$, $Fe(NO_3)_2 \cdot 9H_2O$, and $CuCO_3 \cdot Cu(OH)_2 \cdot H_2O$ (Wako Pure Chem. Ind.) at 673 K for 4 h, followed by calcination at 823 K for 4 h in air. TPD apparatus used here was basically the same as that described in the literature.[11] Desorption chromatograms of water were obtained from the difference of the chromatograms recorded with two thermal conductivity detectors located at upper and at lower stream of the cold trap at 77 K for the removal of water vapor. The detector downstream gave chromatograms of oxygen.

References

1) S. Yamauchi, *Yuki Gosei Kagaku*, **18**, 602 (1960); M. D. Thomas, *J. Am. Chem. Soc.*, **42**, 862 (1920).
2) Y. Moro-oka, Y. Takita, and A. Ozaki, *J. Catal.*, **27**, 177 (1972).
3) T. Seiyama, K. Nita, T. Maehara, N. Yamazoe, and Y. Takita, *J. Catal.*, **49**, 164 (1977).
4) Y. Takita, K. Iwanaga, N. Yamazoe, and T. Seiyama, *Oxidation Commun.*, **1**, 135 (1980); Y. Takita, F. Hori, N. Yamazoe, and T, Seiyama, *J. Catal.*, **90**, 232 (1984).
5) M. Misono, K. Sakata, and Y. Yoneda, *7th Intern. Congr. Catal.*, B27.
6) M. Iwamoto and S. Kagawa, *J. Phys. Chem.*, **87**, 903 (1983).
7) USP 2904580.
8) Y. Takita, T. Tashiro, Y. Saito, and F. Hori, *J. Catal.*, in press. Y. Takita, T. Yokoo, F. Hori, N. Yamazoe, and T. Seiyama 43rd National Meeting of the Chemical Society of Japan, Tokyo, March 1981 Abstr., No. 2L08; Y. Takita, T. Tashiro, F. Hori, N. Yamazoe, and T. Seiyama 47th National Meeting of the Chemical Society of Japan, Kyoto, April 1983, Abstr., No. 1N11.
9) M. Egashira, M. Nakashima, and S. Kawasumi, *J. Chem. Soc. Chem. Commun.*, **1981**, 1047.
10) M. Iwamoto, Y. Yoda, M. Egashira, and T. Seiyama, *J. Phys. Chem.*, **80**, 1989 (1976).
11) Y. Amenomiya and R. J. Cvetanovic, *J. Phys. Chem.*, **67**, 144, 2046, 2705 (1963).

UV and Visible Fluorescences of CF_3 Radicals Produced by the Two-photon Decomposition of CF_3Br and Their Radiative Lifetimes

Nobuaki WASHIDA,* Osamu HORIE,† and Karl H. BECKER†

Division of Atmospheric Environment, The National Institute for Environmental Studies, P. O. Tsukuba-gakuen, Ibaraki 305

†*Physikalische Chemie, FB9, Bergische Universität-gesamthochschule Wuppertal, Gaussstrasse 20, D-5600 Wuppertal, Federal Republic of Germany*

(Received December 5, 1984)

Synopsis. The UV and visible emission bands of the CF_3 radical were observed in the two-photon decomposition of CF_3Br using KrF excimer laser (248 nm) radiation. Very short radiative lifetimes (shorter than 40 and 50 ns for the UV and visible bands, respectively) were obtained.

Knowledge of the excited states of the CF_3 radical is important in both semiconductor-device fabrication[1] and regarding ozone depletion in the stratosphere.[2] Two emission bands of CF_3 radicals were observed in the UV (170—320 nm) and visible (400—750 nm) regions by the VUV (100—140 nm) photolysis of CF_3X molecules (X=H, Cl, Br) recently.[3] In the present study, the observation of the UV and visible emissions of CF_3, produced by the two-photon decomposition of CF_3Br, were investigated using KrF excimer laser light (248 nm). Also, measurements of the radiative lifetimes of both emission bands were attempted. Since both UV and visible emission bands of CF_3 were observed in the photolysis of CF_3Br by the Kr resonance line (123.6 nm) in the previous study, these emission bands can be produced by the two-photon photodecomposition of CF_3Br by the KrF excimer laser (248 nm).

$$CF_3Br + 2h\nu(248\text{ nm}) \longrightarrow CF_3^* + Br \qquad (1)$$

Further, if the radiative lifetimes of both bands are longer than the experimental response, these values can be obtained directly using a laser pulse.

The KrF excimer laser (Lamda Physik EMG 102) beam was focussed in a stainless steel fluorescence cell through a quartz lens. The emission was collected at a right angle to the laser beam (using an optical system consisting of three quartz lenses) and was dispersed with a 0.35-m monochromator (McPherson Model 270). Since fluorescence was measured in the UV and visible regions, two gratings (1200 grooves/mm) blazed at 250 and 500 nm were used. A glass filter (Schott Glaswerke, GG 475, transmission longer than 470 nm) was used in the measurement of the visible emission spectrum. Fluorescence signals were detected with a photomultiplier (EMI 9635 and 9558B for UV and visible, respectively) and processed by a boxcar integrator (PAR 162).

When laser light was focussed through a quartz lens in the CF_3Br gas, a very bright-yellow emission was visible from the cell. The measured UV emission band is shown in Fig. 1a. The pressure of CF_3Br in the cell was kept at 133 Pa and the gas was slowly pumped using a rotary pump. The discrete emission band observed in the region of 200—225 nm corresponds to the UV emission band of CF_3.[3] The spectral profile is quite similar to that observed previously and separations of the characteristic progression (shown by arrows, 1000—1050 cm^{-1}), correspond to the ν_1 mode of CF_3.[3] The emission appearing at 193 nm should originate from the resonance fluorescence of the excited carbon atoms,[4] $C(3^1P^0 \xrightarrow{193\text{ nm}} 2^1D)$, after the resonance absorption from $C(^1S)$, $C(3^1P^0 \xleftarrow{248\text{ nm}} 2^1S)$. The excited carbon atom, $C(^1S)$, might be produced during the multi-photon decomposition of CF_3Br. The strong emission band (starting at 220 nm) corresponds to the $CF(A^2\Sigma \rightarrow X^2\Pi)$ system.[5] Essentially, the UV emission band of CF_3 should extend to 300 nm, having a maximum at 240 nm. In the present experimental system, however, the emission band of the $CF(A \rightarrow X)$ system was too strong and the UV band of CF_3 can be identified only in the region from 200 to 220 nm. The strong emission band of the $CF_2(^1B_1 \rightarrow {}^1A_1)$ system was observed in the region from 250 to 350 nm and an unidentified strong emission band was present up to 450 nm.

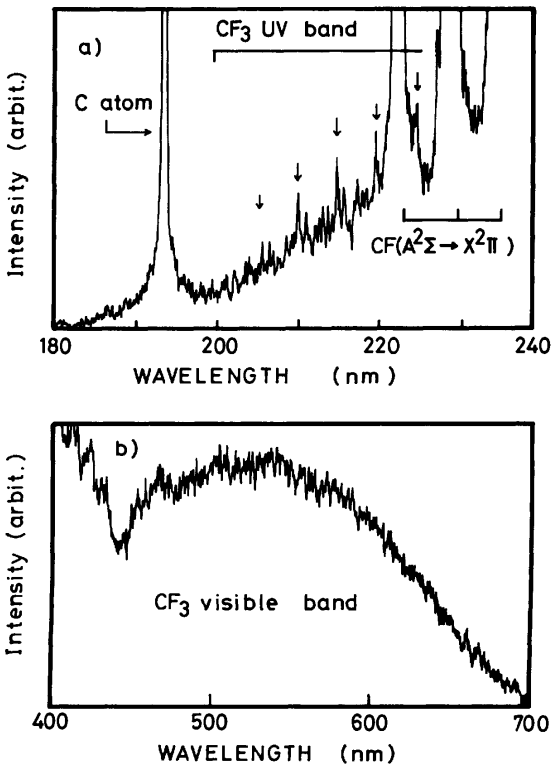

Fig. 1. Emission spectra of the UV (a) and visible (b) bands of CF_3 produced in the two-photon decomposition of CF_3Br by the KrF excimer laser (248 nm) radiation.

The observed visible emission-band spectrum is

shown in Fig. 1b. The continuous emission band (devoid of structure) in the region from 450 to 700 nm is also the same as that observed previously.[3] Since both UV and visible bands were observed, a two-photon decomposition of CF_3Br occured by Reaction (1), although other excited species (such as C, CF, and CF_2) were produced in this system.

The measurements of the radiative lifetimes were carried out at 210 nm for UV and 600 nm for the visible band (under 1 nm of spectral resolution). Fluorescence signals detected by photomultipliers were digitized by a transient digitizer (Tektronix R7912, 1 ns of time resolution) and processed by a minicomputer (DEC, LSI 11). Since the pulse of the KrF laser was 16 ns (fwhm) and the time response of the photomultipliers was about 25 ns (fwhm), radiative lifetimes could be obtained if the lifetime was longer than 50 ns (reliable value should be longer than 100 ns). The apparent radiative lifetimes measured at 27—667 Pa of CF_3Br were 30—40 ns for the UV band and 40—50 ns for the visible band. These lifetime values are shorter than the reliable instrumental time response. Therefore, it is concluded that radiative lifetimes for the UV and visible bands are shorter than 40 and 50 ns, respectively. No significant pressure dependence of the lifetime was observed for both measurements.

Very short radiative lifetimes were obtained for UV and visible band emissions of CF_3. Results are reasonable for the allowed transition of a polyatomic molecule. Using theoretical calculations[3] regarding the CF_3 electronic states, the UV band has been tentatively assigned to a Rydberg state (D_{3h} structure) emitting to the ground state ($2A'_1 \rightarrow 1A''_2$), while the visible band is thought, based on emission quenching experiments, to arise from transitions from the 1E' and/or $2A_2''$ Rydberg states (D_{3h}) to a repulsive state ($1A_1'$). The fluorescence quantum yields of the UV and visible band from the photolysis of CF_3Br at 124 nm were determined to be 1 and 5%, respectively.[3] It is possible that the predissociation occurs in both the upper states by the coupling of the potential curves of the lower electronic states. Short radiative lifetimes were obtained.

Recently, lifetime measurements regarding the UV and visible emission bands of CF_3 were carried out by two groups using synchrotron-radiation tequniques[6] and pulsed VUV laser (121 nm) radiation.[7] The former obtained fluorescence lifetimes of 14—17 ns for both the UV and visible bands and the later gave those of 15±3 and 18±3 ns for the UV- and the visible-band emissions, respectively.

The financial support by the "Sonderforschungsbereich 42/Deutsche Forschungs Gemeinschaft" is gratefully acknowledged.

References

1) a) C. M. Melliar-Smith and C. J. Mogab, "Thin Film Processes," ed by J. L. Vossen and W. Kern (Academic, New York, 1978); b) J. W. Coburn, *Plasma Chem. & Plasma Processing* **2**, 1 (1982).

2) F. S. Rowland and M. J. Molina, *Rev. Geophys. Space Phys.* **13**, 1 (1975); "Chlorofluoromethanes and the Stratosphere," ed by R. D. Hudson, NASA Reference Publication 1010 (1977).

3) M. Suto and N. Washida, *J. Chem. Phys.*, **78**, 1007 (1983); M. Suto and N. Washida, *ibid* 1012 (1983); M. Suto, N. Washida, H. Akimoto, and M. Nakamura, *ibid.* 1019 (1983); N. Washida, M. Suto, S. Nagase, U. Nagashima, and K. Morokuma *ibid* 1025 (1983); M. Suto and L. C. Lee, *J. Chem. Phys.* **79**, 1127 (1983).

4) M. Umemoto, H. Shinohara, N. Nishi and R. Shimada, *J. Photochem.*, **20**, 277 (1982).

5) R. W. B. Pearse and A. G. Gaydon, "The Identification of Molecular Spectra" 4th ed. (Chapman and Hall, London 1976) p. 89.

6) C. R. Quick, Jr., J. J. Tiee, J. Press, and R. E. Weston Jr. *Chem. Phys. Lett.*, **114**, 371 (1985).

7) R. W. Dreyfus and L. Urbach, *Chem. Phys. Lett.* **114**, 376, (1985).

Decomposition of Solid Potassium Nitrate by Incident 100 keV Ions†

Katsutoshi FURUKAWA and Shin-ichi OHNO*
Department of Chemistry, Japan Atomic Energy Research Institute, Tokai-mura, Ibaraki 319-11
(Received January 16, 1985)

Synopsis. Potassium nitrate was bombarded at 100 keV energy with ion beams extracted from a discharge of D_2, He, N_2, and O_2, and the yield for the formation of nitrite ion was determined: $G(NO_2^-)$=1.8, 1.8, 0.5, and 0.5, respectively. The results suggest that the reaction takes place *via* electronic excitations.

Whereas a lot is known about chemical reaction induced by ionizing radiations, very little information exists about chemical reaction induced by energetic particles having energies of 1 to 100 keV. Ions at keV energies have been used to initiate chemical reactions in gaseous methanol,[2,3] crystalline nitrate,[4] and condensed simple gases (H_2O, CH_4, CO).[5,6] The results in these low energy ion-impact experiments were interpreted as due to elastic collisions of incident ion with atoms leading to atomic displacements in the target molecules. Ions at higher energies lose energy more and more in inelastic collisions leading to electronic excitations of the molecule. Puglisi *et al.*, thus, studied chemical effects of elastic and inelastic collisions of 15—100 keV ions with benzene.[7]

In the present work, 100 keV ions were used to initiate the decomposition of potassium nitrate. Potassium nitrate was chosen because its radiolytic behavior toward ionizing radiations was well known: The only radiolytic products reported are nitrite ions and oxygen. The objectives of this work were to obtain the nitrite ion yields for 100 keV ions and to see the effect of the nature of bombarding ions on the decomposition yield.

Experimental

The sample to be irradiated was about 80 mg of polycrystalline potassium nitrate (Koso Chemical Co., Inc, Analytical Grade), pressed into a disk of the diameter of 10 mm, and mounted onto the sample holder by means of clamps. It was irradiated at ambient temperature in vacuum (*ca.* 10^{-5} Pa) with energetic ions. Ions were produced by discharge of D_2, He, N_2, and O_2 in a radio-frequency source,[8] extracted and accelerated at desired energies and were focussed through an aperture of 8 mmϕ onto the sample. The current density of the ion beam was measured by a Faraday cage and was 10 μA cm^{-2} throughout this work. Composition of the ionic species from each gas was analyzed magnetically; *i.e.*, D_2: D^+ (47%), D_2^+ (19%), and D_3^+ (34%); He: He^+ (99%); N_2: N^++N_2^{2+} (6%), N_2^+ (94%); and O_2: O^+ (17%), O_2^+ (82%), and O_3^+ (1%).

After irradiations, the samples were dissolved in water and the concentration of nitrite ions produced was determined spectrophotometrically[9] by adding 1-naphthylamine and sulfanilic acid. The molar absorption coefficient used was 35000 mol^{-1} dm^3 cm^{-1} at 520 nm.

†Chemical Reactions Induced by Energetic Particles. II.[1]

Results and Discussion

The yields of nitrite ion as a function of incident ion dose are shown in Fig. 1 for the bombardment with 100 keV ions. The rapid initial decomposition is followed by a decline in rate. At lower bombarding energies, *e.g.* 20, 50, and 80 keV, somewhat lower values for the initial yield were obtained, though the shape of the yield-dose curves remained unchanged.

From the initial slope of the curves in Fig. 1, the *G*-value for the formation of nitrite ions per 100 eV of the energy absorbed may be calculated. The results are included in Table 1, together with the $G(NO_2^-)$'s reported in the literature for other radiation sources.

On the other hand, we have calculated the electronic (S_e) and nuclear (S_n) stopping power of KNO_3 for these 100 keV ions according to the method of Lindhard *et al.*[10-12] The ratio S_e/S_n gives a relative amount of electronic and nuclear (elastic) energy deposition. Some relevant values of $S_e/(S_e+S_n)$ are included in Table 2. There may be seen a correlation between $G(NO_2^-)$ value and $S_e/(S_e+S_n)$ value. It should be remembered that ionizing radiations, *e.g.* α, β,

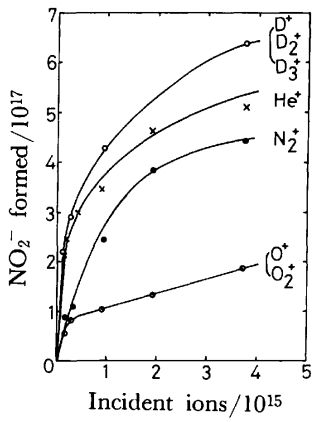

Fig. 1. Yield-dose curves for various 100 keV ions incident on potassium nitrate. Current density: 5 μA/0.5 cm^2.

TABLE 1. COMPARISON OF $G(NO_2^-)$ FROM KNO_3 OBTAINED BY VARIOUS RADIATIONS.

i) This work (100 keV)

D^+,D_2^+,D_3^+	He^+	N_2^+	O^+,O_2^+
1.8±0.2	1.8±0.2	0.5±0.1	0.5±0.2

ii) Literature values

10 keV He^+	3.4 MeV α	1.5 MeV e^-	^{60}Co γ
1.54[4]	2.2[13]	1.48[14]	1.46[15]

Table 2. Some values of $S_e/(S_e+S_n)$ for the ions traversing KNO_3.

Energy/keV	Ion			
	D^+	He^+	N^+	O^+
100	1.0	0.99	—	—
50	0.99	0.97	0.67	0.58
20	0.98	0.91	0.42	0.39

*) It is assumed that a molecular ion traversing a solid decomposes into atomic fragments. Thus, in the calculation of stopping power, a 100 keV-N_2^+ ion, for example, is regarded as two 50 keV-N^+ ions.

and γ rays and protons, lose most of their energy by electronic excitations. Thus, it may be concluded that the energetic ion-induced decomposition of nitrate leading to the formation of nitrite is mainly through electronic excitations.

Moreover, it is interesting to compare the yield-dose curve for oxygen-ion bombardment with that for nitrogen-ion bombardment. As the concentration of oxygen increases due to implantation, the yield for nitrite ion diminishes. This fact suggests that a nitrate ion-reforming reaction from nitrite ion and oxygen-containing species take place:[13]

$$NO_2^- + 1/2\,O_2(O, O^+, O^-, O_2^-, \text{or } O_3) \longrightarrow NO_3^- \quad (1)$$

The yield-dose curve for deuterium ion should be compared to that for helium ion. The difference in yield at higher doses (shown in Fig. 1) may be ascribed to the elimination of the oxygen-containing species (Reaction 1) by the implanted deuterium ion.

In conclusion, it was found that electronic excitations play an important role in ion-induced decomposition of potassium nitrate and that the effect of different bombarding ion is to accelerate or decelerate the nitrate reforming thermal reaction.

References

1) Part I: S. Ohno and K. Furukawa, *Bull. Chem. Soc. Jpn.*, **58**, 1100 (1985).
2) T. Kotoyori, M. Takahashi, and A. Ichinose, *Bull. Chem. Soc. Jpn.*, **44**, 2893 (1971).
3) E. Arai and M. Takahashi, *Radiochim. Acta*, **26**, 179 (1979).
4) S. R. Logan and W. J. Moore, *J. Phys. Chem.*, **67**, 1042 (1963).
5) R. A. Haring, A. Haring, F. S. Klein, A. C. Kummel, and A. E. de Vries, *Nucl. Instrum. Methods*, **211**, 529 (1983).
6) R. A. Haring, A. W. Kolfschoten, and A. E. de Vries, *Nucl. Instrum. Methods*, **B2**, 544 (1984).
7) O. Puglisi, G. Marletta, A. Torrisi, G. Foti, and L. Torrisi, *Radiat. Eff.*, **65**, 11 (1982).
8) K. Furukawa and S. Ohno, To be published in JAERI-M Report.
9) F. D. Snell and C. T. Snell, "Colorimetric Methods of Analysis," Vol. 2, D. Van Nostrand, New York (1955), p. 802.
10) J. Lindhard and M. Scharff, *Phys. Rev.*, **124**, 128 (1961).
11) J. Lindhard, M. Scharff, and H. E. Schiott, *Mat. Fys. Medd. Dan. Vid. Selsk*, **33**, No. 14 (1963).
12) J. F. Ziegler, "The Stopping and Ranges of Ions in Matter," Pergamon Press, New York (1980), Vol. 5.
13) A. R. Jones and R. L. Durfee, *Radiat. Res.*, **15**, 546 (1961).
14) E. R. Johnson, *J. Phys. Chem.*, **66**, 755 (1962).
15) J. Cunningham and H. G. Heal, *Trans. Faraday Soc.*, **54**, 1355 (1958).

Phosphorescence from Biacetyl and Benzophenone Surfaces by Collision with the T_1 State of Benzene

Shigeru OHSHIMA,† Tamotsu KONDOW,* and Kozo KUCHITSU
Department of Chemistry, Faculty of Science, The University of Tokyo, Bunkyo-ku, Tokyo 113
(Received January 23, 1985)

Synopsis. Benzene molecules in the lowest-excited triplet state, T_1, were allowed to collide with biacetyl and benzophenone surfaces, and phosphorescence from the surface due to energy transfer from the T_1 state of benzene was observed. The possibility of application of this method to detection of metastable species is discussed.

The T_1 state of benzene (3.5 eV [1]) is known to transmit its excitation energy efficiently to the T_1 state of biacetyl in the gas phase causing phosphorescence [2]. The quantum yields of gas-phase phosphorescence are reported to be 0.23 and 0.9, and the energies of the T_1 states are 2.53 and 3.0 eV for biacetyl [3] and benzophenone [4], respectively. This phenomenon can be extended to a gas-solid system by use of a phosphor surface, instead of a phosphor gas, as an energy acceptor. Since such an energy transfer occurs exclusively on the surface and is expected to depend on the spin multiplicity, observation of phosphorescence from the surface has potential applicability, for example, to detection of low-lying metastable states. In the present note, we report observation of phosphorescence from biacetyl and benzophenone surfaces in collision with metastable benzene molecules.

Experimental

A schematic diagram of the apparatus is shown in Fig. 1. An effusive beam of benzene through a multichannel array A with a pushing pressure of 2—3 Torr (1 Torr=133.322 Pa) was excited by electron impact (2—20 eV) to the T_1 state [5]. The electron gun and the excitation region was magnetically shielded with μ-metal. Either biacetyl or benzophenone was deposited continuously on an alumimum surface cooled at 77 K from nozzle B. The metastable benzene molecules were allowed to collide on the phosphor surface after traveling 17 cm. The emission from the surface was detected through an interference filter having a band-pass of 10 nm. The filter was so chosen that the wavelength of the maximum transmittance of the filter coincided with that of the maximum intensity of the resulting emission, *i.e.*, band pass filters of 520-nm (Toshiba KL-52) and 440-nm (Toshiba KL-44) for biacetyl and benzophenone, respectively. Charged species produced concurrently were removed by an electrostatic deflector (see Fig. 1).

For measurement of the time dependence of the emission intensity, the molecular beam was excited by a pulsed electron beam with a pulse width of 70 μs and a repetition rate of 10 ms. The data were accumulated in a Hewlett-Packard 5480A multichannel analyzer for 2 h. For measurement of the excitation function, the emission intensity was recorded as a function of electron impact energy, where the electron beam was not pulsed. A part of the fluorescence from the benzene molecules produced in the excitation region was estimated and eliminated from the observed emission; for the purpose a quartz window, shown in Fig. 1, was placed on the beam path.

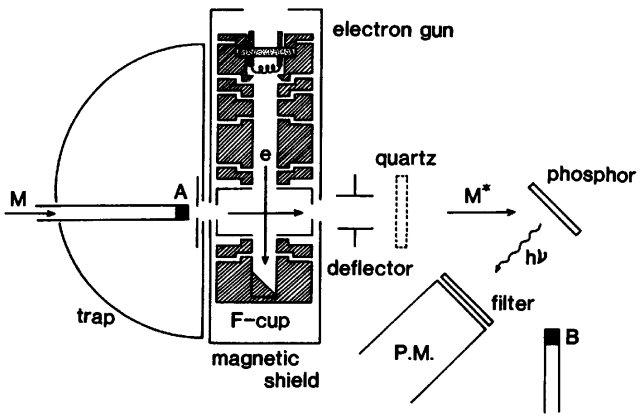

Fig. 1. A schematic diagram of the apparatus. A and B are multichannel slits for introducing benzene (M) and phosphor molecules, respectively, into the chamber. The emission from the phosphor surface is detected by a photomultiplier tube, PM. A quartz window is placed on the beam path when the contribution of stray light from the excitation region is estimated.

The signals at each impact energy were collected for 200 s, so that statistical errors were reduced to less than 6%. The absolute scale of the impact energy was calibrated by the threshold energy of the $N_2(C—B)$ transition [6].

Results and Discussion

The time-dependence curve of the emission from biacetyl surface is made of one sharp peak at $t\simeq 0$ ms and one broad peak at $t\simeq 0.6$ ms. The sharp peak arises from the photons produced in the excitation region, because (1) the peak appears at a time much shorter than the time of flight of the metastable molecules, and (2) only this peak is observed when no phosphor is deposited on the surface. Almost identical time dependence was obtained when benzophenone was used as a phosphor.

The emission forming the broad peak has maximum intensity at 520 nm for biacetyl and at 440 nm for benzophenone. Each wavelength coincides with that of the intensity maximum in the phosphorescence spectrum of the corresponding phosphor. Furthermore, the time of flight of the metastable benzene molecule agrees approximately with the time corresponding to the maximum intensity of the broad peak. These results indicate that the impinging metastable molecules to the target surface excite the phosphor by the $T—T$ energy transfer, which arises the broad peak, *i.e.*, the phosphorescence.

The shape of the broad peak is reproduced by

†Present address: Department of Chemistry, Faculty of Science, Toho University, Funabashi, Chiba 274.

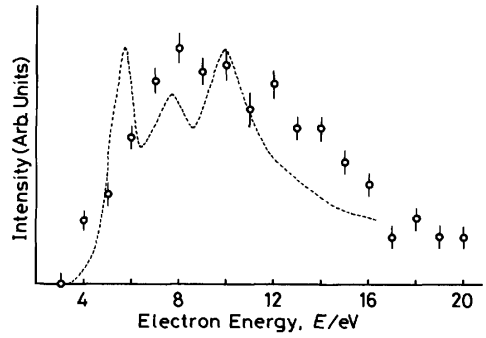

Fig. 2. Intensity of the phosphorescence (open circles) produced by collision of metastable benzene molecules on benzophenone surface (77 K) as a function of electron-impact energy. The broken line is the excitation function measured by Auger electron emission from sodium surface [7]. The ordinate is in arbitrary units.

assuming the velocity distribution of the metastable benzene molecules as

$$N(v) \propto v^4 \exp[-Mv^2/2kT], \quad (1)$$

where v and M are the velocity and the mass of benzene molecule, respectively. In addition, the phosphorescence is assumed to decay exponentially with a lifetime τ. The lifetime thus estimated, 1.0±0.2 ms, is much shorter than that for polycrystalline biacetyl (about 2 ms [2]). By optical excitation of polycrystalline biacetyl the excitation occurs in the bulk so that the measured lifetime corresponds to that of the phosphor molecules in the bulk. In contrast, the lifetime, τ, determined in the present measurement corresponds to that of the phosphor molecules on the surface, because the excitation energy of the T_1 state is transmitted directly to the phosphor surface.

Figure 2 shows the excitation function of the emission obtained by using benzophenone deposited on aluminum at 77 K. The excitation function rises in the vicinity of 3—4 eV, makes a broad maximum at 8—12 eV and falls off. This excitation function agrees qualitatively with that measured by Smyth *et al.* [7] by detecting Auger electron emission from sodium surface. In spite of the limited resolution ($\Delta E \simeq$ 2 eV) of the electron-impact energy in the present measurement, the general shape of the present excitation function provides another support that collision of the metastable benzene molecules is the main origin of the emission from the phosphor surface. A similar excitation function was obtained when biacetyl was used as a phosphor, where the signals were about 25% of those from benzophenone. The less intense signals from biacetyl is probably an indication that the phosphorescence quantum yield from biacetyl is about 25% of that from benzophenone [3,4]. On the basis of the reported cross sections for the formation of metastable benzene and $N_2(A^3\Sigma_u^+)$ molecules [8,9] and a comparison of the measured phosphorescence from metastable benzene molecules with that from the $N_2(A^3\Sigma_u^+)$ molecules, the phosphorescence yield from biacetyl surface is estimated to be on the order of 10^{-3}—10^{-4}. A more detailed study using a supersonic nozzle beam of metastable molecules is in progress [10].

We are indebted to Mr. H. Kume for his assistance in the estimation of the phosphorescence quantum yield. This work was supported by a Grant-in-Aid from the Ministry of Education, Science and Culture.

References

1) H. Ishikawa and W. A. Noyes, Jr., *J. Chem. Phys.*, **37**, 583 (1962).
2) J. C. D. Brand and A. W. H. Mau, *J. Am. Chem. Soc.*, **96**, 4380 (1974).
3) S. P. McGlynn, T. Azumi, and M. Kinoshita, "Molecular Spectroscopy of the Triplet State," Prentice Hall, Englewood Cliffs, N. J., 1969.
4) J. B. Birks, "Photophysics of Aromatic Molecules," Wiley, New York, 1970.
5) J. P. Doering, *J. Chem. Phys.*, **67**, 4065 (1977).
6) T. G. Finn, J. F. M. Aarts, and J. P. Doering, *J. Chem. Phys.*, **56**, 5632 (1972).
7) K. C. Smyth, J. A. Schiavone, and R. S. Freund, *J. Chem. Phys.*, **61**, 4747 (1974).
8) C. I. M. Beenakker, F. J. De Heer, and L. J. Oosterhoff, *Chem. Phys. Lett.*, **28**, 324 (1974).
9) D. C. Cartwright, S. Trajmar, A. Chutjian, and W. Williams, *Phys. Rev.* A, **16**, 1041 (1977).
10) T. Kondow, T. Hirooka, K. Suzuki, T. Nagata, and K. Kuchitsu, "Atomic Collision Research in Japan," Progress Report, **9**, 104 (1983).

Synthesis and Magnetism of Trinuclear Copper(II) Complexes with a Salen-like Schiff Base and a Tertiary Diamine

Makoto HANDA, Hisashi ŌKAWA,* and Sigeo KIDA
Department of Chemistry, Faculty of Science, Kyushu University 33, Hakozaki, Higashiku, Fukuoka 812
(Received November 28, 1984)

Synopsis. Trinuclear Copper(II) complexes [{Cu(sb)}$_2$Cu(da)](ClO$_4$)$_2$ have been synthesized by the use of a copper(II) complex with a salen analog ([Cu(sb)]) and a diamine (da) such as bpy or phen. Cryomagnetic investigations revealed the operation of an antiferromagnetic spin-exchange interaction ($-J$=26—78 cm^{-1}) between the adjacent copper ions.

Binuclear copper(II) complexes of the type [Cu(sb)CuX$_2$] (H$_2$sb denotes salen-like Schiff bases; H$_2$salen=*N*,*N*′-di-salicylideneethylenediamine) have been synthesized and magnetically studied by Gruber *et al.*[1] Recently Patel and Bhattacharya[2] have reported the synthesis of binuclear copper(II) complexes of the type [Cu(sb)Cu(da)](ClO$_4$)$_2$ by the use of a diamine (da) such as 2,2′-bipyridyl (bpy) or 1,10-phenanthroline (phen). According to them, the magnetic moments of the complexes at room temperature fall in the range 0.83—1.19 BM†, which are considerably lower than the moments of [Cu(sb)CuX$_2$].[1] The configuration around the copper coordinated by [Cu(sb)] and da must be much distorted to tetrahedron because of a steric hinderance between these ligands.[1] Since antiferromagnetic spin-exchange interaction generally becomes weaker when the >Cu<$\overset{O}{\underset{O}{}}$>Cu< configuration is distorted from a coplane,[3] such low magnetic moments (which suggest a fairly strong antiferromagnetic spin-exchange interaction) observed for [Cu(sb)Cu(da)](ClO$_4$)$_2$ seem quite unusual. In this study we have reinvestigated the synthesis of the complexes by the use of [Cu(salen)], *N*,*N*′-disalicylidene-1,2-propanediaminatocopper(II) ([Cu(salpn)]), or *N*,*N*′-bis(5-methylsalicylidene)ethylene-diaminatocopper(II) ([Cu(5-Mesalen)]) as [Cu(sb)] and bpy or phen as da. Contrary to the Patel and Bhattacharya's result,[2] we have obtained the complexes of the type [{Cu(sb)}$_2$Cu(da)](ClO$_4$)$_2$. The characterization and the magnetism of the complexes have been reported in this paper.

Experimental

Syntheses. The synthesis of the complexes was carried out in nearly the same way as that of the literature.[2] However, the products obtained by the method often contaminated with some impurities. It was found in this study that the same complexes were obtained without the contamination of impurities when [Cu(sb)], [Cu(H$_2$O)$_6$](ClO$_4$)$_2$, and da were reacted in the 2:1:1 mole ratio.

Magnetic Measurements. Magnetic susceptibilities were measured by the Faraday method in the temperature range 80—300 K. The apparatus was calibrated by the use of [Ni(en)$_3$]S$_2$O$_3$.[4]

Results and Discussion

The elemental analyses were invariably consistent with the formulation of [{Cu(sb)}$_2$Cu(da)](ClO$_4$)$_2$ (see Table 1). No complexes of the stoichiometry [Cu(sb)Cu(da)](ClO$_4$)$_2$ as reported in the literature[2] were obtained in spite of our all efforts. We believe that [{Cu(sb)}$_2$Cu(da)](ClO$_4$)$_2$ is the most stable among possible oligonuclear complexes when [Cu(sb)] and da are utilized as the ligands. It is to be noted that tetranuclear complexes [Cu(sb)Cu(ta)]$_2$(ClO$_4$)$_4$ are obtainable when a triamine (ta) is utilized instead of a diamine.[5]

The sketetal band near 1525 cm^{-1} of [Cu(sb)] shifted to 1540 cm^{-1} in [{Cu(sb)}$_2$Cu(da)](ClO$_4$)$_2$, suggesting that the phenolic oxygens are acting as the bridges in the present complexes.[6] Magnetic moments (per copper atom) at room temperature are lower than the spin-only value, implying an operation of antiferromagnetic spin-exchange interaction. The plausible structure is supposed to be trinuclear as shown in Fig. 1, since such a structure has been demonstrated for [{Cu(sb)}$_2$M(H$_2$O)$_2$](ClO$_4$)$_2$.[7]

TABLE 1. ELEMENTAL ANALYSES, MAGNETIC MOMENTS AT ROOM TEMPERATURE, AND MAGNETIC PARAMETERS OF COMPLEXES

	Found/% (Calcd/%)				g	J/cm^{-1}	μ_{eff}/BM (T/K)
	C	H	N	Cu			
[{Cu(salen)}$_2$Cu(bpy)](ClO$_4$)$_2$·H$_2$O	46.03 (46.01)	3.32 (3.49)	7.90 (7.67)	17.1 (17.4)	2.07	−30	1.70(297.6)
[{Cu(salen)}$_2$Cu(phen)](ClO$_4$)$_2$·H$_2$O	47.09 (47.17)	3.49 (3.42)	7.29 (7.50)	16.7 (17.0)	2.05	−70	1.55(297.8)
[{Cu(salpn)}$_2$Cu(bpy)](ClO$_4$)$_2$·H$_2$O	47.10 (47.00)	3.69 (3.76)	7.43 (7.47)	17.0 (17.0)	2.09	−32	1.72(297.8)
[{Cu(salpn)}$_2$Cu(phen)](ClO$_4$)$_2$·H$_2$O	48.26 (48.11)	3.56 (3.69)	7.36 (7.32)	17.0 (16.6)	2.05	−78	1.60(297.6)
[{Cu(5-Mesalen)}$_2$Cu(bpy)](ClO$_4$)$_2$	48.46 (48.70)	4.06 (3.91)	7.28 (7.41)	16.6 (16.8)	2.09	−66	1.68(297.8)
[{Cu(5-Mesalen)}$_2$Cu(phen)](ClO$_4$)$_2$	49.57 (49.77)	4.09 (3.83)	7.01 (7.25)	16.5 (16.6)	2.09	−26	1.74(297.6)

† 1BM=9.274078(36)×10^{-24} Am^2.

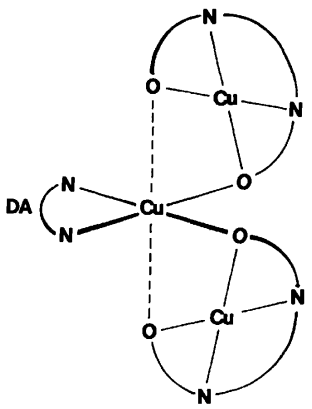

Fig. 1. Schematic representation of trinuclear structure for $[\{Cu(sb)\}_2Cu(da)]^{2+}$.

The magnetic susceptibilities of the complexes were examined in the temperature range 80—300 K. Based on the spin Hamiltonian, $\mathcal{H}=-2J(\hat{S}_1\cdot\hat{S}_2+\hat{S}_2\cdot\hat{S}_3)$, the susceptibility equation for the linear trinuclear system is given by

$$\chi_A=\frac{Ng^2\beta^2}{12kT}\times\frac{\exp(2J/kT)+10\exp(3J/kT)+1}{\exp(2J/kT)+2\exp(3J/kT)+1}+N\alpha,$$

where J is the exchange integral between the adjacent copper ions and other symbols have their conventional meanings. As exemplified in Fig. 2, the magnetisms of the complexes can be well explained with this equation. The magnetic parameters determined by the best-fit technique are given in Table 1, together with the moments at room temperature. Thus, the magnetical investigations clearly demonstrate the trinuclear structure for the present complexes.

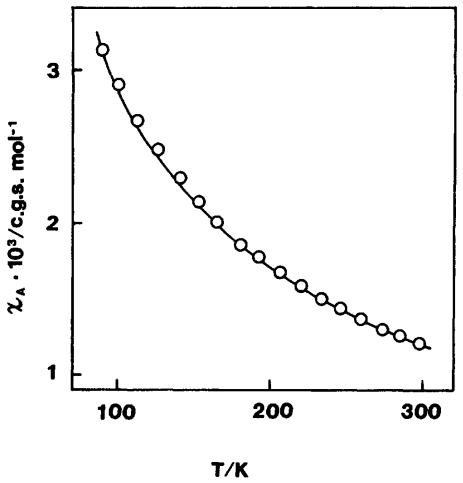

Fig. 2. Temperature variation of magnetic susceptibility of $[\{Cu(salen)\}_2Cu(bpy)](ClO_4)_2\cdot H_2O$. Solid curve is drawn on the basis of the expression in the text using the parameters, $J=-30\,cm^{-1}$, g=2.07, and $N\alpha=0$.

References

1) S. J. Gruber, C. M. Harris, and E. Sinn, *Inorg. Chem.*, **7**, 268 (1968).
2) K. V. Patel and P. K. Bhattacharya, *J. Chem. Soc., Dalton Trans.*, **1982**, 359.
3) R. M. Countrymann, W. T. Robinson, and E. Sinn, *Inorg. Chem.*, **13**, 2013 (1974).
4) N. F. Curtis, *J. Chem. Soc.*, **1961**, 3147.
5) M. Handa, A. Honda, Z. J. Zhong, H. Ōkawa, and S. Kida, *Inorg. Chim. Acta*, in press.
6) C. M. Harris and E. Sinn, *J. Inorg. Nucl. Chem.*, **30**, 2723 (1968).
7) J. M. Epstein, B. N. Figgis, A. H. White, and A. G. Willis, *J. Chem. Soc., Dalton Trans.*, **1974**, 1954.

A Fairly Effective Environment Substance $[Co(sep)]^{3+}$ Ion in the Pfeiffer Effect of Some Oxalato Complexes of Chromium(III)

Katsuhiko MIYOSHI, Yukio SAKAMOTO, Yoshihisa TODA, and Hayami YONEDA*

Department of Chemistry, Faculty of Science, Hiroshima University, Higashi-senda-machi, Naka-ku, Hiroshima 730

(Received December 27, 1984)

Synopsis. A chiral complex ion $[Co(sep)]^{3+}$ (sep= 1,3,6,8,10,13,16,19-octaazabicyclo[6.6.6]eicosane) was found to displace the chiral equilibrium between Δ and Λ enantiomers greatly for moderately optically labile metal complexes $[Cr(ox)_2(acac)]^{2-}$ and $[Cr(ox)_2(gly)]^{2-}$ in dioxane-water mixtures.

When an optically labile and racemic complex is mixed with a certain chiral compound (called an environment substance hereafter) in solution, new optical activity due to the initially racemic complex is sometimes induced. This phenomenon is referred to as the Pfeiffer effect,[1] and has been ascribed to a shift in a chiral equilibrium between two enantiomers of the racemic complex. Several organic compounds have been so far reported to induce the equilibrium shift. Nordquist[2] was probably the first to study the Pfeiffer effect in which a dissymmetric metal complex, *e.g.*, resolved $[Co(en)_3]^{3+}$(en=ethylenediamine), was used as an environment substance. Pollock *et al.*[3] have also examined this complex as an environment substance to $[Ni(acac)_3]^-$ (acac=acetylacetonate ion) in water. However, the above two studies did not afford direct evidence that the chiral equilibrium was actually displaced by chiral $[Co(en)_3]^{3+}$ ion.[4a] Subsequently, Yoneda and coworkers[4,5] unambiguously demonstrated that one enantiomer of $[Cr(ox)_3]^{3-}$ (ox=oxalate dianion) was enriched at a rate comparable to its racemization rate in the presence of resolved *cis*-$[Co(X)(Y)(en)_2]^{n+}$-type complexes (X and/or Y=anionic unidentate ligand) as well as $[Co(phen)_3]^{3+}$ (phen= 1,10-phenanthroline). The enantiomeric excess (ee) attained with these chiral complexes, however, amounts to only a few per cent, despite the expectation that these cationic complexes associate with $[Cr(ox)_3]^{3-}$ more strongly than do usual organic environment substances such as *d*-cinchoninium ion. We report herein that an optically active cation complex $[Co(sep)]^{3+}$ (sep=1,3,6,8,10,13,16,19-octaazabicyclo[6.6.6]eicosane) derived from resolved $[Co(en)_3]^{3+}$ serves as a fairly effective environment substance to some oxalato complexes of Cr(III) in dioxane-water mixtures.

Experimental

Preparation of Complexes. Perchlorate salts of Λ-$[Co(en)_3]^{3+}$, Λ-$[Co(d\text{-pn})_3]^{3+}$ (*d*-pn=(S)-propylenediamine), and Λ-$[Co(sep)]^{3+}$ employed as an environment substance were available from our previous works.[6] Λ-$[Co(phen)_3]^{3+}$ was obtained as a chloride salt as before.[4a] Racemic complexes $K_2[Cr(ox)_2(acac)]$ and $K_2[Cr(ox)_2(gly)]$ (gly=glycinate anion) were prepared as described in the literature,[7,8] and their purity was checked by ion-exchange chromatography and/or their absorption spectra. They were resolved by the methods applied to the corresponding Co(III) complexes.[9,10] The $\Delta\varepsilon$ values of -3.40 mol^{-1} dm^3 cm^{-1} (at 545 nm) and $+1.23$ mol^{-1} dm^3 cm^{-1} (at 533 nm) were obtained for Δ-$[Cr(ox)_2(acac)]^{2-}$ and Λ-$[Cr(ox)_2(gly)]^{2-}$, respectively. Since these complexes were moderately optically labile, their recrystallization did not lead to improved optical purity, and hence no further attempt was made to obtain correct $\Delta\varepsilon$ values. The correct $\Delta\varepsilon$ value for the gly complex must be much higher than was obtained above. Absolute configurations were assigned to these complexes on the criterion that the Λ enantiomers have a positive main CD component at the first d-d transition region.[11]

Detection of the Pfeiffer Effect. The degree and direction of the equilibrium shift attained in the racemic Cr(III) complexes were determined in exactly the same manner as in the previous studies.[4a,12] Sample solutions were prepared in volumetric flasks (10 cm^3) to which 3 cm^3 of dioxane had been added, so that they contained the racemic Cr(III) complex in 8 mmol dm^{-3} and the chiral environment substance in 30 mmol dm^{-3}. CD spectra of these solutions were recorded as quickly as possible after the environment substance was removed by passing them through a cation-exchange column.

Results and Dicussion

Figure 1 shows the CD spectra recorded for initially racemic complexes $[Cr(ox)_2(acac)]^{2-}$ and $[Cr(ox)_2(gly)]^{2-}$ after they had been mixed with Λ-$[Co(sep)]^{3+}$ in dioxane-water mixtures. These spectra are the same in pattern as those of the respective complexes resolved separately. Thus, it is evident that the Δ enantiomer is enriched for both complexes in the presence of Λ-$[Co(sep)]^{3+}$. If the $\Delta\varepsilon$ of -3.40 mol^{-1} dm^3 cm^{-1} at 545 nm is adopted for the pure Δ-$[Cr(ox)_2(acac)]^{2-}$, the ee is estimated to be 10.9%, which is fairly high. A high ee is probably attained for the gly complex also, though a correct CD intensity for its pure enantiomer is not known. On the other hand, when Λ-$[Co(en)_3]^{3+}$ from which Λ-$[Co(sep)]^{3+}$ is derived is employed as an environment substance, the Δ enantiomer is similarly enriched for both complexes,[13] but the ee's are very low; an ee of 0.4% is estimated for the acac complex.

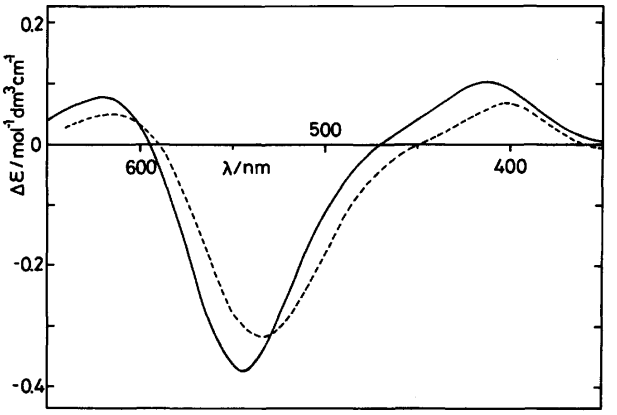

Fig. 1. CD spectra induced for $[Cr(ox)_2(acac)]^{2-}$ (solid curve) and $[Cr(ox)_2(gly)]^{2-}$ (dotted curve) with Λ-$[Co(sep)]^{3+}$ as an environment substance.

TABLE 1. ABSOLUTE CONFIGURATIONS OF ENANTIOMERS ENRICHED BY THE PFEIFFER EFFECT

Environment[a] Substance	Racemic Complex $[Cr(ox)_2(acac)]^{2-}$	$[Cr(ox)_2(gly)]^{2-}$
$[Co(sep)]^{3+}$	Δ	Δ
$[Co(en)_3]^{3+}$	Δ	Δ
$[Co(d\text{-pn})_3]^{3+}$[b]	Λ	Λ
$[Co(phen)_3]^{3+}$	Λ	Λ

a) All have a Λ configuration. b) A mixture of *fac-lel*$_3$ and *mer-lel*$_3$ isomers.

Since the ee's attained with Λ-$[Co(d\text{-pn})_3]^{3+}$ and Λ-$[Co(phen)_3]^{3+}$ were also low (at most 1.4%), only the direction of the equilibrium shift was determined. In Table 1 are listed absolute configurations of the enantiomers of the two Cr(III) complexes enriched by the Pfeiffer effect. Table 1 indicates that Λ-$[Co(en)_3]^{3+}$ and Λ-$[Co(sep)]^{3+}$ interact with the Δ enantiomer more favorably than with the Λ enantiomer for the two Cr(III) complexes. This is consistent with the earlier observation that the Δ enantiomers of $[Co(ox)_2(acac)]^{2-}$ and $[Co(ox)_2(gly)]^{2-}$ are eluted faster on usual ion-exchange chromatography with Λ-$[Co(en)_3]^{3+}$ or Λ-$[Co(sep)]^{3+}$ as an eluent.[14,15] On the other hand, the Λ enantiomers of the two Cr(III) complexes are favored by Λ-$[Co(d\text{-pn})_3]^{3+}$ and Λ-$[Co(phen)_3]^{3+}$ (Table 1), suggesting that the mode of chiral discrimination is different at least between the former two environment substances and the latter two.

In our previous work,[14] it was proposed that both chiral $[Co(en)_3]^{3+}$ and $[Co(sep)]^{3+}$ ions discriminate between Λ and Δ enantiomers of a usual complex anion with the C_2 axis directed to the anion to form hydrogen bonds to the anion (C_2 access). If the Δ anion is favored by Λ-$[Co(en)_3]^{3+}$ or Λ-$[Co(sep)]^{3+}$ in the C_2 access, it is a reasonable observation that the Λ anion is favored by Λ-$[Co(d\text{-pn})_3]^{3+}$ which "uses" the C_3 axis predominantly owing to the steric hindrance due to methyl groups.[16] The interaction mode of $[Co(phen)_3]^{3+}$ seems complicated,[17] since it has no hydrogen atom available for the interaction with the anion complex.[18]

Finally, it is noteworthy that the efficiency of chiral discrimination is surprisingly enhanced when the environment substance $[Co(en)_3]^{3+}$ is capped covalently with alkyl groups along its C_3 axis to form $[Co(sep)]^{3+}$. This may be partly attributed to the resulting conformational rigidity of the environment substance[19] and/or to a greater affinity of the anion complex for $[Co(sep)]^{3+}$ than for $[Co(en)_3]^{3+}$, as exemplified by their association constants with *d*-tartrate and bis(μ-*d*-tartrato)-diantimonate(III) anions in water.[6] However, it is more tempting to suppose that chiral $[Co(en)_3]^{3+}$ can also "use" the C_3 axis to favor the enantiomer opposite to that favored by it in the C_2 access, its discrimination efficiency being thereby extremely low. By contrast, since $[Co(sep)]^{3+}$ is forced to "use" the C_2 axis only, it serves not only as an effective environment substance in the Pfeiffer effect, but also as an effective eluent in the chromatographic resolution of several anion complexes.[20]

References

1) For recent reviews, see, S. Kirschner, N. Ahmad, C. Munir, and R. J. Pollock, *Pure Appl. Chem.*, **51**, 913 (1979); S. Kirschner and I. Bakker, *Coord. Chem. Rev.*, **43**, 325 (1982).

2) P. E. R. Nordquist, Ph. D. Thesis, University of Minnesota, 1964.

3) R. J. Pollock, S. Kirschner, and S. Policec, *Inorg. Chem.*, **16**, 522 (1977).

4) a) K. Miyoshi, Y. Wada, and H. Yoneda, *Inorg. Chem.*, **17**, 751 (1978); b) *idem, Chem. Lett.*, **1977**, 319.

5) K. Miyoshi, Y. Matsumoto, and H. Yoneda, *Inorg. Chem.*, **20**, 1057 (1981).

6) U. Sakaguchi, A. Tsuge, and H. Yoneda, *Inorg. Chem.*, **22**, 1630, 3745 (1983).

7) W. T. M. Andriessen and M. P. Groenewege, *Inorg. Chem.*, **15**, 621 (1976).

8) T. W. Kallen and R. E. Hamm, *Inorg. Chem.*, **16**, 1147 (1977).

9) F. P. Dwyer, I. K. Reid, and A. M. Sargeson, *Aust. J. Chem.*, **18**, 1919 (1965).

10) K. Yamasaki, J. Hidaka, and Y. Shimura, *Bull. Chem. Soc. Jpn.*, **42**, 119 (1969).

11) This assignment is followed by the conclusion that Δ-$[Ni(phen)_3]^{2+}$ forms a less-soluble diastereomer with the Δ enantiomer of both $[Cr(ox)_2(acac)]^{2-}$ and $[Co(ox)_2(acac)]^{2-}$, and Λ-$[Co(ox)_2(en)]^{+}$ does with the Λ enantiomer of both $[Cr(ox)_2(gly)]^{2-}$ and $[Co(ox)_2(gly)]^{2-}$.

12) K. Miyoshi, K. Watanabe, Y. Toda, and H. Yoneda, *Bull. Chem. Soc. Jpn.*, **56**, 3845 (1983).

13) It has been recently demonstrated that the Δ enantiomer is enriched for tris(2,6-pyridinedicarboxylato)terbium(III) in the presence of Λ-$[Cr(en)_3]^{3+}$ in dioxane–water mixtures; see, J. S. Madaras and H. G. Brittain, *Inorg. Chem.*, **19**, 3841 (1980); F. Yan, R. A. Copeland, and H. G. Brittain, *Inorg. Chem.*, **21**, 1180 (1982).

14) U. Sakaguchi, I. Yamamoto, S. Izumoto, and H. Yoneda, *Bull. Chem. Soc. Jpn.*, **56**, 153 (1983).

15) A. Tatehata, M. Iiyoshi, and K. Kotsuji, *J. Am. Chem. Soc.*, **103**, 7391 (1981); A. Tatehata, Y. Ejima, and K. Kotsuji, 29th Symposium on Coordination Chemistry, Hamamatsu, October, 1979, Abstr. No. 1B01.

16) In accord with this observation, Λ-$[Co(ox)_2(gly)]^{2-}$ is eluted faster on ion-exchange chromatography when the chiral eluent used is Λ-$[Co(d\text{-chxn})_3]^{3+}$ (*d*-chxn=(1*S*,2*S*)-cyclohexanediamine) which "uses" the C_3 axis exclusively owing to the presence of cyclohexane rings; see Ref. 14.

17) Λ-$[Cr(ox)_3]^{3-}$ and Λ-$[Co(ox)_3]^{3-}$ are similarly enriched in the presence of Λ-$[Co(phen)_3]^{3+}$; see Ref. 4a.

18) A. Tatehata, K. Andoh, M. Fujita, and Y. Asaba, 33rd Symposium on Coordination Chemistry, Osaka, October, 1983, Abstr. No. 1PA13.

19) It is informative to note that all the racemic complexes for which the equilibrium shifts have been confirmed are with no exception composed of planar ligands such as ox^{2-}, gly^{-}, $acac^{-}$, phen, 2,2′-bipyridine, 8-hydroxy-5-quinolinesulfonate^{2-}, and 2,6-pyridinedicarboxylate^{2-}. The ligand rigidity might be a necessary condition for the development of the Pfeiffer effect.

20) Y. Sakamoto, Y. Toda, K. Miyoshi, and H. Yoneda, 34th Symposium on Coordination Chemistry, Nagaoka, October, 1984, Abstr. No. 3C13.

The Crystal Structures of a Dicopper(II) Complex Containing Two N_4-Macrocyclic Rings Connected with an Ethylene Chain

Masahiro MIKURIYA, Kosuke HAMADA, Sigeo KIDA,* and Ichiro MURASE†

Department of Chemistry, Faculty of Science, Kyushu University 33, Hakozaki, Higashi-ku, Fukuoka 812

†*Laboratory of Chemistry, College of General Education, Kyushu University 01, Ropponmatsu, Chuo-ku, Fukuoka 810*

(Received January 17, 1985)

Synopsis. The crystal structure of diaqua {7,7′-ethylenebis[2,12-dimethyl-3,7,11,17-tetraazabicyclo[11.3.1]-heptadeca-1(17),2,11,13,15-pentaene]}dicopper(II) perchlorate dihydrate was determined by a single-crystal X-ray diffraction method. The complex assumes an extended conformation with the intramolecular Cu···Cu separation 7.081(2) or 6.985(2) Å.

Recently, Murase *et al.* reported the synthesis and characterization of a binuclear copper(II) complex with bis(macrocycle), $Cu_2(dap)(ClO_4)_4$ (dap=7,7′-ethylenebis[2,12-dimethyl-3,7,11,17-tetraazabicyclo[11.3.1]-heptadeca-1(17),2,11,13,15-pentaene]), as shown in Fig. 1.[1] Molecular models showed many structural possibilities between two extremes of open(extended) conformation and closed(bent) conformation. The ESR spectra in DMF frozen solution suggested that the two copper(II) ions are located in a proximity and the two coordination planes are of a face-to-face or half-opened clam shell structure. The present X-ray study was undertaken to reveal the structure of this complex in crystal.

Experimental

The $Cu_2(dap)(ClO_4)_4$ complex was prepared by the method previously reported.[1] Crystals suitable for an X-ray study were obtained from a dilute aqueous solution after standing one year. The unit-cell parameters and intensities were measured on a Rigaku AFC-5 automated four-circle diffractometer with graphite-monochromated Mo$K\alpha$ radiation (λ=0.71069 Å) at 21±1 °C.

Crystal Data: $Cu_2(C_{32}H_{46}N_8)(ClO_4)_4\cdot 4H_2O$, FW=1139.72; triclinic; $P\bar{1}$; a=14.894(2), b=15.144(2), c=10.734(1) Å; α=91.04(1), β=108.80(1), γ=87.22(1)°; D_m=1.64, D_c=1.65 g cm^{-3}; Z=2; μ(Mo$K\alpha$)=12.4 cm^{-1}, crystal dimensions: 0.23×0.28×0.50 mm^3.

The intensity data were collected by the 2θ—ω scan technique with a scan rate of 2° min^{-1}. A total of 15954 reflections with $2\theta<62°$ were collected. The intensity data were corrected for the Lorentz and the polarization effects, but not for absorption. Independent 6564 reflections with $|F_o|>3\sigma(|F_o|)$ were considered as "observed" and were used for the structure analysis. The structure was solved by the direct methods and refined by the block-diagonal least-squares method. In the course of refinement, it became apparent that the oxygen atom of the perchlorate ion, O(4A), is subjected to disorder. The oxygen atom was divided between two positions with an occupancy factor 0.5 on the basis of a difference Fourier map. Hydrogen atoms were inserted in their calculated positions and included in the refinement. In the least-squares refinement the weighting scheme, $w=(8.82+|F_o|+0.0086|F_o|^2)^{-1}$ was employed. The final discrepancy factors were $R_1=\sum||F_o|-|F_c||/\sum|F_o|=0.081$ and $R_2=[\sum w(|F_o|-|F_c|)^2/\sum w|F_o|^2]^{1/2}=0.123$.

The atomic scattering factors and the anomalous dispersion corrections were taken from the International Tables for X-Ray Crystallography.[2] All the calculations were carried out on the FACOM M-200 computer at the Computer Center of Kyushu University by the use of a local version of the UNICS-III programs.[3] The final positional and thermal parameter with their estimated standard deviations are given in Table 1. The atomic coordinates, the thermal parameters and the F_o-F_c tables have been deposited as a Document No. 8531 at the Office of the Editor.

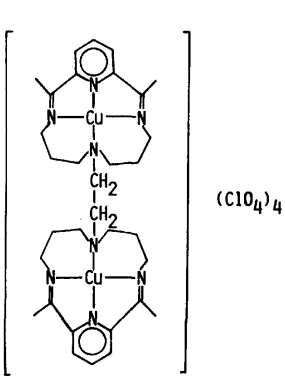

Fig. 1. Chemical structure of $Cu_2(dap)(ClO_4)_4$.

Results and Discussion

The crystal contains two crystallographically inde-

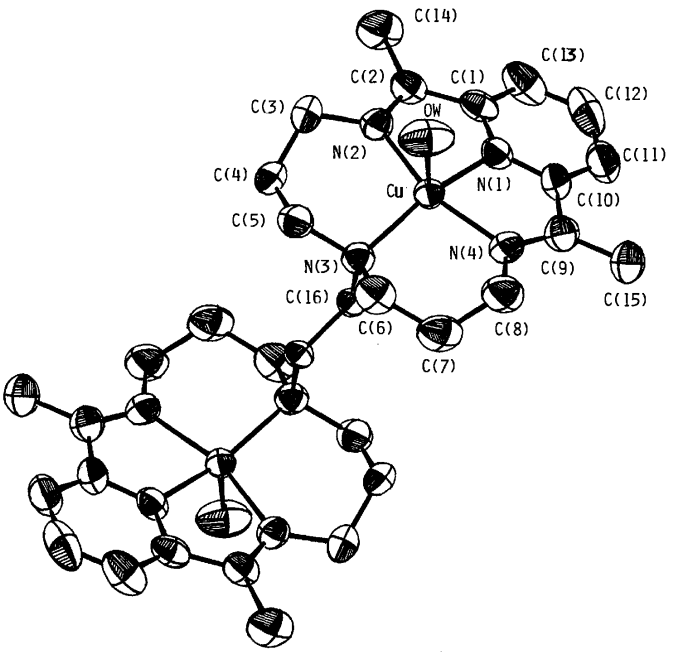

Fig. 2. Molecular structure of $[(Cu_2(dap)(H_2O)_2]^{4+}$ with thermal ellipsoids. Distances (l/Å): Cu-N(1) 1.915(6), 1.904(7); Cu-N(2) 2.013(6), 2.023(10); Cu-N(3) 2.010(7), 1.988(6); Cu-N(4) 2.003(8), 2.001(7); Cu-OW 2.255(8), 2.237(8). Angles (ϕ/°): N(1)-Cu-N(2) 79.7(3), 80.3(4); N(1)-Cu-N(4) 80.2(3), 79.7(3); N(2)-Cu-N(3) 100.4(3), 99.1(3); N(3)-Cu-N(4) 98.1(3), 99.0(3) for molecules A and B, respectively.

pendent binuclear molecules; they are denoted by A and B. Their structures are essentially the same. Both molecules are centrosymmetric about the mid-point of the central ethylene group connecting the two macrocyclic rings. The molecular structure is shown in Fig. 2. The coordination geometry of each copper atom is a distorted square pyramid. Each basal plane is formed by four nitrogen atoms, which are coordinated to Cu with Cu–N bond lengths, 1.904—2.023 Å, of the macrocyclic ring. The fifth coordination site is occupied by a water oxygen atom with Cu–O distance of 2.255(8) or 2.237(8) Å. The basal atoms around each copper atom deviate from the mean plane within ±0.2 Å and Cu(A) and Cu(B) are displaced by 0.23 Å and 0.24 Å, respectively, from the basal-mean planes toward water molecules.

The structures of the macrocyclic moieties are similar to that of the analogous mononuclear copper(II) complex, $Cu(CR)Cl(NO_3)\cdot 2H_2O$ (CR=2,7,12-trimethyl-3,7,11,17-tetraazabicyclo[11.3.1]heptadeca-1(17),2,11,-13,15-pentaene).[4]

Both binuclear molecules assume an extended conformation and the intramolecular Cu···Cu distances are 7.081(2) Å and 6.985(2) Å for molecules A and B, respectively. The shortest intermolecular Cu···Cu distance is 8.059(2) Å (Cu(A)···Cu(B)($x, y-1, z$)). The water molecules (two per complex molecule) are trapped in the space of the crystal lattice. The perchlorate ions are hydrogen bonded with the coordinated or crystal water molecules.

This structure dose not accord with that presumed from the ESR spectra. But, this is not surprising, because in solution, free rotation about the central ethylene group is possible and may give rise to the closed conformation allowing the two copper atoms to array close to each other.

References

1) I. Murase, K. Hamada, and S. Kida, *Inorg. Chim. Acta*, **54**, L171 (1981); I. Murase, K. Hamada, S. Ueno, and S. Kida, *Synth. React. Inorg. Met. Org. Chem.*, **13**, 191 (1983).

2) "International Tables for X-Ray Crystallography," Kynoch Press, Birmingham (1974), Vol. IV.

3) S. Kawano, *Rep. Comp. Cent. Kyushu Univ.*, **16**, 113 (1983); T. Sakurai and K. Kobayashi, *Rep. Inst. Phy. Chem. Res.*, **55**, 69 (1979).

4) M. R. Caira, L. R. Nassimbeni, and P. R. Woolley, *Acta Crystallogr., Sect., B*, **31**, 1334 (1975).

Behavior of Trifluoroacetohydrazonoyl Bromide in Basic Media

Kiyoshi TANAKA,* Seiji MAENO, and Keiryo MITSUHASHI
Department of Industrial Chemistry, Seikei University, Musashino-shi, Tokyo 180
(Received September 11, 1984)

Synopsis. The bromide **1** was treated with sodium methoxide or phenoxide to give exclusively the corresponding substituted product. The predominant formation of the substituted products was also recognized with regard to various amines. However, the reaction with triethylamine proceeded more complicatedly to give the products *via* reduction process together with a trace amount of the dimer of *N*-phenyl-*C*-(trifluoromethyl)nitrilimine.

It is well known that hydrazonoyl halides, when treated with a base such as triethylamine or alkoxide, are converted into the corresponding nitrilimines which, in the absence of a reactive dipolarophile, result in the head-to-tail dimerizations to the corresponding tetrazines.[1] And only when treated with soft nucleophiles such as thiolates, hydrazonoyl halides are known to undergo the substitutions.[2-4] As a part of studies on the fluorinated nitrilimines,[5,6] we now wish to report the behavior of *N*-phenyltrifluoroacetohydrazonoyl bromide (**1**) toward bases such as alkoxides and amines.[7]

The bromide **1** was treated with sodium methoxide or phenoxide in methanol to give the corresponding substituted product **3** or **4** in 64 or 36% yield, respectively (Scheme 1). The reaction with sodium methoxide was next carried out in the presence of excess methyl acrylate to give a 56% yield of the 1,3-dipolar cycloadduct, 5-methoxycarbonyl-1-phenyl-3-trifluoromethyl-2-pyrazoline (**5**), as well as a 38% yield of **3**. These results indicate that the nitrilimine **2** is generated on treatment of **1** with sodium methoxide. Therefore, the substituted product **3** is thought to be formed entirely or partially *via* **2**. In this case, the usually observed dimerization of **2** was not detected at all.

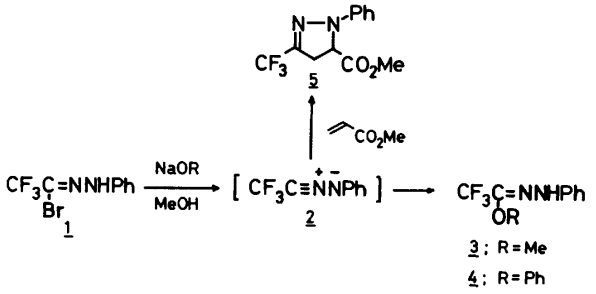

Scheme 1.

The predominant formation of the substituted products was also recognized with regard to amines. Aniline or diethylamine was allowed to react with **1** to afford *N*-phenyl- or *N,N*-diethyltrifluoroacetamide phenylhydrazone (**6** or **7**) in 49 or 89% yield, respectively. Similarly, the reaction with *N*-methylpyrrolidine proceeded smoothly to give the pyrrolidinium salt **8** in 79% yield. The IR spectrum of **8** shows the band at 1614 cm^{-1} due to the C=N group, no absorption owing to the ammonium salt (–$\overset{|}{N}H^+$) being observed.[8] The salt is relatively unstable and gradually decomposes on storing for several weeks.

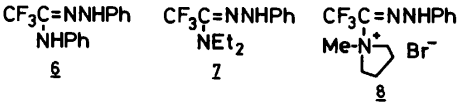

On the other hand, the reaction with triethylamine was found to be more complicated to give trifluoroacetaldehyde phenylhydrazone (**9**) (16%), 1-phenyl-3-(trifluoromethyl)pyrazole (**10**) (16%), and the acetamide **7** (7%) together with a trace amount of 1,4-diphenyl-3,6-bis(trifluoromethyl)-1,4-dihydro-1,2,4,5-tetrazine (**11**) (Scheme 2). The products **7**, **9**, and **10** were identified by

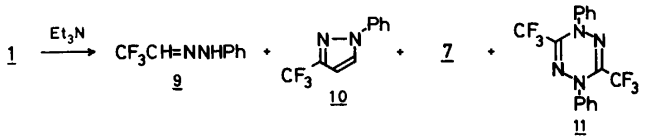

Scheme 2.

comparing their physical and spectral data with those of the authentic samples. Regarding the structure of **11**, the MS spectrum and elemental analysis indicate the dimer of **2** and the UV spectrum (λ_{max} 267 nm, log ε=4.23; 275 nm(sh), log ε=4.22) supports the 1,2,4,5-tetrazine ring.[9] The formation of **7**, **9**, and **10** is quite curious. However, a similar reduction is reported by Knunyants and his co-workers in the reaction of trifluoroacetyl chloride with triethylamine which affords trifluoroacetaldehyde and 4-diethylamino-1,1,1-trifluoro-3-buten-2-one derived from once formed *N,N*-diethylvinylamine.[10] The products **7**, **9**, and **10** may be formed through a similar reduction. That is, **1** is reduced with triethylamine to give **9** and *N,N*-diethylvinylamine. *N,N*-Diethylvinylamine is trapped with **2** to produce the unstable 5-diethylamino-1-phenyl-3-trifluoromethyl-2-pyrazoline which undergoes breakdown to **10** and diethylamine.[11] Diethylamine thus formed reacts with **1** to give **7**, as shown above.

In summary, it is found that the nucleophilic substitution of the bromide **1** is predominant over the dimerization of the nitrilimine **2** *in situ* formed. It should be also noted that the nitrilimine **2** dimerizing with great difficulty is in sharp contrast to the nitrilimine **12** with a similar electron-withdrawing group such as benzoyl[12] or ethoxycarbonyl group[9] which easily dimerize to the corresponding tetrazines.

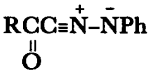

12

Experimental

The IR spectra were recorded on a JASCO IRA-1 spec-

trometer and ^{1}H NMR spectra were measured with a JEOL JNM-PMX 60 spectrometer using tetramethylsilane as an internal standard, the chemical shifts being given in δ ppm downfield. The MS spectra were obtained on a Finnigan 4023 GC-MS DS spectrometer. The UV spectra were observed with a Hitachi 340 spectrometer. The bromide **1** was prepared by the method reported in our previous papers.[5,7]

Reaction of 1 with Sodium Methoxide. A solution of 1.00 g (3.7 mmol) of **1** in 10 cm^3 of methanol was added dropwise to a solution of 0.61 g (11.3 mmol) of sodium methoxide in 20 cm^3 of methanol. After stirring at room temperature for 0.5 h, the solvent was removed. To the residue was added 100 cm^3 of ethyl ether and the mixture was washed with water and brine, dried over magnesium sulfate, and evaporated to leave crude **3** which was purified by distillation to give 0.52g (64%) of pure **3**, bp 80°C/2mmHg (1mmHg=133.322 Pa), ^{1}H NMR (CCl_4) δ=3.96 (q, J=2 Hz, 3H), 6.6—7.4 (m, 5H), and 7.6 (br.s, 1H), IR (neat) 1643 (C=N) and 1115 cm^{-1} (CF_3).

Found: C, 49.37; H, 3.98; N, 12.75%. Calcd for $C_9H_9F_3N_2O$: C, 49.55; H, 4.16; N, 12.84%.

In a similar manner, the reaction of **1** (1.00 g) with sodium phenoxide (1.30 g, 11.2 mmol) in methanol (30 cm^3) was carried out to give a mixture of **4** and **3**. The mixture was submitted to column chromatography (silica gel, hexane–chloroform; 8:1) to give 0.38 g (36%) of **4** and 40 mg (5%) of **3**. The hydrazonate **4** was further purified by bulb-to-bulb distillation (bath temperature 123—125°C, 1 mmHg), ^{1}H NMR (CCl_4) δ=6.6—7.5 (m, 10H) and 7.6 (br.s, 1H), IR (neat) 3330 (NH), 1638 (C=N), and 1159, 1125 cm^{-1} (CF_3).

Found: C, 60.11; H, 3.71; N, 9.77%. Calcd for $C_{14}H_{11}F_3N_2O$: C, 60.00; H, 3.96; N, 10.00%.

Reaction of 1 with Sodium Methoxide in the Presence of Methyl Acrylate. A solution of **1** (1.00 g, 3.7 mmol) in 10 cm^3 of methanol was added dropwise to a mixture of methyl acrylate (0.97 g, 11.3 mmol) and sodium methoxide (0.40 g, 7.4 mmol) in 20 cm^3 of methanol and the mixture was stirred at room temperature for 24 h. The usual workup gave 0.57 g (56%) of **5** and 0.31 g (38%) of **3**. **5**, mp 60—61°C (lit,[5] mp 60—61.5°C). Spectral data are consistent with those of our authentic sample.

Reaction of 1 with Diethylamine. A mixture of diethylamine (3 cm^3) and **1** (1.00 g) in 10 cm^3 of toluene was stirred at room temperature for 4 h. The residue obtained by the usual workup was chromatographed over silica gel (hexane–chloroform; 4:1) to give 0.86 g (89%) of **7** which was further purified by distillation, bp 103—104°C/4 mmHg, ^{1}H NMR (CCl_4) δ=1.13 (t, 6H), 2.96 (q, 4H), 6.6—7.4 (m, 5H), and 8.5 (br.s, 1H), IR (neat) 3290 (NH), 1602 (Ph and C=N), and 1139, 1109 cm^{-1} (CF_3).

Found: C, 55.68; H, 6.26; N, 16.03%. Calcd for $C_{12}H_{16}F_3N_3$: C, 55.59; H, 6.22; N, 16.21%.

The reaction with aniline was similarly performed at 100°C for 7 h to give **6** in 49% yield, mp 66.5—67.5°C (hexane) (lit,[6] mp 66.5—67.5°C).

Reaction of 1 with N-Methylpyrrolidine. *N*-Methylpyrrolidine (3 cm^3) was added dropwise to a solution of 2.00 g (7.5 mmol) of **1** in 10 cm^3 of toluene holding the temperature below 20°C. After stirring for 2 h, the deposited white crystals were collected on a filter, washed with hexane, and dried to give 2.09 g (79%) of **8**, mp 72°C (dec.), ^{1}H NMR ($CDCl_3$) δ=1.84 (m, 4H), 2.46 (s, 3H), 2.62 (m, 4H), 6.9—7.5 (m, 5H), and 8.0 (br.s, 1H), IR (KBr) 3355 (NH), 1614 (C=N), and 1179, 1129 cm^{-1} (CF_3).

Found: C, 44.08; H, 4.66; N, 11.84%. Calcd for $C_{13}H_{17}BrF_3N_3$: C, 44.33; H, 4.86; N, 11.93%.

Reaction of 1 with Triethylamine. A mixture of 2.00 g (7.5 mmol) of **1** and 6 cm^3 of triethylamine in 10 cm^3 of toluene was stirred at room temperature for 23 h. To the reaction mixture was added 100 cm^3 of ethyl ether and the mixture was washed with water and brine, dried over magnesium sulfate, and evaporated. The residue was chromatographed over silica gel (hexane–chloroform; 7:1) to give 0.22 g (16%) of **9**, 0.25 g (16%) of **10**, 0.13 g (7%) of **7**, and 30 mg (2%) of **11**. Spectral data of **7** are consistent with those obtained above. **9**, mp 69—71°C (lit,[5] mp 69—73°C), ^{1}H NMR (CCl_4) δ=6.5—7.3 (m, 6H) and 7.6 (br.s, 1H).

10, ^{1}H NMR (CCl_4) δ=6.60 (d, J=2.5 Hz, 1H), 7.2—7.8 (m, 5H), and 7.83 (d, J=2.5 Hz, 1H), IR (neat) 3135 (=CH), 1605 (Ph and C=N), and 1166, 1130 cm^{-1} (CF_3).

Found: C, 56.36; H, 3.27; N, 13.15%. Calcd for $C_{10}H_7F_3N_2$: C, 56.61; H, 3.33; N, 13.20%.

11, mp 118—120°C (hexane), ^{1}H NMR ($CDCl_3$) δ=7.37 (s), IR (KBr) 1612 (C=N) and 1138, 1104 cm^{-1} (CF_3), MS (CI, m/z) 372 $(M)^+$ and 401 $(M+C_2H_5)^+$, UV λ_{max}^{EtOH} (log ε) 267 (4.23) and 275 nm (sh, 4.22).

Found: C, 51.47; H, 2.69; N, 15.25%. Calcd for $C_{16}H_{10}F_6N_4$: C, 51.62; H, 2.71; N, 15.05%.

References

1) R. Huisgen, R. Grashey, and J. Sauer, "Cycloaddition Reactions of Alkenes," in "The Chemistry of Alkenes," ed by S. Patai, Wiley-Interscience, New York, N. Y. (1964); A. S. Shawali and C. Párkányi, *J. Heterocyclic Chem.*, **17**, 833 (1980).

2) I. T. Barnish and M. S. Gibson, *J. Chem. Soc., C*, **1970**, 854.

3) T. Bacchetti, *Gazz. Chim. Ital.*, **91**, 866 (1961).

4) F. L. Scott and J. B. Aylward, *Tetrahedron Lett.*, **1965**, 841.

5) K. Tanaka, S. Maeno, and K. Mitsuhashi, *Chem. Lett.*, **1982**, 543.

6) K. Tanaka, T. Igarashi, S. Maeno, and K. Mitsuhashi, *Bull. Chem. Soc. Jpn.*, **57**, 2689 (1984).

7) Part VI on "Applications of the fluorinated 1,3-dipolar compounds as building blocks of the heterocycles with fluorine groups." Part V: K. Tanaka, S. Maeno, and K. Mitsuhashi, *J. Heterocyclic Chem.*, in press.

8) For the formation of ammonium salts from hydrazides and amines, see H. Feuer and L. F. Spinicelli, *J. Org. Chem.*, **42**, 2091 (1977).

9) R. Huisgen, E. Aufderhaar, and G. Wallbillich, *Chem. Ber.*, **98**, 1476 (1965).

10) A. M. Platoshkin, Yu. A. Cheburkov, and I. L. Knunyants, *Izv. Akad. Nauk SSSR, Ser Khim.*, **1969**, 112; *Chem. Abstr.*, **70**, 114541c (1969).

11) For the breakdown of 5-amino-2-pyrazolines, see R. Fusco, G. Bianchetti, and D. Pocar, *Gazz. Chim. Ital.*, **91**, 1233 (1961).

12) A. S. Shawali and A. O. Abdelhamid, *Bull. Chem. Soc. Jpn.*, **49**, 321 (1976).

Dichlorotetrakis(isocyanide)dipalladium(I) Containing a Metal-Metal Bond[1)]

Yasuhiro YAMAMOTO* and Hiroshi YAMAZAKI
The Institute of Physical and Chemical Research, Wako, Saitama 351-01
(Received November 21, 1984)

Synopsis. The structure of $[\{PdCl(t\text{-}BuNC)_2\}_2]$ has been determined by X-ray diffraction. A metal-metal bond joins two Pd atoms, each of which possesses an essentially square-planar coordinate site. The photochemical reaction of $[\{PdCl(RNC)_2\}_2]$ in CH_2Cl_2 led to a cleavage of the metal-metal bond to give *trans*-$[PdCl_2(t\text{-}BuNC)_2]$.

Metal clusters attract considerable attention as plausible models of surfaces in heterogeneous catalysts.[2)] Binuclear complexes are the simplest units which can provide information on the metal-metal interactions. Previously we reported that the electrochemical reductions of *cis*-$[PtCl_2(RNC)_2]$ gave $[\{PtCl(RNC)_2\}_2]$ **1** containing a metal-metal bond.[3)] This finding prompted us to reexamine the structure of $[\{PdCl(t\text{-}BuNC)_2\}_2]$, assigned to chloride bridged structure.[4)]

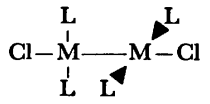

1: M = Pt
2X: M = Pd

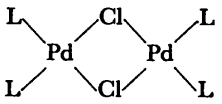

2

When we were preparing the paper on the X-ray crystallographic analysis of $[\{PdCl(t\text{-}BuNC)_2\}_2]$ **2a**, we knew of the study on crystal structure of $[\{PdI(MeNC)_2\}_2]$ **3** described by Balch and his co-workers.[5)] We report here the X-ray analysis of **2a** and the characterization of related complexes having aromatic isocyanides as ligands.

Experimental

The isocyanides,[6)] $PdCl_2(RNC)_2$,[7)] and $[\{PdCl(RNC)_2\}_2]$[7)] were prepared according to the literature.

$PdCl_2(2,6\text{-}Me_2C_6H_3NC)_2$: IR (Nujol): 2205, 2172 cm^{-1} (N≡C). Found: C, 49.15; H, 4.18; N, 6.37%. Calcd for $C_{18}H_{18}N_2Cl_2Pd$: C, 49.17; H, 4.13, N, 6.37%.

$PdCl_2(2,6\text{-}Me_2\text{-}4\text{-}BrC_6H_2NC)_2$. IR (Nujol): 2224, 2205 cm^{-1} (N≡C). Found: C, 36.17; H, 2.73; N, 4.59%. Calcd for $C_{18}H_{16}N_2Cl_2Br_2Pd$: C, 36.19; H, 2.70; N, 4.69%.

$[\{PdCl(2,6\text{-}Me_2C_6H_3NC)_2\}_2]$ **2b**. IR (Nujol): 2155 cm^{-1}. (N≡C). ^1H NMR($CDCl_3$): δ=2.53 (s, CH_3), 7.2 (aromatic protons). Found: C, 53.50; H, 4.46; N, 6.84%. Calcd for $C_{36}H_{36}N_4Cl_2Pd_2$: C, 53.49; H, 4.49; N, 6.93%.

$[\{PdCl(2,6\text{-}Me_2\text{-}4\text{-}BrC_6H_2NC)_2\}_2]$ **2c**. IR (Nujol): 2154 cm^{-1} (N≡C). ^1H NMR ($CDCl_3$): δ=2.50 (s, CH_3), 7.31 (aromatic protons). Found: C, 38.19; H, 2.95; N, 4.92%. Calcd for $C_{36}H_{32}N_4Br_4Cl_2Pd_2$: C, 38.47; H, 2.87; N, 4.98%.

$[Pd_2(2,6\text{-}Me_2C_6H_3NC)_6](PF_6)_2(2C_6H_6)$ **4b**. IR (Nujol): 2194, 2173 cm^{-1}. UV (CH_2Cl_2): λ 264 (49230), 325 sh nm. Found: C, 54.78; H, 4.40; N, 5.74%. Calcd for $C_{66}H_{66}N_6P_2F_{12}Pd_2$: C, 54.82; H, 4.60; N, 5.81%.

$[Pd_2(2,6\text{-}Me_2\text{-}4\text{-}BrC_6H_2NC)_6](PF_6)_2$ **4c**. IR (Nujol): 2170 cm^{-1} (N≡C). UV(CH_2Cl_2): λ 275(58640), *ca.* 335 sh nm. Found: C, 36.75; H, 2.75; N, 4.82%. Calcd for $C_{54}H_{48}N_6Br_6P_2F_{12}Pd_2$: C, 36.79; H, 2.74; N, 4.77%.

X-Ray Data and Structure Determination. Crystal data: space group C_c. a=12.665(2), b=14.449(2), c=18.402(3) Å, β=102.94(1)°, V=3282(9) Å^3. Z=4. R=0.060 for 2588 reflections. The choice of the space group C_c was justified on the basis of the successful refinement of the struture. Intensity data were collected with the crystals mounted in a nitrogen filled capillary. The positions of the palladium atoms were determined from Patterson maps. Subsequent difference Fourier maps and cycles of block-diagonal least-squares refinement revealed the positions of the remaining nonhydrogen atoms. The scattering factors were taken from "International Table for X-Ray Crystallography" (1974). The two *t*-butyl groups displayed disorder. The Pd and Cl, and C-N-C groups were refined anisotropically and other nonhydrogen atoms isotropically. The final difference synthesis showed no peaks higher than 0.4 e Å^{-3}.

Results and Discussion

The dimeric complexes $[\{PdCl(RNC)_2\}_2]$ (**2a**: R=*t*-Bu; **2b**: R=2,6-$Me_2C_6H_3$; **2c**: R=2,6-Me_2-4-BrC_6H_2) were prepared by the reaction of $Pd_2(dba)_3(CHCl_3)$, isocyanide and dichlorobis(isocyanide)palladium(II) in a 1:4:2 ratio. They are yellow and stable. The IR spectra showed a peak near 2155 cm^{-1} due to terminal isocyanide groups. The reaction of **2b** with 2,6-xylyl isocyanide in the presence of NH_4PF_6 took place readily to give $[Pd_2(2,6\text{-}Me_2C_6H_3NC)_6](PF_6)_2$ **4b** quantitatively.

The photochemical reaction of **2a** in CH_2Cl_2 was monitored by the electronic spectra. The band at 307 nm in **2a** decreased with the photolysis time and finally the spectrum was in good agreement with that of *trans*-$[PdCl_2(t\text{-}BuNC)_2]$, indicating a cleavage of a metal-metal bond. The band at 307 nm was assigned as a σ-σ^* transition.

$$[\{PdCl(t\text{-}BuNC)_2\}_2] \xrightarrow[CH_2Cl_2]{h\nu} \textit{trans}\text{-}[PdCl_2(t\text{-}BuNC)_2]$$

Similar σ-σ^* transitions connected with metal-metal bonds have also been observed in the same range with $[\{PtCl(2,4\text{-}t\text{-}Bu_2\text{-}6\text{-}MeC_6H_2NC)_2\}_2]$ **1d**[3)] [324 nm(CH_2Cl_2)] and $[Pd_2(MeNC)_6](PF_6)_2$ **5** [302 nm(CH_2Cl_2)].[8)]

Crystal Structure of **2a**.[9)] The crystal structure is shown in Fig. 2. Typical bond lengths and angles are given in Table 1. A metal-metal bond joins the two Pd atoms, each of which possesses essentially a square-planar coordinate geometry with the Pd-Pd bond occupying one of the coordination sites. The overall geometry is nearly D_{2d} symmetry. The Pd(1)-Pd(2) bond length of 2.532(2) Å is similar to those [2.533(1) and 2.531(9) Å] found in **3** and **5**, and somewhat shorter than those [2.563(2) and 2.561(2) Å] found in **1d**. The dihedral angle between the two $PdClC_2$ coordination planes is 82.7°, compared with those (85.3 and 86.4°) in **3** and **5**. The Cl-Pd-Pd-Cl unit is nearly linear. The Pd-Pd-Cl angles are 176.7

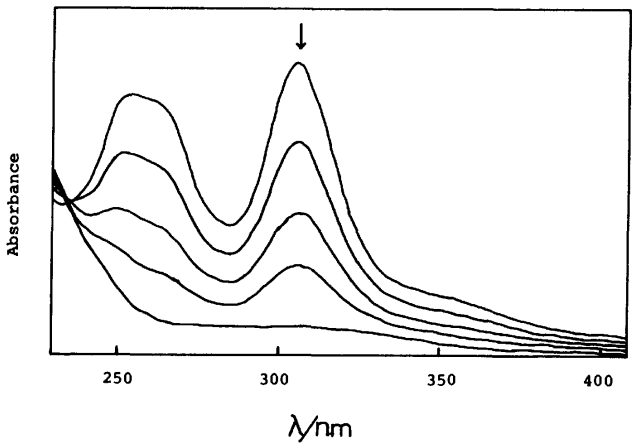

Fig. 1. Electronic spectrum of $[PdCl(t\text{-}BuNC)_2]_2$ in CH_2Cl_2 as a fnction of photolysis time.

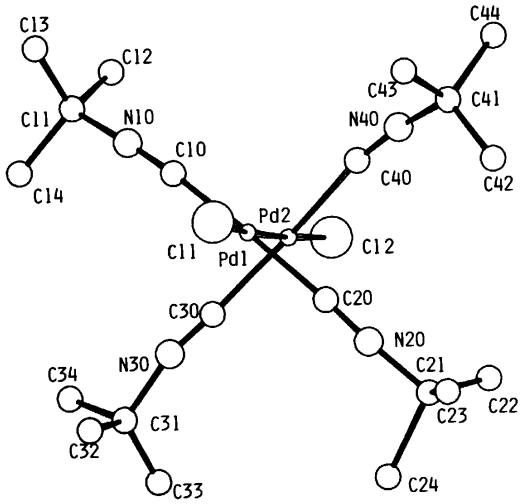

Fig. 2. A perspective drawing of $[PdCl(t\text{-}BuNC)_2]_2$ with the numbering scheme.

(2) and 177.4(2)°. The Pd-Cl bond lengths of 2.403 (9) and 2.416(9)Å, are longer than those [2.300(2) and 2.302(2)Å] of *cis*-$[PdCl_2(c\text{-}C_6H_{11}NC)_2]$.[10] This arises from the high trans effect of Pd-Pd bond. Similar behavior of terminal halide-metal bonds trans to metal-metal bonds has been noted in **3**.[5] The equatrial isocyanide ligands bend away from the axial Cl ligand giving rise to values of 97.2° for the mean C-Pd-Cl angle and 83.0° for the mean C-Pd-Pd angle. A similar distortion has been observed in **1d**, **3**, and **5**, where the averages of C-M-Cl (or equatrial C) angles are 93.8, 95.2, and 95.0°, the averages of C-M-M angles are 85.5, 84.7, and 85.0°, respectively. Thus, the type of the complexes $[\{PdCl(RNC)_2\}_2]$ was revised to the structure **2a** involving terminal halogens and a metal-metal bond.

A list of the final F_o—F_c table, bond lengths and angles (Table 1), and temperature factors are deposited as Document No. 8523 at the office of Bull. Chem. Soc. Jpn.

Table 2. Positional parameters for $[\{PdCl(t\text{-}BuNC)_2\}_2]$[a]

ATOM	X	Y	Z
PD1	0(0)	1126(1)	2500(0)
PD2	1659(2)	1119(1)	3564(1)
CL1	−1538(6)	1052(6)	1464(3)
CL2	3281(6)	1063(6)	4548(4)
N10	−794(16)	−102(13)	3649(11)
C10	−515(16)	321(13)	3194(10)
C11	−1052(21)	−580(18)	4293(14)
N20	1117(14)	2586(12)	1695(9)
C20	730(16)	2029(13)	1986(11)
C21	1811(23)	3264(20)	1435(17)
N30	372(19)	2572(16)	4261(13)
C30	831(24)	2082(21)	4010(16)
C31	−30(21)	3385(18)	4622(15)
N40	2382(17)	−209(15)	2433(11)
C40	2104(25)	189(21)	2849(16)
C41	2484(24)	−514(20)	1697(15)
C12	0(3)	−107(3)	473(2)
C13	−177(2)	−133(2)	413(2)
C14	−151(2)	22(2)	472(2)
C22	300(6)	307(5)	167(4)
C23	128(7)	330(6)	57(5)
C24	158(6)	430(5)	192(4)
C22A	262(5)	274(4)	108(3)
C23A	99(5)	382(4)	83(3)
C24A	240(5)	384(4)	210(3)
C32	−112(8)	355(7)	405(5)
C33	61(7)	417(6)	475(5)
C34	−16(5)	307(4)	540(4)
C32A	43(5)	428(4)	442(3)
C33A	−130(5)	336(4)	435(3)
C34A	33(5)	329(4)	546(3)
C42	271(3)	28(2)	121(2)
C43	141(3)	−85(3)	130(2)
C44	349(5)	−134(4)	198(3)

a) Positional parameters from Pd1 to C41 atoms are multiplied by 10^4 and those from C12 to C44 atoms, by 10^3.

References

1) Studies on interactions of isocyanides with transition metal complexes 28. For the preceeding paper, see Y. Yamamoto and H. Yamazaki, *J. Organomet. Chem.*, **282**, 191 (1985).

2) a) R. Ugo, *Catal. Rev.*, **11**, 225 (1975); b) E. L. Muetterties, *Bull. Chem. Soc. Chim. Berg.*, **84**, 959 (1975); c) E. L. Muetterties, *ibid.*, **85**, 451 (1976).

3) Y. Yamamoto, K. Takahashi, and H. Yamazaki, *Chem. Lett.*, **1985**, 201.

4) S. Otsuka, Y.Tatsuno, and K. Ataka, *J. Am. Chem. Soc.*, **93**, 6705 (1971).

5) N. M. Rutherford, M. M. Olmstead, and A. L. Balch, *Inorg. Chem.*, **23**, 2833 (1984).

6) H. M. Walborsky and G. E. Niznik, *J. Org. Chem.*, **37**, 187 (1972).

7) M. F. Rettig, E. A. Kirk, and P. M. Maitlis, *J. Organomet. Chem.*, **111**, 113 (1976).

8) T. D. Miller, M. A. St. Clair, M. K. Relnking, and C. P. Kubiak, *Organometallics*, **2**, 767 (1983).

9) The following programs were used: T. Sakurai and K. Kobayashi, UNICS III(1978).

10) Y. Kitano and T. Hori, *Acta Crystallogr., Sect. B.*, **37**, 1919 (1981).

A Facile Synthesis of 3-(1-Benzyloxymethyl-3-hydroxypropyl)-2,5-piperazinedione

Masanori YAMAURA, Khalid Khan SADOZAI, and Juji YOSHIMURA*
Laboratory of Chemistry for Natural Products, Faculty of Science, Tokyo Institute of Technology, Nagatsuta, Midori-ku, Yokohama 227
(Received January 7, 1985)

Synopsis. The title compound, a key intermediate for a total synthesis of bicyclomycin, was obtained from γ-butyrolactone through eight steps in *ca.* 4.4% overall yield.

Bicyclomycin,[1] an antibiotic having unique structure[2] and biological activity, was recently synthesized in racemic[3] and optically active[4] forms. In these syntheses, the pathway in which the carbon-substituent is introduced into the 2,5-piperazinedione ring was adopted for the construction of racemic bicyclic skeleton. However, another pathway in which a precursor having a suitable carbon chain is cyclized into 2,5-piperazinedione[5] should be used for the synthesis of optically active skeleton, though many reaction steps are necessary. This paper describes a synthesis of racemic title compound (**12**) from γ-butyrolactone as an attempt of the latter pathway.

γ-Butyrolactone was converted into the racemic mixture of 2-methoxy-3-methoxycarbonyltetrahydrofuran (**1**) by the known method[6] in 82% yield. Reduction of **1** with lithium aluminum hydride (LAH) gave quantitatively the corresponding alcohol (**2**), which was converted into 3-benzyloxymethyl-2-hydroxytetrahydrofuran (**4**) in a good yield, by successive *O*-benzylation (**3**) and partial hydrolysis with 0.1 M (M=mol dm^{-3}) hydrochloric acid–dioxane (1:1) at room temperature.

Reaction of **4** in methanol with ammonia and hydrogen cyanide gave the corresponding amino nitrile (**5**) in 72% yield, and that with *p*-methoxybenzylamine instead of ammonia gave **6** in 85% yield. The structures of **5** and **6** were confirmed by ^{1}H NMR after conversion into acetates (**7** and **8**), respectively. While, the reaction of **4** with ammonium carbonate and sodium cyanide gave the corresponding hydantoin (**9**). However, the hydantoin ring could not be opened by refluxing with barium hydroxide for a long period. Hydrolysis of **5** in aqueous methanol with hydrochloric acid, and *N*-chloroacetylation of the product gave the expected product (**10**) and a lactone (**11**) in 23 and 31% yields, respectively. Successive treatment of **10** with sodium iodide for halogen exchange and with methanolic ammonia gave one of the two possible racemates of the corresponding 2,5-piperazinedione (**12**) as crystals in 24% yield. A similar treatment of **11** gave also **12** in 9% yield. The structure of **12** was confirmed by ^{1}H and ^{13}C NMR, after conversion into the corresponding *N,N',O*-triacetyl derivative (**13**).

Experimental

Melting points were determined with a Yanagimoto micro melting-point apparatus, and were not corrected. ^{1}H and ^{13}C NMR spectra were recorded with a JEOL JMN PS-100 and a JEOL FX-90Q spectrometers, respectively, in $CDCl_3$ with tetramethylsilane as the internal standard.

3-Hydroxymethyl-2-methoxytetrahydrofuran (2). Reduction of **1** (5.8 g, 39 mmol) in dry ether with LAH (3.0 g, 79 mmol) by the usual manner, and purification of the product on a column of silica gel (chloroform–hexane 3:1) gave **2** (5.1 g, 99%) as a syrup. ^{1}H NMR: δ 4.94 and 4.86 (each d, 1H, $J_{2,3}$=5.0 and 2.0 Hz, H-2), 4.05—3.65 (m, 2H, H-5), 3.54 (d, 2H, $J_{3,1'}$=8.0 Hz, CH_2OH), 3.36 (s, 3H, OMe), 2.7—1.8 (m, 4H, H-3,4 and OH). Anal. ($C_6H_{12}O_3$) C, H.

3-Benzyloxymethyl-2-methoxytetrahydrofuran (3). Benzylation of **2** (47.0 g, 350 mmol) in dry DMF with sodium hydride (18.8 g, 390 mmol) and benzylchloride (47.3 g, 370 mmol) by the usuel manner, and distillation of the product gave oily **3** (73.5 g) in 95% yield. Bp 119—125 °C/1 Torr (1 Torr=133.322 Pa). Anal. ($C_{13}H_{18}O_3$) C, H.

3-Benzyloxymethyl-2-hydroxytetrahydrofuran (4). Partial hydrolysis of **3** (5.0 g, 23 mmol) in dioxane (100 cm^3) with 0.1 M hydrochloric acid (100 cm^3) at room temperature for 2 days, and purification of the product on a silica-gel column (hexane–ethyl acetate 7:3) gave syrupy **4** (4.5 g, 96%). Anal. ($C_{12}H_{16}O_3$) C, H.

2-Amino-3-benzyloxymethyl-5-hydroxypentanenitrile (5). To a solution of **4** (10.0 g, 48 mmol) in abs methanol (80 cm^3) saturated with ammonia at 0 °C was added hydrogen cyanide (3.9 g, 144 mmol), the mixture was kept at room temperature for 72 h, and then evaporated. The residue was purified on a silica-gel column (chloroform–methanol 5:1) to give **5** (8.1 g, 72%) as a colorless syrup. The usual *N*-acetylation of **5** in methanol with acetic anhydride, and purification of the product on a preparative TLC (chloroform–ethyl acetate 1:1) gave syrupy 2-scetamido-3-benzyloxymethyl-5-hydroxypentanenitrile (**7**) in 89% yield. ^{1}H NMR: δ 7.35 (s, 6H, Ph and NH), 5.3—5.0 (m, 1H, H-2), 4.55 (s, 2H, CH_2Ph), 3.9—3.5 (m, 4H, H-5 and CH_2OBn), 2.70 (bs, 1H, OH), 2.45—2.15 (m, 1H, H-3), 1.93 and 1.87 [each s (1:1), 3H, Ac)], 1.9—1.5 (m, 2H, H-4). Anal. ($C_{15}H_{20}N_2O_3$) C, H, N.

3-Benzyloxymethyl-5-hydroxy-2-(p-methoxybenzylamino)pentanenitrile (6). A similar treatment of **4** (2.3 g, 11 mmol) with hydrogen cyanide (0.90 g, 33 mmol) and *p*-methoxybenzylamine (1.7 g, 12 mmol) to **5**, and purification of the product on a silica-gel column (chloroform–methanol

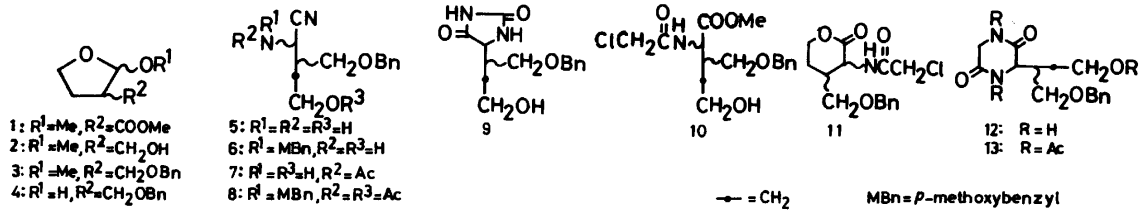

7:1) gave **6** (3.3 g, 85%) as a colorless syrup. The usual acetylation of **6** in pyridine with acetic anhydride, and purification of the product on a preparative TLC (hexane–ethyl acetate 3:2) gave syrupy 5-acetoxy-3-benzyloxymethyl-2-[*N*-(*p*-methoxybenzyl)acetamido]pentanenitrile (**8**) in 65% yield. ^{1}H NMR: δ 7.42 and 7.39 (each s, 5H, Ph), 7.24, 7.16, 6.95 and 6.93 (each d, 4H, J=8.5 Hz, MBn), 5.45—5.15 (m, 1H, H-2), 4.9—3.4 (m, 6H, H-5, CH_2OBn and CH_2 in MBn), 4.54 and 4.52 (each s, 2H, CH_2Ph), 2.2—1.6 (m, 3H, H-3 and 4), 2.19 and 2.13 (each s, 3H, OAc), 2.04 and 2.01 (each s, 3H, NAc). Anal. ($C_{25}H_{30}N_2O_5$) C, H, N.

*5-(1-Benzyloxymethyl-3-hydroxypropyl)-2,4-imidazolidinedione (**9**).* A mixed solution of **4** (1.0 g, 4.8 mmol) in ethanol (40 cm^3), ammonium carbonate (4.3 g, 44.7 mmol) and sodium cyanide (0.48 g, 9.8 mmol) in water (40 cm^3), was heated for 5 h at 60 °C, poured into ice–water, and extracted with chloroform. The usual processing of the extract gave a crude syrup, which was purified on a column of silica gel (chloroform–methanol 9:1) to give **9** (540 mg) in 41% yield. ^{1}H NMR: δ 7.38 and 7.34 (each s, 5H, Ph), 4.78 (bs, 2H, NH and OH), 4.59 and 4.48 (each s, 2H, CH_2Ph), 4.28 and 4.40 (each d, 1H, $J_{3,1'}$=2.5 and 3.0 Hz, H-3), 3.8—3.5 (m, 2H, H-3′), 3.32 and 3.28 (each d, 2H, J=3.0 Hz, CH_2OBn), 2.6—2.2 (m, 1H, H-1′), 1.7—1.4 (m, 2H, H-2′). Anal. ($C_{14}H_{18}N_2O_4$) C, H, N.

*Methyl 3-Benzyloxymethyl-2-chloracetemido-5-hydroxypentanoate (**10**) and 3-Benzyloxymethyl-2-chloroacetamido-5-pentanolide (**11**).* A mixed solution of **5** (16.0 g, 68 mmol) in methanol (40 cm^3), methanol (40 cm^3) saturated at 0 °C with hydrogen chloride and water (2.4 g, 130 mmol) was kept at room temperature for 48 h, filtered, and the filtrate was evaporated to one third volume, again filtered, and the filtrate was evaporated. The usual *N*-chloroacetylation of the residue in benzene (120 cm^3) and ether (40 cm^3) with potassium carbonate (28.0 g, 203 mmol) in water (200 cm^3) and chloroacetyl chloride (15.4 g, 136 mmol) in benzene (20 cm^3) at 0 °C, and separation of the products on a column of silica gel (benzene–ethyl acetate 7:3) gave **11** (6.5 g, 31%) and **10** (5.5 g, 23%) as colorless syrups.

11: ^{1}H NMR: δ 7.56 and 7.16 (each d, 1H, $J_{2,NH}$=7.0 and 8.0 Hz, NH), 7.40 (s, 5H, Ph), 4.9—4.6 (m, 1H, H-2), 4.52 and 4.49 (each s, 2H, CH_2Ph), 4.45—4.25 (m, 2H, H-5), 4.07 and 3.97 (each s, 2H, CH_2Cl), 3.6—3.3 (m, 2H, CH_2OBn), 3.1—2.7 (m, 1H, H-3), 2.4—1.9 (m, 2H, H-4). Anal. ($C_{15}O_{18}O_4NCl$) C, H, N.

10: ^{1}H NMR: δ 7.86 and 7.75 (each bd, 1H, $J_{2,NH}$=8.0 and 7.0 Hz, NH) 7.35 (s, 5H, Ph), 4.9—4.7 (m, 1H, H-2), 4.44 (s, 2H, CH_2Ph), 4.27 and 4.25 (each t, 2H, $J_{4,5}$=6.5 Hz, H-5), 4.07 and 4.04 (each s, 2H, CH_2Cl), 4.05 (bs, 1H, OH), 3.71 (s, 3H, OMe), 3.6—3.3 (m, 2H, CH_2OBn), 2.6—2.2 (m, 1H, H-3), 2.0—1.7 (m, 2H, H-4). Anal. ($C_{16}H_{22}O_5NCl$) C, H, N.

*3-(1-Benzyloxymethyl-3-hydroxypropyl)-2,5-piperazinedione (**12**).* A solution of **10** (700 mg, 2.0 mmol) and 3 equimolar sodium iodide in acetone (20 cm^3) was refluxed for 3 h, evaporated to a half volume, poured into water, and then extracted with ethyl acetate. The usual processing of the extract gave a crude syrup, which was treated for 12 h at room temperature with methanol (10 cm^3) saturated with ammonia to give crude **12**. It was crystallized from methanol-ether and recrystallized from methanol–water. Yield, 24% (140 mg), mp 204—205 °C. Anal. ($C_{15}H_{20}N_2O_4$) C, H, N.

*3-[3-Acetoxy-1-(benzyloxymethyl)propyl]-1,4-diacetyl-2,5-piperazinedione (**13**).* The usual acetylation of **12** (100 mg, 0.34 mmol) in DMF (20 cm^3) with acetic anhydride (2 cm^3) and catalytic amount of 4-(dimethylamino)pyridine, and purification of the product on a column of silica gel (hexane–ethyl acetate 7:3) gave syrupy **13** (62 mg, 43%). ^{1}H NMR: δ 7.28 (s, 5H, Ph), 5.32 (d, 1H, $J_{3,1'}$=7.5 Hz, H-3), 4.97 (d, 1H, $J_{6a,6b}$=18.0 Hz, H-6a), 4.73 (s, 2H, CH_2Ph), 4.3—3.9 (m, 3H, H-6b and 3′), 3.6—3.35 (m, 2H, CH_2OBn), 2.54 and 2.51 (each s, 6H, NAc×2), 2.01 (s, 3H, OAc), 2.2—1.5 (m, 3H, H-1′ and 2′); ^{13}C NMR: 171.3s, 171.1s and 170.0s (C=O×3), 167.8s and 166.9s (C-2 and 5), 137.0s, 128.4d, 127.9d and 127.7d (aromatic), 73.4t, 69.5t and 61.4t (CH_2Ph, CH_2OBn and C-3′), 58.9d (C-3), 47.1t (C-6), 39.3d (C-1′), 28.3t (C-2′), 26.4q, 26.7q and 20.8q (Ac×3). Anal. ($C_{21}H_{26}N_2O_7$) C, H, N.

References

1) T. Miyoshi, N. Miyairi, H. Aoki, M. Kohsaka, H. Sakai, and H. Imanaka, *J. Antibiot.*, **25**, 569 (1972); S. Miyamura, N. Ogasawara, H. Otsuka, S. Miwayama, H. Tanake, T. Take, T. Uchiyama, H. Ochiai, K. Abe, K. Koizumi, K. Asao, K. Matsuki, and T. Hoshino, *ibid.*, **25**, 610 (1972).

2) Y. Tokuma, S. Koda, T. Miyoshi, and Y. Morimoto, *Bull. Chem. Soc. Jpn.*, **47**, 18 (1974); H. Maag, J. F. Blount, D. L. Coffen, T. V. Steppe, and F. Wong, *J. Am. Chem. Soc.*, **100**, 6786 (1978).

3) S. Nakatsuka, K. Yamada, K. Yoshida, O. Asano, Y. Murakami, and T. Goto, *Tetrahedron Lett.*, **24**, 5627 (1983).

4) R. M. Williams, R. W. Armstrong, and J.-S. Dung, *J. Am. Chem. Soc.*, **106**, 5748 (1984); J. Yoshimura, M. Yamaura, T. Suzuki, and H. Hashimoto, *Chem. Lett.*, **1984**, 2157.

5) L. V. Dunkerton and R. M. Ahmed, *Tetrahedron Lett.*, **21**, 1803 (1980); C. Shin, Y. Sato, and J. Yoshimura, *ibid.*, **22**, 2401 (1981); T. Fukuyama, B. D. Robins, R. A. Sachleben, *ibid.*, **22**, 4155 (1981); P. Yates and J. H. Hoare, *Can. J. Chem.*, **61**, 519, 1397 (1983).

6) C. R. Hutchinson, *J. Org. Chem.*, **39**, 1854 (1974); F. Korte and H. Machleidt, *Chem. Ber.*, **88**, 1684 (1955).

NAD(P)$^+$-NAD(P)H Model. 54. Free Radical Mechanism for the Reductive Debromination of *vic*-Dibromides to Alkenes

Shinro YASUI,* Kaoru NAKAMURA,† and Atsuyoshi OHNO†
Tezukayama Junior College, Gakuen-Minami, Nara 631
†*Institute for Chemical Research, Kyoto University, Uji, Kyoto 611*
(Received January 30, 1985)

Synopsis. *vic*-Dibromides undergo reductive debromination with a model of NAD(P)H, *N*-benzyl-1,4-dihydronicotinamide, to afford the corresponding alkenes quantitatively. Stereochemistry of the reduction suggests that the reaction involves a free radical intermediacy.

Whether the reduction with NAD(P)H or its model compounds proceeds through a multi-step (electron-transfer) mechanism or through a one-step (hydride-transfer) mechanism has been a subject of current discussion.[1] There are several reports on reactions in which a model of NAD(P)H acts as a one-electron donor; it acts even as a radical-chain initiator in the reaction of bromotrichloromethane to chloroform,[2a] radical polymerization of acrylamide,[2b] and dediazoniation of arene diazonium salts.[2c] These reactions have been invoked to support the multi-step mechanism which involves initial one-electron transfer process. Nevertheless, since these reactions are not initiated by any provocations other than one-electron transfer onto the substrates, the models may be compelled to act as a one-electron donor in these reactions. Therefore, in order to obtain the definitive proof for the intrinsic ability of dihydropyridine derivatives as a one-electron donor, an alternative reaction system that is known to be susceptible both for one-electron and two-electron reductions should be taken.

A variety of reductants[3-5] as well as electrochemical reduction[6] convert *vic*-dibromide into the corresponding alkene by reductive debromination. Studies on the stereochemistry of these reductions have demonstrated that two-electron reductants such as iodide and hydride ions mainly give rise to concerted *anti*-elimination resulting in stereoselective formations of *trans*- and *cis*-alkenes from *meso*- (or *erythro*)- and *dl*- (or *threo*)-isomers, respectively. On the other hand, one-electron reductants such as copper(I) and iron(II) generate free radical species, which then give thermodynamically more stable alkenes predominantly[7,8] Thus, the reductive debromination of *vic*-dibromide is supposed to be an useful tool to diagnose whether a model of NAD(P)H acts as a one-electron donor or a hydride donor.

Results and Discussion

The results from the reactions of *vic*-dibromides **1a—c** with a model of NAD(P)H, *N*-benzyl-1,4-dihydronicotinamide (BNAH), are summarized in the Table. The table shows that *meso*- (or *erythro*)-bromide gave the *trans*-alkene (*trans*-**2**) quantitatively under anaerobic conditions with excess BNAH. On the other hand, the alkene from the *dl*-bromide is contaminated by a small amount of the *cis*-isomer (*cis*-**2**) under the same conditions. The results can be interpreted in terms of a free radical intermediacy in the course of the reaction. That is, **1** accepts one electron from BNAH and eliminates a bromide ion, and thus generated free radical species **3** can rotate around the central C–C bond to afford thermodynamically more stable isomer of the alkene predominantly.[8] A plausible reaction path is illustrated in the Scheme.

It has been reported that triphenylphosphine generates a carbanion from 1,2-dibromo-1-nitro-2-phenylethane (**5**) on its 1-position through the abstraction of a bromonium ion, which may afford the isomerized product.[9] However, the situation is not applicable to the present system, because BNAH is not a so strong nucleophile as triphenylphosphine and the substrates employed presently are not so electron deficient as **5**. Interestingly, an amine such as triethylamine gave rise to β-elimination of hydrogen bromide instead of reductive debromination.

Reductions under aerobic conditions also supports

TABLE 1. REDUCTIVE DEBROMINATION OF *VIC*-DIBROMIDES WITH BNAH[a]

Dibromide	Atmosphere	React. time/h	Conv. /%	Yield/%[b] *trans*-**2**	*cis*-**2**	*trans*-**4**	*cis*-**4**
meso-**1a**	N_2	2	92	100	0	0	0
meso-**1a**[c]	N_2	28	75	98	0	Trace	Trace
meso-**1a**[d]	N_2	24	46	80	0	Trace	Trace
meso-**1a**	O_2	2.5	98	28	0	8	56
dl-**1a**	N_2	7	100	100	Trace	0	0
erythro-**1b**	N_2	3	96	96	0	0	4
erythro-**1b**	Air	3	47	66	0	0	28
meso-**1c**[e]	N_2	4	100	90	0	0	0
dl-**1c**[f]	N_2	2	58	52	26	0	0
dl-**1c**[f]	O_2	2	84	27	20	52	Trace

a) The reactions were carried out with 5.0×10^{-2} mmol of **1** and 1.5×10^{-1} mmol of BNAH in 1 cm^3 of MeCN at 323 K in the dark unless otherwise indicated. b) Based on **1** consumed. c) 1.0×10^{-1} mmol of BNAH was used. d) 5.0×10^{-2} mmol of BNAH was used. e) In DMSO. f) At 343 K.

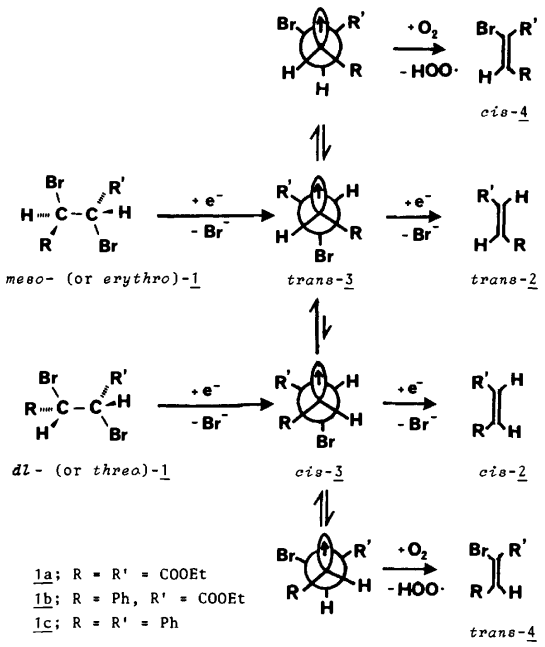

Scheme 1.

the participation of a free radical intermediacy: an oxygen molecule, which is an effective free radical scavenger, suppresses the debromination and β-elimination of hydrogen bromide predominates. Thus, as illustrated in the scheme, a free radical **3** generated is immediately trapped by an oxygen molecule to form a peroxide, which subsequently undergoes β-elimination of hydrogen peroxide in *anti*-direction to give the corresponding bromoalkene (**4**) without isomerization.[10]

BNAH promoted neither interconversion between *trans*-**2** and *cis*-**2** nor between *meso*- (or *erythro*)-**1** and *dl*-**1** under the reaction conditions. It was also confirmed that BNAH does not convert **4** to **2**.

Stoichiometry of the present reduction is noteworthy. The completion of the reduction requires more than two equivalents of BNAH against **1**, which excludes the possibility that BNAH releases a hydride ion in one step. Unfortunately, the fate of the cation radical produced from BNAH is not clear at present.

In conclusion, BNAH acts as a one-electron reductant in the reductive debromination of *vic*-dibromides even though it has a potential to behave as a hydride-ion donor. The present finding supports our previous proposal that the reduction with NAD(P)H-models involves initial one-electron transfer process.

In addition, the reductive debromination of *vic*-dibromides is an useful procedure for the purification of alkenes or the protection of alkenyl groups. The present reaction system is available for these procedures, since the conversion of the reaction and the yields of the products are satisfactory under anaerobic conditions with a little excess of BNAH. The process is much simpler than those so far reported.[4,5]

Experimental

Materials. Diethyl *dl*-dibromosuccinate (*dl*-**1a**)[11] and *dl*-1,2-dibromo-1,2-diphenylethane (*dl*-**1c**)[12] were prepared by bromination of diethyl maleate and *cis*-stilbene, respectively. Diethyl *meso*-dibromosuccinate was prepared by esterification of the corresponding acid. Ethyl *erythro*-α,β-dibromohydrocinnamate (*erythro*-**1b**) and *meso*-**1c** were commercially available (Tokyo chemical industry Co., Ltd.). NMR, IR, and GC-MS spectra of these compounds were satisfactory.

General Procedure. To a solution of 5.0×10^{-2} mmol of **1** in 0.5 cm³ of acetonitrile was added, using a syringe, a solution of 1.5×10^{-1} mmol of BNAH in 0.5 cm³ of acetonitrile through a silicone-rubber stopper. The mixture was left at 323 K in the dark for an appropriate time: then a 0.20-cm³ aliquot of the mixture was quenched with 1 cm³ of water. The aliquot was extracted with 1 cm³ of benzene containing *p*-diethoxybenzene as an internal standard for VPC analysis. The organic layer was analyzed on a Yanaco G-180 gas chromatograph (OV-17 column). Identification of products was done by comparison of IR, NMR, and GC-MS spectra of isolated products with those of the corresponding authentic smaples.

References

1) a) A. Ohno, H. Yamamoto, and S. Oka, *J. Am. Chem. Soc.*, **103**, 2041 (1981) and references cited therein; b) M. F. Powell and T. C. Bruice, *ibid.*, **105**, 7139 (1983); c) B. W. Carlson and L. L. Miller, *ibid.*, **105**, 7453 (1983); d) M. M. Kreevoy and I. H. Lee, *ibid.*, **106**, 2550 (1984).

2) a) J. L. Kurz, R. Hutton, and F. H. Westheimer, *J. Am. Chem. Soc.*, **83**, 584 (1961); b) S. Shinkai, T. Tsuno, Y. Asatani, and O. Manabe, *Chem. Lett.*, **1982**, 1439; c) S. Yasui, K. Nakamura, and A. Ohno, *J. Org. Chem.*, **49**, 878 (1984); d) S. Fukuzumi, Y. Kondo, and T. Tanaka, *J. Chem. Soc., Perkin Trans. 2*, **1984**, 673.

3) K. Fukunaga and H. Yamaguchi, *Synthesis*, **1981**, 879 and references cited therein.

4) T. Endo, Y. Saotome, and M. Okawara, *J. Am. Chem. Soc.*, **106**, 1124 (1984).

5) D. Landini, L. Milesi, M. L. Quadri, and F. Rolla, *J. Org. Chem.*, **49**, 152 (1984).

6) a) K. M. O'Connell and D. H. Evans, *J. Am. Chem. Soc.*, **105**, 1473 (1983); b) O. R. Brown, P. H. Middleton, and T. L. Threlfall, *J. Chem. Soc., Perkin Trans. 2*, **1984**, 955.

7) a) I. M. Mathai, K. Schug, and S. I. Miller, *J. Org. Chem.*, **35**, 1733 (1970); b) W. K. Kwok and S. I. Miller, *J. Am. Chem. Soc.*, **92**, 4599 (1970).

8) It may be claimed that the cis/trans ratio of the product, alkene, is determined also by relative stabilities of rotamers of the intermediate, property of the leaving atom (group), or bulkiness and charge of counter cation(s). Although such a point is not investigated in detail in the present study, this does not interfere our present discussion. It is important for the present study to point out that the intermediate has a chance to change its conformation.

9) C. J. Devlin and B. J. Walker, *J. Chem. Soc., Perkin Trans. 1*, **1972**, 1249.

10) The free radical species with such a structure has been supposed along the reductive debromination of *erythro*- and *threo*-2,3-dibromo-3-methylpentane with sodium naphthalenide: W. Adam and J. Arce, *J. Org. Chem.*, **37**, 507 (1972).

11) H. R. Ing and W. H. Perkin, Jr. *J. Chem. Soc.*, **125**, 1814 (1924).

12) R. E. Buckles, W. E. Steinmetz, and N. G. Wheeler, *J. Am. Chem. Soc.*, **72**, 2496 (1950).

Effects of Reduction Conditions on the Catalytic Activity of Rhodium Supported on TiO_2 for the Hydrogenation of Carbon Monoxide: Favorable Metal-Support Interaction

Hiroshi FUJITSU,* Nobuhide IKEYAMA,† Yasunobu SHIGAKI,† and Isao MOCHIDA

Research Institute of Industrial Science,

†*Department of Molecular Technology Graduate School of Engineering Sciences, Kyushu University 86, Kasuga 816*

(Received November 16, 1984)

Synopsis. Catalytic activity of Rh/TiO_2 was influenced significantly by reduction conditions, the maximum activity per weight being obtained by reduction at 400°C for 2 h, in spite of limited adsorption abilities against reactant gases. The nature of Rh/TiO_2 is sensitively modified to develop the most favorable metal-support interaction.

Designs of novel catalysts for $CO-H_2$ reaction have been extensively investigated for these years.[1] The roles of support and additive may be one of the most influential factors to be considered for this purpose. Titania is one of the most interesting supports to modify the catalytic activity and selectivity,[2-5] since Tauster *et al.*[6] reported SMSI as for the reduced adsorption abilities of group VIII metals supported on the oxide after the reduction at higher temperatures (above 500°C). Vannice *et al.*[7] claimed that the turnover frequency on such catalysts was enhanced by the higher reduction temperatures because of SMSI, however the activity per weight was rather similar to that reduced at lower temperature.[8] It has been scarecely attempted yet to find catalysts of better practical performance in spite of a number of studies on SMSI concept.[5,7] Kikuchi *et al.*[9] reported recently that Ru supported on rutile of large surface area showed the larger activity per weight at the SMSI than that at the non-SMSI state.

The present authors are going to report significant effects of the reduction temperature and time on the catalytic activity of Rh on TiO_2 for the $CO-H_2$ reaction to find the most active catalyst.

The most favorable extent of the reduction for the highest catalytic activity per weight must exist, since electron transfer from the support is profoundly influenced by the reductive heat-treatment.[10]

Experimental

Rh/TiO_2 was prepared by the impregnation of $RhCl_3-3H_2O$ on TiO_2 (Aerosil Inc, P-25, 50 m^2/g) using a methanol solution (Rh: 4.6 wt%). The catalytic reaction was carried out at 200 and 250°C, using a circulating reactor (vol. 800 ml) with a fixed catalyst bed (0.5 g cat, diluted with 5 g SiC), through which a reactant gas of CO and H_2 (their partial pressures were 26.7 and 53.3 KPa, respectively) flowed. Before the reaction, the catalyst was reduced in situ, and evacuated at 200°C for 1 h. During the reaction, products except for methane were trapped at liquid nitrogen temperature. The reactant gases and methane were analyzed with a gas chromatograph (Molecular Sieve 13 X, 1m) by the sampling at proper intervals during the reaction. Other trapped products were analyzed after the reaction with a gas chromatograph (Porapack Q, 1m, for CO_2; VZ-10, 2m, for hydrocarbons).

Reaction rates were calculated from the conversion of CO. The catalytic reacation was repeated three time at least giving well-reproduced rates and product distributions.

Adsorption of CO, H_2 and O_2 on the catalyst was measured volumetrically using the same reactor.

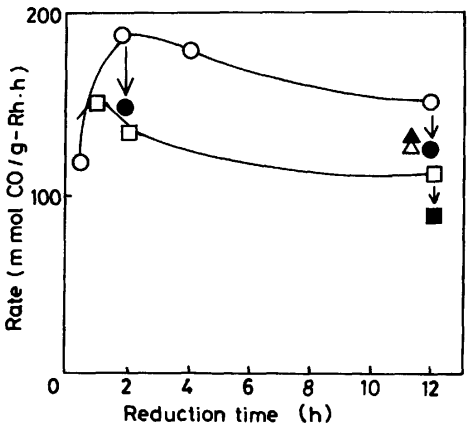

Fig. 1. Effects of reduction conditions and oxygen preadsorption on the catalytic activity of Rh/TiO_2. cat: 0.5 g/5 g SiC, P_{H_2}/P_{CO}=26.7/53.3(KPa), reaction temp: 200°C, reduction temp: 200°C (△,▲), 400°C (○,●), 500°C (□,■), open: without oxygen preadsorption, colsed: after the oxygen pre-adsorption.

Results and Discussion

Catalytic activities at 200°C depended very much on the reduction conditions, both temperature and time, as shown in Fig. 1. The reduction at 400°C for 2 h (catalyst-400) provided the highest activity per weight among the reduction conditions examined. Longer time at the same temperature decreased the rate considerably. The catalyst reduced at 500°C (catalyst-500) showed the maximum activity by the reduction for 1 h and gradual decreases of activity with longer times to give the lowest activity by 12 h. In contrast, the reduction at 200°C (catalyst-200) provided constant activities independent on the reduction time. Such activity differences due to the reduction conditions were more marked in the reaction at 250°C (Table 1).

More long-chain hydrocarbons ($>C_5$) were obtained over the catalysts reduced at both 400 and 500°C when the product distributions were compared.

Table 2 summarized the effects of reduction conditions on the adsorption abilities against H_2, CO and O_2 at room temperature. The reduction at 200°C provided *ca.* 0.5 of both H/Rh and CO/Rh atomic ratios regardless the reduction time. These ratios decreased markedly by increasing the reduction temperature. The smallest values on the catalyst-500 indicate the definite SMSI as reported in the literature.[6] In contrast, adsorption ability of the catalyst against O_2

Table 1. Effects of the reduction temperature and oxygen adsorption on the catalytic activity of Rh/TiO_2 at 250 °C[a]

Redn. temp	Reaction rate	
°C	m mol CO/g-Rh·h	
	Virgin	After O_2 adsorption[b]
200	1180	1200
400	1350	900
500	970	680

a) cat.(4.6 wt % Rh): 0.5 g/5 g SiC, reduction time: 2h P_{H_2}/P_{CO}=26.7/53.3 KPa. b) 20.0 KPa O_2 was pre-adsorbed at room temperature, followed by evacuation at 200 °C-1 h.

Table 2. Adsorption abilities of the catalysts against H_2, CO and O_2

Redn. temp	Adsorption		
°C-h	H/Rh[a]	CO/Rh[b]	O/Rh[c]
200- 2	0.54	0.52	0.48
-12	0.54	0.51	—
400- 2	0.23	0.32	0.53
-12	0.11	0.23	—
500- 2	0.05	0.08	0.50
-12	0.02	0.06	—

a) Room temp, P_{H_2}=1.3—93.3 KPa. b) Room temp, P_{CO}=26.7 KPa. c) Room temp, P_{O_2}=20.0 KPa.

was not influenced by the reduction conditions to show almost constant values of O/Rh ratio as reported by Meriaudeau *et al.*[11]

The oxygen adsorption at room temperature provided remarkable effects on the catalytic activity, depending strongly on the reduction temperatures of the catalysts as shown in Fig. 1 and Table 1. The reaction rates over the catalysts-400 and -500 at 200 and 250 °C were decreased by the oxygen adsorption by *ca.* 20 and 30%, respectively, whereas no retardation was observable with the catalyst-200. The product distribution was not effected by the oxygen adsorption.

It may be the most significant observation in the present study that the catalyst reduced at 400 °C for 2 h exhibited the highest catalytic activity per g-Rh. The interaction between Rh and TiO_2 which allowed the maximum activity per g-Rh can be defined as FMSI (Favorable Metal Support Interaction), its search being a practical target in the catalyst design. The reduction at 400 °C for 2 h may compromise most favorably the extents of reduction and dispersion of Rh as well as electron-donating ability of supporting TiO_2.[10] The hydrogenation activity of such a catalyst was rather low to increase the yields of longchain hydrocarbons.

The activity per g-catalyst is the product of the activity of an active site and its number on the catalyst surface. The latter has been proposed to be estimated from the amounts of hydrogen adsorption (H/Rh ratio).[5,7,8] However, it is suspicious that the ratio reflects its accurate number. The nature of the metal catalyst is suggested to be modified significantly by the support according to the pretreatment conditions.

The balanced activation abilities against H_2 and CO of Rh modified through FMSI may provide the maximum activity where the number of the active sites is rather unchanged. Such a FMSI may be possible between Rh metal and properly reduced titania by dehydration and hydrotreatment.

Reference

1) Catalysis Society of Japan Ed., "C_1 Chemistry," Kodansha Scientific Inc., Tokyo (1984).
2) B. Imelik, C. Naccache, G. Coudurier, H. Praliaud, P. Meriaudeau, P. Gallezot, G. A. Martin, and J. C. Vedrine Ed., "Metal-Support and Metal-Additive Effects in Catalysis," Elsevier (1982).
3) M. Ichikawa, *Bull. Chem. Soc. Jpn.*, **51**, 2268, 2278 (1978).
4) E. L. Kugler, *ACS Prep., Div. Petrol. Chem.*, **25**, 564 (1980).
5) M. A. Vannice and R. L. Gartern, *J. Catal.*, **66**, 242 (1980).
6) S. L. Tauster, S. C. Fung and R. L. Garten, *J. Am. Chem. Soc.*, **100**, 170 (1978).
7) M. A. Vannice, "Pan-Pacific Synfuels Conference, Abstract," Vol. 1., (1982), p. 208.
8) T. Uchijima and K. Kunimori, *J. Surf. Sci. Soc. Jpn.*, **5**, 332 (1984).
9) E. Kikuchi, H. Nomura, M. Matsumoto, and Y. Morita, "Pan-Pacific Synfuels Conference, Abstract," Vol. 1, (1982), p. 216.
10) I. Mochida, K. Tsuji, K. Suetsugu, H. Fujitsu, and K. Takeshita, *J. Phys. Chem.*, **84**, 3159 (1980); I. Mochida, K. Suetsugu, H. Fujitsu and K. Takeshita, *ibid.* **87**, 1524 (1983), *Chem Lett.*, **1983**, 177.
11) P. Meriaudeau, O. H. Ellestad, M. Dufanx, and C. Naccache, *J. Catal.*, **75**, 243 (1982).

Rate Coefficient for $H+C_2H_2 \rightleftarrows C_2H+H_2$

William GARDINER,* Tsuneo TANZAWA, Tohru KOIKE,† and Kihei MORINAGA†
Department of Chemistry, University of Texas, Austin, Texas 78712 U. S. A.
†*Department of Chemistry, National Defense Academy, Hashirimizu, Yokosuka 239*
(Received November 27, 1984)

Synopsis. The rate coefficient expressions $k=10^{13.78}$ exp(−99 kJ/RT) cm^3 mol^{-1}s^{-1} for $H+C_2H_2 \rightarrow C_2H+H_2$ and $k=10^{13.05}$ exp(−12 kJ/RT) cm^3 mol^{-1} s^{-1} for $C_2H+H_2 \rightarrow H+C_2H_2$ were proposed after correcting for errors in previously reported data analyses of shock tube data on C_2H_2 pyrolysis.

The homogeneous thermal decomposition of C_2H_2 proceeds by chain reactions in which one of the important elementary reactions is

$$H + C_2H_2 \longrightarrow C_2H + H_2. \quad (1)$$

Rate coefficients for this reaction can be derived by analysing C_2H_2 decomposition rate data with the aid of computer modeling. In one of such studies, Tanzawa and Gardiner[1] (TG1) fitted laser-schlieren profiles of the density gradients in C_2H_2–Ar mixtures heated by incident shock waves to temperatures in the range 1700—3400 K. In another, Koike and Morinaga[2] (KM) fitted 216 nm absorption profiles of C_4H_2 appearance from C_2H_2–Ar mixtures heated to temperatures in the range 1800—2600 K in incident shock waves. In a modeling study in which a number of experiments were interpreted with a single mechanism[3] (TG2), a temperature-independent value for the rate coefficient of the reverse reaction $k_{-1}=10^{13.54}$ cm^3 mol^{-1}s^{-1} was reported to fit the experimental results. This value is higher than the k_{-1} value $10^{12.4}$ cm^3 mol^{-1}s^{-1} of KM by a factor much larger than the anticipated experimental error bounds. In order to discover the source of this difference, the procedures used in both data analyses were reexamined. As described below, the apparent discrepancy resulted from transcriptional errors in manuscript preparation and in an incorrect thermochemical data record for C_2H. When these corrections were made, it became clear that the KM and TG1 experiments are in close agreement about the rate of Reaction (1).

For the conditions of C_2H_2 decomposition in shock waves, Reaction (1) proceeds in the forward direction during the time of rate measurements. In the data analysis of TG2, the forward rate coefficient k_1 was input as an Arrhenius expression for the computer modeling. As it was noticed that this expression implied fairly constant values of the reverse rate coefficient k_{-1}, it was decided to report a temperature-independent k_{-1} valid for the range of the TG1 experiments rather than the Arrhenius expression of k_1. (The computer programs used in all studies discussed here used essentially identical mathematical procedures and include both the forward and reverse directions of all reactions, the reverse reaction rate coefficients being computed from the forward reaction rate coefficients using the equilibrium constant implied by the thermochemical properties of the reacting species.) Unfortunately, in preparing the TG2 manuscript for publication, the preexponential factor of the k_1 expression $10^{13.54}$ cm^3 mol^{-1} s^{-1} was assigned to k_{-1} instead of the value $10^{12.75}$ cm^3 mol^{-1} s^{-1} that was actually found to be typical of the k_{-1} values implied by k_1 expressions that provided good fits to the TG1 data.

In analysing their data, KM adopted the more convenient reverse reaction $C_2H+H_2 \rightarrow H+C_2H_2$ as input even though the direction in which reaction proceeded during their measurements was $H+C_2H_2 \rightarrow C_2H+H_2$ as in the TG1 experiments. By adjusting k_{-1} to fit their data, the value $k_{-1}=10^{12.4}$ cm^3 mol^{-1} s^{-1} was found to be optimal, still a factor of two smaller than the corrected TG2 value and still outside the error limits of both studies. The source of the remaining discrepancy was found on investigation to be a faulty thermochemical data record for the species C_2H. While this record was faulty at first in both the TG2 and KM computer programs, it affected the data analysis only through computing the value of k_1 from k_{-1}, and thus distorted only the KM computations. When the correct C_2H thermochemistry was used, it was found that the optimal k_{-1} values for fitting the KM data became quite close to the corrected TG2 result. Over 2000 K, $k_{-1}=10^{12.88}$ cm^3 mol^{-1} s^{-1} gave very close match to the KM data, while at lower temperatures $k_{-1}=10^{10.18}$ exp(115 kJ/RT) was required. A comparison with the KM data is shown in Fig. 1. It can be seen that the inconsistent k_{-1} expression for lower temperatures is actually very close to higher-temperature result; There seems to be some unappreciated systematic error at lower temperatures, which has no effect upon the analysis presented here. Arrhenius expressions can be derived for k_1 and k_{-1} by combining room temperature

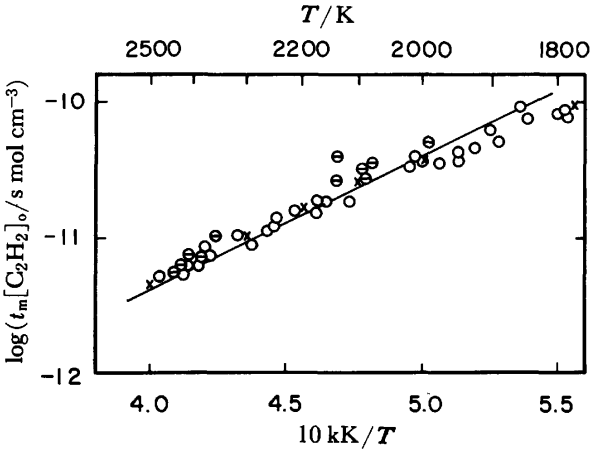

Fig. 1. Comparison of computed and measured rate parameters for 216 nm absorption change. For definition of t_m, see Ref. 2.
○: C_2H_2/Ar=3.2/96.8, ⊖: C_2H_2/H_2/Ar=2.0/2.2/95.8, and ×: computed for C_2H_2/Ar=3.2/96.8. All data points are from Ref. 2.

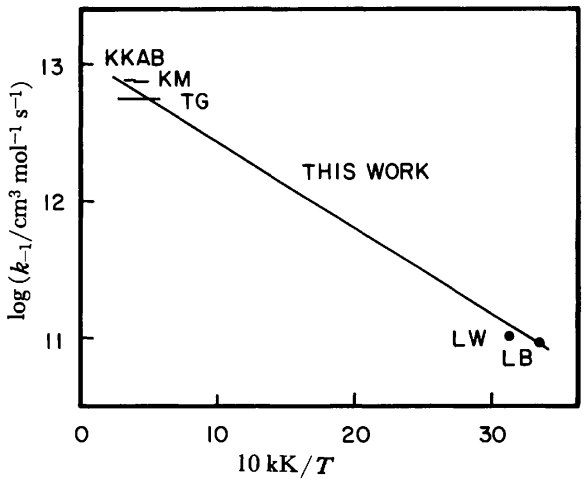

Fig. 2. Arrhenius graph for $C_2H+H_2 \rightarrow C_2H_2+H$. KKAB=Ref. 11, KM=Ref. 2, TG=Ref. 1, LW=Ref. 4, LB=Ref. 5, and THIS WORK=$10^{13.05}$ exp(−12 kJ/RT) $cm^3 mol^{-1} s^{-1}$.

measurements of k_{-1} with a representative value for k_{-1} at 2800 K of $10^{12.75}$ $cm^3 mol^{-1} s^{-1}$. Lange and Wagner[4] reported $k_{-1}=10^{11}$ $cm^3 mol^{-1} s^{-1}$ at 320 K, while Laufer and Bass[5] reported $10^{10.96}$ $cm^3 mol^{-1} s^{-1}$ at 298 K. The Arrhenius expression $k_{-1}=10^{13.05}$ exp(−12 kJ/RT) $cm^3 mol^{-1} s^{-1}$ accounts for the 50-fold increase in rate coefficient between 300 and 2800 K. (Fig. 2) The corresponding expression for k_1 is $10^{13.78}$ exp(−99 kJ/RT) $cm^3 mol^{-1} s^{-1}$. These two expressions are thermochemically compatible with one another providing that JANAF[6] thermochemistry is used for all species except that $\Delta H^\circ_{f0}(C_2H)=531$ kJ/mol as derived by Okabe and Dibeler.[7]

The only other study known to us in which fairly direct determination of k_1 or k_{-1} is asserted is that of Yampol'skii *et al.*[8] Their expessions, however, are more than an order of magnitude higher than the consensus of the 5 studies shown in Fig. 2, and apparently result from contamination by unidentified catalytic pathways for isotope exchange.

Aside from Reaction (1), the reaction mechanisms used by KM and TG2 differ in that TG2 included the reaction

$$H + C_2H_2 \longrightarrow C_2H_3 \qquad (2)$$

using a rate coefficient reported by Payne and Stief,[9] while KM used instead the M-dependent form for the reverse reaction

$$C_2H_3 + M \longrightarrow C_2H_2 + H + M \qquad (-2)$$

and a theoretical rate coefficient derived by Benson and Haugen.[10] While reactions of C_2H_3 become important in C_2H_2 thermal decomposition only at temperatures well below those of the TG1 and KM experiments, we nonetheless repeated the TG2 computations using Reaction (−2) and the Benson and Haugen rate coefficient expression. No significant differences were seen. We note, however, that while the rate of Reaction (2) is predicted to be more or less the same by both the Payne and Stief and the Benson and Haugen expressions for the conditions of the TG1 and KM experiments, they do diverge for other conditions and must be adopted with care for simulation purposes.

Subsequent to the TG2 and KM publications, the thermal decomposition of C_2H_2 produced from thermal decomposition of C_2H_4 was studied by Kiefer *et al.*[11] For their conditions, Reaction (1) proceeds predominantly in the reverse direction, and the laser-schlieren gradients they measured proved to be sensitive to k_{-1}. Their result $k_{-1}=10^{12.87}$ $cm^3 mol^{-1} s^{-1}$, for the temperature range 2600—3000 K, is seen to be in good agreement with the expression derived here. Reference is made to their paper for extensive discussion of the effect of subsequent reactions for their and the TG1 experimental conditions.

Our reexamination of the rate coefficient for this important reaction was stimulated by discussions with J. H. Kiefer and J. Warnatz. Finantial support was provided by the U. S. Army Research Office and the Robert A. Welch Foundation.

References

1) T. Tanzawa and W. C. Gardiner, Jr., "17th Int. Symp. Combust.," The Combustion Institute, Pittsburgh (1979), p. 563.
2) T. Koike and K. Morinaga, *Bull. Chem. Soc. Jpn.*, **54**, 530 (1981).
3) T. Tanzawa and W. C. Gardiner, Jr., *J. Phys. Chem.*, **84**, 236 (1980).
4) W. Lange and H. Gg. Wagner, *Ber. Bunsenges. Phys. Chem.*, **79**, 165 (1975).
5) A. H. Laufer and A. M. Bass, *J. Phys. Chem.*, **83**, 310 (1979).
6) D. R. Stull and H. Prophet, "JANAF Thermochemical Tables," 2nd Ed., NSRDS-NBS 37 (1971).
7) H. Okabe and V. H. Dibeler, *J. Chem. Phys.*, **59**, 2430 (1973).
8) Yu. P. Yampol'skii, K. P. Lavrovskii, Yu. V. Masksimov and V. M. Rybin, *Kinetics and Catalysis*, **15**, 9 (1974).
9) W. A. Payne and L. J. Stief, *J. Chem. Phys.*, **64**, 1150 (1976).
10) S. W. Benson and G. R. Haugen, *J. Phys. Chem.*, **71**, 1735 (1967).
11) J. H. Kiefer, S. A. Kapsalis, M. Z. Al-Alami, and K. A. Budach, *Comb. Flame*, **51**, 79 (1983).

Measurement of Ultralow Interfacial Tension in the Vicinity of Critical Solution Temperature

Makoto ARATONO* and Kinsi MOTOMURA
Department of Chemistry, Faculty of Science, Kyushu University 33, Fukuoka 812
(Received January 24, 1985)

Synopsis. A new apparatus adopting the sessile drop technique has been designed to measure the ultralow interfacial tension between two liquids of a binary mixture. The equilibrium interfacial tension of the mixture of isobutyric acid and water has been determined near its upper critical solution temperature up to the value of 0.02 $\mu N\,m^{-1}$.

When two liquids are practically immiscible with each other, the properties and structure of the interface between the liquids have been clarified by measuring the dependence of interfacial tension on temperature and pressure and evaluating the thermodynamic quantities of interface formation.[1-3] When two liquids are practically miscible and have the critical solution temperature, however, thermodynamic investigations of the interface are scarce.[4-9] This may be attributable to the difficulty of the precise measurement of ultralow interfacial tension at temperatures near the critical solution temperature. In the present study, we made an apparatus for measuring the ultralow interfacial tension and determined the equilibrium interfacial tension values near the critical solution temperature.

Experimental

Materials. Isobutyric acid (Nakarai's guaranteed reagent) was distilled fractionally at atmospheric pressure and the middle fraction was used for the experiments. The sample was found to be 99.9% pure by gas-liquid chromatography with a 3 m long and 3 mm in diameter column packed with Unisole 400 (Gaskuro Kogyo Inc.). The doubly distilled water was further distilled after refluxing with alkaline permanganate.

Interfacial Tension Measurement. The measurements of the interfacial tension between the two phases in equilibrium near the upper critical solution temperature T_c of binary liquid mixture under atmospheric pressure were carried out by a new sessile drop method. Figure 1 shows the sessile drop cell which was mounted in the jacketed vessel made of acrylate resin. The temperature control of the cell is an important matter in the present study. To minimize a fluctuation in temperature, the whole system was placed in the air thermostat. In result, the temperature of the cell measured by the Beckmann thermometer was found to be constant within ±0.002 K. The sessile drop was formed in the following way. The binary mixture (80—100 ml) having a composition close to the critical one in the cell was vigorously stirred by a rotor (a) for about 30 min at the desired temperature and permitted to stand for from 1 to 7 h to separate completely into the water-rich (b) and acid-rich (c) phases. Then a part of the upper layer solution was sucked up into the syringe (d) by the plunger (e) and then the optical flat (f) attached to the bottom of syringe was dipped into the lower layer solution. At this stage, the sessile drop (g) was formed on the surface of the optical flat by pushing the plunger by rotating micrometer (h) and located by the level adjuster in the position which permits to take its photograph. By the use of the camera with the bellows of about five magnification and the light ray parallel to the optical axis, we could have a clear, enlarged, and undistorted profile.

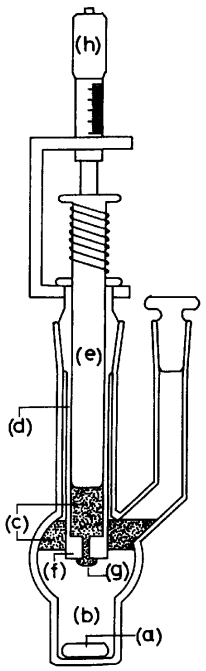

Fig. 1. Cross sectional view of a quartz sessile drop cell. (a): Rotor, (b): water-rich phase, (c): acid-rich phase, (d): syringe, (e): plunger, (f): optical flat, (g): sessile drop, (h): micrometer.

The interfacial tension γ was calculated by making use of the following equation[10,11]

$$\gamma = (1/2)g\Delta d a^2 \quad (1)$$

where g is the acceleration of gravity and Δd the density difference between two conjugate solutions. The values of Δd were available from the literature.[12] The capillary constant a^2 is correlated to the dimensions of the image on the negative film by the relation

$$a^2 = r^2 f(h/r), \quad (2)$$

where r is the radius of the drop in the equatorial plane, h the distance from the apex to the plane, and $f(h/r)$ the function of h/r. The values of h and r were determined by Nikon measurescope (model II) with the precision of ±1 μm. The experimental error of the interfacial tension did not exceed two percent of the obtained value.

Figure 2 shows the time dependence of interfacial tension. It can be seen that the equilibrium value can be obtained within a few minutes. Therefore, the drop was stood for about 15 min and photographed.

Results and Discussion

The γ *vs.* $T-T_c$ curves are shown in Fig. 3; the value of T_c determined by making use of the mutual solubility curve[13] has been used. It is seen from Fig. 3 that the value of γ decreases monotonously with rising

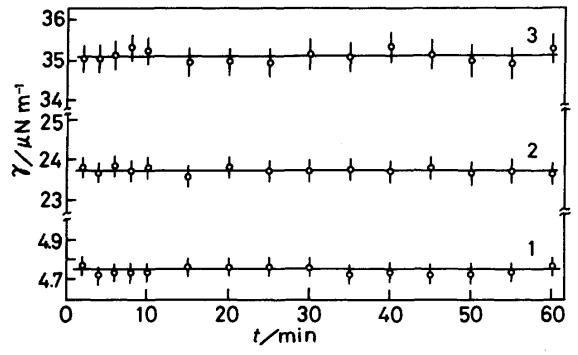

Fig. 2. Interfacial tension *vs.* time curves. 1: $T-T_c$=−0.708 K, 2: −2.365, 3: −3.175.

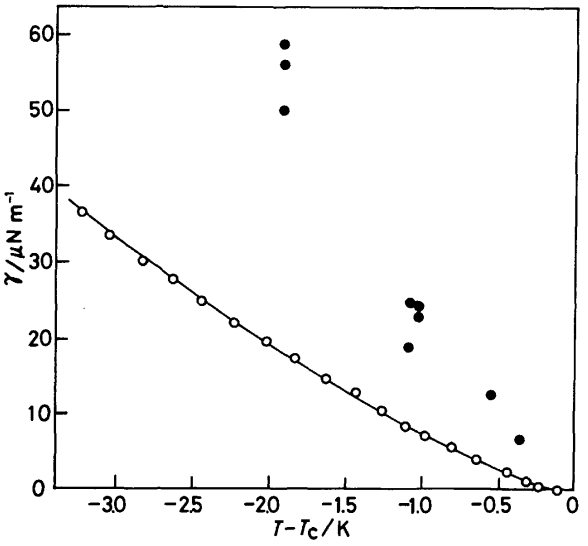

Fig. 3. Interfacial tension *vs.* temperature curve. (○): Present study, (●): data from reference 9.

temperature and approaches zero at the critical solution temperature. This is the behavior expected for the binary liquid mixture which has the upper critical solution temperature. Further it is worth noting that the value varies from 35 to 0.02 μN m^{-1} in the narrow temperature range in $T-T_c$ from −3.2 to −0.1 K. The closed symbols in Fig. 3, the γ values of Howland *et al.*,[9] are larger than ours and show considerable scatter. In addition, the lowest value of the former is found to be significantly high compared to the one of the latter. Taking into account that the capillary rise method employed by Howland *et al.* is unsuitable in principle for measuring the ultralow interfacial tension, the above results may indicate that the sessile drop method of the present study provides the ultralow interfacial tension values accurate enough to consider the behavior of the interface between the two phases of binary liquid mixture near the critical solution temperature.

It has been shown that the dependence of γ on temperature at constant pressure gives useful information regarding the entropy of interface formation.[1,4] It is supposed, therefore, that the formation of the interface from the two phases of binary liquid mixture in equilibrium near the upper critical solution temperature is attended by an increase in entropy and the entropy of interface formation is reduced to zero at the upper critical solution temperature. Further discussion will be made in the separate paper.[13]

The present work was supported by a Grant-in-Aid for Scientific Research No. 59470005 from the Ministry of Education, Science and Culture.

References

1) K. Motomura, *J. Colloid Interface Sci.*, **64**, 348 (1978).
2) K. Motomura, *Adv. Colloid Interface Sci.*, **12**, 1 (1980).
3) K. Motomura, H. Iyota, M. Aratono, M. Yamanaka, and R. Matuura, *J. Colloid Interface Sci.*, **93**, 264 (1983).
4) D. Atack and O. K. Rice, *Discuss. Faraday Soc.*, **15**, 210 (1953).
5) B. E. Sundquist and R. A. Oriani, *J. Chem. Phys.*, **36**, 2604 (1962).
6) C. Warren and W. W. Webb, *J. Chem. Phys.*, **50**, 3694 (1969).
7) A. W. Wims, J. V. Sengers, D. McIntyre, and J. S. Sherenshefsky, *J. Chem. Phys.*, **52**, 3042 (1970).
8) R. B. Heady and J. W. Cahn, *J. Chem. Phys.*, **58**, 896 (1973).
9) P. G. Howland, N. C. Wong, and C. M. Knobler, *J. Chem. Phys.*, **73**, 522 (1980).
10) J. F. Padday, "Surface and Colloid Science," ed by E. Matijević, Wiley, New York (1969), Vol. 1, p. 101.
11) J. F. Padday, *Phil. Trans. R. Soc. London A*, **269**, 265 (1971).
12) S. C. Greer, *Phys. Review A*, **14**, 1770 (1976).
13) M. Aratono and K. Motomura, to be submitted.

Determination of the Stability Constants of Crown Ether Complexes with Protonated Amines by Solvent Extraction

Hideyuki NOGUCHI,* Masatoshi NAGAMATSU, and Masaki YOSHIO
Department of Industrial Chemistry, Faculty of Science and Engineering, Saga University, Honjyo, Saga 840
(Received September 27, 1984)

Synopsis. Stability constants of crown ether complexes with protonated primary amines were determined by the solvent extraction method. Stability constants between protonated amines(AH^+) and 18-crown-6(L), log K_{AHL}, were found to be 0.4, 0.15, 0.1, −0.05, and −0.1 for protonated methylamine, ethylamine, propylamine, butylamine, and *iso*-propylamine at 25.0 °C, respectively.

Accurate determination of stability constants of small values are more difficult than those of higher values.[1] Here, we propose a method for the determination of stability constants. The method has been successfully applied to determing especially small values of stability constants between 18-crown-6 and protonated primary amine. Crown ether in an organic phase is extracted by complexation with primary amine hydrochloride (or sodium chloride etc.) in the aqueous phase, which can not be extracted into the organic phase. So, stability constants of crown ether with protonated primary amines can be determined by the analysis of the extraction equilibria.

In this paper, we describe the method for the determination of stability constant by back extraction, and discuss the results with data obtained in other literature.[3-5]

Theory

The following equations may be written for the extraction system composed of crown ether, water, organic solvent, and salts, such as potassium chloride, sodium chloride and ammonium chloride, which can not be extracted into the organic phase at the limited pH range.

$$L \rightleftharpoons L_o \qquad K_{d,L} = [L]_o/[L] \tag{1}$$

$$M^+ + L \rightleftharpoons ML^+ \qquad K_{ML^+} = [ML^+]/([M^+][L]) \tag{2}$$

$$C_{M^+} = [M^+] + [ML^+] \tag{3}$$

$$C_L = [L] + (V_o/V)[L]_o + [ML^+] \tag{4}$$

where subscript "o" denotes the organic phase, $K_{d,L}$, K_{ML^+}, C_{M^+}, C_L, V_o, and V show the distribution coefficient of the crown ether, stability constant of crown ether complex (ML^+) in the aqueous phase, total concentration of M^+ and L, volume of organic and aqueous phase, respectively. In the case of protonated amines, the symbol AH^+ is used instead of M^+. Eq. 5 can be obtained when C_{M^+} is much larger than C_L.

$$\log C_L = \log [L]_o + \log (V_o/V + K_{d,L}^{-1}(1 + K_{ML^+}C_{M^+})) \tag{5}$$

Log C_L against log $[L]_o$ plot should show a straight line of slope 1. Therefore, K_{ML^+} can be calculated from the value at the intercept of the log C_L axis. Thus, the stability constants can be determined under constant ionic strength by the method.

Experimental

A typical procedure was as follows. 25 ml of aqueous solution containing 0.5 mol dm^{-3} primary amine hydrochloride and 18-crown-6(5×10^{-5}—2×10^{-3} mol dm^{-3}) was mixed with 10 ml of 1,2-dichloroethane and shaken for 1 day in a thermostated bath at 25.0 °C. The concentration of alkali metal chloride or ammonium chloride were the same as in the above case except for the potassium ion, which was 0.1 mol dm^{-3}. The concentration of the 18-crown-6 in the organic phase was measured spectrophotometrically after extraction with potassium picrate.[2] The adjustment of the pH was made with dilute hydrochloric acid and lithium hydroxide solution. No other reagents and buffers were used during the experimental runs.

Results and Discussion

In order to check the validity of the Eq. 5, 18-crown-6, water, 1,2-dichloroethane and metal salt (KCl, NaCl, or NH_4Cl) system was chosen. It was found that cations (K^+, Na^+, NH_4^+) and anion(Cl^-) are not extracted into the 1,2-dichloroethane phase at least over the pH range of 3.5—6.0.

Distribution coefficient of 18-crown-6($K_{d,L}$) was determined to be 1.12 at 25.0 °C.

Plots of C_L against log $[L]_o$ are shown in Fig. 1. Linear relationships were obtained as expected from Eq. 5. The calculated values of log K_{ML^+} are found to be 2.08, 0.63, and 0.97 for potassium, sodium, and ammonium complexes with 18-crown-6 under the ionic strength 0.5 (0.1 in the case of KCl). These values agreed very closely with those in the literature,[3,4] in which 2.03, 0.8, and 1.23 were reported for the values of the respective complexes.

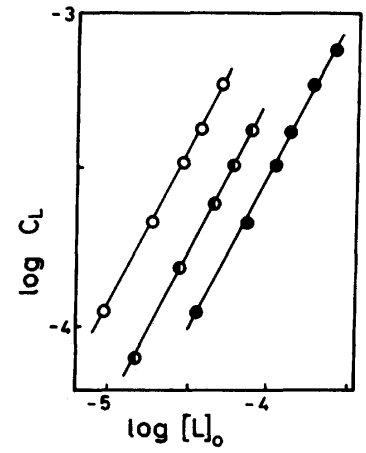

Fig. 1. log C_L *vs.* log $[L]_o$ plots in the presence of 0.1 mol dm^{-3} KCl(○), 0.5 mol dm^{-3} NH_4Cl(◐), and NaCl(●).

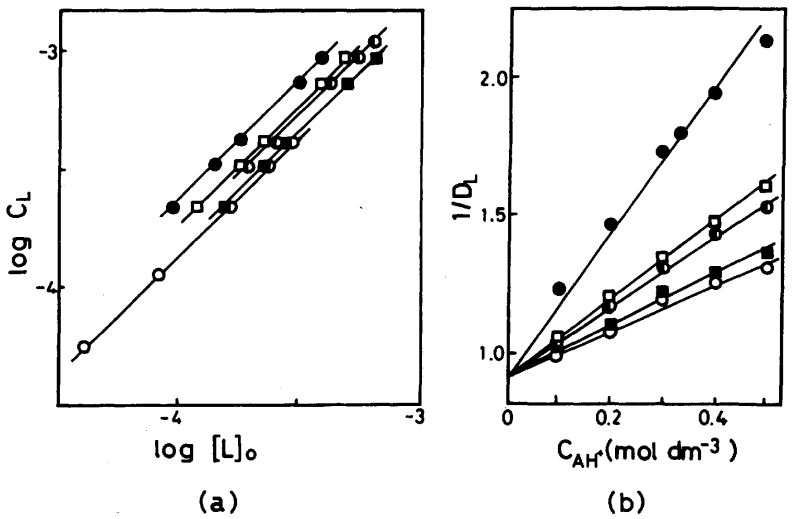

Fig. 2. log C_L *vs.* log $[L]_o$ and $1/D_L$ *vs.* C_{AH^+} plots for protonated primary amines.
(a)$C_{AH^+}=0.5$ mol dm^{-3}, (b) $C_L=2.4\times10^{-4}$ mol dm^{-3}.
●: methylamine, □: ethylamine, ◐: propylamine, ■: buthylamine, ○: isopropylamine

Methods for the determination of accurate stability constants having small values are very limited and such small values of stability constants sometimes contain errors.

Our method proposed here would, especially, be valid for the determination of stability constants of small values, because the concentration of crown ether in the organic phase can be determined accurately. The accuracy increases when the crown ether distributes more equally between both phases. The determination of stability constants of 18-crown-6 complexes with several protonated amines were then attempted. The experimental conditions are the same as those described before. Plots of log C_L against log $[L]_o$ are shown in Fig. 2a for protonated primary amines. Each plot has a straight line with a slope of 1. The result shows that the extraction system can be expressed by Eqs. 1—4.

The log K_{AHL} values obtained are 0.4, 0.15, 0.1, −0.05, and −0.1 for protonated methylamine, ethylamine, propylamine, butylamine, and isopropylamine at a constant ionic strength (0.5).

The values obtained by Larson *et al.*[5] for protonated amine–18-crown-6 are obviously higher than the data obtained by us. Their values obtained by the glass electrode measurement may contain some errors. They determined the stability constants by the measurement of the pH difference before and after adding 18-crown-6 to the system containing an amine and the corresponding amine hydrochloride. For example, the pH difference for the trimethylamine system is only 0.074 pH units according to our calculation by using the stability constant 5.5 (log $K_{AHL}=0.74$) given by them. They reported that the uncertainties are equivalent to an error in pH of about ±0.02 pH units. This means that the stability constants especially for weak complexes such as 18-crown-6-protonated trimethylamine, contains about ±30% errors.

Another approach for the determination of stability constants is as follows. Equation 6 can be obtained by using Eqs. 1—4 and distribution ratio of crown ether, ($D_L=[L]_o/([L]+[AHL^+])$).

$$\frac{1}{D_L}=\frac{1}{K_{d,L}}+\frac{K_{AHL}C_{AH^+}}{K_{d,L}} \qquad (6)$$

Plot of $1/D_L$ against C_{AH^+} should show a straight line and the intercept at $C_{AH^+}=0$ should show the value of $K_{d,L}^{-1}(=0.89)$. Hence, K_{AHL} can be also calculated from the slope analysis. The plot of $1/D_L$ *vs.* C_{AH^+} for protonated primary amines at fixed C_L (2.4×10^{-4} mol dm^{-3}) is shown in Fig. 2b. The extrapolation to $C_{AH^+}=0$ shows $1/K_{d,L}$, then the extraction mechanism could be expressed by Eqs. 1—4. Log K_{AHL} values obtained from this method agreed well with those obtained (deviations are within ±0.03) by the method under constant ionic strength.

References

1) H. Rossotti, "The Study of Ionic Equilibria," Longman (1978), p. 71
2) C. J. Pedersen, *J. Am. Chem. Soc.*, **92**, 391 (1970).
3) R. M. Izatt, R. E. Terry, B. L. Haymore, L. D. Hansen, N. K. Dalley, A. G. Avondet, and J. J. Christensen, *J. Am. Chem. Soc.*, **98**, 7620 (1976).
4) H. K. Frensdroff, *J. Am. Chem. Soc.*, **93**, 600 (1971).
5) J. L. Roberts, R. E. McClintock, Y. El-Omrani, and J. W. Larson, *J. Chem. Eng. Data*, **24**, 79 (1979).

Crystal and Molecular Structure of a Triply-thiolate-bridged Binuclear Cobalt(III) Complex, $[Co_2\{SCH(CH_2CH_2NH_2)_2\}_3](ClO_4)_3 \cdot H_2O$

Masahiro MIKURIYA,* Sigeo KIDA, Shigehiro UENO, and Ichiro MURASE†

Department of Chemistry, Faculty of Science, Kyushu University 33, Hakozaki, Higashi-ku, Fukuoka 812

†*Laboratory of Chemistry, College of General Education, Kyushu University 01, Chuo-ku, Fukuoka 810*

(Received February 8, 1985)

Synopsis. The crystal structure of tris[μ-(1,5-diamino-3-pentanethiolato)-*N*,*N*′, μ-*S*]-dicobalt(III) perchlorate monohydrate was determined by the single-crystal X-ray diffraction method. The binuclear complex has a novel type of binuclear structure in which the two cobalt atoms are bridged by three thiolate sulfur atoms forming a face-shared bioctahedron.

Metal compounds with thiolate ligands are now regarded as an important class of complex in the field of bioinorganic chemistry.[1] A number of compounds containing metal atoms bridged by thiolate sulfur have been reported, but little effort has been devoted toward the isolation of discrete binuclear metal complexes as yet.[2] Recently, Murase *et al.* reported the synthesis of binucleating ligand, 1,5-diamino-3-pentanethiol (Hdpet), and its binuclear complexes, $[M_2(dpet)_2](ClO_4)_2$ (M=Ni, Pd) and $[Co_2(dpet)_3](ClO_4)_3$.[3] Based on the analytical, spectral and magnetic data, they concluded that the cobalt(III) complex possesses a binuclear structure in which the two cobalt atoms are bridged by three thiolate sulfur atoms forming a face-shared bioctahedron. To our knowledge, this is the first example of a triply-thiolate-bridged binuclear cobalt(III) complex. In this study, we have confirmed the structure of $[Co_2(dpet)_3](ClO_4)_3$ by the single-crystal X-ray diffraction method.

Experimental

Black crystals of $[Co_2(dpet)_3](ClO_4)_3 \cdot H_2O$ were prepared by method previously reported.[3] A crystal with dimensions of 0.20×0.40×0.42 mm was used for the X-ray analysis. The unit-cell parameters and intensities were measured on a Rigaku AFC-5 automated four-circle diffractometer with graphite-monochromated Mo$K\alpha$ radiation (λ=0.71069 Å) at 23±1 °C.

Crystal Data: $Co_2(C_5H_{13}N_2S)_3(ClO_4)_3 \cdot H_2O$, F.W.=833.93, monoclinic; $P2_1/c$; a=11.101(4), b=28.619(6), and c=10.692(2) Å; β=113.66(2)°; V=3111(1) Å^3; D_m=1.78, D_c=1.78 g cm^{-3}; Z=4.

The intensity data were collected by the 2θ—ω scan technique with a scan rate of 4° min^{-1}. Three standard reflections were monitored every 100 reflections, and their intensities showed a good stability. A total of 5960 reflections with 2θ<50° were collected. The intensity data were corrected for the Lorentz and the polarization effects, but not for absorption. Independent 4439 reflections with $|F_o| \geq 3\sigma(F_o)$ were considered as "observed" and were used for the structure analysis.

The structure was solved by the direct method. Refinement was carried out by the block-diagonal least-squares method. Hydrogen atoms were inserted in their calculated positions and included in the refinement. The final R value was $R=\sum||F_o|-|F_c||/\sum|F_o|=0.071$. Final difference Fourier map was featureless except for three peaks of 1.26—1.78 e/Å^3 in the vicinity of the sulfur atoms, S(A), S(B), and S(C). All the calculations were carried out on the FACOM M-200 computer in the Computer Center of Kyushu University by the use of a local version[4] of the UNICS-III and the ORTEP programs. The final positional and thermal parameters with their estimated standard deviations are given in Table 1. The coordinates and isotropic temperature factors of the hydrogen atoms, the anisotropic thermal parameters of the non-hydrogen atoms, bond lengths and bond angles, and the F_o—F_c tables have been deposited as a Document No. 8528 at the Office of the Editor.

TABLE 1. FRACTIONAL POSITIONAL PARAMETERS (×10^4) AND THERMAL PARAMETERS OF NON-HYDROGEN ATOMS WITH THEIR ESTIMATED STANDARD DEVIATIONS IN PARENTHESES

Atom	x	y	z	B_{eq}/Å^2
Co(1)	3072(1)	1011(1)	6343(1)	2.6
Co(2)	1301(1)	1362(1)	7586(1)	2.7
Cl(A)	4922(2)	3612(1)	7489(2)	4.3
Cl(B)	−975(2)	2037(1)	10025(3)	4.7
Cl(C)	−2659(2)	293(1)	6781(3)	4.5
S(A)	2417(2)	1732(1)	6555(2)	3.2
S(B)	975(2)	830(1)	5926(2)	3.7
S(C)	3171(2)	949(1)	8487(2)	3.4
OW	3417(8)	−1097(3)	10014(8)	7.3
O(A1)	5217(9)	3479(5)	8803(8)	10.0
O(A2)	4759(20)	3246(4)	6631(13)	17.0
O(A3)	5935(14)	3845(5)	7403(14)	13.2
O(A4)	3850(13)	3865(7)	6988(11)	18.0
O(B1)	260(10)	2198(5)	10733(13)	11.9
O(B2)	−1829(11)	2178(5)	10568(12)	12.1
O(B3)	−945(14)	1573(4)	9930(16)	13.1
O(B4)	−1388(15)	2181(7)	8714(12)	16.5
O(C1)	−1713(7)	286(3)	6209(9)	6.9
O(C2)	−2365(10)	610(4)	7830(12)	10.5
O(C3)	−3890(8)	421(4)	5750(9)	8.6
O(C4)	−2849(15)	−153(4)	7123(13)	11.9
N(1A)	4952(7)	1222(3)	6964(8)	4.0
N(2A)	1897(8)	1818(3)	9145(8)	4.1
N(1B)	2802(8)	1071(3)	4385(7)	4.3
N(2B)	−343(7)	1730(3)	6625(8)	4.6
N(1C)	3639(8)	349(3)	6310(8)	4.1
N(2C)	346(7)	986(3)	8471(8)	4.2
C(1A)	5229(9)	1715(4)	6747(10)	4.5
C(2A)	4966(10)	2065(3)	7648(10)	4.5
C(3A)	3840(10)	1976(3)	8024(10)	4.4
C(4A)	3420(11)	2368(3)	8679(10)	4.9
C(5A)	2172(11)	2300(4)	8877(11)	5.1
C(1B)	1563(11)	1269(4)	3353(9)	5.2
C(2B)	381(11)	982(9)	3171(9)	5.4
C(3B)	−198(10)	1046(4)	4242(10)	5.2
C(4B)	−811(11)	1501(4)	4238(10)	5.6
C(5B)	−1366(9)	1561(4)	5321(11)	5.4
C(1C)	4230(12)	78(4)	7598(13)	6.1
C(2C)	3305(12)	−30(4)	8195(13)	5.9
C(3C)	2899(13)	349(4)	8941(12)	5.9
C(4C)	1649(12)	262(4)	9090(12)	5.5
C(5C)	1073(10)	654(4)	9592(9)	4.6

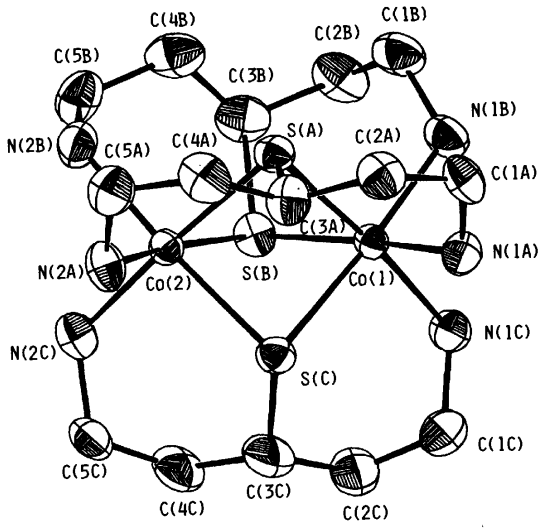

Fig. 1. A perspective view of $[Co_2(dpet)_3]^{3+}$ ion. Selected bond lengths (l/Å) and angles (ϕ/°) are: Co(1)-Co(2) 2.955(2), Co(1)-S(A) 2.229(3), Co(1)-S(B) 2.247(3), Co(1)-S(C) 2.257(3), Co(2)-S(A) 2.229(3), Co(2)-S(B) 2.256(3), Co(2)-S(C) 2.243(3), Co(1)-N(1A) 2.013(8), Co(1)-N(1B) 2.000(8), Co(1)-N(1C) 2.003(8), Co(2)-N(2A) 2.008(8), Co(2)-N(2B) 1.997(8), Co(2)-N(2C) 1.996(10); Co(1)-S(A)-Co(2) 83.04(9), Co(1)-S(B)-Co(2) 82.03(8), Co(1)-S(C)-Co(2) 82.09(8).

Results and Discussion

The crystal structure consists of discrete binuclear clusters, $[Co_2(dpet)_3]^{3+}$, perchlorate ions and crystal water molecules. A perspective view of the complex ion, $[Co_2(dpet)_3]^{3+}$, is shown in Fig. 1. As has been anticipated, the complex ion consists of two distorted octahedra sharing the face formed by the three thiolate sulfurs.

The Co-S bond lengths (2.229—2.257 Å) fall in the range of those of other cobalt(III)-mercaptide complexes.[5] The Co-N bond lengths (1.996—2.013 Å) are significantly longer than those of ordinary cobalt(III)-amine complexes. The observed lengthening seems to be due to the trans influence of the thiolate sulfur coordination as was observed for cobalt(III) complexes containing 2-aminoethanethiol.[5]

The Co-Co distance is 2.955(2) Å and the Co-S-Co angle 82.0—83.1°. For some tri(μ-hydroxo)dicobalt(III) complexes Co-Co distances of 2.55—2.58 Å, and Co-O-Co angles of 81—86° were reported.[6] Thus, the substitution of the thiolate sulfur for the hydroxo oxygen leads to an appreciable lengthening of the metal-metal separation.

The water molecules and perchlorate ions are in the vicinity of the amino groups of the dpet ligands by hydrogen bonds.

References

1) E. I. Stiefel, *Prog. Inorg. Chem.*, **22**, 1 (1977); C. G. Kuehn and S. S. Isied, *Prog. Inorg. Chem.*, **27**, 153 (1980).

2) S. L. Rose, R. E. Hoskin, J. E. Cavanaugh, C. J. Smith, and E. L. Blinn, *Inorg. Chim. Acta*, **40**, 7 (1980).

3) I. Murase, S. Ueno, and S. Kida, *Bull. Chem. Soc. Jpn.*, **56**, 2748 (1983).

4) S. Kawano, *Rep. Comput. Cent. Kyushu Univ.*, **16**, 113 (1983); T. Sakurai and K. Kobayashi, *Rep. Inst. Phys. Chem. Res.*, **55**, 69 (1979); C. K. Johnson, Report No. 3794, Oak Ridge National Laboratory, Oak Ridge, Tennessee (1965).

5) R. C. Elder, L. R. Florian, R. F. Lake, and A. M. Yacynych, *Inorg. Chem.*, **12**, 2690 (1973); H. C. Freeman, C. J. Moore, W. G. Jackson, and A. M. Sargeson, *Inorg. Chem.*, **17**, 3513 (1978); M. J. Heeg, R. C. Elder, and E. Deutsch, *Inorg. Chem.*, **19**, 554 (1980).

6) P. Andersen, *Acta Chim. Scand.*, **21**, 243 (1967); G. S. Mandel, N. S. Mandel, R. E. Marsh, and W. P. Schaefer, *Acta Crystallogr., Sect B.*, **33**, 700 (1977); G. H. Searle and T. W. Hambley, *Aust. J. Chem.*, **35**, 1297 (1982).

Electrogenerated Acid-catalyzed Cyclization of Isoprenoids

Kenji UNEYAMA, Akihiro ISIMURA, and Sigeru TORII*
Department of Industrial Chemistry, School of Engineering, Okayama University, Okayama 700
(Received January 24, 1985)

Synopsis. Biogenetic-type cyclization of some isoprenoids (geranyl phenyl sulfone, methyl geranate, pseudoionone, and 6,10-dimethyl-2,5,9-undecatrien-4-one) has been performed by use of an electrogenerated acid in 1,2-dichloroethane.

The biogenetic cyclization of polyisoprenoids to cyclic terpenoids has been performed by the action of strong acids such as boron trifluoride, tin(IV) chloride, and concentrated sulfuric acid.[1] For instance, pseudoionone is converted into ionone in concentrated sulfuric acid[2] and geranyl phenyl sulfone in concentrated sulfuric acid–acetic acid[3] or stannic tetrachloride in dichloromethane.[4] The requirement of a large amount of bases to neutralize the strong acid is unfavorable for the practical process.

Recently, the electrogenerated acid (EGA) has been recognized as a powerful acid-catalyst for epoxide ring opening,[5] acetalization[6] cyanation,[7] and conversion of nerolidol to bisaborol.[8] We describe an EGA-catalyzed cyclization of polyisoprenoids, demonstrating that a very small quantity of the EGA does promote the cyclization and the neutralization is easy for workup.

The electrolysis of **1a** (500 mg) in a distilled 1,2-dichloroethane (DCE) in the presence of lithium perchlorate (50 mg) and tetraethylammonium perchlorate (50 mg) was performed by use of platinum foil electrodes in an undivided cell. Constant current (1.7 mA/cm^2) was passed for 25 min (0.04 F/mol). If it is assumed that a proton of EGA is produced by one-electron oxidation of a trace amount of water existed in the solvent employed,[9] the amount of the EGA must be very small since 0.04 F/mol of electricity is enough to complete the cyclization. Therefore, a few drops of pyridine can neutralize the solution. The yield (95%) is comparable to that (87—94%) obtained in concentrated sulfuric scid.[3]

Lithium perchlorate is an essential electrolyte for generation of EGA, but tetraethylammonium perchlorate was employed as a coelectrolyte so as to get an enough conductivity of the solution. The use of tetraethylammonium perchlorate or tetraethylammonium tosylate alone is less effective for the purpose. 1,2-Dichloroethane is highly effective solvent while mixing of about 7% of more polar solvent such as ethyl acetate (81%, 0.8 F/mol), acetone (73%, 1.0 F/mol), and THF (42%, 2.1 F/mol) as a cosolvent resulted in decrease of both yield and reaction rate.

In order to elucidate the behavior of the EGA in this cyclization, two types of electrolysis procedure were examined. On electrolyzing the solution in the absence of **1a** (0.5 F/mol), and then adding **1a** in the pre-electrolyzed solution and allowing to react at 55 °C for 20 min, **2a** was obtained in almost the same yield (92%) as compared with that (95%) obtained in the electrolysis in the presence of **1a**. However, at the lower temperature (20 °C), both electrolysis procedures revealed a marked difference as shown in Table 1 (entry 5 and 7), clearly demonstrating that the cyclization proceeds faster on electrolyzing in the presence of a substrate. The EGA would be concentrated during the electrolysis at the anode surface to make the proximity of the anode extremely acidic so that the cyclization proceeds even with a small amount of EGA.[9]

TABLE 1. EGA CATALYZED CYCLIZATION OF **1a**[a]

Entry	Electrolyte[b]	Temp °C	F/mol	**2a** %	**1a** %
1	$LiClO_4$–Et_4NClO_4	55	0.04	95	0
2	Et_4NClO_4	55	1.6	15	38
3	Et_4NOTs	55	2.0	trace	71
4	$LiBF_4$–Et_4NClO_4[e]	55	1.0	54	15
5	$LiClO_4$–Et_4NClO_4	20	2.1	60	0
6[c]	$LiClO_4$–Et_4NClO_4	55	0.5	92	0
7[d]	$LiClO_4$–Et_4NClO_4	20	2.1	12	80

a) Substrate (0.36 mmol) in 8 ml of DCE. b) Electrolyte (50 mg for each). c) Pre-electrolyzed conditions (0.5 F/mol). d) Pre-electrolyzed conditions (2.1 F/mol). e) Because of the low solubility of $LiBF_4$ in DCE, Et_4NClO_4 was employed as a coelectrolyte.

The cyclization of **1a** and **1b**[10] proceeds successfully by the EGA catalysis [95% (α:β:γ=86:9:5) and 88% (α:γ=89:11)], respectively. Also pseudoionone **1c** afforded ionone in 57% yield. α-Damascone **2d**[11] was prepared in 30% yield from **1d**. In contrast, geraniol **1e** behaved somewhat differently and dehydrative cyclization occurred exclusively rather than the desired cyclization leading to the formation of a mixture of limonene and terpinolene (78%, limonene:terpinolene =36:64). And cyclization of **3** provided **4** (72%, α-H$_9$:β-H$_9$=34:64).[12]

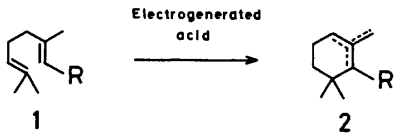

1 2

1a R = CH_2SO_2Ph
b CO_2Me
c $CH{=}CHCOCH_3$
d $COCH{=}CHCH_3$
e CH_2OH

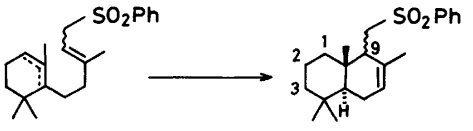

3 4

Experimental

Boiling points are indicated by an air bath temperature and uncorrected. The IR spectra were obtained with a JASCO IRA-1 spectrometer. ^{1}H-NMR spectra were measured with a JNM FX-100 spectrometer at 100 MHz in $CDCl_3$ using Me_4Si as an internal standard. Substrates **1a**,[13] **1b**,[10] **1d**,[11] and **3**[12] were prepared as reported in the literatures. Geraniol and pseudoionone were the samples which were manufactured in Kuraray Co. Ltd., to which the authors are grateful. 1,2-Dichloroethane and ethyl acetate were refluxed over P_2O_5 and distilled. THF was refluxed over NaOH and then $LiAlH_4$, and finally distilled from a sodium-benzophenone drying system. Acetone was stirred over dry $MgSO_4$ for overnight, filtered, and distilled. Electrolytes, $LiClO_4$, Et_4NClO_4, $LiBF_4$, and Et_4NOTs were commercially available and dried under the reduced pressure. A typical electrolysis is described below and the products, **2a**,[2,3] **2b**,[10] **2c**, **2d**,[11] and **4**[12] were idientified in comparison with the authentic samples.

Electrolysis of ***1a*** *in a 1,2-Dichloroethane-$LiClO_4$-Et_4NClO_4 system.* A solution of **1a** (500 mg, 1.8 mmol) $LiClO_4$ (50 mg), and Et_4NClO_4 (50 mg) dissolved in 1,2-dichloroethane (8 ml) was added in a beaker-type (10 cm in height and 3 cm in diameter) undivided cell settled with two platinum foil electrodes (2×1.5 cm^2) and electrolyzed at 55 °C under a constant current (1.7 mA/cm^2) for 25 min (0.04 F/mol). Saturated $NaHCO_3$ was added to the electrolysis mixture. After evaporation of the solvent under reduced pressure, the residue was extracted with ether three times. The combined extracts were washed with brine, dried (Na_2SO_4), and concentrated *in vacuo*. The residue was chromatographed (SiO_2, hexane:AcOEt=20:1) to give **2a** as a mixture (476 mg, 95%, isomer ratio α:β:γ=86:9:5). The pure γ-isomer of **2a** was obtained by column chromatography, and β-isomer was recrystallized from a mixture of α- and β-isomers. The structures of α- and β-isomers were identified in comparison with the authentic samples.[2,3]

*1,1-Dimethyl-3-methylene-2-(phenylsulfonylmethyl)cyclohexane (γ-**2a**)*: bp 113—115 °C/1.9 Pa; IR (neat) 3060, 2930, 2860, 1645 (C=C), 1443, 1300 (SO_2), 1136 (SO_2), 910, 730 cm^{-1}; ^{1}H NMR ($CDCl_3$) δ 0.80 (s, 3H, CH_3), 0.92 (s, 3H, CH_3), 1.20—1.70 (m, 4H, CH_2), 2.02 (t, J=6 Hz, 2H, CH_2), 2.45 (dd, J_1=8.3 Hz, J_2=3.6 Hz, 1H, CH), 3.24 (dd, J_1=14.6 Hz, J_2=3.7 Hz, 1H, CH_2), 3.42 (dd, J_1=14.6 Hz, J_2=8.3 Hz, CH_2), 4.60 (br s, 1H, =CH_2), 4.77 (br s, 1H, CH_2), 7.50—8.10 (m, 5H, ArH). Found: C, 69.25; H, 8.13%. Calcd for $C_{16}H_{22}O_2S$: C, 69.03; H, 7.96%.

The authors are grateful to the Ministry of Education, Science, and Culture for a financial support by a Grant-in-Aid (No 57118002 and 59550596).

References

1) W. S. Johnson, *Accounts Chem. Res.*, **1**, 1 (1968); E. E. van Tamelen, *ibid.*, **1**, 11 (1968).
2) W. Kimel, J. D. S, Surmatis, J. Weber, G. O. Chase, N. W. Sax, and A. Ofner, *J. Org. Chem.*, **22**, 1611 (1957).
3) S. Torii, K. Uneyama, and M. Isihara, *Chem. Lett.*, **1975**, 479.
4) T. Kato, H. Takayanagi, T. Uyehara, and Y. Kitahara, *Chem. Lett.*, **1977**, 1009.
5) K. Uneyama, A. Isimura, K. Fujii, and S. Torii, *Tetrahedron Lett.*, **24**, 2857 (1983); K. Uneyama, N. Nisiyama, and S. Torii, *ibid.*, **25**, 4137 (1984).
6) S. Torii and T. Inokuchi, *Chem. Lett.*, **1983**, 1349.
7) S. Torii, T. Inokuchi, and T. Kobayasi, *Chem. Lett.*, **1984**, 897.
8) K. Uneyama, Y. Masatsugu, T. Ueda, and S. Torii, *Chem. Lett.*, **1984**, 529.
9) S. Torii," Electroorganic Synthesis Part I, Oxidation Methods and Applications," Verlag Chemie, Weinheim (1985).
10) P. A. Stadler and P. Overhansli, *Helv. Chim. Acta*, **42**, 2597 (1959); V. A. Smit, A. V. Semenovskii, P. F. Vlad, and V. F. Kucherrov, *Izv. Akad. Nauk SSSR, Otd. Khim. Nauk*, **1962**, 312.
11) K. H. Schulte-Elte, H. Strickler, F. Gautschi, W. Pichenhagen, M. Gadola, J. Limacher, B. L. Muller, F. Wuffli, and G. Ohloff, *Ann. Chem.*, **1975**, 484; Y. Nakatani, K. Kubota, R. Tahara, and Y. Shigematsu, *Agr. Biol. Chem.*, **38**, 1351 (1974).
12) S. Torii, K. Uneyama, I. Kawahara, and M. Kuyama, *Chem. Lett., 1978*, 455.
13)P. A. Grieco and Y. Masaki, *J. Org. Chem.*, **39**, 2135 (1974).

Reactions of Aromatic Azido, Azo, Azoxy, and Hydrazo Compounds with Diphosphorus Tetraiodide

Hitomi SUZUKI,* Hiroyuki TANI, and Shigeko ISHIDA
Department of Chemistry, Faculty of Science, Ehime University, Bunkyo-cho, Matsuyama 790
(Received February 16, 1985)

Synopsis. On treatment with diphosphorus tetraiodide in boiling benzene followed by aqueous work-up, the title nitrogen-containing compounds undergo a reductive cleavage of the nitrogen–nitrogen bond, giving the corresponding amines in low to good yields.

Diphosphorus tetraiodide (P_2I_4) is a long-known halogen derivative of diphosphine, but its potential as a reagent for organic synthesis has received attention only recently. It possesses a high affinity for oxygen and exhibits a unique ability to deoxygenate and dehydrate a variety of oxygen-containing functionalities.[1] As for the reaction of P_2I_4 with nitrogen-containing compounds, we have already reported the dehydration of aldoximes[2] and amides[3] to nitriles, coupling of carboxylic acids and amines into amides,[4] and dehydrative cyclization of 2-amino alcohols to aziridines.[5] In the present paper, we wish to report a new feature of this reagent to cleave the nitrogen–nitrogen bond of aromatic azido, azo, azoxy, and hydrazo compounds in a reductive way, giving the corresponding amines in various yields.

When heated with P_2I_4 in dry benzene for several hours under nitrogen, aryl azides lost a molecule of nitrogen and aqueous work-up of the reaction mixture afforded the corresponding aromatic amines in low to good yields. Aroyl and arenesulfonyl azides reacted similarly to give the respective amides. The results are summarized in Table 1.

$$\begin{matrix} ArN_3 \\ ArCON_3 \\ ArSO_2N_3 \end{matrix} \xrightarrow[2.\ H_2O]{1.\ P_2I_4/C_6H_6,\ \Delta} \begin{matrix} ArNH_2 \\ ArCONH_2 \\ ArSO_2NH_2 \end{matrix}$$

While aryl azides were smoothly converted to aromatic amines within a short reaction time under mild conditions, aroyl azides needed more time for complete conversion. 4-Methylbenzenesulfonyl azide was quite slow to be transformed into sulfonamide; even after 50 h refluxing in benzene, appreciable amounts of the substrate remained unchanged. In these reactions, hindered as well as functionalized azides could be reduced cleanly with moderate ease.

On a similar treatment with diphosphorus tetraiodide, azobenzene, azoxybenzene, and hydrazobenzene underwent a reductive cleavage of the nitrogen–nitrogen bond, giving aniline in *ca.* 30—40% yields. The reaction was accompanied by the extensive formation of as yet unidentified, powder-like substance of pale yellow color as a common by-product. The typical results are summarized in Table 1.

$$\begin{matrix} ArN{=}NAr \\ ArN{=}NAr \\ \downarrow O \\ ArNHNHAr \end{matrix} \xrightarrow[2.\ H_2O]{1.\ P_2I_4/C_6H_6,\ \Delta} ArNH_2$$

When these reactions were carried out in the presence of 4-methoxybenzoic acid or benzyl alcohol, the major products obtained were 4-methoxybenzanilide and *N*-benzylated aniline respectively.

$$C_6H_5N{=}NC_6H_5 + 4\text{-}CH_3OC_6H_4CO_2H \xrightarrow[2.\ H_2O]{1.\ P_2I_4/C_6H_6,\ \Delta,\ 5h} 4\text{-}CH_3OC_6H_4CONHPh \quad 56\%$$

$$C_6H_5N_3 + C_6H_5CH_2OH \xrightarrow[2.\ H_2O]{1.\ P_2I_4/C_6H_6,\ \Delta,\ 6h} C_6H_5NHCH_2C_6H_5 + C_6H_5N(CH_2C_6H_5)_2 \quad 54\% \quad 9\%$$

TABLE 1. REACTION OF AROMATIC AZIDO, AZO, AZOXY, AND HYDRAZO COMPOUNDS WITH DIPHOSPHORUS TETRAIODIDE

Substrate	Reaction time/h	Product	Yield/%[a]
Phenyl azide	5	Aniline	86[b]
4-Chlorophenyl azide	7	4-Chloroaniline	75
4-Methoxyphenyl azide	4	4-Methoxyaniline	13
4-Nitrophenyl azide	8	4-Nitroaniline	63
2-Methylphenyl azide	6	2-Methylaniline	45
4-Azidobiphenyl	10	4-Aminobiphenyl	53
2,6-Dimethylphenyl azide	11	2,6-Dimethylaniline	40
Benzoyl azide	4	Benzamide	61
4-Methoxybenzoyl azide	4	4-Methoxybenzamide	20
4-Nitrobenzoyl azide	6	4-Nitrobenzamide	53
4-Methylbenzenesulfonyl azide	50	4-Methylbenzenesulfonamide	57
Azobenzene	2	Aniline	27[b]
4,4'-Dichloroazobenzene	2	4-Chloroaniline	31[b]
Azoxybenzene	2	Aniline	28[b]
Hydrazobenzene	2	Aniline	41[b]

a) Yields were based on the isolated compounds and not optimized. All products are known and identified by comparison with authentic specimens. b) Yields were determined by GLC using $C_{14}H_{30}$ as internal standard.

The transformation of the title nitrogen-containing compounds into the corresponding amines may be easily accomplished by conventional methods based on the reduction with hydride reagents or catalytic hydrogenolysis. However, most of these methods are not compatible with compounds containing activated carbon–carbon multiple bond, carbonyl, ester, nitro, or cyano groups, to which P_2I_4 is known to be inert.

Although nothing can be said as yet about the scope and synthetic utility of the present reaction, one may expect its potential as a means for the selective reduction of azido, azo, azoxy, and hydrazo groups in the presence of other reducible functionalities. Reaction with aliphatic analogues has not been studied yet.

Experimental

Materials. Solvents were dried and distilled under nitrogen before use. Diphosphorus tetraiodide (P_2I_4) was prepared according to the previously reported procedure.[2,6] Thin layer chromatography was performed using Kieselgel 60 HF_{254} (Merck).

Reaction of Azides with P_2I_4. To a solution of aryl azide (aroyl azide or arenesulfonyl azide) (2.0 mmol) in dry benzene (20 ml) was added P_2I_4 (1.2 mmol) in one portion under nitrogen and the mixture was heated with stirring under a gentle reflux. The progress of the reaction was monitored by GLC. After appropriate hours, the reaction mixture was allowed to cool and 10% sodium carbonate solution was added. The organic phase was extracted with ether, dried over sodium sulfate, and evaporated to give the corresponding amine or amide.

Reaction of Azo, Azoxy, and Hydrazo Compounds with P_2I_4. Each of the above nitrogen-containing compounds (1.0 mmol) was dissolved in dry benzene (10 ml) containing tetradecane (1.0 mmol) as internal standard. P_2I_4 (1.2 mmol) was added to the solution and the resulting mixture was stirred under reflux for 2 h. As the reaction went on, a pale yellow powder-like substance gradually deposited on the wall of reaction vessel. It was almost insoluble in ordinary solvents. The reaction was quenched by the addition of 10% sodium carbonate solution and the organic phase was extracted with ether, dried over sodium sulfate and evaporated. The product yields were determined by GLC.

Reaction of P_2I_4 with Azobenzene and Aryl Azide in the Presence of Benzoic Acid or Benzyl Alcohol. To a solution of one of the above nitrogen-containing compounds (1.0 mmol) in dry benzene (10 ml) was added 4-methoxybenzoic acid (1.0 mmol) or benzyl alcohol (1.0 mmol) followed by P_2I_4 (1.2 mmol) and the resulting mixture was heated to reflux with stirring under nitrogen. After appropriate hours, the reaction was quenched by the addition of water and the reaction mixture was worked up as described above. Products were recrystallized from aqueous ethanol and identified by comparison with authentic samples.

References

1) For reviews, see: H. Suzuki and H. Tani, *Yuki Gosei Kagaku Kyokai Shi*, **43**, 76 (1985); A. Krief, Aldrich Technical Information **191** (1981).

2) H. Suzuki, T. Fuchita, A. Iwasa, and T. Mishina, *Synthesis*, **1978**, 905; *Nippon Kagaku Kaishi*, **1979**, 91.

3) H. Suzuki and N. Sato, *Nippon Kagaku Kaishi*, **1981**, 392.

4) H. Suzuki, J. Tsuji, Y. Hiroi, N. Sato, and A. Osuka, *Chem. Lett.*, **1983**, 449.

5) H. Suzuki and H. Tani, *Chem. Lett.*, **1984**, 2129.

6) H. Suzuki and T. Fuchita, *Nippon Kagaku Kaishi*, **1974**, 1679.

Regioselective Monoalkylation of Ketones with Allylic Nitro Compounds

Noboru ONO,* Isami HAMAMOTO, and Aritsune KAJI*
Department of Chemistry, Faculty of Science, Kyoto University, Kyoto 606
(Received February 18, 1985)

Synopsis. Lithium enolates from 2-methylcyclohexanone and *p*-methylacetophenone react with allylic nitro compounds in the presence of triethylborane (2 equiv) and $Pd(PPh_3)_4$ (5 mol%) to give monoallylated compounds regioselectively.

Palladium-catalyzed allylic alkylations are extremely useful synthetic reactions, with allylic acetates being among the most commonly used allylic compounds.[1] Recently, allylic nitro compounds have been demonstrated to react with stabilized nucleophiles such as carbanions from active methylene compounds, amines or sulfinate ions in a similar way.[2,3] In this paper we wish to report the allylic alkylation of allylic nitro compounds with the less stabilized nucleophiles such as enolates from ketones, which will expand the scope of the allylic alkylation.

The reaction of various enolates (**1**) from 2-methylcyclohexanone with 3-methyl-3-nitro-1-butene (**2**) was carried out under the conditions summarized in Table 1. The results are also summarized in this table.

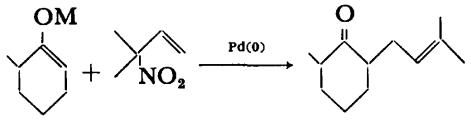

(1)

1 **2** **3**

M = Li, Li + $2BEt_3$, ZnCl, MgCl, CdCl, $SnBu_3$, $SiMe_3$

The reaction of the lithium enolate with **2** did not give the allylated compound (**3**) in good yield even if a catalytic system [bis(dibenzylideneacetonato)palladium+1, 2-bis(diphenylphosphino)ethane, $Pd(dba)_2$-dppe] which allowed the alkylation of allylic acetates with lithium enolates[4] was used. However conversion of the counter cation from lithium to boron or zinc enhanced the reactivity of the present reaction.[5] Thus, 6-methyl-2-prenylcyclohexanone (**3**) was prepared in 62% or 45% yield by the reaction with the boron or zinc enolate, respectively, where the regiochemistry of the enolate was preserved and the nucleophile attacked at the less hindered site predominantly.[6] Although enol stannates are reported to be reactive to palladium-catalyzed reaction of allylic acetates,[7] they are inert to **2**.[8] *p*-Methylacetophenone (**4**) was also monoalkylated to give **5** and **5'** in the similar way. (Eq. 2).

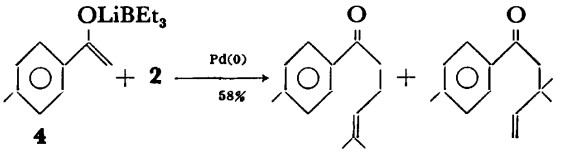

(2)

4 **5** (90 : 10) **5'**

Table 1. Reaction of metal 6-methylcyclohexenolates with **2**

M	Catalyst[a]	Yield of **3** %[b]
Li	A	11
Li	B	24
Li+$2BEt_3$	A	70 (62)[c]
Li+$2BEt_3$	None	0
ZnCl	A	52 (45)[c]
MgCl	A	0
CdCl	A	3
$SnBu_3$	A	0
$SiMe_3$	A	0

a) A: $Pd(PPh_3)_4$ (5 mol%) B: $Pd(dba)_2$+dppe (3 mol%). b) Yields were determined by GLC. c) Isolated yields.
All reactions were carried out at room temperature for 20 h in dry THF.

Although compounds **3** and **5** can be prepared by the reaction of the corresponding acetate, the use of allylic nitro compounds as allylic electrophiles has also its own merits over the conventional alkylating agents. Allylic nitro compounds can be prepared by different methods from those for preparation of other alkylating agents.[2,3] Furthermore, electrophiles can be introduced regioselectively at the α-position of the nitro compounds. For example, 2-nitro-2-butene (**5**) was readily converted into allylic nitro compound (**6**) by very simple procedures as shown in Eq. 3, where the isomerization of **5** and the Michael addition of the resultant allylic nitro compound to methyl acrylate took place simultaneously. Alkylation of **1** with **6** gave the monoalkylated product, **7**, in good yield.[9]

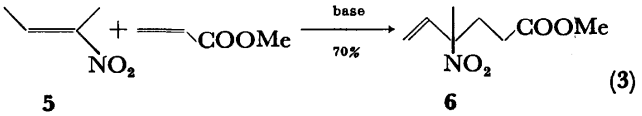

(3)

5 **6**

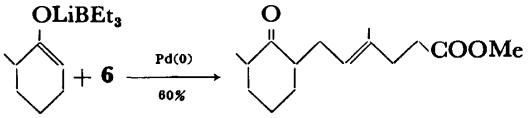

(4)

7

Introduction of a vinyl group to nitroalkanes also provides a useful method for the preparation of allylic nitro compounds.[2] Ethyl 2-methyl-2-nitro-3-butenoate (**9**) was prepared by this procedure. Alkylation of **4** with **9** gave the monoalkylated compound, **10**, in 65% yield with high regio-and stereoselectivity. The products **5** and **10** are good precursors of terpenoids such as curcumene and dehydrolancenol, respectively.

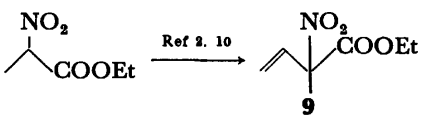

(5)

9

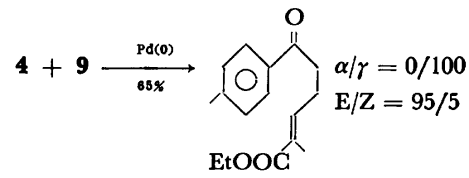

(6)

10

Experimental

Preparation of Allylic Nitro Compounds. Allylic nitro compounds, **2**[9] and **9** were prepared by the Michael addition of the corresponding nitro compounds to phenyl vinyl sulfoxide and the subsequent termolysis.[2,10] **9**: IR (neat) 1340, 1540, 1730 cm^{-1}, NMR ($CDCl_3$) δ 1.36 (3H, t, J=8 Hz), 1.84 (3H, s), 4.22 (2H, q, J=8 Hz), 5.30 (1H, d, J=10 Hz), 6.28 (1H, dd, J=10 and 17 Hz). 4-Methyl-4-nitro-5-hexenoate (**6**) was prepared as follows: A solution of 2-nitro-2-butene (**5**, 1.01 g, 10 mmol), methyl acrylate (1.03 g, 12 mmol) and tetramethylguanidine (0.233 g, 2 mmol) in 10 ml of acetonitrile was kept at room temperature for 24 h. The reaction mixture was poured into water and extracted with diethyl ether. The usual work-up followed by distillation with Kugelrohr gave **6**, 1.31 g (70%), bp 150 °C/1 mmHg (1 mmHg=133.322 Pa). IR (neat) 1370, 1535, 1720 cm^{-1}, NMR ($CDCl_3$) δ 1.64 (3H, s), 2.26 (4H, m), 3.60 (3H, s), 5.20 (1H, d, J=17 Hz), 5.24 (1H, d, J=10 Hz), 6.12 (1H, dd, J=17 and 10 Hz). Found: C, 51.28; H, 6.99; N, 7.48. Calcd for $C_8H_{13}NO_4$: C, 51.32; H, 6.94; N, 7.48.

Reaction of 2-Methylcyclohexanone with 2. Preparation of 3: The lithium enolate of 2-methylcyclohexanone was prepared according to the literature[5] by using *n*-BuLi (1.6 M (1 M=1 mol dm^{-3}) in hexane, 0.683 ml, 1.1 mmol), diisopropylamine (0.11 g, 1.1 mmol) and THF (3 ml). Triethylborane (1 M in hexane, 2 ml) was added to the lithium enolate at −75 °C and stirred for 35 min at this temperature. To the above solution was added a solution of **2** (0.115 g, 1 mmol) and $Pd(PPh_3)_4$ (0.058 g, 0.05 mmol) in THF (1 ml). The reaction mixture was warmed to room temperature and stirred for 20 h, then worked up in the usual way after destroying Et_3B by adding 3 M NaOH (1 ml) and H_2O_2 (30%, 0.5 ml). Pure **3** was isolated by column chromatography (silica gel/benzene–hexane), 0.11 g (62%). IR (neat) 1700 cm^{-1}, NMR ($CDCl_3$) δ 0.98, 1.05 (3H, d, J=7 Hz), 1.2—1.6 (10H, m), 1.60 (3H, s), 1.68 (3H, s), 4.9—5.2 (m, 1H). The ratio of **3**/other isomers was determined by GLC to be 98/2. The spectral data were in good agreement with those of the literature.[5] Other metal enolates were preapard according to the literature[5] and the reaction of them with **2** was carried out in the same way. The yield of **3** was determined by GLC or isolation of pure product. Following compounds were prepared by this procedure.

5: The reaction starting from *p*-methylacetophenone (0.403 g, 3 mmol) gave the mixture of **5** and **5′** (0.35 g, 58%), bp 120—130 °C/1 mmHg. IR (neat) 1700 cm^{-1}, NMR ($CDCl_3$) δ 1.60 (3H, s), 1.64 (3H, s), 2.36 (3H, s), 2.42 (2H, t, J=8 Hz), 2.92 (2H, m), 5.0—5.3 (1H, m), 7.2 (2H, m), 7.8 (2H, m). The regio isomer **5′**; NMR ($CDCl_3$) δ 1.16 (6H, s), 2.36 (3H, s), 2.4 (2H, s), 4.8—5.1 (2H, m), 5.8—6.2 (1H, m), 7.2 (2H, m), 7.8 (2H, m). MS of **5**+**5′**, Found: m/z 202.1348. Calcd for $C_{14}H_{18}O$: M, 202.1295.

7: The reaction using 2-methylcyclohexanone (0.336 g, 3 mmol) gave **7**, 0.455 g (60%). IR (neat) 1710, 1720 cm^{-1}, NMR ($CDCl_3$) δ 0.98, 1.04 (3H, d, J=8 Hz), 1.60, 1.64 (3H, s), 1.2—2.6 (14H, m), 3.65, 3.67 (3H, s), 5.0—5.4 (1H, m). This is the mixture of the cis and trans 2,6-isomers whose ratio is about 65/35 by GLC and NMR. Although exact ratio of *E/Z* was not determined, the *E*-isomer was predominant. Found: 252.1712. Calcd for $C_{15}H_{24}O_3$: M, 252.1724.

10: The reaction in 3 mmol scale gave **10**, 0.51 g (65%). IR (neat) 1690, 1710 cm^{-1}, NMR ($CDCl_3$) δ 1.22 (3H, t, J=8 Hz), 1.85 (3H, s), 2.38 (3H, s), 2.46 (2H, q, J=8 Hz), 3.00 (2H, t, J=8 Hz), 4.20 (2H, q, J=8 Hz), 6.82 (1H, t, J=8 Hz), 7.22 (2H, m), 7.80 (2H, m). Found: 260.1423. Calcd for $C_{16}H_{20}O_3$: 260.1411.

The *E/Z* ratio was determined by GLC and NMR to be 95/5.

References

1) Reviews: J. Tsuji, *Yuki Gosei Kagaku Kyokai Shi*, **41**, 619 (1983); B. M. Trost, *Acc. Chem. Res.*, **13**, 38 (1980). Various kinds of allylic substrates have been used as allylic electrophiles, see also the following paper and references therein, B. M. Trost and R. S. Christopher, *J. Org. Chem.*, **49**, 468 (1984).

2) N. Ono, I. Hamamoto, and A. Kaji, *J. Chem. Soc., Chem. Commun.*, **1982**, 821 and Abstract, 13th Syposium on Organometallic Chemistry, Kyoto, (1983), p. 238.

3) R. Tamura and L. S. Hegedus, *J. Am. Chem. Soc.*, **104**, 3727 (1982); R. Tamura, K. Hayashi, M. Kakihana, M. Tsuji, and D. Oda, *Chem. Lett.*, **1985**, 229.

4) J. C. Fiaud and J. J. Malleron, *J. Chem. Soc., Chem. Commun.*, **1981**, 1159.

5) E. Negishi and R. A. John, *J. Org. Chem.*, **48**, 4098 (1983), in which similar tendency of the rate enhancement of the reaction with allylic acetates was reported. It is not clear about the structure of the enolate formed by the addition of triethylborane to the lithium enolate, but transmetallation from lithium to boron should occur to some extent.

6) The regiochemistry of the present reaction is affected by mainly two factors, steric and electronic effects. Secondary ketones gave only γ-substitition product as in Eq. 1 and primary ketones gave some amounts of α-substitution product as in Eq 2. This selectivity in the present reaction is higher than that in the reaction with stabilized nucleophiles.[2,3]

7) B. M. Trost and E. Keinan, *Tetrahedron Lett.*, **21**, 2591 (1980).

8) This difference may be due to the difference of catalytic spieces between the reaction of allylic nitro coompounds and allylic acetates. The catalysis in the former reaction involves the nitro group which deactivates the reaction with enol stannates.

9) Allylic alkylation of allylic nitro compounds with enolates of ketones is limited to tretiary nitro compounds. For example, the reaction of **1** with primary or secondary allylic nitro compounds resulted in recovery of 2-methylcyclohexanone.

10) R. Tanikaga, H. Sugihara, K. Tanaka, and A. Kaji, *Synthesis*, **1977**, 299.

Abnormal Methyl Radicals on Alumina Surfaces

John David BARNES, Mahendra Aruind TRIVEDI, Duro Abimbola ODUWOLE, and Barrie WISEALL
Department of Chemistry, City of London Polytechnic, Jewry Street, London EC3N 2EY.
†*Department of Chemistry, Queen Mary College, Mile End Road, London El 4NS.*
(Received April 17, 1984)

Synopsis. The ESR spectrum of abnormal methyl radicals on alumina surfaces is found to be symmetrical at low surface coverages. Possible mechanisms for the formation of these radicals are presented.

Fujieda *et al.*[1] have interpreted the ESR spectra of methyl radicals produced by the photolysis of methane adsorbed on alumina surfaces as indicating that the three methyl protons are not equivalent and that one is interacting more strongly with the surface than the other two. In an earlier paper[2] concerned with the stabilisation of abnormal methyl radicals (Me_{ab}) on silica gel surfaces we suggested that this observation was due to concentration effects arising from the relatively high surface coverages employed and that strongly caged adsorbate molecules are precursors of the abnormal radical. The present study examines this problem in more detail and suggests a possible mechanism for the production of Me_{ab}.

Chromatographic grade neutral activated alumina powder, Brockmann grade 1, was obtained from British Drug House (BDH). Prior to sample preparation, alumina powder was heated in air at 537 K to oxidize and remove any organic impurities; it was then dehydrated at a predetermined temperature (T_d) for 4 h *in vacuo*. Excess iodomethane was adsorbed onto the surface at room temperature and the sample pumped off for 1 h. The samples were sealed in Vitreosil/Pyrex ESR cells as previously described.[3-6] Methyl radicals were produced by UV photolysis at 77 K using a medium pressure Hanovia lamp. ESR measurements were made on a Decca X-3 spectrometer employing a microwave frequency of 9270.28±0.01 MHz with a reflection cavity fitted with a proton resonance probe for field determination and modulated at 100 kHz.

A preliminary study showed that Me_{ab} radicals could be obtained only from strongly pumped off alumina samples prepared above a T_d of 673 K and were not stable above 77 K. Contrary to the observation of Fujieda, the Me_{ab} radical ESR spectrum was found to be symmetrical with approximate line intensities of 1:5:5.5:1 and line widths of 0.211, 0.143, 0.132, and 0.198 mT respectively from low to high field. The Me_{ab} radical concentration at first increased with photolysis time but eventually attained a steady state. The yield as a function of T_d is shown in Fig. 1 and confirms that these radicals are not produced on samples prepared below a T_d of 673 K even after prolonged photolysis. Their absence may be attributed either to the lack of sites of stabilization for the radicals and/or to the lack of sites of absorption for the iodmethane. Since molecular water remains strongly adsorbed onto alumina surfaces up to 573 K,[7,8] it is possible that at the lower temperature iodomethane molecules cannot be strongly adsorbed in the first step and are completely removed in the pump-off process. The Me_{ab} radical

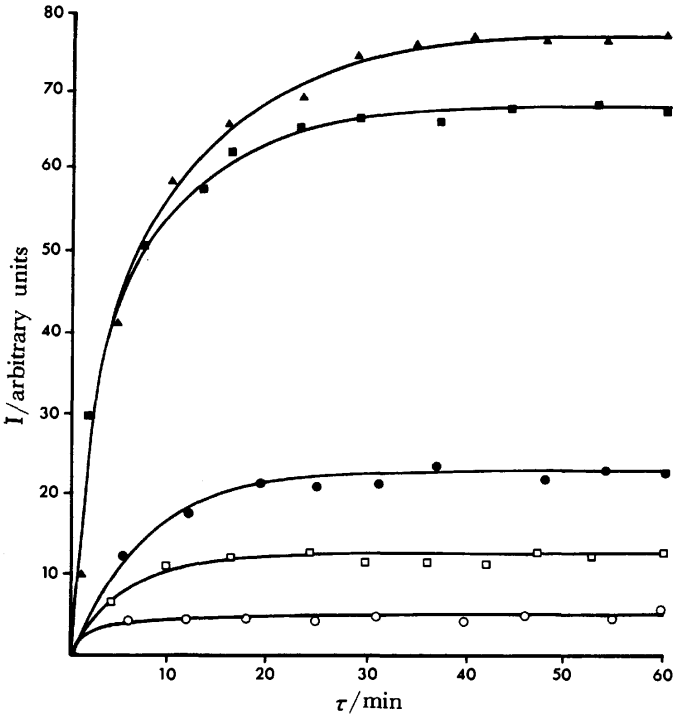

Fig. 1. The yield of abnormal methyl radicals at 77 K on alumina surfaces pretreated at various temperatures. I is the integrated signal intensity of the low field line in the methyl radical spectrum and τ is the photlysis time.
T_d; ■: 1173 K, ▲: 1073 K, ●: 973 K, □: 873 K, ○: 773 K.

yield increased with T_d from 673 K to 1073 K and then decreased at 1173 K. On increasing the T_d abve 673 K, although the surface hydroxyls which are thought to be the sites of adsorption may decrease[9] the surface sites of stabilisation would increase and result in a higher concentration of Me_{ab} radicals. However, at 1173 K, bulk movement in the alumina matrix may result in the sintering of pore walls, a reduction in pore volume and a large reduction in surface area which must reduce the number of sites of stabilization.

The formation of Me_{ab} radicals on alumina surfaces can be accounted for in two ways. The first involves the sites of adsorption and it is suggested that iodomethane is more strongly adsorbed by those surface hydroxyls remaining on the surface. The stronger adsorption may result in a change of planar methyl in iodomethane to nonplanar methyl, which on UV photolysis yields Me_{ab} radicals. If this was true, then since alumina surfaces have at least 5 different types of surface hydroxyl group[7] it should be possible to observe 5 different types of Me_{ab} radical and to vary their relative concentrations with T_d.

The second and more likely possibility involves the sites of stabilization of the radical once formed. Normal methyl radicals (Me_n, a=2.3 mT) produced

during photolysis stabilise upon electron deficient aluminium ions exposed during dehydration of the surface to exhibit a single Me_{ab} radical spectrum (a =2.08 mT). The attraction of the unpaired electron of the Me_n radical closer to the site of stabilisation, effectively changes the ESR characteristics of the methyl radical spectrum. Support for this mechanism is found in the work of Fujita *et al.*[10] who suggest that a reduction in the hyperfine splitting constant indicates charge transfer to the environment.

The production of Me_{ab} may be represented schematically as:

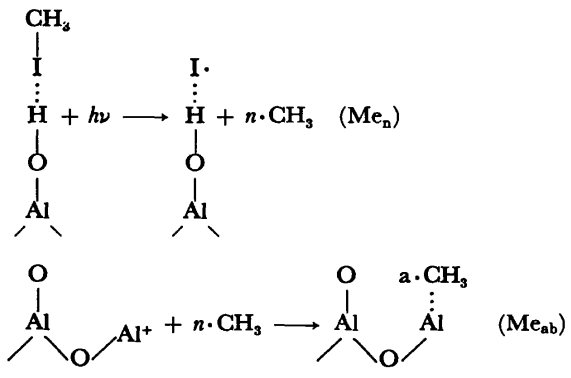

References

1) S. Fujieda. M. Setaka, and T. Kwan, *Chem. Lett.*, **1972**, 43.
2) D. A. Oduwole and B. Wiseall, *Bull. Chem. Soc. Jpn.*, **53**, 3037 (1980).
3) J. Turkevich and Y. Fujita, *Science*, **152**, 1619 (1966).
4) M. Fujimoto, H. D. Gesser, B. Garbutt, and A. Cohen, *Science*, **154**, 381 (1966).
5) P. K. Wong and J. E. Willard, *J. Phys. Chem.*, **72**, 2623 (1968); G. R. Joppien and J. E. Willard, *ibid.*, **78**, 1391 (1974).
6) G. B. Garbutt, H. D. Gesser, and M. Fujimoto, *J. Chem. Phys.*, **48**, 4065 (1968); G. B. Garbutt and H. D. Gesser, *Can. J. Chem.* **48**, 2685 (1970).
7) J. B. Peri, *J. Phys. Chem.*, **69**, 211; 220 (1965).
8) D. J. Norfolk and T. Swan, *J. Chem. Soc. Faraday Trans.* **73**, 1454 (1977).
9) F. H. Van Cauwelaert, J. R. Van Assche, and J. B. Utterhoeven, *J. Phys. Chem.*, **74**, 4329 (1970).
10) Y. Fujita, T. Katsu, and M. Sato, *J. Chem. Phys.*, **61**, 4307 (1974).

Preparation of Hexafluorodisilane and Reactions of Hexafluorodisilane and Hexachlorodisilane with Sulfur Trioxide

Bettadapura Srinivasaiah SURESH and Doddaballapur Krishnamurthy PADMA*

Department of Inorganic and Physical Chemistry, Indian Institute of Science, Bangalore 5600 12, India

(Received July 15, 1983)

Synopsis. Hexafluorodisilane has been prepared by the fluorination of hexachlorodisilane or hexabromodisilane by potassium fluoride in boiling acetonitrile, in yields approximating 45 and 60% respectively. Hexafluorodisilane has been characterised by infrared spectral data, vapour density measurements and analytical data. Both hexafluorodisilane and hexachlorodisilane are found to react with sulfur trioxide when heated to 400 °C for 12 h. The products of reaction are silicon tetrafluoride, silica and sulfur dioxide with hexafluorodisilane while hexachlorodisilane in addition gives rise to hexachlorodisiloxane.

The chemistry of hexahalodisilanes is interesting because of the presence of Si–Si bond and Si–X (halogen) bond which can undergo oxidation and cleavage. The bond energy of Si–Si bond is relatively weak when compared to C–C bond and therefore it undergoes homolytic cleavage on application of thermal energy. However, the Si–Si bond is thermodynamically favoured to undergo oxidation and this happens in reactions involving phosphine and phosphetane oxides[1,2] as well as phosphine sulfides.[3] In these cases, the hexachlorodisilane gets oxidised to hexachlorodisiloxane in the case of the oxides and to hexachlorodisilathiane with the sulfides. Therefore, it was of interest to see the action of sulfur trioxide on hexafluorodisilane and hexachlorodisilane.

In the reported methods for the preparation of Si_2F_6[4,5] disproportionation occurs and the product is contaminated with mixed halide fluorides. In the present modified procedure, based on the synthetic procedures evolved in this laboratory,[6,7] wherein the hexachlorodisilane or hexabromodisilane is treated with potassium fluoride in boiling acetonitrile, considerable improvement in the yields and purity are noted. Hexachlorodisilane and hexabromodisilane are prepared by standard methods.[8,9] The procedural details of preparation of Si_2F_6 and the reaction of sulphur trioxide on these hexahalodisilanes are given below.

Experimental

A Preparation of Hexafluorodisilane (Si_2F_6). Hexachlorodisilane (≈12.0 g) or hexabromodisilane (≈24 g), prepared and purified by standard methods,[8,9] is dissolved in 1,2-dichloroethane (20 ml) and added dropwise to a suspension of potassium fluoride (finely ground and dried at 110 °C in vacuum for 20 h) in boiling acetonitrile held in a three necked flask provided with a dropper, reflux condenser (with an outlet for the evolved gas) and a nitrogen inlet. The exit of the condenser is connected to two traps T_1 and T_2 maintained at −40 °C and liquid nitrogen temperature respectively. The addition is done slowly (about 2 h) and then the contents of the flask are allowed to reflux for a further period of 30 min in a slow stream of nitrogen. At the end of this period, heating and nitrogen flow are stopped, trap T_2 containing the solidified product gas is disconnected from the assembly. The uncondensable gases are removed at the pump and the solid is then allowed to sublime into a previously evacuated dry glass globe.

The infrared spectrum of the gaseous sample was recorded and the impurities SiF_4 and HCl were removed by low temperature fractional distillation (sublimation point of SiF_4=−95.7 °C, boiling point of HCl=−85 °C and of Si_2F_6=−18.4 °C). The infrared spectrum of the purified sample exhibits all the reported bands[10] of Si_2F_6 along with an absorption band at 1030 cm^{-1} characteristic of SiF_4, is as following, Observed: 420 (s), 440 (m), 520 (w), 740 (w), 840 (s), 850 (vs), 860 (s), 875 (m), 910 (w), 975—1010 (vvs, br) 1030 (SiF_4), 1060 (w), 1180 (m). (The intensities of the absorption bands are given in parentheses; vvs=very very strong, vs=very strong, s=strong, m=medium, w=weak and br=broad). The sample is found to contain more than 90% of Si_2F_6, remaining being SiF_4 as impurity as seen from the gas density measurements and chemical analysis. The compound; preparation mode (a) Si_2Cl_6 (b) Si_2Br_6; vapour density (reported, found); chemical analysis (Si(%): calcd, found, F(%): calcd, found); purity and yields are given below. a) Si_2F_6; Si_2Cl_6 and KF; (7.74,[4] 7.30); (33.01, 32.41; 66.99, 67.59),>90%; ≈45%. b) Si_2F_6; Si_2Br_6 and KF; (7.75,[4] 7.39); (33.01, 32.59, 66.99, 67.40); >93%; ≈60%. The yield of hexafluorodisilane is found to be approximately 45% with hexachlorodisilane and 60% with hexabromodisilane. This increase in yield can be attributed to the decreased bond energy of Si–Br bond compared to Si–Cl bond.

B. Reaction of Hexafluorodisilane with Sulfur Trioxide. Hexafluorodisilane (≈0.200 g, ≈1.1 m moles) containing some silicon tetrafluoride (≈10%) is condensed in a reaction vessel cooled by liquid nitrogen. Sulfur trioxide (≈0.240 g, 3.0 m moles) is condensed on to this and the reactant gases allowed to attain room temperature by withdrawing the coolant. At room temperature for 12 h no reaction occurred. Even at 300 °C the infrared spectrum shows only the reactants. The contents of the reaction vessel are then heated to 400 °C for 12 h. A white solid deposit is observed at the bottom and sides of the reaction vessel. The gas-phase infrared spectrum shows complete absence of the absorption bands of hexafluorodisilane and presence of enhanced absorption bands of SO_2,[11] 520 (s), 1150 (s), 1360 (vs), and SiF_4,[12] 1030 (s). The spectrum also shows the absence of any other compound such as hexafluorodisiloxane and sulfuryl fluoride.

The white solid in the reaction vessel is found to be silica by infrared spectroscopy. This is further confirmed by chemical tests. The solid dissolves rapidly in aqueous hydrofluoric acid to give fluorosilicic acid. The latter is identified by the formation of a white precipitate (K_2SiF_6) when potassium chloride solution is added.

C. Reaction of Hexachlorodisilane with Sulfur Trioxide. Sulfur trioxide (≈0.240 g; ≈3.0 m mole) is taken in an evacuated reaction vessel. Into this hexachlorodisilane (≈0.538 g, ≈2.0 m moles) is condensed and then the reactants are brought to room temperature. As the condensed hexachlorodisilane melts it dissolves in sulfur trioxide to form a clear colourless liquid. This is kept for 12 h at room temperature and the gas phase infrared spectrum is taken

which shows unreacted hexachlorodisilane. This is the case up to 300 °C. The reactants are then heated at 400 °C for 12 h. The infrared spectrum of the gaseous products now show the presence of hexachlorodisiloxane, sulfur dioxide and silicon tetrachloride. Sulfur dioxide and silicon tetrachloride are removed from the reaction mixture by low temperature fractional distillation. The gas phase infrared spectrum of the remaining products in the reaction vessel show the presence of only hexachlorodisiloxane,[13] 480 (s), 640 (vs), 1130 (vs), and complete absence of hexachlorodisilane.[14] The volatile hexachlorodisiloxane is removed from the reaction vessel by slow pumping till the gas phase does not show any absorption bands. It is observed that no other nonvolatile higher polychlorosiloxanes are present in the reaction vessel, except a white solid deposit at the bottom of the reaction vessel. The solid is found to be silica.

It is important to mention that these compounds are moisture sensitive and strictly anhydrous conditions have to be maintained.

The experimental results indicate that Si_2F_6 has been prepared in improved yields and greater purity. Mixed halides of silicon are not produced.

Both hexafluoro- and hexachloro-disilane have been found to undergo complete reaction with sulfur trioxide at 400 °C in 12 h. The products of reaction with Si_2F_6 are silicon tetrafluoride, sulfur dioxide and silica while hexachlorodisilane in addition gives rise to hexachlorosiloxane. With hexachlorodisilane some oxidation of the Si–Si bond occurs to form siloxane (Si–O–Si) linkage. However, with hexafluorodisilane no such oxidation is observed possibly because the nucleophilic attack on silicon by oxygen through a barrier of highly electronegative fluorine atoms occurs less predominantly at 400 °C and cleavage takes an upper hand. It has also been shown in the present investigation that higher molecular weight polysiloxanes, whose formation requires radical type cleavage and recombination, are not formed. This observation suggests the formation of the products *via* cleavage and disproportionation in both the cases.

References

1) K. Naumann, G. Zon, and K. Mislow, *J. Am. Chem. Soc.*, **91**, 2788 (1969).
2) K. E. DeBruin, G. Zon, K. Naumann, and K. Mislow, *J. Am. Chem. Soc.*, **91**, 7027 (1969).
3) G. Zon, K. E. DeBruin, K. Naumann, and K. Mislow, *J. Am. Chem. Soc.*, **91**, 7023 (1969).
4) W. C. Schumb and E. L. Gamble *J. Am. Chem. Soc.*, **54**, 583 (1932).
5) M. Schmeisser, *Angew. Chem., Int. Ed, Engl.*, **3**, 700 (1964).
6) D. K. Padma, V. Subrahmanya Bhat, and A. R. Vasudeva Murthy, *J. Fluorine Chem.*, **11**, 187 (1978).
7) D. K. Padma, B. S. Suresh, and A. R Vasudeva Murthy, *J. Fluorine. Chem.*, **14**, 327 (1979).
8) W. C. Schumb and E. L. Gamble, *Inorg. Synth.*, **1**, 42 (1939).
9) W. C. Schumb, *Inorg. Synth.*, **2**, 98 (1946).
10) P. L. Timms, R. A. Kent, T. C. Ehlert, and J. C. Margsane, *J. Am. Chem. Soc.*, **87**, 2824 (1965).
11) R. D. Shelton, A. H. Nielsen, and W. H. Fletcher, *J. Chem Phys.*, **21**, 2178 (1953).
12) J. Heicklen and V. Knight, *Spectrochim Acta*, **20**, 295 (1964).
13) K. Hamada, *J. Fluorine Chem.*, **7**, 385 (1976).
14) Y. Morino, *J. Chem. Phys.*, **24**, 164 (1956).
15) E. Hengge, "Halogen Chemistry" ed by V. Gutman Academic Press, London, 1967 Vol. 2, p. 199.
16) H. W. Kohlschutter and H. Mattner, *Z. Anorg. Allg. Chem.*, **282**, 169 (1955).

Interaction between 1,1′-Biacenaphthene-2,2′-diyl and Dibromomethane. Decay Kinetics in Mixed Solvents

Harumichi KOBASHI* and Hiroshi MASAMOTO
Department of Chemistry, Faculty of Engineering Gunma University, Kiryu, Gunma 376
(Received December 17, 1984)

Interaction of the triplet biradical, 1,1′-biacenaphthene-2,2′-diyl (BR) with dibromomethane has been examined by means of transient absorption measurements and kinetic analysis. The absorption spectrum of BR in CH_2Br_2 shows a red shift compared with those in other solvents with various polarities. The spectral result indicates that the red shift is not due to effect of solvent polarity but due to existence of weak electronic interaction acting directly between BR and CH_2Br_2. The nonlinear dependence of decay rates of BR upon $[CH_2Br_2]$ is interpreted in terms of a simple kinetic model of solvation based on solvent replacement between cage and bulk.

In a previous paper, it was reported that BR interacts with halogenated compounds to cause intersystem crossing (ISC) through spin-orbit (SO) interaction enhanced by heavy atoms, prior to chemical reactions.[1] At the same time, a complex formation

BR

between BR and the quencher C_2H_5I was suggested from a result of only kinetic analysis for decay rates of BR as a function of $[C_2H_5I]$. However, no spectroscopic evidence for the complex formation was obtained, because the intensity of BR absorption became too weak to observe the spectrum of the complex with increasing the quencher concentration. For the type II biradicals, on the other hand, it has been considered that a complex formation does not contribute to the enhancement of ISC induced by di-*t*-butyl nitroxide or oxygen through spin-spin interaction.[2] BR has two aromatic rings which are apt to form electron donor-acceptor (EDA) complexes with several quenchers. Therefore, in order to elucidate the decay behavior of BR, it will be important to examine whether direct electronic interaction concerns the biradical decay or not.

In this paper we examine in detail the interaction between BR and CH_2Br_2 in the wide range of $[CH_2Br_2]$, since the decay time of BR lies in a measurable time range of our experimental apparatus even in neat solvent of CH_2Br_2. Results give spectral evidence for the existence of an electronic interaction different from solvent polarity effect. In addition, a simple solvation model is proposed for interpreting the decay rates as a function of $[CH_2Br_2]$.

Experimental

The transient absorption spectra were observed by means of a 347 nm ruby-laser photolysis at room temperature.[3] For kinetic analysis, the decay times of BR were measured at several temperatures controlled by circulating thermostated water into a cell holder.

trans-Dimer of acenaphthylene (t-D) as a source material of BR was synthesized and purified by the same methods as described before.[3] Commercially available dibromomethane (Wako, GR grade) was taken out from an ampoule and immediately used without further purification. Zone-refined benzophenone (BP) was used as a triplet sensitizer. The concentrations of t-D and BP were both *ca.* 4×10^{-3} M (1 M=1 mol dm^{-3}). All solutions were degassed by the freeze-pump-thaw method.

Results and Discussion

Figure 1 shows time-resolved absorption spectra obtained for the BP-t-D system in several solvents, where the absorbances in the wavelength region $\leq$400 nm observed at the earlier time after excitation are omitted for simplicity. The initially observed absorptions at 530 nm and around 450 nm are due to ^{3}BP and ^{3}t-D, respectively.[3] After disappearance of ^{3}BP and ^{3}t-D, BR exhibits characteristic absorption bands at 379±1 nm in toluene (dielectric constant at 20 °C: ε=2.38), pyridine (ε=13.23), chlorobenzene (ε=5.71), and dichloromethane (ε=9.14) as well as in benzene (ε=2.28), dichloromethane, and 1,4-dioxane (ε=2.29) reported previously.[1,3] Although no spectra are given here, BR also shows the absorption maxima at 379±1 nm both in 1,2-dichloroethane (ε=10.66) and bromobenzene (ε=5.39). In dibromomethane solvent (ε=7.04), however, the absorption of BR is red-shifted by *ca.* 5 nm (Fig. 1(5)). Then, it is clear that the red shift is not due to the effect of solvent polarity but due to a weak electronic interaction between BR and CH_2Br_2. An origin of the interaction is probably charge-transfer (CT) interaction as in the systems of anthracene–CCl_4 and *etc.*[4] The quenching of BR by CH_2Br_2 in both CH_2Cl_2 and C_6H_6 were followed by lifetime measurements at 380 nm over the wide range of $[CH_2Br_2]$. Figure 2 shows the Stern-Volmer plots in C_6H_6. Each quenching curve bends downward similar to that by C_2H_5I in C_6H_6 but the deviation from a straight line is remarkable only in

much higher concentration region for the quencher CH_2Br_2 than for C_2H_5I. In the present case, therefore, an influence of change of medium properties by the addition of CH_2Br_2 could not be neglected for analyzing the quenching curve. Then, it is supposed that a complex formation is unrealistic, although the curvatures fit fairly well to Eq. 4 in Ref. 1 based on the complex formation mechanism. In order to obtain a more precise information about this circumstance, highly resolved absorption spectra around 380 nm were measured in mixed solvents of CH_2Cl_2 plus CH_2Br_2 and C_6H_6 plus CH_2Br_2 as well as in CH_2Cl_2, C_6H_6, and CH_2Br_2. The results are given in Fig. 3. The spectrum of BR shows gradual red-shift with increasing $[CH_2Br_2]$ in each solvent system (CH_2Cl_2 or C_6H_6). But, no spectrum with two absorption peaks indicating firmly the simultaneous existence of both free and complexed BR was observed in the mixed solvents of any composition of CH_2Br_2 so far as we examined (at 3, 5, and 10 M of CH_2Br_2). Hence, it seems plausible to consider that the red shift and nonlinear quenching curves are due to a

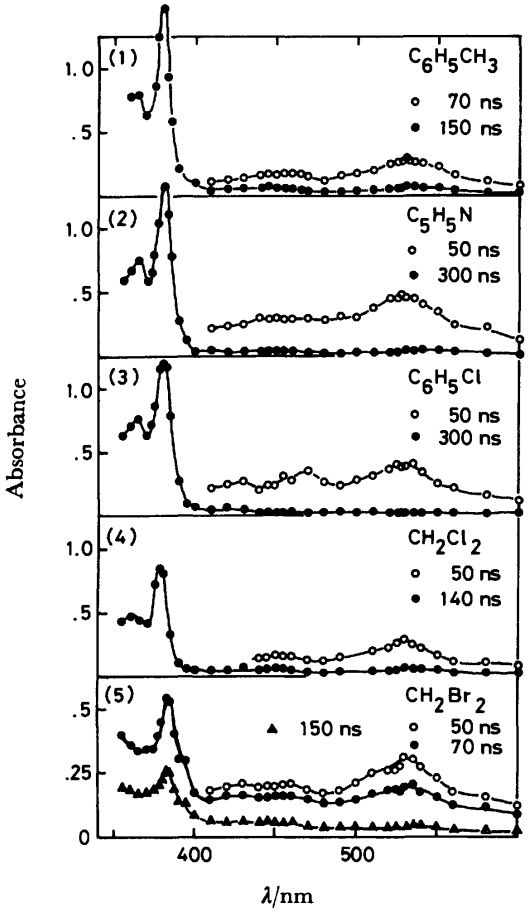

Fig. 1. Transient absorption spectra obtained in the solvents; (1) toluene, (2) pyridine, (3) chlorobenzene, (4) dichloromethane, and (5) dibromomethane. Delay times after the start of laser excitation are indicated in the figure.

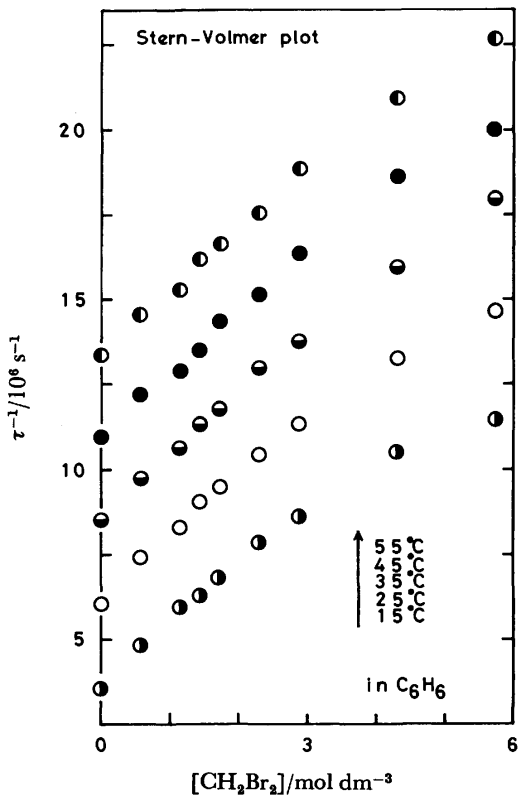

Fig. 2. Stern-Volmer plots for the CH_2Br_2/C_6H_6 system observed at several temperatures. The origin of ordinate is shifted upward by 2.5 each in the order of measurements at 15, 25, 35, 45, and 55 °C.

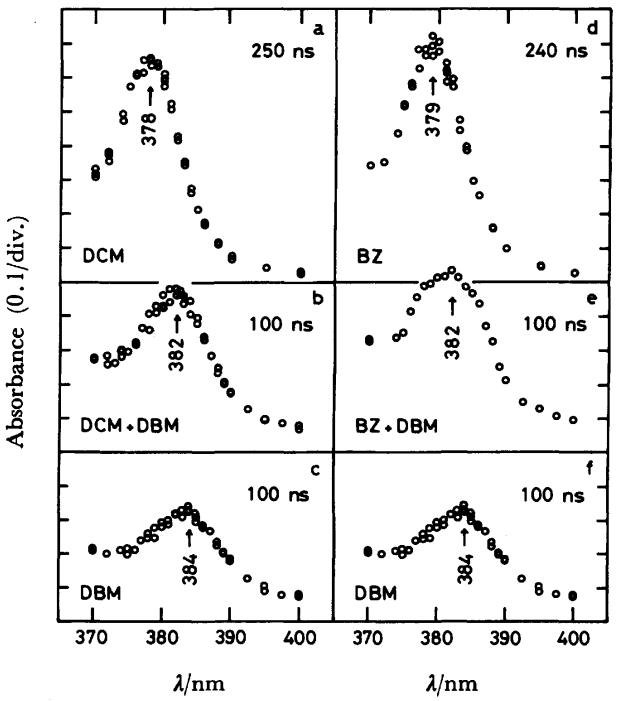

Fig. 3. Absorbance spectra of BR in (a) CH_2Cl_2, (b) CH_2Cl_2+(10 M) CH_2Br_2, (c) CH_2Br_2, (d) C_6H_6, (e) C_6H_6+(10 M) CH_2Br_2, and (f) CH_2Br_2: DCM=CH_2Cl_2, BZ=C_6H_6, DBM=CH_2Br_2. Delay times after the start of laser excitation are indicated in the figure.

continuous change of properties of medium surrounding BR but not due to formation of a complex with fixed geometry and stoichiometry.

Then, we employ a simple solvation model developed below for analyzing the decay behavior of BR in the mixed solvents. We assume the following conditions in the model: (i) The decay rate constant of BR (τ^{-1}) is determined by the composition of a solvent cage surrounding BR, as expressed by Eq. 1.

$$\tau^{-1} = \theta_A\tau_A^{-1} + \theta_B\tau_B^{-1} \quad (1)$$

where τ_A and τ_B are the lifetimes of BR in neat solvent A and B, respectively and θ_A and θ_B denote the mole fractions of component solvents A and B, respectively, in the solvent cage. Namely, Eq. 1 indicates the additivity between τ_A^{-1} and τ_B^{-1}. (ii) The solvent composition of the cage is proportional to that of the bulk solution in an equilibrium state of solvation;

$$\theta_A/\theta_B = K(\chi_A/\chi_B), \quad (2)$$

where χ_A and χ_B are the mole fractions of A and B, respectively, in the bulk solution and K is the proportionality constant. Equation 2 can be derived by assuming a solvent replacement between one component molecule (A or B) in the solvent cage and another component one (B or A) in the bulk. This situation is schematically shown as follows:

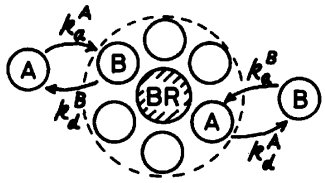

where k_a^i and k_d^i are the rate constants of solvation (or association) to BR and escape (or dissociation) from the cage, respectively, for i-th component molecule. When the equilibrium as to the solvent replacement is attained, the rate of solvation will be equal to the rate of escape for each component under the given conditions; *i.e.*, $k_a^A\theta_B[A]=k_d^A\theta_A[B]$ or $k_d^B\theta_B[A]=k_a^B\theta_A[B]$. These two equations are rearranged to Eq. 3;

$$\frac{\theta_A}{\theta_B} = \frac{k_a^A}{k_d^A}\cdot\frac{\chi_A}{\chi_B} = \frac{k_d^B}{k_a^B}\cdot\frac{\chi_A}{\chi_B}. \quad (3)$$

Therefore, K in Eq. 2 is equal to k_a^A/k_d^A or k_d^B/k_a^B. By combining Eq. 1 with Eq. 2 using the relations $\theta_A+\theta_B=1$ and $\chi_A+\chi_B=1$, one can obtain Eq. 4,

$$\frac{1}{\tau} = \frac{1}{\tau_B} + \frac{K\chi_A}{1+(K-1)\chi_A}\left(\frac{1}{\tau_A}-\frac{1}{\tau_B}\right). \quad (4)$$

Equation 4 shows that τ^{-1} is a nonlinear function of χ_A, involving only one unknown parameter K if τ_A and τ_B values are known. Rearrangement of Eq. 4 yields the following linear expressions with respect to $X(\equiv\chi_A/\chi_B)$, which are mathematically equivalent to one another.

$$(\tau^{-1}-\tau_B^{-1})^{-1} = (\tau_A^{-1}-\tau_B^{-1})^{-1}\{1+(KX)^{-1}\} \quad (5)$$

$$X^{-1}(\tau^{-1}-\tau_B^{-1}) = K(\tau_A^{-1}-\tau^{-1}) \quad (6)$$

$$X(\tau^{-1}-\tau_B^{-1})^{-1} = (\tau_A^{-1}-\tau_B^{-1})^{-1}(X+K^{-1}) \quad (7)$$

Equation 5 is identical in form to those derived by Ketelaar *et al.* for analyzing EDA complex formation[5] and by Ware *et al.* for exciplex formation.[6] Equation 6 is formally identical to those employed by Foster *et al.* for EDA complex systems[7] and by Rayner and Wyatt for an acid-base equilibrium in the excited state.[8] Equation 7 has also the same form as that described by Scott for EDA complexes.[9] These equations are very useful, since they do not need the knowledge about τ_A value.

Here, we analyze the decay times of BR using Eqs. 5, 6, and 7, because we can estimate the lifetime of BR in neat CH_2Br_2 simultaneously with K.[10] It was found that the observed lifetimes (τ) in the solvent systems of CH_2Br_2 (component A)/C_6H_6 (component B) and CH_2Br_2 (A)/CH_2Cl_2 (B) follow the relations, Eqs. 5, 6, and 7 with correlation factors better than those in the complex formation model. The results obtained for the CH_2Br_2/C_6H_6 mixture are shown in Fig. 4. By using the method of weighted least square,[11] each K and τ_A values obtained from these plots are, as a matter of course, in agreement with one another. Table 1 lists the parameter values obtained at several temperatures. According to the van't Hoff equation, the temperature dependence of K yields ΔH (-6.4 ± 1.1 kJ mol^{-1}) and ΔS (-14 ± 4 J mol^{-1} K^{-1}) for the solvation of CH_2Br_2 in the place of C_6H_6. In the CH_2Br_2 (A)/CH_2Cl_2 (B) mixture, K and τ_A values were also estimated to be 2.5 ± 0.2 and 70 ± 6 ns respectively at 20 °C.

The estimated τ_A values for both solvent systems agree with each other and are in fair agreement with the observed τ_A (84 ± 3 ns at 25 °C).[12] Therefore, the kinetic model used here is consistent. The small values of ΔH and ΔS seem to support that this model is more appropriate than the (1:1) complex forma-

Table 1. K and τ_A (in ns) values in the CH_2Br_2(A)/C_6H_6(B) system at several temperatures (t in °C)

t	K	τ_A
15	2.6 ± 0.3	71 ± 8
25	2.6 ± 0.5	64 ± 10
35	2.2 ± 0.5	62 ± 11
45	2.0 ± 0.5	60 ± 10
55	1.9 ± 0.5	58 ± 13

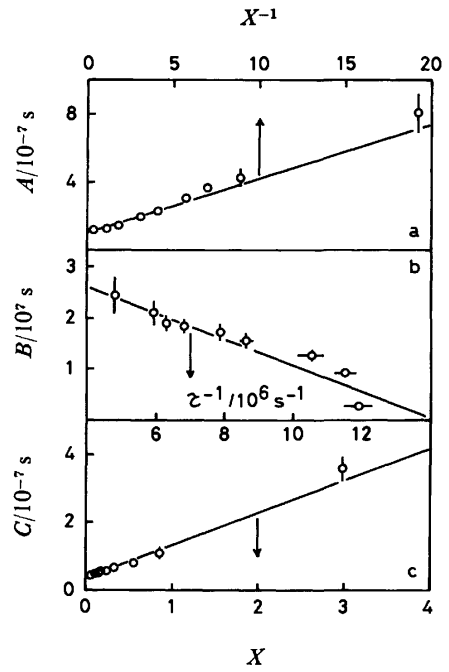

Fig. 4. Plots of the relations corresponding to Eqs. 5, 6, and 7 for the CH_2Br_2/C_6H_6 system at 15 °C. The abbreviated functions in the ordinate:
(a) $A=(\tau^{-1}-\tau_0^{-1})^{-1}$; (b) $B=X^{-1}(\tau^{-1}-\tau_0^{-1})$;
(c) $C=X(\tau^{-1}-\tau_0^{-1})^{-1}$.

tion model which, in most cases, accompanies rather large values of ΔH(*ca.* 20 kJ mol^{-1}) and ΔS(*ca.* 40 J K^{-1} mol^{-1}).[7] It is then implied that BR is likely to be solvated by CH_2Br_2 approximately 2.5 times stronger than by C_6H_6 or CH_2Cl_2, since K is *ca.* 2.5 in both solvent systems at ordinary temperatures. A different approach to solvation has been done for fluorescence frequency shift and quenching in mixed solvents by Lippert and Moll[13] and Kokubun[14] based on the Langmuir adsorption isotherm. They derived a kinetic equation which has also the same form as the present Eq. 5, if ψ or [Q] in their expression is replaced by X.

It should be noted further that a change in hydrodynamic properties of solvent mixtures is not negligible when the viscosity and molecular volume of A are largely different from those of B. If K is replaced by $(\eta_A V_A/\eta_B V_B)\exp \gamma_A$, Eq. 4 becomes identical to the expression derived by Stevens *et al.* based on the cage displacement model.[15] Here, η_i and V_i are the viscosity coefficient and the molecular volume of i-th component solvent, respectively, and γ_A is the index of preferential solvation of A in place of B. In the present cases, $\eta_A V_A/\eta_B V_B=1.26$ for A=CH_2Br_2 and B=C_6H_6 at 25 °C and $\eta_A V_A/\eta_B V_B=2.53$ for A=CH_2Br_2 and B=CH_2Cl_2 at 20 °C. By using these values, $\gamma_A=0.72$ for the CH_2Br_2/C_6H_6 system and $\gamma_A=-0.011$ for the CH_2Br_2/CH_2Cl_2 system are obtained. Accordingly, the preferential solvation by CH_2Br_2 should be taken into account for the BR quenching in the CH_2Br_2/C_6H_6 system and need not almost completely for that in the CH_2Br_2/CH_2Cl_2 system, in addition to the change of hydrodynamic properties.

As for BR decay, an important fact is that there exists the direct electronic interaction between BR and CH_2Br_2, which is able to cause the red shift of the BR spectrum but not so strong as a complex formation is confirmed spectroscopically. In conclusion, it is considered that the BR quenching is enhanced by SO interaction[1] perturbed by the weak electronic interaction, probably CT interaction, between BR and CH_2Br_2 in the solvent cage.

One of the authors (H.K.) expresses his thanks to Prof. Hiroshi Kokubun at Tohoku University for valuable suggestions in setting the kinetic model and to Prof. Haruo Shizuka at this laboratory for kind advice.

References

1) H. Kobashi, R. Kondo, H. Ikawa, and T. Morita, *Bull. Chem. Soc. Jpn.*, **57**, 1197 (1984).
2) J. C. Scaiano, *Tetrahedron*, **38**, 819 (1982); M. V. Encinas and J. C. Scaiano, *J. Photochem.*, **11**, 241 (1979).
3) H. Kobashi, H. Ikawa, R. Kondo, and T. Morita, *Bull. Chem. Soc. Jpn.*, **55**, 3013 (1982).
4) W. R. Ware and C. Lewis, *J. Chem. Phys.*, **57**, 3546 (1972) and references therein.
5) J. A. A. Ketelaar, C. van de Stolpe, A. Goudsmit, and W. Dzcubas, *Recl. Trav. Chim. Pays-Bas Belg.*, **71**, 1104 (1952).
6) W. R. Ware, D. Watt, and J. D. Holmes, *J. Am. Chem. Soc.*, **96**, 7853 (1974).
7) R. Foster, D. Ll. Hammick, and A. A. Wardley, *J Chem. Soc.*, 3817 (1953); R. Foster, "Organic Charge-Transfer Complexes," Academic Press, London (1969), Chap. 6.
8) D. M. Rayner and P. A. H. Wyatt, *J. Chem. Soc., Faraday Trans. 2*, **70**, 945 (1974).
9) R. L. Scott, *Recl. Trav. Chim. Pays-Bas Belg.*, **75**, 787 (1956).
10) This analysis allows us to compare the estimated τ_A value with the observed one. Analysis by Eq. 4 was not chosen for fear that the observed lifetime τ_A in CH_2Br_2 might involve the contribution of the decay time of precursor ^{3}t-D.
11) A. Yoshimura, *Journal of the Association of Personal Computer for Chemists*, **6**, 133 (1984). Thanks are due to Dr. A. Yoshimura at Osaka University for sending us a revised program.
12) The small difference between the estimated and observed τ_A values might be due to a little contribution of the decay rate of ^{3}t-D.
13) E. Lippert and F. Moll, *Z. Elektrochem.*, **58**, 718 (1954).
14) H. Kokubun, *Bull. Chem. Soc. Jpn.*, **42**, 919 (1969).
15) B. Stevens, K. L. Marsh, and M. A. Sylvia, *J. Phys. Chem.*, **88**, 669 (1984), and references cited therein.

X-Ray Photoelectron Diffraction (XPED) Studies on Metal Oxide Surfaces. (I) Analysis of the XPED Patterns from TiO_2(001) and α-Al_2O_3(0001) by the Single Scattering Calculation

Koji TAMURA,* Masanori OWARI, Masahiro KUDO, and Yoshimasa NIHEI
Institute of Industrial Science, University of Tokyo,
7-22-1 Roppongi, Minato-ku, Tokyo 106
(Received January 5, 1985)

X-Ray photoelectron diffraction (XPED) measurements were applied to the (001) surface of TiO_2 rutile and the (0001) surface of α-Al_2O_3 in order to examine the applicability of XPED to metal oxides. Obtained XPED patterns were compared with the results of theoretical calculations based on a single scattering model. The calculated patterns from both oxides agreed with the experimental patterns. It was revealed from theoretical calculations that the four oxygen atoms in the unit cell of TiO_2 made different contributions to the XPED pattern which reflected different atomic environments. The same calculation was also made on titanium in TiO_2, and on aluminum and oxygen in Al_2O_3. This clarified the contributions of nonequivalent sites of emitter atoms to the main peaks in the experimental XPED patterns. In comparison with the crystal structures, some peaks could be attributed to some specific emitters or specific emitter-scatterer pairs. This analysis was found to be useful to interpret experimental XPED patterns, and is expected to be applied to the analysis of the structures of surfaces or interfaces related to such phenomena as selective desorption or substitution of specific site of atoms.

It is known that angular distributions of XPS intensities from single crystals exhibit fine structures [1—4]. This modulation of photoelectron intensities is caused by the diffraction effect of photoelectrons excited in a single crystal by X-ray radiation, and is called X-ray photoelectron diffraction (XPED). Since XPED patterns reflect atomic arrangements, structural information regarding material can be obtained from an XPED measurement. The information derived from an XPED measurement can be summarized as 1) symmetry and orientation of the crystal surface [5,6], 2) atomic sites in the crystal [7—12], 3) crystal regularity [5,13], and 4) adsorption structure [14—16]. The influence of crystal symmetry and orientation on the XPED patterns have been investigated in detail by the present authors using GaAs(110) and Ge(110) [6]. The knowledge obtained in that study was then used to characterize such systems as the epitaxially grown Au overlayers on the GaAs(110) surface [5].

The XPED studies on a compound mixed crystal $Ga_{1-x}Al_xAs$ [9] showed correspondence between XPED patterns and the sites of photoelectron emitter atoms in the crystal, which indicated that XPED patterns can be regarded as finger prints of atomic sites. This method, therefore, can be used to determine the atomic sites of the foreign atoms in the crystal surface layers [11,12]. In the case of Au/GaSb interface [7], it was concluded that gold atoms occupy the equivalent atomic sites to gallium atoms.

XPED can further be used to estimate the crystal structural regularity. For example, measurements on the ion-bombarded GaAs(110) surface [5] made it possible to evaluate the crystal regularity and the thickness of the disordered layers in the surface region.

XPED can also provide information about the adsorption structure on the surface. The adsorption site of oxygen on the O/c(2×2)Cu(001) [14,15] and the bond orientation of adsorbed CO on the CO/Ni-(001) [16] have been reported.

The purpose of this study is to apply XPED to metal oxides and to investigate their surface structures. Metal oxides are used in many fields as solar cells, sensors, electronic devices, catalysts, absorbents and substrates for crystal growth. It is, therefore, very important to sufficiently characterize the surface structure and the chemical state of the oxide in order to control and reproduce their properties.

In general, in order to obtain structural information regarding the crystal surface, low energy electron diffraction (LEED) or reflection high energy electron diffraction (RHEED) have been used. However, in the case of the metal oxide, these conventional diffraction methods cannot be effectively used due to several reasons. First, they cannot distinguish the contribution from each component. This means that they are not suitable for the analysis of the complicated changes which occur on such samples as metal oxides. Secondly, these metal oxides suffer from severe charge-up problems because of irradiation of high-density primary electron beams. Thirdly, they generally require rather long-range ordering to obtain explicit diffraction patterns.

On the other hand, XPED does not have these drawbacks. Therefore, it can be expected that by using this new method, useful information can be provided regarding the surface structures of metal oxides.

In this study, the XPED patterns for metal oxides were obtained and compared with the results of theoretical calculations. The metal oxides selected for this study were the (001) surface of TiO_2 rutile and the (0001) surface of α-Al_2O_3, which are of great importance in connection with catalysts and have been investigated by many other methods [17—19].

Experimental

Apparatus. All experiments were performed with an angle-resolved X-ray photoelectron spectrometer [6,20] with an aperture in front of the entrance lens of the hemispherical analyzer in order to restrict the solid angle of photoelectron detection. The position-sensitive detection system compensates for the reduced photoelectron intensity due to the restriction of the solid angle. The angular scans were automatically performed using a two-axis sample rotation manipulator. The direction of the normal of the surface was defined as a polar angle of θ=0°, and the direction parallel to the surface was θ=90° [10]. The mean divergence of the acceptance angle was 1.3° along the polar-angle scan and 2.0° perpendicular to the polar-angle scan. The pressure during all measurements was kept below 5×10^{-9} Torr†. Al $K\alpha$ radiation was used to excite photoelectrons.

Samples. A (001) oriented TiO_2 single crystal (10×10×1 mm; Murakami Engineering Co. Ltd) was mechanically polished using a diamond polishing powder. A (0001) oriented Al_2O_3 single crystal (8×9×0.5 mm; Kyoto Ceramic Co. Ltd) had been polished beforehand. Both samples were chemically etched in HCl and in NaOH, and were thoroughly rinsed with distilled water. Before measurements, both samples were annealed in vacuum at 773 K for 50 min and at 823 K for 20 min, respectively, to reduce contaminations. It was confirmed by XPS that there were no carbon nor other impurities after the surface cleaning. Although a slight charge-up effect was observed on both samples, it did not cause any problems on the XPS spectrum shape and intensity.

Results and Discussion

TiO_2(001). (a) XPED Patterns from Oxygen Atoms: The azimuthal dependences of Ols emission from TiO_2(001) are shown in Fig. 1(a). The crystal structure of TiO_2 rutile [21] is also shown as the inset in Fig. 1. The polar angle θ=39° was chosen since the preliminary polar dependence measurement at ϕ=45° showed an intensity maximum at around θ=39°. As for the azimuthal angle, ϕ=0° is defined on the (010) plane and was determined by considering the symmetry property of the crystal. As can be seen in this XPED pattern, the photoelectron intensity maxima were observed at ϕ=0° (This angle is equivalent to 90° by the symmetry of the crystal.) and at ϕ=45°. The peaks at ϕ=45° are relatively sharp, whereas the peaks at ϕ=0° and 90° are broad. The results of the theoretical calculations based on the single scattering model [22] are also shown in Fig. 1(b) as a comparison with those obtained from the experiments. Although the relative intensities of peaks are somewhat different, the calculated XPED pattern reproduces the features of the experimental XPED pattern very well.

There are four kinds of atomic sites which are occupied by oxygen atoms in the unit cell of the TiO_2 crystal, as is shown in Fig. 1. Generally, the atomic arrangements surrounding these oxygen atoms are not equivalent to each other on the occasion of the photoelectron diffraction, though

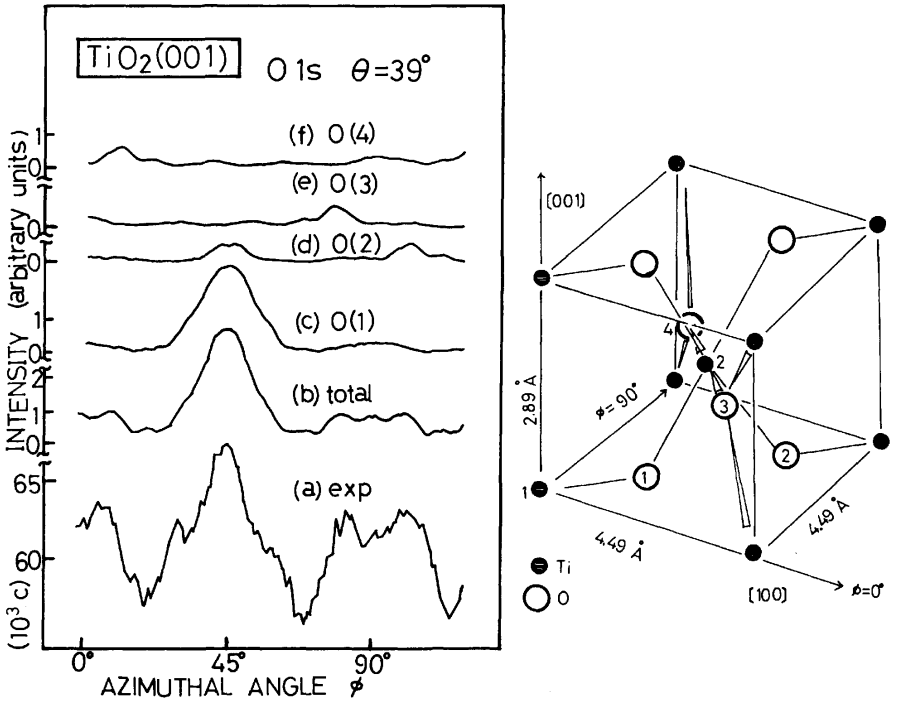

Fig. 1. XPED patterns of Ols from TiO_2(001) and crystal structure. (a) Experimental pattern. (b) Total calculated pattern. (c)—(f) Calculated patterns for each site of oxygen atom.

† 1 Torr ≈ 133.322 Pa.

these four sites become equivalent by rotating the arrangements by some multiples of 90°. As an XPED pattern is known to vary according to the environment of the photoelectron emitter atom, each XPED pattern from nonequivalent atomic sites should be different. An experimentally observed pattern is regarded as the sum of each pattern, and the contribution of each site can not be decomposed. On the other hand, in the theoretical calculation, XPED patterns from these four atomic sites can be individually obtained. The calculated XPED patterns from oxygen atoms in the different sites are shown in Fig. 1 (c—f). The four oxygen atomic sites O(1)—O(4) indicated for each pattern correspond to those shown in the crystal structure.

By comparing the individual calculated patterns with the total calculated pattern (b), it is easily understood that the peak at an azimuthal angle ϕ=45° is mainly due to the photoelectrons from oxygen atom O(1) and slightly to those from the oxygen atom O(2), and also understood that no contribution is made by the oxygen atom O(3) or O(4) at this angle. A similar comparison is also possible for other peaks. The peak at ϕ=12° was revealed to be constructed due to the contribution of oxygen atom O(4), and the peak at ϕ=78° by oxygen atom O(3).

The peak at ϕ=45° will be discussed in more detail in order to understand the origin of this peak. It is known that strongly peaked forward scattering is dominant in the scattering of electrons in metals with kinetic energies about 1000 eV [23,24]. The cause for this effect is that the magnitude of the atomic-scattering factor $f_j(\theta_j)$ is very strongly peaked in the forward direction, and that in this direction the scattering phase shift is rather small. The calculated polar dependence of Ols emission from oxygen atom O(1) at ϕ=45° showed an intensity maximum at θ=39°. This direction (θ,ϕ)=(39°,45°) is almost the same as that of the vector O(1)→Ti(2) in TiO_2. Taking all these facts into account, it is concluded that the experimental peak at ϕ=45° in the azimuthal pattern (Fig. 1(a)) originates mainly from the forward scattering of photoelectrons from the oxygen atom O(1) by the titanium atom Ti(2).

(b) XPED Patterns from Titanium Atoms: In Fig. 2 the azimuthal dependences of Ti2p emission at polar angle θ=39° are shown for TiO_2(001). As is seen in the experimentally obtained XPED pattern (Fig. 2 (a)), there are sharp and strong peaks at ϕ=0° and ϕ=±45°. The results of calculations are also shown in Fig. 2 (b) and they reproduce the features and the relative intensities of the experimental XPED patterns very well. In a TiO_2 crystal, these are two nonequivalent Ti atomic sites as are shown in Fig. 1. The calculated XPED patterns for each site of titanium atom are also shown in Fig. 2 (c—d). It is evident from these results that both emitter atoms Ti(1) and Ti(2) significantly contribute to all of the main peaks at ϕ=0° and ϕ=±45°, which is different

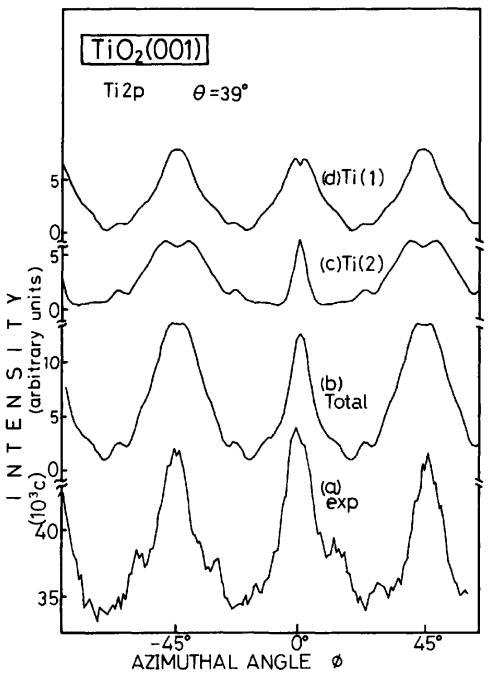

Fig. 2. XPED patterns of Ti2p from TiO_2(001). (a) Experimental pattern. (b) Total calculated pattern. (c), (d) Calculated patterns for each site of titanium atom.

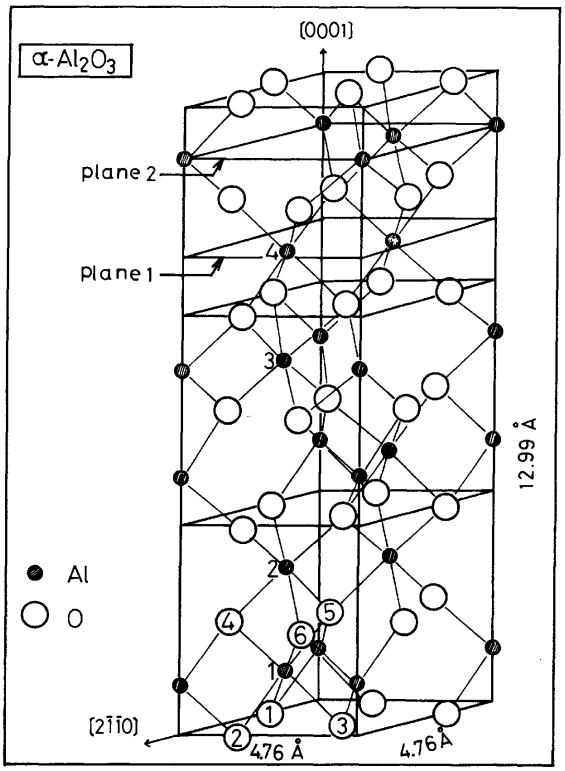

Fig. 3. Crystal structure model of α-Al_2O_3.

from the case of oxygen.

$Al_2O_3(0001)$. (a) XPED Patterns from Aluminum Atoms: The crystal structure of α-Al_2O_3 is shown in Fig. 3. The atomic positions of aluminum atoms and oxygen atoms in the hexagonal unit cell of α-Al_2O_3 were calculated from the results of X-ray diffraction measurement [25]. In an α-Al_2O_3 crystal, aluminum atoms are displaced about 0.2 Å upward or downward from the ideal plane along the c-axis. This displacement was taken into account in the theoretical calculation. On the other hand, the displacement of oxygen atoms in the c-plane was neglected. The azimuthal dependences of Al2s emission at polar angle θ=50° relative to surface normal are shown in Fig. 4. In the experimental XPED pattern (a), there are six peaks at −90°, −60°, −30°, 0°, 30°, 60°, whose shapes and relative intensities are not equal each other. Because of the symmetry of the crystal, ϕ=−90° is equivalent to ϕ=30°. In this figure, azimuthal angle ϕ=0° was on the (01$\bar{1}$0) plane of the hexagonal system. The result of the theoretical calculations is also shown in Fig. 4 (b). Though only single scattering was taken into account, the calculated results agreed well with the experimental results.

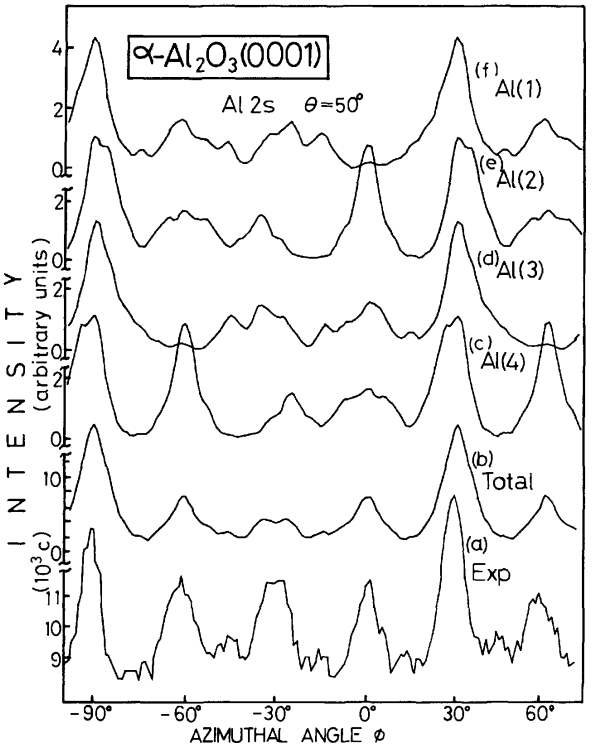

Fig. 4. XPED patterns of Al2s from α-Al_2O_3(0001). (a) Experimental pattern. (b) Total calculated pattern. (c)—(f) Calculated patterns for each site of aluminum atom.

There are four nonequivalent Al atomic sites in an α-Al_2O_3 crystal which are denoted as Al(1)—Al(4) as are shown in Fig. 3. Calculated XPED patterns for these four aluminum atoms are shown as Fig. 4(c)—(f), respectively. By comparing these calculated XPED patterns with the experimental pattern, it is easily seen how each peak in the experimental XPED pattern is constructed. The peak at ϕ=30° is constructed by the contribution of all four emitter atoms and this peak becomes rather a strong one. On the other hand, the peak at ϕ=0° is constructed mainly by the contribution of emitter atom Al(2) and the peak at ϕ=−60° is constructed mainly by the contribution of emitter atom Al(4), and these two peaks become relatively weak.

It is interesting to note the peak at ϕ=−30°. The

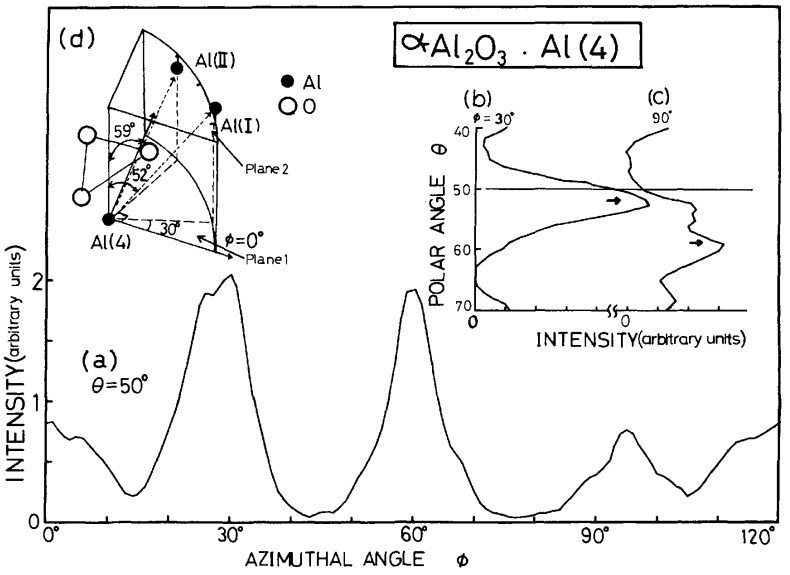

Fig. 5. XPED patterns calculated for aluminum atom Al(4) in α-Al_2O_3. (a) Azimuthal dependences. (b), (c) Polar dependences. (d) Atomic arrangement.

experimentally obtained peak is symmetrical and the top of the peak is flat. The comparison with each calculated pattern revealed that all four emitter atoms contribute to this peak and that the peak positions of each pattern deviated from $\phi=-30°$ to a higher or lower azimuthal angle. The peak shapes of patterns due to aluminum atoms Al(1) and Al(3) or due to aluminum atoms Al(2) and Al(4) are in the relation of a mirror symmetry about $\phi=-30°$. Thus, the total shape of these four patterns becomes a symmetrical one.

The relation between the direction from the emitter atom to the scatterer atom and the XPED pattern is discussed below by use of aluminum atom Al(4) (as an example). Figure 5 shows the calculated results for aluminum atom Al(4) and its atomic environment. The bottom curve (a) shows the azimuthal dependence at $\theta=50°$, and in the upper right, the polar dependences at some azimuthal angles are shown (b—c). In the same figure, some of the surrounding atoms of the emitter atom are also illustrated (d) where the emitter atom Al(4) is on a plane 1, and the scatterer atoms Al(I) and Al(II) are located almost on a plane 2. More strictly, the aluminum atom Al(I) displaces upward and Al(II) downward from a plane 2, as was mentioned before (also see Fig. 3). In the azimuthal dependence (a), there is a strong peak at $\phi=30°$, and this azimuthal

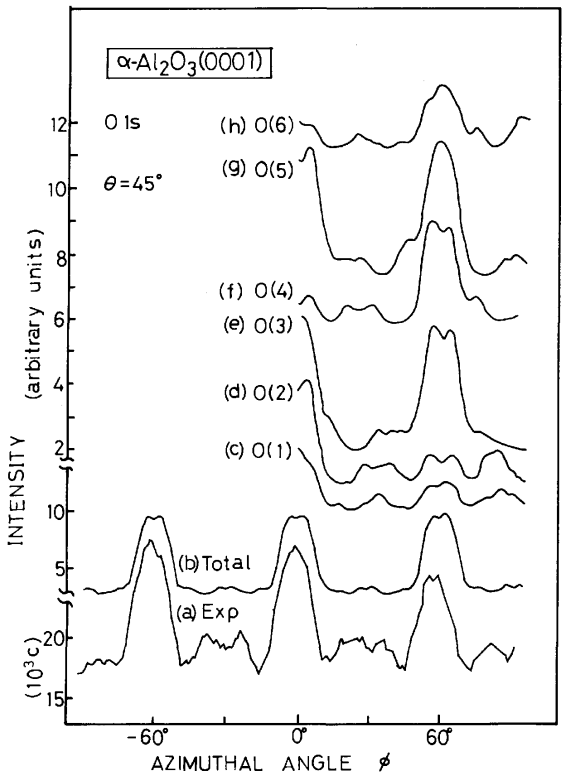

Fig. 6. XPED patterns of O1s from α-Al_2O_3 (0001). (a) Experimental pattern. (b) Total calculated pattern. (c)—(h) Calculated patterns for each site of oxygen atom.

direction is the direction from emitter atom Al(4) to the scatterer atom Al(I). The polar dependence at $\phi=30°$ (Fig. 5(b)) shows the peak at $\theta=52°$. This direction $(\theta,\phi)=(52°,30°)$ coincides with the direction from emitter Al(4) to scatterer Al(I). From this fact, the peak in curve (a) at $\phi=30°$ can be attributed to the forward-scattering peak by the emitter Al(4) and the scatterer Al(I).

On the other hand the shoulder at $\phi=90°$ in curve (a) has a different character. As shown in (d), the azimuthal angle $\phi=90°$ corresponds to the direction from Al(4) to Al(II). The polar angle of this direction is 59°, which leads to the appearance of a peak at $\theta=59°$ in the polar dependence curve (c). From this analysis it is understood that the small hump at $\phi=90°$ in the curve (a) at $\theta=50°$ is just the skirt of the forward-scattering peak which arises from the combination of the emitter Al(4) and the scatterer Al(II).

(b) XPED Patterns from Oxygen Atoms: Azimuthal dependences of O1s emission from α-Al_2O(0001) at polar angle $\theta=45°$ are shown in Fig. 6. As seen in this figure, strong peaks were found at $\phi=0°$, and $\phi=\pm60°$. The results of the theoretical calculations are also shown in Fig. 6(b). The comparison between these results showed that each main peak in the experimental pattern was reproduced by theoretical calculations. For the oxygen atoms in an α-Al_2O_3 crystal, there are six nonequivalent atomic sites, and these six atomic sites O(1)—O(6) correspond to those shown in Fig. 3. The calculated patterns obtained from each emitter atom O(1)—O(6) are shown in Fig. 6(c—h). It is evident that the main peaks in the experimental pattern are constructed by the contributions of some specific emitters.

As shown above, clear XPED patterns for the constituent elements on the metal oxide surfaces were obtained on which structural analysis is generally not easy because of the charge-up problem. A calculation based on the single scattering model explains the experimental results. It is found that the comparison of the total XPED pattern with each pattern from nonequivalent sites of atoms clarified the origin of XPED patterns. Therefore, such a comparison is useful in interpreting the experimental XPED patterns, and some main peaks were, for example, interpreted as the forward-scattering peaks from a specific emitter atoms by the surrounding scatterer atoms. When selective substitution or desorption takes place, some of the peaks in the experimental XPED patterns which are related to the specific sites of atoms appear and/or disappear. It is expected that the XPED analysis can be applied to the characterization of the surface or interface resulting from the reaction on the metal oxide surface. This is very difficult or impossible to be analyzed by other techniques.

References

1) K. Siegbahn, U. Gelius, H. Siegbahn, and E. Olson, *Phys. Scr.*, **1**, 272 (1970).
2) C. S. Fadley and S. Å. L. Bergström, *Phys. Lett. A*, **35**, 375 (1971).
3) J. Brunner and M. Thüler, *Helv. Phys. Acta*, **51**, 21 (1978).
4) M. Kudo, M. Owari, Y. Nihei, Y. Gohshi, and H. Kamada, *Jpn. J. Appl. Phys.*, **17**, Suppl. 17-2, 275 (1978).
5) M. Kudo, N. Koshizaki, M. Owari, Y. Nihei, and H. Kamada, *Hyoumen Kagaku*, **1**, 48 (1980).
6) M. Owari, M. Kudo, and Y. Nihei, *J. Electron Spectrosc.*, **22**, 131 (1981).
7) N. Koshizaki, M. Kudo, M. Owari, Y. Nihei, and H. Kamada, *Jpn. J. Appl. Phys*, **19**, L349 (1980).
8) Y. Nihei, M. Owari, N. Koshizaki, M. Kudo, and H. Kamada, *Proc. Japan Acad.*, **56B**, 654 (1980).
9) Y. Nihei, M. Owari, M. Kudo, and H. Kamada, *Jpn. J. Appl. Phys.*, **20**, L420 (1981).
10) M. Owari, P.-X. Jien, M. Kudo, Y. Nihei, and H. Kamada, *Bunko Kenkyu*, **32**, 103 (1983).
11) J. M. Adams, S. Evans, and J. M. Thomas, *J. Am. Chem. Soc.*, **100**, 3260 (1978).
12) S. Evans, E. Raftery, and J. M. Thomas, *Surf. Sci.*, **89**, 64 (1979).
13) M. Owari, M. Kudo, Y. Nihei, and H. Kamada, *Jpn., J. Appl. Phys.*, **19**, 1203 (1980).
14) S. Kono, C. S. Fadley, N. F. T. Hall, and Z. Hussain, *Phys. Rev. Lett.*, **41**, 117 (1978).
15) S. Kono, S. M. Goldberg, N. F. T. Hall, and C. S. Fadley, *Phys. Rev. Lett*, **41**, 1831 (1978).
16) L. G. Petersson, S. Kono, N. F. T. Hall, C. S. Fadley, and J. B. Pendry, *Phys. Rev. Lett.*, **42**, 1545 (1979).
17) C. C. Change, *J. Appl. Phys.*, **39**, 5570 (1968).
18) T. M. French and G. A. Somorijai, *J. Phys. Chem.*, **74**, (1979).
19) R. H. Tait and R. V. Kasowski, *Phys. Rev. B*, **20**, 5178 (1979).
20) M. Kudo, Y. Nihei, and H. Kamada, *Rev. Sci. Instrum.*, **49**, 756 (1978).
21) W. G. Wyckoff, "Crystal Structures," Interscience Publishers Inc., New York (1948), Chap. IV p5.
22) M. Owari, M. Kudo, Y. Nihei, and H. Kamada, *J. Electron Spectrosc. Relat. Phenom.*, **34**, 215 (1984).
23) S. Kono, S. M. Goldberg, N. F. T. Hall, and C. S. Fadley, *Phys. Rev. B*, **22**, 6085 (1980).
24) J. B. Pendry, "Low Energy Electron Diffraction," Academic, London (1974), Chap. 2.
25) R. E. Newnham and Y. M. De. Haan, *Z. Krist.*, **117**, 235 (1962).

The Curve Fitting Analysis of D.c. and A.c. Voltammograms of a Two-step Surface-redox Reaction. The Application to the Surface-redox System of Adriamycin Adsorbed on a Pyrolytic Graphite Electrode

Kenji KANO, Tomonori KONSE, and Tanekazu KUBOTA*
Gifu Pharmaceutical University, 6-1 Mitahora-higashi 5-Chome, Gifu 502
(Received February 21, 1985)

A theoretical study of the two-step surface-redox reaction ($O_{ad}+n_1e \rightleftharpoons S_{ad}$, $S_{ad}+n_2e \rightleftharpoons R_{ad}$) was performed using d.c. voltammetry. A new method based on a non-linear least-squares curve fitting of cyclic d.c. and a.c. voltammograms was proposed for determining electrochemical parameters and was successfully applied to the surface-redox system of the quinone moiety of adriamycin adsorbed on a pyrolytic graphite electrode.

Recently, research regarding redox modified electrodes has been a very active field in electrochemistry and a wealth of reports have been published concerning applications to electroanalysis, electrocatalysis, and electrochromic devices (for reviews, see Refs. 1—3). In order to analyze the electrochemical behavior of surface-attached redox materials associated with biological, pharmaceutical, and chemical fields, a two-step electron-transfer surface-redox reaction mechanism seems to be very important. Numerous studies have been carried out regarding this type of electrode reaction.[4-8] However, there is little literature pertinent to the kinetic treatment of this mechanism. Kakutani and Senda have recently reported a theory of the a.c. polarization and a.c. voltammetry of the mechanism[7] and showed that a.c. voltammetry is a powerful technique for determining electrochemical kinetic parameters.[8] Alternatively, cyclic d.c. voltammetry has been widely used for the characterization of the electrochemical behavior of a modified electrode.[1-3] Analyses regarding cyclic d.c. voltammetry are, thus, very important. As far as we know, however, theoretical studies of cyclic d.c. voltammetry regarding two-step surface-redox reactions are limited to an electrochemically reversible system[4,6,7] and also to a reversible electrochemical reactions coupled with irreversible chemical reactions.[4]

In this paper, we report on a theoretical study regarding a two-step surface-redox reaction in d.c. voltammetry and also a useful method for the analysis of cyclic d.c. and a.c. voltammograms by means of non-linear least-squares curve fitting for determining the electrochemical kinetic parameters. The application of our methods to a surface-redox system of adriamycin (antitumor anthracycline antibiotics) adsorbed on a pyrolytic graphite electrode is discussed in detail.

Theoretical Treatment of D.c. Voltammetry for the Case of Two-step Surface-redox Reaction

Let us now consider a two-step surface-redox reaction:

$$\begin{aligned} O_{ad} + n_1e &\rightleftharpoons S_{ad} \quad \text{(1st step)} \\ S_{ad} + n_2e &\rightleftharpoons R_{ad} \quad \text{(2nd step)}, \end{aligned} \tag{1}$$

where all the electrochemical species (O, S, and R) are strongly adsorbed on the electrode surface. The quantities of O, S, and R due to a mass transfer from (to) the electrode surface to (from) the solution are negligibly small compared with those of the adsorbed reactants. Thus,

$$\Gamma_o + \Gamma_s + \Gamma_r = \Gamma_t = \text{const.} \tag{2}$$

Here Γ_j (j=o, s, or r) is the surface concentration of the adsorbed reactant j per unit area, and Γ_t is the total surface concentration. For the above system, theoretical studies of the reversible d.c.[4,6,7] and a.c.[7] voltammetries have already been reported. Our formulation for Scheme (1) is therefore for the d.c. voltammogram of a quasi-reversible case.

Assuming that the surface-redox reaction occurs only among the adsorbed reactants, the faradaic current, i, is given by

$$i = i(1) + i(2) \tag{3a}$$

$$i(1) = n_1FA\,d\Gamma_o/dt \tag{3b}$$

$$i(2) = -n_2FA\,d\Gamma_r/dt, \tag{3c}$$

where $i(1)$ and $i(2)$ are the faradaic currents of the first and second electron-transfer steps, respectively, and A is the electrode area. The electrode potential, E, can now be written as

$$E = E_i + vt, \tag{4}$$

E_i and v being the initial potential and the sweep rate, respectively. The current-potential-surface

concentration characteristics can, thus, be expressed by the Butler-Volmer equation:[1,7,9]

$$i(1) = n_1FAk_{sap}(1)\{\Gamma_s \exp[(1-\alpha_1)n_1F(E-E'_{o1})/RT] - \Gamma_o \exp[-\alpha_1 n_1F(E-E'_{o1})/RT]\} \quad (5a)$$

$$i(2) = n_2FAk_{sap}(2)\{\Gamma_r \exp[(1-\alpha_2)n_2F(E-E'_{o2})/RT] - \Gamma_s \exp[-\alpha_2 n_2F(E-E'_{o2})/RT]\}. \quad (5b)$$

In these equations, $k_{sap}(1)$ and $k_{sap}(2)$ are, respectively, the apparent rate constants of the first and second steps at the formal standard redox potentials, E'_{o1} and E'_{o2}, corresponding to the redox couples O_{ad}/S_{ad} and S_{ad}/R_{ad}. The transfer coefficient with regard to the (cathodic) electron-transfer of the j-th step is expressed by α_j (j=1 or 2).

Combination of Eqs. 2 to 5 may lead to current potential characteristics for linear potential sweep voltammetry. Assuming $n_1=n_2=n$ (for convenience), we define the semiquinone formation constant, K, as follows:

$$K = [S_{ad}]^2/[O_{ad}][R_{ad}] = \exp[nF(E'_{o1}-E'_{o2})/RT]. \quad (6)$$

Differential equations (as dimensionless functions) are easily written as Eqs. 7a and 7b using the above equations,

$$\psi(1) = i(1)RT/n^2F^2vA\Gamma_t = m(1)[(1-f_o-f_r)(\rho/\sqrt{K})^{1-\alpha_1} - f_o(\rho/\sqrt{K})^{-\alpha_1}] = df_o/d\rho \quad (7a)$$

$$\psi(2) = i(2)RT/n^2F^2vA\Gamma_t = m(2)[f_r(\rho\sqrt{K})^{1-\alpha_2} - (1-f_o-f_r)(\rho\sqrt{K})^{-\alpha_2}] = -df_r/d\rho, \quad (7b)$$

the current being defined by

$$\psi = iRT/n^2F^2vA\Gamma_t = \psi(1) + \psi(2), \quad (7c)$$

where

$$f_j = \Gamma_j/\Gamma_t \quad (j=o, r) \quad (8a)$$

$$m(j) = k_{sap}(j)RT/nFv \quad (j=1, 2) \quad (8b)$$

$$\rho = \exp[nF(E-E'_o)/RT]. \quad (8c)$$

Here $E'_o(=(E'_{o1}+E'_{o2})/2)$ is the formal standard redox potential of the redox couple O_{ad}/R_{ad}. Other symbols have their usual meanings. Solving Eqs. 7a and 7b, we obtain values for f_o and f_r. Thus, ψ can be calculated using Eq. 7c where $\psi(1)$ and $\psi(2)$ are easily evaluated by introducing f_o and f_r into the original Eqs. 7a and 7b.

Two sets of the differential Eqs. 7a and 7b were solved using a standard fourth-order Runge-Kutta method.[10] The initial conditions are $f_o=0$ and $f_r=1$ at $\rho\to 0$ for the anodic curve, and $f_o=1$ and $f_r=0$ at $\rho\to\infty$ for the cathodic curve. The calculation was carried out with an NEC 8001 personal computer.[11]

Let us also assume that the adsorbed reactants undergo homogeneous intermolecular interactions (written by Frumkin's a-parameter[12]). Thus, E'_{o1}, E'_{o2}, $k_{sap}(1)$, and $k_{sap}(2)$ are now given by[7]

$$E'_{o1} = E_{o1} + (RT/n_1F)\ln[B_s(1)/B_o(1)] \quad (9a)$$

$$E'_{o2} = E_{o2} + (RT/n_2F)\ln[B_r(2)/B_s(2)] \quad (9b)$$

$$k_{sap}(1) = k_s(1)B_o(1)^{\alpha_1-1}B_s(1)^{-\alpha_1}\exp(-a\theta) \quad (10a)$$

$$k_{sap}(2) = k_s(2)B_s(2)^{\alpha_2-1}B_r(2)^{-\alpha_2}\exp(-a\theta). \quad (10b)$$

In these equations, $B_j(1)$ and $B_j(2)$ (j=o, s, or r) are the adsorption coefficients of the species j at E_{o1} and E_{o2}, respectively. The E_{o1} and E_{o2} stand for the standard redox potentials of the redox couples O/S and S/R in the bulk solution, respectively, θ being the total surface coverage (Γ_t/Γ_t^{max}; Γ_t^{max} is the maximum value of the total surface concentration). Note that when $k_{sap}(1)=k_{sap}(2)=k_{sap}$, the k_{sap} dependence on θ is given by

$$k_{sap} = k_{sap}(\theta\to 0)\exp(-a\theta), \quad (10c)$$

where $k_{sap}(\theta\to 0)$ means k_{sap} at $\theta\to 0$.

Figure 1 shows the m ($=m(1)=m(2)$) dependence of the normalized anodic voltammograms at K=1 and α ($=\alpha_1=\alpha_2$)=0.5. There is a positive shift of the peak potential, $E_{p,a}$, with decreasing m. Figure 2 depicts the K dependence of the normalized voltammograms under the conditions of m=0.5 and α=0.5. As in the case of a reversible system[4,7] there is only one peak

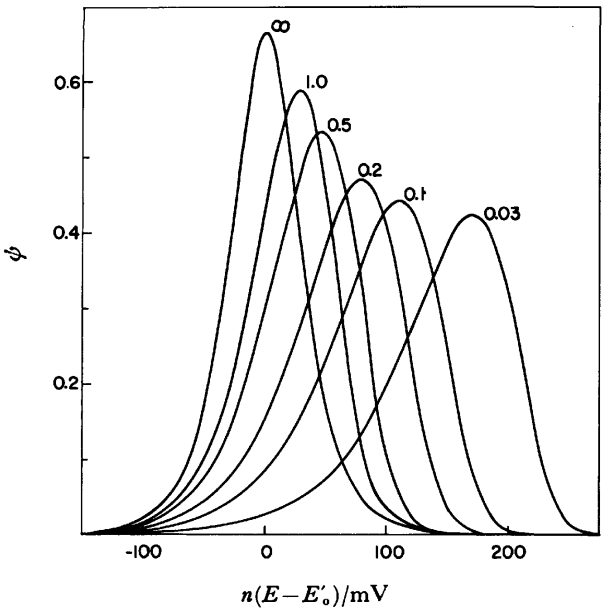

Fig. 1. The dependence of m on the normarized d.c. anodic voltammograms at K=1.0 and α=0.5. The m value is indicated on each curve.

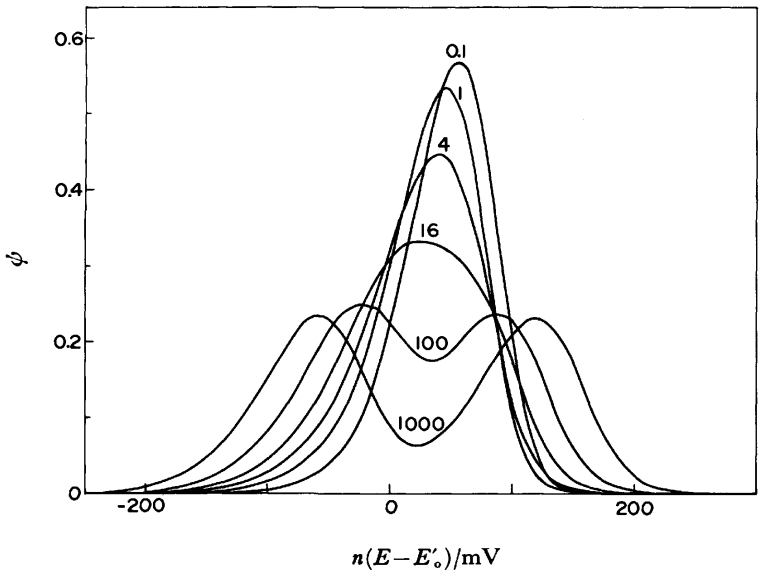

Fig. 2. The dependence of K on the normarized d.c. anodic voltammograms at $m=0.5$ and $\alpha=0.5$. The K value is indicated on each curve.

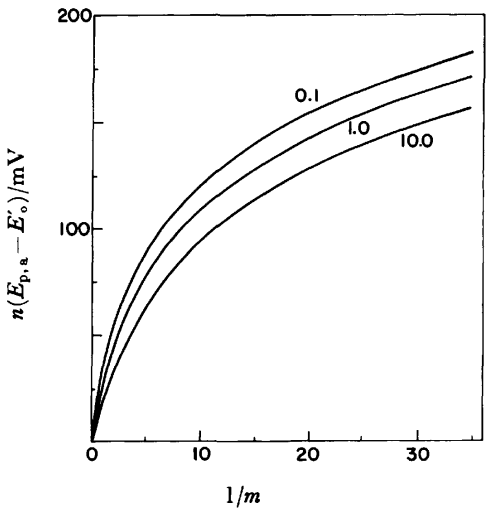

Fig. 3. Variation of $n(E_{p,a}-E'_o)$ with $1/m$ for $\alpha=0.5$ and $K=0.1$, 1.0, and 10.0. The value of K is indicated on each curve.

for $K\leq16$, but two peaks are obtained for $K>16$. Also, Eqs. 7a to 7c indicate that the cathodic curve, having $m(1)=a$, $m(2)=b$, $K=c$, and $\alpha=d$, and the anodic curve, having $m(1)=b$, $m(2)=a$, $K=c$, and $\alpha=1-d$, are symmetrical about the C_2 axis which is vertical to the curve plane and goes through the point of $\rho=1$ ($E=E'_o$) and $\psi=0$ ($i=0$). Accordingly, when $m(1)=m(2)$ and $\alpha=0.5$ (conditions necessary to experimentally obtain cathodic and anodic voltammograms in a C_{2h} symmetry) both the waves are symmetrical about the point of $E=E'_o$ and $i=0$.

The change of $n(E_{p,a}-E'_o)$ with m is shown in Fig. 3 for various K's at $\alpha=0.5$. Using the working curves like those in Fig. 3, k_{sap} can be estimated from the observed $E_{p,a}-E'_o$ value[13], provided that n and K can be obtained by the other methods, and that $k_{sap}(1)=k_{sap}(2)=k_{sap}$ and of $\alpha_1=\alpha_2=0.5$ are kept. The latter situation can be verified by checking whether or not the average of the cathodic and anodic peak potentials, $(E_{p,a}+E_{p,c})/2$, is independent of v and Γ_t and equal to E'_o,[13] and also whether the peak currents, the half-peak widths, and the electricities of the cathodic and anodic waves coincide with each other. Needless to say, the K as well as E'_o can be estimated from the reversible d.c. voltammogram.[4,7]

The above method is, however, only based on information regarding peak potentials. Furthermore, if an estimation of K is difficult, the above method can not be used. Thus, we propose here a non-linear least-squares analysis of the d.c. voltammograms for the determination of kinetic parameters.[14,15] In the following section we will discuss the results concerning the characterization of the electrochemical behavior of adriamycin adsorbed on a pyrolitic graphite electrode.

Experimental

Adriamycin hydrochloride and all other chemicals used have been described elsewhere.[16] The electrochemical measurements were performed mostly as described in previous papers.[16,17] Positive feedback circuits were used for ohmic drop compensation. Electrodes, used as working electrodes, were fabricated using cylindrical rods of pyrolytic graphite carbon (Tomoe Co., Osaka), and were sealed onto glass tubing by heat-shrinkable Teflon tubing. The pyrolytic graphite electrode was cleaved with a razor blade to produce a basal-plane surface and was first polished with silicon carbide paper (No. 1000) and then with a diamond paste in order to prepare a smooth shiny surface. The electrode was ultrasonically cleaned in ethanol. The geometrical area of the electrodes were

0.126 cm^2. The freshly prepared pyrolytic graphite electrode was immersed into an electrolysis solution containing adriamycin for 1—3 min under stirring at an initial potential, E_i. After standing for 0.5—2 min, a d.c. voltage scan was started from E_i, a saturated calomel electrode (SCE) being used as a reference electrode. A sodium acetate (0.2 mol dm^{-3})-nitric acid buffer (pH 4.54, ionic strength 0.5 with potassium nitrate) was used as the base solution. Most experiments were performed in solutions containing $2—6\times10^{-6}$ mol dm^{-3} of adriamycin.

The electrode surface was cleaned after several potential scans because of an aging effect which may have some relation to the stability of the reduced adriamycin[16,17] as well as the electrode.

Results and Discussion

Cyclic D.c. Voltammetry. Figure 4 shows the cyclic d.c. voltammogram of adriamycin adsorbed on a pyrolytic graphite electrode (recorded from $E_i=-0.30$ V at $v=10$ mV s^{-1}). A symmetric pair of cathodic and anodic waves was observed at −0.5 V. This wave is ascribed to the redox reaction of the quinone moiety of the adsorbed adriamycin.[16] When the voltammograms were recorded at $v\leq50$ m V s^{-1}, the peak heights of cathodic and anodic waves, $i_{p,c}$ and $i_{p,a}$, coincided with each other and were proportional to v at a given Γ_t.[18] The electricities of cathodic and anodic waves, Q_c and Q_a, also agree well with each other within the experimental error. The peak potentials ($E_{p,c}$ and $E_{p,a}$) and the half-peak widths ($\Delta E_{p/2,c}$ and $\Delta E_{p/2,a}$) are −0.498 V and 54—55 mV, respectively, for both the cathodic and anodic waves, and are independent of v and Γ_t. This electrochemical behavior should be interpreted in terms of a d.c. reversible two-step surface-redox reaction as shown in Scheme (1), where $n_1=n_2=1$.[8,16] According to the theory of a reversible two-step surface-redox reaction, we have estimated the K value to be 0.244±0.085 from the half-peak widths.[19]

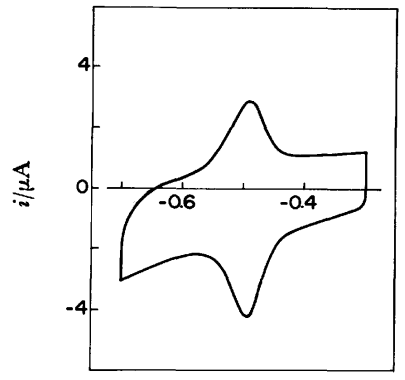

E/V *vs.* SCE

Fig. 4. Cyclic d.c. voltammogram of adriamycin adsorbed on a pyrolytic graphite electrode. Voltage scanning was done with $v=10$ mV s^{-1} after stirring for 1 min at $E_i=-0.3$ V in 5.52×10^{-6} mol dm^{-3} adriamycin solution.

Under the conditions of $v>100$ mV s^{-1}, a discrepancy occurs between $E_{p,a}$ and $E_{p,c}$, and the ΔE_p ($=E_{p,a}-E_{p,c}$) becomes larger with an increase in v. Figure 5 shows the cyclic d.c. voltammogram recorded at $v=9000$ mV s^{-1}, the current being corrected for the base. This is a typical quasi-reversible voltammogram: ΔE_p comes out 59 mV. Nevertheless, the same values between $i_{p,a}$ and $i_{p,c}$, and also between $\Delta E_{p/2,a}$ and $\Delta E_{p/2,c}$ can be within the experimental error at a given v and Γ_t. The $(E_{p,a}+E_{p,c})/2$ value is independent of v and Γ_t and agrees well with E_o', which is equal to $E_{p,a}$ or $E_{p,c}$ of the reversible waves. These facts suggest that $k_{sap}(1)=k_{sap}(2)=k_{sap}$, and $\alpha_1=\alpha_2=\alpha=0.5$.

Based on the above consideration, we analyzed the voltammogram shown in Fig. 5 by means of a non-linear least-squares analysis using two parameters, k_{sap} and K, at $E_o'=-0.498$ V, $Q=5.94$ μC[20] ($\Gamma_t=2.44\times10^{-10}$ mol cm^{-2}),[18] and $\alpha=0.5$.[21] The refined parameters are $k_{sap}=503\pm19$ s^{-1} and $K=0.229\pm0.023$. The resultant regression curve is depicted in Fig. 5 as a broken curve. Table 1 gives the regression results of the voltammograms at various Γ_t and v. We can see that although k_{sap} decreases with an increase in Γ_t, K is almost independent of Γ_t and stays within 0.211±0.099. This is in good agreement with the K estimated from the reversible voltammograms. This indicates the effectiveness of the non-linear least-squares curve fitting analysis of d.c. voltammograms.

In addition, a one-parameter curve fitting was also

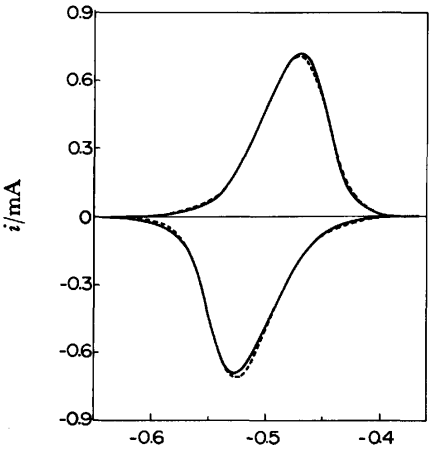

E/V *vs.* SCE

Fig. 5. Cyclic d.c. voltammogram of adriamycin adsorbed on a pyrolytic graphite electrode. Voltage was scanned with $v=9000$ mV s^{-1} after stirring for 1 min at $E_i=-0.3$ V in 1.84×10^{-6} mol dm^{-3} adriamycin solution. The current is corrected for the base current. The broken line represents the regression curve calculated under the conditions of $k_{sap}=503$ s^{-1}, $K=0.229$, $\alpha=0.5$, $E_o'=-0.498$ V *vs.* SCE, and $Q=5.94$ μC.

TABLE 1. k_{sap} AND K VALUES OF ADRIAMYCIN ADSORBED ON A PYROLYTIC GRAPHITE ELECTRODE ESTIMATED BY MEANS OF CYCLIC D.C. VOLTAMMETRY

Γ_t / 10^{-10} mol cm^{-2}	v / V s^{-1}	k_{sap} / s^{-1}	K
1.72	4.0	532	0.104
2.44	9.0	503	0.229
2.72	8.0	519	0.062
3.14	4.0	320	0.280
3.33	9.0	358	0.187
4.20	4.0	239	0.290
6.30	4.0	167	0.325

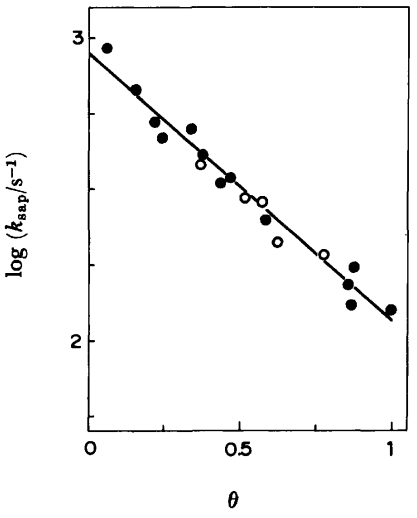

Fig. 6. Surface coverage dependence of the log k_{sap} values estimated by one-parameter curve fitting (K= 0.211) of cyclic d.c. (●) and of a.c. (○) voltammograms. The solid line represents the regression result; *i.e.* log k_{sap}[=log $k_{sap}(\theta\rightarrow 0)-a\theta/2.303$]=2.94−0.882$\theta$ (r=0.983).

carried out using a constant K value of 0.211 (the average value obtained by two-parameter fitting). A linear log k_{sap} *vs.* θ (surface coverage) plot for the refined k_{sap} is depicted in Fig. 6 (closed circles); the linearity seems to be quite good. These results prove the adequacy of Eq. 10c for the adsorbed adriamycin; *viz.* the interaction among the adsorbed reactants is homogeneous, and the reactants obey Frumkin's adsorption isotherm. The negative log k_{sap} *vs.* θ plot indicates an attractive interaction.

A.c. Voltammetry. Figure 7 shows the real and imaginary components of the a.c. voltammogram of the adsorbed adriamycin, recorded at 100 Hz (a.c. frequency, f). The imaginary component is less than the real component and has two peaks. The peak potential of the real component and the valley potential between the two imaginary component peaks coincide with each other and also with the E_o'

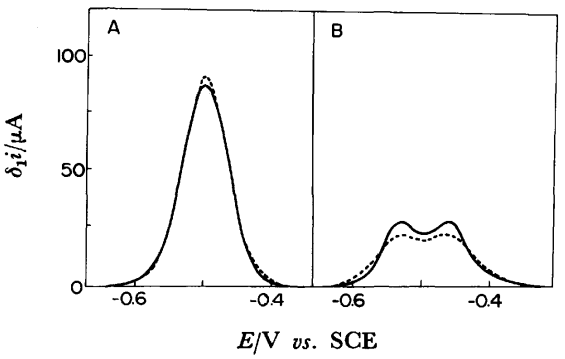

Fig. 7. (A) Real component and (B) imaginary component of a.c. voltammograms of adriamycin adsorbed on a pyrolytic graphite electrode. D.c. voltage sweep was done with v=20 mV s^{-1} after stirring 3 min at E_i=−0.3 V in 1.84×10^{-6} mol dm^{-3} adriamycin solution. Amplitude of the superimposed a.c. voltage was 10 mV peak-to-peak and the a.c. frequency was 100 Hz. The current is corrected for the base current. The broken lines represent the regression curves calculated under the conditions of k_{sap}=194 s^{-1}, K=0.199, α=0.5, E_o'=−0.498 V *vs.* SCE, and Q=13.37 μC.

TABLE 2. k_{sap} AND K VALUES OF ADRIAMYCIN ADSORBED ON A PYROLYTIC GRAPHITE ELECTRODE ESTIMATED BY MEANS OF A.C. VOLTAMMETRY

Γ_t / 10^{-10} mol cm^{-2}	f / Hz	k_{sap} / s^{-1}	K
2.63	100	415	0.135
3.69	100	238	0.217
4.12	200	311	0.137
4.48	100	225	0.156
5.50	100	194	0.199

estimated from d.c. voltammetry. This result makes it possible to set $k_{sap}(1)=k_{sap}(2)=k_{sap}$ and α=0.5, and agrees well with the situation derived from the d.c. voltammetry (previously described). The theory of a.c. voltammetry[7] tells us that the a.c. frequency dependence of the current ratio of the real and imaginary components at the E_o' and a constant Γ_t leads to information regarding kinetic parameters. In case of solid electrodes, however, it is a quite difficult matter to always obtain a constant Γ_t. This renders the experiment regarding the frequency dependence of a.c. voltammograms at a given Γ_t difficult. Here, we have analyzed the a.c. voltammogram by a direct non-linear least-squares analysis[15] according to the theory of a.c. voltammetry.[7,22] Using the same procedure as that regarding an analysis of the d.c. voltammograms, we have used two parameters, k_{sap} and K, for the simulation. The analysis of the voltammograms (Fig. 7) results in k_{sap}=194±12 s^{-1} and K=0.199± 0.028, at E_o'=−0.498 V, Q=13.37 μC[20] (Γ_t= 5.50×10^{-10} mol cm^{-2}),[18] and α=0.5.[23] The broken lines in Fig. 7 represent regression curves. The

TABLE 3. ELECTROCHEMICAL DATA OF ADRIAMYCIN ADSORBED ON A PYROLYTIC GRAPHITE ELECTRODE AND ON A MERCURY ELECTRODE AT pH 4.54

Electrode	E'_o / V *vs.* SCE	Γ_t^{max} / 10^{-10} mol cm^{-2}	$k_{sap}(\theta\rightarrow 0)$ / 10^3 s^{-1}	K	a
Pyrolytic Graphite[a)]	−0.498	7.21	0.870	0.211	2.03
Mercury[b)]	−0.450	1.10	19.8	0.132	1.66

a) This work. b) Ref. 16.

refined parameters, thus obtained, are shown in Table 2. It was found that an increasing Γ_t becomes a decreasing k_{sap}; however, K is almost independent of Γ_t. The average value of K (0.169±0.037) agrees with that estimated by d.c. voltammetry. We have also simulated a.c. voltammograms with only one parameter, k_{sap}, by setting K=0.211. In Fig. 6, a linear graph of log k_{sap} *vs.* θ (open circles) for the refined k_{sap} is given. The agreement between the k_{sap} values obtained by d.c. and a.c. voltammetries is quite good. The results now verify that the curve fitting analysis of d.c. and a.c. voltammograms is a useful technique for determining electrochemical kinetic parameters.

Table 3 summerizes the electrochemical data regarding the adriamycin adsorbed on a pyrolytic graphite electrode as well as that regarding a hanging mercury drop electrode (HMDE), reported in a previous paper.[16] The E'_o value at a pyrolytic graphite electrode is more negative by 48 mV than at an HMDE. This difference can be attributed to a disagreement in the adsorption energies on the electrodes, as predicted by Eqs. 9a and 9b. Nevertheless, the K's obtained for the two electrodes are almost the same, and less than unity, indicating the semiquinone formation reaction to be unfavorable thermodynamically at pH 4.54.[17] Note that the Γ_t^{max} value at a graphite electrode is almost 7 times as large as that at an HMDE, the former being determined by using the geometrical surface area. The "effective" surface area of the pyrolytic graphite electrode, however, is postulated to be no more than tenfold the geometrically calculated surface area. This assumption causes us to believe that the adsorption state of adriamycin on a pyrolytic graphite electrode is essentially the same as that on an HMDE; that is, the aromatic ring of the adsorbed adriamycin must be oriented parallel to the basal-plane of a pyrolytic graphite electrode. The agreement of the values of the Frumkin's α-parameter derived from the two electrodes may support the above consideration. In turn, it was also found that the $k_{sap}(\theta\rightarrow 0)$ value, *i.e.* extrapolated k_{sap} value at $\theta\rightarrow 0$, evaluated using a pyrolytic graphite electrode is markedly small compared with that at an HMDE. Similar results were observed for flavin-adenine dinucleotide adsorbed on a graphite electrode[5b,24] and on an HMDE.[8c]

As a conclusion we may say that the thermodynamic and kinetic informations concerning a two-step surface-redox reaction system can be successfully evaluated by means of a direct non-linear least-squares analysis of d.c. as well as a.c. voltammograms. Particularly, note that in these analyses we do not need (necessarily) information regarding K values, since K can be treated as one of the parameters. The viewpoint that a cyclic d.c. voltammetry has been widely used for the study of the surface-redox reaction would make it noteworthy that the kinetic information can be obtained from the theoretical analysis of the d.c. voltammetry.

The authors wish to express their sincere thanks to professor Mitsugi Senda and Dr. Tadaaki Kakutani, Kyoto University, for their valuable advice and discussion on this study. This work was supported in part by a Grant-in-Aid for Scientific Research (No. 59390012) from the Ministry of Education, Science and Culture.

References

1) E. Laviron, "Electroanalytical Chemistry," ed by A. J. Bard, Marcel Dekker, New York (1982), Vol. 12, pp. 53—157.

2) "Polymer Complex 8-Polymer Functional Electrodes," (in Japanese), ed by M. Senda, M. Aizawa, and N. Oyama, Gakkai Press Center, Tokyo (1983).

3) R. W. Marray,"Electroanalytical Chemistry," ed by A. J. Bard, Marcel Dekker, New York (1984), Vol. 13, pp. 191—368.

4) U. Plicon and E. Laviron, *J. Electroanal. Chem.*, **71**, 143 (1976).

5) a) H. Huck, *Z. Physikal. Chem.* NF., **120**, 39 (1980); b) L. Gorton and G. Johansson, *J. Electroanal. Chem.*, **113**, 151 (1980).

6) R. Vallot, A. N'Diaye, A. Bermont, C. Jakubowicz, and L. T. Yu, *Electrochim. Acta*, **25**, 1501 (1980); H. Huck, *Ber. Bunsenges. Phys. Chem.*, **85**, 221 (1981).

7) T. Kakutani and M. Senda, *Bull. Chem. Soc. Jpn.*, **53**, 1942 (1980).

8) a) T. Kakutani, K. Kano, S. Ando, and M. Senda, *Bull. Chem. Soc. Jpn.*, **54**, 884 (1981); b) T. Ikeda, S. Ando, and M. Senda, *Bull. Chem. Soc. Jpn.*, **54**, 2189 (1981); c) T. Kakutani, T. Katasho, and M. Senda, *Bull. Chem. Soc. Jpn.*, **56**, 1761 (1983).

9) E. Laviron, *J. Electroanal. Chem.*, **101**, 19 (1979); T. Kakutani and M. Senda, *Bull. Chem. Soc. Jpn.*, **52**, 3256 (1979).

10) H. Margenau and G. M. Mupphy, "The Mathematics of Physics and Chemistry," the 2nd Japanese ed by T. Sato and M. Kunimune, Kyoritsu Press, Tokyo (1961), p. 534.

11) Our "basic" computer program is distributed upon request.

12) The value of the a-parameter is positive for attraction and negative for repulsion.

13) Strictly speaking, $E_{p,a}$ and $E_{p,c}$ correspond to the peak potentials of the anodic and/or cathodic waves for $K \leq 16$, and also to the valley potentials between two peaks of anodic and/or cathodic waves for $K > 16$.

14) The "basic" program pertinent to the non-linear least-squares analysis was rewritten from that found in the literature[15] with some modification, and combined with a program for the numerical solution of the d.c. voltammogram. Our program is distributed upon request.

15) Y. Tanaka and Y. Yamaoka, "Microcomputer Guide for Chemist," (in Japanese) 2nd ed by Nankodo Press, Tokyo (1983), pp. 114—119. In this program, the criterion for convergence of parameters is $1-[SS(n)/SS(n-1)] \leq 0.001$, where $SS(n)$ is the residual sum of squares for the n-th iteration.

16) K. Kano, T. Konse, N. Nishimura, and T. Kubota, *Bull. Chem. Soc. Jpn.*, **57**, 2383 (1984).

17) K. Kano, T. Konse, and T. Kubota, *Bull. Chem. Soc. Jpn.*, **58**, 424 (1985).

18) The value of Γ_t was estimated from the electricity, Q, using the relation, $Q=(n_1+n_2)FA\Gamma_t$, where $n_1=n_2=1$ for the redox of the quinone moiety and A is the "geometric" surface area of a pyrolytic graphite electrode.

19) Equation 40 in Ref. 7 was used for the estimation of K, where $\alpha+\beta=1$ and $n=1$.

20) The Q value is the average of Q_a and Q_c of the d.c. voltammogram.

21) In curve-fitting analysis of the voltammogram in Fig. 5, the observed currents were measured at every 10 mV from -0.600 V to -0.380 V from the anodic wave (23 points) and from -0.410 V to -0.650 V for the cathodic wave (25 points). The initial conditions for numerical solution were set as $f_o=0$ and $f_r=1$ at -0.650 V for the anodic wave and $f_o=1$ and $f_r=0$ at -0.360 V for the cathodic wave. The initial parameters were roughly estimated as follows: K was evaluated from the $\Delta E_{p/2}$ of the reversible d.c. wave[19] and k_{sap} was estimated from the ΔE_p by using the working curves like those in Fig. 3 (see text). In a simulation of these voltammograms, the parameters set under the above conditions usually converged at an iteration of no more than 5 cycles.

22) See Eqs. 34a and 34b in Ref. 7 for the analytical solutions of the real and imaginary components of the a.c. voltammograms.

23) In a simulation of the voltammograms in Fig. 7, the observed currents of the real and imaginary components were measured at every 10 mV from -0.360 V to -0.620V (27 points for each component). The initial parameters were estimated as follows: K was the value (0.211) obtained by d.c. voltammetry (see text), and k_{sap} was estimated (to be 234 s^{-1}) using the ratio of the real component current to the imaginary one at $E=E_o'$, according to Eq. 37 in Ref. 7 under the assumpsion of $K=0.211$. In a simulation of these voltammograms, the parameters converged at an iteration of no more than 5 cycles.

24) The authors of Ref. 5b have treated this system as a "one-step" surface-redox reaction and reported the standard electron-transfer rate constant to be about 1 s^{-1}. A reanalysis of the cyclic d.c. voltammograms of Fig. 1 in Ref. 5b by the curve-fitting method proposed in this paper has revealed that $k_{sap}=1.8\ s^{-1}$ and $K=7.6$, under the assumption that $k_{sap}(1)=k_{sap}(2)=k_{sap}$ and $\alpha_1=\alpha_2=0.5$.

Electric and Magnetic Properties of a Neutral Radical, 2-Cyano-10-methyl-5-phenazinyl

Kunio AWAGA, Tadashi SUGANO, and Minoru KINOSHITA*
The Institute for Solid State Physics, The University of Tokyo, Roppongi, Minato-ku, Tokyo 106
(Received March 8, 1985)

The temperature dependence of electric conductivity, static magnetic susceptibility and ESR absorption, and electronic absorption spectra at room temperature have been measured on an organic neutral radical, 2-cyano-10-methyl-5-phenazinyl (NMPN). NMPN is found to be more conductive than the neutral radicals studied previously. The room temperature conductivity of powder NMPN is of the order of $10^{-7}\,\Omega^{-1}\,cm^{-1}$ and the activation energy is 0.36 eV. The absorption spectra and the magnetic susceptibility measurements indicate that the NMPN molecules form pairing array with considerably large interpair interaction in the solid state. The absence of the triplet fine structure in the ESR spectrum also suggests the existence of the interpair interaction. From these, the magnetic behavior of NMPN is interpreted in terms of the alternating antiferromagnetic Heisenberg model with temperature dependent alternation.

The electrical conduction of organic solids has been a matter of concern for long time and the efforts to find out highly conducting materials among the organic solids composed of one kind of molecules have been continued. Especially, the conduction of aromatic hydrocarbons represented by anthracene has been studied in detail.[1] However, it is known that most of them show the conductivity of less than $10^{-10}\,\Omega^{-1}\,cm^{-1}$ at room temperature and the activation energy of several eV (1 eV/molecule≒96.48 kJ mol^{-1}). One of the reasons for poor conductivity is that in the ground state no carriers can exist because the component molecules take the closed shell structure.

In this regards, the electrical conduction of a neutral free radical, which has intrinsically one unpaired electron giving the expectancy of becoming a carrier, has been interested in. Table 1 (a)—(c) shows the electric conductivities of the neutral radicals studied previously.[2-4] Contrary to expectation, they exhibit poor conductivity in spite of the presence of unpaired electrons. The reason for this is considered to be as follows. These radicals are characterized commonly by having protective substituents to stabilize the unpaired electron.[5,6] The protective substituents must obstruct the interactions between the unpaired electrons and therefore the unpaired electrons would be localized on each site of radical molecules. Above consideration is supported by the fact that the magnetic behavior of these radicals follow the Curie-Weiss law with small Weiss constants, representing the localized character of spins. Taking it the other way round, it would be predicted that using a planar radical molecule leads to increase of the interactions and to improvement of the conductivity.

To confirm this prediction, we have chosen 2-cyano-10-methyl-5-phenazinyl(commonly called *N*-methylphenazyl-2-nitrile; abbreviated as NMPN hereafter) shown in Fig. 1 as an experimental sample, which has planar molecular structure and is stabilized mainly by the intramolecular delocalization of the unpaired electron. We have investigated the electric conductivity and further, to make the properties of NMPN clearer, the temperature dependence of the magnetic susceptibility and the electron spin resonance signals, and the absorption spectra at room temperature have been measured.

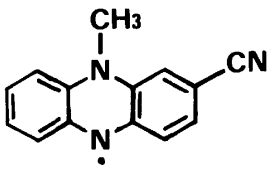

Fig. 1. The molecular structure of NMPN (2-cyano-10-methyl-5-phenazinyl).

In this paper, we characterize the electric and magnetic properties of NMPN using the results of the above experiments and discuss the electric conductivity of NMPN. From these, we suggest the way to improve the electric conductivity of a neutral free radical.

Experimental

NMPN was prepared by the method of McIlwain.[7] The crude NMPN obtained was purified by recrystallization from chloroform or a mixture of chloroform and diethyl ether, followed by washing with diethyl ether continuously (Found: C, 76.36; H, 4.36 N, 19.31%, Calcd for $C_{14}H_{10}N_3$: C, 76.35; H, 4.58; N, 19.08%). The purified samples were kept in a freezer, because they were gradually damaged when kept at room temperature.

The d.c. electric conductivity of compressed polycrystals was measured in a vacuum using the standard two-probe technique with the aid of Ag paint for electrodes.

The magnetic susceptibility was measured by using a Faraday balance on a powder sample of about 50 mg. The details of the apparatus have been described previously.[8] The measurement was taken over the con-

tinuous temperature range of 4—295 K.

A Cary model 14 spectrophotometer was used for measurements of the electronic absorption spectra of an ethanol solution and a solid sample suspended in liquid paraffin. The spectra were measured at room temperature in the range of 5000—30000 cm^{-1}.

Temperature dependence of X-band electron spin resonance (ESR) spectra from 10 to 300 K were performed on a JES-FE1X spectrometer with an Oxford Instruments ESR-900 variable temperature helium gas flow cryostat. In every measurement the modulation width was kept within 0.1 G (1 G=10^{-4}T) in order to prevent lineshape distortion due to over modulation.

Electrical and Magnetic Properties

Electric Conductivity. Figure 2 shows a plot of logarithm of the conductivity at absolute temperature T *vs.* $1/T$ for two specimens which were prepared in different butches. The discrepancy between the temperature dependence of the two specimens is within the experimental error. The conductivity at room temperature is of the order of $10^{-7}\,\Omega^{-1}\,cm^{-1}$. Below 350 K, the linear relation between logarithm of the conductivity and $1/T$ is established well. Above 350 K, the conductivity decreases abruptly. After keeping the samples above this temperature, the intensity of ESR signals vanishes almost completely. Therefore, the decrease of conductivity would be ascribed to the decomposition of radical molecules. In other words, the relatively high conductivity of NMPN observed below 350 K is attributable to the existence of an unpaired electron on each molecule.

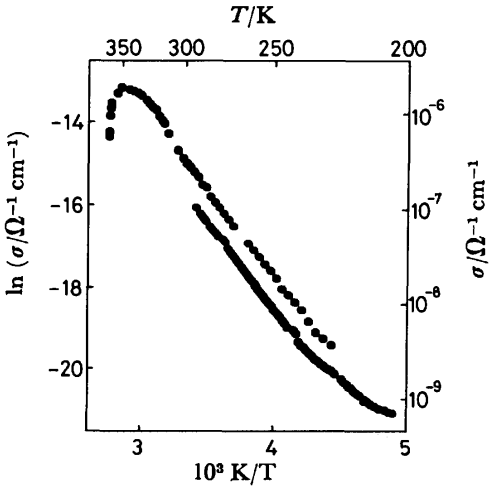

Fig. 2. Specific conductivity of NMPN for two specimens.

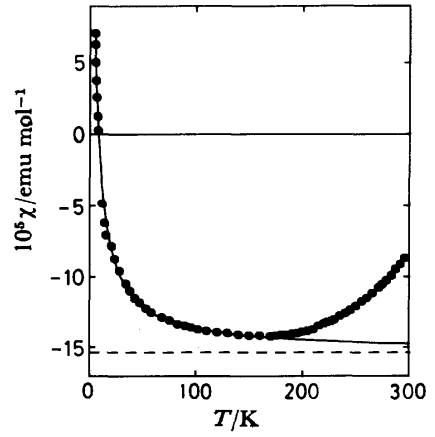

Fig. 3. Temperature dependence of total magnetic susceptibility of NMPN. The dashed line represents the diamagnetic susceptibility. The solid curve represents the paramagnetic one due to impurities.

The activation energy is computed from the change of conductivity as a function of temperature using the equation

$$\sigma = \sigma_0 \exp(-\Delta/k_B T), \quad (1)$$

where σ is the specific conductivity at T, σ_0 is a constant, k_B is the Boltzmann constant and Δ is the activation energy. The slope below 350 K corresponds to the activation energy of 0.36 eV. NMPN shows relatively high conductivity and low activation energy among the organic solids composed of one kind of molecules.

Table 1 shows the comparison of the electric conductivity of NMPN and that of the neutral free radicals investigated previously.[2-4] The latter radicals are stabilized by the protective substituents.[5,6] The conductivity of NMPN is higher than that of the other radicals by more than three orders of magnitude. The activation energy of NMPN is about a half as large as the others. The prediction made in the introductory section thus seems to be fulfilled.

Magnetic Susceptibility. Temperature dependence of the molar magnetic susceptibility of NMPN is shown in Fig. 3. In the high temperature region, the susceptibility decreases with decreasing temperature, and after passing a minimum it increases in the low temperature region. The diamagnetic contribution is evaluated by assuming that the susceptibility change in the low temperature region is dominated by the paramagnetic susceptibility due to impurities

Table 1. The comparison of the electric conductivity of the neutral radicals

		$\sigma_{25\,°C}$ / $\Omega^{-1}\,cm^{-1}$	Δ / eV	σ_0 / $\Omega^{-1}\,cm^{-1}$
(a)	DPPH (single crystal)	2×10^{-10}	0.75	10^{3}
(b)	Galvinoxyl	4×10^{-14}	0.72	0.07
(c)	Banfield and Kenyon's radical	3×10^{-15}	1.2	10^{5}
(d)	NMPN	3×10^{-7}	0.36	0.35

(a) in Ref. 4. (b), (c) in Ref. 3. (d) This work.

and/or defects which follows the Curie-Weiss law. The diamagnetic susceptibility thus obtained is -153×10^{-6} emu mol^{-1} [9] which is indicated by the dashed line in Fig. 3. The Curie-Weiss susceptibility with the Curie constant of 1.70×10^{-3} emu K mol^{-1}, corresponding to a spin concentration ($S=1/2$) of 0.45%, and with the Weiss constant of -2.66 K, is shown in Fig. 3 by the solid curve.

The intrinsic paramagnetic susceptibility χ_P, after correction for the diamagnetic and the Curie-Weiss parts have been made, is plotted as a function of temperature in Fig. 4. χ_P appears to increase exponentially from about 150 K. This shows existence of relatively strong antiferromagnetic interactions between the unpaired electrons and of the thermally accessible magnetic excitation state. By assuming that the antiferromagnetic interactions are limited only within a pair of spins, the temperature dependence of χ_P may be analyzed by the singlet-triplet model. The temperature dependence of the singlet-triplet susceptibility χ_{st} is given by

$$\chi_{st} = \frac{N_A g^2 \mu_B^2}{k_B T} \frac{1}{3+\exp(J/k_B T)}, \qquad (2)$$

where N_A is the Avogadro constant, μ_B is the Bohr magneton, g is the g-value and J is the energy separation between the ground singlet state and the excited triplet state. The solid curves (a), (b), and (c) in Fig. 4 are theoretical curves of the singlet-triplet model for $J=0.11$, 0.12, and 0.13 eV, respectively. The temperature dependence of magnetic susceptibility of NMPN is found to fit only qualitatively to the singlet-triplet susceptibility, but does not fit quantitatively for any value of J. Such discrepancy between χ_P and χ_{st} has also been observed in various charge transfer complexes and the following explanations have been suggested.

1) The change in the intermolecular distance by thermal expansion.[10]

2) The phonon induced interaction between magnetic excitons.[11,12]

3) The existence of interpair interaction (*i.e.*, alternating antiferromagnetic chain).[13–17]

Further discussion will be given below by taking account of the results of the absorption spectra and the ESR measurements.

Electronic and ESR Spectra

Absorption Spectra. The temperature dependence of χ_P suggests that, within the first approximation, NMPN molecules exist in the solid as what is called "radical pair" formed by the charge transfer interaction.[18] In order to confirm the existence of the charge transfer interaction, absorption spectra were measured for an ethanol solution and a solid sample at room temperature. The comparison is shown in Fig. 5. The broad band at about 9000 cm^{-1} in the solid spectrum is much enhanced in comparison with that of the solution spectrum. Therefore, we could attribute this band to the charge transfer band. A weak absorption appears like shoulder at about 12000 cm^{-1}. Such a structure of a CT-band is also observed in Würster's blue perchlorate and alkali metal-TCNQ(7,7,8,8-tetracyano-*p*-quinodimethan) which are known as Mott insulators. Lyo has given two explanations for this phenomenon.

1) The effect of long-range Coulomb interaction.[19]

2) The charge transfer between pairs.[20]

On the basis of the experimental results of susceptibility and ESR, we will take the latter explanation in the later sections.

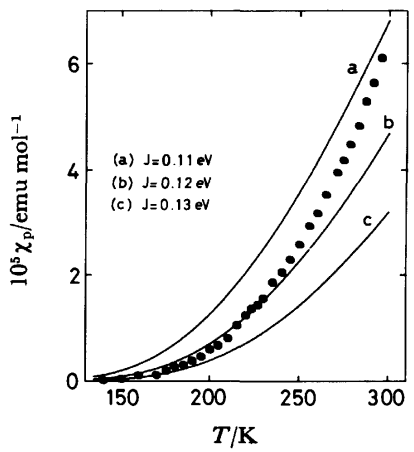

Fig. 4. Intrinsic paramagnetic susceptibility of NMPN. The solid curves are theoretical fits as explained in the text.

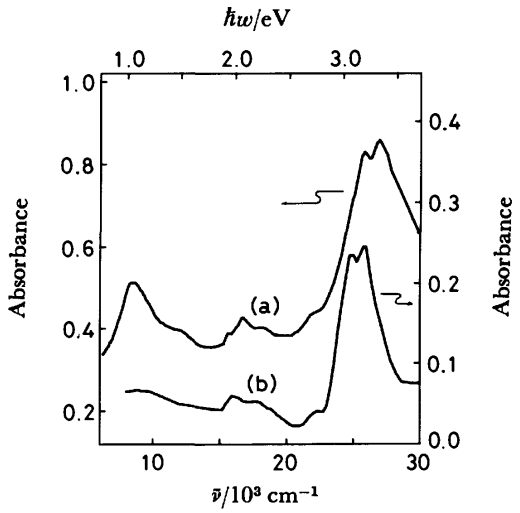

Fig. 5. Absorption spectra of NMPN at room temperature. (a): Powder sample suspended in liquid paraffin, (b): solution in ethanol.

The other absorption bands of solid NMPN correspond well to those of the solution spectrum except for blue shift of the strong absorption at about 27000 cm^{-1}. This blue shift would be explained by either the solvent effect or the coupling of CT and LE transitions.[21]

ESR Absorption. The ESR spectra observed on the powder sample at various temperatures are shown in Fig. 6, in which the three signals at lower temperatures are magnified by ten times. Asymmetric lineshape of the spectra in the high temperature region is due to g-value anisotropy. The g-value anisotropy disappears with broadening of the linewidth at low temperatures. Temperature dependence of the peak-to-peak linewidth ΔH_{pp} is shown in Fig. 7. Below 140 K, ΔH_{pp} increases abruptly with decrease of temperature and becomes constant at 80 K. Thus,

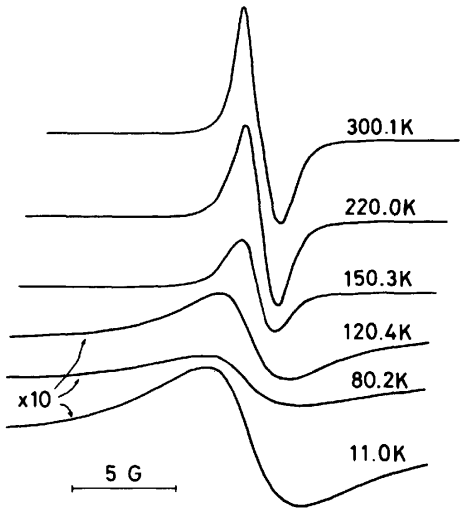

Fig. 6. ESR signals on powder sample at various temperatures.

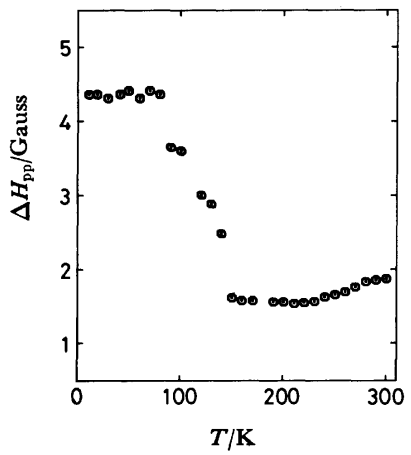

Fig. 7. Temperature dependence of ESR peak-to-peak linewidth, ΔH_{pp}.

the temperature dependence of ΔH_{pp} may be separated into the following three temperature regions.

In the high temperature region ($T>140$ K), the narrow linewidth signal, which increases in intensity with increasing temperature, is dominant. From the results of the static magnetic susceptibility, the observed ESR signals in this region should represent the spins excited thermally across the magnetic gap. The g-value anisotropy stands up with increasing temperature. Because the peak-to-peak linewidth in Fig. 7 is affected by the g-value anisotropy, we cannot place much significance on the variation of the linewidth in this temperature region. However, the true linewidth seems to depend little on temperature or to become narrower a little with increasing temperature.

In the low temperature region ($T<90$ K), the broad linewidth signal without g-value anisotropy, which increase in intensity with decreasing temperature, is dominant. These signals represent paramagnetic impurities observed in the susceptibility measurements. Their temperature independent linewidth suggests that the spins on the impurities are localized. The fact that the two kinds of signals observed in the high and low temperature regions have the same g-value suggests that the paramagnetic impurities are the localized spins on the monomer radicals, which have failed to form a pair structure during crystallization.

In the middle temperature region, the observed signals result from the two kinds of signals being piled up and therefore originate from the two kinds of spins discussed above. With decreasing temperature the linewidth increases abruptly and main contribution to the observed signals varies from the narrower signal to the broader one.

In order to examine whether or not the magnetic excited state is described by the triplet spin Hamiltonian:

$$\mathscr{H} = D\left(S_z^2 - \frac{2}{3}\right) + E(S_x^2 - S_y^2), \tag{3}$$

which represents the dipolar interaction in an isolated spin pair, we have tried to find out fine structure signals and $\Delta m = \pm 2$ transitions. The measurements were carefully done on the powder samples over the range of 90—300 K, but we could not find out both of them. This fact indicates that the spin system in NMPN is not simply described by an assembly of noninteracting spin pairs of Hamiltonian (3).

Analysis of Magnetic Susceptibility

The Model to be Used. From the experimental results described in the preceding sections, the

NMPN molecules are considered to be paired off, within the first approximation, by the charge transfer interaction in the solid state. Because this interaction needs the overlapping of the molecules and NMPN exhibits relatively high conductivity, it is reasonable to assume that the NMPN molecules form linearly stacking columns in the solid. The results of the ESR experiments suggest the existence of the interpair interaction. The discrepancy between the temperature dependence of the magnetic susceptibility observed and the singlet-triplet statistics would also be attributed to the interpair interactions as mentioned above. As a matter of course, this interpair interaction is weaker than the intrapair one, but seems to be so strong that the spin system in NMPN is not represented by the spin Hamiltonian (3). Therefore, the spins on the NMPN molecules are to be interpreted by a linear alternating antiferromagnetic Heisenberg model. As mentioned in a previous section, one of the explanations for the side band in the CT absorption region is also due to the coexistence of the intra- and interpair charge transfer interactions. The interpair charge transfer makes the two pair spins singlet just like the intrapair interaction.

Analysis. The Hamiltonian of the linear alternating antiferromagnetic Heisenberg model is given by

$$\mathscr{H} = \sum_{i=1}^{N/2} (J_1 \boldsymbol{S}_{2j}\boldsymbol{S}_{2j+1} + J_2 \boldsymbol{S}_{2j-1}\boldsymbol{S}_{2j}) = J_1 \sum_{i=1}^{N/2} (\boldsymbol{S}_{2j}\boldsymbol{S}_{2j+1} + \gamma \boldsymbol{S}_{2j-1}\boldsymbol{S}_{2j}) \quad (4)$$

where J_1 and J_2 are the alternating interactions along the chain (assumed as $J_1 > J_2 > 0$) and $\gamma = J_2/J_1$ is a parameter which conveniently measures the degree of alternation. When $\gamma=1$, the linear Heisenberg model is obtained, whereas when $\gamma=0$ the system breaks up into an assembly of noninteracting spin pairs.

Bulaevskii calculated the spectrum of triplet excitations of alternating chain of spins with the above Hamiltonian (4), by using the Hartree-Fock approximation.[13,14] His model has been used frequently in approximate theoretical treatments of a variety of phenomena. For example, it has been applied to charge-transfer salts,[22-24] to spin dynamics,[25] and to the uniform Heisenberg chain.[26]

On the other hand, Duffy and Barr[16] and Bonner *et al.*[17] have made exact calculations of the susceptibility on finite alternating antiferromagnetic Heisenberg spin-1/2 chains. The extrapolation of their results to $N \to \infty$ shows a good numerical agreement with the corresponding curves calculated from the model of Bulaevskii, especially at low temperatures.

In our case, the temperature region examined falls into the low temperature regions of these models. Therefore, we use the results of Bulaevskii for the analysis of the temperature dependence of the intrinsic paramagnetic susceptibility in Fig. 4. Bulaevskii has derived the following approximate equation at low temperatures ($0.033 < k_B T/J_1 < 0.25$)

$$\chi = \frac{N_A g^2 \mu_B^2 a(\gamma)}{k_B T} \exp\left(\frac{-J_1 \Delta(\gamma)}{k_B T}\right), \quad (5)$$

where $a(\gamma)$ and $\Delta(\gamma)$ are γ dependent parameters whose values are given by him.[14] For any value of γ, the relations of $0 < a(\gamma) < 1$, $0 < \Delta(\gamma) < 1$ are to be satisfied. Although the plot of $\log(\chi_P T)$ *vs.* $1/T$ (not shown) gives rise to a linear relation between them, the regression yields contradictory values of $a(\gamma)$ and $J_1\Delta(\gamma)$ as follows

$$a(\gamma) = 3.8, \quad J_1\Delta(\gamma) = 0.15\,\text{eV}.$$

This contradiction could originate in the temperature dependence of the alternation parameters, J_1 and/or γ. When both J_1 and γ are temperature dependent, each of J_1 and γ cannot be determined uniquely from our susceptibility measurements, but the possible combinations of (J_1, γ) can be determined so as to reproduce the observed value of χ_P at T by using Eq. 5. In Fig. 8, the determined combinations are plotted as a function of temperature over the range of J_1 from 0.10 to 0.16 eV. A curved plane is obtained for the possible set of parameters (J_1, γ, T). When J_1 is assumed to be constant, γ increases with increasing temperature. Such behavior of γ means that the spin system varies from the singlet-triplet model to Heisenberg one with increasing temperature. When γ is assumed to be constant contrariwise, J_1 decreases with increasing temperature. Thus, the

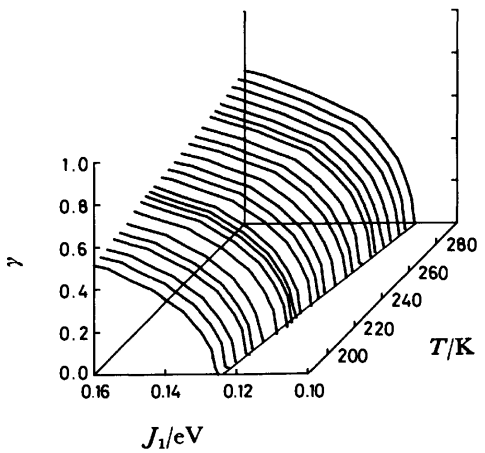

Fig. 8. Temperature variation of possible combination of (J_1, γ). The curves are not smooth, because the numerical values of $a(\gamma)$ and $\Delta(\gamma)$ in Eq. 5 are given for the values of γ in every 0.1 step.[14]

curved plane in Fig. 8. seems to be reasonable phenomenologically. In other words, the observed temperature dependence of χ_p could be explained by the linear alternating antiferromagnetic Heisenberg model with the rational temperature dependence of the alternation parameters. We expect the value of γ to be somewhat large (*e.g.*, 0.3—0.5) in NMPN on the basis of the absence of the fine structure and the transitions of $\Delta m=\pm 2$ in the ESR measurements.

Such temperature dependence of the alternation parameters resembles the prediction made by the theoretical studies of the spin-Peierls transition. It is known from these studies that the presence of the spin-lattice[24,27,28] or spin-phonon[22,27,28] interactions in an uniform chain system results in a phase transition to an alternating chain, indicating temperature dependence of alternation parameters. This predicted temperature dependence is similar to that observed in our material. The decompositions of the radical molecules above room temperature prevent us from getting the information about the phase transition and therefore we cannot apply the theory of the spin-Peierls transition to our problem at present. However, we preferably think that the spin-lattice or spin-phonon interaction plays an important role in the magnetic behavior of our material.

Comparison of NMPN and NEP

The comparison of properties of organic solids whose components have similar molecular structure is important in chemistry, especially for molecular designing. 10-Ethyl-5-phenazinyl (NEP) is a member of the phenazinyl family and has well been studied. Therefore NMPN and NEP are compared with each other below.

NEP was investigated by Hausser[31] and Hausser and Murrell[32] first. They discovered the charge transfer absorption in the near IR region. Sakata and Nagakura[33] measured the temperature dependence of the CT-band intensity and of the magnetic properties in detail. They found that the properties of NEP were explained as the isolated spin pairs almost quantitatively. The existence of the charge transfer interactions is thus common to the two radicals. In ESR studies of NEP, however, the fine structure and the transitions of $\Delta m=\pm 2$ are found[33] and therefore its magnetic excited state is described by the spin Hamiltonian (3). The comparison of the two radicals is summarized in Table 2.

Table 2. The comparison of NMPN and NEP

	NMPN	NEP[a]
$h\nu_{CT}$/eV	1.08	1.38
J/eV	0.11[b]	0.04
Fine structure and transition of $\Delta m=\pm 2$	not observed	observed

a) in Ref. 33. b) The magnetic excitation gap at room temperature calculated from Eq. 2.

The most remarkable difference is the magnitude of the interpair interactions. The ESR behaviour of NEP is described by the spin Hamiltonian of noninteracting pair, whereas that of NMPN is not. This difference would arise from the steric factor. The steric hindrance due to the ethyl group in NEP seems to be so large that the interpair interactions are prevented. This difference has something in common with that of the crystal structures of *N*-methylphenazinium(NMP)-TCNQ and other *N*-alkylphenazinium-TCNQ complexes. NMP-TCNQ is a famous organic conductor and forms segregated columns in the crystal. NMP molecules in the columns stack uniformly.[34] On the other hand, NEP_2-$TCNQ_2$ crystallizes in mixed stacks with σ-bonded dimers of $(TCNQ)_2^{2-}$.[35] *N*-butylphenazinium (NBP)-TCNQ[36] and NBP-F_4TCNQ[37] comprise -AADD- type mixed stacks. Replacement of the methyl group of NMP by a larger alkyl group therefore seems to hinder the interactions beyond the intradimer ones.

The maximum position of the CT-band of NMPN is lower than that of NEP by about 0.30 eV. In terms of the Hubbard model,[38] it is known that when the on-site Coulomb repulsion U is much larger than the transfer integral t the position of the CT-band maximum is almot determined only by U.[39] Therefore, the relation of the on-site Coulomb repulsion of the two radicals is established as;

$$U_{NMPN} < U_{NEP}.$$

It is likely that the nitrile group in NMPN extends the conjugation system of the phenazinyl frame and the extention decreases the on-site repulsion.

The magnetic excitation gap J of NMPN is about three times as large as that of NEP at room temperature. This gap is approximated by the equation $J=(1/2)(U^2+16t^2)^{1/2}-U/2$. The difference of U is not so large that the following relation of the intrapair hopping integrals would be established;

$$t_{NMPN} > t_{NEP}.$$

The Electric Conductivity of Neutral Radicals

Finally, we discuss the way to obtain more conductive neutral radicals by referring to the electric conductivity of NMPN. As described in a previous section, NMPN is much more conductive than the other neutral radicals which are thought to be stabilized by the protective subtituents and is placed in the most conductive class of organic solids

composed of one kind of molecules. In comparison with recent "organic metals", however, the conductivity of NMPN is still much poor.

The factors which raise the conductivity of NMPN are summarized as follows.

1) The existence of the unpaired electron on the each molecule.

2) The planar molecular structure giving the expectancy of large molecular overlaps.

3) The small substituent.

It is clear from our studies that the second and the third factors are necessary conditions to give neutral radicals higher conductivity. These factors mean that the neutral radical should be stabilized not by the protective substituents, but by the intramolecular delocalization energy of unpaired electron.

On the other hand, the conductivity of NMPN would be suppressed by the following factors.

1) The nonuniform interactions between unpaired electrons which are localized, to some extent, within a pair.

2) The electron localization due to the fully-occupied Hubbard band with large U (Mott insulator).

In order to produce new neutral radicals having higher conductivity than that of NMPN, these factors should be improved. One of the possibilities for improvement is to find neutral radicals containing heavy atoms that are expected to have interactions comparable with or beyond the intrapair ones. In this case, we could further expect the effect of interchain interaction, if the heavy atoms are properly chosen. The problem of electron localization would also be relaxed, to some extent, by introducing heavy atoms with large polarizability and large van der Waals radius, because such heavy atoms would reduce the magnitude of U and increase the transfer integral. Another way to reduce the electron localization is to make a mixed crystal of a neutral radical and a closed shell compound, which has molecular structure similar to the radical molecule and has HOMO or LUMO of energy nearly equivalent to the nonbonding molecular orbital of the neutral radical. In such a crystal, if exist, it would be possible that the nonbonding MO of the neutral radicals and HOMO or LUMO of the closed shell molecules make the band partially filled, in which electrons or holes are delocalized. In the case of NMPN, the mixed crystal of NMPN and phenazine or 5,10-dialkyl-5,10-dihydrophenazine could be a possible candidate.

The authors are thankful to Professor Kazuo Morigaki and Dr. Izumi Hirabayashi of Institute for Solid State Physics for the kindness in putting the ESR spectrometer at their disposal. This work was in part supported by the Grant-in-Aid for Scientific Research (Nos. 58118003, 58470003, and 59112003) from the Ministry of Education, Science and Culture.

References

1) For a review see F. Gutmann and L. E. Lyons, "Organic Semiconductor," J. Wiley, New York (1967).

2) D. D. Eley and H. Inokuchi, *Z. Electrochem.*, **63**, 29 (1959).

3) D. D. Eley and M. R. Willis, "Symposium on Electrical Conductivity in Organic Solids," ed by H. Kallmann and M. Silver, Interscience Pub., London (1961), p. 257.

4) H. Inokuchi, Y. Harada, and Y. Maruyama, *Bull. Chem. Soc. Jpn.*, **35**, 1559 (1962).

5) D. E. Williams, *J. Am. Chem. Soc.*, **89**, 4280 (1967).

6) D. E. Williams, *Mol. Phys.*, **16**, 145 (1969).

7) H. McIlwain, *J. Chem. Soc.*, **1937**, 1704.

8) M .Takahashi, T. Sugano, and M. Kinoshita, *Bull. Chem. Soc. Jpn.*, **57**, 26 (1984).

9) We employed in this report the c.g.s. electromagnetic units for magnetic susceptibility, in the interest of comparison with values in references. The χ values given in emu mol^{-1} are converted into the SI units of $m^3\,mol^{-1}$ by multiplying the factor of $4\pi\times10^{-6}$.

10) Y. Sato, M. Kinoshita, M. Sano, and H. Akamatu, *Bull. Chem. Soc. Jpn.*, **43**, 2370 (1970).

11) H. M. McConnell and Z. G. Soos, *J. Chem. Phys.*, **40**, 586 (1964).

12) D. B. Chesnut, *J. Chem. Phys.*, **41**, 472 (1964).

13) L. N. Bulaevskii, *Zh. Eksp. Teor. Fiz.*, **44**, 1008 (1963) (*Sov. Phys. **JETP**,* **17**, 684 (1963)).

14) L. N. Bulaevskii, *Fiz. Tverd. Tela (Leningrad)*, **11**, 1132 (1969) (*Sov. Phys. Solid State*, **11**, 921 (1969)).

15) Z. G. Soos, *J. Chem. Phys.*, **43**, 1121 (1965); *ibid.*, **46**, 253 (1967).

16) W. Duffy, Jr. and K. P. Barr, *Phys. Rev.*, **165**, 647 (1968).

17) J. C. Bonner, H. W. J. Blöte, J. W. Brag, and I. S. Jacobs, *J. Appl. Phys.*, **50**, 1810 (1979).

18) N. Mataga and T. Kubota, "Molecular Interactions and Electronic Spectra," Marcel Dekker, Inc., New York (1970), P. 275.

19) S. K. Lyo, *Phys. Rev. B*, **18**, 854 (1978).

20) S. K. Lyo, *Phys. Rev. B*, **18**, 5835 (1978).

21) T. Yamazaki and K. Kimura, *Bull. Chem. Soc. Jpn.*, **44**, 298 (1971).

22) E. Pytte, *Phys. Rev. B*, **10**, 4637 (1974).

23) S. Etemad and E. Ehrenfreund, *AIP Conf. Proc.*, **10**, 1499 (1973); S. K. Khanna, E. Ehrenfreund, E. F. Rybaczewski, and S. Etemad, *AIP Conf. Proc.*, **10**, 1509 (1973).

24) G. Beni, *J. Chem. Phys.*, **58**, 3200 (1973).

25) T. Todani and K. Kawasaki, *Prog. Theor. Phys.*, **50**, 1216 (1973).

26) L. N. Bulaevskii, *Zh. Eksp. Teor. Fiz.*, **43**, 968 (1962) (*Sov. Phys. **JETP**,* **16**, 685 (1963)).

27) P. Pincus, *Solid State Commun.*, **9**, 1971 (1971).

28) G. Beni and P. Pincus, *J. Chem. Phys.*, **57**, 3531 (1972).

29) J. Y. Dubois and J. B. Carton, *J. Phys. (Paris)*, **35**, 371 (1974).

30) E. Pytte, *Phys. Rev. B*, **10**, 2039 (1974).

31) K. H. Hausser, *Z. Naturforsh., Teil A*, **11**, 20 (1956).

32) K. H. Hausser and J. N. Murrell, *J. Chem. Phys.*, **27**, 500 (1957).
33) T. Sakata and S. Nagakura, *Bull. Chem. Soc. Jpn.*, **42**, 1497 (1969).
34) C. J. Fritchie Jr., *Acta Crystallogr.*, **20**, 892 (1966); B. Morosin, *Phys. Lett. A*, **53**, 455 (1975).
35) B. Morosin, H. J. Plastas, L. B. Coleman, and J. M. Stewart, *Acta Crystallogr., Sect. B*, **34**, 540 (1978).
36) D. Gundel, H. Sixl, R. M. Metzger, N. E. Heimer, R. H. Harms, H. J. Keller, D. Nöthe, and D. Wehe, *J. Chem. Phys.*, **79**, 3678 (1983).
37) R. M. Metzger, N. E. Heimer, D. Gundel, H. Sixl, R. H. Harms, H. J. Keller, D. Nöthe, and D. Wehe, *J. Chem. Phys.*, **77**, 6023 (1982).
38) J. Hubbard, *Proc. R. Soc. London, Ser. A*, **276**, 278 (1963); *ibid.*, **281**, 401 (1964).
39) I. Sadakata and E. Hanamura, *J. Phys. Soc. Jpn.*, **34**, 882 (1973).

 © 1985 The Chemical Society of Japan Bull. Chem. Soc. Jpn., 58, 1894—1898 (1985) [Vol. 58, No. 7

Conformation and Coordination Behavior of Zinc(II) Complex with Cyclo(L-methionyl-L-histidyl)

Yoshitane KOJIMA,* Ken HIROTSU,* Tetsushi YAMASHITA, and Toshio MIWA
Department of Chemistry, Faculty of Science, Osaka City University, Sugimoto, Sumiyoshi-ku, Osaka 558
(Received December 3, 1984)

The crystal structure of a zinc(II) complex with cyclo(L-methionyl-L-histidyl) shows that all four ligands coordinated tetrahedrally to a Zn^{2+} ion have a folded conformation, with the imidazole ring facing the piperazine ring in each ligand. The calculation from α-β coupling constant data (obtained by ^1H NMR measurement) of the histidyl residue of cyclo(L-methionyl-L-histidyl) linked to a Zn^{2+} ion shows that the ratio of a folded conformation to an unfolded one is 61:39 in D_2O.

Several metal complexes with cyclic dipeptides[1] have been used as simple model compounds for studying metallo-proteins and -enzymes, in which metal ions link to the functional groups in the side chains of the peptides, but not to the amide groups in the main chain. Especially, the limited conformations[2] of the peptides with the imidazole rings show the important effects on the formations and conformations of the metal complexes.

In this paper, the conformation and coordination behavior of the $[Zn(CMH)_4]^{2+}$ [abbreviated as CMH for cyclo(L-methionyl-L-histidyl)] ion are examined using X-ray structure analysis, NMR (^1H and ^{13}C) and molecular-weight measurements. A preliminary communication on the structure of this zinc(II) complex with CMH has already been published.[1b] The numbering scheme of a CMH moiety is given below:

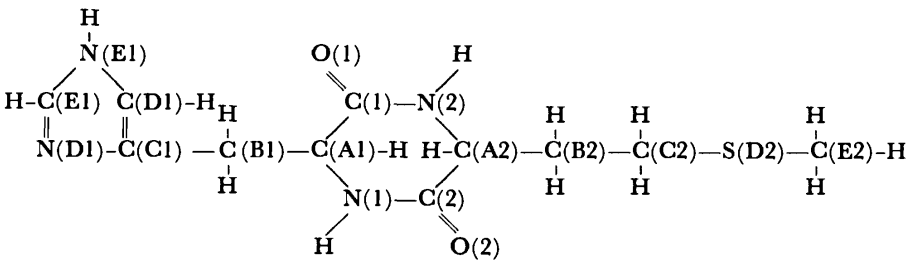

Experimental

Materials. CMH was prepared according to the methods reported earlier.[1a] Zinc(II) sulfate (obtained commercially) was used without further purification.

Preparations of Zinc(II) Complexes. A mixture of CMH (1.40 mmol) and zinc(II) sulfate (0.35 mmol) was completely dissolved in hot water (5 ml) with stirring. After standing at room temperature for a few days, a formed precipitate was filtered off. mp; 232—234°dec., Yield; 63%. Found: C, 41.51; H, 5.22; N, 17.49%. Calcd for $Zn(C_{11}H_{16}N_4O_2S)_4SO_4 \cdot 2H_2O$: C, 41.65; H, 5.24; N, 17.66%.

X-Ray Measurement. X-Ray analysis: $Zn(C_{11}H_{16}N_4O_2S)_4 \cdot SO_4 \cdot 10H_2O$, M=1414.9, monoclinic, space group $P2_1$, a=15.143(2), b=20.586(4), c=11.007(2) Å, β=97.89(1)°. Z=2.

With the use of 2692 uniquely observed reflections, the structure was solved by MULTAN[3a] and refined anisotropically to R=0.062 (R_w=0.071).[3b] The absolute configuration was determined by reference to the known configuration of L-histidine moiety. Fractional atomic coordinates and B_{eq} values are listed in Table 1. Tables of observed and calculated structure factors, bond distances and angles, anisotropic temperature factors, atomic parameters of hydrogen atoms, and hydrogen bonds are kept at the chemical society of Japan. (Document No. 8526)

Other Measurements. ^1H and ^{13}C NMR data were obtained in D_2O at 50°, using sodium 3-trimethylsilyl-1-propanesulfonate as an internal reference. The ^1H NMR investigation of CMH were carried out with the aid of spin decoupling methods. The amide protons were replaced by deuterium in D_2O. The molecular weights of zinc(II) complexes with CMH were measured in H_2O at 42°, using urea as a standard material. A JEOL FX-100 (for ^1H and ^{13}C NMR spectra), a PS-100 (for ^1H NMR spectra), and a Knauer Vapor-Pressure Osmometer (for molecular weight) were used for the measurements of the samples.

Results and Discussion

A Zn^{2+} ion is coordinated tetrahedrally by four N (E1) atoms of the imidazolyl groups of the histidyl residues of peptides exclusively (see Fig. 1). The N-Zn-N angles are all within 3.5° from 109.5° and the average distance of four independent Zn-N bonds is 2.01(1) Å, which is comparable to the values found

in other tetrahedral complexes.[4] The complex ion, except for the terminal $-CH_2SCH_3$ groups, has an approximate D_2 symmetry since three pseudo two-fold axes bisect the N-Zn-N angles.

Selected dihedral angles of the CMH moieties of the complex and the free CMH molecule are given in Table 2.[5] The orientation of imidazole rings to the piperazine rings is determined by the dihedral angles around C(A1)-C(B1) and C(B1)-C(C1) bonds. The values of χ_1^1 and χ_1^2 show that all CMH moieties have a same conformation concerning the piperazine and imidazole rings. The imidazole rings are folded back over the piperazine rings to have the intimate contacts between these two rings. Recent X-ray crystallographic studies of cyclic dipeptides such as cyclo(L-histidyl-L-histidyl),[6] CMH,[5] and cyclo(L-

Table 1. Fractional atomic coordinates and isotropic temperature factors for non-hydrogen atoms with estimated standard deviations in parentheses[a]

Atom	x	y	z	B_{eq}	Atom	x	y	z	B_{eq}
Zn	0.1869(1)	0.5000(1)	0.0302(2)	2.34(5)	C(B1)C	0.437(1)	0.3002(8)	0.104(2)	3.1(6)
S(D2)A	0.2378(4)	0.3869(4)	−0.3291(8)	8.3(3)	C(C1)C	0.366(1)	0.3488(8)	0.117(2)	3.5(6)
N(1)A	0.4501(9)	0.6011(7)	−0.384(1)	3.6(5)	C(D1)C	0.329(1)	0.3977(9)	0.045(2)	3.4(6)
N(D1)A	0.2809(9)	0.6108(6)	−0.235(1)	2.8(4)	C(E1)C	0.268(1)	0.4001(9)	0.204(2)	3.6(6)
N(E1)A	0.2530(8)	0.5489(7)	−0.082(1)	2.7(4)	C(2)C	0.577(1)	0.4124(8)	0.302(2)	2.7(5)
N(2)A	0.5181(9)	0.4892(7)	−0.266(1)	3.0(4)	C(A2)C	0.585(1)	0.4658(8)	0.210(2)	2.5(5)
C(1)A	0.533(1)	0.5436(8)	−0.206(2)	3.1(6)	C(B2)C	0.528(1)	0.5229(8)	0.237(2)	3.8(6)
C(A1)A	0.500(1)	0.6092(9)	−0.258(2)	3.3(6)	C(C2)C	0.576(2)	0.570(2)	0.303(4)	15.(2)
C(B1)A	0.442(1)	0.6443(9)	−0.176(2)	3.3(6)	C(E2)C	0.650(2)	0.657(1)	0.145(2)	8.(1)
C(C1)A	0.358(1)	0.6083(8)	−0.152(2)	2.4(5)	O(1)C	0.5305(8)	0.3777(6)	−0.071(1)	4.5(4)
C(D1)A	0.341(1)	0.5708(9)	−0.055(2)	2.9(5)	O(2)C	0.6011(8)	0.4214(6)	0.411(1)	4.8(4)
C(E1)A	0.221(1)	0.5766(9)	−0.188(1)	3.1(5)	S(D2)D	0.0392(4)	0.3479(3)	0.2761(5)	4.6(2)
C(2)A	0.430(1)	0.5463(9)	−0.446(2)	3.9(6)	N(1)D	0.0133(9)	0.6276(7)	0.503(1)	3.2(4)
C(A2)A	0.469(1)	0.4808(9)	−0.388(2)	4.4(7)	N(D1)D	0.1835(9)	0.6136(7)	0.336(1)	3.3(5)
C(B2)A	0.403(1)	0.428(1)	−0.395(2)	6.9(9)	N(E1)D	0.1607(8)	0.5572(7)	0.172(1)	2.8(4)
C(C2)A	0.333(2)	0.444(1)	−0.320(2)	6.3(8)	N(2)D	−0.0931(8)	0.5515(7)	0.335(1)	3.0(4)
C(E2)A	0.283(2)	0.314(2)	−0.281(3)	12.(1)	C(1)D	−0.088(1)	0.6111(9)	0.307(2)	3.9(6)
O(1)A	0.5779(8)	0.5451(6)	−0.099(1)	4.2(4)	C(A1)D	−0.026(1)	0.6592(8)	0.390(2)	3.3(6)
O(2)A	0.3867(9)	0.5449(8)	−0.546(1)	6.9(5)	C(B1)D	0.047(1)	0.6857(8)	0.320(2)	3.3(6)
S(D2)B	−0.1672(4)	0.7351(3)	−0.1001(6)	6.6(2)	C(C1)D	0.104(1)	0.6341(8)	0.273(2)	2.9(5)
N(1)B	−0.2490(8)	0.4724(6)	−0.192(1)	3.1(4)	C(D1)D	0.093(1)	0.5986(8)	0.172(1)	2.8(5)
N(D1)B	−0.0304(9)	0.4172(7)	−0.189(1)	3.4(5)	C(E1)D	0.216(1)	0.5662(8)	0.272(2)	2.8(5)
N(E1)B	0.0708(8)	0.4655(7)	−0.055(1)	2.9(4)	C(2)D	0.010(1)	0.5647(9)	0.529(2)	4.1(6)
N(2)B	−0.1979(8)	0.5544(7)	−0.001(1)	3.3(5)	C(A2)D	−0.039(1)	0.5151(9)	0.439(2)	4.9(7)
C(1)B	−0.2059(9)	0.4933(9)	0.030(1)	2.8(5)	C(B2)D	0.022(1)	0.4637(9)	0.398(2)	4.0(6)
C(A1)B	−0.229(1)	0.4425(8)	−0.072(2)	2.6(5)	C(C2)D	−0.031(1)	0.4087(9)	0.340(2)	3.4(6)
C(B1)B	−0.154(1)	0.3925(8)	−0.067(1)	2.7(5)	C(E2)D	0.098(2)	0.312(1)	0.412(2)	7.3(9)
C(C1)B	−0.064(1)	0.4210(8)	−0.084(1)	2.3(5)	O(1)D	−0.1280(8)	0.6382(6)	0.209(1)	3.7(4)
C(D1)B	−0.002(1)	0.4498(8)	0.002(2)	2.7(5)	O(2)D	0.0495(9)	0.5410(7)	0.626(1)	6.5(5)
C(E1)B	0.054(1)	0.4455(9)	−0.171(2)	3.2(6)	S	0.2837(3)	0.7419(2)	0.5324(4)	3.0(1)
C(2)B	−0.248(1)	0.5342(9)	−0.221(2)	4.0(6)	O(1)	0.2342(9)	0.7846(6)	0.600(1)	5.7(5)
C(A2)B	−0.209(1)	0.5824(8)	−0.125(1)	2.7(5)	O(2)	0.3783(8)	0.7456(6)	0.582(1)	5.0(4)
C(B2)B	−0.120(1)	0.6123(8)	−0.152(2)	3.9(6)	O(3)	0.2544(8)	0.6756(6)	0.5452(9)	3.4(4)
C(C2)B	−0.087(1)	0.669(1)	−0.084(2)	5.3(7)	O(4)	0.2666(9)	0.7589(6)	0.403(1)	4.9(4)
C(E2)B	−0.126(2)	0.785(1)	0.026(2)	10.(1)	OW(1)	−0.3554(8)	0.3765(6)	−0.337(1)	4.7(4)
O(1)B	−0.1956(8)	0.4742(5)	0.137(1)	3.6(4)	OW(2)	−0.2550(8)	0.3445(7)	0.174(1)	5.6(5)
O(2)B	−0.2704(9)	0.5542(7)	−0.326(1)	6.3(5)	OW(3)	0.532(1)	0.2499(7)	−0.176(2)	7.3(6)
S(D2)C	0.6766(4)	0.6049(3)	0.2716(6)	6.1(2)	OW(4)	0.0920(9)	0.7193(6)	0.694(1)	5.6(5)
N(1)C	0.5541(9)	0.3518(7)	0.257(1)	3.2(5)	OW(5)	0.7663(9)	0.4697(8)	0.492(1)	6.7(5)
N(D1)C	0.3257(8)	0.3495(7)	0.218(1)	3.3(5)	OW(6)	−0.1314(9)	0.3701(7)	−0.394(1)	6.1(5)
N(E1)C	0.2684(8)	0.4296(6)	0.104(1)	2.9(5)	OW(7)	0.357(1)	0.2568(9)	0.396(2)	9.6(7)
N(2)C	0.5622(9)	0.4484(6)	0.080(1)	3.0(4)	OW(8)	0.507(1)	0.747(1)	0.425(2)	10.2(8)
C(1)C	0.546(1)	0.3898(8)	0.042(2)	2.7(5)	OW(9)	−0.235(1)	0.6649(7)	−0.465(1)	7.0(6)
C(A1)C	0.536(1)	0.3338(8)	0.127(1)	2.7(5)	OW(10)	0.199(2)	0.733(1)	0.953(2)	13.2(9)

a) B_{eq} is the equivalent temperature factor calculated from corresponding anisotropic temperature factors.*

* W. C. Hamilton, *Acta Crystallogr.*, **12**, 609 (1959).

leucyl-L-histidyl)[7] with at least one histidyl residue indicate that these dimers also have the folded conformation, although the χ_1^2 values are nearly +90° and are different by about 180° from those in the $[Zn(CMH)_4]^{2+}$ ion.

The piperazine rings (A and B) are intramolecularly connected to the C and D piperazines through two -NH···O=C hydrogen bonds, respectively, to give the hydrogen-bonded dimers which may behave like bidentate ligands. The formation of these dimers forces χ_1^2 to have nearly −90° when the folded conformations between the imidazole and the piperazine rings are maintained, since χ_1^2=+90° causes a large conformational change of the complex ion, which make the intramolecular hydrogen bonds between the piperazine rings impossible. Interestingly, the conformations of the $-CH_2-CH_2-S-CH_3$ groups are not only different from each other but also different from that of free CMH as given in Table 2, reflecting a large conformational flexibility of this group.

The crystal structure of $[Zn(CMH)_4]\ SO_4 \cdot 10H_2O$ is shown in Fig. 1. The complexes are linked by a complex system of many hydrogen bonds. There is no hydrogen bond which directly connects the complex ions. All of N(1), N(2), N(D1), O(1), and O(2) atoms except O(2)A and O(2)D participate in hydrogen bonds as donors or acceptors. There are two >C-H···O=C< type short contacts other than typical hydrogen bonds described above: C(E1)B···O(2)D of

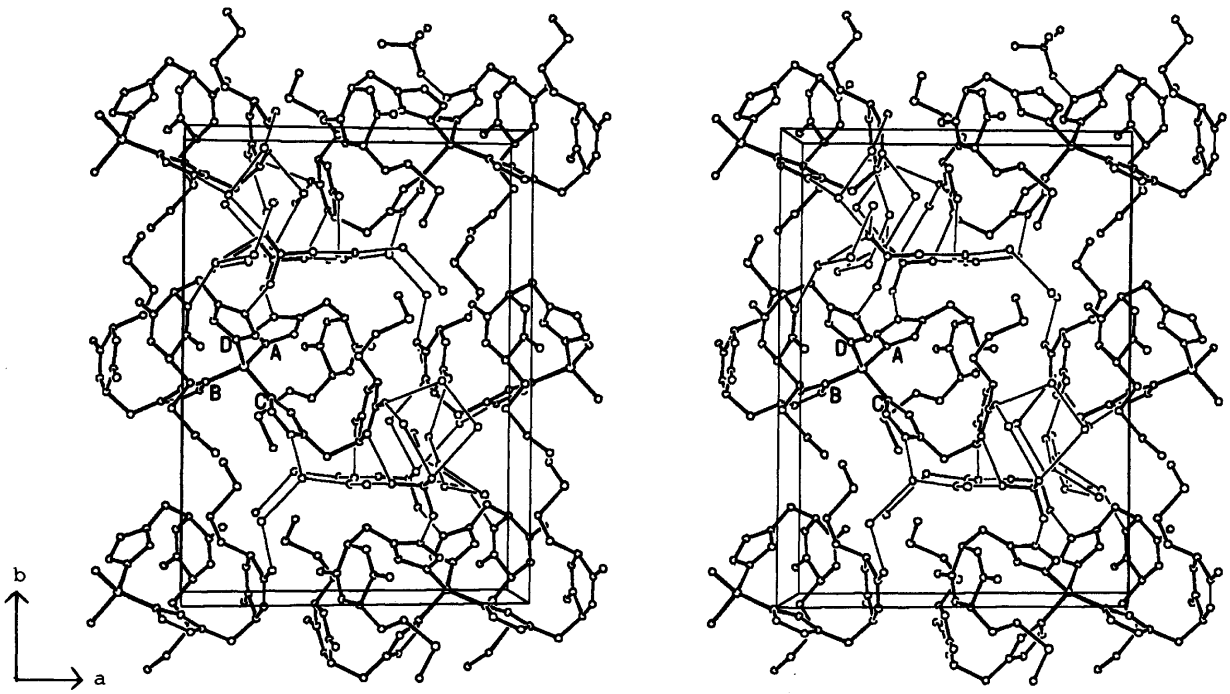

Fig. 1. Crystal structure of $Zn[cyclo(L\text{-methionyl-L-histidyl})]_4SO_4 \cdot 10H_2O$.

TABLE 2. SELECTED DIHEDRAL ANGLES (°) OF THE CYCLO(L-METHIONYL-L-HISTIDYL) MOIETIES IN THE ZINC(II) COMPLEX AND THE CYCLO(L-METHIONYL-L-HISTIDYL) MOLECULE

		Complex				CMH molecule
		A	B	C	D	
C(2)-N(1)-C(A1)-C(1)	ϕ_1	3	1	1	9	−2
N(1)-C(A1)-C(1)-N(2)	ψ_1	0	−7	−5	−6	3
C(A1)-C(1)-N(2)-C(A2)	ω_1	−1	1	9	−6	1
C(1)-N(2)-C(A2)-C(2)	ϕ_2	−1	10	−8	14	−7
N(2)-C(A2)-C(2)-N(1)	ψ_2	4	−15	4	−10	8
C(A2)-C(2)-N(1)-C(A1)	ω_2	−6	11	−1	−1	−4
N(1)-C(A1)-C(B1)-C(C1)	χ_1^1	64	65	68	66	56
C(A1)-C(B1)-C(C1)-N(D1)	χ_1^2	−83	−102	−104	−94	89
N(2)-C(A2)-C(B2)-C(C2)	χ_2^1	65	−68	−134	−70	70
C(A2)-C(B2)-C(C2)-S(D2)	χ_2^2	174	−57	49	175	−163
C(B2)-C(C2)-S(D2)-C(E2)		60	162	75	71	79

Estimated standard deviations are 1—2°.

Table 3. ^{1}H NMR data of cyclo(L-methionyl-L-histidyl) and its zinc(II) complex in D_2O at 50 °C

Compound	Chemical shifts (ppm), $\delta(\Delta\delta^{a)})$								
	C(A1)-H	C(B1)-H[b] high	C(B1)-H[b] low	C(D1)-H	C(E1)-H	C(A2)-H	C(B2)-H	C(C2)-H	C(E2)-H
CMH	4.40	3.01	3.28	6.97	7.71	4.08	1.11—1.84[c]	2.15	2.03
$Zn(CMH)_4^{2+}$[d]	4.47 (0.07)	3.13 (0.12)	3.34 (0.06)	7.06 (0.09)	8.04 (0.33)	4.16 (0.08)	1.30—1.85[c]	2.13 (−0.02)	1.99 (−0.04)

a) $\Delta\delta=\delta$[zinc(II) complex ion]$-\delta$(free ligand). b) C(B1)-H(β-protons) and C(A1)-H(α-proton) fragments of histidyl residues exhibit an ABX spin system, in which A and B are the β-protons and X is the α-proton. c) Complex and unresolved signals were given for C(B2)-H at this region. d) $Zn(CMH)_4SO_4\cdot 2H_2O$ was used for the measurement.

2.97(2) Å and C(E1)D···O(2)A of 3.08(2) Å.[8] It is noticeable that O(2)A and O(2)D atoms free from hydrogen bonds take part in this interaction as proton acceptors.

Table 3 shows the proton chemical shifts of CMH and its zinc(II) complex ion. β-Methylene protons [C(B2)-H; δ=1.11—1.84] of the methionyl residue of CMH absorbs at higher fields than those (δ= 2.10—3.00) of cyclo(L-methionyl-L-methionyl)[1a] because of the magnetic anisotropy of imidazole ring, suggesting that CMH prefers a folded form.[2a] Although the peaks of β-methylene protons [C(B2)-H] of CMH and $[Zn(CMH)_4]^{2+}$ ion are complex and unresolved, the values of the chemical shifts are used for explaining the conformation of $[Zn(CMH)_4]^{2+}$ ion. The small difference between the chemical shift (δ=1.11—1.84) of β-methylene protons [C(B2)-H] of CMH and those (δ=1.30—1.85) of $[Zn(CMH)_4]^{2+}$ ion suggests a possibility for the complex ion to have a folded form.

Table 4 shows α-β coupling constants and side-chain conformations for CMH and its zinc(II) complex in D_2O. These data indicate that the side-chain conformations of CMH and its zinc(II) complex are 67 and 61% for a folded form, respectively, showing the preference of a folded one in aqueous solution.

Table 4. α-β Coupling constants and side chain conformations of cyclo(L-methionyl-L-histidyl) and its zinc(II) complex ion in D_2O at 50 °C

Compound	α-β Coupling constant, Hz		Side chain conformation[a]		
	$J_{\alpha h\beta}$	$J_{\alpha l\beta}$	F	U_I	U_{II}
CMH	4.7	4.1	67	14	19
$Zn(CMH)_4^{2+}$[b]	4.9	4.6	61	18	21

a) Expressed in %; for notations see Ref. 2. b) $Zn(CMH)_4SO_4\cdot 2H_2O$ was used for the measurement.

Also, Table 3 indicates the downfield shift ($\Delta\delta$= 0.09 and 0.33) for C(D1)-H and C(E1)-H of $[Zn(CMH)_4]^{2+}$ ion from those of CMH, respectively. Table 5 shows the up- or down-field shifts ($\Delta\delta$=−1.4, −2.1, 3.4, and 1.0) for C(B1), C(C1), C(D1), and C(E1) carbons of $[Zn(CMH)_4]^{2+}$ ion from those of CMH, respectively. Moreover, Tables 3 and 5 show no distinct shifts for the methine protons [C(A1)-H and C(A2)-H], the methionyl residue protons [C(B2)-H, C(C2)-H, and C(E2)-H], the piperazine ring carbons [C(A1), C(A2), C(1), and C(2)], and the methionyl residue carbons [C(B2), C(C2), and C(E2)] of zinc(II) complex ion from those of CMH. These results reveal that the Zn^{2+} ion links exclusively to the imidazolyl groups of the histidyl residues.

We would also like to infer which N(D1 or E1) atom of the imidazolyl group coordinates to the Zn^{2+} ion in aqueous solution. Iyer *et al.*[9] previously reported that the N(D1) atom of the imidazolyl group coordinates to the Zn^{2+} ion in DMSO-d_6 from their NMR studies of the zinc(II) complexes with cyclohepta- and cyclooctapeptides though their results are similar to those for our zinc(II) complex. As shown in Fig. 1, the X-ray structure of the $[Zn(CMH)_4]^{2+}$ ion indicates that the N(E1) atom of the imidazolyl group of CMH links to the Zn^{2+} ion. Speculation regarding the CPK model also supports a possibility for the N(E1) atom of imidazolyl groups to coordinate to the Zn^{2+} ion. These results introduce a conclusion that the N(E1) atom of CMH coordinates to the Zn^{2+} ion in an aqueous solution (as

Table 5. ^{13}C NMR data of cyclo(L-methionyl-L-histidyl) and its zinc(II) complex ion in D_2O at 50 °C

Compound	Chemical shifts (ppm), $\delta(\Delta\delta^{a)})$										
	C(1)	C(A1)	C(B1)	C(C1)	C(D1)	C(E1)	C(2)	C(A2)	C(B2)	C(C2)	C(E2)
CMH	171.9	57.6	33.1	133.8	121.2	138.5	171.4	56.1	35.3	30.4	16.7
$Zn(CMH)_4^{2+}$[b]	172.0 (0.1)	57.3 (−0.3)	31.7 (−1.4)	131.7 (−2.1)	124.6 (3.4)	139.5 (1.0)	171.2 (−0.2)	56.2 (0.1)	35.2 (−0.1)	30.4 (0.0)	16.7 (0.0)

a) $\Delta\delta=\delta$[zinc(II) complex ion]$-\delta$(free ligand). b) $Zn(CMH)_4SO_4\cdot 2H_2O$ was used for the measurement.

opposed to that of Iyer *et al.*). However, further studies of similar complexes are necessary for determining which N(D1 or E1) atom of the imidazolyl group coordinates to the Zn^{2+} ion in an aqueous solution.

The values (381 and 412 for 0.0246 and 0.0591M, respectively) of the molecular weight obtained for $[Zn(CMH)_4]SO_4 \cdot 2H_2O$ are smaller than the theoretical value (1233/2=617) given in the dissociation of this complex to a monomeric complex ion and a sulfate one. These results suggest that the above complex ion has the following dissociative equilibrium;

$$[Zn(CMH)_4]^{2+} \rightleftharpoons [Zn(CMH)_3]^{2+} + CMH \rightleftharpoons [Zn(CMH)_2]^{2+} + 2CMH \text{ } etc.$$

The authors wish to thank Mr. Junichi Gohda for the measurements of the elemental analyses. We are also indebted to the Crystallographic Research Center, Institute for Protein Research, Osaka University, for computer calculations.

References

1) a) Y. Kojima, T. Yamashita, Y. Ishino, T. Hirashima, and T. Miwa, *Bull. Chem. Soc. Jpn.*, **56**, 3841 (1983); b) Y. Kojima, N. Ishio, T. Yamashita, and K. Hirotsu, *Chem. Lett.*, **1983**, 1365; c) Y. Kojima, *Transition Met. Chem.*, **4**, 269 (1979). d) Y. Kojima, T. Yamashita, Y. Ishino, T. Hirashima, and K. Hirotsu, *Chem. Lett.*, **1983**, 453; e) E. Ettore, V. Guantieri, A. M. Tamburro, and L. de Nardo, *Inorg. Chim. Acta*, **32**, L39 (1979).

2) a) K. D. Kopple and M. Ohnishi, *J. Am. Chem. Soc.*, **91**, 962 (1969); b) Y. Imanishi, *Adv. Polymer Sci.*, **20**, 1 (1976).

3) a) G. Germain, P. Main, and M. M. Woolfson, *Acta Crystallogr., Sect. B.*, **26**, 274 (1970); M. M. Woolfson, *ibid., A.*, **33**, 219 (1977); b) W. R. Busing, K. O. Martin, and H. S. Levy, "A Fortran Crystallographic Least Square Program," USAEC Report ORNL-TM-305, Oak Ridge National Laboratory, Oak Ridge, TN, (1965).

4) B. K. S. Lundberg, *Acta Crystallogr.*, **21**, 901 (1966); M. M. Harding and S. J. Cole, *ibid.*, **16**, 643 (1963); C. A. Bear, K. A. Duggan, and H. C. Freeman, *ibid., Sect. B.*, **31**, 2713 (1975); W. D. Horrocks, Jr., J. N. Ishley, and R. R. Whittle, *Inorg. Chem.*, **21**, 3265 (1982); C. I. H. Ashby, C. P. Cheng, E. N. Duesler, and T. L. Brown, *J. Am. Chem. Soc.*, **100**, 6063 (1978).

5) M. Bressan, F. Marchiori, and G. Valle, *Int. J. Pept. Protein Res.*, **23**, 104 (1984). The crystal structure of cyclo-(L-mehionyl-L-histidyl)·monohydrate was independently solved by us and will be published elsewhere. The dihedral angles listed in Table 2 are from our data with two times smaller standard deviations than those of Bressan *et al.*

6) Y. Kojima, T. Yamashita, S. Nishide, K. Hirotsu, and T. Higuchi, *Bull. Chem. Soc. Jpn.*, **58**, 409 (1985).

7) a) I. Tanaka, T. Iwata, N. Takahashi, and T. Ashida, *Acta Crystallogr., Sect. B.*, **33**, 3902 (1977); b) M. Cortrait and M. Ptak, *ibid., Sect. B.*, **34**, 528 (1978); c) R. Ramani, K. Venkatesan, and R. E. Marsh, *J. Am. Chem. Soc.*, **100**, 949 (1978); d) C-F. Lin and L. E. Webb, *ibid.*, **95**, 6803 (1973).

8) a) J. Donohue in "Structural Chemistry and Molecular Biology," ed by A. Rich, N. Davidson, and W. H. Freeman, San Francisco, **1968**, p. 443; b) B. C. Wang and B. M. Craven, *J. Chem. Soc., Chem. Commun.*, **1971**, 290.

9) K. S. Iyer, J.-P. Laussac, S.-J. Lau, and B. Sakar, *Int. J. Pept. Protein Res.*, **17**, 549 (1981); K. S. Iyer, J.-P. Laussac, and B. Sarkar, *ibid.*, **18**, 468 (1981).

 © 1985 The Chemical Society of Japan Bull. Chem. Soc. Jpn., 58, 1899—1902 (1985)

Differential Pulse Polarographic Determination of Lead Using Coprecipitation with Hafnium Hydroxide

Joichi UEDA* and Chikako KITA

Department of Chemistry, Faculty of Education, Kanazawa University, Marunouchi, Kanazawa 920

(Received January 28, 1985)

A differential-pulse polarographic determination of trace amounts of lead using coprecipitation with hafnium hydroxide has been studied. Hafnium hydroxide is effective as a collector of lead and makes 2.5 to at least 1250 μg of lead coprecipitate quantitatively from 100—500 cm^3 of sample solution. The formed precipitate is easily dissolved with hydrochloric acid and the presence of hafnium does not affect to the polarogram of lead. The effects of twenty-three diverse ions such as aluminium, zinc, cadmium, chromium(III), manganese(II), cobalt, and nickel were examined, and it was found that the presence of tin(IV), copper, and iron(III) interfered with the determination, even in small amounts. The recommended procedure for the determination is as follows. To a sample solution containing lead, 5 mg of hafnium is added and the pH is adjusted to about 10 with 1:1 aqueous ammonia. Then, the precipitate is filtered with a glass filter and dissolved with 2 cm^3 of concd hydrochloric acid. After the solution is diluted to 25 cm^3 with distilled water and deaerated with pure nitrogen for 5 min, lead is determined by the current peak height at −0.41 V.

The methods for the determination of trace amounts of lead by a combined coprecipitation-polarography have frequently been studied, and several coprecipitants such as hydroxides of beryllium,[1] aluminium,[2,3] iron(III),[4,5] thorium,[6] and zirconium,[7] or carbonates of calcium[8] and strontium[9] or sulfides of nickel,[10] copper,[11] and zinc[12] or barium chromate[13] have been proposed for a concentration of trace amounts of lead. The majority of these coprecipitants except hydroxides of zirconium and thorium, however, have more or less their individual disadvantages: It is difficult to dissolve the precipitates, the recovery of lead is not so good or the polarogram of lead is affected by the presence of the coprecipitants. This time, we have investigated a new collector of lead, and have found that hafnium hydroxide is excellent. That is, hafnium hydroxide can not only quantitatively collect lead as well as zirconium hydroxide,[7] but it can also quantitatively coprecipitate lead from a wider pH range than zirconium. Furthermore, it dissolves easier than zirconium hydroxide. In this work, we have also tried to filter the precipitate by means of suction with a glass filter and have obtained good results; shortening of the filtration time without the loss of the precipitate and simplifying the filtration procedure. This paper describes the fundamental conditions for the collection of trace amounts of lead by coprecipitation with hafnium hydroxide and a differential pulse polarographic determination of lead.

Experimental

Apparatus. A Yanagimoto model p-1000 polarograph was used for the differential-pulse polarographic measurements. It was operated in a three-electrode configuration with a dropping-mercury electrode, a saturated calomel reference electrode and a platinum counter electrode. A Hitachi-Horiba model M-5 glass electrode pH meter was used for the pH measurements.

All measurements were carried out at 25.0±0.1 °C and the solutions were deaerated with pure nitrogen for 5 min before the polarographic analysis. Voltage scans were made from −0.25 to −0.65 V at a rate of 10 mV s^{-1}, a modulation amplitude of 100 mV and a drop time of 1 second.

Reagents. *Standard Lead Solution*: A solution containing about 1 mg cm^{-3} of lead was prepared by dissolving guaranteed reagent-grade lead nitrate in a small amount of nitric acid and diluting with distilled water. The solution was standardized by the complexometric titration using Xylenol Orange as an indicator. This solution was diluted as required.

Hafnium Solution: A solution containing about 5 mg of hafnium was prepared by dissolving hafnium chloride (Nakarai Chemicals Co.) in 2 mol dm^{-3} hydrochloric acid. The solution was standardized by the complexometric back titration with a standard solution of thorium using Xylenol Orange as an indicator.

1:1 aqueous ammonia and 1 mol dm^{-3} hydrochloric acid were used for pH adjustments.

All the other reagents used were of guaranteed reagent grade.

Recommended Procedure. To a sample solution (100—500 cm^3) containing 2.5—1250 μg of lead, 5 mg of hafnium is added and the pH is adjusted to about 10 with 1:1 aqueous ammonia. Then, this solution is allowed to stand for more than 10 min. The precipitate is filtered by suction using a 3G4 glass filter, washed with aqueous ammonia of pH 10, and dissolved with 2 cm^3 of concd hydrochloric acid (with two 1 cm^3 portions of concd hydrochloric acid in about 5 min intervals). After the solution is diluted to 25 cm^3 with distilled water and deaerated with pure nitrogen for 5 min, the polarogram is recorded from −0.25 to −0.65 V. Lead is determined by the current peak height at −0.41 V.

Results and Discussion

Supporting Electrolyte. As a result of the investigation of various acids (such as hydrochloric, nitric, sulfuric, and perchloric acid), the most

suitable supporting electrolyte was found to be hydrochloric acid in respect to the shape of the polarograms of lead and the ease of dissolution of hafnium hydroxide. So, hydrochloric acid was chosen as the supporting electrolyte for further studies. Then, the effect of the concentration of this acid on the current peak height was studied. As shown in Fig. 1, the current peak height was gradually decreased with increasing amounts of hydrochloric acid; however, a maximum and almost constant value was obtained over a concentration range from 0.5 to 2 mol dm^{-3} of hydrochloric acid. Accordingly, an acidity of 1 mol dm^{-3} was used in this experiment and obtained the highest current peak height.

In Table 1, the relation between the concentration of hydrochloric acid and the time required for the dissolution of hafnium hydroxide is also shown. From this, it can be seen that hafnium hydroxide is dissolved easily by the use of hydrochloric acid whose concentration is more than 3 mol dm^{-3}. In this Table, the results of experiments with zirconium hydroxide is also appended.

Effect of pH on Coprecipitation. The effect of the pH on the coprecipitation of lead with hafnium hydroxide was studied for a solution (100 cm^3) containing 20 μg of lead. The pH values were adjusted with 1:1 aqueous ammonia and 1 mol dm^{-3} hydrochloric acid. The results are shown in Fig. 2. The pH range in which about 100% recovery of lead was observed was found to be 7.0—11.5, which was wider by about 4 times than that of zirconium hydroxide.[7] In this experiment, a pH of about 10 was adopted for the coprecipitation with hafnium hydroxide.

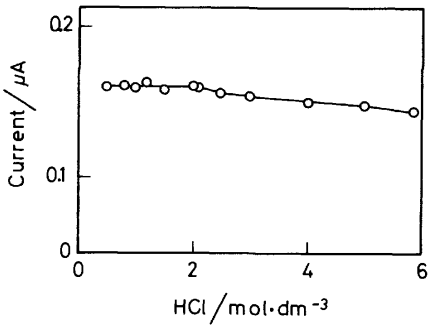

Fig. 1. Effect of the concentration of supporting electrolyte.
Pb: 20 μg/25 cm^3, Hf: 5 mg/25 cm^3, temperature: 25.0±0.1 °C.

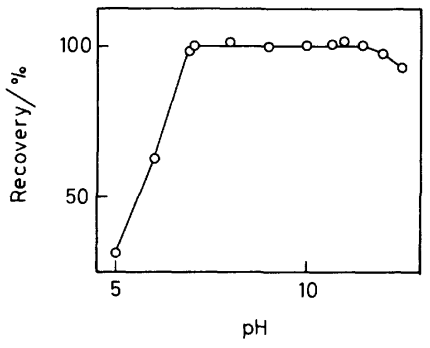

Fig. 2. Effect of pH on coprecipitation.
Pb: 20 μg/25 cm^3, Hf: 5 mg/25 cm^3, supporting electrolyte: 1 mol dm^{-3} HCl, temperature: 25.0±0.1 °C.

Effect of the Amount of the Coprecipitant. The effect of the hafnium concentration on the coprecipitation was studied with a solution (100 cm^3) containing 20 μg of lead and various amounts of hafnium. As the result, lead could be quantitatively collected by adding from 2 mg to at least 20 mg of hafnium.

Effect of Volume of Sample Solution. The relation between the recovery percentage of lead and the volume of the sample solution was studied by the recommended procedure, using various volumes (100—900 cm^3) of sample solutions which contain 20 μg of lead. The recovery percentage was approximately 100% when volumes from 100 to 500 cm^3 were used. However, in the case of using a volume of more than 500 cm^3, the percentage decreased considerably.

Effect of Aging of Precipitate on Lead Recovery. The relation between the recovery of lead and the aging time of the precipitate was investigated. The results indicated that the recovery of lead reached almost 100% at about 10 min after the precipitate was formed. After that, this percentage remained almost constant for at least 10 h. Then, the effect of the aging temperature of precipitate on the recovery of lead was also studied. It was found that almost a 100% recovery was always obtained within a temperature range from room temperature to 90 °C. In this experiment, therefore, the aging of the precipitate was carried out for more than 10 min at room temperature.

TABLE 1. RELATION BETWEEN CONCENTRATION OF HYDROCHLORIC ACID AND DISSOLUTION TIME OF PRECIPITATES

Concentration of HCl/mol dm^{-3}	$Hf(OH)_4$ min	$Zr(OH)_4$ min
1	*ca.* 2.5	*ca.* 50
2	*ca.* 1	*ca.* 12
3	*ca.* 10 s	*ca.* 3
6	*ca.* 5 s	*ca.* 1
9	(A)	*ca.* 1
12	(A)	*ca.* 0.5

10 mg of hafnium or zirconium was taken and 1 cm^3 of hydrochloric acid was used. (A): Precipitate dissolved instantaneously.

Filtration of Precipitate. In this experiment, we tried to filter the precipitate by means of suction using a glass filter and were able to considerably shorten the filtration time without any loss of precipitate. Also, the filtration and dissolution procedures of the precipitate were simplified. Whether the loss occurs or not by suction was examined by a comparison of the recovery of lead obtained by suction with that obtained by natural filtration (using Toyoroshi No. 5A filter paper). It was confirmed that almost the same recoveries were obtained for the both cases.

Calibration Curves. The calibration curves which were prepared by the recommended procedure were shown in Fig. 3. A linear relationship between the current peak height and the concentration was maintained over the range of 0.1—50 μg cm^{-3} for lead. In the absence of 5 mg of hafnium, the calibration curves were also prepared. It was recognized that the obtained curves were the same as the one which was prepared in the presence of hafnium. The reproducibility of the method, expressed by the relative standard deviation of the current peak heights which were obtained from ten repeated determinations, was 1.2% for 20 μg in 100 cm^3 sample solution. In order to investigate the temperature effect on the current peak height, a series of polarograms were also recorded at different temperatures. With a rise of temperature, the potential of the current peak shifted to more negative values and the current peak height increased. In this case, the temperature coefficient was calculated as 1.0%.

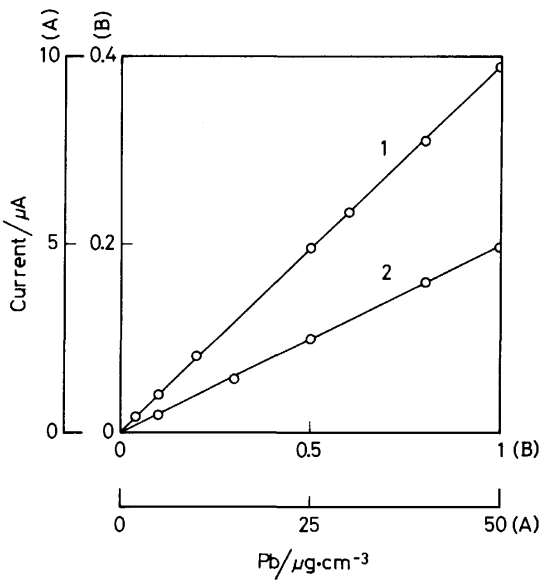

Fig. 3. Calibration curves.
Supporting electrolyte: 1 mol dm^{-3} HCl, Hf: 5 mg/25 cm^3, temperature: 25.0±0.1 °C, 1: utilize scale (A), 2: utilize scale (B).

Effect of Diverse Ions. The effect of twenty-three diverse ions on the determination of 20 μg of lead were examined by the application of the recommended procedure. The results are summarized in Table 2. Lead could be determined within a 5% error in the presence of 5 mg each of 8 cations, such as alkali metals, alkaline earth metals, aluminium, lanthanum, and molybdenum(VI), 0.5 mg each of 3 cations such as zinc, manganese(II), and nickel, and 0.1 mg each of 5 cations such as antimony(III), bismuth(III), cadmium, chromium(III), and cobalt. Tin(IV), copper, and iron(III), however, interfered with the determination even if they were present in a small amounts.

References

1) K. Kida, M. Abe, S. Nishigaki, and T. Kusaka, *Bunseki Kagaku*, **10**, 1217 (1961).
2) M. Sato, *Nippon Kagaku Zasshi*, **80**, 1453 (1959).
3) L. S. Studenskaya, K. F. Vorozhbitskaya, L. V. Kamaeva, and T. B. Gorodentseva, *Trudy vses. nauchno-issled. Inst. standard. Obraztsov*, **4**, 167 (1968); *Anal. Abstr.*, **18**, 2267 (1970).
4) K. Itsuki and M. Nagao, *Bunseki Kagaku*, **8**, 800 (1959).
5) K. Itsuki, B. Kobayashi, and K. Nishino, *Bunseki Kagaku*, **8**, 804 (1959).
6) S. Ueda, K. Fujihara, H. Miyakawa, and Y. Yamamoto, *Nippon Kagaku Zasshi*, **92**, 979 (1971).

Table 2. Effect of diverse ions

Ion	Amount added / mg	Recovery / %
Li^+	5.0	99.0
Be^{2+}	5.0	103.1
Mg^{2+}	5.0	104.0
Ca^{2+}	5.0	100.4
Ba^{2+}	5.0	100.1
Al^{3+}	5.0	98.0
Ga^{3+}	1.0	100.0
In^{3+}	0.05	97.0
Sn^{4+}	0.02	110.0
Sb^{3+}	0.1	99.2
Bi^{3+}	0.1	102.0
Cu^{2+}	0.02	94.8
Zn^{2+}	0.5	100.0
Cd^{2+}	0.1	98.0
La^{3+}	5.0	100.0
Zr^{4+}	1.0	100.0
Th^{4+}	1.0	100.0
Cr^{3+}	0.1	101.0
Mo(VI)	5.0	99.1
Mn^{2+}	0.5	98.0
Fe^{3+}	0.02	93.7
Co^{2+}	0.1	98.3
Ni^{2+}	0.5	101.0

20 μg of lead was taken.

7) W. Yoshimura, *Bunseki Kagaku*, **22**, 1346 (1973).
8) B. Visintin, S. Monteriolo, and S. A. Giuseppi, *Ann. Idrol.*, **1**, 212 (1963); *Anal. Abstr.*, **12**, 3575 (1965).
9) F. K. Baev, *Uch. Zap. Rostovsk. Univ.*, **40**, 163 (1958); *Anal. Abstr.*, **7**, 1286 (1960).
10) S. Yokosuka, *Bunseki Kagaku*, **4**, 99 (1955).
11) A. A. Fedorov, F. A. Ozerskaya, R. D. Malinina, Z. M. Sokolova, and F. V. Linkova, *Sb. Trud. Tsentr. Nauch-issled. Inst. Chern. Metallurg.*, **19**, 7 (1960); *Anal. Abstr.*, **9**, 2284 (1962).
12) L. E. Gorn, *Gigiena i Sanit.*, **3**, 41 (1955); *Chem. Abstr.*, **49**, 9724 (1955).
13) T. Yanagihara, N. Matano, and A. Kawase, *Bunseki Kagaku*, **8**, 576 (1959).

 © 1985 The Chemical Society of Japan Bull. Chem. Soc. Jpn., 58,1903—1912 (1985)

Gas Chromatography-Mass Spectrometry of Trimethylsilylated Imino Derivatives of Alanine

Katsuhiro KAWASHIRO,* Shiro MORIMOTO, and Hideyuki YOSHIDA
Department of Chemical Engineering, Faculty of Engineering, Tokushima University, Minamijosanjima, Tokushima 770
(Received December 4, 1984)

Trimethylsilylation of seven imino derivatives of alanine with *N,O*-bis(trimethylsilyl)trifluoroacetamide in acetonitrile was studied. The imino derivatives include 2,2′-iminodipropionitrile (**1**), 2,2′-iminodipropionamide (**2**), 2,2′-iminodipropionic acid (**3**), 2-(1-cyanoethylamino)propionamide (**4**), 2-(1-cyanoethylamino)-propionic acid (**5**), 2-(1-carbamoylethylamino)propionic acid (**6**), and 3,5-dimethyl-2,6-piperazinedione (**7**). The reaction products were identified by gas chromatography–mass spectrometry. Under the present reaction conditions (at 100 °C for 30 min), hydrogen atoms of carboxyl and carbamoyl groups and an imide hydrogen were readily replaced by the trimethylsilyl (TMS) group, but imino hydrogens were not replaced because of the steric hindrance of *N*-substituent group. For the carbamoyl group, only one hydrogen was replaced. Consequently, **1** was not trimethylsilylated. Furthermore, no definite trimethylsilylation products were obtained for **4**. Upon electron impact at 70 eV, **2**, **3**, and **5**—**7** gave rather simple spectra with molecular (M^+) and M −15 (loss of CH_3) ions characteristic of TMS derivatives. A fragment, M−117 (loss of COOTMS) or M −116 (loss of CONHTMS), was very prominent for **2**, **3**, **5**, and **6**. Other important ions such as *m/z* 70 were noted. Preparations and properties of some of the imino derivatives are also described.

In recent years, gas chromatography–mass spectrometry (GC–MS) has become a useful method for unequivocal identification of nonvolatile compounds such as amino acids and related compounds after their conversion into suitable volatile derivatives. Of numbers of such volatile derivatives,[1] the trimethylsilyl (TMS) derivative has received great interest because of its simple preparation and both good gas chromatographic and mass spectral properties.

In our previous paper[2] the presence of certain imino derivatives of alanine (Ala) in the polymerization product of 2-aminopropionitrile (2-APN) was suggested by ion-exchange chromatography. Ion-exchange retention data, however, are generally not sufficient to identify unequivocally amino acids and related compounds present in complex reaction mixtures. This has led us to study the GC–MS of the imino derivatives of Ala as shown in Fig. 1, after conversion into their TMS derivatives. The main reason for choosing the TMS derivative is that TMS groups can be readily introduced into functional groups such as carboxyl, hydroxyl, amino, carbamoyl groups, *etc.* with an easily available reagent such as *N,O*-bis(trimethylsilyl)trifluoroacetamide (BSTFA). Because of the absence of an acid or a base no hydrolysis takes place during trimethylsilylation; this makes it possible to distinguish, for example, between acid and amide groups present in the molecules. In this respect the TMS derivative has an advantage over the *N*-trifluoroacetyl alkyl ester derivative, preparations of which generally involve an esterification catalyzed by HCl.

Leimer *et al.*[3] have reported a comprehensive study of the complete mass spectra (electron impact at 70 eV), and the general fragmentation pathways for TMS derivatives of protein amino acids. The GC–MS of TMS derivatives of nonprotein amino acids such as

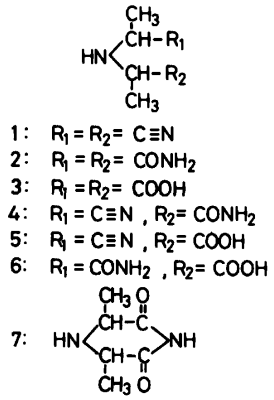

Fig. 1. Imino derivatives of Ala.

N-substituted amino acids, however, has far less been studied. In the previous paper,[4] we have reported GC–MS of TMS derivatives of some iminodicarboxylic acids including 2,2′-iminodipropionic acid (**3**).

This paper describes trimethylsilylation of imino derivatives of Ala as shown in Fig. 1 with BSTFA, and mass spectra of the resultant TMS derivatives upon electron impact at 70 eV. The imino derivatives include 2,2′-iminodipropionitrile (**1**), 2,2′-iminodipropionamide (**2**), (**3**), 2-(1-cyanoethylamino)propionamide (**4**), 2-(1-cyanoethylamino)propionic acid (**5**), 2-(1-carbamoylethylamino)propionic acid (**6**), and 3,5-dimethyl-2,6-piperazinedione (**7**). The structures of **1**—**7** are shown in Fig. 1. Preparations, ion-exchange chromatography, and lability in aqueous solutions are also described for **1**—**7**.

Results and Discussion

Preparations and Properties of 1—7. Of **1**—**7**, symmetrical compounds such as **1**—**3** were easily pre-

pared according to the method of Dubsky.[5] Compound **4** was prepared for the first time in a 40% yield in the following way:[6]

$$CH_3CHO\cdot NaHSO_3 + H_2NCH(CH_3)CONH_2 + NaCN \xrightarrow{0\,^\circ C} \mathbf{4}$$

However, preparations of unsymmetrical compounds such as **5** and **6**, were rather difficult.[7]

Karrer *et al.*[8] have reported preparation of **5**, which involved partial hydrolysis of **1** *via* an imidate derivative. In the present study, a product of mp 188—189 °C was obtained according to their method. Although the results of elemental analysis suggested the formation of **5**, spectral data were not consistent with the structure of **5**. IR spectrum showed no C≡N absorption near at 2250 cm^{-1}, but two strong absorptions due to $\nu_{C=O}$ were observed at 1680 and 1710 cm^{-1}, characteristic positions of an imide structure. The ^1H NMR spectrum of the product is rather simple, and equivalence of both two methyl (δ=1.20) and methine (3.45) protons suggests a cyclized imide structure as shown in Fig. 2. On the basis of these spectral data, the product was determined to be not **5**, but its isomer **7**. Repeated preparations gave the same product. Although the mechanism of the formation of **7** from **1** is not well understood, this reaction may be speculated as shown in Scheme 1.[9] A longer elution time of the product on ion-exchange chromatography

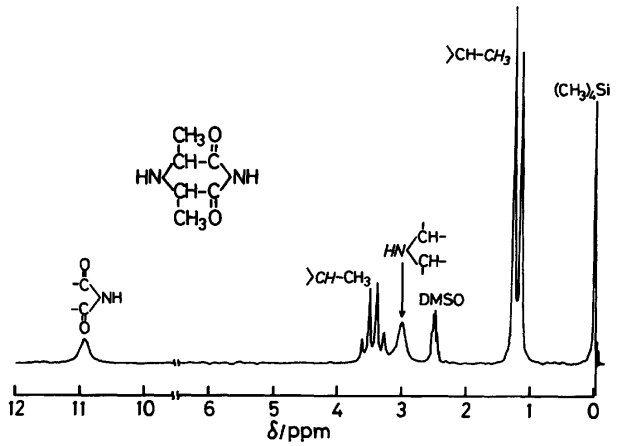

Fig. 2. ^1H NMR spectrum of the product obtained from **1** (DMSO-d_6).

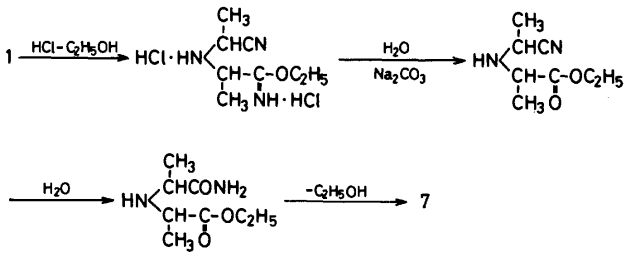

Scheme 1. Possible route for the formation of **7** from **1**.

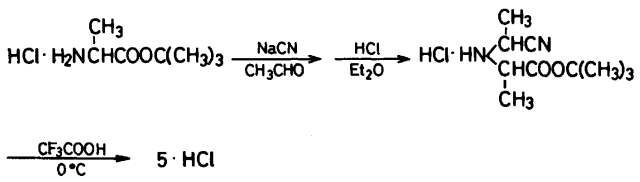

Scheme 2. Synthetic route for **5**.

(158 min, Table 1) revealed that it was of a basic nature rather than of an acidic nature. This is an additional evidence for the imide structure.

Compound **5** was successfully synthesized by the Strecker reaction and subsequent removal of the *t*-butyl group as shown in Scheme 2. An intermediate, *t*-butyl 2-(1-cyanoethylamino)propionate, was isolated as its hydrochloride (mp 120—122 °C), which was characterized by ^1H NMR spectrum and elemental analysis. Addition of CF_3COOH (TFA) to it gave a very hygroscopic hydrochloride of **5** with removal of the *t*-butyl group.[10] On ion-exchange chromatography, the product exhibited a single peak with a very short elution time (57 min, Table 1); the elution behavior was consistent with an acidic nature of **5**. After conversion into the TMS derivative, the product was further characterized by GC-MS which revealed the presence of both M^+ (*m/z* 214) and M−15 (*m/z* 199) ions corresponding to the mono-TMS derivative (Table 3).

Although two methods[5,11] have been reported for the preparation of **6**, they have individual disadvantages.[12] In the present study, **6** was prepared by partial hydrolysis of **2**. Compound **2** was found to be hydrolyzed to give **3** *via* an intermediate **6** in a hot dilute aqueous solution. The yield of **6** reached a maximum after 1 d at 100 °C, when starting compound **2** disappeared almost completely. After separation by ion-exchange chromatography, **6** was obtained as the monohydrate.

Table 1 gives elution times and color constants of **1**—**7** except **3** on ion-exchange chromatography using an amino acid analyzer. Compound **3** is known to be ninhydrin-negative.[8,13,14] Data of some related compounds such as Ala, alaninamide (Ala-NH_2), and 2-APN are also included. With buffer system A (pH 3.25—pH 5.28, buffer change of 30 min), elution orders of imino derivatives of Ala were similar to those of imino derivatives of glycine (Gly) reported previously.[6] With buffer system B (pH 3.25 alone), elution of basic components was retarded significantly, and **7** was found not to be eluted as a peak. The elution order of 2-APN and Ala-NH_2 reversed with the two buffer systems. As shown in Table 1,[15] **2a** and **6a** exhibited a single peak. On the other hand, the separation between diastereomers was observed for both **2b** and **6b**. It is noted that the peaks of **2a** and **6a** corresponded to the second peaks of **2b** and **6b**, respectively.

Table 1. Elution times and color constants of imino derivatives of Ala and related compounds on ion-exchange chromatography[a)]

Imino derivative	Elution time/min[b,c)] A	B	Relative color constant[d)]
1	54		1.03
5	57		0.65
6	60, 66		0.095
Ala	98		1.00
4[e)]	112, 131		0.63
7	158	—	0.17
2	206, 240	294, 363	0.70
2-APN	221	390	1.05
NH_3	249	348	0.96
Ala-NH_2	276	379	1.05

a) Column: 0.25ϕ×50 cm (Aminex A-4). Conditions of chromatography are shown in the Experimental section. b) Buffer systems A and B refer to pH 3.25—5.28 buffer with buffer change of 30 min, and to pH 3.25 buffer alone, respectively. c) In the cases of **2** and **6**, the separation between diastereomers was observed for **2b** and **6b**, whereas **2a** and **6a** gave a single peak. The peaks of **2a** and **6a** corresponded to the second peaks of **2b** and **6b**, respectively. d) Color constant of Ala: 124.9 μmol^{-1}. In the cases of **2** and **6**, color constants were calculated for **2a** and **6a**, respectively. e) The separation between diastereomers was observed.

Lability of α-amino nitriles in dilute aqueous solutions is well known.[6,16,17] Figure 3 shows the time course of decomposition of **1**, **4**, and **5** in both H_2O and the buffer solutions of pH 3.25 at room temperature. Lability increased in the order of **4**, **1**, and **5** in both solutions and the decomposition was more rapid in the buffers (pH 3.25) than in aqueous solutions. α-Aminonitriles **1**, **4**, and **5** decomposed with the formation of 2-APN, Ala-NH_2, and Ala, respectively. Consequently, the decomposition may be explained in terms of the reverse Strecker reaction as follows:[6]

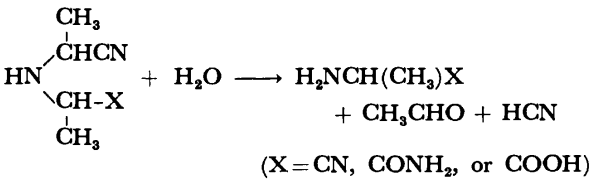

On decomposition, **4** and **5** gave almost stoichiometric amounts of Ala-NH_2 and Ala, respectively, and no other ninhydrin-positive products were found. In contrast, a significant amount of NH_3 was released in the case of **1** as shown Fig. 4. The formation of NH_3 can be explained in terms of the decomposition of the unstable intermediate, 2-APN, as follows:

$$H_2NCH(CH_3)CN + H_2O \longrightarrow NH_3 + CH_3CHO + HCN$$

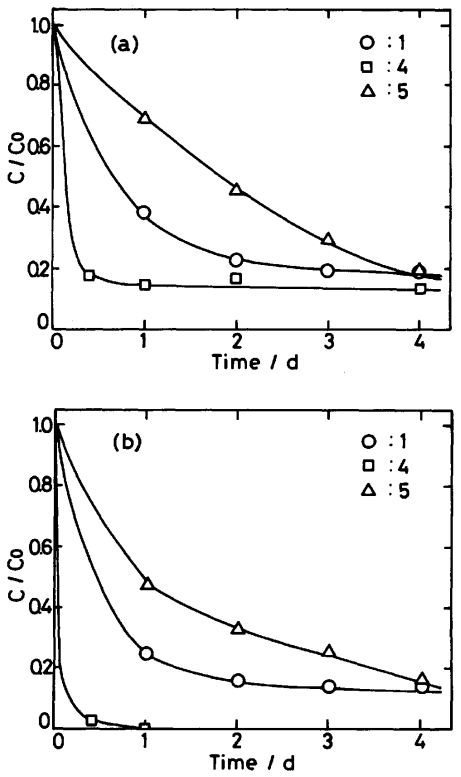

Fig. 3. The time course of decomposition of **1**, **4**, and **5** in aqueous solutions at room temperature. Initial concentration (C_0) is 1 mM (1 M = 1 mol dm^{-3}) for **4** and **5**, but 0.5 mM for **1**. a: H_2O. b: Citrate buffer solution of pH 3.25.

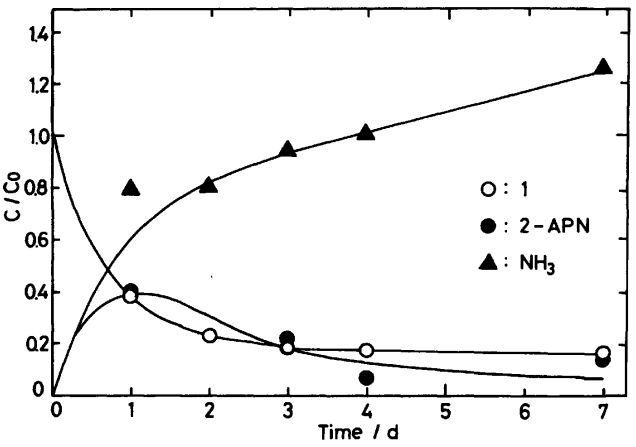

Fig. 4. The time course of decomposition of **1** in aqueous solution at room temperature. C_0: 0.5 mM.

There were some differences in decomposition of **1**, **4**, and **5**. As shown in Fig. 3a, **5** decomposed irreversibly according to the pseude first-order kinetics,[18] whereas **1** and **4** appeared to reach equilibria after 2 and 1 d, respectively. In the buffer solution of pH 3.25, **4** decomposed completely after 1 d (Fig. 3b); this fact indicates that the equilibrium was shifted greatly to the decomposition-product side with a decrease in

pH. In aqueous solutions, α-amino nitriles **1**, **4**, and **5** were found to be more labile than the corresponding imino derivatives of Gly reported previously.[6] Therefore, when these α-amino nitriles are to be analyzed with an amino acid analyzer, freshly prepared aqueous sample solutions should be charged on the analyzer as promptly as possible.

Trimethylsilylation and Gas Chromatography. When trimethylsilylation was performed in BSTFA-CH_3CN (1:1, v/v)[19] at 100 °C for 30 min, completely clear solutions were obtained for **1**—**7**. This observation suggests the formation of the corresponding TMS derivatives. In general, active hydrogens such as NH (imino), COOH, $CONH_2$, and NH (imide), were expected to be replaced by TMS groups. The GC-MS of the derivatized products revealed that among the active hydrogens, the imino NH could not be trimethylsilylated under the present conditions because of the steric hindrance of the *N*-substituent group.[4] Consequently, **1** having only imino NH as an active hydrogen was not trimethylsilylated. Nevertheless, free **1** was eluted most rapidly on GC because of its high volatility (Table 2). In contrast, some GC peaks were observed for **4**, but any definite trimethylsilylation products could not be identified, suggesting the decomposition of **4** during derivatization.

Table 2 gives retention times of trimethylsilylated imino derivatives of Ala on GC and the number of TMS groups introduced into them. A fused silica capillary column (OV-101 FS-WCOT, 0.35 mmφ×25 m) had advantages over a packed column (3 mmφ×1 m, 1.5% OV-101 on Chromosorb G HP) in terms of the good separation and the absence of decomposition of TMS derivatives. As shown in Table 2, separation between diastereomers of **3** was rather poor as compared with those of **2** and **6**. However, almost base line separation between the diastereomers was achieved when an SE-30 fused silica capillary column (FS-WCOT, 0.35 mmφ×25 m) was used.

Table 2. Retention times of trimethylsilylated imino derivatives of Ala on GC[a]

Parent compound	Number of TMS group	Retention time/min[b]
1	0	6.6
2	2	23.7, 24.7
3	2	16.8, 17.0
4[c]	—	—
5	1	11.1
6	2	20.1, 20.9
7	1	14.6

a) Initial temp: 100 °C. Initial hold: 5 min. Program rate: 5 °C/min. Final temp: 250 °C. Injector temp: 250 °C. Column: OV-101 fused silica capillary (0.35 mmφ×25 m). Retention time of phenanthrene: 25.9 min. b) In the cases of **2**, **3**, and **6**, the separation between diastereomers was observed for **2b**, **3b**, and **6b**, whereas **2a**, **3a**, and **6a** gave a single peak. The peak of **3a** corresponded to the first peak of **3b**. On the other hand, the peaks of **2a** and **6a** corresponded to the second peaks of **2b** and **6b**, respectively. c) No definite trimethylsilylation products were detected.

There was a difference in the elution behavior between **3a** and **3b**. Two GC peaks were eluted for **3b**, indicating separation between the diastereomers, which were proved on the basis of mass spectral data. On the other hand, a single peak was observed for **3a**, which corresponded to the first peak of **3b**. From these findings, it is evident that **3b** is a mixture of the diastereomers whereas **3a** is a racemate (*R,R*-+*S,S*-) or meso-form (*R,S*-). Similarly, two peaks were eluted for **2b**, while a single peak was observed for **2a**. It is noted, however, that the peak of **2a** corresponded to the second peak of **2b**. The reversed elution order of the diastereomers may be attributable to the nature of the carbamoyl groups, because it seems reasonable to assume no inversion of the two asymmetric centers during the preparation of **2a** from **3a**. Similar elution behavior of diastereomers was also found for **6a** and **6b**. For **2** and **6**, their elution behavior was well consistent with that on ion-exchange chromatography (Tables 1 and 2). Karrer and Appenzeller have reported that 2,2′-iminodipropionic acid (mp 233 °C) prepared by acid hydrolysis of **1**, was not a racemate, but a meso-form or a mixture of these two forms, by comparing its melting point with those of authentic samples.[13,20] The fact that **6a** prepared from **3a** as the starting material exhibited a single GC peak in the present study,[21] is not consistent with the results obtained by Karrer and Appenzeller. If **3a** is a meso-form, **6a** must become a mixture of the diastereomers. This discrepancy needs to be investigated further.

Figure 5 shows the time course of trimethylsilylation of **2b** at 100 °C, as a typical example. The peak area ratio of the di-TMS derivative to an internal standard (phenanthrene) becomes almost constant after 20 min, and its conversion into a more highly

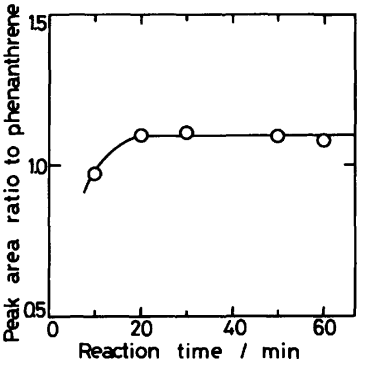

Fig. 5. The time course of trimethylsilylation of **2b** at 100 °C (**2b**: 50 μmol, BSTFA: 0.25 ml, CH_3CN: 0.25 ml, phenanthrene: 3.0 mg).

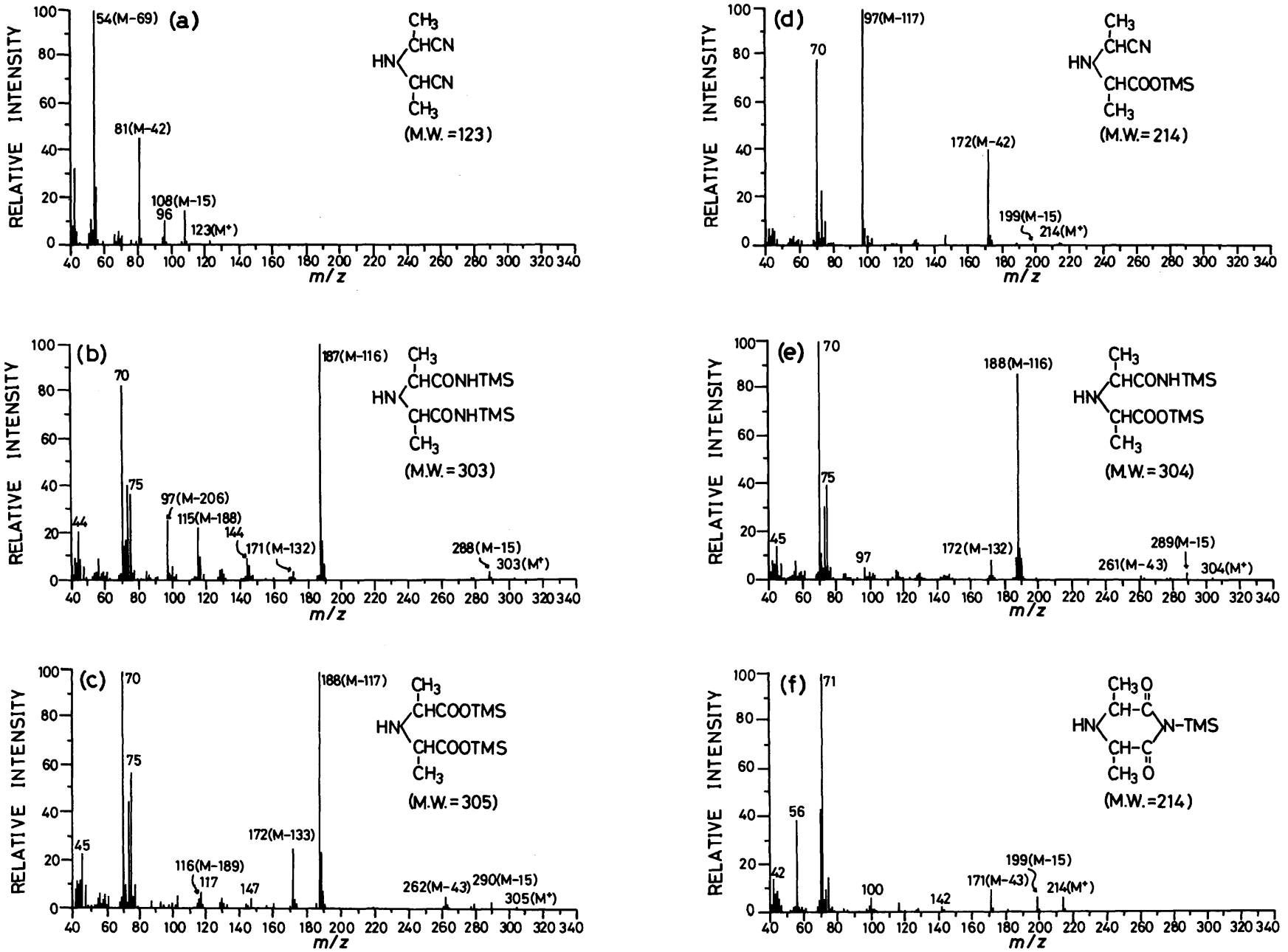

Fig. 6. Mass spectra of trimethylsilylated imino derivatives of Ala. a: **1**, b: **2**, c: **3**, d: **5**, e: **6**, and f: **7**.

trimethylsilylated derivative was not observed under the present conditions. Compound **7** having an imide NH also exhibited similar behavior on derivatization. Trimethylsilylation of **3b** was found to be more facile than **2b**. Therefore, derivatization of the functional groups present in the imino derivatives of Ala (except the imino NH) may be taken as completed under the present conditions (at 100 °C for 30 min).

Mass Spectra. Figures 6a—f present mass spectra of trimethylsilylated products for **1**—**3** and **5**—**7**. No TMS groups were introduced into **1**, as described above. Some characteristic ions are listed in Table 3. Both M^+ and M−15 ions are present in all the spectra.

For **2**, **3**, and **5** which have either a carboxyl or carbamoyl group, the most important ions arise from the M^+ by the loss of a COOTMS or CONHTMS group (α-cleavage to the imino nitrogen) with charge retention on the amine fragments. That the carbon-carbon bond adjacent to the nitrogen is preferentially cleaved is well known for amino acids and related compounds.[3,4] Thus both **3** and **5**, and **2** are characterized by the prominent M−117 (COOTMS) and M−116 (CONHTMS) ions, respectively. These fragments resulted from the α-cleavage constitute base peaks. The predominance of the fragments can be explained in terms of their stabilization due to resonance. There are two possibilities of α-cleavage for **6**, which has both carboxyl and carbamoyl groups (Scheme 3). As shown in Table 3, the M−116 ion is about 10 times abundant than the M−117 ion. This fact indicates that the CONHTMS group is more preferentially split off from the M^+ than the COOTMS. The elementary compositions of both the M−116 and M−117 ions were confirmed by hgh-resolution mass measurement.

For **5**, there are also two possibilities of α-cleavage, the loss of COOTMS and CN, with charge retention on the amine fragment. As shown in Fig. 6d, the M−117 (COOTMS) ion at m/z 97 constitutes a base peak, whereas the M−26 (CN) ion at m/z 188 has a relative intensity of less than 1%. This fact indicates that the cleavage of the carbon-carbon bond adjacent to the cyano group is very difficult. The increased stability of the bond compared with those adjacent to electron-withdrawing functional groups such as carbonyl, has been explained by McLafferty.[22]

As is expected, for **1** having two cyano groups no cleavage of the carbon-carbon bond adjacent to the cyano group, is observed. However, instead of the cleavage, the following fragmentation becomes significant, which accounts for the presence of a rather intense M−15 ion (rel. intensity, 14.2%) for **1** without

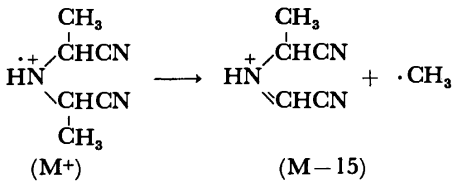

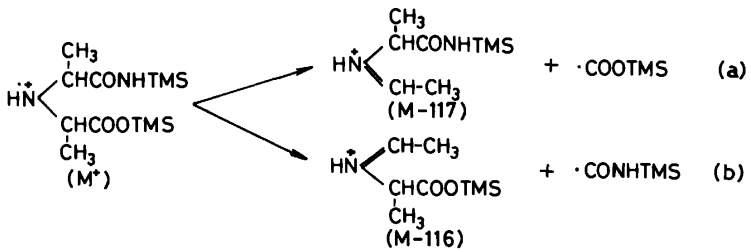

Scheme 3. Two possible α-cleavages for **6**.

TABLE 3. CHARACTERISTIC IONS OF TRIMETHYLSILYLATED IMINO DERIVATIVES OF Ala

Parent compound	Number of TMS group	m/z[a]						
		M^+	M−15	M−42	M−43	M−116	M−117	Others
1	0	123 (1.3)	108 (14.2)	81 (45.0)	—	—	—	54 (100)
2	2	303 (0.4)	288 (3.4)	261 (0.3)	—	187 (100)	186 (0.4)	115[M−118], (22.0) 97[M−206], (25.2) 70 (82.3)
3	2	305 (1.3)	290 (3.0)	—	262 (5.0)	189 (23.2)	188 (100)	172[M−133], (25.0) 116[M−189], (3.1) 70 (99.3)
5	1	214 (0.7)	199 (0.3)	172 (30.0)	—	98 (7.4)	97 (100)	70 (70.2)
6	2	304 (0.3)	289 (2.4)	—	261 (1.1)	188 (86.7)	187 (9.1)	172[M−132], (8.2) 97[M−207], (4.8) 70 (100)
7	1	214 (6.2)	199 (6.1)	—	171 (9.5)	98 (0.5)	97 (1.1)	71, 70 (100) (43.8)

a) Values in parentheses indicate relative intensity.

TMS groups. A base peak at *m/z* 54 corresponds to M−69 (NHCH(CH$_3$)CN), indicating that the N-C bond between the imino nitrogen and methine carbon is cleaved with charge retention on the 1-cyanoethyl fragment. Two ions characteristic of the nitrile, the M−27 (HCN) at *m/z* 96 and M−42 (CH$_3$+HCN) at *m/z* 81, are observed. The latter ion also appears at *m/z* 172 for **5**, indicating the presence of a -CH(CH$_3$)-CN group in the molecule. For **7**, the M$^+$ ion is rather intense because of its cyclic structure. An ion at *m/z* 71 constitutes a base peak, which may result from the following cleavage:

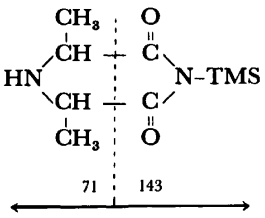

As is expected, the 70 eV spectrum of **3** becomes slightly complicated as compared with the corresponding 20 eV spectrum reported previously,[4] although similar characteristic ions are present. In the 70 eV spectrum, ions in the low mass region such as *m/z* 70, 73, and 75, become significant, whereas the M+1 ion which was larger than the M$^+$ in the 20 eV spectrum is not seen.

As shown in Fig. 6c, **3** having two carboxyl groups gives characteristic ions such as M−43 (CH$_3$+CO), M−133 (CH$_3$+CO+(CH$_3$)$_3$SiOH), and M−189 (COOTMS+CH$_2$=Si(CH$_3$)$_2$). Analogous characteristic ions are observed for **2**, which has two carbamoyl groups (Fig. 6b). Ions at *m/z* 261 and 171 were determined to be M−42 (CH$_3$+CNH) and M−132 (CH$_3$+CNH+(CH$_3$)$_3$SiOH), respectively. Although an ion at *m/z* 170 corresponds to M−131 (CH$_3$+CNH+(CH$_3$)$_3$SiNH$_2$), this is far less significant than the M−132 ion. A prominent ion at *m/z* 115 was determined to be M−188 (CONHTMS+CH$_2$=Si(CH$_3$)$_2$). This fact indicates that the ion results from the α-cleavage fragment (M−116) by the loss of a neutral species, CH$_2$=Si(CH$_3$)$_2$. The elementary composition of an ion at *m/z* 97 was determined to be C$_5$H$_9$N$_2$, which corresponds to M−206 (CONHTMS+CH$_2$=Si(CH$_3$)$_2$+H$_2$O). Consequently, this ion arises most likely from the M−188 ion by the loss of H$_2$O. The fragmentation may be depicted as shown in Scheme 4.

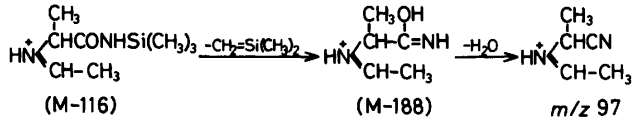

Scheme 4. Proposed fragmentation to the *m/z* 97 for **2**.

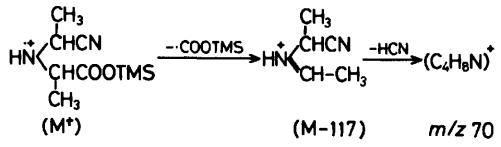

Scheme 5. Proposed fragmentation to the *m/z* 70 for **5**.

As is expected, the ions characteristic of both **2** and **3** (except M−42 and M−133) are observed for **6**, which has both carboxyl and carbamoyl groups. In this case, ions at *m/z* 116 and 115 were determined to be M−188 (CONHTMS+CH$_2$=Si(CH$_3$)$_2$) and M−189 (COOTMS+CH$_2$=Si(CH$_3$)$_2$), respectively. The ion *m/z* 97 corresponds to M−207 (COOTMS+CH$_2$=Si(CH$_3$)$_2$+H$_2$O) and, therefore, results from the M−189 by the loss of H$_2$O. Most of the characteristic ions described above were confirmed by high-resolution mass measurement.

In the low mass region, a very prominent ion at *m/z* 70 appears in most of the spectra (except **1**); this is a base peak for **6**. Generally, this unusual ion is not found for the TMS derivatives of common amino acids. High-resolution mass measurement revealed that it had an elementary composition of C$_4$H$_8$N without a silicon atom. Since the *m/z* 70 ion corresponds to M−144 (COOTMS+HCN) for **5**, its formation may be depicted as shown in Scheme 5. Similarly, for **2** and **3**, the *m/z* 70 ion arises most likely from the *m/z* 97 (M−206) and *m/z* 116 (M−189) by the loss of neutral species, HCN and HCOOH, respectively. For **6**, both the two fragmentations are possible for the formation of the *m/z* 70 ion.

In the previous paper,[4] tri-TMS derivative of **3** exhibited an abundant ion at *m/z* 70. In the present study, under forced derivatization conditions, **6** was found to give a small amount of the tri-TMS derivative along with the di-TMS derivative. The tri-TMS derivative also gave a prominent *m/z* 70 ion upon electron impact.[23] These observations indicate that imino derivatives of Ala (except **1**) generally exhibit a very prominent ion at *m/z* 70, whether their imino NHs are trimethylsilylated or not. Consequently, the presence of this ion can be used as a method of detecting them by GC-MS.

Experimental

All the melting points were determined with a Yanagimoto micro melting point apparatus and were not corrected. ^{1}H NMR spectra were measured with a Hitachi R-24B spectrometer using tetramethylsilane or sodium 2,2-dimethyl-2-silapentane-5-sulfonate as an internal standard. IR spectra were taken with a Hitachi 285 infrared spectrophotometer. Ala and 2-bromopropionic acid used as starting materials were of (*RS*)-form.

2,2'-Iminodipropionitrile (1). Compound **1** was prepared by the method of Dubsky.[5] Yield, 13%; mp, 65—

66 °C (lit,[5] 68 °C). Found: C, 58.29; H, 7.31; N, 34.14%. Calcd for $C_6H_9N_3$: C, 58.52; H, 7.37; N, 34.12%.

2,2'-Iminodipropionic Acid (3). ***3a***: Compound **1** was hydrolyzed with 6 M† HCl (at 100 °C for 6 h)[5] and then the product was isolated as a zinc salt to remove Ala produced by a side reaction. The free acid was obtained by decomposition of the salt with H_2S in aq solution. Yield, 25%; mp (dec), 239—241 °C (lit,[5] 233—235 °C). Found: C, 44.81; H, 6.96; N, 8.68%. Calcd for $C_6H_{11}NO_4$: C, 44.72; H, 6.88; N, 8.69%.

3b: Compound **3b** was prepared by the reaction of Ala and 2-bromopropionic acid in the presence of NaOH.[14] Yield 32%; mp (dec), 256—258 °C (lit,[14] 250—252 °C). Found: C, 44.56; H, 6.62; N, 8.48%.

2,2'-Iminodipropionamide (2). Compounds **2a** and **2b** were prepared from **3a** and **3b**, respectively, by the method of Dubsky,[5] which involves esterification with methanol and subsequent ammonolysis.

2a: Yield 20%; mp, 133—136 °C (lit,[5] 127 °C). Found: C, 45.11; H, 8.41; N, 26.09%. Calcd for $C_6H_{13}N_3O_2$: C, 45.27; H, 8.23; N, 26.40%.

2b: Yield 41%; mp 135—138 °C. Found: C, 45.01; H, 8.45; N, 26.56%.

2-(1-Cyanoethylamino)propionamide (4). A mixture of acetaldehyde-sodium hydrogensulfite[24] (6.67 g) and H_2O (5 ml) was cooled below 0 °C with stirring, to which was added dropwise a solution of NaOH (1.2 g, 30 mmol) and Ala-NH_2·AcOH[25] (4.45 g, 30 mmol) dissolved in a small amount of H_2O. After the addition was complete, the mixture was stirred for 2h at 0 °C and further for 30 min at room temperature. A solution of NaCN (1.60 g, 33 mmol) in a minimum amount of H_2O was added to it under cooling. After being left overnight at room temperature, the solution was extracted with ethyl acetate (AcOEt) (40 ml×4) and the extract was dried (Na_2SO_4), filtered and then evaporated to give a pale yellowish oil, which solidified on the addition of diethyl ether (Et_2O). Recrystallization was performed from AcOEt–petroleum ether; yield 1.70 g (40%); mp 92—95 °C; IR (KBr) 3410 (NH), 2210 (C≡N), and 1670 cm^{-1} (amide I); ^1H NMR (DMSO-d_6) δ=1.18 (3H, d, J=7.0 Hz, CH_3), 1.47 (3H, d, J=7.0 Hz, CH_3), 2.80—3.92 (2H, m, 2CH), 3.30 (1H, s, NH), and 7.01, 7.27 (2H, br, $CONH_2$). Found: C, 50.91; H, 8.10; N, 29.80%. Calcd for $C_6H_{11}N_3O$: C, 51.05; H, 7.85; N, 29.76%.

As an alternative approach, ammonolysis of methyl 2-(1-cyanoethylamino)propionate was attempted, which was prepared from acetaldehyde-sodium hydrogensulfite, methyl alaninate, and NaCN in a similar manner. However, the product was found to contain a considerable amount of a by-product (Ala-NH_2), which could not be removed by repeated recrystallizations.

2-(1-Cyanoethylamino)propionic Acid (5). *t-Butyl 2-(1-Cyanoethylamino)propionate Hydrochloride*: *t*-Butyl alaninate hydrochloride (mp 143—145 °C; lit,[26] 139—140.5 °C) was prepared by the reaction of *N*-benzyloxycarbonyl-Ala[27] and 2-methylpropene in the presence of H_2SO_4, and subsequent hydrogenation[10] and introduction of dry HCl gas. A mixture of *t*-butyl alaninate hydrochloride (1.0 g, 5.5 mmol), acetaldehyde (0.43 g, 9.8 mmol), and Et_2O (20 ml) was cooled below 0 °C with stirring, to which was added a solution of NaCN (0.49 g, 10 mmol) in a small amount of H_2O. After the addition was complete, stirring was continued for 4 h. The Et_2O layer was separated and then the aq layer was extracted with Et_2O (50 ml×3). The combined Et_2O layer was dried (Na_2SO_4) and filtered. Introduction of dry HCl gas into the Et_2O layer caused crystallization of the hydrochloride, which was recrystallized from ethanol–Et_2O; yield 0.60 g (46%); mp 120—122 °C; ^1H NMR (DMSO-d_6) δ=1.47 (9H, s, $C(CH_3)_3$), 1.54 (3H, d, J=7.1 Hz, CH_3CHCO), 1.65 (3H, d, J=7.1 Hz, CH_3CHCN), 3.93 (1H, q, J=7.1 Hz, CHCO), 4.57 (1H, q, J=7.1 Hz, CHCN), and 7.58 (2H, br, NH_2^+). Found: C, 51.08; H, 8.25; N, 11.94%. Calcd for $C_{10}H_{19}N_2O_2Cl$: C, 51.17; H, 8.16; N, 11.93%.

Removal of the t-Butyl Group: The removal of the *t*-butyl group was carried out with TFA, giving a very hygroscopic product (**5**·HCl). A typical example was as follows. *t*-Butyl 2-(1-cyanoethylamino)propionate·HCl (50 μmol) was dissolved in TFA (0.5 ml) below 0 °C. After being kept for 10 min, the solution was allowed to stand at room temperature for 1 h. Evaporation of the TFA in vacuum gave the product. When a portion of an aq solution of the product was analyzed with the amino acid analyzer, only one peak was eluted (elution time, 57 min; Table 1). The product was also trimethylsilylated with BSTFA–CH_3CN (1:1, v/v) (at 100 °C for 30 min) for GC–MS. GC of the derivatized solution exhibited only one peak with a retention time of 3.1 min (column, 3 mmϕ× 1 m packed with 1.5% OV-101 on Chromosorb G HP; temperature, 100 °C). Its mass spectrum contained both M^+ (m/z 214) and M−15 (m/z 199) ions, indicating the formation of a mono-TMS derivative (mol wt=214) (Table 3).

2-(1-Carbamoylethylamino)propionic Acid (6). Compounds **6a** and **6b** were obtained as monohydrates by partial hydrolysis of **2a** and **2b**, respectively.

6a: A solution of **2a** (0.25 g, 1.6 mmol) in H_2O (45 ml) was heated on a sand bath at 100 °C for 24 h. After evaporation, the residue was extracted with hot methanol (15 ml) to remove **3a**. The methanol was evaporated and then the residue was dissolved in H_2O (3 ml). The solution was charged on a column (2.0 ϕ×5 cm) packed with Amberlite CG-120 (H form). After the column was washed with H_2O, the product was eluted with 1% aq pyridine; yield 0.11 g (38%); mp (dec) 208—209 °C (lit,[5] 210 °C (as **6**·1.5H_2O)). Found: C, 40.68; H, 8.00; N, 15.39%. Calcd for $C_6H_{12}N_2O_3$·H_2O: C, 40.44; H, 7.92; N, 15.72%.

6b: Yield 42%; mp (dec) 196—199 °C; ^1H NMR (TFA) δ=1.87 (6H, d, J=7.2 Hz, $2CH_3$), 4.14—4.73 (2H, m, 2CH), 7.34 and 7.44 (2H, br, $CONH_2$), and 7.82 (2H, br, NH_2^+). Found: C, 40.54; H, 7.61; N, 15.69%.

3,5-Dimethyl-2,6-piperazinedione (7). Into a solution of **1** (1.0 g, 8.1 mmol) in anhydrous ethanol (20 ml) was introduced dry HCl gas under cooling until first-formed white precipitates dissolved completely. The introduction of HCl was continued further for 30 min. The solution was stored in a refrigerator overnight, and then filtered into a flask containing Et_2O (200 ml). The resultant hygroscopic precipitates were collected by filtration, washed with Et_2O, and then dried in vacuum, which were dissolved in H_2O (5 ml). After the addition of Na_2CO_3 (0.86 g, 8.1 mmol), the solution was extracted with Et_2O (30 ml×10). The extract was dried (Na_2SO_4), filtered and then evaporated to give crystals which were recrystallized from AcOEt–petroleum ether; yield 0.21 g (18%); mp 188—189 °C (lit,[5]

† 1 M=1 mol dm^{-3}.

186 °C); IR (KBr) 3250 (imino NH), and 1710 and 1680 cm^{-1} (imide C=O); ^1H NMR (DMSO-d_6) δ=1.20 (6H, d, J=7.2 Hz, $2CH_3$), 3.00 (1H, br, imino NH), 3.45 (2H, q, J=7.2 Hz, 2CH), and 10.92 (1H, br, imide NH). Found: C, 50.42; H, 7.06; N, 19.63%. Calcd for $C_6H_{10}N_2O_2$: C, 50.69; N, 7.09; N, 19.71%.

It is well known that a C≡N group can be easily converted into an amide in hydrobromic acid-acetic acid (HBr-AcOH).[6,17] Treatment of this product with 25% HBr-AcOH (Protein Research Foundation), however, resulted merely in the formation of HBr salt of **7**, which was confirmed by elemental analysis and ^1H NMR spectrum. This is an additional evidence for the absence of a C≡N group in the product.

Ion-exchange Chromatography. Ion-exchange chromatography was carried out with a Sibata amino acid analyzer AA-600 under the following conditions: Column 0.25 ϕ×50 cm packed with Aminex A-4 (Bio-Rad); flow rate of an eluent, 6 ml/h; flow rate of a ninhydrin solution, 3 ml/h; jacket temp, 30 °C. Absorbance at 570 nm was measured by continuous photometry. Sodium citrate buffers of pH 3.25 (0.2 M Na^+) and 5.28 (0.35 M Na^+) were used as eluents (Wako Pure Chemical Industries, Ltd.). Each of imino derivatives of Ala and related compounds was chromatographed separately and its color constant was calculated according to the common H×W method. Ala-NH_2 and 2-APN were prepared as Ala-NH_2·AcOH[25] and 2-APN·1/2 H_2SO_4,[28] respectively, according to the reported methods.

Decomposition of 1, 4, and 5 in Aqueous Media. Both H_2O and pH 3.25 citrate buffer solutions were prepared for **1**, **4**, and **5**. Compound **5**·HCl was obtained from a known amount of *t*-butyl 2-(1-cyanoethylamino)propionate hydrochloride by the treatment of TFA. The concentration of the solutions was 1 mM for **4** and **5**, but 0.5 mM for **1**. The solutions were allowed to stand at room temperature. Portions (0.1 ml) of the solutions were analyzed with the amino acid analyzer (buffer system A) at appropriate time intervals. The reason why the concentration of 0.5 mM was chosen for **1** is that the calibration curve of **1** does not follow Beer's law at a concentration higher than this. Decomposition products were identified by comparing elution times with those of the authentic samples. The other imino derivatives of Ala were stable under the conditions.

Trimethylsilylation. About 25 μmol of each imino derivative was weighed into a 1 ml screw vial. Then, 0.25 ml of BSTFA (Nakarai Chemicals, Ltd.) and 0.25 ml of CH_3CN (Wako Pure Chemical Industries, Ltd., S grade reagent) were added to the vial. It was closed tight with a silicone cap and then heated at 100 °C for 30 min in a Reacti-Therm (Pierce Chemical Company) or in a constant-temperature air bath (Yamato Drying-Oven, DX-58). For the experiments of the time course of trimethylsilylation, the latter was used because of its constant temperature. The derivatized solutions were usually clear, 0.5—1 μl portions of which were injected into a GC column. For GC-MS, about 50 μmol of each imino derivative was trimethylsilylated with 0.4 ml of BSTFA and 0.4 ml of CH_3CN.

GC. GC was carried out with a Hitachi 163 gas chromatograph equipped with a flame ionization detector. The conditions were as follows: Column, 3 mmϕ×1 m (glass) packed with 1.5% OV-101 on Chromosorb G HP (100/120 mesh) (Shimadzu); injector temp, 230 °C. Flow rates of carrier gas (N_2), H_2, and air were 30, 35, and 920 ml/min, respectively. The column oven was operated isothermally at 100 °C for 5 min after injection and then programmed to be heated up to 230 °C at a rate of 5 °C/min. A fused silica capillary column (FS-WCOT, 0.35 mmϕ×25 m, OV-101 or SE-30) (Gasukuro Kogyo Co. Ltd.) was also used instead of the packed column under the following conditions: Flow rate of carrier gas (N_2). 1 ml/min; split ratio, 1:50. Peak area ratios were calculated by a Chromatogram Processor 7000B (System Instrument Corporation).

GC-MS. Mass spectra were obtained with a Varian MAT 312 mass spectrometer which was connected with a Varian 3700 gas chromatograph. Each volatile derivative was chromatographed on a glass column (1.6 mmϕ×1 m) packed with 3% OV-101 on Gas Chrom Q (80/100 mesh) by the use of He as the carrier gas (flow rate, 15 ml/min). The column oven was operated isothermally at 70 °C for 5 min after injection (injector temp, 230 °C) and then programmed to be heated up to 230 °C. The GC-MS combination was operated under the following conditions: Separator temp, 240 °C; energy of electron, 70 eV; accelerating voltage, 3.0 kV; ion source temp, 300 °C. The spectrometer was continuously scanned.

High-Resolution Mass Measurement. High-resolution mass spectra (70 ev) of selected samples were obtained with a JEOL JMS-D 300 mass spectrometer by the use of perfluorokerosene as an internal standard.

We wish to thank Mr. Hideo Mori, Otsuka Pharmaceuticals Co. Ltd., Tokushima Factory, for obtaining low-resolution mass spectra by GC-MS.

References

1) P. Hušek and K. Macek, *J. Chromatogr.*, **113**, 139 (1975).

2) S. Morimoto, K. Kawashiro, H. Yoshida, and K. Sugiura, "The polymerization products of α-aminopropionitrile. The component separation using cation-exchange resin" in "Origin of Life," ed by Y. Wolman, D. Reidel Publishing Company, Dordrecht, Holland (1981), pp. 247—254.

3) K. R. Leimer, R. H. Rice, and C. W. Gehrke, *J. Chromatogr.*, **141**, 355 (1977).

4) K. Kawashiro, S. Morimoto, and H. Yoshida, *Bull. Chem. Soc. Jpn.*, **57**, 2871 (1984).

5) J. V. Dubsky, *Ber.*, **49**, 1045 (1916).

6) K. Kawashiro, S. Morimoto, and H. Yoshida, *Bull. Chem. Soc. Jpn.*, **56**, 792 (1983).

7) In the previous paper (Ref. 6), 2-(cyanomethylamino)acetic acid and 2-(carbamoylmethylamino)acetic acid were prepared by deprotection of *N*-(*p*-methoxybenzyloxycarbonyl)(Z(OMe))-2-(cyanomethylamino)acetic acid with TFA and HBr-AcOH, respectively. The *N*-protected 2-(cyanomethylamino)acetic acid was obtained by introduction of Z(OMe) to the imino nitrogen of ethyl 2-(cyanomethyl)-acetate with *S*-(*p*-methoxybenzyloxycarbonyl)-4,6-dimethyl-2-pyrimidinethiol followed by saponification with aq NaOH. In the present study, attempted preparations of **5** and **6** according to this method were unsuccessful, because introduction of Z(OMe) to the imino nitrogen of ethyl 2-(1-cyanoethylamino)propionate did not take place under the same conditions. This is due to the steric hindrance of the

N-substituent group.

8) P. Karrer, H. Koenig, and R. Legler, *Helv. Chim. Acta*, **24**, 861 (1941).

9) P. G. Pietta, P. Cavallo, and G. R. Marshall, *J. Org. Chem.*, **36**, 3966 (1971). A base-catalyzed elimination of an alcohol leading to a cyclic imide formation is known for *N*-protected asparagine and glutamine esters.

10) G. W. Anderson and F. M. Callahan, *J. Am. Chem. Soc.*, **82**, 3359 (1960).

11) G. Ciamician and P. Silber, *Ber.*, **39**, 3942 (1906).

12) The method of Dubsky (Ref. 5) is difficult to isolate **6** from a reaction mixture and that of Ciamician and Silber (Ref. 11) is very time-consuming.

13) P. Karrer and R. Appenzeller, *Helv. Chim. Acta*, **25**, 595 (1942).

14) K. Kawashiro, S. Morimoto, and H. Yoshida, *Bull. Chem. Soc. Jpn.*, **57**, 1097 (1984).

15) Compound **3** was obtained by the following two methods. Compounds **3a** and **3b** were prepared by acid hydrolysis of **1** and by reaction of Ala and 2-bromopropionic acid (Ref. 14), respectively. Compounds **2** and **6** prepared from **3a** as the starting material were designated as **2a** and **6a**, respectively. Similarly, **2** and **6** from **3b** were designated as **2b** and **6b**, respectively.

16) R. E. Moser and C. N. Matthews, *Experientia*, **24**, 658 (1968).

17) C. Ressler, G. R. Nagarajan, M. Kirisawa, and D. V. Kashelikar, *J. Org. Chem.*, **36**, 3960 (1971).

18) Pseude first-order rate constants at room temperature were found to be 4.17×10^{-1} and 5.31×10^{-1} d^{-1} for H_2O and pH 3.25 buffer solution, respectively.

19) C. W. Gehrke, H. Nakamoto, and R. W. Zumwalt, *J. Chromatogr.*, **45**, 24 (1969).

20) Karrer *et al.* (Ref. 8) once assigned this acid to a racemate on the basis of its degradation with kidney (*R*)-amino acid oxydase.

21) Strictly speaking, GC analysis for **3a** revealed the presence of a small amount (about 3%) of the diastereomers corresponding to the second peak of **3b**. Similarly, **6a** contained about 5% of the diastereomers corresponding to the first peak of **6b**.

22) F. W. McLafferty, *Anal. Chem.*, **34**, 26 (1962).

23) MS (70 eV) *m/z* (rel. intensity) 361(M−CH_3, 3), 260 (M−CONHTMS, 100), 259 (M−COOTMS, 2), 188 (M−CONHTMS−CH_2=Si(CH_3)$_2$, 2), 147 (8), 75 (11), 73 (7), and 70 (31).

24) H. Scheibler and H. Neef, *Ber.*, **59**, 1500 (1926).

25) K. Kawashiro, H. Yoshida, and S. Morimoto, *Bull. Chem. Soc. Jpn.*, **50**, 2956 (1977).

26) E. Taschner, A. Chimiak, B. Bator, and T. Sokolowska, *Justus Liebigs Ann. Chem.*, **646**, 134 (1961).

27) M. Bergmann and L. Zervas, *Ber.*, **65**, 1192 (1932).

28) K. Kawashiro, S. Morimoto, H. Yoshida, and K. Sugiura, *Origins Life*, **8**, 347 (1977).

 © 1985 The Chemical Society of Japan Bull. Chem. Soc. Jpn., 58, 1913—1917 (1985)

The Nature of the Cosolvent Effects of Sugars on the Aqueous Solubilities of Hydrocarbons

Masanobu JANADO* and Yuki YANO†
Department of Food Science, Kyoto Women's University, Kyoto 605
(Received December 19, 1984)

Pentoses (D-arabinose, D-xylose, and D-ribose) and hexoses (D-glucose, D-galactose, and D-mannose) increased appreciably the aqueous solubilities of naphthalene and biphenyl, but all the sugars except ribose caused solubility depression of 1-octanol. Ribose increased most effectively the hydrocarbon solubilities while glucose showed the least effect. Deoxy sugars and methyl glycosides were more effective than the corresponding unsubstituted sugars. As to maltodextrins the solubility-increasing effect per glucose unit is cooperatively enhanced as the number of glucose residue increases. On the basis of these data, it was concluded that the cosolvent effects of the sugars are primarily brought about by their nonpolar interactions with hydrocarbons that occur at the structure-breaking sites of the sugar molecules.

We have previously reported that hexoses decreased to widely different extents the aqueous solubility of 1-octanol.[1] It was also shown that maltose, maltotriose and dextran, but not cellobiose and sucrose, caused solubility increases of 1-octanol and 1-heptanol particularly at high concentrations and that this effect was markedly enhanced as the temperature increased. These results apparently indicate that the cosolvent effects of sugars depend on the configurations of CH and OH groups in the monosaccharide molecules, the type of glycosidic linkages and the molecular size of the oligomers. Inspection of the relevant thermodynamic parameters suggested the presence of the hydrophobic interactions between the solute molecules and the hydrophobic surfaces[2,3] of sugars. We now report the effect of pentoses, hexoses, deoxy sugars, methyl glycosides and maltodextrins on the aqueous solubilities of 1-octanol, benzene, naphthalene and biphenyl, to look further into the nature of the cosolvent effect of sugars.

Experimental

Materials. Hexoses, pentoses and maltose of analytical reagent grade were purchased from Nakarai Chemical Ltd. (Kyoto, Japan) and were used as supplied. Maltotriose and maltopentaose (Nakarai Chemical Ltd.) and maltotetraose and maltohexaose (Seishin Pharm. Ltd., Chiba, Japan) were all analytical reagent grade. All other reagents used including benzene, naphthalene, biphenyl, 1-octanol, 1-butanol, and hexane were analytical reagent grade and were used as supplied.

Solubility Measurement of Aromatic Hydrocarbons and 1-Octanol. The solubilities of benzene, naphthalene, biphenyl and 1-octanol were measured in sugar solutions in the concentration range of 0—50%. As previously pointed out,[4] these aromatic hydrocarbons evaporated rapidly from their saturated aqueous solutions even in tightly closed vials with some air spaces. As a consequence, significantly lower apparent solubilities were often obtained from the solutions which stood for some time after separation from the excess hydrocarbons. This evaporation effect, which is the main source of error, could be practically eliminated by employing the following procedure: An appropriate amount (approximately 10 g) of a sugar solution plus an excess amount of a hydrocarbon was stirred for 6 h and gently shaken for another 18 h in a chamber thermostated within ±0.05°C. After removing a large part of the excess hydrocarbon using a transfer pipet, the mixture was allowed to stand without agitation for 6 h in the thermostated chamber. A portion of clear solution was taken up by a transfer pipet and immediately placed in a 15 ml vial containing a weighed amount of hexane with extreme care being taken not to touch the floating or sedimented residual hydrocarbon. The solubility measurements were made after extracting the solutes into hexane. Benzene, naphthalene and biphenyl were determined by spectrophotometry and 1-octanol by gas chromatography. The average percentage of deviation from the mean never exceeded 2%.

† Present address: Department of Education, Kōgakukan University, Ise 516.

Results

The Cosolvent Effects of Monosaccharides. Figure 1 shows solubilities of 1-octanol, benzene, naphthalene and biphenyl in sugar solutions plotted against the sugar concentrations. The temperature dependence of the cosolvent effects of sugars is summarized in Table 1 for the aromatic hydrocarbons. The results obtained for 1-octanol were omitted here since the relevant data for this solute have been reported elsewhere.[1]

The Cosolvent Effects of Deoxy Sugars and Methyl Glycosides. To examine the effect of OH–H and OH–OCH_3 substitutions and the anomer effect, solubilities of the hydrocarbons were measured in the solutions of fucose, deoxy ribose and α- and β-methyl glycosides. The results are given in Table 2. It is clear that the substitution of one OH group with H and OCH_3 resulted in marked increase in the cosolvent effect, particularly for the large aromatic hydrocarbons. As to the methyl glycosides, β-anomers appear to be more effective than the α-

anomers.

The Cosolvent Effects of Maltodextrins. To examine the effect of molecular size of maltodextrins on their cosolvent effects, solubility of naphthalene was measured in maltodextrin solutions of an identical glucose residue concentration (0.55 M†). Accordingly, the data given in Table 3 represent the cosolvent effect of glucose residue but not that of maltodextrin molecules. The results clearly show that the effect of glucose residue cooperatively increases as the degree of polymerization increases.

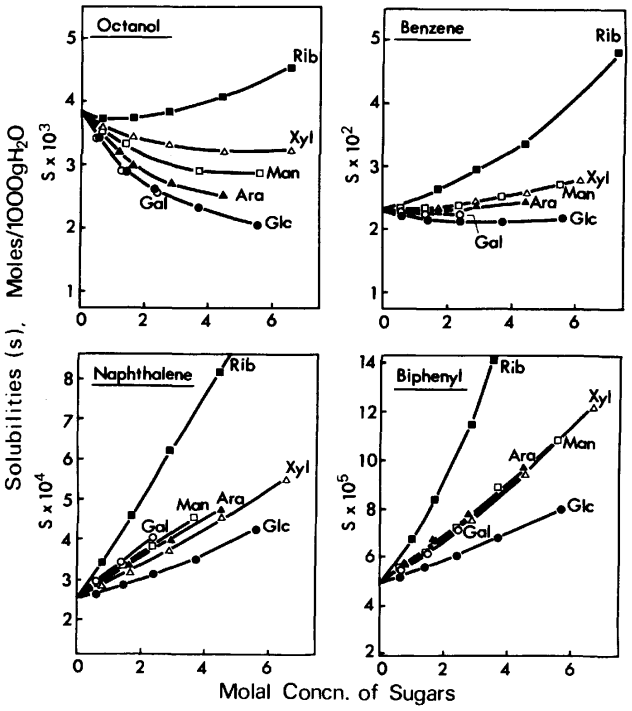

Fig. 1. Solubilities of 1-octanol, benzene, naphthalene, and biphenyl in sugar solutions at 25 °C.

Discussion

The Factors Determining the Cosolvent Effects of Sugars. The solubility plots of 1-octanol and benzene reveal that at low sugar concentrations the solubility-decreasing effect (the negative cosolvent effect) predominates but as the sugar concentration increases it is countervailed by the opposing effect (the positive cosolvent effect) resulting in leveling off or upward curvature of the solubility curves (Fig. 1). In solution of naphthalene and biphenyl the positive cosolvent effect prevails throughout the entire concentration range of sugars. We shall examine the nature of the cosolvent effects of sugars in the light of a current theory put forward by Roseman and Jencks.[5] According to their theory, the cosolvent effect or the transfer free energy of a nonpolar solute from water to a water-cosolvent mixture (ΔF_t) can be written as a sum of the free energy differences of the cavity formation (ΔF^{cav}), of the nonpolar solvent-solute interactions (ΔF_{np}^{int}), and of the polar interactions involving primarily solvent-solute hydrogen bonding (ΔF_p^{int}), in the two solvents. That is,

$$\Delta F_t = \Delta F^{cav} + \Delta F_{np}^{int} + \Delta F_p^{int}. \quad (1)$$

On the basis of extensive data on the cosolvent effects, they concluded that ΔF_t is largely determined by the first two terms, $\Delta F^{cav}+\Delta F_{np}^{int}$, the last term ($\Delta F_p^{int}$) playing a minor role in solution of nonpolar solutes. The important part of their theory is that the primary effect of almost all organic cosolvents is to increase solubilities of nonpolar solutes by making ($\Delta F^{cav}+\Delta F_{np}^{int}$) more favorable. The relative

Table 1. Effect of temperature on the solubilities (S)[a] of aromatic hydrocarbons in concentrated sugar solutions

Sugar(mol kg^{-1} H_2O)	10 °C			25 °C		
	Benzene ($S\times10^2$)	Naphthalene ($S\times10^4$)	Biphenyl ($S\times10^5$)	Benzene ($S\times10^2$)	Naphthalene ($S\times10^4$)	Biphenyl ($S\times10^5$)
D-Glucose(4.5)	1.71	1.82	2.92	2.15	3.83	7.32
D-Galactose(2.0)	1.94	2.02	3.47	2.25	3.80	6.76
D-Mannose(4.7)	2.13	2.46	5.15	2.64	4.89	10.02
D-Arabinose(3.7)	1.96	2.34	4.84	2.42	4.43	8.91
D-Xylose(5.6)	2.21	2.79	5.97	2.70	5.10	10.83
D-Ribose(5.3)	2.94	4.62	10.43	3.69	9.33	20.76
H_2O	2.11	1.39	2.67	2.31	2.52	4.85

a) mol kg^{-1} H_2O.

† 1 M=1 mol dm^{-3}.

magnitude of ΔF^{cav} and ΔF_{np}^{int}, however, has not been evaluated. In the discussion that follows, the cosolvent effects of sugars will be examined in terms of ΔF^{cav} and ΔF_{np}^{int}.

As previously noted,[1] the negative part of the cosolvent effect evident in the solubility plots of 1-octanol and benzene but obscured by the opposing effect in the plots of naphthalene and biphenyl may largely be attributed to the reduction of water activity caused by sugar hydration. One prominent feature of the solubility curves is their remarkable solute-dependence, *e.g.*, while the molar volumes of biphenyl and 1-octanol are comparable, their solubility curves are totally different. This indicates that ΔF_{np}^{int} rather than ΔF^{cav} predominates in the cosolvent effects of sugars. The decrement of the activity coefficients (see Eq. 5) of the solutes on transfer from water to sugar solutions increases in the order, 1-octanol<benzene<naphthalene<biphenyl, indicating that the nonpolar interactions of the hydrocarbons with the sugars are enhanced by the high polarizability and planarity of aromatic rings.[5] The effective nonpolar interactions through Van der Waals' forces can be achieved only when water molecules are excluded and the sugar and hydrocarbon molecules come close to each other. That is, for the effective interaction the water structure around the specific interaction sites of the sugar molecules, presumably the sites where CH density is relatively high, needs to be loose. This contention is consistent with the increased positive-cosolvent effect brought about by the OH-H and OH-OCH_3 substitutions (Table 2). The cooperative effect of glucose residues of maltodextrins (Table 3) may reflect that they form curved nonpolar surfaces, similar to the internal surfaces of the cyclodextrin cavities, that strongly interact with the hydrocarbons.[6]

Relative Magnitude of ΔF_{np}^{int} of Each Sugar. The foregoing evidence indicates that ΔF^{cav} is an important component of ΔF_t and a favorable ΔF^{cav} is prerequisite to the effective nonpolar interaction (ΔF_{np}^{int}) but that the negativity of ΔF_t is largely attributed to the negativity of ΔF_{np}^{int}. If the stoichiometric complex formations between the sugars (S) and biphenyl (B) are assumed, it is possible to estimate the relevant association constants. (Biphenyl was chosen because its ΔF_t values are all negative (Fig. 1)). Let us consider an equilibrium dialysis system in which an aqueous solution of sugar and biphenyl in dialysis bag permeable to water and biphenyl, but not to sugar, is in equilibrium with the external saturated aqueous solution of biphenyl. The equilibrium system can be described by

$$B + \nu S = BS_\nu, \tag{2}$$

where ν is the average number of bound sugar molecules per biphenyl. Provided that ν does not fluctuate greatly,[7] the apparent association constant (K^{app}) can be written as

$$K^{app} = \frac{[BS_\nu]}{[B][S]^\nu}, \tag{3}$$

where [B], [S], and [BS_ν] are the equilibrium molar concentrations. Since [B]=C^o (the molar solubility of biphenyl in the external solvent water) and hence

Table 3. Solubilities (S) (mol kg^{-1} H_2O) of naphthalene in maltodextrin solutions of 0.55 M glucose residue concentration at 25 °C

Maltodextrin	$S \times 10^4$	Maltodextrin	$S \times 10^4$
D-Glucose	2.61	Maltotetraose	3.47
Maltose	3.05	Maltopentaose	3.59
Maltotriose	3.30	Maltohexaose	3.77
H_2O	2.58	—	—

Table 2. Solubilities (S)[a] of 1-octanol and aromatic hydrocarbons in sugar solutions (1 mol kg^{-1}) at 25 °C

Sugar	1-Octanol ($S \times 10^3$)	Benzene ($S \times 10^2$)	Naphthalene ($S \times 10^4$)	Biphenyl ($S \times 10^5$)
D-Glucose	2.89	2.08	2.81	5.33
α-Methyl D-glucoside	3.85	2.53	3.97	7.81
β-Methyl D-glucoside	3.63	2.88	4.24	7.98
D-Galactose	2.94	2.10	3.22	5.64
D-Fucose	nd	2.03	4.07	7.03
α-Methyl D-galactoside	3.66	2.41	4.42	7.88
β-Methyl D-galactoside	3.38	2.47	5.57	9.75
D-Ribose	3.61	2.32	3.78	6.59
2-Deoxy D-ribose	4.43	2.86	4.94	10.12
H_2O	3.83	2.25	2.60	4.94

a) mol kg^{-1} H_2O.

$[BS_\nu]=C-C^\circ$ where C refers to the molar solubility of biphenyl in the sugar solution contained in the dialysis bag, Eq. 3 can be rewritten as

$$\frac{C^\circ}{C}=\frac{1}{1+K^{app}[S]^\nu}. \quad (4)$$

Assuming the activity coefficient of biphenyl in the saturated water solution to be unity,[8] the activity coefficient (f) in a sugar solution is given by

$$f=C^\circ/C. \quad (5)$$

Eq. 4 and Eq. 5 may be combined to yield

$$(1-f)/f=K^{app}[S]^\nu. \quad (6)$$

The term $(1-f)/f$ represents a relative decrement of the activity coefficient of biphenyl upon transfer from water to the sugar solutions. Since the concentration of the added sugar $[S_o]$ is much greater than that of biphenyl (C°), [S] may be replaced by $[S_o]$, and Eq. 6 can be rewritten as

$$\ln[f/(1-f)]=\ln(1/K^{app})-\nu\ln[S_o]. \quad (7)$$

Such an approach can only provide the rough estimates of the interaction parameters (K^{app} and ν), but these values are still quite informative.[9,10] Figure 2 shows the plots of $\ln[f/(1-f)]$ *vs.* $\ln[S_o]$ for all the monosaccharides except glucose for which f is nearly 1 thereby yielding an infinite value of $f/(1-f)$. The values of K^{app} and ν evaluated from Fig. 2 are summarized in Table 4. The results show that each sugar forms 1 to 1 stoichiometric complex with biphenyl and the association constant increases in the order of glucose≪galactose<mannose<xylose<arabinose≪ribose. The difference in K^{app} may reflect the difference in the total surface area of CH group of sugars accessible to water molecule.[11] However, the cooperative enhancement of the positive cosolvent effect of glucose residues of maltodextrins, but not of cellobiose,[1] indicates the importance of the "CH-dense surface," a specific site of sugar molecule where the CH density is the highest, rather than the total CH-surface area.[6]

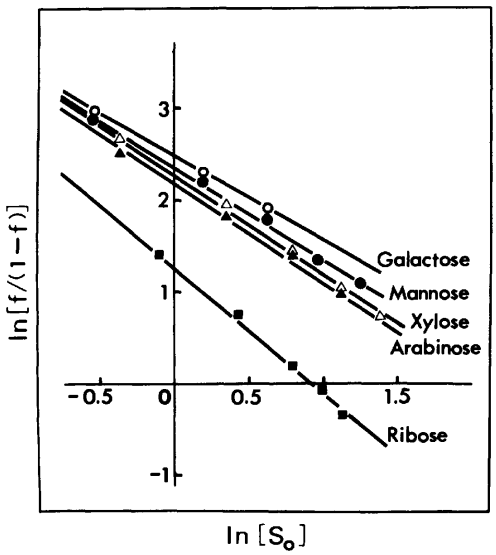

Fig. 2. The plot of Eq. 7.

The Specific Interaction Sites of the Sugar Molecules. The free energy for transfering one mole of the solutes (naphthalene and biphenyl) from pure water to the sugar solutions was calculated from Eq. 8 and summarized in Table 5.

$$\Delta F_t=RT\ln f. \quad (8)$$

The temperature dependence of ΔF_t of the two solutes is negative indicating that their spontaneous transfer from water to the sugar solutions is endothermic and hence entropic in nature. These thermodynamic parameter changes may be interpreted in terms of the "structured water" hypothesis.[12-14] On the other hand, Howarth[15] showed by ^{13}C relaxation time measurements that water is unique in its ability to restrict the motion of hydrophobic part of solute molecules and that the motional restriction accounts for most part of the entropy change on solution.

TABLE 4. THE ASSOCIATION PARAMETERS PERTAINING TO THE SUGAR-BIPHENYL INTERACTIONS

Sugar	ν[a]	$K^{app}\times10$[b]
D-Glucose	0	0
D-Galactose	0.94	0.82
D-Mannose	1.03	0.94
D-Xylose	1.10	1.00
D-Arabinose	1.05	1.13
D-Ribose	1.36	2.86

a) The average number of bound sugar molecules per biphenyl. b) The apparent association constant in $mol^{-1}\,dm^3$.

TABLE 5. TRANSFER FREE ENERGY[a] OF NAPHTHALENE AND BIPHENYL FROM WATER TO THE SUGAR SOLUTIONS

Sugar(mol dm^{-3})	Naphthalene		Biphenyl	
	10 °C	25 °C	10 °C	25 °C
D-Glucose(3.0)	81	−3	182	≈0
D-Galactose(1.6)	−92	−118	−29	−72
D-Mannose(3.0)	−76	−135	−124	−172
D-Arabinose(2.7)	−120	−152	−162	−178
D-Xylose(3.6)	−144	−157	−205	−215
D-Ribose(3.5)	−439	−526	−530	−612

a) cal mol^{-1}.

And according to Roseman and Jencks,[5] the presence of almost all organic cosolvents in water results in a decrease in the number density of hydrogen bonds. Accordingly, it is also possible to attribute the observed positive entropy of the transfer to the increased motional freedom in the sugar solutions relative to that in water. There will be a negative entropy contribution from the nonpolar sugar-aromatic hydrocarbon interaction, but its magnitude is expected to be relatively small. The water structure around the interaction sites of sugar molecules is presumably loose allowing easy access of the hydrocarbons.

It is generally accepted that sugars are structure maker[16-22] with a few exceptions, *e.g.* ribose,[20] and that the extent of hydration depends on the spatial orientations of the individual OH groups.[17,20,21] According to the "specific hydration model"[20] the spacing of equatorial OH groups in a pyranose ring is compatible with the ice-like structure of water thereby enhancing structure of surrounding water. However, ^{17}O NMR study could not distinguish between the hydration properties of glucose, galactose and mannose.[20] It seems that the solubility-increasing effect of the three hexoses as well as their significant differences in the effectivity are not readily explainable in terms of the "specific hydration model" alone. Furtheremore, the structure promoting effect of sugars has been questioned by several authors[23-25] and recently, Miyajima *et al.*[26,27] reported some notable hydration properties of mono- and oligosaccharides which are contrary to what would be expected from the "specific hydration model." Sugar molecules possess many CH groups which will not be compatibly caged in the preexisting network of water without causing serious entropy disadvantage. Recently, the direct evidence for the CH surface-sugar hydrophobicity correlation has been provided by Miyajima *et al.*[11] They showed that the CH and CH_2 surface area of sugars accessible to water molecule is closely correlated with their differential affinity for polystyrene gel.[6] On the basis of the proceeding arguments, we are inclined to conclude that the hydration shell around sugar molecule is quite loose at the vicinity of the "CH-dense surfaces" where the nonpolar sugar-hydrocarbon interactions occur through Van der Waals' forces.

The authors are grateful to Dr. K. Miyajima of Kyoto University for his useful discussions on the stereochemical basis of the hydrophobicity of sugars. This study was supported in part by a Grant-in-Aid for Scientific Research from Ministry of Education, Science and Culture.

References

1) M. Janado and T. Nishida, *J. Solution Chem.*, **10**, 489 (1981).
2) N. V. B. Marsden, *Naturwissenschaften* **64**, 148 (1977).
3) J. L. Neal and D. A. I. Goring, *Can. J. Chem.*, **48**, 3745 (1970).
4) M. Janado, Y. Yano, Y. Doi, and H. Sakamoto, *J. Solution Chem.*, **12**, 741 (1983).
5) M. Roseman and W. P. Jencks, *J. Am. Chem. Soc.*, **97**, 631 (1975).
6) M. Janado and Y. Yano, *J. Solution Chem.*, in press.
7) J. A. Schellman, *Compt. Rend. Trav. Lab. Carlsberg.*, **29**, 230 (1955).
8) W. F. McDevit and F. A. Long, *J. Am. Chem. Soc.*, **74**, 1773 (1952).
9) M. Janado, Y. Yano, and H. Nakamori, *J. Chromatogr.*, **193**, 345 (1980).
10) Y. Yano and M. Janado, *J. Chromatogr.*, **200**, 125 (1980).
11) K. Miyajima, K. Machida, and M. Nakagaki, *Proc. 7th Symp. Solution Chem.*, Wako-shi (Jpn.), Nov., 1984, p. 52; *Bull. Chem. Soc. Jpn.*, in press.
12) H. S. Frank and M. W. Evans, *J. Chem. Phys.*, **13**, 507 (1945).
13) W. Kauzmann, *Adv. Protein Chem.*, **14**, 1 (1959).
14) G. Nemethy and H. A. Scheraga, *J. Chem. Phys.*, **36**, 3401 (1962).
15) O. W. Howarth, *J. Chem. Soc., Faraday Trans, I.* **71**, 2303 (1975).
16) J. B. Taylor and J. S. Rowlinson, *Trans, Faraday Soc.*, **51**, 1183 (1955).
17) M. A. Kabayama and D. Patterson, *Can. J. Chem.*, **36**, 563 (1958).
18) G. E. Walrafen, *J. Chem. Phys.*, **44**, 3726 (1966).
19) F. Franks, J. R. Ravenhill, and D. S. Reid, *J. Solution Chem.*, **1**, 3 (1972).
20) M. J. Tait, A. Suggett, F. Franks, S. Ablett, and P. A. Quickenden., *J. Solution Chem.*, **1**, 131 (1972).
21) F. Franks, D. S. Reid, and A. Suggett, *J. Solution Chem.*, **2**, 99 (1973).
22) A. Suggett, in Water, "A Comprehensive Treatise," ed by F. Franks, Plenum Press, New York (1975), Vol. 4, p. 519.
23) M. V. Ramiah and D. A. I. Goring *J. Polymer Sci. Part C*, **11**, 27 (1965).
24) J. L. Neal and D. A. I. Goring, *J. Phys. Chem.*, **74**, 658 (1970).
25) D. W. James and R. L. Frost, *J. Phys. Chem.*, **78**, 1754 (1974).
26) K. Miyajima, M. Sawada, and M. Nakagaki, *Bull. Chem. Soc. Jpn.*, **56**, 1954 (1983).
27) K. Miyajima, M. Sawada, and M. Nakagaki, *Bull. Chem. Soc. Jpn.*, **56**, 1620 (1983).

Reactions of Trimethylsilyl Cyanide with Tropone, 2-Phenyltropone, and 2-Methoxytropone. Formations of 2-Cyano-1-hydroxytropylidene Derivatives

Katsuhiro SAITO* and Hisashi KOJIMA†

Department of Chemistry, Nagoya Institute of Technology, Gokiso-cho, Showa-ku, Nagoya 466

(Received January 10, 1985)

Reaction of trimethylsilyl cyanide (TMSCN) with tropone and 2-phenyltropone in the presence of a catalytic amount of zinc iodide in dichloromethane afforded silyl ethers of 7-cyano-1,3,5-cycloheptatriene-1-ol (**2a**) and 2-phenyl-7-cyano-1,3,5-cycloheptatriene-1-ol (**2b**), respectively. On the other hand, reaction of TMSCN with 2-methoxytropone gave 2-cyanotropone. Upon hydrolysis, **2a**, and **2b** yielded 2-cyano-1,3,5-cycloheptatrien-1-ol (**3a**) and a tautomeric mixture of 2-cyano-7-phenyl-1,3,5-cycloheptatrien-1-ol (**3b**) and 2-cyano-7-phenyl-3,5-cycloheptadien-1-one (**4b**). Oxidation of **3a** and the tautomeric mixture of **3b** and **4b** with selenium dioxide in dioxane afforded 2-cyanotropone and 2-cyano-7-phenyltropone, respectively.

Reactions of trimethylsilyl cyanide (TMSCN) with carbonyl compounds have attracted much attention from chemists because of their utility in the synthesis of cyanohydrin derivatives and of various compounds which can be derived from the cyanohydrins.[1] TMSCN is known to react with isolated and conjugated carbonyl groups to give 1,2-addition products[1a-e] and 1,4- or 1,6-addition products,[1f] respectively. Tropone derivatives are cyclic conjugated carbonyl compounds with aromaticity and their reactions with organometallic compounds such as Grignard reagents have attracted considerable attention from chemists,[2] however the reported examples of reactions of tropone derivatives with organosilane compounds are relatively few in number.[3] We reacted some tropone derivatives with TMSCN in the presence of a catalytic amount of zinc iodide. Here, we wish to report the result of these reactions.

Results and Discussion

When tropone (**1a**) and 2-phenyltropone (**1b**) were allowed to react with TMSCN in anhydrous dichloromethane in the presence of a catalytic amount of zinc iodide at room temperature for 5 d, silyl ethers of 7-cyano-1,3,5-cycloheptatrien-1-ol (**2a**)

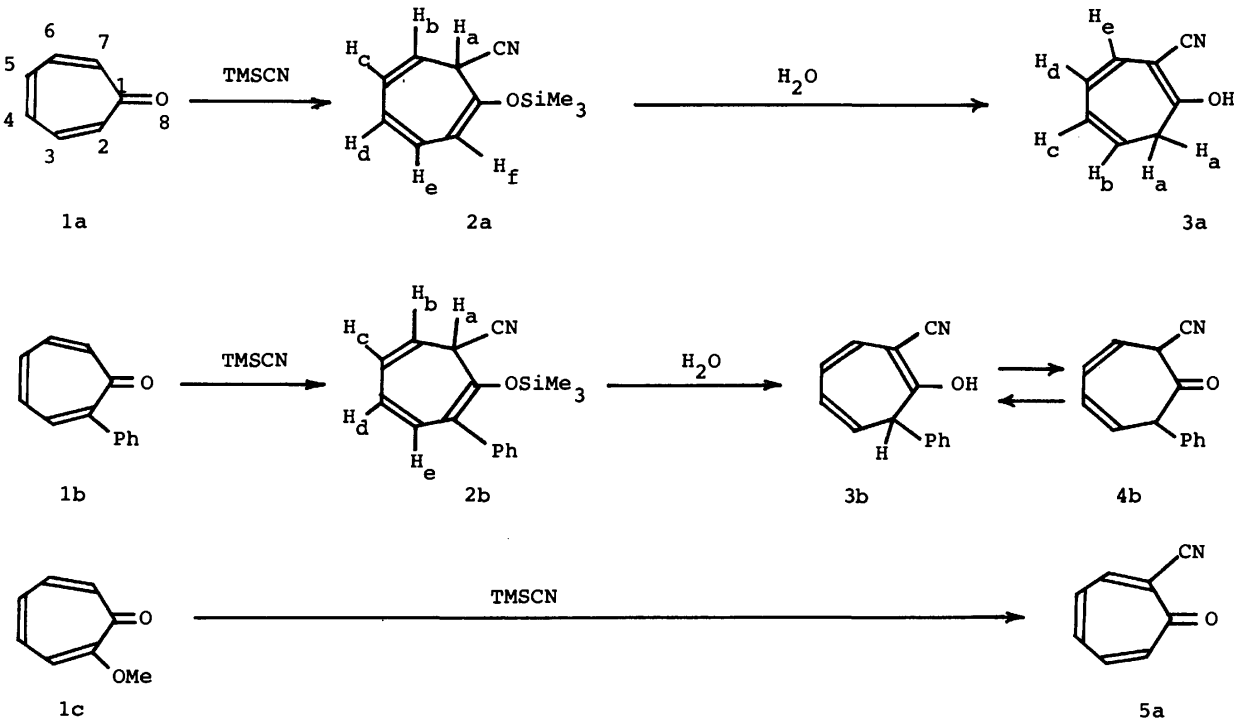

Fig. 1.

† Present address: Okazaki National Research Institutes, National Institute for Basic Biology, Myodaiji-cho, Okazaki 444.

and 2-phenyl-7-cyano-1,3,5-cycloheptatrien-1-ol (**2b**) were obtained in 54 and 59% yields, respectively. On the other hand, the reaction of TMSCN with 2-methoxytropone (**1c**) under the same conditions as above afforded 2-cyanotropone (**5a**) in 84% yield. Upon hydrolysis, **2a** and **2b** gave 2-cyanocycloheptatrien-1-ol (**3a**) and a tautomeric mixture of 2-cyano-7-phenyl-1,3,5-cycloheptatrien-1-ol (**3b**) and 2-cyano-7-phenyl-3,5-cycloheptadien-1-one (**4b**) in 84 and 93% yields, respectively. Oxidation of **3a** and the tautomeric mixture of **3b** and **4b** in dioxane with selenium dioxide afforded 2-cyanotropone (**5a**) and 2-cyano-7-phenyltropone (**5b**) in 54 and 67% yields, respectively.

The structures of **5a**[4a] and **5b**[4b] were confirmed by comparison of their physical properties with the literature values. The structures of the new compounds were deduced on the basis of their physical properties and confirmed by comparison of the physical properties to those of the analogous tropylidene derivatives.[5] The formation of **5a** and **5b** by the oxidation of **3a** and the tautomeric mixture of **3b** and **4b**, respectively, also supports the structures of **3a**, **3b**, and **4b**.

The reaction of **1a** and **1b** with TMSCN can be explained as shown in Fig. 3. The addition reaction of TMSCN to 2- and 8-positions of **1a** and to 7- and 8-positions of **1b** gives the corresponding silyl ethers **2**. It is known that nucleophilic reagents attack the carbon atom at the 2- or 7- position of the tropone moieties.[2] The hydrolysis of **2** affords 7-cyano-1,3,5-cycloheptatrien-1-ol derivatives (**6**), which tautomerize to the corresponding keto-forms **4**, which further tautomerize to **3**. The preferential formations of 1,3,5-cycloheptatrien-1-ol of the type **3** as opposed to the type **6** can be explained by the strong acidity of the methine proton attached to the carbon atom, which has the electron-withdrawing cyano group in **6** compared to that of the methine proton of **3**.

Two possible mechanisms may be considered for

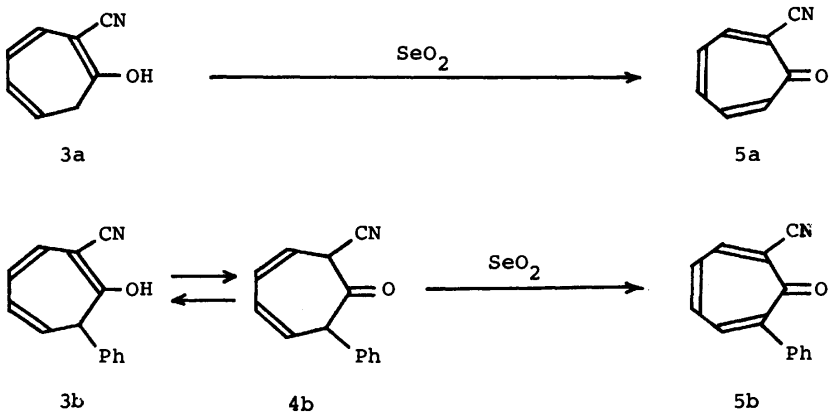

Fig. 2.

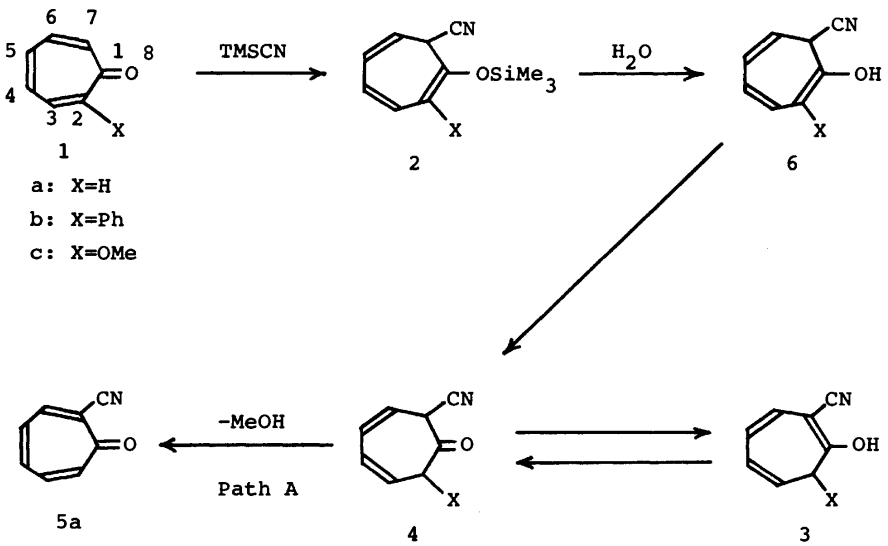

Fig. 3.

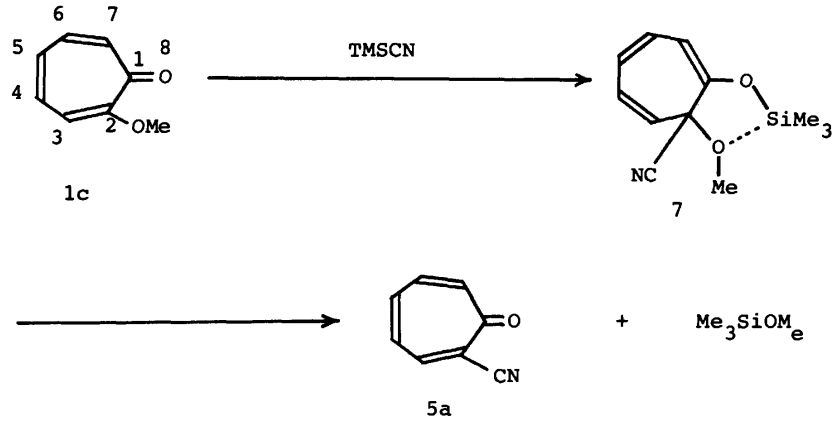

Fig. 4.

the formation of 2-cyanotropone (**5a**) by the reaction of TMSCN with 2-methoxytropone (**1c**). Pathway A involves 2-cyano-7-methoxycyclohepta-3,5-dien-1-one (**4c**) as an intermediate, which is formed through the same reaction path as that described above *via* the silyl ether derivative (**2c**) and the 1,3,5-cycloheptatrien-1-ol derivative (**6c**). Elimination of methanol from **4c** affords **5a**. Pathway B involves the intermediate **7**, which is formed *via* 2,8-addition of TMSCN to **1c**. Elimination of trimethylsilyl methoxide from the intermediate **7** leads to the formation of 2-cyanotropone (**5a**).* Pathway B does not need the existence of water for the formation of **5a**. The fact that despite the same anhydrous reaction conditions as those of the reactions of **1a** and **1b** with TMSCN, the silyl ether **2c** could not be detected seems to support pathway B.

Experimental

All the melting points are uncorrected. IR, UV, Mass, and high resolution Mass spectra were measured with DS-701G, Hitachi 220A, Hitachi M-52, and JMS-DX 300 spectrometers, respectively. NMR spectra were recorded with Hitachi R-20B spectrometer with tetramethylsilane as an internal standard. Wakogel C-200 and Wakogel B5F were used for column and thinlayer chromatography, respectively.

Reaction of ***1a*** *with TMSCN.* A mixture of **1a** (1.60 g, 15 mmol), TMSCN (2.97 g, 30 mmol), zinc iodide (100 mg), and anhydrous methylene chloride (20 ml) was stirred at room temperature for 5 d. After filtration, the solvent was evaporated on a rotary evaporator to yield a yellow oil, which was distilled under reduced pressure to yield a colorless oil of **2a** (690 mg, 54%, 0.2 Torr,† 85—90 °C).

2a: Found *m/z*: 205.09393. Calcd for $C_{11}H_{15}NOSi$: 205.09377. Mass *m/z* (rel intensity): 205 (M^+, 9), 190 (34), 131 (42), 103 (100). UV (EtOH): 280 nm (log ε, 3.49). IR (neat): 3030, 2960, 2240, 1620 cm^{-1}. NMR ($CDCl_3$) δ=0.3 (9H, s), 3.41 (H_a, d, *J*=7 Hz), 5.25 (H_b, dd, *J*=7 and 8 Hz), 5.7 (H_c, m), 6.2—6.6 (3H, m, H_d-H_f).

Reaction of ***1b*** *with TMSCN.* A mixture of **1b** (1.82 g, 10 mmol), TMSCN (1.98 g, 20 mmol), zinc iodide (100 mg), and anhydrous methylene chloride (20 ml) was stirred at room temperature for 5 d. After filtration, the solvent was removed on a rotary evaporator to yield a yellow oil, which was chromatographed on silica gel to yield a colorless oil of **2b** (1.65 g, 59%) by pet ether–benzene 1:1.

2b: Found *m/z*: 281.12362. Calcd for $C_{17}H_{19}NOSi$: 281.12362. Mass *m/z* (rel intensity): 281 (M^+, 57), 266 (100), 211 (60). UV (EtOH): 280 nm (log ε, 3.60). IR (neat): 3020, 2960, 2240, 1605 cm^{-1}. NMR ($CDCl_3$) δ=0.0 (9H, s), 4.05 (H_a, d, *J*=7 Hz), 5.57 (H_b, dd, *J*=7 and 8 Hz), 6.28 (H_c, m), 6.61 (2H, m, H_d, H_e), 7.3 (5H, m).

Reaction of ***1c*** *with TMSCN.* A mixture of **1c** (1.36 g, 10 mmol), TMSCN (1.98 g, 20 mmol), zinc iodide (100 mg), and anhydrous dichloromethane (20 ml) was stirred at room temperature for 5 d. The usual treatment of the reaction mixture gave a yellow oil, which was chromatographed on silica gel to yield crystals of **5a** (1.10 g, 84%, mp 139—140 °C, lit,[4a] 138—139 °C) by benzene–ether 1:1.

Hydrolysis of ***2a***. A mixture of **2a** (410 mg, 2 mmol), water (1 ml), and dioxane (5 ml) was stirred at room temperature for 20h. The reaction mixture was extracted with ether and dried over anhydrous sodium sulfate. After filtration, the solvent was removed on a rotary evaporator to yield a colorless crystals of **3a** (220 mg, 83%). Recrystallization from chloroform gave pure crystals of **3a**.

3a: Mp 127—128 °C. Found *m/z*: 133.04879. Calcd for C_8H_7NO: 133.04916. Mass *m/z* (rel intensity): 133 (M^+, 100), 115 (6), 104 (56). UV (EtOH): 283 nm (log ε, 3.67). IR (KBr): 3100, 2220, 1610 cm^{-1}. NMR ($CDCl_3$) δ=2.65 (2H, H_a, d, *J*=7 Hz), 5.40 (H_b, ddd, *J*=2, 7, and 8 Hz), 6.10 (H_c, m), 6.28 (2H, m, H_d, H_e), 6.50 (1H, bs, OH).

Hydrolysis of ***2b***. A mixture of **2b** (850 mg, 3 mmol), water (5 ml), and dioxane (10 ml) was stirred at room temperature for 20h. The reaction mixture was extracted with ether, and dried over anhydrous sodium sulfate. After

* The pathway B was suggested by a referee. We are indebted to the referee for this suggestion.

†1 Torr≈133.322 Pa.

filtration, the solvent was removed on a rotary evaporator to yield a yellow oil, which was chromatographed on silica gel to give a colorless oil of the tautomeric mixture of **3b** and **4b** (590 mg, 93%).

Tautomeric mixture of **3b** and **4b**: Found *m/z*: 209.08268. Calcd for $C_{14}H_{11}NO$: 209.08281. Mass *m/z* (rel intensity): 209 (95), 208 (42), 181 (96), 180 (100). UV (EtOH): 245 nm (log ε, 3.88). IR (neat): 3360, 3040, 2240 2220, 1723, 1600 cm^{-1}. NMR ($CDCl_3$) δ=2.69 (d, J=8 Hz), 3.31 (d, J=7 Hz), 4.35 (bs, OH), 5.8—6.5 (m), 6.9—7.5 (m).

Oxidation of ***3a***. A mixture of **3a** (265 mg, 2 mmol), selenium dioxide (270 mg, 2.4 mmol), and dioxane (5 ml) was refluxed for 30 min. After filtration, the solvent was removed on a rotary evaporator to yield a black tarry material, which was disolved in ethyl acetate, washed with aqueous saturated sodium hydrogencarbonate and water, and dried over anhydrous sodium sulfate. After filtration, the solvent was removed on a rotary evaporator to yield a brown solid, which was thin-layer chromatographed on silica gel using benzene–ether 1:1 as a developing solvent to give crystals of **5a** (R_f=0.45, 125 mg, 54%).

Oxidation of the Tautomeric Mixture of ***3b*** *and* ***4b***. A mixture of the tautomeric mixture of **3b** and **4b** (315 mg, 1.5 mmol), selenium dioxide (200 mg, 1.8 mmol), and dioxane (10 ml) was refluxed for 40 min. The reaction mixture was treated as usual to give a black tarry material, which was thin-layer chromatographed on silica gel using benzene–ether 8:2 as a developing solvent to give crystals of **5b** (R_f=0.40, 210 mg, 67%, mp 134—135 °C, lit,[4b] 134—135 °C).

The authors are indebted to Professor Paul G. Gassman of University of Minnesota, Professor Toshio Mukai of Tohoku University, and Professor Takashi Toda of Utsunomiya University for their fruitful suggestions.

References

1) a) D. A. Evans, J. M. Hoffman, and L. K. Truesdale, *J. Am. Chem. Soc.*, **95**, 5822 (1973); b) H. Neef and R. Muller, *J. Pract. Chem.*, **315**, 367 (1973). c) J. K. Rasmussen and S. M. Heilmann, *Synthesis* **1978**, 219; d) P. G. Gassman, K. Saito, and J. J. Talley, *J. Am. Chem. Soc.*, **102**, 7613 (1980); e) P. G. Gassman and J. J. Talley, *ibid.*, **102**, 1214 (1980); *Tetrahedron Lett.*, **1978**, 3773; f) K. Utimoto, M. Obayashi, Y. Shishiyama, M. Inoue, and H. Nozaki, *ibid.*, **21**, 3889 (1980).

2) T. Nozoe, T. Mukai, and I. Murata, *Proc. Jpn. Acad.*, **29**, 169 (1953); R. D. Haworth and P. B. Tinker, *J. Chem. Soc.*, **1955**, 911; T. Mukai, *Bull. Chem. Soc. Jpn.*, **31**, 852 (1958); T. Nozoe, T. Mukai, T. Asao, *ibid.*, **33**, 1452 (1960); T. Mukai, H. Tsuruta, and T. Nozoe, *Tetrahedron Lett.*, **1966**, 1063; Z. Goldshmidt and S. Antebi, *ibid.*, **1978**, 1225.

3) R. Gompper and W. Reiser, *Tetrahedron Lett.*, **1976**, 1263; K. Saito, H. Kojima, T. Okudaira, and K. Takahashi, *Bull. Chem. Soc. Jpn.*, **56**, 175 (1983).

4) a) T. Nozoe, S. Seto, and S. Masamune, *Proc. Jpn. Acad.*, **28**, 483 (1952); b) K. Kikuchi, *Bull. Chem. Soc. Jpn.*, **34**, 1610 (1961).

5) C. H. Jutz, I. Rommel, I. Lengyel, and J. Feeney, *Tetrahedron*, **22**, 1809 (1966); A. S. Kende, *Tetrahedron Lett.*, **1967**, 2661; C. H. Bushweller, M. Sharp, and S. J. Weiniger, *ibid.*, **1970**, 453; T. Toda, K. Saito, and T. Mukai, *ibid.*, **1972**, 1981; T. Sasaki, K. Kanematsu, K. Kobayashi, and M. Sugiura, *J. Am. Chem. Soc.*, **97**, 355 (1975); K. Saito, Y. Omura, and T. Mukai, *Chem. Lett.*, **1980**, 349.

The Facile Synthesis of Dihydrofurans by the Oxidation of Olefins with Tris(2,4-pentanedionato)manganese(III)

Hiroshi NISHINO
Department of Chemistry, Faculty of Science, Kumamoto University, Kurokami, Kumamoto 860
(Received January 21, 1985)

Eleven olefins were oxidized with tris(2,4-pentanedionato)manganese(III) at the reflux temperature to give the corresponding 3-acetyl-2-methyl-4,5-dihydrofurans in good yields. The oxidation of 9-benzylidene-9,10-dihydroanthracene under the same reaction conditions did not produce the corresponding dihydrofuran, but 9-[α-(1-acetyl-2-hydroxy-1-propenyl)benzylidene]-9,10-dihydroanthracene. When 1,1-diphenylethene was oxidized at room temperature, 3-acetyl-2-hydroperoxy-2-methyl-5,5-diphenyltetrahydrofuran was obtained in a high yield. The effects of the solvent and the additives on the yield of dihydrofuran, the comparable reactivities of other (2,4-pentanedionato)metal complexes, such as Co(III), Cr(III), Fe(III), and Cu(II), and the reaction mechanism are discussed.

In previous papers it was reported that the reaction of malonic acid with olefins in the presence of manganese(III) acetate, $Mn(OAc)_3$, gave spirobi-γ-lactones,[1] while a similar reaction of malonamide yielded 2-buten-4-olides and/or 1*H*-pyrrol-2(5*H*)-ones.[2] The formation of these lactones and lactams can be explained by a proposed mechanism based on the generation of radicals from malonic acid and malonamide.[2] The reactions of β-dicarbonyl compound with olefins in the presence of $Tl(OAc)_3$,[3] $Pb(OAc)_4$,[4] $Mn(OAc)_3$,[5] AgO, and PbO_2[6] have also been reported to give dihydrofurans. The yields of dihydrofurans, however, were not always satisfactory, and it seems possible to improve the yields by using tris(2,4-pentanedionato)manganese(III), $Mn(acac)_3$, in a donor solvent such as acetic acid, which can complex manganese(III) ions. This is because Mn(III) complexes generally tend to undergo a rapid exchange of ligands (ligand-exchange reaction),[7] and hence $Mn(acac)_3$ will be easily decomposed in the donor solvent to form $\cdot CH(COCH_3)_2$ radicals directly. This radical should react with olefins in the reaction mixture to produce the corresponding dihydrofurans. The present author was interested in this active property of Mn(III) complexes and investigated the title reaction. It is known in general that $Mn(acac)_3$ can be used as a catalyst in a polymerization reaction[8] and as one-electron-transfer oxidant in coupling reactions of phenols[9] or thiophenols.[10]

Results and Discussion

When 1,1-diphenylethene (**1a**) was oxidized with $Mn(acac)_3$ in acetic acid at the reflux temperature, it gave 3-acetyl-2-methyl-5,5-diphenyl-4,5-dihydrofuran (**2a**), together with a small amount of benzophenone (**3a**). The reaction was repeated in various solvents, but it was found that acetic acid was the best of all, as is shown in Table 1. The effects of various additives were then examined. The addition of acetic anhydride to the reaction mixture decreased the yield of **2a**, but the reaction time was shortened considerably (Table 2, Entry 2). When β-dicarbonyl compounds were added to the reaction mixture, they still gave **2a** predominantly, thus proving that $Mn(acac)_3$ is a more active species than the $\cdot CH(CO_2H)_2$, $\cdot CH(CONH_2)_2$, and $\cdot CH(CO_2Et)_2$ radicals (Table 2, Entries 3—5).[1,2]

When **1a** was oxidized with $Mn(acac)_3$ at room temperature for 12 h, **2a** (6%) and 3-acetyl-2-hydroperoxy-2-methyl-5,5-diphenyltetrahydrofuran (**8**; 89%) were isolated from the reaction mixture. The structure of **8** was determined on the basis of its spectral data. The treatment of **8** with acetic anhydride gave the corresponding (acetyldioxy)tetrahydrofuran **9**. The same oxidation under a nitrogen atmosphere

Table 1. Oxidation of 1,1-diphenylethene (**1a**) with $Mn(acac)_3$ in various solvents[a,b]

Entry	Solvent	Reaction time / h	Recovery / %	Product/yield/%[c] **2a**	**3a**
1	Acetic acid	2.5[d]	3	89	2
2	Propionic acid	1[d]	35	60	5
3	Acetylacetone	1	32	53	
4	Acetone	24	38	18	23
5	Methanol	24	30	15	24
6	DMSO	24	18		12
7	Benzene	24	53	16	15

a) The reaction was carried out at the reflux temperature. b) **1a** (1 mmol) and $Mn(acac)_3$ (2 mmol) were employed. c) The yields are based on the amount of **1a** used. d) Minutes.

Table 2. Oxidation of 1,1-diphenylethene (**1a**) with $Mn(acac)_3$ in the presence of some additives in boiling acetic acid

Entry	Additive	Molar ratio of **1a**: additive: $Mn(acac)_3$	Time / s	Recovery / %	Product/yield/%[a]		
					2a	**12**[b]	**13**[c]
1	None	1 : 0 : 2	150	3	89		
2	Ac_2O	1 : 20 : 2	10	17	73		
3	$CH_2(CO_2H)_2$	1 : 1 : 2	10	14	75	2	
4	$CH_2(CONH_2)_2$	1 : 4 : 2	10	22	50		9
5	$CH_2(CO_2Et)_2$	1 : 4 : 2	10	9	90		

a) The yields are based on the **1a** used. b) 3,3,8,8-Tetraphenyl-2,7-dioxaspiro[4.4]nonane-1,6-dione.[1] c) 2-Carbamoyl-4,4-diphenyl-2-buten-4-olide.[2]

for 27 h yielded **2a** (27%) and **8** (67%).

Similar reactions of **1a** were carried out by using $Co(acac)_3$, $Cr(acac)_3$, $Fe(acac)_3$, and $Cu(acac)_2$ instead of $Mn(acac)_3$. In the case of $Co(acac)_3$, the reaction gave **2a** (66%), but the reaction took more than 1 h. The reaction with the other oxidants did not occur in boiling acetic acid. It seems that these complexes are stable under the present reaction conditions.

The reactions of 1,1-bis(4-methoxyphenyl)ethene (**1b**), 2-phenylpropene (**1c**), styrene (**1d**), acenaphthylene (**1e**), 1,1,2-triphenylethene (**1f**), 1,1-bis(4-methoxyphenyl)-2-phenylethene (**1g**), 1,1,2-tris(4-methoxyphenyl)ethene (**1h**), 9-benzylidene-9*H*-xanthene (**1i**), 9-benzylidene-9,10-dihydroanthracene (**1j**), and 1-heptene (**1k**) with $Mn(acac)_3$ were also carried out in acetic acid to yield the corresponding dihydrofurans **2b—i** and **2k**, except for **1j** (Fig. 1 and Table 3). In the cases of **1g** and **1h**, acetoxyethenes **4g** and **4h** were mainly produced rather than the dihydrofurans **2g** and **2h**. For the reaction of **1j** with $Mn(acac)_3$, the corresponding dihydrofuran was not isolated, but 9-[α-(1-acetyl-2-hydroxy-1-propenyl)benzylidene]-9,10-dihydroanthracene (**7j**) was obtained. The dienone **7j** was heated with $Mn(OAc)_3$ in acetic acid in the hope obtaining the corresponding dihydrofuran.[11] However, this was not formed, and the products were found to be **10** and **11** (Scheme 1). The absorption bands at 395, 374, 355, and 338 nm in the UV spectrum of **10** are similar to those of anthracene, and the ^{1}H-NMR and the IR spectrum showed that a 1-acetyl-2-hydroxy-1-propenyl group remained intact. Thus, the structure of **10** was determined to be 9-(1-acetoxy-2-acetyl-3-hydroxy-1-phenyl-2-butenyl) anthracene. The ^{13}C-NMR spectrum of **11** (R=Ac) indicated the structure of 9-acetoxy-9-(2-acetyl-3-oxo-1-phenyl-1-butenyl)-9,10-dihydroanthracene.

The mechanism for the formation of the dihydrofurans can be depicted as involving the α,α′-diketo radical, which is generated directly by the thermolysis of $Mn(acac)_3$ (Scheme 2).[5] It appears that acetic acid as a donor solvent facilitates the ligand-exchange reaction of $Mn(acac)_3$, while the addition of acetic

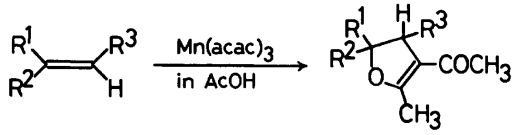

1a–k **2a–i,k**

a: $R^1=R^2=Ph$, $R^3=H$
b: $R^1=R^2=4\text{-}MeOC_6H_4$, $R^3=H$
c: $R^1=Me$, $R^2=Ph$, $R^3=H$
d: $R^1=Ph$, $R^2=R^3=H$
e: $R^1, R^3=$, $R^2=H$
f: $R^1=R^2=R^3=Ph$
g: $R^1=R^2=4\text{-}MeOC_6H_4$, $R^3=Ph$
h: $R^1=R^2=R^3=4\text{-}MeOC_6H_4$
i: $R^1, R^2=$, $R^3=Ph$
j: $R^1, R^2=$, $R^3=Ph$
k: $R^1=C_5H_{11}$, $R^2=R^3=H$

3a,b **4g–i**

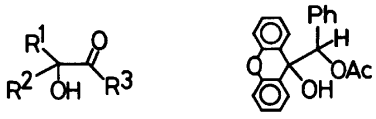

5g,h **6**

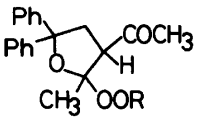

8: R=H
9: R=Ac

Fig. 1.

Table 3. Oxidation of olefins with $Mn(acac)_3$ in boiling acetic acid

Entry	Substrate	Molar ratio of 1 : $Mn(acac)_3$	Time / min	Recovery / %	Product/yield/%[a]				
1	**1a**	1 : 2	2.5	3	**2a** (89)	**3a** (2)			
2	**1b**	1 : 2	1	5	**2b** (88)	**3b** (5)			
3	**1c**	1 : 2	3		**2c** (97)				
4	**1d**	1 : 2	3		**2d** (75)				
5	**1e**	1 : 3	5	4	**2e** (70)				
6	**1f**	1 : 6	3	57	**2f** (41)				
7	**1g**	1 : 4	3	2	**2g** (29)		**4g** (56)	**5g** (5)	
8	**1h**	1 : 4	3		**2h** (13)		**4h** (57)	**5h** (14)	
9	**1i**	1 : 4	3	3	**2i** (44)		**4i** (21)	**6** (23)	
10	**1j**	1 : 2	3						**7j** (70)
11	**1k**	1 : 2	3		**2k** (12)				

a) The yields are based on the amount of the substrate used.

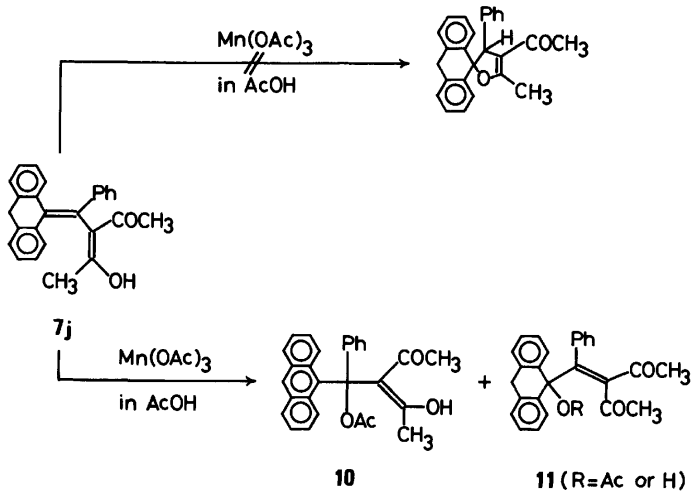

Scheme 1.

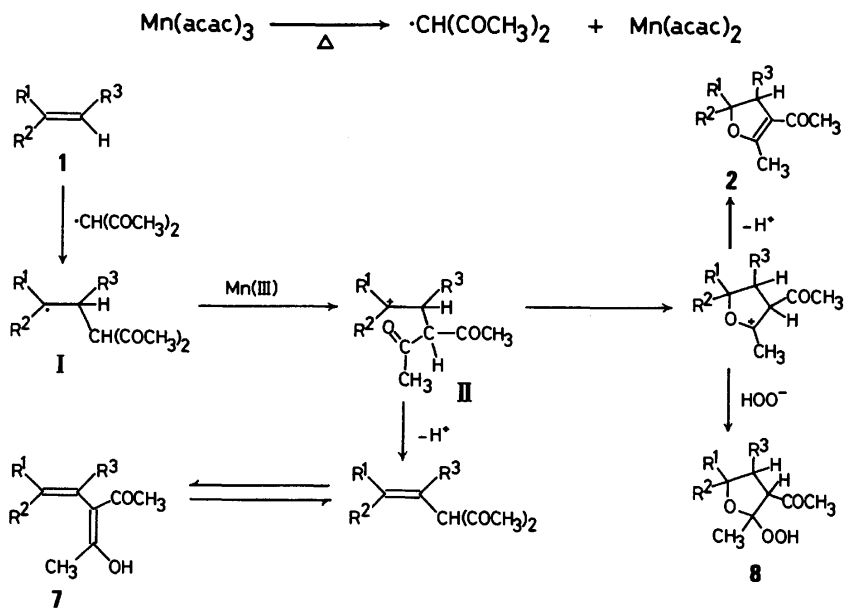

Scheme 2.

anhydride or β-dicarbonyl compounds accelerates the thermolysis of $Mn(acac)_3$, as in the oxidation of olefins with $Mn(OAc)_3$ in the presence of acetic anhydride.[12] The reason for the failure to cyclize **7j** to the corresponding dihydrofuran is not evident. However, it could be pointed out that the cyclization may occur at the stage of the carbonium ion **II** and that one of the oxygen functions and the C-1 in **7j** are too far apart to ring-closure.

The reaction of olefins with acetylacetone in the presence of $Mn(OAc)_3$ by the method of Heiba and Dessau[5] gave dihydrofurans in similar yields. In their method, an excess of acetylacetone was needed, and the reaction took more than 10 min. In the present author's method, however, only a stoichiometrical amount of $Mn(acac)_3$ was required for the synthesis of dihydrofurans, except in the case of trisubstituted olefins **1f—i**. Moreover, the oxidation with $Mn(acac)_3$ was completed within 3 min.

The reaction of $Mn(acac)_3$ with olefins is most successful when ethenes containing an aryl group are used. This is primarily due to the electronic effect of the aryl group, which could stabilize the intermediate radical **I** and the cation **II**. Alkyl-substituted olefin **1k** gave the lowest yield. The yields of dihydrofurans from trisubstituted olefins **1f—i** range from moderate to poor. It should be pointed out that the furans are always formed by the attack of the α,α′-diketo radical on the less substituted carbon in ethenes. This is probably attributable to steric reasons.

Thus, it has been shown that the reaction of $Mn(acac)_3$ with aryl-substituted olefins is a useful method for the preparation of substituted dihydrofurans.

Experimental

Measurements. The melting points are uncorrected. The IR spectra were taken on a JASCO A-102 infrared spectrometer, and the IR spectral data are expressed in cm^{-1}. The ^1H- and ^{13}C-NMR spectra were recorded on a Hitachi Perkin-Elmer R-24 spectrometer and a JEOL FX-100 spectrometer at room temperature. The chemical shifts are recorded in the δ scale, relative to TMS as an internal standard. The mass spectra were obtained with a JEOL JMS-DX-300 mass spectrometer using a direct-insertion probe at an ionizing voltage of 70 eV. The UV spectrum is measured on a Hitachi 220A spectrophotometer in a methanol solution.

Materials. The $Mn(acac)_3$ and olefins (**1a—c, f—j**) were prepared according to the method described in the literature.[2,13] The $Co(acac)_3$, $Cr(acac)_3$, $Fe(acac)_3$, $Cu(acac)_2$, and olefins (**1d, e,** and **k**) were obtained from commercial samples of the Wako Pure Chemical Industries, Ltd.

Oxidation of Olefins with $Mn(acac)_3$. A typical procedure for the oxidation of olefins with $Mn(acac)_3$ was as follows. To a heated solution of olefin (1 mmol) in acetic acid (25 cm^3), the amount of $Mn(acac)_3$ shown in Table 3 was added. The solution was then heated under reflux until the brown color of the Mn(III) ion disappeared (within 3 min). The solvent was removed *in vacuo*, and the residue was triturated with 2 M (1 M=1 mol dm^{-3}) hydrochloric acid and then extracted with chloroform. The products were separated on TLC (Kieselgel 60G), with chloroform as the developing solvent. The yields are summarized in Table 3.

Oxidation Products. 3-Acetyl-2-methyl-5,5-diphenyl-4,5-dihydrofuran (2a): Yellow liquid; bp 180—185 °C/133 Pa (bath temperature); IR ($CHCl_3$) 1667 (C=O) and 1620 (C=C); ^1H-NMR ($CDCl_3$) δ=2.13 (3H, s, $COCH_3$), 2.32 (3H, t, J=1.2 Hz, CH_3), 3.61 (2H, q, J=1.2 Hz, CH_2), and 7.13—7.50 (10H, m, ArH). Found: *m/z* 278.12918. Calcd for $C_{19}H_{18}O_2$: M, 278.13068.

3-Acetyl-5,5-bis(4-methoxyphenyl)-2-methyl-4,5-dihydrofuran (2b): Colorless needles (from benzene/light petroleum); mp 96.0—96.5 °C; IR ($CHCl_3$) 1664 (C=O); ^1H-NMR ($CDCl_3$) δ=2.28 (3H, s, $COCH_3$), 2.30 (3H, t, J=1.2 Hz, CH_3), 3.55 (2H, q, J=1.2 Hz, CH_2), 3.73 (6H, s, 2×OCH_3), and 6.69—7.27 (8H, m, ArH). Found: C, 74.24; H, 6.49%. Calcd for $C_{21}H_{22}O_4$: C, 74.55; H, 6.55%.

In the oxidation of **1a** and **1b**, small amounts of benzophenone (**3a**) and 4,4′-dimethoxybenzophenone (**3b**) were also obtained.

3-Acetyl-2,5-dimethyl-5-phenyl-4,5-dihydrofuran (2c): Yellow liquid; bp 160—165 °C/133 Pa (bath temperature).[6]

3-Acetyl-2-methyl-5-phenyl-4,5-dihydrofuran (2d): Yellow liquid; bp 140 °C/133 Pa (bath temperature).[4]

7-Acetyl-8-methyl-cis-6b,9a-dihydroacenaphtho[1,2-b]furan (2e): Pale orange needles (from benzene/hexane); mp 149.7—150.2 °C; IR ($CHCl_3$) 1660 (C=O) and 1622 (C=C); ^1H-NMR ($CDCl_3$) δ=2.07 (3H, d, J=1.2 Hz, CH_3), 2.26 (3H, s, $COCH_3$), 5.12 (1H, br. d, J=7.8 Hz, H-6b), 6.20 (1H, d, J=7.8 Hz, H-9a), and 7.15—7.80 (6H, m, ArH). Found: C, 81.35; H, 5.67%. Calcd for $C_{17}H_{14}O_2$: C, 81.58; H, 5.64%.

3-Acetyl-2-methyl-4,5,5-triphenyl-4,5-dihydrofuran (2f): Colorless microcrystals (from benzene/light petroleum); mp 139.5—140.5 °C; IR ($CHCl_3$) 1665 (C=O) and 1622 (C=C); ^1H-NMR (CCl_4) δ=1.80 (3H, s, $COCH_3$), 2.40 (3H, d, J=1.2 Hz, CH_3), 4.98 (1H, q, J=1.2 Hz, >CH-), and 6.70—7.69 (15H, m, ArH). Found: C, 84.65; H, 6.33%. Calcd for $C_{25}H_{22}O_2$: C, 84.71; H, 6.26%.

Oxidation Products of 1g. 3-Acetyl-5,5-bis(4-methoxyphenyl)-2-methyl-4-phenyl-4,5-dihydrofuran (2g): Colorless liquid; IR ($CHCl_3$) 1664 (C=O); ^1H-NMR ($CDCl_3$) δ=1.89 (3H, s, $COCH_3$), 2.42 (3H, d, J=1.2 Hz, CH_3), 3.47 (3H, s, OCH_3), 3.66 (3H, s, OCH_3), 4.97 (1H, q, J=1.2 Hz, >CH-), and 6.36—7.60 (13H, m, ArH). Found: *m/z* 414.18228. Calcd for $C_{27}H_{26}O_4$: M, 414.18311.

1-Acetoxy-2,2-bis(4-methoxyphenyl)-1-phenylethene (4g): Colorless microcrystals (from ethanol); mp 103.0—103.5 °C (lit,[2] mp 101—102 °C).

2-Hydroxy-2,2-bis(4-methoxyphenyl)-1-phenylethanone (5g): The ^1H-NMR and IR spectral data were in agreement with those of an authentic sample.[2]

Oxidation Products of 1h. 3-Acetyl-4,5,5-tris(4-methoxyphenyl)-2-methyl-4,5-dihydrofuran (2h): Colorless liquid; IR ($CHCl_3$) 1664 (C=O); ^1H-NMR ($CDCl_3$) δ=1.90 (3H, s, $COCH_3$), 2.45 (3H, d, J=1.2 Hz, CH_3), 3.57 (3H, s, OCH_3), 3.61 (3H, s, OCH_3), 3.73 (3H, s, OCH_3), 4.94 1H, q, J=1.2 Hz, >CH-), and 6.41—7.55 (12H, m, ArH).

Found: *m/z* 444.19165. Calcd for $C_{28}H_{28}O_5$: M, 444.19368.

1-Acetoxy-1,2,2-tris(4-methoxyphenyl)ethene (4h) and 2-Hydroxy-1,2,2-tris(4-methoxyphenyl)-1-ethanone (5h): These ^{1}H-NMR and IR spectral data were compatible with those of authentic samples.[2]

Oxidation Products of 1i. 4-Acetyl-5-methyl-3-phenylspiro[furan-2(3H), 9'-xanthene] (2i): Colorless prisms (from aqueous ethanol); mp 141 °C; IR ($CHCl_3$) 1665 (C=O); ^{1}H-NMR ($CDCl_3$) δ=1.74 (3H, s, $COCH_3$), 2.68 (3H, d, J=1.2 Hz, CH_3), 4.44 (1H, q, J=1.2 Hz, >CH-), and 6.57—7.57 (13H, m, ArH). Found: C, 81.56; H, 5.59%. Calcd for $C_{25}H_{20}O_3$: C, 81.50; H, 5.47%.

9-(α-Acetoxybenzylidene)-9H-xanthene (4i): Colorless plates (from ethanol); mp 156—157 °C; IR ($CHCl_3$) 1758 (OAc); ^{1}H-NMR ($CDCl_3$) δ=2.04 (3H, s, OAc) and 6.49—8.00 (13H, m, ArH). Found: C, 80.26; H, 4.95%. Calcd for $C_{22}H_{16}O_3$: C, 80.47; H, 4.91%.

9-(α-Acetoxybenzyl)-9-xanthenol (6): The ^{1}H-NMR and IR spectra were identical with those of an authentic sample.[2]

Oxidation Product of 1j. 9-[α-(1-Acetyl-2-hydroxy-1-propenyl)benzylidene]-9,10-dihydroanthracene (7j): Colorless microcrystals (from ethanol); mp 181.3—181.8 °C; IR ($CHCl_3$) 3600—3200 (OH) and 1600 (C=O); ^{1}H-NMR ($CDCl_3$) δ=1.64 (6H, s, 2×CH_3), 5.09 (2H, s, CH_2), 7.20 (5H, s, Ph), 7.40—8.38 (8H, m, ArH), and 17.02 (1H, s, OH). Found: C, 85.09; H, 6.12%. Calcd for $C_{26}H_{22}O_2$: C, 85.21; H, 6.05%.

Oxidation of 1a with Mn(acac)$_3$ in the Presence of Additives. To a heated solution of **1a** and an additive in acetic acid (25 cm^3), Mn(acac)$_3$ was added (see Table 2). The mixture was then heated under reflux and worked-up according to the procedure previously described.

When malonic acid was used in the reaction mixture, 3,3,8,8-tetraphenyl-2,7-dioxaspiro[4.4]nonane-1,6-dione (**12**)[10] was formed as a by-product. The reaction using malonamide gave **2a**, together with 2-carbamoyl-4,4-diphenyl-2-buten-4-olide (**13**).[2]

Oxidation of 1a with Mn(acac)$_3$ at Room Temperature. The olefin **1a** (1 mmol) and Mn(acac)$_3$ (2 mmol) were stirred in acetic acid (25 cm^3) at room temperature for 12 h. The subsequent treatment of the reaction mixture by the above method yielded **2a** (6%) and **8** (89%).

3-Acetyl-2-hydroperoxy-2-methyl-5,5-diphenyltetrahydrofuran (8): Colorless prisms (from ethanol); mp 161—162 °C; IR ($CHCl_3$) 3600—3200 (OH) and 1696 (C=O); ^{1}H-NMR ($CDCl_3$) δ=1.26 (3H, s, CH_3), 2.28 (3H, s, $COCH_3$), 2.81 (3H, m, $-CH_2-CH<$), 4.20 (1H, s, OH), 7.28 (5H, s, Ph), and 7.26—7.70 (5H, m, Ph); ^{13}C-NMR ($CDCl_3$) δ=209.244 (s, C=O), 143.047 (s, ArC), 140.520 (s, ArC), 128.515 (d, ArC), 128.308 (d, ArC), 128.017 (d, ArC), 127.401 (d, ArC), 126.697 (d, ArC), 125.814 (d, ArC), 98.131 (s, C-2), 85.158 (s, C-5), 52.487 (d, C-3), 32.143 (t, C-4), 29.736 (q, $CO\underline{C}H_3$), and 24.687 (q, CH_3); MS *m/z* (rel intensity), 312 (M^+, 1), 279 (65), 182 (60), 105 (100), 77 (100), and 43 (100). Found: C, 72.93; H, 6.39%. Calcd for $C_{19}H_{20}O_4$: C, 73.06; H, 6.45%.

Reaction of 8 with Acetic Anhydride. The product **8** (101.4 mg) was heated under reflux in acetic anhydride (20 cm^3) for 4 h. The solvent was then removed under reduced pressure, and the residue was triturated with 2 M HCl (20 cm^3). The aqueous solution was extracted with chloroform, and the products were separated on TLC.

2-Acetyldioxy-3-acetyl-2-methyl-5,5-diphenyltetrahydrofuran (9): 57.7 mg, 50%; colorless needles (from ethanol); mp 117.5—118.0 °C; IR ($CHCl_3$) 1754 (OAc) and 1701 ($COCH_3$); ^{1}H-NMR ($CDCl_3$) δ=1.70 (3H, s, CH_3), 2.11 (3H, s, OAc), 2.25 (3H, s, $COCH_3$), 2.73—3.06 (3H, m, $-CH_2-CH<$), 7.22 (5H, s, Ph), and 7.15—7.65 (5H, m, Ph); MS *m/z* (rel intensity), 354 (M^+, 10), 279 (73), 180 (100), 105 (100), and 43 (100). Found: C, 71.00; H, 6.31%. Calcd for $C_{21}H_{22}O_5$: C, 71.17; H, 6.26%.

Oxidation of 1a with (2,4-Pentanedionato) Metal Complexes. The olefin **1a** (1 mmol) and Co(acac)$_3$ (2 mmol) were heated under reflux in acetic acid (25 cm^3) until the dark green color of the Co(III) ion turned to the pink color of the Co(II) ion (for 1 h). The change in the color of the reaction mixture was monitored by means of TLC. The mixture was then treated by the procedure described above, and **1a** (13% recovered) and **2a** (66%) were obtained. The reaction of **1a** (1 mmol) with Cr(acac)$_3$, Fe(acac)$_3$, and Cu(acac)$_2$, respectively (2 mmol of each), under reflux for 4 h in acetic acid, did not give **2a** (**1a** was recovered in 92, 89, and 85% yields, respectively).

The Attempt of Cyclization of 7j with Mn(OAc)$_3$. The **7j** compound (0.5 mmol) was oxidized with Mn(OAc)$_3$ (2 mmol) in acetic acid (25 cm^3). The mixture was heated under reflux for 10 min and then treated by the above method. However, the cyclization reaction did not occur (**7j** was recovered in a 3% yield), and **10** and **11** were obtained instead of the corresponding dihydrofuran.

9-(1-Acetoxy-2-acetyl-3-hydroxy-1-phenyl-2-butenyl)anthracene (10): 45%; colorless microcrystals (from benzene/ethanol); mp 245.5—246.5 °C; UV(MeOH) λ_{max}nm (log ε), 338 (3.59), 355 (3.89), 374 (4.10), and 395 (4.12); IR ($CHCl_3$) 3600—3200 (OH), 1728 (OAc), and 1600 (C=O); ^{1}H-NMR ($CDCl_3$) δ=1.64 (6H, s, 2×CH_3), 2.17 (3H, s, OAc), 7.27 (5H, s, Ph), 7.44—8.65 (9H, m, ArH), and 17.05 (1H, s, OH). Found: C, 79.05; H, 5.85%. Calcd for $C_{28}H_{24}O_4$: C, 79.22; H, 5.70%.

9-Acetoxy-9-(2-acetyl-3-oxo-1-phenyl-1-butenyl)-9,10-dihydroanthracene (11; R=Ac): 29%; colorless needles (from benzene/hexane); mp 152—153 °C; IR ($CHCl_3$) 1747 (OAc) and 1680 ($COCH_3$); ^{1}H-NMR ($CDCl_3$) δ=2.13 (9H, s, OAc and 2×$COCH_3$), 3.24 (2H, s, CH_2), 6.8—7.5 (13H, m, ArH); ^{13}C-NMR ($CDCl_3$) δ=200.875 (s, $\underline{C}OCH_3$), 167.996 (s, $O\underline{C}OCH_3$), 144.338 (s, C=C), 138.937 (s, ArC), 136.560 (s, ArC), 134.621 (s, ArC), 131.187 (d, ArC), 130.102 (s, C=C), 128.721 (d, ArC), 127.636 (d, ArC), 127.167 (d, ArC), 126.814 (d, ArC), 126.697 (d, ArC), 124.316 (d, ArC), 81.372 (s, $-\underset{|}{\overset{|}{\underline{C}}}-$), 49.520 (t, CH_2), 31.292 (q, $CO\underline{C}H_3$), and 21.722 (q, $OCO\underline{C}H_3$); MS *m/z* (rel intensity), 424 (M^+, 7), 366 (5), 333 (8), 291 (100), 273 (27), and 249 (25). Found: C, 79.05; H, 5.87%; *m/z* 424.16835. Calcd for $C_{28}H_{24}O_4$: C, 79.22; H, 5.70%; M, 424.16746.

9-(2-Acetyl-3-oxo-1-phenyl-1-butenyl)-9,10-dihydro-9-anthrol 11; R=H): 14%; liquid; IR ($CHCl_3$) 3600—3100 (OH) and 1680 (C=O); ^{1}H-NMR ($CDCl_3$) δ=2.21 (6H, s, 2×$COCH_3$), 2.53 (1H, br. s, OH), 3.08 (2H, s, CH_2), 6.75—7.55 (13H, m, ArH).

Reaction of Olefins with Acetylacetone in the Presence of Manganese(III) Acetate (Heiba's Method).[9] To a heated solution of olefin (1 mmol) and acetylacetone (4 mmol) in acetic acid (25 cm^3), Mn(OAc)$_3$ (4 mmol) was added. The solution was heated under reflux until the brown color of the Mn(III) ion disappeared. The reaction mixture was then treated by the procedure described above. The prod-

ucts were separated on TLC, and the structure of the compound was determined by means of the ^{1}H-NMR and IR spectra. **2a** (88%) and **3a** (2%) from **1a** (10% recovered); **2b** (89%) from **1b**; **2c** (69%) from **1c**; **2d** (36%) from **1d**; **2e** (55%) from **1e**; **2f** (39%) and **6f** (2%) from **1f** (50% recovered); **2g** (22%), **4g** (38%), and **5g** (10%) from **1g**; **4h** (28%), **5h** (15%), **6h** (2%), and 2,3,3-tris(4-methoxyphenyl)-2-propenal (6%)[2] from **1h**; **2i** (25%) and **6i** (18%) from **1i**; **7j** (67%) from **1j**.

The author would like to thank Mr. Hiromichi Matsuura of the Wakunaga Pharmaceutical Co., Ltd., Hiroshima, for his measurements of the mass spectra. Thanks are also due to Mr. Teruyoshi Marunaka and Mr. Yasunori Sudo of the Taiho Pharmaceutical Co., Ltd., Tokushima, for their measurements of the mass and ^{13}C-NMR spectra.

References

1) N. Ito, H. Nishino, and K. Kurosawa, *Bull. Chem. Soc. Jpn.*, **56**, 3527 (1983).
2) H. Nishino, *Bull. Chem. Soc. Jpn.*, **58**, 217 (1985).
3) K. Ichikawa, S. Uemura, and T. Sugita, *Tetrahedron*, **22**, 407 (1966).
4) K. Ichikawa and S. Uemura, *J. Org. Chem.*, **32**, 493 (1967).
5) E. I. Heiba and R. M. Dessau, *J. Org. Chem.*, **39**, 3456 (1974).
6) M. Hájek, P. Šilhavý, and J. Málek, *Collect. Czech. Chem. Commun.*, **44**, 2393 (1979).
7) H. Taube, *Chem. Rev.*, **50**, 69 (1952).
8) K. Uehara, T. Nishi, Y. Kataoka, and N. Murata, *Kogyo Kagaku Zasshi*, **70**, 1945 (1967).
9) M. J. S. Dewar and T. Nakaya, *J. Am. Chem. Soc.*, **90**, 7134 (1968).
10) T. Nakaya, H. Arabori, and M. Imoto, *Bull. Chem. Soc. Jpn.*, **43**, 1888 (1970).
11) K. Kurosawa, *Bull. Chem. Soc. Jpn.*, **42**, 1456 (1969); K. Nogami and K. Kurosawa, *ibid.*, **47**, 505 (1974).
12) E. I. Heiba, R. M. Dessau, and W. J. Koehl, Jr., *J. Am. Chem. Soc.*, **91**, 138 (1969).
13) M. N. Bhattacharjee, M. K. Chaudhuri, and D. T. Khathing, *J. Chem. Soc., Dalton Trans.*, **1982**, 669.

ESR and ENDOR Studies of Cation Radicals Derived from Benzodipyran Compounds. Structure and Dynamic Behavior of Heterocyclic Ring in Tocopherol (Vitamin E)

Kazuo MUKAI,* Yuichi UEMOTO, and Kazuhiko ISHIZU
Department of Chemistry, Faculty of Science, Ehime University, Matsuyama 790
(Received February 8, 1985)

ESR and ENDOR spectra of cation radicals of benzodipyran compounds were measured in CH_2Cl_2, and the proton hyperfine coupling constants were correctly determined for each radical. From detailed analysis of the temperature dependence of hyperfine coupling of β- and γ-methylene protons in the heterocyclic ring, the equilibrium conformation of the β-methylene group and activation energy for the conformational interconversion have been determined. The structure of the heterocyclic ring was compared with those of α-tocopherol (vitamin E) model previously obtained by X-ray analysis. The result suggests that the solution and crystal conformations of the heterocyclic ring are distinctly different.

It is well recognized that tocopherols (vitamin E) are localized in cellular membranes and have function as an antioxidant by protecting unsaturated lipids from peroxidation.[1,2] The ESR studies of the "tocopheroxyl" neutral radicals (6-chromanyloxyl radicals from tocopherol) are biologically interesting since they are involved in antioxidant action of vitamin E. Therefore, in recent years, several investigators including present authors have studied the ESR spectra of α-, β-, γ-, and δ-tocopheroxyl radicals and their model compounds in detail.[3-9] The proton hyperfine coupling constants were determined correctly, and the methyl-substitution effects on the unpaired spin distribution and radical stability of the tocopheroxyl radicals have been discussed.[7,9]

Recently, Ingold *et al.* have reported absolute rate constants, k_1, for the reaction of α-tocopherol and some related phenols (for example, 4-methoxy-2,3,5,6-tetramethylphenol) with peroxyl radicals (ROO·).[11-14] By comparing the k_1 value for α-tocopherol with those found for structually related phenols that lacked the 6-membered heterocyclic ring, they suggested that the structure of this ring was largely responsible for the high reactivity of α-tocopherol. In a previous paper, from the results of the ENDOR measurements of α-tocopheroxyl and its model, we reported that each of the two β- and γ-methylene protons in the heterocyclic ring shows an equivalent hyperfine coupling (see Fig. 1).[6] This suggests that the two carbon atoms C-4 and C-3 in the heterocyclic ring are coplanar with the aromatic ring. The result is inconsistent with the X-ray structure of α-tocopherol model, which shows that the dihedral angle, θ_γ, between the C_3–C_4 bond and the aromatic ring is 11.1 and 11.9°.[11,13] However, in a previous work, the clear ENDOR spectra of the α-tocopheroxyl and its model radicals were observable in the comparatively high and narrow temperature range (from −25 to −35 °C for α-tocopheroxyl and from −40 to −55 °C for α-tocopheroxyl model), because these radicals are not so stable and dimerize at low temperature region.

In the present paper, we have succeeded in measuring ESR and ENDOR spectra of cation radicals obtained by the oxidation of benzo[1,2-*b*:4,3-*b*′] and [1,2-*b*:4,5-*b*′]dipyran compounds **1** and **2** (see Fig. 1), which have heterocyclic ring common to that of tocopherols, in $AlCl_3$–CH_2Cl_2 mixtures. The proton hyperfine coupling constants were correctly determined for each radical, and further the temperature dependence of the hyperfine coupling constants has been studied in detail. From the results, the electronic structure of the cation radicals and the conformation and dynamic behavior of the heterocyclic ring have been discussed.

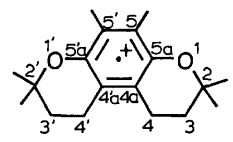

(1)

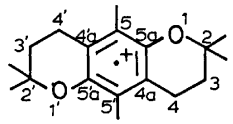

(2)

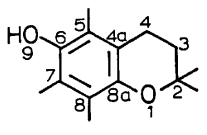

α -Toc. model

Fig. 1. Molecular structures of benzo[1,2-*b*:4,3-*b*′] and [1,2-*b*:4,5-*b*′]dipyran cation radicals **1** and **2** and α-tocopherol model, and the atomic numbering system.

Experimental

Preparation of Specimens. 2,3- and 2,5-dimethylhydroquinones were prepared according to the method of Nilsson *et al.*[15] Benzo[1,2-*b*:4,3-*b'*] and [1,2-*b*:4,5-*b'*]dipyran compounds (**1**; mp 101—102 °C and **2**; mp 196—197 °C) were synthesized by condensation of 2-methyl-3-buten-2-ol to the corresponding alkylhydroquinone, according to the method of Nilsson *et al.*[16]

Measurements. The ESR measurements were carried out using a JES-FE-2XG spectrometer equipped with a Takeda-Riken microwave frequency counter. The *g*-values were measured relative to the value of Li-TCNQ powder, calibrated with $(KSO_3)_2NO$ (g=2.0054).[17] The ENDOR spectra were recorded by a JES-EDX-1 spectrometer, operated with 80 Hz magnetic field modulation. All the ESR and ENDOR spectra have been measured in a sealed, degassed system.

Results and Discussion

ESR and ENDOR Spectra of Benzodipyran Cation Radicals 1 and 2. The cation radicals **1** and **2** were prepared by the oxidation of the corresponding benzodipyran compounds in an $AlCl_3$–CH_2Cl_2 solution. The ESR spectra of the **1** and **2** are shown in Figs. 2 and 3, respectively. The ESR spectra are complex and exhibit line-width alternation phenomena. This is due to the hindered rotation of the heterocyclic ring in radicals **1** and **2**. The g_{iso}-values of these cation radicals observed in CH_2Cl_2 at −105 °C are given in Table 1.

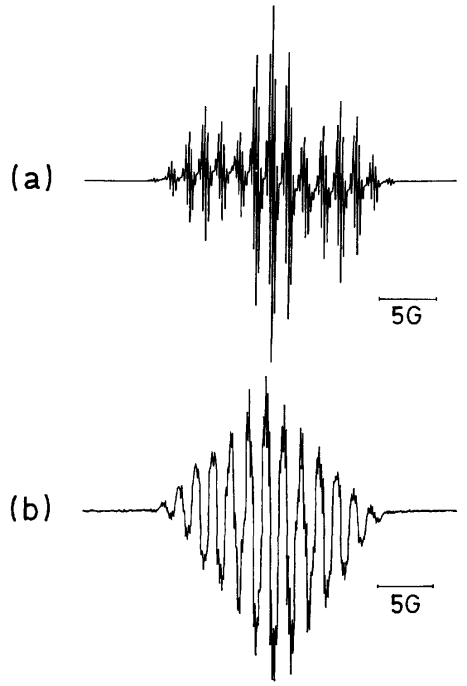

Fig. 2. ESR spectrum of cation radical **1** in CH_2Cl_2 at (a) 20 °C and (b) −100 °C.

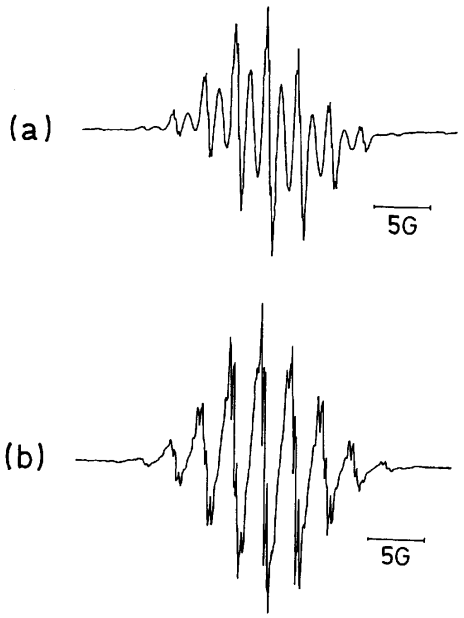

Fig. 3. ESR spectrum of cation radical **2** in CH_2Cl_2 at (a) 20 °C and (b) −100 °C.

Table 1. Hyperfine couplings (a_1^H) (in gauss) and spin densities (ρ_1) of benzodipyran cation radicals **1** and **2** in CH_2Cl_2

		$a_{5,5'}^{CH_3}$	$a_{4,4'}^{CH_2}$	$a_{3,3'}^{CH_2}$	$a_{2,2'}^{CH_3}$	T/°C	g_{iso}-values
1	ENDOR	1.547[a]	4.910, 1.547	0.285	0.046	−40	
		1.547	5.024, 1.444	0.389, 0.199	0.040[c]	−105	2.00367[d]
	ρ(Exptl)	0.0573	0.0932[b]	—	—	−105	
	ρ(Calcd)	0.0731	0.0787	—	—		
2	ENDOR	2.981	2.412	0.237	0.041	−40	
		2.986	2.452, 2.349	0.355, 0.141	0.038[c]	−105	2.00368
	ρ(Exptl)	0.1106	0.0593[b]	—	—	−105	
	ρ(Calcd)	0.0976	0.0548	—	—		

a) Experimental errors ±0.010 G. 1 G = 10^{-4} T. b) Spin densities at C-4a,4'a. c) It is not clear at present whether the smallest hyperfine coupling $a_{2,2'}^{CH_3}$ is due to two or four methyl groups at C-2,2'. d) Experimental errors ±0.00005.

ENDOR measurements of the cation radicals were performed on several samples under slightly different conditions of oxidation, varying the concentration of the benzodipyran precursors and the amount of $AlCl_3$. The ENDOR spectra of the cation radicals were observed in the broad temperature range −105 to −40 °C. Figures 4 and 5 show ENDOR spectra of cation radicals **1** and **2** in CH_2Cl_2, respectively, where the free proton frequency ν_0 (13.8 MHz) is shown by an arrowhead in the diagram.

The ENDOR spectrum of **1** clearly shows six different proton hyperfine splittings at −105 °C, as shown in Fig. 4(b). The spectrum changed explicitly by increasing temperature, and showed four different hyperfine splittings at −55 °C (see Fig. 4(a)). The cation radical **2** also shows notable temperature dependence of the ENDOR spectrum. The temperature dependence of the hyperfine couplings observed for the cation radicals **1** and **2** is shown in Figs. 6 and 7, respectively, and the hyperfine coupling constants obtained at −105 and −40 °C are summarized in Table 1.

If all the proton hyperfine couplings due to 5-CH_3, 4-CH_2, 3-CH_2, 2-$(CH_3)_2$ are different from each other, we can expect seven different hyperfine couplings for both the cation radicals **1** and **2**, as a maximum, assuming the free rotation of CH_3 groups. In our ENDOR measurements, we could resolve six different hyperfine splittings for both the

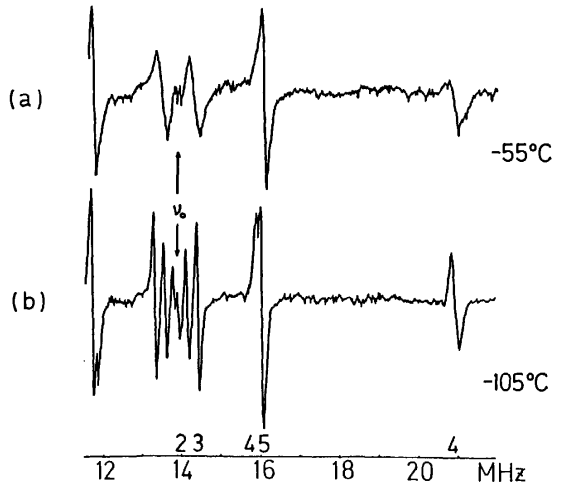

Fig. 4. ENDOR spectrum of cation radical **1** in CH_2Cl_2 at (a) −55 °C and (b) −105 °C.

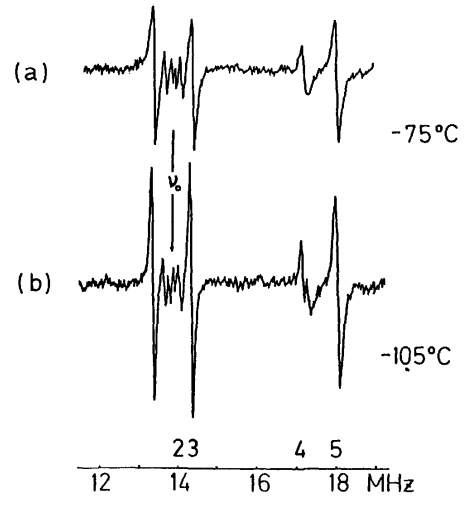

Fig. 5. ENDOR spectrum of cation radical **2** in CH_2Cl_2 at (a) −75 °C and (b) −105 °C.

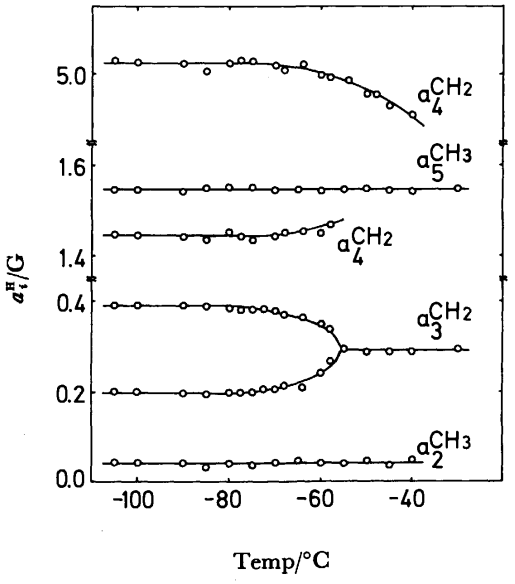

Fig. 6. Temperature dependence of the hyperfine couplings of cation radical **1** in CH_2Cl_2.

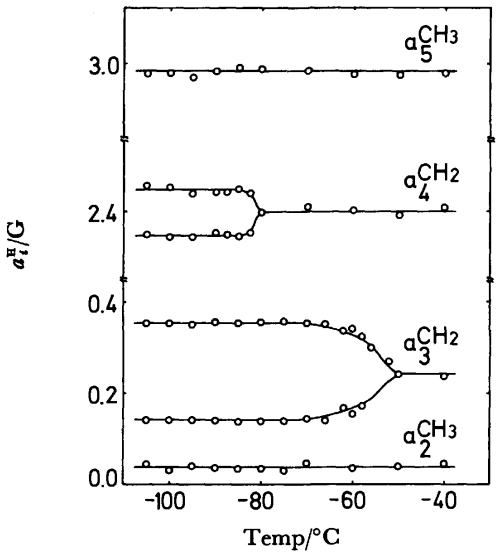

Fig. 7. Temperature dependence of the hyperfine couplings of cation radical **2** in CH_2Cl_2.

cation radicals **1** and **2**. Assignments of the hyperfine couplings have been performed, taking the temperature dependence of the hyperfine couplings (see Figs. 6 and 7) and the result of the McLachlan MO calculations (see Table 1), as described in the following section, into account.

McLachlan Molecular Orbital Calculations. McLachlan spin densities (ρ_i^π) of benzodipyran cation radicals were calculated, using the same parameters for the oxygen atom and methyl group ($\alpha_{O_1}=\alpha_{O_{1'}}=\alpha+2.0\beta$, $\beta_{C_{3a}-O_1}=\beta_{C_{3'a}-O_{1'}}=1.0\beta$, $\alpha_{C_{4a}}=\alpha_{C_{4'a}}=\alpha-0.06\beta$, $\alpha_{C_5}=\alpha_{C_{5'}}=\alpha-0.1\beta$, $\lambda=1.2$) as those used for the vitamin E radical (α-tocopheroxyl).[6] The results of McLachlan MO calculations (see Table 1) were found to be in satisfactory agreement with the "experimental" spin densities evaluated from the hyperfine coupling constants.

Conformation of β-Methylene Group in Benzodipyran Cation Radicals 1 and 2. The magnitude of the β-proton hyperfine coupling can often be calculated using Heller-McConnell's equation.[18]

$$a_\beta^H = \langle B_0 + B_2 \cos^2\theta \rangle \rho_i^\pi , \quad (1)$$

where ρ_i^π is the spin density on the carbon atom to which an alkyl group is attached and θ is the dihedral angle between the axis of the $2p_z$ orbital and the aliphatic C–H bond of the alkyl group. B_0 and B_2 are empirical parameters and were taken to be 0 and 54 G respectively, in Eq. 1. Consequently, the experimental values of the spin densities at C-5 and C-5′ carbon atoms were estimated from the methyl proton coupling, assuming the free rotation of the methyl group, $\langle\cos^2\theta\rangle=1/2$. On the other hand, in the ENDOR spectra for the cation radical **2** in CH_2Cl_2, two kinds of hyperfine couplings ($a_4^{CH_2}=2.452$ G and $a_4^{CH_2}=2.349$ G) (1 G=10^{-4} T) attributable to the magnetically inequivalent β-methylene protons were recorded at −105 °C. They collapsed into a single line as the temperature was raised to −80 °C (see Fig. 7). Therefore, in the case of the present cation radical **2**, one may expect that a rotation of the β-methylene residue would be tightly rocked at low temperatures. This is indeed true, because the temperature dependence of the β-proton coupling constant has been found to be negligible for the above cation radical **2** in the temperature range from −105 to −90 °C, as shown in Fig. 7. Consequently, the dihedral angles, θ_A and θ_B, of the inequivalent β-protons, were calculated to be 28.9 and 31.1° for **2**, respectively, assuming the sum of the two dihedral angles is $\pi/3$. The result suggests that the dihedral angle, θ_γ, between the C_3–C_4 bond and the aromatic ring is 1.1° (see Fig. 8). The experimental values of the spin densities at C-4a and C-4′a carbon atoms were estimated using Eq. 1.

Similarly, the dihedral angles (θ_A and θ_B) and the experimental spin densities of the cation radical **1** were calculated from the observed β-methylene hyperfine splittings (5.024 and 1.444 G) at −105 °C, assuming $\theta_A+\theta_B=\pi/3$. These values are listed in Tables 1 and 2.

As listed in Table 2, the values of dihedral angles (θ_A and θ_B) observed for **1** are very different from those observed for **2**. The above change in dihedral angles will be due to the difference in the steric repulsion forces between the β-methylene protons at C-4 and at C-4′ in **1** and between the β-methylene protons at C-4 and neighboring methyl protons

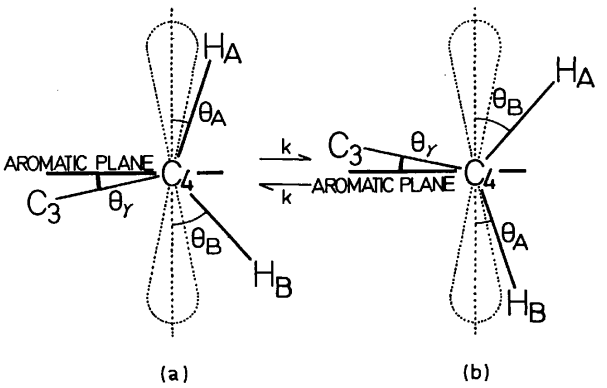

Fig. 8. Possible equilibrium conformations of the β-methylene group in cation radicals **1** and **2** in CH_2Cl_2.

Table 2. Dihedral angles (θ_A, θ_B and θ_γ) and activation energies of **1**, **2**, **3**, and α-tocopherol model

	θ_A/°	θ_B/°	θ_γ/°	$\frac{E_{act}}{kJ\ mol^{-1}}$	Solvent
1	2.4	57.6	27.6[b]	19.0±2.7	CH_2Cl_2
2	28.9	31.1	1.1[b]	32.8±4.6	CH_2Cl_2
3[a]	27.6	32.4	2.4[c]	25.9±1.7[c]	Toluene
α-Tocopherol model	—	—	11.1[d] 11.9	—	Solid state

a) 7-*t*-Butyl-2,2,5-trimethyl-6-chromanyloxyl (**3**). b) Calculated assuming $\theta_\gamma=|\theta_A-\theta_B|/2$. c) From Ref. 19. d) There are two different molecules in the unit cell. From Ref. 13.

at C-5′ in **2**.

As described in a previous section, Burton and Ingold have reported that the dihedral angle, θ_γ, between the aromatic ring and the C_3–C_4 bond is 11.1 and 11.9°, from an X-ray crystallographic analysis of α-tocopherol model.[13] In the α-tocopherol model and the above cation radical **2**, the steric repulsion force between the β-methylene protons at C-4 and the neighboring methyl protons (at C-5 in α-tocopherol model and at C-5′ in **2**) will be similar to each other, and thus the conformation of the heterocyclic ring in **2** is considered to be similar to that of the α-tocopherol model. However, the value of the dihedral angle (θ_γ=1.1°) in **2** is different from those (θ_γ=11.1 and 11.9°) in α-tocopherol model. On the other hand, very recently, we have succeeded in measuring the ENDOR spectrum of a new stable tocopheroxyl radical **3** (7-*t*-butyl-2,2,5-trimethyl-6-chromanyloxyl) (see Table 2) in toluene.[19] It was found that the two β-methylene protons in the heterocyclic ring become magnetically inequivalent at low temperature (<−72 °C). The observed dihedral angles are θ_A=27.6° and θ_B=32.4°, and θ_γ is calculated to be 2.4°. These values are very similar to those of the cation radical **2**, because the steric repulsion force between the β-methylene protons at C-4 and the neighboring methyl protons is equivalent in **2** and **3**. These results suggest that the solution structure of the heterocyclic ring attached to the aromatic ring is similar to each other and the crystal and solution conformations of the heterocyclic ring are distinctly different.

Dynamic Behavior of Heterocyclic Ring. As described in a previous section, in the ENDOR spectra of the cation radical **2** in CH_2Cl_2, two signals attributable to the two inequivalent splittings of the β-methylene protons ($a_4^{CH_2}$=2.452 G and $a_4^{CH_2}$=2.349 G) were recorded at −105 °C. The β-methylene proton hyperfine coupling constants remain almost unchanged upon warming from −105 to −85 °C. They collapsed into a single line ($a_4^{CH_2}$=2.401 G) as the temperature was raised to −80 °C (see Fig. 7). Similar behavior has been observed for γ-methylene protons.

In such a case, we can calculate the activation energy E_{act} for the conformational interconversion of the heterocyclic ring, applying the Gutowsky-Holm equation.[20–22] In a four-jump dynamic process, the separation $\Delta\omega$ on the two ENDOR lines at T K due to β- or γ-methylene protons is given by

$$\Delta\omega = (\Delta w_{max}^2 - 8k^2)^{1/2} \quad (2)$$

where $\Delta\omega_{max}$ is the two limiting values of the splitting constants of β- or γ-methylene protons and equals to $\gamma_e|(a_A^{CH_2}-a_B^{CH_2})/2|$, and $k=1/2\tau$. Here, τ is the mean life time of each conformation.

With the aid of this relation we have obtained k at different temperatures for cation radical **2** in CH_2Cl_2. However, in the case of the β-methylene protons, the value of $\Delta\omega_{max}$(=0.103 G=0.289 MHz) is very small and thus the change of the $a_4^{CH_2}$ values occurs in the narrow temperature range (−85—−80 °C). Therefore, the E_{act} value was obtained from the temperature dependence of γ-methylene proton hyperfine couplings ($a_3^{CH_2}$). Figure 9 shows the Arrhenius plots of $\log k$ *vs.* $1/T$ for **2** from which E_{act} was determined. The observed activation energy E_{act}=32.8±4.6 kJ mol^{-1}. On the other hand, in the case of cation radical **1**, the value of $\Delta\omega_{max}$(=3.580 G=10.033 MHz) for β-methylene hyperfine coupling is very large and the coalescence temperature is higher than the temperature where the ENDOR observation is possible. Therefore, the E_{act} was calculated from the temperature dependence of γ-methylene proton hyperfine couplings, as performed for cation radical **2**. The activation energy obtained is E_{act}=19.0±2.7 kJ mol^{-1}. As described in a previous section, in the cation radical **2** and the tocopheroxyl radical **3** (7-*t*-butyl-2,2,5-trimethyl-6-chromanyloxyl), the steric repulsion force between the β-methylene protons at C-4 and the neighboring methyl protons will be similar to each other, and thus we can expect similar E_{act} values for **2** and **3**. However, the activation energy, E_{act} obtained in the present work for **2** is slightly larger than that (25.9±1.7 kJ mol^{-1}) reported for such an interconversion in **3**.[19]

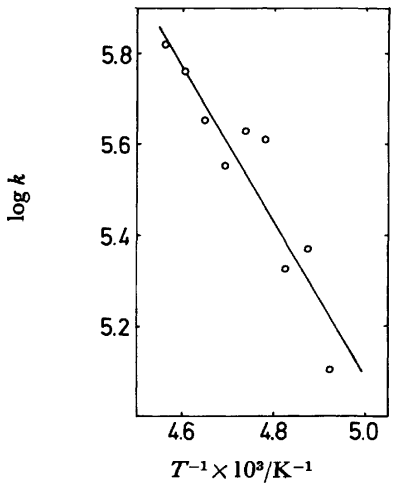

Fig. 9. The Arrhenius plot of the rate constant for the conformational interconversion process of the heterocyclic ring of cation radical **2** in CH_2Cl_2.

References

1) P. Schudel, H. Mayer, and O. Isler, "The Vitamins," 2nd ed, ed by W. H. Sebrell, Jr. and R. S. Harris, Academic Press, New York (1972), Vol 5, pp. 168—218.

2) M. L. Scott, "The Fat-Soluble Vitamins," ed by H. F.

DeLuca, Plenum Press, New York (1978) pp 133—210.
3) D. H. Kohl, J. R. Wright, and M. Weissman, *Biochim. Biophys. Acta*, **180**, 536 (1969).
4) W. Boguth and H. Niemann, *Biochim. Biophys. Acta*, **248**, 121 (1971).
5) T. Ozawa, A. Hanaki, S. Matsumoto, and M. Matsuo, *Biochim. Biophys. Acta*, **531**, 72 (1978).
6) K. Mukai, N. Tsuzuki, K. Ishizu, S. Ouchi, and K. Fukuzawa, *Chem. Phys. Lipids*, **29**, 129 (1981).
7) K. Mukai, N. Tsuzuki, S. Ouchi, and K. Fukuzawa, *Chem. Phys. Lipids*, **30**, 337 (1982).
8) J. Tsuchiya, E. Niki, and Y. Kamiya, *Bull. Chem. Soc. Jpn.*, **56**, 229 (1983).
9) M. Matsuo and S. Matsumoto, *Lipids*, **18**, 81 (1983).
10) K. Mukai, K. Takamatsu, and K. Ishizu, *Bull. Chem. Soc. Jpn.*, **57**, 3507 (1984).
11) G. W. Burton, Y. Le Page, E. J. Gabe, and K. U. Ingold, *J. Am. Chem. Soc.*, **102**, 7792 (1980).
12) G. W. Burton and K. U. Ingold, *J. Am. Chem. Soc.*, **103**, 6472 (1981).
13) T. Doba, G. W. Burton, and K. U. Ingold, *J. Am. Chem. Soc.*, **105**, 6505 (1983).
14) G. W. Burton, L. Hughes, and K. U. Ingold, *J. Am. Chem. Soc.*, **105**, 5950 (1983).
15) J. L. G. Nilsson, H. Sievertsson, and H. Selander, *Acta Pharm. Suecica*, **5**, 215 (1968).
16) J. L. G. Nilsson, H. Sievertsson, and H. Selander, *Acta Chem. Scand.*, **22**, 3160 (1968).
17) J. J. Windle and A. K. Wiersma, *J. Chem. Phys.*, **39**, 1139 (1963).
18) C. Heller and H. M. McConnell, *J. Chem. Phys.*, **32**, 1535 (1960).
19) K. Mukai, K. Takamatsu, and K. Ishizu, sent for publication.
20) H. S. Gutowsky and C. H. Holm, *J. Chem. Phys.*, **25**, 1228 (1956).
21) C. Morczyskowski, K. Möbius, and M. Plato, *J. Magn. Reson.*, **17**, 202 (1975).
22) M. Iwaizumi, S. Kita, M. Kohno, and T. Isobe, *Bull. Chem. Soc. Jpn.*, **53**, 1745 (1980).

Nucleophilic Substitution of Tricoordinate Sulfur Atom of Sulfonium Salt with Retention of Configuration.[1] Different Stereochemistry of Substitution by Amidate Anions

Katsuaki KIKUCHI, Naomichi FURUKAWA,* Masaru MORIYAMA,† and Shigeru OAE*,††
Department of Chemistry, The University of Tsukuba, Sakura-mura, Niihari-gun, Ibaraki 305
(Received February 12, 1985)

Optically active *N*-substituted *S*-(*o*-methoxyphenyl)-*S*-phenylsulfilimines were obtained in moderate yields upon simple treatment of a mixture of *o*-methoxyphenyl phenyl sulfide and *t*-butyl hypochlorite in the presence of *l*-menthol and followed by amidate anions. Although some sulfilimines (*N*-tosyl-, *N*-benzoyl-, and *N*-(chloroacetyl)sulfilimines) were found to be rich in *S*-configuration around the sulfur atom, the others (*N*-(dichloroacetyl)-, *N*-(trichloroacetyl)-, and *N*-(trifluoroacetyl)sulfilimines) were found to be rich in *R*-configuration around the sulfur atom. In the displacement of *l*-menthyloxy group on the sulfur atom of the incipiently formed *l*-menthyloxysulfonium salt with *p*-toluenesulfonamidate, benzamidate, and chloroacetamidate anions, the respective *N*-acylsulfilimines of *S*-configuration were obtained by substitution with inversion of configuration, while *N*-acylsulfilimines having *R*-configuration were obtained by substitution of the same *l*-menthyloxysulfonium salt by polyhaloacetamidate anions such as dichloroacetamidate, trichloroacetamidate, and trifluoroacetamidate anions, with retention of configuration.

The mechanism of nucleophilic substitution reaction at the tricoordinate sulfur atom has been a subject of considerable interest.[2] One of the important problems is the structure of the transition state or the intermediate and the stereochemical course of the nucleophilic substitution on the sulfur atom. The nucleophilic substitution of the tricoordinate sulfur atom has been suggested to proceed *via* formation of a sulfurane type intermediate of trigonal bipyramidal structure shown below, and the stereochemistry of the substitution which involves the initial formation of a σ-sulfurane is believed to be determined by the relative orientation of the attacking nucleophile and the leaving group. In the hypervalent σ-sulfurane, the apical bond is presumed to be made up with a *p*-orbital, and hence is longer and more polar than the basal bond which is composed mainly of sp^2 hybrid.

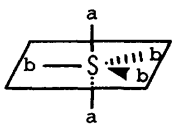

NUCLEOPHILE	LEAVING GROUP	STEREOCHEMISTRY
a	a	INVERSION
b	b	INVERSION
a	b	RETENTION
b	a	RETENTION

Fig. 1. The relation between the stereochemistry and the orientation of the nucleophile and the leaving group.

Therefore both the entering nucleophile and the leaving group are considered to be placed at apical positions in the nucleophilic substitution on the tricoordinate sulfur atom. When there is no special interaction between the entering nucleophile and the leaving group, both groups will be placed at the apical positions of opposite directions, inversion of configuration on the sulfur atom will be the rational course.

Inversion of configuration would also be resulted, if both entering and leaving groups would occupy the basal positions.

However, this orientation is quite unlikely, since both entering and leaving groups are relatively more polar and their bonds are longer than others and hence should be placed at the apical rather than at the basal positions at the transition state of the nucleophilic substitution on the tricoordinate sulfur atom. Meanwhile, if there is any special interaction between the entering nucleophile and the leaving group, in the resulted sulfurane type intermediate, the nucleophile which enters from the apical position and the leaving group at the basal position may turn their positions by pseudorotation before placing the entering nucleophile at a basal position and extruding the leaving group from an apical position, retention of configuration is expected to be observed (Fig. 1).

Since the first example of inversion at the sulfur atom was found in the transesterification of a chiral sulfite,[3] numerous instances of nucleophilic substitution reaction have been demonstrated to occur with inversion of configuration on the sulfur,[4] and this is

† Present address; Pharm. Reserch Center, Kanebo. Ltd., Miyakojima-ku, Osaka 534.
†† Present address; Okayama University of Science, Ridai-cho, 1-1, Okayama 700.

believed to be the most common stereochemical course for the nucleophilic substitution (ligand exchange) on the sulfur atom. However, there have been a few cases in which retention of configuration has been observed in the nucleophilic substitution on the tricoordinate sulfur atom. Oae *et al.* were the first who observed that optically active methyl *p*-tolyl sulfoxide labeled with ^{18}O undergoes the oxygen exchange with that of dimethyl sulfoxide without any loss of optical activity, *i.e.*, the retention of configuration on the sulfur atom.[5] In this case a dipole-dipole interaction between the two sulfoxide linkages is considered to keep the two ligands at nearly 90° angle throughout the ligand exchange. Since then the retention of configuration in nucleophilic substitution has also been observed in the several reactions, such as in the conversion of chiral sulfoxides into the corresponding sulfilimines in the reactions with *N*-sulfinyl-*p*-toluenesulfonamide,[6] *N,N'*-ditosylsulfur diimide,[7] and *p*-toluenesulfinylnitrene[8] as reagents. Moreover, the reaction of an optically active amidothiosulfite with mercury(II) chloride leading to the optically active aminosulfinyl chloride was shown to proceed with retention of configuration at the sulfur center.[9]

Recently, a few other reactions also have been reported to proceed with retention of configuration on the sulfur atom.[10]

In all these reactions involving the trigonal bipyramidal intermediates, formation of four-membered ring by a special interaction between leaving and entering groups at the apical and basal positions is generally believed to be the main factor responsible for the retention mechanism.

Recently, we have reported that optically active (*S*)-(−)-*S*-(*o*-methoxyphenyl) (or *o*-methylphenyl)-*S*-phenyl-*N*-tosylsulfilimine was obtained by simple treatment of an equimolar mixture of *l*-menthol and the corresponding sulfide at first with *t*-butyl hypochlorite and subsequent addition of sodium *N*-*p*-toluenesulfonamidate at a low temperature, as shown in Fig. 2. When we used some other nucleophiles instead of the amidate anion, we were able to obtain other optically active diaryl tricoordinate sulfur compounds; namely, when hydroxide anion was used, the corresponding (*S*)-(−)-sulfoxide of inverted configuration was obtained whereas in the teatment of malonate anion, the corresponding inverted (+)-sulfonium ylide was also obtained.[11] In all these reactions, optically active *l*-menthyloxysulfonium chloride is presumed to be formed as the incipient intermediate (Fig. 2). This method has now become a simple and hence the most general preparative method to synthesize optically active (*o*-substituted aryl) phenyl tricoordinate sulfur compounds. However, when such polyhaloacetamidates such as dichloro-, trichloro-, and trifluoroacetamidate anions were used instead of *p*-toluenesulfonamidate anion, we have obtained unexpectedly the corresponding sulfilimines each having excess of the R-configuration in good yields.[1] In this papar we wish to report this new type of nucleophilic substitution at the tricoordinate sulfur atom and the mechanism of this unusual stereochemistry.

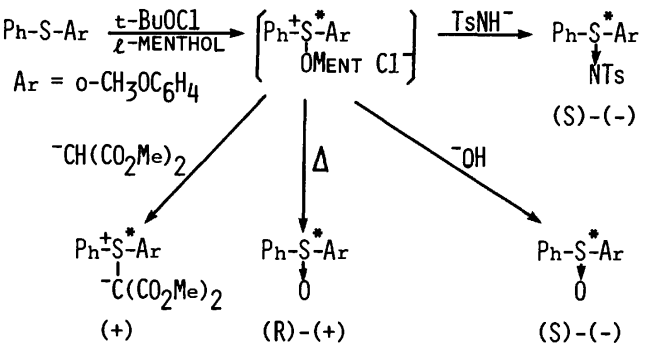

Fig. 2. Asymmetric syntheses of some optically active tricoordinate sulfur compounds.

Results and Discussion

Unsymmetrical *S,S*-diarylsulfilimines were obtained in moderate yields by treating an equimolar mixture of *l*-menthol and the corresponding sulfide first with *t*-butyl hypochlorite and subsequently with amidate anions as shown in Scheme 1.

The *N*-tosylsulfilimines (**3a** and **g**), *N*-benzoylsulfilimine (**3b**), and *N*-(chloroacetyl)sulfilimine (**3c**) thus obtained showed minus sign of optical rotation, and *N*-(polyhaloacetyl)sulfilimines such as *N*-(dichloroacetyl)-(**3d**), *N*-(trichloroacetyl)-(**3e**), and *N*-

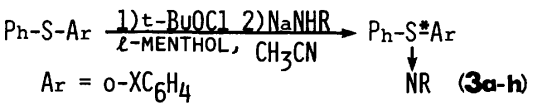

Scheme 1.

Table 1. Asymmetric syntheses of *N*-substituted *S*-(*o*-methoxyphenyl)-*S*-phenylsulfilimines (**3a—h**)

	X-	R	Yield/%	$[\alpha]_D$/°	e.e./%
3a	CH_3O-	Ts	47	−39.0	40.4[a]
3b	CH_3O-	COPh	65	−17.3	27.3
3c	CH_3O-	$COCH_2Cl$	47	−45.5	35.5
3d	CH_3O-	$COCHCl_2$	34	+11.7	12.5
3e	CH_3O-	$COCCl_3$	72	+26.4	47.2
3f	CH_3O-	$COCF_3$	53	+35.4	47.2
3g	CH_3-	Ts	72	−14.4	35.1[a]
3h	CH_3-	$COCF_3$	96	+20.9	26.4

a) This value was calculated optical purity.

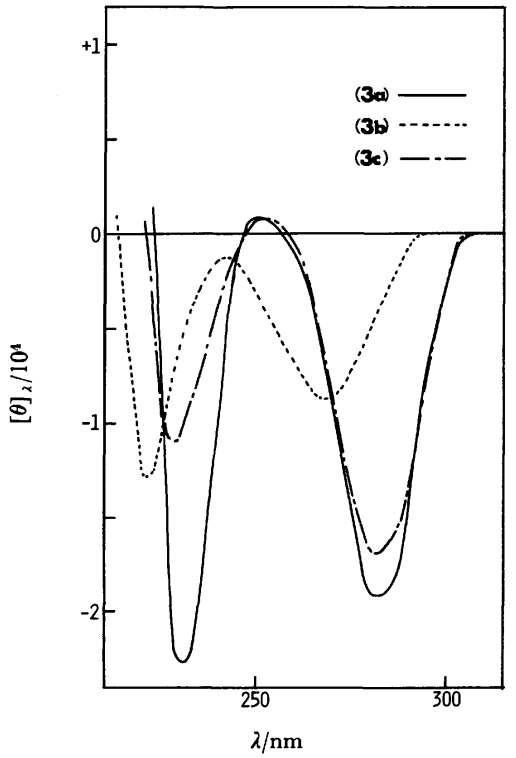

Fig. 3a. CD spectra of (*S*)-(−)-*S*-(*o*-methoxyphenyl)-*S*-phenyl-*N*-tosyl-(**3a**), (*S*)-(−)-*N*-benzoyl-(**3b**), and (*S*)-(−)-*N*-(chloroacetyl)-(**3c**) sulfilimines.

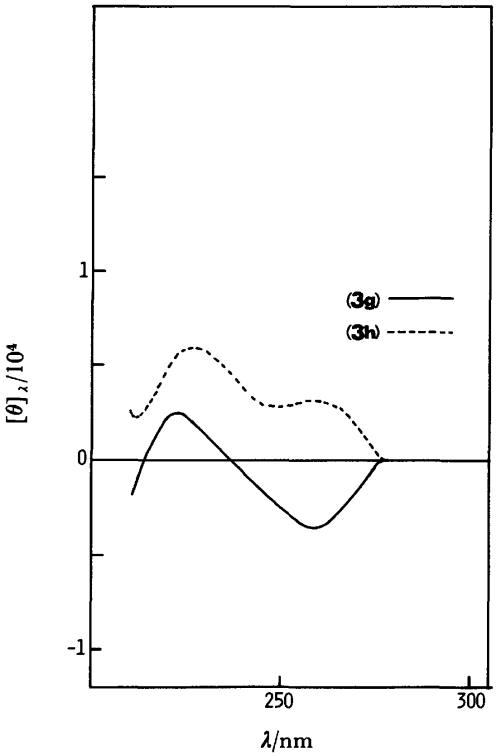

Fig. 3c. CD spectra of (*S*)-(−)-*S*-(*o*-methylphenyl)-*S*-phenyl-*N*-tosylsulfilimine (**3g**) and (*R*)-(+)-*N*-(trifluoroacetyl)sulfilimine (**3h**).

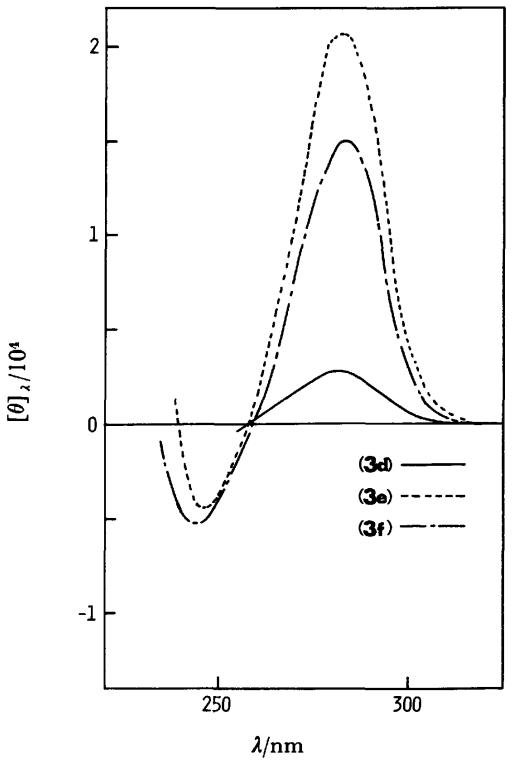

Fig. 3b. CD spectra of (*R*)-(+)-*S*-(*o*-methoxyphenyl)-*S*-phenyl-*N*-(dichloroacetyl)-(**3d**), *N*-(trichloroacetyl)-, (**3e**), and *N*-(trifluoroacetyl)-(**3f**) sulfilimines.

(trifluoroacetyl)sulfilimines (**3f** and **h**) showed plus sign of optical rotation. The configurations of these sulfilimines were determined by comparing their circular dichroism (CD) spectra with that of (−)-**3a** which was determined to be of *S*-configuration by X-ray crystallographic analysis.[12] The CD spectra of these sulfilimines, thus obtained, are shown in Fig. 3. Meanwhile, the configurations of sulfilimines (**3b—f**) were also determined by comparing the optical rotations with those of the authentic samples. The authentic samples were prepared by acylating of optically active (*S*)-(−)-S-(*o*-methoxyphenyl)-*S*-phenylsulfilimine formed upon treatment of (*S*)-(−)-*S*-(*o*-methoxyphenyl)-*S*-phenyl-*N*-tosylsulfilimine with concd sulfuric acid, as shown in Scheme 2. The sulfilimines thus obtained are listed in Table 2. The assignment of the configuration of each of these sulfilimines (**3b—f**) determined by the CD spectrum was in good agreement with the result obtained by comparison with the optical rotation of the authentic sample.

Based on these observations the sulfilimines having minus optical rotations (**3a—c** and **g**) obtained in this reaction, are considered to have the *S*-configuration, while those having plus optical rotations (**3d—f** and **h**) are determined to have the *R*-configuration. Thus, the sulfilimines prepared by treatment of the *l*-menthyloxysulfonium salt (**2**) with such amidate

Table 2. Syntheses of authentic samples

4 $[\alpha]_D$/°	Acylating reagent		Sulfilimines R	Yield/%	$[\alpha]_D$/°	Mp θ_m/°C
−194	$(PhCO)_2O$	**3b**	PhCO	55	−76	99—99.5
−187	$ClCH_2COCl$	**3c**	$ClCH_2CO$	86	−89	Oil
−33	$Cl_2CHCOCl$	**3d**	Cl_2CHCO	62	−16	116—118
−33	$(Cl_3CCO)_2O$	**3e**	Cl_3CCO	35	−13	122—124
−187	$(F_3CCO)O$	**3f**	F_3CCO	75	−76	Oil

anions as *p*-toluenesulfonamidate, benzamidate, and chloroacetamidate have in excess of those of the *S*-configuration, while the sulfilimines prepared by the reaction of **2** with amidate anions having highly electron-withdrawing acyl groups such as dichloroacetamidate, trichloroacetamidate, and trifluoroacetamidate have in excess of those of the *R*-configuration. In order to scrutinize the stereochemistry of these substitutions, we have made an attempt to isolate the key intermediate, namely *o*-methoxyphenylphenyl-*l*-menthyloxysulfonium salt and investigated the stereochemical course of the nucleophilic substitution of the sulfonium salt with various amidate anions. *o*-Methoxyphenylphenyl-*l*-menthyloxysulfonium salt was obtained as perchlorate (**2**) by treating an equimolar mixture of *o*-methoxyphenyl phenyl sulfide and *l*-menthol, at first with *t*-butyl hypochlorite and subsequent addition of silver perchlorate as shown in Scheme 3. The sulfonium salt (**2**) thus obtained was found to be a mixture of two

Table 3. Diastereomer ratio of *l*-menthyloxysulfonium perchlorate

Solvent	Temperature/°C	Yield/%	*R*/*S*
CH_3CN	−40	84	75/25
THF	−60	36	75/25
$(CH_3)_2O$	−60	67	58/42
CH_2Cl_2	−60	89	78/22
CH_2Cl_2	−80	67	84/16

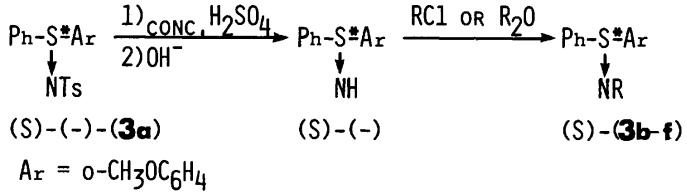

Scheme 2.

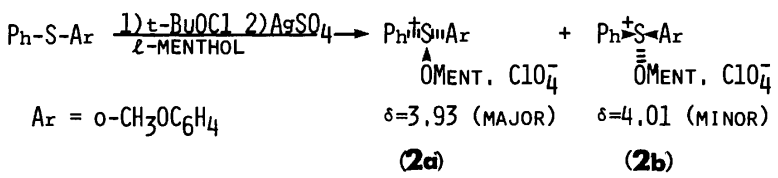

Scheme 3.

Table 4. Reaction of amidate anions with *l*-menthyloxysulfonium perchlorate (**2**)[a)]

R/*S* of 2	Solvent	R	Yield/%	$[\alpha]_D^{20}$/°	e.e./%	o.p./%
83/17	CH_3CN-DMF	Ts	5	−43	44	60
70/30	CH_3CN	$COCH_2Cl$	58	−9	7	18
78/22	CH_3CN	$COCHCl_2$	51	+5	5	9
83/17	CH_3CN	$COCCl_3$	39	+16	44	66
83/17	CH_3CN	$COCF_3$	60	+33	40	58

a) Reaction temperature was −35 °C.

diastereomers, since the sulfonium salt (**2**) has two chiral centers, namely the sulfonium sulfur atom and the carbon atom of *l*-menthyloxy group attached to the oxygen atom. The ratio of the two diastereomers thus obtained was determined by the ^{1}H NMR integration of the peaks of *o*-methoxyl groups appeared at δ 3.93 for the major diastereomer and δ 4.01 for the minor one. However, the diastereomeric ratio of 2 was found to change with the change of solvent and reaction temperature in the treatment with *t*-butyl hypochlorite as shown in Table 3. When an amidate anion was added into the acetonitrile solution of the sulfonium salt (**2**), the corresponding sulfilimine was obtained as summarized in Table 4. Their optical yields are rather low, however, the stereochemical course for the substitution is in good agreement with the result obtained from the direct asymmetric induction shown in Table 1; namely, the corresponding *N*-tosyl-(**3a**) and *N*-(chloroacetyl)sulfilimine (**3c**) have the *S*-configuration, and *N*-(dichloroacetyl)-(**3d**), *N*-(trichloroacetyl)-(**3e**), and *N*-(trifluoroacetyl)sulfilimines (**3f**) show the *R*-configuration. These observations clearly indicate that the *l*-menthyloxysulfonium salt (**2**) is the key intermediate in the asymmetric reaction as shown in Scheme 1.

Table 5. Optical yields of asymmetric syntheses of sulfilimines (**3a—f**)

	R	e.e./%	o.p./%
3a	Ts	40.4	81
3b	COPh	27.3	55
3c	$COCH_2Cl$	35.5	71
3d	$COCHCl_2$	12.5	25
3e	$COCCl_3$	47.2	94
3f	$COCF_3$	47.2	94

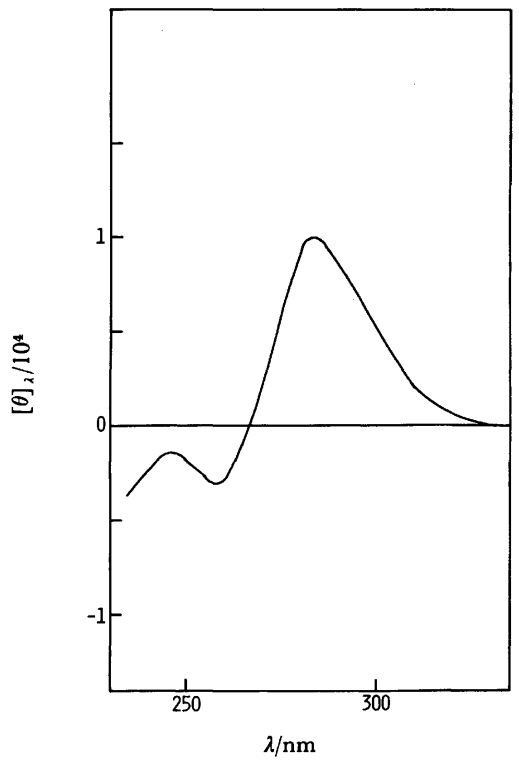

Fig. 4. CD spectra of (*l*-menthyloxy)(*o*-methoxyphenyl)phenylsulfonium perchlorate (**2**).

When *t*-butyl hypochlorite was added at −40°C into the acetonitrile solution of the equimolar mixture of sulfide (**1**) and *l*-menthol, namely under the same conditions as the results shown in Table 1 and the ratio of the two diastereomers was found to be 75 : 25. Thus, the optical yields in the asymmetric syntheses of these sulfilimines shown in Table 1 have been determined and the results are summarized in Table 5. The CD spectrum of *l*-menthyloxysulfonium perchlorate (**2**) is shown in Fig. 4. From the CD curve, the configuration around the sulfur atom of the *l*-menthyloxysulfonium perchlorate (**2**) was determined to be excess of the *R*-configuration, in accordance with the result reported previously by us.[11a] Therefore, the sulfilimines having the opposite sign of the Cotton effect to that of the sulfonium perchlorate (**2**), namely, *N*-tosyl-(**3a**), *N*-benzoyl-(**3b**), and *N*-(chloroacetyl)sulfilimines (**3c**) are undoubtedly obtained through the inversion process. When the sulfilimines showing the same sign of the Cotton effect to that of the sulfonium perchlorate (**2**), namely *N*-(dichloroacetyl)-, (**3d**), *N*-(trichloroacetyl)-(**3e**), and *N*-(trifluoroacetyl)-sulfilimines (**3f**) are obviously formed through the retention process stereochemically. Thus, it appears that the retention process predominates over the inversion process when the more acidic amidate anion is used. Accordingly, some reported pK_a values for the conjugated acids of amides which were used in this experiment have been sought out, as shown in the following, namely $PhCONH_3^+$=−1.55,[13] $ClCH_2CONH_3^+$−3.21,[14] *p*-$TolSO_2$ NH_3^+=−3.3,[15] $Cl_2CHCONH_3^+$<−6.4.[14]

These data sugggest that the stereochemistry of substitution of the *l*-menthyloxysulfonium salt with the amidate anion seems to be related to the acidity of the amide. Namely, the ordinary amidate anion seems to substitute *l*-menthyloxy group of *l*-menthyloxysulfonium salt with inversion of the configuration, while the more acidic amidate anion seems to undergo substitution with retention of the configuration.

The effect of temperature on the stereochemistry of the reaction was also examined. In order to fix the *R*/*S* ratio of the intermediate, *i.e.*, the *l*-menthyloxysulfonium ion, *t*-butyl hypochlorite was added under a certain fixed conditions. Then, after changing the temperature of the whole mixture,

sodium trifluoroacetamidate was added into the system as shown in Scheme 4. The enantiomeric excess of the *N*-(trifluoroacetyl)sulfilimine thus obtained has been found to decrease with the increase of the reaction temperature as shown in Table 6. The decrease of *R/S* ratio with the increase of temperature could be resulted by the thermal racemization of the intermediate sulfonium salt. However, since the *R/S* ratio was found not to change from −30 °C to 42 °C, the thermal racemization cannot be responsible (Table 7). Furthermore, the sulfonium salt (**2**) did not undergo any racemization even under keeping at 61.5 °C for 1 h.

Only at a somewhat higher temperature (80.1°C,1 h), it decomposed completely to form the corresponding sulfoxide but no thermal racemization was observed. Another possibility is the intervention of the concurrent inversion process.

At a low temperature (−40°C), trifluoroacetamidate anion may attack the sulfur atom of the sulfonium salt (**2**) interacting with a basal ligand to offer the sulfilimine (**3f**) of only the retained configuration (stereoselectivity is over 94%), and at a higher temperature (22°C), the ratio (*R/S*) of retention to inversion path decreased to roughly 75 : 25.

This result suggests that the substitution with retention of configuration is more sensitive to the effect of temperature than that with inversion. This would mean that the substitution with retention proceeds through a more rigid transition state than the inversion process. Indeed the plots of *R/S* ratio against the reaction temperature, gave a value of energy difference between the retention and the inversion process for trifluoroacetamidate anion as $\Delta\Delta G^{\ddagger}=4.9$ KJ mol^{-1} (Fig. 5).

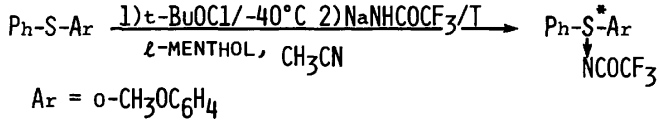

Scheme 4.

Table 6. Temperature effect on reaction path

T/°C	Yield/%	$[\alpha]_D$/° (*c*, $CHCl_3$)	e.e./%	Ratio of (ret/inv)
−40	47	+35.5 (1.06)	47.2	97 : 3
+4	50	+20.6 (1.02)	27.0	77 : 23
+20	23	+19.3 (1.07)	25.1	75 : 25

Table 7. Thermal change on R/S ratio of *l*-menthyloxysulfonium perchlorate (**2**)

Temp/°C	R_S-R_C/S_S-R_C[a)]
−30±2	75/25
0±2	75/25
+20±2	75/25

a) Diastereomer ratio was determined by ^{1}H NMR in $CDCl_3$.

Mechanism. It has become quite clear from all the observations that the retention process is the main path of the nucleophilic substitution when the nucleophile used is the amidate anion bearing an acidic proton, and proceeds through a more rigid transition state than the inversion process. The most plausible mechanism for this process is as shown in Fig. 6. When *t*-butyl hypochlorite is added to an equimolar mixture of *l*-menthol and *o*-methoxyphenyl (or *o*-methylphenyl) phenyl sulfide, the corresponding *l*-menthyloxysulfonium ion is obtained. This sulfonium ion is a mixture of two diastereomers, *i.e.*, R_S—R_C and S_S—R_C, however in excess of the kinetically favored R_S—R_C conformer. When the ordinary amidate anion such as *p*-toluenesulfonamiate, benzamidate, or chloroacetamidate, attacks the sulfur atom along an apical direction, *i.e.*, the back side of the leaving group, namely *l*-menthyloxy group of the sulfonium ion at another apical direction, the reaction proceeds *via* formation of a σ-sulfurane as the key intermediate, in which both attacking and leaving groups are placed

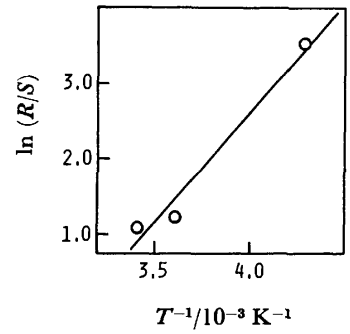

Fig. 5. The retention/inversion plots against the reaction temperature.

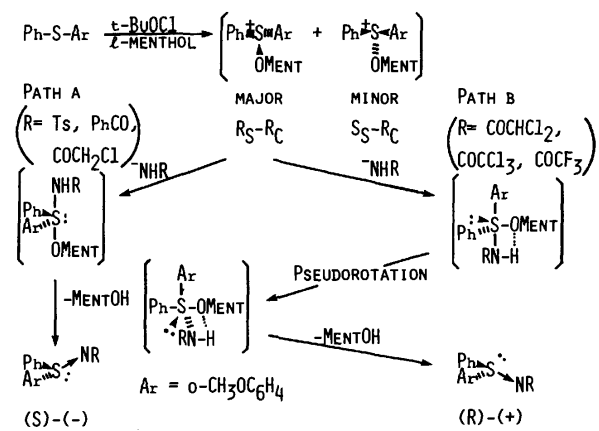

Fig. 6. Reaction mechanisms.

at apical-apical positions respectively, to result in the formation of the sulfilimine of inverted configuration on the sulfur, (path a). However, when the amidate anion, which has an acidic proton such as in dichloro, trichloro-, or trifluoroacetamidate anion, attacks the sulfur atom along an apical direction, there would be a substantial interaction between the amidate and the leaving group, *i.e.*, *l*-menthyloxy group of the sulfonium ion, and even during and after pseudorotation, the interaction would hold both groups at nearly perpendicular around the sulfur atom till the final release of *l*-menthyloxy group from the apical direction.

Thus the retention of configuration on the sulfur is resulted. This study has thus revealed that hydrogen bonding plays an important part in fixing the geometry of the entering nucleophile and the leaving group in the incipiently formed σ-sulfurane and leads the nucleophilic substitution on tricoordinate sulfur to proceed with retention of configuration.

Experimental

General. All melting points were uncorrected. IR spectra were recorded on a JASCO A-3 spectrometer. ^{1}H NMR spectra were recorded on a Hitachi Perkin-Elmer R-20 and R-600 spectrometers. Optical rotations were measured by a JASCO DIP-140 spectrometer. Circular dichroism spectra were recorded on a JASCO J-20 spectrometer.

Elemental analyses were carried out at the Chemical Analysis Center of this University.

Sulfides. The sulfides were prepared by decomposition of the diazonium salt of *o*-substituted anilines in the presence of thiophenol, as described previously.[16] Their boiling points were 146 °C (399 Pa) for *o*-methoxyphenyl sulfide (lit,[11a] 130—135 °C (266 Pa)) and 117—118 °C (399 Pa) for *o*-methylphenyl phenyl sulfide (lit,[11a] 120—125 °C (266 Pa)).

t-Butyl Hypochlorite. *t*-Butyl hypochlorite was prepared by chlorination of *t*-butyl alcohol by aqueous sodium hypochlorite in the presence of acetic acid as described before.[17]

(R)-(+)-S-(o-Methoxyphenyl)-S-phenyl-N-(trifluoroacetyl)-sulfilimine (3f). A mixture of *o*-methoxyphenyl phenyl sulfide (0.66 g, 3.05 mmol), *l*-menthol (0.559 g, 3.58 mmol), and dry pyridine (0.227 g, 3.50 mmol) was dissolved in 20 ml of dry acetonitrile. Into the well-stirred solution kept at −40 °C, at first *t*-butyl hypochlorite (0.388 g, 3.57 mmol) in 4 ml of dry acetonitrile and then sodium trifluoroacetamidate (prepared by treating trifluoroacetamide (0.511 g, 4.52 mmol) with 60% sodium hydride (0.18 g, 4.51 mmol)) was added. After the whole mixture was strirred at the temperature for 2 h, it was warmed up to room temperature.

Then into the reaction mixture was added aqueous dil. $Na_2S_2O_3$ and the aqueous solution was extracted with chloroform.

The residue was chromatographed on silica gel by elution with hexane–ethyl acetate (7:3). Yield was 0.527 g (53%); colorless crystals; mp 109—114 °C; $[\alpha]_D^{20}$=+35.4° ($CHCl_3$, c=1.06). The enantiomeric excess of the sulfilimine was determined by NMR using Eu(hfc) as shift reagent to be 47±5%; IR (KBr) 1630 (C=O); ^{1}H NMR ($CDCl_3$) δ=3.83 (3H,s,*o*-CH_3O-), 6.8—8.2 (9H,m, aromatic protons); Found; C, 54.45; H, 3.65; N, 4.24%. Calcd for $C_{15}H_{12}F_3NO_2S$; C, 55.04; H, 3.70; N, 4.28%.

Other optically active sulfilimines (**3a—h**) were obtained by the same procedure as described above.

(S)-(−)-S-(o-Methoxyphenyl)-S-phenyl-N-tosylsulfilimine (3a). Optically active **3a** was prepared by a similar method as described above except for using sodium *p*-toluenesulfonamidate (prepared by treating *p*-toluenesulfonamide with sodium methoxide and recrystallized from ethanol-methanol) instead of sodium trifluoroacetamidate. Yield was 47%; colorless crystals; mp 156—158 °C; $[\alpha]_D^{20}$=−40° C ($CHCl_3$, c=1.00); 41% o.p.;[11a] IR (KBr), 995(S-N); ^{1}H NMR ($CDCl_3$) δ=2.32 (3H, *p*-CH_3-), 3.70 (3H,s,*o*-CH_3O-), 6.78-8.20 (13H,m, aromatic protons).

(S)-(−)-S-(o-Methoxyphenyl)-S-phenyl-N-benzoylsulfilimine (3b). Yield was 40%; colorless crystals; mp 115.5—118 °C; $[\alpha]_D^{25}$=−17° ($CHCl_3$, c=1.03); 27±5% e.e; IR (KBr), 1590 (C=O); ^{1}H NMR ($CDCl_3$) δ=3.80 (3H,s,*o*-CH_3O-), 6.82—8.47 (14H,m, aromatic protons).

(S)-(−)-S-(o-Methoxyphenyl)-S-phenyl-N-(chloroacetyl)sulfilimine (3c). Yield was 47%; colorless crystals; mp 122—125 °C; $[\alpha]_D^{20}$=−45.5° ($CHCl_3$, c=0.994); 35±5% e.e; IR (KBr), 1590 (C=O); ^{1}H NMR ($CDCl_3$) δ=3.88 (3H,s,*o*-CH_3O-), 4.24 (2H,s,$ClCH_2$-), 6.84—8.13 (9H,m, aromatic protons); Found; C, 58.48; H, 4.49; N, 4.51%. Calcd for $C_{15}H_{14}ClNO_2S$; C, 58.53; H, 4.58; N, 4.55%.

(R)-(+)-S-(o-Methoxyphenyl)-S-phenyl-N-(dichloroacetyl)-sulfilimine (3d). Yield was 34%; colorless crystals; mp 116.5—120 °C; $[\alpha]_D^{20}$=−11.7° ($CHCl_3$, c=3.78 (3H, s,*o*- IR (KBr) 1600 (C=O); ^{1}H NMR ($CDCl_3$) δ=3.78 (3H,s,*o*-CH_3O-), 6.25 (1H,s,Cl_2CH-), 6.83—8.17 (9H,m, aromatic protons); Found; C, 52.60; H, 3.78; N, 4.09%. Calcd for $C_{15}H_{13}Cl_2NO_2S$; C, 52.64; H, 3.82; N, 4.09%.

(R)-(+)-S-(o-Methoxyphenyl)-S-phenyl-N-(trichloroacetyl) sulfilimine (3e). Yield was 72%; colorless crystals; mp 121—122 °C; $[\alpha]_D^{20}$=+26.4° ($CHCl_3$, c=0.85); 47±5% e.e.; IR (KBr) 1625 (C=O); ^{1}H NMR ($CDCl_3$) δ=3.90 (3H,s,*o*-CH_3O-), 6.85—8.23 (9H,m, aromatic protons); Found; C, 47.80; H, 3.14; N. 3.77%. Calcd for $C_{15}H_{12}Cl_3NO_2S$; C, 47.82; H, 3.21; N, 3.71%.

(S)-(−)-S-(o-Methylphenyl)-S-phenyl-N-tosylsulfilimine (3g). Yield was 72% (2.8 ml of *N,N*-dimethylformamide was added to 28 ml of acetonitrile solution as reaction solvent); colorless crystals; mp 102—103 °C; $[\alpha]_D^{25}$=−14.4° ($CHCl_3$, c=2.07); 35%o.p.[11a]; IR (KBr), 955 (S-N); ^{1}H NMR ($CDCl_3$) δ=2.36 (6H,s,*o*-CH_3- and *p*-CH_3-), 7.02—8.04 (13H,m, aromatic protons)

(R)-(+)-S-(o-Methylphenyl)-S-phenyl-N-(trifluoroacetyl) sulfilimine (3h). Yield was 96%; colorless crystals; mp 64—65°C; $[\alpha]_D^{25}$=+21° ($CHCl_3$, c=1.32); 26±5%e.e.; IR (KBr), 1640 (C=O); ^{1}H NMR ($CDCl_3$) δ=2.66 (3H,s,*o*-CH_3O-), 7.25—8.04 (9H,m, aromatic protons); Found; C, 57.91; H, 3.92; N, 4.46%. Calcd for $C_{15}H_{12}F_3NOS$; C, 57.87; H, 3.88; N, 4.49%.

Circular Dichroism Spectra. CD spectra shown in Fig. 3a, 3b, and 3c were all recorded in methanol solution.

Sulfilimines of which CD spectra were measured, have following optical rotations. (**3a**), $[\alpha]_D^{20}$=−25.5° ($CHCl_3$)

c=1.19); (**3b**), $[\alpha]_D^{20}$=−17.3° ($CHCl_3$, c=1.03); (**3c**), $[\alpha]_D^{20}$=−43.6° ($CHCl_3$, c=2.34); (**3d**), $[\alpha]_D^{20}$=+4.8° ($CHCl_3$, c=2.34); (**3e**), $[\alpha]_D^{20}$=+26.4° ($CHCl_3$, c=0.85); (**3f**), $[\alpha]_D^{20}$=+35.4° ($CHCl_3$, c=1.06); (**3g**), $[\alpha]_D^{25}$=−14.4° ($CHCl_3$, c=2.07); (**3h**), $[\alpha]_D^{25}$=+20.9° ($CHCl_3$, c=1.32).

Syntheses of Authentic Samples. *(S)-(−)-S-(o-Methoxyphenyl)-S-phenyl-N-(trifluoroacetyl)sulfilimine (3f) from (S)-(−)-S-(o-Methoxyphenyl)-S-phenylsulfilimine.* To a benzene solution (10 ml) of (*S*)-(−)-S-(*o*-methoxyphenyl)-S-phenylsulfilimine[11a] $[\alpha]_D^{25}$=−187° (96%o.p) (0.253 g 1.09 mmol) and dry pyridine (0.088 g, 1.12 mmol) stirred in an ice bath, trifluoroacetic anhydride (0.258 g, 1.23 mmol) was added slowly. After stirring the mixture for 1 h, the solution was washed with 10% aqueous NaOH, water, dried ($MgSO_4$), and evaporated under vacuum. The remained oily product was chromatographed on silica gel eluted with benzene: ethyl acetate=2 : 1. Yield was 0.263 g (75%); colorless oil; $[\alpha]_D^{25}$=−13.1° ($CHCl_3$, c=1.02). The IR spectrum and the ^1H NMR spectrum are identical to those of the sulfilimine obtained previously.

Other authentic sulfilimines were obtained by similar methods as described above. The acylating reagents and the results are summarized in Table 2.

(1-Methyloxy)(o-methoxyphenyl)phenylsulfonium perchlorate (2). A mixture of *o*-methoxyphenyl phenyl sulfide (0.228 g, 1.05 mmol) and *l*-menthol (0.194 g, 1.24 mmol) was dissolved in 25 ml of dry acetonitrile. Into the well-stirred solution kept at −40°C, at first *t*-butyl hypochlorite (0.125 ml, 1.05 mmol) and then silver perchlorate (0.228 g, 1.10 mmol) were added. After colorless precipitates (silver chloride) appeared, $Na_2S_2O_3$ and water were added and the solution was filterd. The filterate extracted with chloroform, was washed with water, dried ($MgSO_4$). The chloroform solution was poured into a large amount of ether. Oily product was precipitated and the ethereal layer was removed by decantation. After reprecipitation several times, the oily product was evaporated under reduced pressure. Yield was 0.153 g (31%); colorless oil; R_S-R_C: S_S-R_C=75:25. IR (NaCl), 1070 (ClO_4); ^1H NMR ($CDCl_3$) δ=0.46—2.00 (m, menthyl group protons), 3.93 (s,*o*-CH_3O-(R_S-R_C)), 4.01 (s,*o*-CH_3O-(S_S-R_C)), 6.92—8.15 (m, aromatic protons); Found; C, 58.65; H, 6.74%. Calcd for $C_{23}H_{31}ClO_6S$; C, 58.65; H, 6.63%.

Reactions of Sodium Amides with (1-Methyloxy)(o-methoxyphenyl)phenylsulfonium Perchlorate (2). Typical procedure is as following: The sulfonium salt (**2**) (0.239 g, 0.506 mmol) (*R*/*S*=83/17) was dissolved in 10 ml of dry acetonitrile and strirred at −35 °C. Into the well-stirred solution, sodium trichloroacetamidate (prepared from trichloroacetamide (0.168 g, 1.04 mmol) and 60% sodium hydride (0.041 g, 1.03 mmol)) was added at the temperature. After stirring for 20 min, water was added and extracted with chloroform. The extract was dried and evaporated under vacuum. The oily product was chromatographed on silica gel by elution with benzene-ethyl acetate (2:1). Yield was 0.028 g (39%); colorless crystals; $[\alpha]_D^{19}$=+16° ($CHCl_3$, c=1.1); 44%e.e.; 66% optical yield. The IR and the ^1H NMR spectra of sulfilimines obtained by above method are identical to those of the sulfilimines obtained previously.

Temperature Effect. A mixture of *o*-methoxyphenyl phenyl sulfide (0.215 g, 0.993 mmol) and *l*-menthol (0.195 g, 1.25 mmol) was dissolved in dry acetonitrile (15 ml).

Into the well-stirred solution kept at −40 °C, *t*-butyl hypochlorite (0.125 ml, 1.05 mmol) was added. The reaction mixture was allowed to be set at a certain temperature (−40°, +2, or +22 °C) and then sodium trifluoroacetamidate (prepared as described before) was added. Further work up procedure was the same as described before.

References

1) Preliminary communication see, S. Oae, K. Kikuchi, M. Moriyama, and N. Furukawa, *Chem. Lett.*, **1982**, 1723.

2) For reviews or books see J. G. Tillett, *Chem. Rev.*, **76**, 747 (1976); S. Oae "Organosulfur Chemistry," Kagakudojin, Kyoto (1982); D. J. Cram, J. Day, D. C. Garwood, D. R. Rayner, D. M. von Shrilts, T. R. Williams, A. Nudelman, F. G. Yamagishi, R. E. Booms, and M. R. Jones, *Int, J. Sulfur Chem., C*, **7**, 103 (1972); S. Oae, and N. Furukawa "Sulfilimines and Related Derivatives," ACS Monograph, **179**, Am. Chem. Soc., Washington D. C. (1983).

3) H. Phillips, *J. Chem. Soc.*, **127**, 2552 (1925).

4) M. Mikolajczyk and J. Drabowicz, "Chiral Organosulfur Compounds," in "Topics in Stereochemistry Vol. 13," ed by N. L. Allinger, E. L. Eliel, and S. H. Wilen, John Wiley and Sons (1982).

5) S. Oae, M. Yokoyama, M. Kise, and N. Furukawa, *Tetrahedron Lett.*, **1968**, 4131.

6) B. W. Christensen and A. Kjaer, *J. Chem. Soc., Chem. Commun.*, **1969**, 934; F. G. Yamagishi, D. R. Rayner, E. T. Zwicker, and D. J. Cram, *J. Am. Chem. Soc.*, **95**, 1916 (1973).

7) B. W. Christensen, *J. Chem. Soc., Chem. Commun.*, **1971**, 597.

8) T. J. Maricich and V. L. Hoffman, *Tetrahedron Lett.*, **1972**, 5309; *J. Am. Chem. Soc.*, **96**, 7770 (1974).

9) M. Mikolajczyk and J. Drabowicz, *J. Chem. Soc., Chem. Commun.*, **1974**, 774.

10) J. Drabowicz, B. Bujnicki, and M. Mikolajczyk, *J. Org. Chem.*, **46**, 2788 (1981); R. Annunziata, M. Cinquini, and S. Colonna, *J. Chem. Soc., Perkin Trans. 1*, **1975**, 404.

11) a) M. Moriyama, T. Yoshimura, N. Furukawa, T. Numata, and S. Oae, *Tetrahedron*, **32**, 3003 (1976); b) M. Moriyama, K. Kuriyama, T. Iwata, N. Furukawa, T. Numata, and S. Oae, *Chem. Lett.*, **1976**, 363.

12) M. Koshibe, Y. Matsuura, and M. Kakudo, 36th. National Meeting of the Chemical Society of Japan, Osaka, April 1977, Abstr., No. 4M31.

13) J. T. Edward and S. C. R. Meacock, *J. Chem. Soc.*, **1957**, 2000.

14) T. Higuchi, C. H. Barnstein, H. Ghassemi, and W. E. Peretz, *Anal. Chem.*, **34**, 400 (1962).

15) W. E. Truce, D. P. Tate, and D. N. Burge, *J. Am. Chem. Soc.*, **82**, 2872 (1960).

16) M. J. Mintz and C. Walling, *Org. Synth.*, Coll. Vol., 5, 184, (1973).

 © 1985 The Chemical Society of Japan Bull. Chem. Soc. Jpn., 58, 1942—1945 (1985) [Vol. 58, No. 7

A Convenient Route to 2-Lithio-1,3-butadiene from Chloroprene *via* 2-Stannyl-1,3-butadiene

Eiji WADA, Shuji KANEMASA, Isamu FUJIWARA, and Otohiko TSUGE*
Research Institute of Industrial Science, and Department of Molecular Science and Technology, Interdisciplinary Graduate School of Engineering Sciences, Kyushu University, Kasugakoen, Kasuga 816
(Received February 22, 1985)

A convenient route to 2-lithio-1,3-butadiene from chloroprene *via* a 2-stannyl-1,3-butadiene is presented, and the regioselective additions to a variety of carbonyl groups are demonstrated.

Introduction of a 1,3-butadienyl unit to a molecule is important in organic synthesis as the diene moiety can be used usefully to construct a stereochemically defined six-membered ring. One of the most useful reagents along this purpose is 1-methylene-2-propenylmagnesium chloride which is easily accessible in a large quantity from an industrial material, chloroprene.[1] However, a serious disadvantage is a poor regioselectivity in the additions to carbonyl groups. In most reported cases, it reacts at both the α- and γ-positions and major products are usually the γ-adducts,[2] while its cross coupling reactions with alkyl halides[3] and the Michael reactions take place in a highly regioselective manner at the α-position.[4]

Recently it has been reported that 2-lithio-1,3-butadiene reacts with several aldehydes mainly at the α-position.[5] However, this reagent was prepared only in a fair yield from the Shapiro reaction of trisylhydrazone (2,4,6-triisopropylphenylsulfonylhydrazone) of methyl vinyl ketone, its use in organic synthesis having been quite limited.

The present work aims at opening a more convenient and efficient route to 2-lithio-1,3-butadiene from chloroprene, and also knowing the degree of α-regioselectivity of this reagent in the reactions with some other types of carbonyl compounds.

Results and Discussion

The Grignard reagent **1**, prepared from chloroprene and metal magnesium in the presence of zinc chloride in dry tetrahydrofuran (THF) was transmetalated with chlorotributyltin affording an excellent yield of 2-(tributylstannyl)-1,3-butadiene **2**, which had been previously synthesized from the Grignard reagent of 4-chloro-1,2-butadiene with the stannyl reagent.[6] The tin-lithium exchange reaction was examined in dry THF at −78 °C using butyllithium, and 2-lithio-1,3-butadiene **3** generated was allowed to react with a variety of carbonyl compounds as shown in Scheme 1.

Treatment of **2** with an equivalent of butyllithium in dry THF, at −78 °C for 0.5 h, provided a deep red-colored solution of **3** to which was then

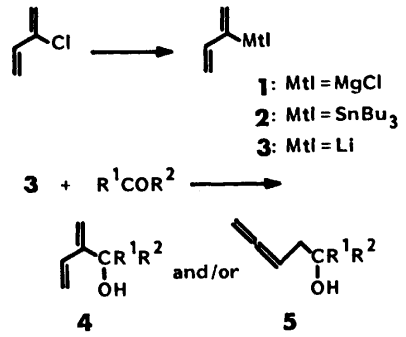

Scheme 1.

added an equivalent of benzaldehyde in THF. The mixture was quenched, after 0.5 h at the same temperature, with an ice-cold ammonium chloride solution. The crude product which was obtained in 80% yield by the filtration through a short column over silica gel was found to be a mixture of two isomeric alcohols, the 2-methylene-3-buten-1-ol **4a** as an α-adduct and the 3,4-pentadien-1-ol **5a** as a γ-adduct, in 9:1 ratio.

Table 1 summarizes the results obtained from the reactions of **3** with other carbonyl compounds under similar conditions. Aliphatic aldehydes, whichever with a straight alkyl chain or a bulky substituent, α,β-unsaturated aldehydes carrying a variety of substituents at the β-position, and acetophenones all smoothly reacted with **3** providing the corresponding alcohols **4b**—**4i** and/or **5b**—**5i** in satisfied yields. The α-selectivity was found excellent in all cases, no γ-adducts being even detected by GLC or ^{1}H-NMR analyses in some cases (the reactions leading to exclusive formation of **4b**, **4c**, **4e**, and **4g**). To be noteworthy is the high α-selectivity toward acetophenones because the Grignard reaction of **1** has shown a very poor afinity at the α-position to this aromatic ketone (**4h**:**5h**=12~19:88~81). Even benzophenone which is known to afford only the γ-adduct **5j** in the Grignard reaction produced a mixture of comparable amounts of **4j** and **5j**, while their separation was unsuccessful.

The present method offers an alternative for the preparation of **3** and seems more convenient and effi-

Table 1. Reactions of 2-lithio-1,3-butadiene **3** with carbonyl compounds[a)]

Carbonyl compounds	Products			Yield/%[b)]		Products from **1**	
	4, 5	R^1	R^2	**4+5**	**4 : 5**	Yield/%	**4 : 5**
PhCHO	**a**	H	Ph	80	91 : 9 (46%, 93 : 7)[c)]	73[d)] 68[e)]	39 : 61[d)] 30 : 70[e)]
$Me(CH_2)_5CHO$	**b**	H	$Me(CH_2)_5$	61	Only **4b**		
Me_3CCHO	**c**	H	Me_3C	61	Only **4c**		
CH_2=CHCHO	**d**	H	CH_2=CH	59	96 : 4		
MeCH=CHCHO (t)	**e**	H	MeCH=CH (t)	80	Only **4e**		
PhCH=CHCHO (t)	**f**	H	PhCH=CH (t)	76	19 : 1 (32%, 81 : 19)[c)]	84[f)]	7 : 9[f)]
Me_2C=CHCHO	**g**	H	Me_2C=CH	45	Only **4g**		
PhCOMe	**h**	Me	Ph	70	9 : 1	63[d)] 45[e)]	19 : 81[d)] 12 : 88[e)]
p-$MeOC_6H_4COMe$	**i**	Me	*p*-$MeOC_6H_4$	78	95 : 5		
PhCOPh	**j**	Ph	Ph	73	1 : 1	92[d)]	Only **5j**[d)]

a) Conditions: **2** : *n*-BuLi : R^1COR^2 = 1 : 1 : 1 in dry THF at −78 °C. b) Isolated yields. The isomer ratio was determined by GPLC or ^{1}H-NMR. c) Ref. 2a. d) Ref. 1. f) Our unpublished results.

cient than the Shapiro procedure. It is certain that this method stimulates the wide applications of the industrial material, chloroprene, in organic synthesis. We have recently developed a new [6.6] annelation method by the diene-transmissive Diels-Alder reaction equivalent of 2-methylene-3-buten-1-ols which were prepared by the Grignard reactions of chloroprene.[2b)] These carbinols are now being employed in a research directed toward the [6.5] annelation processes by the sequence of Diels-Alder reaction and Nazarov cyclization or Diels-Alder cycloaddition and electrocyclic reaction.

Experimental

General. IR spectra were recorded on a JASCO IRA-1 or a JASCO A-102 IR spectrometer. ^{1}H-NMR spectra were taken with a Hitachi R-40 (90 MHz) or a JEOL FX-100 instrument (100 MHz) and ^{13}C-NMR spectra on a JEOL FX-100 spectrometer at 25.04 MHz. Chemical shifts are expressed in part per million downfield from tetramethylsilane as an internal standard. Mass spectra were measured with a JEOL JMS-01SG-2 mass spectrometer at 70 or 40 eV of ionization energy. Elemental analyses were obtained with a Hitachi 026 CHN micro analyzer. GPLC analysis was performed on a Yanagimoto gas chromatograph YANACO G-2800 model equipped with a hydrogen flame ionization detector (column: SE 30, 3 mm×2 m). Micro vacuum distillation was carried out with a Shibata GTO-250R Kugelrohr distilling apparatus, and boiling points are all uncorrected. For preparative column chromatography, either of Wakogel C 300 or Silicagel 60 (Merck, 70—230 mesh) was used. Solvents were evaporated with a Tokyo Rikakikai rotary evaporator type V at 0 °C to room temperature unless otherwise stated.

Materials. Tetrahydrofuran as a reaction solvent was distilled over lithium aluminum hydride prior to its use. Chloroprene was purified by distillation under nitrogen stream from the xylene solution also immediately before it was used. Anhydrous zinc chloride was obtained by the crystallization of commercial material from dioxane containing a small amount of zinc powder. Metal magnesium (turning), chlorotributyltin, and butyllitium (15% in hexane) are commercially available and were used without further purification. The carbonyl compounds which are also all commercially available were purified by distillation or crystallization.

2-(Tributylstannyl)-1,3-butadiene **2**. To a solution of **1**, prepared from chloroprene (21 g, 0.187 mol), magnesium (5 g, 0.206 g atom), anhydrous zinc chloride (1.2 g) in dry tetrahydrofuran (80 ml) according to the reported method,[1)] was added dropwise a solution of chlorotributyltin (55.3 g, 0.17 mol) in tetrahydrofuran (80 ml) at −12 to −10 °C. After heated under reflux for 0.5 h, the mixture was treated with aqueous solution of ammonium chloride at 0 °C. The tetrahydrofuran was condensed *in vacuo*, the residue extracted with ether, the ether dried over anhydrous magnesium sulfate, and finally evaporated *in vacuo*. The liquid obtained was distilled under vacuum giving 51.6 g (89%) of pure **2** as a colorless liquid: bp 92—95 °C (93 Pa) (lit,[6)] bp 80—90 °C (53 Pa)).

General Procedure for the Preparation of 2-Lithio-1,3-butadiene **3** *and its Reactions with Carbonyl Compounds.* To a solution of **2** (1.25 g, 3.64 mmol) in dry tetrahydrofuran (9 ml), was added butyllithium (2.25 ml, 3.6 mmol) at −78 °C under nitrogen and then the mixture was stirred for 0.5 h during which time the color of solution gradually turned deep red. When carbonyl compounds (3.6 mmol) in tetrahydrofuran (2 ml) was added by the use of a syringe, the red color immediately faded away. The mixture was stirred for 0.5 h at the same temperature and treated with ice-cold ammonium chloride solution. Organic products were extracted with ether (20 ml×2), the ether dried over magnesium sulfate, and then evaporated *in vacuo*. The residue was chromatographed through a short column packed with silica gel. The first fraction containing tetrabutyltin as an undesired product was eluted with hexane and disregarded. After all the tin compound was removed out, the second fraction was collected using hexane–ether (3:1) for the low-boiling products or hexane–

ethyl acetate (9:1) for the nonvolatile products. At this moment, the isomer ratios between **4** and **5** were determined by GPLC and/or ^{1}H-NMR analyses. The combined yields as well as the isomer ratios for **4** and **5** are given in Table 1.

Although the 2-methylene-3-buten-1-ols **4a** to **4i** could be separated and purified through repeated chromatographic operations over silica gel in a long column (15 mm×400 mm) using hexane–ether (20:1) or hexane–ethyl acetate (9:1) as an eluent, no authentic samples of allenic alcohols **5** were obtained because of the too poor formation and the contamination by the major products **5**. The formation of **5** was, however, confirmed on the basis of the analysis of ^{1}H-NMR spectra for the crude reaction mixtures. The separation of either **4j** or **5j** which was yielded from benzophenone was unsuccessful.

The spectral data and elemental analyses for the products are given below. Some of the products were transformed to their derivatives which were then submitted for elemental analyses.

2-Methylene-1-phenyl-3-buten-1-ol ***4a***: Colorless viscous oil; IR (neat) 3350 cm^{-1} (OH); ^{1}H-NMR ($CDCl_3$) δ=2.82 (1H, br. s, OH), 4.97 (1H, d, $J_{4-3\,(cis)}$=11.2 Hz, one of 4-H), 5.11 (1H, d, $J_{4-3\,(trans)}$=17.8 Hz, the other of 4-H), 5.22 (1H, s, 1-H), 5.30 (2H, s, 2-(CH_2=)), 6.23 (1H, dd, J_{3-4}=17.8 and 11.2 Hz, 3-H), and 7.23 ppm (5H, m, Ph); ^{13}C-NMR ($CDCl_3$) δ=73.78 (d, 1-C), 115.25, 115.49 (each t, 4-C and 2-($\underline{C}H_2$=)), 126.89, 127.62, 128.31 (each d, *o*-, *m*-, and *p*-C of Ph), 135.81 (d, 3-C), 142.00 (s, 1-C of Ph), and 147.56 ppm (s, 2-C); MS *m/z* (rel. intensity, %) 160 (M^+, 33), 142 (16), 129 (10), 115 (11), 107 (83), 105 (28), 91 (18), 79 (base peak), 78 (18), and 77 (64).

Found: *m/z* 160.0880. Calcd for $C_{11}H_{12}O$: M, 160.0888. ^{1}H-NMR ($CDCl_3$) of the isomeric alcohol **5a**: δ=2.36 (m, CH_2) and 4.60 ppm (m, =CH_2). The ratio of **4a**:**5a**=9:1.

3-Methylene-1-decen-4-ol ***4b***: Colorless oil; IR (neat) 3330 cm^{-1} (OH); ^{1}H-NMR ($CDCl_3$) δ=0.87 (3H, t, Me), 1.05—1.80 (10H, m, CH_2), 2.47 (1H, br. s, OH), 4.37 (1H, t, J_{4-5}=5.7 Hz, 4-H), 5.04 (1H, d, $J_{1-2\,(cis)}$=11.0 Hz, one of 1-H), 5.10, 5.18 (each 1H, s, 3-(CH_2=)), 5.29 (1H, d, $J_{1-2\,(trans)}$=17.9 Hz, the other of 1-H), and 6.31 ppm (1H, dd, J_{2-1}=17.9 and 11.0 Hz, 2-H); ^{13}C-NMR ($CDCl_3$) δ=14.13 (q, 10-C), 22.71, 25.88, 29.34, 31.92, 36.50 (each t, 5-, 6-, 7-, 8-, and 9-C), 71.63 (d, 4-C), 113.78 (t, 3-($\underline{C}H_2$=)), 114.08 (t, 1-C), 136.30 (d, 2-C), and 149.40 ppm (s, 3-C); MS *m/z* (rel. intensity, %) 168 (M^+, 5), 151 (9), 97 (29), 84 (98), and 83 (base peak).

Elemental analysis was carried out with an authentic sample of the *p*-nitrobenzoate of **4b** (pale yellow oil).

Found: C, 67.98; H, 7.35; N, 4.57%. Calcd for $C_{18}H_{23}NO_4$: C, 68.12; H, 7.31; N, 4.41%.

2,2-Dimethyl-4-methylene-5-hexen-3-ol ***4c***: Colorless viscous oil; IR (neat) 3450 cm^{-1} (OH); ^{1}H-NMR ($CDCl_3$) δ=0.90 (9H, s, *t*-Bu), 2.10 (1H, br. s, OH), 4.10 (1H, s, 3-H), 4.99 (1H, dd, $J_{6-5\,(cis)}$=11.2 and J_{gem}=1.2 Hz, one of 6-H), 5.10, 5.27 (each 1H, br. s, 4-(CH_2=)), 5.34 (1H, dd, $J_{6-5\,(trans)}$=17.6 and J_{gem}=1.2 Hz, the other of 6-H), and 6.34 ppm (1H, br. dd, J_{5-6}=17.6 and 11.2 Hz, 2-H); ^{13}C-NMR ($CDCl_3$) δ=26.46 (q, Me of *t*-Bu), 35.50 (s, 2-C), 78.86 (d, 3-C), 113.82 (t, 4-($\underline{C}H_2$=)), 115.67 (t, 6-C), 138.28 (d, 5-C), and 148.58 ppm (s, 4-C).

Elementary analysis was performed with an authentic sample of the *p*-nitrobenzoate of **4c** (pale yellow prisms from hexane, mp 46—47 °C).

Found: C, 66.64; H, 6.66; N, 4.90%. Calcd for $C_{16}H_{19}NO_4$: C, 66.42; H, 6.62; N, 4.84%.

4-Methylene-1,5-hexadien-3-ol ***4d***: Colorless viscous oil; bp 75 °C (439 Pa); IR (neat) 3500 cm^{-1} (OH); ^{1}H-NMR ($CDCl_3$) δ=2.48 (1H, br. s, OH), 4.86 (1H, d, J_{3-2}=5.5 Hz, 3-H), 4.96—5.50 (6H, m, 1-H (2H), 6-H (2H), and 4-(CH_2=) (2H)), 5.93 (1H, ddd, J_{2-1}=17.5 and 10.0 and J_{2-3}=5.5 Hz, 2-H), and 6.32 ppm (1H, dd, $J_{5-6\,(trans)}$=17.5 and $J_{5-6\,(cis)}$=11.0 Hz, 5-H); ^{13}C-NMR ($CDCl_3$) δ=72.32 (d, 3-C), 114.91 (t, 4-($\underline{C}H_2$=)), 115.10, 115.64 (each t, 1- and 6-C), 135.86 (d, 5-C), 139.03 (d, 2-C), and 147.21 ppm (s, 4-C).

This compound **4d** polymerized in the oven of mass spectrometer, showing some higher fragment peaks than that for the parent ion.

The elemental analysis was carried out with an authentic sample of the *p*-nitrobenzoate of **4d** (pale yellow viscous oil).

Found: C, 64.88; H, 5.15; N, 5.59%. Calcd for $C_{14}H_{13}NO_4$: C, 64.86; H, 5.05; N, 5.40%.

^{1}H-NMR ($CDCl_3$) of the isomeric alcohol **5d**: δ=2.23 (m, CH_2) and 4.64 ppm (m, =CH_2).

(E)-3-Methylene-1,5-heptadien-4-ol ***4e***: Colorless viscous oil; bp 100 °C (399 Pa); IR (neat) 3350 cm^{-1} (OH); ^{1}H-NMR ($CDCl_3$) δ=1.70 (3H, dd, J_{7-6}=5.0 and J_{7-5}=0.5 Hz, Me), 2.46 (1H,br. s, OH), 4.80 (1H, d, J_{4-5}=5.5 Hz, 4-H), 5.00—5.92 (6H, m, 1-H (2H), 3-(CH_2=) (2H), 5-H, and 6-H), and 6.30 ppm (1H, $J_{2-1\,(trans)}$=17.5 and $J_{2-1\,(cis)}$=10.0 Hz, 2-H); ^{13}C-NMR ($CDCl_3$) δ=17.67 (q, 7-C), 72.17 (d, 4-C), 114.12 (t, 3-($\underline{C}H_2$=)), 114.71 (t, 1-C), 127.81 (d, 5-C), 132.25 (d, 6-C), 136.06 (d, 2-C), and 147.84 ppm (s, 3-C); MS *m/z* (rel. intensity, %) 124 (M^+, 5), 110 (18), 106 (11), 95 (36), 91 (13), 81 (15), 80 (17), 79 (13), and 71 (base peak).

Found: *m/z* 124.0878. Calcd for $C_8H_{12}O$: M, 124.0888.

(E)-4-Methylene-1-phenyl-1,5-hexadien-3-ol ***4f***: Colorless viscous oil; IR (neat) 3330 cm^{-1} (OH); ^{1}H-NMR ($CDCl_3$) δ=2.82 (1H, br. s, OH), 4.97 (1H, d, J_{3-2}=6.5 Hz, 3-H), 5.00—5.50 (4H, m, 6-H (2H) and 4-(CH_2=) (2H)), 6.20 (1H, dd, J_{2-3}=6.5 and J_{2-1}=16.0 Hz, 2-H), 6.32 (1H, dd, $J_{5-6\,(trans)}$=17.5 and $J_{5-6\,(cis)}$=11.2 Hz, 5-H), 6.58 (1H, dd, J_{1-2}=16.0 Hz, 1-H), and 7.10—7.40 ppm (5H, m, Ph); ^{13}C-NMR ($CDCl_3$) δ=71.97 (d, 3-C), 115.00 (t, 6-C and 4-($\underline{C}H_2$=)), 126.45, 127.58, 128.45 (each d, *o*-, *m*-, and *p*-C of Ph), 130.35, 130.93 (each d, 1- and 2-C), 135.81 (d, 5-C), 136.54 (s, 1-C of Ph), and 147.26 ppm (s, 4-C); MS *m/z* (rel. intensity, %) 186 (M^+, 26), 142 (15), 134 (11), 133 (base peak), 131 (14), 129 (13), 128 (11), 115 (49), 107 (21), 105 (39), 104 (24), 103 (25), 95 (23), and 91 (52).

Found: *m/z* 186.1048. Calcd for $C_{13}H_{14}O$: M, 186.1044.

^{1}H-NMR ($CDCl_3$) of the isomeric alcohol **5f**: δ=4.66 ppm (m, =CH_2). The ratio of **4f**:**5f**=19:1.

6-Methyl-3-methylene-1,5-heptadien-4-ol ***4g***: Colorless viscous oil; IR (neat) 3300 cm^{-1} (OH); ^{1}H-NMR ($CDCl_3$) δ=1.72 (6H, s, Me), 2.18 (1H, br. s, OH), 4.90—5.40 (6H, m, 1-H (2H), 3-(CH_2=) (2H), 4-H, and 5-H), and 6.29 ppm (1H, dd, $J_{2-1\,(trans)}$=18.0 and $J_{2-1\,(cis)}$=11.0 Hz, 2-H); ^{13}C-NMR ($CDCl_3$) δ=18.02, 25.58 (each q, Me), 68.26 (d, 4-C), 113.71 (t, 3-($\underline{C}H_2$=)), 114.45 (t, 1-C), 126.80 (d, 5-C), 136.13 (s, 6-C), 136.23 (d, 2-C), and 148.58 ppm (s, 3-C); MS *m/z* (rel. intensity, %) 138 (M+, 4), 123 (8), 120 (5), 105 (15), 95 (30), 91 (17), 85 (base peak), 83 (37), 80 (26), 79 (18), 77 (17), and 67 (20).

Found: *m/z* 138.1043. Calcd for $C_9H_{14}O$: M, 138.1044.

3-Methylene-2-phenyl-4-penten-2-ol ***4h***: Colorless viscous

oil; IR (neat) 3420 cm^{-1} (OH); ^{1}H-NMR ($CDCl_3$) δ=1.66 (3H, s, Me), 2.24 (1H, br. s, OH), 4.94 (1H, dd, $J_{5-4\,(cis)}$= 11.0 and J_{gem}=1.2 Hz, one of 5-H), 5.24 (1H, dd, $J_{5-4\,(trans)}$= 17.5 and J_{gem}=1.2 Hz, the other of 5-H), 5.31, 5.34 (each 1H, s, 3-(CH_2=)), 6.09 (1H, dd, J_{4-5}=17.5 and 11.0 Hz, 4-H), and 7.00—7.60 ppm (5H, m, Ph); ^{13}C-NMR ($CDCl_3$) δ=29.53 (q, Me), 76.12 (s, 2-C), 111.93 (t, 3-($\underline{C}H_2$=)), 116.51 (t, 5-C), 125.33, 126.99, 128.20 (each d, *o*-, *m*-, and *p*-C of Ph), 135.56 (d, 4-C), 146.09 (s, C-1 of Ph), and 151.89 ppm (s, 3-C); MS *m/z* (rel. intensity, %) 174 (M^+, 22), 159 (12), 131 (20), 130 (13), 129 (10), 121 (78), 115 (12), 105 (25), 91 (18), 77 (21), and 43 (base peak).

Found: *m/z* 174.1032. Calcd for $C_{12}H_{14}O$: M, 174.1044.

^{1}H-NMR ($CDCl_3$) of the isomeric alcohol **5h**: δ=1.53 (s, Me), 2.50 (m, CH_2), and 4.60 ppm (m, =CH_2). The ratio of **4h**:**5h**=9:1.

3-Methylene-2-(p-methoxyphenyl)-4-penten-2-ol ***4i***: Colorless viscous oil; IR (neat) 3450 cm^{-1} (OH); ^{1}H-NMR ($CDCl_3$) δ=1.67 (3H, s, Me), 2.31 (1H, br. s, OH), 3.76 (3H, s, *p*-MeO), 4.93 (1H, dd, $J_{5-4\,(cis)}$=11.0 and J_{gem}=1.8 Hz, one of 5-H), 5.24 (1H, dd, $J_{5-4\,(trans)}$=17.5 and J_{gem}=1.8 Hz, the other of 5-H), 5.32 (2H, br. s, 3-(CH_2=)), 6.09 (1H, dd, J_{4-5}=17.5 and 11.0 Hz, 4-H), 6.78, and 7.29 ppm (each 2H, m, Ar); ^{13}C-NMR ($CDCl_3$) δ=29.29 (q, Me), 55.11 (q, *p*-MeO), 75.68 (s, 2-C), 111.35 (t, 3-($\underline{C}H_2$=)), 113.49 (d, 3-C of Ar), 116.12 (t, 5-C), 126.60 (d, 2-C of Ar), 135.61 (d, 4-C), 138.20 (s, 1-C of Ar), 152.13 (s, 3-C), and 158.47 ppm (s, 4-C of Ar); MS *m/z* (rel. intensity, %) 204 (M^+, 7), 152 (99), 135 (17), 108 (55), 77 (12), and 43 (base peak).

Found: C, 75.89; H, 7.95%. Calcd for $C_{13}H_{16}O_2$: C, 76.44; H, 7.90%.

Found: *m/z* 204.1191. Calcd for $C_{13}H_{16}O_2$: M, 204.1149. ^{1}H-NMR ($CDCl_3$) of the isomeric alcohol **5i**: δ=1.53 (s, Me), 2.50 (m, CH_2), and 4.61 ppm (m, =CH_2). The ratio of **4i**:**5i**=20:1.

2-Methylene-1,1-diphenyl-3-buten-1-ol ***4j*** *and 1,1-Diphenyl-3,4-pentadien-1-ol* ***5j***: These alcohols were obtained as the 1:1 mixture whose separation was unsuccessful. The ^{1}H- and ^{13}C-NMR spectra of the mixture were analyzed by the comparison with the spectra of the authentic sample of **5j** which was prepared from the reaction of **1** with benzophenone.[1] **4j**: ^{1}H-NMR ($CDCl_3$) δ=2.88 (1H, s, OH), 4.68 (1H, s, one of 2-(CH_2=)), 4.98 (1H, dd, $J_{4-3\,(cis)}$=11.0 and J_{gem}=1.7 Hz, one of 4-H), 5.30 (1H, dd, $J_{4-3\,(trans)}$=17.7 and J_{gem}=1.7 Hz, the other of 4-H), 5.41 (1H, s, the other of 2-(CH_2=)), 6.22 (1H, dd, J_{3-4}=17.7 and 11.0 Hz, 3-H), and 7.00—7.50 ppm (10H, m, Ph); ^{13}C-NMR ($CDCl_3$) δ= 83.02 (s, 1-C), 117.89 (t, 2-($\underline{C}H_2$=)), 118.13 (t, 4-C), 128.40, 128.87, 129.05 (each d, *o*-, *m*-, and *p*-C of Ph), 137.15 (d, 3-C), 147.42 (s, 1-C of Ph), and 152.53 ppm (s, 2-C). **5j**: ^{1}H-NMR ($CDCl_3$) δ=2.70 (1H, s, OH), 2.97 (2H, dt, J_{2-3}= 7.4 and J_{2-5}=2.8 Hz, 2-H), 4.57 (2H, br. dt, J_{5-3}=6.2 and J_{5-2}=2.8 Hz, 5-H), 4.93 (1H, dt, J_{3-2}=7.4 and J_{3-5}=6.2 Hz, 3-H), and 7.00—7.50 ppm (10H, m, Ph); ^{13}C-NMR ($CDCl_3$) δ=41.80 (t, 2-C), 74.50 (t, 5-C), 77.55 (s, 1-C), 84.83 (d, 3-C), 125.99, 126.81, 128.05 (each d, *o*-, *m*-, and *p*-C of Ph), 146.13 (s, 1-C of Ph), and 210.30 ppm (s, 4-C).

We would like to thank Toyo Soda Co., Ltd., for giving us a generous gift of chloroprene.

References

1) S. Nunomoto and Y. Yamashita, *J. Org. Chem.*, **44**, 4788 (1979).

2) a) K. Kondo, S. Dobashi, and M. Matsumoto, *Chem. Lett.*, **1976**, 1077; b) O. Tsuge, E. Wada, S. Kanemasa, and H. Sakoh, *ibid.*, **1984**, 469 and 709. See also Ref. 1.

3) S. Nunomoto, Y. Kawakami, and Y. Yamashita, *J. Org. Chem.*, **48**, 1912 (1983).

4) K. J. Shea and P. Q. Pham, *Tetrahedron Lett.*, **24**, 1003 (1983).

5) P. A. Brown and P. R. Jenkins, *Tetrahedron Lett.*, **23**, 3733 (1982).

6) C. A. Aufdermarsh, Jr., *J. Org. Chem.*, **29**, 1994 (1964). The same procedure to ours was presented by M. Mizuno, T. Ohta, M. Kawanishi, T. Hitomi, and S. Kojima, 49th National Meeting of the Chemical Society of Japan, Tokyo, April 1984, Abstr., No. 2Z07.

Alkylation and Oxidation of 6,7-Dihydro-6-methyl-5*H*-dibenzo-[*b*,*g*][1,5]thiazocine. Selective Oxidation of the Sulfide Moiety by Transannular Participation of the Amino Group

Katsuo OHKATA, Kohichi TAKEE, and Kin-ya AKIBA*
Department of Chemistry, Faculty of Science, Hiroshima University
Higashisenda-machi, Naka-ku, Hiroshima 730
(Received February 23, 1985)

6,7-Dihydro-6-methyl-5*H*-dibenzo[*b*,*g*][1,5]thiazocine (**7**) was prepared by cyclization of the corresponding amino alcohol using thionyl chloride in acetonitrile. Methylation of **7** gave *N*,*N*-dimethyl derivative (**8**) as the sole product. Treatment of **7** with various oxidizing reagents, however, afforded the corresponding sulfoxide (**9**) and/or *N*-oxide (**13**), and sulfone (**14**) depending on the kind of reagent. Oxidation of **7** with sodium periodate furnished *N*-oxide (**13**) in 72% yield as a major product along with sulfoxide (**9**) in 12% yield, while **9** was obtained as a major product (76%) by oxidation with sodium hypochlorite together with a small amount of methoxysulfonium derivative (**15**) in aqueous methanol. The acceleration in oxidation of **7** compared with diphenyl sulfide as well as production of **15** is ascribed to the transannular participation of the amino group with the chlorosulfonio group or intermediacy of a sulfurane. In addition, structural features of **9** and **15** have been investigated by means of ^{1}H NMR and evidence for the transannular interaction between the two heteroatoms is presented.

Previously, one of us reported that the selectivity of alkylation of compounds containing both sulfur and nitrogen atoms is dependent upon the structure of the compounds and also the properties of reagents.[1] During the investigation, we invoked the presence of equilibrium between the sulfonioamine (**1**) and the ammoniosulfurane (**2**) or the formation of the latter (Eq. 1). No positive evidence for Eq. 1, however, could be obtained by ^{1}H NMR and UV spectroscopy even for **3** and **4**, where the two heteroatoms are designed to come closely. This was ascribed to the congestion among methyl groups.[1a]

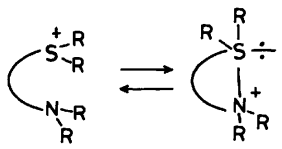

(1)

1 **2**

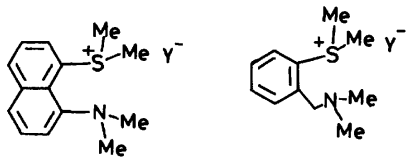

3 **4**

On the other hand, Young and Hsieh proposed that a sulfurane intermediate with S–N bonding was required to account for the kinetic behavior in oxidation of methionine.[2] Moreover, Musker *et al.* also invoked such a sulfurane intermediate in the iodine oxidation of 5-methyl-1-thia-5-azacyclooctane on the basis of their kinetic investigation.[3]

In this paper, we wish to describe selective methylation and oxidation of 6,7-dihydro-6-methyl-5*H*-dibenzo[*b*,*g*][1,5]thiazocine (**7**) in which frontal congestion between the two heteroatoms can be got around. The corresponding ammonium salt (**8**) was obtained exclusively in the methylation and the oxidation took place predominantly on the sulfur where transannular participation of the amino group is proposed.

Results and Discussion

6,7-Dihydro-6-methyl-5*H*-dibenzo[*b*,*g*][1,5]thiazocine (**7**) and its ammonium salt (**8**) were prepared by a suitable modification of the procedure developed by Mehta and his coworkers[4] as illustrated in path A and the sulfoxide (**9**) in path B by Tanaka *et al.*[5] (Scheme 1). These contain the sulfide, the sulfoxide, and the amino groups, which are susceptible to electrophilic reactions.

Methylation of the Title Compound (7). Methylation of **7** with various reagents (MeI, MeI/HgI_2, $Me_3O^+BF_4^-$, MeI/$AgBF_4$, and FSO_3Me) gave the ammonium salt (**8**) as the sole product, which was identified on the basis of spectral comparisons with an authentic sample.[4] The spectral data and the reaction conditions are summarized in Table 1. The results are, on the whole, independent of the method of methylation and are contrary to those obtained for other substrates, where selective methylation took place on the amino and the sulfide groups according to the kind of reagent.[1] The observed spectra result from two kinds of conformer (BC and TB) in every case as reported by Mehta and coworkers.[4,6] Furthermore, reaction of the ammonium sulfide (**10**) with Meerwein's reagent ($Me_3O^+BF_4^-$) does not proceed, whereas *o*-(methylthio)benzylammonium salt (**12**) is smoothly converted into the corresponding sulfonium salt (**4**) under the same conditions (Scheme 2).[1a] The results indicate that the reactivity at the

sulfide function in **7** is extremely decreased due to the delocalization of a lone-pair electrons over two benzene rings.

Oxidation of the Title Compound (7). Due to relatively small difference between the oxidation potentials of sulfide and amine, considerable difficulty was expected for selective oxidation of the title compound (**7**), *i.e.*, oxidation potential in cyclic voltammetry is +1.81 V ($Ag/AgNO_3$) for diphenyl sulfide and +1.92 V ($Ag/AgNO_3$) for *N*,*N*-dibenzylmethylamine.[7] The results of oxidation of **7** with some reagents are illustrated in Scheme 3.

The reactive position clearly depends on the kind of oxidizing reagent. Oxidation of **7** with sodium periodate afforded a mixture of sulfoxide (**9**: 12%) and *N*-oxide (**13**: 72%), the latter is very polar with a low R_f value on silica gel and is an extremely hygroscopic compound. In the oxidation of **7** with hydrogen peroxide in refluxing acetic acid, sulfoxide (**9**) was not obtained but sulfone (**14**) was a sole product. Reaction of **7** with aqueous sodium hypochlorite at −78 °C in methanol solution afforded sulfoxide (**9**) in 76% yield. It is noteworthy that the oxidation at room temperature furnished methoxysulfonium derivative (**15a**) in a very small amount besides the major product (**9**: 47%). The structure of **9** was confirmed by an alternative synthesis developed by Tanaka *et al.* as shown in path B of Scheme 1.[5a] Structural assignment to **13** and **14** is based upon the spectral data and their chemical behavior in comparison with **9**.

It is noteworthy that the amino sulfide (**7**) was oxidized to **9** accompanied with a small amount of methoxysulfonium derivative (**15a**) smoothly with aqueous hypochlorite in methanol under the same conditions where diphenyl sulfide was inert. The structure of **15a** was assigned as methoxyammoniosulfurane on the basis of spectral analogy to that of **15b** obtained by methylation of **9**.[8a,c] Both the acceleration in oxidation of **7** and the formation of **15a** are understandable in terms of the intermediacy of ammoniochlorosulfurane such as **16a**. A similar chloride (**16b**) was obtained by treatment of **9** with thionyl chloride in benzene solution as a stable species in quantitative yield, and **16b** was converted to **16c** as relatively nonhygroscopic crystals by exchange of the counter anion using ammonium hexafluorophosphate.[8a] The S-chloro derivaives (**16b,c**) were easily hydrolyzed to give protonated amino sulfoxide which was converted back to **9** by neutralization.

It is therefore reasonable to consider that the S-chloro intermediate (**16a**) may react with water or methanol competitively to produce the final products in the aqueous methanol solution. The acceleration of the oxidation of 1,5-thiazocine with iodine has been ascribed to the presence of an analogous sulfurane, but such an intermediate has not been

Table 1. Methylation of amino sulfide (**7**) with various reagents to afford dimethylammonium salt (**8**)

Reagent	Reaction conditions: Solvent	Temp °C	Reaction time/h	Yield %	Counter anion	Solvent	^{1}H NMR (δ): BC conformer N-Me(6H)	BC conformer CH_2(4H)	TB conformer N-Me(6H)	TB conformer CH_2(4H)	Aromatic
MeI/$AgBF_4$	CH_3CN	r.t.	4	50	BF_4^-	CD_3CN	2.58(s) 3.55(s)	4.43 and 5.60 (ABq, J=13 Hz)	3.00(s)	4.10 and 4.70 (ABq, J=14 Hz)	7.00—7.98 (m, 8H)
Me_3OBF_4	CH_2Cl_2	r.t.	4	90	BF_4^-	CD_3CN	2.58(s) 3.55(s)	4.43 and 5.60 (ABq, J=13 Hz)	3.00(s)	4.10 and 4.70 (ABq, J=14 Hz)	7.00—7.98 (m, 8H)
MeI	CH_3CN	r.t.	24	63	I^-	CD_3CN	2.73(s) 3.73(s)	4.68 and 5.77 (ABq, J=13 Hz)	3.16(s)	4.36 and 4.81 (ABq, J=14 Hz)	7.07—8.00 (m, 8H)
FSO_3Me	CH_3NO_2	r.t.	3	—	FSO_3^-	CD_3CN	2.60(s) 3.60(s)	4.46 and 5.63 (ABq, J=13 Hz)	3.02(s)	4.11 and 4.70 (ABq, J=14 Hz)	7.10—7.90 (m, 8H)
MeI/HgI_2	CH_3CN	82	5	22	HgI_3^-	DMSO-d_6	2.64(s) 3.67(s)	4.63 and 5.70 (ABq, J=13 Hz)	3.08(s)	4.37 and 4.70 (ABq, J=14 Hz)	7.20—7.90 (m, 8H)

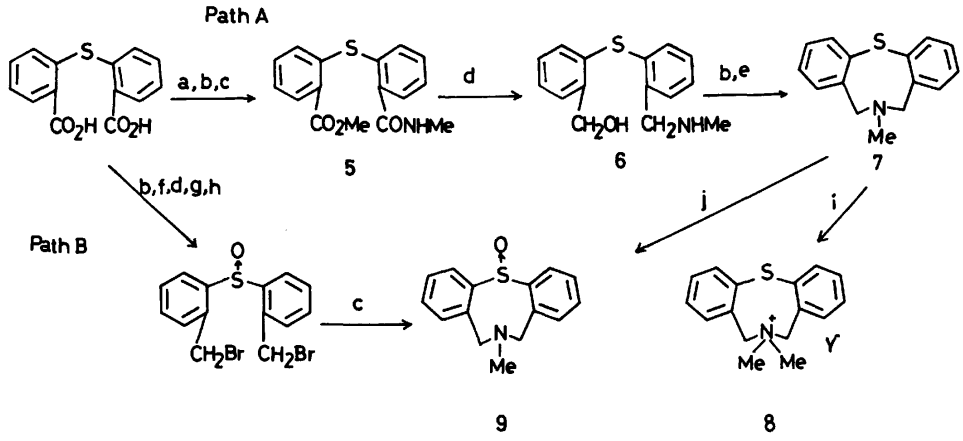

a), Reagents and conditions: (a) H_2SO_4, aq MeOH; (b) $SOCl_2$; (c) $MeNH_2$; (d) $LiAlH_4$; (e) KOH, MeOH; (f) MeOH; (g) PBr_3; (h) H_2O_2; (i) Methylating reagents ($Y=I^-$, BF_4^-, SO_3F^-, and HgI_3^-); (j) NaOCl, aq MeOH.

Scheme 1.[a)]

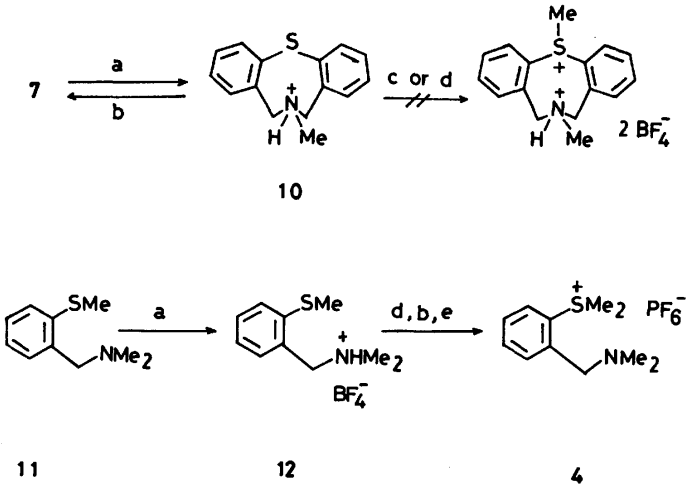

a), (a) HBF_4; (b) $NaHCO_3$; (c) $Me_3O^+BF_4^-$; (d) MeI/$AgBF_4$; (e) KPF_6/NH_4Cl.

Scheme 2.[a)]

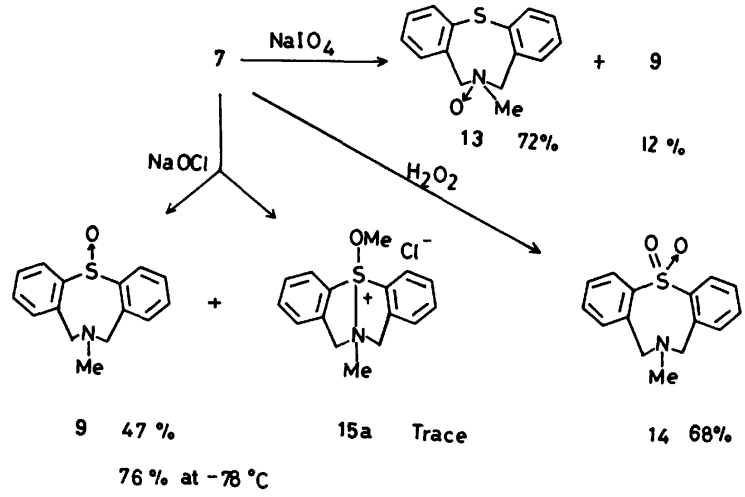

Scheme 3.

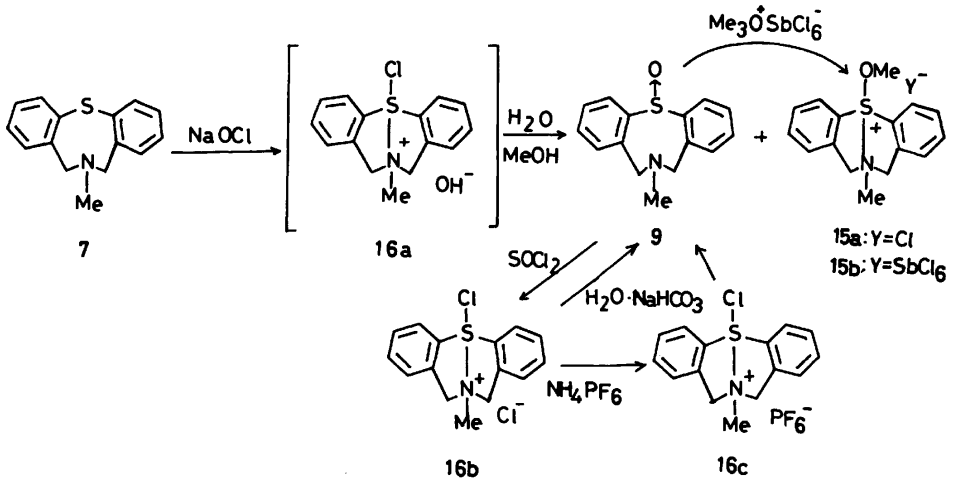

Scheme 4.

isolated so far.[3]

Structural Considerations of 9 and 15. There are some structural problems of **9** concerning the conformation of eight-membered ring and the relative stereochemistry around the sulfur atom. From theoretical and experimental investigations on conformational properties of 1,4-cyclooctadiene systems, it was concluded that the boat-chair (BC) conformer is significantly more stable than the twist-boat (TB) and boat-boat (BB) conformers,[9] but the TB conformer is of considerable importance in the heteroatom containing systems.[10] In the present system, sulfoxide (**9**) does not show any temperature dependence in ^{1}H NMR spectrum from −75 to 110 °C which indicates that only a single conformer is present for **9**, while both conformers exist for amino sulfide (**7**) and also for dimethylammonio sulfide (**8**) as reported by Tanaka *et al.* and Mehta *et al.*, respectively.[4,5] In the ^{1}H NMR spectrum of **9**, benzyl protons appear as a broad singlet at δ 3.88 in $CDCl_3$ solution but as a distinct AB quartet (J=15 Hz) at δ 3.18, 3.42 in benzene-d_6 solution. The proton-decoupled carbon spectrum features only eight lines, which reveals the presence of a single conformer for **9**. This spectral feature of **9** in solution is consistent with TB or BB conformer according to the criticism for such a conformer which was investigated in detail by Ollis *et al.*[10a] and Renaud *et al.*[10b] However the relative stereochemistry at the sulfur atom could not be completely determined by such a spectral consideration.

The unambiguous structure of **9** and **15b** in the solid state was determined by X-ray analysis on a single crystal (Fig. 1).[8a,c] The sulfur has distorted trigonal bipyramidal configuration and O, S, and N atoms are colinear with the angle of 179.5 and 175.0 ° for **9** and **15b**, respectively. The N···S distances are 2.593 and 2.207 Å for **9** and **15b** respectively and are very much shorter than the sum of van der Waals radii (3.35 Å) and longer than that of covalent radii (1.74 Å). It is concluded that there is a weak but definite attractive interaction between the electron-deficient sulfur and the donating amino group, which is strong enough to keep **9** and **15** in the unfavorable distorted BB conformation with TBP

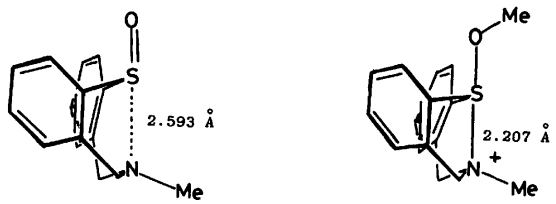

Fig. 1. Structure of **9** and **15**.

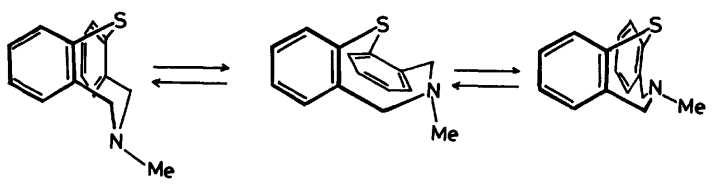

configuration at the sulfur. This is maintained also in solution as was exemplified by ^{1}H NMR study.[8,11,12]

In conclusion, the present investigation offers strong evidence for the formation of ammoniosulfuranes as intermediates in the oxidation of the sulfur of **7**, methionine, and 5-methyl-1-thia-5-azacyclooctane.[2,3]

Experimental

All the melting points are uncorrected. IR spectra were obtained with a Hitachi 215 grating IR spectrophotometer. ^{1}H NMR measurements were carried out on a Varian T-60 instrument and a Hitachi R-90H FT instrument, using tetramethylsilane as the internal reference. Mass spectra were measured with Hitachi RMU-6L spectrometer.

2-(Methoxycarbonyl)phenyl 2-(Methylcarbamoyl)phenyl Sulfide (5). Treatment of 2-(methoxycarbonyl)phenyl 2-carboxyphenyl sulfide (1.98 g, 6.88 mmol), which was prepared according to the literature,[4] with excess thionyl chloride (10 ml) gave a yellowish oil under refluxing for *ca.* 2 h. To a solution of the oil in 30 ml of ether was added an aqueous methylamine solution (in excess). The reaction mixture was poured into water after stirring for 2 h and extracted with dichloromethane. The organic layers were dried ($MgSO_4$) and concentrated to yield 1.41 g (68%) of the amide ester (**5**), mp 125—126 °C (hexane–dichloromethane); ν_{max} (KBr) 3260, 1705, and 1630 cm^{-1} ; ^{1}H NMR ($CDCl_3$) δ=2.78 (d, J=5 Hz, 3H), 3.92 (s, 3H), 6.70—7.62 (m, 7H), and 7.63—8.08 (m, 2H).

Found: C, 63.70; H, 4.94; N, 4.78%. Calcd for $C_{16}H_{15}NO_3S$: C, 63.77; H, 5.02; N, 4.65%.

2-(Hydroxymethyl)phenyl 2-(Methylaminomethyl)phenyl Sulfide (6). To a solution of 2.23 g (7.41 mmol) of **5** in benzene (20 ml) was added phosphorus pentachloride (1.55 g, 7.43 mmol) and the mixture was heated at reflux for 1 h. After removal of benzene, the residue was dissolved in THF (30 ml) and added to a suspension of lithium aluminium hydride (1.6 g, 41 mmol) in the same solvent (20 ml). The mixture was stirred at 0 °C for 30 min and at room temperature for 35 h before the excess hydride was carefully decomposed with water. The solution was filtered and the filtrate was concentrated to yield 1.61 g (84%) of amino alcohol (**6**) as a colorless oil; ^{1}H NMR (CCl_4) δ=2.17 (s, 3H), 3.64 (s, 2H), 3.72 (s, 2H), 4.52 (s, 2H), and 6.65—7.80 (m, 8H). The product was crystallized as a hydrochloride; mp 221—223 °C (lit,[4] mp 216—219 °C); ν_{max} (KBr) 3360, 2920, 2760, and 1035 cm^{-1}; ^{1}H NMR (CD_3OD) δ=2.85 (s, 3H), 4.33 (s, 2H), 4.70 (s, 2H), 4.76 (s, 2H), and 6.90—7.74 (m, 8H).

*6,7-Dihydro-6-methyl-5*H*-dibenzo*[b,g]*[1,5]thiazocine (7).* To a solution of amino alcohol (**6**) (1.0 g, 3.86 mmol) in 100 ml of benzene was added 10 ml of thionyl chloride and the mixture was heated at reflux for 2.5 h. After concentration of the reaction mixture, the residue was dissolved in 50 ml of ethanol and treated with potassium hydroxide (2.2 g) in 50 ml of the same solvent for 1 h at reflux temperature. Workup in the ordinary manner gave 0.77 g (83%) of a yellow oil. A pure sample of **7** was isolated by preparative TLC (silica gel; benzene–ethyl acetate (1:1)). Recrystallization from petroleum ether afforded a colorless solid of **7**, mp 65—66 °C (lit,[5] mp 68—69 °C); ν_{max} (KBr) 2875 cm^{-1}; ^{1}H NMR ($CDCl_3$, at 35 °C) δ=2.11 (s, 3H), 3.31—5.07 (br s, 4H), 6.90—7.30 (m, 6H), and 7.41—7.72 (m, 2H); ^{1}H NMR (CD_3OD, at −49.5 °C) δ=1.92 (s, Me for BC form), 2.23 (s, Me for TB form), 3.84 and 5.02 (ABq, J=14 Hz, CH_2 for BC form), 3.67 (br s, CH_2 for TB form), 7.08—7.49 (m, 6H), and 7.60—7.84 (m, 2H). BC/TB=2/1 at 49.1 °C.

*6,7-Dihydro-6,6-dimethyl-5*H*-dibenzo*[b,g]*[1,5]thiazocinium Salt (8).* To a solution of amino sulfide (**7**) (50 mg, 0.21 mmol) in acetonitrile (1 ml) was added 40 mg (0.28 mmol) of methyl iodide dissolved in the same solvent (1.5 ml). The mixture was stirred at room temperature for 24 h. After evaporation of the solvent, a yellow solid (40 mg, 63%) of **8a** was obtained. By using different solvents and methylating reagents under the same procedure, the other salts (**8b—e**) were obtained. The ^{1}H NMR spectral data and reaction conditions are collected in Table 1.

Oxidation of Amino Sulfide (7) with Sodium Periodate.

*6,7-Dihydro-6-methyl-5*H*-dibenzo*[b,g]*[1,5]thiazocine 6-Oxide (13).* A solution of **7** (224 mg, 0.93 mmol) in methanol (25 ml) was treated with sodium periodate (248 mg, 1.16 mmol) in water (5 ml) for 10 d. After ordinary workup, 219 mg of yellow residue was obtained. Thin layer chromatography of the residue on silica gel (ethyl acetate) gave 13.5 mg (12%) of **9** and 82.5 mg (72%) of **13** as a colorless solid. Recrystallization of **13** from dichloromethane–hexane afforded a pure sample, mp 175—177 °C (hygroscopic); ν_{max} (KBr) 905 cm^{-1}; ^{1}H NMR ($CDCl_3$) BC/TB=1/2.8, for BC form: δ=2.80 (s, 3H), 3.79 and 5.74 (ABq, J=14 Hz, 4H), and 7.00—8.00 (m, 8H); for TB form: 3.20 (s, 3H), 4.46 and 4.93 (ABq, J=16 Hz, 4H), and 7.00—8.00 (m, 8H); Mass (m/z) 257 (M^+), 241 (M^+−16), and 211 (M^+−46).

Found: C, 66.82; H, 6.15; N, 5.11%. Calcd for $C_{15}H_{15}NSO+0.7H_2O$: C, 66.77; H, 6.08; N, 5.19%.

Oxidation of Amino Sulfide (7) with Hydrogen Peroxide.

*6,7-Dihydro-6-methyl-5*H*-dibenzo*[b,g]*[1,5]thiazocine 12,12-Dioxide (14).* A mixture of **7** (209 mg, 0.87 mmol) and 30% hydrogen peroxide (2.5 ml) in acetic acid (5 ml) was heated at reflux for 1.5 h. After ordinary workup and recrystallization from hexane–dichloromethane, 159.6 mg (68%) of **14** was obtained as a colorless solid; mp 170—174 °C: ν_{max} (KBr) 1305 and 1125 cm^{-1}; ^{1}H NMR ($CDCl_3$) δ=1.97 (s, 3H), 3.95 and 5.62 (ABq, J=15 Hz, 4H), 7.06—7.71 (m, 6H), and 7.87—8.28 (m, 2H).

Found: C, 65.68; H, 5.52; N, 4.97%. Calcd for $C_{15}H_{15}NSO_2$: C, 65.91; H, 5.53; N, 5.12%.

*Oxidation of Amino Sulfide (7) with Sodium Hypochlorite. 6,7-Dihydro-6-methyl-5*H*-dibenzo*[b,g]*[1,5]thiazocine 12-Oxide (9).* To a solution of **7** (352 mg, 1.46 mmol) in 7 ml of methanol was added 10% aqueous sodium hypochlorite (2.72 g, 3.65 mmol) at −78 °C. The mixture was stirred for 1 h at the same temperature before the mixture was poured onto ice and extracted with dichloromethane. The organic layers were washed with water, dried, and evaporated to yield yellow solids. Recrystallization of the solids from benzene–hexane gave **9** (284 mg, 76%) as colorless crystals, mp 113—115 °C; ν_{max} (KBr) 1065 and 1015 cm^{-1}; ^{1}H NMR ($CDCl_3$) δ=2.56 (s,

3H), 3.88 (s, 4H), 6.98—7.67 (m, 6H), and 8.08—8.35 (m, 2H); ^{1}H NMR (C_6D_6) δ=2.02 (s, 3H), 3.18 and 3.42 (ABq, J= 15 Hz, 4H), 6.58—7.32 (m, 6H), and 8.50—8.67 (m, 2H); ^{13}C NMR (CD_3CN) δ=41.9 (q), 58.6 (t), 125.3 (d), 127.3 (d), 129.4 (d), 130.4 (d), 140.2 (s), and 145.8 (s); Mass (*m/z*) 257 (M^+), 241 (M^+ −16), 226 (M^+ −31), and 197 (M^+−60).

Found: C, 69.82; H, 5.91; N, 5.50%. Calcd for $C_{15}H_{15}NOS$: C, 70.01; H, 5.88; N, 5.44%.

Oxidation of **7** with sodium hypochlorite at room temperature for 15.5 h afforded sulfoxide (**9**) (47%) as a major product together with a small amount of methoxysulfonium salt (**15a**). The latter was isolated in 4% yield by evaporation of the filtrate followed by trituration of the residue twice with benzene. The structure was assigned by spectral comparison with an analogous sample (**15b**) obtained by methylation of **9** as described below.

*6,7-Dihydro-6-methyl-12-methoxy-5*H*-dibenzo*[b,g]*[1,5]-thiazocinium Hexachlorantimonate (15b).* A mixture of sulfoxide (**9**) (512 mg, 1.99 mmol) and trimethyloxonium hexachloroantimonate (787 mg, 1.99 mmol) in dichloromethane (10 ml) was stirred at room temperature for 15 h under argon atmosphere. The mixture was filtered and the filtrate was concentrated to furnish 588 mg (49%) of **15b**. A pure sample of the salt (**15b**) was obtained by recrystallization from acetonitrile–ether: mp 148—151 °C: ν_{max} (KBr) 1445 and 993 cm^{-1}, ^{1}H NMR (CD_3CN) δ=2.77 (s, 3H), 3.92 (s, 3H), 4.25 (s, 4H), 7.35—7.80 (m, 6H), and 7.92—8.15 (m, 2H).

Found: C, 31.82; H, 2.98; N, 2.30%. Calcd for $C_{16}H_{18}NSOSbCl_6$: C, 31.67; H, 2.99; N, 2.31%.

*12-Chloro-6,7-dihydro-6-methyl-5*H*-dibenzo*[b,g]*[1,5]thiazocinium Chloride (16b).* To a solution of **9** (639 mg, 2.49 mmol) in dry benzene (14 ml) was added dropwise a solution of thionyl chloride (1 ml) in the same solvent (2 ml) under nitrogen atmosphere. The mixture was stirred at room temperature for 2.5 h and filtered. The yellowish solids were washed with dry benzene and ether successively before drying under an inert gas. There was obtained a colorless hygroscopic chloride (**16b**, 739 mg, 95%). ^{1}H NMR ($CDCl_3$) δ=3.13 (s, 3H), 4.70 (s, 4H), 7.22—8.02 (m, 6H), and 8.23—8.63 (m, 2H).

*12-Chloro-6,7-dihydro-6-methyl-5*H*-dibenzo*[b,g]*[1,5]thiazocinium Hexafluorophosphate (16c).* To a stirred suspension of **16b** in anhydrous dichloromethane (10 ml) prepared from **9** (517 mg, 2.01 mmol) was added ammonium hexafluorophosphate (1.31 g, 8.04 mmol). The mixture was stirred at room temperature for 17 h prior to filtration. The filtrate was diluted with dry ether to afford 288 mg (34%) of **16c** as a colorless solid: mp 145—155 °C (dec); ν_{max} 1470 and 820 cm^{-1}; ^{1}H NMR (CD_3CN) δ=3.13 (s, 3H), 4.59 and 4.72 (ABq, J=15.6 Hz, 4H), 7.30—8.05 (m, 6H), and 8.27—8.65 (m, 2H).

Found: C, 42.82; H, 3.62; N, 3.59; Cl, 8.65%. Calcd for $C_{15}H_{15}NSClPF_6$: C, 42.72; H, 3.58; N, 3.32; Cl, 8.41%.

Hydrolysis of **16b** or **16c**, followed by neutralization with sodium hydrogencarbonate, reverted back to amino sulfoxide (**7**) in quntitative yield.

N,N-Dimethyl-2-(methylthio)benzylamine (11). To a stirred suspension of lithium aluminium hydride (2.93 g, 75 mmol) in anhydrous tetrahydrofuran (100 ml) was added dropwise a solution of *N,N*-dimethyl-2-(methylthio)-benzamide[13] (4.88 g, 25 mmol) in the same solvent (50 ml). The mixture was stirred at 0 °C for 1 h and at room temperature for 6 d before the excess hydride was carefully decomposed with water. Workup in the predescribed manner gave 3.72 g (**11**, 82%) of a colorless oil:[1a] ν_{max} (neat) 1465 cm^{-1}; ^{1}H NMR ($CDCl_3$) δ=2.22 (s, 6H), 2.40 (s, 3H), 3.45 (s, 2H), and 6.87—7.40 (m, 4H); Mass (*m/z*) 181 (M^+) and 166 (M^+−15).

Dimethyl[2-(dimethylaminomethyl)phenyl]sulfonium Hexafluorophosphate (4). Treatment of **11** (1.03 g, 5.70 mmol) with 42% aqueous tetrafluoroboric acid (1.9 ml, 9.3 mmol) in acetonitrile (25 ml) gave 1.03 g (71%) of *N,N*-dimethyl-2-(methylthio)benzylammonium salt (**12**) as colorless crystals, mp 122—125 °C: ν_{max} (KBr) 1443 and 1068 cm^{-1}; ^{1}H NMR (CD_3CN) δ=2.54 (s, 3H), 2.84 (s, 6H), 4.38 (s, 2H), and 7.23—7.67 (m, 4H).

Treatment of **12** (1.03 g, 4.05 mmol) with methyl iodide (1.73 g, 12 mmol) and silver tetrafluoroborate (2.34 g, 12 mmol) in acetonitrile (10 ml) afforded 2.77 g of the sulfonium salt as yellow crystals: ^{1}H NMR (CD_3CN) δ=2.98 (d, J=5 Hz, 6H), 3.25 (s, 6H), 4.70 (d, J=5 Hz, 2H), 7.77—8.12 (m, 3H), and 8.12—8.50 (m, 1H).

The salt was neutralized with aqueous sodium hydrogen carbonate to give a colorless precipitate. The mixture was treated with an aqueous solution (10 ml) of potassium hexafluorophospate (10 g) and ammonium chloride (2 g) at room temperature for 1 h. After the usual workup, 742 mg (57%) of **4** was obtained as a colorless oil: ^{1}H NMR ($CDCl_3$) δ=2.23 (s, 6H), 3.10 (s, 6H), 3.63 (s, 2H), 7.27—7.82 (m, 3H), and 7.84—8.20 (m, 1H).

Found: C, 38.95; H, 5.52; N, 4.31%. Calcd for $C_{11}H_{18}NSPF_6$: C, 38.71; H, 5.32; N, 4.10%.

The authors are indebted partially to a Grant-in Aid for Scientific Research (No. 57430006) administered by the Ministry of Education, Science, and Culture of Japanese Government.

References

1) a) Y. Ohara, K. Akiba, and N. Inamoto, *Bull. Chem. Soc. Jpn.*, **56**, 1508 (1983); b) K. Akiba, Y. Ohara, and N. Inamoto, *Bull. Chem. Soc. Jpn.*, **55**, 2976 (1982); c) K. Akiba, Y. Ohara, and N. Inamoto, *Heterocycles*, **6**, 13 (1977).

2) P. R. Young and L. -S. Hsieh, *J. Am. Chem. Soc.*, **100**, 7121 (1978).

3) J. D. Doi and W. K. Musker, *J. Am. Chem. Soc.*, **103**, 1159 (1981).

4) L. E. Brieaddy, B. S. Hurlbert, and N. B. Mehta, *J. Org. Chem.*, **46**, 1630 (1981).

5) a) S. Tanaka, H. Watanabe, and Y. Ogata, *Yakugaku Zasshi*, **93**, 997 (1973); b) S. Tanaka, K. Hashimoto, H. Watanabe, and K. Sakaguchi, *Chem. Pharm. Bull.*, **21**, 1683 (1973).

6) In accordance with the nomenclature used in the literature,[4] the description "BC", "TB", and "BB" refer to "boat chair", "twist boat", and "boat boat" conformations in eight-membered ring.

7) C. K. Mann and K. K. Barnes, "Electrochemical Reactions in Nonaqueous Systems," Marcel Dekker, Inc., New York, (1970) p. 279, 383.

8) a) K. Akiba, K. Takee, K. Ohkata, and F. Iwasaki, *J. Am. Chem. Soc.*, **105**, 6965 (1983); b) K. Ohkata, K. Takee,

and K. Akiba, *Tetrahedron Lett.*, **24**, 4859 (1983); c) F. Iwasaki and K. Akiba, *Acta Crystallogr., Sect. B*, **41**, (1985), accepted for publication.

9) N. L. Allinger, J. F. Viskocil, Jr., U Burkert, and Y. Yuh, *Tetrahedron*, **32**, 33 (1976).

10) a) R. P. Gellatly, W. D. Ollis, and R. N. Sutherland, *J. Chem. Soc., Perkin Trans. 1*, **1976**, 913; b) R. N. Renaud, J. W. Bovenkamp, R. R. Fraser, and J. -L. Roustan, *Can. J. Chem.*, **55**, 3456 (1977).

11) a) C. Picard, L. Cazaux, and J. Jaud, *J. Chem. Soc., Perkin Trans. 2*, **1981**, 1554; b) C. Cohen-Aldad, M. S. Lehmann, P. Becker, L. Parkanyi, and A. Kalman, *J. Chem. Soc., Perkin Trans. 2*, **1984**, 191.

12) Attractive interaction between the sulfonio and the amino groups was evaluated theoretically by *ab initio* calculation: K. Morokuma, M. Hanamura, and K. Akiba, *Chem. Lett.*, **1984**, 1557.

13) E. W. Clelland and C. E. Salkeld, *J. Chem. Soc.*, **1936**, 1143.

Restricted Rotation Involving the Tetrahedral Carbon. LVII. Stereodynamics of 9-(2-Alkylphenoxy)-1,4-dimethyltriptycenes[1)]

Gaku YAMAMOTO* and Michinori ŌKI
Department of Chemistry, Faculty of Science, The University of Tokyo, Bunkyo-ku, Tokyo 113
(Received February 26, 1985)

1,4-Dimethyl-9-phenoxytriptycene and its derivatives carrying a methyl, isopropyl, or *t*-butyl group in the *o*-position of the phenoxyl moiety were synthesized and their dynamic NMR behavior was studied. These molecules are considered to constitute a bevel gear system with a two-toothed and a three-toothed wheels and the dynamic NMR behavior is best explained in terms of gear rotation. The *o*-isopropyl derivative, for example, shows the energy barriers of 17.2 and 10.8 kcal† mol^{-1} for the $ap \rightleftarrows \pm sc$ and $+sc \rightleftarrows -sc$ gearing processes, respectively. The population of the $\pm sc$ rotamer increases with the bulkiness of the *o*-alkyl group: The steric congestion among the *o*-alkyl group, the oxygen atom, and the *peri*-methyl group is severer in *ap* than in $\pm sc$. Results of molecular mechanics calculations on these molecules are discussed.

In the course of our studies on restricted rotation about the bridgehead-to-substituent bond in 9-substituted triptycene derivatives,[2)] we have been interested in the stereodynamics of 9-benzyltriptycene (**1**) and its various derivatives.[3–7)]

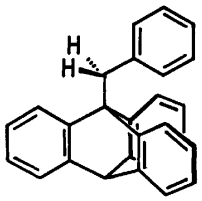

1

Compound **1** adopts a conformation in which the plane of the phenyl group is coplanar with the bridgehead-to-methylene bond and thus constitutes a meshed bevel gear with a two-toothed and a three-toothed wheels. Dynamic NMR studies of singly *peri*-substituted 9-(2-methylbenzyl)triptycenes (**2**)[6)] and 9-(2,4,6-trimethylbenzyl)triptycenes (**3**)[7)] revealed that these molecules behave as dynamic gears: Gear rotation is the lowest energy process and gear slippage has a higher barrier. Mislow *et al.*[8)] made detailed molecular mechanics studies on the stereodynamics of **1**, 9-(2,6-dimethylbenzyl)triptycene, and its 1-methyl derivative, which are complementary to our results.

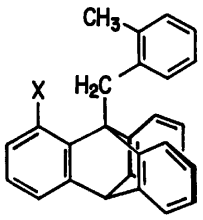

2

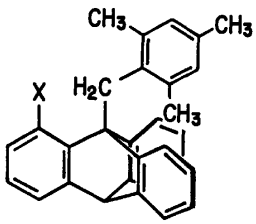

3

† 1 cal=4.184 J.

It was reasonably expected that observation of gear rotation could be extended to systems where the methylene group in 9-(arylmethyl)triptycenes is replaced by a heteroatom group such as O, NH, and so on, and that it would be of interest to see how the stereodynamics of these compounds differs from that of the carbon analogs. We report here NMR studies on the stereodynamics of 1,4-dimethyl-9-phenoxytriptycene (**4**) and its derivatives (**5**—**7**) carrying an alkyl group in the *o*-position of the phenoxyl moiety.[9)] We discuss also the results of molecular mechanics calculations on these molecules.

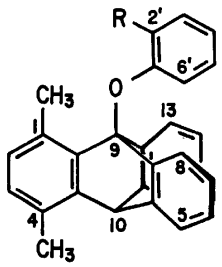

4: R=H
5: R=CH_3
6: R=$CH(CH_3)_2$
7: R=$C(CH_3)_3$

Results and Discussion

Syntheses. The triptycenes **4**—**7** were synthesized by reactions of 9-aryloxyanthracenes (**8**—**11**) with 3,6-dimethylbenzyne. The anthracenes were obtained by Ullmann reactions from 9-bromoanthracene and appropriate phenols[10)] (Method A). Compounds **9** and **10** were prepared also by

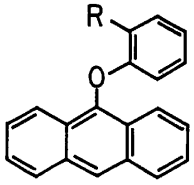

8: R=H
9: R=CH_3
10: R=$CH(CH_3)_2$
11: R=$C(CH_3)_3$

condensation of anthrone with the corresponding phenols in the presence of acid catalyst by the analogy of the recent report on the syntheses of 9-alkoxyanthracenes from anthrone and alcohols[11] (Method B). An attempt at the synthesis of **11** by the second method was not successful probably because of partial dealkylation under the reaction conditions.

NMR Spectral Studies. On the analogy of the behavior observed in 9-(2-methylbenzyl)triptycenes (**2**),[6] the stereodynamic behavior of **5—7** is expected to be explained in terms of the gear rotational circuit shown in Fig. 1.

Molecules of **5—7** exist as one of the three stable conformers, *ap*, $+sc$, and $-sc$, in which the *o*-alkyl group points toward outside of the triptycene skeleton. Conformers with the *o*-alkyl group pointing inwards, *ap'*, $+sc'$, and $-sc'$, are very unstable and populated too little to be detected, but serve as intermediates in the interconversion among the stable conformers by gear rotation (GR). The $+sc$ rotamer changes to *ap'* by a GR step in which the aryl group passes over a *peri*-hydrogen. We refer to this step as GR(H). As *ap'* is unstable, the molecule immediately changes to $-sc$ by further GR(H). Thus $+sc$ and $-sc$ interconvert by two successive GR(H) steps. In order for the $+sc$ rotamer to convert to *ap*, it should first change to $-sc'$ by passing of the aryl group over the *peri*-methyl group, which we refer to as GR(CH_3), and then to *ap* by GR(H). GR(CH_3) should naturally have a higher energy barrier than GR(H) and therefore the $ap \rightleftharpoons \pm sc$ process should show a higher overall barrier than the $+sc \rightleftharpoons -sc$ process.

From the discussion above, the following behavior is expected in the dynamic NMR spectra. At low temperatures where both processes are frozen on the NMR time scale, the *ap* and $\pm sc$ rotamers are separately observed, and the chiral nature of the $\pm sc$ rotamer is proved by the diastereotopicity of a prochiral group such as $-CX_2Y$, if the molecule carries such a group. At an intermediate temperature range, the situation is realized where the $+sc \rightleftharpoons ap' \rightleftharpoons -sc$ occurs fast on the NMR time scale but the $+sc \rightleftharpoons -sc' \rightleftharpoons ap$ (and $-sc \rightleftharpoons +sc' \rightleftharpoons ap$) process is still slow.[12] In such circumstances, two rotamers are separately observed but the $\pm sc$ rotamer appears achiral in the NMR spectra. At higher temperatures where both processes occur fast on the NMR time scale, identity of the rotamers is lost and a coalesced signal is observed.

The 2'-isopropyl derivative (**6**) serves as a typical example. In the ^1H NMR spectrum at ambient temperature, two sets of signals are observed in an intensity ratio of *ca.* 1:2 corresponding to the presence of two types of rotamers, *ap* and $\pm sc$ (Table 1). Among the four singlets due to the aromatic methyl groups appearing at δ 2.0—3.0, the highest-field one is reasonably assigned to the 1-methyl group of the $\pm sc$ rotamer because this methyl group is susceptible to the diamagnetic ring current of the benzene ring in the aryloxyl moiety. Then the other signals can be uniquely assigned as shown in Table 1 on the basis of the relative intensities and the coalescence behavior observed upon raising the temperature: The major isomer is assigned to $\pm sc$. Validity of the rotamer assignment in **6** is further confirmed by the low temperature NMR behavior of **6** described below. The isopropyl-methyl signals consist of two doublets, one from *ap* and the other from $\pm sc$, indicating that the *gem*-dimethyl groups

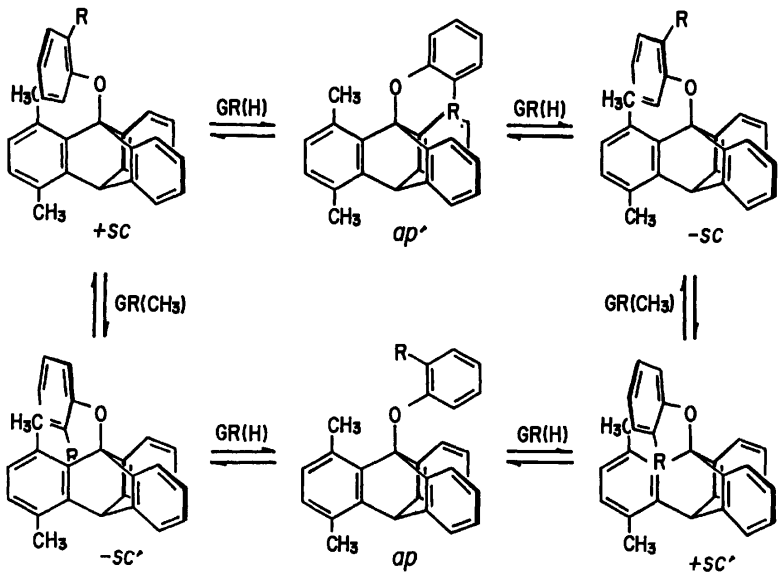

Fig. 1. Gear rotational circuit for 9-(2-alkylphenoxy)-1,4-dimethyltriptycenes.

are isochronous not only in *ap* but also in ±*sc*.

These spectral features are just those expected at intermediate temperatures mentioned above. Upon raising the temperature, the two sets of signals coalesce into an averaged set of signals, reflecting the increase of the interconversion rate between the *ap* and ±*sc* rotamers. Lineshape analysis of the 1- and 4-methyl proton signals obtained at 60 MHz in a chlorobenzene solution at five temperatures between 51 and 80 °C gave the rate constants for the process. The kinetic parameters obtained therefrom are shown in Table 2.

Meanwhile, upon lowering the temperature, the doublet signal assigned to the isopropyl-methyl group of the ±*sc* rotamer splits into two equally intense doublets, the other nonaromatic signals remaining intact. This feature suggests the slow-down of the $+sc \rightleftarrows -sc$ process. The spectral change was studied at 400 MHz because no explicit splitting was observed at 60 MHz. At −81 °C in dichloromethane-d_2, the isopropyl-methyl signals appeared as three doublets at δ=1.52, 1.48, and 1.46 with an intensity ratio of 29:29:42 indicating the presence of ±*sc* and *ap* in a ratio of 58:42.[13] Lineshape analysis of these signals in the temperature range of −60 to −25 °C afforded the rate con-

Table 1. 400 MHz ^{1}H NMR data of 9-aryloxy-1,4-dimethyltriptycenes (**4**—**7**) in $CDCl_3$[a]

Compd	Rotamer	Pop %	1-CH_3	4-CH_3	10-H	5,16-H	8,13-H	2′-R	6′-H
4			2.779	2.443	5.630	7.426 d (7.1)	7.250 d (7.1)	7.38 br	6.54 br
5	*ap*	56	2.902	2.432	5.637	7.441 d (7.1)	7.140 d (7.7)	2.701	6.229 d (8.1)
	±*sc*	44	2.035	2.552	5.621	7.363 ad (≈7)	≈7.44 br	2.679	6.570 d (8.1)
6	*ap*	35	2.890	2.426	5.637	7.437 d (8.1)	7.134 d (7.6)	1.461 d 4.050 sep (6.8)	6.195 d (8.3)
	±*sc*	65	2.090	2.550	5.618	7.406 dd (7.6, 1.7)	≈7.4 br	1.511 d 3.921 sep (6.8)	6.600 dd (7.8, 1.1)
7	±*sc*	>98	2.139	2.556	5.617	7.291 d (7.1) 7.439 d (7.1)	6.916 d (7.6) 8.014 d (7.6)	1.754	6.651 dd (8.3, 1.2)

a) Obtained at 21—24 °C. Aromatic protons are omitted except for those shown in the Table. Chemical shifts are given in δ. Signals are singlets unless otherwise stated; ad: apparent doublet, br: broad, d: doublet, dd: double doublet, sep: septet. In parentheses are coupling constants in Hz. The digital resolution of 0.24 Hz should be allowed for.

Table 2. Dynamic NMR data of 9-aryloxytriptycenes (**4**—**7**) and a related compound (**15**)

Compd	Process	Rds[a]	Signal Obsd	T_c °C	$\Delta G^{\ddagger}(T)$ kcal mol^{-1} (°C)	$\Delta H^{\ddagger}$ kcal mol^{-1}	$\Delta S^{\ddagger}$ cal mol^{-1} K^{-1}	K[b]	MF[c] MHz	Solvent
4	*ap*→±*sc*	GR(H)	1,4-CH_3	<−101	<8.0				400	CD_2Cl_2
5	*ap*→±*sc*	GR(CH_3)	1-CH_3	≈90	18.1 (60)	18.7±0.3	1.8±1.4	0.92	60	C_6H_5Cl
			4-CH_3	57						
	$+sc \rightleftarrows -sc$	GR(H)	8,13-H	≈−30	10.5 (−30)				400	$CDCl_3$
6	*ap*→±*sc*	GR(CH_3)	1-CH_3	87	18.2 (60)	17.2±1.5	−3.0±4.3	2.0	60	C_6H_5Cl
			4-CH_3	59						
	$+sc \rightleftarrows -sc$	GR(H)	$CH(CH_3)_2$	≈−45	11.7 (−45)	10.8±0.2	−4.0±1.0		400	CD_2Cl_2
			8,13-H	≈−10	11.8 (−10)					
7	$+sc \rightleftarrows -sc$	GR(H)	5,16-H	≫60	≫16.0				400	$CDCl_3$
			8,13-H	>120	>19.5				60	CCl_2CCl_2
15	*ap*→±*sc*	GR(CH_3)	CH_2	98	20.0 (98)			1.2	60	$C_6D_5CD_3$
	$+sc \rightleftarrows -sc$	GR(H)	CH_2	14	14.1 (14)				60	$C_6D_5CD_3$

a) Rate-determining step. b) $[\pm sc]/[ap]$ at around T_c. c) Magnetic field strength.

stants for the $+sc \rightleftarrows -sc$ interconversion and the Eyring parameters therefrom (Table 2).

The 2′-methyl compound (**5**) shows a similar spectral feature as **6** does. Each of the 1- and 4-methyl groups gives rise to two singlets with an intensity ratio of 56:44 at ambient temperature. From the chemical shift criteria mentioned above, the major isomer is assigned to *ap* (Table 1). These signals coalesce on raising the temperature and lineshape analysis of the spectra at six temperatures between 39 and 73 °C affords the kinetic parameters for the $ap \rightleftarrows \pm sc$ process in **5** as shown in Table 2.

As compound **5** has no NMR sensor groups which would definitely detect the $+sc \rightleftarrows -sc$ process, no clear information is easily obtained for the process in **5**. The spectra of the aromatic protons give some information on this point, which is described later.

In the ^{1}H NMR spectrum of the 2′-*t*-butyl derivative (**7**) at ambient temperature, a single peak is observed for each of the 1-methyl, 4-methyl, and 2′-*t*-butyl groups. The chemical shifts of the signals due to the 1- and 4-methyl groups are very similar to those of the corresponding signals in the $\pm sc$ rotamers of **5** and **6**.[14] This strongly suggests that **7** exists almost exclusively as the $\pm sc$ rotamer. The 400 MHz spectrum of the aromatic proton region is rather simple and is easily analyzed: The spectrum consists of three sets of ABCD four-spin systems and one AB-quartet, indicating that the two unsubstituted *o*-benzeno bridges are not equivalent. This clearly confirms that **7** exists solely as $\pm sc$ rotamer and further that the $+sc \rightleftarrows -sc$ process is frozen at ambient temperature. The spectrum was completely analyzed by use of the double resonance technique and the signals were assigned as shown in Scheme 1 by assuming that the lowest-field signal should derive from 13-H and the highest-field one from 6′-H. No significant change in the lineshape was observed up to 60 °C and thus the energy barrier to the $+sc \rightleftarrows -sc$ gearing, *i.e.* GR(H), in **7** is concluded to be considerably higher than 16 kcal mol^{-1}. The value is still conservative. In the 60 MHz spectra, the doublet at δ 8.01 assigned to 13-H appears clearly separated from the other aromatic signals, and shows no significant change of its appearance up to 120 °C, indicating that the energy barrier to GR(H) is higher than 19.5 kcal mol^{-1}.

The aromatic proton spectra of **5** and **6** are far more complex than that of **7**, because **5** and **6** consist of two types of rotamers, *ap* and $\pm sc$. In these compounds, change in the lineshape in the aromatic region owing to the $+sc \rightleftarrows -sc$ process was observed over a wide range of temperature, from −60 °C up to room temperature. Signals ascribed to 8-H and 13-H of the $\pm sc$ rotamer of **6** appearing at δ 7.90 and *ca.* 6.9 at −81 °C broadened on raising the temperature and coalesced at about −10 °C. The free energy of activation is roughly estimated to be 11.8±0.5 kcal mol^{-1} using the approximate equation.[15] The value is consistent with the kinetic data obtained from the lineshape analysis of the isopropyl-methyl signals. The 2′-methyl compound (**5**) shows a similar signal broadening at somewhat lower temperatures than **6** does. The *peri*-protons coalesce at about −30 °C, which gives a rough ΔG^* value of 10.5±0.5 kcal mol^{-1} for the $+sc \rightleftarrows -sc$ process.

The transition state for the GR(H) step in the $+sc \rightleftarrows -sc$ process would be represented by **12**. The severest steric interaction occurs between the face of the aryl group and the opposing *peri*-hydrogen. The

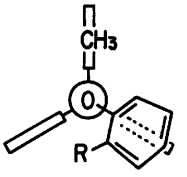

12a : R = CH_3
12b : R = $CH(CH_3)_2$
12c : R = $C(CH_3)_3$

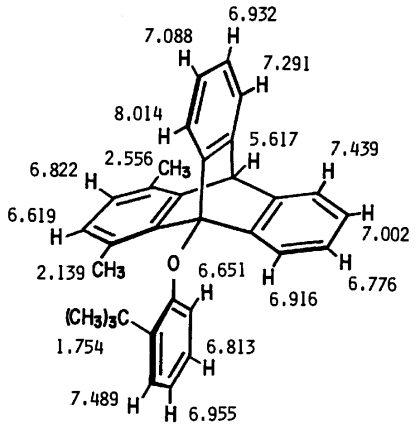

Scheme 1.

energies of **12a** and **12b** will be similar because the *o*-substituent R can adopt a conformation in which an α-hydrogen directs towards the triptycene skeleton, but the energy of **12c** will be considerably higher than those of **12a** and **12b**, because R has no α-hydrogen in **12c**. Therefore it may be reasonable that the energy barriers to the $+sc \rightleftarrows -sc$ process are similar for **5** and **6** but that for **7** is higher than those for **5** and **6**. Similarity of the GR(CH_3) barriers between **5** and **6** may be similarly understood.

It should be pointed out that the interconversion between *ap* and $\pm sc$ in **5** and **6** can occur by several other pathways. One group of such pathways involves an "isolated rotation" (IR) of the aryl group, which corresponds to slippage of the gear[4]: *ap*

changes to *ap'* by IR and then to $+sc$ (or $-sc$) by GR(H), or *ap* changes first to $+sc'$ (or $-sc'$) by GR(H) and then to $+sc$ (or $-sc$) by IR. In both pathways, IR is rate-determining. Inspection of molecular models, however, immediately suggests that the energy barrier to IR would be far higher than that to GR(CH_3) because the steric hindrance during the process is far larger. The transition state

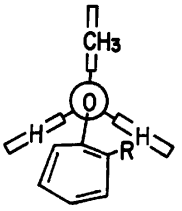

13

for IR seems something like **13** (the one for $ap \rightleftarrows ap'$ is illustrated), in which the severest interactions occur between the *o*-groups (R or H) and the *peri*-hydrogens. The congestion around the *o*-substituent is far severer than that in the transition state for GR(H) or GR(CH_3), and thus the energy barrier to IR should be significantly dependent on the bulkiness of the *o*-substituent R. The similar barrier heights observed in **5** and **6** therefore strengthen the impression from the molecular model considerations that the pathways involving IR are not the lowest energy process for the $ap \rightleftarrows \pm sc$ interconversion.[16]

The possibility that any process involving the configurational inversion of the oxygen atom might be responsible for the dynamic NMR behavior is rejected by the facts that the $+sc \rightleftarrows -sc$ and $ap \rightleftarrows \pm sc$ processes are separately observed and that the energy barrier to the former process is far lower than that to the latter.[17]

Temperature dependence of the ^1H NMR spectra of the 9-phenoxy compound (**4**) was studied as well at 400 MHz. In this molecule, the interconversion between *ap* and $\pm sc$ is attained by a single GR(H) step. At ambient temperature, one singlet is observed for each of the methyl groups, suggesting that the interconversion among rotamers is fast on the NMR time scale. The singlet at δ 2.44 is unambiguously assigned to the 4-methyl group by nuclear Overhauser effect (NOE) experiments: Upon irradiation of this signal, the bridgehead proton signal at δ 5.63 enhances its intensity by *ca.* 20%, while it remains intact on irradiation of the signal at δ 2.78. Even at -101 °C either of the methyl signals remains a singlet though somewhat broadened because of the slow-down of the process. Broadening of the 1-methyl signal is considerably larger than the 4-methyl signal and the peak height of the former is about a half of that of the latter at -101 °C. The larger broadening of the 1-methyl signal is reasonable because it should split into two peaks with a larger chemical shift difference than the 4-methyl signal on the analogy of the behavior found in **5** and **6**. Energy barrier to this process is estimated to be less than 8 kcal mol^{-1}.

Close inspection of the aromatic proton region of the spectra of **4** reveals an interesting phenomenon. Signals ascribed to two *o*-protons of the phenoxyl moiety appear as two multiplets at δ 6.32 snd 7.52 at -101 °C. The anisochrony of the *o*-protons remains even at room temperature, although the signals show considerable broadening. This means that any

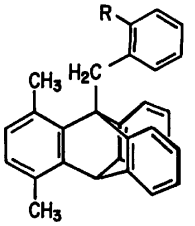

14 : R = H
15 : R = CH_3

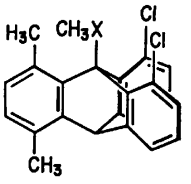

16 : X = O
17 : X = CH_2

process which exchanges the magnetic environments of the two protons has a considerably high energy barrier of more than 15 kcal mol^{-1}. The to-and-fro gearing process ($+sc \rightleftarrows ap' \rightleftarrows -sc$) by two GR(H) does not average out the chemical shifts of the two protons. Either of two processes, GR(CH_3) and IR, can explain the observed dynamic NMR behavior. Differentiation between the two as the lower energy process is not possible at the present stage. Detailed studies along this line are in progress.

In Table 2 are included the data for 1,4-dimethyl-9-(2-methylbenzyl)triptycene (**15**).[6] The rather small difference in the energy barriers between **5** and **15**, in both of those for GR(CH_3) and GR(H), is intriguing when one considers the large difference in the barriers to rotation about the triptycyl-X bond found in compounds **16** and **17**, where X is O and CH_2, respectively. The energy barriers to the $ap \rightleftarrows \pm sc$ process, in which the methyl group in the 9-substituent eclipses one of the *peri*-chlorines in the transition state, were 11.8 and 20.2 kcal mol^{-1} for **16** and **17**, respectively.[1,18]

As discussed in detail in the previous paper,[1] two main factors should be considered which govern the difference in rotational barriers between C–C and C–O bonds: (1) Three pairs of eclipsing interactions in the transition state for C–C rotation *vs.* one pair for C–O rotation, and (2) the difference in

TABLE 3. ROTAMER EQUILIBRIA OF 5 AND 6

Compd	Solvent	Temp Range °C	ΔH° kcal mol^{-1}	ΔS° cal mol^{-1} K^{-1}	K_{273}[a]
5	$CDCl_3$	−24—58	0.73±0.17	2.1±0.6	0.77
6	CD_2Cl_2	−30—20	0.64±0.15	3.2±0.6	1.57

a) [±*sc*]/[*ap*].

bond length between C–C and C–O. The former factor operates to lower the C–O barrier. In the 9-CH_3X system (**16** and **17**), the former factor contributes more strongly than the latter, resulting in the large barrier difference. In the aryl-X compounds (**5** and **15**), the latter factor would act to raise the C–O barrier, because the shorter C–X bonds increase the steric interaction between the face of the aryl group and the opposing *peri*-group (H or CH_3) in the transition state, while the effect would be less important in the ground state. Thus the second factor partly compensates the former factor to result in the small difference in the barriers.

Rotamer Equilibria. As shown in Table 1, the rotamer distribution is highly dependent on the *o*-alkyl group. Population of the *ap* rotamer steeply decreases as the *o*-alkyl group becomes bulkier. The van't Hoff parameters for **5** and **6** are given in Table 3.

Inspection of molecular models of 9-phenoxytriptycene indicates that the inner *o*-hydrogen in the phenoxyl moiety locates very closely to and thus strongly interacts with the triptycene skeleton. When a methyl group is present at a *peri*-position of the triptycene skeleton, it sterically interacts with the oxygen atom at the bridgehead. In the *ap* rotamer, the aryl group is pushed down into the notch made by the two *o*-benzeno bridges due to the buttressing effect of the *peri*-methyl group, which results in the destabilization of this isomer, but such an effect does not work in the ±*sc* rotamer. Presence of an alkyl group in the *o*-position increases the congestion and enhances the destabilization. Therefore, as the bulkiness of the *o*-alkyl group increases, the *ap* rotamer would be steeply destabilized, resulting in the increase in the population of the ±*sc* rotamer.

These situations seem to be reflected in ^{1}H NMR spectra (Table 1). In the spectra of **5** and **6**, a doublet signal ascribed to 6′-H appears at the highest-field part of the aromatic proton region (*ca.* δ 6.2). No such signal is observed in the spectrum of **7**, in accordance with the absence of *ap* in **7**. The corresponding proton in the ±*sc* rotamer appears at a lower field of *ca.* δ 6.6 in **5**—**7**. The buttressing effect should push the proton into the shielding region of the flanking benzene rings in the *ap* rotamer.

Although the rotamers of **4** are not separately observed at room temperature or even at the lowest temperature examined (−101 °C), the populations can be roughly estimated from the averaged chemical shift of the 1-methyl signal. If it is assumed that the chemical shift of the 1-methyl protons for each rotamer is the same as that in **5**, *i.e.* δ 2.04 for ±*sc* and δ 2.90 for *ap*, the averaged value of δ 2.78 observed at 24 °C predicts the population of *ap*-**4** to be about 85% at this temperature. Predominance of the *ap* rotamer in **4** may be consistent with the extrapolation of the tendency observed in **5**—**7**, though the value seems somewhat larger than expected judging from the fact that, in the carbon analogs **14** and **15**, the population of *ap* decreases only slightly on going from **14** to **15** (54% in **14** at −50 °C in $CDCl_3$–CS_2 (2:3)[3a] and 50% in **15** at −33 °C in $CDCl_3$[6]).

TABLE 4. STERIC ENERGIES BY MM2 CALCULATIONS

Compd	Rotamer		Rel. Energy kcal mol^{-1}	Calcd Popul.[a] %
4	*ap*		0	97.8
	±*sc*		2.67	2.2
5	*ap*		0	97.6
	±*sc*		2.63	2.4
	ap′		9.08	
	±*sc*′		10.81	
6	*ap*	**19a**	0	95.1
		20a	0.18	
		21a	2.94	
	±*sc*	**19b**	2.35	4.9
		20b	2.21	
		21b	2.15	
7	*ap*		1.21	6.2
	±*sc*		0	93.8

a) At 300 K. Statistical factors of conformers are properly taken into account.

Molecular Mechanics Calculations. In order to understand the dependence of rotamer equilibria upon the *o*-alkyl group in more detail, we performed molecular mechanics calculations on **4**—**7** using the MM2 force field.[19] Relative steric energies of conformers are compiled in Table 4.

In any of the stable rotamers of **4**—**7**, the plane of the aryl moiety is coplanar with the C_9–O bond: The dihedral angles C(9)–O–C(1′)–C(6′) are less than ±3°, except for +*sc*-**7** where it is −6.6°. Two *o*-benzeno

bridges flanking the aryl group bend away from each other, the dihedral angle C(1′)-O-C(9)-C being *ca.* 65°. The C(9)-O-C(1′) angles are around 121°, widening by about 10° from the standard C(sp^3)-O-C(sp^2) angle of 110.8°.

As for the conformation of the *o*-alkyl group, the conformation **18** in which a hydrogen or a methyl

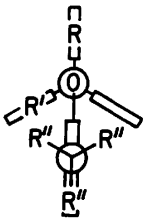

R or R′ = CH_3
R″ = H or CH_3

18

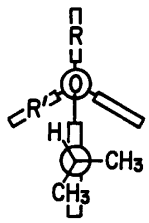

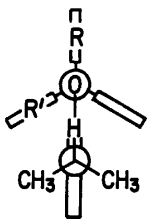

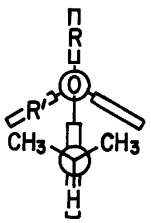

19 **20** **21**

a : R = CH_3, R′ = H
b : R = H, R′ = CH_3

group eclipses 3′-C was calculated to be the most stable in either rotamer of **5** and **7**. In *ap*-**6**, the lowest-energy conformation is **19a** in which one of the methyl group is perpendicular to the plane of the benzene ring. Conformation **20a** is slightly less stable than **19a**. **21a** in which the methine hydrogen eclipses 3′-C is far less stable, because the *gem*-dimethyl groups are very close to the *peri*-methyl group. In +*sc*-**6**, on the other hand, **19b**, **20b**, and **21b** have almost the same energy.[20]

Steric energies of the unstable rotamers with the *o*-alkyl group pointing inwards, *ap′* and ±*sc′*, were calculated for **5**. *ap′*-**5** was shown to be less stable by 9.08 kcal mol^{-1} than *ap*-**5**, and ±*sc′*-**5** less stable by 8.18 kcal mol^{-1} than ±*sc*-**5**.

As is evident from Table 4, the steric energy of the ±*sc* rotamer relative to the corresponding *ap* one decreases on going from **5** to **6**, and in the *t*-butyl derivative **7**, ±*sc* is more stable than *ap*. The tendency that the ±*sc* rotamer becomes more and more populous as the *o*-substituent becomes bulkier is reproduced by calculation, but the quantitative agreement between the experiment and the calculation is very poor.

These discrepancies might be partly ascribed to solvent effects and/or some other factors which affect the relative energies of rotamers but are not reproduced by molecular mechanics calculations. One of such possibilities is the C-H···π attractive interaction, which might operate between the *peri*-methyl and the aryl groups in the ±*sc* rotamer.[21] However, most of the discrepancies should be attributed to the intrinsic properties of the force field used. Overestimation of the steric energies of the ±*sc* rotamers, especially by overestimating the repulsive interaction between the *peri*-methyl group and the flanking aryl group in ±*sc*, seems to be the most probable origin. Similar situations were encountered by Mislow *et al.* in their molecular mechanics studies on the stereodynamics of 9-(arylmethyl)triptycenes.[8] They found that the repulsive interaction between a benzene ring and a hydrogen which protrudes into the π-cloud of the benzene ring is overestimated in the calculations of the transition states for GR in 9-(arylmethyl)triptycenes and also for the ring flipping in [2.2]metaparacyclophane. Such overestimation seems to operate in the calculations of conformational equilibria as well.[8]

It has become evident that the MM2 force field does not satisfactorily reproduce the conformational equilibria in our present compounds. Improvement of the force field and/or the calculation methodology is necessary to obtain satisfactory results on the ground states and to further extend the calculations to the energy surfaces of the dynamic processes, and is under investigation.[22]

Experimental

Materials. Yields, melting points, and the analytical data are compiled in Table 5. Melting points are not corrected.

General Procedure for the Synthesis of 9-Aryloxyanthracenes. Method A. A mixture of 2.57 g (10 mmol) of 9-bromoanthracene and 30 mmol of an appropriate phenol was heated at 220—230 °C for 4 h together with 1.0 g of potassium hydroxide and 0.3 g of copper powder. The reaction mixture was extracted with dichloromethane and the extract was washed with aqueous sodium hydroxide to remove the unreacted phenol and then with water, dried over magnesium sulfate and concentrated. The residue was chromatographed on silica gel with benzene-hexane as the eluent. Recrystallization of the eluate from tetrahydrofuran-hexane gave pure compounds. ^1H NMR data of the anthracenes are given in Table 6.

Method B. A mixture of 3.88 g (20 mmol) of anthrone and 100 mmol of a phenol in 100 mL of toluene containing 1.0 mL of concentrated sulfuric acid was heated under reflux for 150—180 h using a Dean-Stark water collector. The reaction mixture was washed with aqueous sodium hydroxide and then with water, dried over magnesium sulfate, and concentrated. Chromatography on silica gel followed by recrystallization gave the anthracenes as above.

TABLE 5. YIELDS, MELTING POINTS, AND ANALYTICAL DATA

Compd	Method	Yield %	Mp θ_m/°C	Found (%) C	Found (%) H	Calcd (%) C	Calcd (%) H
8	A	14	131—132[a]				
9	A	30	140—141	88.47	5.58	88.70	5.67
	B	36					
10	A	17	161—162	88.63	6.15	88.42	6.45
	B	38					
11	A	7	202—203	88.37	6.59	88.31	6.79
4		28	202—203	90.04	5.64	89.80	5.92
5		29	193—194	89.51	6.02	89.65	6.23
6		31	162—163	89.33	6.64	89.38	6.78
7		33	224—225	89.00	6.74	89.26	7.02

a) Lit: 132—133 °C (Ref. 10).

TABLE 6. ^{1}H NMR DATA OF ANTHRACENES IN $CDCl_3$ AT *ca.* 35 °C[a]

Compd	R	2′-R	6′-H	10-H	Other Aromatic Protons
8	H	b)	b)	8.35 s	6.6—7.6(9H), 7.8—8.2(4H)
9	CH_3	2.71 s	6.00m	8.34 s	6.6—7.0(2H), 7.1—7.6(5H), 7.8—8.2(4H)
10	$CH(CH_3)_2$	1.55 d 3.90 sep (J=6.9 Hz)	5.99m	8.35 s	6.6—7.0(2H), 7.1—7.6(5H), 7.8—8.2(4H)
11	$C(CH_3)_3$	1.76 s	6.00m	8.36 s	6.6—7.0(2H), 7.2—7.6(5H), 7.8—8.2(4H)

a) Obtained at 90 MHz. Chemical shifts are given in δ. b) Not identified.

General Procedure for the Synthesis of 9-Aryloxy-1,4-dimethyltriptycenes. A solution of 830 mg (5 mmol) of 3,6-dimethylanthranilic acid[23] in 20 mL of 1,2-dimethoxyethane (DME) and a solution of 1.0 mL (*ca.* 7.5 mmol) of isopentyl nitrite in 10 mL of DME were added dropwise during the course of 1 h to a boiling solution of 2.0 mmol of 9-aryloxyanthracene in 20 mL of DME so that an excess of isopentyl nitrite was always present in the reaction mixture. The reaction mixture was heated under reflux for further 30 min and concentrated. Chromatography of the residue on silica gel with hexane as the eluent followed by recrystallization from tetrahydrofuran-hexane gave the desired triptycene as colorless crystals.

Spectral Measurements. ^{1}H NMR spectra at ambient temperature and below were obtained on a JEOL GX-400 spectrometer operating at 399.65 MHz in the pulse FT mode. Temperatures were read as digital outputs from the variable temperature accessory and are not corrected. Dynamic NMR spectra above room temperature were obtained on a Hitachi R-20B spectrometer at 60.0 MHz in the CW mode, and temperatures were calibrated using ethylene glycol.[24] Measurements of some of the spectra at ambient temperature as well as the nuclear Overhauser effect experiments were made on a Varian EM-390 spectrometer at 90.0 MHz in the CW mode.

Computer Simulations. Theoretical spectra were obtained on a HITAC M-280H computer system at the Computer Center of The University of Tokyo (CCUT) using a modified version of the DNMR3 program by Binsch.[25] Temperature dependence of the isopropyl-methyl signals of **6** was analyzed as a 3-spin 3-site system (ABX $\rightleftarrows$ BAX $\rightleftarrows$ C_2Y) instead of a 7-spin 3-site system ($A_3B_3X \rightleftarrows B_3A_3X \rightleftarrows C_6Y$), regarding a methyl group as a single nucleus. In this case, the rate constant for the $\pm sc \rightarrow ap$ process, *i.e.* ABX$\rightarrow C_2Y$ and BAX$\rightarrow C_2Y$, was assumed to be 0.001 s^{-1} throughout the temperature range of −60 to −25 °C (see Ref 13). The spectra of the 1- and 4-methyl groups in **5** and **6** were simulated as a 2-spin 2-site system (AB $\rightleftarrows$ CD), regarding again a methyl group as a single nucleus.

Molecular Mechanics Calculations. Calculations were performed on the HITAC M-280H computer system using the MM2 program in the CCUT Program Library. Original parameters in the program were used as they were except for the bond length and the stretching force constant for C(sp^2)-C(sp^2), which were modified so that they represented aromatic carbons (l_o=1.3937 Å, k_s=8.067 mdyn[††] $Å^{-1}$). Only one set of torsional parameters were newly added: $V_1=V_2=V_4=0$, V_3=0.403 kcal mol^{-1} for C(sp^2)-C(sp^3)-O-C(sp^2).

The authors are grateful to Professors N. L. Allinger and E. Ōsawa for their helpful discussion, and to Dr. G. Izumi of Nippon Kayaku Co., Ltd. and Mr. S. Murata of Institute for Molecular Science for the measurements of the 400 MHz ^{1}H NMR spectra.

†† 1 dyn=10^{-5} N.

References.

1) Part LVI: G. Yamamoto and M. Ōki, *Bull. Chem. Soc. Jpn.*, **58**, 1690 (1985).

2) M. Ōki, *Angew. Chem., Int. Ed. Engl.*, **15**, 87 (1976).

3) a) F. Suzuki and M. Ōki, *Tetrahedron Lett.*, **1974**, 2845; *Bull. Chem. Soc. Jpn.*, **48**, 596 (1975); b) M. Kono, H. Kihara, N. Nakamura, F. Suzuki, and M. Ōki, *ibid.*, **52**, 1682 (1979); M. Ōki, M. Kono, H. Kihara, N. Nakamura, *ibid.*, **52**, 1686 (1979).

4) G. Yamamoto, *J. Mol. Struct.*, **126**, 413 (1985).

5) G. Yamamoto and M. Ōki, *Chem. Lett.*, **1979**, 1251; *Bull. Chem. Soc. Jpn.*, **54**, 473 (1981).

6) G. Yamamoto and M. Ōki, *Chem. Lett.*, **1979**, 1255; *Bull. Chem. Soc. Jpn.*, **54**, 481 (1981).

7) G. Yamamoto and M. Ōki, *J. Org. Chem.*, **48**, 1233 (1983).

8) R. B. Nachbar, Jr., W. D. Hounshell, V. A. Naman, O. Wennerström, A. Guenzi, and K. Mislow, *J. Org. Chem.*, **48**, 1227 (1983).

9) Preliminary results have been reported: G. Yamamoto and M. Ōki, *Chem. Lett.*, **1984**, 97.

10) W. Theilacker, U. Berger-Brose, and K.-H. Beyer, *Chem. Ber.*, **93**, 1658 (1960).

11) W. H. Pirkle and J. M. Finn, *J. Org. Chem.*, **48**, 2779 (1983).

12) In this temperature range, the *ap* rotamer may be in dynamic equilibrium with $\pm sc'$ although the situation is not detected by NMR because the population of $\pm sc'$ is extremely low. Similarly, the GR(H) barrier in $ap \rightleftarrows \pm sc'$ is not obtained experimentally.

13) The ratio does not necessarily represent the equilibrium populations at −81 °C: The data in Table 3 indicate that the value corresponds to the equilibrium populations at about −30 °C. The $ap \rightleftarrows \pm sc$ process is very slow in this temperature range and the equilibrium might not have been attained during the NMR measurements. The nonequilibrium state, however, does not affect the analysis of the $+sc \rightleftarrows -sc$ process.

14) Nuclear Overhauser effect experiments confirmed that the low-field signal at δ 2.56 derives from 4-CH_3: irradiation of this signal enhances the intensity of the 10-H signal at δ 5.62 by *ca.* 20% while irradiation at δ 2.14 does not change the 10-H signal intensity.

15) D. Kost, E. H. Carlson, and M. Raban, *J. Chem. Soc., Chem. Commun.*, **1971**, 656.

16) Molecular mechanics studies would afford some information on these points but are still pending for several reasons discussed in the later section.

17) For further discussion on this point, see Ref. 1.

18) G. Yamamoto and M. Ōki, *Bull. Chem. Soc. Jpn.*, **57**, 2219 (1984).

19) N. L. Allinger, *J. Am. Chem. Soc.*, **99**, 8127 (1977); N. L. Allinger and Y. H. Yuh, *QCPE*, No. 395.

20) For conformational analysis of an isopropyl group in substituted cumenes and related compounds, see for example: A. Mannschreck and L. Ernst, *Chem. Ber.*, **104**, 228 (1971); C. Roussel, A. T. Balaban, U. Berg, M. Chanon, R. Gallo, G. Klatte, J. A. Memiaghe, J. Metzger, D. Oniciu, and J. Pierrot-Sanders, *Tetrahedron*, **39**, 4209 (1983); J. C. Schug and J. W. Viers, *ibid.*, **40**, 3971 (1984).

21) See for example: S. Zushi, Y. Kodama, K. Nishihata, K. Umemura, M.Nishio, J. Uzawa, and M. Hirota, *Bull. Chem. Soc. Jpn.*, **53**, 3631 (1980).

22) For example, the use of smaller values for the van der Waals radius (r^*) of an sp^2-carbon was found to improve the situation. When the radius of 1.50 Å was used instead of the original value of 1.94 Å, the energy difference between *ap*-**5** and $\pm sc$-**5** was 1.45 kcal mol^{-1} favoring *ap*-**5**. It is however uncertain whether the single change of $r^*(sp^2\text{-C})$ gives the totally consistent results not only for the energy differences of rotamers but also for the molecular geometries.

23) S. Gronowitz and G. Hansen, *Arkiv Kemi*, **27**, 145 (1967); M. S. Newman and J. A. Cella, *J. Org. Chem.*, **38**, 3482 (1973).

24) A. L. Van Geet, *Anal. Chem.*, **40**, 2227 (1968).

25) G. Binsch, *Top. Stereochem.*, **3**, 97 (1968); D. A. Kleier and G. Binsch, *QCPE*, No. 165.

Hydrogenation of Pyrene and Catalytic Interconversion of Hydropyrenes

Masahiro MINABE* and Katsuko NAKADA
Department of Industrial Chemistry, Faculty of Engineering, Utsunomiya University, Ishiicho, Utsunomiya 321
(Received December 10, 1984)

Reexamination on the hydrogenation of pyrene (**1**) with Raney nickel catalyst under atmospheric pressure afforded a mixture of 4,5-di- (**2**), 4,5,9,10-tetra- (**3**), 1,2,3,6,7,8-hexa- (**4**), and 1,2,3,3a,4,5-hexahydropyrene (**5**). The relative amount of each product at the initial reaction stage was determined by time–yield relation of the products. The formation sequence of the products is discussed with reference to the hydrogenations of **2**—**5**: **4** may be formed independent of **2**, and **2** is converted to **3**. Hydropyrene **5** may be produced from **1** mainly through the same σ-adsorbed species which also leads to **2**. The hydrogenation of **1** with palladium and platinum catalysts gave similar results as with nickel. With nickel and palladium catalysts the hydrogenation of **1** was faster than that of 4*H*-cyclopenta[*def*]phenanthrene (**9**). However, with platinum the hydrogenation of **1** was slower than that of **9**. Catalytic interconversion of **2**—**5** was examined at 240 °C under an argon pressure of 90 kg cm^{-2}. Hydroarene **2** was easily dehydrogenated, and **3** and **5** were interconverted to a fair extent. Therefore, **2**, **3**, and **5** may be good hydrogen donor solvents for coal liquefaction.

The catalytic hydrogenation of polycyclic aromatic hydrocarbons (PAHs) has been investigated extensively from both stereochemical and mechanistic standpoints.[1,2] The products are of interest both as synthetic intermediates,[1] and because of their carcinogenic properties.[1,3,4] In addition, partially hydrogenated PAHs have recently been used as hydrogen donor solvents in coal liquefaction.[5] For our continuing study of PAHs having active methylene such as fluorene,[6] we have compared the reactivity of hydrogenation of PAHs possessing active methylene with that of PAHs possessing no active methylene such as pyrene (**1**). The hydrogenation of **1** is of interest in particular from the following three viewpoints. One of those is the hydrogenation sequence. It has been known that the hydrogenation of **1** gives 4,5-di- (**2**),[7] 4,5,9,10-tetra- (**3**),[8] 1,2,3,6,7,8-hexa- (**4**),[9] 1,2,3,3a,4,5-hexa- (**5**),[9] isomeric deca- (**6**, **7**),[10] and perhydropyrenes (**8**)[11] under various reaction conditions (Scheme 1).[12] Although the previous papers have studied the function of temperature and pressure in addition to catalysts, the hydrogenation sequence was not so clear.[10] This is because the change of the yield of each product has not yet been examined as a function of reaction time. The study of the hydrogenation of **1** with respect to the reaction time may shed light on the reaction pathway and be useful to uncover the reaction conditions to obtain specific hydroarenes.

A second consideration is the relative reactivity of **1** among PAHs. For example, the rate of hydrogenation of **1** to **2** with palladium-on-carbon catalyst has been reported to be comparable to the rate of the hydrogenation at the 8,9-double bond of 4*H*-cyclopenta[*def*]phenanthrene (**9**).[13] We have recognized in the study of the hydrogenation of **9**[14] that the reduction of **1** is slower than that of **9** when platinum oxide is used as catalyst. The abnormality of palladium as a catalyst in the platinum group metals has been pointed out in the hydrogenation of aromatic compounds[15,16] and cycloolefins.[17] The abnormality may be caused by the fact that palladium in particular adsorbs reactants very weakly[18] and the rate- and product-controlling steps of hydrogenation with palladium may differ from that of hydrogenation with platinum.[19]

The third interest concerns the ability of **2**—**5** as hydrogen donor solvents in coal liquefaction. Mochida *et al.* have reported the effectiveness of hydrogenated pyrene mixture as the solvent.[20] The direct coal liquefaction occurs mainly by radical hydrogen transfer, and hence, the ability of hydrogen transfer of the solvent may play an important role in the coal liquefaction process. The hydrogen donat-

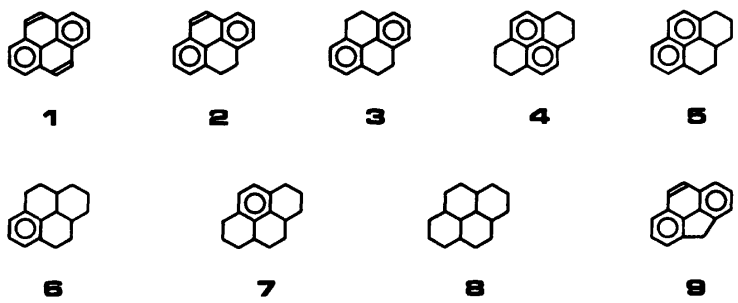

Scheme 1.

ing property of partially hydrogenated aromatics has been determined by disproportionation of the substrate or by the reaction of substrate with hydrogen acceptor as the cases of cyclohexene,[21] naphthalene,[22] phenanthrene,[23] and anthracene[12] derivatives. With regard to the partially hydrogenated pyrenes, no reports describing such reactions are limited to a few examples.[24]

The present paper deals with the hydrogenation of **1** under mild conditions to indicate the reaction pathway of **1**. Also, it examines the competitive hydrogenation of **1** and **9**. Finally, it considers the catalytic interconversion of hydropyrenes, **2**—**5** to clarify the ability of these compounds as hydrogen donors.

Results and Discussion

Hydrogenation of **1** in the presence of Raney nickel (W-7) was carried out in ethanol at room temperature under atmospheric pressure of hydrogen to afford **2**, **3**, **4**, and **5** as illustrated in Fig. 1. In addition, more highly hydrogenated arenes, **6**—**8**, were detected in small amounts, but they were not further studied. Also, the hydrogenations of **2**—**5** were examined under similar conditions. The relative amount of each product at the initial reaction stage was determined by a known procedure[15,25] (Table 1). The rate constant of the conversion of each substrate was roughly estimated from time-conversion relation, based on the assumption that the reaction followed zero-order kinetics in reactant till its complete conversion.

The results suggest that **2** and **4** are mainly formed from **1**, and the main portion of **2** is converted gradually into **3**. Hydroarene **4** is formed independent of the formation of **2**. The interconversion of hydropyrenes except **3** may be negligible under these conditions as is explained later. Therefore, the adsorption of the planar molecule **1** onto the catalyst surface (A) could take place in two different manners; namely at the C_4–C_5 bond (B) and at the biphenyl ring system (C)[26] (Scheme 2). Either the half-hydrogenated state (D) at the C_4 atom may undergo desorption to give **2**, or may be converted to the adsorption state (E)[19] at the biphenyl ring moiety to afford **5** by subsequent hydrogenation. In a similar manner, **2** can give **3** *via* (F) and **3** may be hydrogenated slowly to **4** and **5** through hydrogen transfer. Absorbate (C) may yield **4** and **5** *via* (G) and (H), respectively. The process to **5** through (H) may be a minor route in the hydrogenation of **1** because **5** is thermodynamically less stable than **4** as is explained later.[26]

The hydrogenation of **1** was also carried out in

Table 1. Relative amount of **2**—**7** formed in the hydrogenation of pyrene and hydropyrenes with Raney nickel at initial stage

Reactant	Relative amount/mol%				Rate constant
	2	**3**	**4**	**5**	mol s^{-1} g-cat.$^{-1}$
1	39	6	37	12	2.3×10^{-7}
2		78	7	6	9.3×10^{-8}
3			58	32	2.2×10^{-9}
4	90(for **7**)				5.4×10^{-10}
5	53(for **7**)		44(for **6**)		2.0×10^{-9}
1[a]	64	6	19	11	
1[b]	32	18	14	8	

a) With Pd-C. b) With PtO_2.

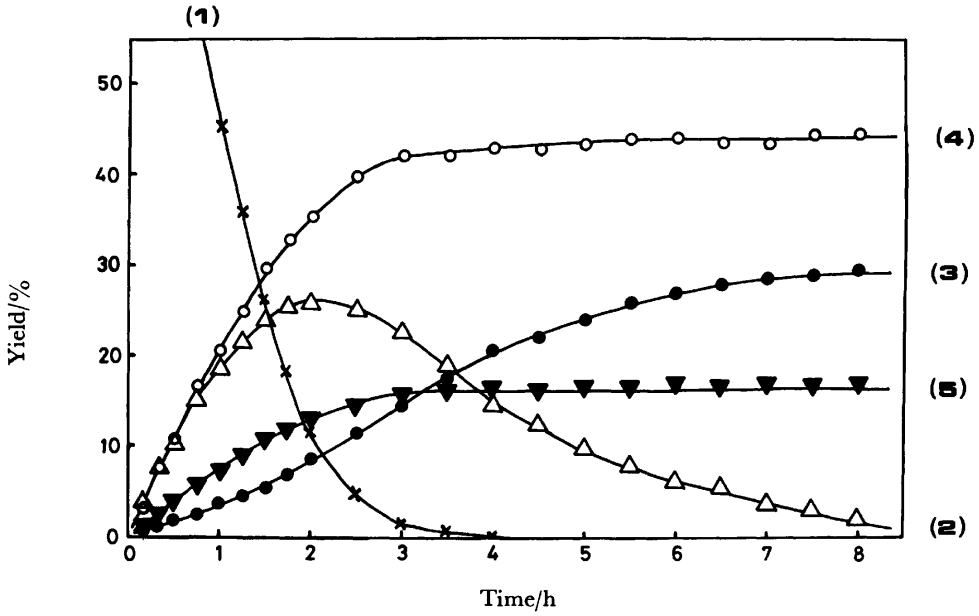

Fig. 1. Figure 1. The process of hydrogenation of **1**.
—×— (**1**); —△— (**2**); —●— (**3**); —○— (**4**); —▼— (**5**).

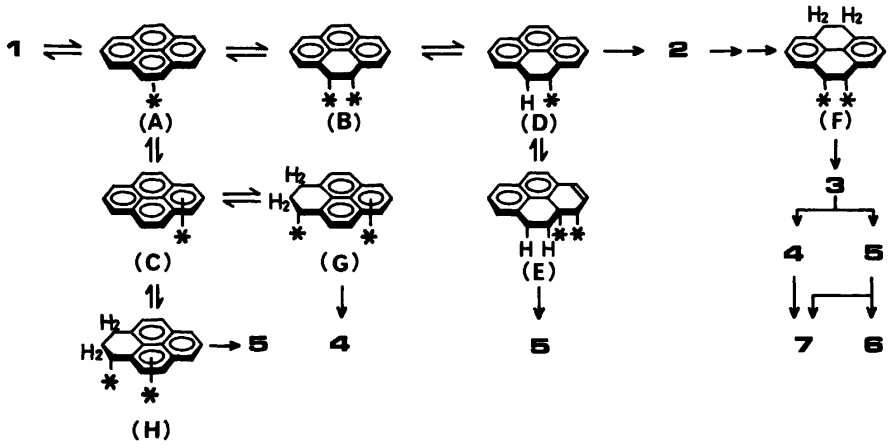

Scheme 2. The presumptive sequence of hydrogenation of **1**. (The asterisk shows the active surface of catalyst.)

TABLE 2. HYDROGENATION OF **1** WITH SOME CATALYSTS

Catalyst	Product distribution/%					$k(\mathbf{1})/k(\mathbf{9})$[a]
	1	**2**	**3**	**4**	**5**	
R-Ni(W-7)	45	19	4	21	7	1.37
Pd-C(10%)	46	33	4	11	5	1.74
PtO_2	50	22	5	6	3	0.75
Mo-Co	47	11	3	24	14	

a) Relative conversion of **1** and **9**.

the presence of palladium-on-carbon or platinum catalyst at 50 °C under a hydrogen pressure of 5 kg cm^{-2} (1 kg cm^{-2}=98066.5 N m^{-2}) to afford **2**—**8**. Table 2 shows the product distribution at about 50% conversion of **1**. The distribution with Mo-Co catalyst was estimated by comparison of the NMR data described elsewhere[27] with the NMR spectra of an authentic mixture of pure **1**—**5**. Since the overall trend of the yield is similar to the case of Raney nickel, the reaction sequence in the presence of palladium or platinum catalyst may be explained as in the case of the nickel catalyst. The palladium catalyst in particular gives **2** in relatively high yield (Table 1). On the contrary, significant amounts of **6**—**8** are formed with the platinum catalyst in analogy with the example of **9**.[14]

The relative reactivity of **1** and **9** was examined by a competitive method. The hydrogen pressure was maintained as constant as possible during the reaction in order to remove the factor of hydrogen pressure.[16,28,29] The reactions followed zero-order kinetics in reactants till about half-conversion of reactants. Table 2 shows that **1** is more reactive than **9** over the nickel and palladium catalysts, in contrast to hydrogenation using platinum.

The ratio of conversion of **1** and **9** may be regarded as the overall results of two factors. One is the adsorption equilibrium of each reactant and the other is the rate factor of each adsorbed species. If the adsorbed species of one reactant disturbs the adsorption of the other reactant, the rate of the latter reactant estimated by the competitive method may be less than that determined independently. Therefore, the ratio of conversion in Table 2 may differ from that obtained independent hydrogenations of **1** and **9**. Nevertheless, the difference of the ratio due to the catalyst is thought in some degree to indicate the difference of reactivities of each component. The real reason could be complex, but **9** is presumed to be more reactive than **1**, because **9** is strained owing to the five-membered ring. In fact, **9** is known to give an 8,9-dihydro derivative by treatment with sodium in ethanol[13] and to give 8,9-dibromide by the action of bromine.[30]

TABLE 3. CATALYTIC INTERCONVERSION OF HYDROPYRENES[a]

Reactant	Product distribution/%				
	1	**2**	**3**	**4**	**5**
1	99	1			
2	70	25	2	2	1
3	48	18	4	20	8
3[b]	97	3	*	*	*
3[c]	*	1	99	*	*
4	20	9	1	58	9
5	19	7	1	21	48

a) Reaction was carried out with platinum at 240 °C under an argon pressure of 90 kg cm^{-2} for 10 h. The asterisk shows that trace amount (<0.4%) was detected by GLPC. b) 240 °C, 9 kg cm^{-2}, 3 h. c) 50 °C, 90 kg cm^{-2}, 50 h.

Catalytic interconversion of hydropyrenes, **2**—**5**, was examined at 240°C under an argon pressure of 90 kg cm^{-2} with platinum catalyst (Table 3). Dehydrogenation takes place due to increase of the resonance stability by aromatization. Easily dehydrogenated reactants such as **2** or **3** may be good hydrogen donors. The thermodynamical stability

of **4** compared with that of **5** would be supported by the fact that **4** was easily formed from **5**, as contrasted with the yield of **5** from **4**. Consequently, the interconversions of **3** and **5** occur easily. This is the reason why **2**, **3**, and **5** may be good hydrogen donors for coal liquefaction solvent.

Experimental

All melting points are uncorrected. The ^{1}H NMR (in CCl_4), IR (KBr-disk), UV (in cyclohexane), and mass spectra were recorded using the same apparatus as described elsewhere.[14]

The distribution of products was examined by GLPC with a GC-8A gas chromatograph (Shimadzu) equipped with a column (3 mmϕ, 1 m) containing Dexsil 300GC (5%) on Chromosorb WAW (80—100 mesh) at 195 °C under 1 kg cm^{-2} of nitrogen. Each peak area of **1** (retention time; 9.5 min), **2** (7.2 min), **3** (4.6 min), **4** (6.3 min), **5** (5.8 min), **6** (3.4 min), and **7** (3.8 min) was compared using TR-2217 integrator (Takeda Riken). The competitive hydrogenation of **1** and **9** was also examined by the same gas chromatograph containing Silicone OV-17 (5%) as liquid phase at 165 °C. Each peak area of **1** (8.8 min) and **9** (3.8 min) was compared with that of tetracosane (13.5 min) as an internal reference.

The catalysts used in this experiment were the same as those described elsewhere.[14]

Hydrogenation of 1 over Palladium-on-Carbon. 400-mg of Pd-C (10%) suspended in AcOEt (5 ml) was pretreated at 50±1 °C under hydrogen pressure of 5 kg cm^{-2} for 1 h. A solution of **1** (202 mg, 1 mmol) in AcOEt (25 ml) was added to the suspension. After 4 purges with hydrogen, the mixture was stirred at 50 °C and 5 kg cm^{-2}. A small amount (*ca.* 0.2 ml) of the mixture was taken out, filtered, and submitted to GLPC after 30 min, 1 h, and additionally every 1 h.

After 7 h, the test portion showed the proportion to be **1** (46%), **2** (33%), **3** (4%), **4** (11%), **5** (5%), and others (1%). All the mixtures were filtered and evaporated to dryness, and the residues chromatographed on an alumina column (200 g, 16 mmϕ, 120 cm) with hexane. The rate of effusion was 1.2 min ml^{-1}, and the eluate was collected as 10-ml units. Fraction from 840 to 1140 ml gave 21.4 mg (10%) of **4**: mp 131—132 °C (from hexane) (lit,[9] mp 132—134 °C); NMR, δ=1.99 (4H, q, J=6.5 Hz), 3.02 (8H, t), and 6.95 (4H, s); UV, λ_{max} 235 (log ε 4.81), 286 (3.87), 309 (4.15), 315 (3.71), 323 (3.32), and 330 nm (3.49). Fraction between 1240 and 1490 ml afforded 5.8 mg (3%) of **3**: mp 135—137 °C (hexane) (lit,[8] mp 135—136 °C); NMR,[26] δ=2.85 (8H, s) and 6.96 (6H, s); UV, λ_{max} 215 (log ε 4.59), 270 (4.18), and 280 nm (4.27). Fraction at 1490—2050 ml gave 11.0 mg (5%) of **5**: mp 104—106 °C (hexane) (lit,[9] mp 105 °C); NMR, δ=1.25—3.26 (11H, m) and 6.89—7.46 (5H, m); UV, λ_{max} 227 (log ε 4.78), 233 (4.93), 285 (3.80), 294 (3.70), 311 (3.17), and 325 nm (3.21). Fraction between 2130 and 3640 ml afforded 52.6 mg (26%) of **2**: mp 131—132 °C (hexane) (lit,[7] mp 132 °C); NMR,[26] δ=3.24 (4H, s) and 7.23—7.67 (8H, m); UV,[7] λ_{max} 217 (log ε 4.63), 260 (4.67), 282 (4.17), 287 (4.13), 299 (4.00), 319 (3.03), and 335 nm (3.19). Fraction at 3830—4440 ml gave 90.0 mg (45%) of **1**, mp 149 °C.

In addition, fraction ranging from 540 to 840 ml afforded an oil (9.9 mg) which was determined as a mixture of **4**, **6**, **7**, and **8** by means of GC-MS.

Hydrogenation of 1 over Platinum. A 50.2-mg portion of platinum oxide in AcOEt (5 ml) was treated with hydrogen for 1 h at 5 kg cm^{-2}. A solution of **1** (101 mg, 0.5 mmol) in AcOEt (20 ml) was added to the vessel and the mixture was stirred at 50 °C under hydrogen pressure of 5 kg cm^{-2}.

Hydrogenation of 1 over Raney Nickel. A mixture of **1** (202 mg, 1 mmol) in HOEt (40 ml) was shaken with Raney nickel catalyst (W-7, 0.4 g as alloy) at room temperature under hydrogen at atmospheric pressure. The composition of the mixture was determined by GLPC as is shown in Fig. 1.

Hydrogenation of 2. Compound **2** (40.8 mg, 0.2 mmol) in HOEt (15 ml) was shaken with Raney nickel (W-7, 0.2 g) in a similar manner to **1**. The distribution of the test portion was **2** (trace), **3** (76%), **4** (9%), and **5** (6%) after 3 h and was **3** (74%), **4** (11%), and **5** (6%) after 10 h.

Hydrogenation of 3. A solution of **3** (41.2 mg, 0.2 mmol) in HOEt (15 ml) was allowed to react in the presence of Raney nickel (W-7, 0.75 g). The test portion showed the proportion to be a mixture of **3** (86%), **4** (8%), **5** (4%), **6** (1%), and **7** (1%) after 3 h and to be **3** (42%), **4** (33%), **5** (trace), **6** (7%), and **7** (11%) after 23 h.

Hydrogenation of 4. A mixture of **4** (41.6 mg, 0.2 mmol) in HOEt (15 ml) was treated with Raney nickel (W-7, 1 g) in a similar manner to **1**. The distribution of the mixture was as follows: **4** (89%), **6** (1%), and **7** (7%) after 3 h and **4** (62%), **6** (2%), and **7** (32%) after 27 h.

Hydrogenation of 5. Compound **5** (41.6 mg, 0.2 mmol) in HOEt (15 ml) was shaken with Raney nickel (W-7, 1 g) as above. The proportion of the mixture was **5** (72%), **6** (12%), and **7** (15%) after 3 h and **5** (5%), **6** (40%), and **7** (49%) after 19 h.

Competitive Hydrogenation of 1 and 9. Over Raney Nickel. A mixture of **1** (51.1 mg, 0.26 mmol), **9** (45.1 mg, 0.24 mmol), and tetracosane (31.0 mg) in HOEt (30 ml) was shaken with Raney nickel (W-7, 0.6 g) at room temperature under hydrogen at atmospheric pressure. Every 15 min, a small portion was taken out and submitted to GLPC.

Over Palladium-on-Carbon. A mixture of **1** (50.5 mg, 0.25 mmol), **9** (50.3 mg, 0.27 mmol), tetracosane (35.5 mg), and Pd-C catalyst (10%, 600 mg, pretreated with hydrogen at 50 °C under 5 kg cm^{-2} for 1 h) in EtOAc (30 ml) was stirred at 50 °C and 5 kg cm^{-2} of hydrogen.

Over Platinum Catalyst. Platinum oxide (50.1 mg) in AcOEt (5 ml) was pretreated with hydrogen at 50 °C for 1 h under 5 kg cm^{-2}. A mixture of **1** (50.8 mg, 0.25 mmol), **9** (47.5 mg, 0.25 mmol), and tetracosane (34.5 mg) in AcOEt (25 ml) was poured into the solution, and all was stirred at 50 °C under a hydrogen atmosphere of 5 kg cm^{-2}.

Catalytic Interconversion of Hydropyrenes. General Procedure. About 1-mg portion of platinum oxide (1.0—1.5 mg) was placed in a tube (0.5 mmϕ, 6 cm), cyclohexane (0.1 ml) was added, and it was stirred at 50 °C under 5 kg cm^{-2} of hydrogen pressure for 1 h. Reactant (0.05 mmol per 1 mg of PtO_2) was added with cyclohexane (0.4 ml). After purge by argon, the top of the tube was extended to 12 cm in length with a diameter of *ca.* 0.1 mm. The reaction tube was placed in an autoclave which contained hexane

(20 ml), and it was maintained at 240—250 °C under an argon pressure of 85—95 kg cm^{-2} during 10 h. Upon cooling the mixture, the content was submitted to GLPC. A part (<3%) of the reaction mixture flowed out into outer hexane; the proportion of the hexane solution was similar to that of the reaction mixture.

We wish to thank Professor Takashi Toda and Mr. Masaaki Yoshida, Utsunomiya University for their valuable discussion.

References

1) E. Clar, "Polycyclic Hydrocarbons," Academic Press, London (1964).
2) P. N. Rylander, "Catalytic Hydrogenation over Platinum Metals," Academic Press, New York (1967).
3) "Particulate Polycyclic Organic Matter," ed by Committee on Biologic Effects of Atmospheric Pollutants, National Research Council, National Academy of Sciences, Washington (1972): translated into Japanese by N. Ishinishi and Y. Kodama, Tokyo Kagaku Dozin, Tokyo (1981).
4) J. P. Lowe and B. D. Silverman, *Acc. Chem. Res.*, **17**, 332 (1984).
5) D. D. Whitehurst, "Coal Liquefaction Fundamentals," Symp. Ser., No. 139, Am. Chem. Soc., Washington (1980).
6) The previous paper: M. Minabe, M. Yoshida, and O. Kimura, *Bull. Chem. Soc. Jpn.*, **58**, 385 (1985).
7) E. A. Coulson, *J. Chem. Soc.*, **1937**, 1298.
8) T. Sato, E. Yamada, Y. Okamura, T. Amada, and K. Hata, *Bull. Chem. Soc. Jpn.*, **38**, 1049 (1965).
9) J. M. L. Cameron, J. W. Cook, and W. Graham, *J. Chem. Soc.*, **1945**, 286.
10) W. Treibs and G. Mann, *Chem. Ber.*, **91**, 1910 (1958).
11) K. Smeykal and G. Zimmermann, *J. Prakt. Chem.*, **15**, 105 (1962).
12) I. Kagehara, *Bull. Chem. Soc. Jpn.*, **6**, 241 (1931).
13) T. Horaguchi, R. Yamazaki, and T. Abe, *Bull. Chem. Soc. Jpn.*, **53**, 494 (1980).
14) M. Minabe, Y. Yamamoto, M. Yoshida, K. Nakada, and K. Suzuki, *Bull. Chem. Soc. Jpn.*, **57**, 725 (1984).
15) S. Nishimura, S. Ohbuchi, K. Ikeno, and Y. Okadâ, *Bull. Chem. Soc. Jpn.*, **57**, 2557 (1984).
16) P. N. Rylander and D. R. Steele, *Engelhard Ind. Tech. Bull.*, **3**, 19 (1962); **5**, 113 (1964).
17) S. Siegel and B. Dmuchovsky, *J. Am. Chem. Soc.*, **84**, 3132, 3136 (1962).
18) T. Chihara and K. Tanaka, *J. Catal.*, **80**, 97 (1983).
19) S. Siegel and G. V. Smith, *J. Am. Chem. Soc.*, **82**, 6082, 6087 (1960).
20) I. Mochida, K. Otani, Y. Korai, and H. Fujitsu, *Chem. Lett.*, **1983**, 1025. Also see; I. Mochida, K. Tamaru, Y. Korai, H. Fujitsu, and K. Takeshita, *Carbon*, **20**, 231 (1982); I. Mochida, Y. Moriguchi, T. Shimohara, Y. Korai, H. Fujitsu, and K. Takeshita, *Fuel*, **61**, 1014 (1982).
21) E. A. Braude, R. P. Linstead, and P. W. D. Mitchell, *J. Chem. Soc.*, **1954**, 3578..
22) A. C. Buchanan, III, A. S. Dworkin, and G. P. Smith, *J. Org. Chem.*, **47**, 603 (1982).
23) J. R. Durland and H. Adkins, *J. Am. Chem. Soc.*, **59**, 135 (1937); **60**, 1501 (1938).
24) D. H. Paskovich and N. C. Das, *J. Chem. Soc., Chem. Commun.*, **1967**, 39.
25) S. Nishimura, *Yuki Gosei Kagaku Kyokai Shi*, **30**, 36 (1972).
26) P. P. Fu, H. M. Lee, and R. G. Harvey, *J. Org. Chem.*, **45**, 2797 (1980).
27) See Ref. 20. The picture has a broad peak at δ=0.8 ppm, but it can't be explained.
28) H. A. Smith, D. M. Alderman, Jr., C. D. Shacklett, and C. M. Welch, *J. Am. Chem. Soc.*, **71**, 3772 (1949).
29) I. V. Kalechits and A. S. Nakhmanovich, *Dokl. Akad. Nauk. SSSR*, **148**, 835 (1963); *Chem. Abstr.*, **59**, 3737 (1963).
30) M. Yoshida, M. Minabe, and K. Suzuki, *J. Org. Chem.*, **44**, 3029 (1979).

Rotational Isomerism in Fluorene Derivatives. IX. Restricted Rotation about the C(9)-C(9′) Bonds in 9(or 9′)-Substituted 2-Methyl-9,9′-bifluorenyls[1]

Shoji KAJIGAESHI,* Akiko NISHIDA, and Shizuo FUJISAKI
Department of Industrial Chemistry, Faculty of Engineering, Yamaguchi University, Tokiwadai, Ube 755
(Received December 24, 1984)

Several 9(or 9′)-substituted 2-methyl-9,9′-bifluorenyls were prepared and the restricted rotation about the C_{sp^3}–C_{sp^3} bonds in these compounds were investigated by DNMR. In these cases, nonequivalent gauche conformers were observed at low temperatures. Barriers (ΔG^*) for the forward and backward interconversions were slightly increased in agreement with the bulkiness of the 9(or 9′)-substitutents.

Previously, we have discussed the conformations of 9-(9-fluorenyl)-9-(2-substituted 9-fluorenyl)fluorene derivatives[2] (**1**) and 9-aryl-9-(2-methyl-9-fluorenyl)-fluorene derivatives[3] (**2**) concerning the restricted rotation about the C_{sp^3}–C_{sp^3} bonds on the basis of their DNMR behavior.

This work was undertaken to examine the restricted rotation about the C_{sp^3}–C_{sp^3} bonds in 9(or 9′)-substituted 2-methyl-9,9′-bifluorenyl derivatives (**3**). These compounds have a simpler skeleton than **1** or **2**, such as 9,9′-unsubstituted[4] (**3a**), 9-bromo-[4] (**3b**), 9′-hydroxy-[4] (**3c**), 9-methoxy-[4] (**3d**), 9′-methoxy- (**3e**), 9-ethoxy-[4] (**3f**), 9′-ethoxy[4] (**3g**), 9-propoxy- (**3h**) and 9-isopropoxy-2-methyl-9,9′-bifluorenyl (**3i**).

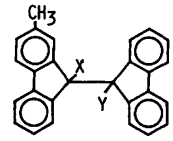

3

	X	Y		X	Y
3a:	H	H	**3f**:	OC_2H_5	H
3b:	Br	H	**3g**:	H	OC_2H_5
3c:	H	OH	**3h**:	$O(CH_2)_2CH_3$	H
3d:	OCH_3	H	**3i**:	$OCH(CH_3)_2$	H
3e:	H	OCH_3			

Results and Discussion

The compounds **3h** and **3i** were prepared by refluxing **3b** with 1-propanol and 2-propanol, respectively. The ^{1}H-NMR data of **3** at room temperature are shown in Table 1.

It has been noted that bifluorenyl has a gauche geometry in the solid state, and the same gauche conformation prevails in solution judging from the magnitude of the H(9)–H(9′) vicinal coupling constant in its ^{1}H-NMR spectrum.[5] We have also reported that rotational isomerization in **1** or **2** may occur by interconversion between two stable gauche conformers of these compounds.[2,3]

TABLE 1. ^{1}H-NMR DATA OF **3** IN $CDCl_3$: δ

Compd	2-CH_3	9- or 9′-H	9- or 9′-Substituent	Aromatic proton
3a	2.26[s]	4.76[s]		6.60—7.68[m]
3b	2.28[s]	5.11[s]		6.96—7.68[m]
3c	2.21[s]	4.69[s]	2.45[s]	6.80—7.48[m]
3d	2.24[s]	4.70[s]	2.85[s]	6.60—7.54[m]
3e	2.22[s]	4.62[s]	2.87[s]	6.59—7.53[m]
3f	2.26[s]	4.76[s]	1.16[t] 2.98[q]	6.78—7.64[m]
3g	2.26[s]	4.77[s]	1.16[t] 2.97[q]	6.72—7.68[m]
3h	2.31[s]	4.78[s]	0.91[t] 1.41—1.79[m] 2.88[t] 2.90[t]	6.67—7.63[m]
3i	2.22[s]	4.64[s]	0.94[d] 0.96[d] 3.10[m]	6.62—7.50[m]

Recently, Olah *et al.*[6] have determined the energy barriers for the interconversion of the equivalent gauche conformers of the symmetrical 9,9′-disubstituted 9,9′-bifluorenyl derivatives (**4**) by complete line-shape analysis of the DNMR spectra of the protons in aromatic regions. We have now obtained the energy barriers for the rotation about the C_{sp^3}–C_{sp^3} bonds in **3** from the line-shape analysis of their DNMR spectra due to the protons of the 2-methyl group; this does not directly hinder rotation about the central bonds. The observed and simulated ^{1}H-NMR spectra of **3c** are shown in Fig. 1 as a typical example.

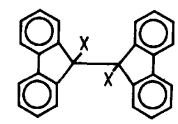

X=H, Me, Cl, Br

4

In Fig. 1, the 2-methyl signal (δ=2.21) which is observed as a singlet at room temperature gradually broadens when the temperature is lowered, and is completely split into two nonequivalent singlets (δ=2.56 and 1.84) at −75 °C. That is, two different conformers which are caused by restricted rotation about the C(9)–C(9′) bond can be observed at low

temperature.

Figure 2 shows the conformations concerned with rotation about the C(9)–C(9′) bond in **3c**, and their interconversion processes by Newman projection formulas. The conformation B (+*ac*), D(*sp*), and F(−*ac*) should be unstable forms because of their eclipsed geometries. An examination of the molecular model suggests that anti conformation E(−*sc*) is also unstable on account of the steric interaction between the 1- and 1′-protons as well as the 8- and 8′-protons in the two fluorene moieties. Consequently, the observed conformations at low temperature are attributed to the gauche forms A(*ap*) and C(+*sc*). In this case, it is reasonable to assume that the methyl group in conformation A which is located in a shielding zone of the other

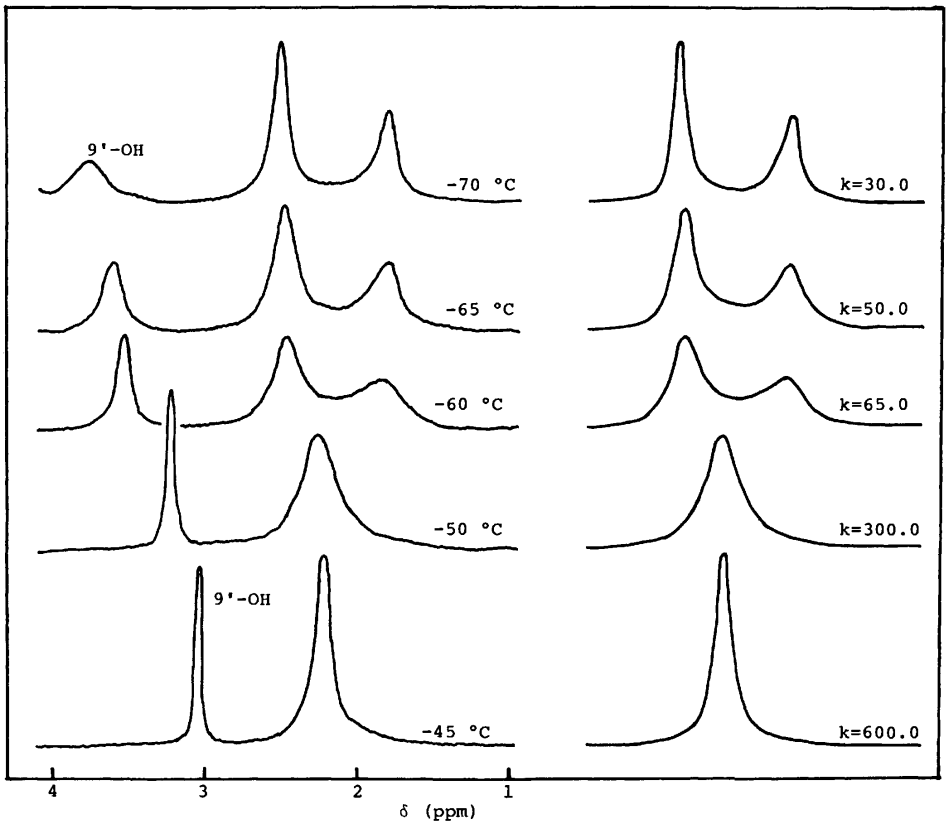

Fig. 1. Obserbed (left) and calculated (right) spectra of 2-CH_3 in **3c** at various temperature.

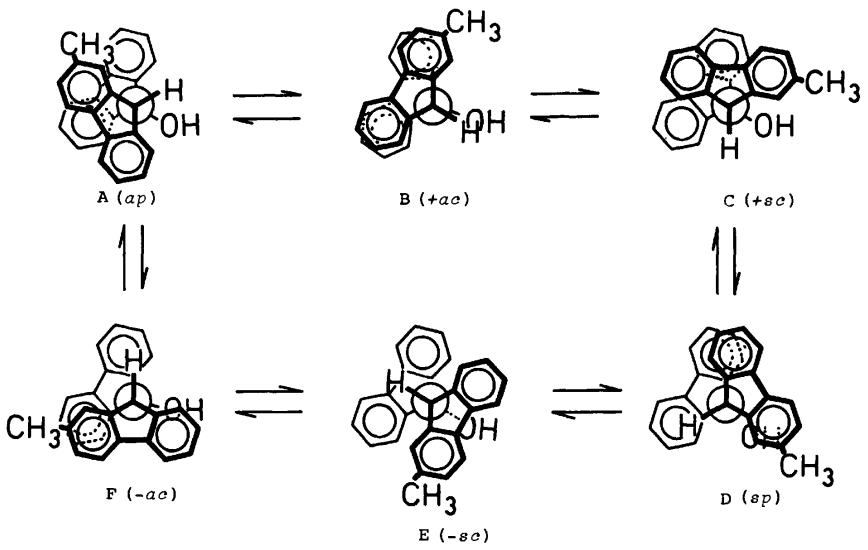

Fig. 2. Stereoisomerization process of **3c** by rotation about the C(9)–C(9′) bond.

fluorene moiety gives ^{1}H-NMR signal at a high field, and the methyl group in C located in a deshielding zone of the other's gives the signal at low field. Thus, the singlet at δ=1.82 is assigned to the methyl signal of A and the singlet at δ=2.52 is assigned to that of C. Furthermore, the equilibrium constant $K(N_A/N_C)$ for the equilibria C$\rightleftharpoons$A was found to be 0.54—0.73 from the intensity ratio of the two methyl signals.

Interconversion between the two gauche conformers, A and C, can occur by two different pathways, *via* the fully eclipsed form B, or *via* the anti form E. But irrespective of the pathways, the observed dynamic behavior can be viewed as a rocking motion from one gauche form to the other. The rotational energy profile for **3c** is illustrated graphically in Fig. 3. The same convincing argument is applicable to the other deirvatives in the series of **3**.

In the ^{1}H-NMR spectra of the derivatives **3** at low temperature, signal intensities of the methyl groups observed at the higher magnetic field were always smaller than that observed at the lower magnetic field. As shown in Fig. 2, it turned out that the conformer A in which the 2-methyl group of **3** is located above the other fluorene moiety is less stable than the conformer C, and the conformational equilibrium between A and C favors C. Therefore, it can be expected that there would be appreciable π-π repulsive interaction between the phenyl moiety with an electron-donating methyl group and the other fluorene moiety.

The activation parameters for internal rotation in **3** obtained from the line-shape analysis of their DNMR spectra due to the methyl groups are listed in Table 2, together with the equilibrium constants between the two rotamers at low temperature.

Steric interactions are obviously responsible for the observed barriers. In fact, as shown in Table 2, the free energies of activation ($\Delta G^{\ddagger}$) for rotation about the C(9)-C(9′) bonds in **3** were slightly increased as the size of 9- or 9′-substituents (X or Y) increased, except for the OH in **3c**. Particularly, 9-alkoxy-2-methyl 9,9′-bifluorenyls gave the magnitudes of the rotational barriers (A→C and/or C→A) in the following order, $\Delta G^{\ddagger}_{3i} > \Delta G^{\ddagger}_{3h} \approx \Delta G^{\ddagger}_{3f} > \Delta G^{\ddagger}_{3d}$.

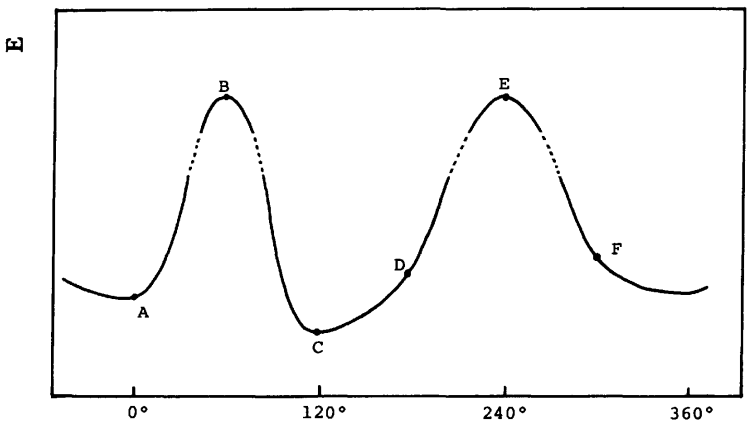

Fig. 3. Rotational energy profile for **3c**.

Table 2. Equilibrium constants and activation parameters of the A$\rightleftharpoons$C systems of **3** at 25 °C

		A⟶C			C⟶A		
		$\Delta H^{\ddagger}$	$\Delta S^{\ddagger}$	$\Delta G^{\ddagger}$	$\Delta H^{\ddagger}$	$\Delta S^{\ddagger}$	$\Delta G^{\ddagger}$
Compd	$K(N_A/N_C)$	kcal/mol[a]	e.u.[b]	kcal/mol[a]	kcal/mol[a]	e.u.[b]	kcal/mol[a]
3a	0.54	9.4	−4.5	10.4	9.4	−5.8	10.8[c]
3b	0.60	9.3	−4.5	10.7	9.3	−5.5	11.0
3c	0.73	10.6	1.6	10.1	10.6	0.9	10.3
3d	0.60	10.0	−3.1	10.9	10.0	−4.1	11.2
3e	0.73	11.3	2.2	10.6	11.3	1.6	10.8
3f	0.60	10.2	−5.2	11.7	10.2	−6.2	12.0
3g	0.60	10.7	−3.4	11.7	10.7	−4.4	12.0
3h	0.60	10.8	−2.5	11.6	10.8	−3.5	11.9
3i	0.66	9.2	−11.2	12.5	9.2	−12.0	12.7

a) 1 cal=4.18 J. b) 1 e.u.=4.18 JK^{-1}·mol^{-1}. c) $\Delta G^{\ddagger}_{240\,°C}$ of **3a** was obtained as 9.9 kcal/mol in Ref. 6.

Experimental

The ^{1}H-NMR spectra were recorded on a JEOL-MH-100 spectrometer with a JEOL model JES-VT-3 variable temperature controller. The chemical shifts are expressed in ppm, with tetramethylsilane as the internal standard. Dynamic NMR spectra were analyzed by using a modified version of the computer program DNMR3.[7] The melting points of the compounds obtained are uncorrected.

*2-Methyl-9-propoxy-9,9'-bifluorenyl (**3h**).* A solution of **3b** (0.21 g, 0.5 mmol) in 1-propanol (3 ml) was refluxed for 30 min. Solvent was distilled off and the residue was chromatographed on alumina using benzene as eluent. The crude product was recrystallized from acetone to give **3h** (0.16 g, 80%) as slight yellow crystals; mp 135—136 °C. ^{1}H-NMR ($CDCl_3$) δ=0.91 (3H, t, J=7 Hz, $(CH_2)_2C\underline{H}_3$), 1.4—1.79 (2H, m, $CH_2C\underline{H}_2CH_3$), 2.31 (3H, s, CH_3), 2.88, 2.90 (2H, two t, J=7 Hz, $C\underline{H}_2CH_2CH_3$), 4.78 (1H, s, CH), 6.67—7.63 (15H, m, aromatic protons).

Found: C, 89.69; H, 6.63%. Cacld for $C_{30}H_{26}O$: C, 89.51; H, 6.51%.

*9-Isopropoxy-2-methyl-9,9'-bifluorenyl (**3i**).* A solution of **3b** (0.21 g, 0.5 mmol) in 2-propanol (3 ml) was refluxed for 30 min. After the same procedure as above, **3i** (0.15 g, 75%) was obtained as slight yellow crystals; mp 141—142 °C. ^{1}H-NMR ($CDCl_3$) δ=0.94, 0.96 (6H, two d, J=6 Hz, $CH(C\underline{H}_3)_2$), 2.22 (3H, s, CH_3), 3.10 (1H, m, J=6 Hz, $C\underline{H}(CH_3)_2$), 4.64 (1H, s, CH), 6.62—7.50 (15H, m, aromatic protons).

Found: C, 89.54; H, 6.52%. Calcd for $C_{30}H_{26}O$: C, 89.51; H, 6.51%.

References

1) Part VIII of this series: A. Nishida, Y. Yoshimoto, H. Fukuda, S. Fujisaki, and S. Kajigaeshi, *Nippon Kagaku Kaishi*, **1984**, 1409.

2) S. Kajigaeshi, S. Fujisaki, I. Aizu, and H. Hara, *Bull. Chem. Soc. Jpn.*, **52**, 3569 (1979).

3) S. Fujisaki, A. Nagashima, H. Hara, and S. Kajigaeshi, *Nippon Kagaku Kaishi*, **1976**, 1874.

4) S. Kajigaeshi, T. Akahoshi, Y. Tanaka, S. Fujisaki, and M. Mashihara, *Nippon Kagaku Kaishi*, **1973**, 762.

5) D. A. Dougherty, F. M. Llort, K. Mislow, and J. F. Blount, *Tetrahedron*, **34**, 1301 (1978).

6) G. A. Olah, L. D. Field, M. I. Watkins, and R. Malhotra, *J. Org. Chem.*, **46**, 1762 (1981).

7) a) G. Binsch, *J. Am. Chem. Soc.*, **91**, 1304 (1969); b) H. Kihara, *JAPC*, **4**, 9 (1983).

Oxidation of Lipids. VIII. Synergistic Inhibition of Oxidation of Phosphatidylcholine Liposome in Aqueous Dispersion by Vitamin E and Vitamin C

Etsuo NIKI,* Akira KAWAKAMI, Yorihiro YAMAMOTO, and Yoshio KAMIYA
Department of Reaction Chemistry, Faculty of Engineering, The University of Tokyo, Hongo, Bunkyo-ku, Tokyo 113
(Received January 23, 1985)

Vitamin E acted as an efficient antioxidant in the oxidation of soybean phosphatidylcholine liposome in an aqueous dispersion initiated by free radicals generated initially either in the aqueous phase or in the lipid phase. Vitamin E decayed linearly with time, and when it was exhausted, the oxidation proceeded rapidly at a similar rate to that in the absence of vitamin E. Vitamin C was also effective by itself in scavenging radicals in an aqueous phase, but it could not scavenge the radicals efficiently in a lipid bilayer. However, when vitamin E was located in phosphatidylcholine bilayer, the addition of vitamin C into an aqueous phase prolonged the period of suppression of oxidation and vitamin C reduced the rate of decay of vitamin E markedly even when the radicals were generated initially in the lipid region. Vitamin C was predominantly consumed linearly at first and vitamin E began to decay after vitamin C was exhausted. It was suggested that vitamin C could regenerate vitamin E by reacting with vitamin E radical during the oxidation of phosphatidylcholine liposome in an aqueous dispersion as observed in a homogeneous solution.

Vitamin E is now accepted to function as a chain-breaking antioxidant during the non-enzymatic oxidation of lipids *in vivo*.[1-5] It scavenges the chain-carrying peroxyl radicals very quickly[6-12] and a small concentration of vitamin E protects the biomembranes from peroxidation efficiently. Vitamin E is also popular as a natural and safe antioxidant for foods. A synergistic inhibition of oxidation by the combination of vitamin E and vitamin C has long been suggested[10,13-22] and it has been found experimentally that vitamin E radical reacts with vitamin C,[21,22] glutathione,[22,23] and cysteine.[23] We have recently found[10] that, when both vitamin E and vitamin C are present, the oxidation of methyl linoleate solution is suppressed quite efficiently and that vitamin E remains almost unchanged while only vitamin C is consumed at the initial stage and vitamin E is consumed after vitamin C is exhausted. A question still remains whether vitamin C which resides largely in an aqueous phase can interact with vitamin E radical that must be located in a lipid phase in heterogeneous liposome system or *in vivo*. We wish to report here the evidence that shows the synergistic inhibition of oxidation by vitamin E and vitamin C in the oxidation of soybean phosphatidylcholine (PC) as a bilayer liposome in an aqueous dispersion.

Experimental

Commercial soybean PC purchased from Daigo Chemicals Co. (Osaka) was purified with alumina and silica-gel columns. The purified PC gave only one spot on thin-layer chromatography and no conjugated diene was observed before oxidation. The composition of fatty acids in PC measured by gas-liquid chromatography after hydrolysis and esterification with HCl-methanol was as follows: palmitic acid 12.1, stearic acid 1.6, oleic acid 9.6, linoleic acid 69.6, and linolenic acid 7.1 mol%. Dimyristoyl PC was purchased from Sigma Chemical Co. 2,2′-Azobis(2-amidinopropane) dihydrochloride (AAPH) and 2,2′-azobis(2,4-dimethylvaleronitrile) (AMVN) were used as a water-soluble and oil-soluble radical initiator respectively. Both AAPH and AMVN were provided by Wako Chemicals (Tokyo) and used as received. These water-soluble and lipid-soluble initiators enable us to generate radicals initially outside or within the bilayer as requested and initiate free radical chain oxidation at a constant rate, which is essential for the fundamental and quantitative study.

Vitamin E (*d*-α-tocopherol) was kindly supplied from Eisai Co. (Tokyo) and commercial vitamin C (L-ascorbic acid) was used as received.

The liposome was prepared as follows as reported previously.[11] PC and oil-soluble additives such as AMVN and vitamin E were dissolved in chloroform and the solution was taken into a small flask. Chloroform was removed by evacuation on a water aspirator using a rotary vacuum evaporator to obtain a thin film on a flask wall. Appropriate amount of 0.1 M (M=mol dm^{-3}) NaCl aqueous solution was added and the film was slowly peeled off by shaking to obtain a white and milky liposome solution. It must be noted that the liposome we have prepared in this study is a multilamellar vesicles.

The oxidation was carried out at either 37 or 50 °C under air in a Pyrex glass ampoule. The reaction conditions such as temperature and concentrations of substrate, initiator, and additives were determined so as to obtain appropriate rates of oxidation and disappearance of reactants. The reaction mixture was agitated with a magnetic stirrer. The rate of oxygen uptake was measured continuously in an automatic recording gas absorption apparatus with a pressure transducer.[10] In some oxidations, the rate of build-up of conjugated diene was followed spectrometrically at 233 nm. Since linoleic acid is the major fatty acid in soybean PC and its oxidation gives conjugated diene hydroperoxides quantitatively,[24-29]

this spectrometric analysis should give a good measure of the rate of oxidation. Since the extinction coefficient of conjugated diene is large, $\varepsilon=28000\ M^{-1}\,cm^{-1}$, the rate of oxidation can be followed at very early stages.

The rates of consumption of vitamin E and vitamin C were followed by high performance liquid chromatography (HPLC).[10] A Finepak SIL C18 column was used and methanol was delivered as an eluent at 1 $cm^3\ min^{-1}$. Vitamin C (eluted at 2.7 min) was measured at 275 nm and vitamin E (eluted at 7.7 min) was measured at 290 nm.

Results

When water soluble AAPH is used as a radical initiator, the radicals are formed initially in an aqueous phase, whereas water-insoluble and oil-soluble AMVN incorporated into PC bilayers generates free radicals within the lipid region. In both cases, the soybean PC liposome was oxidized smoothly at a constant rate without any noticeable induction period with long kinetic chain length, suggesting that the free radicals initially formed either in aqueous phase or in lipid phase induce the autoxidation of liposome similarly as observed previously.[11] In the absence of radical initiator, the rates of oxygen uptake and conjugated diene formation and that of vitamin E disappearance were negligibly small. Figure 1 illustrates the profile of oxygen uptake during the oxidations of soybean PC

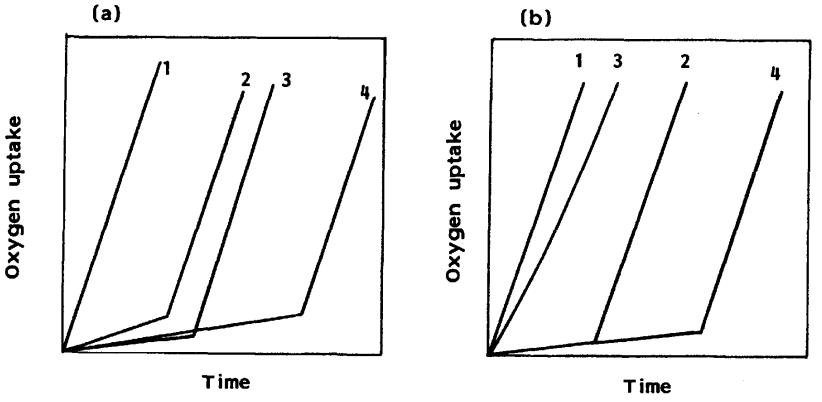

Fig. 1. Profile of the oxygen uptake during the oxidations of soybean PC liposome in aqueous dispersions initiated with (a) water soluble AAPH and (b) lipid soluble AMVN, respectively.
1: without antioxidant; 2: with vitamin E; 3: with vitamin C; 4: with both vitamin E and vitamin C

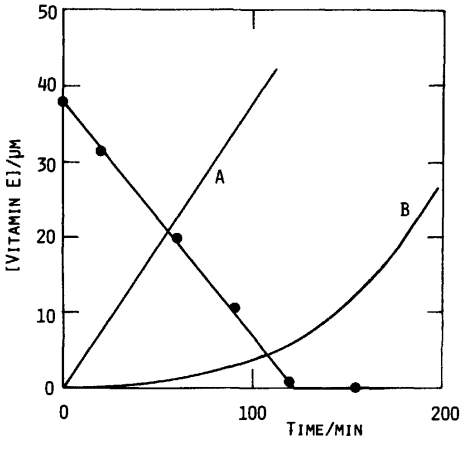

Fig. 2. Consumption of vitamin E (●) during the oxidation of 20 mM soybean PC liposome in 0.1 M NaCl aqueous dispersion at 37 °C under air, [AAPH]=50 mM, [vitamin E]=36.8 μM. Lines A and B show oxygen uptake without and with vitamin E, respectively.

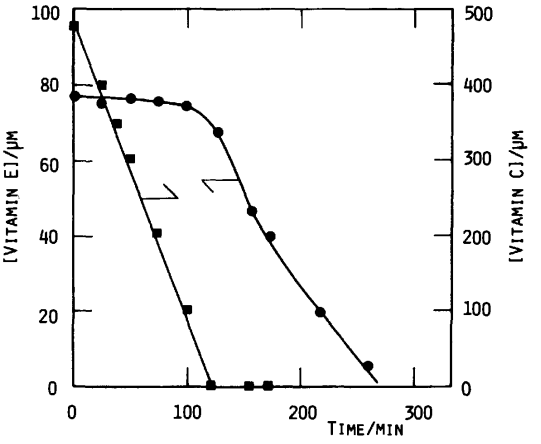

Fig. 3. Consumption of vitamin E (●) and vitamin C (■) during the oxidation of 22 mM soybean PC liposome in 0.1 M NaCl aqueous dispersion initiated with 50 mM AAPH at 37 °C under air, [vitamin E]=77 μM, [vitamin C]=480 μM.

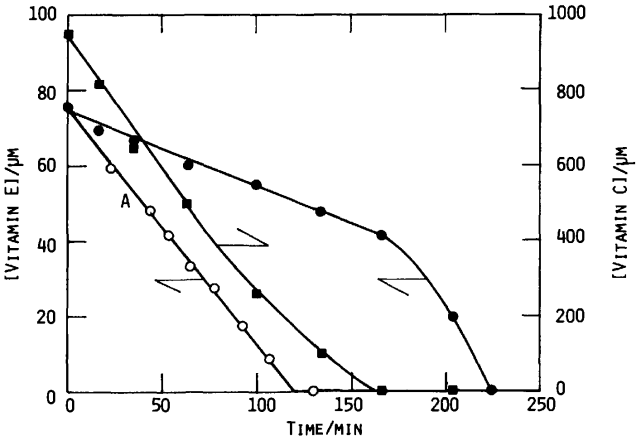

Fig. 4. Consumption of vitamin E (●) and vitamin C (■) during the oxidation of 20 mM soybean PC liposome in 0.1 M NaCl aqueous dispersion initiated with 4.0 mM AMVN at 50 °C under air, [vitamin E]=77 μM, [vitamin C]=950 μM. Line A (○) shows the rate of decay of vitamin E in the absence of vitamin C.

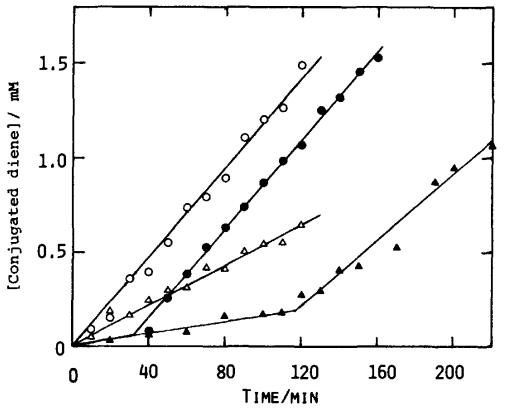

Fig. 5. Formation of conjugated diene in the oxidation of 10.7 mM soybean PC liposome dispersed in 10 cm³ of 0.1 M aqueous NaCl at 50 °C under air initiated with 2.53 mM AMVN.
○, without antioxidant; ●, with 14.5 μM vitamin E; △, with 929 μM vitamin C; ▲, with 14.5 μM vitamin E and 929 μM vitamin C.

liposome initiated with AAPH and AMVN.

Oxidations Initiated with AAPH. When vitamin E or vitamin C was added in the oxidation of PC liposome initiated with AAPH, the rate of oxygen uptake was suppressed markedly as observed in the oxidation of methyl linoleate in homogeneous solution[10] or in water dispersion.[9,11] As shown in Fig. 2, vitamin E was consumed linearly with time and after all of vitamin E was consumed the oxidation proceeded rapidly at a similar rate to that in the absence of vitamin E. Figure 3 shows that, when both vitamin E and vitamin C were present, vitamin C was consumed first linearly with time but vitamin E remained almost constant at the initial stage and then it was consumed after vitamin C was exhausted.

Oxidations Initiated with AMVN. When oil-soluble AMVN was incorporated into liposome and the initiating radicals were generated within the liposomal lipid region, the oxidation of PC liposome proceeded smoothly at a constant rate and oxygen uptake was suppressed efficiently by a small amount of vitamin E which was also incorporated into lipid bilayer (Fig.1b). Vitamin E decayed linearly with time as shown in Fig. 4 (Line A). However, although vitamin C alone added to an aqueous phase retarded the oxidation, it did not produce a clear induction period (Fig. 1b) which was observed when the oxidation was initiated with water-soluble AAPH (Fig. 1a). As shown in Fig. 5, similar results were observed when the rate of oxidation was followed by the formation of conjugated diene. These results show that, as observed previously in the oxidation of methyl linoleate micelle in aqueous dispersions,[9] vitamin C can not scavenge the radicals in the bilayer as efficiently as it scavenges radicals in aqueous phase.

When vitamin E and vitamin C were located in bilayer and in aqueous phase, respectively, the induction period was lengthened markedly as shown in Figs. 1b and 5. Furthermore, it must be pointed out that the rate of oxidation during the induction period was much smaller than that in the presence of vitamin C alone. Figure 4 shows how vitamin E and vitamin C decayed with time when both vitamins were present in the oxidation of PC liposome initiated with AMVN. Interestingly, the rate of consumption of vitamin E in liposome was reduced markedly by vitamin C in an aqueous phase even though the radicals were generated initially in the lipid region. When all of vitamin C was consumed, vitamin E began to decrease at a similar rate to that in the absence of vitamin C.

Discussion

Both vitamin E and vitamin C can scavenge peroxyl radicals when they are accessible and interact.[10] However, Fig. 1b indicates that vitamin C can not efficiently scavenge peroxyl radicals formed from AMVN and PC within liposomal lipid region, probably because AMVN is buried in the bilayer and the peroxyl radicals from both AMVN and PC are not accessible to vitamin C.

The results shown in Fig. 3 that vitamin C retards the rate of consumption of vitamin E during the

oxidation of PC liposome initiated with AAPH suggest that vitamin C scavenges the initiating radicals from AAPH in an aqueous phase directly before they attack liposome or that vitamin C regenerates vitamin E by reacting with vitamin E radical as observed in homogeneous solution.[10] Probably some combination of these reactions may be involved. The use of water soluble initiator AAPH does not permit us to differentiate which reaction is more important.

On the other hand, the results of oxidation initiated with lipid soluble AMVN give us more information concerning the cooperative and synergistic inhibition of oxidation by vitamins E and C. The results in Figs. 1 and 5 show that, although vitamin C can not scavenge chain-carrying peroxyl radicals within liposomal lipid region efficiently, vitamin C can prolong the induction period in the presence of vitamin E. This strongly supports the interaction of vitamin C in an aqueous phase and vitamin E radical in the lipid region. Apparently, vitamin C is more accessible to vitamin E radical than to peroxyl radicals in the lipid region, since the phytyl side chain of vitamin E must be buried in the lipid region and polar chromanyloxyl head group must be located near the membrane surface.

In contrast to the oxidation initiated with AAPH (Fig. 3), vitamin E did not remain constant but it was consumed gradually (Fig. 4) even though some vitamin C was present in an aqueous phase. This may imply that vitamin C in an aqueous region can not react with vitamin E radical in the lipid layer as efficiently as in the homogeneous system and/or that vitamin E radical reacts with another peroxyl radical (Reaction 3)[30] faster than it reacts with vitamin C (Reaction 2).

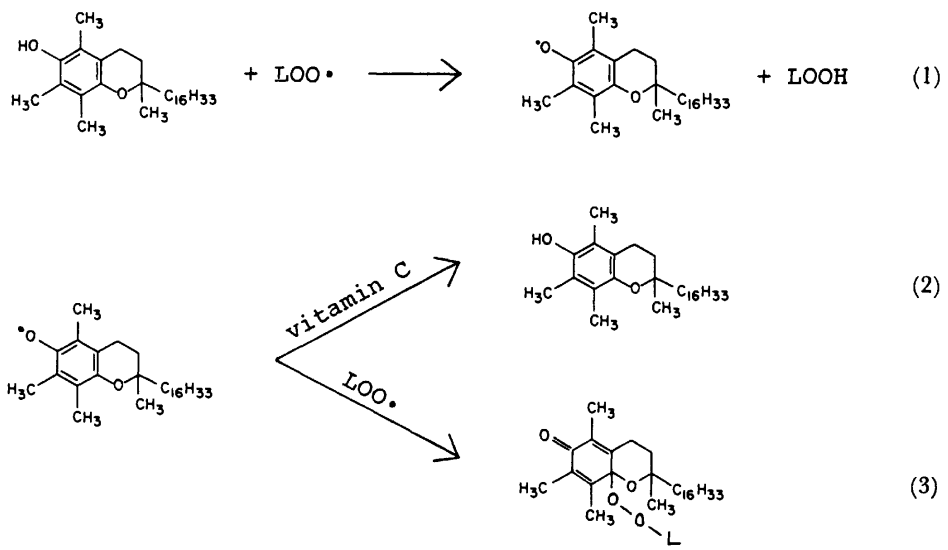

Furthermore, the synergistic inhibition of oxidation of methyl linoleate micelle by the combination of vitamin C and 2,2,5,7,8-pentamethyl-6-chromanol (PMC, a vitamin E model) observed previously[32] supports the interaction of vitamin E radical with vitamin C. Vitamin C acts as an efficient antioxidant for the oxidation of methyl linoleate micelle in 0.01 M Triton X-100 aqueous dispersion initiated with AAPH. On the other hand, when AMVN was used as an initiator and the radicals were generated initially in the oil region, vitamin C could not act as an antioxidant. However, even in this case, vitamin C was found to lengthen the suppression period when PMC was located in the methyl linoleate micelle.

It must be also noteworthy that ESR spectrum of vitamin E radical disappeared quite rapidly when it reacted with vitamin C.[22] It was also found by ESR study and absorption spectroscopy that galvinoxyl, a stable phenoxyl radical, which was incorporated into dimyristoyl PC liposome could react with vitamin C in an aqueous phase.[23]

The results and discussion given above strongly suggest that vitamin C can contribute to the synergistic inhibition of oxidation and to the regeneration of vitamin E by reacting with vitamin E radical during the oxidation of PC liposome in an aqueous dispersion as well as in the homogeneous solution.

As shown in Figs. 1b and 5, vitamin C could retard, although slightly, the oxidation of soybean

PC liposome initiated with AMVN. This probably indicates that vitamin C could interact with peroxyl radicals at the membrane surface and/or that vitamin C could penetrate into the membrane slowly. It must be noteworthy that the liposome prepared in this study by soybean PC alone without choresterol may be more leaky than real biomembranes. In biological systems, the oxygen radicals generated in a lipid region must be scavenged by vitamin E while those present in an aqueous region must be scavenged by water soluble antioxidants such as vitamin C, uric acid, and cysteine, and the synergistic inhibition by vitamin E and vitamin C must contribute to maintaining the vitamin E level and also its antioxidant activity in biological membranes.

References

1) "Tocopherol, Oxygen, and Biomembranes," ed by C. de Duve and O. Hayaishi, Elsevier, Amsterdam (1978).
2) "Vitamin E," ed by M. J. Machlin, Marcel Dekker, New York (1980).
3) A. L. Tappel, "Free Radicals in Biology," ed by W. A. Pryor, Academic Press, New York (1980) Vol. IV, p. 1.
4) L. A. Witting, "Free Radicals in Biology," ed by W. A. Pryor, Academic Press, New York (1980) Vol. IV, p. 295.
5) "Biology of Vitamin E," ed by R. Porter and J. Whelan, Pitman, London (1983).
6) M. G. Simic, "Autoxidation in Food and Biological Systems," ed by M. G. Simic and M. Karel, Plenum Press, New York (1980), p. 17.
7) G. W. Burton and K. U. Ingold, *J. Am. Chem. Soc.*, **103**, 6472 (1981), and references cited therein.
8) E. Niki, R. Tanimura, and Y. Kamiya, *Bull. Chem. Soc. Jpn.*, **55**, 1551 (1982).
9) Y. Yamamoto, S. Haga, E. Niki, and Y. Kamiya, *Bull. Chem. Soc. Jpn.*, **57**, 1260 (1984).
10) E. Niki, T. Saito, A. Kawakami, and Y. Kamiya, *J. Biol. Chem.*, **259**, 4177 (1984).
11) Y. Yamamoto, E. Niki, Y. Kamiya, and H. Shimasaki, *Biochim. Biophys. Acta*, **795**, 332 (1984).
12) L. R. C. Barclay, S. J. Locke, J. M. MacNeil, J. VanKessel, G. W. Burton, and K. U. Ingold, *J. Am. Chem. Soc.*, **106**, 2479 (1984).
13) C. Golumbic and H. A. Mattill, *J. Am. Chem. Soc.*, **63**, 1279 (1941).
14) A. L. Tappel, *Geriatrics*, **23**, 97 (1968).
15) W. M. Cort, *J. Am. Oil Chem. Soc.*, **51**, 321 (1974).
16) A. H. Natahaus and A. E. Kitabchi, *Biochim. Biophys. Acta*, **399**, 244 (1975).
17) L. H. Chen, M. S. Lee, W. F. Hsing, and S. H. Chen, *Int. J. Nutr. Res.*, **50**, 156 (1980).
18) H. W. Leung, M. J. Vang, and R. D. Mavis, *Biochim. Biophys. Acta*, **664**, 266 (1981).
19) L. J. Machlin, and E. Gabriel, *Ann. New York Acad. Sci.*, **355**, 98 (1980).
20) E. Niki, T. Saito, and Y., Kamiya, *Chem. Lett.*, **1983**, 631.
21) J. E. Packer, T. F. Slater, and R. L. Willson, *Nature*, **278**, 737 (1979).
22) E. Niki, J. Tsuchiya, R. Tanimura, and Y. Kamiya, *Chem. Lett.*, **1982**, 789.
23) J. Tsuchiya, T. Yamada, E. Niki, and Y. Kamiya, *Bull. Chem. Soc. Jpn.*, **58**, 326 (1985).
24) H. W. S. Chen and G. Levett, *Lipids*, **12**, 99 (1977).
25) E. N. Frankel, W. E. Neff, W. K. Rohwedder, B. Khambay, R. F. Garwood, and B. C. L. Weedon, *Lipids*, **12**, 908 (1977).
26) N. A. Porter, L. S. Lehman, B. A. Weber, and K. J. Smith, *J. Am. Chem. Soc.*, **103**, 6447 (1981).
27) D. K. Park, J. Terao, and S. Matsushita, *Agric. Biol. Chem.*, **45**, 2071 (1981).
28) Y. Yamamoto, E. Niki, and Y. Kamiya, *Bull. Chem. Soc. Jpn.*, **55**, 1548 (1982).
29) Y. Yamamoto, E. Niki, and Y. Kamiya, *Lipids*, **12**, 870 (1982).
30) Although the product of the reaction 3 has been suggested,[31] it has not been identified quantitatively. We are currently working to isolate and identify the product of the reaction 3.
31) J. Winterle, D. Dulin, and T. Mill, *J. Org. Chem.*, **49**, 491 (1984).
32) E. Niki, A. Kawakami, Y. Yamamoto, J. Tsuchiya, and Y. Kamiya, *J. Biol. Chem.*, **260**, 2191 (1985).

Studies of Unusual Amino Acids and Their Peptides. XVII.[1,2] The Synthesis of Peptides Containing *N*-Carboxymethyl Amino Acids. II[3,4]

Toshifumi MIYAZAWA,* Shin'ichi HIRAMATSU, Yasuhiro TSUBOI, Takashi YAMADA, and Shigeru KUWATA

Department of Chemistry, Faculty of Science, Konan University, Okamoto, Higashinada-ku, Kobe 658

(Received February 23, 1985)

The synthetic routes were investigated to four kinds of tetrapeptides made up of three usual amino acid residues and one *N*-carboxymethyl (Cm-) amino acid residue. The application of vacuum distillation made the isolation of a Cm-amino acid diester more convenient and efficient compared with the chromatographic methods which had been used previously. The efficiency of peptide bond formation at the imino group of a Cm-amino acid by the acid chloride method was remarkably improved under suitable reaction conditions. In the elongation of the peptide chain from a peptide containing a Cm-amino acid at the C-terminal position, the coupling efficiency was usually poorer than that in the case of the corresponding peptide composed only of the usual amino acid residues, and it depended greatly on the coupling methods, the 1-ethyl-3-(3-dimethylaminopropyl)carbodiimide–1-hydroxybenzotriazole method being generally the most desirable.

In our previous publications,[3,5,6] we have reported on the preparation of *N*-carboxymethyl (Cm-) amino acids (**I**, R′=H) and their derivatives using the corresponding usual amino acids as the starting materials. Cm-amino acids are simple-structured members of a group of unusual amino acids represented by the general structural formula of **I**.

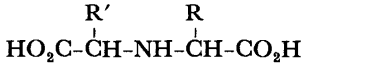

I

These amino acids (**I**) have been found in increasing numbers in nature, *e.g.*, in many marine animals and in crown gall tumors, and have recently been receiving more attention.[7,8] Furthermore, a series of synthetic peptides containing substituted Cm-amino acids have recently been demonstrated to be active as inhibitors of angiotensin-converting enzyme,[9] thermolysin,[10] enkephalinase,[11] and malate dehydrogenase.[12]

In Part I[3] of this series, we dealt with some basic problems in the synthesis of peptides containing Cm-amino acids, *e.g.*, the protection of the carboxyl and the imino groups of a Cm-amino acid, and the peptide bond formation at its carboxyl groups and imino group. As an extension of this work, the present paper will deal with the synthetic routes to four kinds of tetrapeptides (**9**, **15**, **19**, and **20**) made up of three usual amino acid residues (Pro, Val, and Phe) and one Cm-amino acid residue (CmVal),[13] the latter occupying four different positions in the peptide chains. These tetrapeptides were intended as the starting materials for a cyclic peptide model containing a Cm-amino acid.[14] The peptide chains were lengthened mainly from the dipeptide (**7**), which contained the Cm-amino acid at the C-terminal position and was protected by three kinds of selectively removable groups. Such a way of peptide chain elongation has not yet been attempted, and it has often been demonstrated that the efficiency of peptide bond elongation from a peptide containing a Cm-amino acid residue as either the amino or the carboxyl component is much poorer than that in the case of the corresponding usual peptide.

Preparation of Tetrapeptide **9**. According to the route adopted in the previous study,[3] Z-CmVal-OEt (**4**) was coupled with H-Pro-Val-OBu^t by the DCC, DCC-HOBt, or EDC method, to afford the tripeptide **5** (Scheme 1). For this purpose, **4** was prepared first *via* the H-Val-OEt→**2**→**3**→**4** route,[3] and later *via* a new route, H-Val-OEt→**1**→**3**→**4**. The debenzyloxycarbonylation of **5** was accomplished by hydrogenation, using Pd on carbon as the catalyst in the absence of any acid. It is noteworthy that the resulting product, **6**, though having a free imino group, was stable at room temperature for a long period of time, like the diesters of Cm-amino acids.[5] Then, **6** was coupled with Z-Phe-OH by the acid chloride method. Though the coupling efficiency by this method had generally been far from satisfactory,[3] the improvement of the procedure described below gave the tetrapeptide **9** in a fairly good yield (60%).

As an alternative to the desired tetrapeptide (**9**), the route *via* the dipeptide **7**, which contains CmVal as the C-terminal residue and is useful as a key compound for the preparation of two other tetrapeptides (**15** and **19**) as well, was examined next. For

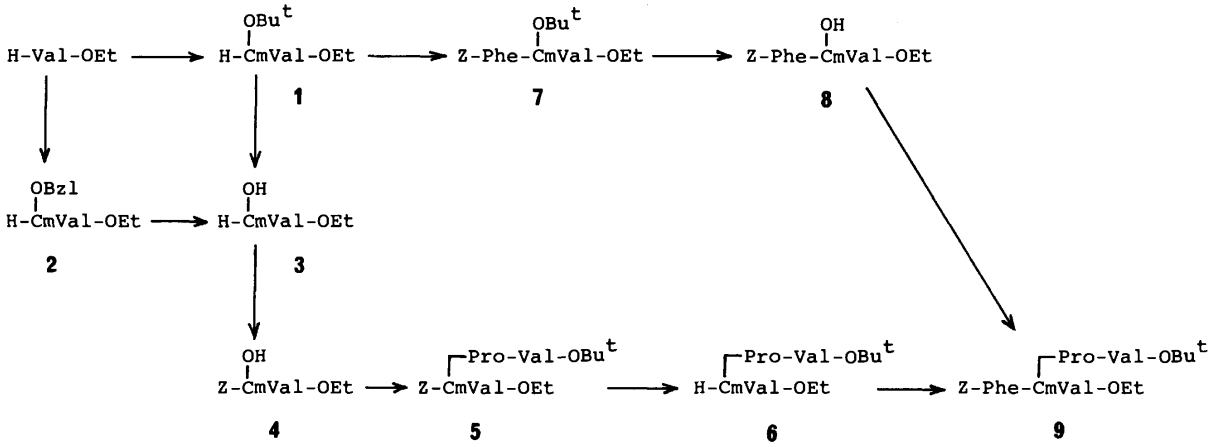

Scheme 1.

that purpose, the Cm-valine ethyl *t*-butyl ester **1** was prepared according to the general procedure described previously,[5] using ethyl valinate and *t*-butyl bromoacetate in the presence of triethylamine (TEA). Though the purification of Cm-amino acid diesters had hitherto been carried out by silica-gel column chromatography or TLC,[5] **1** was found to be isolable by means of vacuum distillation, thus making it possible to prepare such Cm-amino acid diesters as **1** more conveniently and in quantity.

As stated in the previous papers[3,5] the imino group of a Cm-amino acid has a remarkably poor reactivity, showing that the attempted couplings of Z-Phe-OH with a diester of Cm-valine by several conventional condensation methods all ended in failure, except by the acid chloride method. The coupling efficiency by the last method, however, was rather poor (*ca.* 40%). Recently we have attempted to overcome this difficulty by the use of the high pressure technique in the couplings of Z-amino acids with Cm-amino acid diesters by means of the *N*-hydroxysuccinimide ester method.[16] The application of high pressure (10 kbar) enabled some of the coupling reactions to be carried out so as to give much higher yields than at atmospheric pressure, while the coupling yields remained low in some reactions between relatively bulky amino acid residues. Moreover, a large-scale preparation at high pressure must be attended with some difficulties under the present conditions. Accordingly, the optimum reaction conditions for the coupling by the acid chloride method was investigated in the reaction of Z-Phe-Cl with the Cm-valine diester **1**; it was revealed that the best yield of **7** (84%) was obtained by the use of 2 to 3 equivalents of Z-Phe-Cl and by conducting the reaction at 0 °C from beginning to end instead of at 0 °C for several hours and thereafter at room temperature.[3]

The removal of the *t*-butyl group from **7** was carried out by treating **7** with hydrogen chloride in ethyl acetate for a few hours, without causing any damage to the coexistent Z group. Then, as an attempt to elongate the peptide chain from a C-terminal Cm-amino acid residue, the de-*t*-butylated product **8** was coupled with H-Pro-Val-OBu^t by means of the EDC or EDC–HOBt method. The yield of the reaction, **8**→**9**, (45%) as conducted according to the EDC method, was poorer than that of the corresponding reaction, **4**→**5**, (66%) under comparable conditions. This illustrates the large steric hindrance of a peptide containing a Cm-amino acid compared with that of a Cm-amino acid itself. On the other hand, the application of the EDC–HOBt method to the present coupling gave **9** in a good yield (80%). The superiority of this coupling method seems to be a general trend in the preparation of peptides containing Cm-amino acids, as will be indicated below by several examples.

The optical rotation of the product (**9**) obtained from **8** and H-Pro-Val-OBu^t by the EDC or EDC–HOBt method was identical with that of the product obtained *via* the first-mentioned route (**4**→**5**→**6**→**9**). No racemization occurs during the segment coupling at the carboxyl group in the glycine moiety of a Cm-amino acid residue, as might be expected. On the other hand, when we compare the overall yields of the tetrapeptide **9** starting from ethyl valinate *via* the two routes mentioned above, it is apparent that the route *via* the dipeptide **7** is more desirable, so much the more because the route *via* Z-CmVal-OEt (**4**) contains more steps (H-Val-OEt→**2**→**3**→**4** or H-Val-OEt→**1**→**3**→**4**).

Preparation of Tetrapeptide 15. For the preparation of the tetrapeptide **15**, the following two routes were examined starting from the dipeptide **7** mentioned above: (i) **7**→**10**→**11**→**12**→**15** and (ii)

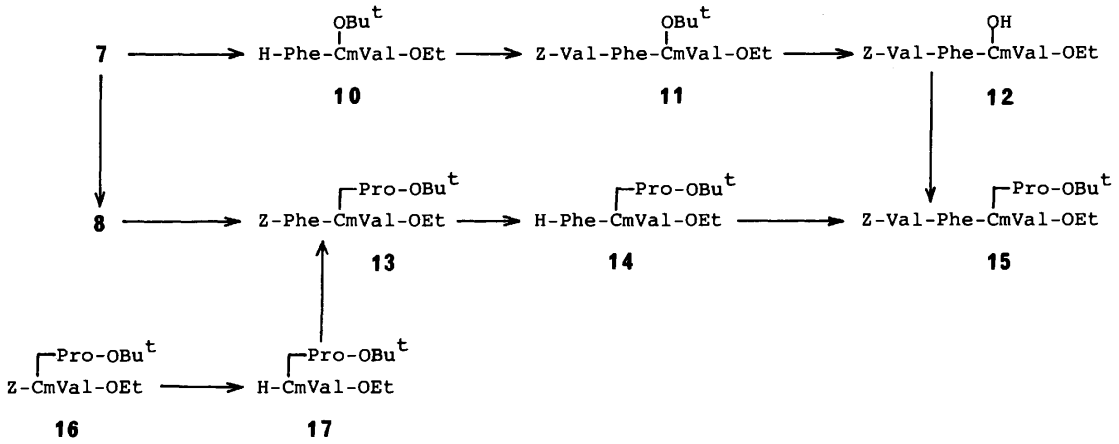

Scheme 2.

7→8→13→14→15 (Scheme 2). The elongation of the peptide chain at the N-terminal residue of a peptide containing a C-terminal Cm-amino acid residue has not previously been attempted. In the (i) route, the Z group of **7** was first removed, and the resulting product (**10**) was coupled with Z-Val-OH by several methods. Generally, the coupling efficiency was less satisfactory than that of the corresponding coupling, Z-Val-OH+H-Phe-Val-OBu^t, under comparable conditions (see Experimental). This presumably indicates the extention of the influence of the bulkiness of the Cm-amino acid to the amino group of the adjacent amino acid residue. Thus, the coupling method and conditions had a profound influence on the coupling efficiency. The *N*-hydroxysuccinimide ester method in dioxane gave only a 25% yield after 3 d, while it gave a 46% yield in dichloromethane. The mixed anhydride method and the EDC method gave better yields (45 and 54% respectively). The best yield (70%) was obtained by the EDC-HOBt method. The comparison of the yields of the couplings of Z-Val-OSu and Z-Ala-OSu with **10** in dichloromethane under comparable reaction conditions (46 and 65% respectively) also reveals the influence of the steric hindrance. Then the removal of the *t*-butyl group from **11** was attained as in the **7→8** step to give **12**. The coupling of **12** with H-Pro-OBu^t was carried out by the EDC-HOBt method, thus obtaining the desired tetrapeptide **15** in a 61% yield.

On the other hand, in the (ii) route, **8** was first coupled with H-Pro-OBu^t by means of the EDC-HOBt method to give the tripeptide **13** in a 65% yield. This yield was somewhat better than that of the corresponding coupling of the tripeptide **12** with H-Pro-OBu^t described above. The tripeptide **13** was also prepared *via* another route. The dipeptide **16**[3] was debenzyloxycarbonylated by hydrogenation as usual to give **17**, and this was then coupled with Z-Phe-Cl by the improved procedure described above (77% yield). The product thus obtained was identical with that obtained by the (ii) route. Then the tripeptide **13** was debenzyloxycarbonylated by hydrogenation, and the resulting **14** was coupled with Z-Val-OH by several methods. The yields were 34% for the *N*-hydroxysuccinimide ester method, 41% for the mixed anhydride method, and 51% for the EDC-HOBt method. These yields were rather poor compared with those of the corresponding coupling of Z-Val-OH with **10**. This presumably reflects the difference in the bulkiness of the two amino components containing the Cm-amino acid (**14** *vs.* **10**).

The final products (**15**) obtained *via* the two routes, (i) and (ii), were identical. On the other hand, a comparison of the overall yields (from the dipeptide **7**) of the tetrapeptide **15** obtained by the EDC-HOBt method *via* Routes (i) and (ii) revealed that the (i) route (43%) was somewhat better than the (ii) route (33%).

Preparation of Tetrapeptides 19 and 20. As is shown in Scheme 3, the tripeptide **11** was debenzyloxycarbonylated by hydrogenation to give **18**, which was then coupled with Z-Pro-OH by several different methods. The yields were 26% for the *N*-hydroxysuccinimide ester method, 44% for the mixed anhydride method, and 77% for the EDC-HOBt method. In this case also, the last method was the most desirable one. The yields were generally comparable with those of the preceeding step, **7→10→11**. Moreover, there was a close resemblance in the relationship between the coupling method and the coupling efficiency in both cases.

The tetrapeptide **19** was also prepared in a 59%

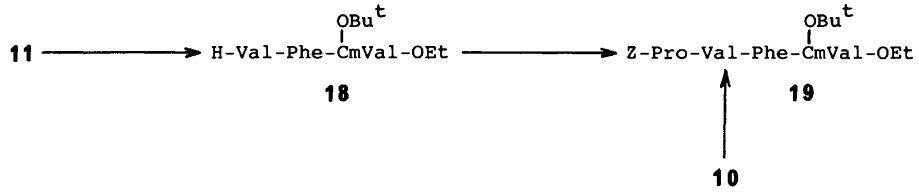

Scheme 3.

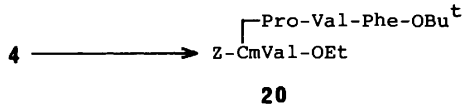

Scheme 4.

yield by the coupling of Z-Pro-Val-OH with **10** by the EDC-HOBt method. This yield was poorer than that of the corresponding coupling of Z-Val-OH with **10**, but the overall yield *via* the **7**→**10**→**19** route (segment coupling) was somewhat better than that *via* the **7**→**10**→**11**→**18**→**19** route (stepwise elongation). The optical rotation of the product obtained by the segment coupling was identical with that of the product obtained by the stepwise elongation, indicating that no racemization occurred.

The EDC coupling of Z-CmVal-OEt (**4**) with H-Pro-Val-Phe-OBu^t, which had been prepared by the stepwise elongation starting from the C-terminal phenylalanine, gave the tetrapeptide **20** in a 55% yield (Scheme 4). This yield was better than that reported previously[3] of the corresponding coupling of **4** with H-Pro-Val-Val-OBzl by the DCC method (37%).

In conclusion, the results obtained in the present work indicate that, in the elongation of the peptide chain from a peptide containing a Cm-amino acid residue, the coupling efficiency is generally poor compared with that in the case of the corresponding peptide composed only of usual amino acid residues, and depends largely on the coupling methods. The EDC-HOBt method is the method of choice.

Experimental

All the melting points are uncorrected. The optical rotations were measured with a JASCO DIP-4 polarimeter. The TLC and preparative TLC were performed on Merck Kieselgel 60 F_{254} and Kieselgel GF_{254} (Type 60) respectively. Merck Kieselgel 60 was used for the column chromatography. The ^{1}H NMR spectra were recorded on a Hitachi R-24B spectrometer.

H-CmVal-OEt (1). To a stirred mixture of H-Val-OEt·TosOH (59.10 g) and TEA (37.96 g) in THF (180 ml) we added, drop by drop, a solution of *t*-butyl bromoacetate[17] (43.58 g) in THF (10 ml) over a period of 2 h. The reaction mixture was then stirred at room temperature for 10 d. The precipitates were subsequently filtered off, and the filtrate was evaporated under reduced pressure. The residue was dissolved in EtOAc, washed with water, and dried over Na_2SO_4. After the solvent had been removed, the residue was distilled under reduced pressure; yield, 29.22 g (61%); oil, bp 85 °C/0.7 Torr (1 Torr=133.322 Pa); $[\alpha]_D^{25}$ −18.0° (*c* 1.0, MeOH); n_D^{22} 1.4345. ^{1}H NMR ($CDCl_3$) δ= 0.96 (6H, d, *J*=6 Hz, $CH(C\underline{H}_3)_2$), 1.26 (3H, t, *J*=7 Hz, $CH_2C\underline{H}_3$), 1.44 (9H, s, $C(C\underline{H}_3)_3$), 1.7—2.2 (1H, m, $C\underline{H}(CH_3)_2$), 2.27 (1H, s, NH), 3.00 (1H, d, *J*=5.5 Hz, $NHC\underline{H}(C_3H_7)CO$), 3.22 (2H, s, $NHC\underline{H}_2CO$), and 4.14 (2H, q, *J*=7 Hz, $C\underline{H}_2CH_3$).

Picrolonate: mp 136.5—138 °C (EtOH); $[\alpha]_D^{25}$ +1.0° (*c* 1.0, MeOH). Found: C, 52.79; H, 6.43; N, 13.35. Calcd for $C_{23}H_{33}N_5O_9$: C, 52.77; H, 6.35; N, 13.38.

DCHA Salt of Z-CmVal-OEt (4). The diester **1** (1.56 g) was treated with 4 M HCl (1 M=1 mol dm^{-3}) in EtOAc (30 ml) at room temperature for 3 h. After the solvent had been removed under reduced pressure, the residue (**3**·HCl) was dissolved in water (11 ml) with $NaHCO_3$ (1.76 g). To the resulting solution, we added a solution of Z-Cl (1.13 g) in ether (2 ml) in 8 portions over a period of 3.5 h. Then the mixture was stirred below 5 °C overnight. After the usual work-up, the raw product was mixed with DCHA (1.09 g) to afford the corresponding salt, which was then recrystallized from hexane; yield, 2.14 g (69%); mp 109.5—110 °C; $[\alpha]_D^{25}$ −40.1° (*c* 1.0, $CHCl_3$). [lit,[3] mp 109.5—110 °C, $[\alpha]_D^{25}$ −39.8° (*c* 1.0, MeOH).]

Z-Pro-Val-OBu^t. This was prepared from Z-Pro-OH and H-Val-OBu^t by the mixed anhydride method using isobutoxycarbonyl chloride in THF; yield, 79%; mp 111—113 °C (EtOAc-petroleum ether); $[\alpha]_D^{23}$ −32.8° (*c* 1.0, DMF). This compound had previously been prepared by the DCC-HOBt method;[18] mp 114—115 °C, $[\alpha]_D^{23}$ −34.3° (*c* 1.0, DMF).

Tripeptide 5. This was prepared from Z-CmVal-OEt (**4**) (recovered from the DCHA salt by treatment in EtOAc with 1 M HCl as usual) and H-Pro-Val-OBu^t (prepared through the debenzyloxycarbonylation of Z-Pro-Val-OBu^t by catalytic hydrogenation in MeOH) by the three different methods described below, according to a previous report.[3] The final purification was performed by preparative TLC on silica gel with benzene-EtOAc (3:1), while recrystallization was done from cyclohexane;

mp 96—97 °C; $[\alpha]_D^{25}$ −107.4° (*c* 1.0, MeOH). Found: C, 63.22; H, 8.23; N, 7.16. Calcd for $C_{31}H_{47}N_3O_8$: C, 63.14; H, 8.03; N, 7.13.

The yields were 54% by the DCC method, 59% by the DCC–HOBt method, and 66% by the EDC method.

Dipeptide **7**. To a stirred solution of **1** (3.65 g) and TEA (1.57 g) in THF (10 ml), we added a solution of Z-Phe-Cl (freshly prepared by the reaction of Z-Phe-OH (10.48 g) with PCl_5 (7.29 g) in ether according to the literature[19]) in THF (20 ml) at 0 °C over a period of 20 min. The mixture was stirred overnight in a thermostatted bath at 0 °C. The precipitates were then filtered off, and the filtrate was evaporated under reduced pressure. The residue was distributed between EtOAc and water, and the separated organic layer was washed successively with 10% citric acid, water, 4% $NaHCO_3$, and water, and dried over Na_2SO_4. After the solvent had been removed under reduced pressure, the residue was purified on a silica-gel column, with hexane–EtOAc (3:1) as the eluent; yield, 6.42 g (84%); syrup, $[\alpha]_D^{25}$ −52.1° (*c* 1.0, MeOH). Found: C, 66.77; H, 7.72; N, 5.05. Calcd for $C_{30}H_{40}N_2O_7$: C, 66.65; H, 7.46; N, 5.18.

De-t-butylation of **7**. **7** (3.81 g) was treated with 4.5 M HCl (9.5 ml) in EtOAc at room temperature for 3.5 h. The oily residue (**8**) obtained after the removal of the solvent under reduced pressure was used for the next reaction without any further purification. On the other hand, a part of this product was converted to the DCHA salt in the usual manner; mp 125—127 °C (EtOAc–hexane); $[\alpha]_D^{25}$ −47.2° (*c* 1.0, MeOH). Found: C, 68.03; H, 8.34; N, 6.30. Calcd for $C_{38}H_{55}N_3O_7$: C, 68.54; H, 8.33; N, 6.31.

Tetrapeptide **9**. a) Into a solution of **8** (prepared from **7** (3.35 g) as described above) and HOBt (0.98 g) in THF (10 ml), we stirred EDC·HCl (1.44 g) at 0 °C. After 15 min, a solution of H-Pro-Val-OBu^t (prepared from Z-Pro-Val-OBu^t (3.00 g) by catalytic hydrogenation) in THF (10 ml) was added, and the reaction mixture was stirred at 0 °C for several hours and then at room temperature overnight. After the mixture had been evaporated under reduced pressure, the residue was dissolved in EtOAc, washed successively with water, 10% citric acid, water, 4% $NaHCO_3$, and water, and dried over Na_2SO_4. The subsequent removal of the solvent afforded a syrup, which was purified on a silica-gel column, with hexane–EtOAc (1:1) as the eluent; yield, 3.63 g (80%); syrup, $[\alpha]_D^{25}$ −76.8° (*c* 1.0, MeOH). Found: C, 64.91; H, 7.91; N, 7.50. Calcd for $C_{40}H_{56}N_4O_9$: C, 65.20; H, 7.66; N, 7.60.

The EDC method in acetonitrile gave the desired compound (**9**) in a 45% yield.

b) The tripeptide **5** (617 mg) was hydrogenated in THF in the presence of 5% Pd-C (150 mg). After the filtration of the catalyst and the removal of the solvent, the residue (**6**) was treated with Z-Phe-Cl (freshly prepared from Z-Phe-OH (877 mg) and PCl_5 (677 mg)) in the presence of TEA (110 mg) in a manner similar to that described for the preparation of the dipeptide **7**. The final purification was performed by preparative TLC on silica gel with benzene–EtOAc (3:2); yield, 466 mg (60%); $[\alpha]_D^{25}$ −76.9° (*c* 1.0, MeOH).

Tripeptide **11**. To a solution of Z-Val-OH (2.26 g) in THF (15 ml), we added EDC·HCl (1.73 g) and HOBt (1.22 g) at 0 °C. After 30 min, a solution of **10** (prepared through the debenzyloxycarbonylation of **7** (4.05 g) by catalytic hydrogenation) in THF (5 ml) was added, after which the reaction mixture was stirred at 0 °C for several hours and then at room temperature overnight. After a work-up similar to that described for the preparation of **9** (Method (a)), the residual syrup was purified on a silica-gel column, with hexane–EtOAc (1:1) as the eluent; yield, 3.37 g (70%); syrup, $[\alpha]_D^{25}$ −55.0° (*c* 1.0, MeOH). Found: C, 65.76; H, 7.85; N, 6.62. Calcd for $C_{35}H_{49}N_3O_8$: C, 65.71; H, 7.72; N, 6.57.

The *N*-hydroxysuccinimide ester method gave a 25% yield in dioxane and a 46% yield in CH_2Cl_2 after 3 d at room temperature. The mixed anhydride method using isobutoxycarbonyl chloride in THF gave a 45% yield, and the EDC method in acetonitrile, a 54% yield.

Z-Val-Phe-Val-OBu^t. Z-Val-OH (1.26 g) and H-Phe-Val-OBu^t (prepared through the debenzyloxycarbonylation of Z-Phe-Val-OBu^t[20] (2.27 g) by catalytic hydrogenation) were reacted in THF (11 ml) by the EDC–HOBt method in the same manner as has been described for the preparation of **11**. The raw product was recrystallized from EtOAc–petroleum ether; yield, 2.52 g (91%); mp 178–179 °C; $[\alpha]_D^{25}$ −46.2° (*c* 1.0, MeOH). [lit,[21] mp 178 °C, $[\alpha]_D$ −45.5° (*c* 1, MeOH).]

The *N*-hydroxysuccinimide ester method in dioxane gave a 72% yield, the mixed anhydride method using isobutoxycarbonyl chloride in THF gave a 78% yield, and the EDC method in acetonitrile gave a 84% yield, under the same reaction conditions as were used for the preparation of **11**.

Z-Ala-Phe-CmVal(OBu^t)-OEt. A sloution of Z-Ala-OSu (222 mg) and **10** (prepared from **7** (308 mg) by catalytic hydrogenation) in CH_2Cl_2 (2 ml) was stirred at room temperature for 3 d. 1-(2-Aminoethyl)piperazine (30 mg) was then added, and the mixture was stirred for an additional hour. After the solvent had been removed under reduced pressure, the residue was dissolved in EtOAc and washed as usual. The final purification was performed by preparative TLC on silica gel with benzene–EtOAc (3:1); yield, 228 mg (65%); syrup, $[\alpha]_D^{25}$ −65.4° (*c* 0.51, MeOH). Found: C, 65.04; H, 7.52; N, 6.80. Calcd for $C_{33}H_{45}N_3O_8$: C, 64.79; H, 7.41; N, 6.87.

Tripeptide **13**. a) **8** (prepared through the de-*t*-butylation of **7** (1.62 g) with HCl in EtOAc as described above) and H-Pro-OBu^t (prepared from Z-Pro-OBu^t (1.01 g) by catalytic hydrogenation) were coupled by the EDC–HOBt method in a manner similar to that described for the preparation of **9** (Method (a)). The final purification was performed on a silica-gel column, with hexane–EtOAc (1:1) as the eluent; yield, 1.24 g (65%); syrup, $[\alpha]_D^{25}$ −64.9° (*c* 1.0, MeOH). Found: C, 65.86; H, 7.56; N, 6.45. Calcd for $C_{35}H_{47}N_3O_8$: C, 65.91; H, 7.43; N, 6.59.

b) The dipeptide **16**[3] (250 mg) was hydrogenated in THF in the presence of 5% Pd-C (55 mg). After the filtration of the catalyst and the removal of the solvent, the residue was treated with Z-Phe-Cl (freshly prepared from Z-Phe-OH (460 mg) and PCl_5 (320 mg)) in the presence of TEA (57 mg) in a manner similar to that described for the preparation of the dipeptide **7**. The final purification was performed by preparative TLC on silica gel with

benzene–EtOAc (3:1); yield, 251 mg (77%); syrup, $[\alpha]_D^{25}$ −64.6° (*c* 1.0, MeOH).

Tetrapeptide 15. a) The tripeptide **11** (3.19 g) was treated with 4 M HCl in EtOAc (15 ml) at room temperature for 1.5 h. After the solvent had been removed under reduced pressure, the oily residue (**12**) was coupled with H-Pro-OBu^t (prepared from Z-Pro-OBu^t (1.67 g)) in THF by the EDC–HOBt method in a manner similar to that described for the preparation of **9** (Method (a)). The final purification was performed on a silica-gel column, with hexane–EtOAc (1:1) as the eluent; yield, 2.23 g (61%); syrup, $[\alpha]_D^{25}$ −78.8° (*c* 1.0, MeOH). Found: C, 65.00; H, 7.91; N, 7.38. Calcd for $C_{40}H_{56}N_4O_9$: C, 65.20; H, 7.66; N, 7.60.

b) The tripeptide **13** (322 mg) was hydrogenated in MeOH in the presence of 5% Pd-C (200 mg). After the filtration of the catalyst and the removal of the solvent, the oily residue (**14**) was coupled with Z-Val-OH (152 mg) in THF (2 ml) by the EDC–HOBt method in a manner similar to that described for the preparation of **9** (Method (a)). The final purification was performed by preparative TLC on silica gel with benzene–EtOAc (3:1); yield, 196 mg (51%); $[\alpha]_D^{25}$ −78.1° (*c* 1.0, MeOH).

The *N*-hydroxysuccinimide ester method in CH_2Cl_2 gave a 34% yield after 3 d at 30 °C, while the mixed anhydride method using isobutoxycarbonyl chloride in THF gave a 41% yield.

Tetrapeptide 19. a) The tripeptide **11** (570 mg) was hydrogenated in MeOH in the presence of 5% Pd-C (400 mg). After the filtration of the catalyst and the removal of the solvent, the oily residue (**18**) was coupled with Z-Pro-OH (266 mg) in THF (3 ml) by the EDC–HOBt method in a manner similar to that described for the preparation of **9** (Method (a)). The raw product was purified by recrystallization from EtOAc–petroleum ether; yield, 506 mg (77%); mp 108—110 °C; $[\alpha]_D^{25}$ −84.1° (*c* 1.0, MeOH). Found: C, 64.98; H, 7.71; N, 7.54. Calcd for $C_{40}H_{56}N_4O_9$: C, 65.20; H, 7.66; N, 7.60.

The *N*-hydroxysuccinimide ester method in CH_2Cl_2 (reactant concentration, 0.34 M) gave a 26% yield after 3 d at room temperature. The mixed anhydride method, using isobutoxycarbonyl chloride in THF, gave a 44% yield (duration and temperature, 3 h at 0 °C and then overnight at 25 °C).

b) Z-Pro-Val-OBu^t (140 mg) was treated with 4 M HCl in EtOAc (2 ml) at room temperature for 1.5 h. After the solvent had been removed under reduced pressure, the residue was coupled with **10** (prepared from **7** (185 mg) by catalytic hydrogenation) in THF (2 ml) by the EDC–HOBt method in a manner similar to that described for the preparation of **9** (Method (a)). Subsequent recrystallization from EtOAc–petroleum ether afforded a pure product; yield, 149 mg (59%); mp 108.5—110 °C; $[\alpha]_D^{25}$ −84.4° (*c* 1.0, MeOH).

Z-Val-Phe-OBu^t. This was prepared from Z-Val-OH and H-Phe-OBu^t by the mixed anhydride method, using isobutoxycarbonyl chloride in THF; yield, 72%; mp 102—103 °C (ether–petroleum ether); $[\alpha]_D^{25}$ −32.5° (*c* 1.0, MeOH). Found: C, 68.79; H, 7.60; N, 6.17. Calcd for $C_{26}H_{34}N_2O_5$: C, 68.70; H, 7.54; N, 6.16.

Z-Pro-Val-Phe-OBu^t. This was prepared from Z-Pro-OH and H-Val-Phe-OBu^t (prepared through the debenzyloxycarbonylation of Z-Val-Phe-OBu^t by catalytic hydrogenation) by means of the EDC–HOBt method in THF; yield, 73%; mp 164—166 °C (EtOAc–petroleum ether); $[\alpha]_D^{25}$ −78.5° (*c* 1.0, MeOH). Found: C, 67.34; H, 7.39; N, 7.74. Calcd for $C_{31}H_{41}N_3O_6$: C, 67.49; H, 7.49; N, 7.62.

Tetrapeptide 20. To a solution of **4** (0.69 g) in THF (5 ml), we added EDC·HCl (0.41 g) at 0 °C. After 20 min, a solution of H-Pro-Val-Phe-OBu^t (prepared through the debenzyloxycarbonylation of Z-Pro-Val-Phe-OBu^t (1.01 g) by catalytic hydrogenation with 5% Pd-C (0.28 g) in THF) in THF (5 ml) was added. After the resulting mixture had been stirred at 0 °C overnight, it was evaporated under reduced pressure. The residue was dissolved in EtOAc, washed successively with water, 10% citric acid, water, 4% $NaHCO_3$ and water, and dried over Na_2SO_4. The subsequent removal of the solvent afforded a syrup (1.19 g). A part of this raw product was chromatographed on preparative layers of silica gel with benzene–EtOAc (1:1); yield, 55% (based on Z-Pro-Val-Phe-OBu^t used); syrup, $[\alpha]_D^{25}$ −101.3° (*c* 0.94, MeOH). Found: C, 65.11; H, 7.77; N, 7.60. Calcd for $C_{40}H_{56}N_4O_9$: C, 65.20; H, 7.66; N, 7.60.

References

1) Part XVI: T. Miyazawa, T. Yamada, S. Kuwata, and H. Watanabe, *Memoirs of Konan University, Science Series*, **31**, 133 (1984).

2) Part IV of "The Chemistry of *N*-Carboxymethyl Amino Acids." For Part III, see Ref. 6.

3) Part I: T. Miyazawa, *Bull. Chem. Soc. Jpn.*, **53**, 3661 (1980).

4) This work was presented in part at the 47th National Meeting of the Chemical Society of Japan, Kyoto, April 1983, Abstr., No. 4H06.

5) T. Miyazawa, *Bull. Chem. Soc. Jpn.*, **53**, 2555 (1980).

6) T. Miyazawa, T. Yamada, and S. Kuwata, *Bull. Chem. Soc. Jpn.*, **57**, 3605 (1984).

7) An opportune review has recently appeared: J. Tempé, "Chemistry and Biochemistry of Amino Acids, Peptides, and Proteins," ed by B. Weinstein, Marcel Dekker, New York (1983), Vol. 7, p. 113. See also M. Drummond, *Nature*, **281**, 343 (1979); P. Guyon, M.-D. Chilton, A. Petit, and J. Tempé, *Proc. Natl. Acad. Sci. U.S.A.*, **77**, 2693 (1980).

8) *Cf.* Ref. 5. Recently Cm-L-serine[5] has been isolated from asparagus shoots; T. Kasai and S. Sakamura, *Agric. Biol. Chem.*, **45**, 1483 (1981).

9) A. A. Patchett, E. Harris, E. W. Tristram, M. J. Wyvratt, M. T. Wu, D. Taub, E. R. Peterson, T. J. Ikeler, J. ten Broeke, L. G. Payne, D. L. Ondeyka, E. D. Thorsett, W. J. Greenlee, N. S. Lohr, R. D. Hoffsommer, H. Joshua, W. V. Ruyle, J. W. Rothrock, S. D. Aster, A. L. Maycock, F. M. Robinson, R. Hirschmann, C. S. Sweet, E. H. Ulm, D. M. Gross, T. C. Vassil, and C. A. Stone, *Nature*, **288**, 280 (1980); M. Vincent, G. Rémond, B. Portevin, B. Serkiz, and M. Laubie, *Tetrahedron Lett.*, **23**, 1677 (1982).

10) A. L. Maycock, D. M. DeSousa, L. G. Payne, J. ten Broeke, M. T. Wu, and A. A. Patchett, *Biochem. Biophys. Res. Commun.*, **102**, 963 (1981).

11) B. P. Roques, M. C. Fournie-Zaluski, D. Florentin, G. Waksman, A. Sassi, P. Chaillet, H. Collado, and J. Costentin, *Life Sci.*, **31**, 1749 (1982); M. C. Fournie-Zaluski, E. Soroca-Lucas, G. Waksman, C. Llorens, J. C. Schwartz,

and B. P. Roques,*ibid.*, **31**, 2947 (1982); M. C. Fournie-Zaluski, P. Chaillet, E. Soroca-Lucas, H. Marcais-Collado, J. Costentin, and B. P. Roques, *J. Med. Chem.*, **26**, 60 (1983).

12) E. T. Maggio and E. F. Ullman, *Biochim. Biophys. Acta*, **522**, 284 (1978); E. F. Ullman, R. A. Yoshida, J. I. Blakemore, E. Maggio, and R. Leute, *ibid.*, **567**, 66 (1979).

13) a) The amino acids and their derivatives used here are all of the L-configuration. b) The following abbreviations are used for Cm-amino acids and their derivatives: CmAA for a Cm-amino acid derived from an amino acid (AA), and X-CmAA-Z for its derivative (X-NC(CH$_2$CO-Y)(R)HCO-Z). In these abbreviations, H of the imino group and/or OH of the carboxyl groups are sometimes omitted. c) Abbreviations given by the IUPAC-IUB Commission (*J. Biol. Chem.*, **247**, 977 (1972)) are used throughout. Additional abbreviations: Z, benzyloxycarbonyl; Bu^t, *t*-butyl; DCC, dicyclohexylcarbodiimide; HOBt, 1-hydroxybenzotriazole; EDC, 1-ethyl-3-(3-dimethylaminopropyl)carbodiimide; TosOH, *p*-toluenesulfonic acid; THF, tetrahydrofuran,; Z-Cl, benzyloxycarbonyl chloride; DCHA, dicyclohexylamine; DMF, *N,N*-dimethylformamide; HOSu, *N*-hydroxysuccinimide.

14) Bottromycin was once said to be a cyclic peptide containing Cm-*t*-leucine.[15a] Its unique structural features still remain of great interest from the viewpoint of the synthetic chemistry of peptides, though a revised structure for it has recently been proposed.[15b]

15) a) Y. Takahashi, H. Naganawa, T. Takita, H. Umezawa, and S. Nakamura, *J. Antibiot.*, **29**, 1120 (1976). b) D. Schipper, *ibid.*, **36**, 1076 (1983).

16) T. Yamada, Y. Manabe, T. Miyazawa, S. Kuwata, and A. Sera, *J. Chem. Soc., Chem. Commun.*, **1984**, 1500.

17) B. Abramovitch, J. C. Shivers, B. E. Hudson, and C. R. Hauser, *J. Am. Chem. Soc.*, **65**, 986 (1943).

18) W. König and R. Geiger, *Chem. Ber.*, **103**, 788 (1970).

19) M. Bergmann, L. Zervas, H. Rinke, and H. Schleich, *Hoppe-Seyler's Z. Physiol. Chem.*, **224**, 37 (1934).

20) E. Wünsch and G. Wandlberger, *Chem. Ber.*, **100**, 160 (1967).

21) Y. Isowa, M. Ohmori, T. Ichikawa, H. Kurita, M. Sato, and K. Mori, *Bull. Chem. Soc. Jpn.*, **50**, 2762 (1977).

α,β-Epoxy Sulfoxides as Useful Intermediates in Organic Synthesis. I. A Novel Synthesis of Dialkyl Ketones and a Synthesis of Aldehydes from Ketones by One Carbon Elongation

Tsuyoshi SATOH, Youhei KANEKO, Takao IZAWA, Kiichi SAKATA, and Koji YAMAKAWA*

Faculty of Pharmaceutical Sciences, Science University of Tokyo, Ichigaya-funagawara-machi, Shinjuku-ku, Tokyo 162

(Received March 12, 1985)

Treatment of α,β-epoxy sulfoxides, prepared from 1-chloroalkyl phenyl sulfoxides with ketones or aldehydes, with sodium benzeneselenolate gives dialkyl ketones or aldehydes in good yields under mild conditions. The mechanism of this reaction and an application of this process to a formal total synthesis of dihydrojasmone are described.

Carbonyl compounds are obviously of most important in synthetic organic chemistry. In the synthesis of ketones with the construction of carbon skeleton, reactions of carboxylic acid or acid halide with organometallic compounds[1] or acid halide with organocopper reagents[2] have extensively been used. Recent years, methods by using organotransition metal catalyst such as palladium are also actively studied.[3] On the other hand, reaction of the "umpolung" reagents involving sulfur compounds acting acyl anion equivalent with alkyl halides or carbonyl compounds is another good method for preparation of carbonyl compounds (Scheme 1).[4] This process, however, has some drawbacks. For example, this reaction usually gives good yields only when primary alkyl halides or active alkyl halides, such as benzyl or allyl halides, are used.

α,β-Epoxy sulfoxides (**4**) were initially reported by Durst in 1969.[5] They are very easily prepared from 1-chloroalkyl phenyl sulfoxide (**1**)[6] and carbonyl compounds (**2**) *via* chlorohydrin (**3**). A few studies on the synthesis of α,β-unsaturated ketones or aldehydes from α,β-epoxy sulfoxides are reported[7] but these interesting compounds have received a scant attention. On the other hand, synthetic methods for a synthesis of α-substituted ketones or aldehydes *via* α,β-epoxy sulfones were reported by Durst[8] and Watt.[9]

Recently, we have found that the β-carbon of α,β-epoxy sulfoxides (**4**) is very reactive to benzeneselenolate to give dialkyl ketones (**5**) or aldehydes (**6**) in excellent yields as shown in Scheme 2.[10] In this paper we describe, in detail, the synthesis of dialkyl ketones and the synthesis of aldehydes from ketones by one carbon elongation through the reaction of α,β-epoxy sulfoxides with sodium benzeneselenolate and an application of this method to a formal total synthesis of dihydrojasmone.

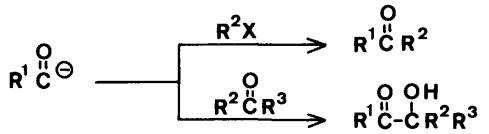

Scheme 1.

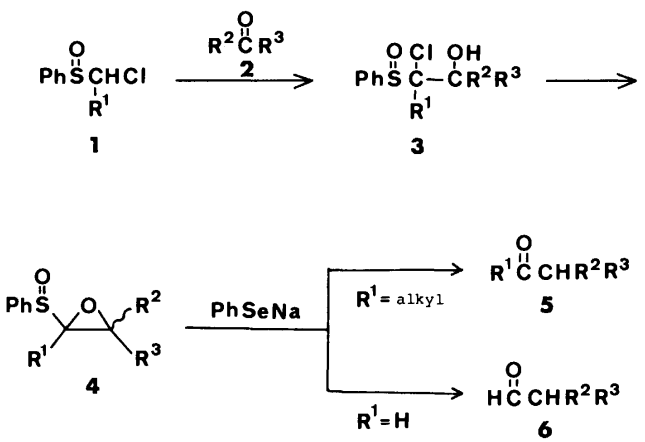

Scheme 2.

Results and Discussion

A Synthesis of Dialkyl Ketones from α,β-Epoxy Sulfoxides. The α,β-epoxy sulfoxide (**4a**) prepared from 1-chloro-2-phenylethyl phenyl sulfoxide and acetaldehyde was treated with three mol equivalents[11] of sodium benzeneselenolate[12] in ethanol under nitrogen for 20 min to give two ketones, 1-phenyl-2-butanone (**5a**) and 1-phenyl-3-phenylthio-2-butanone, in 73 and 18% yields, respectively. The

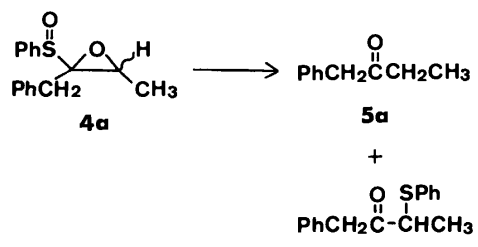

Scheme 3.

mechanism of this reaction is of some interest. The observation that the α,β-epoxy sulfoxide (**4a**) rapidly yields α-sulfenylated carbonyl compounds (1-phenyl-3-phenylthio-2-butanone) along with the desired 1-phenyl-2-butanone (**5a**) implies that the reaction takes place on the pathway as shown in Scheme 4. Benzeneselenolate attacks the β-carbon of **4a** to give 1-phenyl-3-phenylseleno-2-butanone and benzenesulfenate. The α-phenylseleno ketone was attacked by benzeneselenolate to afford 1-phenyl-2-butanone (**5a**) and diphenyl diselenide.[13] On the other hand, the liberated benzenesulfenate is reduced with benzeneselenol to afford benzenethiolate, which attacks the β-carbon of **4a** competitively with benzeneselenolate to give 1-phenyl-3-phenylthio-2-butanone. As the nucleophilicity of selenolate is known to be higher than that of thiolate and the generated thiolate is less than one equivalent, it is thought that the excess

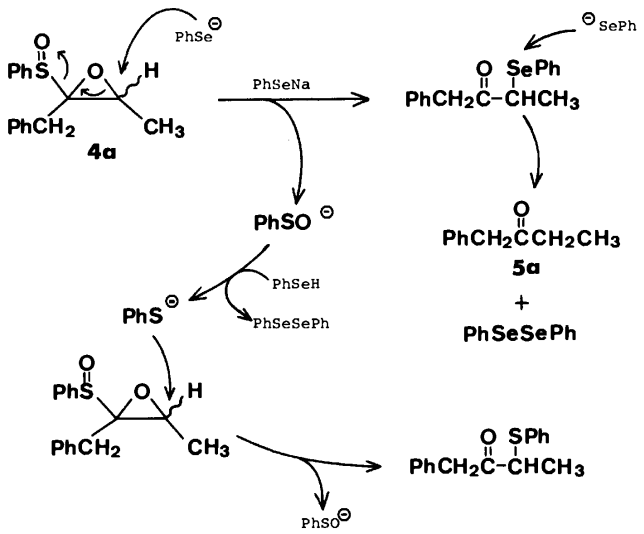

Scheme 4.

Table 1. Preparation of dialkyl ketones from α,β-epoxy sulfoxides and sodium benzeneselenolate

	α,β-Epoxy sulfoxide (**4**) R_1	R_2	R_3	NaSePh mol equiv	Conditions	Ketone **5**		Yield[a] %
4a	$PhCH_2$	CH_3	H	6	r.t. 20 min	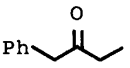	**5a**[16]	92
4b	$PhCH_2$	$CH_3(CH_2)_4$	H	6	r.t. 20 min	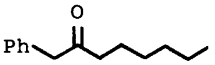	**5b**[17]	92
4c	$PhCH_2$	Ph	H	6	r.t. 3 h	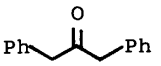	**5c**[16]	80
4d	$PhCH_2$	CH_3	CH_3	10	r.t. 3 h	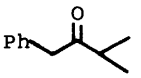	**5d**[18]	86
4e	$PhCH_2$	——$(CH_2)_5$——		12	60 °C, 2 h	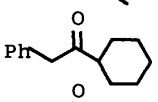	**5e**[19]	90
4f	$CH_3(CH_2)_5$	CH_3	H	6	r.t. 5 min	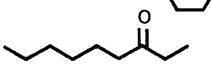	**5f**[20]	80
4g	$CH_3(CH_2)_5$	$CH_3(CH_2)_4$	H	6	r.t. 5 min	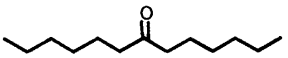	**5g**[16]	89
4h	$CH_3(CH_2)_5$	Ph	H	10	r.t. 20 min	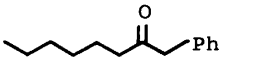	**5h**[17]	94
4i	$CH_3(CH_2)_5$	Cl-C$_6$H$_4$-	H	6	r.t. 20 min	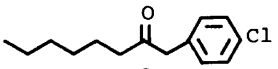	**5i**	85
4j	$CH_3(CH_2)_5$	——$(CH_2)_5$——		14	70 °C, 2 h	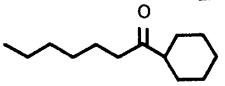	**5j**[21]	83
4k	$(CH_3)_2CH$	——$(CH_2)_5$——		12	reflux 19 h	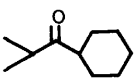	**5k**[22]	84
4l	$(CH_3)_2CH$	—$(CH_2)_2$-C(O,O)-$(CH_2)_2$—		12	reflux 16 h	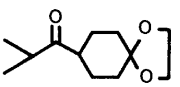	**5l**	89
4m	C$_6$H$_5$-	Cl-C$_6$H$_4$-	H	12	r.t. 50 min	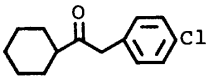	**5m**	98
4n	C$_6$H$_5$-	——$(CH_2)_5$——		12	reflux 16 h	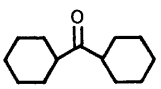	**5n**[22]	75

a) Isolated yield after silica-gel column chromatography.

benzeneselenolate exclusively gives the desired ketone with little sulfenylated carbonyl compound. Actually treatment of **4a** with six mol equivalents of sodium benzeneselenolate gave 92% yield of 1-phenyl-2-butanone (**5a**) along with almost no sulfenylated carbonyl compound.

The results of the reaction of various α,β-epoxy sulfoxides (**4**) with excess sodium benzeneselenolate are summarized in Table 1. As shown in Table 1, various kinds of dialkyl ketones were synthesized in good yields under mild conditions. Di-(secondary alkyl) ketones were also synthesized with no problem though at a higher temperature, a larger amount of sodium benzeneselenolate, and a longer period of reaction time were required. It is worth noting that the unreacted sodium benzeneselenolate is recovered as diphenyl diselenide, which was given by oxidation of benzeneselenolate by air, in nearly quantitative yield.

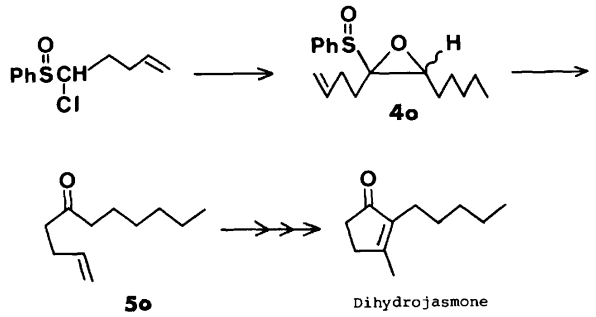

Scheme 5.

This procedure was applied to a formal total synthesis of dihydrojasmone as shown in Scheme 5. Alkylation of chloromethyl phenyl sulfoxide with 4-bromo-1-butene gave 1-chloro-4-pentenyl phenyl sulfoxide in 61% yield. Treatment of this chloride with lithium diisopropylamide followed by hexanal afforded chlorohydrin in 89% yield, which was treated with aqueous potassium hydroxide in methanol to give α,β-epoxy sulfoxide (**4o**) in good yield. The epoxy sulfoxide (**4o**) was treated with six mol equivalents of sodium benzeneselenolate in ethanol at room temperature for 10 min to afford 1-undecen-5-one (**5o**)[14] in 91% yield. This ketone was already converted to dihydrojasmone.[14]

Synthesis of Aldehydes from Ketones by One Carbon Elongation. Many synthetic methods for aldehydes from ketones by one carbon homologation have already been known[15] but they have some advantages and at the same time disadvantages. We have found that the α,β-epoxy sulfoxides (**4**) having hydrogen for R^1 gave aldehydes in excellent yields by the present method. This result means a synthesis of aldehydes (**6**) from ketones (**2**) by one carbon elongation (see Scheme 2). The results of the reaction of α,β-epoxy sulfoxides (**4p—4s**) with sodium benzeneselenolate are summarized in Table 2.

The reaction of **4s** with sodium benzeneselenolate gave 2-methyl-3-phenylthiopropanal (**6s**). This fact may be interpreted as shown in Scheme 6: The α,β-

Table 2. Preparation of aldehydes from ketones via α,β-epoxy sulfoxides

α,β-Epoxy sulfoxide (**4**)		NaSePh mol equiv.	Conditions	Aldehyde (**6**)		Yield[a] %
4p	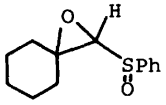	12	50 °C, 15 min	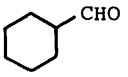	**6p**[16]	80
4q	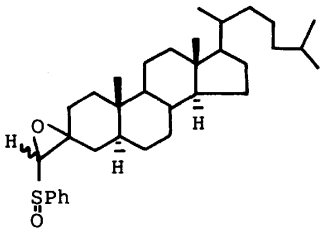	16	60 °C, 1.5 h	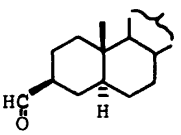	**6q**	96
4r	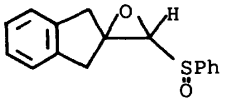	10	r.t. 1 h	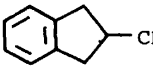	**6r**[23]	90
4s	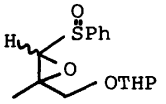	10	r.t. 70 min	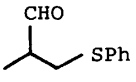	**6s**	75[b]

a) Isolated yield after silica-gel column chromatography. · b) Contamination of a trace of 2-methyl-3-phenylselenopropanal is observed by NMR and mass spectrum.

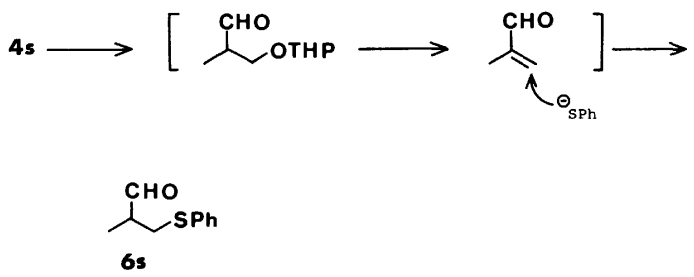

Scheme 6.

epoxy sulfoxide (**4s**) initially gave the aldehyde having tetrahydropyranyloxyl group, which underwent β elimination to afford an enal. Michael addition of benzenethiolate generated from benzenesulfenate (see Scheme 4) to the enal gave the aldehyde having phenylthio group (**6s**).

In conclusion, a novel and versatile procedure for a synthesis of dialkyl ketones and aldehydes has been developed from α,β-epoxy sulfoxides. In regard to the accessibility of the starting material, the simplicity and mildness of the operation, and high yield of the products, the present procedure offers a simple and useful approach to ketones and aldehydes.

Experimental

General. All melting points and boiling points are uncorrected. A Shibata GTO-250 glass tube oven was used for bulb-to-bulb distillation and boiling points are given as the temperature of the heating bath. Infrared (IR) spectra were measured directly on an NaCl plate or in KBr disks with a Hitachi 215 spectrometer. ^{1}H NMR spectra were measured in $CDCl_3$ solution with a JEOL FX-100 puls Fourier-transform spectrometer using Me_4Si as an internal standard. Electron impact mass spectra (MS) were obtained on a Hitachi M-80 double focusing spectrometer at 70 ev by direct insertion. Wako silica gel c-200 containing 2% fluorescence reagent 254 and quartz column were used for column chromatography and the products having UV absorption were detected by ultraviolet irradiation. In experiments requiring dry solvent, THF or ether was distilled from benzophenone ketyl and amines were from calcium hydride.

Preparation of 1-Chloroalkyl Phenyl Sulfoxide. Method A: Alkylation of chloromethyl phenyl sulfoxide with primary alkyl halides (benzyl bromide and 1-iodohexane) was carried out according to Wemple's procedure[6a] to give almost quantitative yield of 1-chloro-2-phenylethyl phenyl sulfoxide [diastereomeric mixture; colorless oil; NMR: δ=2.74 (dd, J=10, 14 Hz), 3.18 (dd, J=10, 14 Hz), 3.58 (dd, J=3, 14 Hz), 3.63 (dd, J=5, 14 Hz), 4.53 (dd, J=3, 10 Hz), 4.67 (dd, J=5, 10 Hz), 7.23 (s), 7.1—7.8 (m)] and 1-chloroheptyl phenyl sulfoxide [diastereomeric mixture; bp 185 °C/1 mmHg†; NMR: δ=0.87 (t, J=6 Hz), 4.39 (dd, J=3.5, 9 Hz), 4.51 (dd, J=3.5, 9 Hz), 7.4—7.8 (m)]. *Method B*: As the alkylation of chloromethyl phenyl sulfoxide with 2-iodopropane or cyclohexyl iodide gave almost no product 1-chloro-2-methylpropyl phenyl sulfoxide and 1-chloro-1-cyclohexylmethyl phenyl sulfoxide were prepared as follows: To a solution of EtONa (55 mmol) in 30 ml of dry EtOH was added thiophenol (50 mmol) followed by isobutyl bromide or cyclohexylmethyl bromide (50 mmol) and the mixture was stirred at room temperature for 3 h. The EtOH was evaporated and the residue was extracted with benzene. The product was distilled to give isobutyl phenyl sulfide (bp 110—114 °C/19 mmHg; 94%) or cyclohexylmethyl phenyl sulfide (bp 117 °C/2 mmHg; 92%). Isobutyl phenyl sulfide (10 mmol) was added to a suspension of *N*-chlorosuccinimide (10.5 mmol) in 30 ml of CCl_4 and the reaction mixture was stirred at room temperature for 2.5 h. The reaction mixture was filtered and the CCl_4 was evaporated. The residue was dissolved with 20 ml of CH_2Cl_2 and cooled to −60 °C. To this solution was added *m*-chloroperbenzoic acid (10 mmol) and the temperature of the reaction mixture was allowed to warm to −40 °C. The reaction mixture was diluted with CH_2Cl_2 and was washed with 10% NaOH followed by sat. aq NH_4Cl. The sulfoxides were separated by flash column chromatography to give 1-chloro-2-methylpropyl phenyl sulfoxide as two diastereomers. Main isomer (a colorless oil; 60%): IR (neat): 1055 (SO) cm^{-1}; NMR: δ=1.14, 1.20 (each 3H, d, J=7 Hz), 2.88 (1H, double septet, J=2, 7 Hz), 4.30 (d, J=2 Hz), 7.4-7.8 (5H, m). Minor isomer (a colorless oil; 25%): IR (neat): 1060 (SO) cm^{-1}; NMR: δ=1.20, 1.24 (each 3H, d, J=7 Hz), 2.40 (1H, octet, J=7 Hz), 4.24 (d, J=7 Hz), 7.4—7.7 (5H, m). Cyclohexylchloromethyl phenyl sulfoxide was synthesized from cyclohexylmethyl phenyl sulfide as similar procedure described above. Main isomer (70% yield): Colorless prisms; mp 86—87 °C; IR (KBr): 1055 (SO) cm^{-1}; NMR: δ=1.0—2.7 (11H, m), 4.31 (1H, d, J=3 Hz), 7.5—7.9 (5H, m). Minor isomer (22% yield): Colorless needles; mp 127—128 °C; IR (KBr): 1060, 1055 (SO) cm^{-1}; NMR: δ=1.0—2.3 (11H, m), 4.24 (1H, d, J=7 Hz), 7.5—7.7 (5H, m). The main isomers were used in this study.

General Procedure for the Preparation of α,β-Epoxy Sulfoxide (4): A synthesis of 2,3-epoxy-1-phenyl-2-phenylsulfinylbutane (**4a**) is described. To a solution of lithium diisopropylamide (3.45 mmol) in dry THF (8 ml) at −70 °C under N_2 was added a solution of 1-chloro-2-phenylethyl phenyl sulfoxide (3 mmol) in 2 ml of dry THF dropwise with stirring. The solution was stirred at −70 °C for 20 min and then acetaldehyde (6 mmol) was added through a syringe and the reaction mixture was stirred for additional 10 min. The reaction was quenched with sat. aq NH_4Cl and the whole was extracted with ether. The products were separated by silica-gel column chromatography (hexane: AcOEt=5:1) to give chlorohydrins (**3a-L**)[24] and (**3a-P**).[24] **3a-L** (40% yield): mp 89—91 °C; IR (KBr): 3360 (OH), 1030 (SO) cm^{-1}; NMR: δ=1.26 (3H, d, J=7 Hz), 3.41, 4.18 (each 1H, d, J=15 Hz), 4.17 (1H, q, J=7 Hz), 7.2—7.8 (5H, m); MS m/z (%): 182 ([M−PhSOH]$^+$, 7), 165 (14), 147 (29), 126 (100), 91 (81). **3a-P** (54% yield): mp 113-115 °C; IR (KBr): 3375 (OH), 1025 (SO) cm^{-1}; NMR: δ=1.40 (3H, d, J=6 Hz), 3.29, 3.42 (each 1H, d, J=15 Hz), 3.83 (1H, q, J=15 Hz), 3.83 (1H, q, J=6 Hz), 7.2—7.8 (5H, m); MS m/z (%): 182 ([M−PhSOH]$^+$, 20), 147 (55), 126 (100), 91 (79); Found: C, 62.21; H, 5.48; S, 10.37; Cl, 11.24%. Calcd for $C_{16}H_{17}SO_2Cl$: C, 62.23; H, 5.55; S,

† 1 mmHg=133.322 Pa.

10.38; Cl, 11.48%. To a solution of **3a-L** (1 mmol) in 12 ml of MeOH was added 30% aq KOH (2.5 ml) dropwise with stirring and the mixture was stirred at room temperature for 1 h. The solution was neutralized by adding NH_4Cl and the MeOH was evaporated. The residue was extracted with ether and the product was purified by silica-gel column chromatography to give 2,3-epoxy-1-phenyl-2-phenylsulfinylbutane (**4a-L**)[25] as colorless oil in 95% yield. IR (neat): 1095, 1055 (SO) cm^{-1}; NMR: δ=1.34 (3H, d, J=6 Hz), 3.05, 3.10 (each 1H, d, J=16 Hz), 3.79 (1H, q, J=6 Hz), 6.9—7.7 (10H, m); MS m/z (%): 272 (M^+, 2), 147 ([M−PhSO]$^+$, 18), 126 (39), 105 (38), 91 (100). Epoxy sulfoxide (**4a-P**)[25] was synthesized from **3a-P** by the similar procedure described above in 98% yield. **4a-P**: IR (neat): 1095, 1055 (SO) cm^{-1}; NMR: δ=1.62 (3H, d, J=6 Hz), 2.45, 3.55 (each 1H, d, J=15 Hz), 2.75 (1H, q, J=6 Hz), 6.9—7.8 (10H, m); MS m/z (%): 272 (M^+, 1.5), 147 ([M−PhSO]$^+$, 20), 126 (49), 105 (40), 91, (100).

2,3-Epoxy-1-phenyl-2-phenylsulfinyloctane (4b). Chlorohydrin **3b-L** (37% yield): Colorless oil; IR (neat): 3375 (OH), 1075, 1020 (SO) cm^{-1}; NMR: δ=0.83 (3H, t, J=6 Hz), 3.38, 4.14 (each 1H, d, J=15 Hz), 3.90 (1H, m), 7.2—7.8 (10H, m). **3b-P** (47% yield): Colorless oil; IR (neat): 3390 (OH), 1075, 1040 (SO) cm^{-1}; NMR: δ=0.87 (3H, t, J=6 Hz), 3.36, 3.50 (each 1H, d, J=14 Hz), 3.52 (1H, m), 7.2—7.9 (10H, m). Epoxy sulfoxide **4b-L** (65% yield): Colorless oil; IR (neat): 1090, 1055 (SO) cm^{-1}; NMR: δ=0.86 (3H, t, J=6 Hz), 1.0—1.7 (8H, m), 3.00, 3.05 (each 1H, d, J=16 Hz), 3.71 (1H, t, J=6 Hz), 7.0—7.7 (10H, m); MS m/z (%): 328 (M^+, trace), 203 (7), 126 (11), 91 (100). **4b-P** (69% yield): Colorless oil; IR (neat): 1090, 1050 (SO) cm^{-1}. NMR: δ=0.89 (3H, t, J=6 Hz), 1.1—2.1 (8H, m), 1.96 (2H, m), 2.54, 3.54 (each 1H, d, J=14 Hz), 2.63 (1H, t, J=6 Hz), 6.8—7.8 (10H, m); MS m/z (%): 328 (M^+, trace), 203 (7), 126 (11), 91 (100).

1,2-Epoxy-1,3-diphenyl-2-phenylsulfinylpropane (4c). Chlorohydrin **3c-L** (37% yield): mp 158—160 °C; IR (KBr): 3320 (OH), 1015 (SO) cm^{-1}; NMR: δ=3.16 4.40 (each 1H, d, J=15 Hz), 5.07 (1H, s), 7.2—8.0 (15H, m); MS m/z (%): 250 (1), 241 (1), 233 (3), 207 (3), 126 (100). **3c-P** (45% yield): Colorless oil; IR (neat): 3350 (OH), 1040 (SO) cm^{-1}; NMR: δ=2.55, 3.30 (each 1H, d, J=15 Hz), 5.41 (1H, s), 7.2—7.8 (15H, m); MS m/z (%): 244 ([M−PhSO]$^+$, 13), 209 (29), 186 (17), 125 (86), 77 (100). Epoxy sulfoxide **4c-L** (50% yield): mp 135.5—136 °C; IR (KBr): 1060 (SO) cm^{-1}; NMR: δ=2.76 (2H, s), 4.87 (1H, s), 7.0—7.7 (15H, m); MS m/z (%): 209 ([M−OhSO]$^+$, 18), 181 (25), 91 (100). **4c-P** (71% yield): mp 112—113 °C; IR (KBr): 1040 (SO) cm^{-1}; NMR: δ=2.66, 3.71 (each 1H, d, J=15 Hz), 3.79 (1H, s), 7.0—7.8 (15H, m); MS m/z (%): 209 ([M−PhSO]$^+$, 19), 181 (28), 91 (100); Found: C, 75.45; H, 5.26; S, 9.69%. Calcd for $C_{21}H_{18}O_2S$: C, 75.42; H, 5.42; S, 9.59%.

2,3-Epoxy-3-methyl-1-phenyl-2-phenylsulfinylbutane (4d). Chlorohydrin **3d** (95% yield): Colorless oil; IR (neat): 3420 (OH), 1090, 1060 (SO) cm^{-1}; NMR: δ=1.25, 1.55 (each 3H, s), 3.30, 3.46 (each 1H, d, J=15 Hz), 7.2—7.8 (10H, m); MS m/z (%): 196 ([M−PhSO]$^+$, 37), 183 (34), 181 (100). Epoxy sulfoxide **4d** (89% yield): mp 81—82 °C; IR (KBr): 1095, 1050 (SO) cm^{-1}; NMR: δ=1.26, 1.83 (each 3H, s), 3.25 (2H, s), 6.6—7.8 (10H, m) MS m/z (%): 286 (M^+, 0.04), 161 (26), 126 (30), 91 (100); Found: C, 71.00; H, 6.30; S, 11.15%; M^+, 286.0997. Calcd for $C_{17}H_{18}O_2S$: C, 71.30; H, 6.34; S, 11.19%; M, 286.1026.

2'-Benzyl-2'-phenylsulfinylspiro[cyclohexane-1,1'-oxirane] (4e). Chlorohydrin **3e** (82% yield): Colorless oil; IR (neat): 3410 (OH), 1090, 1045 (SO) cm^{-1}; NMR: δ=1.0—2.4 (10H, m), 3.35, 3.43 (each 1H, d, J=15 Hz), 7.1—7.8 (10H, m); MS m/z (%): 236 ([M−PhSO]$^+$, 38), 179 (100). Epoxy sulfoxide **4e** (86% yield): mp 61—62 °C; IR (KBr): 1055 (SO) cm^{-1}; NMR: δ=1.2—2.3 (10H, m), 3.24 (2H, s), 6.7—7.7 (10H, m); MS m/z (%): 201 ([M−PhSO]$^+$, 18), 91 (100); Found: C, 73.37; H, 6,76; S, 9.92%. Calcd for $C_{20}H_{22}O_2S$: C, 73.58; H, 6.79; S, 9.82%.

2,3-Epoxy-3-phenylsulfinylnonane (4f). Chlorohydrin **3f-L** (37% yield): mp 62—64 °C; IR (KBr): 3375 (OH), 1085, 1025 (SO) cm^{-1}; NMR: δ=0.93 (3H, t, J=6 Hz), 1.19 (3H, d, J=6 Hz), 1.1—3.0 (10H, m), 4.08 (1H, q, J=6 Hz), 7.5—7.9 (5H, m); MS m/z (%): 250 (2), 126 (100). **3f-P** (52% yield): mp 67—69 °C; IR (KBr): 3360 (OH), 1080, 1035, 1020 (SO) cm^{-1}; NMR: δ=0.89 (3H, t, J=6 Hz), 1.1—2.2 (10H, m), 1.37 (3H, d, J=6 Hz), 4.10 (1H, q, J=6 Hz), 7.4—7.8 (5H, m); MS m/z (%): 241 (1), 126 (100). Epoxy sulfoxide **4f-L** (90% yield): Colorless oil; IR (neat): 1090, 1055 (SO) cm^{-1}; NMR: δ=0.83 (3H, t, J=6 Hz), 0.9—2.0 (10H, m), 1.37 (3H, d, J=6 Hz), 3.73 (1H, q, J=6 Hz), 7.4-7.7 (5H, m); MS m/z (%): 266 (M^+, 4), 141 (12), 126 (29), 57 (100); Found: m/z 266.1353. Calcd for $C_{15}H_{22}O_2S$: M, 266.1339. **4f-P** (92% yield): Colorless oil; IR (neat): 1090, 1050 (SO) cm^{-1}; NMR: δ=0.81 (3H, t, J=6 Hz), 0.9—2.3 (10H, m), 1.77 (3H, d, J=6 Hz), 3.39 (1H, q,J=6 Hz), 7.4—7.7 (5H, m); MS m/z (%): 266 (M^+, 3), 141 (10), 126 (23), 57 (100); Found: m/z 266.1325. Calcd for $C_{15}H_{22}O_2S$: M, 266.1339.

6,7-Epoxy-7-phenylsulfinyltridecane (4g). Chlorohydrin **3g-L** (39% yield): Colorless oil; IR (neat): 3350 (OH), 1075, 1035 (SO) cm^{-1}; NMR: δ=0.83, 0.93 (each 3H, t, J=6 Hz), 3.82 (1H, dd, J=4, 8 Hz), 7.4—7.9 (5H, m); MS m/z (%): 306 (1), 233 (9), 161 (34), 126 (100). **3g-P** (61% yield): Colorless oil; IR (neat): 3375 (OH), 1075, 1035 (SO) cm^{-1}; NMR: δ=0.95 (6H, t, J=6 Hz), 3.70 (1H, dd, J=2, 9 Hz), 7.4-7.8 (5H, m); MS m/z (%): 306 (1), 197 (7), 161 (62), 41 (100). Epoxy sulfoxide **4g-L** (93% yield): Colorless oil; IR (neat): 1090, 1055 (SO) cm^{-1}; NMR: δ=0.84, 0.88 (each 3H, t, J=6 Hz), 3.63 (1H, t, J=6 Hz), 7.4—7.7 (5H, m); MS m/z (%): 322 (M^+, 0.5), 197 (12), 113 (77), 43 (100). **4g-P** (87% yield): Colorless oil; IR (neat): 1090, 1050 (SO) cm^{-1}; NMR: δ=0.81, 0.94 (each 3H, t, J=6 Hz), 3.25 (1H, t, J=6 Hz), 7.4—7.7 (5H, m); MS m/z (%): 322 (M^+, 0.5), 197 (16), 113 (100).

1,2-Epoxy-1-phenyl-2-phenylsulfinyloctane (4h). Chlorohydrin **3h-L** (45% yield): mp 133—134 °C; IR (KBr): 3325 (OH), 1035 (SO) cm^{-1}; NMR: δ=0.89 (3H, t, J=6 Hz), 1.1—2.1 (10H, m), 4.92 (1H, s), 7.24 (5H, s), 7.5—8.0 (5H, m); MS m/z (%)+ 238 ([M−PhSOH]$^+$, 9), 203 (17), 126 (69), 105 (100). **3h-P** (34% yield): mp 99—100 °C; IR (KBr): 3350 (OH), 1035 (SO) cm^{-1}; NMR: δ=0.83 (3H, t, J=6 Hz), 0.9—2.0 (10H, m), 5.29 (1H, s), 7.2—7.9 (10H, m); MS m/z (%): 238 ([M−PhSOH]$^+$, 11), 203 (25), 133 (22), 126 (33), 107 (100). Epoxy sulfoxide **4h-L** (99% yield): mp 55—56 °C; IR (KBr): 1085 1055 (SO) cm^{-1}; NMR: δ=0.80 (3H, t, J=6 Hz), 0.8—1.7 (10H, m), 4.78 (1H, s), 7.1—7.8 (10H, m); MS m/z (%): 328 (M^+, 0.4), 203 ([M−PhSO]$^+$, 14), 91 (100); Found: C, 73.02; H, 7.36; S, 10.00%; M^+, 328.1500. Calcd for $C_{20}H_{24}O_2S$: C, 73.13; H, 7.36; S, 9.76%; M, 328.1496. **4h-P** (95% yield): mp 38—39 °C; IR (KBr): 1085, 1045 (SO) cm^{-1}; NMR: δ=0.84 (3H, t, J=6 Hz), 1.0—2.4 (10H, m), 4.41 (1H, s), 7.3—7.8 (10H, m); MS m/z (%): 328 (M^+, trace), 203 ([M−

PhSO]$^+$, 15), 91 (100); Found: *m/z* 328.1507. Calcd for $C_{20}H_{24}O_2S$: M, 328.1495.

1,2-Epoxy-1-(4-chlorophenyl)-2-phenylsulfinyloctane (4i). Chlorohydrin **3i-L** (41% yield): mp 67—69 °C; IR (KBr): 3230, 1040 (SO) cm^{-1}; NMR: δ=0.90 (3H, t, J=6 Hz), 4.93 (1H, s), 7.28 (4H, s), 7.6—8.0 (5H, m); MS *m/z* (%): 398 (M$^+$, trace), 272 (5), 237 (7), 141 (33), 139 (31), 126 (100). **3i-P** (49% yield): Colorless crystals; mp 114—115 °C; IR (KBr): 3330 (OH), 1045 (SO) cm^{-1}; NMR: δ=0.85 (3H, t, J=6 Hz), 5.43 (1H, d, J=2.5 Hz), 7.2—7.9 (9H, m); MS *m/z* (%): 272 ([M−PhSOH]$^+$, 16), 237 (36), 167 (42), 141 (100). Epoxy sulfoxide **4i-L** (93% yield): Colorless oil; IR (neat): 1090, 1060 (SO) cm^{-1}; NMR: δ=0.81 (3H, t, J=6 Hz), 4.74 (1H, s), 7.0—7.8 (9H, m); MS *m/z* (%): 362 (M$^+$, trace), 237 (14), 125 (100). **4i-P** (90% yield): Colorless crystals; mp 76—77 °C; IR (KBr): 1090, 1050 (SO) cm^{-1}; NMR: δ=0.84 (3H, t, J=6 Hz), 4.38 (1H, s), 7.3—7.8 (9H, m); MS *m/z* (%): 362 (M$^+$, trace), 237 ([M−PhSO]$^+$, 18), 125 (100); Found: C, 66.13; H, 6.32; Cl, 9.89; S, 8.81%. Calcd for $C_{20}H_{23}ClO_2S$: C, 66.19; H, 6.39, Cl, 9.77; S, 9.08%.

2'-Hexyl-2'-phenylsulfinylspiro[cyclohexane-1,1'-oxirane] (4j). Chlorohydrin **3j** (99% yield): Colorless crystrals; mp 73—74 °C; IR (neat): 3345 (OH), 1035 (SO) cm^{-1}; NMR: δ=0.84 (3H, t, J=6 Hz), 7.3—7.8 (5H, m). Epoxy sulfoxide **4j** (76% yield): Colorless oil; IR (neat): 1080, 1045 (SO) cm^{-1}; NMR: δ=0.78 (3H, t, J=6 Hz), 7.4—7.7 (5H, m); MS *m/z* (%): 195 ([M−PhSO]$^+$, 57), 126 (10), 113 (100).

2'-Isopropyl-2'-phenylsulfinylspiro[cyclohexane-1,1'-oxirane] (4k). Colorless crystals; mp 84—85 °C; 94% yield from 1-chloro-2-methylethyl phenyl sulfoxide *via* chlorohydrin (**3k**); IR (KBr): 1050 (SO) cm^{-1}; NMR: δ=0.59, 1.17 (each 3H, d, J=7 Hz), 1.4—2.3 (10H, m), 2.66 (1H, septet, J=7 Hz), 7.3—7.7 (5H, m); MS *m/z* (%): 278 (M$^+$, trace), 262 (1.2), 218 (8), 191 (16), 43 (100); Found: C, 68.89; H, 8.02; S, 11.57%. Calcd for $C_{16}H_{22}O_2S$: C, 69.03; H, 7.97; S, 11.52%.

2''-Isopropyl-2''-phenylsulfinyldispiro[1,3-dioxolane-2,1'-cyclohexane-4',1''-oxirane] (4l). Chlorohydrin **3l** (97% yield): Colorless oil; IR (neat): 3400 (OH), 1040 (SO) cm^{-1}; NMR: δ=1.37, 1.42 (each 3H, d, J=6 Hz), 3.88 (4H, s), 7.3—7.8 (5H, m). Epoxy sulfoxide **4l** (92% yield): Colorless crystals; mp 73—76 °C; IR (KBr): 1090, 1050, 1040 (SO) cm^{-1}; NMR: δ=0.59, 1.16 (3H, d, J=7 Hz), 1.6—2.5 (4H, m), 2.68 (1H, septet, J=7 Hz), 4.01 (4H, s), 7.4—7.7 (5H, m); MS *m/z* (%): 336 (M$^+$, trace), 249 (trace), 211 (55), 99 (100); Found: C, 64.27; H, 7.26; S, 9.60%; M$^+$, 336.1383. Calcd for $C_{18}H_{24}O_4S$: C, 64.26; H, 7.19; S, 9.53%; M, 336.1393.

1,2-Epoxy-2-(4-chlorophenyl)-1-cyclohexyl-1-phenylsulfinylethane (4m). Chlorohydrin **3m-L** (46% yield): Colorless crystals; mp 165—167 °C; IR (KBr): 3350 (OH), 1045 (SO) cm^{-1}; NMR: δ=1.0—2.9 (11H, m), 5.17 (1H, s), 7.2—8.1 (9H, m); MS *m/z* (%): 270 (4), 139 (100). **3m-P** (51% yield): Colorless crystals; mp 164—166 °C; IR (KBr): 3175 (OH), 1015 (SO) cm^{-1}; NMR: δ=0.9—2.6 (11H, m), 5.78 (1H, s), 7.3—7.8 (9H, m); MS *m/z* (%): 270 (10), 252 (15), 217 (63), 78 (100). Epoxy sulfoxide **4m-L** (95% yield): Colorless crystals; mp 131—132 °C; IR (KBr): 1090, 1050 (SO) cm^{-1}; NMR: δ=0.6—1.9 (11H, m), 4.63 (1H, s), 7.2—7.5 (4H, m), 7.5—8.0 (5H, m); MS *m/z* (%): 360 (M$^+$, 0.6), 344 (2), 125 (88), 83 (100); Found: C, 66.43; H, 5.70; Cl, 9.89; S, 8.98%. Calcd for $C_{20}H_{21}ClO_2S$: C, 66.56; H, 5.86; Cl, 9.82; S, 8.88%. **4m-P** (80% yield): Colorless crystals; mp 137—138 °C; IR (KBr): 1090, 1040 (SO) cm^{-1}; NMR: δ=0.6—2.4 (11H, m), 4.42 (1H, s), 7.44 (4H, m), 7.4—7.8 (5H, m); MS *m/z* (%): 344 (trace), 235 (14), 207 (4), 125 (100).

2'-Cyclohexyl-2'-phenylsulfinylspiro[cyclohexane-1,1'-oxirane] (4n). 32% overall yiels from 1-chloro-1-cyclohexylmethyl phenyl sulfoxide and cyclohexanone *via* chlorohydrin (**3n**): Colorless crystals; mp 104—105.5 °C; IR (KBr): 1090, 1055 (SO) cm^{-1}; NMR: δ=0.5—2.5 (methylene-H), 7.3—7.8 (5H, m); MS *m/z* (%): 193 ([M−PhSO]$^+$, 29), 126 (11), 111 (41), 83 (100); Found: C, 71.40; H, 8.15%. Calcd for $C_{19}H_{26}O_2S$: C, 71.66; H, 8.23%.

2'-Phenylsulfinylspiro[5α-cholestane-3,1'-oxirane] (4q). Chlorohydrin **3q-L** (55% yield): Colorless oil; IR (neat): 3430 (OH), 1060 (SO) cm^{-1}; NMR: δ=0.66 (3H, s), 0.89 (6H, d, J=7 Hz), 0.91 (3H, d, J=7 Hz), 0.99 (3H, s), 4.79 (1H, s), 7.62 (5H, s). **3q-P** (39% yield): Colorless oil; IR (neat): 3400 (OH), 1050 (SO) cm^{-1}; NMR: δ=0.66 (3H, s), 0.88 (6H, d, J=7 Hz), 0.91 (3H, d, J=7 Hz), 1.01 (3H, s), 4.30 (1H, s), 7.60 (5H, m). Epoxy sulfoxide **4q-L** (96% yield): Colorless crystals; mp 142—143 °C; IR (KBr): 1050 (SO) cm^{-1}; NMR: δ=0.67 (3H, s), 0.88 (6H, d, J=7 Hz), 0.92 (3H, d, J=7 Hz), 1.04 (3H, s), 3.68 (1H, s), 7.5—7.9 (5H, m); Found: C, 78.03; H, 10.07%. Calcd for $C_{34}H_{52}O_2S$: C, 77.81; H, 9.99%. **4q-P** (94% yield): Colorless crystals; mp 137—140 °C; IR (KBr): 1055 (SO) cm^{-1}; NMR: δ=0.67 (3H, s), 0.89 (6H, d, J=7 Hz), 0.92 (3H, d, J=7 Hz), 1.02 (3H, s), 3.74 (1H, s), 7.5—7.9 (5H, m); Found: C, 77.87; H, 10.03%. Calcd for $C_{34}H_{52}O_2S$: C, 77.81; H, 9.99%.

2'-Phenylsulfinylspiro[indan-2,1'-oxirane] (4r). Chlorohydrin **3r** (86% yield): Colorless crystals; mp 193—195 °C; IR (KBr): 3420 (OH), 1050 (SO) cm^{-1}. Epoxy sulfoxide **4r** (85% yield): Colorless crystals; mp 77—78 °C; IR (KBr): 1060 (SO) cm^{-1}; NMR: δ=3.07, 3.36, 3.52, 3.94 (each 1H, d, J=18 Hz), 4.08 (1H, s), 7.28 (4H, m), 7.5—7.9 (5H, m); MS *m/z* (%): 193 ([M−C_6H_5]$^+$, 0.3), 145 (10), 117 (100); Found: C, 70.93; H, 5.17%. Calcd for $C_{16}H_{14}O_2S$: C, 71.08; H, 5.22%.

1,2-Epoxy-2-methyl-1-phenylsulfinyl-3-(tetrahydropyranyloxy)propane (4s). Chlorohydrin **3s** (99% yield): Colorless oil (about 2:1 diastereomeric mixture); IR (neat); 3340 (OH), 1040 (SO) cm^{-1}. Epoxy sulfoxide **4s** (94% yield): Colorless oil (diastereomeric mixture); IR (neat): 1020 (SO) cm^{-1}; NMR: δ=1.51, 1.76 (s, CH_3).

General Procedure for the Preparation of Dialkyl Ketones (5) or Aldehydes (6) from *α,β-Epoxy Sulfoxides (4)*: A synthesis of 1-phenyl-2-butanone (**5a**) is described. Note that both isomers of the *α,β*-epoxy sulfoxides (**4**) shows almost the same reactivity toward benzeneselenolate. $NaBH_4$(34 mg; 0.9 mmol) was added to a suspension of diphenyl diselenide (140 mg; 0.45 mmol) in 2 ml of EtOH by portions with stirring. After vigorous hydrogen gas evolution ceased, a solution of **4a** (41 mg; 0.15 mmol) in small amount of EtOH was added to the selenolate solution through a syringe under nitrogen. The reaction mixture was stirred at room temperature for 20 min. The reaction mixture was neutralized by NH_4Cl and the EtOH was evaporated. The residue was extracted with ether and, after usual work-up, the product was purified by silica-gel column chromatography followed by bulb-to-bulb distillation (150 °C/15 mmHg) to give 20.5 mg (92%) of 1-phenyl-2-butanone (**5a**). When this reaction was carried out with 3 mol equivalents of sodium benzeneselenolate, 1-phenyl-3-phenylthio-2-butanone (18%) was obtained with 73% of **5a**. 1-Phenyl-3-phenylthio-2-butanone: Colorless oil; IR (neat): 1720 (CO) cm^{-1}; NMR: δ=1.37 (3H, d, J=7 Hz), 3.83 (1H, q, J=7 Hz), 3.92 (2H, s), 7.0—7.5 (10H, m); MS *m/z* (%): 256

(M^+, 18), 147 (19), 137 (100); Found: *m/z* 256.0922. Calcd for $C_{16}H_{16}OS$: M, 256.0921.

1-Phenyl-2-octanone (5b). Colorless oil; IR (neat): 1710 (CO) cm^{-1}; NMR: δ=0.85 (3H, t, J=6 Hz), 2.43 (2H, t, J=6.5 Hz), 3.66 (2H, s), 7.24 (5H, m); MS *m/z* (%): 204 (M^+, 2), 113 (100), 91 (49); Found: *m/z* 204.1512. Calcd for $C_{14}H_{20}O$: M, 204.1513.

1-Cyclohexyl-2-phenylethanone (5e). Bp 135 °C/2.5 mmHg; IR (neat): 1720 (CO) cm^{-1}; NMR: δ=1.0—2.0 (10H, m), 2.44 (1H, m), 3.72 (2H, s), 7.22 (5H, m).

1-(4-Chlorophenyl)-2-octanone (5i). Colorless oil; IR (neat): 1715 (CO) cm^{-1}; NMR; δ=0.86 (3H, t, J=6 Hz), 1.1—1.7 (8H, m), 2.44 (2H, t, J=7 Hz), 3.64 (2H, s), 7.0—7.3 (4H, m); MS *m/z* (%): 238 (M^+, 3), 125 (29), 113 (100); Found: *m/z* 238.1111. Calcd for $C_{14}H_{19}ClO$: M, 238.1122.

1-(4,4-Ethylenedioxycyclohexyl)-2-methyl-1-propanone (5l). Bp 115 °C/3 mmHg; IR (neat): 1715 (CO) cm^{-1}; NMR: δ=1.09 (6H, d, J=7 Hz), 2.50 (1H, m), 2.79 (1H, septet, J=7 Hz), 3.95 (4H, s); MS *m/z* (%): 212 (M^+, 12), 169 (3), 141 (15), 99 (100), 86 (66); Found: *m/z* 212.1387. Calcd for $C_{12}H_{20}O_3$: M, 212.1400.

2-(4-Chlorophenyl)-1-cyclohexylethanone (5m). Mp 97—98 °C; IR (KBr): 1700 (CO) cm^{-1}; NMR: δ=1.0—2.0 (10H, m), 2.42 (1H, m), 3.69 (2H, s), 6.98—7.32 (4H, m); MS *m/z* (%): 236 (M^+, 2), 125 (16), 111 (32), 83 (100); Found: *m/z* 236.0954. Calcd for $C_{14}H_{17}ClO$: M, 236.0967.

3-Formyl-5α-cholestane (6q). Colorless oil; IR (neat): 2720 (CHO), 1740 (CO) cm^{-1}; NMR: δ=0.64 (3H, s), 0.87 (6H, d, J=7 Hz), 0.90 (3H, d, J=7 Hz), 0.96 (3H, s), 9.67 (1H, d, J=2 Hz); MS *m/z* (%): 400 (M^+, 61), 385 (31), 382 (61), 245 (100).

2-Methyl-3-phenylthiopropanal (6s). Colorless oil; IR (neat): 2740 (CHO), 1735 (CO) cm^{-1}; NMR: δ=1.24 (3H, d, J=7 Hz), 2.63 (1H, m), 2.93, 3.33 (each 1H, dd, J=7, 14 Hz), 7.33 (5H, m), 9.71 (1H, d, J=1 Hz); MS *m/z* (%): 180 (M^+, 16), 158 (16), 123 (13), 110 ([M−C_4H_6O]$^+$, 100).

A Formal Total Synthesis of Dihydrojasmone: Alkylation of chloromethyl phenyl sulfoxide with 4-bromo-1-butene in the Method A afforded 61% yield of 1-chloro-4-pentenyl phenyl sulfoxide as an oil; IR (neat): 1640 (C=C), 1085, 1055 (SO) cm^{-1}; NMR: δ=1.6—2.5 (4H, m), 4.50 (dd, J=3, 14 Hz), 4.59 (dd, J=3, 10 Hz), 4.98—5.21 (2H, m), 5.55—5.97 (1H, m), 7.4—7.9 (5H, m); MS *m/z* (%): 228 (M^+, 1), 126 (100). This was treated with LDA in THF at −50 °C for 15 min followed by slight excess hexanal to give chlorohydrins (**3o-L**) and (**3o-P**) in 60 and 29% yield, respectively. **3o-L**: Colorless oil; IR (neat): 3350 (OH), 1080, 1040 (SO) cm^{-1}; NMR: δ=0.83 (3H, t, J=6 Hz), 3.88 (1H, dd, J=3, 7.5 Hz), 4.97—5.24 (2H, m), 5.84 (1H, ddt, J=6, 10, 17 Hz), 7.4—7.9 (5H, m); MS *m/z* (%): 259 ([M−C_4H_9]$^+$, 3), 203 (6), 126 (100). **3o-P**: Colorless oil; IR (neat): 3380 (OH), 1080, 1050 (SO) cm^{-1}; NMR: δ=0.88 (3H, t, J=6 Hz), 3.67 (1H, dd, J=2.5, 9 Hz), 4.88—5.16 (2H, m), 5.74 (1H, ddt, J=6, 10, 17 Hz), 7.4—7.8 (5H, m); MS *m/z* (%): 259 ([M−C_4H_9]$^+$, 1), 203 (5), 126 (100).

These chlorohydrins were treated with aq KOH in MeOH at room temperature for 2 h to give α,β-epoxy sulfoxide (**4o-L**) and (**4o-P**) in 56 and 99% yield, respectively. **4o-L**: Colorless oil; IR (neat): 1090, 1055 (SO) cm^{-1}; NMR: δ=0.89 (3H, t, J=6 Hz), 3.68 (1H, t, J=6 Hz), 4.8—5.0 (2H, m), 5.62 (1H, ddt, J=6, 10, 17 Hz), 7.5—7.8 (5H, m); MS *m/z* (%): 292 (M^+, trace), 167 (5), 126 (11), 83 (48), 55 (100). **4o-P**: Colorless oil; IR (neat): 1090, 1055 (SO) cm^{-1}; NMR: δ=0.94 (3H, t, J=6 Hz), 3.27 (1H, t, J=6 Hz), 4.74—5.02 (2H, m), 5.58 (1H, ddt, J=6, 10, 17 Hz), 7.4—7.7 (5H, m); MS *m/z* (%): 292 (M^+, trace), 167 (4), 126 (11), 83 (55), 55 (100).

The α,β-epoxy sulfoxide (**4o-P**) or (**4o-L**) was treated with 6 mol equivalents of sodium benzeneselenolate in EtOH at room temperature for 10 min. The reaction mixture was neutralized by NH_4Cl and the EtOH was evaporated. After usual work-up, the product was purified by silica-gel column chromatography to give 91% yield of 1-undecene-5-one as an oil. Bp 95 °C/16 mmHg; IR (neat): 1715 (CO), 1645 (C=C) cm^{-1}; NMR: δ=0.88 (3H, t, J=6 Hz), 4.84—5.12 (2H, m), 5.56—6.00 (1H, m); MS *m/z* (%): 168 (M^+, 6), 113 ([M−C_4H_7]$^+$, 86), 83 ([M−C_6H_{13}]$^+$, 50), 43 (100).

The authors are grateful to Dr. S. Saito, Tanabe Seiyaku Co., for elemental analysis and Miss. Sawabe, Mrs. Yamatani, and Miss. Khim of this laboratory for NMR and mass spectral measurement. This work was supported in part by a Grant-in-Aid for Scientific Research No. 59771658 from the Ministry of Education, Science and Culture.

References

1) D. A. Shirley, *Org. React.*, **8**, 28 (1954); M. J. Jorgenson, *ibid.*, **18**, 1 (1970).

2) G. H. Posner, *Org. React.*, **22**, 253 (1975).

3) T. Hirao, N. Yamada, Y. Ohshiro, and T. Agawa, *Chem. Lett.*, **1982**, 1997; C. E. Russell and L. S. Hegedus, *J. Am. Chem. Soc.*, **105**, 943 (1983); J. W. Labadie and J. K. Stille, *Tetrahedron Lett.*, **24**, 4283 (1983); E. Negishi, V. Bagheri, S. Chatterjee. F. Luo, J. A. Miller, and A. T. Stoll, *ibid.*, **24**, 5181 (1983); N. Jabri, A. Alexakis, and J. F. Normant, *ibid.*, **24**, 5081 (1983); J. W. Labadie and J. K. Stille, *J. Am. Chem. Soc.*, **105**, 6129 (1983); E. Negishi and J. A. Miller, *ibid.*, **105**, 6761 (1983); V. P. Baillargeon and J. K. Stille, *ibid.*, **105**, 7175 (1983); J. W. Labadie, D. Tueting, and J. K. Stille, *J. Org. Chem.*, **48**, 4634 (1983); S. Wattanasin and F. G. Kathawals, *Tetrahedron Lett.*, **25**, 811, (1984); M. Kosugi, I. Takano, M. Sakurai, H. Sano, and T. Migita, *Chem. Lett.*, **1984**, 1221; M. Kosugi, I. Hagiwara, T. Sumiya, and T. Migita, *Bull. Chem. Soc. Jpn.*, **57**, 242 (1984); V. Fiandanese, G. Marchese, V. Martina, and L. Ronzini, *Tetrahedron Lett.*, **25**, 4805 (1984).

4) E. J. Corey and D. Seebach, *Angew. Chem., Int. Ed. Engl.*, **4**, 1075, 1077 (1965); B.-T. Grobel and D. Seebach, *Synthesis*, **1977**, 357; T. A. Hase and J. K. Koskimeies, *Aldrichimica Acta*, **14**, 73 (1981), **15**, 35 (1982).

5) T. Durst, *J. Am. Chem. Soc.*, **91**, 1034 (1969).

6) a) K. M. More and J. Wemple, *J. Org. Chem.*, **43**, 2713 (1978); b) G. Tsuchihashi, K. Ogura, S. Iriuchijima, and S. Tomisawa, *Synthesis*, **1971**, 89; c) B. M. Trost and R. A. Kunz, *J. Org. Chem.*, **39**, 2648 (1974); d) H. A. Khan and I. Paterson, *Tetrahedron Lett.*, **1982**, 5083.

7) T. Durst and K.-C. Tin, *Tetrahedron Lett.*, **1970**, 2369; V. Reutrakul and W. Kanghae, *ibid.*, **1977**, 1377; D. F. Taber and B. P. Cunn, *J. Org. Chem.*, **44**, 450 (1979).

8) F. de Reinach-Hirtzbach and T. Durst, *Tetrahedron Lett.*, **1976**, 3677; T. Durst, K.-C. Tin, F. de Reinach-Hirtzbach, J. M. Decesare, and M. D. Ryan, *Can. J. Chem.*, **57**, 258 (1979).

9) M. Adamczyk, E. K. Dolence, D. S. Watt, M. R. Christy, J. H. Reibenspies, and O. P. Anderson, *J. Org. Chem.*, **49**, 1378 (1984).

10) A part of the results of this reaction was reported as a communication. T. Satoh, Y. Kaneko, T. Kumagawa, T. Izawa, K. Sakata, and K. Yamakawa, *Chem. Lett.*, **1984**, 1957.

11) One mol of α,β-epoxy sulfoxide reacts with two mols of sodium benzeneselenolate to give a ketone as shown in Scheme 4.

12) K. B. Sharpless and R. F. Lauer, *J. Am. Chem. Soc.*, **95**, 2697 (1973).

13) H. J. Reich, J. M. Renga, and I. L. Reich, *J. Am. Chem. Soc.*, **97**, 5434 (1975).

14) S. Watanabe, T. Fujita, K. Suga, and M. Haibara, *Aust. J. Chem.*, **35**, 1739 (1982); M. Yamashita, K. Matsumiya, M. Tanabe, and R. Suemitsu, *Bull. Chem. Soc. Jpn.*, **58**, 407 (1985).

15) S. F. Martin, *Synthesis*, **1979**, 633.

16) Commerciaily available ketone. see "The Aldrich Library of NMR Spectra" Aldrich Chemical Company.

17) K. Shankaran, D. G. Talekar, and A. S. Rao, *Synth. Commun.*, **12**, 141 (1982).

18) F. C. Bordwell and J. Almy, *J. Org. Chem.*, **38**, 575 (1973); B. M. Trost and Y. Tamaru, *Tetrahedron Lett.*, **1975**, 3797.

19) S. Inaba and R. D. Rieke, *Tetrahedron Lett.*, **24**, 2451 (1983).

20) Y. Yamamoto, K. Kondo, and I. Moritani, *Bull. Chem. Soc. Jpn.*, **48**, 3682 (1975).

21) B. Lythgoe and I. Waterhouse, *J. Chem. Soc., Perkin Trans. 1*, **1979**, 2429.

22) A. P. Krapcho, D. S. Kashdan, and E. G. E. Jahngen Jr., *J. Org. Chem.*, **42**, 1189 (1977).

23) A. I. Meyers and J. L. Durandetta, *J. Org. Chem.*, **40**, 2021 (1975).

24) We express the diastereomers of the chlorohydrin **(3)** as **L** and **P**. **3-L** is the chlorohydrin having large Rf value (less polar product) on silica gel TLC (hexane-AcOEt mixture as a developing solvent) and **P** means that it is polar chlorohydrin.

25) We express the diastereomers of the α,β-epoxy sulfoxide **(4)** as **L** and **P**. **4-L** and **4-P** are the epoxy sulfoxides derived from the chlorohydrin **3-L** and **3-P**, respectively.

Nucleophilic Aminomethylation of Aldehydes with α-Amino Alkylsilanes

Otohiko TSUGE,* Junji TANAKA, and Shuji KANEMASA
Research Institute of Industrial Science, and Department of Molecular Science and Technology, Interdisciplinary Graduate School of Engineering Sciences, Kyushu University, Kasugakoen, Kasuga 816
(Received March 14, 1985)

Fluoride-induced desilylation of (α-phthalimido-, α-morpholino-, and α-acetamidobenzyl)silanes and a (phthalimidomethyl)silane generates the corresponding α-amino carbanions which add to a variety of aldehydes. The conversion of phthalimido group of the adducts into amino moiety leads to β-amino alcohols. This simple reaction sequence offers a new and general method of nucleophilic aminomethylation.

Removal of a proton from a carbon adjacent to nitrogen leads to an α-amino carbanion synthon which is important for nucleophilic aminomethylation. However, deprotonation at the α-position of amines is generally quite difficult since the α-hydrogen is not highly acidic.[1] When the nitrogen bears a strongly electron-withdrawing substituent or the nitrogen is incorporated in a system in which an anion formed can be stabilized by delocalization, some successful deprotonation has been achieved.[2] Thus, such dipole-stabilized α-amino carbanions[3,4] as α-metalated amides, *N*-nitrosoamines, amidines, amine oxides and such resonance-stabilized α-amino carbanions[5,6] as α-metalated imines, isocyanides are now available and have found wide applications in organic synthesis.

Although not widely developed so far, the use of isolable organometallic compounds with an amino moiety at the α-position offers a fascinating access to the α-amino carbanions. One example is the transmetalation reaction of (α-amino alkyl)tins with alkyllithiums leading to α-amino carbanions of nonstabilized type.[7,8] This method would be useful in organic synthesis if the starting α-amino organometallic compounds are readily available, because the regioselective carbanion generation that is difficult at the α-position of amino substituent could be possible even if some other more acidic hydrogens are present in the same molecule.[9]

It has been recently reported that (α-alkoxybenzyl)-silanes are smoothly desilylated by the action of a fluoride ion forming α-alkoxy carbanions which react with a variety of carbonyl compounds as a useful synthon for nucleophilic hydroxymethylation.[10] As this method has an advantage of regioselective carbanion formation under nearly neutral conditions, its extention to other hetero-substituted silanes has been investigated.

The present paper describes a new approach to nucleophilic aminomethylation using α-aminobenzylsilanes and an aminomethylsilane which carry phthalimido, morpholino, and acetamido moieties as amino substituents.

Results and Discussion

(α-Amino alkyl)silanes were synthesized by the reactions of readily available (α-halo alkyl)silanes with amines as shown in Scheme 1. Thus, (α-phthalimidobenzyl)trimethylsilane **1** and (α-morpholinobenzyl)trimethylsilane **2** were obtained in excellent yields in the reactions of (α-bromobenzyl)trimethylsilane, prepared by the bromination of benzyltrimethylsilane with *N*-bromosuccinimide,[11] with potassium phthalimide and morpholine, respectively. Hydrazinolysis of **1** provided (α-aminobenzyl)trimethylsilane which was then acetylated to give (α-acetamidobenzyl)trimethylsilane **3**. Phthalimidomethyltrimethylsilane **4** was obtained from the reaction of potassium phthalimide with (chloromethyl)trimethylsilane which was commercially available.

α-Amino carbanion formation from the α-aminobenzylsilanes **1**, **2**, and **3** was accomplished by the action of a fluoride ion in such aprotic polar solvents as *N*,*N*-dimethylformamide (DMF) and hexamethylphosphoric triamide (HMPA) at room temperature, and the carbanions generated were attempted to capture with aldehydes as β-amino alcohols.

The reaction of **1** with benzaldehyde (1 equiv) in the presence of cesium fluoride (1 equiv) in dry DMF,

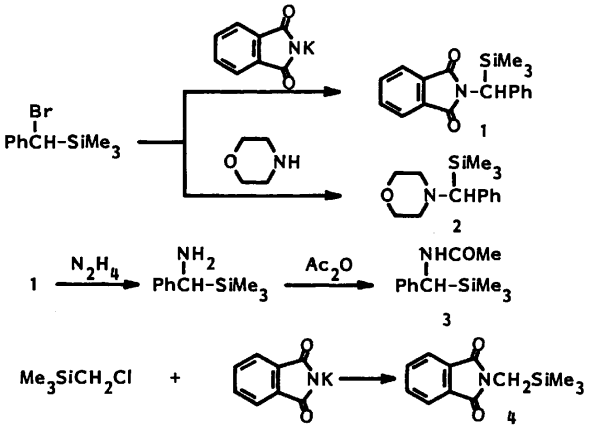

Scheme 1.

at room temperature under nitrogen, furnished a mixture of erythro and threo isomers (1:1) of 1,2-diphenyl-2-phthalimidoethanol **5a** as shown in Scheme 2 and Table 1. Each isomer of **5a** was separable from the other through a flash chromatography over silica gel, their structures being confirmed by their conversion into the known erythro and threo isomers of 2-amino-1,2-diphenylethanol as mentioned later.

The same reaction was carried out as well by the use of a catalytic amount of tetrabutylamonium fluoride (TBAF) under similar conditions. As a solvent, HMPA could be effectively employed, but separation of the solvent from the crude reaction mixture was rather annoying. The reaction in tetrahydrofuran (THF) was found not practical because only a very sluggish reaction occurred in this solvent.

Other aldehydes such as *p*-substituted benzaldehydes (*p*-methyl- and *p*-methoxybenzaldehyde), a heteroaromatic aldehyde (2-furancarbaldehyde), and an α,β-unsaturated aldehyde (cinnamaldehyde) also successfully reacted with **1** under similar conditions giving good to fair yields of the corresponding β-phthalimido-β-phenyl alcohols **5b** to **5e**. In all cases, the ratios of erythro and threo isomers were found to be 1:1, and their separation was carried out without any difficulty through a flash chromatography over silica gel. In the reaction of **1** with an aliphatic aldehyde (butanal), comparable amounts of the desired adduct **5f** and *N*-benzylphthalimide **9** were obtained. The formation of **9** as a protodesilylated product of **1** might be because the aldehyde carries acidic α-hydrogens which could protonate the carbanion species generated from **1** resulting in the formation of **9** and also the decrease of the yield of **5f**. The erythro/threo ratio in this case was 1/2, their separation being easy.

Trapping the α-amino carbanion of **1** with ketones (cyclohexanone and acetophenone), an imine (*N*-benzylideneaniline), and an α,β-unsaturated ester (methyl crotonate) was all unsuccessful. The only

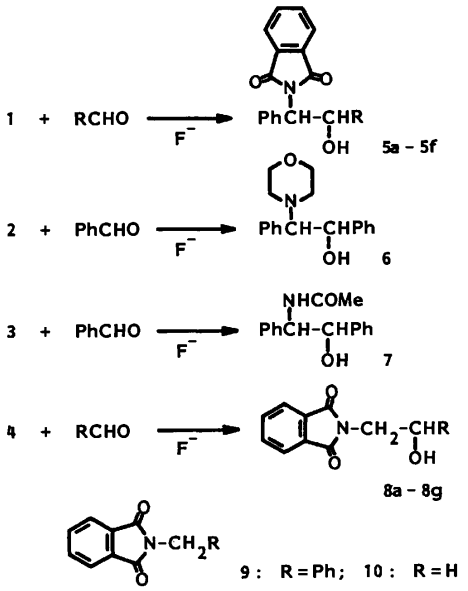

Scheme 2.

Table 1. Reactions of α-aminoalkylsilanes **1**—**4** with aldehydes in the presence of fluoride ion

α-Amino-silanes	Aldehydes	Reaction conditions[a] Fluoride (equiv)	Temp °C	Time h	β-Amino alcohols	R	Yield[b] %	Side products (yield/%)
1	PhCHO	CsF (1)	rt	8	**5a**	Ph	52	
1	PhCHO	TBAF (0.05)	rt	12	**5a**	Ph	62	
1	*p*-MeC_6H_4CHO	CsF (0.1)	rt	12	**5b**	*p*-MeC_6H_4	59	
1	*p*-$MeOC_6H_4CHO$	TBAF (0.05)	rt	16	**5c**	*p*-$MeOC_6H_4$	67	
1	2-furyl-CHO	TBAF (0.05)	rt	6	**5d**	2-furyl	75	
1	PhCH=CHCHO (t)	TBAF (0.05)	rt	12	**5e**	PhCH=CH (t)	74	
1	*n*-PrCHO	TBAF (0.05)	rt	18	**5f**	*n*-Pr	37	**9** (39)
2	PhCHO	CsF (1)	rt	16	**6**		67	
3	PhCHO	TBAF (1)	rt	16	**7**		57	
4	PhCHO	TBAF (0.05×2)	100	6+2	**8a**	Ph	60	**10** (16)
4	*p*-MeC_6H_4CHO	TBAF (0.05×2)	100	2+6	**8b**	*p*-MeC_6H_4	41	**10** (20)
4	*p*-$MeOC_6H_4CHO$	TBAF (0.05×2)	100	2+16	**8c**	*p*-$MeOC_6H_4$	38	**10** (22)
4	2-furyl-CHO	TBAF (0.05×2)	100	2+16	**8d**	2-furyl	49	**10** (20)
4	PhCH=CHCHO (t)	TBAF (0.05×2)	100	2+2	**8e**	PhCH=CH (t)	24	**10** (31)
4	*n*-PrCHO	TBAF (0.05×2)	100	2+8	**8f**	*n*-Pr	36	**10** (26)
4	Me_3CCHO	TBAF (0.05×2)	100	2+2	**8g**	Me_3C	28	**10** (39)

a) In the reactions of **4**, TBAF was added in two portions at the time intervals shown in Table. b) Isolated yields as mixtures of erythro and threo isomers with the ratio of 1:1 in all cases of **5** to **7** except for **5f** which is composed of 1:2 erythro/threo isomers.

isolated product from **1** was **9** in each case.

The phthalimido moiety as an amino substituent could be replaced with others such as a morpholino and an acetamido moiety as well. Thus, the reactions of (α-morpholinobenzyl)- **2** and (α-acetamidobenzyl)-trimethylsilane **3** with benzaldehyde under similar conditions gave satisfied yields of 2-aminoethanols **6** and **7**, respectively, which were unseparable mixtures of erythro and threo isomers (1:1). From these results, it is easily indicated that other dialkylamino substituents might be able to use in the present reaction since the easiness of desilylation of (α-amino-substituted benzyl)silanes seems independent upon the carbanion-stabilizing ability of the amino substituents. Surprising was that even a secondary amide group with a highly acidic NH hydrogen has led to the smooth generation and longtime survival of the α-acetamido carbanion which reacted with the aldehyde leading to **7** with no trace of the corresponding protodesilylated product.

The phthalimidomethylsilane **4**, carrying no anion-stabilizing substituent such as a phenyl in **1**, was only desilylated very slowly at room temperature as shown in Table 2. In addition, the α-amino carbanion generated from **4** showed the preference for the proton abstraction from somewhere forming *N*-methylphthalimide **10** rather than the addition to benzaldehyde giving the 2-aminoethanol **8a**. Although it was certain that the reaction using a catalytic amount of fluoride was more favored for the formation of **8a**, a trouble was that some of the starting **4** remained unchanged even if the reaction time was prolonged. This problem was resolved by the addition of another portion of fresh catalyst (fluoride) sometime in the course of reaction. In this way the yield of **8a** increased up to 60% and that of the undesired product **10** was suppressed down to 16% (Table 2). As the formyl hydrogen in DMF which was used as a solvent was suspected to be a possible proton source for the formation of side-product **10**,[12] a similar reaction in dry HMPA was carried out. However, only nearly identical results were obtained providing no solution to our concern on the proton source.

Table 1 shows the results of reactions of **4** with a variety of aldehydes. Every reaction was performed at 100 °C using two portions of catalytic amounts of TBAF which were added in the intervals of reaction times shown in Table 1. The α-phthalimido carbanion generated from **4** was found also unreactive toward ketones, α,β-unsaturated esters, and imines.

The removal of the phthalimido protecting group of **5** and **8** permits the establishment of a synthetic route of β-amino alcohols *via* a nucleophilic aminoalkylation onto aldehydes. In fact it was found easy to convert the phthalimido group into amino moiety through a hydrazinolysis using hydrazine hydrate. Thus, some of the 2-phthalimidoethanols **5** and **8** that were listed in Table 1 were subjected to the hydrazynolysis (Scheme 3 and Table 3). Both erythro and threo isomers of **5a** and **5f** were separately deprotected giving the erythro and threo isomers of β-amino alcohols **11** and **12**, respectively, in almost quantitative yields. The structures of *erythro*-**11** and *threo*-**11** were confirmed by the comparison of the spectral data and physical properties with those of the authentic samples.

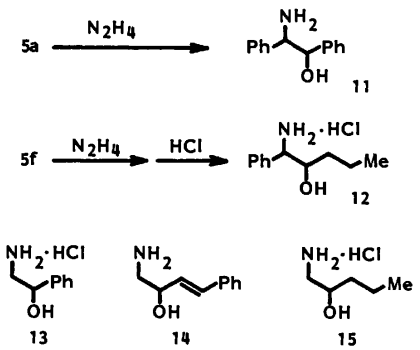

Scheme 3.

Table 2. Reactions of **4** with benzaldehyde under various conditions

Reaction conditions[a]				Products (yield/%)[b]		
Fluoride (equiv)	Solvent	Temp/°C	Time/h	**8a**	**10**	Recovered **4**
TBAF (0.2)	THF	rt	60	2	12	63
TBAF (0.2)	DMF	rt	60	5	37	52
TBAF (1)	DMF	rt	48	10	35	0
TBAF (0.05)	DMF	100	36	41	11	34
TBAF (0.05)	DMF	150	18	30	17	30
CsF (0.05)	DMF	130	4	29	18	0
TBAF (1)	DMF	100	15	38	56	0
TBAF (0.05×2)	DMF	100	6+2	60	16	0
TBAF (0.05×2)	HMPA	100	2+2	58	15	0

a) **4**: benzaldehyde = 1:1.5 in 2 ml of solvents per 1 mmol of **4**. b) All isolated yields.

Similarly other 2-phthalimidoethanols **8a**, **8e**, and **8f** were treated with hydrazine hydrate under reflux in ethanol giving excellent yields of **13**, **14**, and **15**, respectively.

As mentioned above, the reactions of **1** with a variety of aldehydes gave mixtures of comparable amounts of erythro and threo isomers of **5** and these isomers were readily separable by a flash chromatography. The only remarkable difference in the spectral data of *erythro*-**5a** and *threo*-**5a**, whose structures were confirmed by their derivation to the known β-amino alcohols, *erythro*-**11** and *threo*-**11**, is that the hydroxyl proton appears considerably lower in *erythro*-**5a** than in *threo*-**5a** (Table 4).

Table 3. Hydrazinolysis of 2-phthalimidoethanols **5** and **8**

2-Phthalimido-ethanols	Reaction time/h[a]	Products	Yield[b] %
erythro-**5a**	3	*erythro*-**11**	75
threo-**5a**	3	*threo*-**11**	88
erythro-**5f**	2	*erythro*-**12**	96
threo-**5f**	2	*threo*-**12**	95
8a	4	**13**	82
8e	4	**14**	97
8f	2	**15**	99

a) The time for hydrazinolysis under reflux in ethanol. b) All isolated yields.

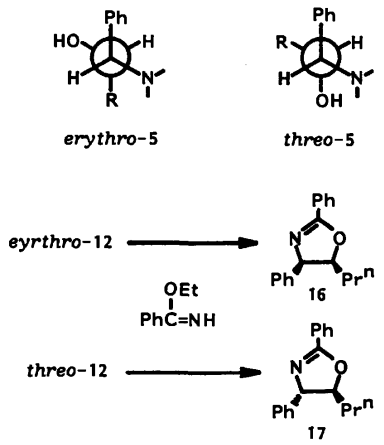

Scheme 4.

In Scheme 4, the most stable conformers for *erythro*-**5** and *threo*-**5** were illustrated. These models show that both the methine hydrogens α and β to the hydroxyl group of *erythro*-**5** look magnetically almost equivalent to those of *threo*-**5**. However, the hydroxyl proton of *threo*-**5** is located close to the adjacent phthalimido moiety so that it may be deshielded to some extent. This is the case observed for *erythro*-**5a** and *threo*-**5a** (R=Ph). Other erythro and threo structures for the similar products **5b** to **5e** were tentatively assigned on the basis of the ^{1}H-NMR spectral data shown in Table 4.

The possibility for intramolecular hydrogen bonding in *threo*-**5a** was confirmed on the basis of the IR spectra taken as the solution in chloroform. For *threo*-**5a**, no essential change of OH stretching vibration was observed between two kinds of solutions of different concentrations: for the solution containing 30 mg of *threo*-**5a** in 1 ml of chloroform, 3728, 3704 (free OH), 3604, and 3464 cm^{-1} (hydrogen-bonded OH); for the solution containing 0.6 mg in 1 ml, 3728, 3705 (free OH), 3516, and 3448 cm^{-1} (hydrogen-bonded OH). However, the last two of four OH absorptions which were observed in the solution containing 30 mg of *erythro*-**5a** in 1 ml of chloroform (3728, 3705 (free OH), 3602, and 3466 cm^{-1} (hydrogen-bonded OH) dissapeared in the spectrum of a diluted solution (0.3 mg in 1 ml, 3730 and 3705 cm^{-1}).

As the ^{1}H-NMR spectra for the two isomers of **5f** were found too close each other, it was impossible to determine the stereostructures only on the basis of the spectral data. Therefore each isomer of **5f** was first converted into **12** (Scheme 3 and Table 3) and then cyclized into each isomeric 2-oxazoline **16** or **17** by the reaction with an imino ether. The isomer **16** showed a coupling constant of 9.7 Hz for J_{4-5} and the other **17** 7.2 Hz, **16** and **17** being assigned as cis and trans isomers, respectively. The propyl hydrogens

Table 4. ^{1}H-NMR data for erythro and threo isomers of **5** [a]

5	*erythro*-**5** (δ, ppm)			*threo*-**5** (δ, ppm)		
	α-CH[b]	β-CH[b]	OH	α-CH[b]	β-CH[b]	OH
5a	5.49 d	5.92 d	2.77 br. s	5.55 d	5.75—5.90 m	3.29 m
5b	5.29 d	5.92 dd	2.69 d [c]	5.53 d	5.73—5.98 m	3.32 m [d]
5c	5.49 d	5.95 d	2.64 br. s [e]	5.55 d	5.87 dd	3.18 d [f]
5d	5.70 d	6.06 dd	2.80 d	5.78 d	5.90 dd	3.40 d
5e	5.33 d	5.56 dd	2.10 br. s [g]	5.30—5.62 m		3.20 m [h]
5f	5.14 d	4.60—4.87 m	2.64 br. s [i]	5.19 d	4.52—4.90 m	2.79 br. d [j]

a) Measured in $CDCl_3$. b) α-CH and β-CH: methine hydrogens α and β to the hydroxyl group. c) 2.21 s (Me). d) 2.21 s (Me). e) 3.64 s (OMe). f) 3.70 s (OMe). g) 6.20 dd and 6.72 d (PhCH=CH). h) 6.10 dd and 6.68 d (PhCH=CH). i) 0.73—1.05 m and 1.20—1.70 m (*n*-Pr). j) 0.72—1.05 m and 1.16—1.78 m (*n*-Pr).

at the 5-position of **16** as well as the methine hydrogen at the 5-position of **17** are both suffering from shielding from the adjacent phenyl plane. As it is known that 2-oxazoline formation from β-amino alcohols and imidic esters takes place with the retention of stereochemistry of the alcohols,[13] one isomer of **5f** which provided **16** can be assigned as *erythro*-**12**, and hence the other of **5f** leading to **17** is *threo*-**12**.

Experimental

General. Melting points were determined on a Yanagimoto micro melting point apparatus and uncorrected. IR spectra were taken with a JASCO A-702 or a JEOL JIR-100 spectrometer. ^{1}H-NMR spectra were recorded on a Hitachi R-40 or a JEOL FX-100 instrument and ^{13}C-NMR spectra were obtained on a JEOL FX-100 spectrometer at 25.05 MHz. Chemical shifts are expressed in parts per million downfield from tetramethylsilane. Mass spectra were measured with a JEOL JMS-01SG-2 spectrometer at 70 eV of ionization energy. Elementary analyses were performed on a Hitachi 026 CHN analyzer. Thin-layer chromatography (TLC) was accomplished on 0.2 mm precoated plates of silica gel 60 F-254 (Merck). Visualization was with ultraviolet light (254 and 365 nm) and iodine. Wakogel C 300 (Wako) and Silicagel 60 (Merck, size: 0.063—0.200 mm) were used for preparative column chromatography. Flash chromatography was carried out on an EYELA EF-10 apparatus using a column (20×180 mm) packed with Silicagel 60 (Merck, size: 0.040—0.063 mm). Micro vacuum distillation was accomplished with a Sibata GTO-250R Kugelrohr distilling apparatus. Solvents were evaporated with a Tokyo Rikakikai rotary evaporator type V.

DMF was purified by a vacuum distillation over alumina under nitrogen and stored on molecular sieves MS-5A. HMPA was also distilled *in vacuo* over calcium hydride under nitrogen and stored on molecular sieves MS-13X. THF was distilled over lithium aluminum hydride immediately prior to its use. Other solvents for reactions as well as for chromatography were used without further purification.

Materials. (α-Bromobenzyl)trimethylsilane (bp 88—92 °C (266 Pa), lit,[11] bp 98—99 °C (532 Pa)) was prepared by the reaction of benzyltrimethylsilane[14] with *N*-bromosuccinimide according to the reported method.[11] (Phthalimidomethyl)trimethylsilane **4** (bp 95—97 °C (100 Pa), lit,[15] bp 117 °C (266 Pa)) was synthesized from both commercially available (chloromethyl)trimethylsilane and potassium phthalimide. Morpholine was used without further purification. Commercial cesium fluoride was dried in a reaction flask under vacuum by heating at about 100 °C. TBAF solution in THF (1 mol dm^{-3}) was dried over molecular sieves MS-5A under nitrogen. Benzaldehyde, butanal, and cinnamaldehyde were purified by distillation. 2-Furancarbaldehyde was passed through a short column packed with alumina immediately before use. Other aldehydes were all used without further purification.

(α-Phthalimidobenzyl)trimethylsilane 1. A mixture of (α-bromobenzyl)trimethylsilane (12.15 g, 0.05 mol) and potassium phthalimide (10.2 g, 0.055 mol) in dry DMF (50 ml) was heated at 140 °C for 3 h. After cooled to room temperature, the reaction mixture was poured into ice-water and extracted with ether (50 ml×2). The ether was dried over magnesium sulfate and evaporated *in vacuo*. The residue was chromatographed over silica gel using hexane–benzene (2:1) as an eluent to give 12.96 g (84%) of **1**: Colorless prisms from hexane; mp 106—107 °C; IR (KBr) 1768, 1712 (CO), 1252, and 845 cm^{-1} (TMS); ^{1}H-NMR ($CDCl_3$) δ=0.15 (9H, s, Me_3Si), 4.66 (1H, s, CH), 7.08—7.30 (5H, m, Ph), and 7.53—7.85 (4H, m, Ar); MS *m/z* (rel. intensity, %) 309 (M^+, 44) and 73 (base peak).

Found: C, 70.04; H, 6.21; N, 4.46%. Calcd for $C_{18}H_{19}NO_2Si$: C, 69.86; H, 6.12; N, 4.53%.

(α-Morpholinobenzyl)trimethylsilane 2. A mixture of (α-bromobenzyl)trimethylsilane (1.2 g, 4.9 mmol) and morpholine (1.3 g, 14.9 mmol) was heated under reflux for 6 h. After cooled to room temperature, the reaction mixture was poured into aqueous potassium hydroxide solution and extracted with ether (10 ml×2). The ether was dried and evaporated *in vacuo*. The residue was distilled on a micro distilling apparatus to give 0.932 g (76%) of **2**: Pale yellow oil; bp 210—215 °C (3325 Pa) (bulb-to-bulb); IR (neat) 1250, 858, and 841 cm^{-1} (TMS); ^{1}H-NMR ($CDCl_3$) δ=−0.09 (9H, s, Me_3Si), 2.35—2.64 (4H, m, CH_2N), 2.79 (1H, s, CH), 3.53—3.78 (4H, m, OCH_2), and 7.01—7.32 (5H, m, Ph); ^{13}C-NMR ($CDCl_3$) δ=−1.17 (q, Me_3Si), 54.82 (t, CH_2N), 66.71 (d, CH), 67.25 (t, NCH_2), 125.58, 127.96 (each d, *o*-, *m*-, and *p*-C of Ph), and 142.00 (s, 1-C of Ph); MS *m/z* (rel. intensity, %) 249 (M^+, 8) and 176 (base peak).

The elementary analysis was carried out with an authentic sample of hydrochloride of **2** (mp 211—212 °C).

Found: C, 58.87; H, 8.70; N, 4.93%. Calcd for $C_{14}H_{24}NOClSi$: C, 58.82; H, 8.46; N, 4.90%.

(α-Acetamidobenzyl)trimethylsilane 3. A mixture of **1** (8.3 g, 0.027 mol) and hydrazine hydrate (100%, 1.5 g, 0.03 mol) in ethanol (100 ml) was heated under reflux for 3 h. Concd hydrochloric acid (3 ml) was added and the resulting mixture was again refluxed for 1 h. After cooled to room temperature, the precipitate separated was removed by filtration and the filtrate was evaporated *in vacuo*. The residue was treated with water, the insoluble material was removed off by filtration, the filtrate was made alkaline with aqueous potassium hydroxide solution, and extracted with dichloromethane (25 ml×2). The dichloromethane was dried and evaporated *in vacuo*. The residue was distilled under vacuum to give 2.9 g (61%) of (α-aminobenzyl)trimethylsilane: Pale yellow oil; bp 114—117 °C (2660 Pa) (bulb-to-bulb); IR (neat) 3380 (NH), 1250, and 840 cm^{-1} (TMS); ^{1}H-NMR ($CDCl_3$) δ=0.03 (9H, s, Me_3Si), 1.56 (2H, br. s, NH_2), 3.52 (1H, s, CH), and 7.04—7.38 (5H, m, Ph); MS *m/z* (rel. intensity, %) 179 (M^+, 22), 106 (98), 105 (62), and 73 (base peak).

The elementary analysis was performed with an authentic sample of hydrochloride of the amine (mp 239—241 °C).

Found: C, 55.87; H, 8.66; N, 6.56%. Calcd for $C_{10}H_{18}NClSi$: C, 55.66; H, 8.41; N, 6.49%.

A mixture of the above amine (0.5 g, 2.8 mmol), triethylamine (0.5 ml), and acetic anhydride (0.5 ml) in dichloromethane (5 ml) was stirred overnight at room temperature and poured into water. The organic material was extracted with dichloromethane (25 ml), the dichloromethane was dried, and evaporated *in vacuo*. The residue

was chromatographed over silica gel using hexane-ethyl acetate (2:1) as an eluent to give 0.41 g (66%) of **3**: Colorless needles from benzene-hexane; mp 137.5—139 °C; IR (KBr) 3270 (NH), 1633 (CO), 1250, 865, and 840 cm^{-1} (TMS); ^{1}H-NMR ($CDCl_3$) δ=0.02 (9H, s, Me_3Si), 2.00 (3H, s, MeCO), 3.60 (1H, d, J=9.0 Hz, CH), 6.00 (1H, br. d, NH), and 6.97—7.32 (5H, m, Ph); MS m/z (rel. intensity, %) 221 (M^+, 30), 178 (20), 106 (41), 104 (19), 79 (20), 77 (21), and 73 (base peak).

Found: C, 65.29; H, 8.61; N, 6.40%. Calcd for $C_{12}H_{19}NOSi$: C, 65.10; H, 8.65; N, 6.33%.

General Procedure for the Reactions of 1 with Aldehydes. The reagents were charged in a reaction flask in the following manner: When cesium fluoride was used, a weighed quantity of cesium fluoride (1—0.1 mmol) was placed in a reaction flask and dried at 100 °C under vacuum. After it was cooled to room temperature, dry DMF (2 ml), aldehydes (1—1.4 mmol), and then **1** (1 mmol) were added. When TBAF was used as a catalyst, to a mixture of **1** (1 mmol) and aldehydes (1—1.4 mmol) in dry DMF (2 ml) was added TBAF (0.05 ml, 0.05 mmol). The resulting mixture was stirred at room temperature under nitrogen for the period of time shown in Table 1. The solvents were all evaporated to dryness under vacuum. The residue was filtered through a short column packed with silica gel using hexane-ethyl acetate (2:1) to give a mixture of two isomeric 2-aminoethanols **5a** to **5f**. The yields as well as the erythro/threo ratios were measured at this stage, the formers of which were listed in Table 1. The separation of isomers was carried out by a flash chromatography over silica gel using hexane-ethyl acetate (5:1) as an eluent.

1,2-Diphenyl-2-phthalimidoethanol **5a**. *erythro*-**5a**: Colorless leaflets from benzene-hexane; mp 184—186 °C; IR (KBr) 3523, 3469, 3425 (OH), and 1708 cm^{-1} (CO); ^{1}H-NMR ($CDCl_3$) δ=2.77 (1H, br. s, OH), 5.49 (1H, d, J_{2-1}=9.0 Hz, 2-CH), 5.92 (1H, d, J_{1-2}=9.0 Hz, 1-CH), and 7.10—7.71 (14H, m, Ph and Ar); MS m/z (rel. intensity, %) 237 (43), 236 (40), 130 (30), 104 (21), 79 (55), and 77 (base peak).

Found: C, 77.05, H; 5.06; N, 4.26%. Calcd for $C_{22}H_{17}NO_3$: C, 76.94; H, 4.99; N, 4.08%.

threo-**5a**: Colorless needles from benzene-hexane; mp 182—184 °C; IR (KBr) 3425 (OH), 1709, and 1697 cm^{-1} (CO); ^{1}H-NMR ($CDCl_3$) δ=3.29 (1H, m, OH), 5.55 (1H, d, J_{2-1}=9.0 Hz, 2-CH), 5.75—5.90 (1H, m, 1-CH), and 7.04—7.90 (14H, m, Ph and Ar); MS m/z (rel. intensity, %) 237 (17), 236 (29), 130 (26), 107 (38), 105 (32), 104 (31), 79 (74), and 77 (base peak).

Found: C, 77.17; H, 4.89; N, 4.11%. Calcd for $C_{22}H_{17}NO_3$: C, 76.94; H, 4.99; N, 4.08%.

^{13}C-NMR ($CDCl_3$) of the mixture of *erythro*-**5a** and *threo*-**5a**: δ=60.86, 62.63 (each d, 2-C), 72.60, and 73.00 (each d, 1-C).

1-(p-Methylphenyl)-2-phenyl-2-phthalimidoethanol **5b**. *erythro*-**5b**: Colorless prisms from benzene-hexane; mp 163—164 °C; IR (KBr) 3545 (OH) and 1709 cm^{-1} (CO); ^{1}H-NMR ($CDCl_3$) δ=2.21 (3H, s, Me), 2.69 (1H, d, J=2.5 Hz, OH), 5.29 (1H, d, J_{2-1}=9.0 Hz, 2-CH), 5.92 (1H, dd, J_{1-2}=9.0 and J_{1-OH}=2.5 Hz, 1-CH), and 6.91—7.74 (13H, m, Ar); MS m/z (rel. intensity, %) 357 (M^+, 5), 238 (17), 237 (base peak), 236 (19), 219 (17), 209 (12), 130 (9), 121 (14), 119 (12), 105 (19), 104 (48), and 91 (38).

Found: C, 77.39; H, 5.39; N, 3.91%. Calcd for $C_{23}H_{19}NO_3$: C, 77.29; H, 5.36; N, 3.92%.

threo-**5b**: Colorless leaflets from benzene-hexane; mp 161—162 °C; IR (KBr) 3450 (OH), 1711, and 1699 cm^{-1} (CO); ^{1}H-NMR ($CDCl_3$) δ=2.21 (3H, s, Me), 3.32 (1H, m, OH), 5.53 (1H, d, J_{2-1}=9.0 Hz, 2-CH), 5.73—5.98 (1H, m, 1-CH), and 6.88—7.82 (13H, m, Ar); MS m/z (rel. intensity, %) 357 (M^+, 4), 238 (17), 237 (base peak), 236 (23), 219 (18), 209 (13), 208 (10), 133 (11), 130 (29), 121 (18), 105 (19), 104 (46), 93 (16), and 91 (25).

Found: C, 77.33; H, 5.38; N, 3.91%. Calcd for $C_{23}H_{19}NO_3$: C, 77.29; H, 5.36; N, 3.92%.

1-(p-Methoxyphenyl)-2-phenyl-2-phthalimidoethanol **5c**. *erythro*-**5c**: Colorless prisms from benzene-hexane; mp 147.5—148.5 °C; IR (KBr) 3460 (OH), 1767, and 1705 cm^{-1}; ^{1}H-NMR ($CDCl_3$) δ=2.64 (1H, br. s, OH), 3.64 (3H, s, MeO), 5.49 (1H, d, J_{2-1}=9.3 Hz, 2-CH), 5.95 (1H, d, J_{1-2}=9.3 Hz, 1-CH), 6.65—6.85, and 7.20—7.78 (13H, m, Ar); MS m/z (rel. intensity, %) 373 (M^+, 4), 356 (13), 238 (15), 237 (89), 236 (17), 219 (22), 209 (13), 137 (base peak), 130 (18), 109 (20), 104 (24), and 94 (14).

Found: C, 74.27; H, 5.17; N, 3.86%. Calcd for $C_{23}H_{19}NO_4$: C, 73.98; H, 5.13; N, 3.75%.

threo-**5c**: Colorless leaflets from benzene-hexane; mp 151—152.5 °C; IR (KBr) 3430 (OH), 1765, and 1700 cm^{-1} (CO); ^{1}H-NMR ($CDCl_3$) δ=3.18 (1H, d, J=6.0 Hz, OH), 3.70 (3H, s, OMe), 5.55 (1H, d, J_{2-1}=8.7 Hz, 2-CH), 5.87 (1H, dd, J_{1-2}=8.7 and J_{1-OH}=6.0 Hz, 1-CH), 6.65—6.81, 7.10—7.43, and 7.56—7.85 (13 H, m, Ar); MS m/z (rel. intensity, %) 373 (M^+, 4), 238 (11), 237 (69), 236 (32), 219 (18), 209 (13), 208 (11), 152 (10), 137 (base peak), 135 (12), 133 (12), 130 (36), 109 (31), 105 (20), 104 (45), and 94 (32).

Found: C, 74.15; H, 5.21; N, 4.01%. Calcd for $C_{23}H_{19}NO_4$: C, 73.98; H, 5.13; N, 3.75%.

1-(2-Furyl)-2-phenyl-2-phthalimidoethanol **5d**. *erythro*-**5d**: Colorless prisms from benzene-hexane; mp 133—134 °C; IR (KBr) 3510 (OH), 1765, and 1708 cm^{-1} (CO); ^{1}H-NMR ($CDCl_3$) δ=2.80 (1H, d, J=4.8 Hz, OH), 5.70 (1H, d, J_{2-1}=9.3 Hz, 2-CH), 6.06 (1H, dd, J_{1-2}=9.3 and J_{1-OH}=4.8 Hz, 1-CH), 6.18 (1H, dd, J=3.6 and 2.2 Hz, 4-H of furyl), 6.31 (1H, br. d, J=3.6 Hz, 3-H of furyl), and 7.20—7.80 (10H, m, Ar and 5-H of furyl); MS m/z (rel. intensity, %) 333 (M^+, 3), 238 (17), 237 (base peak), 236 (40), 219 (14), 130 (16), 104 (16), and 77 (14).

Found: C, 72.33; H, 4.56; N, 4.38%. Calcd for $C_{20}H_{15}NO_4$: C, 72.06; H, 4.54; N, 4.20%.

threo-**5d**: Colorless prisms from benzene-hexane; mp 170—171.5 °C; IR (KBr) 3592 (OH), 1765, and 1704 cm^{-1} (CO); ^{1}H-NMR ($CDCl_3$) δ=3.40 (1H, d, J=6.8 Hz, OH), 5.78 (1H, d, J_{2-1}=8.5 Hz, 2-CH), 5.90 (1H, dd, J_{1-2}=8.5 and J_{1-OH}=6.8 Hz, 1-CH), 6.17 (2H, d, J=2.0 Hz, 3- and 4-H of furyl), and 7.13—7.90 (10H, m, Ar and 5-H of furyl); MS m/z (rel. intensity, %) 237 (50), 236 (63), 219 (12), 209 (14), 208 (14), 180 (11), 153 (17), 133 (29), 132 (13), 131 (10), 130 (88), 105 (42), 104 (base peak), 102 (25), 97 (78), and 77 (91).

Found: C, 72.26; H, 4.62; N, 4.33%. Calcd for $C_{20}H_{15}NO_4$: C, 72.06; H, 4.54; N, 4.20%.

(E)-1,4-Diphenyl-1-phthalimido-3-buten-2-ol **5e**. *erythro*-**5e**: Colorless prisms from benzene-hexane; mp 146—147 °C; IR (KBr) 3473 (OH), 1709, and 1703 cm^{-1} (CO); ^{1}H-NMR ($CDCl_3$) δ=2.10 (1H, br. s, OH), 5.33 (1H, d, J_{1-2}=8.3 Hz, 1-CH), 5.56 (1H, dd, J_{2-1}=8.3 and J_{2-3}= 6.8 Hz, 2-CH), 6.20 (1H, dd, J_{3-2}=6.8 and J_{3-4}=15.8 Hz, 3-CH=),

6.72 (1H, d, J_{4-3}=15.8 Hz, 4-CH=), and 6.90—7.88 (14H, m, Ph and Ar); MS *m/z* (rel. intensity, %) 369 (M^+, 3), 238 (12), 237 (78), 236 (base peak), 219 (12), 133 (29), 130 (38), 116 (11), 105 (19), 104 (28), 103 (12), and 77 (38).

Found: C, 79.26; H, 5.46; N, 3.57%. Calcd for $C_{24}H_{19}NO_3$+ 1/2 C_6H_6: C, 79.39; H, 5.43; N, 3.43%.

threo-**5e**: Colorless leaflets from benzene-hexane; mp 184—186 °C; IR (KBr) 3412 (OH), 1713, and 1697 cm^{-1} (CO); ^{1}H-NMR ($CDCl_3$) δ=3.20 (1H, M, OH), 5.30—5.62 (2H, m, 1- and 2-CH), 6.10 (1H, dd, J_{3-2}=5.4 and J_{3-4}= 16.0 Hz, 3-CH=), 6.68 (1H, d, J_{4-3}=16.0 Hz, 4-CH=), and 7.08—7.92 (14H, m, Ph and Ar); MS *m/z* (rel. intensity, %) 369 (M^+, 4), 238 (14), 237 (87), 236 (base peak), 219 (10), 133 (27), 130 (22), 105 (11), 104 (18), and 77 (23).

Found: C, 78.24; H, 5.26; N, 3.85%. Calcd for $C_{24}H_{19}NO_3$: C, 78.03; H, 5.18; N, 3.79%.

1-Phenyl-1-phthalimido-2-pentanol **5f**. *erythro*-**5f**: Colorless needles from benzene-hexane; mp 115.5—117 °C; IR (KBr) 3493 (OH) and 1705 cm^{-1} (CO); ^{1}H-NMR ($CDCl_3$) δ=0.73—1.05 (3H, m, Me), 1.20—1.70 (4H, m, CH_2), 2.64 (1H, br. s, OH), 4.60—4.87 (1H, m, 2-CH), 5.14 (1H, d, J_{1-2}=6.8 Hz, 1-CH), and 7.12—7.90 (9H, m, Ph and Ar); MS *m/z* (rel. intensity, %) 237 (base peak), 236 (16), 219 (17), 209 (12), 130 (10), 105 (10), 104 (26), and 77 (15).

Found: C, 73.69; H, 6.22; N, 4.55%. Calcd for $C_{19}H_{19}NO_3$: C, 73.77; H, 6.19; N, 4.53%.

threo-**5f**: Colorless needles from benzene-hexane; mp 146.5—148 °C; IR (KBr) 3529, 3490 (OH), 1707, and 1699 cm^{-1} (CO); ^{1}H-NMR ($CDCl_3$) δ=0.72—1.05 (3H, m, Me), 1.16—1.78 (4H, m, CH_2), 2.79 (1H, br. d, *J*=8.0 Hz, OH), 4.52—4.90 (1H, m, 2-CH), 5.19 (1H, d, J_{1-2}=8.7 Hz, 1-CH), and 7.10—7.90 (9H, m, Ph and Ar); MS *m/z* (rel. intensity, %) 237 (base peak), 236 (13), 219 (17), and 104 (12).

Found: C, 73.83; H, 6.28; N, 4.69%. Calcd for $C_{19}H_{19}NO_3$: C, 73.77; H, 6.19; N, 4.53%.

Reaction of **2** *with Benzaldehyde.* Cesium fluoride (152 mg, 1 mmol) was dried in a reaction flask under vacuum at 100 °C. To the falsk, after cooled to room temperature, were added dry DMF (2 ml), **2** (249 mg, 1 mmol), and then benzaldehyde (106 mg, 1 mmol). The mixture was stirred under nitrogen at room temperature for 24 h and then poured into ice-water. The products were extracted with ether (25 ml×2), the ether was dried over magnesium sulfate, and finally evaporated *in vacuo*. The residue was chromatographed over silica gel using hexane-ethyl acetate (3:1) as an eluent to give 190 mg (67%) of the erythro and threo mixture of 2-morpholino-1,2-diphenylethanol **6**, whose separation by a flash chromatography was unsuccessful. The following data were given for the mixture of *erythro*-**6** and *threo*-**6** (1:1) Colorless prisms from benzene-hexane; mp 110—118 °C; IR (KBr) 3500, 3380 (OH), 3100—2800 (CH), 1126, 882, and 712 cm^{-1}; ^{1}H-NMR ($CDCl_3$) δ=2.19—2.80 (4H, m, CH_2N), 4.32 (0.5H, d, J_{2-1}=2.5 Hz, 2-CH), 4.52 (0.5 H, d, J_{2-1}=5.2 Hz, 2-CH), 4.40—4.80 (5H, m, CH_2O and OH), 5.02 (0.5 H, d, J_{1-2}=5.2 Hz, 1-CH), 5.30 (0.5 H, d, J_{1-2}=2.5 Hz, 1-CH), and 6.80—7.38 (10H, m, Ph); ^{13}C-NMR ($CDCl_3$) δ=49.32, 51.90 (each t, CH_2N), 67.00, 67.15 (each t, CH_2O), 70.27, 71.19 (each d, 2-C), 76.46, 76.70 (each d, 1-C), 126.11, 127.28, 127.47, 129.52, 129.61, 132.59, 135.61, and 141.02; MS *m/z* (rel. intensity, %) 177 (13), 176 (base peak), 105 (12), and 91 (13).

Found: C, 76.57; H, 7.47; N, 4.98%. Calcd for $C_{18}H_{21}NO_2$: C, 76.29; H, 7.47; N, 4.94%.

Reaction of **3** *with Benzaldehyde.* To a mixture of **3** (130 mg, 0.59 mmol) and benzaldehyde (70 mg, 0.66 mmol) in dry DMF (1 ml) was added TBAF (0.6 ml, 0.6 mmol). The mixture was stirred under nitrogen at room temperature for 16 h and then poured into ice-water. The products were extracted with ether (25 ml×2), the ether was dried, and evaporated *in vacuo* to give a viscous oily material which solidified on trituration with ether-hexane. Thus obtained colorless solid was found to be the mixture of erythro and threo isomers (1:1) of 2-acetamido-1,2-diphenylethanol **7** (86 mg, 57%), which could not be separated by a flash chromatography. The following data were given for the mixture of *erythro*-**7** and *threo*-**7** (1:1): Colorless solid; IR (KBr) 3360 (OH) and 1650 cm^{-1} (CO); ^{1}H-NMR ($CDCl_3$) δ=1.89, 1.95 (each 0.5×3H, s, COMe), 3.19 (1H, br. s, OH), 4.85—5.30 (2H, m, 1- and 2-CH), 6.42 (1H, br. s, NH), and 6.88—7.32 (10H, m, Ph); MS *m/z* (rel. intensity, %) 149 (83), 148 (18), 107 (22), 106 (base peak), 104 (10), 79 (27), and 77 (25).

Found: C, 75.24; H, 6.73; N, 5.49%. Calcd for $C_{16}H_{17}NO_2$: C, 75.26; H, 6.71; N, 5.49%.

General Procedure for the Reactions of **4** *with Aldehydes.* To a mixture of **4** (1 mmol) and aldehydes (1.5 mmol) in dry DMF (1 ml) was added TBAF (0.05ml, 0.05 mmol) by use of a syringe. The mixture was heated at 100 °C under nitrogen for the time period shown in Table 1 and cooled to room temperature. Another portion of TBAF (0.05 ml) was added and this mixture was again heated under the conditions listed in Table 1. After cooled to room temperature, ice-cold water was added to the mixture which was then extracted with ether (25 ml×2), the ether was dried, and evaporated *in vacuo*. The residue obtained was dissolved in benzene (5 ml) to separate the precipitation of *N*-benzylphthalimide **10** which was filtered off. The filtrate was condensed *in vacuo* and chromatographed over silica gel using hexane-ethyl acetate (2:1) to give 1-substituted 2-phthalimidoethanol **8a** to **8g**. The yields of **8** as well as **10** are listed in Table 1.

1-Phenyl-2-phthalimidoethanol **8a**: Colorless leaflets from benzene-hexane; mp 166—168 °C (lit,[16] mp 164—165 °C); IR (KBr) 3467 (OH) and 1701 cm^{-1} (CO); ^{1}H-NMR ($CDCl_3$) δ=2.92 (1H, d, *J*=5.1 Hz, OH), 3.89 (1H, dd, J_{2-1}=5.0 and J_{gem}=14.0 Hz, one of 2-CH_2), 4.05 (1H, dd, J_{2-1}=7.1 and J_{gem}=14.0 Hz, the other of 2-CH_2), 5.04 (1H, ddd, J_{1-2}=5.0, 7.1 and J_{1-OH}=5.1 Hz, 1-CH), and 7.20—7.92 (9H, m, Ph and Ar).

1-(p-Methylphenyl)-2-phthalimidoethanol **8b**: Colorless needles from benzene-hexane; mp 155—156.5 °C; IR (KBr) 3379 (OH), 1768 and 1711 cm^{-1} (CO); ^{1}H-NMR ($CDCl_3$) δ=2.33 (3H, s, Me), 2.82 (1H, d, *J*=5.0 Hz, OH), 3.85 (1H, dd, J_{2-1}=5.0 and J_{gem}=14.0 Hz, one of 2-CH_2), 4.02 (1H dd, J_{2-1}=7.5 and J_{gem}=14.0 Hz, the other of 2-CH_2), 5.02 (1H, dt, J_{1-2}=5.0, 7.5 and J_{1-OH}=5.0 Hz, 1-CH), 7.04—7.40, and 7.60—7.92 (each 4H, m, Ar); MS *m/z* (rel. intensity, %) 281 (M^+, 7), 190 (15), 162 (15), 161 (base peak), 160 (14), 133 (10), 121 (28), 117 (15), 105 (13), 104 (19), and 91 (15).

Found: C, 72.75; H, 5.46; N, 5.06%. Calcd for $C_{17}H_{15}NO_3$: C, 72.58; H, 5.38; N, 4.98%.

1-(p-Methoxyphenyl)-2-phthalimidoethanol **8c**: Colorless leaflets from benzene-hexane; mp 172—174 °C; IR (KBr) 3470 (OH), 1770, and 1695 cm^{-1} (CO); ^{1}H-NMR ($CDCl_3$)

δ=2.77 (1H, d, J=5.0 Hz, OH), 3.78 (3 H, s, OMe), 3.86 (1H, dd, J_{2-1}=5.0 and J_{gem}=14.5 Hz, one of 2-CH_2), 4.03 (1H, dd, J_{2-1}=7.6 and J_{gem}=14.5 Hz, the other of 2-CH_2), 6.02 (1H, dt, J_{1-2}=5.0, 7.6 and J_{1-OH}=5.0 Hz, 1-CH), 6.85, 7.36 (each 2H, d, J=9.5 Hz, p-$MeOC_6H_4$), and 7.63—7.90 (4H, m, Ar); MS m/z (rel. intensity, %) 297 (M^+, 4), 161 (18), 160 (68), 137 (base peak), 135 (17), 133 (18), 117 (18), 109 (60), 105 (24), 104 (34), and 94 (46).

Found: C, 68.88; H, 5.16; N, 4.96%. Calcd for $C_{17}H_{15}NO_4$: C, 68.68; H, 5.09; N, 4.71%.

1-(2-Furyl)-2-phthalimidoethanol ***8d***: Colorless prisms from benzene-hexane; mp 86—87 °C; IR (KBr) 3400 (OH), 1775, and 1708 cm^{-1} (CO); ^{1}H-NMR ($CDCl_3$) δ=2.80 (1H, d, J=7.0 Hz, OH), 4.00 (1H, dd, J_{2-1}=5.3 and J_{gem}=14.2 Hz, one of 2-CH_2), 4.18 (1H, dd, J_{2-1}=7.6 and J_{gem}=14.2 Hz, the other of 2-CH_2), 5.05 (1H, ddd, J_{1-2}=5.3, 7.6 and J_{1-OH}=7.0 Hz, 1-CH), 6.32 (2H, m, 3- and 4-H of furyl), 7.37 (1H, dd, J=1.8 and 1.2 Hz, 5-H of furyl), and 7.62—7.95 (4H, m, Ar); MS m/z (rel. intensity, %) 257 (M^+, 13), 162 (13), 161 (base peak), 160 (50), 133 (43), 132 (23), 117 (42), 110 (83), 105 (29), 104 (48), and 97 (84).

Found: C, 65.16; H, 4.51; N, 5.62%. Calcd for $C_{14}H_{11}NO_4$: C, 65.36; H, 4.31; N, 5.45%.

(E)-4-Phenyl-1-phthalimido-3-buten-2-ol ***8e***: Pale yellow needles from benzene-hexane; mp 184—186 °C; IR (KBr) 3454 (OH) and 1701 cm^{-1} (CO); ^{1}H-NMR ($CDCl_3$) δ=2.63 (1H, d, J=5.3 Hz, OH), 3.91 (2H, d, J_{1-2}=5.8 Hz, 1-CH_2), 4.65 (1H, dddt, J_{2-1}=5.8, J_{2-3}=6.0, J_{2-OH}=5.3, and J_{2-4}=1.2 Hz, 2-CH), 6.21 (1H, dd, J_{3-2}=6.0 and J_{3-4}=15.8 Hz, 3-CH), 6.68 (1H, dd, J_{4-3}=15.8 and J_{4-2}=1.2 Hz, 4-H), 7.10—7.42 (5H, m, Ph), and 7.58—7.92 (4H, m, Ar); MS m/z (rel. intensity, %) 293 (M^+, 12) 161 (34), 160 (20), 146 (24), 134 (12), 133 (base peak), 115 (14), 105 (12), 104 (12), and 77 (22).

Found: C, 73.56; H, 5.18; N, 4.93%. Calcd for $C_{18}H_{15}NO_3$: C, 73.70; H, 5.16; N, 4.78%.

1-Phthalimido-2-pentanol ***8f***: Colorless prisms from benzene-hexane; mp 86—87.5 °C; IR (KBr) 3508 (OH), 1774, and 1711 cm^{-1} (CO); ^{1}H-NMR ($CDCl_3$) δ=0.76—1.08 (3H, m, Me), 1.21—1.70 (4H, m, 3- and 4-CH_2), 2.52 (1H, br. s, OH), 3.61—4.02 (3H, m, 1-CH_2 and 2-CH), and 7.48—7.83 (4H, m, Ar); MS m/z (rel. intensity, %) 233 (M^+, 2), 190 (14), 162 (11), 161 (base peak), 160 (22), 133 (30), 132 (15), 117 (30), 105 (33), 104 (46), and 77 (36).

Found: C, 67.08; H, 6.39; N, 6.14%. Calcd for $C_{13}H_{15}NO_3$: C, 66.93; H, 6.48; N, 6.00%.

3,3-Dimethyl-1-phthalimido-2-butanol ***8g***: Colorless needles from benzene-hexane; mp 94-95.5 °C; IR (KBr) 3400 (OH), 1770, and 1713 cm^{-1} (OH); ^{1}H-NMR ($CDCl_3$) δ=1.01 (9H, s, Me), 2.47 (1H, d, J=5.8 Hz, OH), 3.46—4.02 (3H, m, 1-CH_2 and 2-CH), and 7.62—7.90 (4H, m, Ar); MS m/z (rel. intensity, %) 247 (M^+, 1), 190 (58), 162 (14), 161 (base peak), 160 (20), 133 (23), 132 (13), 104 (25), and 77 (23).

Found: C, 68.02; H, 6.93; N, 5.78%. Calcd for $C_{14}H_{17}NO_3$: C, 67.99; H, 6.93; N, 5.66%.

General Procedure for the Hydrazinolysis of 5 and 8. A mixture of **5** or **8** (1 mmol) and hydrazine hydrate (100%, 1.5 mmol) in 4 ml of ethanol was heated unnder reflux for a few hours. After a slight excess of concd hydrochloric acid was added, the resulting mixture was again heated under reflux for 0.5 h and then cooled to room temperature. The precipitate separated was filtered off and the filtrate was evaporated *in vacuo*. The residue was dissolved in water (5 ml) to separate some insoluble material which was removed by filtration. Evaporation of the filtrate *in vacuo* gave the hydrochloride of 2-aminoethanols (*erythro*-**12**, *threo*-**12**, **13**, and **15**). Treatment of the filtrate with aqueous potassium hydroxide afforded the free bases (*erythro*-**11**, *threo*-**11**, and **14**). The reaction times and the yields were listed in Table 3.

Identification of the products was accomplished by the comparison of the melting points with those of authentic samples or on the basis of the spectral data of 2-oxazoline derivatives.

erythro-*2-Amino-1,2-diphenylethanol.* erythro-***11***: Colorless needles from ethanol; mp 166.5—168 °C (lit,[17] mp 163 °C); IR (KBr) 3365 and 3298 cm^{-1} (NH and OH); ^{1}H-NMR ($CDCl_3$) δ=1.70 (3H, br. s, NH_2 and OH), 4.15 (1H, d, J_{1-2}=6.2 Hz, 1-H), 4.73 (1H, d, J_{2-1}=6.2 Hz, 2-H), and 7.05—7.20 (10H, m, Ph).

threo-*2-Amino-1,2-diphenylethanol.* threo-***11***: Colorless needles from benzene-hexane; mp 129—131 °C (lit,[17] mp 129 °C); IR (KBr) 3363, 3302, and 3159 cm^{-1} (NH and OH); ^{1}H-NMR ($CDCl_3$) δ=2.00 (3H, br. s, NH_2 and OH), 3.97 (1H, d, J_{1-2}=6.5 Hz, 1-H), 4.63 (1H, d, J_{2-1}=6.5 Hz, 2-H), and 7.00—7.30 (10H, m, Ph).

2-Amino-1-phenylethanol Hydrochloride ***13***: Colorless prisms from ethanol-ether; mp 179—181 °C (lit,[18] mp 176—177 °C); IR (KBr) 3350 and 3000 cm^{-1} (NH and OH); ^{1}H-NMR (DMSO-d_6) δ=2.86 (2H, br. s, CH_2), 4.30 (1H, br. s, OH), 4.63—4.92 (1H, m, 1-H), 7.21 (5H, br. s, Ph), and 8.15 (3H, br. s, NH_3^+).

(E)-1-Amino-4-phenyl-3-buten-2-ol ***14***: This compound **14** was converted into the oxalate whose appearance and melting point are given as follows: colorless prisms from ethanol; mp 235—238 °C (lit,[19] mp 238 °C). The IR and ^{1}H-NMR spectral data are shown for the free base: IR (KBr) 3360 cm^{-1} (NH and OH); ^{1}H-NMR ($CDCl_3$) δ=2.67 (5H, br. s, $C\underline{H}_2N\underline{H}_2$ and OH), 3.95—4.28 (1H, m, 2-H), 6.02 (1H, dd, J_{3-2}=6.0 and J_{3-4}=15.0 Hz, 3-H), 6.50 (1H, d, J_{4-3}=15.0 Hz, 4-H), and 6.95—7.40 (5H, m, Ph).

1-Amino-2-pentanol Hydrochloride ***15***: This compound **15** was converted into 1-benzamido-2-pentanol by the reaction of **15** with benzoyl chloride in the presence of triethylamine. The following data are for the *N*-benzoyl derivative. Colorless leaflets from benzene; mp 111—113 °C (lit,[20] mp 112—113.5 °C); IR (KBr) 3373, 3329 (NH and OH), and 1633 cm^{-1} (CO); ^{1}H-NMR ($CDCl_3$) δ=0.80—1.08 (3H, m, Me), 1.22—1.64 (4H, m, 3- and 4-CH_2), 2.65 (1H, d, J_{OH-2}=4.7 Hz, OH), 3.25 (1H, ddd, J_{1-NH}=4.8, J_{1-2}=8.0, and J_{gem}=13.8 Hz, one of 1-H), 3.70 (1H, ddd, J_{1-NH}=6.5, J_{1-2}=2.7, and J_{gem}=13.8 Hz, the other of 1-H), 3.70—3.95 (1H, m, 2-H), 6.66 (1H, br. s, NH), and 7.26—7.84 (5H, m, Ph).

cis-*2,4-Diphenyl-5-propyl-2-oxazoline* ***16***: The hydrochloride *erythro*-**12** which was obtained according to the general procedure described above was converted into **16** by the following reaction. A mixture of *erythro*-**12** (38 mg, (0.18mmol) and ethyl benzimidate[21] (70 mg, 0.46 mmol) was heated under reflux in 1,2-dichloroethane (5 ml) for 24 h. After cooled to room temperature, the mixture was washed with water twice and the organic layer was dried over magnesium sulfate. The residue which was given by the evaporation of the solution was chromatographed over silica gel using hexane-ethyl acetate (5:1) as an eluent. Colorless oil of **16** (46 mg, 94%) gave the following spectral

data: IR (neat) 1647 cm^{-1} (C=N); ^{1}H-NMR ($CDCl_3$) δ=0.83 (3H, t, J=7.0 Hz, Me), 0.90—1.68 (4H, m, $MeCH_2CH_2$), 4.88 (1H, ddd, J_{5-4}=9.7, J_{5-CH_2}=4.3, and J_{5-CH_2}=9.7 Hz, 5-H), 5.20 (1H, d, J_{4-5}=9.7 Hz, 4-H), and 7.06—7.92 (10H, m, Ph); MS m/z (rel. intensity, %) 265 (M^+, 4), 194 (19), 193 (base peak), 90 (18), 89 (17), and 77 (11).

Found: m/z 265.1466. Calcd for $C_{18}H_{19}NO$: M, 265.1466.

trans-*2,4-Diphenyl-5-propyl-2-oxazoline* **17**: According to the similar procedure mentioned above, colorless oil of **17** was obtained in 92% yield: IR (neat) 1647 cm^{-1} (C=N); ^{1}H-NMR ($CDCl_3$) δ=0.98 (3H, t, J=7.0 Hz, Me), 1.30—2.03 (4H, m, $MeCH_2CH_2$), 4.48 (1H, ddd, J_{5-4}=7.2, J_{5-CH_2}=5.1, and J_{5-CH_2}=7.2 Hz, 5-H), 4.88 (1H, d, J_{4-5}=7.2 Hz, 4-H), and 7.15—8.12 (10H, m, Ph); MS m/z (rel. intensity, %) 265 (M^+, 9), 194 (14), and 193 (base peak).

Found: C, 81.69; H, 7.29; N, 5.52%. Calcd for $C_{18}H_{19}NO$: C, 81.47; H 7.22; N, 5.28%.

References

1) A. I. Shatenshtein and H. A. Gvozdeva, *Tetrahedron*, **25**, 2749 (1969).

2) Recent reviews on α-amino carbanions: D. Seebach, *Angew. Chem.*, **91**, 259 (1979); A. Krief, *Tetrahedron*, **36**, 2531 (1980); J.-F. Biellmann and J.-B. Bucep, *Org. React.*, **27**, 1 (1982).

3) Reviews on dipole-stabilized α-amino carbanions: D. Seebach and D. Enders, *Angew. Chem.*, **87**, 1 (1975); P. Beak and D. B. Reitz, *Chem. Rev.*, **78**, 275 (1978).

4) Related papers published later than 1980: W. Lubosch and D. Seebach, *Helv. Chim. Acta*, **63**, 102 (1980); W. Wykypiel and D. Seebach, *Tetrahedron Lett.*, **21**, 1927 (1980); A. I. Meyers and W. T. Hoeve, *J. Am. Chem. Soc.*, **102**, 7125 (1980); D. Seebach and M. Yoshifuji, *Helv. Chim. Acta*, **64**, 643 (1981); W. Wykypiel, J.-J. Lohmann, and D. Seebach, *ibid.*, **64**, 1337 (1981); N. G. Rodan, K. N. Houk, P. Beak, W. J. Zajdel, J. Chandrasekhar, and P. von R. Schleyer, *J. Org. Chem.*, **46**, 4108 (1981); D. B. Reitz, P. Beak, and A. Tse, *ibid.*, **46**, 4317 (1981); A. I. Meyers, S. Hellring, and W. T. Hoeve, *Tetrahedron Lett.*, **22**, 5115 (1981); A. I. Meyers and S. Hellring, *ibid.*, **22**, 5119 (1981); A. I. Meyers and G. E. Jagdmann Jr., *J. Am. Chem. Soc.*, **104**, 877 (1982); A. I. Meyers and S. Hellring, *J. Org. Chem.*, **47**, 2229 (1982); A. I. Meyers and L. M. Fuentes, *J. Am. Chem. Soc.*, **105**, 117 (1983); M. Al-Asser, P. Beak, D. Hay, D. J. Kempf, S. Mills, and S. G. Smith, *ibid.*, **105**, 2080 (1983); A. I. Meyers, W. F. Rieker, and L. M. Fuentes, *ibid.*, **105**, 2082 (1983); P. D. Edwards and A. I. Meyers, *Tetrahedron Lett.*, **25**, 939 (1984); P. Beak and W. J. Zajdel, *J. Am. Chem. Soc.*, **106**, 1010 (1984); A. I. Meyers, L. M. Fuentes, and Y. Kubota, *Tetrahedron*, **40**, 1361 (1984); A. I. Meyers, P. D. Edwards, W. F. Rieker, and T. R. Bailey, *J. Am. Chem. Soc.*, **106**, 3270 (1984).

5) Reviews on resonance-stabilized α-amino carbanions: U. Schöllkopf, *Angew. Chem.*, **82**, 795 (1970); Th. Kauffmann, *ibid.*, **86**, 715 (1974); D. Hoppe, *ibid.*, **86**, 878 (1974); U. Schöllkopf, *ibid.*, **89**, 351 (1977).

6) Related papers published later than 1980: D. Stafforst and U. Schöllkopf, *Justus Liebigs Ann. Chem.*, **1980**, 28; R. Grigg, J. Kemp, J. Malone, and A. Tangthongkum, *J. Chem. Soc., Chem. Commun.*, **1980**, 648; D. Hoppe and L. Beckmann, *Justus Liebigs Ann. Chem.*, **1980**, 1751; D. Hoppe, R. Follmann, and L. Beckmann, *ibid.*, **1980**, 1765; P. Bey and J. P. Vevert, *J. Org. Chem.*, **45**, 3249 (1980); L. Casella, M. Gullotti, and E. Melani, *J. Chem. Soc., Perkin Trans. 1*, **1982**, 1827.

7) D. J. Peterson, *J. Am. Chem. Soc.*, **93**, 4027 (1971); D. J. Peterson and J. F. Ward, *J. Organomet. Chem.*, **66**, 209 (1974).

8) Generation of a nonstabilized α-amino carbanion by deprotonation with a strong base (*s*-BuLi and *t*-BuOK): H. Ahlbrecht and H. Dollinger, *Tetrahedron Lett.*, **25**, 1353 (1984).

9) It is known that the deprotonation of *N,N*-dialkylbenzylamines with butyllithium occurs at the ortho position of the phenyl ring (F. N. Jones, R. L. Vaulx, and C. R. Hauser, *J. Org. Chem.*, **28**, 3461 (1963); W. H. Puterbaugh and C. R. Hauser, *ibid.*, **28**, 3465 (1963)).

10) O. Tsuge, S. Kanemasa, H. Nagahama, and J. Tanaka, *Chem. Lett.*, **1984**, 1803.

11) C. R. Hauser and C. R. Hance, *J. Am. Chem. Soc.*, **74**, 5091 (1952).

12) B. Banhidai and U. Schöllkopf, *Angew. Chem., Int. Ed Engl.*, **12**, 836 (1973); U. Schöllkopf and H. Beckhaus, *ibid.*, **15**, 293 (1976); R. R. Fraser and P. R. Hubert, *Can. J. Chem.*, **52**, 185 (1974); K. Smith and K. Swaminathan, *J. Chem. Soc., Chem. Commun.*, **1976**, 387.

13) W. S. Johnson and E. N. Schubert, *J. Am. Chem. Soc.*, **72**, 2187 (1950).

14) D. Tzeng and W. P. Weber, *J. Org. Chem.*, **46**, 265 (1981).

15) L. H. Sommer and J. Rockett, *J. Am. Chem. Soc.*, **73**, 5130 (1951).

16) A. Terada, *Nippon Kagaku Zasshi*, **77**, 1265 (1956).

17) J. Weijlard, K. Pfister III, E. F. Swanezy, C. A. Robinson, and M. Tishler, *J. Am. Chem. Soc.*, **73**, 1216 (1951).

18) A. Dornow and H. Eichholtz, *Chem. Ber.*, **86**, 384 (1953).

19) S. Kanao, *Yakugaku Zasshi*, **50**, 911 (1930).

20) G. Fort and A. McLean, *J. Chem. Soc.*, **1948**, 1907.

21) Prepared according to the method of Dox (A. W. Dox, *Org. Syn.*, Coll. Vol. **I**, 6 (1932)). See also Ref. 13.

Vibrational Analysis of Tangled Spectra. I. The Crystal Phase T←S Spectra of Acetophenone[1)]

Kenichi NAKASHIMA† and Motohiko KOYANAGI*
Department of Chemistry, Faculty of Science, Kyushu University 33, Hakozaki Higashi-ku, Fukuoka 812
(Received May 7, 1984)

The $T_{1,2}$←S_0 phosphorescence excitation spectrum of acetophenone has been observed in a crystal at 4.2 K. The observed tangled vibronic structure is a manifestation that two states of different orbital types, $^3\pi\pi^*$ and $^3n\pi^*$, lie close to each other. For the first time, the spectrum has been vibrationally analyzed in terms of the crude adiabatic Born-Oppenheimer vibronic states. The calculation is advanced *via* the following steps: (1) to assume appropriate zero-order vibronic level functions of both electronic excited states in the energy region 0—1000 cm^{-1} above the T_1 phosphorescent origin level, (2) to take into account two different perturbations of vibronic and environmental interactions, (3) to establish a secular equation with two adjustable parameters for the evaluation of the off-diagonal matrix elements, (4) to diagonalize the equation after allocating appropriate values to the parameters, (5) to simulate the T←S spectrum, (6) to compare the simulation spectrum with the observed, (7) to revise several diagonal elements and the parameters if the comparison is not satisfied, and (8) to proceed with steps (1)—(7) until the simulation spectra accord with the observed. The results establish that the lowest excited triplet state of acetophenone in the crystal is $\pi\pi^*$, and that the next one is $n\pi^*$ whose zero-order vibrationless level is postulated to lie at $\approx$400 cm^{-1} higher than $T_1^0(0)$.

Aromatic carbonyls have been very attractive for molecular spectroscopists and photochemists because of the dynamical characteristics in the excited triplet states. There are reported many thereof,[2-21)] and it has generally been accepted that the photochemical reactivity of such a molecule depends strongly upon whether its lowest triplet state is $\pi\pi^*$ or $n\pi^*$ and upon how large the energy separation is.[22,23)] For the state assignments, of course, it is still valuable to vibrationally analyze the T→S emission and, especially, the T←S absorption spectra. Such T←S spectra, however, sometimes become very tangled, reflecting a heavy overlap of different electronic transition absorptions. As regards the tangled spectra of organic molecules, Wessel and McClure have done pioneering (and beautiful) work on the $S_{1,2}$←S_0 absorption spectra of naphthalene,[24)] and their work has been developed by several theoretical investigators.[25-27)] Recently we have also been engaged in analyzing the tangled T←S spectra of benzaldehydes.[28,29)]

Concerning the phosphorescent state of acetophenone in the crystal, there exists a serious discrepancy. On the basis of the intensity of the longest wavelength band (at 382.8 nm) and on the basis of an energy correlation between this and other related molecules, Dym and Hochstrasser concluded that the lowest excited triplet state is $n\pi^*$.[30)] From a study of the polarization and Zeeman effects on the origin band, Tanimoto *et al.* also came to the same conclusion[31)] although they never rejected the alternative $\pi\pi^*$ assignment which has been suggested from a study on dynamical properties of the triplet state by Hirota *et al.*[15)] From the polarization data, on the other hand, Case and Kearns assigned the longest wavelength band as $^3L_a(\pi\pi^*)$←S_0, and the 280 cm^{-1} band as the origin of $^3U(n\pi^*)$←S_0,[32)] reversing the suggestion of Dym and Hochstrasser. A series of works on the zero field magnetic substates of acetophenone by Hirota *et al.* supported this assignment[15,16)] although environments employed were different. On the basis of a study on the phosphorescence of 1% acetophenone in acetophenone-*phenyl-d*$_5$, Koyanagi *et al.* concluded that the phosphorescent state of crystal phase acetophenone is $\pi\pi^*$.[7)] Recently, Souto and Lin have observed the phosphorescence spectra of acetophenone and its derivatives in *p*-dimethoxybenzene[33)] and suggested that the phosphorescent state is $n\pi^*$, preferring Dym and Hochstrasser's assignment[30)] to Case and Kearns'.[32)]

The purpose of this paper is to analyze this tangled spectrum both experimentally and theoretically; and to give a clearcut answer to the controversial issue. The calculation method is based on making up secular equations with many crude BO vibronic state functions. The validity of the treatment will be manifested in comparison with the observed spectra.

Theoretical

The present treatment is, in principle, very simple and essentially the same as that reported elsewhere.[28,29)] Here let us outline the major aspects and show a schematic block diagram of the calculation process (see Fig. 1).

We start with the assumptions that two excited electronic levels T_1^0 and T_2^0 lie close to each other and that there are vibronic and environmental interactions between them. For this system it is no longer

† Present address: Department of Food Science, Nishikyushu University, Kanzaki, Kanzaki-gun, Saga Prefecture 842.

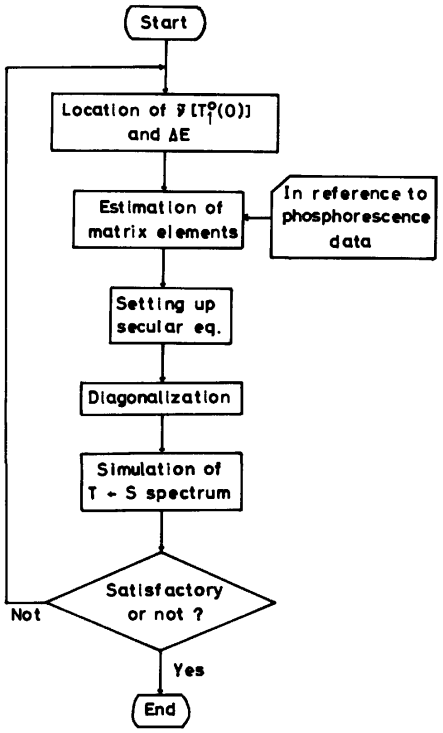

Fig. 1. Block diagram of the calculation process. ΔE is the energy separation between $T_1^0(0)$ and $T_2^0(0)$.

legitimate to use the general perturbation theory. The energies of the perturbed vibronic levels are then obtained by a direct diagonalization of the corresponding part of the energy matrix corrected to the first (or second) order, *i. e.*, by solution of the secular equation:

$$\begin{vmatrix} H_{11}-E & H_{12} & \cdots & H_{1m} & \cdots & H_{1n} \\ \cdot & H_{22}-E & \cdots & \cdot & & \cdot \\ \cdot & \cdots & \cdot & \cdots & & \cdot \\ H_{l1} & \cdots & H_{ll}-E & H_{lm} & \cdots & \cdot \\ \cdot & \cdots & \cdot & \cdots & & \cdot \\ H_{n1} & \cdots & & & & H_{nn}-E \end{vmatrix} = 0, \quad (1)$$

where

$$H_{lm} = \langle l|H_0+H'|m\rangle = \langle l|H_0|m\rangle\delta_{lm} + \langle l|H'|m\rangle(1-\delta_{lm}), \quad (2)$$

and n is the number of vibronic levels considered. H_0 is the Hamiltonian of an idealized problem which can be solved exactly, while H' is the perturbation operator, *i. e.*, vibronic and environmental interactions.

$$H' = H_{\text{vib}} + H_{\text{environment}}. \quad (3)$$

Now, we need to evaluate the matrix elements of the coupling perturbation. If there is no vibronic level degeneracy and the vibronic levels are described by a set of harmonic oscillator wavefunctions, it seems that the calculation is, in principle, straightforward. The zero-order eigenfunctions are given as the crude adiabatic wavefunctions of states T_1^0 and T_2^0. Vibronic interactions, H_{vib}, are in general described as follows:[34]

$$H_{\text{vib}} = \sum_a [\partial V(q, Q)/\partial Q_a]_0 Q_a + 1/2 \sum_a \sum_b [\partial^2 V(q, Q)/\partial Q_a \partial Q_b]_0 Q_a Q_b + \cdots = H_{\text{vib}}(q, Q). \quad (4)$$

Here Q_a and Q_b denote the ath and bth vibrational normal coordinates, respectively. On the other hand, $H_{\text{environment}}$ is given in the point-dipole approximation by[35]

$$H_{\text{environment}} = -(e^2/R_{uv}^3) \sum_r \sum_{f,s} (2Z_r z_{f,s} - X_r x_{f,s} - Y_r y_{f,s}) - (1/2)(e^2/R_{vv}^3) \sum_{f,s} \sum_{g,t} (2z_{f,s} z_{g,t} - x_{f,s} x_{g,t} - y_{f,s} y_{g,t}) = H_{\text{environment}}(q, Q; \xi_1, \Xi_1; \xi_2, \Xi_2; \cdots), \quad (5)$$

where (X_r, Y_r, Z_r) denotes the coordinates of the rth electron of the solute molecule in question, $(x_{f,s}, y_{f,s}, z_{f,s})$ the coordinates of the sth electron of the fth environmental molecule.

For the evaluation of these two types of off-diagonal matrix elements in the acetophenone crystal, we prefer empirical methods to direct calculation. One of the methods is to find other suitable guest/host systems where the energy separation between T_1^0 and T_2^0 is very large. Optical data, if obtainable, will be useful for the evaluation of H_{lm} ($l \neq m$). If there is found no suitable guest/host system, another method is to utilize the spectral data of emissions which originate at the levels in "off-resonance region" and to take several practical assumptions. In the present work we employed this approach because of a failure in finding a suitable host system.

As shown in Eq. 5, $H_{\text{environment}}$ contains a number of solvent (environment) coordinates (ξ_f, Ξ_f) together with the guest molecular coordinates (q, Q). However, we treat this as an "averaged, static" perturbation on the "guest" molecule in question. In other words, we still consider the condensed phase problem in terms of the modulated electronic structure of the one guest molecule:

$$H_{\text{environment}} = H_{\text{environment}}(q, Q) \quad (6)$$

Similar treatments were reported elesewhere.[35,36] This type of perturbation may generally be taken into account for the spectra of molecules in

condensed media with poor site symmetry, and will allow the electrostatic couplings between intramolecular electronic states,[35,37] *e. g.*, direct couplings between T_1 and T_2 zero-point levels of aromatic carbonyls in rigid crystals as has been suggested by Hirota *et al.*[15-17] and Koyanagi *et al.*[38]

Several calculations were carried out for the following two cases: (1) $T_1={}^3\pi\pi^*$ and $T_2={}^3n\pi^*$; and (2) $T_1={}^3n\pi^*$ and $T_2={}^3\pi\pi^*$. Here, let us describe the detailed calculation method for case (1). Similar calculations are possible for case (2) (see the last subsection in "Results and Discussion"). For case (1) the secular determinant was made up using thirty-six crude adiabatic Born-Oppenheimer product functions, of which twenty-seven concern the $T_1(\pi\pi^*)$ electronic state and the others the $T_2(n\pi^*)$ state. For the $T_1(\pi\pi^*)$ state, we took into account eleven nontotally symmetric vibrations with low frequencies, *i. e.*, ν_{45}—ν_{35}; three phosphorescence-active totally symmetric vibrations, *i.e.*, ν_{30}, ν_{29}, ν_{27}, and their combination vibrations.[39] The zero-order vibronic levels of $T_2(n\pi^*)$, are the vibrationless level, three in-plane vibrations (ν_{30}, ν_{29}, ν_{27}), and five low frequency out-of-plane vibrations (ν_{45}—ν_{41}). Several important vibrational modes are listed in Table 1.

Vibronic interaction matrix elements are given assuming Herzberg-Teller couplings.

$$\begin{aligned}&\langle T_1^0(0+\nu_i)|H_{vib}|T_2^0(0+\nu_j)\rangle_{(i\neq j)}\\&=\langle {}^3\pi\pi^*|(\partial V/\partial Q_i)_0|{}^3n\pi^*\rangle\langle i_1|Q_i|i_2\rangle\langle j_1|j_2\rangle\prod_{k\neq i,j}\langle k_1|k_2\rangle\\&+\langle {}^3\pi\pi^*|(\partial V/\partial Q_j)_0|{}^3n\pi^*\rangle\langle j_1|Q_j|j_2\rangle\langle i_1|i_2\rangle\prod_{k\neq i,j}\langle k_1|k_2\rangle\\&=\langle T_1^0(0+\nu_j)|H_{vib}|T_2^0(0+\nu_i)\rangle.\end{aligned}\tag{7}$$

Here $|T_1^0(0+\nu_i)\rangle$, for example, is the eigenstate function for the ν_i vibronic level of $T_1^0(\pi\pi^*)$ and $|k_2\rangle$ is that for the k-normal mode of $T_2^0(n\pi^*)$. The integrals, $\langle i_1|Q_i|i_2\rangle$ and $\langle j_1|Q_j|j_2\rangle$, yield a number of zero-valued matrix elements on the assumption of a set of harmonic oscillators. The overlap integrals, *e. g.*, $\langle i_1|i_2\rangle$ and $\langle j_1|j_2\rangle$, are related to the Franck-Condon factor in the transition $T_2\leftarrow T_1$ (and that in the transition $T_2\leftarrow S_0$ if the molecular structure is assumed to be identical both in the ground and first excited ${}^3\pi\pi^*$ state). The first order perturbation theory for a [weak vibronic coupling/large ΔE] system gives

$$\langle T_1^0(0+\nu_i)|H_{vib}|T_2^0(0)\rangle \propto I(i\leftarrow 0)^{1/2}\Delta E \propto I(0\rightarrow i)^{1/2}\Delta E,\tag{8}$$

where ΔE is the energy separation between $T_1^0(0)$ and $T_2^0(0)$; $I(i\leftarrow 0)$ and $I(0\rightarrow i)$ are the relative intensities of $T_1(0+\nu_i)\leftarrow S_0(0)$ absorption and $T_1(0)\rightarrow S_0(0+\nu_i)$ phosphorescence bands, respectively. Similarly,

$$\begin{aligned}&\langle T_1^0(0+\nu_i)|H_{vib}|T_2^0(0+\nu_j)\rangle_{(i_1\in a'',\ j_2\in a')}\\&\propto I(i\leftarrow 0)^{1/2}\Delta E\langle 0_1|j_2\rangle \propto I(0\rightarrow i)^{1/2}\Delta E\langle 0_1|j_2\rangle,\end{aligned}\tag{9}$$

and so on.

Table 1. A part of acetophenone ground state vibrational frequencies[a]

Mulliken numbering	Mode[b]	$\tilde{\nu}$/cm^{-1}	Designation[c]
a'' spiecies			
ν_{45}	$COCH_3$ torsion	44	a
ν_{44}	CH_3 torsion	125	b
ν_{43}	$COCH_3$ wag	234	c
ν_{42}	ν_{16a}	421	d
ν_{41}	ν_{16b}	471	e
ν_{40}	ν_4	634	f
ν_{39}	ν_{10b}	692	g
ν_{38}	ν_{11}	768	h
ν_{37}	ν_{10a}	847	i
ν_{36}	ν_{17a}	945	j
a' species			
ν_{30}	δ (Ar-$COCH_3$)	204	p
ν_{29}	δ (Ar-C-C)	376	q
ν_{27}	δ (C=O)	597	r
ν_8	ν (C=O)	1684	s

a) Taken from the reported crystal data (Ref. 7). b) The Wilson notation (Ref. 47). c) Band designations for Figs. 2, 4, and 5.

Next let us write more practical assumptions. Two parameters were introduced for the evaluation of the off-diagonal matrix elements. They are f_v and F_e, where the former concerns the vibronic couplings and the latter the environmental couplings. These parameters were then refined in comparison with the simulated and observed spectra. Interaction matrix elements were evaluated from the relative intensity of the corresponding band of the $T_1\rightarrow S_0$ phosphorescence spectrum[7] on the assumption of $\langle T_1^0(0)|H'|T_2^0(0+\nu_i)\rangle=\langle T_1^0(0+\nu_i)|H'|T_2^0(0)\rangle$ (see Eq. 7 for H_{vib}-terms); where H' is given by Eq. 3. The matrix elements $\langle T_1^0(0+\nu_i)|H_{vib}|T_2^0(0)\rangle$ were given as $f_v\times$[the relative intensity of the corresponding vibronic band in the phosphorescence]$^{1/2}$ (see Eqs. 8 and 9); the matrix elements $\langle T_1^0(0+\nu_i)|H_{environment}|T_2^0(0)\rangle$ were given as $F_e\times$[Franck-Condon factor for the phosphorescence band $0\rightarrow\nu_i$]$^{1/2}$. The parameter f_v is common to all the vibronic couplings and the successive quantity in brackets is uniquely determined from the phosphorescence intensity data. This leads to a considerable reduction from a tedious labor of fixing off-diagonal terms in a trial and error method. Similar simplification was carried out for $\langle T_1^0(0+\nu_i)|H_{environment}|T_2^0(0)\rangle$ by using the other parameter F_e.

All the T←S transition intensities were assumed to originate in zero-order transition $T_2^0(n\pi^*;\ 0,0)$ and three Franck-Condon vibronic transitions, $T_2^0(0,0+\nu_{30})$, $T_2^0(0,0+\nu_{29})$, and $T_2^0(0,0+\nu_{27})$, since there has, in general, been accepted the following relation for halogen-free aromatic carbonyls:[8,41]

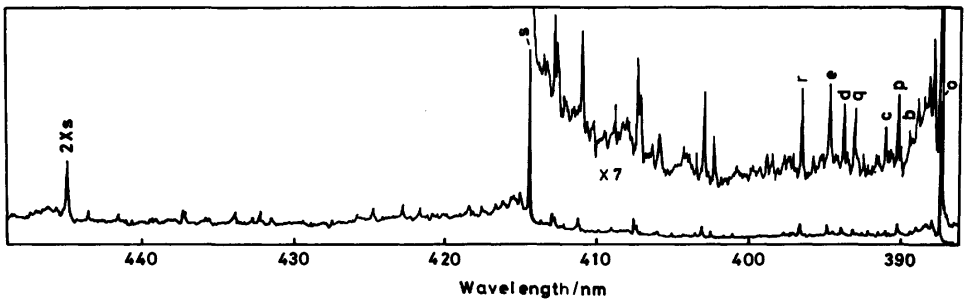

Fig. 2. Phosphorescence spectrum of $\approx 10^{-3}$ M acetophenone in *p*-dimethoxybenzene at 4.2 K. Band notations are difined in Table 1.

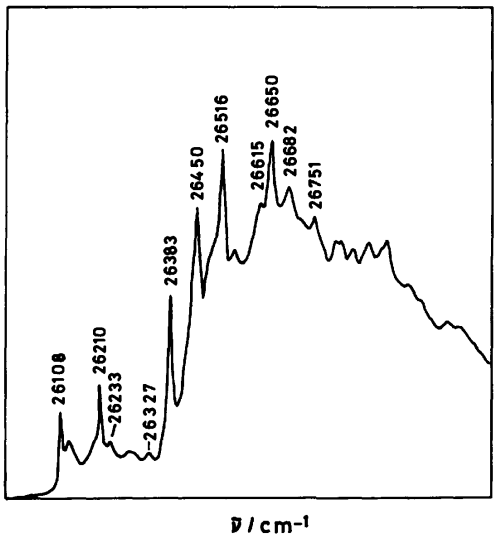

Fig. 3. $T_{1,2}\leftarrow S_0$ phosphorescence excitation spectrum of acetophenone in the crystal at 4.2 K.

$$f(^3n\pi^*\leftarrow S_0) \gg f(^3\pi\pi^*\leftarrow S_0). \quad (10)$$

Here $f(^3n\pi^*\leftarrow S_0)$ and $f(^3\pi\pi^*\leftarrow S_0)$ are the oscillator strengths of $^3n\pi^*\leftarrow S_0$ and $^3\pi\pi^*\leftarrow S_0$ transitions, respectively. The relative intensity ratios of $T_2^0(0,0)$, $T_2^0(0,0+\nu_{30})$, $T_2^0(0,0+\nu_{29})$, and $T_2^0(0,0+\nu_{27})$ were taken to be 1.000, 0.072, 0.051, and 0.086, respectively, as consulting the $T_1(n\pi^*)\rightarrow S_0$ phosphorescence spectrum of acetophenone in *p*-dimethoxybenzene at 4.2 K (Fig. 2).

For the evaluation of the diagonal matrix elements of $T_1^0(0+\nu_i)$, we started off with the same vibrational frequencies as those of the ground state (in other words, we assume almost the same molecular geometry of acetophenone in $^3\pi\pi^*$ as that in S_0),[7] while somewhat different values for the diagonal matrix elements of $T_2^0(0+\nu_i)$ in reference to the $^1n\pi^*\leftarrow S_0$ transition vibrational data in *p*-dimethoxybenzene. The two parameters f_v and F_e were taken to be close to the values employed for the benzaldehyde T←S spectra in acetophenone and methyl benzoate[28] (*e.g.*, f_v=55.0 cm^{-1} and F_e=50.0 cm^{-1} for benzaldehyde in acetophenone).

Each absorption band was assumed to be of a lorentzian with a 10 cm^{-1} full width at half maximum. Any interactions among intra- and intermolecular vibrations were ignored.

Experimental

Acetophenone (Aldrich and Wako Pure Chemical Co., Ltd.) was repeatedly distilled in vacuum. *p*-Dimethoxybenzene (Wako Pure Chemical Co., Ltd.) was purified by vacuum sublimation followed by zone-refining.

The T←S phosphorescence excitation spectrum of acetophenone was observed using crystal samples in which a small amount of benzaldehyde was doped as an effective phosphorescence emitter. The $T_1\rightarrow S_0$ phosphorescence and $S_1\leftarrow S_0$ excitation spectra of acetophenone were also studied at 4.2 K in *p*-dimethoxybenzene single crystals which were prepared by the conventional Bridgman technique (the initial concentration of acetophenone: $\approx 10^{-3}$ M). All the spectra were recorded on a 3/4 m Nalumi Spectrophotometer. Other experimental details were similar to those described previously.[42]

Results and Discussion

Phosphorescence Spectrum of Acetophenone. The phosphorescence spectrum of acetophenone in *p*-dimethoxybenzene at 4.2 K is shown in Fig. 2. The phosphorescent state of acetophenone in *p*-dimethoxybenzene has been assigned to be $n\pi^*$ by Souto and Lin.[33] We confirmed this. However, their vibrational assignment is considerably different from available normal-coordinate analysis data[7,43] and therefore seems to be erroneous especially for several out-of-plane vibrational modes. The present vibrational analysis is essentially based on the data by Koyanagi *et al.*[7] The results are shown in Fig. 2 together with alphabetical band designations whose vibrational notations are given in Table 1. Despite the propose $T_1=^3n\pi^*$ assignment,[33] it is noticeable that there appear several out-of-plane vibrational bands which are weak, but discriminating (see bands *b*—*e* in Fig. 2).

T←S Spectrum of Acetophenone in the Crystal. The T←S excitation spectrum of acetophenone in the crystal is shown in Fig. 3. Sample crystals were prepared to contain $\approx 10^{-3}$ M benzaldehyde since the dopant has been established to be an excellent triplet acceptor in the host.[6] The concentration ratios employed prove that the T←S absorption of the guest is weak enough on the present experimental conditions. Similarity of the T←S phosphorescence excitation spectrum (Fig. 3) to the direct T←S absorption spectrum (*e. g.*, Fig.2 in Ref.31) assures this is the case.

The band at 26108±2 cm^{-1} is taken to be the origin band of the $T_1 \leftarrow S_0$ transition. This assignment is supported by the fact that the band location is in good agreement with the strong phosphorescence origin peak at 26100±2 cm^{-1} which has been observed for the system of acetophenone in acetophenone-*phenyl-d*$_5$.[7] Almost all 20—60 cm^{-1} broad band features attending each prominent peak are assigned to be due to phonons. Main prominent bands are found at 26210, 26383, 26450, 26516, and 26650 cm^{-1}. The higher energy bands become the broader.

Simulated T←S Spectra of Acetophenone in the Crystal. A diagonalization of the matrix was carried out and some parameters were refined. In Tables 2 and 3 we give the final estimates to zero-

TABLE 2. ZERO-ORDER DIAGONAL MATRIX ELEMENTS EMPLOYED[a]

Level	$\Delta\tilde{\nu}$/cm^{-1} [b]	Level	$\Delta\tilde{\nu}$/cm^{-1} [b]	Level	$\Delta\tilde{\nu}$/cm^{-1} [b]
|0>	0	|27>	590	|45*>	50
|45>	70	|40>	600	|44*>	125
|44>	90	|39>	700	|30*>	170
|30>	190	|38>	735	|43*>	195
|43>	245	|37>	835	|29*>	360
|41>	325	|36>	930	|42*>	380
|29>	360	|35>	970	|41*>	430
|42>	445	|0*>	0	|27*>	550

a) For brevity we list only the fundamental vibronic levels. The asterisked states denote the BO vibronic levels of $T_1^0(n\pi^*)$ and the others $T_1^0(\pi\pi^*)$. b) Diagonal matrix elements are calculable on the basis: $|0> \leftrightarrow 26\,150\ cm^{-1}$; $|0^*> \leftrightarrow 26\,555\ cm^{-1}$. The underlined values give the energy separation from the |0*> level.

TABLE 3. OFF-DIAGONAL MATRIX ELEMENTS EMPLOYED[a]

T_1^0	T_2^0								
	|0*>	|30*>	|29*>	|27*>	|45*>	|44*>	|43*>	|42*>	|41*>
|0>	70.00	18.55	17.50	56.42	33.24	55.34	30.68	85.00	41.56
|30>	18.55	4.92	4.64	14.95	8.81	14.66	8.13	22.52	11.01
|29>	17.50	4.64	4.37	14.10	8.31	13.83	7.67	21.25	10.39
|27>	56.42	14.95	14.10	45.47	26.79	44.60	24.73	68.51	33.50
|45>	33.24	8.81	8.31	26.79	0	0	0	0	0
|44>	55.34	14.66	13.83	44.60	0	0	0	0	0
|43>	30.68	8.13	7.67	24.73	0	0	0	0	0
|42>	85.00	22.52	21.25	68.51	0	0	0	0	0
|41>	41.56	11.01	10.39	33.50	0	0	0	0	0
|40>	30.68	8.13	7.67	24.73	0	0	0	0	0
|39>	17.00	4.50	4.25	13.70	0	0	0	0	0
|38>	30.69	8.13	7.67	24.74	0	0	0	0	0
|37>	21.67	5.74	5.42	17.47	0	0	0	0	0
|36>	25.07	6.64	6.27	20.21	0	0	0	0	0
|35>	25.07	6.64	6.27	20.21	0	0	0	0	0
|45+30>	8.50	2.25	2.13	6.85	0	0	0	0	0
|44+30>	13.86	3.67	3.46	11.17	0	0	0	0	0
|43+30>	7.65	2.03	1.91	6.17	0	0	0	0	0
|42+30>	21.25	5.63	5.31	17.13	0	0	0	0	0
|41+30>	10.37	2.75	2.59	8.36	0	0	0	0	0
|45+29>	8.50	2.25	2.13	6.85	0	0	0	0	0
|44+29>	13.60	3.60	3.40	10.96	0	0	0	0	0
|43+29>	7.65	2.03	1.91	6.17	0	0	0	0	0
|42+29>	21.25	5.63	5.31	17.13	0	0	0	0	0
|41+29>	10.37	2.75	2.59	8.36	0	0	0	0	0
|45+27>	8.50	2.25	2.13	6.85	0	0	0	0	0
|44+27>	13.60	3.60	3.40	10.96	9	0	0	0	0

a) In cm^{-1} units.

order energies and interaction values on the assumption of $T_1={}^3\pi\pi^*$.[44] Figure 4(a) shows the location of zero-order levels; and the height of the solid lines represents the relative interaction energies between $T_1^0(0+\nu_i)$ and $T_2^0(0)$ and the height of dashed lines the interactions between $T_1^0(0)$ and $T_2^0(0+\nu_i)$. The longest wavelength band at 26108 cm^{-1} in the simulated T←S spectrum is assigned to the origin band of the $T_1(\pi\pi^*)\leftarrow S_0$ transition as is confirmed by analyzing the eigenvectors given in Table 4. The corresponding state is described by a large component of $|T_1^0(0)>$ and a small part of other zero-order vibronic eigenvectors:

$$\Psi_{T_1(0)} \simeq -0.95|0> + 0.20|0^*> - 0.12|44> + 0.10|42^*>, \quad (11)$$

where $|0>$ and $|0^*>$ represent $|T_1^0(0)>$ and $|T_2^0(0)>$, respectively. There is found considerable $|0^*>$ mixing with $|0>$. This will explain why the origin band of the $T_1\leftarrow S_0$ absorption appears with remarkable intensity despite the proposed $\pi\pi^*$ assignment. The major part of the state function, however, is zero-order function $|0>$. This means that many physical properties for this state are still under the control of the zero-order function $|0>$ except for several optical properties such as the absorption band intensity, polarization, and emission lifetime. The −0.12 value of the expansion coefficient for $|44>$ seems to be due to the second-order coupling through $|0^*>$ as an intermediate level.

The observed bands at 26210 cm^{-1} and 26233 cm^{-1} are assigned as $T_1(0,0+\nu_{45})$ and $T_1(0,0+\nu_{44})$, respectively, since their corresponding state functions contain a large coefficient of either $|45>$ or $|44>$. It should, however, be noted that a considerable mixing of the other zero-order function is also found (see Table 4). These mixings possibly occur *via* second-order vibronic couplings with an intermediate state, $|0^*>$, if the relevant levels (ν_{45} and ν_{44}) are lying close to each other. It is, thus, not surprizing to see that the band $T_1(0,0+\nu_{45})$ is more intense that $T_1(0,0+\nu_{44})$ despite of the reverse magnitude relation of the employed interaction matrix elements, *i.e.*, $|<45|H'$

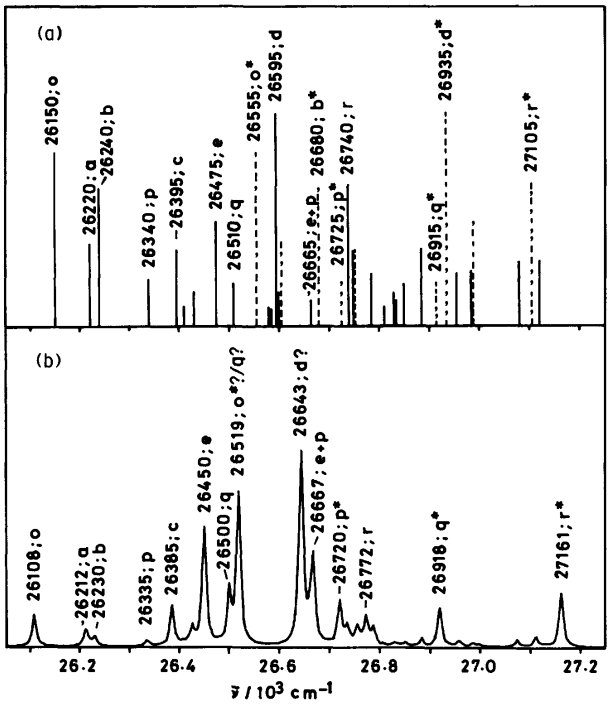

Fig. 4. (a) The zero-order vibronic levels of $T_1^0(\pi\pi^*)$ and $T_2^0(n\pi^*)$. The solid and dashed lines show the zero-order T_1^0 and T_2^0 vibronic levels, respectively. The length of each line shows the relative value of the off-diagonal matrix element between the relevant vibronic level and the zero-order vibrationless level of the counterpart electronic state. (b) Simulated $T_{1,2}\leftarrow S_0$ transition spectrum of acetophenone in the crystal. The bands are assumed to be a lorentzian, each band having a 10 cm^{-1} width.

Table 4. Vibronic eigenfunctions for representative bands of acetophenone in the crystal[a]

BO basis function	State[b] 26108 (26108)	26212 (26210)	26230 (26233)	26335 (26327)	26385 (26383)	26450 (26450)	26519 (26516)	26643 (26650)
$\|0>$	−0.946	−0.159	−0.100	−0.073	0.071	−0.097	0.063	0.086
$\|45>$	−0.081	0.892	−0.427	−0.029	0.053	−0.062	0.050	0.029
$\|44>$	−0.115	0.386	0.889	−0.060	0.101	−0.113	0.089	0.051
$\|30>$	−0.045	0.021	0.021	0.986	0.096	−0.070	0.035	0.037
$\|43>$	−0.029	0.032	0.027	0.056	−0.934	−0.233	0.110	0.046
$\|41>$	−0.031	0.030	0.025	0.031	−0.125	0.766	0.413	0.091
$\|29>$	−0.024	0.008	0.007	0.020	−0.034	0.127	0.554	0.079
$\|42>$	−0.047	0.042	0.034	0.034	−0.108	0.256	−0.516	0.643
$\|0^*>$	0.197	−0.143	−0.110	−0.083	0.220	−0.377	0.428	0.480
$\|42^*>$	0.103	0.016	0.010	−0.031	−0.009	0.003	−0.029	0.050

a) Here the expansion coefficients are shown for only the major BO functions. b) The state functions are denoted by the band energies (eigenvalues). The values in parentheses are the observed data.

$|0^*>|<|<44|H'|0^*>|$. Similarly, from the coefficient analysis, the band at 26327 cm^{-1} is attributed to $T_1(0,0+\nu_{30})$.

Next, let us view the band-crowded region which starts on the lower energy tail of the 26383 cm^{-1} band (Fig. 3). At a glance, there are four prominent bands superimposed on the broadened background: the bands at 26383, 26450, 26516, and 26650 cm^{-1}. Their corresponding state functions are approximately expressed as follows:

$$|26383> \simeq 0.22|0^*> - 0.93|43> - 0.11|42> - 0.13|41> \quad (12)$$

$$|26450> \simeq -0.38|0^*> - 0.23|43> + 0.26|42> + 0.77|41> \quad (13)$$

$$|26516> \simeq 0.43|0^*> + 0.55|29> - 0.52|42> + 0.41|41> \quad (14)$$

$$|26650> \simeq 0.48|0^*> - 0.36|27> + 0.64|42> + 0.26|44^*>. \quad (15)$$

A large mix-up in these state functions is noticeable. The states corresponding to the bands at 26383 and 26450 cm^{-1} have components large enough so that they can safely be attributed to $T_1(0,0+\nu_{43})$ and $T_1(0,0+\nu_{41})$, respectively. However, the other two states do not meet our criterion[28] for unique assignment.[46]

As shown clearly in Table 4, the vibronic state functions are canonically described by a number of crude adiabatic BO state functions and there is considerable environmental mixing between $T_1^0(\pi\pi^*)$ and $T_2^0(n\pi^*)$. The environmental mixing is more prominent in this acetophenone case than in benzaldehyde case,[28] as is rationalized by the easily detectable origin band (see band at 26108 cm^{-1} in Fig. 3).

TABLE 5. VIBRATIONAL FREQUENCIES PROPOSED FOR SEVERAL IMPORTANT MODES OF ACETOPHENONE IN THE EXCITED TRIPLET STATES[a)]

Vibration	Frequency		
	S_0	T_1	T_2
ν_{45}	44	70	50
ν_{44}	125	90	125
ν_{43}	234	245	195
ν_{42}	421	445	380
ν_{41}	471	325	430
ν_{30}	204	190	170
ν_{27}	597	590	550

a) In cm^{-1} units. For comparison, the ground state frequencies taken from the observed values (Ref. 7) were given in the second column. The other frequency values cited were taken on the basis of the present calculation.

We previously gave a CNDO description of $^3n\pi^*$ and $^3\pi\pi^*$ states for benzaldehyde.[28] Similar consideration for acetophenone predicts: (i) the π and π^* orbitals are strongly bonding and antibonding in the C=O region, respectively; (ii) the expectable change in acetyl group bond order brought about by $\pi^* \leftarrow n$ promotion leads to a large reduction in C=O stretching vibrational frequency and a small reduction in C-CH_3 vibrational frequency on going from the ground state to the $n\pi^*$ excited state; and (iii) the large increase in the C-$COCH_3$ bond order is realized consequent to $\pi^* \leftarrow \pi$ promotion, while its small increase on $\pi^* \leftarrow n$ promotion. The prediction (iii) leads us to expect ν_{45} and ν_{43} frequencies increase on going from the ground to the excited states. In Table 5 are summarized several vibrational data employed for the three electronic states. Although ν_{42} essentially belongs to the ring modes, an introduction of a methyl group to the C=O group has been known to bring forth a large mode-mixing between ω(CXO) and so-called Wilson's ν_{16a} modes.[7,47] The mode frequency increase in ν_{43} and ν_{42}, thus, seems to be rationalized to a certain extent. Another notable point in Table 5 is that ν_{41} mode drastically decreases in frequency on going from S_0 to T_1. For the present we cannot explain this.

As regards off-diagonal matrix elements, the values given previously for benzaldehyde[28] are good references. For convenience sake, let us take and compare two representative off-diagonal terms with large values. The prominent values of $\langle T_1^0|H_{\text{environment}}|T_2^0\rangle$ are 36.0, 50.0, and 70.0 cm^{-1} for benzaldehyde/methyl benzoate, benzaldehyde/acetophenone, and acetophenone crystal, respectively, while the largest vibronic interaction matrix elements are 67.5 cm^{-1} (for H-wag), 55.0 cm^{-1} (for H-wag), and 85.0 cm^{-1} (for ν_{42}).

Simulation Spectra for the Reverse Case to the $T_1=^3\pi\pi^*$ Assignment loc. cit. We carried out a series of calculations on the assumption that the lowest excited triplet state of crystal phase acetophenone is of $\pi\pi^*$. Good agreement between the observed and simulated spectra seems to establish our assignment. It is, however, necessary to refer to the results of calculations which we carried out under the reverse assignment, *i.e.*, $T_1=^3n\pi^*$ and $T_2=^3\pi\pi^*$. Figure 5 shows the simulation spectrum where only the two zero-order energies are changed into: $E[T_1^0(n\pi^*;0,0)]=26150$ cm^{-1} and $E[T_2^0(\pi\pi^*;0,0)]=26555$ cm^{-1}: and where all the other parameters are the same as those *loc. cit.*[48] It should be noted that "the spectrum is characterized by the extremely intense T_1 origin band and very weak out-of-plane vibrational bands." This character is, more or less, kept for many other ΔE values except for $|\Delta E|<$ 50 cm^{-1} where the crystal field couplings between the

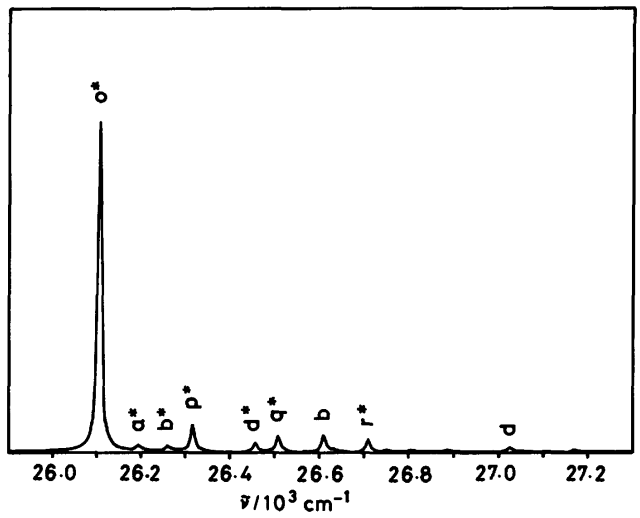

Fig. 5. Hypothetical T←S spectrum of acetophenone. Here $T_1^0 = {}^3n\pi^*$ and $T_2^0 = {}^3\pi\pi^*$ were assumed. $\Delta E = 405\ cm^{-1}$.

zero-order vibrationless levels are considerable so that there appears generally a "doublet" band structure.[50] Similar "$n\pi^*$" type band patterns have also been demonstrated for benzaldehyde T←S spectra in methylcyclohexane.[29,42] In conclusion we do not believe that T_1 is $n\pi^*$ in crystalline acetophenone.

Concluding Remarks

Two different assignments for the lowest excited triplet state of acetophenone in the crystal have been proposed.[5,7,30-32] The present treatment shows that T_1 is $\pi\pi^*$. Almost all observed T←S bands are assignable as $T_1(\pi\pi^*)$ vibronic bands which are strongly coupled with $T_2(n\pi^*)$ origin band.

Many investigators have so far searched for the $n\pi^*$-$\pi\pi^*$ criterion "measures" by which the lowest excited triplet state is discernible: *e.g.*, radiative lifetimes, deuteration shifts, zero-field splittings, spectral band patterns, Zeeman effects, Stark effects, *etc.* (for these problems, see Ref. 54). It seems, however, that there are no decisive "measures" for the criterion. We believe the present treatment could throw a light on the long-time controversial issues.

Lastly , we would like to mention phonons. We have not explicitly taken into account the role of phonon modes in the present theoretical treatment. There remains the problem of deciding whether we should take into account phonons as vibronic coupling modes or Franck-Condon modes. We will refer to this problem in the following paper.[45]

The authors acknowledge helpful discussions with Professor Donald S. McClure (Princeton University) and Professor Lionel Goodman (Rutgers University) at the earliest stage of this work on the vibronic interactions of congested electronic systems, and invaluable suggestions by referees. One of the authors (KN) wishes to express thanks to Professor R. Shimada for his warm hospitality and encouragements in Kyushu University. The calculations reported in this paper have been carried out at the Computation Center of Kyushu University.

References

1) A preliminary report of this work was presented at the National Symposium on Molecular Structure and Molecular Spectroscopy, Aug. 31-Sept. 3, 1983, Sendai, Japan.
2) Y. Kanda, H. Kaseda, and T. Matsumura, *Spectrochim. Acta*, **20**, 1387 (1964).
3) R. Shimada and L. Goodman, *J. Chem. Phys.*, **43**, 2027 (1965).
4) T. Takemura and H. Baba, *Bull. Chem. Soc. Jpn.*, **42**, 2756 (1969).
5) Y. H. Li and E. C. Lim, *Chem. Phys. Lett.*, **7**, 15 (1970).
6) M. Koyanagi and L. Goodman, *J. Chem. Phys.*, **55**, 2959 (1971).
7) M. Koyanagi, R. J. Zwarich, and L. Goodman, *J. Chem. Phys.*, **56**, 3044 (1972).
8) L. Goodman and M. Koyanagi, *Mol. Photochem.*, **4**, 369 (1972).
9) M. Koyanagi and L. Goodman, *Chem. Phys.*, **39**, 237 (1979).
10) H. Hayashi and S. Nagakura, *Mol. Phys.*, **24**, 801 (1972).
11) H. Hayashi and S. Nagakura, *Chem. Phys. Lett.*, **18**, 63 (1973).
12) H. Hayashi and S. Nagakura, *Mol. Phys.*, **27**, 969 (1974).
13) T. H. Cheng and N. Hirota, *Chem. Phys. Lett.*, **13**, 194 (1972).
14) T. H. Cheng and N. Hirota, *J. Chem. Phys.*, **56**, 5019 (1972).
15) T. H. Cheng and N. Hirota, *Mol. Phys.*, **27**, 281 (1974) and references cited therein.
16) S. W. Mao and N. Hirota, *Mol. Phys.*, **27**, 309 (1974).
17) E. T. Harrigan and N. Hirota, *Mol. Phys.*, **31**, 681 (1976).
18) Y. Hirata and N. Hirota, *Mol. Phys.*, **39**, 129 (1980).
19) E. Migirdicyan, *J. Chem. Phys.*, **55**, 1861 (1971).
20) A. Despres, V. Lejeune, and E. Migirdicyan, *Chem. Phys.*, **36**, 41 (1979).
21) A. Despres, V. Lejeune, and E. Migirdicyan, *Chem. Phys.*, **66**, 57 (1982).
22) P. Wagner, A. E. Kemppainen, and H. N. Schott, *J. Am. Chem. Soc.*, **92**, 5280 (1970).
23) P. Wagner, A. E. Kemppainen, and H. N. Schott, *J. Am. Chem. Soc.*, **95**, 5604 (1973).
24) J. Wessel, Ph. D. Thesis, University of Chicago, Chicago, 1971; J. Wessel and D. S. McClure, *Mol. Cryst. Liq. Cryst.*, **58**, 121 (1980).
25) C. A. Langhoff and G. W. Robinson, *Chem. Phys.*, **6**, 34 (1974).
26) H. K. Hong, *Chem. Phys.*, **9**, 1 (1975).
27) J. O. Berg, *Chem. Phys. Lett.*, **41**, 547 (1976).
28) M. Koyanagi, K. Nakashima, and L. Goodman,

Chem. Phys., **92**, 435 (1985). See also Ref. 24 for the theoretical backgrounds of the analysis of tangled spectra.

29) M. Koyanagi and K. Nakashima, *Chem. Phys.*, **90**, 399 (1984).

30) S. Dym and R. M. Hochstrasser, *J. Chem. Phys.*, **51**, 2458 (1969).

31) Y. Tanimoto, T. Azumi, and S. Nagakura, *Bull. Chem. Soc. Jpn.*, **48**, 136 (1975).

32) W. A. Case and D. R. Kearns, *J. Chem. Phys.*, **52**, 2175 (1970). Recently somewhat different polarization data were reported by Tanimoto *et al.* (Ref. 31).

33) M. A. Souto and C. T. Lin, *Chem. Phys.*, **17**, 129 (1976).

34) T. Azumi and K. Matsuzaki, *Photochem. Photobiol.*, **25**, 315 (1977) and references cited therein.

35) M. Koyanagi, *J. Mol. Spectrosc.*, **25**, 273 (1968).

36) G. W. Robinson, *J. Mol. Spectrosc.*, **6**, 58 (1961).

37) G. W. Robinson, *J. Chem. Phys.*, **46**, 572 (1967).

38) M. Koyanagi, K. Higashi, and Y. Kanda, *Chem. Phys. Lett.*, **52**, 184 (1977).

39) Here we employed Mulliken mode numbering (Ref. 40). See also Table 1 for Wilson notations which have been employed in Refs. 7 and 33.

40) R. S. Mulliken, *J. Chem. Phys.*, **23**, 1997 (1955).

41) S. P. McGlynn, T. Azumi, and M. Kinoshita, "Molecular Spectroscoy of the Triplet State," Prentice-Hall, Englewood Cliffs, New Jersey (1969), Chap. 6.

42) L. Goodman, M. Lamotte, and M. Koyanagi, *Chem. Phys.*, **47**, 329 (1980).

43) A. Gambi, S. Giorgianni, A. Passerini, R. Visinoni, and S. Ghersetti, *Spectrochim. Acta*, **36A**, 871 (1980).

44) To simplify the calculation, here we neglected the following type matrix elements: $\langle T_1^0(0+\nu_i)|H_{\text{environment}}|T_2^0(0+\nu_i)\rangle$, where ν_i is an out-of-plane vibrational mode. This integral, in general, leads to minor mixing between the relevant vibronic levels. The magnitude of such mixing, in many cases, is close to that of the mixing between $T_1^0(0)$ and $T_2^0(0)$. This point will be discussed in the succeeding paper (Ref. 45).

45) K. Nakashima and M. Koyanagi, *Bull. Chem. Soc. Jpn.*, the succeeding paper.

46) It is tempting to accept a suggestion that these bands are attributed to $T_1(0,0+\nu_{29})$ and $T_1(0,0+\nu_{42})$, respectively, from the component analysis. For the former, however, we have an explicit calculation band at 26500 cm^{-1} whose state function is expressed as follows:

$$|26500> \simeq 0.25|0^*> - 0.80|29> \\ -0.25|42> + 0.43|41>.$$

47) E. B. Wilson, J. C. Decius, and P. C. Cross, "Molecular Vibration" McGraw Hill, New York (1955).

48) As for off-diagonal vibronic interaction matrix elements, we employed the same values as in case (1) where $T_1={}^3\pi\pi^*$ was assumed. Even if the phosphorescence spectrum of acetophenone in acetophenone-*phenyl*-d_5 is of $n\pi^*$ nature, no big change for the vibronic interaction matrix elements $\langle {}^3n\pi^*|H_{\text{vib}}|{}^3\pi\pi^*\rangle$ will be necessary because the phosphorescence band pattern of acetophenone in acetophenone-*phenyl*-d_5 is considerably similar to that in benzoic acid reported by Nagaoka and Hirota (Ref. 49). Without doubt the phosphorescence in benzoic acid host is of $\pi\pi^*$.

49) S. Nagaoka and N. Hirota, *Bull. Chem. Soc. Jpn.*, **56**, 3381 (1983).

50) Here we completely neglected spin-orbit couplings between ${}^3n\pi^*$ and ${}^3\pi\pi^*$. This seems to be rationalized to a great extent as long as we are concerned with optical spectra in the case of $|\Delta E| > 50\ cm^{-1}$. For $|\Delta E| < 50\ cm^{-1}$, large (8—15 cm^{-1}) spin-sublevel splitting spectra have been observed because of considerable spin-orbit couplings (see Refs. 51—53).

51) H. J. Griesser and R. Bramley, *Chem. Phys.*, **67**, 361, 373, (1982).

52) M. R. Taherian and A. H. Maki, *Chem. Phys.*, **68**, 179 (1982).

53) M. Koyanagi, T. Terada, and Y. Kanda, *J. Chem. Phys.*, to be published.

54) K. Nakashima and M. Koyanagi, *Chem. Phys. Lett.*, **110**, 85 (1984).

Adsorption of Phenol on Surface-modified Carbon Black from Its Aqueous Solution. II. Influence of Surface-chemical Structure of Carbon on Adsorption of Phenol[1)]

Takeo ASAKAWA,*,† Keizo OGINO,†,†† and Kiyoshi YAMABE†††
†*Faculty of Science and Technology, Science University of Tokyo, 2641 Yamazaki, Noda 278*
††*Institute of Colloid and Interface Science, Science University of Tokyo, 1-3 Kagurazaka, Shinjuku-ku, Tokyo 162*
†††*Institute of Industrial Science, The University of Tokyo, 22-1 Roppongi 7-chome, Minato-ku, Tokyo 106*
(Received November 10, 1984)

Samples of electronic conductive carbon black (Lion Akzo Co.) were treated with nitric acid, hydrogen peroxide, dried air, or hydrogen gas. These samples had almost the same specific surface areas and pore volumes, except for the one treated with nitric acid. Phenol gas adsorption and aqueous-phase adsorption were carried out in order to study the adsorption mechanism on these treated samples. During aqueous-phase adsorption, the amount of phenol adsorbed increased with a decrease in the number of surface oxygen compounds on the carbon sample. During gas adsorption, the amount of phenol adsorbed decreased with a decrease in the number of oxygen compounds on the carbon surface. The residual amount of phenol also decreased. In the case of gas adsorption, interactions occur not only between the hydrophobic sites on the carbon and the hydrophobic groups of phenol, but also between the surface functional groups on the carbon and the hydrophilic groups of phenol. In the case of aqueous-phase adsorption, competitive adsorption of phenol with water molecules occurs. Water molecules adsorb, selectively, the surface functional groups on the carbon. Thus, the phenol adsorption due to the hydrophobic interaction on the carbon interferes with this selective adsorption.

Municipal wastewaters and industrial wastewaters, which include various organic compounds, are sources of environmental pollution. The use of solid adsorbents as a medium for removing trace quantities of organic compounds from wastewaters is useful at the time of demanding environmental restrictions and a need for the regeneration of water.[2)]

Activated carbon which has a very large surface area has usually been used for solid adsorbents during wastewater treatment.[2-12)] The carbon produced by usual methods, contains considerable amounts of oxygen chemisorbed on the surface.[13)] It seems that the adsorptive properties of such types of carbon are affected by the amount of chemisorbed oxygen. However, the influence of oxygen compounds on the carbon surfaces regarding the adsorption of organic compounds, has not been studied in detail. In this research, a special carbon black having a very large surface area was used as an adsorbent. Using this sample, four types of surface-modified carbon black were prepared. The amount of phenol adsorbed on the modified forms of carbon black was measured in the gas state and in aqueous solution. On the base of the adsorption data, we discuss the influence of the oxygen compounds on the carbon surfaces upon the adsorption of phenol.

Experimental

Materials. The carbon black used as an adsorbent was Electronic Conductive Carbon Black supplied by Lion Akzo Company, Ltd., Tokyo, Japan. The carbon black was treated with nitric acid, hydrogen peroxide, dried air, or hydrogen gas. The modifications were carried out by a method previously reported.[1)] The modification methods and the typical properties of the modified carbon black samples are shown in Fig. 1 and Table 1.

The phenol used for the adsorption experiment was a reagent grade chemical from Wako Pure Chemical Industries Company, Ltd., Tokyo, Japan, it is more than 99% pure.

Procedures. Phenol Gas Adsorption. Prior to adsorption measurements, all samples were evacuated at 120 °C for 5 h under 1.3×10^{-3} Pa. The amount of phenol adsorbed was measured gravimetrically using a Cahn RG-type electromagnetic microbalance at 25 °C and at $P/P_0=0.080$ (where P and P_0 are equilibrium and saturated pressures respectively). After the adsorption experiment, the samples were outgassed for 12 h under 1.3×10^{-3} Pa at 25 °C and the

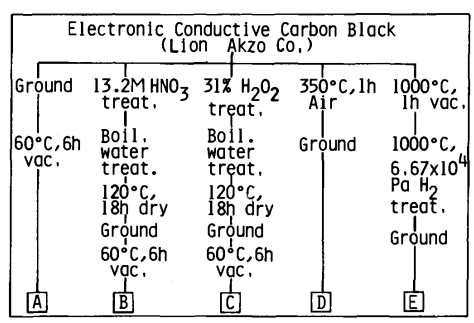

Fig. 1. Surface modifications of carbon black.

Table 1. Properties of surface modified carbon black samples

Carbon black	Surface treatment	Specific surface area[a] $m^2 g^{-1}$	Pore volume[b] $ml g^{-1}$	Ash[c] %
A	Unmodified	886	0.855	0.20
B	13.2 M HNO_3	670	0.562	0.02
C	H_2O_2	826	0.876	0.10
D	Air at 350 °C	959	0.909	0.36
E	H_2	851	0.863	0.25

a) By N_2 BET method. b) Cranston-Inkley method, from 10 to 300 Å pore diameter. c) The ash content was determined with a porcelain crucible, in air.

Table 2. Adsorbed amount and residual amount of phenol on modified carbon black samples

Carbon black	Gas adsorption		Aqueous-phase adsorption
	Adsorbed amount $10^{-5} g m^{-2}$	Residual amount $10^{-5} g m^{-2}$	Freundlich const k[a] $10^{-5} g m^{-2}$
A	33.6	7.2	4.0
B	42.8	17.8	0.9
C	35.0	7.6	2.1
D	32.4	7.4	2.6
E	25.9	5.3	4.8

a) Data from the previous paper.[1]

residual amount of phenol at 25 °C was also measured gravimetrically.

The Weight Decrease of the Carbon Black Samples Heated in Vacuum. After the carbon black samples were outgassed for 18 h under 1.3×10^{-3} Pa at 120 °C, the samples were heated to 1000 °C at a heating rate of 4 °C/min in vacuum. The weight decrease of the samples was measured gravimetrically on the basis of the weight at 120 °C, using the Cahn RG-type electromagnetic microbalance.

Results and Discussion

Adsorbed amounts and residual amounts of phenol on the modified carbon blacks are shown in Table 2. The amount of phenol adsorbed on the modified carbon blacks from its aqueous solution, described in the previous paper, is also shown in Table 2. The amount of phenol adsorbed on the carbons treated with various oxidizing agents, especially with 13.2 M† HNO_3, increased, and the residual amount of phenol also increased. On the other hand, the amount of phenol adsorbed and the residual amount of phenol decreased on the carbon treated with hydrogen gas. In the previous paper it was reported that the amount of phenol adsorbed from an aqueous solution regarding the carbon treated with various oxidizing agents decreased. That regarding carbon treated with hydrogen gas, increased.

The adsorptive properties of forms of carbon are dependent on the pore structure.[6-11] However, Table 1 shows that these modified types of carbon black have almost the same specific surface areas and pore volumes, except for the carbon black treated with nitric acid.

Activated carbon and carbon black produced by the usual methods contain considerable amounts of oxygen and hydrogen chemisorbed on their surfaces.[13] The adsorptive properties of forms of carbon black are presumably affected by the amount of the oxygen and hydrogen on the surface. In order to examine the influence of chemisorbed oxygen and hydrogen on this adsorption, the carbon was evacuated and then heated from 120 to 1000 °C; this treatment decomposed the chemisorbed oxygen and hydrogen. Decomposition products during the heat/evacuation treatment were measured using mass spectrometry. Figs. 2—6 show the variations of mass spectral peaks of the desorbed gas from the modified forms of carbon black with an outgassing temperature up to 1000 °C at a heating rate of 4 °C/min in vacuum. When the samples were heated, the surface compounds decomposed into carbon dioxide, carbon monoxide, water and hydrogen. At higher temperatures, carbon monoxide is more evolved than carbon dioxide. Hydrogen is more difficult to remove than oxygen, but can be removed at very high temperatures.

† 1 M=1 mol dm^{-3}.

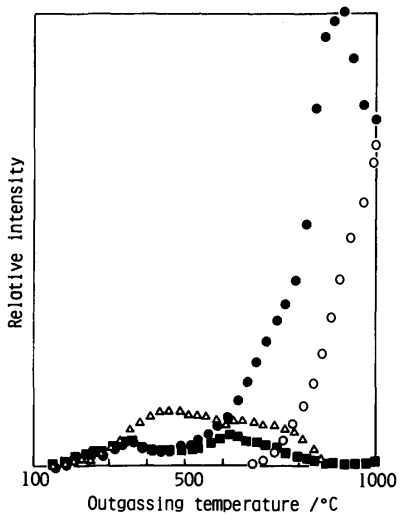

Fig. 2. Variations of mass spectral peaks of the desorbed gas on carbon black A with outgassing temperature up to 1000 °C at a heating rate of 4 °C/min in vacuum. ○: H_2, △: H_2O, ●: CO, ■: CO_2.

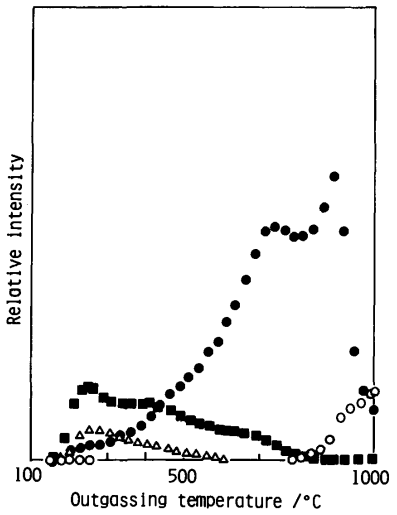

Fig. 4. Variations of mass spectral peaks of the desorbed gas on carbon black C with outgassing temperature up to 1000 °C at a heating rate of 4 °C/min in vacuum. ○: H_2, △: H_2O, ●: CO, ■: CO_2.

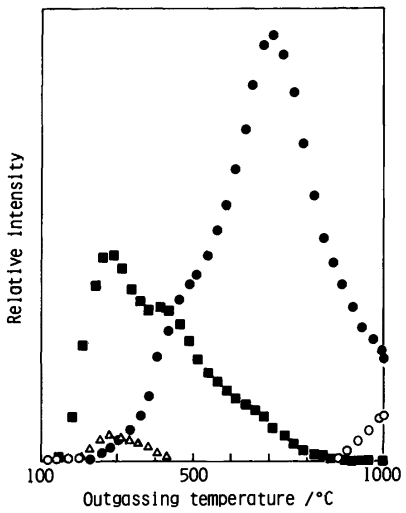

Fig. 3. Variations of mass spectral peaks of the desorbed gas on carbon black B with outgassing temperature up to 1000 °C at a heating rate of 4 °C/min in vacuum. ○: H_2, △: H_2O, ●: CO, ■: CO_2.

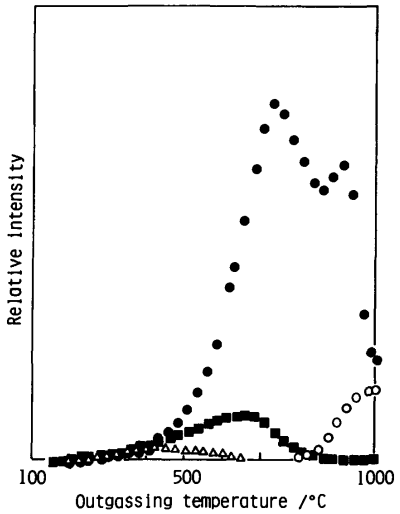

Fig. 5. Variations of mass spectral peaks of the desorbed gas on carbon black D with outgassing temperature up to 1000 °C at a heating rate of 4 °C/min in vacuum. ○: H_2, △: H_2O, ●: CO, ■: CO_2.

The mass spectral peaks of oxygen compounds such as CO and CO_2 from oxidized carbon black, especially from the carbon treated with 13.2 M HNO_3, were very large. However, the mass spectral peaks of H_2 from the oxidized forms of carbon black were low. For the carbon treated with hydrogen gas, the mass spectral peaks of oxygen compounds were very low and the mass spectral peaks of H_2 were rather large. We conclude that the hydrogen gas treatment removes the surface oxygen compounds. Mass spectroscopy showed that they were removed in the forms of H_2O, CO, and CO_2 during the hydrogen gas treatment. The weight decrease of the carbon-black samples heated in vacuum are shown in Table 3. The weight decreases of the oxidized carbon black, especially the carbon treated with 13.2 M HNO_3, were large, while that of the carbon treated with hydrogen gas was small. The weight decrease of various forms carbon, thus, increased along with the increase in the number of surface oxygen compounds.

The relationship between the amount of phenol adsorbed and the weight decrease of the carbon-black

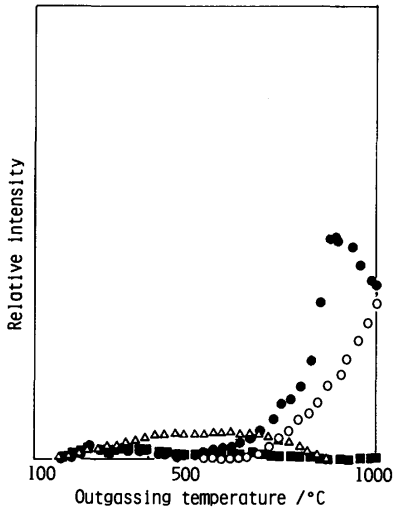

Fig. 6. Variations of mass spectral peaks of the desorbed gas on carbon black E with outgassing temperature up to 1000 °C at a heating rate of 4 °C/min in vacuum. ○: H_2, △: H_2O, ●: CO, ■: CO_2.

Table 3. Weight decrease of modified carbon black samples heated up to 1000 °C at a heating rate of 4 °C/min in vacuum

Carbon black	Weight decrease[a] wt%
A	2.55
B	15.75
C	5.79
D	7.77
E	2.48

a) Based on the weight at 120 °C in vacuum.

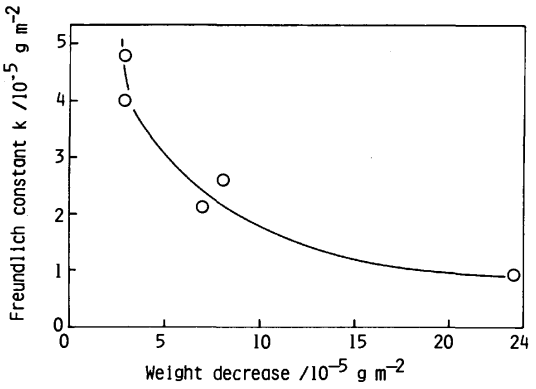

Fig. 7. The relationship between the amount of phenol adsorbed and the weight decrease of the modified carbon black samples in aqueous-phase adsorption.

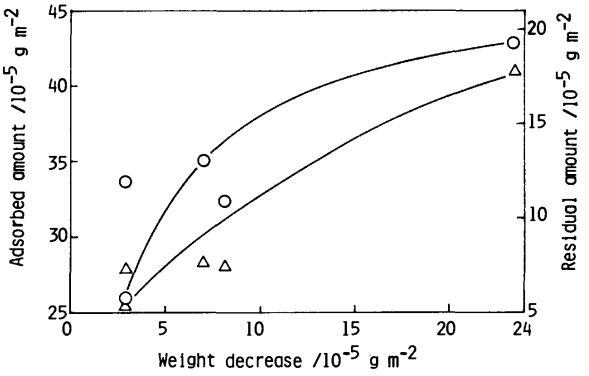

Fig. 8. The relationship between the amount of phenol adsorbed and the weight decrease of the modified carbon black samples in gas adsorption.
○: Adsorbed amount, △: Residual amount.

samples during aqueous-phase adsorption is shown in Fig. 7. In aqueous-phase adsorption, the amount of phenol adsorbed decreased with increasing the amount of the surface oxygen compounds. The relationship between the amount of phenol adsorbed and the weight decrease of the carbon-black samples in gas adsorption is shown in Fig. 8. In gas adsorption, the amount of phenol adsorbed increased with increasing the number of the surface oxygen compounds, and the residual amount of phenol also increased.

From the above results, we propose a model regarding the adsorption mechanism between carbon and phenol (Fig. 9). In the case of gas adsorption, the interactions are not only between the hydrophobic sites on the carbon and the hydrophobic groups of phenol, but also between the surface functional groups on the carbon and the hydrophilic groups of phenol. In the case of aqueous-phase adsorption, there is a competitive adsorption of phenol with water molecules. The adsorption of water may commence by hydrogen bonding to surface oxygen groups.[13] It is thought that the water molecules adsorb selectively to the surface oxygen groups on the carbon because of their large polarity. The water molecules become secondary adsorption centers and retain other water molecules by means of hydrogen bonds.[12] The majority of the surface oxygen groups exist near the edges of fused hexagonal carbon rings or aromatic nuclei that make up the basis structure for carbons.[11,14] As a result, complexes of associated water form at the entrances of the pores of the carbon black. These complexes prevent the phenol adsorption due to the hydrophobic interaction on the carbon and prevent the invasion of phenol into the large surface area within the pores of the carbon. Therefore, the amount of phenol adsorbed on the carbon black in aqueous-phase adsorption decreases upon increasing the number of surface oxygen groups. However, in gas adsorption, the adsorbed amount and the residual amount of phenol on carbon black increased upon

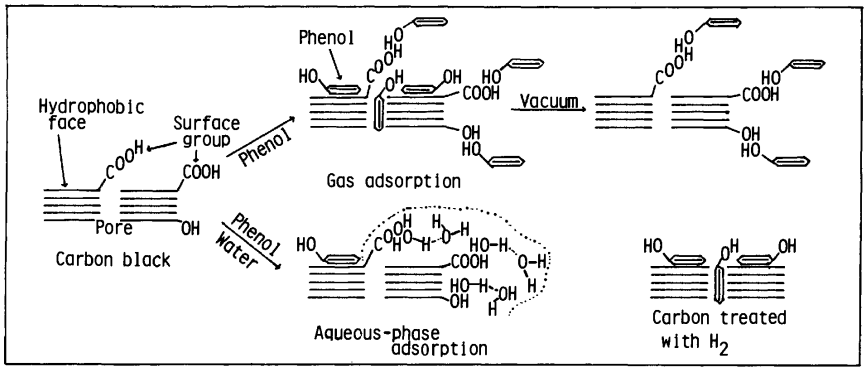

Fig. 9. The model of the adsorption mechanism between carbon and phenol.

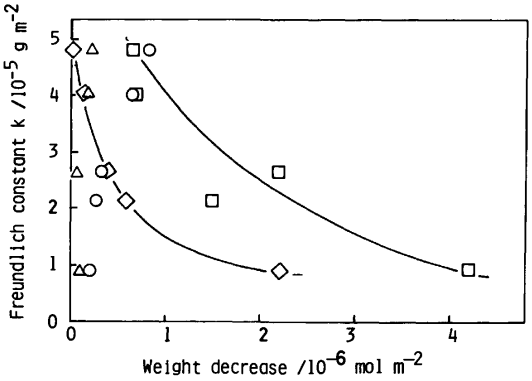

Fig. 10. The effect of surface oxygen compounds on aqueous-phase adsorption of phenol.
○: H_2, △: H_2O, □: CO, ◇: CO_2.

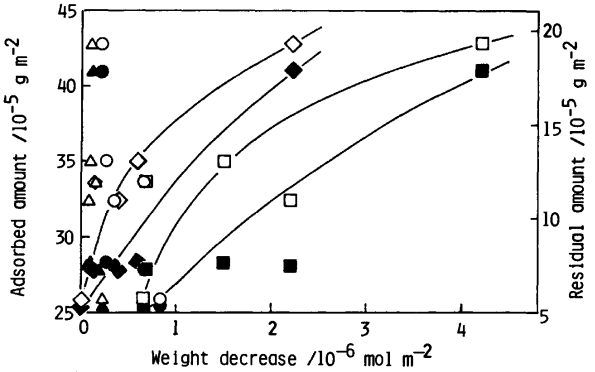

Fig. 11. The effect of surface oxygen compounds on gas adsorption of phenol.
Adsorbed amount: ○; H_2, △; H_2O, □; CO, ◇; CO_2,
Residual amount: ●; H_2, ▲; H_2O, ■; CO, ◆; CO_2.

increasing the number of surface oxygen groups, due to an interaction due to hydrogen bonding to the surface oxygen groups.

In order to investigate the influence of the forms of the surface oxygen groups on the carbon upon the adsorption of phenol, the weight decreases of the carbon for each of the desorbed gases have been evaluated using the mass spectral peaks of the desorbed gases on the modified types of carbon black shown in Figs. 2—6. These results are shown in Table 4. For carbon-black B, the weight decreases according to the desorbed gases, since CO and CO_2 are large and the total weight decrease is also large. For carbon-black C, the weight decreases are rather large for H_2 and H_2O, but the total weight decrease is little. The relationships between the amount of phenol adsorbed on the carbon and the weight decrease of the carbon for each of the desorbed gases are shown in Figs. 10 and 11. In aqueous-phase adsorption, the amount of phenol adsorbed decreased upon increasing the weight decreases based on the gases desorbed as CO and CO_2. In gas adsorption, the amount of phenol adsorbed increased upon increasing the weight decreases based on the gases desorbed as CO and CO_2.

Table 4. The weight decreases of the modified carbon black samples for each of the desorbed gases

Carbon black	Weight decrease mmol g^{-1}				
	H_2	H_2O	CO	CO_2	Total
A	0.58	0.17	0.60	0.11	1.46
B	0.14	0.08	2.82	1.75	4.79
C	0.22	0.08	1.24	0.48	2.02
D	0.33	0.07	2.11	0.38	2.89
E	0.71	0.19	0.56	0.01	1.47

The residual amount of phenol also increased. The variation of the adsorbed amounts on the modified types of carbon black is independent of the weight decreases based on the gases desorbed as H_2 and H_2O in aqueous-phase adsorption and in gas adsorption, because the variation of weight decreases based on the gases desorbed as H_2 and H_2O is little. Suzuki[15] and Walker[16] have reported on the desorbed gases of carbon during the heat/evacuation treatment. The

Table 5. Surface acidities of modified carbon black samples

Carbon black	Surface group (meq g^{-1})				
	I	II	III	IV	Total
A	0.01	0	0.06	0	0.07
B	0.40	0.08	0.41	0	0.89
C	0.06	0.07	0.07	0.02	0.22
D	0.08	0.08	0.09	0.01	0.26
E	0	0.01	0	0.04	0.05

I: Carboxyl group. II: Carboxyl group that occurs as a lactone. III: Phenolic hydroxyl group. IV: Carbonyl group that reacts with the carboxyl group II to form the lactone (or lactol).

weight decrease based on the gas desorbed as CO_2 shows that carboxyl groups and carboxylic anhydrides exist on the carbon. The weight decrease based on the gas desorbed as CO shows that hydroxyl groups, carbonyl groups, and quinone exist on the carbon. Since the weight decrease of H_2O is independent of the variation of the amount of phenol adsorbed, it is thought that the surface oxygen groups are present as anhydrides on the carbon. The surface oxygen groups desorbed as CO and CO_2 are carboxylic anhydrides, carboxyl groups that occur as lactones, quinone, and carbonyl groups. The surface acidity of the modified carbon-black samples, which was estimated by the method of Boehm *et al.*[17,18] in the previous paper, is shown in Table 5. The surface acidity of carbon-black B, especially the surface acidity for carboxyl group, is large. The total weight decrease of carbon-black B is also large. The surface acidity of carbon-black E is less than that for the other types of carbon. The total weight decrease of carbon-black E is also less. The surface acidity of the modified types of carbon black for carbonyl group was less than that for other groups. Therefore, the surface oxygen compounds introduced with the oxidation treatments as carboxylic anhydride and as the carboxyl group that occurs as a lactone are probably dependent on the adsorption of phenol.

Consequently, the adsorption character of the various types of carbon black was found to be dependent on the surface oxygen compounds, especially on the carboxylic anhydrides and on the carboxyl groups that occur as lactones. We conclude that carbon black treated with hydrogen gas exhibits excellent adsorbability in the aqueous-phase adsorption. However, carbon black treated with stronger oxidizing agents exhibits better adsorbability regarding phenol gas adsorption.

The present work was partially supported by a Grant-in-Aid for Environmental Science No. 59030013 from the Ministry of Education, Science and Culture.

References

1) T. Asakawa and K. Ogino, *J. Colloid Interface Sci.*, **102**, 348 (1984).
2) K. Urano, *Yuki Gosei Kagaku Kyokai Shi*, **33**, 333 (1975).
3) K. Ogino, T. Asakawa, K. Yamabe, and H. Takahashi, *Yukagaku*, **31**, 159 (1982).
4) T. Asakawa, K. Ogino, K. Yamabe, and H. Takahashi, *Yukagaku*, **31**, 290 (1982).
5) T. Asakawa and K. Ogino, *Yukgaku*, **33**, 384 (1984).
6) I. Abe, K. Hayashi, and M. Kitagawa, *Yukagaku*, **25**, 145 (1976).
7) I. Abe, K. Hayashi, and M. Kitagawa, *Yukagaku*, **26**, 355 (1977).
8) I. Abe, K. Hayashi, and M. Kitagawa, *Nippon Kagaku Kaishi*, **1977**, 1905.
9) B. R. Puri, S. S. Bhardwaj, and U. Gupta, *J. Indian Chem. Soc.*, **23**, 1095 (1976).
10) D. J. Wilson and A. N. Clarke, *Sep. Sci. Technol.*, **14**, 227 (1979).
11) D. M. Giusti, R. A. Conway, and C. T. Lawson, *J. Water Pollut. Control. Fed.*, **46**, 947 (1974).
12) R. W. Couglin and F. S. Ezra, *Environ. Sci. Technol.*, **2**, 291 (1968).
13) J. R. Dacey, "Solid-Gas Interface," ed by E. A. Flood, Marcel Dekker, New York (1976), Vol. 2, Chap. 34, p. 1007, p. 1012,
14) H. Takahashi, *Kinzoku Kagaku*, **14**, 203 (1978).
15) S. Gao, K. Yamabe, H. Takahashi, and Y. Saito, *Tanso*, **1984**, (No. 119), 207.
16) G. Tremblay, F. J. Vastola, and P. L. Walker, Jr., *Carbon*, **16**, 35 (1978).
17) H. P. Boehm, *Angew. Chem., Int. Ed. Engl.*, **5**, 533 (1966).
18) H. P. Boehm, "Advances in Catalysis," Academic Press, New York (1966), Vol. 16, p. 179.

 © 1985 The Chemical Society of Japan Bull. Chem. Soc. Jpn., 58, 2015—2022 (1985)

Heterogeneous Photocatalytic Decomposition of Phenol over TiO_2 Powder

Ken-ichi Okamoto,* Yasunori Yamamoto, Hiroki Tanaka, Masashi Tanaka, and Akira Itaya†

Department of Chemical Engineering, Faculty of Engineering, Yamaguchi University, Ube 755

(Received November 28, 1984)

The photocatalytic decomposition of phenol in oxygenated aqueous suspensions of lightly-reduced anatase TiO_2, being the most satisfactory among the semiconductors investigated from the standpoint of the photocatalytic activity and stability, has been investigated at the optimum pH 3.5. The products at the initial stage of the reaction were hydroquinone, pyrocatechol, 1,2,4-benzenetriol, pyrogallol, and 2-hydroxy-1,4-benzoquinone. These intermediates underwent further photocatalytic oxidation *via* acids and/or aldehydes finally into CO_2 and H_2O. A reaction scheme involving hydroxyl radicals as real reactive species has been proposed. Although H_2O_2 was formed *via* O_2^- produced by electron trapping of adsorbed oxygen, its concentration remained constant at a low value during the reaction. About 0.7 mole of O_2 was consumed for the consumption of one mole of phenol at the initial stage of the reaction. These results indicated that hydroxyl radicals were formed not only *via* holes but also *via* H_2O_2 from O_2^-. It was interesting from the viewpoint of wastewater treatment that phenol was completely mineralized to CO_2 in the presence of TiO_2 powder under solar irradiation without both aeration and mixing of the solution.

Photocatalytic effects of semiconductors have been of much interest from the view point of solar energy utilization. They have been applied not only to produce useful chemicals,[1] but also to convert pollutants in waste streams to innocuous or less harmful form.[2-8] For example, by heterogeneous photocatalysis of some *n*-type semiconductors such as TiO_2 and ZnO, CN^-, and $Cr_2O_7^{2-}$ in aqueous solutions are converted to CNO^- and Cr^{3+}, respectively.[2,3,5,6] In dilute aqueous solutions, chlorinated hydrocarbons such as $CHCl_3$ and trichloroethylene are completely mineralized to HCl and CO_2.[8] Chlorinated aromatics such as polychlorinated biphenyls also undergo photocatalytic dechlorination to give less harmful products.[2] These facts indicate some potential for phtocatalytic treatment of wastewater utilizing sunlight.

Phenol is a refractory and common compound in industrial wastes, and there is interest in developing a new type of chemical treatment of phenol. Kawaguchi and Uejima have studied on phtocatalytic decomposition of phenol in aqueous suspensions of ZnO.[7] They observed that the decomposition process apparently obeyed the first-order reaction kinetics, and detected hydroquinone and pyrocatechol as the main products. The photocatalytic decomposition process of phenol has not, however, been clarified in detail yet.

In the present paper, the photocatalytic decomposition of phenol was studied at several semiconductor powders. For aqueous suspensions of lightly-reduced anatase, the most satisfactory photocatalyst, the dependence of the reaction rate on pH, partial pressure of O_2 and $[Cu^{2+}]$, the consumption rate of O_2, and variation of $[H_2O_2]$ during the reaction were investigated to clarify the initial steps of the photocatalysis. The intermediate products were investigated to clarify the reaction pathway. The photocatalytic decomposition under solar irradiation was also investigated. The reaction kinetics of the process will be reported elsewhere.[9]

Experimental

Materials. As photocatalysts, TiO_2 (anatase and rutile), ZnO, α-Fe_2O_3, and CdS were used as received from Wako Pure Chemical Co., except for anatase. Anatase powder was reduced in a stream of hydrogen at 520 °C for 6 h. The lightly-reduced anatase had a specific area of 38 $m^2 g^{-1}$, as determined by BET nitrogen adsorption, and was used in this paper except where noted. Cu-deposited anatase powder was prepared by UV-irradiating a deaerated suspension of lightly-reduced anatase in the presence of $CuSO_4$ (0.1 mM (1 M=1 mol dm^{-3})).[10]

All chemicals were of reagent grade (Wako Pure Chemical Co.). Solutions were prepared with distilled deionized water.

Photocatalytic Experiments. The majority of the reaction was carried out in a photochemical reactor which was fitted with a 100 W high-pressure mercury lamp (Ushio Electric Co., UM-102) surrounded by a Pyrex glass thimble. A 0.23 M solution of $CuSO_4 \cdot 5H_2O$ was circulated through the thimble to cool the reaction solution and to help filter out short-wavelength light. The 500 cm^3 reaction vessel formed a gas-tight seal around the lamp and had four ports for gas inlet and outlet, sampling, and pH measurement.

In typical experiments, 2.5 g of catalyst powder was suspended in 400 cm^3 of 1 mM phenol solution by stirring magnetically. A gas was bubbled through this solution at the rate of 220 $cm^3 min^{-1}$. In the experiments using anatase, pH of the solution was adjusted by adding an appropriate amount of a H_2SO_4 or KOH solution to the suspension. In the other experiments, it was not adjusted. During a run, the reaction solution was maintained at

† Present address: Department of Polymer Science and Engineering, Kyoto Institute of Technology, Matsugasaki, Kyoto 606.

25 °C, and *ca.* 3 cm³ samples were taken at given time intervals. After being sampled, the suspensions were centrifuged and the centrifugates were subjected to the analyses.

To measure quantum yield of phenol decomposition, the reaction was also carried out in a rectangular cell at 25 °C. With bubbling oxygen gas slowly and stirring magnetically, 15 cm³ of a 1 mM phenol solution suspended with 95 mg anatase was irradiated through a front side of the cell by a monochromatized and parallel light from a 500 W xenon lamp. The incident light intensity was measured by means of a potassium ferrioxalate actinometer.[11]

Analyses. Phenol and the reaction products were analyzed by means of a high-performance liquid chromatography (Hitachi, 635-A) with a column packed with ODS gel (Toyosoda Co., ODS-120A). An aqueous solution of 50% methanol or 0.2% acetic acid[12] was used as an eluting solvent. Products were identified by comparing both the retention times and the ratios of absorbance monitored at two different wavelengths between samples and standards. Total organic carbon (TOC) content was measured using a TOC analyzer (Shimazu, TOC-10A). COD was measured by the acidic method using a COD analyzer (Bionic Instrument Co., COD-510E). The amount of CO_2 produced was determined either from a reduction in TOC of the reaction solution or as $BaCO_3$ precipitated by passing the effluent gas into a $Ba(OH)_2$ solution. The amount of carbonyl groups produced was measured by treating the reaction solution with a 1 M aqueous HCl solution of 2,4-dinitrophenylhydrazine and following the consumption of hydrazine spectrometrically. H_2O_2 was analyzed spectrometrically using $TiOSO_4$ as the reagent.[13] Zn^{2+} and Ti^{4+} were analyzed spectrometrically using Xylenol Orange and 8-quinolinol, respectively, as the reagents.[14] The partial pressure of O_2 of a bubbled gas was measured using a gaschromatography (Shimazu, TC-4A) with a column packed with silica gel.

Adsorption. 20 cm³ of a 0.5 mM phenol solution and a certain quantity (0.1—3 g) of reduced anatase powder were added to 50 cm³ flask with a tight stopper. After the suspension was magnetically stirred for 10 h at 25 °C, the TiO_2 powder was removed by centrifugation and the absorbance of the solution was measured against a blank solution.

Solar Experiments. In the experiments using sunlight, 10 g of reduced anatase and 1.2 dm³ of 1 mM phenol solution were placed in a rectangular cell with a Pyrex glass cover. As the solution was not stirred during a run, the anatase powder covered the bottom of the cell. The deposited layer of anatase (510 cm² in the surface area) was illuminated with sunlight through the solution layer (2.3 cm in depth). Cu-deposited anatase was also used. The pH of the solution was initially set at 3.5, but it was not controlled during a run. The experiments were carried out in August in Ube located in lattitude 34° north. The temperature of the reaction solution was in the range of 30 to 55 °C. The weather was clear to partly cloudy.

Results and Discussion

Photocatalytic Activity and Stability of Semiconductors. Figure 1 shows reduction of phenol concentration

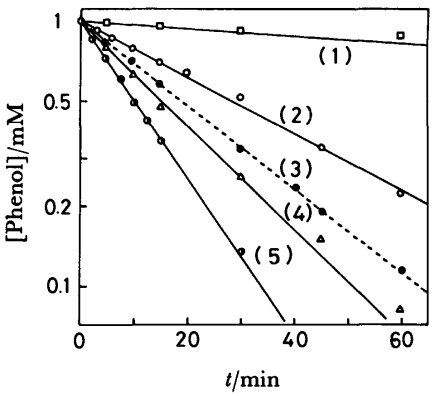

Fig. 1. Reduction of [phenol] with reaction time for the oxygenated aqueous suspensions of semiconductor powders. The ordinate is taken on a log scale.
(1) CdS, (2) anatase at pH 6.5, (3) anatase at pH 3.5, (4) ZnO, and (5) reduced anatase at pH 3.5.

Table 1. Comparison between the photocatalytic activities of semiconductors

Semiconductor	pH	k_{ap}[a]/10^{-4} s^{-1}
None	6.5	0
Rutile TiO_2	6.5	0
Anatase TiO_2	6.5	4.0
Anatase TiO_2	3.5	6.1
Reduced anatase	3.5	10.5—9.2[b]
CdS	—	0.7
α-Fe_2O_3	—	0
ZnO	7	≈7.5

a) $[phenol]_0 = 1.0$ mM. b) The k_{ap} values were scattered in this range between different lots of anatase samples.

with reaction time t for oxygenated aqueous suspensions of several semiconductors. As shown in Fig. 1, the reaction followed the first-order reaction kinetics (Eq. 1) concerning to [phenol].

$$\ln([phenol]/[phenol]_0) = -k_{ap}t \quad (1)$$

The photocatalytic activity of semiconductors was, therefore, compared by use of the values of the apparent rate constant, k_{ap}, shown in Table 1. It was in the order of reduced anatase>ZnO>anatase-(untreated)≫CdS. Rutile used in the present paper did not have the activity at all.

The photochemical stability of anatase and ZnO was checked by measuring the concentration of Ti^{4+} and Zn^{2+} ions dissolved out during the reaction. No trace of Ti^{4+} ions dissolved out was detected for the anatase suspensions, even after the reaction was continued till phenol disappeared completely, indicating that TiO_2 is very stable photochemically in aqueous solutions.[3] On the other hand, a significant quantity of Zn^{2+} was detected for ZnO suspensions; for example $[Zn^{2+}]$=0.93 mM, after the reaction was performed for 1 h. This quantity of Zn^{2+} corresponded to about 1% of ZnO loaded and was roughly equal to

the quantity of consumed phenol. It is known that a ZnO electrode undergoes anodic photocorrosion according to Eq. 2.

$$ZnO + 2h^+ \longrightarrow Zn^{2+} + O^* \quad (2)$$

This reaction occurs in an aqueous solution of formic acid or alchohols as well as in an inert electrolyte solution.[15] ZnO powder is, therefore, not suitable to a photocatalyst for wastewater treatment.

Among the semiconductors investigated here, lightly-reduced anatase was the most satisfactory from the standpoint of the photocatalytic activity and stability. The experiments mentioned below were, therefore, carried out using lightly-reduced anatase.

Effects of pH, Partial Pressure of O_2 and Addition of Cu^{2+}. Figure 2 shows the effect of pH on both the initial reaction rate Ω_0 and k_{ap}. It is noted that pH 3.5 is the optimum for the photocatalytic decomposition of phenol.

As shown in Fig. 3, Ω_0 depended on the partial pressure of O_2 in the bubbled gas, p_{O_2}. Under a N_2 gas bubbled, the reaction hardly occurred. The pattern of Fig. 3 suggests that the reaction rate is controlled by the quantity of O_2 adsorbed on TiO_2 surface in the Langmuir mode;

$$\Omega_0 \propto K_{O_2} p_{O_2}/(1+K_{O_2} p_{O_2}), \quad (3)$$

where K_{O_2} is the equilibrium constant of adsorption of O_2. The solid lines in Fig. 3, which were calculated from Eq. 3 with the K_{O_2} value of 0.11 kPa^{-1}, were in good agreement with the experimental results.

Figure 4 shows variation of the concentration of O_2 dissolved, $[O_2]$, with reaction time. When an anatase suspension without phenol was irradiated with UV-light, a small quantity of O_2 was consumed in the first run. After aeration, the suspension was reirradiated. O_2 was hardly consumed in the second run. After the second run, an appropriate amount of a concentrated phenol solution was added to the suspension to prepare a 1 mM phenol solution. As shown by the line (3) in Fig. 4, O_2 disappeared rapidly in this phenol solution under the UV-irradiation. In the experiments without the preirradiation in the absence of phenol, O_2 disappeared in the similar manner. About 0.7 mole of O_2 was consumed for the consumption of 1 mole of phenol at the initial stage of the reaction, as shown by the dotted lines in Fig. 4.

Table 2 shows the values of quantum yield, ϕ, of the reaction. These values were obtained in the range of the low light intensity where Ω_0 was proportional to it. The reaction proceeded only by light of wavelength shorter than 400 nm, because anatase has a band gap of 3.23 eV (corresponding to 388 nm).[16] The ϕ was almost constant for wavelength shorter than 370 nm, being in agreement with the action spectrum observed for water reduction over platinized

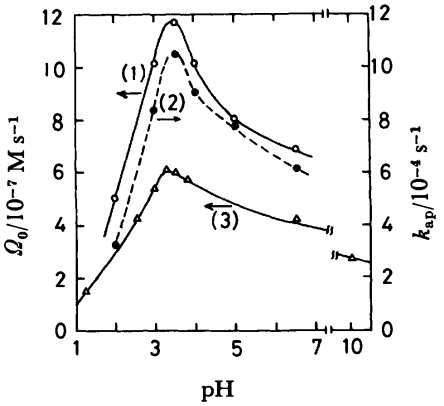

Fig. 2. Effect of pH on both Ω_0 and k_{ap}.
$[phenol]_0 = 1.0$ mM and $p_{O_2} = 101$ kPa.
Anatase: (1) and (2) reduced, (3) untreated.

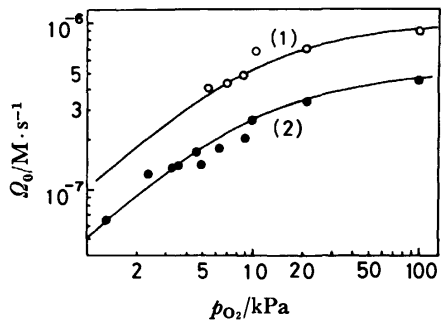

Fig. 3. Effect of p_{O_2} on Ω_0 at pH 3.5.
$[phenol]_0$: (1) 1.0 mM and (2) 0.1 mM.
The solid lines were calculated from Eq. 3 with $K_{O_2} = 0.11$ kPa^{-1}.

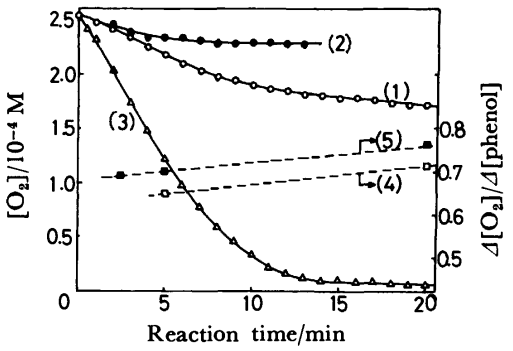

Fig. 4. Variations of $[O_2]$ with reaction time and the consumed mole ratio of O_2 to phenol, $\Delta[O_2]/\Delta[phenol]$, at pH 3.5.
$[phenol]_0 = 1.0$ mM for (3)—(5).
(1) First run in the absence of phenol; (2) second run: after the first run, the suspension was aerated for 5 min prior to the irradiation; (3) third run: after the second run, an appropriate amount of phenol was added to the suspension and it was aerated for 5 min prior to the irradiation; (4) $\Delta[O_2]/\Delta[phenol]$ for the third run; (5) $\Delta[O_2]/\Delta[phenol]$ for experiments without the pre-irradiation in the absence of phenol.

Table 2. Quantum yield of the reaction at pH 3.5[a)]

Wavelength/nm	ϕ/%
430	0
400	1.0
370	10.6
340	11.8

a) For reduced anatase, [phenol] = 1.0 mM, at 25 °C, and in the range of low light-intensity.

anatase.[17)]

For oxygenated aqueous suspensions of anatase, hydroxyl radicals have been considered to be reactive species responsible for the photocatalytic reactions of benzene,[18)] toluene,[19)] benzoic acid,[20)] and so on.[21)] They also seem reactive species responsible for the present reaction, because the photocatalytic decomposition of phenol proceeded *via* its hydroxylated compounds such as hydroquinone and pyrocatechol as will be mentioned in the following section. The initial steps of the photocatalysis are considered as follows.

Judging from the fact that Ω_0 was proportional to the square root of the incident light intensity, as will be reported elsewhere,[9)] the reaction rate was limited by the recombination of photogenerated hole-electron pairs, under the present experimental conditions. The dependence of Ω_0 on p_{O_2} expressed by Eq. 3, therefore, indicates that oxygen adsorbed on anatase surface prevents the recombination of hole-electron pairs by trapping electrons. Superoxide ions are thus formed.[18–23)]

$$O_2(a) + e^- \longrightarrow O_2^{\cdot-} \quad (4)$$

It is likely that H_2O_2 is formed from $O_2^{\cdot-}$ according to the following reactions.[20–22,24)]

$$O_2^{\cdot-} + H^+ \longrightarrow HO_2\cdot \qquad pK_a = 4.88 \quad (5)$$

$$HO_2\cdot + HO_2\cdot \longrightarrow H_2O_2 + O_2 \qquad k = 7.6\times10^5\ M^{-1}\,s^{-1} \quad (6)$$

$$O_2^{\cdot-} + HO_2\cdot \longrightarrow O_2 + HO_2^- \qquad k = 8.5\times10^7\ M^{-1}\,s^{-1} \quad (7)$$

$$HO_2^- + H^+ \longrightarrow H_2O_2 \qquad pK_a = 1.5\times10^{-12} \quad (8)$$

The values of pK_a and k were cited from Ref. 25. It has been suggested that ·OH radicals are formed from H_2O_2 by anyone of the following reactions.[19,22)]

$$H_2O_2 \xrightarrow{h\nu} 2\cdot OH \quad (9)$$

$$H_2O_2 + O_2^{\cdot-} \longrightarrow \cdot OH + OH^- + O_2 \quad (10)$$

$$H_2O_2 + e^- \longrightarrow \cdot OH + OH^- \quad (11)$$

On the other hand, holes react with either H_2O or OH^- adsorbed on anatase surface to give ·OH radicals.[16,18–22)]

$$H_2O(a) + h^+ \longrightarrow \cdot OH + H^+ \quad (12)$$

$$OH^-(a) + h^+ \longrightarrow \cdot OH + OH^- \quad (13)$$

It is ambiguous to what extent the routes of formation of ·OH *via* H_2O_2 are important as compared with ones *via* holes. Mattews has reported that the former routes are negligible as compared with the latter ones.[21)] In order to clarify this point, $[H_2O_2]$ in the reaction solutions was measured under the typical experimental conditions. It increased over first *ca.* 10 min and subsequently remained almost constant at 15 μM. The low value of $[H_2O_2]$ in the steady state suggests that formation of H_2O_2 according to Eqs. 4—8 was in a balance with its decomposition according to Eqs. 9—11. The fact that 0.7 mol of O_2 was consumed for the consumption of 1 mol of phenol is an additional support for the importance of formation of ·OH radicals *via* H_2O_2, as will be mentioned in the following section.

Figure 5 shows the effect of $[Cu^{2+}]$ on both Ω_0 and k_{ap}. A small quantity of Cu^{2+} less than 0.1 mM increased both Ω_0 and k_{ap} by a factor of *ca.* 2, suggesting that the effect is catalytic. On the other hand, a large quantity of Cu^{2+} rather reduced them. It has been observed that Cu^{2+} ions reduce the extent of hole-electron recombination by trapping photogenerated electrons;[10)]

$$Cu^{2+} + e^- \longrightarrow Cu^+ \xrightarrow{e^-} Cu \quad (14)$$

The reduced forms, in turn, prevents the recombination by trapping holes;

$$Cu + h^+ \longrightarrow Cu^+ \xrightarrow{h^+} Cu^{2+} \quad (15)$$

If a small quantity of Cu^{2+} effectively prevents hole-electron recombination even in the oxygenated suspensions, either holes or electrons escaped from the recombination produce ·OH radicals *via* the corresponding routes, resulting in the promotion of the reaction. Because a couple of Eqs. 14 and 15 is the short-circuiting reaction of Cu^{2+},[10,19)] a large quantity

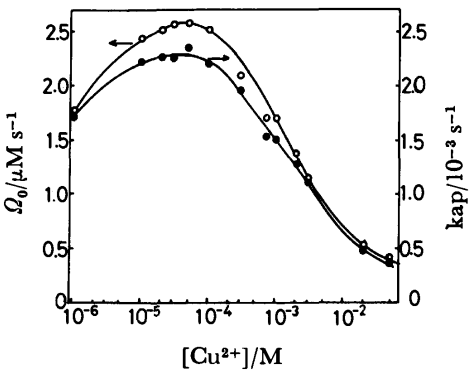

Fig. 5. Effect of $[Cu^{2+}]$ on both Ω_0 and k_{ap} at pH 3.5. $[phenol]_0 = 1.0$ mM and $p_{O_2} = 101$ kPa. With $[Cu^{2+}] = 0$, $\Omega_0 = 0.96$ μM/s and $k_{ap} = 0.92\times10^{-3}\ s^{-1}$.

of Cu^{2+} rather retards the reaction. This is the most probable explanation for the result shown in Fig. 5. An alternative explanation is based on the effect of Cu^{2+} as a catalyst for the Fenton reaction.[26]

$$Cu^{+} + H_2O_2 \longrightarrow \cdot OH + OH^{-} + Cu^{2+}, \quad (16)$$

$$\cdot RHOH + Cu^{2+} \longrightarrow ROH + H^{+} + Cu^{+}, \quad (17)$$

where ·RHOH is a hydroxy adduct of a reactant RH. This effect, however, is unlikely to be significantly responsible for the promotion of the reaction, because the formation of ·OH radicals *via* H_2O_2 seems to occur sufficiently fast even in the abscence of Cu^{2+} ions as mentioned above.

In the oxygenated suspensions, oxygen acts as both a trap for a photogenerated electron and an oxidant for a hydroxy adduct of the reactant (see Eqs. 19—23). In the deaerated suspensions, Cu^{2+} ions probably act in these two modes in place of O_2 according to Eqs. 14 and 17, although formation of ·OH by the routes *via* H_2O_2 does not occur. The values of Ω_0 were 0.20 and 0.28 μM s^{-1} for the deaerated suspensions containg 50 μM and 1 mM of Cu^{2+}, respectively, while the reaction does not occur in the abscence of Cu^{2+}. These values of Ω_0 corresponded to *ca.* 20 and 30% of the value for the oxygenated suspensions without Cu^{2+}. This fact also suggests the importance of the routes of formation of ·OH *via* H_2O_2.

There remains the possibility that photogenerated holes react with phenol adsorbed on anatase to give dihydroxycyclohexadienyl radicals *via* phenol radical cations, as has been recently proposed for the photocatalytic oxidation of benzene by Hashimoto *et al.*[27]

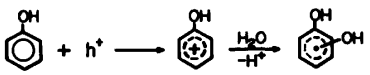

(18)

The energy of holes in the valence band of TiO_2 is about −7.5 eV and is high enough for holes to react easily with H_2O and organic compounds.[28] Therefore, the probability of the reaction of holes with phenol is considered to be roughly proportional to the surface coverage of adsorbed phenol. In the adsorption experiments, a small increase of [phenol] was observed for the solution contacted with a large amount of TiO_2 powder; for example, Δ[phenol]= 0.11 mM for [TiO_2]=50 mg cm^{-3}. This indicates that phenol was hardly adsorbed on TiO_2 powder, as compared with water. Therefore, the path expressed by Eq. 18 is not considered to be significantly responsible for the case of phenol at least.

On the bases of the above-mentioned results and discussion, a mechanism shown in Scheme 1 is proposed for the initial steps of the photocatalysis.

Intermediate Products and Reaction Pathway. The reaction products identified from liquid chromatograms were hydroquinone (abbreviated as HQ), pyrocatechol (CC), 1,2,4-benzenetriol (HHQ), pyrogallol (PG), 2-hydroxy-1,4-benzoquinone (HBQ), and 1,4-benzoquinone (BQ). Many peaks having very short retention times were enhanced with increasing reaction time. These peaks seemed to be attributed to very polar products like aldehydes and carboxylic acids, but were not analyzed in detail.

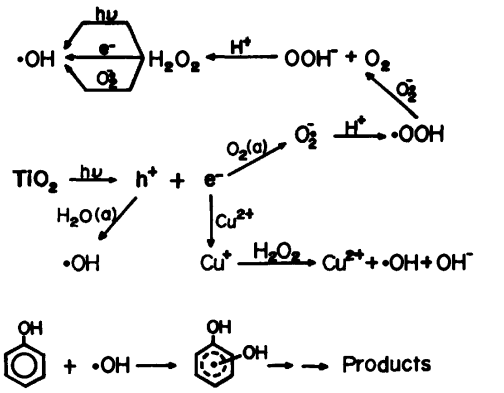

Scheme 1.

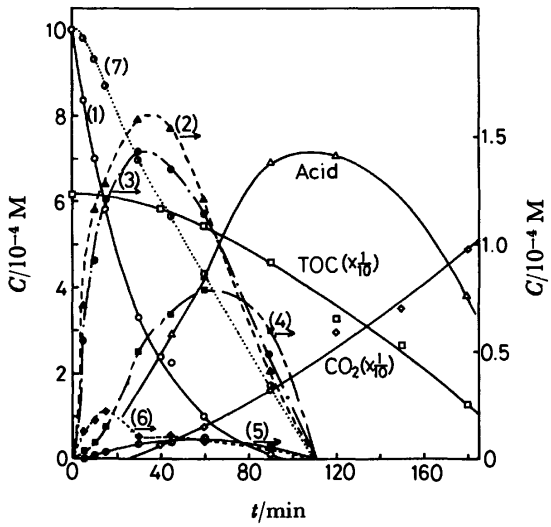

Fig. 6. Variation of concentration of the reaction products and TOC with reaction time at pH 3.5 and p_{O_2} = 101 kPa.
(1) phenol, (2) CC, (3) HQ, (4) HHQ, (5) PG, (6) HBQ and (7) total concentration of the detected aromatic compounds.

Figure 6 shows variation of the concentration of the products and TOC with reaction time. The concentration of acids was obtained from an amount of a KOH solution added to the reaction solution in order to maintain its pH at 3.5. BQ was detected by an amount less than 1 μM till phenol disappeared. At the degrees of conversion of 16, 42, and 80%, the combined amounts of HQ, CC, HHQ, PG, and HBQ corresponded to 90, 68, and 48% of consumed phenol, respectively. With a decrease of the mole ratio of the detected aromatic compounds to consumed phenol, [acids] increased rapidly. These results indicate that

HQ, CC, HHQ, PG, and HBQ are the products at the initial stage of the reaction and undergo further photocatalytic oxidation to yield the very polar intermediate products like carboxylic acids and aldehydes. These aromatic intermediates disappeared in about ten min after disappearence of phenol. After reaching a maximum at that time, [acids] decreased with increasing reaction time. CO_2 began to be detected at the conversion of about 75%. By the reaction for 3 h, about 80% of the carbon quantity of loaded phenol was mineralized to CO_2.

Table 3 shows the distribution of the products for the photocatalytic reaction of HQ, CC, and HHQ. In spite of low conversions, about 50% of consumed pyrocatechol became undetected products having one or two carbonyl groups, suggesting that the attack of ·OH on CC brings about cleavage of benzene ring with a probability of about 50% to yield aldehydes and/or carboxylic acids. Judging from Fig. 6 and Table 3, the reaction pathway shown in Scheme 2 is the most likely. HQ and CC are the major primary products. HHQ is formed as the major secondary product *via* either HQ or CC. PG is formed *via* CC as the minor secondary one. Thus, the photocatalytic decomposition of phenol mainly proceeds *via* its hydroxylated compounds. This is very similar to the case of radiolysis of phenol in aerated aqueous solutions.[29] On the other hand, it is noted that HBQ is formed not only as the minor primary product but also as the minor secondary one *via* either HQ or CC. A possible explanation for these facts is as follows. Hydroxyl radicals react easily with phenol to yield dihydroxycyclohexadienyl radicals.[30] Most of the radicals react with O_2 according to Eqs. 19 and 20. Some of the radicals undergo the unimolecular elimination of water to yield phenoxyl radicals,[30] which react with O_2 to yield HBQ *via* BQ according to Eq. 21.

Table 3. Distribution of the products at the initial stage of the reaction[a)]

Reactant	Conversion	Yield/%					
	%	HQ	CC	HHQ	PG	HBQ	Undetected
Phenol	16.0	33.3	43.6	2.1	0.3	7.9	12.8[b)]
HQ	10.7	—	0	64.8	0	11.1	24.1[b)]
HQ	19.0	—	0	63.3	0	7.5	29.1[b)]
CC	9.8	0	—	33.7	11.8	5.8	48.7[b)]
CC	16.5	0	—	34.0	12.5	4.4	49.1[b,c)]
HHQ	6.2	0	0	—	0	0	100

a) $[\text{reactant}]_0 = 1$ mM, $[TiO_2] = 3.0$ mg cm^{-3}, and at pH 3.5. b) In liquid chromatograms, large peaks with retention times of 5.5 and 3.3 min were observed for the reaction solutions of HQ and CC, respectively. c) The reaction solution contained 0.11 mM of carbonyl groups, which corresponded to 1.3 mole per one mole of CC changed to undetected products.

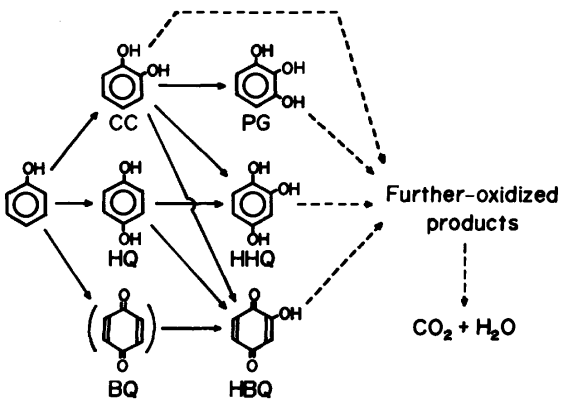

Scheme 2.

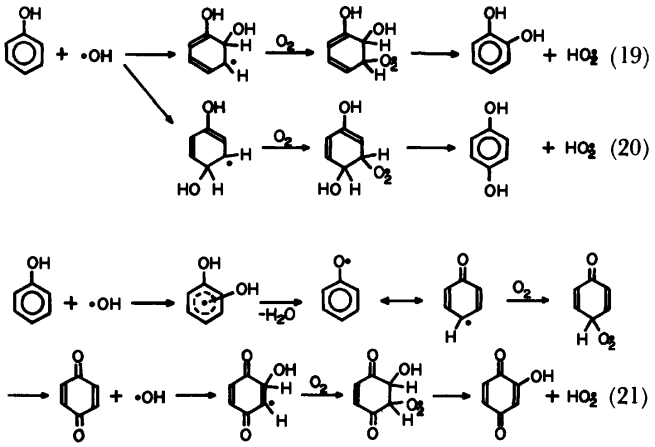

Similar reactions occur for HQ and CC. For example;

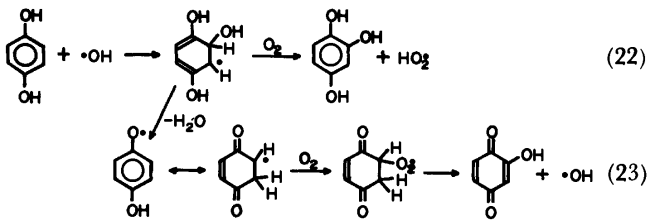

HO_2· radicals produced by Eqs. 19—21 can regenerate ·OH radicals *via* Eqs. 5—11. If the formation of ·OH *via* H_2O_2 according to Eqs. 4—11 is fully operative, 0.67 and 1.05 mole of O_2 will be necessary to consumption of one mole of phenol according to Eqs. 19 and 20 and Eq. 21, respectively. Taking the product distribution shown in Table 3 into account, it is estimated that 0.70 mol of O_2 is consumed for consumption of one mole of phenol. This estimation is in agreement with the experimental result shown in Fig. 4, indicating that the importance of formation of ·OH radicals *via* H_2O_2.

It has been reported that H_2 was not formed for photocatalytic reaction of some organic compounds

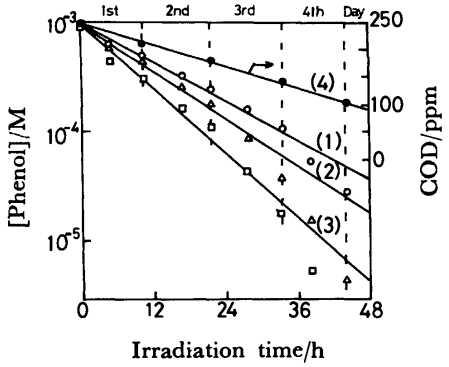

Fig. 7. Reduction of [phenol] and COD with reaction time under solar irradiation.
(1) and (4) anatase; (2) anatase in the presence of Fe^{3+} (50 μM); (3) Cu-deposited anatase.
The experimental conditions are given in the text.

in oxygenated solutions.[8,32] Therefore, the complete decomposition of phenol seems to be expressed by Eq. 24.

$$C_6H_5OH + 7\,O_2 \longrightarrow 6\,CO_2 + 3\,H_2O \qquad (24)$$

Photocatalytic Decomposition under Solar Irradiation. Figure 7 shows reduction of [phenol] and COD under solar irradiation. Control experiments with irradiated solutions with or without Cu^{2+} (50 μM) in the abscence of anatase showed very little decomposition of phenol occurred under these conditions. In the presence of anatase covering the bottom, phenol disappeared according to Eq. 1, without the serious influence of changes in both weather and height of the sun. Phenol was decomposed by the average rate of 8.6 mmol m^{-2} d^{-1} over first two days. By using Cu-deposited anatase powder, the reduction rate was increased appreciably. This catalyst, however, was not useful for wastewater treatment, because Cu deposited were dissolved into the reaction solution according to Eq. 15.

COD was reduced linearly with irradiation time. Since the photocatalytic decomposition proceeded by hydroxylation of phenol and its intermediate products according to Scheme 2, it is reasonable that a reduction in COD is proportional to an amount of ·OH radicals produced and therefore to an irradiation time. It is interesting from the viewpoint of wastewater treatment that phenol is completely mineralized to CO_2 and H_2O in the presence of anatase powder under solar irradiation without both aeration and mixing of the solution.

The present work was partially supported by a Grant-in-Aid for Scientific Research No. 58035042 from the Ministry of Education, Science and Culture.

References

1) A. Fujishima and K. Honda, *Nature*, **238**, 37 (1972); T. Kawai and T. Sakata, *ibid.*, **286**, 474 (1980); T. Kanno, T. Oguchi, H. Sakuragi, and K. Tokumaru, *Tetrahedron Lett.*, **21**, 467 (1980); M. A. Fox, *Acc. Chem. Res.*, **16**, 314 (1983).
2) J. H. Cary, J. Lawrence, and H. M. Tosine, *Bull. Environ. Contam. Toxicol.*, **16**, 697 (1976); J. H. Carey and B. G. Oliver, *Water Poll. Res. J. Canada*, **15**, 157 (1980).
3) S. N. Frank and A. J. Bird, *J. Phys. Chem.*, **81**, 1484 (1977); *idem.*, *J. Am. Chem. Soc.*, **99**, 303 (1977).
4) B. G. Oliver, E. G. Cosgrove, and J. H. Carey, *Environ. Sci. Technol.*, **13**, 1075 (1979).
5) H. Yoneyama, Y. Yamashita, and H. Tamura, *Nature*, **282**, 817 (1979).
6) K. Kogo, H. Yoneyama, and H. Tamura, *J. Phys. Chem.*, **84**, 1705 (1980).
7) H. Kawaguchi and T. Uejima, *Kagaku Kōgaku Ronbunshu*, **9**, 107 (1983).
8) A. L. Pruden and D. F. Ollis, *J. Catal.*, **82**, 404 (1983); C.-Y. Hisao, C.-L. Lee, and D. F. Ollis, *ibid.*, **82**, 418 (1983).
9) K. Okamoto, Y. Yamamoto, H. Tanaka, and A. Itaya, *Bull. Chem. Soc. Jpn.*, **58**, 2023 (1985).
10) M. D. Ward and A. J. Bird, *J. Phys. Chem.*, **86**, 3599 (1982); H. Reiche, W. W. Dunn, and A. J. Bird, *ibid.*, **83**, 2248 (1979).
11) C. A. Parker, *Proc. Roy. Soc. (London)*, **220A**, 104 (1953).
12) For analyses of the reaction products, 0.02% acetic acid solution (pH 3.1) was used from the following reasons; (1) 1,2,4-benzenetriol is unstable in a neutral or alkaline solution, and (2) 2-hydroxy-1,4-benzoquinone was decomposed to compounds with very short retention times (probably on the ODS gel) when neutral water was used as an eluting solvent.
13) H. Pobiner, *Anal. Chem.*, **33**, 1423 (1961).
14) Y. Ishihara, T. Naniwa, S. Yokokura, and S. Uchida, *Japan Analyst*, **17**, 991 (1968); M. Otomo, *Bull. Chem. Soc. Jpn.*, **36**, 1577 (1963).
15) A. Fujishima, T. Kato, E. Maekawa, and K. Honda, *Bull. Chem. Soc. Jpn.*, **54**, 1671 (1981).
16) P. C. Jaeger and A. J. Bird, *J. Phys. Chem.*, **83**, 3146 (1979).
17) A. Mills and George Porter, *J. Chem. Soc., Faraday Trans. 1*, **78**, 3659 (1992).
18) I. Izumi, W. W. Dunn, K. O. Wilbourn, F.-R. F. Fran, and A. J. Bird, *J. Phys. Chem.*, **84**, 3207 (1980).
19) M. Fujihira, Y. Satoh, and T. Osa, *Bull. Chem. Soc. Jpn.*, **55**, 666 (1982).
20) I. Izumi, F. F. Fan, and A. J. Bird, *J. Phys. Chem.*, **85**, 218 (1981).
21) R. W. Matihews, *J. Chem. Soc., Faraday Trans. 1*, **80**, 457 (1984).
22) R. B. Cundall, R. Rudham, and M. S. Salim, *J. Chem. Soc., Faraday Trans. 1*, **72**, 1642 (1976); P. R. Harvey, R. Rudham, and S. Ward, *ibid.*, **79**, 1381 (1983).
23) J-M. Herrmann and P. Pichat, *J. Chem. Soc., Faraday Trans. 1*, **76**, 1138 (1980).
24) G. Munuera, V. Rives-Arnau, and A. Saucedo, *J. Phys. Chem.*, **75**, 736 (1979).
25) D. T. Sawyer and M. J. Gibian, *Tetrahedron*, **35**, 1471 (1979), and the references therein.
26) C. Walling, *Acc. Chem. Res.*, **8**, 125 (1975).
27) K. Hashimoto, T. Kawai, and T. Sakata, *J. Phys.*

Chem., **88**, 4083 (1984).
28) Y. Aikawa, A. Takahashi, and M. Sukigara, *Nippon Kagaku Kaishi* **1984**, 292.
29) S. Hashimoto, T. Miyata, M. Washino, and W. Kawakami, *Environ. Sci. Technol.*, **13**, 71 (1979).
30) G. E. Adams and B. D. Michael, *Nature*, **211**, 293 (1966); G. E. Adams and B. M. Michael, *Trans. Faraday Soc.*, **63**, 1171 (1967); E. J. Land and M. Ebert, *ibid.*, **63**, 1181 (1967).
31) I. Balakvishnam and M. P. Reddy, *J. Phys. Chem.*, **74**, 850 (1970).
32) M. R. St. John, A. J. Furgala, and A. F. Sammells, *J. Phys. Chem.*, **87**, 801 (1983).

 © 1985 The Chemical Society of Japan Bull. Chem. Soc. Jpn., 58, 2023—2028 (1985)

Kinetics of Heterogeneous Photocatalytic Decomposition of Phenol over Anatase TiO_2 Powder

Ken-ichi Okamoto,* Yasunori Yamamoto, Hiroki Tanaka, and Akira Itaya†
Department of Chemical Engineering, Faculty of Engineering, Yamaguchi University, Ube 755
(Received November 28, 1984)

The photocatalytic decomposition of phenol over anatase TiO_2 powder followed the first-order kinetics, upto high conversions, of which the apparent rate constant k_{ap} depended on initial concentration of phenol $[phenol]_0$, $[TiO_2]$, O_2 pressure p_{O_2}, and incident light intensity I. The dependence of the initial reaction rate Ω_0 on $[phenol]_0$ showed characteristic curvature convex to the concentration axis. The p_{O_2} dependence of both Ω_0 and k_{ap} was very similar each other and showed characteristic curvature to the p_{O_2} axis. The dependence of both Ω_0 and k_{ap} on $[phenol]_0$ was affected by the $[TiO_2]$ and I. Both Ω_0 and k_{ap} were proportional to I below *ca.* 1×10^{-5} mol m^{-2} s^{-1} and to $I^{1/2}$ above 2×10^{-5} mol m^{-2} s^{-1}. The activation energy was 10 kJ/mol. The results were satisfactorily explained by the equation;

$$\Omega=\phi_{\cdot OH}I_a^n\frac{K_{O_2}p_{O_2}}{1+K_{O_2}p_{O_2}}\cdot\frac{[phenol]}{[phenol]_0+\beta},$$

where Ω is the reaction rate; $\phi_{\cdot OH}I_a^n$, a parameter related to the formation rate of ·OH radicals or real reactive species; K_{O_2}, the equilibrium constant of Langmuir adsorption of O_2; β, the ratio of the combined first-order rate constant of the reaction of ·OH with species other than organic compounds to the second-order rate constant of the reaction of ·OH with phenol.

In the previous paper,[1] we have reported on the reaction pathway of the photocatalytic decomposition of phenol in oxygenated aqueous suspensions of anatase TiO_2 as follows. Hydroxyl radicals are real reactive species responsible for the reaction. They are formed not only by the reaction of holes with adsorbed H_2O or OH^{-1}, but also *via* H_2O_2 from $O_2^{\cdot-}$ formed by electron trapping of adsorbed O_2. Phenol are decomposed *via* its hydroxylated compounds into the final products of CO_2 and H_2O. It is interesting from the viewpoint of wastewater treatment that phenol is completely mineralized to CO_2 in the presence of TiO_2 powder under solar irradiation without both aeration and mixing of the solution.

In the present paper, effects of initial concentration of phenol, TiO_2 loading, partial pressure of O_2 in a gas bubbled, incident light intensity, and temperature on the reaction rate were investigated at the optimum pH 3.5. A kinetic equation was proposed to explain the experimental results satisfactorily.

Experimental

Lightly-reduced anatase TiO_2 prepared previously[1] was used as a photocatalyst. The experimental procedure was the same as mentioned in the previous paper,[1] except where noted.

The photocatalytic reaction was carried out in two types of photoreactors at pH 3.5. One (named reactor I) was the same as used previously.[1] The other (named reactor II) was a 200 cm^3 beaker with both four pieces of baffles and a water jacket. A quantity of TiO_2 was suspended in 100 cm^3 of a phenol solution by stirring magnetically. Air was bubbled through the suspension at the rate of 50 cm^3 min^{-1}. The suspension was irradiated from the upside of the beaker by a parallel UV-light, which was obtained by passing the light from a 500 W high-pressure mercury lamp (Ushio Electric Co., USH-500D) through both a $CuSO_4$ solution (0.24 M (1 M=1 mol dm^{-3}), 10 cm) and a band-pass filter (Toshiba Co., UVD-25 or UVDIC) and was substantially composed of 366, 334, and 313 nm light. The irradiated area was 27 cm^2 and the depth of the suspensions was 3.5 cm. The light intensity was adjusted by using wire meshes and/or Pyrex glass plates as neutral filters. The suspension was kept at a constant temperature (usually 25 °C) by circulating thermostated water through the jacket.

The average diameter of TiO_2 powder in the suspensions was measured by means of a highly-directional photoprobe.[2]

Results

Effects of Both Initial Concentration of Phenol and Partial Pressure of O_2. The photocatalytic decomposition of phenol followed the first-order reaction kinetics (Eq. 1) upto high conversions.[1]

$$-\ln\left(\frac{[phenol]}{[phenol]_0}\right)=k_{ap}t \qquad (1)$$

where $[phenol]_0$ is initial concentration of phenol; k_{ap}, the apparent first-order rate constant; t, the reaction time. The dependence of initial reaction rate Ω_0 and k_{ap} on $[phenol]_0$ is shown in Figs. 1 and 2, respectively. The k_{ap} depended on $[phenol]_0$, indicating that the reaction was not a simple first-

† Present address: Department of Polymer Science and Engineering, Kyoto Institute of Technology, Matsugasaki, Kyoto 606.

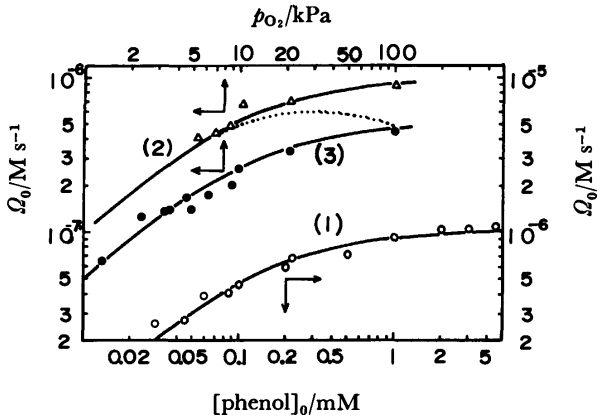

Fig. 1. Dependence of Ω_0 on both [phenol]$_0$ and p_{O_2}.
Reactor I and [TiO_2] = 6.3 mg cm^{-3}. (1) p_{O_2} = 101 kPa; (2) [phenol]$_0$ = 1 mM; (3) [phenol]$_0$ = 0.1 mM.
The solid lines were calculated from Eq. 10 with $\phi_{\cdot OH} I_a^n = 1.12$ μM s^{-1}, $\beta = 0.12$ mM, and $K_{O_2} = 0.11$ kPa^{-1}.
The dotted line was calculated from Eqs. 10 and 17 with $\phi_{\cdot OH} I_a^n = 1.12$ μM s^{-1}, $K_{O_2} = 0.11$ kPa^{-1}, and $k_d/(k_{ph}K_{ph}) = 10$ μM.

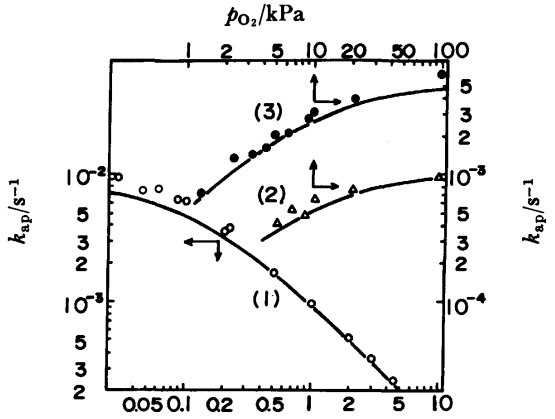

Fig. 2. Dependence of k_{ap} on both [phenol]$_0$ and p_{O_2}.
The experiments were the same as in Fig. 1.
The solid lines were calculated from Eq. 21 with the same values of the parameters as used in Fig. 1.

order one. Figures 1 and 2 also show the dependence of Ω_0 and k_{ap} on the partial pressure of O_2, p_{O_2}, in a bubbled gas, respectively. As has been reported previously,[1] the dependence of Ω_0 on p_{O_2} was represented by Eq. 2.

$$\Omega_0 \propto \frac{K_{O_2} p_{O_2}}{1 + K_{O_2} p_{O_2}} \tag{2}$$

where K_{O_2} is the equilibrium constant of Langmuir adsorption of O_2. It is noted that the dependence of k_{ap} on p_{O_2} was almost the same as that of Ω_0.

As shown in Figs. 3 and 4, the dependence of both

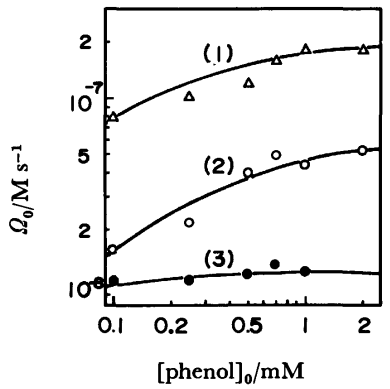

Fig. 3. Dependence of Ω_0 on [phenol]$_0$.
Reactor II and p_{O_2} = 21 kPa. (1) $I = 3.5 \times 10^{-4}$ mol m^{-2}s^{-1} and [TiO_2] = 1.2 mg cm^{-3}; (2) $I = 3.5 \times 10^{-4}$ mol m^{-2}s^{-1} and [TiO_2] = 0.15 mg cm^{-3}; (3) $I = 4.1 \times 10^{-6}$ mol m^{-2}s^{-1} and [TiO_2] = 1.2 mg cm^{-3}. The solid lines were calculated from Eq. 10 with the corresponding set of the parameter values listed in Table 2.

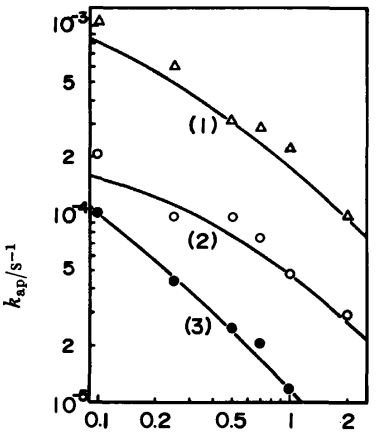

Fig. 4. Dependence of k_{ap} on [phenol]$_0$.
The experiments were the same as in Fig. 3.
The solid lines were calculated from Eq. 21 with the same values of the parameters as used in Fig. 3.

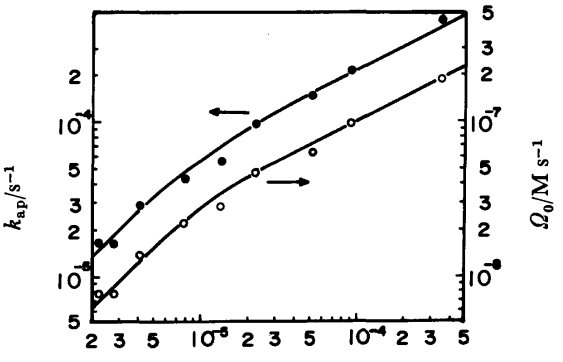

Fig. 5. Light-intensity dependence of both Ω_0 and k_{ap}.
Reactor II, p_{O_2} = 21 kPa, [phenol]$_0$ = 0.5 mM, and [TiO_2] = 2.0 mg cm^{-3}.

Ω_0 and k_{ap} on $[phenol]_0$ depended on light intensity I and $[TiO_2]$.

Effect of Light Intensity. Figure 5 shows light-intensity dependence of both Ω_0 and k_{ap}. Both Ω_0 and k_{ap} were proportional to I below *ca.* 10 μmol m^{-2} s^{-1} and to $I^{1/2}$ *ca.* above 20 μmol m^{-2} s^{-1}. The square-root dependence of Ω_0 in I indicates that the reaction was limited by the recombination of photogenerated hole-electron pairs. The experiments carried out both in the reactor I and without dense neutral filters in the reactor II were in the region of this dependence.

The effective intensity of sunlight was evaluated to be *ca.* 4 μmol m^{-2} s^{-1} from both the Ω_0 value of 1.9×10^{-8} M s^{-1} for $[phenol]_0$=1 mM and the quantum yield of 10% for 366 nm.[1] This is in the region of linear dependence of Ω_0 on I.

Effect of $[TiO_2]$. Figure 6 shows variation of [phenol] with reaction time for the suspensions with different concentrations of TiO_2. When the suspensions were stirred for only 15 min in the dark prior to the reaction, the patterns of the reaction curves observed for the dilute suspensions were quite different from that expected from Eq. 1, as shown by the solid line (3) as an example. On the other hand, when they were stirred for more than 60 min prior to the reaction, such a deviation from Eq. 1 was not observed even for the dilute suspensions, as shown by the solid line (2) as an example. This was related to a change of dispersion state of TiO_2 powder. Table 1 shows the variation of average diameter $\bar{d}_p$ of TiO_2 powder in a suspension during a run. When the suspensions were not stirred sufficiently prior to the reaction, the dispersion state of the powder was much improved by UV-irradiation, probably because of accumulation of surface charge,[3] resulting in gradual increases of the light-absorption rate and consequently of the reaction rate for the dilute suspensions. For the suspensions stirred sufficiently prior to the reaction, a decrease of $\bar{d}_p$ caused by UV-irradiation was not large and was furthermore attained in only several min after light on. Therefore, in this case it hardly affects the reaction curves.

Table 1. Variation of $\bar{d}_p$ of TiO_2 powder in a suspension during a run[a]

$\bar{d}_p$/μm	Stirring conditions
1.88	15 min in the dark
0.98	60 min in the dark
0.76	7 min under UV-irradiation[b]
0.78	20 min under UV-irradiation[b]

a) Reactor II, $[TiO_2]$=0.20 mg cm^{-3} and pH 3.5. The $\bar{d}_p$ was 0.17 μm for the suspension where TiO_2 powder was completely dispersed by use of sodium hexametaphosphate. b) The suspension was stirred for 60 min in the dark prior to UV-irradiation.

The results concerning both Ω_0 and k_{ap} mentioned here were obtained for the suspensions stirred for more than 60 min prior to the reaction.

As shown in Fig. 7, the $[TiO_2]$ dependence of both Ω_0 and k_{ap} was very similar each other. In the high concentration region above 5 mg/cm^3, both Ω_0 and k_{ap} were independent of $[TiO_2]$ at a low light intensity, while they still increased with an increase of $[TiO_2]$ at a high light intensity.

Effect of Temperature. Figure 8 shows the temperature dependence of both Ω_0 and k_{ap}. The activation energy of both Ω_0 and k_{ap} was about

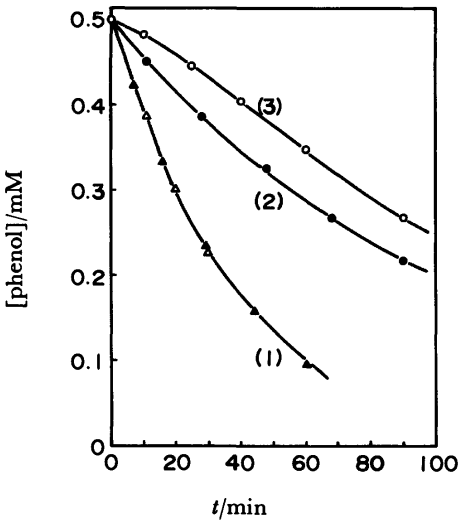

Fig. 6. Effect of stirring time prior to the reaction on the reaction curves.
Reactor II and p_{O_2}=21 kPa. The suspensions were stirred for either 15 min (○ and △) or 60 min (● and ▲) in the dark prior to the reaction.
○ and ●: $[TiO_2]$=0.3 mg cm^{-3}; △ and ▲: $[TiO_2]$ =2.0 mg/cm^3. The solid lines (1) and (2) were calculated from Eq. 1. The solid line (3) was drawn by eyes.

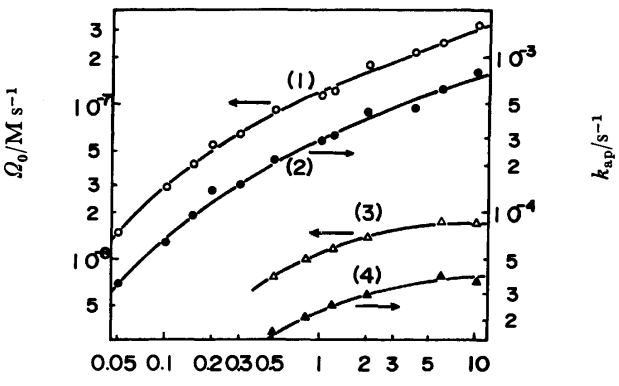

Fig. 7. Dependence of both Ω_0 and k_{ap} on $[TiO_2]$.
Reactor II, $[phenol]_0$=0.5 mM, and p_{O_2}=21 kPa.
(1) and (2): $I=3.5\times10^{-4}$ mol $m^{-2}s^{-1}$; (3) and (4): $I=4.1\times10^{-6}$ mol $m^{-2}s^{-1}$.

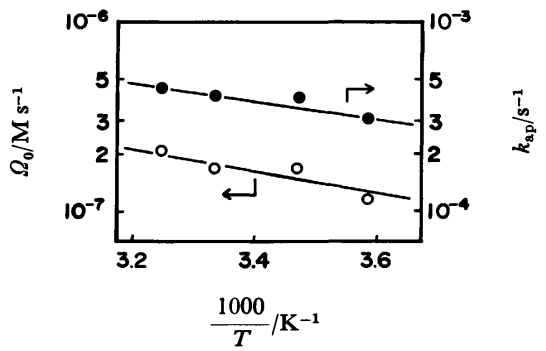

Fig. 8. Temperature dependence of both Ω_0 and k_{ap}. $[phenol]_0=0.5$ mM, $p_{O_2}=21$ kPa, $[TiO_2]=1.2$ mg/cm^3, and $I=3.5\times10^{-4}$ mol m^{-2}s^{-1}.

10 kJ/mol. This value was in the same range as those obtained for oxalic acid (13 kJ/mol)[4] and for formic acid (11 and 17 kJ/mol)[5,6], although being smaller than that obtained for 2-propanol (31 kJ/mol).[7] It was much smaller than that (48 kJ/mol) obtained for oxidation of phenol by means of Fentons' reagent.[8]

Discussion

Influence of Mass Transfer Rate on the Reaction Rate. It is clear from no influence of gas-bubbling rate on both Ω_0 and k_{ap} that mass transfer rate at gas-liquid interface did not affect the reaction rate. On the other hand, there remains the possibility that mass transfer rate at liquid-solid interface might affect the reaction rate, because both Ω_0 and k_{ap} increased with an increase of $[TiO_2]$ upto the highest concentration investigated here at a high light intensity, as shown in Fig. 7. The following consideration, however, objects this possibility.

The reaction rate Ω is expressed by Eq. 3 in terms of volumetric mass transfer coefficient k_sa.

$$\Omega = (k_sa)_A(c_{A,l}-c_{A,s}), \tag{3}$$

where $c_{A,l}$ and $c_{A,s}$ are the concentrations of species A in the bulk liquid and at the external surface of the particles, respectively. For very fine spherical particles k_sa is given by Eq. 4.[9]

$$k_sa = \frac{12\,D\,m_p}{\bar{d}_p^2\rho_p}, \tag{4}$$

where D is diffusion coefficient; m_p, mass of the particles per unit volume of a suspension; ρ_p, density of the particles. If we consider mass transfer of phenol in a dilute suspension with $[TiO_2]=0.12$ mg cm^{-3}, the value of $(k_sa)_{phenol}$ is evaluated to be 0.55 s^{-1}, using $D=8.9\times10^{-6}$ cm^2 s^{-1},[10] $\bar{d}_p=0.77$ μm, and $\rho_p=3.90$ g/cm^3. In the case of an experimental result of $\Omega_0=4\times10^{-8}$ M s^{-1} with $[phenol]_0=0.5$ mM, $I=3.5\times10^{-4}$ mol m^{-2} s^{-1}, and $[TiO_2]=0.12$ mg/cm^3, the ratio of $[phenol]_s/[phenol]_l$ is evaluated to be 0.9998. The similar values of the ratio of $c_{A,s}/c_{A,l}$ are evaluated for other species such as O_2, ·OH, and the intermediate products. This fact indicates that the results mentioned above were not affected by mass transfer rate at liquid-solid interface at all.

Chemical Kinetics. Simple Langmuir-Hinshelwood kinetics have been applied to the photocatalytic reaction of trichloroethylene,[11] chloromethanes[12], halide ions,[13] and aliphatic carboxylic acids.[4,6] In these reports, only the dependence of Ω_0 on initial concentration of the substrates has, however, been investigated. As mentioned above, the photocatalytic decomposition process of phenol had the following important characteristics. (1) Upto the high conversions, the reaction apparently proceeded according to the first-order kinetics with k_{ap} depending on $[phenol]_0$ p_{O_2}, $[TiO_2]$, and I. (2) The dependence of Ω_0 on $[phenol]_0$ showed characteristic curvature convex to the concentration axis. (3) The p_{O_2} dependence of both Ω_0 and k_{ap} was very similar each other and showed characteristic curvature convex to the p_{O_2} axis. (4) The dependence of both Ω_0 and k_{ap} on $[phenol]_0$ was affected by $[TiO_2]$ and I. A chemical kinetic model is proposed as follows, in order to explain these characteristics.

The rate determining step of the reaction is reasonably considered to be the formation of ·OH radicals or real reactive species, because they react very rapidly with phenols; for example, $k=1.4\times10^{10}$ M^{-1} s^{-1} for phenol.[14] The reaction rate is, therefore, given by the product of formation rate of ·OH, $\Omega_{\cdot OH}$, and the probability of the reaction of ·OH with phenol, P_{ph}.

$$\Omega = \frac{-d[phenol]}{dt} = \Omega_{\cdot OH}P_{ph} \tag{5}$$

Judging from the initial steps of the photocatalysis mentioned in the previous paper,[1] $\Omega_{\cdot OH}$ is proportional to the number of hole-electron pairs escaped from the recombination. O_2 adsorbed on TiO_2 surface prevents the recombination by trapping an electron. Therefore, $\Omega_{\cdot OH}$ is reasonably considered to be expressed by Eq. 6.

$$\Omega_{\cdot OH} = \frac{\phi_{\cdot OH}I_a^nK_{O_2}p_{O_2}}{1+K_{O_2}p_{O_2}}, \tag{6}$$

where $\phi_{\cdot OH}$ is a constant related to the yield of formation of ·OH; I_a, rate of light absorption; n, a constant representing the dependence of $\Omega_{\cdot OH}$ on I.

Hydroxyl radicals react with phenol and its intermediates with second-order rate constants of k_{ph} and k_I (k_{I_i} for an intermediate I_i), respectively. They also react with the other species such as electrons and

O_2^- ions[15] with a combined first-order rate constant of k_d.

$$\left.\begin{aligned} \cdot OH + e &\longrightarrow OH^- \\ \cdot OH + O_2^- &\longrightarrow O_2 + OH^- \end{aligned}\right\} \quad (7)$$

The following three cases are assumed concerning the reaction of ·OH with phenol and its intermediates.

Case I. We assume that ·OH radicals react with the species being either in bulk liquid phase or at the interface. Then, P_{ph} is given by Eq. 8.

$$P_{ph} = \frac{k_{ph}[\text{phenol}]}{k_{ph}[\text{phenol}] + \sum_i k_{I_i}[I_i] + k_d}, \quad (8)$$

where the summation of the second term of the denominator is taken over every intermediate. Moreover, we assume that Eq. 9 holds to a fairly good approximation over a long period of reaction time.

$$k_{ph}[\text{phenol}] + \sum_i k_{I_i}[I_i] = k_{ph}[\text{phenol}]_0 \quad (9)$$

Then, Ω is expressed by Eq. 10.

$$\Omega = \phi_{\cdot OH} I_a^n \frac{K_{O_2} p_{O_2}}{1 + K_{O_2} p_{O_2}} \cdot \frac{[\text{phenol}]}{[\text{phenol}]_0 + \beta}, \quad (10)$$

$$\beta = k_d / k_{ph}. \quad (11)$$

Case II. We assume that ·OH radicals react with the species adsorbed on TiO_2 surface in competition with O_2. Then, P_{ph} is given by Eq. 12.

$$P_{ph} = \frac{k_{ph}\theta_{ph}}{k_{ph}\theta_{ph} + \sum_i k_{I_i}\theta_{I_i} + k_d}, \quad (12)$$

where θ_{ph} and θ_{I_i} are the surface coverages of phenol and an intermediate I_i, respectively. Both phenol and its primary intermediates were hardly adsorbed on TiO_2 surface.[1] Moreover, the p_{O_2} dependence of both Ω_0 and k_{ap} was not affected by $[\text{phenol}]_0$. Judging from these facts, Eq. 13 holds.

$$1 + K_{O_2} p_{O_2} \gg K_{ph}[\text{phenol}] + \sum_i K_{I_i}[I_i], \quad (13)$$

where K_{ph} and K_{I_i} are the equilibrium constants of phenol and an intermediate I_i, respectively. Therefore, θ_{ph} and θ_{I_i} is given by Eqs. 14 and 15, respectively.

$$\theta_{ph} = \frac{K_{ph}[\text{phenol}]}{1 + K_{O_2} p_{O_2}} \quad (14)$$

$$\theta_{I_i} = \frac{K_{I_i}[I_i]}{1 + K_{O_2} p_{O_2}} \quad (15)$$

Moreover, we assume that Eq. 16 holds to a fairly good approximation over a long period of reaction time.

$$k_{ph}K_{ph}[\text{phenol}] + \sum_i k_{I_i}K_{I_i}[I_i] = k_{ph}K_{ph}[\text{phenol}]_0 \quad (16)$$

Then, we obtain the same equation as Eq. 10, although in this case β is expressed by Eq. 17 instead of Eq. 11.

$$\beta = \frac{k_d(1 + K_{O_2} p_{O_2})}{k_{ph}K_{ph}} \quad (17)$$

Case III. We assume that ·OH radicals react with the species adsorbed at the sites different from the adsorption sites of O_2. Then, P_{ph} is given by Eq. 12, where θ_{ph} and θ_{I_i} are expressed by Eqs. 18 and 19 instead of Eqs. 14 and 15, respectively.

$$\theta_{ph} = K_{ph}[\text{phenol}] \quad (18)$$

$$\theta_{I_i} = K_{I_i}[I_i] \quad (19)$$

Moreover, we assume Eq. 16 as in Case II. Then, we obtain the same equation as Eq. 10, although in this case β is expressed by Eq. 20.

$$\beta = \frac{k_d}{k_{ph}K_{ph}} \quad (20)$$

Concerning [phenol], Eq. 10 is a first-order kinetic equation with the rate constant k_{ap} expressed by Eq. 21.

$$k_{ap} = \frac{\phi_{\cdot OH} I_a^n K_{O_2} p_{O_2}}{(1 + K_{O_2} p_{O_2})([\text{phenol}]_0 + \beta)} \quad (21)$$

Both Eqs. 10 and 21 have three adjustable parameters of $\phi_{\cdot OH} I_a^n$, K_{O_2}, and β. The solid lines in Fig. 1 were calculated from Eq. 10 with $\phi_{\cdot OH} I_a^n = 1.12\,\mu M\,s^{-1}$, $K_{O_2} = 0.11\,kPa^{-1}$, and $\beta = 0.12\,mM$. These values were determined to give best fit of the calculated lines with the experimental results. The solid lines in Fig. 2

Table 2. Kinetic parameters obtained for various experimental conditions[a]

	Experimental conditions		Kinetic parameters		
	I / mol m^{-2} s^{-1}	$[TiO_2]$ / mg cm^{-3}	$\phi_{\cdot OH} I_a^n$ / M s^{-1}	β / mM	K_{O_2} / kPa^{-1}
(1)	$\approx 10^{-3}$	6.3	1.12×10^{-6}	0.12	0.11
(2)	3.5×10^{-4}	1.2	2.2×10^{-7}	0.15	0.11
(3)	3.5×10^{-4}	0.15	6.8×10^{-8}	0.30	0.11
(4)	4.1×10^{-6}	1.2	1.2×10^{-8}	0.02	0.11

a) (1): Reactor I and $p_{O_2} = 101$ kPa; (2)—(4): Reactor II and $p_{O_2} = 21$ kPa.

were calculated from Eq. 21 with the same values of the parameters. They were in good agreement with the experimental results.

The solid lines in Figs. 3 and 4 were calculated from Eqs. 10 and 21, respectively, with the values of the parameters listed in Table 2. They were also in good agreement with the experimental results obtained for different conditions of I and [TiO_2]. As can be seen from Table 2, there is a tendency that the β value is small for the case with both a high value of [TiO_2] and a low value of I. This is due to the dependence of k_d on both [TiO_2] and I; judging from Eq. 7, k_d is reasonably considered to be reduced with an increase of [TiO_2] and with a decrease of I. Thus, Eq. 10 satisfactorily explains the experimental results.

In Case II, β should depend on p_{O_2}, as expressed by Eq. 17. For the experiments shown in Fig. 2, the value of $k_d/(k_{ph}K_{ph})$ in Eq. 17 was evaluated to be 10 μM using the β and K_{O_2} values (0.12 mM and 0.11 kPa^{-1}, respectively) obtained with p_{O_2}=101 kPa. The relation of Ω_0 *vs.* p_{O_2} for [phenol]=0.1 mM was calculated from Eqs. 10 and 17 with $\phi_{\cdot OH}I_a^n$= 1.12 μM s^{-1}, K_{O_2}=0.11 kPa^{-1} and $k_d/(k_{ph}K_{ph})$=10 μM. As shown by the dotted line in Fig. 1, the calculated relation of Ω_0 *vs.* p_{O_2} is quite different from the experimental one, indicating that Case II is ruled out for the present reaction.

At the present, we have no idea concerning which one between Cases I and III is more appropriate for the present reaction. The Ω_0 values of hydroquinone and pyrocatechol were 70 and 65% of that of phenol observed under the same conditions, respectively, while the reaction of ·OH with phenols has been reported to be diffusion-controlled.[14] Appreciable amounts of undetected compounds having very short retention times in liquid chromatograms were produced at the initial stage of the reaction of hydroquinone and pyrocatechol.[1] Phenol, hydroquinone, and pyrocatechol were hardly adsorbed on TiO_2 powder.[1] Judging from these facts, both Eqs. 9 and 16 appear to be the resonable assumptions.

In order to discuss the dependence of both Ω_0 and k_{ap} on [TiO_2], it is necessary to know the local rate of light absorption of TiO_2 powder in the reactor. At the present, we have no information about it. The experiments are in progress.

The present work was partially supported by a Grant-in-Aid for Scientific Research No. 58035042 from the Ministry of Education, Science and Culture.

References

1) K. Okamoto, Y. Yamamoto, H. Tanaka, M. Tanaka, and A. Itaya, *Bull. Chem. Soc. Jpn.*, **58**, 2015 (1985).
2) M. Tanaka, A. Itaya, and K. Okamoto, *Kagaku Kogaku Ronbunshu*, **10**, 551 (1984); P. H. Calderbank, *Trans. Instn. Engrs.*, **36**, 443 (1958).
3) W. W. Dunn, Y. Aikawa, and A. J. Bird, *J. Am. Chem. Soc.*, **103**, 3456 (1981).
4) J. M. Herrmann, M. N. Mozzanega, and P. Pichat, *J. Photochem.*, **22**, 333 (1983).
5) H. Yoneyama, N. Matsumoto, T. Furusawa, and H. Tamura, *Nippon Kagaku Kaishi*, **1984**, 253.
6) M. Bideau, B. Claudel, and M. Otterbein, *J. Photochem.*, **14**, 291 (1980).
7) P. R. Harvey, R. Rudham, and S. Ward, *J. Chem. Soc., Faraday Trans. 1*, **79**, 1381 (1983).
8) M. Sudo, T. Yonebayashi, and K. Koide, 18th Autumn Meeting of The Society of Chemical Engineers of Japan, Fukuoka, October 1984, Abstr. No.SD210.
9) R. V. Chaudhari and P. A. Ramachandran, *AIChEJ*, **26**, 177 (1980).
10) "Kagaku Kogaku Binran," ed by Inst. Chem. Eng. Jpn., Maruzene (1978), P. 68.
11) A. l. Pruden and D. F. Ollis, *J. Catalysis*, **82**, 404 (1983).
12) C.-Y. Hsiao, C.-L. Lee, and D. F. Ollis, *J. Catalysis*, **82**, 418 (1983).
13) J.-M. Herrmann and P. Pichat, *J. Chem. Soc., Faraday Trans. 1*, **76**, 1138 (1980).
14) G. E. Adams and B. D. Michael, *Trans. Faraday Soc.*, **63**, 1171 (1967); E. J. Land and M. Ebert, *ibid.*, **63**, 1181 (1967).
15) G. Munuera, V. Rives-Arnau, and A. Saucedo, *J. Chem. Soc., Faraday Trans. 1*, **75**, 736 (1979); D. T. Sawyer and M. J. Gibian, *Tetrahedron*, **35**, 1471 (1979).

 © 1985 The Chemical Society of Japan Bull. Chem. Soc. Jpn., 58, 2029—2037 (1985)

Kinetics and Mechanistic Study of the Methanol Homologation with Cobalt-Ruthenium Mixed Catalyst

Kazuhiro WATANABE,* Kiyoshi KUDO, and Nobuyuki SUGITA
Institute for Chemical Research, Kyoto University, Gokanosho Uji, Kyoto 611
(Received January 26, 1985)

The role of each catalyst was examined in detail in the methanol homologation with cobalt-ruthenium mixed catalyst. Cobalt catalyst showed much higher activity for the hydrocarbonylation of methanol than ruthenium. On the other hand, the hydrogenation of acetaldehyde proceeded much more rapidly by ruthenium catalyst. The rate of methanol homologation in 1,4-dioxane with cobalt-ruthenium mixed catalyst system was found to be of the first order with respect to the partial pressure of CO. The *in situ* IR spectra indicated that $[Co(CO)_4]^-$ was an active species for the hydrocarbonylation of methanol and that $[RuI_x(CO)_y]$ existed under the reaction conditions. On the basis of both the kinetic studies and *in situ* IR spectral observations, the reaction mechanism of methanol homologation was fully discussed.

The conversion of synthetic gas to organic chemicals has become an important problem to be solved in both fundamental and applied fields.

Methanol homologation (Eq. 1) with cobalt catalyst, which is one of the most important reactions in the so-called C_1 chemistry, was first reported by Wender and his co-workers in 1949.[1]

$$CH_3OH + CO + 2H_2 \rightarrow CH_3CH_2OH + H_2O \quad (1)$$

Berty's[2] and Mizoroki's[3] groups found independently that the addition of an iodide increased the yield of ethanol. A recent study[4] showed that the covalent CH_3I was more active than the ionic LiI, KI, and $MePBu_3I$. In order to improve the selectivity many studies have been carried out on the effect of solvents[5] and ligands,[6] and that of the addition of ruthenium[7,8] or iron[9] to cobalt catalytic system. From these results, it was revealed that the use of oxygen-containing solvent such as cyclic ether improved the selectivity of ethanol formation and that the optimum mole ratio of ruthenium to cobalt existed.

We found previously that the optimum mole ratio of ruthenium to cobalt depended on the reaction conditions such as the reaction temperature, pressure and H_2/CO.[10]

Up to now, the role of ruthenium as well as the reaction mechanism was not fully elucidated yet. Thus we investigated the mechanism of the methanol homologation with $Co_2(CO)_8$–$RuCl_3$ mixed catalyst from a kinetic study and *in situ* IR observation.

This homologation reaction was accompanied by the side reactions of methanol, as shown in Eqs. 2—4. Therefore, the kinetic experiments

$$CH_3OH + ROH \rightarrow CH_3OR + H_2O \quad (R = CH_3 \text{ or } CH_3CH_2) \quad (2)$$

$$CH_3CHO + 2\,CH_3OH \rightleftarrows CH_3CH(OCH_3)_2 + H_2O \quad (3)$$

$$CH_3OH + CO \xrightarrow{ROH} CH_3COOR \quad (R = H,\ CH_3,\ CH_3CH_2) \quad (4)$$

were carried out in 1,4-dioxane under such reaction conditions that the amounts of by-products could be minimized.

Experimental

Materials. The compounds, $Co_2(CO)_8$, $RuCl_3 \cdot nH_2O$ (Ru content: *ca.* 45 wt%), and methyl iodide were commercially obtained and used without further purification. Methanol and 1,4-dioxane were distilled over a Na-Pb alloy under nitrogen atmosphere. Hydrogen was a commercial material and its purity was above 99.9%. Carbon monoxide was prepared by decomposing formic acid in hot sulfuric acid, and its purity was above 98%.

Procedure. In all kinetic experiments, the reactions were carried out in a glass tube placed in a stainless-steel autoclave (*ca.* 200 ml) equipped with a Teflon stirrer and a Teflon sampling line.

Adequate amounts of the precatalysts ($Co_2(CO)_8$ and $RuCl_3 \cdot nH_2O$) and metyl iodide were dissolved in 1,4-dioxane and this mixture was charged in the autoclave. The air in the autoclave was purged three or four times with CO, and then the solution was pressured with CO and H_2 (total pressure: 150 kg cm^{-2} at room temperature). The vessel was heated to the reaction temperature (160 °C) for 40 min in an oil bath. After the temperature had been kept constant for 30 min, the substrate (methanol or acetaldehyde dimethyl acetal) was pumped into the autoclave with a high pressure injection pump. The mixture of CO and H_2 was introduced to the desired pressure, and stirring of the solution was started with an electromagnetic stirrer (1400 min^{-1}), this time being marked as zero time.

Stirring was stopped from time to time and an aliquot (*ca.* 0.2 ml) was withdrawn through the sampling line into a trap chilled in a dry-ice bath at interval of 10 to 30 min. To keep the pressure constant during the reaction, the consumed gas was supplied from a reservoir in which CO and H_2 had been mixed beforehand in the fixed ratio.

The IR spectra were recorded with Hitachi Model EPI-G3 spectrophotometer under a working pressure of the appropriately mixed gas of CO and H_2 and at the desired temperature (160 °C—180 °C) by using a high pressure IR cell (for *in situ* observation) designed in our laboratory. This high pressure cell consists of 60×70×80 mm block of stainless-steel through which a 30 mm diameter hole bored to form a central capacity for accommodating the window

and the spacer (0.1 mm thick). The cell has optically flat surfaces. The temperature of the cell was monitored with a thermocouple which was inserted into the cell block. Repeated registration of spectrum allowed the reaction to be followed.

Analysis. Products were indentified by comparison of their retention times in the gas-liquid chromatography (GLC) with those of authentic samples (N_2 as carrier gas). A polyethylene glycol 1000 (PEG-1000) column (1.5 m, 3 mm ϕ) was used at 90 °C for the determination of the amounts of products with *m*-xylene as an internal standard.

Results and Discussion

Preliminary Investigation. In 1,4-dioxane solvent, we have explored the optimum reaction conditions for the methanol homologation. Under the optimum reaction conditions, we obtained the high selective formation of ethanol (75 mol%) and high conversion of methanol (67 mol%) as shown in Table 1 (Run 2). The mole ratio of ruthenium to cobalt giving high selectivity of ethanol formation was revealed to be about 0.2 from Table 2. Under the optimum reaction conditions, acetaldehyde dimethyl acetal was the major by-product, and esters (methyl and ethyl acetates) and ethers (dimethyl, ethyl methyl and diethyl ethers) were merely minor by-products. Therefore, the reaction system consisting of $Co_2(CO)_8$–$RuCl_3$ mixed catalyst, methyl iodide and 1,4-dioxane as solvent was chosen for our kinetic studies.

Figure 1 shows that the total amount of acetaldehyde reaches maximum at the early stage of reaction (about 10 min), and then decreases to nearly zero. Here, the total amount of acetaldehyde is the sum of acetaldehyde and its dimethyl acetal formed by dehydration (Eq. 3), and the latter is major. This result indicates that acetaldehyde should be an intermediate for the formation of ethanol. Therefore, the methanol homologation proceeds *via* consecutive steps, that is, the hydrocarbonylation of methanol to acetaldehyde (Eq. 5) followed by the hydro-

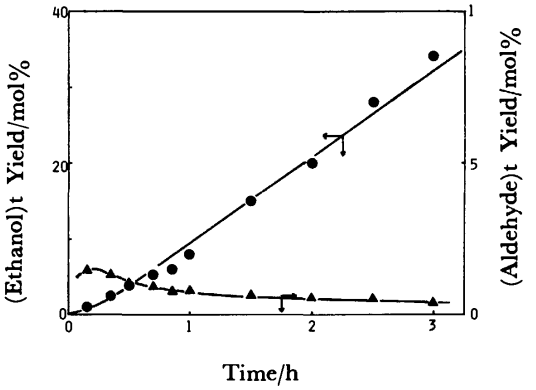

Fig. 1. Methanol homologation catalyzed by cobalt–ruthenium mixed catalyst.
[Ru]/[Co]=0.2. Reaction conditions: see footnote of Table 2.
●: ethanol, ▲: acetaldehyde.

TABLE 1. EFFECT OF TEMPERATURE[a]

Run	T / °C	CH_3OH Conv./%	Yield[b]/%		Select.[c]/%	
			$(Ethanol)_t$[d]	$(Aldehyde)_t$[e]	$(Ethanol)_t$	$(Aldehyde)_t$
1	160	56	34	0.39	60	0.70
2	180	67	50	0.25	75	0.37
3	200	83	38	0.20	46	0.24

a) Total pressure: 240 kg cm^{-2} at room temp ($H_2/CO=2/1$), CH_3OH: 7 M, CH_3I: 0.14 M, 1,4-dioxane: 5 ml $Co_2(CO)_8=(2.0—2.5)\times10^{-2}$ M, $RuCl_3=(0.9—1.0)\times10^{-2}$, Time: 3 h. 1 M=1 mol dm^{-3}. b) Yield=[product] (mol)/charged [CH_3OH] (mol)×100. c) Select.=[Product] (mol)/converted [CH_3OH] (mol)×100. d) $(Ethanol)_t$ = EtOH + EtOMe + 2 EtOEt. e) $(Aldehyde)_t=CH_3CHO+CH_3CH(OCH_3)_2$.

TABLE 2. EFFECT OF RUTHENIUM MOLE RATIO[a]

Run	Added Ru [M]×10^2	Ru/Co	CH_3OH Conv./%	$(Ethanol)_t$		$(Aldehyde)_t$
				Yield/%	Select./%	Yield/%
1	0	—	50	10	21	26
2	0.58	0.1	55	33	59	1.1[c]
3	1.2	0.2	51	43	78	1.1[c]
4	1.7	0.3	56	42	74	0.8[c]
5	2.3	0.4	54	32	64	0.8[c]
6	1.0[b]	—	38	2.8	10	0.9

a) Reaction temperature: 160 °C, Total pressure: 240 kg cm^{-2} at 160 °C ($H_2/CO=2/1$), CH_3OH: 7 M, CH_3I: 0.14 M, 1,4-dioxane: 50 ml, $Co_2(CO)_8=2.8\times10^{-2}$, Time: 3 h. b) $Co_2(CO)_8=0$. c) Maximum amount during the reaction.

genation to ethanol (Eq. 6).

$$CH_3OH + CO + H_2 \rightarrow CH_3CHO + H_2O \quad (5)$$

$$CH_3CHO + H_2 \rightarrow CH_3CH_2OH \quad (6)$$

Figure 2 indicates that the ruthenium catalyst has much lower reactivity for the hydrocarbonylation than the cobalt catalyst. The hydrocarbonylation of methanol seems to be principally catalyzed by the cobalt catalyst.

In order to evaluate the relative activity of the mixed catalytic system, we made three seperate studies on the hydrogenation of acetaldehyde with the cobalt catalyst, the ruthenium catalyst and the mixed catalyst. We chose acetaldehyde dimethyl acetal as the starting substrate, charged it at low concentration and added the equivalent amount of H_2O to the reaction system in order to prevent side reactions such as polymerization of acetaldehyde. Other reaction conditions such as total pressure, partial pressure of CO and H_2, reaction temperature and charged amount of CH_3I were the same as those in the present methanol homologation.

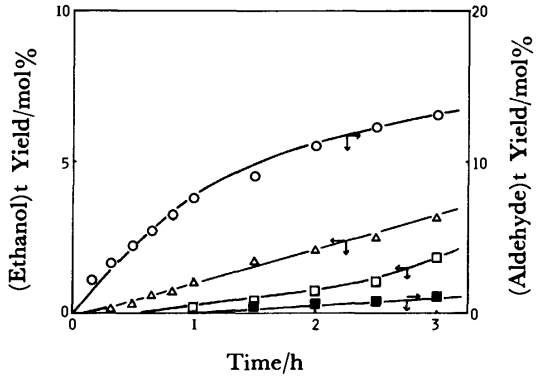

Fig. 2. Methanol homologation by cobalt catalyst and ruthenium catalyst.
Reaction conditions: see footnote of Table 2. ○, △: cobalt catalyst $[Co_2(CO)_8]_0=2.8\times10^{-2}$ M, □, ■: ruthenium catalyst $[RuCl_3]_0=5.6\times10^{-2}$ M. 1 M=1 mol dm^{-3}

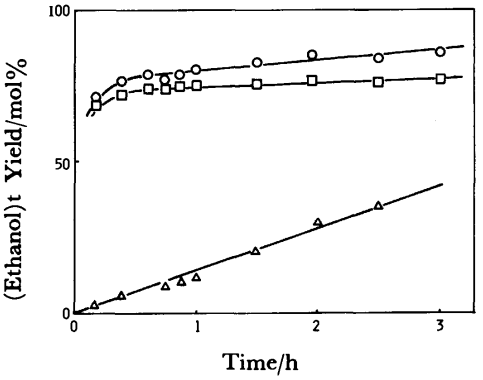

Fig. 3. The hydrogenation of acetaldehyde.
Reaction temperature: 160 °C, total pressure: 240 kg cm^{-2} at 160 °C ($H_2/CO=2/1$), solvent: 1,4-dioxane, substrate: acetaldehyde dimethyl acetal 0.7 M adding H_2O 0.8 M, total volume 70 ml, methyl iodide 0.14 M. ○: $[Co_2(CO)_8]_0=2.8\times10^{-2}$ M and $[RuCl_3]_0=1.1\times10^{-2}$ M, △: $[Co_2(CO)_8]_0=2.8\times10^{-2}$ M, □: $[RuCl_3]_0=1.1\times10^{-2}$ M.

Figure 3 shows that the ruthenium-catalyzed hydrogenation almost completed in 20 min. This rate was much faster than the rate of the cobalt-catalyzed hydrogenation. The hydrogenation rate of acetaldehyde by cobalt-ruthenium mixed catalyst was similar to that by a simple ruthenium catalyst. Hence ruthenium is considered to be the principal catalyst for the hydrogenation of acetaldehyde under the reaction conditions of methanol homologation. This fast hydrogenation should lead to the high selectivity of ethanol.

It has been reported that methyl iodide plays a part as the promoter in the formation of methylcobalt complex from methanol and the cobalt.[3,11,12] We examined the effect of methyl iodide on the hydrogenation of acetaldehyde. Figure 4 reveals that addition of methyl iodide suppresses the rate of the cobalt-catalyzed hydrogenation. We suppose that the result is due to the coordination of iodide to the vacant site

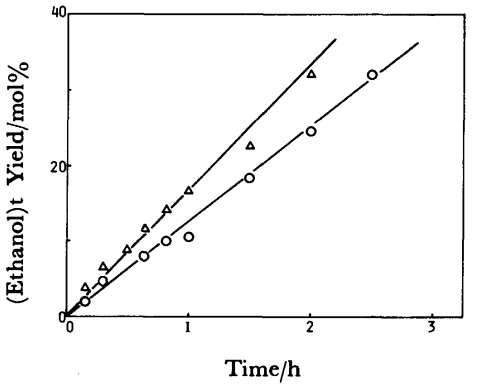

Fig. 4. The effect of methyl iodide on the hydrogenation of acetaldehyde by cobalt catalyst. ○: $[CH_3I]_0=0.14$ M, △: $[CH_3I]_0=0$.

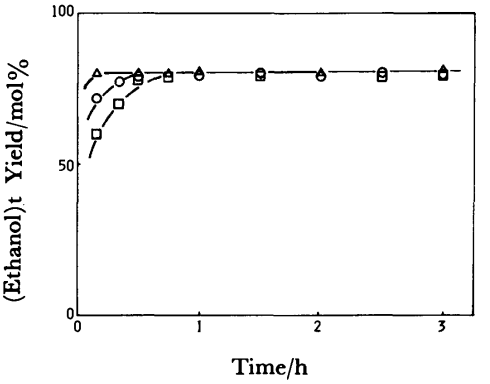

Fig. 5. The effect of methyl iodide on the hydrogenation of acetaldehyde by ruthenium catalyst. △: $[CH_3I]_0/[RuCl_3]_0=3$, ○: $[CH_3I]_0/[RuCl_3]_0=2$, □: $[CH_3I]_0=0$.

of coordinatively unsaturated [$HCo(CO)_3$], which is generally regarded as the active species for the hydrogenation of acetaldehyde. With ruthenium catalyst, the yield of ethanol at 10 min increases with the mole ratio of methyl iodide to ruthenium ([CH_3I]/[Ru]) up to [CH_3I]/[Ru]=2 (Fig. 5). The yield of ethanol becomes independent of the mole ratio when the ratio is higher than 2 (Figs. 3 and 5). This fact suggests that an iodocarbonylruthenium, [$RuI_x(CO)_y$], is an active catalyst for the hydrogenation, where x is supposed to be 2 or 3 from *in situ* IR observation. Therefore, it was found that methyl iodide gave no significant effect on the hydrogenation under the working conditions ([CH_3I]/[Ru]≧5).

Kinetic Study. As shown in Fig. 1, with the cobalt-ruthenium mixed catalyst, the time-yield plot of ethanol production is linear at the low yield of ethanol (less than 30%), and the induction period is less than 10 min. We could thus obtain the initial rate of ethanol production from the slope of the time-yield curve of ethanol. As both ethyl methyl and diethyl ethers were formed rapidly by thermal and/or acid-catalyzed dehydration of alcohols, the amounts of these ethers were included in the amount of ethanol. We investigated the effect of initial concentration of methanol, methyl iodide and ruthenium salt, and that of the partial pressure of CO and H_2 on the rate of formation of ethanol. From Figs. 6 and 7, the rate was found to be apparently of the order between the 0th and 1st in regard to the initial concentration of methyl iodide and ruthenium, and to the partial pressure of H_2. The effect of CO indicates that the insertion of CO to form acyl complex should be an important step, since the rate is of the 1st order in regard to its partial pressure. Figure 8 reveals that the rate with respect to the initial concentration of methanol is higher than the 1st order. With cobalt catalyst, the yield of ethanol at 50 min was less than 1% (Fig. 2), and that the yield of acetaldehyde (including its dimethyl acetal) was approximately proportional to the square of the initial concentration of methanol (Fig. 8). Hence, more than one molecule of methanol should take part in the hydrocarbonylation of methanol.

Determination of in situ *IR Spectra.* In order to obtain detailed information about active species involved in the catalytic cycle, IR spectra of octacarbonyldicobalt and ruthenium trichloride solution were observed under typical conditions (P_{CO}= 60 kg cm^{-2}, P_{H_2}=120 kg cm^{-2} at room temperature, and 160 °C). Since 1,4-dioxane absorbs light at 2000 cm^{-1} region, we chose methanol and hexane as the solvents for these measurements.

In the methanol solution of [$Co_2(CO)_8$], the infrared absorption at 1900 cm^{-1}, which can be ascribed to [$Co(CO)_4$]$^-$ species, was observed under high pressure of the mixture gas at 180—200 kg cm^{-2} in the range of temperature from 20 °C to 160 °C. GLC analysis revealed that the hydrocarbonylation

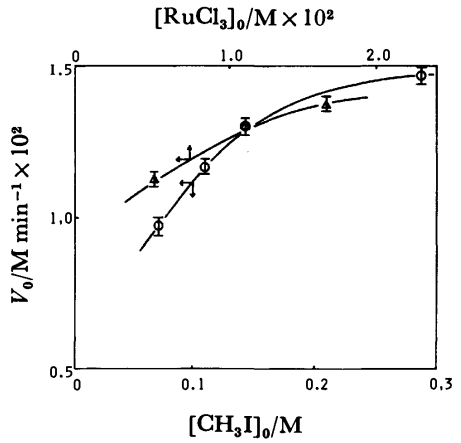

Fig. 6. Plots of v_0 *vs.* [CH_3I]$_0$ and [$RuCl_3$]$_0$.

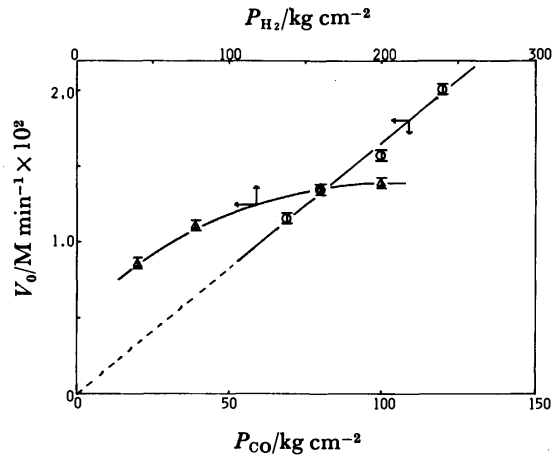

Fig. 7. Plots of v_0 *vs.* P_{CO} and P_{H_2}.

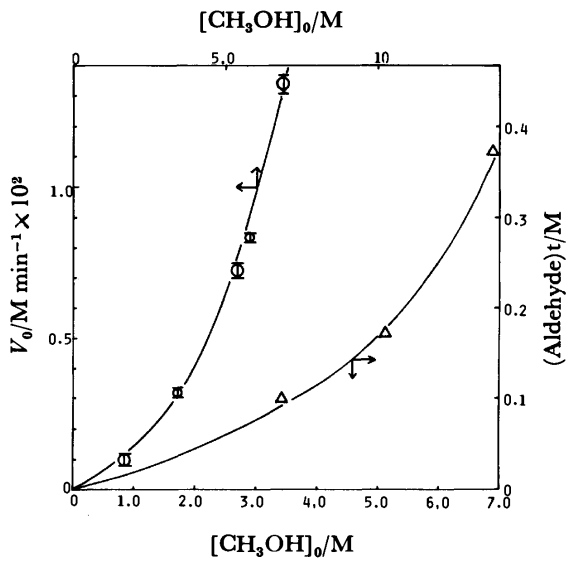

Fig. 8. The effect of the initial concentration of methanol.
◑: the rate of ethanol formation, △: the yield of acetaldehyde at 50 min.

of methanol hardly proceeded under these conditions. When CH_3I was added to this solution, a characteristic absorption at 1900 cm^{-1} was diminished as temperature raised, and ultimately disappeared at the working temperature (160 °C). GLC analysis revealed that the hydrocarbonylation proceeded. These results suggest that the steady-state concentration of $[Co(CO)_4]^-$ species becomes low with the progress of hydrocarbonylation, and that $[Co(CO)_4]^-$ is an active species in the hydrocarbonylation of methanol.

In the hexane solution of $RuCl_3$, the observation of *in situ* IR showed that two kinds of iodocarbonylruthenium species existed under the same conditions as those in the homologation and that chlorocarbonylruthenium complex did not exist. One of the two iodo species is $[RuI_2(CO)_4]$ (2126, 2107, 2096, and 2066 cm^{-1})[13] and the other $[RuI_3(CO)_3]^-$ (2120 and 2050 cm^{-1})[14]. As G. Andlich and his co-workers reported[16] the existence of these iodo species in the carbonylation of dimethyl ether to ethyl acetate, we suppose that one of these iodocarbonylruthenium species is active for the homologation of methanol.

We also prepared a cobalt-ruthenium heterometallic cluster complex ($[RuCo_3(CO)_{12}]^-$) by the reported method[7b] in order to examine the formation of this cluster in the reaction system by *in situ* IR. The results are given in Table 3. It has been known that cobalt-iron heterometallic cluster ($[FeCo_3(CO)_{12}]^-$)[9] and triruthenium cluster ($[Ru_3(CO)_{12}]$)[17] are decomposed into the respective monometallic complexes under high pressure and high temperature. From Table 3, we can conclude that under the reaction conditions a cobalt-ruthenium heterometallic cluster does not remain intact as in the original form, but is decomposed.

Mechanism and Rate Equation. Based on the above results, we propose a reaction mechanism of the homologation of methanol (Scheme 1: the hydrocarbonylation of methanol, Scheme 2: the hydrogenation of acetaldehyde).

TABLE 3. IR SPECTRAL DATA[a]

No.	Complexes	ν(CO) / cm^{-1}
1	$HRuCo_3(CO)_{12}$[b]	2070 vs, 2062 vs, 2050 vs, 2030 s, 2020 vs, 1884 s
2	$Co_2(CO)_8$-$RuCl_3$[c]	2101 s, 2048 s, 2033 s
3	$Co_2(CO)_8$-$RuCl_3$[c,d]	2101 s, 2045 s, 2033 sh, 2022 s, 2001 s
4	$HRuCo_3(CO)_{12}$	2102 s, 2050 s, 2032 s
5	$HRuCo_3(CO)_{12}$[d]	2105 s, 2045 s, 2030 s, 2022 sh, 2001 s

Abbreviations: vs=very strong, s=strong, sh=shoulder. a) CH_3OH: 0.4 ml, hexane: 5 ml, Total pressure: 180 kg cm^{-2} at room temp ($H_2/CO=2/1$), Temperature: 160 °C, $[CH_3I]/[CO]=3$. b) From Ref. 7b. c) [Co]/[Ru] =3. d) After cooling down the solution to room temperature (total pressure 180 kg cm^{-2}).

$$Co_2(CO)_8 + H_2 \overset{K_1}{\rightleftharpoons} 2\,HCo(CO)_4 \quad \text{(I)}$$
1 **2**

$$\mathbf{2} \overset{K_2}{\rightleftharpoons} HCo(CO)_3 + CO \quad \text{(II)}$$
3

$$CH_3OH + \mathbf{2} \overset{K_3}{\rightleftharpoons} [CH_3OH_2]^+[Co(CO)_4]^- \quad \text{(III)}$$
4

$$CH_3OH + HI \overset{K_4}{\rightleftharpoons} CH_3I + H_2O \quad \text{(IV)}$$

$$CH_3I + \mathbf{4} \underset{k_{-5}}{\overset{k_5}{\rightleftharpoons}} CH_3Co(CO)_4 + HI + CH_3OH \quad \text{(V)}$$
5

$$\mathbf{5} + CO \underset{k_{-6}}{\overset{k_6}{\rightleftharpoons}} (CH_3CO)Co(CO)_4 \quad \text{(VI)}$$
6

$$\mathbf{6} + H_2 \xrightarrow{k_7} CH_3CHO + \mathbf{2} \quad \text{(VII)}$$

Scheme 1.

$$RuI_x(CO)_y + H_2 + CH_3OH \overset{K_8}{\rightleftharpoons} [HRuI_x(CO)_y]^-[CH_3OH_2]^+ \quad \text{(VIII)}$$
7

$$CH_3CHO + \mathbf{7} \underset{k_{-9}}{\overset{k_9}{\rightleftharpoons}} [(CH_3CH_2O)RuI_x(CO)_y]^-[CH_3OH_2]^+ \quad \text{(IX)}$$
8

$$\mathbf{8} + H_2 \xrightarrow{k_{10}} CH_3CH_2OH + \mathbf{7} \quad \text{(X)}$$

Scheme 2.

During the heating of the reaction system to the reaction temperature, the charged methyl iodide should have reacted with $[HCo(CO)_4]$ (or $[Co(CO)_4]^-$ which is formed from the dissociation of $[HCo(CO)_4]$) to produce hydroiodic acid. The *in situ* IR spectra suggest that ruthenium chloride (precatalyst) reacts with HI and CO to form iodocarbonylruthenium species.

The disproportionation of $[Co_2(CO)_8]$ was reported[19] to produce the species $[Co(CO)_4]^-$ (Eq. 7). But this disproportionation did not

$$6\,CH_3OH + 3\,Co_2(CO)_8 \rightarrow [Co(CH_3OH)_6]^{2+}([Co(CO)_4]^-)_2 + 4\,CO \quad (7)$$

occur under the present conditions, since no libration of CO was observed in a stoichiometric reaction of methanol with $[Co_2(CO)_8]$.

The equilibrium constant K_4 was found to be 0.464 at 160 °C (calculated from a measured value at 30 °C and ΔH=1.25 kcal† mol^{-1}; ΔH was calculated from

† 1 cal_{th}=4.184 J.

the value of ΔH_f° of each substance cited in the literature).

Since the hydrocarbonylation hardly proceeded in the absence of iodide, the direct conversion of **4** to methylcobalt complex, **5**, (Eq. 8)[12] should be ruled out.

$$\mathbf{4} \longrightarrow \mathbf{5} + H_2O \tag{8}$$

As the hydrogenation of acetaldehyde with the ruthenium catalyst proceeded much more rapidly than with the cobalt catalyst, ruthenium plays a major catalytic role in the hydrogenation, and ruthenium hydride anion, **7**, in Eq. VIII is assumed to be the active species. We do not yet have any obvious evidence for the formation of this complex, but this is analogous to that suggested in a ruthenium-iodine system.[16] Although the number of iodides coordinated to ruthenium is still obscure, Dombek and his coworkers reported[15] that triiodotricarbonylruthenium was inactive for a hydrogenation of CO. Hence, diiodotetracarbonylruthenium is supposed to be the catalyst for the hydrogenation of acetaldehyde.

The initial rate of the production of ethanol, v_o, is derived as follows. Assuming the steady-state concentration for the intermediate **8**, v_o is obtained as Eq. 9. From Eqs. VIII and IX, the steady-state concentration of acetaldehyde is given as Eq. 10.

$$v_o = \frac{k_9 k_{10}[CH_3CHO][\mathbf{7}][H_2]}{k_{-9}+k_{10}[H_2]} \tag{9}$$

$$[CH_3CHO] = \frac{k_7(k_{-9}+k_{10}[H_2])[\mathbf{6}]}{k_9 k_{10}[\mathbf{7}]} \tag{10}$$

By substituting Eq. 10 into Eq. 9, v_o is represented as Eq. 11. Assuming the steady-state conditions for

$$v_o = k_7[\mathbf{6}][H_2] \tag{11}$$

acylcobalt (**6**) and alkylcobalt (**5**) intermediates, the rate equation is derived as Eq. 12, since the concentration of methanol is nearly equal to its initial concentration at the early stage of the reaction, *i.e.*, $[CH_3OH]_o \gg [CH_3I]_o$, [catalyst]$_o$ where the subscript $^\circ$ denotes the initial concentration.

$$v_o = \frac{k_5 k_6 k_7[CH_3I][\mathbf{4}][CO][H_2]}{k_{-5}(k_{-6}+k_7[H_2])[CH_3OH]_o[HI]+k_6 k_7[CO][H_2]} \tag{12}$$

From the equilibrium IV, the concentration of methyl iodide is given as:

$$[CH_3I] = K_4[CH_3OH]_o A/2, \tag{13}$$

where A is given as:

$$A = -1 + \sqrt{1+4[HI]_o/(K_4[CH_3OH]_o)}, \tag{14}$$

and $[HI]_o=[CH_3I]_o-x[RuCl_3]_o$.

The concentration of the intermediate **4**, **5**, and **6** are represented in function of [**2**] as Eq. 15 to Eq. 17 ($K_4'=K_4/2$).

$$[\mathbf{4}] = K_3[\mathbf{2}][CH_3OH]_o \tag{15}$$

$$[\mathbf{5}] = \frac{K_3 K_4' k_5(k_{-6}+k_7[H_2])[CH_3OH]_o^2 A[\mathbf{2}]}{k_{-5}(k_{-6}+k_7[H_2])([HI]_o-K_4'[CH_3OH]_o A)[CH_3OH]_o+k_6 k_7[CO][H_2]} \tag{16}$$

$$[\mathbf{6}] = \frac{K_3 K_4' k_5 k_6[CH_3OH]_o^2 A[\mathbf{2}][CO]}{k_{-5}(k_{-6}+k_7[H_2])([HI)_o-K_4'[CH_3OH]_o A)[CH_3OH]_o+k_6 k_7[CO][H_2]} \tag{17}$$

The total concentration of cobalt complexes is as follows:

$$2[\mathbf{1}]_o = 2[\mathbf{1}] + [\mathbf{2}] + [\mathbf{3}] + [\mathbf{4}] + [\mathbf{5}] + [\mathbf{6}] \tag{18}$$

Since the equilibrium II lies to the left under high pressure of CO, the concentration of **3** can be neglected. By substituting Eqs. 15, 16, and 17 in Eq. 18, the concentration of **2** is represented as the function of [**1**]$_o$ as Eq. 19 using the equilibrium relation derived from I. In Eq. 19, α_1, α_2, and α_3 are denoted as Eqs. 20 to 23.

$$[\mathbf{2}] = (1+\alpha_1+\alpha_2+\alpha_3)K_1[H_2]\{\sqrt{1+16[\mathbf{1}]_o/\{K_1[H_2](1+\alpha_1+\alpha_2+\alpha_3)^2\}}-1\}/4 \tag{19}$$

$$\alpha_1 = K_3[CH_3OH]_o \tag{20}$$

$$\alpha_2 = \frac{K_3 K_4' k_5(k_{-6}+k_7[H_2])[CH_3OH]_o^2 A}{k_{-5}(k_{-6}+k_7[H_2])([HI]_o-K_4'[CH_3OH]_o A)[CH_3OH]_o+k_6 k_7[CO][H_2]} \tag{21}$$

$$\alpha_3 = \frac{k_6[CO]\alpha_2}{k_{-6}+k_7[H_2]} \tag{22}$$

Markó and his coworkers reported[21] that K_1 was small. So, Eq. 19 can be approximately expressed as Eq. 23.

$$[\mathbf{2}] = \sqrt{K_1[H_2][\mathbf{1}]_o}-(1+\alpha_1+\alpha_2+\alpha_3)K_1[H_2]/4 \tag{23}$$

Finally, the rate equation is obtained as Eq. 24 by substituting Eqs. 15 and 23 in Eq. 12.

$$v_o = \frac{K_3K_4'k_5k_6k_7[CH_3OH]_o^2A[CO][H_2]}{k_{-5}(k_{-6}+k_7[H_2])([HI]_o-K_4'[CH_3OH]_oA)[CH_3OH]_o+k_6k_7[CO][H_2]}\{\sqrt{K_1[H_2][\mathbf{1}]_o}-(1+\alpha_1+\alpha_2+\alpha_3)K_1[H_2]/4\} \quad (24)$$

Equation 24 is rearranged as Eq. 25 by substituting Eqs. 20, 21, 22, and 23 into Eq. 24.

$$v_o = \frac{K_3K_4'K_5K_6k_7[CH_3OH]_o^2A\{\sqrt{K_1[H_2][\mathbf{1}]_o}-K_1(1+K_3[CH_3OH]_o)[H_2]/4\}[CO]}{(1+k_7[H_2]/k_{-6})([HI]_o-K_4'[CH_3OH]_oA)[CH_3OH]_o+k_6k_7[CO][H_2]/(k_{-5}k_{-6})} - \frac{K_1K_3^2K_4'^2K_5^2K_6k_7(1+k_7[H_2]/k_{-6})[CH_3OH]_o^4A^2[H_2]^2[CO]}{4\{(1+k_7[H_2]/k_{-6})([HI]_o-K_4'[CH_3OH]_oA)[CH_3OH]_o+k_6k_7[CO][H_2]/(k_{-5}k_{-6})\}^2} - \frac{K_1K_3^2K_4'^2K_5^2K_6^2k_7[CH_3OH]_o^4A^2[H_2]^2[CO]^2}{4\{(1+k_7[H_2]/k_{-6})([HI]_o-K_4'[CH_3OH]_oA)[CH_3OH]_o+k_6k_7[CO][H_2]/(k_{-5}k_{-6})\}^2} \quad (25)$$

From Fig. 7, we conclude that the last term of the right side of Eq. 25 related to the acylcobalt intermediate, **6**, can be neglected and that the rate equation is approximately expressed as Eq. 26.

$$v_o = \left\{\frac{\beta_1\beta_2[CH_3OH]_oA\sqrt{[\mathbf{1}]_o}}{[HI]_o-K_4'[CH_3OH]_oA} - \frac{\beta_2\beta_3(1+K_3[CH_3OH]_o)[CH_3OH]_oA[H_2]^{0.5}}{4([HI]_o-K_4'[CH_3OH]_oA)} - \frac{\beta_1^2\beta_2[CH_3OH]_o^2A^2[H_2]^{0.5}}{4([HI]_o-K_4'[CH_3OH]_oA)^2}\right\}[CO][H_2]^{1.5} \quad (26)$$

where $\beta_1=\sqrt{K_1}K_3K_4'K_5$, $\beta_2=K_6k_7$, $\beta_3=K_1K_3K_4'K_5$ and $[HI]_o=[CH_3I]_o-x[RuCl_3]_o$. From the slope in Fig. 7, we obtained the following value.

$$4.25\times10^4\beta_1\beta_2 - 7.91\times10^5\beta_2\beta_3(1+K_3[CH_3OH]_o) - 9.78\times10^7\beta_1\beta_2 = 1.66\times10^{-4} \quad (27)$$

With respect to $[H_2]$, the rate equation is rewritten as Eq. 28 which agrees with the experimental facts (Fig. 9).

$$v_o/[H_2]^2 = B_1/[H_2]^{0.5} - B_2 \quad (B_1,\ B_2\text{: constants}) \quad (28)$$

The slope and the intercept in Fig. 9 give:

$$\beta_1\beta_2 = 2.81\times10^{-8} \quad (29)$$

$$2.47\times10^3\beta_2\beta_3(1+K_3[CH_3OH]_o) + 3.06\times10^5\beta_1\beta_2 = 3.21\times10^{-6} \quad (30)$$

From the effect of $[CH_3I]_o$ and $[RuCl_3]_o$ (Fig. 6), a value of x to satisfy Eq. 26 is found to be 2.5 from the trial and error method. This value is consistent with the result of the *in situ* IR observation which showed the presence of both diiodo- and triiodo-carbonyl complex of ruthenium (see above). Equation 26 is rearranged as Eq. 31.

$$v_o([HI]_o - K_4'[CH_3OH]_oA)^2/A^2 = B_3([HI]_o-K_4'[CH_3OH]_oA)/4A-B_4 \quad (B_3,\ B_4\text{: constant}) \quad (31)$$

Figure 10 indicates that Eq. 26 explains the experimental results of the initial concentration of methyl iodide and ruthenium. From the slope and the intercept, the following values are obtained.

$$1.90\times10^5\beta_1\beta_2 - 3.54\times10^6\beta_2\beta_3(1+K_3[CH_3OH]_o) = (1.32\pm0.04)\times10^{-3} \quad (32)$$

$$\beta_1^2\beta_2 = (1.23\pm0.02)\times10^{-12} \quad (33)$$

By substituting the value of $\beta_1\beta_2$ and $\beta_1^2\beta_2$ in Eqs. 27, 30, and 32, the values of $\beta_2\beta_3$ $(1+K_3[CH_3OH]_o)$ are found independently from each equation to be 1.15×10^{-9} within the experimental error. The above analysis, therefore, does not conflict with each other. Equation 26 is rewritten as Eq. 34. The plot of $1/$

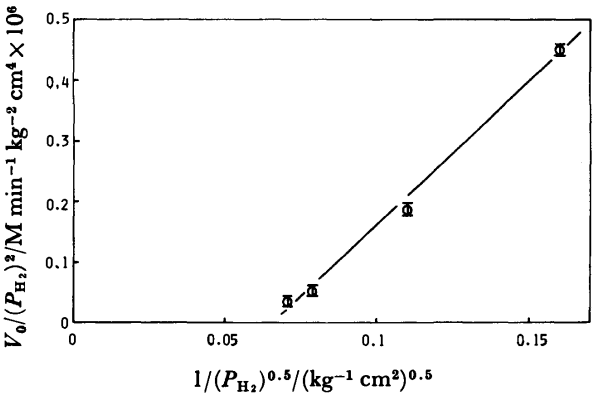

Fig. 9. Plots of $v_0/(P_{H_2})^2$ *vs.* $1/(P_{H_2})^{0.5}$.

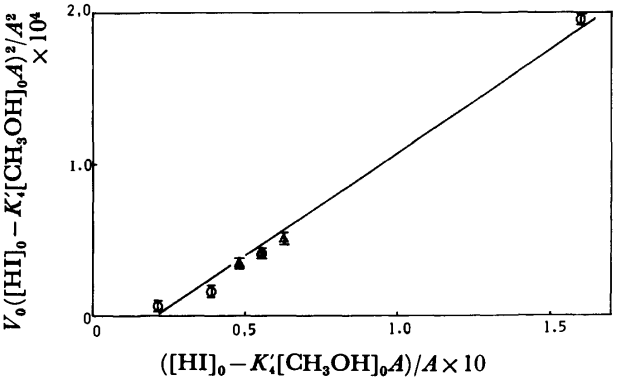

Fig. 10. Plots of v_0 $([HI]_0-K_4'[CH_3OH]_0A)^2/A^2$ *vs.* $([HI]_0-K_4'[CH_3OH]_0A)/A$.
△: $[CH_3I]_0=0.14$ M, ⓘ: $[RuCl_3]_0=1.1\times10^{-2}$ M.

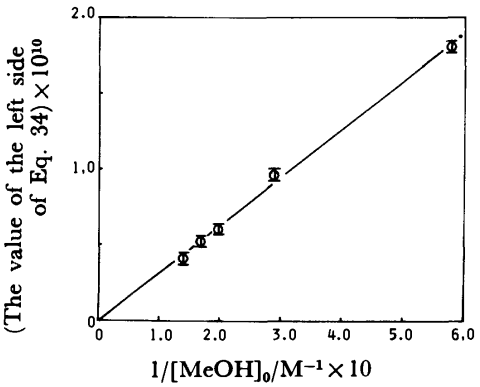

Fig. 11. Plots of the value of the left side of Eq. 34 against $1/[CH_3OH]_0$

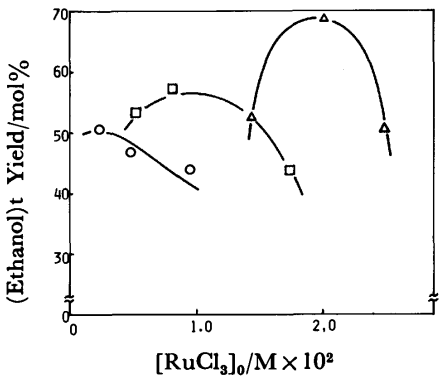

Fig. 12. The effect of the initial concentration of methyl iodide on the methanol homologation by cobalt–ruthenium mixed catalyst.
Reaction temperature: 180 °C, total pressure: 240 kg cm^{-2} at room temperature ($H_2/CO=2/1$), solvent: 1,4-dioxane 5 ml, methanol 2 ml, $[Co_2(CO)_8]_0=(2.3-2.4)\times10^{-2}$ M, Time: 3 h.
○: $[CH_3I]_0=0.07$ M, □: $[CH_3I]_0=0.14$ M, △: $[CH_3I]_0=0.28$ M.

$[CH_3OH]_0$ *vs.* the value of the left side of Eq. 34 is

$$\frac{\beta_1\beta_2B_5}{[CH_3OH]_0}-\frac{\beta_1^2\beta_2A}{4([HI]_0-K_4'[CH_3OH]_0A)}-\frac{v_0([HI]_0-K_4'[CH_3OH]_0A)B_6}{[CH_3OH]_0{}^2A}=\frac{\beta_2\beta_3}{4[CH_3OH]_0}+\frac{\beta_2\beta_3K_3}{4}\quad(B_5,\ B_6\text{: constant})\qquad(34)$$

verified as shown in Fig. 11. From the intercept, the second term of the right side in Eq. 35 related to tetracarbonylcobalt anion, **4**, is neglected. In fact, **4** was not observed by *in situ* IR during the reaction (see above). Therefore, $\beta_2\beta_3$ $(1+K_3[CH_3OH]_0)$ is nearly equal to $\beta_2\beta_3$. The slope in Fig. 11 gives the value of $\beta_2\beta_3$ as:

$$\beta_2\beta_3 = 1.25\times10^{-9} \qquad (35)$$

This value agrees with that obtained above (1.15×10^{-9}). From the above analysis, the values of constants are found as follows: $K_1=(1.83\pm0.1)\times10^{-3}$ [M/(kg cm^{-2})], $K_3K_5=(4.15\pm0.04)\times10^{-3}$ and $K_6k_7=(6.42\pm0.1)\times10^{-4}$ [(kg cm^{-2})·min^{-1}]. From the results reported by Alemdaroğlu and his coworkers,[18] K_1 at 160 °C is calculated to be 2.0×10^{-3} M/kg cm^{-2}. This value is well consistent with the value obtained from the above kinetic analysis.

The rate equation 26 also explains the reason why an optimum concentration of ruthenium exists. When ruthenium is added in excess to this system, the concentration of iodide (HI or CH_3I) is significantly decreased by the coordination of iodide to ruthenium. Consequently, the rate of hydrocarbonylation promoted by iodide is retarded. Figure 12 reveals that the optimum concentration of ruthenium increases with the initial concentration of methyl iodide and that the presence of ruthenium in excess causes the retardation of the hydrocarbonyltion of methanol, resulting in the low yield of ethanol. Thus, the mole ratio of ruthenium to iodide is important for the high yield of ethanol.

All of the above results prove that cobalt principally catalyzes the hydrocarbonylation of methanol while ruthenium only takes part in the hydrogenation of acetaldehyde.

The authors wish to thank Messers. Y. Ichikawa and M. Yasumoto for the contribution of manufacturing the *in situ* high-pressure IR cell and assembling the high-pressure experimental equipment.

References

1) I. Wender, R. Levine, and M. Orchin, *J. Am. Chem. Soc.*, **71**, 4160 (1949).
2) J. Berty, L. Markó, and D. Kallo, *Chem. Tech.*, **3**, 260 (1956).
3) T. Mizoroki and N. Nakayama, *Bull. Chem. Soc. Jpn.*, **37**, 236 (1964).
4) J. G. Lafaya, R. Perron, and Y. Colleuille, *J. Mol. Cat.*, **17**, 339 (1982).
5) W. E. Slinkard, U. S. Patent 4168391 (1979).
6) a) L. H. Slaugh, Ger. Offen. Patent 2625727 (1976). b) L. H. Slaugh and R. D. Mullineaux, *J. Organomet. Chem.*, **13**, 469 (1968). c) Y. Sugi, K. Bando, and Y. Takami, *Chem. Lett.*, **1981**, 63.
7) a) M. Hidai, M. Orisaku, M. Ue, and Y. Uchida, *Chem. Lett.*, **1981**, 143. b) M. Hidai, M. Orisaku, M. Ue, Y. Koyasu, T. Kodama, and Y. Uchida, *Organomettalics*, **2**, 292 (1983).
8) H. F. Schultz and F. Bellstdt, *Ind. Eng. Chem. Prod. Res. Dev.*, **12**, 176 (1973).
9) G. Doyle, *J. Mol. Cat.*, **13**, 237 (1981).
10) K. Kudo and N. Sugita, *Nippon Kagaku Kaishi*, **1982**, 462.
11) H. Barhmann and B. Cornils, "New Syntheses with Carbon Monoxide," ed by J. Falbe, Springer-Verlag, New York (1980) pp. 226
12) I. Wender, *Catal. Rev. -Sci. Eng.*, **14**, 97 (1976).
13) B. F. Johnson, R. D. Johnston, and J. Lewis, *J. Chem.*

Soc. A, **1969**, 792.

14) R. Clton and R. H. Farthino, *Aust. J. Chem.*, **24** 903 (1971).

15) B. K. Warren and B. D. Dombek, *J. Cat.*, **79**, 334 (1983).

16) a) G. Braca, G. Andlich, L. Paladinl, G. Sbrana, and G. Valentil, *Ind. End. Chem. Prod. Res. Dev.*, **20** 115 (1981); b) G. Jenner, H. Kheradmand, A. Kiennenmann, and A. Deluzarche, *J. Mol. Cat.*, **18**, 61 (1983).

17) J. N. Nicolls, D. H. Farrar, P. F. Jackson, B. F. G. Johnson, and J. Lewis, *J. Chem. Soc. Dalton Trans.*, **1982**, 1395.

18) N. H. Alemdaroğlu, J. M. L. Penninger, and E. Oltay, *Monatsh. Chem.*, **107**, 1043 (1976).

19) I. Wender, H. W. Sternberg, and M. Orchin, *J. Am. Chem. Soc.*, **74**, 1216 (1952).

20) A. Slsak, F. Ungváry, and L. Markó, *Organometallics*, **2**, 1244 (1983).

 © 1985 The Chemical Society of Japan Bull. Chem. Soc. Jpn., 58, 2038—2042 (1985) [Vol. 58, No. 7

Cadmium-photosensitized Reaction of γ-Valerolactone and α-Methyl-γ-butyrolactone

Shunzo YAMAMOTO,* Hiroshi TAKAHOSO, Yoshimi SUEISHI, and Norio NISHIMURA
Department of Chemistry, School of Science, Okayama University, 3-1-1, Tsushima-naka, Okayama 700
(Received January 30, 1985)

The cadmium-photosensitized reactions of γ-valerolactone and α-methyl-γ-butyrolactone have been investigated. The obtained products in both cases were carbon monoxide, ethylene, propylene, acetaldehyde, and 2-methyloxetane. The dependence of the yields of ethylene and propylene on the total pressure suggests the existence of a biradical and an energized intermediate. Possible mechanisms are discussed.

While the photochemistry of aliphatic esters and cyclic ketones has been investigated in some detail, there have been only a few quantitative studies on the photo-decomposition of simple aliphatic lactones in the gas phase.

Simonaitis and Pitts[1] investigated the direct photolysis and the mercury-photosensitized decomposition of γ-butyrolactone(BL) in the gas phase and observed that lactone (1) isomerizes to succinaldehyde, (2) decomposes to ethylene, carbon monoxide, and formaldehyde, and (3) decomposes to propylene or cyclopropane and carbon dioxide. They pointed out that succinaldehyde and ethylene are probably singlet-state products, whereas cyclopropane and propylene are probably triplet-state products.

Recent work[2] in our laboratory on BL has shown that quite different products are obtained in mercury- and cadmium- photosensitized reactions. We concluded that the decomposition of lactone takes place through different intermediates, that is, a triplet state of lactone in the mercury-photosensitized reaction and an excited complex between an excited cadmium atom and a lactone molecule in the cadmium-photosensitized reaction. A rational mechanism has been proposed for the mercury-photosensitized reaction. However, the mechanism regarding the cadmium-photosensitized reaction has remained somewhat obscure.

In order to obtain further information on the cadmium-photosensitized reaction of lactone, we investigated the effect of a methyl group in the α- and γ-positions regarding primary processes, quantum yields, and rates of decomposition. In this paper we report on the cadmium-photosensitized reactions of γ-valerolactone(VL) and α-methyl-γ-butyrolactone (ML).

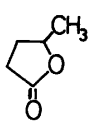

VL

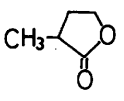

ML

Experimental

The apparatus and techniques were similar to those used previously.[2] An analysis of products was performed using simple fractionation at 77 and 190 K, measurements with a gas burette, and gas chromatography. The light absorbed by cadmium atoms at 326.1 nm was determined by *cis*-2-butene actinometry.[3]

VL (aldrich, 98%) and ML (Tokyo Kasei Ind., E.P. grade) were used after drying using a molecular sieve (5A) and several trap-to-trap distillations. Known amounts of liquid lactone were injected into the reaction cell with a microsyringe and were fully degassed after many careful freeze-pump cycles. *cis*-2-Butene (Nihon Tokushu Gasu K.K., pure grade) snd N_2 (Takachiho Shoji., pure grade) were used as supplied.

The cadmium-photosensitized reaction was carried out at 300 °C in order to obtain a sufficient cadmium vapor pressure. A thermal decomposition occurred at this temperature and yielded carbon dioxide, methylcyclopropane and other minor products. However, the amounts of these products were very small and the influence of the thermal decomposition on the results of the cadmium-photosensitized reaction was negligible.

Results

The major observed volatile products in the cadmium-photosensitized reaction were carbon monoxide, ethylene, propylene and acetaldehyde. These products are different from those obtained during thermal decomposition. Yields of these products increased linearly with reaction time, showing that they are primary products. The quantum yields of carbon monoxide, ethylene, and propylene are shown in Fig. 1 as a function of lactone pressure. All of them decreased with an increasing lactone pressure, showing the existence of a collisional deactivation process. The amount of acetaldehyde was always roughly equal to that of ethylene.

Only small amounts of 2-methyloxetane were obtained for pure lactone systems. In the presence of a large nitrogen pressure, however, we obtained considerably more 2-methyloxetane and found that the yield increased with pressure.

When *cis*-2-butene was added to lactone, the

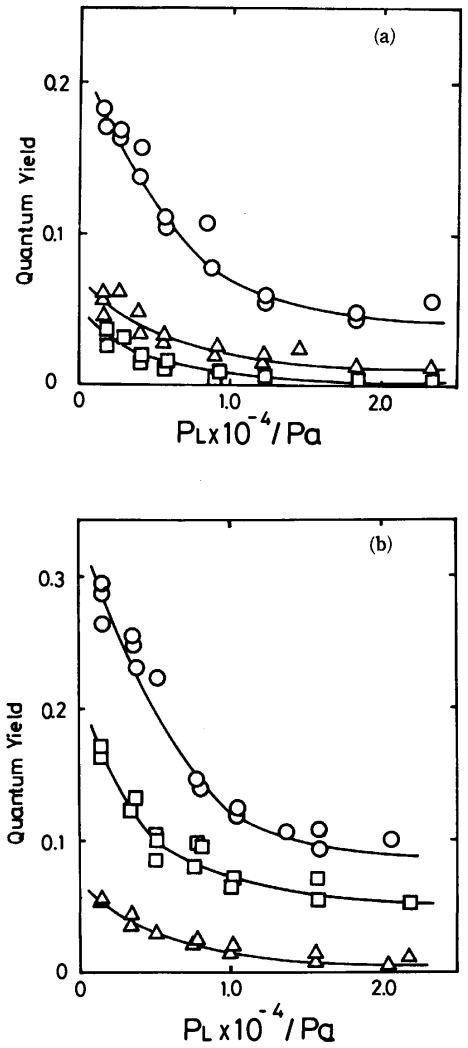

Fig. 1. Pressure dependence of quantum yields of carbon monoxide (○), ethylene (△), and propylene (□) in the cadmium-photosensitized reaction of (a) VL and (b) ML.

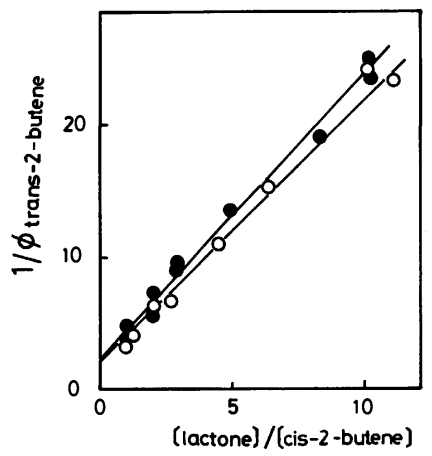

Fig. 2. Plots of the reciplocal of the quantum yield of *trans*-2-butene against the lactone/*cis*-2-butene pressure ratio for VL (●) and ML (○).

quantum yields of the decomposition products decreased as the quantum yield of *trans*-2-butene formation increased. From the slopes of the reciprocal plots of the quantum yield of *trans*-2-butene *vs.* the lactone/*cis*-2-butene ratio (Fig. 2), the quenching efficiencies of VL and ML relative to that of *cis*-2-butene were estimated to be 1.00±0.10 and 1.10±0.10. These values are close to that of BL (0.92±0.10).[2]

Discussion

Simonaitis and Pitts[4] investigated the photolysis of BL, VL, and ML in the liquid phase. They proposed primary processes (1)-(4) to explain major products.

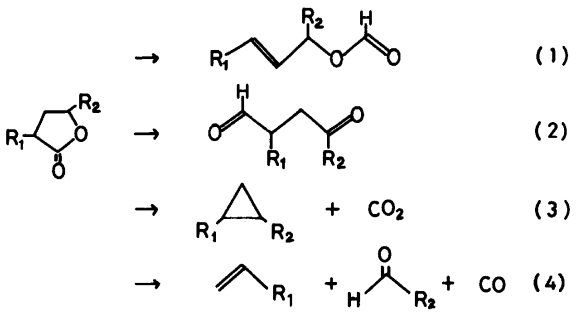

As they pointed out, process (4) is minor regarding liquid-phase photolysis and is important for the vapor-phase photolysis of BL.[1] In the cadmium-photosensitized reactions of BL, VL, and ML, however, products considered to arise from process (4) alone were observed. This suggests the possibility that the cadmium-photosensitized reaction occurs through a different state from those for the direct photolysis.

In the photolysis of *trans*-2,3-dimethylcyclopentanone, Frey and Lister[5] obtained ethylene and butene as well as 1,2-dimethylcyclobutane as products. They pointed out that C_2+C_4 hydrocarbons and 1,2-dimethylcyclobutane are formed by independent pathways and that the former are not formed from a "hot" 1,2-dimethylcyclobutane molecule because (in the latter case) propylene must also be formed. The photolysis of cyclopentanone-2,2,5,5-d_4 gave evidence for the same conclusion.[6] In the present cases, however, ethylene and propylene were observed. Propylene (for VL) and ethylene (for ML) can not be directly formed from the biradicals produced by the elimination of carbon monoxide from VL and ML. This indicates that these products must be formed from "hot" oxetane molecules.

In order to explain the experimental results, the following set of reactions is proposed:

$$Cd(^1S_0) + h\nu(326.1\ nm) \rightarrow Cd^*(^3P_1) \qquad I_a \quad (5)$$

$$Cd^* \rightarrow Cd + h\nu(326.1\ nm) \qquad k_1 \quad (6)$$

$$Cd^* + L \rightarrow CdL^* \qquad k_1 \quad (7)$$

$$CdL^* + L \rightarrow Cd + 2L \qquad k_2 \quad (8)$$

$$CdL^* \rightarrow \alpha(CO + R_1\dot{C}HCH_2CHR_2O\text{-}Cd) \qquad k_3 \quad (9)$$

$$\rightarrow (1-\alpha)\ \text{other processes} \qquad (10)$$

$$R_1\dot{C}HCH_2CHR_2O\text{-}Cd \rightarrow R_1\underline{CHCH_2CHR_2O}^* + Cd \qquad k_4 \quad (11)$$

$$\rightarrow \gamma(R_1CH{=}CH_2 + R_2CH{=}O + Cd) \qquad k_5 \quad (12)$$

$$\rightarrow (1-\gamma)\text{other processes} \qquad (13)$$

$$R_1\underline{CHCH_2CHR_2O}^* \rightarrow R_1CH{=}CH_2 + R_2CH{=}O \qquad k_6 \quad (14)$$

$$\rightarrow R_1CH{=}O + R_2CH{=}CH_2 \qquad k_7 \quad (15)$$

$$R_1\underline{CHCH_2CHR_2O}^* + L \rightarrow R_1\underline{CHCH_2CHR_2O} + L \qquad k_8 \quad (16)$$

$$\rightarrow \text{other processes} \qquad (17)$$

VL; $R_1=H$, $R_2=CH_3$

ML; $R_1=CH_3$, $R_2=H$

Here, CdL* stands for a transient complex between the excited cadmium atom and a lactone molecule. As mentioned previously,[2] since the triplet state of BL lies at about 439 kJ/mol above the ground state, it can not be formed by a reaction of $Cd(^3P_1)$, which has an energy of only 367 kJ/mol. Therefore, we proposed that the complex is formed in the cadmium-photosensitized reaction of BL in order to explain the difference between the mercury- and cadmium-photosensitized reactions. This complex was also assumed for the present cases because the triplet energies of VL and ML are also probably larger than the excitation energy of excited cadmium atom. The formation of an O-Cd bond in Reaction (5) was assumed since the excitation energy of $Cd(^3P_1)$ alone is not sufficient to produce biradical $R_1\dot{C}HCH_2CHR_2O$, as has been shown in a previous paper.[2]

In a pure lactone system, a few minor products other than those previously mentioned were observed (some of them are the same as those observed during thermal decomposition). From their retention times, these minor products seem to be C_4- or higher compounds. Since their gas-chromatogram peaks were very small and overlapped in a complex way, we could not make assignments. In the presence of a large nitrogen pressure, a considerable amount of 2-methyloxetane was obtained (as previously mentioned). In this case, most of the peaks for minor products diminished. These findings indicate that in the presence of a large nitrogen pressure, intermediates seem to be stabilized by collisions with nitrogen molecules and give 2-methyloxetane, while in the pure lactones, most of the intermediates must react with lactone and yield other products (Reaction 17).

From the above mechanism, the following relations can be derived:

$$\frac{1}{\phi_{CO}} = \frac{1}{\alpha} + \frac{1}{\alpha}\frac{k_2}{k_3}[L] \qquad (18)$$

$$\frac{\phi_{CO}}{\phi_{R_2CH=CH_2}} = \left(1+\frac{k_5}{k_4}\right)\left(1+\frac{k_6}{k_7}\right) + \left(1+\frac{k_5}{k_4}\right)\frac{k_8}{k_7}[L] \qquad (19)$$

From plots of $1/\phi_{CO}$ *vs.* lactone pressure (Fig. 3), values of α and k_2/k_3 were obtained for VL and ML. These values are listed in Table 1, together with those for BL. The values of α for VL and ML are similar to that for BL, while the value of k_2/k_3 for VL is somewhat larger than those for ML and BL. This seems to show that the VL complex is a little less stable than those of ML and BL due to a steric hindrance of the methyl group at the γ-position, and more easily decomposes to a cadmium atom and a lactone molecule by collision with lactone molecules.

The quantum yields of carbon monoxide (extrapolated to zero pressure) were 0.31 and 0.37 for VL and ML. These small values suggest that most of the excited lactone that was formed underwent other reaction (Reaction 10). The amount of products volatile at 190 K (other than carbon monoxide, ethylene, propylene, acetaldehyde, and 2-methyloxetane) were negligibly small (see above). Therefore, isomerization to 4-oxopentanal, 2-methylsuccinaldehyde and other substances which were observed in

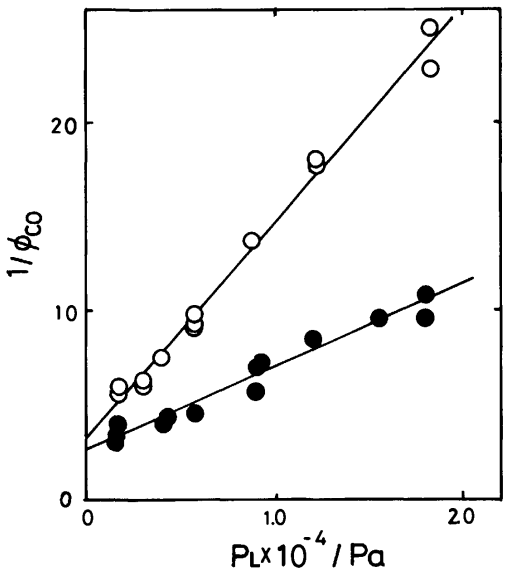

Fig. 3. Plots of $1/\phi_{CO}$ against lactone pressure for VL (○) and ML (●).

TABLE 1. CONSTANT AND RATIO OF RATE CONSTANTS INVOLVED IN Eq. 18

	BL[1]	VL	ML
α	0.27±0.02	0.31±0.02	0.37±0.02
$10^{-4}k_2/k_3$ Pa^{-1}	1.1±0.1	3.6±0.3	1.6±0.1

1) Calculated from the data shown in Ref. 2.

the photolysis of VL and ML in the liquid phase,[4] and the process in which excited lactones lose their energy without forming any products seem to be important (Reaction 10). The ratios of the other reaction (α) are almost equal for three lactones.

It was shown that in the thermal decomposition of 2-methyloxetane, both ethylene and propylene are obtained and the ratio of propylene/ethylene (1.31) is independent of temperature.[7] In our cases, $R_2CH{=}CH_2$ and a part of $R_1CH{=}CH_2$ are possibly formed from a "hot" oxetane as shown in Reactions (14) and (15). If so, the ratio of k_6/k_7 can be set at 1/1.31 for VL and 1.31 for ML. Plots of $\phi_{CO}/\phi_{R_1CH=CH_2}$ *vs.* lactone pressure are presented in Fig. 4. From the intercepts and the slopes of the straight lines, the values of k_5/k_4 and k_8/k_7 were obtained using k_6/k_7 (mentioned above). $k_8/(k_6+k_7)$ can be also calculated from the intercepts and the slopes. These values are listed in Table 2. k_5/k_4 for VL is similar to that for ML and $k_8/(k_6+k_7)$ for VL is considerably larger than for ML. The experimental values of $k_8/(k_6+k_7)$ give $k_d=k_6+k_7$ as $(5.9\pm1.6)\times10^8\ s^{-1}$ for VL and $(3.2\pm1.3)\times10^9\ s^{-1}$ for ML by adopting $8.0\times10^4\ s^{-1}$ as the kinetic collision frequency at 1 Pa and 300 °C and by assuming a collision-deactivation efficiency of unity for lactone.

The excess energy of energized 2-methyloxetane

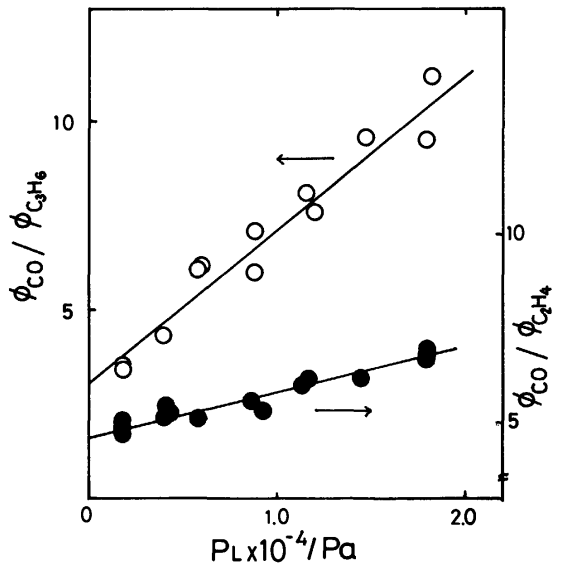

Fig. 4. Plots of $\phi_{CO}/\phi_{C_3H_6}$ (○) for VL and $\phi_{CO}/\phi_{C_2H_4}$ (●) for against lactone pressure.

Table 2. Ratios of rate constants involved in Eq. 19

	VL	ML
k_5/k_4	0.73±0.15	1.0±0.1
$10^4\,k_8/k_7$ Pa^{-1}	2.40±0.30	0.58±0.10
$10^4\,k_8/(k_6+K_7)$ Pa^{-1}	1.36±0.30	0.25±0.10

can be estimated using

$$k_d(E) = A\left(1-\frac{E_a}{E}\right)^{s-1} \tag{20}$$

Here, $k_d(E)$ is the rate constant regarding decomposition when the excess energy is E, A is the frequency factor, E_a is the critical energy, and s is the number of effective oscillators in the molecule. Using experimental values of k_d and substituting $A=10^{14.89}\ s^{-1}$ and E_a=249.8 kJ/mol (taken from the experiment of Hammond and Holbrook[7]) and s=16 (about half of the number of the modes of vibration), the values of E were found to be (410±5) kJ/mol for VL and (444±10) kJ/mol for ML. These excess energies are much larger than the enthalpy changes for the following reaction which are estimated to be 173 and 180 kJ/mol for VL and ML according to thermochemical data given by Benson.[8]

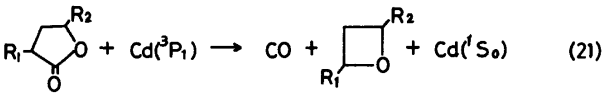

(21)

The estimation of the excess energy is also dependent on the collision-deactivation efficiency and the value of s. For example, an efficiency of 1/10, which is an unlikely small efficiency for lactone, results in a decrease of excess energy by about 34 kJ/mol. If a value of s=14 is adopted, the value of E is found to be 377 kJ/mol for VL. Even in these cases, the excess energy is still much larger than the enthalpy change shown above. Thus, the possibility that the dissociating intermediate is an energized 2-methyloxetane must be eliminated. As has been described in a previous paper,[2] the formation of an O–Cd bond must play an important role in the cadmium-photosensitized reaction of lactone. In order to explain the large rate constant regarding the decomposition of intermediates, we proposed the following intermediate as another possibility:

The excess energy of the above intermediate must be larger than that estimated thermochemically for an energized oxetane because of the additional energy of the O–Cd bond. If this is the case, the "hot" oxetane in the above mechanism should be replaced by this intermediate. It is notable that Eq. 19 holds regarding this case. Unfortunately, since it is difficult to estimate the excess energy of the above intermediate, no quantitative conclusions can be drawn about the thermochemistry.

From the above mechanism, the following relation can be derived:

$$\frac{\phi_{R_1CH=CH_2}}{\phi_{R_2CH=CH_2}} = \frac{k_5}{k_4}\left(\frac{k_6+k_7}{k_7}\right) + \frac{k_6}{k_7} + \frac{k_5k_8}{k_4k_7}[L] \tag{22}$$

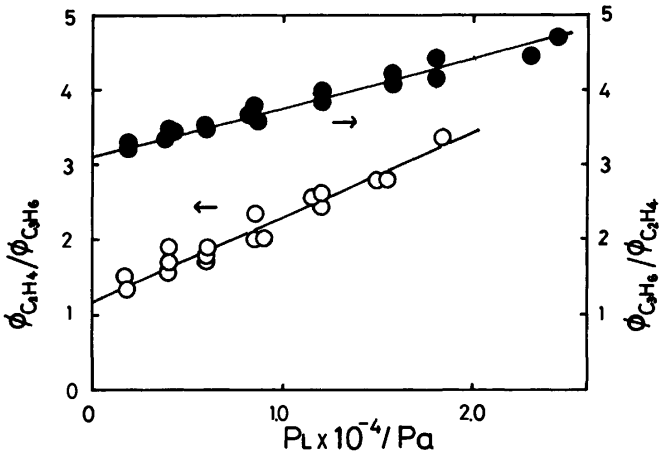

Fig. 5. Plots of $\phi_{C_2H_4}/\phi_{C_3H_6}$ (○) for VL and $\phi_{C_3H_6}/\phi_{C_2H_4}$ (●) for ML against lactone pressure.

From the intercepts and the slopes of the lines shown in Fig. 5, $k_8/(k_6+k_7)$ can be obtained using the following equation:

$$\frac{k_8}{k_6+k_7} = \frac{\text{slope}}{\text{intercept}-k_6/k_7} \tag{23}$$

The values for VL and ML obtained by using 1/1.31 and 1.31 for k_6/k_7 are $(1.79\pm0.30)\times10^{-1}$ and $(0.35\pm0.10)\times10^{-4}$ Pa^{-1}, respectively. These values are in fair agreement with those obtained from Fig. 4 (Table 2). The small discrepancy may be due to the use of these k_6/k_7 values for oxetane instead of those for the above intermediate.

In conclusion, the present results give further evidence for the formation of an O-Cd bond and the presence of an excited complex between the excited cadmium atom and the lactone molecule (discussed in a previous paper[2]).

References

1) R. Simonaitis and J. N. Pitts, Jr., *J. Phys. Chem.*, **75**, 2733 (1971).

2) S. Yamamoto, S. Matsuda, C. Ozaki, H. Takahoso, and N. Nishimura, *Bull. Chem. Soc. Jpn.*, **57**, 3408 (1984).

3) S. Tsunashima and S. Sato, *Bull. Chem. Soc. Jpn.*, **41**, 284 (1968).

4) R. Simonaitis and J. N. Pitts, Jr., *J. Am. Chem. Soc.*, **91**, 108 (1969).

5) H. M. Frey and D. H. Lister, *J. Chem. Soc.* (A), **1970**, 627.

6) R. Srinivasan, *Adv. Photochem.*, **1**, 83 (1963).

7) P. Hammonds and K. A. Holbrook, *J. Chem. Soc., Faraday Trans. 1*, **78**, 2195 (1982).

8) S. W. Benson and H. E. O'Neal, "Kinetic Data on Gas Phase Unimolecular Reactions," NSRDS-NBS, 21 U.S. 1970.

Formaldehyde Electro-oxidation on Copper Metal and Copper-based Amorphous Alloys in Alkaline Media

Ken-ichi MACHIDA and Michio ENYO*
Research Institute for Catalysis, Hokkaido University, Sapporo 060
(Received March 6, 1985)

Copper metal and copper-based amorphous alloys, a-$Cu_{35}Ti_{65}$ and a-$Cu_{33}Zr_{67}$, exhibit a very high and stable activity for the anodic HCHO oxidation in aqueous NaOH and Na_2CO_3. The oxidation current was already observable at electrode potentials as low as 0.1 V (RHE) and, in particular, the HF-treated amorphous alloys gave high current densities around 40 mA cm^{-2} (apparent) at 0.2 V. Kinetic data, roughly first order both in HCHO and OH^- concentration, are in favour of the mechanism in which the oxidation proceeds *via* hydroxymethanolate ion ($HOCH_2O^-$) formed from HCHO and OH^-, producing $HCOO^-$ and H_2: This ion is readily oxidized on the copper metal or copper-based amorphous alloy electrodes. The Tafel slope was in general agreement with the reaction mechanism assuming a rate-determining one-electron transfer step.

Fuel cells which employ organic fuels such as methanol or its derivatives are strongly demanded, especially for uses as small scale transportable electric power sources with improved conveniences in storage and handling of the fuel as compared with hydrogen. A number of investigations on this subject have been carried out about two decades ago,[1-3] but fuel cells of this type which are economically comparable with other electric power sources have not yet been developed. A major difficulty involved in some carbonaceous fuel cells is due to sluggish rate of electro-oxidation of the fuels. Hence, a breakthrough which must be accomplished before developing such fuel cells is concerned with the fabrication of electrodes having high electrocatalytic activity towards the oxidation.

A series of precious metals generally possess high activity compared with other metals for the electro-oxidation of these fuels and most investigations carried out up to this date have been concentrated on them.[2] At the present stage, it appears that the following two directions may be sought for in order to attain fuel cells which are economically more feasible: Thus, (a) the electrocatalytic activity per unit loading of the precious metal should be improved so that its amount of use may be reduced or (b) nonprecious metal electrodes with high electrocatalytic acivity for organic fuels should be developed.

As electrode materials other than precious metals, tungsten carbides[2c] and molybdenum oxides[3c] have been noted, and some workers[4,5] have lately reported that these electrodes have excellent characteristics for the electro-oxidation of methanol or its derivatives. Among methanol derivatives, formaldehyde can readily be electro-oxidized on some nonprecious metals: The present authors have recently reported that a series of IB metals catalyze the anodic HCHO oxidation[6] in alkaline media and suggested a possible use of Cu metal or Cu-based amorphous alloys as electrocatalysts.[6c] In this paper, some further details of the anodic oxidation characteristics in both aqueous NaOH and Na_2CO_3 media are presented and then the reaction mechanism is presented.

Most amorphous alloys prepared by the rapid quench technique generally have a high strength to mechanical stresses. They are also often corrosion resistant because they are essentially in the form of homogeneous solid solutions of the alloying metals and contain no lattice defects, *e.g.* dislocation, grain boundary, *etc.* Their uses as catalysts or electrocatalysts have drawn attentions during the last several years. In the field of electrocatalysis, Kawashima and Hashimoto[7] reported electro-oxidation of methanol and its derivatives in alkaline solutions on a series of Pd-based amorphous alloys such as a-$Pd_{61}Pt_{20}P_{19}$. A number of amorphous Cu–Ti and Cu–Zr alloy specimens with compositions between 30 and 70 wt% Cu have been prepared and the hydrogen absorbability has been studied.[8] The hydrogen evolution reaction property and surface characteristics of HF-treated Cu-based amorphous alloy specimens have been reported in our previous paper.[9]

Experimental

Preparation of Electrodes. The Cu electrodes were prepared from an ordinary Cu plate (0.3 mm in thickness, 99.5% purity) in a rectangular form of 10×5 mm and their surface was etched with dilute nitric acid prior to the electrochemical measurements. The electrodes of Cu-based amorphous alloys were made from alloy ribbons (0.5—1.0 mm wide and *ca.* 20 μm in thickness)† and made porous by treatment with aq HF as described elsewhere.[9] The electrodes were clipped or spot-welded on Ta lead wires which were sealed in Pyrex glass tubings.

Roughness Factor. The roughness factor (*RF*) of the electrodes was evaluated from the double layer capacitance

† Some of these samples were provided by Prof. K. Suzuki and Dr. K. Kai of Tohoku University, to whom our thanks are due.

data measured by a galvanostatic transient method (time scale=1—5 m s) and the assumed value of 18 μF cm^{-2} (true).

Electrochemical Measurements. The cyclic voltammogram and steady-state polarization measurements were carried out in 0.03—3.0 M (M=mol dm^{-3}) NaOH or 0.5 M Na_2CO_3 solutions, which contain various amounts of HCHO (0.003—1.0 M), under a stream of purified Ar gas. The formaldehyde used (GR grade, Nakarai Chemicals, Tokyo) contained 7 wt% CH_3OH. A Ag/AgCl and a pt-Pt RHE were used as reference electrodes, but all the potential values quoted in this report are given on the RHE scale. Details of the cell and other experimental procedures were described previously.[6]

XPS Measurements. Surface analysis of the amorphous Cu-Ti and Cu-Zr alloys was performed using an ESCA apparatus (VG-III) with Mg $K\alpha$ radiation. The binding energy values recorded were calibrated using the $4f_{7/2}$ signal (83.8 eV) from a gold plate which was employed as an internal standard.

Results and Discussion

In NaOH Solutions. The electrocatalytic activity of Cu metal electrodes for the electro-oxidation of HCHO was very high. The rest (open circuit) potential of Cu metal and Cu-based amorphous alloy electrodes was usually observed to be around −50 mV (RHE). Although this value is much more positive than the theoretical oxidation potential of HCHO (−0.22 V *vs.* RHE), it is the most negative potential observed among analogous systems employing various carbonaceous fuels.

Figure 1 shows typical cyclic voltammograms obtained on a Cu plate in 1 M NaOH containing various amounts of HCHO. Even with HCHO of very low concentration (10^{-2} M), the oxidation current was quite significant and it became already noticeable at potentials around 0.1 V. The hysteresis on the cyclic voltammograms, which is very often observed in the electro-oxidation of carbonaceous fuels such as methanol, was small or almost absent in this case under the polarization between 0 and 0.5 V. The decrease of the current density above about 0.4 V observed in 0.01 M HCHO solution may perhaps be attributed, under the short HCHO supply conditions, to the formation of oxide (*e.g.* Cu_2O) on the Cu surface at that potential, which may give rise to the lowering of the electrocatalytic activity. Such a deactivation never took place in solution containing higher amounts of HCHO.

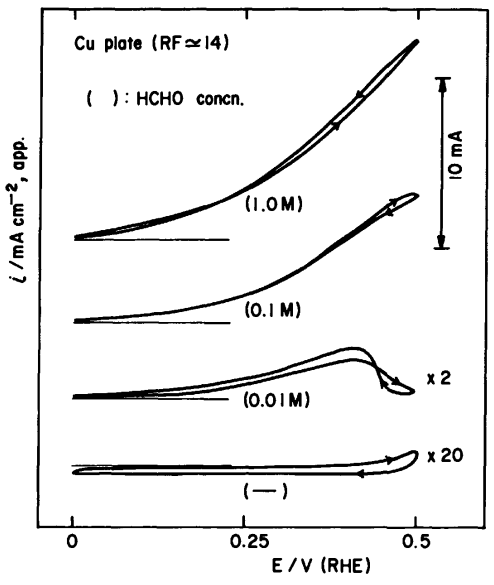

Fig. 1. Typical cyclic voltammograms observed on a Cu plate in 1 M NaOH containing 0.01—1.0 M HCHO at 303 K. Potential sweep rate: 10 mV s^{-1}.

In a previous paper,[9] we have reported that Cu-rich porous layers formed by the treatment with aq HF on the surface of the amorphous Cu-Ti and Cu-Zr alloys show a high electrocatalytic activity for the hydrogen evolution reaction as compared with usual smooth Cu electrodes. Similarly, very high HCHO electro-oxidation currents were observed on the HF-treated amorphous Cu-Ti and Cu-Zr alloy electrodes and, among them, the latter alloy showed more active and hence advantageous electrocatalytic characteristics than the former one. Meanwhile, the HCHO oxidation current on the untreated Cu-based amorphous alloys was very small: This must be due to the existence of inert oxide films, *i.e.* TiO_2 or ZrO_2, covering their surface.

Figure 2 shows cyclic voltammograms observed on the HF-treated amorphous Cu-Ti and Cu-Zr alloys with various *RF* values (given in the parentheses). On the Cu-Ti alloy electrodes, the current-voltage curves have maxima with a peak around 0.35 V in a similar manner as that of the Cu plate at the concentration of 0.01 M HCHO (see Fig 1). On the other hand, the voltammograms on the Cu-Zr alloys have no such maxima and increase monotonously with the potential sweep. In addition, the hysteresis on the voltammograms of these specimens is considerably smaller, and the catalytic activity of the electrodes with analogous *RF* values is much higher, as compared with that of the amorphous Cu-Ti alloy. These observations may suggest a difference in the surface characteristics of the porous Cu layers formed from the Cu-Ti and Cu-Zr alloys by the HF-treatments.

The surface of the Cu-based amorphous alloys was made porous by dissolving the alloy component Ti and Zr out of the alloy matrices with aq HF: It has been observed from SEM pictures that the surface indeed has a porous structure.[9] Nevertheless, the Cu-rich porous layers formed in this way contained a noticeable amount of Ti or Zr residue, as demonstrated in the XPS patterns of the Cu-Ti and Cu-Zr alloys which were observed before and after the HF-

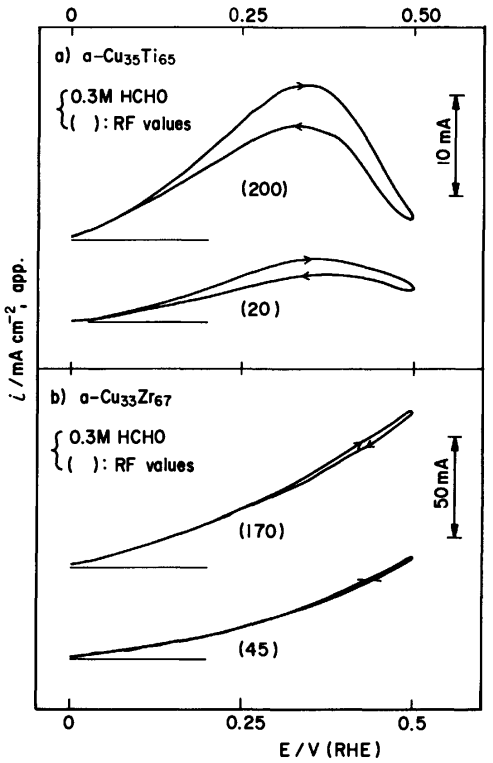

Fig. 2. Cyclic voltammograms observed on the Cu-based amorphous alloy electrodes with several *RF* values in 1 M NaOH containing 0.3 M HCHO at 303 K. Potential sweep rate: 10 mV s^{-1}.

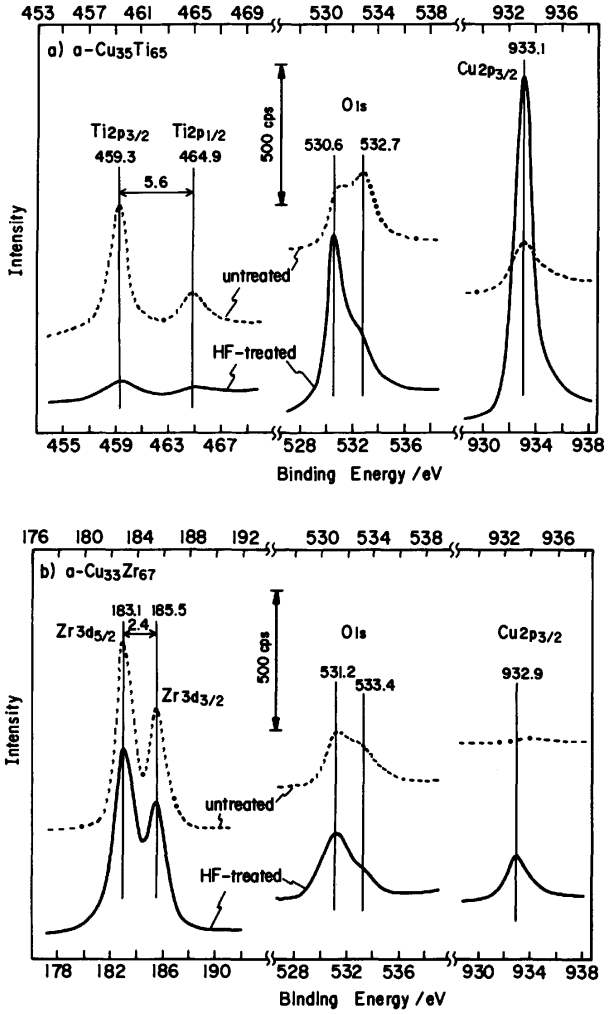

Fig. 3. XPS patterns of the Ti_{2p} (or Zr_{3d}), O_{1s}, and Cu_{2p} electrons on (a) a-$Cu_{35}Ti_{65}$ and (b) a-$Cu_{33}Zr_{67}$ alloys before (broken-lines) and after (solid-lines) the treatment with aq HF.

treatment (shown in Fig. 3).

On both the untreated and HF-treated specimens, spectra derived from strong Ti_{2p} and Zr_{3d} electrons have signals at the binding energy regions of 459—465 and 183—186 eV, respectively: These peak positions agree with those of the titanium of TiO_2 and the zirconium of ZrO_2, respectively. The O_{1s} signals consist of two bands peaking at about 530.6 and 532.7 eV which can respectively be assigned to the oxygens of oxides and hydroxyl groups. The Cu_{2p} signals are attributable to the 2p electrons of the metallic copper and/or Cu_2O. After the HF-treatments, however, the spectrum intensities from Cu_{2p} electrons are considerably increased whereas those of Ti_{2p} or Zr_{3d} electrons decreased.

It can be seen from Fig. 3 that the amounts of the Ti and Zr residue in the resulting Cu-rich layers on the HF-treated amorphous Cu-Ti and Cu-Zr alloys nevertheless differ considerably from each other: The amorphous Cu-Zr alloy gives relatively strong Zr_{3d} signals even after the HF-treatment while this was not the case for Ti in the amorphous Cu-Ti alloys. Thus, the Cu-rich layers formed on the amorphous Cu-Zr alloy still contain an appreciable amount of Zr, and the improved electrocatalytic activity of the amorphous Cu-Zr alloy may be due to this Zr residue. On the other hand, Ti was almost completely lost from the surface of the Cu-Ti alloy and this was probably the reason why the characteristics of the Cu-rich layers on this alloy was rather similar to those of usual Cu plates.

The difference between Cu-Ti and Cu-Zr alloys is again demonstrated in the relationship between the oxidation current density and *RF* values, as shown in Fig. 4 together with results obtained on the Cu metal electrodes. The current increased initially in a proportional way with the *RF* values and the highest value reached on the amorphous Cu-Zr alloy at 0.2 V was around 40 mA cm^{-2}. An analogous shape was also obtained on the Cu-Ti alloy. Although the data were rather erratic, it could be seen in general that the current density was much lower than that on the Cu-Zr alloy. In the region of still higher *RF* values, the current had a tendency to reach a saturation value. This might indicate that not all the surface area of the porous alloy electrodes was any longer used effectively in the oxidation of HCHO: The curve suggests that the electrode with the *RF* value

above 100 is quite satisfactory for the HCHO electro-oxidation.

A kind of "induction period" was seen in Fig. 4 on electrodes with low *RF* values: These were obtained on the electrode without any extensive treatment of the surface. This might indicate that the amorphous alloys became electrocatalytically active only after a significant amount of the inert oxide films (TiO_2 or ZrO_2) was lost from the surface so that their surface became sufficiently rich in Cu.

The electrocatalytic activity was very stable: Large current density values were obtained even after a prolonged time of the steady-state polarization on those electrodes, particularly on the HF-treated amorphous alloys with the porous Cu-rich layers formed on the surfaces. Figure 5 shows the stability of the electrocatalytic activity of Cu metal and Cu-based amorphous alloys at the initial period of the steady state polarization at 0.2 V. No steep decay in the anodic current density, such as those frequently observed in the methanol oxidation on platinum electrodes was recorded. In a long period (several days) polarization, however, a further amount of formaldehyde must be added to the electrolyte in order to maintain the stable current density outputs. This indicated that HCHO would have been decomposed to methanol and formate by the Cannizzaro disproportionation reaction in alkaline media.

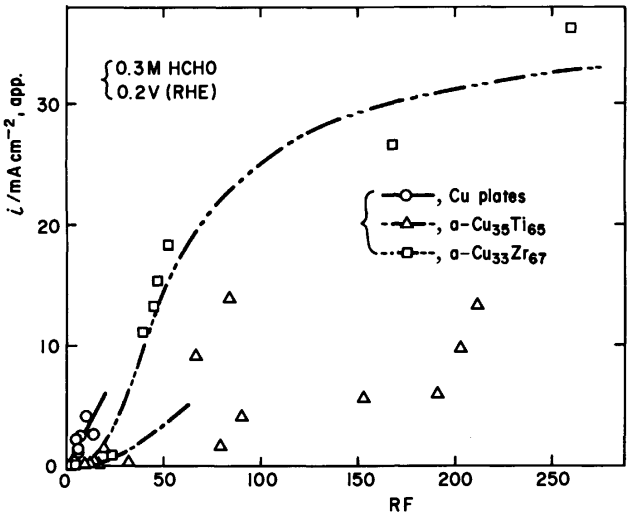

Fig. 4. *RF* value dependences of the anodic current density i on Cu metal and Cu-based amorphous alloy electrodes in 1 M NaOH containing 0.3 M HCHO at 303 K. The i values are read at 0.2 V on the cyclic voltammograms obtained with the potential sweep range of 0—0.5 V and the sweep rate of 10 mV s^{-1}.

In Na_2CO_3 Solutions. If the oxidation of HCHO in alkaline solutions such a NaOH and KOH is complete, yielding CO_2 (and H_2O), the alkali would readily take up CO_2 and form carbonate and then hydrogencarbonate. This means that the cell reaction consumes the alkali metal hydroxide rather like a part of fuels. It is then much more advantageous if the electro-oxidation of HCHO takes place with a reasonable rate in Na_2CO_3 solution. In this case, the fuel cell may be operated at relatively high temperatures so that the hydrogencarbonate is decomposed back to carbonate.

Figure 6 shows typical cyclic voltammograms observed on a Cu plate in 0.5 M Na_2CO_3 solution. As same as those obtained in NaOH solutions, the anodic oxidation current of HCHO was clearly observed at potentials lower than 0.1 V and the rest potential was again negative on the RHE scale. The hysteresis of their voltammograms are very small. The electrocatalytic activity of the Cu-based amor-

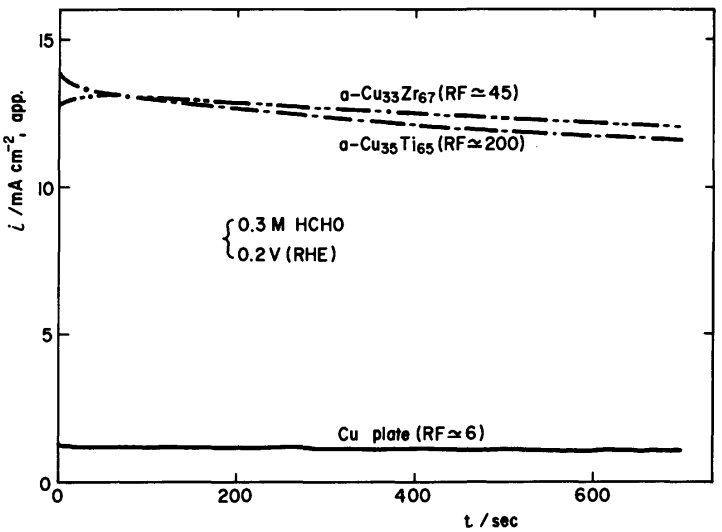

Fig. 5. Time dependences of the anodic current density i under the steady-state polarization at 0.2 V on Cu metal and Cu-based amorphous alloy electrodes in 1 M NaOH containing 0.3 M HCHO at 303 K.

phous alloys was much higher than that of the Cu metal electrodes. Nevertheless, their anodic current outputs were about one order of magnitude smaller than those obtained in NaOH solutions.

The anodic current outputs are maintained practically at constant values for a long period over several days: The Cu-based amorphous alloys with *RF* value of 110—120 constantly give the current density around 3 mA cm^{-2} (see Fig. 7), and thus these alloys are again good candidates for the electrode materials in this type of formaldehyde fuel cells.

Reaction Mechanism. Tafel plots of the anodic polarization currents on the Cu metal and Cu-based amorphous alloys are shown in Fig. 8. It is seen as mentioned already that all the rest potentials are negative to RHE and the catalytic activity is very high. The slopes of the linear portions in their Tafel plots are not much different from the ordinary behaviours of one-electron transfer kinetics, although the behaviour of the amorphous Cu-Ti alloy electrode is somewhat different from the others. The slope values would indicate that the oxidation takes place by a mechanism involving a rate-determining one-electron transfer step.

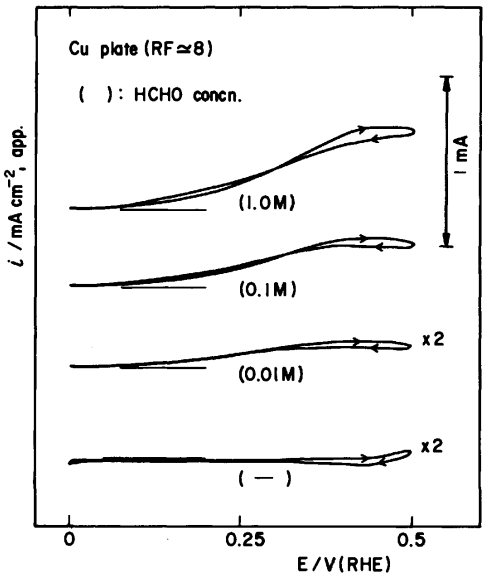

Fig. 6. Typical cyclic voltammograms observed on a Cu plate in 0.5 M Na_2CO_3 (pH=11.5) containing 0.01—1.0 M HCHO at 303 K. Potential sweep rate: 10 mV s^{-1}.

Meanwhile, evolution of hydrogen during the reaction, in spite of more positive electrode potentials than that of the RHE were involved, was reported by some investigators in experiments which are connected with the electroless plating[10c,d] of metals such as Cu: This was also confirmed in the present work.

The number of electrons involved in the electro-oxidation was evaluated from the quantity of electricity required when a given amount of HCHO was completely electro-oxidized at a constant electrode potential. Figure 9 shows a coulometric curve of the anodic HCHO oxidation on a Cu plate electrode. The number obtained was 0.97 equivalents mol^{-1} during the electrolysis at 0.23 V in 1 M NaOH solution. This observation indicates that the reaction is a partial oxidation to $HCOO^-$, along with a co-production of hydrogen.

In Fig. 10 is shown a relation between the anodic current density on the Cu metal electrode and pH of NaOH solutions, 0.03—3.0 M, which contain 0.3 M HCHO. At the lower pH region, the curve obtained was asymptotic to the line with the slope of unity (dashed line in figure): The oxidation reaction may thus be judged to be first order in OH^- in low NaOH

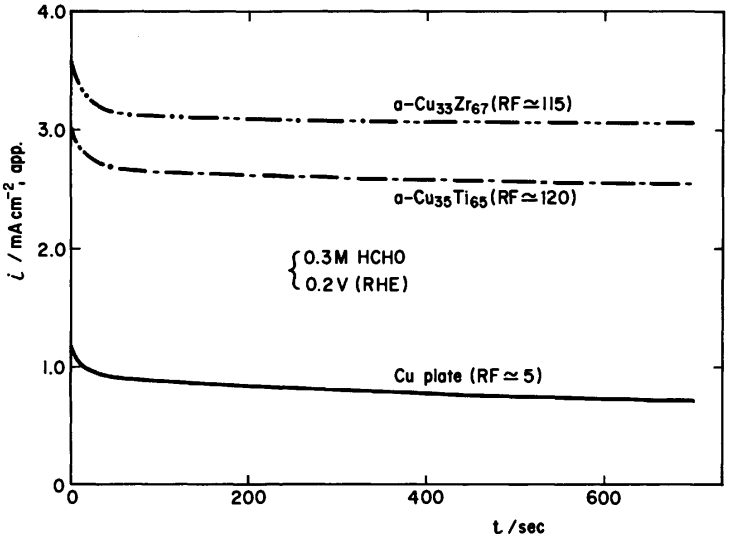

Fig. 7. Time dependences of the anodic current density i under the steady-state polarization at 0.2 V on Cu metal and Cu-based amorphous alloy electrodes in 1 M NaOH containing 0.3 M HCHO at 303 K.

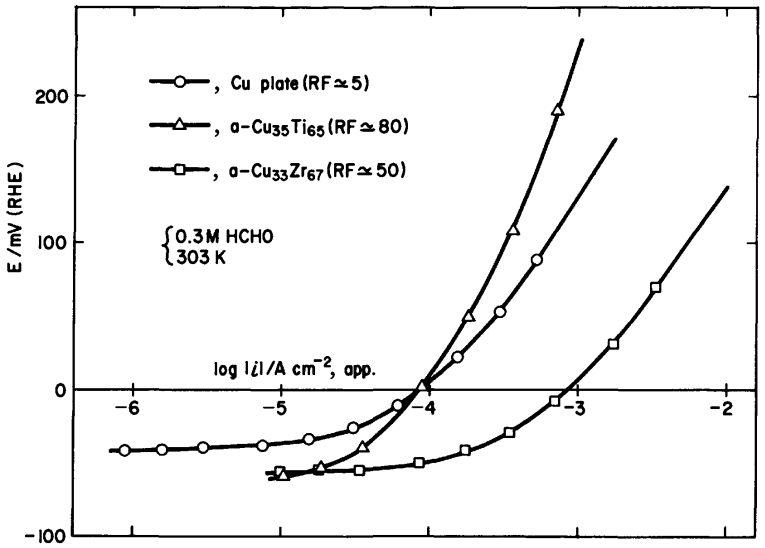

Fig. 8. Anodic polarization behaviors of Cu metal and Cu-based amorphous alloy electrodes in 1 M NaOH containing 0.3 M HCOH at 303 K.

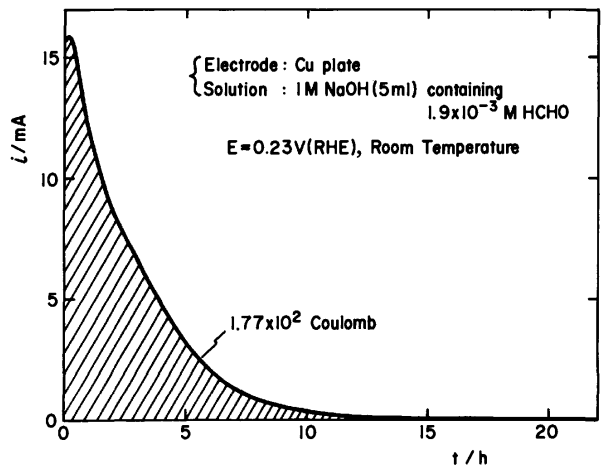

Fig. 9. A coulometric curve of the anodic formaldehyde oxidation on a Cu plate.

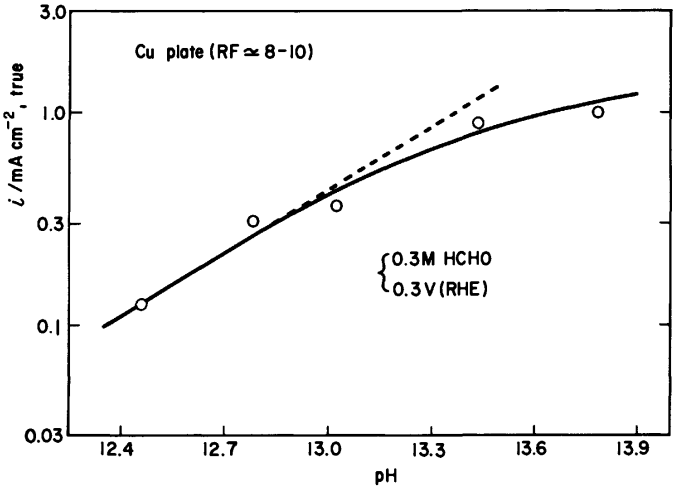

Fig. 10. Anodic current density i *vs.* pH observed on Cu plates in 0.03—3.0 M NaOH solutions containing 0.3 M HCHO at 303 K.

concentration range.

The dependence of the oxidation rate on the HCHO concentration on the Cu metal electrode with a fixed NaOH concentration is shown by open circles in Fig. 11. The log-log plot again yields a smooth bending curve, but it has a general tendency to approach a line with the slope of unity at low concentrations, in a similar manner as in Fig. 10. These observations, *i.e.* the oxidation rate increases with increase both in HCHO or OH^-, are in harmony with the mechanism proposed in the literature[10] that hydroxymethanolate (methyleneglycol) ion, $HOCH_2O^-$, is formed from HCHO in aqueous alkaline solutions, and the anodic HCHO oxidation proceeds *via* this ion.

This reaction scheme means that pH of the alkaline solution should decrease by the addition of HCHO or the equilibrium constant for the formation of $HOCH_2O^-$ can be evaluated from the pH change. In Table 1, the pH values of NaOH solutions observed before and after the addition of the equimolar amounts of HCHO, and the K values thus evaluated are summarized. As an average, K=4.7 M^{-1} was obtained, although the K value at high NaOH concentration (0.298 M) was too high as compared with the other values.

Also presented in Fig. 11 (filled circles) is the relation between the oxidation current and the $HOCH_2O^-$ concentration evaluated from the reactant concentrations and the K value obtained above. It may be seen that the reaction is essentially of the first order with respect to $HOCH_2O^-$ at low concentrations. The decrease of the reaction order in the higher concentration region may require more information

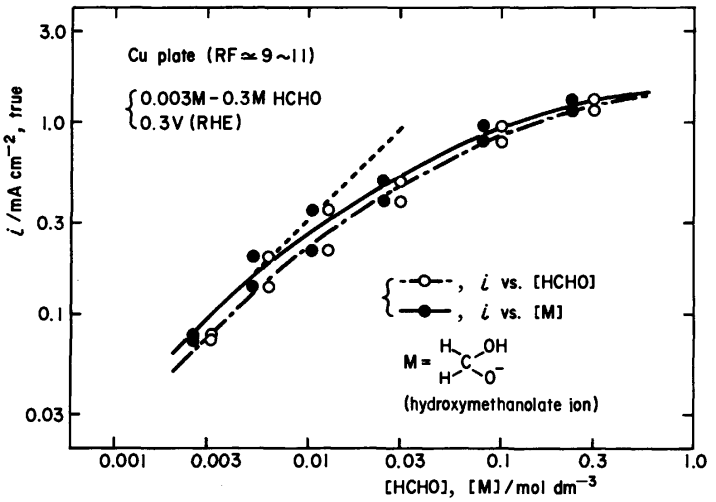

Fig. 11. Anodic current density i *vs.* formaldehyde (open circles) and hydroxymethanolate ion (filled circles) concentration observed on Cu plates in 1 M NaOH at 303 K.

Table 1. Equilibrium constant in the system NaOH-HCHO at room temperature

[NaOH]/M	pH	pH[a)]	K/M
0.016	12.23	12.20	5.0
0.035	12.52	12.46	4.8
0.096	12.90	12.78	4.4
0.298	13.33	13.02	(7.1)
			Av. 4.7

a) Values obtained in the solutions containing HCHO equimolar with the amount of NaOH.

before any definite interpretations be made: It is nevertheless likely that the hydroxymethanolate ion is adsorbed on the electrode surface prior to its discharge and the adsorption gradually approaches a full coverage in this high concentration region.

On the basis of the experimental observation mentioned above, the following reaction scheme may be written:[10)]

$$HCHO + H_2O \rightleftharpoons CH_2(OH)_2 \quad (1)$$

$$CH_2(OH)_2 + OH^- \rightleftharpoons HOCH_2O^- + H_2O \quad (2)$$

$$HOCH_2O^- \xrightarrow{A} HCOOH + H(a) + e \quad (3)$$

$$HCOOH + OH^- \longrightarrow HCOO^- + H_2O \quad (4)$$

$$2H(a) \longrightarrow H_2\uparrow \quad (5)$$

where $\xrightarrow{A}$ denotes the rate-determining step. The experimental observations, namely, the first order reaction both in HCHO and OH^- at low concentrations, the Tafel line which supports rate-determining one-electron transfer step, one electron involved in the overall reaction, and the hydrogen evolution along with the electro-oxidation, may well be explained by this mechanism.

Additional Remarks. As mentioned above, HCHO is not completely oxidized on the Cu-based electrodes to CO_2 and H_2O at potentials which are desirable for practical fuel cell operations. Also, these electrodes are not good electrocatalysts for the oxidation of hydrogen and hence the hydrogen intermediate yields as gaseous H_2 by step (5). It may therefore be necessary for a complete HCHO oxidation that the Cu-based electrodes may be combined with other electrocatalysts which have a high catalytic activity for the oxidation of $HCOO^-$ and of the hydrogen intermediate,

$$HCOO^- \longrightarrow CO_2\uparrow + H^+ + e \quad (6)$$

$$H(a) \longrightarrow H^+ + e \quad (7)$$

Amorphous alloys are noteworthy in this purpose because they may be prepared in uniform solid solutions with various compositions.

In previous reports,[11)] we have reported that several Ti-and Zr-based amorphous alloys of group VIII metals are good electrocatalysts for the evolution or ionization of hydrogen (Eq 7), and also they are expected to be highly active for the oxidation of $HCOO^-$ (Eq 6). Thus, some preliminary experiments[12)] indicated that, while the electrocatalytic activity in the $HCOO^-$ electro-oxidation of Ni- and Pt-based amorphous alloys was relatively low, that of Pd-based amorphous alloys was very high. Furthermore, the electrocatalytic activity of the Pd-based electrodes was much more stable than that of the other alloys. It may be interesting to see if HCHO can be completely oxidized to CO_2 and H_2O using composite electrodes contaning Cu and Pd.

Conclusion

Cu metal and Cu-based amorphous alloy electrodes show very high electrocatalytic activity for the anodic

HCHO oxidation and the oxidation current is already significant at potentials around 0.1 V (RHE). The reaction kinetics have the characteristics such that the oxidation rate is approximately first order in HCHO and OH^-, and the Tafel line suggests a reaction mechanism involving a rate-determining one-electron transfer step. The results indicate that the oxidation proceeds *via* $HOCH_2O^-$ intermediate which is formed from HCHO and OH^-. The oxidation is, however, not of complete one to CO_2 and H_2O and hydrogen is evolved along with the electro-oxidation.

The present work is partly supported by Grants-in-Aid for Scientific Research No. 59045007 from the Ministry of Education, Science, and Culture.

References

1) J. O'M. Bockris and H. Wroblowa, *J. Electroanal. Chem.*, **7**, 428 (1964).

2) a) "Hydrocarbon Fuel Cell Technology," ed by B. S. Baker, Academic Press, New York (1965); b) J. O'M. Bockris and S. Srinivasan, "Fuel Cells: Their Electrochemistry," McGraw-Hill, New York (1969); c) "From Electrocatalysis to Fuel Cells," ed by G. Sandstede, Battelle Seattle Research Center and the University of Washington, New York (1976).

3) a) S. G. Meibuhr, *Electrochim. Acta*, **11**, 1301 (1966); b) R. T. Tischer, *ibid.*, **11**, 1309 (1966); c) S. G. Meibuhr, *ibid.*, **11**, 1325 (1966); d) S. G. Meibuhr, *ibid.*, **13**, 1973 (1968).

4) W. R. Wolfe and K. B. Keating, *J. Electrochem. Soc.*, **121**, 1125 (1974).

5) T. Kudo, G. Kawamura, and H. Okamoto, *J. Electrochem. Soc.*, **130**, 1491 (1983).

6) a) M. Enyo, *J. Electroanal. Chem.*, **186**, 155 (1985); b) M. Enyo, *J. Appl. Electrochem.*, in press; c) K. Machida and M. Enyo, *Chem. Lett.*, **1985**, 75.

7) A. Kawashima and K. Hashimoto, Proc. 4th Int. Conf. on Rapidly Quenched Metals, Sendai, 1982, Abstr. Vol. 2, pp. 1427—1430.

8) A. J. Maeland, L. E. Tanner, and G. G. Libowitz, *J. Less-Common Met.*, **74**, 279 (1980).

9) K. Machida, M. Enyo, K. Kai, and K. Suzuki, *J. Less-Common Met.* **100**, 377 (1984).

10) a) E. Müller and S. Takegami, *Z. Electrochem.* **34**, 704 (1928); b) R. P. Buck and L. R. Griffith, *J. Electrochem. Soc.*, **109**, 1005 (1962); c) M. Saito, *Kinzoku Hyomen Gijutsu (Metal Surface Technology)*, **16**, 300 (1965); d) J. E. A. M. Van Den Meerakker, *J. Appl. Electrochem.*, **11**, 387 (1981).

11) M. Enyo, T. Yamazaki, K. Kai, and K. Suzuki, *Electrochim. Acta*, **28**, 1573 (1983); K. Machida, M. Enyo, I. Toyoshima, K. Miyahara, K. Kai, and K. Suzuki, *Bull. Chem. Soc. Jpn.*, **56**, 3393 (1983); K. Machida and M. Enyo, unpublished data.

12) K. Machida and M. Enyo, to be published.

Reduction Mechanism of 2,3,5-Triphenyltetrazolium Chloride and 1,3,5-Triphenylformazan

Kisaburo UMEMOTO
Department of Pure and Applied Sciences, College of General Education, The University of Tokyo, Komaba, Meguro-ku, Tokyo 153
(Received March 14, 1985)

The reduction mechanism of 2,3,5-triphenyltetrazolium chloride(TTC) and 1,3,5-triphenylformazan was studied by electrochemical, ESR, and spectrophotometric methods. In non-aqueous aprotic solvent, 2,3,5-triphrnyltetrazolium ion was reduced to formazan anion either by two-electron reaction or by disproportionation reaction of tetrazolinyl radical generated by one-electron reduction of TTC. The same formazan anion was generated by one-electron reduction of 1,3,5-triphenylformazan. In the presence of proton donor, the formazan anion was converted to formazan by protonation reaction and cyclic regeneration of formazan was observed in the reduction of formazan. These results indicate that the quantitative determination of reducing materials by using TTC may possibly lead to erroneous evaluation of reductants unless the strength of electron donating property of reductants is established.

Tetrazolium salts have been used for demonstrating dehydrogenase activities,[1-4] for detecting hyperoxide radical,[5-7] and for determination of inorganic reducing materials.[8] Upon reduction tetrazolium salts, generally colorless, are converted to highly colored formazans.

Although tetrazolium salts have merits as qualitative indicators, their use as quantitative reagents has been less successful.[4,5] In the estimation of microbial damage by using TTC, the coloration was dependent on the quality as well as the quantity of microflora.[4] In the examination of using TTC as a quantitative reagent for the determination of hyperoxide, poor reproducibility was revealed in the intensity of the coloration of the solution.[9]

In addition to the ambiguity involved in the quantitative use of tetrazolium salts, there appeared an uncertain relationship between the color of the solution and the reaction intermediate: There has been either or not a relationship between the color of the solution and the intensity of ESR signals.[10,11] Nevertheless, there have been a few works on the systematic studies of the reduction mechanism of tetrazolium salts.[5,11-14]

The purpose of the present work is to elucidate the problem involved in the quantitative use of TTC by clarifying the stepwise reduction pathways of TTC and its formazan.

Experimental

TTC obtained from Tokyo Kasei was recrystallized from mixture of ethanol and diethyl ether and 1,3,5-triphenylformazan of the same source was recrystallized from aqueous ethanol solution under nitrogen. These materials were dried at 70 °C under vacuum. Dimethyl sulfoxide (DMSO) was treated with activated alumina and distilled twice under nitrogen at reduced pressure. Tetraethylammonium perchlorate(TEAP) was prepared according to the usual method.

Absorption spectra were measured with a Hitachi 100-60 spectrophotometer. ESR spectra were measured by a Japan Electron Optics Lab. Co. JES-PE-3X spectrometer. Cyclic voltammograms were recorded with a laboratory made potentiostat.[15] The Pt electrode used for cyclic voltammetry was soaked in aqua regia for 30 s and heated in a blue flame.[15] Controlled potential electrolysis was carried out in an H-type cell equipped with a sintered glass separator. The cathode was a Pt net and the anode was a spiral Pt wire. Potentials were all referred to an SCE equipped with a salt bridge.[15] All experiments were carried out at room temperature (20 °C).

Results and Discussion

Molecular structures and abbreviations of molecular species appeared in this paper are summarized as follows:

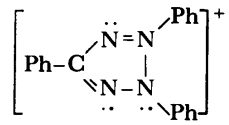

2,3,5-triphenyltetrazolium (R+)

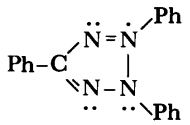

2,3,5-triphenyltetrazolinyl (R·)

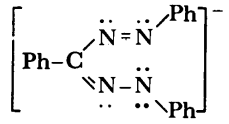

1,3,5-triphenylformazan anion (R−)

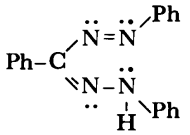

1,3,5-triphenylformazan (RH)

Reduction of TTC. A cyclic voltammogram of TTC is shown in Fig. 1. Two cathodic and two anodic waves were observed. By carrying out the potential reversal immediately after the first cathodic wave, the first redox couple was found to be A/A′.

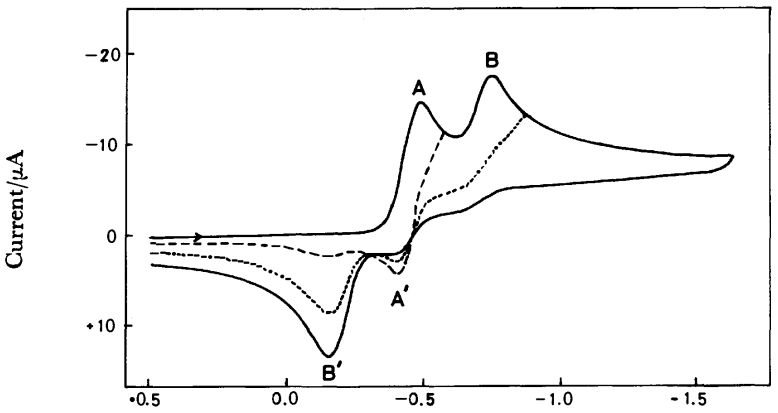

Fig. 1. Cyclic voltammogram of TTC: 1.0×10^{-3} mol dm^{-3} in DMSO containing 0.1 mol dm^{-3} TEAP. Scan rate: 0.05 Vs^{-1}.

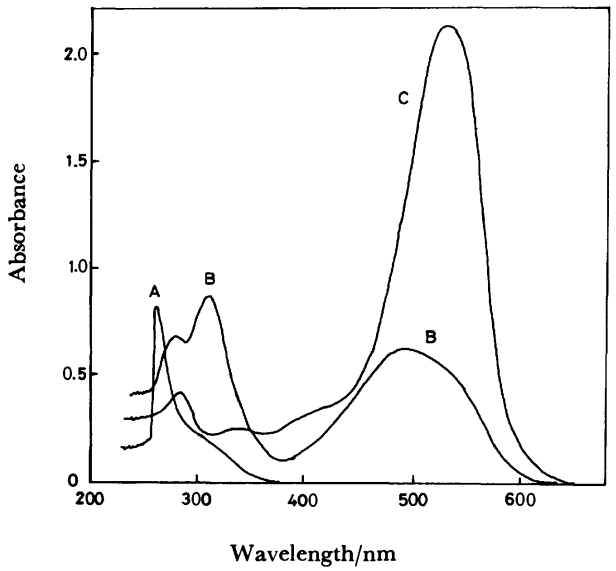

Fig. 2. Absorption spectra of (A): TTC (3.5×10^{-5} mol dm^{-3}), (B): 1,3,5-triphenylformazan (3.2×10^{-5} mol dm^{-3}), and (C): 1,3,5-triphenylformazan anion generated from (A) by controlled potential electrolysis at -1.09 V in DMSO.

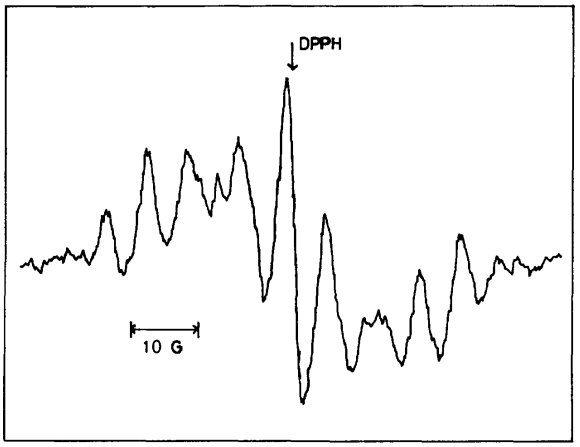

Fig. 3. ESR spectrum of tetrazolinyl radical generated by electrochemical reduction of TTC in DMSO.

The peak potential separation of the first redox couple was *ca.* 70 mV, being close to a reversible one-electron reaction. When constant potential electrolysis at -0.95 V corresponding to the second reduction step was performed to completeness, overall two electrons (1.98 electrons were found by experiment) were found to be required for each molecule of TTC and a highly red colored solution was obtained. The absorption spectrum of the solution is given in Fig. 2 along with absorption spectra of TTC and 1,3,5-triphenylformazan. The absorption band with its maximum at 538 nm was identified to that of formazan anion R^-, since an identical spectrum was obtained when R^- was liberated by adding tetraethylammonium hydroxide to the DMSO solution of 1,3,5-triphenylformazan. Taken together with these results the following stepwise electron transfer reactions are given:

$$R^+ + e \rightleftharpoons R\cdot \quad (1)$$

$$R\cdot + e \longrightarrow R^- \quad (2)$$

In order to obtain a solution of tetrazolinyl radical $R\cdot$, constant potential electrolysis was carried out at -0.55 V corresponding to the first reduction wave. For the complete electrolysis, two electrons (experimentally 1.96 electrons were found), contrary to the probable one electron, were found to be required for each molecule of TTC. The resulted solution was highly red colored and gave no ESR signal, but gave

exactly the same absorption spectrum as that of R^- shown in Fig. 2C. In contrast with the complete electrolysis, the partially electrolyzed solution gave an ESR spectrum as shown in Fig. 3 irrespective of the electrolysis potential being either −0.55 V or −0.95 V. The ESR spectrum was identified to that of 2,3,5-triphenyltetrazolinyl radical.[10,11,16] The same radical was also generated by adding TTC to the solution containing R^- alone. These results provide sufficient evidence for supporting the following equilibrium disproportionation reaction of R·.

$$R\cdot + R\cdot \rightleftharpoons R^+ + R^- \quad (3)$$

Judging from the result that the electron-transfer reaction to the radical (Eq. 2) is observable at the second cathodic wave on the cyclic voltammogram of TTC, the rate of disproportionation reaction is not very fast, since if this rate is too fast, only the first cathodic wave raised twice in height should be observed.

On the absorption spectrum of the solution containing tetrazolinyl radical, any band characteristically attributable to the radical was not observed. However, by subtracting the bands of TTC and formazan anion, a small absorption band was admitted in a range from 300 to 400 nm. Recently, by pulse radiolysis of 2-propanol solution of TTC, the absorption band of transiently lived radical was found to have its maximum at 365 nm.[14] The present observation that the absorption band of the radical was so weak indicates the equilibrium constant of disproportionation reaction (Eq. 3) being large in DMSO.

Cyclic voltammograms obtained in a series of reduction of TTC and subsequent re-oxidation of formazan anion are given in Fig. 4. The peak potentials of formazan anion (curve C) coincided with those of the second anodic wave and the two cathodic waves observed for TTC. In order to verify the probable regeneration of tetrazolium ion, constant potential electrolysis was carried out at +0.20 V. Upon completion of the electrolysis two electrons (experimentally 1.94 electrons were found) were found to be released for each formazan anion, and as shown in Fig. 4D, the original tetrazolium ion was recovered in high efficiency by the following oxidation reaction:

$$R^- - 2e \longrightarrow R^+ \quad (4)$$

In this oxidation reaction, the stepwise two one-electron reactions were not observed as shown in Fig. 4C. The large potential separation of the second redox couple observed for TTC (B/B′ in Fig. 1) indicates a large activation energy being needed for the cyclization of the open chain structure of formazan anion, bringing the potential of electron release of R^- more positive than the oxidation potential of R·. Accordingly, the second electron release would follow immediately after the first electron release of R^- and leaving no place for the accumulation of R· as a reaction intermediate.

Additional support for the reversible interconversion of R^+ and R^- was obtained in the study of absorption spectra. The absorption band of R^+ was substituted by that of R^- on completion of reduction of R^+, and on re-oxidation the absorption band of R^+ was recovered on consumption of that of R^-. The cycle of the complete reduction and oxidation was successively repeated and the interconversion of R^+ and R^- was found to be reproducible in high efficiency.

Formazan anion was stable in unhydrous DMSO, but when proton donors such as water and acids were added into the solution, the anion turned to formazan by the following protonation reaction:

$$R^- + H^+ \longrightarrow RH \quad (5)$$

The absorption spectrum obtained by addition of proton donors into the DMSO solution of R^- agreed

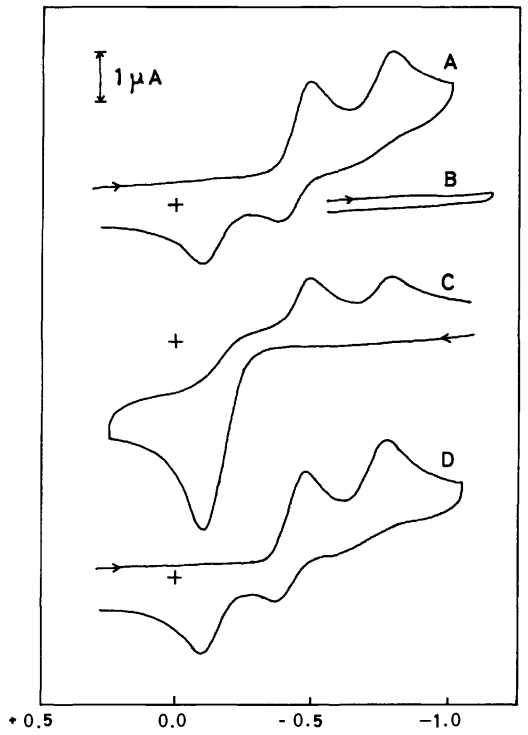

Fig. 4. Cyclic voltammogram of TTC taken (A): Before electrochemical reduction, (B) and (C): After complete electrochemical reduction, and (D): After electrochemical re-oxidation of formazan anion.

well with that of formazan shown in Fig. 2B. The rate of protonation reaction became faster with the stronger acidity of proton donors.

Reduction of 1,3,5-Triphenylformazan. The oxidation of formazan to tetrazolium salts is known to be the most characteristic property of formazan.[1,17-19] The electrochemical oxidation of formazans has been studied in acetonitrile and it was found that formazans are converted to tetrazolium salts with high efficiency.[17-19] However, the electrochemical study of reduction of formazans is quite few.[18] The reason seems to be due to the circumstances that the oxidation of formazans usually affords valuable pathways to prepare tetrazolium salts, while the reduction of formazans has not been praised for the preparative method of their decomposition products, such as hydrazine, amidrazone,amines, and aniline.

As formazan is indeed reducible, the reduction of formazan should be carefully studied, since formazan is the key substance in the analytical use of tetrazolium salt for determining reducing substances.

A cyclic voltammogram of 1,3,5-triphenylformazan is shown in Fig. 5. The first scan showed one cathodic and one anodic waves. Upon sweep reversal at *a* for the second scan additional two cathodic waves appeared at potentials where TTC gave its reduction waves. Constant potential electrolysis at −1.09 V revealed one electron (experimentally 1.06 electron was found) being required for complete electrolysis of each molecule of formazan. After the completion of the electrolysis, a highly red colored solution was obtained and the absorption spectrum as well as the cyclic voltammogram of the solution agreed well with those of formazan anion shown in Fig. 2C and in Figs. 4B and 4C, respectively. Subsequent constant potential electrolysis at +0.20 V revealed two electrons (experimentally 1.91 electrons were found) being released for the complete electrolysis of each formazan anion. After the electrolysis was completed, both the cyclic voltammogram and the absorption spectrum of the solution agreed well with those of TTC. The efficiency of conversion of 1,3,5-triphenylformazan to 2,3,5-triphenyltetrazolium ion was estimated to be over 95%. These results indicate that 1,3,5-triphenylformazan is reduced to formazan anion R^- by one-electron reaction accompanied by the elimination of hydrogen atom as shown below:

$$RH + e \longrightarrow R^- + H \qquad (6)$$

When formazan is reduced in the presence of proton donors, the regeneration of formazan is expected, since the protonation reaction shown by Eq. 5 would follow after the generation of R^-. In order to examine the probable cyclic regeneration of formazan, constant potential electrolysis at −1.09 V was carried out in an aqueous DMSO solution. Water was chosen as the proton donor, since acids were reduced at this potential, while water did not affect the electrolysis. The results are given in Fig. 6. In contrast with the asymptotic approach of the electrolysis current to the background level in unhydrous DMSO, the curent was observed to reach a stationary level in an aqueous DMSO solution, showing a stationary state being attained between the reduction and the regeneration of formazan in an aqueous DMSO solution. After 60 min of electrolysis, the peak heights of the absorption band and the reduction wave of formazan were almost the same with those recorded before the electrolysis was started, indicating that the concentration of formazan was

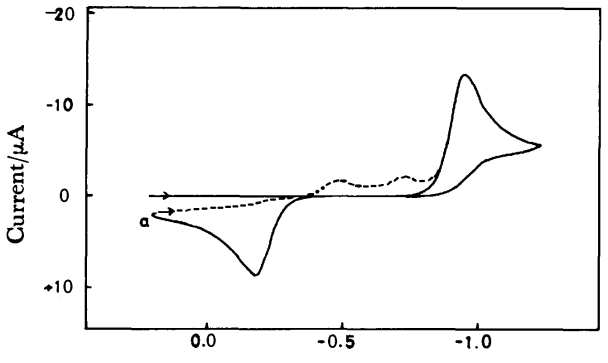

Fig. 5. Cyclic voltammogram of 1,3,5-triphenylformazan: 1.0×10^{-3} mol dm^{-3} in DMSO containing 0.1 mol dm^{-3} TEAP. Scan rate: 0.05 Vs^{-1}.

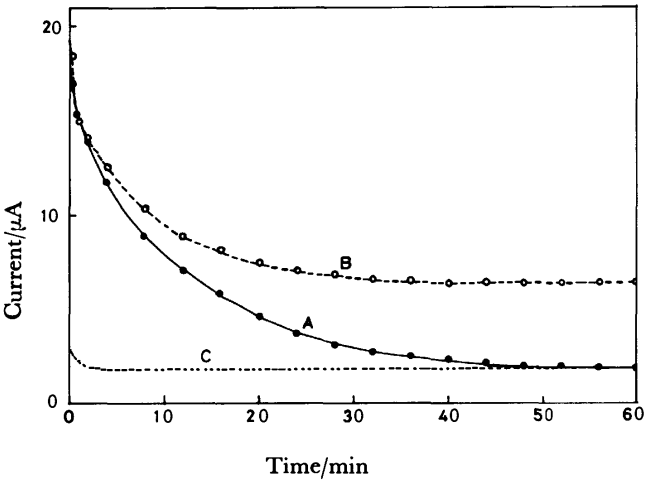

Fig. 6. Current-time curves taken in electrolysis of 1,3,5-triphenylformazan in (A): Unhydrous DMSO, (B): Aqueous DMSO (DMSO : water=92 : 8 in volume), and (C): base current (extrapolated after 10 min.). 1×10^{-7} mol of formazan was taken in *ca.* 4 dm^{-6} of solution containing 0.1 mol dm^{-3} TEAP. Potential: −1.09 V *vs.* SCE.

little affected in spite of formazan being really accepting electrons under conditions examined.

The results presented in this work provide an explanation for the problem encountered in the use of TTC as an electron acceptor. As 1,3,5-triphenylformazan is reduced at a potential (−0.95 V) not far more negative than the second reduction potential of TTC (−0.75 V), a stronger electron donor would reduce not only TTC (according to Eq. 1—4) but also formazan (according to Eqs. 5 to 6). However, the amount of electron donor used for the reduction of formazan is uncertain, since formazan is regenerated by the protonation reaction. The effect of regeneration of formazan depends both on the electron donor and the used solvent system; the stronger the electron donor and the stronger the proton donating property of the solvent system, the more effective the contribution of reduction of formazan, leading to erroneous estimation of electron donors by using TTC. In this sence, the electron donating property of reducing agents should be well established prior to the application of TTC for the particular system.

The author thanks Drs. Ryo Hirasawa and Kazuo Sakamoto for their kind permission and outstanding assistance in using their ESR spectrometer.

References

1) A. W. Nineham, *Chem. Rev.*, **55**, 355 (1955).
2) F. P. Altman and G. R. Butcher, *Histochemie*, **37**, 333 (1973); R. G. Butcher and F. P. Altman, *ibid.*, **37**, 351 (1973); F. P. Altman, *ibid.*, **38**, 155 (1974).
3) P. S. N. Rao and U. B. S. Swami, *Curr. Sci.*, **48**, 818 (1979).
4) V. A. Kalaganov, V. Z. Zakirova, and Z. M. Kartavtseva, *Khim. Tekhnol. Topl. Masel*, **1983**, 40; *CA*, **98**, 146184h (1983).
5) B. H. J. Bielski, G. G. Shiue, and S. Bajuk, *J. Phys. Chem.*, **84**, 830 (1980).
6) I. Saito, T. Matsuura, and K. Inoue, *J. Am. Chem. Soc.*, **105**, 3200 (1983).
7) E. Lee-Ruff, *Chem. Soc. Rev.*, **6**, 195 (1977).
8) A. I. Lazarev, V. I. Lazarev, and I. P. Kharlamov, *Zab. Lab.*, **46**, 291 (1980); *CA*, **93**, 36356e (1980).
9) K. Umemoto and N. Okamura, unpublished data.
10) Y. Deguchi and H. Takagi, *Tetrahedron Lett.*, **33**, 3179 (1967).
11) O. W. Maender and G. C. Russell, *J. Org. Chem.*, **31**, 442 (1966); F. A. Neugebauer and C. A. Russell, *ibid.*, **33**, 2744 (1968).
12) F. A. Neugebauer, *Tetrahedron*, **26**, 4843 (1970).
13) K. M. Dyumaev, G. V. Formin, and Z. K. Kriminskaya, *Khim. Vys. Energ.*, **16**, 558 (1982); *CA*, **98**, 81387e (1983).
14) Z. K. Kriminskaya, K. M. Dyumaev, L. S. Vischipanova, Yu. V. Ivanov, and A. K. Pikaev, *Khim. Vys. Energ.*, **18**, 40 (1984); *CA*, **100**, 174049w (1984).
15) K. Umemoto, T. Saeki, and N. Matsuura, *Bull. Chem. Soc. Jpn.*, **55**, 746 (1982).
16) N. Azuma, K. Mukai, and K. Ishizu, *Bull. Chem. Soc. Jpn.*, **43**, 3960 (1970).
17) M. Lacan, T. Tabakovic, and Z. Cekovic, *Tetrahedron*, **30**, 2911 (1974).
18) I. Tabakovic, M. Trkovnik, and Z. Gruic, *J. Chem. Soc., Perkin Trans. 2*, **1979** 166.
19) V. F. Gryazev, E. S. Karavaeva, I. N. Borukhova, and N. P. Bednyagina, *Khim. Geterosikl. Soedin.*, **1982**, 1274; *CA*, **98**, 4517v (1983).

Adsorption Equilibria of Copper on Octadecylsilica Gel in the Presence of Acetylacetone

Masanao KATO
Department of Materials Science, Faculty of Engineering, Toyohashi University of Technology, Tempaku-cho, Toyohashi 440
(Received December 27, 1984)

The solid-liquid adsorption equilibria of copper with acetylacetone between octadecyl-bonded silica (ODS) gel and aqueous solution were investigated by a batch method at 298±1 K. It is found that a 1:1 complex of copper with acetylacetone is adsorbed on the gel surface.

Some types of chemically modified silica gels have been widely used as stationary phases for high-performance liquid chromatography. Among them, octadecylsilica (ODS) gel has been adopted for reversed phase chromatography, and the chromatographic behavior of various kinds of solute species has been studied in the system using ODS gel. They include studies using metal complexes as solute.[1-7] In these studies, it is well-known that the labile complexes introduced into the column give long tailing on the chromatograms. The phenomena have been explained as the degradation of complex molecules in the separation process; they were supressed by an addition of ligand to the eluent.

The ODS gel has also been used as a solid adsorbent for the preconcentration of trace metals in water.[8-14] In these studies, various complexing agents have been added to the sample solution as a coadsorbent. Metal ions in the samples form complexes with ligand molecules; these were considered to be adsorbed on the gel surface by a hydrophobic interaction with the long alkyl chains on the gel surface.

In these studies, however, the adsorption mechanisms underlying the separation or concentration process were not investigated for the systems containing metal complexes. They have simply been regarded as similar to those involved in the solvent extraction.

It was reported by some workers that an active site on the gel surface behaves as a cation exchanger.[15-17] Although it seems likely that the long alkyl chain on the gel surface plays an important role in the adsorption of metal complexes, these studies indicate that the roles played by the active site can not be neglected. Indeed, Mackey[16] pointed out that iron, copper, manganese, and zinc ions were adsorbed without complexing agent on the ODS gel (Waters) of low coverage.

It is also reported in the kinetic studies of liquid-liquid extraction that the 1:1 complex of copper with several kinds of ligands may be adsorbed at the liquid-liquid interface.[18-19] These studies suggest that the species adsorbed onto ODS gel follow a different mechanism from that involved in liquid-liquid extraction equilibria between two bulk phases, because the octadecyl monolayer on the ODS gel surface may behave as an interface similar to that involved in the solvent extraction or partition systems. Recently, Fardy *et al.*[14] pointed out from the calculation of the concentration of some complexes in the solution containing 8-quinolinol and some metal ions that the 1:1 complexes play dominant roles in the adsorption of copper, manganese and zinc ions on Sep-Pak C_{18} (Waters) which, according to Mackey,[16] adsorbs no metal cation except for iron.

From the above consideration, it can be supposed that the adsorbed species of metal ions on the ODS gel in the presence of some ligands would be much different from that extracted in solvent extraction or liquid-liquid partition of metal complexes. In this study, the adsorption equilibria of copper between the ODS gel and the aqueous phase were investigated in the presence of acetylacetone (2,4-pentanedione). Acetylacetone was chosen for the reasons: (1) the behavior of the ligand and its metal complexes in liquid-liquid partition has been thoroughly investigated; (2) its concentration in the adsorption systems can be changed over a wide range, since its solubility in water is relatively high; and (3) it is stable in water. The second reason aids in making the systems relatively simple, because other solvents like methanol are not required in order to dissolve the insoluble ligands such as 8-quinolinol.

Experimental

Materials. ODS gel (Unisil P-C18, Gasukuro Kogyo) was washed with diluted hydrochloric acid (Special Reagent for Trace Analysis, Kishida Chem.), ultra-pure water (obtained from Milli-Q system, Milipore Corp.), and methanol (Guaranteed reagent, Kanto Kagaku) successively, and then dried.

Acetylacetone (Guaranteed reagent, Kanto Kagaku) was used after distillation. All other reagents were commercially available guaranteed reagents, and were used without further purification.

Apparatus. The pH of the initial and final solutions were measured by a Toyo Kagaku TD-4 pH

meter. The copper concentrations in solutions were determined by atomic absorption spectrometry with a Shimadzu AA-640-12 atomic adsorption spectrometer equipped with GFA-2 graphite furnace atomizer. The concentration of acetylacetone was determined by UV absorbance at 274 nm using a Shimadzu UV-140-02 spectrometer. All the measurements were carried out in a thermostated room at 298±1 K. A box shaker (Itagaki Rika) was employed for equilibration of the adsorption mixtures.

Procedures. Twenty-five cm^3 buffer solutions of 1/15 mol dm^{-3} (CH_3COOH–CH_3COONa–NaOH or $HClO_4$–$NaClO_4$) were introduced into a 100 cm^3 vials, to which stock solution of 1.57×10^{-4} mol dm^{-3} of copper(II) sulfate, and 9.6×10^{-1} mol dm^{-3} of acetylacetone were added. They were filled up to 100 cm^3 with ultra-pure water, and the pH measured.

For the measurements of the adsorption equilibria, 20 cm^3 aliquots were introduced into 50 cm^3 glass centrifuge tubes containing 0.5 g ODS gel. The mixtures were shaken for 10 min at a shaking rate of *ca.* 300 min^{-1}. The equilibrated mixtures were allowed to stand for about 30 min in order to separate the gel from the aqueous phase. The solutions were filtered through a membrane filter of 10 μm pore to remove the gel. The pH and copper concentration of the filtrates were measured.

The ODS gels were washed with a 1 per cent solution of acetylacetone in chloroform in order to elute the adsorbed copper from the gel. Next the gel was rinsed with chloroform until no uv absorption of acetylacetone was observed in the chloroform. After the gel was successively washed with methanol, water, diluted hydrochloric acid (pH 2), and again water; it could then be reused.

The concentration of copper, C, adsorbed on the gel was calculated from the following equation

$$C_{ad} = (C_{in} - C_f)V/m, \quad (1)$$

where subscripts ad, in, and f denote the adsorbed, initial, and filtrate, respectively. V represents the volume of the aqueous phase and m is the mass of the ODS gel.

The distribution ratio, D, was defined by the following equation

$$D = C_{ad}/C_f \quad (2)$$

where the concentration of copper(II) cation in the filtrates are expressed in unit of mol cm^{-3}.

Results and Discussion

The equilibria of adsorption of copper between aqueous phase and ODS gel were attained within 5 min under these experimental conditions of the present investigation. In the measurements, the shaking time was fixed at 30 min, above which the distribution ratios were constant within experimental error.

The adsorption behavior of acetylacetone on the gel is shown in Fig. 1 as a function of initial concentration. The concentration of adsorbed acetylacetone increases linearly with the increasing concentration in the filtrates up to 0.5×10^{-2} mol dm^{-3}. In more concentrated solutions, however, another linearity appears. The distribution ratio tends to decrease with increase of acetylacetone concentration. At low concentrations, it decreases more steeply. The typical concentration of acetylacetone used in the adsorption experiments of copper(II) cation was 1×10^{-2} mol dm^{-3} and the volume of the solutions was 20 cm^3. Under these conditions, the concentration of acetylacetone on the gel is proportional to the initial concentration, and the adsorptive ability of the gel can be regarded as undersaturated.

The adsorption isotherms of acetylacetone obey the Freundlich equation (Fig. 2), but not the Langmuir equation. According to the theoretical consideration,[20] the surface of the ODS gels is not homogeneous, and it has more than two kinds of sites available

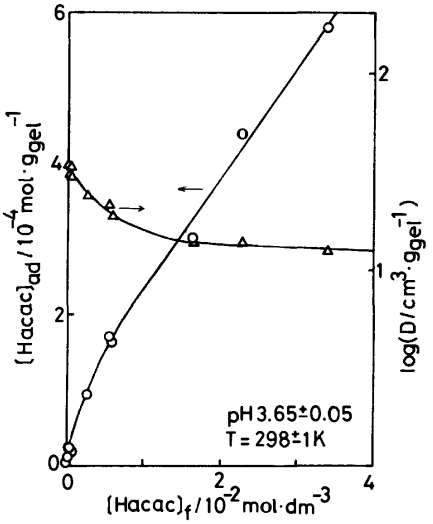

Fig. 1. Adsorption of acetylacetone onto ODS gel. ○ denotes concentration of acetylacetone on ODS gel, and △ is the distribution ratio.

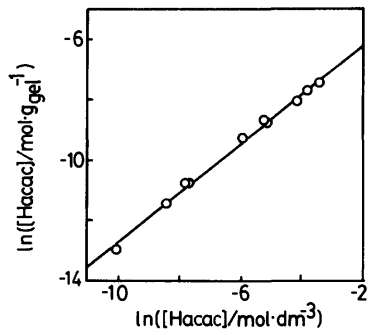

Fig. 2. Analysis of adsorption of acetylacetone by means of Freundlich equation.
$\ln[Hacac]_{ad} = 0.810 \ln[Hacac]_f - 4.60$

for adsorption of acetylacetone. This phenomenon agrees with the results that the gel has a second active site in addition to the hydrophobic site.[15-17] It is expected that these would be the remaining silanols on the surface which can interact *via* hydrogen bonding with acetylacetone, hydrophobic alkyl chains of octadecyl groups bonded on the surface, and the intermediate site among them. According to the information from the manufacturer, the gel used in the present study has uncovered surface silanols.

In Fig. 3, the pH dependence of the adsorption of acetylacetone is illustrated. The adsorption is independent of pH in the region studied. This indicates that acetylacetone is adsorbed on the gel surface as an electrically neutral species.

The dependence of adsorption of copper(II) cation upon the initial concentration is shown in Fig. 4, where the ratios of copper(II) cation concentration to that of acetylacetone are constant. The concentration of copper(II) cation on the gel increased linearly with its initial concentration in the aqueous phase up to 2×10^{-4} mol dm^{-3}, and its adsorption ratio was constant below a copper(II) cation concentration of 1.0×10^{-4} mol dm^{-3}. The ODS gel used in this study has a large ability to adsorb the copper complex, enough to permit experiments at very low copper concentrations of 1.57×10^{-5} mol dm^{-3} (this corresponds to 1 ppm Cu), or up to 3.14×10^{-5} mol dm^{-3} in the experiments of Job's continuous variation method. In this concentration range, 95 per cent of the copper(II) cation was adsorbed.

Now, consider the concentration of copper(II) cation, acetylacetone, and silanol group on the gel surface. The copper concentration on the gel is 6.3×10^{-7} mol g_{gel}^{-1} when the initial concentration is 1.57×10^{-5} mol dm^{-3} and the volume of solution is 20 cm^3, if the copper were completely adsorbed. The concentration of acetylacetone adsorbed is about 3.6×10^{-4} mol g_{gel}^{-1}, when its initial concentration in the aqueous phase is 1.0×10^{-2} mol dm^{-3} and the volume is 20 cm^3, since the adsorption rate is 90 per cent under these experimental conditions. Moreover the total concentration of residual silanol groups on the gel surface is estimated as 1.1×10^{-3} mol g_{gel}^{-1} on the basis of surface silanol concentration[21] and the information from the manufacturer. It is found from the above estimation that the concentration of copper on the gel is much smaller than those of the others, and the concentration change of acetylacetone and surface silanol caused by the adsorption of copper can be neglected. However, the concentration change of acetylacetone in solution or on the gel may significantly influence the adsorption of copper, since the concentration is comparable to that of the surface silanol.

The dependence of the distribution ratio of copper(II) cation upon the acetylacetone concentration and pH are shown in Fig 5. The pH range, in which the distribution ratio regularly increased, shifted to high pH with decrease of ligand concentration. This phenomenon is consistent with that observed in solvent extraction. However, the apparent values of the so-called extraction coefficients,

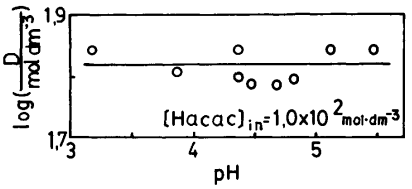

Fig. 3. pH Dependence of adsorption of aceylacetone onto ODS gel. Acetate buffer used.

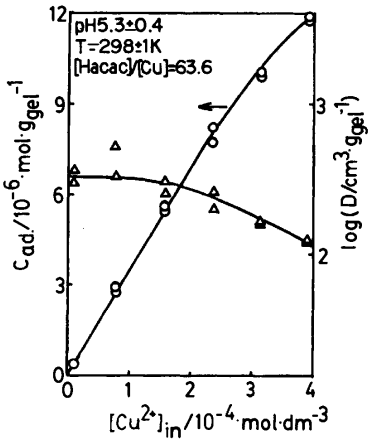

Fig. 4. Concentration dependence of adsorption of copper(II) cation with acetylacetone onto ODS gel. Concentrations of copper on gel are represented by ○, and its distribution ratio, △, respectively.

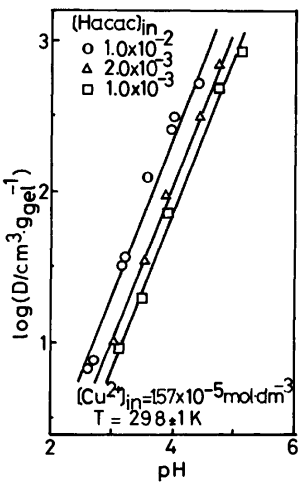

Fig. 5. pH Dependence of adsorption of copper(II) cation with acetylacetone onto ODS gel.

K_{ex}, calculated on the assumption that the ODS gel behaves as one of the phases, were not constant as tabulated in Table 1. K_{ex} is represented as the terms reciprocal to the distribution coefficient of ligand species between two phases, K_L, in the partition mechanism. As shown in Fig. 1, the apparent K_L values also decrease with increase of concentration of acetylacetone. For this reason, it is considered that the activity of the acetylacetone adsorbed on the surface is lowered in the diluted region by the adsorption to the surface silanol groups.[16]

The salt effect on the adsorption was investigated using acetic acid buffer solutions and perchlorate solution at constant pH and ionic strength in order to clarify whether the acetate anion is contained in the adsorbed species. The adsorption ratio was independent of the change of the composition of salts as shown in Fig. 6. Perchlorate anion is well known as one of the weakest ligands and forms no complexes in aqueous solution. The results in this figure suggests that acetate anion is not involved in the adsorption of copper. This fact is supported by the calculation of the degree of complex formation in these mixtures, where the concentration of acetate complex is negligibly small.

In order to determine the chemical composition of the adsorbed species, both the Job's continuous variation method and the molar ratio method were applied. In the Job's continuous varation study, the maximum adsorption was obtained for an equimolar solution. In the molar ratio study, the constant adsorptions were obtained over the equimolar solution. These results suggest that the adsorbed species are composed of one copper(II) cation and one ligand molecule.

The main driving force for the adsorption of the copper(II) cation with acetylacetone onto ODS gel from aqueous media is considered to be the hydrophobic interaction of the acetylacetonato complexes with the alkyl chain bonded on the gel. However, as mentioned above, the adsorption behavior cannot be completely interpreted only by the hydrophobic interaction. That is, it is found in this study that copper(II) cation in the aqueous media is adsorbed on the gel as the charged 1:1 complex of copper(II) cation and acetylacetone. To account for the neutralization of the electric charge of the gel adsorbing copper(II) cation, we may include another interaction of the charged complex with the ODS gel surface, *e. g.*, with residual silanol groups on it, as pointed out by Mackey.[16] At this stage it seems unlikely that the adsorbed 1:1 complexes would immediately exchange with the proton of the surface silanol groups buried under the alkyl chain. If the cation exchange occurs between the charged complex and the surface silanol, the distribution ratio is expressed as follows:

$$D = \frac{K_{ch}\beta_{n-1}K_a^{n-1}}{K_L^{n-1}}[\mathrm{HOSi}]_s\frac{[\mathrm{Hacac}]_{gel}^{n-1}}{[\mathrm{H}^+]^n}, \quad (3)$$

were K_{ch}, β_n, and K_a denote the exchange coefficient between complex and surface silanol, the formation constant of the charged complex, and the dissociation constant of acetylacetone, respectively. s and n indicate the surface and the charge on the copper(II) cation. As the concentration of copper on the gel is much smaller than that of the surface silanol, the concentration of silanol can be regarded as remaining constant. From the equation, it is concluded that if the cation exchange occurs the slope of log D *vs.* pH plot must have a value of nearly two. However, the slope obtained in the present study is close to unity. Therefore, it is reasonable to assume that the adsorption of the copper(II) cation onto the ODS gel can be explained by the partition of a 1:1 complex of copper(II) cation and acetylacetonate anion between the bulk aqueous phase and the alkyl chain layer on the ODS gel as one of the interface. The charge neutralization may be attained between ODS gel adsorbing complexes and anion in the aqueous phase in equilibrated mixtures.

The results obtained in this study may afford basic information essential to an understanding of the mechanism of separation of complexes in liquid

Table 1. Adsorption equilibria of copper(II) cation with acetylacetone onto ODS gel in presence of acetate buffer

$C_{acac,in}/10^{-3}$ mol dm^{-3}	Slope	Log K_{ex}
1.0	1.09	0.935
2.0	1.09	0.739
10.0	1.12	0.226

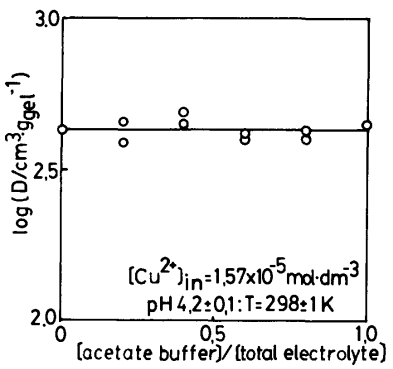

Fig. 6. Dependence of adsorption ratio of copper(II) cation by acetylacetone upon compositions of buffer solution.

chromatography with ODS gel and the concentration of the metal with acetylacetone onto the gel. As mentioned above, this behavior is different from the partition mechanisms in bulk phase for liquid–liquid partition, but similar to the mechanism proposed in explaining the kinetics of partition of metal complex in the interface between two liquid phases.[18,19]

This work was partly supported by Grant-in-Aid for Scientific Research (No. 57740290). from the Ministry of Education, Science, and Culture.

References

1) E. Gaetani, C. F. Laureri, A. Mangia, and G. Paolari, *Anal. Chem.*, **48**, 1725 (1976).
2) A. Mangia, G. Paolari, E. Gaetani, and C. F. Laureri, *Anal. Chim. Acta*, **92**, 111 (1977).
3) G. Schwedt, *Chromatographia*, **12**, 289 (1979).
4) S. Ichinoki and M. Yamazaki, *Bunseki Kagaku*, **31**, E319 (1982).
5) R. C. Gurira and P. W. Carr, *J. Chromatogr.*, **252**, 185 (1982).
6) S. R. Huchins, P. R. Haddad, and S. Dilli, *J. Chromatogr.*, **252**, 185 (1982)
7) J. S. Huber, J. C. Kraak, and H. Veening, *Anal. Chem.*, **44**, 1554 (1972).
8) S. Taguchi and K. Goto, *Talanta*, **27**, 819 (1980).
9) H. Watanabe, K. Goto, S. Taguchi, J. W. McLaren, S. S. Berman, and D. S. Russel, *Anal. Chem.*, **53**, 738 (1981).
10) S. Taguchi, K. Goto, and H. Watanabe, *Talanta*, **28**, 613 (1981).
11) G. L. Mills and J. G. Quinn, *Mar. Chem.*, **10**, 93 (1981).
12) S. Taguchi, C. Yoshikura, and K. Goto, *Bunseki Kagaku*, **31**, 32 (1982).
13) R. E. Sturgeon, S. S. Berman, and S. N. Willie, *Talanta*, **29**, 167 (1982).
14) J. J. Fardy, G. D. McOrist, and T. M. Florence, *Anal. Chim. Acta*, **159**, 199 (1984).
15) O. A. G. J. van der Houwen, R. H. A. Sorel, A. Halshoff, J. Teeuwsen, and A. W. M. Indemans, *J. Chromatogr.*, **242**, 275 (1981).
16) D. J. Mackey, *J. Chromatogr.*, **242**, 275 (1982).
17) S. G. Weber and W. G. Tramposch, *Anal. Chem.*, **55**, 1771 (1983).
18) I. Komasawa, *J. Chem. Eng. Jpn.*, **13**, 204 (1980).
19) M. Cox *Proceedings ISEC '80 paper* 80—118 (1980).
20) T. Kei, "Kyuchaku," Kyoritsu Shuppan, Tokyo (1965), Chapter 3.
21) R. G. Gilpin and M. F. Burke, *Anal. Chem.*, **45**, 1383 (1973).

A Competition between 1,3-Dipolar Cycloaddition and Substitution of Trifluoroacetonitrile Oxide

Kiyoshi TANAKA,* Hideyuki MASUDA, and Keiryo MITSUHASHI
Department of Industrial Chemistry, Seikei University, Musashino-shi, Tokyo 180
(Received September 26, 1984)

Trifluoroacetonitrile oxide reacted with conjugated olefins such as styrenes, indenes, and acyclic conjugated dienes to give not only the cycloadduct but also its linear isomeric oxime. Methyl or phenyl group attached to the unsaturated carbon of the dipolarophiles was found to favor the formation of oxime. Such a concomitant reaction was interpreted in terms of a competition between a concerted cycloaddition and a two-step substitution through an electrophilic attack of nitrile oxide. Similar competitions were also investigated with cyclic conjugated dienes, where the competitive ratio of the products was found to depend on the ring size.

In the reactions of dipolar compounds with olefins or acetylenes, the substitution giving 1,3-addition product has been investigated in connection with the mechanism of 1,3-dipolar cycloaddition.[1,2] The reaction of benzonitrile oxide with phenylacetylene is particularly well documented,[3] and the concomitant formation of diphenylisoxazole and acetylenic oxime was interpreted by the independent two pathways, that is, a concerted cycloaddition and a substitution through an electrophilic attack of nitrile oxide on the triple bond of phenylacetylene.[1,4] As far as literatures show, however, such a substitution is limited only to rather unreactive dipolarophiles such as arylacetylenes and furan.

Previously we have reported the regio- and stereoselectivities in the conventional 1,3-dipolar cycloaddition of trifluoroacetonitrile oxide (**1**) with various olefins and acetylenes.[5] In the present paper,

$$CF_3C{\equiv}N{\rightarrow}O$$
1

we wish to demonstrate a competition between the 1,3-dipolar cycloaddition and the electrophilic substitution in the reaction of the oxide **1** with rather reactive conjugated olefins.[6]

The oxide **1**, generated from trifluoroacetohydroximoyl bromide etherate (**2**) and triethylamine,[5] reacted with styrene to give 5-phenyl-3-trifluoromethyl-2-isoxazoline (**3a**) along with a trace amount of the 1,3-addition product, 1,1,1-trifluoro-4-phenyl-3-buten-2-one oxime (**4a**). In contrast, the reaction with α-methylstyrene and α-phenylstyrene gave the corresponding oximes **4b** and **4c** in preference to the cycloadducts **3b** and **3c**, respectively (Scheme 1 and Table 1). The structures of **3a**—c and **4a**—c were determined on the basis of the elemental analyses and spectral data. Isomeric composition of **4a**—c and their steric configuration were investigated by means of ^{1}H NMR together with GLC. Thus **4a** or **4c** was deduced to be only one isomer and **4b** to consist of two geometric isomers out of four possible ones, respectively. Since **4b** could be hardly separated into

Table 1. Total yields of isoxazolines (**3** or **5**) and oximes (**4** or **6**) and their ratios in the reactions of trifluoroacetonitrile oxide with styrenes and indenes

Product	Total yield, %[a]	Ratio(**3**/**4** or **5**/**6**)[b]
3a, 4a	84	99.5/0.5[c]
3b, 4b	73	33/67
3c, 4c	42	37/63
5a, 6a	53	79/21
5b, 6b	67	37/63
5c, 6c	35	0/100

Numbers of products refer to those in Scheme 1.
a) Isolated yield. b) Determined by ^{1}H NMR analysis of the reaction mixture unless otherwise noted. c) The ratio of the isolated products.

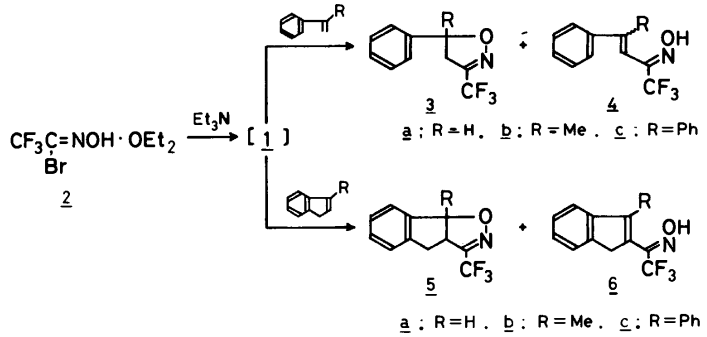

Scheme 1.

the components, its absolute configuration was ambiguous and the components are shown here as **A** and **B**. It should be noted that both the cycloadducts **3** and the oximes **4** are primary products *via* the independent pathways because they were too stable to interconvert under the reaction conditions unless the more drastic conditions were applied. The isoxazolines **3a** and **3b** were converted in high yields into the oximes **4a** and **4b**(**A** and **B**), respectively, through ring-opening by the treatment with lithium diisopropylamide[7] and, conversely, **4b** cyclized on heating at 150 °C to give **3b**. Such an interconversion

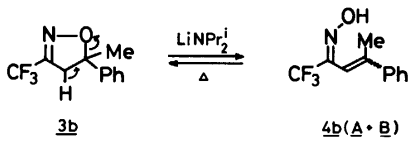

3b 4b(A + B)

might suggest the *E* configuration in respect to C–N double bond of **4**, and **4b-A** and **4b-B** could be the geometrical isomers in respect to C–C double bond. In the case with α-methylstyrene, the effect of the bases was then studied using pyridine and sodium methoxide in place of triethylamine, resulting in no appreciable changes in the ratios of **3b**/**4b** and **4b-A**/**4b-B**, as shown in Table 2.

The concomitant formation of the cycloadducts and the 1,3-addition products was also observed in the reactions of **1** with indenes (Scheme 1). Yields and ratios of these isomers are summarized in Table 1. The reaction of **2** with indene in the presence of triethylamine gave 3a,8a-dihydro-3-trifluoromethyl-4*H*-indeno[2,1-*d*]isoxazole (**5a**) and 2-[2,2,2-trifluoro-1-(hydroxyimino)ethyl]indene (**6a**) in the ratio of 79/21, where their regioisomers were not detected at all. The structure of **5a** was established by the comparable chemical shifts of two methine protons in ^{1}H NMR to those of the 3-phenyl analogue reported in the literature.[8] Singlet olefinic proton of **6a** in ^{1}H NMR supports that the trifluoro(hydroxyimino)ethyl group is attached to 2-position. In analogy with styrenes, methyl and phenyl groups on 3-position of indene ring favor the formation of the oximes. 3-Methylindene gave a mixture of **5b** and **6b** in the ratio of 37/63 and, with 3-phenylindene, the exclusive formation of the oxime **6c** was observed without any detectable amount of the cycloadduct **5c**.

Similarly with acyclic conjugated dienes, the formation of the oximes competed (Scheme 2). In the reaction with 1,3-pentadiene, only the cycloaddition occurred on the monosubstituted double bond to give exclusively **7** in 63% yield. On the other hand, with 2-methyl-1,3-butadiene, the cycloaddition took place on either double bond to afford **8** and **9**, accompanied by the oxime **10** (87% total yield, **8**/**9**/**10**; 48/40/12). The alternative oxime bearing trifluoro(hydroxyimino)ethyl group at 4-position was not detected. Similarly, the reaction with 2,3-dimethyl-1,3-butadiene gave the cycloadduct **11** and the oxime **12** in the ratio of 69/31. The oxime **12** was so unstable as to be cyclodehydrated intramolecularly during the course of isolation by column chromatography (silica gel) to give 4,5-dimethyl-2-trifluoromethylpyridine (**13**). The detailed study on the conversion to the pyridine is now under progress.

The oximes are thought to be formed *via* the addition of **1** toward the double bond giving the zwitterionic intermediate **14** followed by the intra-

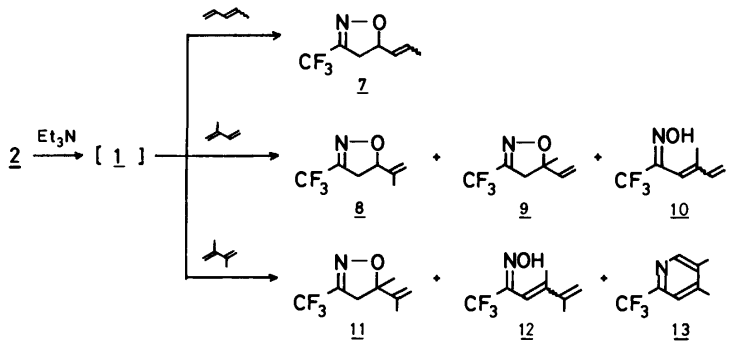

Scheme 2.

TABLE 2. EFFECT OF BASE ON YIELDS AND RATIOS OF THE PRODUCTS **3b** AND **4b** IN THE REACTION OF TRIFLUOROACETONITRILE OXIDE WITH α-METHYLSTYRENE

Base	Yield(**3b**+**4b**), %[a]	Ratio(**3b**/**4b**)[b]	Ratio(**4b-A**/**4b-B**)[b]
Triethylamine	73	33/67	56/44
Pyridine	39	38/62	58/42
Sodium Methoxide	45	37/63	56/44

The reactions were carried out in toluene at room temperature for 3 h.
a) Isolated yield. b) Determined by ^{1}H NMR analysis of the reaction mixture.

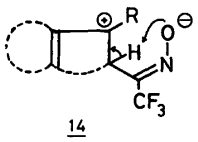

14

molecular proton shift.[9] Caramella *et al.* proposed a competing pathway stabilized by secondary orbital interactions to form oximes by the reactions of benzonitrile oxide with furan or arylacetylenes.[4] Thus the approach of the reagents with alignment, leading to a zwitterionic intermediate, is well stabilized by secondary orbital interactions between the phenyl group of benzonitrile oxide and the furan ring or the aryl group of arylacetylene. However, in the present case of trifluoroacetonitrile oxide **1**, such a stabilizing interaction is unlikely because trifluoromethyl group has no secondary interaction as reported in the Diels-Alder reactions of (trifluoromethyl)ethenes.[10] Therefore, the intermediate **14** might be formed *via* the electrophilic attack of **1** on the double bond owing to the strong electron-withdrawing effect of trifluoromethyl group.[11] The tendency of methyl or phenyl group of dipolarophiles favoring the formation of the oximes may be interpreted by both the steric hindrance which retards the concerted cycloaddition and the electronic effect which stabilizes the intermediate **14**.

A similar competition was further investigated with cyclic conjugated dienes (Scheme 3). While the reaction with cyclopentadiene gave exclusively the cycloadduct **15** in 53% yield, that with 1,3-cyclohexadiene afforded not only the cycloadduct **16** but also the 1,3-addition product **17**, in which trifluoro(hydroxyimino)ethyl group is substituted on the saturated carbon (66% total yield, **16**/**17**; 39/61). The structure of **17** was determined by its ^{1}H NMR and UV spectra. The methine proton (δ=4.07) coupled with the adjacent methylene protons and the absorption at 256 nm (ε=3393) due to conjugated diene strongly support that the trifluoro(hydroxyimino)ethyl group is attached to the saturated carbon. The concerted cycloaddition of nitrile oxide to the double bond in a six-membered ring is known to be slower than that to the one in a five-membered ring[12] and this unreactivity seems to cause the formation of the oxime **17**.

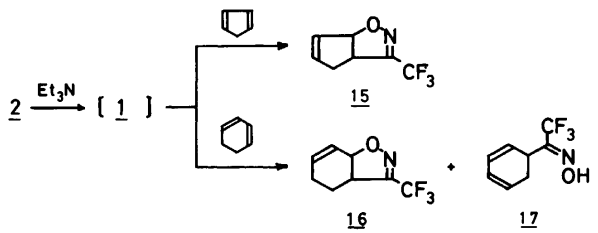

Scheme 3.

Experimental

All melting and boiling points are uncorrected. The IR spectra were recorded on a JASCO IRA-1 spectrometer. The ^{1}H and ^{13}C NMR spectra were measured with JEOL JNM-PMX 60 and -FX 60 spectrometers, respectively, using tetramethylsilane as an internal standard, the chemical shifts being given in δppm downfield. The MS spectra were obtained on a Finnigan 4023 GC-MS DS spectrometer. The UV spectra were observed with a Hitachi 340 spectrometer. The bromide **2** was prepared by the method reported in our previous paper.[5]

Reactions of 2 with Styrenes. To a mixture of **2** (2.64 g, 9.9 mmol) and α-methylstyrene (2.34 g, 19.8 mmol) in 20 cm^3 of toluene was added dropwise a solution of triethylamine (2.7 cm^3) in 10 cm^3 of toluene. The mixture was stirred at room temperature for 3 h. Then hexane was added and the salt, triethylamine hydrobromide, was collected on a filter. The filtrate was washed with water and brine and dried over magnesium sulfate. Removal of the solvent left an oily residue which was a mixture of **3b** and **4b(A+B)**. The residue was distilled (boiling range, 118—119 °C/9 mmHg (1 mmHg=133.322 Pa) to give 1.65 g (73% total yield) of a mixture of **3b** and **4b(A+B)**. The isoxazoline **3b** and **4b(A+B)** were separated by column chromatography (silica gel, hexane and chloroform) followed by preparative GLC: **3b**, ^{1}H NMR (CCl_4) δ=1.73 (s, 3H), 3.23 (q, 2H), 7.3 (s, 5H), IR (neat) 1625 (C=N), 1180 and 1131 cm^{-1} (CF_3).

Found: C, 57.75; H, 4.31; N, 5.92%. Calcd for $C_{11}H_{10}F_3NO$: C, 57.64; H, 4.40; N, 6.11%.

4b-A, ^{1}H NMR ($CDCl_3$) δ=2.29 (d, 3H), 5.87 (q, 1H), 7.2—7.6 (m, 5H), 8.6 (br.s, 1H); **4b-B**, ^{1}H NMR ($CDCl_3$) δ=2.13 (s, 3H), 6.10 (s, 1H), 7.4—7.7 (m, 5H), 8.6 (br.s, 1H).

Found: C, 57.71; H, 4.42; N, 6.05% (for a mixture of **4b(A+B)**). Calcd for $C_{11}H_{10}F_3NO$: C, 57.64; H, 4.40; N, 6.11%.

Similarly, the reactions with styrene and α-phenylstyrene were performed to give the corresponding **3** and **4**. Yields and ratios of these products are summarized in Table 1 and physical and spectral data are as follows: **3a**, bp 85—87 °C/3.5 mmHg (lit,[5] 85—87 °C/3.5 mmHg); **4a**, mp 142—143 °C (hexane-chloroform), ^{1}H NMR ($CDCl_3$) δ=7.1—7.6 (m, 7H), 9.2 (br.s, 1H), IR (KBr) 3320 (OH), 1622 (C=N, C=C), 1105 cm^{-1} (CF_3), MS (CI, *m/z*) 216 $(M+H)^+$, 244 $(M+Et)^+$, ^{13}C NMR ($CDCl_3$), δ=93.8, 112.1, 130.3, 148.6 (CF_3), 110.9 (d, HC=), 127.3, 128.6, 129.3, 135.7 (Ph), 137.3 (d, HC=), 141.5, 143.5, 145.5, 147.6 (C-CF_3).

Found: C, 55.89; H, 3.64; N, 6.45%. Calcd for $C_{10}H_8F_3NO$: C, 55.82; H, 3.75; N, 6.51%.

3c, ^{1}H NMR ($CDCl_3$) δ=3.76 (q, 2H), 7.2—7.8 (m, 10H), IR (neat) 1632 (C=N), 1190 and 1130 cm^{-1} (CF_3).

Found: C, 66.47; H, 4.15; N, 4.39%. Calcd for $C_{16}H_{12}F_3NO$: C, 65.98; H, 4.15; N, 4.81%.

4c, mp 113—114 °C (hexane-chloroform), ^{1}H NMR ($CDCl_3$) δ=6.18 (s, 1H), 7.0—7.4 (m, 10H), 8.6 (br.s, 1H), IR (KBr) 3370 (OH), 1609 (C=N), 1163 and 1093 cm^{-1} (CF_3).

Found: C, 66.12; H, 4.20; N, 4.80%. Calcd for $C_{16}H_{12}F_3NO$: C, 65.98; H, 4.15; N, 4.81%.

Conversion of 3 into 4. A 1.55 mol dm^{-3} solution of butyllithium (3.3 cm^3) in hexane was added dropwise to a solution of 1.00 g (4.7 mmol) of **3a** and 0.52 g (5.1 mmol) of

diisopropylamine in 10 cm³ of tetrahydrofuran cooled in a dry ice-acetone bath. The mixture was allowed to warm to room temperature over a period of 3 h. After stirring at room temperature for an additional 2.5 h, saturated aq ammonium chloride was added to the mixture. The solvent was removed and the resulting aqueous layer was extracted twice with diethyl ether. The ethereal extracts were washed with brine and dried over magnesium sulfate. Removal of the solvent left a residue which was submitted to column chromatography (silica gel, chloroform) to give 0.93 g (93% yield) of **4a**. Thus obtained **4a** was further purified by recrystallization from hexane–chloroform, mp 142—143 °C, ^{1}H NMR and IR spectra are consistent with those obtained above.

The similar treatment of 1.14 g (5.0 mmol) of **3b** with lithium diisopropylamide gave 0.48 g (42%) of a mixture of **4b-A** and **4b-B** in the ratio of 57/43 (^{1}H NMR analysis).

*Conversion of **4b** into **3b**.* A mixture of 1.15 g (5.0 mmol) of **4b** (**4b-A**/**4b-B**; 56/44) and 10 cm³ of chloroform in a sealed tube was stirred at 150 °C for 65 h. The similar procedure to the above afforded 0.68 g (59%) of **3b** and recovered 0.40 g (35%) of a mixture of **4b-A** and **4b-B** in the ratio of 13/87.

*Reactions of **2** with Indenes.* To a mixture of **2** (2.58 g, 9.7 mmol) and indene (3.41 g, 29.4 mmol) in 20 cm³ of toluene was added dropwise a solution of triethylamine (2.8 cm³) in 10 cm³ of toluene. After being stirred at room temperature for 3 h, hexane was added and the deposited salt was filtered out. The filtrate was washed with water and brine, dried over magnesium sulfate, and evaporated to leave an oily mixture of **5a** and **6a** (79/21 by ^{1}H NMR analysis). The oil was distilled (boiling range, 118—119 °C/6 mmHg) to give 1.17 g (53% total yield) of a mixture of **5a** and **6a**. Each isomer was separated by column chromatography (silica gel, hexane and chloroform) and further purification was carried out by recrystallization: **5a**, mp 46—46.5 °C (hexane), ^{1}H NMR ($CDCl_3$) δ=3.37 (d, 2H), 4.25 (dtq, 1H), 6.28 (d, 1H), 7.2—7.6 (m, 4H), IR (KBr) 1605 (C=N), 1160 and 1120 cm^{-1} (CF_3).

Found: C, 58.11; H, 3.54; N, 6.12%. Calcd for $C_{11}H_8F_3NO$: C, 58.16; H, 3.55; N, 6.17%.

6a, mp 170—171 °C (hexane), ^{1}H NMR ($CDCl_3$–DMSO-d_6) δ=3.94 (s, 2H), 7.2—7.5 (m, 4H), 7.64 (s, 1H), 12.6(s, 1H), IR (KBr) 3200 (OH), 1155 and 1122 cm^{-1} (CF_3), MS (CI, *m/z*) 228 $(M+H)^+$, 210 $(M-OH)^+$, 141 $(M-CF_3OH)^+$.

Found: C, 58.17; H, 3.54; N, 6.15%. Calcd for $C_{11}H_8F_3NO$: C, 58.16; H, 3.55; N, 6.17%.

In a similar manner, **5b** and **6b**-c were obtained from the reactions with 3-methyl- and 3-phenylindenes, respectively, and their spectral data are as follows: **5b**, colorless oil, ^{1}H NMR (CCl_4) δ=1.77 (s, 3H), 3.27 (d, 2H), 3.77(tm, 1H), 7.1—7.5 (m, 4H), IR (neat) 1613 (C=N), 1191 and 1131 cm^{-1} (CF_3).

Found: C, 59.49; H, 3.98; N, 5.61%. Calcd for $C_{12}H_{10}F_3NO$: C, 59.75; H, 4.18; N, 5.81%.

6b, mp 115—116 °C (hexane), ^{1}H NMR ($CDCl_3$) δ=2.16 (t, 3H), 3.60 (q, 2H), 7.2—7.6 (m, 4H), 8.9 (s, 1H), IR (KBr) 3250 (OH), 1184 and 1124 cm^{-1} (CF_3).

Found: C, 60.30; H, 3.89; N, 5.62%. Calcd for $C_{12}H_{10}F_3NO$: C, 59.75; H, 4.18; N, 5.81%.

6c, mp 168—169 °C (hexane–chloroform), ^{1}H NMR ($CDCl_3$–DMSO-d_6) δ=3.76 (s, 2H), 7.2—7.6 (m, 9H), 11.8 (s, 1H), IR (KBr) 3310 (OH), 1175 and 1123 cm^{-1} (CF_3).

Found: C, 67.48; H, 3.92; N, 4.52%. Calcd for $C_{17}H_{12}F_3NO$: C, 67.33; H, 3.99; N, 4.62%.

*Reactions of **2** with Acyclic Conjugated Dienes.* To a solution of **2** (5.21 g, 19.6 mmol) and 2,3-dimethyl-1,3-butadiene (3.21 g, 39.1 mmol) in 40 cm³ of diethyl ether was added dropwise a solution of triethylamine (5.5 cm³) in 20 cm³ of diethyl ether. The reaction mixture was stirred at room temperature for 4 h. Then diethyl ether was added and the salt was filtered out. The filtrate was washed with water and brine and dried over magnesium sulfate. The dried organic layer was evaporated to give a mixture of **11** and **12** in the ratio of 69/31 (^{1}H NMR analysis). This mixture was distilled (boiling range, 110—112 °C/40 mmHg) and chromatographed on silica gel with hexane and then chloroform to yield **11** (1.44 g, 38% yield), **12** (0.15 g, 4% yield), and **13** (0.46 g, 13% yield). Each product was further purified by preparative GLC: **11**, ^{1}H NMR (CCl_4) δ=1.53 (s, 3H), 1.81 (d, 3H), 2.87 (dq, 1H), 3.20 (dq, 1H), 4.93 (q, 1H), 5.10 (s, 1H), IR (neat) 1650 (C=C), 1625 (C=N), 1195 and 1139 cm^{-1} (CF_3).

Found: C, 49.68; H, 5.08; N, 7.12%. Calcd for $C_8H_{10}F_3NO$: C, 49.74; H, 5.22; N, 7.25%.

12, ^{1}H NMR (CCl_4) δ=1.86 (s, 3H), 2.00 (s, 3H), 5.14 (s, 1H), 5.31 (s, 1H), 5.73 (s, 1H), 8.7 (br.s, 1H), IR (neat) 3340 (OH), 1630 and 1605 (C=C, C=N), 1195 and 1140 cm^{-1} (CF_3).

Found: C, 49.28; H, 5.16; N, 7.05%. Calcd for $C_8H_{10}F_3NO$: C, 49.74; H, 5.22; N, 7.25%.

13, ^{1}H NMR (CCl_4) δ=2.37 (s, 6H), 7.40 (s, 1H), 8.40 (s, 1H), IR (neat) 1165 and 1132 cm^{-1} (CF_3).

Found: N, 8.00%. Calcd for $C_8H_8F_3N$: N, 8.00%.

In a similar manner to the above, the reactions with 1,3-pentadiene and 2-methyl-1,3-butadiene were carried out to give **7**, **8**, **9**, and **10**, respectively. Spectral data of these products are as follows: **7**, bp 89—90 °C/46 mmHg, ^{1}H NMR (CCl_4) δ=1.77 (d, 3H), 2.6—3.5 (m, 2H), 4.9—6.2 (m, 3H), IR (neat) 1680 (C=C), 1624 (C=N), 1183 and 1134 cm^{-1} (CF_3).

Found: C, 46.44; H, 4.36; N, 7.81%. Calcd for $C_7H_8F_3NO$: C, 46.93; H, 4.50; N, 7.82%.

8, ^{1}H NMR (CCl_4) δ=1.77 (d, 3H), 2.87 (ddq, 1H), 3.27(ddq, 1H), 4.9—5.3 (m, 3H), IR (neat) 1660 (C=C), 1635 (C=N), 1190 and 1140 cm^{-1} (CF_3), MS (CI, *m/z*) 180 $(M+H)^+$, 208 $(M+Et)^+$.

Found: C, 47.46; H, 4.57; N, 7.72% (for a mixture of **8** and **10**). Calcd for $C_7H_8F_3NO$: C, 46.93; H, 4.50; N, 7.82%.

9, ^{1}H NMR (CCl_4) δ=1.55 (s, 3H), 2.82 (dq, 1H), 3.08 (dq, 1H), 5.17 (dd, 1H), 5.30 (dd, 1H), 5.95 (dd, 1H), IR (neat) 1645 (C=C), 1625 (C=N), 1190 and 1140 cm^{-1} (CF_3), MS (CI, *m/z*) 180 $(M+H)^+$, 208 $(M+Et)^+$.

Found: C, 47.12; H, 4.55; N, 7.79%. Calcd for $C_7H_8F_3NO$: C, 46.93; H, 4.50; N, 7.82%.

10, ^{1}H NMR ($CDCl_3$) δ=1.83 (s, 3H), 5.28 (d, 1H), 5.45(d, 1H), 5.72 (s, 1H), 6.48 (dd, 1H), 7.1(br.s, 1H), IR (neat) 3300 (OH), 1605 (C=C, C=N), 1190 and 1140 cm^{-1} (CF_3), MS (CI, *m/z*) 180 $(M+H)^+$, 208 $(M+Et)^+$.

*Reactions of **2** with Cyclic Conjugated Dienes.* To a solution of **2** (2.36 g, 8.9 mmol) and 1,3-cyclohexadiene (2.08 g, 26.0 mmol) in 20 cm³ of toluene, a solution of triethylamine (2.4 cm³) in 10 cm³ of toluene was added. After the reaction mixture was stirred at room temperature for 3 h, hexane was added and the salt was collected on a

filter. The filtrate was washed with water and brine and dried over magnesium sulfate. Removal of the solvent left an oily mixture of **16** and **17** (39/61 by ^{1}H NMR analysis). The oil was distilled (boiling range, 104—105 °C/27 mmHg) to give 1.12 g (66% total yield) of a mixture of **16** and **17**. Each isomer was isolated by preparative GLC; **16**, ^{1}H NMR ($CDCl_3$) δ=1.4—2.3 (m, 4H), 3.3—3.7 (m, 1H), 5.03 (dd, 1H), 5.8—6.5 (m, 2H), IR (neat) 1611 (C=N), 1180 and 1130 cm^{-1} (CF_3).

Found: C, 50.65; H, 4.21; N, 6.87%. Calcd for $C_8H_8F_3NO$: C, 50.27; H, 4.22; N, 7.33%.

17, ^{1}H NMR ($CDCl_3$) δ=2.3—2.6 (m, 2H), 4.07 (ddm, 1H), 5.6—6.2 (m, 4H), 9.2 (br.s, 1H), IR (neat) 3300 (OH), 1189 and 1130 cm^{-1} (CF_3). UV, $\lambda_{max}^{EtOH}(\varepsilon)$ 256 nm (3393).

Found: C, 50.12; H, 4.25; N, 7.32%. Calcd for $C_8H_8F_3NO$: C, 50.27; H, 4.22; N, 7.33%.

Similarly, **15** was obtained from the reaction with cyclopentadiene. **15**, bp 87—89 °C/31 mmHg, ^{1}H NMR (CCl_4) δ=2.7—2.8 (m, 2H), 3.8—4.2 (m, 1H), 5.7—6.1 (m, 3H), IR (neat) 1616 (C=N), 1184 and 1131 cm^{-1} (CF_3).

Found: C, 47.44; H, 3.17; N, 7.80%. Calcd for $C_7H_6F_3NO$: C, 47.47; H, 3.41; N, 7.91%.

References

1) R. Huisgen, *J. Org. Chem.*, **41**, 403 (1976).

2) S. Morrocchi, A. Ricca, and A. Zanarotti, *Tetrahedron Lett.*, **1970**, 3215.

3) S. Morrocchi, A. Ricca, A. Zanarotti, G. Bianchi, R. Gandolfi, and P. Grünanger, *Tetrahedron Lett.*, **1969**, 3329; P. Beltrame, P. Sartirana, and C. Vintani, *J. Chem. Soc. (**B**)*, **1971**, 814; A. Battaglia, A. Dondoni, and A. Mangini, *ibid.*, **1971**, 554; A. Dondoni and G. Barbaro, *J. Chem. Soc., Perkin Trans. 2*, **1974**, 1591.

4) P. Caramella, G. Cellerino, A. C. Coda, A. G. Invernizzi, P. Grünanger, K. N. Houk, and F. M. Albini, *J. Org. Chem.*, **41**, 3349 (1976).

5) K. Tanaka, H. Masuda, and K. Mitsuhashi, *Bull. Chem. Soc. Jpn.*, **57**, 2184 (1984).

6) Part VII in "Applications of the fluorinated 1,3-dipolar compounds as building blocks of the heterocycles with fluorine groups." Part VI: K. Tanaka, S. Maeno, and K. Mitsuhashi, *Bull. Chem. Soc. Jpn.*, **58**, 1841 (1985).

7) For the similar cleavage of isoxazolines, see V. Jäger and H. Grund, *Angew. Chem. Int. Ed. Engl.*, **15**, 50 (1976).

8) G. Bianchi, R. Gandolfi, P. Grünanger, and A. Perotti, *J. Chem. Soc. (**C**)*, **1967**, 1598; M. C. Aversa, G. Cum, and M. Crisafulli, *Gazz. Chim. Ital.*, **98**, 42 (1968); G. Bailo, P. Caramella, G. Cellerino, A. G. Invernizzi, and P. Grünanger, *ibid.*, **103**, 47 (1973).

9) For the similar discussion, see Ref. 4).

10) I. Ojima, M. Yatabe, and T. Fuchikami, *J. Org. Chem.*, **47**, 2051 (1982).

11) M. N. Paddon-Row, C. Santiago, and K. N. Houk, *J. Am. Chem. Soc.*, **102**, 6563 (1980).

12) N. Barbulescu, P. Grünanger, M. R. Langella, and A. Quilico, *Tetrahedron Lett.*, **1961**, 89; K. Bast, M. Christl, R. Huisgen, and W. Mack, *Chem. Ber.*, **106**, 3312 (1973).

A Rationalization of Orientation in Nucleophilic Aromatic Photosubstitution[1,2]

Kiyoshi MUTAI,* Ryoichi NAKAGAKI,† and Hideyuki TUKADA
Department of Chemistry, College of Arts and Sciences, The University of Tokyo
Komaba, Meguro, Tokyo 153
†*Institute for Molecular Science, Myodaiji, Okazaki 444*
(Received December 27, 1984)

Consideration of the relationship between the mechanisms and orientation effects of the nitro group in nucleophilic photosubstitutions of nitroaromatics leads to the proposal of two rules, making use of frontier molecular orbital theory, for interpreting the regioselectivities and determining the reaction mechanisms. The first rule is a summary of previously proposed interpretations, concerning photoreactions accompanying the direct addition of a nucleophile to an excited nitroaromatic substrate. In this case, the regioselectivity is governed by the HOMO of the substrate. The second rule regards reactions involving photoinduced electron transfer, where regioselectivity is LUMO-controlled. The application of these rules is successfully demonstrated for various types of compounds.

As more examples of photoinduced nucleophilic aromatic substitution accumulate, the effects of several substituents on the regioselectivity have attracted great interest.[3] Among the substituents, the nitro group is probably the most extensively studied because of its unusual *meta*-directing effect. For instance, the irradiation of *m*-nitroanisole (**1**) in aqueous organic solvents containing sodium hydroxide gives *m*-nitrophenol (**2**, Eq. 1),[4,5] and 3,4-dimethoxynitrobenzene (**3**) under similar conditions gives a mixture of 3-hydroxy-4-methoxy- (**4**) and 3-methoxy-4-hydroxynitrobenzene (**5**) with a ratio of 370:1 (Eq. 2)[6]

Compound **1** is not hydrolyzed thermally and **3** undergoes thermal

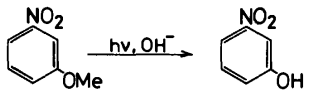

(1)

1 2

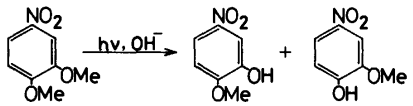

(2)

3 4 5

hydrolysis exclusively at C_4, affording **5** as a sole product. Thus, the orientation directing effect of the nitro group in photochemical nucleophilic substitutions is in remarkable contrast to that in corresponding thermal reactions. It is noteworthy that in such photoreactions, the presence of a good leaving group (such as methoxyl) is not a prevailing factor in the determination of the orientation, as shown in Eq. 2.

On the other hand, when a homologous series of **6** (Eq. 3, R=H or OMe) is irradiated in acetonitrile or methanol, a corresponding series of rearranged products **7** is obtained.[7,8] In these cases, the directing effect of the nitro group is clearly para, though the nitroaromatic moiety in **6** is essentially the same as in **1** or **3**. A quite similar situation is

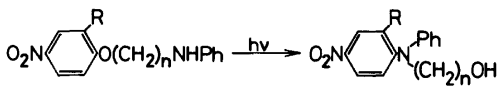

(3)

6, R=H or OMe 7

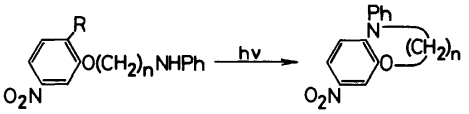

(4)

8, R=H or OMe 9

found in **8** (Eq. 4, R=H or OMe), which gives **9** as the sole isolable product, irrespective of R.[9] Here, again, the nitro group is *para*-directing. These products, **7** and **9**, are also obtained by thermal reactions of **6** and **8** (R=OMe), respectively, catalyzed by a strong base such as sodium hydride or sodium methoxide. Thus, contrary to the cases exemplified in Eqs. 1 and 2, the photoreactions of **6** and **8** show the same regioselectivity as the thermal reactions.

Summarizing the data so far reported, it might be concluded that nitro groups exert two apparently contradicting effects, *meta*- and *para*-orientations, in photosubstitution by a nucleophile.

The present paper has three objectives: (1) to rationalize the two distinct regioselectivities observed for the nitro group; (2) to establish orientation rules based on frontier molecular orbital theory; and (3) to assess the validity of our proposed method by testing its applicability to a variety of cases.

Orientation Rules

Attempts to rationalize the *meta*-favoring regioselectivity of a nitro group have been reported by Fleming[10] using frontier molecular orbital theory and by Epiotis[11] with a more sophisticated procedure. Their conclusions regarding on nucleophilic photosubstitutions are the same in that the reactions are presumed to be HOMO-controlled. Havinga, Cornelisse, and their coworkers have also addressed this problem by attempting to correlate a number

of experimental data with MO calculations.[6,12-16] Unfortunately, according to the interpretations presented by these researchers, it is impossible to explain why apparently conflicting regioselectivities are observed in practically identical nitroaromatics (Eqs. 1—4).

We propose here a rationalization composed of two rules which are based on frontier molecular orbital theory and are applicable to a wide variety of nucleophilic aromatic photosubstitutions. Our rules are as follows;

Rule 1. *HOMO-Controlled Regioselectivity* Nucleophilic photosubstitutions which involve one-step formation of a σ-complex *via direct interaction* between an excited aromatic substrate and a nucleophile are HOMO-controlled (Eq. 5)

$$\mathrm{ArH} + :\mathrm{Nu} \xrightarrow{h\nu} \mathrm{ArH}^* + :\mathrm{Nu} \longrightarrow \sigma\text{-complex} \qquad (5)$$

Rule 2. *LUMO-Controlled Regioselectivity* Nucleophilic photosubstitutions which involve *electron transfer* from a nucleophile to a nitroaromatic substrate and subsequent recombination of the resultant radical ions are LUMO-controlled (Eq. 6).

$$\mathrm{ArH} + :\mathrm{Nu} \xrightarrow{h\nu} \mathrm{ArH}^* + :\mathrm{Nu} \longrightarrow \mathrm{ArH}^{\cdot-} + \mathrm{Nu}^{+\cdot} \longrightarrow \sigma\text{-complex} \qquad (6)$$

Rule 1 is a summary[17] of the essential parts of the conclusions obtained by Fleming,[10] Epiotis,[11] and Havinga.[6] It is based on the assumption that the lowest excited state of an aromatic molecule can be approximated by one electronic configuration in which an electron is promoted from the HOMO to the LUMO. Each level is, thus, singly occupied (Fig. 1). When a nucleophile approaches an excited aromatic substrate with two singly occupied MO's, the dominant orbital interaction is expected to be between HOMO (substrate)-HOMO (nucleophile) and not between LUMO (substrate)-HOMO (nucleophile). Thus, the direct attack of a nucleophile on an excited aromatic substrate is the key step in the reaction. As will be discussed below, the reactions shown in Eqs. 1 and 2 fall under this category.

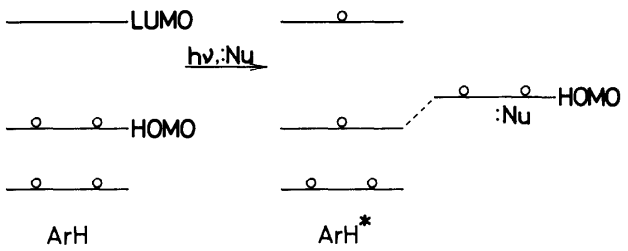

Fig. 1. Schematic illustration of the orientation-determining step, σ-complex formation *via* direct interaction of an excited molecule with a nucleophile. A brokenline denotes the orbital interaction resulting in bond formation. ArH represents an aromatic substrate and Nu a nuleophilic reagent. An asterisk refers to the excited state.

Rule 2 implies an electron-transfer process as a key step in the determination of regioselectivity. This process was originally proposed by Nagakura and Tanaka on the basis of theoretical considerations in 1959[18] regarding the thermal reaction of a nucleophile having a low ionization potential with a substrate having a high electron affinity. The reactions shown in Eqs. 3 and 4 are examples of this category; the formation of a radical ion pair composed of a nitroaryl ether radical anion and an anilino moiety radical cation and the subsequent conversion into a σ-complex (Eq. 6) have been unequivocally confirmed by laser flash photolysis.[9,19,20] As depicted in Fig. 2, in this mechanism, after an initial electron transfer, a strong interaction develops between the singly occupied MO of the nitroaromatic and the singly occupied HOMO of the nucleophile. Since the singly occupied orbital of the aromatic compound corresponds to the LUMO of the ground state, the orientation is LUMO-controlled.

Sample Applications

The rules proposed here neglect all other factors, such as leaving groups and the nature of the nucleophiles, and consider only the effective MO's to govern the regioselectivities. Of course, actual

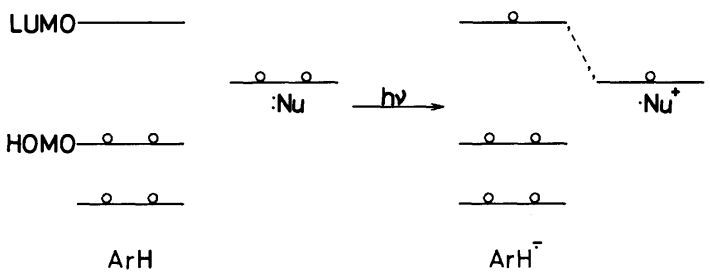

Fig. 2. Schematic illustration of the orientation-determining step, σ-complex formation after photoinduced electron transfer. A broken line denotes the orbital interaction resulting in bond fromation. ArH represents an aromatic substrate and Nu a nucleophilic reagent.

reactions cannot always be interpreted only in terms of frontier MO's; however, the rules are useful in reasoning why specific positions are subject to substitution and in determining whether the reaction mechanism is a "direct attack" or an "electron transfer". Several examples are now discussed.

According to the frontier molecular orbital theory, a nucleophile preferentially attacks the position with the highest frontier electron density (FED) in the corresponding MO's. Here, FED is defined as $FED_i=n_ic^2_{ir}$, where n_i is the number of electrons occupying the ith MO and c_{ir} the coefficient of rth atomic orbital in the ith MO. The FED shown below is calculated by the CNDO/2 approximation, for the displacement of OR with OH.

m-*Alkoxynitrobenzene.* The FED maps of the HOMO and LUMO of *m*-alkoxynitrobenzene are shown in Fig. 3. The FED's of the HOMO are in the order $C_6>C_2>C_3>C_4$. However, the first two positions are less likely to be attacked by a nucleophile on account of the absence of a good leaving group. Thus, photosubstitutions of *m*-nitroanisole have been observed to occur at C_3 with hydroxide ion[4,5] ammonia,[21] methylamine,[4] and cyanide ion[22,23] In case of the photoamination in liquid ammonia, C_6- and C_2-substituted products are minor side products,[21] consistent with the large FED's of the HOMO on these positions and also with the assumption of preferred substitution at the position with a good leaving group.

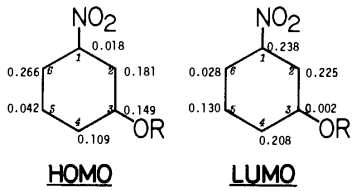

Fig. 3. FED maps of the HOMO and LUMO of *m*-alkoxynitrobenzene.

LUMO-Controlled photosubstitution in *m*-alkoxynitrobenzene analog (**8**, R=H) should occur on either C_2 or C_4 which bear much larger FED's. For steric reason the actual reaction favors the less hindered site C_4 (Eq. 4, R=H).[9] No product suggesting C_3-substitution has been detected.

In connection with the reaction of **8** (R=H), the photochemical behavior of a primary amine analog, 2-(*m*-nitrophenoxy)ethylamine (**10**), studied by Wubbels and his coworkers, is noteworthy (Eq. 7).[24] The structure of the photoproduct (**12**) reveals a *meta*-directing effect of the nitro group, suggesting that the reaction belongs to the category of rule 1, or is HOMO-controlled. Additionally, direct formation of a σ-complex (**11**) from the excited state has unambiguously been confirmed by laser flash photolysis.[25]

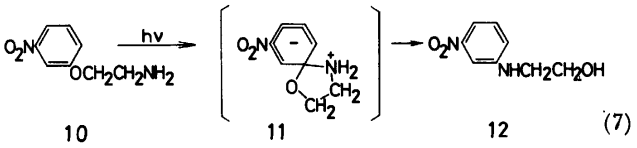

(7)

The significance of the findings should be emphasized because the key step of a direct attack of a nucleophile, requisite for the HOMO-controlled photosubstitutions, has rarely been confirmed spectroscopically, though the scheme itself is generally accepted. Thus, the photorearrangement of **10** is mechanistically and regioselectively in complete accord with the requirement of rule 1, providing strong supporting evidence for its validity.

Differences in the regioselectivity observed between **8** (R=H) and **10** are readily explained in terms of the ionization potential (I_p) of the nucleophilic moieties; the I_p of the primary amino group is higher than that of the anilino group (CH_3NH_2 with I_p=9.64 eV[26] and $PhNHCH_3$ with I_p=7.65 eV[27] are approximate models for nucleophilic moieties in **10** and **8**, respectively). Therefore, in **10** with the high Ip nucleophile, photoinduced electron transfer is highly unfavorable and the reaction must proceed *via* a direct addition to the *m*-nitrophenoxyl moiety, resulting in a HOMO-controlled orientation. Consequently, *m*-nitroanisole undergoes HOMO-controlled photosubstitution with methylamine to yield *N*-methyl-*m*-nitroaniline.[4]

p-*Alkoxynitrobenzene.* Nucleophilic photosubstitutions of *p*-nitroanisole reflect the trifunctional nature of this compound; *ipso* (C_1)-substitution has been observed with hydroxide ion and pyridine,[28] C_4-substitution with hydroxide ion[28] and aliphatic amines,[29] and C_3-substitution with cyanide ion[23] and cyanate ion.[30] It is interesting to note that the orientation strongly depends on the natures of the reaction media and the nucleophiles. An examination of the FED's of the HOMO of this molecule (Fig. 4) readily rationalizes the results; that is, the *ipso* carbon (C_1), *meta*-carbon (C_3), and *para*-carbon (C_4) bear fairly large FED's and, therefore, are all able to accept a nucleophile, if appropriate conditions are provided.

In the LUMO (Fig. 4), the FED's on C_1 and C_4 are the largest and the second largest, respectively. Since

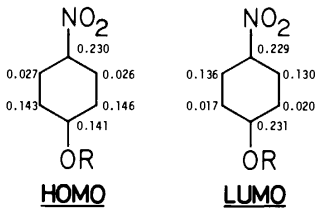

Fig. 4. FED maps of the HOMO and LUMO of *p*-alkoxynitrobenzene.

intramolecular *ipso*-substitution at the NO_2-bearing carbon is sterically inhibited in **6** (R=H), *para*-substitution predominates in its photoreaction (Eq. 3).

3,4-Dialkoxynitrobenzene and Its Isomers. As shown in Fig. 5, the FED's of the HOMO of 3,4-dialkoxynitrobenzene are in the order, $C_3>C_4>C_6>C_1$. As predicted by rule 1, photoreactions with hydroxide ion (Eq. 1),[6] aliphatic amines,[13] and cyanide ion[14] have all been observed predominantly at C_3. These reactions are accompanied by C_4-substituted products,[6,13,16] the formation of which is explained by the high FED as well as the presence of a good leaving group on C_4.

In the LUMO, the FED on the C_4-OR carbon is larger than that on the C_3-OR and photosubstitution has been observed at this position in either **6** (R=OMe)[8] or **8** (R=OMe)[9] (Eqs. 3 and 4).

Furthermore, a good correlation of the FED with experimental results is found in the HOMO-controlled photocyanation of three isomers of dimethoxynitrobenzenes;[31] as shown in Fig. 6, the reaction occurs at the positions with the largest FED in each case.

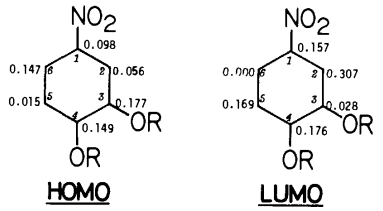

Fig. 5. FED maps of the HOMO and LUMO of 3,4-dialkoxynitrobenzene.

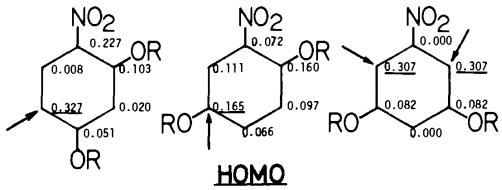

Fig. 6. FED maps of the HOMO of three dialkoxynitrobenzene isomers. The values underlined denote the largest FED's in each ring. Arrows indicate the photocyanated positions.

Photodicyanation of Polymethoxybenzenes. Another example is photocyanation of polymethoxybenzenes in which dicyanated products are obtained (Eqs. 8 and 9).[32] Since the yields of the dicyano derivatives are lower than those of the concomitant monocyano derivatives and the same dicyanodimethoxybenzene is obtained from 1,2,4-trimethoxybenzene as from 1,3-dimethoxybenzene, it is reasonable to suppose that the photocyanation occurs stepwise, that is, a dicyano derivative is formed by cyanation of the corresponding monocyano derivative. For the first step cyanation, an $S_R{}^+{}_N{}^1$ Ar* mechanism[33] has been proposed,[15,16] but the second step should involve direct attack of cyanide ion because of the strong electron-withdrawing nature of the cyano group. Thus, the HOMO of the predominating monocyano derivatives should determine the position of the subsequent cyanation. As illustrated in Eqs. 8 and 9, the second step takes place at the positions bearing the largest FED in each ring.

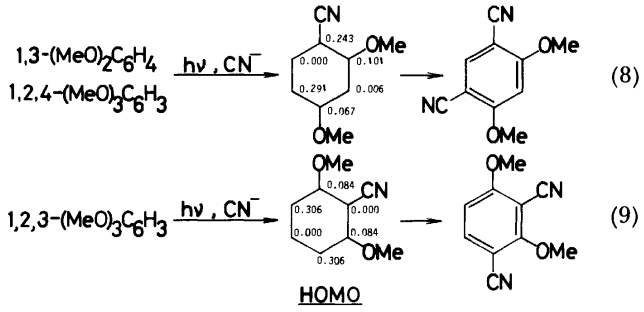

Chloronitrobenzenes. Generally, it is difficult to tell only from the structures of the starting materials and photoproducts whether a reaction belongs to rule 1 or 2, but sometimes the FED data can give a valuable clue to the reaction mechanism. Photoamination of chloronitrobenzenes is such an example.

Photoamination of the three isomers of chloronitrobenzene was carried out in liquid ammonia at −60 °C.[21] As illustrated in Fig. 7, substitution was observed in all isomers at the *para* position to the nitro group. Since the HOMO's of the *o*- and *m*-isomers show very small FED's at the *para* positions (0.012 and 0.040, respectively) and the corresponding LUMO's show the second largest values (0.246 and 0.244, respectively) at these positions the regioselectivity should be regarded as LUMO-controlled. As for the *p*-isomer, the FED on the *para*-carbon is sufficiently large in both MO's and makes it difficult

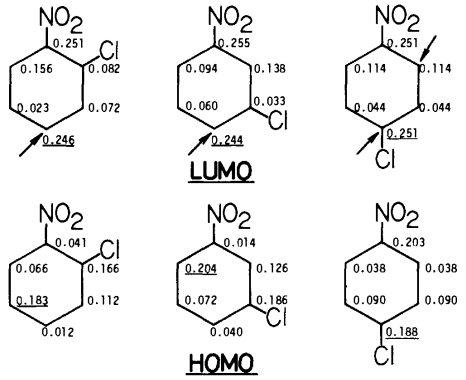

Fig. 7. FED maps of the HOMO and LUMO of chloronitrobenznes. The values underlined show the largest FED in each ring (except C-NO_2 carbons). Arrows denote the positions where photoamination is observed.

to determine which MO dominates the orientation. In this regard, it is noticeable that concurrent *o*-amination is observed as a minor pathway (affording 10% of 2-nitro-5-chloaniline) in contrast to the major pathway (producing *p*-nitroaniline in 45% yield). Examination of the FED maps of *p*-chloronitrobenzene in Fig. 7 suggests that the *o*-amination cannot be HOMO-controlled, because the FED of the HOMO on the *ortho*-carbon (0.038) is too small to allow substitution. Thus, the major part of the photoamination of the *p*-isomer is probably LUMO-controlled, though this conclusion does not completely rule out some concurrent HOMO-controlled process.

In order to obtain further supporting evidence for the electron-transfer mechanism, the key step in the LUMO-controlled reactions, we tried to detect intermediates with the aid of an ESR spectrometer, adopting *p*-chloronitrobenzene as a representative of the isomers. Upon irradiating a solution of this compound in liquid ammonia kept at −70 °C with a high-pressure Hg lamp, a rapid growth of a paramagnetic species was observed. After 10 min of irradiation, a well-defined spectrum with sufficient intensity (Fig. 8) was obtained, which showed slow decay upon cutting off the light. No signal was observed for the solution kept in the dark for the same period. Comparison of the spectral curve obtained with a simulated one, led to an identification of the paramagnetic species as the radical anion of *p*-chloronitrobenzene. Thus, a photoinduced electron transfer was confirmed to take place under similar conditions used for the photoreaction.

All these facts strongly suggest that the photoamination of all three isomers of chloronitrobenzene proceeds, partly if not wholly, *via* electron transfer, thus conforming to rule 2.

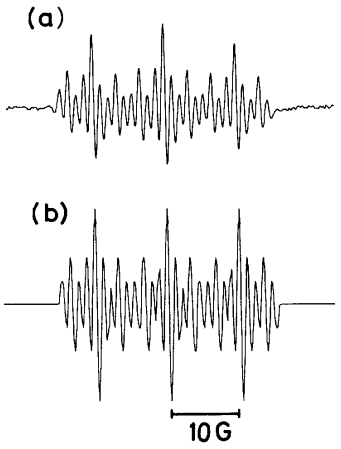

Fig. 8. (a) ESR spectrum of a paramagnetic species formed by irradiation of a solution of *p*-chloronitrobenzene in liquid ammonia. (b) Simulated spectum obtained by employing the following coupling constants; $a_N = 10.4$ G, $a_H(ortho) = 3.40$ G, and $a_H(meta) = 1.20$ G (K. Nakamura, *Bull. Chem. Soc. Jpn.*, **40**, 1 (1967)).

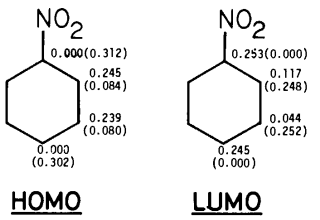

Fig. 9. FED maps of the degenerate HOMO's and LUMO's of nitrobenzene. The values in parentheses belong to nearly degenerate counterparts.

Nitrobenzene. Photoamination of nitrobenzene in liquid ammonia is an example in which the degeneracy of the MO's confuses the assignment of the regio-determining MO. The major reaction takes place at the *para* position to give *p*-nitroaniline in 25% yield.[21] The MO calculation revealed the presence of two pairs of almost degenerate π-MO's, each corresponding to HO and LU levels in energy. Comparison of the FED maps of these MO's (Fig. 9) shows that *p*-amination is explicable either as HOMO- or LUMO-controlled, depending on which HOMO–LUMO pair we choose. Fortunately, it has been reported that the nitrobenzene radical anion is formed upon irradiation of its solution in liquid ammonia,[21] suggesting the occurrence of electron transfer from the solvent to nitrobenzene. Thus, the photoamination of nitrobenzene also proceeds, at least partly, *via* electron transfer.

Concluding Remarks

Although the proposed rules should be regarded as first approximations, they find wide and successful applications to a number of aromatic nucleophilic photosubstitutions. Our present method has, thus, been shown to be useful in interpreting regioselectivities and predicting mechanisms even for polysubstituted aromatics. In addition, the present approach can provide us with a more comprehensive view of photochemical reaction mechanisms than the conventional resonance theory or empirical orientation rules.

It should be noted here that our rules are specifically concerned with the initial stage of nucleophilic photosubstitutions and give no information regarding subsequent reaction pathways. It is also noteworthy that the argument, solely based on MO calculations, does not necessarily identify the reaction mechanism.

Experimental

Calculation. The MO calculations were performed with the CNDO/2 program,[34] adapted by replacing the

original two-center electronic repulsion integrals with the Nishimoto-Mataga approximation,[35] on a Mitsubishi MELCOM COSMO 700 III computer at the University of Tokyo. For all benzene derivatives, it was assumed that the aromatic nucleus has the same structure as the unsubstituted parent,[36] regardless of the positions, numbers, or natures of the substituents. The methoxyl group was approximated by a hydroxyl for convenience of calculation. It was found for some simple anisole derivatives that no significant change in the FED distribution pattern occurred along with this treatment.

ESR Spectra. ESR Spectra were recorded on a Varian E-112 spectrometer equipped with an optical transmission cavity and a variable temperature accessory. Saturated solutions of *p*-chloronitrobenzene in liquid ammonia kept at −70 °C were irradiated with a high-pressure Hg lamp (500 W) through a Pyrex water jacket and a focusing lens.

We are grateful to Professor Koichi Ohno of the University of Tokyo for providing us with the computer program, to Dr. Akinori Inoue for his advice and help in calculation, and to Professor G. L. Closs of the University of Chicago for valuable suggestions. This work was supported by the Joint Studies Program (1984) of the Institute for Molecular Science.

References

1) Preliminary communications: R. Nakagaki, *Yuki Gosei Kagaku Kyokaishi*, **40**, 651 (1982); K. Mutai and R. Nakagaki, *Chem. Lett.*, **1984**, 1537.

2) Part IV of Photoinduced Intramolecular Substitution. Part III of this series, K. Mutai, K. Kobayashi, and K. Yokoyama, *Tetrahedron*, **40**, 1755 (1984).

3) For a review, see: J. Cornelisse and E. Havinga, *Chem. Rev.*, **75**, 353 (1975).

4) E. Havinga and R. O. de Jongh, *Bull. Soc. Chim. Belg.*, **71**, 803 (1962).

5) R. O. de Jongh and E. Havinga, *Recl. Trav. Chim. Pays-Bas*, **85**, 275 (1966).

6) H, C. H. A. van Riel, G. Lodder, and E. Havinga, *J. Am. Chem. Soc.*, **103**, 7257 (1981).

7) K. Mutai and K. Kobayashi, *Bull. Chem. Soc. Jpn.*, **54**, 462 (1981).

8) K. Mutai, K. Yokoyama, S. Kanno, and K. Kobayashi, *Bull. Chem. Soc. Jpn.*, **55**, 1112 (1982).

9) K. Mutai, S. Kanno, and K. Kobayashi, *Chem. Lett.*, **1978**, 931; K. Mutai, K. Kobayashi, and K. Yokoyama, *Tetrahedron*, **40**, 1755 (1984).

10) I. Fleming, "Frontier Orbitals and Organic Chemical Reactions," John Wiley & Sons Inc., New York (1976), p. 223.

11) N. D. Epiotis and S. Shaik, *J. Am. Chem. Soc.*, **100**, 29 (1978); N. D. Epiotis, "Theory of Organic Reactions," Springer-Verlag, New York (1978), p. 171.

12) J. Cornelisse, G. P. de Gunst, and E. Havinga, *Adv. Phys. Org. Chem.*, **11**, 225 (1975).

13) M. E. Kronenberg, A. van der Heyden, and E. Havinga, *Recl. Trav. Chim. Pays-Bas*, **86**, 254 (1967).

14) C. M. Lock and E. Havinga, *Proc. K. Ned. Akad. Wet. B.*, **77**, 15 (1974).

15) E. Havinga and J. Cornelisse, *Pure and Appl. Chem.*, **47**, 1 (1976).

16) J. Cornelisse, G. Lodder, and E. Havinga, *Rev. Chem. Intermed.*, **2**, 23 (1979). See also, J. Cervelló, M. Figueredo, J. Marquet, M. Moreno-Manas, J. Bertrán, and J. M. Lluch, *Tetrahedron Lett.*, **25**, 4147 (1984).

17) For instance, the rule has no requirement for the multiplicity of the reactant in the excited state, as with Epiotis,[11] although van Riel *et al.*[6] proposed an explanation requiring a triplet state for the reacting aromatic substrate.

18) S. Nagakura and J. Tanaka, *Bull. Chem. Soc. Jpn.*, **32**, 734 (1959); S. Nagakura, *Tetrahedron*, **19** *Suppl. 2*, 361 (1963).

19) K. Yokoyama, R. Nakagaki, J. Nakamura, K. Mutai, and S. Nagakura, *Bull. Chem. Soc. Jpn.*, **53**, 2472 (1980).

20) K. Yokoyama, J. Nakamura, K. Mutai, and S. Nagakura, *Bull. Chem. Soc. Jpn.*, **55**, 317 (1982).

21) A. van Vliet, J. Cornelisse, and E. Havinga, *Tetrahedron*, **26**, 1061 (1970).

22) R. L. Letsinger and J. H. McCain, *J. Am. Chem. Soc.*, **88**, 2884 (1966).

23) R. L. Letsinger and J. H. McCain, *J. Am. Chem. Soc.*, **91**, 6425 (1969).

24) G. G. Wubbels, A. M. Holverson, and J. D. Oxman, *J. Am. Chem. Soc.*, **102**, 4848 (1980); G. G. Wubbels and D. W. Celander, *J. Am. Chem. Soc.*, **103**, 7669 (1981).

25) G. G. Wubbels, H. M. van Zeyl, and C. A. G. O. Varma, 185th ACS National Meeting Abstracts, Seattle, WA, March 1983, ORGN 50.

26) K. Kimura, S. Katsumata, Y. Achiba, T. Yamazaki, and S. Iwata, "Handbook of HeI Photoelectron Spectra of Fundamental Organic Molecules," Japan Scientific Societies Press, Tokyo (1981).

27) J. P. Maier and D. W. Turner, *J. Chem. Soc., Faraday Trans. 2*, **1973**, 521.

28) R. L. Letsinger, O. B. Ramsay, J. H. McCain, *J. Am. Chem. Soc.*, **87**, 2945 (1965).

29) M. E. Kronenberg, A. van der Heyden, and E. Havinga, *Recl Trav. Chim. Pays-Bas*, **85**, 56 (1966).

30) J. Hartsuiker, S. de Vries, J. Cornelisse, and E. Havinga, *Recl. Trav. Chim. Pays-Bas*, **90**, 611 (1971).

31) F. J. Wiegerink, unpublished results, cited as Ref. 101 in Ref. 3.

32) J. den Heijer, O. B. Shadid, J. Cornelisse, and E. Havinga, *Tetrahedron*, **33**, 779 (1977).

33) This mechanism is also HOMO-controlled.

34) J. A. Pople and D. L. Beverige, "Approximate Molecular Orbital Theory," McGraw-Hill, New York (1970).

35) K. Nishimoto and N. Mataga, *Z. Phys. Chem. N. F.*, **13**, 140 (1957).

36) O. Bastiansen, L. Fernholt, H. M. Seip, H. Kambara, and K. Kuchitsu, *J. Mol. Struc.*, **18**, 163 (1973).

The Thermal Addition Reactions of Cycloheptatriene with Aromatic *p*-Quinones[1)]

Akira MORI, Hiroaki MAMETSUKA, and Hitoshi TAKESHITA*
Research Institute of Industrial Science, 86, Kyushu University, Kasuga-koen, Kasuga, Fukuoka 816
(Received February 22, 1985)

Thermal addition reactions of cycloheptatriene with several aromatic *p*-quinones gave the Diels-Alder adducts as minor products; the most characteristic feature was the formation of the *vic*-ditropylation products. The mechanism of their formation was clarified to be a sequential ene-reaction and dehydrogenation by means of chemical conversion from the isolated intermediates. Several new other additions, *e.g.*, successive Diels-Alder reactions, were also noted.

Previously, we have reported the characteristic behavior of cycloheptatriene (tropylidene, **1**) in reactions with several carbonyl compounds[2)] and aromatic quinones[3)] upon UV-light irradiations. Under these circumstances, the methylene hydrogens of **1** are extremely reactive toward the hydrogen-abstraction process because of the stability of the resultant symmetrical cycloheptatrienyl (tropyl) radical. In this connections, the thermal behavior of **1** toward aromatic quinones, which are frequently-used dienophiles[4)] and typical oxidizing agents, must also be interesting; once the stable tropyl radical is formed, it may behave differently to give products other than the Diels-Alder adducts. Herein, we wish to report our findings.

Results and Discussion

The Reaction of 1 with p-*Benzoquinone.* When a toluene solution of **1** and *p*-benzoquinone (BQ) was refluxed for 1 h, two products, 1:1-adduct (**2**) and 1:2-adduct (**3**), were isolated, along with some amounts of 1,1′-bi(cyclohepta-2,4,6-trienyl) (bitropyl, **4**)[5)] and BQ and hydroquinone (H_2BQ), which were precipitated as quinhydrone. The **2** was shown to be the ordinary Diels-Alder adduct by the appearance of four cyclopropane ring protons in the ^1H NMR spectrum. The **3** (21% yield)[6)] was shown to be a *vic*-ditropylation product; its ^1H NMR spectrum revealed a symmetrical element in its structure, showed signals ascribable to tropyl groups, and overlapped two olefinic protons. The presence of an enedione chromophore was evidenced by the IR carbonyl stretching vibration absorption peak at ν: 1685 cm^{-1}.

On the other hand, the thermal reaction of **1** and BQ without a solvent gave more complicated results. In addition to **2** (4%), **3** (6%), and **4** (15%), new products (**5**, **6**, and **7**) were isolated after repeated silica-gel column chromatography; another *vic*-ditropylation product, **5** (5%), showed its molecular

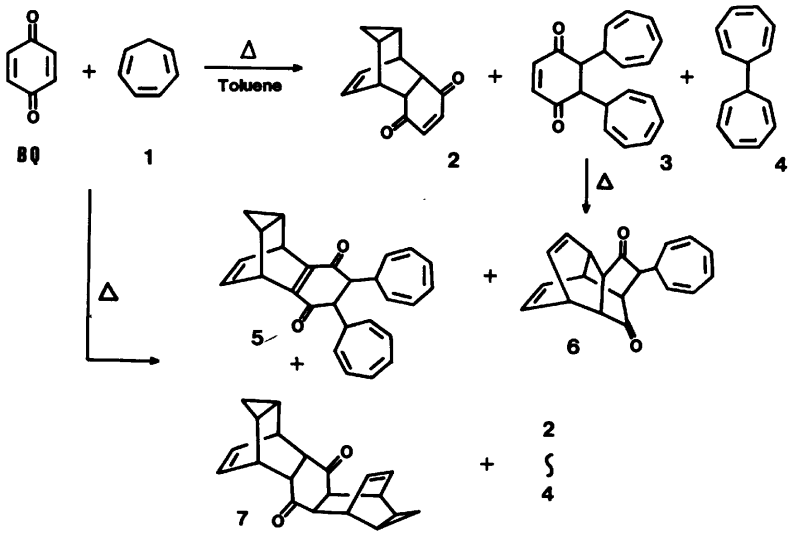

Scheme 1.

weight to be 380, and disclosed four cyclopropane ring protons and an enedione chromophore [ν: 1665, 1582 cm^{-1}]. Therefore, **5** must correspond to the ditropylation product derived from the dehydrogenation products of **2**. A cage compound, **6** (1%), revealed four olefinic protons other than those of the tropyl group in the ^1H NMR spectrum, while a carbonyl absorption at ν: 1730 cm^{-1} in the IR spectrum indicated it to be a strained cycloalkanone derivative. These feature requires the formation of two more C–C bonds. In fact, **6** could be prepared by a thermal isomerization reaction, an intramolecular Diels-Alder process, of **3** by refluxing in **1**.

The structure of the remaining product, **7** (2%), a 1:2-adduct, showed the presence of a symmetrical element in the ^1H- and ^{13}C NMR spectra; it was deduced to be the two-fold Diels-Alder adduct of BQ with the norcaradiene form of **1**. Scheme 1 shows the deduced structures.

The Reaction of 1 with 1,4-Naphthoquinone. When a toluene solution of **1** and 1,4-naphthoquinone (NQ) was refluxed for 12 h, a complicated mixture was obtained. After repeated chromatographic work-ups, the products characterized, besides **4**, were a colorless oil (**8**, 0.6%), yellow needles (**9**, 16%), colorless plates (**10**, 22%), and a yellow oil (**11**, 5%). Their structures were unambiguously determined by NMR spectral analysis; **8** was the ditropylation product, **10** was the Diels-Alder product of NQ and the norcaradiene form of **1**, **9** was the dehydrogenation product of **10**,[7] and **11** was the monotropylated intermediate.

The reaction without any diluent yielded, together with **8** (2%), **9** (10%), **10** (7%), and **11** (1%), two more

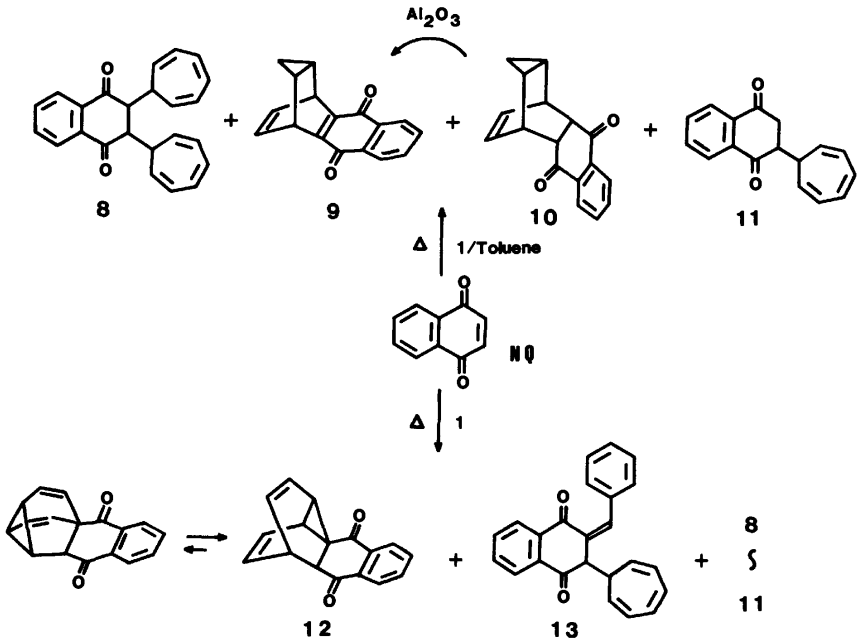

Scheme 2.

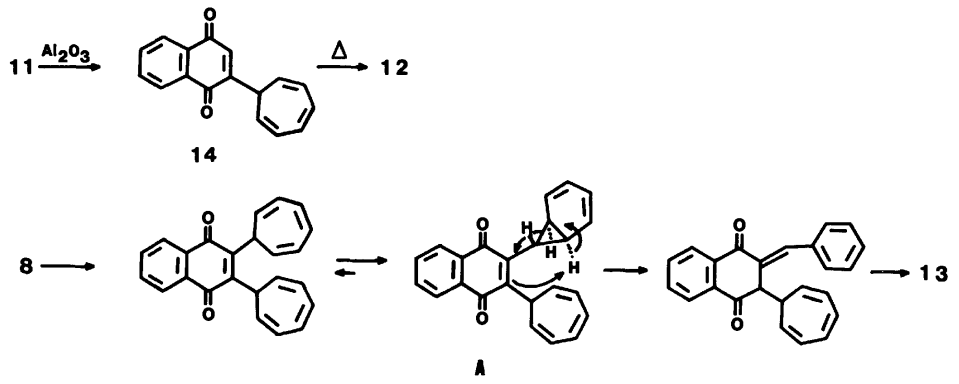

Scheme 3.

by-products, faintly brownish crystals (**12**, 3%) and a colorless oil (**13**, 6%). The **12**[8] was determined to be the intramolecular Diels-Alder product of the dehydrogenated derivative (**14**) of **11**. In fact, the heating of **14**, obtained by placing **11** in contact with a basic alumina, gave **12**. The **13** was deduced to be a benzylidene derivative derived from **8**. Its formation can be explained in terms of a sterically-favored valence tautomerization to the norcaradiene form for one of the tropyl group in dehydrogenated 2,3-ditropyl-1,4-naphthoquinone, **A**, and its isomerization *via* a $2\pi+2\sigma+2\sigma$-process.

The Reaction of 1 with p-*Toluquinone, Phenyl*-p-*benzoquinone, Chloro*-p-*benzoquinone, and 2,6-Dimethyl*-p-*benzoquinone.* When **1** was allowed to react with *p*-toluquinone (TQ) in toluene, two products, a Diels-Alder adduct (**15**, 18%) and a *vic*-ditropylation product (**16**, 14%) were obtained, while without the diluent, again, the formation of an additional compound (**17**, 6%) was observed, together with **4** (1.6%), **15** (15%), and **16** (18%). Similar products (**18**—**21**) were obtained from phenyl-*p*-benzoquinone (PQ), chloro-*p*-benzoquinone (CQ), and 2,6-dimethyl-*p*-benzoquinone (XQ). The structures of these adducts are illustrated in Chart 1.

It is also known to form cycloheptatrienium ion by the action of 2,3-dichloro-5,6-dicyano-*p*-benzoquinone (DDQ) to **1** in an acidic solution,[9] and the formation of two-electron oxidized products from **1** must be important in the organic syntheses. *p*-Tropoquinone (*p*-TRQ), whose oxidation potential is higher than those of the corresponding *p*-benzoquinones,[10] should be interesting from a comparative point of view; in fact, the reaction resulted in the reductive formation of 5-hydroxytropolone (**22**) and 2,10-dihydroxydicyclohepta[*b,d*]furan-3,9-dione (**23**),[11] showing an occurrence of the oxidation of **1** rather than of the addition reaction. On the contrary, *p*-TRQ is known to give the Diels-Alder adducts with cyclopentadiene.[12]

It is well known that **1** gives the Diels-Alder adducts, mostly having a tautomeric norcaradiene form, by reactions with many dienophiles. However, the reaction with aromatic quinones, *e.g.*, *p*-benzoquinones, under the Diels-Alder conditions predominantly yielded the hydrogen-abstraction products, as one can see from the production of quinhydrone. Moreover, the formation of the ditropylation products might also be such a case, for it requires one mole of the dehydrogenation process.

Previously, we have proven the electrocyclic formation of **8** from NQ and **4** under photochemical conditions;[13] the irradiation of NQ and **4** in benzene by means of a high-pressure mercury lamp by cutting off the light shorter in wavelength than 300 nm with a Pyrex glass filter. However, the ditropylation with **4** does not occur under thermal conditions; it merely results in the production of a complicated intractable mixture, and **8** is undetectable. Whatever the mechanisms are, the ditropylation products must be formed *via* a sequential, step-by-step mechanism. In this point, an independent addition reaction of **1** to a monotropylation product like **14** seemed worth trying. Unfortunately, such an experiment went far beyond our expectations; when **14** was heated with **1**, the only product, obtained in a 28% yield from the

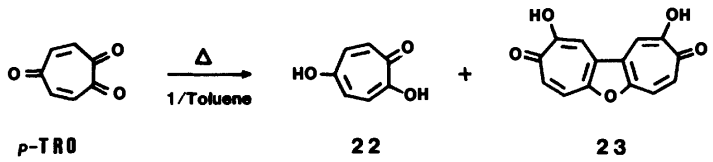

Scheme 4.

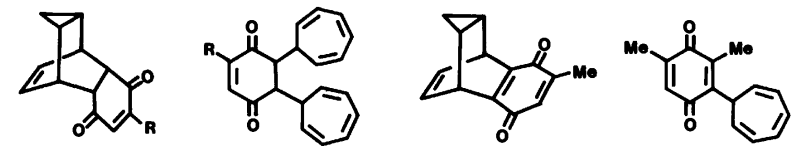

Chart 1.

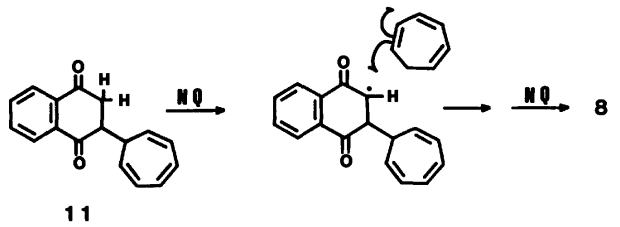

Scheme 5.

mixture, was the barbaralane derivative, **12**. Moreover, when a mixture of **1**, **11**, and NQ was heated to reflux, the products isolated were **8**, **9**, and **10**, while a similar treatment of **11** and NQ in toluene instead formed **9** and **12**; the formation of **12** from **11** and the formation of **9** and **10**, at the same time, proved it easy for NQ-dehydrogenation to occur, though the resultant dehydro intermediates were reluctant to give 1:2-products because of a competitive intramolecular reaction.

In conclusion, it is clear that the quite active methylene group of **1** determines the predominant course of the reaction depending on the nature of the other cycloaddends, *i.e.*, with quinones, the formation of the symmetrical tropyl radical *via* the abstraction of hydrogen is the primarily favored step.

Experimental

All the mps, which were measured by means of a Yanagimoto Micro-mp Apparatus, were uncorrected. The elemental analyses were performed either at the Research Institute or at the Analyses Center, Faculty of Science, Kyushu University. The NMR spectra were measured by means of a JEOL FX 100 Spectrometer in $CDCl_3$ unless otherwise specified, and the chemical shifts are expressed in δ units from the internal Me_4Si. The mass spectra were measured by means of a JEOL OISG-2 Spectrometer. The IR spectra were measured by means of a Jasco IR-A 102 Model Spectrometer. The UV spectra were measured by means of a Hitachi 124 Model Spectrophotometer in methanol. The silica-gel used in this study was Wako Gel C 300.

Thermal Reaction of 1 with BQ. *a)* A toluene solution (8 cm^3) of **1** (2 cm^3) and BQ (1.08 g) was refluxed for 1 h. The mixture was then filtered to remove the insoluble material, from which quinhydrone (375 mg) was isolated. The subsequent evaporation of the filtrate *in vacuo* left a residual mass, which was chromatographed on a silica-gel column, with benzene–ether (8:2) as the eluent, to yield colorless, crystalline **4** (mp 62.5—63.5 °C (lit, [5] 61 °C), 10.4 mg; 0.9%), pale yellow crystalline **2** (mp 113—114 °C, 150.6 mg; 11% [Found: C, 77.83; H, 6.04%. Calcd for $C_{13}H_{12}O_2$: C, 77.98; H, 6.04%. ^{1}H NMR δ=0.04 (1H, dt, J=5.5, 4 Hz), 0.14 (1H, td, J=7, 5.5 Hz), 1.12 (2H, m), 3.02 (2H, t, J=1.5 Hz), 3.48 (2H, ddm, J=4.5, 1.5 Hz), 5.76 (2H, dd, J=4.5, 3.5 Hz), and 6.62 (2H, s). ν: 1665, 1615 cm^{-1}. λ_{max}^{MeOH}: 233 nm (ε=11700)]), and pale yellow crystalline **3** (mp 112—113.5 °C; 205 mg; 21% [Found: C, 82.53; H, 6.21%. Calcd for $C_{20}H_{18}O_2$: C, 82.73; H, 6.25%. ^{1}H NMR δ=1.90 (2H, dt, J=11, 6 Hz), 3.30 (2H, d, J=11 Hz), 5.20 (2H, dd, J=9.5, 6 Hz), 5.27 (2H, dd, J=9.5, 6 Hz), 6.23 (2H, dt, J=9.5, 3 Hz), 6.32 (2H, dt, J=9.5, 3 Hz), 6.59 (2H, s), 6.70 (2H, d, J=3 Hz), and 6.73 (2H, d, J=3 Hz). ν: 1685, 1600 cm^{-1}. λ_{max}^{MeOH}: 234 nm (ε=11100), 266 (4300)]). Additional amounts of BQ (166 mg; 15%) and H_2BQ (72 mg; 7%) were then obtained from the later elutions.

b) A mixture of **1** (20 cm^3) and BQ (3.25 g) was refluxed for 5 h. The mixture was then filtered to remove polymeric materials (3.25 g), and the filtrate was chromatographed on a silica-gel column with benzene–ether (9:1), after the evaporation of the volatile material, to give **5** (pale yellow crystals; mp 161—162 °C; 199 mg; 5% [Found: M^+, 380.1790. Calcd for $C_{27}H_{24}O_2$: 380.1775. ^{1}H NMR δ=0.57 (1H, q, J=7 Hz), 0.80 (1H, dm, J=7 Hz), 1.16 (2H, m), 1.72 (2H, dt, J=10.5, 7 Hz), 3.28 (2H, ddd, J=10.5, 3, 1.5 Hz), 4.22 (2H, m), 5.22 (4H, m), 5.97 (2H, m), 6.2 (4H, m), and 6.65 (4H, m). ν: 1665, 1582 cm^{-1}. λ_{max}^{MeOH}: 257 nm (ε=10500)]), **6** (colorless crystals; mp 198—201 °C; 44 mg; 1% [Found: C, 82.51; H, 6.22%. Calcd for $C_{20}H_{18}O_2$: C, 82.73; H, 6.25%. ^{1}H NMR δ=2.21 (1H, dt, J=10, 7 Hz), 2.38 (1H, d, J=5.5 Hz), 2.79 (1H, ddd, J=9, 5.5, 3 Hz), 3.10 (5H, m), 5.22 (1H, dd, J=9, 7 Hz), 5.66 (2H, t, J=9 Hz), 6.04 (1H, t, J=9 Hz), 6.24 (2H, m), 6.44 (2H, dd, J=9, 7 Hz), and 6.64 (2H, t, J=3 Hz). ν: 1730 cm^{-1}. λ_{max}^{MeOH}: 220 nm (ε=18800), 250 (sh. 6000)]), and **7** (colorless crystals; mp 177—180 °C; 208 mg; 2% [Found: M^+, 292.1475. Calcd for $C_{20}H_{20}O_2$: 292.1462. ^{1}H NMR δ=0.0 (4H, m), 0.9 (4H, m), 2.8 (4H, br. s), 3.25 (4H, m), and 5.87 (4H, dd, J=5, 3 Hz), ν: 1690 cm^{-1}]). The later fractions, eluted with benzene–ether (8:2), contained **2** (4%), **3** (6%), and **4** (15%).

Further Conversion of 3 to 6. A mixture of **3** (107 mg) and **1** (0.7 cm^3) was heated to reflux for 2 h with an occasional check of the reaction by means of thin-layer chromatography. Subsequent silica-gel column chromatography of the mixture, with benzene as the eluent, afforded crystalline **6** (16.5 mg; 18%), whose identity with an authentic sample was established by direct comparisons, and the recovered **3** (15.3 mg; 14%).

Thermal Reaction of 1 with NQ. *a)* A toluene solution (8 cm^3) of **1** (2.1 cm^3) and NQ (1.59 g) was refluxed for 12 h. After the removal of the solvent *in vacuo*, the residue was chromatographed on a silica-gel column, with benzene–ether (9:1) as the eluent, to give **8** (colorless crystals; mp 130—132 °C; 7 mg; 0.6% [Found: C 84.27; H, 5.92%; M^+, 340.1487. Calcd for $C_{24}H_{20}O_2$: C, 84.67; H, 5.93%; M^+, 340.1462. ^{1}H NMR δ=1.88 (2H, dt, J=11, 6 Hz), 3.50 (2H, d, J=11 Hz), 5.29 (4H, m), 6.22 (4H, m), 6.62 (4H, t, J=2.5 Hz), 7.72 (2H, m), and 8.09 (2H, m). ν: 1668, 1595 cm^{-1}]), **9** (yellow needles; mp 188—189 °C; 146 mg; 16% [Found: C, 82.49; H, 4.89%. Calcd for $C_{17}H_{12}O_2$: C, 82.24; H, 4.87%. ^{1}H NMR δ=0.70 (1H, dd, J=7, 6 Hz), 0.93 (1H, dd, J=6, 3.5 Hz), 1.36 (2H, m), 4.58 (2H, m), 6.12 (2H, dd, J=5, 3.5 Hz), 7.7 (2H, m), and 8.12 (2H, m). ^{13}C NMR δ=16.2, 17.8, 35.9, 126.2, 130.0, 132.3, 133.3, 156.2, and 181.7. ν: 1658, 1593 cm^{-1}]), **10** (colorless plates; mp 165—166.5 °C; 408 mg; 22% [Found: C, 81.63; H, 5.69%. Calcd for $C_{17}H_{14}O_2$: C, 81.58; H, 5.64%. ^{1}H NMR δ=0.12 (2H, m), 1.20 (2H, m), 3.23 (2H, dm, J=1.5 Hz), 3.58 (2H, ddd, J=5, 3.5, 1.5 Hz), 5.67 (2H, dd, J=5, 3.5 Hz), 7.66 (2H, m), and

8.00 (2H, m). ν: 1670, 1596 cm^{-1}]), **11** (a yellow oil; 100 mg; 5% [Found: M^+, 250.0993. Calcd for $C_{17}H_{14}O_2$: 250.0993. ^1H NMR δ=2.24 (1H, dt, J=9, 6 Hz), 3.1—3.7 (3H, m), 5.28 (1H, dd, J=10, 6 Hz), 5.40 (1H, dd, J=10, 6 Hz), 6.23 (2H, m), 6.62 (2H, t, J=3 Hz), 7.70 (2H, m), and 8.02 (2H, m). ν: 1694, 1598 cm^{-1}]), and the recovered NQ (423 mg; 26.6%).

b) A mixture of **1** (30 cm^3) and NQ (6.37 g) was heated to reflux for 11 h. After the removal of the solvent by distillation *in vacuo*, the residue was chromatographed on a silica-gel column, with benzene–ether (9:1) as the eluent; together with the already described **8** (128 mg; 2%), **9** (508 mg; 10%), **10** (727 mg; 7%), and **11** (90 mg; 1%), two products, **12** (faintly brown crystals; mp 131—132.5 °C; 151 mg; 3% [Found: C, 82.18; H, 4.89%. Calcd for $C_{17}H_{12}O_2$: C, 82.24; H, 4.87%. ^1H NMR δ=2.48 (1H, dd, J=8.5, 6 Hz), 2.84 (1H, d, J=3 Hz), 3.54 (2H, m), 5.67 (1H, dd, J=9.5, 6 Hz), 5.80 (1H, dd, J=9.5, 6 Hz), 6.06 (2H. dd, J=9.5, 6 Hz), 7.7 (2H, m), and 8.1 (2H, m). ^{13}C NMR δ=30.2, 30.8, 33.6, 38.2, 42.0, 120.2, 121.1, 126.4, 126.6, 126.9, 128.2, 133.9, 134.1, 134.6, 135.2, 195.6, and 195.7. ν: 1700, 1670, 1595 cm^{-1}]), and **13** (a yellow oil; 250 mg; 6% [Found: M^+, 338.1302. Calcd for $C_{24}H_{18}O_2$: 338.1304. ^1H NMR δ=2.26 (2H, dt, J=12, 6 Hz), 4.73 (2H, dd, J=12, 1 Hz), 5.14 (4H, q, J=5 Hz), 6.16 (4H, m), 6.71 (4H, t, J=2.5 Hz), 6.77 (1H, d, J=1 Hz), 7.25 (5H, br. s), 7.7 (4H, m), and 8.0 (4H, m). ^{13}C NMR δ=42.0, 45.6, 123.7, 123.9, 124.9, 125.5, 125.9, 126.8, 127.2, 128.3, 128.8 (4C), 130.9, 131.2, 131.8, 132.2, 133.7, 134.6, 140.0, 151.9, 184.5, and 185.2. ν: 1659, 1596 cm^{-1}]), were isolated.

Thermal Reaction of 1 with TQ. *a)* A toluene solution (8 cm^3) of **1** (2 cm^3) and TQ (1.25 g) was refluxed for 2.5 h. The insoluble solid was then filtered off, the filtrate was evaporated *in vacuo*, and the residue was chromatographed on a silica-gel column, with benzene–ether (8:2) as the eluent, to give **15** (pale yellow needles; mp 81—82 °C; 327 mg; 18% [Found: C, 78.38; H, 6.63%. Calcd for $C_{14}H_{14}O_2$: C, 78.48; H, 6.59%. ^1H NMR δ=0.80 (2H, m), 1.08 (2H, m), 1.98 (3H, d, J=2 Hz), 2.98 (2H, t, J=2 Hz), 3.40 (2H, br. s), 5.68 (2H, dd, J=5, 4 Hz), and 6.46 (1H, q, J=2 Hz). ν: 1660 cm^{-1}. λ_{max}^{MeOH}: 239 nm (ε=8200)]) and **16** (pale yellow crystals, mp 107—108 °C; 172 mg; 14% [Found: C, 82.45; H, 6.80%. Calcd for $C_{21}H_{20}O_2$: C, 82.85; H, 6.63%. ^1H NMR δ=1.80 (2H, m), 1.92 (3H, d, J=1.5 Hz), 3.26 (1H, dt, J=11, 2 Hz), 3.32 (1H, dd, J=11, 2 Hz), 5.20 (4H, m), 6.17 (2H, dt, J=9.5, 3 Hz), 6.28 (2H, dt, J=9.5, 3 Hz), 6.42 (1H, quint, J=1.5 Hz), and 6.67 (4H, t, J=3 Hz). ν: 1680, 1618 cm^{-1}. λ_{max}^{MeOH}: 247 nm (ε=12300)]). From the more polar fractions, eluted with a benzene–ether mixture (7:3), H_2TQ (284 mg) and TQ (241 mg; 19%) were obtained.

b) A mixture of **1** (14 cm^3) and TQ (2.44 g) was heated at 120 °C for 1.5 h. The subsequent removal of the volatile material by distillation *in vacuo* and the silica-gel chromatography of the residue with benzene–ether (9:1) gave **4** (29.5 mg; 1.6%), and **17** (a faintly brown oil; 121 mg; 6% [Found: M^+, 212.0811. Calcd for $C_{14}H_{12}O_2$: 212.0837. ^1H NMR δ=0.66 (1H, q, J=7 Hz), 0.87 (1H, dt, J=7, 3 Hz), 1.24 (2H, m), 2.06 (3H, d, J=1.5 HZ), 4.36 (2H, m), 6.05 (2H, dd, J=5, 4 Hz), and 6.45 (1H, q, J=1.5 Hz). ν: 1650 cm^{-1}. λ_{max}^{MeOH}: 263 nm (ε=12100)]), together with **15** (644 mg; 15%) and **16** (541 mg; 18%). From the later eluent of the benzene–ether mixture (7:3), H_2TQ (1.04 g; 42%) was obtained.

Thermal Reaction of 1 with PQ. A mixture of **1** (3 cm^3) and PQ (416 mg) was heated at 95 °C for 1.5 h. The mixture was then filtered to remove the insoluble solid, the filtrate was evaporated *in vacuo*, and the residue was chromatographed on a silica-gel column, with benzene–ether (9:1) as the eluent, to give **18** (yellow crystals; mp 139—140.5 °C, 59.5 mg; 12.5% [Found: C, 82.20; H, 5.88%. Calcd for $C_{19}H_{16}O_2$: C, 82.58; H, 5.84%. ^1H NMR δ=0.12 (1H, tm, J=4 Hz), 0.24 (1H, tm, J=6 Hz), 1.19 (2H, ddm, J=6, 4 Hz), 3.17 (2H, t, J=3 Hz), 3.52 (2H, m), 5.82 (2H, dd, J=5, 4 Hz), 6.73 (1H, s), and 7.40 (5H, s). ν: 1664 cm^{-1}. λ_{max}^{MeOH}: 228 nm (ε=15600), 307 (7300)]) and **19** (a pale yellow oil; 56.5 mg; 18% [Found: M^+, 366.1607. Calcd for $C_{26}H_{22}O_2$: 366.1619. ^1H NMR δ=2.05 (2H, dt, J=11, 6 Hz), 3.39 (1H, t, J=11 Hz), 3.41 (1H, t, J=11 Hz), 5.70 (4H, dm, J=6 Hz), 6.27 (4H, m), 6.67 (5H, m), and 7.39 (5H, s). ν: 1690, 1595 cm^{-1}. λ_{max}^{MeOH}: 230 nm (ε=13300), 313 (5600)]). The later fractions afforded recovered PQ (99 mg; 24%).

Thermal Reaction of 1 with CQ. A mixture of **1** (5 cm^3) and CQ (1.38 g) was heated at 60 °C for 50 min. After the removal of the volatile material *in vacuo*, the residue thus obtained was chromatographed on a silica-gel column, with benzene–ether (9:1) as the eluent, to give **20** (pale yellow crystals; mp 98—98.5 °C; 368 mg; 16% [Found: C, 66.43; H, 4.76%. Calcd for $C_{13}H_{11}O_2Cl$: C, 66.53; H, 4.72%. ^1H NMR δ=0.12 (1H, tm, J=4 Hz), 0.21 (1H, tm, J=6 Hz), 1.16 (2H, ddm, J=6, 4 Hz), 3.04 (2H, t, J=2 Hz), 3.49 (2H, m), 5.80 (2H, dd, J=4, 3.5 Hz), and 6.81 (1H, s). ν: 1665 cm^{-1}. λ_{max}^{MeOH}: 254 nm (ε=8500)]) and H_2CQ (377 mg; 27%).

Thermal Reaction of 1 with XQ. A toluene solution (2 cm^3) of **1** (2 cm^3) and XQ (1.36 g) was refluxed for 1.5 h. After the subsequent evaporation of the solvent *in vacuo*, the residue was chromatographed on a silica-gel column, with benzene–ether (8:2) as the eluent, to give **4** (30 mg; 6%) and **21** (yellow crystals; mp 90—93 °C; 91 mg; 14% [Found: M^+, 226.0975. Calcd for $C_{15}H_{14}O_2$: 226.0993. ^1H NMR δ=2.05 (3H, s), 2.09 (3H, d, J=2 Hz), 3.16 (1H, t, J=6 Hz), 5.16 (2H, dd, J=9, 6 Hz), 6.17 (2H, dm, J=9 Hz), and 6.62 (3H, m). ν: 1645 cm^{-1}. λ_{max}^{MeOH}: 262 nm (ε=10600)]). Subsequently, H_2XQ (40 mg) and the recovered XQ (663 mg; 49%) were obtained from the polar fractions by elution with benzene–ether (5:5).

Dehydrogenation of 10 to 9. A benzene solution of **10** (35.6 mg) was held on an alumina column for 1 h. Subsequent elution with ether yielded **9** (22.6 mg; 67%).

Dehydrogenation of 11 to 14. The **11** (81 mg) was chromatographed on a basic alumina column with hexane–benzene (1:1) to give **14** (a colorless oil; 58.6 mg; 73% [Found: M^+, 248.0851. Calcd for $C_{17}H_{12}O_2$: 248.0837. ^1H NMR δ=3.64 (1H, td, J=7, 1.5 Hz), 5.41 (2H, dd, J=9.5, 7 Hz), 6.34 (2H, dt, J=9.5, 4 Hz), 6.64 (2H, t, J=4 Hz), 6.84 (1H, d, J=1.5 Hz), 7.75 (2H, m), and 8.1 (2H, m). ν: 1664, 1596 cm^{-1}]).

Further Conversion of 14 to 12. A mixture of **1** (0.5 cm^3) and **14** (30 mg) was heated at 100 °C for 7 h. Subsequent silica-gel column chromatography of the mixture with benzene yielded **12** (8.4 mg; 28%).

Reaction of 14 and 11. A mixture of **1** (0.5 cm^3), **11** (20.5 mg), and **14** (22.8 mg) was heated at 100 °C for 5.5 h. Subsequent silica-gel column chromatography of the mixture with benzene afforded **8** (5.5 mg; 20%) and **12**

(2.5 mg; 16%).

Further Reaction of 11 and NQ. *a)* A mixture of **1** (0.5 cm^3), **11** (16 mg), and NQ (7 mg) was heated at 110 °C for 11 h. Subsequent silica-gel column chromatography of the mixture, with benzene–ether (5:5) as the eluent, yielded **8** (0.7 mg; 6%), together with **9** (1.5 mg) and **10** (2.5 mg).

b) A toluene solution (1 cm^3) of **11** (70.4 mg) and NQ (32.2 mg) was refluxed for 13 h. Subsequent silica-gel column chromatography of the mixture, with hexane–benzene (5:5) as the eluent, yielded **9** (7.4 mg; 11%) and **12** (4.9 mg; 7%).

Thermal Reaction of 1 with p-*TRQ.* A toluene solution of **1** (0.8 cm^3) and *p*-TRQ (545 mg) was heated to reflux for 10 min. The precipitates (287 mg, 56%), removed by filtration and washed with benzene and MeOH, were identical with **23**.[11] From the MeOH washings, **22** (124 mg; 22%) was obtained. From the benzene washings, a trace of **4** was isolated.

References

1) A part of this study has already been reported; H. Takeshita, A. Mori, and H. Mametsuka, *Chem. Lett.*, **1976**, 445, 881. A loss of samples by fire caused delayed publication until the experiments had been repeated.

2) H. Takeshita, A. Mori, and S. Itô, *Bull. Chem. Soc. Jpn.*, **47**, 1767 (1974); H. Takeshita, A. Mori, N. Yamamoto, and T. Fujita, *Kyushu Daigaku Seisan Kagaku Kenkyusho Hokoku*, **66**, 9 (1978).

3) H. Takeshita, A. Mori, M. Funakura, and H. Mametsuka, *Bull. Chem. Soc. Jpn.*, **50**, 315 (1977); A. Mori and H. Takeshita, *Chem. Lett.*, **1975**, 599.

4) K. T. Finley, "The Addition and Substitution Chemistry of Quinones," in the "The Chemistry of the Quinonoid Compounds," in the Series of S. Patai (ed), "The Chemistry of Functional Groups," Wiley-Interscience, New York (1974), p 877.

5) W. von E. Doering and L. H. Knox, *J. Am. Chem. Soc.*, **79**, 352 (1957).

6) The yields of the product were based on the stoichiometry of the quinones required for their formation.

7) For deduction of the stereochemistry, the argument based on the *J* values would necessarily be ambiguous in the bicyclo[2.2.2]octene system. However, the chemical shift differences of the olefinic protons, $\Delta\delta$, between the bicyclooctenes and bicyclooctadienes must provide information. Thus, $\Delta\delta$ for norbornadiene and norbornane is 6.65−5.93=0.72, which could be calculated from the figures given in the literature,[14] but our $\Delta\delta$ value for **9** and **10** is 6.12−5.67=0.45, while for **17** and **15** it is 6.05−5.68=0.37. The differences can probably be explained in terms of the induced ring current effect from the naphthoquinone moiety; therefore, the stereostructures for the products are as depicted. We admit that, in this case, there is no reason why the adducts, which are formed stereospecifically, must have an unfavorable *exo*-configuration against the secondary orbital overlappings.

8) This product is a barbaralane derivative; however, in the ^{1}H and ^{13}C NMR spectra, there is no indication of the occurrence of valence isomerization, which is well known in the case of the parent skeleton.

9) D. H. Reid, M. Fraser, B. B. Molloy, H. A. S. Payne, and B. G. Sutherland, *Tetrahedron Lett.*, **1961**, 530.

10) Currently, we are making a systematic analysis of this subject.

11) H. Takeshita, T. Kusaba, and A. Mori, *Chem. Lett.*, **1982**, 701.

12) M. Hirama, Y. Koyama, Y. Shoji, and S. Itô, *Tetrahedron Lett.*, **1978**, 2289.

13) H. Takeshita, A. Mori, and N. Yamamoto, *Kyushu Daigaku Seisan Kagaku Kenkyusho Hokoku*, **68**, 25 (1978).

14) W. Brügel, "Handbook of NMR Spectral Parameters," Heydon & Son, Ltd., London (1979), Vol. 1, pp. 104—105.

The Pulse-photoconductivity of Poly(*N*-vinylbenzocarbazole)s

Akira ITAYA,* Ken-ichi OKAMOTO, and Shigekazu KUSABAYASHI†
Department of Chemical Engineering, Faculty of Engineering, Yamaguchi University, Tokiwadai, Ube 755
†*Department of Applied Chemistry, Faculty of Engineering, Osaka University, Suita, Osaka 565*
(Received January 25, 1985)

The hole-drift mobility and the carrier-photogeneration efficiency of holes in poly(5-vinylbenzo[*b*]carbazole)(P5VBCz) and poly(7-vinylbenzo[*c*]carbazole)(P7VBCz) films were investigated by means of the time-of-flight method and compared with those in poly(*N*-vinylcarbazole)(PVCz) films. The mobilities of these polymers were nearly equal to each other and smaller than that of PVCz by a factor of *ca.* 1/3. The electric field and temperature dependence of the mobilities fit Gill's empirical equation. The small mobilities of both P5VBCz and P7VBCz were apparently attributable to the small values of the pre-exponential factor, μ_0. The carrier-photogeneration efficiencies, ϕ, of these polymers were larger than that of PVCz by a factor of *ca.* 10. The field dependence of ϕ of these polymers for the excitation of the ^1B_a absorption band was in good agreement with the Onsager theory of geminate recombination. These results indicate that the introduction of bulky and unsymmetric benzocarbazolyl chromophores instead of carbazolyl ones as a pendant group of vinyl polymers is a good modification from the point of view of the carrier-photogeneration, but not from the viewpoint of the carrier transport.

There have been many investigations concerning the electrical conductivity of vinyl polymers with large pendant aromatic groups. Considerable data on the photoconductivity of poly(*N*-vinylcarbazole) (PVCz) have been accumulated because of an interest in highly photoconductive polymers.[1-21] The high photoconductivity of PVCz has been reported to be attributable to both the high efficiency of carrier generation and the ease of carrier migration. The extrinsic carrier-photogeneration *via* nonrelaxed exciplexes has been reported to be predominant for all the excitation bands.[14,20] The hole-drift mobility is described by a hopping mechanism where a hole migrates among pendant chromophores of polymer chains. Therefore, it is of interest to investigate the photoconductivity of vinyl polymers with aromatic chromophores which are more bulky than a carbazolyl chromophore. We have synthesized poly(5-vinylbenzo[*b*]carbazole)(P5VBCz) and poly(7-vinylbenzo[*c*]carbazole)(P7VBCz).[22] The stereoregularity of these polymers depends on the polymerization method. They show the excimer fluorescence, while the monomeric compounds, both 5-ethylbenzo[*b*]-carbazole and 7-ethylbenzo[*c*]carbazole (7EBCz), show no excimer fluorescence in concentrated solutions. This behavior is very similar to that of PVCz.[22,23]

In the present paper, the pulse photoconductivity of P5VBCz and P7VBCz has been investigated in comparison with that of PVCz.

Experimental

The P5VBCz was prepared by the bulk polymerization of purified 5-vinylbenzo[*b*]carbazole in the presence of 2 mol% AIBN in an evacuated sealed tube at 100—105 °C for 68 h.[22] The P7VBCz was prepared by the polymerization of a 0.62 M (1 M=1 mol dm^{-3}) benzene solution of purified 7-vinylbenzo[*c*]carbazole in the presence of 1 mol% AIBN in an evacuated sealed tube at 63 °C for 7 h.[22] The polymers were reprecipitated three times from the 1,2-dichloroethane solution with methanol. The polymer samples were stored in tubes within an argon atmosphere in the dark. Gel-permeation chromatography analysis showed M_n=2.02×10^4 and M_w/M_n=3.63, and M_n=4.72×10^4 and M_w/M_n=3.35, for P5VBCz and P7VBCz respectively. Films were cast on NESA-coated quartz plates from a 1,2-dichloroethane solution and were dried *in vacuo*. A semitransparent gold electrode with a typical area of 1 cm^2 was evaporated on a film to prepare a sandwich-type cell. The film thickness was determined to be 4.3—7.2 μm from the weight and density of a film with a certain known area and/or by a capacitive method. The densities of the films were 1.21 and 1.22 g cm^{-3} for P5VBCz and P7VBCz respectively. The dielectric constants, ε, of P5VBCz and P7VBCz films were determined to be 3.61 and 3.66 respectively from capacitance measurements at the frequency of 1 kHz at 298 K.

The hole-drift mobility and the carrier-photogeneration efficiency of holes were measured with the apparatus described in a previous paper by means of a conventional time-of-flight method in a vacuum of 2.6×10^{-3} Pa.[20,21] A 3 μs light pulse from an air-gap flash was irradiated onto a sample through appropriate narrow band-pass filters. The cautions described in a previous paper[20] were taken in all the procedures in order to get reproducible results.

Results and Discussion

Hole-drift Mobility. For both P5VBCz and P7VBCz, a transient photoresponse was detected only for the illumination of a positively-biased electrode and was attributed to hole transport. It has been reported that PVCz samples with a sequence length of the *N*-vinylcarbazole(VCz) chain of more than *ca.* 10 showed a shoulder of the transient response

* Present address: Department of Polymer Science and Engineering, Kyoto Institute of Technology, Matsugasaki, Kyoto 606.

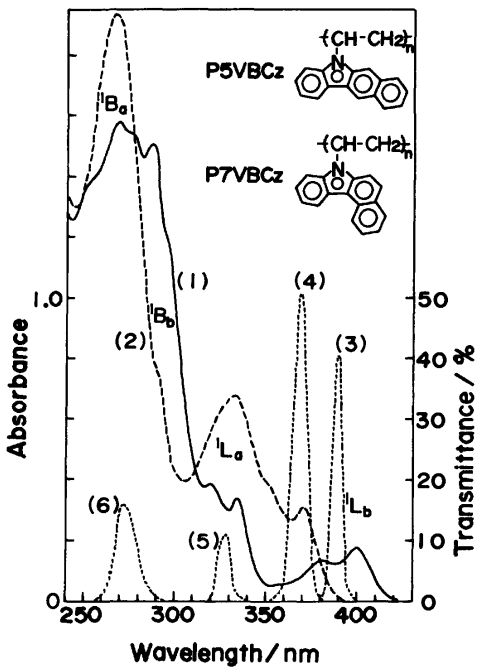

Fig. 1. Absorption spectra of P5VBCz(≈0.12 μm thick) (1) and P7VBCz(≈0.19 μm thick) (2) films, and transmittance of band-pass filters ((3)—(6)).

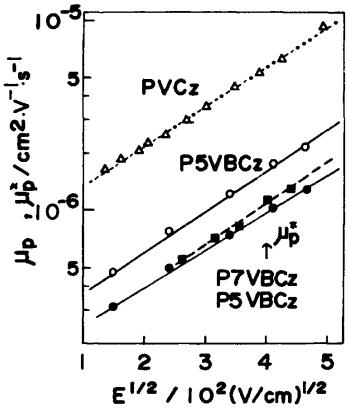

Fig. 2. Field dependence of the hole drift mobility at 339 K.
○,●: P5VBCz, λ_{ex}=270 nm, ■: P7VBCz, λ_{ex}=370 nm, △: PVCz, λ_{ex}=340 nm.

curve.[21] For a P5VBCz sample with a degree the polymerization($\overline{DP}$) of 80, such a shoulder was observed, and the transit time, t_r, was determined from it. For a P7VBCz sample of $\overline{DP}$=180, however, no such shoulder was observed except above 363 K. When no shoulder of the transient response curve was observed, the transit time, t_r^*, was determined from the bilogarithmic plots based on the theory of Scher and Montroll.[24] The hole-drift mobilities calculated from t_r and t_r^* were abbreviated as μ_p and μ_p^* respectively.

Figure 1 shows the absorption spectra of P5VBCz and P7VBCz thin films and the transmittance of the band-pass filters used. The hole-drift mobility was independent of the excitation bands of ^1L_b, ^1L_a, and ^1B_a. The results mentioned below concerning the hole mobility were obtained by the excitation of ^1B_a and ^1L_a absorption bands for P5VBCz and P7VBCz respectively.

The hole-drift mobilities for both polymers depended strongly on both the electric field and the temperature, as is the case with PVCz.[4,12,16,21] Figure 2 shows the electric-field dependence of the hole mobilities of both polymers at *ca.* 339 K. The result for a PVCz sample of $\overline{DP}$=1010 is also shown for the sake of comparison. Straight lines of log μ against the square root of the electric field show that the Poole-Frenkel-type relation holds for these polymers. Under this condition, the hole mobilities of P5VBCz and P7VBCz were nearly equal to each other and about one-thirds as large as that of PVCz. This is not attributable to the difference of the $\overline{DP}$ values, because the mobilities of the PVCz samples prepared by the radical polymerization were reduced by a factor of only two with a decrease in $\overline{DP}$ from 200 to 20.[21]

The electric-field and temperature dependence of the hole mobility of PVCz is expressed by Gill's empirical equation:[4]

$$\mu_p = \mu_0 \exp\{-(\Delta E_0 - \beta\sqrt{E})/kT_{eff}\} \quad (1)$$

$$1/T_{eff} = 1/T - 1/T_0, \quad (2)$$

where k is the Boltzmann constant; E, the electric field; T, the film temperature, and μ_0, ΔE_0, T_0, and β, the characteristic parameters. We have previously reported that the dependence of the mobilities of the copolymers of VCz with styrene(VCz-St copolymer) on both the electric field and the temperature also fit Gill's empirical equation.[21] Figure 3 shows the temperature dependence of the mobilities of P5VBCz and PVCz under various electric fields. The electric-field dependence of the activation energies, ΔE_a, of P5VBCz, P7VBCz, and PVCz is shown in Fig. 4. These figures indicate that the mobilities of the benzocarbazolyl polymers also follow Gill's equation, as is the case with carbazolyl polymers. The values of the parameters obtained are listed in Table 1. There was a remarkable difference in the parameter, T_0, between carbazolyl and benzocarbazolyl polymers. The glass-transition temperatures of P5VBCz and P7VBCz were higher than that of PVCz, while the T_0 values of the benzocarbazolyl polymers were much lower than those of PVCz and VCz copolymers. The T_0 values of the benzocarbazolyl polymers were close to those of polycarbonate molecularly-doped with 7EBCz (522—405 K) reported by Tsutsumi *et al.*[25] It has been suggested that T_0 was related to the freezing-in temperature of the micro motion of chromophores themselves acting as hopping sites;[21,26] their micro motion destroys some structural traps preventing the hole transport and promotes the transport. It has been suggested that the traps which control the hole

transport may be derived from structural defects such as kinks existing at joints between isotactic and syndiotactic sequences.[21] Both P5VBCz and P7VBCz consist of a syndiotactic and isotactic stereoblock structure, as is the case with PVCz.[22] Although both benzo[*b*]carbazole and benzo[*c*]carbazole are bulky compared with carbazole, they both have unsymmetric molecular structure, unlike carbazole. Therefore, the packing between chromophores around the kinks in P5VBCz and P7VBCz may be loose and the chromophores may tend to move to destroy the structural traps at low temperatures as compared with carbazolyl chromophores in PVCz.

The μ_0 values of P5VBCz and P7VBCz were much smaller than that of PVCz, as is shown in Table 1. The μ_0 value of poly(1-vinylpyrene) was close to those of P5VBCz and P7VBCz and much smaller than that of PVCz.[27] Even if a sample with a high value of T_0 tends to have a high value of μ_0, the μ_0 value of PVCz is extremely high. It has been reported that the μ_0 value is related to molecular interaction between chromophores acting as hopping sites[4] and corresponds to the trap-free drift mobility.[19] Therefore, the molecular interaction between carbazolyl chromophores in PVCz is considered to be very strong with regard to the hole transport.

The introduction of bulky and unsymmetric benzocarbazolyl chromophores instead of carbazolyl ones as a pendant group of vinyl polymers results in an increase in the exponential term related to the temperature in Eq. 1, because of the low T_0 values of P5VBCz and P7VBCz. However, the μ_0 values related to the molecular interaction ascribed to properties of the chromophores themselves are much lower for benzocarbazolyl polymers than for PVCz; consequently, the mobilities of both P5VBCz and P7VBCz are smaller than that of PVCz. Therefore, the introduction of benzocarbazolyl chromophores is not a good modification from the point of view of the carrier transport.

Carrier-photogeneration Efficiency. In order to excite the ^1L_b, ^1L_a, and ^1B_a absorption bands, narrow band-pass filters of 390, 330, and 270 nm were used for P5VBCz, and those of 370, 330, and 270 nm, for P7VBCz(Fig. 1). Figure 5 shows the field dependence of the carrier-photogeneration efficiency,ϕ, of P5VBCz and P7VBCz for the various excitation bands at 338 K, including that of PVCz for the sake of

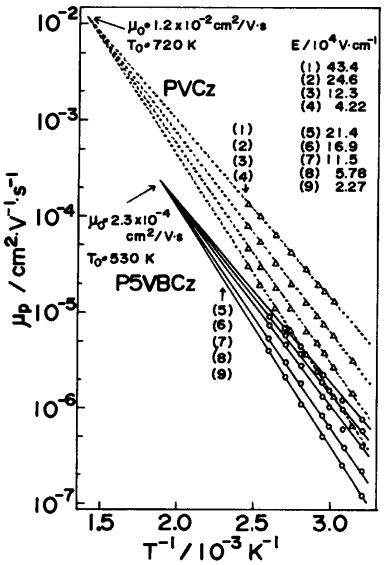

Fig. 3. Dependence of the hole drift mobility on temperature with electric field as a parameter.

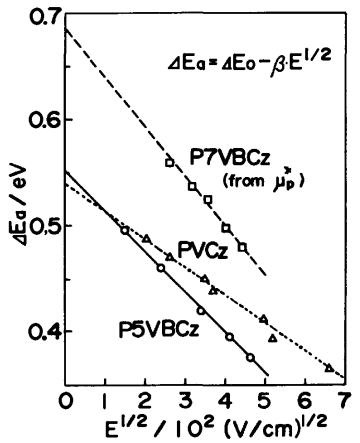

Fig. 4. Dependence of the activation energy ΔE_a on the electric field.

TABLE 1. TRANSPORT PARAMETERS[a] AND GLASS TRANSITION TEMPERATURE, T_g

Sample[b]	μ_0 / 10^{-3} cm²/V·s	T_0 / K	E_0 / eV	β / 10^{-4} eV/$\sqrt{\text{V/cm}}$	T_g / K
P5VBCz	0.23	530	0.55	3.9	>544
PVCz[c]	15	725	0.54	2.6	501
P5VBCz	* 0.14	530	0.54	3.4	>544
P7VBCz	* 0.21	490	0.69	4.7	544
PVCz[c]	* 8.5	730	0.53	2.6	501
VCz-St copolymer[c] (73 mol%)	* 9.0	720	0.57	2.6	—
VCz-St copolymer[c] (50 mol%)	* 5.0	695	0.60	2.8	—

a) *: Values were determined from μ_p^*. b) The values in parentheses show the content of VCz. c) Ref. 21.

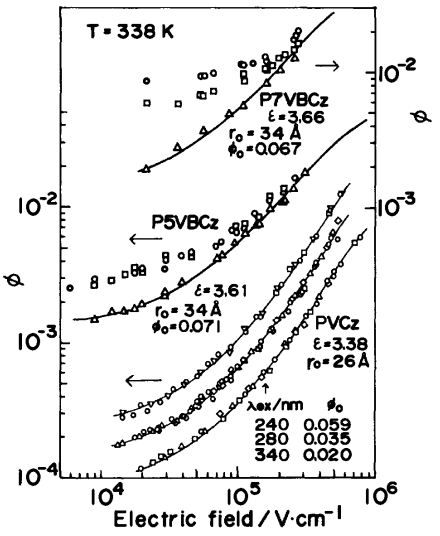

Fig. 5. Field dependence of the carrier-photogeneration efficiency in P5VBCz, P7VBCz, and PVCz films for different excitation bands. The solid lines were calculated from Eq. 1 in Ref. 20 with r_0 and ϕ_0 values presented in the figure. The keys ○, □, and △ present the ^1L_b, ^1L_a, and ^1B_a band excitation, respectively, except for PVCz.

comparison. The ϕ values of P5VBCz and P7VBCz were nearly equal to each other and were much larger than that of PVCz for all the excitation bands.

The solid lines in Fig. 5 were calculated from Eq. 1 in Ref. 20, with an interionic separation r_0 of 34 Å and with a primary yield of the electron-hole pair, ϕ_0, of 0.071 and 0.067 for P5VBCz and P7VBCz respectively; this equation is used in order to calculate the overall carrier-photogeneration efficiency, ϕ, given as the product of ϕ_0 and the dissociation probability, P(E), which is given by the Onsager theory of the geminate recombination of a bound electron-hole pair with r_0. The experimental data for the ^1B_a band were in good agreement with the lines predicted from the Onsager theory, indicating that the extrinsic carrier-photogeneration via an exciplex is predominant for the excitation of a surface layer of a film. However, the experimental data for the ^1L_b and ^1L_a bands did not fit the Onsager theory because of a contribution of another carrier-generation process, one independent of the electric field. On the other hand, the carrier-photogeneration efficiency of PVCz for all the excitation bands fit the Onsager theory, with both ϕ_0 values increasing from 0.02 to 0.059 and r_0 (=26 Å).[20] The large r_0 value of both P5VBCz and P7VBCz is probably attributable to the fact that a large excess energy must be dissipated during the thermalization process from a non-relaxed exciplex state to the ion-pair state because the ionization potential of benzocarbazolyl chromophores is smaller than that of the carbazolyl chromophores.[28]

The results described above show that the introduction of benzocarbazolyl chromophores with a small ionization potential instead of carbazolyl ones is a good modification from the point of view of the carrier-photogeneration.

References

1) P. J. Regensburger, *Photochem. Photobiol.*, **8**, 429 (1968).
2) D. M. Pai, *J. Chem. Phys.*, **52**, 2285 (1970).
3) J. Mort, *Phys. Rev. B*, **5**, 3329 (1972).
4) W. D. Gill, *J. Appl. Phys.*, **43**, 5033 (1972).
5) K. Okamoto, S. Kusabayashi, and H. Mikawa, *Bull. Chem. Soc. Jpn.*, **46**, 2324, 2613 (1973).
6) G. Pfister and D. J. Williams, *J. Chem. Phys.*, **61**, 2416 (1974).
7) P. J. Reucroft and K. Takahashi, *J. Non-Cryst. Solids*, **17**, 71 (1975).
8) K. Okamoto, M. Oda, A. Itaya, and S. Kusabayashi, *Chem. Phys. Lett.*, **35**, 483 (1975).
9) M. Yokoyama, Y. Endo, and H. Mikawa, *Bull. Chem. Soc. Jpn.*, **49**, 1538 (1976).
10) M. Ohnishi, *Jpn. J. Appl. Phys.*, **16**, 1717 (1977).
11) C. H. Griffiths, K. Okumura, and A. Van Laeken, *J. Polym. Sci., Polym. Phys. Ed.*, **15**, 1627 (1977).
12) G. Pfister and C. H. Griffiths, *Phys. Rew. Lett.*, **40**, 659 (1978).
13) P. M. Borsenberger and A. I. Ateya, *J. Appl. Phys.*, **49**, 4035 (1978).
14) A. Itaya, K. Okamoto, and S. Kusabayashi, *Bull. Chem. Soc. Jpn.*, **52**, 2218 (1979).
15) B. Reimer and H. Bässler, *Phys. Status. Solidi A*, **51**, 445 (1979).
16) M. Yamamoto, T. Hamano, K. Yubakami, N. Tsutsumi, and Y. Nishijima, *Rep. Prog. Polym. Phys. Jpn.*, **23**, 559 (1980).
17) N. Tsutsumi, M. Yamamoto, and Y. Nishijima, *Rep. Prog. Polym. Phys. Jpn.*, **24**, 399 (1981).
18) M. Yokoyama, Y. Endo, A. Matsubara, and H. Mikawa, *J. Chem. Phys.*, **75**, 3006 (1981).
19) M. Fujino, H. Mikawa, and M. Yokoyama, *Photogr. Sci. Eng.*, **26**, 84 (1982).
20) K. Okamoto and A. Itaya, *Bull. Chem. Soc. Jpn.*, **57**, 1626 (1984).
21) A. Itaya, K. Okamoto, and S. Kusabayashi, *Polymer J.*, **17**, 557 (1985).
22) K. Okamoto, M. Yamada, A. Itaya, T. Kimura, and S. Kusabayashi, *Macromolecules*, **9**, 645 (1976).
23) A. Itaya, K. Okamoto, and S. Kusabayashi, *Bull. Chem. Soc. Jpn.*, **51**, 79 (1978).
24) H. Scher and E. W. Montroll, *Phys. Rev. B*, **12**, 2455 (1975).
25) N. Tsutsumi, A. Osako, M. Yamamoto, and Y. Nishijima, *Rep. Prog. Polym. Phys. Jpn.*, **25**, 455 (1982).
26) M. Fujino, K. Kanazawa, H. Mikawa, M. Yokoyama, and S. Kusabayashi, *Polym. Preprints, Jpn*, **32**, 516 (1983).
27) A. Itaya and K. Okamoto, unpublished results.
28) M. Yokoyama and H. Mikawa, *Photogr. Sci. Eng.*, **26**, 143 (1982).

Nucleophilic Photoreaction of Chlorobenzene in Methanol as Studied by Emission Spectroscopy

Shin-ichi NAGAOKA, Takeshi TAKEMURA, and Hiroaki BABA*
Division of Chemistry, Research Institute of Applied Electricity, Hokkaido University, Sapporo 060
(Received February 4, 1985)

The photoreaction of chlorobenzene in methanol has been studied by means of emission spectroscopy. Upon irradiation with UV light, chlorobenzene reacts with methanol to form anisole with a quantum yield of 0.049 at 18 °C. Contrary to the case of chlorobenzene, the photoreaction of *p*-dichlorobenzene with methanol is not observed. By combining these results with those of our recent studies on the dual phosphorescence from low-lying triplet states of halogenated benzenes, it is suggested that the photoreaction of chlorobenzene with methanol, which is a nucleophilic substitution reaction, occurs in the $^3(\pi,\sigma^*)$ state. From the temperature dependence of the quantum yield, the activation energy for the nucleophilic photoreaction is estimated to be larger by about 3—4 kcal mol^{-1} than the apparent activation energy for a combination of the nonradiative $^3(\pi,\sigma^*)\rightarrow S_0$ process and the homolytic dissociative process concerning the C–Cl bond in the $^3(\pi,\sigma^*)$ state. It is suggested that the nucleophilic photoreaction contrasts with the radical reaction leading to the dissociation of the C–Cl bond; the latter reaction occurs in the $^3(\pi,\pi^*)$ state as well as in the $^3(\pi,\sigma^*)$ state.

Halogen substitutions in benzene cause significant changes in its phosphorescence spectrum. Benzene exhibits a structured phosphorescence spectrum with a maximum near 370 nm in rigid-glass solution, while chlorobenzene (abbreviated to CB) shows a broad, structureless one with a maximum near 480 nm.[1,2] Lim and Chakrabarti assigned this phosphorescence for CB to an emission originating from a triplet excimer.[2] Recently we studied the phosphorescence emission and the dynamics in the triplet states of CB, *p*-dichlorobenzene (DCB), and *p*-dibromobenzene in 2-methylpentane in the temperature range 70 to 100 K by means of time-resolved emission spectroscopy.[1,3] From the results of these studies we concluded that CB exhibits dual phosphorescence which consists of the structureless spectrum mentioned above and a somewhat structured one with a maximum near 400 nm, and that the former spectrum is not due to the triplet excimer. The phosphorescence properties of the halogenated benzenes were explained in terms of two low-lying triplet states, $^3(\pi,\pi^*)$ and $^3(\pi,\sigma^*)$, as shown in Fig. 1.[1,3] The intersystem-crossing (ISC) quantum yields from the S_1 state to the $^3(\pi,\pi^*)$ and $^3(\pi,\sigma^*)$ states may possibly amount to 0.6 and 0.4 for CB at 77 K, respectively, while for DCB the ISC to the $^3(\pi,\pi^*)$ state predominates, to a great extent, over the ISC to the $^3(\pi,\sigma^*)$ state. The nonradiative decay rate from these triplet states is particularly large at higher temperatures (> 85 K) compared with the corresponding rate of other analogous compounds, *e.g.*, halogenated naphthalenes. Accordingly, a process peculiar to the halogenated benzenes is considered to play an important role in the relaxation from the two triplet states. We suggested that this process corresponds to homolytic dissociation of the C–Cl bond.

On the other hand, the photolysis of halogenated benzenes has been widely studied, because the halogenated compounds are often concerned with environmental pollusion.[4] It is known that the photolysis of CB generates a phenyl radical,[5] which is important as an intermediate in organic radical reactions. Ichimura and Mori suggested that the photolysis of CB in the vapor phase proceeds from the triplet state.[6] Bunce *et al.* showed that a radical reaction occurs in the triplet state of CB in cyclohexane.[7] Soumillion and De Wolf found that upon irradiation benzene and anisole are formed simultaneously in a solution of CB in methanol (MeOH), and they proposed a mechanism involving the triplet excimer for this photoreaction.[8] It is thus inferred that the photoreaction of CB is related to the nonradiative process from the triplet state.

Despite these investigations the relationships among the type of the excited state, the nonradiative

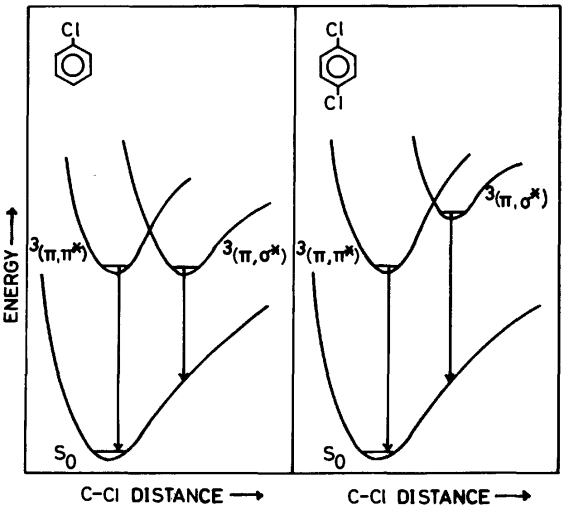

Fig. 1. Schematic sketch of potential curves of the low-lying triplet states of CB and DCB. The $^3(\pi,\sigma^*)\rightarrow S_0$ phosphorescence of DCB can be observed at temperatures higher than 85 K,[3] though it is too weak to be detected at 77 K.[1]

process, and the photoreaction have not fully been explored for halogenated benzenes, although such information is necessary for understanding the detailed mechanism of the photoreaction. Under these circumstances it would be worthwhile to examine the role of the two low-lying triplet states, $^3(\pi,\pi^*)$, and $^3(\pi,\sigma^*)$, in the photochemistry of halogenated benzenes.

From these points of view we have investigated the photoreaction of CB with MeOH by means of emission spectroscopy. One of the reaction products was found to be anisole, as shown by Soumillion and De Wolf,[8] indicating that a nucleophilic substitution reaction takes placae. The quantum yield of the nucleophilic photoreaction was determined, and the temperature dependence of the yield was examined to elucidate the reaction dynamics. The property of this reaction is compared with that of the radical photoreaction leading to the dissociation of the C–Cl bond. It is suggested that the nucleophilic reaction occurs in the $^3(\pi,\sigma^*)$ state, but that the radical reaction occurs in the $^3(\pi,\pi^*)$ state as well as in the $^3(\pi,\sigma^*)$ state. The photochemistry of DCB was also investigated for the sake of comparison.

Experimental

Materials. Chlorobenzene (CB), *p*-dichlorobenzene (DCB) (Wako Pure Chemical Co.), biacetyl, anisole, and *p*-chloroanisole (Nakarai Chemicals, Ltd.) were purified by repeated vacuum sublimation or distillation. Spectroscopic grade methanol (MeOH) and cyclohexane (Wako Pure Chemical Co.) were used without further purification. All sample solutions were degassed by the freeze-pump-thaw method prior to measurements.

Apparatus and Procedure. Unless otherwise stated, experiments were made at room temperature using a 1-cm square quartz cell. Absorption spectra were taken with a Cary 15 or a Hitachi 228A spectrophotometer. Emission and excitation spectra were measured by the photon-counting method, using a high-sensitivity emission spectrophotometer with a Hamamatsu R585 photomultiplier as detector.[9] The emission and excitation spectra were not corrected for the spectral sensitivity of the detector and the spectral intensity of the exciting light, respectively. In the photochemical experiments, unless otherwise stated, irradiation was carried out at 265 nm in the region of the $S_1 \leftarrow S_0$ transition with a bandwidth of 19 nm by the use of light from a system of a 150 W xenon arc and an *f*/4.5 monochromator.

The absolute quantum yield of the photoreaction of CB with MeOH was determined at 18 °C by means of trioxalatoferrate (III) actinometry, using a deaerated MeOH solution of 10^{-3} M (1 M=1 mol dm^{-3}) CB. Before irradiation of the solution, the intensity of fluorescence obtained by excitation at 265 nm was measured. After irradiation for 2 h, the fluorescence intensity was measured again under the same conditions as before to know the increase of the intensity resulting from the irradiation. This intensity increase was then compared with the intensity of the fluorescence from a 10^{-4} M solution of anisole in MeOH to evaluate the concentration of anisole formed by the photochemical reaction. It is to be noted here that the decrease in intensity of the fluorescence of CB need not be taken into account, because this decrease is very small compared with the intensity increase caused by anisole produced. The incident photons were counted after the method established by Hatchard and Parker.[10] These data permit determination of the quantum yield of the photoreaction. The quantum yields of photoreaction at 45, 0, −26 and −44 °C, relative to the yield at 18 °C, were also measured using three types of cryostats. By combining the results with the absolute yield at 18 °C, the absolute quantum yields were obtained for the different temperatures mentioned above.

The fluorescence decay (or the lifetime) was measured on a laser spectrophotomeric system reported previously,[11] using the time-correlated single photon counting method. The frequency of a pulsed dye laser (Molectron DL14) pumped by a nitrogen laser (Molectron UV22) was doubled by KDP crystal. The generated UV pulses, which were used for exciting the sample, have a duration of ≈3 ns. The emission was detected by a Hamamatsu R106 photomultiplier.

Results and Discussion

Photoreaction of CB with MeOH. In Fig. 2(a) the solid curves 1 and 2 represent the fluorescence and fluorescence-excitation spectra of 10^{-3} M CB in MeOH, and the broken curves 1′ and 2′ those of 10^{-3} M

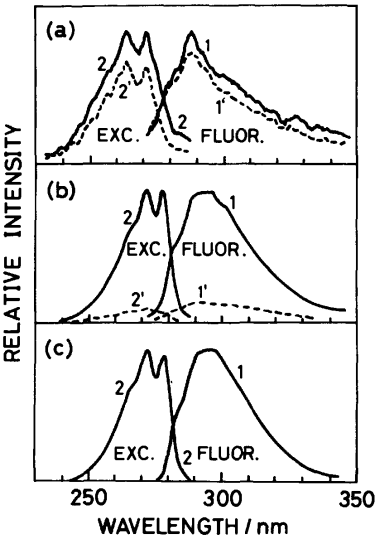

Fig. 2. (a) Fluorescence and fluorescence-excitation spectra of 10^{-3} M CB in MeOH (——) and 10^{-3} M CB in MeOH containing 10^{-2} M biacetyl (– – –). The fluorescence spectra (1 and 1′) were obtained by excitation at 265 nm and the excitation spectra (2 and 2′) by monitoring the emission at 300 nm. The spectra for the two sample solutions were recorded under the same conditions. (b) Same as (a) except that the two sample solutions were irradiated for 10 h. (c) Fluorescence spectrum (1) and fluorescence-excitation spectrum (2) of 10^{-4} M anisole in MeOH.

CB in MeOH containing 10^{-2} M biacetyl. Since the spectra for the two solutions were recorded under the same conditions, it is obvious that the fluorescence of CB is not quenched efficiently by biacetyl. This observation is consistent with the report that the lifetime of the S_1 state of CB is very short (80—800 ps).[12,13] On the other hand, from the latter solution containing biacetyl, strong sensitized biacetyl phosphorescence was observed, indicating that low-lying triplet states of CB are populated to a great extent.

Upon irradiation of the MeOH solution of CB alone, the fluorescence intensity increases with irradiation time, and the fluorescence spectrum undergoes a drastic change. In Fig. 2(b) the solid curves 1 and 2 represent the fluorescence and its excitation spectra for the MeOH solution of CB taken after irradiation for 10 h. These spectra are significantly different in shape and position from spectra 1 and 2 of Fig. 2(a), and are considered to originate from a photoproduct. In fact spectra 1 and 2 of Fig. 2(b) are very similar to the corresponding spectra of anisole in MeOH shown in Fig. 2(c). The fluorescence lifetime of the photoproduct (9.4 ns) also is similar to that of anisole in MeOH (9.8 ns). From these results, it is concluded that CB reacts with MeOH to form anisole upon irradiation. This photoreaction may be assumed to proceed in the excited state *via* a nucleophilic attack by MeOH on the carbon adjacent to the chlorine atom, followed by heterolysis of the C–Cl bond:

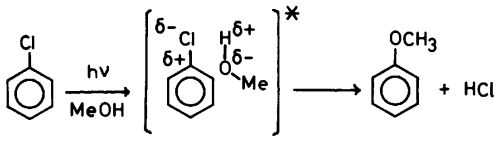

It has been found that photoreactions of alkyl halides in MeOH proceed through similar processes and generate methoxyalkanes.[14] A similar photosolvolysis was also reported for benzyl chloride in *t*-butyl alcohol.[15]

The photoreaction in the MeOH solution of CB is quenched by biacetyl. In Fig. 2(b) the broken curves 1′ and 2′ represent the fluorescence and its excitation spectra of 10^{-3} M CB in MeOH containing 10^{-2} M biacetyl after being irradiated in the same way as the MeOH solution of CB alone. These spectra were recorded under the same conditions as those for the solution without biacetyl, *i.e.*, spectra 1 and 2 of Fig. 2(b). Figure 3 shows the increase of the fluorescence intensity with irradiation time. The open and solid circles refer to the solutions of CB in MeOH in the absence and presence of biacetyl, respectively. It is seen that the efficiency of the photoreaction becomes very low when biacetyl is added to the solution. Since the photoreaction is quenched efficiently by

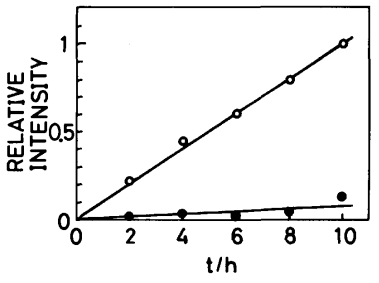

Fig. 3. Increase of the fluorescence intensity with irradiation time for 10^{-3} M CB in MeOH (○) and 10^{-3} M CB in MeOH containing 10^{-2} M biacetyl (●). The intensity was measured by excitation at 265 nm and by monitoring the emission at its intensity maximum.

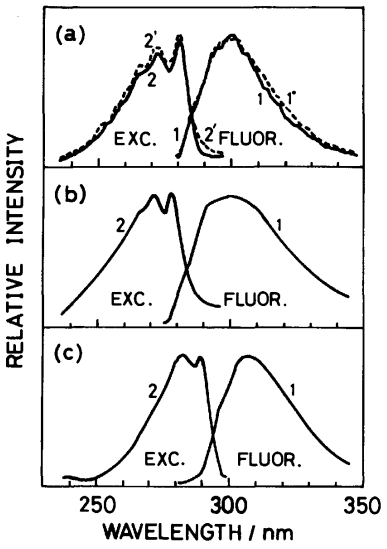

Fig. 4. (a) Fluorescence and fluorescence-excitation spectra of 10^{-3} M DCB in MeOH (——) and those of the same solution after irradiation for 10 h (- - -). The fluorescence spectra (1 and 1′) were obtained at 273 nm and the excitation spectra (2 and 2′) by monitoring the emission at 310 nm. The spectra before and after irradiation were recorded under the same conditions. (b) Fluorescence (1) and fluorescence-excitation (2) spectra of 10^{-3} M DCB in MeOH after irradiation for 3 min with intense light from a 250 W high-pressure Hg lamp. (c) Fluorescence (1) and fluorescence-excitation (2) spectra of 10^{-4} M *p*-chloroanisole in MeOH.

biacetyl in contrast to the case of the fluorescence, this reaction is considered to occur mainly in the low-lying triplet state, $^3(\pi, \pi^*)$ and/or $^3(\pi, \sigma^*)$. Tissot *et al.* also showed that the photohydrolysis of chlorobenzene in aqueous solution involves a triplet state.[16]

Contrary to the case of CB, the nucleophilic photoreaction was not observed for DCB. In Fig. 4(a) the solid curves 1 and 2 show the fluorescence and its excitation spectra of 10^{-3} M DCB in MeOH, and the broken curves 1′ and 2′ the spectra of the same solution after being irradiated under the same

experimental conditions as the solution of CB in MeOH. The solid and broken curves were recorded under the same conditions. If the nucleophilic reaction of DCB occurred in MeOH, the fluorescence and its excitation spectra of DCB should be changed to those of *p*-chloroanisole shown in Fig. 4(c). Actually the spectra of DCB remain essentially unchanged upon irradiation, as is seen in Fig. 4(a). It was found, however, that on irradiating DCB with intense light from a 250 W high-pressure Hg lamp (without being dispersed by a monochromator), the spectra were changed ultimately to those of anisole, as shown in Fig. 4(b). Moreover, during the course of the above irradiation there was no indication that *p*-chloroanisole was formed. These experimental results for DCB can be explained as follows. In the first stage of the photochemical reaction, the homolysis of DCB takes place in MeOH to form CB, as shown by Mansour *et al.*,[17] and then the CB molecule is changed to anisole by the photochemical nucleophilic reaction as described before. It is thus concluded that in the low-lying triplet states of DCB the nucleophilic reaction does not occur at all or proceeds only slowly.

The extent to which each of the $^3(\pi,\pi^*)$ and $^3(\pi,\sigma^*)$ states is involved in the nucleophilic photoreaction depends evidently upon the degree of populating the triplet state concerned. According to our recent study, the ISC quantum yield from the S_1 state to the $^3(\pi,\sigma^*)$ state may possibly amount to 0.4 for CB, but it is essentially zero for DCB in 2-methylpentane at 77 K; that is, the $^3(\pi,\sigma^*)$ state of DCB is populated from S_1 to a far smaller degree than the same state of CB. In either compound, the mutual conversion between the two low-lying triplet states $^3(\pi,\pi^*)$ and $^3(\pi,\sigma^*)$ is negligible at 77 K.[3] In DCB the $^3(\pi,\pi^*)$ state is considered to be significantly lower in energy than the $^3(\pi,\sigma^*)$ state (Fig. 1).[1,3] Accordingly, even if the conversion mentioned above occurs rapidly at high temperature, the $^3(\pi,\sigma^*)$ state of DCB will be populuated *via* $^3(\pi,\pi^*)$ only to a slight degree. It seems reasonable, therefore, to assume that the overall degree of populating the $^3(\pi,\sigma^*)$ state of DCB is much less than that of CB even under the present experimental conditions. This difference in population degree of the $^3(\pi,\sigma^*)$ state between CB and DCB may be the main factor responsible for the difference in reactivity between the two compounds. Thus, the most probable mechanism of the nucleophilic photoreaction of CB with MeOH is that the reaction proceeds from the $^3(\pi,\sigma^*)$ state. Our recent *ab initio* study on the low-lying triplet states of CB also has suggested that the $^3(\pi,\sigma^*)$ state is more favorable to the nucleophilic photoreaction than the $^3(\pi,\pi^*)$ state.[18]

From the phosphorescence and its excitation spectra of the irradiated sample solution of CB in MeOH, which were measured at 77 K after irradiation at room temperature, we noticed formation of benzene in addition to anisole. As mentioned previously, Soumillion and De Wolf also found that benzene and anisole are formed simultaneously upon irradiation of a solution of CB in MeOH, and they proposed a new mechanism which involves formation of a pair of radical ions *via* the triplet excimer.[8] Their argument is based on the suggestion by Lim and Chakrabarti[2] that the phosphorescence from CB in EPA at 77 K is due to the triplet excimer. However, we demonstrated that the phosphorescence is not attributable to the triplet excimer, but that it can be explained in terms of the two low-lying triplet states.[1] It is unlikely, therefore, that the photoreaction proceeds *via* the triplet excimer. This is consistent with the results obtained by Bunce *et al.*[7]

Reaction Quantum Yield and Its Temperature Dependence. The quantum yield of the nucleophilic photoreaction (Φ_{react}) of CB at 18 °C was determined to be 0.049 by means of actinometry. The temperature dependence of Φ_{react} of CB is shown in Fig. 5. The value of Φ_{react} decreases as the temperature is lowerd. The results were analysed under the view that the reaction proceeds from the $^3(\pi,\sigma^*)$ state.

Since the ISC in CB seems to dominate over the other deactivation processes from the S_1 state, the total ISC quantum yield is assumed to be unity. The ISC is considered to take place to both the $^3(\pi,\pi^*)$ and the (π,σ^*) states. At room temperature, the rates of the radiative decays from the two triplet states can safely be regarded as much less than those of the nonradiative decays, so that the radiative decays will be neglected in the following discussion. The rate constants for the nonradiative decay processes and the nucleophilic photoreaction are assumed to change with temperature and to be expressible in the forms of the Arrhenius equation. In order to understand the experimental results, two simple and extreme cases will be discussed. In Case 1, the mutual conversion between the $^3(\pi,\pi^*)$ and $^3(\pi,\sigma^*)$ states is regarded as much slower than the other nonradiative processes from these two triplet states. In Case 2, we assume that just the reverse is the case, namely, that a

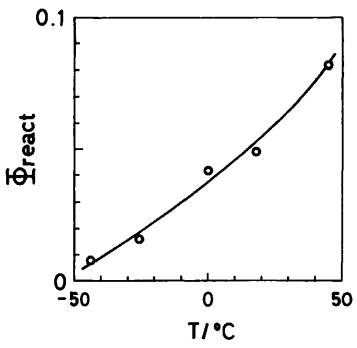

Fig. 5. Temperature dependence of Φ_{react}.

dynamic equilibrium is attained between the two triplet states.

In Case 1, we can show that the following relation holds between Φ_{react} and temperature:

$$\frac{\Phi_{ISC}^{\pi\sigma}}{\Phi_{react}} - 1 \propto \exp\left(\frac{E_r - E_\sigma}{RT}\right), \quad (1)$$

where $\Phi_{ISC}^{\pi\sigma}$ denotes the quantum yield of the ISC to the $^3(\pi,\sigma^*)$ state; E_r is the activation energy of the pseudo first order nucleophilic photoreaction from the $^3(\pi,\sigma^*)$ state, and E_σ represents the apparent activation energy associated with the total rate constant, k_σ, for a combination of the nonradiative $^3(\pi,\sigma^*)\rightarrow S_0$ process and the homolytic dissociative process concerning the C-Cl bond in the $^3(\pi,\sigma^*)$ state.

In Case 2, on some assumptions, the relation between Φ_{react} and temperature is given by

$$\frac{1}{\Phi_{react}} - 1 \propto \exp\left(\frac{E_r - E_\sigma}{RT}\right). \quad (2)$$

The assumptions which have to be introduced are described in the following.

Previously, we suggested that the homolytic dissociative process of the C-Cl bond is dominant in the decay from the two low-lying triplet states of halogenated benzenes in 2-methylpentane above 85 K.[1,3] It is not unreasonable, therefore, to assume that the rate of the homolytic dissociative process of the C-Cl bond is much greater than those of the other nonradiative processes in CB under our experimental conditions. Furthermore, the dissociation of the C-Cl bond of CB is much more likely to occur in the $^3(\pi,\sigma^*)$ state than in the $^3(\pi,\pi^*)$ state, because the C-Cl bond length in the $^3(\pi,\sigma^*)$ state is considered to be significantly longer than that in the $^3(\pi,\pi^*)$ state.[1,3,18] It is thus assumed that k_σ is far greater than the total rate constant for a combination of the nonradiative $^3(\pi,\pi^*)\rightarrow S_0$ process and the homolytic dissociative process concerning the C-Cl bond in the $^3(\pi,\pi^*)$ state. It is further assumed that for CB the ratio of the rate constant for the $^3(\pi,\sigma^*)\rightarrow{}^3(\pi,\pi^*)$ conversion process to the rate constant for the reverse process is not much larger than unity.

Equation 2 (Case 2) is the same as Eq. 1 (Case 1), except that $\Phi_{ISC}^{\pi\sigma}$ is replaced by unity. We attemped to estimate E_r-E_σ from the slopes of the plots of log $[(X/\Phi_{react})-1]$ *vs.* $1/T$ with X varying between 0.1 and 1. The plots of $\log[(X/\Phi_{react})-1]$ *vs.* $1/T$ give nearly straight lines for X between 0.2 and 1, but the plot for $X=0.1$ somewhat deviates from a straight line. Accordingly, we estimated E_r-E_σ only for $0.2 \leqq X \leqq 1$. From the slopes of the straight lines, the values of E_r-E_σ of CB were determined to be (3.9 ± 1.0) and (3.0 ± 0.7) kcal mol^{-1} (1 kcal mol^{-1}= 4.184 kJ mol^{-1}) for $X=0.2$ and 1, respectively, using the least squares method. E_r-E_σ decreases as X increases, but for $0.2 \leqq X \leqq 1$, E_r-E_σ does not depend largely on X. In other words, the two extreme cases, Case 1 and Case 2, lead to similar results for E_r-E_σ. It may thus be said that E_r is larger than E_σ by about 3—4 kcal mol^{-1} in the actual CB molecule.

Comparison between Nucleophilic and Radical Reactions. As described previously benzene as well as anisole is formed by irradiation of CB in MeOH, indicating that the radical photoreaction occurs, besides the nucleophilic one, in the sample solution. We now compare the property of the nucleophilic photoreaction of CB with that of the radical one. Bunce *et al.* showed that the radical reaction occurs in the triplet state of CB in cyclohexane.[7] Examining the photolysis of CB in cyclohexane by a method similar to the one described before, we also concluded that upon irradiation CB in cyclohexane is converted into benzene *via* the low-lying triplet states. In order to know the detailed mechanism of this radical photoreaction, we studied the photolysis of DCB in cyclohexane also.

The fluorescence and its excitation spectra of DCB in cyclohexane are shown in Fig. 6(a). As in the case of CB in MeOH, the fluorescence is not quenched efficiently by biacetyl. Upon irradiation with the intense light from the 250 W high-pressure Hg lamp mentioned previously, the spectra changed drastically. A peak to be assigned to CB was observed at 265 nm in the excitation spectrum, together with peaks of DCB and benzene (Fig. 6(b)). On further irradiation, the fluorescence and its excitation spectra

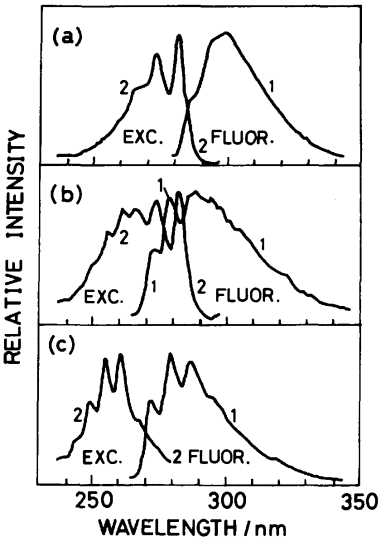

Fig. 6. (a) Fluorescence (1) and fluorescence-excitation (2) spectra of 10^{-3} M DCB in cyclohexane in a 7 mm o.d. cylindrical quartz cell. The fluorescence spectrum was obtained by excitation at 255 nm and the excitation spectrum by monitoring the emission at 310 nm. (b) Same as (a) except that the sample solution was irradiated for 10 min with intense light from a 250 W high-pressure Hg lamp. (c) Same as (b) except that the irradiation time was lengthened to 30 min.

changed finally to those of benzene alone, as may be seen from Fig. 6(c). These results indicate that the radical reaction, including the dechlorination of DCB, takes place upon irradiation. Since this photoreaction is quenched by biacetyl, it is considered to occur in the low-lying triplet states as in the case of the nucleophilic and radical photoreactions of CB. On the other hand, as has already been pointed out, the population degree of the $^3(\pi,\sigma^*)$ state of DCB is considered to be quite small. It is, therefore, reasonable to presume that the radical plotoreaction of DCB takes place in the $^3(\pi,\pi^*)$ state. The radical reaction of CB, therefore, may be supposed to occur in the $^3(\pi,\pi^*)$ state also.

From the foregoing discussion one may suppose that (1) the nucleophilic photoreaction of CB takes place in the $^3(\pi,\sigma^*)$ state, and (2) the radical photoreaction of CB leading to the dissociation of the C–Cl bond may occur both in the $^3(\pi,\pi^*)$ state and in the $^3(\pi,\sigma^*)$ state.

References

1) T. Takemura, Y. Yamada, and H. Baba, *Chem. Phys.*, **68**, 171 (1982).

2) E. C. Lim and S. K. Chakrabarti, *Mol. Phys.*, **13**, 293 (1967).

3) T. Takemura, M. Sugawara, Y. Yamada, and H. Baba, *J. Phys. Chem.*, submitted.

4) A. Gilbert, *Photochem.*, **8**, 362 (1977).

5) J. C. Scaciano and L. C. Stewart, *J. Am. Chem. Soc.*, **105**, 3609 (1983) and references cited therein.

6) T. Ichimura and Y. Mori, *J. Chem. Phys.*, **58**, 288 (1973).

7) N. J. Bunce, J. P. Bergsma, M. D. Bergsma, W. De Graaf, Y. Kumar, and L. Ravanal, *J. Org. Chem.*, **45**, 3708 (1980).

8) J. P. Soumillion and B. De Wolf, *J. Chem. Soc., Chem. Commum.*, **1981**, 436.

9) T. Takemura, M. Aikawa, H. Baba, and Y. Shindo, *J. Am. Chem. Soc.*, **98**, 2205 (1976).

10) C. G. Hatchard and C. A. Parker, *Proc. R. Soc. London, Ser. A*, **235**, 518 (1956).

11) H. Baba, M. Fujita, N. Ohta, and Y. Shindo, *J. Spectrosc. Soc. Jpn.*, **29**, 387 (1980).

12) M. A. Fox, W. C. Nichols, Jr., and D. M. Lemal, *J. Am. Chem. Soc.*, **95**, 8164 (1973).

13) H. Leimann, H. D. Scharf, W. Strassburger, and A. Wollmer, *J. Photochem.*, **21**, 275 (1983).

14) P. J. Kropp, T. H. Jones, and G. S. Poindexter, *J. Am. Chem. Soc.*, **95**, 5420 (1973) and the series subsequent to this paper.

15) S. J. Cristol and B. E. Greenwald, *Tetrahedron Lett.*, **1976**, 2105; S. J. Cristol and T. H. Bindel, *J. Am. Chem. Soc.*, **103**, 7287 (1981).

16) A. Tissot, P. Boule, and J. Lamaire, *Chemosphere*, **13**, 381 (1984).

17) M. Mansour, S. Wawrik, H. Parlar, and F. Korte, *Chem. -Ztg.*, **104**, 339 (1980).

18) S. Nagaoka, T. Takemura, H. Baba, N. Koga, and K. Morokuma, *J. Phys. Chem.*, submitted.

 © 1985 The Chemical Society of Japan Bull. Chem. Soc. Jpn., 58, 2088—2092 (1985) [Vol. 58, No. 7

Kinetic Features of SERS Quenching by Underpotential Deposition (UPD) of Cd and Tl on Ag Electrodes

Tadashi WATANABE,* Osamu KAWANAMI, and Kenichi HONDA†
Institute of Industrial Science, The University of Tokyo, Roppongi, Minato-ku, Tokyo 106
†*Division of Molecular Engineering, Faculty of Engineering, Kyoto University, Yoshida, Sakyo-ku, Kyoto 606*
(Received February 4, 1985)

Surface-enhanced Raman scattering (SERS) in the Ag/pyridine system is quenched through a biphasic kinetics, after completion of submonolayer underpotential deposition (UPD) of Cd. This result is elucidated by invoking a quasi-reversible transformation of the initial SERS-active site into another by an attack, *via* surface diffusion, of deposited Cd, followed by irreversible unimolecular decomposition of the new site. From the SERS quenching data a value of about 10^{-17} cm^2 s^{-1} was derived as the surface diffusion coefficient of Cd on the Ag surface. A similar but somewhat different quenching behavior is observed by UPD of Tl.

A number of authors[1-4] have recently described the use of underpotential deposition (UPD) of foreign metals onto Ag electrodes for mechanistic investigation of the surface-enhanced Raman scattering (SERS).[5] The SERS-quenching effect observed by UPD is generally very drastic, causing nearly perfect intensity loss at metal coverages on the order of several hundredths.[1-3] Moreover, the quenching effect is usually of irreversible nature, *i.e.*, the original SERS intensity is hardly recovered upon reoxidation (stripping) of the deposited foreign metal.[1-4] Such quenching behaviors have been accounted for by invoking an attack or association of the metal atom to some special "SERS-active site," which is supposed to exist on the Ag surface sustaining the SERS effect.

In a more recent work[6] we presented evidence that the SERS-active sites consist of sparingly soluble surface Ag^+ complexes, which are removed from the surface by the action of appropriate ligands forming water-soluble Ag^+ complexes, or are disintegrated through reduction of the Ag^+ centers by application of sufficiently negative potentials. Other workers[7,8] also identify the SERS-active sites with insoluble Ag^+ salts on the electrode surface. Then, as briefly discussed previously,[6] one of the possible mechanisms for the SERS-quenching by UPD may be related to an interaction between the deposited metal atom and the surface Ag^+ complexes. This aspect has been studied in the present work by following the time courses of the UPD itself and of the SERS intensity decrease.

Experimental

A polycrystalline Ag platelet (10×10×1 mm) embedded in a Teflon holder was used as a working electrode in a base electrolyte solution containing 0.1 M KCl and 0.05 M pyridine (1 M=1 mol dm^{-3}). $CdCl_2$ or TlCl was then dissolved to give a metal ion concentration of 2.5×10^{-5} M. The pH values of the Cd^{2+} and Tl^+ solutions were 8.5 and 7.7, respectively. No turbidity was noticed in the Cd^{2+}-containing solution, in contrast to a solution with much higher Cd^{2+} concentration (5×10^{-4} M).[4] The counter and reference electrodes are a Pt wire and a saturated calomel electrode (SCE), respectively.

Stripping voltammetry was used to determine the surface coverage $\theta(E,t)$ for Cd or Tl on tha Ag electrode as functions of potential E and polarization time t in the above-specified electrolyte solution. In this measurement a mirror-finished Ag electrode was employed, the roughness factor of which was estimated to be about 1.5 as in a previous work.[1] The stripping charge Q, corrected for the roughness factor, was converted to θ assuming $\theta=1$ for $Q=420$ μC cm^{-2} (Cd) and 210 μC cm^{-2} (Tl).[9]

The pyridine SERS spectra were recorded over a wavenumber range of 985—1045 cm^{-1}, in which two major vibrational peaks are observed. A single scan required about 6 s. Other details for SERS measurements are the same as in a previous paper,[1] except that a 514.5-nm Ar^+ laser line (100 mW) was used here for excitation.

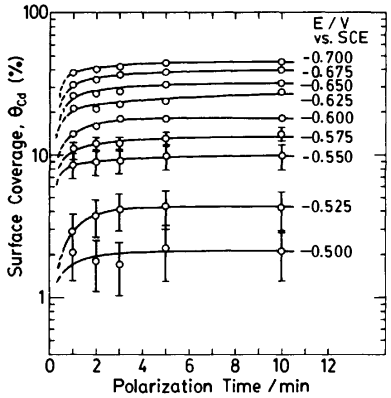

Fig. 1. Effect of electrode potential and polarization time on θ_{Cd} on the Ag electrode surface. $[Cd^{2+}]=2.5\times10^{-5}$ M.

Results and Discussion

UPD of Cd. Figure 1 shows the $\theta_{Cd}(E,t)$ characteristics obtained with a mirror-finished Ag electrode. It is seen that measurable UPD starts at a potential *ca.* 300 mV positive of the thermodynamic deposition potential for the Cd^{2+}/Cd couple (−0.78 V *vs.* SCE at $[Cd^{2+}]=2.5\times10^{-5}$ M). No significant difference was noted between the features of $\theta_{Cd}(E,t)$ in the presence and absence of 0.05 M pyridine. A similar observation is described by Kester[4] for the θ_{Tl} values in the Ag/benzotriazole system. Further, the application of an oxidation-reduction cycle (ORC), leading to roughening of the Ag surface, did not alter the essential feature of $\theta_{Cd}(E,t)$, except for some fourfold increase in the stripping charge Q due to roughening. The most important aspect in Fig. 1 is that the UPD process is practically completed in less than 100 s at each potential. A closer examination of the temporal evolution of θ_{Cd} demonstrated that the effective times for near-completion of UPD were about 40 s and 120 s for Ag electrodes before and after an ORC, respectively.

The SERS quenching effect of Cd UPD was examined as follows. After application of an ORC to a reformation charge of about 20 mC cm^{-2} in an electrolyte solution containing all the three components (pyridine, KCl, and $CdCl_2$), the potential was maintained for 1—2 min at 0.0 V *vs.* SCE to achieve a stationary SERS signal. The potential was then stepped to a negative value, ranging from −0.45 to −0.7 V, and the SERS spectra were thereafter registered every 20 s for about 40 min. Potentials negative of −0.7 V were avoided because of the occurrence of potential-induced irreversible decay of the pyridine SERS.

In a Cd^{2+}-free electrolyte solution, the pyridine SERS intensity was stable for more than 40 min at potentials from 0.0 to −0.7 V. In the presence of 2.5×10^{-5} M Cd^{2+}, a drastic decay of the intensity was observed by stepping the potential to a range of −0.48 to −0.70 V, in correspondence with the occurrence of UPD. In the initial phase of the intensity decay, a change in the SERS spectrum was also noted. These results are summarized in Fig. 2. Here the intensity is represented by the peak height of the totally symmetric vibration at 1007 cm^{-1} (I_{1007}), and the spectral shape by the intensity ratio I_{1007}/I_{1037}. The following features are noticed in this figure: (1) The intensity decay occurs essentially after the completion of Cd UPD, which takes less than 120 s as mentioned above; (2) The intensity decay apparently obeys a biphasic kinetics, with the time constant of the first phase being dependent on the potential (and hence on the θ_{Cd} value), while that of the second phase being practically potential-independent; and (3) The shape of the pyridine SERS spectrum undergoes a change exclusively during the first phase of the decay, and remains nearly unchanged throughout the second phase. The pattern of the spectral change, namely the direction of the change in the peak height ratio, is seen to depend on the potential. Besides such a peak height ratio change, some peak wavenumber shift was also noted (*e.g.*, a shift from 1007 cm^{-1} to 1009 cm^{-1} at −0.7 V within the initial 500 s). A change in the SERS spectrum as well as in the intensity has also been observed by Kester,[4] regarding the quenching of SERS in an Ag/benzotriazole (BTA) system by UPD of Tl, and was ascribed to some unknown effect of deposited Tl on the Ag–BTA interaction.

These results indicate that the SERS quenching in the Ag/pyridine system by UPD of Cd consists in the attack of deposited Cd atom to the initial "SERS-active site (A)" to produce a new site B (which is still SERS-active), followed by a unimolecular decomposition of B into a SERS-inactive site, X. Denoting the time constants of these sequential steps by τ_1 and τ_2, respectively, the quenching process could be represented by the following scheme:

$$A + Cd \xrightarrow{\tau_1} B \xrightarrow{\tau_2} X \qquad (1)$$

By assuming that the SERS activity of B is lower than that of A by a factor α ($0<\alpha<1$), a simple calculation leads to the following formula for the SERS intensity $I(t)$ at time t, normalized by the initial intensity $I(0)$:

$$I(t)/I(0) = e^{-t/\tau_1} + \frac{\alpha\tau_2}{\tau_2-\tau_1}(e^{-t/\tau_2}-e^{-t/\tau_1}) \qquad (2)$$

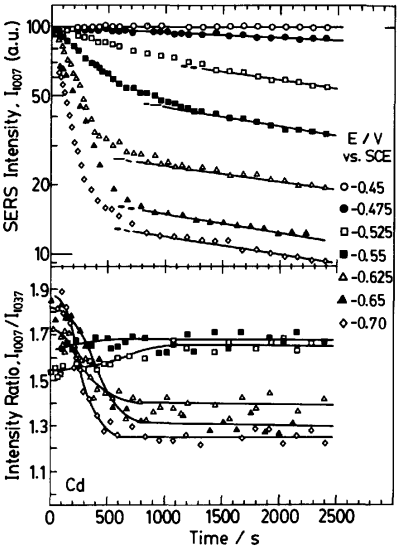

Fig. 2. Time courses of the pyridine SERS intensity (top) and its spectral shape (bottom) after potential steps from 0.0 V to a series of negative values.

Provided that the surface concentration of deposited Cd is sufficiently larger than that of the initial active site A, the first step is regarded as a pseudo-first-order process, with the time constant τ_1 inversely proportional to θ_{Cd}:

$$\tau_1 \propto \theta_{Cd}^{-1} \quad (3)$$

As an example, a result of curve fitting according to Eq. 2 is given in Fig. 3(A) for the decay profile observed at −0.55 V. The experimental points lie fairly well on the simulated curve with τ_1=370 s and τ_2=4860 s. Similar treatments have been conducted on the decay profiles at a series of potentials. In some cases, the curve fittings were not very satisfactory in the very initial phase of the decay; this is probably related to the simultaneous occurrence of spectral change in the initial phase. However, since the extent of the I_{1007}/I_{1037} ratio variation is much smaller (at most *ca.* 35% for E=−0.70 V) than that of the I_{1007} variation itself, we could obtain τ_1 values within a reasonable error range. The τ_1 and τ_2 values thus estimated are summarized in Fig. 3(B) as a function of the reciprocal of θ_{Cd}. It is evident that τ_1 changes in fair agreement with Eq. 3, and that τ_2 is practically constant around 4000—5000 s, suggestive of an intramolecular decay process.

In Fig. 2 we note that the fraction of the SERS intensity lost during the first phase of quenching depends on the electrode potential. Qualitatively this is accounted for as follows. The SERS-active sites are most probably surface Ag^+ complexes having both pyridine molecule(s) and chloride ions as ligands.[6] We could reasonably assume that the composition of

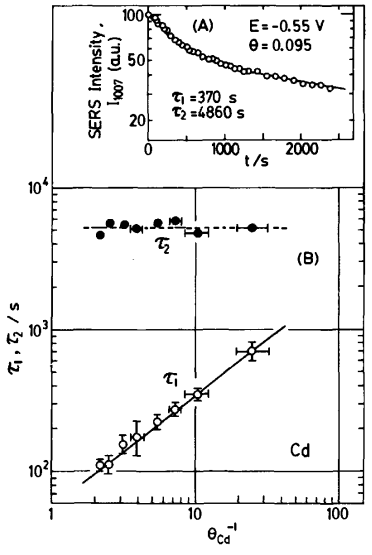

Fig. 3. (A) A typical result of analysis of the SERS intensity decay according to Eq. 2.
(B) Effect of θ_{Cd} on the values of τ_1 and τ_2.

the ligand is a function of the electrode potential, since at least the chloride ions tend to desorb from the surface by negative polarization. Thus the identities of the SERS-active sites A and B, and hence the value of α, should all vary with the electrode potential, leading to the observed potential dependence of the quenching efficiency during the first phase.

If we now assume that the first phase of quenching (interaction between A and Cd) occurs *via* surface diffusion of the deposited Cd atoms, an order-of-magnitude estimate of its diffusion coefficient can be made as follows. The average distance L (cm) between a single active site A and a nearest-neighbor Cd atom at the completion of UPD is roughly the average distance between the Cd atoms, and is thus the reciprocal of the square root of its surface concentration, C_{Cd} (atoms cm^{-2}): $L \simeq C_{Cd}^{-1/2}$. As the Cd atom moves on the surface with a diffusion coefficient D (cm^2 s^{-1}) for a period t (s), the average departure l (cm) from the origin is approximated by $(Dt)^{1/2}$. We then regard the average lifetime τ_1 (s) of the initial active site A as the value of t such that $L \simeq l$; thus $\tau_1 \simeq (DC_{Cd})^{-1}$ or $D \simeq (C_{Cd}\,\tau_1)^{-1}$. Referring to Fig. 3(A) one obtains $D \simeq 2.5\times10^{-17}$ cm^2 s^{-1} from $\tau_1 \simeq 400$ s and $C_{Cd} \simeq 10^{14}$ atoms cm^{-2}. Since several constants related to actual surface geometry have been dropped in this calculation, it would be safe to give $D \simeq 10^{-16}$—10^{-18} cm^2 s^{-1} as a rough estimate. Although there is no data available for the surface diffusion coefficient of Cd on the Ag surface, the range of D deduced above covers remarkably well the homogeneous and heterogeneous surface diffusion coefficients determined recently by field ion microscopic techniques at 25 °C (D in cm^2 s^{-1}): 7.6×10^{-19} for W atom on W(110),[10] 6.8×10^{-18} for Re on W(211),[11] 2.9×10^{-15} for Ta on W(110),[12] 6×10^{-18} for Ir on W(110),[12] and 5.1×10^{-17} for Pt on Pt(110).[13] This could be indirect evidence for the occurrence of surface diffusion of Cd in the first phase of the SERS quenching.

If the first step in Eq. 1 is a simple association between A and Cd, stripping (oxidative removal) of the latter is expected to recover the original SERS intensity. To examine this point we followed the SERS intensity at a Cd-free potential, −0.2 V, before and after the Cd UPD at −0.625 V. By controlling the holding time at −0.625 V, we were able to make the stripping of the deposited Cd either within the first phase or after the quenching had reached deep into the second phase. The results are displayed in Fig. 4. As expected, when the potential was stepped back to −0.2 V after holding it at −0.625 V for 120—600 s, which is substantially within the first phase of the quenching (Fig. 2), the SERS intensity was almost totally recovered. On the contrary, stripping after a 2400-s holding at −0.625 V regenerated the

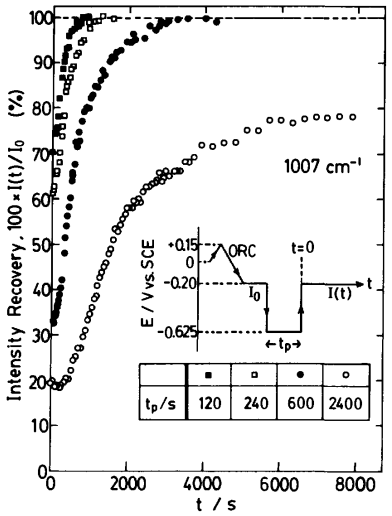

Fig. 4. Recovery of the pyridine SERS intensity observed by Cd stripping from the Ag electrode surface. The inset shows the potential programming.

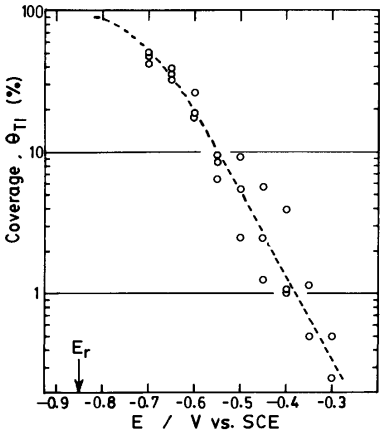

Fig. 5. Stationary Tl coverage on the electrode surface as a function of the electrode potential. $[Tl^+]=2.5\times10^{-5}$ M. E_r denotes the thermodynamic deposition potential.

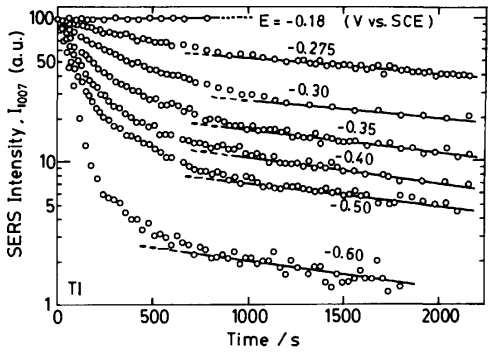

Fig. 6. Time courses of the pyridine SERS intensity after potential steps from 0.0 V to a series of negative values.

original SERS intensity only to *ca.* 80%. The non-recovered fraction (20%) agrees fairly well with that calculated from Fig. 2 by means of Eqs. 1 and 2. These results indicate that the first step in Eq. 1 is of quasi-reversible nature, while the second step is an irreversible decomposition, though we are not yet sure about the actual mechanisms for these processes. Under an assumption that the initial SERS-active sites are sparingly soluble surface Ag^+ complexes having pyridine and Cl^- as ligands,[6] we tentatively propose that the second step of the quenching corresponds to an electron transfer from neutral Cd, being a reduced entity, to a surface Ag^+ center resulting in the disintegration of the Ag^+ complex. This may be in line with an observation by Kester,[4] that deposition of Tl onto the SERS-generating Ag/BTA interface leads to vanishing of BTA molecules from the surface, as evidenced by Auger spectroscopy.

The remarkable slowness of the intensity recovery noted in Fig. 4 suggests that the first phase of the quenching involves, in addition to a simple association between Cd and A, another kind of surface process. For instance, diffusion of state B toward the interior of the electrode bulk (or slight alloying), which could render the Cd atoms resistant to stripping, may be a candidate. This problem is however beyond the scope of the present paper.

The fact that Eq. 3 apparently holds fairly well at Cd surface coverages down to 0.04, or *ca.* 5×10^{13} atoms cm^{-2}, suggests, together with the assumption made in deriving Eq. 3, that the surface concentration of the initial active site A is on the order of 10^{12}—10^{13} sites cm^{-2}. Since a full coverage of pyridine on Ag corresponds to *ca.* 3×10^{14} molecules cm^{-2}, this again confirms the conclusion that the surface population of the SERS-active sites is considerably low.[1-3]

UPD of Tl. A series of similar kinetic measurements have been carried out also for the SERS-quenching effect of underpotentially deposited Tl. The potential dependence of the surface coverage, $\theta_{Tl}(E)$, determined by a procedure described above, is shown in Fig. 5. This result corresponds to a polarization time of 120 s, but we confirmed that the value of θ_{Tl} levels off within 50—100 s, as in the case of Cd UPD. Figure 5 reproduces a well-known tendency[9] that the surface coverage in the UPD region approaches unity as the potential approaches the thermodynamic deposition potential, E_r, which is −0.85 V *vs.* SCE in the present case.

Figure 6 is a counterpart of Fig. 2 (top). The pyridine SERS intensity decays again through a biphasic process, with the time constant of the first phase being dependent on the potential, while that of the second phase being nearly constant. This again

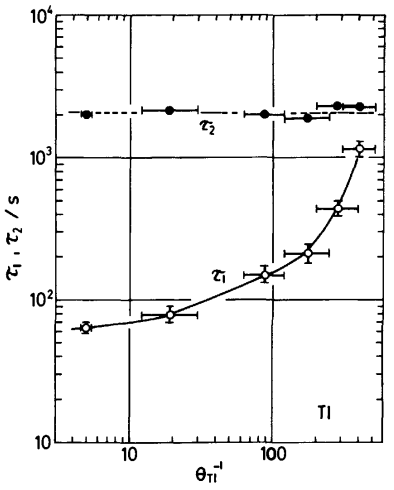

Fig. 7. Effect of θ_{Tl} on the values of τ_1 and τ_2.

suggests the occurrence of a sequential process as in Eq. 1. In comparison with the case of Cd UPD, the general quenching effect of Tl UPD is much more dramatic. For example, at E=−0.4 V, the stationary surface coverage of *ca.* 1% causes the SERS intensity loss of 93% in 2400 s (compare Figs. 5 and 6).

The biphasic decay profiles in UPD of Tl have also been successfully analyzed in terms of Eq. 2, and the τ_1 and τ_2 values thus derived are plotted in Fig. 7 against the reciprocal of θ_{Tl}. It is seen that the value of τ_2 is roughly constant at about 2000 s. The strong dependence of τ_1 on θ_{Tl} indicates that the first phase of quenching takes place *via* an interaction between the deposied Tl and the SERS-active sites. The non-linearity between τ_1 and θ_{Tl}^{-1}, however, suggests that the interaction is of more complicated nature than a simple one-to-one encounter process of the two surface species.

Two major differences were noted between deposited Cd and Tl in quenching the pyridine SERS. First, whereas the UPD of Cd caused a change in the spectrum as well as the intensity in the first phase of the quenching, such a spectral change was not observed by the UPD of Tl within experimental error. This is in contrast with the case of the SERS in the Ag/BTA system,[4] where both intensity and peak frequency underwent a change by UPD of Tl. This would probably reflect a difference in the extent of vibronic state perturbation by the attack of Tl between the two systems. Second, the SERS intensity, once quenched by the UPD of Tl, was hardly recovered by stepping the potential to a sufficiently positive value, irrespective of the holding time at the quenching potential. In the case of UPD of Cd, as stated above, the intensity could be recovered if the quenching had been limited to the first phase. This result suggests that the Tl atom, in an encounter complex such as B in Eq. 1, is bound to the initial SERS-active site so strongly that it apparently undergoes no oxidation within the time range of the present measurements (on the order of 1 h).

So far, the SERS-quenching effect of underpotentially deposited Tl has been reported on the Ag/pyridine[1,3] and Ag/BTA[4] systems. In the former system, and also in the present work, a surface Tl coverage on the order of 1% causes a drastic quenching. In contrast, the SERS signal in the latter system is affected by UPD of Tl only at relatively high surface coverages, and becomes noticeable at potentials negative of −0.5 V *vs.* SCE.[4] Such a difference could qualitatively be accounted for within the framework of the present scheme (Eq. 1), by making a reasonable assumption that there is a difference between the two systems in the stability of the SERS-active site against the attack of Tl. A significantly low value of the solubility product for the Ag^+–BTA salt ($10^{-13.6}$),[14] in comparison with that for the Ag^+–pyridine salt ($10^{-9.8}$), suggests that the strength of the Ag^+–BTA bond is higher than that of the Ag^+–pyridine bond.

The authors are grateful to Prof. Katsumi Niki, Faculty of Engineering, Yokohama National University, for his encouragements during this work, and to Mr. Hiroyuki Katoh for his participation in part of the experiments.

References

1) T. Watanabe, N. Yanagihara, K. Honda, B. Pettinger, and L. Moerl, *Chem. Phys. Lett.*, **96**, 649 (1983).
2) B. Pettinger and L. Moerl, *J. Electron Spectrosc. Relat. Phenom.*, **29**, 383 (1983).
3) T. E. Furtak and D. Roy, *Phys. Rev. Lett.*, **50**, 1301 (1983).
4) J. J. Kester, *J. Chem. Phys.*, **78**, 7466 (1983).
5) T. E. Furtak and R. K. Chang "Surface-Enhanced Raman Spectroscopy," ed by Plenum Press, New York (1981).
6) T. Watanabe, O. Kawanami, K. Honda, and B. Pettinger, *Chem. Phys. Lett.*, **102**, 565 (1983).
7) M. R. Philpott, F. Barz, J. G. Gordon II, and M. J. Weaver, *J. Electroanal. Chem.*, **150**, 399 (1983).
8) T. M. Cotton, D. Kaddi, and D. Iorga, *J. Am. Chem. Soc.*, **105**, 7462 (1983).
9) D. M. Kolb, "Advances in Electrochemistry and Electrochemical Engineering," ed by H. Gerischer and C. W. Tobias, Wiley, New York (1978), Vol. 11, 125—271.
10) G. Ayrault and G. Ehrlich, *J. Chem. Phys.*, **60**, 281 (1974).
11) K. Stolt, W. R. Graham, and G. Ehrlich, *J. Chem. Phys.*, **65**, 3206 (1976).
12) G. L. Kellogg, T. T. Tsong, and P. Cowan, *Surface Sci.*, **70**, 485 (1978).
13) D. W. Bassett and P. R. Webber, *Surface Sci.*, **70**, 520 (1978).
14) J. Pourradier, A. Paillotet, and C. R. Berry, "The Theory of the Photographic Process," ed by T. H. james, Macmillan, New York (1977), 4th Ed., 1—12.

A Method for Preparing A Large Sized, Uniform and Stable Built-up Film of ^{109}Cd Icosanoate as A Radioactive Source by Utilization of an Extremely Small Amount of Substrate Solution

Makio IWAHASHI,* Fujio NAITO,† Norifumi WATANABE, Tsutomu SEIMIYA, Naotake MORIKAWA,** Norio NOGAWA,** Takayoshi OHSHIMA,*** Hirokane KAWAKAMI,*** Kumataro UKAI,*** Isao SUGAI,*** Seiichi SHIBATA,*** Takahiro YASUDA,*** Yoshihiko SHOJI,†† Takeshi SUZUKI,† Teruyasu NAGAFUCHI,† Hiroshi TAKETANI,† Takeshi MATSUDA,††† Yasutaka FUKUSHIMA,††† Manabu FUJIOKA, and Kazuo HISATAKE

Department of Chemistry, Faculty of Science, Tokyo Metropolitan University, Setagaya-ku, Tokyo 158
***Radioisotope Center, The University of Tokyo, Bunkyo-ku, Tokyo 113*
****Institute for Nuclear Study, The University of Tokyo, Tanashi, Tokyo 188*
(Received February 5, 1985)

A stable radioactive source *in vacuo* was obtained by a modified horizontal lifting method of Langmuir-Blodgett (L/B) film. In spite of the slight consumption of the substrate solution (only 2—2.5 ml) for preparing a 15 mm×25 mm sized L/B film containing four molecular layers of ^{109}Cd icosanoate, the deposition of the film was complete. The reliability of the deposited films by this method was confirmed by their radioactivities, deposition ratios and autoradiographs. The condition to obtain a larger sized homogeneous L/B film (20—25 mm×102 mm) was also examined. Two or four molecular layers of nonradioactive Cd icosanote deposited on the L/B film of ^{109}Cd icosanoate did not influence the intensity of the γ-ray of 88.0 KeV. Concequently, it is possible to obtain the high radioactive source by the deposition of the multilayers of ^{109}Cd icosanoate. Spectra of L_2 and L_3 conversion electrons from the ^{109}Cd in its built-up film were also determined. In conclusion, the present depositing method for the L/B film is excellent for the manufacturing the radioactive source and thought to be also applicable for the deposition of other valuable materials.

A Langmuir-Blodgett (L/B) multilayer film is superior to the ordinary vacuum deposition films in the homogeneity of the lateral direction and the uniformity of the thickness together with other advantages of their easy and reliable controllability. The L/B film of soap of a radioactive metal is, therefore, expected to be an excellent radioactive source. There are, however, two problems for the preparation of a high radioactive L/B film by the commonly used depositing method, *i.e.*, the vertical dipping method.[1] One big problem is that a great amount of radioisotope is necessary by the method. Another problem is the contamination by radioactive material on the undesirable side of the substrate plate. To reduce the amount of the radioactive material and prevent the contamination of the back side of the plate in its built-up process, a modified horizontal lifting method was devised and applied to the deposition of ^{109}Cd icosanoate monolayer, combining with an extremely shallow Teflon trough whose inside was treated with oxygen plasma to be hydrophilic. To make sure the reliability of this method, the linear relationship was confirmed between the radioactivity and the deposited amount of the source, and the uniformity of the built-up films was established by the autoradiography. The stability of the source under high vacuum and the influence of the film thickness on the intensity of the γ-ray from ^{109}Cd nucleous were also examined. The built-up film of ^{109}Cd icosanoate was utilized finally as a radioactive source in vacuum.

Experimental

A sample of icosanoic acid (purity of 99.5%, Fulka AG. Swizerland) was dissolved in benzene to make a spreading solution of 1×10^{-3} mol dm^{-3}. 500μCi and 5mCi of carrier-free cadmium-109 were supplied from Amersham (Buckinghamshire, England) as $^{109}CdCl_2$ in 0.1 M HCl. After the isotopic dilution with $CdCl_2$ and the removal of the HCl by distillation from the solutions, the aqueous solutions of radioactive $CdCl_2$ (specific activity of 0.9 or 445mCi mmol^{-1}) were prepared. The pH of the solution was adjusted to be 7—7.8[2] by the addition of a small amount of the aqueous solution of NaOH (electronic grade, Kanto Chemical Co., Tokyo). Iron(III) octadecanoate (the purest grade of Tokyo Kasei Industry Co., Tokyo) was used for the pretreatment of the surfaces of aluminium plates (20 or 25 mm×102 mm×1 mm) and resistive substrate plates (15 mm×25 mm×1 mm or 40 mm×25 mm×1 mm, Japan Fine Co., Tokyo) which were made from a mixture of ruthenium oxide with glass and printed on alumina plates. Water for the underlying ^{109}Cd solution was triply distilled, the second distillation being from alkaline permanganate, and was contained in a very shallow Teflon trough (15 mm×120 mm×0.5 mm or 1mm, 40 mm×200 mm×1 mm, or 20 or 25 mm×280 mm×1 mm) whose inside was hydrophilic by the glow discharge in an oxygen atmosphere,[3] and whose rims remained hydrophobic by protective adhesive tapes. The hydrophilic property of the inside of the trough is very important because an aqueous

† Present address: Department of Applied Physics, Tokyo Institute of Technology, Meguro-ku, Tokyo 152.

†† Present address: Cycrotron Radioisotope Center, Tohoku University, Sendai 982.

††† Present address: National Laboratories for High Energy Physics, Ouhocho, Tsukuba-gun, Ibaragi 305.

†††† Present address: Faculty of General Education, Jissen Women's University, Hino, Tokyo 191.

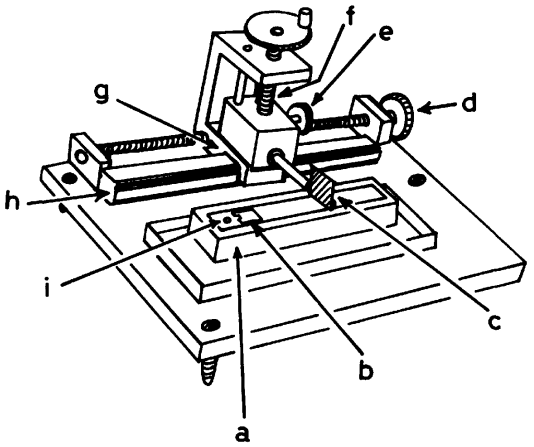

Fig. 1. Apparatus for the deposition of Langmuir-blodgett film. **a** denotes the Teflon trough whose inside is hydrophilic; **b**, Floating barrier (thin mica) coated with paraffin, having a small check at its end for the convenience of setting a small amount of piston oil; **c**, Substrate plate for built-up film; **d**, Wheel for moving the slide unit; **e**, Wheel for turning the substrate plate which was rotated by a hand or a mechanical operation with a motor and gears; **f**, Lifting screw; **g**, Slide unit; **h**, Track rail; **i**, 9-octadecenoic acid drop as a piston oil.

solution on a hydrophobic surface has a large contact angle and does not spread fully on the surface. If the inside of the shallow trough is hydrophobic, a small amount of the aqueous solution, therefore, can not fill the trough. Only 2—2.5 ml of solution was required to fill the small hydrophilic trough and 14—16 ml for the another large troughs. After sweeping the solution surface by a hydrophobic glass barrier treated with dimethyldichlorosilane,[4] a thin mica plate (13.5 mm×15 mm×0.1 mm, 38 mm×50 mm×0.1 mm, 18 mm×25 mm×0.1 mm or 23 mm×30 mm×0.1 mm) coated with paraffin[5] was placed on the surface and used as a movable barrier. As shown in the Fig. 1, the mica plate (b) had a small check at its one end for the convenience of setting a small amount of piston oil drop. The piston oil drop should not contact with the movable barrier because such a contact prevents sometimes the smooth movement of the barrier. The oil drop was set therefore in contact with the end wall of the trough. The floating barrier can move smoothly by the repulsion[6] between the hydrophilic trough and the hydrophobic ends of the movable barrier. A thin Teflon plate or a paper plate coated with paraffin was not suitable for the movable barrier in such the shallow trough because of its warping. The monolayer of ^{109}Cd icosanoate was deposited at the surface pressure of 29.5 mN m^{-1} with 9-octadecenoic acid (the purist grade of Merck AG., Darmstadt, German) using an apparatus shown in Fig. 1. After touching the substrate plate almost horizontally and gently on the monolayer surface from its one end, the plate was turned gradually by a hand or a mechanical operation with a motor and gears, lifted and removed finally from the surface (see Fig. 2). Two molecular layers of the ^{109}Cd icosanoate were deposited on the substrate plate by this process. The repetition of this process produced an additional deposition of two molecular layers. In order to achieve the

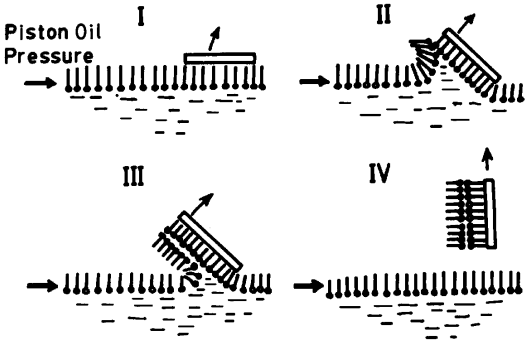

Fig. 2. Scheme of the deposition process of ^{109}Cd icosanoate monolayer on a substrate plate.

complete deposition of the rigid monolayer onto the substrate plate, we should set the plate as close as possible to the end of the floating mica plate: Its possible smallest distance from the mica plate is apparently two times of the length of the substrate plate. This depositing method giving Y-film resembles the horizontal lifting method,[7] which gives X-film, in the first contact of the plate with the monolayer and the vertical dipping method during the gradual turning and removing of the plate. The radioactivity (characteristic γ-ray of 88.032 KeV of ^{109}Cd) of the L/B film was detected with a coaxial Ge (Li) detector (ORTEC Inc. Co., Oak Ridge, USA); a known amount of ^{109}Cd sample was used for the calibration of the radioactivity. LKB2208 Biofilm (Amuko Co. Ltd, Tokyo) was used for the autoradiography of the built-up film obtained.

The stability of the L/B film *in vacuo* was confirmed by the following method. An aluminum plate was fixed in front of the L/B film of the ^{109}Cd icosanoate (the specific activity of 0.9 mCi/mmol) with a 1 mm gap; the whole source, including the plate and the ^{109}Cd film, was set in a vacuum chamber and evacuated to a pressure of 10^{-3} Pa at room temperature (*ca.* 298 K) for a week. After the experiment, the radioactivities of the L/B film and the Al plate were detected, respectively.

Spectra of L_2 and L_3 conversion electrons (84.508 and 84.681 KeV,[8] respectively) from ^{109}Cd source prepared was measured with an INS double forcusing $\pi\sqrt{2}$ air-core β-ray spectrometer[9] and a position sensitive single-wire proportional counter[10] which had the position resolution of 1.3 mm. The momentum resolution of the counter was 0.04%.

Results and Discussion

Figure 3 shows the relationship between the relative radioactivity, R_r, of the two molecular layers of ^{109}Cd icosanoate deposited on the 15 mm×25 mm sized resistive plate and the concentration of the underlying ^{109}Cd solution. The relative radioactivity is defined as the following equation,

$$R_r = \frac{R_{obs}}{R_c}, \quad (1)$$

where R_{obs} denotes the experimental value of radioactivity and R_c, the calculated value assuming the stoichiometric bonding of a ^{109}Cd ion and two icosanoic acid molecules in the deposited L/B film. The characteristic S-shaped curve was obtained and saturated to unity above at the concentration of 1×10^{-4} mol dm.$^{-3}$ The result agrees with that by Petrov *et al.*[2] using the neutron activation analysis of cadmium species. This radioactive saturation indicates that the binding between cadmium ion and the monomolecular film of the fatty acid is complete.

We used therefore the ^{109}Cd solution of 1.2×10^{-4} mol dm^{-3} as the substrate solution for the further experiment.

Figure 4 shows the relationship between the radioactivity and the number of monolayers of ^{109}Cd icosanoate deposited on the resistive plate. A good linearity was obtained. In this fugure the full diamond, whose value is calculated from the specific activity of the $^{109}CdCl_2$, the molecular area of the icosanoic acid on the $CdCl_2$ solution of 1.2×10^{-4} mol dm^{-3} at the pressure of 29.5 mN m^{-1} and the number of layers, agrees exactly with the experimental result. A simular good linearity was observed when using the large resistive plate (40 mm×25 mm),

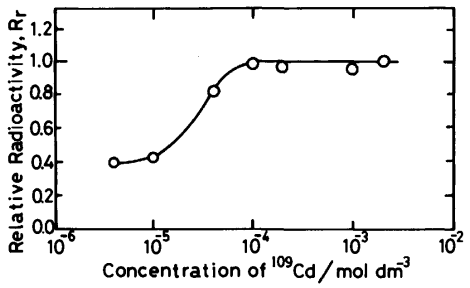

Fig. 3. The relationship between the relative radioactivity, R_r, of the two-molecular layers of ^{109}Cd icosanoate deposited on the 15 mm×25 mm sized resistive plate and the concentration of the underlying ^{109}Cd solution.

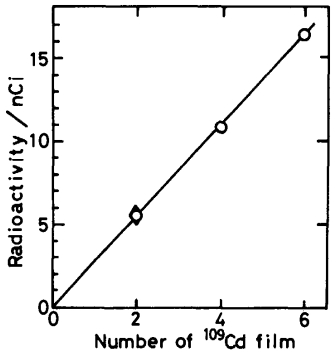

Fig. 4. Relationship between the radioactivity and the number of ^{109}Cd icosanoate monolayers deposited on the 15 mm×25 mm sized resistive plate at 298 K. A full diamond denotes the calculated value.

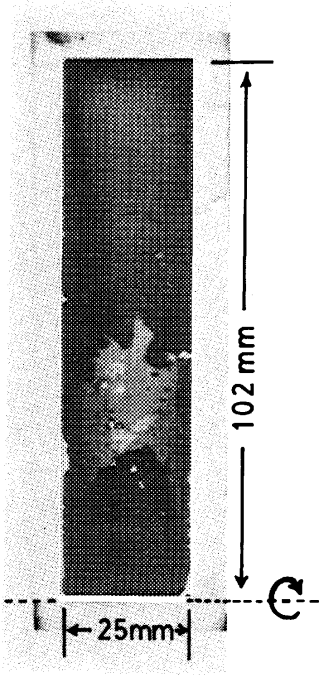

Fig. 5. Autoradiograph of the built-up film of two layers of ^{109}Cd icosanoate monolayer deposited on a 25 mm×102 mm sized almuminium plate. Dotted line denotes the rotation axis of the substrate plate. The dark part expresses the depostion of two layers of monolayers and grayish part, one layer.

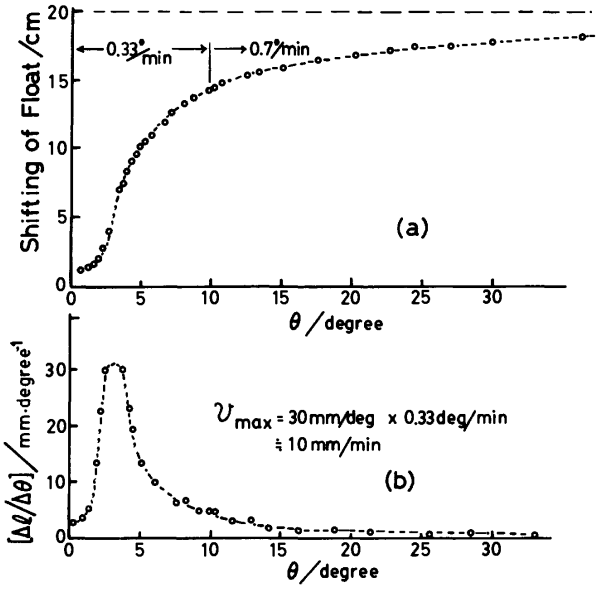

Fig. 6. (a) A typical relationship between a shift of the movable float, l, and an angle, θ, of the turning substrate plate (102 mm in length) to water surface. (b) The relationship between a slope of the tangent to the above curve of (a) and an angle, θ. The largest shift velocity, V_{max}, of the float was obtained to be about 10 min/min at $\theta=ca.$ 3°.

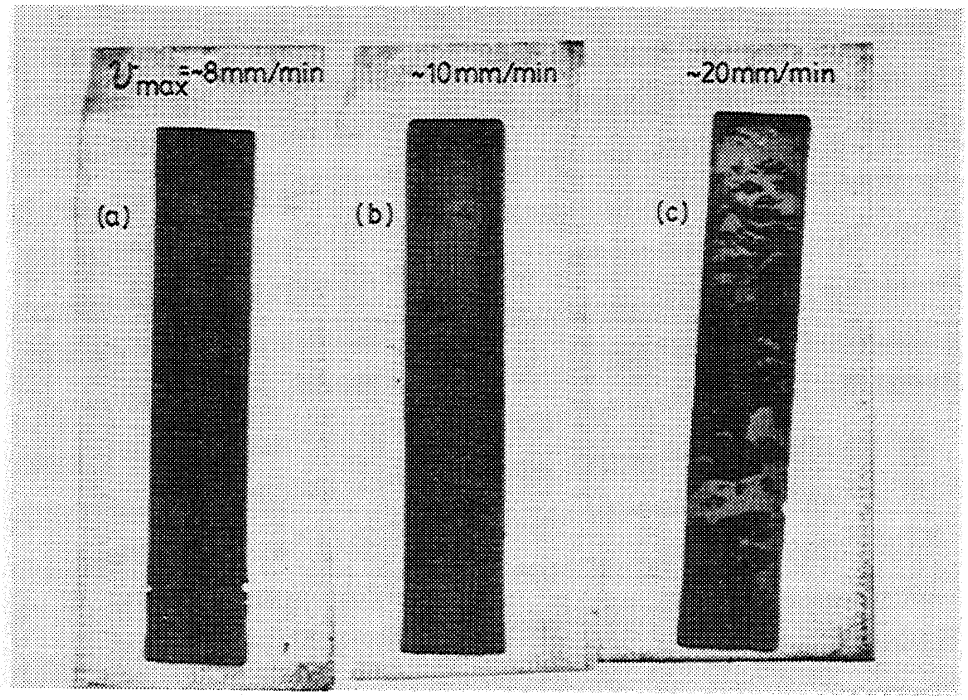

Fig. 7. Autoradiographs of built-up films of two-molecular layers of ^{109}Cd icosanoate deposited on 20 mm × 102 mm sized aluminium plates by various V_{max} values. (a) $V_{max} = \approx 8$ mm min^{-1}. (b) $V_{max} = \approx 10$ mm min^{-1}. and (c) $V_{max} = \approx 20$ mm min^{-1}.

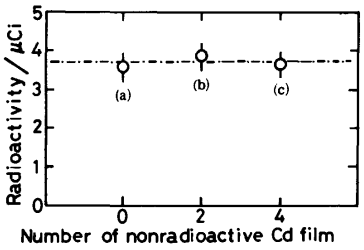

Fig. 8. Radioactivities of three samples of ^{109}Cd icosanoate (two-molecular layers) deposited on the substrate plates. **b** and **c** express the values of radioactivity for the samples containing the additional two and four layers of nonradioactive Cd icosanoate monolayer deposited on the radioactive two layers, while **a** is for the original sample.

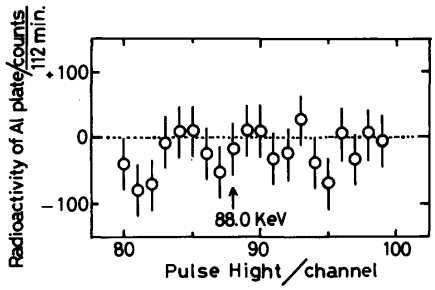

Fig. 9. Radioactivity of Al plate; arrow expresses the peak position of the characteristic γ-ray of ^{109}Cd (88.0 KeV). One channel in the abscissa denotes 1 KeV.

the wide trough and the higher specific active $^{109}CdCl_2$ subsolution. These evidences suggest that the deposition of the ^{109}Cd icosanoate monolayer on the substrate plate was perfectly achieved by this method. This suggestion has been also confirmed by the facts that the trasfer ratio of the ^{109}Cd icosanoate monolayer on the substrate plate was exactly unity and that the autoradiographs taken for these built-up films (15 mm×25 mm or 40 mm×25 mm) deposited by manual operation were entirely uniform. For the larger substrate plate (102 mm in length), however, the deposited film, especially the second layer of the film, peeled off the plate (see Fig. 5) regardless of a careful turning of the plate by the manual operation. Thus we adopted a motor and gears to rotate the substrate plate with a constant angular velocity. Figure 6a shows a typical example of the relationship between a shift of the movable float, l, and an angle, θ, of the turning substrate plate (102 mm in length) to the water surface. By θ being 10° the angular velocity was regurated to be 0.33° min^{-1} and, beyond the angle, 0.7° min^{-1}. Up to 30° the most monolayer (*ca.* 90%) was transfered from water surface to the substrate plate.

A slope of the tangent to the l—θ curve is plotted against θ in Fig. 6b. We can find that the float shifts most significantly at *ca.* 3°. From the $\Delta l/\Delta\theta$ value at

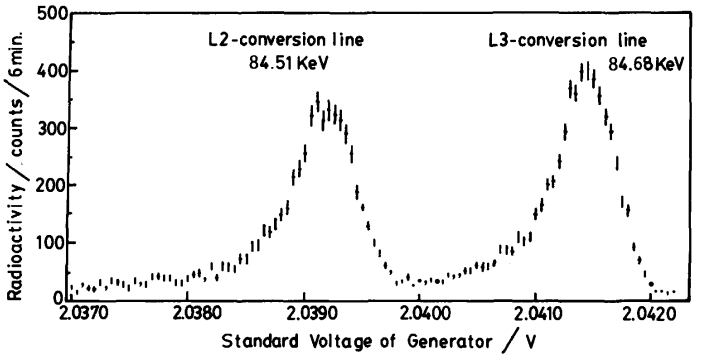

Fig. 10. A spectrum of 88 KeV-L_2 and L_3 conversion electrons (84.508 and 84.681 KeV) from ^{109}Cd source obtained. The source thickness was two-molecular layers; the source activity, 3.7 μ Ci; the source area, 40 mm × 25 mm. SVG (standard voltage of generator[9]) step: 0.00005/V.

this angle and the constant angular velocity (0.33°/min), the largest shift velocity (V_{max}) of the float was calculated to be *ca.* 10 mm min^{-1}. The V_{max} is defined in general by the length of the substrate plate and the angular velocity. The uniformity of the autoradiographs and the deposition ratios of the several built-up films were thus examined to their corresponding V_{max} values. The monolayers were deposited completely at V_{max}<10 mm min^{-1} while the deposited monolayer often peeled off the plate at V_{max}> 10 mm min^{-1}. Several examples are shown in Fig. 7.

In order to obtain a high radioactive source of the L/B film, it is necessary to deposit many number of radioactive molecular film. For such the source, the absorption of the radiation by the films themselves comes into a problem. Figure 8 shows the radioactivities of three samples of the two molecular layers of ^{109}Cd icosanoate (sp. ac. 445 mCi mmol^{-1}) deposited on 40 mm×25 mm sized resistive plate. The second (b) and the third (c) samples contain the additional two and four layers of nonradioactive Cd icosanoate monolayer on the radioactive two hayers, respectively. These three values are almost equal to each other within the experimental error. For the γ-ray of 88.0 KeV, therefore, the influence of its absorption seems to be almost negligible. In addition the result of these constant radioactivities suggests that the additional deposition of the nonradioactive Cd monolayers does not cause the isotope exchange between the ^{109}Cd in the deposited monolayers and the nonradioactive Cd ion in the subsolution in the short period of the additional depositing process (*ca.* 12—3 min).

For the application of the L/B film of ^{109}Cd icosanoate as the radioactive source, its stability *in vacuo* is essential, because the radioactive sources are often used under high vacuum. The test of the stability of the L/B film of ^{109}Cd icosanate (two-molecular layers) *in vacuo* was, threrefore, carried out. After the one week evacuation of the sample at 10^{-3} Pa any reduction of the radioactivity of the L/B film was not observed and the radioactivity was also not detected from the Al plate as shown in Fig. 9. Futhermore, the contents in a liquid nitrogen trap did not show any radioactivity of ^{109}Cd. The stability of the L/B film *in vacuo* was thus confirmed.

Figure 10 shows a spectrum of L_2 and L_3 conversion electrons from the two layers of ^{109}Cd icosanoate (40 mm×25 mm, 3.7μCi). Two peaks due to the above conversion electrons, whose energies are very close each other, were sharp and apparently distinguishable each other. The momentum resolutions obtained from the half-value widths of the peaks were 0.029 and 0.030% for the peaks of L_2 and L_3 conversion electrons, respectively.

The depositing method for the L/B film is excellent, therefore, for preparing the radioactive source and thought to be also applicable for the deposition of other valuable materials.

The authers wish to express their thanks to Prof. Kiyoshige Fukuda and Dr. Hiroo Nakahara of Saitama University for their helpful suggestions and discussions and to Mr. Masateru Kasuya and Mr. Takeo Fujino of INS workshop in The University of Tokyo for their part in constructing the apparatus for the built-up of monolayers. The present work was partially supported by a Grant-in Aid for Scientific Research No. 57460010 from the Ministry of Education, Science and Culture. We thank this supporting agency for making this study possible.

References

1) K. B. Blodgett, *J. Am. Chem. Soc.*, **56**, 1007 (1935); K. B. Blodgett and I. Langmuir, *Phys. Rev.*, **51**, 964 (1939).

2) J. G. Petrov, I. Kuleff, and D. Paltikanov, *J. Colloid Interface Sci.*, **88**, 29, (1982).

3) Osada, *Kagaku To Kogyo*, **36**, 759 (1970).

4) M. Iwahashi, *Hyomen*, **20**, 13 (1982).
5) K. Fukuda and T. Ishii, "Shin Jikken Kagaku Koza," ed by H. Inokuchi, Maruzen Co., Tokyo (1975), Vol. 18, p. 443.
6) J. J. Bikerman, "Physical Surfaces," Academic Press, New York (1970), p. 39.
7) I. Langmuir and V. J. Schaefer, *J. Am. Chem. Soc.*, **60**, 1351 (1938); K. Fukuda, H. Nakahara, and T. Kato, *J. Colloid Interface Sci.*, **54**, 430 (1976).
8) O. Dragoun, V. Brabec, M. Rysavy, J. Plch, and J. Zderadicka, *Z. Phys.*, **A279**, 107 (1976).
9) K. Hisatake, *Genshikaku Kenkyu*, **13**, 21 (1968).
10) Y. Fujita, H. Kawakami, and M. Hosoda, *Nucl. Instru. and Meth.* **196**, 271 (1982).

Complex Formation in Cationic Dye-Organic Anion Systems in Aqueous Solution

Sanyo HAMAI
Department of Physics, Miyazaki Medical College, Kiyotake, Miyazaki 889-16
(Received February 12, 1985)

The interaction between a cationic dye, Methylene Blue (MB), and organic anions (1-naphthalenesulfonate, 2-naphthalenesulfonate, 1-naphthaleneacetate, 2-anthracenesulfonate, 2,7-naphthalenedisulfonate, and 1,3,6-naphthalenetrisulfonate) in aqueous solution has been investigated by means of absorption and fluorescence spectra. The red shifts of the absorption and fluorescence spectra of MB caused by the addition of the organic monoanion are attributed to the 1:1 complex formation between MB and the organic anion. The thermodynamic quantities as well as the equilibrium constants for the complex formation have been determined. From the finding that the absorption spectrum of MB is not affected by the addition of ethanesulfonate, it is concluded that the complex formation is due to the interaction between the MB cation and the aromatic ring in the organic anion. The addition of polyanion (*e.g.*, 2,7-naphthalenedisulfonate) in the low-concentration range accelerates the dimerization of MB; whereas, in the high-concentration range, the formation of the 1:1 complex rather than the MB dimer is dominant. Studies on the complex formation with monoanions have also been made for Rhodamine 6G, Pyronine G, Safranin T, and Crystal Violet, and similar results to that for MB have been obtained.

Studies regarding the interaction between organic cations and organic ions are roughly divided into four categories. The first is the area related to the self-association of a dye in aqueous solution.[1-7] This association is due to an interaction between the organic ions of the same kind having a positive charge. Since the concentration ratio of the dimer to the monomer of the dye increases with an increase in the dye concentration, the electronic absorption of the dye does not follow the Beer-Lambert law.

The second is that related to the adsorption of a cationic dye on the surface of an anionic micelle, an anionic lipid membrane, or a microemulsion.[8-13] This interaction is attributed to the electrostatic attraction between the cationic dye and the anionic micelle, *etc.* Since the adsorption also induces a change in the absorption and/or fluorescence spectrum of the dye, the spectral change can be used for the determination of the critical micelle concentration.[8]

The third is related to a phenomenon known as metachromasy which is observed when an anionic polymer is added into a dye solution.[14-19] This phenomenon is accompanied by a shift of the first electronic absorption band to shorter wavelengths. Inorganic anions have also been reported to cause metachromasy.[20] Metachromasy is mainly elucidated either by the association of dye under the influence of the anionic polymer or by the interaction of dye with added anion.

The fourth is that related to a complex formation between an organic cation and an organic anion. By the addition of *N*-hexadecylpyridinium chloride (below its critical micelle concentration), a solution of 2-naphtholate becomes pale yellow and its fluorescence is quenched.[21] Both the appearance of the color and the fluorescence quenching have been explained in terms of complex formation.

Gicquel *et al.* have studied the complex formation of Crystal Violet with sulfonated azo derivatives by means of resonance Raman and electronic absorption spectra.[22] They suggested that the blue shift of the absorption band of Crystal Violet is related to the approach of the sulfonate group in the azo dye to the central carbon in Crystal Violet.

Solvent effects on the charge-transfer band energies of organic cation–organic anion complexes have been investigated by Beaumont and Davis.[23] Compared with organic cation–iodide complexes, the charge-transfer bands of organic cation–organic anion complexes are notably less solvent sensitive, this insensitivity being particularly marked in cation–neutral molecule complexes.

The pressure effect on the complex formation between 1-methyl-3-(methoxycarbonyl)pyridinium cation and 8-chlorotheophyllinate anion has been studied by Williams.[24] The complex formation of methylviologen with a porphyrin derivative has been pointed out.[25]

Organic charge-transfer salts composed of an organic cation (pyrylium or thiopyrylium) and an organic anion (1,1,3,3-tetracyanopropenide or tricyanomethanide) have been investigated by means of the absorption spectra.[26] The 1,2,3,4,5-pentakis-(methoxycarbonyl)cyclopentadienide anion is also known to form charge-transfer salts with tropylium, 2,4,6-trimethylpyrylium, *N*-methylpyridinium cations, *etc.*[27]

In spite of these studies, there is little information concerning the interaction between organic cations and organic anions. Thus, in selecting cationic dyes as organic cations, we have investigated an interaction between the dyes and the organic anions, naphthalenesulfonates, anthracenesulfonate, *etc.* in

aqueous solutions.

Experimental

Methylene Blue (MB), purchased from Wako, was recrystallized twice from water.[28] Rhodamine 6G obtained from Tokyo Kasei, Pyronine G from Chroma, and Safranin T from Tokyo Kasei were recrystallized twice from ethanol. Crystal Violet from Tokyo Kasei was recrystallized twice from water. Sodium 1-naphthalenesulfonate (1NS) from Tokyo Kasei and sodium 2-naphthalenesulfonate (2NS) from Wako were recrystallized twice from a water–ethanol mixture. Sodium 1-naphthaleneacetate (1NA) from Wako was recrystallized twice from a 1-butanol–hexane mixture. Sodium 2-anthracenesulfonate (2AS) was synthesized from sodium anthraquinone-2-sulfonate,[29] and recrystallized three times from water. Disodium 2,7-naphthalenedisulfonate (NDS) and trisodium 1,3,6-naphthalenetrisulfonate (NTS) were purchased from Tokyo kasei, and recrystallized twice from a water–ethanol mixture.

Absorption spectra were measured with a Hitachi 124 or a Shimadzu 260 spectrophotometer. The fluorescence spectra were recorded on a Shimadzu RF-501 spectrofluorometer equipped with a cooled Hamamatsu R-943 photomultiplier. The spectral response of the spectrofluorometer was determined by the previous method.[30] Measurements were made at 25 °C unless otherwise stated. In order to avoid the concentration change of a dye caused by adsorption on a glass surface, all the glass wares (volumetric flasks, pipets, *etc.*) used for sample preparations were soaked with a dye solution, and then rinsed with water immediately before use.

Results and Discussion

Complex Formation of Methylene Blue (MB) with Sodium 2-Naphthalenesulfonate (2NS). Figure 1 shows the absorption spectra of 10^{-5} M (1 M= 1 mol dm^{-3}) aqueous solutions of MB with varying concentrations of 2NS. The absorption maximum of MB shifted to the red as the concentration of 2NS increased. Below a 2NS concentration of 5×10^{-3} M, an isosbestic point is observed at 680 nm. The spectral change presented in Fig. 1 is attributed to the 1:1 complex formation between MB and 2NS. The possibility that such a spectral change is caused by a change in pH or ionic strengths of the sample solutions can be ruled out from the findings that nearly the same spectral change was observed for buffered solutions at a pH 6.7 (0.033 M potassium dihydrogenphosphate–0.033 M disodium hydrogenphosphate) or solutions containing 0.1 M NaCl. Although the MB dimer exists even at a concentration as low as 10^{-5} M, the concentration ratio of the MB dimer to the MB monomer is calculated to be only 1.5% from the data of the equilibrium constant for the dimerization of MB.[3] Therefore, the effect of the MB dimer on the concentrations of the MB monomer and the complex can be neglected under the conditions of the low concentration of the complex. This explains the appearance of the isosbestic point in the absorption spectra of the MB solutions containing 2NS below 5×10^{-3} M.

The absorption spectrum of MB did not change by the addition of sodium ethanesulfonate up to 0.1 M. This indicates that the interaction between MB and 2NS to form the complex is that between an MB cation and a naphthalene ring in 2NS rather than that between an MB cation and a sulfonate group in

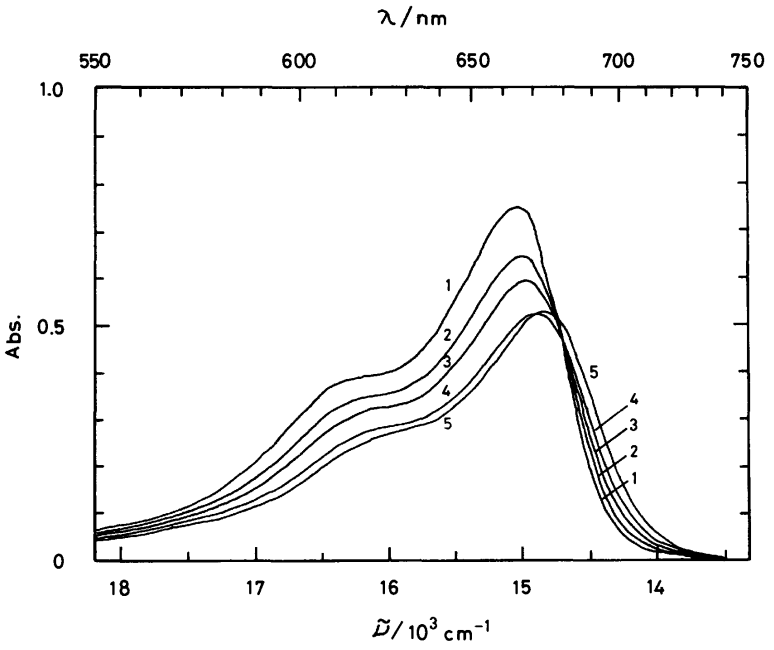

Fig. 1. Absorption spectra of MB (10^{-5} M) in aqueous solution in the presence of 2NS. Concentration of 2NS: 1, 0 M; 2, 10^{-3} M; 3, 2×10^{-3} M; 4, 5×10^{-3} M; 5, 10^{-2} M.

2NS although the attractive force between an MB cation and a sulfonate group may play an important role in the early stage of the complexation. On the other hand, for the complexes formed between Crystal Violet and sulfonated azo derivatives, it has been suggested that the central carbon in Crystal Violet interacts with the sulfonate group in the azo dye.[22] As mentioned above, the maximum of the absorption spectrum of Crystal Violet is shifted to the blue region in contrast to the red shift of the absorption maximum in the MB-2NS system.

When the existence of the dimer of MB is ignored, the absorption-spectrum change can be analyzed by the following equation:[31]

$$\frac{[MB]_0}{A-A_0} = \frac{1}{\varepsilon_1-\varepsilon_0} + \frac{1}{(\varepsilon_1-\varepsilon_0)K'}\frac{1}{[2NS]}, \quad (1)$$

where A and A_0 are the absorbances in the presence and absence of 2NS, $[MB]_0$ is the initial concentration of MB, ε_1 and ε_0 are the molar absorption coefficients of the 1:1 complex, MNS, and MB, K' is the equilibrium constant for the formation of MNS under the assumption of neglecting the MB dimer, and [2NS] is the initial concentration of 2NS. A plot of $[MB]_0/(A-A_0)$ *vs.* 1/[2NS] at 660 nm is shown in Fig. 2 (line (a)). A straight line is obtained with the equilibrium constant $K'=340\ M^{-1}$. In order to evaluate the more precise value of the equilibrium constant, we must take into account the existence of the MB dimer. When such a consideration is made, Eq. 1 becomes

$$\frac{[MB]+[MNS]}{A-A_0'} = \frac{1}{\varepsilon_1-\varepsilon_0} + \frac{1}{(\varepsilon_1-\varepsilon_0)K}\frac{1}{[2NS]}, \quad (2)$$

where [MB] and [MNS] are the concentrations of the MB monomer and MNS, A_0' is the calculated absorbance of [2NS] under the assumption that MNS thoroughly dissociates to MB and 2NS without a variation of the concentration of the MB dimer, and K is the equilibrium constant for the formation of MNS. A_0', [MB], and [MNS] were calculated using the K' value estimated from a plot of Eq. 1 and the literature value of the equilibrium constant for the dimerization of MB.[3] A plot of $([MB]+[MNS])/(A-A_0')$ *vs.* 1/[2NS] at 660 nm is shown in Fig. 2 (line (b)). The plot for Eq.2 also yields a good straight line. From the intercept and the slope, K was determined to be $400\ M^{-1}$, about 15% larger than K' ($=340\ M^{-1}$). Furthermore, we tried to construct a plot for Eq. 2 using K in place of K' for the calculations of A_0', [MB], and [MNS]. However, the new value of K, thus obtained, was identical with the previous value of K obtained by the use of K'.

In order to apply an alternate method which requires no correction for the MB dimer formation, we used a dilute MB solution containing only a negligible amount of the MB dimer, although the experimental error became larger owing to the smaller absorbance of the dilute solution. For a 2×10^{-6} M MB solution, the change in the absorp-

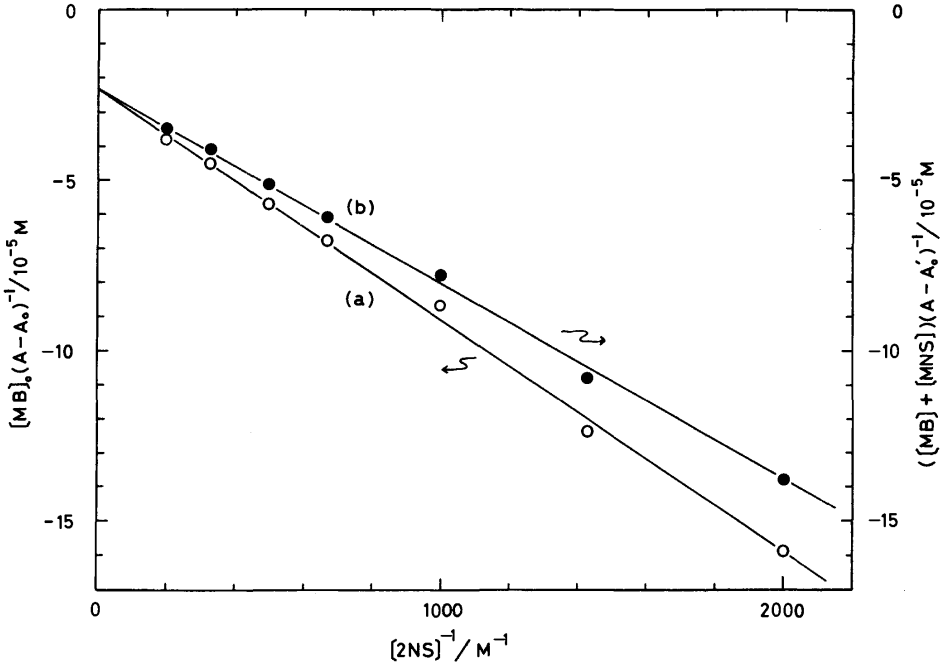

Fig. 2. (a) Plot of $[MB]_0/(A-A_0)$ *vs.* 1/[2NS] at 660 nm. (b) Plot of $([MB]+[MNS])/(A-A_0')$ *vs.* 1/[2NS] at 660 nm.

tion spectrum with the addition of 2NS was very similar to that for the 10^{-5} M MB solution. The equilibrium constant (=410 M^{-1}) evaluated from the absorption-spectrum change for the 2×10^{-6} M solutions was in excellent agreement with that of the 10^{-5} M solutions.

For the fluorescence measurements, 2×10^{-6} M solutions of MB were used to eliminate the reabsorption of fluorescence by the dye. Figure 3 shows the fluorescence spectra of MB in the absence and presence of 2NS which are normalized at the intensity maxima. With the increase in the 2NS concentration, the fluorescence intensity decreases accompanied by the red shift of the spectrum. Such changes in the fluorescence spectrum as well as the absorption spectrum are due to the complex formation between MB and 2NS. From the dependence of the fluorescence intensity on the 2NS concentration, the equilibrium constant for the complex formation was estimated by a similar method to that employed in the absorption study.[31] The equilibrium constant thus obtained is 370 M^{-1}, which agrees reasonably well with those obtained from the change in the absorbance both for the 2×10^{-6} and 10^{-5} M MB solutions. The equilibrium constants determined from the measurements of the absorbance and fluorescence intensity correspond to those in the electronic ground state and the excited state of MB, respectively. The good agreement between the equilibrium constants in the ground and excited state arises from the shortness of the fluorescence lifetime of MB.[32]

Temperature Dependence of the Equilibrium Constant. The temperature dependence of the equilibrium constants obtained from the measurements of the absorption and the fluorescence was examined over a temperature range from 3 to 43 °C. These results are shown in Fig. 4. Good straight-line relationships are obtained with the same slope and intercept for both methods. The enthalpy change ΔH and the entropy change ΔS for the complex formation are determined to be -28 kJ mol^{-1} and -46 J K^{-1} mol^{-1}, respectively.

The positive value of ΔS has been reported for the dimerization of Rhodamine B[33,34] in contrast to the negative value of ΔS usually evaluated for the aggregation of two molecules.[35-37] Generally, ΔS for the complex formation can be divided into two parts, ΔS_c and ΔS_s. Here, ΔS_c is the entropy change for the complexation which does not involve the succeeding reorientation process of solvent molecules, and ΔS_s is the entropy change for the reorientation of solvent molecules immediately after the association between two species. Because an MB cation associates with a negatively-charged 2NS molecule to form a neutral complex MNS, solvating water molecules surrounding an MNS complex may be expected to orient more randomly than those surrounding an uncomplexed, charged MB or 2NS molecule. Such a deduction leads to a positive value of ΔS_s. Our experimental result provides a negative value of ΔS for the complex formation. The implication is that the negative value of ΔS_c may prevail over the positive value of ΔS_s in the MB-2NS system, resulting in a negative value for the net ΔS.

Complex Formation of MB with Other Organic

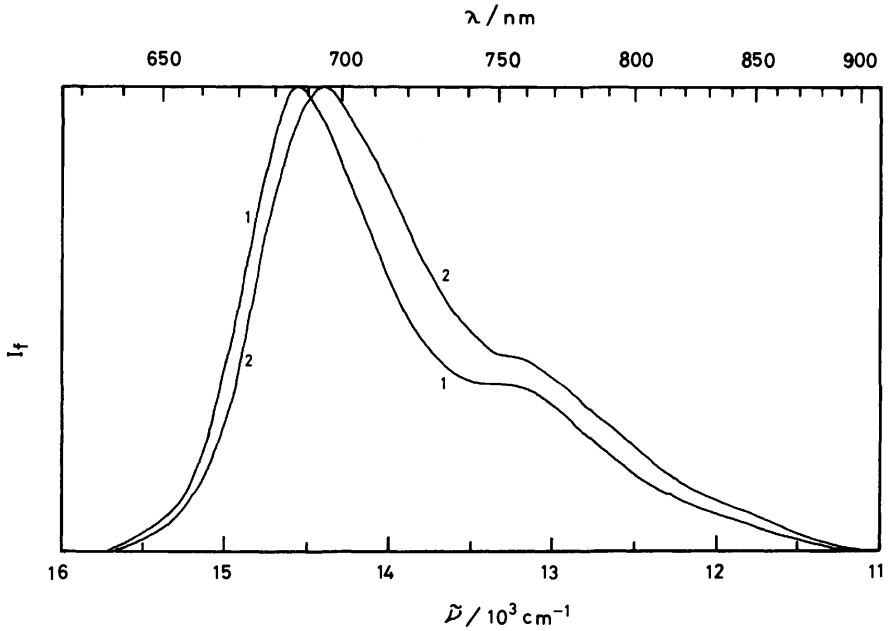

Fig. 3. Normalized fluorescence spectra of MB (2×10^{-6} M) in aqueous solution in the presence of 2NS. Concentration of 2NS: 1, 0 M; 2, 5×10^{-3} M.

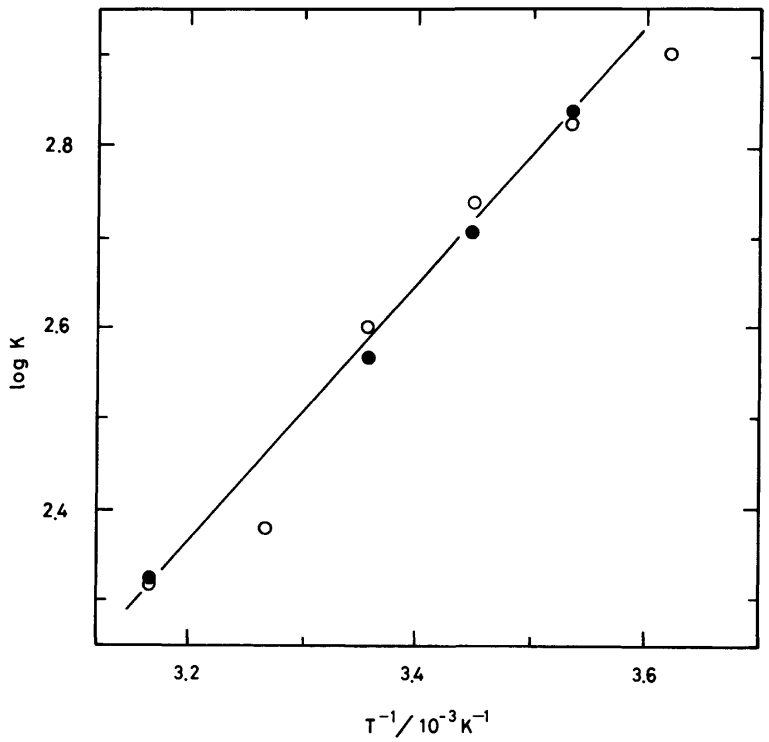

Fig. 4. Temperature dependence of K: (○) data obtained from the absorbance change in the absorption spectra; (●) data obtained from the intensity change in the fluorescence spectra.

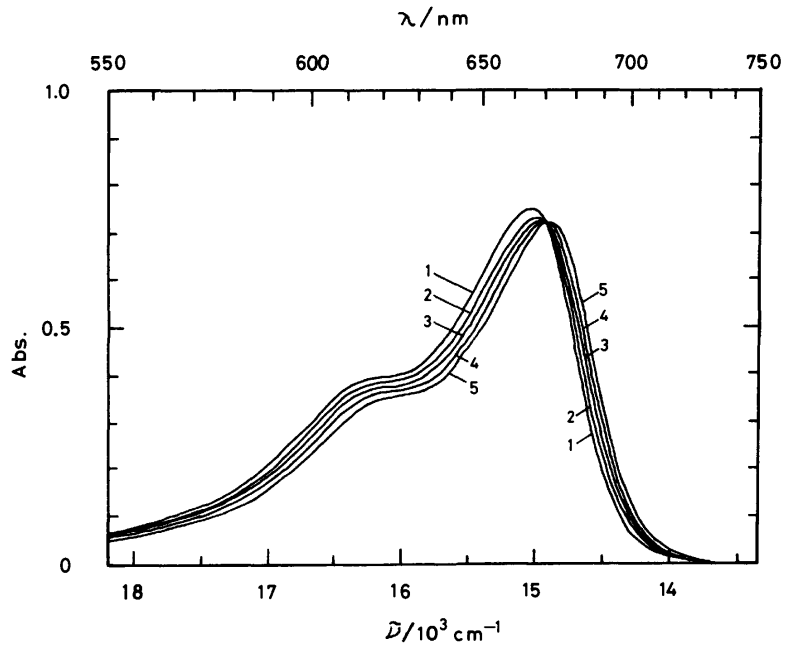

Fig. 5. Absorption spectra of MB (10^{-5} M) in aqueous solution in the presence of 1NS. Concentration of 1NS: 1, 0 M; 2, 2×10^{-3} M; 3, 5×10^{-3} M; 4, 10^{-2} M; 5, 2×10^{-2} M.

Monoanions. In addition to 2NS, the absorption and fluorescence spectra were similarly studied for other organic monoanions, 1-naphthalenesulfonate (1NS), 1-naphthaleneacetate (1NA), and 2-anthracenesulfonate (2AS). Figures 5 and 6 show the absorption spectra of MB solutions containing varying concentrations of 1NS and 2AS, respectively. As in the case for 2NS, both a red shift of an absorption maximum and an isosbestic point are observed on adding the monoanion. The 1:1 complex formation between

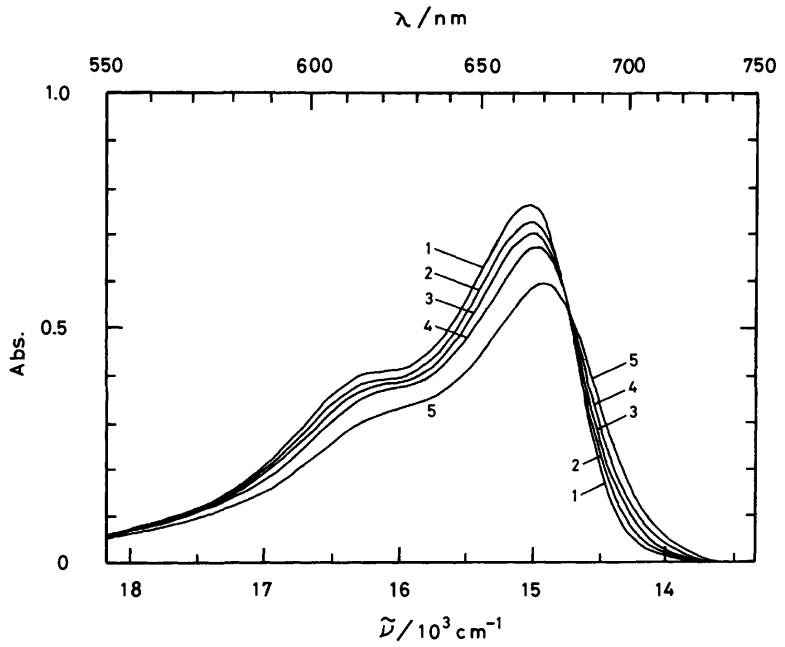

Fig. 6. Absorption spectra of MB (10^{-5} M) in aqueous solution in the presence of 2AS. Concentration of 2AS: 1, 0 M; 2, 2×10^{-5} M; 3, 5×10^{-5} M; 4, 10^{-4} M; 5, 2×10^{-4} M.

MB and the monoanion is responsible for these spectral changes. The equilibrium constants for the complex formation with 1NS, 1NA, and 2AS were determined to be 180, 240, and 7400 M^{-1}, respectively. The markedly large equilibrium constant for 2AS provides evidence that the interaction in the complex formation involves the aromatic ring in the anion.

The fluorescence spectrum of MB in the presence of 1NS is entirely similar to that in the presence of 2NS. In contrast, only the quenching of the MB fluorescence was observed for the MB-2AS system, indicating that the MB-2AS complex is nonfluorescent. The triplet state of the complex, derived primarily from the lowest triplet state of 2AS, may be assumed to lie in energy close to the lowest triplet state of anthracene (14900 cm^{-1}).[38] On the other hand, the energy of the first excited singlet state of the complex is estimated to be $\approx$14400 cm^{-1} from the maximum positions of the absorption and fluorescence of the complex. Since the maximum position of the complex fluorescence was found to be nearly constant irrespective of the kinds of anions, the peak position of the MB-2NS fluorescence was used in the above estimate. From the relationship between the energy levels of the complex, it is suggested that the nonradiative relaxation occurs with high efficiency through the triplet state derived primarily from 2AS.

The values of ΔH for the complex formation with 1NS, 1NA, and 2AS are determined to be -30, -28, and -49 kJ mol^{-1}, respectively, and the values of ΔS for 1NS, 1NA, and 2AS are -53, -47, and -92 J K^{-1} mol^{-1}, respectively. The absolute values of both thermodynamic quantities for 2AS are about two-fold larger than those for 2NS, 1NS, and 1NA. This finding also confirms a much stronger interaction of MB with 2AS possessing the anthracene ring than that with the anions possessing the naphthalene ring.

The addition of sodium benzenesulfonate to an MB solution results in no change in the absorption spectrum of MB within experimental error. The redox potential of MB in aqueous solution has been reported to be +0.011 V.[39] This value is high enough to form an electron donor-acceptor (EDA) complex with an appropriate electron donor. Whether the organic anions form EDA complexes with electron acceptors (tetracyanoethylene and chloranil) or not was not confirmed owing to the insolubility of these acceptors in water; however, the ionization potentials of the organic anions are probably not too different from the corresponding, unsubstituted aromatics which are known to form EDA complexes. In the complexes between MB and the organic anions, it seems to be reasonable that MB is an electron acceptor and the organic anions are electron donors.

Complex Formation of MB with Di- and Trianions. Spectroscopic studies were also made for a dianion, disodium 2,7-naphthalenedisulfonate (NDS) and a trianion, trisodium 1,3,6-naphthalenetrisulfonate (NTS). The absorption spectra of 10^{-5} M MB solutions with varying concentrations of NTS are

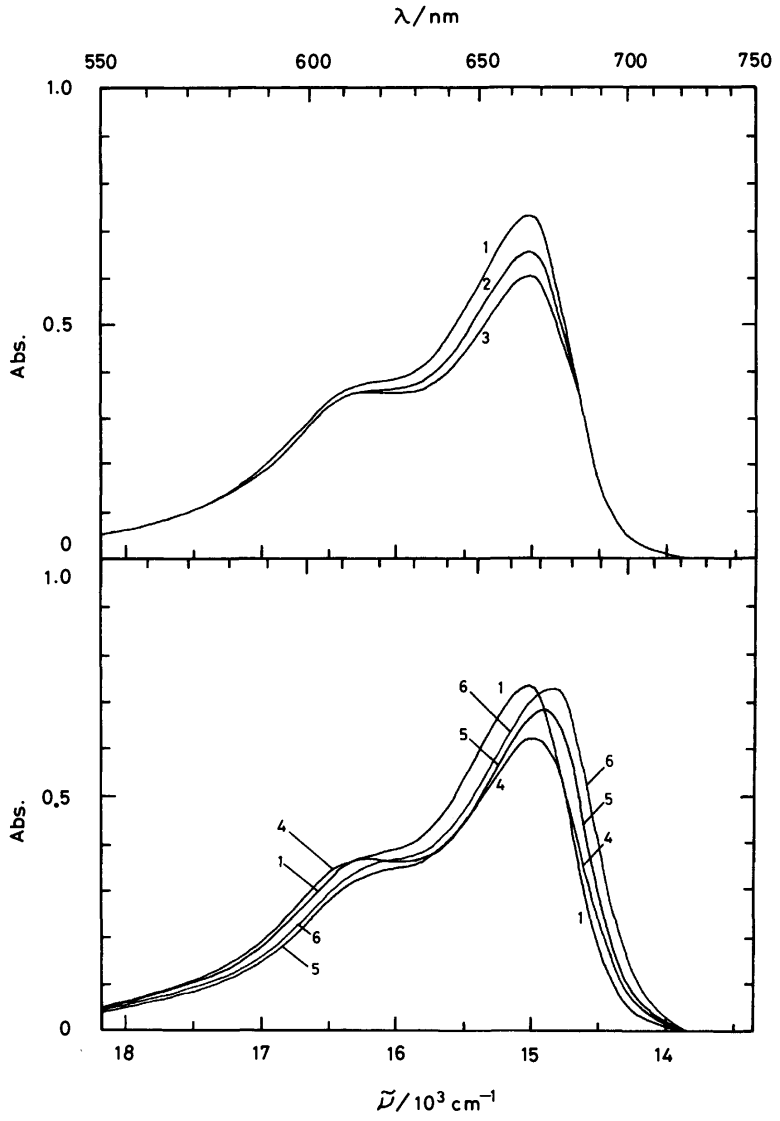

Fig. 7. Absorption spectra of MB (10^{-5} M) in aqueous solution in the presence of NTS. Concentration of NTS: 1, 0 M; 2, 5×10^{-5} M; 3, 2×10^{-4} M; 4, 10^{-3} M; 5, 10^{-2} M; 6, 5×10^{-2} M.

displayed in Fig. 7. Almost the same spectral change as in Fig. 7 was observed upon adding NDS. In contrast to the case of the monoanion (2NS, *etc.*), the absorption spectra of MB show a complicated change, exhibiting no isosbestic point. In the low-concentration range of NTS (below 10^{-3} M), the dimer peak appears at ≈610 nm and at the same time the monomer band decreases in intensity without the red shift of the monomer peak at 665 nm. However, as the concentration of NTS is increased above 10^{-2} M, the dimer peak starts to disappear accompanied by the recovery of the intensity and the red shift of the monomer band. In the low-concentration range of NTS, an MB molecule pairing with a sulfonate group substituted in an NTS molecule can easily associate with a neighboring MB molecule pairing with another sulfonate group substituted in the same NTS molecule because of the very close distance between the two MB molecules. The reason why the absorption spectra in the low-concentration range shown in Fig. 7 does not show a simple monomer-dimer equilibrium with an isosbestic point may be explained by the existence of a small amount of the 1:1 complex of MB with NTS and/or the complex of the MB dimer with NTS. Above an NTS concentration of 10^{-2} M, there is little chance that one NTS molecule is surrounded by more than one MB molecule. Under such situations, not the dimer of MB but the 1:1 complex between MB and NTS is formed. The elucidation for the absorption change shown in Fig. 7 is supported by the additional experimental result that, for a dilute (2×10^{-6} M) MB

solution with NTS, the change in the absorption spectra over the whole concentration range of NTS is similar to that of MB solution with 1NS. Nonetheless, the equilibrium constant could not be estimated both for NTS and NDS because of the absence of an isosbestic point in the absorption spectra.

The fluorescence maximum of MB was observed to be shifted to the red with an increase in the concentration of NTS (or NDS), indicating the 1:1 complex formation between MB and NTS (or NDS).

Complex Formation of Other Dyes. Other types of dyes, Rhodamine 6G, Pyronine G, Safranin T, and Crystal Violet were also studied regarding the complex formation with the organic monoanions. The spectral changes in the absorption and fluorescence for all these dyes in the presence of the monoanion are quite similar to those for MB. We ascribe the spectral changes to the 1:1 complexes between the above dyes and the monoanions. No complex formation between Crystal Violet and benzenesulfonate has been reported.[22] With respect to the complex formation with benzenesulfonate as well as with 2NS, *etc.*, the behavior of Crystal Violet resembles that of MB. Irrespective of the difference in the skeletal structure from MB, the equilibrium constants of the dyes other than Rhodamine 6G are comparable with those of MB. The values of ΔH and ΔS for the complex formation of these dyes with the anions of the naphthalene derivatives are in the range from -19 to $-29\,\mathrm{kJ\,mol^{-1}}$ and from -25 to $-57\,\mathrm{J\,K^{-1}\,mol^{-1}}$, respectively. On the other hand, ΔH and ΔS for Rhodamine 6G are in the range from -36 to $-44\,\mathrm{kJ\,mol^{-1}}$ and from -94 to $-120\,\mathrm{J\,K^{-1}\,mol^{-1}}$ respectively. The absolute values of ΔH and ΔS for Rhodamine 6G are significantly larger than those for other dyes, including MB. There still remains a question of why ΔH and ΔS for Rhodamine 6G are strikingly different from those for other dyes.

The author wishes to thank Professor Fumio Hirayama for his valuable discussion.

References

1) K. Bergman and C. T. O'Konski, *J. Phys. Chem.*, **67**, 2189 (1963).
2) E. Braswell, *J. Phys. Chem.*, **72**, 2477 (1968).
3) P. Mukerjee and A. K. Ghosh, *J. Am. Chem. Soc.*, **92**, 6403, 6419 (1970); A. K. Ghosh and P. Mukerjee, *ibid.*, **92**, 6408 (1970).
4) W. Spencer and J. R. Sutter, *J. Phys. Chem.*, **83**, 1573 (1979).
5) E. H. Braswell and J. Lary, *J. Phys. Chem.*, **85**, 1573 (1981).
6) J. Ruprecht and H. Baumgärtel, *Ber. Bunsenges. Phys. Chem.*, **88**, 145 (1984).
7) W. C. Lai, N. S. Dixit, and R. A. Mackay, *J. Phys. Chem.*, **88**, 5364 (1984).
8) P. Mukerjee and K. J. Mysels, *J. Am. Chem. Soc.*, **77**, 2937 (1955).
9) R. Humphry-Baker, M. Grätzel, and R. Steiger, *J. Am. Chem. Soc.*, **102**, 847 (1980).
10) H. Sato, M. Kawasaki, K. Kasatani, N. Nakashima, and K. Yoshihara, *Bull. Chem. Soc. Jpn.*, **56**, 3588 (1983).
11) M. A. J. Rodgers, *J. Phys. Chem.*, **85**, 3372 (1981).
12) T. Handa, C. Ichihashi, I. Yamamoto, and M. Nakagaki, *Bull. Chem. Soc. Jpn.*, **56**, 2548 (1983).
13) N. J. Bridge and P. D. I. Fletcher, *J. Chem. Soc., Faraday Trans. 1*, **79**, 2161 (1983).
14) M. Koizumi and N. Mataga, *Bull. Chem. Soc. Jpn.*, **26**, 115 (1953).
15) N. Mataga and M. Koizumi, *Bull. Chem. Soc. Jpn.*, **27**, 197 (1954).
16) M. K. Pal and M. Schubert, *J. Phys. Chem.*, **67**, 1821 (1963).
17) M. Shirai, Y. Nagaoka, and M. Tanaka, *Makromol. Chem.*, **178**, 1633 (1977).
18) M. Shirai, Y. Murakami, and M. Tanaka, *Makromol. Chem.*, **178**, 2141 (1977).
19) M. Shirai, Y. Nagaoka, and M. Tanaka, *J. Polym. Sci., Polym. Chem. Ed.*, **15**, 1021 (1977).
20) R. B. McKay and P. J. Hillson, *Trans. Faraday Soc.*, **61**, 1800 (1965); M. De Vylder, *J. Chem. Soc., Faraday Trans. 1*, **78**, 137 (1982).
21) 'S. A. Amire and H. D. Burrows, *J. Chem. Soc., Faraday Trans. 1*, **78**, 2033 (1982).
22) J. Gicquel, M. Carles, and H. Bodot, *J. Phys. Chem.*, **83**, 699 (1979).
23) T. G. Beaumont and K. M. C. Davis, *J. Chem. Soc. (B)*, **1968**, 1010.
24) R. K. Williams, *J. Phys. Chem.*, **85**, 1795 (1981); *ibid.*, **88**, 93 (1984).
25) I. Okura, S. Aono, M. Takeuchi, and S. Kusunoki, *Bull. Chem. Soc. Jpn.*, **55**, 3637 (1982).
26) H. Yasuba, T. Imai, K. Okamoto, S. Kusabayashi, and H. Mikawa, *Bull. Chem. Soc. Jpn.*, **43**, 3101 (1970).
27) E. L. Goff and R. B. LaCount, *J. Am. Chem. Soc.*, **85**, 1354 (1963).
28) R. B. McKay and P. J. Hillson, *Trans. Faraday Soc.*, **63**, 777 (1967).
29) P. Ferrero and A. Conzetti, *Helv. Chim. Acta*, **11**, 1152 (1928).
30) S. Hamai, *Bull. Chem. Soc. Jpn.*, **57**, 2700 (1984).
31) S. Hamai, *Bull. Chem. Soc. Jpn.*, **55**, 2721 (1982).
32) H. Merkelo, S. R. Hartman, T. Mar, and G. S. S. Govindjee, *Science*, **164**, 301 (1969).
33) K. K. Rohatgi and G. S. Singhal, *J. Phys. Chem.*, **70**, 1695 (1966).
34) I. L. Arbeloa and P. R. Ojeda, *Chem. Phys. Lett.*, **87**, 556 (1982).
35) F. L. Arbeloa, I. L. Gonzalez, P. R. Ojeda, and I. L. Arbeloa, *J. Chem. Soc., Faraday Trans. 2*, **78**, 989 (1982).
36) S. Iwata, J. Tanaka, and S. Nagakura, *J. Am. Chem. Soc.*, **88**, 894 (1966).
37) G. Briegleb and J. Czekalla, *Z. Elektrochem.*, **58**, 249 (1954).
38) S. P. McGlynn, J. D. Boggus, and E. Elder, *J. Chem. Phys.*, **32**, 357 (1960).
39) P. S. Rao and E. Hayon, *J. Am. Chem. Soc.*, **96**, 1287 (1974).

Proton-induced Quenching of Methoxynaphthalenes Studied by Laser Flash Photolysis and Inclusion Effect of β-Cyclodextrin on the Quenching

Haruo SHIZUKA,* Masaru FUKUSHIMA, Takuya FUJU, Takayoshi KOBAYASHI,† Hiroyuki OHTANI,† and Mikio HOSHINO††

Department of Chemistry, Gunma University, Kiryu, Gunma 376
†*Department of Physics, The University of Tokyo, Hongo, Bunkyo-ku, Tokyo 113*
††*The Institute of Physical and Chemical Research, Wako, Saitama 351*

(Received March 15, 1985)

Proton-induced quenching in both excited singlet and triplet states of methoxynaphthalenes in H_2O–CH_3CN mixtures has been studied by means of laser flash photolysis. Inclusion effect of β-cyclodextrin (βCD) on the proton-induced quenching has been also examined. It is shown that the proton-induced quencing (the rate constant ^1k_q) of 1-methoxynaphthalene (1RH) occurs effectively in the excited singlet state, but not in the triplet state on the basis of the $T_n \leftarrow T_1$ absorption measurements. There is no enhancement of triplet formation *via* the proton-induced quenching since the ^1k_q value obtained by the $T_n \leftarrow T_1$ absorption measurements agrees with that obtained by fluorimetry. It was unsuccessful to observe a protonated σ-complex produced by the excited-state protonation to the naphthalene ring. The 1:1 inclusion complex between 1RH and βCD is produced with the association constant K_g (=27 mol^{-1} dm^3 at 300K). In the presence of βCD, the ^1L_b character of 1RH increases in the fluorescent state and the proton-induced quenching of 1RH markedly decreases, which may be due to inclusion and environmental effects of βCD upon the behavior in the excited state of 1RH. As for 2RH having little or no intramolecular CT character (^1L_a), there is no proton-induced quenching.

Proton association and dissociation in the excited state of aromatic compounds are elementary processes in chemistry. The acid-base properties in the excited state of aromatic compounds are closely related to electronic structure, which is considerably different from that in the ground state. A number of studies on the acidity constants pK_a^* in the excited state of aromatic compounds have been reported showing that the pK_a^* values are significantly different from the acidity constants in the ground state.[1-9] It is well-known that the pK_a^* values can be estimated by means of the Förster cycle,[1-3,10] the fluorescence titration curve,[2,3] and the triplet-triplet absorbance titration curve.[11] These methods involve the assumption that proton transfer in the excited state is very fast, resulting in establishment of an acid-base equilibrium during the lifetime in the excited state.

However, it has been shown recently that proton-induced quenching (^1k_q) is competitive with the proton transfer reaction in the excited state of naphthylamines (that is, simple acid-base equilibrium cannot be attained during the lifetime in the excited state of aromatic amines) and that a dynamic analysis containing the quenching process is, therefore, needed in order to obtain the accurate pK_a^* values.[12] The dynamic analyses by means of nanosecond time-resolved spectroscopy with fluorimetry have been applied to 1-pyrenyl amine,[13] 1-anthrylamine,[14] phenanthrylamines,[15] and naphthols.[16] The Stuttgart group[17] has supported our method to determine the pK_a^* values of naphthylamines. Similar experiments for excited naphthols have been reported by Harris and Selinger.[18] Establishment of prototropic equilibria at moderate acid conditions has been reported in the excited singlet state of 2-naphthol-6,8-disulfonate[19] and in the triplet states of benzophenone[20] and phenyl alkyl ketones.[21] For the triplet state, its lifetime is relatively long enough to accomplish the prototropic equilibrium.[21]

Thus, the proton-induced quenching is a very important process in the prototropic reaction in the excited state. For the quenching mechanism a complex in which a proton is shared between excited 2-naphthylamine and one water molecule[22] or a hydrated naphthylammonium cation in the ground state[23] was assumed as an intermediate for the quenching. However, it has been demonstrated that the proton-induced quenching proceeds *via* electrophilic protonation at one of carbon atoms of the aromatic ring in the excited singlet state, leading to proton exchange (or isotope exchange).[24] An intramolecular CT structure in the excited state is responsible for the quenching.[15,24,25] A linear relationship between the ^1k_q values and the charge densities in the excited state of aromatic compounds has been shown.[25]

In the course of a study on the excited-state proton transfer reaction,[26] we became interested in the proton-induced quenching of methoxynaphthalenes studied by laser flash photolysis in order to establish the proton-induced quenching mechanism. Inclusion effect of βCD on the quenching has been also examined. This work was studied to answer the following questions:
(1) Is there any enhancement of triplet formation induced by the quenching? (2) Is there any proton-induced quenching in the triplet state? (3) Is there any transient produced by protonation in the excited

state? (4) What is the relation between electronic structure and proton-induced quenching? and (5) What about the inclusion efect of βCD upon both the quenching and the fluorescent state?

Experimental

Materials. Both 1- and 2-methoxynaphthalenes were the same as those reported elsewhere.[24] β-Cyclodextrin (Wako) and H_2SO_4 (97%, Wako) were used without further purification. Deionized water was distilled. Acetonitrile (reagent grade) was purified by the usual method.[27] The actual acid contents were determined by titration. Acetonitrile and water mixtures (1:4 or 4:1 by volume) were used as solvents. All samples were thoroughly degassed by freeze-pump-thaw cycles on a high vacuum line.

Absorption and Fluorescence Measurements. Absorption and fluorescence spectra were recorded with a Hitachi 200-10 spectrophotometer and a Hitachi M850 spectrofluorimeter respectively. The spectral corrections for the emission were made.

Nanosecond Laser Flash Experiments. Laser flash photolysis studies were carried out by using a Nd^{3+}-YAG laser equipped with a forth harmonic (266 nm) generator. The duration of a laser pulse was approximately 20 ns. The detection system for measurements of transient spectra consisted of a 150 W xenon lamp (Ushio UXL 150-D) as an analyzing light source, a monochromator (Ritsu Model MC-20N), a photomultiplier (Hamamatsu R758) and a transient memory (Kawasaki Electronica, MR-50E). The analyzing light beam was intensified by a factor of *ca.* 20 during the detection of the transient spectra. The transmitted light beam through a sample cell (10 mm) was led into the entrance slit of the monochromator. The output from the photomultiplier attached to the exit slit of the monochromator was recorded on the transient memory.

Results and Discussion

Proton-induced Quenching of Methoxynaphthalenes Studied by Laser Flash Photolysis. Figure 1 shows the transient absorption spectra of (a) 1-methoxynaphthalene (1RH), (b) 1RH in the presence of acid ($[H_2SO_4]=0.5$ mol dm^{-3}), and (c) 2-methoxynaphthalene (2RH) in CH_3CN-H_2O (4:1) mixtures, obtained by laser flash photolysis at 266 nm. These spectra with peaks of 435 nm (1RH) and 430 nm (2RH) were assigned to those of $T_n \leftarrow T_1$ transitions, since they were the same as the $T_n \leftarrow T_1$ absorption spectra obtained by the triplet sensitization by acetophenone at 337 nm as can be seen in Fig. 1(d). These transient spectra were quenched effectively by dissolved oxygen. The absorbance of the $T_n \leftarrow T_1$ transient spectrum of 1RH was decreased with increasing the concentration of protons without any spectral change [*e.g.*, Fig. 1(b)]. However, for 2RH no change in the $T_n \leftarrow T_1$ absorbance dependent upon the concentration of protons was observed. The Stern-Volmer Plots of A_T^0/A_T *vs.* $[H_3O^+]$ are shown in

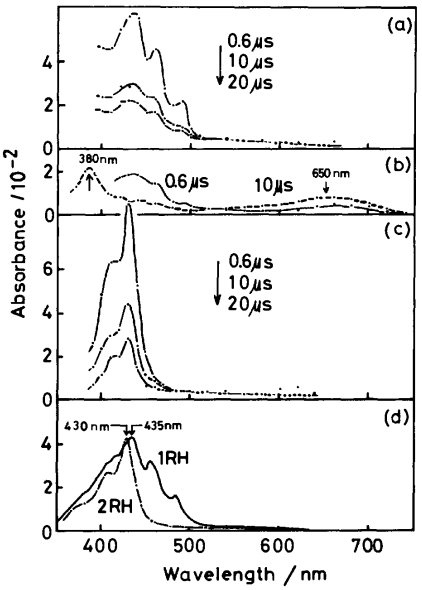

Fig. 1. Transient absorption spectra of (a) 1RH (4.4×10^{-4} mol dm^{-3}), (b) 1RH (4.4×10^{-4} mol dm^{-3}) in the presence of acid ($[H_2SO_4]=0.5$ mol dm^{-3}), and (c) 2RH (1.3×10^{-3} mol dm^{-3}) in H_2O-CH_3CN (1 : 4) mixtures obtained by laser flash photolysis at 266 nm. (d) Reference $T_n \leftarrow T_1$ transient spectra of RH's (2.5×10^{-3} mol dm^{-3}) obtained by triplet sensitization of acetophenone (3×10^{-2} mol dm^{-3}) at 1 μs after laser pulsing at 337 nm.

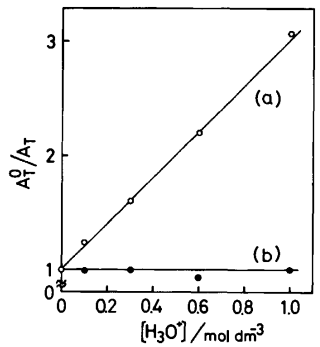

Fig. 2. Plot of A_T^0/A_T of 1RH (a) or 2RH (b) as a function of $[H_3O^+]$. For detail, see text.

Fig. 2(a) and (b) for 1RH and 2RH respectively. Straight lines are obtained indicating that Eq. 1 fairly holds.

$$\frac{A_T^0}{A_T} = 1 + {}^1k_q\tau_0[H_3O^+] \quad (1)$$

where A_T and A_T^0 denote the $T_n \leftarrow T_1$ absorbances at the transient peaks at the delay time=100 ns with and without protons respectively, ${}^1k_q$ the rate constant for the proton-induced quenching in the excited singlet state, and τ_0 the fluorescent life-time of methoxynaphthalenes. From the slope (a) in Fig. 2, the ${}^1k_q$ value is determined to be 1.5×10^8 mol^{-1} dm^3 s^{-1} for

1RH using τ_0=12.6 ns,[24] which is the same as that (1.6×10^8 mol^{-1} dm^3 s^{-1}) obtained by fluorescence intensity measurements[24] within the experimental errors. As for 2RH, the ^1k_q value is very small (less than 1×10^5 mol^{-1} dm^3 s^{-1}). The time trace of the transient $T_n\leftarrow T_1$ absorption monitored at the transient peaks are shown in Fig. 3, which decays with a single exponential function. The triplet lifetimes of 1RH and 2RH are obtained to be 10.2 (±0.4) and 10.2 (±0.2) μs, respectively. The triplet lifetimes were scarcely affected by protons, suggesting that there is little or no proton-induced quenching in the triplet state.

The introduction of electron-donating groups such as amino, hydroxyl, and methoxyl groups into the aromatic ring causes electron migration from the substituents to the ring in the excited singlet state.[28,29] This tendency is enhanced by solvation of the excited species in polar media, and the excited molecule has an intramolecular CT structure. As a result, the basicity of the aromatic ring increases appreciably in the excited state. This is the reason why the intramolecular CT structure is responsible for the proton-induced quenching.[15,24,25] The CT character in the excited species having electron-donating moieties at the α-position of the naphthalene ring is larger than that at the β-position. In contrast, there is no CT character in the lowest triplet state of 1RH, resulting in little or no proton-induced quenching.[24] Therefore, the proton-induced quenching (*i.e.*, protonation to the carbon atoms of the aromatic ring) is attributed to a typical electrophilic reaction.[24,26] A possibility of enhancement of intersystem crossing due to the proton-induced fluorescence quenching was assumed in an early stage of this study.[30] The anion-induced quenching of aromatic compounds is to be the case.[31,32] However, the possibility for enhancement of triplet formation was completely ruled out since the ^1k_q value obtained by the $T_n\leftarrow T_1$ absorbance of 1RH agrees with that fluorimetry[24] as described above. It has been pointed out that there is relatively little correlation between ^1k_q and I_P^* [the ionization potential for the excited singlet state of aromatic compounds ($^1A^*$) estimated from I_P (ionization potential for the gorund state (^1A)) minus $E_A°$ (0-0 transition energy for $^1A^*-{}^1A$)].[24] The quenching mechanism of $^1A^*$ by protons is different from that by inorganic anions X^-. The former involves a chemical interaction (protonation) at one of carbon atoms of the aromatic ring and the latter involves an electron transfer (or charge transfer).[31,32] An electronic interaction between $^1A^*$ and H^+ (or D^+) in the quenching is locally restricted to one of carbon atoms of the aromatic nucleus. This may be due to the following reasons: the radius of the proton (10^{-5} A)[33] is too small to overlap widely with the π-electronic system of $^1A^*$ compared to those of X^- (1.5—3 Å), and electrostatic and covalent interactions between H^+ [or D^+) and the proper carbon atom of $^1A^*$ become large enough to produce bond formation.[24] The experimental results can be accounted for by a schematic energy-state diagram in Fig. 4, showing that the proton-induced quenching ^1k_q occurs in the fluorescent state (^1L_a), but not in the T_1 state.

Unfortunately, the detection of a protonated σ-complex produced by electrophilic attack mainly at position 5 of the excited 1RH was unsuccessful in the present laser flash experiments. This may be due to that the transient σ-complex may have a very weak absorption in the observed wavelength region and/or that its lifetime may be too short to detect the transient absorption. Anyway, it is unknown at the

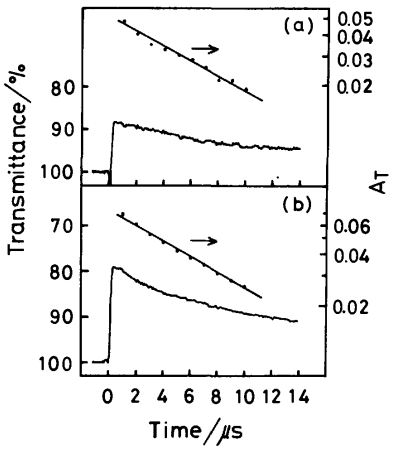

Fig. 3. Time traces of the transient $T_n\leftarrow T_1$ absorptions of 1RH (a) 2RH (b) monitored at 435 and 430 nm respectively, obtained by laser flash photolysis at 266 nm. The semilogarithmic plot of absorbance (A_T) gives a straight line, showing that the triplet species decays with a single exponential function. For the decay kinetics of 1RH, the absorbance (1.26×10^{-2}) due to a transient having a long lifetime was subtracted from the absorbance at 435 nm. Similary, for 2RH the absorbance (2.47×10^{-2}) due to a transient having a long lifetime was substracted from the absorbance at 430 nm. These absorbances may be due to photoproducts of RH.

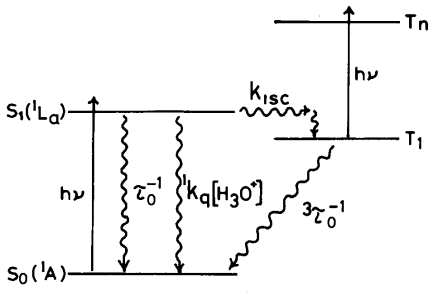

Fig. 4. A schematic energy-state diagram for the proton-induced quenching (^1k_q) of 1RH. For details, see text and Ref. (24).

present stage. A very weak absorption appeared in the longer wavelength region with a peak of 650 nm in the presence of protons, as shown in Fig. 1(b). The buildup time of the transient absorption was about 1 μs. The weak transient spectrum is very similar to that of the cation radical of 1RH.[34] It is obvious that this transient is not produced directly from the excited singlet state of 1RH because the rise (1 μs) and decay (τ_0=12.6 ns) times are different from each other. There was no 650 nm transient formation without acid. Therefore, protons should be needed for formation of the longer wavelength transient. For direct excitation of 2RH, no 650 nm transient was observed. Further investigation on the transient species will be needed in future.

Inclusion Effect of β-Cyclodextrin on Proton-induced Quenching of 1RH. It has been demonstrated that the proton-induced quenching of 1RH proceeds *via* electrophilic protonation at the proper carbon atom of the aromatic ring in the lowest excited singlet state (^1L_a) in polar media, leading to proton exchange or isotope exchange mainly at position 5 (slightly at position 8) of the naphthalene ring.[24] Therefore, it was expected that if position 5 (or position 8) of the naphthalene ring would be protected by β-cyclodextrin the proton-induced quenching might decrease significantly. It is known to produce a 1:1 inclusion complex of β-cyclodextrin (βCD) with naphthalene derivatives.[35,36]

At first, spectroscopic studies of 1RH in the presence of βCD have been carried out. Figure 5(a) shows the absorption spectra of 1RH ([1RH]=1.4×10^{-4} mol dm^{-3}) in a H_2O-CH_3CN (4:1) mixture with(1) and without(2) βCD ([βCD]=2×10^{-2} mol dm^{-3}); the differential spectrum of 1RH with and without βCD ([βCD]=2×10^{-2} mol dm^{-3}) is also depicted in Fig. 5(b). An isosbestic point was observed at 282 nm at various concentrations of βCD, reflecting an equilibrium:

$$1RH + \beta CD \rightleftharpoons (1RH-\beta CD) \quad (2)$$

The association constant in the ground state K_g (=[1RH−βCD]{[1RH][βCD]}$^{-1}$), is calculated by[35]

$$(A_\lambda - A_\lambda^0)/C_\beta = K_g(A_\lambda^\infty - A_\lambda) \quad (3)$$

where C_β represents the concentration of βCD, A_λ^0, A_λ, and A_λ^∞ stand for the absorbances of nil, C_β, and ∞, respectively. Figures 6 shows a plot of $(A_\lambda - A_\lambda^0)/C_\beta$ as a function of A_λ at λ=300 nm at 300 K. The value of K_g is determined to be 27 mol^{-1} dm^3 from the slope.

The fluorescence spectra of 1RH([1RH]=1.4×10^{-4} mol dm^{-3}) (1) with and (2) without βCD ([βCD]=2×10^{-2} mol dm^{-3}) in H_2O-CH_3CN (4:1) mixtures are also shown in Fig. 5(a). In the case of (1), the concentration of the 1RH-βCD complex is estimated to be 4.9×10^{-5} mol dm^{-3} at 300 K, which corresponds to 35% of the total concentration of 1RH

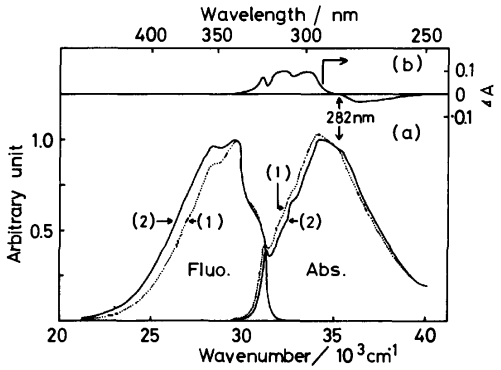

Fig. 5. (a) Absorption and fluorescence spectra of 1RH (1.4×10^{-4} mol dm^{-3}) in H_2O-CH_3CN (4 : 1) (1) with and (2) without βCD ([βCD]=2×10^{-2} mol dm^{-3}). (b) The differential absorption spectrum of 1RH between (1) and (2). For detial, see text.

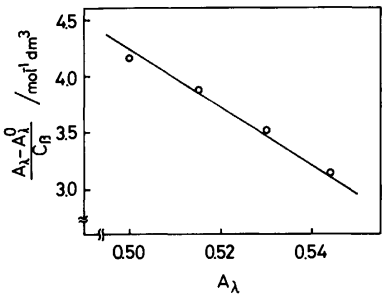

Fig. 6. Plot of $(A_\lambda - A_\lambda^0)/C_\beta$ *vs.* A_λ at 300 K, where λ is 300 nm. For detial, see text.

(1.4×10^{-4} mol dm^{-3}). The maximum concentration of βCD to add to the system is ≈2×10^{-2} mol dm^{-3}, since the molecular weight of βCD is extremely large (1135) and its solubility is restricted. However, the effect of βCD on the fluorescence properties and the proton-induced quenching of 1RH were distinct. The fluorescence intensity at longer wavelengths decreases when βCD is added as shown in Fig. 5. It suggests that the addition of βCD decreases intramolecular CT character (^1L_a) in the excited state. The fluorescence quantum yield and apparent lifetime of 1RH in the presence of βCD (2×10^{-2} mol dm^{-3}) in H_2O-CH_3CN (4:1) were obtained to be 0.38 and 10.6 ns at 300 K, respectively. By addition of βCD to the system, the fluorescence quantum yield slightly decreased compared to that (0.43)[24] of free 1RH, whereas the lifetime became long in comparison with that (8.9 ns)[24] of free 1RH. It is noteworthy that the fluorescence spectrnm of 1RH with βCD is similar to that of free 1RH in less polar or nonpolar media. The vibrational structures of emission from the ^1L_b state (the locally excited state) appear at the shorter wavelengths with a peak of 338 nm. This observation can be explained in terms of a model of the 1RH-βCD inclusion complex, in

which a part of the naphthalene ring of 1RH (*i.e.*, positions 5 and 8) may be included as shown in Eq. 4:

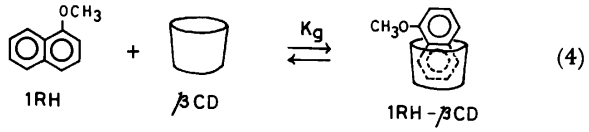

(4)

A similar Corey-Pauling-Kolton molecular model has been proposed recently by Tran and Fendler.[36]

Electron migration from the methoxy group to the naphthalene ring decreases in the excited 1RH-βCD complex, since solvation of the excited 1RH [positions 5 and 8 having large charge densities in the excited state (^1L_a)][24] with polar solvent molecules may be prevented by βCD inclusion. As a result, the 1RH-βCD complex behaves as if it were in less polar media.

The plots of I_0/I *vs.* [H_3O^+] are shown in Fig. 7, where I and I_0 are the fluorescence intensities at 338 nm with and without protons respectively and (a) and (b) denote the absence and presence of βCD ([βCD]=2×10^{-2} mol dm^{-3}) respectively. This result shows that the proton-induced fluorescence quenching of 1RH ($^1k_q=1.1\times10^9$ mol^{-1} dm^3 s^{-1}) decreases markedly in the presence of βCD. This fact shows that the reactive positions [mainly 5 and slightly 8 in the excited state (^1L_a)] of 1RH are efficiently blocked by βCD inclusion. However, the experimental results of the fluorescence and proton-induced quenching cannot be explained only by the effect of the complex formation. In addition to this, one may take into account an environmental effect of βCD upon both fluorescence properties and the proton-induced quenching rate of 1RH, since the 1RH-βCD complex formation is 35% under the experimental conditions as described above. Probably, 1RH may be surrounded by βCD molecules, resulting in that the ^1L_b character of 1RH increases in the excited state. It should be noted that the ^1L_b state (locally excited state) is not susceptible of protons, as shown previously.[24]

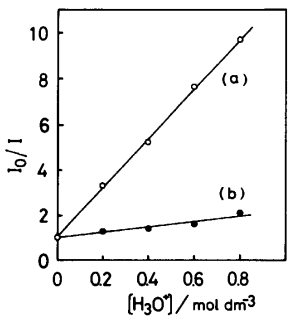

Fig. 7. Plots of I_0/I of 1RH at 338 nm *vs.* [H_3O^+] in H_2O-CH_3CN (4 : 1) (b) with and (a) without βCD ([βCD] = 2×10^{-2} mol dm^{-3}).

Summary

(1) The $T_n\leftarrow T_1$ absorbance of 1RH at 435 nm obtained by laser flash photolysis decreases considerably with increasing the concentration of protons, while its triplet lifetime (10.2 μs) is scarcely affected by protons, showing that the proton-induced quenching occurs in the excited singlet state, but not in the triplet state. There is no enhancement of triplet formation *via* the proton-induced quenching on the basis of the result that the ^1k_q value (1.5×10^8 mol^{-1} dm^3 s^{-1})in H_2O-CH_3CN (1:4) at 300 K obtained by the $T_n\leftarrow T_1$ absorption measurements is nearly equal to that (1.6×10^8 mol^{-1} dm^3 s^{-1}) obtained by fluorimetry[24] within the experimental errors. Unfortunately, the protonated σ-complex cannot be detected under the experimental conditions.

(2) The 1:1 complex between 1RH and βCD is produced with the association constant K_g (27 mol^{-1} dm^3 in H_2O-CH_3CN (4:1) at 300 K). In the presence of βCD (2×10^{-2} mol dm^{-3}) the ^1L_b character of 1RH increases in the fluorescent state and the proton-induced quenching of 1RH markedly decreases. These effects of βCD may be due to not only the inclusion effect of βCD, but also the environmental effect of βCD upon the behavior of the excited 1RH species. The intramolecular CT character (^1L_a) in the excited state of 1RH also decreases by the βCD inclusion.

(3) For 2RH, proton-induced quenching in the lowest excited singlet state is scarcely observed. The difference in the quenching between 1RH and 2RH is caused by that in electronic structures in the excited singlet state; the former has an intramolecular CT structure (^1L_a), but not for the latter (^1L_b). It is confirmed that the intramolecular CT structure in the excited state is responsible for the proton-induced quenching.

This work was supported by a Scientific Research Grant-in-Aid (No. 58470001) of the Ministry of Education. The authors are very grateful to Dr. H. Hiratsuka of Tokyo Institute of Technology for showing us the absorption spectra of the RH cation radicals.

References

1) Th. Förster, *Z. Elektrochem. Angew. Phys. Chem.*, **54**, **42**, 531 (1950).

2) A. Weller, *Ber. Bunsenges. Phys. Chem.*, **56**, 662 (1952); *ibid*, **66**, 1144 (1956).

3) A. Weller, *Prog. React. Kinet.*, **1**, 189 (1961).

4) H. Beens, K. H. Grellmann, M. Gurr, and A. Weller, *Discuss. Faraday Soc.*, **39**, 183 (1965).

5) E. V. Donckt, *Prog. React. Kinet.*, **5**, 273 (1970).

6) E. L. Wehry and L. B. Rogers, In "Fluorescence and Phosphorescence Analyses," ed by D. M. Hercules, Wiley-Interscience, New York, 1966, p.125.
7) S. G. Shulman, In "Modern Fluorescence Spectroscopy," ed by E. L. Wehry, Pleum, New York (1976); Vol. 2, S. G. Shulman, "Fluorescence and Phosphorescence Spectroscopy," Pergamon, Oxford, (1977).
8) J. F. Ireland and P. A. H. Wyatt, *Adv. Phys. Org. Chem.*, **12**, 131 (1976) and a number of references therein.
9) W. Klöpffer, *Adv. Photochem.*, **10**, 311 (1977).
10) Z. R. Grabowski and A Grabowska, *Z. Phys. Chem.* (Wiesbaden), **101**, 197 (1976); Z. R. Grabowski and W. Rubaszewska, *J. Chem. Soc., Faraday Trans. 1*, **73**, 11 (1977).
11) G. Jackson and G. Porter, *Proc. R. Soc. London, Ser. A*, **260**, 13 (1961).
12) K. Tsutsumi and H. Shizuka, *Chem. Phys. Lett.*, **52**, 485 (1977); *Z. Phys. Chem. (Wiesbaden)*, **111**, 129 (1978).
13) H. Shizuka, K. Tsutsumi, H. Takeuchi, and I. Tanaka, *Chem. Phys. Lett.*, **62**, 408 (1979); *Chem. Phys.*, **59**, 183 (1981).
14) H. Shizuka and K. Tsutsumi, *J. Photochem.*, **9**, 334 (1978).
15) K. Tsutsumi, S. Sekiguchi, and H. Shizuka, *J. Chem. Soc., Faraday Trans. 1*, **78**, 1087 (1982).
16) K. Tsutsumi and H. Shizuka, *Z. Phys. Chem. (Wiesbaden)*, **122**, 129 (1980).
17) F. Hafner, J. Wörner, U. Steiner, and M. Hauser, *Chem. Phys. Lett.*, **72**, 139 (1980).
18) C. M. Harris and B. K. Selinger, *J. Phys. Chem.*, **84**, 891, 1366 (1980).
19) S. G. Schulman, L. S. Rosenberg, and W. R. Vincent, Jr., *J. Am. Chem. Soc.*, **101**, 139 (1979).
20) D. M. Rayner and P. A. H. Wyatt, *J. Chem. Soc., Faraday Trans. 2*, **70**, 945 (1974).
21) H. Shizuka and E. Kimura, *Can. J. Chem.*, **62**, 2041 (1984).
22) Th. Förster, *Chem. Phys. Lett.*, **17**, 309 (1972).
23) S. G. Schulman and R. J. Sturgeon, *J. Am. Chem. Soc.*, **99**, 7209 (1977).
24) H. Shizuka and S. Tobita, *J. Am. Chem. Soc.*, **104**, 6919 (1982); S. Tobita and H. Shizuka, *Chem. Phys. Lett.*, **75**, 140 (1980).
25) H. Shizuka and K. Tsutsumi, *Bull. Chem. Soc. Jpn.*, **56**, 629 (1983).
26) H. Shizuka, *Acc. Chem. Res.*, **18**, 000 (1985).
27) A. Weissberger, E. S. Proskauer, J. A. Riddich, and E. E. Troops Jr., "Organic Solvents," Wiley-Interscience, New York, (1955), p435.
28) N. Mataga, *Bull. Chem. Soc. Jpn.*, **36**, 654 (1963).
29) S. Suzuki, T. Fujii, and K. Sato, *Bull. Chem. Soc. Jpn.*, **45**, 1937 (1972); H. Suzuki and H. Baba, *ibid.*, **40**, 2199 (1967).
30) H. Shizuka, Y. Ishii, and T. Morita, *Chem. Phys. Lett.*, **62**, 408 (1979).
31) H. Shizuka, M. Nakamura, and T. Morita, *J. Phys. Chem.*, **84**, 989 (1980).
32) H. Shizuka and H. Obuchi, *J. Phys. Chem.*, **86**, 1297 (1982).
33) Protons exist in aqueous solution as hydronium ions. However, protonation proceeds *via* proton transfer involving only the movement of a nucleus as has been stated by Bell: R. P. Bell, "The Proton in Chemistry," Chapman and Hall, London, (1973).
34) H. Hiratsuka, Unpublished results.
35) T. Yorozu, M. Hoshino, M. Imamura, and H. Shizuka, *J. Phys. Chem.*, **86**, 4422 (1982).
36) C. D. Tran and J. H. Fendler, *J. Phys. Chem.*, **88**, 2167 (1984).

Dopant Structure in $FeCl_3$-doped Polyacetylene Studied by X-Ray Absorption Spectroscopy and X-Ray Photoelectron Spectroscopy

Kiyotaka ASAKURA, Isao IKEMOTO,† Haruo KURODA,* Takaaki KOBAYASHI,†† and Hideki SHIRAKAWA††

Department of Chemistry and Research Center for Spectrochemistry, Faculty of Science, The University of Tokyo, Hongo, Bunkyo-ku, Tokyo 113

††*Institute of Material Science, University of Tsukuba, Sakura-machi Niihari-gun, Ibaragi 305*

(Received March 18, 1985)

The dopant structure in $FeCl_3$-doped polyacetylene was studied from the analysis of Fe K-edge EXAFS and XANES, measured by use of synchroton radiation. It is concluded that Fe atom is surrounded by four Cl atoms with Fe–Cl distance of 2.19—2.20 Å, and the dopant exists in the state of $[FeCl_4]^-$. The following mechanism is proposed for the doping process:

$$(CH)_x + 2yxFeCl_3 \rightarrow [CH(FeCl_4^-)_y]_x + yxFeCl_2$$

It is also shown that the chlorination of polyacetylene occurs significantly on performing a "heavy doping."

When doped with a suitable electron donor or acceptor, polyacetylene becomes metallic with an electrical conductivity more than 12 orders of magnitude higher than that of the undoped state.[1] A wide variety of dopants has been tested to see their effects on the electrical properties. However, little has been known on the electronic states and geometrical structures of dopants in the doped polyacetylenes. When a polyacetylene film is immersed into a nitromethane solution of $FeCl_3$, $FeCl_3$ is taken into the polyacetylene film to give electrical conductivity of, at most, 10^2 S cm^{-1}.[2,3] The state of the dopant in the $FeCl_3$-doped polyacetylene was studied by means of Mössbauer spectroscopy and ESR, but there were some contradictions among the conclusions given by different authors.[4–7]

The doping of polyacetylene is often compared with the formation of the graphite intercalation compound. In the case of the graphite intercalation compound with $FeCl_3$, the intercalated $FeCl_3$ layer was reported to have a structure more or less similar to that in anhydrous $FeCl_3$.[8] On the other hand, available experimental data suggest that the dopant state in $FeCl_3$-doped polyacetylene is quite different from this case.[4–7] Thus it seemed to be of great interest to elucidate the dopant structure in a $FeCl_3$-doped polyacetylene. We report here the results of the analysis of the extended X-ray absorption fine structure (EXAFS) and X-ray absorption near-edge structure (XANES) of Fe K-edge measured on $FeCl_3$-doped polyacetylene films. They provide a most direct evidence that the dopant exists in the state of $[FeCl_4]^-$. Curious behaviors were found for a heavy doping with $FeCl_3$. Namely, Fe K-edge jump decreased in spite of the increase of apparent dopant content, and the electrical conductivity of the film decreased on increasing apparent dopant content. We will also discuss the origin of this phenomenon.

Experimental

Polyacetylene films of cis-rich form were prepared by the previously reported method.[9] $FeCl_3$-doping was carried out by immersing polyacetylene films into a nitromethane solution of $FeCl_3$ as described elsewhere.[3] $FeCl_3$ had been kept *in vacuo* for several hours before use. Nitromethane was well dried over $CaCl_2$ and distilled before it was used as the solvent. Films of different dopant content were obtained by changing the immersing period and/or $FeCl_3$ concentration of the solution. The dopant contents and electrical conductivities of the prepared samples are listed in Table 1. The dopant content given there is the apparent value which is calculated from the weight uptake of a polyacetylene film in the doping process assuming that the dopant exists entirely in the form of $FeCl_3$. In reality, the dopant exists as $[FeCl_4]^-$, not as $FeCl_3$, and furthermore, the weight increase is partly due to the chlorination of polyacetylene, particularly in the case of heavy doping as we will show later. Thus the values of dopant content in Table 1 should be taken only as a measure of doping degree. Figure 1 shows the change of electrical conductivity as a function of dopant content, where the points indicated as **A**, **B**, C, and **D** correspond to Samples **A**, **B**, C, and **D**, respectively.

The specimens for the measurements of X-ray absorption spectrum were prepared in the following way. In an Ar-

Table 1. The dopant content and conductivity of $FeCl_3$-doped polyacetylene sample

Sample	Dopant concent[a] / % mol/(CH) mol	Conductivity / S/cm
Sample **A**	2.4	10—80
Sample **B**	8.7	700—800
Sample **C**	13.0	0.4—200
Sample **D**	7.4	700

a) Dopant content was calculated from the weight uptake of the polyacetylene assuming all the dopant was in the form of $FeCl_3$.

† Present address: Department of Chemistry, Faculty of Science, Tokyo Metroporitan University, Fukasawa, Setagaya-ku, Tokyo 158.

filled gloved box, a doped polyacetylene film was cut into several pieces of appropriate size and folded up several times to give a thickness suitable for X-ray absorption measurement, and then sandwiched between two pieces of adhesive tape to keep it in the folded state and, at the same time, to prevent the sample from a direct exposure to the atmosphere. The samples prepared by this way were stored in an Ar-filled Schlenk flask until just before they were used for the measurements.

Preliminary EXAFS experiments were done by use of an in-laboratory EXAFS spectrometer combined with a high-power rotating-anode X-ray generator (RIGAKU RU-1000).[10] Through these experiments, we checked the effects of sealing the sample with adhesive tapes, the appropriate sample thickness, and the homogeneity of the dopant distribution in a doped film. The final data of X-ray absorption spectrum were taken by use of synchrotron radiation emitted from the 2.5 GeV storage ring of the Photon Factory in the National Laboratory for High-energy Physics (KEK-PF), employing the EXAFS facilities at BL-10B.[11] X-Rays were monochromatized with a Si(311) channel-cut crystal. The intensity of the incident beam, I_0, and that of the transmitted beam, I, were measured with the ionization chambers which were placed before and after the sample, respectively, the gas filled in an ionization chamber being N_2 for I_0 and Ar for I. Most of X-ray absorption measurements were done at room temperature. The measurement at low temperature (10 and 80 K) was done only for Sample **D**, which was regarded to be a representative sample having a high electrical conductivity. X-Ray photoelectron spectra were taken with McPherson ESCA 36 electron spectrometer by empolying Mg $K\alpha$ (1253.6 eV) as the stimulating radiation. In order to avoid the effects of directly exposing the sample to air, a sample which has been kept in an Ar-filled vessel was transferred to the spectrometer by use of an Ar-filled gloved box which was directly connected to the spectrometer. The gases coming out from a sample were analyzed by use of JEOL JMS-D300 mass spectrometer. For the purpose to check the inhomogeneity of Fe distribution in a $FeCl_3$-doped polyacetylene film, we carried out the electron probe microanalysis by use of JEOL EPXMA TYPE JXA-5, the intensity distribution of Fe $K\alpha$ fluorescent X-ray being observed.

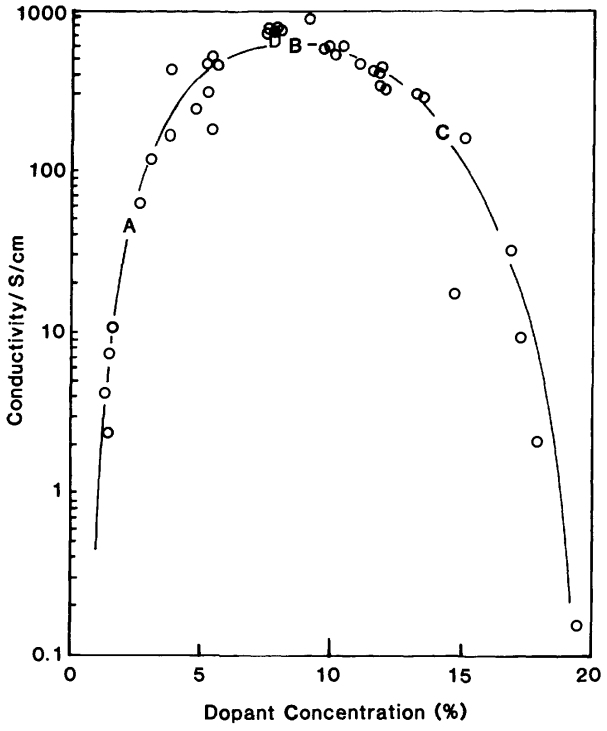

Fig. 1. Conductivity of $FeCl_3$-doped polyacetylene as a function of dopant concentration y. **A**, **B**, and **C** in the figure correspond to samples **A**, **B**, and **C**, respectively.

Results and Discussion

In the preliminary EXAFS experiments, we noted that Fe K-edge jump was significantly lower in the case of Sample **C** than what was expected from its apparent dopant content, it being even lower than those observed for Samples **A**, **B**, and **D**, and furthermore, it was found to vary as we examined different portions of Sample **C**. Since the latter fact indicated that the distribution of Fe is considerably inhomogeneous in this sample, we examined the Fe distribution in the film by use of an electron probe microanalyzer (EPMA). The image of Fe $K\alpha$ fluorescent X-ray showed that Fe distribution was indeed quite inhomogeneous, having Fe-rich regions and Fe-less regions within a film. On the other hand, the films of lower dopant content (Samples **A**, **B**, and **D**) were found to have a homogeneous Fe distribution. The reason for this anomarous behavior of Sample **C** will be discussed later.

As a typical example of the Fe K-edge absorption spectra measured by use of synchrotron radiation, the spectrum of Sample **D** at 80 K is shown in Fig. 2. The spectrum shows a sharp pre-edge peak attributable to ls-3d transition and several peaks near Fe K-edge,

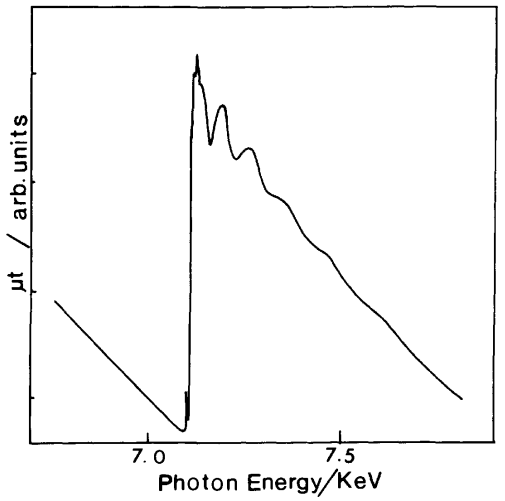

Fig. 2. Fe K absorption spectrum of Sample **D** at 80 K.

which are followed by EXAFS of a relatively simple structure. Spectral shape was found to be almost the same for all other samples of $FeCl_3$-doped polyacetylene.

We extracted EXAFS oscillation $\chi(k)$ from the observed spectra by the following method.[12] The smoothly-varying component $\mu_s(\lambda)$, was estimated by fitting an observed spectrum using the cubic spline method. The free atom absorption coefficient, $\mu_o(\lambda)$, in the region of 50—60 eV from the edge was taken to be equal to the difference between μ_s and the background absorption μ_b which was determined by a smooth extrapolation from the preedge region by use of Eq. 1.

$$\mu_b(\lambda) = \mathbf{A} + \mathbf{C}\lambda^3 + \mathbf{D}\lambda^4 \quad (1)$$

The μ_o value in other region was estimated by extrapolating the μ_o values in the above-mentioned region assuming that the wavelength dependence of μ_o was describable with the Victoreen's equation, the parameters of which were taken from the literature.[13] The photon energy E was converted to the photoelectron wave number k by Eq. 2.

$$k = \sqrt{2m(E-E_o)}/\hbar \quad (2)$$

where E_o is the ionization threshold. Then the EXAFS oscillation was calculated by using Eq. 3.

$$\chi(k) = (\mu-\mu_s)/\mu_o \quad (3)$$

Using thus extracted $\chi(k)$, we performed a Fourier transformation of $k^3\cdot\chi(k)$ over the region, $4 \leqq k \leqq 12$ Å^{-1}.

Figure 3 shows the Fourier transform of the EXAFS data of Sample **D** at 80 K. It shows only one prominent peak with the maximum at about 1.8 Å. This peak can be attributed to the nearest-neighbor Cl atoms surrounding Fe atom. No peak which is attributable to Fe-C or Fe-Fe, can be found even in the Fourier transform of the EXAFS data at 10 K. The Fourier transforms of the EXAFS data of all other samples (Samples **A**, **B**, and **C**) were also nearly the same as that of Sample **D**, exhibiting again only one prominent peak attributable to Fe-Cl.

Assuming the first shell to be due to Fe-Cl bond, we carried out the curve-fitting analysis by use of the following equation based on the single scattering theory.

$$k^3\chi(k) = (N/R^2)k^2F(k)\exp(-2k^2\sigma^2)\sin[2kR+\phi(k)] \quad (4)$$

where N is the coordination number, R the interatomic distance, $F(k)$ the back-scattering amplitude function, σ the Debye-Waller factor, $\phi(k)$ the phase shift function. The back-scattering amplitude function $F(k)$ and the phase shift function $\phi(k)$ were empirically determined from the analysis of the EXAFS data of the model compound, $[N(C_2H_5)_4][FeCl_4]$. Treating N, R, and σ as fitting parameters, their best-fit values were determined by means of the nonlinear least square technique. Figure 4 shows the calculated and observed $k^3\cdot\chi(k)$ curves for Sample **D**. The R and N values obtained by the curve-fitting analysis are listed in Table 2. For all samples of $FeCl_3$-doped polyacetylene, Fe-Cl bond length was found to be 2.19—2.20 Å. The obtained coordination numbers were somewhat different from sample to sample within the range of 3—4. But this difference is not likely to be intrinsic since a relatively large error is generally expected for a coordination number determined from the EXAFS data measured at room temperature. Because the EXAFS data obtained at lower temperature have better quality, the coordination number 3.9—4.0 obtained from the 80 K and 10 K EXAFS data of Sample **D**, is most reliable and can be taken as the actual coordination number. Thus we can conclude that, in the $FeCl_3$-doped

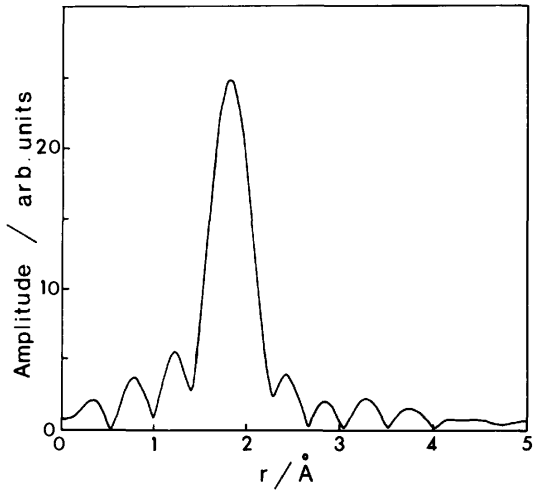

Fig. 3. Fourier transform of $k^3\cdot\chi(k)$ of the 80 K EXAFS data of Sample **D**.

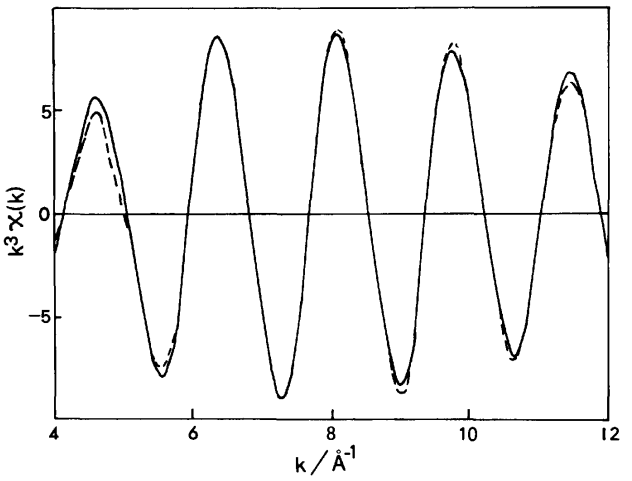

Fig. 4. The calculated (——) and observed (- - -) $k^3\cdot\chi(k)$ curves for Sample **D**.

polyacetylene, Fe atom is surrounded by four Cl atoms with Fe-Cl distance of 2.19—2.20 Å.

There are several kinds of the chemically stable ion of the type $[FeCl_x]^{y-}$, which are $[FeCl_4]^-$, $[FeCl_4]^{2-}$, $[FeCl_6]^{3-}$, and $[FeCl_6]^{4-}$. The Fe-Cl distances which have been determined from the crystal structure analysis are given in Table 3. Note that Fe-Cl distance is nearly the same for a given kind of the anion irrespective of the kind of the counter cation. In other words, it is almost determined by the valence state of Fe and the Cl coornination number. The data shown in Table 3, indicate that the Fe-Cl distance of 2.19 Å is the one characteristic of $[FeCl_4]^-$. Another ion which has the coordination number of 4, is $[FeCl_4]^{2-}$, but its average Fe-Cl distance is about 2.3 A. Therefore the results of the analysis of the Fe K-edge EXAFS data of $FeCl_3$-doped polyacetylenes indicate that the dopant is in the state of $[FeCl_4]^-$. As we have mentioned, Sample **C** has a very inhomogeneous Fe distribution. However, its Fe K-edge EXAFS data gave also the same conclusion. This means that the Fe-containing chemical species existing in the Fe-rich regions of this sample is also in the state of $[FeCl_4]^-$.

As it is known, XANES is determined by the local electronic state surrounding the X-ray absorbing atom, and reflects the valency state and the local symmetry around the X-ray absorbing atom.[23,24] Although a detailed analysis of XANES is rather complicated, one can use XANES just as a fingerprint of the local structure and electronic state. In Fig. 5, the Fe K-edge XANES spectrum of Sample **D** measured at 80 K is compared with the corresponding spectra of $[Co(NH_3)_6][FeCl_6]$, $[N(C_2H_5)_4]_2[FeCl_4]$, and $[N(C_2H_5)_4][FeCl_4]$, in which the local structure surrounding Fe is $[FeCl_6]^{3-}$, $[FeCl_4]^{2-}$, and $[FeCl_4]^-$, respectively. The sharp pre-edge peak in the spectrum of Sample **D** arises from 1a—3d transition and is characteristic of a tetrahedrally-coordinated ion like $[FeCl_4]^-$. Furthermore, the structures above the absorption edge are also similar to the ones found for $[N(C_2H_5)_4][FeCl_4]$. XANES spectra of other $FeCl_3$-doped samples are also nearly the same as that of Sample **D**. Thus the Fe K-edge XANES of $FeCl_3$-doped polyacetylene indicates that the local state surrounding Fe corresponds to $[FeCl_4]^-$ in agreement with the conclusion derived from EXAFS data. Summarizing all the results mentioned above, we can definitely conclude that, in a $FeCl_3$-doped polyacetylene, the dopant exists mainly in the state of $[FeCl_4]^-$,

Table 2. Results of the analysis of EXAFS data by using the empirical parameters[a)]

Sample	Bond length l/Å	Coordination No.
Sample **A**	2.200	2.9
Sample **B**	2.195	3.3
Sample **C**	2.195	4.2
Sample **D**	(T=300 K) 2.199	3.5
Sample **D**	(T= 80 K) 2.200	3.9
Sample **D**	(T= 10 K) 2.200	4.0

a) The phase shift and amplitude functions obtained from the analysis of the room-temperature EXAFS data of $[N(C_2H_5)_4][FeCl_4]$, assuming Fe-Cl distance as 2.18 Å and coordination number as 4, were used except for the analyses of the 80 K and 10 K EXAFS data of Sample **D**, for which the empirical parameters derived from the 80 K EXAFS data of $[N(C_2H_5)_4][FeCl_4]$.

Table 3. Fe-Cl bond lengths in $[FeCl_2]^{y-}$ ions

Type	Salt	Bond length l/Å	Ref
$[FeCl_4]^{2-}$	$(C_5H_5S_2)_2[FeCl_4]$	2.313 (av.)	14
	$(C_5H_5S_2)_2[FeCl_4]$	2.33 (av.)	15
	$\{[Fe(\eta^5\text{-}C_5H_5)(CO)_2]_3SbCl\}_2$		
	$[FeCl_4]CH_2Cl_2$	2.302 (av.)	16
	$[N(CH_3)_4]_2[FeCl_4]$	2.292	17
$[FeCl_4]^-$	$[As(C_6H_5)_4[FeCl_4]$	2.19	18
	$[FeCl_2(DMSO)_4][FeCl_4]$	2.162	19
	$Na[FeCl_4]$	2.196	20
	$[PCl_4][FeCl_4]$	2.185	21
$[FeCl_6]^{4-}$	$NaK_3[FeCl_6]$	2.5100	22
$[FeCl_6]^{3-}$	$[Co(NH_3)_6][FeCl_6]$	2.3926	22

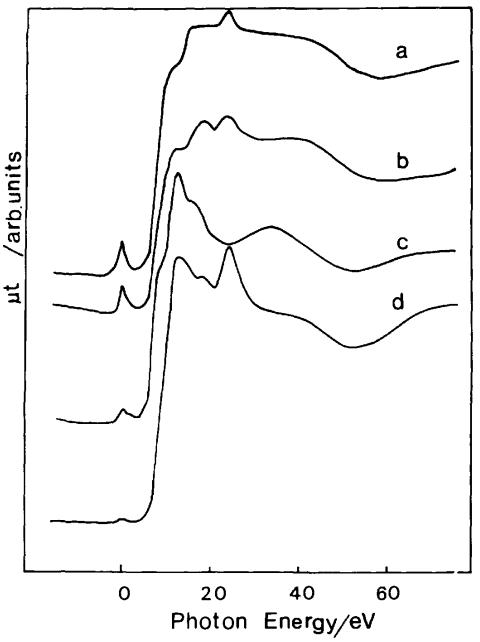

Fig. 5. XANES spectra of (a) Sample **D**, (b) $[N(C_2H_5)_4][FeCl_4]$, (c) $[N(C_2H_5)_4]_2$ $[FeCl_4]$ and (d) $[Co(NH_3)_6][FeCl_6]$. The photon energy is measured from the transition energy of the pre-edge peak E_d of each sample. The transition energies of the pre-edge peaks of Sample **D**, $[N(C_2H_5)_4][FeCl_4]$, $[N(C_2H_5)_4]_2$ $[FeCl_4]$ and $[Co(NH_3)_6]$ $[FeCl_6]$ are 7104.8, 7104.8, 7103.0, and 7104.5 eV, respectively.

not in the state of $FeCl_3$ nor in the state of $[FeCl_4]^{2-}$. This conclusion is consistent with the recent studies by Mössbauer spectroscopy.[4,5]

The dopant state revealed by the present study, is quite different from that in the graphite intercalation compound, where ther intercalated $FeCl_3$ takes a layer structure somewhat similar to the one in anhydrous $FeCl_3$, having a partial charge transfer between graphite and $FeCl_3$ layers.[8] Since the dopant exists as $[FeCl_4]^-$, we propose the following doping mechanism for the $FeCl_3$-doped polyacetylene. In a separate experiment, we have studied the solute structure in a nitromethane solution of $FeCl_3$ by use of Fe K-edge EXAFS, and found that $[FeCl_4]^-$ exists in the nitromethane solution beside another iron-containing species.[25] The latter is likely to be a solvated octahedral chloro complex,[25] which we tentatively denote as $[FeCl_2]^+$. Possibly the following electrolytic dissociation had taken place in the nitromethane solution to yield $[FeCl_4]^-$.

$$2FeCl_3 \rightarrow [FeCl_4]^- + [FeCl_2]^+ \quad (5)$$

Therefore it is most likely that, when a polyacetylene film is immersed into the nitromethane solution of $FeCl_3$, $[FeCl_2]^+$ is reduced by the electron transfer from polyacetylene to form $FeCl_2$ which might remain in the solution or precipitate from the solution, and only $[FeCl_4]^-$ ions enter into the space surrounded by positively-charged polyacetylene chains.

As shown in Fig. 1, it has been generally observed that the electrical conductivity of $FeCl_3$-doped polyacetylene initially increases with dopant content, but decreases when the apparent dopant content exceeds about 10 mol% on performing a heavy doping. Among the samples taken up in the present study, Sample **C** was the one prepared under the condition of heavy doping. In fact, the apparent dopant content of this sample was 13 mol%, which is considerably higher than that of Sample **D**. However, the magnitude of Fe K-edge jump was found to be lower in comparison with Sample **D**. As we have already mentioned, the magnitude of Fe K-edge jump varies from portion to portion on the film of Sample **C**. We confirmed also by means of electron probe microanalysis(EPMA), that Fe distribution is quite inhomogeneous in this sample. To clarify the origin of these anomalous behaviors of a heavily-doped sample, we examined the X-ray photoelectron spectra of $FeCl_3$-doped polyacetylene films. As shown in Fig. 6, Samples **A** and **B** exhibit a single C 1s peak accompanied by a high-binding-energy tail, whereas the C 1s spectrum of Sample **C** splits into two peaks, indicating the presence of two different kinds of C atom. The Cl 2p spectra of $FeCl_3$-doped polyacetylenes are shown in Fig.7 together with the corresponding spectrum of $[N(C_2H_5)_4][FeCl_4]$. Note that the Cl 2p spectrum of Sample **A** very much resembles that of $[N(C_2H_5)_4][FeCl_4]$, but the Cl 2p spectrum of Sample **C** exhibits a quite strange shape, indicating the presence of two different kinds of Cl atoms. The observed binding energies of C 1s and Cl 2p peaks are listed in Table 4. The binding energy of the main C 1s peak is 284.1 eV both for Sample **A** and Sample **B**, which is in good agreement with the C 1s binding energy of an undoped *trans*-polyacetylene. Since the C 1s spectrum of Sample **C** is clearly composed of two components, we carried out a deconvolution into two components and determined the energy splitting and the intensity ratio of the high-binding-energy com-

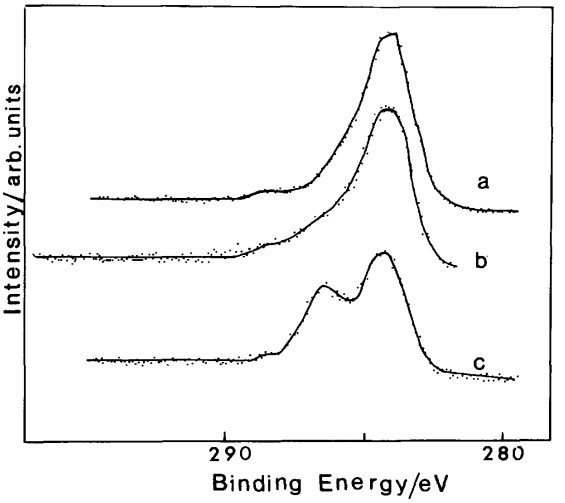

Fig. 6. XPS C_{1s} spectra of (a) Sample **A**, (b) Sample **B**, and (c) Sample **C**.

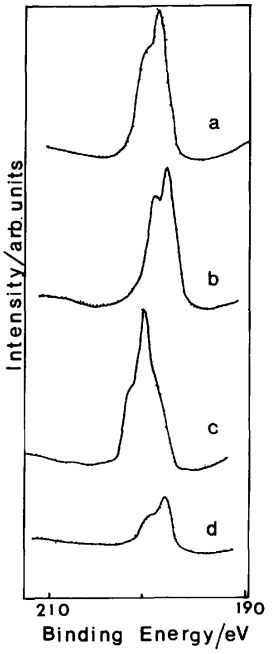

Fig. 7. XPS Cl_{2p} spectra of (a) Sample **A**, (b) Sample **B**, (c) Sample **C**, and (d) $[N(C_2H_5)_4][FeCl_4]$.

TABLE 4. XPS RESULTS OF $FeCl_3$-doped POLYACETYLENE FILMS

Sample	C_{1s}			Cl_{2p}		
	Binding energy		Intensity ratio	Binding energy		Intensity ratio
	C-1	C-2	C-2/C-1	Cl-1	Cl-2	Cl-2/Cl-1
	eV			eV		
Sample **A**	284.1	—	—	198.3	—	—
Sample **B**	284.1	—	—	198.2	—	—
Sample **C**	284.4	286.2	0.39	198.6	200.2	0.35

ponent to the low-binding-energy component. A deconvolution into two components was also done on the Cl 2p spectrum. The results are given in Table 4. Hereafter we denote the low-binding-energy component of the C 1s peak as C-1 and the high-binding-energy component as C-2. In the same way, we denote the low-binding-energy and high-binding-energy components of the Cl 2p spectrum as Cl-1 and Cl-2, respectively.

We noted that the shape of C 1s spectrum as well as that of Cl 2p spectum changed when Sample **C** was kept *in vacuo* for a long period (see Figs. 8 and 9). This means that the intensity ratio of the two components of each spectrum changes with time. In Fig. 10, we have plotted the intensity of each component as a function of the time for which the sample had been kept *in vacuo*. Note that the intensity of the C-2 component of the C 1s specrum decreased while that of the C-1 component increased with time, and at the same time, the intensity of the Cl-2 component of the Cl 2p spectrum showed a significant decrease with time while no appreciable

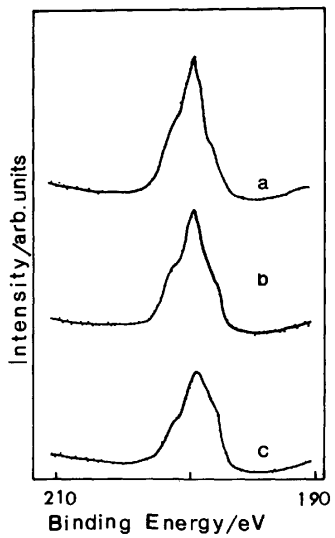

Fig. 9. Time dependence of the Cl_{2p} spectra of Sample **C**; (a) 11 h, (b) 25 h, (c) 50 h.

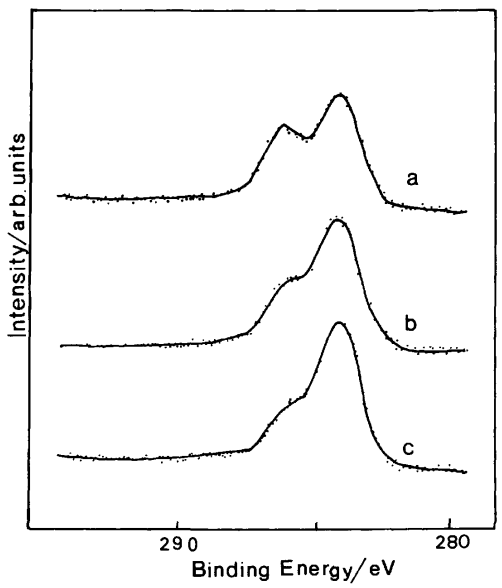

Fig. 8. Time dependence of the C_{1s} spectra of Sample **C**; (a) 10 h, (b) 24 h, and (c) 49 h.

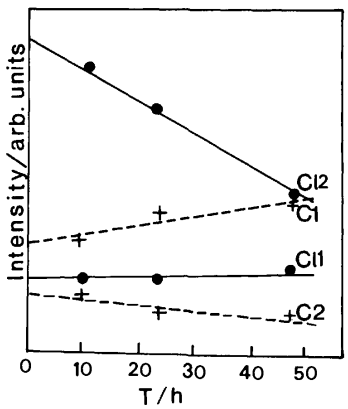

Fig. 10. Time dependence of the intensities of the decomvoluted components of Cl_{2p} and C_{1s} peaks. C-1 and C-2 denote the lower and higher binding energy components of the C_{1s} peaks, respectively. C-1 and Cl-2 denote the lower and higher binding energy components of Cl_{2p} peaks, respectively.

change was found for the intensity of the Cl-1 component. We examined the gases which coming from the sample during the above-mentioned process by use of mass spectroscopy and found that the main chemical species was HCl.

Summarizing the above-mentioned experimental data, we can derive the following conclusion. Since the intensities of the C-2 and Cl-2 components decrease in parallel to each other, they are likely to be associated with the same origin. The Cl $2p_{3/2}$ binding energy of the Cl-2 component, 200 eV, is the value that is usually found for a Cl atom forming C–Cl bond, and the C 1s binding energy of the C-2 component is the one that is expected for a C atom of C–Cl bond.[28] Thus the C-2 and Cl-2 components are likely to be associated with the C–Cl bond which has been formed as a result of the chlorination of polyacetylene chain. At present, we do not know about the mechamism of the chlorination taking place in the process of a heavy $FeCl_3$ doping. Possibly, when a polyacetylene film already saturated with $[FeCl_4]^-$ with apparent dopant content above 10 mol%, is further kept in a nitromethane solution of a high $FeCl_3$ concentration, the chlorination of polyacetylene chain takes place in some way within the doped region and the Fe containing species of the reaction products escapes from the polyacetylene film into the solution. Thus the weight increase in this process is not due to an increase of $[FeCl_4]^-$ content, but is mainly due to chlorination. This explains the reason why the magnitude of Fe K-edge jump is markedly smaller than what is expected from the apparent dopant content, and why the electrical conductivity decreases on a heavy doping.

The above-described phenomenon is similar in some respects to the one found for a heavy doping with bromine.[29] In this case, the addition of bromine to polyacetylene chain significantly takes place, resulting in an abrupt decrease of electrical conductivity. It is also known that HBr comes out from such a heavily Br-doped film when kept *in vacuo*.

Finally we wish to point out that, in the case of Sample **B** whose dopant content is just around 10 mol%, the shape of the Cl 2p spectrum is a little different from what is expected for $[FeCl_4]^-$. There seems to be a contribution of the component corresponding to Cl-2. In other words, the chlorination is likely to take place to a small extent even in a relatively-light $FeCl_3$ doping.

The authors would like to express their thanks for the technical advice given by Professor T. Matsushita, Dr. H. Oyanagi and Dr. M. Nomura on the measurements of EXAFS spectra at the Photon Factory. The analyses of EXAFS data were done by use of HITAC M-280H at the Computor Center, The University of Tokyo. This work was supported by the Grant-in-Aid for the Special Project Research on "the Properties of Molecular Assemblies" (No. 58118002), from the Ministry of Education, Science and Culture.

References

1) H. Shirakawa, E. J. Louis, A. G. MacDiarmid, C. K. Chiang, and A. J. Heeger, *J. Chem. Soc., Chem. Commun.*, **1977**, 578.

2) A. Pron, I. Kulszewicz, D. Billaud, and J. Przyluski, *J. Chem. Soc., Chem. Commun.*, **1981**, 783.

3) H. Shirakawa and T. Kobayashi, "Proceeding of International Conference on Physics and Chemistry of Conducting Polymer," Les arcs, France, (1982).

4) H. Sakai, Y. Maeda, T. Kobayashi, and H. Shirakawa, *Bull. Chem. Soc. Jpn.*, **56**, 1616 (1983).

5) Z. Kuoharski, M. Lukasiak, J. Suwalski, and A. Pron, to be published.

6) Y. W. Park, J. C. Woo, W. K. Han, C. H. Choi, T. Kobayashi, and H. Shirakawa, *Solid State Commun.*, **46**, 731 (1983).

7) A. Pron, P. Bernier, D. Billaud, and S. Lefrant, *Solid State Commun.*, **46**, 587 (1983).

8) a) W. Rudorff and H. Schulz, *Z. Anorg. Chem.*, **245**, 121 (1940); b) J. M. Cowley and J. A. Ibers, *Acta Cryst.*, **9**, 421 (1956).

9) T. Ito, H. Shirakawa, and S. Ikeda, *J. Polym. Sci., Polym. Ed.*, **13**, 1943 (1975).

10) Y. Sato, Thesis, The University of Tokyo (1982).

11) H. Oyanagi, T. Matsushita, M. Ito, and H. Kuroda, *KEK Report* **83—30**, (1984).

12) K. Asakura, M. Nomura, and H. Kuroda, *Bull. Chem. Soc. Jpn.*, **58**, 1543 (1985).

13) "International Tables for X-ray Crystallography III," ed by C. H. Macgillavry, G. D. Rieck, and K. Lonsdale, Kynoch Press (1962).

14) R. Mason, E. D. Mckensie, G. B. Robertson, and G. A. Rusholme, *J. Chem. Soc., Chem. Commun.*, **1969**, 56.

15) H. C. Freeman, G. H. Milburn, C. E. Nockolds, P. Hemmerich and K. H. Knauer, *J. Chem. Soc., Chem. Commun.*, **1969**, 56.

16) Trinh-Toan and L. F. Dahl, *J. Am. Chem. Soc.*, **93**, 2654 (1971).

17) J. W. Lauher and J. A. Ibers, *Inorg. Chem.*, **14**, 348 (1975).

18) B. Zaslow and R. E. Rundle, *J. Phys. Chem.*, **61**, 490 (1975).

19) M. J. Bennett, F. A. Cotton, and P. L. Weaver, *Acta Cryst.*, **23**, 581 (1967).

20) R. R. Richards and N. W. Gregory, *J. Phys. Chem.*, **69**, 239 (1965).

21) T. J. Kistenmacher and G. D. Stucky, *Inorg. Chem.*, **7**, 2150 (1968).

22) J. K. Beattje and C. J. Moore, *Inorg. Chem.*, **21**, 1292 (1982).

23) F. W. Kutzler, *SSRL Report*, **80/01**, (1981).

24) N. Kosugi, T. Yokoyama, K. Asakura, H. Kuroda, *Chem. Phys.*, **19**, 249 (1984).

25) H. Kuroda, N. Kosugi, K. Asakura, H. Ishii, M. Nomura, *Photon Factory Activity Report* **82/83**, VI-36, (1984).

26) The method of the deconvolution of the XPS peaks was described elwewhere.[27] The standard peaks used for Cl_{2p} and C_{1s} were the Cl_{2p} peak of $[N(C_2H_5)_4][FeCl_4]$ and C_{1s} peak of *trans*-polyacetylene, respectively.

27) I. Ikemoto, M. Yamada, T. Sugano, and H. Kuroda, *Bull. Chem. Soc. Jpn.*, **53**, 1871 (1980).

28) D. T. Clark, D. Kilcast, D. B. Adams and W. K. R. Musgrave, *J. Electron. Spec.*, **6**, 117 (1975).

29) I. Ikemoto, Y. Cao, M. Yamada, H. Kuroda, I. Harada, H. Shirakawa, and S. Ikeda, *Bull. Chem. Soc. Jpn.*, **55**, 721 (1982).

Active and Selective Transport of Alkali Metal Ions through a Polyelectrolyte Complex Membrane Consisting of Glycol Chitosan and the Sulfate of Poly(vinyl alcohol)

Yasuo KIKUCHI* and Naoji KUBOTA
Faculty of Engineering, Ōita University, 700-Dannoharu, Ōita 870
(Received December 6, 1984)

Polyelectrolyte complex (PEC) membranes consisting of glycol chitosan and the sulfate of poly(vinyl alcohol) have been prepared. The membrane of the polyelectrolyte complex under a 50% humidity prepared in a 4% hydrochloric acid solution was stable in basic and acidic solutions. The membranes of the PECs under a 90% humidity prepared at pH 1.0 were not stable in an alkaline solution. The active and selective transport of K^+ and Na^+ were observed in the PEC membrane prepared in a 4% hydrochloric acid solution. The transport behavior of alkali metal ions through this membrane was much affected by the hydrogen-ion concentration, which acted as a driving force. A proton-pump mechanism was suggested for the acive transport of Na^+ and K^+. It was also suggested that the affinity of the carrier and changes in both the chemical and physical properties of the PEC membrane with the hydrogen-ion concentration controlled the selective transport through the membrane.

The specific transport of ions is a common function of a biomembrane. An active transport process is usually defined as one that can bring about a flow of a substance against an electrochemical potential gradient of the substance; the name implies that specific biological activity is involved in the process described by Rosenberg.[1] That is to say, the dissipation function is smaller than zero. This is observed in the active and selective transport of metal ions through a protoplasmic liquid[2-4] and synthetic membranes carrying a fixed functional group.[5-7] Research into such synthetic membranes is an important objective in the field of macromolecules. Active and selective transport through a polyelectrolyte complex membrane carrying a fixed functional group has not yet been investigated. However, for several polyelectrolyte complexes[8-10] we have reported that the polyelectrolyte complex membranes consisting of [2-(diethyl-amino)ethyl]dextran hydrochloride, sodium carboxymethyl dextran, and the sulfate of poly (vinyl alcohol) were capable of the active and selective transport of alkali metal ions.[11,12] This paper will deal with the similar phenomena of membranes consisting of glycol chitosan and the sulfate of poly (vinyl alcohol).

Experimental

Glycol chitosan (GC)(nitrogen content, 4.32%; inherent viscosity, 1.79 dl/g in a 0.1 M†NaCl solution at 25 °C) and the sulfate of poly(vinyl alcohol)(PVSK)(sulfur content, 18.91%; inherent viscosity, 0.67 dl/g in a NaCl solution at 25 °C) were used.

The reaction was carried out in a hydrochloric acid solution, 4% (v/v) and pH 1.0, considering the conformational change in the materials. The polyelectrolyte complex (PEC) was not formed at hydrogen-ion concentrations above pH 4.0. The GC solution (2 g/L) or PVSK (2 g/L) solution was added dropwised to a PVSK or GC solution, and the pH values of both solutions were adjusted to that of a 4% hydrochloric acid solution, pH 1.0 at about 22 °C at a rate of 50 ml/30 min under stirring.[11] A water-insoluble PEC was thus obtained. After being left to stand for 30 min, the PEC was washed with the hydrochloric acid solution, water, and then methanol. Then it was separated by centrifugation and dried at room temperature until a constant weight was attained. The details of the expermental conditions were described in a previous paper.[11]

The PEC was dissolved in a ternary solvent mixture (HCl/1,4-dioxane/H_2O, 16:47:37 wt-%). The solution was poured onto a Teflon plate; about 2 d latter the solvent was removed at room temperature. In addition, a uniform and yellowish transparent film was obtained on the Teflon plate by further evaporating of the solvent under 50 or 90% humidity for one or 2 d. The thickness of the membrane was about 100 μm. The resistence of the membranes against acid and base were examined by immersing them in a acidic (0.1 M HCl) or an alkaline solution (0.1 M NaOH). A PMMA cell consisting of two chambers was used in the active and selective transport. The membrane, having an effective area of 4.0 cm^2,was fixed tightly with rubber between two chambers of the cell.[12] The cell was then immersed in a constant-temperature bath set at 30 °C. The concentrations of the alkali metal ions, K^+ and Na^+, in both the left and right sides of the cell (chambers) were measured by means of atomicabsorption spectrophotometer.

Results and Discussion

The experimental conditions for the PEC prepared before and after the coagulation of PEC and the mole ratio of the reactive group S(PVSK) to that of N(GC) in the mixture solution before and after the coagulation of the PEC produced are given in Table 1. The details of the experimental conditions were described

† 1 M=1 mol dm^{-3}.

TABLE 1. PREPARATION OF POLYELECTROLYTE COMPLEXES

Sample code	Concentration of hydrogen ions	Order in mixing	Molar ratio of reactive group of S(PVSK) to that of N(GC) in the mixture
1-A	4v/v% HCl	PVSK $\xrightarrow{\text{into}}$ GC solution	1.00
1-a	4v/v% HCl	PVSK $\xrightarrow{\text{into}}$ GC solution	1.57
1-B	4v/v% HCl	GC $\xrightarrow{\text{into}}$ PVSK solution	3.61
1-b	4v/v% HCl	GC $\xrightarrow{\text{into}}$ PVSK solution	2.49
2-A	pH 1.0	PVSK $\xrightarrow{\text{into}}$ GC solution	0.83
2-a	pH 1.0	PVSK $\xrightarrow{\text{into}}$ GC solution	1.30
2-B	pH 1.0	GC $\xrightarrow{\text{into}}$ PVSK solution	2.52
2-b	pH 1.0	GC $\xrightarrow{\text{into}}$ PVSK solution	1.62

The polyelectrolyte complexes (PEC) of 1-A, 1-B, 2-A, and 2-B were prepared before the starting point of coagulation. The molar ratios of S/N at the starting point of coagulation were 1.04, 3.57, 0.89, and 2.39 respectively. The PECs of 1-a, 1-b, 2-a, and 2-b were prepared after the end point of coagulation. The molar ratios of S/N at the end point of coagulation were 1.51, 2.56, 1.24, and 1.67 respectively. The concentration of glycol chitosan (GC) and that of sulfate of poly(vinyl alcohol) (PVSK) were both 2.0 g/l. GC: Nitrogen content 4.32%, inherent viscosity 1.79 dl/g, in 0.1 M NaCl solution at 25 °C. PVSK: Sulfur content 18.91%, inherent viscosity 0.67 dl/g, in 1 M NaCl solution at 25 °C.

TABLE 2. STABILITIES OF MEMBRANES IMMERSED IN ACIDIC (0.1 M HCl) AND ALKALINE (0.1 M NaOH) SOLUTIONS

Sample code[a)]	Acidic solution	Alkaline solution
1-A	○	△
1-a	○	△
1-B	○	△
1-b	○	○
2-A	—	—
2-a	—	—
2-B	○	×
2-b	○	×

a) Sample code corresponds to that in Table 1. The PEC membranes were prepared under 50% humidity. ○: Stable, △: Slightly unstable, ×: Soluble in alkaline solution, —: Soluble in water

TABLE 3. STABILITIES OF MEMBRANES IMMERSED IN ACIDIC (0.1 M HCl) AND ALKALINE (0.1 M NaOH) SOLUTIONS

Sample code[a)]	Acidic solution	Alkaline solution
1-A	○	×
1-a	○	△
1-B	○	×
1-b	○	△
2-A	—	—
2-a	—	—
2-B	△	×
2-b	△	×

a) Sample code corresponds to that in Table 1. The membranes were prepared under 90% humidity. ○: Stable, △: Slightly unstable, ×: Soluble in alkaline solution, —: Soluble in water.

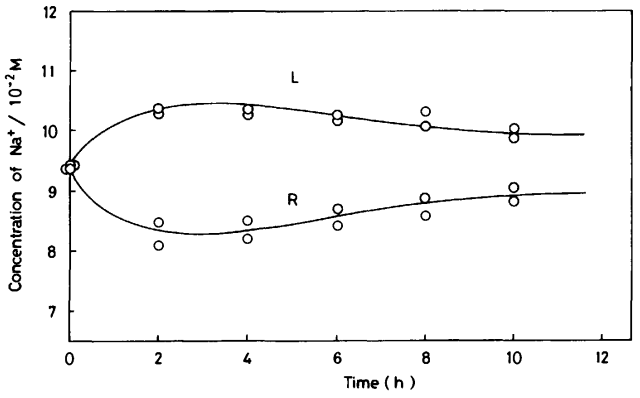

Fig. 1. Time-transport curve of Na^+ of the active transport at 30 °C.

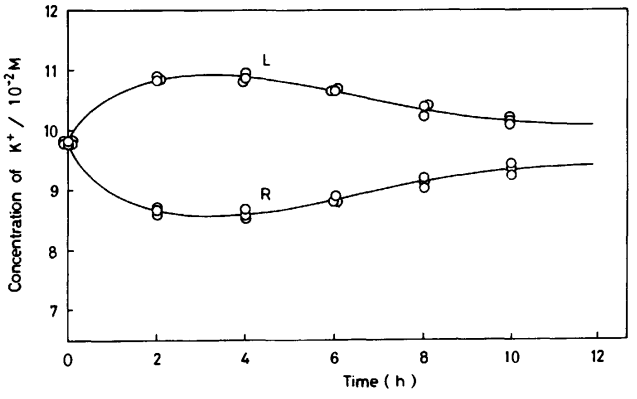

Fig. 2. Time-transport curve of K^+ of the active transport at 30 °C.

in a previous paper.[11]

The properties of the membranes in acidic and basic solutions are shown in Tables 2 and 3 respectively. The membranes formed under 50 and 90% humidity except for 2-A and 2-a, which were formed at pH 1.0, resisted an acidic solution. On the other hand, the membranes except 1-b formed in a 4% hydrochloric acid solution at 50% humidity were not resistant to a basic solution. The 1-b membrane was not damaged in either a 0.1 M NaOH or 0.1 M hydrochloric acid solution, even after 5 d. This membrane was used in the study of the transport of alkali metal ions. The sulfur and nitrogen contents in the PEC used to prepare the membrane were 9.55 and 3.73% respectively. The active-transport experiment was carried out at 30 °C. The concentration of the Na^+ or K^+ ion both the left and right sides of the cell was kept identical initially. In the left side, the cell also contained HCl, while the right-side cell contained NaOH or KOH.

Figures 1—2 show the concentration change in the Na^+ or K^+ ion against the reaction time in both cells at pH 1.0 through the membrane. The concentration of alkali metal ions in the left-side cell, which was acidic, increased up to a maximum and then decreased with the reaction time, while the change in the right-side cell was just the reverse. A back transfer of the concentrated alkali metal ions was due to the decrease in the hydrogen ion concentration on the left side. The changes in the concentration of Na^+ in the NaOH system were somewhat smaller than those of K^+ in the KOH system.

As is shown in Figs 3—4, the transport ratio[13], $([M^+]_{max}-[M^+]_o/[M^+]_o)\times 100$, of the alkali metal ions (Na^+, K^+) was proportional to the concentration of hydrogen ions in the left-side cell. Since the initial concentration of the alkali ion was originally the same in both left and right cells, the increase in the alkali concentration in the left cell suggests the active transport of the alkali metal ion through the membrane. It is of important significance in saving energy and resources that a PEC membrane carrying a fixed functional group is capable of the active transport of alkali metal ions. The difference in the transport ratios of Na^+ and K^+ against the hydrogen-ion concentration of the two systems are hardly discernible in hydrogen-ion concentrations below pH 2.0, whereas that of Na^+ is larger than that of K^+ in hydrogen-ion concentrations above pH 1.0. The transport rate,[13] $[M^+]_{max}-[M^+]_o/T_{max}$ in Mh^{-1} was proportional to the initial hydrogen-ion concentration. The pH values in the left- and right-side cells changed with the passing of time.

The change in the pH in both side cells is shown in Fig. 5. A maximum in the alkali metal-ion concentration appeared because of the neutralization of the aqueous solution in both cells. Accordingly, the driving force for transport was a gradient of the hydrogen-ion concentration. This pH change is attributed to a transfer of H^+, OH^- and alkali metal ions as well as the Cl^- ion[6] in both side cells. A proton-pump mechanism was considered for the concentration of alkali-metal ions.[5]

Selective transport from the right-side cell to the left-side cell through the membrane was observed under a 0.05 M concentration of both NaOH and KOH solutions in the right-side cell and at different hydrogen-ion concentrations in the left-side cell at 30 °C. The ratios of the transported ions the selectivity,[5,6] were calculated from the following equation:

$$\text{Selectivity} = \frac{[K^+]_{Lt}/[K^+]_{R,o}}{[Na^+]_{Lt}/[Na^+]_{R,o}}$$

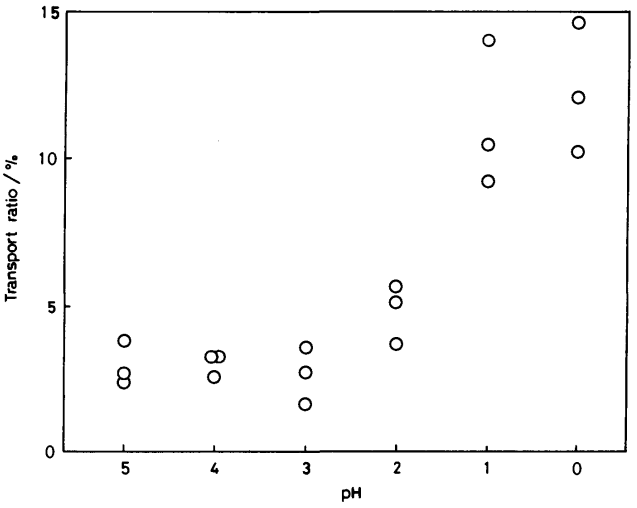

Fig. 3. Influence of hydrogen ion concentrations on the transport ratio of Na^+ ion at 30 °C.

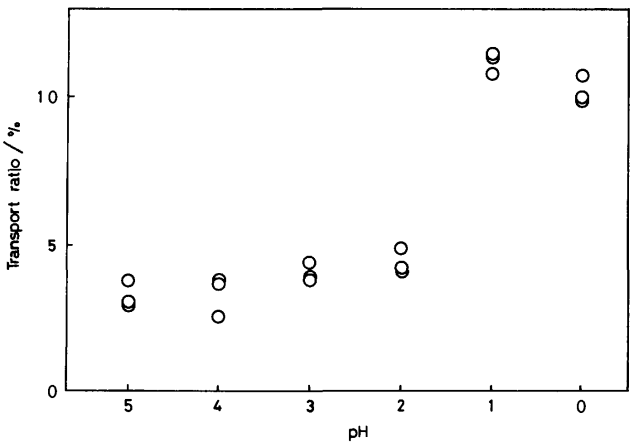

Fig. 4. Influence of hydrogen ion concentrations on the transport ratio of K^+ ion at 30 °C.

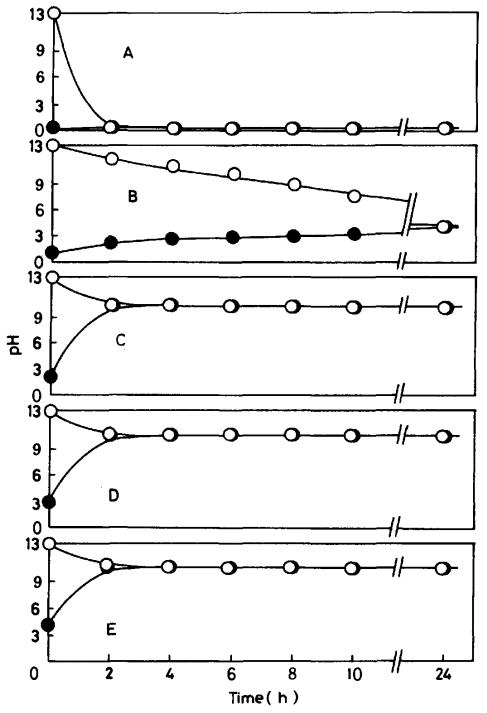

Fig. 5. Changes in hydrogen ion concentration through membrane.
A: 1 M HCl, B: 0.1 M HCl, C: 0.01 M HCl, D: 0.001 M HCl, E: 0.0001 M HCl.

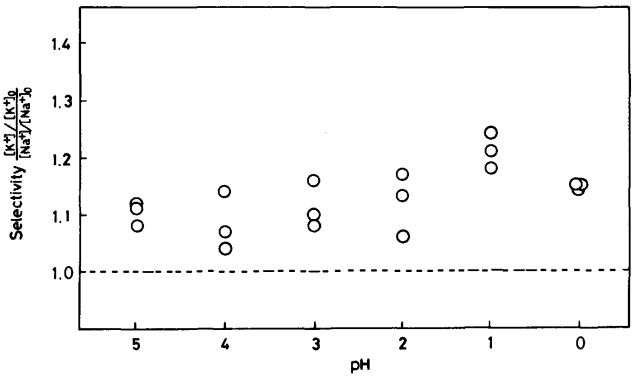

Fig. 6. Influence of hydrogen ion concentrations on selectivities in transport of Na^+ and K^+ ions after 4 h.

The selectivity of the transport through membrane after 4 h at different hydrogen-ion concentrations is shown in Fig. 6. The ratio of the permeated K^+ to the permeated Na^+ changed with the hydrogen-ion concentration. When the initial hydrogen-ion concentration was low, the selectivity was close to unity. In this region, the alkali metal ions diffused without any great or specific interaction with the membrane. In the region where the hydrogen-ion concentration was higher than 1.0×10^{-2} M, more K^+ ions permeated than Na^+ ions. The optimum hydrogen-ion concentration was 1.0×10^{-1} M with 0.05 M concentrations of NaOH and KOH solutions in the right-side cell. These results suggest that the main contributing factor in the selectivity in the transport of alkali metal ions is the hydrogen-ion concentration. The membrane prepared was throughly powdered in a agate mortar with a pestle. The pulverized membrane was then immersed in a basic or acidic solution for about 1 d. The IR spectrum of the pulverized membrane immersed in an acidic solution exhibited the medium absorption a 800—900 cm^{-1}, assigned to the $-SO_3H$ group,[14] but that immersed in a basic solution exhibited only a weak absorption. In addition, that immersed in a basic solution exhibited the medium absorption at 900—940 cm^{-1}, assigned to the $-SO_3$ group.[14] On the acidic side, this characteristic absorption band almost disappeared. From these IR spectra, therefore, it was concluded that the PEC moiety was opened on the alkaline side and closed on the acidic side. Furthermore, this conclusion has been well confirmed by the following experimental results of the lengthing or shrinkage of the membrane immersed in a basic or acidic solution. The horizontal and vertical lengthes of membrane immersed in the pH 1.0 and 13.0 solutions were 25 mm×28 mm and 33 mm×34 mm. When the above membrane, pretreated in a pH 1.0 or pH 13.0 solution, was further immersed in a pH 13.0 or pH 1.0 solution, the lengthes of the above two dimensions varied about 31 mm×34 mm and 30 mm×30 mm respectively, with an error of about 2 mm. That is, the membrane was elongated in a basic solution and shrunk in an acidic solution. In the region where the hydrogen-ion concentration was larger than 1.0×10^{-2} M in the left-side cell, the hydrated K^+ permeated faster than the hydrated Na^+ because of the radius of the hydrated K^+ was shorted than that of the hydrated Na^+ because of the formation of small holes as a result of the closing of the channel in the membrane, whereas that of the hydrogen-ion concentration was smaller. No appreciable selectivity of transport were observed because of the indiscriminate permeation of alkali metal ions owing to the formation of large holes results of the opening of the channel in the membrane. It was suggested that the affinity of the carrier fixed to the membrane, the degree of the opening and closing of the PEC moiety, and the physical properties of the PEC membrane, as well as the hydrogen bonding between -OH and $-OSO_3H$ or $-OSO_3^-Na^+$ groups with the hydrogen-ion concentration, controlled the selective transport through the membrane.[6] Therefore, on the basis of the pH change in the solution we speculate that the PEC membrane achieved the following reaction;

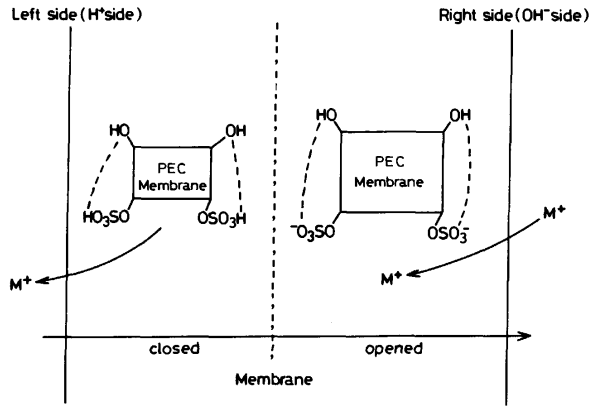

Fig. 7. Tentative mechanism of the transport of Na^+ and K^+ ions.

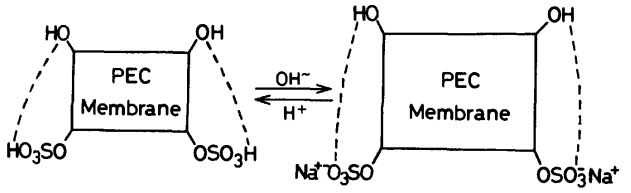

A tentative mechanism of the transport of alkali-metal ions, deduced from the results described above, is shown in Fig. 7. In this system, the hydrogen-ion concentration acted as the driving force and controlling reagent for the properties of the membrane.[5] At first, when a specific functional group, $-OSO_3^-$ in the membrane is on the right-side (OH^- side), metal ions are bound to the sulfate group in an alkaline solution with the changes in both the chemical and physical properties of the PEC membrane described above. Then, the alkali metal ions bound to the sulfate group are transferred through the membrane and are released by the hydrogen-ion or the acidic side. As a result, alkali metal ions are transported from the basic side to the acidic side. We consider that the driving force of the active transport of alkali ions is a gradient of the hydrogen-ion concentration, while the binding of the alkali metal ions to the sulfate group is attributable to the degree of the ring opening of the PEC membrane with hydrogen bonding, which affects the selectivity.[5,6]

The suitable conditions for the formation of the PEC membrane and the PEC membrane of transport for a negative ions have scarcely been elucidated at all. Therefore, further investigation must be carried out clarify the mechanism.

References

1) T. Rosenberg, *Acta. Chem. Scand.*, **2**, 14 (1948).
2) E. M. Choy, D. F. Evance, and E. C. Cussler, *J. Am. Chem. Soc.*, **96**, 7085 (1974).
3) D. K. Shiffer, A. Hochhauser, D. F. Evance, and E. L. Cussler, *Nature*, **250**, 484 (1974).
4) C. J. Pedson, *J. Am. Chem. Soc.*, **89**, 2495 (1967).
5) T. Shimidsu, Y. Yoshikawa, M. Hasegawa, and H. Chiba, *Kobunshi Ronbunshu*, **34**, 753 (1977).
6) T. Shimidsu, M. Yoshikawa, M. Hasegawa, and K. Kawakatsu, *Macromolecules*, **14**, 170 (1981).
7) N. Ogata, K. Sanui, and H. Fujimura, *J. Appl. Polym. Sci.*, **25**, 1419 (1980).
8) Y. Kikuchi and S. Sasayama, *Makromol. Chem.*, **183**, 2153 (1982).
9) Y. Kikuchi and Y. Onishi, *Nippon Kagaku Kaishi*, **1980**, 1157.
10) Y. Kikuchi and Y. Kaseda, *Nippon Kagaku Kaishi*, **1982**, 842.
11) Y. Kikuchi and N. Kubota, *Nippon Kagaku Kaishi*, **1984**, 1986.
12) Y. Kikuchi and N. Kubota, *Nippon Kagaku Kaishi*, **1985**, 111.
13) K. Kakiuchi, K. Fukuda, and S. Suzue, *Polymer Preprint Japan*, **30**, 2312 (1984).
14) M. Tanaka, T. Oba, and S. Toda, "IR Absorption Spectroscopy," Hirokawa, Tokyo (Japan), 1970, p. 39.

Studies on the Electronic Absorption Spectra of 2,2′-Bithienyl and Some of Its Derivatives. A Molecular Orbital Treatment

Rafie H. Abu-Eittah*,† and Fakhreia A. Al-Sugeir
Department of Chemistry, Faculty of Science, University of Kuwait, Kuwait
(Received March 26, 1984)

The electronic absorption spectra of 2,2′-bithienyl and a number of its derivatives have been investigated. The predominant conformer as well as the polarity of the molecule were predicted from the spectrum. Molecular orbital calculations were performed on different conformers of 5-formyl-2,2′-bithienyl and the s-*trans* geometry proved to be the predominant conformer of the molecule. A good agreement is observed between calculated and observed transition energy and intensity.

Bithienyls and their derivatives are important compounds from the biological, pharmaceutical and analytical point of view. Compounds with strong nematocidal activity are derivatives of 2,2′-bithienyl.[1] The absorption spectra of bithienyl[2-4] and substituted bithienyls have been investigated. The transitions observed in the spectra of 5- and 5,5′-substituted 2,2′-bithienyls have been assigned to intramolecular c.t., locally excited and $n\rightarrow\sigma^*$ transitions.

Molecular refraction and dipole moment measurements (in benzene at 25 °C) have shown that the s-*cis*-conformer of 2,2-bithienyl predominates.[6] On the other hand, the apparent polarization and molar Kerr constant[7] and electron diffraction[8] studies indicated that the preferred conformation is defined by an angle of twist ϕ, about the central C–C bond, of 34° from the crystal state.

The investigation of the spectra[9] of the three possible isomeric thienothiophenes as well as the CNDO/2 computations indicated that contribution of the 3d and higher orbitals of sulfur atom has negligible effect on the electronic spectra of sulfur containing composite molecules as was concluded for thiophene. Molecular orbital calculations, using the SCF–MO method, of the UV spectra of thiophene, 3,3′-, 2,3′-, and 2,2′-bithienyls have been described.[10-12] The PPP-approximation has been applied in an SCF study to investigate the barrier to internal rotation of the two isomers of bithienyl.[13] For 3,3′-bithienyl, energy minima were found at about 20° and 150° from the planar form. For the 2,2′-isomer no distinct minima were found.

In this work the electronic absorption spectra of 2,2′-bithienyl and some of its derivatives were investigated. The effect of solvent polarity and refractive index on band maxima and intensity helped in assigning the predominant conformer of the molecule. Molecular orbital calculations were carried out on 5-formyl-2,2′-bithienyl. Results obtained for the transition energies and band intensities agree satisfactorily with experimental results.

Experimental

All the solvents used were BDH-special for spectrocopy grade regents and used without further purifications.

2,2′-Bithienyl was prepared by refluxing a mixture of 2-iodothiophene, copper bronze and *N,N*-dimethylformamide for 22 h.[14] The product was recovered by steam distillation and purified by vacuum distillation (mp 34 °C).

5-Formyl-2,2′-bithienyl was prepared by stirring a mixture of bithienyl, *N,N*-dimethylformamide, dry toluene and phosphoryl chloride. The residue was recrystallized from ethanol (mp 59 °C).[15]

5,5′-Diacetyl-2,2′-bithienyl was prepared by refluxing a mixture of 85% phosphoric acid and 2,2′-bithienyl in acetic anhydride for 1 h. The mixture was cooled while stirring. The separated product was recrystallized from 1,4-dioxane, mp 235 °C (lit,[14] 233—234 °C).

5-Nitro-2,2′-bithienyl: To a solution of bithienyl and acetic anhydride at 0—5 °C fuming nitric acid in acetic anhydride was added. The nitro product was isolated by steam distillation and recrystallized from ethanol as yellow needles (mp 109 °C as reported).[16]

5,5′-Dimethyl-2,2′-bithienyl was prepared by heating a mixture of 2-iodo-5-methylthiophene and copper powder at 200—210 °C for half an hour. The mixture was colled and the product was extracted with boiling chloroform and steam-distilled. The dimethylbithienyl was recrystallized from methanol (mp 67—68 °C as reported 15—17).

5,5′-Dichloro- and 4,5,5′-Trichloro-2,2′-bithienyl: Sulfuryl chloride was added with stirring to a mixture of 2,2′-bithienyl, acetic acid, and aluminium chloride at 40 °C. The mixture was cooled and the separated solid was filtered and crystallized from chloroform (measured mp of the dichloro derivative was 109 °C, that of the trichloro was 103 °C).[18]

The absorption spectra were measured with a Pye Unicam Sp 500 spectrophotometer using 1.0 cm fused silica cells.

Results and Discussion

A. Electronic Absorption Spectra. (i) 2,2′-Bithienyl: The molecule, bithienyl (*R*-*S*), can be treated as a composite molecule consisting of two subsystems, each of which (*R* and *S*) is a thiophene nucleus and both are joined, apparently, by a single bond. The MO's of the composite molecule are built up from those of its subsystems and the excited states result from mutual interaction of the excited states of the subsystems. This interaction is predominant in the planar conformer of bithienyl. As the planarity is distorted, the spectrum of bithienyl will approach that of thiophene.

The calculations of the electronic spectra of sulfur

†Present address: Department of Chemistry, Faculty of Science, King Abdulaziz University, Jeddah, Saudi Arabia.

containing molecules have shown trivial dependence on the inclusion of the 3d or higher atomic orbitals of sulfur atom.[19-21] Microwave spectroscopic, electron and X-ray diffraction data[22-25] on five-membered heterocycles containing sulfur have shown that the bond angle on the sulfure atom is close to 90°, indicating that the σ-bonds result from overlap of the P_x and P_y orbitals of sulfure. Using Slater exponents for sulfur and carbon atomic orbitals, the calculated overlap integral between carbon $2P_z$ and sulfur $3P_z$ is 0.492 while that between carbon $2P_z$ and sulfur $3d_{xz,yz}$ is only 0.109.[26] Figures 1a and 1b show the electronic absorption spectra of bithienyl and that of thiophene. Thiophene spectrum consists of a singlet $\pi \rightarrow \pi^*$ transition with λ_{max} at 235 nm (log ε=4.22) in addition to a long wavelength shoulder in the region of 268 (log ε<1) nm. No discrete absorption band is observed for $n \rightarrow \pi^*$ transition and singlet→triplet transitions were assigned to very weak bands at about 5.63 eV and in the range of 3.90—3.96 eV.[27] On the other hand, the spectrum of bithienyl shows three well defined electronic transitions in the accessible UV region, none of which can be identified as the thiophene electronic transition. This result is an experimental evidence that bithienyl is a "coplanar," "rigid" or "quasi-rigid" molecule. If it were a "freerotator" the probability of getting a perpendicular conformer should be the same as that of getting a planar conformer. The electronic spectrum of the perpendicular conformer would be merely that of thiophene. As Fig. 1 shows the spectrum of bithienyl differs completely from that of thiophene. The planer conformer of bithienyl may be either the s-*cis* (a) or the s-*trans* (b)

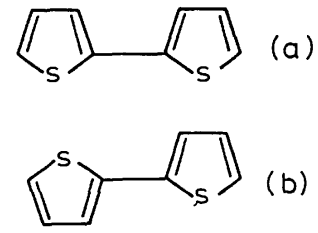

one. The former follows the C_{2v} whereas the latter follows the C_{2h} symmetry point group. Transition probability would be different for the two conformers. The s-*cis* conformer is of much higher dipole moment than the s-*trans* conformer, consequently the electronic transitions of the former should be more affected with solvent polarity than those of the latter. Figure 1 shows a slight shift of λ_{max} with solvent polarity indicating a low polarity of both the ground and excited states.

Many physical studies concerned with the determination of the preferred conformation of 2,2′-bithienyl have been reported. In the solid state, planar *trans* configuration is favored.[28] In gaseous[29] state the angle of twist about the central C–C bond varies between 34—85° from the *cis*-conformer. In solution, the angle of twist is found to be similar to that in gaseous state.[30] However, theoretical consideration favors a near planar structure.[31,32] A molecular orbit-

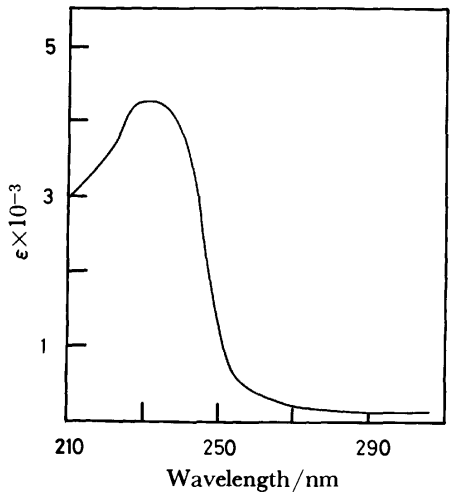

Fig. 1a. Electronic absorption spectrum of thiophene in ethanol.

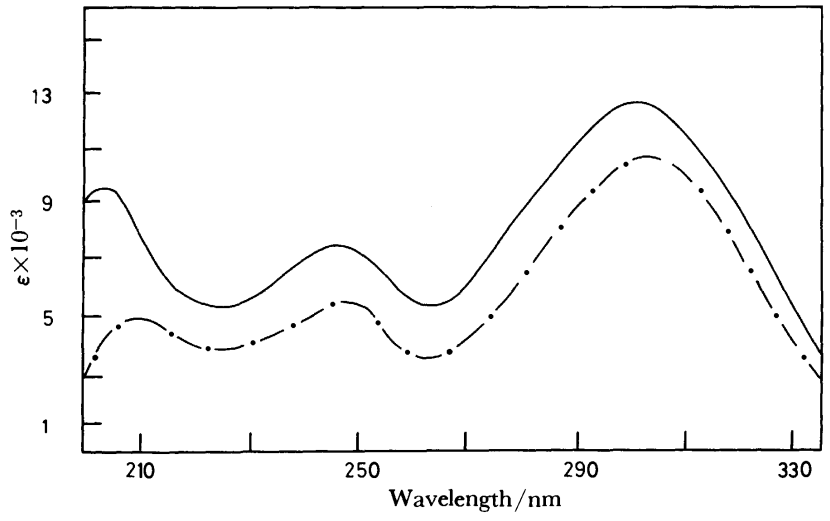

Fig. 1b. Electronic absorption spectra of bithienyl: in cyclohexane (——), in methanol (-·-·-).

Table 1. Numerical values of band maxima and band intensity of 2,2′-bithienyl in different solvents

Solvent	λ_{max}/nm	ε/M^{-1}†cm^{-1}	f
Methanol	303	13440	0.35
	247	7030	0.21
	209	6110	0.11
-2-Butane-01	303	10290	0.26
	248	5360	0.17
N,*N*-Dimethylformamide	305	12480	0.31
Glycerol	305	5820	0.17
	249	3230	0.11
Ethylene glycol	305	12520	0.32
	248	7720	0.23
Cyclohexane	301	13240	0.36
	248	5660	0.22
Hexane	301	13810	0.40
	249	7540	0.25
Heptane	302	13280	0.34
	248	6990	0.22
Decane	304	13320	0.33
	248	6730	0.21
Dodecane	303	10990	0.28
	248	4980	0.11

† 1 M = 1 mol dm^{-3}.

al study of the barrier to internal rotation in bithienyl has shown no distinct energy minima on varying the angle of twist from 0—180°.

The observed three electronic transitions of bithienyl, Fig 1b are $\pi \rightarrow \pi^*$, none of them is localized on a subsystem of the composite molecule. The broad feature of band 1 (lowest energy) as well as the relative blurring of its vibrational components is an evidence that, in solution, bithienyl exists in a number of nearly planar conformers of comparable energy. A statistical distribution is expected to exist between the different conformers. The spectra of 2,2′-bithietyl were investigated in a wide variety of polar and nonpolar solvents (Table 1). In polar solvents, band intensity decreased with the increase of dipole moment and in non-polar solvents band intensity also decreased with the increase of refractive index. On the other hand band maxima slightly increased with the increase of both refractive index and dipole moment.

(ii) Substituted 2,2′-Bithienyl: Figure 2 shows the electronic absorption spectra of 5,5′-dimethyl-, 5,5′-dichloro-, and 4,5,5′-trichloro-2,2′- bithienyls using cyclohexane as a solvent. The features of the spectra are similar to those of the unsubstituted compound. An important observation is the broadness of the lowest energy band in addition to the blurring nature of its vibrational components.

The spectra of 5-formyl- and 5,5′-diacetyl-2,2′-bithienyl are shown in Fig. 3. A significant red shift is observed for the lowest energy transition compared to the unsubstituted compound or to the methyl or halo-substituted bithienyl. This is the result of the strong perturbing effect of the >C=O group which also incrcases the polarity of both the ground and the excited states. The lowest energy transition is apparently red shifted in polar solvent which is an indication of a large

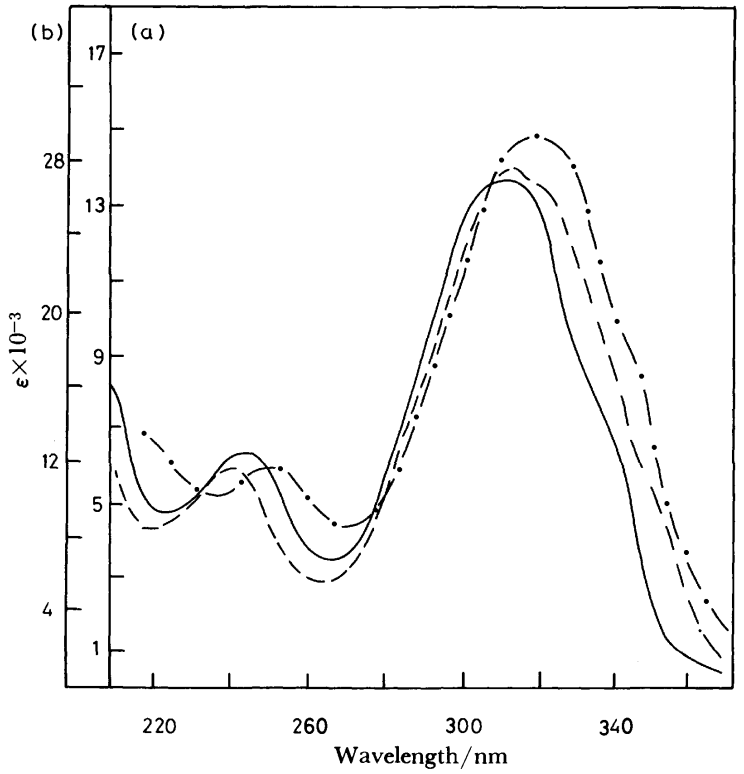

Fig. 2. Electronic absorption spectra of substituted bithienyls in cyclohexane.
5,5′-Dimethyl-2,2′-bithienyl (——); 5,5′-dichloro-2,2′-bithienyl (---) (both on scale a). 4,4,5′-Trichloro-2,2′-bithienyl (-·-·-) (on scale b).

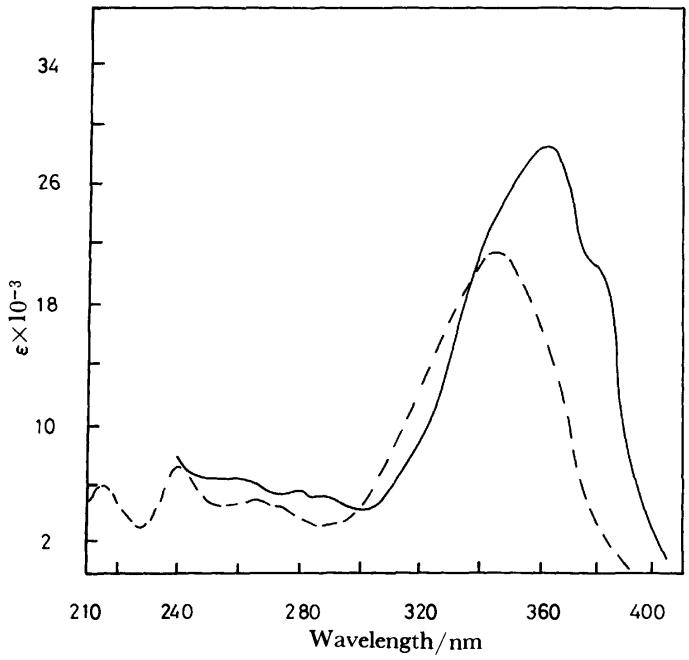

Fig. 3. Electronic absorption spectra of: 5,5′-diacetyl-2,2′-bithienyl in 1,4-dioxane (——); 5-formyl-2,2′-bithienyl in cyclohexane (---).

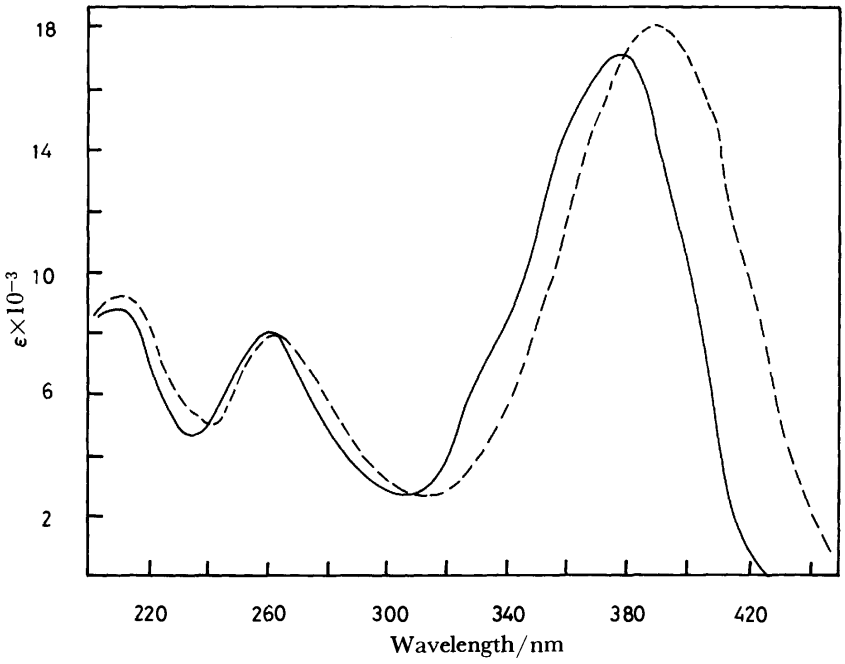

Fig. 4. Electronic absorption spectra of 5-nitro-2,2′-bithienyl: in cyclohexane (——), in methanol (---).

contribution of a polar configuration to the excited state.

Substitution by a nitro group in the 5-position of bithienyl will not affect the coplanarity of the molecule but will reduce its symmetry. Forms as (a) will mainly contribute to the excited states. The interaction between the nitro group and bithienyl nucleus is substantial and is reflected in the spectrum (Fig. 4). Four electronic transitions ($\pi \rightarrow \pi^*$) are observed in the 200—500 nm region. The lowest energy band is substantially red shifted in polar solvent, a characteristic of

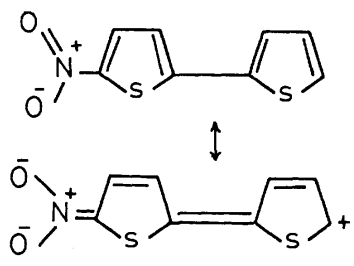

(a)

charge transfer transitions. The highest energy band was not observed in the spectra of any of the studied

Table 2. Numerical values of band maxima and band intensities of some 2,2′-bithienyls

Compound	λ_{max}/nm[a]	ε/M^{-1}cm^{-1}	f
5,5′-Dichloro-	315(317)	13830(17110)	0.38(0.43)
2,2′-Bithienyl	242(241)	5930(5880)	0.20(0.19)
5,5′-Dimethyl-	314(315)	13370(14890)	0.35(0.38)
2,2′-Bithienyl	245(244)	6335(6380)	0.21(0.19)
5-Formyl-	345(354)	21630(20900)	0.47(0.47)
2,2′-Bithienyl	265(268)	5570(4340)	0.21(0.15)
	245(246)	7480(6440)	0.18(0.12)
5-Nitro-	380(391)	17130(18120)	0.36(0.40)
2,2′-Bithienyl	275(264)	6329(7870)	0.16(0.29)
	260	8075	0.28
	212(212)	8730(8910)	—
4,5,5′-Trichloro-	316(320)	29120(18860)	0.76(0.48)
2,2′-Bithienyl	252(252)	11650(6600)	0.54(0.32)
5,5′-Diacetyl-	363(367)	28760(36950)	0.63(0.85)
2,2′-Bithienyl[b]			

a) Values in parentheses are those when methanol was used as a solvent. b) Dioxane is the solvent.

bithienyls except the diacetyl derivative. Table 2 gives the numerical values of band maxima and oscillator strength of the studied compounds.

B. Molecular Orbital Calculations. The method of molecule-in-molecule[34] has been accurately adobted to MO calculations on composite systems such as phenylthiophenes,[35] bithienyls,[32] phenylfurans,[36] and *N*-(2-furylmethylene)aniline.[37] In this work the method is applied for calculations on the different conformers of 5-formyl-2,2′-bithienyl.

The two subsystems of the composite molecule, 5-formyl-2,2′-bithienyl, are 2-thiophenecarbaldehyde (A) and thiophene (B). The molecule-in-molecule method

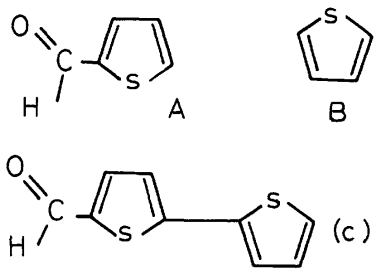

is based on calculating the interaction between the electronic states of subsystems (A) and (B). The SCF-CI[38] state functions were calculated for the two subsystems, results are given in Table 3. The electronic states of 5-formyl-2,2′-bithienyl were calculated for many conformers of the molecule by considering the following interactions between (i) the CI state functions of the subsystems (A) and (B); (ii) the CI state functions of the subsystems and charge-transfer configurations where an electron transfers from (A) to (B) or from (B) to (A) ; (iii) the ground state and the charge-transfer configurations. For the perpendicular conformer the resonance integral $\beta_{22'}$ is zero and interaction of the type (i) are only considered. The state functions and the corresponding energies of the s-*trans* conformer (C) and the perpendicular conformer (planes of thiophene and formylthiophene are perpendicular) are given in Table 4. The variation of transition energies with the angle of rotation around the C_2–$C_{2'}$ bond is given in Table 5.

Table 3. Configuration interaction state functions and the corresponding energies (eV) of 2-thiophenecarbaldehyde and of thiophene

2-Thiophenecarbaldehyde	eV
$\theta_1=0.4306\theta_4^{-1}\theta_5$[a]$+0.3691\theta_4^{-1}\theta_6-0.1119\theta_4^{-1}\theta_7$ $-0.6282\theta_3^{-1}\theta_5+0.5121\theta_3^{-1}\theta_6$	4.22
$\theta_2=0.5196\theta_3^{-1}\theta_5-0.1130\theta_3^{-1}\theta_6-0.7617\theta_4^{-1}\theta_5$ $-0.3214\theta_4^{-1}\theta_7$	4.50
$\theta_3=0.3737\theta_4^{-1}\theta_5+0.5369\theta_4^{-1}\theta_6+0.5122\theta_3^{-1}\theta_5$ $+0.4906\theta_3^{-1}\theta_6$	5.70
$\theta_4=0.1620\theta_4^{-1}\theta_5+0.2459\theta_4^{-1}\theta_6+0.4627\theta_4^{-1}\theta_7$ $+0.8308\theta_3^{-1}\theta_7$	7.16
Thiophene	**eV**
$Y_1=0.9999y_3^{-1}y_4$[b]$-0.0092y_2^{-1}y_5$	5.64
$Y_2=0.8933y_2^{-1}y_4-0.4495y_3^{-1}y_5$	5.93
$Y_3=0.4495y_2^{-1}y_4+0.8933y_3^{-1}y_5$	7.74
$Y_4=0.0092y_3^{-1}y_4+0.9999y_2^{-1}y_5$	8.03

a) $\theta_4^{-1}\theta_5$=Electronic configuration in which an electron transfers from the fourth MO(θ_4) to the fifth MO(θ_5). b) $y_3^{-1}y_4$=Electronic configuration in which an electron transfers from the third MO(y_3) to the fourth MO(y_4).

Table 4. State functions and the corresponding energies (eV) of 5-formyl-2,2′-bithienyl

s-*trans* Conformer	eV
$\Psi_0=0.9821\Gamma-0.0213CR_I+0.1862CR_{II}$	−0.19
$\Psi_{EX,I}=0.4121\theta_2-0.1013\theta_3-0.2819Y_1$ $-0.6042CR_I-0.1743CR_{II}$.	3.53
$\Psi_{EX,II}=0.7052\theta_1+0.6422\theta_2-0.1689Y_3$ $-0.1352CR_I-0.2563CR_{II}$	4.53
$\Psi_{EX,III}=0.4513Y_1-0.2992\theta_1+0.1764\theta_2$ $+0.4172\theta_3+0.2981CR_I-0.6163CR_{II}$	5.01
Perpendicular conformer	**eV**
$\Psi_{EX,I}=0.1292Y_1+0.0293Y_3+0.9893\theta_1-0.0662\theta_2$ $+0.0124\theta_3-0.1203\theta_6$	4.19
$\Psi_{EX,II}=0.1762Y_1-0.0871\theta_1-0.9803\theta_2-0.0412\theta_6$	4.56
$\Psi_{EX,III}=0.7363Y_1-0.0942\theta_1+0.1573\theta_2+0.6421\theta_3$ $-0.0924\theta_4-0.0512\theta_6$	5.53

Γ=Ground configuration, θ_1—θ_6 excited states on subsystem A, Y_1—Y_4 excited states on subsystem B, CR's charge resonance functions.

The oscillator strength was calculated from the equation

$$f = 2.085 \times 10^{-5} M^2 \bar{\nu}$$

where M is the transition moment and $\bar{\nu}$ (cm^{-1}) is the wave number of the electronic transition. M was calculated from

$$\vec{M} = \langle \Psi_0 | \hat{M} | \Psi_E \rangle,$$

where Ψ_0 and Ψ_E are the ground and excited state wave functions, respectively. In the molecule-in-molecule procedure the wave functions have the forms:

$$\Psi_0 = {}_a\Gamma + \sum_n b_n T_n$$

$$\Psi_E = \sum_n c_n A_n + \sum_{n'} d_{n'} T_{n'} + {}_e\Gamma$$

TABLE 5. VARIATION OF TRANSITION ENERGY WITH THE ANGLE OF ROTATION ABOUT THE 2,2′-BOND

Rotation angle/deg	Transition energy/eV	Oscillator strength
30	3.72	1.00
	4.47	0.17
	5.16	0.24
60	4.06	0.51
	4.45	0.20
	5.01	0.05
90	4.19	0.39
	4.56	0.11
	5.53	0.07
120	4.15	0.28
	4.50	0.22
	4.80	0.02
180(s-*trans*)	3.72	0.85
	4.56	0.20
	5.20	0.23
Experimental	3.65	0.47
	4.68	0.22
	5.06	0.18

where A_n is the n-th excited state function and T is the charge-transfer state function. Applying the ZDO approximation

$$\langle \Psi_0|M|\Psi_E\rangle = a\sum_n \langle T|M|A\rangle + \sum_n\sum_{n'} b_n d_{n'}\langle T_n|M|T_{n'}\rangle$$

C. Comparison with Experimental Results: Table 5 gives the values of the transition energy and the oscillator strength computed as a function of the angle of rotation about the C_2–$C_{2'}$ bond together with the experimental values. The results show a good correspondence between the experimental values and the theoretical ones computed for the s-*trans* conformer. An angle of 30° between the planes of the subsystems did not lead to better results than those of the planar conformer. The electronic absorption spectra of 2,2′-bithienyl and some of its derivatives have been investigated in a wide variety of solvents. The important observation is the persistance of the features of the first band (lowest energy) in the spectra of all the studied derivatives. This band is broad, though it corresponds to one electronic transtion, intense and includes a number of blurred vibrational components, though coplanarity of the molecules is not distorted.

A simple way[5] that has been followed in interpreting the spectra of 2,2′- bithienyls is to attribute the observed transitions to: (i) locally excited on a certain subsystem of the composite molecule, (ii) charge transfer from the substituent (X) to the parent molecule or in the opposite direction and (iii) n→π* transitions.

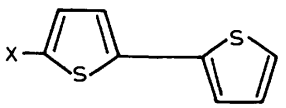

The results of this work prove, on the contrary to what has been previously reported,[5] that the observed transitions are not localized. There is an extensive "mixing" of the state of the subsystems (Table 4) to produce the states of the composite molecule. Also, the slight shift of band maxima with solvent polarity is a proof that none of the observed transitions is a "pure" charge transfer one. The intensity and position for the observed bands indicate that none of them corresponds to n→π* transitions.

Computations on 5-formyl-2,2′-bithienyl indicated that coplanarity of the molecule is not apparently distorted and the interaction between the states of the subsystems, thiophenecarbaldehyde and thiophene, is predominant. The contribution of the charge-transfer configurations (from one subsystem to the other) is significant. The calculated parameters, transition energy and band intensity, as a function of the angle between the planes of the subsystems indicate that the s-*trans* conformer is a good representative of the geometry of the molecule in solutions. It is also evident that the height of the barrier of internal rotation is small since transition energies did not show a wide variation with the angle of rotation.

References

1) J. H. Uhlenbroek and J. D. Bijloo, *Recl. Trav. Chim.*, Pays-Bas, **79**, 1181 (1960).
2) L. Zechmeister and J. W. Sease, *J. Am. Chem. Soc.*, **69**, 273 (1947).
3) H. Wynberg, A. Logothetis, and D. Verploey, *J. Am. Chem. Soc.*, **79**, 1972 (1957).
4) H. Wynberg and A. Bantjes, *J. Org. Chem.*, **24**, 1421 (1959).
5) R. F. Curtis and G. T. Philips, *Tetrahedron*, **23**, 4419 (1967).
6) E. S. Lien and W. D. Kumler, *J. Pharm. Soc.*, **59**, 1685 (1970).
7) M. J. Aroney, H. K. Lee, and R. J. W. Lefevre, *Aust. J. Chem*, **25**, 1561 (1972).
8) A. Almenningen, O. Bastiansen, and P. Svendsos, *Acta Chem. Scand.*, **12**, 1671 (1958).
9) A. Jajiri, T. Asano, and T. Nakajima, *Tetrahedron Lett.* **1971**, 1785.
10) A. J. H. Wachters and D. W. Davies,*Tetrahedron*, **20**, 2841 (1964).
11) D. T. Clark and D. R. Armstrong, *Chem. Commun.*, **1970**, 319.
12) N. Trinajstic and A. Hinchliffe, *Croat. Chem. Acta*, **40**, 163 (1968).
13) A. Skancke, *Acta Chem.Scand.*, **24**, 1389 (1970).
14) H. Wynberg and A. Logothetis, *J. Am. Chem. Soc.*, **78**, 1958 (1956).
15) E. Lescot, Jr., Ng. Ph. Buu. Hoï, and N. D. Xuong, *J. Chem. Soc.*, **1959**, 3234.
16) W. Steinkopf and W. Kohler, *Justus Liebigs Ann. Chem.*, **522**, 17 (1936).
17) W. Steinkopf , R. Leitsmann, A. H. Muller, and H. Wilhelm, *Justus Liebigs Ann. Chem.*, **541**, 260 (1939).
18) T. Sone, K. Sakai and K. Kuroda, *Bull. Chem. Soc. Jpn.*, **43**, 1411 (1970).
19) H. C. Longuet-Higgins , *Trans. Faraday Soc.*, **54**, 173

(1949).
20) A. Jajiri, T. Asano, and T. Nakajima, *Tetrahedron Lett.* **1971**, 1785.
21) M. H. Palmer and R. H. Findlay, *Tetrahedron*, **41**, 4165 (1972).
22) R. Pan-Tan-Luu, L. Bouscasee, É. J. Vincent, and J. Metzger, *Bull. Soc. Chim. France*, **1967**, 3283.
23) E. J. Vincent, R. Pan-Tan-Luu, and J. Metzger, *Bull. Soc. Chim. Fr.*, 3530 (1966).
24) B. Bak, D. Christensen, L. Hansen Nygaard, and J. Rastrup-Aderson, *J. Mol. Spectrosc.*, **7**, 58 (1961).
25) V. Dobyns and L. Pieree, *J. Am. Chem. Soc.*, **85**, 3553 (1963).
26) K. Maida, *Bull. Chem. Soc. Jpn.*, **33**, 308 (1960).
27) M. J. Bielefed and D. D. Fitts, *J. Am. Chem. Soc.*, **88**, 4804 (1966).
28) G. J. Visser, G. J. Heeres, J. Wolters, and C. A. Vos, *Acta Cryst. Sect. B*, **24**, 467 (1968).
29) A. Almenningen, O. Bastiansen, and P. Svendsos, *Acta Chem. Scand.*, **12**, 1671 (1978).
30) C. L. Khetrapol and A. C. Kunwar, *Mol. Phys.*, **28**, 441 (1974).
31) M. J. S. Dewar and N. J. Trinajstic, *J. Am. Chem. Soc.*, **92**, 1453 (1970).
32) R. Abu-Eittah and F. Al-Sugeir, *Int. J. Quantum Chem.*, **13**, 565 (1978).
33) A. Skancke, *Acta Chem. Scand.*, **24**, 1389 (1970).
34) H. C. Longuet-Higgins and J. N. Murrel, *Proc. Phys. Soc.*, **A68**, 601 (1955).
35) R. Abu-Eittah and R. Hilal, *Bull. Chem. Soc. Jpn.*, **49**, 2158 (1976).
36) R. Abu-Eittah, R. Hilal, and M. M. Hamed, *Int. J. Quantum Chem.*, **19**, 383 (1981).
37) R. Abu-Eittah and M. M. Hamed, *Bull. Chem. Soc. Jpn.*, **57**, (1983).
38) R. Pariser and R. G. Parr, *J. Chem. Phys.*, **21**, 466, 767 (1953).

Synthesis and Structure of (Nitroacetato)((7*RS*,14*RS*)-5,5,7,12,12,14-hexamethyl-1,4,8,11-tetraazacyclotetradecane)nickel(II), [Ni(na)(Me$_6$[14]aneN$_4$)]

Haruko Ito† and Tasuku Ito*

Department of Applied Molecular Science, Institute for Molecular Science, Okazaki National Research Institutes, Okazaki 444

(Received February 22, 1985)

Synopsis. The title compound, [Ni(na)(Ma$_6$[14]-aneN$_4$)], has been synthesized by the reaction of α-[Ni-(Me$_6$[14]aneN$_4$)](ClO$_4$)$_2$ with potassium nitroacetate (K$_2$na) in water. X-Ray analysis shows that the complex is a *cis*-NiO$_2$N$_4$ type with the tetraazamacrocycle folded, and that a dianionic nitroacetate (na^{2-}) chelates the nickel(II) with one oxygen atom of the CO_2^- moiety and one oxygen atom of the NO_2^- moiety to form a six membered chelate ring.

Much attention has been paid to the formation of a new C–C bond using CO_2 as carbon source.[1,2] α-Nitro acids, for example, were obtained by the treatment of primary nitroparaffins with CO_2 in the presence of Mg(OCH$_3$)$_2$[3] or MgCl$_2$ and triethylamine.[4] The driving force of the reaction was attributed to the formation of a stable magnesium(II) chelate of α-nitro carboxylate ion during the reaction, since the free anion of α-nitro carboxylate is susceptible to decarboxylation. However, no direct structural evidence has been reported.

Aiming at the deeper understanding of the CO_2 uptake chemistry of this type, we intended in this study to prepare and isolate nitroacetato complex and to know its chemical properties. Another point of interest is the structure of the coordinated nitroacetate ion. There are three possible structures for the nitroacetato chelate, as shown below.

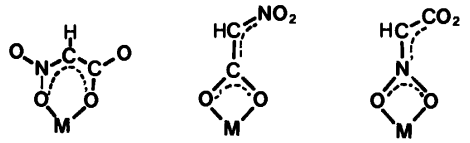

The type (a) is a six-membered chelate like the acetylacetonate. The type (b) and (c) are of four-membered chelate similar to that formed by carboxylate or nitroalkanoate ion, respectively.

The complex, [Ni(na)(Me$_6$[14]aneN$_4$)], was prepared from α-[Ni(Me$_6$[14]aneN$_4$)](ClO$_4$)$_2$[5] and K$_2$na. The complex shows three d-d bands typical of octahedral nickel(II), at 10,200 (ε=23), 17,400 (ε=13), and *ca.* 27000 (shoulder) cm^{-1}. Figure 1 shows an ORTEP view of the complex and the atom numbering system. The complex adopts *cis*-NiO$_2$N$_4$ structure with the tetraazamacrocycle folded, and the na chelate ring was found to take the type (a) structure. The atomic coordinates of non-hydrogen atoms and relevant bond distances and angles are given in Tables 1 and 2, respectively.

The N(A)O(1)O(3)C(B) and the C(A)O(2)O(4)C(B) moieties are planar within experimental errors. These two planes are not coplanar but are tilted each other by 17.3(3)°. The C(A)–C(B) distance (1.421(9)) Å is longer than C–C distances found in acetylacetonate chelates.[6] These facts indicate that the π-electrons are not fully delocalized over the six-membered ring.

The assignments of the N(A) and C(A) atoms are not unique, but they are tentatively assigned to the nitrogen (NO_2^-) and the carbon (CO_2^-) atoms, respectively, on the basis of the examination of the reliability factors and the thermal parameters.[7] No statistical disorder between NO_2^- and CO_2^- was

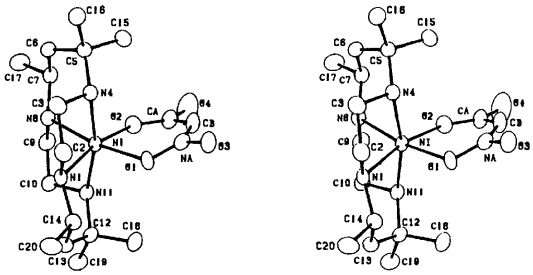

Fig. 1 ORTEP view of [Ni(na)(Me$_6$[14]aneN$_4$)] along with the atom numbering scheme.

Table 1. Fractional coordinates (×10^5) for non-hydrogen atoms

Atom	*x*	*y*	*z*
Ni	21960(3)	3365(4)	11401(6)
O(1)	23870(18)	16340(23)	21753(37)
O(2)	14581(18)	10080(26)	-3284(37)
O(3)	20078(23)	28358(27)	33761(51)
O(4)	7711(35)	21507(41)	-11835(77)
N(1)	31019(20)	-1149(26)	24975(39)
N(4)	17098(21)	-34(29)	31178(42)
N(8)	18444(21)	-9694(28)	2094(40)
N(11)	27789(21)	3819(27)	-7827(41)
N(A)	19293(24)	22615(31)	22177(53)
C(A)	12153(30)	18161(41)	-1774(74)
C(B)	13896(33)	23772(39)	11431(83)
C(2)	29244(27)	-1283(40)	40659(51)
C(3)	22275(28)	-5494(40)	40877(54)
C(5)	10029(26)	-4345(35)	29712(55)
C(6)	9800(27)	-13116(36)	19590(60)
C(7)	11154(28)	-12194(37)	3128(59)
C(9)	20134(30)	-9397(40)	-13879(54)
C(10)	27237(28)	-5824(37)	-14041(52)
C(12)	34870(27)	7794(36)	-6205(52)
C(13)	39344(26)	3363(36)	7356(55)
C(14)	37273(25)	4393(36)	23322(53)
C(15)	5009(28)	3048(40)	22781(64)
C(16)	7966(31)	-7038(41)	45421(61)
C(17)	8859(35)	-21115(48)	-5517(75)
C(18)	34166(32)	18349(39)	-4097(62)
C(19)	38369(31)	6116(46)	-20614(60)
C(20)	43390(28)	1864(46)	35072(61)
O(W)	21064(31)	15192(40)	-40327(59)
O(M)	7908(36)	17755(52)	-38451(81)
C(M)	5184(46)	27424(63)	-46587(113)

† Present address: Department of Chemistry, Aichi Kyoiku University, Kariya, 448.

observed. The uncoordinated oxygen atom, O(3), is involved in intermolecular hydrogen bonds,[8] while the uncoordinated oxygen atom O(4) is not. There seems to be a difference in the ability of the hydrogen bond formation between the oxygen atoms of the CO_2^- and NO_2^- moieties.

The nitroacetato ligand in this complex is fairly stable toward decarboxylation, especially in methanol. The stability is attributed to the formation of the stable six-membered nitroacetato chelate, as has been postulated for the magnesium(II) complex, and to the macrocyclic effect of the ligand Me_6[14]aneN$_4$ that can fold.[9]

Experimental

Materials. α-[Ni(Me_6[14]aneN$_4$)]$(ClO_4)_2$[5] and K_2na[10] were prepared according to the literatures.

[Ni(na)(Me$_6$[14]aneN$_4$)]·CH$_3$OH·H$_2$O. To an aqueous suspension (10 cm^3) of α-[Ni(Me_6[14]aneN$_4$)]$(ClO_4)_2$ (1.08 g, 2 mmole), K_2na (0.45 g, 2.5 mmole) dissolved in a small amount of water was added. The yellow solids disappeared quickly, and blue violet solids were formed. These were filtered and extracted with methanol to remove $KClO_4$. Vacuum evaporation at 30 °C gave blue violet crystals (0.78 g). These were recrystallized from methanol. The elemental analysis was consistent with the above chemical formula. IR (KBr disk, between 1150 and 1600 cm^{-1}): 1580, 1550, 1453, 1392, 1295, and 1170 cm^{-1}.

X-Ray Analysis. A single crystal of [Ni(na)(Me_6[14]aneN$_4$)]·CH$_3$OH·H$_2$O with approximate dimension 0.56×0.42×0.38 mm was used for the X-ray study. Diffraction data were obtained on a Rigaku AFC-5 diffractometer with graphite monochromatized Mo $K\alpha$ radiation. Intensities were corrected for Lorentz and polarization factors. Crystal data are: monoclinic, $P2_1/n$, a=19.710(4), b=14.274(2), c=8.833(1) Å, β=97.13(2)°, V=2466.1(7) Å^3, Z=4, D_x=1.34 g cm^{-3}, μ(Mo $K\alpha$)=0.83 mm^{-1}. The structure was solved by the heavy atom method and refined by block-diagonal least-squares method. The weighting scheme, $w=[\sigma_{count}^2+(0.015|F_o|)^2]^{-1}$, was employed. All the hydrogen atoms except that of hydroxyl group of methanol were located by the difference Fourier syntheses and included in the final refinement with the isotropic temperature factors. The final R indices were R=0.062 and R_w=0.075 for 3344 independent reflections ($2\theta<50°$) with $|F_o|>3\sigma(|F_o|)$.[11] Calculations were carried out on the HITAC M-200H computer at the Computer Center of the Institute for Molecular Science with the Universal Crystallographic Computation Program System, UNICS III.[12]

The present study was partly supported by Grant-in-Aid for Scientific Research No. 58470039 from the Ministry of Education, Science and Culture.

References

1) R. Eisenberg and D. E. Hendriksen, *Adv. Catal.*, **28** 79 (1979).

2) "Organic and Bioorganic Chemistry of Carbon Dioxide," ed by S. Inoue, N. Yamazaki, Kodansha, Tokyo (1981).

3) M. Stiles and H. L. Fiukbeiner, *J. Am. Chem. Soc., 81*, 505 (1959).

4) N. Matsumura, Y. Yagyu, and E. Imoto, *Nippon Kagaku Kaishi*, **1976**, 1801.

5) L. G. Warner and D. H. Busch, *J. Am. Chem. Soc.*, **91**, 4092 (1969); The symbols, α, β, and γ, denote (1*RS*, 4*RS*, 8*RS*, 11*RS*)-, (1*RS*, 4*SR*, 8*RS*, 11*SR*)-, and (1*RS*, 4*RS*, 8*SR*, 11*SR*)-form. The β- and γ-isomers did not react nicely with K_2na, since they can hardly fold to form octahedral complexes.

6) For example, T. Ito, K. Toriumi, F. B. Ueno, and K. Saito, *Acta Crystallogr., Sect B*, **36**, 2998 (1980).

7) If N(A) and C(A) are assinged to carbon and nitrogen, respectively, the reliability factors raised to R=0.064 and R_w=0.078. At the same time, the thermal parameters (B_{eq}) of N(A) and C(A) became too small and too large, respectively, as compared with those of other atoms within the chelate ring.

8) O(3)···O(W)*=2.948(8) Å where O(W) is water of crystallization; O(3)···N(1)*=3.027(6), and O(3)···N(8)*=2.968(7) Å. Key to symmetry operation: (x, y, 1+z) for O(W)*, and (1/2−x, 1/2+y, 1/2−z) for N(1)* and N(8)*.

9) H. Ito and T. Ito, *Bull. Chem. Soc. Jpn.*, **58**, 1755 (1985).

10) W. Steinkopf, *Ber.*, **42**, 3925 (1909).

11) Tables of hydrogen atom coordinates, anisotropic thermal parameters, and observed and calculated structure factors are kept in the office of the Chemical Society of Japan (Document No. 8529).

12) T. Sakurai and K. Kobayashi, *Rikagaku Kenkyusho Hokoku*, **55**, 69 (1979).

Table 2. Relevant bond distances (l/Å) and angles (ϕ/°) with their e.s.d.'s (in parentheses)

Ni	-O(1)	2.079(3)		O(1)	-N(A)	1.275(6)	
Ni	-O(2)	2.061(3)		O(3)	-N(A)	1.305(6)	
Ni	-N(1)	2.124(4)		O(2)	-C(A)	1.262(7)	
Ni	-N(4)	2.150(4)		O(4)	-C(A)	1.262(9)	
Ni	-N(8)	2.119(4)		N(A)	-C(B)	1.345(8)	
Ni	-N(11)	2.167(4)		C(A)	-C(B)	1.422(9)	
O(1)	-Ni	-O(2)	86.4(1)	N(4)	-Ni	-N(8)	87.7(2)
O(1)	-Ni	-N(1)	85.9(1)	N(4)	-Ni	-N(11)	167.7(2)
O(1)	-Ni	-N(4)	85.3(2)	N(8)	-Ni	-N(11)	84.4(2)
O(1)	-Ni	-N(8)	170.8(2)	Ni	-O(1)	-N(A)	123.3(3)
O(1)	-Ni	-N(11)	103.5(1)	Ni	-O(2)	-C(A)	127.3(4)
O(2)	-Ni	-N(1)	167.1(2)	O(1)	-N(3)	-O(3)	116.7(4)
O(2)	-Ni	-N(4)	105.4(2)	O(1)	-N(5)	-C(B)	124.5(5)
O(2)	-Ni	-N(8)	89.6(1)	O(3)	-N(5)	-C(B)	118.9(5)
O(2)	-Ni	-N(11)	83.9(1)	O(2)	-C(A)	-O(4)	120.7(6)
N(1)	-Ni	-N(4)	84.3(2)	O(2)	-C(A)	-C(B)	123.1(5)
N(1)	-Ni	-N(8)	99.4(2)	O(4)	-C(A)	-C(B)	116.1(6)
N(1)	-Ni	-N(11)	87.8(2)	N(A)	-C(B)	-C(A)	126.8(6)

The Determination of a Small Amount of Biological Constituent by the Use of Chemiluminescence. V. An Iron-dyestuff Complex as a Catalyst

Tadashi HARA,* Motohiro TORIYAMA, Kouichi KITAMURA, and Masakatsu IMAKI†
Department of Chemical Engineering, Faculty of Engineering, Doshisha University, Karasuma Imadegawa, Kamigyo-ku, Kyoto 602
†*Horiba Ltd., Kisshoin, Minami-ku, Kyoto 601*
(Received February 26, 1985)

Synopsis. The catalytic activity of the iron(III)-α,β,γ,δ-tetraphenylporphinetrisulfonic acid complex for the chemiluminescence reaction between luminol and H_2O_2 has been found to decrease in the presence of protein. On the basis of this phenomenon, 2×10^{-5}—2×10^{-3} g dm^{-3} bovine serum albumin was determined with the detection limit of 4 ng, lower than that in the previous paper.

It was previously reported[1] by the present authors that the catalytic activity of Cu(II) for the chemiluminescence(CL) reaction between 5-amino-2,3-dihydro-1,4-phthalazinedione(luminol) and hydrogen peroxide(H_2O_2) decreased in the presence of protein, and that the sensitive determination of protein could be carried out on the basis of this phenomenon. In order to make the method of determining protein more sensitive, the use of Co(III) instead of Cu(II) as a catalyst was attempted.[2] The results were slightly improved, but they not very satisfactory, because there was not enough bond formation between Co(III) and a protein molecule.

On the other hand, various dyestuff combination methods have been reported for the determination of a small amount of protein. The dyestuff molecule used for this method generally has several aromatic rings and sulfonic acid groups, which have a high affinity against the residues of lysine, arginine, and histidine, and the amino terminal in a protein molecule.[3] The dyestuff combination method[3,4] could be carried out only by mixing a dyestuff solution with a sample solution and by measuring the absorbance of the mixed soluion. With the object of establishing a highly sensitive method of determining protein by means of the CL method, a metal-complex compounds which had a structure similar to that of a dyestuff in the dyestuff-combination method and which had a catalytic activity for the CL reaction was used in the present study.

Several iron(III) porphine complexes have previously been reported[5] by the present authors to show a high catalytic activity for the CL reaction. Accordingly, the iron(III) α,β,γ,δ-tetraphenylporphinetrisulfonic acid complex([Fe(tpps)]), which contains aromatic rings and sulfonic acid groups in the molecule, was used for the determination of a small amount of protein by means of the CL method. This method was about 50 times as sensitive as the previous method, using the Cu(II) catalyst for the determination bovine serum albumin(BSA) as a model protein.

Experimental

The [Fe(tpps)] was prepared in accordance with Nomura's method.[6] The α,β,γ,δ-tetraphenylporphinetrisulfonic acid was purchased from Dojin Laboratories as its disulfonic acid salt. The absorption spectrum of the solution of the synthesized [Fe(tpps)] was in agreement with that reported by Nomura *et al.* The concentration of the [Fe(tpps)] stock solution was determined by means of an absorbance measurement at 395 nm.

A sample solution containing protein was diluted with a 0.01 mol dm^{-3} phosphate buffer solution(pH 7.2), and to the mixture a definite amount of [Fe(tpps)] stock solution was added to yield 5.7×10^{-9} mol dm^{-3}. The catalytic activity of the [Fe(tpps)] in the mixed solution was measured by mean of the flow-injection-analysis apparatus reported in a previous paper.[5] The ratio of the CL intensity of a protein sample solution to that of a 5.7×10^{-9} mol dm^{-3} [Fe(tpps)] solution was plotted against the amount of protein, and this graph was used as a calibration curve of the protein.

Results and Discussion

Though iron(III) porphine complexes had been reported by the previous authors to show a high catalytic activity for the CL reaction between luminol and H_2O_2, the catalytic activity of [Fe(tpps)] still remained unknown. Therefore, the catalytic activity of [Fe(tpps)] was measured; the results are shown in Fig. 1. [Fe(tpps)] was about 3 times as active as the previous iron(III) porphine complex for the CL reaction. Therefore, the effect of the protein on the catalytic activity of [Fe(tpps)] was examined. Human

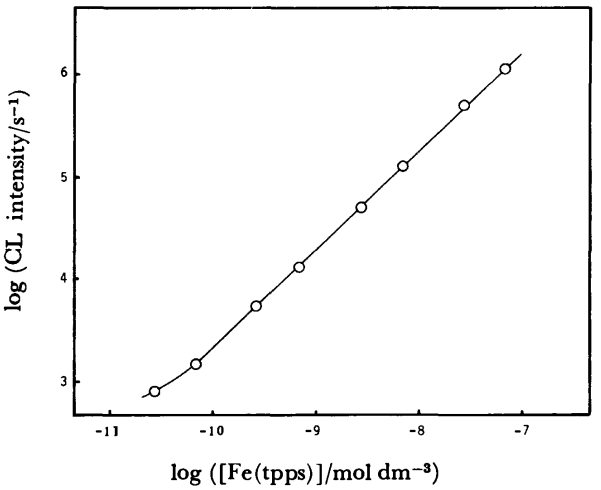

Fig. 1. Calibration curve of [Fe(tpps)].

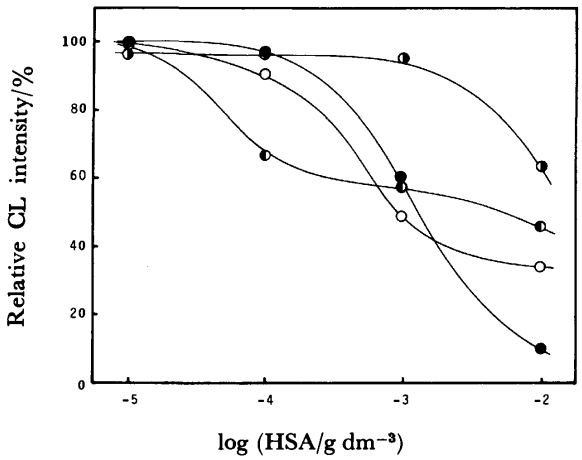

Fig. 2. Effect of pH value on the catalytic activity of [Fe(tpps)].
◐: pH 2.5, ○: pH 7.2, ●: pH 9.1, and ◑: pH 12.1.

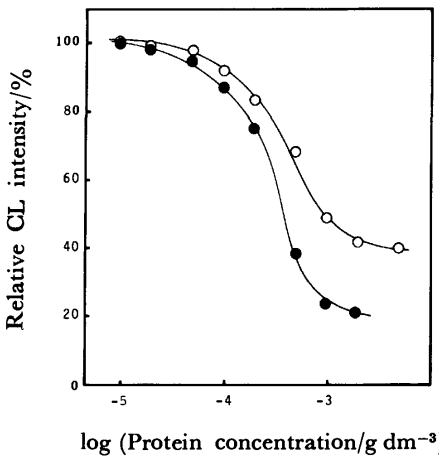

Fig. 3. Calibration curve of HSA and BSA.
○: HSA and ●: BSA.

serum albumin(HSA) was dissolved in a buffer solution and diluted with the same buffer solution as the preceding one, and then to it the [Fe(tpps)] stock solution was added so as to make it 5.7×10^{-9} mol dm^{-3}; this showed a CL intensity of about 10^5 cps, corresponding to the full scale of a photon counter in the absence of any protein. The mixed solution was left standing for 1 h at room temperature, and its catalytic activity was measured. This experiment was carried out at various pH values(Fig. 2). The catalytic acivity of [Fe(tpps)] for the CL reaction was found to decrease in the presence of protein. The change in the catalytic activity in the presence of protein was also found to decrease with an increase in the pH value. However, the CL intensity of a sample solution of less than pH 5 greatly decreased in the absence of protein; moreover, its CL intensity was not so reproducible. Hence, the solution containing [Fe(tpps)] and protein was adjusted to pH 7.2, and its CL intensity was measured.

The change in the catalytic activity of [Fe(tpps)] caused by HSA, BSA, human serum γ-globulin-(HγG), and bovine serum γ-globulin(BγG) was examined. HSA and BSA lowered the catalytic activity, while even 1.0×10^{-3} g dm^{-3} HγG and BγG did not affect the catalytic activiy. It is well known that Methyl Orange, Amido Black 10B, Coomassie Brilliant Blue, and so on, which are used for the dyestuff-combination method, do not react with a protein such as globulin.[3,4] Judging from the effect of the pH on the reaction between [Fe(tpps)] and protein, and the difference in reactivity with various proteins, it may be supposed that the [Fe(tpps)] binds to protein as in the above-mentioned dyestuffs.

The relationship between the reaction time of [Fe(tpps)] with protein and the catalytic activity of [Fe(tpps)] was examined. The CL intensities measured at room temperature at about 1.5 min and 1 h after mixing protein with [Fe(tpps)] were almost the same. Therefore, the CL intensity was measured immediately after a sample solution was mixed with [Fe(tpps)].

Table 1. Coefficient of variation for the determination of protein

HSA concentration/gdm⁻³	CV*/%	BSA concentration/gdm⁻³	CV*/%
0	0.54	0	0.54
2.0×10^{-5}	0.69	2.0×10^{-5}	0.79
2.0×10^{-4}	0.74	2.0×10^{-4}	0.44
2.0×10^{-3}	1.20	2.0×10^{-3}	0.73

* Coefficient of variation.

The calibration curves of HSA and BSA obtained by the present method are shown in Fig. 3, while the coefficient of variation(CV) for the determination of protein is shown in Table 1. The detection limits of HSA and BSA were 10 ng and 4 ng respectively.

In comparison with the previous method using the Cu(II) catalyst, the present method was characterized as follows: 1) about 50 times more sensitive, 2) a rapid reaction between catalyst and protein, 3) no necessity to heat the sample solution, and 4) no response for γ-globulin.

References

1) T. Hara, M. Toriyama, and K. Tsukagoshi, *Bull. Chem. Soc. Jpn.*, **56**, 1382 (1983).
2) T. Hara, M. Toriyama, and K. Tsukagoshi, *Bull. Chem. Soc. Jpn.*, **57**, 289 (1984).
3) K. Sugawara and M. Soejima, "Tanpakushitsu No Teiryoho," Gakkai Shuttsupan Center, Tokyo (1977), pp. 147—165.
4) M. Saitou, M. Kitamura, and M. Niwa, "Rinsho Kagaku Bunseki II," Tokyo Kagaku Dojin, Tokyo (1979), pp. 154—169.
5) T. Hara, M. Toriyama, H. Miyoshi, and S. Syogase, *Bull. Chem. Soc. Jpn.*, **57**, 3009 (1984).
6) T. Nomura and M. Oda, *Bunseki Kagaku*, **28**, 377 (1979).

Regioselectivity of the Coupling of Phenoxyallyllithium with Allylic Electrophiles

Yasuo BUTSUGAN,* Tomokazu GOTO, and Shuki ARAKI
Department of Synthetic Chemistry, Nagoya Institute of Technology, Gokiso-cho, Showa-ku, Nagoya 466
(Received January 14, 1985)

Synopsis. The regioselectivity of the coupling of phenoxyallyllithium with allylic electrophiles was investigated. The allylation pattern corresponded with the hardness of the leaving group and the highest α-selectivity was observed in the reaction with allylic phosphate.

The reaction of heteroatom-substituted allylic anion with electrophiles can lead to two regioisomers, α-attack and γ-attack products (Eq. 1). The

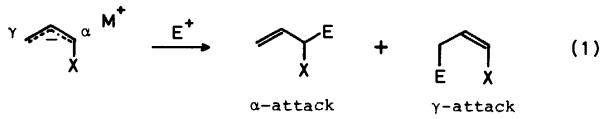

(1)

regioselectivity (α/γ ratio) is a function of a number of factors including the nature of X, and the nature of other substutuents, electrophiles, solvents, and additives.[1] For example, alkyloxyallyl carbanion (X=OR) is reported to yield predominantly γ-attack product by the reaction with alkyl halides, whereas with carbonyl electrophiles α-attack product is formed selectively.[2] In order to define the effect of the leaving group of electrophiles on the α/γ ratio, we examined the reaction of phenoxyallyllithium (**1**) with a series of allylic electrophiles and it was found that the proportion of the α-product increased with increasing hardness of the electrophiles.

To a solution of phenoxyallyllithium (**1**), generated from allyl phenyl ether and butyllithium in tetrahydrofuran-*N*,*N*,*N*′,*N*′-tetramethylethylenediamine, was added allyl halides (**2a**—c), tosylate (**2d**), or phosphate (**2e**) at −78 °C, and the reaction mixture was gradually warmed to room temperature. After stirred for 1 h, the reaction was quenched and the products were extracted with ether. The separation of the α- and γ-products (**3**α and **3**γ) was easily performed by column chromatography on silica gel and the structures were deduced by their elemental and spectral data. It should be noted that the stereochemistry of **3**γ was confirmed to be *Z* by the ^{1}H NMR analysis. The yields of **3**α and **3**γ and the α/γ ratios are summarized in Table 1. The reaction of **1** with allyl iodide predominantly gave the γ-attack product (**3**α/**3**γ=28/72). The proportion of **3**α increased as the hardness of the electrophiles increased, and with allyl diphenyl phosphate the α/γ ratio was reversed (**3**α/**3**γ=53/47). These facts can be reasonably explained by the terms of HSAB principle,[3] that is, the softer halides preferentially attack the softer γ-terminus, while the harder tosylate and the phosphate attack the harder α-position. Similar tendency was also observed in the reactions with prenyl and geranyl compounds (Tables 2 and 3). By the reaction of allylic phosphates (**4**c—**e** and **6**c—**e**), the lesser amount of enol ethers (**5**γ and **7**γ) was formed compared with the reaction of the softer halides (**4a**—**b** and **6a**—**b**). Of the three allylic phosphates (diethyl, diisopropyl, and diphenyl phosphates) which were examined, diphenyl phosphates (**4e** and **6e**) gave the largest α/γ ratio. It is worthwhile to note that all the reactions of **1** with allylic electrophiles (**4** and **6**) gave the products coupled at the α-position of the allylic system, no trace of the products coupled at the γ-position being found. Although the yields of the coupling products (**3**, **5**, and **7**) are not high, considerable amounts (30—50%) of starting electrophiles were recovered in many cases. Furthermore, the coupling products are stable enough under the reaction and separation condi-

Table 1. Reaction of **1** with allyl halides tosylate, and phosphate

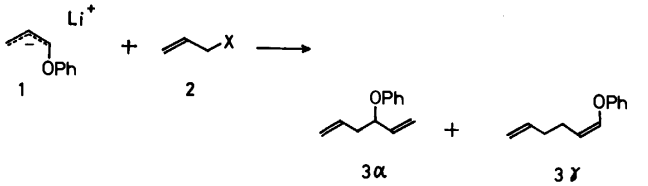

Run	X	Yield/%		**3**α/**3**γ
		3α	**3**γ	
a	I	10	25	28/72
b	Br	21	35	38/62
c	Cl	23	23	50/50
d	OTs	24	25	49/51
e	$OP(O)(OPh)_2$	19	16	53/47

Table 2. Reaction of **1** with prenyl halides and phosphates

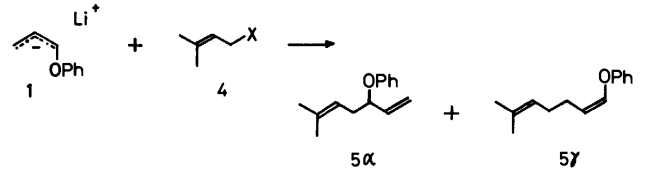

Run	X	Yield/%		**5**α/**5**γ
		5α	**5**γ	
a	Br	17	39	30/70
b	Cl	24	32	42/58
c	$OP(O)(OEt)_2$	36	28	56/44
d	$OP(O)(OPr^i)_2$	26	16	63/37
e	$OP(O)(OPh)_2$	29	10	74/26

Table 3. Reaction of 1 with geranyl halides and phosphates

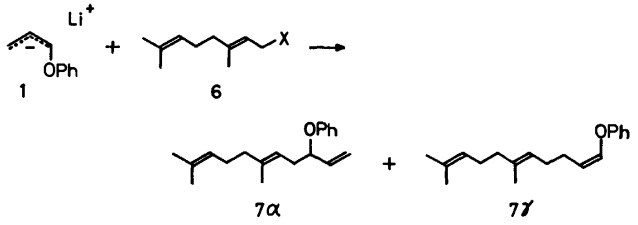

Run	X	Yield/%		7α/7γ
		7α	7γ	
a	Br	13	24	35/65
b	Cl	29	19	61/39
c	$OP(O)(OEt)_2$	26	18	60/40
d	$OP(O)(OPr^i)_2$	20	9	69/31
e	$OP(O)(OPh)_2$	29	12	70/30

tions. Therefore, the isolated yields of the α- and γ-products are considered to reflect the regioselectivity (α/γ ratio).

In summary, it is found that the regioselectivity of the coupling of **1** with allylic electrophiles largely depends on the nature of the leaving group of the electrophile and the highest α-selectivity could be attained by the use of allylic phosphate.

Experimental

General. Infrared spectra were recorded on a JASCO IRA-1 spectrometer. ^1H NMR spectra were recorded on a Hitachi R-24A spectrometer (60 MHz) in CCl_4. Chemical shifts (δ) are recorded in ppm downfield from Me_4Si. Mass spectra were determined using a Hitachi M-52 mass spectrometer at 20 eV. Elemental analyses were performed at the Elemental Analysis Center of Kyoto University.

Reaction of Phenoxyallyllithium (1) with Allylic Electrophiles (2, 4, and 6). The following reaction of **1** and allyl diphenyl phosphate (**2e**)[4] is a representative. To a solution of allyl phenyl ether (419 mg, 3.12 mmol) in THF (12 cm^3) was added a solution of *n*-BuLi in hexane [1.64 M(1 M=1 mol dm^{-3}), 1.85 cm^3, 3 mmol] and then *N,N,N',N'*-tetramethylethylenediamine (0.75 cm^3) at −78 °C. The mixture was stirred at −30——40 °C for 1.5 h. The solution of **1** thus prepared was cooled again to −78 °C and a solution of **2e** (946 mg, 3.26 mmol) in THF (6 cm^3) was added dropwise. The reaction mixture was gradually warmed to room temperature and further stirred for 1 h. After the addition of saturated aqueous ammonium chloride, the products were extracted with ether, washed with brine, and dried (Na_2SO_4). The solvent was evaporated and the residue was chromatographed on silica gel (light petroleum–benzene 10:1) to give 3-phenoxy-1,5-hexadiene (**3α**) (95 mg, 19%) and 1-phenoxy-1,5-hexadiene (**3γ**) (86 mg, 16%). The reactions with prenyl (**4**) and geranyl compounds (**6**) were similarly carried out. Results are summarized in Tables 1 to 3.

3-Phenoxy-1,5-hexadiene (3α): **IR** (neat), 3060, 2900, 1640, 1590, 1580, 1490, 1235, 1165, 980, 915, 745, and 685 cm^{-1}; ^1H NMR 7.38—6.64 (m, 5H, Ph), 6.39—5.51 (m, 2H, olefin), 5.41—4.82 (m, 4H, olefin), 4.82—4.36 (m, 1H, CH), 2.66—2.27 (m, 2H, CH_2); MS *m/z* (rel. intensity) 174 (M^+, 7.8) and 80 (100); Found: C, 82.61; H, 8.16. Calcd for $C_{12}H_{14}O$: C, 82.72; H, 8.10%.

(Z)-1-Phenoxy-1,5-hexadiene (3γ): IR (neat) 3030, 2910, 1665, 1640, 1595, 1490, 1385, 1255, 1220, 1165, 910, 750, and 685 cm^{-1}; ^1H NMR 7.44—6.72 (m, 5H, Ph), 6.28 (d, 1H, *J*=6 Hz, C<u>H</u>(OPh)), 6.09—5.46 (m, 1H, olefin), 5.26—4.53 (m, 3H, olefin), 2.41—2.03 (m, 4H, CH_2); MS *m/z* (rel. intensity) 174 (M^+, 4.7) and 133 (100); Found: C, 83.19; H, 8.19. Calcd for $C_{12}H_{14}O$: C, 82.72; H, 8.10%.

6-Methyl-3-phenoxy-1,5-heptadiene (5α): **IR** (neat) 2930, 1650, 1602, 1590, 1499 1242, 1175, 1035, 992, 930, 755, and 695 cm^{-1}; ^1H NMR 7.33—6.56 (m, 5H, Ph), 6.24—5.54 (m, 1H, olefin), 5.54—4.95 (m, 3H, olefin), 4.70—4.30 (m, 1H, CH), 2.58—2.18 (m, 2H, CH_2), 1.69 (s, 3H, CH_3), 1.61 (s, 3H, CH_3); MS *m/z* (rel. intensity) 202 (M^+, 8.0) and 109 (100); Found: C, 83.71, H, 9.12. Calcd for $C_{14}H_{18}O$: C, 83.12; H, 8.97%.

(Z)-6-Methyl-1-phenoxy-1,5-heptadiene (5γ): IR (neat) 2940, 1670, 1600, 1499, 1394, 1260, 1230, 1170, 1090, 1035, 758, and 695 cm^{-1}; ^1H NMR 7.44—6.72 (m, 5H, Ph), 6.26 (d, 1H, *J*=6 Hz, C<u>H</u>(OPh)), 5.37—4.95 (m, 1H, olefin), 4.95—4.45 (m, 1H, olefin), 2.54—1.85 (m, 4H, CH_2), 1.64 (s, 3H, CH_3), 1.58 (s, 3H, CH_3); MS *m/z* (rel. intensity) 202 (M^+, 7.9) and 133 (100); Found: C, 83.33; H, 9.11. Calcd for $C_{14}H_{18}O$: C, 83.12; H, 8.97%.

(E)-6,10-Dimethyl-3-phenoxy-1,5,9-undecatriene (7α): **IR** (neat) 2940, 1648, 1600, 1590, 1499, 1242, 1175, 1032, 992, 928, 755, and 695 cm^{-1}; ^1H NMR 7.48—6.60 (m, 5H, Ph), 6.16—5.56 (m, 1H, olefin), 5.39—4.97 (m, 4H, olefin), 4.56 (m, 1H, CH), 2.62—2.21 (m, 2H, CH_2), 2.21—1.92 (m, 4H, CH_2), 1.82—1.50 (m, 9H, CH_3); MS *m/z* (rel. intensity) 270 (M^+, 0.8) and 133 (100); Found: C, 84.13; H, 9.82. Calcd for $C_{19}H_{26}O$: C, 84.39; H, 9.69%.

(1Z,5E)-6,10-Dimethyl-1-phenoxy-1,5,9-undecatriene (7γ): **IR** (neat) 2925, 1665, 1595, 1493, 1448, 1386, 1255, 1235, 1225, 1165, 1070, 1025, 750, and 690 cm^{-1}; ^1H NMR 7.42—6.71 (m, 5H, Ph), 6.27 (d, 1H, *J*=6 Hz, C<u>H</u>(OPh)), 5.35—4.55 (m, 3H, olefin), 2.51—1.87 (m, 8H, CH_2), 1.87—1.48 (m, 9H, CH_3); MS *m/z* (rel. intensity) 270 (M^+, 3.1) and 133 (100); Found: C, 84.35; H, 9.91. Calcd for $C_{19}H_{26}O$: C, 84.39; H, 9.69%.

References

1) E. Negishi, "Organometallics in Organic Synthesis," John Wiley and Sons, Inc., 1980, New York, Vol. 1, pp 163—166.

2) D. A. Evans, G. C. Andrews, and B. Buckwalter, *J. Am. Chem. Soc.*, **96**, 5560 (1974); W. C. Still and T. L. Macdonald, *ibid.*, **96**, 5561 (1974); *Idem, J. Org. Chem.*, **41**, 3620 (1976).

3) T-L. Ho, "Hard and Soft Acids and Bases Principle in Organic Chemistry," Academic Press, 1977, New York.

4) J. A. Miller and H. C. S. Wood, *J. Chem. Soc., C*, **1968**, 1837.

Reactions of Vinylphosphonates. 3.[1] One-Pot Synthesis of Dienes and Their Analogues from Vinylphosphonates, Aldehydes and Diethyl Phosphonate

Toru MINAMI,* Shigehumi TOKUMASU, and Ichiro HIRAO
Department of Industrial Chemistry, Kyushu Institute of Technology, Sensuicho, Tobata, Kitakyushu 804
(Received January 24, 1985)

Synopsis. Functionalized dienes and tetraenes were synthesized in 26—63% yields by the one-pot reaction of the phosphoryl-stabilized carbanions, prepared from the Michael addition of diethyl lithiophosphonate to vinylphosphonates, with aromatic aldehydes. A similar reaction using phthalaldehyde gave 2-methylsulfonylnaphthalene (**7**) in 31% yield *via* an intramolecular double Horner-Wittig reaction.

We have previously reported a new synthesis of vinylphosphonates bearing electronegative substituents such as ethoxycarbonyl and cyano groups, and their use in syntheses of functionalized heterocyclic compounds, and olefins, dienes and their analogues.[1,2] In connection with our continuing interest in the synthetic application of the vinylphosphonates, we have now developed an one-pot synthesis of unsaturated systems such as dienes and tetraenes, *etc.* having functionality.

Results and Discussion

The reaction of a phosphoryl-stabilized carbanion **2a**, generated *in-situ* from a Michael addition of diethyl lithiophosphonate to diethyl [1-(methylsulfonyl)vinyl]phosphonate (**1a**), with one equiv of benzaldehyde (**3a**) gave a mixture of 2-methylsulfonyl-1,4-diphenyl-1,3-butadiene (**4a**)(15%), diethyl (2-methylsulfonyl-3-phenyl-2-propenyl)phosphonate (**5a**)(35%), and diethyl [2-diethoxyphosphinyl-1-(methylsulfonyl)ethyl]phosphonate (**6a**)(14%). This result suggests the possibility of an one-pot synthesis of 1,3-dienes and their analogues *via* the double Horner-Wittig reaction.

Accordingly, the reaction of **2a** with an equiv of **3a**, followed by a sequential treatment with an equiv each of lithium diisopropylamide (LDA) and **3a**, afforded the expected **4a** in 63% yield. Similar reactions of **2a** with aromatic aldehydes such as *p*-chlorobenz- (**3b**), cinnam- (**3c**), and 2-thiophenecarbaldehydes (**3d**) gave the corresponding dienes and tetraenes **4b—d** in 42—53% yields. A similar treatment of [1-(ethoxycarbonyl)vinyl]phosphonate **1b** with **3a,d** produced dienes **4e,f**, albeit in low yields.

An application of similar procedures using the phosphonate **1a** to phthalaldehyde successfully gave 2-methylsulfonylnaphthalene (**7**) in 31% yield *via* an intramolecular double Horner-Wittig reaction (Eq. 1).

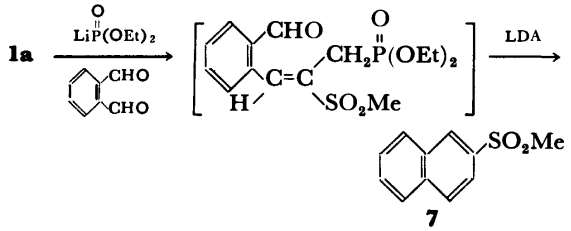

(1)

In contrast to aromatic aldehydes, the one-pot reaction of **1a** with butyraldehyde (**3e**) under similar conditions afforded an unexpected product, diethyl 1,3-hexadienylphosphonate (**8**) in 49% yield, whose formation can not be reasonably accounted for at present. On the other hand, a similar treatment of **1b** with **3e** produced only an 1:1 mixture of diethyl (*E*)-(**9a**) and (*Z*)-(2-ethoxycarbonyl-2-hexenyl)phosphonates (**9b**) in 40% yield.

In conclusion, vinylphosphonates serve as versatile reagents for the one-pot synthesis of dienes, tetraenes,

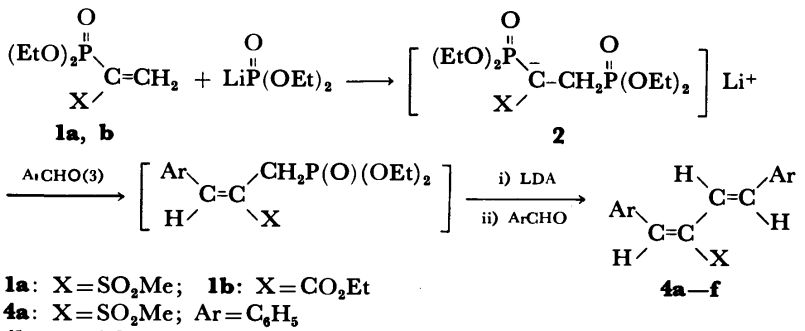

1a: X=SO_2Me; **1b**: X=CO_2Et
4a: X=SO_2Me; Ar=C_6H_5
4b: X=SO_2Me; Ar=*p*-ClC_6H_4
4c: X=SO_2Me; Ar=C_6H_5CH=CH
4d: X=SO_2Me; Ar=2-Thienyl
4e: X=CO_2Et; Ar=C_6H_5
4f: X=CO_2Et; Ar=2-Thienyl

Scheme 1.

and condensed aromatic compounds, which could be useful as synthetic precursors.

Experimental

General. ^{1}H-NMR and ^{13}C-NMR spectra were taken in a $CDCl_3$ solution on a JEOL JNM-FX-60 operating at 60 and 15.04 MHz with Me_4Si as the internal standard. IR spectra were recorded with a Shimadzu IR-408 instrument. Mass spectra were taken with a JEOL DX-300 spectrometer. Melting points were measured in open capillary tubes and are uncorrected.

*Reaction of Diethyl [1-(Methylsulfonyl)vinyl]phosphonate (**1a**) with Benzaldehyde (**3a**) in the Presence of One Equiv. of Diethyl Lithiophosphonate.* To a cooled solution of diethyl lithiophosphonate, prepared from diethyl phosphonate (0.33 g, 2.39 mmol) and butyllithium (2.39 mmol), in THF (20 ml) at −75 °C was added **1a** (0.52 g, 2.15 mmol). The solution was stirred for 0.5 h at this temperature. Then **3a** (0.228 g, 2.15 mmol) was added to the solution and the mixture was stirred at room temperature for 4 h. After a conventional work-up, the residue was chromatographed on a preparative TLC with ether as the eluent to give **4a** (90 mg, 0.317 mmol, 15%), **5a** (0.25 g, 0.753 mmol, 35%), and **6a** (0.11 g, 0.289 mmol, 14%), respectively.

*2-Methylsulfonyl-1,4-diphenyl-1,3-butadiene (**4a**)*: Mp 91—93 °C; IR (KBr): 1300, 1140 cm^{-1}; ^{1}H NMR δ=3.04 (3H, s, Me), 6.70—7.90 (13H, m, olefinic and phenyl H); MS Found: *m/z* 284.0868. Calcd for $C_{17}H_{16}O_2S$: 284.0871 (M^+).

Found: C, 71.74; H, 5.80. Calcd for $C_{17}H_{16}O_2S$: C, 71.80; H, 5.67%.

*Diethyl (2-Methylsulfonyl-3-phenyl-2-propenyl)phosphonate (**5a**)*: Oil; IR (neat): 1300, 1250, 1130, 1020, 960 cm^{-1}; ^{1}H NMR δ=1.30 (6H, t, Me), 3.25 (3H, s, $SO_2\underline{Me}$), 3.40, 3.41 (2H, 2×d, 22.27, 22.12 Hz, P-CH_2), 3.80—4.50 (4H, m, $O\underline{CH_2}CH_3$), 7.10—8.00 (6H, m, olefinic and phenyl H); MS Found: *m/z* 333.0931. Calcd for $C_{14}H_{22}O_5SP$: 333.0926 (M^++1).

*Diethyl [2-Diethoxyphosphinyl-1-(methylsulfonyl)ethyl]phosphonate (**6a**)*: Mp 43—45 °C; IR (KBr): 1310, 1240,1135, 1010, 960 cm^{-1}; ^{1}H NMR δ=1.00—1.70 (12H, m, Me), 2.00—3.00 (3H, m, -$\underline{CH_2}$-$\underline{CH}$), 3.29 (3H, s, $SO_2\underline{Me}$), 3.70—4.60 (8H, m, $O\underline{CH_2}CH_3$); MS *m/z* 380 (M^+).

*General Procedure for the One-Pot Synthesis of 1,3-Dienes **4a—f**.* To a stirred solution of a phosphonate carbanion **2** (3 mmol) in THF (20 ml) at −75 °C was added an aldehyde (3 mmol). After stirring at room temperature for 4 h, the solution was cooled to −75 °C and LDA (3 mmol) in THF (5 ml) was added to the solution. After the solution was stirred at this temperature for 0.5 h, an aldehyde (3 mmol) was added to the solution. The reaction mixture was then stirred at room temperature for 10 h. After a similar work-up, a pure sample of each was obtained by preparative TLC.

*2-Methylsulfonyl-1,4-diphenyl-1,3-butadiene (**4a**)*: Yield 0.54 g (1.90 mmol, 63%).

*2-Methylsulfonyl-1,4-bis(p-chlorophenyl)-1,3-butadiene (**4b**)*: Yield 0.442 g (1.25 mmol, 42%); Mp 149—151 °C; IR (KBr): 1300, 1140 cm^{-1}; ^{1}H NMR δ=3.04 (3H, s, Me), 6.60—7.80 (11H, m, olefinic and phenyl H); MS *m/z* 352, 354, 356 (M^+).

Found: C, 57.83; H, 4.00. Calcd for $C_{17}H_{14}O_2SCl_2$: C, 57.80; H, 3.99%.

*4-Methylsulfonyl-1,8-diphenyl-1,3,5,7-octatetraene (**4c**)*: Yield 0.51 g (1.52 mmol, 51%); Mp 143—145 °C; IR (KBr): 1300, 1120 cm^{-1}; ^{1}H NMR δ=3.00 (3H, s, Me), 6.40—7.80 (17H, m, olefinic and phenyl H); MS *m/z* 336 (M^+).

Found: C, 74.89; H, 6.22. Calcd for $C_{21}H_{20}O_2S$: C, 74.97; H, 5.99%.

*2-Methylsulfonyl-1,4-di(2-thienyl)-1,3-butadiene (**4d**)*: Yield 0.47 g (1.59 mmol, 53%); Mp 123—125 °C; IR (KBr): 1290, 1130 cm^{-1}; ^{1}H NMR δ=3.03 (3H, s, Me), 6.70—8.00 (9H, m, olefinic and aromatic H); MS *m/z* 296 (M^+).

Found: C, 52.68; H, 4.02. Calcd for $C_{13}H_{12}O_2S_3$: C, 52.68; H, 4.08%.

*2-Ethoxycarbonyl-1,4-diphenyl-1,3-butadiene (**4e**)*: Yield 0.218 g (0.786 mmol, 26%); Oil; IR(neat) 1710 cm^{-1}; ^{1}H NMR δ=1.38 (3H, t, Me), 4.34 (2H, q, $\underline{CH_2}CH_3$), 6.50—7.80 (13H, m, olefinic and phenyl H); MS Found: *m/z* 278.1302. Calcd for $C_{19}H_{18}O_2$: 278.1302 (M^+).

*2-Ethoxycarbonyl-1,4-di(2-thienyl)-1,3-butadiene (**4f**)*: Yield 0.248 g (0.855 mmol, 29%); Oil; IR (neat) 1700 cm^{-1}; ^{1}H NMR δ=1.37 (3H, t, Me), 4.32 (2H, q, $\underline{CH_2}CH_3$), 6.50—7.80 (9H, m, olefinic and phenyl H); MS *m/z* 290 (M^+).

Found: C, 62.05; H, 4.88. Calcd for $C_{15}H_{14}O_2S_2$: C, 62.04; H, 4.86%.

*Synthesis of 2-Methylsulfonylnaphthalene (**7**).* The similar reaction of **1a** (2 mmol) with phthalaldehyde (0.268 g, 2 mmol) gave 0.126 g (31%) yield of **7** as white solid: Mp 138—140 °C; IR (KBr) 1290, 1120 cm^{-1}; ^{1}H NMR δ=3.12 (3H, s, Me), 7.20—8.60 (7H, m, aromatic H); MS *m/z* 206 (M^+).

Found: C, 63.64; H, 4.92. Calcd for $C_{11}H_{10}O_2S$: C, 64.06; H, 4.89%.

*One-Pot Reaction of **1a,b** with Butyraldehyd (**3e**). The Reaction Using **1a***: The reaction of **1a** (2 mmol) with **3e** (0.433 g, 6 mmol) gave 0.323 g (49%) yield of **8**: Oil: IR (neat) 1240, 1020, 960 cm^{-1}; ^{1}H NMR δ=1.04 (3H, t, J=7.03 Hz, $CH_2\underline{CH_3}$), 1.32 (6H, t, J=7.03 Hz, $OCH_2\underline{CH_3}$), 1.80—2.50 (2H, m, $\underline{CH_2}CH_3$), 3.70—4.20 (4H, m, $O\underline{CH_2}CH_3$), 5.10—7.60 (4H, m, olefinic H); ^{13}C NMR δ=12.57, 16.12 (d, $^3J_{P\text{-}C}$=6.88 Hz), 25.49, 61.27 (d, $^2J_{P\text{-}C}$=5.16 Hz), 114.34 (d, $^1J_{P\text{-}C}$=191.70Hz), 128.20 (d, $^3J_{P\text{-}C}$=27.51 Hz), 144.77, 148.92 (d, $^2J_{P\text{-}C}$=6.02 Hz). MS Found: *m/z* 218.1075. Calcd for $C_{10}H_{19}O_3P$: 218.1072.

*The Reaction Using **1b***: The reaction of **1b** (0.70 mmol) with **3e** (0.106 g, 1.47 mmol) produced 0.082 g (0.27 mmol, 40%) of an 1:1 mixture of **9a** and **9b**: Oil; IR (neat) 1710, 1250, 1030, 970 cm^{-1}; ^{1}H NMR δ=1.29 (9H, t, J=7.03 Hz, $OCH_2\underline{CH_3}$), 0.60—1.90 (5H, m, =$CHCH_2\underline{CH_2}\underline{CH_3}$), 1.90—3.30 (4H, m, PCH_2- and =$CH\underline{CH_2}CH_2CH_3$), 3.70—4.50 (6H, m, $O\underline{CH_2}CH_3$), 5.85—6.35 (0.5H, m, vinylic H), 6.70—7.15 (0.5H, m, vinylic H); MS Found: *m/z* 292.1413. Calcd for $C_{13}H_{25}O_5P$: 292.1438.

References

1) For the preceding paper in this series, see: T. Minami, K. Nishimura, I. Hirao, H. Suganuma, and T. Agawa, *J. Org. Chem.*, **47**, 2360 (1982).

2) T. Minami, H. Suganuma, and T. Agawa, *Chem. Lett.*, **1978**, 285.

Cobalt-catalyzed Hydroesterification of Formaldehyde Dialkyl Acetals

Kazuhisa MURATA,* Akio MATSUDA, and Takashi MASUDA
National Chemical Laboratory for Industry, Tsukuba Research Center, Yatabe, Tsukuba, Ibaraki 305
(Received January 28, 1985)

Synopsis. $Co_2(CO)_8$-organic amine system was found to be an effective catalyst for the production of alkoxyacetic ester from formaldehyde dialkyl acetals and CO; this is the first example of homogeneous hydroesterification of acetal.

Alkoxyacetic ester is not only a good ether/ester type solvent, but also an important intermediate for preparing ethylene glycol by hydrolysis and hydrogenation. The ester is produced when formaldehyde dialkyl acetals(acetals) are allowed to react with CO in the presence of (solid) acid catalyst (Eq. 1).[1]

$$(RO)_2CH_2 \xrightarrow{CO} ROCH_2COOR \quad (1)$$

$$\xrightarrow{CO/H_2} \mathbf{1}\ (R=Me(\mathbf{a}),\ Et(\mathbf{b}),\ i\text{-}Pr(\mathbf{c})) \quad ROCH_2CHO \quad (2)$$

Also, the ester is obtained by the reaction of formaldehyde with alkyl formate under CO pressure using acid catalyst.[2] In the presence of cobalt catalyst, acetals react with CO/H_2 gas to give alkoxyacetaldehyde (Eq.2).[3] However, in these three processes the yields of product are low. $Co_2(CO)_8$-organic amine system is well known to catalyze the hydroesterification of olefin to give the corresponding carboxylic ester.[4] These findings prompt us to study the cobalt-catalyzed hydroesterification of acetals, yielding alkoxyacetic ester (**1**). We describe here some of our results.

As shown in Table 1, basic solutions prepared *in situ* from $Co_2(CO)_8$ were found to be active catalysts for the hydroesterification of acetals under CO pressure. The reaction proceeded smoothly with no induction period. Ethyl ethoxyacetate (**1b**) was produced from formaldehyde diethyl acetal in 91% yield (*ca.* 910% based on cobalt atom) when the reaction was carried out in dioxane in the presence of γ-picoline under CO pressure of 150 K/cm² at 160 °C (Run 6). Methyl methoxyacetate (**1a**) and isopropyl isopropoxyacetate (**1c**) were obtained from formaldehyde dimethyl acetal and formaldehyde diisopropyl acetal, respectively, in high yields (Runs 4,9). Besides γ-picoline/dioxane(solvent) system, some amine/solvent combinations are also effective (Runs 1—3). The use of γ-picoline solvent was unfavorable(11% yield (**1a**)). The use of CO/H_2 gas in place of CO reduced the yield of **1b**[5] (Run 7).

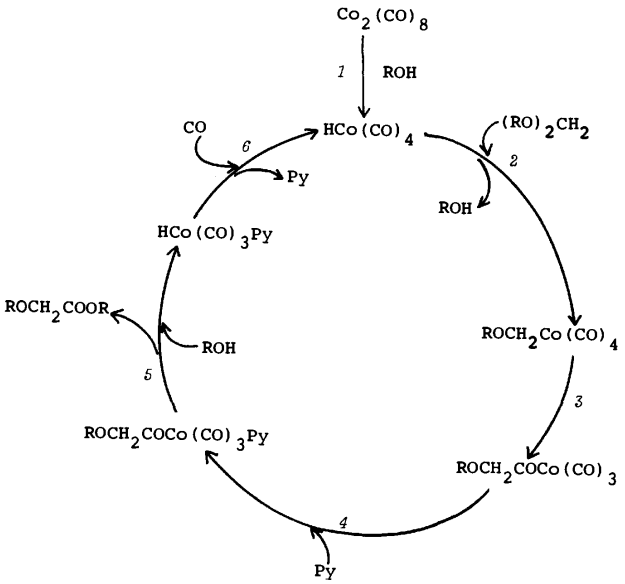

Fig. 1. A possible scheme.

TABLE 1. HYDROESTERIFICATION OF FORMALDEHYDE DIALKYL ACETALS
$Co_2(CO)_8$ 2 mmol, γ-picoline 30 mmol, H_2O 5 mmol, CO 150 Kg/cm² (initial), 160 °C, 5 h.

Run No.	Solvent (mL)		Acetal $CH_2(OR)_2$/alcohol (mmol) /(mmol)	Conv. (%)[a]	Yield of ester/%[b]
1	THF	15	R=Me(50)/MeOH(100)	65	50(**1a**)
2	Benzene	15	R=Me(50)/MeOH(100)	65	57(**1a**)
3	Monoglyme	15	R=Me(50)/MeOH(100)	62	51(**1a**)
4	Dioxane	15	R=Me(50)/MeOH(100)	68	57(**1a**)
5[c]	THF	15	R=Me(50)/MeOH(100)	—	—
6	Dioxane	15	R=Et(40) /EtOH(80)	95	91(**1b**)
7[d]	Dioxane	15	R=Et(20) /EtOH(40)	97	59(**1b**)
8	Dioxane	15	R=Et(40) / —	90	73(**1b**)
9	Dioxane	15	R=i-Pr(40)/i-PrOH(80)	89	46(**1c**)

a) Acetal reacted/acetal initially introduced. b) Ester produced/acetal initially introduced. c) Without γ-picoline.
d) CO 100 Kg/cm², H_2 100 Kg/cm².

Table 2. Effect of some organic amines
$Co_2(CO)_8$ 2 mmol, amine 10 mmol, H_2O 5 mmol, formaldehyde dimethyl acetal 50 mmol, MeOH 100 mmol, THF 15 mL, CO 150 Kg/cm², 160 °C, 5 h.

Run No.	Amine	Conv./%[a]	Yield of ester/**1a**, %
1	Pyridine	40	10
2	Pyridine(40 mmol)	70	50
3	γ-Picoline	54	44
4	β-Picoline	46	28
5	3-Pyridinol	65	47
6	4-Pyridinol	26	12
7	2,4-Lutidine	34	0.4
8	2,4,6-Collidine	13	1.3
9	3-Cyanopyridine	—	—

a) See footnote of Table 1.

Organic amines are essential as catalyst component;[6] the ester, **1a** was not produced at all in the absence of amine (Table 1, Run 5). Pyridine or its derivatives such as γ-picoline, 3-pyridinol are generally favorable (Table 2, Runs 1—6). The yield of ester, **1a** increased with the increase in amine concentration(pyridine 10—60 mmol, γ-picoline 10—30 mmol).

Other metal carbonyl catalysts such as $Rh_4(CO)_{12}$, $Ru_3(CO)_{12}$, $Fe(CO)_5$, $Mo(CO)_6$, and $Cr(CO)_6$ were examined for this reaction of acetals under the same conditions as that of $Co_2(CO)_8$ catalyst, but neither of these catalysts gave carbonylation products.

A possible scheme by which the production of alkoxyacetic ester can be explained, is illustrated in Fig. 1, where pyridine(Py) is used as amine. In this scheme, pyridine participates in alkoholysis step 5, as is the case of the cobalt-catalyzed hydroesterification of olefin.[4] Steps 2 and 3 have been already given in the hydroformylation of acetals (Eq. 2).[3] The absence of EtOH resulted in the appearance of induction period (*ca.* 30 min) and in the drop of **1b** yield (Table 1, Run 8), indicating that, under CO conditions, EtOH takes part in step 1. Based on the scheme, scavenging of $HCo(CO)_4$ from the reaction mixture will stop the catalytic cycle. In fact, when sodium carbonate (4 mmol) is initially added to Run 4(Table 1), the yield of **1a** was only 3%.

Experimental

Materials. Solvents and amines were obtained commercially and used with no further purification. Formaldehyde dimethyl acetal and formaldehyde diethyl acetal were purchased from Tokyo Kasei Kogyo CO., LTD. Formaldehyde diisopropyl acetal was synthesized from aqueous formalin and 2-propanol using *p*-toluenesulphonic acid as catalyst.

Reaction Procedure. A catalyst solution prepared from $Co_2(CO)_8$(2 mmol), amine(10—60 mmol), acetal(40—50 mmol), alcohol(80—100 mmol), and H_2O(5 mmol) in dioxane(15 cm³) was placed in a stainless-steel autoclave (50 cm³), which was subsequently charged with CO (150 Kg/cm²). After the reaction, the vessel was cooled to room temperature and the catalyst solution was analyzed by GLC. Satisfactory spectral data were obtained for alkoxyacetic esters.

This work was supported by National Research and Development(C_1 Chemistry project) of Ministry of International Trade and Industry.

References

1) K. Kumagai, Eur. Pat. Appl., 88529, C07C 69/708.
2) K. Wada, A. Baba, and N. Wada, Jpn. Patent 56-122321.
3) W. Reppe, H. Kröprt, H. J. Pistor, and O. Weissbarth, *Ann. Chem.*, **582**, 87 (1953).
4) A. Matsuda, *Bull. Chem. Soc. Jpn.*, **40**, 135 (1967); ibid., **46**, 524 (1973).
5) $EtOCH_2CH_2OH$(4%), $EtOCH_2CH(OEt)_2$(7%), and trace amount of ethoxyacetaldehyde were detected by GLC analysis as by-products.
6) After the reaction of Run 4 (Table 1), >99% of γ picoline was confirmed by GLC.

N-Nitroso Compounds. IV.[1] Reaction of *N*-Nitrosourea with Thiol. A New Synthesis of Thiocarbamic *S*-Esters

Kitaro Yoshida,* Masayoshi Isobe, Kazuyuki Yano, and Kazuo Nagamatsu
Department of Chemistry, Saitama Medical School, 981 Kawakado, Moroyama, Iruma-gun, Saitama 350-04
(Received March 1, 1985)

Synopsis. Thirteen thiocarbamic *S*-esters have been synthesized in good yield by the reaction of thiol with substituted *N*-methyl-*N*-nitrosourea in anhydrous acetonitrile.

Although several methods have been reported on the preparation of thiocarbamic *S*-esters, the most commonly used ones are those from alkylcarbamoyl chlorides with sodium alkanethiolates,[2a] alkyl thiocyanates with alcohols,[2b] or those using carbonyl sulfide with base,[2a] or carbon monoxide with selenium as a catalyst.[2c] Since the preparation of herbicidal thiocarbamic *S*-esters is of commercial importance, it is significant to explore an alternative route to this class of compounds.

Recently, we have shown that *N'*-substituted *N*-methyl-*N*-nitrosourea readily reacts with aliphatic amines to give "transaminated" urea in substantial yield.[1] Similar S_N2 reactions have also been reported for *N*-alkyl-*N*-nitroso amides with aliphatic primary amines in refluxing dichloromethane.[3] Furthermore, Challis and his co-workers observed a nucleophilic rather than a general base catalysis of imidazole in the hydrolyses of *N*-nitroso-2-pyrrolidone and related compounds in aqueous buffer solution.[4] All of these results are undoubtedly related to an enhanced leaving property of the *N*-nitrosoamino moiety of the substrates. Thus a facile reaction is also expected to occur with other nucleophiles. We have now found that *N*-nitrosourea **1** reacts with various thiols under mild conditions to give the corresponding thiocarbamic *S*-esters **2** in good yields as shown in Scheme 1.

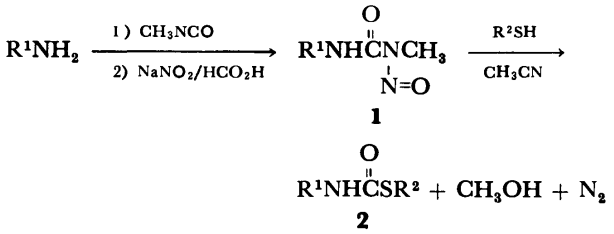

Scheme 1.

We wish to report here a convenient method of the preparation of **2** from primary amines by the use of **1** as a key compound.

Results and Discussion

N-Methylurea ($R^1NHCONHCH_3$) was obtained conventionally[5] through the carbamoylation of starting amine with methyl isocyanate. On treatment of the urea with sodium nitrite in formic acid, an *N*-nitrosated urea **1** was produced exclusively; this was the product from the mononitrosation at the less hindered *N*-position.[6] The crude product **1** was treated with 2 equiv of thiol in anhydrous acetonitrile at 60 °C. Because of the limited solubility and to avoid the hydrolysis of **1**,[7] the use of organic solvent may be of significance. As the reaction proceeded, gas evolution was observed and in most cases, almost all quantity of **1** was consumed within several hours. However, under the same

Table 1. Yields, melting points, and IR data of **2**

Run	R^1(Amine)	R^2(Thiol)	Reaction conditions		**2**		
			Temp/°C	Time/h	Overall Yield/%[a]	Mp(θ_m/°C)	IR(C=O)/cm^{-1}
1	*n*-C_4H_9	Ph	reflux	18	39	oil	1660
2	*cyclo*-C_6H_{11}	*n*-C_4H_9	60	21	77	65—66[b]	1650
3	1-Adamantyl	*n*-C_4H_9	60	2	99	62—64	1670
4	Ph	C_2H_5	60	1	73	69.5—70.0	1680
5	Ph	*n*-C_4H_9	60	1	83	68—70	1670
6	Ph	*i*-C_4H_9	60	0.5	73	105—107	1670
7	Ph	*t*-C_4H_9	60	0.5	12[c]	142—143	1670
8	Ph	$CH_2CH{=}CH_2$	60	1	91	69—70	1680
9	Ph	CH_2CH_2OH	60	0.5	71	72.5—73.5	1660
10	Ph	*cyclo*-C_6H_{11}	60	0.5	86	115.0—115.5	1660
11	Ph	*n*-$C_{10}H_{21}$	r.t.	72	69	62.5—64.0	1680
12	Ph	Ph	reflux	16	89	120—121[d]	1670
13	Ph	*p*-$CH_3C_6H_4$	reflux	16	88	130.0—130.5[e]	1670

a) Isolated Yield. b) 68 °C, Ref. 2b). c) Ref. 8). d) 122—124 °C, Ref. 9). e) 130—132 °C, Ref. 9).

conditions, aromatic thiol did not react with **1** even after a prolonged reaction period, so that an elevated temperature was required. After work up, the thiocarbamic *S*-ester **2** was obtained in the yields of 42—100% (39—99% based on the amine used).[8] The results are summarized in Table 1.

For synthetic purposes, the present method has some advantages in that (i) the direct reaction of **1** with alkanethiol (not sodium alkanethiolates) occurs spontaneously under rather mild conditions; (ii) by-products such as methanol and nitrogen arising from the *N*-methyl-*N*-nitrosoamino fragment can readily be eliminated, so that no tedious work up is necessary (see Experimental); (iii) in addition to the current availability of aromatic amines, it becomes possible to utilize aromatic thiols as well. Thus the present study provides an efficient new route to thiocarbamic *S*-esters.

Experimental

Mps are uncorrected. IR spectra were taken in chloroform solution by a Shimadzu IR-400 spectrophotometer. All the reagents were of commercial grade and used without further purification.

Reaction of 1 with Thiol. An *N'*-substituted *N*-methylurea was prepared in a usual fashion.[5] The urea (10 mmol) was treated by sodium nitrite (20 mmol) in formic acid (10 ml) at 0—5 °C for 1 h. The mixture was poured onto ice-water, and the precipitate formed was collected, washed with cold water, and dried under reduced pressure to yield exclusively *N*-nitrosated urea **1** (77—100% from the amine). The crude product **1** and an excess of thiol (20 mmol) were dissolved in anhydrous acetonitrile (20 ml) and the mixture was stirred at 60 °C with monitoring the reaction by TLC analysis. After **1** was consumed, evaporation of the solvent and the excess thiol under reduced pressure gave **2** in almost pure solid. When a thiol of high boiling point was used, isolation by column chromatography (silica gel, $CHCl_3$–hexane or ether–hexane) was carried out. The IR and ^1H NMR spectra of the crude solid **2** were consistent with the assigned structure. In most cases, the analytical sample was obtained by recrystallization to give a satisfactory elemental analysis within ±0.4% for C, H, N, and S. The yields and some of the physical data of **2** are summarized in Table 1.

References

1) Part III, K. Yoshida, K. Yano, and K. Nagamatsu, *J. Chem. Soc., Parkin Trans. 2*, **1985**, 437.

2) a) H. Tilles, *J. Am. Chem. Soc.*, **81**, 714 (1959); b) R. Riemschneider, *ibid.*, **78**, 844 (1956); c) P. Koch, *Tetrahedron Lett.*, **1975**, 2087.

3) J. Garcia and J. Vilarrasa, *Tetrahedron Lett.*, **1982**, 1127.

4) B. C. Challis and S. P. Jones, *J. Chem.Soc., Perkin Trans. 2*, **1979**, 703; C. N. Berry, B. C. Challis, A. D. Gribble, and S. P. Jones, in "*N*-Nitroso Compounds," ed by R. A. Scanlan and S. R. Tannenbaum, American Chemical Society, Washington, D. C., (1981), p. 101.

5) S. R. Sandler and W. Karo, "Organic Functional Group Preparations," Academic Press, New York (1971), Vol. 2, p. 139.

6) J. K. Snyder and L. M. Stock, *J. Org. Chem.*, **45**, 886 (1980).

7) K. Yoshida and K. Yano, *Bull. Chem. Soc. Jpn.*, **55**, 2200 (1982).

8) The low yield in the reaction with bulky thiol (Run 7, Table 1) may be due to the steric factor around the carbonyl group of **1**.

9) N. Bourne, A. Williams, K. T. Douglas, and T. R. Penkava, *J. Chem. Soc., Perkin Trans. 2*, **1984**, 1827.

Synthesis of Macrocarbocycles Utilizing Intramolecular 1,3-Dipolar Cycloaddition of Nitrile Oxides. Synthesis of (±)-Muscone

Morio Asaoka,* Masayoshi Abe, and Hisashi Takei
Department of Life Chemistry, Tokyo Institute of Technology, Nagatsutacho, Midori-ku, Yokohama 227
(Received March 1, 1985)

Synopsis. Intramolecular 1,3-dipolar cycloaddition of nitrile oxides generated from ω-nitro-1-alkenes gave isoxazoline-fused macrocarbocycles (ring size 12, 14, 15, and 16) in fair to good yields. The 15-membered derivative was converted into (±)-muscone.

In connection with a total synthesis of macrocyclic natural products, we examined intramolecular 1,3-dipolar cycloaddition of silyl nitronates and nitrile oxides generated from ω-nitroalkyl acrylates, and achieved the synthesis of macrolides, (±)-pyrenophorin and (±)-A26771B.[1,2] In this note we will describe intramolecular 1,3-dipolar cycloaddition of nitrile oxides generated from ω-nitro-1-alkenes.[3]

The nitro alkenes **2** were easily prepared from the corresponding aldehydes **1** by the method of Wollenberg and Mille[4] in good yields. Intramolecular 1,3-dipolar cycloaddition was carried out using dilute solution of **2** in benzene or toluene (concentration=1 mmol of **2**/400 ml of solvent) in the presence of 10 equiv of *p*-chlorophenyl isocyanate and triethylamine.[5] We examined the effects of reaction temperature and time using **2c** (Table 1, Run 4—8).

When reaction was carried out in refluxing benzene the reaction was relatively slow and after 15—25 h, desired cyclic compound **4c** was obtained in 31—44% yield (Run 4 and 5). Then the reaction was carried out in refluxing toluene for 15 h. Surprisingly the yield of **4c** dropped to 18% and a large amount (40%) of starting material (**2c**) was recovered. This result suggests that dehydration of nitro compounds with triethylamine and isocyanate is supressed at that temperature presumably because of the instability of *aci*-nitro form at high temperature (Run 6). According to this assumption, the reaction was carried out at 50 °C for 18 h in order to generate the nitrile oxide completely and then at 110 °C for 18 h to give better yield (63%) of **4c** (Run 7). However when the intramolecular addition step was carried out at higher temperature (140 °C) the yield dropped slightly, probably because of decomposition of the product at that temperature. Intramolecular 1,3-

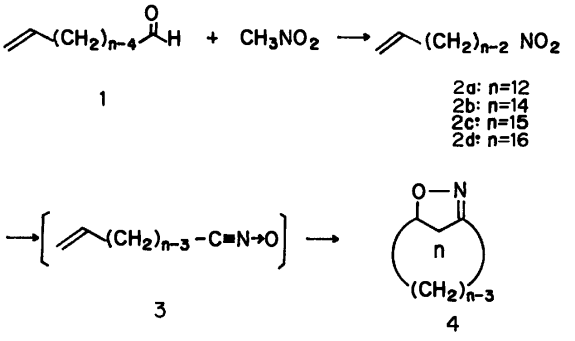

Scheme 1.

Table 1. Intramolecular 1,3-dipolar cycloaddition of nitrile oxides (**3**) derived from **2**

Run	Nitro Olefin	Solvent	Temp and Time	Ring Size	Yield **4**/%
1	**2a**	A	80 °C 18 h	12	21
2	**2b**	A	80 °C 20 h	14	44
3		B	50 °C 18 h and 110 °C 18 h		38
4	**2c**	A	80 °C 15 h	15	31
5		A	80 °C 25 h		44
6		B	110 °C 15 h		18
7		B	50 °C 18 h and 110 °C 18 h		63
8		C	30 °C 20 h and 140 °C 10 h		47
9	**2d**	B	50 °C 18 h and 110 °C 18 h	16	60

Solvent A: Benzene, B: Toluene, C: Xylene.

Table 2. Spectral and physical data of **4a—d**

Compound	NMR ($CDCl_3$), δ	IR (KBr), cm^{-1}	Mp, θ_m/°C
4a	1.30 (14H, broad s), 1.20—1.82 (2H, m), 2.80 (2H, t) 2.14—2.54 (2H, m), 4.26—4.85 (1H, m)	1610 (C=N)	85.5—86.5
4b	1.34 (20H, broad s), 2.26—2.70 (2H, m), 2.80 (1H, d), 2.83 (1H, d), 4.46—4.96 (1H, m)	1605 (C=N)	67.0—68.5
4c	1.43 (22H, broad s), 2.13—2.63 (2H, m), 2.63—2.97 (2H, m), 4.33—4.93 (1H, m)	1615 (C=N)	81.0—82.0
4d	1.82 (24H, broad s), 2.13—2.63 (2H, m), 2.63—2.97 (2H, m), 4.32—4.81 (1H, m)	1610 (C=N)	88.5—90.0

dipolar cycloaddition of alkenenitrile oxides having different chain length was also examined. Nitroalkenes **2b** and **2d**, gave the expected cyclic compounds **4b** and **4d** in 44 and 60% yields, respectively. In the case of **2a** however, the reaction was complex and **4a** was isolated only in 21% yield. The structures of **4a—d** were confirmed by spectral (NMR, IR, and Mass) data and elemental analyses. Their NMR and IR spectral data along with their melting points are listed in Table 2.

In the course of the synthetic studies of macrolides, we have shown that isoxazoline derivatives were easily converted to α,β-unsaturated ketones in high yields by hydrogenolysis under acidic conditions and subsequent dehydration.[1,2,6] Then transformation of the isoxazoline derivative **4c** to (±)-muscone *via* enone **6** was examined. Although hydrogenolysis of **4c** under acidic conditions in the presence of Pd–C showed formation of some by-products, use of PtO_2 as a catalyst gave better results. After hydrogenolysis of **4c** in acetic acid–water under atmospheric pressure of hydrogen at room temperature for 2 d, the resulted crude **5** was treated with methanesulfonyl chloride and triethylamine to give **6** in 45% overall yield from **4c**, which was converted to (±)-muscone **7** in 79% yield by known method.[7]

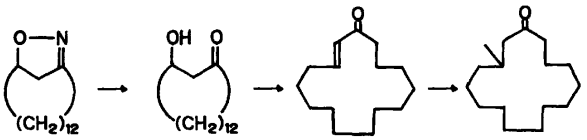

4c **5** **6** **7**

Scheme 2.

Experimental

A Typical Procedure of Intramolecular 1,3-Dipolar Cycloaddition: Nitroalkene **2c** (255 mg, 1 mmol), *p*-chlorophenyl isocyanate (1.52 g, 10 mmol), and triethyamine (4 ml, 10 mmol) were dissolved in 400 ml of dry toluene. The solution was stirred at 50 °C for 18 h and then heated under reflux for 18 h. To the reaction mixture was added isopropylamine (1 ml) at 0 °C and stirred at that temperature for 20 min. After filtration through short pad of celite, the solution was concentrated *in vacuo* and the residue was purified by column chromatography (benzene: ether=50:1) to give 149 mg of **4c**.

trans-*2-Cyclopentadecenone (6)*: A solution of **4c** (66 mg) dissolved in acetic acid (3 ml) and water (0.5 ml) was stirred under H_2 for 2 d in the presence of PtO_2. After removal of catalyst by filtration, solvent was removed under reduced pressure. To the residue dissolved in dry CH_2Cl_2 (2 ml) were added MsCl (124 mg, 1.07 mmol) and triethylamine (0.37 ml, 2.65 mmol) at 0 °C under argon. After 16 h, a small amount of MeOH was added dropwise to the reaction mixture. The mixture was diluted with ether and precipitated salt was removed by filtration. After removal of solvent, the residue was purified by column chromatography (hexane:ether=10:1) to give **6** (28 mg, 45%): IR (NaCl) 1685, 1655 cm^{-1} (C=O) and 1627 cm^{-1} (C=C); NMR (60 MHz, $CDCl_3$) δ=1.05—1.93 (20H, m), 2.07—2.70 (4H, m), 6.10 (2H, d, J=16 Hz), 6.68 (1H, dt, J=16 and 6 Hz).

References

1) M. Asaoka, T. Mukuta, and H. Takei, *Tetrahedron Lett.*, **1981**, 753.

2) M. Asaoka, M. Abe, T. Mukuta, and H. Takei, *Chem. Lett.*, **1982**, 215.

3) Application of intramolecular 1,3-dipolar cyclization of nitrile oxides to the construction of 5—7 membered carbocycles, see; a) V. Jäger and H. J. Gunther, *Angew. Chem. Int. Ed. Engl.*, **16**, 246 (1977); b) A. P. Kozikowski, *Acc. Chem. Res.*, **1984**, 410 and references are cited therein.

4) R. H. Wollenberg and S. J. Miller, *Tetrahedron Lett.*, **1978**, 3219.

5) T. Mukaiyama and T. Hoshino, *J. Am. Chem. Soc.*, **82**, 5339 (1960).

6) Similar transformation has been reported by other groups also; a) R. H. Wollenberg and J. E. Goldstein, *Synthesis*, **1980**, 757; b) A. P. Kozikowski and P. D. Stein, *J. Am. Chem. Soc.*, **104**, 4023 (1982); c) S. H. Amdersen, K. K. Sharma, and K. B. G. Torssell, *Tetrahedron*, **39**, 2241 (1983).

7) a) K. C. Nicolaou, S. P. Seitz, M. R. Pavia, and N. A. Patasis, *J. Org. Chem.*, **44**, 4011 (1979); b) J. Nokami, Y. Kusumoto, K. Jinnai, and M. Kawada, *Chem. Lett.*, **1977**, 715.

Absolute Stereostructure Determination of Cladospolide A Using MTPA Ester Method[1)]

Hiroshi HIROTA,* Akira HIROTA,*,† Heiichi SAKAI,† Akira ISOGAI,†† and Takeyoshi TAKAHASHI

Department of Chemistry, Faculty of Science, The University of Tokyo, Hongo, Bunkyo-ku, Tokyo 113
†Department of Agricultural Chemistry, College of Agriculture, University of Osaka Prefecture, Sakai, Osaka 591
††Department of Agricultural Chemistry, Faculty of Agriculture, The University of Tokyo, Yayoi, Bunkyo-ku, Tokyo 113

(Received March 13, 1985)

Synopsis. The absolute configuration of cladospolide A, a phytotoxic macrolide produced by a fungus *Cladosporium cladosporioides*, was determined as (4*R*,5*S*, 11*R*,2*E*)-4,5-dihydroxy-2-dodecen-11-olide by means of MTPA method.

Cladospolide A (**1**), a novel fungal metabolite, was isolated from culture filtrate of *Cladosporium cladosporioides* FI-113 and showed the inhibitory activity to lettuce seedlings. In the previous papers, we reported cladospolide A was a novel macrolide and its planar structure was shown as (*E*)-4,5-dihydroxy-2-dodecen-11-olide.[2)] The relative stereochemistry of three asymmetric centers of **1** was also established as (4*R*,5*S*,11*R*) or (4*S*,5*R*,11*S*) by X-ray single crystal structure elucidation.[1,3)] We now wish to report here the determination of the absolute configuration of cladospolide A by means of the MTPA method.[4,5)]

The lactone moiety of **1** was transformed into hydroxy ester, methyl (*E*)-4,5,11-trihydroxy-2-dodecenoate (**2**), by treatment with methanolic hydrogen chloride. Isopropylidenation of 1,2-diol part of **2** with acetone in acidic medium gave methyl (*E*)-4,5-(isopropylidenedioxy)-11-hydroxy-2-dodecenoate (**3**), which possesses an acyclic and secondary alcohol structure without steric congestion. To this alcohol (**3**), the MTPA method was applied.[4)] The alcohol (**3**) was transformed into the corresponding (*R*)-(+)-α-methoxy-α-(trifluoromethyl)phenylacetic acid [(*R*)-(+)-MTPA] ester (**4**) and (*S*)-(−)-MTPA ester (**5**) according to Mosher's method.[6)] ^{1}H NMR spectra of **4** and **5** were taken with various molar ratio (0—0.6) of Eu(fod)$_3$-d_{27} to MTPA ester in $CDCl_3$, and the magnitudes of induced chemical shifts of each signal were plotted *versus* molar ratio (Eu(fod)$_3$-d_{27}/MTPA ester). In this range the induced shifts were essentially linear with respect to molar ratio of the reagent and MTPA ester. Lanthanoid induced shift (LIS) values for the selected proton signals of **4** and **5** were given in Table 1. The ΔLIS_{OMe} value for the methoxyl group of MTPA was largely positive (+1.67), while other ΔLIS values were very small. This indicates that the chiral center at $C_{(11)}$ of **3** is in an *R*-configuration according to the generality for the MTPA method.[4)] Then, the stereostructure of cladospolide A was determined as (4*R*,5*S*,11*R*,2*E*)-4,5-dihydroxy-2-dodecen-11-olide (**1**).[7)]

Table 1. Lanthanoid induced shift (LIS) values for the selected proton signals of (*R*)-(+)-MTPA ester (**4**) and (*S*)-(−)-MTPA ester (**5**)

	LIS values of **4**	ΔLIS	LIS values of **5**
$C_{(1)}OOCH_3$	2.85	+0.17	2.68
$C_{(2)}$-H	3.08	+0.25	2.83
$C_{(3)}$-H	2.91	+0.15	2.76
$C_{(4)}$-H	0.63	+0.01	0.62
$C_{(5)}$-H	0.26	+0.05	0.21
$C_{(11)}$-H	1.17	+0.32	0.85
$C_{(11)}$-CH_3	0.63	+0.34	0.29
MTPA-OCH_3	5.05	+1.67	3.38

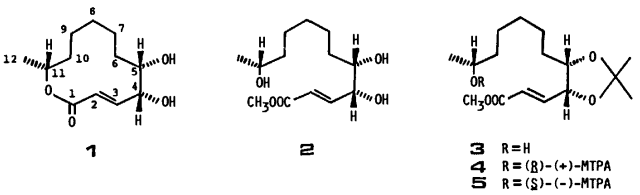

Experimental

General Procedures. Infrared (IR) spectra were measured on JASCO IRA-2 and Hitachi 260-30 spectrometers. Proton and carbon-13 nuclear magnetic resonance (^{1}H and ^{13}C NMR) spectra were taken using Varian EM390 (90 MHz for ^{1}H), JEOL FX-90Q (90 MHz for ^{1}H), JEOL FX-100 (100 MHz for ^{1}H and 25 MHz for ^{13}C), and JEOL MH-100 (100 MHz for ^{1}H) spectrometers. Chemical shifts were expressed in δ (ppm) downfield from tetramethylsilane as an internal standard and coupling constants in Hz. Mass (MS) spectra were run on a JEOL D-300 mass spectrometer operating at 70 eV. Wakogel C-200 (Wako) were used for column chromatography.

*Methyl (4*R*,5*S*,11*R*,2*E*)-4,5,11-Trihydroxy-2-dodecenoate (**2**).* Cladospolide A (**1**; 88 mg) was dissolved in 20 ml methanol saturated with hydrogen chloride. After standing for 1 h, the reaction mixture was concentrated *in vacuo* and extracted with ethyl acetate. The extract was subjected to separation by silica gel (20 g) column chromatography and was eluted with ethyl acetate to afford **2** as an oil (91 mg). **2**: IR (neat) 3400, 1715, and 1665 cm^{-1}; ^{1}H NMR (100 MHz; $(CD_3)_2CO$) δ=1.24 (3H, d, *J*=6 Hz), 3.75 (3H, s), 3.4—4.1 (3H including 2×—OH, m),[8)] 4.2—4.5 (3H including 1×—OH, m),[8)] 6.05 (1H, br d, *J*=15 Hz), 7.05 (1H, dd, *J*=15 and 4.5 Hz); ^{13}C NMR (25 MHz; $(CD_3)_2CO$) δ=24.42 (CH_3), 26.94 (CH_2), 27.02 (CH_2), 30.94 (CH_2), 33.96 (CH_2), 40.60 (CH_2), 52.00 (CH_3), 67.98 (CH), 75.14 (CH), 75.29 (CH), 121.62 (CH), 150.20 (CH), 167.63 (C=O);[9)] MS *m/z* 261 (M+H$^+$; 0.001),[10)] 116 (100).

*Methyl (4*R*,5*S*,11*R*,2*E*)-4,5-(Isopropylidenedioxy)-11-hydroxy-2-dodecenoate (**3**).* Trihydroxy ester (**2**; 80 mg) was

dissolved in dry acetone (20 ml) containing 0.5% 6 M* hydrochloric acid and the mixture was allowed to stand at room temperature for 45 h. The reaction mixture was neutralized with 0.1 M sodium methoxide and evaporated *in vacuo*. The residue was subjected to silica gel (20 g) column chromatographic separation and was eluted with benzene–ethyl acetate (9:1) to afford **3** as an oil (33 mg). **3**: IR (neat) 3450, 1720, 1630 cm^{-1}; ^1H NMR (100 MHz; $CDCl_3$) δ=1.16 (3H, d, J=6 Hz), 1.36 (3H, s), 1.48 (3H, s), 3.70 (3H, s), 4.16 (1H, m), 4.60 (1H, br t, J=4.5 Hz), 6.00 (1H, br d, J=15 Hz), 6.76 (1H, dd, J=15 and 4.5 Hz); ^{13}C NMR (25 MHz; $CDCl_3$) δ=23.60, 25.62, 25.62, 26.32, 28.13, 29.57, 30.53, 39.31, 51.74, 68.18, 77.48, 78.39, 108.93, 122.67, 144.23, 166.55; MS m/z 285 ($M-15^+$; 24), 193 (10), 156 (27), 125 (17), 98 (100). No molecular ion was observed.

(R)-(+)-MTPA Ester (4). A mixture of dry pyridine (0.3 ml), (*R*)-(+)-MTPA chloride (0.05 ml), the substrate alcohol (**3**; 13 mg), and carbon tetrachloride (0.3 ml) was stirred at room temperature for 3 d. Excess amount of *N,N*-dimethyl-1,3-propanediamine (*ca.* 0.1 ml) was added and the mixture allowed to stand for 10 min. It was then extracted with ether, washed (with dil. HCl ×2, saturated aqueous solution of sodium carbonate, and saturated brine ×2), and dried over magnesium sulfate. The filtered ether solution was concentrated, and the reaction product was purified by passing through a silica-gel (*ca.* 5 g) column. Elution with benzene–acetone(5:1) gave 14 mg of (*R*)-(+)-MTPA ester (**4**; 63% yield): an oil, IR (neat) 1740, 1725, and 1660 cm^{-1}; ^1H NMR (90 MHz; $CDCl_3$) δ=1.25 (3H, d, J=6 Hz), 1.38 (3H, s), 1.51 (3H, s), 3.57 (3H, s, OCH_3 at MTPA part), 3.75 (3H, s, $-COOCH_3$), 4.22 (1H, m, $C_{(5)}$-H), 4.64 (1H, td, J=6 and 1 Hz, $C_{(4)}$-H), 5.13 (br q, J=6 Hz, $C_{(11)}$-H), 6.07 (1H, dd, J=16 and 1 Hz, $C_{(2)}$-H), 6.84 (1H, dd, J=16 and 6 Hz, $C_{(3)}$-H), and 7.3—7.6 (5H, m); MS m/z 516 (M^+; 2), 501 (43), 484 (3), 225 (58), 193 (40), 189 (60), 156 (98), and 98 (100); Found: m/z 516.2352. Calcd for $C_{26}H_{35}O_7F_3$: M, 516.2334.

(S)-(−)-MTPA Ester (5). Alcohol (**3**; 14 mg) was treated with (*S*)-(−)-MTPA chloride by the same procedure as above to transform into (*S*)-(−)-MTPA ester (**5**; 15 mg; 62% yield): an oil, IR (neat) 1740, 1725, and 1660 cm^{-1}; ^1H NMR (90 MHz; $CDCl_3$) δ=1.28 (3H, diffused d), 1.38 (3H, s), 1.51 (3H, s), 3.57 (3H, s, $-OCH_3$ at MTPA part), 3.75 (3H, s, $-COOCH_3$), 4.21 (1H, m, $C_{(5)}$-H), 4.64 (1H, br t, J=6 Hz, $C_{(4)}$-H), 5.15 (1H, br q, J=6 Hz, $C_{(11)}$-H), 6.07 (1H, br d, J=15 Hz, $C_{(2)}$-H), 6.84 (1H, dd, J=15 and 6 Hz, $C_{(3)}$-H), and 7.3—7.6 (5H, m); MS m/z 516 (M^+; 2), 501 (36), 484 (6), 225 (60), 193 (38), 189 (91), 156 (96), and 98 (100). Found: m/z 516.2299. Calcd for $C_{26}H_{35}O_7F_3$: M, 516.2334.

* 1 M=1 mol dm^{-3}.

References

1) Preliminary account of this report: A. Hirota, H. Sakai, A. Isogai, Y. Kitano, T. Ashida, H. Hirota, and T. Takahashi, *Agric. Biol. Chem.*, **49**, 903 (1985).

2) A. Hirota, A. Isogai, and H. Sakai, *Agric. Biol. Chem.*, **45**, 799 (1981); A. Hirota, H. Sakai, and A. Isogai, *ibid.*, **49**, 731 (1985).

3) A detail description on the X-ray analysis of cladospolide A (**1**) will be reported elesewhere.

4) S. Yamaguchi and F. Yasuhara, *Tetrahedron Lett.*, **1977**, 89; S. Yamaguchi, F. Yasuhara, and K. Kabuto, *Tetrahedron*, **32**, 1363 (1976).

5) Y. Sugimoto, T. Tsuyuki, Y. Moriyama, and T. Takahashi, *Bull. Chem. Soc. Jpn.*, **53**, 3723 (1980).

6) J. A. Dale, D. L. Dull, and H. S. Mosher, *J. Org. Chem.*, **34**, 2543 (1969).

7) CD spectrum of bis(*p*-chlorobenzoate) of **1** was also taken, and $[\Theta]_{245}$=−23500 was observed, which was coincident with the result from MTPA method; as cladospolide A (**1**) posesses two conformations even in solid state (see Ref. 1 and 3), we estimate it very dangerous to apply dibenzoate chirality rule easily to a derivative of this compound in solution state.

8) Signals of -OH protons were assigned by addition of D_2O in the sample tube.

9) INEPT ($1/4J$, $2/4J$, and $3/4J$) techniques were applied to clarify the multiplicities of these signals.

10) While the molecular ion was not observable, the $(M+H)^+$ ion was abundant, which was given by an ion-molecular reaction: F. W. McLafferty, *Anal. Chem.*, **29**, 1782 (1957).

A Correlation of Electrochemical Oxidation and Ionization Potentials of Group 4B Dimetals

Kunio MOCHIDA,* Atsuko ITANI, Michiyo YOKOYAMA, Tohru TSUCHIYA,† Shelby D. WORLEY,*,†† and Jay K. KOCHI†††

Department of Chemistry, Faculty of Sciences, Gakushuin University, 1-5-1 Mejiro, Tokyo 171
†*National Chemistry Laboratory for Industry, 1-1 Higashi, Yatabe, Ibaraki 305*
††*Department of Chemistry, Auburn University, Alabama 36849, USA*
†††*Department of Chemistry, University of Houston, University Park, Houston, TX 77004, USA*

(Received March 15, 1985)

Synopsis. Correlations of ionization potentials and electrochemical oxidation potentials for group 4B dimetals were obtained.

The reactivity of the metal-metal bond of group 4B dimetals has received considerable interest in comparison with that of carbon-carbon double bond.[1,2] As electron-rich species, metal-metal bonds of group 4B dimetals are subject to cleavage by acids, halogens, metal complexes, and other electrophiles.[1] Since group 4B dimetals have rather low ionization potentials, electron-transfer process in solutions are also possible in which the rate is limited by the ionization potentials of organometals and the electron affinity of electrophiles.[3] In order to predict rates of reactions and the products for such processes, the most fundamental data are the ionization or oxidation potentials of organometals. However, there is only a paper on a correlation of organic oxidation and ionization potentials for group 4B metals.[4] Here we describe such a correlation for group 4B dimetals.

$$R_3M\text{-}M'R_3 \longrightarrow R_3M\text{-}M'R_3^{\dagger} + e \quad (1)$$
$$(M, M' = Si, Ge, Sn)$$

Results and Discussion

The anodic oxidation of group 4B dimetals was examined in acetonitrile solutions with tetraethylammonium perchlorate as a supporting electrolyte and a glassy carbon anode. The reference electrode was Ag/AgCl in acetonitrile. The anodic oxidation of each of the group 4B dimetals was found to be irreversible, suggesting that the dimetal cation radical is unstable. Equation (2) represents a probable mode of decomposition.[5]

$$R_3M\text{-}M'R_3^{\dagger} \longrightarrow R_3M\cdot + {}^{+}M'R_3 \quad (2)$$

Peak potentials (E_p) of group 4B dimetals are listed in Table 1. Since each of these oxidative processes is irreversible, the observed potentials shifted to more positive values relative to $E°$. However, the potentials listed in Table 1 reflect the relative ease of removal of a single electron from the group 4B dimetals examined in this study.

In order to determine if there is a correlation between the anodic oxidation of group 4B dimetals in solution and their ionization potentials, He (I) photoelectron spectra of group 4B dimetals were also examined.

The vapor-phase photoelectron spectra (PES) of some group 4B dimetals have been previously reported by several research groups.[6-8] The lowest-energy band is associated with ionization from the metal-metal σ bonding orbital. Semiempirical calculations for the group 4B dimetals show that a highest occupied molecular orbital (HOMO) is highly localized at the central metal-metal bond ($4a_{1g}$)[6,7] The lowest-energy bands of group 4B dimetals measured in this work are also listed in Table 1.

The threshold or adiabatic ionization energy of the lowest-energy band decreases in the order: Si-Si> Si-Ge>Ge-Ge>Si-Sn>Ge-Sn>Sn-Sn in accord with the metal-metal ionic bond dissociation energy.[9]

The vertical ionization potential correspond to the Frank-Condon transition of the ionic state. Electron detachment from group 4B dimetals in Eq. 1 under these conditions shows a relationship to the electrochemical oxidation potentials in acetonitrile solution as shown in Fig. 1.[4,10]

The plots in Fig. 1 fit the equations E_p=0.91 (IP) −6.08 for permethyl derivatives and E_p=0.78 (IP) −4.82 for perethyl derivatives. The correlation coefficents for the plots are 0.96 and 0.88, respective-

Table 1. Oxidation and ionization potentials of group 4B dimetals

Compound	IP/eV[a]	E_p/V[b]
$Me_3SiSiMe_3$	8.68, 8.69[c]	1.76
$Me_3SiMe_2SiSiMe_3$	8.19[c], 9.14[c]	1.40, 1.76
$Me_3SiGeMe_3$	8.62	1.76
$Me_3GeGeMe_3$	8.60, 8.60[d]	1.70
$Me_3SiSnMe_3$	8.39, 8.32[d]	1.60
$Me_3GeSnMe_3$	8.36, 8.33[d]	1.44
$Me_3SnSnMe_3$	8.20, 8.20[d]	1.28
$Et_3SiSiEt_3$	8.39	1.76
$Et_3SiGeEt_3$	8.24	1.70
$Et_3GeGeEt_3$	8.33	1.48
$Et_3SiSnEt_3$	8.10	1.56
$Et_3GeSnEt_3$	8.05	1.40
$Et_3SnSnEt_3$	7.82	1.24

a) IP is associated with the metal-metal orbitals (vertical IP). b) In acetonitrile solution at 20 °C with glassy carbon anode. c) Ref. 6. d) Ref. 7.

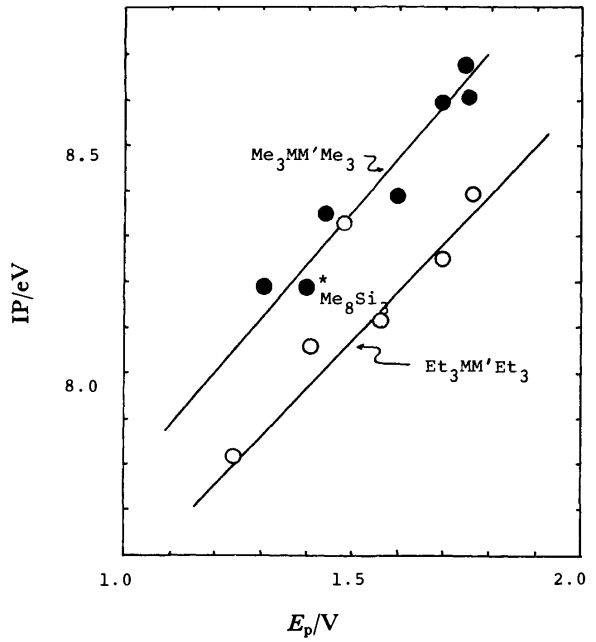

Fig. 1. Relationship between oxidation and ionization potentials of group 4B dimetals.

ly. Each slope is less than unity. It should be realized that these relations result from unstability of dimetal cation radicals and incursion of specific surface effects and solvations. Since the initially formed dimetal cation radicals may decay more rapidly than the time required for the measurement, E_p is a kinetic parameter for the overall oxidation process. The dimetal cation radicals will be strong acids stabilized by hydrogen bonding to the basic solvent, acetonitrile. This solvation will, of course, lower the E_p. These effects should be variable between permethyl derivatives and perethyl derivatives.

This correlation between anodic oxidation of group 4B dimetals in solution and their gas phase ionization potentials should provide interesting criteria for evaluating electron transfer processes involving group 4B dimetals.

Experimental

Materials. $Me_3SiSiMe_3$, bp 112 °C,[13] $Me_3SiMe_2SiSiMe_3$, bp 112 °C/106 mmHg,[14] $Me_3SiGeMe_3$, bp 122 °C,[15] $Me_3GeGeMe_3$, bp 136 °C,[16] $Me_3SiSnMe_3$, bp 144 °C,[17] $Me_3GeSnMe_3$, bp 154 °C,[17] $Me_3SnSnMe_3$, bp 182 °C,[18] $Et_3SiSiEt_3$, bp 100 °C/5.0 mmHg,[19] $Et_3SiGeEt_3$, bp 87 °C/3.0 mmHg,[20] $Et_3GeGeEt_3$, bp 73 °C/0.7 mmHg,[21] $Et_3SiSnEt_3$, bp 77 °C/0.7 mmHg,[22] $Et_3GeSnEt_3$, bp 120 °C/6 mmHg,[23] and $Et_3SnSnEt_3$, bp 160 °C/23 mmHg (1 mmHg=133.322 Pa),[24] were prepared according to the cited literatures.

Photoelectron spectra were obtained with a Perkin-Elmer PS-18 photoelectron spectrometer of Auburn University, using the He (I) resonance line at 21.22 eV as an excitation source. The spectra were calibrated with Ar and Xe as internal standards.

Electrochemical measurements were performed with Bioanalytical System Inc. CV-1B Cyclic Voltammetry Instrument under conditions similar to those described in previous works.[25] The values of E_p were measured in acetonitrile solution containing 0.1 M tetraethylammonium perchlorate (1 M=1 mol dm^{-3}) at 100 mV s^{-1}.

References

1) H. Sakurai, *Kagaku no Ryoiki*, **29**, 36 (1975).
2) R. West, "Comprehensive Organometallic Chemistry," ed by G. Wilkinson, F. G. A. Stone, and E. W. Abel, Pergamon Press, (1982), Vol. 2, p. 365.
3) J. K. Kochi, "Organometallic Mechanism and Catalysis," Academic Press, New York, (1978), part 3.
4) H. C. Gardner and J. K. Kochi, *J. Am. Chem. Soc.*, **97**, 1855 (1975).
5) Mass spectral craking patterns of the group 4B dimetals were examined. At an ionizing voltages of 20 eV, formation of group 4B centered radical in the series Me_3M-$M'Me_3$ (M, M'=Si, Ge, Sn) increased in order Si<Ge<Sn.
6) H. Bock and W. Enßlin, *Angew Chem.*, **83**, 435 (1971).
7) L. Szepes, T. Korányi, G. Nóray-Szabó, A. Modell, and G. D. Distefano, *J. Organomet. Chem.*, **217**, 35 (1981).
8) H. Sakurai, M. Ichinose, M. Kira, and T. G. Traylor, *Chem. Lett.*, **1984**, 1383.
9) The first band of the PES of the group 4B dimetals showed a substantial difference between the adiabatic and vertical *IP* (*e.g.*, 0.75 eV for $Me_3SiSiMe_3$) indicate of a substantial change in geometry upon ionization.
10) A. similar relationship has been observed with hydrocarbons.[11,12]
11) M. Fleischmann and D. Pletcher, *Tetrahedron Lett.*, **1968**, 6255.
12) L. L. Miller, G. D. Nordblom, and E. A. Mayeda, *J. Org. Chem.*, **37**, 916 (1972).
13) K. Oita and H. Gilman, *J. Org. Chem.*, **21**, 1009 (1956).
14) G. R. Wilson and G. A. Smith, *J. Org. Chem.*, **26**, 557 (1961).
15) C. Shaw, F. III; Allred, and L. Albert, *J. Organomet. Chem.*, **28**, 53 (1971).
16) M. P. Brown and G. W. A. Fowles, *J. Chem. Soc.*, **1958**, 2811.
17) H. Schumann and S. Ronecker, *Z. Naturforsch., B* **22**, 452 (1967).
18) T. Harada, *Bull. Chem. Soc. Jpn.*, **15**, 481 (1940).
19) M. G. Voronkov and J. I. Khudobin, *Zeitschrift für Chemie*, **26**, 930 (1956).
20) J. M. Shackelford, H. de Schmertzing, C. H. Henther, and H. Podall, *J. Org. Chem.*, **28**, 1700 (1963).
21) E. J. Bulten and J. G. Noltes, *J. Organomet. Chem.*, **11**, 22 (1968).
22) N. S. Vyazankin, G. A. Razuvaev, E. N. Gladyshev, and S. P. Korneva, *J. Organomet. Chem.*, **7**, 353 (1967).
23) N. S. Vyazankin, E. N. Gladyshev, S. P. Korneva, G. A. Razuvaev, and E. A. Arkhangel'skaya, *Zh. obshch. Khim.*, **38**, 1803 (1968).
24) W. P. Neuman and B. Schneider, *Angew. Chem.*, **76**, 891 (1964).
25) D. T. Sawyer, G. Chiericato, Jr., C. T. Angelis, E. J. Nanni, and T. Tsuchiya, *Anal. Chem.*, **54**, 1720 (1982).

The Reactions of Silicon Phosphate with Alkaline Earth Metal Oxides at High Temperatures[1)]

Eiichi NARITA,* Kazuhiro SANGO,† and Hiroyuki NAITO†
Department of Liberal Arts and Engineering Sciences, Hachinohe National College of Technology, Hachinohe, Aomori 031
†*Mizusawa Industrial Chemicals, Ltd., Chuo-ku, Tokyo 103*
(Received November 26, 1984)

Synopsis. The reactions of $Si_3(PO_4)_4$ with CaO and MgO at high temperatures up to 1150 °C yielded silicon phosphate glass, $Me_3(PO_4)_2$, $Me_2P_2O_7$, and α-cristobalite, depending on the temperature, the heating time, and the $MeO/Si_3(PO_4)_4$ molar ratio (Me: Ca and Mg). These reactions were found to proceed by means of the one-way diffusion of alkaline earth metal oxides into the $Si_3(PO_4)_4$ phase.

The synthesis of SiO_2–P_2O_5 compounds was carried out by Makart[2)] and Liebau *et al.*,[3)] who reported the formations of $Si_3(PO_4)_4$ (hexagonal), SiP_2O_7 (**1**) (hexagonal), SiP_2O_7 (**2**) (monoclinic), SiP_2O_7 (**3**) (tetragonal), and SiP_2O_7 (**4**) (cubic) in the reactions of various SiO_2 compounds with phosphoric acid. However, no information is at present available on the chemical properties of these silicon phosphates. The present authors[4)] have previously prepared silicon phosphates, such as $Si_3(PO_4)_4$, and SiP_2O_7 (**1**, **2**, **3**), by means of the calcination of silica gel impregnated with a small amount of phosphoric acid at temperatures up to 1000 °C; they have thus shown that these phosphates can be used as a satisfactory hardener for silicate adhesives. A kinetic study of the hydrolysis of $Si_3(PO_4)_4$ in aqueous alkaline solutions was also carried out in this connection.[1)] Besides being useful as hardeners of silicate adhesives, silicon phosphates can also be used as binders of various ceramic materials and as raw materials for the production of glass. In this study, we investigated the reaction behaviors of $Si_3(PO_4)_4$ with CaO and MgO at high temperatures.

Experimental

Materials. $Si_3(PO_4)_4$ was prepared by the method reported previously.[1)] The particles were all disk-shaped, 2.2 μm in diameter ×0.9 μm in height. The CaO and MgO were of extra pure grade and were used after calcination at 500 °C for 1 h.

Reactions in the Powder Mixtures. The mixtures of $Si_3(PO_4)_4$ and CaO or MgO were wet with acetone and thoroughly mixed for 30 min in an agate mortar. Then, parts of the powder mixture (0.5—1.5 g) were transferred to a platinum boat, and it was heated at 940 °C in an electric furnace in air. Other parts of the powder mixtures of both systems ($MeO/Si_3(PO_4)_4$ molar ratio=3) were also heated at high temperatures up to 1150 °C with a heating rate of 10 °C min^{-1} in air using a Rigaku Denki Thermoflex TG-DTA apparatus. The reaction products in the samples were determined by means of X-ray diffraction analysis, using a Rigaku Denki Geigerflex D-2F with Ni filtered Cu $K\alpha$ radiation, with 30 kV and 10 mA.

Reactions at the Contact Surface of One-paired Tablets. The diffusion couples, *i.e.*, one-paired tablets, were prepared by a method similar to that used by Kinoshita *et al.*;[5)] about 2 g of $Si_3(PO_4)_4$ powder was pressed into a tablet 10 mm in diameter under a pressure of 640 kg cm^{-2}. A platinum tape (0.1×0.4×10 mm) was placed on the surface of the $Si_3(PO_4)_4$ tablet as a marker. Then, about 2 g of CaO or MgO powder was placed on the tablet, and it was pressed again into a double-layered tablet. After drying over P_2O_5 at room temperature, the diffusion couples were heated at 940 °C for 72 h in a manner similar to that described above. After these diffusion couples had been removed from the furnace, they were separated into two tablets from the border of a platinum marker. The reaction products in the surface layers of the tablets were examined by means of X-ray diffractometry in both the intact-tablet and powdered state.

Results and Discussion

$Si_3(PO_4)_4$–CaO System. The X-ray diffraction patterns of the products obtained in the reaction of the $Si_3(PO_4)_4$–CaO system using the TG-DTA apparatus are shown in Fig. 1. In this system, the reaction occurred at about 850 °C to yield β-$Ca_3(PO_4)_2$ and β-$Ca_2P_2O_7$ as crystalline products. As the temperature increased, the fraction of β-$Ca_2P_2O_7$ increased and that of β-$Ca_3(PO_4)_2$ decreased. At 1150 °C, β-$Ca_2P_2O_7$ and α-cristobalite were crystalline products. The X-ray diffraction lines of all the products were, on the whole, low, and a slight halation was observed in the X-ray diffraction pattern of 2θ=17—25° at 1150 °C. This means that an X-ray amorphous product such as silicon phosphate glass would be formed together with these crystalline products. In this system, no formation of crystalline

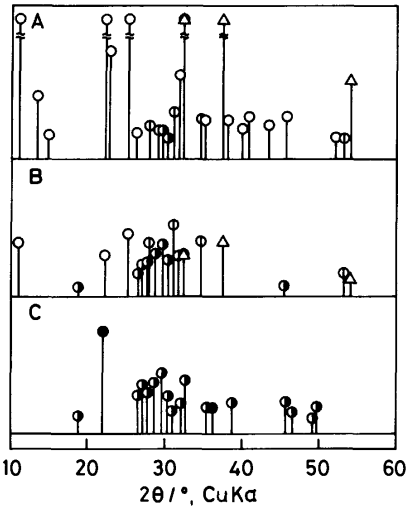

Fig. 1. X-Ray powder diffraction patterns of the mixture of $Si_3(PO_4)_4$–CaO (1 : 3) at the constant rate of heating (10 °C min^{-1}).
○: $Si_3(PO_4)_4$, △: CaO, ⓘ: β-$Ca_3(PO_4)_2$, ◑: β-$Ca_2P_2O_7$, ●: SiO_2(α-cristobalite).
A: 850 °C, B: 950 °C, C: 1150 °C.

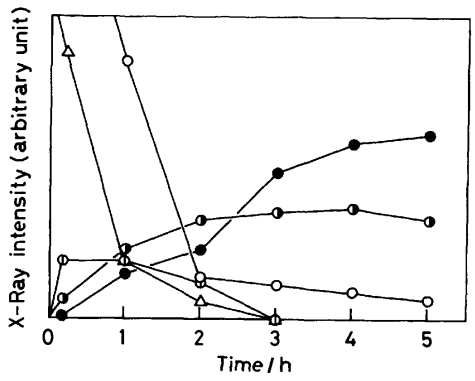

Fig. 2. X-Ray diffraction intensities of the products of $Si_3(PO_4)_4$-CaO reaction (1 : 3) at 940 °C.
○: $Si_3(PO_4)_4$ ($2\theta=11.0°$, 003), △: CaO ($2\theta=37.4°$, 200), ⓘ: β-$Ca_3(PO_4)_2$ ($2\theta=31.0°$, 217), ◑: β-$Ca_2P_2O_7$ ($2\theta=29.6°$, 008), ●: α-cristobalite ($2\theta=21.9°$, 100).

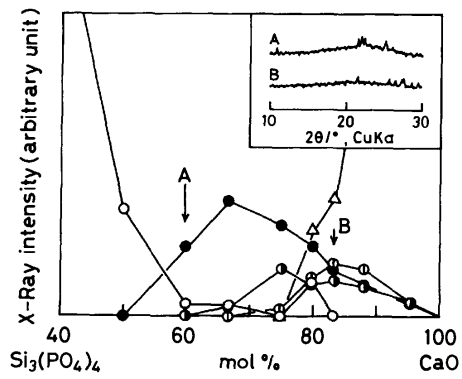

Fig. 3. Relation between CaO-content in the mixtures of $Si_3(PO_4)_4$-CaO and X-ray diffraction intensities of the products after heating at 940 °C for 5 h.
○: $Si_3(PO_4)_4$, △: CaO, ⓘ: β-$Ca_3(PO_4)_2$, ◑: β-$Ca_2P_2O_7$, ●: α-cristobalite.

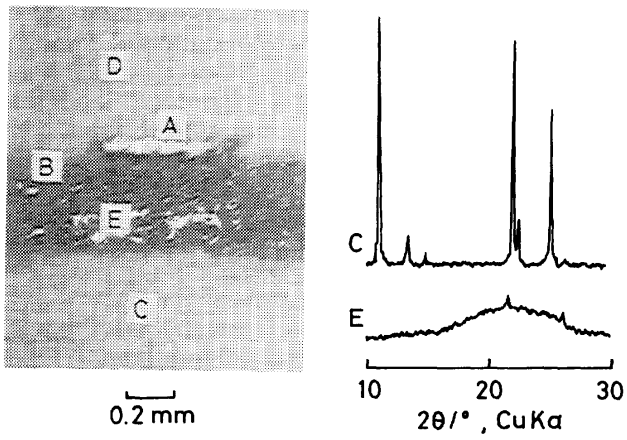

Fig. 4. Micrograph of cross section and X-ray diffraction patterns of the $Si_3(PO_4)_4$-CaO diffusion couple after heating at 940 °C for 72 h.
A: Pt marker, B: Interface before reaction, C: $Si_3(PO_4)_4$ phase, D: CaO phase, E: Product phase.

silicate compounds was observed because the acidity of P_2O_5 is higher than that of SiO_2.[6] The variation in the amounts of the crystalline product with the heating time at 940 °C is shown in Fig. 2. At the first step of the reaction, β-$Ca_3(PO_4)_2$ was formed predominantly. However, the amount of β-$Ca_3(PO_4)_2$ decreased and those of β-$Ca_2P_2O_7$ and α-cristobalite increased with the lapse of time. No changes in the fraction of each product were found after 4 h. Figure 3 shows the relation between the CaO content in the mixtures of the $Si_3(PO_4)_4$-CaO system and the X-ray diffraction intensities of the products, together with the X-ray diffraction patterns of typical products. It was found that the reaction products were also changed by the CaO content. In the region of a low CaO content, β-$Ca_2P_2O_7$ and α-cristobalite were mainly formed as crystalline products. Along with an increase in the CaO content, the fraction of β-$Ca_3(PO_4)_2$ increased and that of α-cristobalite decreased. It was also noticeable that the halation at $\theta=17—25°$ became larger with a decrease in the CaO content.

Figure 4 shows a micrograph of a cross-section of the $Si_3(PO_4)_4$-CaO diffusion couple after the reaction. It can be seen that a semitransparent layer (*E*) about 0.5 mm thick was formed on the side of the $Si_3(PO_4)_4$ phase (*C*). This means that the reactions occurred by means of the one-way diffusion of CaO into the $Si_3(PO_4)_4$ phase. X-ray diffraction revealed that the surface of the $Si_3(PO_4)_4$ tablet was a mixture of trace amounts of β-$Ca_3(PO_4)_2$ and α-cristobalite, along with a large amount of an X-ray amorphous product such as silicon phosphate glass.[6-8] The halation caused by the formation of glass was clearly observed.

$Si_3(PO_4)_4$-MgO System. The reaction behavior of the $Si_3(PO_4)_4$-MgO system was found to be similar to that of the $Si_3(PO_4)_4$-CaO system. In the $Si_3(PO_4)_4$-MgO system, $Mg_3(PO_4)_2$ was observed to be present at higher temperatures than was β-$Ca_3(PO_4)_2$ in the latter system, and the amount of α-cristobalite was lower than in the latter system. In the reaction of the $Si_3(PO_4)_4$-MgO diffusion couple, a semitransparent layer just like the layer (*E*) in Fig. 4 was also observed.

The reactions of silicon phosphates with CaO and MgO were also carried out using SiP_2O_7 (**2**) instead of $Si_3(PO_4)_4$; the results were quite similar to those described above.

The authors wish to thank Professor Taijiro Okabe of the Department of Applied Chemistry, Tohoku University, for his helpful discussion.

References

1) Studies of the Preparation and Utilization of Silicon Phosphates, Part **III**. Part **II**: T. Saeki, E. Narita, and H. Naito, *Bull. Chem. Soc. Jpn.*, **57**, 1591 (1984).
2) H. Makart, *Helv. Chim. Acta*, **50**, 399 (1967).
3) F. Liebau, G. Bissert, and N. Köppen, *Z. Anorg. Allg. Chem.*, **359**, 113 (1968).
4) K. Sango, S. Sato, H. Naito, T. Saeki, T. Matsushita, and E. Narita, *Ind. Eng. Chem. Prod. Res. Dev.*, **23**, 315 (1984).
5) M. Kinoshita and D. Matsuda, *Nippon Kagaku Kaishi*, **1979**, 189.
6) T. Kanazawa, *Kogyo Kagaku Zasshi*, **62**, 182 (1959).
7) T. Kanazawa, *Yogyo Kyokai Shi*, **72**, 87 (1964).
8) T. Kanazawa, H. Kawazoe, and M. Ikeda, *Yogyo Kyokai Shi*, **78**, 121 (1970).

Facile Synthesis of 2-Phenyl-1,2-oxaphospholane and Its Related New Compounds. The Family of Deoxophostones and Deoxothiolphostones

Shiro KOBAYASHI,* Masato SUZUKI, and Takeo SAEGUSA*
Department of Synthetic Chemistry, Faculty of Engineering, Kyoto University, Yoshida, Sakyo-ku, Kyoto 606
(Received February 15, 1985)

Synopsis. 2-Phenyl-1,2-oxaphospholane (**1a**), 2-phenyl-1,2-oxaphosphorinane (**1b**), 2-phenyl-1,2-thiaphospholane (**1c**), and 2-phenyl-1,2-thiaphosphorinane (**1d**) were prepared readily by the reaction of dichlorophenylphosphine with an ω-chloroalkanol or an ω-chloroalkanethiol followed by cyclization with the aid of lithium metal. Compounds **1b—d** have been obtained for the first time.

Recently, we have reported the cationic ring-opening polymerization of a five-membered deoxophostone (2-phenyl-1,2-oxaphospholane, (**1a**)) to give poly (phosphine oxide).[1] During the course of these studies we have found a new facile method to prepare **1a** and its family compounds. The present paper deals with the synthesis of five- and six-membered deoxophostones and their sulfur analogues of deoxothiolphostones,[2] *i.e.*, **1a**, 2-phenyl-1,2-oxaphosphorinane (**1b**), 2-phenyl-1,2,-thiaphospholane (**1c**), and 2-phenyl-1,2-thiaphosphorinane (**1d**).

1a **1b** **1c** **1d**

The synthetic route is given in Scheme 1.

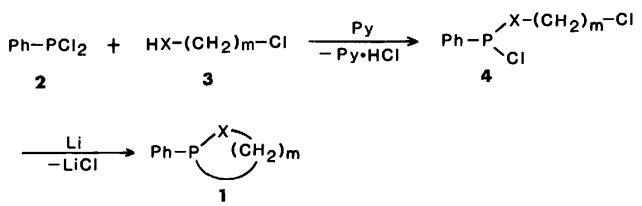

a, X=O; *m*=3 **c**, X=S; *m*=3
b, X=O; *m*=4 **d**, X=S; *m*=4

Scheme 1.

To dichlorophenylphosphine (**2**) with pyridine in tetrahydrofuran (THF) was added an ω-chloroalkanol or ω-chloroalkanethiol **3** and refluxed for 1 h. At this time, The ^{31}P NMR spectrum of the reaction mixture showed a single peak assignable to phosphonochloridite (**4**): **4a**, 175.0 ppm; **4b**, 175.3 ppm; **4c**, 141.7 ppm; **4d**, 141.6 ppm. Without isolation, **4** in THF was reacted with lithium metal. The ^{31}P NMR spectrum of the respective reaction mixture showed many peaks. With adding diethyl ether to the mixture, precipitated insoluble parts which probably consisted of LiCl and polymeric by-products. In the ^{31}P NMR spectrum of the soluble part the peak due to **1** was main. The distillation *in vacuo* gave **1** in a moderate or low yield. ^{31}P, ^{1}H, ^{13}C NMR data as well as MS data supporting the structures of **1a—d** are given in the experimental section.

Few routes to prepare **1a** have previously been reported, which required several steps and the overall yield was lower than that of the present method.[3,5] These methods involve phosphines having a P-H bond which are very stinking and poisonous. On the other hand, the present method is more facile, not necessary to handle stinking phosphines, and more generally applicable to prepare not only **1a** but also **1b—d**. Five-membered deoxothiolphostone **1c** had been known only as a ligand of an Fe-complex.[6] Six-membered deoxophostone **1b** and deoxothiolphostone **1d** have not been known so far. Although the isolated yields are not high, the present study provides the first instance of the isolation of **1b**, **1c**, and **1d**. These new compounds are very attractive reagents which allow investigation of reactivities and stereochemical problems in phosphorus chemistry. The ring-opening polymerization of **1c** and **1d** will be reported soon.[7]

Experimental

^{1}H, ^{13}C, and ^{31}P NMR spectra were recorded on a Hitachi R-20B (^{1}H NMR) or a Hitachi R-900 (^{13}C and ^{31}P NMR) spectrometer. Mass spectra were obtained with JEOL JMS-DX300. THF, diethyl ether, and pyridine were dried respectively over $LiAlH_4$, CaH_2, or KOH, and distilled. Commercially available dichlorophenylphosphine, 3-chloro-1-propanol, and 4-chloro-1-butanol were purified by distillation. 3-Chloro-1-propanethiol was prepared according to the reported procedures.[8] 4-Chloro-1-butanethiol was prepared by the HCl-catalyzed methanolysis[8] of S-(4-chlorobutyl) thioacetate, which was obtained from the substitution reaction[9] of 4-chlorobutyl tosylate with potassium thioacetate; overall yield 38%, bp 89—95 °C (57—65 Torr, 1 Torr=133.322 Pa).

The following all operations were carried out under nitrogen atmosphere.

2-Phenyl-1,2-oxaphospholane ***1a***: To a mixture of dichlorophenylphosphine (2.01 g, 11.2 mmol), pyridine (0.95 ml, 11.8 mmol), and 10 ml of THF was added 3-chloro-1-propanol (1.06 g, 11.2 mmol) in 4 ml of THF at 0 °C. After refluxing for 1 h, the precipitate of pyridinium hydrochloride was removed by filtration. The filtrate was added to 8 ml of THF containing small pieces of lithium metal (0.172 g 24.8 mg-atom) at −78 °C and stirred overnight gradually up to room temperature. THF was evaporated *in vacuo*, and 30 ml of diethyl ether was added to the residue to extract the product. The mixture was well stirred and filtered. After concentration of the filtrate, the residue was

subjected to distillation *in vacuo* to give 0.69 g of **1a** (37% yield), bp 62—65 °C (0.13 Torr)[3]. $^{31}P\{^1H\}$NMR($CDCl_3$) +110.2 ppm (relative to 85% H_3PO_4 external standard); ^1H NMR δ($CDCl_3$) 1.4—2.5 (m, 4H, $PC\underline{H}_2C\underline{H}_2$), 3.6—4.3 (m, 2H, $OC\underline{H}_2$), and 7.1—7.4 ppm (m, 5H, $C_6\underline{H}_5$); $^{13}C\{^1H\}$NMR($CDCl_3$) 23.3 (s, $PC\underline{H}_2$), 32.2 (d, J_{CCP}=20.9 Hz, $PCH_2\underline{C}H_2$) 72.4 (d, J_{COP}=14.0 Hz, $OC\underline{H}_2$), 126.9 (s, P-Ph; δ-C) 128.0 (d, J_{CCP}=14.8 Hz, P-Ph; β-C), 128.1 (s, P-Ph; γ-C), and 144.8 ppm (d, J_{CP}=36.7 Hz, P-Ph; α-C).

These procedures for the preparation of **1a** were similarly applied to those of **1b—d**.

2-Phenyl-1,2-oxaphosphorinane ***1b***: From dichlorophenylphosphine (2.19 g, 12.2 mmol), 4-chloro-1-butanol (1.33 g, 12.2 mmol), pyridine (1.04 ml, 12.8 mmol), and lithium metal (0.186 g 26.8 mg-atom), 0.39 g of **1b** was obtained; 18% yield, bp 76—79 °C (0.55 Torr). $^{31}P\{^1H\}$NMR($CDCl_3$) +111.1 ppm; ^1H NMR δ($CDCl_3$) 1.2—2.4 (m, 6H, $PC\underline{H}_2C\underline{H}_2C\underline{H}_2$), 3.4—3.9 (m, 2H, $OC\underline{H}_2$), and 7.1—7.5 (m, 5H, $C_6\underline{H}_5$); $^{13}C\{^1H\}$NMR($CDCl_3$) 19.3 (d, J_{CP}=3.5 Hz, $PC\underline{H}_2$), 25.5 (d, J_{CCP}=22.6 HZ, $PCH_2\underline{C}H_2$), 27.6 (d, J_{CCOP}=3.5 Hz, $OCH_2\underline{C}H_2$), 63.4 (d, J_{COP}=7.8 Hz, $OC\underline{H}_2$), 127.8 (s, P-Ph; δ-C), 128.6 (d, J_{CCCP}=2.6 Hz P-Ph; γ-C), 129.0 (d, J_{CCP}=14.1 Hz, P-Ph; β-C), and 140.7 (d, J_{CP}=31.4 Hz, P-Ph; α-C); *m/z* 180 (M^+, 69%).

2-Phenyl-1,2-thiaphospholane ***1c***: From dichlophenylphosphine (48 ml, 0.355 mol), 3-chloro-1-propanethiol (39.2 g, 0.355 mol), pyridine (30 ml, 0.371 mol), and lithium metal (4.93 g, 0.710 g-atom), 6.59 g of **1c** was obtained; 10% yield, bp 102—104 °C (0.50 Torr). $^{31}P\{^1H\}$NMR($CDCl_3$) + 22.3 ppm; ^1H NMR δ($CDCl_3$) 1.1—3.1 (m, 6H, $SC\underline{H}_2C\underline{H}_2C\underline{H}_2P$) and 6.8—7.6 (m, 5H, $C_6\underline{H}_5$); $^{13}C\{^1H\}$NMR($CDCl_3$) 28.9 (d, J_{CSP}=7.3 Hz, $SC\underline{H}_2$), 35.2 (s, $PC\underline{H}_2$), 36.0 (d, J_{CCP}=23.2 Hz, $PCH_2\underline{C}H_2$), 128.1 (s, P-Ph; δ-C) 128.1 (d, J_{CCCP}=3.7 Hz, P-Ph; γ-C), 130.0 (d, J_{CCP}=17.1 Hz, P-Ph; β-C), and 140.4 (d, J_{CP}=40.3, P-Ph, α-C); *m/z* 182 (M^+, 100%).

2-Phenyl-1,2-thiaphosphorinane ***1d***: From dichlorophenylphosphine (12.65 g, 0.071 mol), 4-chloro-1-butanethiol (9.52 g, 0.071 mol), pyridine (6.0 ml, 0.074 mol), and lithium metal (0.985 g, 0.142 g-atom), 0.659 g of **1d** was obtained; 5% yield, bp 99—103 °C (0.32 Torr). $^{31}P\{^1H\}$NMR($CDCl_3$) +4.8 ppm; ^1H NMR δ($CDCl_3$) 1.0—3.0 (m, 8H, $SC\underline{H}_2C\underline{H}_2C\underline{H}_2C\underline{H}_2P$) and 6.9—7.8 (m, 5H, $C_6\underline{H}_5$); $^{13}C\{^1H\}$NMR-($CDCl_3$) 20.1 (s, $PC\underline{H}_2$ or $PCH_2CH_2\underline{C}H_2$), 23.5 (d, J_{CCP}=22.6 Hz, $PCH_2\underline{C}H_2$), 24.5 (d, J_{CSP}=10.5 Hz, $SC\underline{H}_2$), 27.8 (s, $PC\underline{H}_2$ or $PCH_2CH_2\underline{C}H_2$), 127.2 (s, P-Ph; δ-C), 128.6 (d, J_{CCCP}=3.5 Hz, P-Ph; γ-C), 130.5 (d, J_{CCP}=14.8, P-Ph; β-C), and 137.1 ppm (d, J_{CP}=32.2 Hz, P-Ph; α-C); *m/z* 196 (M^+, 100%).

References

1) S. Kobayashi, M. Suzuki, and T. Saegusa, *Polymer Bull.*, **4**, 315 (1981); *ibid.*, **8**, 417 (1982); *Macromolecules*, **17**, 107 (1984).

2) A trivial name of "deoxophostone" for **1a** was used by Grayson and Farley.[3] A "phostone" is recognized as a derivative of lactone.[4] We followed logically these naming for new phosphorus heterocycles **1c** and **1d** as "deoxothiolphostones". Then, the inter-relationships are schematically shown as follows:

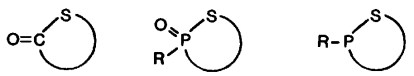

thiollactone thiolphostone deoxothiolphostone

3) M. Grayson and C. E. Farley, *J. Chem. Soc., Chem. Commun.*, **1967**, 830. This literature reported bp of **1a** as 112 °C (0.5 Torr). However, we prepared **1a** according to the present method as well as to this literature's method, distilled it several times, and confirmed that the present bp value is correct.

4) J.-N. Collard and C. Benezra, *Tetrahedron Lett.*, **23**, 3725 (1982).

5) K. Issleib and H.-R. Roloff, *Chem. Ber.*, **98**, 2091 (1965); S. Antczak and S. Trippett, *J. Chem. Soc., Perkin Trans. 1*, **1978**, 1326; F. Mathey and F. Mercier, *J. Chem. Soc., Chem. Commun.*, **1980**, 191.

6) F. Mathey, M.-B. Comarmond, and D. Moras, *J. Chem. Soc., Chem. Commun.*, **1979**, 417.

7) S. kobayashi, M. Suzuki, and T. Saegusa, *Macromolecules*, in press.

8) B. Sjöberg, *Chem. Ber.*, **74**, 64 (1941).

9) J. H. Chapman and L. N. Owen, *J. Chem. Soc.*, **1950**, 579.

Heteropoly Acids Supported on Acidic Ion-exchange Resin as Highly Active Solid-acid Catalysts

Toshihide BABA,* Yoshio ONO,† Tadao ISHIMOTO, Shun-ichi MORITAKA, and Seiichi TANOOKA

Department of Industrial Chemistry, Kochi Technical College, Monobe, Nankoku, Kochi, 783

†*Department of Chemical Engineering, Tokyo Institute of Technology, Ookayama, Meguro-ku, Tokyo, 152*

(Received December 12, 1984)

Synopsis. Heteropoly acids supported on a macroreticular acidic ion-exchange resin shows much higher activity than those supported on activated carbon for the synthesis of methyl *t*-butyl ether and the esterification of acetic acid with 1-pentanol. This high activity can plausibly be attributed to the interaction of heteropoly anions with substrates which are protonated by the protons of the acidic resin.

Heteropoly acids are very effective as catalysts for a variety of acid-catalyzed reactions.[1-4] They can be used as homogeneous as well as heterogeneous catalysts. In order to use them as solid-acids, however, it is desirable to support them on an appropriate carrier, since their surface areas are small. Izumi *at al.*[5] have reported that heteropoly acids supported on silica gel or activated carbon exhibit high catalytic activities for the alkylation of benzene with ethylene, the esterification of acetic acid with ethanol, and the dehydration of 2-propanol. It has also been reported that heteropoly acids and their salts supported on silica or activated carbon are effective in forming methyl *t*-butyl ether (MTBE) from isobutene and methanol in the vapor phase.[6-8] Here, we wish to report that heteropoly acids supported on an acidic ion-exchange resin become very active catalysts for some acid-catalyzed reactions, namely, MTBE synthesis and esterification.

The catalysts were prepared as follows. Heteropoly acid was dissolved in water, and a macroporous acidic resin, Amberlyst-15, was added to the solution. The suspension was kept overnight and then dried by evaporation. The reactions were carried out with a continuous-flow reactor operating at atmospheric pressure. The catalyst was packed in a reactor of silica tubing (10 mm i.d.) placed in a vertical furnace. Liquid reactants were delivered by means of a motor-driven syringe and vaporized in the preheating zone of the reactor containing 10 cm^3 of quartz chips. Isobutene was fed through a flowmeter. The products were analyzed by means of gas chromatography.

TABLE 1. CATALYTIC ACTIVITIES OF HETEROPOLY ACIDS SUPPORTED ON AMBERLYST-15 AND ACTIVATED CARBON

Catalyst	Isobutene conversion/%	Selectivity to MTBE/%
$H_4SiW_{12}O_{40}$/Amberlyst-15	42.0	99.7
$H_3PW_{12}O_{40}$/Amberlyst-15	38.7	99.8
$H_3PMo_{12}O_{40}$/Amberlyst-15	18.0	100
Amberlyst-15	11.0	100
$H_4SiW_{12}O_{40}$/activated carbon	2.1	100

Reaction conditions: 323 K, $W/F=0.50$ g h mol^{-1}, isobutene pressure, 25.3 kPa; methanol pressure, 25.3 kPa; 30 wt% heteropolyacids supported.

In Table 1, the catalytic activities of heteropoly acids (30 wt%) supported on Amberlyst-15 are compared with those of dodecatungstosilicate (TSA) supported on activated carbon and Amberlyst-15 itself. Every heteropoly acid supported on Amberlyst-15 was much more active than Amberlyst-15 itself, TSA supported on the resin being most active. It is also worthy of note that TSA on Amberlyst-15 is far more active than TSA on activated carbon. In all cases, the catalytic activities did not change with time on stream for at least 8 h. The selectivity to MTBE is very close to 100%. The other detectable products are isobutene dimers. No formation of dimethyl ether was observed in any case.

The dependence of the isobutene conversion and the selectivity to MTBE on the amount of supported TSA on Amberlyst-15 is illustrated in Fig. 1. The isobutene conversion increased with the increase in the supported amount and reached a maximum at 30 wt%, where the selectivity to MTBE was 99.7%. The catalysts with less activity showed a 100% selectivity.

The dependence of the isobutene conversion to MTBE on the contact time for the reaction over Amberlyst-15, TSA(30 wt%) on Amberlyst-15, and TSA(30 wt%) on activated carbon, is shown in Fig. 2. The relative activity of the three catalysts was estimated from the rate of the reaction at lower contact times as follows; TSA/activated carbon: Amberlyst-15:TSA/Amberlyst-15=1:13:33. In every case, the isobutene conversion increased with the contact time and approached to a constant value

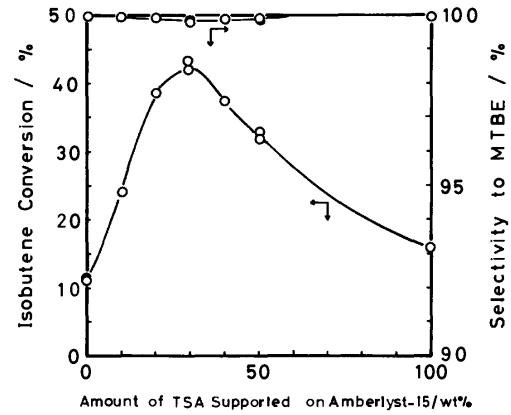

Fig. 1. Change in isobutene conversion and selectivity to MTBE with supported amount of TSA on Amberlyst-15. Reaction conditions: 323 K, $W/F=0.50$ g h mol^{-1}, isobutene pressure 25.3 kPa, methanol pressure 25.3 kPa, nitrogen pressure 50.7 kPa.

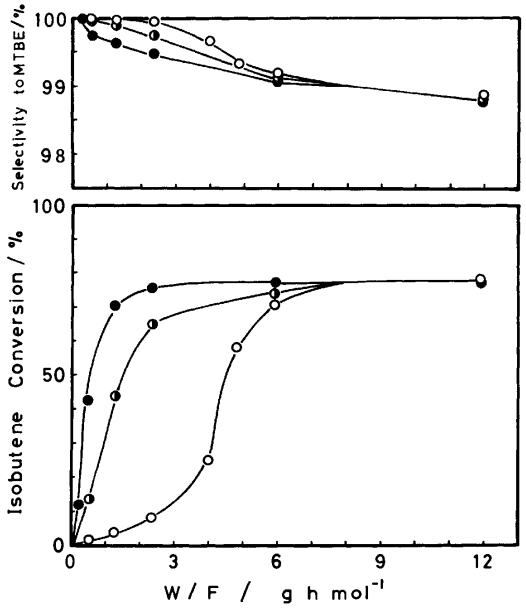

Fig. 2. Effect of contact time on isobutene conversion and selectivity to MTBE. (●): TSA (30 wt%) supported on Amberlyst-15, (○): Amberlyst-15, (◑): TSA (30 wt%) supported on activated carbon. Reaction conditions: 323 K, isobutene pressure 25.3 kPa, methanol pressure 25.3 kPa, nitrogen pressure 50.7 kPa.

because of the limitation by the thermo-dynamic equilibrium.

The reaction temperature was varied in the range of 323—373 K. The highest yield, 57%, was obtained at 333 K. The decrease in the MTBE yield at higher temperatures is due to the limitation by the thermodynamic equilibrium. The selectivity to MTBE was 100% at and below 333 K, but it dropped at higher temperatures as a result of the dimerization of isobutene.

To further test the efficiency of heteropoly acid supported on the ion-exhange resin, the esterification of acetic acid with 1-pentanol to form pentyl acetate in the vapor phase was carried out at 378 K over Amberlyst-15, TSA supported on Amberlyst-15, and TSA supported on activated carbon. As is shown in Fig. 3, the catalytic activity did not change with time on stream in any cases. Heteropoly acid supported on Amberlyst-15 showed a much higher activity for the esterification than the resin itself and also than that supported on activated carbon. Thus, the 1-pentanol conversion over Amberlyst-15 (13.6%) was increased up to 22.4% by supporting TSA(30 wt%) on the resin. The selectivity to pentyl acetate was 100% in every case.

Izumi and his coworkers[1,8] found that heteropoly acids show a much higher catalytic activity for many reactions as homogeneous catalysts than do sulfuric acid or *p*-toluenesulfonic acid and attributed the higher activity to the interaction of heteropoly anions and substrates or protonated substrates. For example, they postulated the existence of a protonated butene-heteropoly anion complex in the hydration of

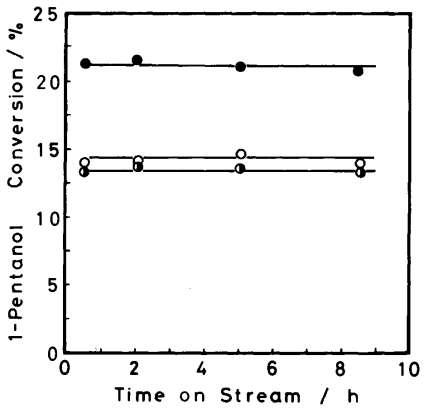

Fig. 3. Change in 1-pentanol conversion in the esterification from acetic acid and 1-pentanol. (●): TSA (30 wt%) supported on Amberlyst-15, (◑): Amberlyst-15, (○): TSA (30 wt%) supported on activated carbon. Reaction conditions: 378 K, $W/F=9.33\times10^{-2}$ g h mol^{-1}, acetic aicd pressure 15.1 kPa, pentyl alcohol pressure 15.1 kPa, nitrogen pressure 70.7 kPa.

1-butene.[1]

The interaction between the heteropoly anion and substrate (or protonated substrate) should be important also in the reactions over hereropoly acids supported on carriers. In the case of heterogeneous systems, it seems of the utmost importance that protons and heteropoly anions exist in close proximity. Protons originating from heteropoly acids naturally satisfy this condition. In addition, in the heteropoly acid/ion-exhanger system, protons originating from the ion-exchanger also can interact with supported heteropoly anions, and they exhibit a higher activity than those of the resin not supported by the anions. This may explain the high activity of heteropoly acid–acid resin composite catalysts.

References

1) Y. Izumi, K. Matsuo, and K. Urabe, "The Chemistry and Uses of Molybdenum, Proceedings, 4th International Conference on Catalysis," Section V-B, Golden (1982), p. 289.

2) M. Misono, "The Chemistry and Uses of Molybdenum, Proceedings, 4th International Conference on Catalysis," Section V-B, Golden (1982), p. 302.

3) I. V. Kozhevnikov and M. I. Matveev, *Applied Catal.*, **5**, 135 (1983).

4) Y. Ono, M. Taguchi, Gerile, S. Suzuki, and T. Baba, "Stud. Surface Sci. Catal.," ed by B. Imelik *et al.*, Elsevier, Amsterdam (1984), in press.

5) Y. Izumi, R. Hasebe, and K. Urabe, *J. Catal.*, **84**, 402 (1984).

6) A. Igarashi, T. Matsuda, and Y. Ogino, *J. Jpn. Pet. Inst.*, **22**, 331 (1979).

7) T. Matsuda, A. Igarashi, and Y. Ogino, *J. Jpn. Pet. Inst.*, **23**, 30 (1980).

8) Y. Ono and T. Baba, Proc. 8th International Congress on Catalysis, Berlin, Vol. 5, Verlag Chemie, Weinheim (1984), p. 405.

9) Y. Izumi, K. Matsuo, and K. Urabe, *J. Mol. Catal.*, **18**, 299 (1983).

 © 1985 The Chemical Society of Japan Bull. Chem. Soc. Jpn., 58, 2157—2162 (1985)

Rate Constants and Mechanism for Reactions of Ketenes with OH Radicals in Air at 299 ± 2K

Shiro HATAKEYAMA,* Shigeo HONDA,† Nobuaki WASHIDA, and Hajime AKIMOTO
Division of Atmospheric Environment, The National Institute for Environmental Studies, P.O. Tsukuba-gakuen, Ibaraki 305
(Received February 26, 1985)

Rate constants for reactions of OH radicals with four kinds of simple ketenes (ketene, methylketene: MK, ethylketene: EK, and dimethylketene: DMK) were measured in 1 atm of air at 299±2 K by use of a competitive reaction method. The photolysis of CH_3ONO in air was used to generate OH radicals. The rate constants for OH reactions obtained are $(1.8\pm0.2)\times10^{-11}$, $(7.6\pm1.4)\times10^{-11}$, $(11\pm3)\times10^{-11}$ and $(10\pm3)\times10^{-11}$ cm^3 $molecule^{-1}$ s^{-1} for ketene, MK, EK, and DMK, respectively. The major product was a carbonyl compound; HCHO from ketene, CH_3CHO from MK, and CH_3COCH_3 from DMK; the yield was ≈80%, 72±17%, and 70±3%, respectively. It is proposed that the reaction proceeded mainly *via* an OH addition to the olefinic carbons of ketenes and the adduct decomposes to give a carbonyl compound and CO as final products in air.

Ketenes are known to be products of ozone-alkene reactions[1] and O(^{3}P)-alkene or alkyne reactions.[2] They are also produced during the combustion of alkynes and alkenes.[3,4] Therefore, a knowledge of oxidation rates of ketenes is significant for modeling the atmospheric life cycle and the combustion of hydrocarbons. However, there have been few reports concerning an experimental investigation of the oxidation of ketenes. Recently, we reported on the reactions of ketenes with O(^{3}P).[5]

Although the OH radical reaction plays an important role in the atmospheric oxidation and combustion processes of ketenes, little has been reported regarding the rate constants of these reactions. Faubel *et al.*[6] reported that the lower limit of the rate constant for ketene+OH is $\approx1.7\times10^{-12}$ cm^3 $molecule^{-1}$ s^{-1}. In computer-modeling studies regarding the combustion of ethylene[3] and acetylene,[4] rate constants of 1.7×10^{-11}[3] and 4.7×10^{-11} cm^3 $molecule^{-1}$ s^{-1},[4] respectively, were adopted without any experimental basis. Rate constants for other substituted ketenes have never appeared in the literature. No experimental study on the mechanism of an OH reaction with ketenes has been reported.

In the work reported here we measured the rate constants for the reactions of OH radicals with four kinds of simple ketenes (ketene, methylketene: MK, ethylketene: EK, dimethylketene: DMK) by use of CH_3ONO photolysis in air as a source of OH radicals. A competitive reaction method was employed. The mechanism for reactions of OH with the ketenes are also discussed in terms of both the linear dependence of the logarithms of the rate constants on the ionization potential and the results of product analyses.

Experimental

Ketene, MK, EK, and DMK were prepared by the pyrolysis of their corresponding dimers at 550 °C,[7] purified by repeated trap-to-trap distillation, and stored at liquid-nitrogen temperature. Dimers of ketene and DMK are commercially available (Tokyo Kasei). Those of MK and EK were prepared by the dehydrochlorination of propionyl chloride and butyryl chloride, respectively, with triethylamine.[8] UV-visible spectra were recorded using a Hitachi 220A spectrometer for given pressures of the ketenes (measured with an MKS Baratron capacitance manometer).

Kinetic measurements were performed in an 11 L cylindrical quartz vessel (120 mm i.d., 1000 mm long), and the changes in the concentration of reactants and products were monitored by means of long-path Fourier-transform infrared spectroscopy (LP-FTIR). The path length was 40 m, and 32 scans at a 1 cm^{-1} resolution were accumulated (≈1 min). The absorptivities (base 10, $Torr^{-1}$ m^{-1} at 30 °C) used were as follows: CH_2CO, 2.11 (2164 cm^{-1}); MK, 2.02 (2140 cm^{-1}); EK, 2.63 (2134 cm^{-1}); DMK, 2.60 (2134 cm^{-1}); HCHO, 0.25 (2780 cm^{-1}, peak to valley); CH_3CHO, 4.05×10^{-2} (2706 cm^{-1}); CH_3COCH_3, 0.173 (1218 cm^{-1}); cyclohexane, 3.31 (2934 cm^{-1}); propylene, 0.384 (912 cm^{-1}). The concentrations of CO and CO_2 were determined by use of calibration curves which were previously reported from this laboratory.[9]

The light source for photolysis was four 20-W black-light lamps (Toshiba FL 20S. BLB, $300<\lambda<400$ nm, $\lambda_{max}=360$ nm) which surrounded the reactor coaxially. The light intensity (measured by the NO_2 photodissociation rate, k_1) was 0.191 min^{-1}. To check for the existence of reactive intermediates such as an OH radical (which can consume ketenes during photolysis) photolyses of ketenes in the presence of 2-methylpropene were also carried out.

OH radicals were generated by the photolysis of methyl nitrite in air, as depicted by following equations.

$$CH_3ONO + h\nu \longrightarrow CH_3O + NO \quad (1)$$

$$CH_3O + O_2 \longrightarrow HO_2 + HCHO \quad (2)$$

$$HO_2 + NO \longrightarrow OH + NO_2 \quad (3)$$

CD_3ONO (in place of CH_3ONO) was also employed for ketene in order to distinguish the product formaldehyde from that produced in reaction 2.

The rate constants were measured on the basis of a competitive reaction method in the presence of cyclohexane or propylene as a reference compound. Typically, CH_3ONO (≈20 mTorr) (1 Torr=133.322 Pa)-ketenes (2—7 mTorr)-reference compound (R.C. 2—7 mTorr) in 1 atm of purified

†On study leave from the University of Tsukuba, Sakura, Ibaraki 305.

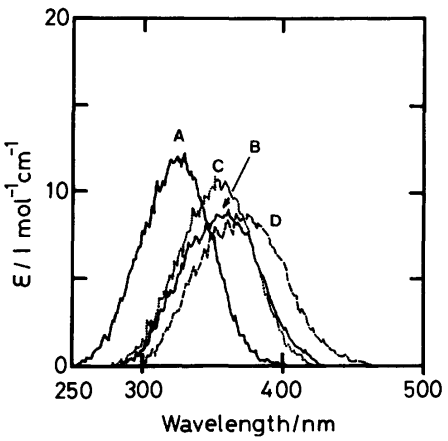

Fig. 1. UV-visible spectra of four kinds of ketenes. A: Ketene, B: methylketene, C: ethylketene, D: dimethylketene.

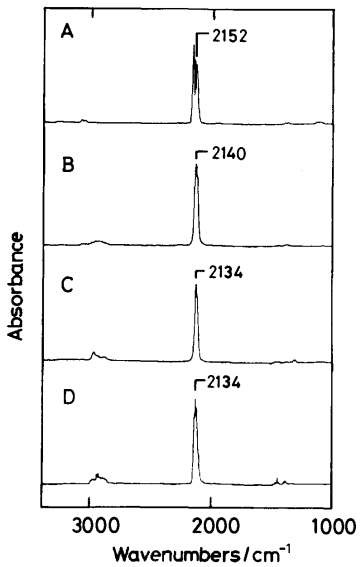

Fig. 2. IR spectra of four kinds of ketenes. A: Ketene, B: methylketene, C: ethylketene, D: dimethylketene.

air was irradiated for 10 min. IR spectra were taken at a constant interval. The reaction temperature was 299±2 K.

Results and Discussion

I. Rate Constants for OH+Ketenes. Figure 1 shows the UV-visible spectra of four kinds of ketenes. The λ_{max} and ε_{max} for ketene, MK, and DMK are in good agreement with those reported earlier.[10-12] That of EK (in a gas phase) has not been measured so far. All of the spectra show diffuse structures. Such structures have been reported for ketene.[13,14] Figure 2 shows the IR spectra of ketenes; the peaks at $\approx$2150 cm^{-1} correspond to the antisymmetric C=C=O stretching bands and were used for the concentration measurements.

An irradiation of the ketenes in 1 atm of air produced a first-order decay of each ketene. In order to check for the possibility that some reactive species, such as an OH radical which consumes ketenes, is produced in the course of photolysis, photolyses in the presence of 2-methylpropene (the rate constant for OH reaction is 5.07×10^{-11} cm^3 $molecule^{-1}$ s^{-1} [15]) were performed. No change in the concentration of 2-methylpropene was observed during 20 min of photoirradiation. Thus, it can be concluded that the decay of each ketene is solely due to photolysis. From the slope of the first-order decay of the ketenes, the photolysis rate constants in this system were calculated to be 9.5×10^{-3}, 3.5×10^{-3}, 3.0×10^{-3}, and 3.1×10^{-3} min^{-1} for ketene, MK, EK, and DMK, respectively.

The rate constants for reactions of the OH radical with ketenes were measured by use of CH_3ONO as a source of OH radicals. Thus, an irradiation of the ketenes-CH_3ONO-R.C. was carried out. The reactions which took place in the system were as follows.

$$\text{OH} + \text{ketenes} \longrightarrow \text{products} \quad (4)$$

$$\text{OH} + \text{R.C.} \longrightarrow \text{products} \quad (5)$$

$$\text{ketenes} + h\nu \longrightarrow \text{products} \quad (6)$$

The decay rate of the ketenes and R.C. are described according to the next equations.

$$-\,\mathrm{d[ketenes]}/\mathrm{d}t = k_4[\mathrm{OH}][\mathrm{ketenes}] + k_6[\mathrm{ketenes}] \quad (7)$$

$$-\,\mathrm{d[R.C.]}/\mathrm{d}t = k_5[\mathrm{OH}][\mathrm{R.C.}] \quad (8)$$

Thus,

$$\ln([\mathrm{ketenes}]_{t_0}/[\mathrm{ketenes}]_t) = k_4\int_{t_0}^{t}[\mathrm{OH}]\mathrm{d}t + k_6(t-t_0) \quad (9)$$

$$\ln([\mathrm{R.C.}]_{t_0}/[\mathrm{R.C.}]_t) = k_5\int_{t_0}^{t}[\mathrm{OH}]\mathrm{d}t \quad (10)$$

From Eqs. 9 and 10 the following equation can be derived.

$$\ln([\mathrm{ketenes}]_{t_0}/[\mathrm{ketenes}]_t) - k_6(t-t_0) = (k_4/k_5)\ln([\mathrm{R.C.}]_{t_0}/[\mathrm{R.C.}]_t) \quad (11)$$

Figure 3 shows a plot of Eq. 11 for four different ketenes. The data, which were obtained during several runs, are almost on the same straight line for each ketene. In this plot, the above photolysis rate constants were used as k_6. From the slopes of those plots and k_5 (cyclohexane: 7.85×10^{-12} cm^3 $molecule^{-1}$ s^{-1}, propylene: 2.51×10^{-11} cm^3 $molecule^{-1}$ s^{-1})[15] k_4 can be calculated. Results are listed in Table 1. The rate constant for MK was measured by use of not only cyclohexane but also propylene as a R.C. The rate constants obtained for the two R.C. agreed well (within experimental error). However, since a large difference in the rate constants between cyclohexane and MK against OH may introduce a systematic error, the rate constant obtained by use of propylene as a R.C. should be more reliable.

In the case of EK and DMK, propylene, the same compound used as the R.C., may be formed during the isomerization of the carbenes produced in the

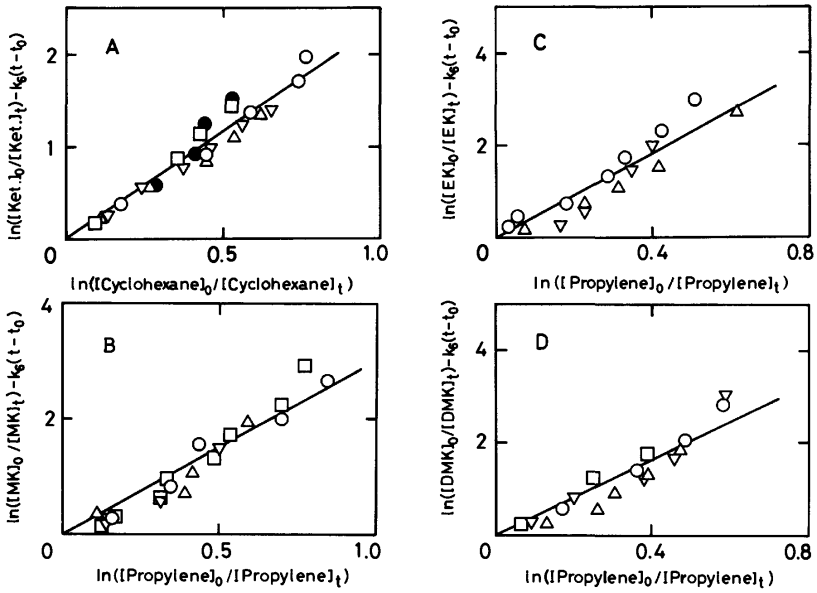

Fig. 3. Plot of Eq. 11 for four kinds of ketenes. Different symbols correspond to different runs. A: Ketene ($CH_3ONO \approx 22$ mTorr-Ketene ≈ 2 mTorr-$C_6H_{10} \approx 2$ mTorr), B: MK ($CH_3ONO \approx 22$ mTorr-MK ≈ 7 mTorr-$C_3H_6 \approx 7$ mTorr), C: EK ($CH_3ONO \approx 23$ mTorr-EK ≈ 6.5 mTorr-$C_3H_6 \approx 7.5$ mTorr), D: DMK ($CH_3ONO \approx 23$ mTorr-DMK ≈ 6.5 mTorr-$C_3H_6 \approx 7.5$ mTorr).

Table 1. Rate constants for the reaction of ketenes with OH radicals

Ketene	Reference Compound	k_4/k_5	$k_4/1\times10^{-11}$ cm^3 molecule^{-1} s^{-1}
Ketene	Cyclohexane[a)]	2.3±0.3	1.8±0.2
MK	Cyclohexane	8.0±1.7	6.4±1.4
MK	Propylene[b)]	3.0±0.5	7.6±1.4
EK	Propylene	4.5±1.1	11±3
DMK	Propylene	4.1±1.1	10±3

a) $k_5=7.95\times10^{-12}$ cm^3 molecule^{-1} s^{-1}.[15] b) $k_5=2.51\times10^{-11}$ cm^3 molecule^{-1} s^{-1}.[15] Estimated errors are 95% confidence limits.

photolysis. However, propylene was not detected during the 20-min photolysis of EK and DMK. This is, perhaps, due to the scavenging of the carbenes by O_2. Thus, the production of propylene can be neglected in our reaction system.

Only one study has previously been reported regarding the rate constants for the reaction of OH with ketene. Faubel *et al.*[6] estimated the lower limit of the rate constant for the OH+ketene reaction to be 1.7×10^{-12} cm^3 molecule^{-1} s^{-1} by means of a discharge flow-MS method in the course of their study on the C_3O_2+OH reaction. OH reactions with other ketenes have never been studied before. Our value for ketene, 1.8×10^{-11} cm^3 molecule^{-1} s^{-1}, is consistent with the lower limit given by Faubel *et al.*,[6] and is in good agreement with the value used in the numerical model study reported by Levy[3] ($\approx1.7\times10^{-11}$ cm^3 molecule^{-1} s^{-1}, no temperature dependence was assumed).

II. Reaction Mechanism of OH+Ketenes. No information is available concerning the mechanism of the reaction of ketenes with OH. In the field of combustion chemistry, the reaction of OH with ketene has been thought to proceed *via* the following reaction[3,4] without any experimental evidence.

$$CH_2CO + OH \longrightarrow HCHO + HCO \qquad (12)$$

In order to get an insight into the mechanism of the reaction, logarithms of the rate constants for OH+alkenes[15] and OH+ketenes were plotted against the ionization potential of alkenes and ketenes[16-18] (Fig. 4), as proposed by Bayes and co-workers.[19] The points for ketenes seem to fall on a straight line (the lower solid line), similar to the points for olefins (the upper solid line). This indicates that the reaction of OH with ketenes proceeds *via* a path similar to that for OH+alkenes (a reaction path on which the charge-transfer surface has an important contribution and the transition state is somewhat polarized). Thus, the reaction of OH with ketenes should proceed *via* addition.

In the reaction of OH with ketene, MK, and DMK, HCHO, CH_3CHO, and CH_3COCH_3 were detected, respectively. Figures 5 and 6 show the amount of acetaldehyde and acetone plotted against the amount of the corresponding ketenes consumed during several runs. The apparently straight lines were obtained in both systems. From the slopes of the lines shown in Figs. 5 and 6 the average ratios of the carbonyl-compounds-formed to ketenes-consumed were calculated to be 0.72±0.17 and 0.70±0.03 for acetaldehyde from MK and acetone from DMK, respectively. Since, in

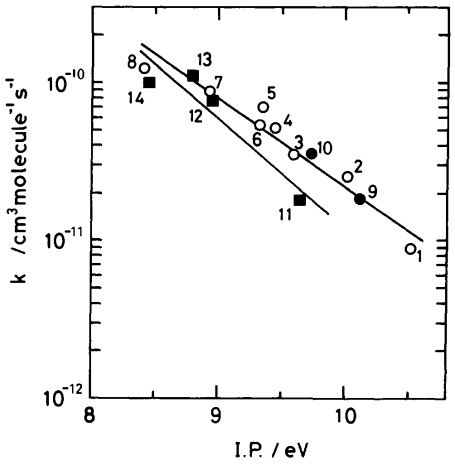

Fig. 4. Log(rate constant) *vs.* ionization potential for alkenes and ketenes. 1: Ethylene, 2: propylene, 3: 1-butene, 4: 2-methylpropene, 5: *trans*-2-butene, 6: *cis*-2-butene, 7: 2-methyl-2-butene, 8: 2,3-dimethyl-2-butene, 9: acrylaldehyde, 10: crotonaldehyde, 11: ketene, 12: methylketene, 13: ethylketene, 14: dimethylketene. Upper solid line was obtained by the least square calculation for compounds 1—10. Lower solid line was obtained by the least square calculation for ketenes.

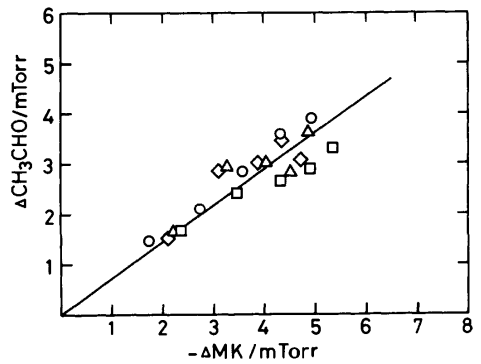

Fig. 5. Concentration of produced acetaldehyde plotted against decreased amount of methylketene. Different symbols correspond to different runs. $[MK]_0$=5.0—6.1 mTorr, $[CH_3ONO]_0$=≈22 mTorr.

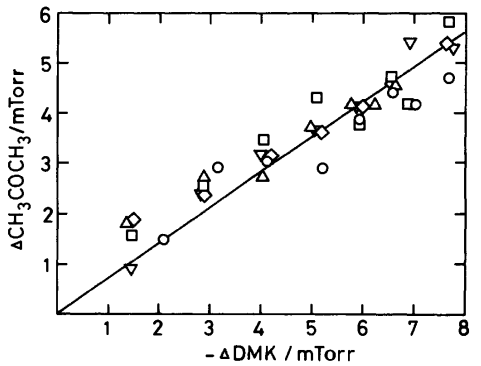

Fig. 6. Concentration of produced acetone plotted against decreased amount of dimethylketene. Different symbols correspond to different runs. $[DMK]_0$= 6.6—7.7 mTorr, $[CH_3ONO]_0$=≈23 mTorr.

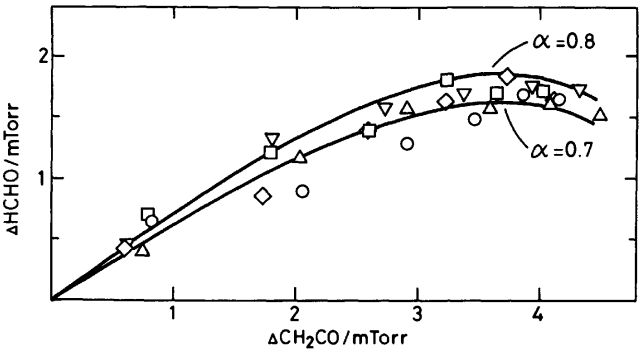

Fig. 7. Concentration of produced formaldehyde plotted against decreased amount of ketene. Different symbols correspond to different runs. $[Ketene]_0$= 4.7—5.4 mTorr, $[CD_3ONO]_0$=≈25 mTorr. Solid lines are the plot of the amount of formaldehyde formed against the amount of consumed ketene calculated by Eqs. 15 and 16 with α=0.8 and α=0.7.

each case, the photolysis of the product carbonyl compounds and the secondary OH reactions of products tend to decrease their yields, the yields estimated above should be taken as lower limits.

For ketene, the plot shows no lineality, and the final yield of formaldehyde is indicated to be much lower (Fig. 7). It is because the OH+HCHO reaction has a rate constant (1.01×10^{-11} cm³ molecule^{-1} s^{-1})[20] comparable to that for OH+ketene; the secondary reaction of OH with formaldehyde (as well as its photolysis) significantly lowers the apparent yield of formaldehyde.

In order to simulate the concentration change of ketene and formaldehyde, the following reaction scheme was used.

$$\text{ketene} + \text{OH} \xrightarrow{k_4} \alpha\text{HCHO} + \text{other products} \quad (4')$$

$$\text{ketene} + h\nu \xrightarrow{k_6} \text{products} \quad (6)$$

$$\text{HCHO} + \text{OH} \xrightarrow{k_{13}} \text{products} \quad (13)$$

$$\text{HCHO} + h\nu \xrightarrow{k_{14}} \text{products} \quad (14)$$

Here α ($\leq$1) is the yield of formaldehyde. Thus, next equations were obtained using a constant OH (OD) radical concentration (≈2×10^8 molecule cm^{-3}), which was measured[21] for about 10 min of irradiations in 5 runs.

$$[\text{ketene}] = [\text{ketene}]_0 \exp\{-(k_4[\text{OH}]+k_6)t\} \quad (15)$$

$$[\text{HCHO}] = \frac{\alpha k_4[\text{OH}][\text{ketene}]_0}{k_{13}[\text{OH}]+k_{14}-k_4[\text{OH}]-k_6} \times [\exp\{-(k_4[\text{OH}]+k_6)t\} - \exp\{-(k_{13}[\text{OH}]+k_{14})t\}] \quad (16)$$

Here $[ketene]_0$ is the initial ketene concentration. The solid lines in Fig. 7 are plots of the amounts of formaldehyde formed against the amounts of consumed ketene as calculated by Eqs. 15 and 16 with α=0.7 and α=0.8 by the use of $k_{13}=1.0\times10^{-11}$ cm³ molecule^{-1} s^{-1} and $k_{14}=2.6\times10^{-5}$ s^{-1}.[22] Most of the experimental points fall between the two lines; thus, we can assume

that the inital yield of formaldehyde in the reaction of OH (OD) with ketene was 70—80%. Therefore, it can be concluded that the reaction of OH with various ketenes at room temperature gives corresponding carbonyl compounds as the main products.

By an *a priori* consideration, the site attacked by an OH can be regarded to be the olefinic carbon of the ketenes, where the electron density is the greatest.[23] The formation of carbonyl compounds from the adduct can be explained in two ways. One is,

$$RR'C{=}C{=}O + OH \longrightarrow \left[\begin{array}{l} RR'C\text{-}C{=}O \\ \quad | \\ \quad OH \end{array}\right]^{\ddagger} \longrightarrow$$

A

$$RR'COH + CO \qquad (17)$$

$$\Delta H = -35.1 \text{ kcal mol}^{-1} \text{ for R,R}' = \text{H}^{24)}$$

Since it is known[26-28] that the RR'COH radical yields RR'CO in the presence of O_2, the formation of formaldehyde, acetaldehyde, and acetone in the reaction of ketene, MK, and DMK, respectively, can be regarded as the products of the reaction of RR'COH radicals with O_2.

The other is the hypothesized route used in the modeling studies[3,4] mentioned above

$$RR'C{=}C{=}O + OH \longrightarrow \mathbf{A} \longrightarrow RR'CO + HCO \qquad (18)$$

$$\Delta H = -31.9 \text{ kcal mol}^{-1} \text{ for R,R}' = \text{H}.^{24)}$$

HCO reacts with O_2 to give $CO+HO_2$, almost exclusively.[25] Thus, the total reaction in air is the same for both cases, as described by the following equation.

$$RR'C{=}C{=}O + OH + O_2 \longrightarrow RR'CO + CO + HO_2 \qquad (19)$$

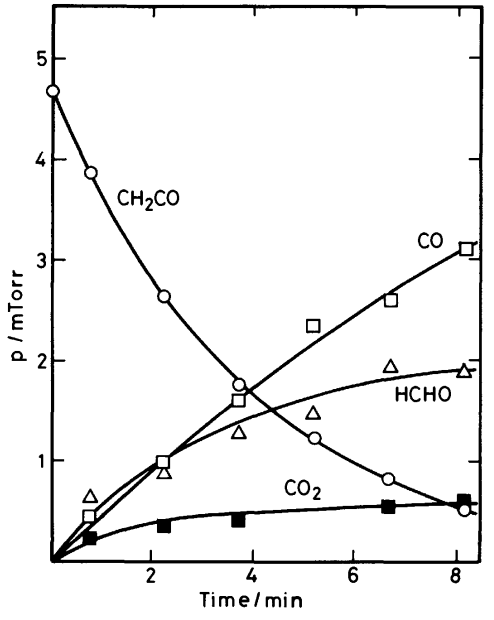

Fig. 8. Typical time profile of the concentration of the reactant and the products in CD_3ONO (22.5 mTorr)-CH_2CO (4.7 mTorr)-air-irradiation system.

The reaction paths in 17 and 18 could not be distinguished in the kinetic experiments and the product analyses performed in this study.

Since **A** is an OH-substituted acetyl radical, the formation of a PAN-type compound ($RR'C(OH)C(O)OONO_2$) can be expected if the radical is stabilized under atmospheric conditions. In the present study, however, no IR band corresponding to PAN-type compounds was detected. Thus, we can assume that the lifetime of **A** is much shorter than the collision interval, even under atmospheric conditions.

Figure 8 shows a typical time profile for the concentration of a reactant and its products in a CD_3ONO-ketene-air-irradiation system. As can be seen in this figure, the CO yield is much higher than CO_2.[29] This strongly supports the above mechanism as being the major pathway. However, the small amount of CO_2 produced may correspond to the pathway of the OH-attack on the carbonyl carbon of the ketenes.

References

1) R. I. Martinez, J. T. Herron, and R. E. Huie, *J. Am. Chem. Soc.*, **103**, 3807 (1981).

2) a) J. R. Kanofsky, D. Lucas, F. Pruss, and D. Gutman, *J. Phys. Chem.*, **78**, 311 (1974); b) F. J. Pruss, Jr., I. R. Slagle, and D. Gutman, *J. Phys. Chem.*, **78**, 663 (1974); c) J. R. Gilbert, I. R. Slagle, R. E. Graham, and D. Gutman, *J. Phys. Chem.*, **80**, 14 (1976).

3) J. M. Levy, *Combust. Flame*, **46**, 7 (1982).

4) C. K. Westbrook, F. L. Dryer, and K. P. Schug, *Combust. Flame*, **52**, 299 (1983).

5) N, Washida, S. Hatakeyama, H. Takagi, T. Kyogoku, and S. Sato, *J. Chem. Phys.*, **78**, 4533 (1983).

6) C. Faubel, H. G. Wagner, and W. Hack, *Ber. Bunsenges. Phys. Chem.*, **81**, 689 (1977).

7) S. Andreades and H. D. Carson, *Org. Synth., Coll. Vol.*, **5**, 679 (1973).

8) J. C. Sauer, *J. Am. Chem. Soc.*, **69**, 2444 (1947).

9) H. Akimoto, H. Bandow, F. Sakamaki, G. Inoue, M. Hoshino, and M. Okuda, *Environ. Sci. Technol.*, **14**, 172 (1980).

10) G. B. Kistiakowsky and B. H. Hahan, *J. Am. Chem. Soc.*, **79**, 2412 (1957).

11) D. P. Chong and G. B. Kistiakowsky, *J. Phys. Chem.*, **68**, 1793 (1964).

12) R. A. Holroyd and F. E. Blacet, *J. Am. Chem. Soc.*, **79**, 4830 (1957).

13) R. N. Dixson and G. H. Kirby, *Trans Faraday Soc.*, **62**, 1406 (1966).

14) A. H. Laufer and R. A. Keller, *J. Am. Chem. Soc.*, **93**, 621 (1971).

15) a) R. Atkinson, K. R. Darnall, A. C. Lloyd, A. M. Winer, and J. N. Pitts, Jr., *Adv. Photochem.*, **11**, 375 (1979); b) R. Atkinson, S. M. Aschman, and J. N. Pitts, Jr., *Int. J. Chem. Kinet.*, **15**, 75 (1983).

16) Ionization potentials of alkenes are from Ref. 17 and those of ketenes are from Ref. 18. Vertical IP was used if available.

17) J. W. Robinson, "Handbook of Spectroscopy", Vol. 1, CRC Press, (1974), pp. 257—511.

18) H. Bock, T. Hirabayashi, and S. Mohmand, *Chem. Ber.*, **114**, 2595 (1981).

19) a) T. M. Lenhardt, C. E. Mcdade, and K. D. Bayes, *J. Chem. Phys.*, **72**, 304 (1980); b) R. P. Ruiz and K. D. Bayes, *J. Phys. Chem.*, **88**, 2592 (1984); c) R. Paltenghi, E. A. Ogryzlo, and K. D. Bayes, *J. Phys. Chem.*, **88**, 2595 (1984).

20) R. Atkinson and W. P. L. Carter, *J. Phys. Chem. Ref. Data*, **13**, 315 (1984).

21) Concentration of OH radical was calculated on the basis of the consumption rate of ketene for 5 runs by use of Eq. 7.

22) The photolysis rate constant in the reaction system employed in this study was calculated by the summation of $\sum_{\lambda} J_{\lambda}\sigma_{\lambda}\phi_{\lambda}$, where J, σ, and ϕ are effective light intensity, absorption cross section, and quantum yield, respectively, by use of the absorption cross section and quantum yield given by Ref. 20.

23) C. E. Dykstra and N. F. Schaefer, III, "The Chemistry of Ketenes, Allenes and Related Compounds," ed by S. Patai, John Wiley & Sons Ltd., New York (1980), Chap. 1.

24) $\Delta H_f°$ values of CH_2CO, OH, HCO, and CO were from H. Okabe, "Photochemistry of Small Molecules," Wiley, New York, 1978, and that of CH_2OH was from J. M. Dyke, A. R. Ellis, N. Honathan, N. Keddar, and A. Morris, *Chem. Phys. Lett.*, **111**, 207 (1984).

25) F. Temps and H. Gg. Wagner, *Ber. Bunsenges. Phys. Chem.*, **88**, 410 (1984).

26) W. P. L. Carter, K. R. Darnall, R. A. Graham, A. M. Winer, and J. N. Pitts, Jr., *J. Phys. Chem.*, **83**, 2305 (1978).

27) N. Washida, *J. Chem. Phys.*, **75**, 2715 (1981).

28) T. Ohta, H. Bandow, and H. Akimoto, *Int. J. Chem. Kinet.*, **14**, 173 (1982).

29) Since CO and CO_2 can be produced by the photochemical reaction of RONO and photodesorption from the cell wall, the contribution of those by-products is corrected in the data shown in Fig. 8 in the following manner. Production rate of CO and CO_2 was estimated as a function of the consumption of nitrite as an average of several runs of photolysis of CH_3ONO or CD_3ONO in air. The yield of CO and CO_2 was estimated by the subtraction of the yield calculated with these functions from the apparent yield.

Preparation of Vanadium-Phosphorus Mixed Oxide (P/V=1) Catalysts and Their Application to Oxidation of Butane to Maleic Anhydride

Tomoaki SHIMODA,† Toshio OKUHARA, and Makoto MISONO*
Department of Synthetic Chemistry, Faculty of Engineering, The University of Tokyo, Hongo, Bunkyo-ku, Tokyo 113
(Received March 28, 1985)

Several vanadium-phosphorus mixed oxides with a P/V ratio=1 have been prepared and the relationships between the structure of catalyst and the catalytic function for the selective oxidation of butane to maleic anhydride were examined. As revealed from XRD, IR, XPS, and redox titration studies, five among them were presumably composed of crystalline single phases, that is, α-$VOPO_4$, β-$VOPO_4$, and $(VO)_2P_2O_7$ as well as unknown phases X_1 and X_2. The valences of the vanadium of these catalysts were close to five, except for $(VO)_2P_2O_7$ (the valence was four). These phases were prepared, respectively, by controlling the kind of precursors and the calcination conditions. The selectivity to maleic anhydride differed markedly among these catalysts, although the rate did not change much when it was normalized to surface area. The selectivity at 440 °C was less than 20% for α- and β-$VOPO_4$, 40% for X_1 and X_2, and 70% for $(VO)_2P_2O_7$. Amorphous phases having V^{4+} were much less selective than $(VO)_2P_2O_7$. No structural changes of the catalysts after use were observed in the cases of α-, β-$VOPO_4$, and $(VO)_2P_2O_7$. Therefore, the effective phase for selective oxidation of butane to maleic anhydride was speculated to be a phase like $(VO)_2P_2O_7$ in which the valence of vanadium is four and the structure is stable under the reaction conditions.

Vanadium-phosphorus mixed oxides are known as catalysts for the selective oxidation of butene to maleic anhydride.[1] Several basic studies have been reported on the active structure of the catalysts,[2] the role of phosphorus,[2-4] and the reaction mechanism.[3] The preferred atomic ratio of phosphorus to vanadium is usually in the range of 1.2 to 2.0.

Recently, certain V-P oxides with a P/V ratio of between 1.0 and 1.2 were found to be efficient catalysts for the selective oxidation of butane, a saturated hydrocarbon, to maleic anhydride.[1,5] Several studies on V-P oxide catalysts in this composition range have also been reported.[6-10] However, in most studies, the V-P oxide catalysts used had various P/V ratios, and they usually contained unknown phases or were mixtures. Therefore, the real active phase for the butane oxidation still remains unclarified, although there are many proposals in patents for the preparation of effective catalysts.[11-14]

It was recently indicated that nearly crystalline phases with P/V ratios close to unity were active and selective for the oxidation of butane.[6,7,10,14] As for V-P oxide with P/V=1, crystalline phases such as α-$VOPO_4$, β-$VOPO_4$, and $(VO)_2P_2O_7$ are known.[15-18] These facts motivated us to study these catalysts in greater detail as an extention of our studies on oxidation catalysts having well-defined bulk structures.

In the present study we attempted (i) to examine more extensively the preparation process of catalysts having single crystalline phases with P/V=1, by using well-defined precursors and (ii) to specify the phase or structure of a catalyst which is efficient for the oxidation of butane. An elucidation of the mechanism of catalytic action and the reason why that phase is effective will be the subjects of following study.

†Present address: Mitsui Petrochemical Industries, Ltd.

Experimental

1. Catalyst Preparation. 1.1. Precursors: Three kinds of V-P-O compounds (P/V=1) with well-defined structures (denoted as P-I, -II, and -III) have been prepared as precursors for catalysts.

(a) $(NH_4)_2[(VO)_2C_2O_4(HPO_4)_2]\cdot 5H_2O$ (P-I). P-I was prepared according to the literature.[19] V_2O_5 powder (0.1 mol) was added gradually with stirring into 400 ml of an aqueous solution of oxalic acid (0.75 mol l^{-1}) at 80 °C. When the solution turned to blue after a few minutes, $NH_4H_2PO_4$ (0.2 mol) was added. A green precipitate was formed while the stirring continued. The precipitate was filtrated, washed with water and acetone, and dried overnight at 100 °C. The obtained solid was confirmed to be $(NH_4)_2[(VO)_2C_2O_4(HPO_4)_2]\cdot 5H_2O$ by comparing X-ray diffraction powder patterns (XRD) with a reference.[19]

(b) NH_4HVPO_6 (P-II). This precursor (P-II) was prepared according to the literature.[15] V_2O_5 powder (0.04 mol) was added to a boiling aqueous solution of $NH_4H_2PO_4$ (0.8 mol in 600 ml H_2O), and boiling was maintained for 30 min. A yellow precipitate was formed after the solution was allowed to stand overnight. The precipitate was filtrated, washed with water and acetone, and dried overnight at 100 °C. The XRD pattern (d/Å: 8.75 (100), 4.60 (2), 4.46 (3.5), 4.41 (3), 4.09 (3), 3.17 (3), 2.95 (15), relative peak intensity in parentheses) indicated that P-II was well crystallized. However, an identification was not made because of the absence of reference data.

(c) $(VO)_2H_4P_2O_9$[20] (P-III-1, 2, and 3). P-III-1 was prepared according to the literature.[14a] V_2O_5 powder (0.1 mol) was added to an aqueous solution (200 ml) of $NH_2OH\cdot HCl$ (0.2 mol, Nakarai Chemicals) and H_3PO_4 (0.2 mol, Koso Chemicals) at 80 °C and was stirred for 1 h, in order to completely reduce V_2O_5. After the solution became a light-blue slurry of about 100 ml, it was evaporated to dryness at 130 °C overnight. A small quantity of water (100 ml) was added to the dried solid and the mixture was boiled for 10 min. A light green precipitate obtained by filtration was washed with water. The structure was confirmed by its XRD pattern with reference to the literature.[20]

P-III-2 was prepared in a similar manner as P-III-I. The

TABLE 1. STARTING MATERIALS OF PRECURSORS

Precursor		Starting Materials
P-I	$(NH_4)_2[(VO)_2C_2O_4(HPO_4)_2]$	V_2O_5, $(COOH)_2$, $NH_4H_2PO_4$
P-II	NH_4HVPO_6	V_2O_5, $NH_4H_2PO_4$
P-III-1	$(VO)_2H_4P_2O_9$	V_2O_5, $NH_2OH \cdot HCl$, H_3PO_4
P-III-2	$(VO)_2H_4P_2O_9$	V_2O_5, $NH_2OH \cdot HCl$, H_3PO_4, $C_3H_4O_3$
P-III-3	$(VO)_2H_4P_2O_9$	V_2O_4, H_3PO_4

only difference was that ethylene carbonate ($C_3H_4O_3$, Nakarai Chemicals) was added to the solution before concentration in order to eliminate Cl.[14b] The XRD pattern was very similar to that of P-III-I; however, the peaks were weaker.

P-III-3 was prepared using V_2O_4. A V_2O_4 powder (0.05 mol, Aldrich) was dissolved into an aqueous solution of H_3PO_4 (0.1 mol in 100 ml H_2O) at 80 °C. The resultant blue solution was concentrated at 80 °C with stirring into a green paste. After the green paste was dried at 100 °C, it was placed into water. A light-blue precipitate was obtained upon filtration and washing with water.

Table 1 summarizes the composition and starting materials of the precursors.

1.2 Calcination of Precursors. The precursors were calcined (a) in streams of O_2 or N_2 in a reactor or (b) in air by use of a muffle furnace.

(a) Each precursor (2—5 g) was calcined in Pyrex-tube reactors (10 or 20 mm in diameter) under the flow of oxygen or nitrogen at a prescribed temperature. The heating rate was controlled by adjusting the power, and the temperature was continuously monitored. The flow rate was 100—200 ml min^{-1}. To avoid any blockage of gas flow due to melting, the heating rate was kept low and a wide reactor diameter was adopted.

(b) In the case of any calcination in air, a muffle furnace was used. The heating rate was about 30 °C min^{-1}.

2. Characterization of Catalysts. 2.1 XRD and IR: XRD powder patterns of precursors and catalysts were recorded using a Rigaku X-ray diffractometer with Cu $K\alpha$ radiation filtered by Ni. The XRD was also measured for the catalysts after use. Infrared spectra were recorded with a spectrometer (JIR-10, FT-IR) using an KBr supporting disc.

2.2 XPS: XPS measurements of fresh and used catalysts were carried out using an ESCA Lab 5 (Vacuum Generator). The excitation was performed with the Mg $K\alpha$ line. Binding energies were referred to the C_{1s} line (285 eV). Samples were evacuated under 10^{-8} Torr (1 Torr=133.3 Pa) at 25 °C in the ESCA chamber.

2.3 Valence of Vanadium: The average oxidation state of vanadium in the catalysts was determined by redox titration.[9] About 0.1 g of each catalyst was dissolved in 100 ml of 2 M† H_2SO_4 at 80 °C. The vanadium (IV or III) content was determined by titration with a solution of $KMnO_4$ (0.1 M). The vanadium (V) content was determined by titration with a solution of a Mohr salt ($FeSO_4 \cdot (NH_4)_2SO_4 \cdot 6H_2O$, 0.1 M) using diphenylamine as an indicator.

2.4 Surface Area: The surface areas of the catalyst were measured by the BET method (N_2 adsorption).

3. Measurement of Catalytic Activity and Selectivity. The oxidation of butane was carried out using a conventional fixed-bed flow reactor at atmospheric pressure. The reactor was a Pyrex tube (10 mm in diameter) and was externally heated by an electric furnace. The feed gas consisted of 1.5 vol% butane, 17 vol% oxygen and nitrogen (balance). The reaction temperature was from 250 °C to 440 °C. Products containing carbon were maleic anhydride (MA), CO and CO_2. No other products (C_2–C_3 aldehydes and carboxylic acids) were detected (less than 1%). The carbon balance at the stationary state was always almost 95—100%. Maleic anhydride was collected by a cold trap and was determined by titration with 0.1 M NaOH.[6] Gaseous products were analyzed by a gas chromatograph. It was confirmed, in some cases, that no products other than MA were trapped.

† 1 M=1 mol dm^{-3}.

Results

1. Effects of Calcination Conditions on the Structure of V–P Oxide Catalysts. 1.1 Calcination in O_2 or Air: The structures of the catalysts obtained by calcination in an O_2 or air flow are summarized in Table 2. The results show that the kinds of precursors, the calcination temperature and the heating rate, all, greatly affect the structure of formed catalysts. For example, a high heating rate caused the formation of β-$VOPO_4$ from P-I, while α-$VOPO_4$ was formed from the same precursor using a low heating rate. At an intermediate heating rate, a mixture of α- and β-phase was obtained.

When P-II was calcined at 550 and 600 °C at a low heating rate, a new XRD pattern (d/Å: 4.72 (40), 4.11 (100), 3.15 (30), relative intensity in parentheses) different from either α-, β-$VOPO_4$ or $(VO)_2P_2O_7$ was observed. A high *S/N* ratio of the XRD peaks, together with the fact that the same XRD patterns were obtained for two samples containing this phase; indicates that this was a single phase. This will be denoted as X_1 in this paper.

The influence of the calcination temperature is seen from the results obtained at a heating rate of 30 °C min^{-1}. The calcination of P-I at 450 °C formed almost an amorphous phase (weak peaks at d/Å : 4.33, 4.17, 3.91, 3.65, 3.50, and 3.10), while after a calcination at 550 or 600 °C, the resultant catalysts were crystalline. This showed that XRD patterns are ascribable to pure β-$VOPO_4$. Changes in the phase with the calcination temperature was also found in the case of P-II. A new phase denoted by X_2 (d/Å : 4.00 (90), 3.66 (45), 3.12 (100), relative intensity in parentheses), was obtained by a low-temperature calcination. X_1 and X_2 were water-soluble and the solution was acidic (pH was 2.37 at about 2 g l^{-1} for X_1 and X_2), while α-, β-$VOPO_4$, and $(VO)_2P_2O_7$ were water-insoluble.

The calcination of P-III-1, 2, containing vanadi-

Table 2. Structures of catalysts obtained by calcination in O_2 or air

Precursor	in	Rate/°C min^{-1}	T/°C	Time/h	Phase formed[a)]	Cat. No.[b)]
P-I	O_2	2.9	600	10	α-$VOPO_4$	1
	O_2	5.0	600	10	$\alpha+\beta$	
	O_2	6.4	550	10	β-$VOPO_4$	2
	O_2	7.0	600	10	β-$VOPO_4$	3
	Air	30	450	20	Unknown	
	Air	30	550	16	β-$VOPO_4$	
P-II	Air	30	450	20	X_2	6
	Air	30	500	20	$X_1+\beta$	
	O_2	3.3	550	10	X_1	
	O_2	3.3	600	10	X_1	5
	O_2	7.5	550	10	$\beta+X_1$	
	Air	30	600	16	β-$VOPO_4$	4
P-III-1	Air	30	450	20	$(VO)_2P_2O_7+X_1$	
	Air	30	600	20	$\beta+(VO)_2P_2O_7+X_1$	
	O_2	3.0	600	10	Unknown$+X_1+X_2+\alpha$	
P-III-2	Air	30	450	20	$X_1+(VO)_2P_2O_7$	
	Air	30	600	20	$X_1+\beta$	

a) In the case of mixtures, the main phases are given in the first place. b) The catalyst numbers are the same as those in Tables 4 and 5.

Table 3. Structures of catalysts obtained by calcination in N_2[a)]

Precursor	Time/h	Phase formed	Cat. No.[b)]
P-I	10	Amorphous	7
P-II	6	Amorphous	8
P-III-1	2	$(VO)_2P_2O_7$	9
P-III-2	2	Unknown	
P-III-3	2	$(VO)_2P_2O_7$	

a) 550°C. heating rate; 10°C min^{-1}. b) The catalyst numbers are the same as those in Tables 4 and 5.

um(IV) in air or O_2 yielded mixed phases. The content of $(VO)_2P_2O_7$ tended to increase as the calcination temperature decreased or the heating rate increased.

1.2 Calcination in N_2: Table 3 shows the results for the calcination at 550°C in N_2 with a heating rate of 10°C min^{-1}. P-I and P-II were converted to amorphous phases, while P-III-1 and P-III-3 readily changed to $(VO)_2P_2O_7$. Less crystalline P-III-2 gave a phase with weak XRD peaks which are not ascribable to $(VO)_2P_2O_7$.

$(VO)_2P_2O_7$ (obtained by the calcination of P-III-1 in N_2) was insoluble in water. However, when it was heated in O_2 (500°C, 2 h), a part of the solid became soluble in the water and the solution became brown. Figure 1 shows the changes of XRD patterns of P-III-1 and P-III-2 due to these processes. After heating P-III-1 in N_2, a typical XRD pattern due to $(VO)_2P_2O_7$ was found (Fig. 1A). The subsequent treatment with O_2 at 500°C caused a partial formation of X_1. By washing with water, the intensity of the XRD peaks due to $(VO)_2P_2O_7$ increased by a factor of about 2; no peaks other than $(VO)_2P_2O_7$ appeared. The changes in the XRD peaks during this procedure were clearer in the case of P-III-2, as shown in Fig. 1B. The weight loss observed by washing with water was about 50% for the latter case.

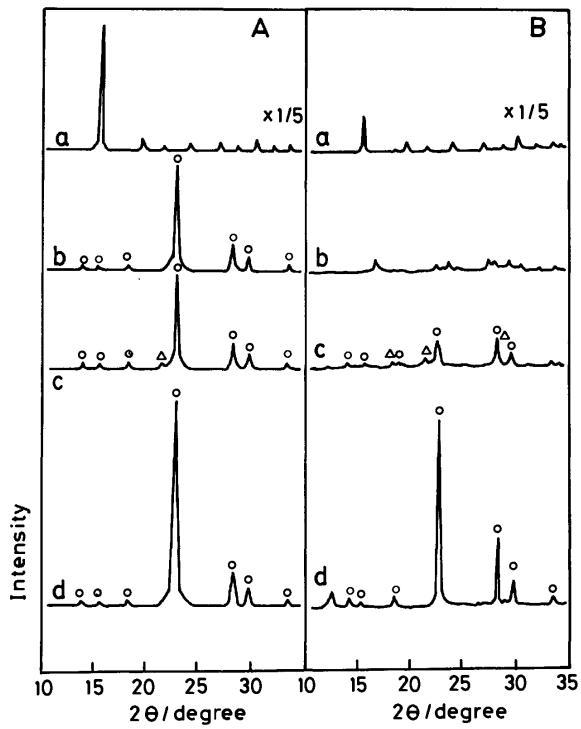

Fig. 1. Changes of XRD patterns by calcination and washing water.
A: P-III-1, B: P-III-2. ○; $(VO)_2P_2O_7$, △; X_1.
a) Precursors, b) After calcination at 550°C in N_2, c) After calcination at 550°C in O_2, d) After washing with H_2O.

2. Characterization of Catalyst. The surface area of catalysts and the valence state of vanadium are summarized in Table 4. The surface area decreased as follows: X_1, X_2>$(VO)_2P_2O_7$>α-$VOPO_4$>Amorphous≥β-$VOPO_4$. The oxidation states were close to five for α-, β-$VOPO_4$, X_1, and X_2 and that of $(VO)_2P_2O_7$ was essentially four. The valence was lower than four after P-I and P-II were heated in N_2 at 550°C.

Typical XRD patterns of these phases are shown

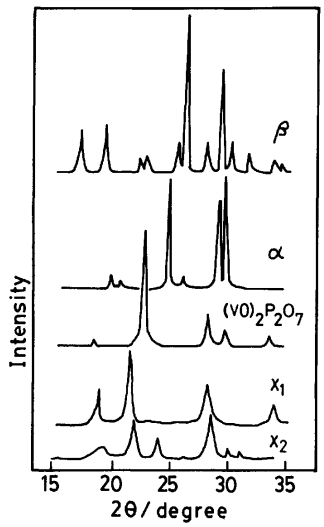

Fig. 2. Typical XRD patterns of V-P oxides prepared.

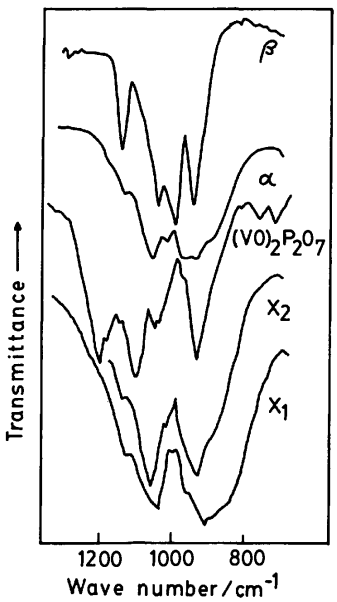

Fig. 3. Infrared spectra of V-P oxides prepared.

in Fig. 2. Figure 3 shows the infrared spectra of the catalysts in the region of 800—1200 cm^{-1}. This region corresponds to the stretching modes of P-O and V=O. The spectra for α-, β-$VOPO_4$ and $(VO)_2P_2O_7$ were in agreement with those reported in the literature.[15,21] The spectra of X_1 and X_2 (1170, 1080, and 955 cm^{-1}) were similar to each other.

XPS spectra of β-$VOPO_4$ and $(VO)_2P_2O_7$ are shown in Fig. 4. The peaks at 526.1 and 519 ev for β-$VOPO_4$ are assigned to $2p_{1/2}$ and $2p_{3/2}$ of vanadium (V) and those at 524.6 and 517.7 eV to $2p_{1/2}$ and $2p_{2/3}$ of vanadium (IV).[22] Although the surfaces of metal oxides are sometimes in more oxidized states than in the bulk, *e.g.*, Fe_2O_3 at the surface of Fe_3O_4,[23] the oxidation states of the catalysts prepared in the present study were very close to those in the bulk. Therefore, it is probable that the crystalline bulk structures were

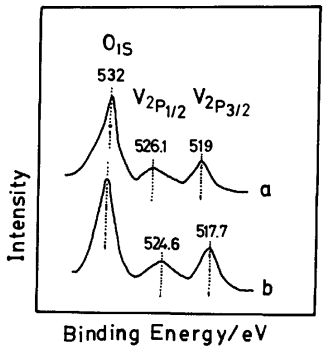

Fig. 4. XPS spectra of β-$VOPO_4$ and $(VO)_2P_2O_7$.
a): β-$VOPO_4$, b): $(VO)_2P_2O_7$.

TABLE 4. SURFACE AREAS AND VALENCE STATES OF VANADIUM OF CATALYSTS

Phase	Surface area/m^2g^{-1}	Valence of Vanadium	Cat. No.
α-$VOPO_4$	5.9	4.97	1
β-$VOPO_4$	3.4	—	2
β-$VOPO_4$	1.7	4.99	3
β-$VOPO_4$	1.3	—	4
X_1	16.0	4.96	5
X_2	14.1	4.96	6
Amorphous	3.8	3.34	7
Amorphous	3.5	3.77	8
$(VO)_2P_2O_7$	7.1	4.02	9
$(VO)_2P_2O_7$[a)]	12.4	4.00	10

a) After O_2-treatment at 500°C, washing with H_2O, and recalcination.

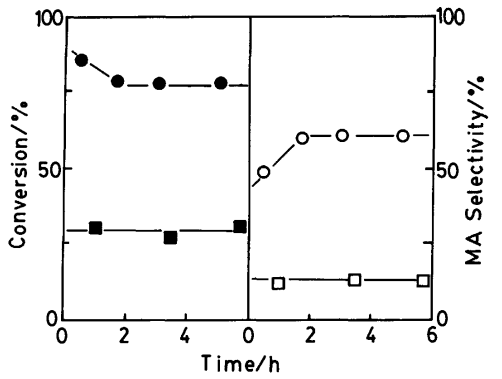

Fig. 5. Activity and selectivity for oxidation of butane at 440°C.
●○; $(VO)_2P_2O_7$, ■□; β-$VOPO_4$.
Reaction conditions; butane 1.5%, O_2 17%, $W/F = 0.67 \times 10^3$ g·h·mol^{-1}.

maintained on the surface of these catalysts. The XPS spectra of β-$VOPO_4$ and $(VO)_2P_2O_7$ did not change after they were used for the oxidation of butane.

3. Catalytic Oxidation of Butane to Maleic Anhydride (MA). Catalysts 1 to 10 (catalyst numbers in Tables 2—4) were used for the oxidation of butane. Typical time courses of the reaction over β-$VOPO_4$ (catalyst 3) and $(VO)_2P_2O_7$ (catalyst 10) are shown in Fig. 5. β-$VOPO_4$ showed a constant conversion and selectivity from the beginning of the reaction. α-$VOPO_4$ (catalyst

TABLE 5. CHANGES OF PHASES AND VALENCE DURING REACTION

Phase	W/F[a]	Conv. %	Rate[b]	Selectivity/C_4-base% CO	CO_2	MA	Phase after reaction[c]	Valence of V[d]	Cat. No.
α-$VOPO_4$	0.67	53	7.8	57	25	18	α-$VOPO_4$	4.99	1
β-$VOPO_4$	0.67	62	9.1	61	21	18	β-$VOPO_4$	—	2
β-$VOPO_4$	0.67	31	4.6	61	25	14	β-$VOPO_4$	4.99	3
β-$VOPO_4$	0.67	14	2.1	53	27	20	β-$VOPO_4$	—	4
X_1	0.67	59	8.7	44	16	40	$\alpha+X_2$	4.97	5
X_2	0.67	52	7.7	41	15	44	$\alpha+X_2$	4.99	6
Amorphous	0.67	61	9.0	69	15	16	$\alpha+\beta$	—	7
Amorphous	0.54	15	2.7	51	5	44	$X_2+\alpha$	—	8
$(VO)_2P_2O_7$	0.33	27	7.9	20	8	72	$(VO)_2P_2O_7$	4.05	9
$(VO)_2P_2O_7$[e]	0.13	35	25.8	23	10	67	$(VO)_2P_2O_7$	4.11	10

a) 10^3g·h·mol^{-1}. b) 10^{-4}mol(g·h)$^{-1}$. c) In the case of mixtures, the main phases are given in the first place. d) After reaction. e) After washing with water (see text).

1) showed a result similar to β-$VOPO_4$. In the case of $(VO)_2P_2O_7$, the activity and selectivity changed slightly at first, and became constant after 2 h. For X_1 and X_2, both the activity and selectivity gradually increased for an initial 3 h. Changes were also observed for amorphous catalysts.

The catalytic activity and selectivity for the oxidation of butane at 440 °C are summarized in Table 5. Data for the stationary state are given in this table. The $(VO)_2P_2O_7$ which was washed and recalcined was most active; however, the catalytic activity was more or less similar when normalized to surface area. The activity of β-$VOPO_4$ was almost proportional to the surface area of the catalysts. In contrast, the selectivity to MA greatly depended on the structure of the catalyst. It was especially high for $(VO)_2P_2O_7$ (about 70%). X_1 and X_2 showed moderate selectivity (40%), and the selectivity was low for α- and β-$VOPO_4$ (20%).

Phase and valence changes of vanadium during the reaction were determined as summarized in Table 5. The XRD patterns changed little after the reaction in the cases of α-, β-$VOPO_4$ and $(VO)_2P_2O_7$. However, X_1 and X_2 changed into mixtures of α-$VOPO_4$ and X_2, for which the compositions were similar. Amorphous phases, catalysts 7 and 8, also changed to mixed phases. The oxidation states of vanadium remained unchanged for α-, β-$VOPO_4$, X_1, X_2 and $(VO)_2P_2O_7$, but those for amorphous phases increased to about five.

Figure 6 shows the effects of W/F on the conversion and the selectivity to MA obtained for $(VO)_2P_2O_7$ and β-$VOPO_4$, where W is the weight of catalyst and F is the flow rate of butane. The selectivity was nearly constant in this range of conversion, although a slight decrease was observed at a low conversion level for $(VO)_2P_2O_7$.

The effects of the reaction temperature on the reaction rate and selectivity are shown in Fig. 7 for $(VO)_2P_2O_7$. The conversion was adjusted to about 40% in order to compare the selectivity, except for the reaction at 250 °C. The rate at 250 °C was so low that a higher conversion was not attained. The selectivity increased as the reaction temperature decreased and was about 90% at 250 °C.

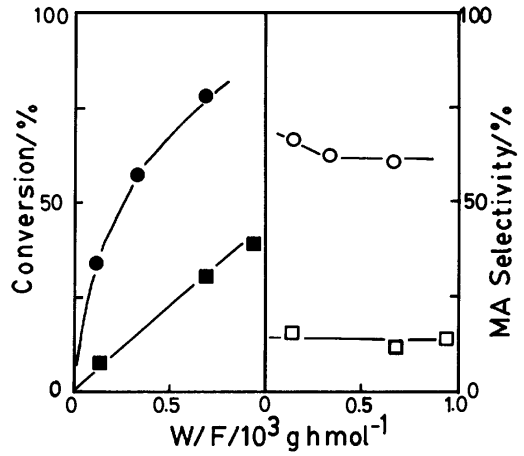

Fig. 6. Effect of W/F on conversion and selectivity to maleic anhydride for oxidation of butane.
●○; $(VO)_2P_2O_7$, ■□; β-$VOPO_4$.
Reaction conditions; 440 °C, butane 1.5%, O_2 17%.

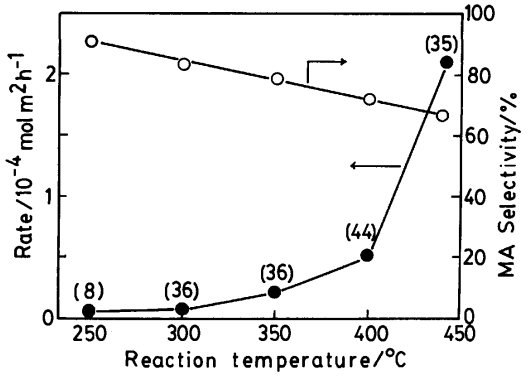

Fig. 7. Effect of reaction temperature on rate and selectivity for oxidation of butane over $(VO)_2P_2O_7$.
Reaction conditions; butane 1.5%, O_2 17%.
Figures in parentheses are % conversions.

The effect of the valence of vanadium on the catalytic properties was examined using catalysts which were prereduced by H_2. Prior to the reaction, β-$VOPO_4$ (catalyst 3) and X_1 were reduced with H_2 in a closed circulation system (200 cm^3) at 400 °C until the average

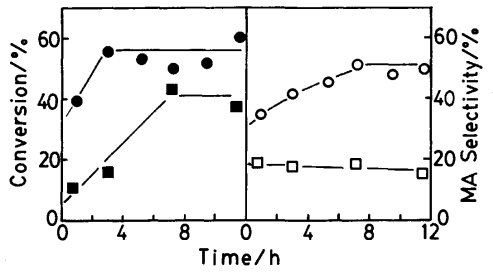

Fig. 8. Variation of activity and selectivity for oxidation of butane over reduced catalysts at 440 °C with reaction time.
Reaction conditions; butane 1.5%, O_2 17%, $W/F = 0.67 \times 10^3$ g·h·mol^{-1}.
●○; reduced X_1, ■□; reduced β-$VOPO_4$.

valence of vanadium became four. After the treatment, the structure of β-$VOPO_4$ and X_1 changed to amorphous. As shown in Fig. 8, the activity increased with the reaction time for both catalysts and became constant at later stage. The rates as well as the selectivity at the steady state were comparable with those of corresponding unreduced catalysts. After the reaction, the reduced β-$VOPO_4$ showed very weak peaks corresponding to β-$VOPO_4$ and the reduced X_1 showed XRD peaks corresponding to α-$VOPO_4$ and $(VO)_2P_2O_7$.

Discussion

1. Structure of V-P Oxides with P/V=1. Several structures have been reported for crystalline phases of V-P mixed oxide catalysts with a P/V ratio close to unity. These phases have recently been reviewed by Delmon and Hodnett.[24] Among them, only α-$VOPO_4$, β-$VOPO_4$, and $(VO)_2P_2O_7$ are structures which were determined by XRD analyses of single crystals.

The phases which have been claimed to be efficient catalysts for the selective oxidation of butane to MA are, for example, phase X of ICI[12] and B phase of Chevron.[11] The XRD powder patterns of X and B closely resemble those of α-$VOPO_4$ and $(VO)_2P_2O_7$, respectively. The phases X_1 and X_2 showed XRD patterns very similar to β^* phase reported by Delmon and Hodnett[8,24,25] and to B′ phase of ICI,[26] respectively. Therefore, so far there have been reported five phases of V-P mixed oxide catalysts (P/V=1), *i. e.*, α-$VOPO_4$, β-$VOPO_4$, $(VO)_2P_2O_7$ (=B phase), X_1 (=β^* phase), and X_2 (=B′ phase). However, it must be kept in mind that catalysts showing similar XRD patterns are often different in crystallinity and purity and sometimes exhibit quite different activity and selectivity.

2. Preparation of Single Crystalline Phases. The preparation processes of the V-P oxides studied in the present work (Tables 2 and 3) are summarized in Fig. 9. As discussed below, these results demonstrate that the factors investigated, *i,e.*, the kind of precursors, the heating rate, the temperature of calcination, and the atmosphere of calcination, are all important factors in determining the resultant structure of catalysts.

2.1 Calcination in the Oxidizing Atmosphere: First of all, it is noteworthy that α- and β-$VOPO_4$ were respectively formed as single phases (judged from XRD powder patterns), by controlling the heating rate. Trifiro *et al.* reported that α-$VOPO_4$ was transformed to β-$VOPO_4$ when α-$VOPO_4$ was heated for a prolonged period at a high temperature,[21] so that β is likely the more stable phase at high temperatures. Bordes and Courtine[15] reported only the formation of β-$VOPO_4$ by the calcination of P-I in O_2. However, the present study has revealed that α-$VOPO_4$ was exclusively formed when the temperature was raised slowly. It is probable that α-$VOPO_4$ is the phase which crystallizes readily at lower temperatures and that once α-phase is formed it is not easily transformed to the β-phase.

P-I tended to melt at 400—450 °C when it was calcined in O_2; sometimes, the gas flow decreased sharply. In these cases, mixtures of α- and β-phases were often obtained. To avoid this phenomenon, we utilized a wide glass tube and raised the temperature gradually while monitoring the rate of gas flow.

Thus, it is important for the preparation of single crystalline phases to control the rate of temperature rise of the calcination process. Trifiro *et al.*[21] also indicated that the heating rate had a significant influence

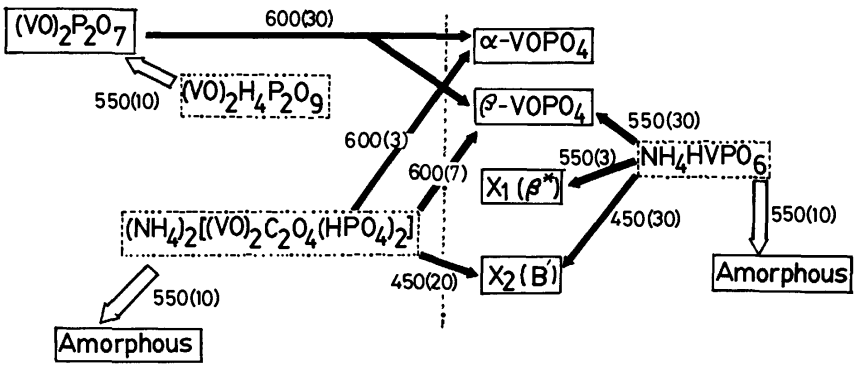

Fig. 9. Preparation processes of V-P oxides.
➡; Calcination in O_2, ⇨; Calcination in N_2.
Figures attached to arrows are calcination temperature and are heating rate (°C min^{-1}, in parentheses).

on the resultant phase.

From P-II (in which vanadium was pentavalent), β-$VOPO_4$, X_1, and X_2 were respectively obtained by controlling the calcination temperature and the heating rate (Table 2). These results are different from those of Bordes and Courtine[15] who reported the formation of α-$VOPO_4$. Probably, the detailed conditions of the preparation were different, although they are not described in their paper. X_1 and X_2 crystallized at lower temperatures and were transformed into β-$VOPO_4$ when calcined at high temperatures. As described above, the X_1 phase showed a XRD pattern similar to the β^* phase which Delmon and Hodnett obtained as mixtures with other phases. They speculated that vanadium in this phase was quadrivalent on the basis of the fact that the fraction of the β^* phase and the average valence state of vanadium changed somewhat in parallel with the calcination time. However, the X_1 phase ($=\beta^*$), which was obtained almost as a single-crystalline phase, has vanadium(V) as determined by redox titration. Although the structures of X_1 and X_2 are not known, it appears probable that they are heteropoly acids with a similar structure (if their solubility in water and the acidic nature of their solutions are considered).

P-III formed mainly $(VO)_2P_2O_7$ by calcination in air; vanadium (IV) was only partially oxidized to vanadium (V) in contrast to P-I. As described below, due to a similarity in structure, P-III is easily transformed to $(VO)_2P_2O_7$. This easy transformation may be the reason why the oxidation of vanadium(IV) took place to a much smaller extent than P-I. By calcination at high temperatures, oxidation proceeded progressively to form β-$VOPO_4$ or X_1. Therefore, it is necessary for a preparation of pure $(VO)_2P_2O_7$ to calcine P-III in the absence of O_2.

2.2 Calcination in the N_2 Flow: The average oxidation states of vanadium in the amorphous phases which were obtained by calcination in N_2 of P-I and P-III were less than four, presumably due to the reduction of catalyst by the NH_3 present in the precursors. Bordes and Courtine[15] reported the formation of $(VO)_2P_2O_7$ from P-I. As described above, the phase formed by the calcination of P-I sensitively varies depending on the calcination conditions.

P-III was transformed into $(VO)_2P_2O_7$ while keeping the valence of vanadium. This is because there was neither a reducing reagent like NH_3 nor an oxidizing reagent. As far as XRD is concerned, $(VO)_2P_2O_7$, thus formed, was pure. According to the structure of P-III determined recently by Torardi and Cababrese,[20] P-III ($(VO)_2H_4P_2O_9$) and $(VO)_2P_2O_7$ have a very similar structure (Fig. 10). This may be the reason why apparently pure $(VO)_2P_2O_7$ was rather easily obtained from P-III.

It was claimed in a patent[13] that a higher yield of MA was obtained by the recalcination of the catalyst

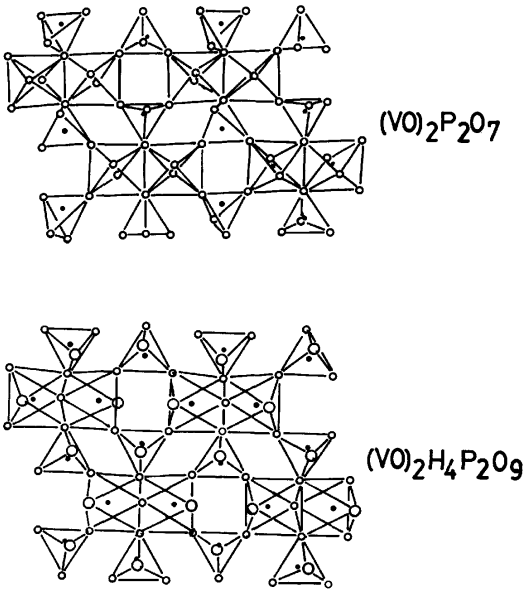

Fig. 10. Structure of $(VO)_2P_2O_7$ and $(VO)_2H_4P_2O_9$.[20]

(probably $(VO)_2P_2O_7$) in air at a high temperature followed by washing with water and calcination at a lower temperature. The present study (Fig. 1) indicates that amorphous or a less-crystalline phase, contained as an impurity, turned to the X_1 phase by calcination in O_2 and that the X_1 phase, thus formed, was washed out, resulting in a highly crystalline and pure $(VO)_2P_2O_7$.

2.3 Purity and Crystallinity: Each α- and β-$VOPO_4$, as well as $(VO)_2P_2O_7$, prepared in this work by carefully controlling the preparation conditions showed sharp XRD peaks of their corresponding structures. IR spectra also agreed with those reported in the literature. Therefore, the purity and crystallinity of all of these catalysts are considered to be of the highest level among the catalysts used in the preceding studies.

The fact that the oxidation states of vanadium were close to four for $(VO)_2P_2O_7$ and five for α- and β-$VOPO_4$ supports this consideration. X_1 and X_2 are likely to have a similar level of purity, as revealed by XRD patterns and IR spectra together with the oxidation state. Furthermore, an XPS analysis showed that the oxidation state of vanadium on the surface was not different from that in the bulk in the cases of β-$VOPO_4$ and $(VO)_2P_2O_7$.

3. Efficient Phase for Catalytic Oxidation of Butane to Maleic Anhydride (MA). The catalytic activity and selectivity to MA of each single phase will be phenomenogically discussed. Chevron found a fair correlation between the MA yield and the content of the B phase ($=(VO)_2P_2O_7$).[11] It was claimed that this phase was the efficient phase, although the highest content of the B phase was obtained at $P/V=1.2$ and the average valence of vanadium was 4.1—4.5.

Later, ICI indicated that phase X ($\fallingdotseq \alpha$-$VOPO_4$) was effective[12] and Delmon's group suggested that the β^* phase was also effective,[8] while their catalysts were

mixtures. Matsuura suggested that both α-$VOPO_4$ and $(VO)_2P_2O_7$ were good catalysts, since the reaction proceeded by the redox cycle between these two phases.[6] Recently, a patent from Mitsubishi Chemical Industry indicated that their catalysts with P/V=1 exhibited a high MA yield and had a $(VO)_2P_2O_7$ structure.[14c]

In our present study, as discussed above, catalysts contained single crystalline phases. The P/V ratios were all unity and the vanadium valences were close to four or five. Moreover, $(VO)_2P_2O_7$ was stable and changed little under the reaction conditions. Structural changes of α- and β-$VOPO_4$ were also negligible. Therefore, it is meaningful to compare the catalytic activity and selectivity of the catalysts as given in Table 5. Table 5 shows that the performance as a catalyst was in the order of $(VO)_2P_2O_7 > X_2$, $X_1 > \alpha$-, β-$VOPO_4$; the selectivity to MA was much better for $(VO)_2P_2O_7$ (catalysts 9 and 10), while the rate normalized to the surface area was more or less similar. The positions of X_1 and X_2 are not certain, since no single phase of X_1 or X_2 was observed after use for a reaction.

A possible reason for the different performances between $(VO)_2P_2O_7$ and α-, β-$VOPO_4$ is the oxidation state of vanadium. However, the prereduced catalysts showed only low selectivities (Fig. 8). Also, the selectivity increased with the reaction time when $(VO)_2P_2O_7$ was formed after reaction and it maintained a low level when β-$VOPO_4$ was formed (Fig. 8). Furthermore, amorphous catalysts having low oxidation states of vanadium also showed low selectivities (Table 5). Thus, catalysts containing vanadium(IV) are not always good catalysts. A certain well-defined structure which is stable under the reaction conditions appears to be necessary. Probably, the $(VO)_2P_2O_7$ catalyst was an efficient catalyst since it consisted of a single crystalline phase in which vanadium(IV) was stable under the reaction conditions. The very high selectivity obtained for $(VO)_2P_2O_7$ at a low temperature (Fig. 7) may be meaningful since the secondary reactions of MA are not significant in this reaction.

Matsuura suggested that the reaction proceeded by a redox cycle between $(VO)_2P_2O_7$ and α-$VOPO_4$.[6] In the present work for purified $(VO)_2P_2O_7$, such a redox cycle was not indicated. Nevertheless, the superiority of $(VO)_2P_2O_7$ is common in the two studies. While Trifiro *et al.*[9,10] also reported that the B-phase ($\fallingdotseq(VO)_2P_2O_7$) showed a good performance, our results were considerably better at high conversion levels. The purity of $(VO)_2P_2O_7$ is a possible reason of this difference. Delmon and Hodnett[8] recently indicated that the β^* phase ($=X_1$) was the efficient phase. The data obtained for the β^* phase were comparable with the X_1 phase in the present study. The X_1 phase was transformed to X_2 and α-$VOPO_4$ during the reaction (Table 5). If one considers the low selectivity of the α-phase, the pure X_2 phase itself could be a fairly good catalyst.

The variations of activity and selectivity of amorphous catalysts 7 and 8 with reaction time are consistent with the concurrent structural changes. When the amorphous catalyst 7 was used as a catalyst, the conversion increased from about 20% (at 3 h) to 60% (after 12 h), and the selectivity to MA decreased from about 30 to about 20%. The steady activity and selectivity were close to those of α-$VOPO_4$. While the conversion was less than 20% (during 15 h) over the catalyst 8, the selectivity to MA gradually increased with time from 25 to 40% (15 h). This is consistent with the result for X_2.

The authors would like to thank Prof. S. Naito and Dr. C. Egawa (The University of Tokyo) regarding the XPS measurement and Mr. M. Kojima, Mr. T. Kurokawa, and Mr. K. Shibata for experimental work at the preliminary stage of this work. A helpful discussion at this stage with Prof. I. Matsuura (presently Toyama University) is also gratefully acknowledged.

References

1) R. L. Varma and D. N. Saraf, *Ind. Eng. Chem., Prod. Res. Dev.*, **18**, 7 (1979).
2) M. Nakamura, K. Kawai, and Y. Fujiwara, *J. Catal.*, **34**, 345 (1974).
3) M. Ai, T. Niikuni, and S. Suzuki, *Kogyo Kagaku Zasshi*, **73**, 165 (1970).
4) L. Morselli, A. Riva, F. Trifiro, M. Zucchi, and G. Emig, *Chim. Ind.*, **60**, 791 (1978).
5) I. Matsuura, *Hyomen*, **20**, 605 (1982).
6) I. Matsuura, Preprints of the 6th Japan-Soviet Catalysis Seminar, 1981 p. 149.
7) I. Matsuura, *Proc. 8th Intern. Congr. Catal. (Berlin)*, **4**, 473 (1984).
8) B. K. Hodnett, P. Permanne, and B. Delmon, *Appl. Catal.*, **6**, 231 (1983).
9) F. Cavani, G. Centi, and F. Trifiro, *Appl. Catal.*, **9**, 191 (1984).
10) F. Cavani, G. Centi, I. Manenti, A. Riva, and F. Trifiro, *Proc. 9th Iberoamerican Symp. Catal., Lisbon*, **1984**, 973.
11) R. A. Schneider (to Chevron Research Co.), U. S. Patent 3864280 (1975).
12) ICI, *Belg.*, **1978**, 867189.
13) S. Kamimura and M. Murayama (to Mitsubishi Chemical Industries Co., Ltd.), *Jpn. Kokai*, **1979**, 161594.
14) a) M. Otake (to Mitsubishi Chemical Industries Co., Ltd.), *Jpn. Kokai*, **1981**, 45815; b) M. Otake (to Mitsubishi Chemical Industries Co., Ltd.), *Jpn. Kokai*, **1981**, 54215; c) M. Otake (to Mitsubishi Chemical Industries Co., Ltd.), *Jpn. Kokai*, **1982**, 111218.
15) E. Bordes and P. Courtine, *J. Catal.*, **57**, 236 (1979).
16) B. Jordan and C. Calvo, *Can. J. Chem.*, **51**, 2671 (1973).
17) R. Gopal and C. Calvo, *J. Solid State Chem.*, **5**, 432 (1972).
18) J. E. Ropbyhoba and C. A. Lnhge, *Izv. Akad. Nauk SSSR*, **23**, 584 (1978).
19) S. Pulvin, M. Ronis and P. Courtine, *C. R. Acad. Sci. Paris, Ser. C.*, **293**, 585 (1976).
20) C. C. Torardi and J. C. Calabrese, *Inorg. Chem.*, **23**, 1308 (1984).

21) G. Centi, I. Manenti, A. Riva, and F. Trifiro, *Appl. Catal.*, **9**, 177 (1984).
22) C. Blaauw, F. Leenhouts, F. Van der Woude, and G. A. Sawatzky, *J. Phys. C*, **8**, 459 (1975).
23) G. Ertl and K. Wandelt, *Surf. Sci.*, **50**, 479 (1975).
24) B. K. Hodnett and B. Delmon, *Appl. Catal.*, **9**, 203 (1984).
25) B. K. Hodnett and B. Delmon, *J. Catal.*, **88**, 43 (1984).
26) G. J. Hutchings and R. Higgins, *U. S. Patent* 4209423 (1980).

Kinetic Studies on the Oxidation of Electrogenerated Mo(V) and Stable Monomeric Mo(V) in Sulfuric Acid Solutions

Kunihiko YOKOI,* Iwao WATANABE,† and Shigero IKEDA†
Department of Chemistry, Osaka Kyoiku University, 3-1-1, Jonan, Ikeda, Osaka 563
†*Department of Chemistry, Faculty of Science, Osaka University, Toyonaka, Osaka 560*
(Received September 21, 1984)

The kinetics of polarographic catalytic reduction of nitrate and perchlorate by electrogenerated transient species of Mo(V) are investigated in 0.1M† sulfuric acid solution. Second-order rate constants for the catalytic reaction with nitrate and perchlorate obtained after Koutecky's treatment are $(2.1\pm0.4)\times10^3$ and $(1.9\pm0.1)\times10^2 M^{-1} s^{-1}$, respectively. Stable Mo(V) species in sulfuric acid solution is studied by spectrophotometry. It is concluded that there exists dimer-dimer-monomer equilibria. The oxidation of the monomer with perchlorate in 14M H_2SO_4 obeys the second-order rate law $-d[monomer]/dt=k[monomer][ClO_4^-]$, where $k=(1.59\pm0.13)\times10^{-1} M^{-1} s^{-1}$. The results indicate that electrogenerated Mo(V) in 0.1M H_2SO_4 is not the same species as the stable monomeric Mo(V) in 14M H_2SO_4.

The electrochemistry of sexivalent molybdenum ions in aqueous acidic solution has been widely investigated.[1-5] It is well known that the polarography of Mo(VI) gives catalytic waves in the presence of nitrate or perchlorate ions, and this phenomenon has been used for the quantitative analysis for Mo(VI).[3,6,7] Some conflict exists concerning the reduction mechanism of Mo(VI) and whether the catalytically active species is Mo(III) or Mo(IV).[2-5] However, recent investigations with coulometry have indicated that the catalytically active species is Mo(V).[1,8,9]

Our polarographic investigations were carried out in sulfuric acid solutions to study oxomolybdenum species. However, no quantitative investigation on the chemical equilibrium and the characteristics of Mo(V) has been reported in sulfuric acid solutions. It is not known whether the catalytically active Mo(V) species can be present as the stable species in bulk solution. The present work was carried out, (1) to obtain the rate constant for the oxidation of electrogenerated Mo(V) with nitrate or perchlorate, (2) to obtain the rate constant for the reaction of Mo(V) in bulk solution with perchlorate for comparison, and (3) to establish the equilibrium of Mo(V) in sulfuric acid solutions.

Experimental

Reagents and Apparatus. All chemicals were of reagent grade and were used without further purification. Polarographic and coulometric instruments employed in this study were the same as reported elsewhere.[10] A Hitachi 124 spectrophotometer was used for absorption measurements.

Procedure. The polarographic current values in this report were measured with RC damping, *i.e.* the average current during the drop life was measured unless otherwise noted. The catalytic current i_c was taken from the difference between the currents measured in the presence and the absence of nitrate or perchlorate at −0.36 V *vs.* SCE. The potential is 95 mV less positive than the half-wave potential of the third wave for Mo(VI) solutions without nitrate or perchlorate.[9]

The Mo(V) solutions were prepared by electrolytic reduction of $2.5-5\times10^{-3}$ M Mo(VI) in 0.1 M H_2SO_4 using a Hg-pool electrode. Oxidation of Mo(V) was initiated by mixing the Mo(V) and perchlorate solutions. Polarographic and spectrophotometric measurements were carried out at (25 ± 0.2)°C.

Results

Polarographic Catalytic Current. Polarograms and reduction mechanisms for Mo(VI) in sulfuric acid solutions were discussed earlier.[9] There are three waves corresponding to the reduction of Mo(VI) to Mo(V) in the polarogram of 0.5 mM Mo(VI) in 0.1 M H_2SO_4. The presence of nitrate or perchlorate enhances the height of the third wave only. Figure 1 shows the relationship between the height of the third wave i_3, which should be proportional to the concentration of the species giving the third wave, and the catalytic current i_c $(=i-i_3)$. When the concentration of Mo(VI) is lower than 0.5 mM, the plot is linear. At higher concentrations, it deviates from the straight line because of the adsorptive behavior of Mo(VI) or Mo(V) at higher concentration. The current amplification by catalytic reaction depends on the concentration of the oxidant as shown in Fig. 2. The ratio of i/i_3 taken at lower concentration of Mo(VI) (5×10^{-5} M) is proportional to the square root of the concentration of nitrate or perchlorate; the second-

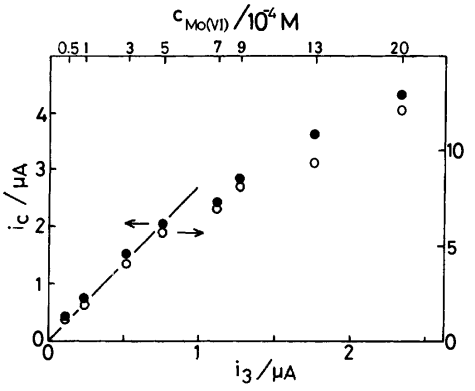

Fig. 1. Dependence of the catalytic current i_c on the height of the third wave i_3 in 0.1 M H_2SO_4: (○) with 20 mM $NaNO_3$; (●) with 50 mM $NaClO_4$.

†1M=1 mol dm^{-3}.

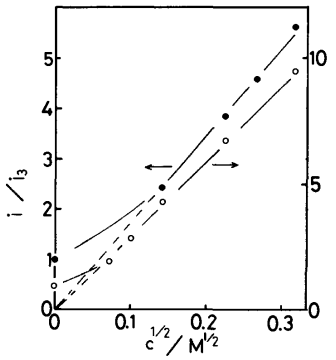

Fig. 2. Dependence of i/i_3 on the square root of the concentration of nitrate (○) and perchlorate (●). $c_{Mo(VI)}=5\times10^{-5}$M.

TABLE 1. SECOND-ORDER RATE CONSTANTS FOR THE POLAROGRAPHIC CATALYTIC REACTION IN 0.1 M H_2SO_4 $c_{Mo(VI)}=5\times10^{-5}$M

	k_c/$M^{-1}s^{-1}$
c_{NaNO_3} 5×10^{-3}—1×10^{-1}M	$(2.1\pm0.4)\times10^3$
$c_{Na_2CrO_4}$ 2×10^{-2}—1×10^{-1}M	$(1.9\pm0.1)\times10^2$

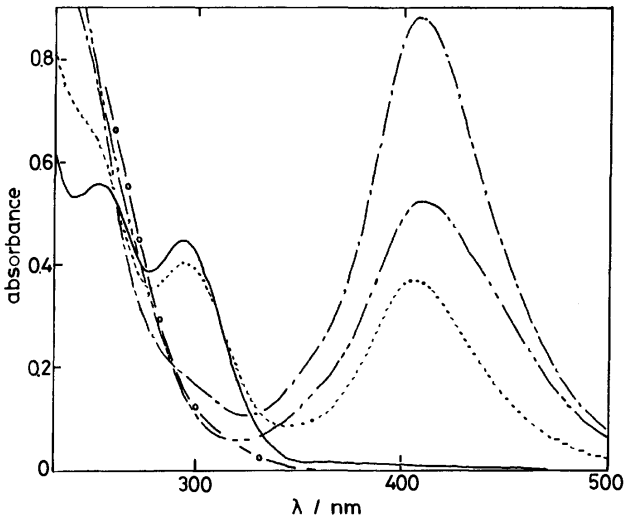

Fig. 3. Absorption spectra of 2.5×10^{-4}M Mo(V) in various concentrations of H_2SO_4: (——) 0.1 M; (------); 7 M; (— — —) 9 M; (— — —) 11 M; (— · —) 15 M. l=1 cm.

order rate constants k_c for the catalytic reduction of nitrate and perchlorate by Mo(V) are obtained by using Koutecky's treatment.[11] Results are listed in Table 1.

Absorption Spectra. Absorption spectra of 2.5×10^{-4}M Mo(V) in various concentration of sulfuric acid solution are shown in Fig. 3. In 0.1 M H_2SO_4, absorption maxima are observed at 254 nm and 293 nm. The spectrum has already been assigned to dimeric Mo(V), $Mo_2O_4^{2+}$.[12,13] When the concentration of sulfuric acid is higher than 3 M, a peak appears at 405 nm. When $c_{H_2SO_4}$ is increased to 9 M, the absorption maxima at 254 nm and 293 nm disappear, and the absorbance of the peak (407 nm) reaches its maximum

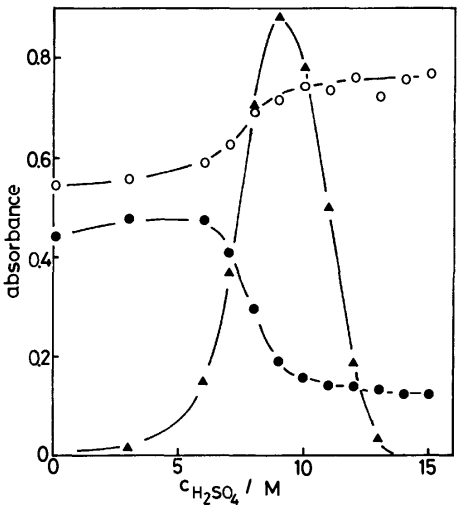

Fig. 4. Effect of the concentration of H_2SO_4 on absorbances of 2.5×10^{-4} M Mo(V) solution at 254nm (○), 293nm (●) and 407nm (▲). l=1 cm.

and the solution looks green-yellow. In 15 M H_2SO_4, there is no absorption in the visible region. The absorbances at 254 nm, 293 nm, and 407 nm vary with $c_{H_2SO_4}$ as shown in Fig. 4. The change of absorbance at 407 nm suggests that three different species of Mo(V) are present in 0.1—15 M H_2SO_4.

Dimer-dimer-monomer Equilibria of Mo(V). In hydrochloric acid solution, dimer-dimer-monomer equilibria of chloro complexes of Mo(V) have been reported.[14,15] However, few study of such equilibria in sulfuric acid solution has been known. Marov *el al.* reported ESR investigations of Mo(V) in sulfuric acid solutions but the precise equilibrium constant could not be obtained[16,17] and no spectrophotometrical investigation of such equilibria has been known. It is well known that the predominant apecies of Mo(V) in 0.1 M H_2SO_4 is dimeric, $Mo_2O_4^{2+}$.[12,13] From the analogy of the equilibria of Mo(V) in hydrochloric acid solution, we expect that the dimer($Mo_2O_4^{2+}$)-dimer-monomer equilibria of Mo(V) in sulfuric acid solution are as follows:

$$D_1 \overset{a}{\rightleftharpoons} D_2 \overset{b}{\rightleftharpoons} 2M \quad (1)$$

$$K_1 = [D_2]/[D_1] \quad (2)$$

$$K_2 = [M]^2/[D_2] \quad (3)$$

$$c_t = 2[D_1] + 2[D_2] + [M] \quad (4)$$

where D_1 means the dimer, $Mo_2O_4^{2+}$, D_2 the other dimer and M is a monomer; K_1 and K_2 are the equilibrium constants and c_t is the total concentration of Mo(V). Spectrophotometric data were treated with Haight's procedure.[14] When $c_{H_2SO_4}$ is lower than 9M, equilibrium a in Eq. 1 should predominate. From the result of Fig. 3 we conclude that only the species of D_2 absorbs at 407 nm; therefore the absorption at 407 nm is,

$$A_{407} = \varepsilon_2[D_2] \quad (5)$$

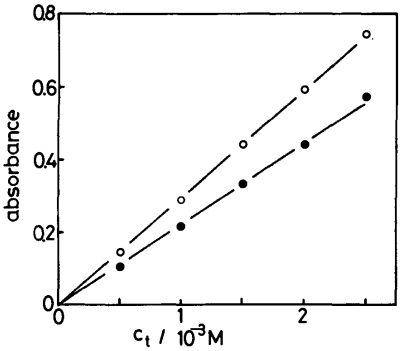

Fig. 5. Dependence of A_{407} on c_t in 7.5 M (●) and 8 M (○) H_2SO_4.

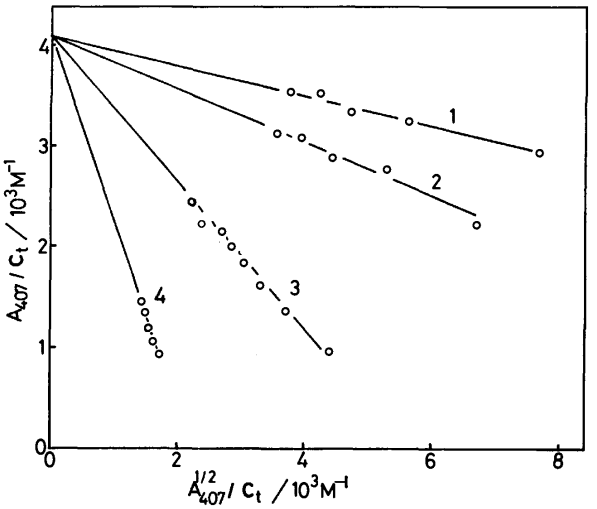

Fig. 6. Dependence of A_{407}/c_t on $A_{407}^{1/2}/c_t$ in H_2SO_4. $c_{H_2SO_4}$: (1) 9 M; (2) 10 M; (3) 11 M; (4) 12 M.

where ε_2 is the molar absorptivity of D_2. Equation 6 follows from Eqs. 2, 4 ([M]=0) and 5.

$$A_{407} = \varepsilon_2 K_1 c_t/2(1+K_1) \quad (6)$$

Therefore, if K_1 is a constant which is independent of c_t, A_{407} should be proportional to c_t when $c_{H_2SO_4}$ is lower than 9 M. The dependence of A_{407} on c_t in 7.5 M and 8 M H_2SO_4 shown in Fig. 5 indicates that D_2 is dimeric.

When $c_{H_2SO_4}$ is higher than 9 M, equilibrium b in Eq. 1 should predominate. In this case,

$$c_t = 2[D_2] + [M] \quad (7)$$

and from Eqs. 3, 5, and 7, we obtain

$$A_{407}/c_t = \varepsilon_2/2 - (\varepsilon_2 K_2/4)^{1/2} A_{407}^{1/2}/c_t. \quad (8)$$

A plot of A_{407}/c_t *vs.* $A_{407}^{1/2}/c_t$ (Fig. 6) gives a straight line with slope $-(\varepsilon_2 K_2/4)^{1/2}$ and intercept of $\varepsilon_2/2$. From the average value of ε_2 (8.17×10^3 $M^{-1}cm^{-1}$) obtained, K_1 and K_2 were calculated for various $c_{H_2SO_4}$ and are listed in Table 2. When $c_{H_2SO_4}$ is higher than 13 M, monomeric Mo(V) is a predominant species.

Oxidation of Monomeric Mo(V) by Perchlorate.

Table 2. Equilibrium constants for dimer(D_1)-dimer(D_2)(K_1) and dimer(D_2)-monomer (M)(K_2) in various concentration of H_2SO_4

$c_{H_2SO_4}$/M	K_1	$c_{H_2SO_4}$/M	K_2/M
3	1.80×10^{-2}	9	1.17×10^{-5}
6	1.71×10^{-1}	10	3.97×10^{-5}
7	5.71×10^{-1}	11	2.28×10^{-4}
7.5	1.28	12	1.71×10^{-3}
8	2.24		

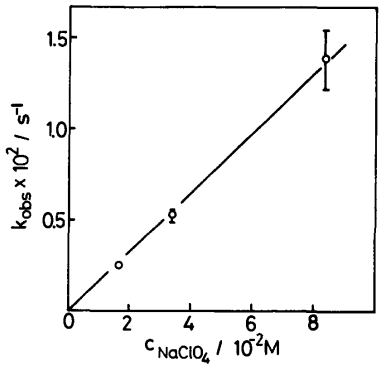

Fig. 7. Dependence of k_{obsd} on the concentration of perchlorate.

The oxidation rate of monomeric Mo(V) by perchlorate was studied by conventional spectrophotometry in the presence of excess perchlorate in 14 M H_2SO_4. The decrease in absorption at 260 nm was used to monitor the reaction. Absorbance at 260nm, A_{260}, is given by

$$A_{260} = \varepsilon_M[M] + \varepsilon_{VI}[Mo(VI)], \quad (9)$$

where ε_M and ε_{VI} are the molar absorptivities of M and Mo(VI), respectively. [M] is given by

$$[M] = (A_{260} - \varepsilon_{VI}c)/(\varepsilon_M - \varepsilon_{VI}), \quad (10)$$

where c=[M]+[Mo(VI)]. A plot of ln[M] *vs.* time was linear to >90% completion. The pseudo-first-order rate constant determined from the plot was linearly dependent on the concentration of perchlorate as shown in Fig. 7. Therefore, the rate law is expressed as

$$-d[M]/dt = k_{obsd}[M] = k[M][ClO_4^-], \quad (11)$$

where k is the second-order rate constant for oxidation of monomeric Mo(V) by perchlorate. The value for k (1.67×10^{-2}—8.33×10^{-2} M perchlorate) was $(1.59\pm0.13)\times10^{-1}M^{-1}s^{-1}$ in 14 M H_2SO_4. The corresponding oxidation by nitrate could not be studied because of the large absorbance of nitrate in the UV region. Oxidation of $Mo_2O_4^{2+}$ by perchlorate is extremely slow[18] and that of the dimer in 9 M H_2SO_4 can not be monitored precisely because the monomer is involved simultaneously. The approximate rate constant obtained is about 1000 times smaller in 9 M H_2SO_4 than in 14 M H_2SO_4.

Discussion

Recent coulometric investigations in the presence

of nitrate and perchlorate have indicated that the catalytically active species is Mo(V).[1,8,9] Paffett and Anson suggested that monomeric Mo(V), $[MoO(OH)(H_2O)_4]^{2+}$, is the catalytically active species,[1] but they did not study the kinetics of the catalytic reaction. Our data on kinetics for the catalytic reaction based on Koutecky's procedure (Table 1) might be compared with data for oxidation of monomeric Mo(V) in bulk solution. However, since such experiments have involved the presence of added ligands which form complexes with Mo(V)[17] or referred to dimeric Mo(V),[18] the direct comparison is not straightforward.

A chloromolybdenum(V) complex in hydrochloric acid solution is involved in dimer-dimer-monomer equilibria.[14,15] In the absence of other complexing ligands, the following equilibria have been considered.

$$2MoO^{3+} \overset{H_2O}{\rightleftharpoons} Mo_2O_3^{4+} + 2H^+ \overset{H_2O}{\rightleftharpoons} Mo_2O_4^{2+} + 2H^+$$

However, no quantitative experiment has been performed.[20] The existence of dimer-dimer-monomer equilibria of Mo(V) is indicated in the present work for sulfuric acid solution. It is not known whether monomeric Mo(V) in 14 M H_2SO_4 is MoO^{3+}. The existence of sulfato complex of monomeric Mo(V), $MoO(HSO_4)_5^{2-}$, has been considered,[16,17] but, detailed structural information can not be obtained at the present stage.

The rate of the reaction involving perchlorate should increase with the activity of hydrogen ion, though the second-order rate constant for oxidation of monomeric Mo(V) with perchlorate in 14 M H_2SO_4 is found to be about 1000 times smaller than that for the reaction of electrogenerated Mo(V) with perchlorate in 0.1 M H_2SO_4 (5×10^{-5}—5×10^{-4} M Mo(VI)). Therefore, monomeric Mo(V) in 14 M H_2SO_4 is not the same species as electrogenerated Mo(V) in 0.1 M H_2SO_4. It has been proposed that a monomeric cation of Mo(V), $[MoO(OH)(H_2O)_4]^{2+}$, is the catalytically active species,[1,10] and this electrogenerated monomer is more reactive than the monomer in bulk solution.

Lahr *et al.* suggested that participation of the MoO^{3+} center might be widespread in catalytic reactions of Mo(V) in aqueous media.[21] In sulfuric acid solutions, both electrogenerated Mo(V) in 0.1 M H_2SO_4 and monomeric Mo(V) in 14 M H_2SO_4 seem to have the MoO^{3+} center, and their oxidation rates with perchlorate are quite different. Thus, other structural characteristic of the catalytically active species of molybdenum having the MoO^{3+} center remains to be established.

References

1) M. T. Paffett and F. C. Anson, *Inorg. Chem.*, **20**, 3967 (1981).
2) I. M. Kolthoff and I. Hodara, *J. Electroanal. Chem.*, **4**, 369 (1962).
3) T. E. Edmonds, *Anal. Chim. Acta*, **116**, 323 (1980).
4) M. G. Johnson and R. J. Robinson, *Anal. Chem.*, **24**, 366 (1952).
5) G. P. Haight, Jr., *Anal. Chem.*, **23**, 1505 (1951).
6) P. Lanza and D. Ferri, *Analyst*, **105**, 379 (1980).
7) G. D. Christian, J. L. Vandenbalck, and G. J. Patriorche, *Anal. Chim. Acta*, **108**, 149 (1979).
8) P. Chalilpoyil and F. C. Anson, *Inorg. Chem.*, **17**, 2418 (1978).
9) K. Yokoi, T. Ozeki, I. Watanabe, and S. Ikeda, *J. Electroanal. Chem.*, **132**, 191 (1982); *ibid.*, **133**, 73 (1982).
10) K. Yokoi, N. Ogawa, I. Watanabe, and S. Ikeda, *J. Electroanal. Chem.*, **153**, 255 (1983).
11) P. Delahay, "New Instrumental Methods in Electrochemistry," Interscience, New York, (1954), p. 100.
12) M. Ardon and A. Pernick, *Inorg. Chem.*, **12**, 2484 (1973).
13) Y. Sasaki and A. G. Sykes, *J. Chem. Soc., Dalton Trans.*, **1974**, 1468.
14) G. P. Haight, Jr., *J. Inorg. Nucl. Chem.*, **24**, 663 (1962).
15) E. I. Stiefel, "Progress in Inorganic Chemistry," ed by S. J. Lippard, John Wiley and Sons, Inc. (1977), Vol. 22, p. 45.
16) I. N. Marov, Yu. N. Dubrov, V. K. Belyaeva, and A. N. Ermakov, *Russ. J. Inorg. Chem.*, **13**, 1262 (1968).
17) I. N. Marov, Yu. N. Dubrov, A. N. Ermakov, and G. N. Martynova, *Russ. J. Inorg. Chem.*, **15**, 1387 (1970).
18) G. R. Cayley, R. S. Taylor, R. K. Wharton, and A. G. Sykes, *Inorg. Chem.*, **16**, 1377 (1977).
19) E.P. Guymon and J. T. Spence, *J. Phys. Chem.*, **70**, 1964 (1966).
20) G. P. Haight and D. R. Boston, *J. Less-Common Met.*, **36**, 95 (1974).
21) S. K. Lahr, H. O. Finklea, and F. A. Schultz, *J. Electroanal. Chem.*, **163**, 237 (1984).

Rate of Complex Formation of Iron(III) with Several β-Diketones in Aqueous Perchlorate Solutions Determined by Solvent Extraction Method

Kazuho INABA,† Nobuyuki ITOH, Yumi MATSUNO, and Tatsuya SEKINE*
Department of Chemistry, Science University of Tokyo, Kagurazaka, Shinjuku-ku, Tokyo 162
(Received February 25, 1985)

The rate of formation of iron(III) complexes with several β-diketones (HA) in aqueous sodium perchlorate solutions has been determined by a solvent-extraction method. The rate was found to be first order with respect to the reagent, and zero to an inverse second order with respect to the hydrogen-ion. From the results, the controlling step has been determined to be the formation of the first complex in aqueous solutions. Three types of unit reactions are suggested for this; (i) $Fe^{3+}+HA_{enol}$, which has an associative character; (ii) $Fe(OH)^{2+}+HA_{enol}$ and; (iii) $Fe(OH)^{2+}+A^-$, both of which has a dissociative character.

In previous studies,[1,2] the rate of complex formation of iron(III) with trifluoroacetylacetone (1,1,1-trifluoro-2,4-pentanedione, Htfa) in aqueous solutions was determined from kinetic data regarding solvent extraction in conjunction with equilibrium data of the complexes in a liquid–liquid system. In the present study, the rate of solvent extraction of iron(III) in aqueous 4 mol dm^{-3} sodium perchlorate solutions with several β-diketones (HA) was measured and the rates of complex formations with the reagents were calculated. Then, the effect of a nucleophilic tendency of the β-diketones on the reaction mechanism was considered. The results are compared with those from previous studies with trifluoroacetylacetone and 2-thenoyltrifluoroacetone (1-(2-thienyl-)-4,4,4-trifluoro-1,3-butanedione, Htta)[1-4] and with other β-diketones.[5]

Experimental

All the experiments were carried out at 298 K in a manner similar to that described in previous papers.[1,2,4] The β-diketones used were: acetylacetone (2,4-pentanedione, Hacac), benzoylacetone (1-phenyl-1,3-butanedione, Hbza), dibenzoylmethane (1,3-diphenyl-1,3-propanedione, Hdbm), benzoyltrifluoroacetone (1-phenyl-4,4,4-trifluoro-1,3-butanedione, Hbfa), and hexafluoroacetylacetone (1,1,1,5,5,5-hexafluoro-2,4-pentanedione, Hhfa). They were obtained from Dojindo Co., Kumamoto, Japan (Hacac, Hbfa, and Hhfa), Tokyo Kasei Co., Tokyo, Japan (Hbza), and Nakarai Chemicals Co., Kyoto, Japan (Hdbm). A portion of an aqueous 4 mol dm^{-3} (H,Na)ClO_4 solution containing iron(III) and an equal volume of carbon tetrachloride containing 5×10^{-5} to 1×10^{-3} mol dm^{-3} of one of the β-diketones were placed in a stoppered glass tube and agitated vigorously for a specific time interval and centrifuged. In some experiments, the two phases were agitated until a distribution equilibrium was established. The organic phase was washed by 4 mol dm^{-3} hydrochloric acid and any iron(III), thus back-extracted, was measured using an atomic absorption method. Any metal in an aqueous phase was also measured in a similar way. The hydrogen-ion concentrations in aqueous solutions were measured using potentiometry and a calibration curve which was obtained by measuring a set of standard perchloric acid solutions of the same ionic medium. Thus results were given in stoichiometric units. Spectrophotometric measurements were also made with acetylacetone complexes in order to determine their stability constants. An acid aqueous iron(III) solution and an aqueous Hacac solution were mixed and left standing until a complex formation equilibrium was reached. Then, the optical absorbance was measured at 440 nm to the reagent blank. The hydrogen-ion concentration was measured in a similar way.

†Present address: National Institute for Environmental Studies, 16-2 Onogawa, Yatabe-machi, Tsukuba-gun, Ibaraki 305.

Statistical

In this paper, the subscript "org" denotes a chemical species in an organic solution; a lack of it denotes species in an aqueous solution. An initial concentration is denoted by the subscript "init".

The acid-dissociation and two-phase distribution constant of a β-diketone and the stability constant of the "n-th" complex are defined as;

$$K_a = [H^+][A^-][HA]^{-1}, \quad (1)$$

$$K_d = [HA]_{org}[HA]^{-1}, \quad (2)$$

$$\beta_n = [FeA_n^{3-n}][Fe^{3+}]^{-1}[A^-]^{-n}. \quad (3)$$

The distribution ratio of metal ions when an equilibrium is established can be written as:

$$\begin{aligned} D &= [Fe(III)]_{org}[Fe(III)]^{-1} \\ &= [FeA_3]_{org}([Fe^{3+}]+\sum[FeA_n^{3-n}])^{-1} \\ &= K_{dm}\beta_3[A^-]^3(1+\sum\beta_n[A^-]^n)^{-1} \\ &= K_{ex}K_d^3K_a^{-3}[A^-]^3(1+\sum\beta_n[A^-]^n)^{-1}, \end{aligned} \quad (4)$$

where K_{dm} is the distribution constant of the tris-complex;

$$K_{dm} = [FeA_3]_{org}[FeA_3]^{-1}, \quad (5)$$

K_{ex} is the extraction constant defined by;

$$K_{ex} = [FeA_3]_{org}[H^+]^3[Fe^{3+}]^{-1}[HA]_{org}^{-3}. \quad (6)$$

From the initial concentration of HA, the hydrogen-ion concentration, and D at equilibrium, the values of β_n, K_{dm}, and K_{ex} can be obtained on the basis of Eq. 4 by a least-squares calculation.

The spectrophotometric data of the aqueous solutions obtained by the equilibrium study were treat-

ed statistically as follows. Under the experimental conditions of the present work, the molar absorption coefficient of the hydrated Fe^{3+} species is negligible and, thus, the optical absorbance can be written as;

$$E = \sum\varepsilon_n[FeA_n^{3-n}] = [Fe^{3+}]_{init} \times \sum\varepsilon_n\beta_n[A^-]^n \times (1+\sum\beta_n[A^-]^n)^{-1}, \quad (7)$$

where ε_n is the molar absorption coefficient of the "n-th" complex. From the initial concentration of HA, the hydrogen-ion concentration and E at equilibrium, β_n and ε_n can be calculated on the basis of Eq. 7.

The constant regarding the hydrolysis of Fe^{3+}, K_h, and that for the keto-enol tautomerism of a β-diketone, K_e, which are used for an analysis of the kinetic data are defined as;

$$K_h = [Fe(OH)^{2+}][H^+][Fe^{3+}]^{-1}, \quad (8)$$

$$K_e = [HA]_{enol}[HA]_{keto}^{-1}. \quad (9)$$

When the rate of complex formation is first order with respect to Fe^{3+} and when the controlling step is the formation of the first complex, the rate can be written as;

$$V = -d[Fe^{3+}]/dt = k_{obsd}[Fe^{3+}]. \quad (10)$$

The concentration of the unreacted Fe^{3+} at a certain time after the start of two-phase agitation can be calculated from the initial concentration of Fe^{3+} and that of extracted species using the following equation;[2]

$$[Fe^{3+}] = [Fe^{3+}]_{Init} - ((\beta_1\beta_3^{-1}[A^-]^{-2}+\beta_2\beta_3^{-1}[A^-]^{-1}+1) \times K_{dm}^{-1}+1) \times [FeA_3]_{org}. \quad (11)$$

Results

Equilibrium Experiments. Since the solvent extraction of iron(III) with the β-diketones proceeded rather slowly, two-phase agitation was continued for 1 h (when Hacac or Hhfa was the extractant) or for 24 h (when Hbza, Hdbm, or Hbfa was the extractant) in order to establish equilibrium. Figure 1 shows a plot of log D *vs.* log $[A^-]$ at equilibrium. The equilibrium constants in Eqs. 3, 5, and 6 were calculated from these data on the basis of Eq. 4 using a least-squares program. The values of β_n and K_{dm}, thus obtained, were somewhat erroneous since the distribution ratio of iron(III) was too high under these conditions. The relative concentrations of the aqueous complexes were too high and the extractability of the tris(β-diketonato) complexes was also too high (K_{dm} was great) to allow an accurate determination of the equilibrium constants. On the other hand, the extraction constant, K_{ex}, could be determined much more accurately. The values of the obtained constants are listed in Table 1.

Figure 2 gives the absorbance of the solutions, normalized to an iron(III) concentration as a function of the ligand anion concentration. By analysing these data on the basis of Eq. 7, β_n and ε_n were obtained (Table 1).

Rate of Complex Formation in Aqueous Solutions. It was reported in a previous paper[9] that a transient maximum appeared in the extraction of copper(II) with several β-diketones. This was explained in terms of the rate of the ketonization of the enol form β-diketones in an aqueous phase being rather low. The same type of transient maximum for extraction was observed with Hhfa in the present study. For this reason, a carbon tetrachloride solution of Hhfa was agitated with an

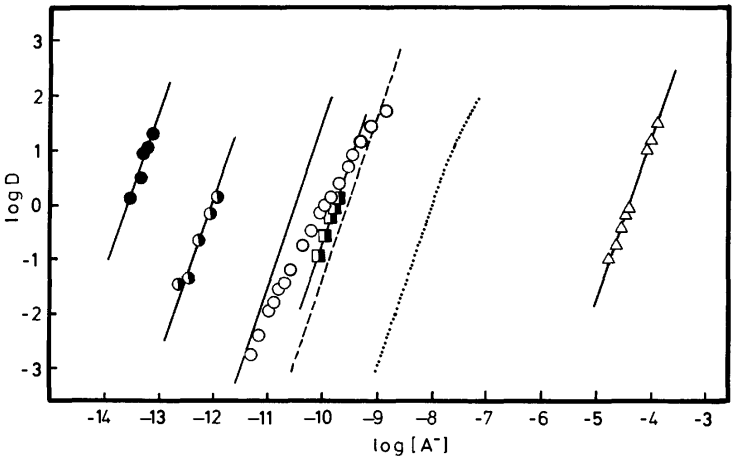

Fig. 1. Extraction curves of iron(III) with $acac^-$ (○), bza^- (◑), dbm^- (●), bfa^- (◨), and hfa^- (△) as a function of ligand concentration into carbon tetrachloride. The solid lines show the slope of +3 which are calculated by introducing the values of K_{ex} in Table 1 into Eq. 4. The dotted and broken lines give the extraction curves of tfa^- and tta^- complexes in Refs. 1 and 3.

Table 1. Equilibrium constants for seven β-diketones and their iron(III) complexes

(a) Equilibrium constants for reagents	Hacac	Hbza	Hdbm	Htfa	Hbfa	Htta	Hhfa
log K_a	−10.1[6]	−9.25[5]	−9.3	−6.61[1]	−6.25[5]	−6.65[5]	−4.5
log K_d	0.25[5]	2.75[5]	5.0	0.41[1]	2.85[5]	1.95[5]	−1.0
log K_e	−0.67[7]	−0.48[8]	(−0.4)*	−2.08[8]	−1.88[8]	−1.88[8]	−3.39[9]

(b) Equilibrium constants for iron(III) complexes	Hacac§	Hbza	Hdbm	Htfa[1]	Hbfa	Htta	Hhfa
log β_1	11.4 11.4†	(11.4)*	(11.4)*	6.7 7.7†	(7.7)*	(7.7)*	2.7
log β_2	20.7 20.8†	(20.8)*	(20.8)*	14.5 14.4†	(14.4)*	(14.4)*	6.8
log β_3	— 26.7†	(26.7)*	(26.7)*	20.3 19.8†	(19.8)*	(19.8)*	9.8
log K_{dm}	4.7	(9.3)**	(14.2)**	4.2	(9.5)**	(9.7)**	3.6
log K_{ex}	0.5	0.3	−2.1	3.1	2.3	4.0[3]	2.7

Hydrolysis constant of iron(III). log K_h=−3.1 (Ref. 10.) † Determined by spectrophotometric method. * Estimated values. ** Calculated from K_{ex}, β_3, K_a, and K_d. § The stability constants of acetylacetonato complexes agree with literature values (Refs. 11, 12.) The molar absorption coefficients of acetylacetonato complexes at 440 nm obtained are; ε_1=540, ε_2=1750, and ε_3=2880, respectively.

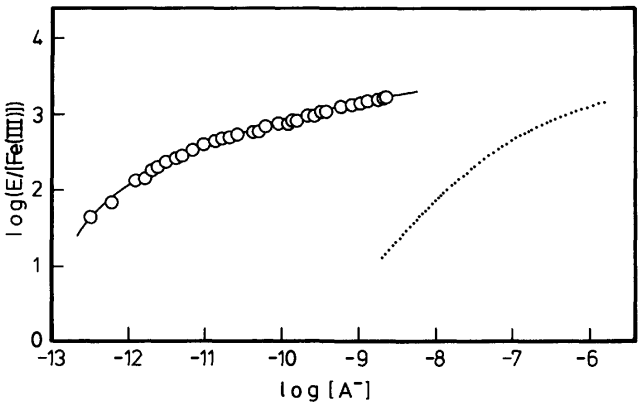

Fig. 2. Optical absorbance (normalized to the iron(III) concentration) of iron(III) complexes with acac⁻ (○) at 440 nm as a function of ligand concentration. The solid curve is calculated by introducing the constants in Table 1 into Eq. 7. The dotted line gives the results of tfa⁻ complexes at 450 nm in Ref. 1.

aqueous perchlorate solution containing no iron(III) for 10 min in order to establish the distribution and ketonization equilibria of the reagent. Then, iron(III) was added to the aqueous phase and kinetic measurements were initiated. The total amount of the iron(III) complexes formed was calculated from the amount of iron(III) extracted into an organic phase, by using Eq. 11. The rate of complex formation was found to be first order with respect to the reagent and zero to an inverse second order with respect to the hydrogen-ion. Figure 3 shows the dependence of the rate of complex formation to the β-diketone concentration; Fig. 4 gives the observed rate constants of the complex formation normalized to the β-diketone concentration in the aqueous phase as a function of the hydrogen-ion concentration. These results could be fitted to the following rate equation;

$$V = [Fe^{3+}][HA](k_A + k_B[H^+]^{-1} + k_C[H^+]^{-2}). \quad (12)$$

The values of the rate constants k_A, k_B, and k_C were obtained by introducing data into Eq. 12 (Table 2). The rate of complex formation with Hacac was too high to determine the rate constant. This is because the solubility of the ligand in an aqueous phase is high and/or the proportion of the enol from to the total amount of reagent in an aqueous phase is also high.

Discussion

In the present study, the ionic concentration in an

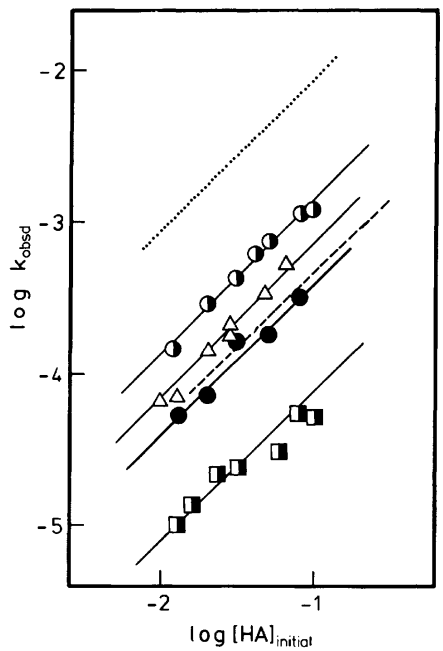

Fig. 3. Dependence of the rate of formation of iron(III) complexes with Hbza (◑), Hdbm (●), Hbfa (◨), and Hhfa (△) on the initial concentration of the reagents. The solid lines show the slope of +1. The dotted and broken lines give the results with Htfa and Htta in Refs. 2 and 4.

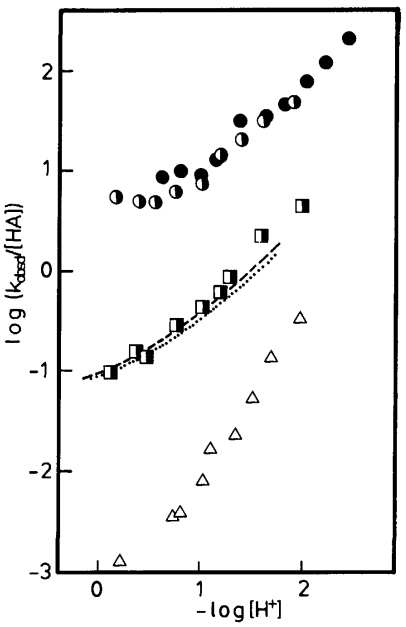

Fig. 4. Dependence of the rate of formation of iron(III) complexes (normalized to the β-diketone concentration in the aqueous phase) with Hbza (◑), Hdbm (●), Hbfa (◨), and Hhfa (△) on the hydrogen-ion concentration. The dotted and broken lines show the results with Htfa and Htta in Refs. 2 and 4.

aqueous phase was kept rather high in order to maintain the activity coefficient of the solutes constant even when for the great charge in the hydrogen-ion concentration was changed. However, the values of the stability constants for acetylacetonato complexes were not very much different from the literature at various ionic concentrations.[11,12]

The stability constants of the iron(III) complexes with bza^-, dbm^-, bfa^-, and tta^- could not be obtained for the reason already mentioned above. However, it can be reasonably assumed that the values of β_n for the bza^- and dbm^- complexes are similar to those of the $acac^-$ complexes, and those of the bfa^- and tta^- complexes to that of the tfa^- complex. In the present work, the estimated values of the stability constants of these four β-diketonato complexes on the basis of this assumption were used for an analysis of the kinetic data.

Since the data fit well with Eq. 12, it is assumed that the following reaction routes are possible.

k_A path:

$$Fe^{3+} + HA_{(enol)} \longrightarrow FeA^{2+} + H^+. \quad (13)$$

k_B path:

$$Fe^{3+} + A^- \longrightarrow FeA^{2+}, \quad (14)$$

and/or

$$[Fe(OH)]^{2+} + HA_{(enol)} \longrightarrow FeA^{2+} + H_2O. \quad (15)$$

k_C path:

$$[Fe(OH)]^{2+} + A^- \longrightarrow FeA^{2+} + OH^-, \quad (16)$$

and/or

$$[Fe(OH)_2]^+ + HA_{(enol)} \longrightarrow [FeA(OH)]^+ + H_2O. \quad (17)$$

Because of the proton ambiguity, two possible reactions are given for both of the k_B and k_C paths. However, from the magnitudes of the rate constants for complex formations, the hydrolysis constant of iron(III), the equilibrium constant for the keto–enol tautomerism, and the acid-dissociation constant of the β-diketone, it was concluded that the route in Eq. 15 was more reasonable except when the reagent was Hhfa. Since the value of K_e of Hhfa, $[Hhfa]_{enol}/[Hhfa]_{keto}$, is much smaller and the acid-dissociation constant is larger than for other β-diketones, the concentration of the ligand, $[A^-]$, in an aqueous phase with this reagent under experimental conditions should be much higher than for the other β-diketones and both the reactions in Eqs. 14 and 15 could be possible. For the k_C path, the reaction in Eq. 16 was determined to be more reasonable since the second hydrolysis constant of Fe^{3+} is very small and, thus, the amount of the $[Fe(OH)_2]^+$ species should be extremely small under the present experimental conditions.

By using K_h of iron(III), K_a and K_e of the β-diketone and k_A, k_B, and k_C in Eq. 12, the rate of each controlling reaction can be written as;

$$V_0 = k_0[Fe^{3+}][HA]_{enol} = k_A \times K_e^{-1} \times (1+K_e)[Fe^{3+}][HA], \quad (18)$$

$$V_1 = k_1[Fe(OH)^{2+}][HA]_{enol} = k_B \times K_h^{-1} \times (1+K_e) \times K_e^{-1}[Fe^{3+}][HA][H^+]^{-1}, \quad (19)$$

$$V_1' = k_1'[Fe^{3+}][A^-] = k_B \times K_a^{-1}[Fe^{3+}][HA][H^+]^{-1}, \quad (20)$$

$$V_2 = k_2[Fe(OH)^{2+}][A^-] = k_C \times K_h^{-1} \times K_a^{-1}[Fe^{3+}][HA][H^+]^{-2}. \quad (21)$$

k_0, k_1, k_1', and k_2 were calculated using the above constants (Tables 1 and 2) using Eqs. 18 to 21. They are listed in Table 3.

Table 2. Summary of rate constants obtained

	Hacac†	Hbza	Hdbm	Htfa[2]	Hbfa	Htta[4]	Hhfa
log (k_A/mol^{-1}dm^{3}s^{-1})	—	0.5	0.5	−1.2	−1.4	−1.2	−3.1
log (k_B/s^{-1})	—	−0.2	−0.2	−1.6	−1.4	−1.5	−3.3
log (k_C/mol dm^{-3}s^{-1})	—	—	—	—	—	—	−4.4

† Too fast to determine.

TABLE 3. RATE CONSTANTS FOR COMPLEX FORMATION OF IRON(III) IN AQUEOUS PERCHLORATE SOLUTIONS AT 298 K

	Hacac†	Hbza	Hdbm	Htfa[2]	Hbfa	Htta[4]	Hhfa*
log (k_0/mol^{-1}dm^{3}s^{-1})	—	1.0	1.0	0.8	0.4	0.6	0.2
log (k_1/mol^{-1}dm^{3}s^{-1})	—	3.4	3.4	3.5	3.5	3.4	3.1
log (k_2/mol^{-1}dm^{3}s^{-1})	—	—	—	—	—	—	3.2

* The rate constant k_1' for the reaction in Eq. 20 is; log (k_1'/mol^{-1}dm^{3}s^{-1})=1.2. † Too fast to determine.

Ishihara, Funahashi, and Tanaka reported that the rate constant and the activation volume for the formation of iron(III) complexes in aqueous solutions with 4-isopropyltropolone, thiocyanate ion, and acetohydroxamic acid.[13,14] They concluded that a reaction of hydrated Fe^{3+} proceeded in all cases by an associative interchange mechanism. That of $[Fe(OH)]^{2+}$ proceeded by a dissociative interchange mechanism. In the present study, the values of k_1 and k_2 (Eqs. 19 and 21) for the reaction of $[Fe(OH)]^{2+}$ are about $10^{3.4}$ with all the β-diketones. These agree well with the above reported values. For this reason, it was concluded that the k_B path could be more reasonably represented by Eq. 15 and the k_C path by Eq. 16. Moreover, the values of k_1 and k_2 agree well with the literature regarding $[Fe(OH)]^{2+}$ with several ligands. Since the mechanisms for these reactions were determined previous papers to be dissociative interchanges from the activation volumes, it should be reasonable to conclude here that the reactions described by Eqs. 15 and 16 also proceed by a mechanism which has a dissociative character.

In reactions of Fe^{3+}, the value of k_0 was greater when the reagent was a weaker acid. This indicates that the rate was higher when the nucleophilic tendency of the reagent was higher and consequently the mechanism should have an associative character. Thus, the mechanism of complex formation of iron(III) with these β-diketones is different when the metal species in the controlling reaction is Fe^{3+} and when it is $[Fe(OH)]^{2+}$.

As described in a previous paper,[2] equilibrium data for complexes formed from products of the controlling reaction are often indispensable in order to make a reasonable analysis of the kinetic data regarding solvent extraction. However, in most previous work regarding the rate of solvent extraction controlled by a complex formation in an aqueous phase, this has not been considered. For example, the rates of solvent extractions and complex formations of iron(III) with β-diketones (except Hdbm) were studied,[5] but no correction was made in the previous work regarding the effect of the complexes formed in the aqueous phase when the kinetic data were analyzed. As can be seen from the previous and present paper, somewhat different conclusions can be drawn from similar experimental data.

When both of the reagents and the complexes are relatively insoluble in water, as those in the present study, the solvent extraction method should be more useful than the spectrophotometric method of the aqueous solution provided that the product is extractable into organic solvents.

The authors are grateful to Miss Akemi Saito for her experimental aid in the early stage of this work.

References

1) T. Sekine and K. Inaba, *Bunseki Kagaku*, **31**, E291 (1982).
2) T. Sekine and K. Inaba, *Bull. Chem. Soc. Jpn.*, **55**, 3773 (1982).
3) T. Sekine and T. Tetsuka, *Bull. Chem. Soc. Jpn.*, **45**, 1620 (1972).
4) T. Sekine, J. Yumikura, and Y. Komatsu, *Bull. Chem. Soc. Jpn.*, **46**, 2356 (1973).
5) Y. Komatsu, H. Honda, and T. Sekine, *J. Inorg. Nucl. Chem.*, **38**, 1861 (1976).
6) T. Sekine, K. Inaba, and O. Takahashi, *Polyhedron*, **3**, 781 (1984).
7) O. Kammori, K. Sato, K. Takimoto, and K. Arakawa, *Bunseki Kagaku*, **15**, 561 (1966).
8) J. C. Reid and M. Calvin, *J. Am. Chem. Soc.*, **72**, 2948 (1950).
9) T. Sekine and N. Itoh, *Bunseki Kagaku*, **33**, E427 (1984).
10) L. Ciavatta and M. Grimaldi, *J. Inorg. Nucl. Chem.*, **37**, 163 (1975).
11) L. G. Sillén and A. E. Martell, "Stability Constants," Spec. Pub. No. 17, The Chemical Society, London (1964).
12) V. V. Fomin, L. I. Averbakh, G. A. Leman, and S. A. Konovalova, *Zh. Neorg. Khim.*, **21**, 1008 (1976). (CA 84:185598)
13) K. Ishihara, S. Funahashi, and M. Tanaka, *Inorg. Chem.*, **22**, 194 (1983).
14) S. Funahashi, K. Ishihara, and M. Tanaka, *Inorg. Chem.*, **22**, 2070 (1983).

The Effect of α-Tocopherol on Polymerization of Methyl Methacrylate

Koe ENMANJI
The Materials Engineering Laboratory of Mitsubishi Electric Corp., Tsukaguchi-Honmachi, Amagasaki 661
(Received January 5, 1985)

Photo- and thermal polymerizations of methyl methacrylate (MMA) in the presence of α-tocopherol were investigated in air or *in vacuo*. α-Tocopherol at higher concentrations inhibits both the photopolymerization of MMA sensitized by benzoin ethyl ether and the thermal polymerization induced by benzoyl peroxide, but at lower concentrations is able to initiate photopolymerization of MMA under aerobic conditions. Spectral data indicate that a fraction of α-tocopherol is incorporated in the produced polymer chain.

α-Tocopherol (αT) (Fig. 1) is known as an oil-soluble antioxidant vitamin, whose action *in vivo* is to quench radicals produced in biological membranes, particularly multivalent unsaturated fatty acid radicals induced through decompositions, and the excited singlet oxygen $^1O_2$. A lot of literature has reported this action,[1,2] but no report is found of the effect on vinyl polymerization. Because the antioxidant property of α-tocopherol is due to the production of semiquinone radical through oxidation of the hydroxyl group having an active hydrogen,[2,3] α-tocopherol is expected to be an inhibitor for vinyl polymerization. A high resolution electron spin resonance study has shown that 6-chromanyloxyl radical is produced by photolytic oxidation of α-tocopherol,[4] but the action of this radical on vinyl monomer has not yet been investigated. The present author has studied the effect of α-tocopherol on the polymerization of methyl methacrylate (MMA) and found that α-tocopherol at high concentrations inhibits the polymerization of MMA as expected but that it is effective at low concentrations for photoinitiation of MMA polymerization in the presence of air.

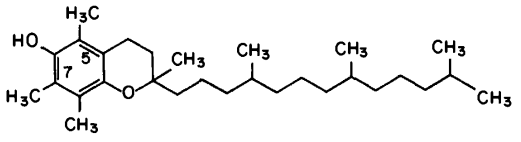

Fig. 1. Chemical structure of α-tocopherol.

Experimental

α-Tocopherol, benzoin ethyl ether (BEE), and benzoyl peroxide (BPO), all of reagent grade (Nakarai Chem. Co.), were used without further purification. MMA was distilled *in vacuo* before use. MMA was placed in a glass ampoule with or without solvent and kept at 25 °C in a thermostat for 30 min, the concentration of dissolved oxygen was confirmed to be 4.5×10^{-4} mol dm^{-3}, and then the ampoule was sealed in atomsphere.

A high pressure mercury lamp was used for photopolymerization and the lights below 300 nm wavelength were cut off with a glass filter (Toshiba, UV-30), if necessary. At a certain reaction time, the polymer solution was poured into methanol, and the conversion of polymer was estimated from the weight of the precipitant required.

Electron spectra were recorded on a Simadzu MPS-5000. Flash photolysis was conducted with a home-made apparatus consisting of a 1 cmφ×10 cm quartz sample tube, two main xenon lamps (Ushio FS-225HMA), a sub xenon flash lamp (Ushio FS-125B), and a spectroscope. The main lamps were

Table 1. Effects of addition of α-tocopherol on the polymerization of methyl methacrylate[a)]

	No.	Air	Reaction temp	Reaction time	Filter[b)]	Concn of initiator (mol dm^{-3})		Concn of α-tocopherol	Conversion of polymer
			°C	h		(BPO)	(BEE)	mol dm^{-3}	%
	1	none	30.6	5.0	none	0	0	0	7.7
	2	none	30.6	3.7	cut	0	0	0	0.0
	3	none	30.6	3.7	cut	0	0	1.45×10^{-4}	1.0
	4	none	30.6	5.0	none	0	0	1.76×10^{-3}	6.4
	5	none	30.6	5.0	none	0	0	4.64×10^{-3}	0.0
	6	+	20	0.5	none	0	4.17×10^{-2}	0	22.3
Photo	7	+	20	0.5	none	0	4.17×10^{-2}	6.37×10^{-4}	15.3
	8	+	20	0.5	none	0	4.17×10^{-2}	6.96×10^{-3}	0.0
	9	+	30.6	4.8	none	0	0	0	0.0
	10	+	30.6	6.3	none	0	0	3.86×10^{-5}	6.4
	11	+	30.6	4.8	none	0	0	9.28×10^{-3}	0.0
	12	+	30.6	4.8	cut	0	0	3.86×10^{-5}	2.1
	13	none	78	0.25		2.48×10^{-2}	0	0	9.0
	14	none	78	0.25		2.48×10^{-2}	0	3.86×10^{-5}	8.5
Thermal	15	none	78	0.25		2.48×10^{-2}	0	4.64×10^{-3}	0.0
	16	+	80	0.25		4.13×10^{-2}	0	0	0.2
	17	+	80	0.25		4.13×10^{-2}	0	4.63×10^{-3}	0.3

a) Light intensity I=80 mW cm^{-2}. b) Cut off below 300 nm.

put parallel with the sample tube, and the sub lamp and spectroscope were put on the elongation of the center axis of sample tube. The sample was kept at room temperature. The concentration of O_2 in MMA was measured with an oxygenelectrode (Yellow Spring Instrument Co., Inc.). The viscosity of polymer acetone solution was measured with an Ubelohde viscosimeter at 30°C.

Results and Discussion

As generally known, MMA monomer is caused to polymerize *in vacuo* by a radical produced by absorption of ultraviolet light below 300 nm wavelength, but the polymerization is hard to proceed under aerobic conditions because the radical is quenched by oxygen. The results of Table 1 were obtained when MMA was photochemically or thermally polymerized in the presence of α-tocopherol under aerobic or anaerobic conditions. Table 1 indicates that α-tocopherol at higher concentrations inhibits the polymerization of MMA by quenching the initiator radical or monomer radical as expected (Nos. 8 and 15). The mechanism of inhibition is thought to be as follows:

$$C_6H_5COOOCOC_6H_5 \xrightarrow{k_d} 2C_6H_5CO_2\cdot, \quad (1)$$

$$C_6H_5CO_2\cdot + M \longrightarrow C_6H_5CO_2M\cdot, \quad (2)$$

$$M_x\cdot + M \xrightarrow{k_p} M_{x+1}\cdot, \quad (3)$$

$$2C_6H_5CO_2\cdot \xrightarrow{2k_t} \text{nonradical products}, \quad (4)$$

$$M_x\cdot + M_y\cdot \longrightarrow M_x + M_y \text{ or } M_{x+y}, \quad (5)$$

$$C_6H_5CO_2\cdot + M\cdot \longrightarrow C_6H_5CO_2M, \quad (6)$$

$$C_6H_5CO_2\cdot + \alpha T \longrightarrow C_6H_5COOH + \alpha T\cdot, \quad (7)$$

$$C_6H_5CO_2\cdot + \alpha T \xrightarrow{k_{inh}} \text{nonradical products}, \quad (8)$$

where M is the monomer and R_i is the rate of initiation. The inhibition rate is expressed by

$$R_{inh} = \frac{k_p[M]R_i}{k_{inh}[\alpha_T]}. \quad (9)$$

Plots of conversion *vs.* reaction time are shown in Fig. 2 for various α-tocopherol concentrations. The value of R_{inh} is close to zero, so that k_{inh} is much larger than k_p.

MMA does not polymerize without α-tocopherol under aerobic conditions, but MMA is photopolymerized in the presence of a small amount of α-tocopherol under an aerobic condition ($[O_2]=4.5\times10^{-4}$ mol dm^{-3}); that is to say, light and α-tocopherol are main initiators for these polymerization reactions. The effect of α-tocopherol on the conversion is shown in Fig. 3. Here, α-tocopherol inhibits to less than 10% of MMA conversion when the α-tocopherol concentration is 1.2×10^{-3} mol dm^{-3} as seen from Fig. 1 and the effect of inhibition may be ignored. The conversion increases in proportion to the square root of the amount of α-tocopherol below 5×10^{-3} mol dm^{-3}, which indicates

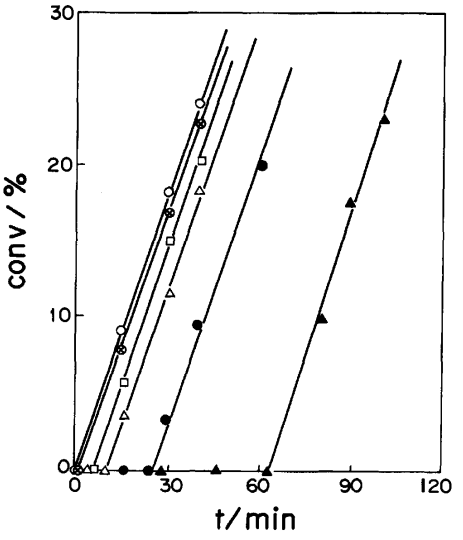

Fig. 2. The relation between conversion and reaction time, concentration of benzoyl peroxide is 2.40×10^{-2} mol dm^{-3} under anaerobic conditions, temperature is 70°C, -○-: [αT]=0, mol dm^{-3}, -×-: [αT]=3.86×10^{-5}, -□-: [αT]=2.32×10^{-4} mol dm^{-3}, -△-: [αT]=6.01×10^{-4} mol dm^{-3}, -●-: [αT]=1.5×10^{-3} mol dm^{-3}, -▲-: [αT]=4.0×10^{-3} mol dm^{-3}.

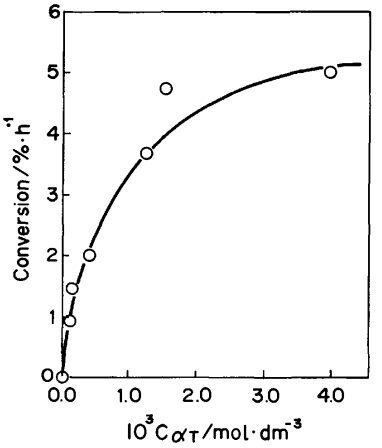

Fig. 3. The relationship between conversion and concentration of α-tocopherol at 30°C under aerobic conditions.
$I=80$ mW cm^{-2}.

that this reaction is on the bimolecular termination mechanism. The logarithm of the conversion is proportional to the logarithm of the intensity of light (the slope is 0.61 as seen from Fig. 4). This fact also supports that this reaction is on the bimolecular termination mechanism.

Next, the conversion was measured at various concentrations of monomer in benzene as a solvent. The results obtained conclude that the conversion is proportional to the concentration of monomer (the slope is 1.19 as seen from Fig. 5). This fact allows the polymerization rate R_p to be written as

$$R_p \propto I^{1/2}C_{MMA}C\alpha_T^{1/2}, \quad (10)$$

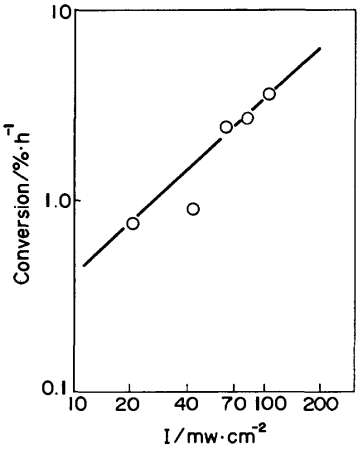

Fig. 4. Plots of conversion *vs.* intensity of light at 30.6 °C under aerobic conditions. Concentration of α-tocopherol is 6.44×10^{-4} mol dm^{-3}.

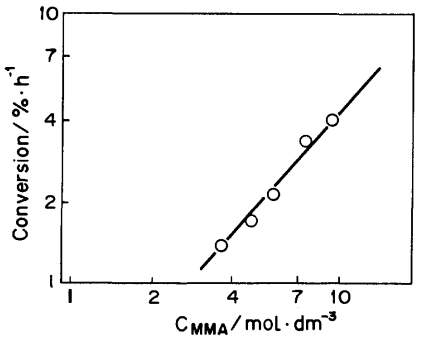

Fig. 5. Plots of conversion *vs.* monomer concentration at 30.6 °C under aerobic conditions. Concentration of α-tocopherol is 6.44×10^{-4} mol dm^{-3}. Intensity of light is 100 mW cm^{-2}.

where I is the intensity of light, C_{MMA} is the concentration of monomer, and $C\alpha_T$ is the concentration of initiator. The temperature dependence of the conversion was also examined (Fig. 6). The conversion reaches a maximum at 50 °C and decreases sharply above 50 °C. The Arrhenius relation holds in the temperature range 5 −50 °C; the activation energy ΔE is estimated as about 33.9 kJ mol^{-1}.

The effect of α-tocopherol as photoinitiator was studied under aerobic conditions. When a methanol solution of α-tocopherol was photoirradiated under aerobic conditions, the optical density at 293 nm decreased with time (Fig. 7). This reaction was found to be first order in α-tocopherol with a rate constant k of 0.024 min^{-1} at 30 °C under aerobic conditions. In contrast, k is 6.4×10^{-3} min^{-1} under anaerobic conditions and 3.9×10^{-3} min^{-1} with the light cut off below 300 nm under aerobic conditions. These results indicate that this reaction needs both oxygen and ultraviolet light. As can be seen from Fig. 6, k and the conversion of MMA decrease above 50 °C. At first glance, the decrease in the conversion might be considered to result from both the increase in the quenching rate

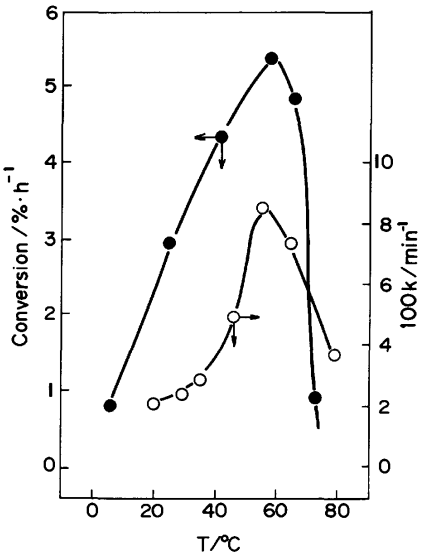

Fig. 6. Temperature dependence of conversion and the photooxidation rate constant. Concentration of α-tocopherol is 6.44×10^{-4} mol dm^{-3}, intensity of light is 100 mW cm^{-2}.
-●-: conversion of MMA, -O-: photooxidation rate of α-tocopherol.

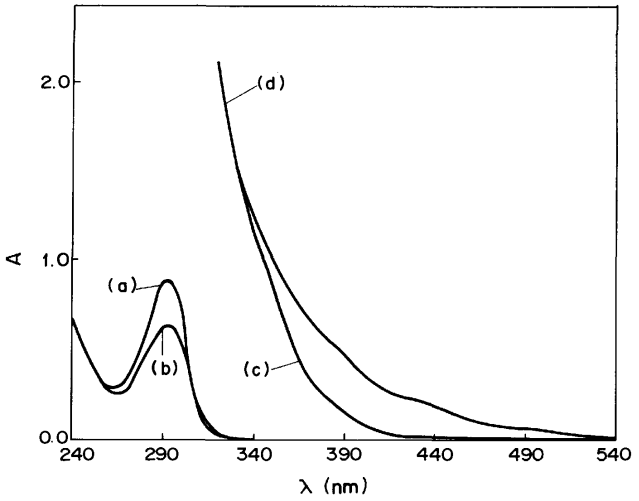

Fig. 7. Spectra of α-tocopherol and photooxidated products.
(a) 2.58×10^{-4} mol dm^{-3} α-tocopherol in methanol, (b) Photoirradiatted (a) for 1.5 h, (c) 3.63×10^{-2} mol dm^{-3} α-tocopherol in methanol, (d) Photoirradiatted (c) for 2 h.

of α-tocopherol radical with temperature and the secrease in the concentration of α-tocopherol radical which initiates the polymerization. However, this mechanism cannot interpret the decrease in the oxidation rate of α-tocopherol above 50 °C. Thus the phenomenon cannot be interpreted with our present knowledge.

Flash photolysis of an α-tocopherol solution in ethanol was examined. Transient spectra were found at 356 nm between 10 and 100 μs and the vanishing rate constant was obtained as 1.55×10^{4} s^{-1}. It may be

thought that the species concerned is the triplet state of semiquinone radical (6-chromanyloxyl radical) of α-tocopherol, because it is generally considered that even the triplet state of chlorophyll a, of which the residence time of the triplet state is the longest among popular molecules is quenched by electron acceptors to a residence time of 10^{-4} s (for example, the quenching rate constant of the triplet state of okitacene is $3.1\times10^{5}\,s^{-1}$).[5] This radical was observed by laser flash photolysis coupled with time resolved ESR.[6]

The mechanism of the photopolymerization of MMA with α-tocopherol is given as follows on the basis of the results obtained:

$$\alpha T \xrightarrow{h\nu} \alpha T\cdot, \quad (11)$$

$$\alpha T\cdot + O_2 \longrightarrow \alpha TO_2\cdot, \quad (12)$$

$$\alpha TO_2\cdot \xrightarrow{k_q} Q(\alpha T\text{-}O_2\text{-}\alpha T), \quad (13)$$

$$\alpha TO_2\cdot + MMA \xrightarrow{k_i} \alpha TO_2\text{-}MMA\cdot, \quad (14)$$

$$MMA_x\cdot + MMA \xrightarrow{k_p} MMA_{x+1}\cdot, \quad (15)$$

$$MMA_x\cdot + MMA_y\cdot \xrightarrow{k_t} MMA_{x+y} \text{ or } MMA_x + MMA_y. \quad (16)$$

The rate of initiation is expressed as

$$v_i = \frac{k_i C_{MMA}}{(k_i C_{MMA}+k_q)}\phi I[1-\exp(-\varepsilon C_{\alpha T} l)], \quad (17)$$

where ϕ is the quantum yield for producing α-tocopherol., Q is the subproduct of the reaction, l is the length of the reactor, and ε is the molecular extinction coefficient. When $C_{\alpha T}$ is small (the light is not perfectly absorbed), Eq. 17 can be reduced to

$$v_i = \frac{k_i C_{MMA}}{(k_i C_{MMA}+k_q)}\phi I\varepsilon C_{\alpha T} l. \quad (18)$$

Further, if $k_i C_{MMA} > k_q$, the following equation is obtained which agrees with the experimental Eq. 1:

$$R_p = \frac{k_p C_{MMA}}{(2k_t)^{1/2}}\phi^{1/2} I^{1/2} C_{\alpha T}^{1/2}(\varepsilon l)^{1/2}. \quad (19)$$

$\alpha TO_2\cdot$ may be a derivative from the 6-chromanyloxyl radical. The chromanyloxyl radical formed would be stabilized by radical delocalization and the most reactive site of the delocalized radical seems to be the C-5 position.[7] Then the initiation point of polymerization may be the C-5 position. Because the polymerized poly(methyl methacrylate) has an absorption band above 400 nm even after purification, it is thought that the oxidative product of α-tocopherol is present at the end of the produced poly(methyl methacrylate). The molecular weight of the polymer produced in the presence of α-tocopherol as a photoinitiator was investigated; the molecular weight was measured by the viscometric method.[8] The results are shown in Table 2, revealing that the presence of α-tocopherol suppresses the increase in the molecular weight.

Table 2. Molecular weight of the poly(methyl methacrylate) produced with α-tocopherol as initiator[a]

$C_{\alpha T}$ / mol dm^{-3}	$[\eta]_{sp}$[b]	$\bar{M}_v$
none	2.00	10.0×10^5
3.66×10^{-5}	1.78	8.6×10^5

a) Bulk polymerization under aerobic conditions, with irradiation by a mercury lamp (80 mW cm^{-2}). b) Measured at 30 °C in acetone with an Ubelohde viscocimeter.

Table 3. Comparison of various vinyl monomers polymerized with α-tocopherol

Temperature is 30.6 °C and lighe intensity is 80 mW cm^{-2} under aerobic conditions

Monomer	$C_{\alpha T}$ / mol dm^{-3}	Conversion / %h^{-1}
Methyl methacrylate	none	0.7
	4.33×10^{-4}	2.0
Styrene	none	0.6
	5.71×10^{-4}	2.2
Ethyl cinnamate	none	0.005
	7.33×10^{-4}	0.052

The effect of α-tocopherol as an initiator on other vinyl monomers were studied. It has been found that α-tocopherol can initiate styrene as well as MMA but hardly initiate ethyl cinnamate (Table 3).

References

1) K. Asada, *Seikagaku*, **48**, 226 (1976).
2) F. Masugi, T. Nakamura, *Tampakushitsu Kakusan Koso*, **21**, 885 (1976).
3) U. Svanholm, K. Bechgaard, and V. D. Parker, *J. Am. Chem. Soc.*, **96**, 2409 (1974).
4) W. Boguth and H. Nieman, *Biochim. Biophys. Acta*, **248**, 121 (1971).
5) H. Sakurai and K. Shima, "Organic Photochemistry," ed by T. Matsuura and H. Nozaki, Nankodo, Tokyo (1970), p. 87.
6) J. K. S. Wan, *J. Photochem.*, **17**, 517 (1981).
7) S. Urano and M. Matsuo, *Lipids*, **11**, 380 (1976).
8) J. Bandrap, "Polymer Handbook," John-Wiely and Sons, New York (1975), p. IV-20.

Preparation of Polyoxa-1,*n*-dithia[*n*](1,1′)ruthenocenophanes and the Structural Studies of Their Metal Complexes

Sadatoshi AKABORI,* Hiroyuki MUNEGUMI, Yoichi HABATA, Sadao SATO,† Kayoko KAWAZOE,† Chihiro TAMURA,† and Masaru SATO††

Department of Chemistry, Faculty of Science, Toho University, Funabashi, Chiba 274
†*Analytical and Metabolic Research Laboratories, Sankyo Co., Ltd., 1-2-58 Hiromachi, Shinagawaku, Tokyo 140*
††*Chemical Analysis Center, Saitama University, Urawa, Saitama 338*

(Received February 16, 1985)

Polyoxa-1,*n*-dithia[*n*](1,1′)ruthenocenophanes were prepared by treatment of 1,1′-ruthenocenedithiol with α, ω-dibromo polyethers. The ruthenocenophanes formed efficiently complexes with soft ions, but not with hard and borderline cations. The ^{1}H- and ^{13}C-NMR spectral data of the silver(I) ion-complexed ruthenocenophanes suggested a partial electron-transfer interaction between the ruthenium atom of the ruthenocene nucleus and the incapsulated silver(I) ion. The crystal structure of the 1:1 complex of 4,7,10,13-tetraoxa-1,16-dithia[16](1,1′)ruthenocenophane with mercury(II) chloride was determined by the X-ray method. The crystals are triclinic, space group $P\bar{1}$, with a=13.722 (3), b=11.678 (4), c=8.179 (2) Å, α=102.69 (3), β=72.82 (2), γ=100.73 (2)°, Z=2, D_x=2.11 g cm^{-3}. The mercury(II) cation and the two chloride ions are situated in the central cavity of the macrocyclic moiety and at the apexes, respectively. The distance between the ruthenium atom of a ruthenocene nucleus and the incapsulated mercury(II) ion is 4.846 (2) Å which is too long for direct metal-metal interaction.

Preparation of a number of crown ethers was first reported by Pedersen twenty years ago.[1] Since that time, a large number and variety of crown, thiacrown and oxathiacrown ethers have been prepared and their complexes with various metal cations and/or organic ammonium cations have been extensively studied.[2] Recently, in order to develop a new functionality, many research groups have attempted to investigate the modified crown ethers.[2] For example, the syntheses of

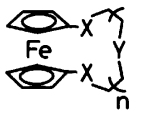

1 : X=Y=S
2 : X=Y=O
3a: X=S, Y=O
3b: X=O, Y=S

many kinds of macrocyclic compounds containing phosphorus, arsenic, and/or other coordinatable atoms have been reported[2] and in this connection, several research groups[3] have reported new-type crown ethers, thiacrown ethers, and oxathiacrown ethers which contain a ferrocene unit as an integral part of a ring member. Although a number of ferroceno crown ethers have already been reported, a crown ether containing a ruthenocene unit is rare.[4,5] Therefore, we wish to report the syntheses of polyoxa-1,*n*-dithia[*n*](1,1′)-ruthenocenophanes, their ability for forming complexes with various metal cations including transition metals, and the crystal structure of the complex of 4,7,-10,13-tetraoxa-1,16-dithia[16](1,1′)ruthenocenophane with mercury(II) chloride.

Syntheses and Spectral Studies. The reaction of 1,1′-dilithioruthenocene (**5**), which was prepared from ruthenocene (**4**) and butyllithium in the presence of *N,N,N′,N′*-tetramethylethylenediamine (TMEDA), with sulfur gave 1,2,3-trithia[3](1,1′)ruthenocenophane (**6**) in a 43% yield. The ^{1}H-NMR spectrum of **6** showed the cyclopentadienyl (Cp) ring protons as a AA′BX pattern at δ 4.05—4.83, supporting the assigned structure. Reduction of **6** with lithium aluminum hydride in boiling ether afforded a 94% yield of ruthenocene-1,1′-dithiol (**7**) as colorless crystals. The ^{1}H-NMR spectrum of **7** showed the Cp ring protons as A_2B_2 pattern at δ 4.47 (t, 4H, J=3.5 Hz) and 4.66 (t, 4H, J=3.5 Hz), and SH protons as a singlet at 2.25 (s, 2H). Also the IR spectrum of **7** showed C–H absorption bands of the Cp rings at 1485 and 3097 cm^{-1} and S–H absorption band at 2500 cm^{-1}. Disodium ruthenocene-1,1′-dithiolate (**8**), which was prepared from the reaction of **7** with aqueous sodium hydroxide in ethanol, was allowed to react with dihalide (**9a**) in aqueous ethanol using highly diluted conditions to give 4,7,10,13-tetraoxa-1,16-dithia[16](1,1′)ruthenocenophane (**10a**) as pale yellow crystals in a 17% yield. In the same manner, the reaction of **8** with dihalide (**9b**) and (**9c**) also gave 4,7,10-trioxa-1,13-dithia[13](1,1′)ruthenocenophane (**10b**) and 4,7-dioxa-1,10-dithia[10](1,1′)-ruthenocenophane (**10c**) in 48 and 23% yields, respectively. The structures of **10a**—c were confirmed as follows. For example, the molecular formula of **10a** was deduced to be $C_{20}H_{18}O_4S_2Ru$ by elemental analysis and mass spectroscopy (M^+, m/z 498). In the ^{1}H-NMR spectrum of **10a**, the resonance for the methylene protons

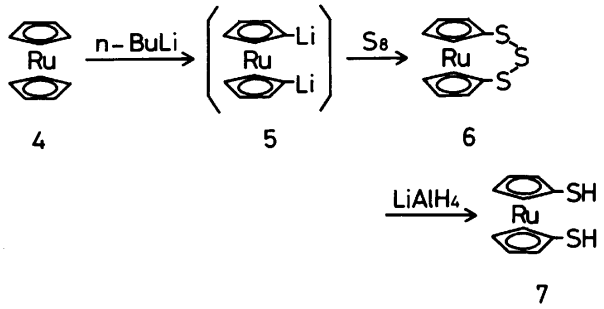

4 5 6 7

attached to the sulfur atom appeared as a triplet (J= 6.3 Hz, 4H) at δ 2.86, in addition to a singlet (12H, OCH_2CH_2) at δ 3.51 and a triplet (J=6.3 Hz, 4H, OCH_2CH_2S) and a pair of triplets (each 4H, J=1.7 Hz, Cp-H, Cp-H) at δ 4.74 and 4.61. The IR spectrum of **10a** displayed absorptions of the ruthenocene ring and ether linkage at 3090, 1470, and 1102 cm^{-1} respectively, but there was no band arising from the S-H group. The electronic spectra of **10a** (λ_{max} 310 nm in CH_3CN) suggest the presence of a ruthenocene nucleus. The structures of other new ruthenoceno crown ethers (**10b**

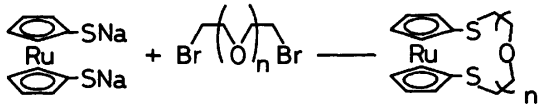

8 9a : n=4, b : n=3, c : n=2 10a : n=4, b : n=3, c : n=2

and **10c**) were also determined by a method similar to that described above.

Complexing Ability. The complexing ability of the crown ether with metal cations depends on several factors. These include cavity size of the ligand, cation diameter, spacial distribution of the ring binding sites, the character of the heteroatoms, and other causes.[6] The complexation of polyoxa-1,*n*-dithia[*n*](1,1′)ferrocenophanes (**3a**) with a variety of metal cations has already been reported in the previous paper.[7] The ferrocenophanes (**3a**) showed a highly complexing ability with silver(I) and thallium(I) ions, while little or negligible with alkali metal, calcium, strontium, and lead cations. These results suggest that the character of the heteroatom is the most important factor in the complexation ability. In order to compare the complexing ability of **10** with that of the corresponding ferrocenophanes (**3a**), the extraction ability of **10** with a variety of metal cations was measured by the method described by Pedersen[8] and the results are summarized in Table 1. The complexing ability of **10** was little or negligible for hard cations (K^+, Cs^+, Rb^+, Li^+, Na^+,

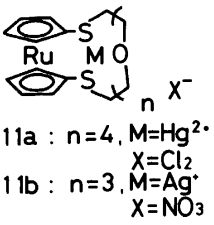

11a : n=4, M=Hg^{2+}, X=Cl_2
11b : n=3, M=Ag^+, X=NO_3

Ca^{2+}, Ba^{2+}, and Sr^{2+}) and borderline cations (Cu^{2+}, Co^{2+}, and Ni^{2+}), but excellent for soft cations (Ag^+, Hg^{2+}, and Tl^+). The results of the extraction ability may be explained by the HSAB rule.[9] That is, the successive displacement of an oxygen atom in the macrocyclic ring of the ruthenocenophane by a sulfur atom, which is softer compared with an oxygen atom, increases the affinity to soft ions. The highly complexing ability of **10** with soft ions compared with the corresponding ferrocenophanes (**3a**) suggests some participation of the ruthenium atom of the ruthenocene nucleus in the process of complexation. It is also interesting that the extraction ability of thallium(I) ion showed a remarkable dependence on the cavity size in the macrocycle of **10**.

The ^{1}H-NMR spectrum of **10** in acetonitrile-d_3 was compared with that measured in the presence of an equivalent amount of silver nitrate. The chemical shift of the ligands (**10**) and the difference in the chemical shift between the free ligands and the complexes are shown in Table 2. The change of chemical shifts of the

Table 1. Percentage of metal picrates extracted from the aqueous to the organic phase[a]

Compd	Ag^+	Hg^{2+}	Tl^+	K^+	Cs^+	Rb^+	Cu^{2+}	Cd^{2+}	Li^+ Sr^{2+}	Na^+ Co^{2+}	Ca^{2+} Ni^{2+}	Ba^{2+}
10a	99	95[b]	2	0	0	0	2	1		0		
10b	99	95[b]	33	0	0	0	2	1		0		
10c	99	30[b]	87	5	3	9	3	1		0		

a) Solvent: Water and dichloromethane (1:1). Concentration of ruthenocenocrown ether: 7×10^{-4} M(1M=1 mol dm^{-3}). Concentration of picric acid: 7×10^{-5} M. Concentration of metal nitrates: 0.1 M. b) Mercury dichloride was used instead of nitrate.

Table 2. Low-field shift of ^{1}H-NMR spectra on addition of silver nitrate to a solution of **10** in acetonitrile-d_3

Compd	Chemical shift/δ				
	Cp-H_α	Cp-H_β	SCH_2	OCH_2	
10a	4.74	4.61	2.86	3.51	3.63
10a+$AgNO_3$	(0.23)[a]	(0.21)	(0.32)	(0.03)	(0.17)
10b	4.76	4.61	2.87	3.61	3.59
10b+$AgNO_3$	(0.15)	(0.16)	(0.21)	(0.11)	(0.09)
10c	4.79	4.62	2.87	3.73	3.65
10c+$AgNO_3$	(0.16)	(0.16)	(0.21)	(0.10)	(0.10)

a) Shift changes are presented in parentheses.

ruthenocenophanes (**10**) on complexation with metal cations seems to be attributable to (i) an electronic field effect caused by a incorporated metal cation, (ii) perturbation of the electron density on the carbon atom through Ag-Ru-ring and/or through Ag-S-ring, and (iii) a factor due to the conformational change on complexation. In the case of the complexes of polyoxa[*n*](1,1′)ferrocenophanes (**2**) with the alkali metal thiocyanates, the differences of the chemical shift between the α- and β-protons of Cp rings depends on the ring size of ligands and the diameter of the incapsulated metal cations.[10] On the contrary, in the ^{1}H-NMR spectrum of the free ligands (**10**) and their silver complexes the chemical shift differences of the α- and β-ring protons were approximately the same, although these signals were remarkably shifted (0.15—0.23 ppm) to down field. If the down field shift is caused by perturbation of the inductive and conjugative effect of the sulfur substituent on coordination to a silver cation through a sulfur atom, the α-protons would be expected to resonate at a lower-field than the β-protons. Therefore, a relatively large down-field shift of the Cp ring protons seems partially to be due to the perturbation of the electron density on the Cp rings by charge transfer from the Ru atom to the Ag(I) ion, although other effects could not be ruled out. In the ^{1}H-NMR spectra of **10**, the methylene protons attached to the sulfur atom showed a large down-field shift (0.21—0.32 ppm), but those attached to the oxygen atom showed a small down-field shift (0.03—0.17 ppm). This finding is in good accord with the HSAB rule,[9] and indicates the presence of a strong coordination of the sulfur atom and a weak coordination of the oxygen atom to the central metal cation. Furthermore, the following finding in the ^{1}H-NMR spectra of **10** is also interesting. The protons of the methylene groups in the free ligands appeared as a triplet (J=*ca.* 6.5 Hz), while the methylene protons in the complexes were shifted to down-field and better resolved as shown in Fig. 1. This result suggests that in the complexes, the silver(I) ion is incapsulated by both sulfur and oxygen atoms in the macrocycle and the complexes takes a more rigid conformation. Similar conclusions were also obtained in the ^{13}C-NMR spectra of the free ligands and their silver complexes of **10** (Table 3). In the spectrum of **10a**, the bridgehead carbon, α-, and β-carbons of the Cp rings and the methylene carbons attached to a sulfur atom showed their resonances at δ 88.1, 77.3, 72.6, and 39.6 ppm, respectively, together with the methylene carbons, which were not rigorously assigned, at δ 71.5, 71.3, and 70.9 ppm. However, when an equimolar amount of silver(I) nitrate were added to an acetonitrile-d_3 solution of **10a**, the ^{13}C-NMR spectrum showed resonances at δ 83.1, 78.7, 74.5, and 40.4 ppm (C_b, C_α, C_β, and CH_2S), together with the resonances of other methylene carbons attached to oxygen atoms at δ 71.2, 71.0, 70.8, and 68.0 ppm. The signal of the bridgehead carbon in **10a** shifted to up-field but those of α- and β-carbons of a ruthenocene nucleus shifted to down-field. These results would be explained by the following effects: (i) The direct electron transfer from the ruthenium atom to the complexed silver(I) ion, (ii) the electron transfer *via* the sulfur atom from the Cp ring to the silver(I) ion, and (iii) a conformational change of the ruthenocenophane on complexation. When silver(I) nitrate was added to a solution of **10a**, the peaks of methylene carbons shifted and became more resolved (four peaks→five peaks). This result is also explained on the basis of the rigid conformation of the macrocycle in the ruthenocenophane (**10a**) as described in the

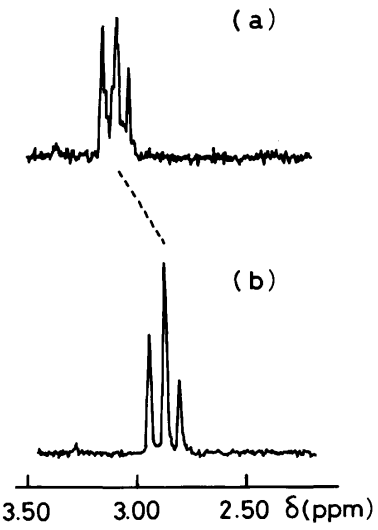

Fig. 1. ^{1}H-NMR Spectra of 10b (b) and the Ag^+ complex of 10b (a).

Table 3. Low-field shift of ^{13}C-NMR spectra on addition of silver nitrate to a solution of **10** in acetonitrile-d_3

Compd	Chemical shift/ppm[a]						
	C_b	Cp-H$_\alpha$	Cp-H$_\beta$	SCH_2		OCH_2	
10a	88.1	77.3	72.6	39.6	71.5	71.3	70.9
10a+$AgNO_3$	(−0.50)[b]	(+1.4)	(+1.9)	(+0.8)		(−0.3 — −1.1)	
10b	89.2	77.0	72.3	39.0	71.4	71.2	70.0
10b+$AgNO_3$	(−8.4)	(+2.4)	(+2.5)	(+1.6)		(−0.1 — −0.15)	
10c	90.4	77.1	72.0	39.6	71.5	70.8	
10c+$AgNO_3$	(−3.6)	(+0.6)	(+2.1)	(+1.1)		(−0.7 — −3.9)	

a) Chemical shifts as δ values. A downfield shift is denoted as a positive value. b) Shift changes are presented in parentheses.

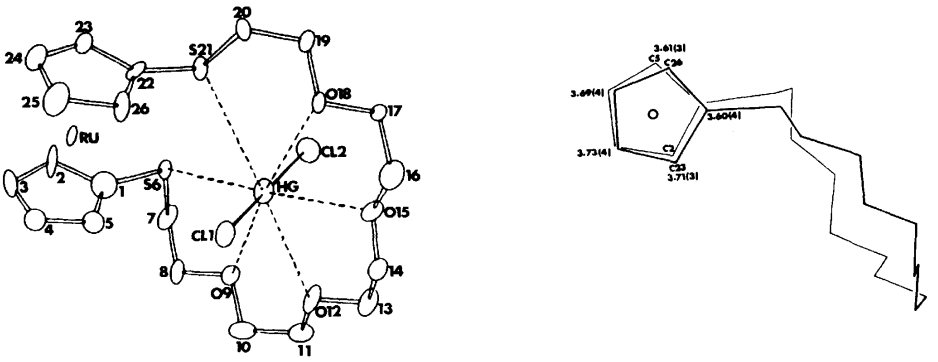

(a) (b)

Fig. 2. (a) ORTEP[20] drawing of the complex with atom numbering scheme. (b) Projection of the organic ligand moiety on the Cp ring containing the C(1) atom. The C·····C distances (Å) between the rings are also given. An open circle denotes the Ru atom.

description of ^{1}H-NMR spectra.

Isolation of Complexes. The 1:1 complexes of **10** with $HgCl_2$ and $AgNO_3$, (**11a**) and (**11b**), respectively, were isolated. In the ^{1}H-NMR spectrum (in CD_3CN) of **11a**, the signals of methylene protons next to a sulfur atom, α-, and β-ring protons of ruthenocene nucleus were shifted down-field only +0.19, +0.03, −0.03 ppm, compared with those of **10a**, respectively. On the other hand, the ^{1}H-NMR spectrum of the complex $Cp_2Ru \cdot HgCl_2$ (**12**) in CD_3CN showed a signal at δ 5.31 corresponding to the Cp-ring protons.[11] The down-field shift of the Cp-ring protons of **12**, compared with those of ruthenocene (**4**), is about +0.7 ppm. Hence, the difference in the chemical shift between the free ligand (**10a**) and the complex (**11a**) seems to be attributable to the inductive and field effects *via* the coordinated sulfur atom by complexation of mercury(II) ion into the crown ether part of the ligand, although a possibility of the weak coordination of the incorporated mercury(II) ion to the Ru atom of ruthenocene nucleus cannot be ruled out. The above explanation was supported by the X-ray crystallographic analysis of **11a** as described below.

Crystal Structure of 11a. The conformation of the complex (**11a**) is illustrated in Fig. 2, which also shows the atom labels used. The positional parameters for non-hydrogen atoms are listed in Table 4. Also, the bond lengths, bond angles and torsion angles are listed in Table 5.

The complex can be divided into two parts: The complexing unit containing dithia-18-crown-6 like moiety which is defined by S(6) to S(21), and the ruthenocene unit. In the complexing unit, the mercury(II) ion and the two chloride ions are situated in the central cavity and at the apexes, respectively. The six heteroatoms (two S and four O atoms) take a slightly distorted half chair form in which O(12) and O(15) deviate by 0.61 and −0.16 Å, respectively, to the side of Cl(1) from the mean plane of the remaining four atoms, S(1), O(9), O(18), and S(21), with a maximum deviation of 0.06 Å at O(9). The mercury(II) ion is situated in the same plane with a deviation of 0.17 Å. The intramolecular atomic distances between the mercury(II) ion and the six heteroatoms are 3.034(6), 3.120(18), 2.888(17), 2.838(17), 3.048(17), 3.330(6) Å with S(6), O(9), O(12), O(15), O(18), and S(21), respectively. These values are longer than the sum of the ionic radius of a mercury(II) ion (1.10 Å) and the van der Waals radius of a sulfur atom (1.85 Å) or O (1.40 Å).[12]

TABLE 4. FRACTIONAL ATOMIC COORDINATES (×10^4), WITH ESTIMATED STANDARD DEVIATIONS IN PARENTHESES

Atom	x	y	z	B_{eq}(Å^2)[a]
HG	2782(1)	1604(1)	3616(1)	2.7
RU	2091(1)	5675(1)	5521(2)	1.4
CL(1)	1408(4)	2014(5)	2814(8)	2.8
CL(2)	4010(5)	984(6)	4506(8)	3.6
C(1)	3477(19)	5165(18)	3624(30)	2.5
C(2)	3684(18)	6405(18)	4268(31)	2.4
C(3)	3014(21)	6981(20)	3846(34)	3.3
C(4)	2405(19)	6173(22)	2956(30)	2.7
C(5)	2685(17)	5017(20)	2751(29)	2.3
S(6)	4059(4)	4021(4)	3920(7)	1.7
C(7)	5188(18)	3956(20)	2040(33)	2.7
C(8)	4907(18)	3430(20)	421(30)	2.4
O(9)	4549(13)	2171(14)	371(21)	2.7
C(10)	4269(21)	1589(25)	−1192(34)	3.6
C(11)	4014(19)	323(23)	−1199(31)	2.9
O(12)	3085(12)	116(14)	230(21)	2.5
C(13)	2785(20)	−1098(20)	260(32)	2.8
C(14)	1765(21)	−1217(20)	1589(30)	2.9
O(15)	1954(12)	−824(13)	3253(20)	2.4
C(16)	1026(17)	−1118(19)	4613(33)	2.6
C(17)	1270(18)	−562(18)	6316(27)	2.1
O(18)	1186(12)	656(12)	6656(20)	2.2
C(19)	1303(19)	1184(19)	8368(29)	2.3
C(20)	1123(17)	2472(19)	8762(28)	2.1
S(21)	2184(4)	3360(5)	7474(7)	2.2
C(22)	1577(18)	4543(19)	7539(28)	2.1
C(23)	1770(18)	5749(19)	8327(29)	2.2
C(24)	1110(19)	6435(20)	8011(34)	2.9
C(25)	472(18)	5666(22)	7052(34)	3.1
C(26)	769(18)	4497(19)	6717(31)	2.4

a) W.C.Hamilton, Atca Cryst., **12**, 609 (1959).

TABLE 5. BOND LENGTHS (l/Å) AND BOND AND TORSION ANGLES (ϕ/°) IN THE ORGANIC LIGAND

1	2	3	4	1-2	1-2-3	1-2-3-4
Dithia-crown moiety						
C(2)	C(1)	S(6)	C(7)	1.43(3)	126(2)	−89(2)
C(5)	C(1)	S(6)	C(7)	1.43(4)	126.3(18)	93(2)
C(1)	S(6)	C(7)	C(8)	1.77(2)	101.8(12)	−73(2)
S(6)	C(7)	C(8)	O(9)	1.83(2)	111.8(19)	−70(2)
C(7)	C(8)	O(9)	C(10)	1.46(4)	110.6(19)	−179(2)
C(8)	O(9)	C(10)	C(11)	1.46(3)	113.8(18)	174.8(17)
O(9)	C(10)	C(11)	O(12)	1.44(4)	110(2)	65(3)
C(10)	C(11)	O(12)	C(13)	1.45(4)	109(2)	179(2)
C(11)	O(12)	C(13)	C(14)	1.48(3)	111.3(17)	−172.5(18)
O(12)	C(13)	C(14)	O(15)	1.41(3)	107(2)	−73(3)
C(13)	C(14)	O(15)	C(16)	1.50(4)	107(2)	−169.5(19)
C(14)	O(15)	C(16)	C(17)	1.42(3)	110.1(14)	−174.5(18)
O(15)	C(16)	C(17)	O(18)	1.46(3)	106.0(17)	79(2)
C(16)	C(17)	O(18)	C(19)	1.51(4)	109.3(16)	173.6(18)
C(17)	O(18)	C(19)	C(20)	1.41(2)	110.4(13)	−175.4(17)
O(18)	C(19)	C(20)	S(21)	1.44(3)	109.4(16)	−71(2)
C(19)	C(20)	S(21)	C(22)	1.52(3)	111.0(17)	158.3(17)
C(20)	S(21)	C(22)	C(23)	1.82(2)	100.0(11)	115(2)
C(20)	S(21)	C(22)	C(26)			−68(2)
S(21)	C(22)	C(23)		1.73(2)	129(2)	
S(21)	C(22)	C(26)			125(2)	
Cyclopentadienyl moiety						
C(1)	C(2)	C(3)	C(4)	1.43(3)	108(2)	−1(3)
C(2)	C(3)	C(4)	C(5)	1.39(3)	110(2)	−1(3)
C(3)	C(4)	C(5)	C(1)	1.37(4)	109.1(18)	2(3)
C(4)	C(5)	C(1)	C(2)	1.43(3)	106.1(19)	−2(3)
C(5)	C(1)	C(2)	C(3)	1.43(4)	107.4(15)	2(3)
C(22)	C(23)	C(24)	C(25)	1.43(3)	110(2)	1(3)
C(23)	C(24)	C(25)	C(26)	1.42(4)	107.9(19)	−2(3)
C(24)	C(25)	C(26)	C(22)	1.41(4)	107.7(18)	2(3)
C(25)	C(26)	C(22)	C(23)	1.44(3)	109(3)	−1(3)
C(26)	C(22)	C(23)	C(24)	1.44(4)	105.7(15)	0(3)

The Cl–Hg–Cl angle is 172.7 (2)° which slightly deviates from the expected 180°. The Hg–Cl bond lengths of 2.327(7) and 2.304(7) Å are in agreement with reported values for the linear Hg–Cl bond.[13] Thus, the mercury(I) ion forms a distorted hexagonal-bipyramidal geometry with the two chloride ions coordinated axially. The organic ligand moiety in present complexing unit has structural similarity compared with that in the complex of $HgCl_2$:1,4-dithia-18-crown-6 (HGDTC).[14] The 13 torsion angles about the chemically corresponding bonds between the both complexes agree well, and the average difference is about 5°. However, in the case of HGDTC the mercury(II) ion interacts with the two sulfur atoms from the outside of the macrocyclic ring because the C–C bridge joining the sulfur atoms directs into the interior of the ring. The Cp rings take an eclipsed conformation to each other and the dihedral angle between the rings is 3.4°. The Ru···C and inter-ring C···C distances of the ruthenocene unit are in the ranges of 2.18(3) to 2.23(3) Å and 3.60(4) to 3.73(4) Å with the average values of 2.21 and 3.67 Å, respectively, and the distances from the Ru atom to the best plane of the Cp rings are 1.84(3) and 1.83(3) Å. These values agree well with those of ruthenocene[15] and [4](1,1′)ruthenocenophane.[16] The distance between the Ru atom of the ruthenocene nucleus and the mercury(II) ion incorporated is 4.846(2) Å which is too long for direct metal–metal interaction, because the sum of the van der Waals radius of the Ru atom and the ionic radius of the Hg^{2+} ion is 3.15 Å[12].

The crystal packings are formed with van der Waals forces; the short intermolecular distances are 3.36(3), 3.49(3), and 3.707(8) Å for C(3)···O(15) (x,1+y,z), Cl(1)···C(16) (−x,−y,1−z), and S(6)···S(6) (1−x,1−y,1−z), respectively.

Experimental

The melting points are uncorrected. The electronic spectra were measured on a Hitachi 340 Spectrometer. The ^{1}H-NMR and ^{13}C-NMR spectra were obtained on a JEOL FX-90Q Spectrometer, TMS being chosen as an internal standard. The mass spectra were taken by using a Hitachi M-80 Spectrometer. The IR spectra were measured on a JASCO DS-701G Diffraction Grating Infrared Spectrophotometer.

Material. All solvents and reagents were used as purchased unless otherwise specified. Ruthenocene, 1,8-dibromo-3,6-dioxaoctane, 1,11-dibromo-3,6,9-trioxaundecane, and 1,14-dibromo-3,6,9,12-tetraoxatetradecane were prepared according to the literatures. Silica gel for thinlayer chromatography utilized Wakogel B-5F.

1,2,3-Trithia[3](1,1′)ruthenocenophane (6). To a mixture

of hexane (3.5 cm³) and TMEDA (3.0 cm³, 0.019 mol) was added a solution of butyllithium (0.024 mol) in hexane (18 cm³) and then a solution of ruthenocene (2.0 g, 8.65 mmol) in hexane (35 cm³) under nitrogen. The mixture was then further stirred for 8 h at room temperature. To the mixture was added 1,2-dimethoxyethane (90 cm³, 0.86 mol) and sulfur (1.72 g, 0.05 mol) and the mixture was then stirred for 12 h at refluxing temperature. After the mixture had been cooled to room temperature, the precipitates were filtered and washed with ether. The filtrate and the washings were combined, washed with 10% aq sodium hydroxide solution and water, and concentrated *in vacuo*. Sublimation of the residue at 130°/1.5 mmHg (1 mmHg=133.322 Pa) gave crude **6**. Recrystallization of the crude material from hexane gave pure **6** as yellow flat plates, mp 183.5—184°C, in 42.7% yield. Found: C, 36.76; H, 2.55%. Calcd for $C_{10}H_8S_3Ru$: C, 36.91; H, 2.48%. MS (70 eV): *m/z* 326 (M^+). ^{1}H-NMR ($CDCl_3$): δ=4.05—4.83 (m, 8H). IR (KBr): 3097 and 1401 cm^{-1}.

Ruthenocene-1,1'-dithiol (7). **6** (1.78 g, 5.47 mmol) was added to ether (107 cm³) containing lithium aluminum hydride (0.05 g, 0.013 mol) under nitrogen. Stirring was continued at refluxing temperature for 3 h, and the mixture was then cooled to ice-water temperature. To the mixture was added dropwise 1.5% aq potassium hydroxide solution (142 cm³) and an aq layer was separated. The aq solution was extracted with three 20 cm³ portions of ether. The aq solution was acidified with concd hydrochloric acid until it became weakly acidic, and then extracted with four 20 cm³ portions of ether. The combined extracts were dried and concentrated to give pure **7** as colorless crystals, mp 116—117°C, in 94% yield. Found: C, 40.54; H, 3.59%. Calcd for $C_{10}H_{10}S_2Ru$: C, 40.66; H, 3.42%. MS (70 eV): *m/z* 296 (M^+). ^{1}H-NMR ($CDCl_3$): δ=2.25 (s, 2H, -SH), 4.47 (t, *J*=3.5 Hz, 4H, Cp-H), and 4.66 (t, *J*=3.5 Hz, Cp-H). IR (KBr): 3097, 2500, and 1419 cm^{-1}.

*General Procedure for Polyoxa-1,*n*-dithia[*n*](1,1')ruthenocenophanes. 4,7-Dioxa-1,10-dithia[10](1,1')ruthenocenophane (10c).* A solution of **7** (1.51 g, 5.12 mmol) in 20% aq sodium hydroxide solution (100 cm³) and a solution of 1,8-dibromo-3,6-dioxaoctane (1.76 g, 6.38 mmol) in 60% ethanol (100 cm³) were added dropwise at the same rate to 60% ethanol (200 cm³) for a period of 3.5 h at refluxing temperature under nitrogen, and then further stirred for 3 h. After the solution had been cooled to room temprerature, 100 cm³ of water was added to the reaction mixture. The solution was extracted with four 30 cm³ portions of ether. The ether extracts were combined, washed with water, and concentrated *in vacuo*. The residual oil was chromatographed by silica gel TLC (using benzene-acetone 10:1 as eluent). The third fraction was eluted with acetone at room temperature, followed by filtration. The evaporation of the solvent gave pale yellow oil which solidified on standing. Recrystallization of the crude material from hexane gave a pure **10c** as yellow needles, mp 101.0—101.5°C, in 23.4%. Found: C, 46.66; H, 5.12%. Calcd for $C_{16}H_{20}O_2S_2Ru$: C, 46.92 ; H, 4.93%. MS (70 eV): *m/z* 410 (M^+). IR (KBr): 3075, 2850, 1410, and 1127 cm^{-1}. UV (MeOH:H_2O=1:1): λ_{max} 320 nm (ε=472).

4,7,10-Trioxa-1,13-dithia[13](1,1')ruthenocenophane (10b). Pale yellow flat plates, 48% yield. Found: C, 47.96; H, 5.48%. Calcd for $C_{18}H_{24}O_3S_2Ru$: C, 47.66; H, 5.68%. MS (70 eV): *m/z* 454 (M^+). IR (KBr): 3090, 2860, 1470, 1416, 1352, 1282, 1115, and 807 cm^{-1}. UV (MeOH:H_2O=1:1): λ_{max} 320 nm (ε=472).

4,7,10,13-Tetraoxa-1,16-dithia[16](1,1')ruthenocenophane (10a). Pale yellow flat plates, mp 46.2—48.0°C, 17% yield. Found: C, 48.48; H, 5.81%. Calcd for $C_{20}H_{28}O_4S_2Ru$: C, 48.26; H, 5.68%. MS (70 eV): *m/z* 498 (M^+). IR (KBr): 3090, 2860, 1480, 1418, 1353, 1286, 1136, and 811 cm^{-1}. UV (MeOH:H_2O=1:1): λ_{max} 320 nm (ε=472).

Complex of 4,7,10,13-Tetraoxa-1,16-dithia[16](1,1')ruthenocenophane (10a) with Mercury(II) Chloride. A solution of **10a** (41 mg, 0.082 mmol) in acetonitrile (1 cm³) was added dropwise to a solution of mercury(II) chloride (22 mg, 0.081 mmol) in acetonitrile (1 cm³). The resulting precipitates were filtered and washed with a small amount of acetonitrile to give a pure 1:1 complex (**11a**), mp 172.0—173.0°C, in 69% yield. Found: C, 31.44; H, 3.75%. Calcd for $C_{20}H_{28}O_2S_2Ru$: C, 31.23; H, 3.68%. IR (KBr): 3090, 2910, 1470, 1411, 1355, 1298, 1102, and 810 cm^{-1}. UV (CH_3CN): λ_{max} 310 nm (ε=455).

Complex of 4,7,10-Trioxa-1,13-dithia[13](1,1')ruthenocenophane (10b) with Silver(I) Nitrate. To a solution of **11b** (30 mg, 0.066 mmol) in acetonitrile was added a solution silver(I) nitrate (11 mg, 0.065 mmol) in acetonitrile (1 cm³). To the mixture was added dropwise 3 cm³ of ether to give colorless precipitates. The precipitates were washed with a small amount of acetonitrile and then ether to give a pure 1:1 complex (**11b**), mp 157.0—157.5°C, in 84% yield. Found: C, 34.51; H, 3.78; N, 2.22%. Calcd for $C_{18}H_{24}NO_5S_2AgRu$: C, 34.67; H, 3.89; N, 2.25%. IR (KBr): 3190, 2920, 2870, 1470, 1450, 1384, 1110, 1025, and 810 cm^{-1}. UV (CH_3CN): λ_{max} 310 nm (ε=403).

Extraction Ability. Extraction ability of the ruthenocenophanes with metal picrate was examined by the method described in the previous paper.[17] The results are summarized in Table 1.

X-Ray Crystal Determination of 11a. A crystal of dimensions 0.5×0.3×0.2 mm obtained from methanol, was used for the intensity measurement. Intensity data were obtained on a Rigaku AFC5 apparatus equipped with a rotating-anode X-ray generator and using a graphite monochrometer (λ(Cu$K\alpha$)=1.5418 Å, $2\theta \geq 128°$) was used. The data were corrected for Lorentz and polarization effects but not for absorption. Among the 3749 unique reflections collected, 3352 were considered to be observed at the 2.0σ (F_o) level.

Crystal Data. $C_{20}H_{28}O_4S_2Cl_2RuHg$, M=769.2. Triclinic, *a*=13.722(3), *b*=11.678(4), *c*=8.179(2) Å, α=102.69(3), β=72.82(2), γ=100.73(2)°, *Z*=2, D_x=2.11 g cm^{-3}, space group $P\bar{1}$.

The structure was solved by the combination of the heavy atom technique and direct methods using MULTAN[18] and refined by block-diagonal least-squares methods. Positions of the hydrogen atoms were estimated from standard geometry. The final refinements with anisotropic temperature factors for the non-hydrogen atoms were reduced the R to 0.089. The anomalous dispersion corrections were applied to the scattering factors of Hg, Ru and Cl.[19]

Thermal parameters for non-hydrogen atoms and observed and calculated structure factors are kept at the Chemical Society of Japan (Document No. 8530).

References

1) C. J. Pedersen, *J. Am. Chem. Soc.*, **89**, 2496 (1967).
2) R. E. Izatt and J. J. Christensen, "Synthetic Multidentate Macrocyclic Compounds," Academic Press, New

York (1977).

3) G. Oepen and F. Vogtle, *Libigs Ann. Chem.*, **1979**, 1094; J. F. Biernat and T. Wilczewski, *Tetrahedron*, **36**, 2521 (1980); A. P. Bell and D. Hall, *J. Chem. Soc., Chem. Commun.*, **1980**, 163; P. J. Hammond, P. D. Beer, and C. D. Hall, *J. Chem. Soc., Chem. Commun.*, **1983**, 1161.

4) A preliminary report: S. Akabori, Y. Habata, H. Munegumi, and M. Sato, *Tetrahedron Lett.*, **25**, 1991 (1984).

5) S. Akabori, H. Munegumi, S. Saito, and M. Sato, *J. Organomet. Chem.*, **272**, C54 (1984).

6) F. De Jong and D. N. Reinhoult, "Stability and Reactivity of Crown-ether Complexes," Academic Press, New York (1981).

7) M. Sato, M. Kubo, S. Ebine, and S. Akabori, *Bull. Chem. Soc. Jpn.*, **57**, 421 (1984).

8) C. J. Pedersen, *Federation Proceedings*, **27**, 1305 (1978).

9) T. Ho, "Hard and Soft Acid and Bases Principle in Organic Chemistry," Academic Press, New York (1977).

10) S. Akabori, Y. Habata, and M. Sato, *Bull. Chem. Soc. Jpn.*, **57**, 68 (1984).

11) This complex was prepared according to the literature: O. Traverso, C. Chiorboli, U. Mazzi, and G. L. Zucchini, *G. Chim. Italiana*, **107**, 181 (1977).

12) L. Pauling, "The Nature of the Chemical Bond," 3rd., ed by Cornell University Press, Ithaca, New York (1960).

13) P. D. Brotherton and A. H. White, *J. Chem. Soc., Dalton Trans.*, **1973**, 2689.

14) N. K. Dalley and S. B. Larson, *Acta Crystallogr., Sect. B*, **37**, 2225 (1981).

15) G. L. Hardgrove and D. H. Templeton, *Acta Crystallogr.*, **12**, 28 (1959).

16) S. Ohba, Y. Saito, S. Kamiyama, and A. Kasahara, *Acta Crystallogr., Sect. C*, **40**, 53 (1984).

17) S. Akabori, Y. Habata, Y. Sakamoto, M. Sato, and S. Ebine, *Bull. Chem. Soc. Jpn.*, **56**, 537 (1983).

18) P. Main, L. Lessinger, M. M. Woolfson, G. Germain, and T. P. Declercq, "MULTAN 74: A System of Computer Programs for the Automatic Solution of Crystal Structures from X-ray Diffraction Data," Universities of York, England, and Louvain, Belgium (1974).

19) "International Tables for X-ray Crystallography," Vol IV, Kynoch Press, Birmingham (1974), p. 72—98 and p. 149—150.

20) C. K. Johnson, ORTEP Report ORNL-3794, Oak Ridge National Laboratory, Tennessee.

Development and Application of Organic Reagents for Analysis. VI.[1] Synthesis and Fluorescence Spectral Properties of 2-(4-Substituted phenyl)benzofurans

Shuzo AKIYAMA,* Hiroyuki AKIMOTO, Shin'ichi NAKATSUJI, and Kenichiro NAKASHIMA
Faculty of Pharmaceutical Sciences, Nagasaki University, 1-14 Bunkyo-machi, Nagasaki 852
(Received February 21, 1985)

A synthesis of fifteen kinds of 2-(4-substituted phenyl)benzofurans (**4**$_n$) was carried out and their fluorescence spectral properties were investigated concerning their applicability as organic reagents for analyses.

In order to develop sensitive and useful fluorogenic reagents, our attention became directed toward the synthesis of derivatives of 2-phenylbenzofuran which were expected to exhibit strong fluorescence due to the presence of a latent *trans*-stilbene skeletone. The synthesis of 2-(4-substituted phenyl)benzofurans (**4**$_n$) was carried out and their fluorescence spectral properties were investigated in order to determine the applicability of **4**$_n$ as reagents for analyses. As shown Scheme 1, the construction of a benzofuran skeletone

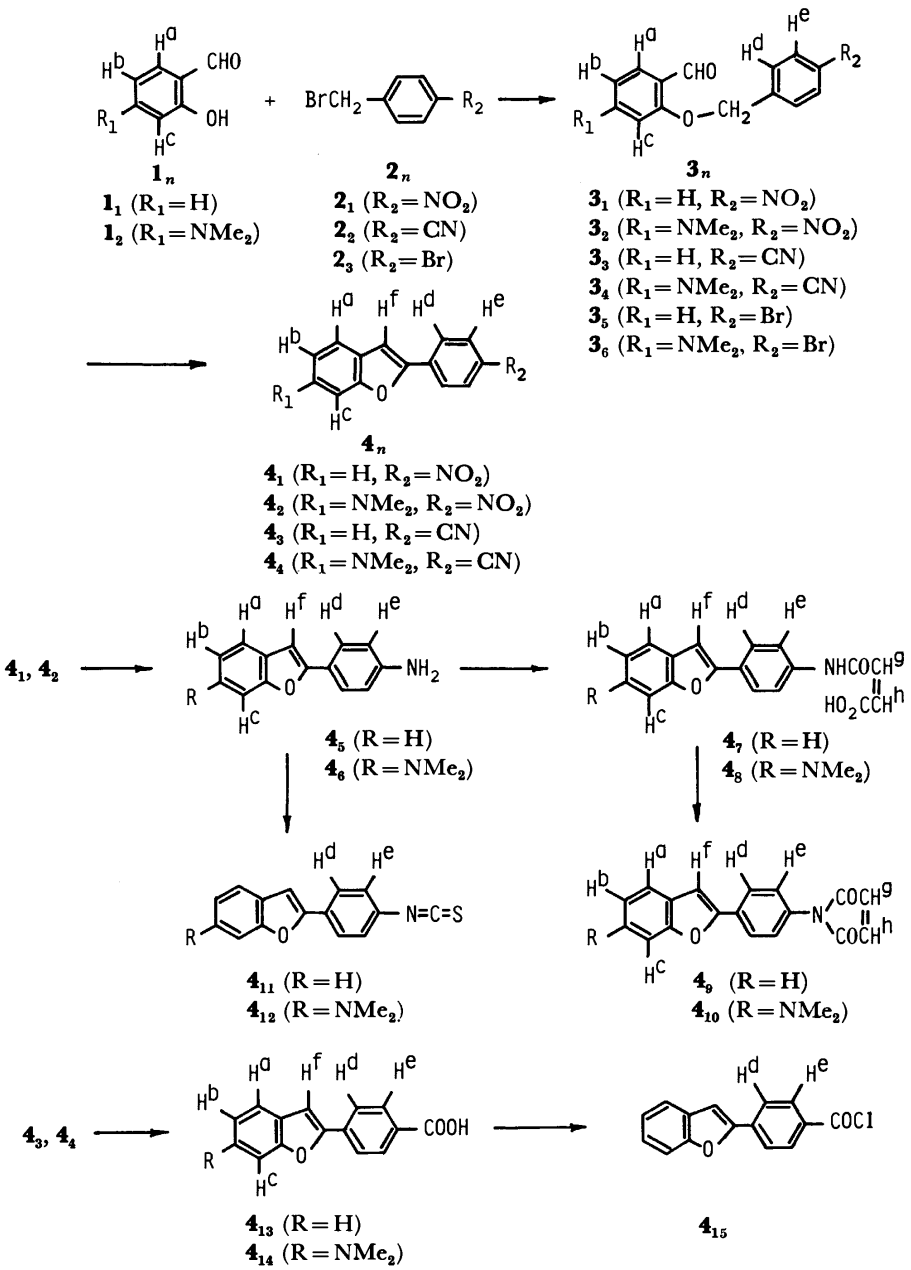

Scheme 1.

of $\mathbf{4}_{1-4}$ was realized by a reaction of salicylaldehydes ($\mathbf{1}_1$ and $\mathbf{1}_2$) with *p*-nitro- and *p*-cyanobenzyl bromides ($\mathbf{2}_1$ and $\mathbf{2}_2$) in the presence of an alkali following cyclization to a furan ring.[2] The nitro compounds ($\mathbf{4}_1$ and $\mathbf{4}_2$) were reduced to corresponding amino compounds ($\mathbf{4}_5$ and $\mathbf{4}_6$). These could be converted to various other compounds ($\mathbf{4}_{7-12}$). In addition, the cyano compounds ($\mathbf{4}_3$ and $\mathbf{4}_4$) were transformed to acids ($\mathbf{4}_{13}$ and $\mathbf{4}_{14}$) and subsequently to the acid chloride ($\mathbf{4}_{15}$).

The electronic absorption and fluorescence spectra of these 2-phenylbenzofuran derivatives were measured and several characteristics were observed.

Results and Discussion

Synthesis of 2-(4-Substituted phenyl)benzofurans ($\mathbf{4}_n$). A synthesis of $\mathbf{4}_n$ was achieved according to Scheme 1. 2-(Benzyloxy)benzaldehydes ($\mathbf{3}_1$, $\mathbf{3}_2$, and $\mathbf{3}_3$) were prepared by the reaction of $\mathbf{1}_n$ with $\mathbf{2}_n$ in the presence of KOH in EtOH (R_2=NO_2) or sodium ethoxide in dimethylformamide(DMF)–EtOH (R_2=CN). 2-(4-Substituted phenyl)benzofurans ($\mathbf{4}_{1-3}$) were obtained from the cyclization of $\mathbf{3}_{1-3}$ in the presence of sodium methoxide in DMF or KOH in DMF.[2] The nitrile ($\mathbf{4}_4$) could be directly synthesized by a reaction of $\mathbf{1}_2$ with $\mathbf{2}_2$ without the isolation of $\mathbf{3}_4$. Cyclizations of the bromides ($\mathbf{3}_5$ and $\mathbf{3}_6$) were unsuccessful under the above conditions.

The nitro compounds ($\mathbf{4}_1$ and $\mathbf{4}_2$) were easily reduced with iron(III) chloride–hydrazine hydrate to yield corresponding amino compounds ($\mathbf{4}_5$ and $\mathbf{4}_6$) in good yields.

From the purpose of the synthesis of the maleimides ($\mathbf{4}_9$ and $\mathbf{4}_{10}$), which could be expected as organic reagents for the selective determination of thiols, $\mathbf{4}_5$ and $\mathbf{4}_6$ were treated with maleic anhydride to give the maleamic acids ($\mathbf{4}_7$ and $\mathbf{4}_8$).[3] The cyclization of $\mathbf{4}_7$ and $\mathbf{4}_8$ in the presence of sodium acetate in acetic anhydride afforded $\mathbf{4}_9$ and $\mathbf{4}_{10}$.

The isothiocyanates ($\mathbf{4}_{11}$ and $\mathbf{4}_{12}$) were obtained by the treatment of $\mathbf{4}_5$ and $\mathbf{4}_6$ with an excess of thiophosgene.[4]

The nitriles ($\mathbf{4}_3$ and $\mathbf{4}_4$) were hydrolyzed with an alkali to give the carboxylic acids ($\mathbf{4}_{13}$ and $\mathbf{4}_{14}$), from which the acid chloride ($\mathbf{4}_{15}$) was derived.

Electronic Absorption Spectral Properties of $\mathbf{4}_n$. The longest wavelength absorption maxima of 2-phenylbenzofurans ($\mathbf{4}_n$) that were observed are given in Table 1. From the data it has become apparent that a dimethylamino substitution in $\mathbf{4}_n$ produces a red shift and a hypsochromic effect.

Fluorescence Spectral Properties. The fluorescence spectra of $\mathbf{4}_n$ were measured and the relative fluorescence intensities were compared with one another (Table 1). Red shifts were observed at the emission maxima (λ_{em}) of the dimethylamino substituted compounds relative to the corresponding unsubstituted ones. The isothiocyanates ($\mathbf{4}_{11}$ and $\mathbf{4}_{12}$) exhibited very little fluorescence and the nitro and *N*-maleimide compounds ($\mathbf{4}_1$, $\mathbf{4}_2$, $\mathbf{4}_9$, and $\mathbf{4}_{10}$) showed almost no fluorescence. These *N*-maleimides ($\mathbf{4}_9$ and $\mathbf{4}_{10}$) when combined with thiols showed strong fluorescence, *e.g.*, the adduct of $\mathbf{4}_9$ with *N*-acetyl-L-cysteine: λ_{ex} 320, λ_{em} 360 nm; the adduct of $\mathbf{4}_{10}$ with *N*-acetyl-L-cysteine: λ_{ex} 346, λ_{em} 470 nm (Fig. 1).[5] The large difference (124 nm) between λ_{ex} and λ_{em} in the latter seems to be an advantageous property as an analytical reagent for practical use. Recently, we have briefly reported on the fluorometric determination of glutathione using $\mathbf{4}_{10}$. This has proved to be useful as a new fluorigenic thiol-selective reagent.[6] Similarly, the isothiocyanates ($\mathbf{4}_{11}$ and $\mathbf{4}_{12}$) reacted with aliphatic amines to afford adducts which emitted strong fluorescence. An application of $\mathbf{4}_{11}$ and $\mathbf{4}_{12}$ to analytical reagents is now in progress.

Table 1. Spectral Data of 2-(4-Substituted Phenyl) Benzofurans

Compound	λ_{max}^{EtOH}	log ε	λ_{em}^{EtOH}	RFI[a]
$\mathbf{4}_1$	357	4.38	—	—
$\mathbf{4}_2$	438	4.34	—	—
$\mathbf{4}_3$	322	4.57	380	100
$\mathbf{4}_4$	392	4.48	512	36
$\mathbf{4}_5$	321	4.56	387	83
$\mathbf{4}_6$	345	4.52	400	71
$\mathbf{4}_9$	310	4.53	—	—
$\mathbf{4}_{10}$	355	4.50	—	—
$\mathbf{4}_{11}$	329	4.73	372	3.2
$\mathbf{4}_{12}$	375	4.59	430	8.5
$\mathbf{4}_{13}$	314	4.54	385	32
$\mathbf{4}_{14}$	366	4.48	465	31

a) Relative fluorescence intensity: the nitrile $\mathbf{4}_3$ is arbitrarily taken as 100 [concentration: 2μM (1 M= 1 mol dm^{-3})].

Experimental

Melting points are uncorrected. The ^{1}H NMR spectra (tetramethylsilane as an internal standard) were recorded on a JEOL FX 90Q spectrometer (chemical shifts given in ppm units). The IR spectra were taken using a JASCO IRA 2 spectrophotometer, the MS using a JEOL JMS-01SG mass spectrometer, and the UV using Hitachi 210 and Shimadzu UV-150 spectrophotometers. The fluorescence spectra were measured with a Shimadzu RF-540 fluorescence spectrophotometer.

4-(Dimethylamino)salicylaldehyde ($\mathbf{1}_2$). Aluminum chloride (18.8 g, 0.14 mol) was added to a solution of *m*-dimethylaminophenol (12.50 g, 0.094 mol) in chloroform (185 ml) and triethyl orthoformate (84 g, 0.57 mol) at room temperature and was mixed for 10 min. After the exothermic reaction had ceased, HCl (10%, 50 ml) was added and stirred to hydrolyze the resulting acetal. The mixture was neutralized with aq sodium hydroxide (10%). The resulting deposit was filtered off through a short column of Celite and washed with $CHCl_3$. The filtrate was combined with a cleaning solution, washed with saturated aq NaCl, dried over $MgSO_4$, and concentrated *in vacuo*. Recrystallization of the product from $CHCl_3$ gave 9.82 g (65%) of $\mathbf{1}_2$, mp 78—79 °C (79—80 °C[7]); ^{1}H NMR ($CDCl_3$): δ=2.81 (s, 6H, NMe_2), 5.8—6.1 (m, 2H, H^a and H^b), 7.13 (s, 1H, H^c), 9.20 (s, 1H, CHO); IR (Nujol): 1640

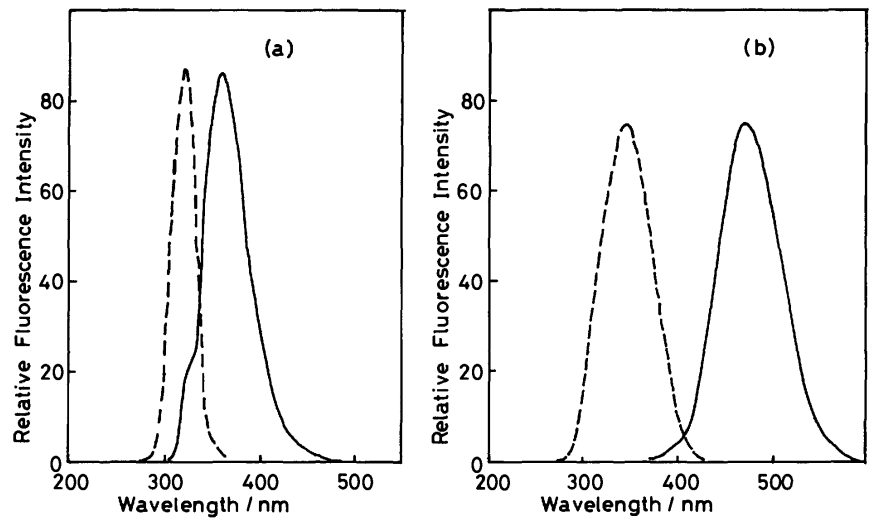

Fig. 1. Fluorescence spectra of the reaction mixtures of $\mathbf{4}_9$ and $\mathbf{4}_{10}$ with *N*-acetyl-L-cysteine (NAC).
(a): adduct of $\mathbf{4}_9$ with NAC; (b): adduct of $\mathbf{4}_{10}$ with NAC.
Procedure: A solution of $\mathbf{4}_9$ or $\mathbf{4}_{10}$ in acetone (0.5 mM 0.5 ml) was mixed with a solution of NAC-0.1 M H_3PO_4 (pH 7.0) (0.5 mM, 10 ml), stood for 1 h at room temperature, and then the fluorescence spectra were measured.

(C=O) cm^{-1}.

4-Dimethylamino-2-(4-nitrobenzyloxy)benzaldehyde ($\mathbf{3}_2$). A solution of KOH (0.40 g, 7 mmol) in EtOH (3 ml) was added to a solution of 4-(dimethylamino)salicylaldehyde ($\mathbf{1}_2$) (1.00 g, 6 mmol) and 4-nitrobenzyl bromide ($\mathbf{2}_1$) in EtOH (12 ml). Then, the mixture was refluxed for 7 h. After the solution had been cooled, the resulting crystals were filtered off, washed with water, and dried *in vacuo*. Then, the crystals were recrystallized from EtOH; 1.02 g, 56%; mp 179—180 °C; ^{1}H NMR ($CDCl_3$): δ=3.06 (s, 6H, NMe_2), 5.27 (s, 2H, CH_2), 6.05 (d, J=3 Hz, 1H, H^c), 6.33 (J=3, 9 Hz, 1H, H^b), 7.44 (d, J=9 Hz, 1H, H^a), 7.64 (d, J=9 Hz, 2H, H^d), 8.25 (d, J=9 Hz, 2H, H^e), 10.23 (s, 1H, CHO); IR (Nujol): 1655 (C=O) cm^{-1}; MS: m/z 300 (M^+). Found: C, 63.91; H, 5.38; N, 9.26%. Calcd for $C_{16}H_{16}N_2O_4$: C, 63.99; H, 5.37; N, 9.33%.

2-(4-Nitrobenzyloxy)benzaldehyde ($\mathbf{3}_1$): Yield, 86%; mp 117 °C (118 °C[8]); ^{1}H NMR ($CDCl_3$): δ=5.28 (s, 2H, CH_2), 6.92—8.32 (m, 8H, aromatic H), 10.52 (s, 1H, CHO); IR (Nujol): 1680 (C=O) cm^{-1}; MS: m/z 257 (M^+). (Found: C, 65.37; H, 4.28; N, 5.60%).

2-(4-Bromobenzyloxy)benzaldehyde ($\mathbf{3}_5$): Yield, 81%; mp 94—94.5 °C; ^{1}H NMR ($CDCl_3$): δ=5.14 (s, 2H, CH_2), 6.95—7.91 (m, 8H, aromatic H), 10.52 (s, 1H, CHO); IR (Nujol): 1685 (C=O) cm^{-1}. Found: C, 57.58; H, 3.79%. Calcd for $C_{14}H_{11}BrO_2$: C, 57.76; H, 3.81%.

4-Dimethylamino-2-(4-bromobenzyloxy)benzaldehyde ($\mathbf{3}_6$): Yield, 36%; mp 126—128 °C; ^{1}H NMR ($CDCl_3$): δ=3.05 (s, 6H, NMe_2), 5.10 (s, 2H, CH_2), 6.04 (d, J=3 Hz, H^c), 6.29 (J=3, 9 Hz, H^b), 7.30 (d, J=9 Hz, 2H, H^e), 7.50 (d, J=9 Hz, 1H, H^a), 7.73 (d, J=9 Hz, 2H, H^d), 10.22 (s, 1H, CHO); IR (Nujol): 1645 (C=O) cm^{-1}. Found: C, 57.40; H, 4.82; N, 4.50%. Calcd for $C_{16}H_{16}BrNO_2$: C, 57.50; H, 4.83; N, 4.19%.

2-(4-Cyanobenzyloxy)benzaldehyde ($\mathbf{3}_3$): Yield, 79%; mp 103—104 °C (105—106 °C[9]); IR (Nujol): 2250 (C≡N), 1685 (C=O) cm^{-1}. (Found: C, 76.01; H, 4.66; N, 6.02%).

6-Dimethylamino-2-(4-nitrophenyl)benzofuran ($\mathbf{4}_2$). A solution of $\mathbf{3}_2$ (0.90 g, 3 mmol) in DMF (6 ml) was added to a solution of sodium methoxide (prepared from Na (69 mg, 3 mmol)) in MeOH (1 ml) and refluxed for 20 min. The crystals ($\mathbf{4}_2$) deposited after adding MeOH (12 ml) to the mixture were filtered off and recrystallized from EtOH: red needles (0.73 g, 86%); mp 209.5—210.5 °C; ^{1}H NMR ($CDCl_3$): δ=3.04 (s, 6H, NMe_2), 6.76 (d, J=9 Hz, 1H, H^b), 6.81 (s, 1H, H^c), 7.10 (s, 1H, H^f), 7.43 (d, J=9 Hz, 1H, H^a), 7.85 (d, J=9 Hz, 2H, H^d), 8.24 (d, J=9 Hz, 2H, H^e); MS: m/z 282 (M^+). Found: C, 67.99; H, 4.97; N, 9.89%. Calcd for $C_{16}H_{14}N_2O_3$: C, 68.08; H, 5.00; N, 9.92%.

2-(4-Nitrophenyl)benzofuran ($\mathbf{4}_1$): Yield, 82% (yellow needles); mp 183.5—184.5 °C (182 °C[8]); ^{1}H NMR ($CDCl_3$): δ= 7.22—8.35 (m, 9H, aromatic H); MS: m/z 239 (M^+). (Found: C, 70.29; H, 3.71; N, 5.85%).

2-(4-Cyanophenyl)benzofuran ($\mathbf{4}_3$): Yield, 72%; mp 143—145 °C (145—146 °C[9]); ^{1}H NMR ($CDCl_3$): δ=7.15—7.97 (m, 5H, aromatic H), 7.69 (d, J=9 Hz, 2H, H^d), 7.93 (d, J=9 Hz, 2H, H^e); IR (Nujol): 2225 (C≡N) cm^{-1}; MS: m/z 219 (M^+). (Found: C, 82.28; H, 4.08; N, 6.44%).

6-Dimethylamino-2-(4-cyanophenyl)benzofuran ($\mathbf{4}_4$). A solution of $\mathbf{1}_2$ (2.00 g, 0.012 mol) in DMF (10 ml) was added to a solution of sodium ethoxide (prepared from Na (0.30 g, 0.013 mol)) in EtOH (8 ml) over a period of 20 min at room temperature. After the mixture had been stirred for 20 min, $\mathbf{2}_1$ (2.62 g, 0.013 mol) in DMF (8 ml) was added. The resulting solution was heated the at 110 °C for 2 h and the EtOH was removed under reduced pressure. The condensed solution was poured into a mixture of ice-cold water (54 g) and MeOH (16 ml) and stirred at 0 °C for 1 h. Deposited crystals were collected, washed with water, and then dried *in vacuo*. Crude $\mathbf{4}_4$ was recrystallized from petroleum benzine (bp 60—80 °C), 1.30 g, 41%: mp 164.5—166 °C; ^{1}H NMR ($CDCl_3$): δ=3.03 (s, 6H, NMe_2), 6.79 (J=3, 9 Hz, 1H, H^b), 6.89 (d, J=3 Hz, 1H, H^c), 7.04 (s, 1H, H^f), 7.42 (d, J=9 Hz, 1H, H^a), 7.63 (d, J=9 Hz, 2H, H^d), 7.83 (d, J=9 Hz, 2H, H^e); IR (Nujol): 2225 (C≡N) cm^{-1}; MS: m/z 262 (M^+). Found: C, 77.86; H, 5.34; N, 10.71%. Calcd for $C_{17}H_{14}N_2O$: C, 77.84; H, 5.38; N, 10.68%.

6-Dimethylamino-2-(4-aminophenyl)benzofuran (4₆). A benzene (20 ml)–MeOH (18 ml) solution of **4₂** (1.00 g, 4 mmol), active carbon (0.08 g) and a catalytic amount of $FeCl_3 \cdot 6H_2O$ was refluxed for 10 min and then hydrazine hydrate (98%) (2.30 g) was added dropwise.[10] The mixture was refluxed for 7 h and filtered off under reduced pressure. A concentrate of the filtrate yielded a crude product which was recrystallized from cyclohexane to afford **4₆** (0.72 g, 81%, orange needles): mp 198.5—200 °C; ^{1}H NMR ($CDCl_3$): δ= 2.98 (s, 6H, NMe_2), 6.68 (s, 1H, H^c), 6.71 (d, J=9 Hz, 2H, H^e), 6.80 (d, J=9 Hz, 1H, H^b), 7.25 (s, 1H, H^f), 7.35 (d, J=9H, 1H, H^a), 7.59 (d, J=9 Hz, 2H, H^d): IR (KBr): 3420, 3340 (NH_2) cm^{-1}; MS: m/z 252 (M^+). Found: C, 76.42; H, 6.34; N, 11.11%. Calcd for $C_{16}H_{16}N_2O$: C, 76.16; H, 6.36; N, 11.10%.

2-(4-Aminophenyl)benzofuran (4₅): Yield, quantitative; mp 150—151 °C (152—154 °C[11]); ^{1}H NMR ($CDCl_3$): δ=3.81 (broad s, 2H, NH_2), 6.67—7.70 (m, 9H, aromatic H); IR (KBr): 3440, 3340 (NH_2) cm^{-1}; MS: m/z 209 (M^+). (Found: C, 80.64; H, 5.31; N, 6.72%).

N-[4-(2-benzofuranyl)phenyl]maleamic Acid (4₇). A mixture of **4₅** (0.50 g, 2.4 mmol) and maleic anhydride (0.23 g, 2.4 mmol) in $CHCl_3$ (5 ml) was stirred for 3 h at room temperature. The deposited crystals were filtered off, washed with a small amount of $CHCl_3$, and then recrystallized from EtOH to afford **4₇** (0.64 g, 86%, orange crystals): mp *ca.* 238.5 °C (dec.); ^{1}H NMR (DMSO-d_6): δ=3.59 (broad s, 1H, NH), 6.31 (d, J=12 Hz, 1H, H^g or H^h), 6.53 (d, J=12 Hz, 1H, H^g or H^h), 7.21—7.95 (m, 9H, aromatic H), 10.52 (s, 1H, COOH); IR (KBr): 1695 (COOH), 1625 (CONH) cm^{-1}; MS: m/z 307 (M^+). Found: C, 70.32; H, 4.21; N, 4.57%. Calcd for $C_{18}H_{13}NO_4$: C, 70.35; H, 4.26; N, 4.56%.

N-[4-(6-Dimethylamino-2-benzofuranyl)phenyl]maleamic Acid (4₈): Yield, 84%; mp 219.5—221 °C; ^{1}H NMR (DMSO-d_6): δ=2.95 (s, 6H, NMe_2), 3.80 (broad s, 1H, NH), 6.32 (d, J=12 Hz, 1H, H^g or H^h), 6.52 (d, J=12 Hz, 1H, H^g or H^h), 6.71—7.45 (m, 4H, H^{a-c} and H^f), 7.76 (s, 4H, $H^{d,e}$), 10.56 (s, 1H, COOH); IR (KBr): 1695 (COOH), 1620 (CONH) cm^{-1}; MS: m/z 350 (M^+). Found: C, 68.56; H, 5.14; N, 7.88%. Calcd for $C_{20}H_{18}N_2O_4$: C, 68.56, H, 5.18; N, 8.00%.

N-[4-(6-Dimethylamino-2-benzofuranyl)phenyl]maleimide (4₁₀): A mixture of **4₈** (1.17 g, 3.3 mmol) and sodium acetate (0.03 g, 0.3 mmol) in acetic anhydride (18 ml) was refluxed and cooled in an ice bath. The deposited crystals of **4₁₀** were collected and washed with water while the filtrate was neutralized with aq NaOH (20%) and extracted with $CHCl_3$ (30 ml×2). The organic phase was washed with saturated aq NaCl, dried over $MgSO_4$, and concentrated *in vacuo* to afford **4₁₀**. The combined products were recrystallized from acetone to give reddish purple crystals (0.51 g, 46%): mp 203—204 °C; ^{1}H NMR ($CDCl_3$): δ=3.01 (s, 6H, NMe_2), 6.84 (s, 2H, $H^{g,h}$), 6.68—7.91 (m, 8H, aromatic H); IR (Nujol): 1710 (C=O) cm^{-1}; MS: m/z 332 (M^+). Found: C, 72.15; H, 4.81; N, 8.28%. Calcd for $C_{20}H_{16}N_2O_3$: C, 72.28; H, 4.85; N, 8.43%.

N-[4-(2-Benzofuranyl)phenyl]maleimide (4₉): Yield, 45%, mp 250.5—251.5 °C; ^{1}H NMR ($CDCl_3$): δ=6.87 (s, 2H, $H^{g,h}$), 7.06 (s, 1H, H^f), 7.45 (d, J=9 Hz, 2H, H^d or H^e), 7.20—7.88 (m, 4H, *o*-disubstituted benzene H), 7.95 (d, J=9 Hz, 2H, H^d or H^e); IR (Nujol): 1710 (C=O) cm^{-1}; MS: m/z 289 (M^+). Found: C, 74.52; H, 3.80; N, 4.81%. Calcd for $C_{18}H_{11}NO_3$: C, 74.43; H, 3.83; N, 4.84%.

4-(6-Dimethylamino-2-benzofuranyl)phenyl Isothiocyanate (4₁₂). A benzene solution of thiophosgene (1 ml) was added to a solution of **4₆** (1.00 g, 4 mmol) in acetone (10 ml). The mixture was refluxed for 1 h and cooled in an ice bath. The crystals which were separated were filtered off and recrystallized from cyclohexane to afford yellow leaflets (0.56 g, 48%). mp 140—140.5 °C; ^{1}H NMR ($CDCl_3$): δ=3.01 (s, 6H, NMe_2), 6.67—7.44 (m, 4H, aromatic H), 7.22 (d, J=9 Hz, 2H, H^d), 7.77 (d, J=9 Hz, 2H, H^e); IR (Nujol): 2070, 2110, 2280 (N=C=S) cm^{-1}; MS: m/z 294 (M^+). Found: C, 69.45; H, 4.79; N, 9.44; S, 10.90%. Calcd for $C_{17}H_{14}N_2OS$: C, 69.39; H, 4.79; N, 9.52; S, 10.89%.

4-(2-Benzofuranyl)phenyl Isothiocyanate (4₁₁): Yield, 45%; mp 127—129.5 °C; ^{1}H NMR ($CDCl_3$): δ=7.26 (d, J=9 Hz, 2H, H^d), 7.01—7.76 (m, 5H, benzofuran ring H), 7.81 (d, J=9 Hz, 2H, H^e); IR (Nujol): 2170, 2150 (N=C=S) cm^{-1}; MS: m/z 251 (M^+). Found: C, 71.82; H, 3.55; N, 5.44; S, 12.86%. Calcd for $C_{15}H_9NOS$: C, 71.69; H, 3.61; N, 5.57; S, 12.76%.

4-(2-Benzofuranyl)benzoic Acid (4₁₃). A solution of **4₃** (0.30 g, 1.3 mmol) and powdered KOH (1.00 g, 18 mmol) in ethylene glycol (25 ml) was refluxed for 6 h, cooled to room temperature, and poured into a mixture of ice-water (50 ml) and concd HCl (0.5 ml). The deposited crystals were filtered off, washed with water, and dried *in vacuo*. Any crude crystals were recrystallized from EtOH to give colorless needles (0.27 g, 83%). mp *ca.* 293 °C (dec) (301—302 °C[12]); ^{1}H NMR (DMSO-d_6): δ=7.19—7.75 (m, 5H, benzofuran ring H), 8.04 (s, 4H, $H^{d,e}$); IR (Nujol): 1680 (C=O) cm^{-1}; MS: m/z 238 (M^+). (Found: C, 75.54; H, 4.14%).

4-(6-Dimethylamino-2-benzofuranyl)benzoic Acid (4₁₄): Yield, 59%; mp *ca.* 157 °C (dec); ^{1}H NMR (DMSO-d_6): δ=3.39 (s, 6H, NMe_2), 6.80 (d, J=9 Hz, 1H, H^b), 6.90 (s, 1H, H^c), 7.39 (s, 1H, H^f), 7.46 (d, J=9 Hz, 1H, H^a), 7.88 (d, J=9 Hz, 2H, H^d), 8.01 (d, J=9 Hz, 2H, H^e); IR (Nujol): 1675 (C=O) cm^{-1}; MS: m/z 281 (M^+). Found: C, 72.43; H, 5.43; N, 4.92%. Calcd for $C_{17}H_{15}NO_3$: C, 72.58; H, 5.37; N, 4.98%.

4-(2-Benzofuranyl)benzoyl Chloride (4₁₅). A mixture of **4₁₃** (1.00 g, 4.2 mmol) and thionyl chloride (25 ml) was refluxed for 15 min and concentrated *in vacuo*. Purification of the residue by recrystallization from cyclohexane gave **4₁₅** as light yellow needles (1.01 g, 94%). mp 159—160 °C; ^{1}H NMR ($CDCl_3$): δ=7.18—7.69 (m, 5H, benzofuran ring H), 7.95 (d, J=9 Hz, 2H, H^d), 8.18 (d, J=9 Hz, 2H, H^e); IR (Nujol): 1760, 1725 (C=O) cm^{-1}; MS: m/z 256 (M^+). Found: C, 70.49; 3.47; Cl, 13.58%. Calcd for $C_{15}H_9ClO_2$: C, 70.19; H, 3.53; Cl, 13.81%.

The present work was partly supported by Grant-in-Aid for Scientific Research (No. 58470031) from the Ministry of Education, Science, and Culture.

References

1) For Part V, see K. Nakashima, T. Ando, T. Nakamizo, and S. Akiyama, *Chem. Pharm. Bull.*, in press.

2) *Cf.*, O. Dann, G. Bergen, E. Demant, and G. Volz, *Justus Liebigs Ann. Chem.*, **749**, 68 (1971).

3) *Cf.* Y. Kanaoka, M. Machida, Y. Ban, and T. Sekine, *Chem. Pharm. Bull.*, **15**, 1738 (1967).

4) *Cf.*, S. Goya, A. Takadate, T. Tanaka, and F. Nakashima, *Yakugaku Zasshi*, **100**, 289 (1980).

5) The structures of these adducts (1:1) isolated are now investigated.

6) K. Nakashima, H. Akimoto, K. Nishida, S. Nakatsuji, and S. Akiyama, *Talanta*, **32**, 167 (1985).

7) Farbenfabriken Baeyer A.-G., Brit. 775312 (1957); *Chem. Abstr.*, **52**, 434e (1957).
8) K. B. L. Mathur and H. S. Mehra, *J. Chem. Soc.*, **1960**, 1954.
9) W. Sahm, E. Schinzel, and P. Jürges, *Justus Liebigs Ann. Chem.*, **1974**, 523.
10) *Cf.*, T. Hirashima and O. Manabe, *Chem. Lett.*, **1975**, 259.
11) K. Chamberlain and G. A. Carter, *Pestic Sci.*, **11**, 526 (1980).
12) A. Horn, E. Schinzel, W. Sahm, and G. Roesch, Ger. Offen, 2400656 (1974); *Chem. Abstr.*, **82**, 45068n (1975).

Pyrolyse und Eigenschaften von Tris(2,3-epoxypropyl)- und Tris(2,3-epoxy-3-methylpropyl)-1,3,5-triazin-2,4,6(1*H*,3*H*,5*H*)-trion[1)]

Choichiro SHIMASAKI,* Masanori TAKEUCHI, Junichiro TSUTUGUCHI, Koichi SHIMIZU, und Hisato YAMAKAWA

Fakultät für Ingenieurwissenschaften, Universität Toyama, Nakagawasonomachi, Takaoka, Toyama 933

(Eingangsdatum: 5. Januar 1985)

Die Pyrolyse von Tris(2,3-epoxypropyl)-1,3,5-triazin-2,4,6(1*H*,3*H*,5*H*)-trion (**1**) [zwei Razem-Modifikationen: Typus (*R*,*R*,*R*)/(*S*,*S*,*S*) Schmp. 103—104 °C (**1a**); Typus (*R*,*R*,*S*)/(*S*,*S*,*R*) Schmp. 156—157 °C (**1b**)] und Tris(2,3-epoxy-3-methylpropyl)-1,3,5-triazin-2,4,6(1*H*,3*H*,5*H*)-trion (**2**) wurde bei thermischen Analysen untersucht. Der Spaltungsmechanismus durch Elektronenschlag von **1** und **2** wurde massenspektrometrisch untersucht. Die thermische Zersetzungsreaktion verläuft via die Bildung von 5-gliedrige Ringe (Oxazolidinon Ring) und dem Schmelzzustand. Eine kinetische Rechnung der thermischen Zersetungsreaktion auf Grund von DTA Kurven hat gezeigt, daß die Aktivierungsenergien der Zersetzungsreaktionen von **1a**, **1b**, und **2** jeweils 114,170, und 146 kJ mol^{-1} sind. Der Hauptspaltungsmechanismus für der Zersetzung mit dem Elektronenschlag von **1** und **2** besteht aus fünf Spaltungsstilen. Der hochauflösende Massenspektrometrie bestätigte die Zusammensetzung einer großen Anzahl von Spitzen in niederauflösenden Massenstrahlenspektren. Mittels der Kernresonanzspektroskopie läßt sich auch Spinentkopplungen und Lösungsmitteleinflüsse bei **1** und **2** untersuchen.

Einige Forschungen[2)] wurden über die Reaktivität von Tris(2,3-epoxypropyl)-1,3,5-triazin-2,4,6(1*H*,3*H*,-5*H*)-trion (**1**) ausgeführt, das Industriewichtigkeit und Strukturinteresse hat: zwei Razem-Modifikationen **1a** und **1b** wurden ergeben. Obwohl die zwei Strukturen mit IR Spektren[3)] registriert wurden, wurden Untersuchungen über thermische Analysen, wie DTA, nicht ausführlich durchgeführt.

In der jetzigen Abhandlung wurden die thermische Zersetzungsreaktion mit DTA und die Zersetzung mit dem Elektronenschlag zusammengefaßt. Außerdem wurde die Kernmagnetischenresonanzen, die Kopplungskonstanten, und die Lösungsmitteleinflüsse von **1** und Tris(2,3-epoxy-3-methylpropyl)-1,3,5-triazin-2,4,6(1*H*,3*H*,5*H*)-trion (**2**) gemessen.

Durchführung der Experimente

Materialien. **1** wurde von Nissankagaku A. G. erhalten. Es wurde zweimal mit Chloroform rekristallisiert. Die Trennung von **1a** und **1b** von ein ander wurde gleich nach der Methode von Price *et al.*[4)] ausgeführt. **2** wurde aus 2-Chlormethyl-2-methyloxiran und Cyanursäure mit Tetramethylammoniumchlorid als Katalysator, gemäß der Methode von Literatur,[5)] synthetisiert. Die Ergebnisse der physikochemischen Eigenschaften von **1** und **2** sind in Tabelle 1 zusammengestellt.

Apparate und Verfahren. DTA Kurven wurden an der Luft bei verschiedenen Aufheizgeschwindigkeiten mit einem Mitamura-DTA-Apparat aufgenommen. Für DTA und DSC wurde α-Al_2O_3 als Bezugsmittel gebraucht. IR Spektren wurden mittels eines JASCO IRA-I aufgenommen. ^{1}H und ^{13}C NMR-Spektren wurden mit einem JEOL JNM-FX 90 QFT Spektrometer aufgenommen. Als Lösungsmittel wurden deuteriertes Chloroform, Dimethylsulfoxid, und Pyridin, und schweres Wasser verwendet. Tetramethylsilan wurde als innere Standardsubstanz verwendet. Massenspektren wurden durch einen JMS-D300 Massenspektrometer mit direkten Probeinjektionen registriert. Schmelzpunkte wurden durch

TABELLE 1. PHYSIKALISCHE EIGENSCHAFTEN VON **1a**, **1b**, UND **2**

Verbindung	Elementaranalyse Gef. (Ber.)/% C	H	N	Schmp. θ_m/°C (Lit.)	α-Epoxid Äquivalent/100g Gef. (Ber.)	M$^+$ *m/z*	IR Spektrum (KBr) cm^{-1} (Lit.)[a)]
	48.15	5.11	13.91	99.1—99.8	0.989(1.009)	297	1686 (1695)
	(48.46	5.09	14.14)	(103.0—104.5)[a)]			980 (976)
1a							840 (847)
							800 (797)
							760 (753)
	47.82	5.21	13.92	153.6—154.1	0.984(1.009)	297	1692 (1695)
	(48.46	5.09	14.14)	(156.0—157.5)[a)]			1560 (1550)
							990 (990)
							925 (930)
1b							895 (897)
							820 (823)
							780 (789)
							750 (755)
	52.85	6.06	12.06	91.1—91.9	0.863(0.885)	339	1700
	(53.09	6.24	12.38)	(89.5—92.0)[b)]			940
2							920
							810
							775

a) H.P. Price und G.E. Schroll, *J. Org. Chem.*, **32**, 2005 (1967). b) Japanisches Patent 46—4745 (1971).

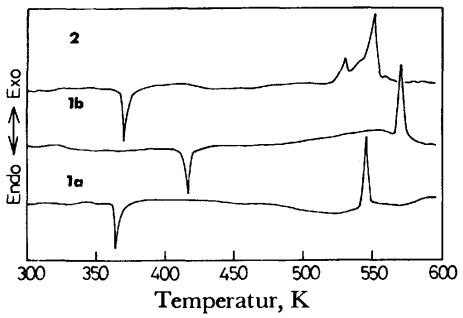

Abb. 1. DTA-Kurven von **1a**, **1b**, und **2** in Luft.

einen Mitamura-Mikroschmelzpunkt-Apparat bestimmt und nicht korrigiert. Für Dünnschicht-Chromatographie wurden Platten mit Kiselgel G nach Stahl (Typ 60) von Merck gebraucht. Elementaranalysen wurden bei der Analysen-Zentrale in der Medizinischen-Pharamazeutischen Universität Toyama durchgeführt. Quantitative Analyse von α-Epoxid wurde durch die HCl-Dioxan Methode durchgeführt.[6]

Ergebnisse und Diskussion

Thermische Analyse. Die DTA Kurven von **1a**, **1b**, und **2** sind in Abb. 1 dargestellt. Die DTA Kurven ergeben in allen drei Proben eine endotherme Spitze durch den Schmelzprozeß und jeweils eine exotherme Spitze bei der thermischen Zersetzung. Aber bei der exothermen Spitze von **2** wurde an der Schulter die parallellaufende Spaltbarkeit des Epoxids beobachtet. Aus dem Resultat der IR-Spektren war es zu erwarten, daß die Spaltung des Epoxids von **1a** und **1b** gleichzeit mit der Ringaufspaltung von Triazin vor sich ging. Bevor die exotherme Spitze entstand, ergaben sich keine thermische Zersetzungen für alle drei Proben.

Die Kinetik der thermischen Zersetzung wurde an der exothermen Reaktion untersucht. Am Anfang wurde die Abhängigkeit der Temperatur des DTA-Maximums von der Aufheizgeschwindigkeit bei der thermischen Zersetzung von **1a**, **1b** , und **2** untersucht. Die Ergebnisse, in Abb. 2 dargestellt, zeigen, daß die Temperatur des DTA-Maximums der thermischen Zersetzung auf die höhere Temperaturseite mit steigender Aufheizgeschwindigkeit verschoben wird. Kissinger[7] leitete die einer thermischen Zersetzungsreaktion entsprechende Gleichung ab

$$\frac{\mathrm{d}\ln(\phi/T_m^2)}{\mathrm{d}(1/T_m)} = -E/R, \qquad (1)$$

wo ϕ für Aufheizgeschwindigkeit steht, T_m für Temperatur des DTA-Maximums, E für Aktivierungsenergie, und R für Gaskonstante. Aus Gl. 1 ersieht man, daß bei kleinen Aktivierungsenergien eine starke Verschiebung des Temperaturmaximums der DTA-Kurve zu erwarten ist. In Abb. 3 ist das $\ln(\phi/T_m^2)-1/T_m$ Diagramm zur Berechnung der Aktivierungsenergie dargestellt. In Tabelle 2 sind die aus Neigung berechneten Aktivierungsenergien der Zersetzungsreaktionen bei den 3 Proben registriert. Der Unterschied zwischen **1a** und **1b** ist vom Temperaturmaximum der DTA-Kurve der Zersetzungsreaktionen abhängig, und der Unterschied zwischen **1** und **2** ist von der Seitenkette des Triazinrings abhängig.

Massenspektren. Der Zersetzungsverlauf kann mittels der entsprechenden Massenspektroskopie direkt verglichen werden. Die Abhängigkeit der Massenspektren von den 3 Proben wurden im Gebiet der Ionisierungsspannung 10—75 eV ausgeführt. Die Basisionenspitze von **2** ist m/z 309, Spitze $(M—CH_2O)^+$. Kein Unterschied zwischen den Massenspektren von **1a** und **1b** wurde erkannt. Die Basisionenspitze von [**1**] ist m/z 99, Spitze $(M/3)^+$, und die Spaltung eines einseiti-

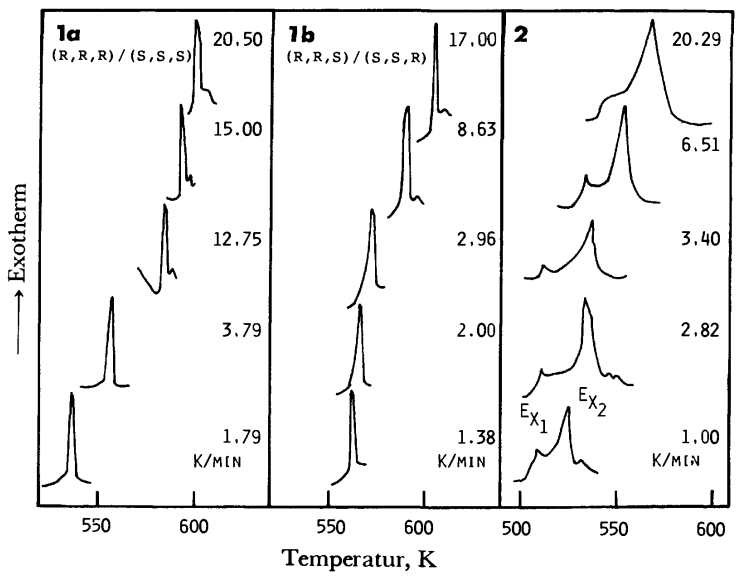

Abb. 2. Abhängigkeit der Temperatur des DTA-Maximums der Aufheizgeschwindigkeit bei der termischen Zersetzung von **1a**, **1b**, und **2**.

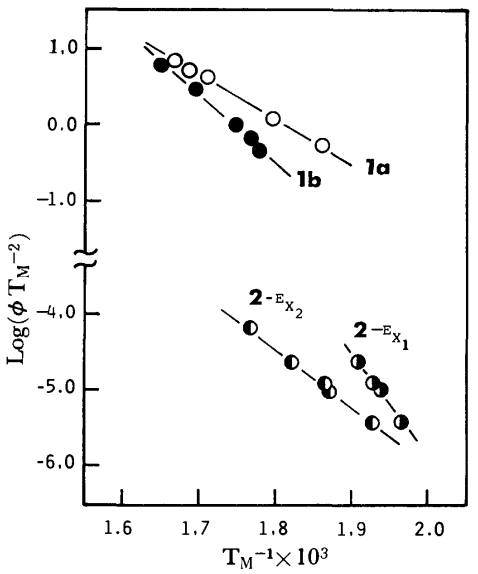

Abb. 3. $\ln(\phi/T_m^2)-1/T_m$ Diagramm zur Berechnung der Aktivierungsenergie nach der Gleichung (1).

TABELLE 2. ZUSAMMENFASSUNG DER KINETISCHEN DATA DER THERMISCHEN ZERSETZUNG VON **1a**, **1b**, UND **2**

Verbindung	$-E/R$[a]	Aktivierungsenergie, E / kJ mol^{-1}	r[b]
1a	5.97	114.4	0.998
1b	8.88	170.1	0.997
2 E_{X_1}	13.17	252.2	0.993
2 E_{X_2}	7.64	146.3	0.998

a) Neigung von gerade Linie. b) Korrelationskoeffizient.

gen Kettenradikals des Triazinrings ist m/z 269, Spitze $(M-28)^+$. Die hochauflösende Massenspektroskopie wurde ausgeführt, um den Spaltungsmechanismus bis in Details zu untersuchen. Die Ergebnisse der Messung sind in Tabelle 3 zusammengestellt.

Aus Tabelle 3 wurde der durch Elektronenschlages erregte Spaltungsmechanismus von **1** und **2** entnommen wie der in Abb. 4 dargestellte. Durch die in Abb. 4 zusammengefaßten Ergebnisse wird erkannt, daß der Hauptspaltungsmechanismus von **1** und **2** aus fünf verschiedenen Spaltungsstilen besteht. Die hierbei auftretenden Spaltungsstile lassen sich in drei Gruppen gliedern:

—Die Spaltung eines einseitigen Kettenradikals des Triazinrings (3 Stile).

—Die Spaltung eines zweiseitigen Kettenradikals des Triazinrings (ein Stil).

—Die Spaltung des Triazinrings; das Ion des Spaltungsprodukts ist gerade $(M/3)^+$.

Bei 1 gab es kein metastabiles Ion (m*), aber bei **2** wurde m* an den Stellen 215.0 und 186.7 erkannt. Diese metastabilen Ionen entsprechen den Prozessen m/z 339→m/z 270 und m/z 309→m/z 240 in Abb. 5. Neben den komplizierteren, bereits aufgeführten Spaltungsmechanismen aus dem Seitenkettenradikal ist die Spitze von $(M/3)^+$—d.h. die Spaltung des Triazinrings—bekannt, die auf Grund ihrer chemischen Zusammensetzung einen wesentlich einfacheren Abbaumechanismus hat. Es gelang uns, mit Hilfe einiger Beispiele, ein Spaltstücksion $(M/3)^+$ aus Isocyanuratderivate (**3**)

TABELLE 3. MASSENSTRAHLENSPEKTREN VON **1** UND **2**

Tris(2,3-epoxypropyl)isocyanurat (1)

m/z[a]	Relative Intensität[b]	Sigma/%[c]	Gefundenes Molekulargewicht	U.S.[e]	Wahrscheinliche Ionenzusammensetzung
87.0	18.2	1.27	87.0210(87.0318)[d]	2.0	$C_3H_5NO_2$
99.0	100.0	7.02	99.0253(99.0318)	3.0	$C_4H_5NO_2$
130.0	27.5	1.93	130.0323(130.0249)	3.5	$C_3H_4N_3O_3$
156.0	38.1	2.67	156.0277(156.0405)	4.5	$C_5H_6N_3O_3$
199.0	9.4	0.66	199.0505(199.0588)	5.0	$C_7H_9N_3O_4$
211.0	6.9	0.48	211.0579(211.0588)	6.0	$C_8H_9N_3O_4$
225.0	9.5	0.66	225.0776(225.0744)	6.0	$C_9H_{11}N_3O_4$
237.0	19.6	1.37	237.0703(237.0744)	7.0	$C_{10}H_{11}N_3O_4$
239.0	19.4	1.36	239.0937(239.0900)	6.0	$C_{10}H_{13}N_3O_4$
242.0	9.3	0.65	242.0789(242.0771)	5.5	$C_9H_{12}N_3O_5$
269.0	63.3	4.44	269.1084(269.1005)	6.0	$C_{11}H_{15}N_3O_5$
297.0	20.2	1.41	297.0944(297.0954)	7.0	$C_{12}H_{15}N_3O_6$

Tris(2,3-epoxy-3-methylpropyl)isocyanurat(2)

m/z[a]	Relative Intensität[b]	Sigma/%[c]	Gefundenes Moleculargewicht	U.S.[e]	Wahrscheinliche Ionenzusammensetzung
96.0	53.6	1.63	96.0444(96.0447)[d]	3.5	C_5H_6NO
113.0	39.0	1.19	113.0081(113.0474)	3.0	$C_5H_7NO_2$
170.0	34.1	1.04	170.0494(170.0561)	4.5	$C_6H_8N_3O_3$
200.0	26.8	0.82	200.0915(200.0666)	4.5	$C_7H_{10}N_3O_4$
222.0	17.1	0.51	222.0844(222.0873)	6.5	$C_{10}H_{12}N_3O_3$
240.0	24.4	0.74	240.0888(240.0978)	5.5	$C_{10}H_{14}N_3O_4$
252.0	17.6	0.53	252.0844(252.0978)	6.5	$C_{11}H_{14}N_3O_4$
270.0	17.6	0.53	270.1052(270.1083)	5.5	$C_{11}H_{16}N_3O_5$
292.0	17.1	0.51	292.1179(292.1290)	7.5	$C_{14}H_{18}N_3O_4$
309.0	85.4	2.59	309.1474(309.1317)	7.0	$C_{14}H_{19}N_3O_6$
339.0	46.3	1.37	339.1428(339.1422)	7.0	$C_{15}H_{21}N_3O_6$

a) Molekular-Ion, unterstrichen. b) Relative Intensität der Basisionenspitze der Spektren als 100. c) Spitzenhöhe im Prozent der Gesamtionization. d) Berechnete Werte. e) U.S.=Unsättigungsgrad.

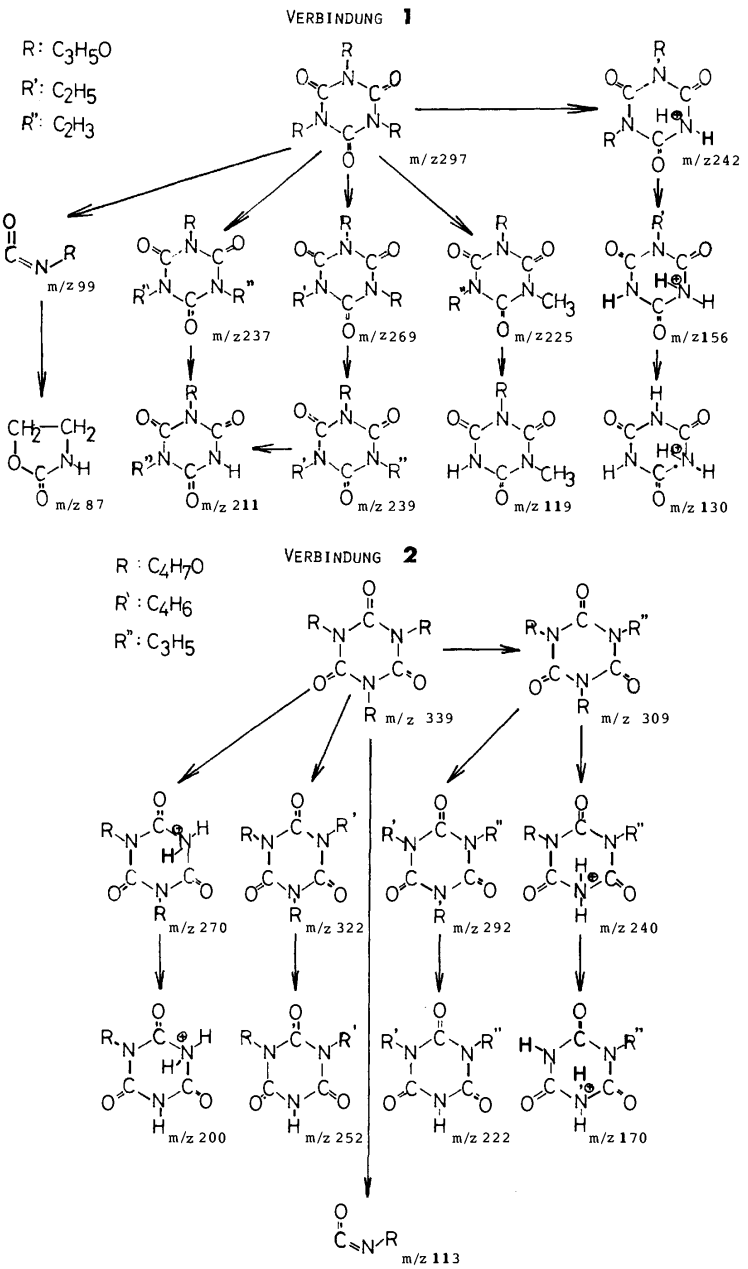

Abb. 4. Hauptspaltungsmechanismus des Elektronenschlages von **1** und **2**.

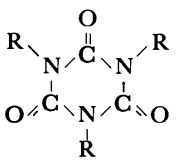

3

zu erhalten, wo die Proben die folgenden waren: R=-H, $-CH_3$, $-CH_2CH_2OH$, $-CH_2CH{=}CH_2$, $-CH_2CH_2CONH_2$, $-CH_2C_6H_5$, $-CH_2CH(OH)CH_2OH$, und -Cl. Alle Proben haben die Spitze von $(M/3)^+$ gegeben.

NMR-spektren. Die ^1H NMR-Spektren von **1** und **2** ergeben eine Reihe interessanter Erscheinungen; das Spektrum des reinen **1** besteht aus einem komplizierten Multiplett mit relativ breiten Banden. In vielen Fällen waren die Bandlagen abhängig vom Lösungsmittel und man kann sich dieses Effektes bedienen, um komplizierte Spektren zu vereinfachen. Daher wurden die ^1H NMR-Spektren von **1** in $CDCl_3$, $(CD_3)_2SO$, und C_5D_5N (deuteriertes Pyridin) gemessen. Wir können die Vereinfachung der Spektren durch C_5D_5N deutlich erkennen. In $CDCl_3$ erschienen die Signale der Epoxidenprotonen H_A und H_B als zwei Quadruplette im Abstand von 2.701 und 2.839 ppm, in $(CD_3)_2SO$ im Abstand von 2.599 und 2.751 ppm, und in C_5D_5N als zwei Singulette im Abstand von 2.708 und 2.743 ppm. Dies ist ein besonders schönes Beispiel der Induktionsverschiebung für **1** in aromatischen Lösungen. Das Spektrum von **1** ist ABX-Typ.

Bei 100 MHz ergab das Spektrum von **1** kompliziertere Signale. Die Spinentkopplungen ließen

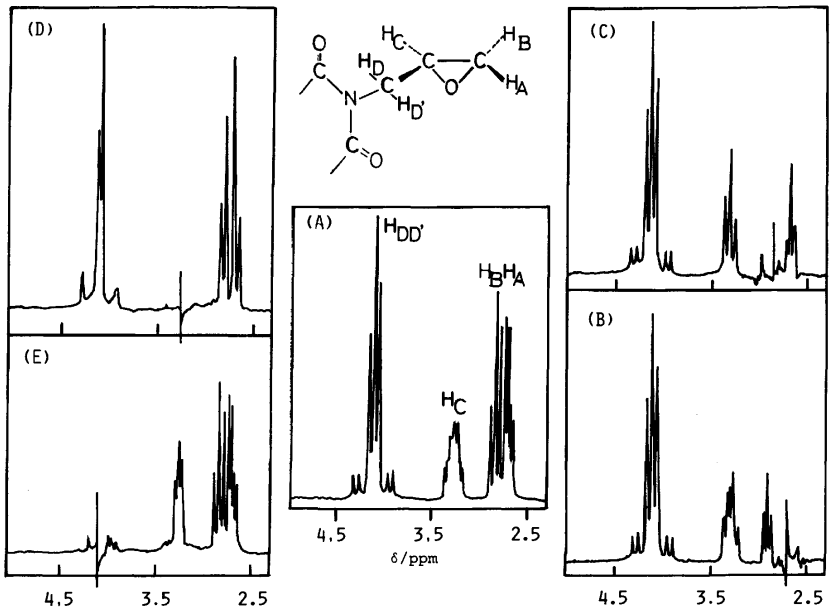

Abb. 5. ^{1}H NMR-Spektrum von **1** bei 100 MHz. Darüber die Signale bei teilweiser Spinentkopplung.
A) ^{1}H NMR-Spektrum von **1** bei 20 proz. Lösung in $CDCl_3$, B) Spinentkopplung von H_A in Spektrum-(A), C) Spinentkopplung von H_B in Spektrum-(A), D) Spinentkopplung von H_C in Spektrum-(A), E) Spinentkopplung von $H_{D,D'}$ in Spektrum-(A).

TABELLE 4. CHEMISCHE VERSCHIEBUNGEN IN VERSCHIEDENEN LÖSUNGSMITTELN UND KOPPLUNGSKONSTANTEN IN $CDCl_3$ VON **1** UND **2**

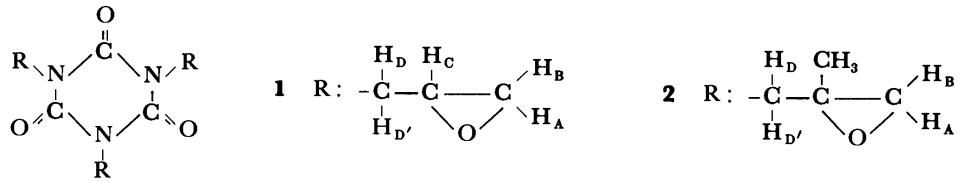

Verbindung	Chemische Verschiebungen (Vielfeltigkeit)[a] δ/ppm					Kopplungskonstanten/Hz						Losungsmittel
	H_A	H_B	H_C	CH_3	H_D,$H_{D'}$	J_{AB}	J_{AC}	J_{BC}	J_{CD}	$J_{CD'}$	$J_{DD'}$	
	2.701 (Q)	2.839 (T)	3.271 (M)		4.114 (H)	4.83	2.42	4.61	4.83	5.27	14.06	20.0% $CDCl_3$
1	2.708 (S)	2.743 (S)	3.363 (M)		4.174 (O)							19.8% C_5D_5N
	2.599 (Q)	2.751 (T)	3.169 (M)		3.940 (H)							19.5% $(CD_3)_2SO$
	2.590 (Q)	2.703 (D)		1.392 (S)	4.162 (M)	4.84					14.06	20.6% $CDCl_3$
2	2.576 (T)	2.913 (D)		1.364 (S)	4.276 (M)							20.2% C_5H_5N

a) S: Singulett, D: Dublett, T: Triplett, Q: Quartett, H: Heptett, O: Oktett, M: Multiplett.

sich auch bei komplizierteren Molekülen anwenden. Darüber hinaus wurden die Signale von **1** bei teilweiser Spinentkopplung gemessen. In Abb. 5 wurden die Spektren von **1** in $CDCl_3$ nach teilweiser Spinentkopplung wiedergegeben. Die Bandgruppen im Spektrum dieser Verbindung wurden so weit voneinander getrennt, daß es möglich war, alle Signale einzeln zu sättigen und die Veränderung bei den übrigen Bändern zu beobachten. Die drei Kopplungskonstanten, J_{AB}, J_{AC}, und J_{BC}, in substituierten Ethylenoxiden (**4**), sind von Reilly und Swalen[8] für eine Reihe von Verbindungen bestimmt worden. Die gefundenen Werte liegen bei J_{AB}=5.8±0.5, J_{AC}=2.2±0.5, und J_{BC}=4.6±0.5.

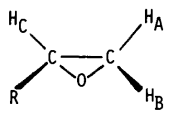

4

Die Ergebnisse der chemischen Verschiebungen und der Kopplungskonstanten von **1** und **2** sind in Tabelle 4 zusammengestellt. Tabelle 4 zeigt, daß die Werte

TABELLE 5. ^{13}C-CHEMISCHE VERSCHIEBUNGEN IN ppm AUF VERSCHIEDENEN LÖSUNGSMITTELN

Verbindung	δ/ppm C=O	(1)	(2)	(3)	(4)	Lösungsmittel	Konzentration/%
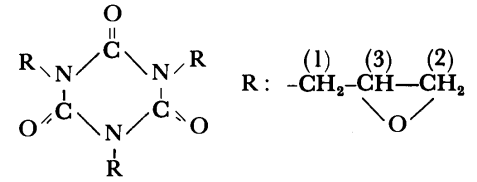	149.489	46.345	44.734	48.586		$CDCl_3$	20.0
	148.611	46.148	44.978	48.927		C_5D_5N	19.8
	148.952	45.319	43.978	48.488		$(CD_3)_2SO$	19.5
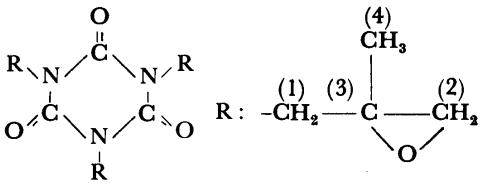	148.904	52.316	45.831	54.364	19.844	$CDCl_3$	20.6
	149.489	52.365	46.221	54.607	19.844	C_5D_5N	20.2

der Kopplungskonstanten J_{AB}, J_{AC}, und J_{BC}, mit den Werten von Reilly und Swalen übereinstimmen. Bei teilweiser Spinentkopplung übt die Spinentkopplung des Protons A von **1** einen Einfluß auf die Werte der Kopplungskonstante J_{BC} aus; im Proton B beeinflussen J_{CD} und $J_{CD'}$, im Proton C J_{AB} und $J_{DD'}$, und in Protonen D und D' J_{AB}. Die Zuordnung der Spektren wird dadurch erleichtert, daß die Kopplungskonstanten wenig von der Art der Spinentkopplung abhängig sind. Die gefundenen Werte in $CDCl_3$ liegen bei J_{AB}=4.83, J_{AC}=2.42, J_{BC}=4.61, J_{CD}=4.83, $J_{CD'}$=5.27, und $J_{DD'}$= 14.06 Hz.

Die Bandlagen einiger ^{13}C Kernresonanzspektren von **1** und **2** sind in Tabelle 5 angegeben. Die chemische Verschiebung von ^{13}C-Signalen ist nicht von den Lösungsmitteln abhängig.

Die Materialien in der vorliegenden Arbeit wurden von Nissankagaku A.G. angeboten. Für die Bedienung der Apparatur zur Anfertigung der Mass und NMR-Spektren haben sich in dankenswerterweise Fräulein M. Shinoda und Herr K. Yoneyama zur Verfügung gestellt. Herrn Prof. S. Takeuchi danken wir bestens für wertvolle Hinweise.

Literaturen

1) Nachricht X von "Untersuchungen über Zersetzung und Bildung von triazinserien Verbindungen." Nachricht IX von dieser Serien: C. Shimasaki, K. Yamakuro, F. Takeuchi, N. Oki, A. Uchida, und M. Oonishi, *Nippon Kagaku Kaishi*, **1983**, 82.

2) M. Budnowski, *Kunststoffe*, **55**, 641 (1965); T. Ishikawa und J. Watanabe, *Nippon Kagaku Kaishi*, **1980**, 852.

3) M. Budnowski, *Angew. Chem.*, **80**, 851 (1968).

4) H. P. Price und G. E. Schroll, *J. Org. Chem.*, **32**, 2005 (1965).

5) Japanisches Patent 46-4745 (1971).

6) F. T. Weiss, "Determination of Organic Compounds: Methods and Procedures." Wiley-Interscience, New York (1970).

7) H. E. Kissinger, *Anal. Chem.*, **29**, 1702 (1957).

8) C. A. Reilly und J. D. Swalen, *J. Chem. Phys.*, **32**, 1378 (1960).

Reactions of α-Lithiatd 4*H*-1-Benzothiopyran-4-one and 1,2-Dihydrocyclopenta[*b*][1]benzothiopyran-9(3*H*)-one Derivatives

Ichiro HIRAO, Masahiko YAMAGUCHI,* Takashi TERADA, and Koichi HASEBE
Department of Industrial Chemistry, Kyushu Institute of Technology, Sensui-cho, Tobata-ku, Kitakyushu 804
(Received January 14, 1985)

Treatment of 5- and 7-methoxy-2-methyl-4*H*-1-benzothiopyran-4-one with lithium diisopropylamide followed by electrophiles gave 2-substituted 4*H*-1-benzothiopyran-4-ones. Utilizing this reaction, 3-substituted 6- and 8-methoxy-1,2-dihydrocyclopenta[*b*][1]benzothiopyran-9(3*H*)-ones were also synthesized, and several compounds showed potential analgesic and anti-inflammatory activities.

In our previous synthetic studies on heterocyclic compounds directed to the development of biologically active substances, we prepared polycyclic derivatives of 1-alkyl-4-pyridone[1] and 4-pyrone,[2] which have a common 6-membered cyclic structure with nitrogen or oxygen atom at 1-position and a carbonyl group at 4-position. Recently, we found that a sulfur analogue, 1,2-dihydro-8-methoxycyclopenta[*b*][1]benzothiopyran-(3*H*)-one (**8**), possesses analgesic and anti-inflammatory activities. In order to examine the activities of the related compounds, we devised an α-lithiation reaction of this heterocyclic system. The present report describes the reaction of the lithiated 4*H*-1-benzothiopyran-4-ones with electrophiles.

The starting materials, 7- and 5-methoxy-2-methyl-4*H*-1-benzothiopyran-4-one (**3** and **4**) or 8- and 6-methoxy-1,2-dihydrocyclopenta[*b*][1]benzothiopyran-9(3*H*)-one (**8** and **9**), are synthesized from *m*-methoxybenzenethiol (**1**) and ethyl acetoacetate (**2**) or ethyl 2-oxo-1-cyclopentanecarboxylate (**7**), respectively, by the condensation in polyphosphoric acid at 80 °C.[3] Each isomer is separable by chromatography on silica gel. The assignment is based on the NMR spectra. Thus, a triplet with 8 Hz of the coupling constant at δ 7.4 was observed for **4** and **8**, indicating the presence of 1,2,3-trisubstituted aromatic ring, while the other isomers **3** and **9** showed a broad singlet at δ 6.9.

Benzothiopyranones **3**, **4**, **8**, and **9**, thus obtained, were treated with lithium diisopropylamide (LDA) and lithiation ocurred smoothly. The reaction with several alkyl halides and aldehydes gave the corresponding benzothiopyranones **5**, **6**, **10**, and **11** (Scheme 1 and 2). The results are summarized in Tables 1 and

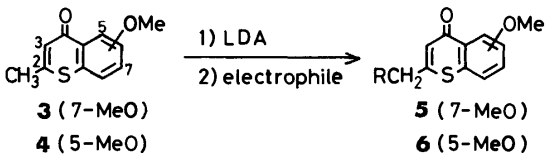

3 (7-MeO)
4 (5-MeO)
5 (7-MeO)
6 (5-MeO)

Scheme 1.

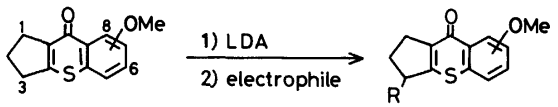

8 (8-MeO)
9 (6-MeO)
10 (8-MeO)
11 (6-MeO)

Scheme 2.

TABLE 1. SYNTHESIS OF 2-SUBSTITUTED 7- AND 5-METHOXY-4*H*-1-BENZOTHIOPYRAN-4-ONES

Substrate	Electrophile	Product	R	Yield/%
3	MeI	**5a**	Me	57
	CH_2=$CHCH_2Br$	**5b**	CH_2=$CHCH_2$	43
	$C_2H_5O_2CCH_2Br$	**5c**	$C_2H_5O_2CCH_2$	70
	PhCHO	**5f**	PhCH(OH)	67
	p-$MeOC_6H_4CHO$	**5g**	*p*-$MeOC_6H_4CH(OH)$	63
	3,4-$(OCH_2O)C_6H_3CHO$	**5h**	3,4-$(OCH_2O)C_6H_3CH(OH)$	58
4	PhCHO	**6f**	PhCH(OH)	71
	p-$MeOC_6H_4CHO$	**6g**	*p*-$MeOC_6H_4CH(OH)$	21

TABLE 2. SYNTHESIS OF 3-SUBSTITUTED 8- AND 6-METHOXY-1,2-DIHYDROCYCLOPENTA [*b*][1] BENZOTHIOPYRAN-9(3*H*)-ONES

Substrate	Electrophile	Product	R	Yield/%
8	MeI	**10a**	Me	70
	$C_2H_5O_2CCH_2Br$	**10c**	$C_2H_5O_2CCH_2$	69
	EtI	**10d**	Et	43
	$PhCH_2Br$	**10e**	$PhCH_2$	40
	PhCHO	**10f**	PhCH(OH)	60
	O_2	**10i**	HO	17
9	$C_2H_5O_2CCH_2Br$	**11c**	$C_2H_5O_2CCH_2$	65
	O_2	**11i**	HO	15

2. In general, the reaction ocurred at C-2 methyl carbon for **3** and **4**, and at 3-position for **8** and **9**. However, a small amount of mixture of other products, presumable compounds formed by alkylation at C-3 carbon, was also detected in methylation and allylation of **3**.

When attentions are paid on β-sulfur substituted α,β-unsaturated carbonyl moiety of these benzothiopyranones, the present process can be classified as the γ-alkylation of enone system. As β-sulfur substituted enones are reported to give α,α-dialkylated products,[4] this synthesis provides a novel example of γ-alkylation. In contrast, carbon-carbon bond formation at γ-position of α,β-unsaturated carbonyl compounds possessing nitrogen[5] or oxygen[6] substituents are well known (Fig. 1).

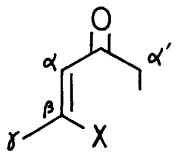

X = RO, RS, R_2N

Fig. 1.

Though the lithiation of **3** was performed at −78 °C in THF-HMPA, lithiated **4** was unstable under these reaction conditions. After the examination of the conditions including bases and solvents, the lithiation was achieved in toluene-HMPA at −78 °C, and addition to aldehydes gave the alcohols **6**. The alkylation, however, was ineffective even in this solvent system.

The lithiated **8** and **9** are treated with electrophiles in THF-HMPA at 0 °C to give 3-substituted 1,2-dihydrocyclopenta[*b*][1]benzothiopyran-9(3*H*)-ones **10** and **11** in good yields. The possibility of the lithiation at 1-position could be excluded for **8** and **9** from the following observations. Thus, 2-ethyl-3-methyl-5-methoxy-4*H*-1-benzothiopyran-4-one (**12**), synthesized from ethyl 2-methyl-3-oxopentanoate, was treated with LDA in toluene-HMPA at −78 °C followed by benzaldehyde, and 2-(2-hydroxy-1-methyl-2-phenylethyl)-3-methyl-5-methoxy-4*H*-1-benzothiopyran-4-one (**13**) was isolated as a mixture of diastereomers. The structure was determined by ^{1}H-NMR. Disappearance of a triplet (δ 1.26) of **12**, and observation of a couple of doublets at δ 1.06 and 1.40 in **13** show that the addition ocurred at the methylene carbon of C-2 ethyl group and not at C-3 methyl carbon (Scheme 3.).

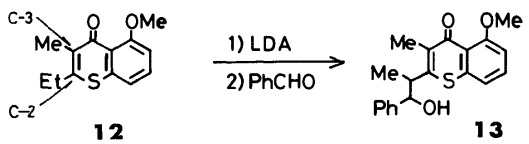

Scheme 3.

Oxygenation of lithiated **8** and **9** was also perfomed by introducing gaseous oxygen at 0 °C followed by the reduction of the resulted peroxide with sodium sulfite[7] to give 6- and 8-methoxy-1,2-dihydro-3-hydroxycyclopenta[*b*][1]benzothiopyran-9(3*H*)-one (**10i** and **11i**). Several attempts to improve the yields, however, were unsuccessful.

Esters **10c** and **11c** were further converted to the corresponding carboxylic acids **10j** and **11j** by treating with lithium hydroxide in refluxing THF-H_2O for 2 h.

Compounds **8**, **10a**, and **10d** showed a potent analgesic activities by the acetic acid induced writhing method. ED_{50}: **8**; 11.5 mg/Kg. **10a**; 5.8 mg/Kg. **10b**; 12.5 mg/Kg. And **8** showed an anti-inflammatory activities against carragenan-induced rat paw edma. ED_{50}: 30 mg/Kg.

Experimental

The melting points are uncorrected. ^{1}H-NMR spectra were obtained with JEOL JNM-FX-60. Chemical shift values are given in ppm relative to internal Me_4Si. IR spectra were performed with Shimadzu IR-408. High resolution mass spectra were taken with JEOL JMS-DX-300. Elemental analyses were performed with Yanagimoto CHN Corder, MT-2 type. Silica gel chromatographies were conducted on Wako gel B5F or C-200 (Wako Pure Chemical Industries LTD.).

7-Methoxy-2-methyl-4H-1-benzothiopyran-4-one (3) and 5-Methoxy-2-methyl-4H-1-benzothiopyran-4-one (4). These compounds were synthesized from *m*-methoxybenzenethiol (**1**) and ethyl acetoacetate (**2**) according to the reported method[3] in 28 and 26% yield, after the separation by silica gel chromatography with ethyl acetate:hexane=1:1 as the eluent. **3**: mp 121 °C (benzene-hexane), lit,[8] mp 118—119.5 °C. ^{1}H-NMR ($CDCl_3$) δ=2.40 (3H, d, J=1 Hz), 3.88 (3H, s), 6.75 (1H, d, J=1 Hz), 6.8—7.1 (2H, m), and 8.39 (1H, dd, J=1, 8 Hz). IR (KBr) 1630, 1600, 1260, and 850 cm^{-1}. Found: C, 63.78 H, 4.99%. Calcd for $C_{11}H_{10}O_2S$: C, 64.06; H, 4.89%. **4**: mp 83 °C (benzene-hexane). ^{1}H-NMR ($CDCl_3$) δ=2.34 (3H, d, J=1 Hz), 3.96 (3H, s), 6.69 (1H, d, J=1 Hz), 6.90 (1H, dd, J=1, 8 Hz), 7.08 (1H, dd, J=1, 8 Hz), and 7.46 (1H, t, J=8 Hz). IR (KBr) 1610, 1260, and 1030 cm^{-1}. Found: C, 64.29; H, 4.99%. Calcd for $C_{11}H_{10}O_2S$: C, 64.06; H, 4.89%.

1,2-Dihydro-8-methoxycyclopenta[b][1]benzothiopyran-9(3H)-one (8), 1,2-Dihydro-6-methoxycyclopenta[b][1]benzothiopyran-9(3H)-one (9). Synthesized from **1** and ethyl 2-oxo-1-cyclopentanecarboxylate (**7**) as above (20 and 20% yield). **8**: mp 137 °C (benzene-hexane). ^{1}H-NMR ($CDCl_3$) δ=1.8—2.4 (2H, m), 2.7—3.2 (4H, m), 3.86 (3H, s), 6.93 (1H, brs), 7.00 (1H, dd, J=2.5, 9 Hz), and 8.43 (1H,dd, J=1, 9 Hz). IR (KBr) 1590, 1240, and 1020 cm^{-1} Found: C, 66.91; H, 5.12%. Calcd for $C_{13}H_{12}O_2S$: C, 67.22, H, 5.29%. **9**: mp 155 °C (benzene-hexane). ^{1}H-NMR ($CDCl_3$) δ=1.8—2.4 (2H, m), 2.7—3.1 (4H, m), 3.95 (3H, s), 6.89 (1H, dd, J=1.5, 8 Hz), 7.08 (1H, dd, J=1.5, 8 Hz), and 7.42 (1H, t, J=8 Hz). IR (KBr) 1605, 1460, 1270, 1040, and 800 cm^{-1}. Found: C, 67.30; H, 5.11%. Calcd for $C_{13}H_{12}O_2S$: C, 67.22, H, 5.21%.

2-Ethyl-3-methyl-7-methoxy-4H-1-benzothiopyran-4-one (12). The compound **12** was synthesized as described above from ethyl 2-methyl-3-oxopentanoate in 16% yield. **12**: mp 110 °C (benzene-hexane). ^{1}H-NMR ($CDCl_3$) δ=1.26 (3H, t, J=7 Hz), 2.17 (3H, s), 2.63 (2H, q, J=7 Hz), 3.94 (3H, s), 6.85 (1H, dd, J=1.5, 8 Hz), 7.12 (1H, dd, J=1.5, 8 Hz), and 7.40 (1H, t, J=8 Hz). IR (KBr) 1610, 1270, 1040, and 800 cm^{-1}. Exact mass

Found: *m/z* 234.0715. Calcd for $C_{13}H_{14}O_2S$: M, 234.0715.

*Reaction of Lithiated **3** with Alkyl Halides and Aldehydes. General Procedure*: Under a nitrogen atmosphere, to a THF (1 ml) solution of diisopropylamine (50 mg, 0.5 mmol) was added butyllithium in hexane (0.32 ml, 0.5 mmol) at −78 °C. After 5 min, **3** (103 mg, 0.5 mmol) in THF (2 ml) and HMPA (1 ml) were added successively. The mixture was stirred for 5 min and an alkyl halide (1.5 mmol) or an aldehyde (0.6 mmol) in THF (2 ml) was added. After 15—30 min at the temperature, the reaction was quenched with saturated aqueous ammoinum chloride, and the products were two times extracted with ethyl acetate. The combined extracts were washed with water and brine, dried over Na_2SO_4. Removal of the solvents *in vacuo*, and chromatography on silica gel (eluent; ethyl acetate:hexane=1:1) gave the product **5**.

*2-Ethyl-7-methoxy-4H-1-benzothiopyran-4-one (**5a**)*: mp 61 °C (ether-hexane). ^{1}H-NMR ($CDCl_3$) δ=1.28 (3H, t, J=7 Hz), 2.61 (2H, q, J=7 Hz), 3.83 (3H, s), 6.72 (1H, s), 6.86 (1H, brs), 6.93 (1H, dd, J=2, 8 Hz), and 8.31 (1H, dd, J=1, 8 Hz). IR (KBr) 1620, 1600, 1260, 1230, 1050, and 1020 cm^{-1}. Found: C, 65.17; H, 5.35%. Calcd for $C_{12}H_{12}O_2S$: C, 65.43; H, 5.49%.

*2-(3-Butenyl)-7-methoxy-4H-1-benzothiopyran-4-one (**5b**)*: mp 65 °C (ether-hexane). ^{1}H-NMR ($CDCl_3$) δ=2.1—2.9 (4H, m), 3.84 (3H, s), 4.8—5.2 (2H, m), 5.5—6.2 (1H, m), 6.74 (1H, s), 6.8—7.1 (2H, m), and 8.35 (1H, dd, J=1, 8 Hz). IR (KBr) 1610, 1600, 1250, and 840 cm^{-1}. Found: C, 68.21; H, 5.76%. Calcd for $C_{14}H_{14}O_2S$: C, 68.26; H, 5.73%.

*2-(2-Ethoxycarbonylethyl)-7-methoxy-4H-1-benzothiopyran-4-one (**5c**)*: mp 126 °C (benzene-hexane). ^{1}H-NMR ($CDCl_3$) δ=1.26 (3H, t, J=7 Hz), 2.3—3.1 (4H, m), 3.87 (3H, s), 4.16 (2H, q, J=7 Hz), 6.78 (1H,s), 6.93 (1H, s), 6.99 (1H, dd, J=2, 8 Hz), and 8.35 (1H, dd, J=2, 8 Hz). IR (KBr) 1725, 1620, 1600, and 1240 cm^{-1}. Found: C, 61.42; H, 5.72%. Calcd for $C_{15}H_{16}O_4S$: C, 61.43; H, 5.52%.

*2-(2-Hydroxy-2-phenylethyl)-7-methoxy-4H-1-benzothiopyran-4-one (**5f**)*: mp 129 °C (benzene-hexane). ^{1}H-NMR ($CDCl_3$) δ=2.94 (2H, d, J=6 Hz), 3.81 (3H, s), 4.33 (1H, brs), 5.04 (1H, t, J=6 Hz), 6.7—7.0 (3H, m), 7.0—7.5 (5H, m), and 8.18 (1H, dd, J=1, 8 Hz). IR (KBr) 3300, 1610, 1600, 1560, 1050, 830, 760, and 710 cm^{-1}. Found: C, 68.70; H, 4.87%. Calcd for $C_{18}H_{16}O_3S$: C, 69.21; H, 5.16%.

*2-[2-Hydroxy-2-(p-methoxyphenyl)ethyl]-7-methoxy-4H-1-benzothiopyran-4-one (**5g**)*: mp 114 °C (benzene-hexane). ^{1}H-NMR ($CDCl_3$) δ=1.84 (1H, brs), 3.00 (2H, d, J=7 Hz), 3.80 (3H, s), 3.88 (3H, s), 5.00 (1H, t, J=7 Hz), 6.79 (1H, s), 6.8—7.1 (4H, m), 7.32 (2H, d, J=8 Hz), and 8.34 (1H, dd, J=1, 8 Hz). IR (KBr) 3400, 1600, 1230, and 835 cm^{-1}. Found: C, 66.55; H, 5.32%. Calcd for $C_{19}H_{18}O_4S$: C, 66.65; H, 5.30%.

*2-[2-Hydroxy-2-(3,4-methylenedioxyphenyl)ethyl]-7-methoxy-4H-1-benzothiopyran-4-one (**5h**)*: mp 162 °C (ethanol-ether-hexane). ^{1}H-NMR ($CDCl_3$) δ=2.97 (2H, d, J=7 Hz), 3.88 (3H, s), 4.58 (1H, brs), 4.97 (1H, t, J=7 Hz), 6.79 (2H, s), 6.8—7.1 (4H, m), 7.32 (2H, d, J=8 Hz), and 8.34 (1H, dd, J=1, 8 Hz). IR (KBr) 3400, 1600, 1230, and 835 cm^{-1}. Found: C, 66.55; H, 5.32%. Calcd for $C_{19}H_{16}O_5S$; C, 66.65; H, 5.30%.

*Reaction of Lithiated **4** with Aldehydes.* The reaction was carried out as described above except that toluene was used as the reaction solvent instead of THF, and ethyl acetate:hexane=3:1 was used for chromatography.

*2-(2-Hydroxy-2-phenylethyl)-5-methoxy-4H-1-benzothiopyran-4-one (**6f**)*: mp 84 °C (benzene-hexane). ^{1}H-NMR ($CDCl_3$) δ=2.87 (2H, d, J=6 Hz), 3.79 (3H, s), 4.55 (1H, brs), 4.98 (1H, t, J=6 Hz), 6.5—6.9 (2H, m), and 6.9—7.5 (7H, m). IR (KBr) 3400, 1600, 1270, and 1040 cm^{-1}. Found: C, 69.28; H, 5.48%. Calcd for $C_{18}H_{16}O_3S$: C, 69.21; H, 5.16%.

*2-[2-Hydroxy-2-(p-methoxyphenyl)ethyl]-5-methoxy-4H-1-benzothiopyran-4-one (**6g**)*: mp 138 °C (benzene-hexane). ^{1}H-NMR ($CDCl_3$) δ=1.73 (1H, brs), 2.94 (2H, d, J=7 Hz), 3.79 (3H, s), 3.93 (3H, s), 4.99 (1H, t, J=7 Hz), 6.71 (1H, s), 6.7—7.0 (1H, m), 6.87 (2H, d, J=7 Hz), 7.18 (1H, dd, J=1.5, 8 Hz), 7.31 (2H, d, J=7 Hz), and 7.44 (1H, t, J=8 Hz). IR (KBr) 3400, 1610, 1260, and 1040 cm^{-1}. Found: C, 66.45; H, 5.41%. Calcd for $C_{19}H_{18}O_3S$: C, 66.65; H, 5.30%.

*Reaction of Lithiated **8** with Electrophiles. General Procedure*: Under a nitrogen atmosphere, diisopropylamine (1 mmol) was suspended in THF (1 ml) at 0 °C. A hexane solution (0.64 ml) of butyllithium (1 mmol) was added and the solution was stirred at 0 °C for 5 min. Then, **8** (232 mg, 1 mmol) was added in one portion followed, after 10 min, by HMPA (2 ml). The mixture was stirred for 10 min. An alkyl halide (3 mmol) or aldehyde (1.1 mmol) in THF (2 ml) was added, and stirring was continued for additional 40—60 min. The reaction was quenched by the addition of saturated aqueous ammonium chloride. The products were extracted twice with ethyl acetate, washed with brine, and dried over Na_2SO_4. The solvents were evaporated *in vacuo*, and the residue was chromatographed on silica gel using ethyl acetate-hexane (1:1) as the eluent.

*1,2-Dihydro-3-methyl-8-methoxycyclopenta[b][1]benzothiopyran-9(3H)-one (**10a**)*: mp 103 °C (benzene-hexane). ^{1}H-NMR ($CDCl_3$) δ=1.31 (3H, d, J=7 Hz), 1.4—2.6 (2H, m), 2.6—3.1 (2H, m), 3.1—3.6 (1H, m), 3.96 (3H, s), 6.90 (1H, dd, J=1.5, 8 Hz), 7.13 (1H, dd, J=1.5, 8 Hz), and 7.44 (1H, t, J=8 Hz). IR (KBr) 1610, 1590, 1450, 1260, and 1040 cm^{-1}.

*1,2-Dihydro-3-ethyl-8-methoxycyclopenta[b][1]benzothiopyran-9(3H)-one (**10d**)*: mp 131 °C (benzene-hexane). ^{1}H-NMR ($CDCl_3$) δ=0.98 (3H, t, J=7 Hz), 1.4—2.5 (4H, m), 2.6—3.4 (3H, m), 3.94 (3H, s), 6.90 (1H, dd, J=1.5, 8 Hz), 7.11 (1H, dd, J=1.5, 8 Hz), and 7.42 (1H, t, J=8 Hz). IR (KBr) 1610, 1590, 1260, and 1040 cm^{-1}. Found: C, 68.92; H, 6.43%. Calcd for $C_{15}H_{16}O_2S$: C, 69.20; H, 6.19%.

*3-Benzyl-1,2-dihydro-8-methoxycyclopenta[b][1]benzothiopyran-9(3H)-one (**10e**)*: mp 131 °C (benzene-hexane). ^{1}H-NMR ($CDCl_3$) δ=1.5—2.3 (2H, m), 2.6—3.1 (5H, m), 3.2—3.8 (1H, m), 3.92 (3H, s), 6.86 (1H, dd, J=1.5, 8 Hz), 7.07 (1H, dd, J=1.5, 8 Hz), 7.23 (5H, s), and 7.39 (1H, t, J=8 Hz). IR (KBr) 1615, 1260, and 1035 cm^{-1}. Found: C, 73.86; H, 5.77%. Calcd for $C_{20}H_{18}O_2S$: C, 74.50; H, 5.63%.

*1,2-Dihydro-3-(α-hydroxybenzyl)-8-methoxycyclopenta[b][1]-benzothiopyran-9(3H)-one (**10f**)*: mp 98—105 °C (benzene-hexane). ^{1}H-NMR ($CDCl_3$) δ=1.4—2.0 (2H, m), 2.4—3.0 (2H, m), 3.5—4.0 (1H, m), 3.86 (3H, s), 4.4—5.0 (2H, m), and 6.6—7.6 (8H, m). IR (KBr) 3400, 1590, 1260, 1040, 760, and 700 cm^{-1}. Found: C, 71.06; H, 5.32%. Calcd for $C_{20}H_{18}O_3S$: C, 70.98; H, 5.36%.

*1,2-Dihydro-3-ethoxycarbonylmethyl-8-methoxycyclopenta[b]-[1]benzothiopyran-9(3H)-one (**10c**)*: mp 97 °C (benzene-hexane). ^{1}H-NMR ($CDCl_3$) δ=1.28 (3H, t, J=7 Hz), 1.4—3.1 (6H, m), 3.3—4.0 (1H, m), 3.94 (3H, s), 4.19 (2H, q, J=7 Hz), 6.89 (1H, dd, J=1.5, 8 Hz), 7.08 (1H, dd, J=1.5, 8 Hz), and 7.41 (1H, t, J=8 Hz). IR (KBr) 1720, 1600, 1260, 1170, 1040, 790, 770, and 690 cm^{-1}. Found: C, 63.63: H, 6.04%. Calcd for $C_{17}H_{18}O_4S$: C, 64.13; H, 5.70%.

*1,2-Dihydro-3-hydroxy-8-methoxycyclopenta[b][1]benzothiopyran-9(3H)-one (**10i**)*: The compound was synthesized by in-

troducing gaseous oxygen to the solution of lithiated **8** for 20 min at 0 °C followed by the reductive treatment with aqueous sodium sulfite. Mp 182 °C (dichloromethane-hexane). ^{1}H-NMR ($CDCl_3$) δ=1.8—3.2 (4H, m), 3.34 (1H, brs), 5.0—5.4 (1H, m), 6.88 (1H, dd, J=1, 8 Hz), 6.97 (1H, dd, J=1, 8 Hz), and 7.40 (1H, t, J=8 Hz). IR (KBr) 3400, 1605, 1585, 1040, and 795 cm^{-1}. Exact mass, Found: m/z 248.0559. Calcd for $C_{13}H_{12}O_3S$: M, 248.0507.

Reaction of Lithiated 9 with Electrophiles. The reaction was carried out as described for **8**.

1,2-Dihydro-3-ethoxycarbonylmethyl-6-methoxycyclopenta[b]-[1]benzothiopyran-9(3H)-one (11c): mp 82 °C (benzene-hexane). ^{1}H-NMR ($CDCl_3$) δ=1.29 (3H, t, J=7 Hz), 1.4—3.1 (6H, m), 3.3—4.0 (1H, m), 3.86 (3H, s), 4.20 (2H, q, J=7 Hz), 6.91 (1H, brs), 6.98 (1H, dd, J=1, 9 Hz), and 8.37 (1H, dd, J=1, 8 Hz). IR (KBr) 1730, 1600, 1025, and 760 cm^{-1}. Found: C, 64.17; H, 5.67%. Calcd for $C_{17}H_{18}O_4S$: C, 64.13; H, 5.70%.

1,2-Dihydro-3-hydroxy-6-methoxycyclopenta[b][1]benzothiopyran-9(3H)-one (11i): mp 184 °C (benzene-hexane). ^{1}H-NMR ($CDCl_3$) δ= 1.6—3.0 (4H, m), 3.37 (1H, brs), 3.89 (3H, s), 5.0—5.2 (1H, m), 7.16 (1H, dd, J=2.5, 9 Hz), 7.39 (1H, d, J=2.5 Hz), and 8.27 (1H, d, J=9 Hz). IR (KBr) 3400, 1590, and 1230 cm^{-1}. Exact mass, Found: m/z 248.0523. Calcd for $C_{13}H_{12}O_3S$: M, 248.0508.

Reaction of Lithiated 12 with Benzaldehyde. The reaction was performed as depicted in the synthesis of 5-methoxy-4*H*-1-benzothiopyran-4-one **6**.

2-(2-Hydroxy-1-methyl-2-phenylethyl)-5-methoxy-3-methyl-4H-1-benzothiopyran-4-one (13): oil. ^{1}H-NMR ($CDCl_3$) δ=1.06 (1.5H, d, J=7 Hz), 1.40 (1.5H, d, J=7 Hz), 1.99 (1.5H, s), 2.23 (1.5H, s), 3.22 (1H, brs), 3.2—3.9 (1H, m), 3.93 (3H, s), 4.81 (0.5H, d, J=6 Hz), 4.94 (0.5H, d, J=4 Hz), and 6.7—7.8 (8H, m). IR (KBr) 3400, 1600, 1265, 1045, 765, and 700 cm^{-1}. Exact mass, Found: m/z 339.1113. Calcd for $C_{20}H_{19}O_3S$: M-1, 339.1055.

Hydrolysis of 10c. A solution of **10c** (760 mg, 2.4 mmol) in THF (10 ml) and 4 M[†] lithium hydroxide (30 ml) was refluxed for 2 h. On cooling, the mixture was acidified with 6 M hydrochloric acid and the products were extracted twice with a mixture of THF and ethyl acetate (1:2). The combined extracts were washed with brine, dried over Na_2SO_4, and concentrated *in vacuo*. The residue was chromatographed on silica gel using ethyl acetate as the eluent to give 3-carboxymethyl-1,2-dihydro-8-methoxycyclopenta[*b*][1]benzothiopyran-9(3*H*)-one (**10j**) (420 mg, 60%): mp 202 °C (dichloromethane-hexane). ^{1}H-NMR (d_6-DMSO) δ=1.4—3.0 (6H, m), 3.4—4.0 (1H, m), 3.85 (3H, s), 5.76 (1H, brs), 6.9—7.3 (2H, m), and 7.50 (1H, t, J=8 Hz). IR (KBr) 3700, 2500, 1720, 1270 and 1030 cm^{-1}. Found: C, 61.60; H, 5.11%. Calcd for $C_{15}H_{14}O_4S$: C, 62.05; H, 4.86%.

Hydrolysis of 11c. The reaction was carried out as described above except that the products were extracted with ethyl acetate, and chromatographed with ethyl acetate-hexane (1:1) to give 3-carboxymethyl-1,2-dihydro-6-methoxy-cyclopenta[*b*][1]benzothiopyran-9(3*H*)-one (**11j**) (58% yield): mp 200 °C (benzene-hexane). ^{1}H-NMR ($CDCl_3$-d_6-DMSO) δ=1.4—2.0 (2H, m), 2.0—3.0 (4H, m), 3.91 (3H, s), 3.5—4.0 (1H, m), 5.39 (1H, brs), 7.0—7.1 (2H, m), and 8.37 (1H, d, J=9 Hz). IR (KBr) 3700, 2400, 1715, 1570, 1540, and 1240 cm^{-1}. Exact mass, Found: 290.0545. Calcd for $C_{15}H_{14}O_4S$: M, 290.0612.

The authors are deeply indebted to Dr. Ryuzo Ueno and his staff of Ueno Pharmaceutical Company, Ltd., for the assay.

[†] 1 M = 1 mol dm^{-3}.

References

1) I. Hirao, M. Yamaguchi, and Y. Kawazoe, *Memoirs Kyushu Inst. Tech., Eng.*, **14**, 13 (1984); I. Hirao, M. Yamaguchi, N. Takefuji, and Y. Fujikura, *ibid*, **14**, 17 (1984); I. Hirao, M. Yamaguchi, N. Takefuji, and Y. Kawazoe, *ibid*, **14**, 23 (1984); I. Hirao, M. Yamaguchi, T. Fujimoto, N. Nishino, Y. Kawazoe, and T. Araki, *ibid*, **14**, 29 (1984).

2) I. Hirao, M. Yamaguchi, and M. Hamada, *Synthesis*, **1984**, 1076.

3) F. Bossert, *Justus Liebigs Ann. Chem.*, **680**, 40 (1964).

4) R. B. Gammill and T. A. Bryson, *Synthesis*, **1976**, 401. An example of α'-alkylation is reported; R. B. Gammill and T. A. Bryson, *Tetrahedron Lett.*, **1975**, 3793.

5) For example; M. Yoshimoto, N. Ishida, and T. Hiraoka, *Tetrahedron Lett.*, **1973**, 39; T. A. Bryson and R. B. Gammill, *ibid*, **1974**, 3963; J. E. Telschow and W. Reusch, *J. Org. Chem.*, **40** 862 (1975); M. Yamamoto and N. Sugiyama, *Bull. Chem. Soc. Jpn.*, **48**, 508 (1975); Y. L. Chen, P. S. Marino, G. M. Little, D. O'Brien, and P. L. Huesmann, *J. Org. Chem.*, **46**, 4643 (1981).

6) For example; A. B. Smith, III and R. M. Scarborough, Jr., *Tetrahedron Lett.*, **1978**, 4193; M. Koreeda and Y. P. L. Chen, *ibid*, **1981**, 15.

7) H. H. Wasserman and B. H. Lipshutz, *Tetrahedron Lett.*, **1975**, 1731.

8) H. Nakazumi and T. Kitao, *Bull. Chem. Soc. Jpn.*, **50**, 939 (1977).

Synthesis and Thermal Decomposition of Di-*t*-Butyl Peroxydicarbonate

Takeshi KOMAI* and Kazuo MATSUYAMA
Chemicals and Explosives Research Laboratory, Nippon Oil & Fats Co., Ltd., Taketoyo, Chita-gun, Aichi 470-23
(Received February 25, 1985)

Di-*t*-butyl peroxydicarbonate(DBPD) has been synthesized in a novel route and thermally decomposed at 40—70 °C. The decomposition exhibits first-order kinetics and the values of $\Delta H^{\ddagger}$ and $\Delta S^{\ddagger}$ are 122 kJ mol^{-1} and 46 J K^{-1} mol^{-1}, respectively. 2-Methyl-2-propanol is obtained quantitatively as a decomposition product and the rates are a little dependant on the viscosities of solvents, normal alkanes. The mechanism that involves the initial scission of the O–O bond is discussed and the values of the rates and the activation parameters of DBPD are compared with those of diacetyl peroxide and dibenzoyl peroxide.

Dialkyl peroxydicarbonates (**1**) are useful low-temperature initiators of polymerization for vinyl chloride and other monomers.[1] The decomposition rate of di-

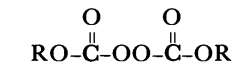

(**1**)

isopropyl peroxydicarbonate in benzene containing styrene at 54 °C is equal to that of dibenzoyl peroxide in the same medium at 82 °C.[2] However, based on the overall activation energy for the decomposition, 118 kJ mol^{-1}, closer to the values (121 to 126 kJ mol^{-1}) reported for dibenzoyl peroxide, Strain and coworkers[3] proposed that the primary rate-determing step was the same for both peroxides, homolytic cleavage of the peroxide bond.

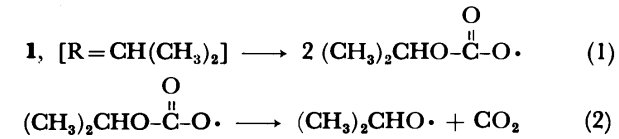

(1)

(2)

McBay and Tucker[4] examined the thermal decomposition products of peroxydicarbonates in several solvents at 140 °C, and proposed a different decomposition scheme.

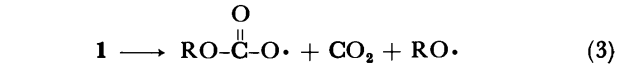

(3)

A more recent study[5] of dicyclohexyl peroxydicarbonate (**1**, R=C_6H_{11}) indicated that it was decomposed by the homolytic one-bond fission (Eq. 1) and the decarboxylation of the generated alkoxycarboxyl radical (Eq. 2) was negligible at 50 °C, compared to the reaction with solvent or bimolecular disproportionation.

One of the complexities of the decomposition mechanisms of peroxydicarbonates is that the homolytic decomposition is accompanied with the induced decomposition. For instance, the α-hydrogen atom of dicyclohexyl peroxydicarbonate is abstracted easily by the alkoxycarboxyl radical.[5]

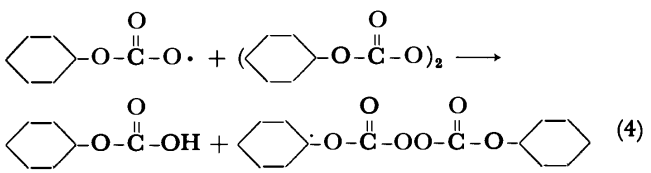

(4)

The amounts of homolytic (Eq. 1) and induced decompositions (Eq. 4) are nearly equal at 0.1 M† in benzene solution.[5] Hence, we have supposed that di-*t*-alkyl peroxydicarbonate (**I**, R=*t*-alkyl) which lacks the α-hydrogen atom in the alkyl group is more suitable for clarifying the homolytic decomposition mechanisms than primary or secondary analogues. For this purpose, we have synthesized di-*t*-butyl peroxydicarbonate (**I**, R=*t*-C_4H_9, DBPD) and measured the decomposition rates and products at 40—70 °C.

Results and Discussion

Synthesis. Di-primary and secondary alkyl peroxydicarbonates have been synthesized by conventional reactions between alkyl chloroformates and hydrogen peroxide in aqueous alkali solution.[6] However, in the case of the synthesis of DBPD the yield is low because *t*-butyl chloroformate is unstable under the reaction conditions.[7] We synthesized DBPD in a novel route from 2-(*t*-butoxycarbonyloxyimino)-2-phenylacetonitrile (Boc ON) (**2**) and hydrogen peroxide in the presence of dicyclohexyl 18-crown-6 (18-Crown-6) equivalent to potassium hydroxide at 2 °C (See Experimental).

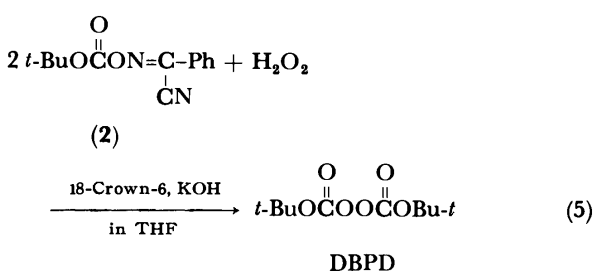

(5)

DBPD

This procedure was also applied for the synthesis of di-*t*-butyl peroxymonocarbonate with using *t*-butyl hydroperoxide in place of hydrogen peroxide. In this case, 18-Crown-6 was not necessary.

Kinetics and Products of Decomposition. Decomposition products of DBPD in cumene detected by gas chromatography were 2-methyl-2-propanol, 1,1,2,2-tetramethyl-1,2-diphenyl-ethane and a small amount of *t*-butyl α,α-dimethylbenzyl carbonate. In dodecane and chlorobenzene containing 0.1 M cyclo-

† 1 M=1 mol dm^{-3}.

Table 1. Decomposition products of DBPD

Temp °C	Solvent	Initial concd of DBPD/M	Products/M *t*-BuOH	*t*-BuOCO$_2$CMe$_2$Ph	(PhCMe$_2$)$_2$
50	PhCHMe$_2$	0.0203	0.0400	ca. 0.0006	0.0104
50	PhCHMe$_2$	0.201	0.436	ca. 0.014	0.105
50	*n*-C$_{10}$H$_{22}$	0.0200	0.0442	—	—
40	PhCl (0.1 M *c*-C$_6$H$_{12}$)	0.0212	0.0443	—	—

Table 2. Rate constants for thermal decomposition of DBPD

Solvent	Viscosity[a] cP	Initial concd of DBPD/M	Temp °C	$10^5 k_{obsd}$[b] s^{-1}
Cumene	0.613	0.0203	40	0.722±0.012
Cumene	0.560	0.0203	50	3.12±0.07
Cumene	0.560	0.201	50	3.78±0.12
Cumene	0.490	0.0203	60	11.6±0.3
Cumene	0.440	0.0203	70	49.0±0.4
Hexane	0.235	0.0229	50	3.29±0.03
Decane	0.623	0.0215	50	3.23±0.03
Octadecane	2.29	0.0209	50	3.10±0.07

a) Viscosity of cumene was obtained from *Beilstein III*, **5**, p. 879 and those of *n*-alkanes from Ref. 12. b) Rate constants and their standard deviations were calculated by the method of least squares.

hexane, 2-methyl-2-propanol and unidentified products were obtained. Table 1 summarizes the products data on DBPD decomposition. Thermal decomposition rates were measured by following the disappearance of DBPD by the iodometric titration. The data exhibit first-order kinetics over the temperature range employed (40—70 °C).

Table 2 summarizes the rate constants for the decomposition in cumene and other solvents. When the decomposition is carried out over a ten fold variation in the initial concentration, the rate constant of the reaction increases approximately 20%. This indicates that the data of Table 2 are not pure unimolecular first-order but involving some induced decomposition.

Using the method of Nozaki and Bartlett[8] an attempt was made to separate the induced decomposition (k_i) and the unimolecular decomposition (k_d) by the following equation.

$$-\frac{d[DBPD]}{dt} = k_d[DBPD] + k_I[DBPD]^{3/2} \quad (6)$$

The values of k_d=2.77×10^{-5} s^{-1} and k_i=3.47×10^{-5} M$^{-1/2}$ s^{-1} are obtained. In the decomposition of dicyclohexyl peroxydicarbonate (**I**, R=C$_6$H$_{11}$) in benzene at the same temperaure (50 °C), the values of k_d=3.9×10^{-5} s^{-1} and k_i=1.39×10^{-4} M$^{-1/2}$ s^{-1} were reported.[5] For the decomposition of dibenzoyl peroxide the values of k_d=3.3×10^{-5} s^{-1} and k_i=4.3×10^{-5} M$^{-1/2}$ s^{-1} were reported in both benzene and toluene at 80 °C.[8] From these results it can be understood that the ratio of the induced decomposition of DBPD to the unimolecular one is similar to that of dibenzoyl peroxide, but its value is 1/3-fold of that of dicyclohexyl peroxydicarbonate.

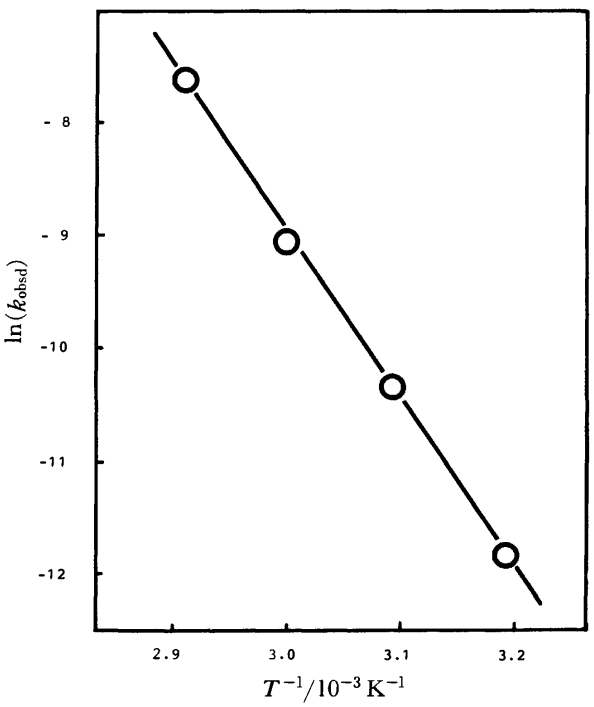

Fig. 1. Arrhenius plot for decomposition of 0.0203 M DBPD in cumene.

Figure 1 shows an Arrhenius plot for the decomposition of DBPD of 0.0203 M in cumene in the range of 40—70 °C. Table 3 indicates the relative rate at 50 °C and the activation parameters of the DBPD together with those of dibenzoyl peroxide and diacetyl peroxide.

The formation of above-mentioned products and the observed kinetic data can be understood in terms of the reactions in Scheme 1.

TABLE 3. RELATIVE RATES AND ACTIVATION PARAMETERS WITH DECOMPOSITION OF DBPD, DIACETYL AND DIBENZOYL PEROXIDE

Peroxide	Solvent	Relative rate at 50°C	Activation parameter ΔH^*/kJ mol^{-1}	ΔS^*/JK^{-1} mol^{-1}
DBPD	Cumene	43	122	46
Diacetyl[a]	Toluene	1.8	130	44
Dibenzoyl[b]	Acetophenone	1.0	126	19

a) See Ref. 9. b) See Ref. 10.

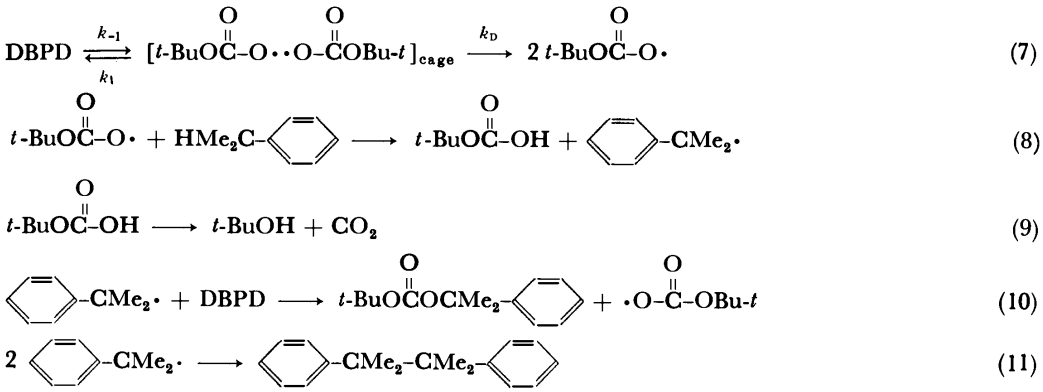

Scheme 1.

Niki and Kamiya decomposed di-*t*-butyl diperoxyoxalate in a cumene–benzene mixture at 45 °C and obtained 5.8% of di-*t*-butyl peroxide as the cage product, 4.4% of acetone and 90.8% of 2-methyl-2-propanol.[11]

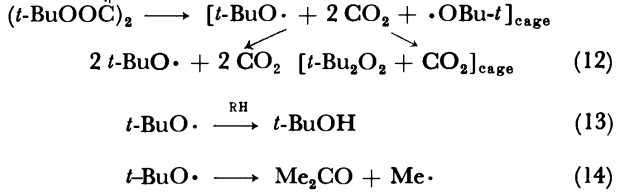

In the case of DBPD decomposition 2-methyl-2-propanol was nearly quantitaively obtained, but acetone, β-scission product of *t*-butoxyl radical (Eq. 14) was not detected (Table 1). Furthermore, di-*t*-butyl peroxide, as the cage product of two *t*-butoxyl radicals (Eq. 12) and di-*t*-butyl peroxymonocarbonate, that of *t*-butoxyl and *t*-butoxycarboxyl radicals, also were not detected. These results show that *t*-butoxyl radical is not present under the experimental conditions. Accordingly DBPD decomposes with one-bond homolysis, and the decarboxylation of the resulting *t*-butoxycarboxyl radical does not compete with hydrogen abstraction from cumene. This agrees with Van Sickle's results.[5]

The solvent viscosity dependence of the observed rate is one of the methods of separating the concerted and stepwise mechanisms for the peroxide decomposition. The relationship[12] between the observed rate constant (k_{obsd}) and the solvent viscosity (η) is written as

$$\frac{1}{k_{obsd}} = \frac{1}{k_1} + \frac{k_{-1}}{k_1 A_D}\left(\frac{\eta}{A_v}\right)^{\alpha} \qquad (15)$$

TABLE 4. CAGE RETURN OF PEROXIDES

Peroxide	Temperature °C	f_r
DBPD[a]	50	0.04
Diacetyl[b]	80	0.28
Dibenzoyl[c]	80	0.02

a) In decane. b) In octane (See Ref. 13). c) In 2,2,4-trimethylpentane (See Ref. 13).

where k_1 is the rate constant for bond homolysis; k_{-1} is the rate constant for cage return; A_D and A_v are Arrhenius preexponential factors for solute diffusion and self-diffusive flow of solvent, respectively, and α is a proportionality constant between the activation energies for the above-mentioned diffusion and flow ($E_D=\alpha E_v$), set equal to 0.5 for the calculation. The fraction (f_r) of geminate radicals which combine to reform the parent peroxydicarbonate is defined as

$$f_r = \frac{k_{-1}}{k_{-1}+k_D} = 1 - \frac{k_{obsd}}{k_1} \qquad (16)$$

The value of the rate constant for bond homolysis (k_1) of DBPD is estimated to be 3.37×10^{-5} s^{-1} from the intercept of a plot of $1/k_{obsd}$ *vs.* $(\eta/A_v)^{0.5}$ using the values in Table 2 and Ref. 12. The value of f_r in decane can be calculated from Eq. 16. The obtained data are presented in Table 4 with those of dibenzoyl and diacetyl peroxides.[13] The values of $f_r>0.1$ have been expected for the peroxides which decompose with one-bond fission. The value of $f_r=0.04$ for DBPD may suggest its two-bond concerted fission. However, dibenzoyl peroxide which decomposes with one-bond fission also has very low f_r value (Table 4). Pryor[13] proposed that a

larger activation barrier exists for the combination of benzoyloxyl radicals than for acetoxyl radicals. In the case of DBPD, the resonance structures can be written for geminate pair.

$$[2\ t\text{-BuOCO}_2\cdot] \longleftrightarrow [t\text{-BuOCO}_2^-,\ t\text{-BuOCO}_2^+] \longleftrightarrow [t\text{-BuOCO}_2^-,\ Me_3C^+O\text{-}C(=O)\text{-}O]$$

We believe that the solvent viscosity effect test is not a sure method for distinguishing between one-bond and concerted two-bond fission.

The decomposition rate of DBPD is 43 and 24 fold faster than those of dibenzoyl and diacetyl peroxides at 50 °C, respectively (Table 3). However, the activation enthalpies of these three peroxides are almost the same values (*ca.* 125 kJ mol^{-1}), which support the above-mentioned one-bond fission of DBPD (Eq. 7). Hammett's σ_p values of alkoxycarbony,[14] benzoyl and acetyl groups are 0.310, 0.459, and 0.509, respectively. Those of methoxyl, phenyl and methyl groups are −0.37, −0.01, and −0.170, respectively.[15] The alkoxycarbonyl or methoxyl group is the most electron-donating substituent, respectively, in the above-mentioned two sequences, but the difference of electron-donating ability among the substituents in each sequence is small. We suppose that the faster decomposition rate of DBPD than those of diacetyl and dibenzoyl peroxides arises not only from the simply electrostatic repulsion between the peroxyl oxygen atoms, but also from the structural factor of *t*-butoxycarboxyl group.[16]

t-Butyl α,α-dimethylbenzyl carbonate is produced by radical induced decomposition of DBPD (Eq. 10). It is clear from the effects of initial peroxide concentration on the rate and product (Table 1 and 2). But its amount is small. On the other hand, the yield of a radical coupling product, 1,1,2,2-tetramethyl-1,2-di-phenylethane (Eq. 11) is *ca.* 50%. Thus, di-primary or secondary alkyl peroxydicarbonates accept two types of induced decompositions, one is the attack to the peroxyl bond and the other is the abstraction of the α-hydrogen atom on the alkoxyl group.

Experimental

IR and NMR spectra were recorded on a JASCO A-3 and a JEOL JNM-MH-100 spectrometer, respectively. GC analysis was carried out by a Shimadzu GC-6A gas chromatograph using two columns: PEG 20 M, 5% on Shimalite AW-DMCS, 2 m; Silicon GE SE-30, 5% on Shimalite W, 0.5 m. GC-MS spectra were recorded on a JEOL JMS-D300 mass spectrometer.

Materials. 2-(*t*-Butoxycarbonyloxyimino)-2-phenylacetonitrile (Boc-ON) was obtained from Protein Research Foundation. Potassium hydroxide, THF, acetone, 2-methyl-2-propanol, cyclohexane, petroleum ether and dicyclohexyl-18-crown-6 (18-Crown-6) were the products of Wako Pure Chemical Ind. Co. Di-*t*-butyl peroxide was the product of Nippon Oil & Fats Co., Ltd. Cumene, chlorobenzene, cyclohexane, hexane, decane and octadecane, pure grade, obtained commercially, were stirred for several hours with concentrated sulfuric acid, washed with 10% sodium hydrogencarbonate and distilled water, dried with drying agents and distilled through a 24-in Vigreux column. The sample of 1,1,2,2-tetramethyl-1,2-diphenylethane was prepared by the literature method.[17] Purities of these materials were checked by melting point, IR, NMR, and/or GC analysis.

Di-t-Butyl Peroxydicarbonate. To a solution of dicyclohexyl-18-crown-6 (18-Crown-6)(81.9 g, 0.22 mol) in THF (200 cm^3) was added the fine powder of potassium hydroxide (14.5 g, 0.22 mol). After being stirred at room temperature till the powder was dispersed completely, 50% hydrogen peroxide (27.2 g, 0.40 mol) in THF (200 cm^3) was added dropwise to the mixture at 5 °C. Then the mixture was added dropwise at 2 °C for 15 min to Boc-ON (50.8 g, 0.20 mol) in THF (200 cm^3) and the reaction mixture was stirred again at 20 °C for 5 h. After petroleum ether (400 cm^3) was added to the reaction mixture the precipitate formed was filtered. The filtrate was washed four times with water (100 cm^3) and dried over anhydrous Na_2SO_4, and then the solvent was evaporated. The oily residue was crystallized twice from ether by cooling in Dry Ice-acetone to give di-*t*-butyl peroxydicarbonate (DBPD) as white crystals in 8.4% yield. On titration for active oxygen, the purity of the product was shown to be 98.4%. mp 32—34 °C (lit,[7] mp 28—30 °C); IR (CCl_4): 1820 (C=O) and 1795 cm^{-1} (C=O); ^{1}H NMR ($CDCl_3$): δ=1.58 (1H, s, *t*-CH_3). Found: C, 50.57; H, 7.98% Calcd for $C_{10}H_{18}O_6$: C, 51.27; H, 7.75%.

Di-t-Butyl Peroxymonocarbonate. To a suspension of the fine powder of potasium hydroxide (13.2 g, 0.20 mol) in THF (120 cm^3) there was added 80.5% *t*-butyl hydroperoxide (44.8 g, 0.40 mol), and stirred at room temperature till the powder was dispersed completely. Then to the mixture there was added dropwise Boc-ON (24.6 g, 0.10 mol) in THF (100 cm^3) at 30 °C for 1 h and stirred at 35 °C for 6 h. After petroleum ether (200 cm^3) was added to the reaction mixture, the precipitate formed was filtered. The filtrate was washed with 5% NaOH (50 cm^3) and water (50 cm^3), respectively twice, and dried over anhydrous Na_2SO_4, and the solvent was evaporated. The crude product was distilled through a short Vigreux column at 48—50 °C under decreased pressure of 0.9 mmHg (1 mmHg=133.322 Pa) (lit,[18] bp 46—47 °C at 0.47 mmHg) to give di-*t*-butyl peroxymonocarbonate (DBPM); IR (Neat): 1785 (C=O) and 1760 cm^{-1} (C=O); ^{1}H NMR (CCl_4): δ=1.46 (1H, s, *t*-CH_3) and (1H, s, Peroxyl *t*-CH_3). Found: C, 62.59; H, 6.93% Calcd for $C_9H_{18}O_4$: C, 62.84; H, 6.71%.

Kinetic Procedure. A weighed sample of DBPD was dissolved in a known volume of the solvent. Samples (generally 4 cm^3) of solution were pipetted into test tubes. The solutions were exhaustively evacuated, and the tubes were sealed in an atmosphere of nitrogen. The evacuation procedure consisted of cooling in a Dry Ice-acetone bath, evacuation on an oil pump and warming to 10 °C. This was repeated three times before sealing. The tubes were completely immersed in an oil thermostat regulated to ±0.05 °C. At successive time intervals, tubes were removed from the constant temperature bath and immersed in a Dry Ice-acetone bath. Then the concetration of DBPD in the solution was measured by iodometry titration. The reaction were followed up to 75—80% decomposition and exhibited first-order kinetics. The titration procedure involved the use of a

mixture (20:2) of isopropyl alcohol and acetic acid as the solvent, and saturated potassium iodide as the source of iodine. After boiling of 3 min for liberation of iodine, the iodine was titrated to a starch end point with 0.01 N thiosulfate for the dilute solution and 0.1 N thiosulfate for the concentrated solution. The values for the observed first-order rate constants and their standard deviations were calculated from the first-order rate equation using the method of least squares. The values for the activation parameters and their standard deviations were calculated from absolute rate equation of Eyring using the method of least squares.

Decomposition Products. DBPD in solutions was decomposed completely at 40 °C for 130 h and at 50 °C for 40 h and the solutions were analyzed by gas chromatography and mass spectrometer. Effluent peaks were identified by comparing retension times with those of authentic samples and by GC-MS spectra; product, *m/z* (rel. intensity); 2-methyl-2-propanol, 49 (100), 41 (17), and 31 (25); *t*-butyl α,α-dimethylbenzyl carbonate, 236 (M^+, 10), 180 (57), 162 (20), 119 (100) and 57 (65); 1,1,2,2-tetramethyl-1,2-diphenylethane, 238 (M^+, 4), 119 (100) and 91 (22). Cyclohexane and decane were added as internal standards, and the response factors were determined for the identified products with the column of PEG 20 M. The factor of *t*-butyl α,α-dimethylbenzyl carbonate was estimated by comparing its peak with that of 1,1,2,2-tetramethyl-1,2-diphenylethane taking into account the difference of the molecular weight. Di-*t*-butyl peroxide and DBPM were not detected from the gas chromatograph using the columns of PEG 20 M (DBPM was decomposed through the measurement.) and Silicone GE-SE-30 (DBPM was not decomposed through the measurement.) in comparision with the authentic samples.

References

1) M. Yamada, K. Kitagawa, and T. Komai, *Enbi to Polyma*, **11**, 38 (1971).
2) S. G. Cohen and D. B. Sparrow, *J. Am. Chem. Soc.*, **72**, 611 (1950).
3) F. Strain, W. E. Bissinger, W. R. Dial, H. Rudoff, B. J. DeWitt, H. C. Stevens, and J. H. Langston, *J. Am. Chem. Soc.*, **72**, 1254 (1950).
4) H. C. McBay and O. Tucker, *J. Org. Chem.*, **19**, 869 (1954).
5) D. E. Sickle, *J. Org. Chem.*, **34**, 3446 (1969).
6) R. Hiatt, "Organic Peroxides II," ed by D. Swern, John Wiley & Sons, Inc., New York (1971), Chap. 8.
7) H. N. Friedlander, U. S. Patent 2728756 (1955).
8) K. Nozaki and P. D. Bartlett, *J. Am. Chem. Soc.*, **68**, 1868 (1946).
9) M. Levy, M. Steinberg, and M. Szwarc, *J. Am. Chem. Soc.*, **76**, 5978 (1954).
10) A. T. Blomquist and A. J. Buselli, *J. Am. Chem. Soc.*, **73**, 3883 (1954).
11) E. Niki and Y. Kamiya, *J. Org. Chem.*, **38**, 1403 (1973).
12) W. A. Pryor and K. Smith, *J. Am. Chem. Soc.*, **92**, 5403 (1970).
13) W. A. Pryor, E. H. Morkved, and H. T. Bickley, *J. Org. Chem.*, **37**, 1999 (1972).
14) M. Charton, *J. Org. Chem.*, **28**, 3121 (1963).
15) E. Imoto, "Kagaku-hanno Niokeru Heiko To Sokudo," Tokyo Kagaku Dogin, Tokyo (1967), p. 149.
16) O. Kikuchi, A. Hiyama, H. Yoshida, and K. Suzuki, *Bull. Chem. Soc. Jpn.*, **51**, 11 (1978).
17) E. H. Farmer and C. G. Moore, *J. Chem. Soc.*, **1951**, 131.
18) P. D. Bartlett and H. Sakurai, *J. Am. Chem. Soc.*, **84**, 3269 (1962).

Synthesis and Molecular Structure of the 2:1-Cycloadduct of 1-Methoxy-2-benzopyrylium-4-olate with Acenaphthylene

Jiro Toyoda, Toshikazu Ibata,* Hatsue Tamura, Kazuhide Ogawa, Tsuyoshi Nishino,† and Matsuji Takebayashi†

Institute of Chemistry, College of General Education, Osaka University, Toyonaka, Osaka 560

†*Department of Chemistry, Faculty of Science and Technology, Kinki University, Higashi-osaka, Osaka 577*

(Received March 5, 1985)

The $Cu(acac)_2$-catalyzed decomposition of *o*-methoxycarbonyl-α-diazoacetophenone in the presence of acenaphthylene gave a 2:1-cycloadduct of the corresponding carbonyl ylide, 1-methoxy-2-benzopyrylium-4-olate, with acenaphthylene along with *exo*- and *endo*-1:1-adducts. The molecular structure of the 2:1-adduct was determined by means of X-ray analysis. The colorless crystals of the adduct are triclinic with the space group $P\bar{1}$, and with the unit-cell dimensions of $a=12.104(2)$, $b=12.477(3)$, $c=9.112(2)$ Å, $\alpha=102.98(3)$, $\beta=110.16(2)$, $\gamma=70.65(1)°$, and $Z=2$. The structure was determined by direct methods and refined by block-diagonal least-squares methods. All hydrogen atoms were revealed by a difference-Fourier synthesis, and further least-squares refinement gave the final R value of 0.057 for 3681 observed reflections. The configurations of methine protons obtained by X-ray methods are compatible with the NMR coupling pattern of the adduct.

1,3-Dipolar cycloadditions of carbonyl ylide with acetylenic, ethylenic, and carbonyl compounds have been studied extensively from the theoretical and synthetic interests.[1] The authors have reported that 1-methoxy-2-benzopyrylium-4-olate (**3**) gave 1,3-dipolar cycloadducts with carbonyl compounds in the $Cu(acac)_2$-catalyzed decomposition of *o*-methoxycarbonyl-α-diazoacetophenone (**1**).[2] In the previous study of this series, the yields of *exo*- and *endo*-1:1-adducts (**4a** and **4b**) of (**3**) with acenaphthylene were reported to be not so high.[3] This may be attributed to the competitive reactions of the 1:1-adducts (**4**) and acenaphthylene toward the carbonyl ylide intermediate (**3**). In order to investigate the possibility of the reaction of the 1:1-adducts with (**3**), the decomposition of *o*-methoxycarbonyl-α-diazoacetophenone (**1**) was reexamined in the presence of acenaphthylene giving the expected 2:1-adduct (**5**), of which the structure was determined by X-ray analysis.

Experimental

The ^1H NMR and ^{13}C NMR spectra of the 2:1-adduct were measured on a Brucker NMR spectrometer, model MA 360 in $CDCl_3$, using TMS as an internal standard.

The Cu(acac)₂-catalyzed Decomposition of (1) in the Presence of Acenaphthylene. A benzene solution of **1** (6 mmol) was added drop by drop into a benzene solution of acenaphthylene (6 mmol) and $Cu(acac)_2$ (0.6 mmol) at 80 °C under stirring in N_2 atmosphere. The reaction products were isolated by column chromatography on silica gel using benzene as an eluent. Colorless crystals (**5b**; 1.56 mol, 26%) were obtained besides the *exo*- (**4a**; 16%) and *endo*-1:1-adducts (**4b**; 25%): (**5b**); colorless crystals; mp 165—166 °C; IR (KBr) 1709 cm^{-1} (C=O); ^1H NMR ($CDCl_3$) $\delta=3.50$ (s, 3H, OCH_3), 4.04 (dd, 1H, Ha, $J_{a,b}=6.7$, $J_{a,4}=1.3$ Hz), 4.05 (s, 3H, OCH_3), 4.39 (dd, 1H, Hb, $J_{a,b}=6.7$, $J_{b,c}=1.3$ Hz), 4.67 (d, 1H, Hc, $J_{b,c}=1.3$ Hz), 5.19 (s, 1H, Hd), 6.28 (d, 1H, H_{17}, $J_{17,18}=7.8$ Hz), 6.95 (t, 1H, H_{18}, $J_{17,18}=J_{18,19}=7.8$ Hz), and 7.1—8.0 (m, 11H, Ar); ^{13}C NMR ($CDCl_3$) 48.56 (d, C_2), 50.27 (q, C_{22}), 53.65 (q, C_{32}), 61.52 (d, C_{13}), 80.83 (s, C_{15}), 86.90 (d, C_{14}), 88.20 (d, C_{23}), 107.63 (s, C_1), 119.82 (s, C_{31}), 191.44 (s, C_{24}), and 21 signals in the region of $\delta=118.69$—145.68. Found: C, 76.21; H, 4.87%. Calcd for $C_{32}H_{24}O_6$: C, 76.18; H, 4.80%.

Table 1. Crystal data of the 2:1-adduct

Crystal system Space group	Triclinic $P\bar{1}$
a	12.104(2) Å
b	12.477(3)
c	9.112(2)
α	102.98(3)°
β	110.16(2)
γ	70.65(1)
V	1209.3(2) Å^3
Z	2
Dm	1.386 Mg m^{-3}
Dx	1.377 Mg m^{-3}
μ(Cu $K\alpha$)	0.79 mm^{-1}
Scan method	θ—2θ
Scan speed in ω	4° min^{-1}
Scan width	$1.4°+0.15°\tan\theta$
Background	2×4 s
2θmax(Cu $K\alpha$)	125°
No. of Reflections	3863 3681(except $\|F_o\|=0$)
Crystal size	0.3×0.3×0.2 mm^3

X-Ray Crystal Analysis of 5. The crystal data of **5** are listed in Table 1 along with the experimental details. The X-ray intensity data were measured on a Rigaku four-circle diffractometer with Ni-filtered Cu $K\alpha$ radiation. The number of nonzero reflections used in the structural determination were 3681.

The space group $P\bar{1}$ was confirmed by a statistical distribution of E values and a successful refinement of the structure.

Using 300 reflections with $|E|\geq 1.78$, the crystal structure was determined by direct methods with the MULTAN 78 program.[6] The E-map computed with the phase set of the highest combined figure of merit (2.708) revealed the positions of all the non-hydrogen atoms. The isotropic refinement, followed by anisotropic refinement reduced R to 0.094. The hydrogen atoms were located on a difference map and their positional parameters were refined together with isotropic thermal parameters, while the other atoms were refined anisotropically by block-diagonal least-squares. The final R value was 0.057. The function minimized was

Table 2-A. Atomic positional ($\times 10^4$) and thermal parameters for the non-hydrogen atoms of the 2:1-adduct

Atom	x	y	z	B_{eq}/Å^2
O(1)	2670(1)	8299(1)	2403(2)	4.4
O(2)	2269(1)	7013(1)	3473(2)	3.6
O(3)	1454(1)	4343(1)	1636(2)	3.5
O(4)	2434(1)	4038(1)	4174(2)	3.8
O(5)	852(1)	3225(1)	2746(2)	4.2
O(6)	5202(1)	3755(1)	3527(2)	4.9
C(1)	2137(2)	7401(2)	2030(3)	3.6
C(2)	738(2)	7809(2)	1292(3)	3.5
C(3)	93(2)	8967(2)	2002(3)	3.7
C(4)	146(2)	10052(2)	2031(3)	4.7
C(5)	−613(3)	10983(2)	2782(4)	5.6
C(6)	−1397(2)	10841(2)	3456(3)	5.0
C(7)	−1476(2)	9730(2)	3429(3)	4.3
C(8)	−2215(2)	9419(2)	4083(3)	4.7
C(9)	−2177(2)	8300(2)	3970(4)	4.8
C(10)	−1399(2)	7395(2)	3211(3)	4.4
C(11)	−663(2)	7666(2)	2577(3)	3.5
C(12)	−712(2)	8822(2)	2692(3)	3.6
C(13)	298(2)	6926(2)	1779(3)	3.4
C(14)	1469(2)	6287(2)	2972(3)	3.4
C(15)	2199(2)	5128(2)	2303(3)	3.3
C(16)	2674(2)	5294(2)	1052(3)	3.5
C(17)	3043(2)	4392(2)	−50(3)	4.0
C(18)	3435(2)	4580(2)	−1203(3)	4.7
C(19)	3447(2)	5671(3)	−1285(3)	5.0
C(20)	3056(2)	6582(2)	−219(3)	4.5
C(21)	2686(2)	6403(2)	966(3)	3.7
C(22)	3949(2)	8003(2)	3235(4)	5.7
C(23)	3167(2)	4540(2)	3732(3)	3.6
C(24)	4223(2)	3597(2)	3317(3)	3.8
C(25)	3951(2)	2480(2)	2609(3)	3.8
C(26)	4863(2)	1507(2)	2307(3)	4.7
C(27)	4561(3)	492(2)	1633(4)	5.4
C(28)	3366(3)	456(2)	1216(4)	5.7
C(29)	2449(2)	1420(2)	1497(3)	4.9
C(30)	2751(2)	2432(2)	2237(3)	3.8
C(31)	1834(2)	3505(2)	2693(3)	3.5
C(32)	−162(2)	4152(2)	2999(3)	5.0

Table 2-B. Atomic potential ($\times 10^3$) and thermal parameters for the hydrogen atoms of the 2:1-adduct

Atom	x	y	z	B/Å^2
H(a)	57(2)	777(2)	14(3)	1.7(5)
H(4)	77(2)	1011(2)	158(3)	3.3(6)
H(5)	−52(2)	1178(2)	284(3)	3.2(6)
H(6)	−192(2)	1151(2)	404(3)	3.5(6)
H(8)	−269(2)	1011(2)	477(3)	3.6(6)
H(9)	−270(2)	811(2)	441(3)	2.8(6)
H(10)	−141(2)	653(2)	319(3)	3.5(6)
H(b)	−6(2)	638(2)	88(3)	1.7(5)
H(c)	127(2)	616(2)	395(3)	1.4(4)
H(17)	295(2)	363(2)	2(3)	1.6(5)
H(18)	365(3)	390(3)	−198(4)	5.5(8)
H(19)	379(2)	579(2)	−202(3)	3.1(6)
H(20)	306(3)	739(2)	−29(3)	4.1(7)
H(221)	443(3)	744(2)	253(3)	4.2(8)
H(222)	419(3)	859(2)	360(4)	5.0(7)
H(223)	405(3)	763(3)	422(4)	5.4(8)
H(d)	347(2)	510(2)	462(3)	2.1(5)
H(26)	566(2)	158(2)	260(3)	3.5(6)
H(27)	523(3)	−19(2)	155(4)	4.5(7)
H(28)	311(2)	−30(2)	66(3)	3.5(6)
H(29)	158(2)	137(2)	122(3)	3.5(6)
H(321)	−62(3)	441(3)	212(4)	6.3(9)
H(322)	−70(3)	392(2)	338(4)	4.6(7)
H(323)	14(2)	478(2)	379(3)	3.2(6)

$\sum w(|F_o|-|F_c|)^2$ with the following weighting scheme: $w=1/(\sigma(F_o)^2+0.0063|F_o|+0.0006|F_o|^2)$. All the atomic scattering factors were taken from the "International Tables for X-ray Crystallography." The computations were carried out on an ACOS-S900 computer at the Crystallographic Research Center, Institute for Protein Research Laboratory, Osaka University using "The Universal Crystallographic Computing System-Osaka." Table 2 lists the final atomic and thermal parameters with their estimated standard deviations. The table of the best planes is deposited as Document No. 8534 at the Office of the Editor of Bull. Chem. Soc. Jpn. The bond distances and angles are given in Figs. 3 and 4. The atom numbering is also shown in these figures.

Results and Discussion

Reaction of o-Methoxycarbonyl-α-diazoacetophenone (1) with Acenaphthylene. The ^{1}H NMR spectrum of the 2:1-adduct (**5b**) has signals of four nonaromatic methine protons Ha, Hb, Hc, and Hd at δ 4.04 (dd), 4.39 (dt), 4.67 (d), and 5.19 (s), respectively.

The coupling patterns of protons Ha, Hb, and Hc are quite similar to those of methine protons of *exo*-1:1-adduct (**4a**).[3] This means that each pair of protons Ha–Hb and Hb–Hc locates on adjacent carbons in a similar stereochemistry observed in **4a** and that Hd is on a carbon having no vicinal proton. Therefore the 2:1-adduct is assumed to be the 1,3-dipolar cycloadduct of **3** on carbonyl group of *exo*-1:1-adduct (**4a**). This assumption was confirmed by the fact that the yield of **5b** decreased to 3% with the increase of the yields of **4a** and **4b** (25 and 34%, respectively) when 10 molar excess

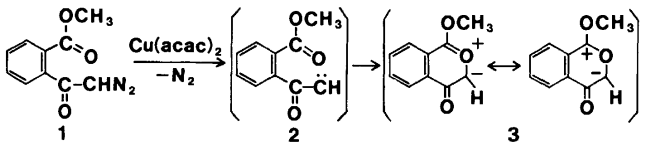

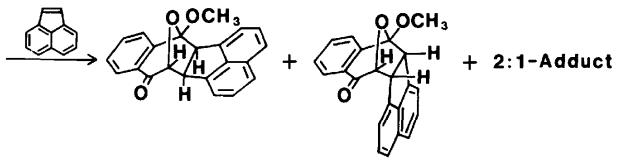

4a + 3 ⟶ 5

Scheme 1.

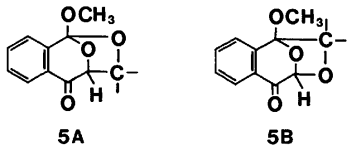

Scheme 2.

of acenaphthylene was used. The finding that the decomposition of **1** in the presence of **4a** gave the same 2:1-adduct (**5**) along with the dimers of **3**[4] is also consistent with the above consideration. On the other hand, the reaction of **3** with *endo*-1:1-adduct (**4b**) in a similar procedure did not give the 2:1-adduct but gave dimers of **3**. This indicates the poor 1,3-dipolarophilicity of the *endo*-1:1-adduct toward **3** in comparison with the reactivity of the *exo*-1:1-adduct (**4a**).

The reaction site of the 1:1-adduct (**4a**) in this reaction is assumed to be carbonyl group.[2,5] The CPK model of **4a** and **4b** reveals that the *endo*-adduct (**4b**) does not allow the approach of the carbonyl ylide (**3**) to the carbonyl group of **4b** due to the structural crowdedness caused by adjacent *o*-phenylene and acenaphthenylene groups.

In general, two regio-isomers (**5A** and **5B**) are possible in the cycloaddition of the carbonyl ylide (**3**) with carbonyl compounds. Of these, **5A** agrees with the ^{13}C NMR spectrum which shows a signal of quartanary carbon (C_{31}) of orthocarboxylate, at very low field (119.82 ppm). Four stereoisomers (**5a—d**) and their enantiomers are feasible in the **5A**-type adducts as is shown in Fig. 1. The stereoisomers **5a**, **5b**, **5c**, and **5d** are described as *RRR*, *RRS*, *RSR*, and *RSS*, respectively in *R–S* description, depending upon the stereochemistry at C_{14}, C_{15}, and C_{23}. The isomers **5a** (*RRR*) and **5b** (*RRS*) have the same stereochemistry at both C_{14} and C_{15}, but different at C_{23}. The **5c** (*RSR*) and **5d** (*RSS*) are also in the same relationship. The isomers **5a** (*RRR*) and **5c** (*RSR*) have the same

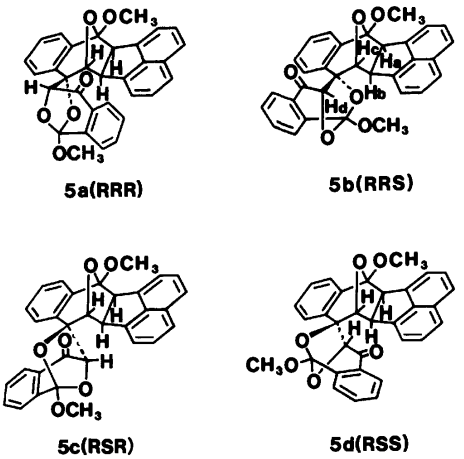

Fig. 1. Possible structures of the 2:1-adduct (**5**).

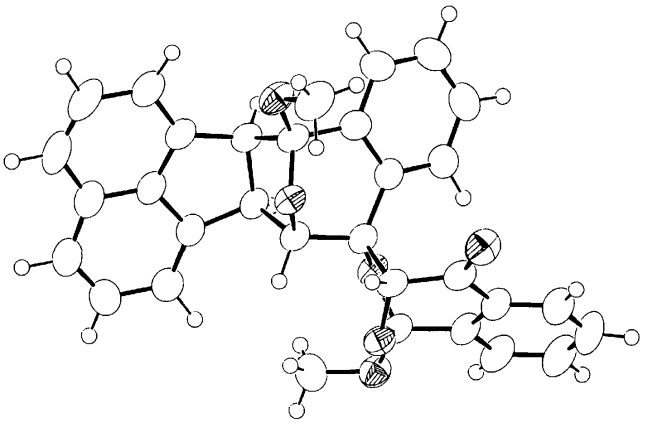

Fig. 2. Stereodrawing of the 2:1-adduct (**5b**).

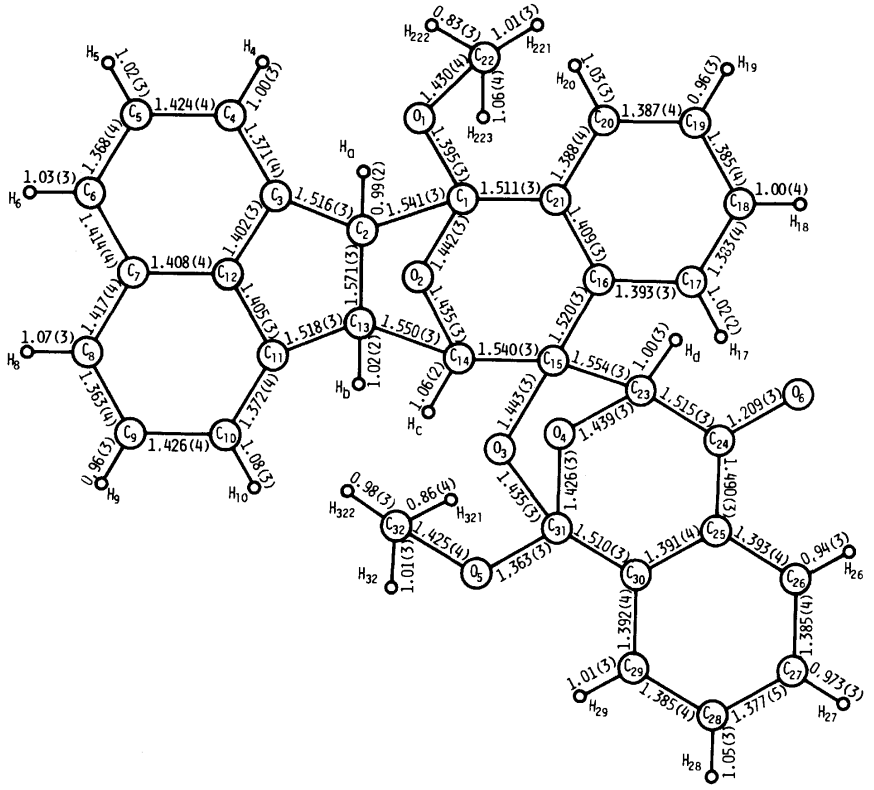

Fig. 3. Bond distances of the 2:1-adduct (**5b**).

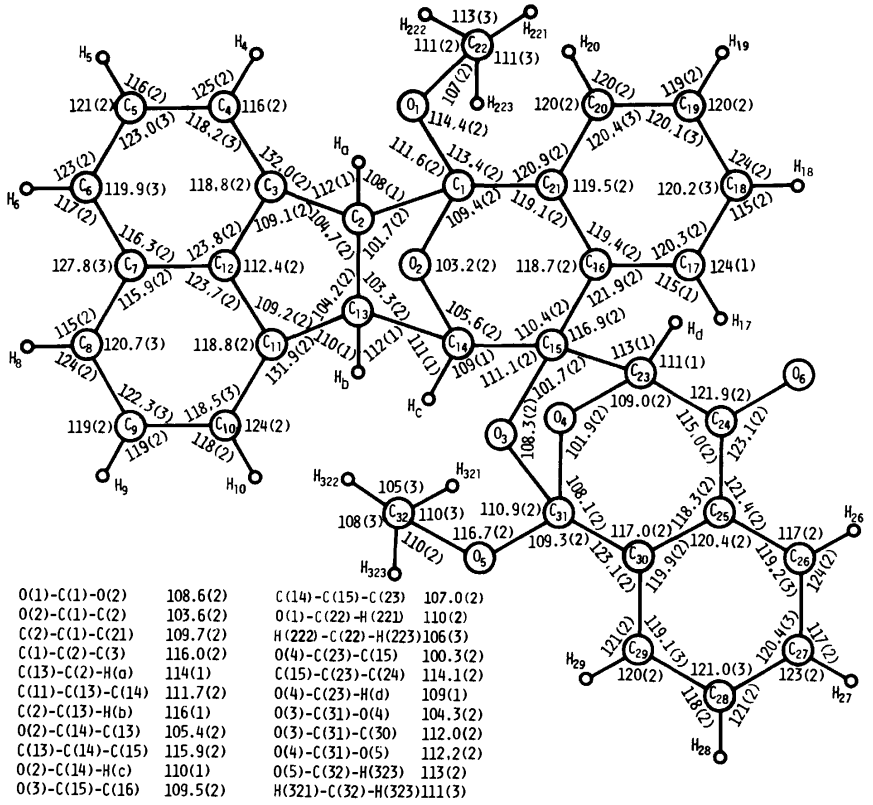

O(1)-C(1)-O(2)	108.6(2)	C(14)-C(15)-C(23)	107.0(2)
O(2)-C(1)-C(2)	103.6(2)	O(1)-C(22)-H(221)	110(2)
C(2)-C(1)-C(21)	109.7(2)	H(222)-C(22)-H(223)	106(3)
C(1)-C(2)-C(3)	116.0(2)	O(4)-C(23)-C(15)	100.3(2)
C(13)-C(2)-H(a)	114(1)	C(15)-C(23)-C(24)	114.1(2)
C(11)-C(13)-C(14)	111.7(2)	O(4)-C(23)-H(d)	109(1)
C(2)-C(13)-H(b)	116(1)	O(3)-C(31)-O(4)	104.3(2)
O(2)-C(14)-C(13)	105.4(2)	O(3)-C(31)-C(30)	112.0(2)
C(13)-C(14)-C(15)	115.9(2)	O(4)-C(31)-O(5)	112.2(2)
O(2)-C(14)-H(c)	110(1)	O(5)-C(32)-H(323)	113(2)
O(3)-C(15)-C(16)	109.5(2)	H(321)-C(32)-H(323)	111(3)

Fig. 4. Bond angles of the 2:1-adduct (**5b**).

stereochemistry at C_{14} and C_{23}, but different at C_{15}. In these isomers the stereochemistry at C_{31} is prescribed by that at C_{23}. Therefore, there is no need to describe the stereochemistry at C_{31}.

Molecular Structure. The molecular structure of **5** determined by the X-ray analysis is given in Figs. 2—4. The results indicate that **5** has the *RRS*-structure (**5b**), which is one of the four possible structures deduced from the NMR data. The CPK-model inspection shows that the approach of **3** to the carbonyl group of the *exo*-1:1-adduct (**4a**) in the manner to give **5b** is that of the most favorable in stereochemistry. The present compound has two benzene-fused bicyclo[3.2.1]-ring systems, 8-oxabicyclo[3.2.1]-2-octene and 7,8-dioxabicyclo[3.2.1]octa-2-ene-4-one, which are combined in spiro form. Their corresponding dihedral angles are similar to each other as shown in the deposited Table. This conformation is also similar to that of the *exo*-adduct (**6**) between **3** and *N*-methylmaleimide.[7] The bond distances and angles of the 2:1-adduct (**5b**) except the C(2)-C(13) bond distance are comparable to those of **6**. The C(2)-C(13)

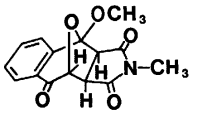

6

bond distance, 1.571 Å, in the acenaphthene ring of **5b**, is considerably longer than the corresponding one (1.545 Å) of the acenaphthene-chloranile molecular complex,[8] while the bond distance is comparable to the corresponding ones (1.567, 1.562 Å) of the *cis*-dimer of acenaphthylene.[9] Two of the intramolecular distances (O···H) between the bridged oxygen atoms and the methyl-hydrogen atoms are shorter than the van der Waals distance as shown in Table 3.

Table 3. Intramolecular distances between the bridged oxygens and the methyl hydrogens

O(2)···H(221)	3.24(3) Å
O(2)···H(222)	3.47(3)
O(2)···H(223)	2.36(4)
O(4)···H(321)	3.44(3)
O(4)···H(322)	3.66(3)
O(4)···H(323)	2.54(3)

Coupling Constant. In general, coupling constants of the vicinal protons depend mainly on the dihedral angles and an equation was proposed by Karplus to express the relationship between them.[10] The torsion angles Ha-C(2)-C(13)-Hb and Hb-C(13)-C(14)-Hc were found to be 3.8° and −97.6°, respectively, according to the present X-ray crystal structure determination. The substitution of these torsion angles in the Williamson-Johnson's equation[11] gave calculated values of coupling constants, $J_{a,b}$=10.0 Hz and $J_{b,c}$=−0.11 Hz, which are fairly in accord with the observed values $J_{a,b}$=6.7 Hz and $J_{b,c}$=1.3 Hz.

The coupling between ^{13}C and H separating by three bonds has recently been reported to be useful for the

determination of conformation of rigid cyclic systems[12] and an equation (Eq. 1) to calculate the $J(^{13}C, H)$ using the value of the dihedral angles has been reported by Wasylishen and Schaefer.[13]

$$^{3}J(^{13}C,H) = 4.26 - 1.00\cos\theta + 3.56\cos 2\theta \quad (1)$$

The coupling constants $^{3}J(^{13}C_{14}\text{-Hd})$=4.83 Hz and $^{3}J(^{13}C_{23}\text{-Hc})$=3.60 Hz calculated by application of the torsion angles, $C_{10}\text{-}C_{15}\text{-}C_{23}\text{-Hd}$=33.4° and $C_{23}\text{-}C_{15}\text{-}C_{14}\text{-Hc}$=43.0°, to the equation 1 are consistent with the observed values, $^{3}J(^{13}C_{14}\text{-Hd})$=4.96 Hz and $^{3}J(^{13}C_{23}\text{-Hc})$=2.76 Hz. This also supports the structure of the 2:1-adduct (**5b**).

Anisotropic Effect of Benzene Ring. The ^{1}H NMR spectrum of the 2:1-adduct (**5b**) has a doublet signal of an aromatic proton (H_{17}) at a little higher field (δ 6.28) than the signals of the usual aromatic protons. The high field shift may be attributed to the anisotropic effect of ring current of benzene. The X-ray study indicates that the aromatic hydrogen, H_{17}, locates close to the benzene ring ($C_{25}\text{-}C_{30}$); the perpendicular drawn from the H_{17} to the plane of the benzene ring ($C_{25}\text{-}C_{30}$) has a length of 2.60 Å, and the distance from the foot of the perpendicular to the center of the benzene ring is 1.96 Å.[7] The estimation of the ring current effect according to the Johnson-Bovey's ring current effect map[14] indicates that the high field shift of H_{17} is δ 0.56 ppm. This may assign the signal at δ 6.28 to H_{17}.

The authors indebt to Dr. Masami Sawada and Mr. Yoshio Takai of ISIR of Osaka University for their fruitful discussion and measurement of NMR spectra.

References

1) R. Huisgen, *Angew. Chem. Int. Ed. Engl.*, **16**, 572 (1977); and references cited therein.
2) T. Ibata and J. Toyoda, *Chem. Lett.*, **1983**, 1453.
3) T. Ibata, K. Jitsuhiro, and Y. Tsubokura, *Bull. Chem. Soc. Jpn.*, **54**, 240 (1981).
4) The X-ray crystallography of the dimer is now under progress.
5) M. Bękhazi and J. Warkentin, *J. Am. Chem. Soc.*, **105**, 1289 (1983); and references cited therein.
6) P. Main, S. E. Hull, L. Lessinger, G. Germain, J.-P. Declercq, and M. M. Woolfson, "A System of Computer Programs for the Automatic Solution of Crystal Structures from X-ray Diffraction Data," MULTAN 78, University of York (1978).
7) H. Tamura, T. Ibata, and K. Ogawa, *Bull. Chem. Soc. Jpn.*, **57**, 926 (1984).
8) I. J. Tickle and C. K. Prout, *J. Chem. Soc., Perkin Trans., 2*, **1973**, 724.
9) T. R. Welberry, *Acta Crystallogr., Sect. B.* **27**, 360 (1971).
10) M. Karplus, *J. Chem. Phys.*, **30**, 11 (1959).
11) One of the modified Karplus equation: K. L. Williamson and W. S. Johnson, *J. Am. Chem. Soc.*, **83**, 4623 (1961).
12) S. Takeuchi, J. Uzawa, H. Seto, and H. Yonehara, *Tetrahedron Lett.*, **1977**, 2943.
13) R. Wasylishen and T. Schaefer, *Can. J. Chem.*, **50**, 2710 (1972).
14) C. E. Johnson, Jr. and F. A. Bovey, *J. Chem. Phys.*, **29**, 1012 (1958).

Vacuum UV Photolyses of Some Bichromophoric Alkenes Possessing Hydroxyl or Methoxycarbonyl Group

Yoshihisa INOUE,* Kazuyoshi GOAN, and Tadao HAKUSHI
Department of Applied Chemistry, Himeji Institute of Technology, 2167 Shosha, Himeji, Hyogo 671-22
(Received April 8, 1985)

The direct photolyses at 185 nm of some naturally occurring and related bichromophoric alkenes possessing hydroxyl or methoxycarbonyl group at an allylic, homoallylic, or remote position gave the geometrical isomers as the major photoproducts detectable on gas chromatography. The isomerization yield was highly sensitive to the functional group introduced and its position; allylic alkenols gave poor yields, while both functionalization at a remote position and esterification of the hydroxyl group improve the photoisomerization yield.

The vacuum UV light has recently been used extensively in the investigation of the photochemistry of simple unsaturated compounds like alkenes and alkynes in solution phase.[1,2] With simple alkenes, a wide variety of novel singlet photobehavior *via* π,π^*, π, R(3s), and π,σ^* excited states has been reported to occur upon direct excitation in the vacuum UV, although the cis-trans photoisomerization, where accessible, is the dominant process in most cases.[1,2] On the other hand, much less effort has been done in order to reveal the effects of an additional functional group upon the fundamental photobehavior of simple alkenes, except for the works by Srinivasan[3] and by us.[4] The investigations on the photochemistry of bichromophoric alkenes not only afford insights into the nature of the excited double bond but also extend the scope and limitations of the vacuum UV photochemistry.

In this paper we report our results on the direct photolyses at 185 nm of bichromophoric alkenes possessing a hydroxyl or methoxycarbonyl group at an allylic, homoallylic, or remote position.[5] The bichromophoric alkenes examined in the present work are *trans*-2-buten-1-ol(**1t**), *cis*-3-hexen-1-ol or "leaf alcohol"[6] (**2c**), geraniol (**3t**), nerol (**3c**), methyl oleate (**4c**), methyl elaidate (**4t**), *cis*-3-hexenyl acetate (**5c**), and neryl acetate (**6c**). Most of these are naturally occurring products or their immediate derivatives, and, therefore, the present work will shed light on this relatively unexplored region of photochemistry/natural product chemistry.

Another purpose of this paper is to test the suitability of water as a solvent for the vacuum UV photolysis by using water-soluble alkenols. The solvent available in the vacuum UV has long been restricted to the nonpolar, aprotic saturated hydrocarbons and even an alcohol such as methanol as a polar, protic solvent cannot be used due to the extinction coefficient of several handreds in this wavelength region,[7] whereas water is almost transparent at 185 nm.[7]

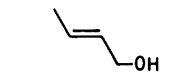

1t

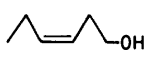

2c

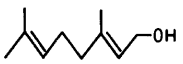

3t

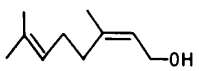

3c

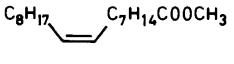

4c

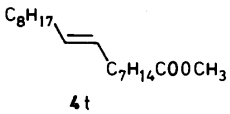

4t

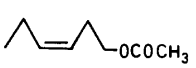

5c

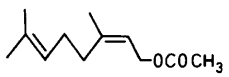

6c

Results and Discussion

Photoisomerization. The direct irradiations of the bichromophoric alkenes **1—6** were performed at 185 nm in pentane and/or in water under a nitrogen atmosphere to give the geometrical isomers as the major photoproducts detected by GC analysis and the other valence isomers were not detected in significant yields. The isomerization yield varied drastically depending upon the functional group introduced and its position and also upon the solvent used. The isomerization yields at low and moderate conversions are listed in Table 1.

The direct photolyses of the allylic alcohols **1t**, **3t**, and **3c** in pentane afforded the corresponding geometrical isomers only in poor yields below 40%, while the homoallylic alcohol **2c** gave somewhat improved yield. The irradiation of **1t** or **2c** in water resulted merely in a similarly low or much reduced yield. From the mechanistic point of view, it is noted that no valence isomers other than cis-trans isomer were produced in significant yields and that the prolonged irradiations of **2c** in water led to the accumulated deposition of white precipitate, which was not characterized chemically due to the limited sample availability but is inferred to be water-insoluble polymeric

TABLE 1. DIRECT cis-trans PHOTOISOMERIZATION AT 185 NM OF SOME BICHROMOPHORIC ALKENES

Alkene (10 mM)	Solvent	Irradiation time/min	Conversion /%	Isomerization yield/%[a]
1t	Pentane	10	26	16
		20	36	20
	Water	10	14	24
		30	41	17
2c	Pentane	10	21	51
		20	40	41
	Water	10	30	18
		20	46	19
		60	86	6[b]
3t	Pentane	10	15	36
		20	27	34
3c	Pentane	10	15	27
		20	26	28
4c	Pentane	10	13	98
		20	27	79
4t	Pentane	10	18	91
		20	30	76
5c	Pentane	10	17	84
		20	29	72
6c	Pentane	10	12	28
		20	21	25

a) Chemical yield based on alkene consumed. b) Water-insoluble polymeric product was produced as white precipitate.

product. Above results suggest that the major process which occurred upon photolysis of the alkenols **1**—**3** is not the geometrical photoisomerization but the polymerization initiated probably by some radicals generated by the high-energy radiation in the vacuum UV. However, since analogous radical process which competes well with the cis-trans isomeization has not been reported in the photochemistry of simple acyclic alkenes,[1,2] this unexpected photobehavior must originate from the special electronic feature of the alkenols. The presence of oxygen atom at a weakly interactable, especially β, position may change the excitation profile of the alkenes significantly. The $\pi_{C=C} \rightarrow \sigma^*_{\pi CH_2}$ charge-transfer excitation is tentatively proposed as an electronic transition responsible for the radical formation,[3,8-10] since, in both semiempirical and *ab initio* calculations, the π atomic orbital ($\sigma_{\pi CH_2}$) of allylic CH_2 group has shown to mix readily with the π molecular orbital ($\pi_{C=C}$) of C=C bond. In particular, an oxygen atom β to C=C bond may lower the level of the σ^*_π orbital through further participation of its lone-pair electrons to the above mixing. The resulting electronic configuration with a reduced C-H bond order may facilitate the fission of the allylic C-H bond, giving rise to hydrogen and allylic radicals. The introduction of a hydroxyl group into an allylic position of alkene reduces the bond dissociation energy of the allylic C-H bond by 30—40 kJ mol^{-1}.[11] This may also facilitate the allylic bond fission in conjunction with the stabilization of the resulting allylic radical by the electron-donating hydroxyl group. The reason for much reduced isomerization yield upon photolysis

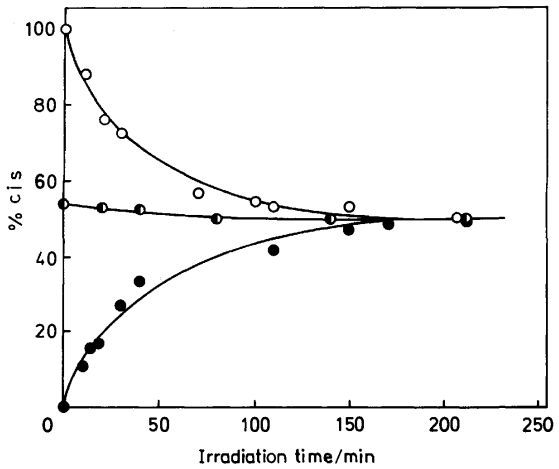

Fig. 1. Percent of the *cis*-isomer (**4c**) in **4** recovered on direct photolysis of **4** at 185 nm in pentane; initial composition: (○) 100% **4c**; (○) 54% **4c**; 46% **4t**; (●) 100% **4t**.

of **2c** in water is not necessarily clear, but the nucleophilic trapping by water of π, 3s Rydberg excited state of alkene may consume the alkene affording addition products, *i.e.* diols,[12] as has been shown by Kropp *et al.* in the direct photolyses of tri- and tetrasubstituted alkenes at >200 nm,[1] and the possibility is not regorously ruled out that the use of a highly polar solvent may change the population of the excited states generated, which leads to different distribution of products.

In sharp contrast to the alkenols, methyl oleate **4c** and methyl elaidate **4t**, possessing a methoxycarbonyl group at a remote position, interconverted mutually in excellent yields upon direct irradiation, as is the case with simple alkenes.[1,2] Although the major reason for the facile isomerization in this particular case is probably the functionalization at a remote position in **4**, it is also expected that the methyoxycarbonyl group may improve the isomerization yield. Indeed *cis*-hexenyl acetate **5c** prepared by esterification of hexenol **2c** gave the trans-isomer **5t** in fairly improved yield as compared with **2c**. However this method is no longer applicable for the allylic alcohol. Neryl acetate **6c** isomerized photochemically only in low yields which are comparable with those for nerol **3c** itself. Thus the attempt to improve the photoisomerization yield by esterification is successful only for the alkenols possessing a hydroxyl group at a homoallylic or more remote position.

Photostationary State. Since the mutural photoisomerization between oleate **4c** and elaidate **4t** was highly efficient, the irradiation at 185 nm was prolonged up to 3 h in order to obtain the *cis/trans* ratio at the photostationary state, $(c/t)_{pss}$. As can be seen from Fig. 1, the prolonged irradiation of any given compositions of **4c** and **4t** afforded the identical ultimate value of 50% cis or $(c/t)_{pss}$ of 1.0. Since the reported molar extinction coefficients of **4c** and **4t** at

Table 2. Photostationary state *cis/trans* ratios on direct photoisomerizations at 185, 214, and 229 nm of methyl oleate **4c** and methyl elaidate **4t** in pentane

Excitation wavelength, nm	$(c/t)_{pss}$
185	1.0
214	1.2
229	0.43

185 nm are 12800 and 11600 $M^{-1}cm^{-1}$, respectively,[13] the decay ratio from the excited singlet (^1p) to **4c** an **4t**, k_{dc}/k_{dt}, is calculated, from the equation $(c/t)_{pss}=(\varepsilon_t/\varepsilon_c)(k_{dc}/k_{dt})$,[14] to be 1.1, which is reasonable for an acyclic alkene.

Similar prolonged irradiation of pentane solutions of a given mixture of **4** was run at 214 and 229 nm by using zinc and cadmium lamps, respectively. The photostationary states were attained at both wavelengths affording the $(c/t)_{pss}$ ratios listed in Table 2. The present $(c/t)_{pss}$ values obtained in the direct excitations of **4** at 185 and 214 nm are much higher than those reported for the semiconductor photosensitization, $(c/t)_{pss}=0.20—0.44$,[15,16] and for the triplet photosensitization, $(c/t)_{pss}=0.21—0.74$,[16] of the same compound, and therefore the direct photoisomerization merits synthetic application.

Experimental

General. Infrared spectra were obtained on a Jasco A-100 spectrometer. Mass spectra were recorded at 70 eV using a Hitachi RMU-6E instrument. ^1H NMR spectra were obtained on a Jeol JMX-60 sepctrometer in chloroform-*d* solution containing 1% tetramethylsilane as an internal standard. Gas chromatographic analyses of the photolyzates from **1**, **2**, **3**, **5**, and **6** were performed on a Yanaco G-180 or G-1800 instrument equipped with a System Instruments Chromatocorder 11 using columns of 20% PEG-20M (1.5 m) at 100 °C, 20% PEG-20M (1.5 m) at 120 °C, 20% PEG-20M (1.5 m) at 180 °C, 10% DEGS (3 m) at 120 °C, and 10% APL (65 cm) at 100 °C, respectively; the internal standards employed for pentane (water) solutions were cyclooctane (*t*-butyl alcohol), cyclooctane (*t*-butyl alcohol), dodecane, dodecane, and undecane, respectively. Liquid chromatographic analyses of the photolyzates from **4** were run on a Yanaco L-4000W instrument equipped with a Yanaco M-315 UV monitor, operated at 205 nm, and a Waters Data Module M730 using a 25 cm column of ODS-T with a water/methanol (2/98) eluent at a flow rate of 1.0 mL min^{-1}; the internal standard added after irradiation was *trans*-2-octene. Under the above conditions, the cis-trans isomers of **1—6** and the internal standard were seprated satisfactorily in each case.

Materials. Commercially available *trans*-2-buten-1-ol (**1t**), *cis*-3-hexen-1-ol (**2c**), geraniol (**3t**), and nerol (**3c**) (all from Tokyo Kasei) were fractionally distilled prior to use. Methyl oleate (**4c**) and methyl elaidate (**4t**) (both from Tokyo Kasei) were used without further purification.

cis-3-Hexenyl acetate (**5c**) and neryl acetate (**6c**) were prepared from the corresponding alcohols **2c** and **3c**. To a stirred mixture of **2c** or **3c** (0.07 mol) and *N,N*-dimethylaniline (0.07 mol) in dry ether (100 mL) was added dropwise acetyl choride (0.07 mol), and the mixture was heated to reflux for 2 h. The subsequent workup and fractional distillation gave the product **5c** or **6c** in 90—95% yield. **5c**: bp 105 °C/130 Torr†; MS *m/z* 142 (M^+); IR (neat) 3020, 2960, 2875, 1745, 1660, 1240, 1040 cm^{-1}; ^1H NMR δ=4.9—5.6 (m, 2H), 3.93 (t, 2H), 1.8—2.6 (m, 4H), 1.98 (s, 3H), 0.95 (t, 3H). **6c**: bp 115 °C/13 Torr; MS *m/z* 196 (M^+); IR (neat) 3025, 2970, 2930, 2850, 1740, 1675, 1235, 1030, 960, 830 cm^{-1}; ^1H NMR δ=4.8—5.5 (m, 2H), 4.47 (d, 2H), 2.0—2.2 (m, 7H), 1.67 (m, 9H).

Photolysis. A pentane or aqueous solution containing an alkene **1—6** (10 mM)†† and an internal standard (2—3 mM) was charged in a Suprasil tubing (1 cm o.d.) and bubbled with nitrogen gas for 10 min at 0 °C. The solution was irradiated at room temperature by using a 30-W mercury resonance lamp made of Suprasil (Eikosha), the light path being flushed with nitrogen gas; the effective radiation in the present case is the 185 nm resonance line, since another intense resonance line at 254 nm is not absorbed by the alkenes **1—6**. The photolyses at 214 and 229 nm were conducted by using 16-W zinc and cadmium resonance lamps (Philips), respectively.

Identification. The photoproducts from **1t**, **2c**, **3**, **4**, **5c**, and **6c** were identified by the comparison of GC retention time of the product with that of the authentic specimen obtained commercially or prepared independently, using a couple of columns of different polarity. The authentic specimens of *trans*-3-hexen-1-ol (**2t**)(Nakarai), **3c**, **3t**, **4c**, **4t**, and geranyl acetate (**6t**)(Nakarai) were commercially available. *trans*-3-Hexenyl acetate (**5t**) was prepared from the corresponding alcohol **2t** according to the esterification procedure mentioned above. The pure specimen of *cis*-2-buten-1-ol (**1c**) was isolated from the photolyzate of **1t**. Preparative-scale irradiation of a pentane solution of **1t** (50 mM) were performed for 5 h with continuous bubbling of nitrogen gas and stirring in an immersion-well reactor (130 mL) using the same lamp. The solvent was distilled fractionally and the residue obtained was trap-to-trap distilled. The trap-distillate was subjected to preparative gas chromatography to give the pure product of **1c**. **1c**: IR (neat) 3350, 3030, 2930, 2880, 1660, 1035, 980, 900 cm^{-1}; ^1H NMR δ=5.57 (m, 2H), 4.17 (d, 2H), 2.5 (br, 1H), 1.67 (d, 3H). **5t**: IR (neat) 3030, 2960, 2930, 2870, 1740, 1660, 1240, 1040, 965, 900 cm^{-1}; ^1H NMR δ=5.2—5.5 (m, 2H), 3.99 (t, 2H), 1.8—2.5 (m, 4H), 2.00 (s, 3H), 0.95 (t, 3H).

Generous support of this work by a grant from the Shorai Foundation for the Promotion of Science and Technology (Grant No. 005) is gratefuly acknowledged.

References

1) P. J. Kropp, *Org. Photochem.*, **4**, 1 (1979); *Molec. Photochem.*, **9**, 39 (1979).

2) Y. Inoue and T. Hakushi, *Kagaku to Kogyo (Science and Industry)*, **56**, 78, 116, 165 (1982).

3) R. Srinivasan, J. Studebaker, and K. H. Brown, *Tetrahedron Lett.*, 1955 (1979); R. Srinivasan, J. A. Ors, T.

† 1 Torr=133.322 Pa.

†† 1 M=1 mol dm^{-3}.

Baum, L. S. White, and A. R. Rossi, *J. Am. Chem. Soc.*, **102**, 5297 (1980); R. Srinivasan, L. S. White, A. R. Rossi, and G. A. Epling, *ibid.*, **103**, 7299 (1981); W. J. Leigh and R. Srinivasan, *ibid.*, **104**, 4424 (1982); *ibid.*, **105**, 514 (1983).

4) Y. Inoue, N. Matsumoto, T. Hakushi, and R. Srinivasan, *J. Org. Chem.*, **46**, 2267 (1981).

5) Since typical absorption coefficients for simple alcohols and carboxylic esters are much smaller (by factors of 20—100) than those for simple alkenes (Ref. 8), more than 95% of the incident light is absorbed by the olefinic chromophore and the photoreaction is initiated by the excitation of a π electron. Indeed, no specific difference is seen between simple and bichromophoric alkenes at least above 205 nm, where only a tail of the major absorption band around 185 nm is observed.

6) For recent reviews on the biosynthesis and chemistry of leaf alcohol, see: A. Hatanaka, *Bull. Inst. Chem. Res., Kyoto Univ.*, **61**, 180 (1983); *J. Synth. Org. Chem., Jpn*, **39**, 142 (1981).

7) M. B. Robin, "Higher Excited States of Polyatomic Molecules," Vol. 1, Academic, New York, 1974, p. 254.

8) Reference 7, Vol. 2, Chap. 4; and the references cited therein.

9) M. B. Robin, R. R. Hart, and N. A. Kuebler, *J. Chem. Phys.*, **44**, 1803 (1966); M. B. Robin, H. Basch, N. A. Kuebler, B. E. Kaplan, and J. Weinwald, *ibid.*, **48**, 5037 (1968).

10) F. H. Watson, Jr., A. T. Armstrong, and S. P. McGlynn, *Theor. Chim. Acta*, **16**, 75 (1970); F. H. Watson, Jr. and S. P. McGlynn, *ibid.*, **21**, 309 (1971).

11) R. T. Sanderson, "Chemical Bonds and Bond Energy," Academic, New York, 1976, Chap. 10.

12) Under the GC conditions employed, these diols, even if produced, are absorbed on the column. No effort was done to detect the diols.

13) R. G. Binder, L. A. Goldblatt, and T. H. Applewhite, *J. Org. Chem.*, **30**, 2371 (1965).

14) Y. Inoue, S. Takamuku, and H. Sakurai, *J. Phys. Chem.*, **81**, 7 (1977).

15) K. Mizumoto, A. Kabumoto, C. Pac, and S. Yanagida, 25th Symposium on Photochemistry, Abstract, p. 257 (1984).

16) S. Yanagida, K. Mizumoto, A. Kabumoto, C. Pac, and K. Yoshino, 5th International Conference on Photochemical Conversion and Storage of Solar Energy, Abstract, p. 181 (1984).

Molecular Complexes of Hydroxy Host Systems with Alcohols. X-Ray Crystal Structures of 1,1,6,6-Tetrakis(2,4-dimethylphenyl)-2,4-hexadiyne-1,6-diol–Ethanol (1:2), 1,1-Bis(2,4-dimethylphenyl)-2-butyn-1-ol–Ethanol (1:1), and 9-(1-Propynyl)-9-fluorenol–Methanol (1:1)

Fumio Toda,* Koichi Tanaka, and Thomas C. W. Mak*†

Department of Industrial Chemistry, Faculty of Engineering, Ehime University, Matsuyama 790

†*Department of Chemistry, The Chinese University of Hong Kong, Shatin, New Territories, Hong Kong*

(Received April 10, 1985)

The structures of a 1:2 molecular complex(I) of 1,1,6,6-tetrakis(2,4-dimethylphenyl)-2,4-hexadiyne-1,6-diol with ethanol, a 1:1 complex(II) of 1,1-bis(2,4-dimethylphenyl)-2-butyn-1-ol with ethanol, and a 1:1 complex (III) of 9-hydroxy-9-(1-propynyl)fluorene with methanol have been determined by X-ray crystallography. The crystal data are: I, $C_{42}H_{50}O_4$, $P\bar{1}$, a=8.249(3), b=9.522(5), c=14.803(8)Å, α=100.95(4), β=110.82(4), γ=113.08(3)°, Z=1, and R_f=0.105 for 1834 observed Mo $K\alpha$ data; II, $C_{22}H_{28}O_2$, $P\bar{1}$, a=8.142(2), b=11.281(3), c=12.262(4)Å, α=102.76(2), β=97.08(2), γ=111.19(2)°, Z=2, and R_f=0.073 for 2104 data; III, $C_{17}H_{16}O_2$, $P2_1/a$, a=8.641(5), b=10.883(5), c=30.63(2)Å, β=92.88(4)°, Z=8, R_f=0.154 for 1885 data. The crystal structures of I and II are closely related and both feature planar hydrogen-bonded $(OH)_4$ rings centered at centrosymmetric sites. In III, the fluorene and methanol molecules belong to two independent sets, and the molecular components in each set are alternately linked by hydrogen bonds to form infinite zigzag chains parallel to the a axis.

Previously, we reported that 1,1,4,4-tetraphenyl-2-butyne-1,4-diol (**1**) and 1,1,6,6-tetraphenyl-2,4-hexadiyne-1,6-diol (**2a**) form 1:1 and 1:2 crystalline inclusion compounds with various guest molecules, which show the presence of strong hydrogen bonds *via* their IR spectra.[1,2] X-Ray single-crystal analysis of the complexes **1**·$(CH_3)_2CO$[2] and **2a**·$(CH_3)_2CO$[3] disclosed that the acetone moiety is included in a channel and surrounded by phenyl groups, being bound to the anti-oriented OH groups of the host through hydrogen bonding.

If surrounding of the guest species by phenyl rings is important for the stabilization of the complex, an effective host molecule might be derived by employing a more bulky aromatic substituent. Proceeding along this line of reasoning, we subsequently found that 1,1,6,6-tetrakis(2,4-dimethylphenyl)-2,4-hexadiyne-1,6-diol (**2b**) forms a stable 1:2 complex (I) with ethanol, even though **2a** fails to do so. The complexation Phenomenon is potentially useful for the isolation of ethanol from aqueous solution. However, complex I turned out to be too stable for the extraction of ethanol by the usual method, and it appeared that the 2,4-dimethylphenyl group might hinder the escape of ethanol molecules from the channels in the crystalline complex.

We then designed 1,1-diphenyl-2-propyn-1-ol (**3a**), 1,1-bis(2,4-dimethylphenyl)-2-propyn-1-ol (**3b**), and 1,1-bis(2,4-dimethylphenyl)-2-butyn-1-ol (**3c**) as potentially useful host molecules which would include ethanol more loosely than **2b** because one side of the molecular skeleton is opened. Actually, we did find that ethanol can easily be removed from its complexes with **3b** and **3c** by evaporation, even though **3a** does not include ethanol. Another variation in the design of related host systems is achieved by making the two aromatic rings coplanar, as in 9-(1-propynyl)-9-fluorenol (**4**), which has been shown to be an effective reagent for extracting ethanol from its aqueous solution.[4]

In order to test the above hypotheses and as part of our continuing studies on the synthesis and structural characterization of inclusion compounds, we have determined the crystal structures of I, a 1:1 complex (II) of **3c** with ethanol, and a 1:1 complex (III) of **4** with methanol, which are reported in the present paper. The analogous ethanol adduct turned out to be too unstable for X-ray analysis.

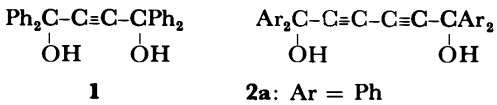

1 **2a**: Ar = Ph; **b**: Ar = 2,4-dimethylphenyl

3a: Ar = Ph; R = H

b: Ar = 2,4-dimethylphenyl; R = H

c: Ar = 2,4-dimethylphenyl; R = Me

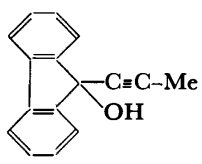

4

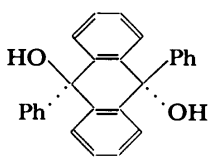

5

Experimental

1,1-Bis(2,4-dimethylphenyl)-2-propyn-1-ol (3b). A solution of Na (49 g) in liquid NH_3 (1.5 l) was stirred at −33 °C for 3 h in the presence of a catalytic amount of $Fe(NO_3)_3 \cdot 9H_2O$. The resulting $NaNH_2$ suspension was cooled to *ca.* −60 °C and acetylene gas bubbled through it for 2 h, and then a solution of 2,2′,4,4′-tetramethylbenzophenone (380 g) in THF (500 ml) was added and stirred for 2 h. The residue left after the evaporation of NH_3 was decomposed with dil HCl and extracted with ether. The ether solution

Table 1. Data collection and processing parameters

Complex	I	II	III
Molecular formula	$C_{42}H_{50}O_4$	$C_{22}H_{28}O_2$	$C_{17}H_{16}O_2$
Molecular weight	618.85	324.46	252.31
Cell constants	a=8.249(3)Å α=100.95(4)°	a=8.142(2)Å α=102.76(2)°	a=8.641(3)Å β=92.88(3)°
	b=9.522(5) β=110.82(4)	b=11.281(3) β=97.08(2)	b=10.883(4) V=2877(2)Å^3
	c=14.803(8) γ=113.08(3)	c=12.262(4) γ=111.19(2)	c=30.63(1) Z=8
	V=923.6(8)Å^3 Z=1	V=998.3(4) Z=2	
Density (flotation in KI/H_2O)	1.11 g cm^{-3}	1.09 g cm^{-3}	1.18 g cm^{-3}
Density (calcd)	1.113 g cm^{-3}	1.079 g cm^{-3}	1.165 g cm^{-3}
Space Group	$P\bar{1}$	$P\bar{1}$	$P2_1/a$
Absorption coefficent	0.65 cm^{-1}	0.63 cm^{-1}	0.70 cm^{-1}
Crystal size	0.50×0.50×0.50 mm	0.48×0.44×0.42 mm	0.50×0.42×0.38 mm
Scan type and speed		ω—2θ; 2.02—8.37 deg min^{-1}	
Scan range		1° below $K\alpha_1$ to 1° above $K\alpha_2$	
Background counting	stationary counts for one-half of scan time at each end of scan		
Collection range	$h,\pm k,\pm l$; $2\theta_{max}$=45°	$h,\pm k,\pm l$; $2\theta_{max}$=50°	$h,k,\pm l$; $2\theta_{max}$=45°
Unique data measured	2095	2777	2784
Observed data with $\lvert F_o\rvert>3\sigma(\lvert F_o\rvert)$, n	1834	2104	1885
Number of variables, p	206	231	175
$R_f=\sum\lvert\lvert F_o\rvert-\lvert F_c\rvert\rvert/\sum\lvert F_o\rvert$	0.105	0.073	0.154
Constant g in weighting scheme $w=[\sigma^2(F_o)+g\lvert F_o\rvert^2]^{-1}$	0.001	0.002	0.002
$R_g=[\sum w(\lvert F_o\rvert-\lvert F_c\rvert)^2/\sum w\lvert F_o\rvert^2]^{1/2}$	0.152	0.098	0.185
$S=[\sum w(\lvert F_o\rvert-\lvert F_c\rvert)^2/(n-p)]^{1/2}$	3.664	1.714	2.626
Residual extrema in final difference map	+0.49 to −0.23 e Å^{-3}	+0.47 to −0.21 e Å^{-3}	+0.69 to −0.42 e Å^{-3}

was washed with water and dried over Na_2SO_4. Evaporation of the solvent gave crude **3b**, recrystallization of which from benzene resulted in pure **3b** (350 g, 87%) as colorless needles, mp 61—63 °C, NMR ($CDCl_3$), 6.9—7.8 (6H, m, Ar), 2.83 (1H, s, =CH), 2.57 (1H, s, OH), 2.30 (6H, s, Me), and 2.02 (6H, s, Me). Found: C, 86.11; H, 7.48%. Calcd for $C_{19}H_{20}O$: C, 86.32; H, 7.63%.

Recrystallization of **3b** in ethanol gave a 1:1 complex which melted at 40—48 °C. NMR ($CDCl_3$) 6.9—7.8 (6H, m, Ar), 3.68 (2H, q, J=6.8 Hz, CH_2), 2.83 (1H, s, CH), 2.30 (6H, s, Me), 2.02 (6H, s, Me), and 1.21 (3H, t, J=6.8 Hz, Me). Found: C, 81.15; H, 8.37%, Calcd for $C_{21}H_{26}O_2$: C, 81.25; H, 8.44%.

1,1-Bis(2,4-dimethylphenyl)-2-butyn-1-ol (3c). To a $NaNH_2$ suspension prepared from Na (49 g) and liquid NH_3 (1.5 l), 1,2-dichloropropane (80 g) was added and stirred for 1 h. To this solution, 2,2′4,4′-tetramethylbenzophenone (140 g) dissolved in THF (200 ml) was added and stirred for 2 h. The residue left after the evaporation of NH_3 was decomposed with dil HCl and extracted with ether. The ether solution was washed with water and dried over Na_2SO_4. Evaporation of the solvent gave crude **3c** as an oil, crystallization of which from ethanol yielded a 1:1 complex (140 g, 76%), II, colorless prisms, mp 64—65 °C. NMR ($CDCl_3$) 6.8—7.7 (6H, m, Ar), 3.68 (2H, q, J=6.8 Hz, CH_2), 2.27 (6H, s, Me), 1.98 (6H, s, Me), 1.82 (3H, s, Me), and 1.21 (3H, t, J=6.8 Hz, Me). Found: C, 85.89; H, 5.70%. Calcd for $C_{22}H_{28}O_2$: C, 86.12; H, 5.68%.

1,1,6,6-Tetrakis(2,4-dimethylphenyl)-2,4-hexadiyne-1,6-diol (2b). A solution of **3b** (100 g) and CuCl (10 g) in acetone (500 ml) containing pyridine (50 ml) was stirred under O_2 atmosphere for 12 h. When 3 M† HCl (500 ml) was added to the reaction mixture, **2b** crystallized out. Recrystallization from benzene gave pure **2b** as colorless prisms (90 g, 90%), mp 192—193 °C. NMR ($CDCl_3$) 6.90—7.73 (12H, m, Ar), 2.29 (12H, s, Me), and 1.98 (12H, s, Me,). Found: C, 86.47; H, 7.44%. Calcd for $C_{38}H_{38}O_2$: C, 86.65; H, 7.27%.

Recrystallization of **2b** from ethanol resulted in a 1:2 complex, **I**, which does not have a clear mp. NMR ($CDCl_3$) 6.90—7.73 (12H, m, Ar), 3.68 (4H, q, J=6.8 Hz, CH_2), 2.29 (12H, s, Me), 1.98 (12H, s, Me), and 1.21 (6H, t, J=6.8 Hz, Me). Found: C, 81.39; H, 7.87%. Calcd for $C_{42}H_{50}O_4$: *c*, 81.51; H, 8.14%.

X-Ray Data Collection. All three complexes turned milky upon exposure to air, and each selected crystal was therefore enclosed in an alcohol atmosphere inside a 0.5 mm Lindemann glass capillary. Determination of the crystal class and orientation matrix was performed on a Nicolet R3m four-circle diffractometer according to established procedures[5] using graphite-monochromatized Mo $K\alpha$ radiation (λ=0.71069 Å). Accurate unit-cell parameters were derived from a least-squares fit of the angular settings for 25 reflections in the range 14°<2θ<18°. Reflection intensities were recorded at an ambient laboratory temperature of 22 °C, and three standards monitored every 50 data measurements showed only random fluctuations within ±2% of their mean values. The crystal data and processing parameters for I—III are sumarized in Table 1.

Structure Determination and Refinement

The raw intensities were processed with the learnt-profile procedure,[6] and redundant and equivalent reflections were averaged to yield a set of structure amplitudes following corrections for Lorentz and polarization factors. No absorption correction was applied. For each complex the statistical distributions of the normalized structure factors strongly favoured a

† 1 M=1 mol dm^{-3}.

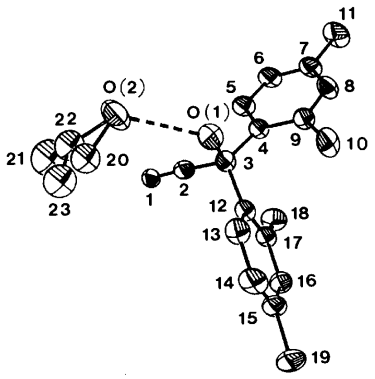

Fig. 1. Perspective view and atom labelling of the asymmetric unit in I. Both orientations of the disordered ethyl group are shown, and the broken line represents an O(1)···O(2) hydrogen bond.

centrosymmetric space group, and structure solution was achieved by direct phase determination based on negative quartets.[7]

In complex I, the 1,1,6,6-tetrakis(2,4-dimethylphenyl)-2,4-hexadiyne-1,6-diol molecule is situated at a center of symmetry, and the carbon atoms of the ethanol molecule exhibit two-fold orientational disorder as illustrated in Fig. 1. The disordered atoms C(20)–C(23) were assigned half weight and isotropic temperature factors, whereas the remaining non-hydrogen atoms were varied anisotropically. The aromatic H atoms were generated geometrically (C–H bond length fixed at 0.96Å) and allowed to ride on their respective parent C atoms.

In complex II the methyl group of the ethanol moiety is two-fold disordered and was accordingly represented by two isotropic "half-carbon" atoms. Anisotropic thermal parameters were assigned to all other non-hydrogen atoms. The aromatic H atoms were treated with the riding model, and the methyl groups were handled as rigid groups in including the contribution of the hydrogen atoms with isotropic temperature factors.

In complex III, there exist two sets of crystallographically independent molecules in the unit cell. In view of the unfavourable data-to-parameter ratio in this structure, all non-hydrogen atoms were refined isotropically except those belonging to the 1-propynyl and hydroxyl groups and the methanol molecules. To further reduce the number of variables, the benzene rings of the fluorene moiety were treated as regular hexagons of edge 1.395Å. The aromatic H atoms were assigned isotropic temperature factors and allowed to ride on their respective parent C atoms.

Computations were performed on a Data General Corporation Nova 3/12 minicomputer using the SHELXTL program package.[8] Analytic expressions of atomic scattering factors were employed, and anomalous dispersion corrections were incorporated.[9] Blocked-cascade least-squares refinement[10] converged to the R indices and parameters listed in Table 1.

Results and Discussion

Perspective views, each with atom labelling, of the asymmetric units in complexes I, II, and III are shown in Figs. 1, 2, and 3, respectively. The final atomic parameters are listed in Tables 2—4. The dimensions of the **3c** host molecule in II closely match the corresponding values for one-half of molecule **2b** in I, and those for the two independent **4** molecules in III are in satisfactory agreement (Table 5).

In the crystal structure of I (Fig. 4), the hexadiynediol molecule **2b** occupies a centrosymmetric site at the center of the unit cell, and its hydroxyl groups are linked by hydrogen bonds to neighboring ethanol molecules, generating a layer structure which features $(OH)_4$ rings centered at a second set of centrosymmetric sites at (0,0,1/2). The dimensions of the planar, hydrogen-bonded $(OH)_4$ ring are: O(1)···O(2)=2.723(8)Å, O(1)···O(2)′=2.669(7)Å, and O(2)···O(1)···O(2)′=84.2(2)°, where the primed superscript denotes the symmetry

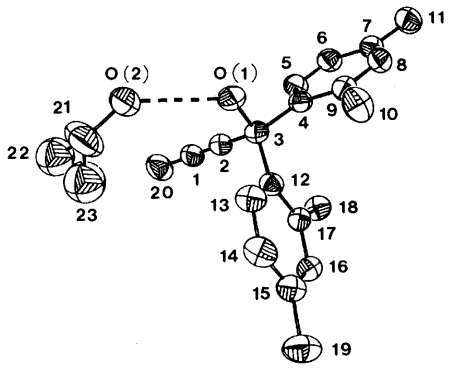

Fig. 2. Perspective view and atom labelling of the two molecular components in II. Both orientations of the disordered methyl group are shown, and the O(1)···O(2) hydrogen bond is represented by a broken line.

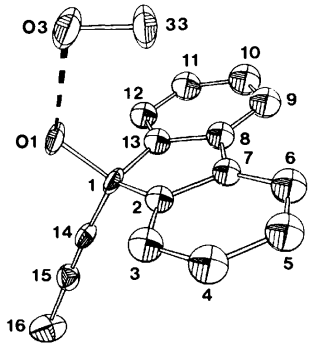

Fig. 3. Perspective view and atom labelling of one set (Type A) of molecular components in III, the O(1)···O(3) hydrogen bond being shown as a broken line. Atom labels for the other fluorene and methanol molecules (Type B) in the asymmetric unit are derived by incrementing the numbering of the corresponding oxygen and methanol carbon atoms by 1, and that of the remaining carbon atoms by 16.

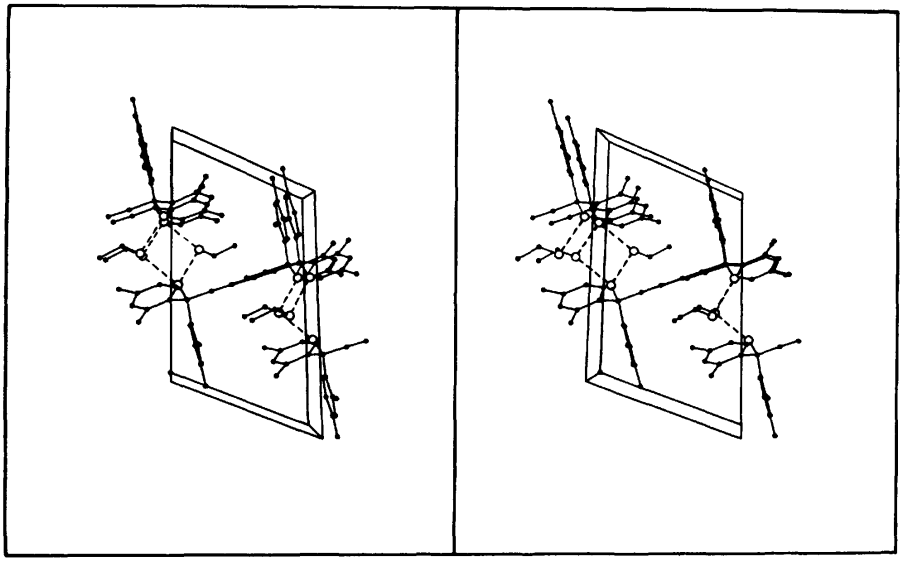

Fig. 4. Stereo view of the crystal structure of the 1:2 adduct (I) of 1,1,6,6-tetrakis(2,4-dimethylphenyl)-2,4-hexadiyne-1,6-diol (**2b**) with ethanol. The origin of the unit cell lies at the lower left corner, with a pointing towards the reader, b slantwise from left to right, and c upwards. The disordered ethyl group is shown in one of its two orientations, and hydrogen bonds are represented by broken lines.

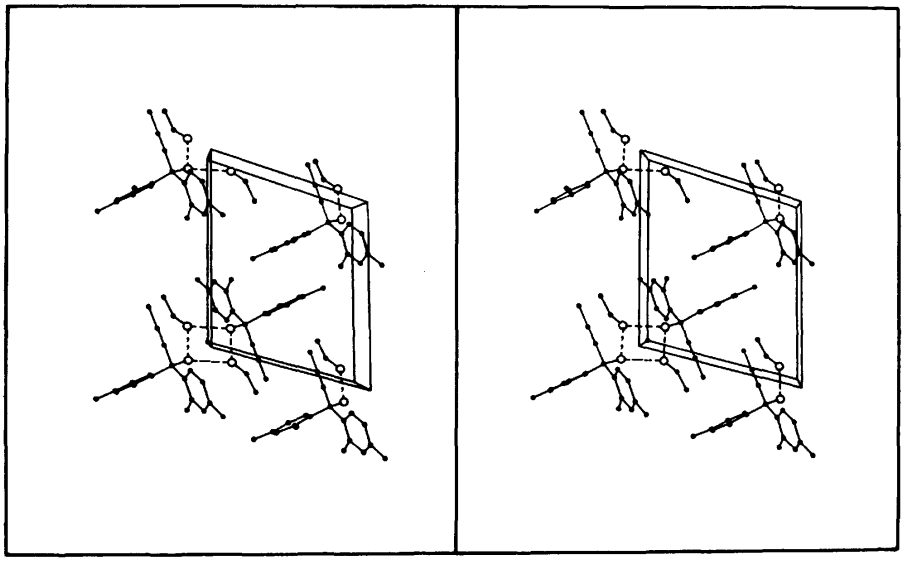

Fig. 5. Stereo view of the crystal structure of the 1:1 adduct (II) of 1,1-bis(2,4-dimethylphenyl)-2-butyn-1-ol (**3c**) with ethanol. The origin of the unit cell lies at the lower left corner, with a pointing towards the reader, b slantwise from left to right, and c upwards. The disordered methyl group of the ethanol molecule is shown in one of its two half-populated sites, and hydrogen bonds are represented by broken lines.

transformation ($-x$, $-y$, $1-z$). In the crystal lattice, van der Waals' contacts between the hydrophobic groups occur mainly across the (001) set of planes, midway between which are located the $(OH)_4$ rings and acetylenic functions.

In the crystal structure of II (Fig. 5), two butynol (**3c**) and two enthanol molecules are likewise alternately linked into a planar, hydrogen-bonded $(OH)_4$ ring centered at (1/2, 0, 0), with dimensions O(1)···O(2)= 2.700(5) Å, O(1)···O(2)′=2.686(4) Å, and O(2)···O(1)···O(2)′=91.9(1)°, where the primed superscript indicates the transformation ($1-x$, $-y$, $-z$). The crystal lattice thus comprises a packing of clearly discernible "dimeric" $(butynol\text{-}ethanol)_2$ aggregates.

The salient features common to the crystal structures of I and II are the effective utilization of crystallographic inversion centers and the occurrence of hydrogen-bonded $(OH)_4$ rings, which have been found

Table 2. Atomic coordinates (× 10^4) and thermal parameters[a] (Å²×10^3) for complex I

Atom	x	y	z	U_{eq}/U
O(1)	72(5)	516(4)	3762(3)	69(2)*
C(1)	4272(7)	4228(5)	4658(3)	56(3)*
C(2)	2996(7)	2837(6)	4044(4)	58(3)*
C(3)	1287(6)	1162(5)	3276(4)	52(2)*
C(4)	2005(6)	−45(5)	3015(3)	49(2)*
C(5)	3968(7)	358(6)	3634(4)	64(3)*
C(6)	4648(7)	−745(6)	3475(4)	68(3)*
C(7)	3389(7)	−2285(6)	2735(4)	63(3)*
C(8)	1449(7)	−2680(6)	2130(4)	65(3)*
C(9)	685(7)	−1649(6)	2229(4)	56(3)*
C(10)	−1523(7)	−2260(7)	1521(4)	79(3)*
C(11)	4148(10)	−3499(8)	2604(5)	98(4)*
C(12)	61(6)	1449(5)	2329(4)	50(2)*
C(13)	−1720(7)	1399(7)	2233(4)	68(3)*
C(14)	−2787(8)	1761(7)	1421(5)	81(3)*
C(15)	−2160(8)	2166(7)	735(4)	70(3)*
C(16)	−440(7)	2175(6)	820(4)	64(3)*
C(17)	737(7)	1867(5)	1621(4)	53(3)*
C(18)	2639(8)	1970(7)	1645(4)	72(3)*
C(19)	−3374(10)	2570(8)	−136(5)	105(4)*
O(2)	442(9)	2029(6)	5638(4)	126(4)*
C(20)	−437(21)	3150(16)	5640(10)	87(4)
C(21)	1479(34)	4609(28)	6446(18)	143(8)
C(22)	1110(27)	3808(23)	6181(13)	96(5)
C(23)	−834(25)	3906(21)	5795(12)	109(5)

a) Asterisk indicates equivalent isotropic temperature factor U_{eq} calculated as one-third of the trace of the orthogonalized U matrix. The exponent of the istropic temperature factor takes the form: $-8\pi^2 U \sin^2\theta/\lambda^2$.

Table 3. Atomic coordinates (× 10^4) and thermal parameters[a] (Å²×10^3) for complex II

Atom	x	y	z	U_{eq}/U
O(1)	4788(3)	1319(2)	1133(2)	80(1)*
C(1)	3226(5)	3181(3)	−152(3)	73(2)*
C(2)	3546(4)	2764(3)	621(3)	66(1)*
C(3)	4087(4)	2293(3)	1580(3)	59(1)*
C(4)	2484(4)	1555(3)	2064(3)	59(1)*
C(5)	739(4)	1235(3)	1479(3)	69(1)*
C(6)	−763(5)	542(3)	1841(3)	73(2)*
C(7)	−586(5)	131(3)	2808(3)	69(2)*
C(8)	1177(5)	430(3)	3380(3)	69(2)*
C(9)	2714(4)	1137(3)	3037(3)	63(1)*
C(10)	4539(5)	1405(4)	3740(4)	89(2)*
C(11)	−2202(5)	−601(4)	3234(4)	92(2)*
C(12)	5642(4)	3512(3)	2463(3)	56(1)*
C(13)	7418(4)	3632(3)	2537(3)	70(2)*
C(14)	8843(5)	4740(4)	3249(3)	77(2)*
C(15)	8583(5)	5784(3)	3918(3)	69(2)*
C(16)	6807(4)	5660(3)	3843(3)	62(1)*
C(17)	5339(4)	4559(3)	3125(3)	55(1)*
C(18)	3471(4)	4569(4)	3087(3)	72(2)*
C(19)	10153(6)	6993(4)	4677(4)	100(2)*
C(20)	2841(6)	3685(4)	−1101(3)	99(2)*
O(2)	6536(6)	1340(3)	−601(4)	144(2)*
C(21)	7894(8)	2199(6)	−935(6)	144(4)*
C(22)	7497(18)	2781(14)	−1782(13)	144(4)
C(23)	7878(21)	3383(16)	−944(14)	168(5)

a) Asterisk indicates equivalent isotropic temperature factor U_{eq} calculated as one-third of the trace of the orthogonalized U matrix. The exponent of the istropic temperature factor takes the form: $-8\pi^2 U \sin^2\theta/\lambda^2$.

Table 4. Atomic coordinates (× 10^4) and thermal parameters[a] (Å²×10^3) for complex III

Atom	x	y	z	U_{eq}/U
Type A molecules				
O(1)	591(8)	6636(6)	1270(3)	56(3)*
C(1)	1452(13)	5512(9)	1178(4)	49(4)*
C(2)	420(8)	4607(6)	975(3)	48(3)
C(3)	−406(8)	4658(6)	573(3)	64(4)
C(4)	−1311(8)	3661(6)	430(3)	75(4)
C(5)	−1390(8)	2612(6)	690(3)	73(4)
C(6)	−563(8)	3561(6)	1093(3)	71(4)
C(7)	342(8)	3558(6)	1235(3)	49(3)
C(8)	1284(9)	3746(7)	1632(2)	55(3)
C(9)	1585(9)	3012(7)	2000(2)	75(4)
C(10)	2582(9)	3431(7)	2340(2)	87(5)
C(11)	3277(9)	4583(7)	2313(2)	79(4)
C(12)	2976(9)	5317(7)	1945(2)	61(4)
C(13)	1979(9)	4899(7)	1604(2)	53(3)
C(14)	2783(14)	5865(10)	917(4)	42(4)*
C(15)	3827(15)	6088(10)	707(4)	52(5)*
C(16)	5158(16)	6342(14)	423(5)	85(6)*
O(3)	−2449(10)	6520(7)	1502(3)	83(4)*
C(33)	−2972(16)	5317(11)	1507(5)	76(6)*
Type B molecules				
O(2)	5161(8)	3396(7)	3729(3)	62(3)*
C(17)	6054(12)	4485(10)	3827(4)	50(4)*
C(18)	5057(8)	5418(6)	4030(3)	48(3)
C(19)	4352(8)	5318(6)	4428(3)	69(4)
C(20)	3478(8)	6291(6)	4580(3)	75(4)
C(21)	3309(8)	7366(6)	4334(3)	84(5)
C(22)	4014(8)	7467(6)	3936(3)	82(4)
C(23)	4888(8)	6493(6)	3784(3)	50(3)
C(24)	5719(9)	6312(7)	3395(3)	61(4)
C(25)	5907(9)	7089(7)	3040(3)	74(4)
C(26)	6794(9)	6710(7)	2696(3)	107(5)
C(27)	7492(9)	5554(7)	2708(3)	95(5)
C(28)	7304(9)	4777(7)	3063(3)	68(4)
C(29)	6417(9)	5156(7)	3407(3)	55(3)
C(30)	7440(14)	4204(11)	4080(4)	54(5)*
C(31)	8605(16)	3994(11)	4302(4)	56(5)*
C(32)	10035(16)	3692(16)	4559(5)	91(7)*
O(4)	2030(10)	3403(8)	3508(4)	89(4)*
C(34)	1497(17)	4657(12)	3420(5)	88(6)*

a) Asterisk indicates equivalent isotropic temperature factor U_{eq} calculated as one-third of the trace of the orthogonalized U matrix. The exponent of the istropic temperature factor takes the form: $-8\pi^2 U \sin^2\theta/\lambda^2$.

previously in related complexes such as the 1:1 adduct of 9,10-diphenyl-9,10-dihydro-r-9,t-10-anthracenediol (**5**) with 1,4-butanediol.[12] In both structures the environment around the ethyl carbon atoms of the ethanol molecule is relatively spacious, especially in I, allowing for the equal population of two energetically similar orientations. Interestingly, two neighboring CH_3–C≡C– groups in II are related by inversion and play the same role as a –C≡C–C≡C– fragment in I (see Figs. 4 and 5), and the structural relationship is analogous to that between the crystalline adducts **5**·2CH_3OH[13] and **5**·$HO(CH_2)_4OH$,[12] in which a pair of oppositely oriented methanol molecules are topologically equivalent to a 1,4-butanediol species.

Figure 6 illustrates the crystal structure of III, which

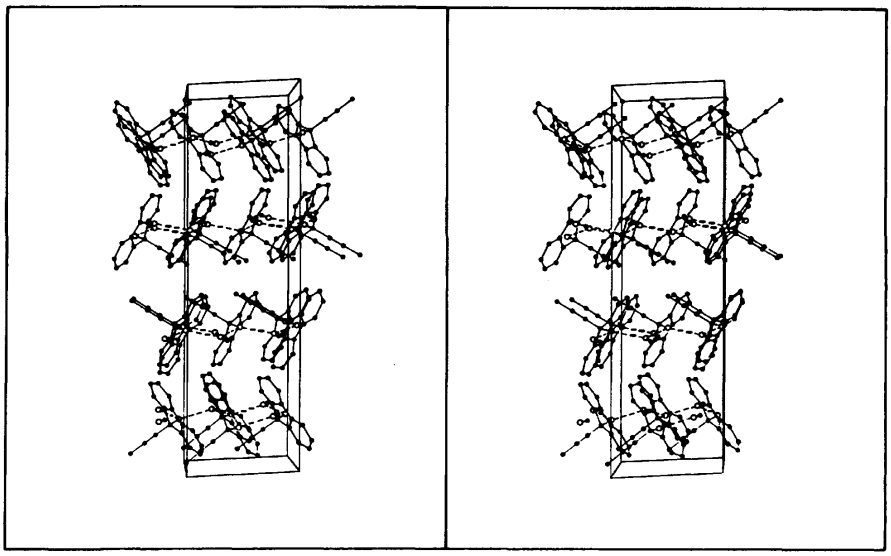

Fig 6. Stereo view of the crystal structure of the 1:1 adduct (III) of 9-hydroxy-9-(1-propynyl)fluorene (**4**) with methanol. The origin of the unit cell lies at the upper right corner, with a pointing from left to right, b towards the reader, and c downwards. Hydrogen bonds are represented by broken lines.

Table 5. Selected bond distances (l/Å) and angles (ϕ/°) in the host molecules

	I	II
C(3)-O(1)	1.447(7)	1.449(5)
C(3)-C(4)	1.533(9)	1.539(5)
C(3)-C(12)	1.555(7)	1.553(3)
C(3)-C(2)	1.494(5)	1.476(5)
C(2)-C(1)	1.208(5)	1.189(6)
C(1)-C(1)′	1.347(7)	—
C(1)-C(20)	—	1.451(6)
O(1)-C(3)-C(4)	107.0(4)	105.3(2)
O(1)-C(3)-C(12)	109.2(4)	108.8(3)
O(1)-C(3)-C(2)	107.5(4)	107.5(3)
C(4)-C(3)-C(12)	115.3(4)	115.4(3)
C(2)-C(3)-C(4)	111.9(4)	113.0(3)
C(2)-C(3)-C(12)	105.6(4)	106.5(2)
	III, Molecule A	III, Molecule B*
C(1)-O(1)	1.47(1)	1.44(1)
C(1)-C(2)	1.45(1)	1.49(1)
C(1)-C(13)	1.52(1)	1.53(1)
C(1)-C(14)	1.49(2)	1.43(2)
C(14)-C(15)	1.16(2)	1.21(2)
C(15)-C(16)	1.50(2)	1.47(2)
O(1)-C(1)-C(2)	110.0(8)	109.5(8)
O(1)-C(1)-C(13)	109.7(8)	110.4(9)
O(1)-C(1)-C(14)	107.5(8)	111.4(9)
C(2)-C(1)-C(13)	102.8(7)	100.0(8)
C(2)-C(1)-C(14)	114.9(9)	114.0(9)
C(13)-C(1)-C(14)	111.7(9)	111.0(9)

*Values matching those in molecule A are displayed. To obtain the atom numbers for O and C atoms in molecule B, add 1 and 16, respectively, to those shown in Fig. 3.

contains two independent sets of fluorene (**4**) and methanol molecules; the molecular species in each set are linked by hydrogen bonds to form infinite zigzag chains parallel to the a axis. The measured parameters of the two independent systems of hydrogen-bonded chains are: O(1)···O(3)=2.76(1)Å, O(1)···O(3)^{i}=2.70(1)Å, O(3)···O(1)···O(3)^{i}=124.0(4)°, O(1)···O(3)···O(1)^{ii}=119.5(4)°, O(4)···O(2)···O(4)^{iii}=122.9(4)°, and O(2)···O(4)···O(2)^{iv}=122.6(4)°, where the superscripts i, ii, iii, and iv denote the symmetry transformations ($^{1}/_{2}+x$, $^{1}/_{2}-y$, z), ($-^{1}/_{2}+x$, $1^{1}/_{2}-y$, z), ($^{1}/_{2}+x$, $^{1}/_{2}-y$, z) and ($-^{1}/_{2}+x$, $^{1}/_{2}-y$, z) respectively. With reference to Figs. 3 and 6, it is noted that the hydrogen-bonded chains generated from Type A fluorene [O(1)-C(16)] and methanol molecules [O(3)-C(33)] lie close to the planes z=1/8 and 5/8, whereas similar chains belonging to the other system are in the proximity of the planes z= 3/8 and 7/8. The van der Waals' contacts between hydrophobic groups thus occur mainly accross the (004) set of planes.

Elucidation of the crystal structures of the complexes I, II, and III in the present study provides a rationale for the formation of analogous alcohol adducts by the relevant host species **2b**, **3c**, and **4**. In each instance the alkyl group of the alcohol guest component is accommodated in a spacious void, so that its substitution by a more bulky alcohol would not be expected to significantly affect the overall pattern of molecular packing and hydrogen bonding.

The authors gratefully acknowledge financial support for this work by the Ministry of Education (Grant No. 56460040) and the Ming Yu Cultural Foundation (Grant No. 636011000).

References

1) F. Toda and K. Akagi, *Tetrahedron Lett.*, **1968**, 3695.
2) F. Toda, K. Tanaka, H. Hart, D. L. Ward, H. Ueda, and T. Ōshima, *Nippon Kagaku Kaishi*, **1983**, 293.
3) F. Toda, D.L. Ward, and H. Hart, *Tetrahedron Lett.*, **22**, 3865 (1981).

4) F. Toda, K. Tanaka, G. Ulibarri Daumas, and M. C. Sanchez, *Chem. Lett.*, **1983**, 1521.

5) R. A. Sparks, "Crystallographic Computing Techniques," ed by F. R. Ahmed, Munksgaard, Copenhagen (1976), pp. 452—467.

6) R. Diamond, *Acta Crystallogr., Sect. A*, **25**, 43 (1969).

7) G. T. DeTitta, J. W. Edmonds, D. A. Langs, and H. Hauptman, *Acta Crystallogr., Sect. A*, **31**, 472 (1975).

8) G. M. Sheldrick, "Computational Crystallography," ed by D. Sayre, Oxford University Press, New York (1982), pp. 506—514.

9) "International Tables for X-Ray Crystallography," Kynoch Press, Birmingham (1974), Vol. IV, pp. 55—60, 99—101, 149—150.

10) J. W. Schilling, "Crystallographic Computing," ed by F. R. Ahmed, Munksgaard, Copenhagen (1970), pp. 201—204.

11) Tables of anisotropic thermal parameters, atomic parameters for hydrogen atoms, and structure factors have been deposited as Document No. 8540 at the Office of the Chemical Society of Japan.

12) F. Toda, K. Tanaka, and T. C. W. Mak, *J. Incl. Phenom.*, in press.

13) F. Toda, K. Tanaka, S. Nagamatsu, and T. C. W. Mak, *Israel J. Chem.*, in press.

Studies of the Formation of Complexes of Np(V) with Inorganic Ligands by Means of Solvent Extraction with 2-Thenoyltrifluoroacetone and 1,10-Phenanthroline. II. Fluoro, Sulfato, and Phosphato Complexes

Yasushi INOUE* and Osamu TOCHIYAMA
Department of Nuclear Engineering, Faculty of Engineering, Tohoku University, Aramaki-aza-aoba, Sendai 980
(Received December 6, 1984)

The formation constants of the complexes of Np(V) with fluoride, sulfate, and phosphate have been determined in 1 mol dm^{-3} $NaClO_4$ at 25 °C by means of the solvent-extraction method using 2-thenoyltrifluoroacetone and 1,10-phenanthroline. Extractions at various pH values revealed that $H_2PO_4^-$ and HPO_4^{2-} participate in the complex formation of Np(V).

The study of the complex formation of quinquevalent uranides (U, Np, Pu, and Am) with a variety of ligands in aqueous solutions is important for understanding both the systematics and the nuclear chemical applications of these elements. Among uranides, neptunium is the only element which has a quinquevalent state which is stable enough to permit a study of complex formation in aqueous solutions.[1] Recent compilations[2-5] indicate a general lack of reliable data on the complex formation of Np(V), especially with inorganic ligands.

Previously,[6-8] the formation constants of the complexes of Np(V) with some organic ligands and the carbonate ion have been determined by means of the solvent-extraction method using 2-thenoyltrifluoroacetone (TTA) and methyltrioctylammonium[9] or TTA and 1,10-phenanthroline(phen).[10] Inorganic anions, such as fluoride, chloride, nitrate, sulfate, and phosphate, are also important ligands in both natural and artificial systems. The present authors aimed to determine the formation constants of Np(V) complexes with these ligands by means of solvent extraction with TTA and phen. Among these anions, however, chloride and nitrate cannot be studied since they are expected to form only very weak complexes with Np(V). The complex formation of Np(V) with only fluoride, sulfate, and phosphate has, therefore, been investigated.

Experimental

The neptunium-239 tracer was prepared by milking from ^{243}Am by the method of Sill;[11] it was then adjusted to the quinquevalent state by evaporation to dryness and dissolution in water.[12] To avoid any possible contamination by any complex-forming substances or by neptunium with a valence state other than quinquevalent (which might be introduced during milking), the following back-extraction procedure was adopted. The ^{239}Np tracer was first extracted into an organic (3-methyl-1-butanol or dichloromethane) solution containing the desired concentrations of TTA and phen. A 4-cm^3 portion of this organic solution containing ^{239}Np was then mechanically shaken for 15 min (140 times/min) at 25±1 °C in a glass tube with the same volume of an aqueous solution containing 1 mol dm^{-3} sodium perchlorate, buffer reagents (a proper mixture of 0.1 mol dm^{-3} of 2-morpholinoethanesulfonic acid monohydrate(MES) and 0.1 mol dm^{-3} of tris(hydroxymethyl)aminomethane (THAM)), and a variable concentration of a complex-forming reagent. After phase separation, a 1-cm^3 portion of each phase was pipetted into a counting tube and the γ-activity of each phase was measured with a well-type NaI(Tl) scintillation counter. The remaining part of the aqueous phase was used for the pH measurement. The reagents and apparatus used in the experiments were those previously described.[8]

Results

The distribution ratio of Np(V) in the absence of complexing agents, D_0, can be represented by:[10]

$$D_0 = K_{ex}[HT]_o[phen]_o^m/[H^+], \quad (1)$$

where HT and phen denote the neutral forms of TTA and phen; K_{ex}, the extraction constant; m, the number of molecules of phen in the extracted species, and o, the organic phase. The concentration of HT in the organic phase, $[HT]_o$, is related to the total added concentration of TTA (C_{TTA}) by means of the following equations:

$$\begin{aligned} C_{TTA} &= [HT]_o + [HT] + [T^-] \\ &= [HT]_o(1+1/K_{DR} + K_a/K_{DR}[H^+]), \end{aligned} \quad (2)$$

where:

$$K_a = [H^+][T^-]/[HT] = 10^{-6.46}(\mu=0.1, 25°C),^{12} \quad (3)$$

and

$$K_{DR} = [HT]_o/[HT], \quad (4)$$

for 3-methyl-1-butanol;

$$K_{DR} = 10^{1.63}(\mu=1.0, 20°C),^{13}$$

and for dichloromethane;

$$K_{DR} = 10^{1.81}(\mu=0.1, 25°C).^{13}$$

The concentration of phen in the organic phase, $[phen]_o$, can be assumed to be equal to the total added concentration of phen, C_{phen}, under the conditions adopted in the experiment.

Under some experimental conditions, the effect of complexation with the TTA anion must be taken into consideration. The corrected distribution ratio, D_0', which is obtained experimentally in the absence of

complexing agents other than the TTA anion, can be expressed by the following equation:

$$D_0' = D_0/a, \tag{5}$$

$$a = 1 + \sum\beta_n^T[T^-]^n, \tag{6}$$

where β_n^T is the overall formation constant of the neptunium complex with the TTA anion. Equations 2—4 can be used for the estimation of $[T^-]$. The values of log β_1^T=2.89 and log β_2^T=5.48[14] were used for the calculation. As will be discussed later, uncertainties in the values of K_a, K_{DR}, and β_n^T give systematic errors to the calculation of the formation constants of Np(V) complexes through the conditional constant a in Eq. 6. Therefore, the total concentration of TTA was taken to be as low as was practicable in order to give values of a close to 1 (the largest value of a used in this study was 1.24). The complex formation of Np(V) with MES, THAM, or phen can be ignored under the conditions adopted in this experiment, because the change in the total concentration of MES plus THAM from 0.05 to 0.2 mol dm^{-3} has no effect on the distribution ratio of Np(V).

The distribution ratio of Np(V) in the presence of fluoride or sulfate can be expressed by:

$$D = D_0/(a+\sum\beta_n[L]^n), \tag{7}$$

where [L] is the concentration of F^- or SO_4^{2-} and where β_n is the overall formation constant of the complex of Np(V) with the ligand L (the charges of the ions are omitted for the sake of simplicity):

$$\beta_n = [ML_n]/[M][L]^n, \tag{8}$$

where M=NpO_2^+.

By substituting Eq. 5 into Eq. 7, we obtain:

$$1/D = 1/D_0' + \sum(\beta_n/D_0'a)[L]^n. \tag{9}$$

By using this equation, the β_n values can be obtained, together with D_0', from the analysis of the $1/D$ *vs.* [L] plots.

Figures 1 and 2 show the plots of log D *vs.* log ([L]/mol dm^{-3}) for fluoride and sulfate respectively. In each series of experiments, the distribution ratios were obtained in a medium buffered at a constant pH. Since the pH of the aqueous phase before and after shaking changed only slightly, the pH's of the aqueous phase at equilibrium (after shaking) differed from each other by less than 0.1 unit in each series. Because log D_0 changes with the pH according to Eqs. 1 and 2, the experimental values of D were corrected to those at a constant pH using the extraction curves which were obtained experimentally.[10] Although the value of a in Eqs. 5 and 6 may also change with the pH because of the change in $[T^-]$, the value of a was assumed to be constant in each series of experiments, since the experimental conditions were such that $\sum\beta_n^T[T^-]^n<1$. As the degree of dissociation of HF and HSO_4^- is fairly large in solutions within the pH range studied (pK_a=2.96 for HF and pK_a=1.10 for HSO_4^-),[4] the concentrations of F^- and SO_4^{2-} were taken as equal to the added concentrations of NaF and Na_2SO_4 respectively. The distribution of any species containing fluoride or sulfate in the organic phase was neglected.

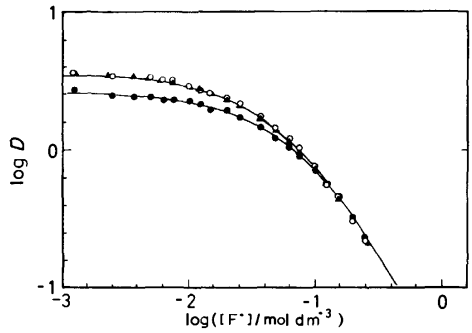

Fig. 1. Plots of log D *vs.* log([F^-]/mol dm^{-3}). Conditions: (○): No. 1, (▲): No. 2, (●): No. 3 in Table 1.

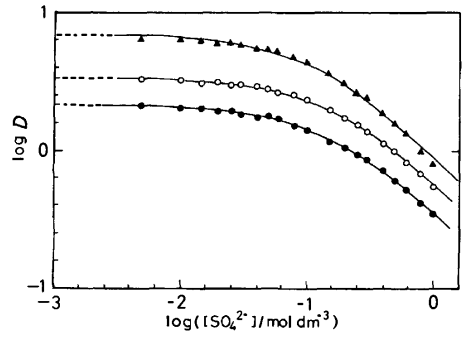

Fig. 2. Plots of log D *vs.* log([SO_4^{2-}]/mol dm^{-3}). Conditions: (○): No. 4, (▲): No. 5, (●): No. 6 in Table 1.

To check the validity of the assumptions mentioned above, different kinds of organic diluents, 3-methyl-1-butanol and dichloromethane, and different pHs were adopted in different series of experiments.

The plots in Figs. 1 and 2 were analyzed to obtain the best fit to Eq. 9 as follows:

Equation 9 is equivalent to a linear function:

$$y = f(x), \tag{10}$$

where:

$$y = 1/D, \tag{11}$$

$$f(x) = 1/D_0' + \sum(\beta_n/D_0'a)x^n, \tag{12}$$

and:

$$x = [L]. \tag{13}$$

A set of data (x_i, y_i) (19—20 points) was analyzed by the

least-squares method to determine the β_n and D_0' values. Since the counting-time of the γ-activity was set to make the relative statistical errors of the total counts approximately constant (0.01—0.02), the residuals of the observed ratios, y, were expected to be proportional to the value of $1/D$, judging from error-propagation rules. Although the observed values of $1/D$ are not error-free, these values give a good basis for estimating the weight of the observation. Therefore, the least-squares fitting was carried out to minimize the following sum of the weighted squares of the residuals:

$$S = \sum\{y_i - f(x_i)\}^2/y_i^2. \quad (14)$$

The results of the analyses are shown in Table 1. Two series of experiments (Nos. 1 and 2) were carried out to check the reproducibility of the experiment, while others were carried out under different conditions in order to check if the unknown factors govern the distribution behavior of Np(V). Although the differences in β_n values were slightly larger than the standard deviations obtained from each series of experiments, the results agreed well with each other and enabled us to analyze the data altogether. Since Eq. 9 can be rearranged to:

$$aD_0'/D - (a-1) = 1 + \sum\beta_n[\mathrm{L}]^n, \quad (15)$$

the least-squares study was carried out between:

$$y = Y \equiv aD_0'/D - (a-1), \quad (16)$$

$$f(x) = 1 + \sum\beta_n x^n, \quad (17)$$

and:

$$x = [\mathrm{L}]. \quad (18)$$

The plots of log Y *vs.* log([L]/mol dm^{-3}) are shown in Figs. 3 and 4. The solid lines show the best fit of the data to Eq. 15, while the dashed lines show the contribution of each species of Np(V). The formation constants thus obtained are listed in Table 1.

In the presence of phoshate as a complexing agent, there is a possibility of the formation of different types of complexes, and the $1/D$ ratio can be expressed as:[8]

$$1/D = 1/D_0' + \sum(\beta_n'/D_0'a)[\mathrm{H_2L}]^n + \sum(\beta_n/D_0'a)[\mathrm{HL}]^n, \quad (19)$$

where H_2L and HL denote $H_2PO_4^-$ and HPO_4^{2-} respectively. The overall formation constants and dissociation constants are given by these equations:

$$\beta_n' = [\mathrm{M(H_2L)}_n]/[\mathrm{M}][\mathrm{H_2L}]^n, \quad (20)$$

$$\beta_n = [\mathrm{M(HL)}_n]/[\mathrm{M}][\mathrm{HL}]^n, \quad (21)$$

$$K_i = [\mathrm{H}][\mathrm{H}_{3-i}\mathrm{L}]/[\mathrm{H}_{4-i}\mathrm{L}], \quad (22)$$

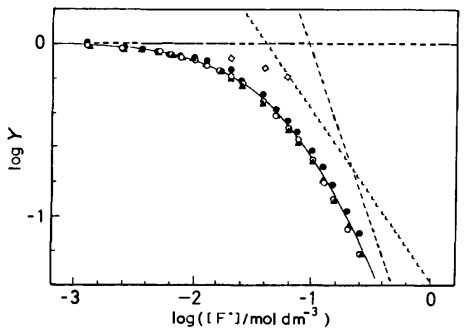

Fig. 3. Plots of log Y (Eq. 16) *vs.* log([F$^-$]/mol dm^{-3}). Conditions: (○): No. 1, (▲): No. 2, (●): No. 3 in Table 1, (◇): reproduced from Ref. 15, log D_0= −0.66.

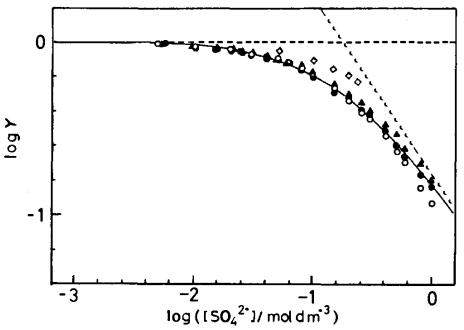

Fig. 4. Plots of log Y (Eq. 16) *vs.* log([SO$_4^{2-}$]/mol dm^{-3}). Conditions: (○): No. 4, (▲): No. 5, (●): No. 6 in Table 1, (◇): reproduced from Ref. 15, log D_0= −0.66.

TABLE 1. EXPERIMENTAL RESULTS FOR Np(V)-FLUORIDE AND Np(V)-SULFATE SYSTEMS

Ligand	No.	pH	a	log(β_n/mol^{-n}dm^{3n})	
				n=1	n=2
F^-	1	6.63	1.00	1.38±0.01	2.17±0.01
	2	6.64	1.00	1.42±0.01	2.14±0.01
	3	7.62	1.14	1.34±0.01	1.98±0.01
	Mean			1.39±0.03	2.07±0.03
SO_4^{2-}	4	6.60	1.00	0.70±0.03	
	5	7.50	1.02	0.84±0.03	
	6	7.47	1.10	0.76±0.01	
	Mean			0.76±0.02	

1,2,4,5: C_{TTA}=1×10^{-4} mol dm^{-3}, C_{phen}=1×10^{-2} mol dm^{-3} in 3-methyl-1-butanol.
3,6: C_{TTA}=1×10^{-3} mol dm^{-3}, C_{phen}=1×10^{-2} mol dm^{-3} in dichloromethane.

where pK_1=1.70, pK_2=6.46, and pK_3=10.79.[4] Equation 19 may then be written as:

$$1/D = 1/D_0' + \sum(B_n'/D_0'a)[\mathrm{H_2L}]^n, \quad (23)$$

where:

$$B_n' = \beta_n' + \beta_n K_2^n/[\mathrm{H}]^n, \quad (24)$$

or:

$$1/D = 1/D'_0 + \sum(B_n/D'_0 a)[\mathrm{HL}]^n, \quad (25)$$

where:

$$B_n = \beta'_n[\mathrm{H}]^n/K_2^n + \beta_n. \quad (26)$$

Nine series of experiments were carried out to obtain the plot of log D *vs.* log([$H_2PO_4^-$]/mol dm^{-3}) or the plot of log D *vs.* log([HPO_4^{2-}]/mol dm^{-3}). The pH of the aqueous phase after shaking changed from the initial pH by less than 0.2 unit in each series of experiments; the experimental values of D were corrected to those at a constant pH using the experimental extraction curves which were obtained experimentally. The concentration of a particular species of phosphate was calculated at the pH of interest according to the following relationship:

$$C_L = [H_3PO_4] + [H_2PO_4^-] + [HPO_4^{2-}] + [PO_4^{3-}]$$
$$= [H_3PO_4](1 + K_1/[H^+] + K_1K_2/[H^+]^2 + K_1K_2K_3/[H^+]^3). \quad (27)$$

Some of the plots of log Y (Eq. 16) *vs.* log([HPO_4^{2-}]/mol dm^{-3}) are shown in Fig. 5 as illustrations. The values of B'_n and B_n obtained at various pH's are shown in Table 2, together with the experimental conditions used. Each series of experiments comprised 18 to 20 points of the data-set, and the standard deviations of the values of B'_n and B_n were less than 0.02. Since values of B'_n and B_n show the dependence on the pH in the opposite way, it can be concluded that both, and only, $H_2PO_4^-$ and HPO_4^{2-} ions form considerably stable complexes with Np(V). As the value of B'_n or B_n is a function of the pH, as is expressed by Eq. 24 or 26, a set of B'_n or B_n can be treated by the same least-squares method as explained before to determine the values of β'_n and β_n. Figure 6 shows the results of the least-squares fitting of the values of B_n to Eq. 26; the values of β'_n and β_n thus obtained are listed in Table 3. The fairly large standard deviations of the values can be ascribed to the rather restricted pH range studied, since a pH value than 4.5 is too high to allow the formation of a considerable amount of complexes of Np(V) with the $H_2PO_4^-$ ion. Moreover, uncertainties may be brought about in the observed values since the fraction of Np(V) in a particular chemical form is a quite complex function of both the total concentration of phosphate (C_L) and the pH. In

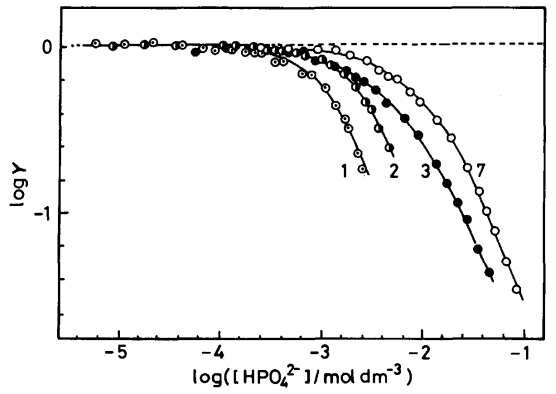

Fig. 5. Plots of log Y (Eq. 16) *vs.* log([HPO_4^{2-}]/mol dm^{-3}).
Conditions: See Table 2.

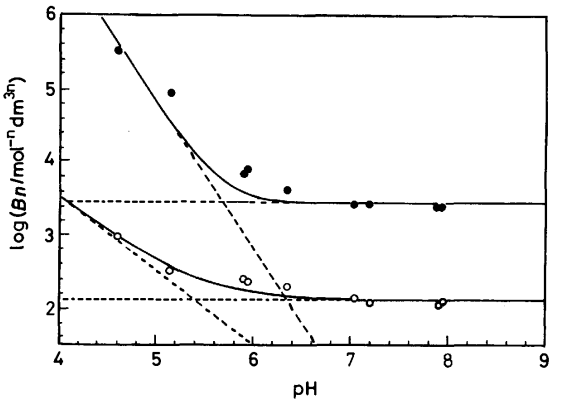

Fig. 6. Plots of log(B_n/mol^{-n}dm^{3n}) *vs.* pH for HPO_4^{2-} ligand.
○: $n=1$, ●: $n=2$. Solid lines (composites of the dashed lines) are the results of the least-squares treatment.

TABLE 2. APPARENT CONSTANTS OBTAINED FOR THE Np(V)-PHOSPHATE SYSTEM

No.	pH	C_{TTA} / mol dm^{-3}	log D'_0	a	log(B_n/mol^{-n}dm^{3n}) *vs.*[$H_2PO_4^-$]		log(B_n/mol^{-n}dm^{3n}) *vs.*[HPO_4^{2-}]	
					$n=1$	$n=2$	$n=1$	$n=2$
1	4.60	2.0×10^{-3}	0.09	1.00	1.10	1.77	2.96	5.49
2	5.14	1.0×10^{-3}	0.29	1.00	1.17	2.28	2.49	4.92
3	5.90	1.0×10^{-2}	0.43	1.03	1.83	2.69	2.39	3.81
4	5.94	2.5×10^{-4}	0.45	1.00	1.83	2.85	2.35	3.89
5	6.34	1.0×10^{-4}	0.38	1.00	2.14	3.36	2.26	3.60
6	7.02	1.0×10^{-4}	0.71	1.00	2.69	4.53	2.13	3.41
7	7.20	1.0×10^{-4}	0.79	1.01	2.80	4.89	2.06	3.41
8	7.90	1.0×10^{-3}	0.52	1.24	3.48	6.23	2.04	3.35
9	7.94	1.0×10^{-4}	0.79	1.03	3.55	6.32	2.07	3.36

1,2,4-7,9: 3-methyl-1-butanol, 3,8: dichloromethane.
1,2,4-9: C_{phen}=1×10^{-2} mol dm^{-3}, 3: C_{phen}=2×10^{-2} mol dm^{-3}.

Table 3. Formation constants of Np(V)-complexes

Ligand	Method	Conditions	$\log(\beta_n/\text{mol}^{-n}\text{dm}^{3n})$		Ref.
			$n=1$	$n=2$	
F^-	TTA-phen	μ=1.0, 25°C	1.39±0.03	2.07±0.03	This work
	DNNS[a]	μ=2.0, 25°C	0.99±0.03		(15)
SO_4^{2-}	TTA-phen	μ=1.0, 25°C	0.76±0.02		This work
	DNNS[b]	μ=2.0, 25°C	0.45±0.04		(15)
	DNNS[c]	μ=2.0, 25°C	0.19±0.02		(16)
	coppt.[d]	$\mu\simeq$1.5, 20°C	1.04±0.4		(18)
$H_2PO_4^-$	TTA-phen	μ=1.0, 25°C	1.04±0.18	1.87±0.29	This work
	cix.	μ=0.2, 20°C	0.81		(20)
HPO_4^{2-}	TTA-phen	μ=1.0, 25°C	2.11±0.09	3.43±0.16	This work
	cix.	μ=0.2, 20°C	2.85		(20)
	coppt.[e]	μ=0.1, 20°C	2.90±0.11		(18)
	cix.[f]	μ=0.1, 25°C	2.36±0.42		(21)
PO_4^{3-}	coppt.	μ=1.0, 20°C	5.78±0.25		(18)

TTA-phen: solvent extraction with TTA plus phen, DNNS: solvent extraction with DNNS, coppt.: coprecipitation, cix.: cation exchange.
a) $[F^-]$: 0.02—0.06 mol dm^{-3}, b) $[SO_4^{2-}]$: 0.05—0.25 mol dm^{-3}, c) $[SO_4^{2-}]$: 0.05—0.3 mol dm^{-3}, d) $[SO_4^{2-}]$: 0.15—0.6 mol dm^{-3}, e) $[(NH_4)_2HPO_4]_t$: 0.05—0.34 mol dm^{-3}, f) $[HPO_4^{2-}]\simeq C_L$: 0.001—0.01 mol dm^{-3}.

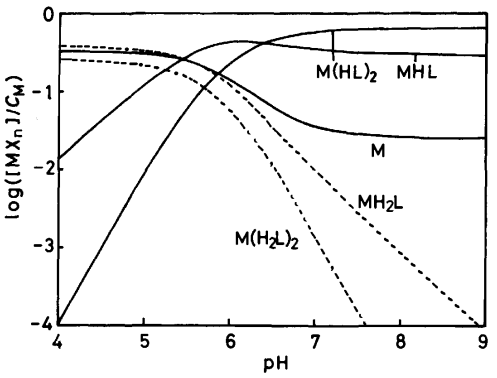

Fig. 7. Logarithmic diagram of the Np(V)-phosphate system at C_L=0.1 mol dm^{-3}.
M=NpO_2^+, H_2L=$H_2PO_4^-$ and HL=HPO_4^{2-}.

the presence of C_L=0.1 mol dm^{-3}, for instance, the fraction of Np(V) in the form of a particular phosphate complex changes as a function of the pH, as is shown in Fig. 7, which was constructed by using the formation constants obtained in the present study.

Discussion

Table 3 lists the formation constants obtained in this study, together with the values reported by other workers.

Rao *et al.*[15] have studied the complexing of Np(V) with F^-, SO_4^{2-}, and some other inorganic anions by the solvent-extraction method using 3,7-dinonylnaphthalenesulfonic acid (DNNS) as the extractant. Their values are smaller than the present values. Figures 3 and 4 show their extraction curves, which have been constructed by the present authors from the table in the original paper. Although they stated that the pH was maintained around 5 in their experiment, there was no description of the pH at equilibrium after the extraction. Since they used a stock solution of Np(V) in $HClO_4$ without any buffer, the aqueous phase might possibly be more acidic than expected. This may lead to the overestimation of $[F^-]$ by neglecting the association into HF. Since the distribution ratios of Np(V) were small even in the absence of the ligands (D=0.219 in the presence of 0.4 mol dm^{-3} DNNS), the range of the distribution ratio they measured was too narrow to obtain reliable formation constants (the percentages of the extraction of Np(V) varied within the small range from 18% to 11%).

Halperin and Oliver[16] repeated the experiment on the sulfate complexing of Np(V) by the same method and under conditions almost equal to those adopted by Rao *et al.*[15] Although they used the same technique, they obtained a considerably smaller value than that reported by Rao *et al.*; the discrepancy is outside the limits of experimental error. We suspect that the starting solution of Np(V) might have contained chemical species other than NpO_2^+, such as peroxide, since Halperin and Oliver used H_2O_2 as a reductant. If such kinds of species are not extractable into the organic phase, this will give systematic errors and lead to a lower formation constant. Hydrogen peroxide has been found to cause unusual behavior in neptunium when used as a redox reagent.[12,17]

Moskvin and Poznyakov[18] studied the complexing of Np(V) with SO_4^{2-}, SO_3^{2-}, HCO_3^-, HPO_4^{2-}, *etc.* by means of coprecipitation with iron(III) hydroxide at pH 8.5. As for the sulfate complex, they have reported a larger value than the present one, though the discrepancy is within the limits of experimental error. The main difficulty in their coprecipitation method is that the distribution ratio of Np(V) in the absence of complexing agents is too high to obtain reliable data, since the distribution ratio was determined from the difference in the activities of the centrifugate and a control (original) solution. The percentage of the adsorption is reported to around 95% and cannot be

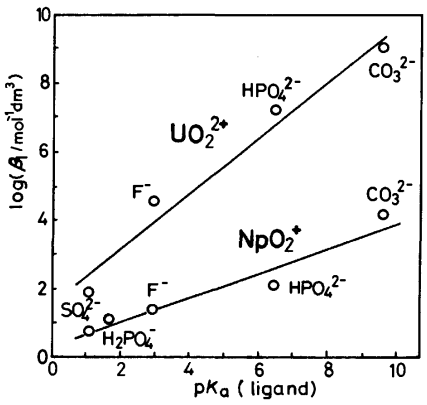

Fig. 8. Correlation between 1:1 chelate formation constants of UO_2^{2+} or NpO_2^+ and pK_a.

controlled, in contrast to the case with the solvent-extraction system adopted in this report.

The failure by Al-Niaimi *et al.*[19] to observe fluoride and sulfate complexing can be ascribed to the low fluoride and sulfate concentrations they used.

As for the formation constants of phosphate complexes, despite the large standard deviations in the present study, they may be considered to be more reliable than those listed in Table 3.

Moskvin *et al.*[18,20] obtained their values in a still more limited pH region (at pH 4.8—6.7 in Ref. 20 and at pH 8.5 in Ref. 18). Their formation constants for the complexes of Np(V) with $H_2PO_4^-$ and HPO_4^{2-} are not very different from the present values. However, if we accept the reported formation constant of the Np(V)-PO_4^{3-} complex, the main species of Np(V) at pH 8.5 should be $NpO_2PO_4^{2-}$, and the formation constants of Np(V)-HPO_4^{2-} complexes cannot be obtained at this pH.

Rees and Daniel[21] have determined the formation constant of the Np(V)-HPO_4^{2-} complex. They measured the distribution of Np(V) between the aqueous phase and a cation-exchange resin at pH 7.5. In their calculation, the concentration of HPO_4^{2-} was assumed to be equal to the total phosphate concentration at this pH. The agreement with the present value is reasonable, since Np(V) forms only a one-to-one complex with HPO_4^{2-} under the conditions they adopted (pH 7.5, $C_L=10^{-3}$—10^{-2} mol dm^{-3}).

In Fig. 8, the formation constants of the Np(V)-complexes with inorganic anions (including CO_3^{2-} by Ref. 8) obtained in the present study are compared with those of the UO_2^{2+}-complexes,[4,22] because UO_2^{2+} is also a dioxo cation of similar type. The good correlation of the stabilities of the Np(V)-complexes with the pK_a values of the ligands implies that all these complexes are formed by the interaction of a hard acid and a hard base.

In conclusion, since the present experiment was conducted to ensure the formation of various chemical species by covering a fairly wide range of ligand concentrations and pH's, the resultant formation constants can be used reliably to estimate the behavior of Np(V) in widely different natural or artificial systems.

References

1) Y. Inoue and O. Tochiyama, *Technology Reports, Tohoku Univ.*, **47**, 263 (1982).
2) S. K. Patil, V. V. Ramakrishna, and M. V. Ramaniah, *Coord. Chem. Rev.*, **25**, 133 (1978).
3) G. A. Burney and R. M. Harbour, "Radiochemistry of Neptunium," **NAS-NS-3060** (1974).
4) A. E. Martell and R. M. Smith, "Critical Stability Constants," Plenum Press, New York (1977).
5) S. Jensen, "Migration Phenomena of Radionuclides into the Geosphere," Harwood Academic Publishers for the Commission of the European Communities, New York (1982).
6) Y. Inoue, O. Tochiyama, and T. Takahashi, *Radiochim. Acta*, **31**, 197 (1982).
7) Y. Inoue and O. Tochiyama, *Polyhedron*, **2**, 627 (1983).
8) Y. Inoue and O. Tochiyama, *Bull. Chem. Soc. Jpn.*, **58**, 588 (1985).
9) Y. Inoue, O. Tochiyama, and I. Oda, *J. Inorg. Nucl. Chem.*, **41**, 1375 (1979).
10) Y. Inoue and O. Tochiyama, *Radiochim. Acta*, **31**, 193 (1982).
11) C. W. Sill, *Anal. Chem.*, **38**, 802 (1966).
12) Y. Inoue and O. Tochiyama, *J. Inorg. Nucl. Chem.*, **39**, 1443 (1977).
13) J. Stary and H. Freiser, "IUPAC Equilibrium Constants of Liquid-Liquid Distribution Reactions, Part IV: Chelating Extractants," Pergamon Press, Oxford (1978).
14) J. Gross and C. Keller, *J. Inorg. Nucl. Chem.*, **34**, 725 (1972).
5) P. R. Vasudeva Rao, N. M. Gudi, S. V. Bagawde, and S. K. Patil, *J. Inorg. Nucl. Chem.*, **41**, 235 (1979).
16) J. Halperin and J. H. Oliver, *Radiochim. Acta*, **33**, 29 (1983).
17) Y. Inoue, O. Tochiyama, and N. Shinohara, *Technology Reports, Tohoku Univ.*, **42**, 387 (1977).
18) A. I. Moskvin and A. N. Poznyakov, *Russ. J. Inorg. Chem.*, **24**, 1357 (1979).
19) N. S. Al-Niaimi, A. G. Wain, and H. A. C. Mckay, *J. Inorg. Nucl. Chem.*, **32**, 2331 (1970).
20) A. I. Moskvin and V. F. Peretrukhin, *Sov. Radiochem.*, **6**, 196 (1964).
21) T. F. Rees and S. R. Daniel, *Polyhedron*, **3**, 667 (1984).
22) A. I. Moskvin, A. M. Shelyakina, and P. S. Perminov, *Russ. J. Inorg. Chem.*, **12**, 1756 (1967).

The Bound Ligand Effect in the Complexation Kinetics of Some Anionogallium(III) Complexes

Shinkichi YAMADA* and Motoharu TANAKA†

Laboratory of Analytical Chemistry, Faculty of Engineering, Shizuoka University, Johoku, Hamamatsu 432

†*Laboratory of Analytical Chemistry, Faculty of Science, Nagoya University, Chikusa-ku, Nagoya 464*

(Received February 4, 1985)

The formation rate of some anionogallium(III) complexes (GaA) with 4,5-dihydroxy-1,3-benzenedisulfonate (H_2L^{2-}) in the presence of thiocyanate ion has been studied spectrophotometrically by a stopped-flow technique. The rate law is expressed as $d[GaL^-]/dt = k_{Ga}[Ga^{3+}][H_2L^{2-}] + k_{GaOH}[GaOH^{2+}][H_2L^{2-}] + k_{Ga(OH)_2}[Ga(OH)_2^+][H_2L^{2-}] + k_{GaNCS}[GaNCS^{2+}][H_2L^{2-}]$, with $k_{Ga} = 10^{1.23}$ $M^{-1}s^{-1}$ (M=mol dm^{-3}), $k_{GaOH} = 10^{3.36}$ $M^{-1}s^{-1}$, $k_{Ga(OH)_2} = 10^{4.37}$ $M^{-1}s^{-1}$, and $k_{GaNCS} = 10^{3.90}$ $M^{-1}s^{-1}$ at 25 °C and I=0.50M. The enhanced reactivity of GaA as compared to that of Ga^{3+} is attributable to the labilizing effect of the bound ligand A on the rate of loss of coordinated water molecules at GaA. Together with the additional formation rate constants of monoisothiocyanato- and monooxalatogallium(III) with 2-hydroxy-2,4,6-cycloheptatrien-1-one, this labilizing effect is quantitatively discussed in terms of the electron-donating ability of the ligand.

From the mechanistic consideration on the formation constants of metal complexes,[1,2] it has been shown that, taking into account the statistical factor arising from the number of water molecules available for exchange, the water exchange rate constant at MA ($k_{MA}^{-H_2O}$) is expressed as

$$\log (k_{MA}^{-H_2O}/\text{number of } H_2O \text{ in MA}) = \log (k_M^{-H_2O}/\text{number of } H_2O \text{ in M}) + \gamma E(A) \quad (1)$$

where E(A) refers to the electron donor constant[3] of the ligand A and γ is a constant characteristic of the metal ion M.

In the preceding paper,[4] we have studied the kinetics and mechanism of the complex formation of monohydroxo-, monoacetato-, monothiocyanato-, monoazido-, and monofluorozinc(II) complexes with 1,10-phenanthroline and found that the labilizing effect of the bound ligand on the rate of loss of coordinated water molecules is quantitatively described by Eq. 1. Recently, we have shown[5] that Eq. 1 can predict the bound ligand effect of the multidentate-ligand complexes of nickel(II). In the system, the value of the effective E(A) for a multidentate ligand is given by the summation of E(X) of each donor atom X involved in A which is corrected for the effect of vicinal functions. This effective E(A) value is particularly useful in the estimation of the γ parameter for a hard metal ion such as gallium(III): The number of bound ligands suitable for kinetic measurements is limited due to their small formation constants with gallium(III) ion in acidic medium.

To understand how the rate of loss of coordinated water molecules at GaA is labilized by the presence of the coordinated ligand A, we have studied the complexation kinetics described as

$$GaA + H_2L^{2-} \xrightarrow{k_{GaA}} GaAL(\text{and/or } GaL^- + A) + 2H^+, \quad (2)$$

$$GaA + HL \xrightarrow{k_{GaA}} GaAL(\text{and/or } GaL^{2+} + A) + H^+, \quad (3)$$

where A is a bound ligand such as hydroxide, thiocyanate or oxalate. H_2L^{2-} and HL refer to tiron (4,5-dihydroxy-1,3-benzenedisulfonate) and tropolone (2-hydroxy-2,4,6-cycloheptatrien-1-one), respectively. With these two entering ligands, we have already described the thermodynamic and kinetic results on the complexation reaction of the gallium(III) ion and provided definite mechanistic information on the reaction of this cation, on the basis of values of activation volume obtained by a high-pressure stopped-flow technique.[6]

Experimental

The solutions of gallium(III) perchlorate, tropolone, tiron, and sodium thiocyanate were prepared as described elsewhere.[4,6] Sodium oxalate of primary standard quality (Wako-junyaku) was used without further purification. All experiments were carried out in a room thermostated at 25.0±0.5 °C. Temperature of the reaction solution was controlled to within ±0.1 °C. Ionic strength was maintained at 0.50 M with sodium perchlorate. Reaction rates were followed by a stopped-flow spectrophotometer equipped with a data processor. The changes in absorbance at 305 nm and 313 nm, wavelength of the maximum absorption of the 1:1 Ga(III)-tiron and Ga(III)-tropolone complexes respectively, were accumulated to obtain high S/N curves. Other experimental details are described elsewhere.[4,6]

Results

Reaction of Gallium(III) Ion with Tiron. Gallium(III) ion forms a 1:1 complex with tiron in acidic solution where the concentration of gallium(III) is in large excess over that of the ligand:[6]

$$Ga' + H_2L^{2-} \underset{k_{r(H)}}{\overset{k_{f(H)}}{\rightleftharpoons}} GaL^- + 2H^+ \quad (4)$$

where $k_{f(H)}$ is a second-order conditional rate constant involving the concentration of hydrogen ion for the formation of the complex and $k_{r(H)}$ is a pseudo-first-order conditional rate constant involving the concentration of hydrogen ion for the dissociation of the com-

plex. Then the kinetic equation for this reaction is described by

$$d[GaL^-]/dt = k_{f(H)}[Ga'][H_2L^{2-}] - k_{r(H)}[GaL^-] = k_{f(H)}C_L[Ga'] - k_{o(H)}[GaL^-] \quad (5)$$

where [Ga'] denotes the total concentration of gallium(III) not combined with the ligand L^{4-} (aqua and hydroxo gallium ions), and $C_L=[H_2L^{2-}]+[GaL^-]$ and $k_{o(H)}=k_{f(H)}[Ga']+k_{r(H)}$.

Integration of Eq. 5 gives

$$\ln \frac{k_{f(H)}C_L[Ga']}{k_{f(H)}C_L[Ga'] - k_{o(H)}[GaL^-]} = \ln \frac{A_\infty - A_0}{A_\infty - A_t} = k_{o(H)}t,$$

where A_0, A_t, and A_∞ are the absorbances at 305 nm for reaction systems at reaction time 0, t, and ∞, respectively. The rate plot of $\ln\{(A_\infty-A_0)/(A_\infty-A_t)\}$ *vs.* t was linear for over 90% of the reaction. The conditional rate constant involving the concentration of hydrogen ion $k_{o(H)}$ determined from the slope of this plot is correlated with $k_{f(H)}$ and $k_{r(H)}$ by the following relations:

$$k_{o(H)} = k_{f(H)}[Ga'] + k_{r(H)}$$

$$k_{f(H)}/k_{r(H)} = K_{GaL}{}^{H_2L}/(\alpha_{Ga(OH)}[H^+]^2)$$

where $K_{GaL}{}^{H_2L}=[GaL^-][H^+]^2[Ga^{3+}]^{-1}[H_2L^{2-}]^{-1}$ and $\alpha_{Ga(OH)}=1+K_{GaOH}[H^+]^{-1}+K_{GaOH}K_{Ga(OH)_2}[H^+]^{-2}$. Employing the values of $K_{GaL}{}^{H_2L}$ and $K_{GaOH}=[GaOH^{2+}][H^+][Ga^{3+}]^{-1}$ previously determined[6] and $K_{Ga(OH)_2}=[Ga(OH)_2{}^+][H^+][GaOH^{2+}]^{-1}$ reported,[7] the values of $k_{f(H)}$ and $k_{r(H)}$ were calculated as in Table 1.

TABLE 1. CONDITIONAL RATE CONSTANTS FOR THE COMPLEXATION OF GALLIUM(III) WITH TIRON[a]

$-\log([H^+]/M)$	$k_{o(H)}$ / s^{-1}	$k_{f(H)}$ / $10^2 M^{-1}s^{-1}$	$k_{r(H)}$ / s^{-1}
1.530	3.07	1.23	1.70
1.566	3.16	1.38	1.62
1.606	2.98	1.42	1.39
1.642	2.98	1.52	1.27
1.691	3.12	1.74	1.17
1.733	3.29	1.96	1.09
1.797	3.38	2.19	0.92
1.860	3.54	2.46	0.78
1.931	3.85	2.84	0.66
2.022	4.50	3.52	0.55
2.150	5.74	4.74	0.43
2.152	5.47	4.52	0.41
2.215	6.29	5.29	0.36
2.255	6.93	5.88	0.34
2.282	7.01	5.98	0.31
2.362	8.92	7.70	0.29
2.433	10.23	8.90	0.25
2.458	10.42	9.09	0.23
2.566	14.68	12.90	0.22
2.649	18.14	16.00	0.20
2.675	18.97	16.75	0.19
2.757	24.05	21.29	0.18
2.769	23.05	20.41	0.17
2.779	23.06	20.42	0.16
2.790	24.05	21.31	0.16

a) $C_{Ga}=1.12\times10^{-2}$ M, $C_{H_2L}=1.08\times10^{-4}$ M, I=0.50 M, 25 °C.

The increase of the conditional rate constant $k_{f(H)}$ with decreasing concentration of hydrogen ion is attributable to the hydrolyzed species of gallium(III).[8] Thus

$$d[GaL^-]/dt = \{k_{Ga}[Ga^{3+}] + k_{GaOH}[GaOH^{2+}] + k_{Ga(OH)_2}[Ga(OH)_2{}^+]\} \times [H_2L^{2-}] - k_{r(H)}[GaL^-] \quad (6)$$

and

$$k_{f(H)}\alpha_{Ga(OH)} = k_{Ga} + k_{GaOH}K_{GaOH}[H^+]^{-1} + k_{Ga(OH)_2}K_{GaOH}K_{Ga(OH)_2}[H^+]^{-2}.$$

The values of the rate constants for these three reaction paths were determined from the plot of $k_{f(H)}\alpha_{Ga(OH)}$ *vs.* $[H^+]^{-1}$ as shown in Fig. 1 and they are given in Table 2.

The conditional rate constant for the dissociation of the complex, $k_{r(H)}$, is found to be correlated with the concentration of hydrogen ion as

$$k_{r(H)} = 10^{-1.29} + 10^{1.75}[H^+].$$

Reaction of Isothiocyanatogallium(III) with Tiron. Under the conditions where only $GaNCS^{2+}$ is responsible for the reaction of the gallium(III)–thiocyanate complex, the complexation reaction of gallium(III) complexes with tiron is considered to proceed as in Scheme 1.

With the total concentration of thiocyanate ion much

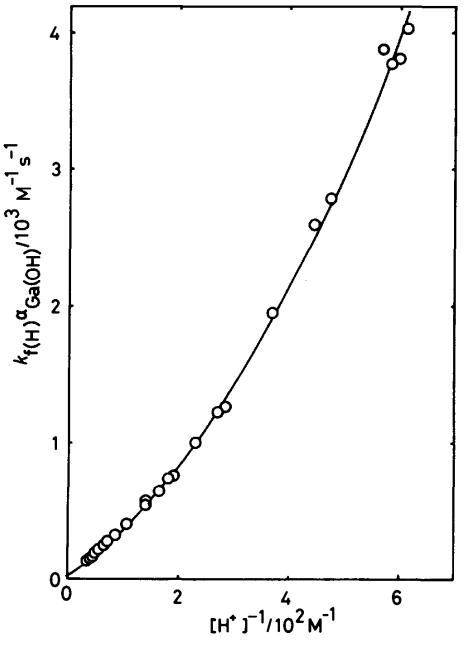

Fig. 1. Plot of $k_{f(H)}\alpha_{Ga(OH)}$ *vs.* $[H^+]^{-1}$.
The solid line is the curve calculated with the values obtained by a least-squares procedure.

TABLE 2. VALUES OF RATE CONSTANTS FOR THE COMPLEXATION REACTION OF GALLIUM(III) WITH VARIOUS ENTERING LIGANDS AT 25 °C

Entering ligand(L^{n-})[a]	I	$\log(k_{Ga}/M^{-1}s^{-1})$	$\log\{(k_{Ga}^{-H_2O}/s^{-1})/6\}$	Ref.
Tiron(H_2L^{2-})	0.5	1.23	0.95	This work
Tropolone(HL)	0.5	1.58	1.30	6
NSAL(HL^-)	0.1	2.61	1.06	18
PCV(H_3L^-)	0.2	1.84	1.56	19
SAL(HL^-)	0.1	2.83	1.28	20
SXO(H_2L^{2-})	0.1	2.84	1.29	21
		$\log(k_{GaOH}/M^{-1}s^{-1})$	$\log\{(k_{GaOH}^{-H_2O}/s^{-1})/5\}$	
Tiron(H_2L^{2-})	0.5	3.36	3.16	This work
Tropolone(HL)	0.5	3.91	3.71	6
NSAL(HL^-)	0.1	3.81	2.76	18
PCV(H_3L^-)	0.2	3.94	3.74	19
SAL(HL^-)	0.1	4.53	3.48	20
SXO(H_2L^{2-})	0.1	4.08	3.03	21
		$\log(k_{Ga(OH)_2}/M^{-1}s^{-1})$	$\log\{(k_{Ga(OH)_2}^{-H_2O}/s^{-1})/4\}$	
Tiron(H_2L^{2-})	0.5	4.37	4.26	This work
NSAL(HL^-)	0.1	4.56	4.06	18
SAL(HL^-)	0.1	5.30	4.80	20
		$\log(k_{GaNCS}/M^{-1}s^{-1})$	$\log\{(k_{GaNCS}^{-H_2O}/s^{-1})/5\}$	
Tiron(H_2L^{2-})	0.5	3.90	3.70	This work
Tropolone(HL)	0.5	3.12	2.92	This work
		$\log(k_{Ga(ox)}/M^{-1}s^{-1})$	$\log\{(k_{Ga(ox)}^{-H_2O}/s^{-1})/4\}$	
Tropolone(HL)	0.5	3.27	3.16	This work

a) Ligand abbreviation: NSAL for 5-nitrosalicylic acid, PCV for Pyrocatechol Violet, SAL for salicylic acid, and SXO for Semixylenol Orange.

$$
\begin{array}{l}
Ga(OH)_2^+ + H_2L^{2-} \xrightarrow{k_{Ga(OH)_2}} GaL^- \\
\quad\downarrow\uparrow K_{Ga(OH)_2} \\
GaOH^{2+} + H_2L^{2-} \xrightarrow{k_{GaOH}} GaL^- + H^+ \\
\quad\downarrow\uparrow K_{GaOH} \\
Ga^{3+} + H_2L^{2-} \xrightarrow{k_{Ga}} GaL^- + 2H^+ \\
\quad\downarrow\uparrow K_{GaNCS} \\
GaNCS^{2+} + H_2L^{2-} \xrightarrow{k_{GaNCS}} \\
\qquad [Ga(NCS)L]^{2-}(\text{and/or } GaL^- + SCN^-) + 2H^+
\end{array}
$$

Scheme 1.

higher than that of tiron (see Fig. 2), $GaNCS^{2+}$ would be certainly in equilibrium with aquagallium(III) during the reaction. The formation of a small amount of a mixed-ligand complex such as $[Ga(NCS)L]^{2-}$ may be anticipated. However, the coordination of tiron being quantitative at $-\log[H^+]=2.3$ (see Table 1), the kinetic equation for this reaction scheme is described as

$$
\begin{aligned}
d[GaL^-]/dt &= k_{f(H,SCN)}[Ga'][H_2L^{2-}] \\
&= \{k_{Ga}[Ga^{3+}] + k_{GaOH}[GaOH^{2+}] \\
&\quad + k_{Ga(OH)_2}[Ga(OH)_2^+] \\
&\quad + k_{GaNCS}[GaNCS^{2+}]\}[H_2L^{2-}] \qquad (7)
\end{aligned}
$$

where,

$$
k_{f(H,SCN)} = \frac{k_{f(H)}\alpha_{Ga(OH)} + k_{GaNCS}K_{GaNCS}[SCN^-]}{\alpha_{Ga(OH)} + K_{GaNCS}[SCN^-]}
$$

and $K_{GaNCS}=[GaNCS^{2+}][Ga^{3+}]^{-1}[SCN^-]^{-1}$ is the formation constant of the inner-sphere complex of isothiocyanatogallium(III).

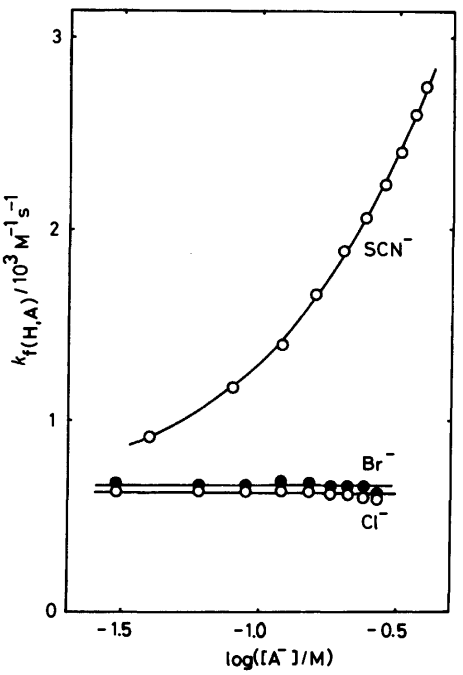

Fig. 2. Plot of $k_{f(H,A)}$ *vs.* $\log[A^-]$.
Conditions: $C_{Ga}=1.12\times10^{-2}$ M, $C_L=1.08\times10^{-4}$ M, and $-\log[H^+]=2.32\pm0.02$ for $A^-=SCN^-$; $C_{Ga}=1.12\times10^{-2}$ M, $C_L=1.01\times10^{-4}$ M, and $-\log[H^+]=2.28\pm0.01$ for $A^-=Cl^-$; $C_{Ga}=1.12\times10^{-2}$ M, $C_L=1.11\times10^{-2}$ M, and $-\log[H^+]=2.28\pm0.01$ for $A^-=Br^-$; all at 25 °C and $I=0.50$ M.

The increase of $k_{f(H,SCN)}$ at constant pH with increasing concentration of SCN^- is attributable to the enhanced reactivity of $GaNCS^{2+}$. From the plot of $k_{f(H,SCN)}$ *vs.* log[SCN^-] (Fig. 2), the k_{GaNCS} value was determined by a least-squares procedure to be $k_{GaNCS}=10^{3.90}$ $M^{-1}s^{-1}$ with $K_{GaNCS}=10^{0.11}$ M^{-1} at 25 °C and I=0.50 M.

In the presence of chloride and bromide, the conditional formation rate constants $k_{f(H,Cl)}$ and $k_{f(H,Br)}$ did not change with increasing total concentration of A up to 0.27 M as shown in Fig. 2. This is most probably due to the small formation constant K_{GaA} for these complexes.[9,10]

Reaction of Isothiocyanatogallium(III) with Tropolone. Gallium(III) ion quantitatively forms the 1:1 complex with tropolone (HL) in acidic solution (−log[H^+]= 0.6—1.3) where the concentration of gallium(III) ion is in large excess over that of the ligand. Under such conditions, the complexation reaction and the kinetic equation for the formation of the (tropolonato)gallium(III) (GaL^{2+}) is expressed as[6]

$$Ga' + HL' \xrightarrow{k_{f(H)}} GaL^{2+} + H^+ \quad (8)$$

$$\begin{aligned} d[GaL^{2+}]/dt &= k_{f(H)}[Ga'][HL'] \\ &= k_{f(H)}\alpha_{Ga(OH)}\alpha_{HL(H)}[Ga^{3+}][HL] \\ &= \{k_{Ga}[Ga^{3+}] + k_{GaOH}[GaOH^{2+}]\}[HL]. \end{aligned} \quad (9)$$

where [Ga′]=[Ga^{3+}]+[$GaOH^{2+}$] and [HL′]=[HL]+ [H_2L^+] =(1+K_{H_2L}[H^+])[HL]=$\alpha_{HL(H)}$[HL].

As in the reaction with tiron, the conditional rate constant $k_{f(H,SCN)}$ increased with increasing concentration of thiocyanate ion. At −log[H^+]=1.25, the values of $k_{f(H,SCN)}$ obtained at various thiocyanate concentrations (C_{SCN}=0.04—0.40 M) were analyzed with the following equation

$$k_{f(H,SCN)}\alpha_{HL(H)} = \frac{k_{f(H)}\alpha_{HL(H)}\alpha_{Ga(OH)} + k_{GaNCS}K_{GaNCS}[SCN^-]}{\alpha_{Ga(OH)} + K_{GaNCS}[SCN^-]}$$

and the k_{GaNCS} value was determined to be $10^{3.12}$ M^{-1} s^{-1} with $K_{GaNCS}=10^{0.47}$ M^{-1} at 25 °C and I=0.50 M. The k_{GaNCS} value obtained with tiron as an entering ligand is higher than this value. This may be due to the partial formation of [Ga(NCS)(OH)]$^+$ at higher pH where kinetics with tiron was carried out.

Reaction of Oxalatogallium(III) with Tropolone. Under the conditions where only $Ga(ox)^+$ is present as the gallium(III)–oxalate complex, the reaction of the gallium(III) complex with tropolone can be expressed as[6]

$$Ga' + HL' \xrightarrow{k_{f(H,ox)}} Ga(ox)L(\text{and/or } GaL^{2+} + ox^{2-}) + H^+ \quad (10)$$

and the kinetic equation is described as

$$d[Ga(ox)L]/dt = k_{f(H,ox)}[Ga'][HL'] \quad (11)$$

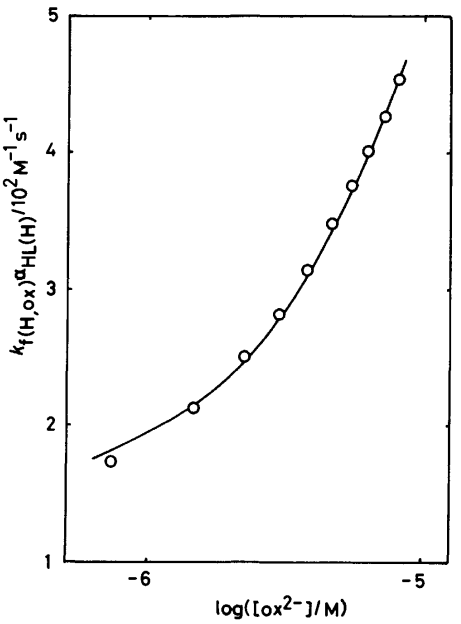

Fig. 3. Plot of $k_{f(H,ox)}$ *vs.* log[ox^{2-}].
Conditions: $C_{Ga}=2.81\times10^{-2}$ M, $C_L=1.03\times10^{-4}$ M, $C_{ox}=1.00\times10^{-3}$—1.00×10^{-2} M, −log[H^+]=1.056± 0.002, at 25 °C and I=0.50 M.

where [Ga′]=[Ga^{3+}]+[$GaOH^{2+}$]+[$Ga(ox)^+$]. Then we obtain

$$k_{f(H,ox)}\alpha_{HL(H)} = \frac{k_{f(H)}\alpha_{HL(H)}\alpha_{Ga(OH)} + k_{Ga(ox)}K_{Ga(ox)}[ox^{2-}]}{\alpha_{Ga(OH)} + K_{Ga(ox)}[ox^{2-}]}$$

where $K_{Ga(ox)}$=[$Ga(ox)^+$][Ga^{3+}]$^{-1}$[ox^{2-}]$^{-1}$ is the formation constant for the inner-sphere complex of monooxalatogallium(III).

At constant pH, the values of $k_{f(H,ox)}$ obtained at various oxalate concentrations were analyzed as a function of [ox^{2-}] by a least-squares procedure.[11] The solid line in Fig. 3 was calculated with $K_{Ga(ox)}=10^{4.44}$ M^{-1} and $k_{Ga(ox)}=10^{3.27}$ $M^{-1}s^{-1}$ at 25 °C and I=0.50 M. The value of $k_{f(H)}\alpha_{HL(H)}\alpha_{Ga(OH)}$ obtained (1.50×10^2 M^{-1} s^{-1}) compares favorably with the value calculated (1.59×10^2 $M^{-1}s^{-1}$) from the relation of $k_{f(H)}\alpha_{HL(H)}\alpha_{Ga(OH)}$= $k_{Ga}+k_{GaOH}K_{GaOH}$[H^+]$^{-1}$ and the values of k_{Ga}, k_{GaOH}, and k_{GaOH} previously determined.[6]

Discussion

On the basis of the values of activation volume, we have shown[6] that the complexation of gallium(III) is accommodated within the framework of a dissociative-interchange mechanism.[12] For the complexation reactions dissociatively activated, the values of k_M/K_{os} and k_{MA}/K_{os} (apart from a statistical factor which is not far from unity,[13] where K_{os} is the formation constant of an outer-sphere complex) are not very different from the values of $k_M{}^{-H_2O}$ and $k_{MA}{}^{-H_2O}$, respectively.[14,15] We calculated rate constants, $k_{Ga}{}^{-H_2O}$ and $k_{GaA}{}^{-H_2O}$, for our system and others. The results are summarized in Table 2 in which are also given the second-order rate

TABLE 3. BOUND LIGAND EFFECTS OF GaA COMPLEXES

A	E(A)	R(A)[a]
H_2O	0.00	0.00
OH^-	1.65	2.07±0.26
$(OH)_2^{2-}$	3.30	3.28±0.21
SCN^-	1.83	2.19±0.57
ox^{2-}	1.70	1.86

a) $R(A)=\log(k_{GaA}{}^{-H_2O}/\text{number of } H_2O \text{ in GaA})-\log(k_{Ga}{}^{-H_2O}/6)$.

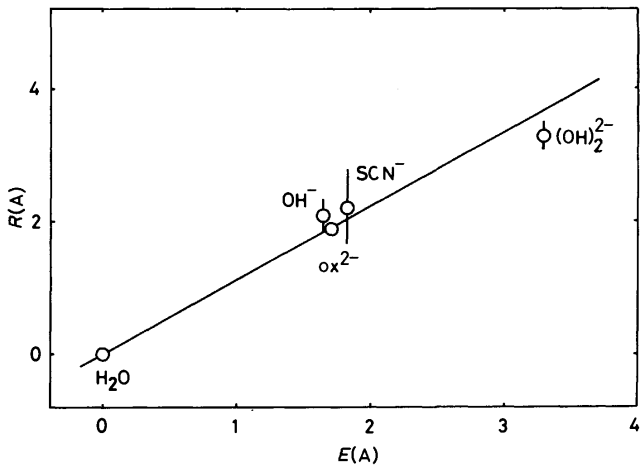

Fig. 4. Plot of R(A) *vs.* E(A).
$R(A)=\log(k_{GaA}{}^{-H_2O}/\text{number of } H_2O \text{ in GaA})-\log(k_{Ga}{}^{-H_2O}/6)$.

constants for complexation reactions. K_{os} were calculated from the Fuoss equation[16] with the distance of closest approach=5 Å, assuming that a negatively charged group removed from the eventual coordination site is unimportant in the calculation of K_{os} values.[17]

With the water exchange rate constant calculated, the bound ligand effect of GaA on the water exchange rate can be estimated by the difference between $\log(k_{GaA}{}^{-H_2O}/\text{number of } H_2O \text{ in GaA})$ and $\log(k_{Ga}{}^{-H_2O}/6)$, which is shown in Table 3 under the heading of R (A). In this Table, the values of E (A) for the monodentate ligands are taken from Ref. 3 and the value for oxalate is the effective E(A) which is given by $E(ox^{2-})=2E(OAc^-)-2\Delta E_{OO}$.[5] Since the donor-donor interaction between hydroxo ligands coordinated to gallium(III) may be anticipated to be small, the value of E ($2OH^-$) is assumed to be $2E$ (OH^-).

The positive values of R(A) indicate that the coordinated ligands do have the expected libilizing effect on the water exchange rate at GaA. If this labilizing effect is attributable to the electron donation from the ligand to the gallium(III) ion, the bound ligand effect could be quantitatively predicted by Eq. 1. Then the plot of R(A) *vs.* E(A) should yield a straight line with an intercept of zero. The value of γ for gallium(III) was estimated from the slope of Fig. 4 to be 1.1. As stated previously,[4,22] a hard metal ion[23] such as Ga(III) has higher γ value than less hard metal ions such as Co(II) (γ=0.47), Ni(II) (γ=0.40), and Zn(II) (γ=0.30). This implies that the harder the metal ion, the more sensitive is the water exchange rate to the electron-donating ability of the ligand already attached.

References

1) M. Tanaka, *J. Inorg. Nucl. Chem.*, **35**, 965 (1973).
2) M. Tanaka, *J. Inorg. Nucl. Chem.*, **36**, 151 (1974).
3) J. O. Edwards, *J. Am. Chem. Soc.*, **76**, 1540 (1954).
4) S. Yamada, K. Ohsumi, and M. Tanaka, *Inorg. Chem.*, **17**, 2790 (1978).
5) S. Yamada, T. Kido, and M. Tanaka, *Inorg. Chem.*, **23**, 2990 (1984).
6) S. Yamada, A. Iwanaga, S. Funahashi, and M. Tanaka, *Inorg. Chem.*, **23**, 3528 (1984).
7) V. A. Nazarenko, V. P. Antonovich, and E. M. Nevskaya, *Zhur. Neorg. Khim.*, **13**, 1574 (1968).
8) Distinction between reaction paths with proton ambiguity is made by checking the reasonableness of the rate constants calculated (see Ref. 6).
9) L. G. Sillén and A. E. Martell, "Stability Constants of Metal-Ion Complexes," the Chemical Society, London (1964); Supplement No. 1, the Chemical Society, London (1971).
10) E. Högfeldt, "Stability Constants of Metal-Ion Complexes," IUPAC Chemical Data Series, No. 21, Pergamon Press, Oxford (1982).
11) pK_a values for oxalic acid are taken from "Critical Stability Constants," ed by A. E. Martell and R. M. Smith, Plenum Press, New York (1977), Vol. 3. The value of $\alpha_{HL(H)}$ was calculated with the protonation constant K_{H_2L} previously determined.[6]
12) C. H. Langford and H. B. Gray, "Ligand Substitution Processes," W. A. Benjamin, New York (1965).
13) J. Neely and R. Connick, *J. Am. Chem. Soc.*, **92**, 3476 (1970).
14) D. W. Margerum, G. R. Cayley, D. C. Weatherburn, and G. K. Pagenkopf in "Coordination Chemistry," ed by A. E. Martell, American Chemical Society, Washington DC (1978), ACS Monogr. No. 174, Chap. 1.
15) M. Tanaka, *Inorg. Chim. Acta*, **76**, L243 (1983).
16) R. M. Fuoss, *J. Am. Chem. Soc.*, **80**, 5059 (1958).
17) J. C. Cassatt and R. G. Wilkins, *J. Am. Chem. Soc.*, **90**, 6045 (1968).
18) B. Perlmutter-Hayman, F. Secco, E. Tapuhi, and M. Venturini, *J. Chem. Soc., Dalton Trans.*, **1980**, 1124.
19) R. Corigli, F. Secco, and M. Venturini, *Inorg. Chem.*, **18**, 3184 (1979).
20) B. Perlmutter-Hayman, F. Secco, E. Tapuhi, and M. Venturini, *J. Chem. Soc., Dalton Trans.*, **1977**, 2220.
21) Y. Kawai, T. Takahashi, K. Hayashi, T. Imamura, H. Nakayama, and M. Fujimoto, *Bull. Chem. Soc. Jpn.*, **45**, 1417 (1972).
22) M. Tanaka and S. Yamada, *J. Chem. Soc., Chem. Commun.*, **1976**, 178.
23) S. Yamada and M. Tanaka, *J. Inorg. Nucl. Chem.*, **37**, 587 (1975).

Stereoselective Interaction of Chiral Metal Complexes in Solution as Studied by Chromatography. I. Modes of Chiral Discrimination and Optical Resolution of Anion Complexes

Katsuhiko MIYOSHI, Yukio SAKAMOTO, Atsuko OHGUNI, and Hayami YONEDA*
Department of Chemistry, Faculty of Science, Hiroshima University, Higashi-senda-machi, Naka-ku, Hiroshima 730
(Received March 1, 1985)

Chromatographic resolution of some anion complexes, $[Co(ox)_2(en)]^-$, C_1- and C_2-*cis*(*N*)-$[Co(ox)(gly)_2]^-$, $[Co(ox)_2(gly)]^{2-}$, and $[Co(ox)_2(acac)]^{2-}$ (ox=oxalate ion, en=ethylenediamine, gly=glycinate ion, and acac=acetylacetonate ion), was attempted on an ion-exchange column using as chiral selectors several optically active cation complexes such as $[Co(en)_3]^{3+}$, $[Co(sep)]^{3+}$, $[Co(pn)_3]^{3+}$, $[Co(chxn)_3]^{3+}$, $[Co(acac)(en)_2]^{2+}$, and $[Co(gly)(en)_2]^{2+}$ (sep=1,3,6,8,10,13,16,19-octaazabicyclo[6.6.6]icosane, pn=propylenediamine, and chxn=*trans*-1,2-cyclohexanediamine). The elution orders and degrees of optical resolution attained were interpreted on the basis that chiral discrimination is effected along either the C_3 (or pseudo C_3) axis or the C_2 (or pseudo C_2) axis of the respective complexes; the cation complex faces the anion complex with its N–H protons hydrogen-bonded to the coordinated oxygen atoms of the anion complex along the (pseudo) C_3 or C_2 axis. Plausible association models were proposed, which indicate that homochiral (*i.e.*, *Δ*-*Δ* or *Λ*-*Λ*) and heterochiral (*i.e.*, *Δ*-*Λ* or *Λ*-*Δ*) combinations are favored when the cation complex directs its C_3 and C_2 axes to the anion complex, respectively, regardless of which axis (C_3 or C_2) of the anion complex is directed to the cation complex. Most of the experimental data are consistently explained within the framework of the association models proposed.

Several attempts have been made to resolve metal complex anions into optical isomers by chromatography.[1] However, only few examples are known in which optically active metal complex cations are utilized as chiral selectors, and thus the mechanism of chiral discrimination between complex cation and anion in solution has not yet been elucidated clearly. For example, Tatehata *et al.*[2] have succeeded in complete resolution of $[Co(ox)_2(gly)]^{2-}$ (ox=oxalate dianion and gly=glycinate anion) on the DEAE-Sephadex A-25 column with *Λ*-$[Co(en)_3]^{3+}$ cation (en=ethylenediamine) employed as an eluent, the *Δ* anion complex being eluted faster. They proposed an association model for a favorable pair, *Λ*-$[Co(en)_3]^{3+}$-*Δ*-$[Co(ox)_2(gly)]^{2-}$, in which *Λ*-$[Co(en)_3]^{3+}$ faces the anion complex along its C_3 axis (C_3 access) with its three N–H protons triply hydrogen-bonded to the three oxygen atoms of different chelate rings of $[Co(ox)_2(gly)]^{2-}$. This model well explains fairly strong association between the two complex ions (association constant K_A=480 $mol^{-1}dm^3$ at μ=0.01),[2] but it is not clearly demonstrated why the *Δ* anion complex associates more favorably with *Λ*-$[Co(en)_3]^{3+}$ than the antipode does. Furthermore, this model fails to account for the fact that the reversed elution order is obtained for $[Co(ox)_2(gly)]^{2-}$ when the eluent used is *Λ*-$[Co(d\text{-chxn})_3]^{3+}$ (*d*-chxn=(1*S*,2*S*)-1,2-cyclohexanediamine) which can also direct the C_3 axis like *Λ*-$[Co(en)_3]^{3+}$ to the anion complex, as seen later in Table 1.

Subsequently, Sakaguchi *et al.*[3] attempted to elucidate the discrimination mechanism more generally by employing as chiral selectors various cation complexes which had some structural characteristics restricting their possible interaction modes. A similar allowance was made for the selection of anion complexes to be examined. Some of the results they obtained are listed in Table 1. Based on these elution orders (*i.e.*, favorable pairs), they assumed that favorable pairs are formed between those chiral cation and anion complexes which have the same handedness of chelate rings when viewed along the axis that each complex directs to the counterpart complex upon association. However, it is not easily accepted that the overlapping of chelate rings rather than the interionic hydrogen bonding takes a major part in chiral discrimination between these amine complexes and oxalato or amino acidato complexes. In fact, the mechanism they proposed leads to a somewhat strange assertion that $[Co(en)_3]^{3+}$ always "uses" its C_2 axis to recognize the chirality of the anion complexes. In addition, the elution orders of $[Co(ox)_2(en)]^-$ obtained with *Δ*-$[Co(sep)]^{3+}$ (sep=1,3,6,8,10,13,16,19-octaazabicyclo[6.6.6]icosane) and *Δ*-$[Co(l\text{-chxn})_3]^{3+}$ (*l*-chxn=(1*R*,2*R*)-1,2-cyclohexanediamine) are opposite to those predicted by their proposal.

TABLE 1. ENANTIOMERS OF SOME ANION COMPLEXES WHICH FORM FAVORABLE PAIRS WITH Δ CATION COMPLEXES

	Δ-$[Co(en)_3]^{3+}$	*Δ*-$[Co(sep)]^{3+}$	*Δ*-$[Co(l\text{-chxn})_3]^{3+}$
$[Co(edta)]^-$	*Λ*	*Λ*	*Δ*
$[Co(ox)_2(en)]^-$	*Δ*	*Λ*[a]	*Δ*[a]
$[Co(ox)_2(gly)]^{2-}$	*Λ*	*Λ*	*Δ*
$[Cr(mal)_3]^{3-}$	*Λ*	*Λ*	*Δ*
fac-$[Co(\beta\text{-ala})_3]$	*Δ*[a]	*Λ*	*Δ*

edta=ethylenediaminetetraacetate ion and mal=malonate ion.
a) Erroneously determined in Ref. 3 and thus corrected here.

As presented above, no satisfactory explanation has been so far afforded for the elution orders (or favorable pairs formed between chiral complex cations and anions) determined by chromatography. It is a main purpose of the present study to elucidate the detailed mechanism by which chiral discrimination is effected

between these complex cations and anions bearing a hydrogen-bonding ability.

Experimental

Preparation of Metal Complexes. Appropriate salts of *Δ* isomers of $[Co(en)_3]^{3+}$, $[Co(sep)]^{3+}$, $[Co(sen)]^{3+}$ (sen=1,1,1-tris(((2-aminoethyl)amino)methyl)ethane), $[Co(l\text{-chxn})_3]^{3+}$, $[Co(l\text{-pn})_3]^{3+}$, (*l*-pn=(*R*)-propylenediamine), $[Co(gly)(en)_2]^{2+}$, $[Co(acac)(en)_2]^{2+}$, and *cis*-$[Co(NO_2)_2(en)_2]^+$ were available from the previous works[3,4] and/or were prepared by well-established methods. $[Co(sar)(en)_2]^{2+}$[5] (sar=sarcosinate anion), $[Co(\beta\text{-ala})(en)_2]^{2+}$[6] ($\beta$-ala=$\beta$-alaninate anion), and $[Co(N,N'\text{-Me}_2\text{-en})(en)_2]^{3+}$[7] ($N,N'$-Me$_2$-en=$N,N'$-dimethylethylenediamine) were also prepared as racemates of appropriate salts by the literature methods. Racemic $[Co(gly)(N,N'\text{-Me}_2\text{-en})(en)]^{2+}$ and $[Co(\beta\text{-ala})(N,N'\text{-Me}_2\text{-en})(en)]^{2+}$ were newly prepared as perchlorate salts by allowing $[Co(Cl)(gly)(OH_2)(en)]Cl$[8] and $[Co(Cl)_2(\beta\text{-ala})(en)]$,[9] respectively, to react with an equivalent amount of N,N'-Me$_2$-en in dimethyl sulfoxide at 60 °C for 5 h. The precipitates which formed upon addition of acetone were purified and converted to perchlorate salts by ion-exchange chromatography. Found: C, 19.73; H, 5.09; N, 14.31%. Calcd for $[Co(gly)(N,N'\text{-Me}_2\text{-en})(en)](ClO_4)_2=C_8H_{24}N_5O_{10}Cl_2Co$: C, 20.01; H, 5.04; N, 14.59%. Found: C, 21.60; H, 5.24; N, 13.93%. Calcd for $[Co(\beta\text{-ala})(N,N'\text{-Me}_2\text{-en})(en)](ClO_4)_2=C_9H_{26}N_5O_{10}Cl_2Co$: C, 21.87; H, 5.30; N, 14.17%.

Following anion complexes were also available from the previous work[3] and/or were prepared as described in the literature; $[Co(ox)_2(en)]^-$, $[Co(ox)_2(gly)]^{2-}$,[10] $[Co(ox)_2(acac)]^{2-}$,[10] and C_1- and C_2-*cis*(*N*)-$[Co(ox)(gly)_2]^-$.[11] They were found all chromatographically pure. The first two complexes were resolved by conventional methods.[10,12]

The absolute configuration has been assigned to most of the above complexes; the *Δ* isomers have a negative main CD component at the first d-d transition region except for $[Co(sep)]^{3+}$[13] and $[Co(sen)]^{3+}$,[14] the *Δ* isomers of which have a positive component.

Chromatographic Experiments. Two types of experiments were carried out in essentially the same manner as in the previous work[3] to determine the enantiomers of anion complexes which associate favorably with various types of *Δ* cation complexes.

Type (a) Experiment: The SP-Sephadex C-25 resin saturated with a *Δ* complex cation was packed in a glass column (12 mm i.d. ×170 mm). At the end of the column was placed a small amount of the resin (Na^+ form) to adsorb the complex cation eluted slightly during the chromatographic run. A racemic complex anion (0.3 cm^3 in 30 mmol dm^{-3}) was loaded on the top of the column and was eluted with 30% aqueous ethanol solution. The elution rate was regulated at 0.3 cm min^{-1} with a peristaltic pump. The eluate was fractionally collected, and absorption and circular dichroism spectra of each fraction (2 cm^3) were recorded on a Shimadzu UV-240 spectrophotometer and a Jasco J-40CS spectropolarimeter, respectively at ambient temperatures. The elution curves were obtained in this way when necessary, but the degree of resolution was generally so low that only the elution orders were determined for the most cases. Care was taken to ensure that the elution order was determined by the chirality of the complex cation in the resin, but not of the resin matrix.[15] It is the late-eluted enantiomer that interacts favorably with the *Δ* cation complex in the resin. Similar experiments were carried out for some racemic cation complexes on the QAE-Sephadex A-25 column saturated with an optically active $[Co(ox)_2(en)]^-$ or $[Co(ox)_2(gly)]^{2-}$ ion.

Type (b) Experiment: The same procedures as before[3,16] were applied to measure the retention volumes of some anion complexes. A racemic anion complex (20 μl in 0.1 mol dm^{-3}) was loaded with a syringe on the top of the IEX-520-SIL (anion-exchange resin) column and was eluted with an aqueous solution containing a *Δ* cation complex as a chloride salt in 10 mmol dm^{-3}. The column size was 4 mm i.d. ×150 mm and the elution rate was regulated at 0.5 cm^3 min^{-1} with a Jasco BIP-1 pump for HPLC. The eluate was guided to a flow cell to detect the anion complex at an appropriate wavelength with a Shimadzu UV-140 spectrophotometer. The retention volumes thus recorded were found to be reproducible to within at least ±0.1 cm^3. When necessary, two enantiomers of the anion complex were chromatographed separately to estimate respective retention volumes V_R.

Results and Discussion

In Table 2 are summarized enantiomers of anion

Table 2. Enantiomers of anion complexes which form favorable pairs with *Δ* cation complexes

	C_2^-		C_3^-	$C_2^-+C_3^-$	
	$[Co(ox)_2(en)]^-$	C_2-*cis*(*N*)-$[Co(ox)(gly)_2]^-$	C_1-*cis*(*N*)-$[Co(ox)(gly)_2]^-$	$[Co(ox)_2(gly)]^{2-}$	$[Co(ox)_2(acac)]^{2-}$
C_2^+					
Δ-$[Co(sep)]^{3+}$	*Λ*[a,b]	*Λ*	*Λ*	*Λ*[a]	*Λ*
Δ-$[Co(acac)(en)_2]^{2+}$	*Λ*[c]	*Λ*	*Λ*	*Λ*[c]	*Λ*[c]
Δ-*cis*-$[Co(NO_2)_2(en)_2]^+$	*Λ*[d]	*Λ*	*Λ*	*Λ*[d]	*Λ*
C_3^+					
Δ-$[Co(l\text{-chxn})_3]^{3+}$	*Δ*[a,b]	*Δ*	*Δ*	*Δ*[a]	*Δ*
Δ-$[Co(l\text{-pn})_3]^{3+}$	*Λ*	*Λ*	*Δ*	*Δ*	*Δ*
$C_2^+ + C_3^+$					
Δ-$[Co(en)_3]^{3+}$	*Δ*[a,c,e]	*Δ*[e,f]	*Λ*[f]	*Δ*[a,g]	*Λ*[c]
Δ-$[Co(gly)(en)_2]^{2+}$	*Δ*[c,e]	*Λ*[e]	*Λ*	*Λ*[c]	*Λ*[c]
Δ-$[Co(sen)]^{3+}$	*Λ*	*Λ*	*Λ*	*Λ*	*Λ*

a) Also reported in Ref. 3. b) Erroneously determined in Ref. 3. c) Also reported in Ref. 17. d) Also reported in Ref. 19. e) Very low resolution attained. f) Also reported in Ref. 18. g) Ref. 2.

complexes which are eluted later in the type (a) experiment with *Δ* cation complexes employed as chiral selectors. Thus, it is these enantiomers that form favorable pairs with the *Δ* cation complexes. Some of the favorable pairs listed in Table 2 have been already reported by Tatehata *et al.*[17,18] and Sakaguchi *et al.*[3] Most of their results are reproduced by our present study, but those for $[Co(ox)_2(en)]^-$ obtained with *Δ*-$[Co(sep)]^{3+}$ and *Δ*-$[Co(l\text{-chxn})_3]^{3+}$ are at variance with the present results. Then, the elution order was determined repeatedly for $[Co(ox)_2(en)]^-$ with a longer column, leading to the conclusion that the two elution orders (or favorable pairs) were erroneously determined by Sakaguchi *et al.*

Structural Characteristics of Complexes. The cation complexes used as chiral selectors in the present study are *Δ*-$[Co(en)_3]^{3+}$, *Δ*-$[Co(sep)]^{3+}$, *Δ*-$[Co(sen)]^{3+}$, *Δ*-$[Co(l\text{-chxn})_3]^{3+}$, *Δ*-$[Co(l\text{-pn})_3]^{3+}$ (a mixture of *fac*-lel_3 and *mer*-lel_3 isomers), *Δ*-$[Co(acac)(en)_2]^{2+}$, *Δ*-$[Co(gly)(en)_2]^{2+}$, and *Δ*-*cis*-$[Co(NO_2)_2(en)_2]^+$. It is likely that interionic hydrogen bonds play a major role in association of these amine complex cations with complex anions such as $[Co(ox)_2(en)]^-$, $[Co(ox)_2(gly)]^{2-}$, and $[Co(ox)_2(acac)]^{2-}$. If inter-chelate repulsion is taken into account, hydrogen bonds are intimately formed between amino protons of the cation complex and coordinated oxygen atoms of the anion complex along either the (pseudo) C_3 or the (pseudo) C_2 axis of the respective complexes. That is, we assume that chiral discrimination between these complex cations and anions is effected along either the C_3 or the C_2 axis.

$[Co(sep)]^{3+}$ is covalently capped along both sides of the C_3 axis.[13] Thus, this complex can form hydrogen bonds to the anion complex only along its C_2 axis. Then, we say that $[Co(sep)]^{3+}$ belongs to the C_2^+ group complex and "uses" the C_2 axis only in association with the anion complex (C_2^+ access). $[Co(acac)(en)_2]^{2+}$ and *cis*-$[Co(NO_2)_2(en)_2]^+$ are also classified as the C_2^+ group, since they are expected to approach the anion complex along their C_2 axis from the side of their en rings so as to avoid the electrostatic repulsion between the negatively charged acac or NO_2 groups and the negative charge on the complex anion. On the other hand, $[Co(l\text{-chxn})_3]^{3+}$ and $[Co(l\text{-pn})_3]^{3+}$ are regarded as the C_3^+ group complex, since they are expected to direct the (pseudo) C_3 axis to the anion complex (C_3^+ access) owing to the presence of chxn or CH_3 groups on the chelate rings which will block the C_2^+ access. It is easily accepted that both C_2^+ and C_3^+ accesses are possible for $[Co(en)_3]^{3+}$ and $[Co(gly)(en)_2]^{2+}$, which thus belong to the $(C_2^+ + C_3^+)$ group. $[Co(sen)]^{3+}$ is also regarded as the $(C_2^+ + C_3^+)$ group complex, since it is capped covalently along one side of the C_3 axis, but the other side is available for hydrogen bonds to the anion complex.[14]

The anion complexes are also classified into three groups on the basis of the axis which they "use" in association with the cation complexes. For these anion complexes, charge localization on chelate rings is taken into account to determine the site and the direction of ion association.[3] Thus, $[Co(ox)_2(en)]^-$ and C_2-*cis(N)*-$[Co(ox)(gly)_2]^-$ belong to the C_2^- group complex, while C_1-*cis(N)*-$[Co(ox)(gly)_2]^-$ belongs to the C_3^- group, since three oxygen atoms are disposed triangularly along the pseudo C_3 axis in the last complex. $[Co(ox)_2(gly)]^{2-}$ as well as $[Co(ox)_2(acac)]^{2-}$ is, on the other hand, regarded as the $(C_2^- + C_3^-)$ group if the coordinated oxygen atoms of the acac ligand are available for the hydrogen-bonding interaction with amine complex cations.

Analysis of Favorable Pairs. As is evident in Tables 1 and 2, a typical C_2^+ group cation, *Δ*-$[Co(sep)]^{3+}$ forms favorable pairs always with the Λ anion complexes, whereas a typical C_3^+ group cation, *Δ*-$[Co(l\text{-chxn})_3]^{3+}$ does always with the *Δ* anion complexes. In other words, homochiral (*i.e.*, *Δ*-*Δ* or *Λ*-*Λ*) and heterochiral (*i.e.*, *Δ*-*Λ* or *Λ*-*Δ*) combinations are favored when the cation complex "uses" the C_3 and C_2 axes, respectively, regardless of which axis (C_3 or C_2) of the anion complex is directed to the cation complex. In fact, both *Δ*-$[Co(acac)(en)_2]^{2+}$ and *Δ*-*cis*-$[Co(NO_2)_2(en)_2]^+$ which belong to the C_2^+ group form favorable pairs with the Λ anion complexes.[19] *Δ*-$[Co(l\text{-pn})_3]^{3+}$ which has been tentatively classified as the C_3^+ group, however, favors unexpectedly a heterochiral combination (*Δ*-*Λ*) with the C_2^- group anions such as $[Co(ox)_2(en)]^-$ and C_2-*cis(N)*-$[Co(ox)(gly)_2]^-$. This is probably because the C_2^+ access of $[Co(l\text{-pn})_3]^{3+}$ can not be fully blocked by the CH_3 groups on the pn chelates.

For the $(C_2^+ + C_3^+)$ group cations, a heterochiral (*Δ*-*Λ*) combination is certainly favored in the interaction with the C_3^- and $(C_2^- + C_3^-)$ group anions, but the favorable pairs with the C_2^- group anions are not amenable to generalization. It should be noted here

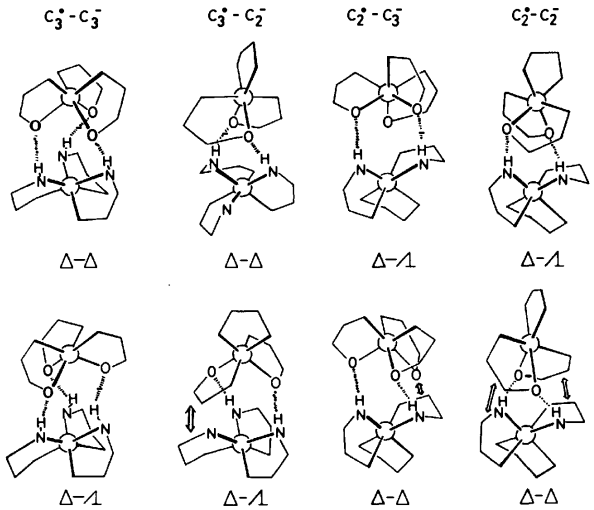

Fig. 1. Association models of $C_n^+ - C_m^-$ interaction modes between *Δ* cation complex and *Δ* or *Λ* anion complex. Favorable pairs are shown at the upper part.

that the degrees of resolution attained with Δ-$[Co(en)_3]^{3+}$ and Δ-$[Co(gly)(en)_2]^{2+}$ are very low, particularly for the C_2^- group anions. This implies that the (C_2^++C_3^+) group cations use both of the C_2 and C_3 axes in association with the anion complexes; they favor a heterochiral combination in the C_2^+ access, while they favor a homochiral one in the C_3^+ access, overall discrimination efficiency being thereby low. By contrast, $[Co(sen)]^{3+}$ always favors a heterochiral combination, though it has been classified above as the (C_2^++C_3^+) group cation.

Association Models. We now propose association models which explain consistently all the experimental data given in Table 2. In constructing the models, two acceptable assumptions were made; hydrogen-bonding interaction prevails between complex cation and anion, and these hydrogen bonds are formed intimately along either the (pseudo) C_3 or the (pseudo) C_2 axis of the respective complexes. All the possible interaction modes (C_3^+—C_3^-, C_3^+—C_2^-, C_2^+—C_3^-, and C_2^+—C_2^-) are depicted in Fig. 1, where C_n^+—C_m^- refers to the interaction in which complex cation and anion "use" the C_n and C_m axes, respectively on association. Each complex is assumed here to have five-membered bidentate chelates such as en, gly, or ox. Favorable pairs are drawn at the upper part, and the anion complex is located above the Δ cation complex in each pair where interionic hydrogen bonds are shown by dotted lines.

In the C_2^+—C_3^- and C_2^+—C_2^- interaction modes, favorable pairs are heterochiral (Δ-Λ or Λ-Δ), since inter-chelate repulsion is anticipated for the homochiral pair, as indicated by arrows. On the other hand, a favorable pair is homochiral (Δ-Δ or Λ-Λ) in the C_3^+—C_2^- mode because of the presence of similar interchelate repulsion in the heterochiral pair. In the C_3^+—C_3^- mode, such repulsion is not anticipated for either pair. However, the strength of the interionic hydrogen bond may be different between the two diastereomeric pairs; it depends greatly on the spacial disposition of the interacting atoms (H and O). A close examination of the two pairs in the C_3^+—C_3^- mode reveals that lone pair electrons on the O atoms of the anion complex are more favorably disposed in the homochiral pair for the hydrogen bonding with axial N-H protons of the cation complex than in the heterochiral pair, when the cation complex assumes the lel_3 conformation. Thus, a favorable pair is also homochiral in the C_3^+—C_3^- mode.

Tatehata *et al.*[2] supposed, on the contrary, that a favorable pair was heterochiral in the C_3^+—C_3^- mode, since they assumed that both $[Co(en)_3]^{3+}$ and $[Co(ox)_2(gly)]^{2-}$ use the (pseudo) C_3 axis in association. If so, favorable pairs formed with Δ-$[Co(l\text{-chxn})_3]^{3+}$ could not be accounted for, as discussed in Introduction. It should be pointed out here that discrimination efficiency may be very low in the C_3^+—C_3^- mode for conformationally labile complexes such as $[Co(en)_3]^{3+}$ and $[Co(gly)(en)_2]^{2+}$, since only a small difference in the strength of the interionic hydrogen bond is expected between the two diastereomeric pairs if the cation complex is conformationally labile.

In this way, the association models proposed here demonstrate that homochiral and heterochiral combinations are favored when the cation complex "uses" the C_3 and C_2 axes, respectively, in conformity with the experimental data listed in Table 2.

Now, if the above generalization is accepted as valid, favorable pairs formed with the (C_2^++C_3^+) group cations are analyzed in more detail. For $[Co(en)_3]^{3+}$, for example, all of the four modes, C_3^+—C_3^-, C_3^+—C_2^-, C_2^+—C_3^-, and C_2^+—C_2^- are possible in the interaction with the (C_3^-+C_2^-) group anions such as $[Co(ox)_2(gly)]^{2-}$ or $[Co(ox)_2(acac)]^{2-}$. The former two modes favor a homochiral combination, while the latter two favor a heterochiral one. The C_3^+—C_3^- mode is likely to contribute appreciably to the overall interaction between $[Co(en)_3]^{3+}$ and $[Co(ox)_2(gly)]^{2-}$ or $[Co(ox)_2(acac)]^{2-}$, but discrimination efficiency of this mode is low owing to the conformational lability of $[Co(en)_3]^{3+}$. Thus, the resulting favorable pair is eventually determined by the C_2^+ access which favors a heterochiral combination; the contribution due to the C_2^+—C_3^- and C_2^+—C_2^- modes surpasses that due to the C_3^+—C_3^- and C_3^+—C_2^- modes. Similarly, the C_2^+—C_3^- mode predominates over the C_3^+—C_3^- mode in the discriminating interaction of $[Co(en)_3]^{3+}$ with the C_3^- group anion like C_1-*cis(N)*-$[Co(ox)(gly)_2]^-$.

With the C_2^- group complex anion, the C_3^+—C_2^- and C_2^+—C_2^- modes contribute to chiral discrimination. It is not obvious in Fig. 1 which mode contributes more effectively. As a result, overall discrimination efficiency should be extremely low; the former mode barely predominates over the latter, a homochiral pair being eventually favored slightly over a heterochiral pair. The results obtained for $[Co(gly)(en)_2]^{2+}$ are analyzed similarly, though the C_2^+—C_2^- mode seems to predominate accidentally over the C_3^+—C_2^- mode in the interaction with C_2-*cis(N)*-$[Co(ox)(gly)_2]^-$ (C_2^-).

$[Co(sen)]^{3+}$ which also belongs to the (C_2^++C_3^+) group, however, always favors a heterochiral combination. This suggests that $[Co(sen)]^{3+}$ uses the C_2 axis more frequently than the C_3 axis,[4] probably because this complex is covalently capped along one side of the C_3 axis, while both of the two sides are available for hydrogen bonding in $[Co(en)_3]^{3+}$ which behaves as a typical (C_2^++C_3^+) group cation. In short, $[Co(sen)]^{3+}$ behaves as if it were a prototype of the C_2^+ group cation.

Effect of N-*Methylation on Chiral Discrimination.* In order to account for the favorable pairs formed with $[Co(en)_3]^{3+}$ or $[Co(gly)(en)_2]^{2+}$, we have made an assumption that both of the C_3^+ and C_2^+ accesses are

Table 3. Enantiomers of complex cations which form favorable pairs with Λ-$[Co(ox)_2(en)]^-$ and Λ-$[Co(ox)_2(gly)]^{2-}$

	C_2^- Λ-$[Co(ox)_2(en)]^-$	$C_2^-+C_3^-$ Λ-$[Co(ox)_2(gly)]^{2-}$
$[Co(en)_3]^{3+}$	Λ[b]	Δ
$[Co(N,N'\text{-}Me_2\text{-}en)(en)_2]^{3+}$ [a]	$\Lambda(RR)$[b,c]	$\Delta(SS)$[c]
$[Co(gly)(en)_2]^{2+}$	Λ[b]	Δ
$[Co(\beta\text{-}ala)(en)_2]^{2+}$	Λ[b]	Δ
$[Co(sar)(en)_2]^{2+}$ [a]	$\Lambda(R)$[b,c]	$\Delta(S)$[c]
$[Co(gly)(N,N'\text{-}Me_2\text{-}en)(en)]^{2+}$ [a]	$\Delta(SS)$[c]	$\Delta(SS)$[c]
$[Co(\beta\text{-}ala)(N,N'\text{-}Me_2\text{-}en)(en)]^{2+}$ [a]	$\Delta(SS)$[c]	$\Delta(SS)$[c]

a) Isomers having CH_3 group(s) parallel to the pseudo C_3 axis. b) Very low resolution. c) *R* and *S* in the parentheses donote the configurations around the N atoms coordinated to Co(III).

involved in the interaction of these cation complexes. Then, if either of the two accesses is prohibited, say, by *N*-methylation of amino groups of the en or gly ligand, the discrimination mechanism would be drastically affected. With this expectation in mind, *N*-methyl derivatives of $[Co(en)_3]^{3+}$, $[Co(gly)(en)_2]^{2+}$, and $[Co(\beta\text{-ala})(en)_2]^{2+}$ were chromatographed on the QAE-Sephadex column saturated with Λ-$[Co(ox)_2(en)]^-$ or Λ-$[Co(ox)_2(gly)]^{2-}$ ion. The late-eluted enantiomers, *i.e.*, those forming favorable pairs with these Λ anion complexes are listed in Table 3.

With Λ-$[Co(ox)_2(en)]^-$ ion (C_2^-), both of the C_3^+—C_2^- and C_2^+—C_2^- modes are possible for $[Co(en)_3]^{3+}$, $[Co(gly)(en)_2]^{2+}$, and $[Co(\beta\text{-ala})(en)_2]^{2+}$. Since the former mode barely predominates over the latter, favorable pairs are homochiral, and the degrees of resolution are very low, as discussed earlier. For $[Co(N,N'\text{-}Me_2\text{-}en)(en)_2]^{3+}$ and $[Co(sar)(en)_2]^{2+}$ which have CH_3 group (s) parallel to the pseudo C_3 axis,[20] favorable pairs with $[Co(ox)_2(en)]^-$ are still homochiral, suggesting that the C_3^+ access is not prohibited in these *N*-methylated complexes. In other words, only two NH_2 groups are involved in the C_3^+—C_2^- mode (see Fig. 1), and the amino group of gly or β-ala is not effectively utilized in the C_3^+—C_2^- mode.

On the contrary, $[Co(gly)(N,N'\text{-}Me_2\text{-}en)(en)]^{2+}$ and $[Co(\beta\text{-ala})(N,N'\text{-}Me_2\text{-}en)(en)]^{2+}$ favor a heterochiral combination with $[Co(ox)_2(en)]^-$ and discrimination efficiency exhibited is not so low. This indicates that the CH_3 group located parallel to the pseudo C_3 axis renders the C_3^+ access impossible in these complexes, provided that the CH_3 group is present on the amino group of en but not of gly or β-ala. Thus, favorable pairs of the two cation complexes with $[Co(ox)_2(en)]^-$ are governed by the C_2^+—C_2^- mode which survives and favors a heterochiral combination, and thus the degree of resolution attained should not be so low.

With Λ-$[Co(ox)_2(gly)]^{2-}$ ($C_2^-+C_3^-$), all of the four modes are possible for $[Co(en)_3]^{3+}$, $[Co(gly)(en)_2]^{2+}$, and $[Co(\beta\text{-ala})(en)_2]^{2+}$. Since the contribution of the C_3^+—C_3^- mode to chiral discrimination is negligible for these conformationally labile complexes, favorable pairs are governed by the C_2^+ access which favors a heterochiral combination. Then, even if the C_3^+—C_3^- and C_3^+—C_2^- modes are prohibited by *N*-methylation favorable pairs remain heterochiral. Instead, discrimination efficiency should be improved. In fact, the degree of resolution is found to be higher for $[Co(gly)(N,N'\text{-}Me_2\text{-}en)(en)]^{2+}$ and $[Co(\beta\text{-ala})(N,N'\text{-}Me_2\text{-}en)(en)]^{2+}$ than for $[Co(gly)(en)_2]^{2+}$ and $[Co(\beta$-

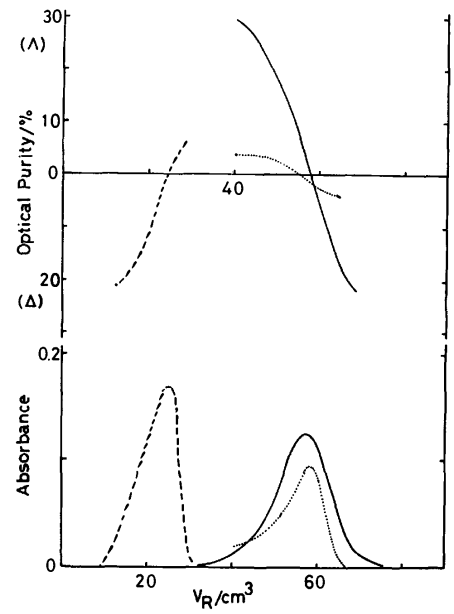

Fig. 2. Elution curves and plots of optical purity obtained for $[Co(ox)_2(en)]^-$ with Δ-$[Co(sep)]^{3+}$ (---), Δ-$[Co(l\text{-}chxn)_3]^{3+}$ (——), and Δ-$[Co(en)_3]^{3+}$ (···) employed as chiral selectors.

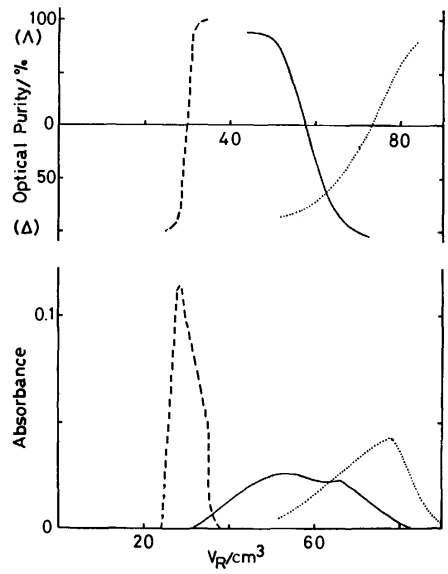

Fig. 3. Elution curves and plots of optical purity obtained for C_1-*cis*(*N*)-$[Co(ox)(gly)_2]^-$ with Δ-$[Co(sep)]^{3+}$ (---), Δ-$[Co(l\text{-}chxn)_3]^{3+}$ (——), and Δ-$[Co(en)_3]^{3+}$ (····) employed as chiral selectors.

ala)$(en)_2]^{2+}$, respectively. In this way, our assumption that both of the C_3^+ and C_2^+ accesses are involved in the (C_2^++C_3^+) group cation complexes, is verified experimentally.

Elution Curves. In Figs. 2 and 3 are shown the elution curves of $[Co(ox)_2(en)]^-$ (C_2^-) and C_1-*cis(N)*-$[Co(ox)(gly)_2]^-$ (C_3^-), respectively, obtained by the type (a) experiment with Δ-$[Co(sep)]^{3+}$ (C_2^+), Δ-$[Co(l\text{-}chxn)_3]^{3+}$ (C_3^+), and Δ-$[Co(en)_3]^{3+}$ (C_2^++C_3^+) ions as chiral selectors. Also plotted is the optical purity of each fraction of the eluate as a function of a retention volume V_R. It is seen that fairly good resolution is attained for both anion complexes with Δ-$[Co(sep)]^{3+}$ and Δ-$[Co(l\text{-}chxn)_3]^{3+}$, for which only the C_2^+ and C_3^+ accesses are possible, respectively. A comparison between Figs. 2 and 3 indicates that better resolution is attained for C_1-*cis(N)*-$[Co(ox)(gly)_2]^-$ (C_3^-) than for $[Co(ox)_2(en)]^-$ (C_2^-) with both cation complexes. This observation suggests that the C_2^+—C_3^- mode contributes more effectively to chiral discrimination than the C_2^+—C_2^- mode, and the C_3^+—C_3^- mode does than the C_3^+—C_2^- mode, provided that the C_3^+—C_3^- mode is of conformationally rigid complexes.

On the other hand, $[Co(en)_3]^{3+}$ certainly serves as a moderately good chiral selector for C_1-*cis(N)*-$[Co(ox)(gly)_2]^-$ (C_3^-), but it hardly discriminates the chirality of $[Co(ox)_2(en)]^-$ (C_2^-); the C_3^+—C_3^- mode is negligible as compared with the C_2^+—C_3^- mode for the former C_3^- complex, while the C_3^+—C_2^- and C_2^+—C_2^- modes contribute almost equally but oppositely to chiral discrimination for the latter C_2^- complex. Similarly, $[Co(en)_3]^{3+}$ is expected not to serve as a good selector for another C_2^- anion complex, C_2-*cis(N)*-$[Co(ox)(gly)_2]^-$.[18] The finding that the degree of resolution attained for C_1-*cis(N)*-$[Co(ox)(gly)_2]^-$ (C_3^-) with $[Co(en)_3]^{3+}$ is comparable to that attained with $[Co(sep)]^{3+}$ or $[Co(l\text{-}chxn)_3]^{3+}$, is consistent with the above assertion that discrimination efficiency is comparatively high in the C_2^+—C_3^- mode. If the C_3^+—C_2^- mode as well as the C_3^+—C_3^- mode of conformationally labile $[Co(en)_3]^{3+}$ is not effective, as mentioned above, $[Co(en)_3]^{3+}$ is expected to serve as a moderately effective selector for the (C_2^-+C_3^-) and particularly for the C_3^- group anions; the contribution of the C_2^+ access overwhelmingly surpasses that of the C_3^+ access in the discriminating interaction of conformationally labile $[Co(en)_3]^{3+}$ with these anion complexes. In fact, Tatehata *et al.*[18] have found that several anion complexes which we can classify as the C_3^- or (C_2^-+C_3^-) group anions, are completely resolved by usual ion-exchange chromatography with $[Co(en)_3]^{3+}$ employed as an eluent, though on a somewhat longer column.

In Figs. 4 and 5 are shown similar elution curves obtained by the type (a) experiment with Δ-$[Co(gly)(en)_2]^{2+}$(C_2^++C_3^+) and Δ-$[Co(acac)(en)_2]^{2+}$ (C_2^+) cations as chiral selectors. It is confirmed that $[Co(gly)(en)_2]^{2+}$ discriminates the chirality of $[Co(ox)_2(en)]^-$ (C_2^-) to a much lesser extent than $[Co(acac)(en)_2]^{2+}$ which uses the C_2 axis only and thus is expected to serve as a good selector. In fact, even $[Co(en)_3]^{3+}$ is less effective than $[Co(acac)(en)_2]^{2+}$ (Fig. 2). On the other hand, when the anion complex uses the C_3 axis only like C_1-*cis(N)*-$[Co(ox)(gly)_2]^-$ (C_3^-), the degree of resolution attained with $[Co(gly)(en)_2]^{2+}$ is almost comparable to that obtained with $[Co(acac)(en)_2]^{2+}$. This is again because the C_2^+—C_3^- mode is effective, but the C_3^+—C_3^- mode of conformationally labile $[Co(gly)(en)_2]^{2+}$ does not contribute appreciably

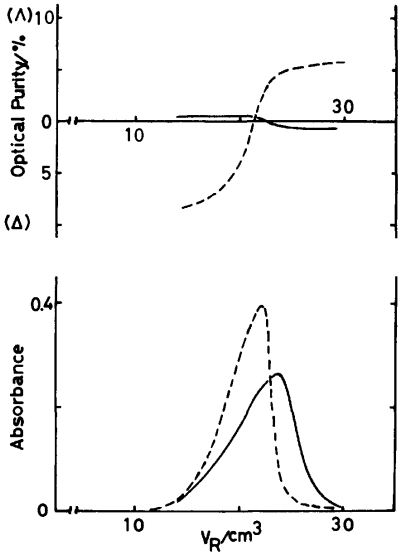

Fig. 4. Elution curves and plots of optical purity obtained for $[Co(ox)_2(en)]^-$ with Δ-$[Co(acac)(en)_2]^{2+}$ (---) and Δ-$[Co(gly)(en)_2]^{2+}$ (——) employed as chiral selectors.

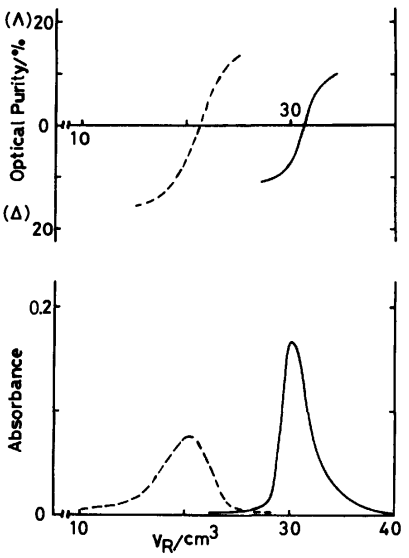

Fig. 5. Elution curves and plots of optical purity obtained for C_1-*cis(N)*-$[Co(ox)(gly)_2]^-$ with Δ-$[Co(acac)(en)_2]^{2+}$ (----) and Δ-$[Co(gly)(en)_2]^{2+}$ (——) employed as chiral selectors.

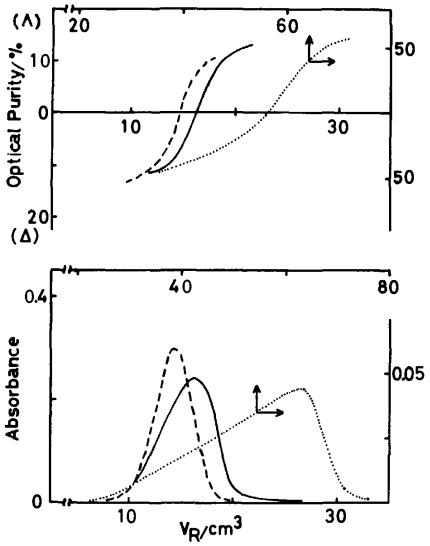

Fig. 6. Elution curves and plots of optical purity obtained for $[Co(ox)_2(gly)]^{2-}$ with Δ-$[Co(acac)(en)_2]^{2+}$ (----), Δ-$[Co(gly)(en)_2]^{2+}$ (——), and Δ-$[Co(en)_3]^{3+}$ (····) employed as chiral selectors.

to chiral discrimination, as discussed above. It is notable that $[Co(gly)(en)_2]^{2+}$ gives a greater retention volume V_R to C_1-*cis(N)*-$[Co(ox)(gly)_2]^-$ (C_3^-) than does $[Co(acac)(en)_2]^{2+}$ (C_2^+). This suggests that the C_3^+—C_3^- mode of $[Co(gly)(en)_2]^{2+}$ contributes appreciably to the overall interaction with the C_3^- anion complex.

Figure 6 shows the elution curves of $[Co(ox)_2(gly)]^{2-}$ obtained similarly with Δ-$[Co(en)_3]^{3+}$, Δ-$[Co(gly)(en)_2]^{2+}$, and Δ-$[Co(acac)(en)_2]^{2+}$ employed as a chiral selector. It is evident there that $[Co(gly)(en)_2]^{2+}$ is as effective as $[Co(acac)(en)_2]^{2+}$ in chiral discrimination of a typical (C_2^-+C_3^-) group anion, $[Co(ox)_2(gly)]^{2-}$, as expected. It is probably the difference in electric charge on the selectors that is responsible for generally lower optical resolution attained with $[Co(gly)(en)_2]^{2+}$ and $[Co(acac)(en)_2]^{2+}$ than with $[Co(en)_3]^{3+}$. The retention volumes V_R of $[Co(ox)_2(gly)]^{2-}$ obtained with these bivalent complexes are actually much smaller than that obtained with $[Co(en)_3]^{3+}$. By the same reason, univalent *cis*-$[Co(NO_2)_2(en)_2]^+$ does not serve as a good selector, though it uses the C_2 axis exclusively.

It is worthy of note here that some experimental results relevant to our present study have been reported. Miyoshi *et al.*[21] have found that Λ-*cis*-$[Co(X)(Y)(en)_2]^{n+}$-type complexes (X and/or Y=anion ligand) displace the chiral equilibrium of $[Cr(ox)_3]^{3-}$ in favor of its Δ enantiomer in dioxane-water mixtures. They have claimed that this phenomenon is successfully utilized to assign the absolute configuration to *cis*-$[M(X)(Y)(diamine)_2]^{n+}$-type complexes. Since these complexes are prototypes of the C_2^+ group cations, they should always favor a heterochiral combination, as is actually the case. Another experimental result to be noted is that the Δ enantiomer is enriched when

Table 4. Retention volumes V_R and separation factors α of $[Co(ox)_2(gly)]^{2-}$ obtained by HPLC

eluent	V_R/cm³		α
	Λ	Δ	
Δ-$[Co(sep)]Cl_3$	19.2	24.0	1.25
Δ-$[Co(l\text{-}chxn)_3]Cl_3$	15.2	11.9	1.28
Δ-$[Co(en)_3]Cl_3$	13.7[a]	14.3[a]	1.04

a) Determined by eluting resolved enantiomers separately.

a racemic mixture of tris(2,6-pyridinedicarboxylato)-terbium(III) is mixed with Λ-$[Cr(en)_3]^{3+}$ in dioxane-water mixtures.[22] Since the lanthanoid complex has an approximate D_3 symmetry and is regarded as the (C_2^-+C_3^-) group anion, all of the four interaction modes are possible. However, the contribution of the C_3^+—C_3^- mode is expected to be small because of the conformational lability of $[Cr(en)_3]^{3+}$. Consequently, the favorable pair should be heterochiral, as explained repeatedly.

Optical Resolution by HPLC. The above-mentioned discussions lead us to conclude that highly charged cation complexes which use the C_3 axis only and are conformationally rigid or which use the C_2 axis only, can recognize the chirality of anion complexes effectively, while those which use the two axes simultaneously do not in general serve as a good selector. However, the type (a) experiment is inherently not suitable for the practical resolution of anion complexes, since so-called ion-exclusion effect due to the negatively charged functional groups in the resin tends to diminish the chance of the anion complex to interact with the chiral cationic selector adsorbed in the resin.[23] In fact, very small retention volumes are obtained for all the anion complexes in the type (a) experiments. Then, we attempted to resolve $[Co(ox)_2(gly)]^{2-}$ by usual ion-exchange chromatography (type (b) experiment) with three cation complexes, Δ-$[Co(sep)]^{3+}$ (C_2^+), Δ-$[Co(l\text{-}chxn)_3]^{3+}$ (C_3^+), and Δ-$[Co(en)_3]^{3+}$ (C_2^++C_3^+) used as a chiral eluent. The retention volumes V_R and separation factors α obtained are given in Table 4.

The V_R values tell us that $[Co(en)_3]^{3+}$ and $[Co(chxn)_3]^{3+}$ which can use the C_3 axis bear a greater elution ability for $[Co(ox)_2(gly)]^{2-}$ than does $[Co(sep)]^{3+}$ which uses the C_2 axis only. That is, the C_3^+ access contributes to the overall interaction with the anion complex to a greater extent than the C_2^+ access. This seems to hold also for the interaction with C_1-*cis(N)*-$[Co(ox)(gly)_2]^-$ (Fig. 3) and $[Co(ox)_2(en)]^-$ (Fig. 2). On the other hand, a much higher α value is obtained with Δ-$[Co(sep)]^{3+}$ (α=1.25) which uses the C_2 axis only and with Δ-$[Co(l\text{-}chxn)_3]^{3+}$ (α=1.28) which uses the C_3 axis only than with Δ-$[Co(en)_3]^{3+}$ (α=1.04) which uses both of the C_3 and C_2 axes. This observation is in perfect agreement with what is predicted by our association models shown in Fig. 1. Tatehata *et*

al.,[2] nevertheless, succeeded in complete resolution of $[Co(ox)_2(gly)]^{2-}$ with chiral $[Co(en)_3]^{3+}$ employed as an eluent on a very long column (1300 mm long) of the DEAE-Sephadex A-25 resin and the α value is estimated to be *ca.* 1.08 from the elution curves. Therefore, if optically active $[Co(sep)]^{3+}$ or $[Co(chxn)_3]^{3+}$ is used in place of $[Co(en)_3]^{3+}$, much more efficient resolution of this anion complex should be achieved.

References

1) H. Yoneda, *J. Chromatogr.*, **313**, 59 (1984).

2) A. Tatehata, M. Iiyoshi, and K. Kotsuji, *J. Am. Chem. Soc.*, **103**, 7391 (1981).

3) U. Sakaguchi, I. Yamamoto, S. Izumoto, and H. Yoneda, *Bull. Chem. Soc. Jpn.*, **56**, 153 (1983).

4) U. Sakaguchi, A. Tsuge, and H. Yoneda, *Inorg. Chem.*, **22**, 1630, 3745 (1983).

5) M. Fujita, Y. Yoshikawa, and H. Yamatera, *Bull. Chem. Soc. Jpn.*, **50**, 3209 (1977).

6) M. Kojima, H. Takayanagi, and J. Fujita, *Bull. Chem. Soc. Jpn.*, **50**, 1891 (1977).

7) J. A. Hearson, S. F. Mason, and R. H. Seal, *J. Chem. Soc., Dalton Trans.*, **1977**, 1026.

8) N. Matsuoka, J. Hidaka, and Y. Shimura, *Bull. Chem. Soc. Jpn.*, **39**, 1257 (1966).

9) This complex was prepared by the same procedures as applied to the preparation of $[Co(gly)(Cl)(OH_2)(en)]Cl$ using β-ala in place of gly.

10) F. P. Dwyer, I. K. Reid, and A. M. Sargeson, *Aust. J. Chem.*, **18**, 1919 (1965).

11) N. Matsuoka, J. Hidaka, and Y. Shimura, *Bull. Chem. Soc. Jpn.*, **40**, 1868 (1967); *Inorg. Chem.*, **9**, 719 (1970).

12) J. H. Worrell, *Inorg. Chem.*, **10**, 870 (1971).

13) I. I. Creaser, J. MacB. Harrowfield, A. J. Herlt, A. M. Sargeson, J. Springborg, R. J. Geue, and M. R. Snow, *J. Am. Chem. Soc.*, **99**, 3181 (1977).

14) J. E. Sarneski and F. L. Urbach, *J. Am. Chem. Soc.*, **93**, 884 (1971); H. Okazaki, U. Sakaguchi, and H. Yoneda, *Inorg. Chem.*, **22**, 1539 (1983).

15) Y. Yoshikawa and K. Yamasaki, *Coord. Chem. Rev.*, **28**, 205 (1979).

16) K. Miyoshi, M. Natsubori, N. Dohmoto, S. Izumoto, and H. Yoneda, *Bull. Chem. Soc. Jpn.*, **58**, 1529 (1985).

17) A. Tatehata, Y. Ejima, and K. Kotsuji, 29th Symposium on Coordination Chemistry, Hamamatsu, October, 1979, Abstr. No. 1B01.

18) A. Tatehata, K. Andoh, M. Fujita, and Y. Asaba, 33rd Symposium on Coordination Chemistry, Osaka, October, 1983, Abstr. No. 1PA13.

19) A. Tatehata, H. Fukui, M. Iiyoshi, and K. Kotsuji, 37th National Meeting of the Chemical Society of Japan, Tokyo, April, 1978, Abstr. No. 4J14.

20) Several diastereomers are possible in each of these *N*-methylated complexes. In the present study, however, a racemic mixture of the most stable isomers is used; $\Lambda(R)$ (or $\Lambda(RR)$) and $\Delta(S)$ (or $\Delta(SS)$) isomers which have CH_3 group(s) parallel to the pseudo C_3 axes.

21) K. Miyoshi, Y. Matsumoto, and H. Yoneda, *Inorg. Chem.*, **20**, 1057 (1981); K. Miyoshi, K. Watanabe, Y. Toda, and H. Yoneda, *Bull. Chem. Soc. Jpn.*, **56**, 3845 (1983).

22) J. S. Madaras and H. G. Brittain, *Inorg. Chem.*, **19**, 3841 (1980); F. Yan, R. A. Copeland, and H. G. Brittain, *Inorg. Chem.*, **21**, 1180 (1982).

23) In this respect, the type (a) experiment should be applied to the resolution of electrically neutral complexes such as *mer*- and *fac*-$[Co(\beta\text{-ala})_3]$ (see, for example, S. Yamazaki and H. Yoneda, *Inorg. Nucl. Chem. Lett.*, **15**, 195 (1979) and T. Yukimoto and H. Yoneda, *J. Chromatogr.*, **210**, 477 (1981)). Chromatographic resolution of these neutral complexes is now in progress with chiral metal complexes employed as selectors, and the results will be reported soon as Part II of this series.

Preparation and Characterization of [Co(acetylacetonato)(diamine or 2,2′-bipyridyl)-(aminoalkylphosphine)]$^{2+}$. Crystal Structure of (+)$^{CD}_{531}$-*Λ*-*fac*(*N*)-(Acetylacetonato){(1*R*,2*R*)-1,2-cyclohexanediamine}{(2-aminoethyl)-diphenylphosphine}cobalt(III) Perchlorate, [Co($C_5H_7O_2$)-($C_6H_{14}N_2$)($C_{14}H_{16}NP$)](ClO_4)$_2$

Masakazu TAKATA, Kazuo KASHIWABARA, Haruko ITO,† Tasuku ITO,† and Junnosuke FUJITA*
Department of Chemistry, Faculty of Science, Nagoya University, Chikusa-ku, Nagoya 464
†*Department of Applied Molecular Science, Institute for Molecular Science, Myodaiji, Okazaki 444*
(Received March 28, 1985)

Nine new cobalt(III) complexes of the types, [Co(acac)(L)(edpp)]$^{2+}$ (L=ethylenediamine(en), (1*R*,2*R*)-1,2-cyclohexanediamine(*RR*-chxn), 2,2′-bipyridyl(bpy)), [Co(acac)(L′)(empp)]$^{2+}$ (L′=en, bpy), and structurally related [Co(acac)(bpy)(en)]$^{2+}$ were prepared and resolved into optical isomers, where acac, edpp, and empp denote an acetylacetonate ion, (2-aminoethyl)diphenylphosphine, and (2-aminoethyl)methylphenylphosphine, respectively. The molecular structure of (+)$^{CD}_{531}$-[Co(acac)(*RR*-chxn)(edpp)](ClO_4)$_2$ was determined by single-crystal X-ray analysis. Crystal data; monoclinic, $P2_1$, a=19.562(3)Å, b=16.882(1)Å, c=9.696(1)Å, β=91.22(1)°, V=3201.3(6)Å^3, Z=4. Three nitrogen donor atoms in the complex ion are arranged in the facial mannar (*fac*(*N*)) and the absolute configuration of the complex ion is *Λ*. The structures of other complexes were assigned by comparing the ^{1}H NMR and circular dichroism spectra with those of the *fac*(*N*)-*Λ*-[Co(acac)(*RR*-chxn)(edpp)]$^{2+}$ complex. The complexes containing a 1,2-diamine yielded selectively the *fac*(*N*) isomer, whereas those containing bpy the *mer*(*N*) isomer.

In our recent studies on cobalt(III)–tertiary phosphine complexes, we have often observed stereoselective formation of a particular geometrical isomer.[1–7] This seems to arise from the steric effect of bulky substituents on a phosphorus donor atom and/or the strong trans effect of a phosphine ligand. In this paper, we have extended the study to cobalt(III) phosphine complexes of the type, [Co(acac)(L)(L′)]$^{2+}$ (L= en, *RR*-chxn, bpy; L′=edpp, empp), where one of the two acac ligands in [Co(acac)$_2$(L′)]$^+$ [6,8] is replaced by the typical chelate ligand with nitrogen donor atoms L. The abbreviations used here are as follows; acac=acetylacetonate ion, en=ethylenediamine, *RR*-chxn=(1*R*,2*R*)-1,2-cyclohexanediamine, bpy=2,2′-bipyridyl, edpp=(2-aminoethyl)diphenylphosphine, empp=(2-aminoethyl)methylphenylphosphine.

Experimental

Phosphine ligands, edpp[9] and empp,[8]* were prepared according to the reported methods and handled under a nitrogen atmosphere until they formed cobalt(III) complexes. Absorption, circular dichroism (CD), and ^{1}H NMR spectra were recorded on a Hitachi 323 spectrophotometer, a Jasco J-40CS spectropolarimeter, and a Jeol JNM-PMX 60 spectrometer, respectively.

Preparation of the Complexes. fac(N)-*[Co(acac)(en)(edpp)]Br$_2$·2H$_2$O*: To a methanol solution (160 cm^3) of [Co(acac)(en)$_2$]Br$_2$[11] (2.5 g, 5.7 mmol) were added edpp (1.17 g, 5.1 mmol) in methanol (10 cm^3) and active charcoal (*ca.* 0.2 g). The solution was stirred at room temperature overnight and then filtered. The filtrate was diluted with water (2 dm^3, pH *ca.* 4 with HCl) and mixed with diethyl ether (500 cm^3) to extract free edpp into the ethereal layer. The aqueous layer was applied on a column (2.5×120 cm) of SP-Sephadex C-25. By elution with 0.2 mol dm^{-3} NaCl, three red bands containing [Co(acac)(en)$_2$]$^{2+}$, [Co(acac)(en)(edpp)]$^{2+}$, and [Co(acac)(edpp)$_2$]$^{2+}$ developed in this order. The second eluate containing [Co(acac)(en)(edpp)]$^{2+}$ was collected and concentrated to *ca.* 200 cm^3 under reduced pressure at 45 °C and mixed with an aqueous solution (30 cm^3) of NaB(C_6H_5)$_4$ (1 g) to give a red precipitate. The precipitate was filtered, washed with water, and then dissolved in a mixture of methanol (500 cm^3) and water (500 cm^3). The solution was applied on a column (2.5×10 cm) of Dowex 1×8 (Br^- form). The eluate was evaporated to dryness under reduced pressure, and the residue was crystallized from water. Yield: 420 mg (13%). Found: C, 39.07; H, 5.55; N, 6.85%. Calcd for $C_{21}H_{35}N_3O_4PBr_2Co$: C, 39.21; H, 5.48; N, 6.53%. The complex is soluble in water and methanol.

fac(N)-*Λ*-*[Co(acac)(RR-chxn)(edpp)](ClO_4)$_2$* *and* fac(N)-*Δ*-*[Co(acac)(RR-chxn)(edpp)](PF_6)$_2$·1.5H$_2$O*: A mixture of [Co(acac)$_3$][12] (5.0 g, 14 mmol), *RR*-chxn (3.2 g, 28 mmol), and active charcoal (*ca.* 0.2 g) in methanol (350 cm^3) was stirred at 25 °C overnight, and filtered. The filtrate was diluted with water (2 dm^3) and applied on a column (5×10 cm) of SP-Sephadex C-25. After red-violet [Co(acac)$_2$(*RR*-chxn)]$^+$ had been eluted from the column with 0.05 mol dm^{-3} NaCl, red [Co(acac)(*RR*-chxn)$_2$]$^{2+}$ was eluted with 0.2 mol dm^{-3} NaCl. The eluate was concentrated to *ca.* 150 cm^3 under reduced pressure at 45 °C. On addition of $NaClO_4$ (5 g) in water (50 cm^3) the concentrate gave a precipitate of a mixture of *Δ*- and *Λ*-[Co(acac)(*RR*-chxn)$_2$](ClO_4)$_2$, which was filtered, washed with a small amount of water, and air-dried. Yield: 5.4 g. A mixture of [Co(acac)(*RR*-chxn)$_2$](ClO_4)$_2$ (0.90 g, 1.5 mmol), edpp (0.35 g, 1.5 mmol), and active charcoal (*ca.* 0.1 g) in methanol (100 cm^3) was stirred overnight at room temperature. The resulting solution was filtered and subjected to column chromatography in the same way as for the en complex. By elution with 0.2 mol dm^{-3} NaCl, the starting complex, and the *Λ*-(FI) and *Δ*-(FII) isomers of the

*The notation of the absolute configurations, *R* and *S*, for the chiral phosphorus atom of a free ligand is reversed upon coordination to the cobalt(III) ion.[10] In this paper, we use the same notation for a coordinationg phosphine ligand as that when it is free.

desired complex were eluted separately in this order. The eluate containing FI was diluted ten times with water, applied again on a column (1×10 cm) of SP-Sephadex C-25, and the adsorbed complex was eluted with 1 mol dm^{-3} $NaClO_4$. The eluate was saturated with $NaClO_4$, and the complex was extracted with chloroform. The chloroform was separated and evaporated to dryness. The residue was crystallized from a mixture of methanol and water (1:1). Yield (FI, *Λ*-isomer): 94 mg (9%). Found: C, 42.55; H, 5.21; N, 5.62%. Calcd for $C_{25}H_{37}N_3O_{10}PCl_2Co$: C, 42.87; H, 5.32; N, 6.00%.

The formation of the other isomer (FII(*Δ*)) was poor (*ca.* 1/3 of the *Λ*-isomer), so that the procedure was repeated several times. The combined eluate containing FII was concentrated to a small volume and mixed with excess $NaPF_6$ to yield a red precipitate, which was recrystallized from a mixture of methanol and water (1:1). Found: C, 36.49; H, 4.52; N, 5.32%. Calcd for $C_{25}H_{40}N_3O_{3.5}P_3F_{12}Co$: C, 36.69; H, 4.93; N, 5.13%. Both complexes FI and FII are soluble in water and methanol.

fac(N)-*Δ*(R),*Λ*(S)-*[Co(acac)(en)(empp)]*$Br_2 \cdot 2H_2O$ *and* fac(N)-*Δ*(S),*Λ*(R)-*[Co(acac)(en)(empp)]*$Br_2 \cdot 1.5H_2O$: These complexes were prepared from $[Co(acac)(en)_2]Br_2$ (0.48 g, 1.05 mmol) and rac-empp (0.18 g, 1.07 mmol) by a method analogous to that for $[Co(acac)(en)(edpp)]^{2+}$. By elution with 0.1 mol dm^{-3} Na_2SO_4, the starting complex, and the *Δ(R),Λ(S)*-(FI) and *Δ(S),Λ(R)*-(FII) isomers of the desired complex were eluted separately in this order. Each eluate containing the empp complex was evaporated to dryness under reduced pressure, and the complex was extracted with ethanol. The extract was applied on a column (1×5 cm) of Dowex 1×8 (Br^- form), and the effluent was evaporated to dryness. The residue was dissolved again in methanol (5 cm^3) and then mixed with diethyl ether (3 cm^3). The solution was stored in a refrigerator, yielding crystals of the complex. Yield: FI (*fac(N)-Δ(R),Λ(S)* isomer), 24 mg (4%); FII (*fac(N)-Δ(S),Λ(R)* isomer), 35 mg (6%). Found for FI: C, 33.26; H, 5.30; N, 7.22%. Calcd for $C_{16}H_{33}N_3O_4PBr_2Co$: C, 33.07; H, 5.72; N, 7.23%. Found for FII: C, 33.88; H, 5.40; N, 7.30%. Cacld for $C_{16}H_{32}N_3O_{3.5}PBr_2Co$: C, 33.59; H, 5.64; N, 7.34%. The complexes are soluble in water and methanol.

mer(N)-*[Co(acac)(bpy)(edpp)]*$(PF_6)_2$: An *N,N*-dimethylformamide solution (100 cm^3) containing $[Co(acac)(bpy)_2](ClO_4)_2$[13] (440 mg, 0.66 mmol) and edpp (153 mg, 0.67 mmol) was stirred at room temperature overnight. The resulting solution was diluted with 5% aqueous acetic acid (3 dm^3), and the free edpp ligand was extracted with diethyl ether (500 cm^3). The aqueous layer was applied on a column (2.5×50 cm) of SP-Sephadex C-25. By elution with 0.2 mol dm^{-3} NaCl, three reddish brown bands containing $[Co(acac)(bpy)_2]^{2+}$, $[Co(acac)(bpy)(edpp)]^{2+}$, and $[Co(acac)(edpp)_2]^{2+}$ were eluted successively. The eluate of the second band was collected and evaporated to *ca.* 50 cm^3 under reduced pressure. On addition of $NaPF_6$ the concentrate gave a reddish brown precipitate, which was filtered and recrystallized from acetone (5 cm^3) by adding water (3 cm^3). Yield: 80 mg (15%). Found: C, 41.96; H, 3.69; N, 5.19%. Calcd for $C_{29}H_{31}N_3O_2P_3F_{12}Co$: C, 41.79; H, 3.75; N, 5.19%. The complex is soluble in methanol and acetone, but hardly in water.

mer(N)-*Δ*(R),*Λ*(S)-*[Co(acac)(bpy)(empp)]*$(PF_6)_2$ *and* mer(N)-*Δ*(S),*Λ*(R)-*[Co(acac)(bpy)(empp)]*$(PF_6)_2 \cdot 1.5H_2O$: These complexes were prepared by a method similar to that for $[Co(acac)(bpy)(edpp)]^{2+}$ using $[Co(acac)(bpy)_2](ClO_4)_2$ (612 mg, 0.91 mmol) and empp (153 mg, 0.92 mmol). By SP-Sephadex C-25 column chromatography, the eluate containing a mixture of *Δ(R),Λ(S)*- and *Δ(S),Λ(R)*-isomers of *mer(N)*-$[Co(acac)(bpy)(empp)]^{2+}$ was obtained from the second band, the small first and large third bands containing $[Co(acac)(bpy)_2]^{2+}$ and $[Co(acac)(empp)_2]^{2+}$, respectively. The second eluate was diluted with water (1 dm^3) and applied again on a column (2×15 cm) of SE-Toyopearl.[14] The adsorbed band was separated into two (FI and FII in the elution order) by elution with 0.3 mol dm^{-3} NaBr. Each eluate was concentrated to *ca.* 50 cm^3 under reduced pressure, and then mixed with NH_4PF_6 (20 mg) to yield an orange precipitate, which was recrystallized from methanol and water (1:1). Yield: FI(*mer(N)-Δ(R), Λ(S)* isomer) 40 mg (6%). FII (*mer(N)-Δ(S), Λ(R)* isomer) 20 mg (3%). Found for FI: 37.28; H, 3.71; N, 5.43%. Calcd for $C_{24}H_{29}N_3O_2P_3F_{12}Co$: C, 37.37; H, 3.79; N, 5.45%. Found for FII: C, 35.91; H, 3.64; N, 5.32%. Calcd for $C_{24}H_{32}N_3O_{3.5}P_3F_{12}Co$: C, 36.11; H, 4.04; N, 5.26%. These complexes are soluble in water and common organic solvents such as alcohols, acetone, and chloroform.

[Co(acac)(bpy)(en)]$(PF_6)_2$: An aqueous solution containing $[Co(CO_3)_3]^{3-}$ was prepared from $KHCO_3$ (10 g, 100 mmol) and $CoCl_2 \cdot 6H_2O$ (3.5 g, 15 mmol) according to a literature method.[15] The solution was diluted with water (400 cm^3) and then mixed with a solution of bpy (1.8 g, 12 mmol) in methanol (50 cm^3). The solution was stirred at room temperature for 2 h, and then en·H_2CO_3[15] (1.7 g, 14 mmol) was added with stirring. After 30 min the solution was stirred at 50 °C for 30 min. The resulting red solution was diluted 100 times with water and applied on a column (5×15 cm) of SP-Sephadex C-25. By elution with 0.03 mol dm^{-3} NaCl, red fractions containing complexes with the +1 charge were collected and concentrated to *ca.* 100 cm^3 under reduced pressure. On addition of $NaBF_4$ (13 g) the concentrate yielded a light brown precipitate of $[Co(CO_3)(bpy)_2]BF_4$, which was filtered off. The filtrate was mixed with additional $NaBF_4$ (5 g), and the mixture was kept at 0 °C for a while, yielding a red precipitate of $[Co(CO_3)(bpy)(en)]BF_4$ (5.8 g). The precipitate was filtered and washed with a small amount of cold water. To an aqueous solution (50 cm^3) of $[Co(CO_3)(bpy)(en)]BF_4$ (0.8 g, 1.9 mmol) were added acetylacetone (0.5 cm^3) and acetic acid (0.3 cm^3). The mixture was stirred at 50 °C for 3 h and then filtered. The filtrate was diluted with water (1 dm^3) and applied on a column (2×50 cm) of SP-Sephadex C-25. The desired red complex was eluted from the column with 0.2 mol dm^{-3} NaCl. The eluate was concentrated to *ca.* 50 cm^3 under reduced pressure. The concentrate was mixed with NH_4PF_6 (50 mg) to yield a red precipitate, which was recrystallized from methanol and water (3:1). Yield: 165 mg (13%). Found: C, 30.70; H, 3.30; N, 8.47%. Calcd for $C_{19}H_{23}N_4O_2P_2F_{12}Co$: C, 30.74; H, 3.49; N, 8.43%. The complex is soluble in methanol, but hardly in water.

Optical Resolution of the Complexes. Optical resolution of the complexes was carried out by an SP-Sephadex C-25 column-chromatographic method using a column (2.5×120 cm) and 0.2 mol dm^{-3} $Na_2[Sb_2(d\text{-tartrate})_2]$ as an eluent.[16] For $[Co(acac)(bpy)(en)]^{2+}$ and isomers FI and FII of $[Co(acac)(bpy)(empp)]^{2+}$, the resolution was complete, while it was incomplete for $[Co(acac)(en)(edpp)]^{2+}$, $[Co(acac)(bpy)(edpp)]^{2+}$, and isomer FII of $[Co(acac)(en)(empp)]^{2+}$. However, the first several fractions of the band containing each of these three complexes showed a con-

stant $\Delta\varepsilon/\varepsilon$ value, and were subjected to CD measurements. No resolution was achieved for isomer FI of [Co(acac)(en)(empp)]$^{2+}$.

The eluate containing the resolved complex was diluted 20 times with water and applied on a column (0.7×5 cm) of SP-Sephadex C-25. After the column had been washed with water, the adsorbed complex was eluted with 1 mol dm^{-3} NaCl, and the effluent was used for CD measurements. The complex concentration in the effluent was determined by measuring the optical density of the first absorption band.

X-Ray Analysis. X-Ray analysis of $(+)^{CD}_{531}$-[Co(acac)(*RR*-chxn)(edpp)](ClO$_4$)$_2$ (FI) was performed. Crystal Data: monoclinic, $P2_1$, a=19.562(3) Å, b=16.882(1) Å, c=9.696(1) Å, β=91.22(1)°, V=3201.3(6) Å^3, Z=4, D_m=1.45 g cm^{-3}, D_c=1.45 g cm^{-3}, μ(Mo $K\alpha$)=0.832 mm^{-1}. A specimen with dimensions 0.50×0.45×0.45 mm^3 was used for the X-ray work. Diffraction data were collected on a Rigaku AFC-5 diffractometer with graphite monochromatized Mo $K\alpha$ radiation. Within the range $2\theta<60°$, 5053 independent reflections with $|F_o|\geq 3\sigma(|F_o|)$ were obtained. In order to determine the absolute configuration, intensity data for Bijvoet pair reflections were also collected up to 2θ=35°. The intensity data were corrected for Lorentz-polarization effects, and for absorption.

The calculations of the structure analysis were performed on a HITAC M-180 computer at the Computer Center of the Institute for Molecular Science with the Universal Crystallographic Computation Program System UNICS III.[17] The structure was solved by the direct method (MULTAN). The positions of all the hydrogen atoms were identified in subsequent difference-Fourier maps. The structure was refined by a block-diagonal least-squares method with anisotropic thermal parameters for non-hydrogen atoms and isotropic for hydrogens. The weighting scheme, $w=[\sigma^2_{count}+(0.015|F_o|)^2]^{-1}$, was employed. At the final stage, refinements were carried out on two enantiomeric models, $\Lambda(R,R)$ and $\Lambda(S,S)$, using 6577 intensities including the Bijvoet pair reflections. The R and R_w values were reduced to 0.052 and 0.065, respectively, for the $\Lambda(R,R)$ configuration, whereas the values were 0.060 and 0.074 for the $\Lambda(S,S)$ model, respectively. Thus application of the R-factor ratio test[18] showed that the $\Lambda(S,S)$ model can be rejected at the 99.5% confidence level. This result is consistent with the fact that *RR*-chxn was used for the preparation of the complex.

Table 1 lists the atomic parameters for non-hydrogen atoms. Complete lists of observed and calculated structure factors, hydrogen atomic parameters, and thermal parameters for non-hydrogen atoms are preserved by the Chemical Society of Japan (Document No. 8539).

Results and Discussion

In general, it is difficult to prepare octahedral complexes comprising of three different kinds of bidentate ligands in good yield.[16,19] The [Co(acac)(en)(edpp)]$^{2+}$ complex was obtained in a 13% yield by reaction of [Co(acac)(en)$_2$]$^{2+}$ with edpp in methanol in the presence of active charcoal. The complex was also obtained by a similar reaction between [Co(acac)$_2$(en)]$^+$ and edpp in a yield of less than 10%. However, no desired complex was formed by reaction of

Table 1. Atomic parameters of Λ-*fac(N)*-[Co(acac)(*RR*-chxn)(edpp)](ClO$_4$)$_2$. positional parameters are multiplied by 10^5 and thermal parameters are given by the equivalent temperature factors (Å^2)

Atom	x	y	z	B_{eq}
Co(1)	11337(4)	0(6)	53278(8)	3.6
P(1)	18895(10)	−7307(11)	65140(18)	4.1
N(1)	4679(28)	6878(31)	42367(50)	4.1
N(2)	3809(27)	−1224(31)	66428(47)	3.9
N(3)	15258(30)	9215(33)	63600(51)	4.6
O(1)	7463(22)	−8876(25)	44141(39)	4.0
O(2)	18174(23)	1970(25)	40163(43)	4.5
C(1)	−2267(35)	5150(38)	47683(65)	4.0
C(2)	−1715(36)	4792(36)	62779(65)	4.1
C(3)	−8275(43)	3021(44)	70134(74)	5.5
C(4)	−13612(40)	9202(50)	65306(98)	6.6
C(5)	−14359(45)	9172(54)	49246(104)	7.3
C(6)	−7633(40)	11132(41)	42677(79)	5.3
C(7)	8891(38)	−10660(39)	31467(63)	4.4
C(8)	13923(41)	−7050(43)	23726(64)	5.0
C(9)	18376(37)	−1428(41)	28210(65)	4.6
C(10)	4213(51)	−16868(59)	25111(78)	7.4
C(11)	24227(45)	1174(59)	19384(77)	6.8
C(12)	22606(46)	7966(49)	68042(89)	6.7
C(13)	23086(41)	238(51)	76205(87)	6.6
C(14)	16066(39)	−14966(39)	77259(67)	4.5
C(15)	10050(37)	−18874(41)	74613(65)	4.6
C(16)	7686(46)	−24618(46)	83954(73)	5.8
C(17)	11857(45)	−26535(43)	95103(65)	5.6
C(18)	17969(41)	−22478(51)	97233(68)	5.9
C(19)	20033(39)	−16791(44)	88455(65)	4.9
C(20)	25060(39)	−12127(47)	54871(72)	5.3
C(21)	31300(47)	−8608(61)	52285(108)	8.1
C(22)	35846(53)	−12781(89)	42317(122)	11.3
C(23)	34009(55)	−19966(77)	37312(94)	9.2
C(24)	27989(57)	−23397(70)	39975(93)	8.9
C(25)	23436(48)	−19351(54)	48720(82)	7.1
Co(2)	61671(5)	−19423(5)	93969(8)	3.6
P(2)	68874(10)	−11961(11)	81994(18)	4.2
N(4)	55249(29)	−26472(30)	104676(48)	4.0
N(5)	53647(27)	−17839(29)	81572(44)	3.7
N(6)	64996(31)	−28459(32)	83036(54)	4.6
O(3)	58277(24)	−10804(26)	103960(39)	4.4
O(4)	69023(23)	−21807(26)	106056(43)	4.6
C(26)	48280(33)	−24716(40)	99896(62)	3.8
C(27)	48532(35)	−24022(38)	84650(61)	4.0
C(28)	41339(36)	−2211(45)	77983(70)	4.9
C(29)	36379(44)	−28281(53)	82793(92)	6.7
C(30)	35980(40)	−28746(53)	97813(84)	6.2
C(31)	43062(40)	−30879(50)	103974(75)	5.7
C(32)	60264(39)	−9093(41)	116501(69)	4.9
C(33)	65883(43)	−12205(45)	123000(67)	5.5
C(34)	70168(37)	−18120(43)	117525(68)	4.9
C(35)	56017(59)	−2727(58)	123328(85)	8.6
C(36)	76599(46)	−20717(57)	124989(95)	7.7
C(37)	72134(44)	−27211(48)	77758(79)	6.0
C(38)	72233(41)	−19135(49)	70362(80)	5.9
C(39)	65568(35)	−3859(39)	71517(65)	4.2
C(40)	59575(36)	21(43)	74663(64)	4.7
C(41)	57253(42)	6084(46)	66515(69)	5.2
C(42)	60911(45)	8411(48)	55153(88)	6.4
C(43)	66986(44)	4692(51)	51710(76)	6.1
C(44)	69471(36)	−1627(48)	59953(72)	5.1
C(45)	75846(40)	−7704(50)	91984(81)	5.8
C(46)	82083(45)	−11725(66)	93507(96)	7.7
C(47)	87457(52)	−8184(78)	101676(119)	9.9
C(48)	86146(66)	−1415(97)	108233(115)	11.9

TABLE 1. (Continued)

Atom	x	y	z	B_{eq}
C(49)	80149(69)	2832(68)	106904(107)	10.4
C(50)	74742(57)	−284(60)	98728(87)	8.3
CL(1)	90564(9)	−21127(11)	54618(21)	5.3
CL(2)	59853(9)	−48456(13)	2741(24)	6.3
CL(3)	56553(13)	−26520(18)	46145(20)	7.9
CL(4)	93010(13)	−39501(18)	7(21)	8.1
O(7)	85498(36)	−26661(40)	56674(87)	10.0
O(8)	95948(51)	−25490(49)	49365(129)	14.7
O(9)	88440(47)	−14655(40)	47306(105)	13.1
O(10)	92984(65)	−18032(59)	67305(114)	17.7
O(11)	64845(41)	−42649(47)	4688(90)	11.0
O(12)	62964(53)	−55137(41)	131(118)	13.8
O(13)	54577(52)	−50131(86)	9874(115)	17.4
O(14)	56988(77)	−44388(70)	−7565(154)	21.3
O(15)	57313(38)	−18717(46)	51665(55)	9.6
O(16)	52032(45)	−26082(72)	35010(69)	13.2
O(17)	62494(50)	−28967(54)	40037(106)	13.8
O(18)	53895(47)	−31531(52)	56733(69)	11.5
O(19)	90841(56)	−46236(85)	6047(71)	18.4
O(20)	97053(60)	−41106(74)	−10267(78)	15.7
O(21)	87525(65)	−36405(95)	−5666(179)	22.9
O(22)	96545(72)	−35055(76)	9701(78)	17.1

$[Co(acac)_2(edpp)]^+$ and en. Other edpp and empp complexes were prepared by methods analogous to that for $[Co(acac)(en)(edpp)]^{2+}$ from $[Co(acac)(diamine\ or\ bpy)_2]^{2+}$ and the phosphine ligand. The $[Co(acac)(bpy)_2]^{2+}$ complex reacted with the phosphine ligand in the absence of active charcoal to give [Co(acac)(bpy)(phosphine)]$^{2+}$, while the corresponding bis(diamine) complexes did not react under the same conditions.

There are two possible geometrical isomers, *fac(N)* and *mer(N)*, for $[Co(acac)(N\text{-}N)(N\text{-}P)]^{2+}$, where N-N and N-P represent diamine or bpy and aminoalkylphosphine chelate ligands, respectively (Fig. 1). Each of the geometrical isomers has a pair of enantiomers, *Δ* and *Λ*, when all the chelate ligands are achiral, and can have a pair of diastereomers, *Δ(R)(Λ(S))* and *Λ(R)(Δ(S))*, when a chiral ligand is contained. Both [Co(acac)(en)(edpp)]$^{2+}$ and [Co(acac)(bpy)(edpp)]$^{2+}$ formed only one of the two possible geometrical isomers as evidenced by column chromatography. The same isomer of [Co(acac)(en)(edpp)]$^{2+}$ was also yielded selectively by the reaction of edpp with $[Co(acac)_2(en)]^+$ in place of $[Co(acac)(en)_2]^{2+}$. Each of [Co(acac)(*RR*-chxn)(edpp)]$^{2+}$, [Co(acac)(en)(empp)]$^{2+}$, and [Co(acac)(bpy)(empp)]$^{2+}$ yielded two isomers. However, the isomers were a pair of diastereomers with the same geometrical configuration, *fac(N)* or *mer(N)*. (*vide infra*) Thus the [Co(acac)(N-N)(N-P)]$^{2+}$-type complex forms selectively only one of two possible geometrical isomers.

In order to assign geometrical structures of the complexes, a crystal of $(+)_{531}^{CD}$-[Co(acac)(*RR*-chxn)(edpp)]$(ClO_4)_2$ (FI) was subjected to X-ray analysis. There are two crystallographically independent but chemically equivalent complex ions (**1** and **2**). Figure 2 shows a stereoview of complex **1** and the numbering scheme of the atoms. The complex ion has three nitrogen donor atoms arranged in a facial manner and is assigned as the *fac(N)* isomer shown in Fig. 1. The absolute configuration of the complex ion is *Λ*. The selected bond distances and angles for complex **1** are listed in Table 2. The Co(1)-P distance of 2.224(3) Å (Co(2)-P: 2.234(3) Å) is slightly shorter than those found in *trans(Cl,Cl),cis(P,P)*-$[CoCl_2(edpp)_2][CoCl_4]$ (2.255(3) Å)[4], *trans(NCS,NCS),cis(P,P)*$[Co(NCS)_2(edpp)_2]Br\cdot 3H_2O\cdot(CH_3)_2CO$ (2.270 Å)[20], and *cis(NCS,NCS), trans-*

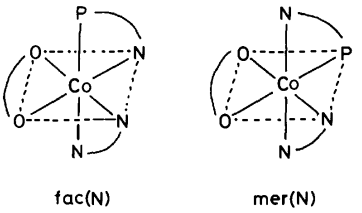

Fig. 1. Geometrical isomers of $[Co(acac)(N\text{-}N)(N\text{-}P)]^{2+}$.

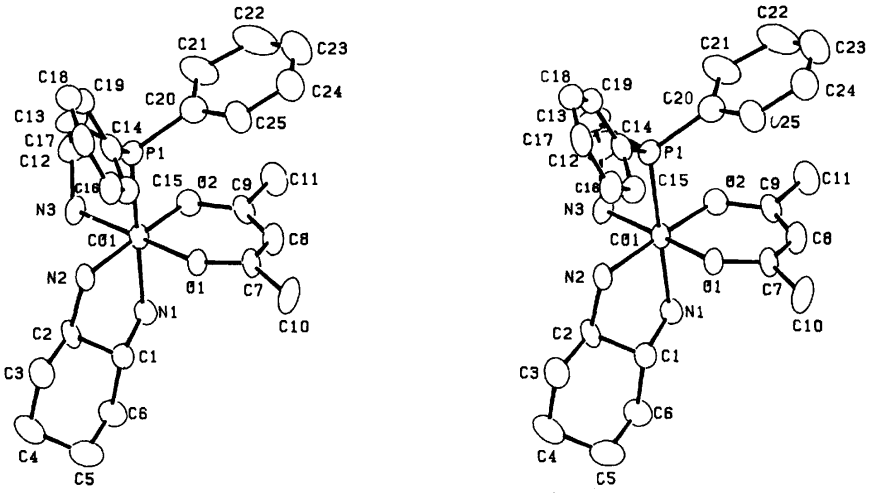

Fig. 2. A stereoview for complex **1**.

Table 2. Selected bond distances (l/Å) and angles (ϕ/°) for complex **1**

Co(1)-P(1)	2.224(3)	N(1)-C(1)	1.521(14)
Co(1)-N(1)	1.975(8)	N(2)-C(2)	1.487(14)
Co(1)-N(2)	2.037(8)	N(3)-C(12)	1.532(16)
Co(1)-N(3)	1.998(9)	O(1)-C(7)	1.299(11)
Co(1)-O(1)	1.899(7)	O(2)-C(9)	1.295(12)
Co(1)-O(2)	1.886(7)	C(1)-C(2)	1.492(14)
P(1)-C(13)	1.855(13)	C(7)-C(8)	1.385(16)
P(1)-C(14)	1.848(12)	C(8)-C(9)	1.325(16)
P(1)-C(20)	1.778(13)	C(12)-C(13)	1.569(18)
P(1)-Co(1)-N(1)	95.6(3)	Co(1)-P(1)-C(13)	102.0(4)
P(1)-Co(1)-N(2)	178.7(3)	Co(1)-P(1)-C(14)	120.5(4)
P(1)-Co(1)-N(3)	86.6(3)	Co(1)-P(1)-C(20)	114.0(4)
P(1)-Co(1)-O(1)	93.1(2)	C(13)-P(1)-C(14)	105.4(5)
P(1)-Co(1)-O(2)	88.8(2)	C(13)-P(1)-C(20)	108.9(6)
N(1)-Co(1)-N(2)	85.7(3)	C(14)-P(1)-C(20)	105.3(6)
N(1)-Co(1)-N(3)	92.9(3)	Co(1)-N(1)-C(1)	108.0(6)
N(1)-Co(1)-O(1)	85.5(3)	Co(1)-N(2)-C(2)	106.0(6)
N(1)-Co(1)-O(2)	175.5(3)	Co(1)-N(3)-C(12)	112.7(7)
N(2)-Co(1)-N(3)	93.1(4)	Co(1)-O(1)-C(7)	121.8(7)
N(2)-Co(1)-O(1)	87.3(3)	Co(1)-O(2)-C(9)	124.8(7)
N(2)-Co(1)-O(2)	90.0(3)	N(1)-C(1)-C(2)	106.2(8)
N(3)-Co(1)-O(1)	178.3(3)	N(2)-C(2)-C(1)	107.3(8)
N(3)-Co(1)-O(2)	86.1(3)	N(3)-C(12)-C(13)	107.3(10)
O(1)-Co(1)-O(2)	95.6(3)	O(1)-C(7)-C(8)	124.8(10)
		O(2)-C(9)-C(8)	123.5(10)
		P(1)-C(13)-C(12)	105.0(8)

(*P*,*P*)-[Co(NCS)$_2$(edpp)$_2$]Br · CH$_3$OH (2.269Å).[20] The Co(1)-N(2) distance is longer by *ca.* 0.05Å than the mean of Co(1)-N(1) and Co(1)-N(3) distances, indicating trans influence of the P donor atom. Elongations of Co-N bonds due to trans influence of a phosphine ligand have been observed in the above trans-dianiono complexes, and *fac*-[Co{NH$_2$CH$_2$CH$_2$P(CH$_3$)$_2$}$_3$]$^{3+}$[7] and related complexes.[1,3,21] Bond angles around P deviate fairly largely from the tetrahedral angle. In particular, the widening of Co(1)-P(1)-C(14) (120.5(4)Å) is noticeable. This widening may be caused by the steric interaction between the phenyl group containing C(14) and the hydrogen atom(s) on N(1) of *RR*-chxn. The other phenyl group is disposed over the acac ring. (Fig. 3) The angle between the best planes of chelate Co-acac and phenyl rings is 25.6(3)°. The maximum deviations from the best planes of Co-acac and phenyl rings are 0.152Å and 0.04Å, respectively. The distance from C(20) to the best plane of the Co-acac ring is 3.062(8)Å. As shown later, such a stacking structure of the phenyl and acac rings causes a high-field shift of the methine proton signal of acac in ^{1}H NMR spectra. The chelate ring formed by *RR*-chxn takes a typical λ gauche conformation, whereas that formed by edpp an envelope conformation.

Table 3 lists ^{1}H NMR data of the complexes. The *fac(N)*-*Λ*-[Co(acac)(*RR*-chxn)(edpp)]$^{2+}$ isomer (FI) whose structure has been determined shows the methine proton signal of acac at a remarkably high field (5.00 ppm). The high-field shift is attributable to the shielding effect of the phenyl ring disposed over the acac ring.[8] The [Co(acac)(en)$_2$]$^{2+}$ and [Co(acac)$_2$(edmp)]$^+$ (edmp=NH$_2$CH$_2$CH$_2$P(CH$_3$)$_2$) complexes give the corresponding signals at 5.78 ppm,[22] and 5.34 and 5.51 ppm,[8] respectively. The other isomer FII of [Co(acac)(*RR*-chxn)(edpp)]$^{2+}$ also exhibits the methine proton signal at a high field (5.16 ppm) and can be assigned to the same *fac(N)* isomer (*Δ*-isomer). Thus [Co(acac)(*RR*-chxn)(edpp)]$^{2+}$ yields selectively the *fac(N)* geometrical isomer. In the corresponding *mer(N)* isomer, one of the two phenyl groups on P is to be placed above the puckered *RR*-chxn ring. Molecular models show that the *mer(N)* structure brings about a large steric interaction between the phenyl group and the axial hydrogen atoms on nitrogen and carbon atoms of *RR*-chxn. The interaction will render the *mer(N)* isomer unstable.

The methine protons of [Co(acac)(en)(edpp)]$^{2+}$ and isomer FII of [Co(acac)(en)(empp)]$^{2+}$ resonate at a high field, and both complexes are assigned as the *fac(N)* isomer. For *fac(N)*-[Co(acac)(en)(empp)]$^{2+}$, two racemic pairs of diastereomers, *Δ*(*R*),*Λ*(*S*) and *Δ*(*S*),*Λ*(*R*), are possible. (Fig. 4) The former and the latter diastereomers have the phenyl and the methyl groups of empp, respectively over the acac ring. Thus isomer FII of [Co(acac)(en)(empp)]$^{2+}$ is assigned to the racemic pair of *fac(N)*-*Δ*(*R*),*Λ*(*S*) from a high-field shift of the methine proton signal. The other isomer FI of [Co(acac)(en)(empp)]$^{2+}$ shows the methine proton signal at a low field (5.81 ppm), but exhibits the

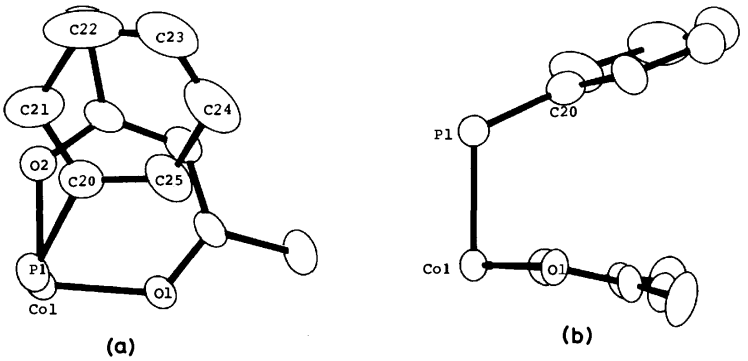

Fig. 3. A stucking structure of the Co-acac and phenyl rings of complex **1**.

TABLE 3. ^{1}H NMR AND ABSORPTION SPECTRAL DATA

Complex	^{1}H NMR[a] (acac)				Absorption[b]	Assignment
	$-CH_3$		=CH-	Solvent		
[Co(acac)(*RR*-chxn)(edpp)]$^{2+}$(FI)	1.69	2.05	5.00	$CDCl_3$	19.9(2.84)	*fac(N)-Δ(RR)*
[Co(acac)(*RR*-chxn)(edpp)]$^{2+}$(FII)	1.67	2.11	5.16	$CDCl_3$	19.9(2.84)	*fac(N)-Δ(RR)*
[Co(acac)(en)(edpp)]$^{2+}$	1.80	2.14	5.14	D_2O	20.0(2.79)	*fac(N)*
[Co(acac)(en)(empp)]$^{2+}$(FI)	2.10	2.13	5.81	CD_3OD	20.8(2.63)	*fac(N)-Δ(R),Λ(S)*
[Co(acac)(en)(empp)]$^{2+}$(FII)	1.67	1.84	4.89	CD_3OD	20.6(2.79)	*fac(N)-Δ(S),Λ(R)*
[Co(acac)(en)$_2$]$^{2+}$	2.17		5.78	D_2O	20.0(2.14)	
[Co(acac)(bpy)(edpp)]$^{2+}$	2.12	2.40	5.99	D_2O	20.9(2.88)	*mer(N)*
[Co(acac)(bpy)(empp)]$^{2+}$(FI)	2.16	2.43	6.03	D_2O	21.5(2.62)	*mer(N)-Δ(R),Λ(S)*
[Co(acac)(bpy)(empp)]$^{2+}$(FII)	2.06	2.21	6.19	D_2O	21.5(2.64)	*mer(N)-Δ(S),Λ(R)*
[Co(acac)(bpy)(en)]$^{2+}$	1.92	2.47	5.83	CD_3OD	19.9(2.23)	

a) δ/ppm from TMS. b) First absorption band peak, $\tilde{\nu}/10^3$cm^{-1}(log ε), solvent: CH_3OH for the bpy complexes and H_2O for the other complexes.

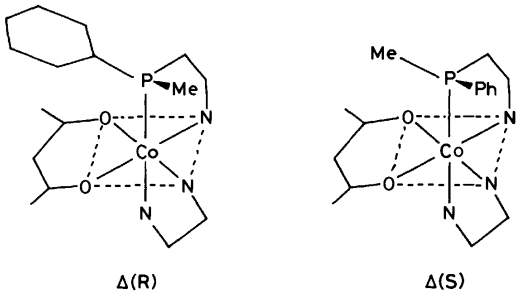

Fig. 4. Diastereomers of *fac(N)*-[Co(acac)(en)(empp)]$^{2+}$.

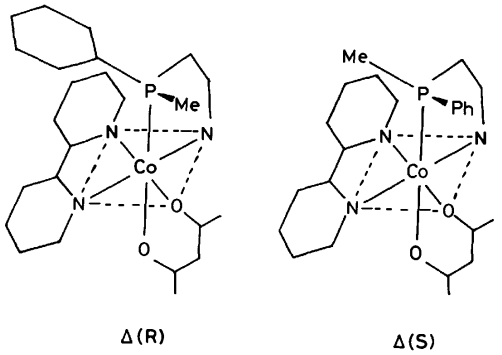

Fig. 5. Diastereomers of *mer(N)*-[Co(acac)(bpy)(empp)]$^{2+}$.

P-CH_3 proton signal at a remarkably high field (1.77 ppm) compared with that of the isomer FII (2.17 ppm). The high-field shift will be attributable to the shielding effect of the pseudo aromatic acac ring. Thus isomer FI can be assigned as the racemic pair of *fac(N)-Δ(S),Λ(R)*. The assignment is supported by absorption spectra of these two isomers. The first absorption band of isomer FI is at a higher energy and smaller in intensity (20800 cm^{-1}, log ε=2.63) than that of isomer FII (20600 cm^{-1}, log ε=2.79), although the spectral patterns are very similar. A similar spectral relation has been observed between the two analogous diastereomers, *Δ(R),Λ(S)* (19700 cm^{-1}, log ε=2.40) and *Δ(S),Λ(R)* (19500 cm^{-1}, log ε=2.62) of [Co(acac)$_2$(empp)]$^+$,[8] the first absorption band of the isomer having the phenyl group disposed over the acac ring being more intense and at lower energy than that of the other isomer. Thus [Co(acac)(en)(empp)]$^{2+}$ also forms selectively the *fac(N)* geometrical isomer (*Δ(R),Λ(S)* (FII), *Δ(S),Λ(R)* (FI)).

All of the bpy complexes, [Co(acac)(bpy)(edpp)]$^{2+}$ and isomers FI and FII of [Co(acac)(bpy)(empp)]$^{2+}$ exhibits the methine proton signal of acac at a low field (5.99—6.19 ppm). The results suggest that the complexes are the *mer(N)* geometrical isomer. When [Co(acac)(bpy)(empp)]$^{2+}$ has the *mer(N)* structure, two racemic pairs of the diastereomers, *Δ(R),Λ(S)* and *Δ(S),Λ(R)* have the phenyl and the methyl groups of empp, respectively over the aromatic bpy ring (Fig. 5). In ^{1}H NMR spectra, isomer FII gives the P-CH_3 proton signal at a remarkably high field (1.20 ppm) compared with that of isomer FI (2.02 ppm). The high-field shift is attributable to the aromatic bpy ring and is more remarkable than that observed for the P-CH_3 protons in *fac(N)*-[Co(acac)(en)(empp)]$^{2+}$ (1.77 and 2.17 ppm), in which the P-CH_3 group is shielded by the pseudo aromatic acac ring. Thus isomer FII of [Co(acac)(bpy)(empp)]$^{2+}$ can be assigned as the racemic pair of *mer(N)-Δ(S),Λ(R)*. As described above, neither P-CH_3 nor acac-CH_3 proton signal of isomer FI shows a high-field shift, and thus the isomer is assigned as the racemic pair of *mer(N)-Δ(R),Λ(S)*. When the bpy complexes take a *fac(N)* structure, a steric interaction arises between the substituent on P and H on C(3) of bpy. The selective formation of the *mer(N)*-bpy complexes, in contrast to the corresponding *fac(N)*-diamine complexes, will be attributable to this steric interaction in the *fac(N)* structure.

Figure 6 shows absorption and CD spectra of isomers FI and FII of [Co(acac)(*RR*-chxn)(edpp)]$^{2+}$. While the absorption spectra are similar, the CD spectra are nearly enantiomeric to each other. Since isomer FI has been determined to have the *Λ* configuration by X-ray analysis, isomer FII is assigned as the *Δ* isomer. The configurational effect(*Λ*) curve estimated by 1/2[$\Delta\varepsilon(\Lambda)-\Delta\varepsilon(\Delta)$][23] is very similar to the CD spectrum of [Co(acac)(en)(edpp)]$^{2+}$ which was obtained

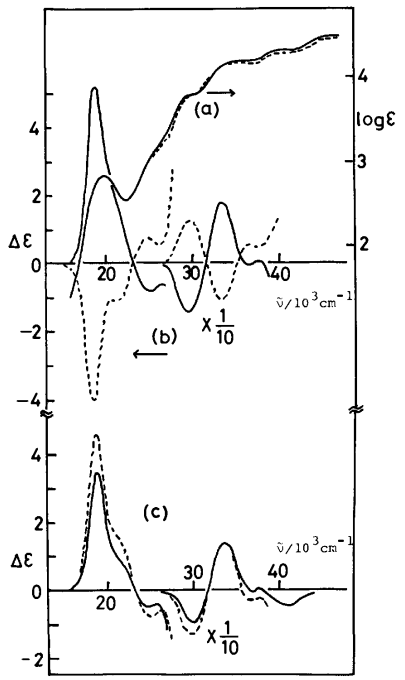

Fig. 6. Absorption (a) and CD (b) spectra of FI (——) and FII (----) isomers of [Co(acac)(*RR*-chxn)(edpp)]$^{2+}$, and the configurational effect (*Λ*) curve estimated by 1/2[Δε(*Λ*)−Δε(*Δ*)] (----) and the CD spectrum of [Co(acac)(en)(edpp)]$^{2+}$ (——) in (c).

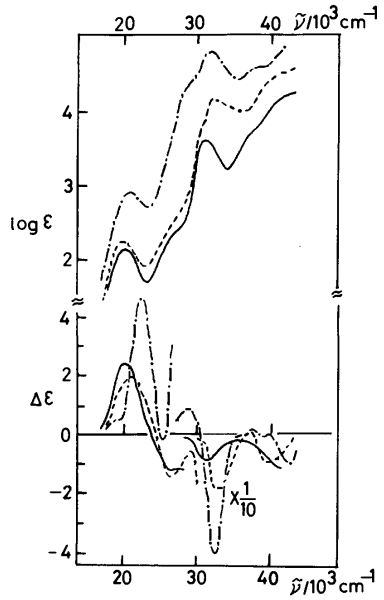

Fig. 7. Absorption and CD spectra of *Λ*-[Co(acac)(en)$_2$]$^{2+}$ (——), [Co(acac)(bpy)(en)]$^{2+}$ (----), and [Co(acac)(bpy)(edpp)]$^{2+}$ (-·-·-).

from the first fraction in SP-Sephadex C-25 column chromatography (see Experimental) (Fig. 6(c)). Thus the en complex given in Fig. 6(c) is assigned to have the *Λ* configuration. In Fig. 7 are compared the absorption and CD spectra of *Λ*-[Co(acac)(en)$_2$]$^{2+}$[24] with those of [Co(acac)(bpy)(en)]$^{2+}$ and [Co(acac)(bpy)(edpp)]$^{2+}$, both bpy complexes being the faster-moving enantiomer in similar SP-Sephadex C-25 column chromatography. Although the absorption intensity and CD strength of the edpp complex are larger than those of the other complexes over nearly the whole spectral region, the spectral patterns are similar among the three complexes. Thus [Co(acac)(bpy)(en)]$^{2+}$ and [Co(acac)(bpy)(edpp)]$^{2+}$ given in Fig. 7 will have the same absolute configuration as *Λ*-[Co(acac)(en)$_2$]$^{2+}$.

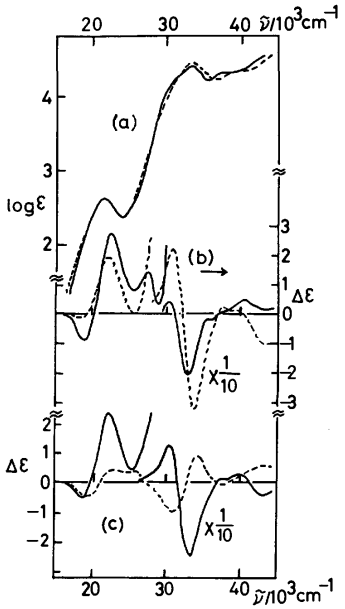

Fig. 8. Absorption (a) and CD (b) spectra of FI (——) and FII (----) isomers of [Co(acac)(bpy)(empp)]$^{2+}$, and the configurational (——) and vicinal (----) effect curves estimated by 1/2[Δε(FI)+Δε(FII)] and 1/2[Δε(FI)−Δε(FII)], respectively, in (c).

Figure 8 shows absorption and CD spectra of isomers FI and FII of [Co(acac)(bpy)(empp)]$^{2+}$. Both isomers were resolved by SP-Sephadex C-25 column chromatography, and the optically active isomers given in Fig. 8 are those eluted faster in chromatography (see Experimental). Both CD spectral patterns (Fig. 8(b)) are similar, and the isomers will have the same absolute configuration for the arrangement of the chelate rings around Co(III). In Fig. 8(c) are given the configurational and vicinal effect curves estimated by 1/2[Δε(FI)+Δε(FII)] and 1/2[Δε(FI)−Δε(FII)], respectively. The configurational effect curve is similar to the CD spectrum of *Λ*-[Co(acac)(bpy)(edpp)]$^{2+}$ in Fig. 7, indicating the same *Λ* configuration for both optical isomers of FI and FII. Since isomers FI and FII of [Co(acac)(bpy)(empp)]$^{2+}$ have been assigned to racemic pairs, *Δ*(*R*),*Λ*(*S*) and *Δ*(*S*),*Λ*(*R*), respectively, on the basis of the ^{1}H NMR spectra, the optical isomers given in Fig. 8 are assigned to have the *Λ*(*S*)(FI) and *Λ*(*R*)(FII) configurations. Accordingly, the vicinal effect curve should be of the (*S*)-empp ligand. The curve is fairly different from those of an analogous (*S*)-$NH_2CH_2CH_2P(C_4H_9)(C_6H_5)$ (ebpp) ligand estimated from CD spectra of [Co(acac)$_2$(ebpp)]$^{+}$[8] and [Co(en)$_2$(ebpp)]$^{3+}$.[7] In order to relate the absolute configura-

tion of chiral phosphorus donor atoms to CD spectra, more CD data of chiral phosphine complexes will be needed.

The authors wish to thank the Ministry of Education for Scientific Research Grant-in-Aid No. 58470032.

References

1) T. Ohishi, S. Ohba, K. Kashiwabara, Y. Saito, and J. Fujita, *Bull. Chem. Soc. Jpn.*, **57**, 877 (1984).
2) T. Ohishi, K. Kashiwabara, and J. Fujita, *Bull. Chem. Soc. Jpn.*, **56**, 1553 (1983).
3) T. Ohishi, K. Kashiwabara, H. Ito, T. Ito, and J. Fujita, *Bull. Chem. Soc. Jpn.*, **56**, 1551 (1983).
4) I. Kinoshita, Y. Yokota, K. Matsumoto, S. Ooi, K. Kashiwabara, and J. Fujita, *Bull. Chem. Soc. Jpn.*, **56**, 1067 (1983).
5) M. Atoh, I. Kinoshita, K. Kashiwabara, and J. Fujita, *Bull. Chem. Soc. Jpn.*, **55**, 3179 (1982).
6) K. Kashiwabara, K. Katoh, T. Ohishi, J. Fujita, and M. Shibata, *Bull. Chem. Soc. Jpn.*, **55**, 149 (1982).
7) I. Kinoshita, K. Kashiwabara, J. Fujita, K. Matsumoto, and S. Ooi, *Bull. Chem. Soc. Jpn.*, **54**, 2683 (1981).
8) K. Kashiwabara, I. Kinoshita, T. Ito, and J. Fujita, *Bull. Chem. Soc. Jpn.*, **54**, 725 (1981).
9) K. Issleib and D. Haferberg, *Z. Naturforsch., Teil B*, **20**, 916 (1965).
10) R. S. Cahn, C. K. Ingold, and V. Prelog, *Angew. Chem., Int. Ed. Engl.*, **5**, 385 (1966).
11) Inorg. Synth., Vol. IX, p. 167. The iodide in the literature was converted to the bromide using Dowex 1X8 (Br^- form).
12) Inorg. Synth., Vol. V, p. 188.
13) K. Kashiwabara, K. Igi, and B. E. Douglas, *Bull. Chem. Soc. Jpn.*, **49**, 1573 (1976).
14) M. Fujita, Y. Yoshikawa, and H. Yamatera, *Chem. Lett.*, **1982**, 432.
15) M. Shibata, *Nippon Kagaku Kaishi*, **87**, 771 (1966).
16) T. Ohishi, K. Kashiwabara, and J. Fujita, *Bull. Chem. Soc. Jpn.*, **56**, 3441 (1983).
17) T. Sakurai and K. Kobayashi, *Rikagaku Kenkyusho Hokoku*, **55**, 69 (1978).
18) W. C. Hamilton, *Acta Crystallogr.*, **18**, 502 (1965).
19) M. Kojima, H. Yamada, H. Ogino, and J. Fujita, *Bull. Chem. Soc. Jpn.*, **50**, 2325 (1977).
20) M. Atoh, K. Kashiwabara, H. Ito, T. Ito, and J. Fujita, *Bull. Chem. Soc. Jpn.*, **57**, 3580 (1984).
21) S. Ohba, Y. Saito, T. Ohishi, K. Kashiwabara, and J. Fujita, *Acta Crystallogr.*, C**39**, 49 (1983).
22) L. J. Boucher, E. J. Battis, and N. G. Paez, *J. Inorg. Nucl. Chem.*, **33**, 1373 (1971).
23) C. T. Liu and B. E. Douglas, *Inorg. Chem.*, **3**, 1356 (1964).
24) L. J. Boucher, *Inorg. Chim. Acta*, **6**, 29 (1972).

Mössbauer, Raman, and DTA Studies on the Structure of BaF_2–ZrF_4–FeF_2 Glasses

Tetsuaki NISHIDA,* Toshiaki NONAKA, and Yoshimasa TAKASHIMA
Department of Chemistry, Faculty of Science, Kyushu University 33, Hakozaki, Higashiku, Fukuoka 812
(Received April 1, 1985)

Structural studies on the ternary BaF_2–ZrF_4–FeF_2 glasses have been performed to elucidate the local structure of the ZrF_4-based glasses which are known to be excellent in the optical transparency and the electric conductivity due to F^- ion. Mössbauer and Raman measurements reveal that iron (Fe^{2+} and Fe^{3+}) plays a structural role similar to that of Ba^{2+} ion surrounded by eight fluorine atoms at the interstitial site of one- or two-dimensional zigzag chains composed of ZrF_6 octahedra. Raman and DTA measurements reveal that the increase in the fraction of BaF_2 causes an increase in the coordination number of Zr from 6 to 7. Mössbauer measurements of $25BaF_2 \cdot 65ZrF_4 \cdot 10FeF_2$ glass at lower temperatures lead to a conclusion that the glass undergoes a phase transition at 225±5K, of which structural change is easily reflected in the isomer shift, quadrupole splitting, and the absorption area. This is supported by the DTA measurement of the same sample at lower temperatures, *i.e.*, the DTA curve consists of two exothermic peaks and a wide endothermic peak observed at about 220—230 K and 180—210 K, respectively.

Zirconium tetrafluoride (ZrF_4)-based glasses discovered by Poulain *et al.*[1] have recently been paid much attention owing to the excellent optical transparency ranging from near UV to middle IR[2–5] and to the relatively high fluoride ion conductivity.[6] The former property makes the ZrF_4-based glasses good candidates for optical waveguide materials and laser windows. Another feature of the glasses lies in the chemical resistancy to fluoridating agents such as HF and F_2.[4] In contrast to the relatively well-studied physical properties of these glasses, the structure has not been well understood. The structure of BaF_2–ZrF_4 glass system was studied by Almeida and Mackenzie[7] by means of IR and Raman spectroscopy. They obtained a conclusion that the structure consists of a two-dimensional zigzag chain in which each zirconium atom is surrounded by six fluorine atoms in octahedral symmetry when the BaF_2 content is not high. The coordination number of Zr has also been reported to be seven when the BaF_2 content is about 50 mol%. A similar conclusion was also obtained by Almeida and Mackenzie in a series of BaF_2–ZrF_2Cl_2 glasses.[8] X-Ray scattering studies of the BaF_2–ZrF_4 glass system was first performed by Coupé *et al.*,[9] and they obtained a conclusion that the glasses consist of three-dimensional network and that the coordination number of Zr is seven or eight. The present study was carried out to know the structure of BaF_2–ZrF_4–FeF_2 glasses by means of Raman spectroscopy, DTA, and Mössbauer spectroscopy which has been used for the structural studies of several glasses, such as borate,[10–12] borosilicate,[13,14] phosphate,[15,16] borophosphate,[17] germanate,[18] and zinc chloride[19] glasses.

Experimental

A series of ZrF_4-based glasses were prepared by fusing individual batches (1.0 g) of BaF_2 (99.9%), ZrF_4 (99.9%), FeF_2 (99.5%), and NH_4F (99.5%) in platinum crucibles at 900 °C for 3—5 min in an electric muffle furnace. Transparent and brown glasses were prepared by quenching the melts in the platinum crucibles with ice-cold water. Mössbauer measurements were performed by a constant acceleration method at various temperatures lower than room temperature using a source of ^{57}Co (10 mCi) diffused into a palladium foil. Metallic iron enriched with ^{57}Fe was used to calibrate the velocity of spectrometer and also as a reference for isomer shift. All the Mössbauer spectra were fitted to Lorenzian lineshapes by the least-squares method. Raman measurements were performed in the 90° scattering configuration at room temperature using a 514.5 nm Ar^+ laser line

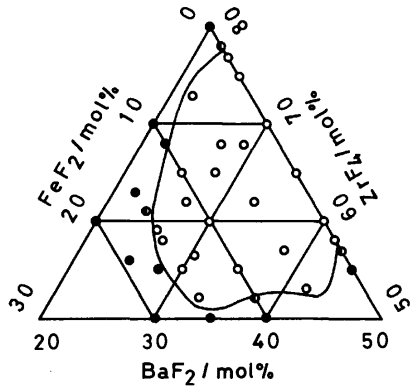

Fig. 1. Glass-forming region for the BaF_2–ZrF_4–FeF_2 system.
(○): Glass, (◐): glass ceramic, (●): crystalline compound.

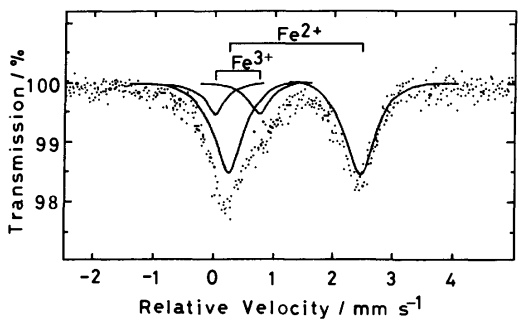

Fig. 2. Mössbauer spectrum for the $25BaF_2 \cdot 65ZrF_4 \cdot 10FeF_2$ glass measured at room temperature.

TABLE 1. MÖSSBAUER AND DTA RESULTS FOR THE BaF_2–ZrF_4–FeF_2 GLASSES

Composition	δ[a]	Δ[b]	Γ[c]	A[d]	T_g[e]	T_c[f]
	mm s^{-1}	mm s^{-1}	mm s^{-1}	%	°C	°C
$25BaF_2 \cdot 65ZrF_4 \cdot 10FeF_2$	1.35	2.20	0.58	77.4	283	322
	0.40	0.73	0.49	22.6		
$30BaF_2 \cdot 60ZrF_4 \cdot 10FeF_2$	1.39	2.19	0.55	53.7	285	337
	0.41	0.95	0.61	46.3		
$35BaF_2 \cdot 55ZrF_4 \cdot 10FeF_2$	1.33	2.19	0.53	43.7	288	343
	0.37	0.86	0.70	56.3		

a) Isomer shift. b) Quadrupole splitting. c) Linewidth. d) Absorption area. e) Glass transition temperature. f) Crystallization temperature.

(100 mW). Slits were opened to 250 μm. Raman spectra were recorded in the HH (||) configuration where the scattered light was analyzed for the vector parallel to that of the incident radiation. DTA measurements of the glasses were performed with a heating rate of 5 °C min^{-1} ranging from −118 °C to 700 °C, and Al_2O_3 powder was used as a reference.

Results and Discussion

The composition region where glass samples were tried to prepare is shown in Fig. 1, in which open circles and closed circles refer to the formation of glass and crystalline sample, respectively and half-closed circles refer to glass ceramic. The glass-forming region of BaF_2–ZrF_4–FeF_2 system is denoted to lie within the area surrounded by a solid line. This is also expressed as 42 mol%≥BaF_2≥22 mol%, 77 mol%≥ZrF_4≥52 mol%, and 15 mol%≥FeF_2≥0. Figure 1 also demonstrates that the glass-forming region of binary BaF_2–ZrF_4 glasses lies in 58—77 mol% ZrF_4, which is relatively well consistent with those reported by Almeida and Mackenzie (52—74 mol%),[7] Poulain *et al.* (60—70 mol%),[20] and Mitachi (58—69 mol%).[21] Mössbauer spectrum of $25BaF_2 \cdot 65ZrF_4 \cdot 10FeF_2$ glass measured at room temperature is shown in Fig. 2, from which we can estimate that most iron species are present as high-spin Fe^{2+} because the isomer shift is larger than 1.0 mm s^{-1}. Figure 2 also indicates that the spectrum contains a weak absorption due to Fe^{3+} of which isomer shift is *ca.* 0.4 mm s^{-1}. Mössbauer parameters for a few ZrF_4-based glasses are shown in Table 1 together with the results of DTA measurements. The errors are estimated to be ±0.01—0.02 mm s^{-1} for the isomer shift, ±0.02 mm s^{-1} or more for the quadrupole splitting and the linewidth, and ±0.5% for the absorption area. The errors are also estimated to be ±1 °C for the glass transition (T_g) and the crystallization (T_c) temperature. Large isomer shift values for Fe^{2+} suggest that each Fe^{2+} ion is surrounded by at least six fluorine atoms and that the chemical bond between iron and fluorine is extremely ionic,[22] because the isomer shift exceeds 1.3 mm s^{-1}. Isomer shift for Fe^{3+} suggests that each Fe^{3+} ion is also surrounded by at least six fluorine atoms. Quadrupole splitting and linewidth are typical of those for the absorption due to Fe^{2+} and Fe^{3+} in glasses. It seems that there is no systematic change in the Mössbauer parameters when the composition is changed. On the other hand, absorption area for the Fe^{2+} shows a distinct decrease with increasing BaF_2 content. This may be due to the increased oxidation atmosphere caused by the addition of BaF_2 into ZrF_4 matrix. (It is generally known that an increase in the basicity of glass matrix brought about by the increased alkali content, *i.e.*, BaF_2 content in the present study, results in an increase in the oxidation state of the transition metal ions in glasses. The present result is well consistent with this idea, and is also supported by the Mössbauer results recently reported by Kawamoto *et al.*[23]) It is also seen from Table 1 that T_g and T_c increase continuously with increasing BaF_2 content. The increase in T_g is also observed in binary BaF_2–ZrF_4 glasses,[7] in which a little higher (5—12 °C) T_g values are reported than those obtained in the present study. Glass transition temperature therefore seems to be reduced by the addition of FeF_2 into the BaF_2–ZrF_4 glasses. Considering that a very similar change in T_g has been observed in germanate glasses with a change in the coordination number of Ge(IV) from 4 to 6,[18] the continuous increases in T_g and T_c observed with the increasing fraction of BaF_2 (Table 1) are ascribed to a successive increase in the coordination number of Zr(IV). The change in the coordination number of Ge(IV) from 4 to 6 in the germanate glasses has also been confirmed by a continuous increase in a parameter of intermolecular force constant, θ^2M, obtained from the temperature dependence of the Mössbauer absorption area.[18] Low temperature measurements of the Mössbauer spectra were then carried out to obtain a structural information on BaF_2–ZrF_4–FeF_2 glasses. The parameter of intermolecular force constant (θ^2M) is known to be expressed by

$$\theta^2M = \frac{3E^2}{kc^2}\left(-\frac{\mathrm{d}\ln f}{\mathrm{d}T}\right)^{-1}, \quad (1)$$

where E and f are Mössbauer transition energy (14.4 keV in the case of ^{57}Fe) and recoil-free fraction, respectively. In the Eq. 1, k is Boltzmann constant and c is the velocity of light. The θ^2M value, in which θ is so-called Debye temperature and M is the mass of Mössbauer nucleus, can therefore be obtained from the slope of the

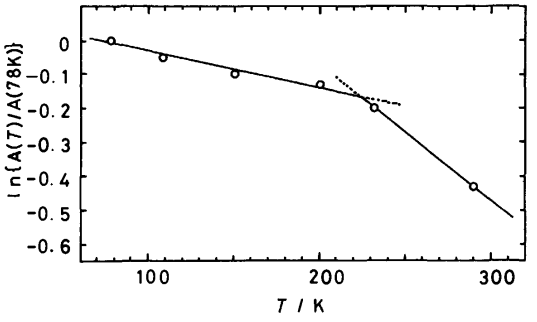

Fig. 3. Change in the absorption area (Fe^{2+} plus Fe^{3+}) with temperature.

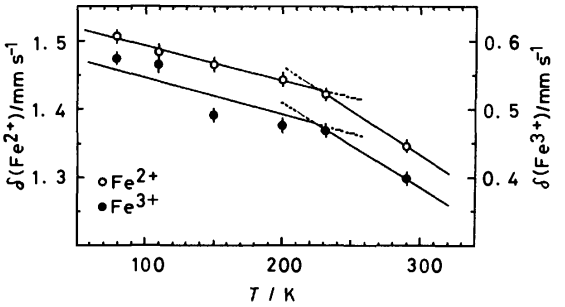

Fig. 4. Change in the isomer shifts of Fe^{2+} and Fe^{3+} with the temperature.

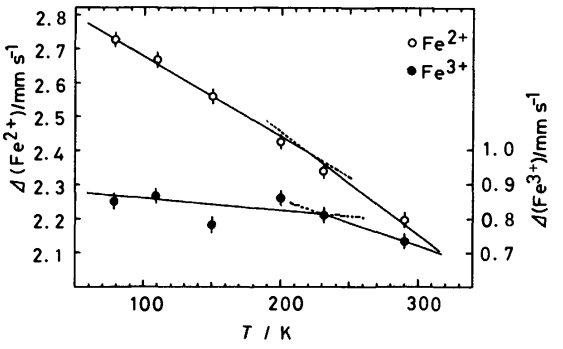

Fig. 5. Change in the quadrupole splittings of Fe^{2+} and Fe^{3+} with the temperature.

absorption area (A) *vs.* temperature (T) plot, because $d\ln f/dT$ can be approximated by $d\ln A/dT$ when a very thin sample is used. The results of the Mössbauer measurements at lower temperatures are shown in Figs. 3—5. The change in the absorption area with temperature is shown in Fig. 3, in which each absorption area is normalized by the area at 78 K. (Total absorption area for Fe^{2+} and Fe^{3+} is plotted in Fig. 3, because the separate plot for Fe^{2+} and Fe^{3+} also gives the same result as Fig. 3) It is obvious from Fig. 3 that the absorption area *vs.* temperature plot gives two straight lines with different slopes, and that the straight lines cross with each other at 224 K. The θ^2M values obtained by dividing $3E^2/kc^2$, *i.e.*, 7.76×10^3 in the present study, with the slope of the individual straight line are 6.9×10^6 and 1.9×10^6 in the temperature ranges of 78—224

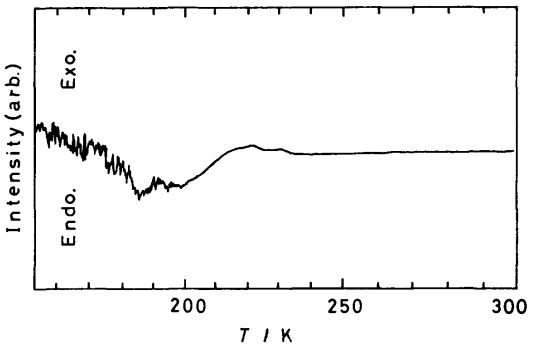

Fig. 6. DTA curve for the $25BaF_2\cdot65ZrF_4\cdot10FeF_2$ glass measured at 155—300 K.

K and 224—290 K, respectively. The drastic change in the θ^2M from 6.9×10^6 to 1.9×10^6 suggests that the intermolecular force between two Zr–F polyhedra is considerably weakened at 224 K, and that iron is present at relatively unstable environment in a sense of lattice dynamics. This leads to a tentative conclusion that iron is present at an interstitial site of Zr–F polyhedra rather than a substitutional site of Zr which is generally considered to be rigid. Large θ^2M value (6.9×10^6) obtained in the temperature range of 78—224 K also supports the conclusion, suggesting that the nature of the chemical bond between iron and fluorine is essentially ionic because the θ^2M values for the ionic compounds are known to be larger than those for the covalent ones ($1—3\times10^6$).[18] The θ^2M value therefore seems to correspond to the intermolecular force between two zigzag chains composed of ZrF_6 octahedra.[7]

The drastic change in the θ^2M observed at 224 K also suggests that the $25BaF_2\cdot65ZrF_4\cdot10FeF_2$ glass undergoes a drastic change in the vibrational mode for some reason such as phase transition. Isomer shifts and quadrupole splittings for Fe^{2+} and Fe^{3+} at lower temperatures are shown in Figs. 4 and 5, and to our surprise these parameters also show distinct changes around 224 K, *i.e.*, at 225 K (isomer shift) and 220—230 K (quadrupole splitting). These Mössbauer results shown in Figs. 4 and 5 lead to a conclusion that a kind of structural change certainly occurs at 225±5 K in the $25BaF_2\cdot65ZrF_4\cdot10FeF_2$ glass, because the plots of isomer shift and quadrupole splitting *vs.* temperature are generally known to give rise to continuous curves similar to straight lines. DTA measurements at lower temperatures were then performed to confirm the structural change. Figure 6 demonstrates a DTA curve for the $25BaF_2\cdot65ZrF_4\cdot10FeF_2$ glass. It is obvious from Fig. 6 that an endothermic reaction occurs at 180—210 K, followed by an exothermic reaction observed around 220—230 K. The DTA curve suggests that a structural change (phase transition) certainly occurs around 225 K, and that the structural change spreads in such a wide region as can be detected by DTA method. It is therefore considered that a reorientation of

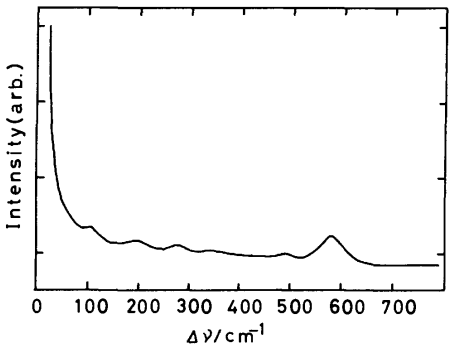

Fig. 7. Raman spectrum for the $30BaF_2 \cdot 60ZrF_4 \cdot 10FeF_2$ glass measured at room temperature.

several ions and atoms, similar to the crystallization at higher temperatures, occurs around 220—230 K.

Almeida and Mackenzie[7] revealed a mutual relationship between Raman peak position and the coordination number of Zr in binary BaF_2–ZrF_4 glasses by comparing each vibrational mode in glasses to that in the corresponding crystalline compounds. Polarized Raman spectrum of $30BaF_2 \cdot 60ZrF_4 \cdot 10FeF_2$ glass measured at room temperature is shown in Fig. 7. According to Almeida and Mackenzie,[7] a distinct peak observed around 580 cm^{-1} is assigned to the symmetric stretching vibrational mode (ν^s) due to four Zr-nonbridging fluorine (-F^-) bands in a ZrF_6 octahedron which constitutes one- or two-dimensional zigzag chain. A weak peak observed around 490 cm^{-1} has been assigned to a symmetric stretching vibration of bridging fluorine atom with which two ZrF_6 octahedra are linked together.[7] In the present study, the symmetric stretching vibrational mode (ν^s) due to the Zr-F^- band is observed at peak positions of 586, 580, and 572 cm^{-1} in $25BaF_2 \cdot 65ZrF_4 \cdot 10FeF_2$, $30BaF_2 \cdot 60ZrF_4 \cdot 10FeF_2$, and $35BaF_2 \cdot 55ZrF_4 \cdot 10FeF_2$ glasses, respectively. This continuous peak shift to the lower frequency region is ascribed to a gradual change in the coordination number of Zr from 6 to 7, because the peak position of the symmetric stretching vibrational mode (ν^s) for the Zr-F^- band is reported to be inversely correlated with the coordination number of Zr and because the peak is observed in the region of 570—600 cm^{-1} in the case of six-coordinated Zr.[7] Almeida and Mackenzie[7] also proved that the increasing fraction of BaF_2 causes a structural change from sheetlike (two-dimensional) zigzag chain to one-dimensional chainlike structure. We can therefore conjecture a structural role of FeF_2 in ZrF_4-based glasses by comparing the peak position of the symmetric stretching vibrational mode for the Zr-F^-band in the binary BaF_2–ZrF_4 glasses[7] with that in the ternary BaF_2–ZrF_4–FeF_2 glasses prepared in the present study. The Raman peaks due to the stretching vibrational mode (ν^s) have been observed at 598 and 580 cm^{-1} in the binary $25BaF_2 \cdot 75ZrF_4$ and $35BaF_2 \cdot 65ZrF_4$ glasses, respectively.[7] Comparison of these results with the peak position of $25BaF_2 \cdot 65ZrF_4 \cdot 10FeF_2$ glass (586 cm^{-1}) prepared in the present study leads to a conclusion that Fe^{2+} plays a structural role similar to that of Ba^{2+}, because the peak position of $25BaF_2 \cdot 65ZrF_4 \cdot 10FeF_2$ glass is almost identical with that of $35BaF_2 \cdot 65ZrF_4$ glass. A little increased peak position of $25BaF_2 \cdot 65ZrF_4 \cdot 10FeF_2$ glass compared to that of $35BaF_2 \cdot 65ZrF_4$ glass *i.e.*, 6 cm^{-1}, is ascribed to the displacement of Ba^{2+} with other metal ions of smaller ionic radii as is also found in the case of SrF_2–ZrF_4 glass.[7] Comparison of the peak position for the $30BaF_2 \cdot 60ZrF_4 \cdot 10FeF_2$ glass (580 cm^{-1}) with that of $40BaF_2 \cdot 60ZrF_4$ glass (577 cm^{-1}) also leads to the same conclusion as in the case of $25BaF_2 \cdot 65ZrF_4 \cdot 10FeF_2$ glass. This is also the case for the $35BaF_2 \cdot 55ZrF_4 \cdot 10FeF_2$ glass in which the corresponding peak (ν^s) is observed at 572 cm^{-1}. This peak position is intermediate between those of $40BaF_2 \cdot 60ZrF_4$ glass (577 cm^{-1}) and $50BaF_2$ $50ZrF_4$ glass (565 cm^{-1}). Coordination number of barium ion has already been reported to be in the range of 8—12 in several barium compounds,[9] and Ba^{2+} is known to be surrounded by eight fluorine atoms in BaF_2.[24] A barium ion is therefore assumed to be surrounded by eight fluorine atoms in one- or two-dimensional zigzag chains composed of ZrF_6 octahedra. The present results obtained from Raman and Mössbauer measurements therefore indicate that Fe^{2+} and Fe^{3+} ions are also surrounded by eight fluorine atoms. As for the coordination number of transition metal higher than six, some review articles[25–27] have been published, in which coordination number 8 is also observed in several metal compounds.

Peak intensity for the Zr-F^- stretching vibrational mode (ν^s) is also considered to give a useful information on the structural change based on the compositional change. In the present study, however, the peak intensity shows a maximum in the $30BaF_2 \cdot 60ZrF_2 \cdot 10FeF_2$ glass, contrary to our general expectation that the peak intensity will increase with increasing fraction of BaF_2. This can be attributed to the change in the coordination number of Zr from 6 to 7, and the fraction of nonbridging fluorine atoms (-F^-) will at least increase in the compositional region in which the coordination number of the central zirconium atom is invariable. Further experiments will be necessary to obtain a more detailed information on the fraction of nonbridging fluorine atoms in ZrF_4-based glasses.

The authors are very grateful to Drs. Toshirou Yagi and Akira Sakai of Kyushu University for their kind help in the Raman measurement and the useful discussion on the results. The present paper is partially supported by a Grant-in-Aid for Scientific Research No. 59740298 from the Ministry of Education, Science and Culture.

References

1) M. Poulain, M. Poulain, and J. Lucas, *Mater. Res. Bull.*, **10**, 243 (1975).
2) C. M. Baldwin, R. M. Almeida, and J. D. Mackenzie, *J. Non-Cryst. Solids*, **43**, 309 (1981).
3) L. G. Van Uitert and S. H. Wemple, *Appl. Phys. Lett.*, **33**, 57 (1978).
4) M. Poulain and J. Lucas, *Verres Refract.*, **32**, 505 (1978).
5) Y. Ohishi, S. Mitachi, T. Kanamori, and T. Manabe, *Phys. Chem. Glasses*, **24**, 135 (1983).
6) D. Leroy, J. Lucas, M. Poulain, and D. Ravaine, *Mater. Res. Bull.*, **13**, 1125 (1978).
7) R. M. Almeida and J. D. Mackenzie, *J. Chem. Phys.*, **74**, 5954 (1981).
8) R. M. Almeida and J. D. Mackenzie, *J. Non-Cryst. Solids*, **51**, 187 (1982).
9) R. Coupé, D. Louer, J. Lucas, and A. J. Leonard, *J. Am. Ceram. Soc.*, **66**, 523 (1983).
10) T. Nishida and Y. Takashima, *J. Non-Cryst. Solids*, **37**, 37 (1980).
11) T. Nishida, T. Shiotsuki, and Y. Takashima, *J. Non-Cryst. Solids*, **41**, 161 (1980).
12) T. Nishida, T. Hirai, and Y. Takashima, *J. Non-Cryst. Solids*, **43**, 221 (1981).
13) T. Nishida, T. Hirai, and Y. Takashima, *Phys. Chem. Glasses*, **22**, 94 (1981).
14) T. Nishida, T. Hirai, and Y. Takashima, *Bull. Chem. Soc. Jpn.*, **54**, 3735 (1981).
15) T. Nishida, T. Shiotsuki, and Y. Takashima, *J. Non-Cryst. Solids*, **43**, 115 (1981).
16) T. Nishida, T. Shiotsuki, and Y. Takashima, *J. Non-Cryst. Solids*, **43**, 123 (1981).
17) T. Nishida, Y. Miyamoto, and Y. Takashima, *Bull. Chem. Soc. Jpn.* **56**, 439 (1983).
18) T. Nishida, M. Katada, and Y. Takashima, *Bull. Chem. Soc. Jpn.*, **57**, 3566 (1984).
19) T. Nishida, A. Nakamura, and Y. Takashima, *Chem. Lett.*, **1984** 1683.
20) M. Poulain, M. Poulain, and J. Lucas, *Rev. Chim. Miner.*, **16**, 267 (1979).
21) S. Mitachi, *Phys. Chem. Glasses*, **23**, 190 (1982).
22) N. N. Greenwood and T. C. Gibb, "Mössbauer Spectroscopy," Chapman and Hall Ltd., London (1971), Chap. 5.
23) Y. Kawamoto, I. Nohara, K. Hirao, and N. Soga, *Solid State Commun.*, **51**, 769 (1984).
24) R. Mühll, S. Andersson, and J. Galy, *Acta Crystallogr., Sect. B*, **27**, 2345 (1981).
25) B. F. G. Johnson, "Transition Metal Chemistry," in "Comprehensive Inorganic Chemistry," ed by J. C. Bailar Jr., H. J. Emeleus, R. Nyholm, and A. F. Trotman-Dickerson," Pergamon Press, Oxford (1973), Vol. 4, Chap. 52.
26) E. L. Muetterties and C. M. Wright, *Quart. Rev.*, **21**, 109 (1967).
27) S. J. Lippard, *Prog. Inorg. Chem.*, **8**, 109 (1967).

The Prediction of Preferred Orientation Planes in X-Ray Powder Diffractometry

Yoshito TAKAKI,* Hiroshi YAMAGUCHI,† and Kazuaki NAKATA
Department of Physics, Osaka Kyoiku University, Tennoji-ku, Osaka 543
†*Department of Earth Science (Mineralogy), Osaka Kyoiku University, Tennoji-ku, Osaka 543*
(Received November 21, 1984)

A method for predicting possible preferred orientation planes in organic and inorganic powders of known crystal structures is presented. The usefulness of this method is demonstrated by applying it to the powders of benzamide, the α-form of 2-pyrazinecarboxamide, benzoic acid, olivine, and the high-temperature form of Li_3PO_4. It should be noted that the existence of preferred orientation axes found in the powders of benzoic acid and Li_3PO_4 can be well explained in terms of zone axes, each formed by two sets of cleavage planes.

A treatment of preferred orientations in X-ray powder diffractometry using an orientation-distribution function for preferentially oriented particles has previously been developed by Uda and Sasa.[1-3] Recently, we extended the above method to include oriented plate-like and needle-like particles in the powder.[4-6]

By using this method, Nakata *et al.*[6] have closely examined the preferred orientations in coarse and fine powders of benzamide and the α-form of 2-pyrazinecarboxamide and have found that the occurrence of preferred orientation planes can be well explained in terms of the layer structure, the layers being linked with each other by weak van der Waals forces. In the above study, the preferred orientation planes for the two substances were found by comparing the observed X-ray powder intensities with those from randomly oriented particles (calculated intensities).

The preferred orientation planes can be easily predicted if one takes into account the well-known fact that cleavages causing preferred orientation effects on X-ray intensities are inherently dependent upon the anisotropic character of the crystal structure and on the strength of bonds between atoms or molecules. From this point of view, we wish here to present a method for predicting possible preferred orientation planes for organic and inorganic powders, the crystal structures of which are known.

Procedure

Prediction of Preferred Orientation Planes for Organic Powders. Organic (molecular) crystals are characterized by the presence of van der Waals bonding as a fundamental type of bonding. Further, strong hydrogen bonds play an important role in the formation of characteristic types of structure in chain structures and in layer structures. Cleavages may then occur along the planes parallel to the chain or to the layer if they are linked by weak van der Waals forces only. Therefore, preferred orientation planes can be predicted by the following procedure:

1) Since cleavages are usually parallel to the planes with simple Miller indices, in our computer calculation (the program is written in N_{88}-BASIC), they are examined for planes (hkl) having interplaner spacings (d-values) larger than 3.0 Å.

2) In a crystal, a plane parallel to (hkl) is represented by:

$$hx + ky + lz = p, \quad (1)$$

where x, y, and z are the fractional coordinates referred to the crystal axes, and where p is a constant.

By varying the value of p, we obtain possible cleavage planes (hkl) from a requirement that the cleavage does not break covalent bonds (molecules) and hydrogen bonds.

3) For each of the possible cleavage planes obtained above, a lattice spacing[7] at right angles to the cleavage plane (D-value, see Fig. 1) is calculated. In this calculation, non-hydrogen-bonded H atoms are omitted since the strength of bonds from an H atom to other atoms is considered to be weak; thus, these bonds do not exert any serious effect on the cleavage. The D-value is used as an indication of the weakness of bonds linking layers of molecules across the cleavage plane.

4) By examining the D values, possible preferred orientation planes are selected.

Prediction of Preferred Orientation Planes for Inorganic Powders. In inorganic crystals, the ionic bond is a fundamental type of bonding linking atoms across a cleavage plane. Therefore, like the lattice spacing, the number of ionic bonds per unit area[8] can also be used as an indication of the weakness of the bonds. In this paper, however, the large D-values are mainly used for selecting preferred orientation planes, since a weak bond is usually accompanied by a large lattice spacing.[7] The following is a procedure for predicting possible preferred orientation planes in inorganic powders:

1) Cleavages are examined for the planes (hkl) with d-values larger than 3.3 Å.

2) Possible cleavage planes are obtained from a requirement that the cleavage does not break covalent bonds.

3) For these cleavage planes, lattice spacings (D-

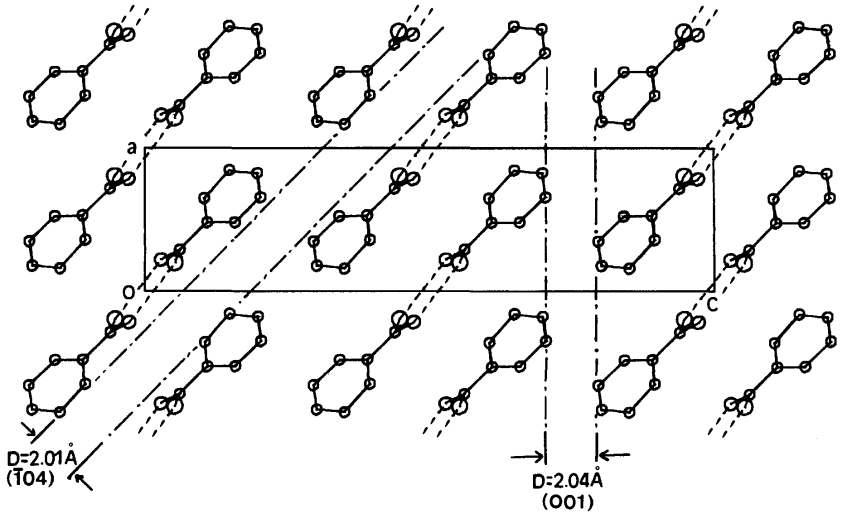

Fig. 1. The crystal structure of benzamide[9] projected along the b axis, showing the cleavages parallel to (001) and ($\bar{1}$04) and their lattice spacings (D-values).

values) are calculated (H atoms are omitted from the calculation).

4) The number of bonds (N) across each cleavage plane in a unit cell is calculated. Within a unit cell, the area of the cleavage plane (S) parallel to (hkl) is also calculated.

5) By examining the values of D (and N/S) and confirming the presence or absence of the sheet of water molecules if the crystal is a hydrate, possible preferred orientation planes are selected.

Prediction of Preferred Orientation Axes. If the crystals obtained from crystal growth are shaped like needles, we must examine the needle axis as a possible preferred orientation axis.[5,6]

In some cases, a zone axis formed by two good cleavage planes coincides with a preferred orientation axis, especially when the zone axis is the needle axis of the crystal, as in the benzoic acid powder. The preferred orientation axis should be examined when the preferred orientations in the powder sample cannot be explained from the cleavage planes predicted by the above procedure.

Application

Benzamide. Crystals[9] are monoclinic, with a=5.607, b=5.046, c=22.053 Å, β=90.66°, and space group $P2_1/c$. Four molecules are contained in a unit cell.

Two possible preferred orientation planes and their D-values, as obtained by the above method, are listed in Table 1. Nakata *et al.*[6] found preferred orientation planes of (001) and ($\bar{1}$04) and explained the occurrence of these planes in terms of the layer structure (Fig. 1). One can see that these two preferred orientation planes are the same as the planes listed in Table 1, and that the two D-values are both larger than 2Å, indicating that the forces linking layers are very weak.

Table 1. Possible preferred orientation planes for benzamide, the α-form of 2-pyrazinecarboxamide and benzoic acid

	hkl	d/Å	D/Å
Benzamide	001	22.05	2.04
	$\bar{1}$04	3.95	2.01
α-Form of 2-pyrazine-carboxamide	100	22.65	1.76
Benzoic acid	$\bar{1}$02	5.16	2.44
	001	21.79	2.33
	100*	5.46	0.44

* The next most possible preferred orientation plane.

α-Form of 2-Pyrazinecarboxamide. The crystals[10] are monoclinic, with a=23.07, b=6.73, c=3.73 Å, and β=101.0° and with the space group $P2_1/a$. Four molecules are contained in a unit cell.

One possible preferred orientation plane (100) was predicted by the present method (Table 1). It is identical with that found by Nakata *et al.*[6] They found also the c preferred orientation axis, which had been predicted from the needle axis.

Benzoic Acid. The crystals[11] are monoclinic, with a=5.510, b=5.157, c=21.973 Å, and β=97.41° and with space group $P2_1/c$. Four molecules are contained in a unit cell.

The three possible preferred orientation planes obtained are listed in Table 1. After the D-values had been examined, the $\bar{1}$02 and 001 planes were selected as the most probable preferred orientation planes. Nakata[12] examined preferred orientations in fine powders and found a great many preferentially oriented needle-like particles with the b axis as the preferred orientation axis and a very small number of plate-like particles with (001) as the preferred orientation plane. The b preferred orientation axis could thus be pre-

TABLE 2. POSSIBLE PREFERRED ORIENTATION PLANES FOR OLIVINE AND THE HIGH-TEMPERATURE FORM OF Li_3PO_4

	hkl	*d*/Å	*D*/Å	*S*/Å^2	*N*	*N*/*S*
Olivine	010	10.19	0.56	28.4	6	0.211
	010	10.49	1.85	30.2	4	0.133
	120	3.98	0.75	79.6	12	0.151
High-temperature	101*	3.84	0.42	82.7	10	0.121
form of Li_3PO_4	011*	4.46	0.30	71.2	16	0.225
	021*	3.59	0.14	88.3	20	0.226
	100*	6.13	0.06	51.9	12	0.231

* The next most possible preferred orientation planes.

dicted as the zone axis formed by the $\bar{1}02$ and 001 cleavage planes.

Olivine. The crystals of forsterite[13] are orthorhombic, with a=4.756, b=10.195, and c=5.981 Å and with space group Pbnm. Four formula units are contained in a unit cell.

One possible preferred orientation plane, along with the values of *D*, *N*, *S*, and *N*/*S*, is listed in Table 2. Yamaguchi *et al.*[14] found that the preferred orientations in powders of olivine from Kaimon-dake can be explained mostly from the 010 preferred orientation plane, in agreement with the prediction of Table 2. Note that the small value of *D*, 0.56 Å, for the plane (010) may support the fact that the cleavage parallel to (010) is imperfect.[13]

High-temperature form of Li_3PO_4. The crystals[15] are orthorhombic, with a=6.12, b=10.53, and c=4.93 Å and with space group Pmnb. Four formula units are contained in a unit cell.

Six possible preferred orientation planes were obtained (Table 2). By examining the *D*-values, the (010) and (120) planes were selected as the most highly probable preferred orientation planes. From a close examination of fine powder samples, Yamaguchi[16] found that the preferred orientations can be explained mainly in terms of the 010 preferred orientation plane and, to some extent, the c preferred orinetation axis. The c preferred orientation axis could also be predicted as a zone axis formed by the 010 and 120 cleavage planes.

References

1) M. Uda, *Z. Anorg. Allg. Chem.*, **350**, 105 (1967).
2) Y. Sasa and M. Uda, *J. Solid State Chem.*, **18**, 63 (1976).
3) M. Uda and Y. Sasa, *J. Solid State Chem.*, **46**, 121 (1983).
4) Y. Takaki and H. Yamaguchi, *Yogyo Kyokai Shi*, **90**, 34 (1982).
5) A. Kurisu, K. Nakata, H. Yamaguchi, and Y. Takaki, *Mem. Osaka Kyoiku Univ. Ser. III* (in Japanese), **31**, 83 (1983).
6) K. Nakata, H. Sugihara, S. Mori, H. Yamaguchi, and Y. Takaki, *Bull. Chem. Soc. Jpn.*, **57**, 3395 (1984).
7) C. S. Hurlbut, Jr., "Mineralogy," 17th ed, J. Wiley and Sons, New York (1959), p. 149.
8) A. N. Mariano and R. M. Beger, *Amer. Mineral.*, **56**, 1867 (1971).
9) C. C. F. Blake and R. W. H. Small, *Acta Crystallogr. Sect. B*, **28**, 2201 (1972).
10) Y. Takaki, Y. Sasada, and T. Watanabé, *Acta Crystallogr. Sect. B*, **13**, 693 (1960).
11) G. Bruno and L. Randaccio, *Acta Crystallogr. Sect. B*, **36**, 1711 (1980).
12) K. Nakata, unpublished data.
13) W. A. Deer, R. A. Howie, and J. Zussman, "Rock-Forming Minerals," Longmans (1962), Vol. 1, p. 2.
14) H. Yamaguchi, K. Akatsuka, A. Kurisu, Y. Takaki, and M. Setoguchi, Annual Meeting of Mineralogical Society of Japan, Tsukuba, June 1982, Abstr., No. 36.
15) J. Zemann, *Acta Crystallogr.*, **13**, 863 (1960).
16) H. Yamaguchi, unpublished data.

The Electric Properties of VO_2 Thin Films Doped with Other Metal Oxides under Water Vapor

Yoshiya KERA,* Tadashi OONISHI, Hisateru IMORI, and Shigeharu KIDA
Department of Applied Chemistry, Faculty of Science and Engineering, Kinki University, Higashiosaka, Osaka 577
(Received February 14, 1985)

The electric property of a pure VO_2 thin films, prepared from a vanadium naphthenate by thermal decomposition, was examined preliminarily under various inorganic gas atmospheres, H_2O, H_2, O_2, N_2O, and NO_2, at 20—200 °C. Only in the case of the H_2O adsorption, did the conductivity-temperature curve change reversibly; in the other cases it changed irreversibly. With respect to the VO_2 films doped with Na_2O, ZrO_2, Cr_2O_3, and TiO_2, similarly, the conductivities changed reversibly with the water vapor adsorbed; the extent and the manner of these changes differed rather greatly depending upon the kind of metal oxides doped. In the Zr–VO_2 film, which had a large conductivity (σ) and its gap ($\Delta\sigma$) at the transition point (T_t=60 °C) relative to the pure VO_2 film, the electric property was almost unaffected by water-vapor adsorption. In the cases of the Cr- and Ti–VO_2 films, with quite small σ and $\Delta\sigma$ values relative to the pure VO_2 film, on the contrary, the ln σ—$1/T$ curves decreased parallelly to less than about one-half of that under a vacuum throughout the temperature range. With the Na–VO_2 film, the σ—$1/T$ curve measured under water vapor gradually nears that under a vaccum with the elevation of the temperature to 200 °C. From the comparisons of the effects of the electric properties of these doped films on the water vapor adsorbed, the structural features of the films, especially the contact states in the boundary layer, were deduced favorably. Furthermore, a possibility of the application to a switching element working at about 60 °C was suggested for the Zr–VO_2 film, and that to a fume sensor working at a temperature less than 200 °C, for the Cr- and Ti–VO_2 films.

Many solid-state physisists and chemists have been interested in vanadium oxide compounds because these compounds show a metal-semiconductor transition.[1-9] We have previously proposed a more convenient method for the preparation of a VO_2 thin film[10] by improving the Sekiya-Matsushita method.[11] Furthermore, we prepared VO_2 thin films doped with various metal oxides and compared their electric properties. The conductivity and also the extent of the conductivity gap, which was observed at the transition point in the pure VO_2 film, were largely affected by the metal-oxide additions. Based on the conductivity changes, the structural features, especially in the grain boundary of these VO_2 films, were discussed.[10]

In the present paper, the electric properties of the VO_2 films doped and undoped with other metal oxides under various atmospheres, especially under water vapor, will be examined in detail in order to obtain further information about the structures and the contact states of the particles in the grain boundary. In fact, the conductivity-temperature curve was considerably affected by the water vapor adsorbed physically, depending upon the kinds of metal oxides doped. The structural features of these doped VO_2 films will be discussed favorably based on these findings, and finally a possibility of their application to a solid state sensor will be suggested.

Experimental

1) Materials and Procedures. Vanadium naphthenate (containing *ca.* 3 wt% of vanadium(IV) ion; Harima Kasei Co., Ltd.) was dissolved in 1-butanol to prepare 10 wt% of the solution. A thin film of vanadium oxide (VO_2 thin film) was formed on a Pyrex glass plate by the following procedures. The glass plate was cut in the size of 11×24 mm^2; on both ends there had previously been deposited gold film (7 mm in width) as an electrode in order to keep a good ohmic contact during the conductivity measurements. Three droplets of the vanadium naphthenate solution were placed on the plate, after which it was dried at 20 °C in air for 1 h. The plate was then inserted into a furnace kept at 600 °C for 20 min to decompose the vanadium naphthenate and then rapidly taken out into the air for cooling. A nitrogen gas stream, bubbled in water kept exactly at 21.5 °C, was introduced into the funace during the decomposition.[10]

Upon the preparation of the VO_2 thin films containing other metal oxides, such as Na_2O, TiO_2, Cr_2O_3, and ZrO_2, these oxides ($NaOCH_3$ in the case of Na_2O), weighed exactly, were added to a 10 wt% 1-butanol solution of vanadium naphthenate and then ground well with an agate mortar in order to dissolve them fully. Then, the solution containing the metal oxides was dropped onto the glass plate with the gold electrodes and subsequently decomposed by the procedures used in the case of the pure VO_2 thin film. The concentrations of these metal oxides added to vanadium oxide were in the range of 40—60 atom%; [(M)/(V)]×100.

2) Measurements. The electric conductivity was measured by the usual two-probe method under various gas atmospheres and under an evacuation below 10^{-3} mmHg†. The pressure measurement was carried out by the use of a mercury manometer at a relatively high pressure and by the use of a Pirani gauge, Shimazu Model PM-12, at lower pressures. In the measurements of the conductivity, the temperature was elevated from 20 to 200 °C at the constant speed of 4.5 °C/min by the use of a programable controller, Yokogawa Model PC-182. The relationship between the conductivity and the temperature was determined exactly by means of an automatic measurement system; both the potential difference between the ends of the VO_2 thin film and the thermoelectric power generated in the AC-thermocouple attached to the film were amplified simulteneously by means of microvoltmeters, Ookura Denki Model AM-2002, and then introduced, at intervals of 1 °C, into a microcomputer, Sharp Model Mz-80K2E, *via* a 12-bit A/D-convertor, Hoowa

† 1 mmHg≈133.322 Pa.

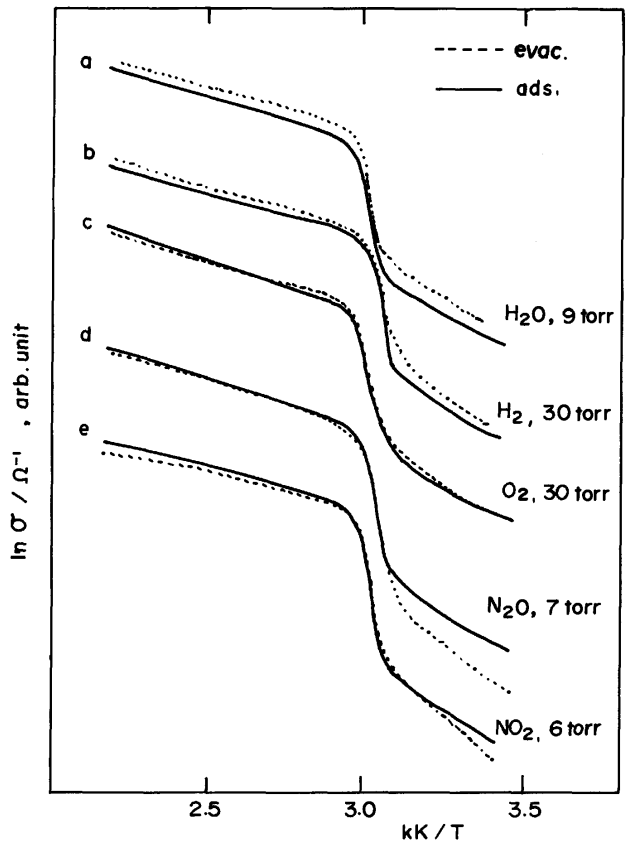

Fig. 1. The $\ln\sigma - 1/T$ curves for the pure-VO_2 thin film measured under various inorganic gas atmospheres; the blank curves are given to each curve with dotted lines, which have been measured under the vacuum before the each measurement. The measurements were repeated alternatively by the use of the same film in the sequence of a→e.

Sangiyo Model ADL-1224.

Results and Discussion

1) Conductivity Changes of Pure VO_2 Thin Film under Various Gas Atmospheres at 20—200°C. The temperature dependence of the conductivity (σ) for the pure VO_2 thin film measured under various inorganic gas atmospheres in the range of 20—200°C are summarized in Fig. 1, in which the ln σ values are plotted against $1/T$. In Curve a, the dotted and full lines denote the curve measured under the vacuum at 10^{-3} torr and under water vapor (p=9 Torr[†]) respectively. After the measurement of Curve a, the σ values for Curve b were measured repeatedly under a H_2 atmosphere (p=30 Torr). Similarly, the σ values under O_2 (p=30 Torr), N_2O (p=7 Torr), and NO_2 (p= 7 Torr) were successively measured, as is shown by Curve c, d, and e respectively. By comparing these σ values with the corresponding values under the vacuum, it is known that the σ decreases with the water-vapor adsorption at all temperatures. The σ decreases just a little under H_2 at all temperatures, but, on the contrary, it rather increases under N_2O at temperatures lower than the transition point (T_t). Under O_2 and NO_2, however, the σ does not change remarkably.

[†] 1 Torr≈133.322 Pa.

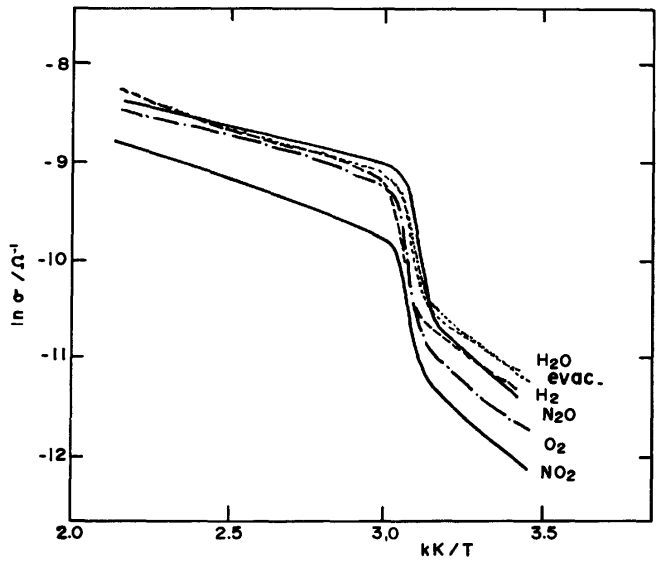

Fig. 2. The comparisons of the blank curves given in Fig. 1: "evac." indicates the curve for the pure-VO_2 film measured at the very initial under the vacuum, and "H_2O" that measured under the vacuum after the experiment under water vapor. "O_2", "N_2O", and "NO_2" also indicate the same meanings. They were successively measured in the order of "evac.", "H_2O", "O_2", "N_2O", and "NO_2", as mentioned in Fig. 1.

TABLE 1. THE CONDUCTIVITIES (σ_h AND σ_l) JUST ABOVE AND BELOW T_t AND THE ACTIVATION ENERGIES (E_h AND E_l) AT THE TEMPERATURES ABOVE AND BELOW T_t, ESTIMATED FROM THE LN$\sigma - 1/T$ CURVES UNDER THE VACUUM AFTER THE INORGANIC GAS ADSORPTIONS, *i.e.*, FROM THE Evac. CURVES IN Fig. 2

Samples	$\sigma_h/10^{-4}\Omega^{-1}$	E_h/eV	$\sigma_l/10^{-4}\Omega^{-1}$	E_l/eV
"Evac."	1.04	0.074	0.34	0.18
"H_2O"	1.04	0.082	0.31	0.21
"H_2"	1.04	0.084	0.28	0.18
"O_2"	0.97	0.068	0.22	0.23
"N_2O"	1.15	0.056	0.27	0.23
"NO_2"	0.54	0.084	0.15	0.24

The $\sigma - 1/T$ curves, a—e, of Fig. 1 are summarized in Fig. 2, where "Evac." indicates the ln $\sigma - 1/T$ curve measured first of all under the vacuum and "H_2" the curve measured also under the vacuum after measurement under water vapor. Similarly, "H_2", "O_2", and "N_2O" have similar meanings. The curve for "NO_2" was measured similarly under the vacuum after the measurement of Curve e in Fig. 1. The electric conductivities just above and below the transition point, σ_h and σ_l, were evaluated approximately by extrapolating linearly the curves above and below T_t in Fig. 2 to the transition point, and the activation energies for the conductions above and below T_t, E_h, and E_l, from the inclination of the corresponding curves. These values are summarized in Table 1. The conduc-

tivity of the pure VO_2 thin film is known to be recovered almost to the initial value by evacuation after measurement under water vapor, but not after those under the other gases, H_2, O_2, N_2O, and NO_2. Therefore, only in the case of the H_2O molecule, a physical adsorption onto the interface among the VO_2 particles (or in the grain boundary) is suggested. Furthermore, the water molecules adsorbed physically could be deduced to affect only the mobility in the grain boundary, because of the parallel change in the $\sigma-1/T$.

The σ was affected just a little under the atmospheres of H_2 and O_2, but in both cases it decreased irreversibly after the measurements under these gases, especially rather largely at temperatures lower than T_t. A series of vanadium oxides, which are generally shown by the formulae; V_nO_{2n+1} and V_nO_{2n-1}, have been reported[12] in which the electric conductivities vary greatly with the n.[9] Therefore, the boundary layer of the pure VO_2 film is expected to be composed of various vanadium oxide compounds, unlike as in the n: *e.g.*, one compound in the grain boundary is mainly affected by the O_2 adsorption, and the other compounds in the other part, by the H_2 adsorption, so as to make the σ values decrease similarly. Under the atmosphere of N_2O, which easily releases oxygen atoms near 200 °C, the grain boundary might be oxidized by it so that the σ is increased irreversibly. In the case of NO_2, we can not explain the irreversible decrease in the σ.

2) Dependence upon Water Vapor of the Electric Property of the VO_2 Thin Films Doped with Other Metal Oxides. The electric property of the pure VO_2 thin film under water vapor are shown again in Fig. 3 as the ln $\sigma-1/T$ curves, a—c. Curve a indicates the curve measured under the vacuum and Curve c, that measured in the air after the film has stood for a long time in a desiccator which had not been kept in a good state. Curve b and c were changed reversibly to Curve a after the evacuation, so their deviation from Curve a can be expected to be caused by water vapor adsorbed physically onto the boundary layer.

With respect to a Na-VO_2 thin film (Na: 40 atm%), the conductivity was measured under the vacuum and also under water vapor, as is shown by the ln $\sigma-1/T$ curves, a and b respectively, in Fig. 4. Curve c indicates the curve measured in the air after the Na-VO_2 film has stood for 2 d in the air. Curves b and c are changed reversibly to Curve a by the evacuation after the measurement. Therefore, the deviations of Curves b and c from Curve a seem to be caused by water vapor adsorbed weakly (or condensed) onto the boundary layer. The extents of the deviations tend to decrease with the elevation of the temperature, nearing zero with the elevation up to near 200 °C in Fig. 4. This finding may suggest that the film is composed of various sizes of particles of the Na-V-O compounds; that the water molecules, which condense into micro-pores formed by the contact of the particles with so many varied types, are desorbed step-by-step with the elevation of the

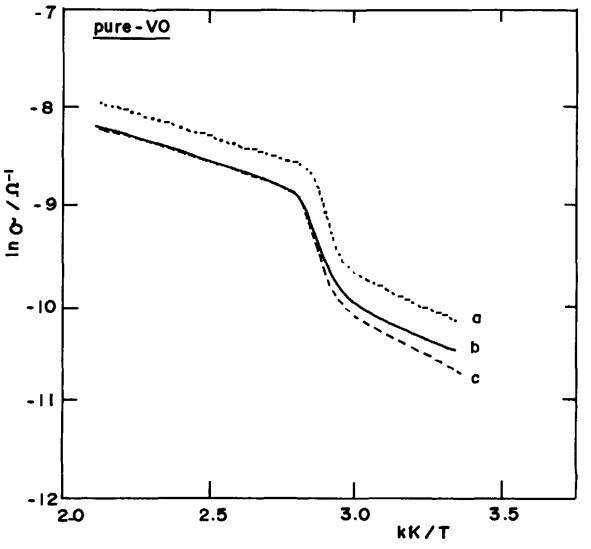

Fig. 3. Changes in the ln $\sigma-1/T$ curve for the pure-VO_2 thin film with water vapor adsorbed physically; a: blank, b: under H_2O (saturated at 20 °C). Curve c indicates the curve measured under the air after keeping it for a long time in a desiccator being not so good in the preservation.

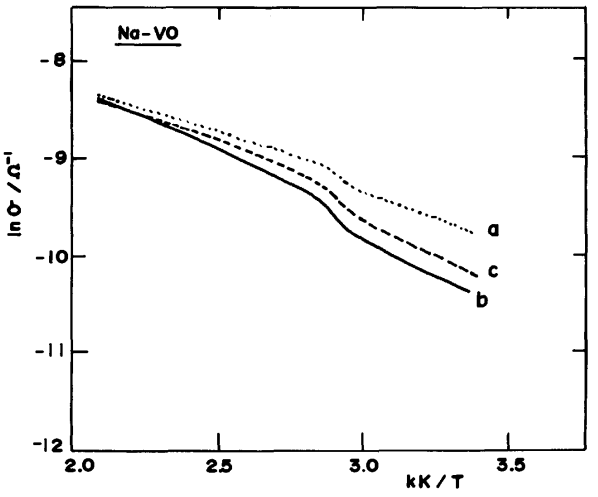

Fig. 4. Changes in the ln $\sigma-1/T$ curve for the Na-VO_2 thin film (Na: 40 atom%) with water vapor adsorbed physically; a: under vacuum, b: under H_2O (saturated at 20 °C). Curve c indicates the curve measured under the air after standing it in the air for 2 d.

temperature, and, further, that the σ-difference varies in proportion to the quantity of the water molecules remaining in the layer.

With respect to a Cr-VO_2 (Cr: 60 atom%) and a Ti-VO_2 (Ti: 40 atm%) thin film, the ln $\sigma-1/T$ curves are shown in Figs. 5 and 6 respectively. From a comparison of Curves a and b, it can be seen that both the Cr- and Ti-VO_2 films are affected considerably by water vapor adsorbed over all the temperature range, 20—200 °C. Curve c in Figs. 5 and 6 indicates the curves measured under the air after the films have been kept in the desiccator for a long time. In

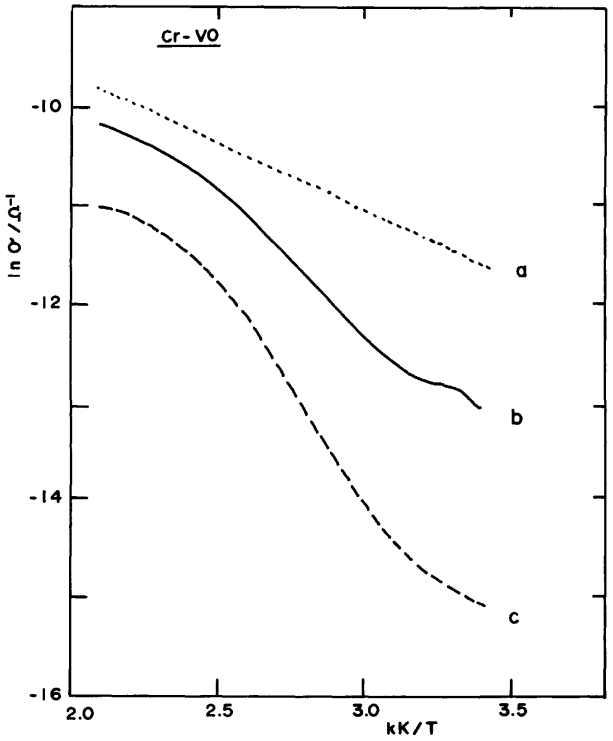

Fig. 5. Change in the $\ln\sigma - 1/T$ curve for the Cr-VO_2 thin film (Cr: 60 atom%) with water vapor adsorbed physically; a: under vacuum, b: under H_2O vapor (saturated at 20 °C). Curve c indicates the curve measured under the air after keeping it for a long time in a desiccator being not so good in the preservation.

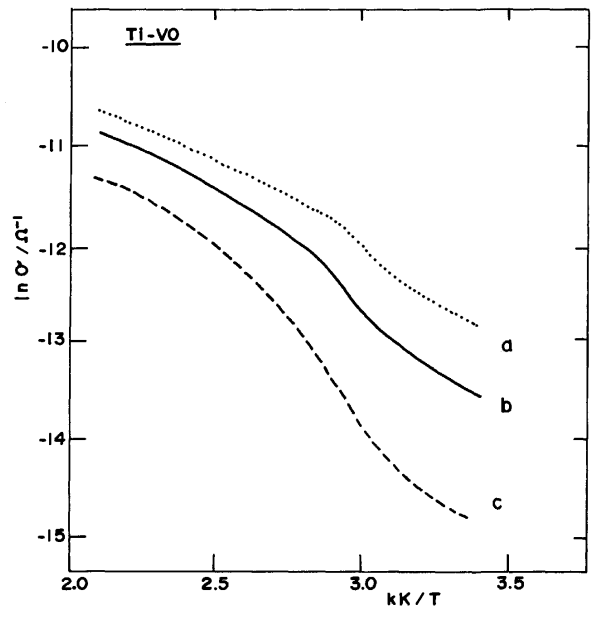

Fig. 6. Changes in the $\ln\sigma - 1/T$ curve for the Ti-VO_2 thin film (Ti: 40 atom%) with water vapor adsorbed physically; a: under vacuum, b: under H_2O vapor (saturated at 20 °C). Curve c indicates the curve measured under the air after keeping it for a long time in a desiccator being not so good in the preservation.

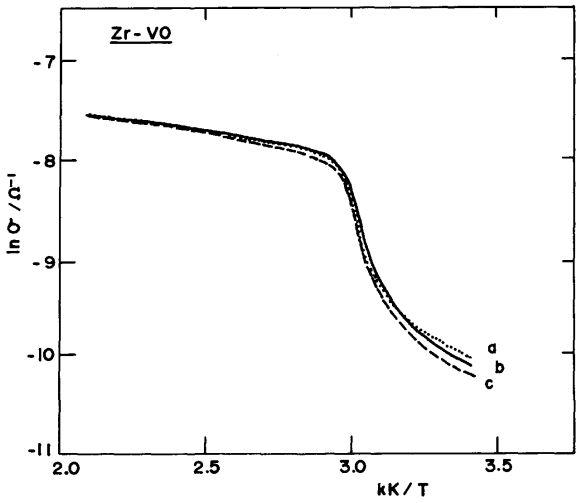

Fig. 7. Change in the $\ln\sigma - 1/T$ curve for the Zr-VO_2 thin film (Zr: 60 atom%) with water vapor adsorbed physically; a: under vacuum, b: under H_2O vapor (saturated at 20 °C). Curve c indicates the curve measured under the air after keeping it for a long time in the desiccator being not so good in the preservation.

both cases, Curves b and c were also changed reversibly to Curve a by evacuation. In the Cr- and Ti-VO_2 it was suggested previously that amorphous (or very small crystalline) Cr_2O_3 and TiO_2 particles, mixed with some vanadium oxides, were formed at the grain boundary and, further, that the apparent conductivities are controlled by that of the grain parts.[10] We can understand easily from such suggestions that the σ values of those films are affected rather greatly by the water vapor adsorbed physically.

With respect to a Zr-VO_2 thin film (Zr: 60 atom%), the conductivity was measured under the vacuum and water vapor, as is shown by the $\ln\sigma - 1/T$ curves, a and b, respectively in Fig. 7. In this case, the σ value was almost entirely unaffected by water vapor; also, when it was left standing for a long time in the desiccator it was not preserved in a so good state (*cf.* Curve b and c respectively). Curves b and c were also changed reversibly to Curve a. The formation of a grown (or crystallized) ZrO_2 particle mixed with vanadium oxide at the grain boundary was shown previously by X-ray diffraction; further, it was suggested that the electric properties of the VO_2 particles themselves appeared more strongly, because the conductivity in the grain boundary was high relative to the inner bulk of the VO_2 particles.[10] On the basis of the suggestion that the conductivity is mainly controlled by the bulk of the VO_2 particles rather than by the grain parts in the Zr-VO_2 film, it can be understood why the conductivity is almost unaffected by the water vapor adsorbed.

For these doped VO_2 films, the conductivities, σ_h and σ_l and the apparent activation energies, E_h and E_l, were estimated similarly from the $\ln\sigma - 1/T$ curves in Figs. 3—7, as is shown in Table 2. The data for the Cr-

TABLE 2. DEPENDENCE UPON WATER VAPOR OF THE ELECTRIC CONDUCTIVITIES OF THE VO_2 THIN FILMS DOPED WITH VARIOUS METAL OXIDES

Samples	$\sigma_h/10^{-4}\Omega^{-1}$	E_h/eV	$\sigma_l/10^{-4}\Omega^{-1}$	E_l/eV
Pure-VO_2				
Evac.	1.57	0.089	0.66	0.113
H_2O	1.37	0.089	0.54	0.118
Na-VO_2				
Evac.	1.09	0.083	0.94	0.092
H_2O	0.80	0.119	0.64	0.138
Zr-VO_2				
Evac.	3.42	0.036	0.79	0.152
H_2O	3.67	0.034	0.79	0.178
Ti-O_2				
Evac.	0.076	0.116	0.054	0.142
H_2O	0.049	0.148	0.030	0.160

VO_2 film have been omitted from the table because the transition point could not be seen clearly on the film, but a large effect of adsorbed water vapor can be qualitatively found in Fig. 5. The ratio of the $\sigma(H_2O)$ value to the σ(Evac.) value is about 0.85 in both σ_h and σ_l for the pure VO_2 film, while the ratios between the values about 1.0 and 0.6 for the Zr- and Ti-VO_2 films respectively. Thus, the effect of water-vapor adsorption on the conductivity clearly tends to decrease upon the addition of ZrO_2, while, on the contrary, it is considerably extended by the addition of TiO_2.

These results may be summarized as follows. The changes in the electric properties with various gases, especially with the water-vapor adsorption, were confirmed to be related not only to the chemical properties of the compounds existing in the grain boundary, but also to the states of the contact between the particles. In other words, the states of the VO_2 particles grown and their contact states at the grain boundary, by which the electric property is apparently controlled, could be favorably varied by selecting the kind of metal oxide and its contents.

The Zr-VO_2 thin film may be applied to a switching element working near 60 °C, because of its stability in relation to water vapor in the air; on the other hand, the Cr- and Ti-VO_2 thin films may be applied to a fume sensor working at temperatures from 20—200 °C because of their showing rather large changes of the water vapor adsorbed reversibly, although further studies will be needed to increase the sensitivity. In the case of the Na-VO_2 film, the σ value changed delicately with the temperature under water vapor, so we can not make any suggestions about its application, although considering the structural features of the grain boundary of the VO_2 thin films gives important information.

References

1) N. F. Mott, *Proc. Phys. Soc. London, Sec A.*, **62**, 416 (1949); *Rev. Modern Phys.*, **40**, 677 (1968).
2) J. B. Goodenough, *Phys. Rev.*, **177**, 1442 (1960).
3) S. Westman, *Acta Chem. Scand.*, **15**, 217 (1961).
4) H. W. Verleur, A. S. Barker, Jr., and C. N. Berglund, *Phys. Rev.*, **172**, 172 (1968).
5) D. Adler, *Rev. Modern Phys.*, **40**, 714 (1968).
6) D. B. Mcwhan, T. M. Rice, and J. P. Remeika, *Phys. Rev. Lett.*, **23**, 1384 (1969).
7) G. J. Hyland, *J. Solid State Chem.*, **2**, 318 (1970).
8) C. J. Hearn, *J. Phys. C: Solid State Phys.*, **5**, 1317 (1972).
9) S. Kachi, T. Takada, Y. Bando, K. Kosuge, H. Okinaka, and K. Nagasawa, FELITES: *Proc. Intern. Conf., Jpn*, 563 (1970).
10) Y. Kera, H. Imori, S. Kida, and K. Degawa, *Bull. Chem. Soc. Jpn.*, **57**, 2069 (1984).
11) T. Sekiya and T. Matsushita, *Yogyo-Kyokaishi (Japan)*, **85**, 13 (1977); *Report Gov. Ind. Res. Inst., Nagoya*, **27**, 92 (1978).
12) G. Anderson, *Acta Chem. Scand.*, **8**, 1599 (1954).

The Crystal and Molecular Structure of *N*-Ethylcarbazole†

Toshihiko KIMURA,†† Yasushi KAI, Noritake YASUOKA,††† and Nobutami KASAI*
Department of Applied Chemistry, Faculty of Engineering, Osaka University, Yamadaoka, Suita, Osaka 565
(Received February 27, 1985)

N-Ethylcarbazole crystallizes in the orthorhombic system, space group Pbca with fairly large unit cell dimensions of a=7.971(1), b=24.615(3), c=56.587(5) Å, D_m=1.17 g cm^{-3}, D_c=1.168 g cm^{-3} for Z=40. The structure was solved by the direct method and refined anisotropically by the least-squares procedure, R=0.062 for 5134 non-zero reflections. Five crystallographically independent molecules are not different from each other, the carbazole group is planar, and the ethyl group attached to the nitrogen atom is almost perpendicular to the carbazole ring. In the crystal, each carbazole ring makes a similar angle with the a axis [52 to 55°].

Recently, intrinsic and extrinsic photoconductivities of *N*-ethylcarbazole has been extensively studied by H. Mikawa and his co-workers[1] in conncetion with those of poly(*N*-vinylcarbazole).[2] In order to obtain a basic information to elucidate the correlation between the structure and photoconductivity, the crystal structure analysis of *N*-ethylcarbazole has been carried out.

Experimental

A large single crystal, grown from melt in a Bridgeman furnace,[3] was supplied by H. Mikawa and his co-workers of this university. A crystal with approximate dimensions of 0.3×0.35×0.31 mm was cut out and coated with collodion in order to prevent sublimation during the X-ray experiment.

The crystal was mounted on a Rigaku automated, four-circle diffractometer. Nickel-filtered Cu $K\alpha$ radiation was used. Unit-cell dimensions were determined by the least-squares fit of 2θ values of 22 high angle reflections.

Crystal Data: $C_{14}H_{13}N$, M=195.27, orthorhombic, space group Pbca (No. 61), a=7.791 (1), b=24.615 (3), c=56.587 (5) Å, V=11104 (2) Å^3, D_m=1.17 g cm^{-3} (by flotation in an aqueous solution of $ZnCl_2$), D_c=1.168 g cm^{-3} for Z=40, μ (Cu $K\alpha$)= 5.80 cm^{-1}.

Integrated intensities were measured on the diffractometer by the θ—2θ scan technique. The 2θ scan rate and scan width were 4° min^{-1} and $\Delta 2\theta$=(2.0+0.7 tanθ)°, respectively. Backgrounds were measured for 7.5 s before and after the scan of each peak. Intensities of five standard reflections were measured after every 52 reflections, $|F|$ values of which changed about 3 to 5% with time. Their changes could be expressed approximately by a fifth order equation, the coefficients of which were determined from the intensity changes of three stronger reflections, 080, 0,0,16, and 600, and the observed $|F|$ values were corrected with time. A total of 6993 independent (5215 non-zero) reflections was collected up to 2θ=110°. Usual Lorentz and polarization corrections were made but absorption and extinction corrections were ignored.

Solution of the Structure and Refinement

The crystal data show that the corresponding space group is Pbca and 40 molecules are contained per unit cell. The asymmetric unit consists of 5 independent molecules.

The structure could be established by the direct method using *MULTAN* program.[4] Of the 32 choices of the starting sets, only one gave the figure of merit larger than 0.8. The $|E|$ map was then computed using the phases based on this starting set. 54 peaks out of 75 high peaks in the $|E|$ map revealed non-hydrogen atoms of three independent molecules out of five and also parts of the ethyl and carbazole moieties of the other molecules. The successive Fourier synthesis could locate all of the remaining non-hydrogen atoms.

The structure was refined anisotropically by the block-diagonal least-squares procedure (*HBLS* V).[5] The function minimized was $\sum w(\Delta F)^2$, where w=1. Hydrogen atoms except those of the methyl groups were located on a difference Fourier map, which were refined isotropically. In the final cycle of the refinement the R index decreased to 0.062 for 5134 non-zero reflections. Final atomic coordinates with equivalent temperature factors[6] are listed in Table 1.††††

Atomic scattering factors for non-hydrogen atoms were taken from International Tables for X-Ray Crystallography, Vol. IV,[7] and those of hydrogen atoms from Stewart and co-workers.[8]

All the Computations were carried out mainly on a NEAC 2200-700 computer at the Computation Center and at the final stage on an ACOS 850 computer at the Crystallographic Research Center, Institute for Protein Research, Osaka University.

Results and Discussion

Molecular Structure. Since five independent molecules do not differ significantly from each other, only the structure of the molecule 1 is depicted in Fig. 1, with the numbering scheme of atoms. Bond lengths and bond angles in five molecules are given in Table 2.†††††

†Presented at the Tenth Congress of the International Union of Crystallography, Amsterdam (1975).

††Present address: Photographic Research and Developement Laboratory, Konishiroku Photo Ind. Co. Ltd., Sakuramachi, Hino, Tokyo 191.

†††Present address: Himeji Institute of Technology, Shosha, Himeji, Hyogo 671-22.

††††Tables of anisotropic thermal parameters, atomic coordinates of hydrogen atoms and observed and calculated structure factors are deposited at the Chemical Society of Japan, Document No. 8533.

†††††Deposited at the Chemical Society of Japan, Document No. 8533.

TABLE 1. FINAL ATOMIC COORDINATES OF *N*-ETHYLCARBAZOLE WITH ESTIMATED STANDARD DEVIATIONS IN PARENTHESES

a) Non-hydrogen atoms

Atom	*x*	*y*	*z*	B_{eq}/Å^2	Atom	*x*	*y*	*z*	B_{eq}/Å^2
N(100)	0.3233(4)	0.41703(13)	0.13319(6)	4.6	C(312)	0.1145(6)	0.28523(17)	0.05090(7)	5.0
C(101)	0.4112(5)	0.40700(16)	0.11243(7)	4.4	C(313)	−0.0027(7)	0.32490(17)	0.04540(8)	5.9
C(102)	0.3807(6)	0.36841(18)	0.09521(8)	5.9	C(314)	−0.1279(6)	0.31603(18)	0.02891(8)	5.9
C(103)	0.4872(7)	0.36735(21)	0.07609(9)	7.6	C(315)	−0.1409(5)	0.26683(17)	0.01753(7)	4.9
C(104)	0.6184(7)	0.40381(22)	0.07409(9)	7.0	C(316)	−0.0245(5)	0.22619(15)	0.02259(6)	3.7
C(105)	0.6504(6)	0.44167(18)	0.09127(8)	5.3	C(370)	0.3517(6)	0.18566(18)	0.05579(8)	5.3
C(106)	0.5450(5)	0.44390(16)	0.11072(7)	4.0	C(380)	0.5039(6)	0.20720(21)	0.04334(9)	7.0
C(111)	0.3944(5)	0.46114(16)	0.14424(7)	4.3	N(400)	−0.0242(5)	0.44367(15)	0.20091(6)	5.6
C(112)	0.3469(6)	0.48760(17)	0.16492(7)	5.2	C(401)	0.0721(5)	0.40287(18)	0.21029(7)	4.8
C(113)	0.4382(6)	0.53245(18)	0.17170(8)	5.8	C(402)	0.0558(7)	0.34685(20)	0.20761(8)	6.3
C(114)	0.5768(6)	0.55029(17)	0.15914(8)	5.6	C(403)	0.1684(8)	0.31417(21)	0.21931(9)	7.7
C(115)	0.6272(6)	0.52346(16)	0.13882(7)	4.9	C(404)	0.2951(7)	0.33545(23)	0.23331(9)	7.8
C(116)	0.5353(5)	0.47853(15)	0.13123(7)	3.9	C(405)	0.3112(6)	0.39060(22)	0.23612(7)	6.4
C(170)	0.1583(6)	0.39463(18)	0.13926(8)	5.5	C(406)	0.1992(5)	0.42500(18)	0.22457(7)	5.0
C(180)	0.0152(6)	0.42576(20)	0.12829(10)	7.0	C(411)	0.0339(6)	0.49224(18)	0.20955(7)	5.4
N(200)	0.1800(4)	0.09878(14)	0.42261(6)	5.0	C(412)	−0.0257(7)	0.54428(21)	0.20522(10)	7.7
C(201)	0.0986(5)	0.05792(17)	0.43441(7)	4.9	C(413)	0.0560(9)	0.58659(22)	0.21578(11)	9.5
C(202)	0.1362(6)	0.03274(21)	0.45601(8)	6.9	C(414)	0.1947(9)	0.57813(23)	0.23034(10)	9.5
C(203)	0.0294(8)	−0.00807(23)	0.46361(9)	8.0	C(415)	0.2560(7)	0.52651(22)	0.23458(8)	7.4
C(204)	−0.1070(7)	−0.02505(20)	0.45036(9)	7.3	C(416)	0.1743(6)	0.48251(19)	0.22411(7)	5.4
C(205)	−0.1436(6)	−0.00093(17)	0.42926(8)	5.8	C(470)	−0.1822(6)	0.43554(21)	0.18842(8)	6.7
C(206)	−0.0404(5)	0.04091(16)	0.42092(7)	4.5	C(480)	−0.3300(6)	0.43108(23)	0.20520(9)	7.3
C(211)	0.0995(5)	0.10749(16)	0.40137(7)	4.5	N(500)	0.1906(5)	0.28059(14)	0.33122(7)	5.8
C(212)	0.1407(6)	0.14301(17)	0.38320(8)	5.6	C(501)	0.2851(6)	0.27188(17)	0.35128(8)	5.7
C(213)	0.0422(7)	0.14239(19)	0.36337(9)	6.4	C(502)	0.2694(7)	0.29519(19)	0.37376(9)	6.7
C(214)	−0.0966(6)	0.10866(19)	0.36132(8)	6.2	C(503)	0.3828(8)	0.27928(22)	0.39068(9)	8.0
C(215)	−0.1388(6)	0.07398(17)	0.37948(8)	5.2	C(504)	0.5081(7)	0.24275(22)	0.38622(9)	7.8
C(216)	−0.0394(5)	0.07277(15)	0.39981(7)	4.1	C(505)	0.5254(6)	0.21951(20)	0.36415(9)	6.9
C(270)	0.3410(6)	0.12253(21)	0.42920(9)	6.5	C(506)	0.4123(6)	0.23432(17)	0.34629(8)	5.4
C(280)	0.4873(6)	0.09255(23)	0.41845(10)	7.8	C(511)	0.2499(6)	0.24685(17)	0.31357(8)	5.5
N(300)	0.2000(4)	0.18948(12)	0.04151(6)	4.2	C(512)	0.1910(7)	0.24082(20)	0.29050(9)	7.0
C(301)	0.1394(5)	0.15101(15)	0.02581(7)	4.1	C(513)	0.2737(8)	0.20527(23)	0.27600(9)	8.3
C(302)	0.2002(6)	0.09864(17)	0.02182(8)	5.3	C(514)	0.4115(8)	0.17573(21)	0.28425(10)	8.3
C(303)	0.1169(7)	0.06783(17)	0.00532(9)	6.5	C(515)	0.4715(7)	0.18157(19)	0.30681(9)	6.8
C(304)	−0.0203(7)	0.08780(19)	−0.00673(8)	6.5	C(516)	0.3889(6)	0.21767(17)	0.32199(8)	5.5
C(305)	−0.0820(6)	0.13942(18)	−0.00282(8)	5.5	C(570)	0.0314(7)	0.31002(20)	0.33027(9)	7.1
C(306)	−0.0003(5)	0.17197(15)	0.01385(6)	3.9	C(580)	−0.1157(7)	0.27405(23)	0.33681(11)	8.7
C(311)	0.1015(5)	0.23559(15)	0.03932(6)	3.7					

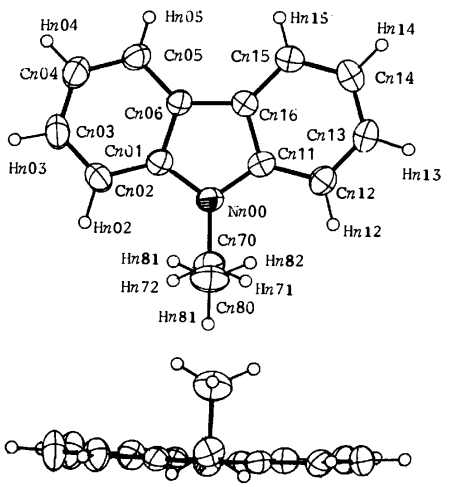

Fig. 1. Molecular structure of *N*-ethylcarbazole (*ORTEP* drawing).[11]
Non-hydrogen atoms are drawn as thermal ellipsoids with 30% probability level and hydrogen atoms as spheres with $B=1.0$ Å^2.
(a) Plan. (b) Side view.

The carbazole moiety is approximately planar (Fig. 1(b)), and no significant difference has been observed between chemically-equivalent bond lengths and bond angles. Average values of bond lengths and bond angles are compared in Table 3 with those of carbazole[9] and *N*-vinylcarbazole.[10] All of the corresponding lengths and angles in the three compounds show accordances within the limit of errors.

In each of the present *N*-ethylcarbazole molecule, the C(*n*01)-N(*n*00)-C(*n*70) angle [av. 125.3°] is equal to the corresponding C(*n*11)-N(*n*00)-C(*n*70) angle [av. 124.5°] and the N(*n*00)-C(*n*01)-C(*n*02) [av. 129.7°] equal to the N(*n*00)-C(*n*11)-C(*n*12) [av. 129.8°]. The ethyl group attached to the nitrogen atom is almost perpendicular to the carbazole plane [av. 87.8°]. On the other hand, in *N*-vinylcarbazole the ethylenic bond planes in two independent molecules make angles of 14.0 and 2.6° with the carbazole planes. The C(01)-N-C(70) angle [128.6(7) or 130.6(7)°] is, therefore, much larger than the C(11)-N-C(70) angle[122.9(7) or

TABLE 3. COMPARISON OF AVERAGE BOND LENGTH AND BOND ANGLES IN CARBAZOLE RING

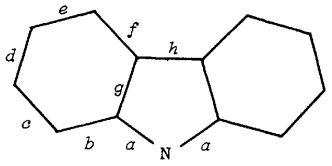

	N-Ethyl-carbazole[a]	*N*-Vinyl-carbazole[10]	Carbazole[9]
Bond lengths[l/Å][b]			
a	1.372(8)	1.393(2)	1.394
b	1.391(6)	1.404(7)	1.404
c	1.365(6)	1.378(8)	1.374
d	1.367(8)	1.389(8)	1.394
e	1.374(6)	1.385(7)	1.392
f	1.385(6)	1.388(2)	1.391
g	1.386(4)	1.401(3)	1.408
h	1.437(9)	1.442(7)	1.479
Bond angles[ϕ/°][b]			
aa	109.0(2)	108.3(1)	108.4
ab	129.8(3)	129.6(4)	128.4
ag	108.8(2)	109.0(4)	109.7
bg	121.5(2)	121.5(6)	121.9
bc	118.1(1)	117.0(5)	115.6
cd	121.2(2)	122.1(7)	123.9
de	121.1(2)	120.8(8)	120.1
ef	119.3(2)	118.6(9)	117.9
fh	134.4(2)	133.0(6)	133.3
fg	118.8(1)	120.1(9)	120.6
gh	106.7(2)	106.9(4)	106.1

a) Present study. b) Average: $\bar{x}=\sum x_i/n$, where x_i is the individual bond length or angle observed, and n is the number of chemically equivalent structural parameters. Estimated standard deviation of average: $\sigma(\bar{x})=\{\sum(x_i-\bar{x})^2/n(n-1)\}^{1/2}$

TABLE 4. INTERMOLECULAR ATOMIC CONTACTS LESS THAN 3.6 Å[l/Å]

C(270)···C(301)[a]	3.518(6)	C(105)···C(180)[b]	3.552(7)
C(370)···N(200)[a]	3.551(5)	C(380)···C(315)[b]	3.457(7)
C(380)···N(200)[a]	3.566(6)	C(380)···C(480)[b]	3.445(8)
		C(505)···C(580)[b]	3.466(8)

key, a: 0.5+x, y, 0.5−z,
b: 1+x, y, z.

121.2(7)°].[10] The carbazole molecule has crystallographic mirror symmetry about the plane, vertical to the C(06)-C(16), which includes the N and H atoms.[9]

Crystal Structure. Figure 2 shows the crystal structure of *N*-ethylcarbazole projected along the a axis. Carbazole rings of the five independent molecules make similar angles with the a axis, the angles ranging from 36.1 to 38.3°. It is remarkable that no pair of neighboring molecules, in which the π-electron clouds of the carbazole rings overlaps, is found. All the molecules contact with each other by the van der Waals force (Table 4). The closest intermolecular distance between non-hydrogen atoms is observed between molecules directly related by the glide plane [C(405)(x, y, z)···C(480)(1+x, y, z)=3.445(8) Å]. In

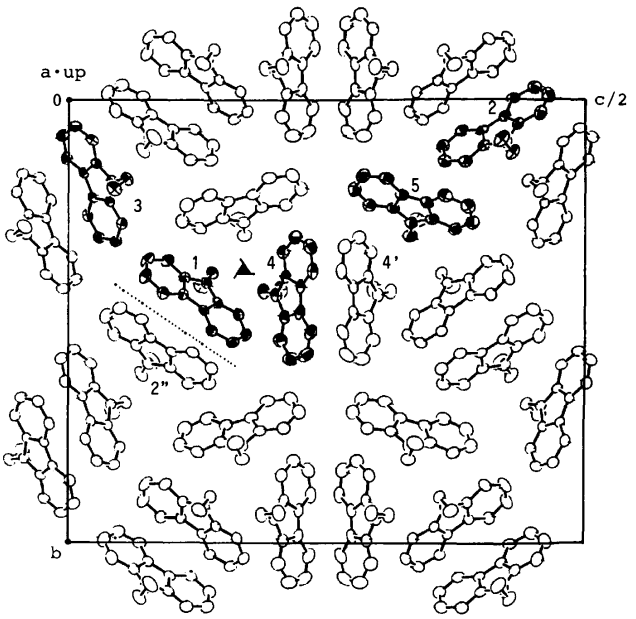

Fig. 2. Crystal structure of *N*-ethylcarbazole (*ORTEP* drawing).[11]
Non-hydrogen atoms are drawn as thermal ellipsoids with 30% probability level. Hydrogen atoms are omitted for clarity. Atoms belong to the five molecules in an asymmetric unit are drawn as ellipsoids with principal and enveloping ellipses whereas others only with enveloping ellipses.
Local pseudo symmetries are also given.

the packing of molecules the following pseudo-symmetries can be locally observed besides the crystallographic symmetry operations: 1) a local pseudo a-glide plane, expressed by a broken line in Fig. 2, between the molecules 1 (x, y, z) and 2'' (−x, 0.5+y, 0.5−z) and 2) a local pseudo three-fold screw axis parallel to the a axis among the molecules 4 (x, y, z), 1 (x, y, z), and 5 (0.5+x, y, 0.5−z).

The authors wish to express their deep thanks to Professor Hiroshi Mikawa and his co-workers of Osaka University for the supply of crystals and helpful discussions. Thanks are also due to Miss Nobuko Kanehisa who helped the authors at the final stage of the computations and *ORTEP* drawings.

References

1) K. Kato, M. Yokoyama, and H. Mikawa, *Bull. Chem. Soc. Jpn.*, **47**, 1795 (1974); K. Kato, T. Nogami, M. Yokoyama, and H. Mikawa, *Chem. Lett.*, **1974**, 1097.

2) M. Yokoyama, S. Shimokihara, A. Matsubara, and H. Mikawa, *J. Chem. Phys.*, **76**, 724 (1982).

3) K. Kato, M. Yokoyama, K. Okamoto, S. Kusabayashi, H. Mikawa, K. Yoshihara and S. Nagakura, *Mol. Cryst. Liq. Cryst.*, **28**, 37 (1974).

4) G. Germain, P. Main, and M. M. Woolfson, *Acta Crystallogr., Sect. A*, **27**, 368 (1971).

5) T. Ashida, *HBLS* V, "The Universal crystallographic Computing System-Osaka," The Computation Center, Osaka Univ., 1973, p. 55.

6) W. C. Hamilton, *Acta Crystallogr.*, **12**, 609 (1959).
7) International Tables for X-Ray Crystallography, Vol. IV, Kynoch Press, Birmingham (1974), p. 71.
8) R. F. Stewart, E. R. Davidson, and W. T. Simpson, *J. Chem. Phys.*, **42**, 3175 (1965).
9) M. Kurahashi, M Fukuyo, A. Shimada, A. Furusaki, I. Nitta, *Bull. Chem. Soc. Jpn.*, **42**, 2174 (1969).
10) K. Tsutsui, K. Hirotsu, M. Umesaki, M. Kurahashi, A. Shimada, T. Higuchi, *Acta Crystallogr., Sect. B*, **32**, 3049 (1976).
11) C. K. Johnson, *ORTEP* II, Report ORNL-5138, Oak Ridge National Laboratory, Tennessee (1976).

Crystal Structures of Complexes between Hexacyanobutadiene and Tetramethyltetrathiafulvalene and Tetramethylthiotetrathiafulvalene

Chuji KATAYAMA, Masako HONDA, Hiroaki KUMAGAI, Jiro TANAKA,*
Gunzi SAITO,†† and Hiroo INOKUCHI†
Department of Chemistry, Faculty of Science, Nagoya University, Chikusa-ku, Nagoya 464
†*Institute for Molecular Science, Myodaiji, Okazaki 444*
(Received March 6, 1985)

Hexacyanobutadiene(HCBD) forms two kinds of molecular complexes with tetramethyltetrathiafulvalene (TMTTF) one kind with tetramethylthiotetrathiafulvalene(TTMTTF). The crystal structures of these complexes and neutral TTMTTF are determined by X-ray analyses. $(TMTTF)_2$·HCBD is composed of 2:1 donor and acceptor, and TMTTF exists as a dimer cation stacked along the c axis. HCBD anions are included in the cavity of the dimer stack directing their molecular planes parallel to the stacking axis. TMTTF·HCBD is composed of 1:1 donor and acceptor, and has segregated cation and anion stacks with the interplanar spacing of 3.61 Å in TMTTF and 3.43 Å in HCBD columns. TTMTTF·HCBD is shown to have a regular segregated column with a partial charge transfer. Neutral TTMTTF has a non-planar conformation. The C=C and C–S bond lengths of the donors in free and complexed states are correlated with the degree of the charge transfer in these four complexes, and linear relationships are found between these two quantities.

Hexacyanobutadiene (HCBD) is one of the strongest electron acceptors[1,2] and is expected to give charge-transfer complexes.[3] A weak or medium electron donor may form a nominally neutral, weak complex or a segregated mixed valence complex, and a good electron donor may crystallize as an ionic complex. Single crystals of HCBD complexes with tetramethyltetrathiafulvalene (TMTTF) and tetramethylthiotetrathiafulvalene (TTMTTF) were prepared and two complexes of TMTTF·HCBD were obtained; one is 2:1 and the other is 1:1 donor to acceptor ratio. TTMTTF·HCBD formed a crystal of 1:1 ratio.[4]

The crystal structures of these three complexes and that of free TTMTTF were analyzed and the molecular structures of the donors are discussed based on the structural data and the electronic structures of the complexes. This information will be used for the interpretation of the physical properties of these complexes in the succeeding paper.[5]

Experimental

Preparation of HCBD Complexes. HCBD was prepared by the method of Webster.[1] The product was identified by mass and infrared spectra. Molecular complexes of HCBD with TMTTF and TTMTTF were obtained by mixing hot acetonitrile solutions of the donor and the acceptor in the same flask. Complex crystals were grown in the refrigerator for overnight. Two complexes of TMTTF·HCBD were obtained; $(TMTTF)_2$·HCBD crystal is a hexagonal prism of dark green color with the (100), (001), and (20$\bar{1}$) faces and

TABLE 1. CRYSTALLOGRAPHIC DATA

	$(TMTTF)_2$·HCBD	TMTTF·HCBD	TTMTTF·HCBD	TTMTTF
Chemical formula	$C_{30}H_{24}N_6S_8$	$C_{20}H_{12}N_6S_4$	$C_{20}H_{12}N_6S_8$	$C_{10}H_{12}S_8$
$D:A$	2:1	1:1	1:1	—
FW	725.10	464.61	592.89	388.73
Space group	C2/m	C2/m	C2/c	$P2_1/n$
a/Å	18.266(2)	12.8016(10)	30.161(3)	15.668(1)
b/Å	9.813(1)	21.6196(9)	4.046(1)	7.804(1)
c/Å	9.501(1)	4.0223(3)	23.414(2)	14.010(2)
β/°	102.741(8)	108.062 (7)	117.48 (1)	106.16 (1)
V/Å^3	1661.0 (3)	1058.4 (2)	2534.7 (5)	1645.5 (4)
Z	2	2	4	4
d_{obd}/g/cm^3	1.46	1.46	1.53	1.56
d_{cald}/g/cm^3	1.45	1.46	1.55	1.57
R	0.042	0.049	0.051	0.053
$2\theta_{max}$/°	126	126	126	126
No. of non-zero unique data	1398	867	1954	2593
Crystal size/mm	0.15×0.16×0.35	0.18×0.03×0.38	0.09×0.02×1.11	0.15×0.15×0.75
μ(Cu $K\alpha$)/cm^{-1}	50.46	41.24	64.94	95.89
transmission factor	—	0.48—0.88	0.56—0.88	0.23—0.24
λ(Cu $K\alpha$)/Å	1.5418	1.5418	1.5418	1.5418
Diffractometer	Rigaku automated four-circle diffractometer			

††Present address: The Institute for Solid State Physics, The University of Tokyo, Minato-ku, Tokyo 106.

it is composed of two donor and one acceptor molecules. TMTTF·HCBD is a one to one complex and the crystal is a thin plate showing golden luster with the (010) face. TTMTTF·HCBD is a complex of 1:1 donor to acceptor ratio. The crystal is a black rod elongated along the b axis with the (100) and (001) faces. TTMTTF is a crystal of an orange color.

Crystal Structure Analysis. The X-ray diffraction data were collected by use of an automated four-circle diffractometer, Rigaku AFC-5, set on a rotating anode X-ray generator, Rigaku RU-200, with a graphite monochromated Cu radiation (Cu $K\alpha$=1.5418 Å). Composition of the complexes and crystallographic data are listed in Table 1 together with experimental results. Crystal structures were solved by the Monte-Carlo direct method[6] using MULTAN 78 program system[7] and were refined on F^2 by the full-matrix least-squares program with the analytical absorption correction.[8] Atomic scattering factors were taken from International Tables for X-ray Crystallography.[9] ORTEP[10] was used for drawing of the molecular and crystal structures. Anisotropic temperature factors were used for the refinement of the non-H atoms. All H atoms were located from difference Fourier maps and were refined with the isotropic temperature factors equivalent to that of the bonded carbon atoms.

TABLE 2. POSITIONAL PARAMETERS ($\times 10^5$) AND EQUIVALENT ISOTROPIC THERMAL PARAMETERS WITH *e.s.d.*·*s* IN PARENTHESES

$B_{eq}=8/3\pi^2\,\Sigma_i\Sigma_j U_{ij}a_i^*a_j^*\boldsymbol{a}_i\boldsymbol{a}_j$

$(TMTTF)_2$·HCBD	*x*	*y*	*z*	$B_{eq}/10^2$Å^2
S(1T)	96259(2)	14820(5)	18134(5)	361(1)
S(1S)	110011(2)	14838(5)	46333(5)	363(1)
C(2T)	100197(14)	0	26349(29)	332(5)
C(2S)	105983(14)	0	38324(29)	331(5)
C(5T)	89724(10)	6802(23)	4445(19)	373(4)
C(5S)	116945(9)	6788(20)	59327(19)	353(4)
C(7T)	84727(15)	15830(32)	−6179(29)	506(6)
C(7S)	122269(11)	15963(28)	69202(25)	456(5)
C(1H)	47425(31)	0	29424(52)	672(13)
C(2H)	46652(37)	0	43994(95)	368(20)
C(3H)	51840(86)	0	44859(156)	668(42)
C(4H)	40245(34)	0	20302(65)	748(16)
N(5H)	34378(31)	0	13096(68)	1009(20)
C(6H)	39600(20)	0	48834(53)	604(11)
N(7H)	33436(19)	0	48574(46)	703(11)
C(8H)	53331(31)	0	22304(62)	727(14)
N(9H)	58042(29)	0	16119(71)	1075(21)
H(7TA)	80186(206)	16151(340)	−4435(368)	506(*)
H(7TB)	85438(203)	14584(352)	−13482(417)	506(*)
H(7TC)	85130(179)	24481(359)	−3186(361)	506(*)
H(7SA)	125490(185)	11348(334)	76103(371)	456(*)
H(7SB)	119961(173)	21975(326)	74169(337)	456(*)
H(7SC)	125284(173)	20557(319)	64045(344)	456(*)

TMTTF·HCBD	*x*	*y*	*z*	$B_{eq}/10^2$Å^2
S(1T)	60682(5)	7525(2)	44756(19)	439(12)
C(2T)	50000	3252(15)	50000	387(14)
C(5T)	54966(20)	14739(10)	47499(71)	416(13)
C(7T)	61570(28)	20240(13)	44037(99)	546(14)
C(1H)	100000	8854(18)	100000	579(17)
C(2H)	103272(34)	2408(20)	97292(123)	371(16)
C(4H)	108346(32)	12375(15)	93115(99)	648(16)
N(5H)	114953(34)	15415(19)	87695(123)	959(18)
C(6H)	113099(32)	0	88601(114)	545(17)
N(7H)	120839(29)	0	81156(120)	660(18)
H(7TA)	57603(282)	24047(167)	40748(927)	546(*)
H(7TB)	64115(286)	19878(182)	26558(1005)	546(*)
H(7TC)	667571(291)	20795(167)	63197(1007)	546(*)

TTMTTF·HCBD	*x*	*y*	*z*	$B_{eq}/10^2$Å^2
S(1T)	71636(2)	4812(25)	5681(2)	441(6)
C(2T)	75781(10)	17452(92)	2956(13)	423(10)
S(3T)	81991(2)	9580(25)	8075(2)	467(6)
C(4T)	80996(10)	−6435(87)	14264(11)	417(10)
C(5T)	76137(10)	−9137(81)	13073(13)	397(10)
S(6T)	85864(2)	−19848(32)	21441(3)	585(6)
C(7T)	91302(16)	−5853(175)	21057(31)	820(19)
S(8T)	74547(2)	−27064(23)	18628(2)	479(6)
C(9T)	68145(14)	−14583(111)	15845(19)	529(12)
C(1H)	96597(15)	32813(120)	4486(22)	672(15)
C(2H)	97823(22)	40292(166)	−666(40)	354(19)
C(3H)	100246(38)	50158(252)	3042(40)	521(27)
C(4H)	92272(15)	13140(130)	1787(19)	656(15)
N(5H)	88842(15)	−3543(139)	−82(22)	878(18)
C(6H)	95059(13)	30266(117)	−7507(19)	595(13)
N(7H)	92192(11)	18758(114)	−12022(15)	701(13)
C(8H)	98246(18)	40467(139)	11038(26)	766(18)
N(9H)	99356(22)	46245(175)	16244(28)	1212(27)
H(7TA)	93702(218)	−14596(1519)	24433(285)	820(*)
H(7TB)	91220(219)	14855(1617)	20224(301)	820(*)
H(7TC)	91485(209)	−12314(1593)	16872(279)	820(*)
H(9TA)	66996(167)	−26332(1239)	18392(230)	529(*)
H(9TB)	68022(175)	8788(1331)	15671(231)	529(*)
H(9TC)	66353(169)	−24514(1292)	11843(239)	529(*)

TTMTTF	*x*	*y*	*z*	$B_{eq}/10^2$Å^2
S(1T)	39724(6)	23842(13)	38353(6)	451(6)
S(1S)	24083(6)	25540(10)	49006(6)	386(6)
C(2T)	31612(22)	39841(46)	35640(23)	341(10)
C(2S)	25140(22)	40872(44)	40250(23)	326(10)
S(3T)	32809(6)	54067(14)	26398(6)	425(6)
S(3S)	17043(6)	56958(11)	38157(6)	377(6)
C(4T)	44253(25)	49656(53)	28540(26)	427(11)
C(4S)	14590(19)	53447(41)	49568(23)	291(9)
C(5T)	47454(25)	35967(56)	34091(29)	444(12)
C(5S)	17739(19)	39035(43)	54491(22)	292(9)
S(6T)	50307(7)	62301(15)	22418(7)	552(7)
S(6S)	7194(5)	67389(11)	52944(6)	378(6)
C(7T)	51368(34)	82070(65)	29217(40)	530(14)
C(7S)	11845(43)	87948(60)	51112(44)	599(17)
S(8T)	58328(7)	28321(23)	36560(10)	706(7)
S(8S)	14824(5)	31580(11)	64922(6)	345(6)
C(9T)	60759(38)	20495(99)	48926(47)	669(18)
C(9S)	25413(29)	24609(80)	72705(34)	551(14)
H(7TA)	51446(368)	88533(905)	23555(457)	530(*)
H(7TB)	55284(394)	80184(857)	35902(459)	530(*)
H(7TC)	45726(403)	86923(869)	28828(425)	530(*)
H(7SA)	8786(394)	93550(879)	53160(446)	599(*)
H(7SB)	9245(358)	88295(845)	44091(439)	599(*)
H(7SC)	18573(395)	87813(837)	53580(408)	599(*)
H(9TA)	66091(481)	17677(1032)	50768(538)	669(*)
H(9TB)	60311(510)	30263(1071)	51073(581)	669(*)
H(9TC)	57379(476)	10515(1104)	49221(518)	669(*)
H(9SA)	27525(384)	14515(911)	68986(439)	551(*)
H(9SB)	24593(400)	19582(883)	77948(499)	551(*)
H(9SC)	29532(394)	33655(925)	73350(445)	551(*)

* The B_{eq} of hydrogen atoms were assumed to be the same with the values for the attached C atoms.

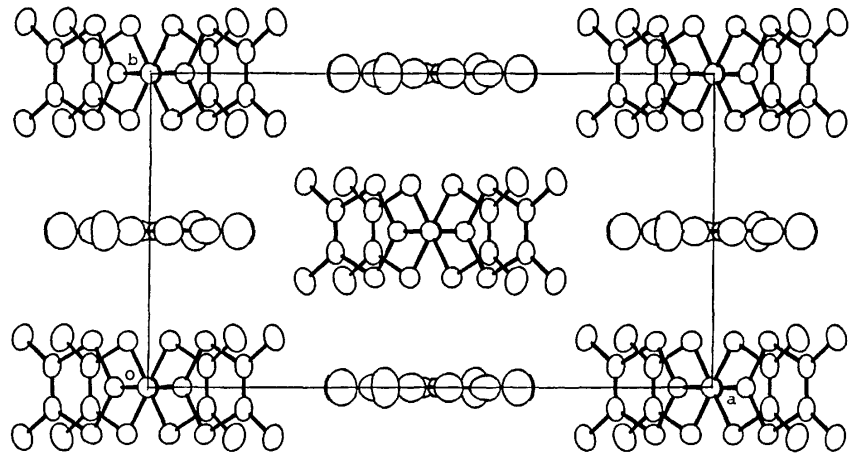

Fig. 1. Crystal structure of $(TMTTF)_2 \cdot HCBD$ projected along the c axis.

The final atomic parameters are listed in Table 2. All computations were carried out at the Computation Center of Nagoya University. The complete F_o—F_c data and the anisotropic temperature parameters are deposited as Document No. 8535 at the Office of the Editor of Bull. Chem. Soc. Jpn.

Results and Discussion

Crystal Structure. $(TMTTF)_2 \cdot HCBD$: Crystal of $(TMTTF)_2 \cdot HCBD$ is composed of two donor and one acceptor molecules. The TMTTF molecules form a dimer, and the stacking axis is parallel to the c axis as shown in Fig. 1. HCBD molecules are included in the channels surrounded by the TMTTF columns and they are lined up without face to face stacking. A crystallographic two-fold axis penetrates the center of HCBD molecule and the molecules are disordered with a pseudo D_{2h} symmetry. The molecular plane of HCBD, which lies on a crystallographic mirror plane, is perpendicular to the plane of TMTTF molecule. The other mirror plane bisects the TMTTF molecule through the long axis.

In most donor-acceptor complexes having a segregated column, the stacking of both donor and acceptor molecules occur along the same direction; however, the present crystal shows different arrangement. It is conceivable that a large polarizability of HCBD parallel to the molecular plane may stabilize the charge resonance interaction in the dimer column of TMTTF. In the literature there are several examples in which the aromatic ring planes are arranged in the crystal parallel to the stacking axis of organic radicals.[11] From the bond length of the central C=C bond of TMTTF and the band position of the electronic spectra,[5] it is suggested that an oxidation occurs by transferring an electron in the ground state from one of the TMTTF dimer to the HCBD molecule. Accordingly the crystal is composed of $(TMTTF_2)^+ \cdot (HCBD)^-$. The interplanar spacing in the dimer is 3.53 Å and that between the dimer is 3.69 Å.

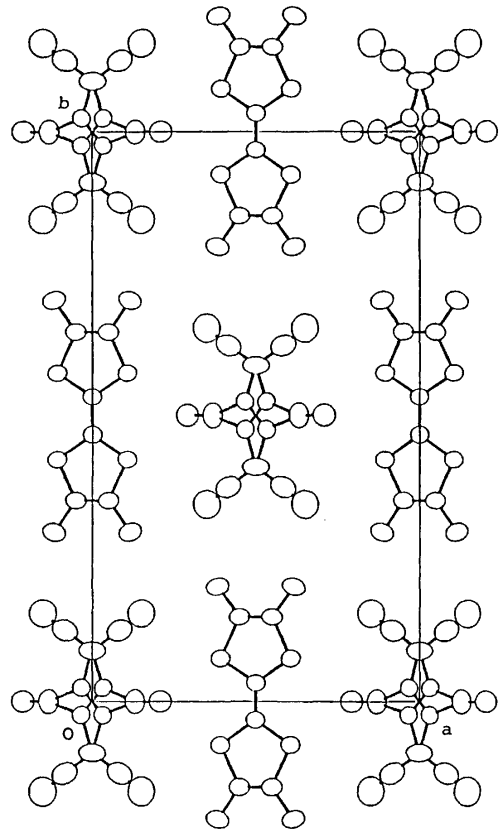

Fig. 2. Crystal structure of TMTTF·HCBD projected along the c axis.

TMTTF·HCBD: The crystal composition is one donor and the one acceptor. They are stacked in segregated columns extending along the c axis (Fig. 2). A mirror plane parallel to the (010) bisects the central C–C bonds of TMTTF and HCBD. A crystallographic two-fold axis penetrates the center of these molecules. The HCBD molecule is disordered in the positions of carbon atoms of the central C–C bond. As will be discussed in the next section, the charge transfer from TMTTF to HCBD seems to be complete, therefore this crystal has segregated columns com-

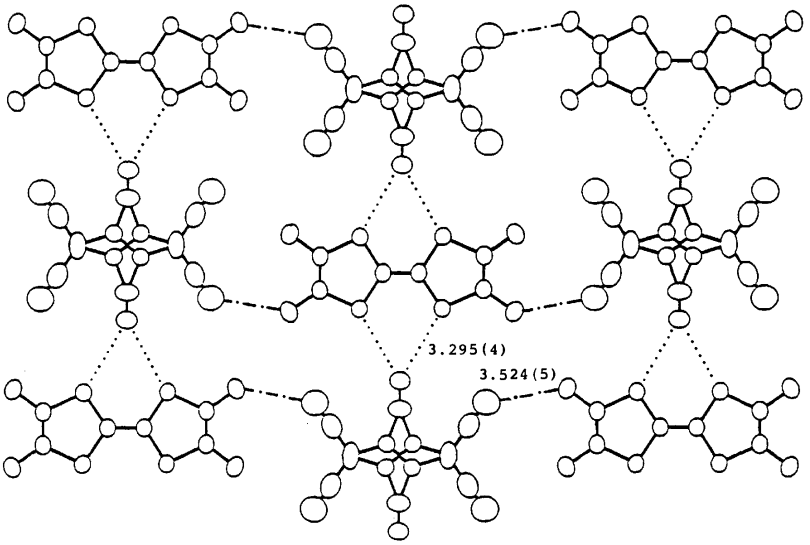

Fig. 3. The network of TMTTF and HCBD molecules projected onto the (101) plane. Close intermolecular distances are illustrated.

posed of ionic constituents. Such a structure of DA complex is known in the case of HMTTF·TCNQF$_4$.[12] The interplanar distance is 3.61 Å in the TMTTF cation column, which is a mean value of the inter- and intra-dimer distances in (TMTTF)$_2$·HCBD. The corresponding distance for HCBD anion is 3.43 Å. The Coulomb force between the charges of the same sign is repulsive for close contact of the same molecules; however, the covalent or the charge resonance interaction will favour a short interplanar distance. The actual molecular packing is determined by a balance of these repulsive and attractive interactions. The inter-column interaction between HCBD and TMTTF molecules is evident in the composite diagram of the (101) plane (Fig. 3). The closest contact is that between S···N with the distance of 3.295 (4) Å, which is shorter than the van der Waals distance of 3.35 Å, and two-dimensional network is formed.

TTMTTF·HCBD: The complex is made of the donor and the acceptor with 1:1 ratio, and they form segregated stacks along the b axis as shown in Fig. 4. Both the donor and the acceptor are stacked in one-dimensional regular lattice, and the spacing between the planes of adjacent TTMTTF molecules is 3.63 Å. The degree of the charge transfer from the donor to the acceptor is a partial one as will be discussed in the next section from the bond lengths. It is inferred that both the donor and the acceptor columns are in mixed valence state. The centers of the molecules are coincident with a center of symmetry of the crystal. The central carbon atoms in HCBD are disordered around the inversion center. There are several close distances between TTMTTF and HCBD in different columns, and they are S···S 3.510(1) Å where the van der Waals distance is 3.70 Å. In the polarized reflection spectra, there is some indication of the inter-column interaction.[5]

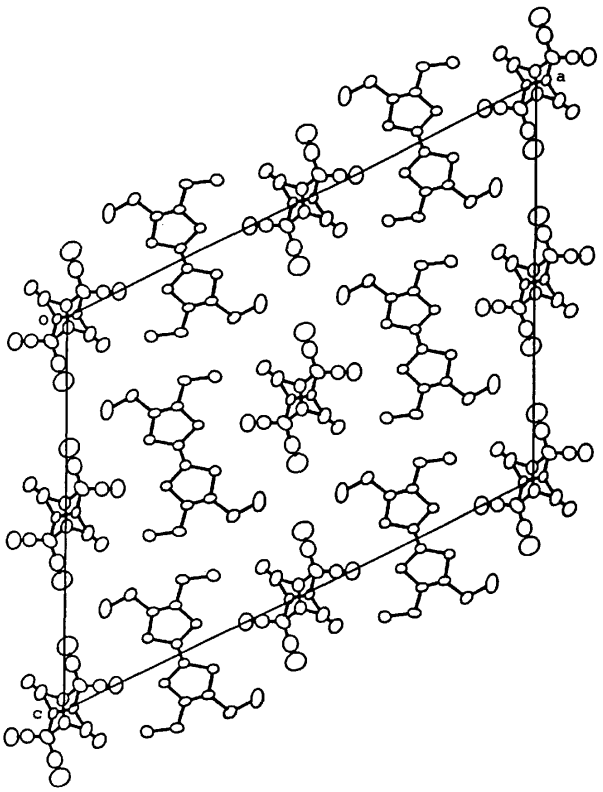

Fig. 4. Crystal structure of TTMTTF·HCBD projected onto the (010) plane.

TTMTTF: The arrangement of the molecules is projected onto the (010) plane as shown in Fig. 5. There are close contacts between S atoms of methylthio groups arranged along [10$\bar{1}$] ranging about 3.54—3.57 Å.

Molecular Structure. ORTEP drawings and important bond lengths are shown for the donor molecules in different crystals in Figs. 6—10. Several papers have been published in which the bond lengths

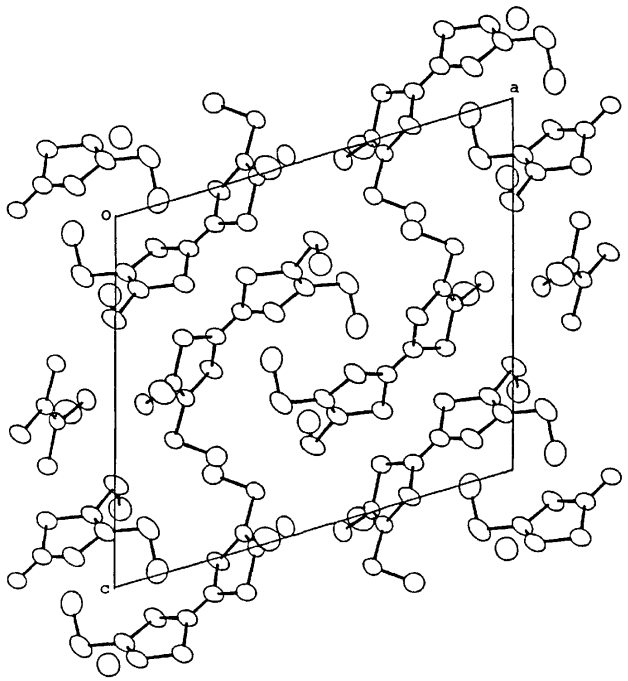

Fig. 5. Crystal structure of TTMTTF projected onto the (010) plane.

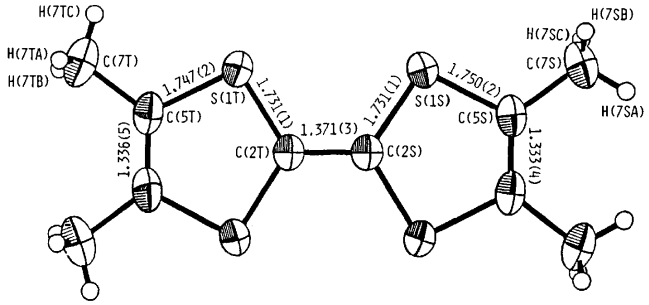

Fig. 6. Molecular structure of TMTTF in $(TMTTF)_2$ ·HCBD crystal.

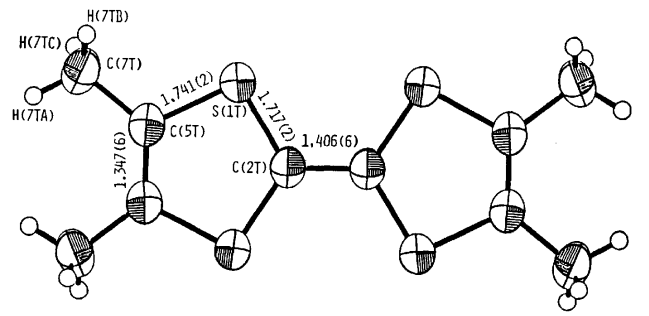

Fig. 7. Molecular structure of TMTTF in (TMTTF)·HCBD crystal.

of TTF analogues are discussed with reference to charges in the molecule.[11] We take the bond lengths of TTF[13] and TTMTTF and their salts TTF perchlorate,[14] and TTMTTF·AsF_6[15] as standards of the neutral and ionic species and draw the correlation diagram between the bond length and the degree of charge transfer as shown in Figs. 11 and 12. The results

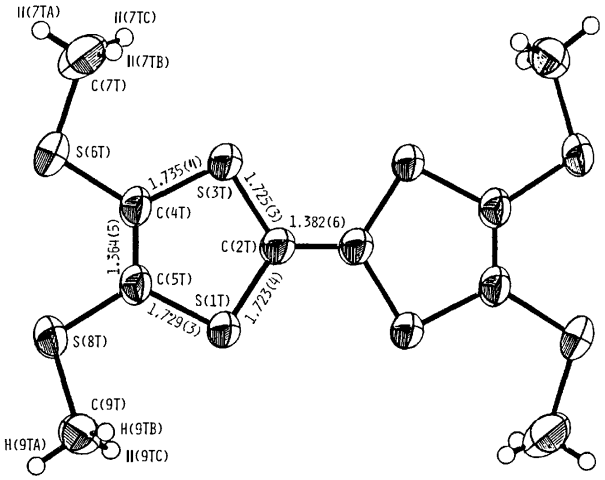

Fig. 8. Molecular structure of TTMTTF in (TTMTTF)·HCBD crystal.

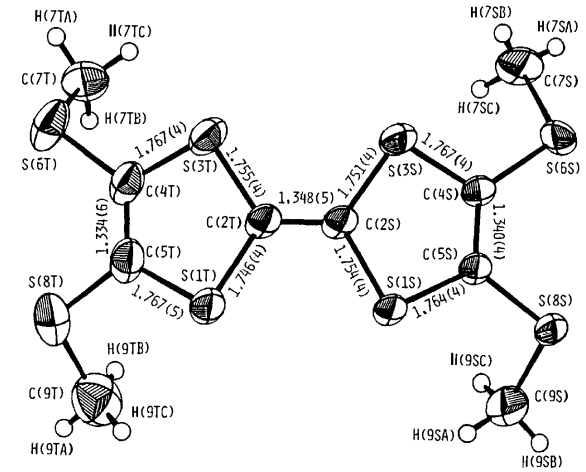

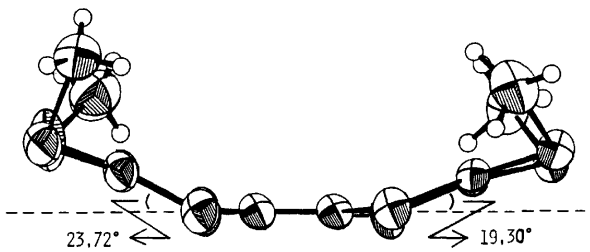

Fig. 9. Molecular structure of neutral TTMTTF (a) and the side view (b).

of the present crystal analysis clearly show that the charges of TMTTF in TMTTF·HCBD is one (ρ=1.0) and that of in $(TMTTF)_2$·HCBD is a half (ρ=0.5) and the value in TTMTTF·HCBD is ρ=0.4—0.6. The standard deviations of the present results are rather small as compared to the published data. We quote here the values for the crystals in which the ρ value is well established by chemical stoichiometry and by other means. They are TTF·TCNQ[16] $(TMTTF)_2$·Br,[17] $(TMTTF)_2$·BF_4 (at 100 K),[18] $(TMTTF)_2$·SCN,[19] HMTTF·TCNQ.[20] The strain caused by substituent groups or benzene ring fusion might be significant in

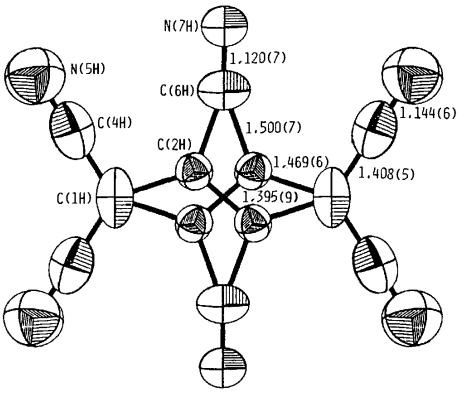

Fig. 10. Molecular structure of HCBD in (TMTTF)·HCBD crystal.

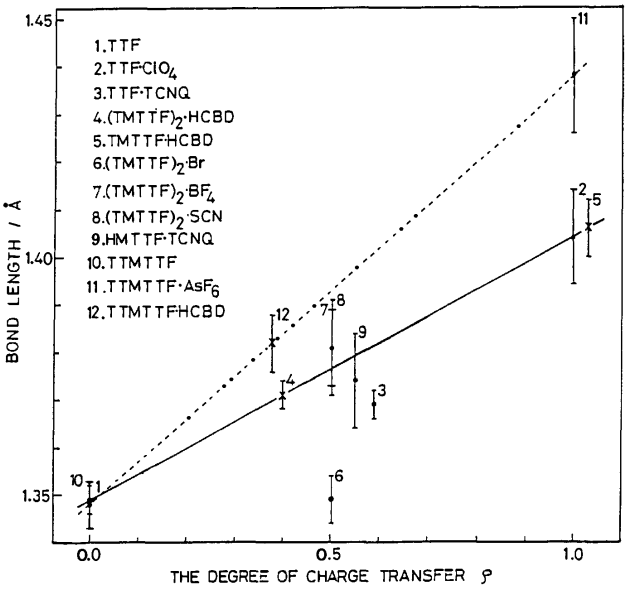

Fig. 11. The relation between the length of the central C=C bond and the degree of cherge transfer in TMTTF complexes (——) and TTMTTF complexes (---). The vertical line at each point illustrates the standard deviation.

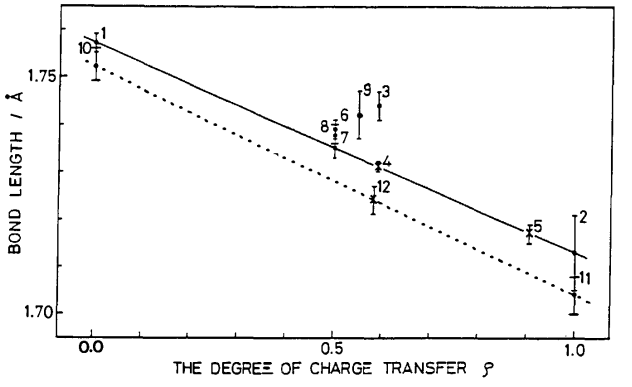

Fig. 12. The relation between the bond length (C–S) and the degree of charge transfer in TMTTF complexes (——) and TTMTTF complexes (----). The vertical line at each point illustrates the standard deviation.

changing the central C=C bond distance in dibenzotetrathiafulvalene series. In spite of this, the correlation between the bond lengths and the charge density seems to be useful for assessment of the electronic structure of the TTF type donors when the accuracy of structural analysis is sufficiently high.

The molecular structure of HCBD in the crystal of TMTTF·HCBD is illustrated in Fig. 10. However, the precise structure of HCBD is difficult to ascertain because the molecule is disordered in all complexes. It is remarkable that all C–C bond lengths in butadiene skelton are longer than normal values, presumably because all cyano groups will take electrons from the central carbon bonds.

The free TTMTTF molecule has a bent structure (Fig. 9b), in which all methylthio groups and the attached carbon atoms are displaced significantly from the central ring plane. The tilt angles are about 20° in both ends. The terminal C–S–C bonds are strongly bent, and the bond angles are in the range of 101—104°. It is of interest that the molecule is planar in the partial ionic column of TTMTTF·HCBD complex, because the planar conformation will be favoured by the charge resonance interaction.

This research was supported by the grant in aids of special research project on properties of molecular assemblies (No. 59112003) from the Ministry of Education, Science and Culture.

References

1) O. W. Webster, *J. Am. Chem. Soc.*, **86**, 2898 (1964).
2) M. L. Kaplan, R. C. Haddon, F. B. Bramwell, F. Wudl, J. H. Marshall, D. O. Cowan, and S. Gronowltz, *J. Phys. Chem.*, **84**, 427 (1980).
3) F. Wudl, and E. W. Southwick, *J. Chem. Soc., Chem. Commun.*, **1974**, 254.
4) G. Saito, T. Enoki, H. Inokuchi, H. Kumagai, C. Katayama, and J. Tanaka, *Mol. Cryst. Liq. Cryst.*, **120**, 345 (1985).
5) J. Tanaka, H. Kumagai, S. Akhtar, G. Saito, T. Enoki, and H. Inokuchi, to be published.
6) A. Furusaki, *Acta Crystallogr., Sect. A*, **35**, 220 (1979).
7) P. Main, S. E. Hull, L. Lessinger, G. Germain, J. P. Declercq, and M. M. Woolfson, MULTAN 78, (1978). Univs. of York, England, and Louvain, Belgium.
8) C. Katayama, N. Sakabe, and K. Sakabe, *Acta Crystallogr., Sect. A*, **28**, S207 (1972).
9) "International Tables for X-ray Crystallography," Kynoch Press, Birmingham, (1974), Vol. IV.
10) C. K. Johnson, ORTEP, (1965). Report ORNL-3794, Oak Ridge National Laboratory, Tennessee.
11) T. J. Kistenmacher, T. E. Phillips, D. O. Cowan, J. P. Ferraris, A. N. Bloch, and T. O. Poehler, *Acta Crystallogr., Sect. B*, **32**, 539 (1976).
12) J. B. Torrance, J. J. Mayerle, K. Bechgaard, B. D. Silverman, and Y. Tomkiewicz, *Phys. Rev. B*, **22**, 4960 (1980).
13) W. F. Cooper, N. C. Kenny. J. W. Edmonds, A. Nagel, F. Wudl, and P. Coppens, *J. Chem. Soc., Chem. Commun.*, **1971**, 889.

14) K. Yakushi, S. Nishimura, T. Sugano, H. Kuroda, and I. Ikemoto, *Acta Crystallogr., Sect. B*, **36**, 358 (1980).
15) Y. Higuchi *et al.*, private communication.
16) T. J. Kistenmacher, T. E. Phillips, and D. O. Cowan, *Acta Crystallogr., Sect. B*, **30**, 763 (1974).
17) J. L. Galigné, B. Liautard, S. Peytavin, G. Brun, J. M. Fabre, E. Tarreilles, and L. Giral, *Acta Crystallogr., Sect. B*, **34**, 620 (1978).
18) J. L. Galigné, B. Liautard, S. Peytavin, G. Brun, M. Maurin, J. M. Fabre, E. Tarreilles, and L. Giral, *Acta Crystallogr., Sect. B*, **35**, 1129 (1979).
19) J. L. Galigné, B. Liautard, S. Peytavin, G. Brun, M. Maurin, J. M. Fabre, E. Tarreilles, and L. Giral, *Acta Crystallogr., Sect. B*, **35**, 2609 (1979).
20) D. Chasseau, G. Comberton, J. Gaultier, and C. Hauw, *Acta Crystallogr., Sect. B*, **34**, 689 (1978).

Electronic Structures of 3,4:3′,4′-Bis(tetramethylene)-2,2′,5,5′-tetrathiafulvalene-TCNQ and 3,4:3′,4′-Bis(tetramethylene)-2,2′,5,5′-tetrathiafulvalene-1,4-Dihydro-1,4-bis(dicyanomethylene)-triptycene Complex Crystals

Shamim AKHTAR, Jiro TANAKA,* Kazuhiro NAKASUJI,† and Ichiro MURATA†
Department of Chemistry, Faculty of Science, Nagoya University, Chikusa-ku, Nagoya 464
†*Department of Chemistry, Faculty of Science, Osaka University, Toyonaka, Osaka 560*
(Received March 19, 1985)

Experimental results of the polarized reflection spectra and the calculated absorption spectra of 3,4:3′,4′-bis(tetramethylene)-2,2′,5,5′-tetrathiafulvalene (OMTTF)–TCNQ and OMTTF–1,4-dihydro-1,4-bis(dicyanomethylene)triptycene(DBTCNQ) crystals are discussed by developing approximate theoretical models, based on the CT mechanism. The electronic structures conform well that, OMTTF–TCNQ is a neutral crystal whereas, OMTTF–DBTCNQ is ionic. Furthermore, the temperature dependent spin susceptibilities imply the former as diamagnetic and the latter as a regular Heisenberg antiferromagnet.

Recently many scientists show keen interests in the field of highly conducting charge-transfer (CT) complexes. In this regard, complexes of TCNQ as the acceptor and TTF as the donor are the most widely investigated. In this class of complexes, the donor (D) and the acceptor (A) form segregated columns of their own in a mixed valence state[1] ($DD^+DD^+\cdots$ and $AA^-AA^-\cdots$). They are characterized by metallic conductivity ($\sigma\sim10^2$—10^3 $ohm^{-1}cm^{-1}$) and an intense reflectance in the infrared region. Discovery of such high conductivities in the quasi-one-dimensional materials stimulated people greatly to design, synthesize and subsequently to investigate into the CT complexes of the new derivatives of TTF and TCNQ. Many attempts were successful[2] although lots of the crystals were found to belong to another category. Here, the complexes are of the simplest stoichiometry (1:1) and they form mixed stacks of alternating donors and acceptors either in the neutral (···DADADA···) or in the ionic ($\cdots D^+A^-D^+A^-\cdots$) forms and consequently exhibit insulating to semiconductive behavior ($\sigma\sim10^{-9}$—10^{-3} $ohm^{-1}cm^{-1}$). The overlap between D and A hybridizes these states so that the solids in this class are only nominally neutral (**N**) or nominally ionic (**I**) in their ground states.[3]

In this paper we shall report on the electronic spectra and electronic structures of two such mixed stack complex crystals with OMTTF as the common donor. Figure 1 shows their molecular structures. The first crystal is the OMTTF–TCNQ[4] which has been suggested to be neutral from the structural analysis.[5] The second one is a new complex[6] between OMTTF and DBTCNQ.[7] The polarized reflection spectra and hence the calculated absorption spectra by Kramers-Kronig transformation[8] are presented and theoretical interpretations are made with a special emphasis on the CT bands. It has been found that OMTTF–DBTCNQ is an ionic complex,[6] accordingly the ESR measuerments are performed to find its spin susceptibility. The results of the optical and magnetic studies are interpreted in terms of the CT mechanism based on the calculations of the interactions between the MOs of the donor and the acceptor.

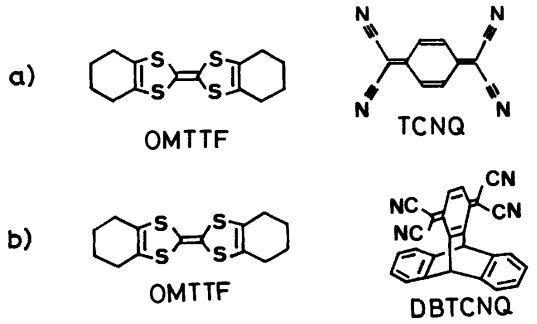

Fig. 1. Molecular structures of (a) OMTTF–TCNQ and (b) OMTTF–DBTCNQ.

Experimental

The crystals of OMTTF–TCNQ and OMTTF–DBTCNQ were of needle shape and lustering surfaces. In the structural analysis,[5] OMTTF–TCNQ crystal is reported as triclinic, $P\bar{1}$. In one of our previous papers,[1] we have reported the cell constants in a different way: $a'=b$, $b'=c$, $c'=a$, $\alpha'=\beta$, $\beta'=\gamma$, and $\gamma'=\alpha$, the dashed parameters being of our previous paper. OMTTF–DBTCNQ on the other hand, is monoclinic, C2/c.[6] The lattice parameters are: $a=18.535$ Å, $b=14.417$ Å, $c=14.906$ Å, $\beta=98.890°$, $Z=4$ and there exists one distorted C_6H_6 (solvent) per molecular complex. The oscillation/Weissenberg photographs were used to select suitable crytal faces for the spectral measurements.

Optical Spectra. The polarized reflection spectra on the (100) plane of OMTTF–TCNQ single crystal have been observed in the range of 3000—35000 cm^{-1} by a reflection spectrophotometer designed in our laboratory. Similar measurements on the (010) plane of OMTTF–DBTCNQ were performed in the range of 5000—25000 cm^{-1}. For both the crystals spectral measurements, one parallel to the needle axis and the other perpendicular to it, were made. Corresponding absorption spectra were then calculated by the Kramers-Kronig transformation.[8] The crystal oscillator strength along the α-axis was evaluated as:

$$f^{\alpha} = 4.32 \times 10^{-9}\int n_{\alpha}(\nu)\varepsilon_{\alpha}(\nu)d\nu \qquad (1)^{9,10}$$

where, ν is the wave number, n_α and ε_α are the α-components of the refractive index and the molar extinction coefficient, respectively.

ESR Measurements. The ESR absorptions were observed by a Varian-E 112 X-band spectrophotometer at 100 KHz field modulation. Measurements were made at the field strength of 3248 Gauss and care was taken with the microwave power so as to prevent saturation effect, if any, of the ESR signal especially at low temperatures. At least 20 single crystals of OMTTF-DBTCNQ and 3 of OMTTF-TCNQ were used due to their size factors. In the crystal setting of both the crystals, the needle axes were kept approximately perpendicular to the magnetic field direction. The absolute intensities of the ESR absorptions were obtained by integration of the derivative curves. Temperature dependent ESR were observed in the range of 1.6—293 K with an accuracy of ±1 K. The spin susceptibility was calculated by comparing the measured intensity with that observed for DPPH and then with spin susceptibility of the latter.[11]

Results and Discussion

Electronic Spectra. *a) OMTTF-TCNQ Crystal:* The polarized reflection spectra parallel and perpendicular to the crystal c-axis as observed on the (100) plane are shown in Fig. 2. In this spectra, there are two low energy bands and two other humps in the //c component. The corresponding absorptions calculated by the K-K transformation[8] are represented by Fig. 3. In the //c spectra, the lowest absorption arises near 5000 cm^{-1} and the second one which is very sharp, in the region of 17200 cm^{-1}. There are also a number of feeble absorptions but all in the high energy side. The $\perp$c component, on the other hand, shows almost no absorption over a wide range of the observed spectra. Therefore, a comparative study between these two spectra reveals that, both the bands of 5000 and 17200 cm^{-1} are absolutely polarized along the c-axis of the crystal. At this stage, a close look into the crystal packings as depicted in Figs. 4 (a) and 4 (b) will provide an important clue to characterize them: The molecular components, OMTTF and TCNQ, stack alternately along the c-axis with the average molecular planes almost perpendicular to it (interplanar distance, 3.53 Å). Therefore, it would be appropriate to suggest these two as the CT bands where OMTTF donates its electrons to the TCNQ molecule: the first absorption is due to the first charge transfer, CT_1 and the second one is due to the second charge transfer, CT_2. In the photoelectron spectra, TMTTF showed closely situated two levels at 6.40 eV (b_{1u}) and 7.99 eV (a_{1u}) which are about 12800 cm^{-1} (1.59 eV) apart.[13] Therefore, in OMTTF-TCNQ, if the CT band from the HOMO is found at 5000 cm^{-1}, the CT_2 band appearing at 17200 cm^{-1} may be assigned to the transition from the second HOMO of OMTTF, because, energy separation (12200 cm^{-1}) between these two bands is close to the difference in energy of the first and second HOMOs in the TMTTF molecule.

In order to estimate the CT state energy, secular

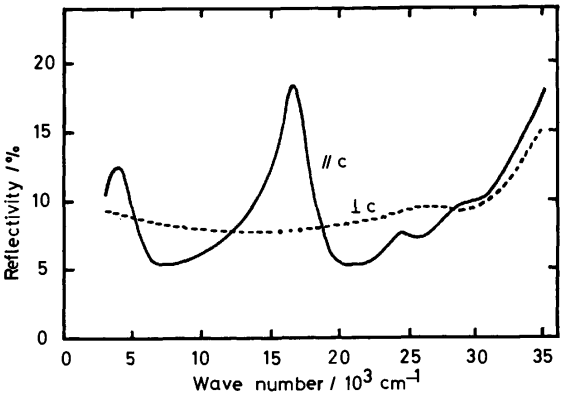

Fig. 2. Polarized reflection spectra of the OMTTF-TCNQ crystal on the (100) plane.

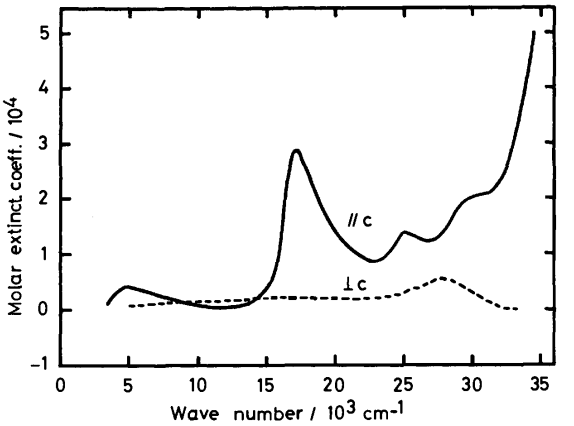

Fig. 3. Calculated absorption spectra of OMTTF-TCNQ on the (100) plane.

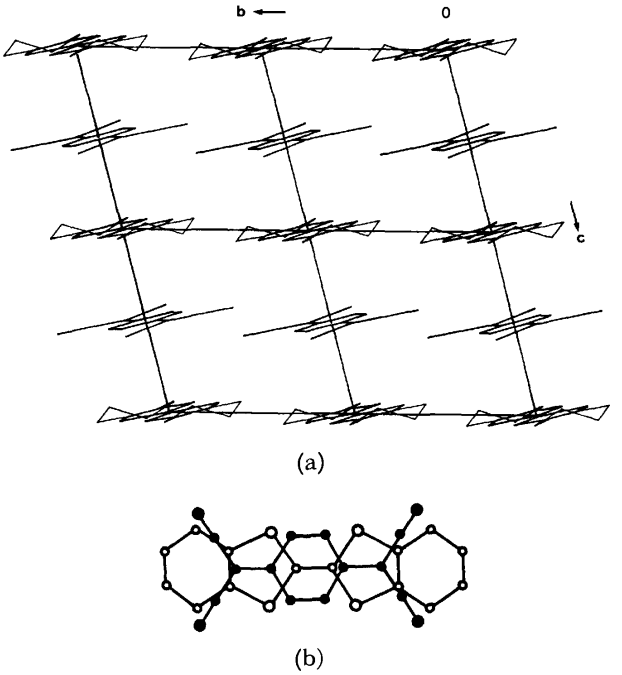

Fig. 4. (a) Projection figure of the OMTTF-TCNQ crystal onto (100). (b) Mode of overlap of the component molecules in the crystal.

TABLE 1. VALUES OF IONIZATION POTENTIAL(I_P), ELECTRON AFFINITY(E_A), COULOMB(C)/MADELUNG(M) ENERGY, POLARIZATION ENERGY(P), CT CONFIGURATION ENERGY(Δ) AND THE CALCULATED MIXING COEFFICIENTS a AND b OF THE CRYSTALS

Complex	Transition type	I_P (eV)	E_A (eV)	C/M (eV)	P (eV)	Δ (eV)	a	b
OMTTF-TCNQ	CT_1	6.5	2.80	2.96	0.2	0.54	0.995	0.103
	CT_2	8.0	2.80	2.95	0.2	2.05	0.981	0.196
OMTTF-DBTCNQ	back CT	6.5	2.85	3.84	0.7	0.89	0.130	0.992

equation of the following form may be solved. Considering the ground configuration at the zero level and the CT configuration energy to be denoted as Δ, the equation follows:

$$\begin{vmatrix} \Delta - E & 2t_{Ak,DI} \\ 2t_{Ak,DI} & -E \end{vmatrix} = 0 \qquad (2)$$

In this equation, Δ may be defind as:

$$\Delta = I_p - E_A - C - P \qquad (3)$$

where, I_P is the ionization potential, E_A the electron affinity, C the Coulomb potential in the DA pair and P is the polarization energy (positive) of the crystal. Again, $t_{Ak,DI}$ is the transfer integral and may be related to the overlap integral, $S_{Ak,DI}$, approximately as:

$$t_{Ak,DI} = KS_{Ak,DI}\left(\frac{W_{Ak}+W_{DI}}{2}\right) \qquad (4)^{1,12)}$$

where, W_{Ak} and W_{DI} are the respective MO energies and K is a semiempirical constant lying in the range of 1.0—2.0.

For the crystal of OMTTF-TCNQ ionization energies that are yet to explore, were approximated to be 6.5 eV (I_p^1) and 8.0 eV (I_p^2) with reference to those of TMTTF.[13,14] From the MO calculations by Pariser-Parr-Pople method, the two transitions in this crystal may be considered as: CT_1:$D_7 \rightarrow A_9$ and CT_2:$D_6 \rightarrow A_9$, subscript denoting the number of MO counted from the bottom in the concerned molecule. The associated orbital overlaps ($S_{A9,D7}$ and $S_{A9,D6}$) are 0.00367 and 0.02315 so that, transfer integrals may be estimated as t_1=−0.0290 and t_2=−0.2125 eV provided K=1.7 in Eq. 4. Moreover, considering Ohno-Klopman's approximations Coulomb energies as calculated are 2.96 eV (CT_1) and 2.95 eV (CT_2). Now, if we assume that the polarization energy (unknown yet) be as small as 0.2 eV, Δ in Eq. 3 may be estimated as 0.54 eV (Δ_1) and 2.05 eV (Δ_2). Therefore, solving the respective secular equations our theoretical CT transition energies obtained are 0.55 and 2.22 eV which are fairly comparable to the observed values of 0.62 and 2.13 eV, respectively. To estimate approximately the contribution of these CT states to the crystal ground state, mixing coefficients a and b in the wave function,

$$\Psi_G = a\Psi_0 + b\Psi_1 \qquad (5)^{15)}$$

were calculated and are shown in Table 1. Respective magnitudes of a and b thus suggest that, in the ground state crystal of OMTTF-TCNQ is mostly neutral and, in its CT interaction, contribution of the CT_2 is more than that of the CT_1. The observed and the calculated degrees of charge transfer, oscillator strengths and the stabilization energy as displayed in Table 3 are in reasonable agreement. The larger value of the degree of charge transfer of CT_2 than that of CT_1 indicates that the former configuration is quite significant in the CT interaction. Following the theoretical calculations, CT stabilization energy in the ground state is found to be 2.02 kcal mol^{-1}† of which ≈93% (1.88 kcal mol^{-1}) is accounted as the contribution of the CT_2 configuration. The large f_2 of the CT_2 transition may be attributed as due to the allowed character of the transition from the second HOMO(D_6) of OMTTF to the LUMO(A_9) of TCNQ. In contrary, CT_1 transition seems to be of forbidden type as can be decided by the difference in the symmetry of the HOMO and the LUMO, because, the transfer integral between the molecular orbitals of different symmetry will be negligibly small. Nevertheless, both the CT_1 and CT_2 configurations stabilize the crystal ground state only to a certain extent, so that the crystal as a whole is almost neutral in its ground state.

b) OMTTF-DBTCNQ Crystal: Presence of two benzene rings in the DBTCNQ molecule creates a novelty in the crystal of OMTTF-DBTCNQ. One would notice interestingly that, in the crystalline state OMTTF and DBTCNQ form linear stacks in an alternating fashion along the c-axis (average interplanar distance ≈3.60 Å) in a pattern such that the molecular planes of OMTTF and TCNQ moiety of DBTCNQ are almost parallel (Figs. 5 (a) and 5 (b)). As compared with the mode of overlapping in OMTTF-TCNQ crystal, there is a lateral shift of TCNQ moiety along its short axis. By comparing its powder spectra with those of $K^+DBTCNQ^-\cdot 2H_2O$ and $OMTTF^+BF_4^-$, Nakasuji *et al.*[6] suggested that OMTTF-DBTCNQ is an ionic complex. In this paper polarized electronic spectra will conform the assignments of the spectra and the ionic ground state.

The observed reflection spectra polarized parallel and perpendicular to the crystal c-axis are shown in Fig. 6 and the corresponding absorption spectra in Fig. 7. In the absorption spectra, the ⊥ c component

†1 cal_{th}=4.184 J.

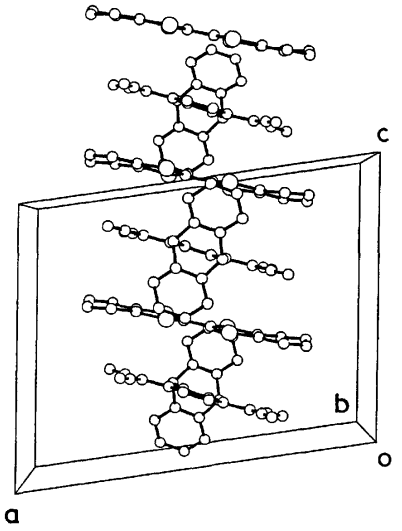

(a)

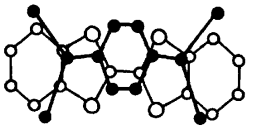

(b)

Fig. 5. (a) Crystal packing of OMTTF and DBTCNQ on the (010) plane. Solvent molecules (C_6H_6) have been excluded for clarity. (b) Mode of overlapping of the OMTTF molecule and the TCNQ moiety in the crystalline state.

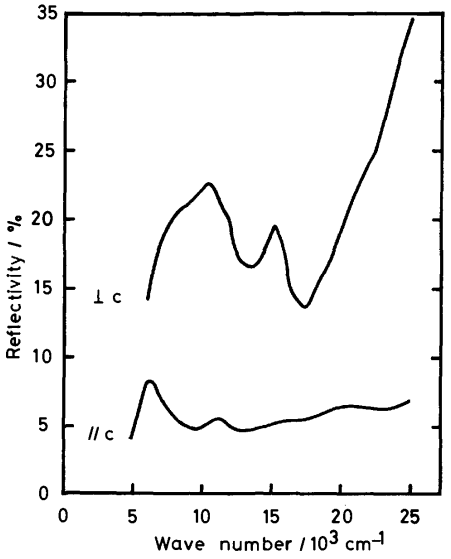

Fig. 6. Reflection spectra of OMTTF-DBTCNQ on the (010) plane.

shows its first absorption in the region of 11800 cm^{-1} which may be suggested as due to the first local excitation (LE_1) in the TCNQ moiety of DBTCNQ, since in solution the first excitation in $TCNQ^-$ has been observed[16] near 12000—13000 cm^{-1}. At the similar energy region (≈11800 cm^{-1}) there is a small absorption also in the //c spectra which may be interpreted

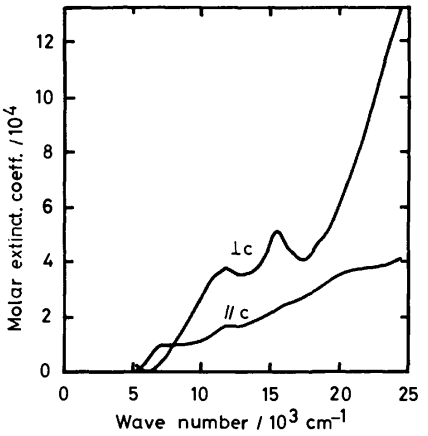

Fig. 7. Calculated absorption spectra of OMTTF-DBTCNQ crystal on the (010) plane.

as the perpendicular component of the former absorption. This is justified because, the molecular planes of OMTTF and TCNQ moiety are not exactly perpendicular to the c-axis, rather inclined to it (roughly by 10—15°). The next absorption at around 15400 cm^{-1} in the ⊥ c spectra may be interpreted as due to a local excitation in $OMTTF^+$ since an absorption at 17000 cm^{-1} of this cation radical has been observed in its powder spectra[6] and also one of the local excitations in TTF^+ has been found near 18000 cm^{-1}.[17] Ultimately, the lowest absorption of 7200 cm^{-1} in the //c component indicates its unique polarization in a direction which is close to the stacking axis. Therefore, it is typical of the CT band and the ionicity in the complex strongly suggests it to be associated with the "back charge transfer" where, an electron transfer occurs from the HOMO of the $TCNQ^-$ moiety to the LUMO of the $OMTTF^+$ radical.

Using the P-P-P method we have performed MO calculations of OMTTF-DBTCNQ also which referred to $\phi_9 \rightarrow \theta_7$ as the CT transition. Here, ϕ and θ are the HOMO and LUMO of DBTCNQ anion and OMTTF cation respectively and the subscripts denote the numbers of MOs in the ions. In addition, considering Ohno-Klopman's approximations, overlap integral calculated was 0.00721 so that the transfer integral may be estimated as t=—0.0573 eV at the value of K=1.7.

In the case of ionic crystals, we like to prefer back CT configuration energy, Δ', to be defind as:

$$\Delta' = M + P + E_A - I_P \qquad (6)$$

Here, M represents the negative of the crystal Madelung energy and the other parameters have the similar significances as in Eq. 3. From the very difference in the redox potentials of TCNQ and DBTCNQ of 0.18 and 0.23 V, respectively, electron affinity of the latter may be assumed to be increased by only 0.05 eV from that of TCNQ, *i.e.*, E_A(DBTCNQ)=2.85 eV. To have an estimation of the crystal Coulomb energy we have computed Madelung energy of OMTTF-DBTCNQ by the

Ewald method[18] following Metzger's expressions.[19] The computation program written here was tested with NaCl, $TMPD^+$-$TCNQ^-$ and $TMPD^+$-ClO_4^- and all of them have shown good coincidence with those calculated by Metzger.[19,20] For the OMTTF-DBTCNQ crystal, detailed charge distributions at different atom positions were calculated by the P-P-P method and they are represented in Table 2. Two runs, at η=15.00 and η=20.00, were made with this charge distribution model and the results are shown in Table 2. Thus the estimated Madelung energy of magnitude of 3.846±0.002 eV may merely be as enough as to ionize a DA pair since, $I_P - E_A \simeq 3.65$ eV is our guess about this complex. Therefore, to find an approximate fit to the observed spectra we have considered $\Delta' \simeq 0.89$ eV which needed obviously a polarization energy of 0.7 eV. This amount is larger than that of the neutral crystal of OMTTF-TCNQ and also seems to be reasonable because, polarization energies of TTF and its methyl-substituted derivatives lie in the range of 0.9—1.4 eV and that of TCNQ is 2.1 eV.[14]

Table 2. Delocalized atomic charge distributions (by P-P-P method), convergence parameter(η) and the computed Madelung energy of OMTTF-DBTCNQ

Atom No.[a]	Atomic charge/|e|	η	Madelung energy (eV mol^{-1})
1	0.093		
2	0.176		
3	0.027		
4	0.031		
5	0.173	15.00	−3.84401
6	−0.067		
7	−0.072		
8	−0.055		
9	−0.195		
10	−0.010	20.00	−3.84754
11	−0.008		
12	−0.043		
13	−0.050		

a) For numbering, see below.

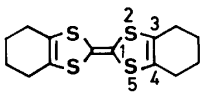

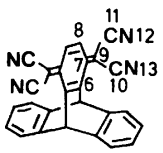

The large value of b (Table 1) of the OMTTF-DBTCNQ crystal suggests a highly ionic ground state. Our calculated degree of charge transfer and oscillator strength (based on an ionic complex) are comparable with the observed data (Table 3) and all of them suggest an ionic ground state of the OMTTF-DBTCNQ crystal with an additional stabilization (ΔE=0.33 kcal mol^{-1}) due to the back charge transfer.

Spin Susceptibility: In the ESR measurements, crystal of OMTTF-TCNQ showed only a feeble room temperature absorption with an approximate g of 2.0015. Moreover, in the range of 2.8—300 K no phase transition was found to occur. The observed spin susceptibility was of the order of 10^{-8} emu mol^{-1} most of which may be due to the contamination of crystals with certain paramagnetic impurities.

The ionic crystal, on the other hand, exhibited a single line absorption in the range of 1.6—293 K except a little distortion at 1.6 K. This is because, at low temperatues, ESR intensity shows a small Curie-like upturn which is characteristic of the extrinsic Curie-impurities commonly found in organic salts. However, g value of this crystal was found to be 2.066 at room temperature and increased only by 0.3% at 4.2 K.

The spin susceptibility of OMTTF-DBTCNQ was calculated from the observed intensity and it was corrected by subtracting the contribution of Curie-impurity which showed the Curie constant, C= 7.82×10^{-3} emu K mol^{-1}. The resulting temperature dependence is shown by solid circles as in Fig. 8. A finite spin value near T=0 and presence of a rounded maximum in the temperature dependent spin susceptibility lead to suggest that, OMTTF-DBTCNQ is a typical example of the regular Heisenberg antiferromagnet.[21] An approximate Hamiltonian for such a one-dimensional Heisenberg regular chain is given by:

$$H = \sum_{i=1}^{N} J \boldsymbol{S}_i \cdot \boldsymbol{S}_{i+1} \qquad (7)^{22}$$

where, J represents equal interaction with both the neighbors along the chain and $\boldsymbol{S}_i$ is the spin vector of the ith radical. For a regular Heisenberg antiferro-

Table 3. Calculated and observed transition energies(ΔE^i_{CT}), degrees of charge transfer(b_i^2), oscillator strengths(f_i) and the stabilization energies(ΔE) in the ground states of the crystals

Complex		CT_1[a]			CT_2			
		ΔE^1_{CT}	b_1^2	f_1	ΔE^2_{CT}	b_2^2	f_2	ΔE
		cm^{-1}	%		cm^{-1}	%		kcal mol^{-1}
OMTTF-TCNQ	calcd	4438	1.1	0.020	17915	3.7	0.266	2.02
	obsd	5000	3.2	0.065	17200	10.1	0.706	
OMTTF-DBTCNQ	calcd	7424	1.6	0.049				0.33
	obsd	7200	4.4	0.133				

a) For OMTTF-DBTCNQ, back CT.

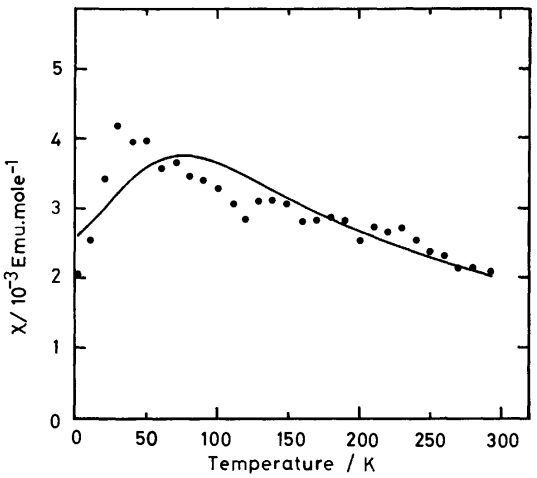

Fig. 8. Temperature dependent spin susceptibility of the OMTTF-DBTCNQ crystal. Solid circles are the experimental points and the solid line is the Bonner-Fisher susceptibility at $J=0.005$ eV.

magnet Soos[23] has expressed the exchange energy as:

$$J = 2|t|^2/\Delta E_{CT} \quad (8)$$

provided, $\Delta E_{CT} \gg t$. Here, t is Mulliken's CT integral and ΔE_{CT} the energy of CT transition. Our observed spin susceptibility fits moderately well to the Bonner-Fisher model[24] which is calculated for $J=0.005$ eV by using the formulation of Torrance *et al.*;[25] solid line in Fig. 8 represents the calculated values. This value of J is comparable, at least in order, to the expected value of 0.007 eV which may be obtained from equation (8) using our estimated values of t and CT transition energy.

Thus, from so far we have investigated, we find a quite good correlation between the magnetic behaviors and the electronic structures of the two crystals. The OMTTF-TCNQ with two CT transitions and a nearly diamagnetic behavior identifies itself as an almost neutral crystal and probably it has a high energy triplet above its singlet ground state. On the other hand, OMTTF-DBTCNQ is characterized by a single CT transition due to the back charge transfer and magnetically behaves as a simple regular Heisenberg antiferromagnet with a small exchange interaction between the ion radicals along its infinite chain. These facts suggest that OMTTF-DBTCNQ is a highly ionic crystal and the ionicity in the ground state approaches almost to unity. In particular, this OMTTF-DBTCNQ is the third CT crystal as reported yet,[26] with a nearly fully ionic ground state and it follows regular Heisenberg antiferromagnetism strictly over a wide range of temperature.

The authors thank the Instrument Center, Institute for Molecular Science, Okazaki, for the use of a Varian spectrophotometer. This research was supported by the grant in aids of special research project on properties of molecular assemblies (No. 59112003) from the Ministry of Education, Science and Culture.

References

1) J. Tanaka, M. Tanaka, T. Kawai, T. Takabe, and O. Maki, *Bull. Chem. Soc. Jpn.*, **49**, 2358 (1976).
2) M. R. Bryce and L. C. Murphy, *Nature*, **309**, 119 (1984).
3) J. B. Torrance, A. Girlando, J. J. Mayerle, J. I. Crowley, V. Y. Lee, P. Batail, and S. J. Laplaca, *Phys. Rev. Lett.*, **47**, 1747 (1981).
4) Y. Ueno and M. Okawara, *Chem. Lett.*, **1974**, 1135.
5) D. Chasseau, J. Gaultier, J. M. Fabre, and L. Giral, *Acta Crystallogr., Sect. B*, **38**, 1632 (1982).
6) K. Nakasuji, M. Nakatsuka, H. Yamochi, I. Murata, S. Harada, N. Kasai, K. Yamamura, J. Tanaka, G. Saito, T. Enoki, and H. Inokuchi, to be published.
7) K. Nakasuji, H. Yamochi, I. Murata, K. Yamamura, and S. Inagaki, *J. Org. Chem.*, **48**, 2384 (1983).
8) R. K. Ahrenkiel, *J. Opt. Soc. Am.*, **61**, 1651 (1971).
9) M. Tanaka, *Bull. Chem. Soc. Jpn.*, **50**, 2881 (1977).
10) J. Tanaka and M. Tanaka, *Mol. Cryst. Liq. Cryst.*, **52**, 221 (1979).
11) W. Duffy Jr. and D. L. Strandburg, *J. Chem. Phys.*, **46**, 456 (1967).
12) J. Tanaka and C. Tanaka, *Mol. Cryst. Liq. Cryst.* **126**, 121 (1985).
13) R. Gleiter, M. Kobayashi, J. Spanget-Larsen, J. P. Ferraris, A. N. Bloch, K. Bechgaard, and D. O. Cowan, *Ber. Bunsenges. Phys. Chem.*, **79**, 1218 (1975).
14) N. Sato, K. Seki, and H. Inokuchi, *J. Chem. Soc. Faraday Trans. 2*, **77**, 1621 (1981).
15) R. S. Mulliken, *J. Am. Chem. Soc.*, **74**, 811 (1952).
16) R. H. Boyd and W. D. Phillips, *J. Chem. Phys.*, **43**, 2927 (1965); Y. Iida, *Bull. Chem. Soc. Jpn.*, **42**, 71 (1969).
17) F. Wudl, G. M. Smith, and E. J. Hufnagel, *Chem. Commun.*, **1970**, 1453.
18) P. P. Ewald, *Ann. Physik*, **64**, 253 (1921); C. Kittel, "Introduction To Solid State Physics," 2nd ed., John Wiley & Sons, Inc. (1956), pp. 571—75.
19) R. M. Metzger, *J. Chem. Phys.*, **57**, 1870 (1972).
20) R. M. Metzger, *J. Chem. Phys.*, **57**, 1876 (1972).
21) D. J. Klein and W. A. Seitz, *Phys. Rev. B*, **10**, 3217 (1974).
22) B. M. Hoffman and R. C. Hughes, *J. Chem. Phys.*, **52**, 4011 (1970).
23) Z. G. Soos, *Ann. Rev. Phys. Chem.*, **25**, 121 (1974).
24) J. C. Bonner and M. E. Fisher, *Phys. Rev.*, **135**, 640 (1964).
25) J. B. Torrance, Y. Tomkiewicz, and B. D. Silverman, *Phys. Rev. B*, **15**, 4738 (1977), Ref. 60.
26) Z. G. Soos, H. J. Keller, K. Ludolf, J. Queckbörner, D. Wehe, and S. Flandrois, *J. Chem. Phys.*, **74**, 5287 (1981).

 © 1985 The Chemical Society of Japan Bull. Chem. Soc. Jpn., 58, 2285—2288 (1985)

NMR Study of Molecules in Anisotropic Systems. II.† 1a,2a,3e,4e,5e,6e- and 1e,2e,3e,4e,5e,6e-Hexachlorocyclohexanes Dissolved in Nematic Liquid Crystals

Hideaki FUJIWARA,* Naoto SHIMIZU, Tatsuya TAKAGI, and Yoshio SASAKI
Faculty of Pharmaceutical Sciences, Osaka University, 1-6 Yamada-oka, Suita, Osaka 565
(Received April 20, 1985)

NMR spectra of the titled compounds (α- and β-BHC) have been measured in nematic solvents and analyzed. Vibrational corrections were important for the full interpretation of the observed direct couplings. The order parameters showed that the BHC molecules orient most preferably with their six-membered rings parallel to the optic axis of the nematic solvents. Molecular structure of α-BHC derived from the direct couplings corresponds well with those determined by the X-ray method on a crystal and calculated by the MNDO MO method. For β-BHC, however, discrepancies are found with the crystallographic structure, suggesting molecular deformations in the crystal state. Principal axes have been determined for the order matrix and compared with those for the moment of inertia. The difference between the two principal axis systems in α-BHC is interpreted as due to a steric repulsive effect between the two axial chlorine atoms and the solvent molecules.

NMR spectroscopy of molecules dissolved in anisotropic systems, such as liquid crystals, provides unique informations of direct spin-spin couplings and anisotropies in chemical shifts.[1,2] The direct couplings can give accurate structures of molecules in mobile state, *e.g.*, the r_α structures of benzene determined from NMR spectroscopy in ZLI1167 and from electron diffraction in gas phase agree well with each other.[3] The accurate determination also makes it possible to examine experimentally environmental effects on molecular structure, *i.e.*, the effect of solvent[4] as well as that of the phase under investigation[5] which may be gas, liquid (liquid crystal), or solid. A nematic solvent ZLI1167 is reported[4] as an ideal solvent for benzene derivatives which gives rise to negligible distortion on the molecular structure, whereas it has a weak basic character as revealed with some organotin compounds.[6] Anisotropic environment may also induce a specific molecular deformation of anisotropic nature, which is considered responsible to the observation of dipolar or quadrupolar coupling constants even for molecules with high symmetry such as T_d or O_h.[7] All these properties of the solvents originate from solute-solvent molecular interactions and are of wide interests in view of the similar situations met by molecules dissolved in membrane systems with biological importance.

In the present study, benzene hexachloride (BHC) molecules are taken up which have a flexible framework compared to the rigid benzene ring, and their molecular structures and preferred orientations determined by the NMR spectroscopy. The results are discussed by comparing the principal axes of the moment of inertia and those of the order matrix and by comparing molecular structures derived from several physicochemical methods. The isomers treated here are 1a,2a,3e,4e,5e,6e- and 1e,2e,3e,4e,5e,6e-hexachlorocyclohexane, *i.e.*, α- and β-BHC, respectively.

†See Ref 16 for I.

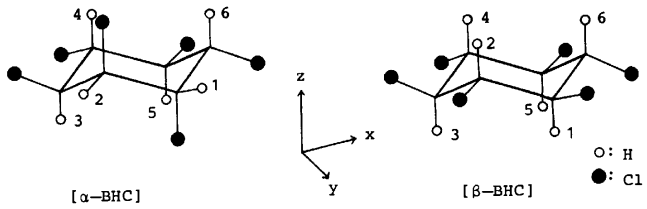

Experimental

α- and β-BHC (City Chemical Co., USA) were recrystallized several times from ethanol. Nematic solvents ZLI1167 and ZLI1132 (Merck) were used without any special purification. NMR spectra were recorded on a Hitachi R-900M FT spectrometer operating at 90 MHz and at 34.1 °C. Concentrations of the samples were 1 wt% for α-BHC in ZLI1167, and less than 1 wt% (saturated) for β-BHC in ZLI1167 and in ZLI1132. A data point of 16k was used in all measurements and the spectral width and the number of fid's accumulated were 2700 Hz and 3500 for α-BHC, 3150 Hz and 4400 for β-BHC in ZLI1167, and 4950 Hz and 4500 for β-BHC in ZLI1132. Typical line widths were 6 Hz for α-BHC, and 8 Hz (in ZLI1167) and 15 Hz (in ZLI1132) for β-BHC. The sample tube was not rotated when ZLI1132 was used as a solvent.

Spectral analysis was carried out by a computer program LAOCN3 modified to apply to the oriented system.[8] The observed direct couplings were corrected for harmonic vibrations by the program VIBR[9] and processed to the program SHAPE[10] to derive the order and the structural parameters. Principal axes of the moment of inertia were calculated by the program XYZ.[11] All these calculations were achieved with an ACOS System 1000 computer at the Computation Center in Osaka University. Diagonalization of the order matrix was done by a Basic program on a NEC personal computer.

Results and Discussion

Spectral Analysis Leading to the Order and the Structural Parameters. α-BHC belongs to the C_2 point group and gives AA'BB'CC' spin spectra in oriented state, including three chemical shifts and nine

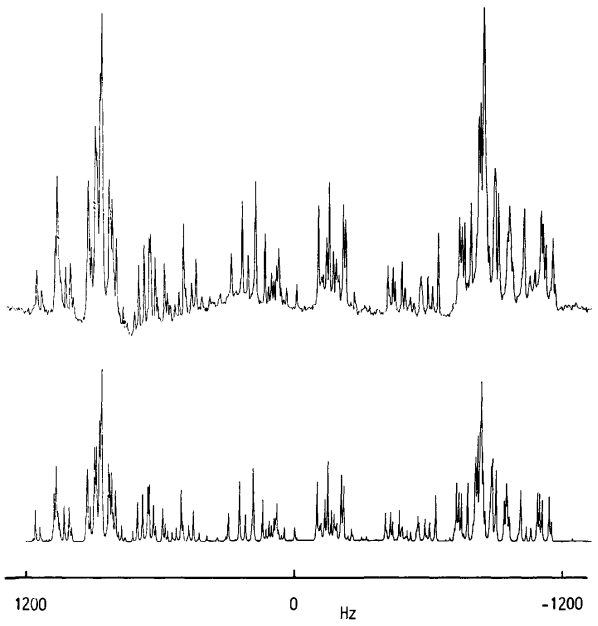

Fig. 1. ^{1}H NMR spectra of α-BHC observed (upper) and simulated (lower) in ZLI1167.

TABLE 1. NMR SPECTRAL PARAMETERS OF α-BHC IN NEMATIC SOLUTION OF ZLI1167[a)]

Direct couplings:[b)]		Indirect couplings:[18)]
D_{12}= 553.95±0.05	(567.61)	J_{12}= 3.28
D_{13}= 69.37±0.04	(70.02)	J_{13}=−0.49
D_{14}= 29.37±0.04	(29.01)	J_{14}= 0.26
D_{15}= −5.20±0.05	(−5.22)	J_{15}=−0.38
D_{16}= −86.46±0.04	(−90.05)	J_{16}= 3.28
D_{34}=−238.41±0.03	(−242.15)	J_{34}= 10.90
D_{35}= 380.74±0.02	(371.60)	J_{35}=−0.23
D_{36}= 11.10±0.03	(9.74)	J_{36}=−0.05
D_{45}=−188.24±0.04	(−190.53)	J_{45}= 10.24
Chemical shifts:[c)]		
$\nu_1-\nu_3$= 1.33±0.06		
$\nu_1-\nu_4$=62.82±0.06		

a) In units of Hz at 90 MHz. b) Probable errors are given and in parenthese listed are D_{ij}'s corrected for harmonic vibrations. c) Positive frequency toward low field side.

TABLE 2. STRUCTURAL AND ORDER PARAMETERS OF α-BHC IN NEMATIC PHASE ZLI1167 AT 34.1 °C

	Without vibration corrections	With vibration corrections
Distance ratios:		
r_{12}/r_{45}	=0.803±0.003	0.818±0.004
r_{13}/r_{45}	=1.212±0.008	1.226±0.008
r_{14}/r_{45}	=1.334±0.004	1.382±0.006
r_{15}/r_{45}	=1.208±0.007	1.258±0.005
r_{16}/r_{45}	=0.785±0.006	0.795±0.007
r_{34}/r_{45}	=0.988±0.003	1.001±0.003
r_{35}/r_{45}	=0.848±0.005	0.869±0.005
r_{36}/r_{45}	=1.297±0.009	1.293±0.009
Order parameters:[a)]		
S_{xx}	=−0.0720±0.0017	−0.0791±0.0014
S_{zz}	= 0.0834±0.0014	0.0902±0.0009
S_{xz}	= 0.0028±0.0008	0.0010±0.0009

a) r_{45}=3.092Å assumed.

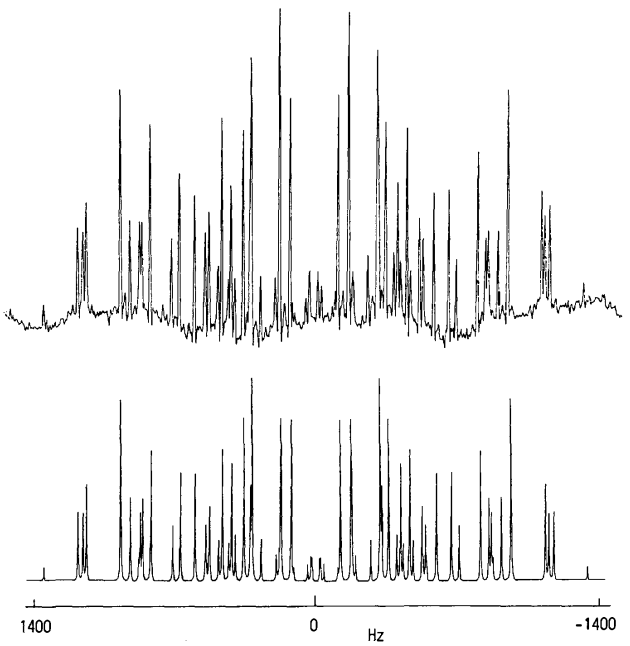

Fig. 2. ^{1}H NMR spectra of β-BHC observed (upper) and simulated (lower) in ZLI1167.

direct couplings as independent variables besides the indirect couplings which are usually substituted by those determined in isotropic media. The spectral pattern observed in ZLI1167 (Fig. 1) is characteristic and the spectral analysis is not laboring. Iteration was made on 96 lines in a final step and rms error between the observed and the simulated frequencies was 0.3 Hz. The results are summarized in Table 1. Order and structural parameters were calculated from the direct couplings (D_{ij}) by the use of SHAPE and they are listed in Table 2, where rms error between the observed and the recalculated D_{ij} values is zero since nine unknown parameters (three order parameters and six structural parameters) are determined from nine experimental data.

β-BHC has the C_{3v} symmetry and gives AA'A''-A'''A''''A''''' spectra in nematic solvents, including one chemical shift and three direct couplings as independent variables. The spectra observed in ZLI1167 (Fig. 2) and ZLI1132 resemble each other and are analyzed easily (Table 3). Iterations were made on 62 lines (in ZLI1167) and 43 lines (in ZLI1132), and rms errors were 0.3 Hz (in ZLI1167) and 0.5 Hz (in ZLI1132). Calculations of the order and the structural parameters from experimental D_{ij} values are summarized in Table 4. Since only one order parameter and one structural parameters are variable independently against three data of D_{ij}, the system is overdetermined. Least squares fits, however, resulted in only partial agreement between the experimental and the recalculated D_{ij}'s, and the rms errors remained large in both nematic solvents used here, *i.e.*, 0.99 Hz in ZLI1167

TABLE 3. NMR SPECTRAL PARAMETERS OF β-BHC IN NEMATIC SOLUTIONS OF ZLI1167 AND ZLI1132[a)]

	in ZLI1167	in ZLI1132
Direct couplings:[b)]		
D_{12}	−188.23±0.01 (−191.18)	313.28±0.03 (318.18)
D_{13}	236.99±0.01 (230.98)	−395.83±0.03 (−385.80)
D_{14}	−17.66±0.02 (−17.44)	29.95±0.05 (29.59)
Indirect couplings:[18)]		
J_{12}	10.58	
J_{13}	−0.20	
J_{14}	−0.20	

a) In units of Hz at 90 MHz. b) Probable errors are given and in parentheses listed are D_{ij}'s after vibration correction.

TABLE 4. STRUCTURAL AND ORDER PARAMETERS OF β-BHC IN NEMATIC SOLUTIONS OF ZLI1167 AND ZLI1132

	Without vibration corrections	With vibration corrections
	In ZLI1167	
r ratios:		
r_{13}/r_{12}	0.857±0.001	0.8755±0.0003
r_{14}/r_{35}	1.317±0.001	1.3291±0.0002
Order parameter:[a)]		
S_{zz}	0.0714±0.0007	0.07584±0.00004
rms error/Hz	0.99	0.01
	In ZLI1132	
Distance ratios:		
r_{13}/r_{12}	0.855±0.001	0.8737±0.0002
r_{14}/r_{12}	1.317±0.001	1.3279±0.0002
Order parameter:[a)]		
S_{zz}	−0.1223±0.0006	−0.12668±0.00001
rms error/Hz	1.56	0.03

a) r_{12}=3.092Å assumed.

and 1.56 Hz in ZLI1132 (Table 4).

Corrections for Harmonic Vibrations. It was unexpected that the D_{ij} values observed for the simplest β-BHC were not reproduced well in the above calculation. Model calculations were attempted assuming anisotropic molecular deformations, *e.g.*, C_{2h} symmetry, under the uniaxial orienting system, but they all resulted in unrealistic (very large) deformations. This is the case for both of the nematic solvents used, one of which (ZLI1132) orients parallel to and another (ZLI1167) perpendicular to the external magnetic field. Therefore, corrections for vibrations are considered necessary before invoking to a special molecular deformation. Although such corrections are very small and frequently negligible for the H-H direct couplings, they are known to become important in some cases for a full analysis of the direct couplings, *e.g.*, in cyclopropane[12)] D_{15} is reduced by 1.2 Hz after such correction. Valence force constants which are necessary for the vibrations are not available for BHC itself. Therefore, necessary date are cited from a general valence force field for secondary chlorides[13)] after a dimensional modification to mdyn/Å.††[14)] Calculations of the vibrational corrections are included also in Tables 3 and 4. Rms errors between the experimental and the recalculated D_{ij} values are reduced in great deal and are virtually zero for both of the nematic solvents, supporting successful corrections (Table 4). Vibrational corrections are also applied to α-BHC (Table 1), for which structural parameters change slightly after the correction but not the rms error since the number of unknown parameters equals to that of the experimental data (Table 2).

††dyn=10^{-5}N.

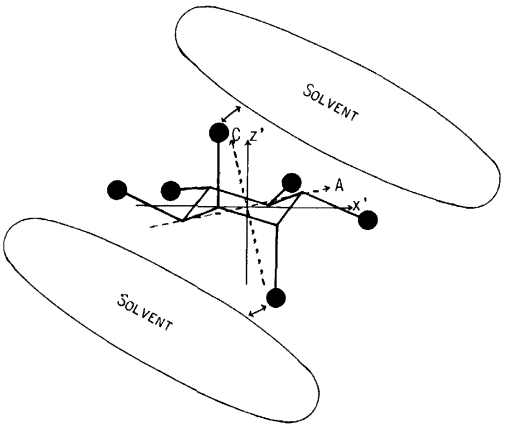

Fig. 3. Principal axis systems for the order matrix (solid line) and for the moment of inertia (dashed line) in α-BHC.
Only Cl atoms are depicted (●).

Orientational Probability from the Order Matrix. As seen from the sign of the order parameters, BHC molecules are most easily oriented like that the *z* axis directs perpendicular to the external magnetic field in ZLI1167 but parallel to it in ZLI1132. When orientation is expressed relative to the optic axis of the nematic solvent, all order parameters need be multiplied by -2 in ZLI1167 which itself orients perpendicular to the external field. Therefore, most probable orientation of the BHC molecules is that their *z* axis is perpendicular to the optic axis in both nematic solvents.

For α-BHC, an off-diagonal element S_{xz} remains non-zero. This S_{xz} is, however, able to be reduced to zero by an appropriate redefinition (rotation) of the cartesian coordinates, *i.e.*, by a diagonalization of the order matrix.[15)] In case of α-BHC such an appropriate rotation is the one that makes $S_{x'z'}=\sum_{pq}\mathrm{COS}\theta_p\mathrm{COS}\theta_q S_{pq}$ ($p,q=x, y, z$) equal zero where θ means the angle between the new (x',y',z') and the old (x,y,z) axes. The new axes are found to be close to the old ones, resulting $S_{x'x'}=-0.08582$ and $S_{z'z'}=0.09799$ for the principal values. Principal axes are also defined with the moment of inertia. They are depicted in Fig. 3 by dashed lines (*A* and *C* axes), *B* axis coinciding with *y* axis which is the molecular C_2 axis. In case of β-BHC, principal axes of the order matrix agree with those of the moment of inertia because of its C_{3v} symmetry. For δ-BHC, where only one chlorine atom is located at an axial position and others are at equatorials, these two

TABLE 5. MOLECULAR STRUCTURE OF α-BHC DETERMINED FROM SEVERAL PHYSICO-CHEMICAL METHODS

Ratio	NMR	MNDO[a]	X-ray[b]	Cyclohexane[c]
r_{12}/r_{45}=	0.818	0.825	0.82	0.815
r_{13}/r_{45}=	1.226	1.237	1.25	1.234
r_{14}/r_{45}=	1.383	1.364	1.28	1.344
r_{15}/r_{45}=	1.258	1.232	1.24	1.234
r_{16}/r_{45}=	0.795	0.821	0.75	0.815
r_{34}/r_{45}=	1.001	0.997	1.00	1.000
r_{35}/r_{45}=	0.870	0.843	0.82	0.839
r_{36}/r_{45}=	1.284	1.303	1.31	1.305

a) optimized value of r_{45}=3.094Å. b) from ref. 20, r_{45}= 2.983Å. c) calculated from data by gas electron-diffraction study[19], r_{45}=3.092Å.

TABLE 6. MOLECULAR STRUCTURES OF β-BHC DETERMINED FROM SEVERAL PHYSICO-CHEMICAL METHODS

Ratio	NMR ZLI1167	NMR ZLI132	MNDO[a]	X-ray[b]	Cyclohexane[c]
r_{13}/r_{12}=	0.876	0.874	0.945	0.74	0.839
r_{14}/r_{12}=	1.329	1.328	1.376	1.24	1.306

a) r_{12}=3.038Å. b) From Ref. 21, r_{12}=3.238Å. c) From Ref. 19, r_{12}=3.092Å.

axis systems have been found virtually coincident in a multiple quantum NMR study.[16] In case of α-BHC, two axial chlorine atoms make the *C* axis depart from the *z* axis. But the *z'* axis was not found to deviate considerably from the *z* axis. This is probably because there exists a steric stress effect between the axial chlorine atoms and the solvent molecules, which prevents the *C* axis from being directed perpendicular to the solvent molecules (Fig. 3). A difference of 11° was observed between the two axis systems as shown in Fig. 3.

Solution Structure of the BHC Molecules. Molecular structures are calculated from the observed direct couplings. The direct couplings have been corrected for harmonic vibrations, and hence r_α structure is derived. The results are compared with those determined from other physicochemical methods in Tables 5 and 6, where distance ratios are listed which are derived accurately in the NMR method. In these Tables, NMR means solution structure oriented in nematic phase, X-ray means crystallographic structure, and MNDO means the optimized structure according to the MNDO MO calculation[17] which is listed in place of the unavailable gas-phase structure. These structures corresponds well to each other, supporting reliability of the NMR method adopted here. It is rather difficult to find any dependency of the structure on the phase of investigation in case of α-BHC, but for β-BHC proton distances are seen to be relatively elongated along the *z* axis in crystal state. Such deformation is expected to come from molecular interactions characteristic in crystal states which will be well reflected to the framework of protons located at an outermost sphere of the molecule.

The author (HF) is grateful to Professors P. Diehl and H. Boesiger for sending lists of VIBR and SHAPE.

References

1) J. W. Emsley and J. C. Lindon, "NMR Spectroscopy Using Liquid Crystal Solvents," Pergamon Press, Oxford (1975).
2) C. L. Khetrapal, A. C. Kunwar, A. S. Tracey, and P. Diehl, in "NMR Basic Principles and Progress," ed by P. Diehl, E. Fluck, and R. Kosfeld, Springer, Heidelberg (1975), Vol. 9.
3) P. Diehl and W. Niederberger, *J. Magn. Reson.*, **9**, 495 (1973).
4) P. Diehl, H. Boesiger, and H. Zimmermann, *J. Magn. Reson.*, **33**, 113 (1979).
5) See for example: H. Fujiwara, A. Kawamura, T. Takagi, and Y. Sasaki, *J. Am. Chem. Soc.*, **105**, 125 (1983).
6) H. Fujiwara and Y. Sasaki, *J. Chem. Soc., Chem. Commun.*, **1981**, 35.
7) Ref. 1) chap. 4 and E. E. Burnell and C. A. de Lange, *J. Chem. Phys.*, **76**, 3474 (1982).
8) H. Fujiwara, K. Takahashi, and Y. Sasaki, *J. Magn. Reson.*, **41**, 171 (1980).
9) P. Diehl and W. Niederberger, *J. Magn. Reson.*, **9**, 495 (1973).
10) P. Diehl, P. M. Henrichs, and W. Niederberger, *Mol. Phys.*, **20**, 139 (1971).
11) QCPE program No. 178, Indiana University.
12) N. J. D. Lucas, *Mol. Phys.*, **22**, 233 (1971).
13) W. H. Moore and S. Krimm, *Spectrochim. Acta*, **29A**, 2025 (1973).
14) A torsional constant for C-C-C-C is approximated by that for cyclohexane: C. D. Chalk, B. G. Hutley, J. McKenna, L. B. Sims, and I. H. Williams, *J. Am. Chem. Soc.*, **103**, 260 (1981), and a bend-bend constant for Cl-C-C-Cl is set to 0.150 which gives smaller rms error in β-BHC.
15) J. M. Anderson, *J. Magn. Reson.*, **4**, 231 (1971).
16) H. Fujiwara, N. Shimizu, T. Takagi, Y. Sasaki, and K. Takahashi, *J. Magn. Reson.*, in press.
17) a) M. S. Dewar and W. Thiel, *J. Am. Chem. Soc.*, **99**, 4907 (1977); b) M. S. Dewar and H. S. Rzepa, *J. Compt. Chem.*, **4**, 158 (1983).
18) K. Hayamizu, O. Yamamoto, K. Kushida, and S. Satoh, *Tetrahedron*, **28**, 779 (1972).
19) H. J. Geise, H. R. Buys, and F. C. Mijlhoff, *J. Mol. Struct.*, **9**, 447 (1971).
20) G. Smith, C. H. L. Kennard, and A. H. White, *Cryst. Struct. Commun.*, **5**, 683 (1976).
21) G. Smith, C. H. L. Kennard, and A. H. White, *J. Chem. Soc., Perkin Trans.*, **1976**, 614.

Studies of "Manganese Cycle" for Gasification of Solid Carbon Resources. I. Formation and Hydrolysis of Manganese Carbides and Their Repetition

Hiroyasu IWAHARA,* Hiroyuki UCHIDA, and Satoshi MIZOGUCHI
Department of Environmental Chemistry and Technology, Faculty of Engineering, Tottori University, Koyama-cho, Tottori 680
(Received March 16, 1985)

A new carbide method based on "Manganese Cycle" was studied in order to produce new fuel gas. This process consists of four steps; (i) carbide production from Mn_2O_3 and solid carbon sources, (ii) fuel gas production by means of hydrolysis of the carbide, (iii) spontaneous oxidation of $Mn(OH)_2$ with air to Mn_2O_3, and (iv) regeneration of the carbide from Mn_2O_3 and new carbon sources. In this process, manganese is used as a recyclable medium for gas production, and hydrogen and hydrocarbons (C_1–C_5) are obtained by hydrolysis. Carbon monoxide generated during the formation of the carbide is also utilizable. The addition of Li_2CO_3 was effective for the carbide reproduction.

Recently, much thought has been given to the development of new energy sources replaceable for fossil fuels. And also, many investigators have studied the effective utilization of coal or the other solid carbon sources, which have been wasted or poorly utilized. Production of salt-like carbides and their hydrolysis to obtain hydrocarbons is one of the prospective methods for the gasification of solid carbon sources. Although carbide technology for acetylene production was one of important chemical industries, very high temperature (>2000 °C) is necessary to produce calcium carbide and, nowadays, the technology is unprofitable for the production of organic raw materials. It is desirable to research other salt-like carbides which can be prepared at much lower temperatures.

Tamers[1,2] has proposed the process for total synthesis of benzene by using lithium carbide as the intermediator. His process consists of four steps; (1) production of Li_2C_2 (at 1000 °C), (2) hydrolysis of Li_2C_2 to produce C_2H_2, (3) regeneration of Li from its hydroxide or oxide, and (4) conversion of C_2H_2 to benzene.

Manganese carbides may be another candidate for such a recyclable fuel production medium. Mn_3C is produced at about 1000 °C and hydrolyzed at room temperature to evolve hydrogen and methane ($Mn_3C+6H_2O \rightarrow 3Mn(OH)_2+H_2+CH_4$).[3] The formation and stability of the manganese carbides have been studied by many workers.[4–10] Recently, Christopher[11] has proposed that iron-manganese carbides can be used to produce liquid hydrocarbons by the hydrolysis at high temperature. In his process, since iron(III) chrolide was used to promote the formation of iron-manganese carbide, the latter may be difficult to recycle. And the necessity of the repeated quenching process of the carbides (Mn_3C+Fe_3C) makes the process complicated.

We propose "Manganese Cycle" to produce new fuel gas. As shown in Fig. 1, this process consists of four steps:

(i) Carbide production from Mn (or oxides) and solid carbon sources.

$$x\,Mn + y\,C \longrightarrow Mn_xC_y \qquad (1)$$

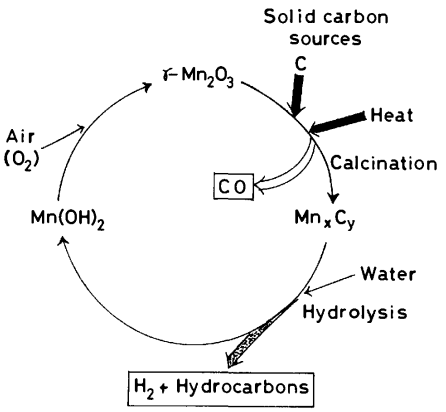

Fig. 1. Schematic illustration of "Manganese Cycle" for gasification of solid carbon resources.

or

$$x\,MnO_z + (y+xz)C \longrightarrow Mn_xC_y + xz\,CO \qquad (2)$$

(ii) Fuel gas production by means of the hydrolysis of the carbide.

$$Mn_xC_y + H_2O \longrightarrow H_2 + \text{hydrocarbons} + x\,Mn(OH)_2 \qquad (3)$$

(iii) Spontaneous oxidation of $Mn(OH)_2$ to Mn_2O_3.

(iv) Regeneration of the carbides from Mn_2O_3 and new carbon sources (the same process as Eq. 2).

Consequently, we can obtain hydrogen and hydrocarbons with hydrolysis of the carbides and, in addition, carbon monoxide during the production of the carbides. Since the manganese source can be recycled, we have only to charge the solid carbon sources and water to this process.

In the present study, we investigated this new carbide method with respect to the formation of manganese carbides, their hydrolysis for gas production and the recycle of manganese in the process.

Experimental

As the starting materials, manganese powder (purity 99.00—99.98%) and graphite powder were used. They were

Table 1. Formation of manganese carbides and the volume of gas evolved by hydrolysis at 50 °C

No.	Mn/C (charged)	Calcining Temperature/°C	Time/h	Produced carbide[a]	Gas volume[b]/$cm^3 g^{-1}$
1	1.5	800	15	◎ Mn_7C_3, △ Mn_5C_2	197.8
2	2.0	800	15	○ Mn_7C_3, ○ Mn_5C_2	206.4
3	2.5	800	15	○ Mn_5C_2, ○ $Mn_{23}C_6$	200.9
4	2.5	1000	3	◎ Mn_5C_2, ▲ Mn_3C	218.8
5	3.0	1000	3	○ $Mn_{15}C_4$, ○ Mn_5C_2, △ Mn_3C	172.6

a) Observed phase by X-ray diffraction: The symbols indicate the relative intensity (◎>○>△>▲). b) Volume of gas at 25 °C and 1 atm(101.3 kPa) evolved by hydrolysis. Strong Weak

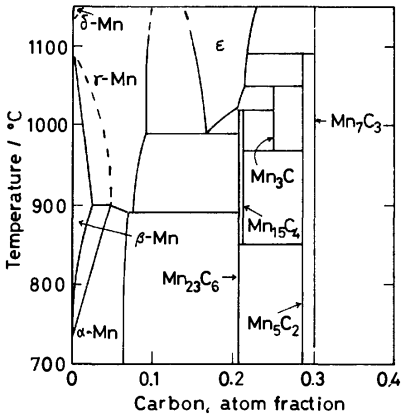

Fig. 2. Manganese-carbon phase diagram.[7]

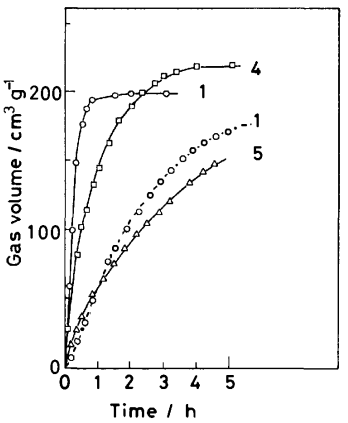

Fig. 3. The volume of evolved gas during hydrolysis. ---: Hydrolyzed at 50 °C, ---: hydrolyzed at 18 °C. (The volume of the gas is converted to a dry basis at 25 °C, and at 101.3 kPa, and the sample No. in the figure is same as in Table 1)

mixed and pressure molded at 400 kg cm^{-2} into the cylindrical form (dia; 14 mm). Test specimens were set in a ceramic tube and calcined at 500—1000 °C in vacuum (0.4—2.0 Torr†) for 3—15 h. After the calcination, specimens were cooled by removing the ceramic tube from the furnace. The carbides thus obtained were identified by X-ray powder diffraction (Fe-$K\alpha$) and subjected to hydrolysis test.

The hydrolysis experiment was carried out by using a gas burette. Since $Mn(OH)_2$, the precipitate by hydrolysis, absorbs oxygen to form γ-Mn_2O_3, the gas burette was purged with dry nitrogen gas before the hydrolysis. The evolved gas was analyzed by gas chromatography (Yanagimoto, Rapid Gas Analyzer G-1001).

Results and Discussion

Formation of Carbides and Their Hydrolysis. The calcined products obtained by the above described method were the mixtures of carbides and carbon, the composition of which depended on the firing temperature and the ratio of the starting materials. Typical examples of the products are shown in Table 1. We obtained different kinds of carbide including Mn_5C_2, Mn_7C_3, $Mn_{15}C_4$, Mn_3C, and $Mn_{23}C_6$ by changing the ratio of Mn to C(Mn/C=1.5—3.0) in the starting material and the calcining temperature (500—1000 °C). Figure 2 shows the currently accepted manganese-carbon phase diagram.[7] Our results exhibited almost mixed phase probably due to insufficient equilibrium time and a rather slow cooling rate.

Some workers have reported the hydrolysis of Mn_3C[3,8], Mn_5C_2,[8] and Mn_7C_3.[10] However, the volume and the composition of the evolved gas were not so clear for some carbides. The volume of evolved gas during hydrolysis of our products (cm^3 per 1 g of the product, at 25 °C and 1 atm†) is also shown in Table 1. Figure 3 shows the increase in the gas volume with time. These carbides could be hydrolyzed more rapidly at 50 °C than at room temperature. While the decomposition of the carbides containing $Mn_{15}C_4$ (calcined at 1000 °C) were rather slow, the hydrolysis of Mn_5C_2 and Mn_7C_3 took place very easily at 50 °C. A hard and dense sinter was observed in the case of No. 5 product. The maximum gas volume evolved was about 220 $cm^3 g^{-1}$ for the product mainly composed of Mn_5C_2. After the hydrolysis, gray precipitate, whose X-ray diffraction gave a broad and weak lines corresponding to $Mn(OH)_2$, was observed in all cases. This precipitate changed gradually dark brown colored γ-Mn_2O_3 on exposure to air.

Compositions of the Gas Evolved. The composition of the product gases was analyzed by gas chromatography and results are shown in Table 2. The calcined product mainly composed of Mn_5C_2 (No. 4 in Table 1) evolved hydrogen, methane, ethane, propane and a small amount of ethylene. On the other hand, much more varieties of hydrocarbons could be detected

†1 Torr=133.322 Pa.

†1 atm=101.3 KPa.

TABLE 2. COMPOSITION OF THE GAS EVOLVED BY HYDROLYSIS AT 50 °C

Carbide	Composition/%[a]										
	H_2	CH_4	C_2H_4	C_2H_6	C_3H_6	C_3H_8	i-C_4H_{10}	n-C_4H_{10}	x	y	Mn/C[b]
No. 1(Mn_7C_3 rich)	48.13	37.43	0.21	9.52	0.22	2.91	0.08	0.24	1.659	0.675	2.46
No. 4(Mn_5C_2 rich)	51.48	36.89	0.10	7.57	—	0.93	—	—	1.519	0.550	2.76

a) Residual gas (1—3%) is air. b) Ratio of Mn to C in the caribide calculated assuming Eq. 4.

in the case of No. 1 product mainly composed of Mn_7C_3. In this experiment, trace amount of C_5-hydrocarbons were sometimes detected. Such composition for our No. 1 product was in good agreement with that for Mn_7C_3 reported Hajek *et al.*[10]

Kor[8] has reported the composition of the evolved gas from the hydrolysis of Mn_5C_2 at 20 °C. His analysis by mass spectrometry found hydrogen, methane, ethane, and propane. And he has also reported that the ratio of Mn to C (Mn/C) calculated from the composition of the product is 2.4 or 2.7 for Mn_5C_2. Then we calculated the ratio of Mn to C by a similar way. The reaction equation of the hydrolysis of the carbide, Mn_xC_y, can be written as Eq. 4 assuming that the precipitate is only composed of $Mn(OH)_2$.[8]

$$\begin{aligned} Mn_xC_y + a\,H_2O \longrightarrow\ & x\,Mn(OH)_2 + p\,H_2 \\ & + q\,CH_4 + r\,C_2H_4 + s\,C_2H_6 + t\,C_3H_6 \\ & + u\,C_3H_8 + v\,C_4H_8 + w\,C_4H_{10} \end{aligned} \quad (4)$$

The values of x and y were calculated from the gas composition and results are shown in Table 2. Mn/C was 2.76 for the carbide mainly composed of Mn_5C_2 (No. 4 in Table 1). This value was larger than the stoichiometric ratio (2.5) for Mn_5C_2. However, a similar result was shown by Kor[8] (Mn/C=2.7) and our gas composition was also coincident with his report. This may be ascribed to the existence of Mn_3C or to the existence of the high valency state Mn in the precipitate. Mn/C was 2.46 for the No. 1 carbide mainly composed of Mn_7C_3. Since Mn_5C_2 phase could be also observed in this specimen, the value of Mn/C may become somewhat higher than the stoichiometric ratio (2.33) for Mn_7C_3.

Furthermore, by substituting the values of x, y, p, q, $\cdots$, v, and w into Eq. 4, the theoretical gas volume evolved from 1 g of the produced carbide can be calculated. For example, from the values of p=0.4813, q=0.3743, $\cdots$, w=0.0024 for the No. 1 product in Table 2, the amount of gas was 0.9874 mole ($p+q+\cdots+w$) per one mole of Mn_xC_y (x=1.659, y=0.675). Therefore, the theoretical gas volume is calculated to be 243 $cm^3\,g^{-1}$ (at 25 °C) for the No. 1 product. The volume of gas obtained in our experiment (197.8 $cm^3\,g^{-1}$) was lower than this value and the yield may be 81%. In the literature,[10] the experimentally observed volume for Mn_7C_3 hydrolyzed at 80 °C was 208 $cm^3\,g^{-1}$ and their predicted value was 213 $cm^3\,g^{-1}$. Our yield might be somewhat higher than 81% if we took account of the liquid phase products, which we did not analyze in the experiment. The analysis of the liquid product is in progress.

Recycle of Manganese. After the hydrolysis, the precipitate was filtrated and γ-Mn_2O_3 thus obtained was subjected to the second production of the carbide. The mixture of γ-Mn_2O_3 and graphite in a stoichiometric composition corresponding to Mn_3C was calcined at 1000 °C in vacuum. Unfortunately, only very small amounts of the carbides were formed in this procedure and the gas volume evolved by the hydrolysis was only 9.8 $cm^3\,g^{-1}$ for 50 h firing specimen. The X-ray diffraction patterns of calcined exhibited only MnO and graphite(unreacted starting material). The reduction of MnO with carbon has been studied by many workers.[12–16] According to Ikeda and Terayama,[16] the reduction of MnO with graphite into Mn_7C_3 began at about 1050 °C in argon atmosphere and the addition of Fe_2O_3 lowered the reduction temperature. If one can find more effective additives for the reduction of MnO, the yield of the carbides may be increased. We added firstly the alkaline carbonates to the specimen. γ-Mn_2O_3 (prepared from $MnCl_2$ and KOH), graphite and alkaline carbonate were mixed and pelletized with hydrostatic pressure of 2×10^3 kg cm^{-2}. In these experiments, the compositions of starting materials were decided by assuming that following reactions took place to form $(Mn_3C)_x(M_2C_2)_y$.

$$3/2Mn_2O_3 + 11/2C \longrightarrow Mn_3C + 9/2\,CO \quad (5)$$

$$M_2CO_3 + 4C \longrightarrow M_2C_2 + 3CO\ (M=K, Na, Li) \quad (6)$$

The specimens were calcined at 1000 °C in vacuum.

Typical results are shown in Table 3. The addition of Na_2CO_3 and K_2CO_3 did not promote the production of the carbide. However, Li_2CO_3 was very effective promoter for carbide formation. For example, when Li/Mn=0.35 (No. 11 in Table 3), the main product after 12 h calcination at 1000 °C was Mn_7C_3 and the volume of gas evolved by hydrolysis at 50 °C was 193 $cm^3\,g^{-1}$, which was close to that obtained for the carbide made from metallic Mn and graphite. Li_2C_2 could not be detected in the products by X-ray diffraction. The composition of product gas was similar to that shown in Table 2. Since neither the appearance of acetylene nor the increase in C_2-hydrocarbon could be detected in this gas, it was considered that the product might not contain Li_2C_2 and that the gas was evolved by hydrolysis of Mn_7C_3.

Effect of Li_2CO_3 on Carbide Formation. In order

Table 3. Formation of manganese carbide from γ-Mn_2O_3 with and without additives

No.	Composition	Time/h	Product[a]	Gas volume[b]/$cm^3 g^{-1}$
6	$(Mn_2O_3)_3\ C_{11}$	50		9.8
7	$(Mn_2O_3)_{1.05}(Na_2CO_3)_{0.30}C_{5.05}$	12	◎ MnO	7.3
8	$(Mn_2O_3)_{1.05}(K_2CO_3)_{0.30}C_{5.05}$	12		8.5
9	$(Mn_2O_3)_{1.35}(Li_2CO_3)_{0.10}C_{5.35}$	12	○ MnO, △ Mn_7C_3	96.0
10	$(Mn_2O_3)_{1.20}(Li_2CO_3)_{0.20}C_{5.20}$	12	○ Mn_7C_3, ▲ MnO	164.5
11	$(Mn_2O_3)_{1.05}(Li_2CO_3)_{0.30}C_{5.05}$	12	◎ Mn_7C_3	193.0

a) Observed phase by X-ray diffraction: The symbols are same as in Table 1. b)Volume of gas at 25 °C and 1 atm(101.3 kPa) evolved by hydrolysis at 50 °C.

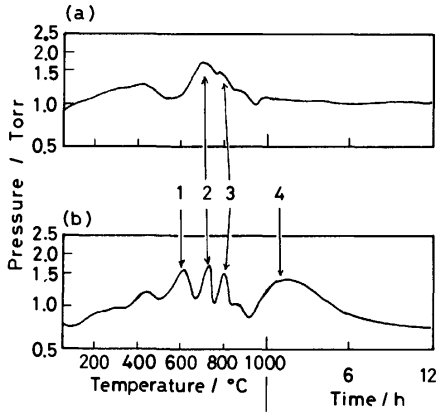

Fig. 4. Change in the total pressure during calcination.*
(a) Mn_2O_3+C ($(Mn_2O_3)_3C_{11}$), (b) Mn_2O_3+Li_2CO_3+C ($(Mn_2O_3)_{1.05}(Li_2CO_3)_{0.30}C_{5.05}$).
* Specimen is heated up to 1000 °C at the heating rate of 200 °C h^{-1} and kept at 1000 °C for 12 h.

to obtain an information about the effect of Li_2CO_3 on the production of Mn_7C_3, the variation of pressure during the calcination was monitored by a vacuum meter (ULVAC, GP-1S). The specimen in the ceramic tube was heated up to 1000 °C at the heating rate of 200 °C h^{-1} and then kept at 1000 °C for 12 h. Since the ceramic tube was evacuated with a vacuum pump at a constant pumping speed, the evolution of gas(CO) could be detected as the increase in the pressure.

Figure 4 shows the change in the total pressure during the calcination with and without addition of Li_2CO_3. In the heating process, appreciable pressure peaks were observed in the temperature range between 600 and 900 °C (peaks 2, 3) in both cases. The peaks 2 and 3 correspond probably to the following reaction steps (Eqs. 7 and 8) since γ-Mn_2O_3 can be reduced to MnO by graphite at these temperatures without Li_2CO_3.[17]

$$Mn_2O_3 + 1/3C \longrightarrow 2/3Mn_3O_4 + 1/3CO \text{ (peak 2)} \quad (7)$$

$$2/3Mn_3O_4 + 2/3C \longrightarrow 2MnO + 2/3CO \text{ (peak 3)} \quad (8)$$

$$Mn_2O_3 + C \longrightarrow 2MnO + CO \quad (9)$$

When Li_2CO_3 was added to the sample ((b) in Fig. 4), additional increases in the pressure were observed at 600 °C (peak 1) and at 1000 °C (peak 4). The peak 1 may be ascribed to the evolution of CO[18] because Li_2CO_3 is easily decomposed to Li_2O at 600 °C in vacuum.

$$Li_2CO_3 + C \longrightarrow Li_2O + 2CO \quad (10)$$

Since the formation of Mn_7C_3 was confirmed after this calcination, the peak 4 should correspond to a reduction step of MnO into Mn_7C_3 which was catalyzed by lithium or Li-compounds ($7MnO+10C \xrightarrow{(Li)} Mn_7C_3+7CO$). Li_2C_2 or metallic lithium should be an effective reducing agent against MnO. Although Li_2C_2 was not detected in the product, appreciable amount of metallic lithium was observed in the ceramic tube after the calcination. Therefore following reaction steps including Li as an intermediator may be possible at peak 4.

$$Li_2O + C \longrightarrow 2Li + CO \quad (11)$$
(1000 °C, under vacuum[2])

$$MnO + 2Li \longrightarrow Mn + Li_2O \quad (12)$$

$$7Mn + 3C \longrightarrow Mn_7C_3 \quad (13)$$

Other posssible reaction steps including Li_2C_2 as an intermediator may be also followed by Eq. 11.

$$2Li + 2C \longrightarrow Li_2C_2\ (950\ °C^{2)}) \quad (14)$$

$$2MnO + Li_2C_2 \longrightarrow 2Mn + 2Li + 2CO \quad (15)$$

$$7Mn + 3C \longrightarrow Mn_7C_3 \quad (16)$$

Anyway, it can be said that lithium is a good catalyzer for reducing MnO to Mn_7C_3, and that "Manganese-Cycle" proposed by us is one of promising methods for the production of hydrogen and hydrocarbons. Carbon monoxide gas during the production of the carbides could be also utilizable. The detailed studies are in progress.

Conclusion

A new carbide method based on "Manganese-Cycle" was studied. In this process, the fuel gas containing hydrogen and hydrocarbons (C_1–C_5) was obtained by the hydrolysis of manganese carbides. And carbon monoxide could also be obtained during the production of the carbides. γ-Mn_2O_3, by-product of the hydrolysis, was

recycled as the manganese source effectively by adding Li_2CO_3 in order to promote the carbide formation.

We would like to thank the staffs of the Laboratory in Tottori Gas Co. for their cooperation in analyzing the gas.

The present work was partially supported by a Grant-in Aid for Developmental Scientific Research No. 567500551 from the Ministry of Education, Science and Culture.

References

1) M. A. Tamers, U. S. Patent, 4009219 (1977).
2) M. A. Tamers, *Science*, **193**, 231 (1976).
3) W. R. Myers and W. P. Fishel, *J. Am. Chem. Soc.*, **67**, 1962 (1945).
4) K. Kuo and L. E. Person, *J. Iron Steel Inst., London* **178**, 39 (1954).
5) M. Isobe, *Sci. Inst. Rep. Tohoku Univ.*, **A3**, 468 (1951).
6) J. P. Bouchaud and R. Fruchart, *Bull. Soc. Chim. Fr.*, **1964**, 1579.
7) R. Benz, J. F. Elliott, and J. Chipman, *Metall. Trans.*, **4**, 1449 (1973).
8) G. J. W. Kor, *Metall. Trans. B*, **108**, 397 (1979).
9) W. M. Dawson and F. R. Sale, *Metall. Trans. A*, **11A**, 1849 (1980).
10) B. Hajek, P. Karen, and V. Borzed, *Collect. Czech. Chem. Commun. (CSK)*, **48**, 2740 (1983).
11) M. Christopher, U. S. Patent, 4110082 (1978).
12) W. D. Grimsley, J. B. See, and R. P. King, *J. S. Afr. Inst. Min. Metall.*, **77**, 51 (1977).
13) A. Koursaris and J. B. See, *J. S. Afr. Inst. Min. Metall.*, **79**, 149 (1979).
14) A. G. Bodpianov and G. N. Kojebinikov, *Meralli.*, **1980**, 28.
15) K. Terayama and M. Ikeda, *J. Japan Inst. Metals*, **46**, 1138 (1982).
16) M. Ikeda and K. Terayama, *Rep. Toyama Univ.*, **34**, 24 (1983).
17) J. P. Coughlin, *U. S. Bureau of Mines. Bull.*, **1954**, 542.
18) V. C. Kröger and E. Fingas, *Z. Anorg. Allgem. Chem.*, **212**, 269 (1933).

NMR Studies of Picolyl-type Carbanions. VIII.[1,2] Anions Produced by Reactions of Alkyl-substituted Pyridines with Butyllithium

Kazuyori KONISHI,* Hiroshi MATSUMOTO,† Katsuhiro SAITO,† and Kensuke TAKAHASHI†

The Industrial Technology Center of Mie Prefecture, Takajaya-komori-cho, Tsu 514

†*Nagoya Institute of Technology, Gokiso-cho, Showa-ku, Nagoya 466*

(Received December 27, 1984)

The ^{1}H and ^{13}C NMR spectra have been observed for the anions, produced from methyl-, ethyl-, and isopropylpyridines, in tetrahydrofuran (THF). Two kinds of anions are formed concomitantly by lithium-proton exchange and addition of butyllithium from 2-ethyl-, 2-isopropyl-, 4-methyl-, and 4-ethylpyridines. The former reaction tends to occur at the substituent bonded to the position adjacent to nitrogen, and the latter one occurs at the position adjacent to nitrogen without substituent. In the anions formed by the exchange from 2- and 4-ethylpyridines, a specific ring proton is coupled to the α-carbon, and, further, the *ortho*- or *meta*-protons (or -carbons) in the latter anion are nonequivalent respectively at room temperature. The α-carbons in these anions are virtually sp^2-hybridized.

It has recently been reported that two kinds of anions are produced by exchange and addition reactions of methyl-substituted quinolines with and without a 2-methyl group, with butyllithium, respectively, and that the former anions are picolyl-type carbanions, but the latter ones are ionic species having two of three basic characteristics on picolyl-type carbanions.[3] We now take up methyl-, ethyl-, and isopropylpyridines having at least two reaction sites (*i.e.*, the 2- and 6-positions) adjacent to nitrogen in a molecule, and present here some observations of the anions prepared from them.

Experimental

The starting materials, except for 2-, 3-, and 4-isopropylpyridines, used in this study were commercially available. 2- and 4-Isopropylpyridines were prepared by heating pyridine (10.60 g, 134 mmol) and 2-iodopropane (23.21 g, 137 mmol) at 200—240 °C for 16 h in an autoclave. A crude mixture (2.716 g) was obtained after removal of the recovered starting materials by distillation (101 kPa). A part of the mixture (1.267 g) was separated with thin-layer chromatography on silica gel using benzene–ether as a developing solvent to give 2-isopropylpyridine (R_f=0.71, 375 mg, 5%) and 4-isopropylpyridine (R_f=0.54, 515 mg, 7%). The structure of each pyridine derivative was confirmed by comparison of its physical properties with those of the authentic samples.[4,5] 3-Isopropylpyridine was prepared from 3-isopropenylpyridine by the method reported by Brown *et al.*[4] These starting materials were used after dried over calcium hydride and vacuum distilled.

The preparation of the anions was carried out *in vacuo*. About 1—3 mmol of a starting material was reacted with the equimolecular amount of butyllithium in hexane at 0—5 °C. After the completion of the reaction, all the volatile materials were trapped out and dried THF was introduced into the system. By solvent exchange, the solution became red or red-brown. The solution was then transferred into a NMR sample tube, and the tube was sealed off. The ^{1}H NMR spectra were measured at 200, 60, and 60 MHz on an Varian XL-200, Hitachi R-20B, and R-24B spectrometers respectively, and the ^{13}C spectra were measured at 50.3 MHz on a Varian XL-200. The proton and carbon chemical shifts were eval-

Table 1. The proton chemical shifts of the anions, in THF at 200 MHz, in ppm

Anion	Assignment 2-H	3-H	4-H	5-H	6-H	CH	CH_2		CH_3		
1 a		5.62	6.02	4.80	6.86		2.52				
b		5.42	6.13	4.70	6.81	3.11			1.41		
c[e]		5.35	5.83	4.42	6.82				1.45	1.54	
2 a	a)	4.22	5.78	4.33			1.29[b]		a)		0.89
b	a)	4.17	5.80	4.36			1.28[b]	a)	1.03		0.86
c[e]	3.54	4.01	5.80	4.28		2.02	1.28[b]		1.01	1.05	0.88
3 a	a)		5.52	4.26	6.41		1.27[b]		a)		0.86
b	a)		5.52	4.29	6.41		1.26[b]	a)	1.01		0.85
c[e]	3.63[c]		5.54	4.35	6.40	2.21	1.30[b]		0.96		0.85
4 a	a)	4.26	5.65		6.32		1.27[b]		a)		0.86
b	a)	4.29	5.71		6.36		1.26[b]	a)	0.92		0.85
c[e]	3.48	4.30	5.79		6.42	2.25	1.30[b]		0.96		0.85
5 a	6.39	5.28		5.28	6.39		2.64				
b	6.21	5.18		4.98	6.45	2.70			1.37		
c[e]	6.38	5.07		5.07	6.38				d)		
6 a	a)	4.03		4.26	6.57		1.28[b]		1.57		0.85
b	a)	4.07		4.31	6.57		1.27[b,c]	a)	0.97		0.86
c[e]	3.53	4.10		4.34	6.56	2.14	1.27[b]		0.98		0.87

a) Chemical shifts are not available because of overlapping of the large solvent peak. b) Center peak of complex multiplet. c) Assignment uncertain. d) Overlapping of large peaks. e) In THF-d_8.

TABLE 2. THE CARBON CHEMICAL SHIFTS OF THE ANIONS, IN THF AT 50.3 MHz, IN ppm

Anion	Assignment 2-C	3-C	4-C	5-C	6-C	CH	CH_2				CH_3		
1 a	164.1	116.1	131.5	97.1	148.7		57.2						
b	155.9	109.9	132.0	95.1	149.6	66.9 (=C<)					12.5		
c[b]	161.2[a]	110.7	129.0	91.7	149.8	74.7					20.2	14.2	
2 b	57.2	97.3	127.2	87.3	161.5		35.6	28.3	24.3	31.7	14.7		15.0
c[b]	57.5	94.7	127.3	83.4	166.1	37.0	35.0	28.5	24.4		25.5	23.2	15.1
3 a	62.2	106.6	121.9	89.5	146.9		34.1	29.9	24.8		23.6		15.0
b	61.8	113.0	119.4	89.5	147.0		33.9	29.7	24.8	29.8	14.1		15.0
c[b]	60.6	117.5	117.9	89.4	146.9	34.0	34.0	29.6	24.8		23.6	22.9	15.1
4 a	57.3	98.7	128.9	96.8	147.9		35.5	28.6	24.5		19.4		15.0
b	57.5	98.7	127.6	105.4	147.0		35.1	28.6	24.5	28.1	18.1		15.0
c[b]	57.7	99.1	125.8	110.3	145.0	32.7	35.4	28.8	24.6		25.4	25.1	15.1
5 a	143.8	109.9	149.8	109.9	143.8		65.8						
b	141.7	111.3	150.2[a]	103.6	144.4	74.4					12.8		
6 a	58.0	96.8	133.5	93.0	150.1		35.5	28.5	24.5		21.6		15.0
b	57.8	95.2	140.0	91.7	150.2		35.4	28.5	24.5	29.3	15.0		15.0
c[b]	57.6	93.9	144.6	90.7	150.2	34.2	35.6	28.6	24.5		23.8	23.4	15.0

a) Assignment uncertain. b) In THF-d_8.

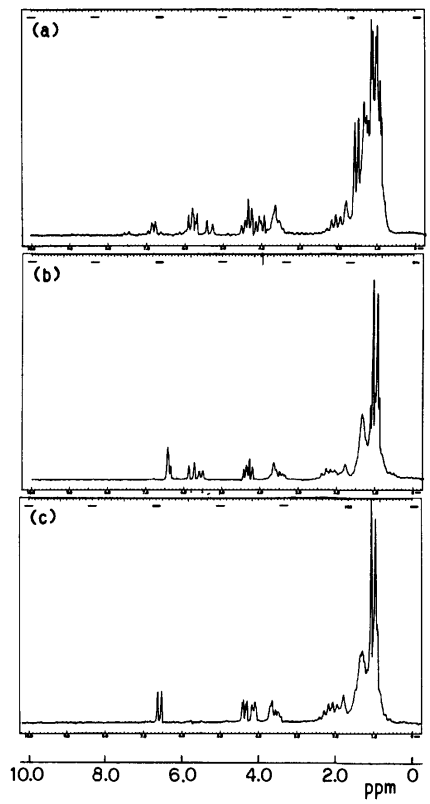

Fig. 1. ^1H spectra of the anions in THF-d_8 at 60 MHz; (a) **1c** and **2c**, (b) **3c** and **4c**, and (c) **6c**.

uated with the higher-field solvent peak of THF used as an internal reference and then converted to δ_H and δ_C values from TMS by taking 1.79 and 26.4 ppm respectively.

Results and Discussion

Typical ^1H NMR spectra of the anions produced from 2-, 3-, and 4-isopropylpyridines are shown in Figs. 1(a)—(c) respectively, and a typical ^{13}C spectrum of the anions produced from 2-ethylpyridine is shown in Fig. 2. The ^1H and ^{13}C NMR chemical-shift data are given in Tables 1 and 2 respectively.

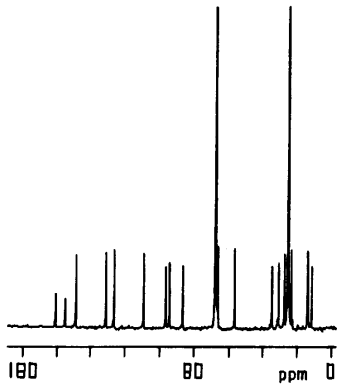

Fig. 2. ^{13}C spectrum of **1b** and **2b** in THF at 50.3 MHz.

First, it can be seen from Fig. 1 (a) that two kinds of anions, **1c** and **2c** (Scheme 1), are formed concomitantly by lithium-proton exchange and addition of butyllithium. In Fig. 2, eighteen signals, except for two large solvent peaks, are attributable to two kinds

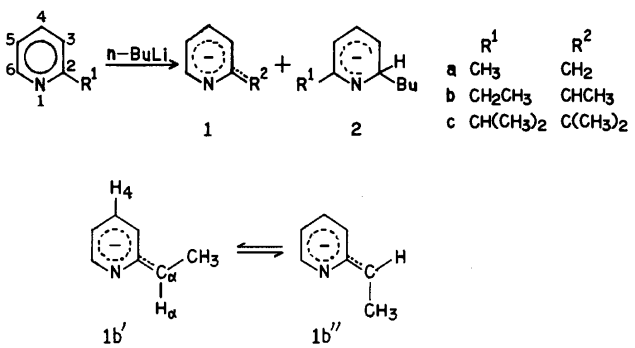

Scheme 1.

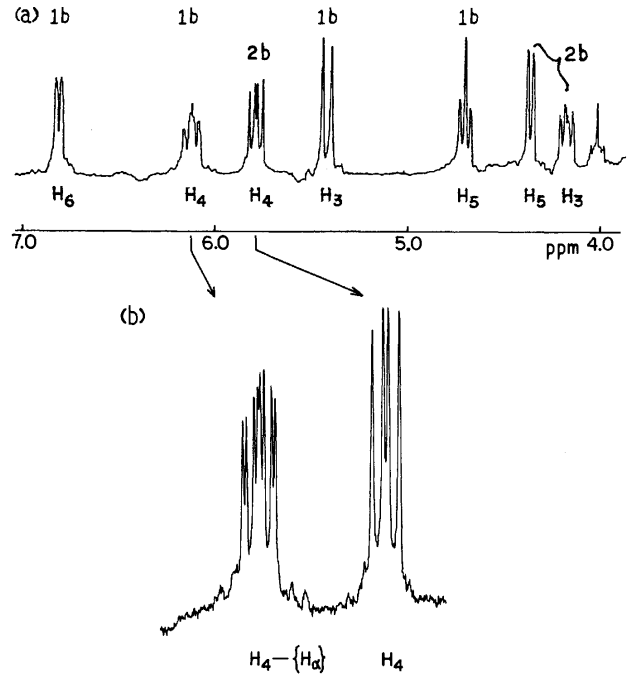

Fig. 3. (a) ^1H spectrum of the ring proton region of **1b** and **2b** in THF at 200 MHz, and (b) the expanded spectrum of the 4-proton peaks, where the 4-H of **1b** is decoupled to the α-H.

of anions, **1b** and **2b**. Thus, 2-ethyl- and 2-isopropylpyridines undergo both exchange and addition. 2-Methylpyridine appears to undergo only exchange to give **1a**, but, in a large scale preparation,[6] the presence of a small amount of **2a** was confirmed from a detailed inspection of the ^1H spectrum. Each of these two reactions occurs at a specific position as shown in Scheme 1. In any event, the 2-substituted pyridines undergo exchange to give **1**. The proportion of **1c** relative to **2c** is smaller than that of **1b** relative to **2b**, where **1b** and **2b** are in the ratio about 1:1. These facts indicate that the proton-releasing power of the α-carbon in the 2-substituted pyridines decreases in the order of methyl-, ethyl-, and isopropylpyridines.

In the ^{13}C spectra of **1**, the 5-carbon signal of each anion appears at a higher field in the order of **1a**, **1b**, and **1c**. The 5-carbon chemical shift is a well-defined index of negative charge delocalization, leading to the resonance stabilization, as stated before.[7] In the above order, therefore, these anions tend to take the resonance stabilization in a molecular plane. The resonance stabilization is enhanced by the α-positioned methyl group.

A typical ^1H spectrum of the ring proton region of **1b** and **2b**, prepared concomitantly from 2-ethylpyridine, is shown in Fig. 3. On the four signals assigned to **1b**, decoupling experiments show that the 4-H is coupled to the α-H with a coupling constant of 1.1 Hz.[8] This kind of long-range coupling was previously observed for **1a** at lower temperature.[9] Clearly, the α-carbon of **1b** is virtually sp^2-hybridized. These four signals for **1b** are attributable to the **1b'** isomer (Scheme 1). The presence of the **1b''** isomer could not be confirmed.[10] In **1c** and **2c**, the two methyl carbons bonded to the α-carbon of each anion show magnetic nonequivalence. The chemical shift difference between the two for **1c** is 6 ppm. This magnitude is appreciably larger than that for **2c** ($\Delta\delta_c$=2.3 ppm), whose α-carbon is in a sp^3 configuration.

Second, the 3-substituted pyridines undergo addition to give **3** and **4** (Scheme 2) concomitantly, but fail to do exchange. In **3c** and **4c**, as shown in Fig. 1 (b), the signals appearing as doublets at δ 5.54 and 5.79 are attributable to the 4-protons of **3c** and **4c** respectively. The ratio of the two peak areas is about 1:1.8,

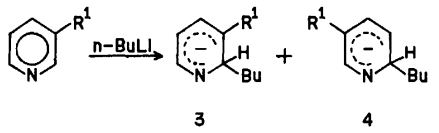

Scheme 2.

indicating that **3c** and **4c** are present in this ratio. In **3b** and **4b**, however, the ratio is about 1:1. This suggests that the 3-isopropyl group may tend to hinder the addition reaction occurring at the 2-position in the steric sense as compared with the 6-position.

Third, 4-methyl- and 4-ethylpyridines produce **6a** and **6b** (Scheme 3) together with **5a** and **5b** as by-products respectively. Further, 4-isopropylpyridine appears to produce **6c** only, as shown in Fig. 1(c), but the presence of a slight amount of **5c** was confirmed from a detailed inspection of the spectrum. In any

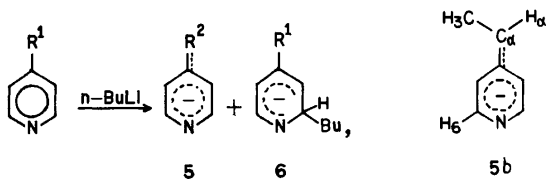

Scheme 3.

event, the 4-substituted pyridines undergo exchange with difficulty, as compared with the 2-substituted ones. It was reported before by Zoltewicz *et al.* that 4-methylpyridine was more acidic than 2-methylpyridine.[11] This implies that the proton-releasing power of the 4-methyl carbon is stronger than that of the 2-methyl one, that is, 4-methylpyridine tends to undergo exchange. In practice, however, **1a** is rather formed with ease as described above. This lithium-proton exchange reaction tends to occur at the substituent bonded to the position adjacent to nitrogen. This experimental result agrees with the observation of the anions produced from 2,4,6-trimethylpyridine,[1,9] and gives support to the view that the ring nitrogen (not α-carbon) can be regarded as the site where the anion–cation interaction takes place mainly in picolyl-

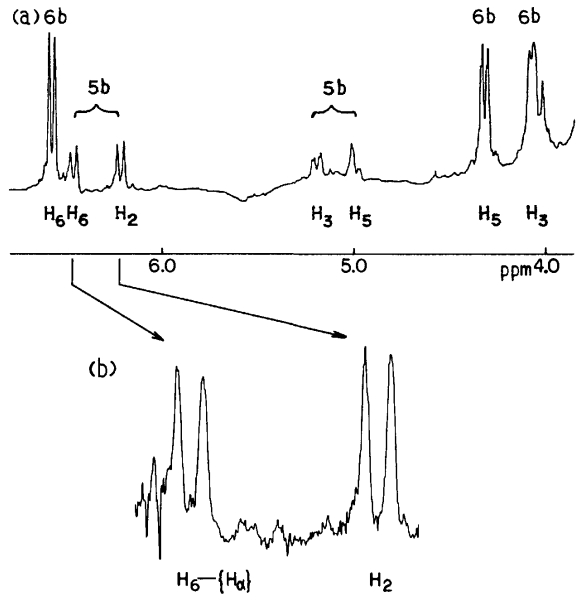

Fig. 4. (a) ^{1}H spectrum of the ring proton region of **5b** and **6b** in THF at 200 MHz, and (b) the expanded spectrum of the 6- and 2-proton peaks of **5b**, where the 6-H is decoupled to the α-H.

type carbanions with lithium as a counter ion.[3] The addition reaction also occurs at the position adjacent to nitrogen without substituent.

On the signals assigned to **5b** in Fig. 4, the *ortho*-protons (3- and 5-H) or *meta*-protons (2- and 6-H) are nonequivalent respectively at room temperature. Similar nonequivalence was observed before by Takahashi *et al.* for the α-methylbenzyl carbanion.[12] The *ortho*- or *meta*-carbons are also nonequivalent. This nonequivalence is explained by the restricted rotation around the bond between the ring and the α-carbon, caused by the resonance stabilization. Further, decoupling experiments show that the 6-H is coupled to the α-H (Scheme 3), and that the four signals appearing as doublets are attributable to the 6-, 2-, 3-, and 5-protons respectively in the upfield direction. The α-carbon of **5b**, as well as **1b**, is virtually in a sp^2 configuration.

In conclusion, two interesting facts should be noted. One is that two kinds of anions are formed concomitantly by lithium-proton exchange and addition of butyllithium from 2-ethyl-, 2-isopropyl-, 4-methyl-, and 4-ethylpyridines. The former reaction tends to occur at the substituent bonded to the position adjacent to nitrogen, and the latter one occurs at the position adjacent to nitrogen without substituent. Another is that a specific ring proton is coupled to the α-carbon in the anions formed by the exchange from 2- and 4-ethylpyridines, and, further, that the *ortho*- or *meta*-protons (or -carbons) in the latter anion are nonequivalent respectively at room temperature. The α-carbons in these anions are virtually sp^2-hybridized.

References

1) Part VII in this series: K. Konishi, A. Yoshino, M. Katoh, H. Matsumoto, K. Takahashi, and H. Iwamura, *Chem. Lett.*, **1982**, 169.

2) K. Konishi and K. Takahashi, Preprint presented at the 30th Symposium on Organometallic Chemistry, Kyoto, November 1983, 4.

3) K. Konishi and K. Takahashi, *Bull. Chem. Soc. Jpn.*, **56**, 1612 (1983).

4) H. C. Brown and W. A. Murpheny, *J. Am. Chem. Soc.*, **73**, 3308 (1951).

5) Y. Wakatsuki and H. Yamazaki, *Synthesis*, **1976**, 26.

6) About 100 mmol of 2-methylpyridine was reacted with the equimolecular amount of butyllithium in hexane at 0—5 °C.

7) K. Konishi and K. Takahashi, *Bull. Chem. Soc. Jpn.*, **50**, 2512 (1977).

8) T. E. Hogen-Esch and W. L. Jenkins, *J. Am. Chem. Soc.*, **103**, 3666 (1981).

9) K. Takahashi, K. Konishi, M. Ushio, M. Takaki, and R. Asami, *J. Organomet. Chem.*, **50**, 1 (1973).

10) W. L. Jenkins, C. F. Tien, and T. E. Hogen-Esch, *J. Polym. Sci., Polym. Lett. Ed.*, **16**, 501 (1978).

11) J. A. Zoltewicz and L. S. Helmick, *J. Org. Chem.*, **38**, 658 (1973).

12) K. Takahashi, M. Takaki, and R. Asami, *Org. Magn. Reson.*, **3**, 539 (1971).

 © 1985 The Chemical Society of Japan Bull. Chem. Soc. Jpn., 58, 2298—2303 (1985) [Vol. 58, No. 8

Effect of High Surface Coverage on the Rate of Methanol Oxidation at Platinum Electrode

Hiroshi MATSUI* and Takeo HISANO
Department of Applied Chemistry, Faculty of Engineering, The University of Tokushima, Minami-josanjima-cho, Tokushima 770
(Received January 23, 1985)

The rates of the methanol oxidation and the CO_{ad} formation at Pt electrodes in solutions of CH_3OH+ 0.5 mol dm^{-3} H_2SO_4 were investigated under the conditions minimizing the harmful effect of impurities. Under the particular conditions, the both rates decreased remarkably towards zero at a limiting coverage of about 0.8. Namely, the CO_{ad} hindered both the formation of the CO_{ad} itself and the oxidation of methanol *via* some unidentified intermediate other than CO_{ad}. This fact was explained by assuming an aggregate with two vacant sites indispensable for the CO_{ad} formation and the methanol oxidation to CO_2.

It is well known[1-4] that the stationary-state rates of the methanol oxidation on platinum electrodes in acid media increase and, in succession to a maximum, decrease with an increase in the methanol concentration, and that the decrease is remarkable at low potentials and high methanol concentrations. Similar maxima and the subsequent decreases of rate are also observed on each system of formaldehyde,[5] ethanol,[6] ethylene,[7,8] and so on. For the case of ethylene, Bockris *et al.*[8] gave an explanation on the basis of their hydroxyl-radical mechanism. Bagotzky *et al.*[1] however, observed variations in the rate of the methanol oxidation with potential differing from those predicted by the hydroxyl-radical mechanism. Biegler *et al.*[4] related the retardation of the methanol oxidation to the effect of high surface coverage with adsorbate formed from methanol, while Bagotzky *et al.*[1] showed that it also occurred even at low coverages. Breiter[9] proved that the presence of chloride ion, even in its very low concentrations, resulted in the inhibition of the methanol oxidation. Belanger[10] also reported similar effects of several anions such as nitrate as well as halogen ions.

In short, there were certain serious disagreements among groups of workers about the experimental data, particularly about the rates in the range of medium to limiting coverages. Thus it appeared of necessity to establish in the first place reliable data that were practically uninfluenced by impurities.

The data obtained with such a particular attention were different from those of the previous workers[1,4] in certain respects, *e.g.*, whether there were stationary-state rates in the methanol oxidation to CO_2. Above all, the rates of the formation of the adsorbate, CO_{ad}, and the overall oxidation of methanol decreased remarkably, in many cases towards zero, as soon as the coverage with CO_{ad} attained to a limiting value of 0.8, though the definition of the coverage here differed from that adopted by the previous investigators.[1,4] The phenomenon was explained by assuming that at the high coverage the CO_{ad} would damage the aggregates, each consisting of two vacant sites, indispensable for the formation of the CO_{ad} itself and for the oxidation of methanol *via* some unidentified intermediate other than CO_{ad}.

Experimental

The cells, electrodes, reagents, and the procedures were the same as those described in the previous paper.[11]

The coverages with adsorbate, θ_1 and θ_2, were expressed as

$$\theta_1 = (Q_H^0 - Q_H)/Q_H^0 \quad (1)$$

$$\theta_2 = Q^{ox}/(Q^{ox})_{max} \quad (2)$$

where Q_H^0 was the electric quantity required to cover fully the electrode surface with a monolayer of adsorbed hydrogen atoms in the absence of the carbon-containing adsorbate, Q_H was that in the presence. Q^{ox} was the quantity required to oxidize an amount of the adsorbate, and $(Q^{ox})_{max}$ was the maximum Q^{ox}. Q_H and Q_H^0 were determined by the conventional hydrogen-deposition method, in which the scan rates of potential were 20 and 100 V s^{-1} at the concentrations of methanol below and above 0.3 mol dm^{-3}, respectively. Q^{ox} and $(Q^{ox})_{max}$ were determined by the method described previously.[11]

In order to minimize the disturbing effect of adsorbed impurities on the rate of methanol oxidation, the temperature was lowered to 0°C, and roughened electrodes were used. Under these conditions, the decrease of Q_H^0 due to the adsorption of impurities did not exceed 3% within the oxidation time of 400 s.

The potentials were referred to the reversible hydrogen electrode in 0.5 mol dm^{-3} H_2SO_4, and the current densities were expressed for the unit true surface area, which was determined by the hydrogen-deposition method.

Results and Discussion

As seen in Fig. 1, the rate of oxidation never became stationary within about 400 s at the methanol concentrations above about 0.1 mol dm^{-3}. Although longer times resulted eventually in stationary rates, then Q_H^0 decreased more than 3% and the disturbing effect of impurities became perceptible. Figure 2 shows the time dependence of the CO_{ad} coverage under the same conditions as in Fig. 1. The coverage reached an approximately constant value of 0.8 at

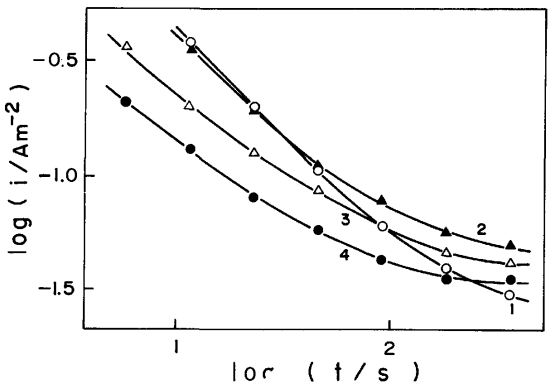

Fig. 1. Variation in oxidation rate with time (CH_3OH+0.5 mol dm^{-3} H_2SO_4, 0.6 V, 0 °C). Methanol: (1) 3.0; (2) 1.0; (3) 0.1; (4) 0.03 mol dm^{-3}.

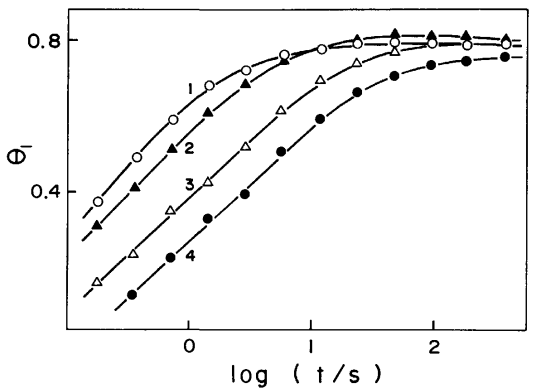

Fig. 2. Variation in surface coverage with time (CH_3OH+0.5 mol dm^{-3} 0.6 V, 0 °C). Methanol: (1) 3.0; (2) 1.0; (3) 0.1; (4) 0.03 mol dm^{-3}.

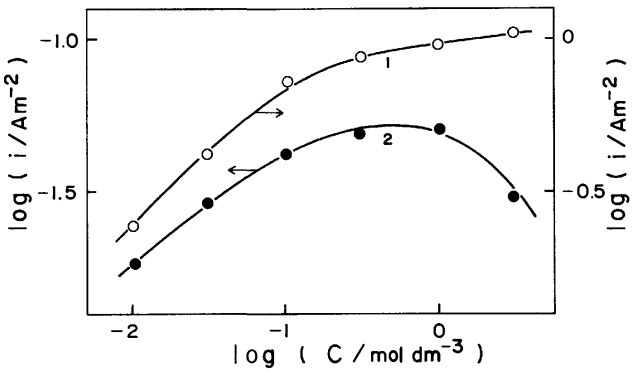

Fig. 3. Variation in oxidation rate at 360 s with methanol concentration (CH_3OH+0.5 mol dm^{-3} H_2SO_4, 0 °C). Potential: (1) 0.75; (2) 0.60 V.

all the methanol concentrations of 0.03—3 mol dm^{-3}. Respective curves in Fig. 3 show the typical rate-variations with the methanol concentration. The current densities plotted were ones at a particular time of 360 s when the coverages had already become stationary. Retarding of the oxidation rate at higher concentrations is obvious, and it becomes remarkable at lower potentials. These trends are in consistent with the observations by Bagotzky,[1] Biegler[4] *et al.* Contrary to their observations, however, the rates were not always stationary.

It is known[1,4,12] that the decay of current observed in the initial stage of the methanol oxidation at constant potentials is associated with the formation and accumulation of adsorbates. In order to know the time dependence of the oxidation rate uninfluenced by such a nonstationary current, i_N, subtraction of i_N from the observed current is necessary; the remainder is denoted hereafter by i_R. The present authors[11] showed that the formation and oxidation of the adsorbate that is experimentally identifiable could be written as

$$CH_3OH_{sol} = CO_{ad} + 4H^+ + 4e \quad (3)$$

$$CO_{ad} + H_2O = CO_2 + 2H^+ + 2e \quad (4)$$

Because part of the adsorbates formed are simultaneously oxidized unless the potential is very low, i_N at every moment solely contributes to the increase in the CO_{ad} coverage, θ_2. Expressing the mole number of CO_{ad} at its saturated coverage by N_s, and the Faraday constant by F,

$$i_N = 4FN_s d\theta_2/dt \quad (5)$$

according to Eq. 3. The i_N can also be expressed in terms of an electric quantity, Q_s^{ox} required to oxidize N_s moles of CO_{ad} to CO_2.

$$Q_s^{ox} d\theta_2/dt = 2FN_s d\theta_2/dt \quad (6)$$

From Eqs. 5 and 6,

$$i_N = 2Q_s^{ox} d\theta_2/dt \quad (7)$$

The time dependence of $i_R/(1-\theta_1)$ under the same conditions as those in Fig. 1 is shown in Fig. 4. Strictly speaking, no stationary rate was seen. In the course of the gradual fall of current, the coverages attained to a constant limiting value of about 0.8 at all the methanol concentrations when the potential was 0.6 V. The solid circle on each curve indicates the time at which the coverage attains to 0.75, and the time became shorter with an increase in the methanol concentration.

Relations between $i_R/(1-\theta_1)$ and θ_1 at various methanol concentrations and at a constant potential of 0.6 V are shown in Fig. 5. The fall of the rate became extremely remarkable with an increase of the coverage in its range of about 0.75 to 0.80. At the concentration of 0.03 mol dm^{-3}, the coverage could not reached 0.8, and no further fall of current could be measured. Because the rate of Reaction 3 is relatively small at low concentrations and exponentially decreases with an increase in θ_1, the coverage would be unable to come up to 0.8 within the limited measurement time. The electrode potential also exerted an effect upon the value

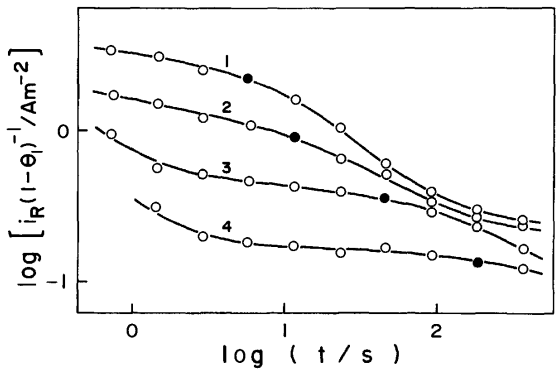

Fig. 4. Variation in oxidation rate with time (CH_3OH+0.5 mol dm^{-3} H_2SO_4, 0.6 V, 0°C). Methanol: (1) 1.0; (2) 0.3; (3) 0.1; (4) 0.03 mol dm^{-3}. Solid circle indicates when coverage attains to *ca.* 0.75.

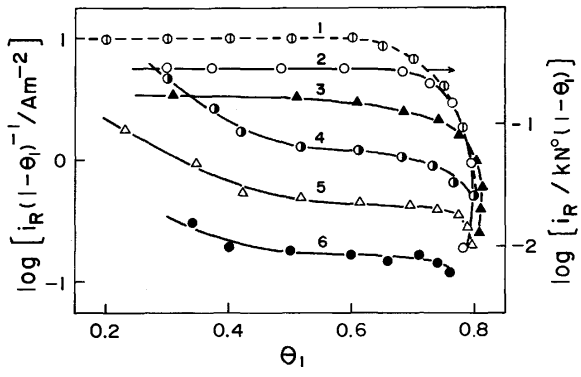

Fig. 5. Variation in oxidation rate with coverage (CH_3OH+0.5 mol dm^{-3} H_2SO_4, 0.6 V, 0°C). Methanol: (2) 3.0; (3) 1.0; (4) 0.3; (5) 0.1; (6) 0.03 mol dm^{-3}; Curve 1: theoretical.

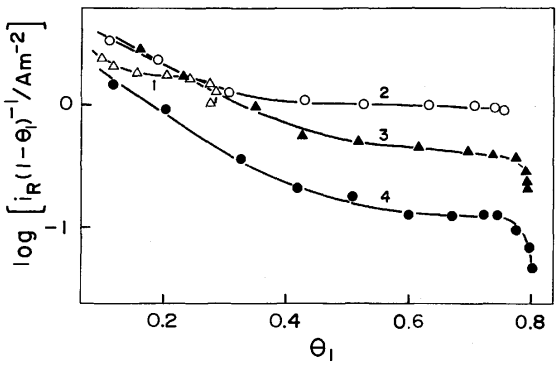

Fig. 6. Variation in oxidation rate with coverage (0.1 mol dm^{-3} CH_3OH+0.5 mol dm^{-3} H_2SO_4, 0°C). Potential: (1) 0.75; (2) 0.65; (3) 0.60; (4) 0.55 V.

of limiting coverage and the subsequent rate fall as illustrated in Fig. 6. Limiting coverages were 0.75 at 0.65 V, 0.3 at 0.75 V, and intermediate values ranging from 0.75 to 0.3 at the potentials from 0.65 to 0.75 V. In every case of higher potentials above 0.65 V, the current hardly continued falling after the limiting coverage, though an indication of the fall was observed. A potential increase accelerates the oxidation of the

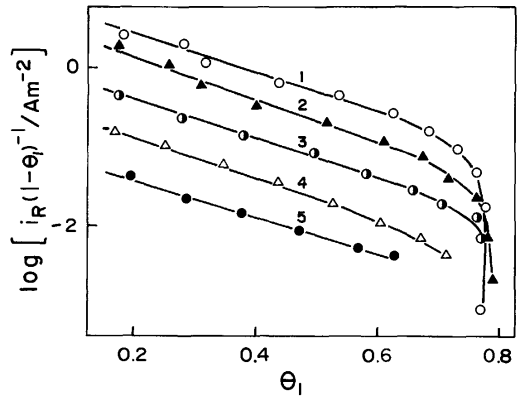

Fig. 7. Variation in CO_{ad} formation rate with coverage at 0.4 V (CH_3OH+0.5 mol dm^{-3} H_2SO_4, 0°C). Methanol: (1) 3.0; (2) 1.0; (3) 0.3; (4) 0.1; (5) 0.03 mol dm^{-3}.

CO_{ad} exponentially,[13] but doesn't the formation so much.[1,4] Therefore, the both rates would become balanced at a coverage lower than 0.8.

Similar remarkable falls of the rate of CO_{ad} formation took place whenever the coverage approached a limiting coverage of about 0.8 as shown in Fig. 7. The formation currents, i_F, were ones, except for Curve 2, corrected for the simultaneous oxidation of CO_{ad} by the method described in the preceding paper.[11] Coincidence in the value of the limiting coverages between the methanol oxidation and the CO_{ad} formation suggests that their causes would be similar.

Rate Fall before and after the Coverage of 0.8. As shown above, both the rates of the CO_{ad} formation and the overall methanol oxidation under the particular conditions markedly decrease, in some cases towards zero, immediately after the CO_{ad} coverage attains to a limit of about 0.8. A few explanations[1,4,7,8] have been given for the decrease in the oxidation rate at high coverages before the limits, but not an explanation for the unusual fall after the limiting coverage of 0.8. The definition of the coverage adopted here differs from those used by previous workers;[1,4] the value of 1 in their definition corresponds to about 0.8 in ours.

We have the data proving the oxidation rate of the CO_{ad} itself to be very small at its high coverages compared with the rate of the overall methanol oxidation to CO_2, the detail of which will be reported before long. Therefore, we are with Breiter *et al.*[12,14,15] about the opinion that different paths of CO_2 production exist in parallel. And we consider that at high coverages methanol is oxidized to CO_2 mostly without passing through the intermediate CO_{ad}.

Generally, such an adsorbate as is hard to react further can diminish the rate of an electrode reaction down to zero at a high coverage, if the adsorbate hinders sterically the approach of reactant species to the vacant sites adjacent to the preoccupied site, or if it prevents the availability of a site-aggregate that is indispensable for the electrode reaction to occur. The

CO_{ad} formed in the methanol oxidation is unlikely to exert the steric hindrance, because the coverage with the CO_{ad} formed from an aqueous solution of CO[16,17] is able to attain to 1. The aggregate-damaging effect is now under intensive investigation[18–20] in connection with the catalytic activity of an electrode modified with adatoms. This effect is operable provided the following conditions are satisfied.

(1) For the reaction under consideration to occur, an aggregate consisting of some of the vacant sites is necessary.

(2) The aggregate-damaging adsorbates are uniformly distributed on the surface.

(3) One molecule of the adsorbate occupies less sites than has one aggregate.

The CO_{ad} forming in the methanol oxidation can satisfy these requirements, the reasons are as follows.

(1) It would be reasonable to consider that the CO_{ad} formation takes place in a series of successive stages at which 4 hydrogen atoms of a methanol molecule are abstracted. Thus one or more sites are necessary in addition to the site(s) for the CO_{ad} eventually formed. Such site-aggregates would also be required for another path of the methanol oxidation to CO_2, though any stable intermediate is not yet experimentally identified.

(2) When the potential and the methanol concentration were below 0.5 V and 1 mol dm^{-3} respectively, no oxidation of methanol to CO_2 took place, and therefore the currents for the CO_{ad} formation, i_F, were directly measurable. The plots of log i_F $(1-\theta_1)^{-1}$ *vs* θ_1 were approximately linear within the limits of $0.1<\theta_1<0.75$ (Fig. 7), and expressed as

$$i_F = k(1-\theta_1)\exp(-3.84\,\theta_1) \qquad (8)$$

where k is a potential dependent constant. This experimental rate equation is substantially the same as the theoretical one[21] derived on the assumption that the heat of adsorption on a uniform surface increases linearly with an increase in the coverage. In other words, the CO_{ad} formation will occur in order of the increasing heat of adsorption, which will result in a uniform distribution of the CO_{ad}. At higher potentials above 0.5 V, an approximately uniform distribution would also be expected.

(3) Gilman *et al*[13,17] reported that the CO_{ad} formed from an aqueous solution of CO showed two states of binding with Pt surface atoms, *i.e.*, one-site (or linear) and two-site (or bridged) adsorptions. Since the value of 2 $(Q_H^0-Q_H)/Q^{ox}$ represents the number of sites occupied by one CO_{ad}, the number can be determined from the slope of plots, Q^{ox}/Q_H^0 *vs.* $(Q_H^0-Q_H)/Q_H^0$, the latter equals to θ_1. Figure 8 shows the case in which the methanol concentration is 1 mol dm^{-3} and the potential 0.35—0.75 V. The number of sites, 1.89, indicates that most adsorbates at $\theta_1<$ about 0.6 are the bridged type, and the number 1.08 that the adsorbates at about $0.6<\theta_1<0.8$ are mainly linear type.

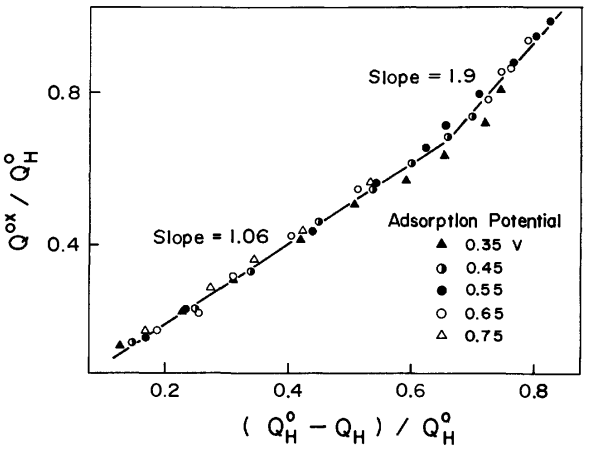

Fig. 8. Variation in Q^{ox} with coverage (1 mol dm^{-3} CH_3OH+0.5 mol dm^{-3} H_2SO_4, 0 °C).

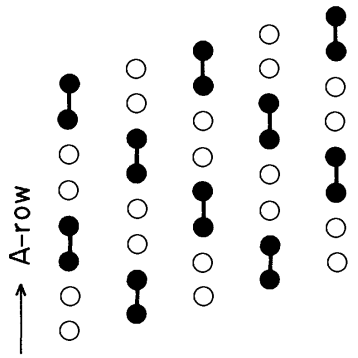

Fig. 9. Uniform distribution of bridged CO_{ad} at $\theta_1=0.5$ under minimum repulsion among CO_{ad} molecules.

To sum up, the CO_{ad} probably has such an aggregate-damaging effect as diminishes the rates of both the methanol oxidation to CO_2 and the further formation of CO_{ad} itself at its high coverage less than 1.

It is shown below first that the number of the aggregates, each consisting of 3 or more adjacent vacant sites, should be reduced to zero at $\theta_1=0.5$, if the bridged CO_{ad} species are distributed uniformly. And then that the linear adsorbates forming at $\theta_1>0.6$ should make all the aggregates consisting of two vacant sites each vanish at the coverage of 0.8.

The actual surface of the Pt electrodes used in the experiment was a mixture of crystal faces with the different indices and not a completely flat plane. However it can be represented by an orderly gathering of parallelograms as a simplest approximation, the apices representing the lattice sites (Fig. 9). In Fig. 9, rows of the nearest sites are called A-rows, and those of the next nearest ones B-rows.

A bridged CO_{ad} is considered[22] to be attached with its carbon atom to a pair of Pt sites. Since the atomic radius of Pt is larger than that of C, it must be energetically favorable for a bridged CO_{ad} to occupy those two sites which are nearest with each other. Thus

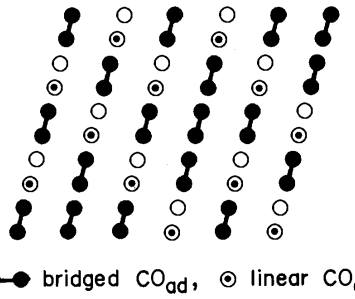

Fig. 10. An example of vacant-site distribution when coverage with bridged CO_{ad} (●—●) is 0.6 and that with linear CO_{ad} (⊙) 0.2.

the adsorbates will preferentially line up in the A-rows.

The negative value of the exponent, $-3.84\,\theta_1$, in Eq. 8, indicates that there are mutual repulsions between the CO-adsorbates, the adsorbed methanol molecules, or the both species, and that the repulsions make the adsorption energy of the CO_{ad} increasingly high with an increase in θ_1. In an A-row, the bridged CO_{ad} should align at intervals of some vacant sites in order to make the mutual repulsion small. If the maximum amount and the minimum repulsion of the adsorbates over the whole surface are required, every two pairs of sites situated directly abreast with a CO_{ad} should always be vacant as shown in Fig. 9. In this distribution of the adsorbates, the number of the aggregates with 3 or more adjacent vacant sites each is zero at $\theta_1=0.5$. However the experiment shows that the rate of the methanol oxidation does not fall to zero at the coverage of 0.4 to 0.75. It can thus be concluded that the number of sites in the aggregate indispensable to the oxidation of methanol to CO_{ad} or CO_2 is probably 2.

By assuming that the respective adsorbates at $\theta_1 \leq 0.6$ and >0.6 are exclusively bridged and linear types, the number of the remaining aggregates with two vacant sites each, A_2, can be deduced in the following way. Although the uniform distribution of the bridged adsorbates is probable at $\theta_1=0.5$ as shown in Fig. 9, a local irregularity cannot be avoidable at $\theta_1=0.6$. The distribution of the solid circles in Fig. 10 gives an example. At this coverage, A_2 is equal to a half of the remaining vacant sites, *i.e.*, $(1-0.6)\,S_t/2$; S_t is the total number of sites on the electrode surface. When $\theta>0.6$ and the linear adsorbates are distributed as uniformly as possible (Fig. 10), one linear adsorbate damages one aggregate. Consequently, A_2 is expressed as

$$A_2 = (1-0.6)S_t/2 - M_1 \qquad (9)$$

where M_1 is the number of the linear adsorbates, and equal to $(\theta_1-0.6)\,S_t$. Then the expression 9 becomes

$$A_2 = S_t(0.8-\theta_1) \qquad (10)$$

If i_R, the current for the oxidation of methanol to CO_2, is proportional to A_2, then

$$\log i_R(1-\theta_1)^{-1} = \log (kS_t) + \log (0.8-\theta_1)(1-\theta_1)^{-1} \qquad (11)$$

This theoretical equation shows that the rate of the oxidation decreases towards zero as θ_1 approaches 0.8, as indicated by Curve 1 of Fig. 5. This is in substantial agreement with the experimental fact. The rate decreases in the CO_{ad} formation at 0.8 can also be explained in the same way.

To sum up, the aggregate consisting of two vacant sites is indispensable for the formation of CO_{ad} and the overall oxidation of methanol. The CO_{ad} exerts the aggregate-damaging effect at the coverages of about 0.8, leading to the decrease of the both rates towards zero.

Additional Remarks about the Coverages by Different Definitions. As described above, the maximum coverage with the CO_{ad} varies according to whether the starting species, from which the CO_{ad} is formed, is methanol or carbon monoxide in a solution. Generally speaking, the maximum coverage with a particular adsorbate does not always take an invariable value even if the adsorbates are identical, which are eventually formed from different starting species *via* different paths. It is therefore not appropriate to use the following coverages, θ_2 and θ_3, for the purpose of comparison of the coverage values, unless the starting and the adsorbate species are respectively the same. In such cases, the coverage defined by Eq. 1 should be used.

$$\theta_3 = (Q_H^0 - Q_H)/[Q_H^0 - (Q_H)_{min}] \qquad (12)$$

where Q_H and Q_H^0 are previously stated when θ_1 is defined, and $(Q_H)_{min}$ are for the maximum amount of adsorbate, and $[Q_H^0-(Q_H)_{min}]$ corresponds to the maximum number of available hydrog hydrogen sites.

References

1) V. S. Bagotzky and Yu. B. Vassilyev, *Electrochim. Acta*, **12**, 1323 (1967).
2) O. A. Khazova, Yu. B. Vassilyev, and V. S. Bagotzky *Electrokhimiya*, **1**, 82 (1965).
3) A. N. Frumkin, *Electrochim. Acta*, **9**, 465 (1964).
4) T. Biegler and D. F. A. Koch, *J. Electrochem. Soc.*, **114**, 904 (1967).
5) D. F. A. Koch, Proc. 1st Austral. Conf. on Electrochemistry, Pergamon, Oxford (1965): cited in Ref. 1.
6) A. R. Blake, A. T. Kuhn, and J. G. Sunderland, *J. Electrochem. Soc.*, **120**, 492 (1973).
7) H. Wroblowa, B. J. Piersma, and J. O'M. Bockris, *J. Electroanal. Chem.*, **6**, 401 (1963).
8) B. J. Piersma, and E. Gileadi, "Modern Aspect of Electrochemistry," ed by J. O'M. Bockris, Plenum press, New York (1966) Vol. 4, p. 149.
9) M. W. Breiter, *Electrochim. Acta*, **9**, 827 (1964).
10) G. Belanger, *Can. J. Chem.*, **50**, 1891 (1972).
11) H. Matsui, T. Hisano, and T. Terazawa, *Bull. Chem. Soc. Jpn.*, **58**, 911 (1985).
12) O. A. Petrii, "Adsorption of Organic Compounds on Electrodes," ed by B. B. Damaskin, O. A. Petrii, and V. V.

Batrakov, Plenum press, New York (1971) p. 351, 458, and 463.
13) V. N. Kamath and Hira Lal, *J. Electroanal. Chem.*, **19**, 249 (1968) ; *ibid.*, **24**, 125 (1970).
14) M. W. Breiter, "Modern Aspects of Electrochemistry," ed by J. O'M. Bockris and B. E. Conway, Plenum press, New York (1975) Vol. 10, p. 161.
15) M. W. Breiter, *Discussions Faraday Soc.*, **45**, 79 (1968).
16) S. Gilman "Electroanalytical Chemistry," ed by A. J. Bard, Marcel Dekker Inc., New York, (1967) Vol. 2 p. 161.
17) S. Gilman, *J. Phys. Chem.*, **66**, 2657 (1962); **67**, 78 (1963); **67**, 1898 (1963); **68**, 70 (1964); **70**, 2880 (1966).
18) R. R. Adzic, D. N. Simic, A. R. Despic, and D. M. Drazic, *J. Electroanal. Chem.*, **65**, 587 (1975).
19) N. Furuya and S. Motoo, *J. Electroanal. Chem.*, **78**, 243 (1977); **98**, 195 (1979); **99**, 19 (1979).
20) H. Matsui, *Denkikagaku*, in press.
21) D. O. Hayward and B. M. W. Trapnell "Chemisorption," Butterworths, London (1964) p. 93.
22) G. Kohlmayer and P. Stonehart, *Electrochim. Acta*, **18**, 211 (1973).

Crystal Structure of 6-[6(e)-Carbamoyltetrahydro-2(e)-pyranyl]-8-oxa-6-azabicyclo[3.2.1]octan-7-one

Takashi YAMANE,* Hiroto NANAYAMA, Tamaichi ASHIDA,
Kazuhiko HASHIMOTO,† and Hiroshi SUMITOMO†
Department of Applied Chemistry, Faculty of Engineering, Nagoya University, Chikusa-ku, Nagoya 464
†Faculty of Agriculture, Nagoya University, Chikusa-ku, Nagoya 464
(Recieved March 18, 1985)

The structure of the dimerization product of bicyclic oxalactam, 8-oxa-6-azabicyclo[3.2.1] octan-7-one, was determined by the X-ray diffraction method. The final R value was 0.062 for 2009 reflections. The structure suggests that the cationic oligomerization of the bicyclic oxalactam proceeds through the C^5-N^6 scission, differing from the cases of other common lactams.

Cationic oligomerization of optically active bicyclic oxalactam, 8-oxa-6-azabicyclo[3.2.1]octan-7-one (abbreviated as BOL), produces the oligomer mixture.[1] The GPC analysis showed that the main product is the dimer, $(BOL)_2$. On the basis of IR and NMR data, an equatorial orientation of the BOL moiety with respect to the tetrahydropyran ring has been expected.[1] Therefore, the anticipated structure of $(BOL)_2$ and the dimerization mechanism are deduced as Eq. 1. It

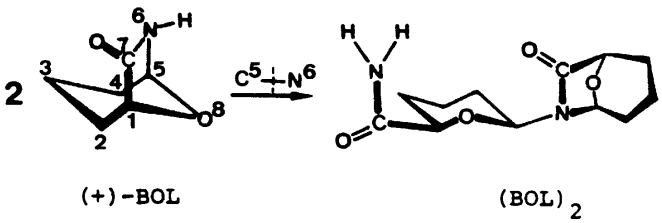

Eq. 1.

shows that the reaction proceeds through the C^5-N^6 scission of the oxaamide unit in BOL, though the N^6-C^7 scission is generally observed in the cases of other common lactams. In order to confirm the molecular structure and to elucidate the oligomerization mechanism, the crystal structure of $(BOL)_2$ has been studied by the X-ray diffraction method.

Results and Discussion

Crystal Data. $C_{12}H_{18}N_2O_4$, M.W.=254.29, $P2_1$, a=10.814(1), b=9.964(1), c=11.975(2) Å, β=101.44(1)°, U=1264.6(3) Å^3, Z=4, D_m=1.33, D_x=1.333 gcm^{-3}, μ(Cu $K\alpha$)=8.6 cm^{-1}. Intensity data with $2\theta \leq 120°$ were collected on a Rigaku four-circle diffractometer using graphite-monochromated Cu $K\alpha$ radiation (λ=1.5405 Å). The structure was solved by the use of *MULTAN* 78.[2] The refinement was carried out by the block-diagonal least-squares method.[3] The function minimized was $\sum w(|F_o|-|F_c|)^2$, and the weighting scheme at the final stage of the refinement was $w=[\sigma^2(F_o)-1.566|F_o|+0.079|F_o|^2]^{-1}$ for $|F_o|>0$, and w=1.016 for $|F_o|=0$. The final R value is 0.062 for 2009 independent reflections. All the scattering factors were taken from the International Tables for X-Ray Crystallography, Vol. IV.[4] The final atomic parameters with equivalent temperature factors are listed in Table 1.* The bond distances and angles are given in Fig. 1,

TABLE 1. FINAL FRACTIONAL COORDINATES(×10^4) AND EQUIVALENT ISOTROPIC TEMPERATURE FACTORS, WITH THEIR ESTIMATED STANDARD DEVIATIONS IN PARENTHESES

Atom	x	y	z	B_{eq}[5]/Å^2
C(1)A	3616(3)	1888(4)	4375(3)	4.2(1)
C(2)A	3924(4)	2661(4)	3403(4)	5.1(2)
C(3)A	3450(5)	1921(6)	2264(4)	7.2(3)
C(4)A	2142(5)	1336(5)	2222(5)	7.9(3)
C(5)A	2056(3)	710(4)	3356(4)	5.2(2)
C(7)A	4071(3)	441(4)	4358(3)	3.7(1)
C(62)A	1796(3)	−3500(3)	4091(3)	3.4(1)
C(63)A	1593(3)	−4051(4)	2886(3)	4.2(1)
C(64)A	2671(4)	−3643(3)	2323(4)	5.0(2)
C(65)A	2839(3)	−2119(4)	2376(3)	4.5(2)
C(66)A	3007(3)	−1664(3)	3605(3)	3.5(1)
C(67)A	677(3)	−3789(3)	4644(3)	3.5(1)
N(6)A	3082(2)	−229(3)	3760(3)	3.6(1)
N(69)A	−22(3)	−2776(3)	4835(3)	4.2(1)
O(8)A	2295(2)	1717(3)	4211(3)	5.6(1)
O(71)A	5113(3)	13(3)	4754(2)	5.9(1)
O(61)A	1983(2)	−2076(2)	4104(2)	3.5(1)
O(68)A	443(2)	−4951(3)	4854(2)	5.1(1)
C(1)B	3370(4)	−59(5)	9318(3)	5.8(2)
C(2)B	3861(4)	748(4)	8431(4)	5.2(2)
C(3)B	3655(5)	26(5)	7350(4)	6.7(2)
C(4)B	2365(5)	−601(5)	7039(4)	7.6(2)
C(5)B	2000(3)	−1271(5)	8074(5)	6.6(2)
C(7)B	3855(4)	−1481(4)	9392(3)	5.2(2)
C(62)B	1861(3)	−5499(4)	9096(3)	4.0(1)
C(63)B	1642(3)	−6076(4)	7894(3)	4.6(2)
C(64)B	2686(4)	−5634(3)	7293(4)	5.0(2)
C(65)B	2784(3)	−4114(4)	7330(3)	4.4(2)
C(66)B	3002(3)	−3633(4)	8556(3)	4.0(1)
C(67)B	804(3)	−5870(4)	9681(3)	4.5(2)
N(6)B	3018(3)	−2187(3)	8660(3)	4.2(1)
N(69)B	162(3)	−4858(4)	10021(3)	4.6(1)
O(8)B	2062(3)	−268(4)	8950(4)	8.5(2)
O(71)B	4839(4)	−1888(4)	9963(4)	9.3(2)
O(61)B	1988(2)	−4078(3)	9097(2)	4.0(1)
O(68)B	564(3)	−7042(3)	9818(3)	7.2(2)

*The anisotropic thermal parameters, the parameters of H atom and the tables of the observed and the calculated structure factors are kept as Document No. 8537 at the Office of the Chemical Society of Japan.

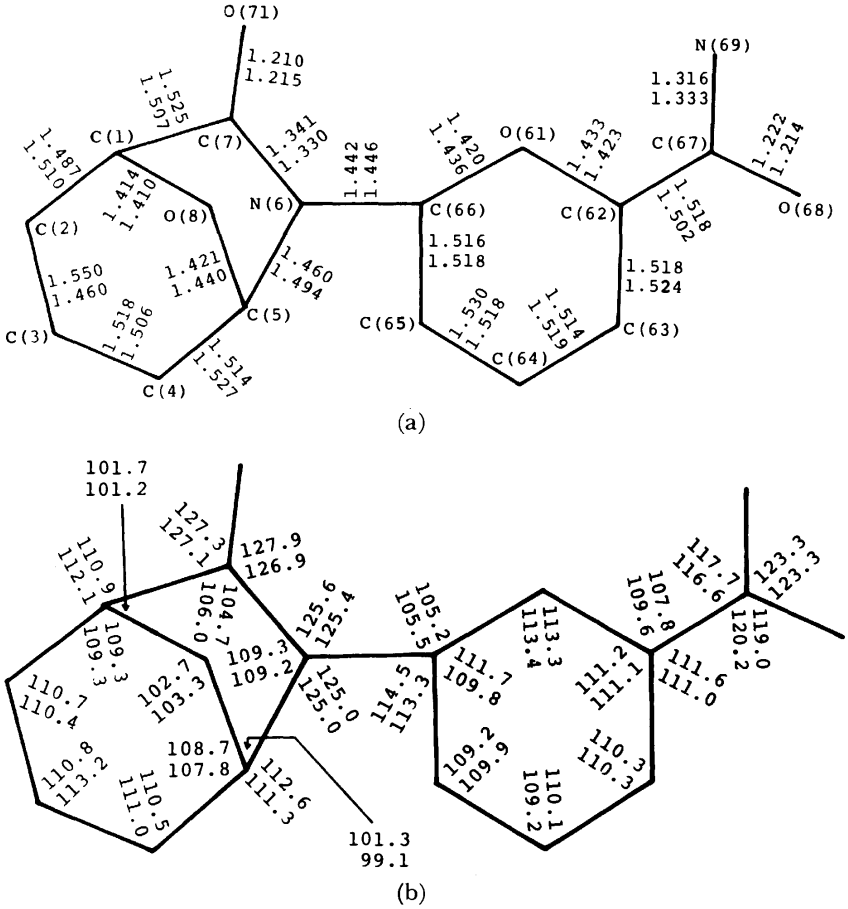

Fig. 1. (a) Bond distances (l/Å), (b) bond angles (ϕ/°) for molecule **A** (upper) and molecule **B** (lower). The estimated standard deviations are 0.005—0.007 Å for bond distances and 0.3—0.4° for bond angles.

with the numbering scheme of the atoms. Two independent molecules, **A** and **B**, are included in the asymmetric unit. The overall structure of the two molecules are almost the same. However, the thermal motion of molecule **B** is slightly larger than that of molecule **A**, as a whole. The bond distances and angles between the two molecules are in good agreement with each other, except for the C(2)–C(3) distance. An *ORTEP II*[6] drawing of molecule **A** is shown in Fig. 2. This shows that the tetrahydopyran ring takes a chair conformation, and ascertains that both the amide and the BOL moiety are equatorial with respect to the tetrahydropyran ring. This structure confirms the anticipated structure, and supports the presumed reaction mechanism of Eq. 1 that the cationic oligomerization of BOL proceeds through the C^5–N^6 scission of the oxaamide unit.

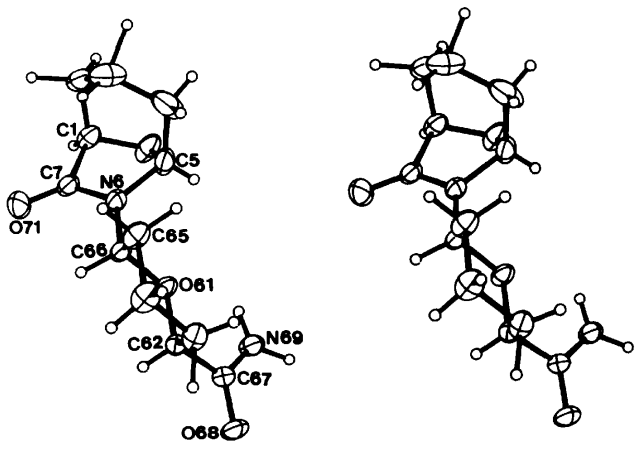

Fig. 2. Stereodrawing of molecule **A**. Atoms are drawn with 50% probability thermal ellipsoids.

The most interesting conformational feature of the molecule is the anticlinal conformation (ac^+) around the N(6)–C(66) bond. From the spectral data, the C(7)–N(6) bond was speculated to take g^- conformation to the C(66)–O(61) bond, leading to the formation of the intramolecular hydrogen bond between N(69) and O(71). However, the torsion angle of C(7)–N(6)–C(66)–O(61) is 118.4(3)° for **A** and 104.8(4)° for **B**, and the intramolecular hydrogen bond is not made. In this structure the C(5) is g^- to the O(61) and g^+ to the C(65) around the N(6)–C(66) bond. The torsion angles of the main skeleton which is of interest in consider-

TABLE 2. HYDROGEN BONDS(THE ESTIMATED STANDARD DEVIATIONS ARE IN PARENTHESES)

D*	A*	D···A	<D—H···A	Symmetry code of A
N(69)**A**	O(8)**A**	2.952(5)Å	155(2)°	$-x,-0.5+y,1-z$
N(69)**A**	O(68)**A**	2.877(5)	134(2)	$-x,0.5+y,1-z$
	O(61)**A**	2.588(4)	107(2)	—
N(69)**B**	O(8)**B**	2.940(6)	165(2)	$-x,-0.5+y,2-z$
N(69)**B**	O(68)**B**	2.930(5)	121(2)	$-x,0.5+y,2-z$
	O(61)**B**	2.581(4)	115(2)	—

* D means a protan donor and A a proton acceptor.

ing the model structure of the polymer of BOL synthesized by the anion polymerization are: C(1)-C(7)-N(6)-C(66), −173.5(3)° for **A** and −171.0(3)° for **B**; N(6)-C(66)-O(61)-C(62), −176.8(2)° for **A** and −177.6 (3)° for **B**; C(66)-O(61)-C(62)-C(67), −179.8(2)° for **A** and 178.6(3)° for **B**; O(61)-C(62)-C(67)-N(69), 11.5 (4)° for **A** and 2.8 (5)° for **B**. Therefore the conformation around the N(6)-C(66), C(66)-O(61) and O(61)-C(62) bonds can be described as an ac^{+}-*t*-*t* conformation.

Hydrogen bonds are listed in Table 2. The fairly distorted bifurcated hydrogen bonds are observed between N(69) and O(61), and between N(69) and O(68). The former is intramolecular and the latter is intermolecular. One of the reasons for the distorsions is considered to be the formation of the five-membered ring by the N(69)···O(61) hydrogen bond.

The authors would like to thank Toyota Physical and Chemical Research Institute for financial support.

References

1) K. Hashimoto and H. Sumitomo, *J. Polym. Sci., Polym. Chem. Ed.*, **22**, 1733 (1984).

2) P. Main, S. E. Hull, L. Lessinger, G. Germain, J.-P. Declercq and M. M. Woolfson, "*MULTAN* 78, A System of Computer Programs for the Automatic Solution of Crystal Structures from X-ray Diffraction Data," University of York, England, and Louvain, Belgium (1978).

3) T. Ashida, "*UNICS-NAGOYA*," Nagoya University, Nagoya, Japan, 65 (1981).

4) "International Tables for X-Ray Crystallography," Vol. IV, Kynoch Press, Birmingham (1974).

5) W. C. Hamilton, *Acta Crystallogr.*, **12**, 609 (1959).

6) C. K. Johnson, "*ORTEP-II*," *Report ORNL*-5138, Oak Ridge National Laboratory, Tennessee, USA (1976).

Photocatalytic Isomerization of Butenes over ZnO and SnO_2

Sukeya KODAMA,* Masaaki YABUTA, Masakazu ANPO, and Yutaka KUBOKAWA
Department of Applied Chemistry, University of Osaka Prefecture, Sakai, Osaka 591
(Received April 1, 1985)

It has been found with ZnO as well as TiO_2 that 2-butene is much more reactive than 1-butene for their photocatalytic isomerization. Although both *cis-trans* and double bond isomerizations take place on ZnO, only *cis-trans* isomerization occurs over SnO_2. The photocatalytic isomerizations were suppressed drastically in the presence of NO. From those results together with the ESR studies the following conclusions emerge: a butene molecule interacts with the photoformed O^- to form a radical species as a result of fission of the C=C bond; the photocatalytic isomerization proceeds *via* such a radical intermediate; the lack of the reactivity of 1-butene appears to be explicable on such basis.

In order to understand the photocatalysis of metal oxides, it seems necessary to investigate on a wide range of the photocatalytic reactions, other than the oxidation and reduction reactions. From such standpoint we have investigated the photocatalytic isomerization of butenes over TiO_2 and ZnO with the result that in the case of TiO_2 2-butene is more reactive than 1-butene.[1] A continued study concerning the isomerization over ZnO has revealed that it is unnecessary to propose an intermediate different from that for the isomerization over TiO_2. Essentially the same features have been observed with both ZnO and TiO_2. Similar works have been extended to SnO_2.[2] In addition to those results, the present paper deals with the ESR studies which provide information on the active species as well as an intermediate in the photocatalytic isomerization of butenes. Furthermore, its mechanism has been worked out.

Experimental

All the butenes used in the present work as well as NO were of extrapure grade from the Takachiho Kagakukogyo Co. ZnO (Kadox 25, 10 m^2g^{-1}) was obtained from New Jersey Zinc Co. SnO_2 (8.6 m^2g^{-1}) was prepared from hydrolysis of $SnCl_2$ with aqueous ammonia. Both ZnO and SnO_2 were subjected to oxygen treatment for one hour at 560°C followed by evacuation at the same temperature. Butenes of about 4.0 kPa were introduced over the catalysts (ZnO 0.6 g, SnO_2 2.0 g) which had been spread on the quartz cell window, having a surface area of *ca.* 32 cm^2. The photoisomerization was carried out by UV irradiation from a high pressure mercury lamp (Toshiba, SHL-100UV) with and without a filter (Toshiba, UV-D33S) shading the visible and infrared regions. Gas samples were taken at definite intervals and analyzed gas chromatographically using a dimethylsulfolane column. ESR measurements were carried out with JES-ME-1 (X-band). Mn^{2+} ions in MgO powder were used for *g* value and sweep calibration.

Results

Continued work concerning the isomerization of 1-butene over ZnO at 0°C was carried out in the dark and under UV irradiation with and without the filter with the results shown in Fig. 1. No enhancement of the isomerization by UV irradiation was found. Figure 2 shows the results on the isomerization of *trans*-2-butene over ZnO at 0°C. It is found that both isomerizations to *cis*-2-butene and 1-butene are enhanced by UV irradiation. From those results the following conclusions emerge: the enhancement of the isomerizations of 2-butene under UV irradiation arises from photocatalytic effects and not thermal effects by the radiation from the lamp; 1-butene is unreactive for

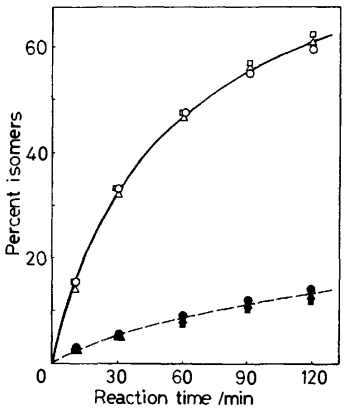

Fig. 1. Isomerization of 1-butene over ZnO at 0°C.
Solid curve: *cis*-2-butene; broken curve: *trans*-2-butene.
○, ●: Under UV without filter; △, ▲: under UV with filter; □, ■: in the dark.

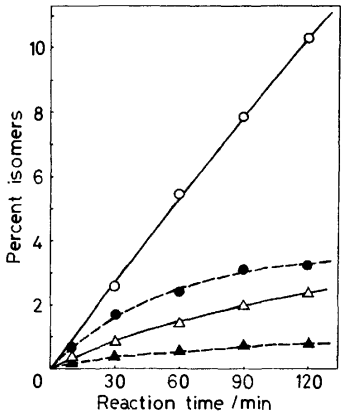

Fig. 2. Isomerization of *trans*-2-butene over ZnO at 0°C.
Solid curve: under UV with filter; broken curve: in the dark. ○, ●: *cis*-2-Butene; △, ▲: 1-butene.

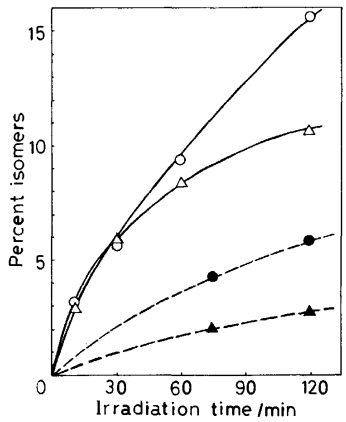

Fig. 3. Photoisomerization of *cis*-2-butene over ZnO at 0°C.
Solid curve: without NO; broken curve: with NO of 1.3 kPa. O, ●: *trans*-2-Butene; △, ▲: 1-butene.

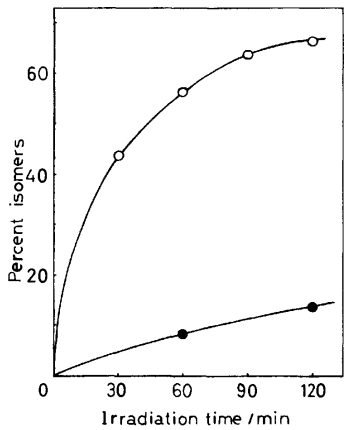

Fig. 4. Photoisomerization of *cis*-2-butene to *trans*-2-butene over SnO_2 at 40°C. O: Without NO; ●: with NO of 1.3 kPa.

photocatalytic isomerization. Thus, the conclusion obtained with TiO_2 that 2-butene is much more reactive than 1-butene holds for ZnO. Its general applicability is confirmed. As shown in Fig. 3, the photocatalytic isomerization of *cis*-2-butene is suppressed by the presence of NO.

Similar studies have been extended to SnO_2. The results are shown in Fig. 4. It should be noted that only *cis-trans* isomerization proceeds, without double bond migration. The isomerization is again restrained in the presence of NO.

When NO molecules were adsorbed onto the catalyst, which had been treated in vacuum, the ESR spectrum due to the adsorbed NO molecules was observed at 77 K.[3] UV irradiation of the catalyst in the presence of NO at 77 K led to the appearance of a new signal shown in Fig. 5, which was thermally unstable and it disappeared completely on raising the temperature up to 300 K. This new spectrum is characterized by *g* value of 2.002 with hyperfine splitting of *ca.* 35 G† for N^{14}.

† 1 G≈10^{-4}T.

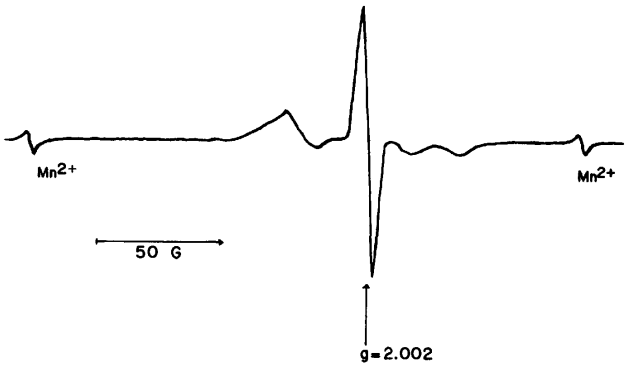

Fig. 5. ESR spectrum of photoformed NO_2^{2-} anion radicals adsorbed on ZnO (0.20 g) at 77 K. Amount of photoformed NO_2^{2-} is 8.6×10^{-7} mol.

These values are similar to those for NO_2^{2-} species adsorbed on the surface of ZnO, though the hyperfine splitting of 35 G is slightly smaller.[3b] As described previously,[4] UV irradiation of ZnO at 77 K *in vacuo* leads the formation of O^- anion radicals. Accordingly, it is expected that the photoformed O^- species reacts with NO to produce NO_2^-, which is transformed to NO_2^{2-} by electron trapping. This assumption is strongly supported from the results of ESR measurements. From these results, it is concluded that the spectrum shown in Fig. 5 can be assigned to NO_2^{2-}. Thus, the reaction of photoformed O^- with NO is confirmed. Since the photocatalytic isomerization is suppressed by the presence of NO as described above, it is suggested that interaction of butene molecules with photoformed O^- is involved in its photocatalytic isomerization.

The catalyst exhibited the ESR spectrum due to the presence of Zn^+ and bulk O^- species after the pretreatment in vacuum.[5] When 1-butene was admitted onto the catalyst, a new ESR spectrum was observed neither at 77 K nor at room temperature, except for a slight weakening of the signal due to O^- species. On UV irradiation of the catalyst in the presence of butene at 77 K, a new ESR signal appears as shown in Fig. 6. It shows a doublet hyperfine splitting separated by *ca.* 22 G. This splitting is comparable to the 17—22 G splitting due to one β-hydrogen in alkyl or alkene radicals.[6] Further triplet hyperfine splitting with *ca.* 7 G is similar to that for two α-hydrogens in alkene cation radicals adsorbed on zeolite surfaces.[7] When the temperature was raised up to around 300 K, this signal disappeared irreversibly without appearance of any new signals. In addition to such hyperfine splitting, the number of hyperfine components, *i.e.*, a doublet of triplet and their intensity ratio together with a *g* value of 2.0014 suggest that a radical species, $CH_2\dot{-}CH-CH_2-CH_3$, is formed on ZnO under UV irradiation.

Discussion

The fact that 2-butene is much more reactive than

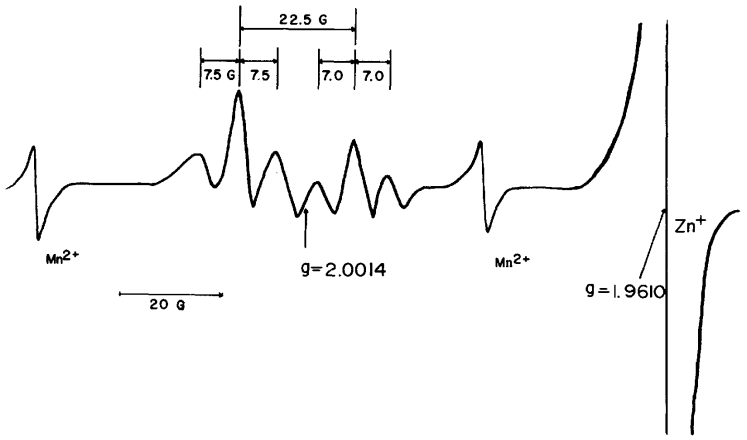

Fig. 6. ESR spectrum of photoformed butene radicals at 77 K.
Amount of 1-butene adsorbed on ZnO (0.20 g) is 1.2×10^{-5} mol g^{-1}.

1-butene is unexplicable by π-allyl intermediates, which has been proposed for the isomerization of butenes over ZnO and Al_2O_3.[8] This suggests that an intermediate different from π-allyl species is involved in the photocatalytic isomerization. In the previous works[9] it has been shown that fission of the C=C bond of alkenes is induced by its interaction of photoformed O^- or $[M^{(n-1)+}—O^-]$ pairs. Furthermore, the ESR studies described above demonstrate clearly that the photoformed O^- species interacts with a butene molecule to form a radical species. Accordingly, it might be concluded that a radical species is involved as the intermediate in the photocatalytic isomerization. Thus, the following reaction scheme is proposed for the 2-butene isomerization:

$$\begin{array}{l} CH_3\text{-}CH{=}CH\text{-}CH_3 \xrightarrow{h\nu} CH_3\text{-}CH{=}CH\text{-}CH_3 \longrightarrow \\ O^{2-}\ M^{2+}\ OH^- \qquad\quad O^-\ M^+\ OH^- \end{array}$$

$$\begin{array}{l} \overset{1}{CH_3}\text{-}\overset{2}{CH}\text{-}\overset{3}{CH}\text{-}\overset{4}{CH_3} \xrightarrow{[I]} CH_3\text{-}CH\text{-}CH_2\text{-}CH_3 \longrightarrow \\ \quad\vdots\ \cdot \qquad\qquad\qquad\quad \vdots \\ O^-\ M^+\ OH^- \qquad\quad O^-\ M^{2+}\ O^{2-} \end{array}$$

$$\begin{array}{l} CH_2\text{-}CH\text{-}CH_2\text{-}CH_3 \longrightarrow CH_2{=}CH\text{-}CH_2\text{-}CH_3 \\ \quad\vdots \qquad\qquad\qquad\quad \\ OH^-M^{2+}\ O^{2-} \qquad OH^-\ M^{2+}\ O^{2-} \end{array}$$

The photoformed O^- or $[M^{(n-1)+}—O^-]$ pairs interact with a butene molecule to form the radical [I] as a result of opening of the C=C bond. When the radical reverts to butene, the *cis-trans* isomerization is expected to occur. In fact, Morikawa *et al.*[10] have proposed that such radical species adsorbed on porous Vycor glass play a significant role in the photocatalytic *cis-trans* isomerization of butenes on it.

In case where the double bond migration proceeds *via* a radical intermediate, the presence of hydrogen atoms appears to be the prerequisite for its occurrence. If H atoms are present on the surface, H atom addition to C atom at the position 3 of the radical [I] will occur. This will be followed by removal of H atom from CH_3 group by the O^- species because of its high efficiency for hydrogen abstraction. Thus, 1-butene is formed. In the above reaction scheme it is assumed that H atoms are supplied from the surface OH groups, although there is no evidence for this postulate. In this case the acidity of the OH groups as well as the concentration of electrons available for the neutralization of protons would determine to what extent the double bond migration occurs. The photoformed electrons trapped as M^+ ions are used for the neutralization of protons. At present it is unclear whether or not the difference in the selectivity of the isomerization between ZnO and SnO_2 described above is explicable on the basis of such a concept. A further study is necessary to settle this problem. It is to be noted that trace amounts of the OH groups are enough to bring about the isomerization in the case of a concerted mechanism where the removal and addition of H atom proceed with a similar rate.

In the case of the isomerization of 1-butene, in contrast to the case of 2-butene where opening of the C=C bond brings about only one type of the adsorbed radical, two types of the adsorbed radicals may be expected to be formed:

$$\begin{array}{ll} \dot{C}H_2\text{-}CH\text{-}CH_2\text{-}CH_3 & CH_2\text{-}\dot{C}H\text{-}CH_2\text{-}CH_3 \\ \quad\vdots & \quad\vdots \\ \quad M^+ & \quad M^+ \\ \text{(primary radical)} & \text{(secondary radical)} \end{array}$$

Although for the primary radical the removal and addition of H atom may be possible, for the secondary radical only regeneration of 1-butene may take place. Since it is well-known that the secondary radical is more stable than the primary one, the secondary radical is expected to participate in the reaction. Accordingly, in the case of 1-butene occurrence of the isomerization is not expected, in agreement with the experimental results. Finally it should be noted that the unusual feature of the photocatalytic isomerization, *i.e.*, the lack of the reactivity of 1-butene is explicable on the basis of

the concept that an intermediate where one unpaired electron remains uninteracted with the surface is involved in the reaction.

References

1) S. Kodama, M. Yabuta, and Y. Kubokawa, *Chem. Lett.*, **1982**, 1671.

2) C. Kemball, H. F. Leach, and I. R. Shannon, *J. Catal.*, **29**, 99 (1973); M. Itoh, H. Hattori, and K. Tanabe, *ibid.*, **43**, 192 (1976); J. Herrmann, J. Disdler, and P. Pichat, *J. Chem. Soc., Faraday Trans. 1*, **77**, 2815 (1981).

3) a) J. H. Lunsford, *J. Chem. Phys.*, **46**, 4347 (1967); b) J. H. Lunsford, *J. Phys. Chem.*, **72**, 2141 (1968); c) J. H. Lunsford, *ibid.*, **72**, 4163 (1968).

4) M. Anpo and Y. Kubokawa, *J. Phys. Chem.*, **88**, 5556 (1984).

5) K. M. Sancier, *J. Catal.*, **5**, 314 (1966); J. H. C. Van Hooff, *ibid.*, **11**, 277 (1968).

6) R. W. Fessenden and R. H. Schuler, *J. Chem. Phys.*, **39**, 2147 (1963); J. E. Wertz and J. R. Bolton, "Electron Spin Resonance Elementary Theory and Practical Applications," McGraw-Hill Book Co., New York (1972).

7) S. Shin, *J. Catal.*, **36**, 238 (1975).

8) C. C. Chang, W. C. Conner, and R. J. Kokes, *J. Phys. Chem.*, **77**, 1957 (1973); J. H. Lunsford, L. W. Zingery, and M. P. Rosynek, *J. Catal.*, **38**, 179 (1975).

9) M. Anpo, I. Tanahashi, and Y. Kubokawa, *J. Chem. Soc., Faraday Trans. 1*, **78**, 2121 (1982); M. Anpo, N. Aikawa, S. Kodama, and Y. Kubokawa, *J. Phys. Chem.*, **88**, 2569 (1984).

10) A. Morikawa, M. Hattori, K. Yagi, and K. Otsuka, *Z. Phys. Chem. (Frankfurt am Main)*, **104**, 309 (1977).

Polarization in Light-scattering by Aerosol

Akiyoshi MATSUZAKI
The Institute of Space and Astronautical Science, Komaba 4-6-1, Meguro-ku, Tokyo 153
(Received April 5, 1985)

The polarization of the light scattered by aerosol has been studied by the theoretical calculation based on the Mie scattering theory. The present calculation obtains the polarization of the light scattered by aerosol as a function of size parameter, *i.e.* $x=2\pi r/\lambda$, where r and λ are the radius of aerosol and the wavelength of the scattered light, respectively, for various refractive indexes. These results give the useful informations for the experimental study on the size-growth in aerosol formation by the measurement of the scattered light polarization. The characteristic of the scattered light intensity, which is usually used as a kind of concentration parameter in the study on aerosol formation, is also discussed.

The investigation on aerosols, which are small particles floating in the atmosphere, is of great importance in view of chemical reaction and environmental science. For example, aerosol formation includes heterogeneous reactions, *i.e.*, gaseous molecules and solid, gas and liquid, or liquid and solid. On the other hand, in view of environmental science, the stratospheric aerosol is known to affect the radiation balance in the atmosphere. Consequently, it is very important with the relevance to the climate problem. Its property and formation mechanism are the up-to-date targets.

In the study on aerosol, the scattered light intensity is usually used as a kind of concentration parameter. Namely, the property of aerosol, *e.g.* the size, the refractive index, *etc.*, has been studied by the measurement of the polarization and the angular distribution of the scattered light. However, in fact, these show the complex dependence on the size and the refractive index of aerosol and the wavelength of the scattered light. In this situation, the present work made the theoretical calculation of the polarization of the scattered light for some typical aerosol models with the aid of the Mie scattering theory.[1] The property of the scattered light intensity is also discussed with the experimental and theoretical results.

Experimental

The experimental system is schematically shown in Fig. 1. The N_2 laser with 25 Hz of repetition causes aerosol formation in the reaction cell (sphere glass with 25 cmϕ), which is filled with approx. fifty Torr† of carbon disulfide vapor. The polarized radiation of a He-Ne laser is introduced coaxially with the N_2 laser radiation, and the light scattered by the aerosol formed and the carbon disulfide vapor was measured in the direction perpendicular to the He-Ne

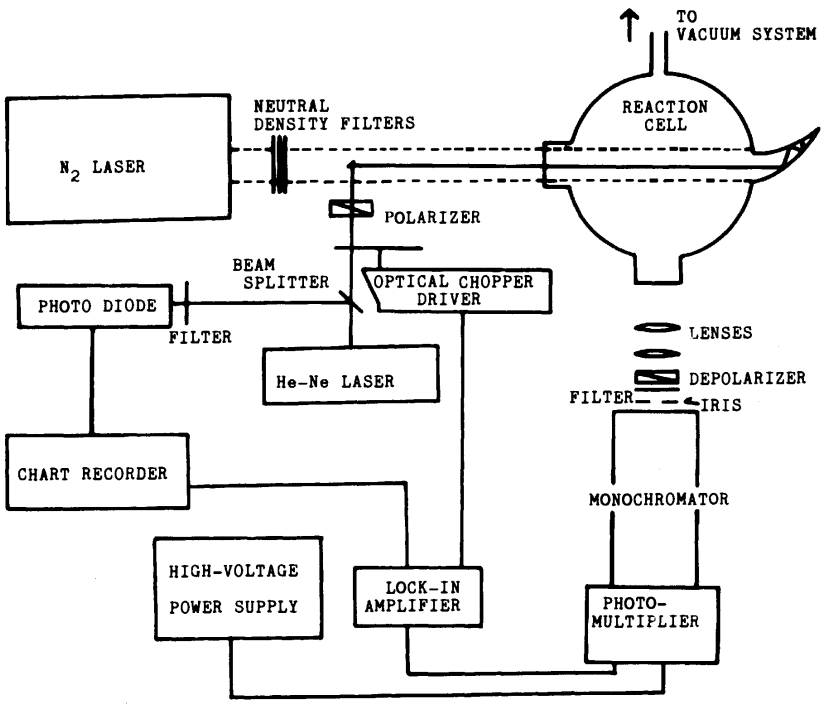

Fig. 1. Block diagram of experimental apparatus.

† 1 Torr=133.322 Pa.

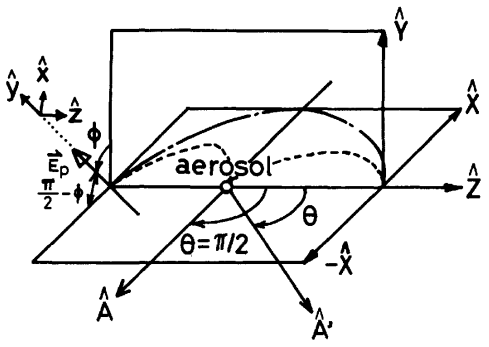

Fig. 2. Definition of the laboratory coordinate $(\hat{X},\hat{Y},\hat{Z})$ and the electric vector coordinate $(\hat{x},\hat{y},\hat{z})$. The angle between $\hat{Y}$ and $\hat{y}$ is ϕ. $\hat{A}$ and $\hat{A}'$ have the angles of $(\pi/2)$ and θ with the $\hat{Z}$-axis, respectively.

laser beam. Namely, lenses and an iris introduce the scattered light into a monochromator (f=200 mm) after the depolarization, then a photomultiplier detects it. The modulation of the He–Ne laser radiation with an optical chopper allows the measurement with a good signal-to-noise ratio by using a lock-in-amplifier detecting system. Carbon disulfide (Wako reagent grade) was used after the vacuum distillation.

Method of Theoretical Calculation

Definitions of Axes. For the convenience to describe these theoretical and experimental examinations, Figure 2 defines the laboratory-fixed axes $(\hat{X},\hat{Y},\hat{Z})$, the electric-vector-fixed axes $(\hat{x},\hat{y},\hat{z})$ and the angular parameters. The $\hat{Z}$-axis is coincident with the incident laser-beam axis. The directions of observation, *i.e.* $\hat{A}$ and $\hat{A}'$, are on the $\hat{X}$–$\hat{Z}$ plane and have the angles of $(\pi/2)$ and θ with the $\hat{Z}$-axis, respectively. The electric vector $\vec{E}_p$ of the incident laser beam is expressed in term of the $\vec{E}_p$-fixed axes $(\hat{x},\hat{y},\hat{z})$. The $\hat{z}$-axis is in the same direction as the $\hat{Z}$-axis. The angle between the $\hat{y}$-axis and the $\hat{Y}$-axis is ϕ. For example, the Rayleigh-scattering angular distributions for the incident light polarized with ϕ=0° and 90° are shown by the dashed-solid line and the dashed line, respectively, in Fig. 2.

Outline of the Mie Scattering Theory. The exact solution to the scattering problem for a sphere radius r at wavelength λ was given by Mie in 1908,[1] elaborated by Debye,[2] and thereafter arranged by van de Hulst.[3] The problem is to obtain three dimensional solutions for Maxwell's equations for the electric and magnetic fields inside and outside a spherical region of radius r and the refractive index m at the frequency ω. By seperating the variables, solutions of the scalar wave equation $\nabla^2\psi+k^2m^2\psi=0$, where k is the wavenumber $(2\pi/\lambda)$, can be written in the spherical coordinates as:

$$\psi_{l,n} = \begin{cases}\cos l\phi \\ \sin l\phi\end{cases} P_n^l(\cos\theta)\left\{\sqrt{\frac{\pi}{2mkr}}\,Z_{n+1/2}(mkr)\right\}, \tag{1}$$

where Z represents either J- or H-solutions of Bessel's equation, P_n^l Legendre polynominals. A plane-incident scalar wave can be written:

$$u_0 = \exp(i\omega t)\cos\phi\sum_1^\infty(-)^n\frac{2n+1}{n(n+1)}P_n^1(\cos\theta)j_n(kr), \tag{2}$$

$$v_0 = \exp(i\omega t)\sin\phi\sum_1^\infty(-)^n\frac{2n+1}{n(n+1)}P_n^1(\cos\theta)j_n(kr). \tag{2'}$$

The corresponding spherical Bessel functions are written by j_n and h_n. The scattered wave therefore contains only terms with l=1 and the scalar functions u and v can be written as:

$$u = \exp(i\omega t)\cos\phi\sum_{n=1}^\infty(-a_n)(-i)^n\frac{2n+1}{n(n+1)}P_n^1(\cos\theta)h_n(kr), \tag{3}$$

$$v = \exp(i\omega t)\sin\phi\sum_{n=1}^\infty(-b_n)(-i)^n\frac{2n+1}{n(n+1)}P_n^1(\cos\theta)h_n(kr). \tag{3'}$$

The Mie solution process is one of finding a set of complex numbers a_n and b_n (Mie coefficients):

$$a_n = \frac{S_n'(y)S_n(x)-mS_n(y)S_n'(x)}{S_n'(y)[S_n(x)+iC_n(x)]-mS_n(y)[S_n'(x)+iC_n'(x)]}, \tag{4}$$

$$b_n = \frac{mS_n'(y)S_n(x)-S_n(y)S_n'(x)}{mS_n'(y)[S_n(x)+iC_n(x)]-S_n(y)[S_n'(x)+iC_n'(x)]}. \tag{4'}$$

These complex-valued coefficients, functions of the refractive index m, $x=2\pi r/\lambda$ and $y=mx$ provide the full solution to the scattering problem. Here, S_n and C_n can be represented, as follows, with the Bessel functions $J_{n+1/2}(\rho)$ and the Neumann functions $N_{n+1/2}(\rho)$:

$$S_n(\rho) = \sqrt{\pi\rho/2}J_{n+1/2}(\rho), \tag{5}$$

$$C_n(\rho) = -\sqrt{\pi\rho/2}N_{n+1/2}(\rho). \tag{5'}$$

The prime denotes differentiation with respect to the argument. The Mie coefficients give directly some important integrated quantities: The excitation, scattering and absorption efficiencies. The efficiency factors are defined as follows: The energy removed from an incident wave with energy flux density I_0 is $\pi r^2Q_eI_0$, Q_e being the extinction efficiency; the energy which reappears as scattered energy is $\pi r^2Q_sI_0$, Q_s being the scattering efficiency; the energy absorbed is $\pi r^2Q_aI_0$, Q_a being the absorption efficiency. These all can be written in terms of the Mie coefficients:

Extinction efficiency

$$Q_e = (2/x^2)\sum_1^\infty(2n+1)\mathrm{Re}(a_n+b_n), \tag{6}$$

Scattering efficiency

$$Q_s = (2/x^2)\sum_1^\infty(2n+1)\{|a_n|^2+|b_n|^2\}, \tag{7}$$

Absorption efficiency $Q_a = Q_e - Q_s$. (8)

Results and Discussion

The relationships between Q_s and the size of the aerosol particle are calculated for several refractive indices $1.5+im_{IM}$, m_{IM}=0, 0.01, 0.1, 1, 10, as shown in Fig. 3. Since x is the size parameter defined by $x=2\pi r/\lambda$ with an aerosol radius r and wavelength λ, x is proportional to r for a constant wavelength. Figures 4(a)—(f) show the angular distributions, *i.e.* θ-dependence, for x=0.01, 0.1, 1, 1.5, 2, 2.5 with m=1.55+0i. These figures indicate that, with the increase of x, (1) the forward scattering becomes predominant, (2) the perpendicular and parallel components of the scattered light intensities against the electric vector of the incident light, *i.e.* $I_\perp$ and $I_{/\!/}$, respectively, become greater and greater, (3) there is the intensity inversion between $I_\perp$ and $I_{/\!/}$ for the large x range, while $I_{/\!/}$ is always equal to or smaller than $I_\perp$ for $x\leq 1.5$, and (4) $I_\perp$ and $I_{/\!/}$ becomes oscillatory. The intensity inversion between $I_\perp$ and $I_{/\!/}$ causes the large variation of the polarization. The polarization is defined by $P=(I_\perp-I_{/\!/})/(I_\perp+I_{/\!/})$. Figure 5 shows the plot of P as a function of x. The polarization is nearly constant, *i.e.* approx. 1, for the range $x\leq 1.2$, then decreases steeply and gets to approx. −0.6 for

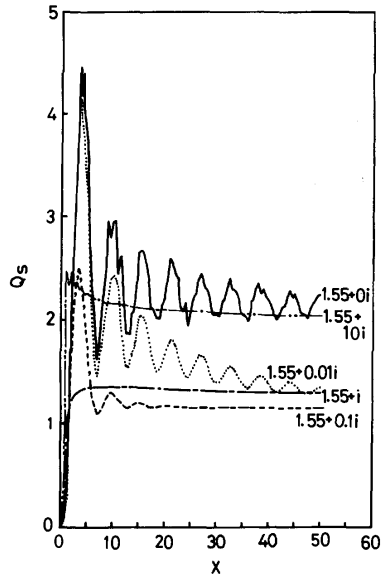

Fig. 3. The scattered light intensity Q_s versus the size-parameter x for $m=1.55+im_{IM}$, where m_{IM}=0, 0.01, 0.1, 1, 10.

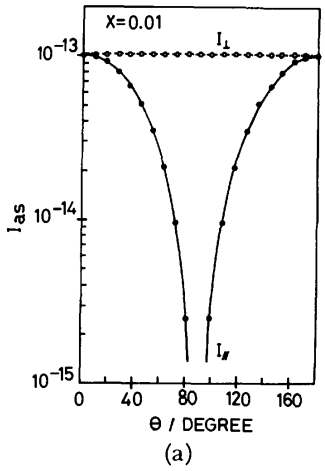

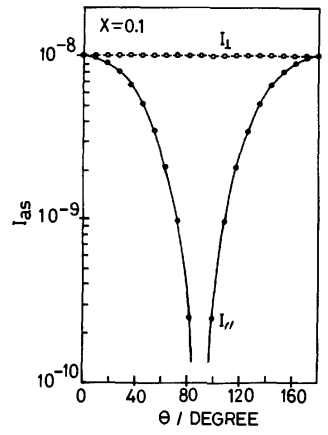

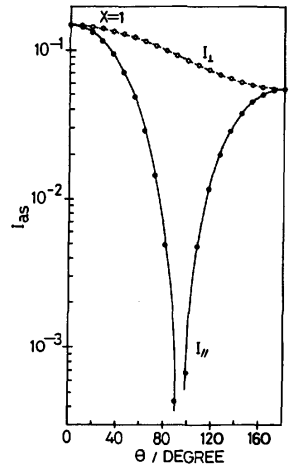

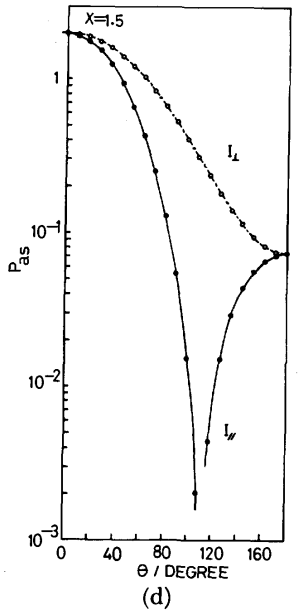

(Fig. 4. Continued on the next page)

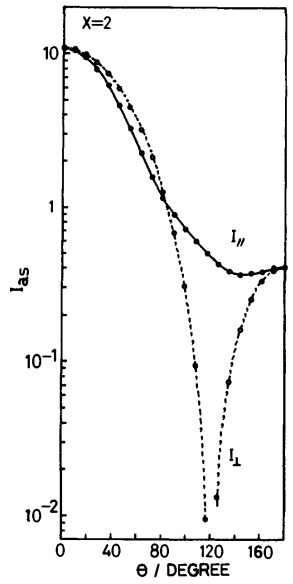

(e)

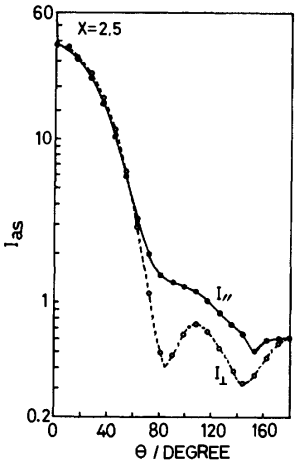

(f)

Fig. 4. The polarized scattered light intensities as a function of θ. $m=1.55+0i$.
(a) $x=0.01$, (b) $x=0.1$, (c) $x=1$, (d) $x=1.5$, (e) $x=2$, (f) $x=2.5$.

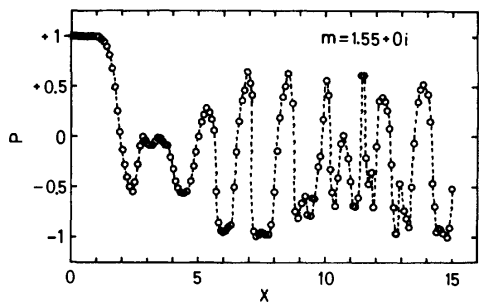

Fig. 5. Polarization P as a function of x, where $m=1.55+0i$.

$1.2 \leq x \leq 2.3$, and oscillates with the periods of $1 \leq x \leq 2$ and the amplitudes of $0.3 \leq P_{\text{peak-to-peak}} \leq 1.5$ for the range of $x \geq 2.3$. Therefore, as a function of the angle ($\phi - 90°$), the scattered light intensity in the direction of $\theta = 90°$

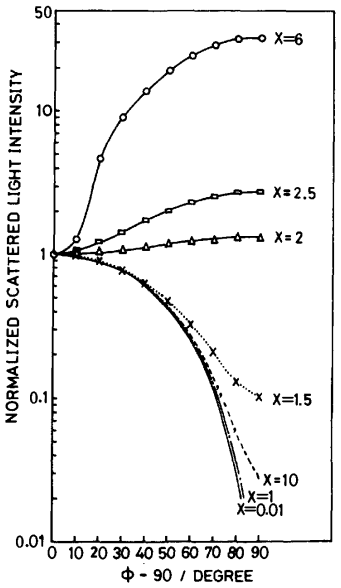

Fig. 6. The scattered light intensity calculated theoretically as a function of ($\phi - 90°$). $\theta = 90°$.

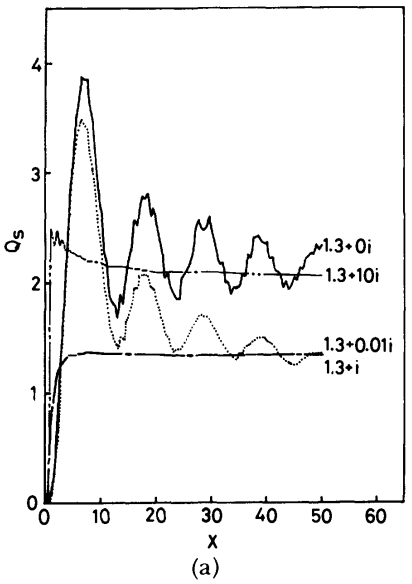

(a)

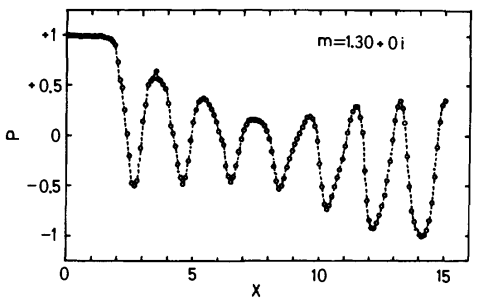

(b)

Fig. 7. (a) Scattered light intensity Q_s as a function of size parameter x for $m=1.3+im_{IM}$, where $m_{IM}=0, 0.01, 1, 10$, (b) Polarization P as a function of size parameter x, for $m=1.3+0i$.

can be theoretically estimated as shown in Fig. 6.

Furthermore, the scattering cross section Q_s and

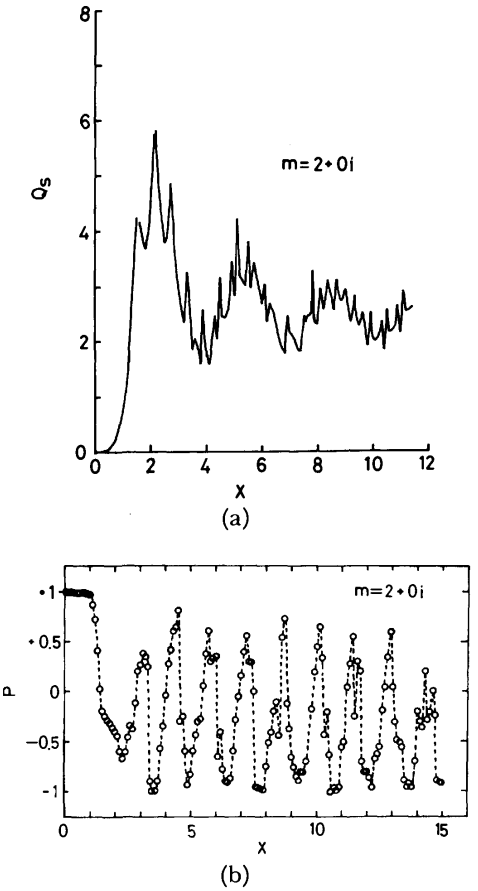

Fig. 8. (a) Scattered light intensity Q_s as a function of size parameter x, (b) Polarization P as a function of size parameter x, for $m=2.0+0i$.

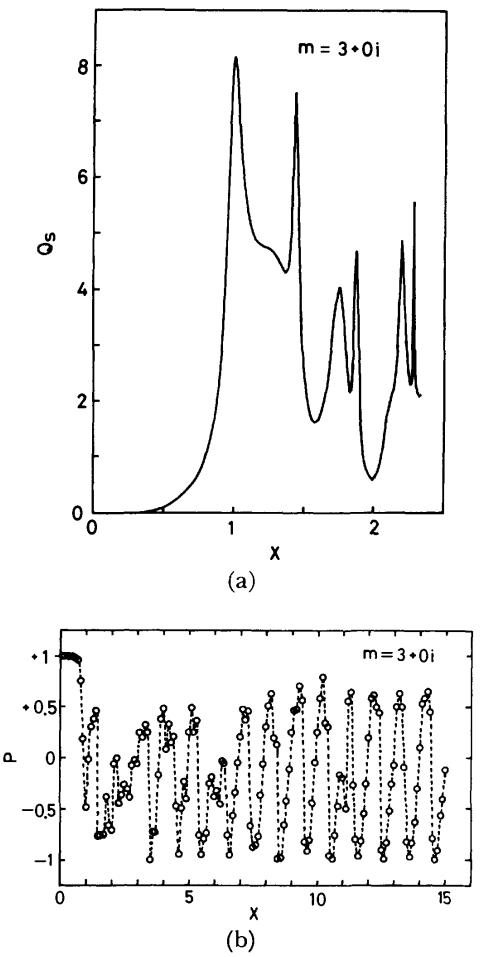

Fig. 9. (a) Scattered light intensity Q_s as a function of size parameter x, (b) Polarization P as a function of size parameter x, for $m=3.0+0i$.

the polarization P were also calculated for various indices, *i.e.* $m=1.3+im_{IM}$ ($m_{IM}=0$, 0.01, 1, and 10), $m=2+0i$, and $3+0i$, as shown in Figs. 7(a) and (b), 8(a) and (b), and 9(a) and (b), respectively. The essential shapes of the scattering extinction coefficients Q_s are similar for 1.3—2.0 of the real refractive index m_R, but Q_s becomes oscillatory with the increase in the real refractivity. The period becomes shorter. On the other hand, Q_s for $m_R=3$ has the different shape from those of $m_R=1.3$, 1.5, and 2. We can recognize the consistent characteristics of the polarizations for $m_R=1.3$, 1.5, 2, and 3. Namely, the steep decreasing of the polarization appears at smaller values of the size-parameter with the increase of the real refractive index. Furthermore, the polarization becomes oscillatory with the increase in the real refractive index.

The measurement of polarization has been used for experimental study on the size-growth in photoexcitation-induced aerosol formation.[4] However, the present study strongly suggests the caution for using this technique. Namely, since the polarization oscillates and becomes the same value for various size parameters, we cannot in general determine the size parameter from the polarization. In this view, the measurement of the angular distribution, *i.e.* θ-dependence, can be accounted much better for the study on the size-distribution of aerosol, as inferred from Figs. 4(a)—(f). Nevertheless, the polarization will be very useful for the judgement whether the scattering by the aerosol can be approximately expressed by the Rayleigh scattering[5] or not, *i.e.* the polarization is equal to 1 or not. As the application of it, this paper describes the experiments of the scattered-light polarization in laser-induced aerosol formation from gaseous CS_2.

In laser-induced aerosol formation, the light intensity scattered by the aerosol formed varies with time. The time evolution of the scattered light intensity in Fig. 10(a) is typical.[6] The scattered light intensity for the incident light polarized by the angle of $(90°-\phi)$ varies as a function of the angle $(90°-\phi)$, as shown by the open circles in Fig. 10(b). This ϕ-dependence was invariant for this time range. The dashed line in Fig. 10(b) is the curve of $\cos^2(90°-\phi)$, whose intensity is normalized to be 450 at $\phi=90°$. The experimental results agree well with the $\cos^2(90°-\phi)$ curve. By the comparison with the theoretical result shown in Fig. 6, the scattered light by the aerosol formed under the present experimental condition can be approximately expressed by the Rayleigh scattering theory. On the

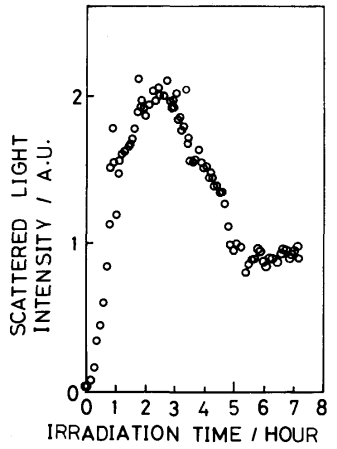

(a)

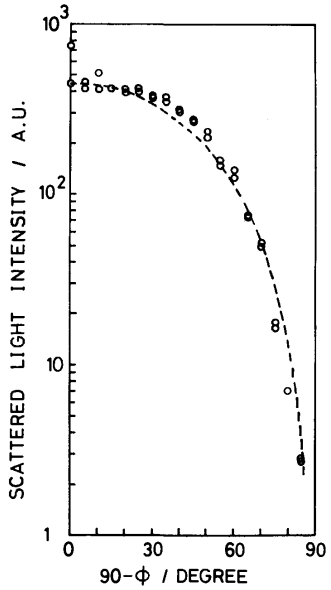

(b)

Fig. 10. (a) Scattered light intensity as a function of N_2-laser irradiation time. The CS_2 pressure is 50 Torr. The intensity of the N_2-laser beam was reduced by nuetral density filters. (b) Scattered light intensity as a function of $(90°-\phi)$. The dashed line is the curve of $\cos^2(90°-\phi)$.

other hand, the scattered light shows different behavior for the experiment with much more intense excitation N_2-laser beam, as shown in Fig. 11. In this case, the time-evolution of the scattered light intensity is quite different from that shown in Fig. 10(a). The polarization is less than 1 and varies with time. Therefore, in Fig. 11, the radius of the aerosol particle is large and the scattered light behavior cannot be expressed by the Rayleigh scattering theory.

The scattered light intensity has been extensively used as a kind of concentration variable. Since the scattered light intensity can be expressed by $\pi I_0 \int_{-\infty}^{+\infty} r^2 Q_s N(r) dr$, it depends upon the radius and concentration of aerosol. If the aerosol is small enough, the scattering intensity behavior is in the Rayleigh scattering range, *i.e.* it can be expressed as:

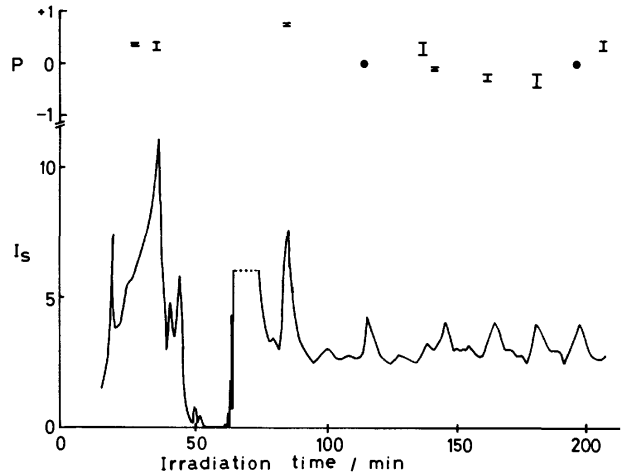

Fig. 11. The polarization P and scattered light intensity I_s as a function of N_2-laser irradiation time.

$$I = \frac{\omega^4}{c^4 R^2} \alpha^2 (1+\cos^2\theta) N(r) I_0, \tag{9}$$

$$I = \frac{\omega^4 r^6}{c^4 R^2} \left(\frac{m^2-1}{m^2+2}\right)^2 (1+\cos^2\theta) N(r) I_0, \tag{9'}$$

where R is the distance from the aerosol, ω the frequency of the scattered light, and c the light velocity. The polarizability α can be expressed by

$$\alpha = \frac{3}{4\pi N_s}\left(\frac{m^2-1}{m^2+2}\right), \tag{10}$$

where N_s is the total number of molecules per volume, and m is the nondimensional refractive index of molecules. Equation 9′ suggests that the scattered light intensity is proportional to the number of aerosol, $N(r)$, and the sixth power of the aerosol radius. Therefore, for the Rayleigh scattering range, the scattered light intensity can be expressed by $I=c_1 r^6 N(r)=c_2 v^2 N(r)$, where c_1 and c_2 are constants, $N(r)$ the number density, v the volume of aerosol, as a kind of extensive variable. Since the total number of molecules in the aerosol, N_m, can be considered proportional to the volume v, the scattered light intensity can also be expressed by $I=c_3 N_m^2 N(r)$, where c_3 is a constant. Thus the *trajectory tracing approach*[6] is applicable by using the scattered light intensity for the Rayleigh scattering range. On the other hand, more complicated process will be required for the case shown in Fig. 11. Nevertheless, since the maximum entropy method used in the *trajectory tracing approach*[6] is a kind of nonlinear spectrum analysis, it can make the analysis of the oscillatory behavior of the scattered light intensity for the size-parameter range, where Q_s increases with the size-parameter, even if it is out of the Rayleigh scattering range.

References

1) G. Mie, *Ann. Phys.*, **25**, 377 (1908).

2) P. Debye, *Ann. Phys.*, **30**, 59 (1909).
3) H. C. van de Hulst, "Light Scattering by Small Particles," Wiley, New York, (1957), p. 470.
4) T. Sato, T. Yabuzaki, and T. Ogawa, *J. Appl. Phys.*, **21**, 1599 (1982).
5) L. Rayleigh, *Proc. Lond. Math. Soc.*, **10**, 4 (1879).
6) A. Matsuzaki, *Chem. Lett.*, **1983**, 1149.

The Iodine-127 Nuclear Quadrupole Resonance of Several Iodine Complexes with Sulfur-containing Organic Molecules

Hiromitsu TERAO,* Hiroshi SAKAI,† and Hisao NEGITA††

Department of Chemistry, Faculty of Education, Tokushima University, Minamijosanjima-cho, Tokushima 770
†*Research Reactor Institute, Kyoto University, Kumatori-cho, Sennan-gun, Osaka 590-04*
††*Department of Chemistry, Faculty of Science, Hiroshima University, Naka-ku, Hiroshima 730*

(Received April 15, 1985)

The ^{127}I NQR spectra of 1,4-dithiane-2I_2, thiane-I_2, 1,4-thioxane-I_2, and 1,3,5-trithiane-I_2 are reported. Two distinct iodine atoms are observed in the former three complexes, whereas only one iodine atom is present in the last-named complex. The charge densities on the donors and the iodine atoms are obtained according to the Townes-Dailey approximation. The order of donor strength toward the iodine molecule is: thiane>1,4-thioxane>1,4-dithiane≫1,3,5-trithiane. The thioethers can compete with amines in terms of the donor strength to iodine molecules. The no-bond ionic structure of the ground state is less important in the thioether–iodine complexes than in amine–iodine complexes. The positive temperature coefficients found previously in a few similar complexes of amines are observed for the terminal iodine atoms of 1,4-dithiane-2I_2, thiane-I_2, and 1,4-thioxane-I_2. This phenomenon is ascribed to the increasing shift of the dative structure to the no-bond covalent structure with the rise in the temperature.

Many n-σ-type charge-transfer (CT) complexes, such as amine–halogen and amine–interhalogen, have been successfully investigated by means of the halogen[1-4] and the nitrogen[4,5] nuclear quadrupole resonance (NQR). This method makes it possible to estimate the charge distribution on the atom related directly to the CT interaction from the quadrupole coupling constant ($e^2q_{zz}Q/h$). It has been indicated that, for strong n-σ complexes, 0.2—0.3 electrons transfer from the amine to the halogen molecule; further, the bridging halogen atom bonded to a nitrogen atom is charged positively, while the terminal halogen atom, on which the transferred charges mostly exist, is charged negatively.

Sulfur-containing organic molecules (thioethers) also can act as electron donors to iodine molecules. X-Ray-crystal-structure investigations were carried out for 1,4-dithiane-2I_2[6] and dibenzyl sulfide-I_2.[7] In each structure, a strong n-σ CT bond is found between the donor S atom and the iodine molecule; *i.e.*, one atom of each iodine molecule is bonded to the sulfur atom, while the remaining one is free from the intermolecular bonding, and the S···I_A–I_B arrangement is almost linear. The S···I bond is shorter than the sum of the respective van der Waals radii, while the I_A–I_B bond is longer than the I–I bond in solid I_2.

It is of interest to compare the CT interaction in intermolecular S···I bonds with that in N···I bonds on the basis of the charge distribution. We tried to observe the ^{127}I NQR for several thioether–iodine complexes: 1,4-dithiane–iodine (1:2) (DT-2I_2), thiane–iodine (1:1) (TH-I_2), and 1,4-thioxane–iodine (1:1) (TO-I_2), and 1,3,5-trithiane–iodine (1:1) (TT-I_2).

The most interesting feature of the halogen NQR in the amine–halogen complexes is the positive temperature coefficient found for terminal halogen atoms;[1,2,4] it has been suggested that this is due to a vibronic coupling effect.[2] The temperature dependence of the ^{127}I (1/2—3/2) transition frequency is precisely measured to investigate whether or not the same phenomenon is observed in the present compounds.

Experimental

Preparation of the Samples. All the chemicals were obtained commercially and were used without further purification. The TH-I_2 complex was prepared by mixing approximately stoichiometric amounts of the components in chloroform. The dark brown crystalline product was precipitated by then concentrating and cooling the solution. The product was filtered, washed, and dried in air. The product decomposed slowly in air. The iodine content was analyzed by means of iodimetry. (Found: I, 70.5%. Calcd for $C_5H_{10}S$-I_2: I, 71.5%). The orange-red TO-I_2 was prepared in hexane in the same manner. The stoichiometry was determined by means of elemental analysis. (Found: C, 13.2; H, 2.4; I, 67.5%. Calcd for C_4H_8OS-I_2: C, 13.4; H, 2.3; I, 70.9%). The purple crystalline complex of DT-2I_2 was obtained by adding a saturated iodine solution of carbon tetrachloride to a dithiane solution of the same solvent. (Found: C, 7.7; H, 1.4; I, 80.8%. Calcd for $C_4H_8S_2$-2I_2: C, 7.7; H, 1.3; I, 80.8%). The red crystalline complex of TT-I_2 was prepared in chloroform by a procedure similar to that used for the TH-I_2 complex. The complex easily decomposed to its components within 10—15 min in air at room temperature. (Found: I, 64.0%. Calcd for $C_3H_6S_3$-I_2: I, 64.7%).

NQR Measurement. The NQR spectra were observed on an oscilloscope using an externally quenched superregenerative Lecher-line oscillator similar to that described by Schawlow,[8] but incorporating minor changes. Temperature variation was attained by immersing the sample tube in a copper container, placed in a Dewar vessel filled with petroleum ether, and by then cooling the petroleum ether with dry ice or liq. N_2. The accuracy of the measurements was estimated to be within ±0.01 MHz in frequency and ±1 K in temperature.

Results and Discussion

Table 1 lists the resonance frequencies observed at 77 and 298 K, with the signal-to-noise ratios shown in parentheses. These are assigned to the ^{127}I (1/2—3/2)

TABLE 1. ^{127}I NQR FREQUENCIES IN IODINE-SULFUR-CONTAINING ORGANIC MOLECULE COMPLEXES[a)]

Compound	Frequency/MHz		$(d\nu/dT)_{T=273\,K}$	Assignment
	77K	298K	KHz/K	
1,4-Dithiane-2I_2	377.81(6)	374.83(3)	−16.5	I_A(1/2—3/2)
	233.37(2.5)	238.02(2)	+25.4	I_B(1/2—3/2)
Thiane-I_2	377.82(10)	373.69(1.5)	−23.4	I_A(1/2—3/2)
	197.22(10)[b)]	200.99(2)[b)]	+24.2	I_B(1/2—3/2)
	394.43(4)[b)]	401.98(1.5)[b)]	—	I_B(3/2—5/2)
1,4-Thioxane-I_2	374.78(2.5)	370.46(1.5)	−23.4	I_A(1/2—3/2)
	220.58(5)	226.01(1.5)	+30.0	I_B(1/2—3/2)
1,3,5-Trithiane-I_2	322.14(10)	320.39(1.5)	−9.8	I(1/2—3/2)

a) The numbers in parentheses are the signal-to-noise ratios as measured on an oscilloscope. b) $e^2q_{zz}Q/h$ and η are 1314.8 MHz and 0.004 at 77 K, and 1339.9 MHz and 0.000 at 298 K.

transitions except for the resonance line with the highest frequency in TH-I_2, corresponding to the ^{127}I (3/2—5/2) transition. The existence of two resonance lines in DT-2I_2, separated in frequency by about 140 MHz, is consistent with its crystal structure, which has the S···I_A-I_B arrangement.[6)] Since it is well established that the terminal iodine atom I_B is negatively charged compared to the bridging iodine atom I_A, the lower frequency line can be assigned to the I_B atom, and the higher line, to the I_A atom. The similarity of the NQR spectrum in TH-I_2 or TO-I_2 to that in DT-2I_2 suggests that the S···I_A-I_B arrangement also exists in both complexes. The O atom as well as the S atom in the TO molecule can act as the donor atom, though no solid complexes with the O···I_A-I_B arrangement have yet been observed. However, the proximity of the ^{127}I NQR frequencies of TO-I_2 to those of DT-I_2 and TH-I_2 may show that not the O atom, but the S atom, acts as the donor atom toward the iodine molecule in TO-I_2.

On the other hand, only a single line is observed in TT-I_2; this suggests that all I atoms are equivalent in their crystals. This fact and the molar ratio of its component molecules (1:1) predict the existence of endless chains consisting of alternating TT and iodine molecules in the solid state of TT-I_2. Probably, the CT interaction is of a weak n-σ type. The resonance frequency in TT-I_2 is close to the 332 MHz[3)] of the ^{127}I (1/2—3/2) transition observed for the phenazine-I_2 complex, which contains a N···I-I···N bridge in its structure.[9)]

It has previously been pointed out that a three-center four-electron bonding scheme[1,10–13)] gives a good approximation for describing the bonding in trihalide anions, amine-halogen complexes, and bis(amine)-halogen cations. Therefore, we consider only the pure p_σ bond orbitals for the bonding of I atoms in the present compounds. Then we can estimate the charge density on the iodine atoms and, hence the transferred charges from the donor to the acceptor, according to the Townes-Dailey approximation:[14)]

$$\rho = 1 - (e^2q_{zz}Q/h)/(e^2q_{at}Q/h), \quad (1)$$

TABLE 2. CHARGE DISTRIBUTIONS IN SEVERAL CT COMPLEXES OF IODINE WITH SULFUR-CONTAINING ORGANIC MOLECULES

Complex	Charge on I_A	Charge on I_B	Charge on S
1,4-Dithiane-2I_2	+0.10	−0.32	+0.22
Thiane-I_2	+0.10	−0.43	+0.33
1,4-Thioxane-I_2	+0.09	−0.36	+0.27
1,3,5-Trithiane-I_2	−0.06		+0.06

where $e^2q_{zz}Q/h$ is the observed quadrupole coupling constant, where $e^2q_{at}Q/h$ is the atomic quadrupole coupling constant, which equals the value of 2292.7 MHz for ^{127}I, and where ρ stands for the charge density localized on the iodine atom.

When the frequencies attributable to both the ^{127}I (1/2—3/2) and ^{127}I (3/2—5/2) transitions are obtained, the exact values of the $e^2q_{zz}Q/h$ and the asymmetry parameter (η) are derived from the eigen-value table for a nuclear spin, I=5/2. The $e^2q_{zz}Q/h$ and η values are given in the margin of Table 1 for the I_B atom of TH-I_2. In the other cases, where only the ^{127}I(1/2—3/2) transition is observed, we obtain the $e^2q_{zz}Q/h$ value by putting η=0 into the following relation, which holds for $\eta \leq 0.1$:

$$\nu(1/2-3/2) = \frac{3}{20}(e^2q_{zz}Q/h)\left(1+\frac{5}{54}\eta^2\right) \quad (2)$$

It is safe to neglect η in Eq. 2 for the purposes of the present calculation because of the expected small η value and the much smaller contribution to the resonance frequency of the second term than the first. Obviously, the η value is very small for the I_B atom of TH-I_2, and also for the iodine atoms of the amine-iodine complexes,[3,15–17)] corresponding to the present type of complexes.

The charge densities on the iodine and sulfur atoms, as calculated from the values of $e^2q_{zz}Q/h$ at 77 K, are listed in Table 2. In accordance with the prediction from the delocalized three-center bonding, the terminal iodine I_B has negative charges, and the bridging iodine I_A, small positive charges. The small negative charge on the iodine atom of TT-I_2 indicates a weak CT interaction. We may estimate the order of donor

strengths toward the iodine molecule from the amounts of the positive charges localized on the donors:

$$TH > TO > DT \gg TT.$$

The bonding of the complexes is alternatively described in terms of Mulliken's valence-bond expression[18] of a charge-transfer model. As is well known, the ground-state wave function is written as:

$$\Psi_N = a\Psi(D,X_2) + b\Psi(D^+-X_2^-). \quad (3)$$

This equation is satisfactory for a weak CT complex. Bowmaker and Hacobian[1] expanded Eq. 3 in the following form for the strong n-σ complex by considering that the two X atoms in D-X_2 are in inequivalent positions:

$$\Psi_N = a\Psi(D,X_2) + b\alpha\Psi(D^+-XX^-) + b\beta\Psi(D^+X^-X) + c\Psi(DX^+X^-) \quad (4)$$

where the first and fourth terms refer to the no-bond structures, and the second and third, to the dative structures. The fourth structure, regarded as a resonance hybrid with the second structure, is introduced into Eq. 4 because the D^+-X bond must have a partial ionic character if D^+ has a greater affinity than the X atom. This term is more important than the third because the bridging halogen atoms of the complexes have positive charges.

For further discussion, we plot the charges on the I atoms against those on the S donors in Fig. 1. The results of several amine-iodine complexes are also shown in this figure. Unfortunately, the ^{127}I NQR results for the strong n-σ type of amine-iodine complexes have been obtained imperfectly; the frequencies of only the bridging iodine atom are observed, mainly because of the weakness of the resonance intensities of the terminal halogen atoms. However, a few data on the amine-iodine complexes obtained from the ^{129}I Mössbauer-effect measurements[15-17] are available for this purpose.

Though the quantity of data is restricted, it is found from the charges on the donors that the S donor is almost as strong as the N donor in its donor strength toward the iodine molecule. When the donor strength increases in each set of the S···I_A-I_B and N···I_A-I_B complexes, the negative charge on the I_B atoms increases linearly, whereas the charge on the I_A atoms is maintained at an almost constant value. It is, therefore, obvious that transferred charges from the donor are mostly localized on the terminal iodine atom. This shows that the weight of the fourth term in Eq. 4 is maintained to about a constant value from complex to complex in each set of complexes, while the third term is practically negligible. Thus, we can calculate the weight of each structure in Eq. 4 from the charge densities, neglecting the third structure. The weights

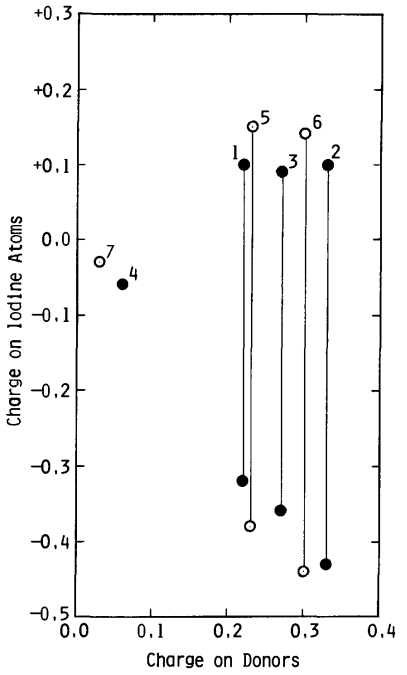

Fig. 1. Plot of the charges on I atoms *vs.* the charges on donors. ●: S donor; ○: N donor. 1) 1,4-Dithiane-$2I_2$, 2) Thiane-I_2, 3) 1,4-Thioxane-I_2, 4) 1,3,5-Trithiane-I_2, 5) Pyridine-I_2,[15,17] 6) Triethylamine-I_2,[17] 7) Phenazine-I_2.[3,16]

of the first (no-bond covalent), the second (dative), and the fourth (no-bond ionic) structures are 68, 22, and 10% for DT-$2I_2$, 57, 33, and 10% for TH-I_2, and 64, 27, and 9% for TO-I_2, respectively. Both positive charges on I_A and negative ones on I_B are larger in their absolute values for the N-atom donors than for the S-atom donors when the donor strengths are about the same. Those results indicate that the contribution of the fourth term in Eq. 4 is smaller for the S-atom donor-iodine complexes than for the N-atom donor-iodine complexes. The ionic structure of the ground state is less important in the former than in the latter. This is reasonable, because the N^+ has a larger electron affinity than the S^+.

The temperature dependence of the resonance frequency due to the ^{127}I (1/2—3/2) transition was observed in the range of from the temperature of liquid N_2 to room temperature. The results for the present complexes are shown in Figs. 2 and 3, while the temperature coefficients at 273 K of the frequency curves are listed in the fourth column of Table 1. It is found that all terminal iodine atoms of DT-$2I_2$, TH-I_2, and TO-I_2 have positive temperature coefficients; this is in accordance with the results previously reported for the terminal halogens of pyridine-ICl,[2] 4-methylpyridine-ICl,[2] and 3,5-dibromopyridine-Br_2.[1]

This tendency can be qualitatively realized from Eq. 4. As the temperature is raised, the increasing excitation of molecular vibrations will weaken the weaker intermolecular CT-bond rather than the intramolecular I-I bond; the contribution of the dative

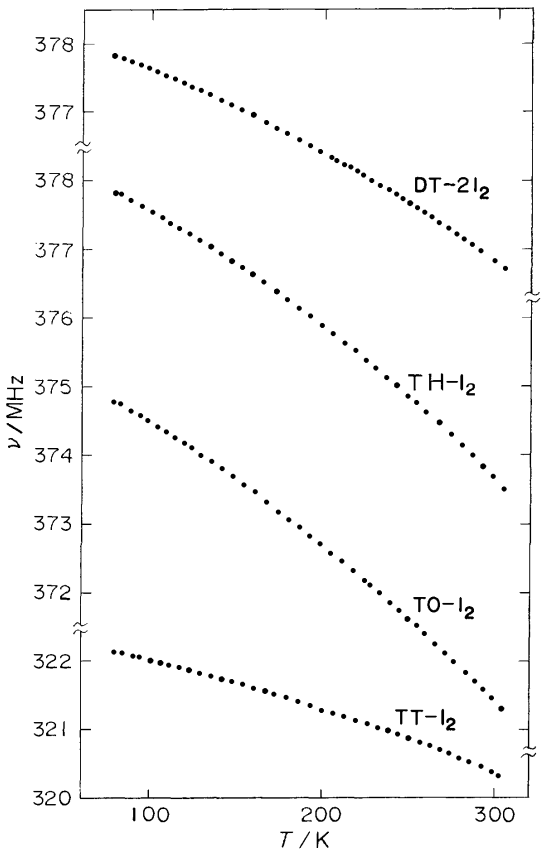

Fig. 2. Temperature dependence of the ^{127}I(1/2—3/2) NQR frequencies of the bridging iodine atoms. DT: 1,4-dithiane, TH: Thiane, TO: 1,4-thioxane, TT: 1,3,5-trithiane.

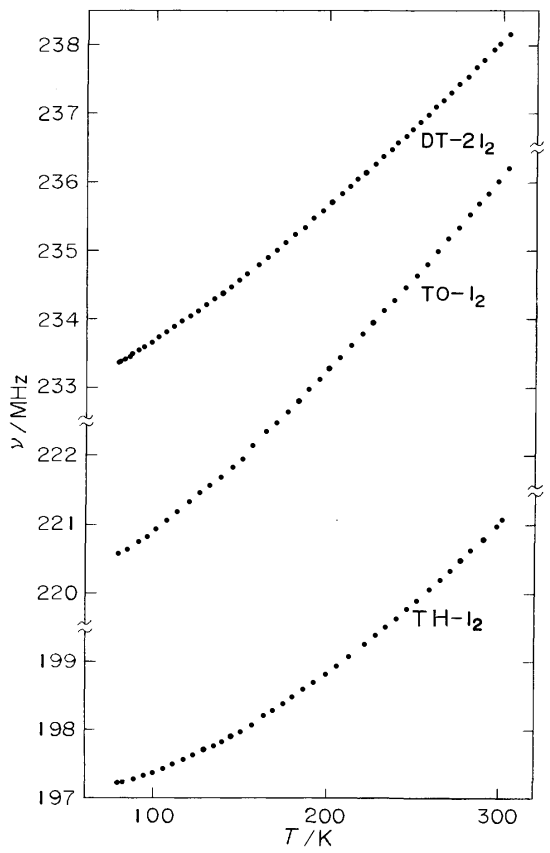

Fig. 3. Temperature dependence of the ^{127}I(1/2—3/2) NQR frequencies of the terminal iodine atoms. DT: 1,4-dithiane, TH: Thiane, TO: 1,4-thioxane.

structure will, consequently, decrease with the increase in the temperature. As has been seen previously, the dative structure is approximated by the second structure in Eq. 4, while neglecting the third structure. The contribution of the no-bond covalent structure is larger than that of the no-bond ionic one. Further, the contribution of the no-bond ionic structure is kept at about a constant value even if the donor strength is changed. Accordingly, it is mainly the no-bond covalent structure that increases its contribution with an increase in the temperature. The conversion of the second structure to the first one reduces the negative charge (and hence the p_z-electron populations) of the I_B atom, holding the charge density of the I_A atom constant. Since the decrease of p_z-electron populations of the iodine atom results in the increase of the value of its electric-field gradient (eq_{zz}), the resonance frequency increases from Eq. 2. The frequency of the I_B atom thus increases with the temperature, as in the present case, if the frequency increase due to the decrease of the dative structure described above overcomes the normal decrease in frequency[19] which is caused by the averaging of eq_{zz} following the increasing molecular vibrations.

The authors wish to express their thanks to Dr. Tsutomu Okuda of Hiroshima University for his helpful suggestions.

References

1) G. A. Bowmaker and S. Hacobian, *Aust. J. Chem.*, **22**, 2047 (1969).
2) H. C. Fleming and M. W. Hanna, *J. Am. Chem. Soc.*, **93**, 5030 (1971).
3) R. Brüggemann, F. Reiter, and J. Voitländer, *Z. Naturforsch., A*, **27**, 1525 (1972).
4) G. A. Bowmaker, *J. Chem. Soc., Faraday Trans., 2*, **72**, 1964 (1976).
5) G. V. Rubenacker and T. L. Brown, *Inorg. Chem.*, **19**, 392 (1980); G. V. Rubenacker and T. L. Brown, *ibid.*, **19**, 398 (1980).
6) G. Y. Chao and J. D. McCullough, *Acta Crystallogr.*, **13**, 727 (1960).
7) Chr. Rømming, *Acta Chem. Scand.*, **14**, 2145 (1960).
8) A. L. Schawlow, *J. Chem. Phys.*, **22**, 1211 (1954).
9) T. Uchida, *Bull. Chem. Soc. Jpn.*, **40**, 2244 (1967).
10) G. A. Bowmaker and S. Hacobian, *Aust. J. Chem.*, **21**, 551 (1968).
11) S. G. W. Ginn and J. L. Wood, *Trans. Faraday Soc.*, **62**, 777 (1966).
12) R. Brüggemann and J. Voitländer, *Theor. Chim. Acta*, **34**, 301 (1974).
13) E. E. Havinga and E. H. Wiebenga, *Recl. Trav. Chim. Pays-Bas*, **78**, 724 (1959).

14) C. H. Townes and B. P. Dailey, *J. Chem. Phys.*, **17**, 782 (1949); C. H. Townes and B. P. Dailey, *ibid.*, **20**, 35 (1952).
15) S. Bukshpan, C. Goldstein, T. Sonnino, L. May, and M. Pasternak, *J. Chem. Phys.*, **62**, 2606 (1975).
16) S. Ichiba, H. Sakai, H. Negita, and Y. Maeda, *J. Chem. Phys.*, **54**, 1627 (1971).
17) H. Sakai, Y. Maeda, S. Ichiba, and H. Negita, *J. Chem. Phys.*, **72**, 6192 (1980).
18) R. S. Mulliken and W. B. Person, "Molecular Complexes," John Wiley & Sons, New York (1969).
19) H. Bayer, *Z. Phys.*, **130**, 227 (1951).

Voltammetric Studies of the Metal-Ligand Interaction in Low-valent Metal-Olefin π-Complexes. II. Palladium(0) and Platinum(0) Complexes with Olefin-Diimine Mixed Ligands

Naoyuki Ito, Tetsuo Saji,* and Shigeru Aoyagui
Department of Chemical Engineering, Tokyo Institute of Technology, Ohokayama, Meguro-ku, Tokyo 152
(Received February 4, 1985)

Cyclic voltammograms for the reduction of Pd^0 and Pt^0 complexes with mixed ligands of diimine and olefin exhibit, respectively, two or four reversible one-electron steps. The half-wave potentials of each step give a straight line with a slope of 1.0, when plotted against the half-wave potentials of diimine ligands, and a slope smaller than 0.2, when plotted aganist the half-wave potentials of olefinic ligands. The half-wave potentials of the complexes are affected only a little by the difference in the central metal. These findings lead to the conclusion that each LUMO of these complexes is dominated by the diimine π*-orbital, though it is higher-lying than the olefinic π*-orbital in free ligands.

The changes in the molecular structure and electronic state that olefinic compounds may suffer when they are coordinated to transition metals may be worthy of note in connection with their reactions catalyzed by these metals. Usually, the former change can be detected by X-ray diffraction and the latter by absorption spectroscopy. Besides these, the specific contribution of voltammetry to the latter purpose is promising because it provides information on the ionization potential and the electron affinity, *viz.* the HOMO and LUMO energies, in contrast to absorption spectroscopy which provides information on the intramolecular relative energy levels. Knowledge of the HOMO and LUMO energies will make it possible to determine the behaviour of the frontier electron which has a dominant effect on the chemical reactivity.

Voltammetric and IR studies of $[M(0)_2(dibenzylideneacetone)_3]$(M=Pd and Pt; dibenzylideneacetone= 1,5-diphenyl-1,4-pentadien-3-one) in Part I of this seires have led to the conclusion that each LUMO of these complexes is twofold degenerate and delocalized over a π-framework composed of a metal and three phenyl-substituted olefinic moieties.[1] This paper deals with the voltammetry of mixed ligand complexes, [M(0)LoLc] (M=Pd and Pt; Lo=olefinic ligand; Lc=diimine ligand), with a hope that we can discuss the change of LUMO of Lo caused by coordination.

Experimental

Ethenetetracarbonitrile (tcne), (*E*)-2-butenedinitrile (fn), dimethyl fumarate (dmf), dimethyl maleate (dmm), diethyl fumarate (def), 1,10-phenanthroline (phen) and 2,2′-bipyridine (bpy) were supplied by Tokyo Chemical Industries, maleic anhydride (ma) by Wako Pure Chemical Industries and 4,7-diphenyl-1,10-phenanthroline (dφphen) by Kanto Chemical Industries. 4,4′-Dimethyl-2,2′-bipyridine (4-dmbpy), 5,5′-dimethyl-2,2′-bipyridine (5-dmbpy), and 4,4′,5,5′-tetramethyl-2,2′-bipyridine (tmbpy) were gifts of Dr. Y. Ohsawa who prepared them by the literature method.[2]

[Pd(0)Lo(bpy)] (Lo=ma, dmf, and dmm) were prepared by methods found in the literature,[3] and other palladium complexes by similar methods. Platinum complexes were prepared by the same methods as the corresponding palladium complexes, except that the reaction mixtures were slightly heated until their colors turned yellow. The complexes were characterized by elemental analyses on C, H, and N.

The half-wave potential was identified with the midpoint of the cathodic peak potential (E_{pc}) and the anodic one (E_{pa}) of a cyclic voltammogram. The reversibilities of redox steps were judged on the basis of the separation (ΔE_p) beween the E_{pc} and the E_{pa} and the ratio of the anodic peak current to the cathodic one. The base solution was 0.2 M (1M=1 mol dm^{-3}) tetrabutylammonium perchlorate (TBAP) in ethylene glycol dimethyl ether (DMeE). Neutral alumina (ICN W200) was added to the test solutions except for tcne, ma, and dφphen, which are strongly adsorbed on alumina. Voltammetric measurements were carried out at −30±2 °C with a scan rate of 0.1 V s^{-1}, unless otherwise noted. Other experimental procedures have been previously described.[4] IR spectra were recorded with KBr plates on a Hitachi 295 IR spectrometer operated at 25 °C.

Results and Discussion

The ν(C-N) frequencies for [Pd(0)LoLc] with Lo= tcne and fn, and Lc=bpy and dφphen, and [Pt(0)Lo-(dφphen)] with Lo=tcne and fn fall within 2100—2240 cm^{-1}, as those of other complexes of similar structure generally do.[5,6] They are lower than the ν(C-N)

Table 1. Half-wave potentials for the reduction of free ligands ($E^{red}_{1/2,L}$) in 0.2 M TBAP-DMeE at −30 °C, scan rate 0.1 V s^{-1}

Ligand	$-E^{0/-}_{1/2,L}$/V[a]	$-E^{-/2-}_{1/2,L}$/V[a]
tcne	0.358	1.433[b]
ma	1.580[b]	—
fn	2.028[b]	—
dmf	2.033	—
def	2.062	—
dmm	2.450[b]	—
dφphen	2.526	2.923[b]
phen	2.667	3.264[b]
bpy	2.766	3.368
4-dmbpy	2.823	3.388
5-dmbpy	2.899	3.504
tmbpy	2.963	3.558[b]

a) ±5 mV *vs.* Ag/$AgNO_3$(sat.). b) Cathodic peak potential.

frequencies of free olefin ligands, *i.e.* 2262 cm^{-1} for tcne and 2246 cm^{-1} for fn. The same lowering has been reported concerning the ν(C=O) frequencies of [Pd(0)LoLc] with Lo=dmm and dmf, and Lc=bpy and phen.[3] These findings may be evidence for the metal-to-olefin charge transfer and/or the back-donating bond operating in these complexes.

Cyclic voltammograms for the reduction of free ligands (L) exhibited, respectively, one or two one-electron steps judged on the basis of ΔE_p. Some of these steps were reversible and others irreversible, in the sense that they had no current peaks in reversal scans. Table 1 lists the reversible half-wave potentials of $L^{0/-}$ ($E^{0/-}_{1/2,L}$) and $L^{-/2-}$ ($E^{-/2-}_{1/2,L}$). For irreversible steps, E_{pc} values are shown instead of $E_{1/2,L}$ values. All of the ligands studied gave no oxidation steps within the available potential range.

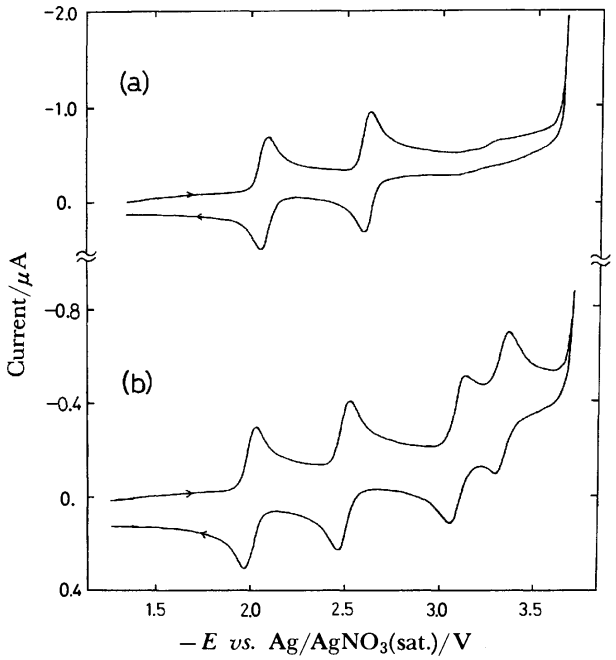

Fig. 1. Cyclic voltammograms for 0.3 mM of (a) [Pd(fn)(bpy)] and (b) [Pd(fn)(dφphen)] in 0.2 M TBAP-DMeE at −30 °C, scan rate 0.1 V s^{-1}.

Cyclic voltammograms for the reduction of complexes (C) gave four one-electron steps for complexes with dφphen as Lc. Otherwise, two are given as shown in Fig. 1. The reversible steps may be tentatively assigned to $C^{0/-}$, $C^{-/2-}$, $C^{2-/3-}$, and $C^{3-/4-}$. No oxidation steps were observed. Table 2 summarizes the voltammetric results on complexes.

The characteristic features of Tables 1 and 2 are follows:

(1) Each $E^{0/-}_{1/2,C}$ is by 0.4—0.9 V more positive than the corresponding $E^{0/-}_{1/2,L}$ of Lc ($E^{0/-}_{1/2,Lc}$), and by 0.1—1.5 V more negative than the $E_{1/2,L}$ of Lo ($E^{0/-}_{1/2,Lo}$).

(2) The $E^{0/-}_{1/2,C}$ and $E^{-/2-}_{1/2,C}$ for the Pt complexes are by 0.1 V more positive than the corresponding Pd complexes.

(3) The $E^{2-/3-}_{1/2,C}$ and $E^{3-/4-}_{1/2,C}$ of dφphen complexes are independent of type of metal.

(4) The $E^{0/-}_{1/2,C}-E^{-/2-}_{1/2,C}$ values are nearly identical with the $E^{0/-}_{1/2,Lc}-E^{-/2-}_{1/2,Lc}$ values, which suggests that the coordinated Lc in a C^{2-} should be of the form Lc^{2-}.[7]

Figure 2 shows $E^{red}_{1/2,C}$ *vs.* $E^{0/-}_{1/2,L}$ plots for [M(0)-(dmf)Lc] (M=Pd and Pt) with Lc=tmbpy, 5-dmbpy, 4-dmbpy, and bpy. The straight lines were drawn in accordance with the following equation:[8]

$$E_{1/2,C} = E_{1/2,L} + \text{const.}, \quad (1)$$

Table 2. Half-wave potentials for the reduction of [M(0)LoLc] ($E^{red}_{1/2,C}$) in 0.2 M TBAP-DMeE at −30 °C, scan rate 0.1 V s^{-1}

M	Lo	Lc	$-E^{0/-}_{1/2,C}$/V[a]	$-E^{-/2-}_{1/2,C}$/V[a]	$-E^{2-/3-}_{1/2,C}$/V[a]	$-E^{3-/4-}_{1/2,C}$/V[a]
Pd	tcne	dφphen	1.776	2.089[b]	—	—
Pd	ma	dφphen	1.989	2.505	3.077	3.309
Pd	fn	dφphen	2.006	2.501	3.091	3.328
Pd	dmf	dφphen	2.052	2.568	3.126	3.354
Pd	def	dφphen	2.047	2.568	3.162	3.389
Pd	dmm	dφphen	2.081	2.589	3.134	3.373
Pt	tcne	dφphen	1.669	2.158	2.895[b]	—
Pt	fn	dφphen	1.884	2.389	3.060[c]	3.290
Pt	dmf	dφphen	1.942	2.482	3.130[c]	3.355[c]
Pd	dmf	phen	2.139	2.746		
Pd	dmf	bpy	2.157	2.740		
Pd	dmf	4-dmbpy	2.226	2.782		
Pd	dmf	5-dmbpy	2.257	2.839		
Pd	dmf	tmbpy	2.341	2.926		
Pd	tcne	bpy	1.845[b]	—		
Pd	ma	bpy	2.088	2.641		
Pd	fn	bpy	2.115	2.661		
Pd	def	bpy	2.160	2.758		
Pd	dmm	bpy	2.191	2.759		
Pt	dmf	bpy	2.032	2.650		
Pt	dmf	tmbpy	2.217	2.836		

a) ±5 mV vs. Ag/$AgNO_3$(sat.). b) Cathodic peak potential. c) Scan rate 0.25 V s^{-1}.

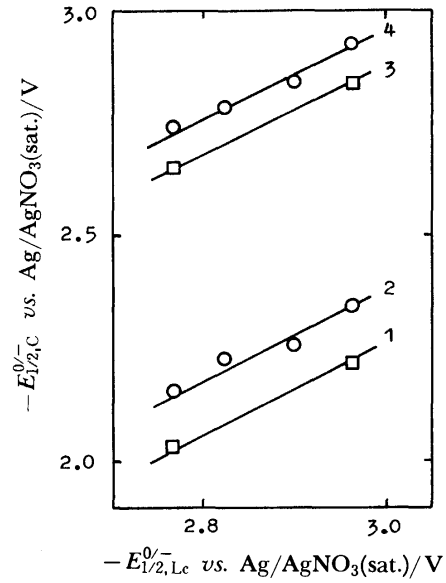

Fig. 2. $E^{0/-}_{1/2,C}$ *vs.* $E^{0/-}_{1/2,Lc}$ for (1) [Pt(dmf)Lc] and (2) [Pd(dmf)Lc], and $E^{-/2-}_{1/2,C}$ *vs.* $E^{-/2-}_{1/2,Lc}$ for (3) [Pt(dmf)Lc] and (4) [Pd(dmf)Lc] with Lc=bpy, 4-dmbpy, 5-dmbpy and tmbpy.

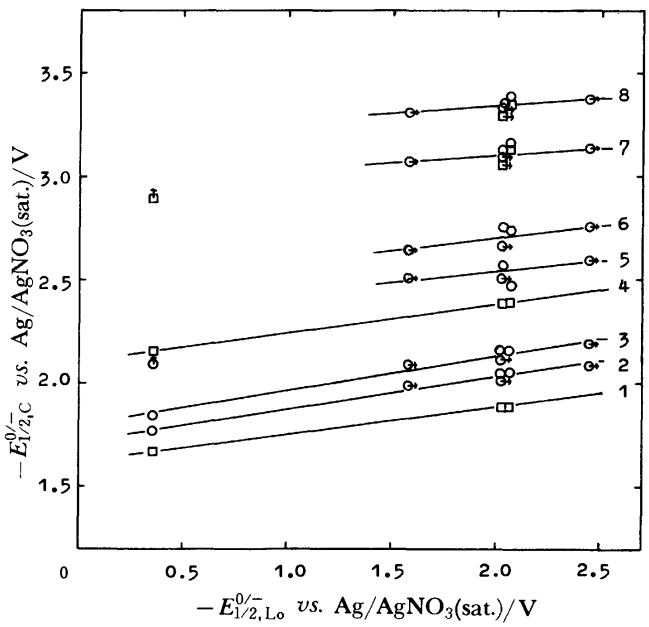

Fig. 3. $E^{0/-}_{1/2,C}$ *vs.* $E^{0/-}_{1/2,Lo}$ for (1) [PtLo(dφphen)], (2) [PdLo(dφphen)] and (3) [PdLo(bpy)], $E^{-/2-}_{1/2,C}$ *vs.* $E^{0/-}_{1/2,Lo}$ for (4) [PtLo(dφphen)], (5) [PdLo(dφphen)] and (6) [PdLo(bpy)], (7) $E^{2-/3-}_{1/2,C}$ *vs.* $E^{0/-}_{1/2,Lo}$ for (□) [PtLo(dφphen)] and (○) [PdLo(dφphen)], and (8) $E^{3-/4-}_{1/2,C}$ *vs.* $E^{0/-}_{1/2,Lo}$ (□) [PtLo(dφphen)] and (○) [PdLo(dφphen)] with Lo=tcne, ma, fn, dmf, def and dmm. Experimental points with horizontal and vertical arrows are plotted with cathodic peak potentials for olefinic ligands and complexes, respectively. The arrows show the direction in which reversible half-wave potentials are located.

which was derived by assuming that the redox orbital is a ligand π*-orbital. Figure 3 shows $E^{red}_{1/2,C}$ *vs.* $E^{0/-}_{1/2,Lo}$ plots for [M(0)Lo(dφphen)] and [Pd(0)Lo(bpy)] with Lo=tcne, dmf, and def. The experimental points of Fig. 2 obey Eq. 1. The straight lines of Fig. 3, however, are only tentative, because experimental points for appropriate $E^{0/-}_{1/2,Lo}$ values are lacking. However, it is evident that $E^{red}_{1/2,C}$ *vs.* $E^{0/-}_{1/2,Lo}$ has a positive slope of 0.1—0.2, when the experimental points for the irreversible $Lo^{0/-}$ steps of ma, fn, and dmm are taken into consideration. These findings, together with features (2) and (4) of Tables 1 and 2, lead to the conclusion that the two electrons added to [M(0)LoLc] occupy the LUMO of this complex, which is dominated by a diimine ligand π*-orbital. Unfortunately, the lack of data on reversible $E^{red}_{1/2,Lo}$ makes it difficult to assign the third and fourth steps of [M(0)Lo(dφphen)] which molecular orbital an electron occupies a molecular orbital mainly of an olefinic orbital character or a diimine orbital one. However, taking into account $E^{0/-}_{1/2,Lo}$ values of ma, fn and dmm, the coordination of tri and tetra-anions of dφphen can be concluded for the following reasons: First, the third and fourth steps cannot be ascribed to the reduction of coordinated Lo's because [M(0)(dmf)(bpy)] and [M(0)(dmf)(phen)] exhibit no such steps. Secondly, $E^{2-/3-}_{1/2,C}$ and $E^{3-/4-}_{1/2,C}$ do not depend on $E^{0/-}_{1/2,Lo}$ or the type of metal at all. This suggests that the redox orbital in these steps should be localized on the coordinated dφphen molecules.

Strikingly, the excess electrons of [M(0)LoLc] occupy the Lc π*-orbitals inspite of the fact that they are higher-lying than the Lo π*-orbitals in a free ligand, *e.g.* the $E^{0/-}_{1/2,Lo}$ of tcne is by 2.4 V more positive than the $E^{0/-}_{1/2,Lc}$ of bpy. One of the probable reasons may be the stabilization of the diimine π*-orbitals caused by coordination, and the instabilization of the olefin π*-orbitals. Although the same stabilization is seen in [M(0)(bpy)$_3$] (M=Cr and Mo),[8] the stabilization energy is considerably greater in [M(0)LoLc] than in [M(0)(bpy)$_3$]. This may be due to the coexistance of Lo operating as an electron acceptor. This is suggested by the finding that the IR spectra of the Lo is shifted to lower frequencies upon coordination. The instabilization of the olefin π*-orbital, on the other hand, can be ascribed to the structural change of the olefin ligand caused by coordination. Such a change is suggested by the experimental finding that the olefin C-C bond distance is longer in the complex than in the free ligand, probably due to a decrease in π-conjugation caused by the metal-to-ligand back donation.[9] A similar π-conjugation decrease in [M(0)$_2$(dibenzylideneacetone)$_3$] (M=Pd and Pt) was discussed in Part I.[1] Also, X-ray and neutron diffraction studies of [Pt(0)(tcne)(PPh$_3$)$_2$] show that the configuration around the ethylene carbons is essentially tetrahedral. Consequently, the ligand-metal bond is equivalent to that of the two metal-alkyl σ-bonds.[10]

References

1) N. Ito, T. Saji, and S. Aoyagui, *J. Electroanal. Chem.*, **144**, 153 (1983).

2) G. M, Badger and W. H. F. Sasse, "Advances in Heterocyclic Chemistry," ed by A. R. Karit, Academic Press, New York (1963), Vol. 2, p. 180

3) T. Ito, S. Hasegawa, Y. Takahashi, and Y. Ishii, *J. Organomet. Chem.*, **73**, 401 (1974).

4) N. Ito, T. Saji, K. Suga, and S. Aoyagui, *J. Organomet. Chem.*, **229**, 43 (1982).

5) M. Herberhold, "Metal π-complexes," Elsevier, Amsterdam (1972) Vol. 2, p. 263.

6) T. G. Groshens, B. Henne, D. Bartak, and K. J. Klabunde, *Inorg. Chem.*, **20**, 3629 (1981).

7) T. Saji and S. Aoyagui, *J. Electroalal. Chem.*, **110**, 329 (1980).

8) T. Saji and S. Aoyagui, *J. Electroanal. Chem.*, **63**, 405 (1975).

9) V. Graves and J. H. Lagowski, *Inorg. Chem.*, **15**, 577 (1976); D. W. Clark and K. D. Warren, *J. Organomet. Chem.*, **162**, 83 (1978); S. Evans, J. C. Green, and S. E. Jackson, *J. Chem. Soc., Faraday Trans., 2*, **68**, 249 (1972).

10) M. L. H. Green, "Organometallic Compounds," Methuen, London (1968) Vol. 2, p. 16—18.

The Viscosities and Molal Volumes of *t*-Butyl Alcohol in Metal Chelate Electrolyte Solutions

Kouzou Yoshitani
Faculty of General Education, Gifu University, Yanagido, Gifu 501-11
(Received February 23, 1985)

The Viscosities and molal volumes of *t*-butyl alcohol (*t*-BuOH) in aqueous solutions of $[Fe(phen)_3]Cl_2$, $[Co(phen)_3]Cl_3$ (phen=1,10-phenanthroline), $[Co(en)_3]Cl_3$ (en=ethylenediamine), tetraphenylphosphonium chloride ($(C_6H_5)_4PCl$), tetramethylammonium chloride (Me_4NCl), tetraethylammonium chloride (Et_4NCl), and tetra-*n*-butylammonium bromide ($(n\text{-}Bu)_4NBr$) were measured at 25 °C, and solute–solvent interactions characteristic of the metal chelate cations were investigated. The apparent molal volumes of *t*-BuOH in the solutions of $[Fe(phen)_3]^{2+}$ are larger than those in the $(n\text{-}Bu)_4N^+$ and $[Co(phen)_3]^{3+}$ solutions. The hydrophobicity of $[Fe(phen)_3]^{2+}$ is not so strong because of the aromaticity of the ligand. The same can be said for $[Co(phen)_3]^{3+}$. However, on the interaction between $[Co(phen)_3]^{3+}$ and *t*-BuOH, the charge-dipole interaction and hydrophobic interaction act cooperatively to stabilize this pair through the overlap of the solvation spheres.

The solute–solvent interactions of such metal chelate ions as $[Fe(phen)_3]^{2+}$ have been studied by means of their thermodynamic,[1–4] transport,[5–6] and kinetic[7] properties. From the viscosity study, $[Fe(phen)_3]^{2+}$ and $[Fe(bpy)_3]^{2+}$ (bpy=2,2′-bipyridine) were found to be hydrophobic-structure-making ions, though their hydrophobicity is weaker than that of the tetraalkylammonium ions at the equivalent level of the partial molal volumes.[5] $[Fe(phen)_3]^{2+}$ was found to show a large salting-in effect through hydrophobic interaction on the nonelectrolytes, such as nitrobenzene, toluene, benzene, and $[Co(acac)_3]$ (Hacac=2,4-pentanedione).[2–4] It was also found that the racemization rate of the trivalent metal chelate cation, $[Co(phen)_3]^{3+}$, by the electron-transfer mechanism is strongly affected by the structural change of water on the addition of *t*-BuOH.[7] In the present study, solute–solvent and solute–solute interactions of the metal chelates were examined through the viscosities and the apparent molal volumes of *t*-BuOH in aqueous solutions of these metal chelate electrolytes.

Experimental

The metal chelate electrolytes, $[Fe(phen)_3]Cl_2 \cdot 7H_2O$,[5] $[Co(phen)_3]Cl_3 \cdot 6H_2O$,[8] and $[Co(en)_3]Cl_3 \cdot H_2O$[9] were prepared by the literature methods and recrystallized twice from water. The tetraalkylammonium salts (Tokyo Kasei Kogyo Co., Ltd.) were purified by the methods described in the literature.[10] The tetraphenylphosphonium chloride (Merck) was used without further purification. The purities of the salts were checked by analysis. The *t*-BuOH was reagent grade (Nakarai Chemicals, Ltd.) and was used without further purification. The water was distilled from an alkaline permanganate solution. The concentrations of the electrolytes were determined by potentiometric titrations of the halide ions with $AgNO_3$ standard solutions just prior to use.

Ubbelohde viscometers with flow times for water at 25 °C of about 590 and 690 s were used. The kinetic-energy corrections for the viscometers were found to be negligible within the limits of experimental error. All the viscosity measurements were carried out in a 25.00±0.03 °C constant-temperature water bath controlled to ±0.005 °C. The flow times were measured with a stop watch and were reproducible to ±0.1 s.

The densities were measured with a digital densimeter (Anton Paar, Model DMA-02D). The thermostated bath was kept at 25.00±0.03 °C and controlled to ±0.002 °C. The densimeter was calibrated by the use of dry air and distilled water, and checked by measuring the densities of the aqueous *t*-BuOH solutions.[11] The errors in the density measurements were estimated to be within $\pm 2 \times 10^{-6}$ g cm^{-3}.

Results

The relative viscosities, η_r, of the aqueous solutions of *t*-BuOH in the presence of the electrolytes could be represented by the following equation over the range of *t*-BuOH concentrations from 0.2 to 1.5 mol dm^{-3}:

$$\eta_r = \eta/\eta^\circ = 1 + BC + DC^2, \quad (1)$$

where η_r represents the relative viscosity of the ternary solution (*t*-BuOH–electrolyte–water) with respect to the electrolyte solution used as the solvent, where η and η° are the viscosities of the ternary solution and the solvent respectively, and where C is the molar concentration of *t*-BuOH. The B coefficient is a function of the solute–solvent interaction, and the D coefficient represents the contribution of the solute–solute interaction to the relative viscosity.

Taking pure water as the reference solvent, the relative viscosity can be represented as follows:

$$\eta/\eta_w = \eta^\circ/\eta_w + B'C + D'C^2, \quad (2)$$

where η_w is the viscosity of pure water, and where B' and D' are $B\eta^\circ/\eta_w$ and $D\eta^\circ/\eta_w$ respectively. These equations differ in their reference states. In the present study, Eq. 2 was used, because B' reflects the differences more clearly than B. The B' and D' coefficients obtained by the least-squares method are given in Table 1. The B coefficient of *t*-BuOH in pure water at 25 °C is in good agreement with the literature value.[12]

The apparent molal volumes, ϕ_v, of *t*-BuOH in the electrolyte solutions were calculated from the density data.[11] The partial molal volumes at infinite dilution in aqueous electrolyte solutions, V^∞, were obtained by

Table 1. B' and D' coefficients of Eq. 2 for t-BuOH in various electrolyte solutions

Electrolyte	C / mol dm^{-3}	B' / mol^{-1} dm^3	D' / mol^{-2} dm^6
(Pure water)		0.372 (0.373)[a]	0.108
$[Fe(phen)_3]Cl_2$	0.06683	0.404	0.111
	0.09669	0.421	0.113
$[Co(phen)_3]Cl_3$	0.07251	0.427	0.113
	0.09386	0.443	0.117
$[Co(en)_3]Cl_3$	0.08320	0.385	0.115
	0.1267	0.394	0.121
Ph_4PCl	0.07839	0.391	0.107
	0.1136	0.404	0.109
Bu_4NBr	0.05095	0.395	0.105
	0.1019	0.417	0.111
Et_4NCl	0.09815	0.383	0.109
	0.1684	0.392	0.114
Me_4NCl	0.1648	0.373	0.114
	0.2031	0.378	0.110
NaCl	0.1034	0.379	0.103
NaBr	0.09996	0.378	0.102

a) Ref. 12.

Table 2. Partial molal volumes of t-BuOH in various electrolyte solutions

Electrolyte	C / mol dm^{-3}	V^∞ / cm^3 mol^{-1}
(Pure water)		87.83 (87.90)[a]
$[Fe(phen)_3]Cl_2$	0.04985	87.59
	0.09828	87.38
$[Co(phen)_3]Cl_3$	0.09386	87.18
	0.2246	86.20
$[Co(en)_3]Cl_3$	0.04818	87.71
	0.09636	87.72
Ph_4PCl	0.04595	87.58
	0.1004	87.39
Bu_4NBr	0.05095	87.45
	0.1008	87.01
Et_4NCl	0.04910	87.57
	0.09815	87.37
Me_4NCl	0.08120	87.59
	0.1172	87.60
NaCl	0.1034	87.85
NaBr	0.09996	87.88

a) Ref. 11.

fitting the apparent molal volumes to this equation:

$$\phi_v = V^\infty + A_v C + B_v C^2, \quad (3)$$

where C is the molar concentration of t-BuOH and where A_v and B_v are the fitting parameters. The V^∞ and fitting parameters, A_v and B_v, were obtained by the least-squares method and are given in Table 2.

Discussion

In the presence of the electrolyte, the viscosity B' coefficient of t-BuOH increases with an increase in the concentration of the electrolyte, as is shown in Fig. 1. The increase in the B', coefficient can be attributed to the t-BuOH–electrolyte interaction and the obstruction effect.[13] Of course, it is difficult to evaluate these two effects separately, but it can be assumed that it is proportional to the volume fraction and, therefore, to the partial molal volume of the electrolyte, by analogy with the obstruction effect in conductance and diffusion.[13] Therefore, the B' coefficients in various electrolyte solutions at 0.1 mol dm^{-3} are plotted against the partial molal volumes of the electrolytes in Fig. 2, which shows that the B' coefficients increase with an increase in the partial molal volumes of electrolytes in pure water. The plot for $(C_6H_5)_4PCl$ falls on the line connecting plots for pure water, NaCl, Me_4NCl, and $[Co(en)_3]Cl_3$. The plot for $[Fe(phen)_3]Cl_2$ does not deviate markedly from the line.

Here, the B' coefficients can not be divided into the

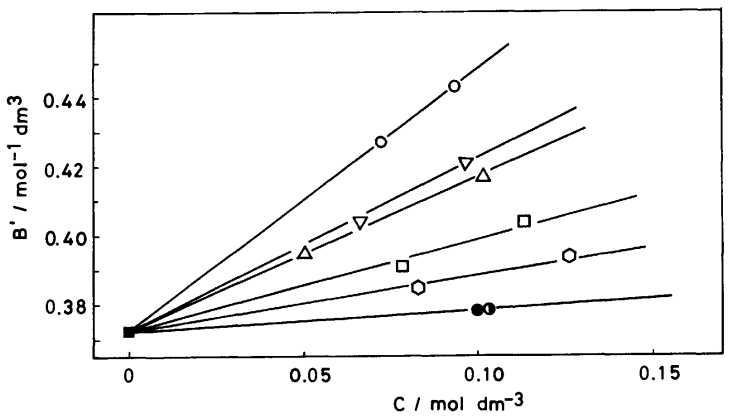

Fig. 1. Dependence of B′ coefficient of t-BuOH on electrolyte concentration.
■: In pure water, ◑: in NaCl solution, ●: in NaBr solution, ○: in $[Co(en)_3]Cl_3$ solution, □: in $(C_6H_5)_4PCl$ solution, △: in Bu_4NBr solution, ▽: in $[Fe(phen)_3]Cl_2$ solution, □: in $[Co(phen)_3]Cl_3$ solution.

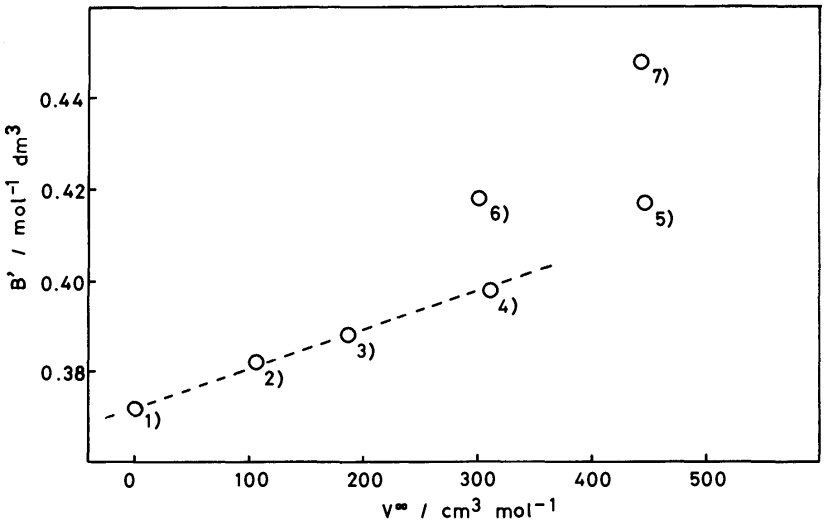

Fig. 2. Relation between B' coefficient of *t*-BuOH in electrolyte solution (0.1 mol dm^{-3}) and partial molal volume of electrolyte in water.
1): In pure water, 2): Me_4NCl,[a] 3) $[Co(en)_3]Cl_3$,[b] 4): $(C_6H_5)_4PCl$,[c] 5): $[Fe(phen)_3]Cl_2$,[d] 6): Bu_4NBr,[a] 6): $[Co(phen)_3]Cl_3$.[b]
Partial molal volumes of electrolytes in water were taken from references: a) Ref. 18), b) Ref. 19), c) Ref. 20), d) Ref. 1).

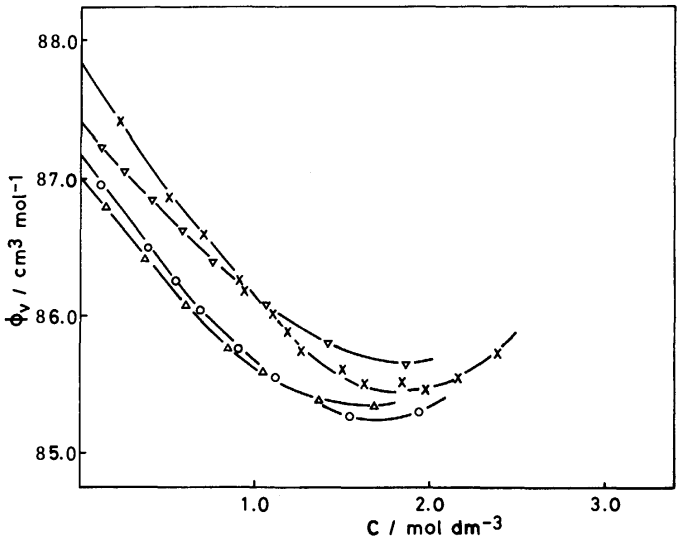

Fig. 3. Apparent molal volumes of *t*-BuOH in water and electrolyte solutions.
×: In pure water, ▽: in $[Fe(phen)_3]Cl_2$ solution (0.09828 mol dm^{-3}), ○: in $[Co(phen)_3]Cl_3$ solution (0.09386 mol dm^{-3}), △: in Bu_4NBr solution (0.1008 mol dm^{-3}).

contributions of the cation and the anion, but it may be safely assumed that the cationic contributions are the main factor in the large difference of the B' coefficients between the solutions of $(n\text{-Bu})_4NBr$ and $(C_6H_5)_4PCl$, or $[Fe(phen)_3]Cl_2$ and $[Co(phen)_3]Cl_3$.

The larger B', coefficient of *t*-BuOH in the $(n\text{-Bu})_4N^+$ solution was attributed to the strongly hydrophobic interaction.[11,14–16] The smaller B' value for $(C_6H_5)_4P^+$ means that the hydrophobicity becomes weak upon the introduction of the aromatic character.[5,17] The same can be said for the hydrophobicity of $[Fe(phen)_3]^{2+}$.

The large B' coefficient in the solution of $[Co(phen)_3]^{3+}$ compared with that in the $[Fe(phen)_3]^{2+}$ solution needs to be explained other than in terms of the hydrophobicity, because the hydrophobicity of $[Co(phen)_3]^{3+}$ should be weaker than $[Fe(phen)_3]^{2+}$ because of its trivalent charge. On the other hand, it seems that the ion-dipole interaction by the trivalent

charge of the ion can not cause the large B' coefficient by itself, because the B' coefficient is not so large in the solution of the trivalent ion with much smaller volumes of $[Co(en)_3]^{3+}$.

As is shown in Fig. 3, the ϕ_v of *t*-BuOH decreases with an increase in the concentration of *t*-BuOH and reaches a minimum at about 1.9 mol dm^{-3} in pure water. This minimum corresponds to the composition of the maximum structure of the solution.[11] For the case of ϕ_v in the $(n\text{-}Bu)_4N^+$ solution the minimum in ϕ_v shifts to a lower concentration as a result of the cooperative effect of *t*-BuOH and $(n\text{-}Bu)_4N^+$. In the solution of $[Fe(phen)_3]^{2+}$, the minimum shifts only a little, which indicates that such a cooperative action does not occur for the pairs of $[Fe(phen)_3]^{2+}$ and *t*-BuOH.

When the V^∞ values of *t*-BuOH in electrolyte solutions of about 0.1 mol dm^{-3} in Table 2 are compared, the V^∞ values are nearly equal in alkali halide solutions, slightly smaller in Me_4N^+, and smallest in $(n\text{-}Bu)_4N^+$, compared with the V^∞ value in pure water. Such a trend can be expected from the effects of these ions on the water structure, but the fairly small V^∞ value in $[Co(phen)_3]^{3+}$ can not be explained from the structural property. The most probable explanation for the V^∞ and B' values of *t*-BuOH in $[Co(phen)_3]^{3+}$ is that $[Co(phen)_3]^{3+}$ attracts *t*-BuOH in the vicinity of the hydrophobic ligands by means of such long-range forces as the charge-dipole interaction.[3] After that, the van der Waals interaction between *t*-BuOH and $[Co(phen)_3]^{3+}$ becomes effective and the overlap of the hydration sphere occurs.[3] This also causes the large B' coefficient of *t*-BuOH in the solution of $[Co(phen)_3]^{3+}$.

From the above observations, it may be concluded that the hydrophobic interaction between the $[Fe(phen)_3]^{2+}$ ion and the aliphatic solute of *t*-BuOH is weak because of the aromatic character of the ligands. However, for the pair of the $[Co(phen)_3]^{3+}$ ion and *t*-BuOH, the cooperative action of ion-dipole and hydrophobic interaction is very effective in stabilizing the water structure.

The author wishes to thank Professor Yuroku Yamamoto and Dr. Manabu Yamamoto of Hiroshima University for their helpful discussions.

References

1) K. Yoshitani, M. Yamamoto, and Y. Yamamoto, *Bull. Chem. Soc. Jpn.*, **56**, 1978 (1983).
2) E. Iwamoto, M. Yamamoto, and Y. Yamamoto, *Inorg. Nucl. Chem. Lett.*, **10**, 1069 (1974).
3) E. Iwamoto, Y. Hiyama, and Y. Yamamoto, *J. Solution Chem.*, **6**, 371 (1977).
4) E. Iwamoto, Y. Tanaka, H. Kimura, and Y. Yamamoto, *J. Solution Chem.*, **9**, 841 (1980).
5) Y. Yamamoto, T. Tominaga, and T. Tagashira, *Inorg. Nucl. Chem. Lett.*, **11**, 825 (1975).
6) Y. Yamamoto, E. Sumimura, K. Miyoshi, and T. Tominaga, *Anal. Chim. Acta*, **64**, 225 (1973).
7) M. Yamamoto, Y. Uwate, and Y. Yamamoto, *Inorg. Nucl. Chem. Lett.*, **12**, 713 (1976).
8) P. Pfeiffer and Br. Werdelmann, *Z. Anorg. Allg. Chem.*, **263**, 31 (1950).
9) J. B. Work, *Inorg. Synth.*, **2**, 221 (1946).
10) B. E. Conway, R. E. Verrall, and J. E. Desnoyers, *Trans. Faraday Soc.*, **62**, 2738 (1966).
11) L. Avêdikian, G. Perron, and J. E. Desnoyers, *J. Solution Chem.*, **4**, 331 (1975).
12) T. T. Herskovits and T. Kelly, *J. Phys. Chem.*, **77**, 381 (1973).
13) R. A. Robinson and R. H. Stokes, "Electrolyte Solutions," 2nd. ed, Butterworths, London (1959).
14) J. E. Desnoyers, G. Perron, J. P. Morel, and L. Avêdikian, "Chemistry and Physics of Aqueous Gas Solutions," ed by W. A. Adams, The Electrochemical Society, Princeton, N. J. (1975).
15) C. de Visser, G. Perron, and J. E. Desnoyers, *J. Am. Chem. Soc.*, **99**, 5894 (1977).
16) J. E. Desnoyers, G. Perron, S. Leger, B. Y. Okamoto, T. H. Lilley, and R. H. Wood, *J. Solution Chem.*, **7**, 165 (1978).
17) C. Jolicoeur, N. D. The, and A. Cabana, *Can. J. Chem.*, **49**, 2008 (1971).
18) F. J. Millero, "Water and Aqueous Solutions, Structure, Thermodynamics and Transport Processes," ed by R. A. Horn, Wiley-Interscience, New York (1972), Chap. 13.
19) The ϕ_v values of $[Co(en)_3]Cl_3$ and $[Co(phen)_3]Cl_3$ were determined over a range of concentrations (0.01—0.05 mol dm^{-3}) The V^∞ values were obtained by fitting the ϕ_v values to the Redlich-Mayer equation:[18]
$$\phi_v = V^\infty + 27.45C^{1/2} + b_vC,$$
while the parameters, V^∞ and b_v, for $[Co(en)_3]Cl_3$ (187.4 cm^3 mol^{-1} and -15.8 cm^3 dm^3 mol^{-2} and for $[Co(phen)_3]Cl_3$ (441.8 cm^3 mol^{-1} and -50.1 cm^3 dm^3 mol^{-2}) were determined by the least-squares method.
20) C. Jolicoeur, P. R. Philip, G. Perron, P. A. Leduc, and J. E. Desnoyers, *Can. J. Chem.*, **50**, 3167 (1972).

The Solution Chemistry of Organotin Compounds. IV. Thermodynamic Parameters of the Complex Formation between $MeSnCl_3$ and Alkyl Sulfoxides Determined from Titration Calorimetry

Hideaki FUJIWARA,* Fumihiko SAKAI, Akio KAWAMURA, Naoto SHIMIZU, and Yoshio SASAKI
Faculty of Pharmaceutical Sciences, Osaka University, 1-6 Yamada-Oka, Suita, Osaka 565
(Received March 11, 1985)

Calorimetric titration data have been analyzed to determine thermodynamic parameters of the interacting system. The system studied is $MeSnCl_3$ plus dialkyl sulfoxide in CH_2Cl_2 and a nonlinear least squares method is utilized to simulate the titration curve. The 1:1 and 1(acid):2(base) complexes are found to coexist in solution, and the effect of alkyl chain length on the complex formation is examined. The complex formation proceeds most favorably under the total carbon number of four, and inductive and steric effects are considered to operate in a compensating way. Entropy changes on the reactions are discussed with the aid of molecular theory of thermodynamic functions, and a new method is suggested that affords the number of solvent molecules released on the complex formation.

Thermodynamic parameters are essential for the discussion of molecular interactions such as complex formation between acids and bases. These parameters are most often determined from the van't Hoff plot after measuring equilibrium constants at different temperatures.[1] However, titration calorimetry may be best suited for such studies, because those parameters are determined precisely and readily from the direct observation of the heat evolved or absorbed on reaction. For the analysis of such titration data it is frequently encountered that more than one type of reaction needs be dealt with concurrently.[2] This arises from the fact that concentration of solute studied is relatively high and the infinite dilution approximation is not applicable. This seems to be a main reason of rather small number of reports regarding the titration calorimetry. Hitherto, a trial and error method has been reported[3] and applied[4] to the complex formation of several organometallic compounds with bases. The authors have established a simulation program for the analysis of concentration dependence of NMR parameters, which optimizes adjustable parameters by means of a nonlinear least squares method under the several types of equilibrium.[5-7] This program is extended in this paper to apply to the titration calorimetry and the complex formation of $MeSnCl_3$ with dialkyl sulfoxides is examined. The sulfoxides used are as follows:

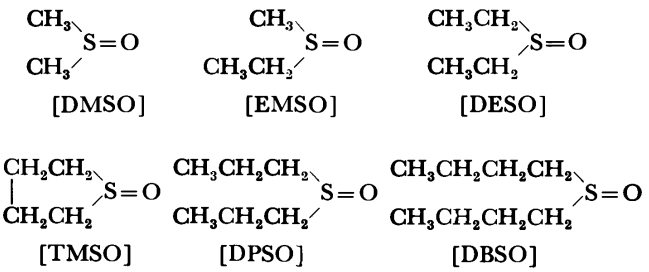

Experimental

An isothermal isoperibol titration calorimeter Model 550 (Tronac Inc.) was used under the isothermal mode at 25 °C. Calibration of the energy equivalent of the reaction solution is unnecessary under this mode. Total sample volume was 50.0 ml and about 2 ml of titrant was added in increment of 0.1315 ml. Solution of the base was added titrimetrically to the solution in vessel containing the tin compound by *ca.* 0.05 mol dm^{-3}. Heat necessary to compensate for the reaction enthalpy was measured in 15 s. after an addition of the titrant. Titration and the subsequent data collection were controlled by the Programmer C-930. Heat of solution of the base was also measured by adding the titrant to the solvent without tin compound in the same manner. Differential heat of these two runs was set to the effective heat of complex formation and analyzed by the computer program. Errors were also estimated in the program for each parameter as equal to the 95% confidence range which makes the σ^2(see Eq. 4 below) larger by 1.96 times, and they were also tested by repeated experiments (more than 3 runs).

$MeSnCl_3$ was synthesized from Me_2SnCl_2 using catalytic reagents[8] and sublimed at *ca.* 30 °C after distillation. EMSO, DESO, and DPSO were synthesized from the corresponding sulfides according to a scheme:[9]

$$R_1R_2S + NaIO_4 \longrightarrow R_1R_2SO + NaIO_3$$

Sulfoxides were dried over BaO and distilled under reduced pressure after decantation. All operations of the purification and sample preparation were done in dry boxes.

Analysis of Calorimetric Titration Data

Effective heat of the complex formation determined experimentally q_{expt} is expressed as the differential heat between the titration q_{titrn} and the dilution q_{diln} (Fig. 1): $q_{expt}=q_{titrn}-q_{diln}$. The heat q in each incremental step in the succesive titration experiment can be integrated to give the integrated heat Q, for which following eq holds after i-th step of titration.

$$Q_{expt,i} = Q_{titrn,i} - Q_{diln,i} \quad (1)$$

On the other hand, integrated heat of the complex formation such as in Eq. 2 is calculated according to Eq. 3:

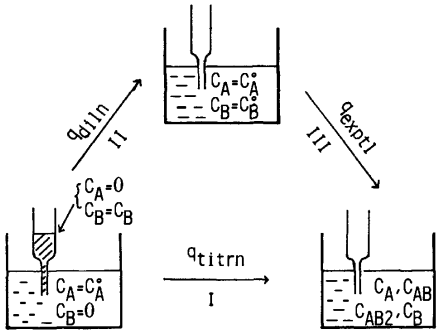

Fig. 1. Heat of titration (step I) can be divided into two parts, *i.e.*, heat of dilution q_{diln} in step II and heat of complex formation q_{exptl} in step III: $q_{titrn}=q_{diln}+q_{exptl}$.

$$\left.\begin{array}{ll} A + B = AB & K_1, \Delta H_1^\circ \\ AB + B = AB_2 & K_2, \Delta H_2^\circ \end{array}\right\}, \quad (2)$$

$$Q_{calcd,i} = (\Delta H_1^\circ \cdot C_{AB} + \Delta H_2^\circ \cdot C_{AB_2}) \cdot V_i, \quad (3)$$

where ΔH_1° and ΔH_2° are the molar enthalpies for the reactions in Eq. 2, and V_i is the volume of solution, *i.e.*, $V_i=V_0+i\cdot\Delta V$, V_0 being the initial volume of the titrated solution and ΔV the incremental volume added in each step. Molarity of the complexes AB and AB_2, C_{AB} and C_{AB_2}, are obtained by solving Eqs. of the chemical equilibrium. In this way, the problem is how to reproduce well the experimental data (Eq. 1) by adjusting K_1, K_2, ΔH_1°, and ΔH_2° in Eq. 2. For this purpose, standard deviation σ as expressed by Eq. 4 needs be minimized by optimizing the four parameters, and to this end a least squares method is surely superior than a trial and error method.

$$\sigma = [\sum_{i=1}^{n} (Q_{expt.i} - Q_{calcd,i})^2/(n-p)]^{1/2} \quad (4)$$

In above equation n is the total number of titration steps and p is the number of adjustable parameters. In our previous case of NMR titration experiments,[5-7] chemical shift or coupling constant (ϕ) is expressed as $\phi_{calcd}=(\phi_A\cdot C_A+\phi_B\cdot C_B+\phi_{AB_2}\cdot C_{AB_2})/C_A^\circ$ instead of Eq. 3 in the present case. Therefore, the method is easily modified to the present case.[10]

Among various kinds of nonlinear least squares analysis, we have adopted a version of so-called DFP (Davidon-Fletcher-Powell) method, which belongs to a variable metric method. This algorithm is widely accepted as one of the most sophisticated search technique, and it appears to be independent of the number of variables involved.[11] The superiority of the DFP method itself is also approved in the MO calculation with geometrical optimization[12] where a large number of variables are usually included but the derivatives of the minimized function are available. However, when we utilized a version of this algorithm, some drawbacks were encountered. A search process failed frequently in improving the variable parameters when started from initial values far from the final ones under the three- or four-parameter simulation. In the original DFP algorithm, an updating formula 5 is used to find a Hessian matrix

$$H_{j+1} = H_j + \delta\cdot\delta^T/\delta^T\cdot\gamma - H_j\gamma\cdot\gamma^T H_j/\gamma^T H_j\gamma, \quad (5)$$

appropriate for the next step. Fletcher[13] demonstrated that use of this equation together with the linear search is unsuccessful in special circumstances and proposed an improved algorithm where the updating formula is switched appropriately between Eq. 5 and the complementary one:

$$H_{j+1} = (I-\delta\gamma^T/\delta^T\gamma)H_j(I-\gamma\delta^T/\delta^T\gamma) + \delta\delta^T/\delta^T\gamma. \quad (6)$$

In the present study the improved algorithm is incorporated and the failure of improving parameters stated above is circumvented.

Results and Discussion

Calorimetric titration curves are depicted in Fig. 2

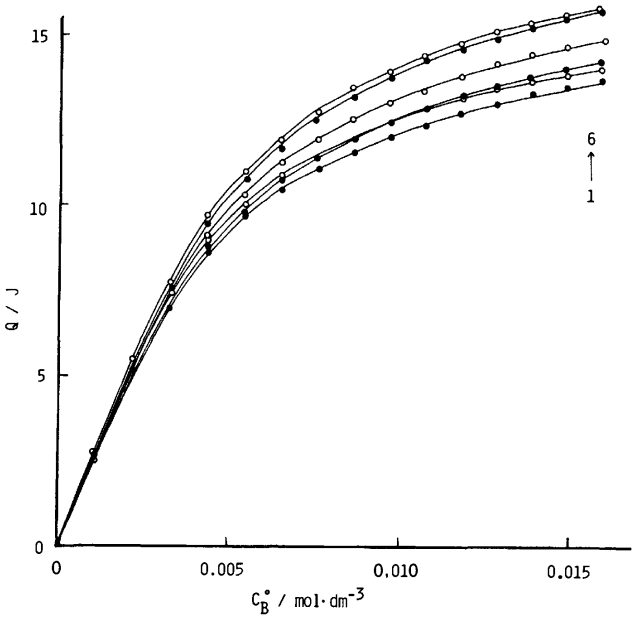

Fig. 2. Calorimetric titration curves for the $MeSnCl_3$ plus alkyl sulfoxide systems in CH_2Cl_2.
Solution of sulfoxide is added titrimetrically into that of $MeSnCl_3$ at 25 °C. Sulfoxides used are: DMSO(1), EMSO(3), DESO(5), TMSO(6), DPSO(4), DBSO(2). C_B° is the initial concentration of sulfoxide and Q the integrated heat of complex formation.

Table 1. Analysis of calorimetric titration data of $MeSnCl_3$ plus DMSO system under some models of chemical equilibrium

Model		K/dm^{3}mol^{-1}	ΔH°/kJ mol^{-1}	σ/J
I	A+B=AB	log K=2.42	ΔH°=−90.8	0.30
II	A+2B=AB_2	log K=7.51	ΔH°=−81.3	1.79
III	A+B=AB	log K_1=3.83	ΔH_1°=−48.0	0.03
	AB+B=AB_2	log K_2=2.00	ΔH_2°=−40.1	

TABLE 2. EQUILIBRIUM AND THERMODYNAMIC PARAMETERS DERIVED FROM CALORIMETRIC TITRATION DATA FOR $MeSnCl_3$ PLUS SULFOXIDE IN CH_2Cl_2 AT 25 °C[a)]

Base	log K_1	log K_2	$-\Delta H_1^\circ$	$-\Delta H_2^\circ$	$-\Delta S_1^\circ$	$-\Delta S_2^\circ$	σ[b)]
DMSO	3.83±0.03	2.00±0.01	48.0±0.2	40.1±0.3	87.7±1.2	96.2±1.1	0.03
EMSO	3.93±0.04	2.18±0.01	47.8±0.3	42.1±0.2	85.2±1.8	99.5±0.8	0.03
DESO	4.13±0.04	2.31±0.01	48.5±0.2	45.1±0.2	83.6±1.5	107.6±0.8	0.03
TMSO	4.13±0.05	2.34±0.01	50.3±0.3	43.5±0.2	89.8±2.0	101.1±0.9	0.04
DPSO	4.12±0.04	2.21±0.01	49.1±0.2	42.3±0.2	85.8±1.4	99.7±0.8	0.03
DBSO	3.94±0.05	2.14±0.01	48.7±0.3	38.2±0.2	88.0±1.9	87.1±0.9	0.04

a) The subscript 1 is used for the reaction of A+B=AB and 2 is for that of AB+B=AB_2. Units used are $dm^3\,mol^{-1}$ for K, $kJ\,mol^{-1}$ for ΔH°, and $J(K\,mol)^{-1}$ for ΔS°. b) Standard deviation between the experimental and recalculated heat of reaction in unit of J.

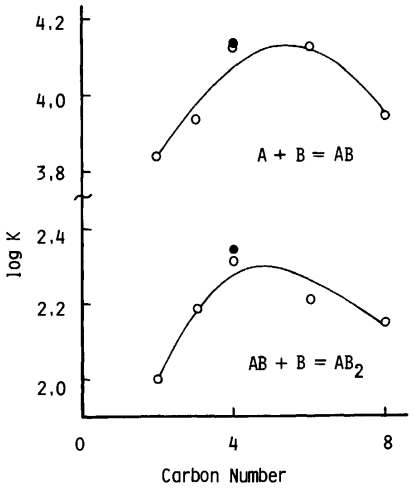

Fig. 3. Dependence of log K on the carbon number of sulfoxide.
●: Indicates data point of TMSO.

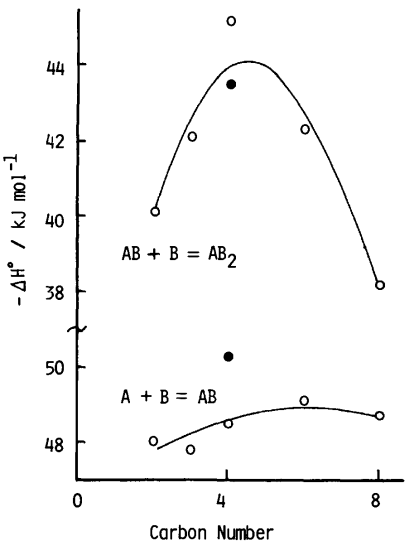

Fig. 4. Dependence of $-\Delta H^\circ$ on the carbon number of sulfoxide.
●: Indicates data point of TMSO.

for the $MeSnCl_3$ plus sulfoxide systems in CH_2Cl_2. Analysis of such experimental data basing on a few models of chemical equilibrium which may occur is

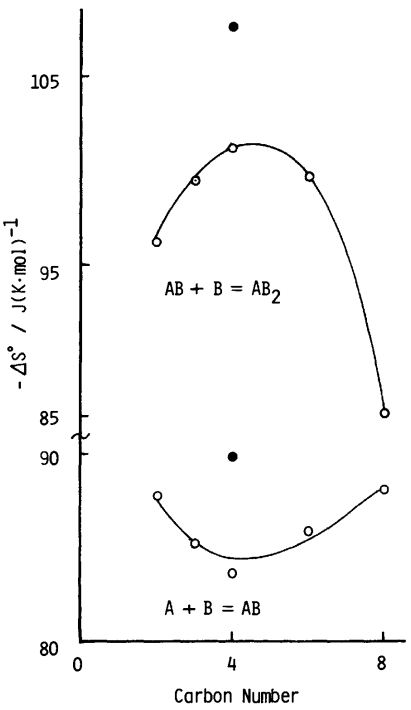

Fig. 5. Dependence of $-\Delta S^\circ$ on the carbon number of sulfoxide.
●: Indicates data point of TMSO.

compared in Table 1 for the DMSO system typically. It is clear that 1:1 and 1(acid):2(base) complexes are formed in solution. Analysis under the model III in Table 1 is summarized in Table 2 for all the systems studied here, including error limit estimated from the program and repeated runs whichever is larger. Equilibrium constants, enthalpies, and entropies are plotted in Fig. 3 to 5 against the total number of carbon atoms in the alkyl groups in sulfoxide. It is interesting to note that the complexes AB and AB_2 are most stable for the sulfoxide with the carbon number of four (Fig. 3). For the 2nd step of the complex formation, $-\Delta H^\circ$ and $-\Delta S^\circ$ also show the similar dependency on the carbon number (Figs. 4 and 5). This means that the enthalpy term contributes positively but the entropy term negatively in the 2nd step. That is, the dependency comes out of the enthalpy term. Introduction of a methylene group into the substituent of the functional

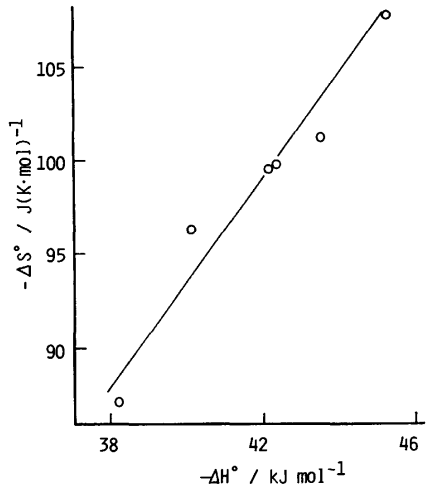

Fig. 6. Enthalpy-entropy compensation relation for the reaction of AB+B=AB_2. A=$MeSnCl_3$ and B=alkyl sulfoxide.

S=O group will increase the electron-donating ability of the functional group through an effect such as called "hyperconjugation." On the contrary, increase in the number of methylene groups will induce the steric hindrance, weakening the chemical bond between Sn and S=O.[14] This steric effect is, however, not such a strong and specific one as to disturb the enthalpy-entropy compensation relation as revealed in Fig. 6 for the 2nd step.

In contrast to the 2nd step of the complex formation, the results are not straightforwardly explained in the 1st step. That is, the entropy change is oppositely dependent on the carbon number (Fig. 5), and the enthalpy change is not clearly dependent on this number (Fig.4).[15] The 1st step of the complex formation is considered entropy-dependent, because the trend in reactivity in Fig. 3 is consistent with that in the entropy term and because difference in the enthalpy term is small among the sulfoxides listed in Fig. 4. Only an exception is TMSO, for which enhanced reactivity surely comes from the enthalpy term.

Entropy change on the complex formation is generally expressed by the difference in standard entropies of the components, *e. g.*, $\Delta S^\circ_{calcd}=S^\circ_{AB}-(S^\circ_A+S^\circ_B)$ for A+B=AB. The entropies can be calculated from molecular theory of thermodynamic functions, and it is composed of several contributions of translational, rotational, vibrational, and internal rotational parts, *i.e.*, $S^\circ=S^\circ_{tr}+S^\circ_r+S^\circ_v+S^\circ_{fir}-(S_f-S)$.[16] This value of ΔS°_{calcd} is considered to correspond to the gas-phase value of ΔS°. Such calculations have been applied precisely to various chemical reactions and equilibria to approve the third-law of thermodynamics, and the results are also useful for the discussion of internal motions in the relevant substances.[17] Although similar discussion should be applicable to the case of complex formation,

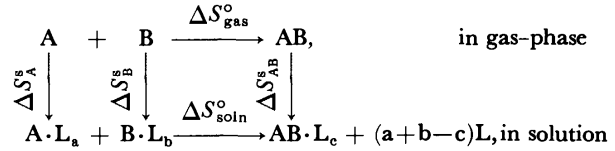

Fig. 7. Entropy changes related to the complex formation in gas phase and in solution.
The species A, B, and AB are assumed solvated weakly by the solvent L, and the numbers of solvation are a, b, and c, respectively, the related entropies of solution being denoted by ΔS^s's.

those studies are very limited in number.[18] This is probably because only the enthalpy change is interested and the entropy one is overlooked. However, if the entropy is measured carefully in gas phase, the result can be compared with the calculation. As an example, $\Delta S^\circ=-166.9$ J K^{-1} mol^{-1} determined for the complex formation of $B(CH_3)_3$ with NH_3 in gas phase at 100° C[19] can be interpreted by the moment of inertia and vibration-spectral data of each species, calculated value being -168.9 J K^{-1} mol^{-1}.[20]

For the present case of $MeSnCl_3$ plus sulfoxides, experimental values of ΔS° are measured in solution and the values will not correspond with the calculated ones, and also exact calculations of the vibrational and the internal rotational entropies are prevented by a lack of necessary physicochemical constants. However, it is interested to compare the experimental values with the calculated ones which include predominant parts, *i.e.*, translational and rotational ones, of the entropies. The calculated value is -253.1 J K^{-1} mol^{-1} against the observed one of -87.7 for A+B=AB, and is -259.8 against -96.2 for AB+B=AB_2 when B is DMSO. Since the vibrational and the internal rotational contributions are very small for the simple molecule such as DMSO, the entropy changes observed in CH_2Cl_2 are said to be about 1/3 of the net entropy changes in gas phase. If, as in a model calculation described in the previous paper,[21] DMSO is assumed to be solvated by one molecule of CH_2Cl_2 and the latter be released on the complex formation, the entropy changes are reduced in absolute value to -19.2 for A+BS=AB+S and -25.5 for AB+BS=AB_2+S. Therefore, experimental entropies can be said to indicate the solvation number of 0.7 or the release of solvent molecules by 0.7 mol on the complex formation of both A+B=AB and AB+B=AB_2. In these calculations entropies are also estimated by assuming different geometries of the complexes as well as the solvated species, but the result does not change considerably. This situation may be discussed more precisely by a thermodynamic cycle as shown in Fig. 7. The entropy change in solution ΔS°_{soln} is expressed as follows:

$$\Delta S^\circ_{soln} = \Delta S^\circ_{gas} + (\Delta S^s_{AB} - \Delta S^s_A - \Delta S^s_B) + (a+b-c)S^\circ_L \quad (7)$$

where S°_L means the entropy of solvent.[22] Therefore,

a+b−c, the number of solvent molecules released on the complex formation, is seen to be obtained from the Eq.:

$$a+b-c = \{\Delta S^{\circ}_{soln} - \Delta S^{\circ}_{gas} - (\Delta S^{s}_{AB} - \Delta S^{s}_{A} - \Delta S^{s}_{B})\}/S^{\circ}_{L}. \quad (8)$$

This number may be interpreted as reflect the solvation number judged from the entropy effect. It is, however, not easy to estimate exactly the entropy of solution for the complex, *i. e.*, ΔS^{s}_{AB}. Usually ΔS°_{gas} is more negative than ΔS°_{soln} as is shown in above case. Therefore, if the entropies of solution ΔS^{s}'s are smaller than ΔS°_{gas} in absolute value or if ΔS^{s}_{AB} almost cancells out with $\Delta S^{s}_{A}+\Delta S^{s}_{B}$, above equation is simplified as:

$$a+b-c = (\Delta S^{\circ}_{soln} - \Delta S^{\circ}_{gas})/S^{\circ}_{L}. \quad (9)$$

From this equation and by putting ΔS°_{calcd} in place of ΔS°_{gas}, a+b−c is calculated as 0.6 for $MeSnCl_3$ plus DMSO in CH_2Cl_2, in consistent with above preliminary calculations. In this way, entropy changes in the complex formation is expected to give a number of solvent molecules released on the reaction. Further study is under way including other systems.

References

1) M. D. Joesten and L. J. Schaad, "Hydrogen Bonding," Marcel Dekker, New York, 1974.

2) For a simple case of A+B=AB, see: T. F. Bolles and R. S. Drago, *J. Am. Chem. Soc.*, **88**, 5730 (1966).

3) Y. Farhangi and D. P. Graddon, *J. Organomet. Chem.*, **87**, 67 (1975).

4) D. P. Graddon and B. A. Rana, *J. Organomet. Chem.*, **136**, 19 (1977).

5) H. Fujiwara, F. Sakai, and Y. Sasaki, *J. Phys. Chem.*, **83**, 2400 (1979).

6) H. Fujiwara, F. Sakai, M. Takeyama, and Y. Sasaki, *Bull. Chem. Soc. Jpn.*, **54**, 1380 (1981).

7) H. Fujiwara, F. Sakai, and Y. Sasaki, *J. Chem. Soc. Perkin Trans. 2*, **1983**, 11.

8) H. W. Jung, R. Maul, S. Kintopf, N. Kloss, and R. Knapp, Ger. Patent: 2437586 (1975), also see *Chem. Abstr.*, **83**, 1040n (1975).

9) N. J. Leon and C. R. Johnson, *J. Org. Chem.*, **27**, 282 (1962).

10) Activity coefficients were assumed to be unity because of the lack of necessary data for the alkyl sulfoxides. They would be easily incorporated into the computer program by expressing activities as an appropriate function of the analytical concentration.

11) D. A. Pierre, "Optimization Theory with Applications," John Wiley, New York, (1969), p. 320.

12) R. C. Bingham, M. J. S. Dewar, and D. H. Lo, *J. Am. Chem. Soc.*, **97**, 1285 (1975) and M. J. S. Dewar and W. Thiel, *ibid.*, **99**, 4907 (1977). Fletcher's improvement is not included therein.

13) R. Fletcher, *Compt. J.*, **13**, 317 (1970).

14) That such a steric effect surely acts when a carbon number exceeds two in each alkyl substituent may be seen from a molecular model of the complex AB_2 assuming a bent form for S=O···Sn (angle=≈120°). Such a bent form has been observed in some tin halide complexes with DMSO and DMF: L. A. Aslanov, V. M. Ionov, V. M. Attiya, A. B. Permin, and V. S. Petrosyan, *Zhur. Strukt. Khim.*, **19**, 109 (1978).

15) The authors suggest that a weak solvation of the complex AB has obscured a clear dependency.

16) G. Herzberg, "Molecular Spectra and Molecular Structure. II. Infrared and Raman Spectra of Polyatomic Molecules," Van Nostrand, New York, 1945.

17) S. C. Schumann and J. G. Aston, *J. Chem. Phys.*, **6**, 480 (1938) and the references cited therein.

18) Only a case known to the authors is an ion-pair formation: R. Fujishiro, G. Wada, and R. Tamamushi, "Yoeki no Seishitsu. II," (in Japanese), Tokyo-Kagaku-Dojin, (1968) p. 136, and references cited therein.

19) H. C. Brown, "Boranes in Organic Chemistry," Cornell Univ. Press, (1972).

20) If methyl groups become restricted in rotation in the complex, the calculated value is reduced by an amount of $-(S_f-S)$ for these groups, and if the NH_3 fragment can rotate around the N-B bond, it is increased by $S_{fir}-(S_f-S)$. But these effects are not included here because of a lack of necessary data.

21) Part III, H. Fujiwara, F. Sakai, Y. Mikawa, and Y. Sasaki, *Bull. Chem. Soc. Jpn.*, **58**, 1741 (1985).

22) $S^{\circ}_{L}=270.3$ J K^{-1} mol^{-1} for CH_2Cl_2 from: S. W. Benson, "Thermochemical Kinetics," John Wiley, New York, (1968), Japanese ed by H. Sakurai, T. Fueno, and M. Kira, Hirokawa, Tokyo.

X-Ray Photoelectron Spectra and Electrical Conductivities of One-dimensional Halogen-bridged Pd(II)-Pt(IV) and Ni(II)-Pt(IV) Mixed-valence Complexes

Masahiro YAMASHITA,* Ichiro MURASE, Tasuku ITO,† Yoshiki WADA,†
Tadaoki MITANI,† and Isao IKEMOTO††

Laboratory of Chemistry, College of General Education, Kyushu University, Ropponmatsu, Fukuoka 810
†*Institute for Molecular Science, Okazaki National Research Institutes, Myodaiji, Okazaki 444*
††*Department of Chemistry, Faculty of Science, Tokyo Metropolitan University, Setagaya-ku, Tokyo 158*

(Received April 13, 1985)

The X-ray photoelectron spectra have been measured for the one-dimensional halogen-bridged metal-alternated mixed-valence complexes, $[Pd^{II}(en)_2][Pt^{IV}X_2(en)_2](ClO_4)_4$ (X=Cl, Br, and I) and $[Ni^{II}(en)_2][Pt^{IV}X_2(en)_2](ClO_4)_4$(X=Cl and Br), along with their parent complexes, $[Pd(en)_2]Cl_2$, $Ni(en)_2Cl_2$, and $[PtCl_2(en)_2]Cl_2$. As the bridging halogen changes from Cl to I, the binding energies of the Pt(IV)4f levels become lower while those of M(II) (M=Pd and Ni) levels become higher, each gradually approaching to the M(III) binding energies (M=Pt, Pd, or Ni), respectively. Comparing the binding energies of the Pt(IV)4f levels in these hetero-metal mixed-valence complexes with those previously reported for the homo-metal halogen-bridged Pt(II)-Pt(IV) mixed-valence complexes having the same bridging halogens, the reductive trend of the oxidation states of Pt(IV) is found to be significantly suppressed by the metal alternation. In accord with this result, the activation energies obtained from the electrical conductivities are fairly larger than those of the homo-metal Pt(II)-Pt(IV) mixed-valence complexes. Their magnitudes are in the order of Pd^{II}-Pt^{IV}>Ni^{II}-Pt^{IV}>Pt^{II}-Pt^{IV}, suggesting that the electron-electron repulsion energy on M(II) ions plays an important role in mixed-valence states.

Various kinds of halogen-bridged one-dimensional M(II)-M(IV) mixed-valence complexes of Pt, Pd, and Ni have created a greater current interest in the field of low-dimensional chemistry and physics.[1-4] So far, we have prepared about one hundred compounds with a general formula of $[M^{II}(AA)_2][M^{IV}X_2(AA)_2]Y_4$ (M=Pt, Pd and Ni; X=Cl, Br and I; $(AA)_2$=(diamines)$_2$, linear-tetramines, and tetraaza-macrocycles; Y=ClO_4, BF_4 *etc.*).[5-9] Although these complexes exhibit a considerable variety of semiconducting properties, they can be well characterized by a common feature; the electrical,[10-12] optical,[13-15] and vibrational properties[16-18] are closely correlated with the degree of the oxidation states of the M(II) and M(IV) ions. This has been clearly demonstrated by the X-ray photoelectron spectra[19-22] and XANES.[23] From the results of the X-ray diffraction measurements,[24-31] the oxidation states of metal ions were found to be systematically dependent on the ratio between M(IV)-X and M(II)···X distances, which is influenced by the kinds of metals, bridging halogens, counter ions, and in-plane ligands.

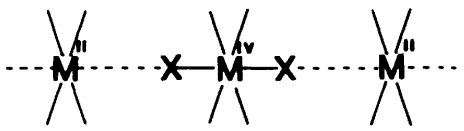

For example, as the bridging halogen ions change from Cl to I, the ratio between M(IV)-X and M(II)···X distances approaches unity.[31] At the same time, the oxidation states of the M(II) and M(IV) metal ions almost become tervalent states. These characteristic behaviors have been theoretically elucidated by energy-band calculations by Whangbo and Foshee[32] using the extended Hückel method and recently by Nasu[33-35] on the basis of an extended Peierls-Hubbard model. According to Nasu's model, the oxidation states of metal ions are determined by three physical parameters: the distortion energy due to the displacement of a halogen ion from the midpoint between adjacent metal ions, the transfer energy between metal ions, and the electron-electron (e-e) repulsion energy on metal ions. In a preceding paper,[36] it has been confirmed that the metal (M) and halogen ions (X) dependences on intervalence charge transfer transitions along the chains can be interpreted in terms of these parameters, including the e-e repulsion energy on the adjacent metal ions.

In order to obtain more detailed information regarding the mixed-valence states in one-dimensional complexes of this type, we have measured the X-ray photoelectron spectra and single-crystal electrical conductivities of the hetero-metal mixed-valence complexes, $[Pd(en)_2][PtX_2(en)_2](ClO_4)_4$(X=Cl, Br, and I) and $[Ni(en)_2][PtX_2(en)_2](ClO_4)_4$ (X=Cl and Br) (hereafter, they are abbreviated to Pd(II)-X-Pt(IV) and Ni(II)-X-Pt(IV)). The X-ray photoelectron spectra of their parent complexes, $[Pd(en)_2]Cl_2$, $Ni(en)_2Cl_2$[37] and $[PtCl_2(en)_2]Cl_2$ have also been measured as references. The metal alternation is expected to add two different types of energy to the one-dimensional M-X-M system. One is due to the alternating ionization energies and the other is due to the alternating electron-electron repulsive energies on metal sites.

Experimental

Materials. The M(II)-X-Pt(IV) complexes were synthesized by methods previously described.[5,8,38] Single crystals of the Pd(II)-X-Pt(IV) complexes were grown from dilute perchloric acid solutions, while those of the Ni(II)-X-Pt(IV) complexes were obtained from aqueous solutions containing $NaClO_4$.

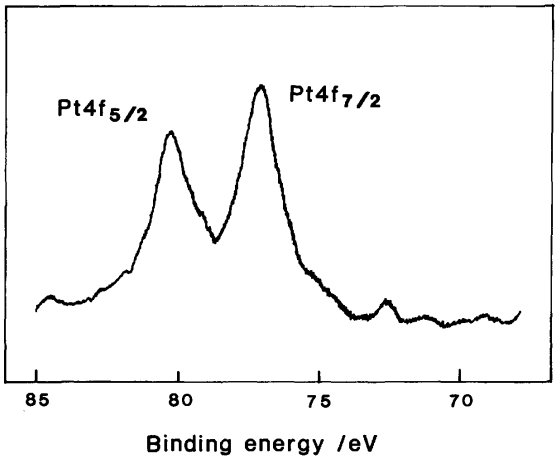

Fig. 1. X-Ray photoelectron spectra of Pt4f in [Pd(en)$_2$][PtCl$_2$(en)$_2$](ClO$_4$)$_4$.

X-Ray Photoelectron Spectra. The X-ray photoelectron spectra were obtained on a SHIMADZU ESCA 750 using Mg$K\alpha$ exciting radiation at room temperature, the source vacuum being $\approx 10^{-7}$ Torr.† The spectra were calibrated by the emission from the Cls line (285.0 eV). The absolute energy of emitted electrons, however, may not be so meaningful in the present study because it is not free from possible systematic errors due to charging-up. Thus, in this paper, we will refer only to a relative energy with respect to the reference signals for the parent complexes.

Electrical Conductivities. Single-crystal d.c. conductivities along the needle axis were measured in a temperature range below 100°C by the two-probe method. Silver paste was used as the electrode material.

Results and Discussion

As a probe for an examination of the oxidation states of metal ions in metal-alternated mixed-valence complexes, we measured the binding energies of Pt(IV)4f, Pd(II)3d, and Ni(II)2p levels in the Pd(II)-X-Pt(IV), Ni(II)-X-Pt(IV) and their parent complexes. In Fig. 1, the X-ray photoelectron spectrum of Pt(IV)4f levels in the Pd(II)-Cl-Pt(IV) complex is shown as an example. The peak energies of the doublet correspond to the binding energies of the 4f$_{7/2}$ and 4f$_{5/2}$ levels of Pt(IV). All the Pt(IV)4f spectra observed in the metal-alternated mixed-valence complexes, including the reference complexes, are quite similar, but the magnitudes of their binding energies show a characteristic dependence on the kind of the constituent metal and halogen ions. The observed binding energies of the Pt(IV)4f$_{7/2}$ and Pd(II)3d$_{5/2}$ levels for the Pd(II)-X-Pt(IV) complexes and for the Pt(IV)4f$_{7/2}$ and Ni(II)2P$_{3/2}$ levels of the Ni(II)-X-Pt(IV) complexes are listed in Table 1, along with those for reference states of the parent complexes.

In this table, it is immediately noticed that the binding energy of the Pt(IV)4f$_{7/2}$ level shifts to a lower

† 1 Torr≈133.322 Pa.

Table 1. Binding energies /eV

(i) Pd(II)-Pt(IV)	Pd3d$_{5/2}$	Pt4f$_{7/2}$
[Pd^{II}(en)$_2$]Cl$_2$	338.6	—
[Pt^{IV}Cl$_2$(en)$_2$]Cl$_2$	—	75.8
[Pd(en)$_2$][PtCl$_2$(en)$_2$](ClO$_4$)$_4$	338.6	75.8
[Pd(en)$_2$][PtBr$_2$(en)$_2$](ClO$_4$)$_4$	338.7	75.6
[Pd(en)$_2$][PtI$_2$(en)$_2$](ClO$_4$)$_4$	338.9	75.4
(ii) Ni(II)-Pt(IV)	Ni2p$_{3/2}$	Pt4f$_{7/2}$
Ni^{II}(en)$_2$Cl$_2$	855.6	—
[Ni(en)$_2$][PtCl$_2$(en)$_2$](ClO$_4$)$_4$	856.1	75.8
[Ni(en)$_2$][PtBr$_2$(en)$_2$](ClO$_4$)$_4$	856.4	75.6

energy while those of the Pd(II)3d$_{5/2}$ and Ni(II)2p$_{3/2}$ levels shift to higher energies by changing halogen ions in order of X=Cl, Br, and I. Such a trend is the same as that previously observed for homo-metal M(II)-M(IV) mixed-valence complexes.[19-22] This can be interpreted in terms of the difference of magnitudes of the charge-transfer dependence on the ionic radius of the bridging halogens.[36] The energy shifts of the Pt(IV)4f$_{7/2}$ level in the metal-alternated Pd(II)-X-Pt(IV) complexes from the reference energy of [Pt^{IV}Cl$_2$(en)$_2$]Cl$_2$ yield 0.0, −0.2, and −0.4 eV for X=Cl, Br, and I, respectively. These values are remarkably smaller than −0.3, −0.7, and −1.0 eV for the Pt(IV)4f$_{7/2}$ level in the homo-metal Pt(II)-X-Pt(IV) complexes.[19] Such a suppression of the reductive trend of the Pt(IV)4f binding energy due to the alternated substitution of Pd ions indicates that the alternated core-potentials in the Pd-X-Pt chain structure give a fairly large effect on the mixed-valence states constituted by the metal d electron. Since there is a considerable energy difference between the Pd-4d and Pt-5d levels, the 4d-5d

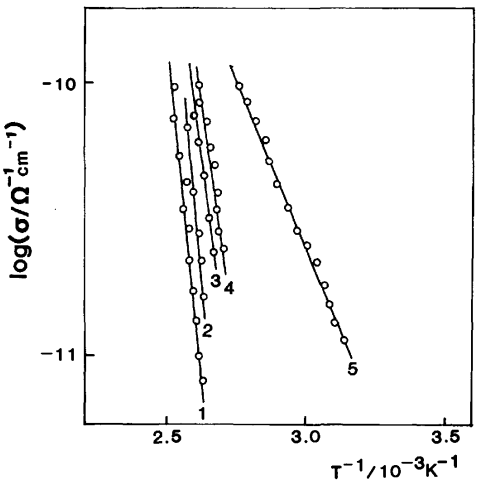

Fig. 2. Electrical conductivities of [M(en)$_2$][PtX$_2$(en)$_2$](ClO$_4$)$_4$.
1) [Pd(en)$_2$][PtCl$_2$(en)$_2$](ClO$_4$)$_4$, 2) [Ni(en)$_2$][PtCl$_2$(en)$_2$](ClO$_4$)$_4$, 3) [Pd(en)$_2$][PtBr$_2$(en)$_2$](ClO$_4$)$_4$, 4) [Ni(en)$_2$][PtBr$_2$(en)$_2$](ClO$_4$)$_4$, 5) [Pd(en)$_2$][PtI$_2$(en)$_2$](ClO$_4$)$_4$.

TABLE 2. ELECTRICAL CONDUCTIVITIES (σ) AND ACTIVATION ENERGIES (ΔE) OF $[M^{II}(en)_2][M^{IV}X_2(en)_2](ClO_4)_4$

	X	Ni(II)-Ni(IV)[a]	Pd(II)-Pd(IV)[b]	Pt(II)-Pt(IV)[b]	Ni(II)-Pt(IV)	Pd(II)-Pt(IV)
σ[c]	Cl	1.3×10^{-8}	2.0×10^{-12}	2.0×10^{-15}	3.2×10^{-17}*	4.0×10^{-18}*
ΔE[d]		0.5	0.8	1.4	1.8	2.1
σ[c]	Br	—	1.2×10^{-8}	3.0×10^{-11}	8.4×10^{-14}*	1.4×10^{-15}*
ΔE[d]		—	0.5	0.8	1.3	1.3
σ[c]	I	—	—	1.8×10^{-8}	—	4.5×10^{-11}
ΔE[d]		—	—	0.4	—	0.6

a) Ref. 6, b) Ref. 12, c) $\Omega^{-1}cm^{-1}$, d) eV The * mark denotes the values of the room-temperature electrical conductivities obtained by an extrapolation.

charge transfer in the Pd(II)-X-Pt(IV) complexes is thought to be considerably smaller compared with the resonance 5d-5d charge transfer in the Pt(II)-X-Pt(IV) complexes. The decrease in the charge transfer, therefore, provides for the smaller energy shift of the Pt(IV)$4f_{7/2}$ level, indicating that the oxidation state of the Pt(IV) species remains close to the quadrivalent state. A similar interpretation can hold for the change in the Pt(IV)$4f_{7/2}$ binding energy in the Ni(II)-X-Pt(IV) complexes. Thus, it may be concluded that the metal alternation in the mixed-valence complexes leads to a suppression of the mixing of d_{z^2} orbitals between adjacent metal ions.

The metal alternation effect is expected to cause a change in the semiconducting properties of the mixed-valence complexes. The experimental results of the electrical conductivities of M(II)-X-Pt(IV) complexes along the chain are presented as a function of temperature in Fig. 2. Their behaviors suggest a hopping-type of electron-conduction with a thermal-activation energy ΔE. Upon assuming this conduction mechanism, estimated activation energies can be determined as summarized in Table 2, together with conductivities at room temperature. For complexes indicated by an * mark, we used room-temperature conductivities obtained by extrapolation. In this table, for comparison, we also list data concerning the homo-metal M(II)-M(IV) mixed-valence complexes of Pt, Pd, and Ni.

It is found that the activation energies decrease in the order of Cl>Br>I for X in both Pd(II)-X-Pt(IV) and Ni(II)-X-Pt(IV) complexes. This tendency is also coincident with those observed in homo-metal mixed-valence complexes. Such a ΔE behavior can be qualitatively interpreted in terms of a small polaron model,[39] whose activation energy is closely correlated with the degree of the charge transfer between M(II) and M(IV) ions; the smaller the charge transfer, the larger the binding energy of the polaron. This may be the reason why the activation energies are in the order of Cl>Br>I.

It is interesting to note that the activation energies in changing metal ions increase in the order of Pd(II)-Pt(IV)>Ni(II)-Pt(IV)>Pt(II)-Pt(IV) for the same bridging halogen ions. The relation, M(II)-X-Pt(IV)>Pt(II)-X-Pt(IV) (M=Pd and Ni), that is, the activation energies of the metal-alternated complexes are larger than those of the regular Pt(II)-Pt(IV) mixed-valence complexes, may be naturally understood assuming a smaller charge-transfer energy in the metal-alternated complexes, as described before regarding the M-dependence of the Pt(IV)$4f_{7/2}$ binding energy. However, the order of Pd(II)-X-Pt(IV)> Ni(II)-X-Pt(IV) is rather peculiar because the ionization energy of a Ni ion is much larger than that of a Pd ion and, thereby, it gives a smaller charge transfer, suggesting an opposite relation regarding the activation energy to the experimental results. In order to interpret such a characteristic nature of the metal-alternated complexes, we have to take into account another contribution arising from metal alternation. In the M(II) species of M(II)-X-M(IV) complexes, electron-electron (e-e) repulsion energy is much larger for M= Ni(II) than for M=Pd(II). This surpassed the effect brought about by a change in the ionization energy, resulting in the observed relation concerning ΔE, Pd-(II)-X-Pt(IV)>Ni(II)-X-Pt(IV). Such an important role of the e-e repulsive energy in mixed-valence complexes has been emphasized in a previous paper.[36] For a more concrete discussion, we need information regarding the crystal structures of alternated-metal complexes, which is now under investigation. The optical results will be reported elsewhere.

This work was supported by the Joint Studies Program (1983—1984) of the Institute for Molecular Science.

References

1) J. S. Miller and A. J. Epstein, *Prog. Inorg. Chem.*, **20**, 1 (1976).
2) I. F. Shchegolev, *Phys. Status Solidi A*, **12**, 9 (1972).
3) R. J. H. Clark, "Mixed-Valence Compounds," ed by D. B. Brown, Reidel, Dordrecht (1982), p. 271.
4) H. J. Keller, Extended Linear Chain Compound, J. S. Miller, Plenum Press, New York (1982), Vol. 1.
5) N. Matsumoto, M. Yamashita, and S. Kida, *Bull. Chem. Soc. Jpn.*, **51**, 2334 (1978).
6) M. Yamashita, Y. Nonaka, S. Kida, Y. Hamaue, and R. Aoki, *Inorg. Chim. Acta*, **52**, 43 (1981).
7) M. Yamashita, H. Ito, K. Toriumi, and T. Ito, *Inorg. Chem.*, **22**, 1566 (1983).
8) M. Yamashita, I. Murase, T. Ito, T. Mitani, and I. Ikemoto, 49th National Meeting of the Chemical Society of Japan, Tokyo, April 1984, Abstr. No. 1035.

9) M. Yamashita and I. Murase, *Inorg. Chim. Acta*, **97**, L43 (1985).
10) T. W. Thomas and A. E. Underhill, *J. Chem. Soc. A*, **1971**, 512.
11) L. V. Interrante and K. W. Browall, *Inorg. Chem.*, **13**, 162 (1974).
12) Y. Hamaue, R. Aoki, M. Yamashita, and S. Kida, *Inorg. Chim. Acta*, **54**, L13 (1981).
13) H. Tanino and K. Kobayashi, *J. Phys. Soc. Jpn.*, **52**, 1446 (1983).
14) G. C. Papavassiliou and A. D. Zdetsis, *J. Chem, Soc., Faraday Trans. 2*, **76**, 106 (1980).
15) H. Tanino, N. Koshizuka, K. Kobayashi, M. Yamashita, and K. Hoh, *J. Phys. Soc. Jpn.*, **54**, 483 (1985).
16) R. J. H. Clark and M. L. Franks, *J. Chem. Soc., Dalton*, **1977**, 198.
17) R. J. H. Clark, M. L. Franks, and W. R. Trumble, *Chem. Phys. Lett.*, **41**, 287 (1976).
18) N. Ohta, M. Kozuka, K. Nakamoto, M. Yamashita, and S. Kida, *Chem, Lett.*, **1978**, 843.
19) M. Yamashita, N. Matsumoto, and S. Kida, *Inorg. Chim. Acta*, **31**, L381 (1978).
20) M. Yamashita, H. Ito, K. Toriumi, and T. Ito, 32th Meeting on Coordination Compounds, Nagasaki, October 1982, Abstr. No. 2B10.
21) M. Yamashita and T. Ito, *Inorg. Chim. Acta*, **87**, L5 (1984).
22) M. Yamashita, I. Murase, and I. Ikemoto, *Bull. Chem. Soc. Jpn.*, in press.
23) H. Tanino, H. Oyanagi, M. Yamashita, and K. Kobayashi, *Solid State Commun.*, **53**, 953 (1985).
24) B. M. Craven and D. Hall, *Acta Crystallogr.*, **14**, 475 (1961).
25) N. Matsumoto, M. Yamashita, and S. Kida, *Bull. Chem. Soc. Jpn.*, **51**, 3514 (1978).
26) N. Matsumoto, M. Yamashita, S. Kida, and I. Ueda, *Acta Crystallogr., Sect. B*, **35**, 1458 (1978).
27) H. Endres, H. J. Keller, R. Martin, H. N. Gung, and U. Treagar, *Acta Crystallogr., Sect. B*, **35**, 1885 (1979).
28) P. E. Franwick and J. L. Huckaby, *Inorg. Chem.*, **21**, 3067 (1982).
29) M. Tanaka, I. Tsujikawa, K. Toriumi, and T. Ito, *Acta Crystallogr., Sect. B*, **38**, 2793 (1982).
30) M. Yamashita, K. Toriumi, and T. Ito, *Acta Crystallogr., Sect. C*, in press.
31) N. Matsumoto, M. Yamashita, I. Ueda, and S. Kida, *Mem. Fac. Sci., Kyushu Univ. Ser. C*, **11**, 209 (1978).
32) M. -H. Whangbo and M. J. Foshee, *Inorg. Chem.*, **20**, 113 (1981).
33) K. Nasu, *J. Phys. Soc. Jpn.*, **52**, 3865 (1983).
34) K. Nasu, *J. Phys. Soc. Jpn.*, **53**, 302 (1984).
35) K. Nasu, *J. Phys. Soc. Jpn.*, **53**, 427 (1984).
36) Y. Wada, T. Mitani, M. Yamashita, and T. Koda, *J. Phys. Soc. Jpn.*, in press.
37) $Ni(en)_2Cl_2$ is formulated as $[Ni_2Cl_2(en)_4]Cl_2$, which consists of chloro-bridged cation dimers of *cis*-$[NiCl(en)_2]^+$ and uncoordinated Cl^- anions (*Inorg. Chem.*, **18**, 804 (1979)).
38) G. C. Papavassiliou and D. Layek, *Z. Naturforsch.*, **37b**, 1406 (1982).
39) G. Whitfied and P. B. Shaw, *Phys Rev., B*, **14**, 3346 (1976).

Photoregulated Ion-binding to Azobenzene-linked Ethylenediamines and Iminodiacetic Acids[1)]

Seiji SHINKAI,* Shinichiro NAKAMURA, Mikio NAKASHIMA, Osamu MANABE,* and Masakazu IWAMOTO

Department of Industrial Chemistry, Faculty of Engineering, Nagasaki University, Nagasaki 852

(Received November 21, 1984)

New photoresponsive complexones bearing two iminodiacetic acid units or ethylenediamine units at the two sides of an azobenzene through CH_2 or $(CH_2)_2$ (AzoIDA(n=1,2) and AzoED(n=1,2), respectively) have been synthesized. The CH_2 and $(CH_2)_2$ spacers were selected in order to examine the influence of the spacer length on the intramolecular cooperativity for the two ligands in the cis-isomers to coordinate to one metal ion. The thermal cis-to-trans isomerization of AzoIDA was efficiently suppressed by Zn(II) and Cu(II) while that of AzoED was suppressed only by Cu(II). The rate suppression supports the formation of the intramolecular chelate complexes with the metal ion. The measurements of ESR spectra of the cis-isomer·Cu(II) complexes indicated that the square-planar structure of the complexes is somewhat distorted and probably close to a lozenge. The stability constants (K_s) were determined by a displacement method. The K_s values for the cis-isomers were generally greater than those for the trans-isomers, and the K_s for n=2 series increased more clearly. In particular, the K_s for *cis*-AzoED(n=2)+Cu(II) was improved by 43.8 fold. The photoresponsive change in the stability constants suggests a possible application of the present system as light-driven ion pumps for heavy metal ions.

Azobenzene derivatives which exhibit photoinduced reversible cis-trans isomerism have frequently been employed as a photoantenna to control physical and chemical functions of membranes,[2-5)] microemulsions,[6)] synthetic polymers,[7-9)] polypeptide chains,[10,11)] cyclodextrins,[12,13)] and crown ethers.[14-18)] The ideas are all associated with the photoresponsive, large geometrical change between *trans*- and *cis*-azobenzene. These systems are interesting not only as candidates for the storage of light energy but also as models of natural photoresponsive systems mediating the conversion of light into other forms of energy.

The purpose of our investigation has been to control the functions of a crown ether family by light, which would lead to photoresponsive ion extraction and light-driven ion-transport across membranes.[18)] We and others have synthesized several photoresponsive crown ethers, but the research effort has mainly been devoted toward photoresponsive binding of alkali and alkaline earth metal ions.[14-20)] In contrast, very few precedents exist for photoresponsive binding of heavy metal ions. Irie *et al.*[21)] synthesized a thioindigo derivative with ethylene glycol chains which exhibits photoresponsive affinity with Ag(I), Hg(II), Cu(II), *etc.* We synthesized azobenzene-capped and azopyridine-capped thiacrown ethers which exhibit affinity with Cu(II) and Hg(II).[22)] Blank *et al.*[23)] extended this concept to a complexone, 4,4′-bis[bis(carboxymethyl)-aminomethyl]azobenzene(AzoIDA(n=1)). It is known that the stability constants (K_s) of complexones are efficiently increased through cooperative binding of plural ligand groups.[24-26)] Thus, the *cis*-isomer of AzoIDA(n=1) (*i.e.*, *cis*-AzoIDA(n=1)) which can form an intramolecular complex with a single metal ion gives the K_s greater than the trans-isomer of AzoIDA-(n=1) (*i.e.*, *trans*-AzoIDA(n=1)). Blank *et al.*[23)] established on the basis of a polarographic method that *cis*-AzoIDA(n=1) forms a 1:1 metal/AzoIDA complex with Zn(II). On the other hand, we recently studied the photoresponsive behavior of a copper complex of 4,4′-bis(1-oxa-4,10-dithia-7-azacyclododec-7-ylmethyl)azobenzene (**1**).[27)] The most noteworthy result in this paper is that the Cu(I) complex is capable of binding O_2 in a partially reversible manner only when **1** is photoisomerized to the *cis*-form. Therein, we found that both *trans*- and *cis*-**1** bind two copper ions to form the 1:1 copper/crown complex. The finding suggests that the two crown ether rings act quite independently and that most probably, two nitrilo nitrogens of *cis*-AzoIDA(n=1) are too far to bind intramolecularly to one metal ion.

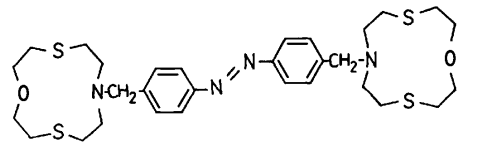

1

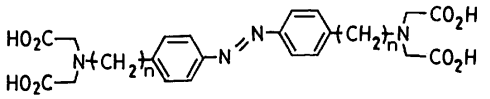

trans-AzoIDA(n=1,2)

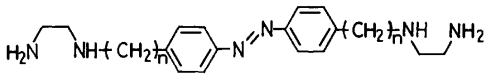

trans-AzoED(n=1,2)

It occurred to us that if appropriate spacers are inserted between azobenzene and iminodiacetic acid, two nitrilo nitrogens may be able to coordinate intramolecularly to one metal ion. Examination of Corey-Pauling-Koltun (CPK) molecular models of AzoIDA-(n=1,2) suggests that (i) four carboxy groups in *cis*-AzoIDA(n=1) favorably occupy the tetrahedral coordination sites and it is fairly difficult for two nitrilo

nitrogens to coordinate to one metal ion and (ii) four carboxy groups in *cis*-AzoIDA(n=2) possibly be placed in either (tetrahedral and planar) coordination structure and two nitrilo nitrogens can interact with one metal ion. We thus synthesized AzoIDA(n=1,2) and AzoED(n=1,2) and examined whether or not metal affinities of these azobenzene-linked ligands change in response to photoinduced trans-cis isomerization. We employed Zn(II) and Cu(II) as metal ions, because Zn(II) is classified as a relatively "hard" metal ion and adopts the tetrahedral coordination, whereas Cu(II) is a "soft" metal ion and favors the square-planar coordination.

Experimental

Materials. *trans*-AzoIDA(n=1) and *trans*-AzoIDA(n=2) were synthesized by the reaction of iminodiacetic acid with 4,4′-bis(chloromethyl)azobenzene and 4,4′-bis(2-chloroethyl)azobenzene, respectively.

trans-*4,4′-Bis[bis(carboxymethyl)aminomethyl]azobenzene-(*trans-*AzoIDA*(n=*1*)).* 4,4′-Bis(chloromethyl)azobenzene (0.28 g; 1.0 mmol) in 40 ml of methanol and iminodiacetic acid (0.54 g; 4.1 mmol) in 50 ml of water containing K_2CO_3 (0.80 g; 5.79 mmol) were mixed and refluxed for 21 h. The progress of the reaction was followed by TLC. Methanol was removed from the reaction mixture by evaporation under reduced pressure. The residual solution was turbid (probably owing to monosubstituted compound). It was filtered after treatment with active charcoal, and orange crystals precipitated from the filtrate on the addition of NaCl were recovered by filtration. The crystals were dissolved in water and reprecipitated by adding concd HCl; mp 225.5—226.5 °C (lit,[23] 208—209 °C), yield 38%. Found: C, 55.03; H, 5.06; N, 11.67%. Calcd for $C_{22}H_{24}N_4O_8$: C, 55.93; H, 5.12; N, 11.86%. IR (KBr): ν_{OH} 3000 cm^{-1}, $\nu_{C=O}$ 1725 cm^{-1}, $\nu_{N=N}$ 1635 cm^{-1}. NMR (Me_2SO-d_6): NCH_2CO, δ=3.50, 8H; $ArCH_2N$, 3.99, 4H; aromatic protons, 7.63 and 7.91, 4H each.

trans-*4,4′-Bis[2-[bis(carboxymethyl)amino]ethyl]azobenzene-(*trans-*AzoIDA*(n=*2*)).* First, *trans*-4,4′-bis(2-hydroxyethyl)azobenezene was prepared from 1-(2-hydroxyethyl)-4-nitrobenzene. 1-(2-Hydroxyethyl)-4-nitrobenzene (5.0 g; 29.9 mmol) in 30 ml of ethanol and NaOH (1.3 g; 32.5 mmol) in 6 ml of water were mixed in a 100 ml flask, and zinc powder (16.1 g; 0.246 mol) was added to the stirred solution. The reaction mixture was refluxed for 1 h. The hot solution was filtered and the solid was washed with ethanol. To the combined solution air was introduced for 2 h. After filtration, ethanol in the filtrate was removed under reduced pressure, and the residual solution was diluted with water. The precipitate was recovered by filtration and recrystallized from ethanol; mp 140.5—142.5 °C, yield 75%. Found: C, 70.84; H, 6.80; N, 10.34%. Calcd for $C_{16}H_{18}N_2O_2$: C, 71.09; H, 6.71; N, 10.36%. IR(KBr): ν_{OH} 3240—3340 cm^{-1}, $\nu_{N=N}$ 1580 cm^{-1}. NMR (Me_2SO-d_6): Ar-CH_2, δ=2.82, 4H; CH_2O, 3.68, 4H; OH, 4.69, 2H; aromatic protons, 7.41 and 7.79, 4H each.

trans-4,4′-Bis(2-hydroxyethyl)azobenzene was converted to *trans*-4,4′-bis(2-chloroethyl)azobenzene by treatment with thionyl chloride. *trans*-4,4′-Bis(2-hydroxyethyl)azobenzene (3.0 g; 11.1 mmol) was heated in 30 ml of thionyl chloride for 4 h in the presence of one drop of *N,N*-dimethylformamide. The progress of the reaction was followed by TLC. The hot solution was filtered using a glass filter and evaporated to dryness *in vacuo*. The residual crystals were recrystallized from benzene; mp 120—121 °C, yield 91%. Found: C, 62.22; H, 5.23; N, 9.03%. Calcd for $C_{16}H_{16}N_2Cl_2$: C, 62.55; H, 5.25; N, 9.12%.

trans-AzoIDA(n=2) was synthesized in a manner similar to *trans*-AzoIDA(n=1); mp 215 °C (dec), yield 35%. Found: C, 57.76; H, 5.75; N, 10.98%. Calcd for $C_{24}H_{28}N_4O_8$: C, 57.59; H, 5.64; N, 11.19%. IR(KBr): ν_{OH} 2960—3020 cm^{-1}, $\nu_{C=O}$ 1725 cm^{-1}, $\nu_{N=N}$ 1630 cm^{-1}. NMR(Me_2SO-d_6): $ArCH_2$ and NCH_2, δ=2.92 and 2.94, 4H each; NCH_2CO, 3.55, 8H; aromatic protons, 7.49 and 7.86, 4H each.

trans-*4,4′-Bis[(2-aminoethyl)aminomethyl]azobenzene(*trans-*AzoED* (n=*1*)).* 4,4′-Bis(chloromethyl)azobenzene (1.00 g; 3.58 mmol) in 100 ml of acetonitrile was added slowly (for 75 min) into stirred acetonitrile solution (200 ml) of ethylenediamine (4.31 g; 7.17 mmol) containing finely powdered K_2CO_3 (9.90 g; 71.6 mmol). The mixture was refluxed for 2 h and the completion of the reaction was confirmed by TLC. The hot solution was filtered to remove KCl and K_2CO_3, the filtrate being evaporated to dryness. The residue was crystallized by benzene-diisopropyl ether. The crystals were dissolved in hot water, the insoluble material removed by filtration, and the filtrate was acidified by concd HCl. On cooling, *trans*-AzoED(n=1) was recovered as its tetrahydrochloride salt; mp>300 °C, yield 35%. Found: C, 45.21; H, 6.36; N, 17.93%. Calcd for $C_{18}H_{30}N_6Cl_4$: C, 45.78; H, 6.40; N, 17.79%. IR(KBr): ν_{NH} 2890—3030 and 2735—2770 cm^{-1}, $\nu_{N=N}$ 1585 cm^{-1}.

trans-*4,4′-Bis[2-[(2-aminoethyl)amino]ethyl]azobenzene(*trans-*AzoED*(n=*2*)).* This compound was synthesized from *trans*-4,4′-bis(2-chloroethyl)azobenzene and ethylenediamine in a manner similar to *trans*-AzoED(n=1) and isolated at its tetrahydrochloride; mp 279—281 °C, yield 63%. Found: C, 46.89; H, 6.88; N, 16.40%. Calcd for $C_{20}H_{34}N_6Cl_4 \cdot 0.66H_2O$: C, 46.89; H, 6.95; N, 16.40%. IR(KBr): ν_{NH} 2735—2770 and 2890—3030 cm^{-1}, $\nu_{N=N}$ 1560 cm^{-1}.

Measurements of ESR Spectra. The ligand (1.00×10^{-3}M[†]) in the buffer solution (pH 9.02) was irradiated by UV light and then mixed with an equal amount of the buffer solution containing $CuSO_4$(1.00×10^{-3} M). ESR spectra were measured at −50 °C with JEOL-JES-FE-1X and simulated by using a computer program made by Dr. M. Iwamoto. The ligand after photoirradiation was a mixture of trans- and cis-isomer (see Table 1). We first made a simulation of the ESR spectra of trans-isomer·Cu(II) complexes and reduced these spectra from the observed ESR spectra. The remaining spectra thus obtained were regarded to be those of "pure" cis-isomer·Cu(II) complexes and analyzed by computer simulation.

Photoisomerization and Kinetic Measurements. A 100-W high-pressure Hg-lamp with a color glass filter ($330<\lambda<380$ nm) was used for the trans-to-cis photoisomerization. The thermal cis-to-trans isomerization was followed spectrophotometrically at 30 °C by monitoring the appearance of the absorption maximum of trans-isomers. The details of the method have been described.[16,17] The thermal isomerization of *cis*-AzoIDA(n=1) in the presence of metal ions was very slow. At [Zn(II)]/[AzoIDA(n=1)]=1.0, for example, the $(A_\infty-A_0)/(A_\infty-A_t)$ after 48 h was only 1.014. We

[†] 1 M=1 mol dm^{-3}.

thus calculated the first-order rate constant (k) for this system from about 2% change in the optical density. Other systems gave much greater spectral changes, so that the k values could be determined by a usual first-order rate equation.

Estimation of Stability Constants. A displacement method was employed to estimate the stability constants of AzoIDA(n=1,2) and AzoED(n=1,2).[28] Eriochrome Black T (EBT) and 1-(2-pyridylazo)-2-naphthol (PAN) were used as indicators for Zn(II)- and Cu(II)-complexes, respectively: log K_{EBT}=10.4 for Zn(II) and log K_{PAN}=12.6 for Cu(II).[29,30] The employed wavelengths were 650 nm for EBT-Zn(II) and 550 nm for PAN-Cu(II). For an equilibrium in Eq. 1, one can derive Eq. 2 where K_e is the displacement equilibrium constant and K_I and K_s are the stability constants of I (indicator) and L (ligand), respectively.[28]

$$\text{I}\cdot\text{M(II)} + \text{L} \overset{K_e}{\rightleftharpoons} \text{I} + \text{L}\cdot\text{M(II)} \quad (1)$$

$$K_s = K_e \cdot K_I \quad (2)$$

As the indicators have the stability constants greater than 10^{10} M^{-1}, one can consider that the indicator and the metal ion (added in a 1:1 mole ratio) totally exist as the complex form. Thus, the degree of the spectral change induced by ligand addition is readily ascribed to the production of the free indicator. From this spectral change one can estimate the K_e for trans-isomers.[28] In the present system, however, one should pay attention to the possibility that AzoIDA and AzoED may form L·M(II)$_2$ in addition to L·M(II). In order to obviate this problem we employed excess L over M(II) (see Tables 4 and 5).

The analysis of the spectral change induced by the addition of the cis/trans mixture is more complex. The magnitude of the spectral change (ΔOD_{photo}) can be regarded as the sum of ΔOD_{trans} and ΔOD_{cis}. That is,

$$\Delta OD_{photo} = \frac{\text{trans}\%}{100}\cdot\Delta OD_{trans} + \frac{\text{cis}\%}{100}\cdot\Delta OD_{cis} \quad (3)$$

Since trans%, cis%, and ΔOD_{trans} are known, one can estimate ΔOD_{cis} which corresponds to hypothetical ΔOD induced by the "pure" cis-isomer. By using ΔOD_{cis} thus estimated, we calculated K_e and K_s for cis-isomers.

In a separate study, we determined the K_s for iminodiacetic acid and ethylenediamine by a titration method and a displacement method.[28,31] The K_s values determined by two different methods agreed with the satisfactory accuracy (see Tables 4 and 5). The K_s values determined by the displacement method are therefore reliable.

Results and Discussion

Effects of Metal Ions on Photo and Thermal Isomerization. The spectroscopic properties of AzoIDA and AzoED are summarized in Table 1. These compounds gave two absorption bands at around 330 nm and 427 nm, which are attributed to π-π* and n-π* transition, respectively. The photoisomerization was carried out using a 100-W high-pressure Hg-lamp equipped with a colored glass filter (330<λ<380 nm). In aqueous solution buffered to pH 9.02, the isomerization reached a photostationary state after 5 min.

Table 1. Spectroscopic properties and photoisomerization of AzoIDA and AzoED[a]

Ligand	λ_{max}/nm		ε_{max} of π-π*	*cis/trans*
	π-π*	n-π*	/cm^{-1}M^{-1}	
trans-AzoIDA(n=1)	329	428	25200	61/39
trans-AzoIDA(n=2)	332	426	24000	63/37
trans-AzoED(n=1)	333	427	19400	66/34
trans-AzoED(n=2)	333	426	19300	67/33

a) pH 9.02 with 0.01 M NH_3 buffer, μ=0.10 with KCl.

The cis/trans ratios are collected in Table 1. The cis concentration at the photostationary was not affected in the presence of an equimolar amount of $ZnSO_4$. In the dark in the absence of metal ions, the cis-isomers isomerized, although very slowly, to the corresponding trans-isomers and the initial spectra of the trans-isomers were regenerated. The appearance of the absorption maximum of the trans-isomers satisfied a first-order rate equation for up to three-half lives. The first-order rate constants (k) were obtained by analyzing the time-dependence.

We previously investigated the metal effect on the photoresponsive behaviors of azobis(benzocrown ether)s.[17,32] It has been found that in the presence of metal ions which can form intramolecular 1:2 metal/crown sandwich-type complexes with cis-isomers, the rate of the thermal cis-to-trans isomerization is suppressed. This novel phenomenon is attributed to the "lock-in" effect of metal ions flanked by two crown rings. That is, an additional free energy of activation is required for the cis-to-trans isomerization process, which reflects the need to disrupt favorable interactions between the metal ion and the crown ethers. In contrast, such an inhibitory effect was not seen for an analogous photoresponsive crown ether in which crown ether groups are linked to the two sides of an azobenzene *via* methylene spacers (*i.e.*, CrCH_2-*p*-C_6H_4-N=NC_6H_4-*p*-CH_2Cr where Cr denotes monoaza-15-crown-5).[33] Probably, free-rotating methylene spacers act as an absorber of the geometrical change occurring at the N=N bond. One may conclude, therefore, that the "lock-in" effect is operative only in fairly rigid molecules.

In AzoIDA and AzoED, ligand groups are linked to an azobenzene *via* methylene or ethylene spacers. Nevertheless, we observed that the rates of thermal cis-to-trans isomerization are efficiently inhibited by Zn(II) and Cu(II). The inhibitory effect of Zn(II) is illustrated in Fig. 1. The rates for AzoIDA were strongly inhibited by Zn(II) and the plots provided a minimum at [Zn(II)]/[AzoIDA]=1.0. This may be taken as evidence that both *cis*-AzoIDA(n=1) and *cis*-AzoIDA(n=2) form intramolecular 1:1 metal/ligand complexes: that is, two intramolecular iminodiacetate moieties coordinate to one Zn(II) ion. This finding is in agreement with the conclusion obtained from a polarographic study.[23] The slight rate increase at

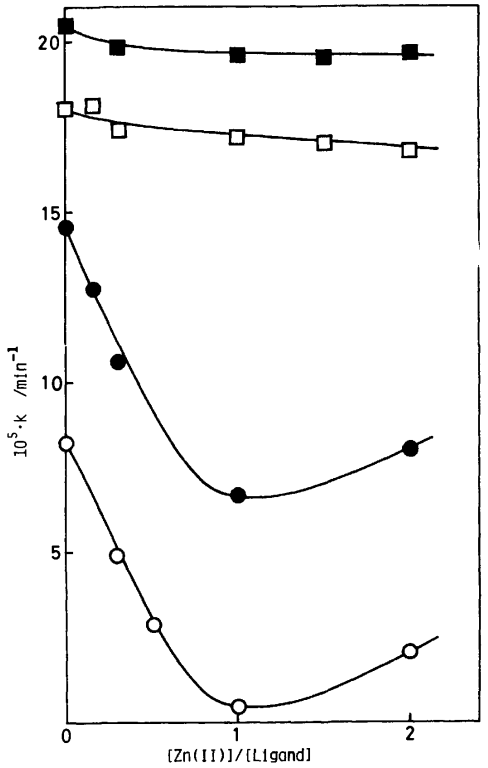

Fig. 1. Influence of added $ZnSO_4$ on the first-order rate constants for the thermal cis-to-trans isomerization. 30 °C, pH 9.02 with 0.01 M NH_3 buffer, μ= 0.10 with KCl, [ligand]=1.67×10^{-5} M.
○: AzoIDA(n=1), ●: AzoIDA(n=2), □: AzoED(n= 1), ■: AzoED(n=2).

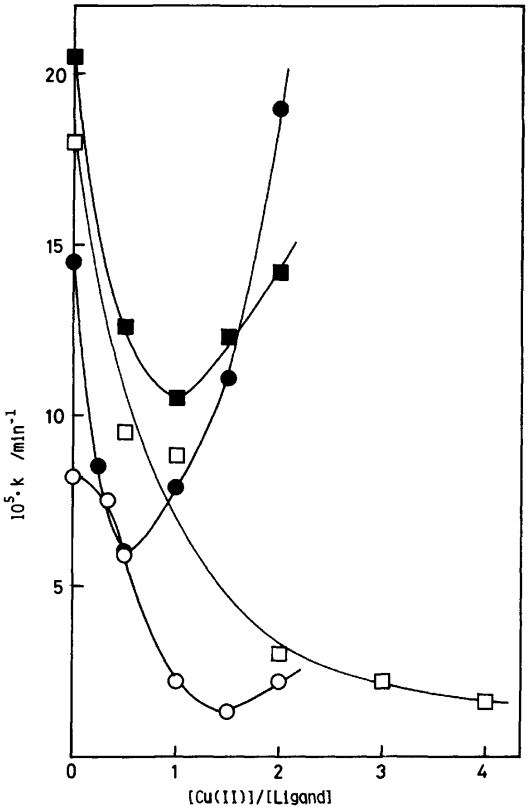

Fig. 2. Influence of added $CuSO_4$ on the first-order rate constants for the thermal cis-to-trans isomerization. The reaction conditions and symbols are identical to those in Fig. 1.

TABLE 2. PSEUDO-FIRST-ORDER RATE CONSTANTS(k) FOR THE THERMAL CIS-TO-TRANS ISOMERIZATION[a]

Ligand	$10^5 \cdot k$/min^{-1}		
	No metal	Zn(II)[b]	Cu(II)[b]
AzoIDA(n=1)	8.2	0.5	2.2
AzoIDA(n=2)	14.5	6.7	7.9
AzoED(n=1)	18.0	17.2	8.8
AzoED(n=2)	20.5	19.6	10.5

a) 30 °C, pH 9.02 with 0.01 M NH_3 buffer, μ=0.1 with KCl, [ligand]=1.67×10^{-5} M. b) [Zn(II) or Cu(II)] /[ligand]=1.00.

[Zn(II)]/[AzoIDA]>1 may be attributed either to the catalytic effect of Zn(II) on the thermal isomerization through the Zn(II)-azo interaction[27,35] or to the electrostatic repulsion between two Zn(II) ions[32] if *cis*-AzoIDA·$Zn(II)_2$ is formed at [Zn(II)]>[AzoIDA]. In contrast, the rates of AzoED were scarcely affected by Zn(II). The marked difference between AzoIDA and AzoED is probably rationalized in terms of low affinity of "soft" ethylenediamines with "hard" Zn(II) ion. In fact, AzoED gave the K_s much smaller than AzoIDA (*vide post*).

The k values at [Zn(II)]/[ligand]=1.0 are summarized in Table 2. The k observed for *cis*-AzoIDA(n=1)+ Zn(II)(5×10^{-6} min^{-1}) is the smallest rate constant we have ever observed: thus, extra free energy of activation ($\Delta\Delta G^{\ddagger}=\Delta G^{\ddagger}_{\text{no metal}}-\Delta G^{\ddagger}_{\text{Zn(II)}}$) required to disrupt the interaction between Zn(II) and the iminodiacetate moieties is roughly estimated to be 7.1 kJ mol^{-1}. This value is comparable with those required to disrupt the interaction between *cis*-azobis(benzocrown ether)s and alkali metal ions (2.5—7.1 kJ mol^{-1}).[17,32] The fact that the thermal isomerization of *cis*-AzoIDA is efficiently inhibited in spite of the presence of the spacers suggests that the Zn(II)iminodiacetate interaction should be stronger than the alkali metal-crown interaction, because the inhibitory effect in the latter system has disappeared in the presence of the spacers.[33]

The effect of Cu(II) on the thermal cis-to-trans isomerization is illustrated in Fig. 2. The most distinct difference from Fig. 1 is that Cu(II) can suppress not only the thermal isomerization of *cis*-AzoIDA but also that of *cis*-AzoED. Conceivably, "soft" Cu(II) can interact with the ethylenediamine moieties more strongly. However, the k values for *cis*-AzoIDA are still smaller than those for *cis*-AzoED. It is interesting to note that the ligand which has the relatively small rate constant gives the large K_s (see Table 5).

Here, one may notice that the plots in Fig. 2 are more complex than those in Fig. 1 and the rate minimum does not always appear at [Cu(II)]/[ligand]=1.0. The complexity is associated with overlapping of two

contrasting effects of Cu(II): that is, an inhibitory effect due to intramolecular chelation and an accelerative effect due to interaction between Cu(II) and the azo linkage.[27,34] We have examined the catalytic effect of various metal ions on the thermal cis-to-trans isomerization of *cis*-azobenzene derivatives.[27,35] Among metal ions tested therein, Cu(II) exerted the greatest accelerative effect while Zn(II) acted as very weak catalyst.

The plots of k *vs.* [Cu(II)]/[ligand] for *cis*-AzoIDA-(n=1), *cis*-AzoIDA(n=2), and *cis*-ED(n=2) provided a minimum, whereas the plot for *cis*-AzoED(n=1) decreased monotonously with increasing Cu(II) concentration. It is also seen from Fig. 2 that after experiencing a minimum, the rate constants for n=2 series are enhanced at high Cu(II) concentrations. In contrast, the accelerative effect of Cu(II) ion is scarcely operative on n=1 series. Examination of CPK models suggests that the intramolecular complexes with the n=1 cis-isomers are more rigid than the corresponding complexs with the n=2 cis-isomers. In fact, the complexes of n=2 series showed a considerable flexibility due to ethylene spacers. The absence of the accelerative effect on n=1 series implies, therefore, that in *cis*-azobenzenes rigidified through metal complexation, the thermal isomerization is rather insusceptible to the metal catalysis.

ESR Spectra of cis-Isomer·Cu(II) Complexes. Subsequently, we measured the ESR spectra of *cis*-isomer·Cu(II) complexes in order to obtain a further insight into the coordination structure. Practically, the ESR spectra were measured for the mixture of trans- and cis-isomers. The process we obtained the spectra of "pure" cis-isomer·Cu(II) complexes is following (Fig. 3): first, we measured the ESR spectra of trans-isomer·Cu(II) complexes and then eliminated this spectra from the observed spectra taking trans% at the photostationary state (see Table 1) into account. The remaining spectra which can be regarded as those of "pure" cis-isomer·Cu(II) complexes were analyzed by computer simulation. The results are summarized in Table 3 and Fig. 4.

Examination of Table 3 and Fig. 4 reveals that basically, all Cu(II) complexes adopt square-planar or octahedral coordination, but the xy planes are somewhat distorted from a neat square-planar structure because the third g value is required in order to fully simulate the spectra. Probably, the xy planes of the cis-isomer·Cu(II) complexes are more or less close to a lozenge.

With respect to g_1 in *cis*-AzoIDA, the g_1 for n=1 is somewhat greater than that for n=2, while the reverse is true in *cis*-AzoED. This difference may be rationalized in connection with the spacer effect. Provided that the nitrilo nitrogens in *cis*-AzoIDA(n=1) cannot coordinate to central Cu(II) because of steric hindrance, it serves as a tetradentate ligand. In this case, the g_1 for *cis*-AzoIDA(n=1) reflects the axial coordination of solvent or buffer base(NH_3). On the other hand, *cis*-AzoIDA(n=2) possibly serves as a hexadentante ligand owing to the flexibility increased by the ethylene spacers, and the g_1 would reflect the axial coordination of intramolecular ligand groups. In fact, *cis*-AzoIDA(n=1) shows an ESR pattern characteristic of square-planar coordination, whereas that of *cis*-AzoIDA(n=2) is rather close to octahedral coordination. It is very likely, therefore, that the distance from central Cu(II) to the intermolecular ligand is longer than that to the intramolecular one. On the other hand, *cis*-AzoED(n=2) has the g_1 greater than *cis*-AzoED(n=1). Since *cis*-AzoED series act as tetradentate ligands, the g_1 values are definitely governed by

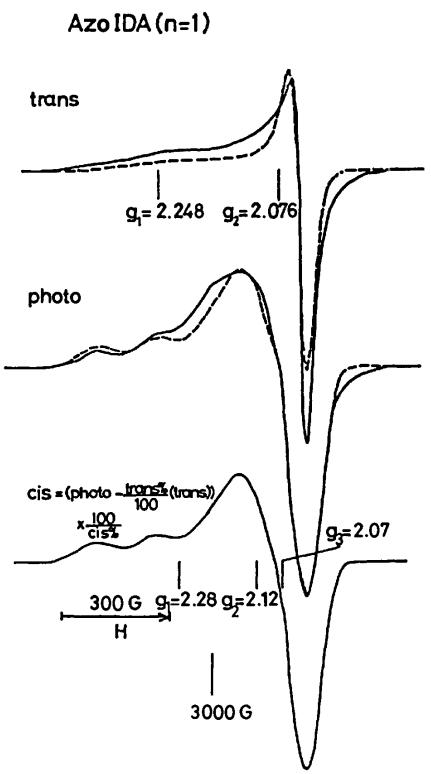

Fig. 3. ESR simulation of the "pure" *cis*-AzoIDA(n=1)·Cu(II) complex. The spectrum of *trans*-AzoIDA(n=1)·Cu(II) could be simulated by using two g values. The spectrum of *cis*-AzoIDA-(n=1)·Cu(II) was obtained by subtracting this spectrum from photo spectrum observed under photoirradiation.

TABLE 3. ESR PARAMETERS FOR THE cis-isomer·Cu(II) COMPLEXES[a]

Ligand	g value		
	g_1	g_2	g_3
cis-AzoIDA(n=1)	2.28	2.12	2.07
cis-AzoIDA(n=2)	2.23	2.15	2.06_5
cis-AzoED(n=1)	2.20	2.10	2.05_5
cis-AzoED(n=2)	2.34	2.10	2.05_2

a) −50 °C, [ligand]=5.00×10^{-4} M, [$CuSO_4$]=5.00×10^{-4} M, pH 9.02 with 0.01 M NH_3 buffer, μ=0.1(KCl).

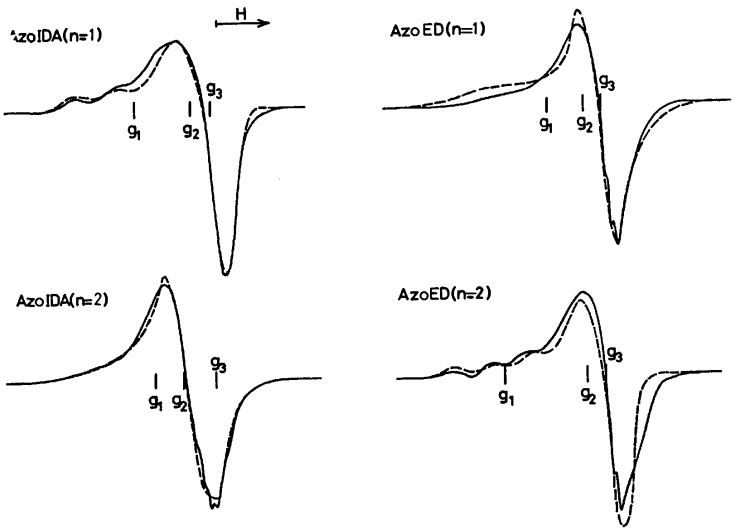

Fig. 4. ESR spectra (solid line) and simulated spectra (dotted line) of the Cu(II) complexes with the photoirradiated ligands. The g values inserted in the figure are those determined for the "pure" cis-isomer·Cu(II) complexes. −50 °C, [ligand]=5.00× 10^{-4} M, pH 9.02 with 0.01 M NH_3 buffer, μ=0.1(KCl).

Table 4. Displacement equilibrium constants (K_e) and stability constants (K_s) of AzoIDA and AzoED for Zn(II)[a]

Ligand	K_e		$10^{-8}\cdot K_s/M^{-1}$	
	dark or trans-isomer	cis-isomer	dark or trans-isomer	cis-isomer
$HN(CH_2COOH)_2$	1.71×10^{-3}	—	0.43[b]	—
AzoIDA(n=1)	0.230	0.327	57.8	82.1
AzoIDA(n=2)	1.86	3.30	467	829
$H_2N(CH_2)_2NH_2$	8.36×10^{-5}	—	0.021[c]	—
AzoED(n=1)	1.10×10^{-3}	1.95×10^{-3}	0.28	0.49
AzoED(n=2)	4.00×10^{-3}	0.0188	1.00	4.72

a) pH 9.02 with 0.01 M NH_3 buffer, μ=0.10 with KCl, [EBT]=[$ZnSO_4$]=3.00×10^{-6} M, [ligand]=1.50×10^{-5} M. b) K_s=2.75×10^7 M^{-1} from titration. c) K_s=1.26×10^6 M^{-1} from titration.

Table 5. Displacement equilibrium constants (K_e) and stability constants (K_s) of AzoIDA and AzoED for Cu(II)[a]

Ligand	K_e		$10^{-9}\cdot K_s/M^{-1}$	
	dark or trans-isomer	cis-isomer	dark or trans-isomer	cis-isomer
$HN(CH_2COOH)_2$	7.32×10^{-4}	—	2.91[b]	—
AzoIDA(n=1)	0.0163	0.0226	64.9	89.9
AzoIDA(n=2)	0.0180	0.0376	71.7	150
AzoED(n=1)	1.18×10^{-4}	7.70×10^{-4}	0.47	3.06
AzoED(n=2)	3.02×10^{-4}	0.0132	1.20	52.5

a) pH 9.02 with 0.01 M NH_3 buffer, μ=0.10 with KCl, [PAN]=[$CuSO_4$]=3.14×10^{-6} M, [ligand]=3.05×10^{-4} M. b) K_s=4.79×10^9 M^{-1} from titration.

the axial coordination of solvent or buffer base. The g_1(=2.34) for *cis*-AzoED(n=2) much greater than others is characterized by the elongation of the distance from Cu(II) to the axial ligand. This may be induced by the stable coordination of the ethylenediamine moieties in the xy plane which is brought forth by the ethylene spacers. In fact, the K_s for *cis*-AzoED(n=2) was much greater than that for *cis*-AzoED(n=1) (*vide post*).

These findings consistently suggest that the structure of the cis-isomer·Cu(II) complexes is significantly affected by the spacer length.

Photoresponsiveness of Stability Constants. The stability constants (K_s) were determined according to a displacement method[28] and are summarized in Tables 4 and 5 together with the displacement equilibrium constants (K_e). Since one of our objects is to

specify whether or not the amine nitrogens in AzoIDA can contribute to the complex formation, we evaluated the K_s at pH 9.02 where they are mostly dissociated.[31] As reference ligands, we employed Eriochrome Black T (EBT) and 1-(2-pyridylazo)-2-naphthol(PAN) for Zn(II) and Cu(II), respectively. Further details of the experimental methods and measurement conditions are described in Experimental and footnotes to Tables 4 and 5. In order to give full assurance to this method, we determined the K_s for iminodiacetic acid and ethylenediamine by a titration method.[28,31] The K_s values determined by two different methods agreed within the allowable error (see Tables 4 and 5). Therefore, the displacement method with EBT and PAN is reliable enough to make discussions on the photoirradiation effect. Here, note that we have defined K_s= [M(II)·AzoIDA(or AzoED)]/[M(II)][AzoIDA(or AzoED)].

Blank *et al.*[23] who first synthesized AzoIDA(n=1) reported that (i) *cis*-AzoIDA(n=1) forms an intramolecular 1:1 metal/ligand complex with Zn(II), (ii) the K_s for *cis*-AzoIDA(n=1)+$ZnSO_4$ determined in aqueous solution (no buffer) is $1.1\times10^5\,M^{-1}$, and (iii) *trans*-AzoIDA (n=1) scarcely interacts with Zn(II). The last conclusion sounds a little strange, because it has been established that iminodiacetic acid and its derivatives usually have the K_s of 10^7—$10^9\,M^{-1}$.[31] As shown in Table 4, the K_s values for AzoIDA+Zn(II) determined in buffered (pH 9. 02) aqueous solution lie between 8.13×10^9—$1.16\times10^{11}\,M^{-1}$ and those for AzoED+Zn(II) between 3.0×10^7—$4.64\times10^8\,M^{-1}$.[36] As for the association with Zn(II), the marked photoresponsive difference reported by Blank *et al.*[23] could not be realized under the present conditions. Detailed examination of Table 4 indicates, however, that the K_s values for AzoIDA(n=1), AzoIDA(n=2), and AzoED(n=1) are enhanced by 1.4—1.8 fold by photoirradiation, and that for AzoED(n=2) is further enhanced (4.7 fold). The slight but perceptible improvement in *cis*-AzoED(n=2) may be ascribed to superiority of the ethylene spacer over the methylene spacer to form the intramolecular complexes.

It is known that Zn(II) absolutely favors the tetrahedral coordination. On the other hand, the ESR studies established that all Cu(II) complexes tested herein adopt the planar coordination. Examination of CPK models suggests that one can easily make the molecuar models of either tetrahedral or planar coordination from n=2 series, whereas it is pretty difficult to make the molecular models of planar coordination from n=1 series without any steric distortion. One may expect, therefore, that the effect of the spacer length appears more clearly in the association with Cu(II). As recorded in Table 5, the photoinduced K_s increases are relatively small for AzoIDA(1.4-fold for n=1 and 2.1-fold for n=2). The lack of the spacer effect is probably rationalized as follows: the K_s values for *cis*-AzoIDA are primarily governed by the interaction with four carboxyl groups and the interaction with the amines exerts only the additional stabilization effect. Thus, the K_s values are scarcely changed by the spacer length. In contrast, the distinct spacer effect was observed for AzoED: the photoirradiation increases the K_s values for AzoED(n=1) and AzoED(n=2) by factors of 6.5 and 43.8, respectively, and the K_s for *cis*-AzoED-(n=2) is 17 times greater than that for *cis*-AzoED(n=1). The K_s for *cis*-AzoED is crucially governed by whether or not the four nitrogens can coordinate intramolecularly to one Cu(II) ion. In other words, when the coordination of two nitrogens close to the benzene ring accompanies some steric distortion (probably, *cis*-AzoED(n=1) is the case), it directly leads to the lowering of K_s. Consequently, *cis*-AzoED(n=2) having the longer spacer becomes more advantageous in the intramolecular complexation to one Cu(II) ion. These findings suggest that in order to realize the large spacer effect, the heteroatom which has a straightforward influence on the complex formation should be placed next to the spacer moiety.

Conclusion. The present study has demonstrated that the stability constants for typical complexones such as iminodiacetic acid and ethylenediamine can be photocontrolled by means of induced structural changes arising from the photoisomerization of azobenzene. Although several examples for photoresponsive binding of alkali and alkaline earth metal ions have been reported, few examples ever exist for photoresponsive binding of heavy metal ions. This study newly suggests, although the reversibility of the photoinduced isomerization in the presence of metal ions is not fully studied in this paper, possible applications of photoresponsive complexones to ion-extraction, ion transport, light-driven ion pumps, *etc.*

We thank Mr. Yoshihiro Honda and Miss K. Ueda for technical assistance. This work was supported by the Grant-in-Aid for the Special Project Research on the Properties of Molecular Assemblies (No. 59212033) from the Ministry of Education, Science and Culture.

References

1) Photoresponsive Crwon Ethers. 16.
2) K. Kano, Y. Tanaka, T. Ogawa, M. Shimomura, Y. Okahata, and T. Kunitake, *Chem. Lett.*, **1980**, 421.
3) M. Irie, A. Menju, and K. Hayashi, *Nippon Kagaku Kaishi*, **1984**, 227.
4) A. Kumano, O. Niwa, T. Kajiyama, M. Takayanagi, K. Kano, and S. Shinkai, *Chem. Lett.*, **1983**, 1327.
5) J. Anzai, H. Sasaki, K. Shimokawa, A. Ueno, and T. Osa, *Nippon Kagaku Kaishi*, **1984**, 338.
6) D. Balasubramanian, S. Subramani, and S. Kumar, *Nature (London)*, **254**, 252 (1975).
7) C. D. Eisenbach, *Makromol. Chem.*, **179**, 2489 (1978).
8) M. Irie and K. Hayashi, *J. Macromol. Sci., Chem.*, **A13**, 511 (1979).
9) F. Agolini and F. P. Gay, *Macromolecules*, **3**, 349 (1979).
10) A. Ueno, K. Takahashi, J. Anzai, and T. Osa, *J. Am.*

Chem. Soc., **103**, 6410 (1981).
11) O. Pieroni, J. L. Houben, A. Fissi, P. Costantino, and F. Ciardelli, *J. Am. Chem. Soc.*, **102**, 5913 (1980).
12) A. Ueno, H. Yoshimura, R. Saka, and T. Osa, *J. Am. Chem. Soc.*, **101**, 2779 (1979).
13) A. Ueno, R. Saka, and T. Osa, *Chem. Lett.*, **1979**, 841.
14) N. Shiga, M. Takagi, and K. Ueno, *Chem. Lett.*, **1980**, 1021.
15) J. Anzai, H. Sasaki, A. Ueno, and T. Osa, *J. Chem. Soc., Chem. Commun.*, **1983**, 1045.
16) S. Shinkai, T. Nakaji, Y. Nishida, T. Ogawa, and O. Manabe, *J. Am. Chem. Soc.*, **102**, 5860 (1980).
17) S. Shinkai, T. Nakaji, T. Ogawa, K. Shigematsu, and O. Manabe, *J. Am. Chem. Soc.*, **103**, 111 (1981).
18) For a comprehensive review see S. Shinkai and O. Manabe, "Host Guest Complex Chemistry III," ed by F. Vögtle and E. Weber, Springer-Verlag, Berlin, 1984, p. 67.
19) I. Yamashita, M. Fujii, T. Kaneda, S. Misumi, and T. Otsubo, *Tetrahedron Lett.*, **1980**, 541.
20) J.-P. Desvergne and H. Bouas-Laurent, *J. Chem. Soc., Chem. Commun.*, **1978**, 403.
21) M. Irie and M. Kato, *J. Am. Chem. Soc.*, **107**, 1024 (1985).
22) S. Shinkai, Y. Honda, K. Ueda, and O. Manabe, *Bull. Chem. Soc. Jpn.*, **57**, 2144 (1984).
23) M. Blank, L. M. Soo, N. H. Wasserman, and B. F. Erlanger, *Science*, **214**, 70 (1981).
24) G. Schwarzenbach, E. Kampitsch, and R. Steiner, *Helv. Chim. Acta*, **28**, 828 (1945).
25) R. Leppkes, F. Vögtle, and F. Luppertz, *Chem. Ber.*, **115**, 926 (1982).
26) F. Vögtle, H. Schäfer, and C. Ohm, *Chem. Ber.*, **117**, 955 (1984).
27) S. Shinkai, K. Shigematsu, Y. Honda, and O. Manabe, *Bull. Chem. Soc. Jpn.*, **57**, 2879 (1984).
28) T. Sakaguchi and K. Ueno, "Kinzoku Chelates," Nankodo, Tokyo, 1971, p. 290.
29) K. Ueno, "Chelate Tekitei-Ho," Nankodo, Tokyo, 1960, p. 94.
30) D. Betteridge, Q. Fernando, and H. Freiser, *Anal. Chim. Acta*, **35**, 294 (1963).
31) T. Ando, *Bull. Chem. Soc. Jpn.*, **35**, 1395 (1962).
32) S. Shinkai, T. Ogawa, Y. Kusano, O. Manabe, K. Kikukawa, T. Goto, and T. Matsuda, *J. Am. Chem. Soc.*, **104**, 1960 (1982).
33) S. Shinkai, K. Shigematsu, Y. Kusano, and O. Manabe, *J. Chem. Soc., Perkin Trans. 2*, **1981**, 3279.
34) D. P. Fisher, V. Piermattie, and J. C. Dabrowiak, *J. Am. Chem. Soc.*, **99**, 2811 (1977).
35) S. Shinkai, T. Kouno, Y. Kusano, and O. Manabe, *J. Chem. Soc., Perkin Trans. 1*, **1982**, 2741.
36) These K_s values are somewhat greater than those determined for iminodiacetic acid and ethylenediamine. The reason is not clear at the present time but a similar trend was observed for analogous ligands:[37] that is, the K_s values of 1,3- and 1,4-bis[bis(carboxymethyl)amino]cyclohexane for Mg(II) and Ca(II) are greater by 10—10^2 fold than those of iminodiacetic acid. One possible rationale is that these *trans*-isomers may form the polymeric, intermolecular complexes.
37) G. Schwarzenbach and H. Ackermann, *Helv. Chim. Acta*, **32**, 1682 (1949); D. L. Wright, J. H. Holloway, and C. N. Reilley, *Anal. Chem.*, **37**, 884 (1965).

The Crystal and Molecular Structure of *syn*-[2.2](1,4)-Anthracenophane and Its Photoisomer

Toshihiro TOYODA, Nobutami KASAI,*,† and Soichi MISUMI*

The Institute of Scientific and Industrial Research, Osaka University, Ibaraki, Osaka 567

†*Department of Applied Chemistry, Faculty of Engineering, Osaka University, Suita, Osaka 565*

(Received March 18, 1985)

Molecular structure of *syn*-[2.2](1,4)anthracenophane (**1**) and its photoisomer (**2**) have been determined by means of X-ray diffraction; **1**, monoclinic, space group A2, a=25.539(2), b=8.152(1), c=20.561(3) Å, β=106.03(1)° (−149 °C), Z=8; **2**, monoclinic, space group $P2_1/c$, a=8.065(6), b=12.963(9), c=19.580(5) Å, β=91.46(5)°, Z=4. The structure of **1** was solved by the vector search method and **2** by the direct method. Both structures were refined including all hydrogen atoms by the block-diagonal least-squares procedure: R=0.053 and 0.043 for 4413 and 2003 observed reflections for **1** and **2**, respectively. Two anthracene nuclei, connected by ethylene bridges at the 1 and 4 positions, in each of the two independent molecules (A and B) of **1** are approximately parallel. However, their overlappings differ slightly. In the photoisomer **2** the two anthracene nuclei are bound by newly formed bonds at the 9 and 10 positions: bond distances are 1.628(5) and 1.637(5) Å whereas the corresponding nonbonded distance in **1** are 3.312(6) and 3.301(6) Å (A molecule) and 3.357(6) and 3.366(6) Å (B molecule).

Previously, the preparation of *syn*-[2.2](1,4)anthracenophane (**1**), its photoisomer (**2**), and *anti*-[2.2](1,4)-anthracenophane (**3**) by pyrolysis of ammonium base and interesting photochemical interconversion of **1** and **2** have been reported.[1]

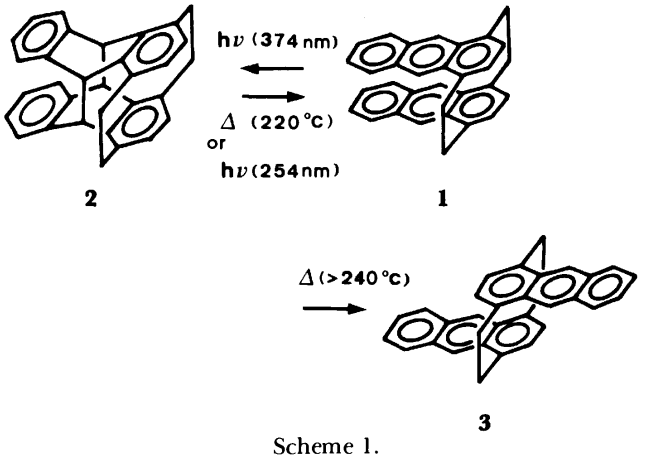

Scheme 1.

Each of the anthracenophane isomers contains anthracene nuclei with ethylene bridges at their 1- and 4-carbon atoms. They are of special interest for studying transannular electronic interaction and steric effect. Spectral properties of these isomers have been studied. The *syn*-[2.2](1,4)anthracenophane, **1**, shows an excimer fluorescence spectrum, with shorter life time, in longer wavelength region than the other anthracenophane, *anti*-[2.2](1,4)anthracenophane, **3** and [2.2](1,4)-(9,10)anthracenophane, and anthracene excimer.[2] On the other hand, [2.2](9,10)anthracenophane gives no fluorescence spectrum. The comparison of these fluorescence spectra indicates distinctly that the nonbonded distance between the active sites, 9- and 10-positions, of two anthracene nuclei is the most important factor to solve a relationship between the excimer structure and fluorescence spectrum.

As the structure difference of the molecules before and after the photoisomerization is also of much interest, this paper deals with the X-ray crystal structure analysis of *syn*-[2.2](1,4)anthracenophane†† and its photoisomer.††† A brief account of the *syn*-anthracenophane structure[3] and a profile of both structures[4] have been reported.

Experimental

Crystal Data. (**1**) *syn*-Anthracenophane, $C_{32}H_{24}$, M=408.5, monoclinic, space group A2, a=25.344(5), b=8.1340(2), c=20.743(4) Å, β=104.80(15)°, V=4238.9(15) Å^3, D_m=1.29 g cm^{-3}, D_c=1.280 g cm^{-3} for Z=8 (room temperature); a=25.539(2), b=8.152(1), c=20.561(3) Å, β=106.03(1)°, V=4114.3(9) Å^3, D_c=1.319 g cm^{-3} for Z=8 (−149 °C). (**2**) Photoisomer, $C_{32}H_{24}$, M=408.5, monoclinic, space group $P2_1/c$, a=8.065(5), b=12.963(9), c=19.580(5) Å, β=91.46(5)°, V=2046.3(12) Å^3, D_m=1.32 g cm^{-3}, D_c=1.323 g cm^{-3} for Z=4 (room temperature).

Oscillation and Weissenberg photographs determined the possible space group for *syn*-anthracenophane as A2 (No. 5), Am (No. 8), or A2/m (No. 12) (absent reflections; hkl: $k+l=2n+1$) and that for photoisomer as $P2_1/c$ (No. 14) (absent reflections; $h0l$: $l=2n+1$, $0k0$: $k=2n+1$). Unit-cell dimensions and reflection intensities were measured on a Rigaku automated four-circle diffractometer using Mo $K\alpha$ radiation (λ=0.71069 Å).

The θ—2θ scan technique was employed for the intensity data collection at a 2θ rate of 2° min^{-1}. The scan width was from $\{2\theta(\alpha_1)-0.7\}$ to $\{2\theta(\alpha_2)+0.7\}$°. Backgrounds were measured for 10 s at both ends of a scan. Three standard reflections measured after every 50 reflections to monitor the stability and orientation of the crystal showed no significant decay throughout the data collection.

syn-Anthracenophane: The intensity measurement was first carried out at room temperature, but later at −149 °C, in a dark room in order to avoid the photochemical cycloaddition of the present compound. The low temperature data were used for the structure analysis. In total 4477 independent

††Called as *syn*-anthracenophane hereafter.

†††Called as photoisomer hereafter.

reflection data were collected ($2\theta \leqq 100°$), of which 4413 could be observed ($|F_o| \leqq 3\sigma(F_o)$). Low temperature was attained by the gas flow method of liquid nitrogen.

Photoisomer: A total of 3740 independent reflections was measured at room temperature($2\theta \leqq 100°$), of which 2003 were non-zero reflections.

Intensity data of both crystals were corrected for usual Lorents and polarization effects but not for absorption [μ(Mo $K\alpha$)=0.767 and 0.785 cm^{-1} for *syn*-anthracenophane and photoisomer, respectively.]

Structure Solution and Refinement

The structures of *syn*-anthracenophane and photoisomer were solved by the Patterson function and direct method, respectively. Both structures were refined anisotropically by the block-diagonal least-squares procedure (*HBLS* V).[5]

syn-*Anthracenophane*: The unit-cell has a short b axis and contains eight molecules. Of the three possible space groups, Am and A2/m could be excluded by considering the packing of molecules with expected dimensions. The structure was then solved by assuming the space group as A2, which was later proved correct by the structure determined. Trials to establish the structure by the *MULTAN* program[6] were not successful. The deduction of the structure was then carried out by translational and rotational operations in the Patterson function with the idealized model structure constructed by referencing the structure of a similar compound, [2.2](9,10)anthracenophane.[7] The position of one of the two independent molecules (A molecule) in an asymmetric unit could be deduced. The other molecule (B molecule) was located on the Fourier map computed by using atomic parameters of carbon atoms of the A molecule. Hydrogen atoms of the two molecules were located by geometrical consideration, and they were refined isotropically. Final R index was 0.053 for observed reflections. The weighting scheme used at the final stage of the refinement was $w=\{\sigma^2(F_o)+0.04756|F_o|+0.00017|F_o|^2\}^{-1}$, where σ is the standard deviation obtained from the counting statics. The final atomic parameters are listed in Table.††††

Photoisomer: From the Wilson plot average temperature factor and scale factor were obtained. The $\sum_2$ formula was applied to 795 normalized structure factor magnitudes $|E|$'s($|E| \leqq 1.2$) in order to establish the phase relationship by the symbolic addition method.[9] One of the two E maps, respectively synthesized by two possible sets of signs of 277 reflections, could locate the 32 carbon atoms. The structure was first refined isotropically. Anisotropic temperature factors were then assigned for the carbon atoms, and the structure was refined with unit weight. Hydrogen atoms located on the difference Fourier map was in-

††††Tables of observed and calculated structure factors and anisotropic thermal parameters are kept at the Chemical Society of Japan, Document No. 8541.

Table 1. Final atomic coordinates of *syn*-[2.2](1,4)-anthracenophane with their estimated standard deviations in parentheses

a) Carbon atoms

Atom	x	y	z	B_{eq}/Å²[8]
1C(1)	0.34434(14)	1.3132(5)	0.33565(17)	2.0
1C(2)	0.39834(14)	1.2430(5)	0.33140(18)	1.8
1C(3)	0.44068(15)	1.2253(5)	0.38840(18)	2.0
1C(4)	0.48142(14)	1.1033(5)	0.39351(18)	2.1
1C(5)	0.47983(13)	1.0001(5)	0.34089(18)	1.8
1C(6)	0.50651(15)	0.8313(5)	0.35561(18)	2.1
1C(7)	0.44529(14)	1.0426(5)	0.27460(17)	1.7
1C(8)	0.44964(14)	0.9668(5)	0.21576(19)	2.1
1C(9)	0.41507(14)	1.0063(5)	0.15174(18)	1.9
1C(10)	0.41999(15)	0.9317(5)	0.09131(20)	2.4
1C(11)	0.38644(16)	0.9751(6)	0.03029(20)	2.6
1C(12)	0.34552(15)	1.0947(6)	0.02559(18)	2.3
1C(13)	0.33909(14)	1.1692(5)	0.08213(19)	2.1
1C(14)	0.37345(14)	1.1284(5)	0.14715(18)	1.9
1C(15)	0.36918(14)	1.2036(5)	0.20664(19)	2.0
1C(16)	0.40378(14)	1.1654(5)	0.27024(17)	1.7
2C(1)	0.30823(15)	1.1841(6)	0.36180(21)	2.6
2C(2)	0.33370(14)	1.0158(6)	0.37244(20)	2.4
2C(3)	0.36721(16)	0.9736(6)	0.43398(20)	2.7
2C(4)	0.40771(16)	0.8533(6)	0.44054(19)	2.6
2C(5)	0.41612(15)	0.7737(5)	0.38504(19)	2.2
2C(6)	0.47157(15)	0.7064(5)	0.38660(19)	2.3
2C(7)	0.37414(14)	0.7865(5)	0.32266(19)	2.1
2C(8)	0.37439(15)	0.6909(5)	0.26684(19)	2.2
2C(9)	0.33597(15)	0.7094(5)	0.20368(19)	2.2
2C(10)	0.33774(15)	0.6169(6)	0.14577(20)	2.4
2C(11)	0.29984(17)	0.6386(6)	0.08531(19)	2.7
2C(12)	0.25813(16)	0.7580(6)	0.07823(20)	2.8
2C(13)	0.25560(15)	0.8510(5)	0.13250(20)	2.5
2C(14)	0.29393(14)	0.8316(5)	0.19710(20)	2.2
2C(15)	0.29250(15)	0.9263(6)	0.25312(21)	2.4
2C(16)	0.33192(14)	0.9098(5)	0.31597(20)	2.1
3C(1)	0.22445(13)	0.8118(5)	0.41690(17)	1.7
3C(2)	0.20205(13)	0.6419(5)	0.42137(16)	1.5
3C(3)	0.18701(14)	0.5980(5)	0.47816(16)	1.7
3C(4)	0.14626(14)	0.4789(5)	0.47577(16)	1.7
3C(5)	0.11935(13)	0.4026(5)	0.41635(17)	1.6
3C(6)	0.06214(14)	0.3389(5)	0.40717(17)	1.9
3C(7)	0.14425(13)	0.4128(5)	0.36095(16)	1.4
3C(8)	0.12787(13)	0.3112(5)	0.30399(17)	1.6
3C(9)	0.15190(13)	0.3192(5)	0.25049(16)	1.5
3C(10)	0.13452(14)	0.2177(5)	0.19206(17)	1.8
3C(11)	0.15882(15)	0.2291(5)	0.14078(17)	2.0
3C(12)	0.20230(15)	0.3422(5)	0.14500(17)	2.0
3C(13)	0.21965(14)	0.4422(5)	0.19980(17)	1.8
3C(14)	0.19468(13)	0.4349(5)	0.25429(16)	1.5
3C(15)	0.21092(13)	0.5396(5)	0.31032(17)	1.6
3C(16)	0.18644(13)	0.5323(5)	0.36393(16)	1.4
4C(1)	0.18238(13)	0.9531(5)	0.41925(16)	1.6
4C(2)	0.12441(13)	0.8899(5)	0.40495(16)	1.5
4C(3)	0.09974(14)	0.8702(5)	0.45540(17)	1.8
4C(4)	0.05865(14)	0.7510(5)	0.45137(17)	1.9
4C(5)	0.04143(13)	0.6501(5)	0.39648(16)	1.6
4C(6)	0.01851(13)	0.4822(5)	0.40222(17)	1.9
4C(7)	0.05659(13)	0.6936(5)	0.33557(16)	1.5
4C(8)	0.03466(13)	0.6125(5)	0.27435(17)	1.6
4C(9)	0.05411(13)	0.6408(5)	0.21774(16)	1.5
4C(10)	0.03438(14)	0.5500(5)	0.15632(17)	1.9
4C(11)	0.05653(15)	0.5731(5)	0.10385(17)	2.0
4C(12)	0.09982(15)	0.6869(5)	0.10900(17)	2.1
4C(13)	0.11950(14)	0.7760(5)	0.16635(18)	1.8
4C(14)	0.09690(13)	0.7579(5)	0.22268(16)	1.6
4C(15)	0.11767(13)	0.8421(5)	0.28337(17)	1.6

Table 1. (continued)

a) Carbon atoms Atom	x	y	z	B_{eq}/Å^2 [28]
4C(16)	0.09869(13)	0.8135(5)	0.34022(16)	1.4

b) Hydrogen atoms Atom	x	y	z	B/Å^2
1H(1)	0.3205(14)	1.352(5)	0.2908(17)	2.0(8)
1H(1)	0.3481(15)	1.403(6)	0.3637(18)	2.2(8)
1H(3)	0.4381(14)	1.285(5)	0.4288(17)	1.8(8)
1H(4)	0.5072(14)	1.075(6)	0.4400(17)	2.1(8)
1H(6)	0.5438(15)	0.845(6)	0.3906(18)	2.0(8)
1H(6)	0.5117(15)	0.783(6)	0.3162(18)	2.4(9)
1H(8)	0.4783(14)	0.881(6)	0.2188(17)	2.0(8)
1H(10)	0.4496(15)	0.848(6)	0.0954(19)	2.6(9)
1H(11)	0.3946(17)	0.917(6)	−0.0082(20)	3.2(10)
1H(12)	0.3228(16)	1.125(6)	−0.0200(19)	2.8(9)
1H(13)	0.3076(15)	1.237(6)	0.0773(18)	2.2(9)
1H(15)	0.3403(14)	1.285(5)	0.2038(17)	1.9(8)
2H(1)	0.2688(15)	1.192(6)	0.3288(18)	2.5(9)
2H(1)	0.3014(15)	1.216(6)	0.4059(18)	2.6(9)
2H(3)	0.3687(16)	1.045(6)	0.4734(19)	2.6(9)
2H(4)	0.4370(15)	0.838(6)	0.4862(18)	2.6(9)
2H(6)	0.4956(15)	0.678(6)	0.4358(18)	2.4(9)
2H(6)	0.4697(15)	0.589(6)	0.3610(18)	2.1(8)
2H(8)	0.4052(15)	0.615(6)	0.2684(18)	2.2(8)
2H(10)	0.3679(16)	0.539(6)	0.1504(19)	2.7(9)
2H(11)	0.2990(16)	0.570(6)	0.0436(19)	3.0(10)
2H(12)	0.2286(16)	0.777(6)	0.0288(19)	3.1(10)
2H(13)	0.2245(16)	0.936(6)	0.1244(19)	2.6(9)
2H(15)	0.2633(15)	1.009(6)	0.2466(18)	2.4(9)
3H(1)	0.2343(13)	0.823(5)	0.3715(16)	1.5(7)
3H(1)	0.2564(14)	0.825(5)	0.4537(17)	1.5(8)
3H(3)	0.2001(14)	0.660(5)	0.5220(17)	1.8(8)
3H(4)	0.1293(14)	0.461(5)	0.5132(17)	1.8(8)
3H(6)	0.0588(14)	0.270(6)	0.4448(17)	1.9(8)
3H(6)	0.0514(14)	0.266(5)	0.3656(17)	2.0(8)
3H(8)	0.0972(14)	0.231(5)	0.3006(17)	1.6(8)
3H(10)	0.1017(14)	0.137(5)	0.1895(17)	1.6(8)
3H(11)	0.1425(15)	0.167(6)	0.1005(17)	2.0(8)
3H(12)	0.2184(14)	0.358(5)	0.1079(17)	2.0(8)
3H(13)	0.2505(14)	0.520(6)	0.2021(17)	1.8(8)
3H(15)	0.2400(14)	0.617(5)	0.3102(17)	1.6(8)
4H(1)	0.1875(14)	1.034(5)	0.3868(17)	1.5(8)
4H(1)	0.1953(14)	1.000(6)	0.4654(17)	1.7(8)
4H(3)	0.1171(14)	0.904(5)	0.5009(17)	1.6(8)
4H(4)	0.0490(14)	0.708(6)	0.4916(17)	1.8(8)
4H(6)	0.0058(14)	0.484(6)	0.4444(17)	2.0(8)
4H(6)	−0.0108(14)	0.453(5)	0.3670(17)	1.8(8)
4H(8)	0.0040(15)	0.533(6)	0.2693(16)	1.8(8)
4H(10)	0.0028(14)	0.478(5)	0.1528(17)	1.7(8)
4H(11)	0.0395(15)	0.513(6)	0.0619(17)	1.9(8)
4H(12)	0.1135(15)	0.702(6)	0.0718(18)	2.0(8)
4H(13)	0.1477(14)	0.852(5)	0.1691(17)	1.6(8)
4H(15)	0.1465(14)	0.919(5)	0.2886(17)	1.5(8)

cluded in the refinement with isotropic temperature factors. Finally, the refinement converged with R= 0.043 for non-zero reflections. The atomic parameters are given in Table 2.††††

Atomic scattering factors for the carbon and hydrogen atoms were first taken from those of T. Suzuki[10] and at the final stage from International Tables for X-Ray Crystallography.[11] Computations were done mainly on a NEAC2200-700 computer at the Computation Center, Osaka University. At the final stage, an ACOS 850 computer was used at the Crystallographic

Table 2. Final atomic coordinates of photoisomer with their estimated standard deviations in parentheses

a) Carbon atoms Atom	x	y	z	B_{eq}/Å^2 [28]
1C(1)	0.5658(5)	0.6523(3)	0.18364(18)	4.3
1C(2)	0.6090(5)	0.5722(3)	0.23769(17)	3.5
1C(3)	0.6838(5)	0.4802(3)	0.21957(18)	4.1
1C(4)	0.7840(5)	0.4260(3)	0.26534(19)	4.1
1C(5)	0.8091(5)	0.4631(3)	0.33203(17)	3.5
1C(6)	0.9665(5)	0.4346(3)	0.37175(19)	4.2
1C(7)	0.7095(4)	0.5435(3)	0.35370(16)	3.1
1C(8)	0.7413(4)	0.5932(3)	0.42317(16)	3.2
1C(9)	0.5854(4)	0.6405(3)	0.44930(17)	3.1
1C(10)	0.5401(5)	0.6327(3)	0.51739(18)	3.7
1C(11)	0.3995(5)	0.6817(3)	0.5391(2)	4.6
1C(12)	0.3022(5)	0.7379(3)	0.4932(3)	4.8
1C(13)	0.3448(5)	0.7440(3)	0.4250(2)	4.0
1C(14)	0.4870(4)	0.6959(3)	0.40282(18)	3.3
1C(15)	0.5435(4)	0.7020(3)	0.33049(17)	3.2
1C(16)	0.6081(4)	0.5982(3)	0.30726(17)	3.0
2C(1)	0.7089(5)	0.7356(3)	0.17642(18)	4.2
2C(2)	0.8556(5)	0.7151(3)	0.22452(17)	3.5
2C(3)	0.9896(5)	0.6583(3)	0.20284(18)	4.2
2C(4)	1.0902(5)	0.6048(3)	0.24955(18)	4.1
2C(5)	1.0571(4)	0.6070(3)	0.31902(17)	3.5
2C(6)	1.1120(5)	0.5171(3)	0.36365(19)	4.2
2C(7)	0.9419(4)	0.6786(3)	0.34201(16)	3.06
2C(8)	0.8879(4)	0.6785(3)	0.41543(16)	3.1
2C(9)	0.8322(4)	0.7850(3)	0.43581(17)	3.2
2C(10)	0.8700(5)	0.8283(3)	0.49908(18)	3.8
2C(11)	0.8150(5)	0.9267(3)	0.5147(2)	4.7
2C(12)	0.7206(5)	0.9815(3)	0.4676(3)	5.0
2C(13)	0.6830(5)	0.9383 3)	0.4043(2)	4.3
2C(14)	0.7351(4)	0.8400(3)	0.38880(17)	3.2
2C(15)	0.6921(4)	0.7867(3)	0.32211(17)	3.3
2C(16)	0.8408(4)	0.7330(3)	0.29429(17)	3.1

b) Hydrogen atoms Atom	x	y	z	B/Å^2
1HA(1)	0.455(5)	0.690(3)	0.1938(18)	3.6(9)
1HB(1)	0.559(5)	0.615(3)	0.1388(18)	3.4(9)
1H(3)	0.691(5)	0.457(3)	0.1685(17)	3.1(9)
1H(4)	0.852(5)	0.366(3)	0.2484(19)	4.0(10)
1HA(6)	1.012(5)	0.369(3)	0.3561(18)	3.7(10)
1HB(6)	0.943(5)	0.424(3)	0.4238(18)	3.5(9)
1H(8)	0.788(4)	0.537(3)	0.4571(16)	2.4(8)
1H(10)	0.613(5)	0.592(3)	0.5510(18)	3.4(9)
1H(11)	0.374(5)	0.674(3)	0.5893(19)	3.8(10)
1H(12)	0.193(5)	0.773(3)	0.5077(19)	4.0(10)
1H(13)	0.271(5)	0.780(3)	0.3895(17)	3.0(9)
1H(15)	0.440(4)	0.723(3)	0.3004(16)	2.1(8)
2HA(1)	0.753(5)	0.737(3)	0.1283(17)	3.0(9)
2HB(1)	0.658(5)	0.807(3)	0.1865(17)	3.0(9)
2H(3)	1.003(5)	0.649(3)	0.1526(18)	3.2(9)
2H(4)	1.180(5)	0.559(3)	0.2338(18)	3.8(10)
2HA(6)	1.225(5)	0.483(3)	0.3436(19)	4.1(10)
2HB(6)	1.149(5)	0.542(3)	0.4125(19)	3.8(10)
2H(8)	0.985(4)	0.656(3)	0.4486(16)	1.8(8)
2H(10)	0.939(5)	0.786(3)	0.5341(18)	3.2(9)
2H(11)	0.832(5)	0.958(3)	0.5625(19)	4.8(11)
2H(12)	0.677(5)	1.052(3)	0.4813(19)	4.5(11)
2H(13)	0.619(5)	0.977(3)	0.3668(18)	3.7(10)
2H(15)	0.643(5)	0.839(3)	0.2878(17)	2.9(9)

Research Center, Institute for Protein Research, Osaka University.

Results and Discussion

Molecular Structure. Perspective views (*ORTEP* drawing)[12] of *syn*-anthracenophane and photoisomer molecules with atom labelling, are shown in Figs. 1 and 2, respectively. Bond distances and bond angles of both compounds are listed in Table 3.

syn-*Anthracenophane*: As seen in Fig. 1, the feature of the molecular structure is that two anthracene nuclei are closely placed in nearly parallel. All of the four anthracene nuclei in two crystallographically independent A and B molecules have normal bond distances and bond angles. However, each of the ethylene-bridged benzene rings is boat-shaped as those in [2.2]paracyclophane[13] and layered paracyclophanes.[14]

The four C_{sp^3}–C_{sp^3} bonds of ethylene bridges, 1Cl–2Cl [1.588(6)Å], 1C6–2C6[1.597(6)Å], 3Cl–4Cl[1.585(5)Å], and 3C6–4C6[1.598(5)Å] are elongated by 0.02 to 0.04Å than the corresponding bonds of [2.2](9,10)anthracenophane[7] and [2.2]paracyclophane.[13]

As side view of each molecule is presented in Fig. 3, in which nonbonded intramolecular atomic distances between anthracene nuclei are given. As shown in Figs. 1 and 3 the structure of the present compound demonstrates that all the anthracene nuclei are approximately in parallel position suitable for forming an excimer and that two anthracene nuclei are mutually overlapped well in the A molecule whereas less in the B molecule. The nonbonded interatomic distances between the two pairs of active sites, C8 and C15 in the largely overlapped A molecule [1C8···2C8= 3.312(6) and 1C15···2C15=3.301(6)Å] are shorter than the van der Waals contact. On the other hand, the less overlapped B molecule shows slightly longer interatomic distances between the corresponding carbon atoms, 3C8···4C8[3.357(6)Å] and 3C15···4C15[3.366(5)Å], which are longer than the 3C7···4C8[3.302(5)Å] and 3C16···4C15[3.256(5)Å], owing to larger mutual displacement of the two anthracene nuclei along their longer axis. However, all of them are longer than the corresponding ones of [2.2](9,10)anthracenophane [both 2.772(3)Å][7] but shorter than that of anthracenophane excimer [~3.5Å].[2] These nonbonded distances between two sp^2 carbon atoms are relatively shorter than the van der Waals distance, which shows considerable overlap between the two $2p_x$ orbitals easy to form a covalent bond. It can be said that the *syn*-anthracenophane molecule has the structure ready for the isomerization to their photoisomers, and *vice versa*.

Photoisomer: The feature of the structure is that, in addition to the ethylene bridge, the 1C8–2C8 and 1C15–2C15 bonds connect the upper and lower dihydroanthracene nuclei tightly, and the end benzene rings are not in parallel (Fig. 4). The 1C8–2C8 and

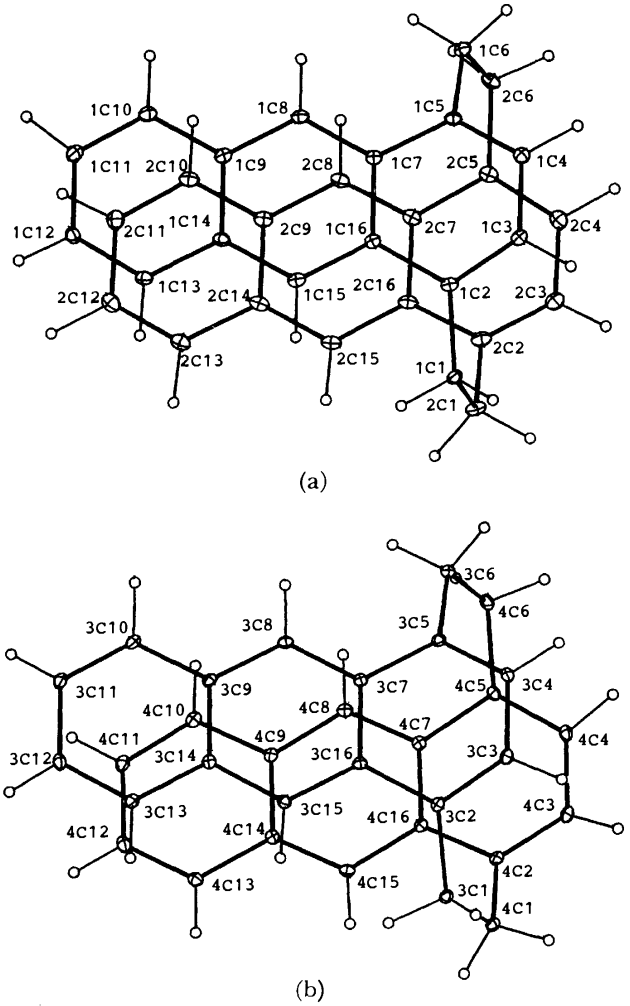

Fig. 1. A. perspective view(*ORTEP* drawing)[12] of *syn*-[2.2](1,4) anthracenophane molecules.
(a): A molecule, (b): B molecule
Non-hydrogen atoms are expressed by thermal ellipsoids with 10% probability level. Hydrogen atoms are drawn as spheres with B=1 Å^2.

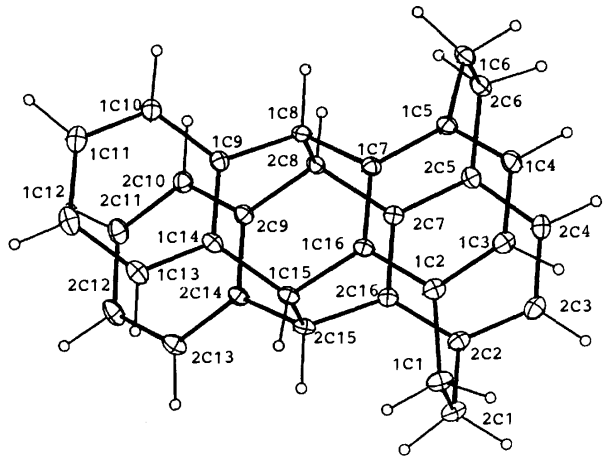

Fig. 2. A perspective view[12] of *syn*-[2.2](1,4) anthracenophane photoisomer molecule.
Non-hydrogen atoms are expressed by thermal ellipsoids with 10% probability level. Hydrogen atoms are drawn as spheres with B=1 Å^2.

Table 3. Bond distances and bond angles of *syn*-anthracenophane and photoisomer with their estimated standard deviations in parentheses

	Syn-anthracenophane			Photoisomer	
	A molecule		B molecule		
Bond distances[l/Å]					
1C2–1C3	1.365(5)	3C2–3C3	1.374(5)	1C2–1C3	1.387(5)
1C3–1C4	1.422(5)	3C3–3C4	1.414(5)	1C3–1C4	1.383(5)
1C4–1C5	1.363(5)	3C4–3C5	1.374(5)	1C4–1C5	1.401(5)
1C5–1C7	1.446(5)	3C5–3C7	1.452(5)	1C5–1C7	1.389(5)
1C7–1C16	1.442(5)	3C7–3C16	1.441(5)	1C7–1C16	1.400(5)
1C2–1C16	1.448(5)	3C2–3C16	1.447(5)	1C2–1C16	1.404(5)
2C2–2C3	1.361(6)	4C2–4C3	1.364(5)	2C2–2C3	1.383(5)
2C3–2C4	1.405(6)	4C3–4C4	1.416(5)	2C3–2C4	1.392(5)
2C4–2C5	1.380(6)	4C4–4C5	1.367(5)	2C4–2C5	1.393(5)
2C5–2C7	1.430(5)	4C5–4C7	1.453(5)	2C5–2C7	1.396(5)
2C7–2C16	1.453(5)	4C7–4C16	1.436(5)	2C7–2C16	1.412(5)
2C2–2C16	1.438(6)	4C2–4C16	1.452(5)	2C2–2C16	1.394(5)
1C1–1C2	1.517(5)	3C1–3C2	1.511(5)	1C1–1C2	1.517(5)
1C5–1C6	1.528(5)	3C5–3C6	1.513(5)	1C5–1C6	1.518(5)
2C1–2C2	1.508(6)	4C1–4C2	1.518(5)	2C1–2C2	1.520(5)
2C5–2C6	1.511(6)	4C5–4C6	1.506(5)	2C5–2C6	1.518(5)
1C1–2C1	1.588(6)	3C1–4C1	1.585(5)	1C1–2C1	1.589(5)
1C6–2C6	1.597(6)	3C6–4C6	1.598(5)	1C6–2C6	1.599(5)
1C7–1C8	1.390(5)	3C7–3C8	1.401(5)	1C7–1C8	1.521(5)
1C8–1C9	1.405(5)	3C8–3C9	1.401(5)	1C8–1C9	1.500(4)
1C14–1C15	1.399(5)	3C14–3C15	1.402(5)	1C14–1C15	1.501(5)
1C15–1C16	1.396(6)	3C15–3C16	1.411(5)	1C15–1C16	1.516(4)
2C7–2C8	1.389(5)	4C7–4C8	1.395(5)	2C7–2C8	1.513(4)
2C8–2C9	1.403(6)	4C8–4C9	1.405(5)	2C8–2C9	1.509(4)
2C14–2C15	1.396(6)	4C14–4C15	1.394(5)	2C14–2C15	1.510(5)
2C15–2C16	1.408(6)	4C15–4C16	1.403(5)	2C15–2C16	1.501(4)
1C8···2C8	3.312(6)	3C8···4C8	3.357(5)	1C8–2C8	1.628(4)
1C15···2C15	3.301(6)	3C15···4C15	3.366(5)	1C15–2C15	1.637(5)
1C9–1C10	1.420(6)	3C9–3C10	1.425(5)	1C9–1C10	1.395(5)
1C10–1C11	1.357(6)	3C10–3C11	1.366(5)	1C10–1C11	1.376(5)
1C11–1C12	1.413(6)	3C11–3C12	1.428(5)	1C11–1C12	1.385(6)
1C12–1C13	1.361(6)	3C12–3C13	1.362(5)	1C12–1C13	1.390(6)
1C13–1C14	1.421(5)	3C13–3C14	1.435(5)	1C13–1C14	1.385(5)
1C9–1C14	1.440(5)	3C9–3C14	1.429(5)	1C9–1C14	1.391(5)
2C9–2C10	1.421(6)	4C9–4C10	1.430(5)	2C9–2C10	1.387(5)
2C10–2C11	1.360(6)	4C10–4C11	1.362(5)	2C10–2C11	1.386(5)
2C11–2C12	1.420(6)	4C11–4C12	1.425(5)	2C11–2C12	1.378(6)
2C12–2C13	1.366(6)	4C12–4C13	1.358(5)	2C12–2C13	1.387(6)
2C13–2C14	1.425(6)	4C13–4C14	1.437(5)	2C13–2C14	1.378(5)
2C9–2C14	1.443(6)	4C9–4C14	1.433(5)	2C9–2C14	1.390(5)
Bond angles[ϕ/°]					
1C2–1C1–2C1	113.1(4)	3C2–3C1–4C1	113.2(3)	1C2–1C1–2C1	111.9(3)
1C1–1C2–1C3	120.5(4)	3C1–3C2–3C3	119.4(4)	1C1–1C2–1C3	120.3(3)
1C1–1C2–1C16	121.4(4)	3C1–3C2–3C16	122.7(4)	1C1–1C2–1C16	120.4(3)
1C3–1C2–1C16	117.1(4)	3C3–3C2–3C16	117.0(4)	1C3–1C2–1C16	117.9(3)
1C2–1C3–1C4	121.9(4)	3C2–3C3–3C4	121.7(4)	1C2–1C3–1C4	121.5(3)
1C3–1C4–1C5	120.8(4)	3C3–3C4–3C5	121.6(4)	1C3–1C4–1C5	119.8(4)
1C4–1C5–1C6	119.0(4)	3C4–3C5–3C6	119.7(4)	1C4–1C5–1C6	119.5(3)
1C4–1C5–1C7	118.5(4)	3C4–3C5–3C7	116.9(4)	1C4–1C5–1C7	118.1(4)
1C6–1C5–1C7	121.7(4)	3C6–3C5–3C7	122.6(4)	1C6–1C5–1C7	120.6(3)
1C5–1C6–2C6	112.6(4)	3C5–3C6–4C6	112.9(3)	1C5–1C6–2C6	113.1(3)
1C5–1C7–1C8	122.6(4)	3C5–3C7–3C8	121.9(4)	1C5–1C7–1C8	120.4(3)
1C5–1C7–1C16	118.1(4)	3C5–3C7–3C16	119.3(3)	1C5–1C7–1C16	120.9(3)
1C7–1C8–1C9	122.2(4)	3C7–3C8–3C9	122.3(4)	1C7–1C8–1C9	110.8(3)
				1C7–1C8–2C8	108.1(3)
				1C9–1C8–2C8	111.8(3)
1C8–1C9–1C10	122.5(4)	3C8–3C9–3C10	122.2(4)	1C8–1C9–1C10	122.6(3)
1C8–1C9–1C14	118.8(4)	3C8–3C9–3C14	118.8(4)	1C8–1C9–1C14	117.1(3)
1C10–1C9–1C14	118.7(4)	3C10–3C9–3C14	119.0(4)	1C10–1C9–1C14	120.3(3)
1C9–1C10–1C11	120.8(4)	3C9–3C10–3C11	120.6(4)	1C9–1C10–1C11	119.9(4)
1C10–1C11–1C12	120.7(5)	3C10–3C11–3C12	120.5(4)	1C10–1C11–1C12	120.0(4)
1C11–1C12–1C13	120.7(4)	3C11–3C12–3C13	120.5(4)	1C11–1C12–1C13	120.3(4)

TABLE 3. (continued)

Syn-anthracenophane				Photoisomer	
A molecule		B molecule			
1C12-1C13-1C14	120.7(4)	3C12-3C13-3C14	120.5(4)	1C12-1C13-1C14	120.1(4)
1C13-1C14-1C15	122.9(4)	3C13-3C14-3C15	121.5(4)	1C13-1C14-1C15	123.1(4)
1C9-1C14-1C13	118.4(4)	3C9-3C14-3C13	118.9(4)	1C9-1C14-1C13	119.4(4)
1C9-1C14-1C15	118.7(4)	3C9-3C14-3C15	119.7(4)	1C9-1C14-1C15	117.6(3)
1C14-1C15-1C16	122.6(4)	3C14-3C15-3C16	121.5(4)	1C14-1C15-1C16	110.6(3)
				1C14-1C15-2C15	111.7(3)
				1C16-1C15-2C15	107.9(3)
1C2-1C16-1C7	119.6(4)	3C2-3C16-3C7	119.1(3)	1C2-1C16-1C7	119.5(3)
1C2-1C16-1C15	121.9(4)	3C2-3C16-3C15	122.0(4)	1C2-1C16-1C15	120.9(3)
1C7-1C16-1C15	118.5(4)	3C7-3C16-3C15	118.9(4)	1C7-1C16-1C15	117.0(3)
1C1-2C1-2C2	112.6(4)	3C1-4C1-4C2	112.3(3)	1C1-2C1-2C2	112.5(3)
2C1-2C2-2C3	120.0(4)	4C1-4C2-4C3	121.6(4)	2C1-2C2-2C3	120.4(3)
2C1-2C2-2C16	120.9(4)	4C1-4C2-4C16	119.6(3)	2C1-2C2-2C16	119.7(3)
2C3-2C2-2C16	118.1(4)	4C3-4C2-4C16	117.4(4)	2C3-2C2-2C16	118.4(4)
2C2-2C3-2C4	121.5(4)	4C2-4C3-4C4	121.8(4)	2C2-2C3-2C4	120.7(4)
2C3-2C4-2C5	121.8(4)	4C3-4C4-4C5	121.7(4)	2C3-2C4-2C5	120.5(4)
2C4-2C5-2C6	120.8(4)	4C4-4C5-4C6	121.7(4)	2C4-2C5-2C6	119.1(3)
2C4-2C5-2C7	117.3(4)	4C4-4C5-4C7	117.6(4)	2C4-2C5-2C7	118.3(3)
2C6-2C5-2C7	120.8(4)	4C6-4C5-4C7	119.4(4)	2C6-2C5-2C7	120.8(3)
1C6-2C6-2C5	112.6(4)	3C6-4C6-4C5	113.0(4)	1C6-2C6-2C5	111.6(3)
2C5-2C7-2C8	121.8(4)	4C5-4C7-4C8	121.7(4)	2C5-2C7-2C18	121.0(3)
2C5-2C7-2C16	119.2(4)	4C5-4C7-4C16	118.8(4)	2C5-2C7-2C16	119.7(3)
2C7-2C8-2C9	122.9(4)	4C7-4C8-4C9	121.6(4)	2C7-2C8-2C9	110.2(3)
				1C8-2C8-2C7	108.5(3)
				1C8-2C8-2C9	112.0(3)
2C8-2C9-2C10	122.9(4)	4C8-4C9-4C10	121.8(4)	2C8-2C9-2C10	123.2(3)
2C8-2C9-2C14	118.3(4)	4C8-4C9-4C14	119.2(4)	2C8-2C9-2C14	117.4(3)
2C10-2C9-2C14	118.8(4)	4C10-4C9-4C14	118.9(4)	2C10-2C9-2C14	119.4(3)
2C9-2C10-2C11	121.2(4)	4C9-4C10-4C11	120.4(4)	2C9-2C10-2C11	120.3(4)
2C10-2C11-2C12	120.5(4)	4C10-4C11-4C12	121.0(4)	2C10-2C11-2C12	120.1(4)
2C11-2C12-2C13	120.0(4)	4C11-4C12-4C13	120.4(4)	2C11-2C12-2C13	119.6(4)
2C12-2C13-2C14	121.6(4)	4C12-4C13-4C14	120.7(4)	2C12-2C13-2C14	120.6(4)
2C13-2C14-2C15	122.7(4)	4C13-4C14-4C15	122.2(4)	2C13-2C14-2C15	123.3(4)
2C9-2C14-2C13	117.8(4)	4C9-4C14-4C13	118.6(4)	2C9-2C14-2C13	119.9(4)
2C9-2C14-2C15	119.5(4)	4C9-4C14-4C15	119.1(4)	2C9-2C14-2C15	116.8(3)
2C14-2C15-2C16	122.0(4)	4C14-4C15-4C16	122.0(4)	2C14-2C15-2C16	111.0(3)
				1C15-2C15-2C14	111.9(3)
				1C15-2C15-2C16	108.6(3)
2C2-2C16-2C7	118.8(4)	4C2-4C16-4C7	119.6(4)	2C2-2C16-2C7	120.2(3)
2C2-2C16-2C15	122.6(4)	4C2-4C16-4C15	121.3(4)	2C2-2C16-2C15	121.4(3)
2C7-2C16-2C15	118.5(4)	4C7-4C16-4C15	118.8(4)	2C7-2C16-2C15	116.4(3)

1C15-2C15 bond distances are 1.628(4) and 1.637(5) Å, which are very long and comparable to that in [9′,10′]-dihydroanthraceno[9,10]dihydroanthracene[1.61(2) Å].[14]

In the [2.2]paracyclophane moiety at one end of the molecule, the C2-C16[1.404(5) and 1.394(5) Å], C5-C7[1.389(5) and 1.396(5) Å], and C7-C16[1.400(5) and 1.412(5) Å] bond distances are clearly shorter than those in *syn*-anthracenophane. Two benzene rings in this moiety deformed in boat form as in *syn*-anthracenophane and other related compounds. The central C_{sp^3}-C_{sp^3} bonds of the ethylene bridges are equal to those in *syn*-anthracenophane.

In the third benzene rings of the dihydroanthracene nuclei, the C9-C10, C11-C12, C13-C14, and C9-C14 bond distances are respectively shorter, whereas the C10-C11 and C12-C13 distances are longer, than the corresponding distances in *syn*-anthracenophane (Table 3). The bond distances [av. 1.387 and 1.384 Å] and bond angles [av. 120 and 120°] in the third benzene rings are contracted to normal values of the benzene molecule by the photoisomerization.

A side view of the molecule, which can be compared with those of *syn*-anthracenophane (Fig. 3), is depicted in Fig. 4 with nonbonded intramolecular atomic distances. The left half of the present molecule, namely the [2.2]orthocyclophane skeleton, has a similar structure as a half of the [9′,10′]dihydroanthraceno-[9,10] dihydroanthracene. The dihedral angle formed by the end benzene rings is 46.6°, which is equal to that of [9′,10′]dihydroanthraceno[9,10]dihydroanthracene [46°]. In the right half of the molecule, namely the tetra-bridged cyclophane skeleton, the nonbonded 1C7····2C[2.580(4) Å] and 1C16····2C16[2.581(4) Å] distances are shorter by about 0.04 Å than that between the upper and lower benzene rings in [2.2.2.2.2.2](1,2,3,4,5,6)cyclophane[2.624 Å], the closest

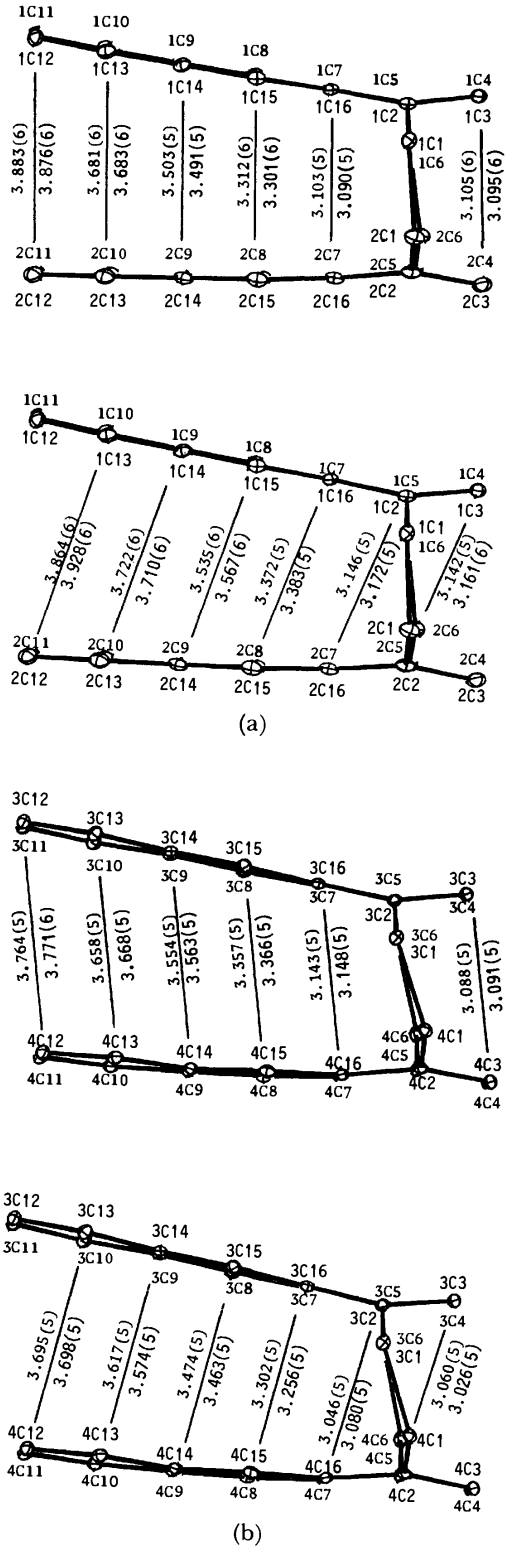

Fig. 3. A side view of *syn*-anthracenophane molecules.[12]
(a): A molecule, (b): B molecule
Hydrogen atoms are omitted for clarity. Nonbonded atomic distances(l/Å) are given with their estimated standard deviations in parentheses.

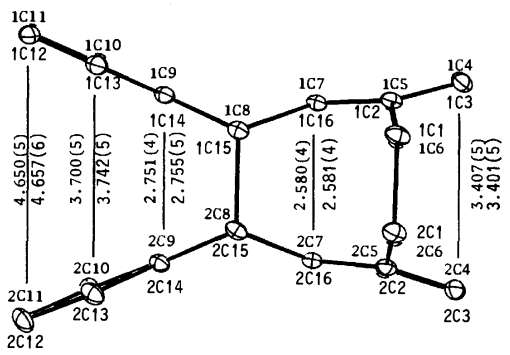

Fig. 4. A side view of *syn*-anthracenophane photoisomer molecules.[12]
Hydrogen atoms are omitted for clarity. Nonbonded atomic distances(l/Å) are given with their estimated standard deviations in parentheses.

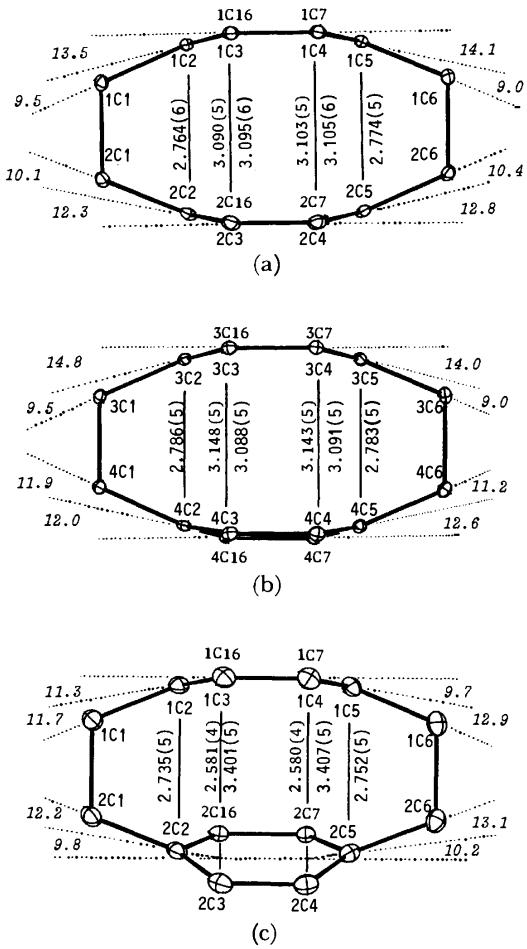

Fig. 5. A comparison of [2.2]paracyclophane moieties in *syn*-anthracenophane and its photoisomer.[12]
Selected interatomic distances [l/Å] are given with their estimated standard deviations in parentheses.
(a): *syn*-Anthracenophane, A molecule, (b): *syn*-Anthracenophane, B molecule, (c): Photoisomer.

distance reported so far. This fact suggests an existence of large strain in the present molecule. One of the chemical proof is that, against the Woodward-Hoffmann rule, by thermal fission of the 1C8–2C8

and 1C15–2C15 bonds the present compound is easily isomerized to *syn*-anthracenophane.

A side view of the [2.2]paracyclophane moiety in the present photoisomer is compared with those of *syn*-anthracenophane in Fig. 5. In the *syn*-anthracenophane the upper and lower benzene rings of this part of the A molecule are parallel and mutually overlapped well (Figs. 3a and 5a), while those of the B molecule not so parallel and not so overlapped well (Figs. 3b and 5b); this difference is caused by a conformational change at ethylene bridges as seen in Fig. 3. Whereas, the [2.2]paracyclophane moiety in the photoisomer shows a large distortion due to the 1C8–2C8 and 1C15–2C15 bonds formation (Figs. 4 and 5c).

Crystal Structure: The packing of molecules in crystals of *syn*-anthracenophane and its photoisomer are respectively given in Figs. 6 and 7 (*ORTEP* drawing).[12] Close intermolecular atomic contacts in these crystals are listed in Table 4.

syn-*Anthracenophane*: Molecules are packed densely. The closest distance between A molecules is 3.400(6) Å and that between B molecules 3.399(5)Å. However, the shortest contact between A and B molecules is 3.539(6)Å, which is slightly longer than the former two.

Photoisomer: A comparatively loose packing of molecules is observed. The closest intermolecular atomic contact is 3.563(7)Å.

The authors are grateful to Miss Nobuko Kanehisa who helped them at the final stage of the computation and for *ORTEP* drawing.

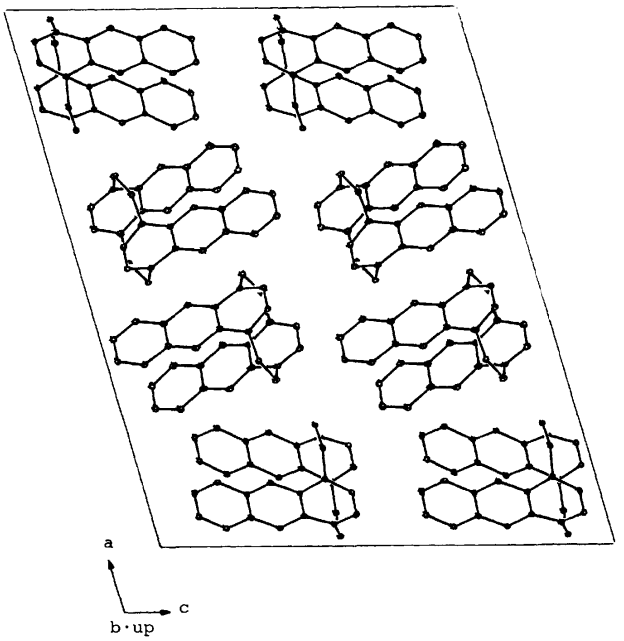

Fig. 6. Crystal structure of *syn*-anthracenophane.[12] Hydrogen atoms are omitted.

TABLE 4. CLOSE INTERMOLECULAR ATOMIC CONTACT[*l*/Å] LESS THAN 3.6 Å WITH THEIR ESTIMATED STANDARD DEVIATIONS IN PARENTHESES

syn-Anthracenophane					
1C1····2C8[a]	3.560(6)	key: a,	x,	$1+y$,	z;
1C12···2C4[b]	3.400(6)	b,	x,	$0.5+y$,	$-0.5+z$;
2C12···3C4[b]	3.539(6)	c,	$-x$,	$-0.5+y$,	$0.5-z$;
3C6····4C10[c]	3.399(6)				
Photoisomer					
1C5····1C11[a]	3.597(5)	key: a,	$1-x$,	$1-y$,	$1-z$.
1C10···1C10[a]	3.563(7)				

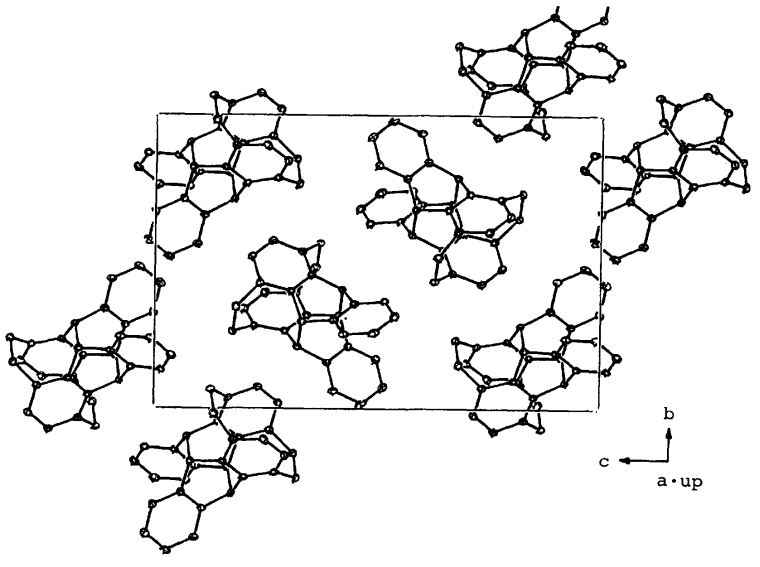

Fig. 7. Crystal structure of *syn*-anthracenophane photoisomer.[12] Hydrogen atoms are omitted.

References

1) T. Toyoda, I. Otsubo, T. Otsubo, Y. Sakata, and S. Misumi, *Tetrahedron Lett.*, **1972**, 1731.

2) T. Hayashi, N. Mataga, Y. Sakata, S. Misumi, and J. Tanaka, *J. Am. Chem. Soc.*, **98**, 5910 (1976); N. Mataga and M. Ottolenghi, "Photophysical Aspects of Exciplexes," in "Molecular Association Vol. 2," ed by R. Foster, Academic Press, London (1979), Chap. 1, pp. 1—78.

3) T. Toyoda and S. Misumi, *Tetrahedron Lett.*, **1978**, 1479.

4) A. Iwama, T. Toyoda, M. Yoshida, T. Otsubo, Y. Sakata, and S. Misumi, *Bull. Chem. Soc. Jpn.*, **51**, 2988 (1978).

5) T. Ashida, *HBLS* V, "Universal Crystallographic Computing System-Osaka," The Computation Center, Osaka University, 1973, p. 55.

6) G. Germain, P. Main, and M. M. Woolfson, *Acta Crystallogr., Sect. A*, **27**, 368 (1971).

7) A. Wada and J. Tanaka, *Acta Crystallogr., Sect. B*, **33**, 355 (1977).

8) W. C. Hamilton, *Acta Crystallogr.*, **12**, 609 (1959).

9) J. Karle and I. L. Karle, *Acta Crystallogr.*, **21**, 849 (1966).

10) T. Suzuki, *J. Phys. Soc. Jpn.*, **13**, 793 (1958).

11) "International Tables for X-Ray Crystallography," Kynoch Press, Birmingham, Vol. IV (1974), p. 71.

12) C. K. Johnson, *ORTEP* II, Report ORNL-5138, Oak Ridge National Laboratory, Tennessee (1976).

13) H. Hope, J. Bernstein, and K. N. Trueblood, *Acta Crystallogr., Sect. B*, **28**, 1733 (1972).

14) M. Ehrenberg, *Acta Crystallogr.*, **20**, 177 (1966).

Bitter Principles of *Ailanthus altissima* Swingle. Conversion of Ailanthone into Shinjulactone C[1)]

Masami Ishibashi, Takahiko Tsuyuki,* and Takeyoshi Takahashi*
Department of Chemistry, Faculty of Science, The University of Tokyo, Hongo, Bunkyo-ku, Tokyo 113
(Received April 13, 1985)

Ailanthone was converted into shinjulactone C with a hexacyclic 1α,12α:5α,13α-dicyclo-9β*H*-picrasane skeleton. The key reaction consists of an intramolecular ionic [4+2] cycloaddition between a pentadienyl cation and an olefin.

In the course of studies on the bitter principles of Simaroubaceous plants, we obtained three new compounds possessing modified picrasane skeletons, shinjudilactone,[2)] shinjulactone B,[3)] and shinjulactone C (**1**),[2)] from *Ailanthus altissima* Swingle (Japanese name: Shinju or Niwaurushi). Structures of these new quassinoids were determined by single crystal X-ray diffraction analyses. These migrated picrasane skeletons are very interesting from the biogenetical view points and stimulated us to study on the backbone-rearrangement reactions leading to the modified picrasanes. Since it seems possible that these migrated quassinoids are biogenetically derived from ailanthone (**2**),[4)] a main quassinoid of this plant, chemical conversions of ailanthone (**2**) into the migrated picrasanes were investigated. In previous papers[2,5)] we have reported a transformation of ailanthone (**2**) into shinjudilactone through benzilic acid rearrangement. This paper deals with chemical conversion of ailanthone (**2**) into shinjulactone C (**1**) with a novel 1α,12α:5α,13α-dicyclo-9β*H*-picrasane skeleton.

A conceivable biogenetic pathway from ailanthone (**2**) to shinjulactone C (**1**) *via* intermediates **A** and **B** is shown in Scheme 1. An inversion of a chiral center at C-9 position must occur prior to the cycloaddition of $\Delta^{12(13)}$-double bond in ring C with a pentadienyl cation in ring A. If the inversion of 9α-H into 9β-H occurs and both B and C rings adopt boat forms, the rings A and C would be sterically very close to each other enough to overlap π-orbitals.

According to these considerations, chemical conversion of ailanthone (**2**) into shinjulactone C (**1**) was investigated. Prior to the intramolecular cycloaddition, the compound which corresponds to the hypothetical intermediate **A** or **B** has to be prepared from ailanthone (**2**). For this purpose there seem to be three problems to be examined; i) an isomerization of $\Delta^{13(21)}$-exocyclic double bond into $\Delta^{12(13)}$ endocyclic double bond, ii) a selective oxidation of the hydroxyl group at C-1 position, and iii) an inversion of the stereochemistry of the hydrogen atom at C-9 position.

In regard to the third problem J. Polonsky *et al.* described that when glaucanol (**3**) was heated in pyridine, the inversion of 9α-H occurred to afford a 9β-H derivative (**4**).[6)] According to this procedure, an isomerization of ailanthone (**2**) was examined. But on heating in pyridine under reflux for 10 h, **2** produced isoailanthone (**5**) in 67% yield.[2)] Though it was shown that the isomerization proceeded without an inversion of the C-9 position, this experiment corresponds to giving a solution to the problem i discussed above. However the heating of ailanthone (**2**) in pyridine was continued for longer time to furnish a complex mixture, from which shinjulactone C (**1**) was obtained in 5—8% yield together with isoailanthone (**5**; 30—40% yield) and many unidentified by-products. Since the reaction was carried out in atmosphere, isoailanthone (**5**) or other intermediates must suffer autoxidation, which was supported by the following experiment; neither ailanthone (**2**) nor isoailanthone (**5**), on heating in argon atmosphere, yielded shinjulactone C (**1**). The reaction carried out in atmosphere was shown to yield so many by-products by HPLC examination and the separation of them was

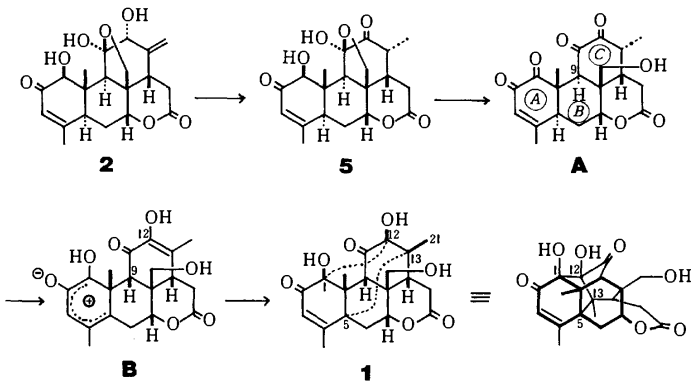

Scheme 1.

found to be so difficult that any attempts to isolate intermediates corresponding to **A** or **B** were not successful.

Instead of the isolation of intermediates, a stepwise conversion from ailanthone (**2**) into shinjulactone C (**1**) was then investigated. First examination concerned a direct oxidation of the hydroxyl group at C-1 of ailanthone (**2**). But oxidation of **2** with Jones reagent afforded unidentified polar products, while oxidation of ailanthone (**2**) with lead tetraacetate or manganese dioxide gave an 11,12-seco aldehyde (**6**);[4] this suggested that the protection of hydroxyl groups in C ring was required.

On heating in pyridine ailanthone triacetate (**7**)[7] isomerized to enol acetate (**8**), which was also obtained by acetylation of isoailanthone (**5**). Partial hydrolysis of the acetates (**7** and **8**) was examined under several conditions, but it was found that the selective removal of the acetyl group at C-1 was not easy. Under alkaline conditions ($NaHCO_3$, NH_3, *etc.*) the hydrolysis reactions did not proceed cleanly, probably owing to the opening of δ-lactone in D ring and an isomerization to α-diketone (**C**-type) in A ring, the latter being proposed in the case of 6-acetoxyisophorone (**9**).[8] Heating might cause a backbone rearrangement in C ring.[2,5] Acidic hydrolysis of the triacetate (**7**) afforded 1,12-di-*O*-acetylailanthone (**10**) and 12-*O*-acetylailanthone (**11**), but the 1-hydroxy-12,20-di-*O*-acetyl derivative was not obtained.

Discrimination of the hydroxyl group at C-1 from those in C ring was accomplished as follows (Scheme 2). Treatment of ailanthone (**2**) with *t*-butyldimethylsilyl chloride in the presence of imidazole in *N,N*-dimethylformamide[9] afforded a monosilyl derivative (**12**; 91% yield), which underwent acetylation to give a monosilyl diacetate (**13**; 92% yield). On heating in pyridine, **13** isomerized to a monosilyl enol acetate (**14**; 95% yield). ^{1}H NMR spectrum of **14** showed a signal due to vinyl methyl protons (δ 1.79, 3H, s; $C_{(13)}$-CH_3) instead of signals due to *exo*-methylene (δ 5.14 and 5.20, each 1H, s; $C_{(21)}$-H) and a proton (δ 5.45, 1H, s; $C_{(12)}$-H) attached to a carbon atom with an acetoxyl group for **13**. Signals due to a proton attached to a carbon atom with a siloxyl group appeared at δ 3.97 (1H, s; $C_{(1)}$-H) in ^{1}H NMR spectra of both **13** and **14**. ^{13}C NMR spectrum of **13** showed a signal at δ 198.9 due to a carbonyl carbon atom at C-11 position, while a signal due to a hemiacetal carbon atom was observed at δ 108.5 for **12**. From these results the structure of the monosilyl diacetate (**13**) was firmly established. Then the deprotection of the monosilyl enol acetate (**14**) was carried out by a treatment with AcOH–H_2O–THF (2:1:1) at room temperature to afford 1-hydroxy enol acetate (**15**; 85% yield based on the consumed **14**). Jones oxidation of **15** gave an α-diketone (**16**; 80% yield). This compound corresponds to a diacetate of the intermediate **A** shown in Scheme 1.

Now the α-diketone (**16**) in hand was transformed into 12,20-di-*O*-acetylshinjulactone C (**17**) by heating in pyridine under reflux for 9 h in 22% yield, which was shown to be completely identical with a specimen (**17**) derived from natural shinjulactone C (**1**). Alkaline hydrolysis of **17** afforded shinjulactone C (**1**) in *ca.*

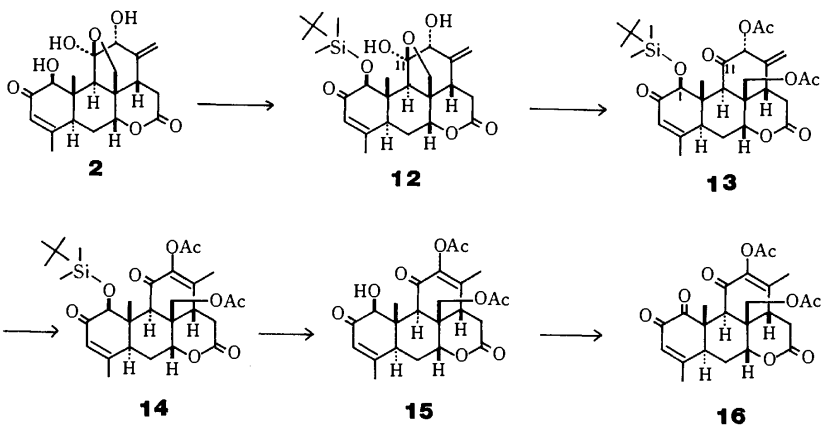

Scheme 2.

90% yield.

The reaction from the α-diketone (**16**) to the diacetate (**17**) could be explained by an inionic [4+2] cycloaddition of class B,[10] which was proposed for a transformation from perezon (**18**) to pipitzol (**19**).[11] The reaction process from **16** to **17** through an intermediate **D** is depicted in Scheme 3.

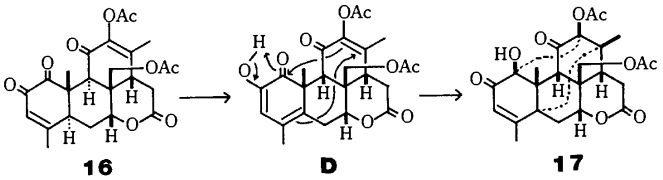

16 **D** **17**

Scheme 3.

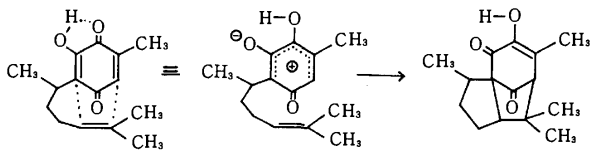

18 **19**

Experimental[12]

Reaction of Ailanthone (2) with Pyridine. Ailanthone (**2**; 60 mg) was heated in pyridine (5 ml) under reflux for 19 h. After evaporation under reduced pressure, the reaction mixture was separated by preparative TLC developed with 10% methanol-chloroform to give isoailanthone (**5**; 30—40%) and shinjulactone C (**1**; 5—8%) together with many unidentified by-products. After recrystallization from acetone, **1** was identified with a natural specimen by mp, TLC, HPLC, ^{1}H NMR, and IR. The yields were estimated by HPLC examination (column: Nucleosil 10-CN; solvent system: hexane-THF, 3:2; flow rate: 0.8 ml/min; retention times were 11.5, 13.2, and 23.1 min for **1**, **2**, and **5**, respectively).

Oxidation of Ailanthone (2) with Manganese Dioxide. A solution of ailanthone (**2**; 19 mg) in ethyl acetate (20 ml) was treated with manganese dioxide (120 mg) for 3 d at room temperature. After the usual work-up, the reaction mixture was subjected to a separation by preparative TLC developed with methanol-chloroform (1:19) to afford a mixture (13 mg) of an aldehyde (**6**) and a hemiacetal (**20**) in *ca.* 1:1 ratio.[4]

1β,12,20-Triacetoxypicrasa-3,12-diene-2,11,16-trione (8). i) Ailanthone triacetate (**7**; 497 mg) in pyridine (10 ml) was heated under reflux for 10 h. After evaporation of the solvent under reduced pressure, the reaction mixture was purified by a column chromatography eluted with 3% methanol-chloroform to give an enol acetate (**8**; 369 mg). ii) Ailanthone (**2**; 26 mg) in pyridine (5 ml) was heated under reflux for 11 h. After cooling, acetic anhydride (5 ml) and a catalytic amount of 4-dimethylaminopyridine were added to the reaction mixture. Standing at room temperature for 6 d followed by the usual work-up afforded the enol acetate (**8**; 23 mg), mp 153—156 °C (acetone-hexane); IR (Nujol) 1745, 1705, 1685, 1230, and 1140 cm^{-1}; UV (EtOH) 240 nm (ε 17000); ^{1}H NMR (400 MHz; $CDCl_3$) δ=1.33 (3H, s; $C_{(10)}$-CH_3), 1.82 (3H, s; $C_{(13)}$-CH_3), 1.98 (3H, br s; $C_{(4)}$-CH_3), 2.07, 2.09, and 2.23 (each 3H, s; CH_3CO-), 3.25 (1H, s; $C_{(9)}$-H), 4.13, and 4.59 (each 1H, d, J=12.5 Hz; $C_{(20)}$-H), 4.61 (1H, br s; $C_{(7)}$-H), 5.25 (1H, s; $C_{(1)}$-H), and 6.08 (1H, br s; $C_{(3)}$-H); MS *m/z* (%) 502 (M^+; 2), 460 (30), 418 (100), and 400 (20); Found: *m/z* 502.1807. Calcd for $C_{26}H_{30}O_{10}$: M, 502.1837.

Acidic Hydrolysis of Ailanthone Triacetate (7). A solution of the triacetate (**7**; 590 mg) in 1.5 M (1 M=1 mol dm^{-3}) sulfuric acid-THF (each 10 ml) was refluxed for 5 h. After extraction with dichloromethane, the organic layer was dried over magnesium sulfate and evaporated to give a residue. Purification by a silica-gel column chromatography eluted 3% methanol-chloroform afforded 1,12-di-*O*-acetylailanthone (**10**; *ca.* 120 mg), 12-*O*-acetylailanthone (**11**; *ca.* 120 mg), and ailanthone (**2**; 155 mg) in succession. **10**: Mp 266—268 °C (chloroform-acetone); IR (Nujol) 3420, 1735, 1705, and 1675 cm^{-1}; ^{1}H NMR ($CDCl_3$) δ=1.35 (3H, s), 2.04 (6H, s), 2.24 (3H, s), 3.55 and 3.93 (each 1H, d, J=8 Hz), 4.49 (1H, t, J=3 Hz), 5.25 (1H, s), 5.32 (1H, s), 5.38 (1H, s), 5.49 (1H, s), and 6.10 (1H, m); MS *m/z* (%) 460 (M^+; 2), 418 (88), 358 (94), 247 (63), 151 (100), and 60 (86); Found: *m/z* 460.1768. Calcd for $C_{24}H_{28}O_9$: M, 460.1733. **11**: Mp 221—224 °C (acetone); IR (Nujol) 3200, 1730, 1670, and 1240 cm^{-1}; ^{1}H NMR ($CDCl_3$) δ=1.20 (3H, s), 2.03 (3H, br s), 2.07 (3H, s), 3.56 and 3.94 (each 1H, d, J=8 Hz), 4.07 (1H, br s), 4.52 (1H, *t*, J=3 Hz), 5.10 (1H, br s), 5.30 (2H, s), 5.51 (1H, s), 6.15 (1H, m), and 7.66 (1H, s); MS *m/z* (%) 418 (M^+; 24), 358 (14), 328 (23), 313 (18), 247 (22), 151 (32), and 60 (100); Found: *m/z* 418.1632. Calcd for $C_{22}H_{26}O_8$: M, 418.1627.

1-O-t-Butyldimethylsilylailanthone (12). Ailanthone (**2**; 402 mg) was treated with *t*-butyldimethylsilyl chloride (806 mg; 5.0 equiv) in the presence of imidazole (950 mg; 13 equiv) in DMF (12 ml) at room temperature for 18 h. After addition of water, the reaction mixture was extracted with dichloromethane. The organic layer was washed with 2 M hydrochloric acid and then with a saturated solution of sodium hydrogencarbonate, dried over magnesium sulfate, and evaporated under reduced pressure. The residue was subjected to separation by a silica-gel column chromatography eluted with 15—30% ethyl acetate-ether to give the starting ailanthone (**2**; 12 mg) and a monosilyl derivative (**12**; 480 mg), mp 234—236 °C; IR (KBr) 3450, 3250, 1730, 1685, 1660, and 840 cm^{-1}. ^{1}H NMR ($CDCl_3$) δ=0.15 and 0.16 (each 3H, s), 1.05 (9H, s), 1.25 (3H, s), 1.95 (3H, br s), 3.52 and 3.90 (each 1H, d, J=8 Hz), 4.01 (1H, s), 4.26 (1H, s), 4.50 (1H, t, J=2.5 Hz), 5.22 and 5.31 (each 1H, br s), 5.99 (1H, m); ^{13}C NMR ($CDCl_3$) δ=−4.1q, −2.5q, 10.1q, 19.1s, 22.4q, 25.7t, 26.7q, 26.7q, 26.7q, 34.5t, 43.0d, 43.5d, 45.2s, 45.6s, 47.2d, 71.6t, 78.0d, 79.3d, 86.0d, 108.5s, 120.7t, 126.3d, 143.4s, 159.4s, 169.3s, and 195.1s; MS *m/z* (%) 490 (M^+; 3), 475 (3), 433 (55), and 57 (100); Found: *m/z* 490.2383. Calcd for $C_{26}H_{38}O_7Si$: M, 490.2385.

1β-t-Butyldimethylsiloxy-12α,20-diacetoxypicrasa-3,13(21)-diene-2,11,16-trione (13). The monosilyl derivative (**12**; 480 mg) was acetylated with acetic anhydride (5 ml) and pyridine (15 ml) at 70 °C for 18 h. After the usual work-up, purification with a silica-gel column chromatography eluted with ethyl acetate-ether (1:3) afforded a monosilyl diacetate (**13**; 519 mg), mp 182—184 °C (ether-hexane); IR (Nujol) 1750, 1690, 1230, and 845 cm^{-1}; ^{1}H NMR ($CDCl_3$) δ=−0.14, −0.10 (each 3H, s), 0.84 (9H, s), 1.14 (3H, s), 1.83 (3H, br s), 2.00 and 2.07 (each 3H, s), 3.97 (1H, s), 3.80 and 4.31 (each 1H, d, J=12 Hz), 4.57 (1H, br s), 5.14 and 5.20 (each 1H, s), 5.45 (1H, s), and 5.85 (1H, br s); ^{13}C NMR ($CDCl_3$) δ=−3.7, −3.3,

10.6, 18.8, 20.6, 21.0, 21.9, 25.9, 26.5, 26.5, 26.5, 30.7, 40.1, 41.6, 42.6, 46.4, 51.1, 65.0, 76.0, 77.9, 86.9, 114.5, 126.9, 140.5, 158.3, 168.9, 169.9, 170.1, 196.5, 198.9; MS *m/z* (%) 574 (M^+; 0.3), 559 (5), 517 (100), 475 (10), 457 (10), 415 (15), and 207 (8); Found: *m/z* 574.2618. Calcd for $C_{30}H_{42}O_9Si$: M, 574.2598.

1β-t-Butyldimethylsiloxy-12,20-diacetoxypicrasa-3,12-diene-2,11,16-trione (14). The monosilyl diacetate (**13**; 75 mg) was heated in pyridine (5 ml) under reflux for 11 h. After evaporation under reduced pressure, the reaction mixture was purified by a silica-gel column chromatography eluted with ethyl acetate-ether (1:3) to give a monosilyl enol acetate (**14**; 71.5 mg), mp 210—213 °C (ether-hexane); IR (Nujol) 1740, 1710, 1690, 1240, and 845 cm^{-1}; ^1H NMR ($CDCl_3$) δ=−0.12 and 0.07 (each 3H, s), 0.90 (9H, s), 1.24 (3H, s), 1.79 (3H, s), 1.93 (3H, br s), 2.08 and 2.20 (each 3H, s), 3.97 (1H, s), 4.60 (1H, t, J=2.5 Hz), 4.19 and 4.68 (each 1H, d, J=12 Hz), and 5.98 (1H, m); MS *m/z* (%) 574 (M^+; 0.1), 559 (3), 517 (100), 475 (10), 457 (18), and 207 (18); Found: *m/z* 574.2648. Calcd for $C_{30}H_{42}O_9Si$: M, 574.2598.

12,20-Diacetoxy-1β-hydroxypicrasa-3,12-diene-2,11,16-trione (15). The monosilyl enol acetate (**14**; 457 mg) was treated with AcOH (10 ml), H_2O (5 ml), and THF (5 ml) at room temperature for 22 h. The reaction mixture was evaporated and separated by a silica-gel column chromatography eluted with 30—80% ethyl acetate-ether to give the starting monosilyl enol acetate (**14**; 147 mg) and 1-hydroxy enol acetate (**15**; 210 mg), mp 173—175 °C (acetone); IR (KBr) 3430, 1740, 1675, 1220, and 1030 cm^{-1}; ^1H NMR ($CDCl_3$) δ=1.16 (3H, s), 1.86 (3H, s), 1.97 (3H, br s), 2.11 and 2.26 (each 3H, s), 3.30 (1H, s), 3.97 (1H, d, J=3.5 Hz), 4.47 (1H, d, J=3.5 Hz), 4.21 and 4.61 (each 1H, d, J=12 Hz), 4.59 (1H, br s), and 6.07 (1H, br s); MS *m/z* (%) 460 (M^+; 3), 418 (18), 400 (23), 358 (40), 151 (90), and 60 (100); Found: *m/z* 460.1741. Calcd for $C_{24}H_{28}O_9$: M, 460.1734.

12,20-Diacetoxypicrasa-3,12-diene-1,2,11,16-tetrone (16). 1-Hydroxy enol acetate (**15**; 210 mg) was treated with Jones reagent (in excess) in acetone (30 ml) at 0 °C for 30 min. After addition of 2-propanol (*ca.* 3 ml) and sodium hydrogencarbonate (*ca.* 1 g), the reaction mixture was filtered through Florisil (Wako, 100—200 mesh; *ca.* 5 g) and evaporated to a concentrated solution, to which brine and dichloromethane were added. After extraction with dichloromethane, the organic layer was subjected to purification by a silica-gel column chromatography eluted with 3% methanol-chloroform to afford an α-diketone (**16**; 167 mg), mp 160—164 °C (dichloromethane-hexane); IR (KBr) 2910, 1740, 1695, 1220, and 1040 cm^{-1}; UV (EtOH) 245 nm (ε 9100); ^1H NMR ($CDCl_3$) δ=1.41 (3H, s), 1.89 (3H, s), 2.04 (3H, br s), 2.11 and 2.25 (each 3H, s), 3.52 (1H, s), 4.25 and 4.65 (each 1H, d, J=12 Hz), 4.56 (1H, t, J=2.5 Hz), and 6.23 (1H, m); ^{13}C NMR ($CDCl_3$) δ=14.2, 16.0, 20.0, 20.6, 22.4, 25.6, 30.3, 38.5, 41.0, 43.1, 44.8, 51.5, 61.9, 76.9, 129.0, 141.4, 143.2, 164.1, 167.9, 168.5, 170.2, 185.5, 187.5, and 198.5; MS *m/z* (%) 458 (M^+; 60), 430 (12), 416 (100), 398 (30), 356 (45), 151 (70); Found: *m/z* 458.1586. Calcd for $C_{24}H_{26}O_9$: M, 458.1576.

12,20-Di-O-acetylshinjulactone C (17). The α-diketone (**16**; 51 mg) was heated in pyridine (5 ml) under reflux for 9 h. After evaporation, the reaction mixture was separated by preparative TLC developed with ethyl acetate-ether (1:1) to give 12,20-diacetylshinjulactone C (**17**; 11 mg), whose ^1H NMR, IR, and mass spectra and optical rotation were completely identical with those of a specimen (**17**) obtained by acetylation of natural shinjulactone C (**1**).

Hydrolysis of 12,20-Di-O-acetylshinjulactone C (17). To a solution of the diacetate (**17**; 2.8 mg) in methanol (2 ml), 0.24 M potassium methoxide-methanol solution (0.1 ml) was added and the reaction mixture was stirred at room temperature for 1 h. After addition of 2 M hydrochloric acid (*ca.* 1 ml), the reaction mixture was evaporated to give a residue, which was subjected to purification by preparative TLC developed by 10% methanol-chloroform to afford shinjulactone C (**1**; 2.1 mg).

The authors wish to thank Mr. Kazuhiro Matsushita of JEOL Co., Ltd. for measurement of ^1H NMR spectrum at 400 MHz.

References

1) A preliminary account of this report: M. Ishibashi, T. Tsuyuki, T. Takahashi, *Tetrahedron Lett.*, **24**, 4843 (1983).

2) M. Ishibashi, T. Tsuyuki, T. Murae, H. Hirota, T. Takahashi, A. Itai, and Y. Iitaka, *Bull. Chem. Soc. Jpn.*, **56**, 3683 (1983).

3) T. Furuno, M. Ishibashi, H. Naora, T. Murae, H. Hirota, T. Tsuyuki, T. Takahashi, A. Itai, and Y. Iitaka, *Bull. Chem. Soc. Jpn.*, **57**, 2484 (1984).

4) H. Naora, M. Ishibashi, T. Furuno, T. Tsuyuki, T. Murae, H. Hirota, T. Takahashi, A. Itai, and Y. Iitaka, *Bull. Chem. Soc. Jpn.*, **56**, 3694 (1983).

5) M. Ishibashi, T. Tsuyuki, T. Murae, and T. Takahashi, *Chem. Pharm. Bull.*, **30**, 1917 (1982).

6) J. Polonsky, CL. Fouquey, and A. Gaudemer, *Bull. Soc. Chim. Fr.*, **1964**, 1818.

7) J. Polonsky and J.-L. Fourrey, *Tetrahedron Lett.*, **1964**, 3983.

8) A. W. Fort, *J. Org. Chem.*, **26**, 332 (1961).

9) A. J. Caruso, J. Polonsky, and B. S. Rodriguez, *Tetrahedron Lett.*, **23**, 2567 (1982).

10) R. B. Woodward and R. Hoffmann, "The Conservation of Orbital Symmetry," Academic Press, New York (1970), p. 86.

11) P. Joseph-Nathan, V. Mendoza, and E. Garcia, *Tetrahedron*, **33**, 1573 (1977) and references cited therein.

12) General procedures are the same as described in the preceding papers.[4,13]

13) M. Ishibashi, S. Yoshimura, T. Tsuyuki, T. Takahashi, A. Itai, and Y. Iitaka, *Bull. Chem. Soc. Jpn.*, **57**, 2885 (1984).

Electrochemical Epoxidation and Carbon-Carbon Bond Cleavage for the Preparation of 3-Methyl-4-oxo-2-phenyl-4*H*-1-benzopyran-8-carboxylic Acid from 3-Methyl-2-phenyl-8-(1-propenyl)-4*H*-1-benzopyran-4-one

Kenji UNEYAMA, Yosinori MASATSUGU, and Sigeru TORII*

Department of Industrial Chemistry, School of Engineering, Okayama University, Okayama 700

(Received April 15, 1985)

Electrooxidative carbon-carbon bond cleavage is useful for the preparation of 3-methyl-4-oxo-2-phenyl-4*H*-1-benzopyran-8-carboxylic acid (**1b**) from 3-methyl-2-phenyl-8-(1-propenyl)-4*H*-1-benzopyran-4-one (**2**). Olefin **2** was transformed into 3-methyl-8-(1,2-epoxypropyl)-3-methyl-2-phenyl-4*H*-1-benzopyran-4-one (**3**) by the electrochemical bromohydrination in an MeCN–H_2O–H_2SO_4–NaBr–(Pt) system followed by treatment of aqueous sodium hydroxide (94%). The epoxide **3** was electrooxidized in an MeOH–H_2SO_4–(C) system, affording 8-formyl-3-methyl-2-phenyl-4*H*-1-benzopyran-4-one (**4**) in 83% yield. Hydrogen peroxide oxidation of **4** in refluxing 2-butanone gave **1b** in 86% yield.

Among the flavone derivatives, 2-piperidinoethyl 3-methyl-4-oxo-2-phenyl-4*H*-1-benzopyran-8-carboxylate (**1a**) has been used as a drug for prostatitis.[1] Several syntheses have been proposed where carboxyl group of salicylic acid was employed as a source of 8-carboxyl group of **1b**.[2] Carbon-carbon bond cleavage methods of propenyl group of 3-methyl-2-phenyl-8-(1-propenyl)-4*H*-1-benzopyran-4-one (**2**)[3] and 1-(3-propenyl-2-hydroxyphenyl)propanone with potassium permanganate and dichromate[4,5] are also known. Unfeasibility of the waste heavy metal in industry prompted us to study non-heavy metal oxidation method.

Chemoselective electrooxidative cleavage of a carbon-carbon double bond of the propenyl group would be promising. However, very few example has been known so far on one-step carbon-carbon double bond cleavage. Electrooxidation of stilbene[6] in an MeOH–NH_4Cl–(Pt) system and isoeugenol[7] in an H_2O–KOH–(PbO_2) system give the corresponding aromatic aldehyde in 45 and 77% yield, respectively. Yield of the reaction is not satisfactory and alkaline media are not usable for the present purpose because of instability of **2** in the media. Oxygenation of carbon-carbon double bond followed by carbon-carbon bond cleavage leading to aldehyde is an alternative method. Dimethoxy compounds[8] and α-hydroxy ketones[9] are electrochemically cleaved but their preparation from olefins is not accessible. 1,2-Diols and epoxides are promising precursors of the desired aldehydes and can be prepared from the corresponding halohydrins whose electrochemical preparations are intensively studied. On this basis, we have studied an electrochemical preparation and carbon-carbon bond cleavage of epoxide **3** and glycol **6a**, as precursors of **1b**. (Scheme 1).

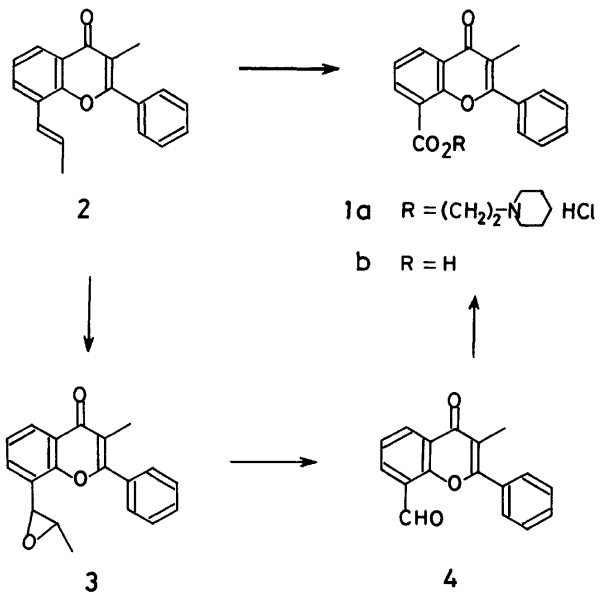

Scheme 1.

Electrooxidation of 2. The olefin **2** was prepared as described in literatures.[10] Aqueous acetonitrile containing sodium bromide was found to be an excellent medium for the epoxidation of isoprenoids,[11] cyclohexene,[12] and isosafrole.[13] Because of the low solubility of **2** in aqueous acetonitrile, tetrahydrofuran was employed as a cosolvent. In an MeCN–THF–H_2O (5:2:2)–NaBr–(Pt) system, a constant-current-density electrolysis (3.3 mA cm^{-2}) was conducted at room temperature in an undivided cell, affording **3** in 48% yield along with the dibromide **5a** in 9% yield. When 5—10 F mol^{-1} of electricity were passed, the starting material **2** was consumed completely but the material balance was poor due to the formation of the unidentified products. The reactivity of the double bond of propenyl group of **2** was found to be lower than those of isoprenoids and isosafrole due to meta-carbonyl group. Therefore, pH of the electrolysis solution was kept at an acidic side to affect bromohydrination. The result is shown in Fig. 1.

Electrochemical bromohydrination occurs chemoselectively at the double bond of propenyl group. Yield of **5b** increased sharply and reached to an maximum value (88%) and the amount of electricity required for the conversion of **2** was saved as increase of the concentration of sulfuric acid. Interestingly, the formation of **5a** could be suppressed in a higher concentration of sulfuric acid. [Yield % **3**, **5a**, and **5b** (con-

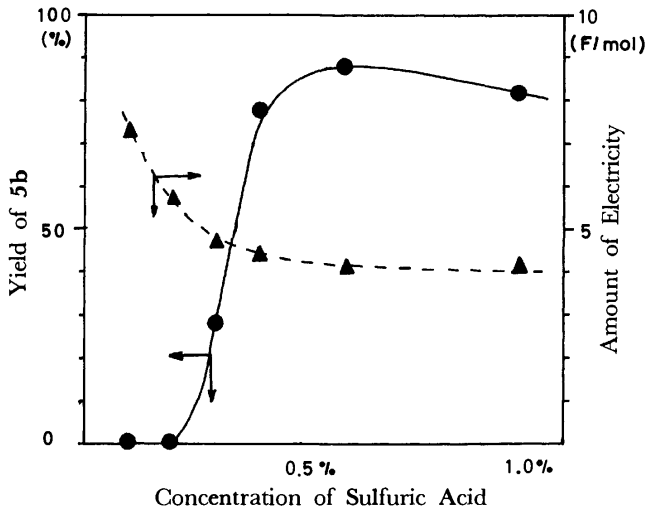

Fig. 1. Effect of the concentration of sulfuric acid for the yield of 5b and the amount of electricity in bromohydrination of **2** in an MeCN-THF-aq H_2SO_4-NaBr-(Pt) system.

centration of sulfuric acid %), 40, 32, 0 (0.1), and 0, 10, 88 (0.6)]. At 45 °C, **2** was soluble in MeCN-aq H_2SO_4 and converted to **5b** effectively in the highest chemical yield and current efficiency (93%, 2.9 F mol^{-1}).

Concentration of sodium bromide is also important. In the epoxidation of isoprenoids, bromide ion is regenerated in situ after epoxidation and thus 0.1—0.5 molar equivalent of sodium bromide to olefin is suitable so as to suppress the formation of the dibromides.[11] On the contrary to this, isosafrole **7** was efficiently electroepoxidized in the presence of 3—4 molar equivalent of sodium bromide because the dibromide **8a** was spontaneously hydrolyzed to the bromohydrin **8b** and finally converted to the epoxide *in situ* under the electrolysis conditions.[13] Hydrolysis of **5a** to **5b** was slow under the electrolysis conditions and therefore, the use of excess amount of sodium bromide should be avoided to minimize dibromination.

The base-catalyzed ring closure of **5b** to **3** proceeded smoothly. Thus, after electrochemical bromohydrination the electrolysis mixture was alkalined with 1 ml of 1 M sodium hydroxide and stirred at room temperature for 1 h, affording **3** in 94% yield.

Electrolysis of 3 and 6a. Glycol **6a** was obtained in 94% yield by the acidcatalyzed ring opening of **3** in THF-10% aq H_2SO_4 at room temperature for 11 h. The electrooxidative carbon-carbon bond cleavage of glycols has been examined in MeOH-Et_4NOTs for cyclic glycols,[14] in MeOH-NaOH for 1,1,2,2-tetraphenyl-1,2-ethanediol,[15] and in H_2O-$NaIO_4$-H_2SO_4 for 2,3-butanediol.[16] At first, electrooxidation of **6a** was examined in an MeCN-aq H_2SO_4-(Pt) system. But, unfortunately the electrooxidative cleavage of **6a** gave **4** in only 60—70% yield. Meanwhile, electrolysis in an MeOH-H_2SO_4-(C) system, the yield of **4** was improved to 91%. At 60 °C with a lower sulfuric acid concentration in MeOH, acetal **9** was formed exclusively (97%). The acetal **9** can be hydrolyzed to **4** in THF-aq H_2SO_4 almost quantitatively.

Comparison of the electrooxidative cleavage of **6a** with the chemical oxidant induced cleavage is shown in Table 1, which clearly reveals the prominent aspect of the electrolysis. Oxidation with sodium periodate proceeds smoothly under very mild conditions. However, the use of the expensive reagent is not economically feasible. Cobalt(II) acetate-catalyzed air oxidation[17] and calcium hypochlorite oxidation[18] under neutral conditions resulted in a disappointed yield.

Next, a direct cleavage of carbon-carbon bond of epoxide **3** was studied. Epoxide **3** was readily and quantitatively transformed into methoxy alcohol **6b** in MeOH-aq H_2SO_4 which was then electrolyzed *in situ*. Acetal **9** was a major product (83%) and **10b** was produced as a side product (8%). Comparison between entries 3 and 4, and entries 6 and 7 (Table 1) indicates that methoxylation on 3-methyl group took place partially at a higher current density. Presumably, electrooxidation of 2-phenyl group would compete with

Table 1. Electrochemical and chemical oxidative transformation of **6a** and **3** into **4** or **9**

Entry	Substrate	Oxidation Methods and Conditions	F/mol	mA/cm²	Product/%[a]			
					4	**9**	**10a**	**10b**
		Electrolysis[d]						
1	**6a**	MeCN-H_2O-0.2 eq H_2SO_4-Et_4NOTs (50 °C)	7.2	3.3	68			
2		MeOH-0.8 eq H_2SO_4 (r.t.)	3.7	1.7	91[b]			
3		MeOH-0.5 eq H_2SO_4 (r.t.)	7.0	0.6	86[b]			
4		MeOH-0.5 eq H_2SO_4 (50 °C)	3.0	3.3	74[b]		6	
5		MeOH-0.15 eq H_2SO_4 (60 °C)	5.6	0.6		97[c]		
6	**3**	MeOH-0.15 eq H_2SO_4 (60 °C)	11.0	0.7		83[c]		8
7		MeOH-0.03 eq H_2SO_4 (60 °C)	4.9	1.7		77[c]		13
		Chemical Oxidation						
8	**6a**	$NaIO_4$, MeOH-H_2O (0—3 °C)[e]			82			
9		$Co(OAc)_2$-O_2, DMF (110 °C)[f]			69			
10		$Ca(ClO)_2$, MeOH-H_2O (65 °C)[g]			27			

a) Isolated yield. b) The mixture was worked up without neutralization. c) After electrolysis, the mixture was neutralized with aq $NaHCO_3$. d) Mole equivalent of H_2SO_4 to substrate. e) 2 eq of $NaIO_4$ to **6a** for 1.5 h. f) 0.3 mole eq of $Co(OAc)_2$ to **6a** for 26 h. g) 4 mole eq of $Ca(ClO)_2$ to **6a** for 7 h.

that of the glycol moiety. Current efficiency of the conversion of **6b** to **9** is lower than that of **6a** to **9**, suggesting the lower reactivity of **6b** than **6a** (entries 5 and 6). In fact, when a 1:1 mixture of **6a** and **6b** was electrolyzed in an MeOH–aq H_2SO_4–(Pt) system (2 mA for 2 d, 3 F mol^{-1} on the basis of a total amount of **6a** and **6b**, **6a** was smoothly converted to **9** in 84% yield, while **6b** was recovered intact (98%).

Oxidation of Aldehyde 4 to Carboxylic Acid 1b. Although electrooxidation of benzaldehyde provides benzoic acid, oxidation of **4** in an MeOH–aq H_2SO_4–(C) system failed and methoxylation at 3-methyl group exclusively occurred leading to the formation of **10b** in 52% yield. In the electrolysis system, the initial electron transfer from 2-phenyl group rather than the trisubstituted aromatic nucleus and the following deprotonation from 3-methyl group would generate a conjugated methyl radical, which suffers methoxylation leading to **10b** by the further one-electron oxidation. Therefore, any oxidations where an initial step occurs on the formyl group rather than aromatic nucleus must be chosen for the present purpose and also because of the instability of **4** in alkaline media, oxidation conditions must be neutral or acidic. Oxidation of **4** with hydrogen peroxide in refluxing 2-butanone proceeded slowly and gave **1b** in 86% yield where supply of hydrogen peroxide at regular time intervals was useful. Nitric acid oxidation of **4** in refluxing benzene also provided **1b** in 85% yield in which concentration of nitric acid plays an important role [Yield (molar concentration of nitric acid); 77% (2 M), 68% (3 M), 85% (4 M), and 59% (6 M)]. Meanwhile, oxidation of **3** with ammonium vanadate–nitric acid[19] in refluxing benzene yielded a mixture of **1b** and **4** (35%).

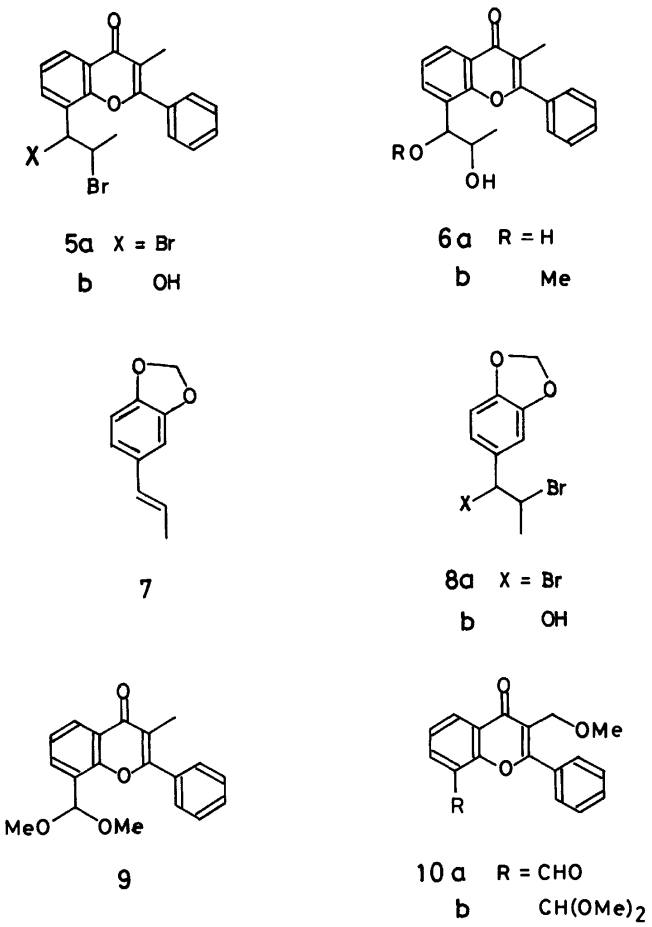

Scheme 2.

Experimental

Melting points and boiling point are uncorrected. The IR spectra were obtained with a JASCO IRA-1 spectrometer. ^{1}H NMR were measured with a JNM FX-100 spectrometer at 100 MHz or Hitachi R-24 spectrometer at 60 MHz in $CDCl_3$ using Me_4Si as an internal standard. Elemental analysis was performed using a Yanaco Model MC-2 micro-determining apparatus. Substrate **2** were supplied from Shiono Koryo Kaisha Ltd., to which the authors are grateful. A regulated DC power was supplied by a Metronix 543B instrument for electrolysis.

8-(1,2-Epoxypropyl)-3-methyl-2-phenyl-4H-1-benzopyran-4-one (3). A mixture of **2** (100 mg, 0.36 mmol) and NaBr (41 mg, 0.4 mmol) dissolved in MeCN (7 ml)–H_2O (1.7 ml) and 1% aq H_2SO_4 (0.3 ml) was electrolyzed in a beaker type undivided cell. A constant current (10 mA, 2.92 F mol^{-1}) was passed at 45 °C for 2 h and 50 min using platinum foils (1.5×2 cm^2) as an electrode. After electrolysis, 1 M NaOH (1 ml) was added to the mixture, which was stirred at room temperature for 1 h. After evaporation of MeCN, the mixture was extracted with AcOEt. The extracts were washed with brine, dried (Na_2SO_4), and concentrated *in vacuo*. The residue was chromatographed (Wako-gel C200, benzene/AcOEt=15/1) to give **3** (99.3 mg, 94%): mp 157.4—159 °C (ether); IR (Nujol) 1632, 1600, 1590, 1136, 761,700 cm^{-1}; ^{1}H NMR ($CDCl_3$) δ=1.48 (3H, d, J=5 Hz, CH_3), 2.18 (3H, s, CH_3), 3.40 (1H, dq, J=5 Hz and 2 Hz, CH), 4.06 (1H, d, J=2 Hz, CH), 7.17—7.80 (7H, m, ArH), 8.15 (1H, dd, J= 8 Hz and 2 Hz, ArH). Found: C, 78.02; H, 5.67. Calcd for $C_{19}H_{16}O_3$: C, 78.07: H, 5.52.

8-(2-Bromo-1-hydroxypropyl)-3-methyl-2-phenyl-4H-1-benzopyran-4-one (5b). Electrolysis of **2** was conducted in the same manner as described for **3** and the mixture was worked up as usual, affording **5b** (125.2 mg, 93%): decomposed at around 160 °C; IR (Nujol) 3300 (OH), 1614, 1595, 1395, 764, 696, 657 cm^{-1}; ^{1}H NMR ($CDCl_3$) δ=1.58 (3H, d, J=7 Hz, CH_3), 2.15 (3H, s, CH_3), 3.00—3.42 (1H, br s, OH), 4.40—4.70 (1H, m, CH), 5.56 (1H, d, J=4 Hz, CH), 7.10—7.75 (6H, m, ArH), 7.85 (1H, dd, J=8 Hz and 2 Hz, ArH), 8.12 (1H, dd, J=8 Hz and 2 Hz, ArH). Found: C, 61.02; H, 4.57. Calcd for $C_{19}H_{17}O_3Br$: C, 61.14; H, 4.59.

8-(1,2-Dibromopropyl)-3-methyl-2-phenyl-4H-1-benzopyran-4-one (5a); mp 128—129.4 °C (ether): IR ($CHCl_3$) 1630, 1607, 1590, 1485, 1450, 1400, 1140 cm^{-1}: ^{1}H NMR ($CDCl_3$) δ=1.79 and 2.05 (3H, d, J=7 Hz, CH_3, a ratio of diastereoisomer= 2:9), 2.20 (3H, s, CH_3), 4.50—5.10 (1H, m, CH), 5.50—5.90 (1H, m, CH), 7.20—7.95 (7H, m, ArH), 8.29 (1H, J=8 Hz and 2 Hz, ArH). Found: C, 52.39; H, 3.74. Calcd for $C_{19}H_{16}O_2Br_2$: C, 52.33; H, 3.70.

8-(1,2-Dihydroxypropyl)-3-methyl-2-phenyl-4H-1-benzopyran-4-one (6a). To a solution of **3** (708.1 mg, 2.42 mmol) in distilled THF (10 ml) was added 10% aq H_2SO_4 (4 ml) at

room temperature and the mixture was stirred for 11 h. The mixture was concentrated *in vacuo* and insoluble materials were removed by filtration. The crystals on filter were washed with water and benzene, dried *in vacuo* to give **6a** (703 mg, 94%): mp 192—193 °C (AcOEt); IR (Nujol) 3400 (OH), 1620, 1605, 1125, 1067, 1025, 763, 700, 660 cm^{-1}; ^1H NMR ($CDCl_3$) δ=1.08 (3H, d, J=8 Hz, CH_3), 2.16 (3H, s, CH_3), 4.08 (1H, m, CH), 5.36 (1H, d, J=4 Hz, CH), 7.20—7.84 (6H, m, ArH), 7.96 (1H, dd, J=8 Hz and 2 Hz, ArH), 8.22 (1H, dd, J=8 Hz and 2 Hz, ArH). Found: C, 73.55; H, 6.00. Calcd for $C_{19}H_{18}O_4$: C, 73.54; H, 5.85.

8-Formyl-3-methyl-2-phenyl-4H-1-benzopyran-4-one (4) and 8-Dimethoxymethyl-3-methyl-2-phenyl-4H-1-benzopyran-4-one (9): Electrolysis of 6a. A solution of **6a** (100 mg, 0.32 mmol) dissolved in H_2SO_4–MeOH solution (25 mM, 10 ml) was electrolyzed in a beaker-type undivided cell. A constant current (5 mA, 3.86 F mol^{-1}) was passed at room temperature for 6 h and 40 min with glassy carbon electrodes (1.21×2.7 cm^2). After evaporation of MeOH under reduced pressure, the residue was dissolved in AcOEt, and the solution was washed with sat. $NaHCO_3$ and brine, dried (Na_2SO_4), and concentrated *in vacuo*. The residue was chromatographed over silica-gel (Wako-gel C200, benzene/AcOEt=11/1) to give **4** (77.7 mg, 91%): mp 119—121.5 °C; IR (Nujol) 1684, 1655, 1623, 1405, 1122, 761, 698, 660 cm^{-1}; ^1H NMR ($CDCl_3$) δ=2.22 (3H, s, CH_3), 7.17—7.87 (6H, m, ArH), 8.20 (1H, dd, J=8 Hz and 2 Hz, ArH), 8.49 (1H, dd, J=8 Hz and 2 Hz, ArH), 10.64 (1H, s, CHO). Found: C, 77.18; H, 4.52. Calcd for $C_{17}H_{12}O_3$: C, 77.26; H, 4.58.

On the other hand, **6a** was electrolyzed in H_2SO_4–MeOH solution (5 mM, 10 ml) under a constant current of 0.67 mA cm^{-2} at 60 °C for 24 h (5.6 F mol^{-1}) using glassy carbon electrodes (1.2×2.5 cm^2). After electrolysis, the reaction solution was neutralized with sat. $NaHCO_3$. The usual workup provided **9** (96.7 mg, 97%): mp 136.5—137.5 °C (ether); IR (Nujol) 1644, 1486, 1404, 1115, 1060, 770, 703, 660 cm^{-1}; ^1H NMR ($CDCl_3$) δ=2.20 (3H, s, CH_3), 3.39 (6H, s, OCH_3), 5.84 (1H, s, ArCH), 7.20—7.80 (6H, s, ArH), 7.90 (1H, dd, J=8 Hz and 2 Hz, ArH), 8.24 (1H, dd, J=8 Hz and 2 Hz, ArH). Found: C, 73.38: H, 5.93. Calcd for $C_{19}H_{18}O_4$: C, 73.54; H, 5.85.

Oxidation of 6a with $NaIO_4$. A solution of $NaIO_4$ (96 mg, 0.45 mmol) in H_2O (3 ml) was dropped to **6a** (70 mg, 0.23 mmol) dissolved in MeOH (4 ml) at 0—3 °C and the mixture was stirred at the temperature for 1.5 h. Ethyl acetate extraction followed by chromatography (Wako-gel C200, benzene/AcOEt=10/1) provided **4** (49.4 mg, 82%).

Oxidation of 6a with $Co(OAc)_2$–O_2. A mixture of **6a** (100 mg, 0.32 mmol) and $Co(OAc)_2$ (17 mg, 0.096 mmol) dissolved in DMF (6 ml) was stirred under oxygen atmosphere at 110—115 °C for 26 h. After addition of water, the organic substance was extracted with AcOEt. The usual workup provided **4** (58.9 mg, 69%).

Oxidation of 6a with $Ca(OCl)_2$. A suspension of $Ca(OCl)_2$ (23 mg, 0.1 mmol) in MeCN (2 ml)–H_2O (1 ml) was added to a solution of **6a** (60 mg, 0.19 mmol) dissolved in MeCN (4 ml)–H_2O (2 ml). After vigorous stirring at 65 °C for 1 h, $Ca(OCl)_2$ (70 mg, 0.3 mmol) suspended in MeCN (2 ml)–H_2O (1 ml) was added again and the mixture was stirred for 2 h. In the same way, $Ca(OCl)_2$ (52 mg, 0.22 mmol) suspended in MeCN (1 ml)–H_2O (1 ml) was added additionally twice and the mixture was stirred for 2 h in each addition. Organic substances were extracted with AcOEt and the usual workup provided **4** (14 mg, 27%) after chromatography.

Electrolysis of 3. A solution of **3** (100 mg, 0.34 mmol) dissolved in H_2SO_4–MeOH solution (5 mM, 10 ml) was stirred at 60 °C for 40 min. And the mixture was electrolyzed under a constant current of 0.67 mA cm^{-2} at 60 °C for 48 h (10.5 F mol^{-1}) using glassy carbon electrodes. After evaporation of MeOH, the residue was dissolved in THF (3 ml). The mixture was added 10% aq H_2SO_4 (2 ml) and stirred at room temperature for 1 h, concentrated *in vacuo*, and extracted with AcOEt. The extracts were washed with sat. $NaHCO_3$ and brine, dried (Na_2SO_4), and concentrated *in vacuo*. The residue was chromatographed (Wako-gel C200, benzene/AcOEt=15/1) to give **4** (75.7 mg, 84%).

8-(2-Hydroxy-1-methoxypropyl)-3-methyl-2-phenyl-4H-1-benzopyran-4-one (6b). The acid-catalyzed ring opening of **3** as described above and the usual workup gave **6b** (quantitatively): mp 151—152 °C (ether); IR (Nujol) 3350 (OH), 1626, 1585, 1397, 1114, 763, 695, 660 cm^{-1}; ^1H NHR ($CDCl_3$) δ=1.14 (3H, d, J=6 Hz, CH_3), 2.13 (3H, s, CH_3), 2.92 (1H, br s, OH), 3.30 (3H, s, OCH_3), 3.95—4.35 (1H, m, CH), 4.85 (1H, d, J=5 Hz, ArCH), 7.20—7.90 (7H, m, ArH), 8.10 (1H, dd, J=8 Hz and 2 Hz, ArH). Found: C, 74.09: H, 6.27. Calcd for $C_{20}H_{20}O_4$: C, 74.06: H, 6.21.

After electrolysis, the reaction mixture was neutralized with sat. $NaHCO_3$. The usual workup and chromatography gave **9** (83%).

3-Methyl-4-oxo-2-phenyl-4H-1-benzopyran-8-carboxylic Acid (1b). Oxidation of 4 with Hydrogen Peroxide: To a solution of **4** (80 mg, 0.30 mmol) in 2-butanone heated to 90—95 °C, 31% of H_2O_2 (1 ml) was added four times at every 10 h intervals. After being stirred for 44 h, H_2O_2 was quenched with $NaHSO_3$. The reaction mixture was acidified with 10% HCl and extracted with AcOEt. The extracts were concentrated *in vacuo*. The residue was dissolved in sat. $NaHCO_3$ and extracted with AcOEt. The aqueous layer was acidified with 10% HCl and extracted with AcOEt. The extracts were dried (Na_2SO_4) and concentrated *in vacuo*. The residue was chromatographed over short silica-gel column (Wako-gel C200, AcOEt/benzene=3/1) to give **1b** (72.4 mg, 85%): mp 226.5—228 °C (AcOEt)(lit,[3a] 227—229 °C); IR (Nujol) 3160 (OH), 1734, 1620, 1218, 1180, 1134, 1025, 785, 763, 700, 678, 664 cm^{-1}; ^1H NMR ($CDCl_3$+CD_3OD=1:2) δ=2.23 (3H, s, CH_3), 7.30—7.65 (5H, m, ArH), 7.70—7.95 (1H, m, ArH), 8.15—8.55 (2H, m, ArH).

Oxidation of 4 with Nitric Acid. A solution of **4** (80 mg, 0.30 mmol) in benzene (2 ml) was added to 4 M HNO_3 (6 ml) and stirred vigorously at 90 °C for 49 h. The reaction mixture was extracted with AcOEt. The extracts were concentrated *in vacuo*. The residue was dissolved in sat. $NaHCO_3$ and extracted with AcOEt. The aqueous layer was acidified with 10% HCl and extracted with AcOEt. The extracts were dried (Na_2SO_4) and concentrated *in vacuo*. The residue was chromatographed over short column (Wako-gel C200, AcOEt/benzene=3/1) to give **1b** (72 mg, 85%).

8-Formyl-3-methoxymethyl-2-phenyl-4H-1-benzopyran-4-one (10a). Mp 146.7—148 °C (ether); IR (Nujol) 1690, 1660, 1623, 1090, 760, 690, 656 cm^{-1}: ^1H NMR ($CDCl_3$) δ=3.50 (3H, s, OMe), 4.37 (2H, s, CH_2), 7.10—8.00 (6H, m, ArH), 8.17 (1H, dd, J=8 Hz and 2 Hz, ArH), 8.45 (1H, dd, J=8 Hz and 2 Hz, ArH), 10.64 (1H, s, CHO). Found: C, 73.71; H, 4.90. Calcd for $C_{18}H_{14}O_4$: C, 73.46; H, 4.79.

8-Dimethoxymethyl-3-methoxymethyl-2-phenyl-4H-1-benzo-

pyran-4-one (10b). Bp 185—186 °C (6.92×10^{-1} Pa): IR(Neat 2950, 1740, 1715, 1650, 1490, 778, 705, 665 cm^{-1}; ^1H NMR ($CDCl_3$) δ=3.37 (6H, s, OMe), 3.50 (3H, s, OMe), 4.36 (2H, s, CH_2), 5.85 (1H, s, CH), 7.25—8.10 (7H, m, ArH), 8.25 (1H, dd, J=8 Hz and 2 Hz, ArH). Found: C, 73.89; H, 6.43. Calcd for $C_{20}H_{20}O_4$: C, 74.06; H, 6.21.

Reference

1) I. Setnikar. M. T. Ravasi, and P. Da Re, *J. Pharmacol Exptl. Therap.*, **130**, 356 (1960); *Chem. Abstr.* **55**, 4764e (1961).

2) P. Da Re, *U. S. Pat.*, 2921070. *Chem. Abstr.*, **54**, 7739h (1960); E. Sianesi, *Ger. Offen*, 2059296; *Chem. Abstr.*, **76**, 140532u (1972).

3) P. Da Re, U. S. Patent, 3350411; *Chem. Abstr.*, **68**, 87159j (1968); S. P. A. Recordati, *Neth. Appl.*, 6410430; *Chem. Abstr.*, **63**, 9717g (1965); N. Mitsumori, H. Suya, S. Houda, and K. Kakamura, *Japan Kokai*, 74-80076; *Chem. Abstr.*, **82**, 111946a (1975).

4) N. Mitsumori, H. Suya, S. Houda, and K. Nakamura, *Japan Kokai*, 74-80035; *Chem. Abstr.*, **82**, 156078k (1975).

5) E. Sianesi, *Ger. Offen*, 2051269; *Chem. Abstr.*, **76**, 99356z (1972).

6) T. Inoue, K. Koyama, T. Matsuoka, and S. Tsutsumi, *Bull. Chem. Soc. Jpn.*, **40**, 162 (1967); T. Inoue and S. Tsutsumi, *Bull. Chem. Soc., Jpn.*, **38**, 661 (1965).

7) F. Fichter and A. Christen, *Helv. Chem. Acta*, **8**, 332 (1925); F. Fichter and M. Rinderspacher, *ibid.*, **10**, 102 (1927).

8) N. L. Weinberg and H. R. Weinberg, *Chem. Revs.*, **68**, 449 (1968); S. Torii, "Electroorganic Syntheses, Methods and Applications, Part 1 Oxidation," Kodansha, Tokyo, Verlag Chemie (Weinheim) (1985). Dimethoxides of olefins can be readily prepared by electrooxidative methoxylation in MeOH-MeONa. However, the electrolysis conditions are not usable for the present purpose.

9) S. Torii, T. Inokuchi, and R. Oi, *J. Org. Chem.*, **47**, 47 (1982); S. Torii, T. Inokuchi, and K. Yoritaka, *J. Org. Chem.*, **46**, 5030 (1981).

10) P. Da Re, *Japan* 41-7953 (1966); T. Takahashi and T. Oshika, *Yakugaku Zasshi* **74**, 48 (1954). The authors are grateful to Shiono Koryo Kaisha Ltd., for the generous supply of the compound **2**.

11) S. Torii, K. Uneyama, M. Ono, H. Tazawa, and S. Matsunami, *Tetrahedron Lett.*, **20**, 466 (1979).

12) S. Torii, K. Uneyama, H. Tanaka, T. Yamanaka, T. Yasuda, M. Ono, and Y. Khomoto, *J. Org. Chem.*, **46**, 3312 (1981).

13) S. Torii, K. Uneyama, and K. Ueda, *J. Org. Chem.*, **49**, 1830 (1984).

14) T. Shono, Y. Matsumura, T. Hashimoto, K. Hibino, H. Hamaguchi, and T. Aoki, *J. Am. Chem. Soc.*, **97**, 2546 (1975).

15) W. Kemula, Z. R.Grabowski, and M. K. Kalinowski, *J. Am. Chem. Soc.*, **91**, 6863 (1969); R. F. Michielli and P. J. Elving, *ibid.*, **91**, 6864 (1969).

16) A. Yoshiyama, T. Nonaka, M. M. Baizer, and T-C Chou, *Bull. Chem. Soc. Jpn.*, **58**, 201 (1985).

17) G. de Vries and A. Schors, *Tetrahedron Lett.*, **1968** 5689.

18) S. O. Nwaukwa and P. M. Keehn, *Tetrahedron Lett.*, **23**, 3135 (1982).

19) I. N. Nazarov, L. D. Bergel'son, I. V. Torgov, and S. N. Ananchenko, *Izvest. Akad. Nauk, SSSR*, **1953**, 889; *Chem. Abstr.*, **49**, 1082 (1955).

A Highly Selective Transannular Route to *trans-trans*-1,2,3,3a,4,-5,9,10,10a,10b-Decahydropyrenes from [2.2]Metacyclophanes

Takeo SATO,* Kozaburo NISHIYAMA, Akira MORITA, and Yoichi IITAKA†
Department of Chemistry, Tokyo Metropolitan University, Setagaya-ku, Tokyo 158
†*Faculty of Pharmaceutical Sciences, The University of Tokyo, Bunkyo-ku, Tokyo 113*
(Received April 23, 1985)

The treatment of [2.2]metacyclophanes with aluminum chloride gave a variety of hydropyrenes as the results of dehydrogenation, cycloisomerization, and disproportionation reactions. With ethylaluminum dichloride, however, a highly selective reaction occurred to give *trans-trans*-1,2,3,3a,4,5,9,10,10a,10b-decahydropyrene. Revised structures were presented for *cis-cis*- and *trans-trans*-decahydropyrenes based on ^{13}C NMR and X-ray crystallographic analyses.

We have reported[1] that the treatment of [2.2]-metacyclophane (**1a**) with aluminum chloride in carbon disulfide gives a variety of hydropyrenes, arising from three types of transannular reactions; 1) dehydrogenation (**2a**, **3a**, and **4a**), 2) cycloisomerization (**5a**), and 3) hydrogenation *via* disproportionation (**6a** and **7a**). The type-1 reaction occurred quite readily

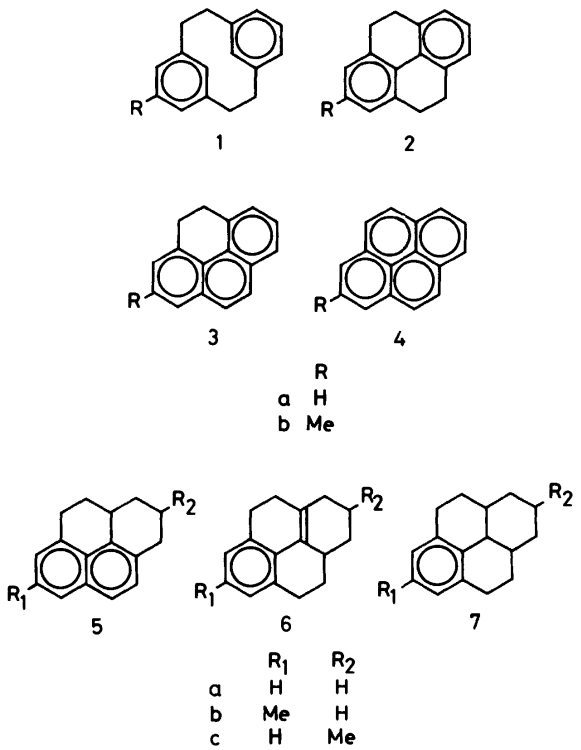

due to an anomalously low anodic potential of **1a**[2] by the action of various one-electron oxidants and other electron-transfer conditions.[3] The selective formation of **5a** through the type-2 reaction was best achieved by the reaction of **1a** with iodine.[4]

In this paper we describe the selective formation of the type-3 products, especially decahydropyrene (*cf.* **7a**) by using ethylaluminum dichloride. We also report the stereochemistry of the decahydropyrene studied by the NMR spectrometry and by the X-ray crystallographic analysis.

The Reaction of [2.2]Metacyclophane with Aluminum Chloride. Baker and co-workers[5] have reported the formation of 1,2,3,3a,4,5-hexahydropyrene (**5a**) by the reaction of **1a** with aluminum chloride in carbon disulfide. When we repeated the reaction we obtained a complex mixture of products, **2a**, **3a**, **4a**, **5a**, **6a**, and **7a**. By carrying out the reaction under various conditions[1] we have shown that the initial products are 1,2,3,3a,4,5,9,10-octahydropyrene (**6a**), **5a**, and 4,5,9,10-tetrahydropyrene (**2a**). Upon further contact with aluminum chloride, 1,2,3,3a,4,5,9,10,10a,10b-decahydropyrene (**7a**) was formed by the disproportionation of **6a**.

Table 1 shows the product ratio obtained from the transannular reaction of **1a** and **1b** with 4 equiv aluminum chloride in carbon disulfide for 3 h at room temperature. The analyses of the products were performed by GC–MS by using an OV-1 column for gas chromatography. When hydrogen chloride was passed through the mixture, the cycloisomerization product **5a** became the major product.

The effect of a substituent at C-5 was then investigated. Under similar conditions as above, 5-methyl-[2.2]metacyclophane (**1b**) also gave a complexed mixture. Compared with **1a**, the yields of **6** and **7** decreased while the yields of **2** and **5** increased marked-

TABLE 1. THE REACTION OF [2.2]METACYCLOPHANE (**1a**) AND (**1b**) WITH $AlCl_3$ OR $AlCl_3$–HCl

Compound	Hydropyrenes/%					
	Tetra-, **2**	Di-, **3**	**4** (Pyrene)	Hexa-, **5**	Octa-, **6**	Deca-, **7**
1a[a]	1	—	20	6	30	43
1a[a,b]	—	—	3	84	12	1
1b	40	10	5	25	18	2
1b[c]	1	—	2	95	2	1

a) Ref. 1. b) $AlCl_3$–HCl reflux. c) $AlCl_3$–HCl room temperature.

ly. For **5**, **6**, and **7**, two isomeric products are possible, namely the b or c types according to the direction of reaction. The ^{1}H NMR of the products showed the presence of an aromatic methyl resonance at around δ 2.2—2.5 and, hence, these were **5b**, **6b**, and **7b** but not **5c**, **6c**, and **7c**. When hydrogen chloride was passed through the mixture the major product was **5b**.

Selective Formation of Decahydropyrene. The Lewis acid strength of ethylaluminum compounds were found to be as follows:[6]

$$AlCl_3 > EtAlCl_2 > Et_2AlCl, Et_3Al$$

While aluminum chloride was too reactive for **1a** to induce a selective disproportionation reaction, **1a** was inert toward triethylaluminum as well as diethylaluminum chloride.

Ethylaluminum dichloride has been generated *in situ* using the following scheme:[7]

$$Et_2AlCl + TiCl_4 \longrightarrow EtAlCl_2 + EtTiCl_3$$

Ethyltitanium trichloride formed was unstable and the evolution of ethylene among others was noticed.[8] As a control experiment, compound **1a** was found to be stable toward titanium tetrachloride.

When compound **1a** was treated with the reagent formed from 3 equiv each of diethylaluminum chloride and titanium tetrachloride in benzene under reflux for 3 h, nearly equal amounts of **2a** and **7a** were produced. Compound **7a** was found to be a single stereoisomer by the ^{13}C NMR spectrum and gas chromatography using an SE-30 column. The stoichiometric consideration requires a hydrogen donor other than **1a** to give **7a** since only two hydrogens are evolved to form **2a** while the formation of **7a** requires four. Presumably, the ethylaluminum reagent is responsible for the hydrogen source to form highly hydrogenated **7a**.

The directional selectivity on the formation of isomeric decahydropyrenes was tested using methyl-substituted [2.2]metacyclophanes, **1b**, **8**, and **9**. It has been found[1,9] that an alkyl substituent on [2.2]metacyclophane exerts different effects according to the position of substitution. With cycloisomerization, for example, a C-5 alkyl group as in **1b** directs the hexahydropyrene formation while preserving a substituted aryl ring. The C-4 and 6 alkyl groups as in **8** and **9** lead the hydrogenation of a substituted aryl ring, presumably through the additional strain effect of the methyl group on the bridging methylene group.[1,9]

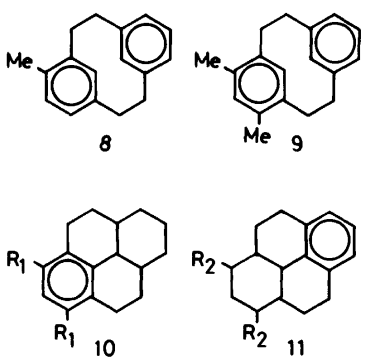

	R_1	R_2
a	Me	H
b	Me	Me

5-Methyl derivative **1b**, upon treatment with 3 equiv diethylaluminum chloride and titanium tetrachloride in benzene, gave an exclusive formation of **7b**, no isomeric **7c** being detected. 4-Methyl derivative **8**, on the other hand, gave a mixture of products **10a** and **11a** in a ratio of 4:6 as analyzed by gas chromatography and ^{1}H NMR. 4,6-Dimethyl derivative **9** gave, under similar conditions, a mixture of **10b** (75%) and **11b** (25%). Here again, the methyl group next to the bridging methylene group forced the formation of the product with a hydrogenated substituted aryl ring similar to the case of cycloisomerization.

In addition to decahydropyrenes, these reactions afforded approximately equal amounts of the corresponding tetrahydropyrenes, **2b**[10] from **1b**, 1-methyl- and 1,3-dimethyl-4,5,9,10-tetrahydropyrenes[10] from **8** and **9**, respectively.

Isomeric structures between **7b** and **7c**, and also **10** and **11**, could be assigned based on both ^{1}H NMR and mass spectrometry. Aromatic methyl compounds, **7b**, **10a**, and **10b** showed singlets around δ 2.2, while aliphatic methyl derivatives **7c**, **11a**, and **11b** showed doublets in the expected region. A base peak in mass spectrometry also gives the difference; namely, base peaks for aromatic methyl and aliphatic methyl compounds were found to be M-15 and M-28, respectively (Table 3).

Stereochemistry of Decahydropyrene. The decahydropyrene **7a** can exist in three stereoisomers, namely *cis-cis*-compound **12a**, *trans-trans*-compound **13a**, and *cis-trans*-**14**. Compounds **12a** and **13a** are *meso* type while **14a** is a *dl*-type.

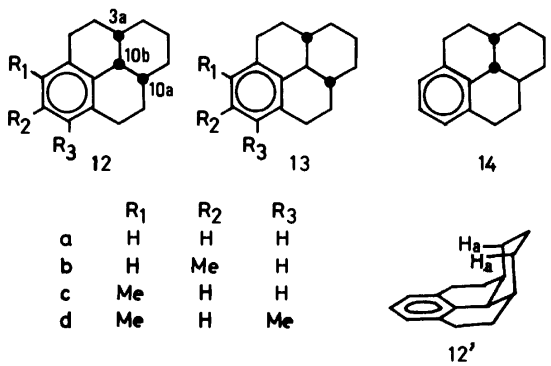

	R_1	R_2	R_3
a	H	H	H
b	H	Me	H
c	Me	H	H
d	Me	H	Me

Lehner and co-worker obtained[11] a decahydropyrene, mp 129 °C, by the hydrogenation of **1a** over rhodium on alumina catalyst and assigned a *trans-trans*-structure **13a** based on the NMR evidence. We obtained[1] a deca-

Table 2. ^{13}C NMR data for decahydropyrenes (**12a**), (**12d**), and (**13a**)—(**13d**)

Compound	Aliphatic Carbons				Aromatic Carbons	
	3a,10a	10b	CH_2	Me	quat.	ArH
12a[a]	35.68	39.75	28.47, 26.06 25.74, 25.24		136.22, 134.12	126.22, 125.00
13a[b]	38.11	47.93	34.29, 30.76 29.14, 25.73		136.11, 135.95	126.13, 125.39
13b	38.47	47.93	34.45, 31.00 29.26, 25.97	21.06	136.07, 135.01 133.02	127.06
13c	38.30 37.45	48.24	34.36, 30.81 30.79, 29.08 27.02, 25.73	19.49	135.76, 134.41 133.53, 126.79	127.20, 126.11
12d	35.64	40.34	28.41, 26.06 24.91, 23.61	19.47	133.60, 133.07 131.82	128.73
13d	37.58	48.47	34.33, 30.75 26.77, 25.58	19.22	135.69, 133.21 131.77	129.99

a) Lehner's decahydropyrene; Ref. 10. b) Our decahydropyrene; Ref. 1: Data reported in Ref. 1 need to be modified as tabulated as pointed out by Hansen *et al.*[12]

Table 3. 1,2,3,3a,4,5,9,10,10a,10b-Decahydropyrenes

Compound	Mp/θ_m/°C	M^+	Base Peak	Formula	Found %		Calcd %	
					C	H	C	H
13a[a]	53.5—54.5	212	184 (M−28)					
13b	93—94	226	211 (M−15)	$C_{17}H_{22}$	89.82	9.97	90.20	9.80
11a	oil	226	198 (M−28)	$C_{17}H_{22}$	90.15	9.73	90.20	9.80
13c	oil	226	211 (M−15)					
13d	97—98	240	225 (M−15)	$C_{18}H_{24}$	89.66	10.01	89.94	10.06
12d	(75—85[b])	240	225 (M−15)	$C_{18}H_{24}$	89.86	10.19	89.94	10.06
11b	oil	240	212 (M−28)					

a) Ref. 1. b) Mp of the mixture, **12d** and **13d**.

hydropyrene, mp 53.5—54.5 °C, by the disproportionation of **1a**. It was also a *meso*-type compound similar to that of Lehner, as examined by ^{13}C NMR. In view of Lehner's results, we tentatively assigned a *cis-cis*-structure **12a**.[1] Later, Hansen *et al.* obtained[12] both of these by the cathodic reduction of tetrahydropyrene **2a** in DMF in the presence of a proton donor. The *dl*-type compound **14** was also reported by Hansen *et al.*[12]

Table 2 summerizes the ^{13}C NMR data for isomeric decahydropyrenes obtained by Lehner *et al.* and by us. The assignment was achieved by an intensity consideration, the off-resonance spectrum, and by a comparison with reported data. Compared with our product, Lehner's decahydropyrene showed a general upfield shift of corresponding resonances. For example, two quaternary carbon resonaces and three out of four methylene carbon resonances showed upfield shifts of 2—8 ppm while aromatic signals were almost similar. The upfield shift of the 10b carbon amounted to almost 8 ppm. This was taken as evidence that Lehner's product had a more congested structure compared to our decahydropyrene.[13] Our product showed a clear triplet in the ^1H NMR spectra, determined at 500 MHz at 1.845 ppm with J=11.3 Hz. This was assigned to the 10b proton which had antiperiplaner vicinal protons (possible only for **13a**, but not for **12a**). From this evidence, we concluded that the assignment must be revised. The Lehner's product was **12a** not **13a**, and our product was **13a** but not **12a**. This assignment appeared to be consistent with the hydrogenation experiment carried out by Lehner for **1a**. They obtained[14] a perhydropyrene possessing *cis-cis*-structure as the partial structure expected from one-sided hydrogenation.

Our decahydropyrenes **7b** and **10a** are best represented by **13b** and **13c**, respectively. The ^{13}C resonances of the 10b carbon for **13b** and **13c** were δ 47.93 and 48.24, respectively, expected from a *trans-trans*-structure. Decahydropyrene **10b**, obtained from **9**, was found to be a mixture of both **12d** and **13d** (mp 75—85 °C as a mixture), almost in equal amounts. These were separated by repeated chromatography on alumina containing silver nitrate. This separated **13d** (mp 97—98 °C) as a fast eluting fraction which was followed by *cis-cis*-compound **12d**. By gas chromatography on OV-1, the elution order was reversed and **12d** became the fast moving fraction. Compound **12d** showed an upfield shift of the 10b carbon resonance by about 8 ppm compared with **13d**. Also, **12d** showed a high-field multiplet in the ^1H NMR at 0.80—1.40 ppm, which in the case of **13d** occurred at 1.05—1.50 ppm. Axial protons Ha in 12′ must be responsible for the upfield shift due to a ring-current

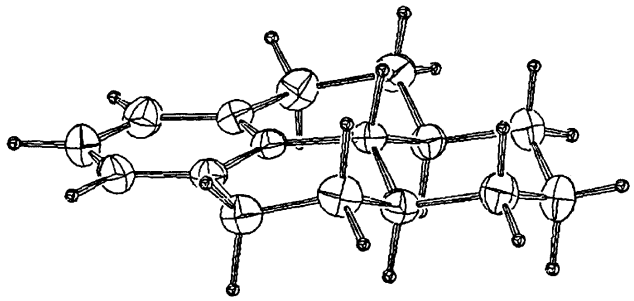

Fig. 1. ORTEP drawing of the structure of **13a**, thermal ellipsoid of 30% probability.

effect.

Conclusive evidence was obtained by the X-ray crystallographic analysis of **13a**. The crystal data for **13a** are as follows: $C_{16}H_{20}$, M=212.32, monoclinic, space group C2/c, a=19.139(15), b=9.970(8), c=15.311(10)Å, β=123.34(9)°, U=2440.8Å^3, Z=8, D_c=1.155 g cm^{-3}. The structure was solved by the direct method. Least-squares refinement of the atomic positional and thermal parameters converged at R=0.06 using 2467 refractions. A view of the molecular structure is shown in Fig. 1.

Experimental

[2.2]Metacyclophane Derivatives. Compounds **1a**,[1] **1b**,[10] and **9**[10] were prepared as described in the literature.

2,11-Dithia-5-methyl[3.3]metacyclophane. α,α'-Dibromo-*m*-xylene was treated with thiourea in ethanol and then with a potassium hydroxide solution to give *m*-xylene-α,α'-dithiol. Benzene solution (600 cm^3) of 4-methyl-α,α'-dichloro-*m*-xylene (17.8 g, 94 mmol), prepared by bischloromethylation of toluene, was dropped slowly into a solution of the dithiol (16 g, 94 mmol) and sodium hydroxide (8 g, 0.2 mol) in benzene (400 cm^3)-ethanol (1000 cm^3) during 72 h under reflux. The solvent was then evaporated, and washed dichloromethane extracts were passed through a silica-gel column. The bis(sulfide) was thus obtained in a 52% yield: pale yellow needles from ethanol-water-hexane, mp 86—88°C: NMR ($CDCl_3$) δ=2.15 (3H, s, Me), 3.6 (8H, m, CH_2), and 6.5—6.9 (7H, m, ArH).

Found: C, 71.24; H, 6.41; S, 22.13%. Calcd for $C_{17}H_{18}S_2$: C, 71.28; H, 6.33; S, 22.39%.

4-Methyl[2.2]metacyclophane (8). The above bis(sulfide) was converted to bis(sulfone), 2,11-dithia-5-methyl[3.3]-metacyclophane 2,2,11,11-tetraoxide, by oxidation with 30% hydrogen peroxide in benzene-acetic acid at room temperature. The pyrolysis of bis(sulfone) at 550°C gave **8** (mp 70—72°C) after chromatography on silica gel: NMR ($CDCl_3$) δ=2.35 (3H, s, Me), 2.05 and 3.07 (8H, m, CH_2), 4.2—4.3 (2H, m, C-8H and C-16H), and 6.9—7.4 (7H, m, ArH).

Found: C, 91.81; H, 8.15%. Calcd for $C_{17}H_{18}$: C, 91.84; H, 8.16%.

The Reaction of 5-Methyl[2.2]metacyclophane (1b) with Aluminum Chloride. The reaction was carried out at room temperature according to the reported method.[1] Analyses of products were carried out by GC-MS using OV-1 (1 m) column. The results are summerized in Table 1.

The Reaction of [2.2]Metacyclophanes with Ethylaluminum Dichloride. a) 1,2,3,3a,4,5,9,10,10a,10b-Decahydropyrenes: As an example the reaction of **1a** with ethylaluminum dichloride is shown. A solution of **1a** (104 mg, 0.5 mmol), diethylaluminum chloride (180 mg, 1.5 mmol), and titanium tetrachloride (285 mg, 1.5 mmol) in benzene (5 cm^3) was stirred at room temperature for 3 h. Column chromatography on alumina eluted with hexane gave **13a** (45 mg, 42%) and **2a** (46 mg, 45%).

Compounds **1b**, **8**, and **9** were treated in a similar manner. Melting points, mass spectra, analytical data, and ^{13}C NMR of decahydropyrenes are shown in Tables 2 and 3.

b) 1-Methyl-4,5,9,10-tetrahydropyrene: The compound was obtained from **8** as an oily material. ^{1}H NMR ($CDCl_3$) δ=2.30 (3H, s, Me), 2.82 (8H, s, CH_2), 6.97 (2H, s, ArH), and 7.05 (3H, s, ArH). Mass spectrum, *m/z* 226.

Found: C, 92.25; H, 7.65%. Calcd for $C_{17}H_{16}$: C, 92.68; H, 7.32%.

Other hydropyrenes were characterized by comparing with the authentic materials reported before.[2,10]

Measurements. ^{1}H NMR spectra were determined on a JEOL GX-500 spectrometer and ^{13}C NMR spectra were measured on a JEOL GX-400 or on a Varian XL-300 spectrometers. X-ray crystallographic analysis was carried out on a Philips automated difractometer (graphite monochromated Cu $K\alpha$ radiation, λ=1.5418Å; θ—2θ scan method, θ_{max} 78°).

References

1) K. Nishiyama, K. Hata, and T. Sato, *Tetrahedron*, **31**, 239 (1975).

2) T. Sato, K. Torizuka, R. Komaki, and H. Atobe, *J. Chem. Soc., Perkin Trans. 2*, **1980**, 561.

3) S. Hayashi and T. Sato, *Bull. Chem. Soc. Jpn.*, **45**, 2360 (1972).

4) T. Yamagishi, K. Torizuka, and T. Sato, *Bull. Chem. Soc. Jpn.*, **55**, 1140 (1982).

5) W. Baker, J. F. W. McOmie, and J. M. Norman, *J. Chem. Soc.*, **1951**, 1114.

6) G. H. Smith and F. J. Hamilton, *J. Phys. Chem.*, **72**, 3567 (1968).

7) C. Beerman, *Angew. Chem.*, **71**, 195 (1959).

8) A. P. Gray, A. B. Callear, and F. H. C. Edgecombe, *Can. J. Chem.*, **41**, 1502 (1963).

9) T. Sato and T. Takemura, *J. Chem. Soc., Perkin Trans. 2*, **1976**, 1195.

10) K. Torizuka and T. Sato, *Bull. Chem. Soc. Jpn.*, **53**, 2411 (1980).

11) E. Langer and H. Lehner, *Monatsh. Chem.*, **104**, 1484 (1973).

12) P. E. Hansen, O. Blaabjerg, and A. Berg, *Acta. Chem. Scand., Ser. B*, **32**, 720 (1978).

13) J. B. Stothers, "Carbon-13 NMR Spectroscopy," Academic Press, New York (1972), Chap. 4, p. 102.

14) E. Langer and H. Lehner, *Tetrahedron Lett.*, **1973**, 1143.

Reactivities of Stable Rotamers. XIV. Reaction of 9-[2-(Substituted Methyl)-6-methylphenyl]fluorene Rotamers with Butyllithium[1)]

Mikio NAKAMURA, Yoshio SUZUKI,† and Michinori ŌKI*,†
Department of Chemistry, School of Medicine, Toho University, Ōta-ku, Tokyo 143
†*Department of Chemistry, Faculty of Science, The University of Tokyo, Bunkyo-ku, Tokyo 113*
(Received April 23, 1985)

The title compounds of which substituents carry atoms with lone-pair electrons have been prepared and their rotamers isolated as stable entities at room temperature. Deprotonation rates of these rotamers with butyllithium in benzene–hexane solution show a striking difference depending upon the substituents and the rotamers. In both *sp* and *ap* series, compounds with a methoxyl group exhibit the largest rate constants, while those with a sulfur substituent show the smallest reactivity. The difference is explained in terms of coordination ability of the heteroatoms toward butyllithium and by taking advantage of the entropy effect at the transition state of lithiation. The difference in reactivities between rotamers is further striking in a sense that the reactions differ in the order; *sp* rotamers show the first-order kinetics while *ap* rotamers obey the second-order kinetics in the substrate. By assuming that the observed rates are the sum of the first-order and the second-order contributions, we estimate the minimum ratios of the first-order rate constants between *sp* and *ap* rotamers, k_1^{sp}/k_1^{ap}, to be >2300 in the methoxyl and dimethylamino derivatives and >240 in the methylthio derivatives.

Understanding of the reactivities of rotational isomers is essential for the improvement of selectivity of a reaction. The estimation of the intrinsic reactivity of a rotamer is, however, hampered by the fact that the fast interconversion among rotamers takes place. Some years ago, we were able to isolate stable rotamers of 9-arylfluorene derivatives at room temperature[2)] and have made it possible to investigate the reactivities of rotational isomers.

Fluorene is an acidic compound because, if it is derpotonated at the 9-position, the 6 π electron system develops which should be stabilized due to the aromaticity.[3)] Thus we first selected the deprotonation of 9-arylfluorene derivatives when we launched the project of the work on reactivity of conformational isomers.

In 9-(2-methoxy-1-naphthyl)fluorene (**1**) the difference in deprotonation rates between the *sp* and *ap* rotamers reached the order of 10^3.[4)] The large difference in reactivities observed in this system attracted our attention. Thus, in a previous paper of this series, we

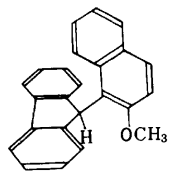

sp-**1**

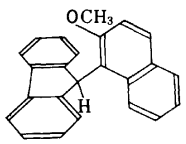

ap-**1**

reported the lithiation of a pair of 9-arylfluorene rotamers which consist of carbon and hydrogen only: The ratio of lithiation rates in the case of 9-(2-methyl-1-naphthyl)fluorene (**2**) was only 7.0 in favor of the *sp* form. The difference can solely be ascribed to the steric effects.[5)] Thus the large difference in lithiation rates in the rotamers of **1** must be ascribed to the existence of the coordinating methoxyl group in a suitable position.

Then it became of interest to see whether a hetero

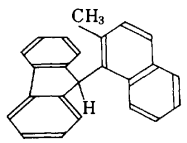

sp-**2**

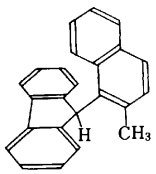

ap-**2**

atom located remotely from the site of the deprotonation can assist the reaction. Thus in order to investigate the effect of the heteroatoms, we have prepared 9-[2-(substituted methyl)-6-methylphenyl]fluorene derivatives. *sp*-Rotamers of compounds **4**, **5**, and **6** were prepared by the nucleophilic substitution reactions of *sp*-**3** with dimethylamine, methanol, or sodium methanethiolate, respectively. *ap*-Rotamers were also prepared from *ap*-**3** in a similar way.

sp-**3** *sp*

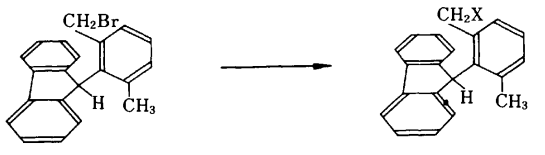

ap-**3** *ap*

4: X = $N(CH_3)_2$
5: X = OCH_3
6: X = SCH_3

In this paper, we wish to report and to discuss the results on deprotonation rates of these rotamers, which showed striking differences from a rotamer to another.

Experimental

9-[2-(Dimethylaminomethyl)-6-methylphenyl]fluorene (4). To a solution of 320 mg of *sp*-**3**[6] in 50 mL of tetrahydrofuran was added 10 mL of 50% aqueous dimethylamine. The mixture was stirred at room temperature for 3 h and then the solvents were evaporated *in vacuo*. The residue was dissolved in 20 mL of ether and dried over sodium sulfate. After evaporation of the solvent, the residue was submitted to silica-gel TLC. Elution with dichloromethane–ethanol (10:1) gave 208 mg (72%) of *sp*-**4**. Recrystallization from hexane–tetrahydrofuran afforded a pure material, mp 87—88 °C. Found: C, 87.89; H, 7.33; N, 4.30%. Calcd for $C_{23}H_{23}N$: C, 88.13; H, 7.40; N, 4.47%. ^{1}H NMR($CDCl_3$) δ=1.10 (3H, s), 2.32 (6H, s), 3.69 (2H, s), 6.02 (1H, s), 6.8—7.5 (9H, m), 7.7—7.9 (2H, m).

To a solution of 130 mg (0.37 mmol) of *ap*-**3** in 50 mL of benzene was added 5 mL of aqueous dimethylamine and 120 mg (0.58 mmol) of silver perchlorate. The mixture was stirred for 20 h at room temperature and then the organic layer was separated. After drying over sodium sulfate, the solvent was evaporated and the residue was submitted to silica-gel TLC (dichloromethane–ethanol (10:1)) to give 52 mg or 44% of *ap*-**4**, mp 90—91 °C, as colorless crystals. Found: C, 87.83; H, 7.15; N, 4.47%. Calcd for $C_{23}H_{23}N$: C, 88.13, H, 7.40; N, 4.47%. ^{1}H NMR ($CDCl_3$) δ=1.51 (6H, s), 2.11 (2H, s), 2.70 (3H, s), 5.44 (1H, s), 7.2—7.5 (9H, m), 7.7—7.9 (2H, m).

9-(2-Methoxymethyl-6-methylphenyl)fluorene (5). Both *sp* and *ap* rotamers were obtained by the treatment of *sp*-**3** and *ap*-**3** with methanol, respectively, as reported previously.[6] mp: *sp* 65—67 °C; *ap* 118 °C.

9-[2-(Methylthiomethyl)-6-methylphenyl]fluorene (6). To a solution of 253 mg (0.72 mmol) of *sp*-**3** in 50 mL of tetrahydrofuran was added 5 mL (11 mmol) of *ca.* 15% aqueous sodium methanethiolate. The mixture was stirred at room temperature for 2 h. After evaporation of the solvent, the residue was dissolved in 20 mL of ether and the solution was dried over sodium sulfate. The ether was evaporated and the resulting oil was submitted to silica-gel TLC. Elution with benzene–hexane (1:1) gave 203 mg (88%) of *sp*-**6**, mp 66—67 °C, as colorless crystals. Found: C, 83.39; H, 6.09; S, 10.41%. Calcd for $C_{22}H_{20}S$: C, 83.50; H, 6.37; S, 10.13%. ^{1}H NMR ($CDCl_3$) δ=1.08 (3H, s), 2.12 (3H, s), 4.00 (2H, s), 5.63 (1H, s), 6.7—7.6 (9H, m), 7.7—7.9 (2H, m).

The *ap*-rotamer of **6** was similarly prepared from *ap*-**3** and sodium methanethiolate in tetrahydrofuran–water solution in 80% yield and was obtained as colorless crystals, mp 76—79 °C. Found: C, 83.52; H, 6.28; S, 10.04%. Calcd for $C_{22}H_{20}S$: C, 83.50; H, 6.37; S, 10.13%. ^{1}H NMR ($CDCl_3$) δ=1.28 (3H, s), 2.45 (2H, s), 2.67 (3H, s), 5.47 (1H, s), 6.7—7.5 (9H, m), 7.7—7.9 (2H, m).

Kinetic Measurement. Following is a typical procedure. A solution of 99.9 mg of *sp*-**4** in 900 μL of benzene-d_6 was prepared. By the use of a microsyringe, 200 μL of this solution (7.08×10^{-5} mol of the substrate) was taken into an NMR sample tube. To each of the 4 samples thus prepared, 300 μL of *ca.* 15% butyllithium in hexane solution was added at −78 °C under a nitrogen atmosphere. These samples were gradually warmed with stirring to make homogeneous solutions. The quantity of butyllithium was determined to be 7.1×10^{-4} mol from the integrated intensity of the signal due to methylene protons alpha to lithium in ^{1}H NMR spectra. Thus the concentration of butyllithium was found to be 10 times as much as that of the substrate. The rates of reactions were determined by monitoring the proton signals due to 4-H and 5-H of the fluorene ring. These protons gave a multiplet signal at δ 8.0—8.2 in the lithiated compound. In each set of the data obtained at 4 different temperatures, a plot of log $(1-x/a)$ *vs.* t gave a good straight line, where a is the initial amount of the substrate and x the amount of the product at time t. The pseudo-first-order rate constants were then obtained by the usual way.

The deprotonation reactions of the other rotamers also obeyed the pseudo-first-order kinetics. The rate constants were similarly obtained at 4 different temperatures. By putting these rate constants into Eyring equation, we obtained the activation parameters for lithiation.

The rates of reactions in the *ap*-rotamers could be followed as in the cases of the *sp*-rotamers. In these cases, however, the treatment of the data assuming the pseudo-first-order kinetics did not give a straight line, but that assuming the rates of second order in the substrate did a straight line.

In all of these reactions, the initial amount of butyllithium was kept constant at 7.1×10^{-4} mol. The reaction temperatures were determined from the difference in chemical shifts between the OH and the methyl signals of methanol in ^{1}H NMR spectra.

Results and Discussion

Rotational Barriers and Rates of Lithiation. Barriers to rotation about C_9–C_{aryl} bond in compounds **4**, **5**, and **6** are expected to be similar to that of compound **3** for the process *sp*→*ap*, since the effect of substituent X in the types, $-CH_2X$,[7] $-COX$,[8] and $-OCOX$,[9] on the barrier to rotation is known to be negligible in the 9-arylfluorene system regardless of the kinds of the substituent X. The barrier to rotation for the process *ap*→*sp* can vary especially when attractive or repulsive interactions are present in the *ap* form between X and fluorene ring.[8,9] Since such effects are not expected in the *ap* forms of the compounds examined in this work, the barriers to rotation are estimated to be E_a=27.1±1.0 kcal mol^{-1} (1 cal=4.18 J) or $\Delta G^{\ddagger}$=28.0±1.0 kcal mol^{-1} at 31.5 °C on the basis of the results reported for compound **3**.

If we take the minimum values of the barrier to rotation, 27 kcal mol^{-1}, the rate constants of interconversion, k_1 and k_{-1}, are calculated to be 3.3×10^{-7} s^{-1}. Since the pseudo-first-order rate constant of lithiation is at least 2×10^{-4} s^{-1} (*sp*-**6**) at 31.5 °C, isomerization of the *sp* rotamer to the *ap* during the lithiation needs not be considered. In the case of *ap* rotamers, however, the rate of isomerization of the *ap* to the *sp* isomer and that of lithiation are comparable and are not very much different from each other especially in the case of *ap*-**6**: the initial rate of lithiation is given by $k^{ap}[ap]_0^2=8.0\times10^{-8}$ mol L^{-1} s^{-1}, which is only 2.4 times larger than the isomerization rate, $k_{-1}[ap]_0=3.3\times10^{-8}$ mol L^{-1} s^{-1}, if the concentration

of the substrate is 0.10 mol L^{-1}. Therefore, partial isomerization of *ap*-**6** to *sp*-**6** may take place under the conditions, which will be followed by the fast lithiation to the product. Raising the temperature increases both k_{-1} and k^{ap}, making the analysis difficult. Thus the rates of lithiation were measured at 31.5 °C only.

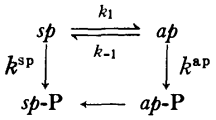

Structure of Lithiated Product. Both *sp* and *ap* rotamers gave identical spectra by lithiation. The structure of the lithiated compound is thought to be **7** where the heteroatom can coordinate to lithium at position 9 to stabilize this form. Such a stabilization is not expected in **8** because of the unfavorable distance between the methoxyl oxygen and the lithium. A piece of experimental evidence supporting this structure is the chemical shifts of the methylene and methyl protons which are connected to the heteroatom. In the lithiated compound derived from **5**, methylene and methyl protons gave broad signals at δ 4.6 and 3.0, respectively, in benzene–hexane (2:3) solutions. These chemical shifts resemble those of the corresponding protons of *sp*-**5**, δ 4.6 and 3.1, in the same solvent system but differ greatly from these of *ap*-**5**, δ 3.3 and 2.6. The results suggest that the methylene and methyl groups in question are located nearly in the plane of the fluorene ring. Although we failed to detect the methyl signals in the NMR spectra of lithiated compounds derived from **4** and **6** owing to the interference of the huge peaks due to solvents, we could find the methylene signals appearing at similar positions as those of the starting *sp* rotamers.

Another piece of evidence for the structure of the lithiated product came from the quenching experiment of it with hydrochloric acid at 0 °C. After the work up procedure as usual, ^{1}H NMR spectrum showed the for-

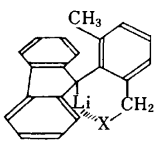

7

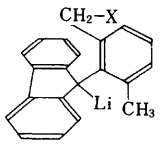

8

mation of the *sp* rotamer as a sole product. Since it is well known that the electrophilic substitution of lithiated compounds in nonpolar solvents such as benzene or hexane proceeds with retention of configuration,[10] the formation of the *sp* rotamer is the direct indication that **7** is the correct structure for the product.

It is difficult to assume that the lithiated structure **7** is directly formed from the *ap* isomers. Instead, the structure **8** will be formed at the first stage and will isomerize to **7** because of the thermal stability of **7**. The barrier to isomerization is expected not prohibitively high in rotation mechanism: The barrier to rotation is known to be reduced as a bulky substituent is introduced to the 9-position of 9-arylfluorenes.[11]

Table 1. Pseudo-first-order rate constants ($\times 10^4$ s^{-1}) of lithiation with temperature (°C) in parentheses of *sp* rotamers[a]

sp-**4**	1.95 (−20.5), 2.93 (−16.2), 12.0 (0.7), 18.8 (4.8)
sp-**5**	1.50 (−24.0), 2.37 (−19.3), 4.96 (−13.7), 7.97 (−9.0)
sp-**6**	2.28 (32.8), 3.29 (37.0), 5.94 (42.6), 10.5 (48.6)

a) Initial concentrations of butyllithium and the substrate were 1.42 and 0.14 mol L^{-1}, respectively.

Table 2. Activation parameters for lithiation of *sp* rotamers

Compound	$\Delta H^{\ddagger}$	$\Delta S^{\ddagger}$
	kcal mol^{-1}	e. u.
sp-**4**	11.7±1.1	−28.9±4.3
sp-**5**	14.6±0.9	−17.1±3.4
sp-**6**	18.5±1.6	−14.8±5.1

a) 1 e.u.=4.18 J K^{-1} mol^{-1}.

Kinetics. Deprotonation reactions were carried out by the addition of a hexane solution of butyllithium into a benzene solution of the substrate. The reaction rates were followed by monitoring ^{1}H NMR signals at low fields. The starting material possessed a multiplet signal at δ 7.7—7.9 due to 4-H and 5-H of the fluorene ring, whereas the product exhibited a doublet signal at δ 8.0—8.2, thanks to the aromatic character of the product anion.

Analysis of the data for the *sp* series of compounds conformed with the pseudo-first-order kinetics. In Table 1 are listed the pseudo-first-order rate constants thus obtained. Putting these rate constants into the Eyring equation afforded the activation parameters for the reaction, which are shown in Table 2.

By contrast, for the *ap*-rotamers, the reaction rates did not obey the pseudo-first-order kinetics but were second order in the substrate. The second order kinetics in the substrate was further confirmed by the change in the initial concentration. Thus the half-life of *ap*-**5** became longer when the less amount of the substrate was used than the original case. Since the rates of lithiation of *ap*-rotamers were very low even at ambient temperature in the concentration range examined, measurement of the rates at higher temperatures is required to obtain the activation parameters. Raising the temperature, however, may cause the isomerization of the *ap* rotamer to the *sp* which will be deprotonated rapidly. Thus the pseudo-second order rate constants were obtained at 31.5 °C only which are listed in Table 3 together with the concentration of the substrates and the relative rates.

Reaction Mechanisms. Before discussing the difference in reactivities among compounds or between rotamers, the reaction mechanisms of each rotamer

TABLE 3. PSEUDO-SECOND-ORDER RATE CONSTANTS OF LITHIATION OF *ap* ROTAMERS AT 31.5 °C AND RELATED DATA[a)]

Compound	Rate Constants	Concentration	Relative Rates
	$mol^{-1}Ls^{-1}$	$mol\ L^{-1}$	
ap-**4**	5.34×10^{-5}	0.10	6.7
ap-**5**	3.20×10^{-4}	0.051	40
	3.38×10^{-4}	0.084	42
ap-**6**	7.98×10^{-6}	0.10	1.0

a) Initial concentration of butyllithium was 1.42 mol L^{-1}.

must be considered. In nonpolar solvents, such as benzene or cyclohexane, butyllithium exists as a hexamer[12] and carbon–lithium bond is mainly covalent. As a result, butyllithium behaves as a bulky reagent. In more polar solvents than hydrocarbons, such as ether or tetrahydrofuran, however, coordination of solvent molecules toward lithium occurs to result in the deaggregation of butyllithium.[12,13] The deaggregation together with the increase in ionic nature of the carbon–lithium bond in the polar solvents makes butyllithium a more reactive species. In fact, a parent hydrocarbon, 9-(2,6-xylyl)fluorene, did not react with butyllithium at 31.5 °C in a benzene–hexane solution even after several days, while it did react instantaneously in tetrahydrofuran solutions at the same temperature.[5] Thus the reaction of *sp* and *ap* rotamers with butyllithium, which occured even in nonpolar solvents is ascribed to the coordination effect of the substituent to the butyllithium and the reaction mechanism must be considered accordingly.

The large negative values of entropy of activation for the reactions of the *sp* series shown in Table 2 suggest that the reactions proceed at least bimolecularly. Deaggregation of butyllithium will take place, when the substrate and butyllithium collide, to form an active species responsible for deprotonation by the assistance of the heteroatom in the substituent. There may be several active species, which differ in the degree of aggregation and are differently contributing to the total reaction. In the second step, the active species deprotonates from the 9-position of the same complex. A plausible structure of the transition state is given by **9** in the case where butyllithium exists as a monomer.

In the case of *ap* rotamers, the reaction path must be different from that of *sp* rotamers because the rates of deprotonation of the *ap* rotamers obeyed the second-order rate law in the substrate. Thus the direct abstraction of 9-H by butyllithium spanning between the substituent and the 9-H as shown by **10** is neglected, since the rate should be first order in the substrate, if it were the case. Inspection of the molecular model also revealed that the distance between the coordinating butyllithium and the 9-H is unfavorable for the reaction to occur, especially when the butyllithium is a monomer. It is, therefore, more reasonable to consider an intermolecular reaction: Coordinated butyllithium

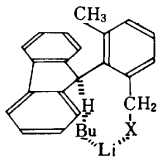

9

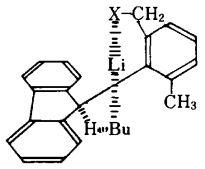

10

abstracts the 9-H of another molecule in the rate-determining step.

Comparison of Reactivities among Compounds. *a)* sp-*Rotamers*: As discussed in the previous section, coordination of the substituent to lithium is very important for the reaction to occur. Then the rate of the reaction of the *sp* rotamer is affected both by the rate constant of deprotonation and the equilibrium constant of deaggregation. If a strong coordination of the heteroatom toward the aggregated butyllithium takes place, it will increase the concentration of active species as well as the ionic character of the lithium–carbon bond: It results in the increase in the rate of deprotonation as well as the equilibrium constant. It is, therefore, reasonable to state that the compound which has a substituent of stronger coordinating ability to lithium ion is much more reactive than the compound carrying a less coordinating substituent.

The rate constants in Table 1 indicate that the oxygen-containing **5** showed the highest reactivity toward butyllithium among the compounds examined at ambient temperature. Nitrogen substitution similarly accelerated the reaction but the sulfur substitution was not so effective as those of the former two compounds. The high reactivities observed in *sp*-**4** and *sp*-**5** relative to that in *sp*-**6** seem to correspond to the generally accepted coordination ability of the heteroatoms concerned toward lithium ions: lithium ions are classified as a typical hard acid[14] and thus tend to make a stronger bond with a hard base such as a nitrogen- or oxygen-containing substituent than a soft base such as a sulfur-containing group.

The recent thermodynamic study by Xu and Smid showed that polyamines such as penta-*N*-methyldiethylenetriamine and hexa-*N*-methyltriethylenetetramine have a higher affinity toward lithium ions than the corresponding oxygen analogs, di- and triethylene glycol dimethyl ether, respectively.[15] These results suggest that the nitrogen-containing substituent has a stronger coordination ability toward lithium ions than the oxygen-containing group and thus are against the order of the reactivities that we observed.

Further inspection of the data in Table 2, however, reveals that *sp*-**4** has the smallest activation enthalpy and the largest negative value of entropy of activation among the compounds examined. The former is ascribed to the strong coordination of the dimethylamino group to butyllithium in the transition state of reaction, being consistent with the thermodynamic

data. The latter could be explained in terms of the orientation of the reactants required in the transition state. Since a dimethylamino group has only one lone pair of electrons, the direction of the lone-pair electrons is important for the effective coordination. Existence of two methyl groups also prohibits certain conformations for steric reasons. As a result, only a limited number of conformations is possible for the dimethylamino group to coordinate to butyllithium. These factors are considered to decrease the entropy of activation. In the case of *sp*-**5**, such a restriction of conformations may not be severe since the methoxyl group has two pairs of electrons and only one methyl group. Thus the apparent reversal in the order of reactivities between **4** and **5** is ascribed to the entropy effect. The activation parameters in Table 2 suggest that the rate constants of *sp*-**4** become larger than those of *sp*-**5** at temperature below −28 °C, where the molecular motion slows down and the rates are controlled mainly by the enthalpy of activation.

b) ap-*Rotamers.* Reactivities of *ap* rotamers are quite similar to those of *sp* rotamers in a sense that *ap*-**5** and *ap*-**6** showed the largest and smallest rate constants, respectively, among the compounds examined at 31.5 °C. The data in Table 3 also showed that the ratio of rate constants, *k*(*ap*-**5**)/*k*(*ap*-**4**), is *ca.* 6.0 which is twice as large as the corresponding ratio in the *sp* series. The difference in the ratio can be explained in terms of the entropy effect as well. The number of conformations possible for the *ap*-form of **4** is more limited than *sp*-**4** because of the presence of the fluorene ring in proximity. As to the C(aryl)-to-C_α(substituent) bond rotation, no conformation is possible in which the C–N bond directs toward the fluorene ring. In addition, any invertomers about the nitrogen atom, in which one or two of the methyl groups directs toward the fluorene moiety may be unstable for the steric reasons. These factors all act to decrease the entropy when lithium ions coordinate to the amino-nitrogen.

Comparison of Reactivities between Rotamers. The most striking feature in the reactivities of rotamers is that they showed different mechanism in the lithiation. Thus the direct comparison of the rate constants between *sp* and *ap* rotamers may be meaningless. For the comparison, let us assume that the observed rate is given by the sum of the first-order and the second-order contributions as described by equations 1 and 2 for the cases of *sp* and *ap* series, respectively. Although it is possible to state that various kinds of reactions, those of butyllithiums of different degrees of aggregation and those of the higher order than the second, can take place, as a rule of thumb, the assumption may be justified.

$$\text{Rate}(sp) = k_1^{sp}[sp] + k_2^{sp}[sp]^2 \quad (1)$$

$$\text{Rate}(ap) = k_1^{ap}[ap] + k_2^{ap}[ap]^2 \quad (2)$$

TABLE 4. PSEUDO-FIRST-ORDER RATE CONSTANTS OF *sp* AND *ap* ROTAMERS AT 31.5 °C

Compound	k_1^{sp} / s^{-1}	k_1^{ap} / s^{-1}	k_1^{sp}/k_1^{ap}
4	1.25×10^{-2}	$<5.3\times10^{-6}$	>2300
5	3.80×10^{-2}	$<1.6\times10^{-5}$	>2300
6	1.95×10^{-4}	$<8.0\times10^{-7}$	>240

where k_1 and k_2 are rate constants of first and second order reactions in the substrate, respectively.

In these equations, the concentration of butyllithium is included in the constants, k_1 and k_2, since it is at least 10 times as much as the concentration of the substrate. In the case of *sp* rotamers, the observed rate obeyed the first-order kinetics, meaning that the first term predominates over the second term in Eq. 1. In the case of *ap* rotamers, in contrast, second term becomes predominant in Eq. 2. Thus we concluded the following two relations, 3 and 4:

$$k_1^{sp} \gg k_2^{sp}[sp] \quad (3)$$

$$k_1^{ap} \ll k_2^{ap}[ap] \quad (4)$$

By considering the data in Table 2 with respect to these relations, we can calculate the maximum values of k_1^{ap} for each *ap* rotamer. In Table 4 are listed these values together with the rate constants of the reaction of the *ap* form at 31.5 °C and the minimum ratios of k_1^{sp}/k_1^{ap}.

It may be possible to obtain the intrinsic k_1 values for *ap* rotamers by measuring the rates at the low concentration range of the substrates, where the second term of Eq. 2 is negligibly small. Present method, which consists of the monitoring of the signals by ^{1}H NMR spectroscopy, however, makes it very difficult to obtain reasonably good results in such a low concentration range. In addition, the reaction of the *ap* form under such conditions may be too slow to be practicable for the measurement, even if we assume that a suitable methodology is found.

This work was supported by a Grant-in-Aid for Scientific Research of the Ministry of Education, Science and Culture, to which our thanks are due.

References

1) Preceding paper: M. Nakamura and M. Ōki, *Chem. Lett.*, **1985**, 255.
2) M. Ōki, *Angew. Chem. Int. Ed. Engl.*, **15**, 87 (1976); M. Nakamura, *Kagaku no Ryoiki*, **30**, 977 (1976); M. Ōki, *Top. Stereochem.*, **14**, 1 (1983).
3) T. Schaefer and W. G. Schneider, *Can. J. Chem.*, **41**, 966 (1963).
4) M. Nakamura and M. Ōki, *Chem. Lett.*, **1975**, 671; M. Ōki, *Acc. Chem. Res.*, **17**, 154 (1984).
5) M. Nakamura, N. Nakamura, and M. Ōki, *Bull. Chem. Soc. Jpn.*, **50**, 1097 (1977).

6) S. Murata, S. Kanno, Y. Tanabe, M. Nakamura, and M. Ōki, *Bull. Chem. Soc. Jpn.*, **55**, 1522 (1982).
7) R. Saito and M. Ōki, *Bull. Chem. Soc. Jpn.*, **55**, 2508 (1982).
8) R. Saito and M. Ōki, *Chem. Lett.*, **1981**, 651; R. Saito and M. Ōki, *Bull. Chem. Soc. Jpn.*, **55**, 3273 (1982).
9) M. Nakamura and M. Ōki, *Chem. Lett.*, **1976**, 651.
10) D. Y. Curtin and W. J. Koehl, Jr., *J. Am. Chem. Soc.*, **84**, 1967 (1968).
11) E. A. Chandross and C. F. Sheley, *J. Am. Chem. Soc.*, **90**, 4345 (1968); T. H. Siddall, III, and W. E. Stewart, *J. Org. Chem.*, **34**, 233 (1969); A. Rieker and H. Kessler, *Tetrahedron Lett.*, **1969**, 505.
12) D. Margerison and J. P. Newport, *Trans. Faraday Soc.*, **59**, 2058 (1963); H. L. Lewis and T. L. Brown, *J. Am. Chem. Soc.*, **92**, 4664 (1970).
13) T. L. Brown, *Adv. Organometal. Chem.*, **3**, 365 (1966); T. L. Brown, *Pure and Appl. Chem.*, **23**, 447 (1970); R. West and R. Waack, *J. Am. Chem. Soc.*, **89**, 4395 (1967); M. M. Exner, R. Waack, and E. C. Steiner, *ibid.*, **95**, 7009 (1973); L. M. Jackman and L. M. Scarmoutzos, *ibid.*, **106**, 4627 (1984); J. F. McCarrity and C. A. Ogle, *ibid.*, **107**, 1805 (1985).
14) T. L. Ho, "Hard Soft Acids and Bases Principle in Organic Chemistry," Academic Press, New York (1977).
15) W. X. Xu and J. Smid, *J. Am. Chem. Soc.*, **106**, 3790 (1984).

Studies with Inorganic Ion-exchange Membranes. I. Effect of Binding Material on the Permeation of Electrolyte Solutions across Titanium Tungstoarsenate Membranes

S. K. SRIVASTAVA,* Satish KUMAR,† and Surendra KUMAR
Department of Chemistry, University of Roorkee, Roorkee-247 667, India
(Received March 19, 1984)

A comparative study of permeability for various electrolytes is made on parchment-, polystyrene-, and Araldite based membranes of titanium tungstoarsenate at 20, 25, 30, and 35 °C. At any given temperature the order of permeability increase is $K^+ > Na^+ > Li^+$ for 1:1 electrolytes and $Ba^{2+} > Ca^{2+} > Mg^{2+}$ for 2:1 electrolytes. Permeability values are higher for parchment-based than polystyrene-based membranes. The diffusion of these electrolyte solutions across Araldite based membrane is almost negligible. Thermodynamic parameters of diffusion process, *viz.*, $\Delta H^{\neq}$, $\Delta S^{\neq}$, $\Delta F^{\neq}$ have been evaluated at 25 °C by applying the theory of absolute reaction rates. $\Delta S^{\neq}$ values are negative for all the cations for both the membranes except that of Li^+ which is positive for parchment-based membranes. $\Delta F^{\neq}$ values are higher for the polystyrene-based than parchment-based membranes.

Inorganic ion-exchange membranes are of vital importance in analytical chemistry[1-6] and also as the models for biological membranes. Literature survey on this topic reveals that a lot of work has been done in the last two decades on the characterization and membrane properties of this class of membranes by various research groups.[7-13] Most of the reports made in this direction deal with the membranes prepared by keeping the same binder but different membrane materials and almost no attempt has been made so far to investigate the effect of binding material on membrane properties by selecting the same membrane material but different binding materials.

We have also been working on the electrochemical properties of inorganic ion-exchange membranes and their possible applications as ion-selective electrode.[14-16] In this communication we report the effect of binding material on the permeability and thermodynamic parameters of the diffusion process, *viz.* ΔS^{*}, ΔH^{*}, ΔF^{*}, across titanium tungstoarsenate membranes with parchment, polystyrene and Araldite as binding material for their preparation.

Experimental

Titanium(IV) chloride (B.D.H), sodium arsenate heptahydrate (E. Merck) and sodium tungstate (AnalR) were used as such. The specimen of Araldite was obtained from Cibatul Limited, India (composition not known). All other chemicals used in this investigation were also of A.R. grade.

Preparation of Titanium Tungstoarsenate. Titanium tungstoarsenate is prepared by adding 0.25 M (1 M=1 mol dm^{-3}) titanium(IV) chloride solution to a mixture of 0.25 M sodium arsenate and 0.25 M sodium tungstate in the volume ratio 2:1:1. The pH of the mixture and titanium(IV) chloride solution was adjusted to one. The precipitate thus obtained was allowed to stand for 24 h at room temperature. It was then washed by decantation with distilled water and afterwards with 2 M nitric acid. The gel, dried at 50 °C, broke down to small particles when immersed in distilled water. The conditions mentioned above are optimum one for the preparation of a stable gel showing good sorption property.

† Institute of Paper Technology, Saharanpur.

A 0.2 g amount of the exchanger material was dissolved in concentrated sodium hydroxide solution and filtered. The residue, titanium hydroxide was dissolved in sulfuric acid and titanium was determined by hydrogen peroxide method, In the filtrate, arsenic was estimated by Volhard's thiocyanate method and tungsten by gravimetry as barium tungstate. The values obtained are Ti=9.51%, W=40.03%, and As=19.98% (the ratio Ti:W:As=1:4:2). The exchange capacity of the material is 0.86 meq g^{-1} (univalent ion) as reported earlier.[17]

Preparation of Membranes Using Different Binding Materials. The homogeneous membranes of titanium tungstoarsenate could not be prepared. Heterogeneous membranes of these compounds employing three different support materials (*i.e.* parchment paper, polysterene and Araldite) were prepared and found to be quite satisfactory.

(i) Preparation of Parchment Paper Impregnated Membrane: The membrane was prepared by impregnated parchment paper with titanium tungstoarsenate. The paper was first soaked in distilled water and then tied carefully on an open glass cylinder. A 0.25 M titanium(IV) chloride (pH=1) solution was filled inside the paper container which was then suspended in a beaker containing a mixture of sodium arsenate and sodium tungstate (prepared by mixing 0.25 M solution each in volume ratio 1:1 at pH=1) for 12 h. The parchment was then taken out and washed repeatedly with distilled water to remove the adsorbed electrolytes. The solutions of titanium(IV) chloride and mixture of sodium arsenate and sodium tungstate were then interchanged and paper was immersed again for another 12 h. The white membrane thus obtained was repeatedly washed with distilled water for complete removal of adsorbed electrolytes.

(ii) Preparation of Polystyrene-based Membrane: Polystyrene granules were heated in a glass tube in a concentrated sulfuric acid bath at 200 °C. The molten mass was allowed to cool down to room temperature and the polystyrene rod, thus obtained was ground to a 50 mesh sieve product. Membranes were obtained by mixing polystyrene and exchanger material in the ratio 1:5 by weight and heating the mass in a die kept in a metallurgical specimen mount press at 110 °C under a pressure of 6000—7000 psi. The optimum quantity of polystyrene to be added was determined by trial. Membranes with 20% polystyrene content were quite stable and did not show any dispersion in salt solutions.

(iii) Preparation of Araldite-based Membranes: A homogeneous mixture of 0.6 g titanium tungstoarsenate and 0.4 g

of Araldite (minimum amount of binder necessary for a stable membrane) was uniformly spread over a piece of filter paper, which was then pressed gently with the help of a glass plate and left to dry overnight. After drying, the membrane of 1.5 cm in diameter was cut manually with the help of a razor and filter paper was also removed from the membrane surface. A large number of membranes were thus prepared and the one which did not have any cracks and was quite smooth and had a thickness of 2 mm was selected for subsequent investigations.

Determination of Permeability. The constant flow method, recommended by Willis,[18] was emplyed for permeability measurements. All experiments were performed with 0.05 M metal chloride solutions and the flow of water as well as solution was maintained at 50 $ml\,h^{-1}$. The conductivity of the lower half cell solution was measured at various time intervals. An increase in initial stages and then a constant value of conductance were observed in almost one hour time. The equilibrium conductance was corrected for conductance of water flowing through the lower half cell.

The concentration of the solution flowing through the lower half cell was computed from calibration curves drawn for this purpose by plotting conductance against concentration. For the evaluation of thermodynamic parameters of diffusion process, the permeability of salt solutions was determined at four tempertures, *viz.* 20, 25, 30, and 35 °C.

Results and Discussion

Permeability of a membrane may be defined as the amount of solute diffusing across it in unit time and unit concentration gradient. The data on permeability of various electrolyte solutions at different temperatures across the parchment- and polystyrene-based membranes are given in Table 1. The permeability across Araldite-based membrane of this compound was found to be negligible and no diffusion of the electrolyte was observed even when the experiments were performed with salt solutions tagged with radioactive isotopes. Thermodynamic parametres for the diffusion process across the membranes, as computed from permeation data at 25 °C, are given in Table 2.

Permeabilities of various electrolytes across the membranes having different binders show the following order:

Parchment-based membranes > Polystyrene-based membranes > Araldite-based membranes.

The diffusion of various salt solutions across the parchment- and polystyrene-based membranes follow the order:

$$K^+ > Na^+ > Li^+ \text{ and } Ba^{2+} > Ca^{2+} > Mg^{2+}$$

The permeation of an electrolyte through a membrane depends upon the charge and size of the diffusing ion, charge on the membrane matrix and its porosity. Over and above this, another factor of prime importance is the exchange capacity of the membrane material and the nature of binder used (in the case of heterogeneous membranes).

The fixed charge on the membrane matrix acts in two ways, firstly it excludes the co-ions from the membrane phase due to electrostatic repulsion and secondly it increases the mobility of counter ions in the membrane phase. Thus the fast moving chloride ions would be exluded from the membrane phase whereas the slow moving cations such as Li^+, Na^+, and Ca^{2+} *etc.* would be attracted towards it. The next two steps in the process of diffusion are the entry of cations into the membrane phase by ion exchange and their diffusion to the other side, through the pores of the membrane.

Table 1. Permeability of univalent and bivalent metal chlorides through titanium tungstoarsenate membranes at different temperatures

Electrolyte	Parchment-based TWA membrane Permeability/$\mu mol\,h^{-1}$				Polystyrene-based TWA membrane Permeability/$\mu mol\,h^{-1}$			
	20 °C	25 °C	30 °C	35 °C	20 °C	25 °C	30 °C	35 °C
LiCl	23.20	30.35	41.50	58.30	1.30	1.70	1.84	2.32
NaCl	38.20	46.25	55.00	62.75	1.64	1.99	2.23	2.50
KCl	82.00	89.00	103.50	121.00	1.99	2.32	2.81	3.27
$BaCl_2$	36.10	42.20	47.75	53.00	0.43	0.45	0.51	0.55
$CaCl_2$	23.10	27.60	31.15	36.20	0.15	0.20	0.24	0.29
$MgCl_2$	8.25	11.15	14.10	17.75	0.05	0.07	0.08	0.99

Table 2. Activation energy and other thermodynamic parameters for electrolyte diffusion through titanium tungstoarsenate membranes at 25 °C

Electrolyte	Parchment-based TWA membrane				Polystyrene-based TWA membrane			
	E_a	ΔH^*	ΔF^*	ΔS^*	E_a	ΔH^*	ΔF^*	ΔS^*
	$kJ\,mol^{-1}$	$kJ\,mol^{-1}$	$kJ\,mol^{-1}$	$J\,mol^{-1}\,K^{-1}$	$kJ\,mol^{-1}$	$kJ\,mol^{-1}$	$kJ\,mol^{-1}$	$J\,mol^{-1}\,K^{-1}$
LiCl	44.98	42.50	37.73	16.00	25.01	22.53	40.46	−60.16
NaCl	23.96	21.48	36.67	−50.97	19.55	11.07	40.07	−77.18
KCl	19.49	17.01	35.00	−60.37	25.53	23.05	39.69	−55.84
$BaCl_2$	19.40	16.92	36.90	−67.05	12.31	9.83	43.72	−113.72
$CaCl_2$	21.13	18.65	37.99	−64.89	31.53	29.05	44.60	−58.18
$MgCl_2$	36.76	34.28	40.24	−20.00	36.47	33.99	48.35	−48.18

This eventually leads to the setting up of an electrical double layer across the membrane and gives rise to equilibrium conditions.

The passage of ions through membranes also depends on the charge and hydration of ions. Multivalent ions will experience a greater electrostatic force than the univalent one. Ions undergoing hydration would affect the permeability in two ways: Firstly by virtue of their size and secondly due to the extent to which the electrical forces of the membrane can pierce through the hydration shell. The position of ions in Holfmeister series should therefore influence the diffusion process and the order of diffusion should be:

$$Cs^+ > Rb^+ > K^+ > Na^+ > Li^+ \text{ and } Ba^{2+} > Ca^{2+} > Mg^{2+}$$

The order of permeability observed with the membranes under discussion, is in agreement with the sequence mentioned above.

It is observed that permeability increases with temperature. Applying Boltzmann distribution law to hydration-dehydration dynamic equilibrium, it can be concluded that at higher temperature considerably higher fraction of the total number of ions would be dehydrated and would possess the excess energy E_a required for permeation. The slope of log P *vs.* $1/T$ (Figs. 1 and 2) gives the activation energy E_a for the process of diffusion and the values obtained for these membranes are listed in Tables 1 and 2.

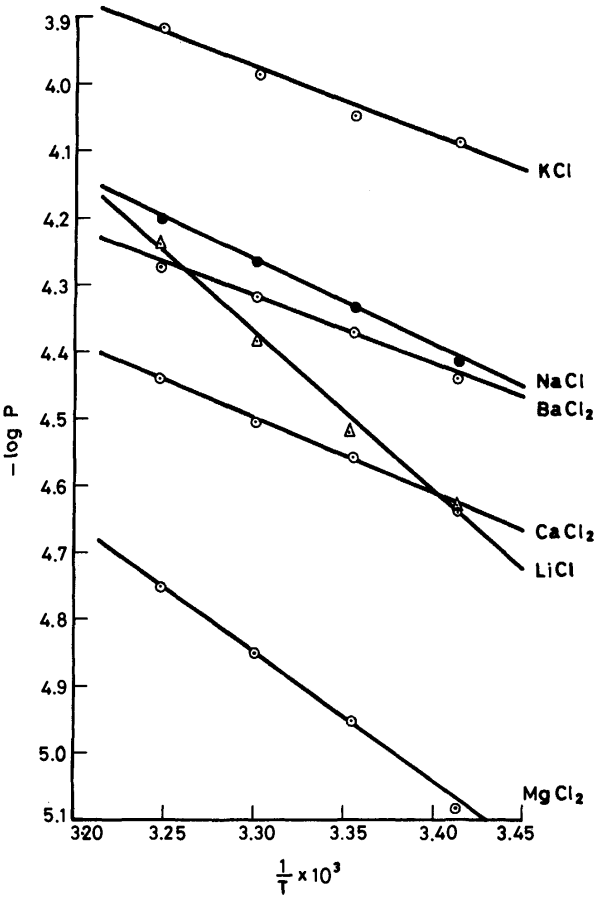

Fig. 1. Plots of log P *vs.* $1/T$ for parchment-based TWA membrane.

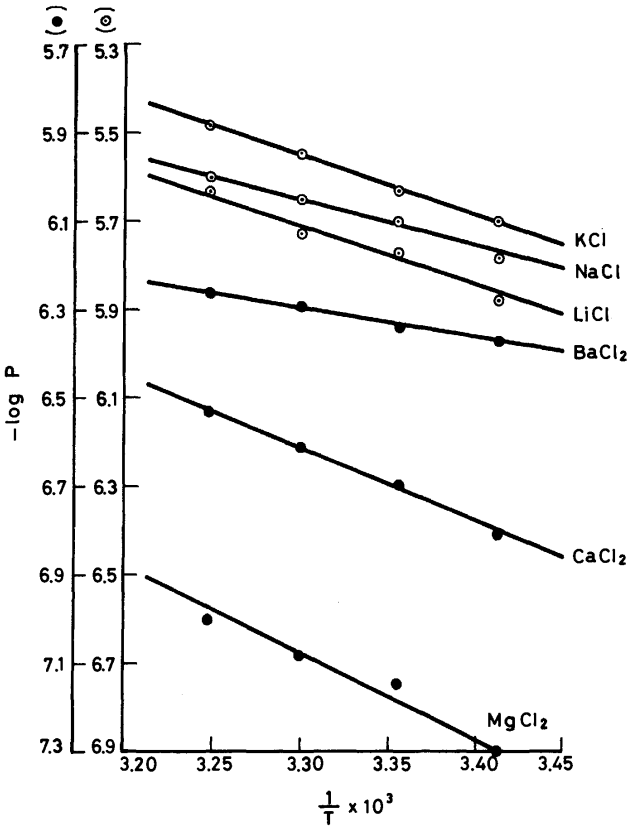

Fig. 2. Plots of log P *vs.* $1/T$ for polystyrene-based TWA membrane.

The theory of absolute reaction rate has been applied to diffusion processes in membranes by several investigators.[19-21] According to Zwolinski *et al.*[19] the permeability P' (cm s^{-1}) is given by the expression

$$P' = \left(\frac{\lambda^2 kT}{\delta h}\right)\exp(-\Delta F^*/RT)$$

where λ is the average distance between two equilibrium positions during the diffusion process, δ is the thickness of the membrane, while other symbols have their usual thermodynamic meanings. The value of free energy of activation can be calculated provided λ is known. This distance can be taken to be the same as the hopping distance, (3×10^{-8} cm) determined by Lai and Mortland.[22]

The ΔH^*, enthalpy of activation is related to E_a by the equation:

$$\Delta H^* = E_a + RT$$

and ΔS^*, the entropy of activation, can be calculated by Gibbs-Helmholtz equation:

$$\Delta F^* = \Delta H^* - T\Delta S^*$$

The values of ΔS^*, ΔF^*, and ΔH^* calculated on the basis of expressions given above are tabulated in Table 2.

It is observed that the values of entropy of activation

are generally negative except for lithium in the case of parchment-based membrane of this compound which exhibits a positive entropy of activation. Similar observations have also been reported by other workers in the case of parchment based ion-exchange membranes.[23] According to Zwolinski *et al.*[19] the values of ΔS^* indicate the mechanism of flow and a large positive ΔS^* is interpreted to reflect the breakage of bonds while low and negative values of entropy of activation indicate that activation is accompanied by a decrease in entropy and this would be possible only if the activated state involved formation of some bonds between the diffusing ion and the membrane material.

According to zone activation theory of Barrer and coworkers[24,25] for permeation of gases through polymer membranes, a high entropy value means either the existence of a large zone of activation or the reversible loosening of ordered segments of the membrane structure on permeation.

The positive value of ΔS^* obtained for Li^+ in the case of parchment-based membrane of this compound indicates that the diffusion of this ion across the membrane generates a greater region of disorder. The negative ΔS^* for other species imply two things:

(i) The permeating ions are partially immobilized in the membrane structure or interfacial region as the activated state involves in the formation of a bond between the diffusing ion and membrane material.

(ii) Permeation across membrane is not the only step which guides the rate, besides other factors are also operative.

A perusal of Table 2 reveals that the energy of activation (E_a) and enthalpy of activation (ΔH^*) values for the diffusion of cations are higher in the case of parchment based membrane except for K^+ and Ca^{2+} ions. The values of ΔF^* are higher for polystyrene-based than the parchment-based membranes for all the cations. ΔF^* may be interpreted as the work involved for the permeating species in overcoming the energy barrier during diffusion. Thus the values (Table 2) reveal that diffusion across polystyrene-based membrane involves more work than the parchment-based membrane of this exchanger material. The data on ΔS^* is higher for parchment-based membrane than polystyrene-based membrane. Higher values of permeability observed across the parchment-based membrane also support the above view-points.

One of authors (S. Kumar) is grateful to Council of Scientific and Industrial Research, India for providing financial assistance for carrying out these investigations.

References

1) K. S. Rajan, D. B. Das, A. J. Casolo, and A. J. Bregman, *Desalination*, **1**, 231 (1966).
2) C. Berger and M. P. Strier, *J. Electrochem. Soc.*, **115**, 230 (1968).
3) D. C. Mueller, P. W. West, and R. H. Mueller, *Anal.Chem.*, **41**, 2038 (1969).
4) M. Mascini, *Analyst*, **98**, 325 (1973).
5) W. E. Linden and R. Costervink, *Anal. Chim. Acta*, **108**, 169 (1979).
6) C. J. Coetzee, *Ion-Selective Electrode Review*, **3**, 105 (1981).
7) W. U. Malik, H. Arif, and F. A. Siddiqi, *Bull. Chem. Soc. Jpn.*, **40**, 1746 (1967).
8) W. U. Malik, S. K. Srivastava, R. K. Gulati, and S. P. Arora, *J. Indian Chem. Soc.*, **56**, 688 (1979).
9) W. U. Malik, S. K. Srivastava, V. M. Bhandari, and S. Kumar, *J. Electroanal. Chem.*, **110**, 181 (1980).
10) G. Alberti, *Albertri Accad. Naze Lincei Rend., Classe Sci. Fis., Mat. Nat.*, **31**, 4276 (1961).
11) N. Lakshminarayanaiah, F. A. Siddiqi, and S. K. Saxena, *Z. Phys. Chem.*, **72**, 298 (1970).
12) F. A. Siddiqi, M. N. Beg, R. Shyam, and R. M. Arshad, *J. Memb. Sci.*, **2**, 365 (1977).
13) M. N. Beg, F. A. Siddiqi, R. Shyam, I. Altaf, and M. Arshad, *Indian J. Chem.*, **20A**, 216 (1981).
14) W. U. Malik, S. K. Srivastava, and A. Bansal, *Anal. Chem.*, **54**, 1399 (1982).
15) S. K. Srivastava, Satish Kumar, C. K. Jain, and Surender Kumar, *Indian J. Chem.*, **22A**, 395 (1983).
16) W. U. Malik, S. K. Srivastava, and A. Bansal, *Indian J. Chem.*, **22A**, 221 (1983).
17) S. K. Srivastava, Satish Kumar, C. K. Jain, and Surender Kumar, *Analyst*, **109**, 151 (1984).
18) G. W. Willis, *Trans Faraday Soc.*, **40**, 520 (1944).
19) B. J. Zwolinski, H. Eyring, and C. E. Reese, *J. Phys. Chem.*, **53**, 1426 (1949).
20) S. Glasston, K. J. Laidler, and H. Eyring, "The Theory of Rate Process," McGraw-Hill, New York (1941).
21) E. K. Schuller, C. A. Dames, and K. J. Laidler, *J. Chem. Phys.*, **17**, 860 (1949).
22) T. M. Lai and M. M. Mortland, *Proc. Am. Soc. Soil Sci.*, **25**, 353 (1960).
23) N. Lakshminarayanaiah, F. A. Siddiqi, and S. K. Saxena, *Z. Phys. Chem. (Frankfurt am Main)*, **72**, 298 (1970).
24) R. M. Barrer and G. Shurron, *J. Polym. Sci.*, **3**, 549 (1968).
25) R. M. Barrer, *Trans. Faraday Soc.*, **38**, 322 (1942).

Stability and Distribution Studies on Semicrystalline Tin(IV) Selenophosphate. Separation of Metal Ions

Syed Ashfaq NABI, Zia Mahmood SIDDIQI,* and Rifaqat A. K. RAO
Department of Chemistry, Faculty of Education, Post Office Box; 18758, University of Sebha, Sebha, Libya
Department of Chemistry, Aligarh Muslim University, Aligarh 202001, India
(Received April 18, 1984)

Tin(IV) selenophosphate has been synthesized by mixing 0.05 mol dm^{-3} aqueous solutions of tin(IV) chloride, sodium selenite and sodium dihydrogenphosphate in 1:1:2 ratio at pH=0. The chemical and thermal stabilities are investigated. A tentative formula has been proposed for tin(IV) selenophosphate on the basis of chemical composition, pH titration, IR spectrum and thermogravimetric anslysis. The distribution coefficients of metal ions have been determined in DMF, DMSO, DMF-HNO_3, and DMSO-HNO_3 media. A number of binary, ternary, and quaternary separations of metal ions have been achieved on the columns of tin(IV) selenophosphate.

Studies on amorphous tin(IV) selenophosphate have been reported.[1] Crystalline products as an ion exchanger are being developed because of its many advantages over amorphous products.[2] Recently semicrystalline tin(IV) selenophosphate has been synthesized in our laboratory.[3] The present paper deals with the studies on semicrystalline tin(IV) selenophosphate beyond its synthesis.

Experimental

Reagents. Tin(IV) chloride (Baker Analyzed; USA), dihydrogenphosphate (BDH, England) and sodium dihydrogenphosphate (BDH, India) were used for the synthesis of tin(IV) selenophosphate. Other chemicals were of analytical reagent grade.

Apparatus. The spectrophotometry and pH measurements were performed using EC spectrophotometer GS 866D and Elico LI-10 pH-meter respectively. Perkin Elmer model 137 spectrophotometer and stanton thermobalance type H_4 were used for Infrared and thermogravimetric analyses.

Synthesis. Two samples of tin(IV) selenophosphate were prepared by earlier method.[3] The condition of synthesis and their few properties are shown in Table 1.

Ion Exchange Capacity. The hydrogen libration capacities of sample P_2 and R_3 with potassium ions were determined by column operations as reported earlier.[3]

Chemical Stability. The chemical stabilities of samples

TABLE 1. SYNTHESIS AND PROPERTIES OF TIN(IV) SELENOPHOSPHATE[3]

Sample No	Condition of synthesis				pH	Appearance of beads after drying at 40 °C	Ion-exchange capacity for K^+ ions meq (dry g)$^{-1}$	X-ray results
	$SnCl_4 \cdot 5H_2O$ mol dm^{-3}	Na_2SeO_3 mol dm^{-3}	$Na_2H_2PO_4$ mol dm^{-3}	Mixing ratio v/v/v				
P_2[a]	0.05	0.05	0.05	1:1:2	0	Brownish shiny	1.32	Amorphous
R_3[b]	0.05	0.05	0.05	1:1:2	0	*ditto*	1.60	Semi crystalline

a) Sample P_2 is unrefluxed product. b) Sample R_3 is refluxed product in 2 mol dm^{-3} H_3PO_4+2 mol dm^{-3} selenious acid (1:1).

TABLE 2. COMPARISON OF THE CHEMICAL STABILITY OF VARIOUS SAMPLES OF TIN(IV) SELENOPHOSPHATE

Solvent	SSP_2[1] (mg 50^{-1} cm^{-3})			P_2(unrefluxed) (mg 50^{-1} cm^{-3})			R_3(refluxed) (mg 50^{-1} cm^{-3})		
	Sn released	Se released	PO_4 released	Sn released	Se released	PO_4 released	Sn released	Se released	PO_4 released
H_2O	0.0	0.0	0.0	0.0	0.0	0.0	0.0	0.0	0.0
2 mol dm^{-3} HNO_3	2.2	1.02	0.0	3.6	3.8	0.0	2.5	0.2	0.0
2 mol dm^{-3} HCl	8.2	6.2	5.1	1.8	10.2	0.15	1.0	0.02	0.13
2 mol dm^{-3} H_2SO_4	0.0	0.22	0.1	0.9	1.0	0.0	0.78	0.01	0.0
4 mol dm^{-3} CH_3COOH	0.0	0.2	0.0	0.0	0.1	0.0	0.0	0.0	0.0
4 mol dm^{-3} HCOOH	0.92	0.10	0.0	0.0	0.2	0.0	0.0	0.02	0.0
4 mol dm^{-3} DMF	—	—	—	0.0	0.0	0.0	0.0	0.0	0.0
8 mol dm^{-3} DMF	—	—	—	0.02	0.1	0.01	0.0	0.0	0.0
4 mol dm^{-3} DMSO	—	—	—	0.0	0.0	0.0	0.0	0.0	0.0
8 mol dm^{-3} DMSO	—	—	—	0.01	0.01	0.0	0.0	0.0	0.0

P_2 and R_3 were determined in several solvents at room temperature. A 0.5 g of the material was equilibrated with 50 cm^3 of the solvent and kept for 24 h with intermittent shaking. Tin(IV), selenium and phosphate ion released in the solution were then determined by standard spectrophotometric methods.[4-6] The results are summarized in Table 2.

Composition. For determination of chemical composition of tin(IV) selenophosphate, 0.5 g of the sample was dissolved in hot concentrated hydrochloric acid. Tin(IV) and selenium were determined spectrophotometrically using hematoxylin and potassium iodide reagents.[4,5] Phosphate ion was determined titrimetrically.[7]

pH-Titrations. pH Titrations for NaCl-NaOH system have been performed on sample R_3. A 0.25 g of the exchanger in hydrogen form was equilibrated with 25 cm^3 of the solution at room temperature. pH-titration curve is shown in Fig. 1.

Thermal Treatment. Thermogravimetric analysis (Fig. 2) of the sample R_3 in hydrogen form was performed at a heating rate of 10 °C min^{-1}. To examine the effect of temperature on the ion-exchange capacity, the material (Sample R_3) was heated at different temperatures in a muffle furnace for 1 h. The results are reported in Table 3.

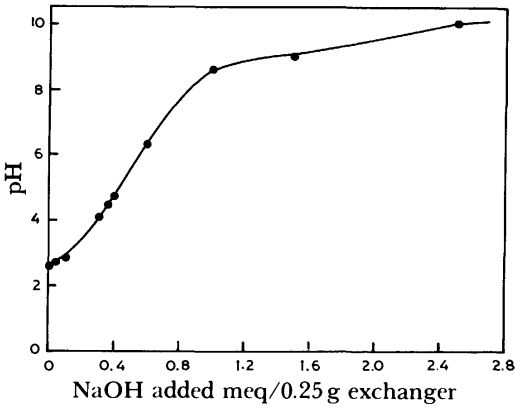

Fig. 1. pH Titration curve of tin(IV) selenophosphate.

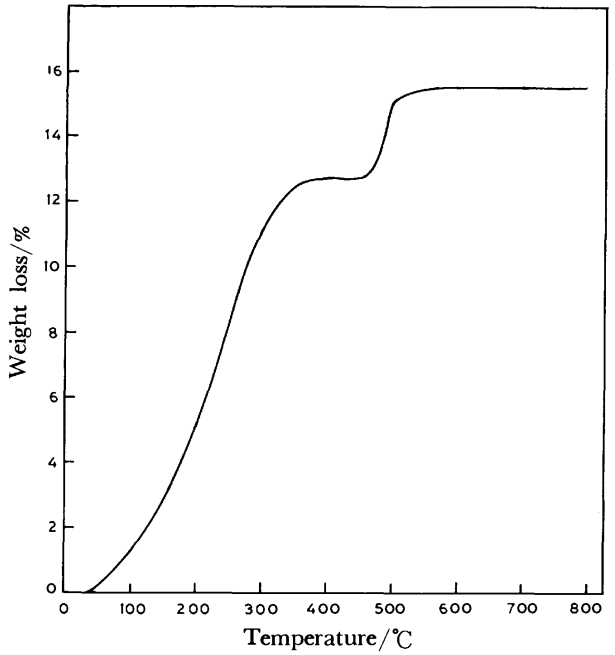

Fig. 2. Thermogram of tin(IV) selenophophate(in H^+ form).

TABLE 3. EFFECT OF DRYING TEMPERATURE ON THE ION-EXCHANGE CAPACITY OF DIFFERENT MATERIALS

Drying temperature °C	Ion-exchange Capacity (meq g^{-1})		
	Tin(IV) phosphate[12]	Tin(IV) Selenite[11]	Tin(IV) Seleno-phosphate
40	1.35	0.75	1.60
100	1.62	0.75	1.63
200	0.82	0.75	1.0
300	0.23	0.75	0.88
400	0.02	0.75	0.70
500	—	0.70	0.64
600	—	0.20	0.38
800	—	—	0.20

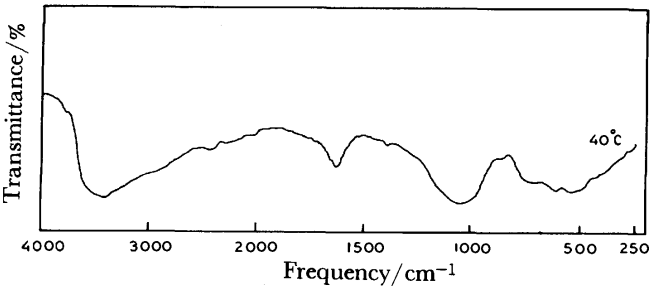

Fig. 3. Infrared spectrum of tin(IV) selenophosphate-(in H^+ form).

IR Analysis. The IR spectrum of sample R_3 dried at 40 °C was obtained by KBr disc method (Fig. 3).

Distribution Coefficients. Distribution coefficients (K_d) of some important metal ions were determined in *N,N*-dimethylformamide (DMF), dimethyl sulfoxide (DMSO) and in mixtures of nitric acid-DMF and nitric acid-DMSO systems as described earlier.[9] The K_d value is defined as following,

$$K_d = \frac{I-F}{F \times W} \times 50$$

where, I is the volume of EDTA consumed by the original solution, F is the volume of EDTA consumed after equilibrium and W is the weight of ion-exchanger in g. The ionic strengths of various metal ion solutions lies between 0.0006 to 0.02. Four mol dm^{-3} DMSO, 4 mol dm^{-3} DMF, and 0.5 mol dm^{-3} HNO_3 were used for distribution studies. The results are given in Tables 4 and 5.

Quantitative Separations. The ion-exchange column was prepared using an earlier method.[10] A 2.0 g of the exchanger (50—100 mesh size) in hydrogen form was taken into a glass column of internal diameter 0.60 cm. Mixture of metal ions was then applied and allowed to pass through the column with a slow rate. The metal ions adsorbed on the exchanger were then eluted with suitable eluting reagent. The flow rate of the effluent was maintained 1 cm^3 min^{-1}, until the metal ions were completely eluted from the column. The metal ions in 10 cm^3 fractions of the effluent were collected and determined either titrimetrically or by standard photometric method.[8] Table 6 describes the separations of metal ions which have been actually achieved on tin(IV) selenophosphate columns.

Results and Discussion

The results of Table 2 show that the samples of

Table 4. Distribution coefficients for some cations on tin(IV) selenophosphate in *N,N*-dimethylformamide and mixed solvent systems

Metal ions	K_d/cm^3 g^{-1}						
	DMF	DMF:HNO_3 (8:2)	DMF:HNO_3 (6:4)	DMF:HNO_3 (4:6)	DMF:HNO_3 (2:8)	HNO_3	H_2O
Mn^{2+}	46±6	25±2	2±1	2±1	2±1	2±1	70±5
Ni^{2+}	28±2	33±5	6±1	2±1	2±1	2±1	1020±30
Cu^{2+}	133±5	101±5	75±2	25±2	2±1	2±1	940±20
VO^{2+}	133±5	250±5	176±5	138±5	43±2	2±1	3900±30
Pb^{2+}	72400±500	72400±500	72400±500	72400±500	72400±500	26±2	8500±50
UO_2^{2+}	500±15	500±15	300±10	200±5	33±2	6±1	9980±100
Fe^{3+}	54±2	145±5	66±5	54±5	44±2	29±2	900±20
Cr^{3+}	900±20	900±20	900±20	900±20	900±20	900±20	—
Th^{4+}	75±5	12±2	9±2	6±2	6±1	4±1	4900±35
Zr^{4+}	7±2	733±16	733±15	341±5	328±5	27±2	9900±100
Cr^{6+}	25±2	25±2	25±2	8±2	00	00	—

Table 5. Distribution coefficients for some cations on tin(IV) selenophosphate in dimethyl sulfoxide and mixed solvent systems

Metal ions	K_d/cm^3 g^{-1}				
	DMSO	DMSO:HNO_3 (8:2)	DMSO:HNO_3 (6:4)	DMSO:HNO_3 (4:6)	DMSO:HNO_3 (2:8)
Mn^{2+}	12±2	2±1	2±1	2±1	2±1
Ni^{2+}	17±2	4±1	3±1	2±1	2±1
Cu^{2+}	69±2	10±2	5±2	5±2	5±2
VO^{2+}	69±2	25±2	12±2	9±2	5±2
Pb^{2+}	79900±500	79900±500	79900±500	79900±500	79900±500
UO_2^{2+}	33±2	33±2	60±2	77±2	77±5
Fe^{3+}	16±2	145±5	116±5	22±2	17±2
Cr^{3+}	650±5	650±5	650±5	650±5	650±5
Th^{4+}	7±2	31±2	21±2	16±2	12±2
Zr^{4+}	47±2	40±2	36±2	29±2	23±2

Table 6. Separations of metal ions achieved on the columns of tin(IV) selenophosphate

S.No.	Separation achieved	Amount loaded	Amount found	Total elution volume	Eluent used[a)]
		μg	μg	cm^3	
1	Cr^{6+}	40	32	30	Water
	Cr^{3+}	500	440	30	1 mol dm^{-3} HNO_3
2	Ni^{2+}	1056	575	70	B
	Fe^{3+}	669	558	60	1 mol dm^{-3} HNO_3
3	Mn^{2+}	682	748	50	A
	Fe^{3+}	669	558	60	1 mol dm^{-3} HNO_3
4	Cr^{6+}	40	38	30	Water
	Cu^{2+}	305	295	40	0.1 mol dm^{-3} HNO_3
	Fe^{3+}	335	357	60	1 mol dm^{-3} HNO_3
5	Mn^{2+}	682	792	50	A
	Cu^{2+}	292	213	40	0.1 mol dm^{-3} HNO_3
	Fe^{3+}	669	570	60	1 mol dm^{-3} HNO_3
6	Ni^{2+}	1056	567	70	B
	Cu^{2+}	292	302	40	0.1 mol dm^{-3} HNO_3
	Fe^{3+}	669	560	60	1 mol dm^{-3} HNO_3
7	Cr^{6+}	40	38	30	Water
	Mn^{2+}	330	294	50	A
	Cu^{2+}	292	343	40	0.1 mol dm^{-3} HNO_3
	Fe^{3+}	669	569	60	1 mol dm^{-3} HNO_3
8	Cr^{6+}	40	38	30	Water
	Ni^{2+}	528	340	70	B
	Cu^{2+}	292	352	40	0.1 mol dm^{-3} HNO_3
	Fe^{3+}	335	312	60	1 mol dm^{-3} HNO_3

A=4 mol dm^{-3} DMF+0.5 mol dm^{-3} HNO_3 (8:2). B=4 mol dm^{-3} DMF+0.5 mol dm^{-3} HNO_3 (2:8).

tin(IV) selenophosphate prepared by these methods are more chemically stable than those prepared earlier.[1] The material becomes more stable when it was refluxed in a mixture of phosphoric acid and selenious acid (sample R_3). Tin (IV) selenophosphate is not affected at all by DMSO and DMF. The pH titration curve however shows bifunctional behaviour of tin(IV) selenophosphate.

A comparison of the ion-exchange capacities of tin(IV) selenophosphate, tin(IV) selenite[11] and tin(IV) phosphate[12] after drying the material at different temperatures are shown in Table 3. Tin(IV) selenophosphate appears to be thermally more stable than tin(IV) phosphate and tin(IV) selenite as it retains reasonable capacity (0.38 meq g^{-1}) upto 600 °C.

The molar composition of tin(IV) selenophosphate shows that tin(IV), selenium and phosphate ion are present in the ratio of 4:1:6.

The thermogram of tin(IV) selenophosphate (Fig. 2) in H^+ form shows continuous loss in weight upto 350 °C. The weight loss upto 200 °C (5%) may be due to the loss of external water molecules. The weight loss from 200 to 350 °C may be due to the loss of water molecules by condensation of OH groups and the conversion of phosphate into pyrophosphate. This process is completed at 450 °C and the ion-exchange capacity of the material coincides with the ion-exchange capacity of tin(IV) selenite (0.70 meq g^{-1}) dried at 500 °C (Table 3). The ion exchange capacity of tin(IV) phosphate is completely lost at this temperature (Table 3). The loss in weight is again observed at about 450 °C. This loss may be referred to the loss of water molecules by condensation of more OH groups and the ion-exchange capacity gradually decreases. After 600 °C the weigt becomes constant due to the formation of oxides and the ion-exchange capacity drops to a negligible value at 800 °C.

IR spectrum of sample R_3 (Fig. 3) in H^+ form shows three strong peaks in the regions of 3500—3000 cm^{-1}, 1700—1500 cm^{-1}, and 1100—900 cm^{-1}. The broad peak in the region 3500—3000 cm^{-1} may be due to presence of water molecules and OH groups. A sharp peak in the region 1700—1500 cm^{-1} with a maximum at 1650 cm^{-1} is characteristics of interstitial water molecules. A third broad peak in the region 1100—900 cm^{-1} may be attributed to HPO_4^{2-} ion.

On the basis of the ion-exchange capacity, pH titration curve, chemical composition and thermogravimetric analysis, the following tentative formula for the tin(IV) selenophosphate may be proposed.

$$[(SnO)_4(OH)(HSeO_3)(H_2PO_4)_6]_n \cdot 4nH_2O \quad (1)$$

If it is assumed that the weight loss (5%) upto 200 °C is due to the removal of external water molecules then the number of water molecules per molecule of exchanger, calculated from the formula given by Alberti[13] are 4. If two hydrogen ions are exchanged at pH 6.5, the ion-exchange capacity calculated from the above formula is 1.48 meq g^{-1} which is in good agreement with the experimental value (1.60 meq g^{-1}). The weight in the temperature range 350—450 °C remains constant (Fig. 2) which is supposed to be due to the conversion of hydrogen phosphate to pyrophosphate. The above formula then can be modified to

$$(SnO)_4(HSeO_3)(P_2O_7)_3 \quad (2)$$

The transformation in this temperature range corresponds to 13.4% loss in weight of the sample. This theoretical value is very close to the weight loss calculated from TGA curve (13% at 400 °C). The ion-exchange capacity therefore at 400 °C should only be due to $HSeO_3$ group of the material. The ion-exchange capacity calculated from formula 2 is 0.80 meq g^{-1} which resembles the experimental ion-exchange capacity (0.70 meq g^{-1} at 400 °C).

The potentiality of tin(IV) selenophosphate has been further investigated for the separation of metal ions. The distribution coefficients (K_d) for some important metal ions have been determined in nitric acid and in some more prospective solvents such as DMF, DMSO, DMF-HNO_3, and DMSO-HNO_3 media. It has been observed that these organic solvents have pronounced effect on the adsorption ability of the material. It is observed that the adsorption of almost all metal ions is very low in DMF and DMSO as compared to water. The K_d values increases as the nitric acid concentration increases in the mixture of DMF and DMSO (Tables 4 and 5). However this effect is more pronounced in the cases of Ni^{2+}, Cu^{2+}, and Mn^{2+}. K_d values become almost negligible with the increased concentration of nitric acid in the mixture. However Pb^{2+} has been found to behave in different manner. The metal ion is strongly adsorbed on tin(IV) selenophosphate in DMSO-HNO_3 and DMF-HNO_3 mixtures. In 0.5 mol dm^{-3} HNO_3 solution the K_d value drops to a negligible value. The peculiar behaviour of Pb^{2+} permits the selective separations of Pb^{2+} from other metal ions in a mixture. A very unique feature which has been noticed regarding this exchanger is that the adsorptions of Cr^{VI} is very low in almost all these media as compared to Cr^{III}. The differential uptake of metal ions in these solvents have been utilized for the separations of some important and valuable metal ions. A number of binary, ternary and quaternary separations have been achieved on the columns of tin(IV) selenophosphate (Table 6).

Tin(IV) selenophosphate may be utilized in the determination of Cr^{VI}/Cr^{III} ratio in sea water which is one of the most important subjects in chemical oceanography.[14] The separations of chromium, nickel, manganese, copper, and iron from one another on columns of tin(IV) selenophosphate suggest the possibility of determination and separation of metal ions in steel, alloys, ores, rocks, and related materials.

The authors are thankful to Prof. W. Rahman,

Chairman, for providing research facilities and to C.S.I.R., New Delhi, for financial assistance to one of us (Z.M.S.).

References

1) S. A. Nabi, A. R. Siddiqi, and R. A. K. Rao, *J. Liquid Chromatog.*, **7**, 1225 (1981).
2) S. A. Nabi and Z. M. Siddiqi, *Bull. Chem. Soc. Jpn.*, **58**, 724 (1985).
3) S. A. Nabi and Z. M. Siddiqi, *Reactive Polymers*, (Communicated).
4) F. D. Snell and C. T. Snell, "Colorimetric Methods of Analysis," Princeton, New Jersey (1959), Vol. IIA, p. 135.
5) Ref. 4 p. 776.
6) Ref. 4 p. 560.
7) N. H. Furman, "Standard Methods of Chemical Analysis," 6th ed, Van Nostrand, Princeton (1962) Vol. I., p. 814.
8) Ref. 4 p. 359.
9) S. A. Nabi, Z. M. Siddiqi, and W. U. Farooqi, *Bull. Chem. Soc. Jpn.*, **55**, 2642 (1982).
10) S. A. Nabi, Z. M. Siddiqi, and R. A. K. Rao, *Separ. Sci. Technol.*, **17**, 1681 (1983).
11) M. Qureshi and S. A. Nabi, *Talanta*, **19**, 1033 (1972).
12) Y. Inoue, *Bull. Chem. Soc. Jpn.*, **36**, 1316 (1963).
13) G. Alberti, P. C. galli, U. Costantino, and E. Rorracca, *J. Inorg. Nucl. Chem.*, **29**, 517 (1967).
14) K. Fujiwara, S. Toda, and K. Fuwa, *Bull. Chem. Soc. Jpn.*, **54**, 3209 (1981).

 © 1985 The Chemical Society of Japan Bull. Chem. Soc. Jpn., 58, 2385—2388 (1985)

Crystal Structure of Potassium Dithizonate†,††

Hiroshi NODA,[1] Lutz Meinhardt ENGELHARDT, Jack MacBean HARROWFIELD, Chaveng PAKAWATCHAI, Jennifer Mary PATRICK, and Allan Henry WHITE*

Department of Physical and Inorganic Chemistry, University of Western Australia, Nedlands, W.A. 6009, Australia

(Received May 14, 1984)

The crystal structure of potassium dithizonate, $K^+[C_6H_5\cdot NH\cdot N\cdot CS\cdot N:NC_6H_5]^-$, has been determined by single crystal X-ray diffraction methods at 295 K and refined by full matrix least squares to a residual of 0.045 for 1101 independent "observed" reflections. Crystals are orthorhombic, Pbca, a=28.942(9), b=13.247(4), c=7.163(3) Å, Z=8. The structure determination is the first carried out on a salt rather than a complex of the anion. The pseudo-planar anion stacks parallel to the ab face of the cell with considerable delocalization evident; as indicated by the above formula, the remaining acidic hydrogen atom is associated with one of the nitrogen atoms.

The well-known analytical reagent dithizone, H_2dz, (A), undergoes both single and double deprotonation, but is best known by way of the numerous, highly-coloured, solvent extractable complexes of the mono-anion, simply referred to usually as the dithizonate anion, Hdz^-.[2]

For such complexes, a variety of linkage isomers is possible and establishment of the coordination mode has demanded the application of X-ray crystallography. In this way, the bidentate N, S chelating form (B) has been established as "usual," though unidentate coordination through sulfur has also been characterized recently in indium(III) dithizonate,[3] in which two bidentate (N,S) and one monodentate (S) ligands are found. All known structures have

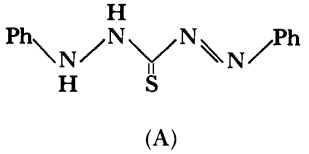

(A)

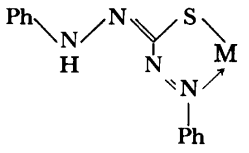

(B)

been determined on compounds of metals which show strong coordinating tendencies and no data has been available for dithizonates which might be regarded as essentially ionic. Accordingly, we have prepared the potassium salt of the monoanion, (1), and report its crystal structure hereunder. Because of its ease of preparation and high solubility in many solvents, it is anticipated that this salt should be of some utility in the preparation of other metal dithizonates.

Synthesis

Because of the ease of oxidation of the ligand, as a routine precaution, all manipulations were carried out under nitrogen using deoxygenated solvents.

Dithizone (2.5 g) was added to a solution of KOH (0.70 g, ≈5% excess assuming 85% purity) in water (3 mL) and the mixture stirred to give a deep orange solution and then a paste as KHdz precipitated. Ethanol (25 mL) was added to dissolve the paste and the solution filtered to remove a small amount of insoluble material. Addition of ether (≈100 mL) to the point of turbidity and standing at room temperature caused the precipitation of clusters of thin, metallic-brown crystals of KHdz. Crystals suitable for X-ray diffraction were obtained from this material, though it could also be recrystallized from ethanol by the addition of ether.

Crystallography

Crystal Data. $C_{13}H_{11}N_4SK$, M=294.4, Orthorhombic, space group Pbca (D_{2h}^{15}, No. 61), a=28.942 (9), b=13.247 (4), c=7.163 (3) Å, U=2746 (2) Å^3. D_c(Z=8)=1.42 g cm^{-3}. F(000)=1216. Monochromatic Mo $K\alpha$ radiation, λ=0.7106$_9$ Å, μ_{Mo}=5.2 cm^{-1}. Specimen: right prism, 0.20×0.40×0.20 mm. T=295 K.

Structure Determination. A unique data set was measured to $2\theta_{max}$=50° using a Syntex P$\bar{1}$ four-circle diffractometer in conventional $2\theta/\theta$ scan mode. 2869 independent reflections were obtained, 1101 with $I>3\sigma(I)$ being considered "observed" and used in the full matrix least squares refinement after analytical absorption correction and solution of the structure by direct methods. Anisotropic thermal parameters were refined; (x, y, z, U_{iso})$_H$ were included constrained at idealized geometries (Exception: the NH hydrogen which was located in a difference map and refined in (x, y, z). Residuals at convergence R, R' (on $|F|$) were 0.045, 0.052, reflections weights being $(\sigma^2(F_0)+0.0005(F_0)^2)^{-1}$. Neutral atom complex scattering factors[4] were used; computation used the X-RAY 76 program system[5] implemented on a Perkin-Elmer 3240 computer by S. R. Hall. Results are presented in the Tables and Figure; atom coordinates for all atoms are given in Table 1, and atom labelling in the Figures.

The lists of structure factors, anisotropic thermal parameters, and non-hydrogen interanion contacts are deposited at the office of the Chemical Society of Japan as Document No. 8504.

Discussion

The result of the structure determination is consistent with the stoichiometry expected for K^+Hdz^-, the

†Material deposited with the editor comprises structure factor amplitudes, thermal parameters and inter-anion contacts.

††Systematic name: Potassium 1,5-Diphenyl-3-mercapto-formazanate.

TABLE 1. ATOM COORDINATES

Atom	Section A			Section B		
	x	*y*	*z*	*x*	*y*	*z*
K	0.28301(5)	0.45023(9)	0.27182(21)			
S	0.31109(5)	0.06809(10)	0.30849(27)			
C	0.3001(2)	0.1944(4)	0.3411(8)			
Ligand						
N(1)	0.3303(1)	0.2681(3)	0.3179(6)	0.2574(1)	0.2368(3)	0.3942(6)
N(2)	0.3729(1)	0.2381(4)	0.2678(8)	0.2267(1)	0.1725(3)	0.4408(6)
H	0.375(2)	0.171(4)	0.251(8)			
C(1)	0.4096(2)	0.3049(4)	0.2592(8)	0.1839(2)	0.2179(4)	0.4974(8)
C(2)	0.4063(2)	0.4010(4)	0.3302(10)	0.1748(2)	0.3211(4)	0.5030(8)
H(2)	0.378(—)	0.424(—)	0.387(—)	0.199(—)	0.367(—)	0.461(—)
C(3)	0.4443(2)	0.4647(5)	0.3206(11)	0.1324(2)	0.3554(5)	0.5618(9)
H(3)	0.443(—)	0.534(—)	0.376(—)	0.128(—)	0.428(—)	0.569(—)
C(4)	0.4849(2)	0.4319(6)	0.2382(11)	0.0986(2)	0.2876(5)	0.6175(9)
H(4)	0.511(—)	0.482(—)	0.232(—)	0.069(—)	0.314(—)	0.657(—)
C(5)	0.4881(2)	0.3356(6)	0.1701(10)	0.1072(2)	0.1871(5)	0.6107(9)
H(5)	0.517(—)	0.318(—)	0.115(—)	0.084(—)	0.139(—)	0.653(—)
C(6)	0.4506(2)	0.2713(5)	0.1801(9)	0.1499(2)	0.1516(5)	0.5521(8)
H(6)	0.453(—)	0.203(—)	0.132(—)	0.156(—)	0.079(—)	0.545(—)

asymmetric unit of the structure comprising one formula unit. The anion is pseudo-planar and approximately parallel to the *ab* face of the cell (Fig. 1(a)); although as discussed below, the central fragment dimensions are indicative of the presence of conjugation, the deviations of the anion from planarity are not confined to the molecular periphery. The plane defined by the $N_2 \cdot CS \cdot N_2$ fragment has σ (defining atoms), 0.047 Å; atom deviations δ N(A2,A1)·CS·N(B1, B2) respectively are 0.041, −0.006, −0.022, −0.021, −0.060, 0.068 Å, with the phenyl ring planes ($\sigma(C_6)$, 0.006, 0.004 Å) having dihedral angles of 14.8, 7.3°

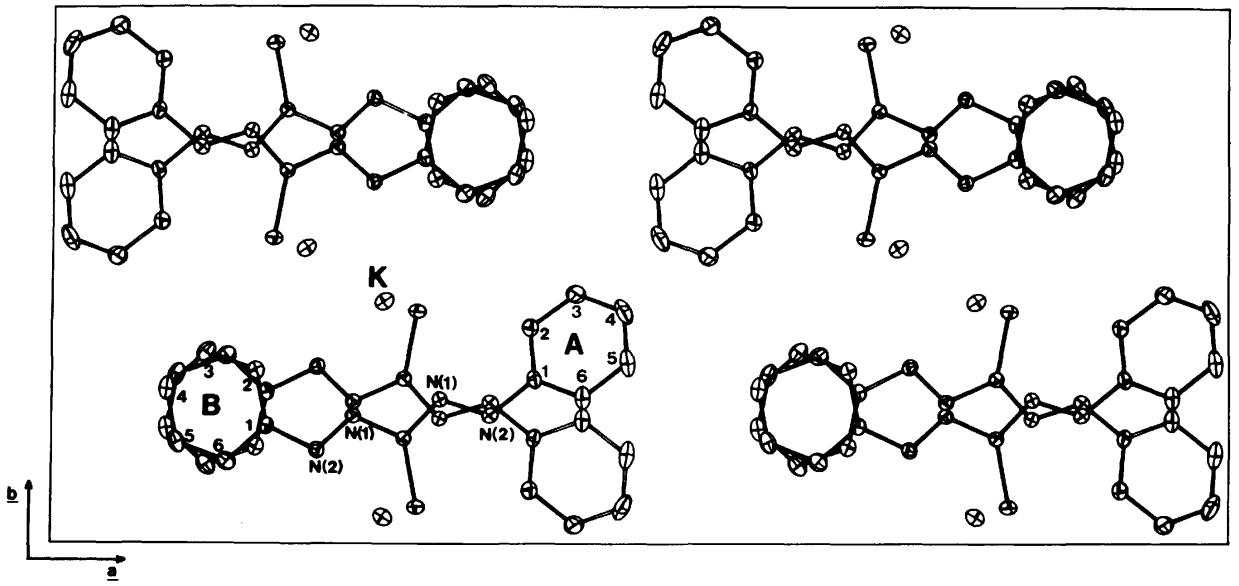

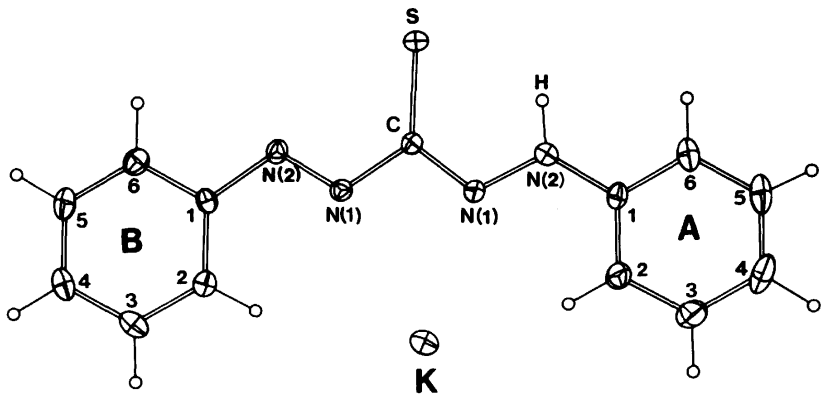

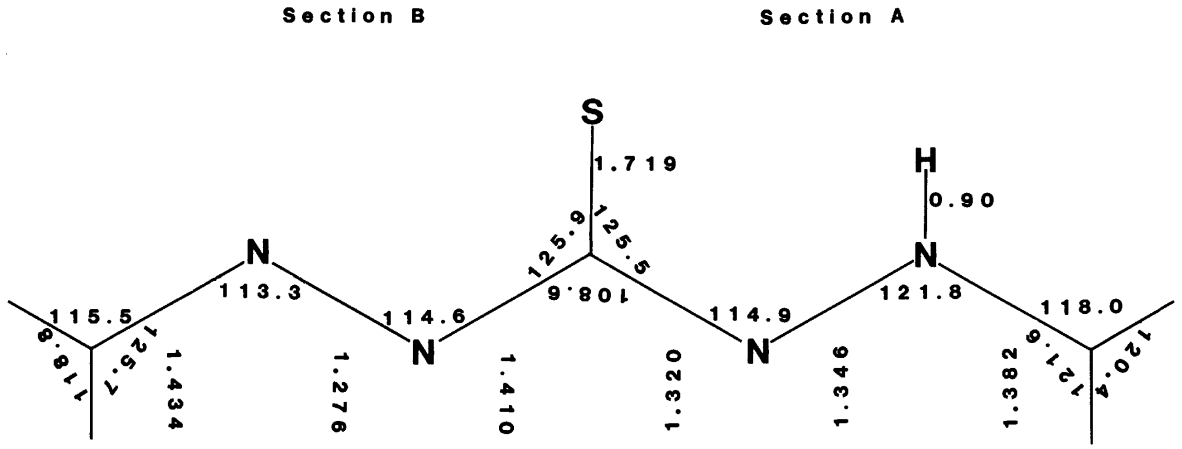

Fig. 1. (a) Unit cell contents, projected down c; 20% thermal ellipsoids are shown for the non-hydrogen atoms.

(b) The asymmetric unit, showing the interaction of the anion with the potassium ion and the location of the acidic hydrogen. Non-hydrogen atom numbering is given, and hydrogen atoms are given arbitrary radii of 0.1 Å.

(c) Non-phenyl anion geometry; distances are in Å and angles in degrees.

Table 2. Potassium environment[a)]

	r	N(B1)	S^{i}	$N(B2^{i})$	S^{ii}	$N(B2^{ii})$
N(A1)	2.793(4)	44.3(1)	147.3(1)	142.6(1)	86.4(1)	84.3(1)
N(B1)	3.052(5)		103.0(1)	136.3(1)	105.7(1)	68.3(1)
S^{i}	3.150(2)			55.7(1)	108.7(1)	82.9(1)
$N(B2^{i})$	3.196(5)				116.9(1)	133.0(1)
S^{ii}	3.426(3)					52.2(1)
$N(B2^{ii})$	3.305(5)					

a) r is the potassium–ligand atom distance (Å); the other entries are the angles (degrees) subtended by the relevant atoms at the metal.
Transformations of the asymmetric unit: i: (1/2−x, 1/2+y,z), ii: (x, 1/2−y, z−1/2).

respectively to the central plane. For the anion non-hydrogen skeletal plane overall, σ is 0.177 Å, with the potassium ion of the asymmetric unit deviating by 1.274 Å; its deviation from the $N_2 \cdot CS \cdot N_2$ plane is −0.906 Å.

The potassium ion environment is sparse (Table 2); an interesting feature is the disposition within the defined asymmetric unit of the two shortest contacts relative to the anion to N(A1,B1), and, because of anion "planarity," the associated contacts to H(A2,B2) of 2.8_8, 2.9_9 Å. Phenyl ring "B," with the smaller dihedral angle to the $N_2 \cdot CS \cdot N_2$ plane, is reasonably coplanar with the associated NN·CS fragment (deviations, 0.01_8, 0.03_8, 0.077, −0.095, although it is clear that there is a twist about the $CS \cdot N_2$ linkage), and the potassium ion deviation is −0.428 Å. Phenyl ring "A"'s association with its NN·CS fragment is less equable (deviations 0.006, −0.191, 0.003, 0.442 Å) and indicative of considerable torsion within the string; the potassium deviation is considerable, being −1.703 Å. It may therefore be assumed that the closeness of the association of the potassium with N(A1), in the situation of a planar anion, results in too close an association with H(A2), with the associated strain being relieved by distortion of the ligand plane. Although the other

Table 3. Anion atom geometries
The two values in each entry are for sections A, B

Atom	Parameter
Distances(l/Å)	
C–S	1.719(5)
C–N(1)	1.320(7), 1.410(7)
N(1)–N(2)	1.346(6), 1.276(6)
N(2)–H	0.90(5)
N(2)–C(1)	1.382(7), 1.434(7)
C(1)–C(2)	1.374(8), 1.394(8)
C(2)–C(3)	1.388(9), 1.373(9)
C(3)–C(4)	1.385(10), 1.386(9)
C(4)–C(5)	1.369(11), 1.356(10)
C(5)–C(6)	1.383(9), 1.388(9)
C(6)–C(1)	1.389(8), 1.376(8)
Angles(ϕ/°)	
N(1)–C–S	125.5(4), 125.9(4)
N(1)–C–N(1)	108.6(4)
C–N(1)–N(2)	114.9(4), 114.6(4)
N(1)–N(2)–C(1)	121.8(5), 113.3(4)
N(2)–C(1)–C(2)	121.6(5), 125.7(5)
N(2)–C(1)–C(6)	118.0(5), 115.5(5)
C(2)–C(1)–C(6)	120.4(5), 118.8(5)
C(1)–C(2)–C(3)	119.4(6), 120.2(5)
C(2)–C(3)–C(4)	120.2(6), 120.3(6)
C(3)–C(4)–C(5)	120.1(6), 119.8(6)
C(4)–C(5)–C(6)	120.1(6), 120.4(6)
C(5)–C(6)–C(1)	119.7(6), 120.5(6)

TABLE 4. COMPARATIVE DITHIZONE GEOMETRIES

	(1)(A)	(3)(A′)	(3)(A)		(2)	(3)(B)		(3)(B′)	(1)(B)
				Distances(l/Å)					
C-S	1.719(5)	1.761(8)	1.754(8),	1.763(8)	1.71				
C-N	1.410(7)	1.410(9)	1.363(10),	1.374(10)	1.34_5	1.328(9),	1.310(8)	1.305(11)	1.320(7)
N-N(H)	1.276(6)	1.274(10)	1.293(8),	1.290(8)	1.29_5	1.326(9),	1.317(10)	1.324(9)	1.346(6)
N(H)-C(aryl)	1.434(7)	1.437(9)	1.403(10),	1.419(10)	1.38_5	1.410(10),	1.407(9)	1.409(12)	1.382(7)
				Angles(ϕ/°)					
N-C-S	125.9(4)	123.5(6)	125.5(5),	125.5(5)	125	123.6(6),	123.4(6)	123.4(5)	125.5(4)
N-C-N	108.6(4)	112.5(7)	110.7(6),	111.1(6)	110				
C-N-N(H)	114.6(4)	114.8(6)	119.5(6),	117.6(6)	115	117.3(6),	116.9(6)	117.2(7)	114.9(4)
N-N(H)-C(aryl)	113.4(4)	112.9(6)	116.0(6),	114.6(6)	122	117.4(6),	122.5(7)	120.6(8)	121.8(5)

Species compared are: (1)(A) Unprotonated section of the present dithizonate anion. (3)(A′) Unprotonated section of the S-coordinated ligand of indium(III) dithizonate. (3)(A) Coordinated sections of the chelate ligands of indium(III) dithizonate. (2) The mean of both (protonated) sections of the parent dithizone molecule. (3)(B) Uncoordinated sections of the chelate ligands of indium(III) dithizonate. (3)(B′) Protonated section of the S-coordinated ligand of indium(III) dithizonate. (1)(B) Protonated section of the present dithizonate anion.

four contacts to the potassium ion are also two pairs of "chelate" type interactions, originating in S,N(B2) combinations, the associated K···H(B6) distances are longer (greater than 3.1 Å) and less relevant. About the sulfur atom, a pair of symmetry related potassium ions is found (S···K(1/2−x, y−1/2, z), (x, 1/2−y, 1/2+z), 3.150 (2), 3.426 (3) Å), with the angle subtended at the sulfur being 80.83 (5)° and K···K, 4.268 (2) Å).

The "acidic" hydrogen atom of the anion is clearly associated with N(A2); as refined, the angles H-N(A2)-N(A1), C(A1) may be slightly unsymmetrical (113(3), 125(3)°) with H···S, 2.34 (5), and H···H(A6), 2.4 Å. The *cis* angles at N(A1) and C(A1) are 114.9 (4), 118.0 (5), slightly greater than their counterparts in section B (114.6(4); 115.5(5)°), with the presence of H presumably a contributing factor, as it also presumably is to the distortions noted above in section A.

In considering geometry and bonding within the ligand, (Table 3), the closest analogues with which comparison might usefully be made appear to be (i) the protonated ligand (2),[6] with a pair of similar halves (average geometry quoted), and (ii) the five-coordinate indium(III) complex, (3),[3] in which a pair of chelating ligands are found with distinctly different geometries for the chelating segment, denoted (A) and the non-chelating (B), and a third ligand which is monodentate S-coordinated, with a protonated section (denoted (B)) and an unprotonated section (A). The geometries of these species are compared in Table 4 with those of sections A and B of the present anion. With certain dimensional exceptions, the present values are comparable with others expected to lie at the extremes of the range. The exceptions are:

(i) The carbon-sulfur distance, comparable with that in the free ligand, but shorter than that in the S-coordinated monodentate ligand of the indium complex (3), and, in parallel, because of electron-pair repulsion effects

(ii) The N-C-N angle again resembles more nearly the value of the free ligand, rather than that of the S-coordinated monodentate ligand;

(iii) The C-N-NH angle in the present complex is less than its counterpart in the protonated section of the monodentate ligand of the indium complex, and nearer the value of the free ligand, presumably assisted by the incorporation of the potassium ion on its opposite side.

The two halves of the ligand suggest a considerable contribution of the resonance form

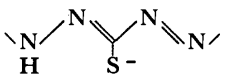

The length of certain bonds, in particular, C-S, (1.719(5) Å) and N(A2)-C(A1), 1.382(7) Å, are indicative of more extensive delocalization, however. A number of non-hydrogen interanion contacts, generated in the stacking apparent in Fig. 1(a) by (x, 1/2−y, 1/2+z), approach 3.3 Å as a lower limit and are suggestive of the possibility of charge-transfer interactions.

We gratefully acknowledge support of this work by a grant from the Australian Research Grant Scheme.

References

1) Visitor from the Shimadzu Corporation, Nakagyo-ku, Kyoto 604, Japan.

2) H. M. N. H. Irving, 'Dithizone,' The Chemical Society, London, (1977).

3) J. McB. Harrowfield, C. Pakawatchai, and A. H. White, *J. Chem. Soc., Dalton Trans.*, **1983**, 1109.

4) "International Tables for X-ray Crystallography," ed by J. A. Ibers and W. C. Hamilton, The Kynoch Press, Birmingham, (1974) Vol. IV, pp. 71ff, 148ff.

5) "The X-RAY System-Version of March, 1976," ed by J. M. Stewart, Technical Report TR-446, Computer Science Center, University of Maryland, U.S.A.

6) M. Laing, *J. Chem. Soc., Perkin Trans. 2*, **1977**, 1248.

 © 1985 The Chemical Society of Japan Bull. Chem. Soc. Jpn., 58, 2389—2394 (1985)

Kinetics and Mechanisms of Oxidations by Metal Ions. V. Oxidation of 4-Oxopentanoic Acid by the Aquavanadium(V) Ion†

Raj Narain MEHROTRA
Department of Chemistry, University of Jodhpur, Jodhpur 342 001, India
(Received January 5, 1984)

The outer sphere oxidation of 4-oxopentanoic acid(4-OPA), studied at 50 °C by aquavanadium(V) ion, is H^+-catalyzed reaction. The reaction has a first-order dependence on each of [V^V], [4-OPA], and [H^+]. The H^+ catalysis can not be ascribed to keto⇌enol equilibrium because of the knowledge that a γ-keto acid is the least enolized amongst keto acids. Hence $V(OH)_3^{2+}$ (aq) ion is the active oxidant. The proposed mechanism, assumed to involve the initial decarboxylation, is supported by the spot test characterization of acetoin as the intermediate oxidation product. Acetoin is further oxidized to two moles of acetic acid which is the final oxidation product. The overall energy of activation($\Delta H_1=26\pm3$ kJ mol^{-1}) is lower than the normal value(84 kJ mol^{-1}) and therefore the highly negative value of the overall entropy of activation($\Delta S_1=-268\pm8$ J K^{-1} mol^{-1}) is considered to be responsible for the observed slowrate of oxidation.

Aquavanadium(V) ions in acid perchlorate solution are milder oxidants in comparison to the other aquametal ions such as Ce^{IV}, Mn^{III}, Co^{III}, Ag^{II} *etc.* However, the redox potential of V^V/V^{IV} couple in acidic solution[1] is about 1 volt and is sufficient for the oxidation of a variety of organic compounds with ease. The subject matter has been reviewed.[2-4]

The equilibrium 1 is considered for explaining the acid catalysis having a first-order dependence in [H^+] in the oxidations by vanadium(V). The protonation equilibrium constant K_1 has been not as yet estimated by physical methods though several studies[5,6] on redox kinetics have consistently suggested that $1 \gg K_1[H^+]$ in solutions of 1—5 mol dm^{-3} perchloric acid.[6]

$$VO_2^+ + H_3O^+ \overset{K_1}{\rightleftharpoons} V(OH)_3^{2+}. \quad (1)$$

Recently, that $K_1=3.4$ dm^3 mol^{-1} at 30 °C was estimated in the oxidation of pyruvic acid.[7] Since this value is of such a magnitude that would render the assumption[5,6] that $1 \gg K_1[H^+]$ erroneous even in dilute acid solutions ≥0.1 mol dm^{-3}. Hence a necessity was felt to have a recheck on this value of K_1. It was only obvious to have a similar substrate and the choice of 4-oxopentanoic acid (here in after abbreviated as 4-OPA) was also motivated by the fact that γ-keto acid is least enolized in comparison to α- and β-keto acids.[8] The choice thus eliminated the complexity of the effect of enolization of the >CO group in the interpretation of the results.

Experimental

Reagents. Stock solution of vanadium(V) was prepared by dissolving ammonium metavanadate (Hopkin & Williams, G. R.) in twice distilled water. To the clear yellow solution was slowly added a calculated amount of standard perchloric acid to have a vanadium(V) solution having 2 mol dm^{-3} perchloric acid. In calculating the amount of perchloric acid, extra amount needed for the protonation reaction 2 was also considered.

$$VO_3^- + 2H^+ \longrightarrow VO_2^+ + H_2O. \quad (2)$$

†Reprints are not available.

The stock vanadium(V) solution was standardised titrimetrically[9] with a standard Fe(II) solution using *N,N*-diphenylsulfamate of barium as the indicator in presence of phosphoric acid.

Solutions of 4-oxopentanoic (E. Merck) and perchloric (E. Merck) acids were prepared by suitable dilutions and standardized against a standard alkali. Solutions of 4-oxopentanoic acid of long standing were discarded.

The stock solution of sodium perchlorate was prepared by neutralising sodium carbonate (BDH, AnalaR) with perchloric acid. The neutralized solution was later boiled to eliminate dissolved carbon dioxide. The solution was standardized gravimetrically.

All other reagents used were of analytical grade and distilled water was once again distilled from an all glass still.

Rate Measurements. The kinetics was studied at constant ionic strength (3 mol dm^{-3}) maintained with sodium perchlorate. Reactant solutions of suitable strength were separately thermostatted in a water bath maintained at the desired temperature (±0.1 °C). The reaction was generally initiated by the quick addition of 4-oxopentanoic acid. However, the rate was not affected when the reaction was initiated with vanadium(V). In all experiments, [4-OPA] ≫[V^V] was used which ensured that k_{obsd}, the pseudo first-order rate constant with respect to vanadium(V), was not affected by any reactive intermediate produced during the course of the reaction.

The disappearance of vanadium(V) was followed with a Beckman DU 2 spectrophtometer at 350 nm.[5,6,10] Absorbance due to vanadium(IV) was negligible at this wave length ($\varepsilon_{350}=1.0$ dm^3 mol^{-1} cm^{-1}).[11]

The values of the pseudo first-order rate constant k_{obsd} were obtained by least square analysis of the slopes of the linear plots of ln (A_t-A_∞) against time where A_t and A_∞ are the absorbance at any time t and at infinite time, respectively. The plots were linear ($r>0.998$) beyond three half-lives. Few runs were repeated in presence of an inert nitrogen atmosphere and the k_{obsd} values so obtained were within the limits of experimental agreement (±3%) with those obtained in the presence of air, and the rate was not affected by the presence of vanadium(IV).

Stoichiometry. The stoichiometry of the complete oxidation reaction was determined under different acidity and atmospheric conditions as are detailed in Table 1. The [V^V] was present in excess and the reaction mixtures were left at 35 °C in a thermostatted water bath till $\Delta[V^V]/\Delta$[4-OPA]

Table 1. Stoichiometries at 35 °C and I=3.0 mol dm^{-3}

$[V^v]$ / mol dm^{-3}	[4-OPA] / mol dm^{-3}	$[H^+]$ / mol dm^{-3}	Unreacted$[V^v]$ / mol dm^{-3}	Atmosphere	$\Delta[V^v]$ / Δ[4-OPA]
0.08	0.010	3.0	0.019	Air	6.1
0.10	0.012	2.0	0.029	N_2	5.9
0.10	0.015	2.0	0.011	Air	5.9
0.12	0.017	3.0	0.013	N_2	6.0
0.14	0.020	1.0	0.021	Air	6.0
0.14	0.022	1.0	0.005	N_2	6.1
					Means: 6.0±0.1

Table 2. Dependence of k_{obsd} on [4-Oxopentanoic acid] at 50 °C. [vanadium(V)]=0.02 mol dm^{-3}, [$HClO_4$]=2.0 mol dm^{-3}, and I=3.0 mol dm^{-3}

[4-OPA] / mol dm^{-3}	10^5k_{obsd}/s^{-1}	10^5k_{obsd}/[4-OPA] / dm^3 mol^{-1} s^{-1}	[4-OPA] / mol dm^{-3}	10^5k_{obsd}/s^{-1}	10^5k_{obsd}/[4-OPA] / dm^3 mol^{-1} s^{-1}
0.11	0.44	4.0	0.72	2.8	3.9
0.18	0.73	4.1	1.03	4.2	4.1
0.36	1.50	4.2	1.32	5.4	4.1
					Means: 4.1±0.1

assumed a constant value (6.0±0.1).

Product Analysis. The oxidation products were repeatedly extracted with ether from the reaction mixtures once $\Delta[V^v]/\Delta$[4-OPA] was constant. The ether solution was slowly evaporated and the liquid left behind was found to smell like acetic acid. The presence of acetic acid was characterized by its usual test with neutral Fe(III) chloride and the spot test with lanthanum nitrate and iodine.[12] Hence the stoichiometry of the reaction is expressed by Eq. 3.

$$CH_3CO(CH_2)_2CO_2H + 6V^v + 3H_2O \longrightarrow 2CH_3CO_2H + CO_2 + 6V^{IV} + 6H^+. \quad (3)$$

Reactive Intermediates. In another series of experiments the reaction mixtures were so prepared as to have large excess of 4-OPA over vanadium(V). The reaction products were repeatedly extracted from the partially oxidized reaction mixtures with ether. In this case acetoin was found to be the product and its presence was confirmed with the specific spot test.[12b] Acetoin is reported to be oxidized to acetic acid *via* biacetyl as the reactive intermediate requiring four equivalents of vanadium(V) per mole of acetoin.[13] The presence of biacetyl as the reactive intermediate could not be confirmed, perhaps, for the reason that it is oxidized at a much faster rate.

In view of the above it is clear that the keto acid is first oxidized to acetoin needing only two equivalents of vanadium(V) per mole. The formation of acetoin could be expressed by Eq. 4.

$$CH_3CO(CH_2)_2CO_2H + 2V^v + H_2O \longrightarrow CH_3COCH(OH)CH_3 + 2V^{IV} + CO_2 + 2H^+. \quad (4)$$

Test for Free Radical. Partially oxidized reaction mixtures which were previously flushed with nitrogen and maintained under nitrogen atmosphere produced polyacrylonitrile upon the addition of monomer acrylonitrile indicating the presence of free radical in the reaction mixtures. The blank experiments in which the monomer was separately added to the solutions of vanadium(V) and the keto acid did not show the formation of polyacrylonitrile. While these experiments are not helpful in identifying the actual free radical species, they did indicate the formation of free radicals during the progress of the reaction.

Table 3. Dependence of k_{obsd} on [$HClO_4$] at different temperatures. [vanadium(V)]=0.02 mol dm^{-3}, [4-OPA]=0.36 mol dm^{-3}, and I=3.0 mol dm^{-3}

[$HClO_4$] / mol dm^{-3}	10^5k_{obsd}/s^{-1} 45°	50°	55°	60°	65 °C
0.5	0.30	0.36	0.43	0.50	0.58
1.0	0.61	0.74	0.84	1.02	1.15
1.5	0.91	1.10	1.27	1.51	1.75
2.0	1.22	1.47	1.67	2.02	2.30
2.5	1.53	1.85	2.11	2.54	2.92

Results

Dependence on [4-OPA]. A twelve fold variation in the initial [4-OPA] was effected to investigate its effect on the k_{obsd}; the results are reported in Table 2. It was found that the plot of k_{obsd} against [4-OPA] was linear with zero intercept indicating that the order with respect to 4-oxopentanoic acid is unity.

Dependence on [H^+]. The effect of initial [H^+] on k_{obsd} was investigated at five different temperatures in the range 0.5—2.5 mol dm^{-3} perchloric acid at a constant ionic strength adjusted with sodium perchlorate to 3.0 mol dm^{-3}. The rate measurements in solutions with [$HClO_4$]<0.5 mol dm^{-3} were not attempted because of the rate of reaction was found to be very slow. The results are reported in Table 3. The plot of k_{obsd} against [H^+] was linear at all temperatures with zero intercept on the rate ordinate as is shown in Fig. 1. Similarly, the plot between k_{obsd} and $-H_0$, the Hammett acidity function,[14] was linear at all the temperatures as is illustrated in Fig. 2. These plots, which are parallel to each other, indicated that slope of plot, 0.84, is independent of temperature. Thus the slope value is nearer to the ideal value of unity expected in this correlation.[15] The H_0 values reported by Day and Wyatt[16] were used.

Effect of Ionic Strength. The effect of ionic

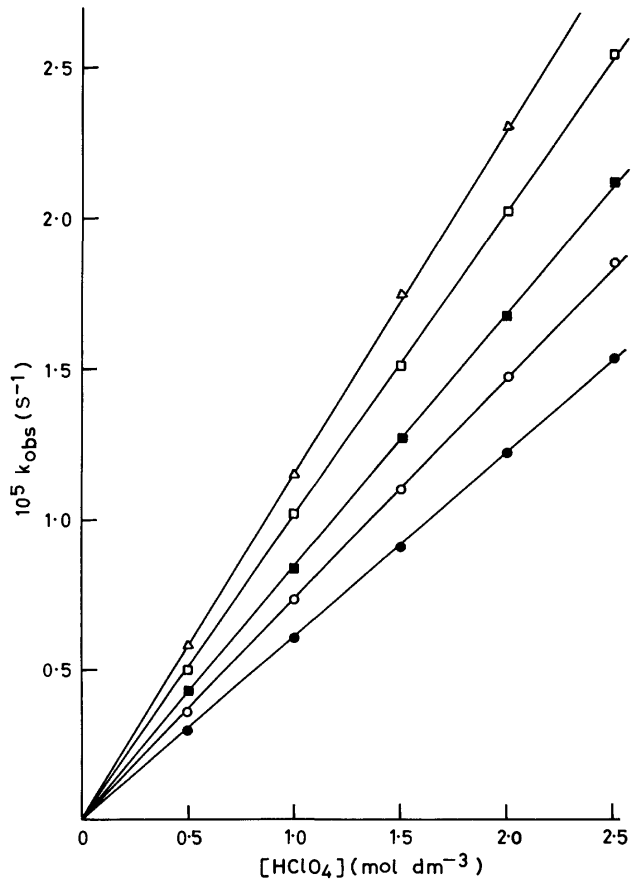

Fig. 1. The linear plots between k_{obsd} and [$HClO_4$] with zero intercepts in solutions of constant ionic strength (3.0 mol dm^{-3}) at 45° (●), 50° (○), 55°(■), 60° (□), and 65° (△). [Vanadium(V)]=0.02 mol dm^{-3} and [4-Oxopentanoic acid]=0.36 mol dm^{-3}.

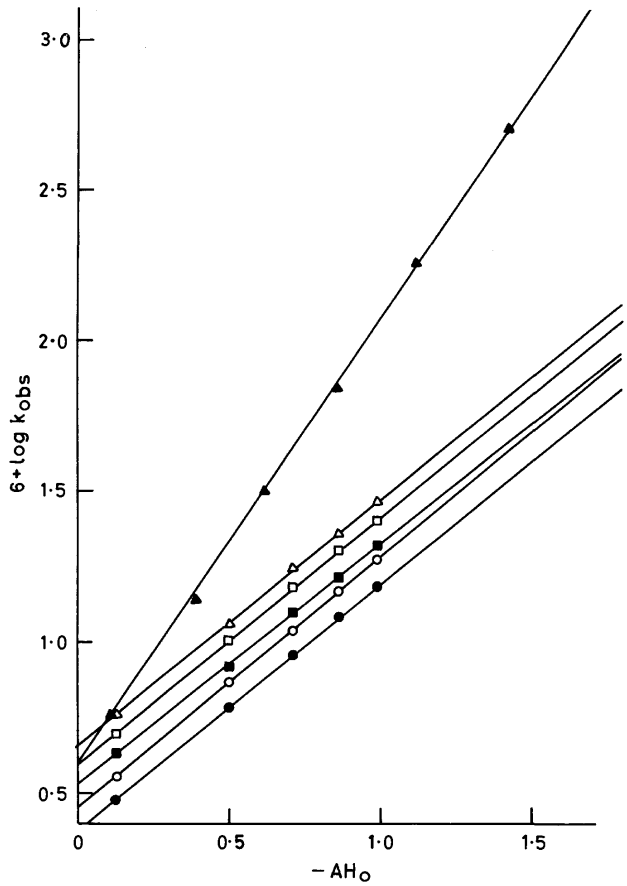

Fig. 2. The linear plots between log k_{obsd} and $-H_0$, the Hammett acidity function, for perchloric acid solutions of a constant ionic strength (3.0 mol dm^{-3}) at 45° (●), 50° (○), 55° (■), 60° (□), and 65° (△) with A=1, and for perchloric acid solution of varying ionic strength at 50° (▲) with A=0.5 [Vanadium(V)]=0.02 mol dm^{-3} and [4-Oxopentanoic acid]=0.36 mol dm^{-3}.

strength on k_{obsd} was investigated by varying the [$NaClO_4$] in the range 0.1—1.0 mol dm^{-3} at a fixed [H^+](2.0 mol dm^{-3}) and [4-OPA] (0.36 mol dm^{-3}) at 50°C. The k_{obsd} was almost independent of ionic strength (10^5 k_{obsd}=1.5±0.1 s^{-1}) indicating that one of the reactants is not charged. Since vanadium(V) species are positively charged[17] in acid solutions>0.1 mol dm^{-3} it is obvious that 4-oxopentanoic acid reacted in the unionized state. A similar conclusion was also derived by considering its pK_a value of 4.5 at 25 °C.[18] The pK_a value indicated that the keto acid is a weak acid and therefore it would largely exist in its undissociated state under the [H^+] used. Moreover, had the anion of the keto acid been reactive a retardation in the rate with increasing [H^+] was expected and was not found.

Discussion

The spectrum of 4-oxopentanoic acid has indicated that any lactol contribution is very small and the keto-form predominates,[19] a fact in conformity with the observation that γ-keto acids are least enolized.[8] Although the formation of enol-lactones is more readily effected in the presence of acid catalysts yet these are less stable,[19] and therefore are not considered to be a major reactive entity. Similarly the keto⇌enol equilibrium has also been excluded from the proposed mechanism because (i) if the rate of keto→enol transformation was rate controlling then the order of the reaction with respect to the oxidant was expected to be zero, and (ii) the very slow nature of the reaction ($10^5 k_{obsd}$/[4-OPA]=4.1±0.1 dm^3 mol^{-1} s^{-1} at 50°C and [$HClO_4$]=2.0 mol dm^{-3}) did not indicate any possibility of the enol as being the reactive entity.

The cationic species of vanadium(V) in acidic aqueous solution are VO_2^+(aq)[20,21] and $V(OH)_4^+$/(aq).[22,23] The existence of $V(OH)_4^+$ as $(VO_2 \cdot H_2O)^+$ has been suggested.[24] The equilibrium between $(VO_2 \cdot 2H_2O)^+$ and its protonated species $V(OH)_3^{2+}$ is shown in equilibrium 5.

In view of the kinetics which has indicated a first-order dependence in each of [V^V], [4-OPA], and [H^+], the following reactions are considered part of the mechanism which is based on the assumption that decarboxylation of the keto acid is the rate determining reaction. The exclusion of the possibility of

the oxidant attacking the >CO group is explained at a later stage of discussion.

$$(VO_2\cdot 2H_2O)^+ + H^+ \overset{K_1}{\rightleftharpoons} V(OH)_3^{2+} + H_2O \quad (5)$$

$$(VO_2\cdot 2H_2O)^+ + CH_3CO(CH_2)_2CO_2H \xrightarrow{k} V^{IV} + CH_3COCH_2\dot{C}H_2 + CO_2 + H^+ \quad (6)$$

$$V(OH)_3^{2+} + CH_3CO(CH_2)_2CO_2H \xrightarrow{k_1} V^{IV} + CH_3COCH_2\dot{C}H_2 + CO_2 + H^+ \quad (7)$$

$$CH_3COCH_2\dot{C}H_2 \xrightarrow{fast} CH_3CO\dot{C}HCH_3 \quad (8)$$

$$CH_3CO\dot{C}HCH_3 + V^V + H_2O \xrightarrow{fast} CH_3COCH(OH)CH_3 + V^{IV} + H^+ \quad (9)$$

$$CH_3COCH(OH)CH_3 + 2V^V \xrightarrow{fast} CH_3COCOCH_3 + 2V^{IV} + 2H^+ \quad (10)$$

$$CH_3COCOCH_3 + 2V^V + 2H_2O \xrightarrow{fast} 2CH_3CO_2H + 2V^{IV} + 2H^+ \quad (11)$$

where reactions 6 and 7 are rate determining, all other reactions are fast. The inclusion of reaction 9 is based on the belief that hydroxylation of free radicals in presence of an oxidant is always a fast process.

The oxidation of acetoin in reaction 10 as a fast one is based on the comparison of the rate constant k_1K_1 with $k_3(=k_{obsd}/4[H^+][\text{acetoin}])$. The value of k_3 is[13] 8.0×10^{-3} $dm^6\,mol^{-2}\,s^{-1}$ compared to k_1K_1 which is 1.32×10^{-6} $dm^6\,mol^{-2}\,s^{-1}$ in solutions of 1.5 mol dm^{-3} perchloric acid and 3 mol dm^{-3} ionic strength at 25 °C. Hence it is seen that the oxidation of acetoin is somewhat 6×10^3 times faster than the rate of oxidation of the keto acid. The inclusion of reaction 10 as the fast one is thus justified. The value of k_1K_1 at 25 °C was obtained by extrapolating the linear plot of ln k_1K_1 and $1/T$. The values of k_1K_1 at different temperatures, Table 4, were obtained by the relation described latter. The actual rate measurements on the oxidation of biacetyl (2,3-butanedione) have as yet not been carried out but it is reported[13] to be much faster than that of acetoin.[13]

The rate of disappearance of $[V^V]$ in terms of reactions 5—11 is given by Eq. 12 which could also be written as Eq. 13.

$$\frac{-d[V^V]}{dt} = \frac{6(k+k_1K_1[H^+])[V^V][\text{4-OPA}]}{1+K_1[H^+]} \quad (12)$$

$$k_{obsd}(1+K_1[H^+]) = 6(k+k_1K_1[H^+])[\text{4-OPA}] \quad (13)$$

Now if it is assumed that $K_1=3.4$ $dm^3\,mol^{-1}$, reported by Sengupta and coworkers in the oxidation of

TABLE 4. VALUES OF k_1K_1 AT DIFFERENT TEMPERATURES AND THE VALUES OF THE ENTHALPY AND ENTROPY OF ACTIVATION

(°C)	45	50	55	60	65
$10^6k_1K_1$ / $dm^6\,mol^{-2}\,s^{-1}$	2.80	3.40	3.89	4.63	5.37

$\Delta H_1=26\pm3$ kJ mol^{-1}
$\Delta S_1=-268\pm8$ J $K^{-1}\,mol^{-1}$

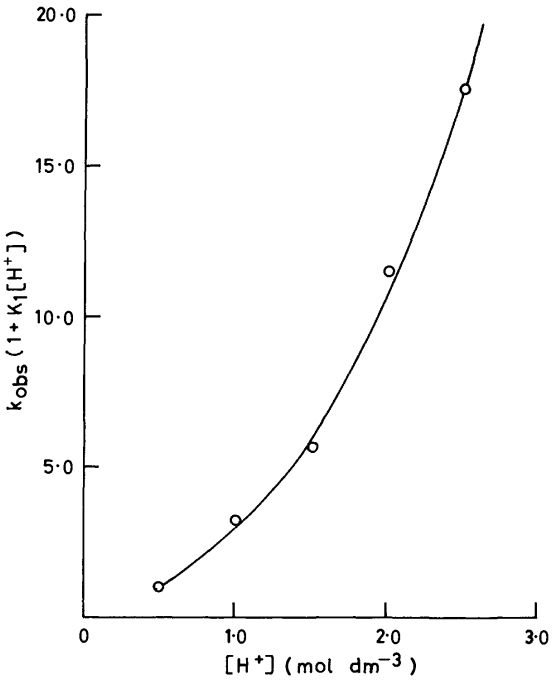

Fig. 3. The plot between k_{obsd} $(1+K_1[H^+])$ and $[H^+]$ at 50 °C with $K_1=3.4\,dm^3\,mol^{-1}$ for perchloric acid solution of constant ionic strength (3.0 mol dm^{-3}). Similar plots were obtained at other temperatures too. [Vanadium(V)]=0.02 mol dm^{-3} and [4-Oxopentanoic acid]=0.36 mol dm^{-3}.

pyruvic acid,[7] then the plot of k_{obsd} $(1+K_1[H^+])$ against $[H^+]$ should be linear with a positive intercept on the rate ordinate. However, when this plot was constructed, Fig. 3, it was found that the plot is not linear indicating that the assumption of the high value of K_1 is at least not correct in the present case.

Next, the application of the assumption[5,6] that $1 \gg K_1[H^+]$ resulted in the linear correlation between k_{obsd} and $[H^+]$ as is shown in Fig. 1. The plot, however, has a zero intercept indicating that $k \ll k_1K_1[H^+]$ *i.e.* $V(OH)_3^{2+}$ is more reactive than VO_2^+ which is rationalized by the assumption that an increase in the effective charge on metal ion increases its oxidizing capability.

The values of $k_1K_1(=k_{obsd}/6[H^+][\text{4-OPA}])$ at different temperatures were calculated from the data given in Table 3. The values so obtained are in Table 4 wherein are also reported the values of the thermodynamic parameters.

Alternate Mechanism. The following sequence of reactions are based on the probability of the initial electron transfer to vanadium(V) from the >CO group of the keto acid.

$$(VO_2\cdot 2H_2O)^+ + H^+ \overset{K_1}{\rightleftharpoons} V(OH)_3^{2+}(aq) + H_2O \quad (5)$$

$$V(OH)_3^{2+} + CH_3CO(CH_2)_2CO_2H \xrightarrow{k_1} CH_3\dot{C}O + \overset{+}{C}H_2CH_2CO_2H + V^{IV} \quad (14)$$

$$CH_3\dot{C}O + V^V + H_2O \longrightarrow CH_3CO_2H + V^{IV} + H^+ \quad (15)$$

$$\overset{+}{C}H_2CH_2CO_2H \longrightarrow CH_3\overset{+}{C}HCO_2H \quad (16)$$

$$CH_3\overset{+}{C}HCO_2H + V^V + H_2O \longrightarrow CH_3CH(OH)CO_2H + V^{IV} + H^+ \quad (17)$$

$$CH_3CH(OH)CO_2H + 2V^V \longrightarrow CH_3CHO + CO_2 + 2V^{IV} + 2H^+ \quad (18)$$

$$CH_3CHO + 2V^V + 2H_2O \longrightarrow CH_3CO_2H + 2V^{IV} + 2H^+ \quad (19)$$

where reaction 14 is the rate determining and the corresponding reaction with VO_2^+(aq) is not included because of the knowledge that VO_2^+(aq) species are not effective oxidant species as had been discussed earlier. The reaction 19 may also not be very correct representation of the oxidation of acetaldehyde because it is just probable that its enol form might be undergoing oxidation as is the case with the oxidation of other aldehydes.[25] Acetaldehyde is the first oxidation product of lactic acid in the oxidation by vanadium(V).[26] The inclusion of fast oxidation of lactic acid in 18 is based on the comparison of k_1K_1 and k_4 ($=k_{obsd}/4[H^+][CH_3CH(OH)CO_2H]$). The value of k_4 is 2.95×10^{-4} dm^6 mol^{-2} s^{-1} against a value of 1.41×10^{-6} dm^6 mol^{-2} s^{-1} for k_1K_1 both at $[HClO_4]=1.0$ mol dm^{-3} at 25 °C.

The rate of disappearance of $[V^V]$ in terms of reactions 5 and 14—19 of course will be given by Eq. 12 and as such the two mechanisms become indistinguishable. However, this alternate mechanism is not well supported by the initial oxidation product detected in the oxidation of the keto acid. Lactic acid, as required by the above mechanism was not the initial oxidation product which was acetoin. Moreover there is no similarity between the observed rate law in Eq. 12 and the one obtained in the oxidation of lactic acid[26] and $Me_2C(OH)COMe$[13] which involved C-C fission similar to reaction 14. Both lactic acid and $Me_2C(OH)COMe$ were oxidized by a path independent of $[H^+]$.

Activation Parameters. The observed enthalpy (ΔH_1) and entropy (ΔS_1) of activation are in Table 4. The ΔH_1 value for the reaction is low compared with the value reported in the oxidation of other organic compounds.[3] Similarly ΔS_1 is highly negative compared to the values obtained in various redox reactions.[3] Since ΔH and ΔS are extensive properties, it is therefore clear that $\Delta H_1=\Delta H°+\Delta H^{\neq}$, and $\Delta S_1=\Delta S°+\Delta S^{\neq}$ where $\Delta H°$, $\Delta S°$, and $\Delta H^{\neq}$, $\Delta S^{\neq}$ are the enthalpy and entropy of activation for reactions 5 and 7 respectively. A negative $\Delta S°$ for the reaction 5 is expected because there is a net increase in the charge on the reactive vanadium(V) species. Similary a negative $\Delta S^{\neq}$ for the reaction 7 is expected because it involves the reaction between polyatomic molecules. Hence the high negative value of ΔS_1 for the combined reactions 5 and 7 is understandable.

The low value of ΔH_1 is probably due to the negative value of either $\Delta H°$ or $\Delta H^{\neq}$. It is also clear that $\Delta H^{\neq}$ cannot be negative hence $\Delta H°$ must be negative which is consistent with the views available in the literature.[27] The negative $\Delta H°$ means that there would be less formation of $V(OH)_3^{2+}$ with increasing temperature, a fact well supported by the report[28] that a 0.2 mol dm^{-3} vanadium(V) solution in 4.4 mol dm^{-3} perchloric acid precipitated vanadium pentaoxide when warmed above 60 °C.

Conclusion. The keto acid is oxidized by the primary attack of the V^V on carboxylic group. That the keto acid is not oxidized at >CO group is concluded on the basis that k_{obsd} is at least one order less than the k_{obsd} value obtained in the oxidation of cyclohexanone under similar conditions of acidity and temperature and concentrations of the substrates. The carboxylic acids, except formic acid,[3] are resistant to the oxidation by vanadium(V) under conditions used in the present study. Thus the relatively easier yet slow oxidation of the keto acid could be ascribed to the presence of >CO group which is apparently not involved in the initial transfer of electron to the oxidant. Whether the >CO group remains in the keto form or is transformed to enol prior to the oxidation is not clear, yet certain conclusions can be derived from certain known facts.

Since the γ-keto acid is least enolised[8] it is suggested that 4-OPA is mainly oxidized in its keto form. The oxidation at >CO group site has been eliminated on the basis of magnitude of k_{obsd} value. A partial order with respect to 4-OPA was expected if the oxidation involved the enol form. However, this would be true only if the equilibrium constant K_e for keto⇌enol equilibrium has a significant value so that $1 \gg K_e$[4-OPA]. Since a strict first-order dependence in 4-OPA is observed, it is clear that K_e has no signifant value and therfore the concentration of the enol form is considered to be kinetically insignificant. The emphasis that 4-OPA is oxidized in the keto form (where keto group remains unreactive) stems out from the fact that one equivalent oxidants generally oxidize a ketone by attacking the >CO group. That the >CO group is not attacked in the present case is another matter.

Thanks are due to Prof. R. C. Kapoor for his interest and encouragement, and to CSIR and UGC for the financial support.

References

Part IV, Raj N. Mehrotra, *Can. J. Chem.* **63**, 663 (1985).

1) D. Benson, "Mechanisms of Oxidation by Metal Ions," Elsevier, London (1976). p. 12.

2) W. A. Waters, *Rev. Chim., (Bucharest)* **7**, 1367 (1962).

3) W. A. Waters, and J. S. Littler in "Oxidation in Organic Chemistry," Part A, ed by K. B. Wiberg, Academic Press, New York (1965) p. 185.

4) D. K. Babel, Rashida Banu, R. Shanker, and G. V. Bakore, *J. Sci. Ind. Res.*, **43**, 250 (1984).

5) C. F. Wells and A. F. M. Nazer, *J. Chem. Soc., Faraday Trans. 2*, **72**, 910 (1976); A. F. M. Nazer and C. F. Wells, *J. Chem. Soc., Dalton Trans.*, **1980**, 1532; A. F. M. Nazer and C. F. Wells, *J. Chem. Soc., Dalton Trans.*, **1980**, 2143.

6) C. F. Wells and L. V. Kuritsyn, *J. Chem. Soc., A*, **1970**, 1372.
7) K. K. Sengupta and H. R. Chatterji, *Inorg. Chem.*, **17**, 2429 (1978).
8) N. N. Melnikov and M. S. Rokitskaya, *J. Gen. Chem. USSR*, **15**, 657 (1945).
9) I. M. Kolthoff and R. Belcher, "Volumetric Analysis," Vol. III, Interscience, New York, (1957) p. 607.
10) J. N. Cooper, H. L. Hoyt, C. W. Buffington, and C. A. Holmes, *J. Phys. Chem.*, **75**, 891 (1971).
11) S. C. Furman and C. S. Garner, *J. Am. Chem. Soc.*, **72**, 1785 (1950).
12) F. Feigl, "Spot Tests in Organic Analysis," Elsevier, Holland (1960), a) p. 369; b) p. 217.
13) J. R. Jones and W. A. Waters, *J. Chem. Soc.*, **1962**, (1629).
14) L. P. Hammett and A. J. Deyrup, *J. Am. Chem. Soc.*, **54**, 2721 (1932).
15) M. A. Paul and F. A. Long., *Chem. Rev.*, **57**, 1 (1957).
16) J. S. Day and F. A. H. Wyatt, *J. Chem. Soc., B*, **1966**, 343.
17) F. J. C. Rossotti and H. Rosotti, *Acta Chem. Scand.*, **10**, 957 (1956); J. Meir and G. Schwarzenbach, *Chimia* (Aarau), **12**, 328 (1958); N. Ingri and F. Brito, *Acta Chem. Scand.*, **13**, 1971 (1959).
18) M. L. Soni, Raj N. Mehrotra, and R. C. Kapoor, *Indian J. Chem.*, **21A**, 196 (1982).
19) "Rodd's Chemistry of Carbon Compounds" ed by S. Coffey, Elsevier, London (1965), Vol. I, Part D, p. 263.
20) M. J. LaSalle and J. W. Cobble, *J. Phys. Chem.*, **59**, 519 (1955).
21) F. J. C. Rossotti and H. Rossotti, *J. Inorg. Nucl. Chem.*, **2**, 202 (1956).
22) J. B. Ramsey, E. L. Colichman, and L. C. Pack, *J. Am. Chem. Soc.*, **68**, 1695 (1946)
23) H. C. Misra and M. C. R. Symons, *J. Chem. Soc.*, **1962**, 4411.
24) Raj N. Mehrotra, *J. Chem. Soc., B*, **1968**, 642.
25) J. R. Jones and W. A. Waters, *J. Chem. Soc.*, **1963**, 352.
26) J. R. Jones, W. A. Waters, and J. S. Littler, *J. Chem. Soc.*, **1961**, 630.
27) L. L. Schaleger and F. A. Long in "Advances in Physical Organic Chemistry," Vol. I, Academic Press, New York, (1963) p. 1.
28) J. S. Littler and W. A. Waters, *J. Chem. Soc.*, **1959**, 3014.

Mono(cyclopentadienyl)titanium(IV) Derivatives with Heterocyclic Thioketones

Om Prakash PANDEY, Soumitra Kumar SENGUPTA,* and Satish Chandra TRIPATHI
Department of Chemistry, University of Gorakhpur, Gorakhpur-273001, India
(Received February 23, 1984)

The reactions of mono(cyclopentadienyl)titanium(IV) trichloride with three important series of heterocyclic thioketones, *viz.*, triazolinethiones 4-amino-, 4-benzylideneamino-, 4-furfurylideneamino-, and 4-salicylideneamino-5-trifluoromethyl-1,2,4-triazoline-3-thiones, thioxoquinazolones (3-methyl-, 3-phenyl-, and 3-(*o*-tolyl)-2-thioxo-4-quinazolones), and oxadiazolethiones (5-phenyl-, 5-(*p*-nitrophenyl), and 5-(*p*-chlorophenyl)-1,3,4-oxadiazole-2-thiones, have been studied in anhydrous dichloromethane. The reaction products have been characterized on the basis of elemental analyses, electrical conductance, magnetic susceptibility and spectral (electronic, infrared, and ^{1}H NMR) data. Proton NMR spectra indicate that there is rapid rotation of the cyclopentadienyl ring around the metal ring axis on the NMR time scale at 28 °C.

Although the preparation of mono(cyclopentadienyl)titanium(IV) trichloride was reported[1] by Gorsich as early as 1960, its coordination behaviour with chelating agents is still practically unknown. Some papers have appeared on mono(cyclopentadienyl)titanium(IV) compounds containing carboxylic acids,[2,3] dithiocarbamates,[4] thiols[5] or β-diketones[6,7] as ligands but they are mostly derived by the oxidation of $cpTiCl_2$ or removal of one cyclopentadienyl moiety from cp_2TiCl_2 derivatives. Recently, some papers appeared dealing with the reactions of $cpTiCl_3$ with dithiocarbamates,[8] Schiff bases,[9] 1,10-phenanthroline,[10] *o*-phenylenebis(dimethylarsine) and 2,2′-bipyridyl.[11] In this paper, we report the syntheses and characterization of mono(cyclopentadienyl)titanium(IV) derivatives containing heterocyclic thioketones as chelating agents. These ligands, containing thioamide bond and capable of undergoing thione-enethiol (HN–C=S⇌N=C–SH) tautomerism, can coordinate to a metal atom through nitrogen or through sulfur or simultaneously through nitrogen and sulfur. The chemistry of transition metal complexes with heterocyclic thioketones continues to be of unabated interest on account of the striking structural features presented by this class of compounds and also due to their biological importance.[12–16]

The structures of the ligands are given below:

(a) Triazolinethione

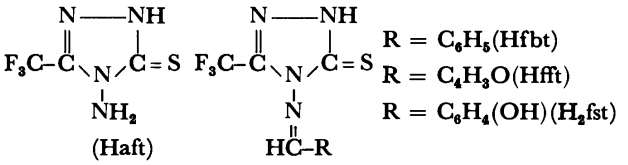

(b) Thioxoquinazolone

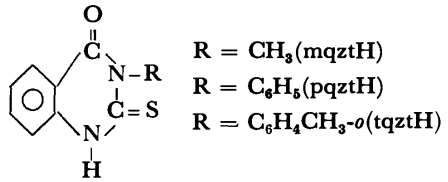

(c) Oxadiazolethione

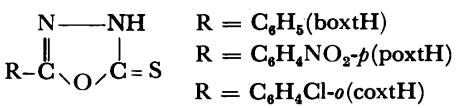

Experimental

The ligands triazolinethiones, thioxoquinazolones, and oxadiazolethiones were prepared as mentioned in literature.[17–19] Mono(cyclopentadienyl)titanium(IV) trichloride was prepared from $(cp)_2TiCl_2$ and $TiCl_4$ in *p*-xylene.[1] Dichloromethane was dried by refluxing it for 30 h over calcium hydride.

Most of derivatives prepared and studied are susceptible to hydrolysis. Hence, all operations were carried out under strictly anhydrous conditions and glass apparatus with standard interchangeable joints was used throughout the work.

Titanium was determined gravimetrically as TiO_2 and chloride as AgCl. Sulphur was estimated as $BaSO_4$. The carbon and hydrogen analyses were carried out at Central Drug and Research Institute, Lucknow.

The details of physical measurements are same as described earlier.[20]

Preparation of Complexes. All these complexes were prepared by taking mono(cyclopentadienyl)titanium(IV) trichloride and respective ligand in appropriate molar ratios and adding about 60 ml of dichloromethane followed by a reflux time of 20—50 h. The solutions were then filtered and their volume reduced to about 20 ml. Further, addition of dry petroleum ether (60—80 °C, ≈20 ml) to the above solution and allowing them to stand for overnight resulted yellow to brown crystals of the products which were filtered and dried in oven at 80 °C.

The details of the amounts of reactants taken for the preparation of complexes, refluxing time, yield and colour of the products are given in Table 1.

Results and Discussion

The analytical data of the complexes are given in Table 1. The methods used for preparation and isolation of these compounds give materials of good purity as supported by their analyses and TLC. All these complexes are coloured. They are thermally stable but decompose above ≈150 °C without melting. They are quite stable in air but their solutions are hydrolyzed on standing. Conductance measurements reveal that they are essentially nonelectrolytes. Magnetic susceptibility values at room temperature show the diamagnetic nature of the complexes. The electronic spectra of all these complexes show a

Table 1. Reactions of (cp)$TiCl_3$ with heterocyclic thioketones in dichloromethane

Reactants	Molar ratio	Refluxing time/h	Product, colour, decomp temp/°C, yield/%	Found(Calcd)				
				C	H	S	Ti	Cl
(cp)$TiCl_3$+Haft	1:1	20	(cp)$TiCl_2$(aft), yellow, 252, 58	26.0 (26.1)	1.7 (1.9)	8.5 (8.7)	13.0 (13.0)	19.2 (19.3)
(cp)$TiCl_3$+Haft	1:2	28	(cp)$TiCl(aft)_2$, brown, 232, 54	25.4 (25.6)	1.7 (1.7)	12.2 (12.4)	9.0 (9.3)	6.8 (6.9)
(cp)$TiCl_3$+Haft	1:3	38	(cp)$Ti(aft)_3$,brown, 280, 62	25.3 (25.3)	1.4 (1.6)	14.2 (14.5)	7.2 (7.2)	— —
(cp)$TiCl_3$+Hfbt	1:1	25	(cp)$TiCl_2$(fbt), yellow, 262, 65	39.3 (39.5)	2.4 (2.4)	6.8 (7.0)	10.5 (10.5)	15.3 (15.6)
(cp)$TiCl_3$+Hfbt	1:2	35	(cp)$TiCl(fbt)_2$, orange, 300, 55	43.2 (43.4)	2.1 (2.4)	9.0 (9.2)	6.7 (6.9)	5.1 (5.1)
(cp)$TiCl_3$+Hfbt	1:3	45	(cp)$Ti(fbt)_3$, orange, 275, 60	45.3 (45.3)	2.2 (2.4)	10.1 (10.3)	5.1 (5.1)	— —
(cp)$TiCl_3$+Hfft	1:1	30	(cp)$TiCl_2$(fft), yellow, 180, 68	35.0 (35.0)	1.8 (2.0)	7.0 (7.1)	10.7 (10.7)	15.9 (15.9)
(cp)$TiCl_3$+Hfft	1:2	40	(cp)$TiCl(fft)_2$, yellow, 210, 65	37.3 (37.5)	1.9 (1.9)	9.2 (9.5)	7.1 (7.1)	5.2 (5.2)
(cp)$TiCl_3$+Hfft	1:3	50	(cp)$Ti(fft)_3$, orange, >300, 50	38.6 (38.8)	2.0 (2.1)	10.7 (10.7)	5.3 (5.3)	— —
(cp)$TiCl_3$+H_2fst	1:1	20	(cp)TiCl(fst), orange, 245, 68	41.2 (41.4)	2.3 (2.5)	7.3 (7.3)	10.9 (11.0)	8.1 (8.1)
(cp)$TiCl_3$+mqztH	1:1	22	(cp)$TiCl_2$(mqzt), yellow, 200, 65	46.0 (46.2)	3.0 (3.3)	8.7 (8.8)	13.0 (13.1)	19.5 (19.5)
(cp)$TiCl_3$+mqztH	1:2	28	(cp)$TiCl(mqzt)_2$, brown, 182, 50	54.2 (54.5)	3.7 (3.7)	12.4 (12.6)	9.3 (9.4)	7.0 (7.0)
(cp)$TiCl_3$+mqztH	1:3	45	(cp)$Ti(mqzt)_3$, orange, >300, 52	59.0 (59.0)	3.8 (4.0)	14.6 (14.7)	7.3 (7.3)	— —
(cp)$TiCl_3$+pqztH	1:1	28	(cp)$TiCl_2$(pqzt), yellow, 165, 68	52.0 (52.1)	3.1 (3.2)	7.3 (7.3)	10.9 (10.9)	16.1 (16.2)
(cp)$TiCl_3$+pqztH	1:2	38	(cp)$TiCl(pqzt)_2$, orange, 295, 58	60.5 (60.5)	3.2 (3.5)	9.7 (9.7)	7.3 (7.3)	5.2 (5.4)
(cp)$TiCl_3$+pqztH	1:3	50	(cp)$Ti(pqzt)_3$, orange, 218, 64	64.4 (64.6)	3.3 (3.6)	11.0 (11.0)	5.4 (5.4)	— —
(cp)$TiCl_3$+tqztH	1:1	28	(cp)$TiCl_2$(tqzt), orange, 248, 58	53.0 (53.2)	3.5 (3.5)	14.0 (14.1)	10.4 (10.6)	15.7 (15.7)
(cp)$TiCl_3$+tqztH	1:2	38	(cp)$TiCl(tqzt)_2$, brown, >300, 62	61.5 (61.5)	3.6 (3.6)	9.0 (9.3)	7.0 (7.0)	5.1 (5.2)
(cp)$TiCl_3$+tqztH	1:3	45	(cp)$Ti(tqzt)_3$, brown, 278, 45	65.6 (65.6)	3.7 (3.8)	10.5 (10.5)	5.0 (5.2)	— —
(cp)$TiCl_3$+boxtH	1:1	22	(cp)$TiCl_2$(boxt), yellow, 162, 60	43.0 (43.1)	2.5 (2.7)	8.8 (8.8)	13.0 (13.2)	19.6 (19.6)
(cp)$TiCl_3$+boxtH	1:2	30	(cp)$TiCl(boxt)_2$, brown, 235, 58	50.1 (50.1)	2.9 (2.9)	12.5 (12.7)	9.4 (9.5)	7.0 (7.0)
(cp)$TiCl_3$+boxtH	1:3	48	(cp)$Ti(boxt)_3$, dark brown, 193, 52	54.0 (54.0)	3.0 (3.1)	14.9 (14.9)	7.3 (7.4)	— —
(cp)$TiCl_3$+poxtH	1:1	28	(cp)$TiCl_2$(poxt), brown, 193, 60	38.4 (38.4)	2.0 (2.2)	7.8 (7.8)	11.6 (11.8)	17.4 (17.4)
(cp)$TiCl_3$+poxtH	1:2	37	(cp)$TiCl(poxt)_2$, orange brown, 188, 54	42.4 (42.5)	2.1 (2.1)	10.7 (10.8)	7.8 (8.0)	5.9 (5.9)
(cp)$TiCl_3$+poxtH	1:3	50	(cp)$Ti(poxt)_3$, yellowish brown, 215, 60	44.4 (44.6)	2.1 (2.1)	12.3 (12.3)	6.0 (6.1)	— —
(cp)$TiCl_3$+coxtH	1:1	28	(cp)$TiCl_2$(coxt), light brown, 214, 60	39.2 (39.4)	2.2 (2.2)	8.0 (8.0)	12.0 (12.1)	26.7 (26.9)
(cp)$TiCl_3$+coxtH	1:2	35	(cp)$TiCl(coxt)_2$, yellowish brown, 186, 52	44.0 (44.1)	2.2 (2.2)	11.2 (11.2)	8.3 (8.3)	18.4 (18.6)
(cp)$TiCl_3$+coxtH	1:3	50	(cp)$Ti(coxt)_3$, brown, 206, 70	46.4 (46.5)	2.2 (2.2)	12.8 (12.8)	6.4 (6.4)	14.1 (14.2)

band in the region 23500—24400 cm^{-1}, which can be assigned[20] to the charge transfer band and is in accordance with the $(n-1)$ d^0 ns^0 electronic configuration of titanium. In additon, the ligands and the complexes show bands around 32000 cm^{-1} which are assigned to $\pi \rightarrow \pi^*$ transition of the azomethine linkages.

Infrared Spectra. *(a) Triazolinethione Derivatives*: The assignments of infrared spectral bands of the ligands and the complexes are based on an earlier study of similar ligands.[21] Organic compounds having a thioamide group (H-N-C=S) give rise to four thio-

amide bands in the IR spectra.[22] These are thioamide band I at about 1500 cm^{-1}, band II at about 1300—1400 cm^{-1}, band III at about 1000 cm^{-1} and band IV at about 700—850 cm^{-1}. These bands have contributions from δ(C-H)+δ(N-H), ν(C=S)+ν(C=N)+ δ(C-H), ν(C-N)+ν(C-S), and ν(C=S) modes of vibrations respectively. In our ligands, these bands appear in the region 1560—1550, 1250, 1090—1080, and 790—780 cm^{-1}. These bands are expected to be affected differently by different modes of coordination after complexation with the metal ions.[21,23,24] However, in our complexes, these bands disappear indicating that mixing of ν(C-N), δ(N-H), and ν(C=S) vibrations may be absent and ligand is coordinating to the metal atom through a deprotonated thiol sulfur atom. A weak band at ≈2550 —2480 cm^{-1} in the spectra of the ligands due to the -SH group vibration, further suggests the thione⇌enethiol tautomerism. However, in the spectra of the complexes, this band disappears indicating the coordination through sulfur after deprotonation. This is further confirmed by the appearance of new band in the far IR region 380—340 cm^{-1} which can be assigned to the ν(Ti-S) vibration.[25]

The bands observed around 3250—3150 (in Haft), 1630 in (Hfbt, Hfft, and H_2fst), 1580—1565 and 1500 cm^{-1} in the spectra of the ligands may be assigned[21] to ν(N-H), ν(C=N) (N-N=C-), ν(C=N) (ring) and ν(C=C) (phenyl) vibrations, respectively. Strong vibrations in the region 1600—1550 cm^{-1} are usually associated with phenyl and C=N groups and it is not usually possible to identify such bands with particular C=C or C=N linkage. However, a stringent assignment of the C=N group can be made by comparing the spectrum of the ligand Haft containing N-NH_2 group with that of the ligands Hfbt, Hfft, and H_2fst in which it is replaced by N-N=CH group. Following this method, the strong band observed around 1630 cm^{-1} is assigned to the ν(C=N) vibration. However, the spectra of the complexes show the shifting of this band to lower frequency (≈25 cm^{-1}) indicating the coordination of the azomethine nitrogen to metal atom. The IR band in the region 3250—3200 cm^{-1} in the ligand Hfat due to ν(NH) of the amino group is shifted towards the lower wave number (≈50 cm^{-1}) in its complexes which indicate[26] the coordination of the amino nitrogen to the metal atom. The bands observed in the region 450—430 cm^{-1} may be assigned[25] to ν(Ti-N).

The ligand H_2fst shows one band at ≈3400 cm^{-1} which may be assigned[26] to ν(OH) of phenolic hydroxyl group. However, in its complex, this band disappears indicating the coordination of phenolic oxygen to the metal atom through deprotonation. The bands at 500 cm^{-1} in the complex can be assigned to ν(Ti-O).[20]

Thus, the infrared spectra reflect that the ligand Haft acts as monobasic bidentate ligand having coordination sites at thiol sulfur and amino nitrogen, the ligands Hfbt and Hfft coordinate through thiol sulfur and azomethine nitrogen and the ligand H_2fst behaves as dibasic tridentate ligand coordinating through thiol sulfur, phenolic oxygen, and azomethine nitrogen.

(b) Thioxoquinazolone Derivatives: The IR spectra of the ligands, 3-substituted 2-thioxo-4-quinazolones, show one sharp band at 3400 cm^{-1} which may be assigned[26] to ν(NH). The δ(NH) mode is observed at 1650 cm^{-1}. However, in the spectra of complexes, these bands disappear indicating the displacement of N-H hydrogen by metal ion. This is further confirmed by the appearance of new bands around 470—440 cm^{-1}, assignable[25] to ν(Ti-N). A sharp band appearing at 1720—1700 cm^{-1} in the ligands may be assigned to ν(C=O) which appears at the same place in the spectra of the complexes, ruling out the possibility of coordination through carbonyl group. The ligands 2-thioxo-4-quinazol-one contains a thioamide group. The four thioamide bands, I, II, III, and IV typical of molecules containing H-N-C=S skeleton are found at ≈1500, 1400—1300, 1000, and 850—700 cm^{-1}, respectively. The appearance of four thioamide bands and the absence of any band near 2500 cm^{-1} (due to ν(S-H)), indicates[16] the existence of the ligands in the thione form. The thioamide III and IV bands, having main contribution from ν(C=S), are shifted towards lower energies in the complexes indicating[21] the coordination of thioxo sulfur to titanium atom. The ν(Ti-S) vibrations appear at 390—360 cm^{-1}. Thus, it becomes evident that the ligands, 3-substituted 2-thioxo-4-quinazolone, act as bidentate chelating agents, coordinating through thione sulfur and amino nitrogen (through deprotonation).

(c) Oxadiazolethione Derivatives: The ligands, 5-substituted 1,3,4-oxadiazole-2-thione, have one phenyl, one oxadiazole rings and >C=S group resulting in the presence of four donor sites (two nitrogen atoms, one oxygen atom and one sulfur atom). Its infrared spectra should, therefore, show characteristic bands of phenyl, oxadiazole rings and of >C=S groups. Although the spectra of the ligand and the complexes are quite complicated owing to the overlap of various bands and the coupling of various modes of vibrations. However, the systematic shifts in the positions of a few bands relative to those present in the spectrum of the ligand, give clue to the mode of bonding in the complexes.

The ν(NH) and δ(NH) vibration bands, which appear in the region 3350 and 1630 cm^{-1} in the ligands, disappear in the complexes indicating[26] the coordination of amino nitrogen to the titanium atom through deprotonation. This is confirmed by the appearance of new bands at about 480—440 cm^{-1}, assignable[25] to ν(Ti-N). The thioamide III and IV vibrations, which have largest contribution from ν(C=S), undergo a red shift in the complexes suggesting the coordination of sulfur atom to the titanium atom in the thione form.[21] The ν(Ti-S) vibrations appear at 400—370 cm^{-1}. The position of IR bands due to phenyl and oxadiazolyl group

(C-O-C)[22] do not change in the complexes indicating the non-coordination of oxygen atom. The above observations indicate that possibly the bonding in titanium complexes is through amino nitrogen and thioxo sulfur.

In addition, absorption bands occurring at ≈3000 cm^{-1} ν(C-H), ≈1430 cm^{-1} ν(C-C), and 1020 cm^{-1} ν(C-H) in all the complexes indicate the presence of cyclopentadienyl ring. All these bands are similar to those of mono(cyclopentadienyl) titanium(IV).[27] Davison and Rakita have pointed out[28] that at 3000 cm^{-1}, η'-C_5H_5 should show four bands whereas η^5-C_5H_5 should show only one. In the complexes, reported in this paper, only one band at 3000 cm^{-1} indicate the pentahapto nature of cyclopentadienyl ring.

^1H NMR Spectra. The proton NMR spectra of some of these complexes have been recorded in deuterated chloroform and *N,N*-dimethyl-formamide. The intensities of all the resonance lines were determined by planimetric integration. The following conclusions can be derived by comparing the spectra of ligands and their corresponding complexes:

(i) A signal in all derivatives at δ≈6.5—6.8 ppm may be assigned to the protons of cyclopentadienyl ring. The value is in the range reported[2] for other (C_5H_5)Ti^{IV} complexes with chelating ligands and is significantly separated from the position of (C_5H_5)$TiCl_3$ (≈7.07 ppm). The appearance of a single, sharp cyclopentadienyl resonance is attributed to rapid rotation of the ring around the metal-ring axis.

(ii) The two kinetic possibilities, *viz.*, metal-centered rearrangement is slow or fast, can be distinguished by the analysis of NMR spectra. In the spectra of 1:3 complexes, (cp)Ti(L)$_3$, two distinct resonance lines for the protons of the ligands are observed which must result from the nonequivalent environments for the different ligands. However in the 1:2 derivatives, (cp)Ti(L)$_2$Cl, the ligand groups are equivalent since one signal have been observed for ligand proton groups.

(iii) In NMR spectra of mercaptotriazoles, the signal due to -SH proton appears at about δ=4.4 ppm which disappears in the corresponding complexes indicating the deprotonation of thiol proton. Further, the ligand H_2fst shows one signal at δ=9.8 ppm due to phenolic proton. This signal disappears in its complex indicating the deprotonation of the phenolic hydroxyl group.

(iv) The spectra of thioxoquinazolone and oxadiazolethione show one sharp signal at δ=4.8—4.9 ppm due to -NH proton which disappear in their corresponding complexes suggesting the coordination of amino nitrogen to titanium atom through deprotonation.

The authors are thankful to the Indian National Science Academy for financial assistance.

References

1) R. D. Gorsich, *J. Am. Chem. Soc.*, **82**, 4211 (1960).
2) P. C. Wailes, R. S. P. Coutts, and H. Weigold, "Organometallic Chemistry of Titanium, Zirconium and Hafnium," Academic Press, New York (1974).
3) A. N. Nesmeyanov, O. V. Nogina, N. A. Lazereva, V. A. Dubovitskii, and B. V. Lokshin, *Izv. Akad. Nauk SSSR, Ser Khim.*, **1971**, 2482.
4) T. A. James and J. A. McCleverty, *J. Chem. Soc., A*, **1970**, 3318.
5) R. S. P. Coutts and P. C. Wailes, *J. Organomet. Chem.*, **84**, 47 (1975).
6) M. J. Frazer and W. E. Newton, *Inorg. Chem.*, **10**, 2137 (1971).
7) R. R. Jain, J. C. Maire, A. Baldy, and B. P. Bachlas, *Indian J. Chem.*, **18A**, 454 (1979).
8) S. Kumar and N. K. Kaushik, *J. Inorg. Nucl. Chem.*, **43**, 2679 (1981).
9) E. C. Alyea and A. Malek, *Inorg. Nucl. Chem. Lett.*, **13**, 587 (1977).
10) A. M. Cardoso, R. J. H. Clark, and S. Moorhouse, *J. Chem. Soc., Dalton Trans.*, **1980**, 1156.
11) R. J. H. Clark, J. A. Stockwell, and J. D. Wilkins, *J. Chem. Soc., Dalton Trans.*, **1976**, 120.
12) C. Preti and G. Tosi, *Austral. J. Chem.*, **29**, 543 (1976); *Canad. J. Chem.*, **54**, 1558 (1976).
13) J. Reedijk, *J. Inorg. Nucl. Chem.*, **35**, 239 (1973).
14) M. R. Gajendragad and U. Agarwala, *Austral. J. Chem.*, **28**, 763 (1975).
15) B. K. Gupta, D. S. Gupta, and U. Agarwala, *Bull. Chem. Soc., Jpn.*, **51**, 2724 (1978).
16) S. K. Sengupta, S. K. Sahni, and R. N. Kapoor, *Synth. React. Inorg. Met. Org. Chem.*, **10**, 269 (1980).
17) T. George, R. Tahilramani and D. A. Dabholkar, *Indian J. Chem.*, 7, 959 (1959).
18) G. R. Dave, *J. Indian Chem. Soc.*, **37**, 595 (1960).
19) R. W. Yong and K. H. Wood, *J. Am. Chem. Soc.*, **77**, 400 (1955).
20) O. P. Pandey, S. K. Sengupta, and S. C. Tripathi, *Synth. React. Inorg. Met. Org. Chem.*, **13**, 867 (1983).
21) B. Singh, Lakshmi and U. Agarwala, *Inorg. Chem.*, **8**, 2341 (1969); B. Singh and U. Agarwala, *J. Inorg. Nucl. Chem.*, **31**, 2575 (1969).
22) C. N. R. Rao, "Chemical Applications of Infrared Spectroscopy," Academic Press, London (1963).
23) J. S. Dwivedi and U. Agarwala, *Indian J. Chem.*, **10**, 652 (1972).
24) B. Singh and K. P. Thakur, *J. Inorg. Nucl. Chem.*, **36**, 1735 (1974).
25) D. M. Adams, "Metal-Ligand and Related Vibrations," E. Arnold, London (1967).
26) K. Nakamoto, "Infrared Spectra of Inorganic and Coordination Compounds," Wiley Interscience, New York (1970).
27) H. P. Fritz, *Adv. Organomet. Chem.*, **1**, 262 (1964).
28) A. Davison and P. E. Rakita, *Inorg. Chem.*, **9**, 289 (1970).

Cyclizations of Dianions from 2-Imino-1,2-diphenylethanone to Oxazolines, Oxazocines, and Oxazonines

Kailash Nath MEHROTRA,* Indra Sen SINGH, and Jalpana ROY
Department of Chemistry, Faculty of Science, Banaras Hindu University, Varanasi-221 005, India
(Received April 16, 1984)

The reaction of 2-imino-1,2-diphenylethanone with sodium in ether and subsequent addition of carbon disulfide or ethyl chloroformate resulted in the formation of 3,4,5-trisubstituted 4-oxazoline-2-thiones and 2-ones, respectively. 1,4-Oxazonines and 1,4-oxazocines were also synthesised from the reaction of 2-imino-1,2-diphenylethanone with sodium in THF followed by addition of dihaloalkanes.

The reported cyclization reactions of anils and dianils leading to the imidazolidine,[1,2] imidazoline,[3] diazocine and diazonine[4] derivatives prompted us to investigate the reactions of dianions from α-imino ketones. This study has led to new, convenient and general synthetic routes to oxazolines, oxazocines and oxazonines. These five-, eight-, and nine-membered heterocycles each containing one oxygen and one nitrogen atoms draw a special attention as potential biologically active compounds.

Results and Discussion

The reaction of (±)-2-(α-phenylethylimino)-1,2-diphenylethanone (**1a**) with sodium in dry ether followed by addition of carbon disulfide gave (±)-3-(α-phenylethyl)-4,5-diphenyl-4-oxazoline-2-thione (**2a**, 49%). The structural assignment of **2a** was made on the basis of its analytical and spectral data. In the above reaction replacing carbon disulfide by ethyl chloroformate gave (±)-3-(α-phenylethyl)-4,5-diphenyl-4-oxazolin-2-one (**3a**, 35%) identified by its analytical and spectral data. Similar treatment of the dianions from 2-imino-1,2-diphenylethanone **1b**—f with carbon disulfide and ethyl chloroformate gave 3-substituted 4,5-diphenyl-4-oxazoline-2-thiones **2b**—**f** and -2-ones **3b**—**f**, respectively. The products have been characterized on the basis of their analytical and spectral data.

Treatment of 2-imino-1,2-diphenylethanone **1d**—**e** with sodium in dry THF and subsequent addition of 1,4-dichlorobutane gave 2,3,4-triaryl-5,6,7,8-tetrahydro-4*H*-1,4-oxazocines **4d**—**e** which were crystallized from hexane.

Similar treatment of the dianions from imino ketones **1d**—**e** with 1,5-dichloropentane gave 2,3,4-triaryl-4,5,6,7,8,9-hexahydro-1,4-oxazonines **5d**—**e** which were recrystallized from hexane. The structural assignments of the products **4d**—**e** and **5d**—**e** were made on the basis of their analytical and spectral data.

When the dianions from imino ketones **1d**—**e** were similarly treated with 1,3-dibromopropane the expected cyclization products 1,4-oxazepines were not obtained and 2-anilino-1,2-diphenyl-4-penten-1-ones (**6d**—**e**) were formed. The products **6d**—**e** have been identified by their analytical and spectral data. One of the three vinyl protons (H_A) appeared downfield as compared to others. An inspection of the models of compounds **6d**—**e** reveals that this proton would be deshielded by the carbonyl group and the nitrogen lone pair. The formation of diazepine derivatives from the reactions of the dianion from benzil dianils with 1,3-dibromopropane and 1,3-diiodopropane,[5] in low yields have been observed due to the steric factors. It has been reported earlier that in the reaction of benzil dianil with sodium in ether followed by addition of 1,3-dichloropropane no diazepine derivative was obtained.[6]

The formation of products **2a**—**f**, **3a**—**f**, **4d**—**e**, **5d**—**e**, **6d**—**e** from 2-imino-1,2-diphenylethanone **1a**—**f** is depicted in the following scheme:

The above reactions involve the initial formation of dianions, by the electron transfer from sodium to 2-imino-1,2-diphenylethanone, which attack carbon disulfide, ethyl chloroformate, 1,3-, 1,4-, and 1,5-dihaloalkanes with elimination of sulfide ions (detected by the formation of lead(II) sulfide with aq lead(II) acetate) or halide ions (detected by the formation of silver halide with aq silver nitrate) or/and ethoxide ions to give rise to the observed products. These reactions provide new, convenient one-pot syntheses of heterocycles which would be difficult to prepare otherwise.

Experimental

Instrumentation. Melting points have been determined in capillaries on Büchi melting point apparatus and are uncorrected. The NMR spectra in $CDCl_3$ were recorded on Varian A-60D and VN 1009 (S-60T) spectrometers with TMS as an internal standard. The IR spectra were measured on a Perkin Elmer 720 spectrophotometer and UV spectra on a Beckman DB-G spectrophotometer.

Materials The 1,2-diketones, amines and dihaloalkanes were obtained from Ega, Chemie, West Germany.

Preparation of 2-Imino-1,2-diphenylethanone 1a—f.
General Procedure From Alkylamines: The starting α-imino ketones **1a**—**c** and **1f** were obtained by keeping an equimolar mixture of benzil and alkylamine in 95% ethanol at room temperature for a week, following the reported method[7] and purified by fractional crystallization from ethanol (78—88%).

From Arylamines. The starting 2-imino-1,2-diphenylethanones **1d**—**e** were obtained by heating an equimolar mixture of benzil and aromatic amine at 150°C for 2—3 h following the reported method[8] and purified by fractional crystallization from ethanol (75—78%).

Preparation of 3-Substituted 4,5-Diphenyl-4-oxazoline-2-thiones 2a—f. *General Procedure*: Sodium pieces (**1g**) were slowly added to dry ether (60 ml) in a three-necked round-

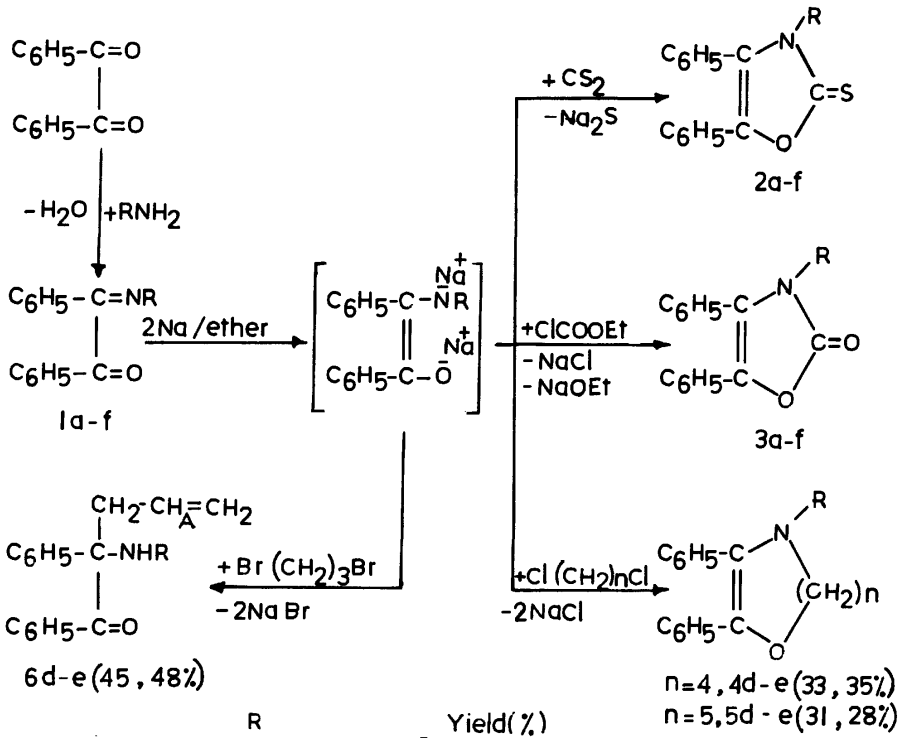

	R	Yield(%) 2	3
a	-CH(CH3)C6H5	49	35
b	-CH2CH2CH3	35	33
c	-CH2CH2CH2CH3	36	35
d	-C6H5	48	45
e	-C6H4CH3(p-)	50	55
f	-CH(CH3)CH3	32	35

Scheme

bottomed flask, fitted with a condenser, a mercury trap and a pressure-equalizing addition funnel, with stirring under a nitrogen atmosphere. A solution of imino ketone (**2g**) in dry ether (10 ml) was added dropwise. Stirring at reflux temperature was continued for 4 h and the contents were allowed to cool. Unreacted sodium pieces were removed by filtration. Dry carbon disulfide (2 ml) was slowly added and the mixture was heated under reflux for 1 h. The ethereal suspension was washed 2—3 times with water and dried over sodium sulfate. The solvent was removed on a rotary evaporator and the residual material was purified by column (neutral alumina, hexane/benzene: 90/10).

*3-(α-Phenylethyl)-4,5-diphenyl-4-oxazoline-2-thione (**2a**).* A yield of 49% was obtained, mp 135—137 °C. UV (Ethanol): 310 (ε 21100) and 223 (22600) nm; IR (Nujol, cm^{-1}): 1165 (ν C=S); NMR ($CDCl_3$, δ): 7.20 (m, 15H, aromatic protons); 6.40 (m, 1H, CH) and 1.70 (bd, 3H, CH_3, J=7 Hz). Found: C, 77.35; H, 5.38; N, 4.21%. Calcd for $C_{23}H_{19}NOS$: C, 77.31; H, 5.32; N, 3.92%.

*4,5-Diphenyl-3-propyl-4-oxazoline-2-thione (**2b**).* A yield of 35% was obtained, mp 128—129 °C. UV (Ethanol): 310 (ε 9740) and 275 (19800) nm; IR (Nujol, cm^{-1}): 1160 (ν C=S); NMR ($CDCl_3$, δ): 7.42 (m, 10H, aromatic protons); 3.80 (t, 2H, N-CH_2, J=7 Hz): 1.60 (m, 2H, C-CH_2); 0.82 (t, 3H, methyl, J=7 Hz). Found: C, 73.55; H, 5.61; N, 4.61%. Calcd for $C_{18}H_{17}NOS$: C, 73.22; H, 5.76; N, 4.74%.

*3-Butyl-4,5-diphenyl-4-oxazoline-2-thione (**2c**).* A yield of 36% was obtained, mp 133—134 °C. UV (Ethanol): 310 nm; IR (Nujol, cm^{-1}): 1180 (ν C=S); NMR ($CDCl_3$, δ): 7.40 (m, 10H, aromatic protons); 3.80 (t, 2H, N-CH_2, J=7 Hz); 1.50 (m, 4H, C-CH_2); 0.80 (t, 3H, methyl, J=7 Hz). Found: C, 73.71; H, 6.10; N, 4.32%. Calcd for $C_{19}H_{19}NOS$: C, 73.78; H, 6.14; N, 4.53%.

*3,4,5-Triphenyl-4-oxazoline-2-thione (**2d**).* A yield of 48% was obtained, mp 228—229 °C (lit,[9] 229 °C). UV (Ethanol): 308 (ε 15700) and 226 (17500) (lit,[10] 308, 225) nm; IR (Nujol, cm^{-1}): 1162 (lit,[11] 1161) (ν C=S); NMR ($CDCl_3$, δ): 7.40 (m, aromatic protons). Found: C, 76.40; H, 4.73; N, 4.51%. Calcd for $C_{21}H_{15}NOS$: C, 76.59; H, 4.55; N, 4.25%.

*4,5-Diphenyl-3-(p-tolyl)-4-oxazoline-2-thione (**2e**).* A yield of 50% was obtained, mp 235—237 °C. UV (Ethanol): 310 (ε 16000) and 225 (22500) nm; IR (Nujol, cm^{-1}): 1162 (ν C=S); NMR ($CDCl_3$, δ): 7.30 (m, 14H, aromatic protons); 2.30 (s, 3H, methyl). Found: C, 76.64; H, 4.65; N, 4.31%. Calcd for $C_{22}H_{17}NOS$: C, 76.96; H, 4.95; N, 4.08%.

*4,5-Diphenyl-3-isopropyl-4-oxazoline-2-thione (**2f**).* A yield

of 32% was obtained, mp 172—173 °C. UV (Ethanol): 310 (ε 18000) and 225 (14300) nm; IR (Nujol, cm^{-1}): 1161 (ν C=S); NMR ($CDCl_3$, δ): 7.51 (m, 10H, aromatic protons); 4.80 (sept, 1H, methine, J=7 Hz); 1.40 (d, 6H, methyl, J=7 Hz). Found: C, 73.60; H, 6.00; N, 5.01%. Calcd for $C_{18}H_{17}NOS$; C, 73.22; H, 5.76; N, 4.74%.

Preparation of 3-Substituted 4,5-Diphenyl-4-oxazolin-2-ones ***3a—f.*** *General Procedure*: In place of carbon disulfide in the above method dry ethyl chloroformate (2 ml) was slowly added and the product was purified by column chromatography as mentioned above.

*3-(α-Phenylethyl)-4,5-diphenyl-4-oxazolin-2-one (**3a**).* A yield of 35% was obtained, mp 155—157 °C. IR (Nujol, cm^{-1}): 1600 (ν C=C), 1750 (ν C=O); NMR ($CDCl_3$, δ): 7.30 (m, 15H, aromatic protons); 4.30 (m, 1H, CH) and 1.40 (bd, 3H, methyl, J=7 Hz). Found: C, 80.65; H, 5.62; N, 4.30%. Calcd for $C_{23}H_{19}NO_2$: C, 80.92; H, 5.61; N, 4.01%.

*4,5-Diphenyl-3-propyl-4-oxazolin-2-one (**3b**).* A yield of 33% was obtained, mp 92—93 °C. UV (Ethanol): 282 (ε 22100) and 221 (29100) nm; IR (Nujol, cm^{-1}): 1610 (ν C=C) and 1745 (ν C=O); NMR ($CDCl_3$, δ): 7.60 (m, 10H, aromatic protons); 3.50 (t, 2H, N-CH_2, J=7 Hz); 1.60 (m, 2H, C-CH_2); 0.80 (t, 3H, methyl, J=7 Hz). Found: C, 77.45; H, 6.20; N, 5.25%. Calcd for $C_{18}H_{17}NO_2$: C, 77.40; H, 6.13; N, 5.01%.

*3-Butyl-4,5-diphenyl-4-oxazolin-2-one (**3c**).* A yield of 35% was obtained, mp 73—75 °C. UV (Ethanol): 286 (ε 17700) and 217 (4350) nm; IR (Nujol, cm^{-1}): 1610 (ν C=C) and 1740 (ν C=O); NMR ($CDCl_3$, δ): 7.50 (m, 10H, aromatic protons); 3.50 (t, 2H, N-CH_2, J=7 Hz); 1.40 (m, 4H, C-CH_2); 0.84 (t, 3H, methyl, J=7 Hz). Found: C, 77.90; H, 6.50; N, 4.63%. Calcd for $C_{19}H_{19}NO_2$: C, 77.79; H, 6.53; N, 4.77%.

*3,4,5-Triphenyl-4-oxazolin-2-one (**3d**).* A yield of 45% was obtained, mp 215—217 °C (lit,[12] 211 °C). UV (Ethanol): 293 (ε 18900) and 226 (14700) (lit,[10] 225, 291.5) nm; IR (Nujol, cm^{-1}); 1600 (ν C=C) and 1750 (lit, [11] 1750) (ν C=O); NMR ($CDCl_3$, δ): 7.40 (m, aromatic protons). Found: C, 80.50; H, 4.62; N, 4.35%. Calcd for $C_{21}H_{15}NO_2$: C, 80.49; H, 4.82; N, 4.47%.

*4,5-Diphenyl-3-(p-tolyl)-4-oxazolin-2-one (**3e**).* A yield of 55% was obtained, mp 224—226 °C. UV (Ethanol): 294 (ε 18900) nm; IR (Nujol, cm^{-1}): 1600 (ν C=C) and 1750 (ν C=O); NMR ($CDCl_3$, δ): 7.42 (m, 14H, aromatic protons); 2.33 (s, 3H, methyl). Mass (m/z): 327. Found: C, 80.75; H, 5.40; N, 4.32%. Calcd for $C_{22}H_{17}NO_2$: C, 80.71; H, 5.23; N, 4.28%.

*3-Isopropyl-4,5-diphenyl-4-oxazolin-2-one (**3f**).* A yield of 35% was obtained, mp 120—124 °C. UV (Ethanol): 286 (ε 15100) and 220 (15400) nm; IR (Nujol, cm^{-1}): 1600 (ν C=C) and 1750 (ν C=O); NMR ($CDCl_3$, δ): 7.50 (m, 10H, aromatic protons); 4.80 (sept, 1H, methine, J=7 Hz); 1.40 (d, 6H, methyl, J=7 Hz). Found: C, 77.80; H, 6.00; N, 5.20%. Calcd for $C_{18}H_{17}NO_2$: C, 77.40; H, 6.13; N, 5.01%.

Preparation of 2,3,4-Trisubstituted-5,6,7,8-tetrahydro-4H-1,4-oxazocines ***4d—e.*** *General Procedure*: A solution containing 2 g of imino ketone (**1d—e**) in dry THF (30 ml) was added dropwise to 2 g of sodium pieces in 30 ml of dry THF under a nitrogen atmosphere and the mixture was stirred for 5—6 h at refluxing temperature. The reaction mixture was allowed to stand at room temperature for 1/2 h. Sodium pieces were removed by filtration. Dry 1,4-dichlorobutane (2 ml) was slowly added and the mixture was heated to reflux for 10—12 h. The excess of THF was removed under reduced pressure and the residual matter was extracted with ether. The ethereal layer was washed 2—3 times with water, dried over sodium sulfate. The solvent was removed on a rotary evaporator and the residual material was purified by column (neutral alumina, hexane) chromatography.

*2,3,4-Triphenyl-5,6,7,8-tetrahydro-4H-1,4-oxazocine (**4d**).* A yield of 33% was obtained, mp 125—126 °C. UV (Ethanol): 352 (ε 10500) and 273 (11500) nm; IR (Nujol, cm^{-1}): 1605 (ν C=C); NMR ($CDCl_3$, δ): 6.90 (m, 15H, aromatic protons); 4.10 (m, 4H, N-CH_2 and O-CH_2); 1.90 (m, 4H, C-CH_2). Mass (m/z): 341. Found: C, 84.10; H, 6.85; N, 3.95%. Calcd for $C_{24}H_{23}NO$: C, 84.42; H, 6.79; N, 4.10%.

*2,3-Diphenyl-4-(p-tolyl)-5,6,7,8-tetrahydro-4H-1,4-oxazocine (**4e**).* A yield of 35% was obtained, mp 128—129 °C. UV (Ethanol): 356 (ε 12000) and 273 (12200) nm; IR (Nujol, cm^{-1}): 1605 (ν C=C); NMR ($CDCl_3$, δ): 7.00 (m, 14H, aromatic protons); 4.00 (m, 4H, N-CH_2 and O-CH_2); 2.20 (s, 3H, methyl); 1.90 (m, 4H, C-CH_2). Mass (m/z): 355. Found: C, 84.20; H, 6.91; N, 4.10%. Calcd for $C_{25}H_{25}NO$: C, 84.47; H, 7.09; N, 3.94%.

Preparation of 2,3,4-Trisubstituted-4,5,6,7,8,9-hexahydro-1,4-oxazonines ***5d—e.*** *General Procedure*: In place of 1,4-dichlorobutane in the above procedure dry 1,5-dichloropentane was slowly added and the product was purified by column chromatography as mentioned above.

*2,3,4-Triphenyl-4,5,6,7,8,9-hexahydro-1,4-oxazonine (**5d**).* A yield of 31% was obtained, mp 141—143 °C. UV (Ethanol): 350 (ε 2370) and 265 (3760) nm; IR (Nujol, cm^{-1}): 1605 (ν C=C); NMR ($CDCl_3$, δ): 6.90 (m, 15H, aromatic protons); 4.00 (m, 4H, N-CH_2 and O-CH_2); 1.80 (m, 6H, C-CH_2). Mass (m/z): 355. Found: C, 84.15; H, 6.95; N, 3.64%. Calcd for $C_{25}H_{25}NO$: C, 84.47; H, 7.09; N, 3.94%.

*2,3-Diphenyl-4-(p-tolyl)-4,5,6,7,8,9-hexahydro-1,4-oxazonine (**5e**).* A yield of 28% was obtained, mp 142—144 °C. UV (Ethanol): 265 and 350 nm; IR (Nujol, cm^{-1}): 1615 (ν C=C); NMR ($CDCl_3$, δ): 7.00 (m, 14H, aromatic protons); 4.00 (m, 4H, N-CH_2 and O-CH_2); 2.20 (s, 3H, methyl); 1.80 (m, 6H, C-CH_2). Found: C, 84.24; H, 7.26; N, 3.90%. Calcd for $C_{26}H_{27}NO$: C, 84.55; H, 7.31; N, 3.79%.

Preparation of 2-Arylamino-1,2-diphenyl-4-penten-1-ones ***6d—e.*** *General Procedure*: In place of 1,4-dichlorobutane, 1,3-dibromopropane was slowly added and the same procedure for purification was followed as described above.

*2-Anilino-1,2-diphenyl-4-penten-1-one (**6d**).* A yield of 45% was obtained, mp 102—104 °C. UV (Ethanol): 250 (ε 25200) nm; IR (Nujol, cm^{-1}): 3370 (N-H) and 1660 (C=O); NMR ($CDCl_3$, δ): 7.00 (m, 16H, aromatic and CH); 5.70 (bs, 1H, NH, D_2O exchangeable); 4.80 (m, 2H, =CH_2); 3.30 (m, 2H, -CH_2). Mass (m/z): 327. Found: C, 84.60; H, 6.41; N, 3.95%. Calcd for $C_{23}H_{21}NO$: C, 84.37; H, 6.46; N, 4.28%.

*1,2-Diphenyl-2-(p-toluidino)-4-penten-1-one (**6e**).* A yield of 48% was obtained, mp 109—110 °C. UV (Ethanol): 250 (ε 23000) nm; IR (Nujol, cm^{-1}): 3355 (NH) and 1660 (ν C=O); NMR ($CDCl_3$, δ): 7.00 (m, 15H, aromatic and CH); 5.50 (bs, 1H, NH, D_2O exchangeable); 4.80 (m, 2H, =CH_2); 3.30 (m, 2H, -CH_2); 2.25 (s, 3H, CH_3). Found: C, 84.10; H, 6.65; N, 3.90%. Calcd for $C_{24}H_{23}NO$: C, 84.42; H, 6.79; N, 4.10%.

We are thankful to professor R. C. Aggarwal for providing the facilities and to C. S. I. R., New Delhi, India for appointing Dr. (Mrs.) Jalpana Roy as Pool Officer under the Scientists' Pool.

References

1) K. N. Mehrotra and G. Prasad, *Indian J. Chem.*, **17B**, 405 (1979).

2) G. Prasad, G. Singh, and K. N. Mehrotra, *Indian J. Chem.*, **19B**, 653 (1980).
3) K. N. Mehrotra and G. Singh, *Synth.*, **1980**, 1001.
4) G. Singh and K. N. Mehrotra, *Heterocycles*, **16**, 1341 (1981).
5) E. J. MacPherson and J. G. Smith, *J. Org. Chem.*, **36**, 2516 (1971).
6) G. Sinqh, Ph. D. Thesis, submitted to Banaras Hindu University, India (1982).
7) R. H-Ramos, A. J. Tebar, R. P-Ossorio, and J. Plumet, *Tetrahedron Lett.*, **1979**, 1355.
8) A. Padwa, *J. Am. Chem. Soc.*, **87**, 4365 (1965).
9) R. Gompper, *Chem. Ber.*, **89**, 1762 (1956).
10) R. Gompper and H. Herlinger, *Chem. Ber.*, **89**, 2816 (1956).
11) R. Gompper and H. Herlinger, *Chem. Ber.*, **89**, 2825 (1956).
12) R. Gompper, *Chem. Ber.*, **89**, 1748 (1956).

 © 1985 The Chemical Society of Japan Bull. Chem. Soc. Jpn., 58, 2403—2406 (1985)

Spectroscopic Studies of Photochemical Reactions in Organic Solids. Photodimerization of *p*-Formylcinnamic Acid

Urmi GHOSH and Tridibendra Narayan MISRA*

Optics Department, Indian Association for the Cultivation of Science, Jadavpur, Calcutta-700 032, India

(Received May 22, 1984)

Raman phonon spectroscopy and electronic absorption and emission spectroscopy have been used to study the mechanism of reaction and the role of electron–phonon coupling in determining the photoreactivity of *p*-formylcinnamic acid (*p*-FCA) in the crystalline state. Raman and infrared spectroscopy in the internal vibration region have been used to characterize the reactant *p*-FCA and the dimeric product *t*-3,*t*-4-bis(*p*-formylphenyl)-*r*-1,*c*-2-cyclobutanedicarboxylic acid. Phonon spectroscopy reveals that the reaction proceeds principally by a heterogeneous mechanism though a homogeneous mechanism in the initial stage of short time domain can not be ruled out. The electronic spectroscopy suggests a strong electron-phonon coupling in the monomer crystal.

Recently Raman phonon spectroscopy has been successfully used to study the mechanism and the kinetics of solid state photoreaction in organic crystals.[1–4] Phonon participation and strong electron–phonon coupling have been shown to be involved in solid state photodimerization reaction of 2,6-dimethyl-*p*-benzoquinone.[3] The study revealed that the reaction is homogeneous in the initial stage but becomes heterogeneous in the later stage.

A new type of crystalline state photodimerization has recently been reported by Nakanishi *et al.*[5,6] in case of some cinnamic acid derivatives. In *p*-FCA, for example, it has been shown that a molecule of water is incorporated in dimer during the photodimerization process. We have used the phonon spectra, sampled as a function of reaction progress, to study this photoreaction to see if the reaction is homogeneous or heterogeneous in the molecular level. The electronic absorption and emission spectroscopy on dimerization reaction progress have been studied. The electronic absorption spectroscopy has also been used to determine the extent of reaction progress. The laser Raman spectroscopy and infrared spectroscopy have been used to obtain intramolecular vibrations of the reactants and the products as well as the partially converted samples. These intramolecular

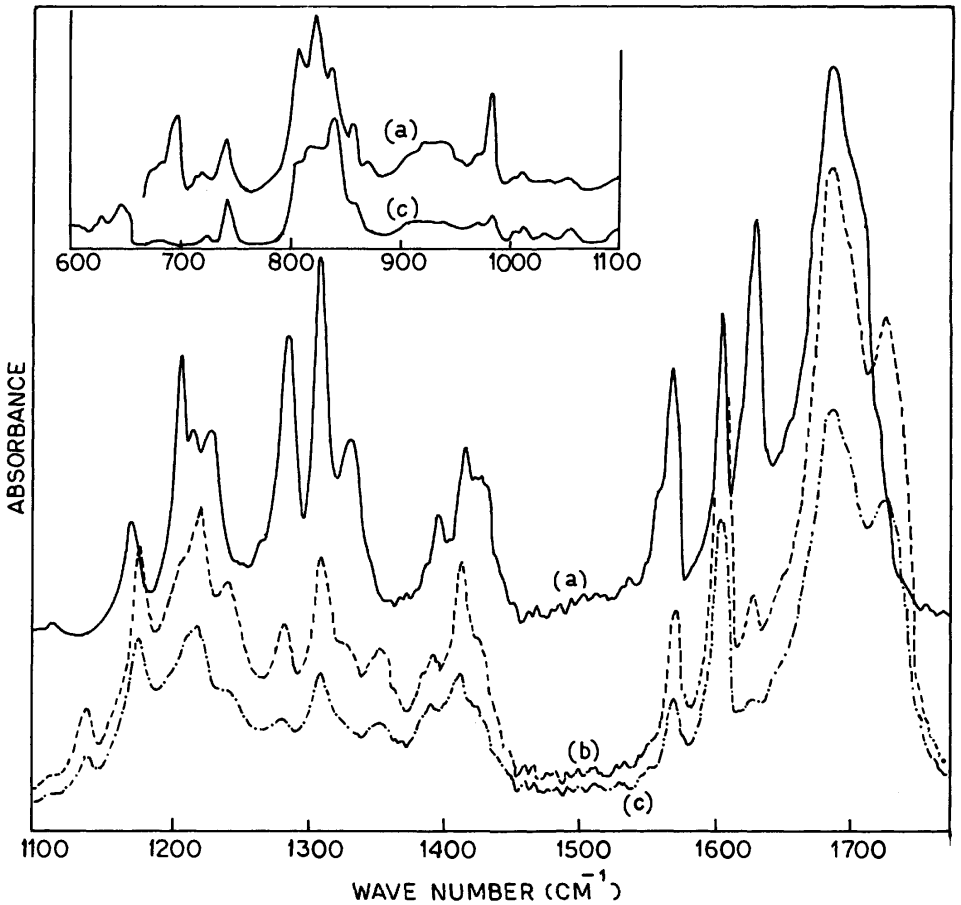

Fig. 1. Infrared absorption spectra of *p*-FCA crystals in KBr pellet as a function of photoreaction progress (a) monomer, (b) exposed for 30 min (c) exposed for 1 h.

vibrations have also been used to characterize the materials as well as to study the mechanism of the reaction. In this paper we report our results.

Experimental

p-FCA prepared as described earlier[6] was further purified by repeated crystallization from ethanol. Crystals were finally grown from ethanol and acetone. Photodimerization was carried out by using a 750 W Xe lamp with the *p*-FCA crystallites dispersed in water in a quartz vessel at room temperature. For the specific set up, almost complete photodimerization was obtained in one hour. The experimental set up was the same as reported earlier.[3] The electronic absorption spectra were run in Shimadzu UV-Vis 210A Spectrophotometer. The emission spectra were run in Perkin-Elmer MPF 44A Spectrofluorimeter. The infrared spectra were run in a KBr pellet on a Beckman Spectrophotometer (Model 4240).

Results and Discussion

Two crystalline modifications of *p*-FCA crystals are known. Crystals grown from ethanol solution are photoreactive and belong to the β-form while γ-form of crystals, obtained from acetone solution, are photostable. The phonon spectra of the two forms are distinctly different as are their reported X-ray diffraction patterns.[6] Nakanishi[6] *et al.* have not observed any phase transition point.

The extent of photodimerization has been monitored by studying the electronic absorption spectra. Monomer *p*-FCA has its absorption maximum at 295 nm in ethanol solution at room temperature whereas the photodimer under similar condition has its maximum at 257 nm.

Characterization of the Reactant and the Product by Infrared and Raman Spectroscopy. The infrared spectra of *p*-FCA crystal before and after photodimerization to different extent are shown in Fig. 1 and the results are summarized in Table 1. The infrared bands observed in partially dimerized crystals were attributed to the monomer if it appeared relatively weaker. Bands present in monomer if appeared in the partially dimerized crystal without losing intensity were attributed to the dimer as existence of some dimer in the monomer crystal can not be ruled out. New bands, of course, were the dimer bands. In monomer crystal, the band at 1624 cm^{-1} which is due to the aliphatic C=C stretching mode is very intense but decreases with the increase of the extent of photodimerization and almost disappears in near complete photodimer crystal. This, indeed, suggests cyclobutane ring formation. The cyclobutane ring breathing vibration around 1000 cm^{-1}, however, has not been observed in the Raman spectrum. Observation of such a Raman active mode has usually been attributed to the confirmation of four center type photopolymerization with cyclobutane ring formation.[4] Absence of such a vibration in the Raman spectrum is however consistent with the structure of the dimer as suggested by Hasegawa *et al.*[6] which is trans, head to head type like β-truxinic acid.

TABLE 1. INFRARED BANDS (IN KBr) OF *p*-FCA CRYSTAL BEFORE AND AFTER PHOTODIMERIZATION

Monomer bands/cm^{-1}	Dimer bands/cm^{-1} (After extensive dimerization)[a]	Inference
698 (ms)		
	720 (w)	D: cyclobutane ring deformation
738 (w)	738 (m)	D
808 (ms)	808 (vw)	M
825 (s)	825 (vw)	M
	843 (s)	D: C-C Skeletal stretch
860 (mw)	860 (vw)	M
875 (w)		M
941 (s, br)	941 (w, vbr)	M
986 (s)	986 (w)	M
1015 (w)	1015 (w)	D
	1036 (w)	D: cyclobutane ring deformation
	1052 (w)	D
1111 (w)		M
	1135 (m)	D
1167 (m)		M
	1170 (m)	D
1202 (s)		M
1214 (ms)		M
	1216 (s)	D
1225 (ms)		M
	1240 (ms)	D: O-H in-plane bending
1282 (vs)	1282 (w)	M
1305 (vs)	1305 (s)	M
1329 (s)		M
	1355 (ms)	D: aliphatic C-H deformation
1393 (s)	1393 (w)	M
	1410 (s)	D
1424 (ms)		M
1564 (vs)	1564 (ms)	M
1599 (ms)	1599 (s)	D
1624 (vvs)		M: aliphatic C=C stretch
1682 (vvs)	1685 (vvs)	D: C=O carboxylic
	1722 (s)	D: C=O formyl

a) m: medium, s: strong, ms: medium strong, w: weak, vw: very weak, vs: very strong, br: broad, mw: medium weak, vbr: very broad, vvs: very very strong. b) M: monomer, D: dimer.

The other infrared features also suggest such a structure of four center type photodimerization in the crystalline state. The bands observed in the dimer at 720, 1035, and 1052 cm^{-1} are possibly the ring deformation vibrations. In such structure of the dimer, the C=O stretching frequency in the carboxyl group and in the formyl group are distinctly resolved, the former possibly is 1722 cm^{-1} and the latter 1685 cm^{-1}. Due to the loss of conjugation through the aliphatic C=C bond, some of the bands are shifted on dimerization. C-C skeletal stretching mode at 825 cm^{-1}, O-H in-plane bending at 1225 cm^{-1} and aliphatic

C-H deformation at 1329 cm^{-1} in monomer shift to 843, 1240, and 1355 cm^{-1} respectively in the dimer.

The Raman spectrum of the dimer is very weak, possibly due to the low value of the polarizability tensor. Intense Raman bands of the monomer are only observed in the partially dimerized sample without any significant change in the band positions.

Electronic Spectral Change on Dimerization Reaction Progress. *p*-FCA in the polycrystalline film at 25 °C show a broad absorption band with λ_{max} at 300 nm. Another band is also observed with λ_{max} at 200 nm. On photoreaction the product dimer in the solid film at 25 °C also shows two broad absorption bands, the 300 nm band is now shifted to 260 nm, the second band at λ_{max} 200 nm does not show any appreciable shift. This band shows a red shift to 210 nm on cooling at 77 K, 260 nm band, however, does not show any appreciable shift on cooling. The solid state absorption spectra are shown in Fig. 2.

Cinnamic acid molecule like benzoic acid is non-fluorescent and only strong phosphorescence emission is observed[7] which, as in benzoic acid, is possibly a $^3\pi,\pi^* \rightarrow S_0$ transition. *p*-Formylcinnamic acid in ethanol solution, on the other hand, is only fluorescent and no phosphorescence emission is observed. The emission spectra of *p*-FCA are shown in Fig. 3, (solid film). In monomer crystal a strong broad fluorescence emission in the 430—550 nm region with λ_{max} at 470 nm is observed at 77 K. This emissive property of *p*-FCA molecule evidently arises because the carbonyl oxygen in the formyl group contributes an additional set of $n\pi^*$ states. Relative energetic position of such states may make the singlet triplet intersystem crossing inefficient. The broad structureless absorption and emission spectra in the crystal at 77 K and the large Stokes' shift (12057 cm^{-1}) between the absorption and emission maxima provide a clear evidence for a strong lattice distortion in the excited state and thus a strong electron phonon coupling. On dimerization reaction progress, the monomer emission

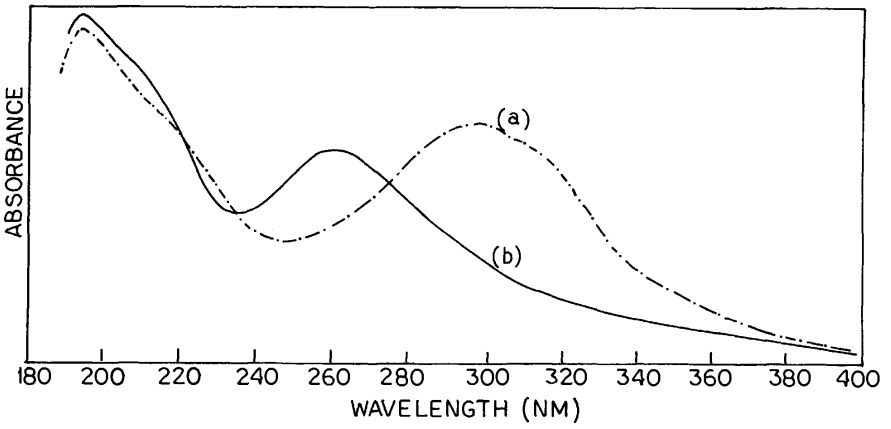

Fig. 2. Solid state absorption spectra at room temperature (a) monomer (b) dimer.

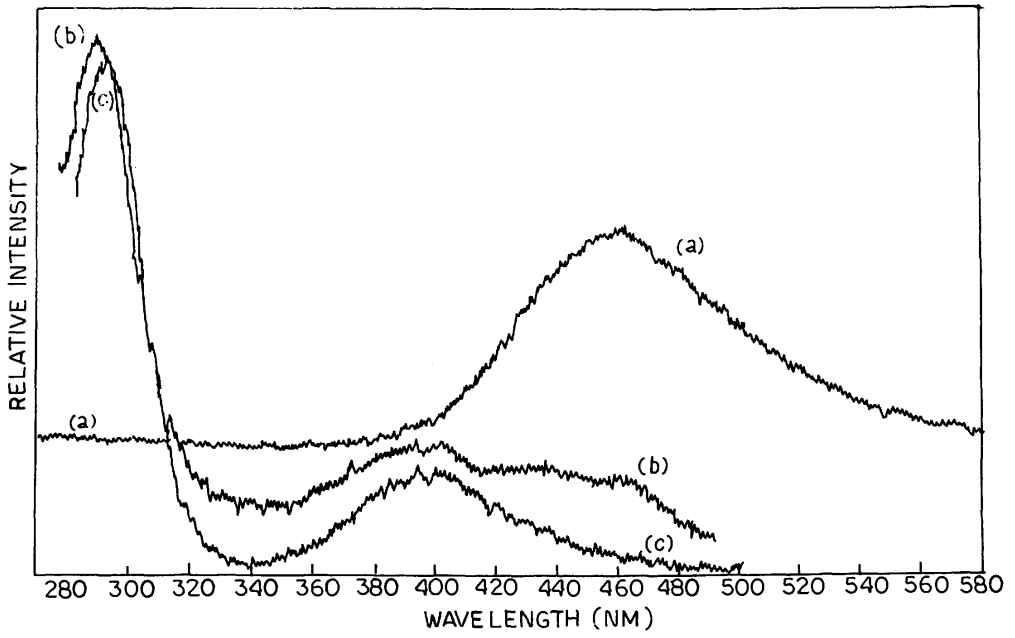

Fig. 3. Emission spectra of solid film of *p*-FCA at 77 K (a) monomer (b) partially dimerized (c) dimer.

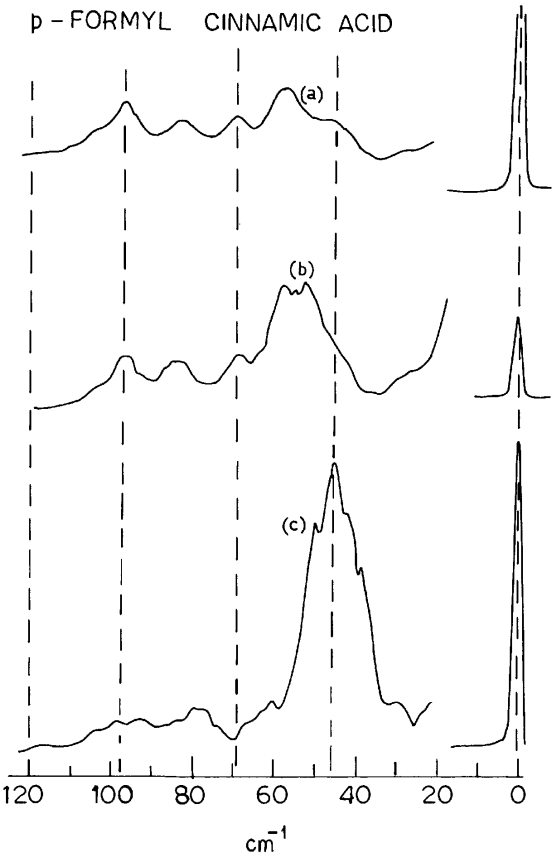

Fig. 4. Raman phonon spectra of *p*-FCA crystal monitored as a function of the photoreaction progress in order of a→c, a being the phonon spectra of the monomer and c that of an extensively dimerized crystal.

intensity decreases and a new emission band system appears on the higher energy side of the monomer crystal emission. This structureless emission band has its λ_{max} at 390 nm. On complete dimerization, only the new emission band, characteristic of the dimer is observed. One interesting feature of the photoproduct emission is that in addition to the emission discussed above another prompt high energy emission is observed with λ_{max} at 290 nm. At this point it is not certain if this double emission arises from the product *t*-3,*t*-4-bis(*p*-formylphenyl)-*r*-1,c-2-cyclobutanedicarboxylic acid molecule or it is some other secondary photoproduct emission.

Phonon Spectral Change on Dimerization Reaction Progress. β-Form of the *p*-FCA crystal is photoreactive. The change in the phonon spectra as the dimerization reaction progress is shown in Fig. 4. The phonon spectrum of the monomer crystal of the β-form obtained from ethanol solution (top) show five distinct phonon bands at 45, 57, 69, 83, and 98 cm^{-1}. In addition two weak phonon bands are observed at 29 and 104 cm^{-1}. On photoirradiation for few minutes slight photodimerization occurs and the phonon spectrum of such crystal (middle) shows some new phonon bands at 31, 52, 55, 63, 87, and 92 cm^{-1}. The monomer phonon bands appear more broad and their intensity is slightly diminished. The broadening of monomer phonon bands may indicate slight shift in frequency of monomer phonons suggesting an amalgamation of phonons in this initial stage of reaction. Appearence of new phonon bands indicates initiation of seggregation of the reaction product. On extensive photodimerization (bottom), the monomer phonon bands appear very weak and new phonon spectrum arise with phonon bands at 29, 39, 43, 45, 50, 60, 63, 67, 74, 77, 87, 92, and 117 cm^{-1}, the 45 cm^{-1} phonon band being most intense in the dimer lattice. Thus the phonon spectrum of the dimerized crystal shows seggregated phonon spectra of the monomer and the dimer lattice. These results suggest that the solid state photoreaction in this crystal is homogeneous in the initial stage but becomes heterogeneous as the concentration of the product increases with reaction progress. The lattice distortion introduced by the product becomes too strong and the product seggregates out, the reactant and the product form their own lattices and no solid solution results.[1,8,9] Further, the existence of the 45 cm^{-1} monomer lattice phonon throughout the reaction progress and its enhanced intensity in the photodimer lattice suggests thet the lattice topology along this phonon coordinate is preserved during the reaction.

This work was partly done in the Chemistry Department, State University of New York at Buffalo. One of the authors (TNM) expresses his thanks to Prof. P. N. Prasad for his kind hospitality and for many valuable discussion. Thanks are also due to Professor M. Hasegawa for a generous gift of the *p*-formylcinnamic acid sample.

References

1) P. N. Prasad, *Mol. Cryst. Liq. Cryst.*, **52**, 63 (1979).
2) D. Dwarkanath and P. N. Prasad, *J. Am. Chem. Soc.*, **102**, 4254 (1980).
3) T. N. Misra and P. N. Prasad, *Chem. Phys. Lett.*, **85**. 381 (1982).
4) J. Swiatkiewicz, G. Eisenhardt, P. N. Prasad, J. M. Thomas, and W. Jones, to be published.
5) F. Nakanishi, H. Nakanishi, T. Tasai, Y. Suzuki, and M. Hasegawa, *Chem. Lett.*, **1984**, 525.
6) F. Nakanishi, H. Nakanishi, M. Tsuchiya, and M. Hesegewa, *Bull. Chem. Soc. Jpn.*, **49**, 3096 (1976).
7) K. Nakamura and S. Kikuchi, *Bull. Chem. Soc. Jpn.*, **41**, 1977 (1968).
8) F. P. Chen and P. N. Prasad, *Solid State Commun.*, **21**, 871 (1977).
9) K. S. Law, Ph. D. Thesis, SUNY/Buffalo (1981).

The Fluorescence Lifetimes of Jet-cooled Alkylnaphthalenes

Teijiro ICHIMURA,* Andrew R. AUTY,† Anita C. JONES,† and David PHILLIPS†
Department of Chemistry, Tokyo Institute of Technology, Ohokayama, Meguro-ku, Tokyo 152
†*The Royal Institution, Albemarle St., London, W1X 4BS, U. K.*
(Received February 22, 1985)

Synopsis. The measured fluorescence lifetime of the origin of jet-cooled 1-methylnaphthalene is close to that of naphthalene, whereas the corresponding lifetimes of the 2-substituted are longer. The fluorescence lifetime decreased with increasing excitation energy; this can be attributed to an increase in the rate of intersystem crossing with vibrational excitation.

Supersonic free jet experiments have been extensively applied to investigate the spectroscopic and molecular dynamical aspects of various size molecules. The supersonic molecular beam prepares isolated gas molecules of low internal temperature, which makes feasible the study of the dynamical behaviour of state selected single vibronic level.

The naphthalene molecule in jet-cooled conditions has recently been investigated by Smalley *et al.*[1] and Rice's group.[2] Many vibronic bands up to about 4000 cm^{-1} from the origin are assigned and intramolecular vibrational relaxation processes have an onset at about 2500 cm^{-1} above the origin. Measurements of fluorescence lifetime and quantum yield led to the radiationless decay rate and the radiationless process is postulated to be intersystem crossing to triplet manifolds, a similar process to that of benzene.

On the other hand, naphthalene derivatives have not been studied well in the jet. Very recently Small's group[3] has observed laser induced fluorescence of jet-cooled 1-methyl- and 2-methylnaphthalene derivatives. They suggested that in the first excited singlet state of 2-methylnaphthalene symmetry reduction-vibronically induced mode mixing should occur.

A previous paper[4] has demonstrated jet-cooled fluorescence excitation spectra associated with 1-methyl-, 2-methyl- and 2-ethylnaphthalene derivatives by monochromatized xenon lamp irradiation. In this paper fluorescence lifetimes were first measured for the origin bands and vibronic bands up to excess vibrational energy of 700 cm^{-1} to study substitution effect on radiative and nonradiative transitions in jet-cooled alkylnaphthalenes.

Experimental

The supersonic free-jet apparatus used in this experiment has been described elsewhere,[5] therefore only a brief description is given here.

The free-jet portion of the apparatus consists of a 50 cm diameter vacuum chamber, through one side of which is inserted a continuously operated supersonic nozzle. A large slit nozzle, 4 mm long and 380 μm wide, was used for these experiments. Back ground pressure in the expansion chamber was maintained in the region of 10^{-3} Torr (1 Torr= 133.322 Pa) by evacuation with a vapour booster (pumping speed 4000 l s^{-1}) backed by a rotary pump. The expansion mixture is argon, at a typical stagnation pressure of 50 Torr. Naphthalene derivatives were seeded into the argon by placing a sample tube heated at 75 °C in the argon feed line to the nozzle, giving a concentration of 2—4 mole%.

Fluorescence excitation spectra were measured by crossing the free jet at 90° with the light of a 450 W Xe lamp, dispersed by a 1 m monochromator with resolution 10 cm^{-1} FWHM. The excitation beam was mildly focused and crossed the jet 5 mm downstream from the slit nozzle. The crossing position is varied by the movement of a lens. Fluorescence was collected, at right angles to the free jet and the excitation beam, by an f/1 lens and focussed *via* a band pass filter (340±20 nm), onto a photomultiplier tube. The signal from the photomultiplier was processed by the photon counting technique. The fluorescence excitation spectrum was corrected for the spectral intensity distribution of the xenon lamp.

Fluorescence lifetimes were determined for each peak of the excitation spectra by the time correlated single photon counting techniques. The excitation source used was the frequency doubled output of a cavity dumped dye laser synchronously pumped by a mode-locked argon ion laser with resolution 3 cm^{-1} FWHM.

Samples of 1-methyl-, 2-methyl-, and 2-ethylnaphthalene were obtained from Aldrich and used without further purification. Stated purities of these samples ranged from 95% to 99%.

Results and Discussion

The positions of the observed origins for π-π^* electronic transitions of 1-methyl-, 2-methyl-, and 2-ethylnaphthalene are 31773, 31705, and 31749 cm^{-1}, respectively.[4] Relative frequencies of some vibronic bands <1000 cm^{-1} are listed in Table 1, together with frequencies and assignments of pertinent naphthalene transitions. Assignments of these naphthalene derivatives are tentative since we do not have reliable information on the vibrational structures of the methyl- and ethylnaphthalene molecules. The prominent Herzberg-Teller origin band 8 ($^1b_{1g}$) at 437 cm^{-1} for naphthalene[1,2] was observed at 422 cm^{-1} in the 1-methylnaphthalene spectrum with slight shift; for the 2-methyl and 2-ethyl derivatives only very weak features were observed at 429 and 421 cm^{-1}, respectively, which are tentatively assigned as the band. Assignments for 1-methylnaphthalene in Table 1 is based on the assumption that relative intensity of the vibronic bands are similar to that of naphthalene. For 2-methyl- and 2-ethylnaphthalene derivatives the frequency change of these vibronic bands is assumed to be small and hence similar to the frequency of 1-methylnaphthalene vibronic bands though relative intensity of the vibronic bands are drastically changed due to mode-mixing.[3,4] The fact that replacement of the 2-methyl group with an ethyl group produces only a minor change in the excitation spectrum is in agreement with the observations of Hopkins *et al.*[6] for jet-cooled alkylbenzenes.

TABLE 1. RELATIVE FREQUENCIES OF S_0—S_1 ABSORPTION BANDS AND FLUORESCENCE LIFETIMES FOR EXCITATION INTO THESE BANDS

	Naphthalene[a]		1-Methyl-Naphthalene		2-Methyl-Naphthalene		2-Ethyl-Naphthalene	
Assignment[b]	$\Delta\nu$/cm^{-1}	τ/ns	$\Delta\nu$/cm^{-1}	τ/ns	$\Delta\nu$/cm^{-1}	τ/ns	$\Delta\nu$/cm^{-1}	τ/ns
	0	299	0	305	0	324	0	364
	—	—	77	324	173	190	35	315
	—	—	—	—	388	235	389	304
$8(b_{1g})^1$	437	317	422	281	429	222	421	259
	—	—	—	—	—	—	450	259
$2(b_{2g})^1$	485	120	485	—	482	194	482	219
	—	—	669	—	—	—	—	—
$8(b_{1g})^14(a_u)^2$	686	300	690	—	686	196	—	—
$8(a_g)^1$	704	309	—	—	719	187	720	—
	—	—	—	—	780	—	—	—
	—	—	822	—	819	—	—	—
	—	—	—	—	872	—	—	—
$7(b_{1g})^1$	911	262	910	—	—	—	—	—
	—	—	—	—	923	—	—	—
	—	—	—	—	—	—	938	—
$7(a_g)^1$	989	290	979	—	977	—	974	—

a) Reproduced from Ref. 2). b) Assignments for alkylnaphthalenes are tentative.

The results of fluorescence lifetime measurements are also shown in Table 1. The fluorescence lifetime of the origin of 1-methylnaphthalene is close to that of naphthalene, whereas the corresponding lifetimes of the 2-substituted are longer. The increase in transition moment of the origin resulting from alkyl substitution is accompanied by an increase in the radiative decay rate of S_1. The observed decrease in the fluorescence decay rate must therefore be due to a decrease in the rate of intersystem crossing in the alkyl substituted naphthalenes. Nonradiative transition in 0-0 bands of the alkylnaphthalenes can not be internal conversion in analogy to naphthalene[2] though the frequency of these 0-0 bands is slightly red-shifted ($\approx$300 cm^{-1}) compared with that of naphthalene.

Reiser and Wright[7] have theoretically predicted that the radiative decay rate increases by a factor of $\approx$2 for 1-methylnaphthalene and $\approx$3 for 2-methylnaphthalene, relative to naphthalene. They have shown these values to be consistent with radiative lifetimes measured in solution. Behlen and Rice[2] have estimated the rate coefficient for radiative decay (k_r) of the S_1 origin of jet-cooled naphthalene to be 9.4×10^5 s^{-1}, and that for intersystem crossing (k_{isc}) to be 2.4×10^6 s^{-1}. On this basis the following values can be predicted: $k_r\approx2\times10^6$ s^{-1}, $k_{isc}\approx1\times10^6$ s^{-1} for the origin of jet-cooled 1-methylnaphthalene and $k_r\approx3\times10^6$ s^{-1}, $k_{isc}\approx1\times10^5$ s^{-1} for 2-methylnaphthalene. The implication is thus that 2-methyl substitution leads to an order of magnitude decrease in the rate of intersystem crossing from the origin level, giving a fluorescence quantum yield of $\approx$1. The effect of 2-ethyl substitution is expected to be similar, and the measured fluorescence lifetime indicates the upper limit for k_r to be 3×10^6 s^{-1} in this case.

For both of the 2-substituted naphthalenes studied, the fluorescence lifetime decreases with increasing excitation energy; this can be attributed to be an increase in the rate of intersystem crossing with vibrational excitation. The marked dependence of decay rate on population of particular vibrational modes which was observed in naphthalene[2] (*e.g.* the sharp increase in k_{isc} on population of the $2(b_{2g})$ mode) was not observed for the 2-substituted molecules, presumably as a result of the mode-mixing which is induced by alkyl substitution.

References

1) S. M. Beck, D. E. Powers, J. B. Hopkins, and R. E. Smalley, *J. Chem. Phys.*, **73**, 2019 (1980), **74**, 43 (1981).
2) a) F. M. Behlen, D. B. McDonald, V. Sethuraman, and S. A. Rice, *J. Chem. Phys.* **75**, 5685 (1981); b) F. M. Behlen and S. A. Rice, *J. Chem. Phys.* **75**, 5672 (1981).
3) J. A. Warren, J. M. Hayes, and G. J. Small, *J. Chem. Phys.* **80**, 1786 (1984).
4) T. Ichimura, A. R. Auty, A. C. Jones, and D. Phillips, *J. Spectrosc. Soc. Japan* **34**, 83 (1985).
5) A. R. Auty, A. C. Jones, and D. Phillips, *Chem. Phys. Lett.*, **112**, 529 (1984).
6) J. B. Hopkins, D. E. Powers, and R. E. Smalley, *J. Chem. Phys.* **72**, 5039 (1980).
7) A. Reiser and T. R. Wright, *J. Chem. Phys.* **59**, 3433 (1973).

Fluorescence Spectra of Anthracene Liquid

Noriko IWASAKI,† Rumiko HORIGUCHI,†† and Yusei MARUYAMA*
Department of Molecular Assemblies, Institute for Molecular Science, Myodaiji, Okazaki 444
†*The Institute for Solid State Physics, The University of Tokyo, Roppongi, Minato-ku, Tokyo 106*
††*Department of Chemistry, Ochanomizu University, Otsuka, Bunkyo-ku, Tokyo 112*
(Received March 8, 1985)

Synopsis. An excimer-like fluorescence band at 470 nm was observed for anthracene liquid. A distinct shoulder at 414 nm was recognized in the absorption spectrum of anthracene liquid. These results suggest the existence of dimeric aggregates in this liquid.

Optical properties of pure organic liquids have been studied in only a very few cases compared with corresponding solids, gases or solutions. Experimental and theoretical difficulties may partly be responsible for this fact. Only benzene and substituted benzenes have been rather extensively studied on the absorption or fluorescence spectra of the liquids.[1]

On the other hand, optical properties of amorphous organic films, which may be regarded as a somewhat frozen-liquid in structure, have recently been studied by several workers, and many interesting characteristics have been revealed.[2] Most prominent features of such amorphous solids are broadening of bands and/or disappearance of Davydov splitting in the absorption spectra[3] and appearance of strong excimer-like emission in the fluorescence spectra.[4,5] The existence of excimer-like fluorescence which is absent in the crystals means that there are significant numbers of dimeric molecular aggregates in these amorphous solids which are more strongly interacting with each other than in the corresponding crystalline solids. The concentration of the dimeric molecular pairs has been tentatively estimated to be 10^{-3} mol/mol or more in an amorphous anthracene film.[5] However, considering the facts that the red-shift and/or the enhancement of long wavelength tail of the lowest absorption band are usually observed in such amorphous films,[6] the dimeric molecular pairs might occur in higher concentrations in a more disordered state, such as a liquid state. In fact, an amorphous anthracene film is colored slightly yellow, although its crystallized film by annealing is colorless in spite of the larger grain size in the latter.

A colorless anthracene crystal turns to yellow liquid on melting in an inactive gas atmosphere, and returns to colorless again on solidifying. This coloration on melting has usually been ascribed to a vibrational hot-band effect[7] or an impurity effect. However, if sufficient numbers of dimeric molecular pairs are prevailing in the liquid, they may contribute to make the color of the liquid yellow, and thus excimer-like emissions could be observed for the liquid anthracene. This point is our main motivation for the present work. Ferguson *et al.* observed the excimer emission from sandwich dimers of anthracene by the photolysis of photodimers of anthracene, and he also proposed the existence of 55° dimers of anthracene.[8] Excimer fluorescence of anthracene has also been observed in amorphous films, in a deformed crystal under high pressure[9] and also in a saturated $CHCl_3$ solution.[10] Pyrene and naphthalene excimer emissions in the liquid state has been reported by Birks.[11] In this note, we report the fluorescence spectra of liquid anthracene and discuss the possibility of the exsistence of the dimeric molecular aggregates as the structural units in such an organic liquid.

Experimental

Anthracene used was purified by recrystallization, sublimation and zone melting. A single crystal was grown with the Bridgman method in a quartz tube sealed off with 0.5 atm He gas and directly used for optical measurements. A larger diameter quartz tube wound by a wire heater was coaxially set with the sample tube for melting. Optical spectra were measured by a conventional technique for stationary fluorescence detection. Light from a 500 W xenon lamp was fed to a monochromator (Bosch-Lomb 1200 G/mm), of which output, 300 nm light, was used for excitation. Fluorescence was detected with a HT VR376 photomultiplier tube through a TEC G-250CT monochromator. Front surface excitation and viewing geometry was mainly used except for the case of meniscus viewing. Other geometries were carefully tested to check the reabsorption effect.

Results and Discussion

Fluorescence intensity of an anthracene crystal gradually decreased with increasing temperature and the total intensity became very low when it was melted. The reducing ratios were different from band to band. Especially, 470 nm band of the crystal most slowly decreased its intensity. A typical fluorescence spectrum of a single crystal at 300 K is shown in Fig. 1(b).

When a crystal in a quartz tube was melted and irradiated by 300 nm exciting light, bluish green fluorescence was emitted from the meniscus which was about 10 mm apart from the irradiated point in the liquid, and it was carried there by total-internal-reflection effects. Its spectrum at 493 K is shown as curve I in Fig. 1(a). The most intense emission in this spectrum is the band around 470 nm which is corresponding to the excimerlike band in the emission spectrum of an amorphous anthracene solid.[4,5] Intensities of monomer emission bands were rather weak in this spectrum because of reabsorption effect. The bulk of the liquid faintly fluoresced in nearly the same color as in the meniscus, but the spectral distribution of the intensity was rather different. Monomer emission bands were rather intensified in the fluorescence spectrum just from the excited region as shown by curve II in Fig. 1. The 386 nm (25906 cm^{-1}) band in this spectrum may be assigned to the 0-0 fluorescence band which corresponds to the 396 nm (25252 cm^{-1}) 0-0 absorption band in the crystalline

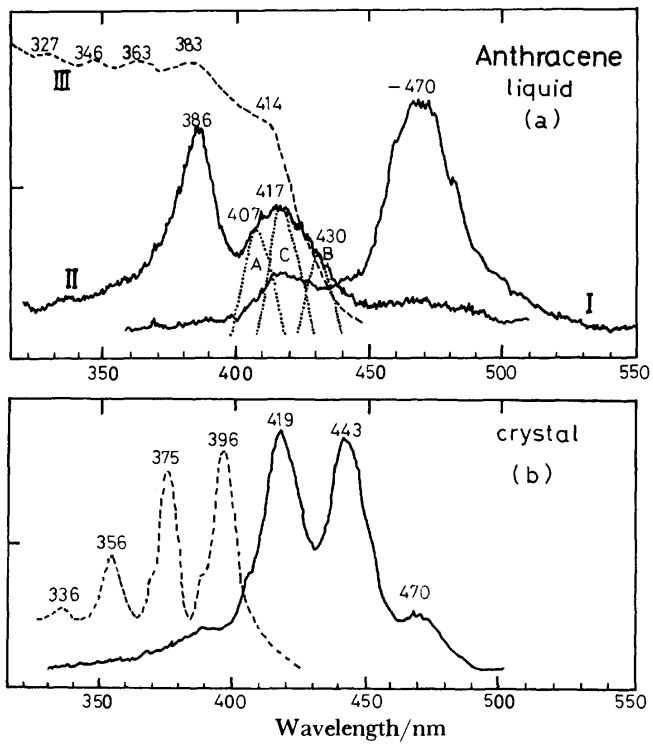

Fig. 1. (a) Fluorescence (full lines I and II) and absorption (in absorbance; dashed line III) spectra of anthracene liquid. Dotted lines show the resolved bands (see the text). (b) Fluorescence (full line) and absorption (in absorbance; dashed line) spectra of anthracne crystal. The absorption sepctrum is of a thin film deposited *in vacuo*.[6]

state. The second band around 417 nm is rather so broad that it could be resolved into three components. A possible procedure for resolving of this band was as follows; assuming the similar vibrational progression in the liquid state as in the crystalline state, the first and second vibronic band peaks could be 407 nm (24570 cm^{-1}) (A) and 430 nm (23256 cm^{-1}) (B) referring to the 386 nm (25907 cm^{-1}) 0-0 band. The halfwidths of these bands were also assumed to be proportional to that of the 386 nm band and the subtraction of these two bands from the observed broad band resulted in the band (C) around 417 nm, as shown in Fig. 1(a).

In order to pursue the origin of the 417 nm band and also to confirm the assignment mentioned above, we tried to observe an absorption spectrum of liquid anthracene, using a ≈50μm thick Pyrex glass cell. This absorption spectrum is shown in Fig. 1(a) together with the fluorescence spectra for convenience of comparison with each other. The 383, 363, 346, and 327 nm absorption bands are recognized to be monomeric vibronic bands. However, the remarkable extra absorption shoulder at 414 nm may be assigned to the dimeric molecular aggregates origin, since it is separated by much larger energy, 1955 cm^{-1}, than the monomer vibrational progression (1450 cm^{-1}) mentioned above. Although the monomer-monomer interactions in a sandwich type geometry in the ground state are usually considered to be repulsive, some configurations might be favourable for attractive interactions because of the reported cluster formation in some molecular beams.[12] Thus, the 417 nm fluorescence band could be assigned to the dimer emission which comes directly from the 414 nm absorption. Then, the 470 nm fluorescence band in the liquid state may be an excimer band which is emitted from the more strongly interacting excimeric molecules in the excited state.

In conclusion, all these observed facts suggest that the existence of fair amounts of dimeric molecular aggregates in the liquid anthracene and these units may also be responsible for the yellow coloration of the liquid, since it has the 414 nm absorption band which is never regarded as a hot band. Further confirmation by the use of time-resolved spectroscopy will appear elsewhere soon.

References

1) R. B. Cundall and S. McD. Ogilvie, "Organic Molecular Photophysics," ed by J. B. Birks, John Wiley & Sons Ltd. London, (1975), Vol. 2, p. 55.
2) H. Bassler, *Phys. Status. Solidi. B*, **107**, 9 (1981).
3) Y. Maruyama and N. Iwasaki, *Chem. Phys. Lett.*, **24**, 26 (1974).
4) H. Muller, H. Bassler, and G. Vaubel, *Chem. Phys. Lett.*, **29**, 102 (1984).
5) Y. Maruyama and K. T-Ichikawa, *Int. J. Quantum. Chem.*, **18**, 587 (1980).
6) Y. Maruyama, K. Machida, N. Iwasaki, and S. Iwashima, *Chem. Lett.*, **1975**, 911.
7) I. Nakada, *J. Phys. Soc. Jpn.*, **20**, 346 (1965).
8) E. A. Chandross, J. Ferguson, and E. G. McRac, *J. Chem. Phys.*, **45**, 3546 (1966).
9) H. Ohigashi, I. Shirotani, H. Inokuchi, and S. Minomura, *Mol. Cryst.*, **1**, 463 (1966).
10) J. K. McVey, D. M. Shold, and N. C. Yang, *J. Chem. Phys.*, **65**, 3775 (1976).
11) J. B. Birks and J. B. Aladekome, *Spectrochim. Acta*, **20**, 15 (1964).
12) P. R. R. Langride-Smith, D. V. Brumbaugh, C. A. Haynam, and D. H. Levy, *J. Phys. Chem.*, **85**, 3742 (1981).

Reactions of Ketene, Methylketene, Ethylketene, and Dimethylketene with Ozone in Air

Shiro HATAKEYAMA,* Shigeo HONDA,† and Hajime AKIMOTO
Division of Atmospheric Environment, The National Institute for Environmental Studies, P.O. Tsukuba-gakuen, Ibaraki 305
(Received March 9, 1985)

Synopsis. Rate constants for reactions with ozone were measured for four kinds of simple ketenes (ketene, methylketene, ethylketene and dimethylketene) in 1 atm of air. The rate constants were obtained as upper limits; $<1\times10^{-21}$, 7×10^{-19}, 1×10^{-18}, and 4×10^{-17} cm^3 molecule^{-1} s^{-1}, respectively. The mechanism of the reactions was proposed to be similar to that for the liquid-phase reaction.

Formation and loss process of oxygen-containing secondary pollutants in the atmosphere is of great interest in the area of atmospheric chemistry. In addition to the well-known oxygen-containing secondary pollutants such as aldehydes, ketones, and carboxylic acids, α-dicarbonyl compounds, ketenes, and peroxides are also observed in the atmosphere. Among these compounds ketenes are known as products of ozone–alkene reactions.[1]

As to the homogeneous loss processes of ketenes in the atmosphere, photolysis and reactions with OH, ozone, and O(^{3}P) should be important. Recently, we reported the reaction of ketenes with O(^{3}P),[2] and with OH.[3] However, little is known about the kinetics of the reactions of ketenes with ozone. To our knowledge, mechanisms of the ozone reactions of ketenes in the gas phase have not been studied so far. For the liquid phase several investigations[4–7] were reported.

In this paper we report the measurement of rate constants for the reactions of ketenes with ozone. The reaction mechanism is also discussed.

Experimental

Ketene, methylketene (MK), ethylketene (EK), and dimethylketene (DMK) were prepared in the same manner as reported before.[2] $^{18}O_2$ (99%) was obtained from Nippon Sanso.

Kinetic measurements were performed both in an 11 L cylindrical quartz vessel (120 mm i.d., 1000 mm long), and in a large volume (6 m^3) smog chamber,[8] whose inner surface is coated with Teflon. The change in the concentration of reactants and products was monitored by means of long-path Fourier transform infrared spectroscopy (LP-FTIR). Path length is 40 m and 221.5 m for the quartz cell and the smog chamber, respectively. Absorptivities used are reported in the previous paper.[3] All the IR spectra were taken at 1 cm^{-1} of resolution. Scans accumulated were 32 times (≈1 min) and 128 times (≈4 min) in the quartz cell runs and in the smog chamber runs, respectively.

Measurements of the rate constant for the reaction of ketene with ozone were performed in the 11 L quartz cell with 2.8 mTorr (1 Torr=133.322 Pa) of ketene and 24—100 mTorr of ozone or with 5.8 mTorr of ozone and 58 mTorr of ketene at room temperature. Those for other ketenes were performed in the smog chamber with ≈0.2 mTorr of ketenes and 1—6 mTorr of ozone at 30±1 °C in the presence of ≈15 mTorr of CH_3CHO as a scavenger of free radicals.

Results and Discussion

Even in the presence of a large excess of ketene (58 mTorr), the decay of ozone (5.8 mTorr) was under detection limit. In the presence of a large excess of ozone (24—100 mTorr), the decay rate of ketene (initial concentration 2.8 mTorr) did not show any dependence on the concentration of ozone as shown in Fig. 1. Thus, the reaction of unsubstituted ketene with ozone is concluded to be very slow. Ketene decay observed in Fig. 1 should be attributed to wall decay of ketene. Decay rate shown in Fig. 1 is three to four times as high as that in the absence of ozone, so it seems that excess ozone enhances the wall decay of ketene. From the results obtained above the upper limit of the rate constant was estimated to be $<1\times10^{-21}$ cm^3 molecule^{-1} s^{-1}. The other ketenes were found to react with ozone more than 100 times faster than ketene. Therefore, the 6 m^3 smog chamber was used as the reactor in order to use much lower concentration of ketenes. Decay of ketenes (initial concentration is about 0.2 mTorr) in the presence of excess ozone (1—6 mTorr) and CH_3CHO (≈15 mTorr) as a scavenger of free radicals was first order. From the dependence of the decay rates on the initial concentrations of ozone as shown in Fig. 2, second order rate constants were calculated to be $(6.7\pm1.9)\times10^{-19}$, $(9.8\pm3.4)\times10^{-19}$, and $(3.7\pm0.5)\times10^{-17}$ cm^3 molecule^{-1} s^{-1} for MK, EK, and DMK respectively. In these plots the intercepts are in good agreement with the wall decay rates of ketenes (filled circles in Fig. 2).

However, stoichiometry of the reaction for three kinds of ketenes are not unity: consumption of ozone is always smaller than that of ketenes in a factor of about 0.7 under the conditions employed for the smog chamber runs and the discrepancy of stoichiometry

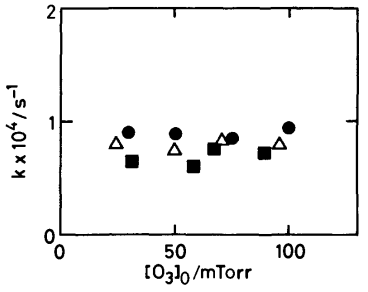

Fig. 1. Dependence of decay rate of ketene on the concentration of ozone. [Ketene]$_0$≅2.8 mTorr.

†On study leave from the University of Tsukuba, Sakura, Ibaraki 305.

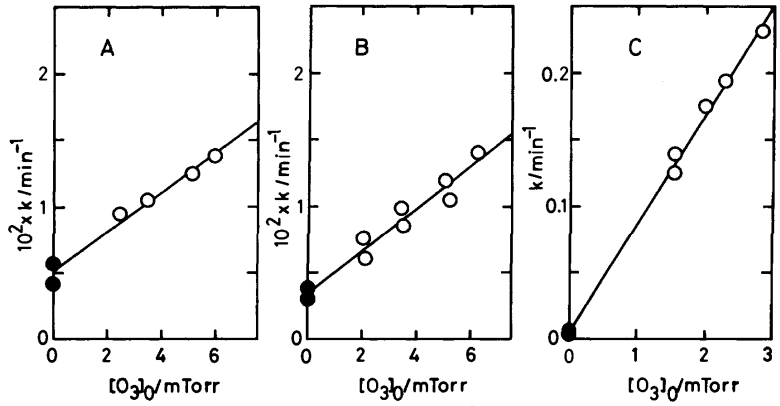

Fig. 2. Dependence of decay rates of MK, EK, and DMK on the concentration of ozone. Solid circles indicate the wall decay. $[Ketene]_0 \cong 0.2$ mTorr.

becomes larger when the concentration of reactants is higher. In the runs with low concentration of ozone and excess ketenes first order decay of ozone was not observed. These facts indicate the contribution of secondary reactions which cannot be prohibited even in the presence of excess CH_3CHO. Thus, the rate constants obtained here may be also regarded as upper limits.

To our knowledge, the gas phase reaction of ozone with ketenes has never been investigated. As for the liquid phase reaction of ozone with ketenes, several reports have been presented.[4,7] In these papers the reaction mechanism is described as follows:

$$RR'C{=}C{=}O + O_3 \longrightarrow RR'\overset{O\diagup\ \diagdown O}{C}\!\!-\!\!\!-\!C{=}O \longrightarrow RR'COO + CO_2 \quad (1)$$

$$RR'COO + RR'C{=}C{=}O \longrightarrow RR'CO + RR'C(\diagup O\diagdown)\!\!-\!\!\!-C{=}O \quad (2)$$

$$RR'C(\diagup O\diagdown)\!\!-\!\!\!-C{=}O \longrightarrow RR'CO + CO \quad (3)$$

In the present study formation of CO, CO_2, and RR'CO (CH_3CHO, C_2H_5CHO, and CH_3COCH_3 from MK, EK and DMK, respectively) was observed, but the stoichiometry of the reaction is not so good enough to discuss the product yields quantitatively. However, the formation of methane, formaldehyde and a small amount of ketene in MK ozone reactions strongly indicates the existence of CH_3CHOO biradical when the mechanism of the decomposition of this biradical,[9] as depicted by following equations, is taken into account.

$$CH_3CHOO \longrightarrow CH_3 + H + CO_2 \quad (4)$$

$$\longrightarrow CH_4 + CO_2 \quad (5)$$

$$\longrightarrow CH_3 + CO + OH \quad (6)$$

$$\longrightarrow CH_2C{=}O + H_2O \quad (7)$$

Radical species formed by the reactions 4 and 6 can consume ketenes, which results in the poor stoichiometry.

An interesting result was obtained in the experiments using $^{18}O_3$ as a reactant. Produced CO_2 mainly consists of $C^{16}O^{18}O$, which supports the occurrence of reaction 1. However, since even a large excess of acetaldehyde cannot trap the biradical (ozonides were not detected), the biradical seems to decompose very quickly and the reaction 2 does not take place in the gas phase.

The authors are grateful to Mr. H. Takagi for his help to conduct experiments using the smog chamber.

References

1) R. I. Martines, J. T. Herron, and R. E. Huie, *J. Am. Chem. Soc.*, **103**, 3807 (1981).
2) N. Washida, S. Hatakeyama, H. Takagi, T. Kyogoku, and S. Sato, *J. Chem. Phys.*, **78**, 4533 (1983).
3) S. Hatakeyama, S. Honda, N. Washida, and H. Akimoto, *Bull. Chem. Soc. Jpn.*, **58**, 2157 (1985).
4) R. Wheland and P. D. Bartlett, *J. Am. Chem. Soc.*, **92**, 6057 (1970).
5) R. M. Moriarty, K. B. White, and A. Chin, *J. Am. Chem. Soc.*, **100**, 5582 (1978).
6) J. K. Crandall, S. A. Sojka, and J. B. Komin, *J. Org. Chem.*, **39**, 2172 (1974).
7) P. S. Bailey, "Ozonation in Organic Chemistry," Academic Press, New York, Vol. 1 (1978), p. 216, Vol. 2 (1982), pp. 401—404.
8) Detail of this smog chamber is described in: H. Akimoto, M. Hoshino, G. Inoue, F. Sakamaki, N. Washida, and M. Okuda, *Environ. Sci. Technol.*, **13**, 471 (1979).
9) J. T. Herron and R. E. Huie, *Int. J. Chem. Kinet.*, **10**, 1019 (1978).

Remarkable Isotope Effect on the Hydrogen-atom Reaction in the Photolysis of D_2-H_2-HI Mixtures at 4 K. A Quantum-mechanical Tunneling Effect

Tetsuo MIYAZAKI
Department of Synthetic Chemistry, Faculty of Engineering, Nagoya University, Chikusa-ku, Nagoya 464
(Received March 22, 1985)

Synopsis. The photolysis of D_2-H_2-HI (0.05 mol%) mixtures has been studied at 4 K by means of ESR spectroscopy. The yield of D atoms decreases sharply upon the addition of a small amount of H_2, while the yield of H atoms increases. The results of the photolysis are similar to those in the radiolysis of D_2-H_2 mixtures at 4 K. The preferential formation of H atoms in the photolysis and radiolysis of the D_2-H_2 mixtures is due to the selective H-atom-abstraction reaction from H_2 by D atoms by means of a quantum mechanical tunneling.

Basic to any theory of the chemical kinetics of elementary reactions is an understanding of the simplest atom-diatomic exchange reaction. A number of experimental and theoretical studies of the reaction of H (or D) with $H_2(D_2)$ in the gas phase have been reported previously.[1] The previous studies, however, have been undertaken above room temperature. Thus, it was difficult to discriminate between the reaction caused by a quantum mechanical tunneling effect and the reaction which proceeds by passing over a potential energy barrier. In order to clarify the tunneling effect, the present author and his colleagues have recently studied the $H_2(D_2)$+H(D) reaction at extremely low temperatures, such as 4.2 and 1.9 K.[2,3]

When solid D_2-H_2 mixtures are irradiated by γ-rays at 4 K, the yields of the trapped D atoms in the radiolysis of D_2 decrease drastically upon the addition of a small amount of H_2, while the yields of trapped H atoms increase.[2] It has been suggested that the remarkable isotope effect on the formation of the D and H atom is to be ascribed to a selective hydrogen-atom reaction caused by a quantum-mechanical tunneling.[2] Since γ-irradiation produces different active species, the selective formation of H atoms in the γ-radiolysis of the D_2-H_2 mixtures may also be explained in terms of activation transfer, such as excitation, charge, and proton transfers, from D_2 to H_2.

In order to verify the remarkable isotope effect on the hydrogen-atom reaction, the reaction of hydrogen atoms produced by the photolysis of HI has been studied here in D_2-H_2 mixtures at 4 K.

Experimental

The H_2 was more than 99.999 mol% pure. The D_2 was more than 99.5 mol% pure. An aqueous solution of HI was vaporized and passed through P_2O_5 to prepare hydrogen iodide. Then, the hydrogen iodide was subjected to trap-to-trap sublimation on a vacuum line several times. The solid sample was made by the rapid cooling of gaseous hydrogen-hydrogen iodide mixtures in a sample tube from room temperature to 4 K. UV illumination was performed at 4 K with a low-pressure mercury lamp. The trapped hydrogen atoms in the irradiated samples were measured at 4 K with a JES-3BX ESR spectrometer at a microwave power level which does not result in the saturation of the signals of the atoms. The relative yields of the H and D atoms were obtained by double integration of the signals, which was performed with a personal computer system. The details of the experimental procedure and the power saturation of the ESR signals had been described in a previous paper.[4]

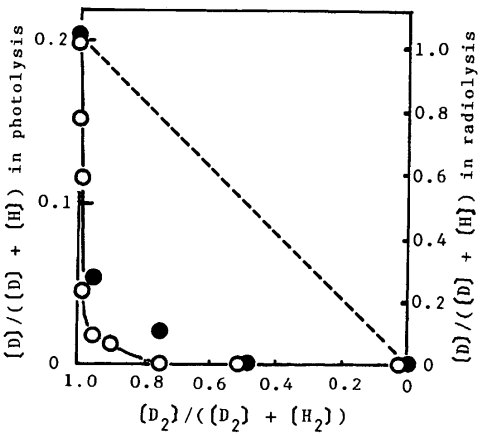

Fig. 1. Fractions of D atom yield in total hydrogen atom yield against fractions of D_2 in D_2-H_2 mixtures at 4 K: (●) D atoms in the UV photolysis of a D_2-H_2-HI(0.05 mol%) mixtures; (○) D atoms in the γ-radiolysis of the D_2-H_2 mixtures.

Results and Discussion

When pure D_2, pure H_2, and D_2-H_2 mixtures containing 0.05 mol% HI are UV-irradiated at 4 K, trapped D and/or H atoms can be observed by means of ESR spectroscopy at 4 K. Figure 1 shows the fraction of the trapped-D-atom yield in the total trapped-hydrogen-atom yield, denoted by closed circles, against a fraction of D_2 in the photolysis of the D_2-H_2-HI (0.05 mol%) mixtures at 4 K. The fraction of the trapped-D-atom yield in the radiolysis of the D_2-H_2 mixtures at 4 K is also shown by open circles. Since the total yields of the trapped D and H atoms are approximately constant over the whole range of D_2 fraction;[5] the D yields decrease sharply upon the addition of H_2, while the H yields increase complementarily. The results in the photolysis are roughly similar to those in the radiolysis. Since the ultraviolet light can be absorbed only by hydrogen iodide in the D_2-H_2-HI mixtures, the possibilities of the excitation, charge, and proton transfers from D_2 to H_2 can be discarded in the photolysis. Thus, the preferential formation

of H atoms in the photolysis can be described by the following schemes of hydrogen-atom reactions:

$$HI \xrightarrow{h\nu} H^* + I \quad (1)$$

$$H^* + D_2(H_2) \longrightarrow HD(H_2) + D(H) \quad (2)$$

$$\searrow H \quad (3)$$

$$D + D_2 \longrightarrow D_2 + D \quad (4)$$

$$D + H_2 \longrightarrow HD + H \quad (5)$$

$$H + D_2 \longrightarrow HD + D \quad (6)$$

$$H + H_2 \longrightarrow H_2 + H \quad (7)$$

Hot H atoms (H*) are produced initially by the photolysis of HI. The hot atoms abstract hydrogen atoms from D_2(or H_2) to produce thermal D(or H) atoms (Reaction 2) or are thermalized to become H atoms (Reaction 3).[4] If the thermal D and H atoms do not react further at 4 K, and if the isotope effect on the hot-atom reaction (Reaction 2) is small, the fraction of the D-atom yields ([D]/([D]+[H])) may be represented by the dotted line in Fig. 1. The large isotope effect on the formation of D and H atoms in the photolysis indicates the secondary reactions of thermal D or H atoms in the D_2–H_2 mixtures at 4 K. All possible reactions of D(H) and D_2(H_2) are represented in Reactions 4—7. Though these reactions have activation energies, the reaction may take place even at 4 K by means of quantum mechanical tunneling reaction.[2,3] Since Reactions 4 and 7 give the same products as the reactants, the large isotope effect is caused by the difference in rate constants between Reactions 5 and 6. Since Reaction 6 is slightly endothermic, the rate of this reaction may be very slow at 4 K.[2] D atoms produced by Reaction 2 react fast with H_2 to form H atoms, as was previously suggested by a theoretical calculation of a tunneling reaction.[3] Thus, it may be concluded that the preferential formation of H atoms in the photolysis and radiolysis of the D_2–H_2 mixtures is due to a selective H-atom-abstraction reaction from H_2 by D atoms.

The author wishes to thank Professor Kenji Fueki at Nagoya University for his encouragement throughout the work. This work was supported in part by a Grant-in-Aid for Scientific Research from the Ministry of Education, Science, and Culture.

References

1) D. G. Truhlar and R. E. Wyatt, *Annu. Rev. Phys. Chem.*, **27**, 1 (1976). The related papers are cited therein.

2) H. Tsuruta, T. Miyazaki, K. Fueki, and N. Azuma, *J. Phys. Chem.*, **87**, 5422 (1983).

3) T. Miyazaki, K. Lee, K. Fueki, and A. Takeuchi, *J. Phys. Chem.*, **88**, 4959 (1984).

4) T. Miyazaki, H. Tsuruta, and K. Fueki, *J. Phys. Chem.*, **87**, 1611 (1983).

5) Though the total yields of hydrogen atoms are approximately constant in the radiolysis of the D_2–H_2 mixtures, the yields in the photolysis are affected by the experimental conditions, such as the cooling process, the sample preparation, and the UV irradiation conditions. Thus, the constancy of the total yields in the photolysis is poorer than that in the radiolysis.

The Determination of the Dissociation Constants of Picric Acid and 2,2′,4,4′,6,6′-Hexanitrodiphenylamine in Ketone-Water Mixtures

Tadashi IWACHIDO,* Shinji OOSAWA,†,†† and Kyoji TÔEI†
College of Liberal Arts, Okayama University, Tsushima, Okayama 700
†*Department of Chemistry, Faculty of Science, Okayama University, Tsushima, Okayama 700*
(Received March 4, 1985)

Synopsis. The acid dissociation constants, K_a, of picric acid and 2,2′,4,4′,6,6′-hexanitrodiphenylamine in acetone, ethyl methyl ketone, and isobutyl methyl ketone were determined in the presence of water. The pK_a values increased remarkably with a decrease in the water content. The pK_a values in water-free ketones were estimated.

Picric acid (HPic) and 2,2′,4,4′,6,6′-hexanitrodiphenylamine (HND) have widely been used as soft acids in the field of analytical chemistry. However, the reported acid dissociation constant values for these substances in ketones lack consistency.[1-5] The aim of the present paper is to determine the dissociation constant values, K_a, of HPic and HND in acetone, ethyl methyl ketone (EMK), and isobutyl methyl ketone (IBMK) as a function of the concentration of water in these solvents, and to show that small quantities of water play a decisive role in acid dissociation. The dissociation constants were determined by means of the spectrophotometric and vapor-pressure osmometric methods.

Experimental

Commercial HND and HPic were recrystallized from acetone and water respectively. The acetone was dried over anhydrous calcium sulfate. The EMK and IBMK were treated with potassium permanganate, washed with a concentrated aqueous potassium carbonate solution and then with water, and dried over anhydrous sodium sulfate for a week or more. These solvents were distilled just before use. The water concentration of the solutions was determined from the absorbances at 1.9 μm. The absorbances of the HND (3×10^{-5} mol dm^{-3}) and HPic (5×10^{-5} mol dm^{-3}) solutions were measured at 430 and 400 nm respectively. The absorbances of the undissociated acid species were evaluated by extrapolating the absorbance-water concentration curves to zero water concentration. The absorbances of the completely dissociated species were approximated by those of the corresponding potassium salts.

Vapor-pressure osmometric measurements of the solutions ($(3-24)\times10^{-2}$ mol dm^{-3}) were done on a Hitachi-Perkin-Elmer Model 115 vapor-pressure osmometer calibrated with 1,2-diphenylethanedione solutions. All the measurements were carried out at 25 °C.

Results and Discussion

The dissociation constant of a weak acid, HA, can be written as:

$$HA \rightleftharpoons H^+ + A^-, \quad (1)$$

$$K_a = [H^+][A^-]/[HA] = C\alpha^2/(1-\alpha), \quad (2)$$

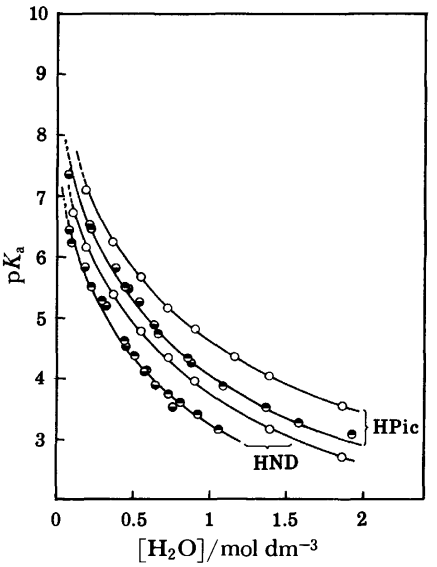

Fig. 1. pK_a *vs.* [H_2O] plots. ○: Acetone, ◓: EMK, ◒: IBMK.

where the brackets denote the molar concentration; C, the total molar concentration of the acid; and α, the degree of dissociation. The absorbance, E, of HA can be expressed as:

$$E = E_{HA}(1-\alpha) + E_A\alpha, \quad (3)$$

where E_{HA} and E_A designate the absorbances of HA and A^- respectively. Taking into account the fact that $[H^+]=[A^-]$, we obtain Eq. 4:

$$K_a = C(E-E_{HA})^2/((E_A-E)(E_A-E_{HA})). \quad (4)$$

In Fig. 1, the pK_a values calculated from E by means of Eq. 4 are plotted against the water concentration. The pK_a values increased markedly with a decrease in the water concentration.

The dissociation constant values in the water-free ketones were determined from pK_a *vs.* $[H_2O]^{1/2}$ plots (Fig. 2) to be pK_a (HPic)=9.3 (acetone), 8.8 (EMK), and 8.8 (IBMK) and pK_a (HND)=8.4 (acetone), 8.0 (EMK), and 8.0 (IBMK). The pK_a value of 9.3 for HPic in acetone is in good agreement with Foltin's value (pK_a=9.2).[1] However, it must be noted that the pK_a values reported by others are much smaller than the present values; Moor reported pK_a values of 3.86 (acetone) and 3.70 (EMK) for HPic;[2] Glover, a pK_a value of 3.3 for HND in acetone;[3] Majersky, pK_a values of 6.04 for HPic in acetone (0.09% water) and 6.54 in EMK (0.16% water);[4] and Majer, a pK_a value of 7.2 for HPic in acetone with a known content of water.[5]

††Present address: Kagawa Prefectural Government, Takamatsu, Kagawa, 761.

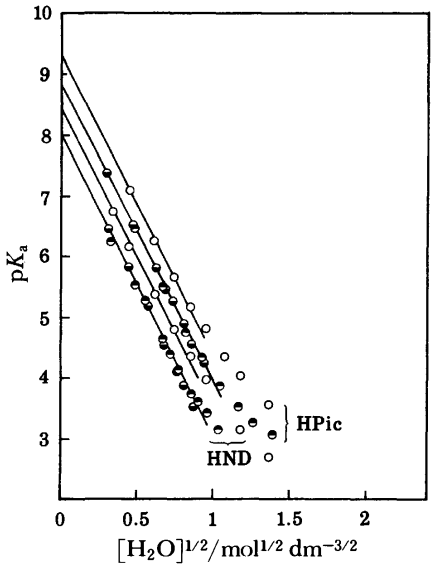

Fig. 2. pK_a *vs.* $[H_2O]^{1/2}$ plots. Symbols: see Fig. 1.

Taking into account the hydration of the solutes, the dissociation of HA can be expressed as:

$$HA_{x(H_2O)} + nH_2O \rightleftharpoons H^+_{y(H_2O)} + A^-_{z(H_2O)}, \quad (5)$$

where $n=x+y+z$. The equilibrium expression is given by:

$$K = [H^+][A^-]/([HA][H_2O]^n), \quad (6)$$

where K refers to the equilibrium constant; the symbols which denote hydration are omitted. Equation 6 can be rearranged as:

$$K_a = [H^+][A^-]/[HA] = K[H_2O]^n. \quad (7)$$

pK_a *vs.* log[H_2O] plots gave straight lines, as is shown in Fig. 3. From the slopes of the lines, the n values were determined to be 4.0±0.1 for all the acid-solvent systems. Since HA and A^- are bulky and hydrophobic in nature, the extent of their hydration is presumably very small or negligible as compared with that of the protons; this leads to the conclusion that the protons exist as $(H_9O_4)^+$ in ketonerich media, as observed in aqueous media.[6]

The dissociation constants can also be determined by means of vapor-pressure osmometry. When a solution and a solvent are placed together in a closed small room, the solvent vapor condenses on the solution, causing a rise in the temperature of the solution. The temperature difference, ΔT, is related to C as follows:

$$\Delta T = K_s(C+b_2C^2 + b_3C^3 + \cdots\cdots), \quad (8)$$

where K_s and b are constants, the values being calibrated with 1,2-diphenylethanedione as a reference substance.

For a dilute solution of electrolytes, Eq. 8 is approximated as:

$$\Delta T = K_s((1+\alpha)C + b_2(1+\alpha)^2C^2). \quad (9)$$

The pK_a values can thus be calculated from ΔT based on Eqs. 2 and 9. The dissociation constants of the potassium salts can also be determined in the same way.

Table 1 summarizes the dissociation constants. In the vapor-pressure osmometric method, the pK_a measurements of weak acids ($pK_a>6$) were unsuccessful because of the limited accuracy of the ΔT of the apparatus. The pK_a values in Table 1 agreed very closely with those obtained by means of the spectrophotometric method (*cf.* Fig. 3). Figures 1—3 and Table 1 show that HND is a stronger acid than HPic in ketone-water media, unlike as in aqueous media (pK_a(HND)= 2.75,[7] pK_a(HPic)=0.29[8]). The dissociation constants of the potassium salts also agreed well with those obtained conductometrically.[9,10]

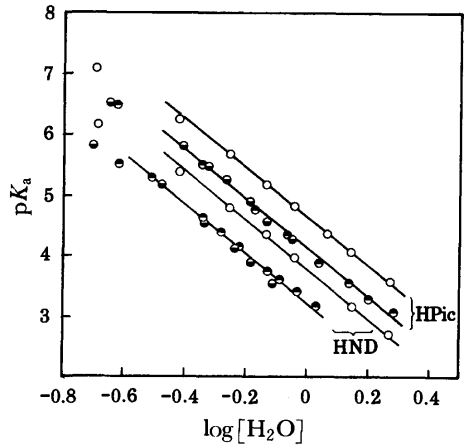

Fig. 3. pK_a *vs.* log[H_2O] plots. Symbols: see Fig. 1.

TABLE 1. pK_a VALUES[a] OBTAINED BY MEANS OF THE VAPOR-PRESSURE OSMOMETRIC METHOD

	[H_2O]/mol dm^{-3}								
	Acetone-H_2O					EMK-H_2O			
Compounds	0.03	1.24	1.29	1.95	4.05	0.03	1.18	2.09	2.52
HND	>6	3.7		2.8		>6	3.3		
K(HND)	2.1					2.2	(2.16)[b]		
HPic	>6		4.4		2.6	>6		3.0	2.6
KPic	2.6	(2.465)[c]							

a) For the K salts, $K_a=[K^+][A^-]/[KA]$. b) Ref. 9 (conductometric). c) Ref. 10 (conductometric).

References

1) M. Foltin and P. Majer, *Collect. Czech. Chem. Commun.*, **43**, 95 (1978).
2) F. J. Moor and I. B. Johns, *J. Am. Chem. Soc.*, **63**, 3336 (1941).
3) D. J. Glover, *J. Am. Chem. Soc.*, **87**, 5275 (1965).
4) P. Majersky and M. Dybalova, *Acta Fac. Rerum Nat. Univ. Comenianae, Chim.*, **24**, 47 (1976).
5) P. Majer, D. Rurikova, and M. Foltin, *Acta Fac. Rerum Nat. Univ. Comenianae, Chim.*, **22**, 1 (1975).
6) For example, R. P. Bell, "The Proton in Chemistry," Chapman and Hall, London (1973), p. 22.
7) D. -W. Fong and E. Grunwald, *J. Phys. Chem.*, **73**, 3909 (1969).
8) R. G. Bates and G. Schwarzenbach, *Experientia* **10**, 482 (1954).
9) T. Iwachido, unpublished work.
10) M. B. Reynolds and C. A. Kraus, *J. Am. Chem. Soc.*, **70**, 1709 (1948).

Electrochemical Reductive Acylation of 2,3-Disubstituted 1-Indenones

Nobuhiro TAKANO,* Noboru TAKENO, Mutsuo MORITA, and Yoshio OTSUJI†
Department of Industrial Chemistry, Muroran Institute of Technology, Mizumoto-cho, Muroran 050
†*Department of Applied Chemistry, College of Engineering, University of Osaka Prefecture, Mozu-Umemachi, Sakai, Osaka 591*
(Received February 8, 1985)

Synopsis. The electrochemical reductive acylation of 2,3-disubstituted 1-indenones in the presence of acetic anhydride in aprotic media such as DMF, DMSO, and acetonitrile gave 2,3-disubstituted 1-acetoxy-1*H*-indenes (**2**) and 1,2-disubstituted 3-acetoxy-1*H*-indenes (**3**) in good yields. The ratios of **2** to **3** in the products were affected by the substituents.

The synthesis of organic compounds using electrochemically generated intermediates is a current topic in synthetic organic chemistry.[1] Previously, we have reported that two reductive acylation products, **2a** and **3a**, are obtained in good yields by the cathodic reduction of 2,3-diphenyl-1-indenone (**1a**) in the presence of acetic anhydride (Scheme 1).[2] As an extension of this synthetically useful reaction, we now wish to report an efficient, one-step synthesis of 2,3-disubstituted 1-acetoxy-1*H*-indenes (**2a—m**) and 1,2-disubstituted 3-acetoxy-1*H*-indenes (**3a—m**) by the cathodic reduction of 1-indenone derivatives (**1a—m**) in the presence of acetic anhydride and discuss the substituent effect on this reaction.

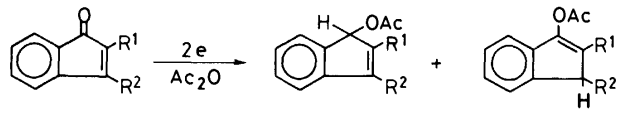

1a-m **2a-m** **3a-m**

a: $R^1 = R^2$ = Ph; **b**: R^1 = Ph, R^2 = 4-MeOPh;
c: R^1 = 4-MeOPh, R^2 = Ph; **d**: R^1 = Ph, R^2 = 4-ClPh;
e: R^1 = Ph, R^2 = Me; **f**: R^1 = Ph, R^2 = Et; **g**: R^1 = Ph, R^2 = *i*-Pr; **h**: R^1 = Ph, R^2 = Benzyl; **i**: R^1 = Ph, R^2 = Cyclohexyl; **j**: R^1 = Ph, R^2 = 1-Naphthyl;
k: R^1 = Me, R^2 = Ph; **l**: R^1 = Et, R^2 = Ph;
m: $R^1 = R^2$ = Me

Scheme 1.

Experimental

The electrolyses were performed in a double cylindrical cell which was divided into the cathode and anode compartments with a sintered glass diaphragm. The working electrode (cathode) was a mercury pool and the auxiliary electrode (anode) was a platinum plate. A 0.1 mol dm^{-3} solution of *n*-Bu_4NBF_4 in DMF was used as both catholyte and anolyte. Acetic anhydride (20 g) and an indenone derivative (0.5 g) were added to the catholyte (100 cm^3). The solution was deoxygenated by bubbling purified N_2 and stirred with a magnetic stirrer. The electrolysis was then carried out at room temperature under controlled potential using a potentiostat and continued until the current dropped to the initial background current. The total electricity passed was measured by use of an integrator. Upon completion of the electrolysis, the catholyte was diluted with water and extracted several times with ether. The combined ether extracts were washed with a saturated $NaHCO_3$ solution and water, dried over Na_2SO_4, and evaporated. The crude products were separated and purified by column chromatography on silica gel using benzene-hexane (1:5) as eluent. The structures of products were confirmed by their IR and NMR spectral data (Table 1).

TABLE 1. NMR AND IR SPECTROSCOPIC DATA FOR ACYLATION PRODUCTS

Product	NMR (CCl_4)δ(ppm, TMS)			IR (Nujol)ν(cm^{-1})	
	-O-Ac	>CH-OAc	>CH-R^2	C=O	C-O
2b	2.00	a)	—	1741	1256
3b	2.33	—	4.90	1774	1174
2c	2.06	a)	—	1736	1250
3c	2.42	—	4.90	1767	1178
2d	1.98	6.92	—	1744	1236
3d	2.33	—	4.86	1762	1200
2e	1.90	6.80	—	1736	1230
3e	2.25	—	3.84[b]	1763	1196
2f	1.92	6.75	—	1734	1230
3f	2.23	—	3.95[c]	1761	1193
2g	1.95	6.70	—	1734	1234
3g	2.30	—	3.93[d]	1761	1200
2h	1.98	a)	—	1735	1227
3h	2.20	—	4.20[e]	1764	1196
2i	1.89	6.68	—	1735	1225
3i	2.20	—	3.84[d]	1764	1200
2j	2.10	a)	—	1733	1221
2k	2.12	6.27	—	1735	1227
3k	2.28	—	4.26	1763	1200
2l	2.12	6.40	—	1737	1227
3l	2.30	—	4.40	1763	1200
2m	2.02	6.10	—	1733	1230
3m	2.31	—	3.23[b]	1761	1200

a) This signal overlaped with that of aromatic ring protons. b) Quartet. c) Triplet. d) Doublet. e) Multiplet.

Results and Discussion

The results of the electrolyses are summarized in Table 2. Only the *O*-acylation products, **2a—m** and **3a—m**, were obtained in good yields under the conditions shown in Table 2. Curphy and co-workers have reported that in the electrochemical reductive acylation of benzophenone under similar conditions, acylation takes place on both carbonyl carbon and carbonyl oxygen atoms.[3] However, in the case of indenone derivatives, *C*-acylation products were not detected at all.

We have shown that the reductive acylation of **1a** to

Table 2. Controlled-potential electrolysis of 1-indenones in the presence of acetic anhydride in DMF

1-Indenone[a]	Electrolysis[b] potential	n	Product[c] Yield	Ratio
	V *vs.* SCE	F/mol	%	**2/3**
1a	−1.20	2.02	98	67/33
1a	−1.30	2.10	97	59/41[d]
1a	−1.30	2.13	96	56/44[e]
1a	−1.80	2.23	82	68/32
1b	−1.35	2.00	98	59/41
1c	−1.30	2.03	95	57/43
1d	−1.20	1.98	98	63/37
1e	−1.40	1.83	87	38/62
1f	−1.40	1.81	86	37/63
1g	−1.40	1.97	89	40/60
1h	−1.40	1.96	88	50/50
1i	−1.40	1.88	79	45/55
1j	−1.30	1.74	97	100/0
1k	−1.40	1.97	48	77/23
1l	−1.40	2.00	52	67/33
1m	−1.60	2.01	57	63/37

a) 1-Indenones were prepared by the methods described in the literatures.[6,7] b) Elecrolysis potentials based on half-wave potentials. c) Isolated yield based on 1-indenones. d) Electrolysis was carried out in DMSO. e) Electrolysis was carried out in acetonitrile.

2a and **3a** is achieved by way of the reaction of the electrogenerated anion radical (**AR**) with acetyl cation and proceeds *via* the ECE mechanism as shown in

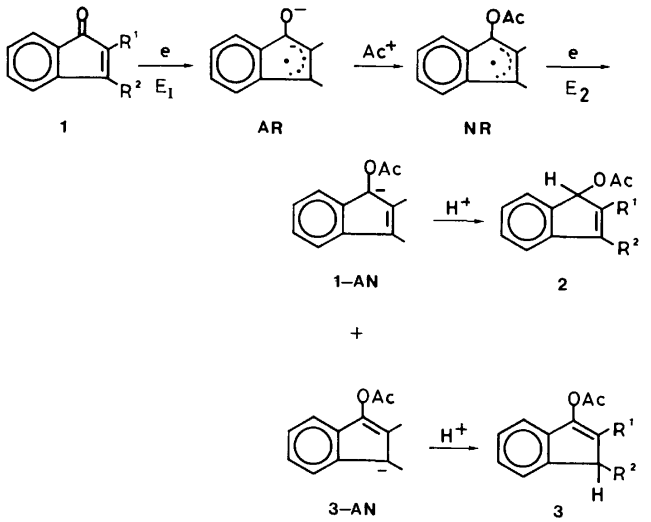

Scheme 2.

Scheme 2.[2] The same mechanism presumably operates for the reductive acylation of the compounds studied in this paper. Support for this mechanism was obtained by observing the voltammetric behavior of the substrates[4] and also by the coulometric analyses of the reactions which showed that the electricity (n) passed during each reaction was very close to two electrons for all the compounds studied (Table 2). Furthermore, the product ratio of **2a** to **3a** in the electrolysis of **1a** at −1.80V where the formation of the dianion of **1a** should predominate was virtually the same as that in the electrolysis at −1.20V where the formation of the anion radical of **1a** should predominate. This result suggests that disproportionation occurs rapidly between the substrate indenone and its electrogenerated dianion if formed, to produce two molecules of the anion radical (**AR**) which is converted into the final products by the reaction with acetyl cation *via* the path way shown in Scheme 2.

The substituent effect on the product ratios in the electrolyses of indenone derivatives is noteworthy. When 3-substituted 2-aryl-1-indenones were used as substrates, alkyl, benzyl, and cyclohexyl substituents at C-3 lowered the ratios of 2,3-disubstituted 1-acetoxy- (**2**) to 1,2-disubstituted 3-acetoxy-1*H*-indenes (**3**) in the products, compared with aryl substituents at the same position (Table 2). This tendency may be explained on the basis of the mechanism of Scheme 2. In this scheme, the second one-electron reduction stage (**NR**→ **1-AN** and/or **3-AN**) is faster than the first one-electron reduction stage (**1**→**AR**), since **NR** is more readily reducible than the starting substrate; $E_1 < E_2$.[5] As a result, the product distribution is most probably considered to be determined at the final protonation stage which depends on the relative electron densities on the reaction centers of **1-AN** and **3-AN**. The inductively electron-donative alkyl substituents at C-3 favor the formation of **3** particularly by increasing the electron density on the reaction center of **3-AN**. On the other hand, the aryl substituents at C-3 favor the formation of **2** particularly by decreasing the electron density on the reaction center of **3-AN**. This is due to the resonance of the aryl groups (Eq. 1).

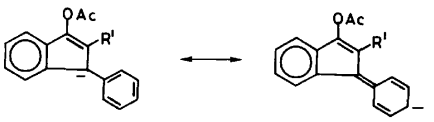

(1)

For **1m** whose substituents at C-2 and C-3 are the electron-donative alkyl groups, the formation of **2** is favored by increasing the electron density on the reaction center of **1-AN**.

References

1) H. Lund, *Denki Kagaku*, **45**, 2 (1977) and references cited therein.

2) N. Takano, N. Takeno, and M. Morita, *Nippon Kagaku Kaishi*, **1983**, 1753.

3) T.J. Curphy, L. D. Trivedi, and T. Layloff, *J. Org. Chem.*, **39**, 3831 (1974).

4) The voltammetric behavior of 2,3-disubstituted 1-indenones (**1b—m**) in DMF was analogous to that of **1a**. Thus the polarograms of indenones in DMF in the absence of acetic anhydride showed two one-electron reduction waves I and II. When acetic anhydride was added to the solution the wave I grew in height at the expense of the wave II. At sufficiently large acetic anhydride concentration the wave I showed a single two-electron wave.

5) G. J. Hoijtink, J. van Schooten, E. de Boer, and W. Y. Aalbersberg, *Recl. Trav. Chim. Rays-Bas*, **73**, 355 (1954).

6) H. Burton and C. W. Shoppee, *J. Chem. Soc.*, **1935**, 1156.

7) N. Takano, N. Takeno, and M. Morita, *Nippon Kagaku Kaishi*, **1984**, 2003.

Reaction of Trimethylsilyl Azide with C=N-O Bond

Kozaburo NISHIYAMA* and Izumi MIYATA
Department of Chemistry, Tokyo Metropolitan University, 2-1-1, Fukasawa, Setagaya, Tokyo 158
(Received March 12, 1985)

Synopsis. Trimethylsilyl azide (TMSA) was reacted with an oxime ester or a Reissert salt in the presence of trimethylsilyl trifluoromethanesulfonate to give tetrazole derivative. The details of these reactions are examined.

Trimethylsilyl azide (TMSA) has a high potential in the synthetic chemistry of heterocycles and azido compounds.[1] We have reported that the decomposition reaction of *gem*-diazidoalkane, which was obtained by a reaction of ketone with TMSA, gave tetrazole derivatives in excellent yields and, therein, imidoyl azide was postulated as a reaction intermediate.[2] As a part of the investigations concerning the reactivities and synthetic utilities of TMSA, we would now like to describe reactions of TMSA with oxime esters or *N*-acyloxy(or *N*-sulfonyloxy)pyridinium(or quinolinium) chloride, which possess C=N-O bonding.

Results and Discussion

When a solution of acetone oxime methanesulfonate (**1a**) and TMSA in acetonitrile was heated to reflux for 24 h, 43% of 1,5-dimethyltetrazole (**2a**), along with trimethylsilyl methanesulfonate, was obtained by the usual work-up of the reaction mixture followed by column chromatography on silica gel. Oxime esters (**1a—g**) with TMSA were treated under various conditions and the results are summarized in the Table 1. From acetone oxime esters (**1a**—c), 1,5-dimethyltetrazole (**2a**) was yielded as the sole product. Acetophenone oxime esters (**1d** and **1e**) and cyclohexanone oxime esters (**1f** and **1g**) were similarly transformed to 5-methyl-1-phenyltetrazole (**2b**) as a major product (a regioisomer, 1-methyl-5-phenyltetrazole (**2c**), was also obtained less than 5%) and 6,7,8,9-tetrahydro-5*H*-tetrazolo[1,5-*a*]azepine (**2d**), respectively. However, the yield of tetrazole **2** obtained from oxime carboxylates with TMSA was not so good, compared with those of oxime sulfonates and TMSA. Even with oxime sulfonates, the addition of trimethylsilyl trifluoromethanesulfonate (TMSOTf) as a catalyst markedly improve the yields of tetrazoles **2** (*vide* Runs 2, 4, and 6). Especially, as shown in runs 3 and 4, such a tendency was more remarkable in benzene. In refluxing dichloromethane, only trace amounts of **2** were obtained, even if TMSOTf was added.

$$\begin{matrix} R_1 \\ R_2 \end{matrix}\!\!>\!C = N\text{-}OX$$

1, a, $R_1 = R_2 = Me$, $X = MeSO_2$
b, $R_1 = R_2 = Me$, $X = p\text{-}MeC_6H_4SO_2$
c, $R_1 = R_2 = Me$, $X = PhCO$
d, $R_1 = Me$, $R_2 = Ph$, $X = MeSO_2$
e: $R_1 = Me$, $R_2 = Ph$, $X = PhCO$
f: $R_1, R_2 = -(CH_2)_5-$, $X = MeSO_2$
g, $R_1, R_2 = -(CH_2)_5-$, $X = PhCO$

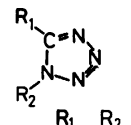

	R_1	R_2
2 a	Me	Me
b	Me	Ph
c	Ph	Me
d	$-(CH_2)_5-$	

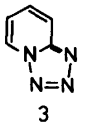

3

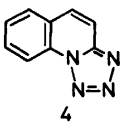

4

Table 1. Reaction of various oxime esters with TMSA[a]

Run	X in		Solvent	Product	Isolated Yield/%
	$Me_2C{=}N\text{-}OX$				
1	$MeSO_2$	(**1a**)	CH_3CN	**2a**	43
2	$MeSO_2$	(**1a**)[b]	CH_3CN	**2a**	95
3	$MeSO_2$	(**1a**)	Benzene	**2a**	0
4	$MeSO_2$	(**1a**)[b]	Benzene	**2a**	69
5	$MeSO_2$	(**1a**)	PhCl	**2a**	98
6	$p\text{-}MeC_6H_4SO_2$	(**1b**)[b]	CH_3CN	**2a**	92
7	PhCO	(**1c**)[b]	CH_3CN	**2a**	42
	$MePhC{=}N\text{-}OX$				
8	$MeSO_2$	(**1d**)[b]	CH_3CN	**2b**	95[c]
9	PhCO	(**1e**)[b]	CH_3CN	**2b**	20[c]
	$(CH_2)_5C{=}N\text{-}OX$				
10	$MeSO_2$	(**1f**)[b]	CH_3CN	**2d**	94
11	PhCO	(**1g**)[b]	CH_3CN	**2d**	84

a) The reactions were carried out at refluxing temperature of the employed solvents for 24 h. b) TMSOTf was used as a catalyst. c) Regioisomer **2c** was contained less than 5%.

In a mechanistic consideration, we assume that the reaction of oxime esters with TMSA takes place *via* a pathway as shown in the Scheme; the Beckmann rearrangement of the oxime esters in the presence of TMSA gives the imidoyl azides, followed by cyclization to tetrazoles **2**. As for the Beckmann rearrangement, a similar reaction in which oxime esters and iodotrimethylsilane afforded imidoyl iodides, has been reported by Yamamoto *et al.*[3] The equilibrium

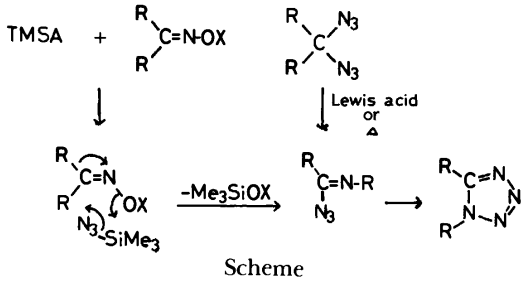

Scheme

between imidoyl azide and tetrazole was well established.[4] According to these investigations, tetrazole form, in most cases, exists predominantly at a low temperature (around room temperature). Thus, 1,5-disubstituted tetrazoles (but not imidoyl azides) were obtained in the reaction of oxime esters with TMSA.

The treatment of *N*-(methylsulfonyloxy)pyridinium chloride, which was prepared from pyridine *N*-oxide and methanesulfonyl chloride *in situ*, with TMSA gave tetrazolo[1,5-*a*]pyridine (**3**) in 29% yield. When acyl chloride instead of sulfonyl chloride was employed, the reaction did not occur. Pyridine *N*-oxide (itself with TMSA) did not give **3**, in contrast to the reaction of pyridine *N*-oxide and sulfonyl azide.[5] Similarly, *N*-(methylsulfonyloxy)quinolinium chloride and TMSA gave tetrazolo[1,5-*a*]quinoline (**4**) in 64% yield. These reactions seem to be modified Reissert reactions.[6,7] The difference in the yields between **3** and **4** may be due to the considerable loss of resonance energy caused by the formation of dihydro intermediates in monocyclic compounds.[8]

In conclusion, TMSA readily reacted with oxime esters or Reissert salts to give tetrazoles (**2**, **3**, and **4**). In these reactions, the sulfonyloxy group was better than an acyloxy group as the leaving group. The temperature dependence, solvent effect, and catalytic effect of TMSOTf were distinctly observed.

Experimental

Melting points are uncorrected. ^{1}H NMR were determined with a Hitachi R-600, Varian XL-100 or XL-300 spectrometer using tetramethylsilane as an internal standard. IR spectra were taken on a Hitachi 260-10 infrared spectrometer and the MS spectra were measured with a JEOL DX-300 spectrometer.

Materials. Trimethylsilyl azide was prepared from chlorotrimethylsilane and sodium azide in dibutyl ether,[1] bp 95—96 °C. Oxime esters (**1a—g**) were synthesized by a reaction of the corresponding oximes with sulfonyl (or acyl) chlorides in the presence of triethylamine or pyridine in benzene according to the reported methods.[9,10] **1a**, mp 46—47 °C (lit,[11] 45—46 °C); **1b**, mp 86—87 °C (lit,[12] 87—88 °C); **1d**, mp 63—64 °C (lit,[9] 64—65 °C); **1e**, mp 98—100 °C (lit,[10] 100—102 °C); **1f**, mp 43—45 °C (lit,[9] 43—45 °C); **1g**, mp 57—58 °C (lit,[13] 58 °C). In addition, these compounds were confirmed by spectroscopic analyses (IR, ^{1}H NMR, and MS). Acetone oxime benzoate (**1c**), pyridine *N*-oxide, quinoline *N*-oxide, and TMSOTf were commercial products and were purified if necessary.

Reaction of Oxime Ester (1a—g) with TMSA. A solution of acetone oxime methanesulfonate (**1a**, 2 g, 13 mmol) and TMSA (2.3 g, 19 mmol) in anhydrous acetonitrile (20 cm^3) was refluxed for 24 h with stirring. After a careful removal of low-boiling substances followed by distillation of trimethylsilyl methanesulfonate (570 mg, 26%), bp 54 °C/3 mmHg (1 mmHg=133.322 Pa), the residue was chromatographed on silica gel using various mixtures of benzene–chloroform and chloroform. Elution with a mixture of benzene–chloroform (1:2) afforded 0.56 g of 1,5-dimethyltetrazole (**2a**, 43%), which was recrystallized from hexane to give colorless needles, mp 72—73 °C (lit,[2] 72—73 °C); ^{1}H NMR ($CDCl_3$) δ=2.50 (s, 3H) and 4.00 (s, 3H); MS, *m/z* 98 (M^+). Elution with chloroform gave the starting sulfonate **1a**. Other oxime esters were treated in a similar manner. The yields of tetrazoles are shown in Table. TMSOTf was used in a range of 0.05—0.1 equiv of oxime esters. From acetophenone oxime ester (**1d**), 5-methyl-1-phenyl- (**2b**) and 1-methyl-5-phenyltetrazole (**2c**), of which ratio was 95:5 from ^{1}H NMR spectrum, δ=2.60 (s, *C*-Me), 4.10 (s, *N*-Me), 7.40 (s), and 7.50 (s), were obtained. After recrystallization from benzene–hexane, only **2b** was isolated, as colorless needles, mp 97—98 °C (lit,[14] 98—99 °C); ^{1}H NMR ($CDCl_3$) δ=2.60 (s, 3H) and 7.50 (s, 5H); MS, *m/z* 161 (M+1). From cyclohexanone oxime esters **1f** and **1g**, 6,7,8,9-tetrahydro-5*H*-tetrazolo[1,5-*a*]azepine (**2d**), recrystallized from hexane, colorless needles, mp 57—58 °C (lit,[2] 57—58 °C); MS, *m/z* 138 (M^+), was obtained.

Reaction of Pyridine (or Quinoline) N-Oxide with TMSA. A mixture of pyridine *N*-oxide (1.0 g, 11 mmol) and methanesulfonyl chloride (1.2 g, 11 mmol) in anhydrous acetonitrile (20 cm^3) was stirred for 3 h at room temperature. TMSA (2.4 g, 11 mmol) was added to the suspension and then the mixture was heated to reflux for 24 h. The dried dichloromethane extract was evaporated and chromatographed on silica gel. Elution with chloroform gave 0.36 g of tetrazolo[1,5-*a*]pyridine (**3**, 29%), recrystallized from ethanol, colorless needles, mp 156—157 °C (lit,[15] 156—158 °C); ^{1}H NMR ($CDCl_3$) δ=7.30 (m, 1H), 7.76 (m, 1H), 8.12 (d, *J*=9.2 Hz, 1H), and 8.92 (d, *J*=6.7 Hz, 1H); MS, *m/z* 120 (M^+). When a reaction of quinoline salt, which was prepared from quinoline *N*-oxide (6 g, 41 mmol) and methanesulfonyl chloride (5.2 g, 45 mmol), was similarly performed for 24 h, the precipitated solid was filtered and the filtrate was concentrated to dryness. Recrystallization of the combined solid gave 4.5 g of tetrazolo[1,5-*a*]quinoline (**4**, 64%) as colorless needles from ethanol, mp 153—155 °C (lit,[16] 155 °C); MS, *m/z* 170 (M^+). ^{1}H NMR ($CDCl_3$) δ=7.73 (m, 1H), 7.88 (d, *J*=9.4 Hz, 1H) 7.90 (m, 1H), 7.97 (m, 1H), and 8.72 (d, *J*=8.0 Hz, 1H).

References

1) K. Nishiyama, *Yuki Gosei Kagaku Kyokai Shi*, **43**, 176 (1985) and references cited herein.

2) K. Nishiyama and A. Watanabe, *Chem. Lett.*, **1984**, 455.

3) Y. Ishida, S. Sasatani, K. Maruoka, and H. Yamamoto, *Tetrahedron Lett.*, **1983**, 3255.

4) For example, M. Tišler, *Synthesis*, **1973**, 123; C. Wentrup and H.-W. Winter, *J. Am. Chem. Soc.*, **102**, 6159 (1980).

5) K. S. Reddy, D. S. Iyenger, and U. T. Bhalerao, *Chem. Lett.*, **1983**, 1745.

6) Review; E. Mosettig, *Org. Reactions*, **8**, 220 (1954).

7) With cyanotrimethylsilane, such Reissert salts gave 2-cyano derivatives. [W. K. Fife, *J. Org. Chem.*, **48**, 1375 (1983).]

8) A. R. Katritzky and E. Lunt, *Tetrahedron*, **22**, 4291 (1969).

9) K. Maruoka, T. Miyazaki, M. Ando, Y. Matsumura, S. Sakane, K. Hattori, and H. Yamamoto, *J. Am. Chem. Soc.*, **105**, 2831 (1983).

10) Z. Gass and F. W. Bope, *J. Am. Pharm. Assoc., Sci. Ed.*, **48**, 186 (1959).

11) M. J. P. Harger, *J. Chem. Soc., Perkin Trans. 1*, **1983**, 2699.

12) C. A. Grob, H. P. Fischer, W. Raudenbusch, and J. Zergeni, *Helv. Chim. Acta.*, **47**, 1003 (1964).

13) Z. Csuros, K. Zech, G. Dely, and E. Zalay, *Acta. Chim. Hung.*, **1**, 66 (1951).

14) P. A. S. Smith, *J. Am. Chem. Soc.*, **76**, 436 (1954).

15) J. H. Boyer, D. I. McCane, W. J. McCarville, and A. T. Tweedie, *J. Am. Chem. Soc.*, **75**, 5298 (1953).

16) L. Garanti and G. Zecchi, *J. Org. Chem.*, **45**, 4767 (1980).

Desulfurization of Thioketones and Thioamides with Diphosphorus Tetraiodide

Hitomi SUZUKI,* Hiroyuki TANI, and Setsuko TAKEUCHI
Department of Chemistry, Faculty of Science, Ehime University, Bunkyo-cho, Matsuyama 790
(Received March 22, 1985)

Synopsis. On heating with diphosphorus tetraiodide in benzene, thioketones undergo reductive desulfurization to afford parent hydrocarbons, while thioamides are slowly converted into nitriles.

Diphosphorus tetraiodide (P_2I_4) exhibits a high affinity for oxygen and thus acts as an excellent deoxygenating and dehydrating agent for various oxygen-containing compounds.[1] However, its ability as a desulfurizing agent has been little studied yet. Only recently, the desulfurization of episulfides to olefins has been reported.[2] In the present paper, we describe the reaction of P_2I_4 with thioketones and thioamides.

Ketones are inert to P_2I_4 in boiling benzene and only in combination with lithium aluminum hydride they are reducible to hydrocarbons.[3] In contrast, thioketones **1** have been found to be moderately reactive and on heating with P_2I_4 in boiling benzene followed by aqueous work-up, they were converted to parent hydrocarbons **2** in good to moderate yields (Table 1). The origin of protons may be sought to a trace of water which is normally present in commercial solvent employed, since the use of less amounts of solvent or thorough drying of solvent led to significantly reduced yields of the reduction products. In some cases, especially when the reactions were performed in a concentrated solution, the desulfurative dimerization of thioketones was found to compete with the reduction, giving olefins **3** as a side product. Geometry of these olefinic products was not determined.

Conventional synthesis of aromatic thioketones involves treatment of the corresponding ketones with

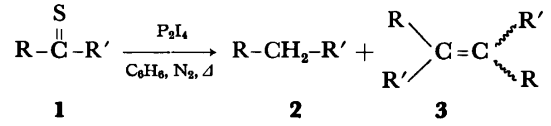

1 **2** **3**

tetraphosphorus decasulfide (P_4S_{10}). When this reaction was carried out in the presence of equimolar amounts of P_2I_4, ketones underwent reduction and reductive dimerization in parallel to give mixtures of hydrocarbons **2** and olefins **3**, usually the latter being predominant. Thus, by this treatment benzophenone was converted into diphenylmethane and tetraphenylethylene in 21 and 35% isolated yields, respectively.

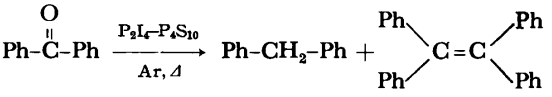

Amides are smoothly dehydrated to nitriles by P_2I_4.[4] In contrast, dehydrosulfurization of thioamides **4** with P_2I_4 proceeded quite slowly in a benzene/triethylamine mixture (10:1) under refluxing conditions, but nitriles **5** were in most cases obtained in high state of purity (Table 2). In the absence of triethylamine, little or no nitriles were formed. Uses of other solvent systems such as DMF, carbon tetrachloride, and heptane in combination with triethylamine or pyridine gave poor results. Aliphatic thioamides were more easily dehydrosulfurized as compared to aromatic ones.

TABLE 1. REDUCTIVE DESULFURIZATION OF THIOKETONES WITH P_2I_4[a]

Thioketone **1**		Reaction time/h	Hydrocarbon **2**	Yield/%[b]
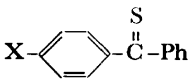	X=H	6	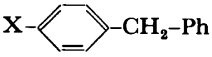	85[c]
	Me	5		52
	Me	5[d]		26[e]
	MeO	7		34
	Cl	4		74
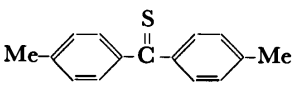		5	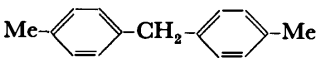	79
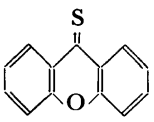		9	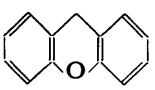	56

a) All reactions were carried out according to the procedure described in Experimental section, except for the case d) where the reaction was conducted in a more concentrated solution. b) Yields refer to the isolated compounds and are not optimized. All products are known and identified by comparison with authentic specimens. c) GLC yield. d) Amount of benzene as solvent was reduced to 5 ml. e) Accompanied by 16% yield of 1,2-diphenyl-1,2-bis(4-methylphenyl)ethylene.

Table 2. Dehydrosulfurization of thioamides to nitriles with P_2I_4

Thioketone **4**		Reaction time/h	Nitrile **5**	Yield/%[a]
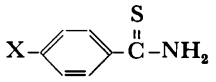	X=H	16	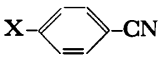	35
	MeO	12		53
	Cl	14		42
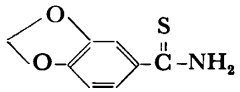		13	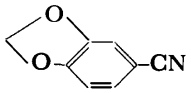	56
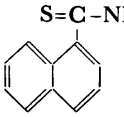		14	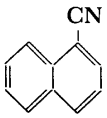	88
$Ph-CH_2-C(=S)-NH_2$		10	$Ph-CH_2-CN$	59
$Ph-CH_2CH_2-C(=S)-NH_2$		10	$Ph-CH_2CH_2-CN$	71

a) Yields refer to the isolated compounds and are not optimized. All products are known and identified by comparison with authentic specimens.

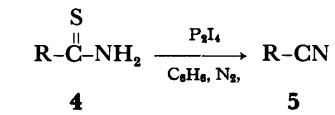

4 **5**

We may conclude that P_2I_4 is not so effective as a desulfurizing agent for thiocarbonyl compounds. However, it exhibits an interesting mode of reductive dimerization with some substrates which, depending on circumstances, may find utility for synthetic purposes.

Experimental

Materials. Thioketones were prepared from ketones and tetraphosphorus decasulfide according to the literature procedure.[5,6] Thioamides were obtained by adding hydrogen sulfide to nitriles in pyridine in the presence of triethylamine, as described in Ref. 7. Products were identified by mass, IR, and ^{1}H-NMR spectra as well as by direct comparison with authentic specimens. All products are known. Separation of hydrocarbon mixture was performed on a fraction preparative liquid chromatograph (Japan Analytical Industry Co, LC-08) using chloroform as solvent.

Reaction of Thioketones 1 with P_2I_4. To a solution of thioketone (1.0 mmol) in benzene (20 ml) was added P_2I_4 (1.0 mmol) and the resulting mixture was heated under reflux for appropriate hours under argon. Then the reaction was quenched by the addition of aqueous sodium hydrogensulfite and the organic phase was separated, washed with water, and dried over sodium sulfate. Removal of the solvent under reduced pressure yielded corresponding product or products, which were purified either by chromatography over silica gel or by recrystallization.

Reaction of Ketones with P_2I_4 in the Presence of P_4S_{10}. A mixture of aromatic ketone (1.0 mmol), P_2I_4 (1.0 mmol), and P_4S_{10} (1.0 mmol) was heated in an oil bath at around 130 °C for 3 h. After cooling the dark brown reaction mixture was extracted with ether and the extract was washed with 10% aqueous sodium sulfite and water, dried over sodium sulfate, and evaporated under reduced pressure. The residue was subjected to preparative liquid chromatography to obtain hydrocarbon component.

Reaction of Thioamides 4 with P_2I_4. To a solution of thioamide (1.0 mmol) in benzene–triethylamine mixture (10:1, 10 ml) was added P_2I_4 (1.0—1.5 mmol) and the resulting mixture was heated under gentle reflux for appropriate hours under nitrogen. After cooling the mixture was washed with 10% aqueous ammonium chloride, the organic phase was extracted with ether, dried over sodium sulfate, and evaporated to leave a residue, which was chromatographed over silica gel, distilled *in vacuo*, or recrystallized from appropriate solvent.

References

1) For reviews, see: H. Suzuki and H. Tani, *Yuki Gosei Kagaku Kyokai Shi*, **43**, 76 (1985); A. Krief, Aldrich Technical Information, 191 (1981).

2) J. R. Schauder, J. N. Denis, and A. Krief, *Tetrahedron Lett.*, **24**, 1657 (1983).

3) H. Suzuki, R. Masuda, H. Kubota, and A. Osuka, *Chem. Lett.*, **1983**, 909.

4) H. Suzuki and N. Sato, *Nippon Kagaku Kaishi*, **1981**, 392.

5) Aromatic thioketones were chosen as substrate because of their handling ease and ready availability.

6) J. W. Scheeren, P. H. J. Ooms, and R. J. F. Nivard, *Synthesis*, **1973**, 149. For a general survey of the chemistry of thiocarbonyl compounds, see F. Duus, "Thiocarbonyl Compounds," in "Comprehensive Organic Chemistry. The Synthesis and Reactions of Organic Compounds," ed by D. N. Jones, Oxford (1979), Vol. 3, pp. 373—487.

7) A. E. S. Fairfull, J. L. Lowe, and D. A. Peak, *J. Chem. Soc.*, **1952**, 742.

Absolute Configuration of Platyphylloside and (−)-Centrolobol

Shinji OHTA, Mika KOYAMA, Tadashi AOKI, and Takayuki SUGA*
Department of Chemistry, Faculty of Science, Hiroshima University, Higashisenda-machi, Naka-ku, Hiroshima 730
(Received March 25, 1985)

Synopsis. The absolute configuration of platyphylloside was established to be *S* by ^{13}C NMR spectroscopy. On the basis of this establishment, the *S*-configuration previously assigned to the chirality at C-3 of (−)-centrolobol was revised to the *R*-configuration.

The absolute configuration of platyphylloside, isolated from the green inner-bark of *Betula platyphylla* Sukatchev var. *japonica* (Japanese name: Shirakamba),[1] has not been assigned yet. In addition, the absolute configuration of (−)-centrolobol ($[\alpha]_D^{25}$ −8.6°) isolated from the heartwoods of *Centrolobium robustum* Mart. is assigned to be *S*[2] on the basis of the empirical rule.[3] However, this rule is not described to be applicable to the compound possessing a phenyl group. This suspicious point necessitated the reexamination of the absolute configuration of (−)-centrolobol, 1,7-bis(4-hydroxyphenyl)-3-heptanol (**5**). We now have established the absolute configuration of platyphylloside by ^{13}C NMR spectroscopy, and this establishment has resulted in the revision of the absolute configuration previously assigned to the (−)-centrolobol.

Results and Discussion

A diarylheptanoid glycoside (**1**) was isolated from the green bark of *B. platyphylla* var. *japonica*. Hydrolysis of **1** with Taka-diastase[4] gave its aglycone (**2**) and glucose. Not only the mp and spectral data (UV, IR, and ^{1}H NMR) of **1** and **2** but also the chemical behaviors of **1** and the EI-MS spectral data of **2** were identical with those reported for platyphylloside and its aglycone, respectively.[1] The glycoside (**1**) was thus confirmed to be platyphylloside, *i.e.*, 1,7-bis(4-hydroxyphenyl)-5-(β-D-glucopyranosyloxy)-3-heptanone. Although the platyphylloside has an asymmetric carbon, however, even the optical rotation, needless to mention the absolute configuration, is not been given in Ref. 1.

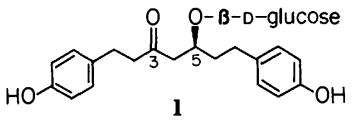

1

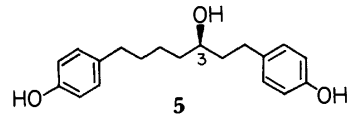

5

The absolute configuration of **1** was established by ^{13}C NMR spectroscopy. On comparison of the ^{13}C NMR chemical shifts of **1** with those of **2**, the larger glycosidation shift (−2.9 ppm) at C-4 than that (−2.3 ppm) at C-6 was observed, as shown in Table 1. Application of the glycosidation shift rule[5] to these shifts indicated the configuration at C-5 of **1** and **2** to be *S*. The validity of this application has been recently confirmed for diarylheptanoid analogs.[6] The similar glycosidation shifts (Table 1) were further observed in comparison of the chemical shifts at C-4 and C-6 of the dimethyl ether (**3**) of **1** with the shifts at those of its aglycone (**4**). This observation supports the *S*-configuration at C-5 of **1** and **2**.

Table 1. ^{13}C chemical shifts (δ_c) of **1**—**4** in C_5D_5N

Carbon No.	1	2	3	4
1	28.8	28.9	28.6	28.7
2	45.5	45.5	45.3	45.4
3	208.8	209.3	208.4	208.9
4	47.8	50.7	47.8	50.9
5	75.0	67.0	75.0	66.8
6	37.6	39.9	37.4	40.0
7	30.7	31.3	30.4	31.2
1′	131.6	131.8	133.3	133.5
1″	132.6	132.8	133.5	134.1
2′	129.5	129.5	129.4	129.4
2″	129.5	129.5	129.4	129.4
3′	115.7	115.8	113.8	114.0
3″	115.7	115.8	113.8	114.0
4′	156.3	156.6[a]	157.9	158.1
4″	156.3	156.4[a]	157.9	158.1
5′	115.7	115.8	113.8	114.0
5″	115.7	115.8	113.8	114.0
6′	129.5	129.5	129.4	129.4
6″	129.5	129.5	129.4	129.4
-OMe			54.9×2	54.9×2
Sugar moiety				
1	102.9		102.7	
2	74.4		74.4	
3	77.7[a]		77.5[a]	
4	71.2		71.0	
5	77.3[a]		77.0[a]	
6	62.3		62.3	

a) These values in any vertical column may be reversed although those given here are preferred.

Compound (**5**), 1,7-bis(4-hydroxyphenyl)-3-heptanol ($[\alpha]_D^{25}$ −8.3°±0.6°), was derived from **2** by conversion of the carbonyl group into the methylene. Thus, the configuration at C-3 of **5** should be *R*. This was supported by the fact that (*R*)-1,7-bis(3,4-dimethoxyphenyl)-3-heptanol (**6**) and (*R*)-1,7-diphenyl-3-heptanol (**7**) were all levorotatory. The physical (mp and $[\alpha]_D$) and spectral (UV, IR, ^{1}H NMR, and EI-MS) data of **5** were identical with those given for (−)-centrolobol,[2] except for the assignment of absolute configuration. Consequently, the *S*-configuration previously assigned to (−)-centrolobol[2] should be revised to the *R*-configuration.

Experimental

The ^{1}H NMR spectra were taken on Hitachi R-600 FT and R-24B NMR spectrometers using TMS as an internal standard. The ^{13}C NMR spectra were obtained on a Hitachi R-42 FT NMR spectrometer (22.6 MHz; δ_{TMS}=0). The EI-MS were obtained on a Shimadzu QP-1000 mass spectrometer at 70 eV. The FD-MS was taken on a JEOL JMS-D 300 mass spectrometer equipped with a silicone emitter; the emitter current was 0—25 mA. The optical rotations were measured on a JASCO DIP-360 Digital Polarimeter using 1-dm cell. Preparative TLC was carried out on a silica-gel plate (Merck 60 GF_{254}; 0.75 mm thick).

Isolation of Diarylheptanoid Glycoside (1). According to the method described in the literature,[1] the glycoside (**1**) (1.624 g) was isolated from the green bark (10.0 kg) of *B. platyphylla* var. *japonica* and it showed the following physical and spectral data: mp 62—64°C (an amorphous solid) (lit,[1] an amorphous solid,* mp 65°C); $[\alpha]_D^{25}$ −14.3°±0.1° (*c* 2.30, MeOH); UV (EtOH) 224 (log ε 4.15), 279 nm (3.54); IR (KBr) ν_{max} 3400 (OH), 1700 (C=O), 1612, 1592, 1515 cm^{-1} (aromatic ring); ^{1}H NMR (CD_3OD) δ=1.57—2.00 (2H, m, -CH_2-), 2.43—2.80 (8H, m, -CH_2-×4), 4.31 (1H, d, *J*=7 Hz, anomeric H), 6.59—7.06 (8H, AA'BB'-type, *J*=8 and 2 Hz, aromatic H); FD-MS *m/z* 499 (M^++Na), 477 (M^++H), 476 (M^+), 296 (M^+−180).

Hydrolysis of 1 with Taka-diastase. To a solution of **1** (191 mg) in H_2O (7.5 cm^3), Taka-diastase (Sankyo Co. Ltd.,[4] 600 mg) dissolved in H_2O (15 cm^3) and then toluene (0.5 cm^3) were added. The reaction mixture was incubated at 33°C for 2 d and extracted with *n*-BuOH. An extract, after removal of the solvent, was purified by preparative TLC with a MeOH-$CHCl_3$-H_2O (10:40:1 v/v) mixture to give 1,7-bis(4-hydroxyphenyl)-5-hydroxy-3-heptanone (**2**) (55 mg): mp 127—129°C (lit,[1] 125—127°C); $[\alpha]_D^{25}$ −1.8°±0.2° (*c* 1.02, MeOH); UV (EtOH) 225 (log ε 4.13), 279 nm (3.52); IR (KBr) ν_{max} 3450, 3340 (OH), 1692 cm^{-1} (C=O); ^{1}H NMR (CD_3OD) δ=3.99 (1H, quin, *J*=6 Hz, >C<u>H</u>OH); EI-MS *m/z* 314 (M^+), 296 (M^+-H_2O). The aqueous liquor obtained in the hydrolysis was lyophilized. A residual substance obtained was acetylated with acetic anhydride-pyridine to give penta-*O*-acetylglucopyranose, which was identified by co-TLC with an authentic sample.

Methylation of 1 and Hydrolysis of Its Dimethyl Ether (3). Methylation of **1** (1.114 g) in MeOH with CH_2N_2 at 0°C gave 1,7-bis(4-methoxyphenyl)-5-(β-D-glucopyranosyloxy)-3-heptanone (**3**) (380 mg): $[\alpha]_D^{25}$ −7.4°±0.1° (*c* 1.57, MeOH). Hydrolysis of **3** (145 mg) with Taka-diastase (900 mg) in the same way as in the case of **1** gave the aglycone (**4**) (26 mg): mp 77—78°C; $[\alpha]_D^{25}$ −7.6°±0.7° (*c* 0.28, MeOH); IR (KBr) ν_{max} 3420 (OH), 1700 cm^{-1} (C=O); ^{1}H NMR ($CDCl_3$) δ=3.77 (6H, s, -OCH_3×2), 4.03 (1H, quin, *J*=6 Hz, >C<u>H</u>OH).

Conversion of 2 to Diarylheptanol (5). Following the method described in the literature,[7] reduction of the carbonyl group of **2** (24 mg) with $TsNHNH_2$ (15 mg) and $NaBH_4$ (100 mg) in MeOH gave compound (**5**) (9 mg): mp 125—126°C (lit,[2] mp 128—130°C); $[\alpha]_D^{25}$ −8.3°±0.6° (*c* 0.34, MeOH); UV (MeOH) 224 (log ε 4.15), 279 (3.59), 285 nm (sh, 3.52); IR (KBr) ν_{max} 3545—3200 (OH), 1615, 1597, 1512 cm^{-1} (aromatic ring); ^{1}H NMR (($CD_3)_2CO$) δ=1.29—1.76 (8H, m, -CH_2-×4), 2.29—2.72 (4H, m, -CH_2-×2), 3.31 (1H, brs, OH), 3.52 (1H, m, >C<u>H</u>OH), 6.66—7.11 (8H, AA'BB'-type, *J*=8 and 2 Hz, aromatic H), 7.92 (2H, brs, Ar-OH×2); EI-MS *m/z* 300 (M^+), 282 (M^+-H_2O). Found: C, 76.11; H, 8.12%. Calcd for $C_{19}H_{24}O_3$: C, 75.97; H, 8.05%.

Preparation of Diarylheptanols (6 and 7). (*S*)-1,7-bis(3,4-Dimethoxyphenyl)-5-hydroxy-3-heptanone (**8**)[6] and (*S*)-1,7-diphenyl-5-hydroxy-3-heptanone (**9**)[8] were converted to their corresponding diarylheptanols (**6** and **7**) in the same way as in the case of **2**. The structures of **6** [mp 63—65°C; $[\alpha]_D^{25}$ −6.0°±2.0° (*c* 0.20, MeOH)] and **7** [mp 44—46°C; $[\alpha]_D^{25}$ −5.7°±2.9° (*c* 0.14, MeOH)] were confirmed by their IR, ^{1}H NMR, and EI-MS spectra.

*It is described[1] that recrystallization of this amorphous solid from EtOH-H_2O gave crystals with mp 189—190°C. However, our attempt at recrystallization failed.

The authors thank Professor Kazumasa Wakabayashi of Shinshu University for his kind arrangement to obtain the green bark of *B. platyphylla* var. *japonica*. They are also grateful to Dr. Teruo Yasui and Mr. Masaya Oka of Kuraray Co. Ltd. for measurement of the FD-MS spectrum.

References

1) M. Terazawa, T. Koga, H. Okuyama, and M. Miyake, *Mokuzai Gakkai Shi*, **30**, 391 (1984).
2) A. A. Craveiro, A. C. Prado, O. R. Gottlieb, and P. C. Welerson de Albuquerque, *Phytochemistry*, **9**, 1869 (1970).
3) J. H. Brewster, *J. Am. Chem. Soc.*, **81**, 5475 (1959).
4) M. Kimura, M. Tohma, I. Yoshizawa, and H. Akiyama, *Chem. Pharm. Bull.*, **16**, 25 (1968).
5) S. Seo, Y. Tomita, K. Tori, and Y. Yoshimura, *J. Am. Chem. Soc.*, **100**, 3331 (1978).
6) S. Ohta, T. Aoki, T. Hirata, and T. Suga, *J. Chem. Soc., Perkin Trans. 1*, **1984**, 1635.
7) L. Caglioti, *Tetrahedron*, **22**, 487 (1966).
8) T. Suga, S. Ohta, T. Aoki, and T. Hirata, *Bull. Chem. Soc. Jpn.*, **56**, 3353 (1983).

Palladium-catalyzed Ketone Synthesis from Acyl Chloride and Organoaluminum Reagents

Kuni WAKAMATSU, Yasuhiro OKUDA, Koichiro OSHIMA,* and Hitosi NOZAKI
Department of Industrial Chemistry, Faculty of Engineering, Kyoto University, Yoshida, Kyoto 606
(Received April 26, 1985)

Synopsis. The reaction of organoaluminum reagents with acyl chloride catalyzed by $Pd(PPh_3)_4$ in tetrahydrofuran provides ketones in fair yields.

During the past decade, a wide variety of organometallics are examined to react with acyl halides to give ketones. Among them, those containing Mg,[1] Mn,[2] Zn,[3] and Cu[4] have been widely used. The transformation of R^1COCl into R^1COR fails, however, by means of plain R_3Al, because they react easily with the resulting ketones. Several attempts have been made to overcome this difficulty. A ketone synthesis reported previously[5] is based on the organometallic reagent generated from trialkylaluminum, bis(acetylacetonato)-copper(II), and triphenylphosphine in 2:1:2 molar ratio. Here we wish to report another effective method for the preparation of ketones from acyl chlorides with organoaluminum reagents in the presence of Pd(0) catalyst.[6]

$$R^1COCl + R_3Al \xrightarrow[THF]{Pd(PPh_3)_4} R^1COR$$

Treatment of benzoyl chloride with triethylaluminum in tetrahydrofuran in the presence of a catalytic amount of $Pd(PPh_3)_4$ gave propiophenone in 70% yield. The uncatalyzed reaction gave <5% yield of propiophenone under the same reaction conditions. Palladium catalyst generated *in situ* from $Pd(OAc)_2$ and triphenylphosphine (1:2) was also efficient for the transformation.[7] Other catalysts such as $RuCl_2(PPh_3)_3$, $NiCl_2(PPh_3)_2$, and $RhCl(PPh_3)_3$ were not effective for this ketone synthesis. The use of tetrahydrofuran as a solvent is critical. In benzen or dichloromethane, the complex mixture was obtained since the resulting ketones were attacked by organoaluminum reagents. The results are summarized in Table 1. Alkynyl and alkenyl groups were introduced selectively in preference to the ubiquitous alkyl substituents on aluminum to give ynones and enones, respectively.

Experimental

The IR spectra were determined on a Shimadzu IR-27-G spectrometer; the mass spectra, on a Hitachi X-80 machine. The NMR spectra were recorded on a Varian EM-390H spectrometer, using TMS as an internal standard. The analyses were performed at the Elemental Analyses Center of Kyoto University. Tetrahydrofuran was dried in benzophenone ketyl and distilled. All the experiments were carried out under an argon atmosphere. Purification of the product was performed by preparative thin-layer chromatography (TLC) or column chromatography on silica gel

TABLE 1. PALLADIUM-CATALYZED ACYLATION OF ORGANOALUMINUM REAGENTS[a]

Entry	RCOCl	Reagent	Product	Yield[b] %
1	PhCOCl	Et_3Al	PhCOEt	70
2	PhCOCl	Me_3Al	PhCOMe	(74)[c]
3	PhCH=CHCOCl	Et_3Al	PhCH=CHCOEt	68
4	CH_2=CH$(CH_2)_8$COCl	Et_3Al	CH_2=CH$(CH_2)_8$COEt	71
5	CH_2=CH$(CH_2)_8$COCl	Me_3Al	CH_2=CH$(CH_2)_8$COMe	59
6	PhCOCl	$C_4H_9C{\equiv}CAlEt_2$	$C_4H_9C{\equiv}CCOPh$	67
7	$C_7H_{15}COCl$	$C_4H_9C{\equiv}CAlEt_2$	$C_4H_9C{\equiv}CCOC_7H_{15}$	65
8	PhCH=CHCOCl	$C_4H_9C{\equiv}CAlEt_2$	$C_4H_9C{\equiv}CCOCH{=}CHPh$	74
9	$C_7H_{15}COCl$	$PhC{\equiv}CAlEt_2$	$PhC{\equiv}CCOC_7H_{15}$	61
10	CH_2=CH$(CH_2)_8$COCl	$C_6H_{13}C{\equiv}CAlEt_2$	$C_6H_{13}C{\equiv}CCO(CH_2)_8CH{=}CH_2$	55
11	CH_2=CH$(CH_2)_8$COCl	$Me_3SiC{\equiv}CAlEt_2$	$Me_3SiC{\equiv}CCO(CH_2)_8CH{=}CH_2$	51
12	PhCOCl	C_4H_9, H, $SiMe_3$, Al^iBu_2	C_4H_9, H, $SiMe_3$, COPh	51
13	CH_2=CH$(CH_2)_8$COCl	C_6H_{13}, H, $SiMe_3$, Al^iBu_2	C_6H_{13}, H, $SiMe_3$, $CO(CH_2)_8CH{=}CH_2$	53

a) The reactions were performed in THF at 0—25 °C. Organoaluminum reagent (1.0—2.0 mmol), acid chloride (1.0 mmol), and $Pd(PPh_3)_4$ (0.05 mmol) were employed. b) Isolated yields unless otherwise stated. c) GLPC yield.

(Merck Kiesel gel 60).

General Procedure for the Preparation of Ketones with Trialkylaluminum: The reaction of benzoyl chloride with triethylaluminum is representative. Triethylaluminum (1.0 M† hexane solution, 2.0 ml, 2.0 mmol) was added to a tetrahydrofuran solution of benzoyl chloride (0.14 g, 1.0 mmol) and $Pd(PPh_3)_4$ (58 mg, 0.05 mmol) at 0 °C under an argon atomosphere. The whole was stirred at 25 °C for 4 h. The resulting mixture was poured into 1 M HCl and extracted with ethyl acetate. The combined organic layer was dried (Na_2SO_4) and concentrated *in vacuo*. Purification by preparative TLC on silica gel (hexane:ethyl acetate=10:1) gave propiophenone (90 mg, 70% yield) as an oil which was identical with the authentic sample.

1-Trimethylsilyl-12-tridecen-1-yn-3-one: Butyllithium (1.6 M hexane solution, 1.3 ml, 2.0 mmol) was added to a solution of trimethylsilylacetylene (0.25 g, 2.5 mmol) in hexane (2.0 ml) at 0 °C. After stirring for 15 min at 0 °C, diethylaluminum chloride (1.0 M hexane solution, 2.0 ml, 2.0 mmol) was added and the resulting mixture was stirred for 15 min at 0 °C. Tetrahydrofuran (3.0 ml), $Pd(PPh_3)_4$ (46 mg, 0.04 mmol), and 10-undecenoyl chloride (0.14 g, 0.7 mmol) were added successively and the whole was stirred for additional 60 min at 25 °C. Workup and purification by silica gel column chromatography gave the desired ketone in 51% yield: Bp 100 °C (bath temp, 2 Torr††); IR (neat) 3080, 2930, 2860, 2150, 2100, 1680, 1640, 1460, 1250, 850, 760 cm^{-1}; NMR (CCl_4) δ=0.25 (s, 9H), 1.08—1.77 (m, 12H), 1.77—2.13 (m, 2H), 2.27—2.57 (m, 2H), 4.83 (d, J=11 Hz, 1H), 4.87 (d, J=18 Hz, 1H), 5.67 (ddt, J=18, 11, 7.5 Hz, 1H). Found: m/z 249.1699. Calcd for $C_{15}H_{25}OSi$: M−CH_3, 249.1678.

18-Nonadecen-7-yn-9-one: Bp 115—120 °C (bath temp, 2 Torr); IR (neat) 3080, 2930, 2850, 2210, 1740, 1680, 1640, 1460, 1160, 1000, 910 cm^{-1}; NMR (CCl_4) δ=0.88 (m, 3H), 1.17—1.80 (m, 23H), 1.80—2.17 (m, 2H), 2.17—2.53 (m, 4H), 4.88 (d, J=12 Hz, 1H), 4.93 (d, J=18 Hz, 1H), 5.73 (ddt, J=18, 12, 7 Hz, 1H). Found: m/z 276.2444. Calcd for $C_{19}H_{32}O$: M, 276.2451.

(Z)-12-Trimethylsilyl-1,12-nonadecadien-11-one: Diisobutylaluminum hydride (1.5 M hexane solution, 1.3 ml, 2.0 mmol) was added to a solution of 1-trimethylsilyl-1-octyne (0.37 g, 2.0 mmol) in hexane (3.0 ml) and ether (1.5 ml) at 25 °C under an argon atmosphere.[8] After stirring for 40 min, tetrahydrofuran (4.0 ml) was added, then $Pd(PPh_3)_4$ (0.04 g, 0.05 mmol) and a solution of 10-undecenoyl chloride (0.14 g, 0.7 mmol) in tetrahydrofuran (3.0 ml) was added. The resulting mixture was stirred for 1.5 h. Workup (1 M HCl, ethyl acetate) and purification by preparative TLC on silica gel (hexane:ethyl acetate=10:1) provided the title compound (0.13 g, 53% yield) as an oil: Bp 115—120 °C (bath temp, 2 Torr); IR (neat) 3080, 2940, 2860, 1675, 1600, 1465, 1250, 850, 760 cm^{-1}; NMR (CCl_4) δ=0.01 (s, 9H), 0.68—0.93 (m, 3H), 0.97—1.67 (m, 20H), 1.70—2.43 (m, 6H), 4.70 (d, J=11 Hz, 1H), 4.75 (d, J=18 Hz, 1H), 5.55 (ddt, J=18, 11, 7 Hz, 1H), 6.5 (t, J=7.5 Hz, 1H). Found: C,75.28; H, 12.09%. Calcd for $C_{22}H_{42}OSi$: C, 75.36; H, 12.07%.

(Z)-1-Trimethylsilyl-1-hexenyl Phenyl Ketone: Bp 110 °C (bath temp, 2 Torr); IR (neat) 2960, 2860, 1655, 1600, 1450, 1250, 840, 710 cm^{-1}; NMR (CCl_4) δ=0.20 (s, 9H), 0.83—1.05 (m, 3H), 1.17—1.55 (m, 4H), 2.17—2.45 (m, 2H), 6.28 (t, J=7.5 Hz, 1H), 7.30—7.93 (m, 5H). Found: m/z 260.1602. Calcd for $C_{16}H_{24}OSi$: M, 260.1595.

References

1) D. A. Shirley, *Org. React.* **8**, 28 (1954); V. Fiandanese, G. Mardhese, V. Matina, and L. Ronzini, *Tetrahedron Lett.*, **25**, 4805 (1984).

2) G. Cahiez, D. Bernard, and J. F. Normant, *Synthesis*, **1977**, 130.

3) a) E. Negishi, V. Bagheri, S. Chatterjie, F-T. Luo, J. A. Miller, and T. Stoll, *Tetrahedron Lett.*, **24**, 5181 (1983); b) R. A. Grey, *J. Org. Chem.*, **49**, 2288 (1984).

4) G. H. Posner, C. E. Whitten, P. E. McFarland, *J. Am. Chem. Soc.*, **94**, 5106 (1972).

5) K. Takai, K. Oshima, and H. Nozaki, *Bull. Chem. Soc. Jpn.*, **54**, 1281 (1981).

6) Negishi has reported about palladium-catalyzed acylation of organoaluminum reagents briefly in the literature 3a. We wish to report here our independent work.

7) Palladium(II) acetate (23 mg, 0.1 mmol) and triphenylphosphine (50 mg, 0.2 mmol) were added to a solution of $^nC_4H_9C{\equiv}CAlEt_2$ (2.0 mmol) in tetrahydrofuran (5.0 ml). Then a solution of benzoyl chloride (0.14 g, 1.0 mmol) in tetrahydrofuran (2.0 ml) was added and the whole was stirred at 25 °C for 3 h. Purification of the product gave the corresponding ketone (0.1 g) in 52% yield. $PdCl_2(PPh_3)_2$ was catalytically as effective as $Pd(PPh_3)_4$.

8) K. Uchida, K. Utimoto, and H. Nozaki, *J. Org. Chem.*, **41**, 2215 (1976).

† 1 M=1 mol dm^{-3}.

†† 1 Torr=133.322 Pa.

New Crossed Aldol Reaction. Reaction of Enamines with Aldehydes Activated by Lewis Acids

Osamu TAKAZAWA,* Kunio KOGAMI, and Kazuo HAYASHI
Kawasaki Research Laboratories, T. Hasegawa Co., Ltd., 335 Kariyado, Nakahara-ku, Kawasaki 211
(Received February 20, 1985)

Synopsis. Enamines react with aldehydes in the presence of Lewis acids such as $BF_3 \cdot OEt_2$ to give the corresponding crossed aldol products in good yields. Reaction of dienamines with aldehydes gives the corresponding β,γ-unsaturated α-(1-hydroxyalkyl) carbonyl compounds.

The aldol reaction is one of the most versatile methods in organic synthesis.[1] In recent years, various useful direct aldol reactions have been reported, most of them being carried out under basic conditions;[2] Mukaiyama and coworkers[3] reported that enol silyl ethers, enol ethers, or enol esters react with carbonyl compounds in the presence of $TiCl_4$ under acidic conditions to give crossed aldol products.

Generally, it is known that the reaction of enamines with aldehydes gives α,β-unsaturated ketones, but that aldols cannot be obtained in this reaction except for some special substances such as chloral.[4] In contrast, we found that a use of Lewis acids allows enamines to react smoothly with aldehydes to give the corresponding aldols in good yields under acidic conditions, as with enol silyl ethers.

In our preceding papers,[5] we reported that enamines react with acetals or trialkyl orthoformates activated by Lewis acids to give the corresponding β-alkoxy or α-dialkoxymethyl carbonyl compounds, respectively. We considered that enamines also would react with aldehydes to afford the corresponding aldols. The reaction of 1-morpholino-1-cyclohexene (**1**) with benzaldehyde (**2**) was first tried. To a dichloromethane solution of a 1.2 molar amount of **2** was added a 1.3 molar amount of $BF_3 \cdot OEt_2$ at −40 °C. Then **1** was added and the reaction mixture was stirred for 0.5 h at room temperature. The aldol product, 2-(α-hydroxybenzyl)-1-cyclohexanone (**3**), was obtained in 92% yield.

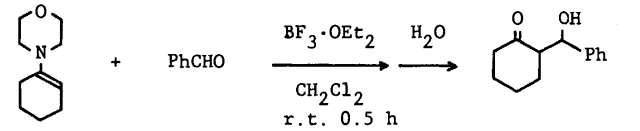

1 **2** **3** 92% (threo/erythro=78/22)

Scheme

The effect of the amount of $BF_3 \cdot OEt_2$ upon the yield of **3** was investigated by using the reaction between **1** and **2** under similar conditions as described above. It was found that the product **3** was obtained in the highest yield when a 1.3 molar amount of $BF_3 \cdot OEt_2$ was applied (Table 1).

TABLE 1. EFFECT OF THE AMOUNT OF $BF_3 \cdot OEt_2$ ON THE YIELD

Molar ratio of $BF_3 \cdot OEt_2$	0.1	0.5	1.0	1.3	2.0
Yield[a] of **3**/%	12	32	78	92	87
threo/erythro	100/0	82/18	73/27	78/22	68/32

a) Isolated yield.

TABLE 2. REACTION OF THE ENAMINE **1** WITH BENZALDEHYDE **2** IN THE PRESENCE OF VARIOUS LEWIS ACIDS

Lewis acid	Reaction conditions Temp/°C	Time/h	Yield[a] of **3** %	threo/erythro
$BF_3 \cdot OEt_2$	r.t.	0.5	92	78/22
$TiCl_4$	r.t.	0.5	83	70/30
$AlCl_3$	r.t.	1	75	92/8
$SnCl_4$	r.t.	0.5	68	75/25
$FeCl_3$	r.t.	5	35	94/6
$ZnCl_2$	r.t.	5	19	100/0
$MgCl_2$	r.t.	5	0	—
LiCl	r.t.	5	0	—

a) Isolated yield.

TABLE 3. EFFECT OF THE STRUCTURE OF THE AMINE MOIETY IN THE ENAMINES

Enamine	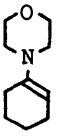 **1**	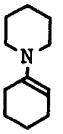 **4**	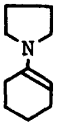 **5**
Yield[a] of **3**/%	92	17	0
threo/erythro	78/22	93/7	—

a) Isolated yield.

TABLE 4. SYNTHESIS OF ALDOLS FROM ENAMINES AND ALDEHYDES IN THE PRESENCE OF $BF_3 \cdot OEt_2$

Enamine	Aldehyde	Product	Yield[a] %	(threo/erythro)
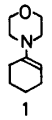 **1**		**8**	85	
	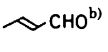 [b]	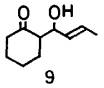 **9**	63	(78/22)
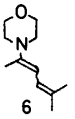 **6**	PhCHO	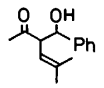 **10**	60	(33/67)
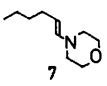 **7**		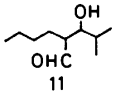 **11**	72	
	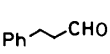	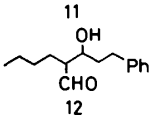 **12**	70	

a) Isolated yield. b) $BF_3 \cdot OEt_2$ was added to a mixture of **1** and crotonaldehyde.

In order to investigate the effect of Lewis acids, reactions of **1** with **2** in the presence of various Lewis acids were then tried according to the procedure

Table 5. Physical properties and analytical data of the aldols

Product	IR	NMR	Found (Calcd)/%	
	cm^{-1}	$\delta(CDCl_3)$ J/Hz	C	H
3, threo	3520	1.1—2.9 (9H, m), 3.95 (1H, s), 4.75 (1H, d, J=9.0),		
	1698	7.26 (5H, s).		
erythro	3550	1.1—2.7 (9H, m), 3.05 (1H, s), 5.37 (1H, d, J=2.5),		
	1698	7.26 (5H, s).		
8	3550	0.88 (3H, d, J=6.0), 1.00 (3H, d, J=6.0),		
	1700	1.2—2.7 (10H, m), 3.30 (1H, s), 3.50 (1H, m).		
9, threo	3450	1.2—2.6 (9H, m), 1.68 (3H, d, J=5.5), 3.55 (1H, s),	71.22	9.68
	1710	4.17 (1H, t, J=7.0), 5.17—6.0 (2H, m).	(71.39)	(9.59)
	965			
erythro	3470	1.2—2.7 (9H, m), 1.68 (3H, d, J=5.5), 3.05 (1H, s),	71.18	9.65
	1705	4.45 (1H, m), 5.25—6.0 (2H, m).	(71.39)	(9.59)
	970			
10, threo	3430	1.32 (3H, d, J=1.5), 1.58 (3H, d, J=1.5), 2.13 (3H, s),	76.91	8.28
	1710	3.28 (1H, broad s), 3.63 (1H, dd, J=10.0 and 8.6),	(77.03)	(8.31)
		4.85 (2H, m), 7.23 (5H, s).		
erythro	3470	1.42 (3H, d, J=1.5), 1.71 (3H, s), 1.98 (3H, s),	76.82	8.25
	1705	3.32 (1H, broad s), 3.58 (1H, dd, J=10.0 and 5.0),	(77.03)	(8.31)
		5.05 (1H, d, J=5.0), 5.27 (1H, d, J=10.0), 7.23 (5H, s).		
11	3430	0.7—2.1 (16H, m), 2.47 (1H, m), 3.07 (1H, broad s),	69.97	11.81
	1720	3.62 (1H, m), 9.73 (1H, m).	(69.72)	(11.70)
12	3320	0.90 (3H, t, J=5.5), 1.1—2.1 (8H, m), 2.33 (2H, m),	76.95	9.41
	1720	2.80 (2H, m), 3.92 (1H, m), 7.22 (5H, s), 9.75 (1H, m).	(76.88)	(9.46)

mentioned above (Table 2). The results described in Table 2 demonstrate that, of the Lewis acids examined, $BF_3 \cdot OEt_2$ exhibits a remarkable effect as compared with the others in respect of the yield of **3**. It is noteworthy that the reaction gave predominantly the *threo*-isomer when $AlCl_3$, $FeCl_3$, or $ZnCl_2$ was used.

Furthermore, the effect of the structure of the amine moiety in the enamines was studied by treating enamines with **2** and $BF_3 \cdot OEt_2$. It was found that **1** realizes an excellent yield (Table 3).

Since it was noted that the combination of morpholine enamine (**1**) and $BF_3 \cdot OEt_2$ is significantly better than other possible combinations (Tables 2 and 3), reactions of morpholine enamines, such as **1**, 2-methyl-5-morpholino-2,4-hexadiene (**6**), or 1-morpholino-1-hexene (**7**), with various aldehydes were tried in the presence of $BF_3 \cdot OEt_2$, and the corresponding aldols were obtained in good yields as shown in Table 4.

In the present reaction, the reverse reaction or the dehydration of aldol would be impossible because of the formation of a stable iminium salt as an intermediate. Furthermore, the acidic reaction medium makes the method useful for compounds that have base-sensitive functional groups. On the other hand, it is known that the reaction of dienoxysilanes with aldehydes in the presence of $TiCl_4$ gives α,β-unsaturated γ-(1-hydroxyalkyl) carbonyl compounds.[3g,6] In contrast to this reaction, the present reaction of a dienamine **6** with **2** in the presence of $BF_3 \cdot OEt_2$ regioselectively afforded β,γ-unsaturated α-(1-hydroxyalkyl) carbonyl compound **10**.

Experimental

Reaction of 1-Morpholino-1-cyclohexene (1) with Benzaldehyde (2) in the Presence of $BF_3 \cdot OEt_2$. To a dichloromethane (20 ml) solution of 1.27 g (12 mmol) of **2** was added 1.85 g (13 mmol) of $BF_3 \cdot OEt_2$ at −40 °C under an argon atmosphere. Then 1.67 g (10 mmol) of **1** was added immediately and the reaction mixture was stirred for 0.5 h at room temperature. The mixture was quenched with water and stirred for 1 h at room temperature. After hydrolysis, the organic layer was separated, washed with a saturated solution of $NaHCO_3$, and dried over $MgSO_4$. After removal of the solvent, the residue was purified by silica-gel column chromatography. Elution with hexane–ether afforded 0.418 g (20%) of *erythro*-2-(α-hydroxybenzyl)-1-cyclohexanone (**3**) and 1.46 g (72%) of *threo*-**3**.

Reactions of a variety of enamines with various aldehydes in the presence of Lewis acids were carried out according to the same procedure, and the yields of the corresponding aldols are listed in Tables 1, 2, 3, and 4. The physical properties and analytical data of the products are shown in Table 5.

The authors wish to express their thanks to Professor Teruaki Mukaiyama, The University of Tokyo for his helpful discussions.

References

1) a) A. T. Nielsen and W. H. Houlihan, *Org. React.*, **16**, 1 (1968); b) H. O. House, "Modern Synthetic Reaction," 2nd ed by W. A. Benjamin, Menlo Park, Calif. (1972) pp. 629—682.

2) T. Mukaiyama, *Org. React.*, **28**, 203 (1982).

3) a) T. Mukaiyama, K. Narasaka, and K. Banno, *Chem. Lett.*, **1973**, 1011; b) T. Mukaiyama, K. Banno, and K. Narasaka, *J. Am. Chem. Soc.*, **96**, 7503 (1974); c) T. Mukaiyama, T. Izawa, and K. Saigo, *Chem. Lett.*, **1974**, 323; d) K. Banno and T. Mukaiyama, *ibid.*, **1975**, 741; e) E. Kitazawa, T. Imamura, K. Saigo, and T. Mukaiyama, *ibid.*, **1975**, 569; f) K. Saigo, M. Osaki, and T. Mukaiyama, *ibid.*, **1975**, 989; g) T. Mukaiyama, *Angew. Chem., Int. Ed. Engl.*, **16**, 817 (1977).

4) a) A. G. Cook, "Enamines," Marcel Dekker, New York (1969) pp. 156, 377; b) P. W. Hickmott, *Tetrahedron*, **38**, 1975, 3363 (1982).

5) a) O. Takazawa and T. Mukaiyama, *Chem. Lett.*, **1982**, 1307; b) O. Takazawa, K. Kogami, and K. Hayashi, *Bull. Chem. Soc. Jpn.*, **57**, 1876 (1984).

6) a) T. Mukaiyama and A. Ishida, *Chem. Lett.*, **1975**, 319, 1201; b) M. Asaoka, N. Sugimura, and H. Takei, *Bull. Chem. Soc. Jpn.*, **52**, 1953 (1979); c) I. Fleming, J. Goldhill, and I. Paterson, *Tetrahedron Lett.*, **1979**, 3205, 3209.

A Facile One-pot Synthesis of Sulfides from Alkyl Halides and Alcohols Using Tetramethylthiourea

Shizuo FUJISAKI, Isamu FUJIWARA, Yasumasa NORISUE, and Shoji KAJIGAESHI*
Department of Industrial Chemistry, Faculty of Engineering, Yamaguchi University, Tokiwadai, Ube 755
(Received February 23, 1985)

Synopsis. Sulfides can be readily prepared under mild conditions by a reaction of tetramethylthiourea with alkyl halides and alcohols in the presence of sodium hydride in satisfactory yields. The scope and limitation of this method are also presented.

The reaction of alkyl halides with Na_2S, leading to symmetrical sulfides, is well known. And, unsymmetrical sulfides are widely synthesized by neucleophilic substitution reaction of alkyl and aryl halides with thiols under basic conditions.[1] Recently, some convenient methods for the preparation of sulfides by the reaction of 2-alkylthio-1,3-benzoxazoles with sodium alkoxide,[2] and 2-alkoxy-1-methylpyridinium salt with thiol in the presence of triethylamine,[3] have been reported.

In the course of our investigation of the reaction of thiocarbamoyl derivatives, we have now found a convenient one-pot preparative method of sulfides (**2**) under mild conditions from alkyl halides and alcohols using tetramethylthiourea (**1**) as starting material which is easily available.

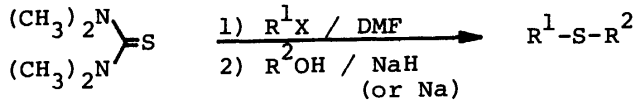

1 **2**

Results and Discussion

The reaction of **1** with alkyl halides in *N,N*-dimethylformamide (or acetonitrile) for 1 h followed by treatment of alcohols in the presence of sodium hydride for 10 min at room temperature gave readily dialkyl sulfides (**2**) in satisfactory yields.

In the case of synthesis of methyl or ethyl sulfide (R^1SCH_3 or $R^2SC_2H_5$), the reagent methanol or ethanol was employed also as a solvent instead of *N,N*-dimethylformamide or acetonitrile, and sodium metal was used instead of sodium hydride. The results are summarized in the Table 1.

The postulated reaction mechanism is shown in the Scheme. Actually, intermediate *S*-alkyltetramethylthiouronium salt (**3**) was obtained as a crystals by the treatment of **1** with alkyl halide in acetone at room temperature for several days in good yield, and then the reaction of **3** with alcohol using sodium hydride in *N,N*-dimethylformamide gave the sulfide **2**. In this reaction, unstable *O*-alkyltetramethyluronium salt (**5**), derived from **3** *via* intermediate **4**, may be undergone nucleophilic attack by alkanethiolate ion to give sulfide **2** and tetramethylurea (**6**).

TABLE 1. SULFIDES (**2**) FROM TETRAMETHYLTHIOUREA, ALKYL HALIDES AND ALCOHOLS USING BASE

R^1-S-R^2	R^1X	R^2OH	Solvent	Base	Yield[a] %	Bp θ_b/°C(Torr) or Mp θ_m/°C	Lit Bp θ_b/°C(Torr) or Mp θ_m/°C
2a CH_3S-*n*-C_8H_{17}	CH_3I	*n*-$C_8H_{17}OH$	CH_3CN	NaH	45	219—221(760)	104—105(20)[4]
2b C_2H_5S-*n*-C_8H_{17}	C_2H_5Br	*n*-$C_8H_{17}OH$	CH_3CN	NaH	40	228—230(760)	108(16)[4]
2c CH_3SCH_2Ph	CH_3I	$PhCH_2OH$	DMF	NaH	65	199—201(760)	195—198(760)[6]
2d $C_2H_5SCH_2Ph$	C_2H_5I	$PhCH_2OH$	DMF	NaH	76	223—224(760)	103(16)[4]
2e $(PhCH_2)_2S$	$PhCH_2Br$	$PhCH_2OH$	CH_3CN	NaH	90	44—45	47[2]
2f 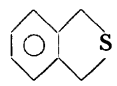	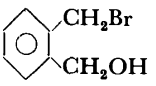		DMF	NaH	65	233—234(760)	94(7)[2]
2g $PhCH_2CH_2SC_2H_5$	$PhCH_2CH_2Br$	C_2H_5OH	DMF	NaH	60	258—260(760)	93—94(5)[2]
2h $PhCH_2SCH_2CH{=}CH_2$	$CH_2{=}CH$-CH_2Br	$PhCH_2OH$	DMF	NaH	76	79—80(6)	—
2i $(CH_2{=}CHCH_2)_2S$	$CH_2{=}CH$-CH_2Br	$CH_2{=}CHCH_2OH$	DMF	NaH	50	27—28(4)	35(6)[5]
2j 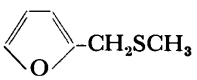	CH_3I	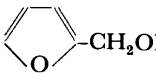	DMF	NaH	56	41—42(7)	—
2c CH_3SCH_2Ph	$PhCH_2Cl$	CH_3OH	CH_3OH	$NaOCH_3$	65	199—201(760)	195—198(760)[6]
2d $C_2H_5SCH_2Ph$	$PhCH_2Cl$	C_2H_5OH	C_2H_5OH	$NaOC_2H_5$	63	223—224(760)	103(16)[4]

a) Yield of isolated product.

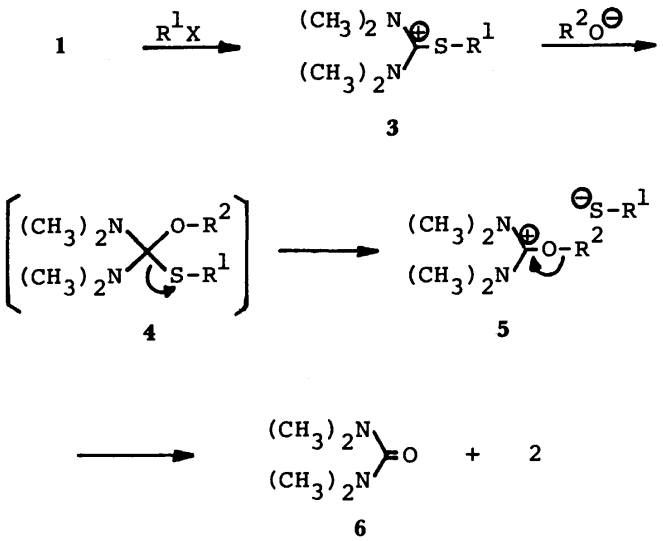

Scheme

These our methods do not use ill-smelling thiols and are applicable to the syntheses of various dialkyl sulfides under mild conditions. Dialkyl sulfides containing heterocyclic moiety, *e.g.*, furfuryl methyl sulfide (**2j**), was also obtained. However, our methods were unsuitable for the syntheses of aryl sulfides and dialkyl sulfides having branched-chain alkyl moiety such as *t*-butyl or isopropyl group because of instability of crowded intermediate **4**. Thiourea could not be used as the reagent instead of tetramethylthiourea since inert imines ($HN{=}C(NH_2){-}SR$) was only obtained from thiourea with alkyl halides.

Experimental

*Typical Procedure for the Syntheses of Sulfides (**2a—2j**) by Use of Sodium Hydride in* N,N-*Dimethylformamide or Acetonitrile. Benzyl Methyl Sulfide (**2c**)*: A solution of **1** (1.0 g, 7.6 mmol) and methyl iodide (1.4 g, 10 mmol) in *N,N*-dimethylformamide (10 ml) was stirred at room temperature for 1 h, and then benzyl alcohol (0.84 g, 7.8 mmol) was added. To the solution was added dropwise sodium hydride (0.5 g, 21 mmol) dispersed in hexane (5 ml) under stirring at room temperature, then the reaction mixture was further stirred for 10 min, and quenched with water. The organic layer was extracted with hexane (3×15 ml), dried with magnesium sulfate, concentrated in a rotatory evaporator and distilled to give benzyl methyl sulfide (**2c**) as colorless oil. Yield 0.68 g (65%); bp 199—201 °C/760 Torr[†] (lit,[6] 195—198 °C/760 Torr).

*Allyl Benzyl Sulfide (**2h**).* Compound **2h** was prepared similarly. ^{1}H NMR (CCl_4) δ=2.92 (2H, d, J=8 Hz, SCH_2-CH=), 3.56 (2H, s, Ph-CH_2S), 5.00, 5.05 (two br. d, J=18 Hz, J=9 Hz, CH=CH_2), 5.50—6.00 (1H, m, CH=CH_2), and 7.22 (5H, br. s, C_6H_5). Found: C, 72.86; H, 7.44%. Calcd for $C_{10}H_{12}S$: C, 73.12; H, 7.36%.

*2-Furfuryl Methyl Sulfide (**2j**).* Compound **2j** was prepared similarly. ^{1}H NMR (CCl_4) δ=2.01 (3H, s, CH_3), 3.55 (2H, s, CH_2), 6.02 (1H, d, J=3 Hz, CH=C-O), 6.16 (1H, dd, J=3 and 2 Hz, CH=CH-O), 7.20 (1H, d, J=2 Hz, =CH-O). Found: C, 56.02; H, 6.39%. Calcd for C_6H_8OS: C, 56.22; H, 6.29%.

*Typical Procedure for the Syntheses of Sulfides (**2c** and **2d**) by Use of Sodium Alkoxide in Alcohol. Benzyl Ethyl Sulfide (**2d**).* A solution of **1** (1.5 g, 11 mmol) and benzyl chloride (1.4 g, 11.1 mmol) in ethanol (10 ml) was refluxed for 4 h. After cooling the solution to room temperature, sodium metal (0.3 g, 13 mmol) was added and the reaction mixture was stirred for 10 min, and then quenched with water. The mixture obtained was worked up as described above **2c** to give **2d** as colorless oil. Yield 1.1 g (63%); bp 223—224 °C/760 Torr (lit,[4] bp 103 °C/16 Torr).

*S-Methyl Tetramethylthiouronium Iodide (**3a**).* Preparation of **3a** was described below as an example of synthetic procedure of **3**. A solution of **1** (4.0 g, 30 mmol) and methyl iodide (4.6 g, 32 mmol) in acetone (50 ml) was allowed to stand for 1 d at room temperature, and then the precipitate deposited was filtered off, washed with acetone (2×5 ml) and dried *in vacuo* to give **3a** as colorless crystals. Yield 7.9 g (96%); mp 177—180 °C (Mp was not given in the literature[7] because of its hygroscopicity).

*Benzyl Methyl Sulfide (**2c**) from **3a** and Benzyl Alcohol.* Preparation of **2c** was described below as an example of synthetic procedure of **2** from **3** and alcohol. To a solution of **3a** (1.0 g, 3.7 mmol) and benzyl alcohol (0.34 g, 3.7 mmol) in *N,N*-dimethylformamide (10 ml) was added dropwise sodium hydride (0.5 g, 21 mmol) dispersed in hexane (5 ml), and then the reaction mixture was stirred at room temperature for 10 min, and quenched with water. The organic layer was extracted with hexane (3×15 ml), dried with magnesium sulfate, concentrated in a rotatory evaporator and distilled to give **2c** as colorless oil. Yield 0.3 g (60%); bp 199—201 °C/760 Torr.

[†]1 Torr=133.322 Pa.

References

1) G. C. Barrett, "Comprehensive Organic Chemistry," ed by D. N. Jones, Pergamon Press, Oxford (1979), Vol. 3, pp. 36—53; and references therein.

2) M. Yamato, Y. Takeuchi, K. Hattori, and K. Hashigaki, *Synthesis*, **1982**, 1014.

3) T. Mukaiyama, S. Ikeda, and S. Kobayashi, *Chem. Lett.*, **1975**, 1159.

4) I. Degani, R. Fochi, and V. Regondi, *Synthesis*, **1979**, 178.

5) Yu. O. Gabel' and L. F. Shepeier, *Zh. Obshch. Khim.*, **21**, 1649 (1951); *Chem. Abstr.*, **46**, 4471 (1952).

6) J. Obermeyer, *Ber.*, **20**, 2926 (1887).

7) Y. Kondo, S. Hirano, and N. Tokura, *J. Chem. Soc., Perkin Trans. 2*, **1979**, 1738.

Rates of Thermal Decomposition of *t*-Butyl Peroxypivalate

Takeshi KOMAI,* Hideyo ISHIGAKI, and Kazuo MATSUYAMA
Chemicals and Explosives Research Laboratory, Nippon Oil & Fats Co., Ltd., Taketoyo, Chita-gun, Aichi 470-23
(Received February 25, 1985)

Synopsis. The kinetics of decomposition of *t*-butyl peroxypivalate in benzene, hexane and mineral spirits were determined iodometrically in the temperature range 50—75°. The decomposition in benzene indicated smaller rate constants and activation parameters than those in hexane or mineral spirits. The solvated transition state in aromatic solvent is discussed on the basis of these results and the previously published data.

The rate constants of decomposition of *t*-butyl peroxypivalate which decomposes with a concerted mechanism have been used as standard of those of other peroxyesters.[1)]

$$(CH_3)_3CC(=O)\text{-}OO\text{-}C(CH_3)_3 \longrightarrow (CH_3)_3C\cdot + CO_2 + \cdot OC(CH_3)_3 \quad (1)$$

However, different values of the activation parameter in the decomposition have been reported by several investigators.[2)] For instance, Lorand and coworkers[2a)] obtained $\Delta H^{\ddagger}=115\,kJ\,mol^{-1}$ and $\Delta S^{\ddagger}=15\,JK^{-1}mol^{-1}$ in cumene, but Fort and Franklin[2b)] reported $\Delta H^{\ddagger}=107\,kJ\,mol^{-1}$ and $\Delta S^{\ddagger}=-11\,JK^{-1}mol^{-1}$ in the same solvent. These conflicting values give rise to some difficulty on studying the decomposition mechanism of peroxyesters.

We measured the rates of the decomposition of *t*-butyl peroxypivalate in benzene, hexane and mineral spirits, and also reevaluated the previously published data.

TABLE 1. RATES OF DECOMPOSITION OF *t*-BUTYL PEROXYPIVALATE

Initial concentration M†	Temperature °C	Rate constant $k\times10^5/s^{-1}$
Solvent: Benzene		
0.10	50	1.03
0.10	55	1.94
0.10	60	3.92
0.21	60	3.89
0.10	65	7.31
0.20	65	7.19
0.10	70	13.0
Solvent: Hexane		
0.10	55	0.842
0.10	60	1.59
0.10	65	3.39
0.10	70	6.19
Solvent: Mineral spirits		
0.10	55	1.01
0.10	60	2.15
0.10	65	4.14
0.10	70	7.58
0.10	75	14.7

† 1M=1 mol dm^{-3}.

Results and Discussion

The rates of the decomposition of *t*-butyl peroxypivalate were determined by following the disappearance of the peroxide with iodometric titration. The results yielded good first order kinetics and were independent of initial peroxide concentration. These ruled

TABLE 2. ACTIVATION PARAMETERS FOR THE DECOMPOSITION OF *t*-BUTYL PEROXYPIVALATE

Solvent	$\Delta H^{\ddagger}$ kJ mol^{-1}	$\Delta S^{\ddagger}$ JK^{-1}mol^{-1}	$k\times10^5$at 60°C/s^{-1}	Rel. rate at 60°C
Hexane	125±3	40± 8	1.59	1.0
Mineral spirits	123±4	33±11	2.15	1.4
Cyclohexane[a)]	123±6	33±17	2.06	1.3
Cumene[b)]	118±1	23±10	2.95	1.6
Benzene	115±1	14± 3	3.82	2.1

a) See Ref. 2a. b) Reevaluated from published data (See Fig. 1.).

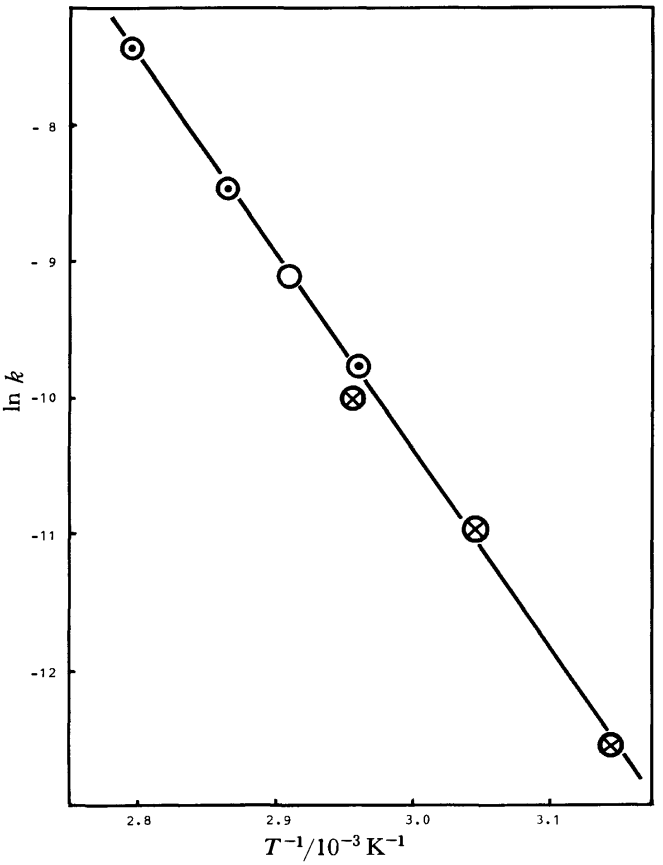

Fig. 1. Arrhenius plot of published data on thermal decomposition of *t*-butyl peroxypivalate in cumene: (⊙) data points of Lorand *et al.*[2a)] (○) data points of Fort *et al.*[2b)] (○) data point of Ernst *et al.*[2c)]

out radical induced decomposition under our experimental conditions. Table 1 shows the obtained data. The activation parameters were calculated from the data of the table and given in Table 2.

We also reevaluated the decomposition rates in cumene using the early published data. The data were plotted in Fig. 1 and the activation parameters were recalculated to be also shown in Table 2. A remarkable good Arrhenius plot in the figure shows that the differences between the activation parameters in each report are due to small systematic errors occurring within each set of experiments.

The rates of homolytic decomposition of *t*-butyl peroxypivalate were affected by solvents. It decomposes about twice faster in polarizable solvents such as benzene and cumene than aliphatic hydrocarbons having low polarizability. This could be explained by strong interactions of the aromatic solvent with *t*-butyl peroxypivalate at the transition state.[3] The observed decreases of the $\Delta H^{\ddagger}$ and $\Delta S^{\ddagger}$ in the aromatic solvents relative to those in the aliphatic hydrocarbons support this solvated transition state. Similar results have been reported in the thermal decomposition of diacyl peroxides,[4] di-*t*-butyl peroxide and *t*-butyl α-(*p*-substituted phenyl) peroxyisobutyrate.[6]

Experimental

t-Butyl peroxypivalate, benzene, hexane and mineral spirits were commercial materials. The rates of decomposition were measured by monitoring the undecomposed peroxyester with iodometric titration. A weighed amount of the peroxyester solution was added to glacial acetic acid solution containing saturated aquous sodium iodide solution and a small amount of iron(III) chloride, and allowed to stand at room temperature for 15 min. Then the iodide liberated was titrated with aquous sodium thiosulfate solution.

References

1) P. D. Bartlett and D. M. Simons, *J. Am. Chem. Soc.*, **82**, 1753 (1960).

2) a) J. P. Lorand, S. D. Chadroff, and R. W. Wallace, *J. Am. Chem. Soc.*, **90**, 5266 (1968); b) R. C. Fort, Jr. and R. E. Franklin, *J. Am. Chem. Soc.*, **90**, 5267 (1968); c) J. A. Ernst, C. Thankachan, and T. T. Tidwell, *J. Org. Chem.*, **39**, 3614 (1974); d) D. D. Tanner, H. Yabuuchi, and H. Lutzer, *Can. J. Chem.*, **55**, 617 (1977).

3) One possibility which is considered as the interactions is an electron transfer from the solvent to the peroxide such as:

$$[(CH_3)_3C\cdot CO_2 : OC(CH_3)_3]^-[\langle\odot\rangle]^+$$

4) a) R. C. Lamb, L. L. Vestal, G. R. Cipau, and S. Debnath, *J. Org. Chem.*, **39**, 2096 (1974); b) J. Koo and G. B. Schuster, *J. Am. Chem. Soc.*, **99**, 6107 (1977).

5) E. S. Huyser and R. M. VanScoy, *J. Org. Chem.*, **33**, 3524 (1968).

6) J. P. Engstrom and J. C. DuBose, *J. Org. Chem.*, **38**, 3817 (1973).

Charge-transfer Complexes of 11,11,12,12-Tetracyanoanthraquinodimethans with Various Donors

Toshio MUKAI,* Takanori SUZUKI, and Yoshiro YAMASHITA
Department of Chemistry, Faculty of Science, Tohoku University, Aramaki, Sendai 980
(Received February 27, 1985)

Synopsis. Titled compounds were found to form charge-transfer (CT) complexes with aromatic hydrocarbons or tetrathiafulvalene (TTF) and the molecular complexes could be isolated.

Since the high electrical conductivity was discovered in the charge-transfer (CT) complex of tetracyanoquinodimethan (TCNQ) and tetrathiafulvalene (TTF),[1] much attention has been paid to CT complexes of electron donors and acceptors such as tetracyano-1,4-naphthoquinodimethan (TCNNQ).[2,3] Recently four groups found facile synthetic methods of 11,11,12,12-tetracyanoanthraquinodimethan (TCNAQ) and its derivatives [4-7] which are dibenzo analogues of TCNQ and promising electron acceptors to form conductive complexes. However, it was reported that TCNAQ failed to form charge-transfer complexes because it is nonplanar due to a steric hindrance between the dicyanomethylene and the hydrogens at C_1, C_4, C_5, and C_8-positions.[5,8] As the first example we report here CT complexes of TCNAQs with various donors.

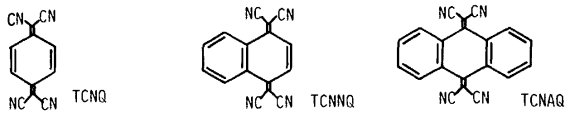

Scheme 1.

When naphthalene, phenanthrene, fluorene, and chrysene were used as donors, only shoulders or end absorptions due to the CT transition were observed. When pyrene, anthracene, perylene, and TTF were used as donors, however, the CT absorption maxima could be observed in the longer wavelength region since they have lower oxidation potentials.[9] These data are summarized in Table 1 together with reduction potentials. Linear correlation is observed between the CT transition energies and reduction potentials except for 1-chloro derivative **1d**, confirming that the absorptions are assigned to the CT transition. The deviation of **1d** from the line can be explained in terms of the larger steric hindrance of the substituent.[7]

In addition to the formation of the CT complexes in solution as described above, TCNAQs were found to form stable molecular complexes in solid state. They were obtained by dissolving TCNAQs and excess donors in dichloromethane. The melting points and colors of the complexes are shown in Table 2. According to elemental analyses, the mole ratio of acceptor to donor was determined to be 1:1 for benzene and diaminodurene, while that for naphthalene, anthracene, phenanthrene, pyrene, and TTF was 2:1. X-Ray analyses of **1e**-benzene complex and **1e**-pyrene complex also support that they are a 1:1 complex and a 2:1 complex, respectively.[10] This ratio is different from that of TCNNQ which is 1:2 for anthracene, phenanthrene, and pyrene.[2] This result may be attributed to the difference of the molecular sizes. Another interesting feature in the formation of the molecular complexes is that TCNAQs form complexes with benzene, while there is no report on the formation of the molecular complexes of TCNQ and TCNNQ with benzene. It should be noted that TCNAQs favorably form molecular complexes in spite of their nonplanar structures. Electical resistivities of complexes of TCNAQs **1b**, e, f, **g** with TTF show that they are insulators.[11] The high resistivities are mainly attributed to the nonplanar structures of TCNAQs.

Experimental

Materials. TCNAQ **1a** and substituted TCNAQs **1b—k** were prepared by our method[7] or Hünig's method.[4] Donors which were commercially available were purified by recrystallization or column chromatography.

Spectra. UV spectra were measured using a Hitachi 340 spectrophotometer. The charge-transfer maxima were measured at room temperature in spectrophotometric grade dichloromethane. The concentration of TCNAQs was ad-

TABLE 1. CHARGE TRANSFER BAND MAXIMA OF TCNAQs WITH DONORS IN CH_2Cl_2[a] AND REDUCTION POTENTIALS

TCNAQ		$E^{red}_{1/2}/V$[b]	Pyrene	Anthracene λmax/nm	Perylene[c]	TTF
H[d]	**1a**	−0.37	470[sh]	486	540	770
2-CH_3[d]	**1b**	−0.38	470[sh]	480	529	690
2-C_2H_5	**1c**	−0.39	470[sh]	478	534	685
1-Cl	**1d**	−0.41	470[sh]	486	540[sh]	700
2-Cl	**1e**	−0.32	490	508	578	740
2-CO_2CH_3	**1f**	−0.31	495	510	594	750
2-CN	**1g**	−0.27	518	532	607	800
2-NO_2	**1h**	−0.24	530	544	630	820
2-$NHCOCH_3$	**1i**	−0.38	495	495	—[e]	690
2-NH_2	**1j**	−0.43	—[e]	—[e]	—[e]	—[e]
2-$N(CH_3)_2$	**1k**	−0.44	—[e]	—[e]	—[e]	—[e]

a) TCNAQs; 6.67×10^{-3} mol dm^{-3}, Donors; 6.67×10^{-2} mol dm^{-3}. b) Ref.7. c) Saturated solution of perylene used; 1.66×10^{-2} mol dm^{-3}. d) Ref. 4. e) No absorption maxima is observed.

TABLE 2. MELTING POINTS AND COLORS OF THE MOLECULAR COMPLEXES

TCNAQ		Mp θ_m/°C (Color)						
		Benzene	Naphthalene	Anthracene	Phenanthrene	Pyrene	TTF	Diaminodurene
H	**1a**	—[a]	—[a]	—[a]	—[a]	—[a]	—[a]	165—300(decomp) (green)
2-CH_3	**1b**	90—95(decomp) (yellow)	—[a]	—[a]	250—255 (orange)	226—227 (red)	200—280 (decomp) (green)	185—188(decomp) (green)
1-Cl	**1d**	—[a]	—[a]	—[a]	—[a]	160(decomp) (red)	—[a]	—[a]
2-Cl	**1e**	110—120(decomp) (yellow)	160—180 (decomp) (yellow)	224—225 (violet)	220—221 (orange)	239—240 (violet)	222—224 (decomp) (green)	198—200(decomp) (green)
2-CO_2Me	**1f**	—[a]	—[a]	—[a]	—[a]	160—240 (decomp) (violet)	247—251 (decomp) (indigo)	138—191(decomp) (green)
2-CN	**1g**	140—150(decomp) (yellow)	160(decomp) (orange)	245—250 (violet)	240—241 (orange)	271—272 (violet)	239—242 (decomp) (green)	188—191(decomp) (green)
2-NO_2	**1h**	—[a]	130—140 (decomp) (orange)	—[a]	217—220 (red)	255—256 (brown)	—[a]	139—140(decomp) (green)
2-$N(CH_3)_2$	**1k**	unstable(violet)	—[a]	—[a]	—[a]	—[a]	—[a]	—[a]

a) These complexes could not be obtained.

justed to 6.67×10^{-3} mol dm^{-3}, and that of donors to 6.67×10^{-2} mol dm^{-3} except perylene in which case a saturated solution of perylene (1.67×10^{-2} mol dm^{-3}) was used because of its low solubility.

Complex Formation. The following is a general procedure to prepare complexes of TCNAQs with donors except benzene.[12] A TCNAQ derivative and an excess donor are dissolved in dichloromethane, and carbon tetrachloride or ethanol is added in order to precipitate a complex and prevent isolation of the excess donor. Concentration of the solvent is needed if crystals do not appear. For example, **1g**-pyrene complex was prepared by the following method. **1g** 100 mg and pyrene 61 mg were dissolved in hot dichloromethane 3 ml and the solution was concentrated to 1 ml. Ethanol 0.5 ml was added and the solution was allowed to stand. Separated red micro-crystals were filtered and washed with hot ethanol.

Analytical data are as follows.[13] Bz: benzene, Nap: naphthalene, Ant: anthracene, Phen: phenanthrene, Pyr: pyrene, DAD: diaminodurene. Found, % (Calcd,† %). **1a**-DAD, C, 76.86; H, 5.07; N, 18.13 (C, 76.90; H, 5.16; N, 17.94). **1b**-Bz, C, 81.98; H, 4.35; N, 14.29 (C, 81.80; H, 4.07; N, 14.13). **1b**-Phen, C, 82.71; H, 3.95; N, 14.02 (C, 82.54; H, 3.71; N, 13.75). **1b**-Pyr, C, 83.19; H, 3.85; N, 13.49 (C, 83.40; H, 3.60; N, 13.36). **1b**-TTF,C, 68.24; H, 3.05; N, 13.22; S, 15.17 (C, 68.55; H, 2.88; N, 13.32; S, 15.25). **1b**-DAD, C, 76.53; H, 5.46; N, 17.23 (C, 77.15; H, 5.43; N, 17.41). **1b**-Pyr, C, 76.59; H, 2.98; N, 11.82; Cl, 8.47 (C, 76.45; H, 2.75; N, 12.74; Cl, 8.06). **1e**-Bz, C, 74.81; H, 3.14; N, 13.44; Cl, 8.50 (C, 74.91; H, 3.17; N, 13.78; Cl, 8.64). **1e**-Nap, C, 74.54; H, 2.97; N, 13.75; Cl, 9.08 (C, 74.54; H, 2.75; N, 13.91; Cl, 8.80). **1e**-Ant, C, 75.59; H, 3.01; N, 13.11, Cl, 8.60 (C, 75.79; H, 2.83; N, 13.09; Cl, 8.28). **1e**-Phen, C, 75.51; H, 2.93; N, 13.12; Cl, 8.47 (C, 75.79; H, 2.83; N, 13.09; Cl, 8.28). **1e**-Pyr, C, 76.29; H, 2.91; N, 12.70; Cl, 8.36 (C, 76.45; H, 2.75, N, 12.74; Cl, 8.06). **1e**-TTF, C, 63.01; H, 2.30; N, 12.71; Cl, 8.36; S, 14.59 (C, 62.65; H, 2.06; N, 12.71; Cl, 8.04; S, 14.54). **1e**-DAD, C, 71.48; H, 4.41; N, 16.69; Cl, 7.45 (C, 71.63; H, 4.61; N, 16.70; Cl, 7.05). **1f**-Pyr, C, 77.30; H, 3.28; N, 12.07 (C, 77.75; H, 3.26; N, 12.09). **1f**-TTF, C, 64.54; H, 2.73; N, 12.05; S, 13.85 (C, 64.64; H, 2.60; N, 12.06; S, 13.81). **1g**-Bz, C, 79.59; H, 3.19; N, 17.21 (C, 79.59; H, 3.22; N, 17.19). **1g**-Phen, C, 80.64; H, 2.92; N, 16.82 (C, 80.37; H, 2.89; N, 16.74). **1g**-Pyr, C, 81.18; H, 2.98; N, 16.26 (C, 80.92; H, 2.81; N, 16.27). **1g**-TTF, C, 66.24; H, 2.14; N. 16.30; S, 13.58 (C, 66.81; H, 2.10; N, 16.23; S, 14.86). **1h**-Phen, C, 74.17; H, 2.50; N, 15.45 (C, 73.97; H, 2.76; N, 15.79), **1h**-Pyr, C, 74.49; H, 2.53; N, 14.69 (C, 74.66; H, 2.69; N, 15.55).

†These values are calculated assuming that the mole ratio of the TCNAQ to donor is 1:1 for Bz, DAD complexes, and is 2:1 for other complexes.

References

1) J. B. Torrance, *Acc. Chem. Res.*, **12**, 79 (1979); R. C. Wheland and J. L. Gillson, *J. Am. Chem. Soc.*, **98**, 3916 (1976).

2) Y. J. I'Haya, T. Yunoki, and N. Suzuki, *Bull. Chem. Soc. Jpn.*, **45**, 1004 (1972).

3) T. Nagami, Y. Kanda, H. Tanaka, and H. Mikawa, *Bull. Chem. Soc. Jpn.*, **54**, 3601 (1981).

4) A. Aumüller and S. Hünig , *Liebigs Ann. Chem.*, **1984**, 618.

5) B. S. Ong and B. Keoshkerian, *J. Org. Chem.*, **49**, 5002 (1984).

6) A. M. Kini, D. O. Cowan, F. Gerson, and R. Möckel, *J. Am. Chem. Soc.*, **107**, 556 (1985).

7) Y. Nishizawa, T. Suzuki, Y. Yamashita, T. Miyashi, and T. Mukai, *Nippon Kagaku Kaishi*, **1985**, 904.

8) S. Yamaguchi, H. Tatemitsu, Y. Sakata, and S. Misumi, *Chem. Lett.*, **1983**, 1229.

9) E. S. Pysh and N. C. Yang, *J. Am. Chem. Soc.*, **85**, 2124 (1963); D. C. Green, *J. Org. Chem.*, **44**, 1476 (1979).

10) "The details will be soon reported elsewhere" by C. Kabuto, Y. Fukazawa, T. Suzuki, Y. Yamashita, T. Miyashi, and T. Mukai.

11) Electrical resistivities were measured as compacted samples at room temperature. **1b**-TTF;$<10^{13}$ Ωcm, **1e**-TTF; 8.2×10^{10} Ωcm, **1f**-TTF; 2.7×10^{13} Ωcm, **1g**-TTF; 5.7×10^{10} Ωcm. We thank Dr. Gunzi Saito at The University of Tokyo for providing the measurement of the resistivities.

12) The benzene complexes were obtained just by recrystallization of TCNAQs from benzene.

13) All of the complexes could not be recrystallized since they easily dissociate into indivisual components by dissolution in solvent. Therefore, some complexes showed unsatisfactory elemental analyses which still establish the mole ratio of the TCNAQs to donors.

Structures of Two New Halochamigrene Derivatives from the Red Alga *Laurencia nipponica* Yamada[1)]

Minoru SUZUKI, Makoto SEGAWA, Teruaki SUZUKI, and Etsuro KUROSAWA*
Department of Chemistry, Faculty of Science, Hokkaido University, Sapporo 060
(Received March 8, 1985)

Synopsis. The structures of two new halochamigrene derivatives isolated from the title alga were determined by chemical and spectral methods.

We have previously reported the structures of the halogenated chamigrene derivatives which have been isolated from the red alga *Laurencia nipponica* Yamada, collected at Soya point, Hokkaido.[2)] Further investigation of this alga has yielded two new metabolites, a halogenated sesquiterpene alcohol **1** and a ketone **2**. We wish to describe herein the structures of these metabolites.

The sesquiterpene alcohol **1**, $C_{15}H_{21}OBr_2Cl$, oil, $[\alpha]_D^{20}$ −24.2° ($CHCl_3$), showed in its ^1H NMR spectrum broad signals at δ 0.99 (3H), 1.17 (3H), 4.27 (1H, m), 4.60 (1H, m), 5.06 (1H), 5.67 (1H), and 6.07 (1H), and a sharp singlet at δ 1.71 (3H). The ^{13}C NMR spectrum revealed no other double bonds, apart from those of an *exo*-methylene group at δ 144.4 (s) and 111.8 (t) and a trisubstituted double bond at 137.2 (s) and 130.9 (d), and hence **1** had to be a bicyclic alcohol. Acetylation of **1** with acetic anhydride and pyridine gave the corresponding acetate **3**, $C_{17}H_{23}O_2Br_2Cl$. Oxidation of **1** with pyridinium chlorochromate in CH_2Cl_2 afforded an α,β-unsaturated ketone which was identical with the natural ketone **2**, $C_{15}H_{19}OBr_2Cl$. The ^1H NMR spectrum of **2** exhibited pairs of signals very similar to those of the dienone **4**,[2)] derived from 2,10-dibromo-3-chlorochamigra-7(14)-en-8-ol (**5**). However, these pairs of signals, when the spectrum was measured at 100°C (in toluene-d_8), collapsed into singlets and the spectral change with temperature variation was reproducible. This fact suggests that the ketone **2** exists as two conformers equilibrated slowly at room temperature. Treatment of **1** with zinc and AcOH in MeOH yielded a monobromo alcohol **6**, $C_{15}H_{21}OBr$, which gave the acetate **7**, $C_{17}H_{23}O_2Br$. The ^1H NMR spectrum of **6** showed the presence of two quaternary methyl groups at δ 0.92 and 1.16 (each 3H, s), a vinyl methyl group at δ 1.60 (3H, br s), an *exo*-methylene group at δ 5.08 and 5.30 (each 1H, s), two olefinic protons at δ 5.38 (1H, m) and 6.17 (1H, d, J=4.5 Hz), and a proton α to hydroxyl group at δ 4.48 (1H, dd, J=4.5, 4.5 Hz), thus indicating that the vicinal bromine and chlorine atoms in **1** were eliminated to form an additional trisubstituted double bond bearing a methyl group. Spin decoupling experiments on the ^1H NMR spectrum of **6** showed the presence of $CH_2{=}\underset{|}{C}{-}CH(OH){-}CH{=}\underset{|}{C}-$ and $-CH_2{-}CH{=}C(CH_3)-$ moieties in the molecule. Comparison of the ^1H NMR spectra of **6** and **7** with those of previously described halochamigrene derivatives coupled with detailed analysis of the spectral data of **2** and **4** allowed us to propose formulae **1** and **2** for the sesquiterpene alcohol and the ketone, respectively. Confirmation of the structures **1** and **2** was obtained by the following chemical correlation with 2,10-dibromo-3-chloro-7,8-epoxychamigrane (**8**), the major metabolite of Atsuta's *L. nipponica*.[3)] Treatment of **8** with zinc and AcOH in MeOH gave three products, **9**, **10**, and **11**. The product **9**, $C_{15}H_{24}OBrCl$, revealed ^1H NMR spectrum very similar to that of **8** except for the chemical shifts of the *gem*-dimethyls and lack of the signal corresponding to the bromomethine proton at δ 4.10. The two signals due to the *gem*-dimethyl group (δ 0.84 and 0.88) in **9** were observed at higher magnetic field region than that (δ 0.96 and 1.10) in **8**, thus indicating that the bromine atom at C-10 of **8** was reduced in a way similar to the case of glanduliferol.[4)] The acid-catalyzed isomerization of **9** with *p*-toluenesulfonic acid in warm benzene gave an alcohol **12**, $C_{15}H_{24}OBrCl$; ν_{max} 3630, 1640, and 910 cm^{-1}. On the other hand, hydrogenation of **1** with PtO_2 in EtOAc gave the hydrogenated product, with evolution of hydrogen bromide, which was identical with **12** in all respects. Consequently, the structures of **1** and **2** were established as (2*S*,3*S*,8*R*)-2,10-dibromo-3-chlorochamigra-7(14),9-dien-8-ol and (2*S*,3*S*)-2,10-dibromo-3-chlorochamigra-7(14),9-dien-8-one, respectively. Conformational analyses of **1** and **2** are in progress.

Experimental

The melting points were uncorrected. The IR spectra were measured on a JASCO A-102 spectrometer and the UV spectra on a Shimadzu UV-240 spectrometer. The ^1H and ^{13}C NMR spectra were recorded on a JEOL JNM-FX 100 spectrometer. TMS was used as an internal reference in $CDCl_3$. The low and

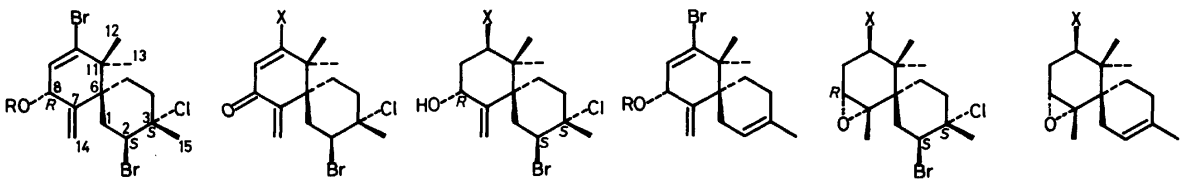

1: R=H
3: R=Ac

2: X=Br
4: X=H

5: X=Br
12: X=H

6: R=H
7: R=Ac

8: X=Br
9: X=H

10: X=Br
11: X=H

high resolution mass spectra were obtained at 70 eV with a JEOL JMS-D300 spectrometer. The optical rotations were measured on a JASCO DIP-140 polarimeter in $CHCl_3$.

Isolation. The detail of the separation of the extracts has been described in the previous paper.[2] The ethyl acetate fraction obtained by alumina column chromatography of the extracts was repeatedly chromatographed on silica-gel column to yield **1** (4% of the extracts) along with two halochamigrene derivatives[2] and *trans*-deacetylkumausyne.[5] From the benzene fraction **2** was isolated in 1.5% yield by repeated silica-gel column chromatography together with kumausallene[6] and *trans*-kumausyne.[5]

1: Colorless oil; $[\alpha]_D^{20}$ −24.2° (*c* 1.88); UV (EtOH), λ_{max} 203 nm (ε 8500); IR (film), ν_{max} 3350, 1640, 1390, 1380, 1367, 1300, 1100, 1045, 990, 910, 860, 810, and 750 cm^{-1}; ^1H NMR, in the text; ^{13}C NMR (25.0 MHz), δ=23.0 (q), 23.5 (q), 24.0 (q), 25.9 (t), 38.6 (t×2), 47.0 (s), 50.1 (s), 60.6 (d), 69.0 (d), 71.7 (s), 111.8 (t), 130.9 (d), 137.2 (s), and 144.4 (s); MS, *m/z* (rel. intensity) 416, 414, 412, 410 (0.2:1:1.5:0.5; M^+), 335, 333, 331 (13:48:37; M^+−Br), 297, 295 (16:17; M^+−Br-HCl), 215 (40; M^+−Br-HCl-HBr), 147 (32), 119 (50), 97 (51), 91 (48), 81 (48), 69 (69), 57 (77), 55 (79), 43 (78), and 41 (100). Found: *m/z* 333.0445. Calcd for $C_{15}H_{21}O^{81}Br^{35}Cl$: M−Br, 333.0445.

2; Pale yellow oil; $[\alpha]_D^{22}$+1.95° (*c* 1.59); UV (EtOH), λ_{max} 262 (ε 9700) and 202 (6200) nm; IR (film), ν_{max} 1670, 1620, 1595, 1390, 1380, 1370, 1320, 1290, 1260, 1220, 1180, 1150, 1100, 1065, 950, 890, 870, and 760 cm^{-1}; ^1H NMR, δ=1.11, 1.14 (total 3H, s), 1.37 (3H, s), 1.69 (3H, s), 4.21 (0.4H, dd, *J*=12, 5 Hz), 4.64 (0.6H, dd, *J*=13, 5 Hz), 5.45 (1H, s), 6.21 (1H, s), 6.52 (0.6H, s), and 6.54 (0.4 H, s); MS, *m/z* 414, 412, 410, 408 (3:16:22:10; M^+), 377, 375, 373 (0.9:2:1; M^+−Cl), 333, 331, 329 (26:100:78; M^+−Br), 296, 294 (9:11; M^+−Br-Cl), 295, 293 (52:53; M^+−Br-HCl), 252, 250 (10:30; M^+−Br-Br), 251, 249 (12:20; M^+−Br-HBr), 215 (41; M^+−Br-Br-Cl), 214 (63; M^+−Br-Br-HCl), 213 (71; M^+−Br-HBr-HCl), 149 (61), 95 (66), 67 (68), and 41 (78). Found: *m/z* 409.9470. Calcd for $C_{15}H_{19}O^{79}Br^{81}Br^{35}Cl$: M, 409.9472.

Acetylation of 1. Acetylation of **1** (19 mg) was carried out with acetic anhydride (0.3 ml) and pyridine (0.3 ml) in the usual manner. The acetylated product was purified by a silica-gel plate to give **3** (17 mg); oil; $[\alpha]_D^{20}$−71.7° (*c* 0.53); IR (film), ν_{max} 1740, 1640, 1230, 1100, 1040, 1010, 990, 930, 920, and 900 cm^{-1}; ^1H NMR, broad and complex signals; MS, *m/z* 458, 456, 454, 452 (0.3:1.1:1.3:0.6; M^+) and 416, 414, 412, 410 (5:25:35:16; M^+−CH_2CO). Saponification of **3** with K_2CO_3 in MeOH gave the original alcohol **1** in quantitative yield.

PCC Oxidation of 1. To a suspended solution of pyridinium chlorochromate (10 mg) in CH_2Cl_2 (0.5 ml) was added a solution of **1** (12 mg) in CH_2Cl_2 (0.5 ml). The mixture was stirred for 40 min at room temperature and then worked up in the usual manner. The resulting oil was chromatographed on a silica-gel plate to afford **2** (10 mg); pale yellow oil; $[\alpha]_D^{23}$ +1.68° (*c* 1.28); whose spectral data were consistent with those of the natural ketone **2**.

Treatment of 1 with Zn-dust-AcOH. To a solution of **1** (10 mg) in MeOH (0.4 ml) was added activated Zn-dust (50 mg) and AcOH (0.04 ml). The mixture was stirred for 70 h at room temperature and then filtered to remove the Zn-dust. The filtrate was extracted with ether. The ethereal solution was successively washed with water, 5% aqueous $NaHCO_3$, and water, and dried over Na_2SO_4. The subsequent removal of the solvent gave a residual oil, which was chromatographed on a silica-gel plate to give **6** (4 mg); crystals; mp 58—59 °C; $[\alpha]_D^{20}$ −95.8° (*c* 0.45); IR ($CHCl_3$), ν_{max} 3600, 3400, 1640, 1010, 990, 915, and 895 cm^{-1}; ^1H NMR, in the text; MS, *m/z* 298, 296 (3:3; M^+) and 280, 278 (56:58; M^+−H_2O).

Acetylation of 6. Acetylation of **6** (3 mg) was carried out with acetic anhydride (0.15 ml) and pyridine (0.15 ml) at room temperature by the usual method to give **7** (3 mg); oil; $[\alpha]_D^{25}$ −103° (*c* 0.25); IR ($CHCl_3$), ν_{max} 1730, 1640, 1230, 1015, 973, and 915 cm^{-1}; ^1H NMR, δ=0.92 (3H, s), 1.18 (3H, s), 1.59 (3H, br s), 2.04 (3H, s), 5.14 (1H, s), 5.30 (1H, m), 5.49 (1H, s), 5.61 (1H, d, *J*=5 Hz), and 6.12 (1H, d, *J*=5 Hz); MS, *m/z* 340, 338 (0.3:0.3; M^+) and 280, 278 (41:42; M^+−CH_3COOH).

Treatment of 8 with Zn-dust-AcOH. To a solution of **8** (46 mg) in MeOH (1.5 ml) was added activated Zn-dust (200 mg) and AcOH (0.15 ml). The mixture was stirred for 6 h at room temperature and then worked up in a manner similar to the case of **1**. The resulting oil was chromatographed on a silica-gel column to give **9** (6 mg); crystals; mp 114—115 °C; $[\alpha]_D^{21}$ +16.8° (*c* 0.46); IR ($CHCl_3$), ν_{max} 1150, 1105, 1090, and 1055 cm^{-1}; ^1H NMR, δ=0.84 (3H, s), 0.88 (3H, s), 1.54 (3H, s), 1.71 (3H, s), 2.97 (1H, dd, *J*=2, 2 Hz), and 4.90 (1H, dd, *J*=12, 6 Hz); MS, *m/z* 338, 336, 334 (0.2:1:0.9; M^+) and 257, 255 (3:13; M^+−Br); **10** (9 mg); oil; $[\alpha]_D^{18}$−81.1° (*c* 0.76); ^1H NMR, δ=0.93 (3H, s), 0.99 (3H, s), 1.31 (3H, s), 1.67 (3H, br s), 2.88 (1H, dd, *J*=2, 2 Hz), 4.38 (1H, dd, *J*=12, 6 Hz), and 5.42 (1H, m); MS, *m/z* 300, 298 (0.7: 0.8; M^+) and 219 (28; M^+−Br); **11** (6 mg); oil; $[\alpha]_D^{21}$−77.5° (*c* 0.46); ^1H NMR, δ=0.76 (3H, s), 0.81 (3H, s), 1.29 (3H, s), 1.67 (3H, br s), 2.89 (1H, dd, *J*=2, 2 Hz), and 5.43 (1H, m); MS, *m/z* 220 (4; M^+).

Isomerization of 9. To a solution of **9** (4 mg) in benzene (0.5 ml) was added a piece of TsOH, and the mixture was stirred for 35 min at 60 °C, cooled, and extracted with ether. The ethereal solution was washed with 5% aqueous $NaHCO_3$ and water, dried over Na_2SO_4, and then evaporated to leave a residual oil, which was chromatographed on a silica-gel plate to give **12** (2 mg); oil; $[\alpha]_D^{18}$−29.4° (*c* 0.19); IR ($CHCl_3$), ν_{max} 3630, 1640, 1300, 1100, and 910 cm^{-1}; ^1H NMR, δ=0.82, 0.94, 1.70 (each 3H, s), 4.32 (1H, m), 4.37 (1H, dd, *J*=13, 4 Hz), 4.93 (1H, s), and 5.59 (1H, s); MS, *m/z* 338, 336, 334 (0.2:0.8:1; M^+) and 320, 318, 316 (0.8:1.3:1; M^+−H_2O).

Hydrogenation of 1. Hyrogenation of **1** (8 mg) was performed in EtOAc over PtO_2-catalyst. After removal of the catalyst and the solvent, the residual oil was chromatographed on a silica-gel plate to give **12** (3 mg); oil; $[\alpha]_D^{23}$−31.9° (*c* 0.31); the spectral data were identical with those of **12** derived from **9**.

References

1) Part 63 of "Constituents of Marine Plants," Part 62; T. Suzuki, M. Suzuki, A. Furusaki, T. Matsumoto, A. Kato, Y. Imanaka, and E. Kurosawa, *Tetrahedron Lett.*, in press.

2) M. Suzuki, M. Segawa, T. Suzuki, and E. Kurosawa, *Bull. Chem. Soc. Jpn.*, **56**, 3824 (1983).

3) T. Suzuki, H. Kikuchi, and E. Kurosawa, *Bull. Chem. Soc. Jpn.*, **55**, 1561 (1982); A. Furusaki, C. Katayama, T. Matsumoto, M. Suzuki, T. Suzuki, H. Kikuchi, and E. Kurosawa, *ibid.*, **55**, 3398 (1982).

4) M. Suzuki, A. Furusaki, and E. Kurosawa, *Tetrahedron*, **35**, 823 (1979).

5) T. Suzuki, K. Koizumi, M. Suzuki, and E. Kurosawa, *Chem. Lett.*, **1983**, 1643.

6) T. Suzuki, K. Koizumi, M. Suzuki, and E. Kurosawa, *Chem. Lett.*, **1983**, 1639.

A New Chamigrane-type Bromo Diether from the Red Alga *Laurencia nipponica* Yamada[1)]

Hajime KIKUCHI,† Teruaki SUZUKI, Minoru SUZUKI, and Etsuro KUROSAWA*
Department of Chemistry, Faculty of Science, Hokkaido University, Sapporo 060
(Received March 8, 1985)

Synopsis. A new halogenated sesquiterpene diether has been isolated from the title alga and its structure was established on the basis of the spectral and chemical evidence.

As part of our studies on the constituents of the red alga *Laurencia nipponica* Yamada ("Ura-sozo") grown in Northern Hokkaido,[2,3)] belonging to the warm current region, we have collected in two locations at Teuri island and Hamamasu. Both specimens displayed the presence of laureatin[4)] (25% and 20% of the extracts) and isolaureatin[4)] (10% and 8%) as the major metabolites. In this paper we report the isolation and the structural determination of a new sesquiterpene bromo diether **1**, which has been obtained as the minor metabolite (0.6%) from the Hamamasu's specimen.

Compound **1**, mp 78—79 °C, $[\alpha]_D^{21}$ −54.8° ($CHCl_3$), was found to have a molecular formula of $C_{15}H_{19}O_2Br$ by high resolution mass spectrometry. The IR spectrum of **1** showed no hydroxyl and carbonyl absorptions, thus indicating that two oxygen atoms in **1** were involved in ether linkages. The ^{13}C NMR spectrum indicated the presence of an *exo*-methylene group at δ 144.2 and 114.6 and a disubstituted vinyl group at 133.9 and 130.1. Tetracyclic nature, including two ether rings, of **1** was demonstrated from the absence of further unsaturation besides the two double bonds. The ^1H NMR spectrum revealed signals at δ 1.02 and 1.14 (each 3H, s) due to two quaternary methyl groups, at 1.24 (3H, s) due to a CH_3–$\overset{|}{C}$–O– grouping, at 4.95 and 5.07 (each 1H, br s) due to an *exo*-methylene group, and at 5.82 (2H, br s) due to a disubstituted vinyl group. Furthermore, the spin decoupling studies indicated the presence of ■–$\underset{|}{\overset{}{CH}}$–$CH_2$–■ grouping at
O–
δ 1.71 (1H, d, J=12 Hz), 2.20 (1H, dd, J=12, 6 Hz), and 4.45 (1H, d, J=6 Hz) and ■–$\underset{|}{\overset{}{CH}}$–$CH_2$–$\overset{|}{C}$=$CH_2$
O–
grouping at 2.39 (1H, dddd, J=14, 14, 2, 2 Hz), 2.66 (1H, dd, J=14, 5 Hz), and 4.06 (1H, dd, J=14, 5 Hz) (■; quaternary carbon).

In view of the above-mentioned partial structural units coupled with comparisons of the spectral data with those of various chamigrane-type sesquiterpenoids, *e.g.* **2** (pacifenol)[5)] and **3**,[6)] which co-occurred in the same alga, it is suggested that formula **1** would be proposed as possible structure for this bromo diether. The structure **1** was confirmed by the following chemical derivation from the known bromo alcohol **4**,[6)] which has also been isolated from *L. nipponica*.

Treatment of **4** with *N*-bromosuccimide in *t*-BuOH and H_2O at room temperature afforded a dibromo compound **5**, $C_{15}H_{20}O_2Br_2$ (*m/z* 394, 392, and 390; M^+), in 90% yield. The IR and ^1H NMR spectra of **5** indicated that the hydroxyl and trisubstituted vinyl groups in **4** disappeared and that an additional ether ring was formed. The formation of the expected diether **5** (not 4-bromo-3,7-epoxy derivative) in the bromonium ion induced cyclization[7)] was supported by the presence of the CH_3–$\overset{|}{C}$(Br)– moiety at δ 1.80 (3H, s) in the ^1H NMR spectrum of **5**. Treatment of **5** with 1 mol dm^{-3} ethanolic potassium hydroxide gave a dehydrobromination product (20% yield) which was identical with natural bromo diether **1** in all respects (IR, ^1H NMR, and MS spectra and undepressed mixed mp). Thus the structure, including the absolute configuration, of the bromo diether is represented by formula **1**.

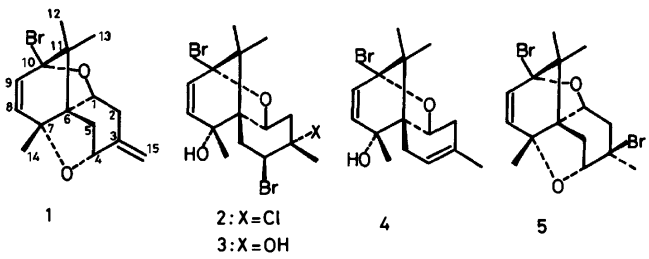

Experimental

All the mps were uncorrected. The IR spectra were measured on a JASCO A-102 spectrophotometer. The ^1H and ^{13}C NMR spectra were recorded on a JEOL JNM-PS-100 and JEOL JNM-FX200 spectrometer, respectively, using tetramethylsilane as an internal reference in $CDCl_3$. The low and high resolution mass spectra were taken at 70 eV with a JEOL JMS-D300 spectrometer. Optical rotations were determined on a JASCO DIP-140 polarimeter in $CHCl_3$. Aluminium oxide (Merck, activity II-III) and silica gel (Merck, Kieselgel 60, 70—230 mesh) were used for column chromatography.

Collection. Algae were collected at Teuri island (Haboro) and Hamamasu (*ca.* 40 km southwest of Rumoi[3)]) early in August 1980.

Isolation. The neutral MeOH extracts (5 g; *ca.* 2% of the half-dried alga), obtained from the Hamamasu's specimen in the usual manner, was fractionated by column chromatography on alumina. The fraction eluted with hexane–benzene (1:1) was rechromatographed on silica-gel column to yield laureatin[4)] (1 g) and isolaureatin[4)] (400 mg) together with deoxyprepacifenol[8)] (25 mg), (3*Z*)-isoprelaurefucin[9)] (170 mg), and spirolaurenone[10)] (40 mg). The fraction eluted with benzene was further submitted to column chromatography on silica gel to give **1** (30 mg) as a crystalline material along with cycloeudesmol[11)] (65 mg). The fraction eluted with benzene–ethyl acetate (10:1) was repeatedly chromato-

†Present address: Tobishi Pharmaceutical Co. Ltd., Koganei 184.

graphed over silica gel to yield pacifenol[5] (100 mg), 2,10-dibromo-3-chloro-α-chamigren-9-ol[12] (10 mg), and laureacetal-A[13] (10 mg). The following fraction eluted with ethyl acetate was submitted to repeated silica-gel column chromatography to afford laureacetal-B[14] (60 mg), 4,10-dibromo-1,10-epoxychamigra-8-ene-3,7-diol[6] (10 mg), and 10-bromo-1,10-epoxychamigra-2,8-diene-4,7-diol[15] (65 mg).

1: Mp 78—79 °C (hexane–diisopropyl ether); $[\alpha]_D^{21}$ −54.8° (*c* 1.43); IR, ν_{max} (Nujol) 1160, 1090, 1050, 1030, 1020, 985, 935, 915, and 865 cm^{-1}; ^1H NMR (100 MHz), in the text; ^{13}C NMR (50.1 MHz), δ=144.2 (s, C3), 133.9 (d, C8 or C9), 130.1 (d, C9 or C8), 114.6 (t, C15), 98.8 (s, C10), 84.7 (s, C7), 81.2 (d, C4), 78.0 (d, C1), 55.5 (s, C6), 47.7 (s, C11), 31.1 (t, C2), 26.9 (t, C5), 23.9 (q, C14 or C13), 23.3 (q, C13 or C14), and 20.1 (q, C12); MS, *m/z* (rel intensity) 312, 310 (0.2; M^+), 297, 295 (1; M^+-CH_3), 231 (9; M^+-Br), 200, 198 (32), 171 (40), 133 (88), 121 (100), 119 (37), 91 (36), 57 (42), 43 (77), and 41 (71). Found: *m/z* 295.0333. Calcd for $C_{14}H_{16}O_2{}^{79}Br$: $M-CH_3$, 295.0333.

Treatment of 4 with NBS in t-BuOH–H_2O. To a soln of **4**[6] (30 mg) in *t*-BuOH (1 ml) and H_2O (1 ml) was gradually added recrystallized NBS (19 mg) at 0 °C. After the mixture had been stirred for 1 h at room temperature, water was added, and the mixture was extracted with ether. The ethereal soln was washed with saturated brine, dried over anhydrous Na_2SO_4, and evaporated to leave an oily substance, which was purified by column chromatography over silica gel to give **5** (34 mg); mp 97—98 °C (hexane–diisopropyl ether); $[\alpha]_D^{23}$ −29.4° (*c* 1.49); IR, ν_{max} (Nujol) 1265, 1160, 1105, 1050, 1040, 1030, 1015, 1005, 982, 958, 950, 935, 925, 910, 880, 865, 815, 765, and 743 cm^{-1}; ^1H NMR (100 MHz), δ=1.03, 1.14, 1.25, 1.80 (each 3H, s), 2.13 (2H, m), 2.33 (1H, br s), 2.43 (1H, s), 3.74 (1H, dd, *J*=10, 9 Hz), 4.26 (1H, dd, *J*=4, 2 Hz), and 5.84 (2H, br s); MS, *m/z* 394, 392, 390 (0.3:0.5:0.3; M^+), 379, 377, 375 (0.3:0.5:0.3; M^+-CH_3), 313, 311 (40; M^+-Br), 231 (5; $M^+-Br-HBr$), 199 (20), 162 (20), 133 (85), 121 (100), 113 (34), 71 (37), 43 (69), and 41 (48).

Conversion of 5 into 1. A soln of **5** (30 mg) in 1 mol dm^{-3} ethanolic KOH (1.5 ml) was refluxed for 2 h and then worked up in the usual way to give an oily product which was further purified by silica-gel column chromatography to yield a crystalline substance (5 mg) (20 mg of **5** was recovered), mp 77—78 °C, $[\alpha]_D^{22}$ −51.0° (*c* 1.21), whose spectral data were consistent with those of natural **1**.

References

1) Part 64 of "Constituents of Marine Plants." Part 63; M. Suzuki, M. Segawa, T. Suzuki, and E. Kurosawa, *Bull. Chem. Soc. Jpn.*, **58**, 2435 (1985).

2) M. Suzuki, M. Segawa, T. Suzuki, and E. Kurosawa, *Bull. Chem. Soc. Jpn.*, **56**, 3824 (1983).

3) M. Suzuki, M. Segawa, H. Kikuchi, T. Suzuki, and E. Kurosawa, *Phytochemistry*, in press.

4) T. Irie, M. Izawa, and E. Kurosawa, *Tetrahedron*, **26**, 851 (1970).

5) J. J. Sims, W. Fenical, R. M. Wing, and P. Radlick, *J. Am. Chem. Soc.*, **93**, 3774 (1971).

6) T. Suzuki, *Chem. Lett.*, **1980**, 541.

7) E. Demole and P. Enggist, *Helv. Chim. Acta*, **54**, 456 (1971).

8) C. Ireland, M. O. Stallard, D. J. Faulkner, J. Finer, and J. Clardy. *J. Org. Chem.*, **41**, 2461 (1976).

9) E. Kurosawa, A. Fukuzawa, and T. Irie, *Tetrahedron Lett.*, **1973**, 4135.

10) M. Suzuki, N. Kowata, and E. Kurosawa, *Tetrahedron*, **36**, 1551 (1980).

11) T. Suzuki, A. Furusaki, H. Kikuchi, and E. Kurosawa, *Tetrahedron Lett.*, **22**, 3423 (1981).

12) W. Fenical, *Phytochemistry*, **15**, 511 (1976).

13) T. Suzuki, A. Furusaki, N. Hashiba, and H. Kurosawa, *Tetrahedron Lett.*, **1977**, 3731.

14) T. Suzuki and E. Kurosawa, *Chem. Lett.*, **1979**, 301.

15) K. Kurata, A. Furusaki, C. Katayama, H. Kikuchi, and T. Suzuki, *Chem. Lett.*, **1981**, 773.

Irreversible Conformational Change of the Complex of Poly(L-lysine) with Methyl Orange upon Irradiation of Light

Hiroyuki YAMAMOTO
Institute of High Polymer Research, Faculty of Textile Science and Technology, Shinshu University, Ueda 386
(Received March 11, 1985)

Synopsis. The effect of light on the chiral complex of poly(L-lysine) (PLL) with Methyl Orange (MO) was studied by means of absorption and circular dichroism (CD) measurements. Upon irradiation, the magnitude of the induced CD of the PLL-MO complex decreased together with a decrease in dimeric dye species. The change was irreversible under dark or visible-light conditions.

Reversible conformational changes induced by light in azobenzene-containing polypeptides in organic solvents have been studied by different groups.[1-3] Conformational changes induced by light in water-soluble poly(L-glutamic acid) (PLG) with photochromic side chains have also been studied by Pieroni *et al.*[4,5] Though a *trans* to *cis* photoconversion in an aqueous solution was lower than in an organic solvent, the photochemical reactions in both solvents were entirely reversible.[4,5]

We have investigated the induced CD of cationic polypeptides and azo dyes[6-9] and wish to report here the effect of light irradiation on the PLL-MO complex in water.

Experimental

The PLL HBr sample used had a polymerization degree of 3260. 4-(4-Dimethylaminophenylazo)benzenesulfonic acid sodium salt (Methyl Orange, MO) was a guaranteed reagent (Wako). A MO solution was prepared in red light and kept in the dark. The final concentrations of MO were 2×10^{-5} mol dm^{-3}, and the ratio of lysyl residues to dye molecules (R/D) was 5. The absorption and CD spectra were measured with a Jasco UVIDEC-1 and a CD J-40A spectrometer. All the following data were reduced to the molar basis of the total dye concentration or the lysyl residue concentration, and were expressed in terms of the ellipticity $[\theta]$ (degree cm^{2}dmol^{-1}) and molar extinction coefficient ε (dm^{3}mol^{-1}cm^{-1}).

Irradiations of the sample solutions were carried out with a mercury lamp (400 W) filtered with narrow-band interference filters (UV-D36A for 360 nm and B-46 for 460 nm) from Toshiba. The light intensity was measured by actinometry.[10]

Results and Discussion

The MO showed a single visible absorption band at 467 nm with ε_{467}=25600 in water (at a neutral pH). Upon complexation with PLL, an additional blue-shifted band was observed at 367 nm due to the dimeric dye species,[11,12] exhibiting an induced CD. The magnitudes of the induced CD of the PLL HBr-MO complex were −128000 (371 nm) and 129000 (359 nm) at pH 6 and R/D=5. Figure 1 shows the time dependence of the absorption spectra of the PLL HBr-MO complex upon irradiation at 360 nm (2.7×10^{19} photons cm^{-2}s^{-1}).[10] The intensity of the absorption band at 367 nm decreased and a new broad band appeared at around 400 nm, together with an increase in the monomeric MO band. The band at around 400 nm has been considered to be due to aggregated MO molecules bound to PLL.[13] After 800 min, the dimeric dye species at 367 nm almost disappeared. Figure 2 shows the time dependence of the CD spectra of the PLL HBr-MO complex under the same experimental conditions. Upon irradiation at 360 nm, the magnitudes of the induced CD in the 300—450 nm region decreased, and the extrema and crossover wave lengths shifted to the shorter wave length region. In agreement with the results of the absorption spectra described above, the induced CD of the PLL HBr-MO complex almost completely disappeared after 800 min. Non-filtered light (1.3×10^{20} photons cm^{-2}s^{-1}) from a mercury lamp caused much faster spectral changes than those of a filtered light and the induced CD disappeared after 10 min. Filtered ultraviolet light (360 nm) caused similar changes after 800 min and visible light (460 nm, 2.1×10^{19} photons cm^{-2}s^{-1}) after 1000 min.

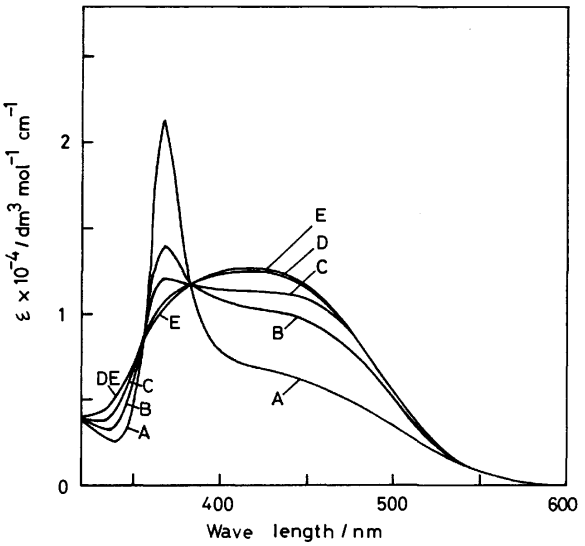

Fig. 1. Absorption spectra of the PLL HBr-MO complex in water at pH 6 and R/D=5 upon irradiation at 360 nm. A: At 0 min, B: after 200 min, C: after 400 min, D: after 600 min, E: after 800 min.

The inherent n-π^* peptide transition of an extended random coiled PLL HBr-MO complex gave an ellipticity value of $[\theta]_{217}$=2500 (based on lysyl residues) at pH 6 and R/D=5 before irradiation. The value decreased to 1000 after irradiation at 360 nm for 800 min. The decrease of the induced CD and n-π^* peptide transition was almost parallel as can be seen from Fig. 2. This observation is the same as for the CD results of water-soluble PLG with azobenzene side chains.[4,5]

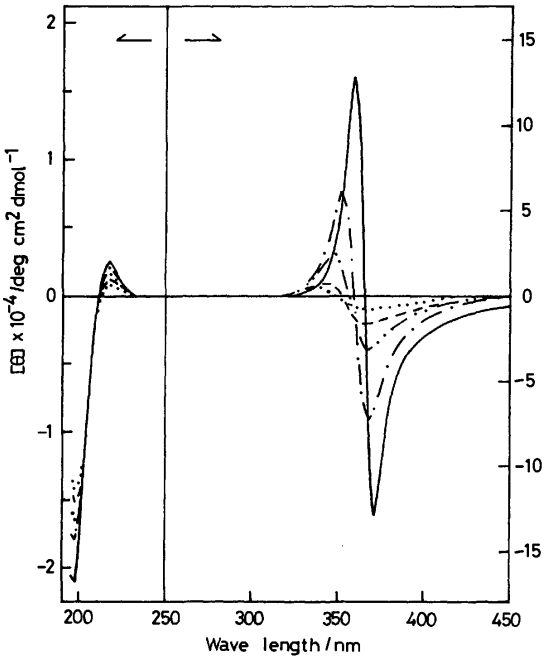

Fig. 2. CD spectra of the PLL HBr-MO complex in water at pH 6 and R/D=5 upon irradiation at 360 nm. ——: At 0 min, —·—: after 200 min, —··—: after 400 min, – – –: after 600 min, ·····: after 800 min.

MO in water does not cause an isomerization from *trans* to *cis* upon irradiation of light.[14] The reason for the spectral changes in Figs. 1 and 2 is due to the change in the interaction mode of the bound dye on the PLL, that is, from dimeric to aggregated and monomeric states. The irradiated sample (at 360 nm) left in the dark or upon re-irradiation by the visible light did not return to its original absorption and CD spectra. Thus, the change in the induced CD spectrum by light is irreversible within several days.

The author wishes to thank Professor Tadao Hayakawa for his encouragement and Miss Ayako Nakazawa for her skillful assistance.

References

1) A. Ueno, J. Anzai, T. Osa, and Y. Kodama, *J. Polym. Sci., Polym. Lett. Ed.*, **15**, 407 (1977).
2) A. Ueno, K. Takahashi, J. Anzai, and T. Osa, *J. Am. Chem. Soc.*, **103**, 6410 (1981).
3) J. L. Houben, O. Pieroni, A. Fissi, and F. Ciardelli, *Biopolymers*, **17**, 799 (1978).
4) O. Pieroni, J. L. Houben, A. Fissi, P. Constantino, and F. Ciardelli, *J. Am. Chem. Soc.*, **102**, 5913 (1980).
5) F. Ciardelli, O. Pieroni, A. Fissi, and J. L. Houben, *Biopolymers*, **23**, 1423 (1984).
6) H. Yamamoto, A. Nakazawa, and T. Hayakawa, *J. Polym. Sci., Polym. Lett. Ed.*, **21**, 131 (1983).
7) H. Yamamoto, A. Nakazawa, T. Hayakawa, and M. Mitsuishi, *Polym. J.*, **16**, 791 (1984).
8) H. Yamamoto, *Makromol. Chem.*, **184**, 1479 (1983).
9) H. Yamamoto, A. Nakazawa, and T. Hayakawa, *Nippon Kagaku Kaishi*, **1985**, in press.
10) H. Kokubun, "Shin Jikken Kagaku Koza," Maruzen, Tokyo (1976), Vol. 4, p. 239.
11) M. Kasha, H. R. Rawls, and M. El-Bayoumi, *Pure Appl. Chem.*, **11**, 371 (1965).
12) M. Hatano, M. Yoneyama, Y. Sato, and Y. Kawamura, *Biopolymers*, **12**, 2423 (1973).
13) T. Takagishi, N. Kuroki, S. Shima, H. Sakai, H. Yamamoto, and A. Nakazawa, *J. Polym. Sci., Polym. Lett. Ed.*, **23**, 329 (1985).
14) H. Yamamoto, Unpublished Data.

A Facile Synthesis of 2-Acyl-3-amino-5-phenacylthio-4-phenylthiophenes from Sodium Cyanophenyldithioacetate and α-Halo Ketones

Toshio FUCHIGAMI,* Zaghloul El-Shahat KANDEEL,†,* and Tsutomu NONAKA
Department of Electronic Chemistry, Graduate School at Nagatsuta, Tokyo Institute of Technology, Nagatsuta, Midori-ku, Yokohama 227
†*Department of Chemistry, Faculty of Science, Cairo University, Giza, A. R. Egypt*
(Received March 18, 1985)

Synopsis. Various kinds of α-halo ketones readily reacted with sodium cyanophenyldithioacetate to provide 2-acyl-3-amino-5-phenacylthio-4-phenylthiophenes in good yields.

In the course of our intensive synthetic studies of heterocyclic compounds,[1,2] we found that 5-acyl-2-alkoxy-4-aminothiazoles were easily prepared by the reaction of potassium (alkoxythiocarbonyl)cyanamide with α-halo ketones (Scheme 1).[1] We have tried to

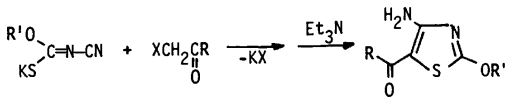

Scheme 1.

extend this process to a facile synthesis of 2-acyl-3-amino-5-mercapto-4-phenylthiophenes (**5**) using α-halo ketones (**2**) and sodium cyanophenyldithioaceate (**1**) instead of (alkoxythiocarbonyl)cyanamide salts as shown in Scheme 2. The starting material **1** was easily prepared from carbon disulfide and phenylacetonitrile in the presence of sodium hydride[3] and without purification the crude **1** was used for the synthesis of **5**.

At first, in a procedure similar to the preparation of 2-acyl-3-aminothiazoles,[1] the reaction was carried out at room temperature using equimolar **1** and phenacyl bromide **2a** and subsequent cyclization was attempted by treatment with triethylamine under slightly warming. The product was not the desired compound **5a** but **6a**.

Since **6a** should be stoichiometrically formed from one mole of **1** and two moles of **2a**, the first condensation reaction was carried out using 2 equiv of **2a** in the presence of an equiv of triethylamine as a dehydrobrominating reagent,[4] and then base-catalyzed cyclization with additional triethylamine was performed. In this case, the thiophene **6a** could be obtained in an excellent yield. The structure of **6a** was confirmed by elemental analysis and spectral studies as follows: The parent peak (*m/z* 429) was observed in MS, and the IR absorption band of a cyano group in the starting **1** disappeared after the reaction, while that of an amino group newly appeared. In addition, the bands of two carbonyl groups (1700 and 1600 cm^{-1}) were also observed.

Thiophenes (**6b—g**) were prepared in good or excellent yields by the similar one-pot reaction from substituted phenacyl halides as shown in Table 1. In this reaction, any aldol condensation to form **7** did not occur and **6** was always a sole product.

Since the reaction proceeds selectively under quite mild conditions, it seems to be useful for the preparation of aminothiophenes having unstable substituents. Although a number of sydnone compounds have been prepared because of their unique electronic structure and biological activities,[5] few works[1b,6] dealing with the successful synthesis of sydnones having heterocyclic substituents have been reported because of the instability of a sydnone ring. From this aspect, the reaction of **1** with 3-aryl-4-(bromoacetyl)sydnone was successfully tried under such mild conditions and pure aminothiophenes (**6h**, **6i**) having a sydnone ring were directly obtained in good yields without purification. In a similar manner, a thiophene derivative (**6j**) having an antipyrine ring was also prepared from the viewpoint of biological activity.

Although our attempts to prepare 3-amino-2-acetylthiophene derivative from α-chloroacetone (**2l**) and **1** failed, the reaction was successfully carried out using 3-chloro-2,4-pentanedione instead of **2l** to provide **6k** in a moderate yield. The product **6k** seemed to be formed by elimination of ketene from the cyclized

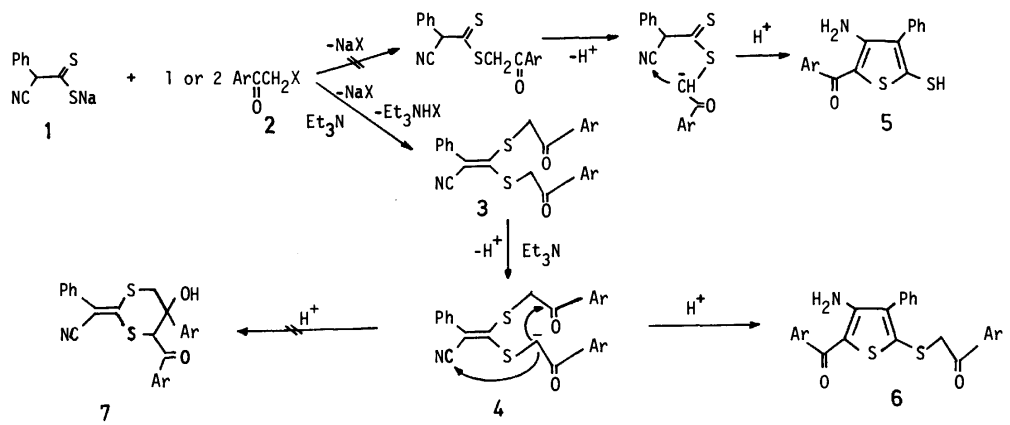

Scheme 2.

Table 1. Synthesis of 2-acyl-3-amino-5-phenacylthio-4-phenylthiophenes (6)[a]

	6 Ar	Yield %	Mp θ_m/°C	MS m/z	IR (KBr) ν_{NH}/cm^{-1}	IR (KBr) $\nu_{C=O}$/cm^{-1}
6a	Ph	Quant	164—165	429(M^+)	3500, 3400	1700, 1600
6b	*p*-ClC_6H_4	Quant	182—183	499(M^++2), 497(M^+)	3520, 3330	1600, 1590
6c	*p*-BrC_6H_4	Quant	179—180	588(M^+), 586(M^+)	3500, 3340	1700, 1600, 1585
6d	*p*-MeC_6H_4	82	133—134	457(M^+)	3520, 3320	1690, 1680, 1610
6e	*p*-$MeOC_6H_4$	97	174—175	489(M^+)	3520, 3340	1675, 1600
6f	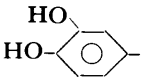	78	247—248(dec)	—[b]	3640, 3480, 3300	1650, 1600
6g	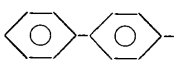	79	182(dec)	581(M^+)	3500, 3350	1680, 1600
6h	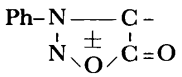	Quant	115(dec)	—[b]	3460, 3400, 3300	1780, 1660, 1580
6i	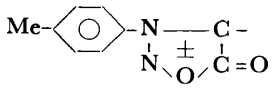	74	143—144(dec)	—[b]	3750, 3660, 3470, 3330	1780, 1670, 1590
6j	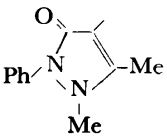	Quant	118—119	—[b]	3500, 3400, 3300	1660, 1640

a) Satisfactory analyses (±0.3% for C,H, and N) were obtained. b) No molecular ion peak was observed.

intermediate as shown in Scheme 3.

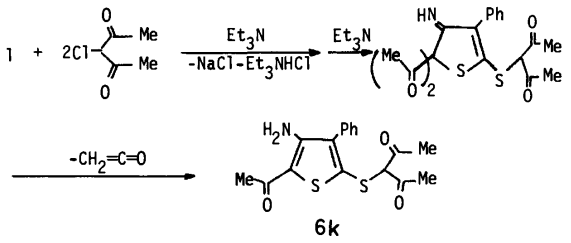

Scheme 3.

Experimental

Typical Procedure for the Preparation of Thiophenes. Preparation of 3-Amino-2-benzoyl-5-phenacylthio-4-phenylthiophene (6a): To a stirred suspension of 2.15 g (10 mmol) of sodium cyanophenyldithioacetate (**1**)[3] and 1.4 ml (10 mmol) of triethylamine in 30 ml of ethanol was gradually added a solution of 4.00 g (20 mmol) of phenacyl bromide in 20 ml of ethanol at room temperature. After about 2 h of stirring, additional triethylamine (1.4 ml) was added and the reaction mixture was refluxed for 1 h or stirred for 10 h at room temperature. The reaction mixture was evaporated to dryness under reduced pressure. The residue was mixed with water, and insoluble solid was collected by filtration. 4.29 g (quant). Recrystallization from DMF-ethanol provided pure **6a** as light yellow needles. Mp 164—165 °C. IR (KBr) 3500, 3400 (ν_{NH}), 1700, and 1600 cm^{-1} ($\nu_{C=O}$). ^{1}H NMR (DMSO-d_6) δ= 3.27 (s, 2H, SC$\underline{H}_2$), 4.70 (s, 2H, N$\underline{H}_2$), and 7.10—8.07 (m, 15H, $C_6\underline{H}_5$). MS: *m/z* 429 (M^+). Found: C, 69.79; H, 4.28; N, 3.27%. Calcd for $C_{25}H_{19}NO_2S_2$: C, 69.90; H, 4.46; N, 3.26%.

Preparation of 2-Acetyl-3-amino-4-phenyl-5-(diacetylmethylthio)thiophene (6k): In a similar manner, **6k** was obtained from 3-chloro-2,4-pentanedione and **1** in 57% yield. Recrystallization from aq ethanol provided pure **6k** as yellow needles. Mp 125 °C. IR (KBr) 3390, 3280, 3200 (ν_{NH}), 1605, 1590 cm^{-1} ($\nu_{C=O}$). ^{1}H NMR (DMSO-d_6) δ=2.22 (s, 3H, C$\underline{H}_3$), 2.40 (s, 6H, C$\underline{H}_3$COCH), 3.44 (broad s, 1H, SC$\underline{H}$), 6.90 (broad s, 2H, N$\underline{H}_2$), and 7.38—7.80 (m, 5H, $C_6\underline{H}_5$). MS: *m/z* 347 (M^+). Found: C, 58.60; H, 4.79; N, 4.14%. Calcd for $C_{17}H_{17}NO_3S_2$: C, 58.77; H, 4.93; N, 4.03%.

We are grateful for valuable discussion with Profs. H.-J. Tien and M.-Y. Yeh of National Cheng Kung University (Republic of China, Taiwan), and thank Mr. C.-S. Chen for doing part of the experiments.

References

1) a) T. Fuchigami and T. Nonaka, *J. Org. Chem.*, **48**, 3340 (1983); b) T. Fuchigami, M.-Y. Yeh, T. Nonaka, and H.-J. Tien, *Bull. Chem. Soc. Jpn.*, **56**, 3851 (1983).

2) F. M. Abdelrazek, N. S. Ibrahim, Z. E. Kandeel, M. H. Elnagdi, *Synthesis*, **1984**, 970.

3) M. Davis, G. Snowling, and R. W. Winch, *J. Chem. Soc. (C)*, **1967**, 124.

4) The open-chain intermediate **3a** which showed IR absorpotion of a cyano group around 2200 cm^{-1} was isolated and it underwent cyclization quantitatively by treatment with triethylamine.

5) a) F. H. C. Stewart, *Chem. Rev.*, **64**, 129 (1964); b) M. Ohta and H. Kato, "Non-benzenoid Aromatics," Academic Press, New York (1969), Vol. 1, p. 117; c) C. G. Newton and C. A. Ramsden, *Tetrahedron*, **38**, 2965 (1982).

6) a) F. H. C. Stewart, *J. Chem. Soc.*, **1963**, 701; b) H.-J. Tien, K. Kanda, A. Chinone, and M. Ohta, *Bull. Chem. Soc. Jpn.*, **46**, 3304 (1973); c) H.-J. Tien and M.-Y. Yeh, *J. Chinese Chem. Soc. (Taipei)*, **24**, 123 (1977); d) M.-Y. Yeh, T. Nonaka, T. Goto, M.-C. Hsu, T. Fuchigami, and H.-J. Tien, *Bull. Chem. Soc. Jpn.*, **56**, 3535 (1983); e) T. Fuchigami, M.-Y. Yeh, T. Goto, T. Nonaka, and H.-J. Tien, *ibid* **57**, 116 (1984); f) T. Fuchigami, T. Goto, M.-Y. Yeh, T. Nonaka, and H. -J. Tien, *ibid.*, **57**, 1362 (1984).

Photochromism of Benzylviologens Containing Methyl Groups on Pyridinium Rings and Embedded in Solid Poly(*N*-vinyl-2-pyrrolidone) Matrix

Hiroyoshi KAMOGAWA* and Masashi SUGIYAMA
Department of Applied Chemistry, Yamanashi University, Takeda 4, Kofu 400
(Received March 18, 1985)

Synopsis. Benzylviologens with 2,2′- and 3,3′-dimethyl groups embedded in poly (*N*-vinyl-2-pyrrolidone) matrix indicate reversible photochromisms with absorption maxima at 605 and 775 nm under light, respectively, which are different from those (610, 570 nm) of conventional benzylviologens.

It is known that viologens embedded in solid poly (*N*-vinyl-2-pyrrolidone)(PVP) matrix undergo rapid reversible photoreductions in the air, which are clearly recognized by a deep color development ascribable to the formation of viologen radical cations (photochromism).[1,2]

The effect of the introduction of the methyl group in 2,2′- and 3,3′-positions of the pyridinium rings on the photochromic behavior of benzylviologens is the object of the present study.

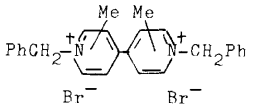

2, 2′-Me **1**
3, 3′-Me **2**

Compounds **1** and **2** were prepared from 2,2′- and 3,3′-dimethyl-4,4′-bipyridyls, respectively, by the Menschutkin Reaction.

Figure 1 indicates the absorption spectra of PVP films containing viologens under exposure to UV light. Table 1 also gives data for photochromic behaviors of these films. Two remarkable features are recognized from these results. The absorption maximum for the colored form of **1**, *i.e.* radical cations, in Fig. 1 is located at 605 nm, which is almost the same as those for conventional viologen radical cations without ring substituents,[3] whereas that for **2** is remarkably red-shifted (775 nm) and the photosensitivity of **2** is lower than **1** (Table 1). This may indicate that the methyl substituents at 3 and 3′ positions of **2** hinder sterically the overlappings of the π-orbitals of the pyridine rings of viologen. The reason of the red-shift is unknown at present time, although the shape of curve III in Fig. 1 is somewhat different from II, which is a typical curve for viologen radical cation.[3] Another feature is that, in the absorption spectrum of the colored form of **1** (II in Fig. 1), no peaks for aggregated forms are recognized, whereas for conventional benzyl viologen dibromide (I) a distinct peak for the aggregated forms (570 nm)[3] is seen under the same film-forming conditions, there by indicating that the presence of 2,2′-methyl groups hinders the aggregation of viologen radical cations to a significant extent.

Accordingly, it is concluded that the introduction of simple methyl groups on the pyridinium rings of viologen dications brings about marked effects on the photochromic behavior in PVP matrix.

TABLE 1. PHOTOCHROMIC BEHAVIORS OF COMPOUNDS **1** AND **2** IN PVP MATRIX

Viologen	Irradiation[a] time/s	Absorption peak/nm	Absorbance[b] /mm^{-1}	Half-recovery[c] /min
Benzyl viologen dibromide	30	610	4.82	30
		570[d]	—	—
1	30	605	4.42	20
2	60	775	2.65	30

a) At a distance of 10 cm from a 75W Hg lamp. b) Reduced to 1 mm of film thickness. c) Recoveries in the dark were complete for all films. d) Peak for aggregate.

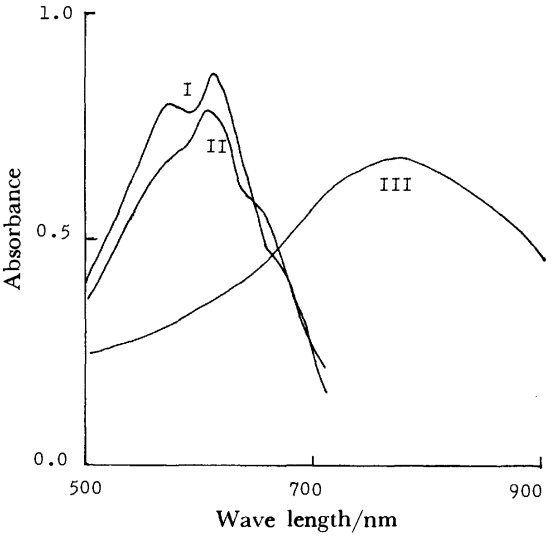

Fig. 1. Color development of viologens in PVP matrix under exposure to UV light.
I: Benzyl viologen dibromide, II: compound **1**, III: compound **2**.
Irradiations of films were carried out at a distance of 10 cm from a 75W Hg lamp. Irradiation times were 30, 30, and 60 s for I, II, and III, respectively.

Experimental

Infrared, ^{1}H NMR, and mass spectra were recorded on a Hitachi 215 spectrophotometer, a JNM-PMX 60 spectrometer, and Hitachi RMU-6 spectrometer, respectively, under standard conditions. Elemental analyses were carried out with a Perkin-Elmer 250 instrument.

2,2′-Dimethyl-4,4′-bipyridyl. A mixture of α-picoline (81 g, 0.87 mol) and sodium metal (1.0 g, 0.043 mol) was first stirred at 20 °C for 48 h with exclusion of moisture and then

kept at 115 °C for 16 h. Oxygen was then bubbled through the mixture kept at 90 °C until the initial dark color disappeared (15 h). The reaction mixture was distilled to remove excess picoline, the residue was crushed to powder with addition of ether (50 ml), and water (2 ml) was added, followed by stirring for 10 min. Ether extraction was then made and the organic layer was dried over anhydrous sodium sulfate, followed by evaporation *in vacuo*. An excess of concd hydrochloric acid was added, the mixture was evaporated, and an equal volume of ethanol was added to the residue. Upon cooling in a refrigerator overnight, the resulting precipitate was filtered and washed with ethanol. Isolation of the product was done by dissolving the precipitate in water (10 ml) and then adding 1 M sodium hydroxide (1 M=1 mol dm^{-3}) solution (10 ml) and ether (50 ml) to effect extraction. The organic layer was washed with water, dried over anhydrous sodium sulfate, and evaporated *in vacuo*. The residue was recrystallized from benzene–hexane to afford crystals of mp 74—75 °C in 2% yield: Found: C, 78.24; H, 6.69; H, 15.07%. Calcd for $C_{12}H_{12}N_2$: C, 78.23; H, 6.57; N, 15.20%. IR (KBr) 3050 (aromatic), 3000—2900 (Me) cm^{-1}. NMR ($CDCl_3$) δ=2.6 (s, 6H, Me), 7.4 (d, 4H, pyridyl), 8.6 (d, 2H, pyridyl). MS (rel. intensity) 185 (M^+, 100).

3,3′-Dimethyl-4,4′-bipyridyl. The same procedure as that for the 2,2′-isomer was employed using β-picoline instead of the α-isomer to afford crystals of mp 120—122 °C in 2% yield: Found: C, 78.17; H, 6.63; N, 15.19%. Calcd for $C_{12}H_{12}N_2$: C, 78.23; H, 6.57; N, 15.20%. IR (KBr) 3050 (aromatic), 3000—2900 (Me) cm^{-1}. NMR ($CDCl_3$) δ=2.1 (s, 6H, Me), 7.0 (d, 2H, pyridyl), 8.6 (d, 4H, pyridyl). MS (rel. intensity) 185 (M^+, 100).

1,1′-Dibenzyl-2,2′-dimethyl-4,4′-bipyridylium Dibromide (1). A solution of 2,2′-dimethyl-4,4′-bipyridyl (2.0 g, 13 mmol) and benzyl bromide (3.9 g, 26 mmol) in anhydrous acetonitrile (40 ml) was heated under reflux for 15 h. The resulting precipitate was filtered and recrystallized from methanol–ether to afford a pale yellow crystals in 87% yield. Found: C, 59.46; H, 4.95; N, 5.20%. Calcd for $C_{26}H_{26}N_2Br_2$: C, 59.33; H, 4.98; N, 5.32%. IR (KBr) 3050 (aromatic), 3000—2900 (CH_3, CH_2) cm^{-1}. NMR (D_2O) δ=3.0 (s, 6H, Me), 6.0 (4H, CH_2), 7.6 (m, 10H, Ph), 8.5 (t, 4H, pyridylium), 9.1 (d, 2H, pyridylium).

1,1′-Dibenzyl-3,3′-dimethyl-4,4′-bipyridylium Dibromide (2). The same procedure as that for **1** was employed using 3,3′-dimethyl-4,4′-bipyridyl instead of the 2,2′-isomer to afford a colorless crystalline powder in 87% yield. Found: C, 59.38; H, 4.89; N, 5.34%. Calcd for $C_{26}H_{26}N_2Br_2$: C, 59.33; H, 4.98; N, 5.32%. IR (KBr) 3050 (aromatic), 3000—2900 (CH_3, CH_2) cm^{-1}. NMR (D_2O) δ=2.3 (s, 6H, Me), 5.9 (s, 4H, CH_2), 7.6 (s, 10H, Ph), 8.1 (m, 2H, pyridylium), 9.0 (d, 4H, pyridylium).

Measurement of Photochromism. *(1) Film Preparation*: A solution of viologen (20 mg) and PVP (500 mg; MW 10000) in water (5 ml) was spread over a glass plate so as to cover an area of 1.2×2 cm. The glass plate was then stored in a desiccator ($CaCl_2$) overnight to make a transparent and almost colorless film. The films thus prepared were stored in a desiccator over saturated aqueous NaBr (RH, 58% at 20 °C) except for exposure to light and measurements of absorption spectra.

(2) UV-irradiation: Films were exposed to light at a distance of 10 cm from a 75 W mercury lamp (Toshiba SHL-100UV-2). Absorption spectra of the irradiated films were measured with a Hitachi 200-10 spectrophotometer. The absorbances thus obtained were reduced to values for 1 mm of film thickness.

References

1) H. Kamogawa, T. Masui, and M. Nanasawa, *Chem. Lett.*, **1980**, 1145.

2) H. Kamogawa, T. Masui, and S. Amemiya, *J. Polymer Sci., Polymer Chem. Ed.*, **22**, 383 (1984).

3) E. M. Kosower and J. L. Cotter, *J. Am. Chem. Soc.*, **86**, 5524 (1964).

The Reaction of Cyclopropenethione with Carbonyl-stabilized Phosphonium Methylides to Yield 2*H*-Pyran-2-thione

Hiroshi YOSHIDA,* Jyun SHIMIZU, Tsuyoshi OGATA, and Kiyoshi MATSUMOTO†
Department of Applied Chemistry, Faculty of Engineering, Shizuoka University, Hamamatsu 432
†*College of Liberal Arts and Sciences, Kyoto University, Kyoto 606*
(Received April 10, 1985)

Synopsis. The reaction of diphenylcyclopropenethione with carbonyl-stabilized triphenylphosphonium methylides (**2**) to yield 2*H*-pyran-2-thiones was studied. It was clarified that electron-releasing substituents increased the reactivity of **2**.

The reactions of carbonyl-stabilized pyridinium and sulfonium methylides with cyclopropenone or cyclopropenethione to yield 2-pyrone derivatives[1,2] are well known. On the other hand the reaction of diphenylcyclopropenone with acyl- or alkoxycarbonyl-stabilized phosphonium methylides yields either 2-pyrone or methylenecyclopropene *via* (3+3)-cycloaddition or Wittig reaction.[1,2] However to our knowledge none of the reaction of diphenylcyclopropenethione (**1**) with carbonyl-stabilized phosphonium methylides (**2**) has been investigated.

In the continuation of our studies on the reaction of cyclopropenone with S-, N-, and P-ylides and imides,[3] we extended our attention to the use of carbonyl-stabilized phosphonium methylides (**2**) which are stable to air and moisture.

Methylides **2** were prepared according to the known methods.[4] Since **1** dimerizes on irradiation,[5] it was treated in the dark. Although a benzene solution of **1** and 1-(triphenylphosphoranylidene)-2-propanone **2a** at reflux gave only a tarry mixture, the reaction at room temperature for 3 d yielded a brown crystalline mass (51%) together with triphenylphosphine in 84% yield after TLC purification. The structure of the product was confirmed to be 3,4-diphenyl-6-methyl-2*H*-pyran-2-thione **3a** on the basis of IR ($\nu_{C=S}$ 1130 cm^{-1}) and NMR spectroscopic studies. The ^{13}C-NMR spectrum of **3a** gave a doublet at δ=111.1 (C^5, $J_{C^5H^5}$=170 Hz) and a quartet at δ=20.2 (C^7, $J_{C^7H^7}$=140 Hz) with long range couplings $J_{C^7H^5}$=3, $J_{C^5H^7}$=4, and $J_{C^5H^5 \text{ and } H^7}$=6 Hz), indicating the presence of the framework:

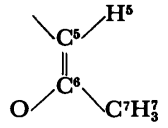

A similar treatment of the carbonyl-stabilized methylides **2b—d** with **1** afforded 2*H*-pyran-2-thiones **3b—d**. The methylides substituted with aroyl groups **2e—i** were less reactive toward **1** than **2a—d**. Thus, the ylides **2e—i** reacted with **1** at toluene reflux to give **3e—i** in moderate yields (Table 1 and 2). The known 2*H*-pyron-2-thione **3f** was obtained in a higher yield than the previously reported (71%).[2] Physical properties are collected in Table 2.

As is evident from the Table 1, increasing the electron releasing power of the substituent R increases the reactivity of **2**. The result correlates well with the reported mechanism for the reaction of cyclopropenone with S- and P-ylides.[1] Thus, the formation of 2*H*-pyran-2-thiones can be explained either by an initial attack on the thiocarbonyl group of **1** by the betaine oxygen atom of **2** or a Michael type addition of the methine of **2** to the C=C bond of **1** followed by isomerization to yield the product.

In conclusion, phosphonium methylides **2** have proven to be convenient reagents for the preparation of 2*H*-pyran-2-thiones in moderate yields.

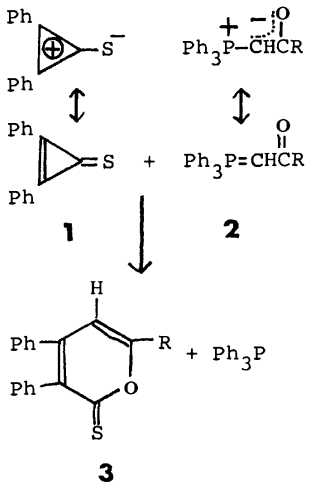

2 3	R
a	Me
b	H
c	NMe_2
d	SMe
e	C_6H_4Me-4
f	C_6H_5
g	C_6H_4Br-4
h	$C_6H_4NO_2$-3
i	$C_6H_4NO_2$-4

Scheme 1.

Experimental

General. Melting points are uncorrected. ^{1}H-NMR spectra were recorded on a Hitachi R-24B (60 MHz) spectrometer using TMS as an internal standard and ^{13}C-NMR spectra on a JEOL JNM FX-60 spectrometer (15.04 MHz).

Materials. Diphenylcyclopropenethione **1** was prepared according to the literature.[6] Phosphonium methylides

Table 1. The reaction of **1** with **2**.

2	Reaction Temp/°C	Conditions Time	Yield **3**/%
2a	25	3d	51
2b	25	4d	39
2c	25	1d	72
2d	25	1d	46
2e	110	6h	74
2f	110	8h	87
2g	110	4d	70
2h	110	6d	39
2i	110	6d	37

TABLE 2. PHYSICAL PROPERTIES OF **3**.

3	Mp θ_m/°C	^{1}H-NMR($CDCl_3$)	MS(M^+)	Found/% (Calcd/%) C	H	N
3a	135—137	2.43(3H, s, Me), 6.43(1H, s, C_6H), 6.8—7.6(10H, m, Ar)	278	77.92	4.87	
				(77.66	5.06	)
3b	148	6.57(1H, d, J=5Hz, C_5H), 6.8—7.4(10H, m, Ar), 7.78(1H, d, C_6H)	264	77.05	4.47	
				(77.24	4.57	)
3c	151—152	3.05(6H, s, 2Me), 5.44(1H, s, C_6H), 6.6—7.2(10H, m, Ar)	307	74.42	5.51	4.37
				(74.24	5.57	4.56)
3d	96—103	2.70(3H, s, Me), 6.70(1H, s, C_6H), 7.0—7.9(10H, m, Ar)	310	69.71	4.65	4.94
				(69.64	4.54	5.15)
3e	194—196	2.28(3H, s, Me), 6.7—7.9(14H, m, Ar)	354	81.16	5.32	
				(81.32	5.11	)
3f	169—170[a]	6.9—7.8(m, Ar)	340			
3g	210—211	6.6—7.9(m, Ar)	419	65.71	3.92	
				(65.87	3.60	)
3h	213—214	6.9—8.1(m, Ar)	385	71.73	3.84	3.52
				(71.67	3.92	3.63)
3i	194—196	6.5—8.4(m, Ar)	385	71.85	3.74	3.90
				(71.67	3.92	3.63)

a) Ref. mp 165—166°C.[2]

2 were obtained by the known methods.[4]

Reaction of 1 with 2. An equimolar mixture of **1** and **2** (**2a—d** in benzene at room temperature and **2e—i** in toluene at reflux temperature) was allowed to react in the dark. The disappearance of **1** was checked by TLC at suitable time intervals. Then, the solvent was removed *in vacuo* to give a crystalline mass. TLC separation over silica gel afforded **3** and triphenylphosphine. Yields and physical properties of **3a—i** are summarized in Tables 1 and 2.

^{13}C-NMR spectroscopic data. **3a**($CDCl_3$) δ=20.2 (q, Me), 111.1 (d, C^5), 127.5 (d), 127.9 (d), 128.0 (d), 128.4 (d), 128.7 (d), 130.6 (d), 136.1 (s), 136.8 (s), 137.0 (s), 147.9 (s), 165.8 (s, C^6), and 198.0 (s, C^2). **3f** ($CDCl_3$) δ=108.5 (d, C^5), 125.7 (d), 127.5 (d), 127.9 (d), 128.1 (s), 128.4 (d), 128.7 (d), 129.0 (d), 130.4 (s), 130.6 (d), 131.3 (d), 136.8 (s), 137.0 (s), 137.4 (s), 147.7 (s), 164.4 (s, C^6), and 196.9 (s, C^2).

References

1) K. T. Potts and J. S. Baum, *Chem. Rev.*, **74**, 189 (1974); K. Matsumoto and Y. Ikemi, *Heterocycles*, **14**, 1445 (1980) and references cited therein.

2) T. Eicher, E. Angerer, and A. Hansen, *Justus Liebigs Ann. Chem.*, **746**, 102 (1971); T. Eicher, U. Sebold, and U. Stegmann, *Tetrahedron Lett.*, **24**, 2977 (1983) and references cited therein.

3) H. Yoshida, S. Sogame, Y. Takishita, and T. Ogata, *Bull. Chem. Soc. Jpn.*, **56**, 2438 (1983).

4) H. J. Bestmann and R. Zimmermann, "Organic Phosphorus Compounds," ed by G. M. Kosolapoff and L. Maier, Wiley-Interscience, New York (1972) Vol. 3.

5) A. Schoenberg and M. Mamluk, *Tetrahedron Lett.*, **1971**, 4993.

6) H. Yoshida, M. Nakajima, and T. Ogata, *Synthesis*, **1981**, 36.

Rapid Spectrophotometric Determination of Chromium(III) with 1-(2-Thiazolylazo)-2-naphthol in Presence of Surfactant

Gogineni V. RATHAIAH and Muppalla C. ESHWAR*
Department of Chemistry, Indian Institute of Technology, Bombay-400 076, India
(Received May 7, 1984)

Synopsis. Chromium(III) reacts with 1-(2-thiazolylazo)-2-naphthol at 80—95 °C in acid media (pH 5.7), in presence of benzoate and sodium dodecyl sulfate. Presence of surfactant increases sensitivity of the complex and reduces heating time to 5 min, thus giving rise to perhaps the most rapid method for absorptiometric determination of chromium(III). The 1:1 complex obeys Beer's law for 0.2 to 2.4 μg of Cr(III) per ml, has molar absorptivity and Sandell sensitivity of 1.46×10^4 dm^3 mol^{-1} cm^{-1} and 3.5 ng cm^{-2} respectively, at 575 nm.

Among various pyridylazo and thiazolylazo derivatives, 1-(2-pyridylazo)-2-naphthol (PAN),[1] 4-(2-pyridylazo)resorcinol (PAR),[2] 4-(2-thiazolylazo)resorcinol (TAR)[3] have been reported for spectrophotometric determination of chromium(III). These methods require 45, 35, and 45 min of heating time respectively, at elevated temperatures. The methods reported by Yotsuyanagi *et al.*[4] Yamamoto[5] with PAR require 130 and 20 min of heating respectively, and the latter method employs hydrogen peroxide to oxidise Cr(III) to Cr(VI). Sodium benzoate has been reported to exert catalytic influence in reducing the heating time for chromium(III)-EDTA reaction.[6] Surfactants find increased application in studies of metal-ligand complexes due to enhanced sensitivity obtained. Hence, the reaction between chromium(III) and 1-(2-thiazolylazo)-2-naphthol (TAN) has been studied in presence of surfactants and benzoate.

Experimental

Apparatus and Reagents. A Spectromom 204 spectrophotometer with matched 10 mm cells was used for all absorbance measurements. The absorption spectra were recorded on a Varian Superscan 3 UV-Visible spectrophotometer. For pH measurements an EC-pH meter (Model 822) was used.

1.923 g of chromium nitrate was dissolved in 250 ml of 2% nitric acid, the solution standardised titrimetrically[7] and diluted as required. A 0.2% (w/v) methanolic solution of TAN was prepared from 1-(2-thiazolylazo)-2-naphthol (Fluka A.G. purum). A buffer solution of pH 5.7 was prepared from 0.5 mol dm^{-3} solutions of sodium benzoate (dissolved in warm water and cooled) and benzoic acid. A 5% (w/v) solution of sodium dodecyl sulfate was prepared with hot water and cooled to room temperature.

General Procedure. An aliquot of solution containing <60 μg of chromium(III) was taken in a 25 ml volumetric flask, added 5 ml of buffer solution, 4 ml of SDS solution and 3 ml of TAN solution. The reaction mixture was heated on a water bath for 5 min around 90 °C, flask cooled to room temperature and contents diluted to 25 ml. The absorbance of the complex was measured at 575 nm against a reagent blank, prepared under identical conditions.

Results and Discussion

Due to inert nature of $[Cr(H_2O)_6]^{3+}$, the reaction between chromium(III) and TAN at room temperature required 24 and 4 h in presence of acetate and benzoate respectively, maximum absorbance being attained in 50% solutions of methanol or *t*-butyl alcohol. Eventhough ionic surfactants dissolved the sparingly soluble complex, it was still necessary to wait for very long intervals of time. For example, in presence of SDS, maximum absorbance was reached only after 38 and 8 h in presence of acetate and benzoate respectively. Hence, the reaction was studied at elevated temperatures in presence of SDS, acetate and benzoate.

Effect of Heating. When the reaction mixture was heated to different temperatures, from 40 to 100 °C, maximum absorbance was observed on heating at ≥80 °C. Hence, reaction mixture was heated at 90 °C.

Complications arose when the time of heating was varied. When the reaction was carried out with 1 ml of 0.1% TAN, time required for complexation was reduced to 30 and 10 min in presence of acetate and benzoate respectively, the resulting complex requiring 50% methanol or *t*-butyl alcohol for dissolution. On further addition of TAN, the complex did not dissolve in any of the water-miscible solvents, but was soluble in some immiscible solvents (max. absorbance in 1-butanol). In latter case, complexation required heating for 60 and 40 min in presence of acetate and benzoate respectively and even then results were not satisfactorily reproducible. However, addition of SDS resulted, besides dissolution of the complex, in a further decrease in reaction time to 4 min at 90 °C both in presence and absence of acetate or benzoate. Hence, reactants were heated for 5 min at 90 °C.

Effect of Sodium Dodecyl Sulfate. On addition of 1 to 8 ml of 5% SDS at least 2 ml of SDS was required for dissolution of the complex, and absorbance remained uneffected with higher volumes. Hence, 4 ml of SDS solution was employed in all studies.

Effect of pH and Benzoate. pH of the solution containing 40 μg of Cr(III) and 4 ml of SDS was varied from 3.0 to 8.0, and maximum absorbance was observed in the pH range 5.4 to 6.2 (Fig. 1, curve a). Hense, pH of 5.7 was maintained in all studies. When attempts were made to maintain the pH with various buffers, only acetate and benzoate buffers were found to be satisfactory and an increase in their concentration resulted in an increase in absorbance of the complex. Maximum absorbance was observed on addition of 1 to 8 ml of 0.5 mol dm^{-3} solutions of benzoate, while further addition of benzoate resulted in a decrease in absorbance. Studies with acetate of different concentrations resulted in lower absorbance. Hence, 5 ml of benzoate buffer was employed in all studies. The increase in sensitivity caused by benzoate may be seen from Fig. 1, curve b, which shows the effect of pH on absorbance in presence of 5 ml of 0.5 mol

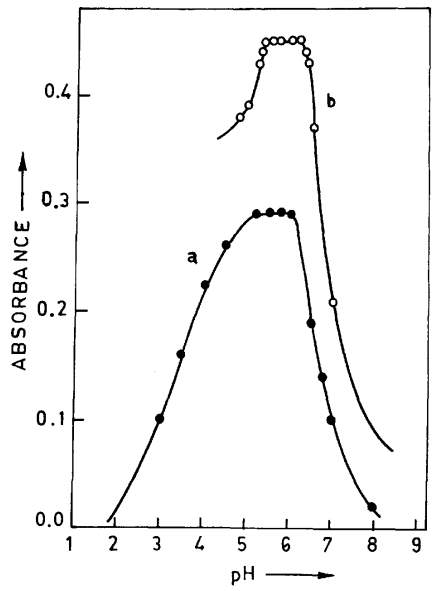

Fig. 1. Effect of pH on Absorbance. See the text for a and b.

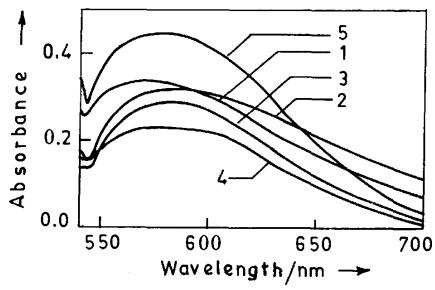

Fig. 2. Absorptin Spectra.
Curves 1, 2, 3, 4, and 5 are as in Table 1 [Cr(III)]=3.077×10 mol dm^{-3}; [TAN]=9.4×10^{-4} mol dm^{-3}; SDS=0.8%; [Benzoate]=[Acetate]=0.1 mol dm^{-3}.

dm^{-3} benzoate.

Effect of Reagent Concentration. Amount of reagent (0.1% TAN) was varied from 0.25 to 8 ml and maximum absorbance observed with ≥5.0 ml. Hence, 3.0 ml of 0.2% TAN was employed for all studies.

Absorption Spectra. Figure 2 gives absorption spectra of different systems *vs.* appropriate reagent blank. Since the complex formed in presence of SDS and benzoate exhibited maximum sensitivity (Table 1) at 575—580 nm, all measurements were made at 575 nm. Reagent blank for all systems exhibited maxium absorbance at 490 nm. All systems were heated for 5 min.

Composition. Composition of the complex established by Job's continuous variation method and mole ratio method, was found to be 1:1, metal to ligand.

Beer's Law, Sensitivity, and Stability. The Cr(III)-TAN-benzoate-SDS complex obeyed Beer's law in the concentration range 5 to 60 μg of chromium(III) per 25 ml. The apparent molar absorptivity of the complex, calculated from Beer's law plot, was 1.46×10^4 dm^3 mol^{-1} cm^{-1} and Sandell sensitivity 3.5 ng cm^{-2}. Table 1 presents sensitivity of complexes obtained by various systems. The complex was found to be stable for 24 h.

Table 1. Sensitivity of the complexes

Sr. No.	Complex	λ_{max}/nm	Sensitivity ng cm^{-2}	ε 10^4 dm^3 mol^{-1} cm^{-1}
1	Cr(III)+TAN+ acetate[a)]	565	4.7	1.09
2	Cr(III)+TAN+ benzoate[a)]	580—590	5.0	1.04
3	Cr(III)+TAN+ SDS	580	5.5	0.95
4	Cr(III)+TAN+ SDS+acetate	580	6.9	0.75
5	Cr(III)+TAN+ SDS+benzoate	575—580	3.5	1.46

a) In 50% *t*-butyl alcohol.

Effect of Diverse Ions. Effect of various ions, usually associated with chromium(III), was studied in the determination of 40 μg of Cr(III) per 25 ml. $EDTA^{4-}$ caused negative interference, while positive interference was shown by Fe(II), Ni(II), Zn(II), and Bi(III) in all proportions. Tolerance limits (in μg) of various ions are: Cl^- Br^-, I^-, 10000; Mg(II) 2500; Ca(II), thiourea, $NH_2OH \cdot HCl$, $N_2H_4H_2SO_4$ 2000; Pt(IV) 1500; Sr(II), Ba(II), Th(IV), CN^- 1000; SCN^- 750; Be(II), Mo(VI), $S_2O_3^{2-}$ 500; Au(III), W(VI), PO_4^{3-} 250; Mn(II), V(V) 200; tartrate, oxalate, Ag(I), Hg(II), Sc(III), Zr(IV), Cr(VI) 100; Pd(II), Ru(III), V(IV) 50; citrate, Co(II), Pb(II), Fe(III), Y(III), Ce(III), Ga(III), Hf(IV), Sb(III), U(VI) 25; In(III) Rh(III) 10. Fluoride was employed to mask Be(II), Sc(III), Zr(IV), and Th(IV), whereas CN^- was employed to mask Mn(II), Co(II), Cu(II), Hg(II), and Fe(III).

Precision and Accuracy. Relative standard deivation and relative mean error, calculated from ten repeat determinations, were found to be ±0.41% and ±0.72% respectively.

Application to Analysis of High Speed Steel. 0.2 g of high speed steel was treated with 15 ml of concd HCl and 5 ml of concd HNO_3, the precipitated tungstic acid filtered off, and filtrate diluted to 100 ml. An aliquot of this was acidified with HCl to 3.5 mol dm^{-3} and iron removed by extraction with mesityl oxide.[8)] Aqueous layer was evaporated to dryness, dissolved in water, pH adjusted to 5.7 and chromium content determined as described in general procedure. From duplicate analysis, amount of chromium was found to be 3.9 and 3.94% against theoretical value of 4.0%. Other constituents of alloy are W=18%, V=1.0% and rest iron.

References

1) S. G. Nagarkar and M. C. Eshwar, *Indian J. Tech.*, **13**, 377 (1975).
2) B. Subrahmanyam and M. C. Eshwar, *Bull. Chem. Soc. Jpn.*, **49**, 347 (1976).
3) B. Subrahmanyam and M. C. Eshwar, *Mikrochim. Acta*, **1976II**, 579.
4) T. Yotsuyanagi, Y. Takeda, R. Yamashita, and K. Aomura, *Anal. Chim. Acta*, **67**, 297 (1973).
5) K. Yamamoto, *Bunseki Kagaku*, **27**, 460 (1978).
6) V. Linder, *Mikrochim. Acta*, **1980I**, 107.
7) A. I. Vogel, "A Text-book of Quantitative Inorganic Analysis," Longman, London (1968) p. 311.
8) V. M. Shinde and S. M. Khopkar, *Separ. Sci.*, **4**, 161 (1969).

Synthesis of New Heterocycles: Condensation of 2-Methyl-4*H*-naphth-[1,2-*d*][1,3]oxazin-4-one with Schiff Bases and Formation of 3-Aryl-2-styrylbenzo[*h*]quinazolin-4(3*H*)-ones

Mandala Satyanarayana REDDY and Chengalvala Venkata RATNAM*
Department of Chemistry, Osmania University, Hyderabad 500 007, India
(Received April 2, 1984)

Synopsis. Condensation of 2-Methyl-4*H*-naphth[1,2-*d*][1,3]oxazin-4-one (**2**) with Schiff bases (**3**) in acetic acid has resulted in 3-aryl-2-styrylbenzo[*h*]quinazolin-4(3*H*)-ones (**4**), characterized by spectral and analytical methods.

As a part of our work on the role of Schiff bases in heterocyclizations[1-8] and with a view to prepare hitherto unreported benzo[*h*]quinazolinones, the condensation of 2-methyl-4*H*-naphth[1,2-*d*][1,3]-oxazin-4-one with Schiff bases has been undertaken and the results are presented below.

The reaction of 1-amino-2-naphthalenecarboxylic acid (**1**)[9] with acetic anhydride under refluxing conditions yielded a colourless crystalline compound with mp 178°, identified as 2-methyl-4*H*-naphth[1,2-*d*][1,3]-oxazin-4-one on the basis of spectral and analytical values. Unlike the lactone bond of 2-methyl-3,1-benzoxazin-4-one,[10] which is vulnerable and is readily hydrolyzed to *N*-acetylanthranilic acid in contact with traces of moisture or on prolonged exposure to atmosphere, the lactone bond of **2** was found to be quite stable.

Condensation of compound **2** with an equimolar proportion of *N*-(*p*-methoxybenzylidene)aniline (**3**, Ar=*p*-methoxyphenyl; Ar′=phenyl) in acetic acid medium at steam bath temperature resulted in a yellow crystalline compound, mp 186° in high yield, characterized on the basis of its microanalytical, mass, IR, and ^{1}H-NMR spectral data as 2-(*p*-methoxystyryl)-3-phenylbenzo[*h*]quinazolin-4(3*H*)-one [**4b**; MS: M^+ at *m/z* 404, IR (KBr): $\nu_{C=O}$ at 1670 cm^{-1}, ^{1}H-NMR ($CDCl_3$): δ 3.7 (*s*, 3H, OCH_3) 6.3 (*d*, 1H, H-7, $J_{7,8}$=15 Hz), 6.7—8.0 (*m*, 14H, H-2 to H-6, H-9 to H-12 and five protons of 3-phenyl), 8.2 (*d*, 1H, H-8, $J_{8,7}$=15 Hz) and 9.1—9.3 (*m*, 1H, H-1)]. The *J* value (15 Hz) of the two olefinic protons (H-7 and H-8) suggested the preferred trans-geometry of the exocyclic double bond. Thus, it is apparent that **4b** is formed by styrylation of 2-methyl group and replacement of ring oxygen in **2** by *N*-phenyl moiety in one step.

This reaction has been extended to eleven other Schiff bases and the product obtained in each case has been characterized as corresponding 3-aryl-2-styrylbenzo[*h*]-quinazolin-4(3*H*)-one (**4a**—l, Scheme 1, Table 1) by analogy, spectral and microanalytical data.

To understand the mechanism of formation of **4**, the reactions of **2** with *p*-methoxybenzaldehyde and separately with aniline have been carried out under identical conditions of the Schiff base reaction. The former reaction resulted in the formation of 1-acetamido-2-naphthalenecarboxylic acid (**5**)[11] characterized by comparing with an authentic sample prepared from 1-amino-2-naphthalenecarboxylic acid and acetic anhydride and spectral data. Compound **5** must have been formed by the addition of elements of water obviously from solvent to the oxazinone ring followed by ring opening.

Oxazinone **2** with aniline gave a compound with mp 192°, characterized as 2-methyl-3-phenylbenzo[*h*]-quinazolin-4(3*H*)-one(**6**) by spectral data [MS: M^+ at *m/z* 286; IR (KBr): $\nu_{C=O}$ at 1675 cm^{-1}, ^{1}H-NMR ($CDCl_3$+DMSO-d_6): δ 2.3 (*s*, 3H, CH_3), 7.4—8.2 (*m*, 9H, aromatic) and 9.0 (*m*, 1H, H_a)] and microanalytical data. Reaction of **6** with *p*-methoxybenzaldehyde in hot acetic acid did not result in the styrylated product **4b**. However, **6** could be converted into **4b** on treatment with **3** (Ar=*p*-methoxyphenyl, Ar′=phenyl) under identical conditions. This result emphasises the superiority of Schiff bases over aldehydes in the styrylation of an active methyl group. Facile styrylation with Schiff base may be possibly due to better leaving ability of the arylamino moiety compared to hydroxyl, from the possible 2-[2-aryl-2-(arylamino)-ethyl]-3-phenyl benzo[*h*]quinazolin-4(3*H*)-one intermediate (**7**).

Based on these results, the formation of **4** from **2** and Schiff base (**3**) is explained on the basis of initial nucleophilic attack by active methyl group through the enamine tautomer. Its attack on the electrophilic carbon of azomethine function and subsequent transformations were described earlier.[7]

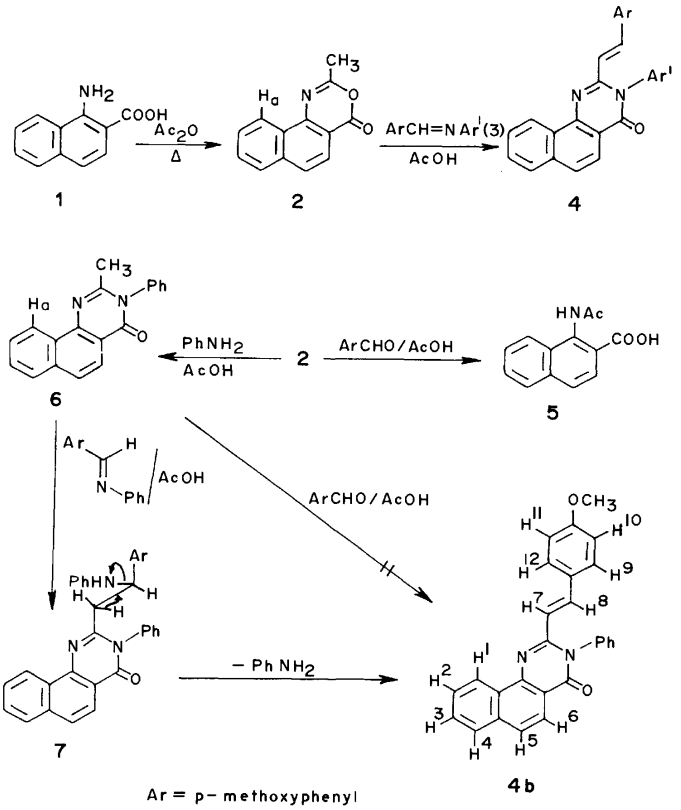

Scheme 1.

TABLE 1. CHARACTERIZATION DATA OF 3-ARYL-2-STYRYLBENZO[*h*]QUINAZOLIN-4(3*H*)-ONES (**4**)

Compd	Ar	Ar′	Mp θ_m/°C	Crystallized from	Yield/%	Mol. formula	C% Found	C% Calcd	H% Found	H% Calcd	N% Found	N% Calcd
4a	C_6H_5	C_6H_5	232	MeOH	80	$C_{26}H_{18}N_2O$	83.13	83.42	4.74	4.81	7.50	7.48
4b	4-$MeOC_6H_4$	C_6H_5	186	MeOH	75	$C_{27}H_{20}N_2O_2$	80.86	80.19	4.92	4.95	6.96	6.93
4c	4-MeC_6H_4	C_6H_5	218	MeOH	74	$C_{27}H_{20}N_2O$	83.65	83.51	5.32	5.15	7.18	7.21
4d	2-$NO_2C_6H_4$	C_6H_5	252	MeOH-CH_2Cl_2	70	$C_{26}H_{17}N_3O_3$	73.98	74.46	4.20	4.06	10.10	10.02
4e	4-ClC_6H_4	C_6H_5	230	MeOH-CH_2Cl_2	76	$C_{26}H_{17}N_2OCl$	77.02	76.37	4.26	4.16	6.90	6.86
4f	C_6H_5	4-$MeOC_6H_4$	233	C_6H_6-MeOH	78	$C_{27}H_{20}N_2O_2$	80.54	80.19	4.88	4.95	6.88	6.93
4g	C_6H_5	4-MeC_6H_4	220	MeOH	82	$C_{27}H_{20}N_2O$	83.14	83.51	5.24	5.15	7.26	7.21
4h	C_6H_5	4-ClC_6H_4	234	C_6H_6-MeOH	81	$C_{26}H_{17}N_2OCl$	76.52	76.37	4.02	4.16	6.90	6.84
4i	4-$MeOC_6H_4$	4-$MeOC_6H_4$	198	C_6H_6-MeOH	76	$C_{28}H_{22}N_2O_3$	77.63	77.42	5.12	5.07	6.38	6.45
4j	4-MeC_6H_4	4-$MeOC_6H_4$	191	MeOH-CH_2Cl_2	73	$C_{28}H_{22}N_2O_2$	80.12	80.38	5.20	5.26	6.76	6.69
4k	4-MeC_6H_4	4-MeC_6H_4	200	MeOH	75	$C_{28}H_{22}N_2O$	83.44	83.58	5.42	5.47	7.05	6.96
4l	4-ClC_6H_4	4-ClC_6H_4	253	MeOH-CH_2Cl_2	70	$C_{26}H_{16}N_2OCl_2$	70.87	70.43	3.68	3.61	6.50	6.33

IR(KBr): All the compounds showed a carbonyl stretching frequency around 1670 cm^{-1}

4a; MS: M^+ at *m/z*: 374; ^{1}H-NMR ($CDCl_3$): δ 6.5(*d*, 1H, olefinic, *J*=15Hz), 7.3—7.7(*m*, 15H, aromatic), 8.2(*d*, 1H, olefinic, *J*=15Hz), and 9.1—9.2(*m*, 1H, aromatic).

4c; MS: M^+ at *m/z*: 388; ^{1}H-NMR ($CDCl_3$): δ 2.3(*s*, 3H, methyl), 6.4(*d*, 1H, olefinic, *J*=15Hz), 7.1—7.8 (*m*, 14H, aromatic), 8.1(*d*, 1H, olefinic, *J*=15Hz), and 9.2(*m*, 1H, aromatic).

4f; MS: M^+ at *m/z*: 404; ^{1}H-NMR ($CDCl_3$): δ 3.8(*s*, 3H, methoxy), 6.6(*d*, 1H, olefinic, *J*=16Hz), 7.0—7.7(*m*, 14H, aromatic), 8.2(*d*, 1H, olefinic, *J*=16Hz), and 9.2(*m*, 1H, aromatic).

4g; MS: M^+ at *m/z*: 388; ^{1}H-NMR ($CDCl_3$): δ 2.5(*s*, 3H, methyl), 6.5(*d*, 1H, olefinic, *J*=15Hz), 7.2—7.7(*m*, 14H, aromatic), 8.2(*d*, 1H, olefinic, *J*=15Hz), and 9.2(*m*, 1H, aromatic).

4h, **4j**, and **4k**; MS: M^+ at *m/z*: 408, 418, and 402 respectively.

Experimental

Melting points are uncorrected. IR spectra were recorded on a Perkin-Elmer infracord 377 Spectrophotometer, ^{1}H-NMR spectra on Varian A-60D instrument using TMS as internal standard and mass spectra on a Perkin-Elmer Hitachi RMU-6L instrument.

1-Amino-2-naphthalenecarboxylic Acid (1): An ethanolic solution of potassium hydroxide (0.5 mol in 56 ml) was added to a boiling solution of 2-methyl-1-nitronaphthalene[12] (0.21 mol in 100 ml) during a period of 6 h and the resulting solution heated under reflux for a further period of 6 h. The mixture was steam-distilled to remove ethanol and then filtered. The filtrate was brought to the neutralization point first with strong acetic acid and then with dilute acetic acid. At first there comes down brown, flocculent precipitates which was discarded. The filtrate on further acidification gave light brown precipitates which was filtered after 2 h. The crude amino acid was purified by repeated dissolution in sodium hydroxide and precipitation with acetic acid, mp 198—199°, yield 10.4 g (26%).

2-Methyl-4H-naphth[1,2-d][1,3]oxazin-4-one (2): A mixture of 1-amino-2-naphthalenecarboxylic acid (3.74 g, 0.02 mol) and acetic anhydride (10 ml) was refluxed for 4 h, the resulting solution concentrated to one third and allowed to stand. The compound that separated was filtered, treated with charcoal and recrystallized from pet. ether (60—80°)-benzene, mp 178°, [MS: M^+ at *m/e* 211, IR (KBr): $\nu_{C=O}$ at 1745 cm^{-1}, ^{1}H-NMR ($CDCl_3$): δ 2.55 (*s*, 3H, CH_3) 7.5—8.2 (*m*, 5H, aromatic) and 8.7—8.9 (*m*, 1H, H_a); Found: C, 73.25; H, 4.32; N, 6.68%; $C_{13}H_9NO_2$ requires C, 73.93; H, 4.26; N, 6.64%].

Condensation of 2 with Schiff Bases (3): *General Procedure.* To a solution of **2** (2 m mol) in acetic acid (2 ml) was added the required Schiff base (**3**; 2 m mol) and the reaction mixture heated on a steam bath for half an hour and left aside for few minutes. The crystalline compound that separated in each case was filtered, washed with a few drops of methanol and recrystallized from appropriate solvent. The characterization data of benzo[*h*]quinazolinones (**4**) thus prepared are given in Table 1.

The acetic acid filtrate on dilution with water and processing the resulting solid gave additional quantities of **4**.

One of the authors (MSR) is thankful to the UGC, New Delhi, India for the award of a teacher fellowship.

References

1) V. Veeranagaiah, C. V. Ratnam, and N. V. Subba Rao, *Indian J. Chem.*, **10**, 133 (1972).
2) A. K. Sarojini, N. Sriramulu, and C. V. Ratnam, *Curr. Sci.*, **41**, 776 (1972).
3) P. Hanumanthu, S. K. V. Seshavatharam, C. V. Ratnam, and N. V. Subba Rao, *Proc. Indian Acad. Sci.*, **84**, 57 (1976).
4) P. Hanumanthu and C. V. Ratnam, *Indian J. Chem.*, **17B**, 349 (1979).
5) P. Hanumanthu and C. V. Ratnam, *Indian J. Chem.*, **15B**, 1019 (1977).
6) V. Bhasker Rao and C. V. Ratnam, *Indian J. Chem.*, **18B**, 409 (1979).
7) M. Satyanarayana Reddy, P. Hanumanthu, and C. V. Ratnam, *Indian J. Chem.*, **21B**, 646 (1982).
8) M. Satyanarayana Reddy and C. V. Ratnam, *Indian J. Chem.*, **22B**, 1100 (1983).
9) I. G. Farbenind, Ger. Patent 622308, Nov. 25, (1935); *Chem. Abstr.*, **30**, 1391 (1936).
10) M. T. Bogert, R. A. Gortner, and C. G. Amend, *J. Am. Chem. Soc.*, **33**, 949 (1911).
11) P. Friedlander and S. Littner, *Ber.*, **48**, 330 (1915).
12) H. E. Fierz-David and E. Mannhart, *Helv. Chim. Acta.*, **20**, 1024 (1937).

Triplet-Triplet Energy Transfer between the Same Molecular Species

Kunio MASUMO† and Nozomu EBARA*
Department of Chemistry, College of Arts and Sciences, The University of Tokyo, Komaba, Meguro-ku, Tokyo 153
(Received January 14, 1985)

A method for obtaining the rate constants for triplet-triplet energy transfer between the same molecular species is presented. It is an improvement on a previously proposed method and comprises an analysis of the phosphorescence decay curve of a mixture of an organic substance and its deuterated homolog. It has been found that the new method gives a good fit to experimental decay curves at 77 and 4.2 K. It was also found that the critical transfer distance between similar molecules is usually smaller than that between differrent molecules.

So far, very few investigations have been reported on the triplet-triplet energy transfer between the same molecular species. Photoselection[1] (or magneto-photoselection[2]), which consists of the measurement of the concentration depolarization of phosphorescence, has been the only investigative method until 1975. These methods, however, had a fatal drawback in that results could not evade the effect of a singlet-singlet transfer whenever it took place.[3]

The isotopic mixture method[4,5] and the ODMR method[6] were developed by one of the authors. The former method was based on the fact that some kinds of organic molecules (H) and their deuterated homologs (D) are quite similar in electronic structures, but are quite different regarding their phosphorescence lifetimes. It consists of analyzing the phosphorescence decay profile of a mixed solution of H and D, where the decay form tends to deviate from a mere superposition of each decay curve when an energy transfer takes place. This method is almost free from the effects of a singlet-singlet transfer since the extent of the initial triplet population is not important in the treatment. However, the analysis is inevitably crude due to the presence of a back transfer which precludes an exact statistical treatment. The latter method makes use of the fact that spin angular momentum must be conserved during an energy transfer. However, the spin-lattice relaxation taking place in a glassy solvent greatly affected the population of each spin sublevel, making a quantitative discussion almost impossible.

The present paper concerns an improvement in the isotopic-mixture method. First, in order to completely exclude any effect due to a singlet-singlet transfer, benzophenone was used as a sensitizer for initial pumping. Second, the experimental decay curves were analyzed by a computer-simulation method, rather than by seeking a solution to the rate equations in a closed form. Thus a more exact statistical treatment is now possible. Moreover, we have taken into account not only the D→H and H→D energy transfers, but also the D→D transfer. The last process may increase the possibility that the exitation on D happens to encounter an H molecule[7,8]. Inhomogeneous widths of the T_1 levels were also taken into consideration in order to account for the temperature dependence of energy-transfer efficiency.

Experimental

The samples used were naphthalene, phenanthrene, and biphenyl (H) together with their perdeuterated homologs (D). Equal molar amounts of H and D were dissolved in methyl methacrylate and deoxygenated by several freeze-thaw cycles. The sample solutions were polymerized at 100 °C for 48 h without an initiator and then annealed at 40 °C for 24 h. The initial concentration was 0.20, 0.15, 0.10 or 0.075 mol dm^{-3} for each component. In each case, benzophenone (0.20 mol dm^{-3}) was added as a sensitizer. The volume contraction according to polymerization was 1/1.27 and contraction by cooling was only a few percent; hence the latter effect was disregarded.

Samples were irradiated at 340 or 350 nm for 20 s using two shutters to excite only the benzophenone, and the total decays of the ensuing phosphorescence, containing H and D components simultaneously, were observed at 77 and 4.2 K. The output signals were accumulated 10—20 times to improve the S/N ratio.

Simulation

Simulation was carried out upon the following assumptions.

1) Solute molecules are randomly distributed in poly(methyl methacrylate) (PMMA); thus, the distribution of the nearest-neighbor distance (R) is[9]

$$\rho(R) = \rho(R, C) = 4\pi CR^2 \exp(-4\pi CR^3/3), \quad (1)$$

where C is the concentration of the solute.

2) The distribution of the mutual orientation is also random; thus, the effect of the orientation on the transfer rate can be ignored.

3) Energy is transferred only to the nearest-neighbor molecule.

4) The sensitization efficiency of benzophenone is the same for H and D.

5) The environment of each molecule was assumed

† Present adress: Asahi Glass Co., Ltd., Research and Development Division; Kanagawa-ku, Yokohama 221.

to be statistically equivalent; that is, a correlation of environments for donor and acceptor molecules was disregarded.[7]

6) The rate constant for energy transfer can be expressed as a product of two terms,

$$k_{ET}(R,\ \Delta E) = k_1(R)\cdot k_2(\Delta E) \tag{2}$$

$k_1(R)$ is approximated[10] as

$$k_1(R) = k_D\exp(\gamma(1-R/R_0)), \tag{3}$$

where k_D is the phosphorescence decay constant of D and γ and R_0 (critical transfer distance) are parameters to be determined. The use of k_D is perfectly arbitrary. k_H (decay constant of H) or any other reference value may be employed instead, whereupon the critical distance changes according to the reference value. However, because of the strong R-dependent nature of the transfer rate, the obtained values of γ and R_0 are not very sensitive to the reference value. $k_2(\Delta E)$ is a function of the triplet energy difference in a donor (excited molecule)-acceptor (nearest-neighbor molecule) pair, $\Delta E=E_{donor}-E_{acceptor}$. It does not depend on whether the molecules are H or D, and can be expressed as

$$\begin{aligned} k_2(\Delta E) &= \exp(\Delta E/kT) && \text{if } \Delta E\leq 0,\\ &1 && \text{if } \Delta E\geq 0. \end{aligned} \tag{4}$$

7) The triplet energy of the solute molecule differs from site to site. Its distribution, $\sigma(E)$, is assumed to follow the spectral form of the 0-0 phosphorescence band (*vide infra*).

Since energy is transferred from molecule to molecule while being dissipated by intramolecular processes, the decay of a D molecule is expressed as

$$f_D(t,\ R,\ \Delta E) = \exp[-(k_D+k_{ET}(R,\ \Delta E))t]. \tag{5}$$

Similarly, the decay of an H molecule is given by

$$f_H(t,\ R,\ \Delta E) = \exp[-(k_H+k_{ET}(R,\ \Delta E))t]. \tag{6}$$

In the following, superfix 0 stands for a group of molecules which are excited by a transfer from benzophenone. Superfix n is for those molecules which are excited by a transfer from group $n-1$.

Decay of the group 0 is

$$f_D^0(t) = \int dR\rho(R) \times \int d\Delta E[\xi_{DD}(\Delta E)+\xi_{DH}(\Delta E)]f_D(t,\ R,\ \Delta E)/2, \tag{7}$$

$$f_H^0(t) = \int dR\rho_D(R)\int d\Delta E\xi_{HD}(\Delta E)f_H(t,\ R,\ \Delta E), \tag{8}$$

where $\xi_{DD}(\Delta E)$, $\xi_{DH}(\Delta E)$, and $\xi_{HD}(\Delta E)$ are the distributions of ΔE for D→D, D→H, and H→D donor-acceptor pairs, respectively, and are

$$\xi_{AB}(\Delta E) = \int \sigma_A(E)\sigma_B(E-\Delta E)dE. \tag{9}$$

$\rho(R)$ is the distribution of the distance to the nearest-neighbor molecule, irrespective of whether it is H or D. $\rho_D(R)$ is the distribution of the distance to the nearest-neighbor D molecule, so that

$$\left.\begin{aligned} \rho(R) &= \rho(R,\ C)\\ \rho_D(R) &= \rho(R,\ C/2) \end{aligned}\right\}, \tag{10}$$

where C is the total concentration. The transfer H→H is disregarded, since the lifetime of H is short; however, it is partly taken into account by using the above ρ_D expression rather than $\rho_D=\rho/2$. We took the arithmetic mean of ξ_{DD} and ξ_{DH} because the probability that the nearest-neighbor molecule is H or D is the same.

Let A^0 be the amount of energy transferred to other molecules in the course of decay (7) and (8), so that

$$A_{DD}^0(t) = \int dR\rho(R) \times \int d\Delta E\xi_{DD}(\Delta E)k_{ET}(R,\ \Delta E)f_D(t,\ R,\ \Delta E)/2, \tag{11}$$

$$A_{DH}^0(t) = \int dR\rho(R) \times \int d\Delta E\xi_{DH}(\Delta E)k_{ET}(R,\ \Delta E)f_D(t,\ R,\ \Delta E)/2, \tag{12}$$

$$A_{HD}^0(t) = \int dR\rho_D(R) \times \int d\Delta E\xi_{HD}(\Delta E)k_{ET}(R,\ \Delta E)f_H(t,\ R,\ \Delta E). \tag{13}$$

In the course of a successive transfer of energy, the decay of group n becomes,

$$f_D^n(t) = [A_{DD}^{n-1}(t) + A_{HD}^{n-1}(t)]*f_D^0(t), \tag{14}$$

$$f_H^n(t) = A_{DH}^{n-1}(t)*f_H^0(t), \tag{15}$$

where

$$A_{DD}^n(t) = [A_{DD}^{n-1}(t) + A_{HD}^{n-1}(t)]*A_{DD}^0(t), \tag{16}$$

$$A_{DH}^n(t) = [A_{DD}^{n-1}(t) + A_{HD}^{n-1}(t)]*A_{DH}^0(t), \tag{17}$$

$$A_{HD}^n(t) = A_{DH}^{n-1}(t)*A_{HD}^0(t). \tag{18}$$

The asterisk * denotes a convolution. The total phosphorescence decay is, then,

$$F(t) = \sum_{n=0}^{\infty}[k_D^r f_D^n(t) + k_H^r f_H^n(t)], \tag{19}$$

where k_D^r and k_H^r are the radiative rate constants of D and H, respectively. Finally, we convolute $F(t)$ with the 20 s square form of the light-sourse intensity $I(t)$

$$G(t) = I(t)*F(t) \tag{20}$$

and then normalize $G(t)$ with respect to the integrated area.

For naphthalene and phenanthrene, the values of

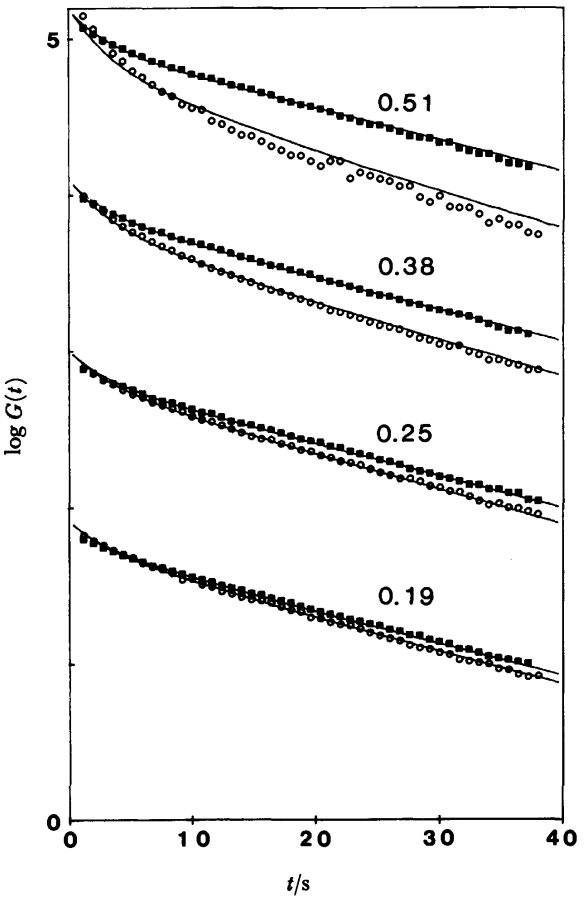

Fig. 1. Decay of naphthalene phosphorescence at 77 K (lower curves) and 4.2 K (upper curves). Total concentrations (mol dm^{-3}) are indicated. Solid lines: calculated ($\gamma=15$, $R_0=13.0$ Å); ○ and ■: experimental.

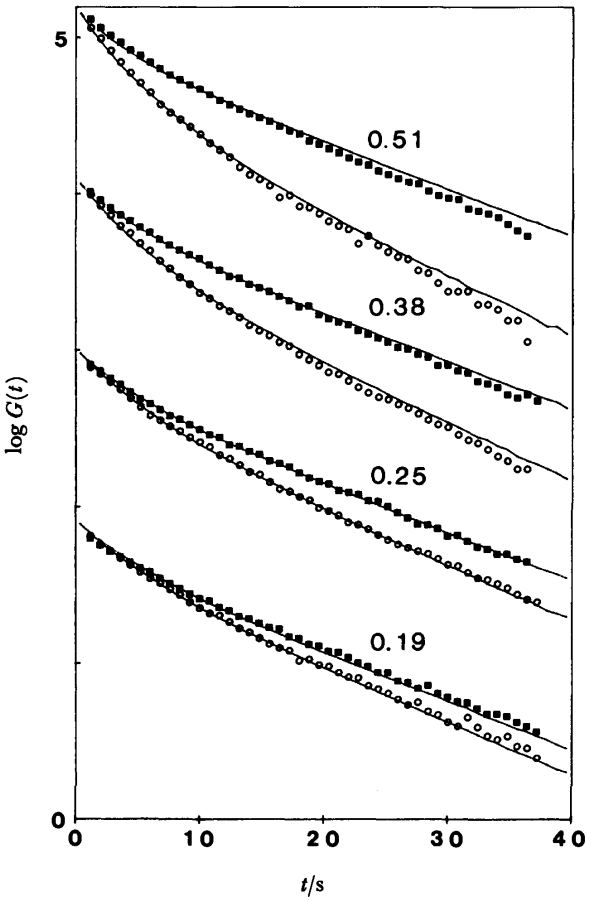

Fig. 2. Decay of phenanthrene phosphorescence at 77 K (lower curves) and 4.2 K (upper curves). Total concentrations (mol dm^{-3}) are indicated. Solid lines: calculated ($\gamma=10$, $R_0=14.5$ Å); ○ and ■: experimental.

Table 1. Phosphorescence lifetimes (s)

Sample	77 K	4.2 K
Naphthalene-d_0	2.3	2.4
Naphthalene-d_8	21.0	21.5
Phenanthrene-d_0	3.3	3.4
Phenanthrene-d_{10}	14.5	14.5
Biphenyl-d_0	3.7	4.4
Biphenyl-d_{10}	10.0	11.2

k_D^r and k_H^r were borrowed from the results of Fischer and Lim[11] (0.0163 s^{-1} and 0.0276 s^{-1} for naphthalene and 0.0215 s^{-1} and 0.0311 s^{-1} for phenanthrene, respectively). Since the values for biphenyl H and D were not available, they were assumed to be equal to each other.

Values of k_H and k_D were measured separately, as displayed in Table 1. They were constant over the whole range of concentrations. For naphthalene and phenanthrene, they were essentially unaffected by the temperature. For biphenyl, on the contrary, both of them increased when the temperature was lowered.

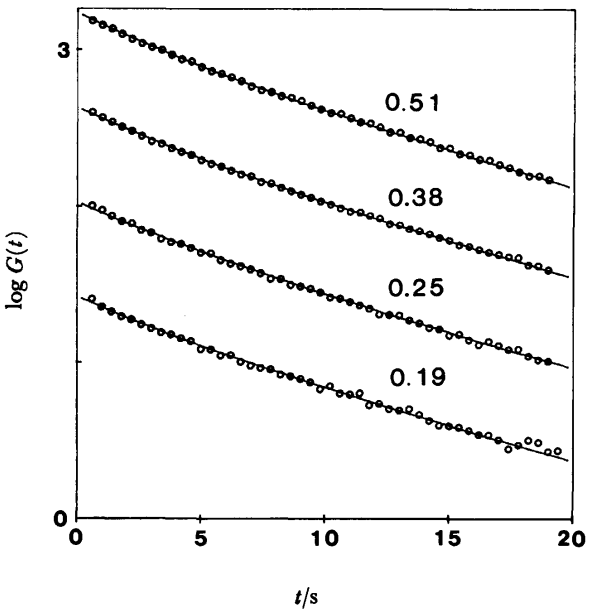

Fig. 3. Decay of biphenyl phosphorescence at 77 K. Total concentrations (mol dm^{-3}) are indicated. Solid lines: calculated ($\gamma=25$, $R_0=8.5$ Å); ○: experimental.

This may be attributed to the structural change which often takes place in labile molecules. Hence, only the curves at 77 K were simulated.

Calculations were carried out up to n=20. The inclusion of higher terms was found to be unnecessary. The results are compared with experiments in Figs. 1—3.

Results and Discussion

Calculations were carrried out by changing γ and R_0 to seek for the best fits to the experimental curves at 77 K. The best fits were obtained by minimizing the square sums of the residuals and, also, by inspecting the uniformity of the distribution of the residuals. Optimal R_0 values are not very sensitive to γ. Changing the latter from 25 to 10 causes a change in the former by only 1.0 Å for naphthalene and no change for phenanthrene (Table 2). A calculation was also carried out by taking account of the exclusion volume for the neighboring molecule within the van der Waals radii, with essentially no effect. This is reasonable since the distribution of R falls off rapidly with decreasing R, whereas the effect of γ has just the reverse trend. However, the distribution of residuals is fairly sensitive to γ; thus, the best values of γ could be obtained and are displayed in Figs. 1—3 and in Table 2.[12]

R_0 of biphenyl is very small. We also measured several donor-acceptor systems, such as carbazole-naphthalene, carbazole-quinoline and carbazole-biphenyl. The values of R_0 were determined to be 16.5, 15.5, and 13.0 Å, respectively. We see that the value for biphenyl is also very small compared to the first two, which are in good agreement with those by Strambini and Galley[13] and by Oginets.[14] Thus, the acceptor property of biphenyl seems to be always poor. Gustav *et al.*[15] have calculated the structure of biphenyl by geometry optimization and have claimed that the molecule is twisted in the ground state by 22.9° about the central bond and is coplanar in the excited singlet and triplet states. If this is the case, the relaxed (planar) triplet biphenyl molecule must transfer its energy to the twisted acceptor molecule in the ground state. This requires an excess energy and renders the transfer less efficient. This may account for the small R_0 value.

It is interesting that the R_0 values for similar molecules are smaller than for different molecules.

Table 2. Values of R_0 (Å)

Sample	γ= 10	15	25	35
Naphthalene	12.5	<u>13.0</u>	13.5	14.0
Phenanthrene	<u>14.5</u>	14.5	14.5	15.0
Biphenyl	8.0	8.5	<u>8.5</u>	9.0

The best values are underlined.

This may reflect a possible requirement that the sum of the Franck-Condon products, corresponding, apart from normalization factors, to the overlap of the S-T absorption spectrum of the acceptor and phosphorescence spectrum of the donor in the treatment of Dexter,[16] should be small due to the small energy difference between the donor molecule and the acceptor molecule.

The fit is somewhat bad for curves of higher concentrations. This may be due to a failure of the assumptions, especially for 5, to hold at high concentrations.

In previous papers,[4,5] the triplet energy difference of H and D had been taken to be equal to the difference of the peak positions of their phosphorescence 0-0 bands; thus only the H→D back transfer had been assumed to be phonon-assisted. If this is true, the phosphorescence decay curves of the mixtures should be steeper at 4.2 K than at 77 K, since transfers to molecules with longer lifetime tend to be inhibited. This contradicted the present experiments and, thus, we have been forced to assume that the phonon-assisted energy transfer takes place in either direction. The phosphorescence spectra of the solutes in PMMA were broad and their band widths did not change even when the temperature was lowered to 4.2 K. Therefore, the widths of the 0-0 bands could be regarded as the inhomogeneous widths of the T_1 levels due to solvation. The Gaussian forms of the bands were regarded to be the distributions functions $\sigma(E)$ of T_1 energies in PMMA. Differences in the peak positions of H and D (that of D is always higher) is 110 cm^{-1} for naphthalene, 60 cm^{-1} for phenanthrene and 110 cm^{-1} for biphenyl. These are smaller than their widths; thus the signs and the values of ΔE differ from site to site and do not depend much on the types of molecules. At 4.2 K, the energy is transferred mainly to sites with lower energies and the effect of temperature is to scramble the transfer sequences. The importance of the energy distribution has recently been stressed with regard to somewhat different aspects of the energy transfer.[17-19]

The values of γ and R_0 obtained from curves at 77 K were used to reproduce curves at 4.2 K. The fits are good, as can be seen from Figs. 1—2; thus, the present method has proven to be of use. In the above-metioned donor-acceptor systems of carbazole-naphthalene, carbazole-quinoline and carbazole-biphenyl, of which the energy differences were larger than their spectral widths, no change was observed in the donor phosphorescence decay curves when the temperature was changed from 77 to 4.2 K. This fact might strongly support our mechanism.

References and Notes

1) N. K. Chaudhuri and M. A. El-Sayed, *J. Chem. Phys.*,

42, 1947 (1965).

2) S. Siegel and L. Goldstein, *J. Chem. Phys.*, **44**, 2780 (1966).

3) Y. Gondo, M. Hirai, T. Iwao, T. Kakibaya, T. Kuroi, H. Nagatomo, and Y. Kanda, *Chem. Lett.*, **1975**, 463.

4) A. Inoue and N. Ebara, *Chem. Lett.*, **1975**, 1137.

5) A. Inoue, H. Chuman, and N. Ebara, *Bull. Chem. Soc. Jpn.*, **51**, 345 (1978).

6) A. Inoue, N. Nishi, M. Kinoshita, and N. Ebara, *Bull. Chem. Soc. Jpn.*, **53**, 2466 (1980).

7) R. Twardowski, J. Kusba, and C. Bojarski, *Chem. Phys.*, **64**, 239 (1982).

8) R. F. Loring, H. C. Andersen, and M. D. Fayer, *J. Chem. Phys.*, **76**, 2015 (1982).

9) Th. Förster, *Ann. Phys.*, **2**, 55 (1948).

10) M. Inokuti and F. Hirayama, *J. Chem. Phys.*, **43**, 1978 (1965).

11) S. F. Fischer and E. C. Lim, *Chem. Phys. Lett.*, **14**, 40 (1972).

12) We may use for $k_1(R)$

$$k_1(R)=k_D(R_0/R)^m,$$

instead of the exponential function. We have calculated for naphthalene with m varying from 8 to 20. The fit was good with quite acceptable values of m=12—16 and R_0= 12.5—13.0 Å.

13) G. B. Strambini and W. C. Galley, *Chem. Phys. Lett.*, **39**, 257 (1976); *J. Chem. Phys.*, **63**, 3467 (1975).

14) V. Ya. Oginets, *Zh. Fiz. Khim.*, **48**, 3030 (1974).

15) K. Gustav, J. Suhnel, and U. P. Wild, *Helv. Chim. Acta*, **61**, 2100 (1978); *Z. Chem.*, **17**, 417 (1977).

16) D. L. Dexter, *J. Chem. Phys.*, **21**, 836 (1953).

17) R. Jankowiak and H. Bassler, *Chem. Phys.*, **79**, 57 (1983).

18) J. R. Morgan and M. A. El-Sayed, *J. Phys. Chem.*, **87**, 200 (1983); *ibid.*, **87**, 383 (1983); *ibid.*, **87**, 2178 (1983).

19) R. Parson and R. Kopelman, *J. Phys. Chem.*, **88**, 2931 (1984).

 © 1985 The Chemical Society of Japan Bull. Chem. Soc. Jpn., 58, 2456—2460 (1985) [Vol. 58, No. 9

Studies of Collectors. VI.[1] Application of β-Diketone-type Surfactants to Ion Flotation

Yoshifumi KOIDE,* Shuichi KITAOKA, and Kimiho YAMADA
Department of Synthetic Chemistry, Faculty of Engineering, Kumamoto University, Kurokami, Kumamoto 860
(Received February 12, 1985)

β-Diketone-type surfactants(2,4-alkanedione, R_nA) were applied as ion-flotation collectors and as extraction reagents. Fe^{3+}, Ga^{3+}, and Cu^{2+} were floated effectively with R_nA as a 1:1 complex from an acidic solution. From a mixture of metal ions(Fe^{3+}, Ga^{3+}, Cu^{2+}, Zn^{2+}, Pb^{2+}, Cd^{2+}, and Ca^{2+}), the Cu^{2+} was floated selectively at pH 6 by R_8A or $R_{12}A$. Then, the metal ions were extracted with R_nA into a benzene layer as coordination-saturated species at regions of a neutral pH. The order of selectivity at pH 6.0 was $Fe^{3+}>Cu^{2+}>\cdots$. The difference between the properties of R_nA as an ion-flotation collector and as an extraction reagent was explained using the HLB value and the surface activity based on the composition of R_nA-metal complexes. The metal ions and R_nA could be recovered from the scum.

Ion flotation has been examined as a method of collecting specific metal ions.[2] However, there are few ion-flotation collectors which exert the flotation effect by adding a small amount. In a previous paper[3] it was shown that complexane-type surfactants formed floatable complexes with heavy metal ions when the HLB(hydrophilic-liphophilic balance) values of the complexes were 4—14. Also, only a trace amount of surfactants remained in the residual solution. Consequently, the mechanism regarding ion flotation might be the complex formation (stability constant) and the flotation of the complex(HLB). Even if a surfactant shows a similar stability constant, the selective removal of a specific metal ion may be achieved using a chelating agent bearing a long alkyl group to regulate its HLB. However, there are few reports concerning flotation using such a chelating agent (surfactant) and the floatability of surfactant-metal complexes. Therefore, the HLB values of floatable complexes must be confirmed using various surfactants. Surfactants are considered to be excellent extraction reagents since their distribution coefficients are large due to a long alkyl group.[4-6]

The enol form of acetylacetone, known as an extraction reagent, behaves as a bidentate univalent anion and forms a stable metal chelate.[6] In this study, in order to obtain further information about the HLB effects on floatability and selectivity, and to clarify the characteristic properties of ion-flotation collectors and extraction reagents, β-diketone-type surfactants(2,4-alkanediones,R_nA) were prepared and applied to an ion-flotion collector and compared with other extraction reagents.

Experimental

Materials. R_nA was prepared by the Claisen condensation of methyl alkanoate with acetone in the presence of a sodium hydride.[7] The crude R_nA was purified by the recrystallization of their copper complexes from 50% of a DMF-water solution and by fractionation at reduced pressure after a decomposition process using 20% sulfuric acid. Abbreviations for various forms of R_nA are R_8A(for 2,4-undecanedione), $R_{12}A$(for 2,4-pentadecanedione) and $R_{18}A$(for 2,4-henicosanedione). A further purification of R_nA gave rather low yields (R_8A 24%, $R_{12}A$ 35%, $R_{18}A$ 48%). The structures of the synthesized R_nA were confirmed by means of their melting points,[7] IR spectra (Shimadzu IR-408), NMR spectra (JEOL JMN-MH-100), and elementary analyses(Yanaco CHN Corder MT-3). Mp: $R_{12}A$, 31.5—33.0 °C (lit,[7] 31—32 °C); $R_{18}A$, 56.0—58.0 °C (lit,[8] 52.5 °C). IR(KBr): ν_{CH} 2920 cm^{-1}, $\nu_{C=O}$ 1640 cm^{-1}. NMR (CCl_4) δ=0.9 (3H, t, CH_3-C-C-), 1.3 (methylene in alkane), 2.0 (3H, CH_3COC-), 2.2 (2H, t, -C-C-CH_2COC-), 3.4 (2H, -CCOCH_2COC-), 5.4 (H, -CC(-O-)=CHCOC-). R_8A Found: C, 70.82; H, 10.84%; Calcd for $C_{11}H_{20}O_2$: C, 71.70; H, 10.94%. $R_{12}A$ Found: C, 74.67; H, 11.82% Calcd for $C_{15}H_{28}O_2$: C, 74.95; H, 11.74%. $R_{18}A$ Found: C,77.63; H, 12.59% Calcd for $C_{21}H_{40}O_2$: C, 77.72; H, 12.42%. Acetylacetone(AA) and dibenzoylmethane(DBM) were obtained from Wako Pure Chemical Industries, Ltd., and benzoylacetone(BzA) was obtained from Kishida Chemical Co., Ltd.

The surface tensions of R_nA solutions were measured on a Du nouy surface-tension balance. R_nA in an alkaline solution lowered the surface tension: 46 dyn (10^{-5}N) cm^{-1} for 10^{-3} mol dm^{-3} of R_8A[critical micelle concentration (cmc) was not observed at below 10^{-3} mol dm^{-3}], 36 dyn cm^{-1} for $R_{12}A$(cmc 5×10^{-4} mol dm^{-3}), and 47 dyn cm^{-1} for $R_{18}A$(cmc 3×10^{-4} mol dm^{-3}). BzA and DBM, known as extraction reagents, scarcely lowered the surface tension. Therefore, the concentration of R_nA in the following ion flotations were always kept below their cmc.

Apparatus and Procedures. The removal of eight kinds of metal ions (Fe^{3+}, Ga^{3+}, Al^{3+}, Cu^{2+}, Zn^{2+}, Pb^{2+}, Cd^{2+}, and Ca^{2+}) was examined by the method of ion flotation and extraction. The concentrations of these metal ions were determined using an atomic absorption spectrophotometer (Hitachi 170—30). The flotation apparatus and procedures were the same as that previously reported.[1] The floatability(%) of a metal ion was calculated using:

$$F = \frac{a_0 - a_1}{a_0} \times 100$$

where a_0 and a_1 denote the initial and final metal-ion concentrations in solution. Extraction was carried out

using a general operation; 100 cm^3 of benzene was added to the 100 cm^3 of metal solution in a separating funnel, and the funnel was shaken for 30 min. The extractability was calculated using the same formula as that regarding floatability.

Results and Discussion

Ion Flotation. The eight kinds of metal ions dissolved in 300 cm^3 of water were floated with a small amount of R_nA, especially $R_{12}A$. The floatable pH ranges for a 10^{-5} mol dm^{-3} solution of specific metal ions using 3×10^{-5} mol dm^{-3} of aqueous $R_{12}A$ were as follows: for Fe^{3+}, pH 4—8; for Ga^{3+}, 4—8; for Al^{3+}, 7—9; for Cu^{2+}, 4—8; for Zn^{2+}, 7—9; for Pb^{2+}, 6—11; for Cd^{2+}, 10—13; and for Ca^{2+}, 12—13. The flotation data for Fe^{3+}, Ga^{3+}, and Cu^{2+} are shown in Fig. 1. The optimum pH for the Cu^{2+} and Fe^{3+} flotations shifted to a lower pH with an increase in the length of the alkyl group, and $R_{12}A$ showed the highest floatability in the series of R_nA. However, DBM(having two phenyl groups) was not so effective and AA(having no long alkyl group) was wholly ineffective. The HLB value of the metal complex is affected by pH since the composition varies with pH.

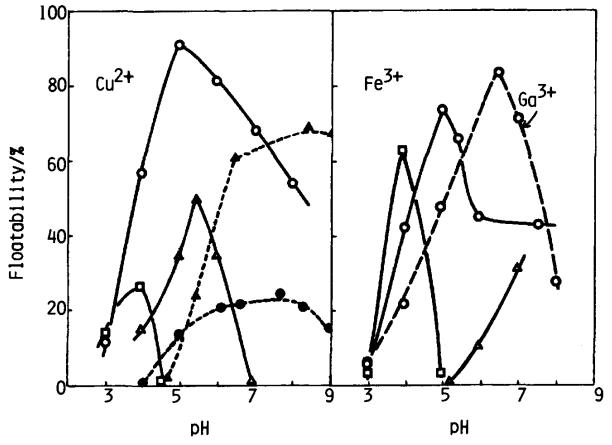

Fig. 1. Flotations for Cu^{2+}, Fe^{3+}, and Ga^{3+}.
Cu^{2+}: 10^{-5} mol dm^{-3}; Fe^{3+}: 10^{-5} mol dm^{-3}; Ga^{3+}: 2.87×10^{-4} mol dm^{-3}; $[R_nA]/[M]=3$. △: R_8A, ○: $R_{12}A$, □: $R_{18}A$, ▲: BzA, ●: DBM.

Then, the metal-ligand ratio of a $R_{12}A$-copper complex was examined. The scum(resulting at pH 5.0 upon adding $R_{12}A$) decomposed with 10% sulfuric acid and the resulting $R_{12}A$ was extracted using chloroform. The amount of $R_{12}A$ was determined by spectrophotometry{Hitachi model 101; ε^{276}, 8360 M^{-1} cm^{-1} (1 M=1 mol dm^{-3}); λ, 276 nm in chloroform}. The mole ratio of $R_{12}A$ and Cu^{2+} was 1:1. The obtained ratio was equal to that obtained by conductometry(Toa CM-7B). For R_nA-copper complex, a 1:1 complex would be present at a lower pH and the complex would be hydrolyzed above pH 5—6 since the hydrolysis constant of a copper(II) ion (pK_1, $I>0$) is 5.4 to 5.8.[9] The HLB values of these complexes calculated using the Oda equation[3,10] are shown in Table 1. High floatabilities were observed over a pH range of 3—4 for hydrophobic $R_{18}A$, 4—6 for less hydrophobic $R_{12}A$, and 5—6 for least hyrophobic R_8A. From these data, it is considered that the floatable complexes are R_8A-CuOH, $R_{12}A$-Cu^+, $R_{12}A$-CuOH, and $R_{18}A$-Cu^+. Their HLB values are in a range of 4—8. Furthermore, the relation between floatability and surface activity at pH 5 is shown in Table 2. The surface tension of 10^{-4} mol dm^{-3} $R_{12}A$ solution was 54 dyn cm^{-1}, and the value in the presence of 3×10^{-4} mol dm^{-3} Cu^{2+}, Fe^{3+}, or Ca^{2+} ion was 65 dyn cm^{-1}, 61 dyn cm^{-1}, or

Table 1. HLB values calcd for R_nA-copper complexes

	R_nA-Cu^+	R_nA-CuOH
R_8A	11	6
$R_{12}A$	8	4
$R_{18}A$	6	3
DBM	9	5

Table 2. Relation between floatability and surface activity at pH 5

Collector	Metal ion	Floatability[a] %	Surface activity: Surface tension[b] dyn cm^{-1}	Surface activity: HLB[c]
$R_{12}A$	none	—	54	5
$R_{12}A$	Cu^{2+}	91	65	8, 4*
$R_{12}A$	Fe^{3+}	74	61	10, 8*
$R_{12}A$	Ca^{2+}	0	54	8
DBM	none	—	68	6
DBM	Cu^{2+}	5	69	9, 5
DBM	Fe^{3+}	24	69	11, 9*
DBM	Ca^{2+}	0	68	9

a) Collector 3×10^{-5} mol dm^{-3}, metal ion 10^{-5} mol dm^{-3}. b) Collector 10^{-4} mol dm^{-3}, metal ion 3×10^{-4} mol dm^{-3}. c) Calculated by the Oda equation.[10] * Hydroxo-metal complex.

54 dyn cm^{-1}, respectively. The copper and iron complexes were considered to be weakly surface-active, and the copper complex would be more hydrophobic than the other. However, the floatability of copper using DBM(having a suitable HLB value) was not so high. The surface tension of a 10^{-4} mol dm^{-3} DBM solution was 68 dyn cm^{-1} and this value was not altered even if metal ions were added. DBM and its complex are presumably surface inactive because of their structural characteristics.

The floatability varies with the concentration of metal ions and the collector. The floatabilities at pH 6.5 for a 2.8×10^{-4} mol dm^{-3} Ga^{3+} solution changed as a function of the $R_{12}A$ concentration and were as follows: 38% with 2.8×10^{-4}mol dm^{-3} $R_{12}A$, 60% with 5.7×10^{-4} mol $dm^{-3}$$R_{12}A$, 82% with 8.2×10^{-4} mol dm^{-3} $R_{12}A$, and 64% with 14.3×10^{-4} mol dm^{-3} $R_{12}A$, respectively.

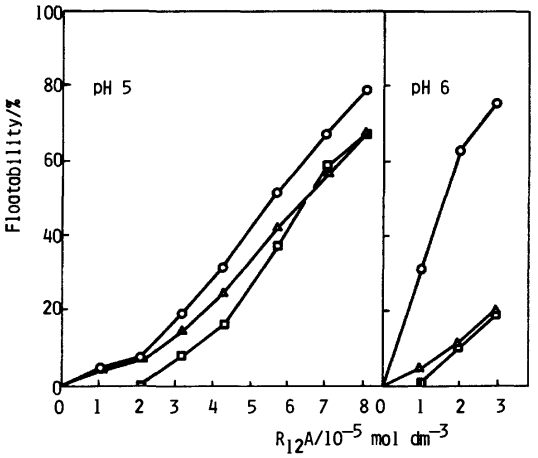

Fig. 2. Selectivity to metal ions.
Mixture of metal ions(Fe^{3+}, Ga^{3+}, Cu^{2+}, Pb^{2+}, Zn^{2+}, Cd^{2+}, and Ca^{2+}: 10^{-5} mol dm^{-3}, respectively). ○: Cu^{2+}, △: Fe^{3+}, □: Ga^{3+}.

The selectivity of these agents to metal ions was examined at pH 5 and 6. A Cu^{2+} ion could be selectively floated with $R_{12}A$ from a mixture of Fe^{3+}, Ga^{3+}, Cu^{2+}, Zn^{2+}, Pb^{2+}, Cd^{2+}, and Ca^{2+}(each a_0 was 10^{-5} mol dm^{-3}) at pH 6.0 as indicated in Fig. 2. However, the selectivity was not obtained at pH 5.0. Moreover, the selectivity was also examined using a 3×10^{-5} mol dm^{-3} solution of BzA, R_8A, $R_{12}A$, $R_{18}A$, and DBM. The floatabilities for Fe^{3+} and Cu^{2+} are indicated in Fig. 3. The Cu^{2+} ion could be selectively floated with R_8A and $R_{12}A$ at pH 6 (floatabilities were 70% and 75%, respectively). However the Cu^{2+} couldn't be floated with the others. The concentration of R_nA was smaller than that of the total metal ions. Therefore, the mole ratio of a R_nA-metal or a R_nA-hydroxo metal complex must be 1:1 at pH 6.0. The HLB values calculated for $R_{12}A$-Cu^+ and $R_{12}A$-CuOH were 8 and 4, as indicated in Table 1. Regarding the complexes of $R_{12}A$-Fe^{2+}, $R_{12}A$-$FeOH^+$, and $R_{12}A$-$Fe(OH)_2$, they were 10, 9, and 8, respectively. Consequently, the more hydrophobic copper complex would be floated selectively.[3] However, the floatabilities of Cu^{2+} using BzA and $R_{18}A$ were very low. The calculated HLB values for the complexes of BzA-Cu^+ and BzA-CuOH were 12 and 7, and for the complexes of $R_{18}A$-Cu^+ and $R_{18}A$-CuOH were 6 and 3 (Table 1), respectively. The BzA complex would be too hydrophilic, while the $R_{18}A$ complex would be too hydrophobic to be floated selectively.

Extraction. Extractability is greatly affected by the distribution coefficient of the extraction reagent corresponding to the HLB value.[4,5] R_nA is expected to be an excellent extraction reagent due to its large distribution coefficent related to its long alkyl group.[4-6] Therefore, extractions for eight kinds of metal ions were examined. The metal ions and the pH range when extracted by benzene (a_0 for 10^{-5} mol dm^{-3} metal ion and 10^{-4}mol dm^{-3} $R_{12}A$) were as follows: for Fe^{3+}, 5.5—11; for Ga^{3+}, 6—8; for

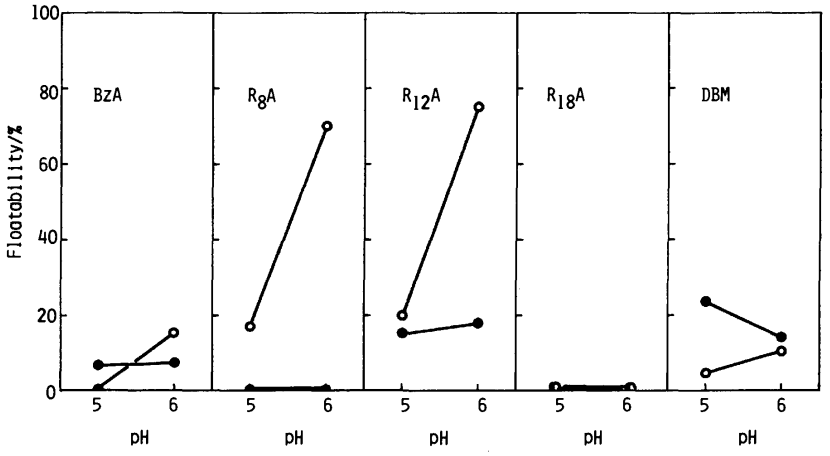

Fig. 3. Selectivity in ion flotation.
Mixture of metal ions(Fe^{3+}, Ga^{3+}, Cu^{2+}, Pb^{2+}, Zn^{2+}, Cd^{2+}, and Ca^{2+}: 10^{-5} mol dm^{-3}, respectively); R_nA: 3×10^{-5} mol dm^{-3}; BzA: 3×10^{-5} mol dm^{-3}; DBM: 3×10^{-5} mol dm^{-3}. ○: Cu^{2+}, ●: Fe^{3+}.

Cu^{2+}, 5.5—11; for Zn^{2+}, 8—12; for Pb^{2+}, 6—11; for Cd^{2+}, 9—13; and for Ca^{2+}, 11—13. Extractions for Cu^{2+} and Ga^{3+} ions are shown in Fig. 4. The extraction efficiencies with R_nA and BzA were more effective than that with AA. Furthermore, the highest extractability was obtained by DBM. The HLB values calculated for DBM, $R_{18}A$, $R_{12}A$, R_8A, BzA, and AA were 5, 3, 4, 6, 7, and 13, respectively. However, the distribution coefficient of DBM must be the largest value in these agents.

The selectivity regarding an extraction was examined using $R_{12}A$. The stability constants of the metal acetylacetone complexes (log K_{MA} and log K_{MA_2}) are arranged in the following order: Fe^{3+}> Ga^{3+}>Cu^{2+}>Zn^{2+}>Pb^{2+}>Cd^{2+}>Ca^{2+}.[11] The selectivity order regarding an extraction from a mixture of seven metal ions at pH 6.0 was the same as the order regarding their stability constants (Fig. 5). A more selective removal of Fe^{3+} was obtained at pH 5 when DBM was employed. The formed metal complex is thought to be uncharged(neutral) because the complex is soluble in benzene. Furthermore, the concentration effect of $R_{12}A$ on the extraction of a Cu^{2+} ion suggested that the mole ratio of R_nA to copper is 2:1. The calculated HLB value for both the complexes{$(R_{12}A)_2Cu$ and $(R_{12}A)_3Fe$} was 1. Therefore, the selectivity is presumably controlled by the stability constant.

Comparison. Ion flotation by using R_8A or $R_{12}A$ was superior to extraction at a lower pH region and inferior around neutral regarding the separation of Cu^{2+}, Fe^{3+}, or Ga^{3+} ion(Fig. 6). The R_nA-metal complex at a lower pH was a 1:1-complex and the ratio of R_nA to metal ions became maximum around a neutral pH. The 1:1-complex must be slightly hydrophilic(HLB, 4—14) and the 2:1- and 3:1-complexes must be more hydrophobic(HLB, 1). The 1:1-complex(which shows a surface-active property) is presumably suitable for ion flotation. Also, coordination-saturated and uncharged complexes of 2:1 and 3:1 are presumably suitable for extraction.

Especially the selective removal for Cu^{2+} ion by the ion-flotation method using R_nA was superior to that by extraction, in spite of a smaller stability constant compared to Fe^{3+} and Ga^{3+} ions.

Recovery. The ion-flotation collector should be recovered almost completely from the residual solution. The residual concentration of $R_{12}A$ was 0.2 ppm after the flotation of Cu^{2+} ions at pH 5, and was below 0.2 ppm after selective removal by the successive addition of $R_{12}A$ at pH 6. Therefore, the additive, $R_{12}A$, remained in an aqueous solution very little and was floated as a scum. The scum was dispersed in benzene; then, the benzene solution was shaken with a 2 mol dm^{-3} solution of mineral acid.

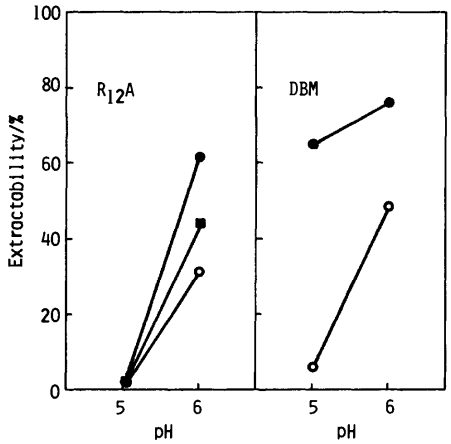

Fig. 5. Selectivity in extraction.
Mixture of metal ions(Fe^{3+}, Ga^{3+}, Cu^{2+}, Pb^{2+}, Zn^{2+}, Cd^{2+}, and Ca^{2+}: 10^{-5} mol dm^{-3}, respectively); $R_{12}A$: 3×10^{-5} mol dm^{-3}; DBM: 3×10^{-5} mol dm^{-3}. ○: Cu^{2+}, ●: Fe^{3+}, □: Ga^{3+}.

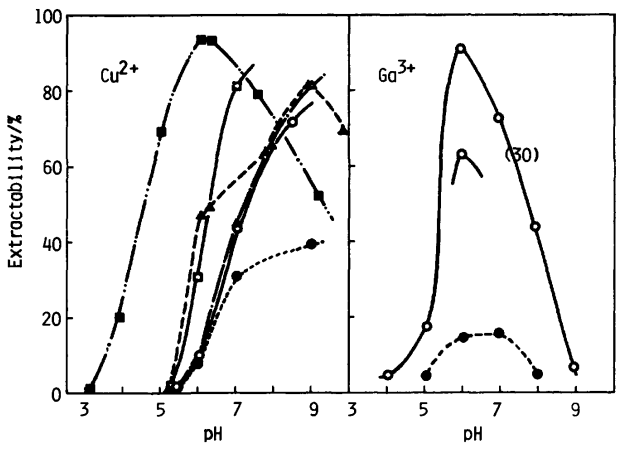

Fig. 4. Extractions for Cu^{2+} and Ga^{3+}.
Cu^{2+}: 10^{-5} mol dm^{-3}; Ga^{3+}: 2.86×10^{-4} mol dm^{-3}; $[R_nA]/[M]=3$, (=30); Solvent: benzene. △: R_8A, ○: $R_{12}A$, □: $R_{18}A$, ●: AA, ▲: BzA, ■: DBM.

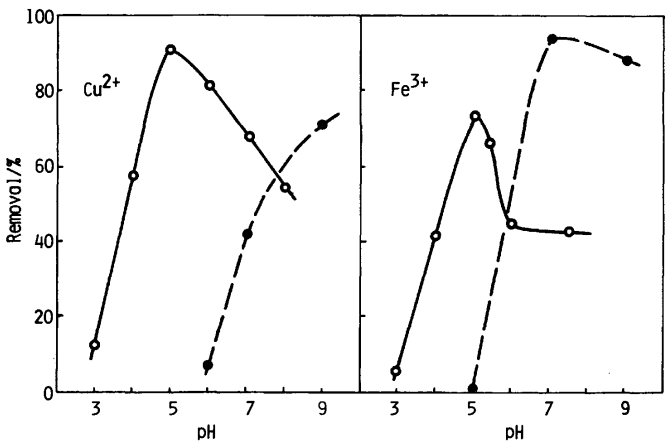

Fig. 6. Removals of Cu^{2+} and Fe^{3+}.
Metal ions: 10^{-5} mol dm^{-3}; $R_{12}A$: 3×10^{-5} mol dm^{-3}.
○: Ion flotation, ●: extraction.

$R_{12}A$ could be quantitatively recovered from the benzene layer, while the Cu^{2+} ions were recovered from an aqueous layer containing a mineral acid.

References

1) Y. Koide, H. Takamoto, K. Matsukawa, and K. Yamada, *Bull. Chem. Soc. Jpn.*, **56**, 3364 (1983).

2) R. Lemlich, "Adsorptive Bubble Separation Techniques," Academic Press, New York and London (1972); T. Sasaki, "Bunri To Seisei," in "Jikken Kagaku Koza," ed by the Chemical Society of Japan, Maruzen, Tokyo (1966), Ser. 2, Vol. 2, Sec. 15, pp. 565—603.

3) Y. Koide, K. Izumi, K. Okuzono, and K. Yamada, *Nippon Kagaku Kaishi*, **1980**, 742.

4) H. Watarai and H. Freiser, *J. Am. Chem. Soc.*, **105**, 189 (1983).

5) K. Haraguchi and H. Freiser, *Inorg. Chem.*, **22**, 1187 (1983).

6) Y. Yamane, *Bunseki Kagaku*, **8**, 264 (1959).

7) F. W. Swamer and C. R. Hauser, *J. Am. Chem. Soc.*, **72**, 1352 (1950).

8) G. T. Morgen and E. Holmes, *J. Chem. Soc.*, **127**, 2891 (1925).

9) J. Burgess, "Metal Ions in Solution," John Wiley & Sons, New York (1979), p. 265.

10) R. Oda and K. Teramura, "Kaimen-kasseizai No Gosei To Sonooyo," Makishoten, Tokyo (1962), p. 501.

11) T. Sakaguchi and K. Ueno, "Kinzokukireto III," Nankodo, Tokyo (1967), p. 62.

 © 1985 The Chemical Society of Japan Bull. Chem. Soc. Jpn., 58, 2461—2463 (1985)

Breathing Vibration of Cyclohexane Ring in Cyclohexanol

Yoshiko TAKEOKA

Department of Chemistry, Otsuma Women's University, Sanban-cho, Chiyoda-ku, Tokyo 102

(Received March 8, 1985)

It was found that the wave numbers of the bands due to the breathing vibration of the cyclohexane ring in the e-conformer are higher than 802 cm^{-1} in the monosubstituted cyclohexane-derivatives having substituents Cl, Br, I, SH, SD and SCH_3, while lower than 802 cm^{-1} in cyclohexanol and fluorocyclohexane. The effect of introducing OH group to the cyclohexane ring upon this band was studied.

The Raman band of cyclohexane due to the breathing vibration of the cyclohexane ring, namely A_{1g} C-C stretching vibration, has been found at 802 cm^{-1} by the studies of fundamental vibration.[1,2] In the Raman spectrum of cyclohexane-derivatives, we can assign a strong band near 800 cm^{-1} to the breathing vibration of the cyclohexane ring, because the Raman band of this vibration is expected to possess the lowest wave number among C-C stretching vibrations and also the strong intensity due to the highest symmetry of this vibration mode. By studying several halogen-derivatives of cyclohexane, it has been found that the wave numbers of the breathing vibration of the ring having substituents in the a-position or the a,a-positions do not remarkably shift from that of cyclohexane, namely, 802 cm^{-1}, and are always lower than that having substituents in the e-position or the e,e-position.[3] This fact could be explained by considering that, in the a- or the a,a-conformer, the carbon-halogen bond is situated nearly vertically to the cyclohexane ring and contributes slightly to the breathing vibration; on the other hand that, in the e- or the e,e-conformer, the carbon-halogen bond is located almost in the same plane as the cyclohexane ring and possesses an important effect upon the breathing vibration.

We have made conformational studies on cyclohexanol,[4] *trans*-2-halocyclohexanols[5] and *trans*-4-halocyclohexanols[6] by infrared spectroscopy. The existence of two mutually convertible isomers, namely the e- and the a-conformers, was found in these molecules as in halogen derivatives of cyclohexane. However, the bands of the breathing vibration for the cyclohexane ring in these molecules were not assigned except *trans*-4-chlorocyclohexanol. It would be interesting to find the bands of the breathing vibration of the ring in these molecules having OH group.

Experimental

The infrared spectra were measured by JASCO model A-302 and Perkin-Elmer model 112 spectrometers. Commercial cyclohexanol was purified by desiccation with calcium oxide and subsequent distillation.

The sample of cyclohexanol was cooled with the mixture of Dry Ice and ethanol. The supercooled solid (phase I) in a cell with potassium bromide windows changed gradually to the ordered solid (phase III) by cooling for about three hours.

Results and Discussion

We have studied the conformational isomers of cyclohexanethiol[7] which is structurally similar to cyclohexanol. It is known that the bands of C-SH stretching vibration have similar wave numbers to those of C-Cl stretching vibration, because of their similar mass. We found that only the e-conformer exists in the true solid of cyclohexanethiol as in that of chlorocyclohexane.

As shown in Table 1, some cyclohexane derivatives having monosubstituent Cl, Br, I, SH, SD and SCH_3

TABLE 1. BANDS OF THE BREATHING VIBRATION IN THE MONOSUBSTITUTED CYCLOHEXANE-DERIVATIVES (cm^{-1})

	Substituente	a-Conformer	e-Conformer	Ref.
Chlorocyclohexane	Cl	807	818 *	3, 8
Bromocyclohexane	Br	806	812 *	9
Iodocyclohexane	I	801	806 *	4, 9
Cyclohexanethiol	SH	802	817 *	7
Cyclohexanethiol-*d*	SD	802	819 *	7
Cyclohexyl methyl sulfide	SCH_3	801	818 *	9
Cyclohexanol	OH		789 *	
Fluorocyclohexane	F		793 *	10

* This band remained in the true solid.

possess the bands of the breathing vibration in the similar wave number region.

The F atom of fluorocyclohexane has a mass similar to OH of cyclohexanol, and the C-F stretching vibration have the bands in the similar region to those of the C-OH stretching vibration. Christian *et al.* showed by the infrared spectra that fluorocyclohexane possesses the e- and the a-conformers in the liquid, while almost only the e-conformer in the true solid (ordered anisotropic phase).[10]

As for cyclohexanol, many studies have been made.[4,9,12,13] It has been known that cyclohexanol has a supercooled plastic solid (disordered phase, phase I) and two true solids (ordered phases, phase II has the transition point at −7.9 °C and the phase III at −28.4 °C).[11]

It is very probable, in view of the results on fluorocyclohexane and cyclohexanethiol, that only or almost only the e-conformer exist in the true solid. However it seems that there is not yet conclusive evidence whether the true solid of cyclohexanol has only one conformer or two conformers. The infrared spectra of cyclohexanol has the very strong bands at 968 cm^{-1} and 1068 cm^{-1} in the true solid (phase II and phase III) and it has been pointed out that the C-O stretching bands for the a- and the e-conformer appear near 960 cm^{-1} and 1060 cm^{-1} respectively in the derivatives of cyclohexanol.[11,13]

The a- and the e-conformers of cyclohexanol exist in the phase I as in the liquid. There are many differences between the infrared spectra of the phase III and that of the phase I.

As shown in Table 2, the infrared spectra of cyclohexanol and fluorocyclohexane have the similarity in the 780 cm^{-1}—1070 cm^{-1} region. Around the 800 cm^{-1} region of the infrared spectra, cyclohexanol has the bands at 789 (m) cm^{-1}, 835 (w) cm^{-1}, 844 (m) cm^{-1}, and 863 (w) cm^{-1} in the liquid, while in the true solid (phase III and according to Ref. 13 also phase II) the bands at 835 cm^{-1} and 863 cm^{-1} disappear, the bands at 789 cm^{-1} and 844 cm^{-1} persist.

TABLE 2. THE SIMILARITY IN THE INFRARED SPECTRA OF CYCLOHEXANOL AND FLUOROCYCLOHEXANE (cm^{-1})

Cyclohexanol		Fluorocyclohexane (Data of Ref. 10)
Liquid	Solid (phase III)	Liquid
789 (m)	787 (m)	793 (m)
835 (w) *		830 (m) *
844 (m)	845 (m)	844 (m)
863 (w) *		865 (m) *
889 (s)	888 (s)	892 (m)
925 (w)	922 (vw)	924 (sh)
		938 (vs) *
	963 (sh)	948 (sh)
968 (vs)	973 (vs)	962 (vs)
1024 (s)	1026 (s)	1016 (vs)
		1024 (vw)
1033 (sh) *		1031 (m) *
	1049 (w)	
1068 (vs)	1067 (vs)	1049 (vs)

* This band disappeared in the true solid.

According to Ref. 10, in the same region of the infrared spectra, fluorocyclohexane has the bands at 793 (m) cm^{-1}, 830 (m) cm^{-1}, 844 (m) cm^{-1}, and 865 (m) cm^{-1} in the liquid, however in the true solid the bands at 830 cm^{-1} and 865 cm^{-1} disappear, the bands at 793 cm^{-1} and 844 cm^{-1} persist like in cyclohexanol. In the true solid of fluorocyclohexane almost only the e-conformer exists as mentioned above, the bands at 793 cm^{-1} and 844 cm^{-1} are assigned to the e-conformer and the bands at 830 cm^{-1} and 865 cm^{-1} to the a-conformer.

By the similarity of the infrared spectra in near 800 cm^{-1} region for cyclohexanol and fluorocyclohexane, the bands at 789 cm^{-1} and 844 cm^{-1} which exist in the true solid of cyclohexanol may belong to the e-conformer and the bands at 835 cm^{-1} and 863 cm^{-1} which disappear in the true solid to the a-conformer. It is very probable that only the e-conformer exists in the true solid of cyclohexanol.

Near 960 cm^{-1} cyclohexanol has one infrared band at 968 (vs) cm^{-1} in the liquid, but according to Ref. 10, fluorocyclohexane has three bands at 962 (vs) cm^{-1}, 948 (sh) cm^{-1}, and 938 (vs) cm^{-1} in the liquid, and only the 938 cm^{-1} band disappears in the true solid. As shown in Fig. 1, the shape of the 968 cm^{-1} band in the liquid cyclohexanol is largely changed in the CS_2 solution from that in the true solid. According to the similarity of the infrared spectra of cyclohexanol to that of fluorocyclohexane, it is very probable that the 968 cm^{-1} band of cyclohexanol consists of three bands in the CS_2 solution and in the liquid, while two bands in the true solid. The 968 cm^{-1} band in the liquid splits in the CS_2 solution and the lower wave number band probably consists of two bands, one of them disappear in the true solid (phase III). Then the band disappearing in the true solid may be assigned to the C-O stretching vibration for the a-conformer of cyclohexanol.

The 789 cm^{-1} band of cyclohexanol and the 793 cm^{-1} band of fluorocyclohexane in the infrared spectra have the very strong intensities in the Raman liquid spectra[10,12] and their intensities are the most strong in each near 800 cm^{-1} region. Therefore the bands at 789 cm^{-1} and 793 cm^{-1} may be assigned to the breathing vibration of cyclohexane ring in the e-conformers of cyclohexanol and fluorocyclohexne respectively.

As shown in Table 1, the wave numbers of the bands due to the breathing vibration of the e-conformer are higher than 802 cm^{-1} in the mono-substituted cyclohexane-derivatives having substituente Cl, Br, I, SH, SD and SCH_3, while lower

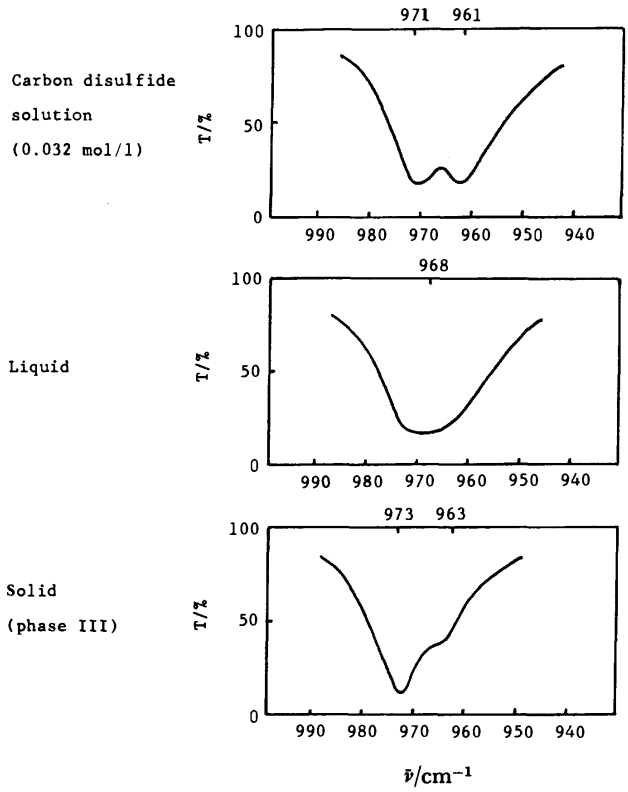

Fig. 1. Change of the 968 cm^{-1} band shape in the infrared spectra of cyclohexanol.

than 802 cm^{-1} in cyclohexanol and fluorocyclohexane. This difference may be due to the fact that the wave numbers for the bands of the C–O and C–F stretching vibrations are higher than 802 cm^{-1}, namely the band of the C–O stretching vibration at 1068 cm^{-1} and the C–F stretching vibration probably at 1049 cm^{-1} in the e-conformer, on the other hand those of the bands of C–Cl, C–Br, C–I, and C–S stretching vibrations are lower than 802 cm^{-1}, namely C–Cl at 733 cm^{-1}, C–Br at 688 cm^{-1}, C–I at 655 cm^{-1}, and C–SD at 757 cm^{-1} in the e-conformers.

As for the breathing vibration, the wave numbers of the bands for the e-conformer differ from those of the band for the a-conformer by about 5—15 cm^{-1} as shown in Table 1. However in the infrared spectra of the liquid, near the 789 cm^{-1} band of cyclohexanol and near the 793 cm^{-1} band of fluorocyclohexane, there are no bands which may be assigned to the breathing vibration for the a-conformers. In these moleculs, the bands at 793 cm^{-1} and 789 cm^{-1} may belong to both the e- and the a-conformer because of the small difference of the wave numbers in the a- and the e-band.

References

1) T. Shimanouchi and K. Kozima, *Nippon Kagaku Zasshi*, **72**, 468 (1951).
2) H. Takahashi, T. Shimanouchi, K. Fukushima, and T. Miyazawa, *J. Mol. Spectrosc.*, **13**, 43 (1964).
3) K. Sakashita, *Nippon Kagaku Zasshi*, **80**, 13 (1959).
4) E. Fujimoto, K. Kozima, and Y. Takeoka, *Bull. Chem. Soc. Jpn*, **44**, 2110 (1971).
5) E. Fujimoto, Y. Takeoka, and K. Kozima, *Bull. Chem. Soc. Jpn*, **43**, 991 (1970).
6) Y. Takeoka, *Bull. Chem. Soc. Jpn*, **35**, 1371 (1962).
7) Y. Takeoka, *J. Mol. Spectrosc.*, **15**, 29 (1965).
8) K. Kozima and K. Sakashita, *Bull. Chem. Soc. Jpn*, **31**, 796 (1958).
9) Y. Takeoka, *Bull. Tokyo Inst. Tech.*, **1964**, No. 57, 39.
10) S. D. Christian, J. Grundnes, P. Klaeboe, E. Torneng and T. Woldbaek, *Acta Chem. Scand.*, **A34**, 391 (1980).
11) K. Adachi, H. Suga, and S. Seki, *Bull Chem Soc. Jpn*, **41**, 1073 (1968).
12) D. W. James, H. F. Shurvell, and R. M. Parry, *J. Raman Spectrosc.*, **5**, 201 (1976).
13) E. Sciesenska and J. Sciesenski, *Mol. Cryst. Liq. Gryst.*, **80**, 19 (1982).

 © 1985 The Chemical Society of Japan Bull. Chem. Soc. Jpn., 58, 2464—2467 (1985) [Vol. 58, No. 9

Molecular Deformation Caused by Hydrogen Bonding and Resonance. 1,3-Dimethyl-2-imidazolidinone

Kunio FUKUSHIMA and Takashi HARAOKA
Department of Chemistry, Faculty of Science, Shizuoka University 836, Oya, Shizuoka 422
(Received March 13, 1985)

The Raman spectra of 1,3-dimethyl-2-imidazolidinone were found to change due to a hydrogen bonding to its nitrogen atoms, especially at low temperatures. The change in the spectra included the unusual change for CH_2 bending vibrations, suggesting that the deformation of the ring of the molecule takes place by hydrogen bonding.

In a preceding paper,[1] one of the present authors reported a remarkable change in the spectra of *N,N'*-dimethylurea in hydrogen-bonding solvents. This change was attributed to the molecular deformation by hydrogen bonding to nitrogen atoms. Further measurements regarding the temperature dependence of the spectra of the substance and an estimation of the enthalpy change of hydrogen bonding supported the idea of molecular deformation.[2] However, in this substance, other probable cause for the change (existence of cis and trans conformers due to an internal rotation around its CO–N axes) is present. In the present study, 1,3-dimethyl-2-imidazolidinone, which has no possibility of cis or trans conformations with respect to its CO–N axes, was adopted. Thus, measurements of Raman spectra were made in the hope of finding some change of the spectra (due to a molecular deformation caused by hydrogen bonding to nitrogen atoms).

Experimental

1,3-Dimethyl-2-imidazolidinone was a commercial product from Tokyo Kasei Co. (grade GR). The Raman

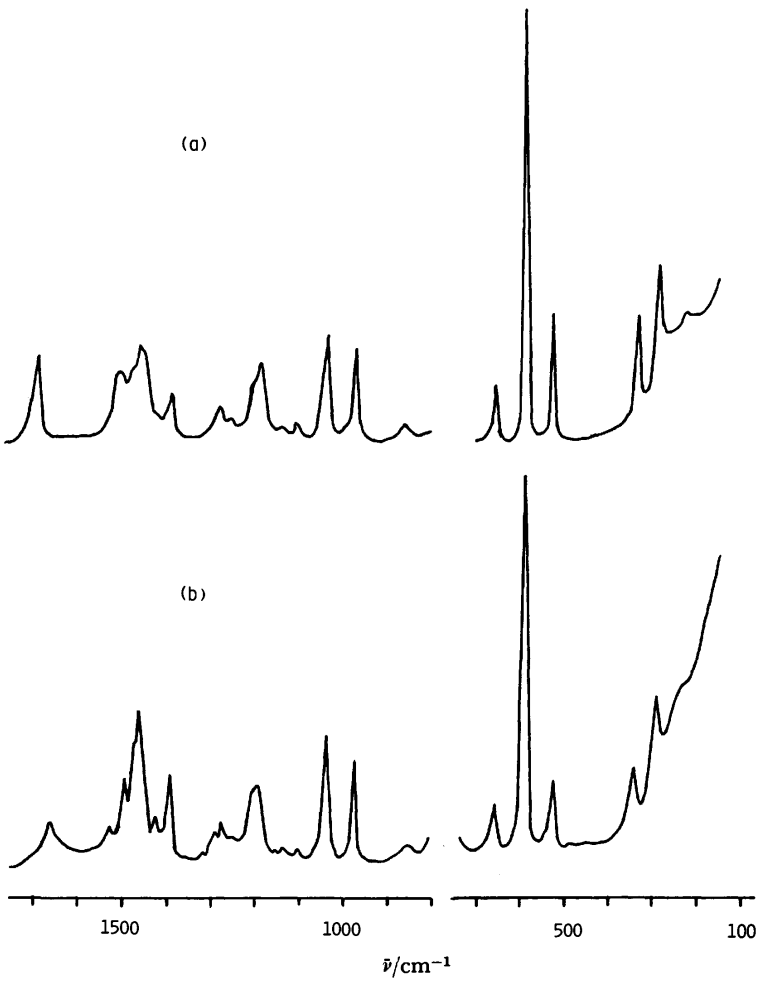

Fig. 1. Raman spectra of 1,3-dimethyl-2-imidazolidinone: (a) pure liquid; (b) aq soln(mixing mol ratio of solute to solvent: 1 : 8.75).

TABLE 1. RAMAN SPECTRA OF 1,3-DIMETHYL-2-IMIDAZOLIDINONE IN SOLUTIONS

Solid		Pure liq			Aq soln*			CCl_4 soln			CH_3CN soln		
$\tilde{\nu}$	I	$\tilde{\nu}$	I	ρ	$\tilde{\nu}$	I	ρ	$\tilde{\nu}$	I	ρ	$\tilde{\nu}$	I	ρ
100	10												
123	46												
153	6												
198	14												
213	10												
235	10												
283	17	283	6		284	4	P				281	4	0.75
329	19	330	4	0.75	338	2	0.75				329	3	0.75
520	28	523	6	0.75	521	3	0.75	520	5	0.75	520	5	0.75
577	40	584	20	0.24	584	21	0.25	580	17	0.17	581	21	0.24
648	21	652	2	0.75	658	3	0.75	651	2	0.59	650	2	0.75
763	100	764	100	0.09	772	100	0.08				764	100	0.11
856	13	858	1	0.75	853	1	0.75				858	1	0.75
963	16	965	5	0.23	972	6	0.24	962	5	0.15	965	6	0.26
					981	sh	?						
986	6	986	1	0.66				984	1	?	984	sh	?
1028	21	1031	5	0.30				1030	4	0.19	1032	6	0.37
					1040	9	0.29						
1070	3												
1093	6	1096	1	0.61	1098	1	0.67	1095	1	0.36	1098	1	0.75
1127	6	1129	1	0.75	1129	1	0.75	1128	1	0.43	1132	1	0.75
1170	44												
1186	7	1184	4	0.35				1180	4	0.18	1184	5	0.38
					1195	sh	?	1195	sh	?	1200	sh	?
		1201	sh	?	1203	6	0.50						
1239	7	1248	1	0.57	1250	1	?	1242	sh	?	1250	sh	?
1266	5	1269	2	0.37	1275	3	P	1269	2	0.16	1274	2	?
1280	7				1293	sh	?				1287	sh	?
1377	8	1384	2	0.31	1384	sh	?	1383	2	?			
					1394	5	0.29						
1406	6												
					1420	1	0.62						
1440	29	1446	sh	?	1446	sh	?	1441	sh	?			
1453	21	1451	5	0.75	1460	12	0.75	1449	5	?			
1465	18	1470	sh	?	1470	sh	?	1463	sh	?			
1473	sh												
1490	19	1494	3	0.67	1491	2	0.65	1488	5	?			
1513	21				1537	sh	?						
1675	24	1684	4	?	1641	6	0.25						
		1695	sh	?				1696	sh	?			

$\tilde{\nu}$: Shift frequency. I: Intensity. ρ: Depolarization ratio. P: Polarized. *: Mixing ratio(solute 1 mol : solvent 71 mols).

spectra were recorded on a Model R-800T Raman spectrometer (Japan Spectroscopic Co.) with an excitation effected by use of a Spectra Physics argon ion laser (Model 165) at 514.5 nm (300 mW). The depolarization ratio was measured with a system consisting of a half-wave plate, a lens, and a polarizer. Room-temperature liquid samples were measured using 0.3-ml Raman cells and crystals, solutions and pure liquids at lower temperatures were measured using an Oxford-type cryostat and liquid nitrogen. Experimental results are shown in Tables 1 and 2 and Figs. 1 and 2.

Results and Discussion

An 1,3-dimethyl-2-imidazolidinone molecule is expected to undergo a molecular deformation due to a deformation of its five-membered ring or the internal rotation of its methyl groups around the N–C axes. The vibrational frequencies of conformers (arising from the internal rotation of methyl groups) do not show any remarkable dependence on the

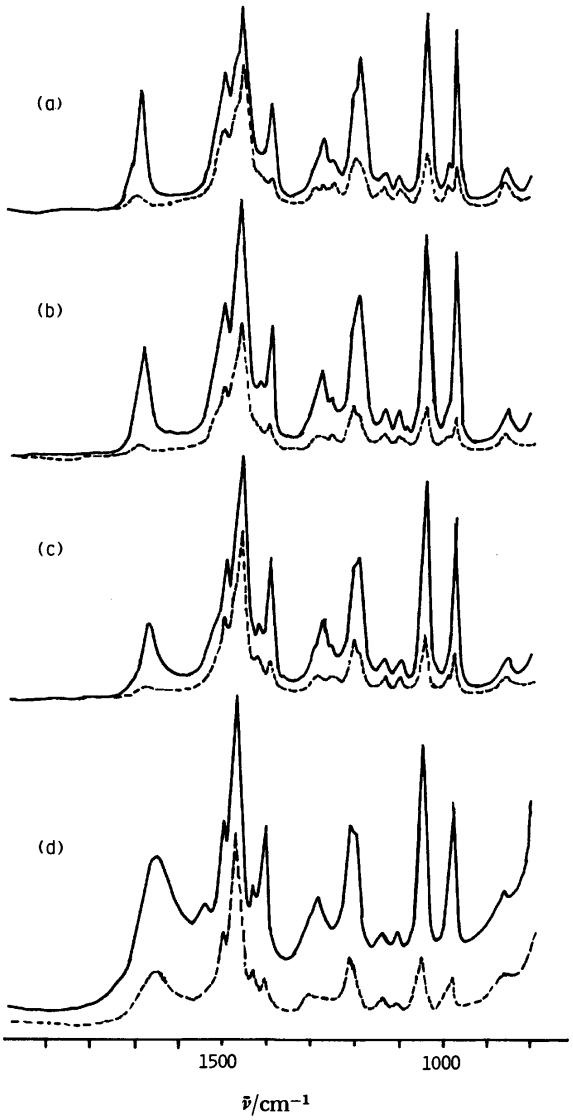

Fig. 2. Raman spectra of aqueous solutions of 1,3-dimethyl-2-imidazolidinone: mixing mol ratio of solute to solvent: (a) 1 : 0.21 (b) 1 : 0.99 (c) 1 : 3.00 (d) 1 : 71.

conformation of the methyl groups. Therefore, a difference among the spectra of the conformers is not expected. On the other hand, the effects of the deformation of the five-membered ring on the vibrational spectra are expected to be very remarkable. The probable causes of the deformation of the ring are the conformational changes due to the internal rotation around the bonds in the ring and that due to a change in the valence angle around the nitrogen atoms. Assuming the above-mentioned conformational change arising from a deformation of the ring, the observed spectral change associated with the state change was interpreted.

(a) Comparison of Liquid Spectra with Those of Solid: As shown in Table 1, there are two groups of bands. One group (1070 cm^{-1}, 1170 cm^{-1}, 1280 cm^{-1}, 1406 cm^{-1}, 1473 cm^{-1}, 1513 cm^{-1}, bands below 235 cm^{-1}) exists in the solid spectra but does not in the liquid spectra. The other (1201 cm^{-1}, 1695 cm^{-1}) exists in the liquid spectra but does not in the solid spectra. In the case of the former, although those below 235 cm^{-1} can be interpreted as due to lattice modes, which are characteristic to crystalline state, the existence of others suggests that a conformation of molecules in the solid state is a little different from that of molecules in a liquid state. The existence of bands of the latter group also supports this interpretation.

(b) Comparison of Liquid Spectra with Those of Solutions of Hydrogen-bonding Solvents: The following frequency shifts were observed to be associated with state changes from pure liquids to aqueous solutions (refer to Table 1 and Fig. 1); 1031 cm^{-1}→1040 cm^{-1}, 1184 cm^{-1}→1195 cm^{-1}, 1384 cm^{-1}→1394 cm^{-1}. The concentration dependency of relative intensities was determined (refer to Fig. 2). In addition, there are Raman bands of pure liquid (1201 cm^{-1} and 1451 cm^{-1}) which increase in intensity in the spectra of aqueous solutions. The 1420-cm^{-1} band appears only for aqueous solutions and the band for a pure liquid (523 cm^{-1}) decreases in intensity for the spectra of aqueous solutions. Similar changes are observed for methanol solutions. The above-mentioned changes do not occur for solutions of non-hydrogen-bonding solvents, of which a few examples (acetonitrile and carbon tetrachloride) are shown in Table 1. The changes are, therefore, considered to be characteristic of solutions of hydrogen-bonding solvents and are interpreted to be caused by the generation of hydrogen-bonded conformers. These arise from the deformation of the conformer which is stable in pure liquid as a result of hydrogen bonding. The Raman bands which appear at the higher frequency side of the pure-liquid bands for solutions of hydrogen-bonding solvents and the bands which appear only in the spectra of solutions of hydrogen-bonding solvents are due to the above-mentioned deformed conformers.

There are two types of hydrogen bonding to 1,3-dimethyl-2-imidazolidinone: Hydrogen bonding to its oxygen atom and that to its nitrogen atoms. In the former, the planarity of the $CH_2(CH_3)NCON$ skeleton by an increase of the double-bond character of the NC bond is expected, while in the latter, a tetrahedral configuration around the nitrogen atom is probable. In solutions of 1,3-dimethyl-2-imidazolidinone dissolved in hydrogen-bonding solvents, the latter situation is considered to be present because the spectra of 1,3-dimethyl-2-imidazolidinone in a hydrochloric acid solution, in which a species having a hydrogen ion attached to its nitrogen and having a tetrahedral configuration around the nitrogen atom is expected to occur, are almost similar to those of 1,3-dimethyl-2-imidazolidinone in an aqueous solution, as shown in Table 2. In connection with this, the remarkable increase in the intensity

TABLE 2. RAMAN SPECTRA OF 1,3-DIMETHYL-2-IMIDAZOLIDINONE IN ACIDS

Pure liq			Aq soln			HCl soln			DCl-D_2O soln		
$\tilde{\nu}$	I	ρ	$\tilde{\nu}$	I	ρ	$\tilde{\nu}$	I	ρ	$\tilde{\nu}$	I	ρ
283	6	?	284	4	P	286	4	P	283	6	P
330	4	0.75	336	2	0.75	338	2	0.75	330	4	0.75
523	6	0.75	520	3	0.75	520	4	0.75	519	6	0.75
584	20	0.24	585	20	0.25	586	23	0.19	583	25	0.23
652	2	0.75	655	2	0.75	656	3	0.75	652	3	0.75
764	100	0.09	767	100	0.08	770	100	0.10	768	100	0.12
858	1	0.75	853	1	0.75	852	1	0.42	851	1	0.66
965	5	0.23	968	6	0.24	969	6	0.24	967	6	0.26
986	1	0.66									
1031	5	0.30									
			1037	7	0.29	1038	8	0.27	1034	6	0.30
1096	1	0.61	1097	1	0.67	1097	w	DP ?	1098	w	DP ?
1129	1	0.75	1129	1	0.75	1129	w	DP ?	1128	w	DP ?
1184	4	0.35							1185	4	0.33
			1190	4	?	1192	sh	?			
1201	sh	?	1202	sh	0.50	1201	5	0.47	1200	sh	?
1248	1	0.57	1250	1	?	1243	sh	?	1248	w	DP ?
1269	2	0.37	1270	2	P	1273	3	?	1273	2	0.24
			1291	sh	?	1287	sh	?	1287	1	0.61
1384	2	0.31	1384	sh	?	1390	4	0.16	1386	3	0.20
			1392	5	0.29						
			1417	1	0.62	1418	w	?			
1446	sh	?	1446	sh	?				1448	7	0.75
1451	5	0.75	1454	9	0.75	1455	9	0.45	1454	7	0.75
1470	sh	?	1470	sh	?						
1494	3	0.67	1491	5	0.65	1490	2	0.52	1491	4	?
1684	4	?	1658	3	0.25	1661	2	0.26	1673	3	0.23
1695	sh	?									

$\tilde{\nu}$: Shift frequency. I: Intensity. ρ: Depolarization ratio. P: Polarized. DP: Depolarized. sh: Shoulder. w: weak. *: Mixing ratio(solute 1 mol : solvent 7 mols).

of the band at 1460 cm^{-1} (CH_2 bending vibration band) in the spectra of aqueous solutions, (whose frequency is different from those of conformers in pure liquid), is interpreted to be due to a valence change of the CH_2 group due to a deformation of the molecular ring caused by a configuration change around the nitrogen atom due to hydrogen bonding.

(c) Spectrum Change Due to Temperature Change: The change in the relative intensity of the bands of a methanol solution at 1195 and 1203 cm^{-1} were observed in a temperature range between −65 °C and room temperature. The former band increased in intensity, while the intensity of the latter decreased. Assuming a Lorentzian curve for the two bands, the overlapping bands were decomposed into two bands by a computer calculation. The enthalpy stabilization about 2 KJ mol^{-1}, of a hydrogen-bonded conformer relative to a non-hydrogen-bonded conformer was obtained. The obtained lower stabilization-enthalpy suggests that the stabilization enthalpy regarding hydrogen bonding is somewhat cancelled by the enthalpy loss due to a deformation around the nitrogern atom.

References

1) K. Fukushima and T. Kawai, *Bull. Chem. Soc. Jpn.*, **54**, 2811 (1981).

2) K. Fukushima and T. Kawai, *J. Mol. Struct.*, **112**, 51 (1984).

 © 1985 The Chemical Society of Japan Bull. Chem. Soc. Jpn., 58, 2468—2471 (1985) [Vol. 58, No. 9

Electronic Spectra of a Simple Trimethine Cyanine Dye Crystal. (3-Dimethylamino-2-propenylidene)dimethylammonium Perchlorate

Masakazu OTSU and Jiro TANAKA*
Department of Chemistry, Faculty of Science, Nagoya University, Chikusa-ku, Nagoya 464
(Received March 25, 1985)

The electronic spectra of the simplest polymethine cyanine dye crystal were studied by measuring the reflection spectra of (3-dimethylamino-2-propenylidene)dimethylammonium perchlorate. The spectra consist of a single peak situated at 32400 cm^{-1} in solution. Davydov splitting is observed in the crystal spectra and it is explained by calculating the dipole-dipole interaction energy and the interaction energy between the transition densities with the Ewald sum method.

(3-Dimethylamino-2-propenylidene)dimethylammonium perchlorate (3-DMP) is the simplest polymethine cyanine dye so far studied. The spectral features and the crystal structure of 3-DMP were studied by Johnson *et al.*[1] and Matthews *et al.*[2] to investigate the orientation of the molecules in a crystal. In our laboratory we continued the study of the reflection spectra and the crystal structures of (5-dimethylamino-2,4-pentadienylidene)dimethylammonium perchlorate.[3,4] A comparative study regarding 3-DMP will be quite interesting.

The reflection spectra of 3-DMP were measured with several crystal faces and the absorption spectra and the optical constant of the crystals were obtained by Kramers-Kronig transformation of the reflectivity. The observed Davydov splitting can be explained by the dipole-dipole interaction energy calculated with the dipole approximation and the Ewald sum of the transition density. The results showed reasonable agreement between theory and experiment.

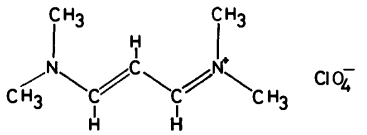

3-Dimethylaminopropenylidenedimethylammonium perchlorate (3-DMP)

Experimental

The material, 3-DMP, was synthesized from propalgyl alcohol. Propynal was obtained by the oxidation of the alcohol with CrO_3 and H_2SO_4.[5] Dimethylamine and the aldehyde reacted to form an adduct[6] and the obtained 3-dimethylamino-2-propenal was refluxed with dimethylammonium perchlorate to give 3-DMP.

Single crystals were obtained from a hot acetic anhydride solution under slow cooling. The crystalline faces are illustrated in Fig. 1. The reflection spectra of the crystals were measured with the (010), ($1\bar{1}0$), and ($11\bar{1}$) faces by a microspectrophotometer developed in this laboratory.

Results and Discussion

The absorption spectrum of 3-DMP measured in an aqueous solution is shown in Fig.2. It consists of a single peak centered at 32400 cm^{-1}. Its origin is considered to be a $\pi\pi^*$ transition of the polymethine chain. From the oscillator strength (f=0.97), the transition moment length is estimated as 1.66 Å. The f value given by Johnson *et al.*[1] is larger by a factor of 3 because of a difference in formulation.

On the (010) face shown in Fig. 3(a), all molecules are aligned along the same direction, and only a single excited state may be found if an intermolecular interaction such as a charge transfer is not concerned.

The reflection spectra were recorded along the

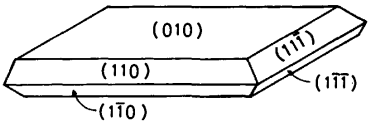

Fig. 1. Crystal habit of 3-DMP.

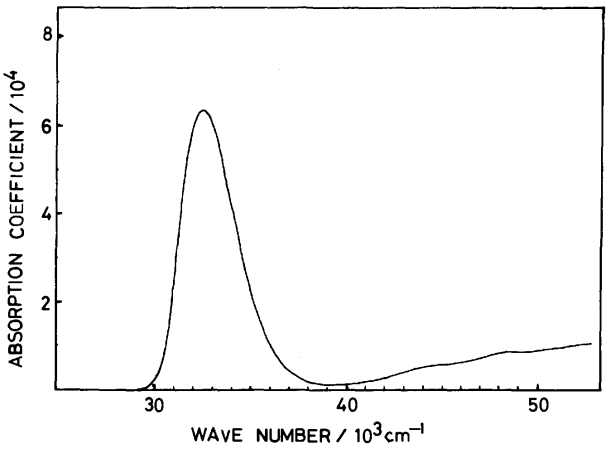

Fig. 2. Electronic absorption spectrum of 3-DMP in aqueous solution.

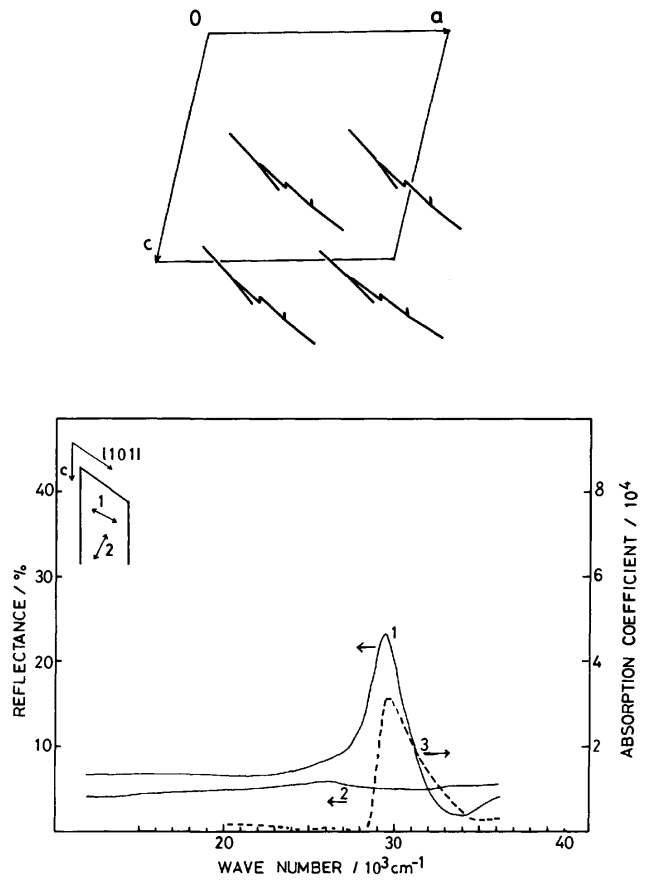

Fig. 3. (a): Projection of molecules onto the (010) face. (b): Crystal reflection spectra parallel to the [101] axis (1) and perpendicular to it (2) and absorption spectrum obtained by K-K transformation for the [101] direction with the (010) face (3).

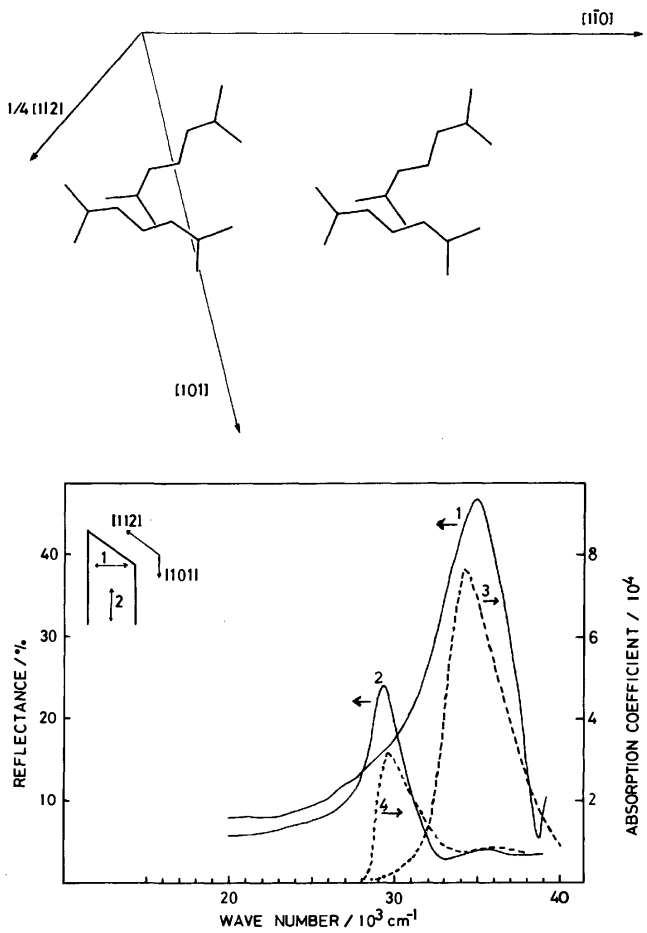

Fig. 4. (a): Projection of molecules onto the (11$\bar{1}$) face. (b): Crystal reflection spectra measured for perpendicular (1) and parallel (2) direction to the [101] axis and absorption spectra obtained by K-K transformation for perpendicular (3) and parallel (4) direction to the [101] axis with the (11$\bar{1}$) face.

molecular axis and perpendicular to it (Fig. 3(b)). A strong peak was found at 29000 cm^{-1} but nothing was found along the perpendicular direction. The K-K transformation gives a single peak situated at 29600 cm^{-1} (Fig. 3(b)).

A projection of the dye molecules onto the (11$\bar{1}$) face is shown in Fig. 4(a). The reflection spectra were measured along the directions parallel and perpendicular to the [101] zone axis. The [101] direction is perpendicular to the b axis, and it has only an ac component. Therefore, a Davydov splitting between the [101] direction and the direction perpendicular to it is expected, and it was actually found. Along the [101] zone axis, a peak was found at 29200 cm^{-1} that is almost coincident with the peak found with the (010) face at 29000 cm^{-1}. A very strong reflection peak was found for the direction perpendicular to the [101] direction at 34800 cm^{-1}. The K-K transformation of the reflectance shows an absorption peak at 34500 cm^{-1} for the perpendicular to the [101] direction which includes the b-axis transition and 29500 cm^{-1} for the [101] zone axis. A large Davydov splitting of 5000 cm^{-1} was found between the ac and b axes components.

The projection of the molecules onto the (1$\bar{1}$0) face is shown in Fig. 5(a). The reflection spectra were measured along the c axis and perpendicular to it parallel to the [110] direction. Along the c axis, no strong peak was detected since the transition moment on the molecule is almost perpendicular to this axis. For the [110] zone axis, both the b and ac axes components were expected and were clearly found at 35300 cm^{-1} and 30200 cm^{-1}. The K-K transformation of these spectra gives absorption maxima at 34600 cm^{-1} and 30000 cm^{-1}.

Using the K-K transformation, the real and imaginary parts of the dielectric constants were estimated (Fig. 6) for the [101] direction and its perpendicular. Large dispersions of the real and imaginary parts were found in the region of a strong absorption band.

The transition moments on the respective faces

were estimated from the intensities of these absorption bands. (Table 1)

A crystal of 3-DMP has four molecules in a unit cell; the crystal symmetry is Cc[2] and the coordinates of these molecules are given by (x,y,z), $(x, -y, 1/2+z)$, $(1/2+x, 1/2+y,z)$ and $(1/2+x, 1/2-y, 1/2+z)$. The molecular exciton state of the crystal is considered to have symmetry of A′ or A″ in the irreducible representation of Cs group. The A′ state is allowed for the ac axis, and the A″ state is active for the b axis direction.

$$\text{A}' \quad \Psi(ac)=\frac{1}{\sqrt{N}}\sum_{i=1}^{n}(\phi_{1i}+\phi_{2i}+\phi_{3i}+\phi_{4i})e^{i\boldsymbol{K}\cdot\boldsymbol{R}_i}$$

$$\text{A}'' \quad \Psi(b)=\frac{1}{\sqrt{N}}\sum_{i=1}^{n}(\phi_{1i}-\phi_{2i}+\phi_{3i}-\phi_{4i})e^{i\boldsymbol{K}\cdot\boldsymbol{R}_i}$$

where ϕ_{1i} represents the molecule in the 1-st site of the i-th unit cell being excited while all other molecules are in the ground state. The summation over i is extended ideally to all N molecules in a cell; however, it is limited in order to give a convergent result. Here $\boldsymbol{R}_i$ is the lattice vector and $\boldsymbol{K}$ is the reciprocal lattice vector.

The calculation of the Davydov splitting was performed using two methods. One was a dipole-dipole approximation to calculate the interaction energy on a particular crystalline surface for molecules with a limited depth and area; namely the summation is taken for molecules within a 20-Å depth and a 100-Å radius. The calculated splitting is shown in Table 1, where the calculated values are compared with the observed ones. Tendencies in the calculated shift are in good agreement with the observed

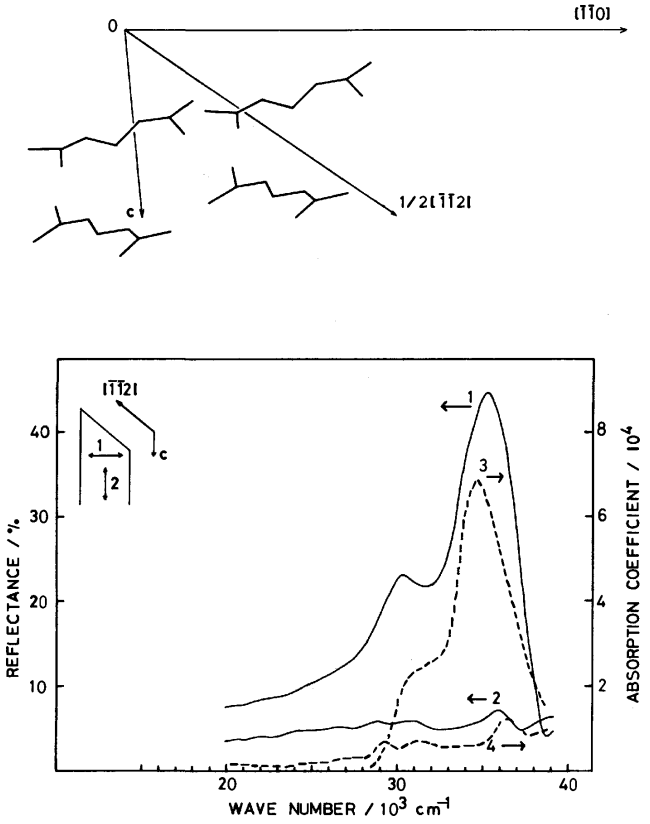

Fig. 5. (a): Projection of molecules onto the (1$\bar{1}$0) face. (b): Crystal reflection spectra measured for perpendicular (1) and parallel (2) to the c axis and absorption spectra obtained by K-K transformation for perpendicular (3) and parallel (4) to the c axis with the (1$\bar{1}$0) face.

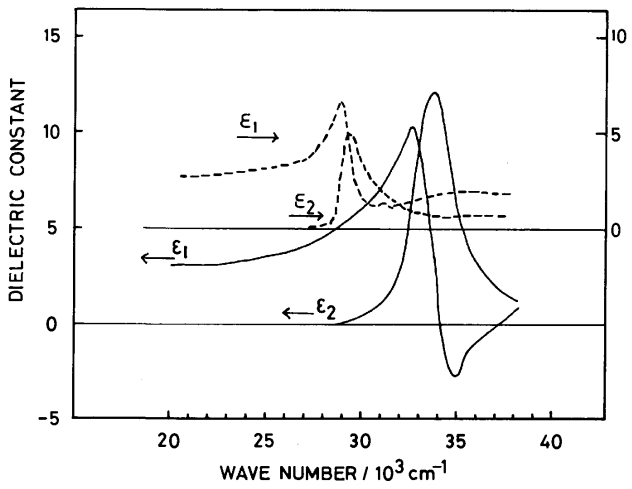

Fig. 6. Real and imaginary parts of dielectric constants for the direction parallel (----) and perpendicualr (——) to the [101] axis on the (11$\bar{1}$) face.

Table 1. Observed excited state and calculated energy levels by dipole-approximation

		Energy levels of crystal excited states/10^3 cm^{-1}		Shift of energy level/10^3 cm^{-1}		f	Transition moment/Å	
Crystal face	Optically active axes	Observed value	Calculated value	Observed value	Calculated value	Observed value	Observed value	Calculated value
(010)	ac	29.6	28.6	−2.8	−3.8	0.40	0.63	0.67
(11$\bar{1}$)	ac	29.5	28.6	−2.6	−3.8	0.42	0.64	0.69
	b	34.5	37.3	+2.1	+4.9	1.77	1.26	1.33
(1$\bar{1}$0)	ac	29.5	28.6	−2.9	−3.8	0.31	0.55	0.22
	b	34.6	36.5	+2.2	+4.1	1.17	1.03	1.03
Free molecule		32.4	(34.1)	—	—	0.97	1.66	(1.50)

values; however, the magnitude is larger by a factor of 1.5~2.3.

It is well known that the dipole approximation exagerates the electrostatic Coulomb interaction, particularly at short distance. In order to more accurately estimate the interaction, the Ewald sum of the Coulomb energies for the transition densities on a molecule was calculated using a program written by Mrs. S. Akhtar of our laboratory. The molecular orbitals concerning the electronic transition were calculated by the Pariser-Parr-Pople method, and the transition densities estimated for a one-electron transition was multiplied by a factor of $\sqrt{2}$ as shown below,

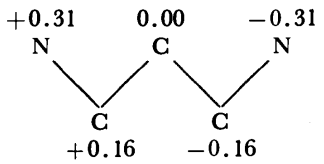

This was because the excited state is described by a linear combination of two one-electron excited configurations. Moreover, these values were multiplied by a factor of 1.12 in order to scale the observed transition moment with the observed value in for a solution. The calculation was performed at the Nogoya University computation center. The result gives a much smaller value compared to the dipole-dipole approximation; the splitting being 3000 cm^{-1} as compared to the observed value of 5000 cm^{-1}.

The oscillator strengths for these crystal transitions were calculated by the oriented gas model and compared with observed values (Table 1). The agreement between theory and experiment is quite reasonable in spite of the simple approach.

The crystal reflection spectra of 3-DMP are characterizad by a single band and its behavior on several crystalline surfaces can be explained well by the excited state of the crystal; the selection rule, the energy shift and the intensities are all explained by the oriented gas model interacting through the electrostatic interaction in the excited state. The results provide a simple example of crystal excited state where no other complication due to a charge transfer or mixing with other highly excited states is significant.

The authors thank to Mrs. S. Akhtar of our laboratory for the help of the calculation. This research was supported by the grant in aid of the special research project on the properties of molecular assemblies (No. 59112003) from the Ministry of Education, Science and Culture.

References

1) B. B. Johnson, P. Gramaccioni, and W. T. Simpson, *Mol. Cryst. Liq. Cryst.*, **28**, 99 (1973).

2) B. W. Matthews, R. E. Stenkamp, and P. M. Colman, *Acta. Crystallogr., Sect. B*, **29**, 449 (1973).

3) N. Sano and J. Tanaka, to be published.

4) M. Honda, C. Katayama, and J. Tanaka, *Acta Cystallogr., Sect. B* to be published.

5) J. C. Sauger, *Org. Syn.* Coll., Vol. 4 **1963**, 813.

6) S. S. Malhotra and M. C. Whiting, *J. Chem. Soc., (London)*, **1960**, 3812.

A New Theorem on an Internal Balance in the State Energy

Makoto Isihara
Department of General Education, Shotoku-Gakuen Women's Junior College, Nakauzura 1-38, Gifu 500
(Received April 17, 1985)

A theorem useful for checking the accuracy of the wave function is presented, which is especially valid and significant for open-shell systems. The theorem connects the kinetic and potential energies of electrons in the up- and down-spin states with one another through an antisymmetric quantity concerned with the spin polarization. Two mutually related derivations of the theorem are shown for the atomic system: One from the hypervirial theorem sets forth the general applicability and the other by the spin-dependent scaling clarifies the variational aspect. The numerical application to restricted and unrestricted analytic self-consistent field wave functions illustrates the sound nature of the theorem. Possibilities of its extension and generalization are touched upon briefly.

The state energy is undoubtedly a quantity of primary importance in the nonempirical calculation of electronic wave functions, not only because the quantity itself is the most fundamental that concerns many physical and chemical properties, but also because the approximate wave function is almost always calculated through the variation principle with the expectation value of the state energy as an indicator of accuracy. However, since the state energy given as an expectation value is of an extremely global character, the accuracy of the wave function cannot be checked enough if one concentrates exclusively on the lowering of the state energy expectation value.

It is, accordingly, quite reasonable to examine an expectation value of some physical quantity other than the state energy, provided that the "exact" value of the quantity is known. This way of checking may work effectively for specific problems under the appropriate choice of the quantity for examination, but it hardly seems to give any feeling for the general situation over various approximate wave functions of different systems.

One can also utilize relations between physical quantities which hold for the exact wave function or in the limit of a specific approximation. Although such relations can be often paraphrased into the form that the expectation value of a relevant composite quantity vanishes, there is qualitative difference between the use of a physical quantity with a known value and that of a physical relation, which is inherently nonempirical and commonly applicable. One of the most typical and important examples is the virial theorem[1-4] which has been frequently used in terms of the virial ratio check.

The virial ratio is, as a matter of course from its global character, not very sensitive in the high stage of approximation. It is true, however, that the virial theorem necessarily holds for the well-optimized wave function even without the gross scaling which forces the approximate wave function to satisfy the theorem. So is that the approximate wave function violating the theorem is more or less ill-behaved.

The usefulness of the virial theorem is mainly due to its intimate association with the state energy. Two dominant constituents of the state energy, the kinetic and potential energies, are subjected to a definite interrelation by the theorem, which is thus regarded as acquanting us with some detail of the state energy, an internal balance therein. Then, is there any other profitable theorem on another internal balance in the state energy?

In this paper we give an affirmative answer to this. The key observation is that a simple expression analogous with the virial relation is to be obtained separately for electrons in the up- and down-spin states. The expression is ready to lead us to a new theorem besides the virial theorem. The constituents participating in the new theorem are the kinetic and potential energies of electrons in the up- and down-spin states. They are connected with one another through an antisymmetric quantity concerned with the spin polarization. The theorem is, therefore, expected to be especially valid and significant in dealing with open-shell systems.

In the subsequent two sections, confining ourselves to the atomic system, we describe the derivation from the hypervirial theorem[5-8] and the derivation by the scaling dependent on the spin. The former is very transparent and clearly sets forth the applicability of the theorem, the latter clarifying the variational aspect. Next, a simple illustrative application is presented to restricted and unrestricted analytic self-consistent field (SCF) wave functions. After short concluding remarks, three appendices follow.

Derivation from the Hypervirial Theorem

Let $\{\phi_{j\sigma}(\boldsymbol{r})\xi_\sigma\}$ be a complete set of orthonormal spin orbitals, ξ_σ being the one-electron spin eigenfunction; σ stands for the one-electron spin state, taking $\uparrow$ (up) or $\downarrow$ (down), and $\boldsymbol{r}$ symbolizes the spatial coordinates with the origin at the atomic center. The notation $\bar{\sigma}$ is used to indicate the spin state opposite to σ in the following. Each of $\{\phi_{j\uparrow}(\boldsymbol{r})\}$ and $\{\phi_{j\downarrow}(\boldsymbol{r})\}$ are assumed to form a complete set of orthonormal spatial orbitals,

though $\phi_{j\sigma}(\boldsymbol{r})$ is not necessarily identical with $\phi_{j\bar{\sigma}}(\boldsymbol{r})$.

Denoting the creation and annihilation operators for the spin orbital $\phi_{j\sigma}(\boldsymbol{r})\xi_\sigma$, respectively, by $a_{j\sigma}^\dagger$ and $a_{j\sigma}$, we can write the atomic electronic Hamiltonian in the second quantized form as

$$H = \sum_\sigma (T_\sigma + V_\sigma + W_{\sigma\sigma} + W_{\sigma\bar{\sigma}}) \tag{1}$$

with

$$T_\sigma = \sum_{jk} t_{jk\sigma} a_{j\sigma}^\dagger a_{k\sigma}, \tag{2}$$

$$V_\sigma = \sum_{jk} v_{jk\sigma} a_{j\sigma}^\dagger a_{k\sigma}, \tag{3}$$

and

$$W_{\sigma\tau} = \frac{1}{2} \sum_{jklm} w_{lm\tau}^{jk\sigma} a_{j\sigma}^\dagger a_{l\tau}^\dagger a_{m\tau} a_{k\sigma}, \tag{4}$$

where

$$t_{jk\sigma} = \int \phi_{j\sigma}^*(\boldsymbol{r})(-\nabla^2/2)\phi_{k\sigma}(\boldsymbol{r})\mathrm{d}v, \tag{5}$$

$$v_{jk\sigma} = \int \phi_{j\sigma}^*(\boldsymbol{r})(-Z/r)\phi_{k\sigma}(\boldsymbol{r})\mathrm{d}v, \tag{6}$$

and

$$w_{lm\tau}^{jk\sigma} = \iint \phi_{j\sigma}^*(\boldsymbol{r}_1)\phi_{l\tau}^*(\boldsymbol{r}_2)(1/r_{12})\phi_{m\tau}(\boldsymbol{r}_2)\phi_{k\sigma}(\boldsymbol{r}_1)\mathrm{d}v_2\mathrm{d}v_1. \tag{7}$$

We abbreviate $|\boldsymbol{r}|$ to r and $|\boldsymbol{r}_1-\boldsymbol{r}_2|$ to r_{12} as usual; $\mathrm{d}v$ stands for the spatial volume element and Z for the atomic number. It holds that

$$W_{\sigma\tau} = W_{\tau\sigma} \tag{8}$$

as a direct consequence of $w_{lm\tau}^{jk\sigma} = w_{jk\sigma}^{lm\tau}$.

Now the hypervirial theorem asserts that an exact stationary state fulfils

$$\langle [H, F] \rangle = 0 \tag{9}$$

for arbitrary choice of an operator F of the system considered.[5-8] The pure bracket means the expectation value in the exact stationary state. Introducing the virial operator for the spin state σ

$$G_\sigma = \sum_{jk} g_{jk\sigma} a_{j\sigma}^\dagger a_{k\sigma} \tag{10}$$

with

$$g_{jk\sigma} = -\frac{\mathrm{i}}{2} \int \phi_{j\sigma}^*(\boldsymbol{r})(\boldsymbol{r}\cdot\nabla + \nabla\cdot\boldsymbol{r})\phi_{k\sigma}(\boldsymbol{r})\mathrm{d}v, \tag{11}$$

we adopt this (or $G_\uparrow \pm G_\downarrow$) as F in the hypervirial theorem. Since $\nabla\cdot\boldsymbol{r}$ is converted into $\boldsymbol{r}\cdot\nabla$ plus a constant, the use of the non-hermitian virial operator containing only $\boldsymbol{r}\cdot\nabla$ is tantamount to that of the present operator under the Hamiltonian which conserves both the numbers of electrons in the up- and down-spin states. We prefer the hermitian form; it just fits the unitary transformation formalism. (See the next section and Appendix II.)

Because G_σ is commutative with $T_{\bar{\sigma}}$, $V_{\bar{\sigma}}$, and $W_{\bar{\sigma}\bar{\sigma}}$, we have only to calculate the commutators of G_σ with T_σ, V_σ, $W_{\sigma\sigma}$, and $W_{\sigma\bar{\sigma}}$. The one-electron commutators are readily found to be

$$[T_\sigma, G_\sigma] = -2\mathrm{i}T_\sigma \tag{12}$$

and

$$[V_\sigma, G_\sigma] = -\mathrm{i}V_\sigma. \tag{13}$$

For the two-electron commutators we have

$$[W_{\sigma\tau}, G_\sigma] = -\mathrm{i}(1+\delta_{\sigma\tau})(W_{\sigma\tau} + X_{\sigma\tau})/2 \tag{14}$$

with

$$X_{\sigma\tau} = \frac{1}{2} \sum_{jklm} x_{lm\tau}^{jk\sigma} a_{j\sigma}^\dagger a_{l\tau}^\dagger a_{m\tau} a_{k\sigma}, \tag{15}$$

where

$$x_{lm\tau}^{jk\sigma} = \iint \phi_{j\sigma}^*(\boldsymbol{r}_1)\phi_{l\tau}^*(\boldsymbol{r}_2)(1/\tilde{r}_{12})\phi_{m\tau}(\boldsymbol{r}_2)\phi_{k\sigma}(\boldsymbol{r}_1)\mathrm{d}v_2\mathrm{d}v_1 \tag{16}$$

with

$$\tilde{r}_{12} = r_{12}^3/(r_1^2 - r_2^2). \tag{17}$$

The property that $x_{lm\tau}^{jk\sigma} = -x_{jk\sigma}^{lm\tau}$ leads to

$$X_{\sigma\tau} = -X_{\tau\sigma} \tag{18}$$

in sharp contrast to $W_{\sigma\tau}$. Because of this antisymmetry it follows that

$$[W_{\sigma\sigma}, G_\sigma] = -\mathrm{i}W_{\sigma\sigma}, \tag{19}$$

but

$$[W_{\sigma\bar{\sigma}}, G_\sigma] = -\mathrm{i}(W_{\sigma\bar{\sigma}} + X_{\sigma\bar{\sigma}})/2. \tag{20}$$

The quantity $X_{\sigma\bar{\sigma}}$ is considered to represent the electronic repulsion potential "filtered" with the factor $(r_1^2 - r_2^2)/r_{12}^2$. It seems proper to refer to this quantity as the spin polarization potential. The point of calculation of the above commutators is given in Appendix I.

It is convenient to define the potential energy operator for the spin state σ as

$$U_\sigma = V_\sigma + W_{\sigma\sigma} + W_{\sigma\bar{\sigma}}. \tag{21}$$

The commutators in the preceding paragraph suffice to give

$$[H, G_\sigma] = -\mathrm{i}(2T_\sigma + U_\sigma + X_{\sigma\bar{\sigma}}), \tag{22}$$

which results in

$$2\langle T_\sigma \rangle + \langle U_\sigma \rangle + \langle X_{\sigma\bar{\sigma}} \rangle = 0 \qquad (\sigma = \uparrow, \downarrow) \tag{23}$$

by virtue of the hypervirial theorem. By the relevant recombination in this set of equations, which is equivalent to using

$$\langle [H, G_\uparrow \pm G_\downarrow] \rangle = 0, \tag{24}$$

we obtain the virial theorem

$$2\langle T\rangle+\langle U\rangle = 0, \tag{25}$$

where

$$T = T_\uparrow + T_\downarrow \tag{26}$$

and

$$U = U_\uparrow + U_\downarrow = V_\uparrow + V_\downarrow + W_{\uparrow\uparrow} + W_{\downarrow\downarrow} + 2W_{\uparrow\downarrow}, \tag{27}$$

and the following theorem independent of the virial one.

$$2\langle \Delta T\rangle + \langle \Delta U\rangle + \langle \Delta X\rangle = 0 \tag{28}$$

with

$$\Delta T = T_\uparrow - T_\downarrow, \tag{29}$$

$$\Delta U = U_\uparrow - U_\downarrow = V_\uparrow - V_\downarrow + W_{\uparrow\uparrow} - W_{\downarrow\downarrow}, \tag{30}$$

and

$$\Delta X = X_{\uparrow\downarrow} - X_{\downarrow\uparrow} = 2X_{\uparrow\downarrow}. \tag{31}$$

We provisionally call this the spin virial theorem for the sake of convenience.

It is evident that the spin virial theorem as well as the virial theorem still holds even if the exact stationary state is replaced with any approximate state $|\Phi\rangle$that satisfies the one-electron hypervirial theorem[9]

$$\langle\Phi|[H,\ a_{j\sigma}^\dagger a_{k\sigma}]|\Phi\rangle = 0 \quad (\text{any } j\sigma, k\sigma). \tag{32}$$

The most representative example is the unrestricted Hartree-Fock (HF) state and the restricted HF state for the closed-shell system. The restricted HF state for the open-shell system, however, does not satisfy the one-electron hypervirial theorem in general, even though it does

$$\langle\Phi|[H,\ a_{j\uparrow}^\dagger a_{k\uparrow}+a_{j\downarrow}^\dagger a_{k\downarrow}]|\Phi\rangle = 0 \quad (\text{any } j,\ k), \tag{33}$$

which is enough for the virial theorem to hold. The application to the approximate state with a specified form is thus often to be considered with respect to the exact limit of the approximation.

Scaling Dependent on the Spin

It is well known the close relation between the virial theorem and the positive gross scaling in the wave function, which can be worded in various manner.[4] The essential point is still the equivalence of the virial theorem to the variational condition upon the scale factor incorporated into the wave function.[2] The corresponding equivalence can be obtained also for the spin virial theorem. Here, in favor of naivety, we show a pedestrian approach starting with the explicit introduction of the spin-dependent scaling in orbitals, though the objective can be reached elegantly with the unitary transformation formalism,[6,8] which is outlined in Appendix II for reference.

Now incorporating the spin-dependent scale factor into orbitals, we define the scaled orbitals as

$$\phi_{j\sigma}(\boldsymbol{r};\ \lambda_\sigma) = \lambda_\sigma^{3/2}\phi_{j\sigma}(\lambda_\sigma \boldsymbol{r}). \tag{34}$$

The orthonormality is preserved;

$$\int \phi_{j\sigma}^*(\boldsymbol{r};\ \lambda_\sigma)\phi_{k\sigma}(\boldsymbol{r};\ \lambda_\sigma)\mathrm{d}v = \delta_{jk}. \tag{35}$$

Soon it is seen to be suitable for our purpose to use the following parameters η and θ instead of $\lambda_\uparrow$ and $\lambda_\downarrow$.

$$\lambda_\sigma = \exp(\eta+\kappa_\sigma\theta) \tag{36}$$

with

$$\kappa_\sigma = \begin{cases} 1 & (\sigma=\uparrow) \\ -1 & (\sigma=\downarrow). \end{cases} \tag{37}$$

The creation and annihilation operators corresponding to the scaled spin orbital $\phi_{j\sigma}^\eta(\boldsymbol{r})\xi_\sigma \equiv \phi_{j\sigma}(\boldsymbol{r};\lambda_\sigma)\xi_\sigma$ are denoted by $a_{j\sigma}^{\eta\theta\dagger}$ and $a_{j\sigma}^{\eta\theta}$, respectively.

We can rewrite T_σ, V_σ, and $W_{\sigma\sigma}$ in the scaled representation simply as

$$T_\sigma = \exp(2(\eta+\kappa_\sigma\theta))\sum_{jk} t_{jk\sigma}a_{j\sigma}^{\eta\theta\dagger}a_{k\sigma}^{\eta\theta}, \tag{38}$$

$$V_\sigma = \exp(\eta+\kappa_\sigma\theta)\sum_{jk} v_{jk\sigma}a_{j\sigma}^{\eta\theta\dagger}a_{k\sigma}^{\eta\theta}, \tag{39}$$

and

$$W_{\sigma\sigma} = \exp(\eta+\kappa_\sigma\theta)\frac{1}{2}\sum_{jklm} w_{lm\sigma}^{jk\sigma}a_{j\sigma}^{\eta\theta\dagger}a_{l\sigma}^{\eta\theta\dagger}a_{m\sigma}^{\eta\theta}a_{k\sigma}^{\eta\theta}, \tag{40}$$

whereas we have

$$W_{\sigma\bar\sigma} = \exp(\eta)\frac{1}{2}\sum_{jklm} w_{lm\bar\sigma}^{jk\sigma}(\theta)a_{j\sigma}^{\eta\theta\dagger}a_{l\bar\sigma}^{\eta\theta\dagger}a_{m\bar\sigma}^{\eta\theta}a_{k\sigma}^{\eta\theta}, \tag{41}$$

where

$$w_{lm\bar\sigma}^{jk\sigma}(\theta) = \iint \phi_{j\sigma}^*(\boldsymbol{r}_1)\phi_{l\bar\sigma}^*(\boldsymbol{r}_2)(1/r_{12}^{\sigma\bar\sigma}(\theta))\phi_{m\bar\sigma}(\boldsymbol{r}_2)\phi_{k\sigma}(\boldsymbol{r}_1)\mathrm{d}v_2\mathrm{d}v_1 \tag{42}$$

with

$$r_{12}^{\sigma\bar\sigma}(\theta) = |\exp(\kappa_{\bar\sigma}\theta)\boldsymbol{r}_1 - \exp(\kappa_\sigma\theta)\boldsymbol{r}_2|. \tag{43}$$

As is implied by the notation, $w_{lm\bar\sigma}^{jk\sigma}(\theta)$ is independent of η, the η-dependence of the matrix element of $W_{\sigma\bar\sigma}$ being completely put into $\exp(\eta)$.

The expansion theorem[10] allows us, without loss of generality, to write the exact or approximate state $|\mathrm{O}\rangle$ as

$$|\mathrm{O}\rangle = \sum_M C_M|M\rangle, \tag{44}$$

where C_M is a numerical coefficient and $|M\rangle$ is a single configuration state

$$|M\rangle = \prod_{j^\sigma\in M} a_{j\sigma}^\dagger|\text{vacuum}\rangle \tag{45}$$

which is characterized by a set M of relevant spin orbital indices. The scaled state is obtained by replacing $a_{j\sigma}^{\eta\theta\dagger}$ with $a_{j\sigma}^{\dagger}$ in the original state;

$$|\eta\theta\rangle = \sum_M C_M |M\eta\theta\rangle \tag{46}$$

with

$$|M\eta\theta\rangle = \prod_{j^\sigma\in M} a_{j^\sigma}^{\eta\theta\dagger}|\text{vacuum}\rangle. \tag{47}$$

The density matrices, $\gamma_{jk\sigma}$ and $\Gamma_{lm\tau}^{jk\sigma}$, are consequently kept unchanged;

$$\gamma_{jk\sigma} = \langle a_{j\sigma}^{\dagger}a_{k\sigma}\rangle_0 = \langle a_{j\sigma}^{\eta\theta\dagger}a_{k\sigma}^{\eta\theta}\rangle_{\eta\theta} \tag{48}$$

and

$$\Gamma_{lm\tau}^{jk\sigma} = \langle a_{j\sigma}^{\dagger}a_{l\tau}^{\dagger}a_{m\tau}a_{k\sigma}\rangle_0 = \langle a_{j\sigma}^{\eta\theta\dagger}a_{l\tau}^{\eta\theta\dagger}a_{m\tau}^{\eta\theta}a_{k\sigma}^{\eta\theta}\rangle_{\eta\theta}, \tag{49}$$

where $\langle\cdots\rangle_0$ and $\langle\cdots\rangle_{\eta\theta}$ are short for the expectation value in $|O\rangle$ and that in $|\eta\theta\rangle$. Thus it follows that

$$\langle T_\sigma\rangle_{\eta\theta} = \exp(2(\eta+\kappa_\sigma\theta))\langle T_\sigma\rangle_0, \tag{50}$$

$$\langle V_\sigma + W_{\sigma\sigma}\rangle_{\eta\theta} = \exp(\eta+\kappa_\sigma\theta)\langle V_\sigma + W_{\sigma\sigma}\rangle_0, \tag{51}$$

and

$$\langle W_{\sigma\bar{\sigma}}\rangle_{\eta\theta} = \exp(\eta)\frac{1}{2}\sum_{jklm} w_{lm\bar{\sigma}}^{jk\sigma}(\theta)\Gamma_{lm\bar{\sigma}}^{jk\sigma} \tag{52}$$

rather straightforwardly.

The differentiation of the above expectation values with respect to η and θ is trivial except that of $\langle W_{\sigma\bar{\sigma}}\rangle_{\eta\theta}$ with respect to θ. Going through

$$\frac{\partial}{\partial\theta}w_{lm\bar{\sigma}}^{jk\sigma}(\theta) = \kappa_\sigma x_{lm\bar{\sigma}}^{jk\sigma}(\theta), \tag{53}$$

where

$$x_{lm\bar{\sigma}}^{jk\sigma}(\theta) = \iint \phi_{j\sigma}^{*}(\boldsymbol{r}_1)\phi_{l\bar{\sigma}}^{*}(\boldsymbol{r}_2)(1/\tilde{r}_{12}^{\sigma\bar{\sigma}}(\theta))\phi_{m\bar{\sigma}}(\boldsymbol{r}_2)\phi_{k\sigma}(\boldsymbol{r}_1)\mathrm{d}v_2\mathrm{d}v_1 \tag{54}$$

with

$$\tilde{r}_{12}^{\sigma\bar{\sigma}}(\theta) = r_{12}^{\sigma\bar{\sigma}}(\theta)^3/(\exp(2\kappa_{\bar{\sigma}}\theta)r_1^2 - \exp(2\kappa_\sigma\theta)r_2^2), \tag{55}$$

we arrive at

$$\frac{\partial}{\partial\theta}\langle W_{\sigma\bar{\sigma}}\rangle_{\eta\theta} = \kappa_\sigma\langle X_{\sigma\bar{\sigma}}\rangle_{\eta\theta}, \tag{56}$$

since $\exp(\eta)x_{lm\bar{\sigma}}^{jk\sigma}(\theta)$ is just the matrix element of $X_{\sigma\bar{\sigma}}$ in the scaled representation;

$$X_{\sigma\bar{\sigma}} = \exp(\eta)\frac{1}{2}\sum_{jklm} x_{lm\bar{\sigma}}^{jk\sigma}(\theta)a_{j\sigma}^{\eta\theta\dagger}a_{l\bar{\sigma}}^{\eta\theta\dagger}a_{m\bar{\sigma}}^{\eta\theta}a_{k\sigma}^{\eta\theta}. \tag{57}$$

After all, we have

$$\frac{\partial}{\partial\eta}\langle T_\sigma\rangle_{\eta\theta} = 2\langle T_\sigma\rangle_{\eta\theta}, \tag{58}$$

$$\frac{\partial}{\partial\theta}\langle T_\sigma\rangle_{\eta\theta} = 2\kappa_\sigma\langle T_\sigma\rangle_{\eta\theta}, \tag{59}$$

$$\frac{\partial}{\partial\eta}\langle V_\sigma + W_{\sigma\sigma} + W_{\sigma\bar{\sigma}}\rangle_{\eta\theta} = \langle V_\sigma + W_{\sigma\sigma} + W_{\sigma\bar{\sigma}}\rangle_{\eta\theta}, \tag{60}$$

and

$$\frac{\partial}{\partial\theta}\langle V_\sigma + W_{\sigma\sigma} + W_{\sigma\bar{\sigma}}\rangle_{\eta\theta} = \kappa_\sigma(\langle V_\sigma + W_{\sigma\sigma}\rangle_{\eta\theta} + \langle X_{\sigma\bar{\sigma}}\rangle_{\eta\theta}). \tag{61}$$

Complete parallelism between the present treatment and the preceding one is quite clear in this step.

Using the above result with the notation defined before, we immediately obtain

$$\frac{\partial}{\partial\eta}\langle H\rangle_{\eta\theta} = 2\langle T\rangle_{\eta\theta} + \langle U\rangle_{\eta\theta} \tag{62}$$

and

$$\frac{\partial}{\partial\theta}\langle H\rangle_{\eta\theta} = 2\langle \Delta T\rangle_{\eta\theta} + \langle \Delta U\rangle_{\eta\theta} + \langle \Delta X\rangle_{\eta\theta}, \tag{63}$$

which show that the variational condition

$$\frac{\partial}{\partial\eta}\langle H\rangle_{\eta\theta} = 0 \tag{64}$$

and

$$\frac{\partial}{\partial\theta}\langle H\rangle_{\eta\theta} = 0 \tag{65}$$

are equivalent to the virial theorem and the spin virial theorem. The exact wave function evidently lets these theorems hold. If θ is excluded out or fixed at zero throughout the treatment, the virial theorem results alone.[11]

Now suppose that one has an approximate wave function violating both or either of the virial theorem and the spin virial theorem. The relevant scaling may be thought to improve the approximate wave function, making it satisfy the theorems; yet, aside from the case that the violation is conspicuous, the approximate wave function will not be improved genuinely with the sole use of the scaling. Here note that the completeness of a set of spin orbitals is assumed in the above, or else the Hamiltonian in the scaled representation inevitably differs from that in the original representation. Therefore, if one starts with an approximate wave function determined with some physical (presumably variational) condition in an incomplete space built of finite spin orbitals, then the scaled wave function may not fulfil the condition with respect to the "scaled" Hamiltonian.

Even in such a case, it is possible to invoke a practical iterative procedure: After the scaling process, calculate a wave function in the space built of the scaled spin orbitals with the predesignated condition, and go back to the scaling process with the calculated wave function as a new nonscaled wave function. This procedure is, however, not recommended as a general way of improving an

approximate wave function in an incomplete space. The determination of η and θ is considerably laborious compared with that of the gross scale factor. It is rather important that the well-optimized, refined wave function is to fulfil the theorems without any scaling treatment. Here we only add that the spin-dependent scaling in a finite basis space necessarily leads us to "different bases for different spins,"[12] which does not match the spin restricted picture.

Illustrative Application

Here we apply the spin virial theorem to several restricted and unrestricted SCF wave functions obtained by the analytic expansion method,[13,14] using the spin virial ratio

$$\Omega_s = -(\overline{\Delta V}+\overline{\Delta W}+\overline{\Delta X})/(2\overline{\Delta T}), \tag{66}$$

where ΔV and ΔW are, respectively, the one- and two-electron components of ΔU. The upper bar means the expectation value for the wave function under consideration. Of course, the spin virial ratio takes unity if the theorem is satisfied. Our aim now is to realize the nature of the theorem rather than to test those wave functions.

For the present application, the above expectation values are reduced to the orbital integrals $t_{jj\sigma}$, $v_{jj\sigma}$, $w^{jj\sigma}_{kk\sigma}$, $w^{jk\sigma}_{kj\sigma}$, and $x^{jj\sigma}_{kk\sigma}$. Further, for the restricted case, we have only to take account of those integrals with which the singly occupied orbital is concerned. The integral of the spin polarization potential can be calculated analytically as well as the others. A few details of the integration are put in Appendix III.

The results are summarized in Tables 1—4. The state considered is ^2S for Li and Na, ^2P for B, and ^4S for N. The basis sets are from Clementi and Roetti's table,[15] unless otherwise specified. For the restricted case, we used the data of expansion coefficients in the published tables[15-17] directly with no SCF recalculation. Hence, the accuracy of the obtained values is a little degraded. The calculated values of the state energy

$$E = \overline{T} + \overline{U} \tag{67}$$

coincide with the published ones in five figures, and the virial ratio

$$\Omega_v = -\overline{U}/(2\overline{T}) \tag{68}$$

remains 1.0000 with the deviation about ± 0.00001, being omitted in Tables 1 and 2. On the other hand, for the unrestricted case, we started with the SCF calculation using Clementi and Roetti's[15] and Weiss'[16] basis sets. Proper accuracy was sustained consistently.

Table 1 shows how the spin virial ratio varies with basis sets for the restricted case. The calculations for B, N, and Na exemplify the varying with the size of a basis set. We see a distinct gap between the single- and double-zeta results, the change being small beyond the double-zeta calculation. As the SCF wave function approaches the HF limit, the spin virial ratio appears to converge to the limit characteristic of the system. This is ascertained by the calculation for Li with different basis sets of fairly large size; the values of Ω_s are almost identical. As mentioned before, the open-shell HF wave function inherently violates the spin virial theorem,[18] so that the limit of convergence is not unity in general. Although the double-zeta results for B and N may look somewhat

Table 1. Varying of the spin virial ratio with basis sets (*Restricted*)

System	Basis	$-E$/a.u.	Ω_s	$\overline{\Delta T}$/a.u.	$-\overline{\Delta V}$/a.u.	$\overline{\Delta W}$/a.u.	$\overline{\Delta X}$/a.u.
B	2s1p	24.498	1.0142	0.7328	3.0267	0.9430	0.5971
	4s2p	24.528	1.0059	0.7466	3.0286	0.9333	0.5933
	5s4p	24.529	1.0061	0.7457	3.0249	0.9320	0.5925
	6s4p	24.529	1.0061	0.7458	3.0251	0.9320	0.5925
N	2s1p	54.269	1.0123	5.5125	20.129	6.2993	2.6683
	4s2p	54.398	1.0057	5.6315	20.128	6.1503	2.6506
	5s4p	54.401	1.0059	5.6289	20.111	6.1406	2.6464
	6s4p	54.401	1.0059	5.6291	20.111	6.1406	2.6464
Na	3s1p	161.12	1.0348	0.2265	3.1869	1.3856	1.3324
	6s2p	161.85	1.0143	0.2629	3.3000	1.4185	1.3481
	7s3p	161.86	1.0134	0.2666	3.3110	1.4215	1.3492
	8s5p	161.86	1.0128	0.2673	3.3154	1.4232	1.3508
Li	6s	7.4327	1.0483	0.2088_4	1.0362	0.3083_9	0.2899_9
	6s W[a]	7.4327	1.0484	0.2087_8	1.0362	0.3083_8	0.2900_0
	6s RSW[b]	7.4327	1.0484	0.2087_8	1.0361	0.3083_5	0.2899_6
	12s RSW	7.4327	1.0484	0.2088_2	1.0362	0.3083_7	0.2899_8

a) Weiss' basis, Ref. 16. b) Roothaan, Sachs, and Weiss' basis, Ref. 17.

strange at first sight, it is easily understood that such results are quite probable and no strange. The spin virial ratio need not to vary in parallel with the state energy and further it now tends to the limit other than unity.

In Table 2 we inquire into the behavior of the spin virial ratio in different systems and in their isoelectronic sequences for the restricted case. The most remarkable feature is that the ratio has comparatively small deviation from unity in the isoelectronic systems of N and B. This is reasonably ascribed to the fact that the influence of the spin restriction is indirect in these systems, the p-symmetry orbital being purely singly occupied. In the Li-isoelectronic sequence we see that the spin virial ratio becomes close to unity as the nuclear charge increases, but this inclination is not general in the results for the other isoelectronic sequences. We should not make such a hasty deduction as "the tighter is the electronic cloud, the less effective is the spin polarization." The change of Ω_s in the isoelectronic sequences is complicatedly affected by the quality of the basis set and the constraint of the spin restriction.

Turning to the unrestricted case, we examine the spin virial ratio in different systems with the variation of the basis set size in Table 3. Again a gap is observed between the single- and double-zeta results. Here, as expected, the limit of convergence is certainly unity. Generally speaking, the unrestricted

Table 2. The spin virial ratio in isoelectronic systems (*Restricted*)

System	Basis	$-E$/a.u.	Ω_s	$\overline{\Delta T}$/a.u.	$-\overline{\Delta V}$/a.u.	$\overline{\Delta W}$/a.u.	$\overline{\Delta X}$/a.u.
Li	6s W	7.4327	1.0484	0.2088	1.0362	0.3084	0.2900
Be^+	6s W	14.277	1.0348	0.7020	2.4292	0.5127	0.4636
B^{2+}	6s W	23.376	1.0266	1.4527	4.3160	0.7079	0.6253
C^{3+}	6s W	34.726	1.0214	2.4566	6.7013	0.9000	0.7828
B	5s4p	24.529	1.0061	0.7457	3.0249	0.9320	0.5925
C^+	5s4p	37.292	1.0094	1.5812	5.3123	1.3347	0.7854
N^{2+}	5s4p	52.816	1.0088	2.6636	8.0576	1.7164	0.9670
O^{3+}	5s4p	71.095	1.0079	3.9963	11.289	2.0898	1.1437
C^-	5s5p	37.709	1.0006	2.8379	12.044	4.3184	2.0468
N	5s4p	54.401	1.0059	5.6289	20.111	6.1404	2.6464
O^+	5s4p	74.373	1.0066	9.1330	29.416	7.8283	3.2019
F^{2+}	5s4p	97.609	1.0063	13.384	40.151	9.4725	3.7405
Na	7s3p	161.86	1.0134	0.2666	3.3110	1.4215	1.3492
Mg^+	7s3p	199.37	1.0186	0.7429	5.4628	2.0662	1.8831
Al^{2+}	7s3p	241.03	1.0194	1.3496	7.6631	2.6050	2.3064
Si^{3+}	6s3p	286.82	1.0186	2.0770	10.024	3.1035	2.6888

Table 3. Varying of the spin virial ratio with basis sets (*Unrestricted*)

System	Basis	$-E$/a.u.	Ω_v	Ω_s	$\overline{\Delta T}$/a.u.	$-\overline{\Delta V}$/a.u.	$\overline{\Delta W}$/a.u.	$\overline{\Delta X}$/a.u.
Li	2s	7.41848	1.00000	1.01539	0.22671	1.05135	0.30658	0.28436
	4s	7.43274	1.00001	1.00052	0.23671	1.06787	0.30848	0.28571
	5s	7.43275	1.00000	1.00081	0.23655	1.06759	0.30844	0.28567
	6s	7.43275	1.00000	1.00050	0.23682	1.06794	0.30845	0.28561
B	2s1p	24.4984	1.00001	1.01424	0.73285	3.02665	0.94295	0.59713
	4s2p	24.5281	1.00001	0.99630	0.79139	3.11632	0.95054	0.58886
	5s4p	24.5293	1.00000	1.00005	0.78189	3.10128	0.94859	0.58885
	6s4p	24.5293	1.00000	1.00005	0.78435	3.10867	0.95035	0.58953
N	2s1p	54.2689	1.00001	1.01235	5.51251	20.1288	6.29935	2.66832
	4s2p	54.4011	1.00002	0.99834	5.89470	20.6020	6.23750	2.59467
	5s4p	54.4038	0.99994	1.00067	5.85057	20.5339	6.22763	2.59731
	6s4p	54.4045	1.00000	1.00002	5.88815	20.6154	6.24400	2.59481
Na	3s1p	161.124	1.00001	1.03479	0.22654	3.18684	1.38561	1.33238
	6s2p	161.850	0.99997	0.98333	0.28987	3.33622	1.42229	1.34385
	7s3p	161.859	1.00000	0.98964	0.27936	3.32259	1.42073	1.34893
	8s5p	161.859	1.00001	0.99977	0.25937	3.28474	1.41352	1.35261

Table 4. The spin virial ratio in isoelectronic systems (*Unrestricted*)

System	Basis	$-E$/a.u.	Ω_v	Ω_s	$\overline{\Delta T}$/a.u.	$-\overline{\Delta V}$/a.u.	$\overline{\Delta W}$/a.u.	$\overline{\Delta X}$/a.u.
Li	6s W	7.43275	1.00001	1.00006	0.23736	1.06859	0.30844	0.28539
Be^+	6s W	14.2775	1.00002	1.00020	0.76390	2.49702	0.51282	0.45610
B^{2+}	6s W	23.3761	1.00001	1.00012	1.54555	4.41571	0.70798	0.61627
C^{3+}	6s W	34.7262	1.00001	1.00006	2.57880	6.83083	0.90001	0.77292
B	5s4p	24.5293	1.00000	1.00005	0.78189	3.10128	0.94859	0.58885
C^+	5s4p	37.2926	0.99999	1.00010	1.64570	5.42579	1.35479	0.77926
N^{2+}	5s4p	52.8163	1.00000	1.00008	2.74665	8.19062	1.73679	0.96007
O^{3+}	5s4p	71.0953	1.00000	1.00003	4.09556	11.4380	2.11001	1.13654
C^-	5s5p	37.7098	0.99994	1.00052	2.93956	12.2831	4.37962	2.02134
N	5s4p	54.4038	0.99994	1.00067	5.85057	20.5339	6.22763	2.59731
O^+	5s4p	74.3764	0.99995	1.00060	9.41548	29.9050	7.91634	3.14616
F^{2+}	5s4p	97.6134	0.99996	1.00048	13.7176	40.6902	9.55958	3.68220
Na	7s3p	161.859	1.00000	0.98964	0.27936	3.32259	1.42073	1.34893
Mg^+	7s3p	199.372	1.00000	0.99302	0.79532	5.52702	2.07072	1.87676
Al^{2+}	7s3p	241.030	1.00000	0.99494	1.44237	7.77862	2.61401	2.29447
Si^{3+}	6s3p	286.821	1.00000	0.99582	2.20720	10.1838	3.11543	2.67239

SCF wave function fulfils the spin virial theorem much more well than the restricted one. It may be interpretable as a reflex of this that the unrestricted calculation often gives excellent estimates for spin-related quantities. As another overall feature we should point out that the unrestricted wave function gives larger $\overline{\Delta T}$ and smaller $\overline{\Delta V}$ than the corresponding restricted one almost exclusively.

Table 4 presents the results for the unrestricted wave functions of the isoelectronic systems of Li, B, N, and Na, complementing Table 2. Though the values of Ω_s in the Na-isoelectronic systems have a little large deviation from unity in comparison with the others, we can say that all the members fulfil the spin virial theorem fairly well, taking it into consideration that the basis set used are optimized for the restricted calculation. Comparison between Tables 2 and 4 manifests that the spin restriction is surly a severe constraint.

Concluding Remarks

The spin virial theorem is thought to have both the practical and conceptual significance. The former results from the validity for examining approximate wave functions, being accorded with our original motivation, and the latter consists in the clear recognition of the fact that the motion of electrons in the different spin state is regulated in the stationary state so as to maintain the specific balance represented by the theorem. This recognition is quite fundamental and no less important than the practicability. It is also to be emphasized that the spin virial theorem as well as the spin polarization potential, which is indispensable for the theorem, is not an artificial but natural conception describing a leading feature of the electronic structure.

The idea of specifying the spin state of an operator in the hypervirial theorem seems to be fruitful. We would like to regard the present theorem as the inception of the spin-related theorems derivable from the hypervirial theorem. Moreover, noting that the virial and the spin virial theorems correspond to the Pauli matrices σ_0 and σ_z, respectively, we have certain possibilities of generalization to the other Pauli matrices with appropriate choice of an operator, provided that the Hamiltonian is not spin-conservative.

An extension of the present theorem to the molecular system is conceptually straightforward, and indeed no essential difficulty is met in the formulation using the hypervirial theorem. Nevertheless, we have much to be considered: There are some nuclear-coordinate derivatives that do not vanish even in an equilibrium position. The actual calculation of the spin polarization potential is, of course, very troublesome.

Finally, we would like to add that the spin virial theorem is completely quantum-mechanical, having no classical counterpart, in striking contrast to the virial theorem.

Appendix I

What is to be noted is that the spin state is specified but that we still have the completeness

$$\sum_j \phi_{j\sigma}(\boldsymbol{r}_1)\phi^*_{j\sigma}(\boldsymbol{r}_2) = \delta(\boldsymbol{r}_1-\boldsymbol{r}_2). \tag{69}$$

By virtue of this, for example, it is found that

$$[T_\sigma,\ G_\sigma] = \sum_{jkl}(t_{jl\sigma}g_{lk\sigma} - g_{jl\sigma}t_{lk\sigma})a^\dagger_{j\sigma}a_{k\sigma}$$
$$= -\frac{i}{2}\sum_{jk}\int \phi^*_{j\sigma}(\boldsymbol{r})[\nabla^2,\ \boldsymbol{r}\cdot\nabla]\phi_{k\sigma}(\boldsymbol{r})dv\, a^\dagger_{j\sigma}a_{k\sigma}. \tag{70}$$

Hence we have only to use the well-known relation

$$[\nabla^2,\ \boldsymbol{r}\cdot\nabla] = 2\nabla^2. \tag{71}$$

Likewise

$$[1/r,\ \boldsymbol{r}\cdot\nabla] = 1/r \tag{72}$$

suffices for the case of V_σ. For the two-electron operator, again by virtue of the above completeness, we have

$$[W_{\sigma\tau},\ G_\sigma] = (1+\delta_{\sigma\tau})\frac{1}{2}$$
$$\times \sum_{jklmn}(w^{jn\sigma}_{lm\tau}g_{nk\sigma} - g_{jn\sigma}w^{nk\sigma}_{lm\tau})a^\dagger_{j\sigma}a^\dagger_{l\tau}a_{m\tau}a_{k\sigma}$$
$$= -(1+\delta_{\sigma\tau})\frac{i}{2}\sum_{jklm}\iint \phi^*_{j\sigma}(\boldsymbol{r}_1)\phi^*_{l\tau}(\boldsymbol{r}_2)[1/r_{12},\ \boldsymbol{r}_1\cdot\nabla_1]$$
$$\times \phi_{m\tau}(\boldsymbol{r}_2)\phi_{k\sigma}(\boldsymbol{r}_1)dv_2dv_1\, a^\dagger_{j\sigma}a^\dagger_{l\tau}a_{m\tau}a_{k\sigma}. \tag{73}$$

Calculating the commutator in the integrand as

$$[1/r_{12},\ \boldsymbol{r}_1\cdot\nabla_1] = (r_1^2 - \boldsymbol{r}_1\cdot\boldsymbol{r}_2)/r_{12}^3$$
$$= (1/r_{12} + (r_1^2 - r_2^2)/r_{12}^3)/2, \tag{74}$$

we reach the resultant.

Appendix II

The crucial point is that the definition of the scaled state with the unitary transformation[6,8]

$$|\eta\theta\rangle = \exp(-i(G_\uparrow + G_\downarrow)\eta - i(G_\uparrow - G_\downarrow)\theta)|O\rangle \tag{75}$$

immediately leads to

$$\frac{\partial}{\partial\eta}\langle\eta\theta|H|\eta\theta\rangle = -i\langle\eta\theta|[H,\ G_\uparrow + G_\downarrow]|\eta\theta\rangle \tag{76}$$

and

$$\frac{\partial}{\partial\theta}\langle\eta\theta|H|\eta\theta\rangle = -i\langle\eta\theta|[H,\ G_\uparrow - G_\downarrow]|\eta\theta\rangle. \tag{77}$$

If the unscaled state $|O\rangle$ is written in the expanded form (Eqs. 44 and 45), we have

$$|\eta\theta\rangle = \sum_M C_M \prod_{j^\sigma\in M} a^\dagger_{j\sigma}(\mu_\sigma)|\text{vacuum}\rangle, \tag{78}$$

where

$$a^\dagger_{j\sigma}(\mu_\sigma) = \exp(-iG_\sigma\mu_\sigma)a^\dagger_{j\sigma}\exp(iG_\sigma\mu_\sigma) \tag{79}$$

with

$$\mu_\sigma = \eta + \kappa_\sigma\theta, \tag{80}$$

because $a^\dagger_{j\sigma}$ is commutative with $G_{\bar\sigma}$ and because

$$\exp(-iG_\sigma\mu_\sigma)|\text{vacuum}\rangle = |\text{vacuum}\rangle. \tag{81}$$

The unitarity allows us to put

$$a_{j\sigma}(\mu_\sigma) = \sum_k u_{jk\sigma}(\mu_\sigma)a_{k\sigma} \tag{82}$$

with

$$u_{jk\sigma}(\mu_\sigma) = \int \phi^*_{j\sigma}(\boldsymbol{r})\phi_{k\sigma}(\boldsymbol{r}:\mu_\sigma)dv, \tag{83}$$

where $\phi_{j\sigma}(\boldsymbol{r}:\mu_\sigma)$ is the spatial orbital associated with $a^\dagger_{j\sigma}(\mu_\sigma)$ and $a_{j\sigma}(\mu_\sigma)$. From the differential equation

$$\frac{\partial}{\partial\mu_\sigma}a_{j\sigma}(\mu_\sigma) = -i[G_\sigma,\ a_{j\sigma}(\mu_\sigma)]$$
$$= i\sum_k g_{jk\sigma}a_{k\sigma}(\mu_\sigma) \tag{84}$$

we can extract the equation for the orbital

$$\frac{\partial}{\partial\mu_\sigma}\phi_{j\sigma}(\boldsymbol{r}:\mu_\sigma) = \frac{1}{2}(\boldsymbol{r}\cdot\nabla + \nabla\cdot\boldsymbol{r})\phi_{j\sigma}(\boldsymbol{r}:\mu_\sigma). \tag{85}$$

It follows immediately that

$$\phi_{j\sigma}(\boldsymbol{r}:\mu_\sigma) = \exp(3\mu_\sigma/2 + \mu_\sigma\boldsymbol{r}\cdot\nabla)\phi_{j\sigma}(\boldsymbol{r}), \tag{86}$$

which is readily proved to be identical with our scaled orbitals.

Appendix III

We can analytically integrate the matrix element of the spin polarization potential

$$P = \iint \rho_1(\boldsymbol{r}_1)\rho_2(\boldsymbol{r}_2)((r_1^2 - r_2^2)/r_{12}^3)dv_2dv_1 \tag{87}$$

rather easily when one of ρ_1 and ρ_2 is spherically symmetric. The analytic integration is not only useful in actual calculation but also instructive because it reveals a latent characteristic of the spin polarization potential. Now we assume ρ_2 is spherically symmetric; $\rho_2(\boldsymbol{r}_2)=\rho_2(r_2)$. Letting the direction of z axis of the second coordinates coincide with that of $\boldsymbol{r}_1$, we change the integration variable θ_2 with r_{12}. Then we have

$$P = 2\pi\int dv_1\int_0^\infty dr_2\rho_1(\boldsymbol{r}_1)\rho_2(r_2)r_1^{-1}r_2(r_1^2 - r_2^2)\int_{|r_1-r_2|}^{r_1+r_2} dr_{12}r_{12}^{-2}$$
$$= I_{r_1>r_2} - I_{r_2>r_1} \tag{88}$$

with

$$I_{r_1>r_2} = 4\pi\int dv_1\rho_1(\boldsymbol{r}_1)r_1^{-1}\int_0^{r_1} dr_2\rho_2(r_2)r_2^2 \tag{89}$$

and

$$I_{r_2>r_1} = 4\pi\int dv_1\rho_1(\boldsymbol{r}_1)\int_{r_1}^\infty dr_2\rho_2(r_2)r_2. \tag{90}$$

These integrals are already familiar. They appear in the calculation of the matrix element of the Coulomb-type electron repulsion integral

$$I = \iint \rho_1(\boldsymbol{r}_1)\rho_2(\boldsymbol{r}_2)(1/r_{12})dv_2dv_1, \tag{91}$$

which can be arranged as

$$I = 2\pi \int dv_1 \int_0^\infty dr_2 \rho_1(r_1)\rho_2(r_2) r_1^{-1} r_2 \int_{|r_1-r_2|}^{r_1+r_2} dr_{12}$$
$$= I_{r_1>r_2} + I_{r_2>r_1} \quad (92)$$

to clarify an intimate connection between P and $I_{..}$ Besides the density built of s-symmetry orbitals we have a few types of spherically symmetric densities, say, the sum like $p_x^2+p_y^2+p_z^2$; the above treatment is widely practical.

References

1) M. Born, W. Heisenberg, and P. Jordan, *Z. Phys.*, **35**, 557 (1926); B. N. Finkelstein, *ibid.*, **50**, 293 (1928).

2) V. Fock, *Z. Phys.*, **63**, 855 (1930).

3) P.-O. Löwdin, *J. Mol. Spectrosc.*, **3**, 46 (1959); this contains a satisfactory bibliography of the fundamental works on the subject up to 1958.

4) S. T. Epstein, "The Variation Method in Quantum Chemistry," Academic Press, New York (1974), Section 20 and the references cited therein.

5) J. O. Hirschfelder, *J. Chem. Phys.*, **33**, 1462 (1960).

6) S. T. Epstein and J. O. Hirschfelder, *Phys. Rev.*, **132**, 1495 (1961).

7) J. O. Hirschfelder and C. A. Coulson, *J. Chem. Phys.*, **36**, 941 (1962).

8) S. T. Epstein, "The Variation Method in Quantum Chemistry," Academic Press, New York (1974), Section 16 and the references cited therein.

9) M. Isihara, *Bull. Chem. Soc. Jpn.*, **54**, 3312 (1981).

10) P.-O. Löwdin, *Phys. Rev.*, **97**, 1471 (1955).

11) The scaling dependent on the spin is a two-parameter scaling as an extension of the usual virial scaling. Aside from miscellaneous incorporations of variation parameters in the early days of quantum chemistry, we have a remarkable example of a several-parameter scaling as an extension of the virial scaling in W. J. Meath and J. O. Hirschfelder, *J. Chem. Phys.*, **39**, 1135 (1963). See Ref. 4 also.

12) "Different bases for different spins" is included in "different bases for different orbitals," which is not very new; for example, M. T. Marron, N. C. Handy, R. G. Parr, and H. J. Silverstone, *Int. J. Quantum Chem.*, **4**, 245 (1970); S. Huzinaga and K. Hirao, *J. Chem. Phys.*, **66**, 2157 (1977).

13) C. C. J. Roothaan, *Rev. Mod. Phys.*, **23**, 69 (1951); *ibid.*, **32**, 179 (1960); C. C. J. Roothaan and P. S. Bagus, *Methods in Compt. Phys.*, **2**, 47 (1963).

14) J. A. Pople and R. K. Nesbet, *J. Chem. Phys.*, **22**, 571 (1954).

15) E. Clementi and C. Roetti, *At. Data Nucl. Data Tables*, **14**, 177 (1974).

16) A. W. Weiss, *Astrophys. J.*, **138**, 1262 (1963).

17) C. C. J. Roothaan, L. M. Sachs, and A. W. Weiss, *Rev. Mod. Phys.*, **32**, 186 (1960).

18) It is, of course, possible for the "sufficient" configuration interaction wave function to satisfy the spin virial theorem, even if the wave function is constructed from restricted spin orbitals.

 © 1985 The Chemical Society of Japan Bull. Chem. Soc. Jpn., 58, 2481—2486 (1985)

Studies on the Hydrous Niobium(V) Oxide Ion Exchanger. I. A Method for Synthesis and Some Properties

Yasushi INOUE,* Hiromichi YAMAZAKI, and Yasuyuki KIMURA
Department of Nuclear Engineering, Faculty of Engineering, Tohoku University, Aramaki, Sendai 980
(Received January 9, 1985)

A comprehensive study of the preparation of hydrous niobium(V) oxide ion exchangers was made using three kinds of niobium solutions: (1) HCl, (2) C_2H_5OH, and (3) H_2SO_4. From a detailed examination of the dependency of the yield, the ion-exchange behavior toward Na^+, the chemical stability, and some other properties, regarding the method for precipitation, it was found that the pyrohydrolysis of the $NbCl_5$ solution was the best method, since the procedure was simple, rapid and reproducible, and the product had a comparatively good ion-exchange property. The product obtained from the H_2SO_4 solution had the largest ion-exchange capacity and was most stable in highly alkaline solutions, but the whole procedure was very tedious. The exchanger prepared from the ethanolic solution had a smaller ion-exchange capacity in a pH region higher than 8. The materials, thus obtained, had at least two kinds of weakly dissociable ion-exchange sites, and the ion-exchange capacity for alkali metal ions decreased in the order of $Li^+>Na^+>K^+$. The aging effect and the chemical stability were also examined.

As has been previously pointed out,[2] hydrous oxide ion exchangers based on various polyvalent metal ions have the serious disadvantage of giving inconsistent results to different investigators, because of the irreproducibility of the synthesis. With this point in mind, the present authours previously studied hydrous titanium(IV) oxide and hydrous tin(IV) oxide for establishing satisfactory synthesis methods.[1,2] Hydrous niobium(V) oxide is expected to have a large ion-exchange capacity (3.2 mequiv/g at pH 12) and to be stable in highly acidic or alkaline solutions.[3] Its ion-exchange properties, however, have not yet been investigated in detail. This material has been prepared using the following methods: (1) the neutralization of the acidic solutions of niobium salts, such as sulfate, chloride, and fluoride,[3-5] (2) the pyrohydrolysis of an $NbCl_5$ solution[6] and, (3) the hydrolysis of a potassium fluoroniobate solution or niobium(V) alkoxide solution.[7,8] These methods, however, are not always suited for synthesizing a large amount of a hydrous niobium(V) oxide. A detailed comparison of these methods must be experimentally made in order to choose the best method since a detailed description of the experimental conditions is lacking in the literature.

The present paper will describe the results of an investigation undertaken to establish the best conditions for the synthesis of the hydrous niobium(V) oxide ion exchanger, together with some of its properties, particularly those with direct bearing on the conditions of the synthesis.

Experimental

Reagents and Apparatus. Niobium(V) chloride and niobium(V) oxide, respectively, were supplied from Mitsuwa Kagaku Yakuhin Kaisha, Ltd. and Shinetsu Kagaku Kogyo Kaisha, Ltd. Hydrofluoric acid was obtained from Hirota Kagaku Kogyo Kaisha, Ltd., and sulfochlorophenol S from Dojindo laboratories. The other chemicals were of the highest purity grades supplied by Wako Pure Chemical Industries, Ltd.

The pH values were measured with a Toa Dempa model HM-6A pH meter. A thermogravimetric analysis was undertaken with a Shimadzu model DT-20B micro thermal analyzer, connected to a Shimadzu model TGC-20H thermal balance. The absorbance was measured with a Hitachi model 124 double-beam spectrophotometer with a 1-cm glass cell.

Synthesis of Hydrous Niobium(V) Oxide. A synthesis was tried for three systems: (a) $NbCl_5$–HCl, (b) $NbCl_5$–C_2H_5OH, and (c) Nb_2O_5–H_2SO_4, as shown in Fig. 1. The concentration of niobium was held constant for each system because of a technical difficulty to make a meaningful variation in the concentration of the niobium from the respective starting materials. In the HCl-system, the starting solution was produced by dissolving 25 g of niobium(V) chloride in 50 cm^3 of concentrated hydrochloric acid, followed by dilution to 1 dm^3 with distilled water. The niobium(V) ethoxide solution was produced by dissolving 25 g of niobium(V) chloride into 200 cm^3 of 99.5% ethanol, followed by dilution to 3 dm^3 with distilled water. In the H_2SO_4-system, the starting solution was obtained by fuming the hydrochloric acid solution or the hydrofluoric acid solution of niobium with 40 cm^3 of concentrated sulfuric acid; the hydrofluoric acid solution was made by dissolving 5 g of niobium(V) oxide in 50 cm^3 of hot 7 mol dm^{-3} hydrofluoric acid.

In the methods from (1) through (6), hydrous niobium(V) oxide was precipitated by pyrohydrolyzing the $NbCl_5$ solution, while in the methods from (7) through (11), the precipitate was obtained by hydrolyzing the $NbCl_5$ solution by the addition of alkaline solutions. In methods (8),(9), and (11), the obtained slurries were refluxed with the mother liquor. In the methods from (12) through (14), the hydrous oxide was precipitated by the dilution of the respective starting solution with distilled water.

After being separated from the mother liquor by a

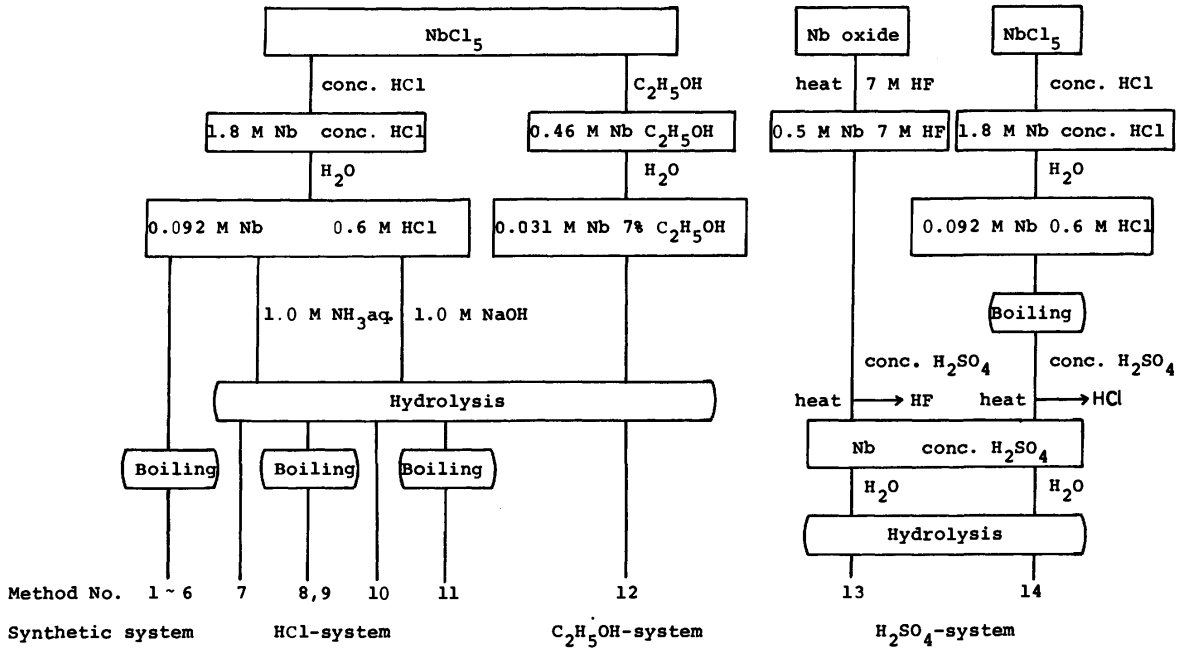

Fig. 1. Scheme of synthesis. (1 M = 1 mol dm^{-3})

combination of decantation and filtration through Toyo No. 1 filter paper under suction, the precipitate was uniformly dispersed into distilled water and filtered again after being completely sedimentated. This procedure was repeated until no chloride or sulfate ion was detected in the filtrate. Then, the precipitate was air-dried at room temperature. The resulting product was then immersed in distilled water to break it down into fine particles, which were subsequently dried again at room temperature. Particles were then ground in a porcelain mortar and sieved to obtain the required particle sizes.

Conditioning. The exchanger of a desired particle size (100—200 mesh) was washed with distilled water to remove any adherent powder. The slurry was poured into a glass tube with glass-wool plugging for column support, and then 0.1 mol dm^{-3} HCl was passed through the column until the pH of the effluent approached that of the influent. Then the column was washed with distilled water until the pH of the effluent became constant. The exchanger in the H^+ form thus prepared was air-dried and stored in a desiccator containing a saturated NaCl solution (relative humidity; 75% at 25 °C). The exchangers were used within 30 d after preparation, unless otherwise noted.

Specific Ion-exchange Capacity and Uptake Curves for Metal Ions. The exchanger (0.5 g) in the H^+ form was immersed into 50 cm^3 of different solutions, prepared by the desired mixed ratio of 0.1 mol dm^{-3} NaCl and 0.1 mol dm^{-3} NaOH, for 7 d at room temperature with intermittent shaking. This was followed by pH measurements and by the determination of the sodium ions. The sodium ions were converted to pure sodium chloride and indirectly determined by titrating the chloride ions. The amount of the ions taken up by the exchanger was evaluated from the difference between the initial and the final concentrations of the ions present in the solutions. The dissolved amount of the exchanger was evaluated from the amount of niobium in the supernatant solution which was determined spectrophotometrically by the sulfochlorophenol S method.[9] The limit of detection was 0.1 wt% of the exchanger used.

Analysis of Cl^- in the Exchanger. A sample of 0.5 g was dissolved by heating with 100 cm^3 of 9 mol dm^{-3} H_2SO_4 in a 500-cm^3 distilling flask, and the HCl evolving therefrom, carried by steam, was absorbed in a slightly alkaline solution and then determined spectrophotometrically using mercury(II) thiocyanate and ammonium iron(III) sulfate as coloring reagents. The limit of detection was 0.01 wt%.

Analysis of Water in the Exchanger. The water content was calculated from the weight loss at 850 °C in the TGA curves which were measured with 5 mg of sample in air at a heating rate of 10 °C min^{-1}.

Density. The apparent density of the exchangers was measured in the usual manner using a 25-cm^3 pycnometer.

Yield of the Exchangers. The yield was calculated on the basis of the recovery of niobium used.

Results and Discussion

Preparation of Hydrous Niobium(V) Oxide as an Ion Exchanger. The conditions for the precipitation, compositions and properties of the hydrous niobium(V) oxides are summarized in Table 1.

(I) Pyrohydrolysis of the Chloride Solution (the methods (1)—(6)): The semitransparent and gelatinous hydrous niobium(V) oxide was precipitated by heating 1 dm^3 of the hydrochloric acid solution of

Table 1. Comparison of various exchangers

Method No.[a]	pH at precipitation	Boiling time / h	Composition	Ion-exchange capacity / mmol Na^+/g		Yield	Density / g cm^{-3}
				pH 8.0	pH 10.0		
1	0.89	0.1	$Nb_2O_5 \cdot 5.3H_2O$	1.6	2.3	0.93	—
2	0.88	0.5	$Nb_2O_5 \cdot 4.7H_2O$	1.6	2.3	0.91	—
3	0.92	1	$Nb_2O_5 \cdot 4.7H_2O$	1.6	2.3	0.90	—
4	0.89	2	$Nb_2O_5 \cdot 4.7H_2O$	1.5	2.2	0.93	2.46±0.01
5	0.85	5	$Nb_2O_5 \cdot 4.6H_2O$	1.3	2.2	0.92	—
6	0.92	24	$Nb_2O_5 \cdot 4.1H_2O$	1.3	2.1	0.85	—
7	2.69	—	$Nb_2O_5 \cdot 6.7H_2O$	1.7	2.3	0.90	—
8	2.58	0.5	$Nb_2O_5 \cdot 6.4H_2O$	1.6	2.1	0.88	—
9	2.51	5	$Nb_2O_5 \cdot 5.5H_2O$	1.6	2.1	0.84	—
10	2.70	—	$Nb_2O_5 \cdot 5.6H_2O$	1.7	2.4	0.71	—
11	2.80	0.5	$Nb_2O_5 \cdot 4.4H_2O$	1.8	2.0	0.84	—
12	—	—	$Nb_2O_5 \cdot 5.7H_2O$	1.5	2.0	0.90	—
13	—	—	$Nb_2O_5 \cdot 4.9H_2O$	1.6	2.6	0.77	—
14	—	—	$Nb_2O_5 \cdot 4.3H_2O$	1.8	2.7	0.70	2.40±0.01

a) The method number corresponds to that in Fig. 1.

niobium in a 3-dm^3 round-bottom flask, equipped with a reflux condenser, for 0.1—24 h. When the precipitate was air-dried at room temperature, it turned into a light-creamy solid.

(II) Neutralization of the Chloride Solution (the methods (7)—(11)): The precipitate was made by hydrolyzing niobium ions in the hydrochloric acid solution with either a 1-mol dm^{-3} NaOH solution or 1-mol dm^{-3} NH_3 aq without refluxing the slurry (the methods (7) and (10)), the precipitate formed at a pH lower than 2.0 was partially lost during washing because of incomplete sedimentation. When the pH at the time of precipitation was higher than 5.0, the yield decreased due to the peptization during washing. When a NaOH solution was used for neutralization, a marked peptization occurred at a pH higher than 6.0 and, then, the yield fell to around zero at a pH higher than 9.0. On the other hand, when NH_3 aq was used, the yield always exceeded 50 per cent at any realizable pH value since the degree of peptization was slight. It can be concluded from the above observations that the desirable pH range at precipitation is 2.5 to 4.0. When the slurries were refluxed (the methods (8), (9), and (11)), the precipitate obtained at a pH as low as 1.0 to 2.0 did not peptize during washing, and the yield exceeded 80 per cent. The air-dried products obtained by the neutralization with NH_3 aq solution were the semitransparent and glassy solid, while those produced by the neutralization with NaOH solution were white, opaque, and brittle like chalk.

(III) Precipitation from Ethanolic Solution of $NbCl_5$: Three cubic decimetres of the starting solution were diluted with distilled water to make total volume 5 dm^3, and it was allowed to stand for 2 d at room temperature. Then, the gelation of the solution took place and, when the precipitate was air-dried, the glassy and semitransparent solid was obtained.

The amount of chloride ions included in the exchanger in the H^+ form synthesized from the HCl-system was below the detection limit (0.01 wt%).

(IV) Precipitation from Sulfuric Acid Solution: The sulfuric solution of niobium was diluted with distilled water to make a total volume of 2 dm^3 and stood for 1 d at room temperature to complete precipitation. The precipitate (air-dried at room temperature) was glassy solid; the solids obtained from methods (13) and (14) were pale purple and light brown, respectivery, in color. The yield in the H_2SO_4-system was appreciably lower than that in the other systems. This is attributable to the lengthy washing of the precipitate due to the difficulty to remove the sulfate ions included in the precipitate.

Ion-exchange Properties. Figure 2 shows the uptake curves for Na^+ of the exchangers prepared by the neutralization of $NbCl_5$ with alkaline solutions (the methods (7), (8), (10), and (11)). These materials were weakly acidic ion exchangers having at least two kinds of dissociable hydrogen atoms, since the inflection points existed in the curves at around pH 8. In the extremely high pH region, the specific ion-exchange capacity decreased with the pH. As will be shown later, this is attributed to the dissolution of a part of the exchanger. This observation was common to all exchangers prepared by any methods except those prepared from the H_2SO_4-system. The uptake curves of the exchangers prepared from methods (8) and (11) indicated that the boiling procedure reduced the ion-exchange capacity in the

whole pH range by a total amount of 0.4 mmol Na^+ g^{-1}, instead, it stabilized the exchanger in alkaline solutions. The stabilization by aging, therefore, is accompanied by the degradation of some of the ion-exchange sites. Figure 3 compares the uptake curves of the exchangers obtained without using alkaline solutions. The ion-exchange capacities of the materials prepared by the pyrohydrolysis of the $NbCl_5$ solution (the methods (1), (3), and (6)) gradually decreased with the length of the boiling period and were slightly smaller than those of the exchangers prepared by the hydrolysis of the $NbCl_5$ solution with alkaline solutions. Furthermore, when the slurries were boiled for longer than 1 h, the degree of the decrease in the ion-exchange capacity in the highly alkaline region became very small, probably due to the stabilization of the exchanger in alkaline solutions. This figure also shown that the exchanger prepared from the H_2SO_4-system had the largest ion-exchange capacity throughout the pH range examined, and that it was most stable in alkaline solutions, since the ion-exchange capacity did not decrease in highly alkaline solutions. The ion-exchange capacities at a pH higher than 9 were appreciably smaller for the exchanger precipitated from the ethanolic solution of $NbCl_5$ than for the materials prepared by the pyrohydrolysis of $NbCl_5$ solution.

Water Content. The water contents in the exchangers are summarized in Table 1. It should be noted that the values in the table are not precise enough to determine the stoichiometry of the compounds since they were obtained during thermal nonequilibrium, the TGA method. However, they are useful for comparative purposes. Table 1 indicates that the water content differs greatly with the synthesis method, that is, 4.5—6.7 mol H_2O per mol Nb_2O_5. As a definite correlation between the water content and the ion-exchange capacity was not observed, it may be considered that a large part of the water does not take part in the ion-exchange reaction.

The exchangers prepared from the H_2SO_4-system have the best property as an ion exchanger, that is, they have the largest ion-exchange capacity and are most stable in alkaline solutions. The method, however, has a serious disadvantage due to a very complicated and lengthy procedure, whereas the synthesis by pyrohydrolysis is very simple. From a practical point of view, the advantages due to the simplicity and rapidity of the procedure in the latter method more than offset the demerits of smaller ion-exchange capacity. Efforts were then concentrated on determining the properties of the exchangers prepared from this system.

Physical Properties. Table 2 shows examples of the size distribution of the particles formed when a gel prepared from method (4) was immersed in water. It is evident from this table that a large part of the exchanger invariably possesses particles large enough for use in column operation. The density of the exchanger in the H^+ form was 2.46±0.01 g cm^{-3}.

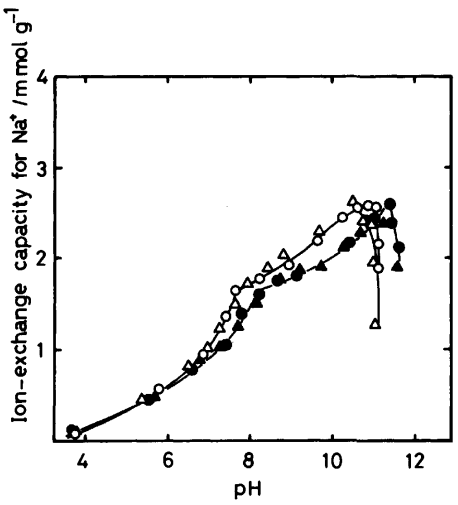

Fig. 2. Uptake curves of various exchangers for Na^+. Method number; ○: (7), ●: (8), △: (10), ▲: (11). The numbers are the same as those in Fig. 1.

TABLE 2. SIZE DISTRIBUTION OF THE EXCHANGER BEFORE GRINDING (THE METHOD (4) IN FIG. 1)

Batch number	Particle size(mesh)/wt%			
	≈42	42—100	100—200	200≈
1	87.7	10.5	1.2	0.2
2	86.4	11.8	1.2	0.6

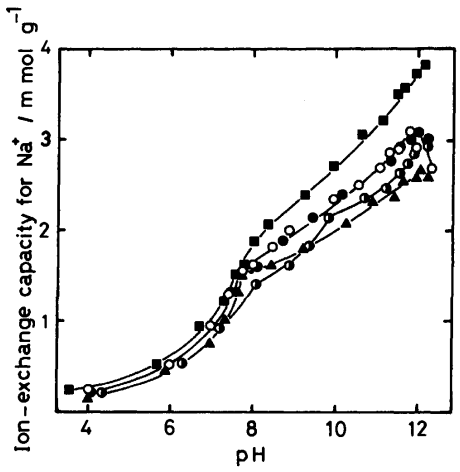

Fig. 3. Uptake curves of various exchangers for Na^+. Method number; ○: (1), ●: (3), ◑: (6), ▲: (12), ■: (14). The numbers are the same as those in Fig. 1.

Chemical Stability. To examine the chemical stability of the exchanger, the amount of niobium dissolved in various reagents was measured using the exchangers prepared by methods (3) and (14). The amount of niobium dissolved in the MOH-MCl solution (M=Li, Na, K) of ionic strength 0.1 is shown in Fig. 4, where the dotted line indicates the detection limit (0.1 wt%). The exchanger prepared from method (3) was stable up to a pH of 10.0, 10.5, or 10.8, respectively, for M=Li^+, Na^+, and K^+. This indicates that the kind of alkali metals in the solution greatly affects the stability of the exchanger. On the other hand, the exchanger prepared from method (14) was fairly stable in an alkaline solution; even at a pH as high as 11.9. Only 0.2 wt% of the exchanger was dissolved. As is shown in Table 3, the exchangers prepared from any method were unstable in a 0.1 mol dm^{-3} NaOH solution, but fairly stable in a 1 mol dm^{-3} NH_3 aq solution. To further examine the stability in various acids, measurements were made of the amount of niobium in typical mineral and organic acids. The results, also shown in Table 3, indicate that both exchangers were very stable against 1 mol dm^{-3} mineral acids but dissolved appreciably into organic acids, particularly into oxalic acid. This fact shows that the exchanger is easily attacked by acids with a strong tendency to complex Nb(V).

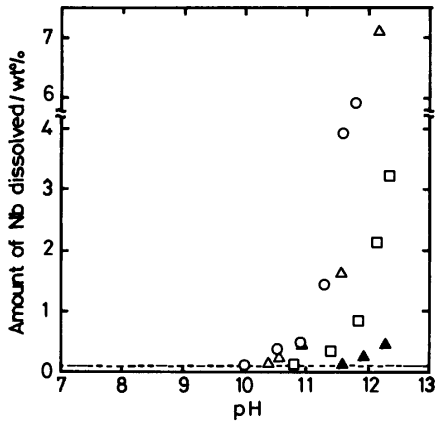

Fig. 4. Chemical stability against MOH-MCl mixed solution (M: Li, Na, K) at room temperature. Cation; ○: Li^+, △: Na^+, □: K^+. Exchanger; open mark: the method (3), filled mark: the method (14). The numbers are the same as those in Fig. 1.

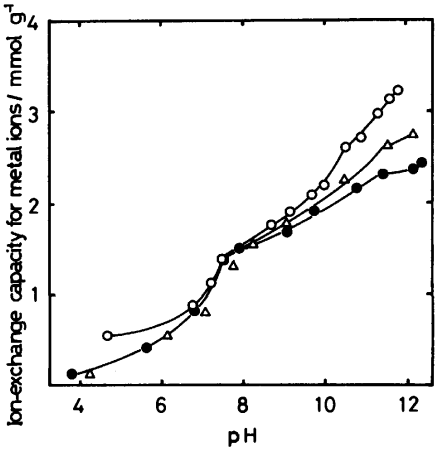

Fig. 5. Uptake curves for various alkali metal ions. Cation; ○: Li^+, △: Na^+, ●: K^+. Exchanger: The method (4) in Fig. 1.

Uptake Curves for Various Alkali Metal Ions. In order to compare the ion-exchange behavior of alkali metal ions, uptake curves were obtained for Li^+ and K^+, as is shown in Fig. 5. The ion-exchange capacities for these cations decreased in the order of $Li^+ > Na^+ > K^+$. This figure also shows that the pH of the inflection point in the curves was independent of the kinds of the exchanging cations and the difference of the ion-exchange capacities was mainly brought about in the pH range higher than that point. This observation can be understood by considering that the weakly dissociable sites are the hydroxyl groups which form olation bonds in the exchanger. When anhydrated cations are exchanged with H^+ from these hydroxyl groups, some of the olation bonds are severed, enhancing the tendency to dissolve into the solution; this tendency is compatible with the order of the ability of alkali metal ions to dissolve the exchanger.

Change in Capacities During Storage. As the hydrous oxide is thermodynamically metastable, the ion-exchange capacity is expected to decrease during storage; in fact hydrous titanium(IV) oxide in the H^+ form was reported to lose its cation-exchange capacity appreciably during storage in air.[10] Figure 6 shows the result for material prepared from method (4), which was stored for 300 d over a saturated NaCl

Table 3. Chemical stability at room temperature[a)]

Solution		Amount of Nb dissolved/wt%	
Reagent	Concentration mol dm^{-3}	Method (3)	Method (14)
NaOH	0.10	41.4	88.3
NH_3 aq	1.0	0.5	0.2
HCl	1.0	<0.1	<0.1
H_2SO_4	0.56	<0.1	<0.1
HNO_3	0.94	<0.1	0.1
Tartaric acid	0.5	6.6	0.5
Oxalic acid	0.5	100	100
Citric acid	0.5	1.4	0.1

a) Exchanger: −100+200 mesh, H^+ form, 0.50 g. Solution: 50 cm^3. Contact time: 7 d.

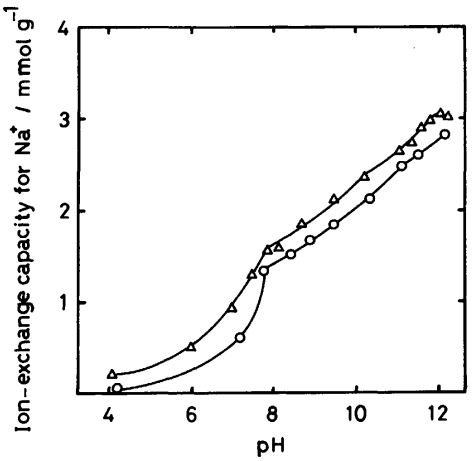

Fig. 6. Effect of storage time on the uptake curves of the method (4) exchanger for Na^+.
△: 30 d after the synthesis. ○: 300 d after the synthesis.

Table 4. Reproducibility of the synthesis (the method (4))

Batch number	Composition	Ion-exchange capacity mmol Na^+/g		Yield
		pH 8.0	pH 10.0	
1[a]	$Nb_2O_5 \cdot 4.7H_2O$	1.5	2.2	0.93
2[a]	$Nb_2O_5 \cdot 4.7H_2O$	1.5	2.2	0.95
3[b]	$Nb_2O_5 \cdot 5.2H_2O$	1.5	2.2	0.98
4[b]	$Nb_2O_5 \cdot 5.2H_2O$	1.5	2.2	0.97

a) Synthesis on the 5th of January in 1981. b) Synthesis on the 6th of October in 1980.

solution. This figure reveals that the ion-exchange capacity in a pH region lower than the inflection point decreased a little during storage. The stability in alkaline solutions was improved slightly. The storage, however, did not affect at all the stabilities of the exchanger in other reagents.

Recommended Synthetic Method. It is concluded that the exchanger precipitated from the concentrated sulfuric acid solution of niobium is best with respect to the ion-exchange capacity and the chemical stability. This method, however, is of no use in preparing a hydrous niobium(V) oxide as an ion exchanger because of the tedious procedure (due to the difficulty in preparing a sulfuric acid solution of niobium in high concentration and the lengthy washing of the precipitate). The method for the pyrohydrolysis of a $NbCl_5$ solution is considered practical since a large amount of pure hydrous niobium(V) oxide can be easily prepared without suffering much from the defects of low ion-exchange capacity and chemical unstability.

In the method regarding pyrohydrolysis, an increase in the boiling period improves the stability for highly alkaline solutions, but reduces the ion-exchange capacity of the product; hence, by a mutual concession between them, method (4), where the $NbCl_5$ solution was thermally hydrolyzed by boiling for 2 h, was chosen as the recommended procedure for synthesizing a hydrous niobium(V) oxide ion exchanger. Table 4 shows the reproducibility of the synthesis by this method. The variation of the water content may be ascribed to the sensitivity of the amount of occluded water to the conditions of the work environment (such as temperature and humidity) since the same water content was observed for exchangers prepared in different batches at a same time. The fluctuation in the yield is a natural consequence of the irregularity in the recovery of a precipitate at the time of repeated washing. As the ion-exchange capacities of the products agree well with each other, a synthesis using method (4) can be regarded as reproducible.

References

1) Y. Inoue and M. Tsuji, *J. Nucl. Sci. Technol.*, **13**, 85 (1976); *Bull. Chem. Soc. Jpn.*, **49**, 111 (1976); **51**, 479 (1978).
2) Y. Inoue and H. Yamazaki, *Bull. Chem Soc Jpn.*, **55**, 3782 (1982); **57**, 1534, 3437 (1984).
3) M. Abe and T. Ito, *Nippon Kagaku Zasshi*, **86**, 55 (1965).
4) M. Qureshi, A. P. Gupte, and T. Khan, *J. Chromatogr.*, **144**, 231 (1977).
5) V. V. Sakharov, N. E. Ivanova, S. S. Korovin, and M. A. Zakharov, *Russ. J. Inorg. Chem.*, **19**, 313 (1974).
6) Y. Kimura, *Bachelor Thesis, Tohoku University, Japan* (1979).
7) V. A. Titova and I. G. Slatinskaya, *Russ. J. Inorg. Chem.*, **12**, 767 (1967).
8) R. W. Lynch, R. G. Dosch, B. T. Kenna, J. K. Johnstone, and E. J. Nowak, IAEA-SM-207 (1975).
9) F. D. Snell, "Photometric and Fluorometric Methods of Analysis Metals Part 2," Wiley-Interscience Publication (1973), pp. 1430.
10) Y. Inoue and H. Yamazaki, *Bull. Chem. Soc. Jpn.*, **53**, 81 (1980).

 © 1985 The Chemical Society of Japan Bull. Chem. Soc. Jpn., 58, 2487—2489 (1985)

Glass Formation Study of Aqueous HX Solutions (X=F, Cl, and Br)

Hitoshi KANNO* and Kenji SATOH
Department of Chemistry, Meisei University, Hino, Tokyo 191
(Received May 2, 1985)

Glass-forming composition regions of aqueous HX solutions (X=F, Cl, and Br) were determined. It was found that oxonium ions play an important role in glass-forming behavior of these solutions. Including the results for HI solution previously reported,[1] the general trends of glass-formation behavior of aqueous HX solutions are summarized.

As an extension of the previous work,[1] we measured the glass-transition temperatures (T_g's) of aqueous HX solutions (X=F, Cl, and Br) as a function of the HX concentration.

The object of this work is two-fold: (1) to see the general trends of glass-formation behavior of aqueous HX solutions, and (2) to find out the reason why the extrapolation of the T_g data of the HI-water system to pure water predicts the glass-transition temperature of glassy bulk water to be around −177 °C, far below the value (−135~−140 °C) expected from the T_g data for other aqueous electrolyte solutions.[2,3]

Experimental

Each sample solution was prepared by simple mixing concentrated HX acid and distilled water by weight. The T_g measurements were carried out in the same way as previously described.[1] Glass formation of the quenched sample solution was visually checked. The abrupt shift of T_g is a good indicator for crystallization or partial crystallization of a quenched sample and therefore can be used for checking glass-formation (crystallization). The upper limit of the glass forming composition range was not established because of the difficulty of obtaining higher concentrated HX solutions (HF>46 wt%, HCl>35 wt%, HBr> 47 wt%).

Results and Discussion

The T_g results for each HX solutions are shown in Figs. 1—3 together with the phase diagrams. Among HX solutions, glass formation of HCl solution has been well studied[4,5] and our results are in good agreement with previous reports.[4,5] Including the results for HI solution which was already reported,[1] we summarized the general trends as follows; (1) except the HF solution, T_g increases almost linearly

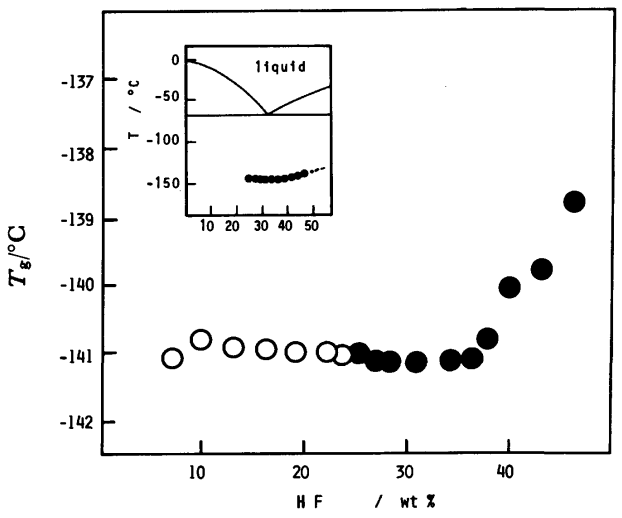

Glass forming region of the HF–H_2O system

Fig. 1. Variation of T_g with solution composition.
The inset shows the phase diagram of the HF-Water system [from J. Timmermans, "Physico Chemical Constants of Binary Systems," Interscience Publishers, New York (1960) vol. 4, p. 439.]
●: T_g in the glass-forming composition region. ○: T_g of the portion remained uncrystallized in the non-glass-forming composition region.

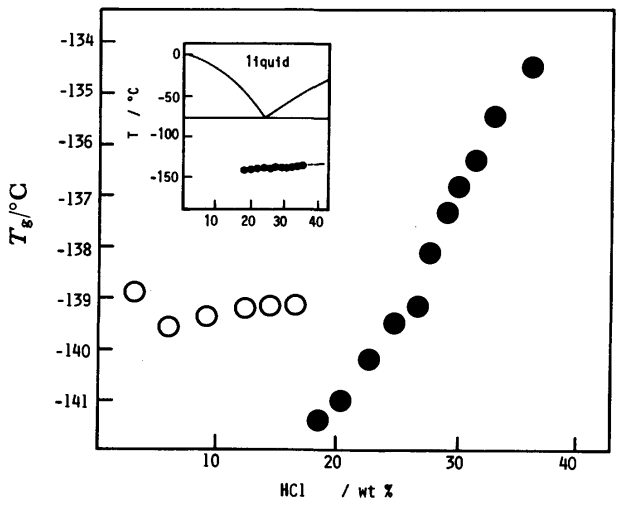

Glass forming region of the HCl–H_2O system

Fig. 2. Variation of T_g with solution composition.
The inset shows the phase diagram of the HCl-Water system [from the same reference as the HF-Water system, p. 446].
●: T_g in the glass-forimng composition region. ○: T_g of the portion remained uncrystallized in the non-glass-forming composition region.

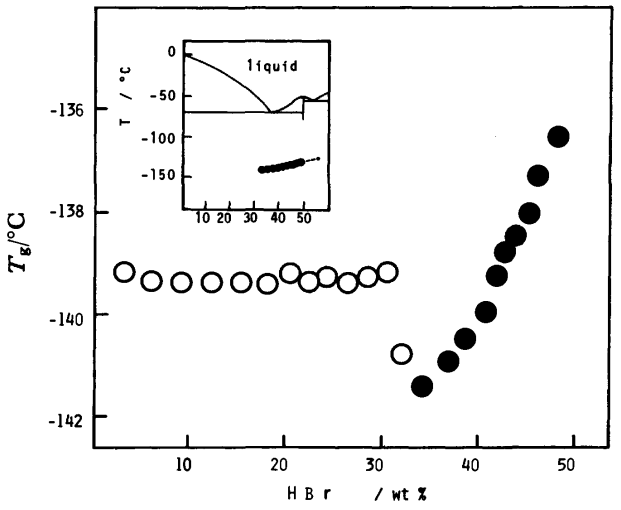

Glass forming region of the HBr–H_2O system

Fig. 3. Variation of T_g with solution composition.
The inset shows the phase diagram of the HBr–Water system [from the same reference as the HF–Water system, p. 461].
●: T_g in the glass-forming composition region. O: T_g of the portion remained uncrystallized in the non-glass-forming composition region.

with HX (in wt%) concentration, (2) the lowest T_g value for each glassy HX solution is about −141 °C, and (3) the first eutectic composition is glass-forming for all HX solutions (X=F, Cl, Br, and I).

Among these trends, the last one is generally observed for most glass forming aqueous solutions.[3] In fact, a binary solution of the eutectic composition is most prone to be glass forming if it has any glass forming composition range.[6]

Glass formation of the HF solution begins from the concentration of about 25 wt% up to ≈46 wt%HF (above which experiment was not made in this study). An interesting point is that T_g is nearly invariant in the concentration range from ≈25 wt% to ≈40 wt% HF and then rises up at higher HF concentrations. Similar behavior has been observed for aqueous LiCl and $MnCl_2$ solutions.[2,7] In these solutions, T_g decreases with water content, then tends to level off at a certain salt concentration and becomes concentration independent of further increase in water content.[2,7,8] There are two possible causes: One is a precursor phenomenon of a phase-separation (liquid–liquid immiscibility)[9,10] and the other the partial crystallization of the solution in the quenching process. In the former case, a homogeneous solution splits into two phases (one is a water-rich phase and the other is a salt-rich one) as the temperature of the solution is lowered.[10] Due to the large thermal instability of the water-rich phase in a high-degree supercooled state, the water-rich liquid phase (possibly dispersed as fine micro-droplets in the solution) crystallizes in the quenching process and only the salt-rich phase is quenched to a vitreous state. In the latter case, the partial crystallization of the solution occurs in the quenching process. As water content increases in the solution, the energy barrier for ice nucleation becomes very low due to the very low stability of bulk supercooled water against ice crystallization.[11] At present it is difficult to determine which is the cause for the observed T_g behavior of the HF solution.

Comparing the solution compositions at which the HX solution becomes glass-forming with the cooling rate of about 600 K min^{-1}, we immediately know that the order of the HX concentration is HF>HBr>HCl>HI, indicating that the HX solution tends to be glass forming with a lower concentration of HX when X^- is a stronger structure breaker: A HI solution is glass-forming at R≃10.2 or less but a HF solution can be vitrified only at R≃3.3 or less (R=moles of water/moles of HX). This glass-forming feature is opposite to the trend for other aqueous electrolyte solutions, which are tend to be glass forming when containing small structure-making ions as a component (or components) of an electrolyte in the solutions.[2] Therefore, we consider that the glass forming ability of aqueous HX solutions should be relevant to oxonium ions in the solutions.

It is now established that oxonium ions in aqueous HX solutions (except X=F) are mostly preserved from a liquid state at room temperatures to a glassy state.[12] On the other hand, ionic dissociations of HNO_3, H_2SO_4, and H_3PO_4 in concentrated aqueous solutions are greatly reduced at low temperatures.[13] In these solutions, Raman bands arising from neutral acid molecules increase in their intensities at low temperatures.[13] Glass formation of aqueous HNO_3 solution begins from 35 wt% HNO_3 (R=6.5) to higher HNO_3 concentrations.[14] The need of higher acid concentration for glass forming of the HNO_3 solution as compared with HX solutions (X=Cl, Br, and I) should be partly due to the decrease of ionization of HNO_3 at low temperatures.

From X-ray and neutron diffraction studies,[15,16] it is concluded that the structure of hydrated oxonium ions in aqueous HCl solutions is trigonal pyramid $OH_3^+(OH_2)_3\cdots(HOH)$, in which three water molecules combine with a H_3O^+ ion through rather strong hydrogen bonds and one water molecule lies at the apex of the $OH_3^+(OH_2)_3$ pyramid. The existence of strong hydrogen bonds between oxonium ions and water molecules is considered to be a good inhibitor to ice nucleation.

The formation of oxonium ions should also be a major cause of the anomalous low T_g prediction for pure bulk water in the T_g data of aqueous HI

solution. When a pure liquid is not glass -forming, estimation of its T_g is made successfully by the extrapolation of the T_g data of binary solution.[2,3,17] Though there have recently been a few reports[18,19] claiming that bulk water can be vitrified, at least partially, by ejecting highly compressed water into cryogenic solvents held at very low temperatures, there has been no reliable T_g datum for bulk glassy water. The estimated T_g for bulk water from the T_g data for binary aqueous solutions is around −138 °C.[2,3] In the cases of HCl and HBr solutions, least-square-curve-fitting calculations give the following formulae:

$T_g = 0.43Y - 150$(°C) for aqueous HCl solution, and

$T_g = 0.37Y - 158$(°C) for aqueous HBr solution,

where Y is wt% of HX. As previously reported,[1] the HI solution predicts T_g for a bulk glassy water to be around −177 °C. Acid strength increases in the order HF>HCl>HBr>HI,[20] and the strength of hydrogen bonds between X^- ions and water molecules is in the order HI>HBr>HCl>HF.[21] In acid solutions, protons move about between water molecules very rapidly.[22] It is well known that the ionic mobility of protons in aqueous solution is about nine times larger than that of lithium ions at 18 °C though the data are at infinite dilution.[23] Thus, knowing that glass transition occurs when diffusion is almost suppressed in a liquid[24] and that ionization of HX in aqueous HX solution is very high even at low temperatures,[12] we expect that the predicted T_g for pure water should reflect the high mobility of protons in the HX solutions. If the expectation is the case, the low T_g for bulk water predicted from the T_g data of aqueous HX solutions is reasonable. The fact that the stronger the HX acid is the lower the predicted T_g for pure water becomes can be taken as a validity of the above explanation. One supporting experimental evidence comes from the observation that the glass transition in a glassy ice crystal, which is claimed to be related to proton movements, occurs at −173 °C.[25] Another, though indirect, evidence is that the T_g data of HNO_3 solution predicts the T_g of pure water to be −144 °C,[14] in parallel with the observation that ionization of concentrated HNO_3 solution is much reduced at low temperatures.[13] However, these data are not so conclusive to warrant our conclusion definitely. Therefore, further experiments are needed before the anomalously low T_g prediction from aqueous HX solutions is fully clarified.

This work was in part assisted by a Grant-in-Aid for Scientific Research from the Ministry of Education, Science and Culture.

References

1) Y. Akama and H. Kanno, *Bull. Chem. Soc. Jpn.*, **55**, 3308 (1982).
2) C. A. Angell and E. J. Sare, *J. Chem. Phys.*, **52**, 1058 (1970).
3) D. H. Rasmussen and A. P. MacKenzie, *J. Phys. Chem.*, **75**, 967 (1971).
4) G. E. Vuillard, *Bull. Soc. Chim. Fr.*, **1954**, 82; *Compt. Rend.*, **241**, 1126 (1955); *Annal. Chim. (Paris)*, **2**, 233 (1957).
5) L. C. S. Shepley and A. B. Bestul, *J. Chem. Phys.*, **39**, 680 (1963).
6) H. Rawson, "Inorganic Glass Forming Systems," Academic Press, London (1967) Chapt. 2.
7) C. A. Angell, E. J. Sare, J. Donnella, and D. R. MacFarlane, *J. Phys. Chem.*, **85**, 1461 (1981).
8) C. A. Angell and E. J. Sare, *J. Chem. Phys.*, **49**, 4713 (1968).
9) S. Y. Hsich, R. W. Gammon, P. B. Macedo, and C. J. Montrose, *J. Chem. Phys.*, **56**, 1663 (1972).
10) J. W. Cahn, *J. Chem. Phys.*, **42**, 93 (1965); J. W. Cahn and R. J. Charles, *Phys. Chem. Glasses*, **6**, 181 (1965).
11) J. Dupuy, J. F. Jal, C. Fierador, P. Chieux, A. Wright, R. Caleczuk, and C. A. Angell, *Nature*, **296**, 138 (1982).
12) H. Kanno and J. Hiraishi, *Chem. Phys. Lett.*, **107**, 438 (1984).
13) H. Kanno and J. Hiraishi, unpublished data.
14) K. Satoh and H. Kanno, *Bull. Chem. Soc. Jpn.*, **55**, 1645 (1982).
15) R. Triolo and A. H. Narten, *J. Chem. Phys.*, **63**, 3624 (1975).
16) H. G. Lee, Y. Matsumoto, T. Yamaguchi, and H. Ohtaki, *Bull. Chem. Soc. Jpn.*, **56**, 443 (1983).
17) C. A. Angell, J. M. Sare, and E. J. Sare, *J. Phys. Chem.*, **82**, 2622 (1978).
18) P. Brüggeller and E. Mayer, *Nature*, **288**, 564 (1980); E. Mayer and P. Brüggeller, *Nature*, **298**, 715 (1981); *J. Phys.Chem.*, **87**, 4744 (1983).
19) J. Dubochet and A. W. McDowell, *J. Micros.*, **124**, RP3 (1981); J. Dubochet, J. Lepault, R. Freeman, J. A. Berriman, and J. U. Homo, *J. Micros.*, **128**, 219 (1982).
20) J. D. Lee, "A New Concise Inorganic Chemistry," Van Nostrand Reinhold Press, Birkshire (1977) Chapt. 5.
21) H. Kanno and J. Hiraishi, *Chem. Phys. Lett.*, **72**, 541 (1980); *J. Phys. Chem.*, **87**, 3664 (1983).
22) B. E. Conway, J. O'M. Bockris, and H. Linton, *J. Chem. Phys.* **24**, 834 (1956).
23) F. A. Cotton and G. Wilkinson, "Advanced Inorganic Chemistry," 4th ed., John Wiley Sons, New York (1980) Chapt. 7.
24) D. Turnbull, *Contemp. Phys.*, **10**, 473 (1969).
25) H. Suga and S. Seki, *J. Non-Cryst. Solids*, **16**, 171 (1974).

 © 1985 The Chemical Society of Japan Bull. Chem. Soc. Jpn., 58, 2490—2493 (1985) [Vol. 58, No. 9

Kinetic Analysis of the High-pressure Diels-Alder Reactions of Tropone with Maleic Anhydride and Norbornene[1)]

Hitoshi TAKESHITA,* Shigeru SUGIYAMA, and Toshihide HATSUI
Research Institute of Industrial Science, 86, Kyushu University, Kasuga-koen, Kasuga, Fukuoka 816
(Received March 12, 1985)

The kinetics of Diels-Alder reactions of tropone with maleic anhydride and norbornene were studied at pressures up to 2000 bar. The activation volumes, obtained from the former at 378.2 K in isopropylbenzene (IPB) and *N,N*-dimethylformamide (DMF), were $\Delta V^{\neq}$(IPB)=−21.4 cm³/mol and $\Delta V^{\neq}$(DMP)=−16.8 cm³/mol. Those from the latter (at 408.2 K) were $\Delta V^{\neq}$(IPB)=−30.0 cm³/mol and $\Delta V^{\neq}$(DMF)=−27.8 cm³/mol. These $\Delta V^{\neq}$ and ΔV showed a large deviation from those of the (6+4)π process of tropone with cyclopentadiene (by le Noble) and a small deviation from those of other typical Diels-Alder reactions to support the concerted cycloaddition mechanism which has been established by the kinetic analysis at atmospheric pressure.

In the field of high pressure organic chemistry, electrocyclic reactions, *e.g.*, Diels-Alder reaction, have been intensively investigated in the last two decades, and the reaction mechanism has been interpreted in terms of the activation parameters obtained by this method.[2,3)] According to general knowledge regarding the activation volume ($\Delta V^{\neq}$) and the reaction volume (ΔV), the concerted reactions show large negative values for their activation volumes; −25 to −35 cm³/mol for Diels-Alder reactions and −18 to −24 cm³/mol for 1,3-dipolar cycloaddition reactions.[3)] $\Delta V^{\neq}/\Delta V$ is in a range between 0.5 and 1.[4)] These values are in contrast to those of a two-step reaction *via* a zwitterionic intermediate in which, $\Delta V^{\neq}/\Delta V$ exceeds unity and $\Delta V^{\neq}$ might be larger than −50 cm³/mol.

Since there should not be much difference in the nature of bond formation among various concerted cycloadditions, such reaction features may be universally recognized in the concerted reactions. However, a remarkable exception has been noticed in a cycloaddition reaction involving tropone (**1**) with cyclopentadiene (CP) in dioxane.[5)] This has been the sole (6+4)π cycloaddition reaction ever studied by means of high-pressure kinetics, from which, a very small $\Delta V^{\neq}$ and ΔV (−7.5 and −4.3 cm³/mol) with a remarkably large $\Delta V^{\neq}/\Delta V$ (1.7) was obtained.[5)] Generally, when $\Delta V^{\neq}$ shows such a small negative value, $\Delta S^{\neq}$ must also be small and negative. However, as far as a kinetic analysis at atmospheric pressure shows, the $\Delta S^{\neq}$ is large and negative.[6)] This result is similar to that obtained in typical concerted Diels-Alder reactions.

These small activation and reaction volumes were interpreted on the basis of an unusually small partial molar volume of **1** which might be attributable to its highly polar structure.

It is true that the chemical properties of **1**, one of the most basic nonbenzenoid aromatic compounds, have been interpreted in terms of a contribution of a delocalized limiting structure (**1a**) with a delocalized 6π structure. Thus, **1** has a large dipole moment. On the other hand, **1** is known to undergo various types of pericycloadditions, such as (2+4)π-,[7)] (4+2)π-,[8)] (4+6)π-,[9)] (6+4)π-,[10)] and (8+2)π cycloaddition[11)] reactions. The concerted nature of its cycloaddition reactions has been accepted after a product analysis and kinetic investigations. Taking these into account, the above-mentioned results regarding (6+4)π cycloaddition of **1** with CP called our attention to whether the extraordinary figures which were obtained should be attributable to the characteristics of **1**, itself, as interpreted by le Noble, or to the special feature of the (6+4)π pericycloaddition of **1**. If the anomalies are due to the observed molar volume of **1** (85.6 cm³/mol; smaller than that calculated from the parachor listings (by 20 cm³/mol), as has been explained),[5)] this might be a good reason for the large dipole moment of **1** (4.17 D[12)]; 4.30 D[13)]). Then, this feature should always be observed in the cycloadditions of tropones.

To verify this point, we carried out Diels-Alder reactions of **1** with two kind of dienophiles: i) polar-, electron-deficient maleic anhydride (**2**) and ii) non-polar-, a strained and rigid bicyclic compound, norbornene (**3**). Each is known to give a single product.[8,14)] Particularly, the selection of the hydrocarbon, **3**, should provide reliable data for comparisons with the le Noble's experiment.

Experimental

Materials. Tropone (**1**) was prepared using Nozoe's procedure,[15)] purified by silica-gel chromatography, and distilled using a Kugelrohr tube *in vacuo*.. The purity was over 99.0%. Maleic anhydride (**2**) was sublimed *in vacuo* to show a mp of 53.5—54.0 °C. Norbornene (**3**) was used without further purification (a commercial Extra-Pure brand of Tokyo Kasei Co.). The adducts, **4** and **5**, were purified by repeated recrystallizations from acetone and pentane, respectively. They showed pertinent melting points, elemental analyses, and IR, NMR, and mass spectra. Isopropylbenzene (IPB) was distilled over Na and *N,N*-

dimethylformamide (DMF) was dried on CaH_2 and distilled *in vacuo*. Both solvents were gas-liquid chromatographically pure.

Kinetic Measurements. All kinetic runs, including the atmospheric runs, were carried out in a pressure vessel with an outlet valve for sampling. The temperature was controlled within 0.5 K and the pressure was measured using a Heise-Bourdon gauge. The initial concentrations of the reactants were *ca.* 0.007 mol/kg for **1** and 0.14 for **2** or **3**. The progress of the reactions was gas-liquid chromatographically monitored with a JEOL JGC-20KFP model gas chromatograph (column: 10%-Silicone XE 60 on Chromosorb W-DMCS) connected to a digital integrator, by observing the change of **1** (in the reaction with **2**) or **5** (in the reaction with **3**). Reliable data were collected after at least 1 h when thermal and pressure equilibrums were achieved. An analysis was performed as a *pseudo*-first-order reaction for **1**. Each reaction was repeated at least three times and second-order rate constants (k) were obtained from the observed rate constants (calculated by least-squares method).

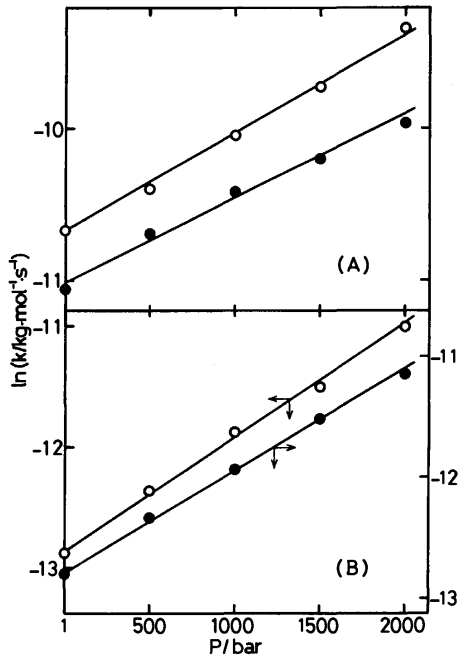

Fig. 1. Pressure Dependence of ln k
(A): **1**+**2** at 378.2 K, (B): **1**+**3** at 408.2 K.
○: in IPB, ●: in DMF

Measurements of the Partial Molar Volumes. The partial molar volume of each substrate (V_i) was determined by an extrapolation of the apparent molar volume (ϕ_i) to infinite dilution (obtained by a measurement of the density with Ostwald's pycnometer at 333.15±0.01 K). For each substrate, ϕ_i was almost constant for the same solvent.

$$\Phi_i = [(1000+M_im_i)/d_{mi}-1000/d]/m_i \quad (1)$$

where the subscript i represents the solute and M the molecular weight. d_{mi} and d are the densities of the solution and a pure solvent, respectively, and m_i is the molality. V_4 in IPB could not be obtained due to the insolubility of **4**.

Results and Discussion

Activation Volume. The rate constants for reactions of **1** with **2** and **3** at various pressures in IPB and in DMF are listed in Table 1. There are good linear correlations between ln k and the pressure in the range of 1 to 2000 bar, exhibited in Fig. 1 (correlation coefficient r: 0.998 and 0.992 for the reactions of **1** with **2** in IPB and in DMF, respectively; 0.997 and 0.999 for **1** with **3** in IPB and DMF, respectively). From Eq. 2 (derived from transition-state theory), $\Delta V^{\neq}$ was obtained and is listed in Table 2, together with the V_i for each compound and the volume profile ($\Delta V^{\neq}/\Delta V$).

$$\Delta V^{\neq} = -RT(\partial \ln k/\partial p)_T \quad (2)$$

The values of $\Delta V^{\neq}$ in Table 2 are large negative figures and (especially for the reaction with **3**) are typical values for Diels-Alder reactions.[2] Therefore, as far as the activation volume is concerned, the

Table 1. Rate constants for the Diels-Alder reaction of **1** with **2** (10^5 k/kg mol^{-1} s^{-1}) and **3** (10^6 k/kg mol^{-1} s^{-1}) under various pressures

Dienophiles	Temperature/K	Pressure/bar	Solvents	
			IPB	DMP
2	378.2	1	2.32±0.02	1.56±0.09
		500	3.03±0.11	2.31±0.02
		1000	4.29±0.29	3.02±0.06
		1500	5.99±0.26	3.69±0.31
		2000	9.02±0.21	4.71±0.25
3	408.2	1	2.55±0.05	2.78±0.05
		500	4.32±0.18	4.40±0.09
		1000	7.07±0.07	6.61±0.02
		1500	9.97±0.09	9.96±0.16
		2000	15.4±0.2	14.3±0.1

Table 2. Partial molar volumes (V_1), activation volumes ($\Delta V^{\neq}$), and reaction volumes (ΔV) for the reaction of **1** with **2** and **3** (in cm^3/mol)

Reactants	Solvent	V_1	V_2 or V_3	V_4 or V_5	ΔV	$\Delta V^{\neq}$	$\Delta V^{\neq}/\Delta V$
1+**2**	IPB	99.8	75.0	—	—	−21.4	—
	DMF	97.0	72.6	144.1	−25.5	−16.8	0.66
1+**3**	IPB	99.8	106.8	173.1	−33.5	−30.0	0.90
	DMF	97.0	106.0	170.9	−32.1	−27.8	0.87

V_1 and ΔV are obtained at 333.15 K, and $\Delta V^{\neq}$ at 378.2 K for **1** and **2**, and at 408.2 K for **1** and **3**.

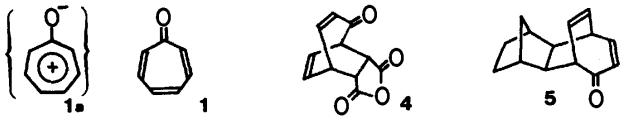

Chart 1

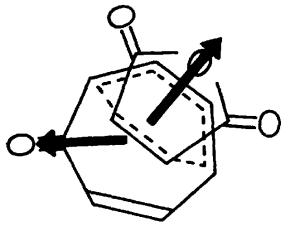

Fig. 2. Schematic Model of Dipoles in the Transition States.

Diels-Alder reaction of **1** clearly falls into a category of the concerted reaction. If one trusts the present results, the electrostriction of **1** must not be as large as has been suggested.

Nevertheless, the negative values for the activation volumes of reaction of **1** with **2** were slightly small. In this case, should the difference in the size of molecule be negligible, it is important that both reactants are equally polar molecules (dipole moments: 4.17 D for **1**[12] and 3.95 D for **2**[16]). In the initial state, **1** and **2** contract due to their high polarity. The polarity should decrease during the transition state, but should not cause a reduction in the volume if one considers a geometry in which the dipole moments of the two components are oriented at large angles with each other (θ=130 to 140°, Fig. 2) in the transition state. In other words, the contracted volumes of the two components are responsible for the small $\Delta V^{\neq}$ in the reaction of **1** with **2**. This conclusion is supported by the observed difference in the activation volumes in the two solvents. The value $\Delta V^{\neq}$(IPB)−$\Delta V^{\neq}$(DMF)=−4.6 cm^3/mol is quite similar to the difference between the sums of the volumes of the reactants in the two solvents ($\Sigma[V_i$(IPB)−V_i(DMF)]=5.2 cm^3/mol). Therefore, the volumes of the transition state are almost same in the two solvents. As the solvent effect on the partial molar volume (V_i) is parallel to the polarity of the reactant and the solvent,[17] the transition state is, therefore, less polar than the initial state.

Reaction Volume and Volume Profile. An analysis of ΔV and $\Delta V^{\neq}/\Delta V$ led to the same conclusion as above. The volume changes and the volume profiles for the reaction of **1** with **3** were the same as those for ordinary Diels-Alder reactions. We also obtained small values for ΔV and $\Delta V^{\neq}/\Delta V$ during the reaction of **1** with **2**. The former can be attributable to the polarity of the reactants and the latter represents a smaller polar transition state than for the product, **4**, as discussed above. Since the dipole moments of **1** and **2** are almost the same, we can assume that the volume reduction of **1** due to polarity is just as large as that of **2**. In this respect, the value of the previously reported partial molar volume of **1** in dioxane[5,18] is too small unless there are some unusual solvent-solute interactions.

Solvent Effect. The reaction rates of **1** with **2** or **3** in solvents having different polarities were slightly different from ordinary Diels-Alder reactions due to an increase in the dielectric constant (36.7 (DMF) from 2.4 (IPB)). The rates changed by only a factor of 1.1 (for the reaction with **3**) and 0.67 (with **2**) at atmospheric pressure. This means: i) the change of polarization is small during the rate-determination step in both reactions, and ii) in the reaction with **2**, the polarity of solvent decreases the rate; *i.e.*, the transition state should be less polar than the initial state. The former (i) seems to conflict with the above discussion concerning volumes, but it does not. Because that depends on the total dipole moment during the transition state. This means that the conclusion regarding the solvent effect is in accord with that for the activation volume.

Activation Energy and Entropy of the Reaction of 1 with 2. For a further determination of the transition state of the cycloaddition of **1** with **2**, atmospheric reactions were examined in IPB and DMF (the rate constants are summarized in Table 3). Arrhenius plots gave good linear correlations (r: 0.997 in IPB and 0.998 in DMF). The activation energy (E_a), activation entropy ($\Delta S^{\neq}$) and activation free energy ($\Delta G^{\neq}$) at 378.2 K are shown in Table 4. The remarkably large negative $\Delta S^{\neq}$ undoubtedly in-

Table 3. The rate constants of the Diels-Alder reaction of **1** with **2** at atmospheric pressure (10^5 k/kg mol^{-1} s^{-1})

Solvent	Temperature/K			
	378.2	388.2	398.2	408.2
IPB	2.32±0.02	3.66±0.08	5.50±0.18	7.36±0.15
DMF	1.56±0.09	2.51±0.01	3.96±0.16	5.54±0.12

Table 4. The activation paraneters for the Diels-Alder reaction of **1** with **2** at 378.2 K

Solvent	E_a/kJ mol^{-1}	$\Delta S^{\neq}$/J mol^{-1} K^{-1}	$\Delta G^{\neq}$/kJ mol^{-1}
IPB	49.7±3.3	−229±9	133±7
DMF	54.8±2.5	−219±7	134±5

dicates a concerted character regarding the reaction. This is parallel to kinetic studies of other Diels-Alder reactions,[19] including those of troponoids.[14,20] In addition, the E_a values, larger in DMF than in IPB, support the proposal that the initial state is more stabilized than the transition state in DMF, *i.e.*, the transition state is less polar than the initial state.

In conclusion, from the reactions with **2** and **3**, it was clarified that in the Diels-Alder reaction of **1**, the activation and reaction volumes are affected by the polarities of the initial state and the transition state. However, they are not negatively small as reported for the reaction of **1** with CP. We will report on studies regarding the (6+4)π cycloaddition of **1** with dienes in order to understand the thermal reactions of tropones.

References

1) Part of the results has been published in a preliminary form: H. Takeshita, S. Sugiyama, and T. Hatsui, *Chem. Lett.*, **1984**, 1855.

2) Reviews: T. Asano and W. J. le Noble, *Chem. Rev.*, **78**, 407 (1978); T. Asano and A. Sera, *Yuki Gosei Kagaku Kyokaishi*, **35**, 535 (1977).

3) Y. Yoshimura, J. Osugi, and M. Nakahara, *Bull. Chem. Soc. Jpn.*, **56**, 680 (1983); Y. Yoshimura, J. Osugi, and M. Nakahara *J. Am. Chem. Soc.*, **105**, 5414 (1983); G. Swieton, J. v. Jouanne, H. Kelm, and R. Huisgen, *J. Org. Chem.*, **48**, 1035 (1983).

4) A few examples of $\Delta V^{\neq}/\Delta V$ larger than 1 were reported in the Diels-Alder reaction of **2** with some dienes, and were explained by the secondary orbital interactions.[16,21]

5) W. J. le Noble and B. A. Ojosipe, *J. Am. Chem. Soc.*, **97**, 5939 (1978).

6) H. Tanida and H. R. Pfaendler (*Helv. Chim. Acta*, **55**, 3062 (1972)) have already shown the (6+4)π cycloaddition of **1** with CP to be concerted by the kinetic analysis; $\Delta S^{\neq}=-146$ J mol^{-1} K^{-1} in dioxane at 373.2 K.

7) In this paper, $(m+n)\pi$ denotes the cycloaddition of $m\pi$ component of **1** with $n\pi$ cycloaddend. For the (2+4)π process, see H. Takeshita, Y. Wada, A. Mori, and T. Hatsui, *Chem. Lett.*, **1973**, 335.

8) T. Nozoe, T. Mukai, T. Nagase, and Y. Toyooka, *Bull. Chem. Soc. Jpn.*, **33**, 1247 (1960); S. Itô, H. Takeshita, and Y. Shoji, *Tetrahedron Lett.*, **1969**, 1815.

9) K. N. Houk, L. J. Luskus, and N. S. Bhacca, *J. Am. Chem. Soc.*, **92**, 6392 (1970).

10) R. C. Cookson, B. V. Drake, J. Hudec, and A. Morrison, *Chem. Commun.*, **1966**, 15; S. Itô, Y. Fujise, T. Okuda, and Y. Inoue, *Bull. Chem. Soc. Jpn.*, **39**, 1351 (1966).

11) M. Oda, M. Funamizu, and Y. Kitahara, *J. Chem. Soc., Chem. Commun.*, **1969**, 737; M. E. Garst, V. A. Roberts, and C. Prussin, *Tetrahedron*, **39**, 581 (1983).

12) T. Nozoe, T. Mukai, and K. Takase, *Proc. Jpn. Acad.*, **28**, 477 (1952).

13) D. J. Berrelli and T. G. Andrews, Jr., *J. Am. Chem. Soc.*, **91**, 5280 (1969).

14) H. R. Pfaendler, H. Tanida, and E. Haselbach, *Helv. Chim. Acta*, **57**, 383 (1974).

15) T. Ikemi, T. Nozoe, and H. Sugiyama, *Chem. Ind. (London)*, **1960**, 932.

16) R. A. Grieger and C. A. Eckert, *Trans. Faraday Soc.*, **66**, 2579 (1970).

17) Partial molar volumes are often observed to be larger in the solvent having small dielectric constant, ε, than in one having large ε,[22] though Grieger and Eckert[16] predicted that partial molar volume decreases with an increase of electrostriction parameter,

$$q_p = \partial[(\varepsilon-1)/(2\varepsilon-1)]/\partial p.$$

18) We have measured the V_1 in dioxane. The figure will be included in a paper of the related subject.

19) J. Sauer, H. Wiest, and A. Mielert, *Chem. Ber.*, **97**, 3183 (1964).

20) For the cycloaddition reactions of troponoids with **2**, the relatively large negative $\Delta S^{\neq}$ values, −189 J mol^{-1} K^{-1} for the reaction of **1** with **2** and −205 J mol^{-1} K^{-1} for 2-chlorotropone with **2** in *p*-cymene at 378.2 K, have been obtained: S. Itô, A. Mori, Y. Shoji, and H. Takeshita, *Tetrahedron Lett.*, **1972**, 2685.

21) K. Seguchi, A. Sera, and K. Maruyama, *Bull. Chem. Soc. Jpn.*, **47**, 2242 (1974).

22) G. Swieton, J. v. Jouanne, H. Kelm, and R. Huisgen, *J. Chem. Soc., Perkin Trans. 2*, **1983**, 37.

 © 1985 The Chemical Society of Japan Bull. Chem. Soc. Jpn., 58, 2494—2501 (1985)

Critical Peptide Size for Insolubility Caused by a β-Sheet Aggregation and Solubility Improvement in Hydrophobic Peptides by Replacement of Alanine Residues with α-Aminoisobutyric Acid Residues[1)]

Mitsuaki NARITA,* Junn-Yann CHEN, Hiroyuki SATO, and Yukio KIM
Department of Industrial Chemistry, Faculty of Technology, Tokyo University of Agriculture and Technology, Koganei, Tokyo 184
(Received March 19, 1985)

In order to demonstrate an important role of a β-sheet aggregation on insolubility of peptides, hydrophobic peptides having partial amino acid sequences found in natural proteins have been prepared by the stepwise elongation and fragment condensation methods. In conformity with the solubility prediction for protected peptides in our previous paper, solubility data indicate that insolubility of peptides appears to begin at octa- or nonapeptide levels. In hydrophobic sequences found in proteins, the structure of peptide backbones, namely, the β-structure clearly plays an important role on insolubility of peptides, but the composition of peptides does not. Solubility improvement in hydrophobic peptides included in α-helical regions of proteins is easily achieved by replacement of Ala residues with Aib residues. High solubility of the peptides containing Aib residues is clearly explained by the observation that replacement of C^{α} hydrogen atoms with methyl groups greatly disturbs β-sheet structures, promoting helical folding in peptides. The great ability of an Aib residue to promote helical folding is distinctly revealed in the peptide fragments included in α-helical regions of proteins as demonstrated before in model oligo(Leu)s.

Peptide fragments having only hydrophobic amino acid residues are often found in signal peptides[2)] and hydrophobic regions of intrinsic membrane proteins.[3)] On the basis of our solubility prediction method in a previous paper,[4)] they are predicted to be extraordinarily less soluble in the solvents used in peptide syntheses and to be less amenable to further elongation of peptide chains. For solubility prediction in the paper,[4)] the peptides **1**—**5** in Fig. 1 were used as representative examples of hydrophobic peptide fragments contained in natural proteins and, as expected, actually found to be extraordinarily less soluble due to their β-sheet aggregations. In Fig. 1, the peptides **1**—**5** have the amino acid sequences corresponding to murine H-2K^{b} [287—294], murine H-2K^{b} [291—298], murine H-2K^{b} [287—298], subtilisin BPN′ [227—235], and T24 human bladder carcinoma oncogene [6—15], respectively.[5-7)] The numbers in brackets in the following trivial names represent the positions of the first and last amino acids from the N-terminals in the intact proteins.[8)]

In this paper, we describe syntheses and IR absorption conformational analyses of the peptides in Fig. 1 and investigate critical chain length for

Boc-Val Ala Val Leu Val_2 Leu Gly-OBzl
1

Boc-Val_2 Leu Gly Ala_2 Ile Val-OBzl
2

Boc-Val Ala Val Leu Val_2 Leu Gly Ala_2 Ile Val-OBzl
3

Boc-Val Ala Gly Ala_3 Leu Ile Leu-OBzl
4

Boc-Leu Val_3 Gly Ala $(Val\ Gly)_2$-OBzl
5

Boc-Val Gly Phe Gly Leu Ile Leu_2-OBzl
6

Boc-Val Ala Val Leu-OBzl
7

Boc-Leu Val_3 Gly-OBzl
8

Boc-Ala_3 Leu Ile Leu-OBzl
9

Boc-Val Leu Gly Ala_2 Ile Val-OBzl
10

Boc-Val Gly Ala $(Val\ Gly)_2$-OBzl
11

Boc-Val_2 Gly Ala $(Val\ Gly)_2$-OBzl
12

Boc-Val_3 Gly Ala $(Val\ Gly)_2$-OBzl
13

Boc-Aib Ala Ile Val-OBzl
14

Boc-Val Ala Gly Ala Aib-OBzl
15

Boc-Gly Ala Aib Ala Leu Ile Leu-OBzl
16

Boc-Val_2 Leu Gly Aib Ala Ile Val-OBzl
17

Boc-Val Ala Gly Ala Aib Ala Leu Ile Leu-OBzl
18

Fig. 1. The amino acid sequences of the peptides **1**—**18** used in this study.

insolubility of hydrophobic peptides caused by the β-sheet aggregation since we postulated that peptides smaller than heptapeptides are readily soluble in the solvents used in peptide syntheses.[4] The peptide **6** in Fig. 1 is further presented as an interesting example to have high solubility in spite of having the β-structure in solution. It has the amino acid sequence corresponding to bacteriorhodopsin [217—224].[9] The peptides **7—13** in Fig. 1 are also presented to investigate the critical chain length for insolubility. They have partial sequences of the peptides **1—5**. Recently, we also demonstrated that replacement of Ala residues with Aib residues in peptides constrained helical folding in the peptides, and that a dramatic change took place in solubility.[10,11] The implications of the strategy of solubility improvement for the chemistry of peptides and proteins were also discussed. The peptides **14—18** in Fig. 1 are presented to demonstrate the usefulness of replacement of Ala residues with Aib residues for solubility improvement in hydrophobic peptides included in α-helical regions of proteins. They have the amino acid sequences in which Ala residues in the peptides **2** and **4** and in their fragments are replaced by Aib residues.

Experimental

General. The uncorrected capillary melting points will be reported. Analytical instruments and conditions were described in the previous paper.[10] The solubility (c=1.0 g/dl) was divided into the following four classes: (A) completely soluble at room temperature, (B) completely soluble at 80 °C or refluxing temperature, (C) partially soluble at 80 °C or refluxing temperature, and (D) nearly insoluble at 80 °C or refluxing temperature.

General Procedure for the Coupling Reaction Using DCC Activation in the Presence or in the Absence of HOBt. DCC (1.1 equiv) was added to an ice-chilled, stirred mixture of a carboxyl component (1.1 equiv) and an amino component (10 mmol) in dichloromethane or DMF (100 ml). The amino components were obtained from a TosOH salt or HCl salt with an equivalent of NMM. When the carboxyl component was a peptide, HOBt (1.2 equiv) was added before the addition of DCC. Peptide chain elongation of lower peptides was performed in dichloromethane, and fragment condensation for the peptides **1—6** and **9—13** was carried out in DMF. The reaction mixture was stirred in an ice-chilled bath for 3 h, at room temperature overnight, and then filtered. The filtrate was concentrated *in vacuo*. The subsequent work-up procedure was essentially the same as those described before.[10,11]

General Procedure for Removal of the Boc Group. Boc-peptide benzyl esters (10 mmol) in 3 M† HCl/AcOEt (40 ml) were stirred in an ice-chilled bath for 1.5 h. Removal of the Boc group from the peptide **2** was carried out in TFA/dichloromethane (1/2, v/v) at room temperature for 1 h. Then, the mixture was concentrated *in vacuo*, followed by the repetition of the addition and removal *in vacuo* of dichloromethane. The residue was used for a subsequent coupling reaction without further purification.

General Procedure for Removal of the Bzl Group. Boc-peptide benzyl esters (7 mmol) were hydrogenated overnight at atmospheric pressure in a mixture of AcOH/MeOH (1/4, v/v) (100 ml) using 5% Pd/C (10 wt%) as a catalyst. After the removal of Pd/C, the filtrate was concentrated *in vacuo*. The residue was washed with water and recrystallized from appropriate solvents.

Results

Syntheses and Solubilities of Hydrophobic Oligopeptides. The typical synthetic procedures are summarized in Scheme. Starting with amino acid benzyl esters as amino components, di- to pentapeptides were prepared by usual stepwise elongation of the peptide chains using DCC activation[12] in dichloromethane. Further chain elongations were performed mainly in DMF by fragment condensation with least danger of racemization using DCC activation in the presence of HOBt.[13] Liberation of the amino group from Boc-peptide benzyl esters was carried out by treatment with 3 M HCl/AcOEt followed by treatment with NMM. Removal of the benzyl group from Boc-peptide benzyl esters was performed by hydrogenolysis using Pd/C as a catalyst in a mixture of MeOH and AcOH. All the soluble peptides were purified by repeated recrystallization, and, as a result of this purification process, each peptide gave a single peak on HPLC. Insoluble peptides were purified by repeated washing with hot MeOH. Synthetic and analytical results of the peptides **1—18** are assembled in Tables 1—3. The amino acid and elemental analyses of the peptides shown in Tables 2 and 3 are in good agreement with the calculated values. Solubility of the peptides **1—18** is also summarized in Table 4. Solubility of the peptides **1—5** was previously examined and found to be extraordinarily less soluble in such solvents as DMSO, NMP, DMA, DMF, and MeOH (Table 4). For these peptides HMPA turned out to be a better solvent than the above (Table 4). On the other hand, the lower oligopeptides **7—11** are easily soluble in these solvents. The peptides **17** and **18**, which are obtained by replacement of Ala residues with Aib residues in the peptides **2** and **4**, respectively, have also high solubility in moderately and highly polar organic solvents. This is in remarkable contrast with the result that the original peptides **2** and **4** are barely soluble in these solvents.

IR Absorption Conformational Analyses of Hydrophobic Peptides in the Solid State and in Dichloromethane. Conformational analyses of hydrophobic peptides in the solid state are interesting for the purpose of elucidating the relationship between

† 1 M=1 mol dm^{-3}.

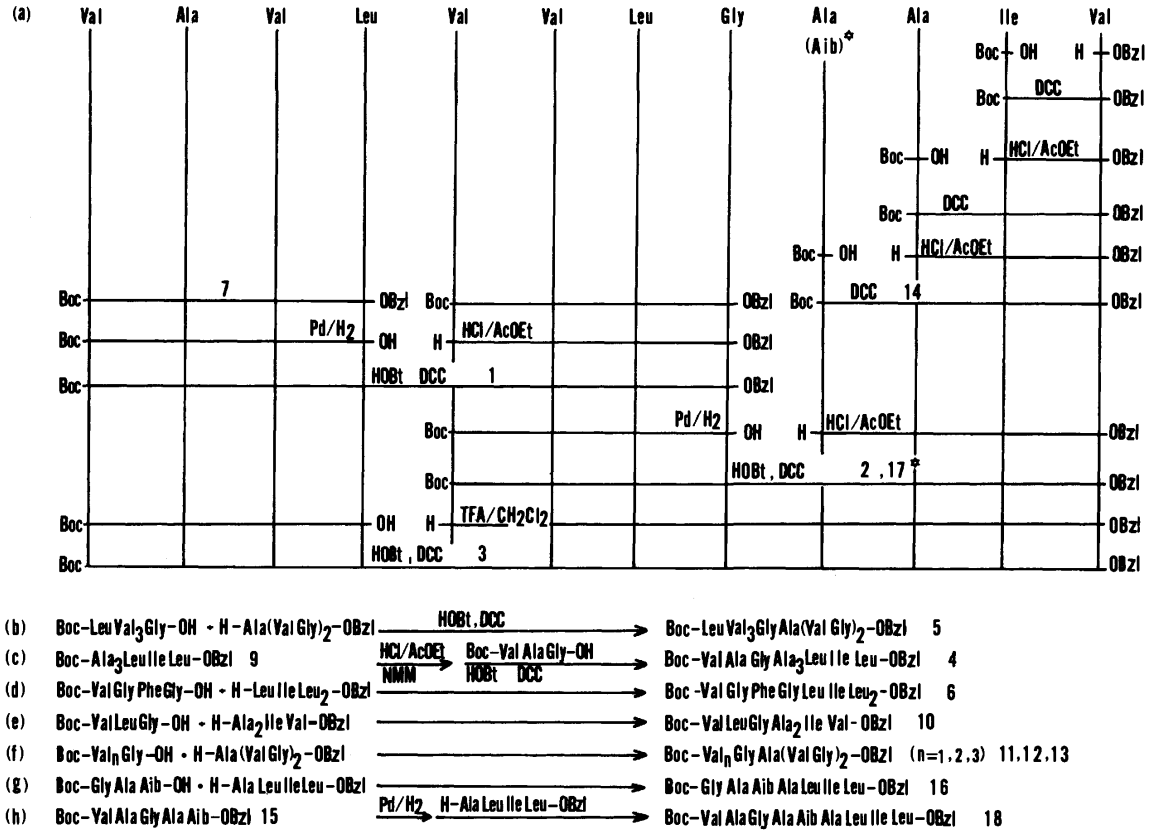

Scheme

TABLE 1. SYNTHETIC RESULTS AND PHYSICAL PROPERTIES OF THE PEPTIDES **1—18**

Compound	Yield/%[a]	Recrystallization solvent	Mp θ_w/°C	$[\alpha]_D^{20}$ (c=1.0, DMF)	Retention time/min
1	88	b)	over 250	c)	c)
2	76	〃	〃	〃	〃
3	81	〃	〃	〃	〃
4	71	〃	〃	〃	〃
5	87	〃	〃	〃	〃
6	74	Ethanol	〃	−33.0	13.6
7	81	AcOEt/hexane	178—180	−29.3	14.8
8	85	Methanol	over 250	−27.8	14.0
9	75	〃	〃	−44.3	14.0
10	83	〃	244—247	−28.5	13.6
11	95	b)	over 250	−19.5	13.1
12	89	〃	〃	c)	c)
13	93	〃	〃	〃	〃
14	76	d)	93—95	−14.3	14.8
15	93	AcOEt/hexane	117—120	−15.0	13.8
16	94	〃	163—165	−36.8	14.3
17	91	Acetone/water	198—201	−22.5	13.9
18	82	AcOEt/hexane	152—155	−26.3	13.7

a) Coupling yields in final steps. b) Purified by washing with hot methanol. c) Not obtained due to insolubility in DMF. d) Purified by Sephadex LH-20 column chromatography.

the conformation and solubility of hydrophobic peptides. Figure 2 shows the IR absorption spectra of the peptides **1**—**6** in the solid state in the most significant spectral regions for the conformational assignments (3600—3200 cm^{-1}, amide A; 1700—1600 cm^{-1}, amide I). As representative examples of the tetra- to hexapeptides, the IR absorption spectra of the peptides **7**—**9** in the solid state are also depicted in Fig. 3. All the peptides show strong bands at 3290—3270 cm^{-1} and 1635—1625 cm^{-1}, assigned to a typical β-sheet structure.[14-16] On the other hand, the IR absorption spectra (Fig. 4) of the peptides **14**—**18** in the solid state, which are obtained by replacement of Ala residues with Aib residues in the peptides **2** and **4** and in their fragments, have shoulder bands at about 3340 cm^{-1} and 1660—

Table 2. Elemental analyses of the peptides **1**—**18**

Compound	Formula	Found (Calcd)/%		
		C	H	N
1	$C_{49}H_{82}N_8O_{11}$	61.28 (61.36)	8.70 (8.62)	11.67 (11.68)
2	$C_{47}H_{78}N_8O_{11}$	60.59 (60.62)	8.60 (8.44)	12.03 (12.04)
3	$C_{66}H_{112}N_{12}O_{15}\cdot H_2O$	59.79 (59.53)	8.63 (8.60)	12.65 (12.62)
4	$C_{49}H_{81}N_9O_{12}$	59.51 (59.55)	8.36 (8.26)	12.72 (12.76)
5	$C_{52}H_{86}N_{10}O_{13}\cdot 1.5H_2O$	57.53 (57.49)	8.33 (8.26)	12.44 (12.89)
6	$C_{54}H_{84}N_8O_{11}\cdot 1.5H_2O$	61.86 (61.87)	8.31 (8.37)	10.86 (10.69)
7	$C_{31}H_{50}N_4O_7$	62.74 (63.03)	8.55 (8.53)	9.59 (9.48)
8	$C_{35}H_{57}N_5O_8\cdot 0.5H_2O$	61.19 (61.38)	8.33 (8.53)	10.63 (10.23)
9	$C_{39}H_{64}N_6O_9\cdot 0.5H_2O$	60.42 (60.84)	8.47 (8.51)	11.05 (10.91)
10	$C_{42}H_{69}N_7O_{10}\cdot 0.5H_2O$	60.05 (59.98)	8.35 (8.39)	11.59 (11.66)
11	$C_{36}H_{57}N_7O_{10}\cdot 0.5H_2O$	57.29 (57.19)	7.72 (7.72)	12.82 (12.95)
12	$C_{41}H_{66}N_8O_{11}\cdot 2H_2O$	55.43 (55.77)	7.53 (7.99)	12.92 (12.69)
13	$C_{46}H_{75}N_9O_{12}\cdot 2H_2O$	55.99 (56.25)	8.04 (8.11)	13.42 (12.84)
14	$C_{30}H_{48}N_4O_7$	62.31 (62.48)	8.62 (8.39)	9.82 (9.71)
15	$C_{29}H_{45}N_5O_8$	58.42 (58.87)	8.03 (7.67)	11.82 (11.84)
16	$C_{42}H_{69}N_7O_{10}$	60.30 (60.63)	8.56 (8.36)	11.53 (11.78)
17	$C_{48}H_{78}N_8O_{18}\cdot H_2O$	59.83 (59.85)	8.69 (8.58)	11.33 (11.63)
18	$C_{50}H_{83}N_9O_{12}\cdot H_2O$	58.84 (58.86)	8.38 (8.40)	12.16 (12.36)

Table 3. Amino acid analyses[a] of the peptides **1**—**18**

Compound	Found (Calcd)					
	Gly	Ala	Val	Leu	Ile	Phe
1	1.09 (1)	1.00 (1)	3.95 (4)	2.12 (2)	—	—
2	1.06 (1)	2.06 (2)	3.00 (3)	0.95 (1)	0.92 (1)	—
3	1.15 (1)	3.17 (3)	5.00 (5)	2.19 (2)	0.98 (1)	—
4	1.00 (1)	4.17 (4)	0.99 (1)	2.17 (2)	0.91 (1)	—
5	3.00 (3)	0.85 (1)	5.07 (5)	1.15 (1)	—	—
6	2.07 (2)	—	1.07 (1)	3.00 (3)	0.96 (1)	0.98 (1)
7	—	1.14 (1)	2.00 (2)	1.00 (1)	—	—
8	1.08 (1)	—	2.97 (3)	1.00 (1)	—	—
9	—	3.27 (3)	—	2.00 (2)	0.93 (1)	—
10	1.04 (1)	1.92 (2)	1.82 (2)	1.00 (1)	0.90 (1)	—
11	3.00 (3)	1.00 (1)	2.87 (3)	—	—	—
12	3.02 (3)	1.00 (1)	3.79 (4)	—	—	—
13	3.00 (3)	1.09 (1)	4.93 (5)	—	—	—
14	—	1.10 (1)	1.00 (1)	—	1.02 (1)	—
15	1.00 (1)	2.07 (2)	0.99 (1)	—	—	—
16	0.90 (1)	1.95 (2)	—	2.06 (2)	1.00 (1)	—
17	1.00 (1)	0.96 (1)	3.00 (3)	1.03 (1)	0.99 (1)	—
18	0.93 (1)	3.01 (3)	0.95 (1)	2.06 (2)	1.00 (1)	—

a) For the peptides **14**—**18**, Aib and Ala peaks often overlapped. The ratio of the peak area for Aib/Ala is 1/50.

TABLE 4. SOLUBILITY PROPERTIES[a] OF THE PEPTIDES **1**—**18** (c=1.0 g/dl)

Compound	Solvent[b]									
	HMPA	NMP	DMSO	DMA	DMF	MeOH	THF	AC	AcOEt	DCM
1	A	C	C	D	D	D	D	D	D	D
2	A	D	C	D	D	D	D	D	D	D
3	C	D	D	D	D	D	D	D	D	D
4	A	B	D	D	D	D	D	D	D	D
5	C	D	C	D	D	D	D	D	D	D
6	A	A	A	A	A	A	A	C	A	B
7	A	A	A	A	A	A	A	B	B	A
8	A	A	A	A	A	B	B	D	D	C
9	A	A	A	A	A	C	D	D	D	D
10	A	A	A	A	A	B	C	D	D	C
11	A	A	A	B	B	C	C	D	D	D
12	A	C	B	D	D	D	D	D	D	D
13	B	C	C	D	D	D	D	D	D	D
14	A	A	A	A	A	A	A	A	A	A
15	A	A	A	A	A	A	A	A	A	A
16	A	A	A	A	A	A	A	A	B	A
17	A	A	A	A	A	A	B	A	C	A
18	A	A	A	A	A	A	A	A	B	A

a) Symbols of A, B, C, and D: see experimental in text. b) Abbreviations: AC, acetone; DCM, dichloromethane. Others, see Ref. 1).

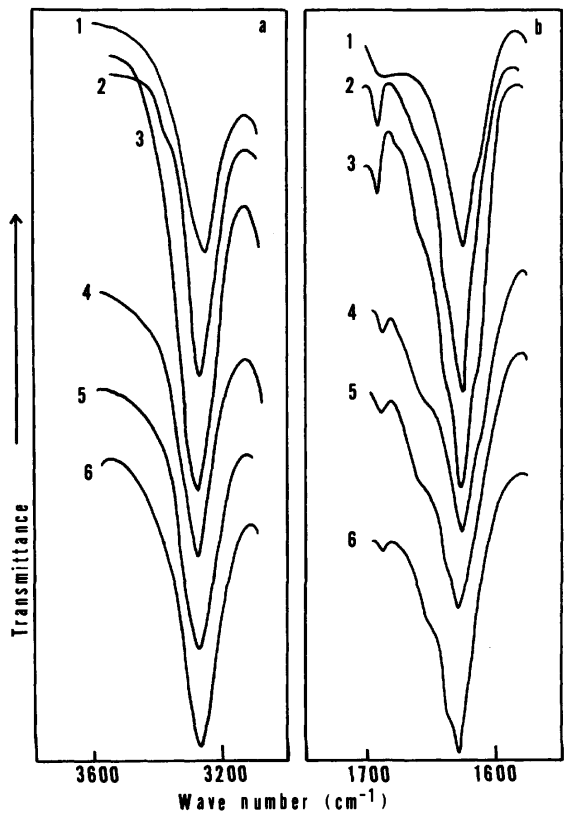

Fig. 2. IR absorption spectra of the peptides **1**—**6** in the solid state.

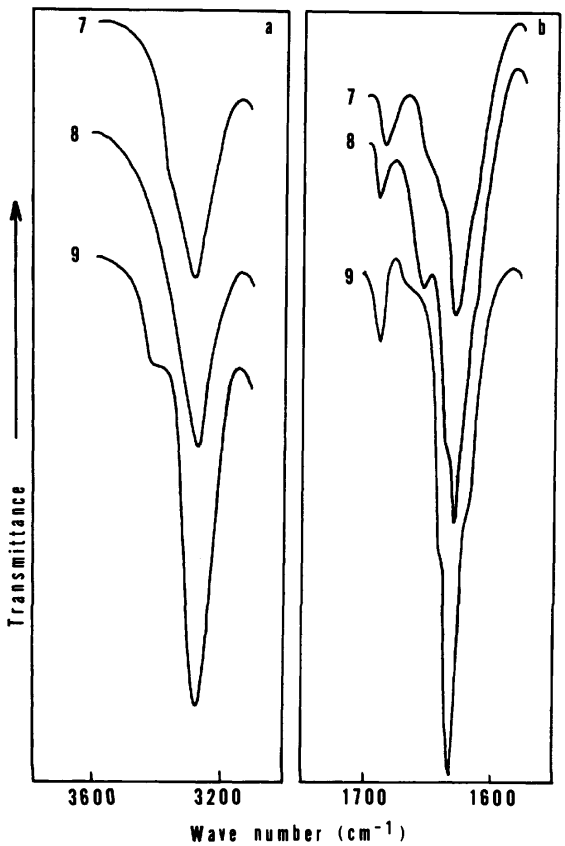

Fig. 3. IR absorption spectra of the peptides **7**—**9** in the solid state.

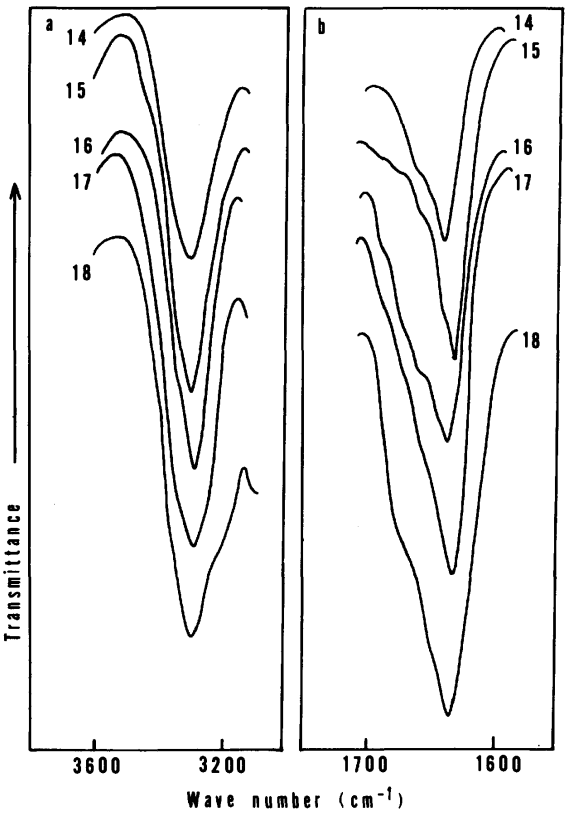

Fig. 4. IR absorption spectra of the peptides **14**—**18** in the solid state.

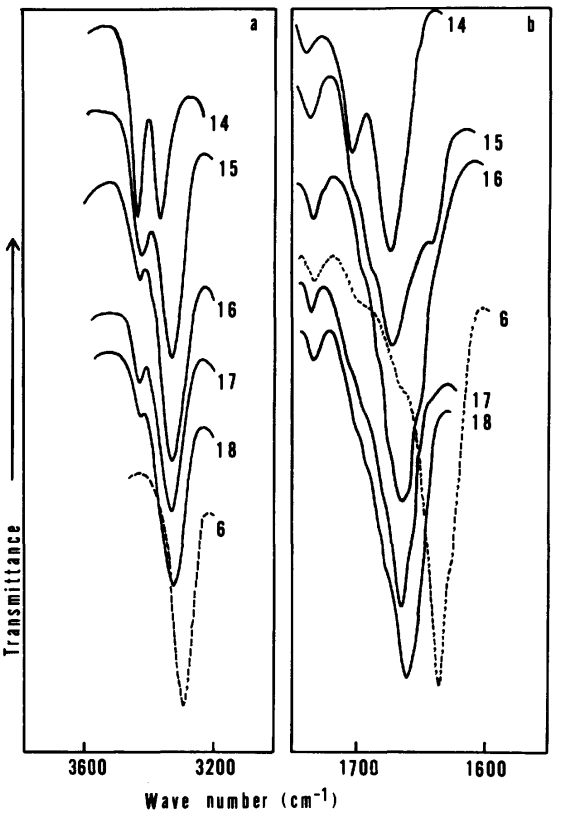

Fig. 5. IR absorption spectra of the peptides **6** and **14**—**18** in dichloromethane.

1650 cm^{-1}, indicating that β-structures are distorted on the Aib residues.

The peptides **6** and **14**—**18** are soluble in dichloromethane and their IR absorption spectra in dichloromethane are presented in Fig. 5. The spectral pattern of the peptide **6** in dichloromethane is essentially the same as that in the solid state. The peptides **14**—**18** in solution, as expected from solubility data and the nature of Aib residues, show no band at about 3280 cm^{-1} and 1630 cm^{-1}, indicating that the restriction of the values of the backbone dihedral angles ϕ and ψ of the Aib residues within the values in the helical regions ($\phi=\pm60\pm20$ and $\psi=\pm40\pm20$)[17] efficiently hinders development of the β-sheet structure. The IR absorption spectrum of the tetrapeptide **14** has two strong bands at 3430 cm^{-1} and 3350 cm^{-1} in the amide A region, indicating the existence of both the nonhydrogen bonding NH and hydrogen bonding NH bonds.[10,11,18] The IR spectrum of the peptide **14** has also a medium-intensity shoulder band at 1708 cm^{-1} and a strong band at 1672 cm^{-1} in the amide I region, assigned to the hydrogen-bonded urethane and free amide carbonyl groups, respectively.[10,11,18] Owing to a strong preference of the Aib residues to form a helical conformation (3_{10}- or α-helix), the peptides **15**—**18** show strong intensity bands at 3325—3320 cm^{-1} and 1672—1660 cm^{-1}, indicating a helical structure (3_{10}- or α-helix), although the frequencies of the amide I region are rather high.[14] Weak or medium intensity bands at 3430—3420 cm^{-1} of the peptides **15**—**18** are also assigned to the nonhydrogen bonding NH bonds, which are attributed to the NH bonds of two or three amino acid residues at the N-terminal portions.

Discussion

Preparation of the peptides **1**—**18** were performed without difficulty by the usual stepwise elongation and fragment condensation methods. The amino component peptide having the Aib residue at the N-terminal, H-Aib-Ala-Ile-Val-OBzl, reacted smoothly with the carboxyl component peptide, Boc-Val_2-Leu-Gly-OH, to produce the peptide **17** in a high yield and the carboxyl component peptide having the Aib residue at the C-terminal, Boc-Val-Ala-Gly-Ala-Aib-OH, also reacted with the amino component peptide, H-Ala-Leu-Ile-Leu-OBzl, to produce the peptide **18** in a high yield, in spite of the fact that the N- and C-terminal Aib residues were sterically hindered.[19] In conformity with the solubility prediction for protected peptides,[4] the β-sheet aggregation caused insolubility in polar solvents of hydrophobic peptides larger than octa- or nonapeptides and, in their preparation, gelation took place along with the reaction. In hydrophobic sequences found in

proteins, the structure of peptide backbones, namely, the β-structure apparently plays an important role on insolubility of peptides, but the structure of peptide side chains, namely, the composition does not.

With respect to the critical chain length for insolubility caused by the β-sheet aggregation, solubility data of the peptides **1**—**13** (Table 4) indicate that insolubility in highly polar solvents of hydrophobic peptides appears to begin at the octa- or nonapeptide levels. Solubility of the octapeptide **6** is rather high in spite of having the β-sheet structure in the solid state (Fig. 3) and 1.0 g of the peptide **6** is easily soluble at room temperature in 100 ml of such solvents as DMSO, HMPA, DMA, DMF, MeOH, and THF. The spectral pattern of the peptide **6** in dichloromethane (Fig. 5) and THF (not shown) is essentially the same as that in the solid state and indicates that the peptide **6** in both solutions exists in the β-sheet aggregation form as reported for a homohexapeptide of Glu(OBzl) in 1,2-dichloroethane.[20] Further development of interpeptide-chain interactions through hydrogen bonding will give rise to severe insolubility as pointed out for model peptides in our previous paper.[21]

Hydrophobic sequences found in natural proteins are expected to be highly organized since hydrophobic amino acid residues have high potentials for the formation of helix- and β-structures.[22] The peptides **1**—**3** are thought to be the partial sequences of a membrane-binding subregion of the murine H-2K^b molecule and the subregion is practically considered to be in the conformation of an α-helix.[23] The peptide **4** is also known to be included in an α-helical region of subtilisin BPN′.[24] On the other hand, the preferred structure, predicted by the Chou-Fasman method,[22] is the β-structure and α-helix for the peptides **1**—**3**, **5**, and **6** and for the peptide **4**, respectively (Table 5). In spite of the disparity between observed and predicted of the conformation, a conformational preference for β-structure formation in the solid state is experimentally demonstrated for the peptides **1**—**6** (Fig. 1). The result is illustrated by the observation that secondary structure formation is dependent on peptide chain length and that critical peptide size for development of the α-helix in the solid state is among decapeptide and pentadecapeptide levels.[25] Therefore, in protein syntheses by fragment condensation methods, the peptide fragments included in α-helical regions of proteins have the β-sheet structure and low solubility before they give rise to helical folding.

Table 5. The preferred structure of the peptides **1**—**6** predicted by the Chou-Fasman method

Compound	P_α	P_β	Preferred structure
1	1.15	1.35	β
2	1.15	1.32	β
3	1.19	1.33	β
4	1.24	1.15	helix
5	1.01	1.29	β
6	1.04	1.23	β

Solubility improvement in hydrophobic peptides included in α-helical regions of proteins is easily achieved by the strategy of replacement of Ala residues with Aib residues.[10,11] The strategy for solubility improvement is based on the restriction of the values of the backbone dihedral angles ϕ and ψ of Aib residues within the values in the region of α- and 3_{10}-helices ($\phi=\pm60\pm20$ and $\psi=\pm40\pm20$). In fact, high solubility of the peptides containing Aib residue is clearly explained by the observation that replacement of C^α hydrogen atoms with methyl groups greatly disturbs β-sheet structures, promoting helical folding in the peptides **14**—**18** (Figs. 4 and 5). The IR spectral patterns of the peptides **14**—**18** in the solid state and in dichloromethane are nearly equivalent to those of the corresponding oligo(Leu)s containing an Aib residue described before.[11] The great ability of an Aib residue to promote helical folding is distinctly revealed in the peptide fragments included in α-helical regions of proteins as demonstrated before in the study of model oligo(Leu)s.[10,11] These results indicate that replacement of a few Ala residues with Aib residues in helical regions of proteins offers the prospect for creating novel proteins in ways not possible by any other method as mentioned previously.[10,11]

References

1) This paper forms Part III of "Peptides and Proteins Containing α,α-Disubstituted α-Amino Acid Residues" series. Part II, M. Narita, K. Ishikawa, H. Sugasawa, and M. Doi, *Bull. Chem. Soc. Jpn.*, **58**, 1731 (1985). The abbreviations for amino acids are those recommended by the IUPAC-IUB Commission on Biochemical Nomenclature *J. Biol. Chem.*, **247**, 977 (1972). Amino acid symbols except for Gly denote the L-configuration. Additional abbreviations used are the following: Aib, α-aminoisobutyric acid residue; Boc, *t*-butoxycarbonyl; OBzl, benzyl ester; DCC, dicyclohexylcarbodiimide; HOBt, 1-hydroxy-1*H*-benzotriazole; TosOH, *p*-toluenesulfonic acid; NMM, *N*-methylmorpholine; DMF, *N*,*N*-dimethylformamide; AcOEt, ethyl acetate; TFA, trifluoroacetic acid; AcOH, acetic acid; MeOH, methanol; DMSO, dimethyl sulfoxide; NMP, *N*-methyl-2-pyrrolidone; DMA, *N*,*N*-dimethylacetamide; HMPA, hexamethylphosphoric triamide; THF, tetrahydrofuran.

2) T. Murachi "Protein, Nucleic Acid and Enzyme," ed by K. Imahori, N. Ui, T. Ohta, and K. Suzuki, Kyoritsu Shuppan, Tokyo (1982), Vol. 27, pp. 794—807.

3) K. Yokoyama, T. Tsuji, and T. Osawa "Protein, Nucleic Acid and Enzyme," ed by K. Imahori, N. Ui, T. Ohta, and K. Suzuki, Kyoritsu Shuppan, Tokyo (1982),

Vol. 27 pp. 985—1004.

4) M. Narita, K. Ishikawa, J. Y. Chen, and Y. Kim, *Int. J. Peptide Protein Res.*, **24**, 580 (1984).

5) J. E. Coligan, T. J. Kindt, H. Uehara, and S. G. Nathenson, *Nature*, **291**, 35 (1981).

6) C. S. Wright, R. A. Alden, and J. Kraut, *Nature*, **221**, 235 (1969).

7) E. P. Reddy, R. K. Reynolds, E. Santos, and M. Barbacid, *Nature*, **300**, 149 (1982).

8) IUPAC-IUB Commission on Biochemical Nomenclature, *Biochemistry*, **6**, 362 (1967).

9) H. G. Khorana, G. E. Gerber, W. C. Herlihy, C. P. Gray, R. J. Anderegg, K. Nihei, and K. Biemann, *Proc. Natl. Acad. Sci. U. S. A.*, **76**, 5046 (1979).

10) M. Narita, M. Doi, H. Sugasawa, and K. Ishikawa, *Bull. Chem. Soc. Jpn.*, **58**, 1473 (1985).

11) M. Narita, K. Ishikawa, H. Sugasawa, and M. Doi, *Bull. Chem. Soc. Jpn.*, **58**, 1731 (1985).

12) J. C. Sheehan and G. P. Hess, *J. Am. Chem. Soc.*, **77**, 1067 (1955); H. G. Khorana, *Chem. Rev.*, **53**, 145 (1953).

13) W. König and R. Geiger, *Chem. Ber.*, **103**, 788 (1970).

14) T. Miyazawa and E. R. Blout, *J. Am. Chem. Soc.*, **83**, 712 (1961).

15) W. H. Moore and S. Krimm, *Proc. Natl. Acad. Sci. U.S.A.*, **72**, 4933 (1975).

16) N. Y. Chirgadze and N. A. Nevskaya, *Biopolymers*, **15**, 627 (1976).

17) G. R. Marshall, "Intra-Science Chemistry Report," ed by N. Kharasch, Gordon and Breach, New York (1971), Vol. 5 pp. 305—316; A. W. Burgess and S. J. Leach, *Biopolymers*, **12**, 2599 (1973); Y. Paterson, S. M. Rumsey, E. Benedetti, G. Nemethy, and H. A. Scheraga, *J. Am. Chem. Soc.*, **103**, 2947 (1981).

18) M. Palumbo, S. D. Rin, G. M. Bonora, and C. Toniolo, *Makromol. Chem.*, **177**, 1477 (1976); E. Benedetti, A. Bavoso, B. D. Blasio, V. Pavone, C. Pedone, C. Toniolo, G. M. Bonora, and M.Crisma, *Int. J. Peptide Protein Res.*, **22**, 385 (1983); E. Benedetti, A. Bavoso, B. D. Blasio, V. Pavone, C. Pedone, M. Crisma, G. M. Bonora, and C. Toniolo, *J. Am. Chem. Soc.*, **104**, 2437 (1982); G. M. Bonora, C. Toniolo, B. D. Blasio, V. Pavone, C. Pedone, E. Benedetti, I. Lingham, and P. Hardy, *J. Am. Chem. Soc.*, **106**, 8152 (1984).

19) M. T. Leplawy, D. S. Jones, G. W. Kenner, and R. C. Sheppard, *Tetrahedron*, **11**, 39 (1960).

20) T. Imae, K. Okahashi, and S. Ikeda, *Biopolymers*, **20**, 2553 (1981).

21) M. Narita, K. Ishikawa, H. Nakano, and S. Isokawa, *Int. J. Peptide Protein Res.*, **24**, 14 (1984).

22) P. Y. Chou and G. D. Fasman, *Biochemistry*, **13**, 211 (1979).

23) J. E. Coligan, T. J. Kindt, H. Uehara, J. Martinko, and S. G. Nathenson, *Nature*, **291**, 35 (1981).

24) C. S. Wright, R. A. Alden, and J. Kraut, *Nature*, **221**, 235 (1969).

25) R. Katakai and Y. Nakayama, *J. Chem. Soc., Chem. Commun.*, **1977**, 805; R. Katakai, *J. Am. Chem. Soc.*, **99**, 232 (1977); C. Toniolo, G. M. Bonora, and M. Mutter, *Int. J. Biolog. Macromolecules*, **1**, 188 (1979).

Functionalized Dithia(2,5)pyridinophanes as Vitamin B_6 Analogues. Synthesis, Properties, and Catalytic Activity for Racemization Reaction

Masaaki IWATA* and Hiroyoshi KUZUHARA
Riken (The Institute of Physical and Chemical Research), Wako, Saitama 351-01
(Received February 6, 1985)

Exploration of synthetic routes to achieve designed vitamin B_6 models on the structural basis of functionalized dithia(2,5)pyridinophanes from pyridoxine hydrochloride was undertaken and the catalyst potency for a racemization reaction was examined in comparison with that of pyridoxal. By the reaction of 3,4′-*O*-isopropylidenepyridoxine 2′,5′-dichloride with α,ω-dithiols, dithia(2,5)pyridinophanes were synthesized in good yields. For dithia[3]paracyclo[3](2,5)pyridinophanes, juncture sulfur atoms were extruded photochemically, whereas 2,(n+3)-dithia[m](2,5)pyridinophanes incompletely extruded sulfur atoms under various conditions. Because of instability and low preparative yield of 15-hydroxy-16-formyl[2]paracyclo[2](2,5)pyridinophane, dithia-containing phanes, (n+9)-hydroxy-(n+10)-formyl-2,(n+3)-dithia[m](2,5)pyridinophanes [**26a** (n=4), **26b** (n=6), **26c** (n=8); m=n+4], 17-hydroxy-18-formyl-2,11-dithia[3]paracyclo[3](2,5)pyridinophane (**27**), and an acyclic congener for **26a**, 5′-deoxy-2′,5′-bis(ethylthio)pyridoxal (**28**), were eventually prepared in high yields by use of manganese dioxide in the presence of a primary amine. It was found on the basis of ^{1}H-NMR spectral analyses that the rotations of pyridine rings in some molecules, **26a**, **26b**, and **27** with ring sizes equal to or less than fourteen were restricted. The racemization potency of **26a—c**, **27**, and **28** for sodium hydrogen L-glutamate demonstrated that these are 1.4- to 1.7-fold more potent than pyridoxal itself under certain conditions (pH 10.0, 25±0.5 °C) until *ca.* 80% completion of the racemization reaction. **26a** was found to be quite stable (no decomposition), but the others, **26b**, **26c**, and **28**, indicated 14, 8, and 12% decomposition, respectively. **27** was so unstable that a 63% decomposition was marked at the time of 56% completion of the racemization reacion.

Racemization, transamination, decarboxylation, replacement, condensation, and elimination of amino acids (depending on the system requirements in the biological systems) are mediated by coenzyme B_6 through a common intermediate, the Schiff base (**1a**).[1] Various chemical model systems for this coenzyme have been devised so far to elucidate the coenzyme function. It is convinced that (a) **1b** mimics all types of reactions *via* **1a**,[2-7] (b) 3-hydroxy-4-pyridinecarbaldehyde[8] and salicylaldehydes[9] may be pyridoxal substitutes, and (c) most of the nonenzymic reactions are catalyzed by metal ions[3c,4,9] and imidazole,[8] or in a cationic micelle without metal ions.[10] The distinct difference between the enzymic and nonenzymic reactions investigated so far is that the former proceeds in a stereospecific manner regarding amino acids (assisted by the protein backbone of the enzyme)[1b-f] and that a stereospecific catalyst is lacking in the latter.[11]

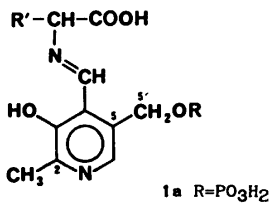

1a R=PO_3H_2
b R=H

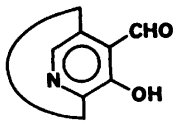

2

Along the line of our continuing interest in chemical congeners to B_6-coenzymes,[9c,12] we started to construct functionalized dithia(2,5)pyridinophanes **2** nearly a decade ago, which were expected to function as a stereospecific vitamin B_6-like catalyst through a mechanism. This includes a bridged chain with a specified length to provide a restricted rotation of the molecule (inducing planar chirality) and functional groups to act in the same way that the catalytic sites of vitamin B_6 do in biological systems. Through a series of experiments since then, this type of molecular design has been found to be very promising regarding alternative enantioselective catalysts. Evidence has been produced in successful studies concerning the optical resolution,[13a-d] the stereoselective racemization of α-amino acids,[13a] enantioselective transamination to α-keto acids,[13e-g] and the stereospecific α-deuteration of α-amino acids.[13h] The present report deals with a synthetic elaboration regarding the exploration of prototypes of pyridoxal-like (dithia)(2,5)pyridinophanes (which are routinely employed now). Also, the properties of the pyridinophanes have been scrutinized and an examination of catalytic activities for the racemization reaction of L-glutamate in terms of racemate catalysts (including the details of preliminary reports)[13a,i,j] was carried out.

Results and Discussion

Synthesis. Syntheses of the target molecules, **21**, **26**, and **27**, were achieved through sequences of

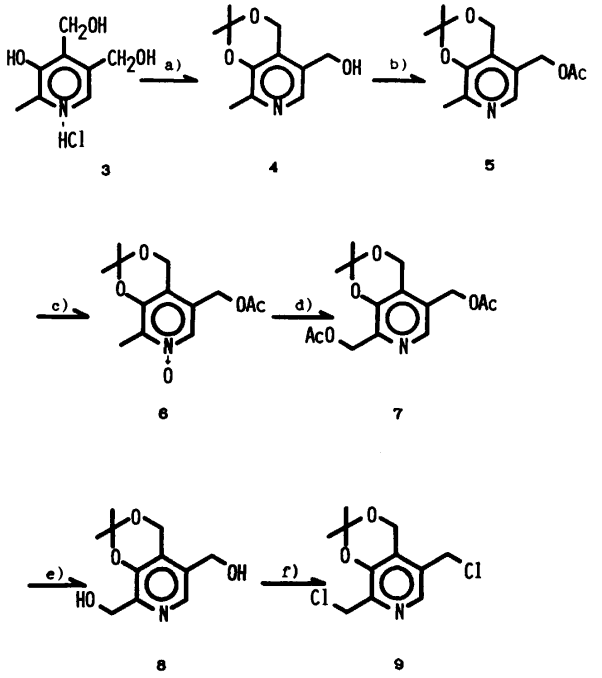

Scheme 1. Modification of C_2- and C_5-Positions of Pyridoxine; (a) i) acetone/HCl, ii) $NaHCO_3$ (Yield of **4**, 95%). (b) Ac_2O–Pyridine (**5**, 93%). (c) *m*-CPBA (**6**, 98%). (d) Ac_2O at 80—90 °C. (e) i) $NaOCH_3$/MeOH, ii) CO_2 (**8**, 83%). (f) i) $SOCl_2$, ii) $NaHCO_3$ (**9**, 98%).

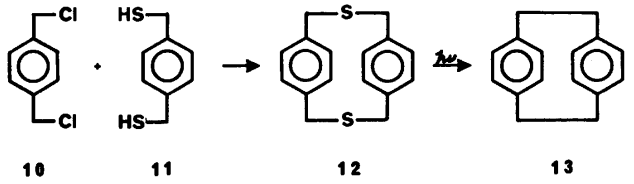

Scheme 2. Preliminary Attempts of Coupling and Photochemical Extrusion of Sulfur Atoms.

reactions which will be described in the following order; (1) modification of the C_2- and C_5-positions of pyridoxine (Scheme 1), (2) the coupling reaction of the modified pyridoxine with α,ω-dithiol (Scheme 3), taking into account preliminary attempts (Scheme 2), (3) the photochemical extrusion of sulfur atoms from the coupling product (Scheme 4) and (4) oxidation with manganese dioxide (Scheme 5).

Modification of the C_2- and C_5-positions of pyridoxine to give the first stable key intermediate (**8**) was attained by a different route from that reported.[14] Pyridoxine hydrochloride (**3**) was treated with dry acetone–hydrogen chloride followed by neutralization with sodium hydrogencarbonate to yield 3,4′-*O*-isopropylidenepyridoxine (**4**)[15] which was converted by acetylation to 5′-acetyl-3,4′-*O*-isopropylidenepyridoxine (**5**) (Scheme 1). Oxidation of **5** with *m*-chloroperbenzoic acid (*m*-CPBA) gave the corresponding *N*-oxide (**6**) in high yield. This was rearranged in a mixture of chloroform and acetic anhydride to 2′-acetoxy-5′-acetyl-3,4′-*O*-isopropylidenepyridoxine (**7**). A hydrolysis of **7** with sodium methoxide in methanol was accomplished to afford a key intermediate, 2′-hydroxy-3,4′-*O*-isopropylidenepyridoxine (**8**)[14] in 70% total yield based on **3**. Another key intermediate **9** was quantitatively obtained by the direct chlorination of **8** with thionyl chloride, after several unsatisfactory attempts with triphenylphosphine–carbon tetrachloride[16] or with thionyl chloride–pyridine. Unfortunately, however, **9** was relatively unstable ($t_{1/2}$ *ca.* 1 d), and, thus, the next coupling reaction had to be executed soon after its preparation.

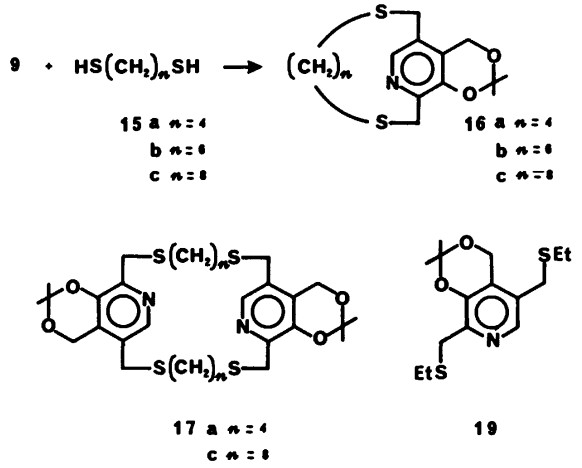

Scheme 3. The Coupling Reaction of the Modified Pyridoxine with α,ω-Dithiol.

In order to prepare bridged compounds connected by heteroatoms from **8** or **9** in good yield, several attempts using *p*-xylene derivatives as model compounds were performed (Scheme 2). The coupling trial employing **8** and α,α'-dichloro-*p*-xylene (**10**) mediated by sodium hydride as a base trigger in dioxane was quite unsuccessful under any condition. Then, in an effort to seek out the appropriate counterparts for the bridge resulted in finding efficient conditions to couple *p*-xylene-α,α'-dithiol (**11**)[17] with **10**. A mixture of **10** and **11** in ethanol was added to sodium ethylate in an ethanol solution (highly diluted).[18] The resulting 2,11-dithia[3.3]-paracyclophane (**12**)[19] had a sulfur atom juncture which may benefit the preparation of [2.2]paracyclophane (**13**) through a photochemical extrusion of the sulfur atoms.[20] Practically, **12** was photochemically desulfurized to **13** by triethyl phosphite in benzene with a high-pressure mercury lamp in 55% yield.

These perspectives through model reactions were put into practice by use of the dichlorides, **9** and **11**, which were successfully coupled to afford 17,18′-*O*-isopropylidene-17-hydroxy-18-hydroxymethyl-2,11-di-

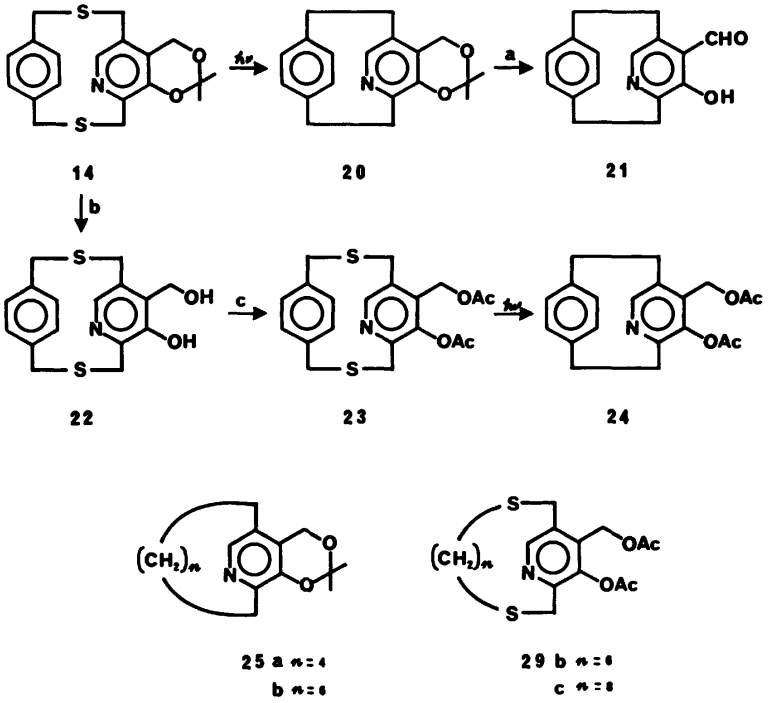

Scheme 4. Photochemical Extrusion of Sulfur Atoms from the Coupling Product; **a** $(C_6H_5)_3C^+BF_4^-$. **b** H_3O^+. **c** Ac_2O–pyridine.

thia[3]paracyclo[3](2,5)pyridinophane (**14**) by a high-dilution method. Likewise, **9** was condensed with α,ω-alkanedithiol (**15**) to give 2,(n+3)-dithia[m](2,5)-pyridinophane (n=4, 6, 8; m=n+4) (**16**) in fairly good yields, with the concomitant formation of the corresponding dimer **17**. The susceptibility of a reactive intermediate **9** to a nucleophilic attack was further exemplified in a condensation with ethanethiol (**18**) to yield 5′-deoxy-2′,5′-bis(ethylthio)-3,4′-*O*-isopropylidenepyridoxine (**19**) (95% based on **8**). This can be a reference open-chain compound relevant to **16a** for a comparison of the catalytic potency.

A photochemical extrusion of the juncture sulfur atoms from **14** yielded **20** (83%) under conditions similar to those aforementioned for **12**. The acetate derivative (**23**) which was obtained through the hydrolysis of **14** was likewise desulfurized to **24** (59%, based on **23**) (Scheme 4). However, this extrusion method regarding the sulfur atom was not satisfactorily applicable to cyclophanes, **16a** and **16b**, and their acetate derivatives **29b**,c (see Experimental). In addition, although the sulfur-extruded cyclophane (**20**) was directly oxidized to the corresponding aldehyde (**21**) by means of a reagent, triphenylmethylium tetrafluoroborate,[21] we had to abandon this type of paracyclophane as a target molecule because of the low yield of **21** (only 7%, based on **20**) and with an unexpected instability ($t_{1/2}$ *ca.* 15d). Therefore, we had to change our tentative target toward direct functionalization as embodied in pyridoxal without desulfurization and with the alternative oxidation method.

Manganese dioxide seemed promising as an alternative oxidant since numerous examples exemplified so far had shown the practical usefulness of this oxidant for the oxidation of α,β-unsaturated alcohols,[22] including pyridoxine derivatives.[23] Therefore, newly prepared active manganese dioxide[24] was applied to the oxidation of the acid-hydrolyzed products of the isopropylidene derivatives (**16b** and **16c**) which are potentially pyridoxine-like. Unfortunately, however, the product yields of **26b** and **26c** remained less than 18 and 16%, respectively. The reason for such low yields might be due to an inadequate preparation of the active manganese dioxide and/or chosen reaction conditions referring to those reported, and/or due to the substrate selectivity of manganese dioxide. A number of trials were carried out which resulted in the conclusion that all these possible causes operated together. The requisite construction of the tentative target encouraged us to develop a new preparative oxidation system.

Recently, we have reported that pyridoxine is oxidized in practical synthetic yield with commercially available manganese dioxide in the presence of a primary amine. We proposed that the oxidation proceeds on the amine-manganese dioxide complex[25] through a probable bimolecular oxidation mechanism.[26,27] The product prepared through the amine-mediated oxidation is the corresponding Schiff base

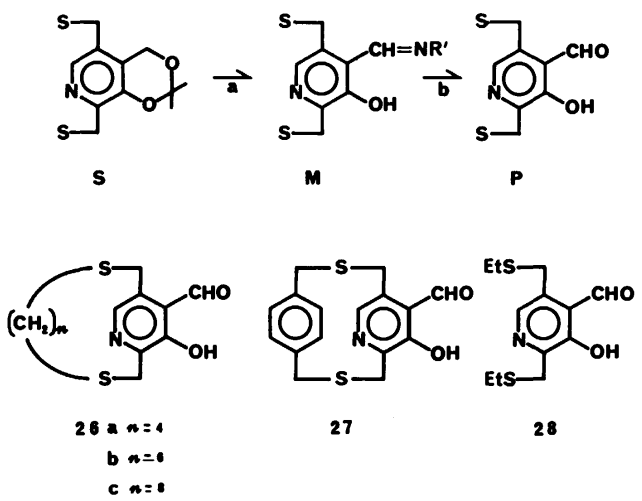

Scheme 5. Oxidation, Mediated by Primary Amine, with Commercial Manganese Dioxide; **a** i) H_3O^+, ii) MnO_2/R'-NH_2. **b** H_3O^+.

Table 1. Effect of amine on MnO_2 oxidation of **16b,c**

Amine[a]	Yield/% of M[b] 16b	16c	Yield/% of P[b] 16b	16c
—	—	—	18(39)[c]	16(71)
$ArNH_2$	49(1.3)	38(1)	—	—
DAPA	—	—	71(1)	51(2)

a) $ArNH_2$; *p*-phenetidine hydrochloride, DAPA; 3-(dimethylamino)propylamine. b) Based on **S**. c) Reaction time (h) is shown in parentheses.

of the pyridoxal. In addition, we have found that Schiff bases prepared from amines with strong basicity can transfer the methylene moiety to amines with relatively weaker basicity.[25] The trend of this transimination is, in principle, compatible to those found by Jencks[28a] and Leussing.[28b] The "basicity-dependent transimination" has been successfully applied to the direct *in situ* resolution of phanes in the treatment of a Schiff base prepared from phane and 3-(dimethylamino)propylamine (DAPA) with an amino sugar.[13a]

These findings made it possible to overcome synthetic problems in the oxidation of the present compounds. The pertinent results are given in Table 1, in which the same remarkable trend as found regarding the oxidation of pyridoxine[25] (that the product yields are increased 4—5 fold in the presence of a primary amine) is substantiated. Likewise, strained compounds like **14** and **16a** and an unstrained molecule **19** (*vide infra*) (**S**) were satisfactorily oxidized (Scheme 5) to corresponding pyridoxal-type compounds (**P**), **26a**—c, **27**, and **28**, by use of DAPA as a coexisting amine (Table 2). It is noteworthy that the juncture sulfur atoms were unaffected during the oxidation process.

Table 2. Synthesis of pyridoxal analogues from the corresponding acetals according to Scheme 5 by use of DAPA as a primary amine

S	Time[a]/h	P	Yield/%[b]
16a	1.5	**26a**	42
16b	1	**26b**	71
16c	2	**26c**	51
14	3	**27**	41
19	1.2	**28**	78

a) Reaction time for conversion of **S** to **M**. b) Based on **S**.

Properties. It is of special interest to scan the properties in the light of the determination of the possible upper-limit length for the restricted rotation depending on the length of the bridged chain and of the general catalytic activity of such modified pyridoxal compounds with heteraphane structures.

In contrast to carba(2,5)pyridinophanes,[29] dithia-(2,5)pyridinophanes offer certain advantages for ^{1}H-NMR spectral studies regarding the restricted rotation as well as the sulfur analogues of metacyclophane.[30] The incorporation of a sulfur atom into the β-position of the benzene ring not only simplified the methylene signals at the α-position by eliminating the complex spin-spin coupling with the other methylene groups, but also shifted them to a sufficiently lower field, allowing them to be observed separately from the other methylene signals.[30] Therefore, the existence of a restricted rotation can be simply judged from an observation of whether or not the proton signal of the α-methylene group of the pyridine ring is split into an AB quartet.

The chemical shifts and coupling constants of the focused α-methylene, formyl, and hydroxyl protons for the final products, **26a**—c and **27**, are summarized in Table 3, and refer to the related simpler compounds, **12**, **13**, and **28**. Chemical shifts of the signals with AB spin systems in Table 3 were adjusted, according to the general method of NMR analysis,[31] based on those observed on the spectral chart. Additionally, signal assignments were elaborated on the basis of numerous reference compounds synthesized through the present study. In Fig. 1, the representative spectral aspect of the methylene proton signals contiguous to heteroatoms and to the pyridine ring is illustrated for the isopropylidene derivatives, **14** and **16a**—c.

The appearance of the spin-spin couplings of the α-methylene protons of **26a,b**, and **27** split into AB quartets is a measure of the restricted rotation of the bridge chain due to an unsymmetrical magnetic field effect on those nuclei. As for the chemical shifts of formyl and hydroxyl protons, it was indicated that the greater conformational strain becomes, the more

TABLE 3. ^{1}H NMR DATA REFERRED TO METHYLENE, FORMYL AND HYDROXYL PROTONS[a)]

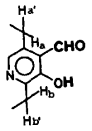

TABLE 3. ^{1}H NMR DATA REFERRED TO METHYLENE, FORMYL AND HYDROXYL PROTONS[a)]

Compd	Size	Ha-C-Ha'		Hb-C-Hb'		CHO	OH	*J*aa'	*J*bb'
12	14	3.82				—	—	—	—
13	12	3.10				—	—	—	—
26a	12	3.68	4.21	3.72	4.27	10.41	11.68	12.3	13.5
26b	14	3.76	4.17	3.78	4.20	10.56	11.68	12.8	14.0
26c	16	3.90		3.99		10.63	11.63	—	—
27	14	3.76	4.26	3.81	4.21	10.43	11.43	14.3	15.8
28		3.90		3.92		10.50	11.53	—	—

a) Measured in $CDCl_3$ at 24°C; δ in ppm and J in Hz.

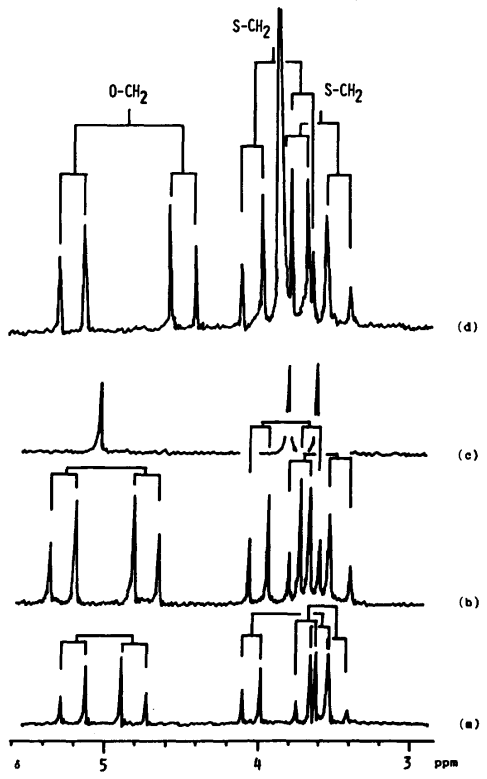

Fig. 1. ^{1}H NMR Spectra of the Methylene Protons between Hetero (O or S) Atoms and the Pyridine Ring; (a) for **16a** (n=4, 12-membered ring), (b) for **16b** (n=6, 14-membered ring), (c) for **16c** (n=8, 16-membered ring), and (d) for **14** (14-membered ring).

an upper-field shift is induced for the formyl proton of **26a**—c, but the hydroxyl protons behave independently. The α-methylene protons of the isopropylidene derivatives **14** and **16a**—**c** (Fig. 1) appear in a separate range, which benefits an ^{1}H-NMR analysis. The same tendency as that of the pyridoxal-type compounds **26a**—**c** and **27** is observable at a glance.

TABLE 4. THE UV-VIS SPECTRAL DATA IN ETHANOL; λ_{max} IN nm (ε IN $M^{-1}\,cm^{-1}$)

26a	**26b**	**26c**	**27**
207 (15000)	206.5 (16100)	208 (14100)	206.5 (19000)
227 (11500) sh	221.5 (13000) sh	223 (10400) sh	241 (8300) sh
247 (8700)	244 (8300) sh	300 (3900)	295 (2100) sh
313 (2800)	301.5 (3100)	348 (2100)	380 (2100)
364 (3800)	361.5 (3700)		

The investigation of the temperature dependence of the spin-spin interaction is a subject related to the practical optical resolution of enantiomers. For this purpose, the ^{1}H-NMR spectra of **14**, **16a**,**b**, and **26b** were recorded in $CDBr_3$ at 10°C intervals up to 120°C while monitoring the AB quartets as markers. Within the temperature range examined, all the AB quartets of the α-methylene protons remained uncolapsed together with unchanged chemical shift differences while participating in the spin-spin interaction. Thus, the conformation of the compounds with the AB quartet signals is found to be fairly rigid and the energy barrier for free rotation is estimated to be more than 15 kcal† mol^{-1}.[30] This suggests that these compounds could be resolved into each enantiomer by appropriate means. A congener of **26** has actually been resolved with an amino sugar.[13a,d]

The UV-VIS spectra of **26a**—c and **27** in ethanol are characterized by a ring strain (Table 4) as well as ^{1}H-NMR spectra. The absorption maxima appear-

† 1 cal_{th}=4.184 J.

Table 5. Racemization potency of pyridinophanes and related compounds for sodium hydrogen L-glutamate (pH 10.0 at 25±0.5 °C)

Catalyst	React. time /h	Final % racemi. completn	Time for 50% completn/h	$k_{obsd} \times 10^4$ min^{-1}	Catalyst dec/%
Pyridoxal	188	84	56	2.09	6.6 (288) [a]
26a	88	80	36	3.19	0 (325)
26b	96	65	37	3.13	14 (307)
26c	188	83	40	2.93	8 (305)
27	96	56	78	1.48	42 (243)
28	96	78	32	(3.58) [b]	12 (305)

a) λ_{max} used for O.D. change measurement. b) Estimated values, based on the plot.

ing at the longest wavelength show distinct red shifts with an augmentation of the extinction coefficient when the ring strain is increased. The red shifts are directly related to the sterically induced nonplanarity of the pyridine ring.[32] The tendency to increase the extinction coefficient with a shortening of the length of the carbon chain, may reflect the increment of the electron density around the formyl chromophore, which, in turn, may positively enforce the catalytic potency of these model compounds.

Catalytic Potency. The catalytic activities of the synthesized pyridinophanes, **26a—c** and **27**, were examined by a measure of the racemization ability for sodium hydrogen L-glutamate as a representative amino acid (chosen for its large rotatory power as in previous work).[9] These were referred to the less modified derivative **28** and pyridoxal as a standard reference. The reaction conditions were set, taking into account the catalyst solubility and those reported[9] (see Experimental). The analyzed results are collected in Table 5 and as a relative measure of catalytic activity, the times for 50% racemization completion are also listed. In addition, the evaluated apparent rate constants for **26b** and **28** are shown on the basis of less-scattered values of k_{obsd} (see Experimental). The results clearly reveal that **26a** is the best catalyst among those investigated. This showed superior properties to those of pyridoxal, with respect to catalytic activity (1.5 fold more active) and to stability (no decomposition) in contrast to an open-chain congener **28**. This compound is highly strained, as shown in ^{1}H-NMR and UV-VIS spectra and, thus, is a promising enantioselective catalyst. Structurally, the same is embodied in **26b** and **27**, but **27** is less active than pyridoxal and outstandingly labile, on one hand. On the other hand, **26b** might have a complex reaction mechanism (suggested by an observation of a nonlinear optical rotation change with considerable catalyst instability). It is of interest to note that less-strained or unstrained compounds, **26c** and **28**, are even more active than pyridoxal with a comparable decomposition each other.

In conclusion, the present results demonstrate that (a) the bridging between C_2- and C_5-positions by suitable chains afforded many advantages over natural vitamin B_6, especially, with respect to catalyst stability and catalytic effectiveness, (b) the π-donor-acceptor interaction between the bridged chain and the pyridine ring decreases the catalytic activity and catalyst stability, and (c) the torsion of the pyridine ring working as an electron sink has no effect on rate enhancement. It would be of interest to extend the present investigation to the construction of better model compounds which might intramolecularly provide suitable groups to efficiently affect the proton abstraction-addition process on the α-carbon of α-amino acid in a transition state.

Experimental

Apparatus. The IR spectra were obtained with a Shimadzu IR-27 spectrophotometer, the UV-VIS measurements (λ_{max}) with a Hitachi 124 spectrophotometer, ^{1}H-NMR spectra with a Varian HA-100D instrument, using TMS as an internal standard, and the optical-rotation measurements with a Perkin-Elmer 241MC polarimeter. The mass spectra (MS) and the exact mass measurements were obtained with a Japan Electron Optics Lab. Model JMS-OISG instrument. The melting points were recorded with a micro-melting apparatus, Yanagimoto Seisakusho, ser. No. 2647. The photochemical reaction was carried out with a high-pressure mercury lamp, UVL-100p (100 W), Rikoh Kagaku Co., Ltd. The elemental analyses were performed by the staff of the Organic Microanalysis Lab. in this Institute.

Materials. Pyridoxine hydrochloride, *m*-chloroperbenzoic acid, thionyl chloride, α,α'-dichloro-*p*-xylene (**10**), triphenylmethylium tetrafluoroborate, triethyl phosphite, 3-(dimethylamino)propylamine (DAPA), α,ω-alkanedithiols (**15a—c**) and ethanethiol were obtained commercially. The preparation of *p*-xylene-α,α'-dithiol (**11**) was performed according to a reported method;[17] 90% yield, colorless crystals, mp 42—44 °C (lit,[33] 46—47 °C). Pyridoxine was prepared by neutralization of the corresponding commercial hydrochloride with sodium hydrogencarbonate followed by azeotropic distillation of water with 1-propanol and by trituration into pyridine. For a separation of the products using column chromatography, Merck Art 7734 (E. Merck,

Darmstadt) silicagel was used. For the detection of the product and for monitoring the reaction by thin-layer chromatography (TLC), a Wakogel B-5 FM (Wako Pure Chem. Ind.) was employed. The following solvent systems were used for column chromatography and TLC unless otherwise stated; benzene:acetone=10:1 v/v (solvent BA1), 9:1 v/v (solvent BA2), 5:1 v/v (solvent BA3), 4:1 v/v (solvent BA4), 5:2 v/v (solvent BA5); chloroform:methanol=95:5 v/v (solvent CM1), 9:1 v/v (solvent CM2). Chemical shift (δ) and coupling constants (J) in ^{1}H-NMR spectrum (in $CDCl_3$) are shown in ppm and Hz, respectively.

Synthesis of 8 from 3 (Scheme 1). The acetonation of pyridoxine hydrochloride (**3**) was achieved by a method reported by Korytnyk and Ikawa[34] in 92% yield. The subsequent treatment of a suspended mixture of 55.1 g of 3,4′-*O*-isopropylidenepyridoxine hydrochloride, colorless crystals, mp 216—217 °C (dec) (lit,[15] 210—212 °C (dec). 217—218 °C (dec)[35]), in water with sodium hydrogencarbonate yielded 45.1 g (96%) of HCl free **4**, mp 118—120 °C (lit, 111—112 °C,[15] 113—115 °C,[35] 108—109 °C[36]), which, in turn, was acetylated by acetic anhydride–pyridine (1:1 v/v) at ambient temperature to give 5′-acetyl-3,4′-*O*-isopropylidenepyridoxine (**5**) in 93% yield, after a usual work-up; colorless liquid, R_f 0.5 (solvent BA3), IR (neat) $\nu_{C=O}$ 1740 cm^{-1}. The corresponding *N*-oxide (**6**) was obtained in 98% yield upon treatment of **5** with a slight molar excess of *m*-chloroperbenzoic acid in chloroform at ambient temperature. This was followed by neutralization with sodium acetate; colorless crystals, recryst, from diisopropyl ether, R_f 0.2 (benzene:acetone 2:1 v/v). In the mixed solution of chloroform and acetic anhydride (4:1 v/v) at *ca.* 50 °C, **6** was rearranged to 2′-acetoxy-5′-acetyl-3,4′-*O*-isopropylidenepyridoxine (**7**), R_f 0.8 (solvent CM1), in 98% yield with column chromatographic separation; colorless viscous liquid (R_f 0.5; chloroform:acetone 93:7 v/v), IR (neat) $\nu_{C=O}$ 1740 and ν_{st} 1420, 1380, 1365, 1220, 1060, 1025, and 855 cm^{-1}. At this stage, it was noted that the lower the reaction temperature was upon mixing an organic solvent such as $CHCl_3$, the better was the product yield and the darkening was less. The hydrolysis of **7** (3.05 g) with sodium (0.6 g) in methanol (40 ml) was followed by neutralization with solid carbon dioxide, then by the evaporation of the solvent and, subsequently, by filtration of the acetone solution, yielded 1.8 g (83%) of 2′-hydroxy-3,4′-*O*-isopropylidenepyridoxine (**8**), R_f 0.3 (solvent CM1); recryst. from acetone–diisopropyl ether, colorless needles, mp 119—122 °C (lit,[15] 110 °C); λ_{max} (EtOH) 281.5 nm; IR (KBr) ν_{OH} 3430, ν_{st} 1420, 1385, 1375, 1290, 1060, 1020, 1010, 900, 860, and 790 cm^{-1}.

Chlorination of 8. Chlorination with triphenylphosphine–carbon tetrachloride[16a] or DMF[16b] was unsuccessful. Then, several trials employing thionyl chloride–pyridine, changing the mole ratio 1:1 to 1:12, suggested that the greater the ratio becomes, the less the product yield of 5′-deoxy-2′,5′-dichloro-3,4′-*O*-isopropylidenepyridoxine (**9**). The reaction was monitored by TLC (R_f of **9**, 0.7 (solvent BA3)). Thus, it was eventually found that when 10—12 ml of thionyl chloride (cooled to 0 °C) was added all at once to 4.5 g of **8** (while being magnetically stirred in an iced-water bath). Stirring was continued for 30 min. The system was then equipped with a drying tube containing anhydrous calcium chloride and any excess of thionyl chloride was removed under reduced pressure. The mixture was neutralized by the addition of sodium hydrogencarbonate solution until no more carbon dioxide was generated and then extracted with ether. After a usual work-up, **9** was obtained in 91% yield (4.78 g) as yellow crystals; mp 89—91 °C. IR (KBr) ν_{st} 1415, 1385, 1380, 1305, 1280, 1250, 1205, 1135, 1060, 855, 760, and 715 cm^{-1}. On a smaller scale, the product yield became quantitative, by supressing decomposition during the work-up. However, **9** seemed to be not so stable that the next reaction was executed immediately after the preparation of **9**.

Attempts of Coupling and Photochemical Extrusion of Sulfur Atom (Scheme 2). Since the condensation of diol (**8**) with α,α'-dichloro-*p*-xylene (**10**) mediated by sodium hydride was unsuccessful in dioxane under any condition, the coupling of **10** with *p*-xylene-α,α'-dithiol (**11**) was examined under basic conditions. After 1.7 g (0.01 mol) of hot **10** in 20 ml of ethanol was rapidly added to a sodium ethylate solution prepared by 0.5 g (0.02 mol) of sodium in 50 ml of ethanol, containing 1.7 g (0.01 mol) of **11** the mixture was warmed for 3 h with stirring and precipitated a white solid (2.6 g) which was not the intended product. After it was filtered off, the filtrate contained a small amount of 2,11-dithia[3.3]paracyclophane (**12**), detected on TLC (R_f 0.6, benzene:cyclohexane 3:2 v/v). Thus, a 16-fold dilution[18] of the above reaction was carried out at ambient temperature to give 0.6 g (22%) of **12**, after chromatography with benzene; recryst. from benzene, mp 236.5—237.5 °C. Calcd for $C_{16}H_{16}S_2$: C, 70.54; H, 5.92; S, 23.54%. Found: C, 70.53; H, 5.70; S, 23.42%. MS *m/z* 272 (M^+) (base peak). ^{1}H-NMR ($CDCl_3$) δ=6.86 (8H, aromatic protons) and 3.82 (8H, $-CH_2-$). IR (KBr) ν_{S-CH} 1423; ν_{st} 1105, 850, 806, 758, 715, and 536 cm^{-1}. λ_{max} (EtOH) 255.5 nm.

According to a reported method,[20] a solution of 0.19 g of **12** and 20 ml of triethyl phosphite in 35 ml of benzene was irradiated using a high-pressure mercury lamp for 6 h while bubbling dry nitrogen gas. After the evaporation of the solvents *in vacuo*, the residue was recrystallized from ethanol to yield 80 mg (55%) of [2.2]paracyclophane (**13**) as colorless fine needles; mp 218—220 °C (lit,[37] 285—287 °C); MS *m/z* 208 (M^+) and 104 (base peak); λ_{max} (EtOH) 225 nm; R_f 0.8 (benzene:cyclohexane 3:2 v/v).

Coupling 9 with α,ω-Dithiols (Scheme 2). In a typical procedure, a mixture of 0.37 g (1.4 mol) of dichloride (**9**) and 0.3 g (1.76 mol) of dithiol (**11**) in 100 ml of ethanol was added (dropwise) over a period of 2.5 h to a 300-ml ethanol solution containing 0.1 g (4 mmol) of sodium in an ice-water bath while bubbling dry nitrogen gas. The mixture was then stirred overnight. After evaporating the ethanol, the residue was triturated with benzene and filtered. The filtrate was chromatographed on a silica-gel column eluted with benzene–acetone (7:2 v/v) then (5:2 v/v) to give 17-hydroxy-18-hydroxymethyl-17,18′-*O*-isopropylidene-2,11-dithia[3]paracyclo[3](2,5)pyridinophane (**14**) as colorless crystals; mp 194—196 °C. Calcd for $C_{19}H_{21}O_2S_2N$: C, 63.48; H, 5.89; S, 17.84; N, 3.90%. Found: C, 63.36; H, 5.92; S, 17.63; N, 3.75%. IR (KBr) ν_{st} 1423, 1406, 1383, 1372, 1295, 1244, 1200, 1135, 1059, 1049, 860, 725, and 543 cm^{-1}. λ_{max} (EtOH) (relative O.D. to the maximum absorption) 258—268 (broad, 0.95), 271.5 (0.97), 281 (1.0), and 306.5 (0.84) nm. ^{1}H-NMR ($CDCl_3$) δ=1.55 and 1.75 (3H each, s,

$C(CH_3)_2$) 3.51 and 3.75 (1H each, AB-q, J=14.9, $-CH_2-S$), 3.75, and 4.05 (1H each, AB-q, J=14.0, $-CH_2-S$), 4.53 and 5.24 (1H each, AB-q, J=16.5, $-CH_2-O$), 3.88 (4H, broad s, $-SCH_2-C_6H_4-CH_2S$), 6.95 (2H, broad d, J=8.0, Ar-H), 7.10 (2H, broad d, J=8.0, Ar-H), and 7.14 (1H, s, Ar_{py}-H). The spectral aspect of the methylene groups is depicted in Fig. 1. MS, metastable peaks appeared at m/z 138.2 for the fragmentation of m/z 197 to m/z 165 and at m/z 113.1 for m/z 166 to m/z 137.

The dropwise addition (3.5 h) of 1.9 g (7.3 mmol) of **9** and 0.82 g (6.6 mmol) of 1,4-butanedithiol (**15a**) in 100 ml of benzene to 400 ml of an ethanol solution containing 0.4 g (14 mmol) of sodium yielded 0.57 g (27% based on **8**) of **16a** and 0.68 g (19%, based on **8**) of the dimer of **16a**, (**17a**), after a similar work-up to the above was eluted with the solvent BA1 for column chromatography.

13-Hydroxy-14-hydroxymethyl-13,14′-*O*-isopropylidene-2,7-dithia[8](2,5)pyridinophane (**16a**); recryst. from diisopropyl ether as colorless crystals; mp 144.5—145.5 °C. R_f 0.55 (solvent BA1). Calcd for $C_{15}H_{21}O_2NS_2$: C, 57.84; H, 6.80; N, 4.50; S, 20.59%. Found: C, 57.59; H, 6.53; N, 4.50; S, 20.62%. IR (KBr) ν_{st} 1408, 1375, 1354, 1295, 1275, 1255, 1235, 1210, 1145, 1130, 1118, 1060, 1050, 855, 780, 730, 685, 665, and 565 cm^{-1}. λ_{max} (EtOH) (M^{-1} cm^{-1}); 211.5 (18900), 235sh (8100), and 303 (7700) nm. ^{1}H-NMR ($CDCl_3$); δ=1.61 (6H, s, $C(CH_3)_2$), 0.6—1.4 (4H, m, $-CH_2-$), 1.8—2.7 (4H, m, $-CH_2-$), 3.51 and 3.68 (1H each, AB-q, J=13.0, $-CH_2S$), 3.62 and 4.05 (1H each, AB-q, J=12.5, $-CH_2S$), 4.85 and 5.21 (1H each, AB-q, J=16.5, $-CH_2O$), and 7.81 (1H, s, Ar-H). The spectral aspect of the methylene signals is shown in Fig. 1. MS; m/z 311 (M+).

The corresponding dimer (**17a**), recryst. from benzene (minor) and diisopropyl ether (major); mp 149.5—150.5 °C. R_f 0.3 (solvent BA1). Calcd for $C_{30}H_{42}O_4N_2S_4$: C, 57.84; H, 6.80; N, 4.50; S, 20.59%. Found: C, 58.12; H, 6.68; N, 4.49; S, 20.59%. IR (KBr) ν_{st} 1410, 1375, 1293, 1250, 1200, 1135, 1063, 1050, and 845 cm^{-1}. λ_{max} (EtOH) (M^{-1} cm^{-1}), 209 (34200), 227.5sh (19000), and 290 (17200) nm. ^{1}H-NMR ($CDCl_3$) δ=1.55 (12H, s, $-C(CH_3)_2$), 1.4—1.6 (8H, m, $-CH_2-$), 2.2—2.6 (8H, m, $-CH_2-$), 3.51 (4H, s, $-CH_2S$), 3.75 (4H. s, $-CH_2S$), 4.95 (4H. s, $-CH_2O$), and 7.88 (2H, s, Ar-H). No signal shift or intensity change was observed until −30 °C in $CDCl_3$. MS: m/z 622 (M^+).

In a similar way, the reaction of 1.325 g (4.8 mmol) of 9 and 0.66 g (4.5 mmol) of 1,6-hexanedithiol (**15b**) in 100 ml of benzene with 400 ml of an ethanol solution containing two molar equiv. of sodium yielded 1.37 g (91%, based on **8**) of 2,9-dithia[10](2,5)pyridinophane (**16b**). This was isolated by silica-gel chromatography eluted with a solvent (BA1) as colorless crystals; R_f 0.5 (solvent BA1). mp 168—170 °C. Calcd for $C_{17}H_{25}O_2NS_2$: C, 60.14; H, 7.42; N, 4.13; S, 18.89%. Found: C, 59.88; H, 7.32; N, 3.86; S, 18.90%. IR (KBr) ν_{st} 1413, 1385, 1377, 1297, 1262, 1242, 1202, 1135, 1065, 1045, and 853 cm^{-1}. λ_{max} (EtOH) (M^{-1} cm^{-1}); 208 (19200), 228sh (8800), and 293 (8300) nm. ^{1}H-NMR ($CDCl_3$) δ=1.57 and 1.63 (3H each, s, $-C(CH_3)_2$), 0.4—1.4 (8H, m, $-CH_2-$), 1.8—2.7 (4H, m, $-CH_2-$), 3.50 and 3.73 (1H each, AB-q, J=13.5, $-CH_2S$), 3.66 and 4.04 (1H each, AB-q, J=12.5, $-CH_2S$), 4.77 and 5.29 (1H each, AB-q, J=16.5, $-CH_2O$), and 7.85 (1H, s, Ar-H). The spectral aspect of the methylene signals is depicted in Fig. 1.

Likewise, the reaction of 1.17 g (4.5 mmol) of **9** and 0.8 g (4.8 mmol) of 1,8-octanedithiol (**15c**) in 100 ml of benzene with 400 ml of an ethanol solution containing 0.21 g (8.96 mmol) of sodium yielded 1.27 g (78%, based on **8**) of 2,11-dithia[12](2,5)pyridinophane (**16c**), 0.26 g (8%, based on **8**) of the dimer of **16c**, **17c** (as colorless crystals), and a pale-yellow viscous liquid. They were isolated by silica-gel column chromatography eluted with a solvent (BA1).

16c showed R_f 0.4 (solvent BA1); mp 68.5—70 °C. Calcd for $C_{19}H_{29}O_2NS_2$: C, 62.09; H, 7.95; N, 3.81; S, 17.44%. Found: C, 62.08; H, 7.82; N, 3.82; S, 17.48%. IR (neat) ν_{st} 1410, 1385, 1875, 1296, 1275, 1240, 1200, 1140, 1062, 1049, and 860 cm^{-1}. λ_{max} (EtOH) (M^{-1} cm^{-1}); 208.5 (18800), 226sh (9700), and 292 (8400) nm. ^{1}H-NMR ($CDCl_3$) δ=1.57 (6H, s, $-C(CH_3)_2$), 0.95—1.5 (12H, m, $-(CH_2)_6-$), 2.40 (2H, t, J=6.5, CH_2-CH_2S), 2.60 (2H, t, J=6.5, CH_2-CH_2S), 3.59 (2H, s, $Ar-CH_2S$), 3.78 (2H, s, $Ar-CH_2S$), 5.01 (2H, s, CH_2O), and 7.92 (1H. s, Ar-H). The spectral aspect of the methylene signals is depicted in Fig. 1.

17c revealed R_f 0.25 (solvent BA1); Calcd for $C_{38}H_{58}O_4N_2S_4$: C, 62.09; H, 7.95; N, 3.81; S, 17.44%. Found: C, 62.80; H, 7.93; N, 3.62; S, 16.36%. IR (neat) ν_{st} 1410, 1385, 1375, 1295, 1275, 1240, 1200, 1138, 1062, 1047, and 856 cm^{-1}. λ_{max} (EtOH) (M^{-1} cm^{-1}); 208.5 (33700), 224.5sh (18400), and 291 (16000) nm. ^{1}H-NMR ($CDCl_3$) δ=1.56 (12H, s, $C(CH_3)_2$), 1.0—1.6 (24H, m, $-(CH_2)_6-$), 2.38 (4H, t, J=7.0, CH_2-CH_2S), 2.52 (4H, t, J=7.0, CH_2-CH_2S), 3.56 (4H, s, $Ar-CH_2S$), 3.79 (4H, s, $Ar-CH_2S$), 4.98 (4H, s, $Ar-CH_2O$), and 7.89 (2H. s. Ar-H).

In a similar treatment of the dichloride (**9**), prepared from 1.0 g (4.45 mmol) of **8**, and 0.9 g (8.9 mmol) of ethanethiol (**18**) in 50 ml of benzene with 200 ml of ethanol solution containing 0.21 g (8.9 mmol) of sodium for 1 h, 5′-deoxy-2′,5′-bis(ethylthio)-3,4′-*O*-isopropylidenepyridoxine (**19**) was prepared in 95% (1.35 g) yield, based on **8**; R_f 0.75 (solvent BA2), as a pale-yellow viscous liquid. Calcd for $C_{15}H_{23}O_2NS_2$: C, 57.47; H, 7.40; N, 4.47; S, 20.45%. Found: C, 57.44; H, 7.33; N, 4.47 S, 20.14%. IR (neat) ν_{st} 1410, 1380, 1370, 1292, 1270, 1236, 1197, 1135, 1055, and 852 cm^{-1}. ^{1}H-NMR ($CDCl_3$) δ=1.22 (3H, t, J=7.3, SCH_2CH_3), 1.25 (3H, t. J=7.3, SCH_2CH_3), 1.54 (6H, s, $C(CH_3)_2$), 2.45 (2H. q, J=7.3, SCH_2CH_3), 2.57 (2H, q, J=7.3, SCH_2CH_3), 3.55 (2H, s, $Ar-CH_2S$), 3.79 (2H, s, $Ar-CH_2$), 4.95 (2H, s, $Ar-CH_2O$), and 7.89 (1H, s, Ar-H).

Photochemical Extrusion of Juncture Sulfur Atoms (Scheme 4). The irradiation of 1.93 g (5.37 mmol) of **14** in a mixture of 350 ml of triethyl phosphite and 150 ml of benzene in an inlet-jacket with a high-pressure mercury lamp at tap-water temperature for 17 h (bubbling dry nitrogen gas throughout) yielded 1.31 g (83%, based on **14**) of [2]paracyclo[2](2,5)pyridinophane (**20**). This was isolated upon evaporation of solvents from the reaction mixture, silica-gel column chromatography eluted with a solvent (BA2). This resulted in a pale-yellow liquid; R_f 0.35 (solvent BA5). MS m/z 295 (M^+) and base peaks at m/z 155 and 182. Exact mass measurement; Calcd for $C_{19}H_{21}O_2N$, 295.157; Found 295.151. IR (neat) ν_{st} 1407, 1383, 1372, 1281, 1242, 1200, 1137, 1058, 1043, 1024, and 858 cm^{-1}. λ_{max} (EtOH) (O.D.); 252sh (0.884); 280sh (0.411), 290 (0.525), and 313.5 (0.515) nm. ^{1}H-NMR ($CDCl_3$) δ=1.32 and 1.68 (3H each, s, $C(CH_3)_2$), 3.00 (center) (8H, AA′BB′-m, $Ar-CH_2-CH_2-Ar$), 4.43 and 4.62 (1H each AB-q, J=16.0, $Ar-CH_2O$), 6.74 (center) (4H, AA′BB′-m, Ar-H),

and 7.39 (1H, s, Ar_{py}-H).

To obtain 17-acetoxy-18-acetoxymethyl-2,11-dithia[3]-paracyclo[3](2,5)pyridinophane (**23**), 0.5 g (1.39 mmol) of **14** was heated at 50 °C for 30 min with 24 ml of 2M-HCl(1 M=1 mol dm^{-3}), followed by neutralization by the addition of sodium hydrogencarbonate after cooling. The precipitate (**22**) was collected by filtration, washed several times with water and dried *in vacuo* over Drierite. The solid was treated with 10 ml of acetic anhydride in 30 ml of pyridine at the ambient temperature for 30 min, followed by evaporation under reduced pressure. After silica-gel chromatography eluted with benzene–acetone (85:15 v/v), the result was 0.45 g (80%, based on **14**) of **23**, as colorless viscous liquid which, then, became crystals by scrubbing; mp 115—116 °C, R_f 0.8 (solvent BA5). Calcd for $C_{20}H_{21}O_4S_2N$: C, 59.53; H, 5.25; N, 3.47; S, 15.89%. Found: C, 59.65; H, 5.29; N, 3.44; S, 15.71%. IR (neat) $\nu_{C=O}$ 1765 and 1740, ν_{st} 1425, 1407, 1370, 1220, 1185, 1027, and 680 cm^{-1}. λ_{max} (EtOH) (M^{-1} cm^{-1}); 207.5 (17800), 215sh (16400), 234sh (8100), 275 (3700), and 297.5sh (2200) nm. ^{1}H-NMR ($CDCl_3$) δ=1.95 (3H, s, $COCH_3$), 2.37 (3H, s, Ar-$OCOCH_3$), 3.81 and 4.09 (1H each, AB-q, J=16.1, Ar_{py}-CH_2-S), 3.83 (2H, s, Ar_{py}-CH_2S), 3.85 (2H, s, Ar-CH_2S), 3.89 (2H, s, Ar-CH_2S), 5.06 and 5.34 (1H each, AB-q, J=12.5, -CH_2O), 7.65 (1H, s, Ar_{py}-H), 6.93 (2H, broad d, J=8.0, Ar-H), and 7.07 (2H, broad d, Ar-H).

23 (0.4 g) in 250 ml of triethyl phosphite was irradiated at tap-water temperature (*ca.* 20 °C) for 9.5 h with a high-pressure mercury lamp. Dry nitrogen was bubbled throughout. After the removal of the solvent *in vacuo*, the residue was chromatographed on a silica-gel column eluted with a solvent (BA5) to give 0.2 g (59%, based on **23**) of 15-acetoxy-16-acetoxymethyl[2]paracyclo[2](2,5)pyridinophane (**24**) as colorless viscous liquid. MS; m/z 339 (M^+) and a base peak at m/z 155. Exact mass measurement; Calcd for $C_{20}H_{21}O_4N$, 339.147. Found, 339.151. IR (neat) $\nu_{C=O}$ 1765 and 1743, ν_{st} 1370, 1226, 1182, 1025, 970, 795, and 720 cm^{-1} λ_{max} (EtOH) (O. D.); 222 (2.73), 287 (0.437), and 307 (0.263) nm. ^{1}H-NMR ($CDCl_3$) δ=1.95 (3H s, $COCH_3$), 2.32 (3H, s, Ar-$OCOCH_3$), 3.09 (center) (8H, AA'BB'-m, -CH_2-CH_2-), 4.83 and 4.91 (1H each, AB-q, J=12.0, CH_2O), 6.71 (center) (4H, AA'BB'-m, Ar-H), and 7.75 (1H, s, Ar_{py}-H).

Photochemical reactions of **16a** (0.2 g) or **16b** (0.5 g) in a solution comprised of 50 ml of benzene and 200 ml of triethyl phosphite at *ca.* 20 °C (by circulating tap-water) under a nitrogen atmosphere for 4 h or 16 h, respectively, resulted in a slight disappearance of the starting materials (R_f 0.55 and 0.5, respectively) on TLC (solvent BA1). However, sulfur-extruded products are unisolable as a result of careful silica-gel chromatography. Then, both isopropylidene-cyclophanes (**16b,c**) were converted to the corresponding acetates **29b,c** in order to examine any alternative possibility regarding the photochemical extrusion of a sulfur atom.

16b (1.6 g, 4.7 mmol) was subjected to the same sequence of procedures as those for the preparation of **23** from **14** to yield 1.8 g (99%, based on **16b**) of 15-acetoxy-16-acetoxymethyl-2,9-dithia[10](2,5)pyridinophane (**29b**) as colorless crystals. These were recryst. from diisopropyl ether after a chromatographic separation by silica gel; R_f 0.6 (solvent BA1), mp 121—122 °C. Calcd for $C_{18}H_{25}O_4NS_2$: C,. 56.37; H, 6.57; N, 3.65; S, 16.72%. Found: C, 56.43; H, 6.54; N, 3.55; S, 16.72%. IR (KBr) $\nu_{C=O}$ 1770 and 1745, ν_{st} 1440, 1405, 1377, 1362, 1301, 1215, 1178, 1153, 1055, 1034, 1010, and 830 cm^{-1}. λ_{max} (EtOH) (M^{-1} cm^{-1}); 205.5 (14400), 221sh (10300), 240sh (5400), and 285 (6100) nm. ^{1}H-NMR ($CDCl_3$) δ=0.4—1.4 (8H, m, -(CH_2)$_4$-), 1.8—2.7 (4H, m, -CH_2CH_2S), 2.03 (3H, s, CH_2OCOCH_3), 2.40 (3H, s, Ar-$OCOCH_3$), 3.79 and 4.11 (1H each, AB-q, J=14.0, Ar-CH_2S), 3.82 (2H, s, Ar-H), 5.22 and 5.41 (1H each, AB-q, J=13.0, Ar-CH_2O), and 8.22 (1H, s, Ar-H).

29b (1.0 g) was irradiated in a solution comprising 50 ml of benzene and 200 ml of triethyl phosphite for 9 h. Dry nitrogen was bubbled throughout. However, the obtained product still included one sulfur atom. 0.15 g of **29b** was recovered by silica-gel chromatography.

16c (0.75 g, 2 mmol) was acetylated by a sequence of procedures similar to those for **23** from **14** to afford 0.79 g (94%, based on **16c**) of 17-acetoxy-18-acetoxymethyl-2,11-dithia[12](2,5)pyridinophane (**29c**) as a pale-yellow viscous liquid. This was isolated by silica-gel column chromatography eluted with a solvent (BA1) (R_f 0.5). Calcd for $C_{20}H_{29}O_4NS_2$: C, 58.37; H, 7.10; N, 3.40%. Found: C, 58.88; H, 6.77; N, 3.41%. IR (neat) $\nu_{C=O}$ 1775 and 1745, ν_{st} 1370, 1220, 1180, and 1028 cm^{-1}. λ_{max} (EtOH) (O.D.); 220sh (0.642), 241sh (0.30), and 283.5 (0.374) nm. ^{1}H-NMR ($CDCl_3$) δ=0.8—1.5 (12H, m, -(CH_2)$_6$-), 2.01 (3H, s, CH_2OCOCH_3), 2.37 (2H, t, J=6.5, CH_2CH_2S), 2.50 (2H, t, J=6.5 CH_2CH_2S), 2.38 (3H, s, Ar-$OCOCH_3$), 3.76 (2H, s, Ar-CH_2S), 3.90 (2H, s, Ar-CH_4S), 5.27 (2H, s, Ar-CH_2O), and 8.33 (1H, s, Ar-H).

29c (0.55 g, 1.3 mmol) in 200 ml of triethyl phosphite was irradiated for 28 h and monitored by TLC. After a work-up followed by a careful silica-gel chromatography eluted with the solvent BA1 (R_f 0.5). gave 80 mg (16%) of a product (R_f 0.45) with a concomitant recovery of the starting material **29c** (50 mg). The product showed MS, m/z 379 (M^+). Exact mass measurement; Calcd for $C_{20}H_{29}O_4NS$, 379.181. Found, 379.188. IR (neat) $\nu_{C=O}$ 1775 and 1750, ν_{st} 1224, 1188, and 930 cm^{-1}. λ_{max} (EtOH) (O.D.); 238sh (0.4) and 277 (0.52) nm. These spectral data suggest that only one sulfur atom is extruded from the starting diacetate **29c**.

Attempts at the oxidation of **20** with triphenylmethylium tetrafluoroborate was carried out as follows:[21] a mixture of 0.95 g (1.2 mmol) of **20** and 3.2 g (3 mol equiv) of triphenylmethylium tetrafluoroborate in 100 ml of dichloromethane was stirred at the ambient temperature under a nitrogen atmosphere for 18 h. This was followed by hydrolysis with a saturated sodium hydrogencarbonate solution. The organic layer was separated, dried over anhydrous magnesium sulfate, filtered through Celite (No. 545) and evaporated to dryness. The residue was chromatographed on a silica-gel column eluted with the solvent BA3 to yield 60 mg (7.4% based on **20**) of 15-hydroxy-16-formyl[2]paracyclo[2](2,5)pyridinophane (**21**) as yellow liquid; R_f 0.9 (benzene–acetone 3:2 v/v) and 0.8 (chloroform). MS; m/z 253 (M^+), 237 (M^+—16), and 225 (M^+—28) and base peaks at m/z 91 and 77. Exact mass measurement; Calcd for $C_{16}H_{15}O_2N$, 253.110. Found, 253.114. ^{1}H-NMR ($CDCl_3$) δ=9.94 (1H, s, CHO).

Oxidation with (Active) Manganese Dioxide (Scheme 5). General Procedure Prior to Oxidation. All the

pyridoxine-type cyclophanediols and related compounds were prepared from corresponding isopropylidene derivatives using acid hydrolysis as follows; the isopropylidene derivatives were heated at *ca.* 70 °C for 1—2 h with 2M-HCl (*ca.* 30 ml/g of the acetal) while being magnetically stirred. The reaction mixture, in which mostly diol hydrochloride was crystallized out as a white solid when the hydrolysis came closer to the terminal point (monitored by TLC), was neutralized with sodium hydrogencarbonate after cooling, followed by the evaporation of any water. The residue was triturated with ethanol and/or pyridine and filtered through Celite (No. 545). The filtrate was evaporated to dryness under reduced pressure to give a colorless solid which was subjected to manganese dioxide oxidation in the presence or absence of amine.

i) *Direct Oxidation with Active Manganese Dioxide.* Newly prepared active manganese dioxide (MnO_2*) (according to the method described by Attenburrow *et al.*)[24] was employed.

When the hydrolyzed product of **16b** (0.4 g, 1.18 mmol) was refluxed with MnO_2* (2.0 g) in chloroform (50 ml) for 23 h, followed by filtration through Celite (No. 545) on 3G sintered-glass filter, washed several times with hot ethanol and pyridine, the combined filtrate was evaporated to dryness and then chromatographed on a silica-gel column eluted with the solvent BA3 to yield 50 mg (14%, based on **16b**) of 16-formyl-15-hydroxy-2,9-dithia[10](2,5)pyridinophane (**26b**) with concomitant recovery of 40 mg (11%) of the starting diol. Obtained **26b** was recrystallized from acetone; R_f 0.75 (solvent BA5), mp 128—130 °C. Calcd for $C_{14}H_{19}O_2NS_2$: C, 56.53; H, 6.44; N, 4.71; S, 21.56%. Found: C, 56.64 H, 6.42; N, 4.39; S, 21.32%. IR (neat) $\nu_{C=O}$ 1653, ν_{st} 2930, 1375, 1295, 1240, 1195, 964, 728, 697, and 670 cm^{-1}. The UV-VIS data are shown in Table 4. ^{1}H-NMR data except for those listed in Table 3; 0.2—1.65 (8H, m, $-(CH_2)_4-$), 1.95—2.75 (4H, m, $-CH_2CH_2S$), and 7.95 (1H, s, Ar-H).

When a mixture of the hydrolyzed product from **16b** (0.4 g, 1.18 mmol) and MnO_2* (1.6 g) in benzene (50 ml) was refluxed with an azeotropic removal of the resulting water using Dean-Stark apparatus for 39 h, followed by filtration and washing as mentioned above, **26b** was obtained by silica-gel chromatography in 18% (50 mg) yield, based on **16b**. with a recovery of 70 mg (20%) of the diol.

After the diol obtained from the hydrolysis of **16c** (0.43 g) was oxidized with MnO_2* (1.5 g) in a mixed solvent of pyridine (5 ml) and chloroform (50 ml) and refluxed for 71 h, the reaction mixture was treated as mentioned above and chromatographed on a silica-gel column eluted with the solvent BA2 to yield 60 mg (16%, based on **16c**) of 18-formyl-17-hydroxy-2,11-dithia[12](2,5)pyridinophane (**26c**) as a pale-yellow liquid. This was crystallized spontanously at the ambient temperature; R_f 0.65 (solvent BA2), mp 68.0—69.5 °C. Calcd for $C_{16}H_{23}O_2NS_2$: C, 59.04; H, 7.12; N, 4.30; S, 19.70%. Found: C, 59.05; H, 7.12; N, 3.90; S, 19.67%. IR (neat) $\nu_{C=O}$ 1655, ν_{st} 2930, 1380, 1248, 1234, and 870 cm^{-1}. The UV-VIS data are listed in Table 4. ^{1}H-NMR data except for those shown in Table 3 are 0.8—1.7 (12H, m, $-(CH_2)_6-$), 2.40 (2H, t, J=7.5, CH_2CH_2S), and 8.04 (1H, s, Ar-H).

ii) *MnO_2* Oxidation in the Presence of* p-*Phenetidine Hydrochloride.* After the diol prepared by the hydrolysis of **16b** (0.3 g, 0.88 mmol) was refluxed with *p*-phenetidine hydrochloride ($ArNH_2$) (0.3 g, 1.6 mmol) and MnO_2* (1.5 g) in a mixed solvent of pyridine (10 ml) and chloroform (40 ml) for 64 h, filtered cooled, through Celite (No. 545) mounted on a 3G sintered-glass filter (the filtrate was evaporated), the residue was chromatographed on a silica-gel column eluted with a solvent BA3 to give 160 mg (39%, based on **16b**) of the Schiff base (**30b**). It comprised **26b** and $ArNH_2$ as red brown crystals, recryst. from benzene-diisopropyl ether; R_f 0.65 (solvent BA3), mp 173—174 °C. Calcd for $C_{22}H_{28}O_2N_2S_2$: C, 63.43; H, 6.77; N, 6.72; S, 15.39%. Found: C, 63.43 H, 6.74; N, 6.66; S, 15.20%. IR (KBr) $\nu_{C=N}$ 1615, ν_{st} 2920, 1510, 1390, 1305, 1292, 1250, 1043, and 836 cm^{-1}. λ_{max} (EtOH) (M^{-1} cm^{-1}); 204 (16200), 228 (15800), 295 (4200), 340sh (10900), 361 (13200), 373 (13300), and 390sh (11000) nm. ^{1}H-NMR ($CDCl_3$) δ=0.55—1.4 (8H, m, $-(CH_2)_4-$), 1.45 (3H t, J=6.95, $-CH_2CH_3$), 2.0—2.7 (4H, m, CH_2CH_2S), 3.80 and 4.25 (1H each, AB-q, J=12.78, $Ar_{py}-CH_2S$), 3.82 and 4.04 (1H each, AB-q, J=14.03, $Ar-CH_2S$), 4.10 (2H, q, J=6.95, OCH_2CH_3), 6.99 (2H, d, J=8.9, Ar-H), 7.40 (2H, d, J=8.9, Ar-H), 7.88 (1H, s, Ar_{py}-H), and 14.45 (1H, s, -OH).

Diol (0.05 g, 0.167 mmol), prepared by the hydrolysis of **16b**, was oxidized with MnO_2* (0.5 g) in the presence of $ArNH_2$ (0.1 g, 0.53 mmol) in a mixed solvent of pyridine (5 ml) and benzene (20 ml) while removing the resulting water (using a the Dean-Stark tube), and gave **30b** (70 mg, 99% yield based on the diol).

Diol (**22**) (0.1 g, 0.313 mmol), prepared by the hydrolysis of **14**, was oxidized with MnO_2* (0.7 g) in the presence of $ArNH_2$ (0.1 g, 0.53 mmol) in benzene (30 ml), refluxed for 12 h while removing the resulting water (using a Dean-Stark tube). The residue, after a work-up as mentioned above, was chromatographed on a silica-gel column eluted with a solvent (BA3) to give 55 mg (40%, based on **22**) of the Schiff base (**31**) composed of **27** and $ArNH_2$, as yellow-red fine needles, recryst. from benzene-diisopropyl ether; R_f 0.6 (solvent BA3), mp 243.5—244.5 °C (dec). Calcd for $C_{24}H_{24}O_2N_2S_2$: C, 66.03; H, 5.54; N, 6.42; S, 14.69%. Found: C, 66.11; H, 5.59; N, 6.27; S, 14.63%. IR (KBr) $\nu_{C=N}$ 1615, ν_{st} 1510, 1390, 1300, 1255, and 820 cm^{-1}. λ_{max} (EtOH) (O.D.); 240sh (0.597), 295sh (0.205), 350sh (0.497), 364 (0.525), and 400sh (0.330) nm. ^{1}H-NMR ($CDCl_3$) δ=1.46 (3H, t, J=7.1, OCH_2CH_3), 3.91 (2H, s, $Ar-CH_2S$), 4.97 (2H, s, $Ar-CH_2S$), 4.12 (2H, q, J=7.1, OCH_2CH_3), 3.85 and 4.08 (1H each, AB-q, J=14.56, $Ar_{py}-CH_2S$), 3.78 and 4.35 (1H each, AB-q, J=14.0, $Ar_{py}-CH_2S$), 6.86—7.46 (8H, m, Ar-H), 7.36 (1H, s, Ar_{py}-H), 9.04 (1H, s, -CH=N), and 14.13 (1H, s, -OH).

iii) *Oxidation with Commercial MnO_2 in the Presence of Amines.* The hydrolysis of each acetal was performed under the conditions mentioned above. The oxidation was carried out under the similar conditions to those described in a previous report,[25] unless otherwise noted. When $ArNH_2$ was used as a coexisting amine, the product was isolated in the form of the corresponding Schiff base (**M** in Scheme 5) by means of silica-gel chromatography. When 3-(dimethylamino)propylamine (DAPA) was employed as a coexistent amine, the resulting Schiff base (**M** in Scheme 5) was hydrolyzed with 0.3 M-HCl, monitored by TLC, followed by extraction with benzene-ethyl acetate. It was then isolated in the form of the corresponding pyridoxal-

type compound (**P** in Scheme 5) by means of silica-gel chromatography.

Diol (**22**), prepared by the hydrolysis of **14** (0.85 g, 2.36 mmol), was oxidized for 3 h with commercial MnO_2[38] (5 g) in the presence of DAPA (1.5 ml) in a mixed solvent of benzene (50 ml) and pyridine (20 ml). This was followed by filtration through Celite (No. 545), washing with hot pyridine, and evaporation of the filtrate. The residue was hydrolyzed with 0.3 M-HCl (40 ml) in benzene–ethyl acetate (1:1 v/v) (20 ml) for 40 min, carefully monitored by TLC (solvent BA2, R_f 0.4 for **27**, and solvent CM2, R_f 0.4 for the Schiff base **M**). The organic layer was separated and passed through a short column to remove the amine and residual water eluted with a solvent (BA2). The eluate was further chromatographed on a silica-gel column to yield 0.31 g (41%, based on **14**) of 18-formyl-17-hydroxy-2,11-dithia-[3]paracyclo[3](2,5)pyridinophane (**27**) as pale-yellow crystals; mp 218—219 °C (start browning near at 204 °C and then decomposed). Calcd for $C_{16}H_{15}O_2NS_2$: C, 60.54; H, 4.76; N, 4.41; S, 20.20%. Found: C, 60.43; H, 4.82; N, 4.39; S, 20.12%. IR (KBr) $\nu_{C=O}$ 1645, ν_{st} 1423, 1410, 1377, 1250, 970, and 723 cm^{-1}. The UV-VIS data are listed in Table 4. ^{1}H-NMR data except for those collected in Table 3 are 3.84 (2H, s, Ar-C$\underline{H}_2$S), 6.84—7.16 (4H, m, Ar-$\underline{H}$), and 7.42 (1H, s, Ar_{py}-$\underline{H}$).

Diol, prepared by the hydrolysis of **16a** (1.1 g, 3.54 mmol), was oxidized with MnO_2 (7.0 g) in the presence of DAPA in a mixed solvent of benzene (50 ml) and pyridine (20 ml) for 1.5 h, followed by filtration, washing with hot pyridine, and an evaporation of the filtrate. The residue in the benzene–ethyl acetate (1:1 v/v) (20 ml) was hydrolyzed with 0.3 M-HCl (60 ml), carefully monitored by TLC (solvent BA2, R_f 0.6 for **26a** and solvent CM2, R_f 0.4 for the Schiff base **M**). The organic layer was treated using the method mentioned above and by a chromatographic separation with silica gel eluted with a solvent (BA4), 0.4 g (42%, based on **16a**) of 14-formyl-13-hydroxy-2,7-dithia-[8](2,5)pyridinophane (**26a**) was obtained as pale-yellow crystals. These were spontaneously crystallized; mp 118—119.5 °C. Calcd for $C_{12}H_{15}O_2NS_2$: C, 53.51; H, 5.61; N, 5.20; S, 23.80%. Found: C, 53.74; H, 5.64; N, 5.03; S, 23.37%. IR (neat) $\nu_{C=O}$ 1655, ν_{st} 1385, 1297, 1240, 1223, 1110, 967, 755, 695, and 675 cm^{-1}. The UV-VIS data are listed in Table 4. ^{1}H-NMR data except for those listed in Table 3; 0.7—1.4 (4H, m, -(C$\underline{H}_2$)$_2$-), 1.6—2.8 (4H, m, SC$\underline{H}_2$C$\underline{H}_2$), and 7.87 (1H, s, Ar_{py}-$\underline{H}$).

Diol, prepared by the hydrolysis of **16b** (1.09 g, 3.22 mmol), in the mixed solvent of benzene (50 ml) and pyridine (20 ml) was oxidized with MnO_2 (7.0 g) in the presence of DAPA (2 ml) for 1 h. This was followed by the hydrolysis of the Schiff base (**M**) with 0.3 M-HCl and a similar work-up to that described above. This yielded 0.68 g (71%, based on **16b**) of **26b**; physical data and elemental analyses are described in section i) of this section.

Diol, propared by the hydrolysis of **16c** (1.14 g, 3.1 mmol), in the mixed olvent of benzene (50 ml) and pyridine (18 ml) was oxidized with MnO_2 (3.5 g) in the presence of DAPA (1.0 ml) for 2 h. This was followed by a similar work-up to that described above and yielded 0.48 g (51%, based on **16c**) of **26c**; physical data and elemental analyses are described in section i) of this section.

Diol, prepared by the hydrolysis of **16c** (0.27 g, 0.825 mmol), in benzene (30 ml), was oxidized with MnO_2 (0.72 g) in the presence of $ArNH_2$ (0.31 g, 1.65 mmol) for 1 h. This produced 0.14 g (38%, based on **16c**) of a Schiff base (**M**) composed of **26c** and $ArNH_2$. This was chromatographically isolated with eluting a solvent (BA3); R_f 0.7 (solvent BA3).

The oxidation of the diol, prepared by the hydrolysis of **16b** (1.33 g, 4.48 mmol), in benzene (100 ml) with MnO_2 (4.6 g) in the presence of $ArNH_2$ (1.7 g, 8.89 mmol) yielded 0.9 g (49%, based on **16b**) of the Schiff base (**M**) comprising **26b** and $ArNH_2$; physical data and elemental analyses are described in section ii) of this section.

The oxidation of the diol, prepared by the hydrolysis of **19** (1.26 g, 4 mmol), with MnO_2 (7 g) in the presence of DAPA (2 ml) in the mixed solvent of benzene (50 ml) and pyridine (20 ml) for 1.2 h, followed by the hydrolysis of the Schiff base (**M**) with 0.3 M-HCl and a similar work-up to that described for the preparation of **26a**. This yielded 0.85 g (78%, based on **19**) of 5′-deoxy-2′,5′-bis(ethylthio)pyridoxal (**28**), as yellow viscous liquid, after chromatography; R_f 0.8 (solvent BA2). Calcd for $C_{12}H_{17}O_2NS_2$: C, 53.11; H, 6.31; N, 5.16; S, 23.63%. Found: C, 53.22; H, 6.24; N, 5.14; S, 23.23%. ^{1}H-NMR ($CDCl_3$) δ=1.25 (6H, t, J=7.5, $SCH_2C\underline{H}_3$), 2.51 (2H, q, J=7.5, $SC\underline{H}_2CH_3$), 2.60 (2H, q, J=7.5, $SC\underline{H}_2CH_3$), 3.90 (2H, s, Ar_{py}-C$\underline{H}_2$S), 3.92 (2H, s, Ar_{py}-C$\underline{H}_2$S), 7.98 (1H, s, Ar_{py}-$\underline{H}$), 10.50 (1H, s, -C$\underline{H}$O), and 11.53 (1H, s, -O$\underline{H}$). IR (neat) $\nu_{C=O}$ 1655, ν_{st} 1380, 1243, and 968 cm^{-1}.

Racemization Reaction. A 0.03 M-borate buffer (pH 10.0) was prapared as follows; 5.73 g (15 mmol) of sodium borate·10H_2O was dissolved in 300 ml of water. A part (60 ml) of the solution was made to be pH 10.0 by adding *ca.* 35 ml of a 0.1 M-NaOH solution and allowed to stand overnight. Then, the pH was readjusted to be 10.0 by adding a 0.1 M-NaOH solution (to become 100 ml).

Sodium hydrogen L-glutamate (18.7 g, 0.1 mol) and 0.5 g (2 mmol) of copper(II) sulfate·5H_2O was mixed in a small amount of water. Then 2 M-NaOH was added to produce a pH of 10. This was then allowed to stand overnight. Then, total volume of the solution was made to be 100 ml by the addition of water and 2 M-NaOH (readjusting the pH to 10.0).

A catalyst solution was prepared as follows; 0.5 mmol of a catalyst was dissolved into a 0.03 M-borate buffer (50 ml) and the pH was readjusted to be 10.0 by adding 2 M-NaOH. Then, the mixture was made to be 100 ml by the addition of *ca.* 50 ml of ethanol.

In a thermostated water bath at 25±0.5 °C, a 2 ml aliquot of an amino acid solution containing copper(II) sulfate (a.a. 1 M, Cu^{+2}, 2×10^{-2} M, pH 10 (NaOH), 25 °C) and a 5 ml aliquot of a catalyst solution (5×10^{-3} M, pH 10 (0.03 M borate buffer), 25 °C) was withdrawn from each stock solution using a pipet. These were mixed in a test tube equipped with a glass stopper and sealed (final molar ratio; a.a.:Cu^{+2}:catalyst=80:1.6:1). The degree of the optical rotation (α_t) was recorded in a standard cell with sodium D-line (589 nm) when the racemization reaction was terminated (every 8 h by the addition of 6 M-HCl all at once). In cases where we found precipitate in a terminated solution, it was filtered through Celite (No. 545) mounted on a 3G4 sintered-glass filter. The filtrate was used for an optical-rotation measurement. The measurement of α_t

continued until the racemization yield (calculated using 100 $(\alpha_0-\alpha_t)/\alpha_0$) became 56—84% (in ten to seventeen aliquots). α_0 is the average magnitude of the initial and the final optical rotation of the amino acid solution in the absence of catalyst. This showed almost no observable difference. The apparent rate constants (k_{obsd}) were calculated (using $2.30(\log \alpha_0-\log \alpha_t)/60t$). It was assumed that the reaction obeys first-order kinetics. The catalyst stability (decomposition percent) was checked by measuring the optical-density change at several specific absorption maxima for a 25-fold diluted aliquot of the reaction mixture terminated by the addition of 6 M-HCl (in the range of 210—450 nm).

In the case of pyridoxal, a plot of $(\log \alpha_0-\log \alpha_t)$ *vs.* time was linearly correlated for 56 h (50% racemization completion). Then the slope was decreased slowly with a linear correlation for 188 h (84% completion, 6.6% decomposition of catalyst at 288 nm). In the case of **27**, the same plot showed a linear relationship for up to 64 h (43% completion) and then leveled off (linearly) for 96 h (56% completion, 42 and 63% decomposition at 243 and 396 nm, respectively). The same plot for **26** was linearly correlated perfectly through measurements lasting 96 h (80% completion, zero percent decomposition at 325 nm). However, **26c** showed the same propensity as that of pyridoxal with a linear relation for 56 h (62% completion). Then it showed a decreased slope until an elapsed time of 188 h (83% completion, 8% decomposition at 305 nm). Additionally, the same plot of **26b** and **28** partly showed a linear correlation (but totally nonlinear) until 96 h (70 and 76% completion respectively, 14 and 26% decomposition at 307 and 385 nm for **26b**, and 12% decomposition at 304.5 nm for **28**, respectively). The reaction of **26c**, **27**, and **28** proceeded with the formation of a preciptate which could be dissolved by the final addition of 6 M-HCl.

We would like to express our thanks to Dr. Haruo Homma and his staff in this Institute for elemental analyses. Dr. Jun Uzawa and Mrs. Tamiko Chijimatsu are greatly appreciated for measurement of ^{1}H-NMR spectra, and Mr. Yasuaki Ezumi, for measurement of mass spectra. We are grateful to Dr. Makoto Ando and Dr. Sakae Emoto for useful discussion.

References

1) a) E. E. Snell and S. J. DiMari, "The Enzyme," 3rd ed, ed by P. D. Boyer, Academic Press, New York (1970), Vol. 2, pp. 335; b) E. A. Boeker and E. E. Snell, *ibid.*, 3rd ed, (1972), Vol. 6, pp. 217; c) E. Adams, *ibid.*, 3rd ed, (1972), Vol. 6, pp. 479; d) L. Davis and D. E. Metzler, *ibid.*, 3rd ed, (1972), Vol. 7, pp. 33; e) A. E. Braunstein, *ibid.*, 3rd ed, (1973), Vol. 9, pp. 379; f) C. Walsh, *Ann. Rev. Biochem.*, **47**, 881 (1978).

2) J. Olivard, D. E. Metzler, and E. E. Snell, *J. Biol. Chem.*, **199**, 669 (1952).

3) a) E. E. Snell and W. T. Jenkins, *J. Cell. Comp. Physiol.*, **54**, Suppl., 1, 161 (1959); b) E. E. Snell, *J. Am. Chem. Soc.*, **67**, 194 (1945); c) D. E. Metzler and E. E. Snell, *ibid.*, **74**, 979 (1952); d) D. E. Metzler, M. Ikawa, and E. E. Snell, *ibid.*, **76**, 648, (1954); e) J. B. Longenecker, M. Ikawa, and E. E. Snell, *J. Biol. Chem.*, **226**, 663 (1957).

4) J. B. Longenecker and E. E. Snell. *J. Am. Chem. Soc.*, **79**, 142 (1957).

5) D. E. Metzler and E. E. Snell, *J. Biol. Chem.*, **198**, 353 (1952).

6) D. E. Metzler, J. B. Longenecker, and E. E. Snell, *J. Am. Chem. Soc.*, **75**, 2786 (1953) and **76**, 639 (1954).

7) a) G. D. Kalyankar and E. E. Snell, *Biochemistry*, **1**, 594 (1962); b) E. Werle and W. Koch, *Biochem. Z.*, **1949**, 319; c) J. W. Thanassi and J. S. Fruton, *Biochemistry*, **1**, 975 (1962).

8) a) T. C. Bruice and R. M. Topping, *J. Am. Chem. Soc.*, **85**, 1480 and 1488 (1963); b) T. C. French, D. C. Auld, and T. C. Bruice, *Biochemistry*, **4**, 77 (1965); c) J. W. Thanassi, A. B. Butler, and T. C. Bruice, *ibid.*, **4**, 1465 (1965); d) D. S. Auld and T. C. Bruice, *J. Am. Chem. Soc.*, **89**, 2083, 2090, and 2098 (1967).

9) a) K. Ohno. I. Sasaji, and M. Hara, Japan Kokai Pat., 295110 (1961); b) S. Yoshikawa, K. Kuga, Y. Ueda, M. Goto, and H. Sugiyama, *Kogyo Kagaku Zasshi*, **70**, 105 (1967); c) M. Ando and S. Emoto, *Bull. Chem. Soc. Jpn.*, **42**, 2624 (1969).

10) H. Kondo, J. Kikuchi, and J. Sunamoto, *Tetrahedron Lett.*, **24**, 2403 (1983).

11) a) Incidental induced stereoselective transamination, owing to diastereoisomeric chelate complex of **1b**, is reported; J. B. Longenecker and E. E. Snell, *Proc. Nat. Acad. Sci. U. S. A.*, **42**, 221 (1956); b) After this work had been completed, publication has been retarded by special reasons. In the meantime, several interesting articles related to stereoselective catalyst based on the independent design of vitamin B_6 derivatives have been reported; S. C. Zimmerman and R. Breslow, *J. Am. Chem. Soc.*, **106**, 1490 (1984) and references cited therein.

12) M. Iwata and S. Emoto, *Bull. Chem. Soc. Jpn.*, **47**, 1687 (1974) and **49**, 1163 (1976).

13) a) H. Kuzuhara, M. Iwata, and S. Emoto, *J. Am. Chem. Soc.*, **99**, 4173 (1977); b) T. Sakurai, H. Kuzuhara, and S. Emoto, *Acta Crystallogr. Sec. B*, **35**, 2984 (1979); c) M. Ando, Y. Tachibana, and H. Kuzuhara, *Bull. Chem. Soc. Jpn.*, **55**, 829 (1982); d) Y. Tachibana, T. Komatsu, M. Ando, and H. Kuzuhara, *ibid.*, **57**, 237 (1984); e) H. Kuzuhara, T. Komatsu, and S. Emoto, *Tetrahedron Lett.*, **1978**, 3563; f) Y. Tachibana, M. Ando, and H. Kuzuhara, *Chem. Lett.*, **1982**, 1765 and 1769; g) *idem*, *Bull. Chem. Soc. Jpn.*, **56**, 2263 (1983); h) *ibid.*, **56**, 3652 (1983); i) M. Iwata, H. Kuzuhara, and S. Emoto, *Chem. Lett.*, **1976**, 983; j) M. Iwata and H. Kuzuhara, *ibid.*, **1981**, 5.

14) W. Korytnyk, S. C. Srivastava, N. Angelino, P. G. G. Potti, and B. Paul, *J. Med. Chem.*, **16**, 1096 (1973).

15) W. Korytnyk and W. Wiedeman, *J. Chem. Soc.*, **1962**, 2531.

16) a) J. M. Downie, J. B. Holms, and J. B. Lee, *Chem. Ind. (London)*, **1966**, 900; b) J. P. H. Verheyden and J. G. Moffatt, *J. Org. Chem.*, **37**, 2289 (1972).

17) C. F. Horn, F. Hostettler, and N. R. Eldred, U. S. Pat., 2696387 (1961); *Chem. Abstr.*, **55**, P 27218d (1961).

18) R. H. Michell, T. Ohtsubo, and V. Boekelheide, *Tetrahedron Lett.*, **1975**, 219.

19) See for nomenclature: F. Voegtle and P. Neumann, *Tetrahedron Lett.*, **1969**, 5329; *Tetrahedron*, **26**, 5847 (1970).

20) a) Boeckelheide, I. D. Reingold, and M. Tuttle, *J. Chem. Soc., Chem. Commun.*, **1973**, 406; b) J. Bruhin and W. Jenny, *Tetrahedron Lett.*, **1973**, 1215.

21) D. H. R. Barton, P. D. Magnus, G. Smith, G.

Streckert, and D. Zurr, *J. Chem. Soc., Perkin Trans. 1*, **1972**, 542.

22) A. J. Fatiadi, *Synthesis*, **1976**, 65 and 133 and references cited therein.

23) a) D. Heyl, *J. Am. Chem. Soc.*, **70**, 3434 (1948); b) A. N. Wilson and S. A. Harris, *ibid.*, **73**, 4693 (1951).

24) J. Attenburrow, A. F. B. Cameron, J. H. Chapman, R. H. Evans, B. A. Hems, A. B. A. Jasen, and T. Walker, *J. Chem. Soc.*, **1952**, 1094.

25) M. Iwata, *Bull. Chem. Soc. Jpn.*, **54**, 2835 (1981).

26) O. H. Wheeler, *Chem. Ind. (London)*, **1965**, 1769.

27) a) H. Kwart and T. J. George, *J. Org. Chem.*, **44**, 162 (1979); b) I. M. Goldman, *ibid.*, **34**, 3289 (1969); c) T. K. Hall and P. R. Story, *J. Am. Chem. Soc.*, **89**, 6759 (1967).

28) a) E. H. Cordes and W. P. Jencks, *J. Am. Chem. Soc.*, **84**, 826 (1962); b) S.-H. Weng and D. L. Leussing, *ibid.*, **105**, 4082 (1983).

29) H. Gerlach and E. Huber, *Helv. Chim. Acta*, **51**, 2027 (1968).

30) T. Sato, M. Wakabayashi, M. Kainosho, and K. Hata, *Tetrahedron Lett.*, **1968**, 4185.

31) W. J. Emseley, J. Feeney, and L. H. Sutcliffe, "High Resolution Nuclear Magnetic Resonance Spectroscopy," Pergamon Press, London (1965), pp. 310.

32) N. L. Allinger, L. A. Freiberg, R. B. Hermann, and M. A. Miller, *J. Am. Chem. Soc.*, **85**, 1171 (1963).

33) A. Koetz, *Ber.*, **33**, 729 (1900).

34) W. Korytnyk and M. Ikawa, "Methods in Enzymology," ed by D. B. MaCormick and L. D. Wright, (1970), Vol. 18 part A, pp. 527.

35) A. Cohen and E. G. Hughes, *J. Chem. Soc.*, **1952**, 4383.

36) J. Baddiley and A. P. Mathias, *J. Chem. Soc.*, **1952**, 2583.

37) D. J. Cram and H. Steinberg, *J. Am. Chem. Soc.*, **73**, 5691 (1951).

38) Manufactured either by Junsei Chem. Co. Ltd., by Wako Pure Chem. Co., or by Kokusan Chem. Co.

 © 1985 The Chemical Society of Japan Bull. Chem. Soc. Jpn., 58, 2515—2518 (1985)

ENDOR Studies of Vitamin E Model Radical. The Solution Structure and Dynamic Behavior of Chromanyloxyl Ring

Kazuo MUKAI,* Kimiko TAKAMATSU, and Kazuhiko ISHIZU
Department of Chemistry, Faculty of Science, Ehime University, Matsuyama 790
(Received March 7, 1985)

ENDOR technique has been used to elucidate the solution structure and dynamic behavior of chromanyloxyl ring in vitamin E radical. We have measured the ENDOR spectrum of a stable vitamin E model radical (7-*t*-butyl-2,2,5-trimethyl-6-chromanyloxyl (**1**)) in toluene in the temperature range −30°—−100 °C. From detailed analysis of the temperature dependence of hyperfine coupling of β-methylene protons in the heterocyclic ring, the equilibrium conformation of the β-methylene group and activation energy, enthalpy and entropy for the conformational interconversion of the heterocyclic ring have been determined. The observed positive temperature dependence of the hyperfine coupling constants ($a_5^{CH_3}$ and a_8^H) may be explained as a consequence of the restricted motion about the C_{8a}–O_1 bond in the chromanyloxyl ring, based on the McLachlan MO calculation.

Tocopherols (vitamin E) are well known as scavengers of lipid peroxide radicals generated in biological membranes.[1,2] The ESR studies of the tocopheroxyl radicals obtained by the oxidation of tocopherols are of biological interest since they are involved in radical-scavenging reactions of tocopherols.[3–6] In a previous paper, we reported the ESR spectra of α-, β-, γ-, and δ-tocopheroxyl and their model compounds in toluene at 20 °C, and found that all the two β-methylene protons at C-4 position are magnetically equivalent.[4] Further, from the results of the ENDOR measurements of α-tocopheroxyl and its model, it was observed that each of the two β- and γ-methylene protons in the heterocyclic ring shows an equivalent hyperfine coupling.[7] This suggests that the two carbon atoms C-4 and C-3 in the heterocyclic ring are coplanar with the aromatic ring. The result is inconsistent with the X-ray structure of α-tocopherol model,[8,9] which shows that the dihedral angle, θ_γ, between the C_3–C_4 bond and the aromatic ring is 11.1° and 11.9° (see Fig. 3).[10] However, in a previous paper, the clear ENDOR spectra of the α-tocopheroxyl and its model radicals were observed in the comparatively high and narrow temperature range (from −25° to −35 °C for α-tocopheroxyl and from −40° to −55 °C for α-tocopheroxyl model), because these radicals are not so stable and dimerize at low temperature region.[7]

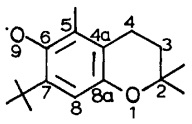

Tocopheroxyl **1**

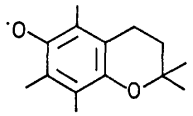

α-Tocopheroxyl model

In the present work, we have measured the ENDOR spectrum of stable vitamin E model radical (7-*t*-butyl-2,2,5-trimethyl-6-chromanyloxyl, hereafter called tocopheroxyl **1**) in toluene in the temperature range −30°—−100 °C. From detailed analysis of the temperature dependence of the hyperfine coupling constants, the conformation and dynamic behavior of the heterocyclic ring in tocopherol in solution have been discussed.

Experimental

The preparation of tocopherol model compound (7-*t*-butyl-2,2,5-trimethyl-6-chromanol) was reported in a previous paper.[11] The tocopheroxyl **1** was obtained by the PbO_2 oxidation of the above tocopherol model compound in toluene under vacuum.

The ENDOR spectra were recorded by a JES-EDX-1 spectrometer, operated with 80 Hz magnetic field modulation.

Results

The ENDOR spectrum of tocopheroxyl **1** was observed in the temperature range −30° to −100 °C. As shown in Fig. 1 and 2, notable temperature effects

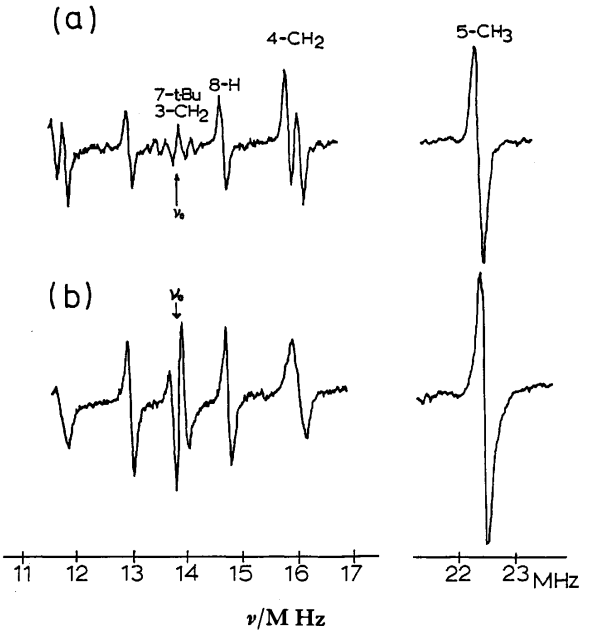

ν/M Hz

Fig. 1. ENDOR spectra of tocopheroxyl **1** in toluene at (a) −94 °C and (b) −72 °C.

Table 1. Hyperfine couplings (a_I^H) (in gauss) and spin densities (ρ_I) of tocopheroxyl **1** in toluene

	$a_5^{CH_3}$	$a_4^{CH_2}$	a_8^H	$a_3^{CH_2}$	a_7^{tBu}	T/°C
ESR	6.05[a]	1.55	0.72	——	—	20
ENDOR	6.086[b]	1.525	0.635	— , 0.073	0.073	−72
	6.074	1.592, 1.448	0.608	0.234, 0.076	0.076	−94
ρ(Exptl.)	0.2250	−0.0376[c]	−0.0225	——	—	−94
ρ(Calcd.)[d]	0.2123	−0.0389[c]	−0.0286	——	—	

a) Experimental errors ±0.04 G. 1G=10^{-4} T. b) Experimental errors ±0.010 G. c) Spin density at C-4a. d) $\beta_{C_{4a}\text{-}O_1}=1.0\,\beta$.

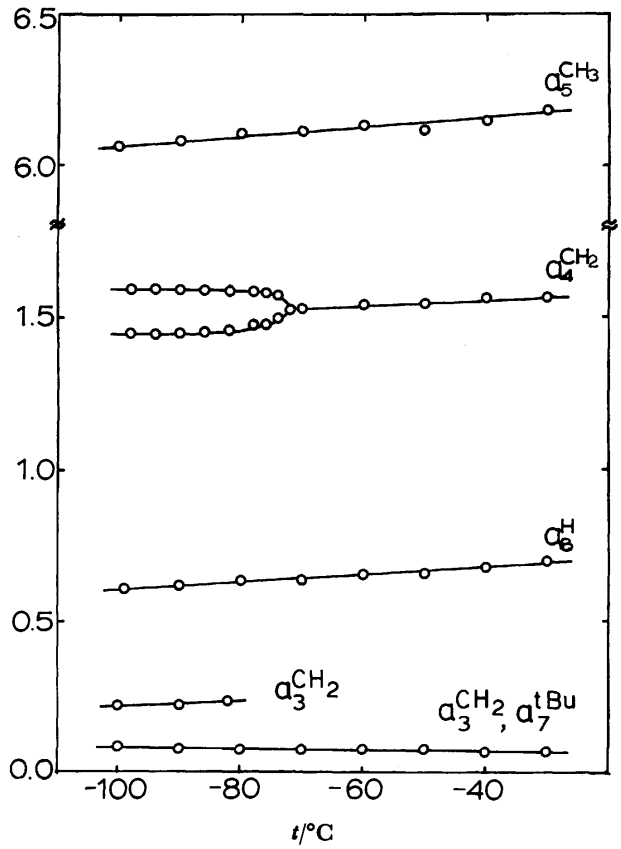

Fig. 2. Temperature dependence of the hyperfine couplings of tocopheroxyl **1** in toluene.

were observed. The ENDOR spectrum at −94 °C (see Fig. 1(a)) clearly shows six different proton hyperfine couplings (6.074, 1.592, 1.448, 0.608, 0.234, and 0.076 G). The larger four hyperfine couplings (6.074, 1.592, 1.448, and 0.608 G) are easily assigned to the protons at C-5, C-4, C-4, and C-8 positions, respectively, taking its ESR hyperfine couplings (see Table 1) into account.[11] By comparing the ENDOR spectrum of **1** with that of α-tocopheroxyl model,[7] the smallest hyperfine coupling of 0.076 G, which has never been observed in the ESR spectrum of **1**, will be assigned to the γ-methylene proton hyperfine coupling at C-3 position and/or *t*-butyl proton at C-7 position. The hyperfine coupling of 0.234 G was tentatively assigned to the γ-methylene proton at C-3. The ENDOR spectrum of **1** remains essentially unchanged upon warming from −100° to −80 °C except for small changes of the hyperfine couplings. When the temperature is increased further, the weak absorption due to γ-methylene proton ($a_3^{CH_2}$=0.234 G) has disappeared at −81 °C, and the two lines of alkyl β-protons ($a_4^{CH_2}$) were gradually merged into a single line at −72 °C, as is shown in Fig. 1(b) and Fig. 2. The values of the hyperfine couplings observed at −72 °C are $a_5^{CH_3}$=6.086, $a_4^{CH_2}$=1.525, a_8^H=0.635, and a_7^{tBu} and/or $a_3^{CH_2}$=0.073 G. These values are listed in Table 1, together with the values of the experimental spin densities (ρ_i) calculated from the hyperfine coupling.[4,11]

Discussion

Conformation of β-Methylene Group in Tocopheroxyl 1. As described in a previous section, in the ENDOR spectrum for the tocopheroxyl **1** in toluene, two signals attributable to the inequivalent splittings ($a_{4A}^{CH_2}$=1.592 G and $a_{4B}^{CH_2}$=1.448 G) of the β-methylene protons were recorded at −94 °C. The inequivalent β-methylene proton splittings have been understood by assuming a tightly rocking model of the methylene group, based on the Heller-McConnell relationship (Eq. 1).[12] In these cases, the sum of the two dihedral angles (θ_A, θ_B) of the inequivalent β-protons is about $\pi/3$. A similar situation probably exists in the present case.

$$a_4^{CH_2} = \langle Q(\theta)\rangle \rho_{4a}, \quad Q(\theta) = B_0 + B_2 \cos^2\theta \qquad (1)$$

where B_0 and B_2 are empirical parameters, and θ is the dihedral angle between the axis of the $2p_z$ orbital and the C–H bond of the β-methylene group. B_0 and B_2 were taken to be 0 and 54 G, respectively, in Eq. 1. Consequently, based on the observed β-methylene proton couplings, and assuming the sum of the two dihedral angles of the inequivalent β-protons is $\pi/3$, the values of the dihedral angles, θ_A and θ_B, were calculated to be 27.6° and 32.4° for **1**, respectively. These values show that the dihedral angle, θ_γ, between the C_3–C_4 bond and the aromatic ring is 2.4° (see Fig. 3). From the results of the estimated dihedral angles, a preferable equilibrium conforma-

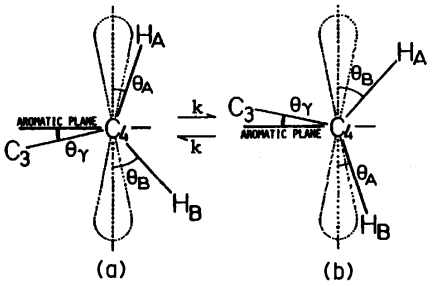

Fig. 3. Possible equilibrium conformations of the β-methylene group in tocopheroxyl **1** in toluene.

tion of C-H and C_3-C_4 bonds was assumed as illustrated in Fig. 3.

On the other hand, as the result of the analysis of the ENDOR spectrum indicates, the two β-methylene protons of **1** show an equivalent hyperfine splitting at higher temperatures. Therefore, the spin density (ρ_{4a}) at the C-4a position was tentatively calculated from $a_4^{CH_2}$=1.525 G at −72 °C, assuming θ=30° for two β-methylene protons in Eq. 1.[7] Using this spin density (ρ_{4a}), the splittings of $a_{4A}^{CH_2}$=1.592 and $a_{4B}^{CH_2}$=1.448 G are found to correspond respectively to angles of θ_A=27.8° and θ_B=32.5°, which add up very nearly to $\pi/3$. These values (θ_A and θ_B) are very similar to those (θ_A=27.6° and θ_B=32.4°) calculated above assuming $\theta_A+\theta_B=\pi/3$.

Very recently, we have succeeded in measuring the ENDOR spectrum of cation radical obtained by the oxidation of benzo[1,2-*b*:4,5-*b*']dipyran, which has heterocyclic ring common to that of tocopherols, in $AlCl_3$-CH_2Cl_2 mixtures.[13] In the cation radical, it was found that the two β-methylene protons in the heterocyclic ring become magnetically inequivalent at low temperature, showing two kinds of hyperfine couplings. The observed dihedral angles are θ_A=28.9° and θ_B=31.1°, and θ_γ is calculated to be 1.1°. These values are very similar to those of the tocopheroxyl **1**, because the steric repulsion force between the β-methylene protons at C-4 and the neighboring methyl protons is equivalent in **1** and the above cation radical. On the other hand, the values of the dihedral angle, θ_γ, (2.4° in **1** and 1.1° in cation radical) in solution are different from those (θ_γ=11.1° and 11.9° in α-tocopherol model[8,9]) in the crystal. The result suggests that the crystal and solution conformations of the heterocyclic ring attached to the aromatic ring in α-tocopherol are different.

Dynamic Behavior of Heterocyclic Ring. In the ENDOR spectra for the **1** in toluene, two signals due to the inequivalent splittings of the β-methylene protons were recorded at −100 °C. The β-methylene proton hyperfine coupling constants remain almost unchanged upon warming from −100° to −90 °C. They collapsed into a single line as the temperature

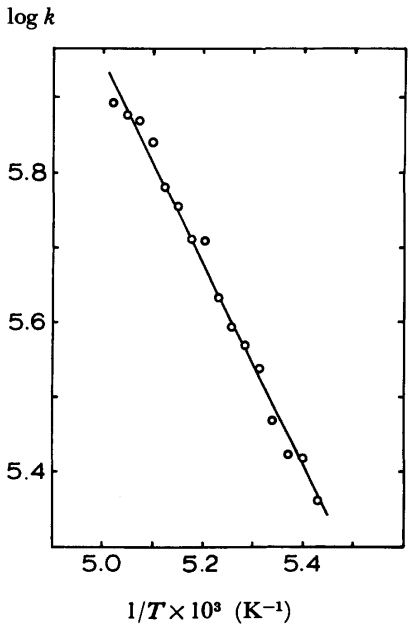

Fig. 4. The Arrhenius plot of the rate constant for the conformational interconversion process of the heterocyclic ring of tocopheroxyl **1** in toluene.

was raised to −72 °C (see Fig. 1 and 2). In such a case, we can calculate the activation energy (E_{act}) for the conformational interconversion of the heterocyclic ring, applying the Gutowsky-Holm equation.[14-16]

In a two-jump dynamic process, in which two nuclear spins of I=1/2 exchange their different hyperfine couplings, the observed separation $\Delta\omega$ of the two ENDOR lines is given by

$$\Delta\omega = (\Delta\omega_{max}^2 - 2k^2)^{1/2} \quad (2)$$

where $\Delta\omega_{max}$ is $\gamma_e|(a_{4A}^{CH_2}-a_{4B}^{CH_2})/2|$, and $a_{4A}^{CH_2}$ and $a_{4B}^{CH_2}$ (measured in Gauss) are the hyperfine coupling constants for the two β-methylene protons observed at −94 °C, and $k=1/\tau$. Here, τ is the mean lifetime of each conformation. We obtained k values as a function of the temperature between −89° and −74 °C.

Dynamic processes of this type can be described by the well-established theories of activated chemical reactions. Empirically the temperature dependence of the rate constant k for such an interconversion is given by the Arrhenius equation.

$$k = A_0 \exp(-E_{act}/RT) \quad (3)$$

where k is the jump rate of Eq. 2. Figure 4 shows the Arrhenius plots of log k *vs.* 1/T for tocopheroxyl **1** from which E_{act} and A_o were determined. The obtained values are E_{act}=25.9±1.7 kJ mol^{-1} and A_o=$5.6\times10^{12\pm0.4}$ s^{-1}. It may be seen that the activation energy, E_{act}, obtained in the present work for **1** is similar to that (29.9 kJ mol^{-1}) reported for such an interconversion in 1,2,3,6,7,8-hexahydropyrene anion radical.[16] From the Eyring theory of the activated

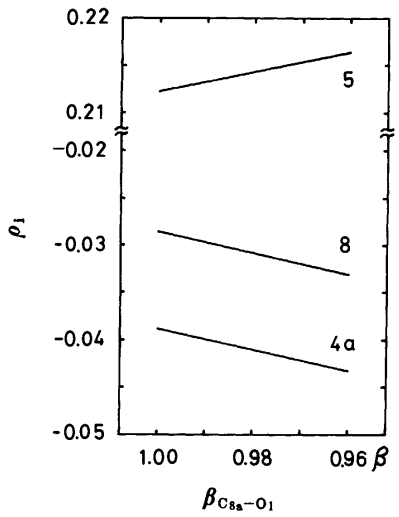

Fig. 5. The variation of the McLachlan spin densities (ρ_i) in tocopheroxyl **1** as a function of the resonance integral $\beta_{C_{8a}-O_1}(=\beta\cos\theta_{CO})$ between O_1 and C_{8a} atoms.

transition state, on the other hand, one obtains

$$k = (kT/h)\cdot\exp(\Delta S^*/R)\cdot\exp(-\Delta H^*/RT) \quad (4)$$

where ΔH^* is the activation enthalpy and ΔS^* is the activation entropy.[15] The thermodynamic quantities ΔH^* and ΔS^* were deduced from plots of ln k/T *vs.* 1/T which yielded straight lines according to Eq. 4. The obtained values are $\Delta H^*=24.2\pm1.7$ kJ mol^{-1} and $\Delta S^*=-5.4\pm3.4$ J mol^{-1} K^{-1}.

Temperature Dependence of the Proton Hyperfine Couplings of the Tocopheroxyl 1. As is shown in Fig. 2, the proton hyperfine couplings, $a_5^{CH_3}$, $a_4^{CH_2}$, and a_8^H, of the tocopheroxyl radical **1** are temperature dependent. These effects are considered to be the restricted motion about the C_{8a}–O_1 bond which causes changes in the unpaired spin density (ρ_i) throughout the radical.[17,18] McLachlan MO calculations successfully predict the changes in the above proton hyperfine couplings from −100° to −30 °C. Following Stone and Carrington,[17] we have used the resonance integral, $\beta_{C_{8a}-O_1}=\beta\cos\theta_{CO}$, as an adjustable parameter to account quantitatively for the changes in the average dihedral angle (θ_{CO}) of the C_{8a} carbon $2p_z$ orbital with respect to the C_{8a}–O_1–C_2 plane. The other Coulomb and resonance integrals employed in the calculations are as follows: $\alpha_{O_1}=\alpha+2.0\beta$, $\alpha_{O_9}=\alpha+1.3\beta$, $\alpha_{C_6}=\alpha-0.1\beta$, $\alpha_{C_{4a}}=\alpha-0.06\beta$, $\alpha_{C_7}=\alpha-0.04\beta$, $\beta_{C_6-O_9}=1.5\beta$, and $\lambda=1.2$, where α and β are, respectively, the standard carbon Coulomb and resonance integrals. These parameters are the same as those used previously for the α-tocopheroxyl radical.[7]

The McLachlan spin densities (ρ_5, ρ_{4a}, and ρ_8) calculated for the tocopheroxyl **1** are plotted against $\beta_{C_{8a}-O_1}$ in Fig. 5. The result indicates that the absolute values of ρ_i increase linearly with increasing the value of $\beta_{C_{8a}-O_1}$. The observed temperature dependence of the hyperfine couplings may be reconciled with the variation of calculated hyperfine couplings since $\beta_{C_{8a}-O_1}$ is expected to decrease with increasing temperature due to increased torsional amplitudes.[17,18] For instance, the change of $\beta_{C_{8a}-O_1}$ required to explain the change (0.118 G) of the methyl hyperfine couplings ($a_5^{CH_3}$) observed between −100° and −30 °C is 0.04 β. Recently, the result of the X-ray analysis of α-tocopherol model was reported by Burton *et al.*; an X-ray structure for α-tocopherol model gives the dihedral angle θ_{CO}= 18.5° and 15.2°.[8–10] Therefore, if we assume that the tocopheroxyl **1** has θ_{CO}=16.9° at −100 °C, the average dihedral angle θ_{CO} at −30 °C is calculated to be 23.5°.

We are very grateful to Mr. Yuichi Uemoto for his kind help in the preparation of 7-*t*-butyl-2,2,5-trimethyl-6-chromanol.

References

1) P. Schudel, H. Mayer, and O. Isler, "The Vitamins," 2nd ed, ed by W. H. Sebrell, Jr. and R. S. Harris, Academic Press, New York (1972), Vol. 5, pp. 168-218.
2) M. L. Scott, "The Fat-Soluble Vitamins" ed by H. F. Deluca, Plenum Press, New York (1978), pp. 133—210.
3) W. Boguth and H. Niemann, *Biochim. Biophys. Acta*, **248**, 121 (1971).
4) K. Mukai, N. Tsuzuki, S. Ouchi, and K. Fukuzawa, *Chem. Phys. Lipids*, **30**, 337 (1982).
5) M. Matsuo and S. Matsumoto, *Lipids*, **18**, 81 (1983).
6) J. Tsuchiya, E. Niki, and Y. Kamiya, *Bull. Chem. Soc. Jpn.*, **56**, 229 (1983).
7) K. Mukai, N. Tsuzuki, K. Ishizu, S. Ouchi, and K. Fukuzawa, *Chem. Phys. Lipids*, **29**, 129 (1981).
8) G. W. Burton, Y. Le. Page, E. J. Gabe, and K. U. Ingold, *J. Am. Chem. Soc.*, **102**, 7791 (1980).
9) T. Doba, G. W. Burton, and K. U. Ingold, *J. Am. Chem. Soc.*, **105**, 6505 (1983).
10) There are two different molecules in the unit cell.
11) K. Mukai, K. Takamatsu, and K. Ishizu, *Bull. Chem. Soc. Jpn.*, **57**, 3507 (1984).
12) C. Heller and H. M. McConnell, *J. Chem. Phys.*, **32**, 1535 (1960).
13) K. Mukai, Y. Uemoto, and K. Ishizu, *Bull. Chem. Soc. Jpn.*, **58**, 1928 (1985).
14) H. S. Gutowsky and C. H. Holm, *J. Chem. Phys.*, **25**, 1228 (1956).
15) C. Borczyskowski, K. Möbius, and M. Plato, *J. Mag. Res.*, **17**, 202 (1975).
16) M. Iwaizumi, S. Kita, M. Kohno, and T. Isobe, *Bull. Chem. Soc. Jpn.*, **53**, 1745 (1980).
17) A. J. Stone and A. Carrington, *Trans. Faraday Soc.*, **61**, 2593 (1965).
18) P. B. Ayscough and R. E. D. McClung, *Mol. Phys.*, **20**, 35 (1971).

 © 1985 The Chemical Society of Japan Bull. Chem. Soc. Jpn., 58, 2519—2522 (1985)

A New Synthetic Method of Alkyl Carbonocyanidate *N*-Oxides

Tomio SHIMIZU,* Yoshiyuki HAYASHI, and Kazuhiro TERAMURA
Department of Color Chemistry and Technology, Faculty of Engineering and Design, Kyoto Institute of Technology, Matsugasaki, Sakyo-ku, Kyoto 606
(Received April 17, 1985)

A thermal decomposition of dimethyl nitromalonate to bis(carbomethoxy)furoxan was observed at about 170 °C. In the presence of dipolarophiles, an intermediate, methyl carbonocyanidate *N*-oxide MeOCOC≡N→O, could be trapped as cycloadducts in good yields by the 1,3-dipolar cycloaddition. Treatment of dimethyl nitromalonate in mesitylene at the refluxing temperature resulted in a formation of methyl 2-(hydroxyimino)-2-(2,4,6-trimethylphenyl)acetate.

1,3-Dipolar cycloaddition reactions using nitrile oxides were one of the versatile methods for the preparation of five-membered heterocycles. Many preparative methods of nitrile oxides have been known so far,[1-8] but each of these methods suffers from some disadvantages; for example, i) many troublesome steps are required for the preparation of a precursor of nitrile oxides, ii) formation of by-products, and iii) a poor yield of the cycloadducts in the reaction with dipolarophiles. The present paper describes a new effective and simple method for the generation of alkyl carbonocyanidate *N*-oxides, ROCOC≡N→O, by a thermal decomposition of dialkyl nitromalonates and the trapping of the intermediate in the presence of dipolarophiles as cycloadducts. Nitromalonates (**1**) can be prepared quantitatively by the nitration of malonates with nitric acid under mild conditions.[9] Dimethyl nitromalonate (**1a**) and diethyl nitromalonate (**1b**) are known to be thermally stable (bp 124 °C/16 mmHg and 134 °C/14 mmHg, respectively).[9]

Results and Discussion

Thermal decomposition of **1** into distinct products is unprecedented to our knowledge, but we found that the thermolysis of **1a** in neat or in decalin at about 170 °C for several hours gave bis(methoxycarbonyl)furazan oxide (furoxan)(**3a**) in 70—75% yields with evolution of CO_2 and methanol. The isolation of the furoxan suggests that methyl carbonocyanidate *N*-oxide (**2a**) is first formed and then is converted into the dimer, **3a**. In the presence of dipolarophiles such as olefins, acetylenes, and nitriles, **2a** could be trapped as 2-isoxazolines (**4a—i**), isoxazoles (**5a** and **5b**), and 1,2,4-oxadiazoles (**6a—g**) respectively in the yields shown in Table 1 (also see Scheme 1). The structures of the products were assigned on the basis of elemental and spectral analyses and comparison of their physical properties with those of authentic specimens. β-Keto esters and 1,3-diketones are known to behave as dipolarophiles *via* a tautomerization into the enol forms.[10] Isoxazoles (**5c—h**) were thus obtained from the reaction of **1a** with several 1,3-dicarbonyl compounds *via* a dehydration of the initial cycloadducts, 5-hydroxy-2-isoxazolines.

A probable mechanism of the formation of **2a** in these reactions would be as follows; **1a** equilibrates with the nitronic acid (**7**), which undergoes an intramolecular substitution with loss of methanol followed by decomposition to give **2a**.

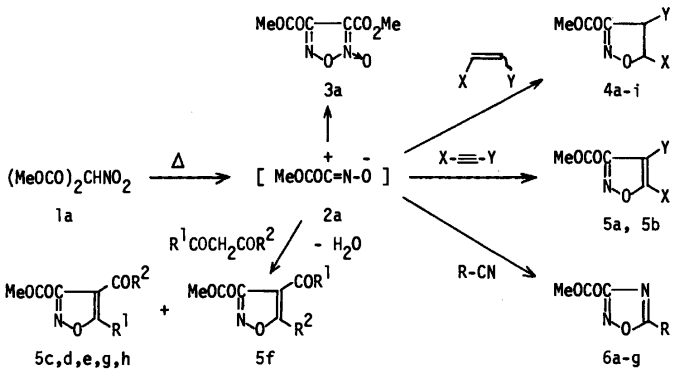

Scheme 1.

TABLE 1. 1,3-DIPOLAR CYCLOADDUCTS FROM THE REACTION OF **1a** WITH DIPOLAROPHILES

Dipolarophile	Reaction[a] condition	Product	Yield %	Mp(Bp) °C
1-Tetradecene	A	**4a** (X=$C_{12}H_{25}$, Y=H)	68	66—68[b]
Allyl *p*-nitrophenyl ether	A	**4b** (X=$CH_2OC_6H_4NO_2$, Y=H)	100	142—143[b]
Allylbenzene	A	**4c** (X=$CH_2C_6H_5$, Y=H)	85	67—68[b]
Cyclooctene	A	**4d** (X, Y=$-C_6H_{12}-$)	88	69—71
Cyclododecene	A	**4e** (X, Y=$-C_{10}H_{20}-$)	55	79—81
Styrene	A	**4f** (X=C_6H_5, Y=H)	86	(110—112/0.2)
iso-Butyl acrylate	A	**4g** (X=$CO_2C_4H_9$, Y=H)	92	(150—151/2)
N-Phenylmaleimide	A	**4h** [X, Y=-CON(Ph)CO-]	90	222—225[b]
Diethyl fumarate	A	**4i** (X=Y=CO_2Et)(trans)	88	(145—147/0.5)
Phenylacetylene	A	**5a** (X=Ph, Y=H)	75	74—76
DMAD[c]	A	**5b** (X=Y=CO_2Me)	80	97—98[b]
Acetylacetone	B	**5c** (R^1=R^2=Me)	30	(95—100/1.5)
Dibenzoylmethane	C	**5d** (R^1=R^2=Ph)	28	111—112
Benzoylacetone	B	**5e** (R^1=Ph, R^2=Me)	43	62—64
		5f (R^1=Me, R^2=Ph)	29	82—85
Ethyl acetoacetate	B	**5g** (R^1=Me, R^2=OEt)	25	(100—120/2)
Ethyl benzoylacetate	C	**5h** (R^1=Ph, R^2=OEt)	20	(150—152/1)
Benzonitrile	C	**6a** (R=Ph)	31	107—108
2,4,6-Trimethylbenzonitrile	C	**6b** (R=C_9H_{11})	15	75—85
4-Methoxybenzonitrile	C	**6c** (R=C_6H_4OMe)	42	156—157
1-Naphthonitrile	C	**6d** (R=$C_{10}H_7$)	12	109—111
Phenylacetonitrile	C	**6e** (R=$CH_2C_6H_5$)	26	75—76
Dodecanenitrile	B	**6f** (R=$C_{11}H_{23}$)	16	50—51
Nonanenitrile	B	**6g** (R=C_8H_{17})	16	35—39

a) A: Refluxing the mesitylene solution of an equimolar mixture of **1a** and dipolarophiles for 20 h; B: Heating the mixture of **1a** and excess amount of dipolarophiles at about 170 °C for 8 h; C: Heating the decalin solution of an equimolar amount of **1a** and dipolarophiles at 170 °C for 20 h. b) **4a**: Lit,[8] mp 66—68 °C; **4b**: lit,[8] mp 142—143 °C; **4c**: lit,[8] mp 60—61 °C; **4h**: lit,[8] mp 223—225 °C; **5b**: lit,[6a] mp 101—102 °C. c) DMAD: Dimethyl acetylenedicarboxylate.

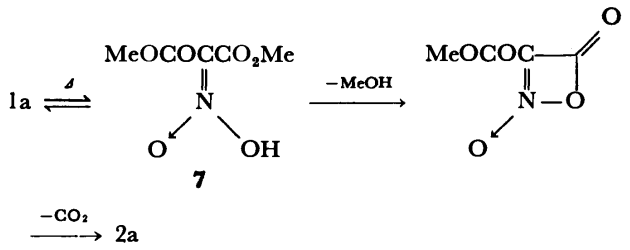

Although the yields of the cycloadducts were not highly dependent on solvents (neat, mesitylene, or decalin), we found that some of aromatic compounds bearing electron-releasing substituents were another acceptor of nitrile oxides. Refluxing a solution of **1a** in mesitylene for 20 h evolved CO_2 and methanol, and methyl 2-(hydroxyimino)-2-(2,4,6-trimethylphenyl)acetate (**8a**) was isolated in 27% yield. Furoxan (**3a**) was not detected in the solution. The structure of **8a** was confirmed by the agreement of the physical properties of **8a** with those of the specimen prepared from the reaction of methyl chloro(hydroxyimino)-acetate (**9**) with mesitylene. Though similar compounds (**8b—f**) were obtained from the reaction of **1a—b** with mesitylene, 1,2,4,5-tetramethylbenzene, pentamethylbenzene, and 3,5-dimethylanisole (see Table 2), 5-(*p*-methoxyphenyl)-3-methoxycarbonyl-1,2,4-oxadiazole (**6c**) or 3-methoxycarbonyl-5-(1,2,3,4-tetramethylphenyl)-1,2,4-oxadiazole (**6h**) was the only isolable compound from the reaction mixture of **1a** and anisole or 1,2,3,4-tetramethylbenzene, respectively.

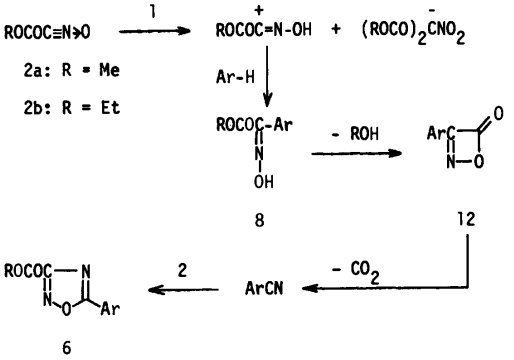

Scheme 2.

The mechanism of the formation of these products can be explained in a fashion as shown in Scheme 2. Nitromalonates are known to be strong carbon-acids.

Protonation of the nitrile oxides (**2**) by nitromalonates would give a carbonium ion followed by electrophilic aromatic substitution to afford **8**. So far only an example of aromatic substitution has been reported using nitrile oxides, although a completely different mechanism of the substitution was suggested.[11] The aromatic substitution described here would provide new aspect of the chemistry of nitrile oxides.

In conclusion, our new reaction provides a simple and useful means of syntheses of isoxazolines, because of economical starting materials, easiness of the removal of by-products (MeOH and CO_2), and high yields of cycloadducts. On the other hand, the less reactive dipolarophiles such as nitriles and 1,3-dicarbonyl compounds gave poor yields of the cycloadducts.

Experimental

Measurements. All melting and boiling points are uncorrected. The ^1H NMR were measured on a Valian T-60A instrument with Me_4Si as an internal standard; chemical shifts are given in δ units and coupling constants (J) are in herz units: s=singlet; d=doublet; t=triplet; q=quartet; m=multiplet; br=broad singlet. All new

Table 2. Reactions of **1a—b** with aromatic compounds

Nitro Malonate	Aromatic Compound	Product	Yield %	Mp θ_m/°C
1a	Mesitylene	**8a** (R=Me, Ar=2,4,6-tetramethylphenyl)	27	131—132
1b	Mesitylene	**8b** (R=Et, Ar=2,4,6-tetramethylphenyl)	20	112—114
1a	1,2,4,5-Tetramethylbenzene	**8c** (R=Me, Ar=2,3.5,6-tetramethylphenyl)	15	210—218
1a	Pentamethylbenzene	**8d** (R=Me, Ar=pentamethylphenyl)	14	188—191
1a	3,5-Dimethylanisole	**8e** (R=Me, Ar=4,6-dimethyl-2-methoxyphenyl)	19	167—169
		8f (R=Me, Ar=2,6-dimethyl-4-methoxyphenyl)	11	
1a	Anisole	**6c**	3	142—145
1a	1,2,3,4-Tetramethylbenzene	**6h** (R=2,3,4,5-tetramethylphenyl)	6	120—121

Table 3. ^1H NMR Spectral data of new compounds (**4—8**)

Adduct	Chemical shift/δ, Solvent: $CDCl_3$
4d	1.1—2.3 (m, 12H), 3.1—3.5 (m, 1H), 3.9 (s, 1H), 4.4—4.8 (m, 1H).
4e	1.0—1.9 (m, 20H), 3.1—3.6 (m, 1H), 3.85 (s, 1H), 3.55—3.95 (m, 1H).
4f	3.13 (dd, 1H, J=9, 18), 3.63 (dd, 1H, J=11, 18), 3.85 (s, 3H), 5.75 (dd, 1H, J=9, 11), 7.3 (s, 5H).
4g	0.93 (d, 6H, J=7), 1.6—2.4 (m, 1H), 3.48 (d, 2H, J=10), 3.87 (s, 3H), 3.97 (d, 2H, J=7), 5.2 (t, 1H, J=10).
5a	3.98 (s, 3H), 6.9 (s, 1H), 7.2—7.6 (m, 3H), 7.6—7.9 (m, 2H).
5c	2.5 (s, 3H), 2.67 (s, 3H), 4.0 (s, 3H).
5d	3.8 (s, 3H), 7.25—8.0 (m, 10H).
5e	2.47 (s, 3H), 4.0 (s, 3H), 7.4—7.9 (m, 5H).
5f	2.53 (s, 3H), 3.66 (s, 3H), 7.3—7.9 (m, 5H).
5g	1.34 (t, 3H, J=7), 2.7 (s, 3H), 4.0 (s, 3H), 4.34 (q, 2H, J=7).
5h	1.3 (t, 3H, J=7), 4.0 (s, 3H), 4.33 (q, 2H, J=7), 7.4—7.7 (m, 3H), 7.85—8.1 (m, 2H).
6a	4.08 (s, 3H), 7.4—7.7 (m, 3H), 8.1—8.3 (m, 2H).
6b	2.27 (s, 6H), 2.34 (s, 3H), 4.07 (s, 3H), 7.0 (s, 2H).
6c	3.9 (s, 3H), 4.05 (s, 3H), 7.0 (d, 2H, J=9), 8.15 (d, 2H, J=9).
6d	4.1 (s, 3H), 7.4—8.2 (m, 5H), 8.4 (dd, 1H, J=2, 7), 9.1 (dd, 1H, J=2, 7).
6e	4.0 (s, 3H), 4.3 (s, 2H), 7.35 (s, 5H).
6f	0.9 (t, 3H, J=7), 1.0—2.1 (m, 16H), 3.0 (t, 3H, J=7), 4.05 (s, 3H).
6g	0.85 (t, 3H, J=7), 1.0—2.1 (m, 12H), 3.0 (t, 3H, J=7), 4.05 (s, 3H).
6h	2.3 (s, 6H), 2.33 (s, 3H), 2.6 (s, 3H), 4.08 (s, 3H), 7.73 (s, 1H).
8a	2.15 (s, 6H), 2.3 (s, 3H), 3.83 (s, 3H), 6.9 (s, 2H), 9.7 (br, 1H, OH).
8b	1.23 (t, 3H, J=7), 2.1 (s, 6H), 2.27 (s, 3H), 4.28 (q, 2H, J=7), 6.87 (s, 2H), 10.0 (br, 1H, OH).
8c	2.04 (s, 6H), 2.23 (s, 6H), 3.83 (s, 3H), 7.0 (s, 1H), 9.5 (br, 1H, OH).
8d*	2.0 (s, 6H), 2.1—2.4 (m, 9H), 3.8 (s, 3H), 12.0 (br, 1H, OH).
8e	2.15 (s, 3H), 2.33 (s, 3H), 3.73 (s, 3H), 3.80 (s, 3H), 6.6 (s, 1H), 6.7 (s, 1H), 10.0 (br, 1H, OH).
8f	2.15 (s, 6H), 3.78 (s, 3H), 3.83 (s, 3H), 6.63 (s, 2H), 10.0 (br, 1H, OH).

* Dissolved in DMSO-d_6.

products gave satisfactory elemental analyses (±0.3% for C, H, and N).

Materials. Dimethyl and diethyl nitromalonate (**1a** and **1b**),[9] and methyl chloro(hydroxyimino)acetate (**9**),[12] were prepared according to the methods described in the literature. Mesitonitrile [mp 49—50 °C (lit,[13] 50 °C)] was prepared in 75% yield from the reaction of mesitaldehyde with hydroxylamine hydrochloride in refluxing ethanol for 10 h. The other chemicals were of commercial origin and used without further purification.

*Thermal Decomposition of **1a—b** to Furoxan.* A decalin solution (10 ml) of **1b** (4.1 g, 20 mmol) was heated in an oil bath (about 170 °C) for several minutes. Gradual evolution of CO_2 (trapped as $CaCO_3$) and ethanol was observed in the course of the reaction. After the mixture was kept at the temperature for 20 h, the solvent was removed from the reaction mixture by distillation. Further distillation under reduced pressure gave a colorless oil (2.2 g yield, bp 110—130 °C/2 mmHg). The oil was found to be a mixture of **1b** and bis(ethoxycarbonyl)furoxan (**3b**) (molar ratio: *ca.* 1:4; yield of **3b**: 78%). Separation of **3b** and **1b** could be accomplished by passing the oil through an alumina column with chloroform. Evaporation of the chloroform eluents gave pure **3b** in 75% yield (1.68 g). **3a** was obtained similarly in 70% yield by decomposition of **1a**.

*Reaction of **1a** with Olefins or Acetylenes. Method A.* A mixture of **1a** (1.77 g, 10 mmol) and a dipolarophile (10 mmol) was refluxed in mesitylene (20 ml) at 160—170 °C for 20 h. Evaporation of the solvent and other low-boiling products from the reaction mixture in a rotary evaporator gave crude product. Crystalline crude products (**4a—e**, **4h**, **5a**, and **5b**) obtained by this method were recrystallized from appropriate solvents (**4a**, **4b**, and **5a** from ethanol; **4c** and **5b** from ethanol–hexane; **4d** from hexane; **4e** from methanol). Oily crude products (**4f**, **4g**, and **4i**) were distilled *in vacuo* to give pure cycloadducts.

*Reaction of **1a** with Nitriles or 1,3-Dicarbonyl Compounds. Method B.* A mixture of **1a** (1.77 g, 10 mmol) and an excess amount of a dipolarophile (*ca.* 20—30 mmol) was heated at about 170 °C for 8 h. The excess dipolarophile was distilled off from the reaction mixture. Crystalline residue was recrystallized from an appropriate solvent: **5e** and **5f** could be separated by fractional recrystallization from ethanol, **6f** from ethanol, and **6g** from hexane. Oily residue was further distilled *in vacuo* and the distillate was passed through an alumina column with chloroform. After evaporation of the chloroform eluent, the fractional distillation of the residue gave pure cycloadducts (**5c** and **5g**).

Method C. An equimolar amount (10 mmol) of **1a** and dipolarophile was heated at about 170 °C in decalin (20 ml) for 20 h. Upon cooling to room temperature, the reaction mixture separated into two layers. After removing a large portion of upper decalin layer by decantation, the residue was distilled *in vacuo* to remove decalin, furoxan **3a**, and the dipolarophile unchanged. Crystalline residue thus obtained was recrystallized from an appropriate solvent (**5d**, **6a**, **6d**, and **6e** from ethanol; **6b** from methanol; **6c** from ethanol–hexane). The oily residue obtained from the reaction with ethyl benzoylacetate was treated similarly as shown in Method B to give pure **5h**.

*Thermal Decomposition of **1a—b** in Aromatic Compounds.* A mixture of **1a** or **1b** (10 mmol) and an aromatic compound (20—30 mmol) was heated in an oil bath at 170 °C for 20 h. Unreacted **1** and aromatic compound were recovered by distillation of the reaction mixture. Crystalline residues obtained from the reactions with 1,2,4,5-tetramethylbenzene, pentamethylbenzene, 3,5-dimethylanisole, and 1,2,3,4-tetramethylbenzene were recrystallized from ethanol (**8e**, **8f**, and **6h**) or carbon tetrachloride (**8c** and **8d**). Oily residues obtained from the reactions with mesitylene and anisole were further distilled *in vacuo* to give viscous oils. The viscous oils were solidified by scraching in hexane to give crystals (**8a**, **8b**, and **6c**).

*Reaction of **8a** with **1a**.* A mixture of **8a** (800 mg, 3.6 mmol) and **1a** (2.0 g, 11 mmol) was heated at 170 °C for 20 h. 1.2 g of **1a** was recovered by distillation of the reaction mixture. Residual oil was passed through an alumina column with chloroform to give crystals, which were recrystallized from methanol to give **6b** in 25% yield (220 mg).

*Reaction of Mesitylene with Methyl Chloro(hydroxyimino)-acetate (**9**).* A mesitylene solution (20 ml) of **9** (1.8 g, 13 mmol) was refluxed untill the evolution of HCl had ceased (after *ca.* 10 h) and removal of excess amount of mesitylene from the reaction mixture afforded reddish oil. The oil was distilled and a viscous fraction (bp 130—150 °C/0.3 mmHg†) was collected, which crystallized partially in a condenser. The fraction was crystallized by scraching in hexane and the crystals were filtered to yield **8a** in 40% yield (1.15 g).

References

1) For reviews, see C. Grundmann and P. Grunanger, "The Nitrile Oxides," Springer-Verlag, New York (1971), pp 31—61.

2) R. Sustmann, R. Huisgen, and H. Huber, *Chem. Ber.*, **100**, 1802 (1967); K. Bast, M. Christ, R. Huisgen, and W. Mack, *ibid.*, **106**, 3312 (1973).

3) L. Gajsler, R. M. Paton, J. H. Hall, and D. J. Harper, *J. Polym. Sci., Polym. Lett. Ed.*, **18**, 635 (1980); M. Arbasino and P. Grunanger, *Ric. Sci., Rend., Sez. A*, **7**, 561 (1964).

4) T. Mukaiyama and T. Hoshino, *J. Am. Chem. Soc.*, **82**, 5339 (1960).

5) G. B. Bachmann and L. E. Strom, *J. Org. Chem.*, **28**, 1150 (1963).

6) K. Harada, E. Kaji, and S. Zen, *Chem. Pharm. Bull.*, **28**, 3296 (1980); b) A. Mckillop and R. J. Kobylecki, *Tetrahedron*, **30**, 1365 (1974).

7) A. Gasco and A. J. Boulton, *Adv. Heterocycl. Chem.*, **29**, 287 (1981) and references cited therein.

8) T. Shimizu, Y. Hayashi, and K. Teramura, *Bull. Chem. Soc. Jpn.*, **57**, 2531 (1984).

9) D. I. Weisblat and D. A. Lyttle, *J. Am. Chem. Soc.*, **71**, 3079 (1949).

10) Ref. 1) p.185.

11) Ref. 1) p.168.

12) I. Adachi, T. Yamamori, and Y. Hiramatsu, Jpn. Tokkyo Koho, 135922 (1978); *Chem. Abstr.*, **90**, 54496t (1979).

13) C. Grundmann and H-D. Frommeld, *J. Org. Chem.*, **30**, 2077 (1965).

† 1 mmHg=133.322 Pa.

 © 1985 The Chemical Society of Japan Bull. Chem. Soc. Jpn., 58, 2523—2525 (1985)

Hydroxylation of Cedrol by *m*-Chloroperbenzoic Acid. Synthesis of an Epimer of the Alleged "Senoxydene"

Motoo Tori, Reiko Matsuda, and Yoshinori Asakawa*

Faculty of Pharmaceutical Sciences, Tokushima Bunri University, Yamashiro Cho, Tokushima 770

(Received April 24, 1985)

Cedrol was hydroxylated by *m*-chloroperbenzoic acid to give four tertiary alcohols and two secondary alcohols, one of which was converted into an epimer of "senoxydene" in four steps.

The hydroxylation of natural products at unactivated positions has been effected by dry ozonization,[1] remote oxidation,[2] the Barton reaction,[3] microbial oxidation,[4] and mammalian metabolism.[5] In 1979, Deno and Meyer reported a method of hydroxylation of the 25-position of a steroidal side chain using hydrogen peroxide and trifluoroacetic acid.[6] Schneider described a practical method of hydroxylation of polycyclic hydrocarbons by *m*-chloroperbenzoic acid (*m*CPBA) yielding tertiary alcohols.[7] However, no examples of the use of *m*CPBA as a reagent for the hydroxylation of natural products have been reported.

We have been studying the oxidation of natural products by not only biological but also chemical methods. The hydroxylation of terpenoids in rabbits has been investigated in these laboratories.[8] We have recently applied *m*CPBA to the hydroxylation of unactivated carbon atoms of triterpenes belonging to the dammarane,[9] lupane,[10] and friedelane[10] classes.

Cedrol(**1**) is a sesquiterpene found in cedar wood. Ourisson and co-workers[11] subjected **1** to dry ozonization which afforded cedrane-2α,8β-diol (**5**) in 79% yield (50% conversion). Moreover, it has been reported by Wang *et al.*[12] that microbial oxidation of **1** produced cedrane-3α,8β-diol (**6**), 8β-hydroxycedran-3-one, and cedrane-3β,8β-diol (**7**).

We became interested in the structure of **1** which is very similar to an epimer of "senoxydene." If we could hydroxylate the 7-position of cedrol (**1**), oxidative bond cleavage and intramolecular aldol condensation would lead to a triquinane skeleton.

In a continuation of our work, the hydroxylation of natural products using *m*CPBA, we have examined the reaction of cedrol (**1**) with this reagent. We now report the products of this reaction as well as the conversion of one of these to an epimer[13] of the alleged "senoxydene."[14]

Cedrol (**1**, 2.2 g) was treated with *m*CPBA (1.2 equiv) in chloroform (75 ml) under reflux for 6 h. The usual work-up and chromatographic separation (see Experimental) afforded three novel compounds (**2**, **3**, and **4**) in addition to the previously known cedrane-2α,8β-diol (**5**),[11] cedrane-3α,8β-diol (**6**),[12,15,16] and cedrane-3β,8β-diol (**7**).[12,15,16] The least polar compound, the diol **2** [IR($CHCl_3$) 3570 and 3450 cm^{-1}; *m/z* 238 (M^+)] had signals characteristic of three tertiary methyl groups [δ 1.35, 1.21, and 0.97 (each s)] and a secondary methyl group [δ 0.87 (d, J=7 Hz)] in its ^1H NMR spectrum. As no resonance due to an oxygenated methine group was observed, it followed that the compound was either cedrane-7β,8β-diol (**2**) or cedrane-5β,8β-diol (**3**). The correctness of the former structure was demonstrated by ^{13}C NMR spectroscopy and $Pb(OAc)_4$ cleavage to the diketone (**8**) [IR($CHCl_3$) 1730 and 1715 cm^{-1}; *m/z* 236 (M^+)].

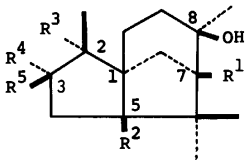

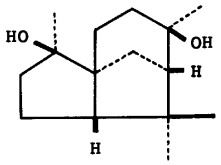

4

1 $R^1=R^2=R^3=R^4=R^5=H$
2 $R^1=OH$, $R^2=R^3=R^4=R^5=H$
3 $R^2=OH$, $R^1=R^3=R^4=R^5=H$
5 $R^3=OH$, $R^1=R^2=R^4=R^5=H$
6 $R^4=OH$, $R^1=R^2=R^3=R^5=H$
7 $R^5=OH$, $R^1=R^2=R^3=R^4=H$

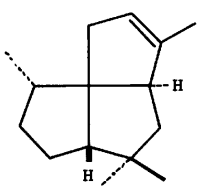

"senoxydene"

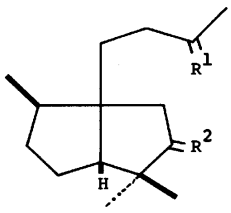

8 $R^1=R^2=O$
13 $R^1=R^2=H$

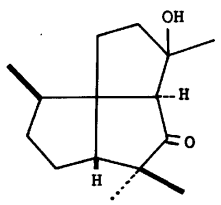

9

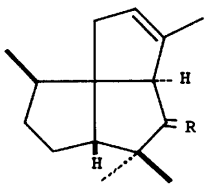

10 R=O
14 $R=H_2$

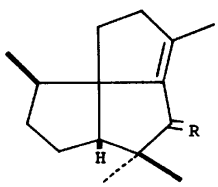

11 R=O
12 $R=H_2$

An analogous argument based on spectroscopic data led to the assignment of structure **3** [IR($CHCl_3$) 3600 and 3550 cm^{-1}; *m/z* 238 (M^+)] to a further product of cedrol oxidation. The ^1H NMR spectrum of the final product, a diol **4** [mp 114 °C; $[\alpha]_D$ +14.1 ° (*c*, 0.28 in $CHCl_3$); IR ($CHCl_3$) 3600 and 3400 cm^{-1}] indicated the presence of four tertiary methyl groups which led directly to structure **4**, cedrane-2β,8β-diol. Dehydration (HCOOH) of **4** gave cedra-2,8-diene,[11] which was obtained by a similar reaction of **5**.[11]

In order to demonstrate the synthetic utility of this method, the diol **2** was transformed into an epimer of the alleged "senoxydene." The glycol **2** was converted to the diketone (**8**) (*vide supra*) which, on treatment with methanolic sodium methoxide, underwent an intramolecular aldol condensation to afford the hydroxy ketone (**9**) [IR(CCl_4) 3600, 3400, and 1720 cm^{-1}; *m/z* 236 (M^+)] in 63% yield. Subsequent dehydration [$SOCl_2$/Py/0 °C] gave an equimolar mixture of enones **10** and **11**, separation of which was effected by column chromatography over silica-gel (EtOAc–hexane gradient as eluent). Upon Huang-Minlon reduction (KOH/NH_2NH_2/diethylene glycol) of **10**, a mixture of olefin **12** and bicyclic hydrocarbon **13** (presumably arising *via* a retro-aldol reaction) was obtained. However, when the preformed hydrazone (NH_2NH_2/diethylene glycol/180 °C/3 h) was subjected to base treatment (KOH/240 °C/9 h/Ar atmosphere) the desired olefin (**14**) ($[\alpha]_D$ −42.5° (*c*, 0.17 in $CHCl_3$)) was isolated in 27% yield after purification. The spectral data were in accord with those reported by Tsunoda *et al.*[13]

In conclusion, cedrol was hydroxylated by *m*CPBA to give cedrane-7β,8β-diol and the transformation of this diol into the optically active triquinane type hydrocarbon, which is the C-2 epimer of "senoxydene," was achieved in four steps.

Experimental

General Procedures. Melting points were determined on a Yanaco Micro Melting Point apparatus (Yanagimoto) and are uncorrected. IR spectra were taken on a Shimadzu IR-27G infrared spectrophotometer. ^1H and ^{13}C NMR spectra were determined on a JEOL JNM GX 400 (400 MHz for ^1H and 100 MHz for ^{13}C) spectrometer in $CDCl_3$ with TMS as internal standard. Low and high resolution mass spectra were obtained on a Shimadzu LKB-9000B and JEOL HX-100 spectrometer, respectively. Precoated silica gel 60 F_{254} (E. Merck) glass supported plates were used for the purposes of analytical (0.25 mm) and preparative (0.5 mm) thin-layer chromatography.

Oxidation of Cedrol (1) by mCPBA. *m*CPBA (2.7 g, 1.2 equiv) was added to a solution of cedrol (**1**, 2.2 g) in chloroform (75 ml) and the mixture was refluxed for 6 h. The cooled solution was washed succesively with 5% Na_2SO_3, 5% $NaHCO_3$, and brine, dried over $MgSO_4$ and the solvent removed to give a residue (2.5 g). Column chromatography over silica gel (155 g, EtOAc–PhH gradient as eluant) gave cedrane-7β,8β-diol (**2**, 36 mg), a mixture of cedrane-3α,8β-diol (**6**), cedrane-3β,8β-diol (**7**), and cedrane-5β,8β-diol (**3**), cedrane-2β,8β-diol (**4**, 49 mg), and cedrane-2α,8β-diol (**5**, 193 mg) as well as unchanged cedrol (**1**, 1.8 g). The mixture of **6**, **7**, and **3** was separated by HPLC (TSK gel; MeOH–H_2O 7:3, 1.2 ml/min) to give **6** (2.5 mg), **7** (1.5 mg), and **3** (33 mg). **2**: mp 95—97 °C (sublime); Found: *m/z* 238.1938. Calcd for $C_{15}H_{26}O_2$: M 238.1933; $[\alpha]_D$=+14.1 ° ($CHCl_3$); IR ($CHCl_3$) 3570—3450 cm^{-1}; ^1H NMR ($CDCl_3$) δ=1.35 (3H, s), 1.21 (3H, s), 0.97 (3H, s), and 0.87 (3H, d, *J*=7 Hz); ^{13}C NMR ($CDCl_3$) δ=85.3 (s), 77.9 (s), 57.3 (d), 49.3 (s), 45.6 (s), 45.5 (t), 42.3 (d), 36.4 (t), 34.8 (t), 31.3 (t), 26.5 (t), 26.1 (q), 25.4 (q), 24.7 (q), and 15.2 (q); MS *m/z* 238 (M^+), 220, 193 (base), 165, 121, 109, and 43. **3**: oil; Found: *m/z* 238.1945. Calcd for $C_{15}H_{26}O_2$: M 238.1933; $[\alpha]_D$=+10.6 ° ($CHCl_3$); IR ($CHCl_3$) 3600—3550 cm^{-1}; ^1H NMR ($CDCl_3$) δ=1.28 (6H, s), 1.10 (3H, s), 0.92 (3H, d, *J*=7 Hz); ^{13}C NMR ($CDCl_3$) 91.9 (s), 75.0 (s), 60.4 (d), 56.0 (s), 46.1 (s), 41.2 (t), 41.0 (d), 36.8 (t), 36.3 (t), 35.1 (t), 31.5 (q), 30.5 (q), 27.1 (t), 23.0 (q), and 16.6 (q); MS *m/z* 238 (M^+), 220, 205, 178 (base), 121, and 43. **4**: mp 114 °C; Found *m/z* 223.1722 ($M-CH_3$)$^+$. Calcd for $C_{14}H_{23}O_2$. M 223.1698; $[\alpha]_D$=+14.1 ° ($CHCl_3$); IR ($CHCl_3$) 3600—3400 cm^{-1}; ^1H NMR ($CDCl_3$) δ=1.31 (3H, s), 1.28 (3H, s), 1.17 (3H, s), and 1.01 (3H, s); ^{13}C NMR ($CDCl_3$) δ=80.9 (s), 75.0 (s), 59.4 (s), 59.1 (d), 53.3 (d), 45.0 (s), 40.3 (t), 39.1 (t), 35.7 (t), 30.5 (q), 30.3 (q), 29.3 (t), 28.6 (q), 23.0 (q), and 22.4 (t); MS *m/z* 223 ($M-CH_3$)$^+$, 220, 205, 151 (base), 93, 43.

Oxidation of Cedrane-7β,8β-diol (2). The diol (**2**, 10 mg) was treated with $Pb(OAc)_4$ (18 mg) in benzene (5 ml) at rt for 2 h and worked up as usual to give 4,4,8-trimethyl-1-(3-oxobutyl)bicyclo[3.3.0]octan-3-one (**8**, 9.3 mg) as an oil. Found: *m/z* 236.1799. Calcd for $C_{15}H_{24}O_2$: M 236.1776; IR ($CHCl_3$) 1730 and 1715 cm^{-1}; ^1H NMR ($CDCl_3$) δ=2.18 (3H, s), 1.09 (3H, s), 0.99 (3H, s), and 0.95 (3H, d, *J*=7 Hz); ^{13}C NMR ($CDCl_3$) δ=223.1 (s), 208.4 (s), 55.4 (d), 48.4 (s), 48.3 (s), 45.9 (t), 44.9 (d), 39.7 (t), 32.8 (t), 30.2 (q), 28.6 (q), 27.6 (t), 25.1 (t), 22.0 (q), and 14.0 (q); MS *m/z* 236 (M^+), 221, 193, 165, 81, and 43.

Intramolecular Aldol Condensation of the Diketone (8). The diketone (**8**, 25 mg) was treated with NaOMe in MeOH [prepared from Na (*ca.* 0.1 g) and MeOH (4.5 ml)] at rt for 3 h. The usual work up and chromatography over silica gel (elution with hexane–EtOAc) afforded 4-hydroxy-4,7,7,11β-tetramethyl-(5α,8β)-tricyclo[6.3.0.0^{1,5}]undecan-6-one (**9**, 16 mg) as an oil. Found: *m/z* 236.1751. Calcd for $C_{15}H_{24}O_2$: M 236.1776; IR ($CHCl_3$) 3600, 3400, and 1720 cm^{-1}; ^1H NMR δ=2.34 (1H, s), 2.22 (1H, dd, *J*=9.5 and 5.5 Hz), 1.45 (3H, s), 1.06 (3H, s), 0.98 (3H, d, *J*=6.5 Hz), and 0.95 (3H, s). ^{13}C NMR δ=226.0 (s), 80.2 (s), 66.2 (d), 59.3 (d), 58.8 (s), 50.8 (s), 43.6 (d), 42.1 (t), 34.3 (t), 32.9 (t), 29.1 (q), 26.0 (q), 23.8 (t), 23.1 (q), and 13.8 (q); MS *m/z* 236 (M^+), 221, 193 (base), 178, 165, and 43.

Dehydration of the Ketol (9). The ketol (**9**, 2.3 mg) was treated with $SOCl_2$ (3 drops) in pyridine (0.6 ml) at 0 °C for 30 min. The usual work up and prep. TLC gave 4,7,7,11β-tetramethyl-(5α,8β)-tricyclo[6.3.0.0^{1,5}]undec-3-en-6-one (**10**, 0.5 mg) [oil; Found: *m/z* 218.1655. Calcd for $C_{15}H_{22}O$:M 218.1671; IR ($CHCl_3$) 1720 cm^{-1}; ^1H NMR δ= 5.33 (1H, brs), 2.84 (1H, brs), 2.71 and 2.12 (each 1H, d, *J*=19.5 Hz), 2.22 (1H, dd, *J*=9 and 6 Hz), 1.75 (3H, s), 1.06 (3H, s), 0.98 (3H, s) and 0.97 (3H, d, *J*=7 Hz); MS *m/z* 218 (M^+), 190, 175, 147 (base), 120, 108, 91, and 55] and

4,7,7,11β-tetramethyl-(8β)-tricyclo[6.3.0.0^{1,5}]undec-4-en-6-one (**11**, 0.6 mg) [oil; IR ($CHCl_3$) 1725 cm^{-1}; ^{1}H NMR δ= 2.05 (3H, brs), 1.04 (6H, s), and 0.94 (3H, d, J=6.6 Hz); MS m/z 218 (M^+), 203, 193 (base), 175, 121, and 43].

Reduction of the Enone (10). The enone (**10**, 18 mg) was heated with hydrazine (0.3 ml) in diethylene glycol (2 ml) at 180 °C for 3h under Ar. After removal of water and excess of hydrazine, the mixture was heated with KOH (50 mg) at 220—240 °C for 9h. The usual work up and chromatography over silica gel afforded 4,7,7,11β-tetramethyl-(5α,8β)-tricyclo[6.3.0.0^{1,5}]undec-3-ene (**14**, 4.7 mg) as an oil. Found: m/z 204.1878. Calcd for $C_{15}H_{24}$: M 204.1878; $[\alpha]_D$=−42.5° ($CHCl_3$, c=0.17); IR ($CHCl_3$) 1460, 1380, 1365 cm^{-1}; ^{1}H NMR ($CDCl_3$) δ=5.09 (1H, brs), 2.59 (1H, brd, J=16.8 Hz), 2.45 (1H, m), 2.02 (1H, brd, J=16.8 Hz), 1.89 (1H, t, J=8.1 Hz), 1.72 (1H, dd, J=13 and 8.5 Hz), 1.65 (3H, brs), 1.43 (1H, dd, J=13 and 4.6 Hz), 0.96 (3H, s), 0.92 (3H, s), and 0.90 (3H, d, J=6.5 Hz); MS m/z 204 (M^+), 189, 161, 147, 133, 123 (base), 105, and 91.

We thank Professor Shô Itô, Tohoku University, for his generous gift of cedrol and Professor Mitsuaki Kodama, of this university, for providing the spectra of the hydrocarbon **14** and helpful discussions. We are also indebted to Dr. Leslie J. Harrison for reading the manuscript. This work was supported in part by a Grant-in-Aid from the Ministry of Health and Welfare.

References

1) Y. Mazur, *Pure & Appl. Chem.*, **41**, 145 (1975).
2) R. Breslow, *Chem. Soc. Rev.*, **1**, 553 (1972).
3) D. H. R. Barton, J. M. Beaton, L. E. Geller, M. M. Pechet, *J. Am. Chem. Soc.*, **82**, 2640 (1960); *ibid.*, **83**, 4076 (1961), and references cited therein.
4) *e.g.* K. Takeda, *Pure & Appl. Chem.*, **21**, 181 (1970).
5) T. S. Santhanakrishnan, *Tetrahedron*, **40**, 3597 (1984).
6) N. C. Deno and M. D. Meyer, *J. Org. Chem.*, **44**, 3383 (1979).
7) W. Müller and H. -J. Schneider, *Angew. Chem., Int. Ed. Engl.*, **18**, 407 (1979).
8) T. Ishida, Y. Asakawa, M. Okano, and T. Aratani, *J. Pharm. Sci.*, **68**, 928 (1979); T. Ishida, Y. Asakawa, T. Takemoto, and T. Aratani, *ibid.*, **70**, 406 (1981); Y. Asakawa, Z. Taira, T. Takemoto, T. Ishida, M. Kido, and Y. Ichikawa, *ibid.*, **70**, 710 (1981); T. Ishida, Y. Asakawa, and T. Takemoto, *ibid.*, **71**, 965 (1982).
9) M. Tori, R. Matsuda, and Y. Asakawa, *Tetrahedron Lett.*, **26**, 227 (1985).
10) M. Tori, R. Matsuda, and Y. Asakawa, *Chem. Lett.*, **1985**, 167.
11) E. Trifilieff, L. Bang, A. S. Narula, and G. Ourisson, *J. Chem. Research (M)*, **1978**, 601.
12) K. C. Wang, L. Y. Ho, and Y. S. Cheng, *J. Chin. Biochem. Soc.*, **1**, 53, (1972).
13) T. Tsunoda, Y. Kabasawa, S. Ito, and M. Kodama, *Tetrahedron Lett.*, **25**, 773 (1984).
14) F. Bohlmann and C. Zdero, *Phytochemistry*, **18**, 1747 (1979).
15) E. Trifilieff, L. Bang, and G. Ourisson, *Tetrahedron Lett.*, **1975**, 4307.
16) We found that the previous assignments[12,15] of these compounds are contrary to each other. Therefore, we have carried out difference NOE experiments for these compounds. When the 3β-proton of **6** was irradiated, an NOE upon the 2β-methyl group was observed. However, no NOE appeared in the case of the 2β-methyl group of **7**, when the 3α-proton was saturated. From these results, **6** was determined to be cedrane-3α,8β-diol and **7** to be cedrane-3β,8β-diol, which is in agreement with Ourisson's results.[15]

Reactions of Ozone with 1-(*m*-Substituted phenylazo)-2-naphthol-6-sulfonic Acids in Aqueous Solutions

Yasuo ONARI
Mie Industrial Research Institute, Takajayakomori-cho, Tsu 514
(Received March 15, 1985)

The substituent effect on the ozone decoloration reactions of 1-(*m*-substituted phenylazo)-2-naphthol-6-sulfonic acids (PANSA) in aqueous solutions was investigated. Both the acidities of PANSA and the variation of the ozone decoloration rates of them increased compared to those of the corresponding 1-(*m*-substituted phenylazo)-2-naphthol-3,6-disulfonic acids (PANDSA). The relationships between the decoloration rates and the indexes(pK_{OH} and σ_m values) of the basicities of the dyes, however, indicated nearly the same characteristics between the data of these two series of dyes, and the ozone decoloration reactions of PANSA appeared to proceed by nearly the same mechanism as those of PANDSA. The changes of the keto–enol ratios of the dyes with their ozone decolorations suggested that the decoloration rates might rise as the reduction rates of their keto–enol ratios increased. It seems likely that the chief organic product that was finally produced in these reactions is oxalic acid.

Because of the toxicity of dye waste, the biological treatment of it is very difficult. Ozone decoloration reactions of dyes have already been applied for the removal of the organic color of the waste water from dyeing industries. However, little is known about the ozonation mechanism of dyes and about the ozone reactivities of them in aqueous media. Ikehata and co-workers[1] have investigated the ozone oxidation products of some azo dyes in water. Matsui *et al.*[2] reported on the ozonation of *p*-aminoazobenzene in aqueous solution. In the previous papers,[3,4] some phenylazonaphthols and naphthylazonaphthols were taken up, and the ozone decoloration reactions of them were investigated. The ozone decoloration rates of these dyes showed the tendency to increase with increasing the electron-withdrawing powers of their substituents. It was also proved that the ozone decolorations of the dyes were accelerated with their substituent sulfo groups. On the basis of these results, the selectivity of the ozone decoloration reactions of a series of phenylazonaphthol dyes was expected to increase with decreasing the number of sulfo groups in their naphthol moieties. Therefore, a series of dyes bearing only one sulfo substituent on each of their naphthol moieties was desired to be taken up for the purpose of the further investigations on the mechanism of the ozone decoloration reactions of azo dyes. The ozone reactivities of seven 1-(*m*-substituted phenylazo)-2-naphthol-6-sulfonic acids(PANSA) were previously investigated using ^{1}H-NMR spectra.[5] In the present work, eight PANSA were examined similarly to eight 1-(*m*-substituted phenylazo)-2-naphthol-3,6-disulfonic acids(PANDSA)[4] so as to throw light mainly on the polar effect of the ozone decoloration rates of them in aqueous media. These observations induce us to know the reaction mechanism more precisely and to see what the difference in the reactivity is between the ozone decoloration of PANSA and that of the corresponding PANDSA.

Experimental

Preparations of the Dyes. The dyes were prepared by the diazotizated-coupling reactions of *m*-substituted anilines with Schaeffer's acid(2-naphthol-6-sulfonic acid) in the ordinary way. They were extracted with 1-butanol from the resulting reaction mixtures followed by purification on a cellulose column using a 2 mol dm^{-3} NH_3 solution saturated with 1-butanol as eluent. And then they were recrystallized from suitable organic solvents for a few times. The properties of the dyes are shown in Table 1.

Measurements. Equipments and measuring methods were the same as those shown in the previous paper.[3] All the chemicals employed for the experiment were special reagent grade. A solution of dye(4×10^{-5} mol dm^{-3}) in 0.5 dm^3 distilled water, the pH and the ionic strength (μ: 0.2) of which were controlled with the Sörensen buffer solution and KNO_3 respectively, was employed for the ozone decoloration reaction. The prepared solution was placed in a 0.5 dm^3 Pyrex gas-washing bottle having a G-2 sintered-glass filter at the bottom of it as a diffuser. Ozonized air(O_3 concn: 1.94 mg dm^{-3}) was continuously supplied into the bottle at a constant flow rate of 2.7 dm^3 min^{-1} through the sintered-glass filter. A part(3.5 cm^3) of the solution was circulated through micro flow-cell of the spectrophotometer with a micropump, and the ozone decoloration of the dye was continuously recorded. Ozonized air was obtained using a Nihon Ozon 0-3-3 electric discharge ozone generator. A Nihon Bunko UVIDEC-1 digital doublebeam spectrophotometer was used for the measurements of the decoloration rates. The visible absorption spectra and the acid dissociation constants of the dyes were obtained on a Hitachi 323 spectrophotometer. Elemental analysis was performed on a Yanaco MT-3 CHN Corder. Fatty acids were measured with a Nihon Bunko FLC 350 high-performance liquid chromatograph equipped with a UVIDEC-100 UV spectrometer as a detector.

Results and Discussion

Acid Dissociation Constants of the Dyes. The acid dissociation constants(pK_{OH}) of the dyes were

Table 1. Properties of the dyes

No.	Constitution	Anal (C/N) Found (Calcd)	λ_{max} (nm)(ε_{max})[a]	pK_{OH}[b]	Keto–enol[c] ratio
1	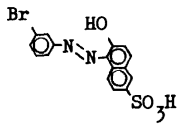	6.99 (6.86)	474 (1.58×10^4)	10.27	2.14
2	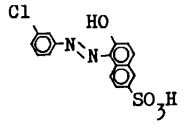	7.00 (6.86)	473 (1.59×10^4)	10.30	2.10
3	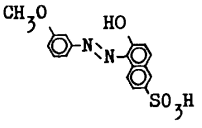	7.37 (7.29)	482 (1.50×10^4)	10.39	2.28
4	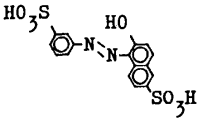	6.86 (6.86)	475 (1.54×10^4)	10.13	2.11
5	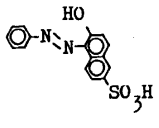	6.89 (6.86)	478 (1.43×10^4)	10.51	2.36
6	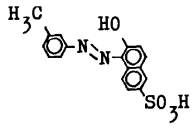	7.39 (7.29)	482 (1.53×10^4)	10.67	2.57
7	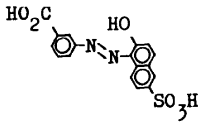	7.40 (7.29)	472 (1.47×10^4)	10.50	2.40
8	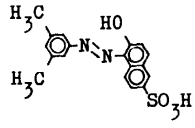	8.00 (7.72)	487 (1.54×10^4)	10.83	2.70

a) Measured in methanol at room temperature. b) Acid dissociation constant of the dye at 21 °C (μ: 0.2 (KNO_3)). c) A_{CO}/A_{OH} value of the dye in distilled water.

determined spectrophotometrically at 21 °C (μ: 0.2 (KNO_3)) in the same manner as that was shown in the previous report.[3] The result is shown in Fig. 1.

The relationship between the pK_{OH} values of PANSA and the Hammett's σ_m values of their substituent groups is shown in Fig. 2. The pK_{OH} values of the dyes showed the tendency to decrease with increasing σ_m values of their substituents, and the regression equation was calculated as follows: $pK_{OH}=10.51-0.62\,\sigma_m$. The result indicated nearly the same tendency as that shown in the pK_{OH} values of PANDSA: $pK_{OH}=10.80-0.91\,\sigma_m$. However, the p$K_{OH}$ values of PANSA were smaller than those of the corresponding PANDSA in contrast to the expectation that was produced from the reduction of the inductive effect of the sulfo substituent in the *ortho*-position to OH. This seemed to be based on the disappearance of another influence (for example, the effect of the negative charge) of the substituent.

The pH Dependence of the Ozone Decoloration Rates of the Dyes. Because of the electrophilic nature of ozone, the ozone decoloration rates of PANSA can be estimated to be accelerated with their proton dissociations. The relationship between the logarithms of pseudo-first-order rate constants($\log k_{obsd}$)

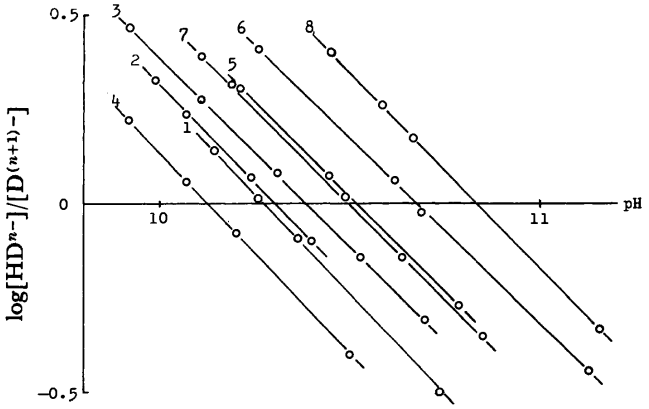

Fig. 1. Relations between log[HD^{n-}]/[D$^{(n+1)-}$] and pH for the determinations of the acid dissociation constants of the dyes at 21 °C (μ: 0.2(KNO_3)).
Number attached to each curve is the same as that given in Table 1.

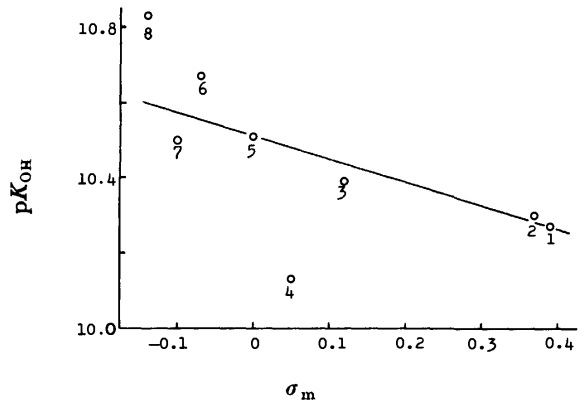

Fig. 2. Relation between the acid dissociation constants of the dyes and the Hammett's σ_m values of their substituents.
pK_{OH}=10.51—0.62 σ_m(n: 6, γ: −0.901).
Number attached to each point is the same as that given in Table 1.

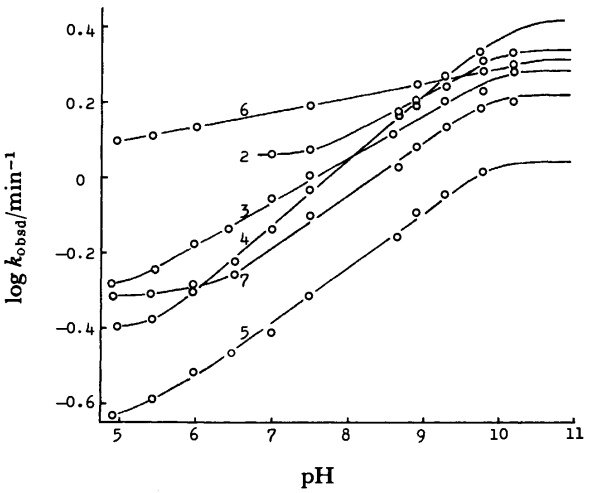

Fig. 3. Relations between the logarithms of pseudo-first-order rate constants and pH for the decoloration reactions of the dyes with ozone at 25 °C.
Number attached to each curve is the same as that given in Table 1.

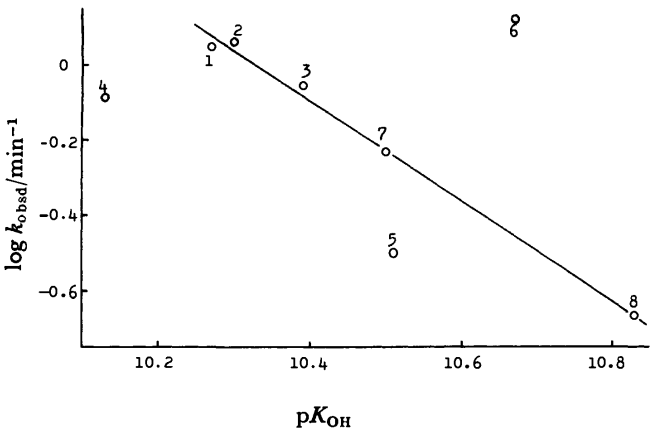

Fig. 4. Relation between log k_{obsd} and pK_{OH} for the decoloration reactions of the dyes with ozone at pH 7.0 and 25 °C.
log k_{obsd}=13.77—1.333 pK_{OH}(n: 5, γ:−0.997).
Number attached to each point is the same as that given in Table 1.

and pH for the ozone decolorations of the dyes is shown in Fig. 3. The log k_{obsd} values of these reactions increased linearly with increasing pH of the solutions in the pH ranges of about the half-neutralization points of the hydroxyl groups of the dyes to 6.0. The slopes of these regression lines were 0.039(NO. 6)—0.171(NO. 4), and the average value of them was 0.119. This average value of the slopes showed nearly the same as those: 0.13 and 0.116 of the results that had been shown in Refs. 3 and 4 respectively. These results suggested that the pH dependence of the decoloration rates was scarcely variable in all the ozone decoloration reactions of those monoazo dyes.

The Relationship between the Basicities of the Dyes and the Ozone Reactivities of Them. In order to reveal the mechanism of these ozone decoloration reactions, the investigation on the pK_{OH} dependence of the decoloration rates was also made in this work. The relationship between log k_{obsd} and pK_{OH} of PANSA is shown in Fig. 4. It showed a good linearity with the exception of 4, 5, and 6(log k_{obsd}=13.77−1.333 pK_{OH}(n=5, γ=−0.997)). The negative slope of this regression line suggested the global process to be nucleophilic. In this case, the variation of log k_{obsd} with pK_{OH} was larger than that shown in the ozone decolorations of the monoazo dyes bearing only sulfo substituents(pH 7.0, log k_{obsd}= 1.955−0.207 pK_{OH})[3] and larger than that shown in the ozone decolorations of PANDSA(pH 7.0, log

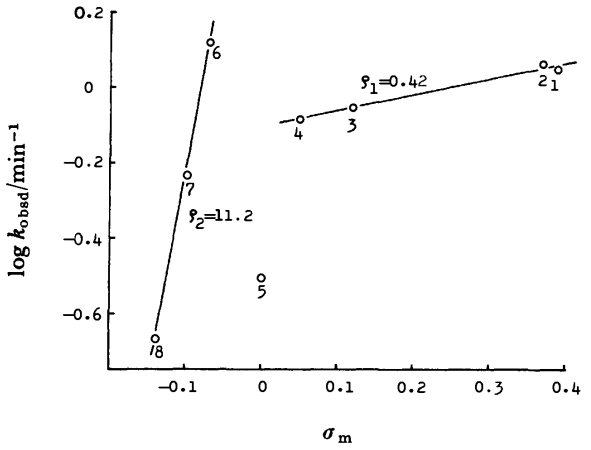

Fig. 5. Hammett plot for the decoloration reactions of the dyes with ozone at pH 7.0 and 25 °C.
Number attached to each point is the same as that given in Table 1.

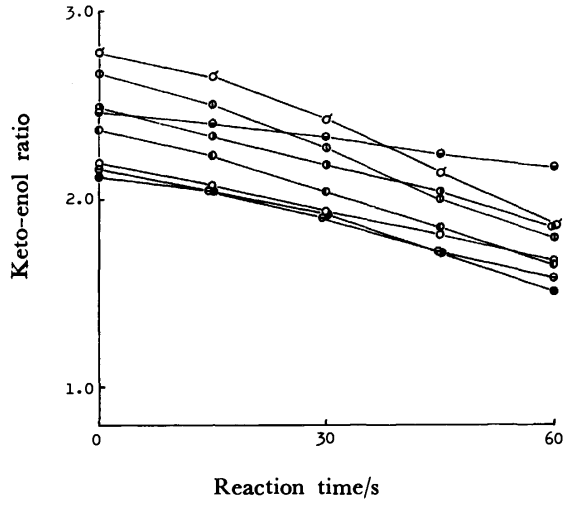

Fig. 6. Changes of the keto-enol ratios with reaction time for the decoloration reactions of the dyes with ozone at pH 7.0 and 25 °C.
●: 1, ⊖: 2, ◐: 3, ○: 4, ◒: 5, ⓘ: 6, ◑: 7, ○: 8.
Number attached to each curve is the same as that given in Table 1.

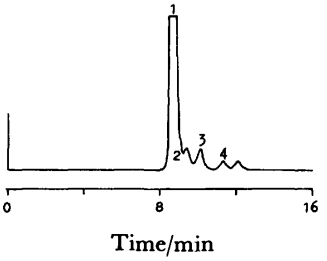

Fig. 7. Typical HPLC chromatogram of the ozone oxidation products of the dye.
Dye: 5, Flow rate: 1 cm^3 min^{-1}, Detector: UV 210 nm.
1: Nitrate, 2: Oxalic acid, 3: Maleic acid, 4: Glyoxylic acid.

k_{obsd}=0.937−0.0911 pK_{OH})[4] as expected.

The relationship between the Hammett's σ_m values and log k_{obsd} for the ozone decolorations of the dyes is shown in Fig. 5. The obtained ρ values were: 0.42(ρ_1) for the dyes bearing the electron-withdrawing groups and 11.2(ρ_2) for those bearing the electron-releasing groups. The positive ρ values indicated that the global process of these reactions was nucleophilic in nature, but $\rho_1<\rho_2$ and the discontinuity in the relationship showed that the electrophilic process played an important role in these ozone decoloration reactions. In the ozone decoloration reactions of these dyes, the variation of the decoloration rates was larger than, but the characteristic of the Hammett plot was similar to, those shown in the ozone decoloration reactions of PANDSA. From these results, the ozone decoloration reactions of these dyes appeared to proceed by nearly the same mechanism as those of PANDSA.

The Changes of the Keto-Enol Ratios of the Dyes with Their Ozone Decoloration Reactions. These dyes exist as the hydroxy azo-keto hydrazo tautomeric equilibria in aqueous solutions. In this work, the effect of the tautomeric equilibria of the dyes on their ozone decoloration rates was investigated. Burawoy and Thompson[6] examined the tautomeric equilibria of arylazonaphthols using electronic spectra, and indicated that the absorption maxima near 480 and 420 nm were due to the keto hydrazo form and the hydroxy azo form respectively. As an index of the tautomeric equilibria, the ratio(A_{CO}/A_{OH}, keto-enol ratio) of the absorbance at the absorption maximum appeared near 480 nm (A_{CO}) to that at the shoulder near 420 nm (A_{OH}) was taken up. The changes of the keto-enol ratios with the ozone decolorations of these dyes are shown in Fig. 6. In the case of the ozone decolorations of PANDSA,[4] the percent residual values of the keto-enol raios after the ozone treatments of PANDSA for 60 s were 50.7—63.4% (average value: 56.3%). The values obtained in this work were 66.9—87.9% (average value: 73.3%). The two couples of dyes; 2, 4 and 5, 7, the initial values of the keto-enol ratios for two dyes of each couple were nearly the same, suggested that the ozone decoloration rates of the dyes increased with increasing the reduction rates of their keto-enol ratios. Therefore, the unexpected behavior of 5 in the Hammett plot (Fig. 5) seemed to be mainly based on the low reduction rate of its keto-enol ratio compared with the reduction rates of those of the others in these ozone decoloration reactions. From these results, initial attack of ozone on the dye molecule was anticipated to take place at the

NC double bond of its keto hydrazo form in a similar manner as described in the ozonolysis of PANDSA.[4]

Oxidation Products of the Dyes. Initial ozone oxidation products of phenylazonaphthol dyes had already been reported in the previous paper.[3] In the present work, fatty acids from the ozonations of these dyes were analyzed by the high-performance liquid chromatograph using a Shodex Ionpak C-811 column (50 cm 8 cm i.d, Showadenko Co., Ltd.) and 0.1% H_3PO_4 as eluent. The typical chromatogram is presented in Fig. 7. In all these reactions, the formations of maleic acid, glyoxylic acid, and oxalic acid were confirmed. Maleic acid seems to be the precursor for glyoxylic acid and oxalic acid, and glyoxylic acid seems to be that for oxalic acid. Consequently, it seems likely that the main organic product that was finally produced in these ozone oxidizing reactions is oxalic acid. Nitrate ion was also detected in the resulting reaction mixtures. This indicates that a part of the azo group of the dye appeared to oxidized to nitrate.

References

1) K. Ishizaki, K. Sakata, S. Shinriki, and A. Ikehata, *Nippon Kagaku Kaishi*, **1979**, 1124.

2) M. Matsui, K. Kobayashi, H. Miyazaki, K. Shibata, and Y. Takase, *Sen-I Gakkaishi*, **37**, 381 (1981).

3) Y. Onari, *Nippon Kagaku Kaishi*, **1978**, 1570.

4) Y. Onari, *Nippon Kagaku Kaishi*, **1983**, 1526.

5) Y. Onari, Presented in part at the 45 th Annual Meeting of the Chemical Society of Japan, April 1982, Abstracts I, P. 246.

6) A. Burawoy, and A. R. Thompson, *J. Chem. Soc.*, **1953**, 1443.

 © 1985 The Chemical Society of Japan Bull. Chem. Soc. Jpn., 58, 2531—2540 (1985)

Ring-cleavage Reactions of Aromatic Hydrocarbons Studied by FT-IR Spectroscopy. I. Photooxidation of Toluene and Benzene in the NO_x-Air System

Hiroshi BANDOW,* Nobuaki WASHIDA, and Hajime AKIMOTO
Division of Atmospheric Environment, The National Institute for Environmental Studies, P.O. Tsukuba-gakuen, Ibaraki 305
(Received February 12, 1985)

The products of the atmospheric photooxidation reactions of toluene and benzene were analyzed quantitatively using long-path FT-IR spectroscopy. Methylglyoxal (only in the case of toluene), glyoxal and maleic anhydride were observed as aromatic ring-cleavage products. In the toluene photooxidation, yields of methylglyoxal, glyoxal, and maleic anhydride were 14±4, 15±4, and 4.0±0.4% (mole/mole), respectively. The formation of small molecules, formaldehyde and formic acid, was observed. It is suggested that the precursor of the ring-cleavage reaction is OH-aromatics-O_2 adducts, and that the α-dicarbonyls and unsaturated γ-dicarbonyls are produced by ring cleavage after cyclization of the OH-aromatics-O_2 adduct. The observation of maleic anhydride is considered as an evidence of the aromatic ring cleavage into C_2 and C_4 fragments. The fraction of the ring cleavage process in the total reaction is 29 and 15—20% in the cases of toluene and benzene, respectively.

Oxidation processes of aromatic hydrocarbons initiated by the reaction of hydroxyl radicals are of fundamental interest in physical chemistry of organic compounds as well as in the development of chemical models of photochemical air pollution.[1-3] For the reactions of OH radicals with an aromatic hydrocarbon such as toluene, the initial reaction can be either abstraction (Reaction 1a) or addition to the aromatic ring (Reaction 1b).

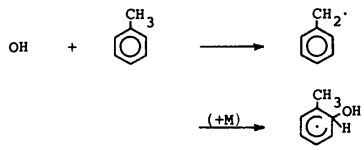

(1a)

(1b)

Studies both by measurements of the rate constant[4-12] and by analysis of reaction products[13-19] indicate that electrophilic addition of the OH radical to the aromatic ring is the dominant reactive pathway (80—93% in the case of toluene) at room temperature over the pressure range from several hundred Pa to 101 kPa (1 atm) total pressure, that side-chain hydrogen abstraction channel is small but significant (7—20% in the case of toluene), and that ring-hydrogen abstraction is a negligible channel. In the presence of O_2 and NO, aromatic aldehydes are produced from radicals obtained by side-chain hydrogen abstraction.[3,13-15,17-19] Under these conditions some of the OH-aromatics adducts yield stable products retaining the aromatic ring[3,14,15,17-19] (including phenols and aromatic nitro compounds) competing with the ring cleavage.[3,17,19-25]

The formation of α-dicarbonyls[17,19,23,24] (glyoxal, methylglyoxal, and biacetyl) in addition to small fragment molecules[3,20-22] (CO, CO_2, formaldehyde, and formic acid) has been reported. These dicarbonyls are typical reaction products caused by the

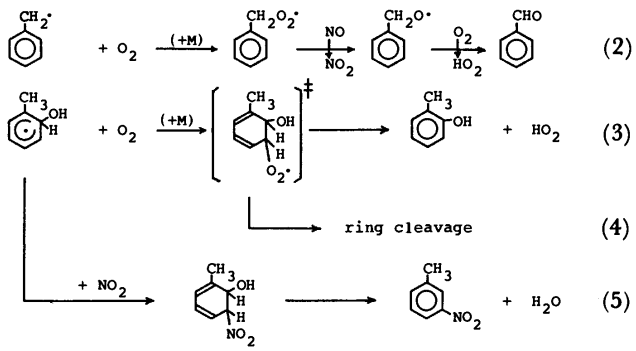

(2)

(3)

ring cleavage (4)

(5)

ring cleavage of cyclic organic compounds as suggested in the oxidation of cycloalkanes.[26,27] Although the importance of ring-cleavage processes in the oxidation of aromatic hydrocarbons has been suggested,[3,17,24] yields and the formation mechanism of dicarbonyls are not clear.

It is well known that aromatic hydrocarbons are important constitutents in polluted atmospheres.[28] The concentration of the total aromatic hydrocarbons is often close to and sometimes higher than that of the total olefins. Recent measurements on the rate constants[4-12,29] for the reaction of hydroxyl radicals with aromatic hydrocarbons indicate that most of aromatic hydrocarbons react with OH faster than paraffins and that highly-alkyl-substituted benzenes are comparable to olefins. Therefore, the elucidation of photooxidation processes of the aromatic hydrocarbons is important to the development of chemical models of photochemical air pollution.[3,30]

In the present study, observations of the reaction products in the photooxidation of aromatic hydrocarbons in the NO_x-air system were carried out using long-path Fourier transform infrared absorption spectroscopy (LP FT-IR), in which products are observed directly without the sampling and preconcentration needed in the GC (gas chromato-

graphy) and GC/MS (gas chromatography/mass spectroscopy) analysis. The major goal of this study is the quantitative analysis of the α-dicarbonyls and unsaturated γ-dicarbonyls to elucidate the mechanism of the ring-cleavage reactions.

In this paper, the reactions of toluene and benzene are reported. Toluene is important as a prototype of the oxidation process of alkylbenzenes.

Experimental

Toluene or benzene, NO, and NO_2 diluted in 1 atm air were irradiated in a reaction chamber and reaction products were measured by LP FT-IR directly. A schematic diagram of the reaction chamber and the LP FT-IR system is shown in Fig. 1. The chamber is a stainless-steel cylinder, 0.5 m inner diameter and 3.55 m long with a volume of 0.79 m^3. Its inner wall is coated by FEP-teflon to minimize wall effects. The chamber is bakable up to 80 °C by circulating hot water through the wall, and evacuable below 1×10^{-6} Torr by an oil-diffusion pump (1500 l s^{-1}) and an oil-rotary pump (950 l min^{-1}). Fourteen

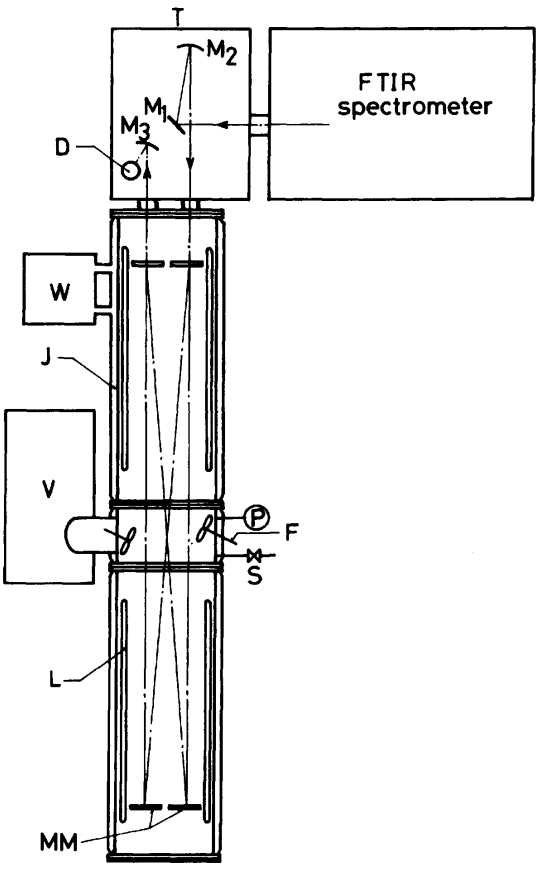

Fig. 1. Schematic diagram of reaction chamber and FT-IR optics.
M_{1-3}: Mirrors, MM: Multi-reflection mirrors, D: Liquid nitrogen cooled MCT detector, L: Black-light lamps, P: Pressure gauge, F: Mixing fans, S: Stopcock for gas inlet, V: Vacuum pumping unit, W: Water bath, J: Water jacket.

black light lamps (40W, Toshiba FL40S BLB) on the inner wall of the chamber were used as a light source. The wavelength distribution of the lamp ranges from 300 to 430 nm with an intensity maximum at about 350 nm. The effective light intensity as measured by the primary photodecomposition rate of NO_2[31] was 0.22 min^{-1}.

An eight-mirror multireflection system (a White cell) is set in the chamber and connected to a Nicolet 7199 FT-IR spectrometer as shown in Fig. 1. The base path between multireflection mirrors is 3.0 m and the number of reflections is 69, giving a total path length of 210.8 m. A liquid nitrogen cooled MCT (Hg-Cd-Te semiconductor) detector was used as an IR detector. The spectral resolution used in the present study was 1 cm^{-1}. IR spectra were recorded by accumulating 128 scans with 3.8 min scanning time.

The air used was supplied by an air purifier (Standard Technology Inc., model SGPU-21), in which hydrocarbons and NO in source air are converted to CO_2, H_2O, and NO_2 by a Pt/Al_2O_3 catalyst at 450 °C and CO_2, H_2O, and NO_2 are removed by a molecular sieves adsorbent. Impurities in the purified air were typically NO_x ($\approx$2 ppb), hydrocarbons (<100 ppbC), CO_2 (<1 ppm), CO (<10 ppb), and H_2O (<10 ppm). Research grade benzene and toluene were used without further purification except degassing. NO and NO_2 (both Research grade, Matheson) were used also without further purification. Standard samples of formaldehyde, formic acid, dimethylglyoxal (biacetyl), and maleic anhydride were prepared by freeze-pump-thaw cycles. Methylglyoxal and glyoxal were desiccated by molecular sieves and P_2O_5, respectively.[32,33] The chemicals used were all from Wako Pure Chemical Ind. except NO and NO_2.

The reaction mixtures were prepared as follows: The amounts of reactant gases were measured by an MKS Baratron capacitance manometer in a known volume in a gas-handling line and the gases were flushed separately by pressurized nitrogen gas into the chamber which was first filled with the matrix air. The total pressure of the reaction mixture thus obtained was 101 kPa (1 atm). The air was stirred by two mixing fans in the chamber during the irradiation.

All runs were made at the temperature 22.5±1 °C controlled by the water circulation system.

Results

A. Photooxidation of Toluene. Formation of formaldehyde, formic acid, glyoxal, methylglyoxal, peroxyacetyl nitrate (PAN), maleic anhydride, and benzaldehyde was observed in the photooxidation of the toluene (4 ppm)-NO (0.17—1.50 ppm)-NO_2 (0.50—1.51 ppm)-air (1 atm) system. These products were identified by using the standard IR absorption spectra of authentic samples as listed in Table 1.

Figure 2 shows an example of the subtraction of spectra in the frequency region of 3000—2700 cm^{-1}. Figure 2a shows the absorption spectrum of products produced in the toluene (4 ppm)-NO (0.17 ppm)-NO_2 (0.50 ppm)-air (1 atm) mixture after 217 min

Table 1. The characteristic band of each product used to determine the concentration

Product		Absorption band	Wavenumber / cm^{-1}
Formaldehyde	HCHO	ν_{C-H}	2781.0, 2778.5
Formic acid	HCOOH	ν_{C-O}	1105.2
Peroxyacetyl nitrate (PAN)	$CH_3C(O)OONO_2$	ν_{C-O}	1160[a]
Glyoxal	$(CHO)_2$	ν_{C-H}	2900—2750
Methylglyoxal	CH_3COCHO	ν_{C-H} in -CHO	2860—2800
Maleic anhydride (MAH)	$\begin{matrix}-CO\\ \|\|\\ -CO\end{matrix}>O$	$\nu_{C=O}$	1805.3, 840.6
Benzaldehyde	C_6H_5CHO	ν_{C-H} in -CHO	2750—2710

a) The standard spectrum of PAN was obtained by the reaction of $CH_3CHO+N_2O_5(NO_3)$ in 101 kPa (1 atm) air.[34] The absolute concentration of PAN was determined by using the reported absorption coefficient.[35]

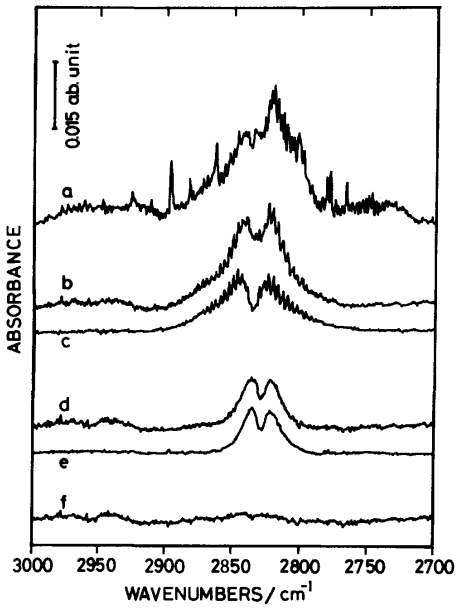

Fig. 2. Typical IR absorption spectrum of the products and spectral subtractions in the frequency region of 2700—3000 cm^{-1} (the region of the C-H stretching). a: Product spectrum from the photooxidation of the toluene (4.00 ppm)-NO(0.17 ppm)-NO_2(0.50 ppm)-air(101 kPa=1 atm) system, after 217 min irradiation. b: Spectrum after subtraction of HCHO, HCOOH, PAN, and benzaldehyde from spectrum (a). C: Spectrum of $(CHO)_2$. d: Difference spectrum, (b) −(c). e: Spectrum of CH_3COCHO. f: Difference spectrum, (d)−(e).

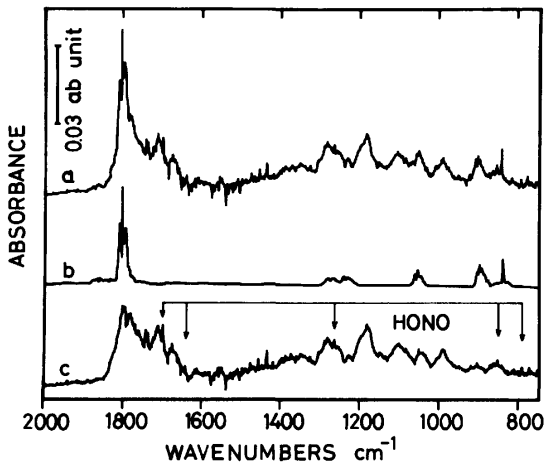

Fig. 3. Absorption spectrum of the products in the frequency region of 800—2000 cm^{-1}. a: Product spectrum under the same condition as in Fig. 2f. b: Spectrum of maleic anhydride. c: Difference spectrum, (a)—(b).

irradiation. In this case, absorption spectra of reactants and H_2O are subtracted. Rotational structure of formaldehyde (2950—2730 cm^{-1}) and broad absorption of benzaldehyde (around 2730 cm^{-1}) are apparent. Subtracting the spectra of formaldehyde, formic acid, benzaldehyde, and PAN from the spectrum (a), the spectrum (b) was obtained. The fine structure in the spectrum (b) corresponds to the absorption of glyoxal whose standard spectrum is shown in spectrum (c). Subtraction of the spectrum of glyoxal from the spectrum (b) gives the spectrum (d) which coincides with the standard spectrum of methylglyoxal, spectrum (e). Spectrum (f) shows the difference spectrum of (d)−(e). No significant absorption remained in the region from 3000 to 2700 cm^{-1} (the frequency region of the C-H stretching mode).

After these spectral manipulations, some absorption bands remained in the frequency region of 2000—800 cm^{-1} as shown in spectrum (a) in Fig. 3. Characteristic bands at 1800 and 900 cm^{-1} and sharp absorption at 840 cm^{-1} are in agreement with the standard spectrum of maleic anhydride (spectrum (b)). Subtraction of spectrum (b) from spectrum (a) gives spectrum (c) shown in Fig. 3. Several bands

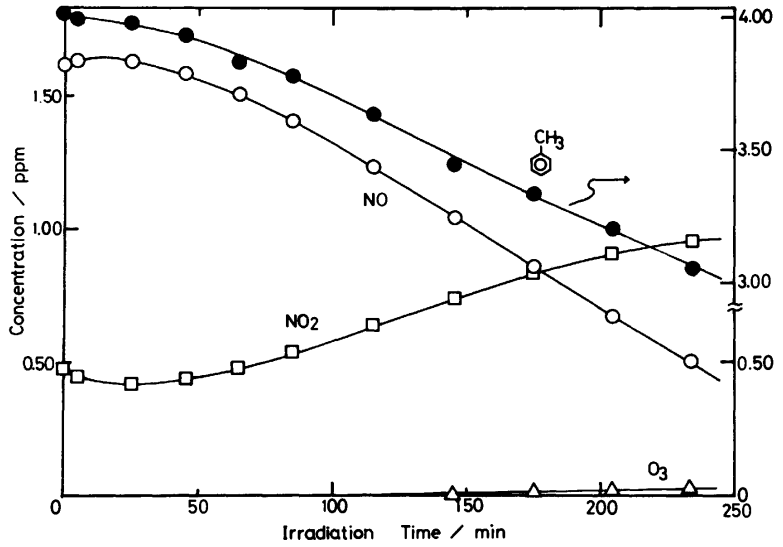

Fig. 4. Concentrations of toluene, NO, NO_2, and O_3 are plotted against the irradiation time. Initial conditions; toluene=4.01 ppm, NO=1.50 ppm, NO_2=0.50 ppm, and air=101 kPa (=1 atm).

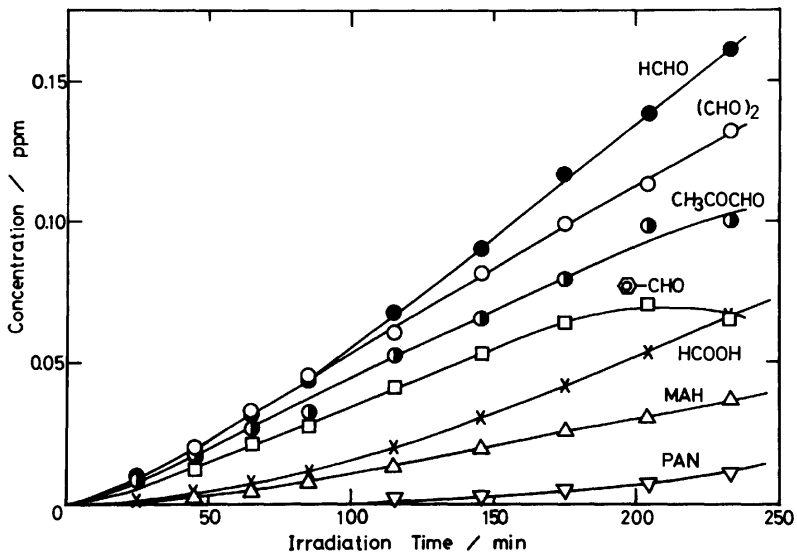

Fig. 5. Dependence of the absolute concentrations of the reaction products on irradiation time. The experimental conditions are the same as the conditions in Fig. 4. MAH: maleic anhydride. PAN: Peroxyacetyl nitrate.

in spectrum (c) can be identified to be HONO,[36] as indicated by the arrows. The remaining spectrum shows intense absorptions at 1800 and 1700 cm^{-1}, which are characteristic of the C=O stretching in carbonyl compounds. The strong absorption around 1800 cm^{-1} is attributable[37] to C=O stretching vibration in a carboxylic acid (not hydrogen-bonded), an anhydride, or a peroxyacyl nitrate. The absorption around 1700 cm^{-1} corresponds[38] to C=O stretching in aldehydes, ketones, dialdehydes, and diketones. However, the spectrum shown in Fig. 3c could not be uniquely identified in the present study.

Figure 4 shows the concentration of reactants (NO, NO_2, O_3, and toluene) plotted against the irradiation time for the photooxidation of the toluene (4.01 ppm), NO (1.50 ppm), NO_2 (0.50 ppm), and air (1 atm) mixture. Change of the concentration of products on the irradiation time is shown in Fig. 5. All these products except PAN are observed from the beginning of the irradiation.

In Fig. 6, the amounts of each product formed are plotted against the amount of toluene consumed.

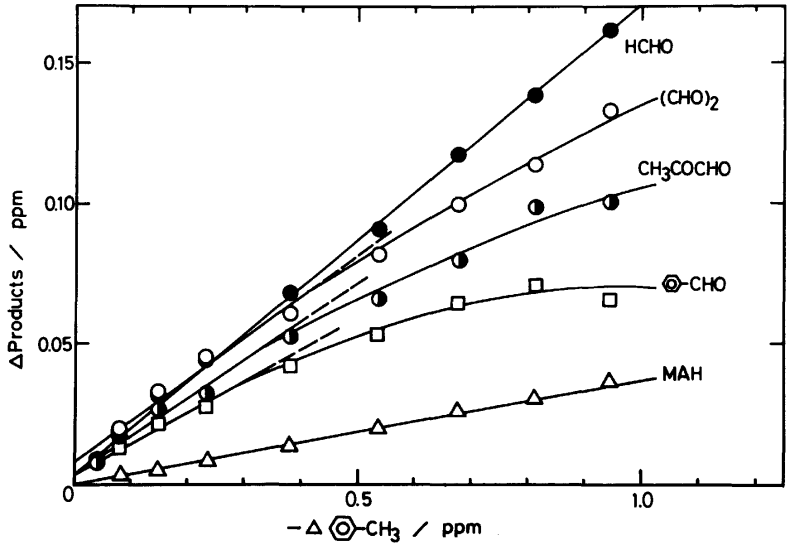

Fig. 6. Concentrations of products are plotted against the toluene consumed.

Table 2. Yields of the primary products in the photooxidation of the toluene-NO_x-air system under three different experimental conditions

	Run No.			
	1	2	3	average[c]
Initial concentration (ppm in 1 atm air)				
Toluene	4.00	4.01	4.00	
NO	0.17	1.50	0.51	
NO_2	0.50	0.50	1.51	
Yield of product[a]				
HCHO	0.15	0.17	0.16	0.16 ± 0.01
$(CHO)_2$	0.20	0.15	0.11	0.15 ± 0.04
CH_3COCHO	0.18	0.14	0.11	0.14 ± 0.04
MAH[b]	0.044	0.039	0.037	0.040±0.004
C_6H_5CHO	0.12	0.11	0.10	0.11 ± 0.01

a) Values were calculated by the least-square fit of four initial points of each run as shown in Fig. 6. b) MAH: maleic anhydride. c) The indicated errors are one standard deviation of three runs.

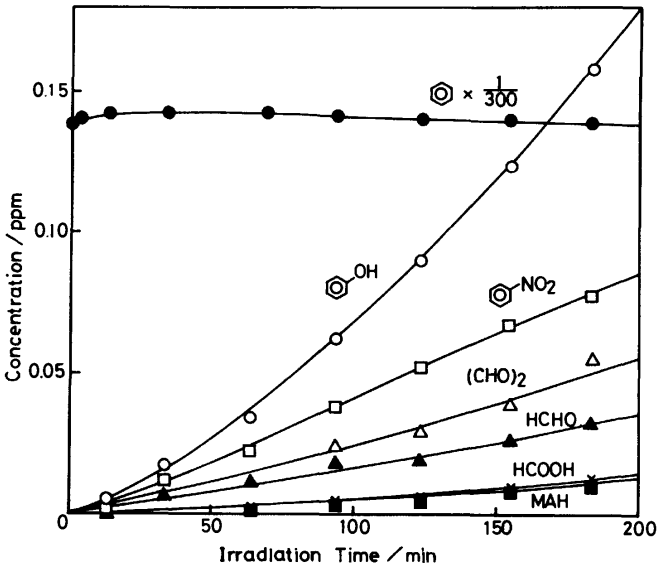

Fig. 7. Concentrations of benzene and reaction products are plotted against the irradiation time. Initial conditions; benzene = 42.65 ppm, NO_2 = 1.50 ppm, and air = 101 kPa (= 1 atm).

Formaldehyde and maleic anhydride increase linearly against toluene consumed, and glyoxal, methylglyoxal, and benzaldehyde show linear increase at the initial stage where toluene consumed is less than 10% of the initial concentration. The plots of formic acid and PAN (not shown) were not straight lines, indicating that both are not primary products. The initial slopes of the products shown in Fig. 6 give the formation yield of each product. Yields of products calculated under three different experimental conditions are listed in Table 2. Values shown in each run were obtained by the least-square fit of four initial points of each run as shown in Fig. 6. The indicated errors are one standard deviation of three runs.

B. Photooxidation of Benzene. In the case of benzene, formation of formaldehyde, formic acid, glyoxal, maleic anhydride, phenol, and nitrobenzene was observed. Since the rate constant for the reaction of OH+benzene is about one-fifth[5,8,11] of that for OH+toluene, this experiment was carried out with a high concentration of benzene. The concentrations of reaction products as a function of irradiation time are shown in Fig. 7. In this case the mixture of 42.7 ppm of benzene, 1.5 ppm of NO_2 in 1 atm air was photolyzed. Since the amount of benzene

consumed was too small to measure, yields of each product could not be determined exactly.

Discussion

A. Photooxidation of Toluene. In the NO–NO_2–air system, the reaction of aromatic hydrocarbon is initiated mainly by OH radicals formed by the photodecomposition of HONO[39] produced in both homogeneous[36] and heterogeneous[40] reactions among NO, NO_2, and H_2O. Further, OH radicals can be produced in a long chain mechanism[41] involving the reaction of HO_2+NO. The effect of the reaction of toluene with oxygen atoms must be considered. $O(^3P)$ is produced in the photodecomposition of NO_2 with the photolysis rate constant of 0.22 min^{-1} in the present chamber, and is readily removed by O_2 under 1 atmospheric air with the rate of 7.4×10^4 s^{-1}.[42a] Using steady state approximation for oxygen atoms, we can roughly estimate the oxygen atom concentration to be at most 2.5×10^6 molecule cm^{-3} under the present experimental conditions. OH radical concentration is in the range of $(1—5)\times10^6$ molecule cm^{-3} under the similar conditions of smog chamber experiments.[40b] Since the rate constant of toluene with OH radicals under 1 atmospheric air is about 6×10^{-12} molecule^{-1} cm^3 s^{-1} [4-12] which is 10^2 times larger than that with $O(^3P)$,[42b-d] the contribution of the reaction of toluene with oxygen atoms can be neglected in the present study.

OH radicals react with toluene by both abstraction (Reaction 1a) and addition (Reaction 1b) reactions. O_2 adds to the benzyl radical produced in Reaction 1a and the peroxyl radical product reacts with NO, and benzaldehyde and benzyl nitrate are eventually produced. The OH-toluene adduct produced in Reaction 1b yields cresols and *m*-nitrotoluene by subsequent reactions. Details of yields and reaction mechanisms for the formation of these high-boiling-point products were reported and discussed previously.[3,14,15,18,19] The addition of OH radicals to toluene is predominantly at the 2-position since *o*-cresol was produced predominantly.[14,15,18]

The low-boiling-point products measured previously are CO, CO_2, formaldehyde, formic acid,[3,20-22] glyoxal, and methylglyoxal.[23,24] Recently C_4 and C_5 compounds and substituted furans were detected in the toluene photooxidation products.[24c,d] In the present study, the formation of maleic anhydride was observed and analyzed quantitatively in addition to these products. Systematic analysis of these low-boiling-point products from various methylbenzenes is crucial to elucidate the mechanisms of ring-cleavage reaction.

Atkinson *et al.*[3] suggested that the OH-toluene adduct produced in Reaction 1b is the precursor of the ring-cleavage reaction. In air, addition of O_2 to the adduct can occur at the 1-, 3-, or 5-position[3] as shown in Reaction 6. According to Atkinson *et al.*,

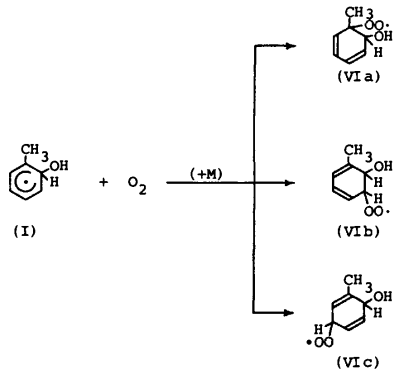

O_2 addition at the 5 position should be the least thermochemically favored, since the double bonds are unconjugated.

Two types of ring-cleavage mechanisms are considered for the OH–toluene–O_2 adduct. The first is a cyclization type of reaction suggested by Atkinson *et al.*[3] For example, in the case of the compound **VIb**, bicyclo[3.2.1] cyclization gives allyl-type radicals, 6,7-dioxabicyclo[3.2.1]octane compounds (DBO[3.2.1]), and both glyoxal and methyl-

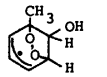

glyoxal can be produced from DBO[3.2.1]. Scheme 1 depicts the reactions which lead to formation of both glyoxals from **VIb** (DBO[3.2.1] is represented formally as **VIIa**↔**VIIb** by its resonance structures). In this scheme glyoxal and methylglyoxal are produced exclusively in Reactions 7a and 7b, respectively. As for the compound **VIa**, the other possible OH–toulene–O_2 adduct, bicyclo[3.2.1] cyclization gives the same allyl radical compound, DBO[3.2.1], as from **VIb**. Therefore, in the bicyclo[3.2.1] cyclization mechanism, the formation ratio of glyoxal to methylglyoxal is governed by the ratio of Reaction 7a to 7b, in other words, the relative probability of oxygen-molecule addition to the alternate radical points (shown as **VIIa** and **VIIb**) in DBO[3.2.1]. When the OH-aromatics–O_2 adducts undergo bicyclo[2.2.2] cyclization process, glyoxal and methylglyoxal can be produced from compounds **VIa** and **VIb**, respectively, as suggested by Atkinson *et al.*[19] In this case, the ratio of glyoxal and methylglyoxal is governed by the ratio of compound **VIa** and **VIb**; *i.e.* position of the O_2 addition in Reaction 6. The bicyclo[2.2.2] intermediate, 2,3-dioxabicyclo[2.2.2]octane compounds (DBO[2.2.2]), might have a lower ring strain energy than the DBO[3.2.1] intermediate, but a radical point and a double bond are isolated. These are conjugated to make an allyl-type radical in the DBO[3.2.1] intermediate. Thus, so far, it is not evident that

either of the DBO[2.2.2] or the DBO[3.2.1] intermediate is more stable.

Another possible ring-cleavage mechanism is a ring opening type of reaction shown in Scheme 2, Reaction 8. For example, glyoxal and compound **VIIc** are produced from compound **VIb** by the mechanism shown in Scheme 2. When the reaction starts from compound **VIa**, methylglyoxal and compound **VIId** are produced. In this case, the ratio of glyoxal and methylglyoxal is governed by the ratio of compounds **VIb** and **VIa**.

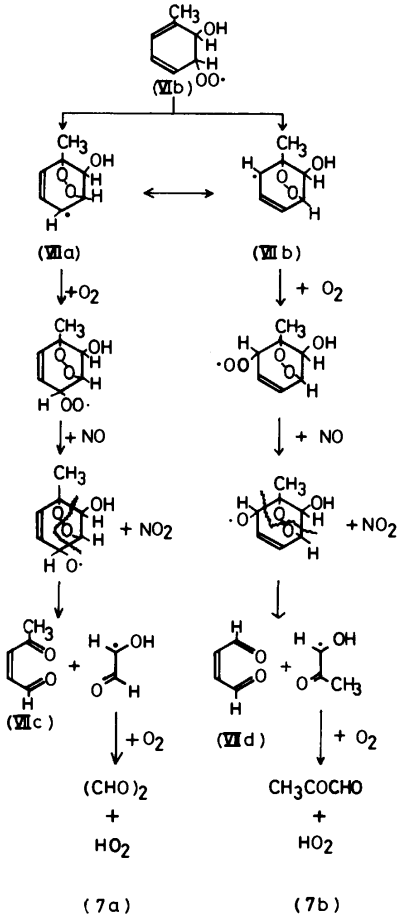

Scheme 1.

As shown in Table 2, the formation ratio of glyoxal to methylglyoxal seems one to one. Recently two groups have reported the yield of these compounds in the toluene photooxidation. Shepson *et al.*[24c] have reported 8.0 and 7.5% yield for glyoxal and methylglyoxal, respectively. The values reported by Tuazon *et al.*[24b] are 0.111±0.013 and 0.146±0.014 for glyoxal and methylglyoxal, respectively. The present result and these recent data clearly show that the formation ratio of glyoxal and methylglyoxal in the toluene photooxidation is almost one to one, although the yield obtained by Shepson *et al.* are little bit smaller than the others. The formation ratio of glyoxal to methylglyoxal, 1:1, can be explained from both the cyclization, Scheme 1, and the ring opening, Scheme 2, mechanisms. In the case of Scheme 1, the probability of O_2 addition to the resonance structures **VIIa** and **VIIb** should be the same in order to explain the formation ratio. While in the case of Scheme 2, the formation ratio of **VIb** to **VIa** in Reaction 6 is to be 1:1.

If glyoxal and methylglyoxal are produced, unsaturated γ-dicarbonyls, compound **VIIc** (*cis*-4-oxo-2-pentenal) and **VIId** (*cis*-2-butenedial), are expected to form as counterparts of ring-cleavage products against glyoxal and methylglyoxal, respectively. In their extensive study of identifying the ring fragmentation products on the photooxidation of toluene, Shepson *et al.*[24c] were successful to detect the compounds **VIIc** and **VIId** using GC/MS, although the apparent yields of these products were quite small, one eighth or less than those of glyoxals. These products might have absorptions in the aldehydic C–H stretching frequency region (2850—2700 cm^{-1}). However, as shown in spectrum (f) in Fig. 2, no significant absorption was observed in this region. This indicates that these products are probably very unstable in the gas phase due to a wall

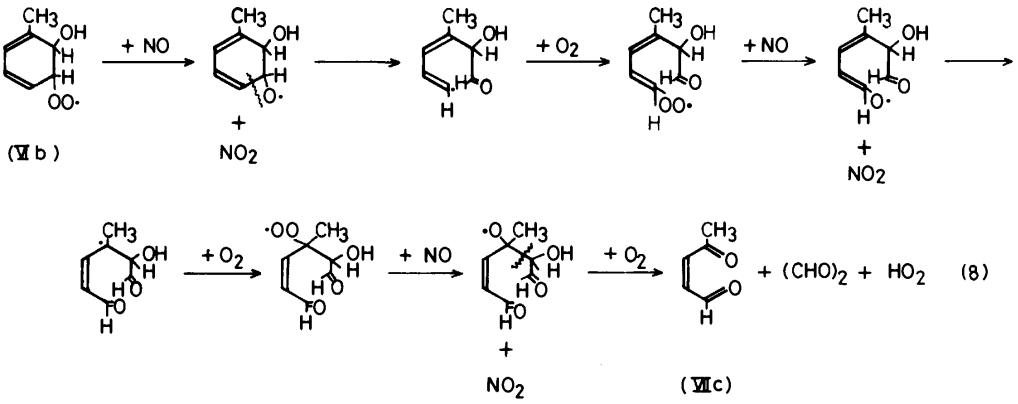

Scheme 2.

loss and also partly due to a photolysis and a reaction with OH radicals.

Maleic anhydride was observed in the present study, and seems a primary product apparently from Fig. 6. However, since the two hydrogen atoms originally attached to the carbons which become carbonyl carbons in maleic anhydride should be removed to form maleic anhydride, it seems unlikely to yield maleic anhydride as a primary product according to the mechanism generally applied to the photooxidation of hydrocarbons.

Maleic anhydride can be produced by the following reactions from *cis*-2-butenedial (compound **VIId**) which is expected to be produced as a counterpart of methylglyoxal. Rate determining step for Reaction 9

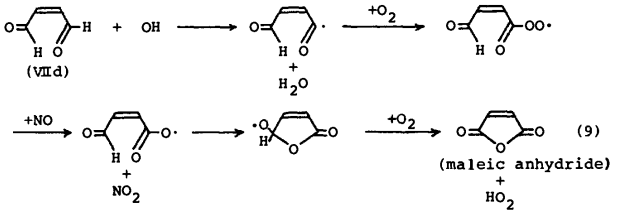

(9)

is considered to be the first step under atmospheric air. The rate constant for the step has been estimated[3] under the assumption that the aldehydic hydrogen in compound **VIId** has a similar reactivity to OH radicals as other aldehydes. The estimated value is 3×10^{-11} molecule^{-1} cm^3 s^{-1}, while the rate constant for the reaction of toluene with OH radicals which would be expected as the rate determining step to produce **VIId** has been measured to be about 6×10^{-12} molecule^{-1} cm^3 s^{-1} [4-12] under 1 atmospheric air. Therefore, only Reaction 9 can not explain the observed linear increase of maleic anhydride against toluene consumption.

Another possible route of the formation of maleic anhydride is the oxidation of *cis*-2-butenedial on the wall surface of the reaction chamber. Recently,

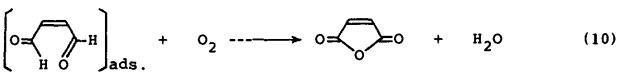

(10)

Dumdei, and O'Brien[24d] reported the observation of 2-butenedial and 4-oxo-2-pentenal among various compounds recovered by solvent extraction from the reaction vessel walls in which the photooxidation of toluene was performed. In the present study, since the gas in the reaction chamber was stirred by fans, *cis*-2-butenedial can collide with the wall in about one minute. Although both Reactions 9 and 10 are probable, at present the mechanism to form maleic anhydride is not clear. A similar reaction mechanism can be considered for *cis*-4-oxo-2-pentenal (compound **VIIc**), with maleic anhydride production by the release of a methyl radical. However, as will be described in a subsequent paper II, maleic anhydride is not produced from *cis*-4-oxo-2-pentenal. As shown in Table 2, the yield of maleic anhydride is about one fourth of yields of both glyoxal and methylglyoxal. This implys that most of the unsaturated γ-dicarbonyls are photodecomposed or consumed by other reactions including adsorption on the reactor surface. In any case, the observation of maleic anhydride suggests the occurrence of the aromatic ring cleavage of toluene into C_2+C_4 fragments.

If the fragmentation of methyl radicals from *cis*-4-oxo-2-pentenal occurs, formaldehyde can be produced as follows:

$$CH_3 + O_2 + M \longrightarrow CH_3O_2 \quad (11)$$

$$CH_3O_2 + NO \longrightarrow CH_3O + NO_2 \quad (12)$$

$$CH_3O + O_2 \longrightarrow CH_2O + HO_2 \quad (13)$$

The formation mechanism of formic acid is not clear although there might be many possible formation routes in secondary reactions involving *cis*-2-butenedial and *cis*-4-oxo-2-pentenal, particularly, in surface reactions. According to Su *et al.*,[43] formic acid can be produced by the photooxidation of formaldehyde. Formic acid might also be produced by the reaction of OH radicals with glyoxal and methylglyoxal.

$$OH + (CHO)_2 \longrightarrow HCO + HCOOH \quad (14)$$

$$OH + CH_3COCHO \longrightarrow CH_3CO + HCOOH \quad (15)$$

Recently, Plum *et al.*[44] reported that the rates of reactions of OH+glyoxal and methylglyoxal are very fast. PAN may be formed from the acetyl radical produced by the photodecomposition of methylglyoxal as suggested by Darnall *et al.*[24a]

In the previous studies,[13-15,18,19] high-boiling-point products formed in the photooxidation or the OH radical reaction with toluene were analyzed. The major products were benzaldehyde and *o*-cresol. The benzaldehyde yield from toluene of 0.11 obtained in the present study is in reasonable agreement with yields obtained previously by the GC analysis.[45] On the other hand, the yield of cresols reported in the previous studies was scattered from 13 to 68%.[46] In the present study, high-boiling-point products except benzaldehyde could not be identified. It is suggested that the fraction of the ring-cleavage process is 29% of toluene consumed and that 71% of total products may be high-boiling-point compounds retaining the aromatic ring[47] (benzaldehyde is 11% and other products including cresols are 60%).

Two possible mechanisms, Scheme 1 and 2, were suggested as the ring-cleavage reaction. In these reactions, the number of NO molecules which are converted to NO_2 when one toluene molecule is consumed are two and four in the cases of Scheme 1 and 2, respectively, including the reaction of $HO_2+NO\rightarrow OH+NO_2$. This number for the pho-

tooxidation of toluene obtained in the previous studies[48,49] are scattered from 1.2 to 2.3 depending upon the experimental conditions. A determination of this number was made in the present reaction chamber. Three measurements were carried out in the toluene (4 ppm) and NO (2 ppm) system.[50] The number obtained from the ratio of toluene consumed to NO consumed in the initial stage (<100 min) were 1.5, 1.5, and 1.6 in these measurements with an average value of 1.5. The number of 1.5 consists of three types of reactions: (1) Formation of benzaldehyde from benzyl radicals produced by the side-chain-hydrogen abstraction (in this case the number is two:[51] (2) Formation of cresols from OH-aromatics adducts (in this case the number is one:[51] (3) Ring cleavage as discussed in the present study. Assuming the fraction of these three types of reactions, (1), (2), and (3), are 11, 60, and 29% of total reaction, respectively, the number in the ring-cleavage reaction can be estimated[52] to be 2.4—2.6. In the ring-cleavage reaction, both α-dicarbonyls and unsaturated γ-dicarbonyls are produced when one toluene molecule is consumed. A part of the unsaturated γ-dicarbonyls is converted to maleic anhydride, and another part of them may be decomposed (including the release of methyl radicals). Therefore, some additional NO should be converted to NO_2 by reaction related to unsaturated γ-dicarbonlys (including the formation of formaldehyde *via* Reactions 11—13). In order to satisfy the estimated number of 2.4—2.6, the preferred number is two rather than four in the reaction related to α-dicarbonyls. Thus, the cyclization mechanism, Reaction 7 is preferred over Reaction 8 as the ring-cleavage mechanism.

B. Photooxidation of Benzene. In the previous work on the photooxidation of benzene, the formation of phenol and nitrobenzene[14,18] and glyoxal[23] were reported as products. In the present study, the formation of formaldehyde, formic acid, and maleic anhydride were observed in addition to the products previously identified. It has been suggested,[14,18] that both phenol and nitrobenzene are produced from the same precursor, OH-benzene adduct.

If phenol and nitrobenzene are the high-boiling-point products and glyoxal is produced by the ring cleavage reaction, the ratio of the high-boiling-point products to the ring-cleavage product can be calculated from the concentration of products shown in Fig. 7. The yields calculated are 80—85% (high-boiling-point products) and 15—20% (ring-cleavage products).

Formaldehyde was detected in the photooxidation of benzene, although the yield is smaller than in the case of toluene. One possible formation route of formaldehyde is the photodecomposition of glyoxal as suggested by Plum *et al.*[44]

$$(CHO)_2 + h\nu \longrightarrow H_2CO + CO \quad (16)$$

The heterogeneous reaction of *cis*-2-butenedial produced as a counterpart of glyoxal might be possible to produce formaldehyde.

References

1) M. C. Dodge, Workshop on Mathematical Modeling of Photochemical Smog, Summary Proceeding, Report EPA-R4-73-010, Environmental Protection Agency, Washington, D. C., 1973.

2) B. J. Finlayson and J. N. Pitts, Jr., *Science*, **192**, 111 (1976).

3) R. Atkinson, W. P. L. Carter, K. R. Darnall, A. M. Winer, and J. N. Pitts, Jr., *Int. J. Chem. Kinet.*, **12**, 779 (1980).

4) D. D. Davis, W. Bollinger, and S. Fischer, *J. Phys. Chem.*, **79**, 293 (1975).

5) D. A. Hansen, R. Atkinson, and J. N. Pitts, Jr., *J. Phys. Chem.*, **79**, 1763 (1975).

6) G. J. Doyle, A. C. Lloyd, K. R. Darnall, A. M. Winer, and J. N. Pitts, Jr., *Environ. Sci. Technol.*, **9**, 237 (1975).

7) A. C. Lloyd, K. R. Darnall, A. M. Winer, and J. N. Pitts, Jr., *J. Phys. Chem.*, **80**, 789 (1976).

8) R. A. Perry, R. Atkinson, and J. N. Pitts, Jr., *J. Phys. Chem.*, **81**, 296 (1977).

9) R. A. Perry, R. Atkinson, and J. N. Pitts, Jr., *J. Phys. Chem.*, **81**, 1607 (1977).

10) A. R. Ravishankara, S. Wagner, S. Fischer, G. Smith, R. Schiff, R. T. Watson, G. Tesi, and D. D. Davis, *Int. J. Chem. Kinet.*, **10**, 783 (1978).

11) F. P. Tully, A. R. Ravishankara, R. L. Thompson, J. M. Nicovich, R. C. Shah, N. M. Kreutter, and P. H. Wine, *J. Phys. Chem.*, **85**, 2262 (1981).

12) J. M. Nicovich, R. L. Thompson, and A. R. Ravishankara, *J. Phys. Chem.*, **85**, 2913 (1981).

13) R. A. Kenley, J. E. Davenport, and D. G. Hendry, *J. Phys. Chem.*, **82**, 1095 (1978).

14) M. Hoshino, H. Akimoto, and M. Okuda, *Bull. Chem. Soc. Jpn.*, **51**, 718 (1978).

15) H. Akimoto, M. Hoshino, G. Inoue, M. Okuda, and N. Washida, *Bull. Chem. Soc. Jpn.*, **51**, 2496 (1978).

16) T. M. Sloane, *Chem. Phys. Lett.*, **54**, 269 (1978).

17) H. Takagi, N. Washida, H. Akimoto, K. Nagasawa, Y. Usui, and M. Okuda, *J. Phys. Chem.*, **84**, 478 (1980).

18) R. A. Kenley, J. E. Davenport, and D. G. Hendry, *J. Phys. Chem.*, **85**, 2740 (1981).

19) R. Atkinson, W. P. L. Carter, and A. M. Winer, *J. Phys. Chem.*, **87**, 1605 (1983).

20) S. L. Kopczynski, *Int. J. Air Water Pollut.*, **8**, 107 (1964).

21) A. P. Altshuller, S. L. Kopczynski, W. A. Lonneman, F. D. Sutterfield, and D. L. Wilson, *Environ. Sci. Technol.*, **4**, 44 (1970).

22) C. W. Spicer and P. W. Jones, *J. Air Pollut. Control Assoc.*, **27**, 1122 (1977).

23) K. Nojima, K. Fukaya, and S. Kanno, *Chemosphere* **3**, 247 (1974).

24) a) K. R. Darnall, R. Atkinson, and J. N. Pitts, Jr., *J. Phys. Chem.*, **83**, 1943 (1979); b) E. C. Tuazon, R. Atkinson, H. MacLeod, H. W. Biermann, A. M. Winer, W. P. L. Carter, and J. N. Pitts, Jr., *Environ. Sci. Technol.*, **18**, 981

(1984); c) P. B. Shepson, E. O. Edney, and E. W. Corse, *J. Phys. Chem.*, **88**, 4122 (1984); d) B. E. Dumdei and R. J. O'Brien, *Nature*, **311**, 248 (1984).

25) H. Takagi, N. Washida, H. Akimoto, and M. Okuda, *Spectrosc. Lett.*, **15**, 145 (1982).

26) H. Takagi, N. Washida, H. Bandow, and M. Okuda, *J. Phys. Chem.*, **85**, 2701 (1981).

27) N. Washida and H. Takagi, *J. Am. Chem. Soc.*, **104**, 168 (1982).

28) a) W. A. Lonneman, T. A. Bellar, and A. P. Altshuller, *Environ. Sci. Technol.*, **2**, 1017 (1968); b) A. P. Altshuller, W. A. Lonneman, F. D. Sutterfield, and S. L. Kopczynski, *ibid.*, **5**, 1009 (1971); c) W. A. Lonneman, S. L. Kopczynski, P. E. Darley, and F. D. Sutterfield, *ibid.*, **8**, 229 (1974); d) W. A. Lonneman, R. L. Seila, and J. J. Bufalini, *ibid.*, **12**, 459 (1978); e) J. Kondo and H. Akimoto, *Adv. Environ. Sci. Technol.*, **5**, 1 (1975); f) T. Chikamoto and K. Sakoda, *J. Jpn. Soc. Air Pollut.*, **12**, 389 (1977); g) E. Häsänen, V. Karlsson, E. Leppämaki, and M. Juhala, *Atmosph. Environ.*, **15**, 1755 (1981).

29) R. Atkinson, K. R. Darnall, A. C. Lloyd, A. M. Winer, and J. N. Pitts, Jr. "Advances in Photochemistry," ed by J. N. Pitts, Jr., G. S. Hammond, K. Gollnick, and D. Grosjean, Interscience, New York, 1979; Vol. 11, pp. 375—488.

30) J. P. Killus, and G. Z. Whitten, *Atmosph. Environ.*, **16**, 1973 (1982).

31) a) C. H. Wu and H. Niki, *Environ. Sci. Technol.* **9**, 46 (1975); b) R. B. Harvey, D. H. Stedman, and W. Chameides, *J. Air Pollut. Control Assoc.*, **27**, 663 (1977).

32) R. Naaman, D. M. Lubman, and R. N. Zare, *J. Chem. Phys.*, **71**, 4192 (1979).

33) R. A. Coveleskie and J. T. Yardley, *J. Am. Chem. Soc.*, **97**, 1667 (1975).

34) J. M. Heuss and W. A. Glasson, *Environ. Sci. Technol.*, **2**, 1109 (1968).

35) a) E. R. Stephens, *Anal. Chem.*, **36**, 928 (1964); b) H. Akimoto, H. Bandow, F. Sakamaki, G. Inoue, M. Hoshino, and M. Okuda, *Environ. Sci. Technol.*, **14**, 172 (1980).

36) a) W. H. Chan, R. J. Nordstrom, J. G. Calvert, and J. H. Shaw, *Environ. Sci. Technol.*, **10**, 674 (1976); b) S. Z. Levine, W. M. Uselman, W. H. Chan, J. G. Calvert, and J. H. Shaw, *Chem. Phys. Lett.*, **48**, 528 (1977).

37) a) N. B. Colthup, L. H. Daly and S. E. Wiberlay, "Introduction to Infrared and Raman Spectroscopy," Academic Press, New York, 1964, pp. 239—268; b) Standard spectra of maleic anhydride, methylmaleic anhydride, and dimethylmaleic anhydride measured in the present study show the absorption by C=O stretching in the frequency region of 1790—1805 cm^{-1}. PAN shows the weak absorption around 1840 cm^{-1}.

38) Standard spectra of glyoxal, methylglyoxal, and biacetyl show the absorption by C=O stretching around 1730 cm^{-1}. 3-Hexene-2,5-dione shows absorption around 1703 cm^{-1}.

39) a) C. H. Wu, C. C. Wang, S. M. Japar, L. I. Davis, Jr., M. Hanabusa, D. Killinger, H. Niki, and B. Weinstock, *Int. J. Chem. Kinet.*, **8**, 765 (1976); b) R. A. Cox and R. G. Derwent, *J. Photochem.*, **6**, 23 (1976/77).

40) a) F. Sakamaki, S. Hatakeyama, and H. Akimoto, *Int. J. Chem. Kinet.*, **15**, 1013 (1983); b) W. P. L. Carter, R. Atkinson, A. M. Winer, and J. N. Pitts, Jr., *ibid.*, **13**, 735 (1981).

41) a) J. Heicklen, K. Westberg, and N. Cohen, "Chemical Reactions in Urban Atmospheres," ed by C. Tuesday; Elsevier, 1971, pp. 54—59; b) A. Gitchell, R. Simonaitis, and J. Heicklen, *J. Air Pollut. Control Assoc.*, **24**, 357 (1974).

42) a) C. L. Lin and M. T. Leu, *Int. J. Chem. Kinet.*, **14**, 417 (1982); b) R. Atkinson and J. N. Pitts, Jr., *J. Phys. Chem.*, **79**, 295 (1975); c) A. J. Colussi, D. L. Singleton, R. S. Irwin, and R. J. Cvetanovic, *ibid.*, **79**, 1900 (1975); d) J. M. Nicovich, C. A. Gump, and A. R. Ravishankara, *ibid.*, **86**, 1684 (1982).

43) F. Su, J. G. Calvert, J. H. Shaw, H. Niki, P. D. Maker, C. M. Savage, and L. D. Breitenbach, *Chem. Phys. Lett.*, **65**, 221 (1979).

44) C. N. Plum, E. Sanhueza, R. Atkinson, W. P. L. Carter, and J. N. Pitts, Jr., *Environ. Sci. Technol.*, **17**, 479 (1983).

45) Yields obtained in the previous studies are 0.073 (Ref. 19), 0.12 (Ref. 3), and 0.15 (Ref. 18).

46) Yields reported are 0.131 (Ref. 19), 0.21 (Ref. 3), and 0.68 (Ref. 18).

47) The ratios of the *o*-cresol/benzaldehyde yields reported previously are 1.8 (Refs. 19 and 3), 2.1 (Ref. 14), and 4.5 (Ref. 18). If these values are used to the estimation of the yield of cresols in the present study, the yields are 20, 23, and 50% of toluene consumed, respectively. The ratio of [benzaldehyde]/[total high-boiling-point products] obtained under the conditions of high NO_2 concentrations (Ref. 15) was about 0.16. Total high-boiling-point products were mostly cresols, nitrocresols, and *m*-nitrotoluene. If this value, 0.16, is used, the yield of total high-boiling-point products can be estimated to be 68% of toluene consumed. This value is in excellent agreement with the value of 71% estimated in the present study.

48) N. Washida, G. Inoue, H. Akimoto, and M. Okuada, *Bull. Chem. Soc. Jpn.*, **51**, 2215 (1978).

49) R. A. Cox, R. G. Derwent, and M. R. Williams, *Environ. Sci. Technol.*, **14**, 57 (1980).

50) For the determination of this number, the conditions in the absence of NO_2 was desired, because the photodecomposition of NO_2 ($NO_2 \rightarrow NO+O$) disturbs the measurement.

51) The formation mechanisms of benzaldehyde (A) and *o*-cresol (B) suggested (Refs. 14, 15, and 48) are

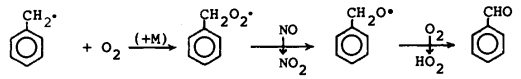

(A)

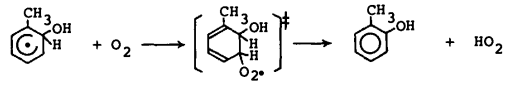

(B)

52) The number, n=2.4 is obtained from the equation; $0.11\times2+0.60\times1+0.29n=1.5$. This number is a lower limit, because in the presence of NO_2, formation of some benzyl nitrate and *m*-nitrotoluene at the expense of benzaldehyde and cresols, observed. Therefore, effective numbers slightly less than 1 and 2 should be used in the above equation. However, even when the photooxidation was carried out in the NO_2–toluene system,[15] yields of benzyl nitrate and *m* nitrotoluene were always less than 10% of benzaldehyde and cresols, respectively. Therefore, the value can be estimated to be 2.4—2.6.

 © 1985 The Chemical Society of Japan Bull. Chem. Soc. Jpn., 58, 2541—2548 (1985)

Ring-cleavage Reactions of Aromatic Hydrocarbons Studied by FT-IR Spectroscopy. II. Photooxidation of *o*-, *m*-, and *p*-Xylenes in the NO_x-Air System

Hiroshi BANDOW and Nobuaki WASHIDA

Division of Atmospheric Environment, The National Institute for Environmental Studies, P. O. Tsukuba-gakuen, Tsukuba, Ibaraki 305

(Received February 12, 1985)

α-Dicarbonyl compounds produced in the photooxidation of *o*-, *m*-, and *p*-xylenes were analyzed quantitatively using long-path FT-IR spectroscopy. Glyoxal, methylglyoxal, and biacetyl were observed in the case of *o*-xylene, and glyoxal and methylglyoxal were observed in cases of *m*- and *p*-xylenes. Yields of glyoxal, methylglyoxal, and biacetyl were 8, 23, and 10% (mole/mole) of *o*-xylene consumed, respectively. Yields of glyoxal and methylglyoxal were 13 and 42% in the case of *m*-xylene, and 24 and 12% in the case of *p*-xylene. These yields could be explained by the ring cleavage of 6,7-dioxabicyclo[3.2.1]octane compounds of OH-aromatics-O_2 adduct. Formations of maleic anhydride was observed in the case of *o*-xylene and it is suggested that maleic anhydride is produced from *cis*-2-butenedial. Formation of 3-hexene-2,5-dione (unsaturated γ-dicarbonyl) was observed from *p*-xylene. The ring-cleavage process accounts for 41, 55, and 36% of the total reaction in *o*-, *m*-, and *p*-xylenes, respectively.

The studies of the mechanism of the ring-cleavage reactions in the photooxidation of benzene and toluene described in part I, are extended to *o*-, *m*-, and *p*-xylenes in the present work. The initial reaction of OH with xylenes also proceeds mainly by addition to aromatic ring (80—98% of the total reaction).[1-4] Also *m*-xylene reacts faster[1,4,5] than either *p*- or *o*-xylene with OH at 298K since meta substitution of the ring enhances electrophilic addition. The formation of α-dicarbonyls, glyoxal, methylglyoxal, and biacetyl (only in the case of *o*-xylene), by xylene-ring-cleavage reaction has been reported.[2,6,7] However, the yields of α-dicarbonyls reported are scattered. For example, in the case of *o*-xylene, the yields of glyoxal, methylglyoxal, and biacetyl per *o*-xylene consumed reported by Nojima *et al.*[6] are 0.2, 4.0, and 1.2%, respectively, the values by Takagi *et al.*[2] are 85, 14, and 26%, respectively, and those by Shepson *et al.*[7c] are 3.4, 11.6, and 8.5%, respectively. Darnall *et al.*[7a] measured only the yield of biacetyl and reported it to be 18% of *o*-xylene consumed. Very large spread of these results might be mainly due to difficulty of handling of α-dicarbonyls. In the previous studies, GC analyses were carried out after a pre-collection of gas-phase products in a solution[6,7c] or by combining with a photoionization mass spectrometer as a detector.[2] The former represents a rather complicated procedure, while the latter requires concentration of a large amount of products, in compensation for the low detectivity of the compounds. Therefore, the direct observation of gaseous products by FT-IR should provide more reliable data on the yield and the ring-cleavage-reaction mechanisms of xylenes.

Experimental

The apparatus and experimental procedures were the same as those mentioned in part I.[8] The experimental conditions were xylene(4 ppm), NO(1.5 ppm), NO_2(0.5 ppm), and air (1 atm=101 kPa) system. Three experiments were carried out for each xylene isomer.

Results

Formaldehyde, formic acid, glyoxal, methylglyoxal, PAN, and tolualdehydes were observed as reaction products in the photooxidation of *o*-, *m*-, and *p*-xylenes. Formation of biacetyl and maleic anhydride was observed only from *o*-xylene. Product spectra (spectra, from which spectra of reactants, xylenes, NO, NO_2, and H_2O were subtracted) and residual spectra (spectra, from which spectra of products mentioned above were subtracted) are shown in Fig. 1 for each of *o*-, *m*-, and *p*-xylenes. Product spectra shown in Fig. 1, (a), (c), and (e), were obtained under the same conversion of xylenes (xylene consumed was about 20%).

Concentrations of each product from *o*-xylene as a function of irradiation time are shown in Fig. 2. Characteristic absorption bands used to determine the absolute concentrations of products are the same as for toluene (Table 1 in part I). The concentration of biacetyl was determined by absorption at 1120 cm^{-1} (in the region of skeletal vibrations), and that of tolualdehydes by absorption at 2730 cm^{-1} which corresponds to the C-H stretching mode of -CHO. The time profiles of formic acid and PAN show that both molecules are secondary products as in the case of toluene. From the slopes of the plots of the concentrations of products formed *versus* *o*-xylene consumed, shown in Fig. 3, yields of products listed in Table 1 were calculated. Yields shown in each run are obtained by the least-square fit of five initial points of each run (as shown in Fig. 3) except the case of tolualdehydes. For tolualdehydes, the least-square fit was done for three initial points. The indicated errors are one standard deviation of three runs.

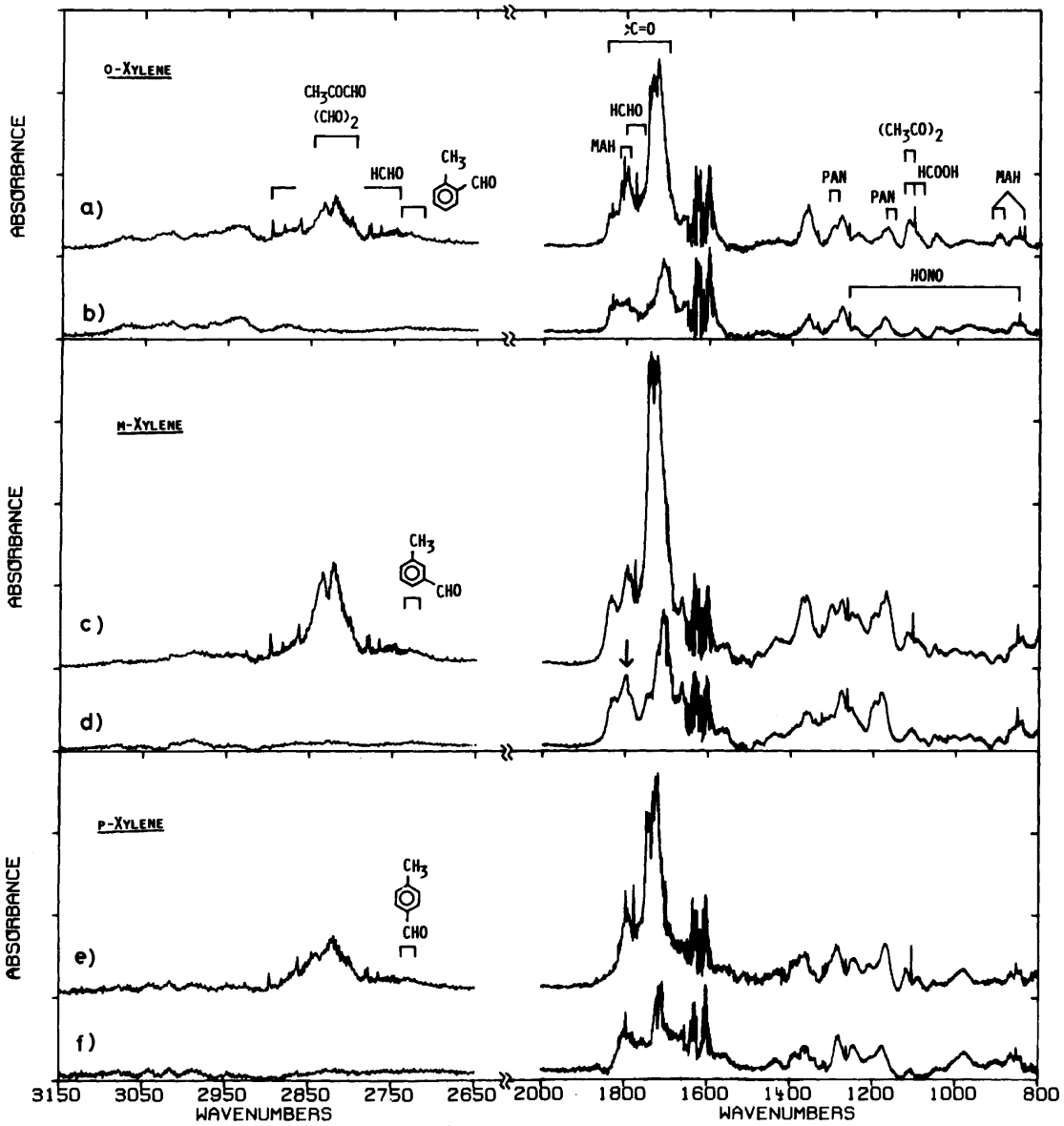

Fig. 1. Product spectra (spectra, from which spectra of xylene, NO, NO_2, and H_2O were subtracted) and residual spectra (spectra, from which spectra of products identified were subtracted).
a) Product spectra in the photooxidation of the *o*-xylene(4 ppm), NO(1.5 ppm), NO_2(0.5 ppm) diluted in 1 atm (=101 kPa) air system. Conversion of *o*-xylene is about 20%. b) Residual spectra after subtraction of products identified (H_2CO, HCOOH, $(CHO)_2$, CH_3COCHO, $(CH_3CO)_2$, maleic anhydride, PAN, and *o*-tolualdehyde). c) Product spectra in the photooxidation of the *m*-xylene(4 ppm), NO(1.5 ppm), NO_2(0.5 ppm) diluted in 1 atm air system. Conversion of *m*-xylene is about 20%. d) Residual spectra after subtraction of products identified (H_2CO, HCOOH, $(CHO)_2$, CH_3COCHO, PAN, and *m*-tolualdehyde). ↓ : See text. e) Product spectra in the photooxidation of *p*-xylene (4 ppm), NO(1.5 ppm), NO_2(0.5 ppm) diluted in 1 atm air system. Conversion of *p*-xylene is about 20%. f) Residual spectra after subtraction of products identified (H_2CO, HCOOH, $(CHO)_2$, CH_3COCHO, PAN, and *p*-tolualdehyde).

Discussion

A. Yields of α-Dicarbonyls and Reaction Mechanism of Ring-cleavage Reaction. As shown in Table 1, product yields of each α-dicarbonyl are varying among the xylenes. For example, the yield of methylglyoxal is the largest for *o*- and *m*-xylene, and that of glyoxal is the largest in the case of *p*-xylene. It is very interesting if the significant variations in yield of α-dicarbonyls among the xylenes can be explained by a unique and simple ring-cleavage mechanism. If such a mechanism will be proved to be applicable as a general rule to other aromatic compounds, it would be very useful for modeling

Table 1. Yield of products[a] (amount of product formed/amount of xylene consumed) in the photooxidation of *o*-, *m*-, *p*-xylene–NO_x–air system[b]

Product \ Run	*o*-Xylene				*m*-Xylene				*p*-Xylene			
	1	2[c]	3	Ave.[d]	4	5	6	Ave.[d]	7	8	9	Ave.[d]
HCHO	0.18	0.13	0.22	0.18±0.04	0.14	0.17	0.19	0.17±0.02	0.19	0.16	0.16	0.17±0.02
$(HCO)_2$	0.07	0.08	0.09	0.08±0.01	0.11	0.12	0.16	0.13±0.03	0.26	0.22	0.23	0.24±0.02
CH_3COCHO	0.23	0.20	0.25	0.23±0.03	0.37	0.44	0.47	0.42±0.05	0.13	0.11	0.14	0.12±0.02
$(CH_3CO)_2$	0.10	0.08	0.12	0.10±0.02								
Maleic anhydride	0.04	0.03	0.05	0.04±0.01								
Tolualdehyde	0.04	0.05	0.05	0.05±0.01	0.03	0.04	0.05	0.04±0.01	0.08	0.08	0.07	0.08±0.01
Total yield of α-dicarbonyls				0.41±0.04				0.55±0.07				0.36±0.03

a) Values were calculated by the least-square fit of five initial points of each run except the case of tolualdehydes (least-square fit of three points). b) Initial conditions of reactants were 4 ppm of xylene, 1.5 ppm of NO, and 0.5 ppm of NO_2 in 1 atm (=101 kPa) air in all runs except run number 2. c) Initial conditions of reactants was 8 ppm of *o*-xylene, 1.5 ppm of NO, and 0.5 ppm of NO_2 in 1 atm air. d) The indicated errors are one standard deviation of three runs.

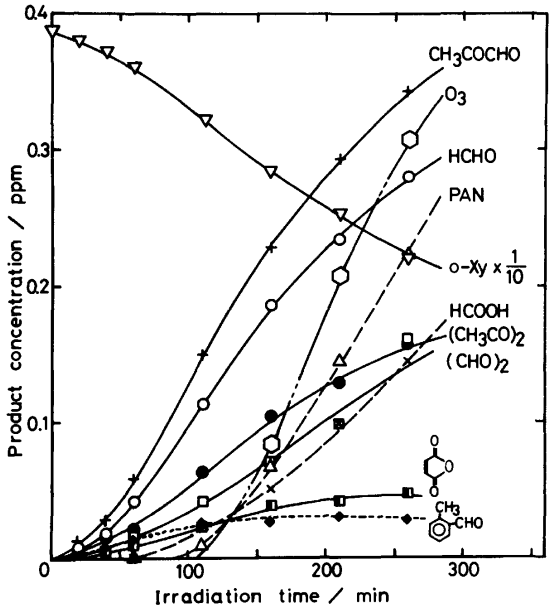

Fig. 2. Concentrations of each product as functions of irradiation time in the case of *o*-xylene.

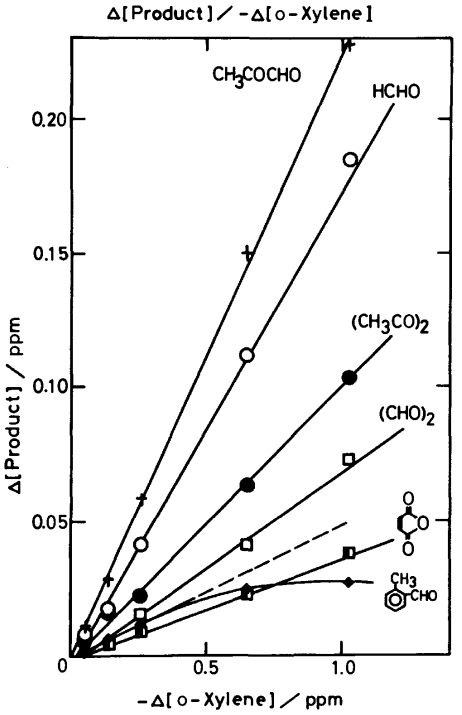

Fig. 3. Concentrations of products are plotted against the concentration of *o*-xylene consumed.

studies of the photooxidation of aromatic compounds.

First, we assume [Assumption I] that the addition of OH to xylene is predominantly at the ortho position.[9] According to the cyclization mechanism described for the ring-cleavage reaction of toluene,[8] the reactions of xylenes are considered to proceed as shown in Scheme 1. In this scheme, allyl-type radicals, 6,7-dioxabicyclo[3.2.1]octane compounds which are produced by bicyclo[3.2.1] cyclization from OH–aromatics–O_2 adducts, are represented by their resonance structures, for example, **Ia**↔**Ib** in the case of *p*-xylene. We consider the example of *p*-xylene first since it is the simplest to follow. Glyoxal and methylglyoxal can be produced with 3-hexene-2,5-dione and 2-methyl-2-butenedial, respectively, and the ratio of the formation of glyoxal and methylglyoxal is governed by the ratio between Reactions 1a and 1b. In the case of *p*-xylene, the formation ratio of glyoxal to methylglyoxal obtained by experiment (see Table 1) is two to one. Therefore, if one takes the bicyclo[3.2.1] cyclization mechanism as the reaction path to yield α-dicarbonyls, the branching ratio of Reaction 1a to 1b should be two to one, that is, the probability of O_2 addition to **Ia** (resonance structure with tertiary radical) and **Ib** (that with secondary radical) of the allyl radicals should be

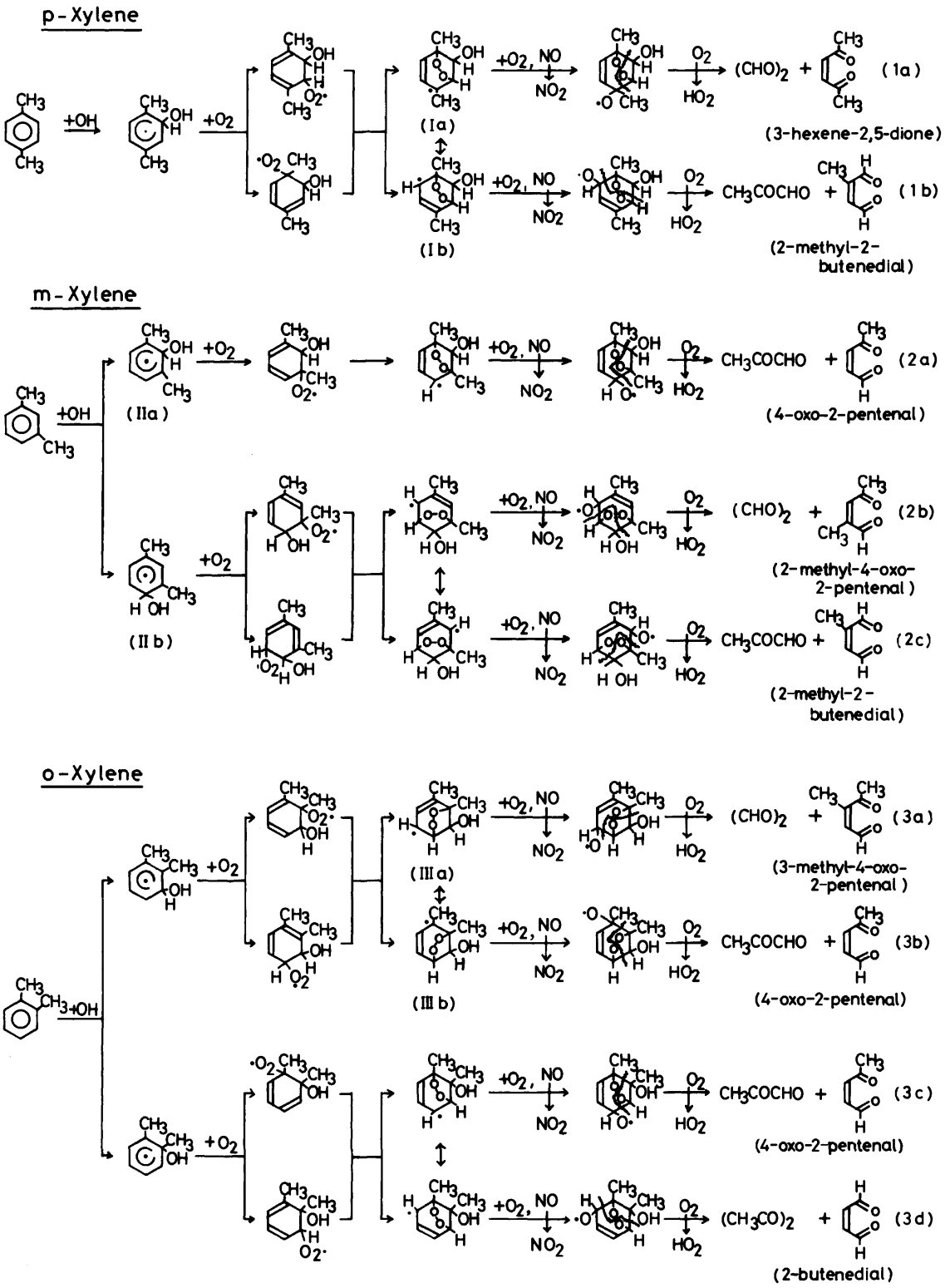

Scheme 1.

two to one. On the other hand, when the resonance structures of the allyl radicals are both secondary radicals, the probability of O_2 addition to the alternate radical points is expected to be the same judging from the case of toluene.[8] This consideration leads us to the second assumption [Assumption II] that the probability of O_2 addition to the resonance structure with tertiary radical is twice as that with secondary radical when the resonance structures of 6,7-dioxabicyclo[3.2.1]octane com-

Table 2. Experimental and calculated[a] values of the ratio of the formation yields of α- and unsaturated γ-dicarbonyls

	$(CHO)_2$	CH_3COCHO	$(CH_3CO)_2$						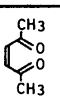
o-Xylene									
Exp.	0.20	0.56	0.24						
Calcd	0.17	0.58	0.25	0.25	0.58	—	0.17	—	—
m-Xylene									
Exp.	0.24	0.76	—						
Calcd	0.25	0.75	—	—	0.50	0.25	—	0.25	—
p-Xylene									
Exp.	0.67	0.33	—						
Calcd	0.67	0.33	—	—	—	0.33	—	—	0.67

a) Calculated by using Assumptions I—III (see text).

pounds consist of both secondary and tertiary radicals, otherwise the probability is the same.

In the case of *m*-xylene, the formation mechanism of glyoxal and methylglyoxal according to Assumption I is also shown in Scheme 1. In the OH-aromatics adducts, **IIa** and **IIb**, the compound **IIa** is produced by the addition of OH to *m*-xylene at the 2-position. The compound **IIb** can be produced by the addition of OH at either the 4- or the 6-position of *m*-xylene. Therefore, if the addition of OH occurs with equal probability, the formation ratio of the compounds **IIa** and **IIb** is one to two. With the assumption of the equal probability of Reactions 2b and 2c under Assumption II the formation ratio of glyoxal to methylglyoxal can be calculated to be 0.33 to 0.67. The experimentally observed formation ratio of glyoxal to methylglyoxal, 0.23 to 0.77, can be explained by introducing the third assumption [Assumption III]: the probability of addition of OH at the 2-position is two times larger than at the other ortho position when the aromatics have methyl groups at 1- and 3-positions simultaneously (*e.g.* *m*-xylene, 1,2,3- and 1,3,4(=1,2,4)-trimethylbenzenes), otherwise the probability is the same. According to Assumption III, the formation ratio of compound **IIa** to **IIb** is one to one and the formation ratio of glyoxal and methylglyoxal was calculated to be 0.25 to 0.75. The value obtained including Assumption III is much closer to the experimental results and assumption III is important to explain the results in cases of trimethylbenzenes as will be described in part III. The formation ratio of α-dicarbonyls obtained by experiments and estimated from Assumptions I—III are listed in Table 2 with estimated yields of unsaturated γ-dicarbonyls.

Reaction mechanisms for the ring-cleavage processes for *o*-xylene are shown also in Scheme 1, and the formation ratios of dicarbonyls obtained by experiments and calculations are listed in Table 2. In the case of *o*-xylene, Assumption II was used to determine the branching ratio of Reactions 3a and 3b (1:2). Table 2 clearly shows that using the same reaction mechanism and the same assumptions which have been introduced to explain the formation ratio of α-dicarbonyls from toluene and *m*- and *p*-xylenes, the ratio from *o*-xylene can be also reproduced well.

The fractions of the ring-cleavage process in the total reaction were 41, 55, and 36% in cases of *o*-, *m*-, and *p*-xylenes, respectively. These values are larger than those of toluene and benzene. The largest fraction from *m*-xylene is reasonable because the addition reaction of OH to the ring is enhanced. This is also evident from the fact that the yields of tolualdehydes which are produced *via* competitive reaction, H-atom abstraction from methyl side chain, are in the reverse order, *i.e.* *p*->*o*->*m*-, as will be discussed later. The reason for the yield of the ring cleavage being larger in *o*-xylene than in *p*-xylene is not clear. However, if the cleavage of the ring occurs in the 6,7-dioxabicyclo[3.2.1]octyloxyl radicals, the distortion energy of the rings should have an effect on the ring cleavage as demonstrated in the photooxidation of C_5–C_7 cycloalkanes.[11] In those molecules, the ring rupture in the vibrationally hot cycloalkyloxyl radicals occurs in order of $C_5>C_7>C_6$ following the order of the strain energy of rings. It is very probable that the distortion energy of the bicyclo compound is larger in the case of *o*-xylene which has adjacent methyl side groups, than in the case of *p*-xylene. Discussions on the distortion energy are given again in paper III.

Yields of α-dicarbonyls obtained in the present study disagree with those obtained in the previous studies by GC analysis.[2,6,7a] In *o*-xylene, for example, reported yields of glyoxal, methylglyoxal and biacetyl by Takagi *et al.*[2] are 0.85, 0.14, and 0.26, respectively. Calculated values from the data by

Nojima *et al.*[6] are 0.002, 0.040, and 0.012, respectively. These data showed quite poor agreement in the yield. Recently, Shepson *et al.*[7c] have carried out an extensive analysis of ring-cleavage products in toluene and *o*-xylene photooxidation. Their reported yields of glyoxal, methylglyoxal and biacetyl are 0.034, 0.116, and 0.085, respectively. Also, Atkinson *et al.*[12] reported the yield of biacetyl (0.137 at 740 torr of air) formed in the NO_x photooxidation of *o*-xylene. The values obtained in the present study (0.08±0.01, 0.23±0.03, and 0.10±0.02 for glyoxal, methylglyoxal and biacetyl, respectively) are in good agreement with those of Shepson *et al.*[7c] and Atkinson *et al.*[12] We believe the direct measurement such as in the present study gives more reliable data of the yield. In *m*- and *p*-xylenes, very low yields of glyoxal, one tenth and one fifth of methylglyoxal, respectively, and the very low absolute yields , only a few percent of the xylene consumed, were reported by Nojima *et al.*[6]

The yield of the high-boiling-point products has been reported only for the photooxidation of *o*-xylene by the use of the GC analysis.[2] The yield of the total high-boiling-point products analyzed was about 17% of *o*-xylene consumed. Therefore, 58% of the total products were accounted for in the case of *o*-xylene; total high-boiling-point products (17%), glyoxal (8%), methylglyoxal (23%), and biacetyl (10%).

B. Residual Spectra of Products and Unsaturated γ-Dicarbonyls. The spectra of unidentified products are shown in the residual spectra (b, d, and f) in Fig. 1. In these, absorptions appearing in the frequency region of 2850—3010 cm^{-1} are due to C–H stretching of hydrocarbons. The absorptions around 1800 cm^{-1} corresponds to the C=O stretching of carboxylic acids, anhydrides, and peroxyacyl nitrates as described in paper I. Formation of maleic anhydride was observed in the case of *o*-xylene. Although Fig. 2 shows a linear increase of maleic anhydride to *o*-xylene consumption, maleic anhydride is considered to be a secondary product produced from *cis*-2-butenedial as proposed in the case of toluene.[8] Under the reaction mechanism mentioned above, only *o*-xylene can yield *cis*-2-butenedial (see Table 2). This also suggests that maleic anhydride is produced from *cis*-2-butenedial. If maleic anhydride is produced from *cis*-2-butenedial, methylmaleic anhydride can be produced from 2-methyl-2-butenedial. However, no significant IR absorption[13] of methylmaleic anhydride was observed. In *m*-xylene, a strong absorption (shown by an arrow) appears at the low frequency side of the absorption around 1800 cm^{-1}. This absorption was always prominent in cases of *m*-xylene and 1,3,5-trimethylbenzene (will be described in part III), and increases strongly upon prolonged irradiation. Although the compounds for this absorption were not identified, it is suggested that more carboxylic acids and/or anhydrides are produced in the photooxidation of *m*-xylene and 1,3,5-trimethylbenzene.

A strong absorption in the frequency region of 1700—1750 cm^{-1} corresponds to the C=O stretching of aldehyde, ketone, dialdehyde, and diketone. If unsaturated γ-dicarbonyls shown in Scheme 1 are present, these compounds should have strong absorption in this region. The noise appearing in the region of 1600—1650 cm^{-1} is caused by the subtraction of the absorption of NO_2. Organic nitrates, which should absorb around 1670, 1280, and 850 cm^{-1}, were not observed as major products.

Absorptions appearing in the frequency region of 1400—800 cm^{-1} are attributable to skeletal vibrations. As described in paper I, absorptions by HONO can also be seen. Spectra in the frequency region of 1400—900 cm^{-1} are expanded and shown in Fig. 4. Spectra (a), (b), and (c) in Fig. 4 are residual spectra of *o*-, *m*-, and *p*-xylene, respectively. In these, the absorption spectrum of HONO was subtracted. Among unsaturated γ-dicarbonyls shown in Scheme 1

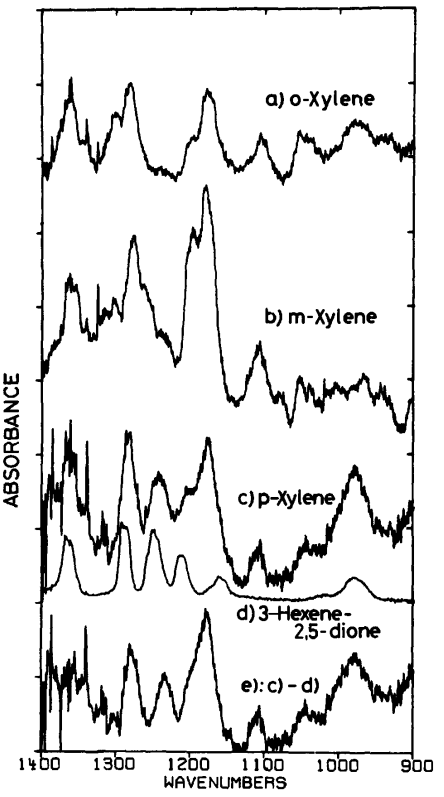

Fig. 4. Residual spectra in the frequency region of 1400—900 cm^{-1}. Conditions are the same as the case in Fig. 1.
a), b), and c) are residual spectra in cases of *o*-, *m*-, *p*-xylenes, respectively. d) Standard spectrum of *trans*-3-hexene-2,5-dione. e) Difference spectrum of c)—d).

and Table 2, 3-hexene-2,5-dione is expected to be the least reactive against OH attack because of an absence of aldehydic hydrogens, taking into account that the loss of unsaturated γ-dicarbonyls is partly due to hydrogen-atom abstraction from -CHO by OH radicals. Takagi *et al.*[14] reported the observation of 3-hexene-2,5-dione by GC/MS method among the compounds collected in a trap at liquid nitrogen temperature from gaseous mixtures of both 1,2,4-trimenthylbenzene and *p*-xylene photooxidation. Thus, in the present study, *in-situ* observation of 3-hexene-2,5-dione was attemped. The standard spectrum of 3-hexene-2,5-dione synthesized by the reaction of acetonylacetone with selenious acid[14,15] is shown in Fig.4(d). Only in the *p*-xylene, spectrum(c), the absorption by 3-hexene-2,5-dione was apparent. Spectrum (e) shows the (c)—(d) difference spectrum. By substraction of the spectrum of 3-hexene-2,5-dione, the yield of 3-hexene-2,5-dione was estimated to be about 8% of the *p*-xylene consumed. The uncertainty of the value is ±100% because of ambiguity of the subtraction. Recently, Tuazon *et al.*[16] investigated the atmospheric chemistry of *cis*- and *trans*-3-hexene-2,5-dione. They report the existence of photoisomerization between the two isomers, and the isomerization was found to account for ≥80% of the total photolysis rate with a photoequilibrium [trans]/[cis] ratio of 0.55±0.05 under their irradiation conditions (25-kW xenon arc solar simulator, NO_2-photolysis rate of 2.1×10^{-3} s^{-1}). According to the vapor-phase IR spectra of the two isomers reported in their study, the spectrum shown in Fig. 4 (d) is *trans*-3-hexene-2,5-dione. In the ring cleavage of *p*-xylene formation of cis isomer is expected primarily, and the cis isomer shows only one strong IR absorption at around 1160 cm^{-1} [16] in the skeletal vibration region. Unfortunately the existence of *cis*-3-hexene-2,5-dione can not be confirmed from Fig. 4(e). It can be, however, assumed that in the present study light intensity is strong enough to establish the photoequilibrium of [trans]/[cis]≃0.5 in 3-hexene-2,5-dione within a few tens min, judging from their data[16] and the NO_2 photodecomposition rate of the present study (3.7×10^{-3} s^{-1}) although the dependence of the photoisomerization rate on wavelength is uncertain. If we take the photoequilibrium into account, the total yield of 3-hexene-2,5-diones should be about three times larger than that of the trans isomer. The yield thus estimated is comparable to that of glyoxal (24±2%), which is a counterpart of 3-hexene-2,5-dione in the ring cleavage of *p*-xylene in Scheme 1.

Syntheses of other unsaturated γ-dicarbonyls, *e.g.* 2-butenedial[17] and 4-oxo-2-pentenal,[18] were attempted. However these compounds were glassy and easily polymerized. Since the purification of these compounds was very difficult, standard spectra of these compounds were not obtained although the residual spectra show the possibility of the presence of unsaturated γ-dicarbonyls.

C. Yields of Tolualdehydes. The formation of *o*-, *m*-, and *p*-tolualdehydes was observed in the photooxidation of *o*-, *m*-, and *p*-xylene, respectively. Since *o*-, *m*-, and *p*-tolualdehydes are formed from *o*-, *m*-, and *p*-methylbenzyl radicals produced by the side-chain hydrogen abstracion by OH radicals, Reactions 4—7, the fractions of the side-chain abstraction channel in the total reaction can be estimated from the yields of tolualdehydes.

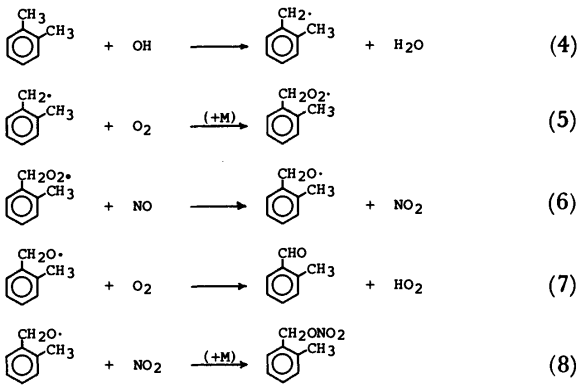

Results are listed in Table 3 together with literature values. The values in the present study were obtained from the yields of tolualdehydes only, and are therefore lower limit, because the amount of other products produced from methylbenzyl radicals such as *o*-, *m*-, *p*-methylbenzyl nitrates (Reaction 8) should account for up to 10%[2] of tolualdehydes produced.

D. Atmospheric Implication. From the photochemical reactivity point of view, ring-cleavage products are important among the compounds produced in the photooxidation of aromatic hydrocarbon. The ring-cleavage products are produced through rather long sequences of reactions involving organic radicals and are often more reactive against photolysis and OH radical attack, which bring forth other radical reaction sequences, than the parent aromatic hydrocarbons. Therefore, the yield of ring-cleavage products such as α-dicarbonyls and unsaturated γ-dicarbonyls is a key for atmospheric photooxidation of aromatic hydrocarbons. Nevertheless, there have been few systematic studies[6,7b] on the yield of α-dicarbonyls from alkylbenzenes, and there is no generalized mechanism for the ring-cleavage reactions so far. This has enforced one to include many branches of reactions and thus to introduce many parameters in model simulation studies of aromatic hydrocarbon photooxidation.

The yield of α-dicarbonyls has been determined systematically for toluene and xylenes in paper I and

Table 3. Fractions of side-chain-abstraction channel in the total reaction of OH+xylenes

	Perry *et al.* (Ref. 1)	Nicovich *et al.* (Ref. 4)	Takagi *et al.* (Ref. 2)	Kenley *et al.* (Ref. 3)	This work
o-Xylene	$0.20^{+0.15}_{-0.10}$	0.04	0.08—0.13		0.05±0.01
m-Xylene	$0.04^{+0.04}_{-0.02}$	0.02			0.04±0.01
p-Xylene	$0.07^{+0.07}_{-0.03}$	0.04		0.15±0.02	0.08±0.01
Method	Temperature dependence of rate constants.	Temperature dependence of rate constants.	GC analysis of tolualdehyde and nitrate.	GC analysis of products.	FT-IR analysis of tolualdehydes.

the present study, and the observed data could be explained by the mechanism depicted as Scheme 1 with Assumptions I—III. Although it is extremely simplified and its validity is still uncertain, the authors believe that it is very useful for predicting the product distribution of the ring-cleavage products and it can provide the most appropriate basis at present of the complex ring-cleavage processes for modeling studies. Indeed, the mechanism seems applicable to other aromatic hydrocarbons as will be demonstrated in the following report, paper III. However, in order to establish more realistic reaction mechanism for the ring-cleavage reactions, extensive analysis of ring-cleavage products is needed including unsaturated γ-dicarbonyls. Further the thermochemical information of the radicals which might involve in the photooxidation of aromatic compounds, such as 6,7-dioxabicyclo[3.2.1]octane and 2,3-dioxabicyclo[2.2.2]octane compounds and their oxygenated radicals, is also needed.

References

1) R. A. Perry, R. Atkinson, and J. N. Pitts, Jr., *J. Phys. Chem.*, **81**, 296 (1977).

2) H. Takagi, N. Washida, H. Akimoto, K. Nagasawa, Y. Usui, and M. Okuda, *J. Phys. Chem.*, **84**, 478 (1980).

3) R. A. Kenley, J. E. Davenport, and D. G. Hendry, *J. Phys. Chem.*, **85**, 2740 (1981).

4) J. M. Nicovich, R. L. Thompson, and A. R. Ravishankara, *J. Phys. Chem.*, **85**, 2913 (1981).

5) A. R. Ravishankara, S. Wagner, S. Fisher, G. Smith, R. Schiff, R. T. Watson, G. Tesi, and D. D. Davis, *Int. J. Chem. Kinet.*, **10**, 783 (1978).

6) K. Nojima, K. Fukaya, S. Fukui, and S. Kanno, *Chemosphere*, **3**, 247 (1974).

7) a) K. R. Darnall, R. Atkinson, and J. N. Pitts, Jr., *J. Phys. Chem.*, **83**, 1943 (1979).
b) E. C. Tuazon, R. Atkinson, H. MacLeod, H. W. Biermann, A. M. Winer, W. P. L. Carter, and J. N. Pitts, Jr., *Environ. Sci. Technol.*, **18**, 981 (1984).
c) P. B. Shepson, E. O. Edney, and E. W. Corse, *J. Phys. Chem.*, **88**, 4122 (1984).

8) H. Bandow, N. Washida, and H. Akimoto, the preceding paper (Part I) in this volume.

9) There is no direct experimental proof that the addition of OH to xylene is predominantly at *o*-position. However, in the case of O(^{3}P)+xylene, Grovenstein and Mosher[10] suggested that the addition of O atoms to xylene is predominantly at *o*-position. Kenley *et al.*[3] reported the formation of $C_6H_3(OH)(CH_3)_2$[2,1,4-] in the reaction of OH+*p*-xylene.

10) E. Grovenstein, Jr. and A. J. Mosher, *J. Am. Chem. Soc.*, **92**, 3810 (1970).

11) H. Takagi, N. Washida, H. Bandow, H. Akimoto, and M. Okuda, *J. Phys. Chem.*, **85**, 2701 (1981).

12) R. Atkinson, W. P. L. Carter, and A. M. Winer, *J. Phys. Chem.*, **87**, 1605 (1983).

13) Since methylmaleic anhydride is commercially available, a standard absorption spectrum can be obtained.

14) H. Takagi, N. Washida, H. Akimoto, and M. Okuda, *Spectrosc. Lett.*, **15** 145 (1982).

15) M. W. Goldberg and P. Müller, *Helv. Chim. Acta*, **21**, 1699 (1938).

16) E. C. Tuazon, R. Atkinson, and W. P. L. Carter, *Environ. Sci. Technol.*, **19**, 265 (1985).

17) K. Alder, H. Betzing, and K. Heimbach, *Liebig's Am. Chem.*, **638**, 187 (1960).

18) J. A. Hirsch and A. J. Szur, *J. Heterocycl. Chem.*, **9**, 523 (1972).

 © 1985 The Chemical Society of Japan Bull. Chem. Soc. Jpn., 58, 2549—2555 (1985)

Ring-cleavage Reactions of Aromatic Hydrocarbons Studied by FT-IR Spectroscopy. III. Photooxidation of 1,2,3-, 1,2,4-, and 1,3,5-Trimethylbenzenes in the NO_x-Air System

Hiroshi Bandow and Nobuaki Washida
Division of Atmospheric Environment, The National Institute for Environmental Studies, P.O. Tsukuba-gakuen, Ibaraki 305
(Received February 12, 1985)

Photooxidation of 1,2,3-, 1,2,4-, and 1,3,5-trimethylbenzenes was carried out in the NO_x-air system. Formation of glyoxal, methylglyoxal and biacetyl was observed in the cases of 1,2,3- and 1,2,4-trimethylbenzenes, and only methylglyoxal was observed from 1,3,5-trimethylbenzene. Yields of glyoxal, methylglyoxal and biacetyl were 7, 18, and 45% and 8, 37, and 11% of trimethylbenzene consumed in cases of 1,2,3- and 1,2,4-trimethylbenzenes, respectively. The reaction mechanism which was used to explain the yields of α-dicarbonyl compounds from toluene and *o*-, *m*-, *p*-xylenes in the preceding paper (part II) has been applied to explain these yields, and has been found to reproduce these yields well. Formation of 3-hexene-2,5-dione was observed only from 1,2,4-trimethylbenzene. The fractions of the ring-cleavage process in the total reaction were 70, 56, and 64% in cases of 1,2,3-, 1,2,4-, and 1,3,5-trimethylbenzenes, respectively. The yields of the ring-cleavage process are discussed.

In the final paper of this series,[1,2] quantitative analysis of ring-cleavage products in the photooxidation of 1,2,3-, 1,2,4-, and 1,3,5-trimethylbenzenes is reported. The rate constants for the reactions of OH+trimethylbenzenes are reported to be very large[3,4,5] (as large as OH+butenes), and the branching ratios for side-chain hydrogen abstractions (estimated to be 2—3% of total reaction[4,6]) are much smaller than in the cases of toluene and xylenes.

The questions addressed in this study are as follows: (1) How large is the fraction of the ring-cleavage process in the total reaction of trimethylbenzenes? (As described in papers I and II, fractions of the ring-cleavage process were in order of *m*-xylene (55%)>*o*-xylene (41%)>*p*-xylene (36%)>toluene (29%)>benzene (15—20%)): (2) Can the formation ratio of α-dicarbonyls (glyoxal, methylglyoxal, and biacetyl) be explained by the cyclization mechanism with three assumptions used in cases of toluene and *o*-, *m*-, *p*-xylenes?: (3) Can formation of unsaturated γ-dicarbonyls be observed? (In the case of 1,2,4-trimethylbenzene, formation of 3-hexene-2,5-dione has been observed by the GC analysis[7]): (4) Are there new specific ring-cleavage products in the photooxidation of trimethylbenzenes?: (5) How consistent are the results for the photooxidation of aromatic hydrocarbons (from benzene to trimethylbenzenes)?

Results

A mixture of trimethylbenzene (4 ppm), NO (1.5 ppm), and NO_2 (0.5 ppm), diluted in 1 atm (=101 kPa) air was irradiated in the reaction chamber as described in paper I.[1] Three experiments were carried out for each 1,2,3-, 1,2,4-, and 1,3,5-trimethylbenzenes.

Product spectra (spectra of reactants and H_2O were subtracted) of each trimethylbenzene are shown by spectrum (a), (c), and (e) in Fig. 1. Residual spectra (spectra of identified products were subtracted from spectrum (a), (c), and (e)) of each trimethylbenzene are shown by spectrum (b), (d), and (f) in Fig. 1. These spectra were obtained under nearly equal (about 20%) conversions of trimethylbenzenes. In all cases, formation of formaldehyde, formic acid, and PAN was observed. α-Dicarbonyls observed are

Table 1. Yield of products[a] (Δproduct/−Δtrimethylbenzene) in the photooxidation of trimethylbenzenes[b]

Product \ Run	1,2,3-Trimethylbenzene				1,2,4-Trimethylbenzene				1,3,5-Trimethylbenzene			
	1	2	3	Ave.[c]	4	5	6	Ave.[c]	7	8	9	Ave.[c]
HCHO	0.17	0.18	0.17	0.17 ±0.01	0.18	0.18	0.17	0.18 ±0.01	0.15	0.15	0.16	0.15±0.01
$(CHO)_2$	0.073	0.071	0.071	0.072±0.001	0.072	0.081	0.081	0.078±0.005	—	—	—	—
CH_3COCHO	0.17	0.18	0.19	0.18 ±0.01	0.38	0.37	0.36	0.37 ±0.01	0.67	0.63	0.63	0.64±0.03
$(CH_3CO)_2$	0.44	0.45	0.47	0.45 ±0.02	0.09	0.11	0.11	0.11 ±0.01	—	—	—	—
Total yield of α-dicarbonyls				0.70 ±0.02				0.56 ±0.02				0.64±0.03

a) Values were calculated by the least-square fit of six initial points of each run. b) Initial concentrations of reactants were 4 ppm trimethylbenzene, 1.5 ppm NO, and 0.5 ppm NO_2 in 1 atm (=101 kPa) air in all runs. c) The indicated errors are one standard deviation of three runs.

glyoxal, methylglyoxal, and biacetyl in cases of 1,2,3- and 1,2,4-trimethylbenzenes, and only methylglyoxal is produced from 1,3,5-trimethylbenzene. Maleic anhydride, which is produced in the reactions of benzene, toluene, and *o*-xylene, was not observed as products of the trimethylbenzenes in significant amounts. Dimethylbenzaldehydes are probably produced, but were not analyzed because of too small yields.

The profile of the product concentrations *versus* irradiation time in the case of 1,2,4-trimethylbenzene is shown in Fig. 2 as an example. Among the products identified, formic acid and PAN were found to be secondary products, like in the cases of toluene and xylenes. As described in paper I,[1] amounts of products formed were plotted against trimethylbenzene consumed. From the slopes of these plots, the yield of each product was determined. Yields of products except formic acid and PAN (secondary products) are listed in Table 1. Values of yield were

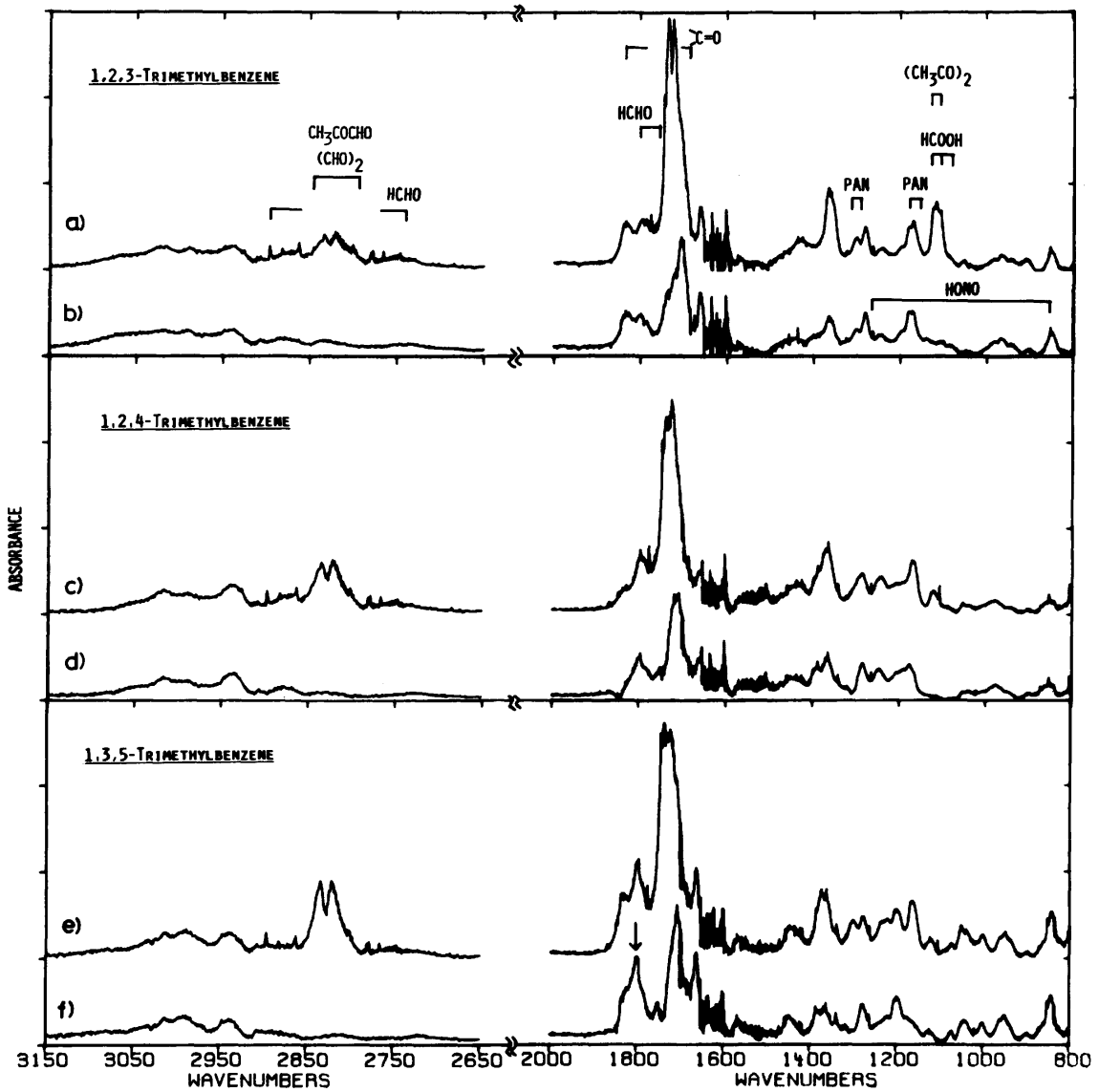

Fig. 1. Product spectra (spectra of reactants were subtracted) and residual spectra (spectra of products identified were subtracted). The initial conditions: [trimethylbenzene]=4 ppm, [NO]=1.5 ppm, and [NO_2]=0.5 ppm in 1 atm (=101 kPa) air.

a) Product spectra in the photooxidation of 1,2,3-trimethylbenzene after 80 min irradiation. Conversion of 1,2,3-trimethylbenzene is 19%. b) Residual spectra after subtraction of products identified (H_2CO, $(CHO)_2$, CH_3COCHO, $(CH_3CO)_2$, PAN, and HCOOH). c) Product spectra in the photooxidation of 1,2,4-trimethylbenzene after 66 min irradiation. Conversion of 1,2,4-trimethylbenzene is 19%. d) Residual spectra after subtraction of products identified (H_2CO, $(CHO)_2$, CH_3COCHO, $(CH_3CO)_2$, PAN, and HCOOH). e) Product spectra in the photooxidation of 1,3,5-trimethylbenzene after 50 min irradiation. Conversion of 1,3,5-trimethylbenzene is 18%. f) Residual spectra after subtraction of products identified (H_2CO, CH_3COCHO, PAN, and HCOOH). ↓: See text.

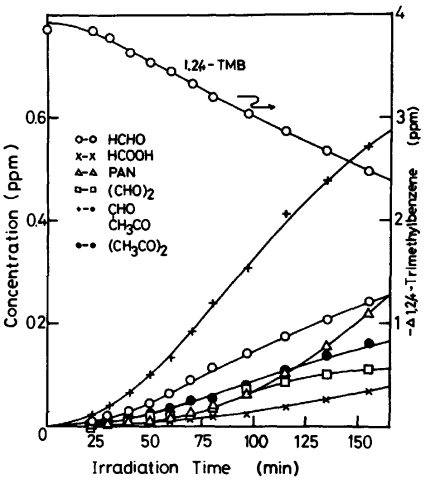

Fig. 2. Concentration of each product as a function of irradiation time in the case of 1,2,4-trimethylbenzene.

calculated by the least-square fit of six initial points of each run. The indicated errors are one standard deviation of three runs. Yields of α-dicarbonyls are fairly large in cases of 1,2,3- and 1,3,5-trimethylbenzenes compared with those of xylenes.

Discussion

A. Yields of α-Dicarbonyls and Reaction Mechanisms. It should be examined whether the yields of α-dicarbonyls shown in Table 1 can be explained by the cyclization mechanism with the assumptions used in cases of toluene and xylenes, as described in paper II.[2] The rules in the reaction mechanism used in paper II are as follows: (1) OH radicals add primarily to the ortho position of each side chain ([Assumption I] in paper II): (2) When the aromatics have side chains ($-CH_3$) at 1- and 3-positions (*e.g.* in *m*-xylene, 1,2,3- and 1,3,4(=1,2,4)-trimethylbenzenes), the probability of OH addition at the 2-position is two times larger than at other ortho position, otherwise the probability is the same ([Assumption III] in paper II): (3) Addition of O_2 to the OH-aromatics adduct occurs predominantly at a position which yields conjugated double bonds (see Reactions 6a and 6b in paper I[1]): (4) The OH-aromatics-O_2 adduct primarily undergoes a cyclization reaction forming a bicyclo-(-O-O-bridge) compound. In this case, formation of 6,7-dioxabicyclo[3.2.1]octane compound (allyl-type radical) is dominant. (In the case of 2,3-dioxabicyclo[2.2.2]octane compound, a radical point and a double bond are not conjugated): (5) The probability of O_2 addition to resonance structure with tertiary radical is two times larger than that to resonance structure with secondary radical when the resonance structures of the allyl-type radical consist of both secondary and tertiary radicals, otherwise the probability of O_2 addition to resonance structures of allyl-type radical is the same ([Assumption II] in paper II): (6) After addition of O_2 to the bicyclo[3.2.1] radical, an alkoxyl-type radical is produced by the abstraction of an O atom by NO: (7) The resulting alkoxyl-type radical undergoes cleavage of the ring, and a 1-hydroxyl-2-oxoalkyl radical (R-C(OH)-CR′=O) and an unsaturated γ-dicarbonyl are produced: (8) The 1-hydroxy-2-oxoalkyl radical undergoes hydrogen abstraction by O_2, and an α-dicarbonyl is produced.

Ring-cleavage reactions of the trimethylbenzenes according to the above rules are shown in Scheme 1. The process of O_2 addition to the OH-aromatics adduct and the formation of 6,7-dioxabicyclo[3.2.1]-octane compound are excluded just for avoiding complication. Formation ratios of α-dicarbonyls obtained by experiments and of α- and unsaturated γ-dicarbonyls calculated using the above rules are listed in Table 2. Branching ratios used in the calculations are as follows: Compound **Ia**:**Ib**:**Ic**= 1:1:1 and **IIa**:**IIb**:**IIc**:**IId**:**IIe**=2:1:1:1:1, according to the number of equivalent positions and Assumptions I and III: Compound **Id**:**Ie**=2:1, **If**:**Ig**=2:1, **IIf**:**IIg**=2:1, **IIh**:**IIi**=2:1, and **IIj**:**IIk**=2:1, according to Assumption II in paper II: One to one is used for all other branching ratios. Yields of α-dicarbonyls obtained by the calculations are in excellent agreement with experimentally observed values. In the

Table 2. Experimental and calculated relative yields of α- and unsaturated γ-dicarbonyls

	$(CHO)_2$	CH_3COCHO	$(CH_3CO)_2$								
1,2,3-Trimethylbenzene											
Exp.	0.10	0.26	0.64								
Calcd	0.11	0.33	0.56	0.56	—	—	0.33	—	—	0.11	—
1,2,4-Trimethylbenzene											
Exp.	0.14	0.66	0.20								
Calcd	0.19	0.67	0.14	—	0.14	0.06	0.11	0.17	0.33	—	0.19
1,3,5-Trimethylbenzene											
Exp.	—	1.0	—								
Calcd	—	1.0	—	—	—	—	—	1.0	—	—	—

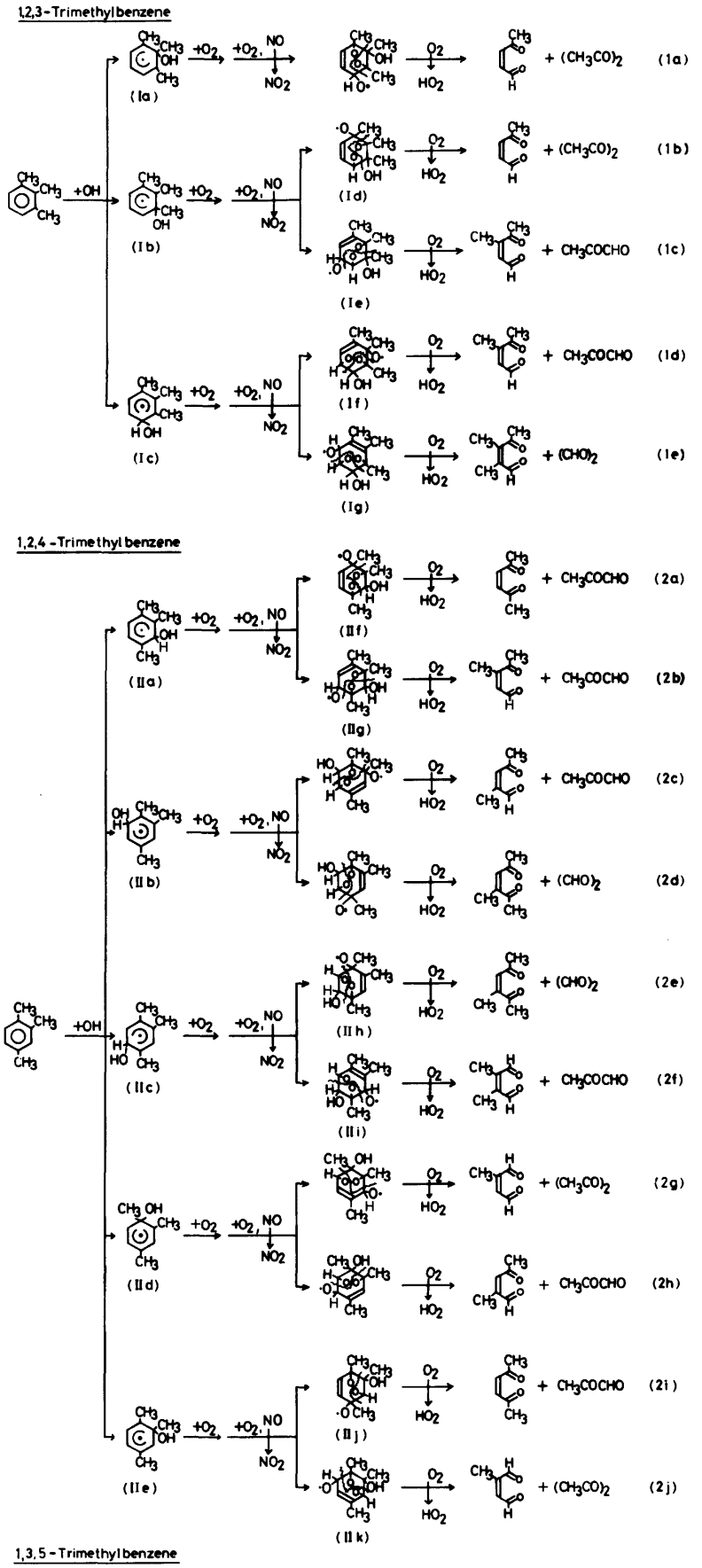
1,2,3-Trimethylbenzene
(Ia)
(Ib)
(Ic)
(Id)
(Ie)
(If)
(Ig)
1,2,4-Trimethylbenzene
(IIa)
(IIb)
(IIc)
(IId)
(IIe)
(IIf)
(IIg)
(IIh)
(IIi)
(IIj)
(IIk)
1,3,5-Trimethylbenzene
+OH
+O2
+O2, NO
NO2
O2
HO2
+ (CH3CO)2 (1a)
+ (CH3CO)2 (1b)
+ CH3COCHO (1c)
+ CH3COCHO (1d)
+ (CHO)2 (1e)
+ CH3COCHO (2a)
+ CH3COCHO (2b)
+ CH3COCHO (2c)
+ (CHO)2 (2d)
+ (CHO)2 (2e)
+ CH3COCHO (2f)
+ (CH3CO)2 (2g)
+ CH3COCHO (2h)
+ CH3COCHO (2i)
+ (CH3CO)2 (2j)
+ CH3COCHO (3)

Scheme 1.

calculations, Assumption III in paper II is crucial. Without this assumption less satisfactory agreement of calculations with experimental values was obtained.[8]

B. Yield of the Ring-cleavage Process. The fractions of the ring-cleavage process in the total reaction are 70, 56, and 64% in cases of 1,2,3-, 1,2,4-, and 1,3,5-trimethylbenzenes, respectively. The percentages in 1,2,3- and 1,3,5-trimethylbenzenes are larger than in the cases of benzene, toluene and xylenes. The value of 56% in 1,2,4-trimethylbenzene is close to 55% in the case of *m*-xylene which shows the largest value of all xylenes. Factors governing the extent of ring cleavage are as follows: 1) The branching ratio between OH addition to the aromatic ring and side-chain hydrogen abstraction: 2) The branching ratio between cyclization of the OH-aromatics-O_2 adduct and the formation of phenols by hydrogen abstraction from the ring by O_2, and the formation of aromatic nitro compounds by the addition of NO_2:[9] 3) The distortion energy of 6,7-dioxabicyclo[3.2.1]octane compound (the alkoxyl-type radical).

As to factor 1, 100%, 85—90%, 90—95%, and 97—98% of total reactions are estimated to proceed through addition in the cases of benzene (no side chain), toluene, xylenes, and trimethylbenzenes, respectively.[4] Therefore, side-chain abstraction might have a slight effect on the yield of ring cleavage, except the case of benzene. Factor 1 alone seems not to explain the large variations of the ring-cleavage yields (15—20% in benzene, 29% in toluene, 36% in *p*-xylene, 41% in *o*-xylene, 55% in *m*-xylene, 56% in 1,2,4-trimethylbenzene, 64% in 1,3,5-trimethylbenzene, and 70% in 1,2,3-trimethylbenzene).

Factor 2 is likely to be important. The probability of cyclization might be governed by the reactivity to electrophilic attack of the carbon with which the end oxygen of the OH-aromatics-O_2 adduct forms a bond. Presumably increase of the number of methyl side chains enhances the probability of cyclization, meta substitution being particularly favorable for electrophilic attack leading to cyclization. The increasing extent of ring cleavage in the order of benzene<toluene<xylenes<trimethylbenzenes, and the large extent of ring cleavage in the cases of *m*-xylene and 1,3,5-trimethylbenzene, might reflect the reactivity of the aromatic ring to electrophilic attack.[10]

After the formation of the 6,7-dioxabicyclo[3.2.1]-octane compound, the distortion energy of this compound would affect the occurrence of the ring cleavage as mentioned in paper II.[2] Although distortion energies of the bicyclo[3.2.1] compounds are not known, the distortion energy is probably larger in the case that the side chains are located adjacent to each other than in the case that side chains are located separately in good symmetry. The larger extent of the ring-cleavage process in the case of 1,2,3-trimethylbenzene as compared with 1,3,5-trimethylbenzene and also in the case of *o*-xylene as compared with *p*-xylene, might be partly due to differences in distortion energy. The fate of the bicyclo compounds when the ring cleavage does not occur is not clear. One possible route is the formation of quinones after rupture of the -O-O- bridge in 6,7-dioxabicyclo[3.2.1]octyloxyl radicals. For example, in the case of *p*-xylene:

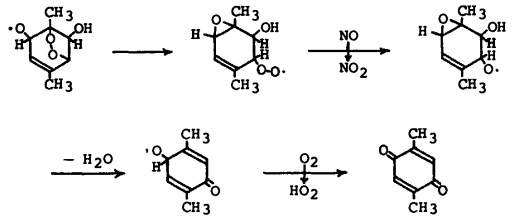

(4)

Formation of small amounts of dimethyl-*p*-benzoquinones have been reported in the photooxidation of *o*-, *m*-, and *p*-xylenes.[11,12] The relative yield of dimethyl-*p*-benzoquinone is the largest for *p*-xylene.[12]

As discussed above, the yield of the ring-cleavage process and the ratio of the α-dicarbonyls formed are governed by several factors. Some features of the ring-cleavage reaction can be explained, although a quantitative evaluation of all factors is not possible at present.

C. Residual Spectra of Products and Unsaturated γ-Dicarbonyls. The spectra of unidentified products are shown in the residual spectra (b,d, and f) in Fig. 1. Absorptions appearing in the frequency region of 2850—3010 cm^{-1} (C-H stretching of hydrocarbons) are stronger than in the case of xylenes. This is probably due to larger yields of unsaturated γ-dicarbonyls (*cf.* Table 2 and Scheme 1) which have more methyl groups.

Residual absorption around 1800 cm^{-1} can be accounted for by C=O stretching of carboxylic acids, anhydrides, and peroxyacyl nitrates. A sharp absorption at 1800 cm^{-1} observed in the case of *m*-xylene is also apparent for 1,3,5-trimethylbenzene (marked by an arrow). No absorptions of maleic anhydride, methylmaleic anhydride, and dimethylmaleic anhydride were observed in this frequency region. Absorption around 1700 cm^{-1} (C=O stretching of aldehyde, ketone, dialdehyde, and diketone) is also present. The large number of overlapping bands in the frequency region of 1700—1850 cm^{-1} shows that there should be a variety of carbonyls present. Sharp absorption at 1670 cm^{-1} is due to organic nitrates which have accompanying bands at 1280 and 850 cm^{-1}.

Absorptions in the region of skeletal vibrations (1400—900 cm^{-1}) are shown on an expanded scale in

Fig. 3. The spectra shown in Fig. 3 are arranged in order of 1,2,3-, 1,3,5-, and 1,2,4-trimethylbenzene: (Note that the order differs from the order in Fig. 1). Spectrum (d) in Fig. 3 shows a standard spectrum of *trans*-3-hexene-2,5-dione. Formation of 3-hexene-2,5-dione in the photooxidation of 1,2,4-trimethylbenzene has been reported in the previous work using the method of GC/MS analysis.[7] In this study, also the formation of 3-hexene-2,5-dione was observed in the case of 1,2,4-trimethylbenzene (spectrum (c) in Fig. 3). Subtraction of the spectrum of *trans*-3-hexene-2,5-dione from spectrum (c) led to an estimated yield of 6% for *trans*-3-hexene-2,5-dione to 1,2,4-trimethylbenzene consumed. According to the study on atmospheric chemistry of *cis*- and *trans*-3-hexene-2,5-dione by Tuazon *et al.*[13] cis and trans isomers of the compound is expected to establish a photoequilibrium with the ratio of [trans]/[cis]≈0.5 under the present experimental conditions.[2] The estimated total yield of 3-hexene-2,5-diones is thus about 18%. The uncertainty of this estimate is ±100% because of the ambiguity of the subtraction. Spectrum (e) shows the difference spectrum (c)—(d).

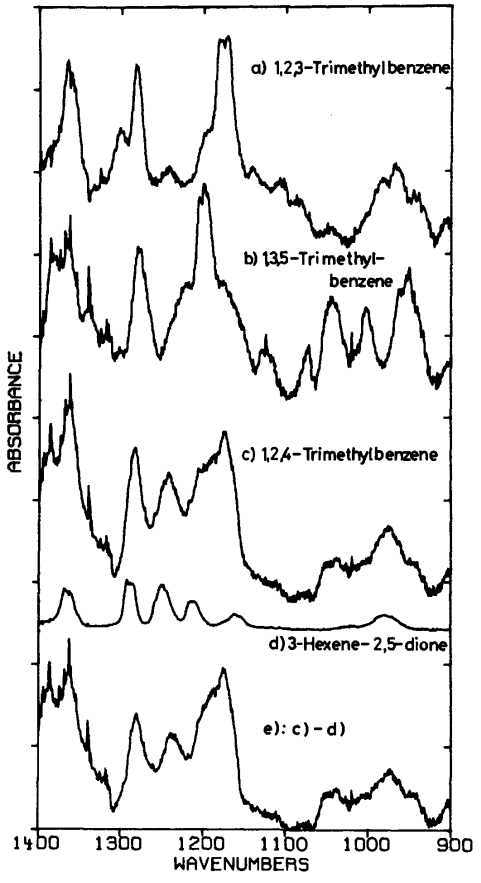

Fig. 3. Residual spectra in the frequency region of 1400—900 cm^{-1}. Conditions are the same as in Fig. 1. a), b), and c) are residual spectra in the cases of 1,2,3-, 1,3,5-, and 1,2,4-trimethylbenzenes, respectively. d) Standard spectrum of *trans*-3-hexene-2,5-dione. e) Difference spectrum of c)−d).

Although no further products except 3-hexene-2,5-dione could be identified in the residual spectra, remaining of C-H stretching vibrations (2850—3010 cm^{-1}), strong absorption around 1700 cm^{-1}, and numerous bands in the region of skeletal vibrations (800—1400 cm^{-1}), suggests the presence of unsaturated γ-dicarbonyls (shown in Table 2 and Scheme 1) in considerable amounts. No unique products of the trimethylbenzenes could be identified.

D. General Conclusions: The Photooxidations of Aromatic Hydrocarbons. This study of eight aromatic hydrocarbons (benzene, toluene, *o*-, *m*-, and *p*-xylenes, 1,2,3-, 1,2,4-, and 1,3,5-trimethylbenzenes) and the conclusions drawn from it may be summarized as follows:

1) Products formed by the ring-cleavage reaction in the photooxidation of aromatic hydrocarbons were analyzed by long-path FT-IR spectroscopy. The advantage of this technique is that products can be observed *in situ*, without the sampling and preconcentration processes which are needed generally in GC and GC/MS analysis. The FT-IR is particularly useful for the quantitative analysis of α-dicarbonyls which cannot be analyzed with reasonable sensitivity by GC even with flame ionization detection.[11] Therefore, reliable yields of α-dicarbonyls were determined for the first time in the present study.

2) The α-dicarbonyls observed in the photooxidation of aromatic hydrocarbons are glyoxal, methylglyoxal, and biacetyl. The relative yields of these products can be explained by a cyclization mechanism of OH-aromatics-O_2 adducts, and cleavage of 6,7-dioxabicyclo[3.2.1]octane compounds. It is suggested that an α-dicarbonyl and an unsaturated γ-dicarbonyl are produced in this process.

3) 3-Hexene-2,5-dione was observed as an unsaturated γ-dicarbonyl in the photooxidation of *p*-xylene and 1,2,4-trimethylbenzene. Formation of maleic anhydride observed in the photooxidation of benzene, toluene, and *o*-xylene is considered as an indirect evidence of the formation of *cis*-2-butenedial (an unsaturated γ-dicarbonyl). Other unsaturated γ-dicarbonyls could not be identified.

4) The fractions of the ring-cleavage process are: 15—20% (benzene); 29% (toluene); 36% (*p*-xylene); 41% (*o*-xylene); 55% (*m*-xylene); 56% (1,2,4-trimethylbenzene); 64% (1,3,5-trimethylbenzene); and 70% (1,2,3-trimethylbenzene). It is suggested that the extent of ring cleavage is governed by the reactivity to electrophilic attack of the OH-aromatics-O_2 adduct, and by the distortion energy of the resulting 6,7-dioxabicyclo[3.2.1]octane compound.

5) Since the formation of fairly large amounts of α- and unsaturated γ-dicarbonyls are expected in the urban atmosphere, studies of the mechanisms of both photolysis and photooxidation of α- and γ-dicar-

bonyls are necessary to develop the chemical models of photochemical air pollution, although the rate constants of the photolysis and OH radical reactions of α-dicarbonyls[14] and 3-hexene-2,5-diones[13] were reported recently.

Throughout this series of investigations, the authors wish to thank Prof. U. Schurath of University of Bonn in Germany and Dr. C. J. Howard of National Oceanic and Atmospheric Administration for helpful suggestions and discussions. We also thank Dr. S. Hatakeyama in our laboratory for helpful discussions. The assistance of H. Takagi in the early stage of this work is gratefully acknowledged.

References

1) H. Bandow, N. Washida, and H. Akimoto, the preceding paper (Part I) in this volume.

2) H. Bandow and N. Washida, the preceding paper (Part II) in this volume.

3) D. A. Hansen, R. Atkinson, and J. N. Pitts, Jr., *J. Phys. Chem.*, **79**, 1763 (1975).

4) R. A. Perry, R. Atkinson, and J. N. Pitts, Jr., *J. Phys. Chem.*, **81**, 296 (1977).

5) R. Atkinson, K. R. Darnall, A. C. Lloyd, A. M. Winer, and J. N. Pitts, Jr., "Advances in Photochemistry," ed by J. N. Pitts, Jr., G. S. Hammond, K. Gollnick, and D. Grosjean, Interscience, New York, 1979, Vol. 11, pp. 375—488.

6) R. A. Kenley, J. E. Davenport, and D. G. Hendry, *J. Phys. Chem.*, **85**, 2740 (1981).

7) H. Takagi, N. Washida, H. Akimoto, and M. Okuda, *Spectrosc. Lett.*, **15**, 145 (1982).

8) The ratios among glyoxal, methylglyoxal and biacetyl were 0.13:0.40:0.47 and 0.23:0.60:0.17 in cases of 1,2,3- and 1,2,4-trimethylbenzene, respectively, when Assumption III in paper II was not used.

9) M. Hoshino, H. Akimoto, and M. Okuda, *Bull. Chem. Soc. Jpn.*, **51**, 718 (1978).

10) Assuming that the probability of forming the 6,7-dioxabicyclo[3.2.1]octane compound increases when the -O-O· attacks the carbon at the ipso position [Assumption IV], the yield of the bicyclo[3.2.1] compound should increase in the cases of *m*-xylene and 1,3,5-trimethylbenzene. For example, in the cases of *o*-, *m*-, and *p*-xylene, the total yield of α-dicarbonyls can be explained if the ratio of the rate of Reactions A to B is 8:1. In the case of *p*-xylene:

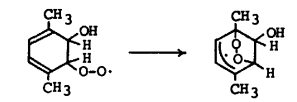

ipso attack (A)

(B)

On this assumption (A:B=8:1), the ratio of the calculated yield of each α-dicarbonyl (Table 2 in paper II and Table 2 in paper III) according to the ring-cleavage mechanism shown in Scheme 1 in paper II and III would vary not more than 10—20%.

11) H. Takagi, N. Washida, H. Akimoto, K. Nagasawa, Y. Usui, and M. Okuda, *J. Phys. Chem.*, **84**, 478 (1980).

12) T. Katou and Y. Hanai, *Bull. Environ. Sci. Technol. Yokohama Natl. Univ.* **2**, 1 (1976).

13) E. C. Tuazon, R. Atkinson, and W. P. L. Carter, *Environ. Sci. Technol.*, **19**, 265 (1985).

14) C. N. Plum, E. Sanhueza, R. Atkinson, W. P. L. Carter, and J. N. Pitts, Jr., *Environ. Sci. Technol.*, **17**, 479 (1983).

Effect of Methyl Substitution in 1,2-Ethanediaminenickel(II) Complexes upon Their Thermal Stabilities

Ryokichi Tsuchiya,† Akira Uehara,* Masatatsu Suzuki, and Akira Matsuda
Department of Chemistry, Faculty of Science, Kanazawa University, Kanazawa 920
†*Kanazawa Women's Junior College, Kanazawa 920*
(Received November 10, 1984)

The enthalpy changes (ΔH) in the reaction of three types of the nickel(II) complexes, $[Ni(AA)_2(H_2O)_2]X_2 \cdot nH_2O$, $[NiX_2(AA)_2]$, and $[Ni(AA)_2]X_2$, with aqueous potassium cyanide solution were calorimetrically measured at 25 °C, where AA denotes a diamine selected from 1,2-ethanediamine (en), *N*-methyl-1,2-ethanediamine (*N*-men), *N,N*-dimethyl-1,2-ethanediamine (*NN*-dmen), *N,N'*-dimethyl-1,2-ethanediamine (*NN'*-dmen), and *N,N,N'*-trimethyl-1,2-ethanediamine (*NNN'*-tmen); X is Cl, Br, I, NO_3, or ClO_4; n=0, 2, or 3. The thermal stabilities of the complexes in the solid state defined by the enthalpy changes (not by the free energy changes) were compared with one another, so that the thermal stabilities of the complexes are highly dependent on numbers and/or positions of *N*-methyl groups on diamines. In the series of $[NiX_2(AA)_2]$ and $[Ni(AA)_2]X_2$ type complexes, the *NN'*-dmen complexes are the most stable. Except for the *NN'*-dmen complexes, as the numbers of *N*-methyl group(s) contained in the diamines increase, the complexes have the tendency to become less stable. The relative thermal stabilities of the present complexes were discussed in terms of the basicities of diamines and steric effect of *N*-methyl groups.

We have systematically studied the structural and thermochemical changes in the course of the solid phase thermal reactions of the nickel(II) complexes containing a variety of diamines.[1] In the preceding paper, the relative thermal stabilites of the octahedral and square planar nickel(II) complexes containing *N,N*- and *N,N'*-diethyl-1,2-ethanediamines were discussed on the basis of their calorimetric data.[2]

In the present study, our interest is focused on the information on the relative thermal stabilities of the nickel(II) complexes containing *N*-methyl, *N,N*(or *N,N'*)-dimethyl, and *N,N,N'*-trimethyl substituted diamines. The diamines selected are 1,2-ethanediamine (en), *N*-methyl-1,2-ethanediamine (*N*-men), *N,N*-dimethyl-1,2-ethanediamine (*NN*-dmen), *N,N'*-dimethyl-1,2-ethanediamine (*NN'*-dmen), and *N,N,N'*-trimethyl-1,2-ethanediamine (*NNN'*-tmen). The enthalpy changes for the following reactions were also estimated; the dehydration ($[Ni(AA)_2(H_2O)_2]X_2 \cdot nH_2O \rightarrow [Ni(AA)_2(H_2O)_2]X_2 + nH_2O$), the dissociation ($[Ni(AA)_2(H_2O)_2]X_2 \rightarrow [Ni(AA)_2]X_2 + 2H_2O$), and the deaquation anation ($[Ni(AA)_2(H_2O)_2]X_2 \rightarrow [NiX_2(AA)_2] + 2H_2O$).

Experimental

Preparation of Complexes. The en,[3] *N*-men, *NN*-dmen, *NN'*-dmen and *NNN'*-tmen[4] complexes were prepared by the known methods or a slight modification thereof, if necessary.

Calorimetric Measurements. In order to discuss the difference in the thermal stabilities of these complexes, the enthalpy changes (ΔH) for the reactions of the accurately weighed complexes in the range of order of 1×10^{-4} mol in the powder state with 100 dm^{-3} of aqueous potassium cyanide solution of 6×10^{-2} mol dm^{-3} were measured with Tokyo Riko TIC-2S isoperibol calorimeter at 25 °C. Three or more measurements were carried out every one sample, and three values within ±0.5 kJ mol^{-1} were averaged. In these reactions, $[Ni(CN)_4]^{2-}$ is formed. The formation constant of $[Ni(CN)_4]^{2-}$(aq) is 31.3 (25 °C)[5], the concentration of Ni^{2+}(aq) remained being calculated to be in the order of 10^{-27} mol dm^{-3}, so that the reactions were concluded to take place completely.

Results and Discussion

Thermal Stability in the en Complexes. Table 1 summarizes the enthalpy changes for the bis(en), bis(*N*-men), bis(*NN*-dmen), bis(*NN'*-dmen) and bis(*NNN'*-tmen) nickel(II) complexes measured. The enthalpy changes for the reaction of $[Ni(en)_2(H_2O)_2]X_2$ (X=NO_3, I, and ClO_4) with aqueous potassium cyanide solution are given as below,

$$[Ni(en)_2(H_2O)_2]X_2(s) + 4CN^-(aq) = Ni(CN)_4^{2-}(aq) + 2en(aq) + 2X^-(aq) + 2H_2O(l),$$

where ΔH=−58.6 kJ mol^{-1} for X=NO_3, ΔH=−60.8 kJ mol^{-1} for X=I and ΔH=−63.4 kJ mol^{-1} for X=ClO_4. By combining the above values with the hydration enthalpies of the respective anions, ΔH_x for the reactions of $X^-(g)=X^-(aq)$ (Table 2),[6] the enthalpy changes for the exchange reaction of anions,

$$[Ni(en)_2(H_2O)_2](NO_3)_2(s) + 2X^-(g) = [Ni(en)_2(H_2O)_2]X_2(s) + 2NO_3^-(g),$$

are calculated. The values thus obtained are 61 kJ mol^{-1} for $X^-=I^-$ and 172 kJ mol^{-1} for $X^-=ClO_4^-$. As was mentioned before, the above enthalpy changes correspond to the difference in the lattice energy between the nitrate and iodide, and between the nitrate and perchlorate, respectively. These results reflect that the iodide and perchlorate are thermally less stable than the nitrate.

The enthalpy changes for the substitution reaction

Table 1. Enthalpy changes for the reaction of nickel(II)–bis(diamine) complexes with CN^- ion (ΔH/kJ mol^{-1})[a]

X \ AA	en	*N*-men	*NN'*-dmen	*NN*-dmen	*NNN'*-tmen
Cl	Oh′	Oh(2) $\xrightarrow{\Delta}$ Oh(0) $\xrightarrow{\Delta}$ Oh′	Oh(3) $\xrightarrow{\Delta}$ Oh′	Oh(2) $\xrightarrow{\Delta}$ Oh(*)[b] $\xrightarrow{\Delta}$ Oh′	Oh(0) $\xrightarrow{\Delta}$ Oh′
	−105.6	−76.6 −95.5 −114.1	−88.8 −124.1	−98.1 −126.5 −153.5	−128.4 −171.2
Br	Oh′	Oh(2) $\xrightarrow{\Delta}$ Oh(0) $\xrightarrow{\Delta}$ Oh′	Oh(2) $\xrightarrow{\Delta}$ Oh′	Oh(2) $\xrightarrow{\Delta}$ Oh(0) $\xrightarrow{\Delta}$ Oh′	Oh(0) $\xrightarrow{\Delta}$ Oh′
	−97.0	−65.3 −71.5 −96.5	−87.3 −106.9	−89.4 −101.4 −141.1	−120.7 −155.6
NO_3	Oh(0) $\xrightarrow{\Delta}$ Oh′	Oh(0) $\xrightarrow{\Delta}$ Oh′	Oh(2) $\xrightarrow{\Delta}$ Oh′	Oh(0) $\xrightarrow{\Delta}$ Oh′	Oh′
	−58.6 −82.0	−63.1 −87.2	−72.7 −105.6	−87.0 −102.6	−143.8
I	Oh(0) $\xrightarrow{\Delta}$ Oh′	Oh(0) $\xrightarrow{\Delta}$ Oh′	Oh(2) $\xrightarrow{\Delta}$ Oh′	Oh(0) $\xrightarrow{\Delta}$ Sq	Oh(0) $\xrightarrow{\Delta}$ Oh′
	−60.8 −73.4	−69.9 −85.3	−67.7 −97.7	−87.8 −117.3	−115.8 −166.8
ClO_4	Oh(0) $\xrightarrow{\Delta}$ Sq	Oh(0) $\xrightarrow{\Delta}$ Sq	Oh(0) $\xrightarrow{\Delta}$ Sq	Oh(0) $\xrightarrow{\Delta}$ Sq	Oh(0) $\xrightarrow{\Delta}$ Sq $\xrightarrow{\Delta}$ Oh′
	−63.4 −76.0	−67.5 −84.6	−86.6 −105.3	−99.1 −105.0	−113.9 −148.0 −151.9

a) Oh(n) designates the octahedral diaquabis(diamine) complex hydrates $[Ni(AA)_2(H_2O)_2]X_2 \cdot nH_2O$, Oh′ the octahedral dianiono-bis(diamine) complexes produced by the anation of the formers, and Sq means $[NiX_2(AA)_2]$ the square-planar bis(diamine) complexes $[Ni(AA)_2]X_2$. b) Oh(*): $[NiCl(NN\text{-dmen})_2(H_2O)]Cl$.

Table 2. The hydration enthalpies, ΔH_x, for the reactions, $X^-(g) = X^-(aq)$ and ΔH_{AA} for $AA(g) = AA(aq)$

ΔH_x/kJ mol^{-1}					ΔH_{AA}/kJ mol^{-1}				
Cl^-	Br^-	NO_3^-	I^-	ClO_4^-	en	*N*-men	*NN'*-dmen	*NN*-dmen	*NNN'*-tmen
−351.5	−318.0	−309.6	−280.3	−225.9	−64.7	−67.1	−79.6	−74.1	−78.2

of the dianiono complexes,

$$[Ni(en)_2Cl_2](s) + 2X^-(g) = [NiX_2(en)_2](s) + 2Cl^-(g),$$

were obtained as ΔH=58 kJ mol^{-1} for X^-=Br^-, ΔH=60 kJ mol^{-1} for X^-=NO_3^-, and ΔH=110 kJ mol^{-1} for X^-=I^-, by using the enthalpy data measured (Table 1) for the octahedral dianiono complexes, $[NiX_2(en)_2]$, where X^- is Cl^-, Br^-, NO_3^-, or I^-, and the ΔH_x values listed in Table 2. These values correspond to the decrements in lattice energies of the dibromo, dinitrato, and diiodo complexes as compared with that of dichloro complex.

From the above enthalpy data, the diagram of enthalpy level for the en complexes can be illustrated as seen in Fig. 1. It is obvious from the figure that the thermal stability decreases in the order, nitrate> iodide>perchlorate in the diaqua series, and dichloro> dibromo>dinitrato>diiodo in the aniono series.

The enthalpy changes for the deaquation-anation,

$$[Ni(en)_2(H_2O)_2]X_2(s) = [NiX_2(en)_2](s) + 2H_2O(g),$$

are also given in Fig. 1. The values were estimated to be ΔH=112 kJ mol^{-1} for X=NO_3 and ΔH=101 kJ mol^{-1} for X=I by combining the heat of vaporization

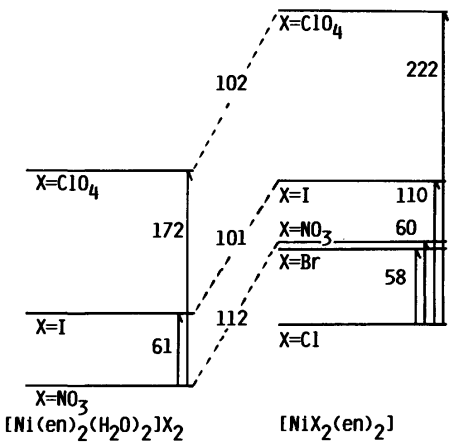

Fig. 1. Enthalpy level diagram for Ni(II)–en complexes (kJ mol^{-1}).

of water, ΔH=44.2 kJ mol^{-1}[17] with the enthalpy data concerned (Table 1). The dissociation enthalpy for the reaction,

$$[Ni(en)_2(H_2O)_2](ClO_4)_2(s) = [Ni(en)_2](ClO_4)_2(s) + 2H_2O(g), \quad \Delta H = 102 \text{ kJ mol}^{-1}$$

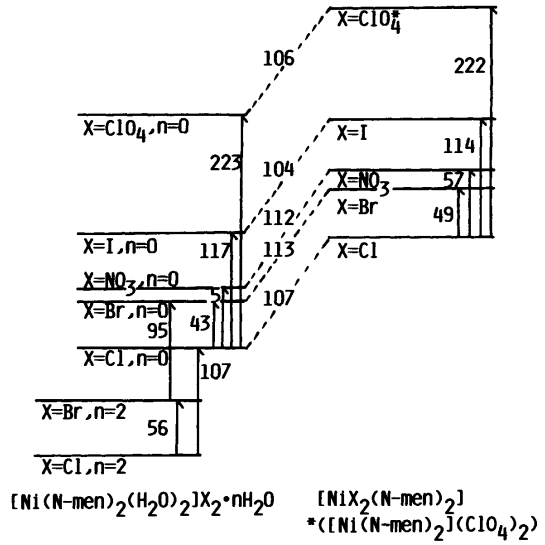

Fig. 2. Enthalpy level diagram for Ni(II)–*N*-men complexes (kJ mol^{-1}).

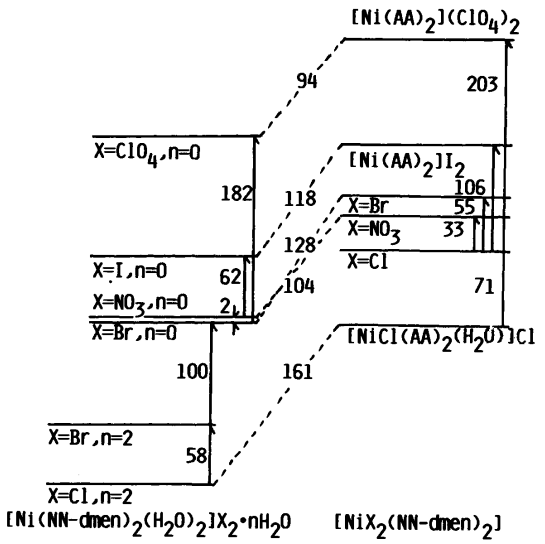

Fig. 3. Enthalpy level diagram for Ni(II)–*NN*-dmen complexes (kJ mol^{-1}).

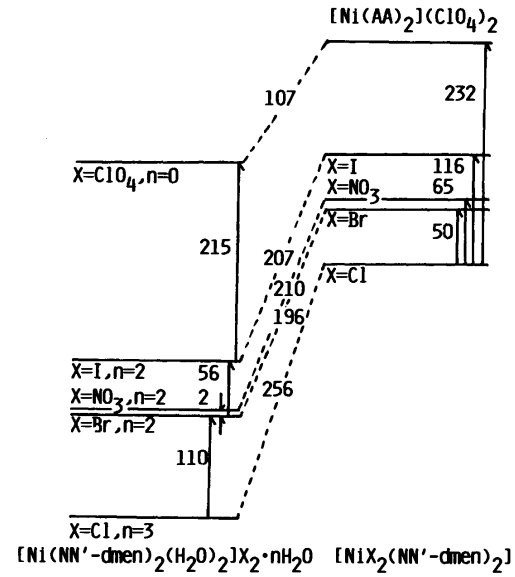

Fig. 4. Enthalpy level diagram for Ni(II)–*NN'*-dmen complexes (kJ mol^{-1}).

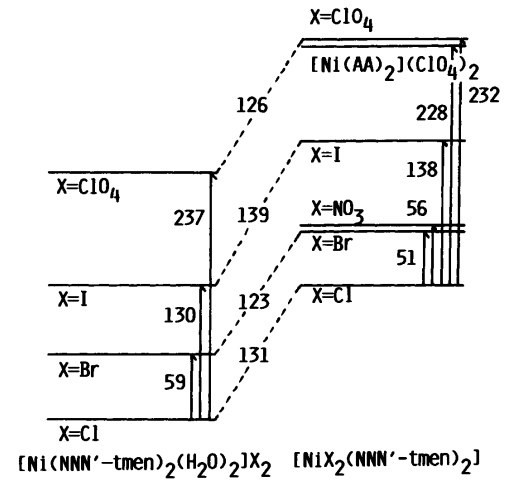

Fig. 5. Enthalpy level diagram for Ni(II)–*NNN'*-tmen complexes (kJ mol^{-1}).

is also shown in Fig. 1.

Thermal Stability in the N-*men Complexes.* The enthalpy changes for the substitutions of counter anion and of aniono ligand, the dehydration, the deaquation-anation, and the dissociation of the *N*-men complexes were calculated in a manner similar to that carried out for the en complexes. The enthalpy level diagram thus obtained is represented in Fig. 2. The figure exhibits that [Ni(*N*-men)$_2$(H$_2$O)$_2$]X$_2$·*n*H$_2$O become thermally less stable in the order, chloride dihydrate>bromide dihydrate (*n*=2), and chloride>bromide>nitrate>iodide> perchlorate (*n*=0); the thermal stabilities of [Ni(*N*-men)$_2$X$_2$] decrease in the order, dichloro>dibromo >dinitrato>diiodo complexes.

Thermal Stability in the NN-*dmen,* NN'-*dmen, and* NNN'-*tmen Complexes.* In the same way as that shown in the *N*-men complexes, the enthalpy level diagrams of the *NN*- and *NN'*-dmen, and *NNN'*-tmen complexes are obtained, which are represented in Figs. 3, 4, and 5, respectively. These figures indicate that the thermal stabilities decrease in the order, chloride>bromide>nitrate>iodide in the diaqua series, and dichloro>dibromo>dinitrato>diiodo in the aniono series except for *NN*-dmen complexes, which are consistent with the orders of the stability

appearing in the *N*-men complexes. The orders of decrement in lattice energy observed in the diaqua and dianiono complexes are parallel to the increasing order of the anionic radii.[8]

Influence of Numbers of N-*Methyl Groups upon Thermal Stability.* The relative thermal stabilities of a series of $[Ni(AA)_2(H_2O)_2]X_2$ can be estimated by comparing the enthalpy changes for the following substitution reaction of diamines:

$$[Ni(AA)_2(H_2O)_2]X_2(s) + 2AA'(g) = [Ni(AA')_2(H_2O)_2]X_2(s) + 2AA(g)$$

For example, the enthalpy change (ΔH) for the reaction,

$$[Ni(en)_2(H_2O)_2](NO_3)_2(s) + 2N\text{-men}(g) = [Ni(N\text{-men})_2(H_2O)_2](NO_3)_2(s) + 2en(g)$$

Table 3. The heats of dissolution of the diamines in aqueous potassium cyanide solution (/kJ mol^{-1})

en	*N*-men	*NN'*-dmen	*NN*-dmen	*NNN'*-tmen
−30.4	−32.9	−45.0	−40.6	−43.8

was calculated as -0.3 kJ mol^{-1} by using the following equation,

$$\Delta H = \Delta H_1 - \Delta H_2 - \Delta H_{en} + \Delta H_{N\text{-men}},$$

where ΔH_1 and ΔH_2 are the enthalpy changes for the following reactions, respectively (Table 1):

$$[Ni(en)_2(H_2O)_2](NO_3)_2(s) + 4CN^-(aq) = Ni(CN)_4^{2-}(aq) + 2en(aq) + 2NO_3^-(aq) + 2H_2O(l) \cdots \Delta H_1$$

$$[Ni(N\text{-men})_2(H_2O)_2](NO_3)_2(s) + 4CN^-(aq) = Ni(CN)_4^{2-}(aq) + 2N\text{-men}(aq) + 2NO_3^-(aq) + 2H_2O(l) \cdots \Delta H_2,$$

and ΔH_{en} and $\Delta H_{N\text{-men}}$ are the heats for the reactions of en(g)=en(aq) and *N*-men(g)=*N*-men(aq), respectively (Table 2). The same procedures as those described above were employed for the calculation of the corresponding enthalpy changes for the reactions of the *NN*-dmen, *NN'*-dmen and *NNN'*-tmen complexes. In these calculations, the enthalpy changes for the reaction of AA(g)=AA(aq) in the various diamine systems should be referred. These values were calculated from the heats of vaporization and the heats of solution. The former heats were estimated from the Trouton's constant and the

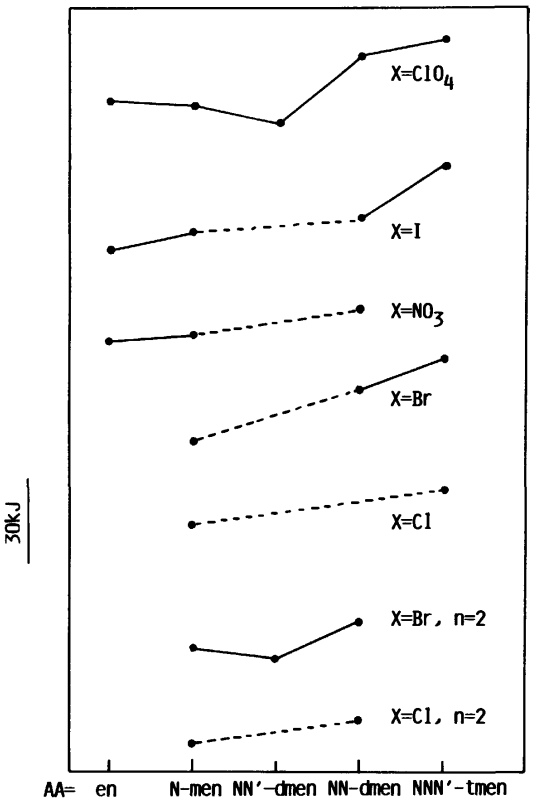

Fig. 6. Enthalpy change diagrams depending upon the displacement of diamines for $[Ni(AA)_2(H_2O)_2]X_2 \cdot nH_2O$ type complexes. The lines to which *n* values are not given are referred to the anhydrates.

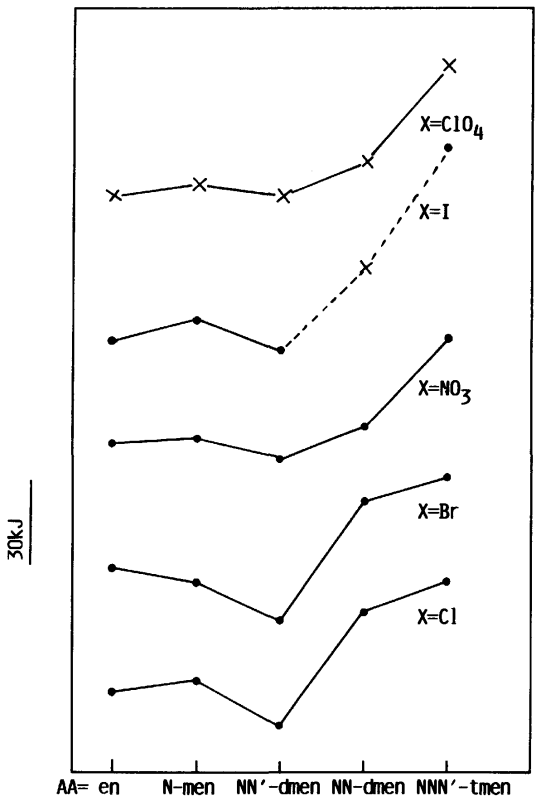

Fig. 7. Enthalpy change diagrams depending upon the displacement of diamines for $[NiX_2(AA)_2]$ (--●--) and $[Ni(AA)_2]X_2$ (--×--) type complexes.

boiling points of diamines within about 5% errors. The latter heats were measured in the concentration of diamine similar to that liberated by the reaction of complexes with CN^- solution. These data measured are listed in Table 3.

Additionally, the enthalpy changes for the substitution reactions of diamines in $[NiX_2(AA)_2]$ and $[Ni(AA)_2]X_2$ were estimated from the data obtained above. The enthalpy change diagrams for $[Ni(AA)_2(H_2O)_2]X_2 \cdot nH_2O$ are depicted in Fig. 6, and those for $[NiX_2(AA)_2]$ and $[Ni(AA)_2]X_2$, in Fig. 7.

The most striking feature is that, in the series of $[NiX_2(AA)_2]$ and $[Ni(AA)_2]X_2$ type complexes, the *NN'*-dmen complexes are the most stable as can be seen in Fig. 7. Except for the *NN'*-dmen complexes, as the number of *N*-methyl groups on diamines increases, the relative thermal stabilities of the complexes generally decrease: namely the complexes become unstable in the order of the en, *N*-men, *NN*-dmen, *NNN'*-tmen complexes (Figs. 6 and 7). This may be partly attributable to an increase of steric repulsion between *N*-methyl groups and the ligands in the apical positions. In the *N*-methyl substituted en complexes, the orientation of methyl group(s) is expected to have an significant influence on the thermal stability of the complexes. In the *NN'*-dmen complexes, two methyl groups are equatorial with respect to the N_4 plane. On the other hand, the *NN*-dmen and *NNN'*-tmen complexes have at least one axial methyl group, which causes a stronger steric repulsion with the ligands in the apical positions than equatorial methyl group and makes the complexes less stable.

The stability of the complexes in the solid state would be mainly dependent not only on the steric interaction but also on the size and shape of the complex cation and the basicity of diamines. In fact, as the numbers of *N*-methyl groups increase, the size of complex cations becomes larger, leading the complexes less stable in the order, en>*N*-men *NN*-dmen>*NNN'*-tmen complexes. This is in line with the results observed in the effect arising from variation of anion size.

So far as the order of the thermal stability between *N*-men and *NN'*-dmen complexes is concerned, however, the interpretation is not so clear only from the steric factor. It has been shown that the formation constant of nickel(II)-*N*-men complex in aqueous solution is larger than that of nickel(II)-*NN'*-dmen complex.[9] In general, the stronger the basicity of the ligand is, the more stable the complex becomes, if no steric hindrance is present within the complex, and the basicity of *N*-men is known to be larger than that of *NN'*-dmen.[10] The observed order of the stabilities between *N*-men and *NN'*-dmen complexes, therefore, is not in harmony with that expected from the formation constant and basicity arguments. In spite of the above discussions, the interpretation on the difference of the thermal stabilities between *N*-men and *NN'*-dmen complexes is not so clear.

References

1) R. Tsuchiya, S. Joba, A. Uehara, and E. Kyuno, *Bull. Chem. Soc. Jpn.*, **46**, 1454 (1973); R. Tsuchiya, E. Kyuno, A. Uehara, S. Joba, and S. Ohba, *Chem. Lett.*, **1976**, 911; H. Nishimoto, T. Yoshikuni, A. Uehara, E. Kyuno, and R. Tsuchiya, *Bull. Chem. Soc. Jpn.*, **51**, 1068 (1978); Y. Ihara and R. Tsuchiya, *Bull. Chem. Soc. Jpn.*, **53**, 1614 (1980).

2) R. Tsuchiya, A. Uehara, and Y. Ohtsuka, *Bull. Chem. Soc. Jpn.*, **55**, 1858 (1982).

3) M. E. Farago, L. M. James, and V. C. G. Trew, *J. Chem. Soc.*, **A1967**, 820.

4) D. M. L. Goodgame and L. M. Venanzi, *J. Chem. Soc.*, **1963**, 616, 5909; S. F. Pavkovic and D. W. Meek, *Inorg. Chem.*, **4**, 1091 (1965).

5) L. G. Sillén and A. E. Martell, Ed., "Stability Constants of Metal-Ion Complexes," The Chemical Society, London (1964).

6) H. F. Halliwell and S. C. Nyburg, *Trans. Faraday Soc.*, **59**, 1126 (1963); V. P. Vasil'ev, E. K. Zolobarev, A. F. Kapustinskii, K. P. Mischenko, E. A. Podgornaya, and K. B. Yatsimirskii, *Russ. J. Phys. Chem.*, **34**, 840 (1960); M. F. C. Ladd and W. H. Lee, *Prog. Solid St. Chem.*, **2**, 378 (1965).

7) F. D. Rossini, D. D. Wagman, W. H. Evans, S. Levine, and I. Jaffe, "Selected Values of Thermodynamic Properties," U. S. Governm. Printing Office, Washington, D. C. (1962), p. 31.

8) V. M. Goldschmidt, *Ber.*, **60**, 1263 (1927); L. Pauling, *J. Am. Chem. Soc.*, **49**, 765 (1927); K. B. Yatsimirskii, Izv. *Akad. Nauk SSSR, Otdel, Khim. Nauk*, **1943**, 398.

9) F. Basolo and R. K. Murman, *J. Am. Chem. Soc.*, **74**, 5243 (1952); **76**, 211 (1954).

10) F. Basolo, R. K. Murman, and Y. T. Chen, *J. Am. Chem. Soc.*, **75**, 1478 (1953); F. Basolo and R. K. Murman, *J. Am. Chem. Soc.*, **74**, 2373 (1952).

 © 1985 The Chemical Society of Japan Bull. Chem. Soc. Jpn., 58, 2561—2568 (1985)

The Stereochemistry of the Six Geometrical Isomers of the Bis(ethylenediamine-*N*-acetato)cobalt(III) Ion, $[Co(edma)_2]^{+}$[1)]

Tomoharu AMA,* Hiroshi KAWAGUCHI, Takaji YASUI, Keiji MATSUMOTO,† and Shun'ichiro OOI†

Department of Chemistry, Faculty of Science, Kochi University, Akebono-cho, Kochi 780
†*Department of Chemistry, Faculty of Science, Osaka City University, Sumiyoshi-ku, Osaka 558*
(Received December 19, 1984)

All of the six geometrical isomers possible in $[Co(edma)_2]^+$ (edma: ethylenediamine-*N*-acetate) were isolated, and the five chiral isomers were resolved into optically active isomers by a column-chromatographic method. Their structures were determined on the basis of the X-ray analysis and the visible absorption, ^1H NMR, and CD spectral data. One of the methylene protons in the glycinate-ring of the facially coordinating edma is stereospecifically exchanged by a deuteron in the basic D_2O solution, and its deuteration rate is influenced by the ligating atoms in the *trans* position. A ^1H NMR method to determine the absolute configurations of the optically active isomers, which contain the stereospecifically deuterated edma, is reported and applied to the $[Co(edma)_2]^+$ systems. The relationship between the absolute configurations and the CD spectral behaviors of these complexes is also discussed.

The ethylenediamine-*N*-acetate anion ($NH_2CH_2CH_2NHCH_2COO^-$: edma) is a terdentate ligand of the N-N-O type. The [Co(N-N-O)$_2$]-type complex provides six geometrical isomers (Fig. 1). Although there have been several reports on this type of complex,[2-7] there have been only a few reports which have dealt with all of the six isomers.[1] In a previous letter[1] we reported the preparation and tentative assignments of the six geometrical isomers for the [Co(edma)$_2$]X complex. In order to confirm these assignments, we have now determined the structure (and the absolute configuration) of one of the isomers by means of X-ray analysis.

It was found that one of the methylene protons in the glycinate-ring of the facially coordinating edma was stereospecifically deuterated in a basic D_2O solution. Optically active edma ($NH_2CH_2CH_2NHC^*HDCOO^-$) was obtained from a stereospecifically deuterated, optically active $[Co(edma)_2]^+$. Further, the isomers of $[Co(edma)_2]^+$, which contain this deuterated edma, were used to determine the absolute configurations on the basis of the ^1H NMR data. In the present paper, this ^1H NMR method to determine the absolute configuration of the complex will be discussed in detail. In addition, the relationship between the absolute configuration and the CD spectral behavior will be discussed.

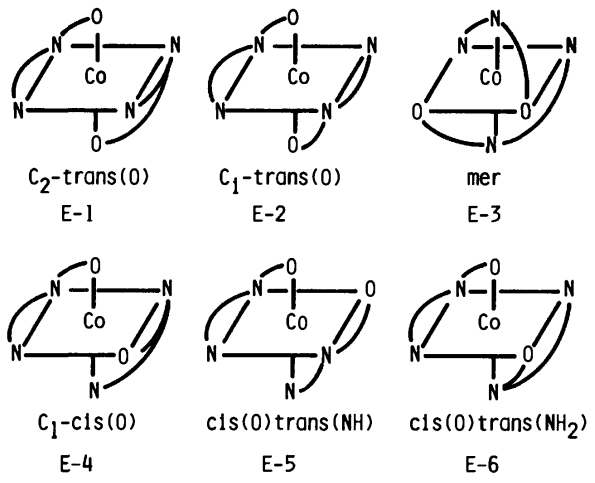

Fig. 1. The six geometrical isomers of the $[Co(edma)_2]^+$ ion.

Experimental

Preparation and Separation of the Isomers of the $[Co(edma)_2]^+$ Ion. The previously reported method[1] was modified for the preparation of the complexes. A solution containing 10 g of ethylenediamine-*N*-acetic acid dihydrochloride dihydrate (Hedma·2HCl·2H$_2$O) in 50 ml of water and solution containing 4.75 g of $CoCl_2 \cdot 6H_2O$ in 30 ml of water were separately passed through an anion-exchange resin (Dowex 1×8, ClO_4^- form) column to convert the chloride ions to perchlorate ions, and then the two solutions were combined. The pH of the combined solution was adjusted to 6—7 with 1 mol dm^{-3} NaOH solution. Lead dioxide (9.0 g) was stirred into the solution in small portions at 50 °C over a 1-h period, the pH of the solution being held at about 6.5. After the insoluble material had then been removed by filtration, the filtrate was charged on an SP-Sephadex column (K^+ form). The adsorbed band was developed by the method described in the previous paper[1] (eluent: 0.1 mol dm^{-3} KCl solution).

The method of preparing the [Co(edma)$_2$]Cl described above (PbO_2-oxidation in a weakly acidic solution) gave better overall yields, especially for E-5 and -6, than the method using $Na_3[Co(CO_3)_3] \cdot 3H_2O$[8] as the starting material (carbonato method[1]). (Under basic conditions, the PbO_2-oxidation method gave low yields for E-3, -5, and -6.)

All of the isomers except for E-2 (the achiral isomer) were optically resolved by the chromatographic method described in the previous paper[1] (eluent: 0.05 mol dm^{-3} K_2Sb_2-(d-tart)$_2$ aqueous solution). The formulas of the optically active complexes (faster eluted isomers) finally obtained are

as follows: $(-)^{CD}_{543}$E-1: $[Co(edma)_2]ClO_4$; $(-)^{CD}_{504}$E-3: $[Co(edma)_2]$-Br; $(+)^{CD}_{534}$E-4: $[Co(edma)_2]Cl\cdot 2H_2O$; $(-)^{CD}_{521}$E-5: $[Co(edma)_2]$-Br; $(+)^{CD}_{509}$E-6: $[Co(edma)_2]Cl\cdot 1.5H_2O$.

The $(-)^{CD}_{521}$E-5 (bromide salt) isomer was converted to a perchlorate salt using QAE-Sephadex (ClO_4^- form) to obtain single crystals suitable for X-ray analysis.

X-Ray Analysis of $(-)^{CD}_{521}$*-[Co(edma)$_2$]ClO$_4\cdot 2H_2O$ (E-5).* *Crystal Data*: Monoclinic, space group $P2_1$, a=11.530(2), b=11.157(2), c=6.489(1) Å, β=96.83(1)°, D_m=1.70 g cm^{-3}, Z=2, D_c=1.72 g cm^{-3}, μ(Mo $K\alpha$)=13.0 cm^{-1}. The unit-cell dimensions were determined from a least-squares analysis of 24 θ values of higher angle reflections (θ=8—14°), as measured on an automated diffractometer by the use of graphite-monochromated Mo $K\alpha$ radiation.

The intensity data ($2\theta<50°$) were collected on the diffractometer by means of the ω-scan method with Mo $K\alpha$ radiation (scan speed, 0.033° s^{-1}; scan width, (1.0+0.4 tan θ)°; background measurement, 10 s at each end of the scan; crystal size, 0.15×0.17×0.15 mm). Of the 1552 independent reflections measured, 1371 with $I>3\sigma(I)$ were used for the structure analysis. No correction was made for absorption.

The crystal structure was solved by the heavy-atom technique. The positional and thermal parameters were refined by the block-diagonal-matrix least-squares method. The minimized function was $\sum w(|F_o|-|F_c|)^2$, where $w=\sigma(F_o)^{-2}$. The large temperature factors found for the O atoms of the ClO_4^- ion were indicative of a disorder of the ion; therefore, the 4 O atoms were treated, in the subsequent least-squares calculation, as a rigid group in which the O atoms lie at the apices of the regular tetrahedron, with a Cl···O distance of 1.426 Å.[9] The parameters of the Cl atom were allowed to vary independently from those of the 4 O atoms.

The atomic scattering factors, with correction for the anomalous dispersion effect for Co and Cl atoms, were taken from Ref. 10. The convergence was attained with R 0.071 and R' ($=[\sum w\Delta F^2/\sum wF_o^2]^{1/2}$) 0.100, whereas R and R' at convergence were 0.070 and 0.098 respectively for the inverted structure. All the parameter shifts in the final cycle of the refinement for either structure were $<0.2\sigma$. The absolute crystal structure was determined by means of the Bijvoet method. Table 1 shows several Bijvoet pairs, which showed a remarkable intensity difference on the Weissenberg photographs taken with Cu $K\alpha$ radiation. The inequality relationship between the intensities of the Bijvoet pair agrees well with that between $|F_c(hkl)|^2$ and $|F_c(h\bar{k}l)|^2$ calculated on the basis of the atomic coordinates (the inverted structure) listed in Table 2. The observed and calculated structure factors, thermal parameters, bond lengths and angles (Table 3), and the projection of the crystal structure along the b axis are preserved by the Chemical Society of Japan (Document No. 8532). The computation was carried out on an ACOS 900 computer at the Crystallographic Research Center, Institute of Protein Research, Osaka University, and a FACOM M180 computer at Osaka City University. The computer programs used were as follows: UNICS,[11] ORTEP,[12] and ORFLS.[13]

Spectral Measurements. The ^{1}H NMR spectra were recorded on a JEOL MH-100 spectrometer, with DSS as the internal standard in D_2O. The visible and UV absorption spectra were recorded on a HITACHI 557 spectrophotometer, while the circular dichroism (CD) spectra were recorded on a JASCO J-22 spectropolarimeter in an aqueous solution.

Measurements of the Deuteration Rate of the G-ring. In order to measure the H-D exchange rate (deuteration rate) of the glycinate-ring (G-ring) $-CH_2-$ in the coordinating

TABLE 1. OBSERVED INEQUALITY RELATIONSHIP BETWEEN THE INTENSITIES OF THE BIJVOET PAIR AND THE $|F_c|^2$ VALUES CALCULATED ON THE BASIS OF THE ATOMIC COORDINATES LISTED IN TABLE 2

$h\ k\ l$	$\lvert F_c(hkl)\rvert^2$	Observed inequality relationship	$\lvert F_c(h\bar{k}l)\rvert^2$
3 1 1	375.2	<	954.8
9 1 1	216.1	<	420.3
$\bar{3}$ 2 1	376.4	>	269.0
$\bar{4}$ 2 1	225.0	<	372.5
4 2 1	139.2	<	338.6
4 1 2	488.4	<	718.2
5 2 1	635.0	>	327.6
$\bar{5}$ 1 2	102.0	<	400.0
$\bar{6}$ 1 2	39.7	<	246.5
$\bar{2}$ 2 2	59.3	<	174.2
$\bar{3}$ 2 2	246.5	<	388.1

TABLE 2. FRACTIONAL COORDINATES AND TEMPERATURE FACTORS FOR $(-)^{CD}_{521}[Co(edma)_2](ClO_4)\cdot 2H_2O$ (E-5). STANDARD DEVIATIONS OF THE LEAST SIGNIFICANT FIGURES ARE GIVEN IN PARENTHESES

Atom	x	y	z	B(eq) or B
Co	−0.3363(1)	−0.69711(0)	−0.1726(2)	1.68(4)
Cl	−0.1958(4)	−0.1520(4)	−0.2863(8)	4.2(1)
N(1)	−0.478(1)	−0.784(1)	−0.138(2)	1.9(3)
N(2)	−0.3636(9)	−0.740(1)	−0.463(2)	2.7(3)
N(3)	−0.197(1)	−0.601(1)	−0.193(2)	2.8(3)
N(4)	−0.231(1)	−0.832(1)	−0.103(2)	2.6(3)
C(1)	−0.531(1)	−0.568(1)	−0.156(2)	1.9(3)
C(2)	−0.567(1)	−0.690(2)	−0.096(2)	2.5(3)
C(3)	−0.513(1)	−0.858(1)	−0.332(2)	2.8(4)
C(4)	−0.487(1)	−0.782(2)	−0.511(2)	3.0(4)
C(5)	−0.242(1)	−0.574(1)	0.165(2)	2.8(4)
C(6)	−0.177(1)	−0.525(1)	−0.013(2)	2.7(4)
C(7)	−0.098(1)	−0.681(2)	−0.230(2)	3.4(4)
C(8)	−0.109(1)	−0.792(2)	−0.081(3)	3.8(5)
O(1)	−0.5941(9)	−0.4813(9)	−0.137(2)	3.0(3)
O(2)	−0.4316(8)	−0.5592(9)	−0.227(2)	2.4(2)
O(3)	−0.2231(7)	−0.5323(8)	0.343(1)	3.4(2)
O(4)	−0.3189(9)	−0.657(1)	0.114(2)	2.2(3)
O(W1)	−0.1924(9)	−0.895(1)	−0.634(2)	3.9(3)
O(W2)	−0.039(1)	−0.399(1)	−0.481(3)	8.4(6)
O(1Cl)	−0.236(2)	−0.269(1)	−0.237(3)	8.9(5)
O(2Cl)	−0.135(2)	−0.154(2)	−0.457(3)	16.(1)
O(3Cl)	−0.293(2)	−0.080(1)	−0.334(2)	5.5(3)
O(4Cl)	−0.132(1)	−0.100(2)	−0.110(3)	15.2(9)

Table 3. Bond length and angles

Bond Lengths (l/Å):			
Co–N(1)	1.94(1)	Co–N(3)	1.95(1)
Co–N(2)	1.94(1)	Co–N(4)	1.95(1)
Co–O(2)	1.90(1)	Co–O(4)	1.90(1)
N(1)–C(3)	1.52(2)	N(3)–C(7)	1.49(2)
N(2)–C(4)	1.49(2)	N(4)–C(8)	1.46(2)
C(3)–C(4)	1.50(2)	C(7)–C(8)	1.58(3)
N(1)–C(2)	1.52(2)	N(3)–C(6)	1.44(2)
C(1)–C(2)	1.48(2)	C(5)–C(6)	1.55(2)
C(1)–O(2)	1.29(2)	C(5)–O(4)	1.29(2)
C(1)–O(1)	1.23(2)	C(5)–O(3)	1.24(2)
Bond Angles (ϕ/°):			
N(1)–Co–N(2)	86.9(5)	N(3)–Co–N(4)	86.8(5)
N(1)–Co–O(2)	87.0(5)	N(3)–Co–O(4)	86.8(5)
Co–N(1)–C(3)	108.7(9)	Co–N(3)–C(7)	109.6(11)
Co–N(2)–C(4)	108.6(9)	Co–N(4)–C(8)	110.7(11)
N(1)–C(3)–C(4)	106(1)	N(3)–C(7)–C(8)	105(1)
N(2)–C(4)–C(3)	107(1)	N(4)–C(8)–C(7)	109(1)
Co–N(1)–C(2)	106.0(9)	Co–N(3)–C(6)	108.8(10)
Co–O(2)–C(1)	113.0(8)	Co–O(4)–C(5)	114.1(10)
N(1)–C(2)–C(1)	112(1)	N(3)–C(6)–C(5)	111(1)
O(2)–C(1)–C(2)	117(1)	O(4)–C(5)–C(6)	116(1)
C(2)–C(1)–O(1)	121(1)	C(6)–C(5)–O(3)	121(1)
O(2)–C(1)–O(1)	122(1)	O(4)–C(5)–O(3)	123(1)
C(2)–N(1)–C(3)	114(1)	C(6)–N(3)–C(7)	116(1)

Bond lengths and angles in the ClO_4^-:
Cl–O = 1.38 – 1.43(2) Å
O–Cl–O = 106 – 112(2)°

edma, an equivolume mixture of 0.1 mol dm^{-3} Na_2CO_3–D_2O and 0.1 mol dm^{-3} $NaDCO_3$–D_2O was used as the solvent; the $-CH_2-$ signals were recorded at prescribed intervals on a ^{1}H NMR spectrometer at 40 °C.

Determination of the Absolute Configuration of the Complexes by ^{1}H NMR. A buffer solution (pH 10) was prepared by adding proper amount of 2 mol dm^{-3} DCl–D_2O to a solution containing 106 mg Na_2CO_3 in 10 cm^3 of D_2O. About 100 mg of $(+)^{CD}_{521}$E-5 was dissolved into the buffer solution, and the temperature of the solution was kept at 40 °C. The deuteration of the G-ring $-CH_2-$ was checked by means of ^{1}H NMR measurements. When the singlet peak arising from the G-ring $-C\underline{H}D-$ increased in intensity in comparison with the AB quartet arising from the G-ring $-CH_2-$ (about 4 h), the solution was acidified to pH 6 with 1 mol dm^{-3} HCl to stop the deuteration reaction. The volume of the solution was adjusted to 20 cm^3 with water, and zinc powder (2 g) was added to the solution. After stirring for 5 min at room temperature, the excess of zinc was filtered off. To the filtrate, 1.5 g of PbO_2 was added, and then the mixture was stirred for 15 min at room temperature. After the solution had been filtered, the filtrate was poured into an SP-Sephadex column (Na^+ form, 2.7 cm×50 cm); then the adsorbed complexes were eluted with a 0.2 mol dm^{-3} NaCl solution. The earlier-eluted band (E-1 and -2) was transferred to another SP-Sephadex column (Na^+ form, 2.7 cm×60 cm) and developed with a 0.1 mol dm^{-3} Na_2Sb_2(d-tart)$_2$ solution by the recycle chromatographic method. The band separated into three bands: red ($(-)^{CD}_{543}$E-1), orange (E-2), and red ($(+)^{CD}_{543}$E-1). Each band of the E-1 enantiomers was once more transferred to another SP-Sephadex column, washed with 1 dm^3 of water, and then eluted out with a 0.2 mol dm^{-3} $NaClO_4$ solution. The eluate was evaporated almost to dryness under reduced pressure, and then 50 cm^3 of ethanol was added to the concentrate to obtain red-orange crystals. The ^{1}H NMR spectra of the E-1 enantiomers are illustrated in Fig. 2.

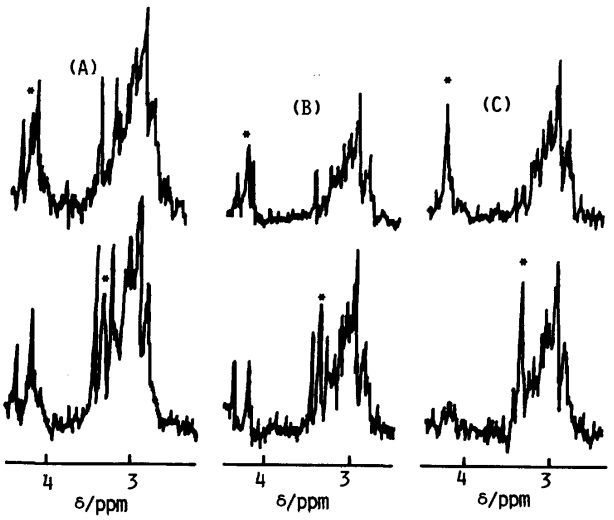

Fig. 2. ^{1}H NMR spectra of $(-)^{CD}_{543}$ and $(+)^{CD}_{543}$E-1 obtained from the deuterated $(+)^{CD}_{534}$E-4, $(+)^{CD}_{521}$E-5, and $(+)^{CD}_{509}$E-6 isomers. Upper: $(-)^{CD}_{543}$E-1. Lower: $(+)^{CD}_{543}$E-1. (A) from $(+)^{CD}_{534}$E-4, (B) from $(+)^{CD}_{521}$E-5, and (C) from $(+)^{CD}_{509}$E-6. (Asterisked peaks: G-ring $-C\underline{H}D-$).

Similarly, the deuterated E-1 enantiomers were obtained from the optically active deuterated E-4 and E-6 isomers. Their ^{1}H NMR spectra are also shown in Fig. 2.

Results and Discussion

Assignments of the Geometrical Isomers. The structural assignments for the six isomers, given in our previous report,[1] are shown in Fig. 1. Although the structures of E-1, -2, -3, and -4 were assigned on the basis of unambiguous evidence, some uncertainty remained as to the tentative assignments for E-5 and -6; E-5 is either *cis*(O)*trans*(NH_2) or *cis*(O)*trans*(NH). The X-ray study which will be shown below revealed that E-5 is *cis*(O)*trans*(NH). (Consequently, E-6 is assigned to *cis*(O)*trans*(NH_2)).

Crystal Structure of $(-)^{CD}_{521}$-[Co(edma)$_2$]$ClO_4 \cdot 2H_2O$ (E-5). Figure 3 shows the absolute configuration of the $(-)^{CD}_{521}$-isomer of E-5. This complex has a distorted octahedral coordination, with two O atoms in the *cis* positions and two secondary N atoms in the *trans* positions: *cis*(O)*trans*(NH). The complex cation has an approximate two-fold axis running through the Co atom and the mid point of the O···O edge. Each coordinating edma contains an asymmet-

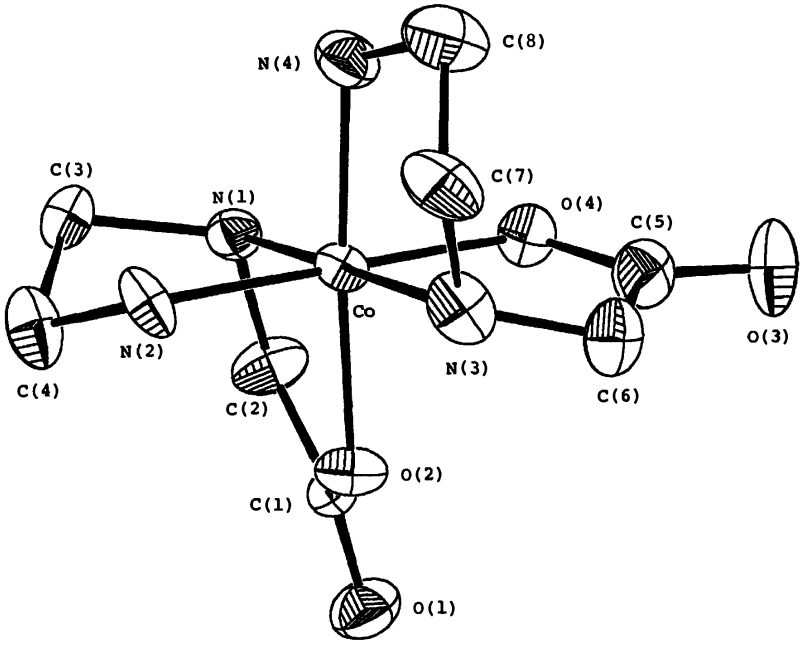

Fig. 3. The structure and absolute configuration of $(-)^{CD}_{\delta\lambda\delta}$E-5 $[Co(edma)_2]^+$ ion in its perchlorate dihydrate crystal.

ric nitrogen whose chirality is *R*. The conformation of the ethylenediamine ring is δ. By modifying the conventional nomenclature,[14] the absolute configuration of this isomer is represented as $\Delta(GG)\Lambda(EE)$ in this paper, where G and E represent the glycinate-ring and the ethylenediamine-ring respectively.

The average Co-N (primary N) and Co-N (secondary N) bond lengths are nearly equal to those found in *u-fac* and *s-fac* $[Co(dien)_2]^{3+}$,[15,16] while the average Co-O bond length is nearly equal to that in $[Co(ida)_2]^-$.[17]

^1H NMR. Table 4 shows the ^1H NMR data of the glycinate methylene protons in the six isomers of the $[Co(edma)_2]^+$ ion. The methylene protons of the G-rings in E-1, -2, -4, -5, and -6, which contain the facially coordinating edma's, appeared as the AB quartet signals. On the other hand, those in E-3 with the meridionally coordinating edma's appeared as a singlet-like signal (slightly splitting) because of a slight difference in chemical shift between the two methylene protons. Such a singlet-like signal has also been observed for the meridionally chelated ring (in-plane G-ring methylenes) of edda in the β-$[Co(edda)(ch)]^{\pm}$ (where ch is ox, mal, or en) ions.[18] The coupling constant of the glycinate geminal protons in the meridionally coordinating edma is 16 Hz, and those in the facially coordinating edma are 18 Hz (Table 4); these findings are consistent with the results of the previous papers.[19-22]

The ^1H-NMR spectra of the facial isomers (E-1, -2, -4, -5, and -6) were measured in 0.5 mol dm^{-3} DCl-D_2O solutions. The ^1H NMR signal of each G-ring in these isomers splits into eight peaks as a result of the $J_{Ha,Hb}$, $J_{N-H,Ha}$, and $J_{N-H,Hb}$ couplings (Fig. 4(A)). The $J_{N-H,Hb}$ and $J_{N-H,Ha}$ values are *ca.* 8 Hz's (lower fields) and 1 Hz's (higher fields) respectively. On the basis of the Karplus equation,[23] the following assignments are possible: the dihedral angles of the protons resonating at higher fields (H-C-N-H) are about 90°, and the protons can be assigned to H_a (inside; Fig. 4 (A)). The angles of the protons (which are assigned to H_b (outside)) resonating at lower fields are about 30°. Similar assignments for the G-ring methylene protons have been made by Legg and Cooke[27] and Schoenberg *et al.*[28] for the edda-Co(III) complexes.

It is known that the methylene protons of the

TABLE 4. ^1H NMR CHEMICAL SHIFTS AND COUPLING CONSTANTS OF THE G-RINGS IN THE $[Co(edma)_2]^+$ COMPLEX IONS

Complex		G-ring $-CH_2-$		
		H_a (δ/ppm)	H_b (δ/ppm)	$J_{H_aH_b}$ (J/Hz)
C_2-*trans*(O)	(E-1)	3.32	4.25	18
C_1-*trans*(O)	(E-2)	3.34	4.05	18
mer	(E-3)	3.85	3.79	16
C_1-*cis*(O)	(E-4)	3.14	4.18	18
		3.36	4.06	18
cis(O)*trans*(NH)	(E-5)	3.41	4.19	18
cis(O)*trans*(NH_2)	(E-6)	3.10	4.06	18

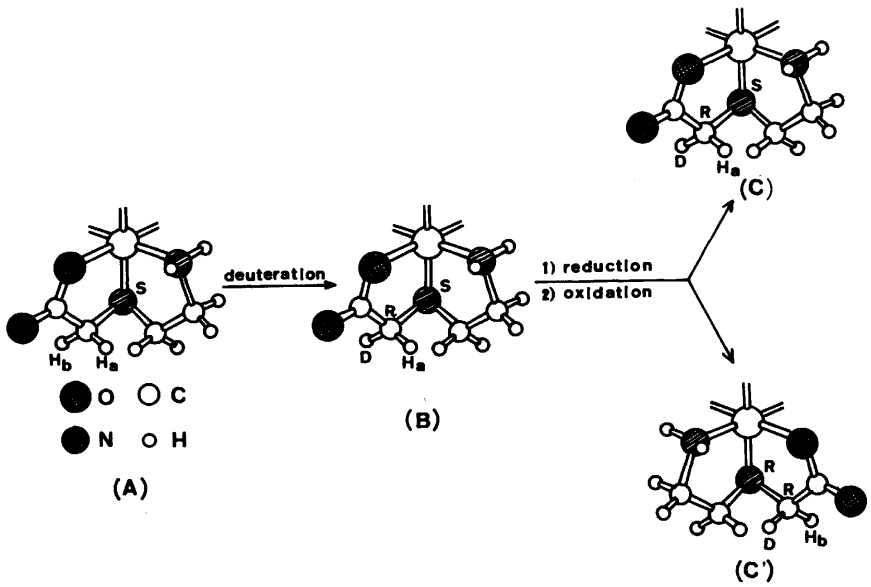

Fig. 4. Chemical environment of the G-ring of the facially coordinating edma.
(A): undeuterated, (B): deuterated, and (C) and (C'): reprepared by oxidizing the reduction product of (B) (See Experimental).

chelating glycinate are deuterated in a basic D_2O solution.[18,21-26] The G-ring methylene protons in the facially coordinated edma are also deuterated; this fact is confirmed from the intensity loss of the AB quartet peaks (Fig. 5). The deuteration occurs stereospecifically in all of the facial isomers; a new singlet appeared between the two higher-field peaks of the AB quartet, with an intensity loss of the AB quartet. In other words, the deuteration rates are different between the two protons; the deuteration of the higher-field proton is much slower than that of the lower-field one. (The new singlet signal disappeared after a long period). Sudmeier and Occupati[26] pointed out that the rate of the deuteration of the inside proton of the facial G-ring is slower than that of the outside proton for the edda-Co(III) complexes. The application of this result to the *fac*-$[Co(edma)_2]^+$ system leads to the conclusion that the two lower-field peaks of the AB quartet arise from the outside proton, which is easily deuterated, while the two higher-field peaks arise from the inside proton (Fig. 4 (B)). These assignments are consistent with those made by the Karplus equation mentioned above.

In a previous paper,[29] we reported that the deuteration rate of the G-ring methylene protons out of the O-Co-O plane which is present in C_1- or C_2-*cis*(*O*)-$[Co(gly)_2(en)]^+$ is smaller than that of the G-ring methylene protons in the O-Co-O plane which is present in C_1-*cis*(*O*)-$[Co(gly)_2(en)]^+$ and that of the G-ring methylene in *trans*(*O*)-$[Co(gly)_2(en)]^+$.

The deuteration rates of the six isomers were measured under the same conditions (40 °C; dissolved in an equivolume mixture of 0.1 mol dm^{-3} Na_2CO_3-D_2O and 0.1 mol dm^{-3} $NaDCO_3$-D_2O). The

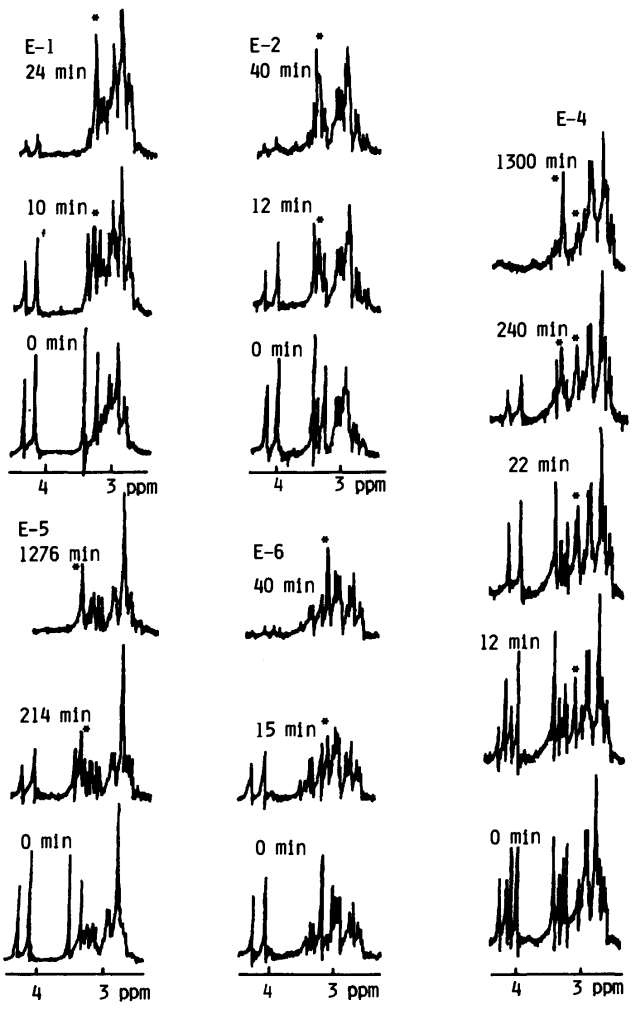

Fig. 5. Changes in ^1H NMR spectra of $[Co(edma)_2]^+$ in basic D_2O solutions. (Asterisked peaks: G-ring -CHD-).

order of the deuteration rates are as follows: C_2-*trans*(O) (E-1)(half-life: *ca.* 15 min)≃*cis*(O)*trans*(NH_2) (E-6)≃C_1-*cis*(O) (E-4; in-plane)≃C_i-*trans*(O) (E-2)≫*cis*-(O)*trans*(NH) (E-5)(*ca.* 190 min)>C_1-*cis*(O) (E-4; out-of-plane) (*ca.* 230 min). This result corresponds well with that obtained for the $[Co(gly)_2(en)]^+$ ion.

The G-ring methylene protons of E-3 (*mer*) are deuterated very slowly; this slow deuteration may arise from the following two effects: (1) from the meridional form (Coleman *et al.*[18] pointed out, for the $[Co(edta)]^-$ ion, that the more strained glycinate-ring meridional to the back-bone ethylenediamine-ring does not prefer to remove one of the methylene protons) and (2) the methylene protons are not situated on the O-Co-O plane.

Determination of Absolute Configurations by ^1H NMR. When the edma ligand coordinates to a cobalt(III) ion in the facial form, the secondary nitrogen (C-NH-C) becomes asymmetric (*R* or *S*) (Fig 4 (A)). Although each isomer of $[Co(edma)_2]^+$ may be expected to provide four diastereomers (*R,R*, *R,S*, *S,R*, and *S,S*), some of them do not exist because of the structural restrictions. For example, the nitrogen atoms in the E-1 isomer can take only the *S,S*(*ΔΔΔ*) or *R,R*(*ΔΔΔ*) chiral configuration. The possible configurations for each geometrical isomer are listed in Table 5.

The $(-)^{CD}_{521}$E-5 isomer, whose structure was determined by the X-ray analysis in this work, has the configuration of *Δ*(GG)*Δ*(EE)(*R,R*). As has been mentioned, one of the G-ring $-CH_2-$ protons in $(+)^{CD}_{521}$E-5 (*Δ*(GG)*Δ*(EE)(*S,S*)) is stereospecifically deuterated in basic D_2O. When the outside proton (H_b in Fig. 4(A)) of $(+)^{CD}_{521}$E-5 is deuterated, the G-ring -CHD- carbon in the facial edma becomes an asymmetric center with the *R* chirality (Fig 4 (B)). It is noteworthy that, when the nitrogen atom of the facially coordinated edma which contains *R* carbon takes the *S* chirality, the undeuterated proton (-CHD-) occupies the inside position (Fig 4 (C)). Using this deuterated edma (containing *R* carbon), the E-1 isomer was prepared and optically resolved (See Experimental section). In the ^1H NMR spectrum of the deuterated $(-)^{CD}_{543}$E-1, a singlet peak due to the G-ring -CHD- appeared between the two lower-field peaks of the AB quartet due to the G-ring $-CH_2-$ (Fig. 2). On the contrary, in the spectrum of the $(+)^{CD}_{543}$E-1, a singlet peak appeared between the two higher-field peaks of the AB quartet. As the chiralities of the asymmetric carbon and nitrogen atoms in the starting material ($(+)^{CD}_{521}$E-5) are *R* and *S* respectively, it is concluded that the asymmetric nitrogens of the coordinating edma's in $(-)^{CD}_{543}$E-1 and $(+)^{CD}_{543}$E-1 should have *R* and *S* chiralities respectively (Fig 4.); the absolute configurations of the $(-)^{CD}_{543}$E-1 and $(+)^{CD}_{543}$E-1 isomers are *ΔΔΔ*(*R,R*) and *ΛΛΛ*(*S,S*) respectively.

TABLE 5. POSSIBLE CONFIGURATIONS AND CD SIGNS OF THE $[Co(edma)_2]^+$ ION

Geometrical isomers	Possible configuration and CD signs	
E-1 C_2-*trans*(O)	*ΔΔΔ*(*R,R*)$(-)^{CD}_{543}$	*ΛΛΛ*(*S,S*)$(+)^{CD}_{543}$
E-2 C_i-*trans*(O)	(*R,S*) (achiral isomer)	
E-4 C_1-*cis*(O)	*ΛΔΔ*(*S*,R*)$(+)^{CD}_{534}$	*ΔΛΔ*(*R*,S*)$(-)^{CD}_{534}$
E-5 *cis*(O)*trans*(NH)	*Δ*(GG)*Δ*(EE)-(*R,R*)$(-)^{CD}_{521}$	*Λ*(GG)*Λ*(EE)-(*S,S*)$(+)^{CD}_{521}$
E-6 *cis*(O)*trans*(NH_2)	*ΔΔΔ*(*R,R*)$(-)^{CD}_{509}$	*ΛΛΛ*(*S,S*)$(+)^{CD}_{509}$

R or *S*: Chirality around the asymmetric nitrogen. *R** or *S**: The asymmetric nitrogen being present on the in-plane (O-Co-O plane) G-ring.

By using the stereospecifically deuterated $(+)^{CD}_{509}$E-6 as a starting material, the $(+)^{CD}_{543}$ and $(-)^{CD}_{543}$E-1 isomers were also obtained, as has been shown in the Experimental section. The ^1H NMR spectra of the $(-)^{CD}_{543}$E-1 and $(+)^{CD}_{543}$E-1 isomers showed a singlet signal due to -CHD- in the lower and higher fields respectively. These signal patterns suggest that the edma ligand contains the *R* asymmetric carbon. Accordingly, the configuration of $(+)^{CD}_{509}$E-6 can be assigned to *ΔΔΔ*(*S,S*) ($(-)^{CD}_{509}$E-6: *ΔΔΔ*(*R,R*)).

Although the *ΛΔΔ*(*S*,R*)E-4 isomer contains both the *R* and *S* asymmetric nitrogens, the in-plane G-ring which contains *S* nitrogen (*S**) is more rapidly deuterated than the out-of-plane G-ring which contains *R* nitrogen, as has been mentioned above. The deuteration was quenched at the time the G-ring containing *S** nitrogen was stereospecifically deuterated. By employing the same method as has been described for the determination of the absolute configuration of E-6, the configurations of the $(+)^{CD}_{534}$E-4 and $(-)^{CD}_{534}$E-4 isomers can be identified as *ΛΔΔ*(*S*,R*) and *ΔΛΔ*(*R*,S*) respectively. The absolute configurations of the facial complexes are summarized in Table 5.

CD Spectra. The CD data of the isomers are summarized in Table 6.

The $E_g(D_{4h})$ component in the first absorption band of E-1 (*trans*-$[Co(N)_4(O)_2]$-type complex) is on a lower-energy side than the $A_{2g}(D_{4h})$.[30] According to the method of ring-pairing proposed by Legg *et al.*[32], the (+) CD component which is related to the E_g transition is assigned to the net *Λ* configuration. Based on the above recognition, Igi and Douglas[3] assigned $(+)^{CD}_{543}$E-1 to the *ΛΔΔ*(net *Λ*) configuration, which is consistent with the result described in our ^1H NMR section. However, the $(+)^{CD}_{534}$E-4 (*cis*-$[Co(N)_4(O)_2]$-type complex) shows (−) CD band in the region related to the $E_g(D_{4h}$: holohedrized symmetry) component (which is at a higher-energy side than the $A_{2g}(D_{4h})$ in the *cis*-$[Co(N)_4(O)_2]$-type), while $(+)^{CD}_{521}$ *Λ*(GG)*Λ*(EE) E-5 shows a CD pattern similar to that of $(+)^{CD}_{534}$E-4.

TABLE 6. CD DATA OF OPTICALLY ACTIVE $[Co(edma)_2]X$

Complex[a]	First Band Region[b]	Second Band Region[b]	Charge-transfer Band Region[b]
$(-)^{CD}_{643}$E-1	18.42(−3.197)	28.33(−1.198)	38.46(+4.156)
	22.27(+2.135)		43.48(−8.621)
$(-)^{CD}_{504}$E-3	17.99(+0.139)	28.09(−1.307)	39.37(+4.984)
	19.84(−1.079)		42.92(−5.162)
	21.93(+2.464)		
$(+)^{CD}_{534}$E-4	18.73(+1.302)	26.18(+0.429)	39.50(−1.19)[sh]
	21.14(−0.930)		45.05(−5.458)
$(-)^{CD}_{521}$E-5	19.19(−2.078)	28.74(−0.787)	38.02(+2.894)
	21.88(+1.454)		45.05(−8.599)
$(-)^{CD}_{509}$E-6	15.83(+0.008)	25.58(+0.110)	38.02(+1.481)
	19.65(−0.335)	28.33(−0.397)	45.25(−17.28)
	22.14(+0.091)		

a) All these isomers are the faster eluted ones (eluent: 0.05 mol dm^{-3} $K_2Sb_2(d\text{-tart})_2$). b) The wave numbers and $\Delta\varepsilon$ values (in parentheses) are given in 10^3 cm^{-1} and mol^{-1} dm^3 cm^{-1} respectively. sh) Shoulder bands.

TABLE 7. ABSORPTION SPECTRAL DATA OF THE SIX ISOMERS OF $[Co(edma)_2]X$

Complex	First Band Region[a]	Second Band Region[a]	Charge-transfer Band Region[a]
E-1	18.87(1.963)	27.86(2.125)	45.46(4.35)
	22.14(1.60)[sh]		
E-2	19.80(1.585)	28.90(1.769)	45.66(4.40)
	21.93(1.56)[sh]		
E-3	21.01(2.279)	28.24(2.240)	45.05(4.31)
E-4	19.96(2.002)	28.01(2.047)	45.46(4.36)
E-5	20.92(1.794)	28.56(1.932)	46.30(4.36)
E-6	20.00(2.061)	28.25(1.855)	45.46(4.33)

a) Wave numbers and log ε values (in parentheses) are given in 10^3 cm^{-1} and mol^{-1} dm^3 cm^{-1} respectively. sh) Shoulder bands.

Although the CD intensity of E-6 in the d-d absorption-band region is very small, the CD band in *ca.* 45000 cm^{-1} is stronger than in the other isomers examined. The low CD intensity in the d-d region probably arises from the counteraction of the vicinal effects due to asymmetric nitrogens against the configurational effect.

The relationship between the CD pattern and the absolute configuration is difficult to account for by the method of ring-pairing for the E-4, -5, and -6 isomers. This is true for the following reasons: (1) The difference in the numbers of the Δ and Λ ring pairs is very small in the present systems (the same as in E-5). (2) The effect of the vicinal CD of asymmetric nitrogen is not negligible compared with that of the configurational CD, though it is difficult to separate the vicinal CD curves from the observed CD. This difficulty results from the geometrical structures of the complexes containing unsymmetrical terdentates.

Absorption Spectra. The absorption spectral data of the six geometrical isomers are listed in Table 7. The first absorption bands of E-1 and -2 show a marked split,[1] which is characteristic of the *trans*(*O*)-$[Co(N)_4(O)_2]$-type,[30,31] and the molar-absorption coefficient of the lower-energy component is larger in E-1 than in E-2. E-1 lacks the center of symmetry, which would give a more intense spectrum than E-2.[32]

The *cis*(*O*)-$[Co(N)_4(O)_2]$-type isomers, E-3, -4, -5, and -6, do not show such a marked split in the first-absorption-band region as the *trans*(O)-type isomers do. The molar-absorption coefficient of the first absorption band is larger in E-3 than in the other five isomers. By stereochemistry, the *mer* isomer is more distorted from a regular octahedron than are the other five isomers, which contains the facially coordinating edma's. The strained structure will give the more intense spectrum.[32,33] An analogous situation is observed for the geometrical isomers of $[Co(ida)_2]^-$[34] and $[Co(ida)(dien)]^+$.[32]

Of the *cis*(O)-type isomers, E-3 exhibits the first absorption maximum in the highest energy region, though the E-3 is the more distorted isomer. This fact may arise from the fact that the molar-absorption coefficient of the $E_g(D_{4h})$ component (on the higher-energy side) is much larger than the $A_{2g}(D_{4h})$ component (on the lower-energy side). In the other *cis*(O) isomers, the $E_g(D_{4h})$ component is not so intense that the absorption maximum may be pulled down to the lower-energy side by the A_{2g} component.

References

1) Part of this work has been reported in: T. Yasui, H. Kawaguchi, and T. Ama, *Chem. Lett.*, **1983**, 1277.

2) Y. Fujii, E. Kyuno, and R. Tsuchiya, *Bull. Chem. Soc.*

Jpn., **43**, 786 (1970).
3) K. Igi and B. E. Douglas, *Inorg. Nucl. Chem. Lett.*, **10**, 587 (1974).
4) M. P. Granchi and B. E. Douglas, *Inorg. Nucl. Chem. Lett.*, **14**, 23 (1978).
5) T. Ohsaka, N. Oyama, S. Yamaguchi, and H. Matsuda, *Bull. Chem. Soc. Jpn.*, **54**, 2475 (1981).
6) J. I. Legg and J. A. Neal, *Inorg. Chem.*, **12**, 1805 (1973).
7) K. Okamoto, J. Hidaka, and Y. Shimura, *Bull. Chem. Soc. Jpn.*, **46**, 475 (1973); **44**, 1601 (1971).
8) H. F. Bauer and W. C. Drinkard, *Inorg. Synth.*, **8**, 202 (1966).
9) B. Berglund, J. O. Thomas, and R. Tellgren, *Acta Cryst allogr., Sect. B*, **31**, 1842 (1975).
10) "International Tables for X-ray Crystallography," Kynoch Press, Birmingham, (1974), Vol. IV.
11) "UNICS," The Crystallographic Society of Japan (1969).
12) C. K. Johnson, ORTEP II, Report ORNL-5138, Oak Ridge National Laboratory, Oak Ridge, TN (1976).
13) "ORFLS," W. R. Busing, K. O. Martin, and H. A. Levy, Oak Ridge National Laboratory Report, ORNL-TM-305.
14) Designated by the IUPAC tentative rule: *Inorg. Chem.*, **9**, 1 (1970).
15) K. Konno, F. Marumo, and Y. Saito, *Acta Crystallogr., Sect. B*, **29**, 739 (1973).
16) M. Kobayashi, F. Marumo, and Y. Saito, *Acta Crystallogr., Sect. B*, **28**, 470 (1972).
17) A. B. Corradi, C. G. Palmieri, M. Nardelli, M. A. Pellinghelli, and M. E. V. Tani, *J. Chem. Soc., Dalton Trans.*, **1973**, 655.
18) P. F. Coleman, J. I. Legg, and J. Steele, *Inorg. Chem.*, **9**, 937 (1970).
19) J. L. Sudmeier, A. J. Senzel, and G. L. Blackmer, *Inorg. Chem.*, **10**, 90 (1971).
20) W. Byers and B. E. Douglas, *Inorg. Chem.*, **11**, 1470 (1972).
21) C. W. Maricondi and C. Maricondi, *Inorg. Chem.*, **13**, 1110 (1974).
22) D. J. Radanovic and B. E. Douglas, *Inorg. Chem.*, **14**, 6 (1975).
23) M. Karplus, *J. Chem. Phys.*, **30**, 11 (1959).
24) D. H. Williams and D. H. Busch, *J. Am. Chem. Soc.*, **87**, 4644 (1965).
25) J. B. Terrill and C. N. Reilley, *Inorg. Chem.*, **5**, 1988 (1966).
26) J. L. Sudmeier and G. Occupati, *Inorg. Chem.*, **7**, 2524 (1968).
27) J. I. Legg and D. W. Cooke, *Inorg. Chem.*, **4**, 1576 (1965).
28) L. N. Schoenberg, D. W. Cooke, and C. F. Liu, *Inorg. Chem.*, **7**, 2386 (1968).
29) T. Ama, H. Kawaguchi, M. Kanekiyo, and T. Yasui, *Bull. Chem. Soc. Jpn.*, **53**, 956 (1980).
30) H. Yamatera, *Bull. Chem. Soc. Jpn.*, **31**, 95 (1958).
31) N. Matsuoka, J. Hidaka, and Y. Shimura, *Bull. Chem. Soc. Jpn.*, **40**, 1868 (1967).
32) J. I. Legg and D. W. Cooke, *Inorg. Chem.*, **5**, 594 (1966).
33) Y. Yoshikawa and K. Yamasaki, *Bull. Chem. Soc. Jpn.*, **45**, 179 (1972).
34) T. Yasui, H. Kawaguchi, N. Koine, and T. Ama, *Bull. Chem. Soc. Jpn.*, **56**, 127 (1983).

 © 1985 The Chemical Society of Japan Bull. Chem. Soc. Jpn., 58, 2569—2571 (1985)

Class Separation of Higher Hydrocarbons by Thin-Layer Chromatography with Flame Ionization Detection

Yojiro YAMAMOTO
Research Center, Maruzen Oil Co., Ltd. 1134-2, Gongendo Satte-cho, Saitama 340-01
(Received March 29, 1985)

3-Aminopropyl or 3-cyanopropyl-bonded silica-gel thin-layer rods (Chromarod NH_2-SII or CN-SII) were prepared and a hydrocarbon class separation of higher hydrocarbons has been investigated by flame ionization detection-thin-layer chromatography (FID-TLC) with those rods as the stationary phase. The resolutions (*Rs*) of the class separation with Chromarod NH_2-SII and CN-SII were compared with those with conventional rods on the market, which were silica-gel-sintered (Chromarod S and SII) and alumina-gel-sintered (Chromarod A) thin-layer rods. An adequate class separation of higher hydrocarbons into Saturates (Sa), Monoaromatics (M-Ar), Diaromatics (D-Ar) and Triaromatics (T-Ar) could be performed by FID-TLC with Chromarod NH_2-SII or CN-SII.

Since heavy oil comprises many kinds of compounds with complicated structures, the isolation of these compounds is impossible. A compositional analysis to determine the content of fractions with similar chemical properties in heavy oil provides an important characterization.

Adsorption column chromatography with silica gel[1] or alumina gel[2] has been generally used for analyzing the composition of heavy oil. Since these methods have, however, such shortcomings as long times for determination and a large quantities of required solvents, high performance liquid chromatography (HPLC) has been recently tried regarding many applications.[3-10] Since Wise *et al.*[5] discovered that alkylamine-bonded silica gels had an advantage for the separation of aromatic ring compounds, these have been widely used for various hydrocarbon class analyses.[8-10] However, this method has not been put to practical use yet due to poor quantitativeness although HPLC has advantages such as a high separating power, and a simple and rapid procedure.

Thin-layer chromatography has a drawback regarding quantitation, although it has such advantages as high separating power, a simple and rapid procedure, and a small quantity of required sample. Recently, this drawback has been corrected due to the development of thin-layer chromatography with flame ionization detection (FID-TLC). This has been widely used for compositional analysis of heavy oil.[11-17] However, a detailed hydrocarbon class separation can not be carried out by FID-TLC, since a stationary phase is limited to silica gel or alumina gel.

In this study, 3-aminopropyl or 3-cyanopropyl bonded silica gel thin layer rods were prepared and the hydrocarbon class separation of higher hydrocarbons has been investigated by FID-TLC with those rods as the stationary phase.

Experimental

Materials. For standard samples, pentacosane, dodecylbenzene, octadecylbenzene, 2,6-dimethylnaphthalene, 1-ethylnaphthalene, acenaphthene, anthracene, phenanthrene, 9,10-dimethylanthracene and chrysene (guaranteed or extra pure reagents obtained from Tokyo Kasei Kogyo) were used. Hexane (chromatographic grade from Wako Pure Chemical Industries) was used as a developing solvent for FID-TLC.

FID-TLC. Iatroscan TH-10 (Iatron Labolatories Inc.) was used for an FID-TLC analysis. Chromarod S and SII (silica-gel-sintered thin-layer rod) and Chromarod A (alumina-gel-sintered thin layer rod) were used as the stationary phase. A chromatopak C-R1A data processor (Shimadzu) was used for FID data collection and treatment. Analytical conditions, such as the weight of a sample loaded in TLC and the combustion in FID were set according to the optimun conditions described in a previous paper.[14] The FID-TLC procedure is described below.

(1) A 1 μl spot of the toluene solution sample (adjusted

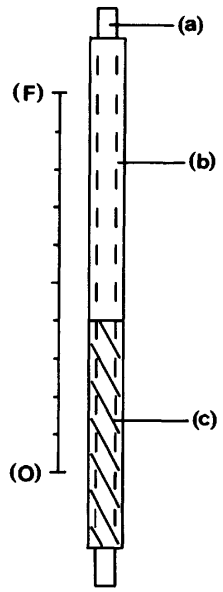

Fig. 1. Schematic picture of thin-layer rod of partially alkyl bonded silica-gel.
(a): Quartz rod, (b): Thin layer of silica gel, (c): Thin layer of alkyl bonded silica gel, (F): Front, (O): Origin.

to a concentration of 5—10 wt%) is placed on the TLC rod with a 1 μl glass capillary.

(2) The rod is developed to 10 cm after it is suspended in a developing tank containing hexane for 5 min.

(3) The rod is dried at room temperature.

(4) The components are determined as the peak area in FID chromatogram.

Preparation of Thin-Layer Rods of Alkyl Bonded Silica-gel. The constructions of the 3-aminopropyl and 3-cyanopropyl bonded silica gel thin-layer rods (Chromarod NH_2-SII and Chromarod CN-SII, respectively) are shown in Fig. 1. These were prepared by the following procedure.[18] Chromarod SII was treated with (3-aminopropyl)triethoxysilane or (3-cyanapropyl)trichlorosilane according to a procedure that is the most popular and convenient for the preparation of bonded phases. It is described in literature.[19,20] The upper portion of the rod was then passed through a hydrogen flame to reform the silica gel layer for detection by FID, as shown in Fig. 1.

Results and Discussion

The characteristics for the hydrocarbon class separation of higher hydrocarbons by FID-TLC with various Chromarods (Chromarod S, SII, A, NH_2-SII, and CN-SII) were examined.

Table 1 shows the R_f values of various standard samples developed with hexane on each Chromarod, and an FID-TLC chromatogram for a standard mixture prepared from pentacosane, octadecylbenzene, 2,6-dimethylnaphthalene and 9,10-dimethylanthracene, which are selected as representatives of Saturates (Sa), Monoaromatics (M-Ar), Diaromatics (D-Ar), Triaromatics (T-Ar), respectively, are shown in Figs. 2 and 3.

From the R_f values of the various standard samples, it is suggested that Sa, M-Ar, D-Ar, and T-Ar can be classified by FID-TLC with every Chromarod. However, Fig. 2 reveals that the separation of Sa, M-Ar, and D-Ar can hardly be carried out with Chromarod A, and that the adequate separation of D-Ar and T-Ar from each other can not be performed even with Chromarod S and SII. On the other hand, an improved separation of these can be carried out by FID-TLC with both Chromarod NH_2-SII and CN-SII, as shown in Fig. 3.

The resolution (Rs) between adjacent peaks in TLC can be calculated using the following equation,

$$Rs = \frac{|(Zx)_2 - (Zx)_1|}{(b_2 + b_1)}$$

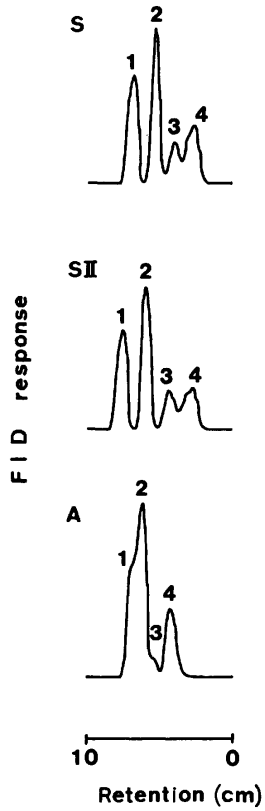

Fig. 2. FID-TLC chromatogram of standard mixture by using Chromarod S, SII, and A.
1: Pentacosane, 2: Octadecylbenzene, 3: 2,6-Dimethylnaphthalene, 4: 9,10-Dimethylanthracene.

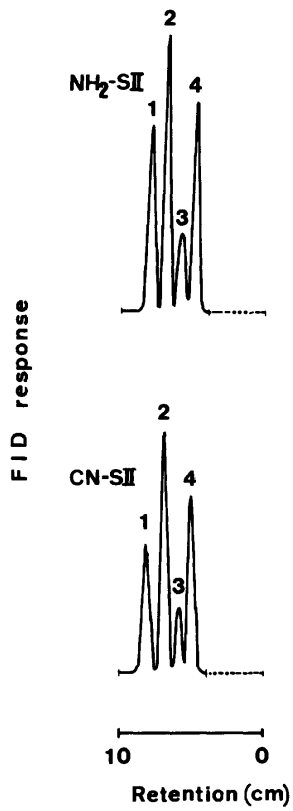

Fig. 3. FID-TLC chromatogram of standard mixture by using Chromarod NH_2-SII and CN-SII.
1,2,3,4: Described in Fig. 2.

Table 1. R_f Values of standard samples on Chromarods

Sample	Hydrocarbon class	S	SII	A	NH_2-SII	CN-SII
Pentacosane	Sa	0.74	0.80	0.76	0.84	0.85
Dodecylbenzene	M-Ar	0.57	0.62	0.66	0.70	0.75
Octadecylbenzene	M-Ar	0.57	0.64	0.68	0.71	0.75
1-Ethylnaphthalene	D-Ar	0.45	0.46	0.57	0.62	0.61
2,6-Dimethylnaphthalene	D-Ar	0.40	0.43	0.59	0.58	0.59
Acenaphthene	D-Ar	0.45	0.41	0.57	0.56	0.62
Anthracene	T-Ar	0.29	0.32	0.42	0.47	0.52
Phenanthrene	T-Ar	0.30	0.36	0.48	0.51	0.52
9,10-Dimethylanthracene	T-Ar	0.26	0.28	0.43	0.44	0.53
Chrysene	P-Ar	0.05	0.06	0.05	<0.4	<0.4

Table 2. Comparison of various Chromarods for resolutions(Rsi) of hydrocarbons

Rsi*	S	SII	NH_2-SII	CN-SII
$Rs1$	1.07	1.09	1.07	1.06
$Rs2$	0.80	0.98	1.00	1.01
$Rs3$	0.56	0.78	1.04	0.89

* The resolution between Sa and M-Ar($Rs1$) M-Ar and D-Ar($Rs2$), and D-Ar and T-Ar($Rs3$).

where $(Zx)_1$ and $(Zx)_2$ are the moved distances of peaks for component-1 and 2, and b_1, b_2 are the half widths of those peaks, respectively.

Following this, the characteristics of the various Chromarods used in this study for the hydrocarbon class separation of higher hydrocarbons by FID-TLC were studied using Rs values as indices. Table 2 gives the results. Rs1, Rs2, Rs3 are the resolutions between Sa and M-Ar, M-Ar and D-Ar, D-Ar and T-Ar, respectively. Since the separation of Sa, M-Ar, and D-Ar could not be carried out with Chromarod A, Chromarod A could not be compared.

Though $Rs1$ values for both Chromarod S and SII are large (1.07 and 1.09, respectively), both the $Rs2$ and $Rs3$ values are small. Especially, the $Rs3$ values for these Chromarods are very small (0.56 and 0.78, respectively). Thus, the Rs values had a tendency to decrease when the number of hydrocarbon aromatic rings increase. That is, it was found that the greater the number of aromatic rings, the more difficult it was to separate the hydrocarbons. On the other hand, the values of $Rs1$, $Rs2$, and $Rs3$ for Chromarod NH_2-SII (1.07, 1.00, and 1.04, respectively) are larger than those for both Chromarod S and SII. This suggests that a more clear separation of each class with Chromarod NH_2-SII can be carried out than with both Chromarod S and SII. The Rs values for Chromarod CN-SII are also larger than those for Chromarod S and SII, though the $Rs3$ value (0.89) is somewhat small compared to that for Chromarod NH_2-SII. Thus, it was found that a clear class separation of hydrocarbon with Chromarod CN-SII could be carried out as well as with Chromarod NH_2-SII.

Consequently, it was proved that an adequate class separation of the higher hydrocarbons into Sa, M-Ar, D-Ar, and T-Ar could be performed by FID-TLC with Chromarod NH_2-SII or CN-SII, which possesed 3-aminopropyl or 3-cyanopropyl-bonded phase.

References

1) ASTM Part **15**, 1289 (1982).
2) H.Iijima, *Sekiyu Gakkai Shi*, **13**, 606 (1970).
3) J. C. Suatoni and R. E. Swab, *J. Chromatogr. Sci.*, **14**, 535 (1976).
4) J. C. Suatoni and H. R. Garber, *J. Chromatogr. Sci.*, **14**, 545 (1976).
5) S. A.Wise, S. N. Chesler, H. S. Hertz, L. R. Hilpert, and W. E. May, *Anal. Chem.*, **49**, 2306 (1977).
6) W. A. Dark and R. R. McGough, *J. Chromatogr. Sci.*, **16**, 610 (1978).
7) G. L. Galya and J. C. Suatoni, *J. Liq. Chromatogr.*, **3**, (2), 229 (1980).
8) J. Chmielowiec and A. E. George, *Anal. Chem.*, **52**, (7), 1154 (1980).
9) T. Katoh, S. Yokoyama, and Y. Sanada, *Fuel*, **59**, 845 (1980).
10) S. Yokoyama, N. Tsuzuki, H. Ucino, T. Katoh, and Y. Sanada, *Nippon Kagaku Kaishi*, **1983**, 405.
11) M. A. Poirier and A. E. George, *ACS, Div. Petrol. Chem., Perp.*, **27**, 973 (1982).
12) M. L. Selucky, *Anal. Chem.*, **55**, 141 (1983).
13) M. A. Poirier and A. E. George, *J. Chromatogr. Sci.*, **21**, 331 (1983).
14) Y. Yamamoto and T. Kawanobe, *Sekiyu Gakkai Shi*, **27**, 269 (1984).
15) Y. Yamamoto and T. Kawanobe, *Sekiyu Gakkai Shi*, **27**, 373 (1984).
16) S. Sawada, T. Takahashi, K.Saitoh, and T. Matsumura, *Nenryo Kyokai Shi*, **63**, 128 (1984).
17) M. A. Poirier, R. Rahimi, and S. M, Ahmed, *J. Chromatogr. Sci.*, **22**, 116 (1984).
18) Y. Yamamoto, Patent pending.
19) R. E. Majors, *J. Chromatogr. Sci.*, **18**, 488 (1980).
20) N. H. C. Cooke and K. Olsen, *J. Chromatogr. Sci.*, **18**, 512 (1980).

 © 1985 The Chemical Society of Japan Bull. Chem. Soc. Jpn., 58, 2572—2576 (1985) [Vol. 58, No. 9

Magnetic and Spectral Properties of Dimeric Copper(II) Phenylpropynoate Complexes

Yoneichiro MUTO,* Ayako SASAKI, Tadashi TOKII, and Michio NAKASHIMA
Department of Chemistry, Faculty of Science and Engineering, Saga University, Saga 840
(Received May 14, 1985)

Dimeric copper(II) phenylpropynoate adducts $[Cu(Ph\text{-}C{\equiv}C\text{-}COO)_2 \cdot L]_2$, where L=benzonitrile, 3,5-dichloropyridine, dimethyl sulfoxide and triphenylphosphine oxide, have been synthesized in order to study the influence of the C≡C group linked to the COO group upon the extent of antiferromagnetic interaction between the two metal ions. Magnetic susceptibility measurements between 80 and 300 K show that the singlet-triplet separation ($-2J$) ranges from 283 to 318 cm^{-1}. The magnetic behavior of the non-adduct compound $Cu(Ph\text{-}C{\equiv}C\text{-}COO)_2$ is interpreted by taking an inter-dimer interaction into consideration.

The relation between the magnetism of copper(II) carboxylate dimers, $[Cu(RCOO)_2 \cdot L]_2$, and their structures or the physicochemical nature of R is still subject to much disputation.[1,2] It was previously shown that the antiferromagnetic interaction in $[Cu(RCOO)_2 \cdot L]_2$ complexes tends to increase as the group R becomes a stronger electron donor.[3,4] Thus, in a number of series of dimeric copper(II) carboxylates, the singlet-triplet separation ($-2J$, a measure of the magnetic interaction) increases as the pK_a of the parent acid RCOOH increases.[3,4] However, there exist a few exceptions to the postulated dependence of $-2J$ upon pK_a; for example, while pK_a of trifluoroacetic acid is lower than that of trichloroacetic acid, the $-2J$ found for $[Cu(F_3CCOO)_2(quinoline)]_2$ (310 cm^{-1})[5] is much higher than that found for $[Cu(Cl_3CCOO)_2(2\text{-chloropyridine})]_2$ (217 cm^{-1}).[6] Recently, Doedens *et al.*[7] have pointed out that, in the series of dimeric copper(II) carboxylate adducts with R=H, CH_3, CF_3, CCl_3, and CBr_3, the $-2J$ decreases as the polarizability of the group R increases. However, recent finding of a very large antiferromagnetic interaction, more than 1000 cm^{-1} in $-2J$, in $[Cu(Ph_3MCOO)_2 \cdot L]_2$ (Ph=phenyl and M=Si and Ge) with the very large polarizability of Ph_3M does not stand for the Doedens' indication.[8] These facts suggest the importance of studying the influence of R on the magnetism of $[Cu(RCOO)_2 \cdot L]_2$ from a variety of viewpoints. Under the situation, we have decided to see the influence of unsaturated systems directly linked to the COO group on magnetism in dimeric copper(II) carboxylates. There are three types of such unsaturated systems: (A) 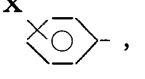 , (B) >C=C<, (C) -C≡C-. Copper(II) carboxylate dimers containing the unsaturated group of type A, *i.e.*, copper(II) arenecarboxylate dimers tend to show lower values of $-2J$ than the related copper(II) alkanoate dimers.[4] Magnetic studies on dimeric copper(II) carboxylates with the unsaturated systems of type B are limited at present. A typical structural and magnetic study in this series is on $[Cu(CH_3CH{=}CHCOO)_2(quinoline)]_2$ which showed a normal value of $-2J$ (333 cm^{-1}).[9] For copper(II) carboxylate dimers with the unsaturated system of type C, no magnetic study has appeared up to date. Based on such a situation, in the present study, six copper(II) phenylpropynoate complexes, $Cu(Ph\text{-}C{\equiv}C\text{-}COO)_2 \cdot 3H_2O$, $Cu(Ph\text{-}C{\equiv}C\text{-}COO)_2$, and $Cu(Ph\text{-}C{\equiv}C\text{-}COO)_2 \cdot L$, where L=benzonitrile (PhCN), 3,5-dichloropyridine (3,5-Cl_2py), dimethyl sulfoxide (DMSO) and triphenylphosphine oxide (Ph_3PO), were prepared and characterized by means of magnetic susceptibility and electronic spectrum measurements. The magnetic properties of $Cu(Ph\text{-}C{\equiv}C\text{-}COO)_2 \cdot L$ complexes were compared with those reported for several other dimeric copper(II) carboxylates. For the sake of discussion, the dimethyl sulfoxide adduct of copper(II) acetate, $Cu(CH_3COO)_2(DMSO)$, was also prepared and investigated.

Experimental

Syntheses. $Cu(Ph\text{-}C{\equiv}C\text{-}COO)_2 \cdot 3H_2O$: Phenylpropynoic acid (12 mmol) was dissolved in 0.25 M sodium hydroxide (100 ml) and the resulting solution was filtered. The solution was neutralized with dilute nitric acid using phenolphthalein as an indicator. When a solution of copper(II) nitrate trihydrate (6 mmol) in water (25 ml) was added to the above solution with stirring, blue crystals precipitated. The crystals were collected, washed repeatedly with water and air-dried at room temperature.

$Cu(Ph\text{-}C{\equiv}C\text{-}COO)_2 \cdot L$: L=PhCN or DMSO: The mixture of $Cu(Ph\text{-}C{\equiv}C\text{-}COO)_2 \cdot 3H_2O$ (1 mmol) and L (5 mmol) in chloroform (60 ml) was stirred for *ca.* 1/2 h at room temperature. The resulting solution was filtered and then concentrated to one-third of its volume. When petroleum ether was added to the solution, green crystals precipitated. The crystals were collected, washed with petroleum ether and dried *in vacuo* at room temperature. L=3,5-Cl_2py or Ph_3PO: A solution of L (1 mmol) in acetone (10 ml) was added to a solution of $Cu(Ph\text{-}C{\equiv}C\text{-}COO)_2 \cdot 3H_2O$ (1 mmol) in acetone (30 ml). The separated green crystals were collected, washed with a 1:2 acetone-petroleum ether mixture and dried *in vacuo* at room temperature.

$Cu(Ph\text{-}C{\equiv}C\text{-}COO)_2$: This non-adduct compound was obtained by dehydrating the hydrate complex at *ca.* 80 °C.

$Cu(CH_3COO)_2(DMSO)$: The mixture of anhydrous copper(II) acetate (5 mmol) and DMSO (13 mmol) in ehanol (70 ml) was heated with stirring for *ca.* 6 h. The

resulting solution was filtered and then allowed to stand overnight at *ca.* 5 °C in a refrigerator. The separated green crystals were collected, washed with benzene and dried *in vacuo* at room temperature.

The results of the elemental analyses are given in Table 1.

Physical Measurements. Magnetic susceptibilities in the temperature range of 80—300 K were determined by the Faraday method. Pascal's constants[10] were used for diamagnetic corrections. The value of 60×10^{-6} cgs emu mol^{-1} (1 cgs emu mol^{-1}=$4\pi\times10^{-6}$ m^3 mol^{-1}) for the temperature-independent paramagnetism ($N\alpha$) per gram ion of copper(II) was used throughout the present study. The cryomagnetic data of Cu(Ph-C≡C-COO)$_2$·3H$_2$O were analyzed in terms of Curie-Weiss law of the form,

$$\chi_A = \frac{Ng^2\beta^2}{4k(T-\theta)} + N\alpha, \quad (1)$$

where θ is Weiss constant and the other symbols have their usual meanings. Plots of χ_A *vs.* T and of $(\chi_A-N\alpha)^{-1}$ *vs.* T are shown in Fig. 1. The cryomagnetic data of the adduct complexes, Cu(Ph-C≡C-COO)$_2$·L, were fitted to the modified Bleaney-Bowers equation (2),

$$\chi_A = \frac{Ng^2\beta^2}{3k(T-\theta')}\left[1+\frac{1}{3}\exp\left(\frac{-2J}{kT}\right)\right]^{-1}\cdot(1-P) + \frac{Ng_i^2\beta^2}{4kT}\cdot P + N\alpha, \quad (2)$$

where P is the mole fraction of the noncoupled copper(II) impurity, g_i is the average g factor for the impurity and θ' represents the Weiss constant for inter-cluster interaction. A fixed value of 2.2 was used for g_i throughout this study. The best-fit parameters, $-2J$, g, P, and θ', were obtained by a nonlinear least-squares fitting procedure. The quality of fit was estimated by means of a discrepancy index, σ_{dis},

$$\sigma_{dis} = \left[\frac{\Sigma(\chi_{obsd}-\chi_{calcd})^2}{\Sigma\chi_{obsd}^2}\right]^{1/2}. \quad (3)$$

The thermal magnetic data are shown in Figs. 2 and 3 as plots of χ_A *vs.* T. The values of $-2J$, g, P, θ', and σ_{dis} are summarized in Table 2.

IR spectra were recorded on a Hitachi 260-10 IR Spectrophotometer as Nujol mulls.

Reflectance spectra were recorded on a Hitachi Recording Spectrophotometer 323.

Results and Discussion

The magnetic susceptibility data of Cu(Ph-C≡C-

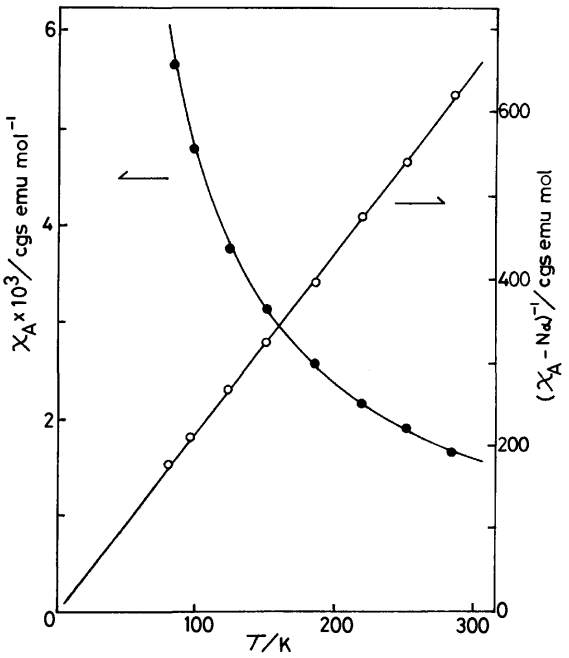

Fig. 1. Temperature dependence of magnetic susceptibilities (●, χ_A; ○, $(\chi_A-N\alpha)^{-1}$) of Cu(Ph-C≡C-COO)$_2$·3H$_2$O.
The solid curve and line were obtained as described in the text.

Table 1. Analytical data

Complex	Found(Calcd) (%)			
	C	H	N	Cu
Cu(Ph-C≡C-COO)$_2$·3H$_2$O	52.82 (53.00)	3.97 (3.95)		15.49 (15.58)
Cu(Ph-C≡C-COO)$_2$	60.96 (61.10)	2.85 (2.85)		18.14 (17.96)
Cu(Ph-C≡C-COO)$_2$(PhCN)	65.22 (65.71)	3.38 (3.31)	2.95 (3.06)	13.92 (13.90)
Cu(Ph-C≡C-COO)$_2$(3,5-Cl$_2$py)	55.32 (55.05)	2.53 (2.61)	2.61 (2.79)	12.57 (12.66)
Cu(Ph-C≡C-COO)$_2$(DMSO)	55.47 (55.61)	3.94 (3.73)		14.80 (14.71)
Cu(Ph-C≡C-COO)$_2$(Ph$_3$PO)	68.34 (68.40)	3.86 (3.98)		10.02 (10.05)
Cu(CH$_3$COO)$_2$(DMSO)	27.81 (27.74)	4.66 (4.65)		24.45 (24.46)

Table 2. Magnetic parameters

Complex	$\frac{-2J}{cm^{-1}}$	g	$P\times10^2$	$\frac{\theta'}{K}$	$\sigma_{dis}\times10^3$
$Cu(Ph\text{-}C\equiv C\text{-}COO)_2(PhCN)$	318	2.27_1	0.20	0	4.15
$Cu(Ph\text{-}C\equiv C\text{-}COO)_2(3,5\text{-}Cl_2py)$	300	2.29_1	1.27	0	6.45
$Cu(Ph\text{-}C\equiv C\text{-}COO)_2(DMSO)$	287	2.26_8	0.48	0	4.96
$Cu(Ph\text{-}C\equiv C\text{-}COO)_2(Ph_3PO)$	283	2.38_4	2.41	0	6.74
$Cu(Ph\text{-}C\equiv C\text{-}COO)_2$	213	2.16_2	7.11	+6.86	5.08
$Cu(CH_3COO)_2(DMSO)$	326	2.25_0	0.32	0	5.66

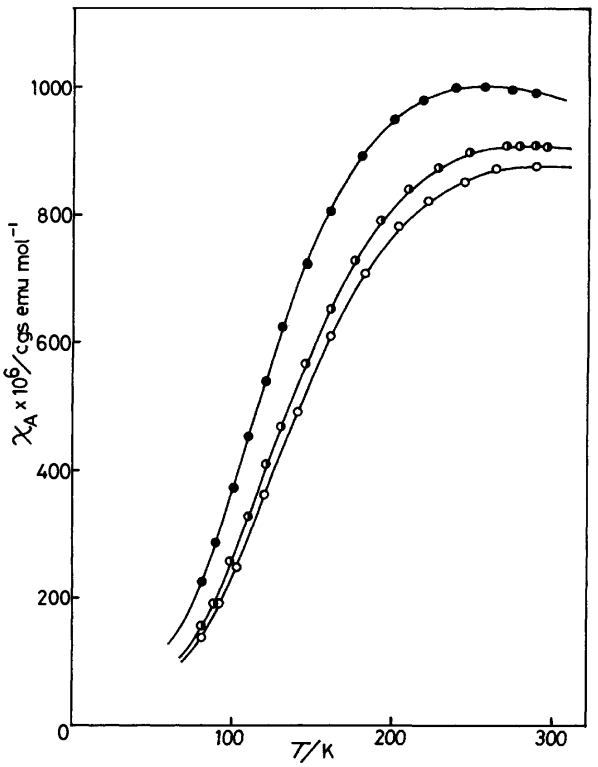

Fig. 2. Temperature dependence of magnetic susceptibilities of $Cu(Ph\text{-}C\equiv C\text{-}COO)_2(DMSO)$ (●), $Cu(Ph\text{-}C\equiv C\text{-}COO)_2(PhCN)$ (◑), and $Cu(CH_3COO)_2(DMSO)$ (○).
The solid curves were obtained as described in the text.

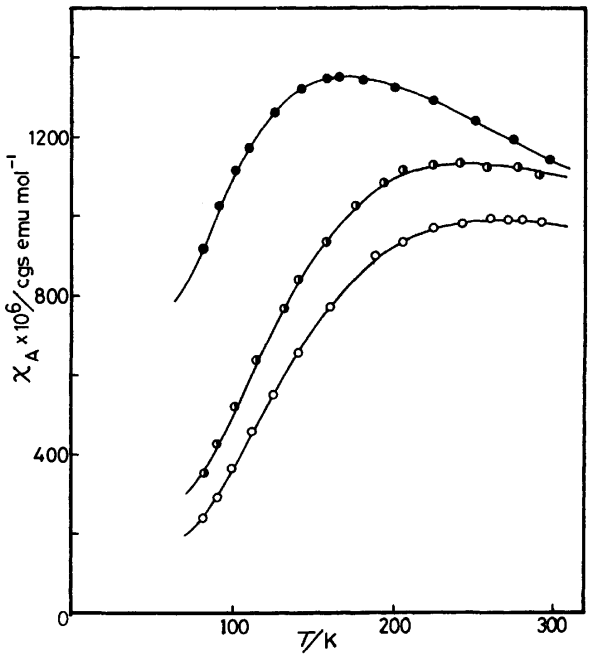

Fig. 3. Temperature dependence of magnetic susceptibilities of $Cu(Ph\text{-}C\equiv C\text{-}COO)_2$ (●), $Cu(Ph\text{-}C\equiv C\text{-}COO)_2(Ph_3PO)$ (◑), and $Cu(Ph\text{-}C\equiv C\text{-}COO)_2(3,5\text{-}Cl_2py)$ (○).
The solid curves were obtained as described in the text.

$COO)_2\cdot3H_2O$ follow the Curie-Weiss law. The best fit of the experimental data to Eq. 1 yields the values of $g=2.19_9$ and $\theta/K=+2.0$ with $\sigma_{dis}=8.55\times10^{-3}$. The effective magnetic moment at 10 °C calculated from the equation, $\mu_{eff}=2.83[(\chi_A-N\alpha)\cdot T]^{1/2}$, is 1.91 BM (1 BM=$9.27\times10^{-24}$ A m^2). These results indicate that this compound does not have a dimeric structure but may have a monomeric structure, as has copper(II) 2-carboxybenzoate dihydrate[11] (μ_{eff}=1.95 BM at 297 K and $\theta/K=-0.6\pm3.3$),[12] or a polymeric structure, as has copper(II) benzoate trihydrate[13] (μ_{eff}=1.97 BM at 293.4 K and $\theta/K=+40$).[14]

The cryomagnetic data observed for the adducts of copper(II) phenylpropynoate prepared in the present study are well represented by Eq. 2 (*cf.* Figs. 2 and 3 and Table 2), indicating that all these adducts have a dimeric structure similar to that found for copper(II) acetate monohydrate.[15] The $-2J$ values of these adducts and those of the corresponding adducts of other dimeric copper(II) carboxylates studied in our laboratory are given in Table 3 along with the pK_a values of their parent carboxylic acids. From Table 3, it can be seen that, in each series of the complexes with the same L, the $-2J$ value decreases as the pK_a value of the parent carboxylic acid becomes smaller. This fact suggests that, in the present phenylpropynoate adducts, the electron-withdrawing nature of the Ph-C≡C group predominantly affects the magnetic interaction. On the other hand, in the present study, the influence of the highly unsaturated

Table 3. Comparison of $-2J$ values for [Cu(RCOO)$_2$·L]$_2$ complexes

R \ L	$-2J$/cm^{-1} PhCN	3,5-Cl$_2$py	DMSO	Ph$_3$PO	p$K_a^{25\,°C}$ of RCOOH[f]
CH_3		349[c]	326[b]	319[e]	4.76
$ClCH_2$	352[a]	340[c]			2.81
Ph-C≡C	318[b]	300[b]	287[b]	283[b]	2.32
Cl_2CH		312[c]			1.29
Cl_3C	224[a]	92[d]			0.08

a) Ref. 23. b) Present work. c) Ref. 22. d) Ref. 24. e) Ref. 25. f) Ref. 26.

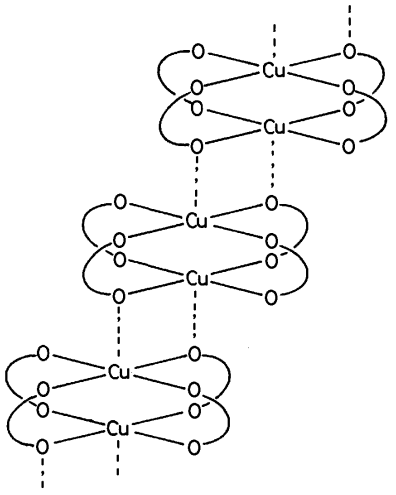

Fig. 4. Schematic representation of polymeric chain structure of copper(II) propionate.[19]

property of the C≡C group directly linked to the COO group on the magnetic interaction could not be detected.

For the non-adduct compound, Cu(Ph-C≡C-COO)$_2$, the best fit of the thermal magnetic data to Eq. 2 gave the value of $-2J$=213 cm^{-1}, a value much lower than those found for the adduct complexes, 283—318 cm^{-1} (*cf.* Table 2 and Fig. 3). Such magnetochemical behavior is in accord with the general trend that, in many dimeric copper(II) carboxylates, the values of $-2J$ for the non-adduct complexes are often lower than those for the corresponding adduct complexes,[4,16] as seen in the case, Cu(C$_2$H$_5$COO)$_2$ (300 cm^{-1})[17]<Cu(C$_2$H$_5$COO)$_2$(py) (350 cm^{-1}).[18] The crystal structure of Cu(C$_2$H$_5$COO)$_2$ is composed of carboxylato-bridged dimers which are linked into one-dimensional polymeric chains by apical Cu-O interaction (*cf.* Fig. 4).[19] Such an apical Cu-O interaction will disturb the superexchange interaction through the carboxylato bridges,[20] leading to the lower value of $-2J$. The low $-2J$ value found for Cu(Ph-C≡C-COO)$_2$, therefore, suggests the presence of apical-to-basal Cu-O-Cu linkages similar to Cu(C$_2$H$_5$COO)$_2$ in this compound. This deduction is further supported by the fact that, among the dimeric compounds in the present study, only the non-adduct compound, Cu(Ph-C≡C-COO)$_2$, showed an appreciably large positive value of θ', θ'/K=+6.86 (*cf.* Table 2). The positive value of θ' is considered to arise from the presence of ferromagnetic spin-spin interaction through the apical-to-basal Cu-O-Cu bonds shown in Fig. 4.

The C≡C stretching vibrations for the non-adduct

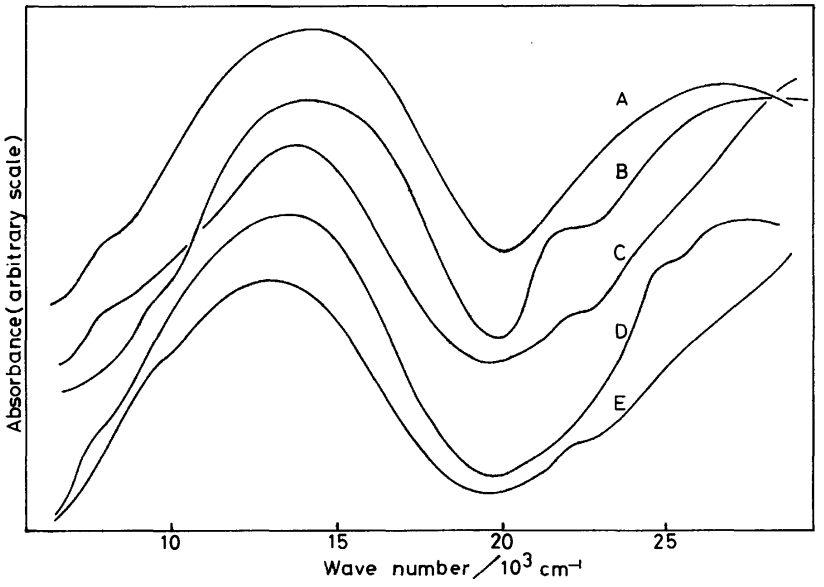

Fig. 5. Reflectance spectra of Cu(CH$_3$COO)$_2$(DMSO) (A), Cu(Ph-C≡C-COO)$_2$(PhCN) (B), Cu(Ph-C≡C-COO)$_2$(3,5-Cl$_2$py) (C), Cu(Ph-C≡C-COO)$_2$(DMSO) (D), and Cu-(Ph-C≡C-COO)$_2$(Ph$_3$PO) (E).

Table 4. Reflectance spectral data

Complex	Band I		New Band		Band II
	$\tilde{\nu}_{max}/10^3$ cm^{-1}				
$Cu(Ph\text{-}C\equiv C\text{-}COO)_2(PhCN)$	14.0	9.5[a]	24.9[a]	22.2[a]	28.3
$Cu(Ph\text{-}C\equiv C\text{-}COO)_2(3,5\text{-}Cl_2py)$	13.8	7.8[a]	24.5[a]		
$Cu(Ph\text{-}C\equiv C\text{-}COO)_2(DMSO)$	13.6	7.8[a]	25.1[a]		28.7
$Cu(Ph\text{-}C\equiv C\text{-}COO)_2(Ph_3PO)$	13.0	8.0[a]	24.5[a]		
$Cu(CH_3COO)_2(DMSO)$	14.2	7.9[a]			26.7

a) Shoulder.

compound (2223 cm^{-1}) and the adduct compounds (2221—2223 cm^{-1}) are almost the same as those for free phenylpropynoic acid (2235, 2200 cm^{-1}). This fact indicates the absence of coordination through the C≡C π system in these dimeric copper(II) compounds.

The reflectance spectra of the present adduct complexes in the range 5000—29400 cm^{-1} show three bands having maxima at 28000—29000 cm^{-1} (so-called Band II), 24000—25000 cm^{-1}, and 13000—14000 cm^{-1} (so-called Band I) with a shoulder at *ca.* 8000 cm^{-1}. The wave numbers of the band maxima ($\tilde{\nu}_{max}$) are listed in Table 4 and their spectral curves are shown in Fig. 5. A remarkable feature of the spectra of these complexes is the appearance of a new band in the range 24000—25000 cm^{-1} which is absent in dimeric copper(II) alkanoate and arenecarboxylate complexes. For comparison, the reflectance spectrum of $Cu(CH_3COO)_2(DMSO)$ ($-2J$=326 cm^{-1}) is given in Fig. 5, which has no such absorption in the 24000—25000 cm^{-1} region. Such a new band has been recently observed for $[Cu(Ph_3GeCOO)_2(DMSO)]_2$ and $[Cu(Me_2PhSiCOO)_2(DMSO)]_2$, where Me=methyl.[8] Since the assignment of d-d bands for dimeric copper(II) carboxylates is still in dispute,[21] finding of such a new band is hoped to serve to elucidate the electronic state of the copper(II) ion in these dimeric systems. From Table 4 and Fig. 5, we can also see that the $\tilde{\nu}_{max}$ value of Band I decreases in the order: PhCN adduct>3,5-Cl_2py adduct>DMSO adduct>Ph_3PO adduct, the order of which is the same as that of the $-2J$ value (*cf.* Table 2). A parallelism exists between the $\tilde{\nu}_{max}$ and $-2J$ values (higher $\tilde{\nu}_{max}$-higher $-2J$). A similar parallelism was previously observed for a series of $[Cu(RCOO)_2\cdot L]_2$ complexes, where R=CH_3, $ClCH_2$, and Cl_2CH, and L=pyridine analogues, and the parallelism was interpreted in terms of the electroneutrality principle.[22]

References

1) R. J. Doedens, *Prog. Inorg. Chem.*, **21**, 209 (1976).

2) R. L. Carlin and A. J. van Duyneveldt, "Magnetic Properties of Transition Metal Compounds," Springer-Verlag, New York (1977), Chap. IV D, p. 86.

3) M. Kato, H. B. Jonassen, and J. C. Fanning, *Chem. Rev.*, **64**, 99 (1964).

4) R. W. Jotham, S. F. A. Kettle, and J. A. Marks, *J. Chem. Soc., Dalton Trans.*, **1972**, 428.

5) J. A. Moreland and R. J. Doedens, *J. Am. Chem. Soc.*, **97**, 508 (1975).

6) J. A. Moreland and R. J. Doedens, *Inorg. Chem.*, **17**, 674 (1978).

7) L. C. Porter and R. J. Doedens, *Inorg. Chem.*, **23**, 997 (1984).

8) M. Kato, T. Taura, O. W. Steward, T. Tokii, Y. Muto, Y. Kushi, and I. Suzuki, 33rd Conference on Coordination Chemistry of the Chemical Society of Japan, Toyonaka, October 1983, Proceedings, p. 494.

9) M. Bukowska-Strzyewska, J. Skoweranda, E. Heyduk, and J. Mrozinski, *Inorg. Chim. Acta*, **73**, 207 (1983).

10) P. W. Selwood, "Magnetochemistry," Interscience Publishers, New York (1956), pp. 78 and 91.

11) M. Biagini Cingi, C. Guastini, A. Musatti, and M. Nardelli, *Acta Crystallogr., Sect. B*, **25**, 1833 (1969).

12) K. E. Hyde, P. L. Bocko, M. Lynch, R. Adams, and G. Kokoszka, *Inorg. Chim. Acta*, **19**, 51 (1976).

13) H. Koizumi, K. Osaki, and T. Watanabe, *J. Phys. Soc. Jpn.*, **18**, 117 (1963).

14) J. Lewis, Y. C. Lin, L. K. Royston, and R. C. Thompson, *J. Chem. Soc.*, **1965**, 6464.

15) J. N. van Niekerk and F. R. L. Schoening, *Acta Crystallogr.*, **6**, 227 (1953).

16) J. Lewis, F. E. Mabbs, L. K. Royston, and W. R. Smail, *J. Chem. Soc., A*, **1969**, 291.

17) R. L. Martin and H. Waterman, *J. Chem. Soc.*, **1957**, 2545.

18) W. E. Marsh, G. O. Carlisle, and M. V. Hanson, *J. Inorg. Nucl. Chem.*, **39**, 1839 (1977).

19) Yu. A. Simonov and T. I. Malinovskii, *Sov. Phys. Crystallogr.*, **15**, 310 (1970).

20) R. L. Beddoes, J. A. Connor, D. Dubowski, A. C. Tones, O. S. Mills, and R. Price, *J. Chem. Soc., Dalton Trans.*, **1981**, 2119.

21) S. Mitra, *Prog. Inorg. Chem.*, **22**, 309 (1977).

22) Y. Muto, T. Tokii, K. Chijiwa, and M. Kato, *Bull. Chem. Soc. Jpn.*, **57**, 1008 (1984).

23) M. Nakashima, M. Mikuriya, and Y. Muto, *Bull. Chem. Soc. Jpn.*, **58**, 968 (1985).

24) H. Horie, M. Nakashima, Y. Muto, M. Kato, and I. Suzuki, 34th Conference on Coordination Chemistry of Japan, Nagaoka, October 1984, Proceedings, p. 476.

25) T. Tokii, T. Ikeda, and Y. Muto, *Bull. Chem. Soc. Jpn.*, **55**, 3925 (1982).

26) L. F. Fieser and M. Fieser, "Text Book of Organic Chemistry," Maruzen Company, Ltd., Tokyo (1952), pp. 157 and 532.

Reduction of Aromatic Ketones or Thioketones with Phenylphosphine

Michiko TAMANO and Jugo KOKETSU*
Department of Industrial Chemistry, College of Engineering, Chubu University, 1200 Matsumoto, Kasugai, Aichi 487
(Received February 7, 1985)

Reactions of certain aromatic ketones or thioketones with phenylphosphine and subsequent addition of diethyl disulfide gave the reduction products of the ketones and *S,S*-diethyl phenylphosphonodithioate or *S,S*-diethyl phenylphosphonotrithioate. A possible intermediate of the phosphine moiety was suggested to be phenylphosphinylidene [PhP=O] or phenylphosphinothioylidene [PhP=S]. The reduction of 10,10′-bianthrone and $\Delta^{10,10'}$-bianthrone resulted in the cleavage of the carbon–carbon single and double bonds and the reduction of the carbonyl groups, respectively.

The reducing properties of the compounds which contain a trivalent phosphorus atom have attracted little attention so far. Because of the affinity of a phosphorus atom for a oxygen atom and its ability to donate hydrogen atoms, primary phosphine is expected to behave as a reducing reagent.

The successful reductions of *N*-chloro-*p*-toluenesulfonamide to *p*-toluenesulfonamide,[1] 1-naphthol to naphthalene,[2] arenesulfonyl chloride to disulfide,[3] and nitro compounds with phosphine to azoxy derivatives[3] and amines[4] have been reported. However, there is no report concerning the reduction of carbonyl or thiocarbonyl compounds with phosphine. The reductions of the carbonyl compounds to alcohols can be achieved by using various reducing reagents such as metal hydrides and dissolving metals, and by catalytic hydrogenations.[5] The complete removal of the oxygen atom from a carbonyl group to give methylene group can be accomplished by well-known Wolf-Kishner[6] and Clemmensen reductions.[7] These methods involve alkaline (Wolf-Kishner) or acidic (Clemmensen) conditions and need drastic heating. The thiocarbonyl groups are also readily reduced with various reducing reagents.[8] Especially, diaryl thioketones are known to be reduced with Zn/HCl to give diarylmethylene.[9] This paper describes our finding about the reduction of aromatic ketones or thioketones with phenylphosphine under mild and neutral conditions.

Results and Discussion

Reduction of anthraquinone (**1**) with $LiAlH_4$[10,11] or $NaBH_4$[12] gives 9,10-dihydro-9,10-anthracenediol, and reduction with Sn/HCl[13] or $SnCl_2$/HCl[14] gives mainly anthrone. Also anthracene was obtained by the reduction of anthraquinone with triphenylsilane,[15] zinc dust/HCl,[16] and HI/AcOH.[17] The conversion of anthraquinone to 9,10-dihydroanthracene was realized by Clemmensen reduction,[18] and reduction with hydriodic acid-phosphorus-iodine[19] and reduction with tetralin in molten $SbCl_3$.[20] Reaction of anthraquinone with two equivalents of phenylphosphine in a sealed ampoule at 140 °C for 3 d and subsequent addition of excess amount of diethyl disulfide gave 91% yield of 9,10-dihydroanthracene and 65% yield of *S,S*-diethyl phenylphosphonodithioate.

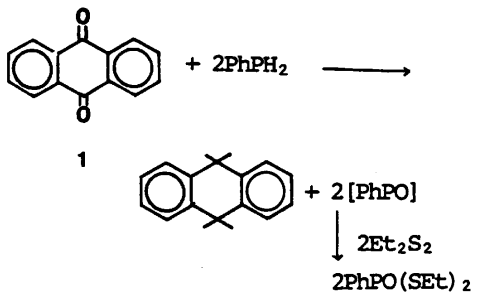

The reduction of this type was carried out successfully with a number of aryl ketones such as 5,12-naphthacenequinone (**2**) and 6,13-pentacenequinone (**3**). By the reaction with equimolar amounts of phenylphosphine, the carbonyl groups of fluorenone (**4**), xanthone (**5**), thioxanthone (**6**), acridinone (**7**), 10-methyl-9(10*H*)-acridone (**8**), and 7*H*-benz[*de*]-anthracen-7-one (**9**) were easily converted to the methylene groups in high yields. Chrysazin(1,8-dihydroxyanthraquinone) (**10**) and anthrarufin(1,5-dihydroxyanthraquinone) (**11**) gave the corresponding anthrones, *i.e.*, 1,8-dihydroxy-9(10*H*)-anthracenone and 1,5-dihydroxy-9(10*H*)-anthracenone, respectively, upon reduction with excess amounts of phenylphosphine.

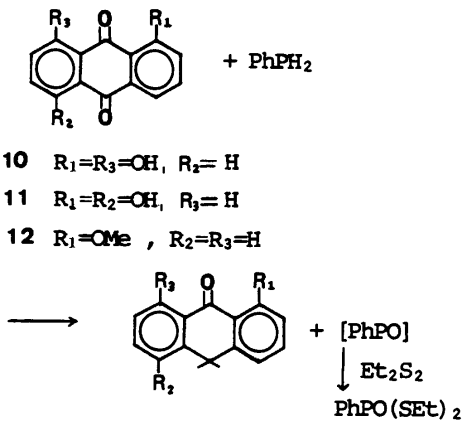

Also, 1-methoxyanthraquinone (**12**) gave 1-methoxy-9(10*H*)-anthracenone. These anthraquinones, in which one or both of the carbonyl groups were protected by hydrogen bonding or by steric hindrance, show strong resistance to the complete removal of the oxygen atoms.

The reduction of 1,4-anthraquinone (**13**) with three molar excess of phenylphosphine and subsequent treatment with excess amounts of diethyl disulfide gave 1,2,3,4-tetrahydroanthracene. *S,S*-Diethyl phenylphosphonodithioate and *S,S*-diethyl phenylphosphonodithioite were separated from the phosphine moiety in 2:1 molar ratio.

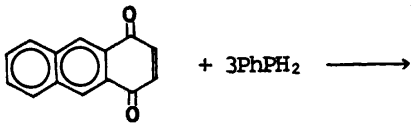

13

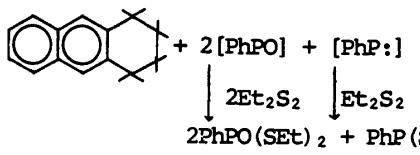

10,10′-Bianthrone (**14**) and $\Delta^{10,10'}$-bianthrone (**15**) were reduced with three and four molar amounts of phenylphosphine to gave 9,10-dihydroanthracene. Also, *S,S*-diethyl phenylphosphonodithioate and *S,S*-diethyl phenylphosphonodithioite were obtained in 2:1 and 1:1 molar ratios, respectively.

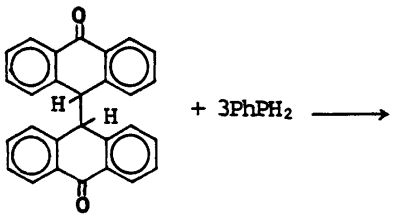

14

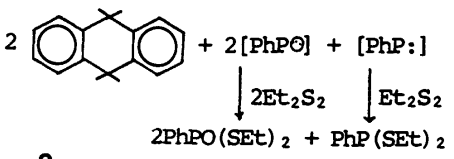

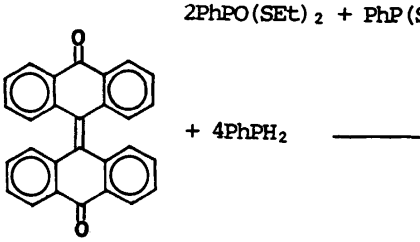

15

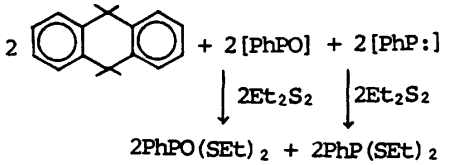

In these reductions, the carbon–carbon single and double bonds were cleaved in addition to the removal of the oxygen atoms from the carbonyl groups.

The reduction of benzophenone (**16**) and acetophenone (**17**) with phenylphosphine gave diphenylmethane and ethylbenzene, respectively. However, the yield of the reduction of acetophenone was very low, and aliphatic ketones could not be reduced with this reagent. Therefore, the intermediate of this reduction must have two aryl rings for stabilization.

Thiocarbonyl groups of 9*H*-xanthenethione (**18**), 9*H*-thioxanthenethione (**19**), 9(10*H*)-acridinethione (**20**), and 10-methyl-9(10*H*)-acridinethione (**21**) were rapidly converted to the methylene groups to give 9*H*-xanthene, 9*H*-thioxanthene, 9,10-dihydroacridine, and 10-methyl-9,10-dihydroacridine, respectively.

With regard to the mechanism of this reduction, a carbonyl or thiocarbonyl group will undergo insertion into the P–H bond of the phenylphosphine to form >CH–XPHPh (X=O or S) as an intermediate. The C–X bond in this intermediate would be cleaved and the hydrogen atom on the phosphorus atom would migrate to the carbonyl carbon atom. Therefore, phenylphosphine would accept an oxygen or a sulfur atom and donate two hydrogen atoms suggesting the intermediary of phenylphosphinylidene [PhP=O] or phenylphosphinothioylidene [PhP=S].

$$>C{=}X + PhPH_2 \longrightarrow >CH{-}XPHPh \longrightarrow >CH_2 + PhP{=}X \quad (X{=}O \text{ or } S)$$

By subsequent addition of diethyl disulfide, these phosphine moieties were trapped as *S,S*-diethyl phenylphosphonodithioate and *S,S*-diethyl phenylphosphonotrithioate.

In the cases of the reduction of 1,4-anthraquinone, 10,10′-bianthrone and $\Delta^{10,10'}$-bianthrone, some part of phenylphosphine acts as a hydrogen donor only and gives phenylphosphinidene [PhP:] as an intermediate, which is converted to *S,S*-diethyl phenylphosphonodithioite by the reaction with diethyl disulfide.

Experimental

General. All the reactions were carried out under an argon atmosphere. Melting points determined with a Yanagimoto micro-melting point apparatus were uncorrected. IR spectra were taken with a Shimadzu IR-430 spectrometer, UV spectra on a Hitachi 200-10 spectrophotometer, ^1H and ^{13}C NMR spectra on a JEOL JNM-FX 60 spectrometer in $CDCl_3$ with tetramethylsilane as an internal standard. MS spectra were recorded on a Hitachi RMU-6L spectrometer. Commercially available carbonyl compounds were used without further purification. 1-Methoxyanthraquinone was prepared from 1-chloroanthra-

quinone according to the method as that reported by Cook and Pauson.[21] 1,4-Anthraquinone was obtained by the reduction of quinizarin with $NaBH_4$ and purified by sublimation.[22] 9*H*-Xanthenethione, 9*H*-thioxanthene-9-thione, 9(10*H*)-aoacridinethione, and 10-methyl-9(10*H*)-acridinethione were prepared by treatment of the corresponding carbonyl compounds with phosphorus pentasulfide.[8] Phenylphosphine was obtained by the reduction of dichlorophenylphosphine with $LiAlH_4$ according to the method described by Pass and Schindlbauer.[23]

Reduction Procedure. A mixture of an aromatic ketone (10 mmol) with phenylphosphine (molar amount used is specified in Table 1) was placed in a sealed ampoule under argon atmosphere, and heated at 140 °C for periods shown in Table 1. The reaction mixture turned into homogeneous pale orange paste. Subsequently, an excess amount (50 mmol) of diethyl disulfide was added to the ampoule, which was resealed and heated at 140 °C for another 24 h. After removal of excess diethyl disulfide, the reduction products were obtained by sublimation under reduced pressure (13.33 Pa/120 °C). From the sublimation residue, *S,S*-diethyl phenylphosphonodithioate or *S,S*-diethyl phenylphosphonotrithioate were distilled. In the reduction of 1,4-anthraquinone, 10,10′-bianthrone, and $\Delta^{10,10'}$-bianthrone. *S,S*-diethyl phenylphosphonodithioate and *S,S*-diethyl phenylphosphonodithioite were separated by column chromatography (silica gel–$CHCl_3$ as eluent) of the distillation mixture. The structures of the reduction products were deduced based on the following analytical and spectroscopic data.

9,10-Dihydroanthracene: White crystals; mp 70—72 °C (lit,[19] 108—110 °C). Spectra data(IR,[24] ^1H,[25] and ^{13}C[26] NMR) matched with the reported data.

5,12-Dihydronaphthacene: Pale yellow needles; mp 210—211 °C; IR (KBr-disk) 3030(w), 2880(w), 1501(w), 1492(w), 1477(m), 1438(w), 767(vs), and 755(vs) cm^{-1}; ^1H NMR ($CDCl_3$) δ=7.24—7.72 (m, 10H), and 4.06 (s, 2H); ^{13}C NMR δ=137.16, 135.73, 132.48, 127.28, 126.31, 125.33, 125.20, and 36.84; UV_{max} (C_2H_5OH) 228 (ε 56200), 260 (ε 2300), 271 (ε 3200), 280 (ε 3020), and 291 nm (ε 2290); MS (70 eV), *m/z* (rel intensity), 230 (M^+, 100), 229 (94), 228 (26), 110 (26), and 109 (90). Found: C, 93.51; H, 6.50%. Calcd for $C_{18}H_{14}$: C, 93.87; H, 6.13%.

6,13-Dihydropentacene: White needles; mp 265—268 °C; IR (KBr-disk) 3055—2750(w), 1595(w), 1485(w), 1440(w), 750(vs), and 740(vs) cm^{-1}; ^1H NMR ($CDCl_3$) δ=7.16—7.78 (m, 12H) and 4.24 (s, 2H); ^{13}C NMR δ=135.93, 133.72, 127.28, 125.33, 125.14, and 37.36; UV_{max} (C_2H_5OH) 234 (ε 105000), 260 (ε 8900), 272 (ε 10200), 281 (ε 9330), and 292 nm (ε 6300); MS (70 eV), *m/z* (rel intensity), 280 (M^+, 100), 270 (72), 278 (56), 140 (33), 79 (39), and 78 (28). Found: C, 93.88; H, 5.62%. Calcd for $C_{22}H_{16}$: C, 94.25; H, 5.75%.

Fluorene: White plate; mp 117—118 °C. All spectroscopic data were identical with those of commercially available sample.

Xanthene: White crystals; mp 98—100 °C (lit,[27] 100.5 °C). All spectroscopic data were identical with those of commercially available sample.

Thioxanthene: White crystals; mp 126—127 °C (lit,[15] 128 °C). IR and ^1H NMR spectra data matched with reported data (IR; Aldrich 627F, ^1H NMR; Aldrich 5, 533 A).

9,10-Dihydroacridine: White crystals; mp 165—167 °C; IR Aldrich 695E.

10-Methyl-9,10-dihydroacridine: White crystals; mp 85—88 °C; IR (KBr-disk) 2960(w), 1585(s), 1460(s), 1152(m), 1110(m), 1032(m), and 742(vs) cm^{-1}; ^1H NMR δ=7.19—6.58

Table 1. Reduction conditions and yields of products

Compd	$PhPH_2$ Equiv	Reaction period	Product from ketone(A)	Yields/% (A)	Yields/% $PhPX(SEt)_2$[a]	Yields/% $PhP(SEt)_2$
(1)	2	3 d	9,10-Dihydroanthracene	91	65	—
(2)	2	3 d	5,12-Dihydronaphthacene	46	36	—
(3)	2	3 d	6,13-Dihydropentacene	32	28	—
(4)	1	3 d	Fluorene	100	76	—
(5)	1	1 d	Xanthene	88	73	—
(6)	1	12 h	Thioxanthene	100	81	—
(7)	1	1 d	9,10-Dihydroacridine	95	79	—
(8)	1	1 d	10-Methyl-9,10-dihydroacridine	81	67	—
(9)	1	3 d	7*H*-benz[*de*]anthracene	56	43	—
(10)	2	3 d	1,8-Dihydroxy-9(10*H*)-anthracenone	13	8	—
(11)	2	3 d	1,5-Dihydroxy-9(10*H*)-anthracenone	17	10	—
(12)	2	3 d	1-Methoxy-9(10*H*)-anthracenone	12	8	—
(13)	3	3 d	1,2,3,4-Tetrahydroanthracene	51	45	22
(14)	3	3 d	9,10-Dihydroanthracene	61	52	31
(15)	4	3 d	9,10-Dihydroanthracene	18	10	8
(16)	1	1 d	Diphenylmethane	96	75	—
(17)	1	5 d	Ethylbenzene	7	trace	—
(18)	1	10 h	Xanthene	93	63	—
(19)	1	10 h	Thioxanthene	90	59	—
(20)	1	10 h	9,10-Dihydroacridine	99	70	—
(21)	1	10 h	10-Methyl-9,10-dihydroacridine	89	52	—

a) X=O for compds 1—17 and X=S for compds 18—21.

(m, 8H), 3.71 (s, 3H), and 3.05 (s, 2H); ^{13}C NMR δ=125.19 (C-1), 118.24 (C-2), 124.54 (C-3), 109.54 (C-4), 121.81 (C-9a), 141.22 (C-4a), 30.65 (C-9), and 30.91 (N-Me); UV_{max} (C_2H_5OH) 210 (ε 10200), 249 (ε 2500), 282 (ε 1120), 355 (ε 1380), and 380 nm (ε 1380); MS (70 eV), *m/z* (rel intensity) 196 (21), 195 (M^+, 100), 194 (28), 181 (35), 180 (81), 166 (26), and 152 (31). Found: C, 86.31; H, 6.68%. Calcd for $C_{14}H_{13}N$: C, 86.12; H, 6.71%.

7H-Benz[de]anthracene: White crystals; mp 70—72 °C; IR (KBr-disk) 3030(m), 2940(w), 2900(w), 1603(m), 1497(s), 1455(m), 1440(s), 765(m), and 752 (s) cm^{-1}; ^{1}H NMR δ=7.29—8.77 (m, 10H) and 4.54 (s. 2H); ^{13}C NMR δ=134.37, 133.33, 131.18, 128.91, 126.67, 126.83, 126.44, 126.18, 125.92, 125.46, 124.42, 123.71, 123.32, 122.73, 120.72, 118.57, and 34.44; UV_{max} (C_2H_5OH) 206 (ε 12300), 223 (ε 14100), 227 (ε 14100), 250 (ε 8500), 256 (ε 8300), 304 (ε 3000), 316 (ε 3700), 330 (ε 4900), and 345 nm (ε 4200); MS (70 eV), *m/z* (rel intensity) 216 (M^+, 53), 215 (100), 213 (21), 107 (15), and 94 (15). Found: C, 94.06; H, 5.51%. Calcd for $C_{17}H_{12}$: C, 94.41; H, 5.59%.

1,8-Dihydroxy-9(10H)-anthracenone: All physical and spectroscopic data were identical with those of an authentic sample.[28]

1,5-Dihydroxy-9(10H)-anthracenone: All physical and spectroscopic data were identical with those of an authentic sample.[28]

1-Methoxy-9(10H)-anthracenone: Reddish orange needles; mp 125—126 °C; IR (KBr-disk) 3050(w), 1660(vs), 1606(vs), 1591(vs), 1454(m), 1438(m), 1305(vs), 1260(s), 1241(m), 1063(s), 731(vs), and 711(vs) cm^{-1}; ^{1}H NMR δ=6.99—8.39 (m, 7H), 4.15 (s, 3H), and 3.92 (s, 2H); ^{13}C NMR δ=156.85 (C-1), 113.38 (C-2), 132.68 (C-3), 119.42 (C-4), 128.91 (C-5), 127.54 (C-6), 126.97 (C-7), 127.41 (C-8), 184.33 (C-9), 27.42 (C-10), 129.88 (C-9a), 140.66 (C-4a), 133.13 (C-8a), and 131.96 (C-10a); UV_{max} (C_2H_5OH) 213 (ε 51300), 256 (ε 57500), 330 (ε 5750), 367 (ε 2880), and 381 nm (ε 1860); MS (70 eV), *m/z*(rel intensity) 224 (M^+, 100), 208 (75), 179 (65), 163 (50), 151 (25), 150 (70), 149 (20), 85 (25), 76 (35), 75 (20), and 63 (29). Found: C, 80.20; H, 5.48%. Calcd for $C_{15}H_{12}O_2$: C, 80.34; H, 5.39%.

1,2,3,4-Tetrahydroanthracene: White lieflets; mp 105—106 °C (lit, 96—105 °C,[29] 103—105 °C[30]); IR(KBr-disk) 3040(w), 2920(s), 2845(m), 2825(w), 1500(m), 1490(w), 1441(w), 970(w), 946(m), and 742(vs) cm^{-1}; ^{1}H NMR δ=7.39—7.60 (m, 6H), 2.92 (s, 4H), and 1.83 (s, 4H); ^{13}C NMR δ=29.83 (C-1), 23.46 (C-2), 127.05 (C-5), 124.88 (C-6), 126.63 (C-9), 136.32 (C-4a), and 132.42 (C-10a); UV_{max} (C_2H_5OH) 228 (ε 33900), 257 (ε7240), 265 (ε 7940), 277 (ε 7940), 285 (ε 7080), and 298 nm (ε3700); MS (70 eV), *m/z* (rel intensity), 182 (M^+, 100), 166 (33), 165 (21), 164 (36), 153 (88), 152 (36), 151 (33), 140 (46), and 114 (21). Found: C, 92.56; H, 7.92%. Calcd for $C_{14}H_{14}$: C, 92.26; H, 7.74%.

Diphenylmethane and Ethylbenzene: All physical and spectroscopic data were identical with those of commercially available materials.

S,S-*Diethyl Phenylphosphonodithioate*: Colorless liquid; bp 106—108 °C/26.66 Pa. Spectra data matched with the reported data.[31]

S,S-*Diethyl Phenylphosphonodithioite*: All physical and spectroscopic data were identical with those of an authentic sample prepared by a standard method.[32]

S,S-*Diethyl Phenylphosphonotrithioate*: Orange liquid; bp 117—120 °C/26.66 Pa. Spectra data matched with the reported data.[33]

References

1) J. R. Bendall, F. G. Mann, and D. J. Prudie, *J. Chem. Soc.*, **1942**, 157.
2) H. Wichelhause, *Ber.*, **38**, 1725 (1905).
3) S. A. Buckler, L. Doll, F. K. Lind, and M. Epstein, *J. Org. Chem.*, **27**, 794 (1962).
4) Th. Weyl, *Ber.*, **39**, 4340 (1906); **40**, 970, 3608 (1907).
5) H. O. House, "Modern Synthetic Reactions," 2nd ed, W. A. Benjamin Inc., Menlo park, Ca (1972), Chap. 1—4.
6) D. Todd. *Org. React.*, **4**, 378 (1948).
7) E. L. Martin, *Org. React.*, **1**, 155 (1942).
8) E. Campaigne, "The Chemistry of the Carbonyl Group," ed by S. Patai, Interscience Publisher, New York (1966), p. 917.
9) A. Schönberg. *Ber.*, **58B**, 1793 (1925).
10) E. Boyland and D. Manson, *J. Chem. Soc.*, **1951**, 1937.
11) R. F. Nystrom and W. G. Brown, *J. Am. Chem. Soc.*, **70**, 3738 (1948).
12) G. S. Panson and C. E. Weill, *J. Org. Chem.*, **22**, 120 (1957).
13) K. H. Meyer, *Org. Synth.*, Coll. Vol. 1, 60 (1956).
14) L. F. Fieser, "Experiments in Organic Chemistry," 3rd ed., D. C. Heath and Company, Boston (1957), p. 60.
15) H. Gilman and J. Diehl, *J. Org. Chem.*, **26**, 4817 (1961).
16) J. T. Traxler, *Synth. Commun.*, **7**, 161 (1977).
17) M. Konieczny and R. Harvey, *J. Org. Chem.*, **44**, 4813 (1979).
18) H. L. Bradlow and C. A. Vander Welf, *J. Am. Chem. Soc.*, **69**, 1254 (1947).
19) R. N. Renaud and J. C. Stephens, *Can. J. Chem.*, **52**, 1229 (1974).
20) A. C. Buchaman, III, A. S. Dworkir, and G. P. Smith, *J. Org. Chem.*, **47**, 603 (1982).
21) J. W. Cook and P. L. Pauson *J. Chem. Soc.*, **1949**, 2725.
22) M. Tamano and J. Koketsu, *Nippon Kagaku Kaishi*, **1984**, 1164.
23) F. Pass and H. Schindlbauer, *Monatsh. Chem.*, **90**, 148 (1959).
24) M. Brigodiot and J. M. Lebas, *J. Mol. Struct.*, **32**, 297 (1976).
25) J. Douris and A. Mathieu, *Bull., Soc. Chem. Fr.*, **1971**, 3365.
26) L. R. Isbrandt, R. K. Jensen, and L. Petrakis, *J. Magn. Reson.*, **12**, 143 (1973).
27) N. Latif and N. Mishriky, *J. Org. Chem.*, **27**, 846 (1962).
28) M. Tamano and J. Koketsu, *Nippon Kagaku Kaishi*, **1982**, 1918.
29) G. Schroeter, *Ber.*, **57**, 2003 (1924).
30) D. I. Davies and C. Waring, *J. Chem. Soc.*, (C), **1968**, 1865.
31) M. Yoshifuji, S. Nakayama, R. Okazaki, and N. Inamoto, *J. Chem. Soc., Perkin Trans. 1*, **1973**, 2065.
32) G. M. Kosolapoff and L. Maier, "Organic Phosphorus Compounds," Vol. 4, Wiley-Interscience, New York (1972), p. 398.
33) S. Nakayama, M. Yoshifuji, R. Okazaki, and N. Inamoto, *J. Chem. Soc., Chem. Commun.*, **1971**, 1186.

 © 1985 The Chemical Society of Japan Bull. Chem. Soc. Jpn., 58, 2581—2585 (1985)

Kinetic Studies of Fast Equilibrium by Means of High-performance Liquid Chromatography. X. Separation of Rotamers of Acetanilides

Masataka MORIYASU,* Kazuko KAWANISHI, Atsushi KATO, Yohei HASHIMOTO, and Makiko SUGIURA

Kobe Women's College of Pharmacy, Motoyamakita-machi, Higashinada-ku, Kobe 658

(Received December 6, 1984)

The restricted rotation about the carbonyl-nitrogen bonds of acetanilides has been investigated by means of high-performance liquid chromatography. The separation of two rotamers (*E*- and *Z*-forms) of acetanilides has been achieved at low temperatures. The presence of a very small amount of the *E*-form has been confirmed for 3-, 4-, and non-substituted acetanilides. The ratios of the *E*- and *Z*-forms in different solvents have also been determined. By combining the HPLC and NMR results, it has been elucidated that the molecular structure of acetanilide in solution can be described in terms of an equilibrium between a large amount of the nearly planar *Z*-form and a small amount of the twisted *E*-form.

In a series of papers,[1-5] we have previously demonstrated that considerably fast equilibria in solutions can be examined by means of high-performance liquid chromatography (HPLC) based on conventional principles. We have entitled the HPLC method "dynamic HPLC"[3] in imitation of "dynamic NMR." We have already separated two rotamers of formanilide at low temperatures and shown that the ratios of rotamers are affected by the solvent composition as well as by the concentration. The present report deals with the separation of various acetanilide derivatives.

Several reports have appeared[6-8] on the NMR study of acetanilides in order to elucidate the conformation, and these results may be summarized as follows. Acetanilide exists as a nearly planar structure, and π-electrons of the benzene ring may be partially delocalized onto the $>N^{+}=C<^{O^{-}}$ moiety, consequently forming an extended partially-conjugated system. The steric hindrance between the benzene ring and the methyl group is so large that acetanilide exists exclusively as the *Z*-form; the presence of the *E*-form has not hitherto been confirmed by NMR. The replacement of *m*-(3-) or *p*-(4-) hydrogen in the benzene ring by a bulky substituent does not bring about any remarkable change in the molecular structure. Contrary to this, when an *o*-(2-) hydrogen is substituted, a drastic change in the molecular structure results. The steric hindrance between the *o*-substituted benzene ring and the carbonyl group is so large that the planar structure is no longer maintained even in the *E*-form rotamer, and eventually the benzene ring deviates from the amide plane and a twisted structure results.[8]

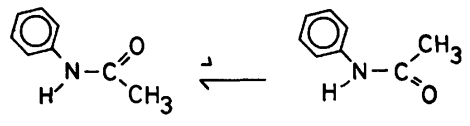

Z-form E-form

Experimental

Reagents. The following acetanilide derivatives were obtained from the market; acetanilide, 2-hydroxyacetanilide, 3-hydroxyacetanilide, 4-hydroxyacetanilide (acetaminophene), 4-ethoxyacetanilide (phenacetin), 2-nitroacetanilide, 3-nitroacetanilide, 4-nitroacetanilide, and *N*-methylacetanilide. The other acetanilides were synthesized by usual procedures from the corresponding aromatic amines and acetic anhydride;[9] 2-methylacetanilide, 3-methylacetanilide, 4-methylacetanilide, 2-ethylacetanilide, 2-isopropylacetanilide, 2,4-dimethylacetanilide, 2,6-dimethylacetanilide, and 2,4,6-trimethylacetanilide.

Apparatus. The HPLC apparatus used in this study is similar to the one described previously.[3] In order to determine the precise ratios of the two rotamers, some modification of the apparatus was made as follows: A column effluent was passed through a narrow stainless-steel tube (0.5 mm in diameter and 10—20 m in length) which was thermostated at 50—100 °C in an air bath (Model ASB-200, Japan Spectroscopic Co., Ltd.) prior to detection by means of a UV detector. This treatment promptly facilitated the attainment of an equilibrium between the two rotamers in the effluent. When the equilibrium is attained in the effluent, the ratio of the two peak areas should reflect the population ratio of the rotamers, irrespective of their absorption coefficients.

The proton NMR spectra of several acetanilides were measured on a Varian XL-200 spectrometer (200.06 MHz) in $CDCl_3$ from 25 to −10 °C.

Results

HPLC of o-Substituted Acetanilides. Various acetanilides were dissolved in chloroform (0.5%), and these sample solutions were submitted to HPLC at different column temperatures. Figure 1 exemplifies the chromatograms of 2-methylacetanilide. A sharp

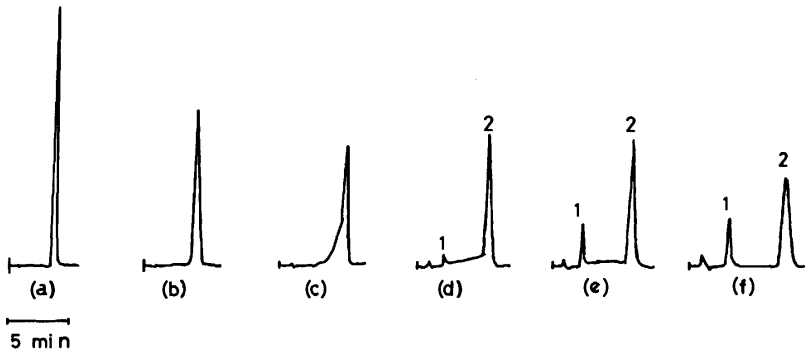

Fig. 1. HPLC chromatograms of 2-methylacetanilide at various temperatures.
Column: Polygosil 60–5 (4.6 mm × 15 cm). Eluent: hexane : 1-propanol : acetic acid = 100 : 10 : 3. Flow rate: 2.0 cm³/min. Detector: UV 254 nm. (a): 20 °C, (b): 0 °C, (c): −20 °C, (d): −30 °C, (e): −40 °C, (f): −50 °C. 1: *E*-form, 2: *Z*-form.

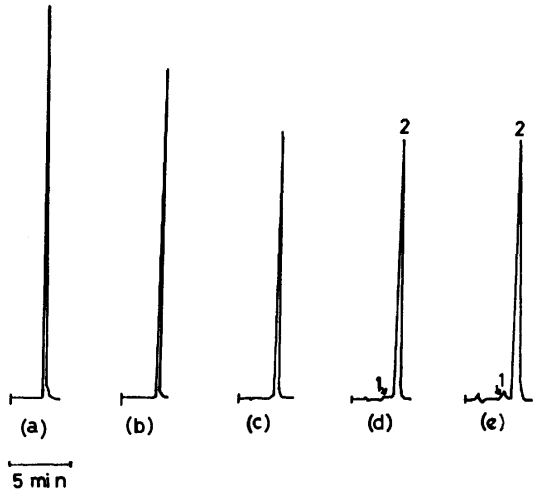

Fig. 2. HPLC chromatograms of 3-methylacetanilide at various temperatures.
For chromatographic conditions, see Fig. 1.
(a): 20 °C, (b): −10 °C, (c): −30 °C, (d): −40 °C, (e): −50 °C. 1: *E*-form, 2: *Z*-form.

peak at room temperature splits into two peaks at low temperatures. The complete baseline separation of the two peaks at −50 °C suggests that interconversion between two rotamers does not take place during chromatography at this temperature. The former and the latter peak in Fig. 1 are attributed to the *E*- and *Z*-forms respectively by comparing the present HPLC results with the NMR data[8] reported by Kessler and Rieker. Other *o*-substituted acetanilides, such as 2-ethylacetanilide and 2-isopropylacetanilide, gave similar chromatographic patterns.

HPLC of Acetanilide, 3-Methylacetanilide, and 4-Methylacetanilide. Figure 2 shows chromatograms of 3-methylacetanilide at various column temperatures. Two rotamers of 3-methylacetanilide were separated by HPLC below −50 °C. The small peak in Fig. 2(e) is not due to impurity but is attributed to the *E*-form for the following reason: When the fraction corresponding to the small peak in Fig. 2(e) was collected and rechromatographed after having been kept at room temperature for some time, equilibrated chromatograms were obtained again. Quite similar chromatograms were obtained when 4-methylacetanilide and acetanilide were chromatographed. Thus, the presence of a very small amount of the *E*-form isomer was confirmed for these acetanilides.

HPLC of Other Acetanilides. When two or more hydrogens of the benzene ring are replaced by bulky substituents, the chromatographic patterns might vary. 2,4-Dimethylacetanilide gave chromatograms quite similar to 2-methylacetanilide. Thus, the equilibrium between *E*- and *Z*-rotamers is determined by the *o*-methyl group, and the *p*-methyl group seems to have little effect on the ratio. 2,6-Dimethylacetanilide and 2,4,6-trimethylacetanilide gave chromatograms similar to 2-methylacetanilide, though the complete separation of two rotamers was achieved at rather higher column temperatures. These results suggest that internal rotation about the carbonyl–nitrogen bond is seriously restricted when both *o*-positions of the benzene ring are occupied by bulky substituents.

Among the various acetanilides tested, only the following did not give the separation of the two rotamers; 2-nitroacetanilide, 3-nitroacetanilide, 4-nitroacetanilide, and *N*-methylacetanilide. This does not necessary mean that the content of the *E*-form is too small to be detected by HPLC, and the following alternative explanations are also possible. (1) The retention times of the two rotamers may happen to be quite similar for these acetanilides under the present HPLC conditions. (2) If the rate of interconversion between the two rotamers is much faster than the rate of separation by HPLC, the two rotamers will not be

Table 1. Percentages of acetanilides existing as *E*-form

Acetanilides	*E*-form/%			
	This work* (HPLC)	Other works		
		(NMR)	Experimental conditions	Ref.
2-Methylacetanilide	18	6	−30 °C, 0.3 mol dm^{-3} in $CDCl_3$	8
2-Ethylacetanilide	24	15	−20 °C, 0.3 mol dm^{-3} in $CDCl_3$	7
2-Isopropylacetanilide	29	25	−20 °C, 0.3 mol dm^{-3} in $CDCl_3$	8
2,4-Dimethylacetanilide	25			
2,6-Dimethylacetanilide	31	26	37 °C, 0.3 mol dm^{-3} in $CDCl_3$	8
		20	room temperature, 2% in CCl_4	20
2,4,6-Trimethylacetanilide	34			
3-Methylacetanilide	2.6			
4-Methylacetanilide	4.0			
Acetanilide	1.9	<1.0	−20 °C, 0.3 mol dm^{-3} in $CDCl_3$	8
		0.1	room temperature, in pyridine	21
2-Hydroxyacetanilide	4.7			
3-Hydroxyacetanilide	1.6			
4-Hydroxyacetanilide	7.3			
4-Ethoxyacetanilide	6.1			

* 25 °C, 0.5% in $CHCl_3$.

Table 2. Percentages of *E*-forms of 2-methylacetanilide, 3-methylacetanilide, 4-methylacetanilide, and acetanilide in different solvents

Solvent	2-Methylacetanilide	3-Methylacetanilide	4-Methylacetanilide	Acetanilide
	E-form/%			
Hexane*	19	2.7	4.1	1.8
Carbon tetrachloride*	18	2.5	4.1	1.7
Benzene	18	2.5	3.8	1.9
Chloroform	18	2.6	4.0	1.9
Diethyl ether	17	2.1	3.7	1.6
1,4-Dioxane	18	2.2	3.7	1.1
Ethyl acetate	17	2.1	3.5	1.5
Acetonitrile	17	1.9	2.8	1.1
Ethanol	16	1.6	2.3	0.7
Methanol	15	1.5	2.1	0.6

0.5% solution, 25 °C. * 0.1% solution.

separated. This phenomenon may occur especially in nitro-substituted acetanilides because the strongly electron-withdrawing nitro group in the benzene ring should reduce the double-bond character of the carbonyl-nitrogen bond. Actually, a decrease in the rotational energy barrier was observed for nitro-substituted formanilides.[10]

The Ratios of the Two Rotamers. Various acetanilides were dissolved in chloroform (0.5%, 25 °C), and the ratios of the two rotamers were determined under the conditions where the complete separation is achieved. The results are summarized in Table 1. The content of the *E*-form was found to increase as the *o*-alkyl group becomes bulkier for *o*-alkyl-substituted acetanilides.

In order to examine the effect of the solvent on the ratios of the two rotamers, 2-methylacetanilide, 3-methylacetanilide, 4-methylacetanilide, and acetanilide were dissolved in a variety of solvents, and the ratios of the two rotamers were determined; the results are shown in Table 2. The population of the *E*-form was found to decrease in the following order; 2-methylacetanilide>4-methylacetanilide>3-methylacetanilide>acetanilide. Table 2 also shows that the population of the *E*-form is high when acetanilides are dissolved in nonpolar solvents, such as chloroform and hexane.

The effect of the concentration was examined on 2-methylacetanilide in chloroform. In contrast to formanilide,[3] the percentage of the *E*-form is insensitive to the concentration. The contents of the *E*-form were calculated to be 18.0, 18.1, and 18.4% at 0.27, 1.1, and 8.6% in molar ratio, respectively.

NMR Measurements. The Proton NMR data hitherto reported have shown that a small amount of the *E*-form exists in the equilibrium state for *o*-substituted acetanilides, while for other acetanilides the presence of the *E*-form has not been confirmed by NMR. When we measured the ^{1}H-NMR spectra of 2-methylacetanilide, 3-methylacetanilide, 4-methylacetanilide, 2-ethylacetanilide, 2-isopropylacetanilide, and acetanilide carefully on a high-field NMR instrument, the following facts were found. A couple of signals corresponding to the *E*- and *Z*-rotamers

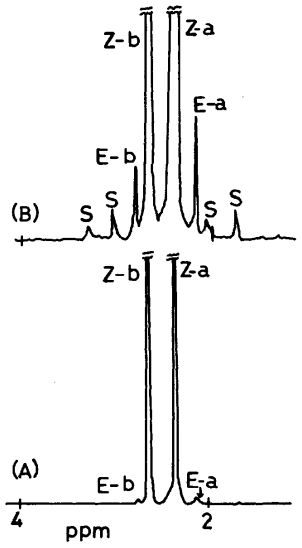

Fig. 3. The ^{1}H-NMR spectra of 3-methylacetanilide at 0 °C.
Sensitivity: (a) ×1, (b) ×5. E: *E*-form, Z: *Z*-form. a: Acetyl protons, b: methyl protons attached on benzene ring. S: spinning side bands.

Table 3. Comparison of NMR and HPLC data on the ratios of *E*-rotamers of acetanilides

	HPLC(25 °C) *E*-form/%	NMR *E*-form/%
2-Methylacetanilide	18	13[a]
3-Methylacetanilide	2.6	2.0[b]
4-Methylacetanilide	4.0	3.2[b]
Acetanilide	1.9	1.6[b]

2% solution. a) 10 °C, b) 0 °C.

appeared for *o*-substituted acetanilides at room temperature. For 4-methylacetanilide, two broad signals were observed at 10 °C; the larger one, at δ 2.15, should be assigned to the acetyl protons of the *Z*-form while the smaller one, at δ 2.05, should possibly corresponds to those of the *E*-form. The decrease in the temperature sharpened both signals (Fig. 3). On the other hand, when the temperature was increased, these signals were broadened; indeed, the smaller one was not recognized at 25 °C. At this temperature, these two signals probably coalesce. Thus, this phenomenon may be interpreted in terms of the interconversion between *E*- and *Z*-forms. 3-Methylacetanilide and acetanilide gave similar results. The percentage of the *E*-form of these acetanilides amounts to only 1—3%. These results are summarized in Table 3, together with the data obtained by HPLC. The two sets of results agree quite well. The NMR data hitherto reported by other authors,[7,8] however, give a smaller content of the *E*-form. We consider that the discrepancy between those results and ours may be interpreted in terms of the low sensitivity of the earlier, relatively low-field NMR instruments, for example, 60 MHz for ^{1}H. When NMR signals are broad and when, in addition, the signal-to-noise ratio is not good, the minor components are apt to be overlooked or sometimes estimated to be too small.

Discussion

The following facts seem noteworthy in considering the rotamer equilibrium of acetanilides in solution: (1) The presence of a considerable amount of the *E*-form in *o*-substituted acetanilides was confirmed by HPLC; this finding was in good agreement with the NMR data hitherto reported. (2) The presence of a very small amount of the *E*-form in several *o*-unsubstituted acetanilides was confirmed for the first time by HPLC. We examined the ^{1}H-NMR spectra of these anilides carefully and found small peaks which were attributable to the *E*-form. Since the content of *E*-form of acetanilide is very low, its detection has not been possible by several spectroscopic methods including NMR. Thus, the studies carried out hitherto by means of ^{1}H-NMR,[8] ^{13}C-NMR,[11] and photoelectron spectroscopy,[12] which has been considered to be a powerful tool for investigating labile equilibria in recent years, have failed to detect the *E*-form. (3) When a hydroxyl group was introduced into the benzene ring, the ratios of the *E*- and *Z*-rotamers were found to be different from those for the corresponding methyl-substituted acetanilides. The following sequence was found for increasing percentages of the *E*-form; 3-hydroxyacetanilide<2-hydroxyacetanilide<4-hydroxyacetanilide. The low percentage of the *E*-form of 2-hydroxyacetanilide may be explained in terms of some intramolecular hydrogen bonding in the *Z*-form.[13-15] (4) The ratios of the *E*- to the *Z*-form are somewhat dependent on the solvents. The percentage of the *E*-form is slightly higher in less polar solvents, although the effect is not so remarkable as that found for formanilide.[3] Furthermore, contrary to formanilide, the ratios of the two forms of 2-methylacetanilide in chloroform were almost unaffected by the concentration. Thus, the ring-dimer formation[16,17] attributable to intermolecular hydrogen bonding does not occur for acetanilides.

The acetyl protons of the *E*-rotamer appear at a higher field than those of the *Z*-rotamer (Table 4) in the ^{1}H-NMR spectra of not only *o*-substituted acetanilides, but also of other acetanilides. These high-field shifts may be due to the ring-current effect of the benzene ring, which suggests a twisted structure of the *E*-rotamer of these acetanilides. A previous ^{1}H-NMR study showed[8] that the *Z*-form of

Table 4. ^{1}H-NMR chemical shifts of the acetyl protons

	E-form δ	*Z*-form δ
2-Methylacetanilide[a)]	1.90	2.20
3-Methylacetanilide[b)]	2.01	2.17
4-Methylacetanilide[b)]	2.02	2.16
Acetanilide[b)]	2.06	2.17

2% solution. a) 10 °C, b) 0 °C.

o-substituted acetanilides has a twisted structure. Contrary to this, the *Z*-forms of the non-*o*-substituted acetanilides have an almost planar structure,[8,18] although the X-ray data of acetanilide indicated[19] that, in the crystalline state, the plane of the aromatic ring deviates slightly from that of the amide group. On the base of these results, the rotamer equilibrium of acetanilides may be described as follows:

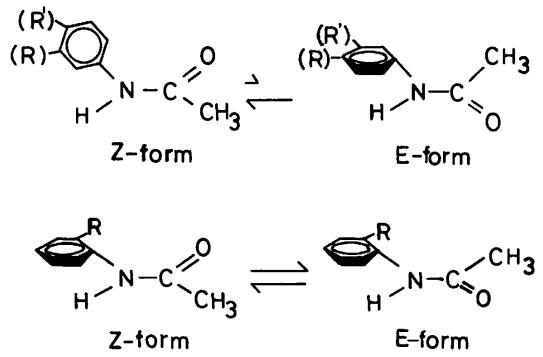

Both *E*- and *Z*-forms of *o*-substituted acetanilides have a twisted structure, because the *o*-substituted benzene ring causes a large steric hindrance if it is located coplanar with the amide plane. Contrary to this, the benzene ring of *o*-unsubstituted acetanilides will cause less steric hindrance. Thus, the *Z*-forms of these acetanilides may allowed to have an almost planar structure. The *E*-forms of these acetanilides, however, cannot have a planar structure, for a methyl group is bulkier than a carbonyl oxygen and the *E*-form will be more crowded than the *Z*-form. In the planar structure of the *Z*-form, since π-electrons in the benzene ring will get delocalized to some extent, a partially extended conjugated system will be formed. Thus, the *Z*-form will be more favoured energetically than the twisted *E*-form. The differences in free energies between the two rotamers ($\Delta G°=-RT\ln K$, K=[*Z*-form]/[*E*-form]) are calculated to be −3.8 and −7.9 kJmol^{-1} for 2-methylacetanilide and 4-methylacetanilide respectively, both in 0.5% solutions in chloroform at 25 °C. The difference between the two $\Delta G°$ values (=4.1 kJmol^{-1}) might be attributed to the difference in resonance energy between the *Z*-forms of the two acetanilides, provided that there is little difference in steric hindrance between the *E*-forms of these two acetanilides.

The authors wish to express their gratitude to Dr. Usha Shome, National Botanical Research Institute, Lucknow, India, who kindly corrects the English description of this paper.

References

1) M. Moriyasu and Y. Hashimoto, *Bull. Chem. Soc. Jpn.*, **53**, 3590 (1980).
2) M. Moriyasu, Y. Hashimoto, and M. Endo, *Bull. Chem. Soc. Jpn.*, **56**, 1972 (1983).
3) M. Moriyasu, K. Kawanishi, A. Kato, and Y. Hashimoto, *Bull. Chem. Soc. Jpn.*, **57**, 1766 (1984).
4) M. Moriyasu, A. Kato, M. Okada, and Y. Hashimoto, *Anal. Lett.*, **17**, 689 (1984).
5) M. Moriyasu, A. Kato, and Y. Hashimoto, *Chem. Lett.*, **1984**, 1181.
6) For the NMR study of the restricted bond rotation of various amides, see the following review and the references cited therein: W. E. Stewart and T. H. Siddall, III, *Chem. Rev.*, **70**, 517 (1970).
7) H. Kessler and A. Rieker, *Z. Naturforsch.*, **22**, 456 (1967).
8) H. Kessler and A. Rieker, *Liebigs Ann. Chem.*, **708**, 57 (1967).
9) L. F. Fieser and K. L. Williamson, "Organic Experiments," 4th ed, ed by D. C. Heath and Company, Toronto (1979), p. 159.
10) C. H. Yoder, J. A. Sandberg, and W. S. Moore, *J. Am. Chem. Soc.*, **96**, 2260 (1974).
11) C. Nagata, K. Ishida, and S. Tanaka, *Nippon Kagaku Kaishi*, **1974**, 395.
12) R. Nakagaki, T. Kobayashi, and S. Nagakura, *Bull. Chem. Soc. Jpn.*, **53**, 901 (1980).
13) M. Zanger, W. W. Simons, and A. R. Gennaro, *J. Org. Chem.*, **33**, 3673 (1968).
14) I. D. Rae, *Can. J. Chem.*, **46**, 2589 (1968).
15) R. J. Bartes-Keith and R. F. W. Cieciuch, *Can. J. Chem.*, **46**, 2593 (1968).
16) A. J. R. Bourn, D. G. Gillies, and E. W. Randall, *Tetrahedron*, **20**, 1811 (1964).
17) L. G. Belinskaya, A. V. Lukashov, and E. S. Efremov, *Izv. Timiryazevsk. S-kh. Akad.*, **1974**, 162; *Chem. Abstr.*, **81**, 119752j (1974).
18) R. A. Russel and H. W. Thompson, *Spectrochim. Acta*, **8**, 138 (1956).
19) C. J. Brown and D. E. C. Corbridge, *Acta Crystallogr.*, **7**, 711 (1954).
20) R. F. C. Brown, L. Radom, S. Starnhell, and I. D. Rae, *Can. J. Chem.*, **46**, 2577 (1968).
21) B. F. Pedersen and B. Pedersen, *Tetrahedron Lett.*, **1965**, 2995.

Volatility of Low-Henry's Constant Contaminants in Water

Shoichi Okouchi* and Sokichi Sasaki
Chemical Laboratory, College of Engineering, Hosei University, Koganei, Tokyo 184
(Received January 10, 1985)

The volatilization rate of low-Henry's constant contaminants (less than about 2 m^3 Pa/mol) from water to the atmosphere was studied, together with the water volatilization rate, using tracer compounds under various mixing conditions. 1-Butanol, 1-pentanol, 1-hexanol, and 1-heptanol were used as the tracer compounds. The volatilization rates of these compounds and water were controlled by a mass-transfer process in the gas phase. The measured parameter was the ratio of the volatilization rate constant of a tracer(i) to that of water, $K_v^{(i)}/K_v^{(H_2O)}$. The obtained ratios agreed with those estimated theoretically. The volatilization rate constant of low-Henry's constant contaminant(i) in environmental water, $K_{v(env)}^{(i)}$, can be estimated by multiplying the ratio, $K_v^{(i)}/K_v^{(H_2O)}$, by the environmental value of $K_{v(env)}^{(H_2O)}$.

The volatilization of contaminants (such as pesticides) from water bodies to the atmosphere can be an important environmental pathway for certain contaminants. The rate equation for the volatilization of a contaminant, i, in water to the atmosphere is given by Eq. 1:

$$-dC_L^{(1)}/dt = K_v^{(1)}(C_L^{(1)} - p^{(1)}/H^{(1)}), \quad (1)$$

where C_L is the concentration of the contaminant in water; t is the time; K_v is the volatilization rate constant; p is the partial pressure of the contaminant in the atmosphere; and H is Henry's constant. The ratio of the volatilization rate constant of a contaminant(i) to the oxygen-reaeration rate constant, $K_v^{(i)}/K_v^{(O_2)}$, has been experimentally determined[1-10] as a parameter for the volatility of contaminants in water. Mackay and Leinonen[11] suggested that the volatilization rate of the volatilized compound is controlled by a mass transfer in the aqueous phase when Henry's constant is greater than about 400 m^3 Pa/mol. However, it is controlled by a mass transfer in the gas phase when Henry's constant is less than about 2 m^3 Pa/mol. In the former case ($H \geq 400$ m^3 Pa/mol), the ratio $K_v^{(i)}/K_v^{(O_2)}$ remains constant, independent of the mixing conditions and the temperature. If the ratio is available, the volatilization rate constant of the contaminant in environmental water, $K_{v(env)}^{(i)}$, can be estimated by multiplying the ratio by the environmental value of $K_{v(env)}^{(O_2)}$. However, the parameter for the volatility in the latter case ($H \leq 2$ m^3 Pa/mol) has been little investigated. Pesticides such as DDT, dieldrin, lindane, parathion, and chlordane correspond to a low-Henry's constant contaminant as an environmental interest, and their pesticide volatilizations from water to the atmosphere have been reported.[9,12-15]

In this work, the volatilization rate of the contaminant which is controlled by a mass transfer in the gas phase was simultaneously measured along with the water volatilization rate, instead of the oxygen reaeration rate. The ratio $K_v^{(i)}/K_v^{(H_2O)}$ was investigated as the parameter for the volatility of low-Henry's constant contaminants in water. As the tracer compounds for the low-Henry's constant contaminants, 1-butanol (H=0.84 m^3 Pa/mol at 298 K), 1-pentanol (H=1.0), 1-hexanol (H=1.3), and 1-heptanol (H=1.6)[16] were used since the concentrations of these compounds and water could be continuously monitored.

Experimental

A schematic diagram of the experimental apparatus is shown in Fig. 1. A dilute aqueous solution of 1-butanol (the tracer for volatilization) which was dissolved into distilled water was prepared in a volatilization vessel (V in Fig. 1), and was then stirred at a constant agitation speed by means of a magnetic stirrer. The vessel was maintained at a constant temperature using the outside-jacket of the vessel. Nitrogen was made to flow through the space above the aqueous solution at a constant rate. The dissolved 1-butanol was volatilized together with the water into the flowing nitrogen as a vapor. The 1-butanol and water concentrations vaporized in the nitrogen were continuously measured by means of a photo-ionization detector (PID in Fig. 1, model PI-101, HNU System, INC., U. S. A.) and a humidity meter (HD in Fig. 1), respectively. The volatilization-rate constant of 1-butanol, $K_v^{(BuOH)}$, was

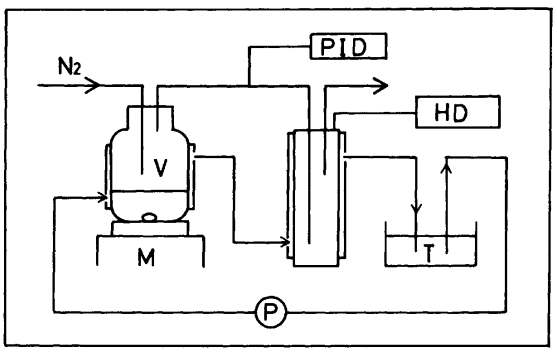

Fig. 1. Schematic diagram of experimental apparatus. V: Volatilization vessel, M: magnetic stirrer, P: pump, T: thermostat, PID: photo-ionization detector, HD: humidity meter.

determined by fitting the concentration data to an integral form of Eq. 1 as $p^{(i)}=0$. That of water, $K_v^{(H_2O)}$, was determined from Eq. 2 using the volatilization rate of water vapor, $F^{(H_2O)}$.

$$K_v^{(H_2O)} = F^{(H_2O)}/(C_{SG}-C_G)V_L, \quad (2)$$

where C_{SG} is the saturated water concentration at the water surface; C_G is the water-vapor concentration in the gas phase; and V_L is the volume of the aqueous solution (0.10 dm^3 in this work).

The same techniques were also used to determine the volatilization-rate constant for 1-pentanol, 1-hexanol, and 1-heptanol with that of water at 298 K.

Results and Discussion

The volatilization-rate constant of 1-butanol, $K_v^{(BuOH)}$, was not affected by the concentration over a range from 0.01 to 0.1 mol dm^{-3}, as was to be expected from Eq. 1. The effects of turbulence in the aqueous phase, which depends on the agitation speed, on $K_v^{(BuOH)}$ and $K_v^{(H_2O)}$ were negligibly small (Fig. 2). On the other hand, both volatilizationrate constants increased with an increase of turbulence in the gas phase, which depends on the nitrogen flow rate, as shown in Fig. 3. In Fig. 4, the values of $K_v^{(BuOH)}$ and $K_v^{(H_2O)}$ are linearly related with a slope of 1.1×10^{-4} ($=K_v^{(BuOH)}/K_v^{(H_2O)}$) at 298 K. Fig. 5 shows the temperature effect on the ratio, $K_v^{(BuOH)}/K_v^{(H_2O)}$, in a temperature range from 288 to 303 K.

From the above data it can be seen that the volatilization rates of both 1-butanol and water were much more affected by turbulence in the gas phase than by that in the aqueous phase. Also, the ratio is highly dependent on temperature. Consequently, the results indicate that the volatilization rates of 1-butanol and water are controlled by a mass-transfer

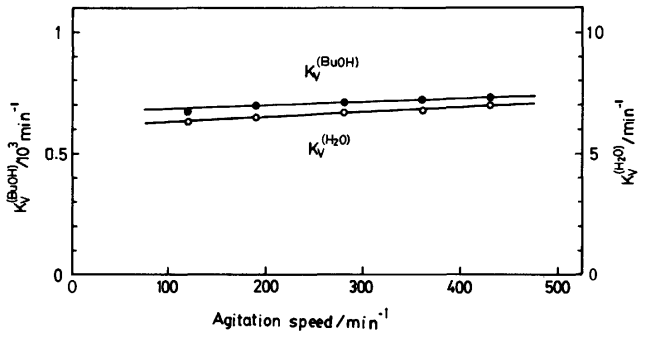

Fig. 2. Effects of turbulence in the aqueous phase (the agitation speed) on $K_v^{(BuOH)}$ and $K_v^{(H_2O)}$ at 298 K. Nitrogen flow rate: 2.0 dm^3 min^{-1}, 1-butanol concentration: 0.05 mol dm^{-3}.

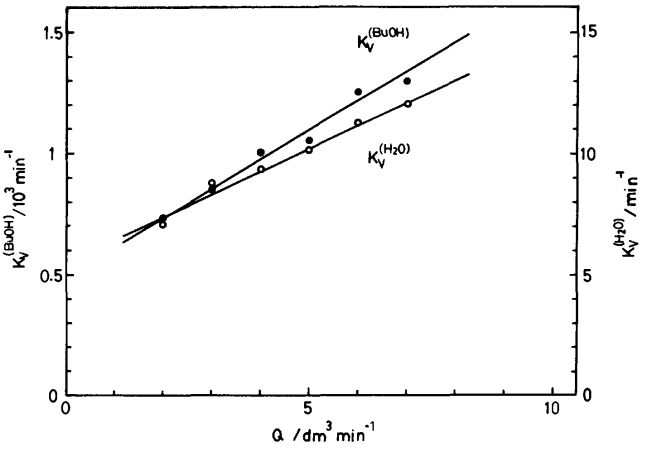

Fig. 3. Effects of turbulence in the gas phase (the nitrogen flow rate) on $K_v^{(BuOH)}$ and $K_v^{(H_2O)}$ at 298 K. Agitation speed: 430 min^{-1}, 1-butanol concentration: 0.05 mol dm^{-1}.

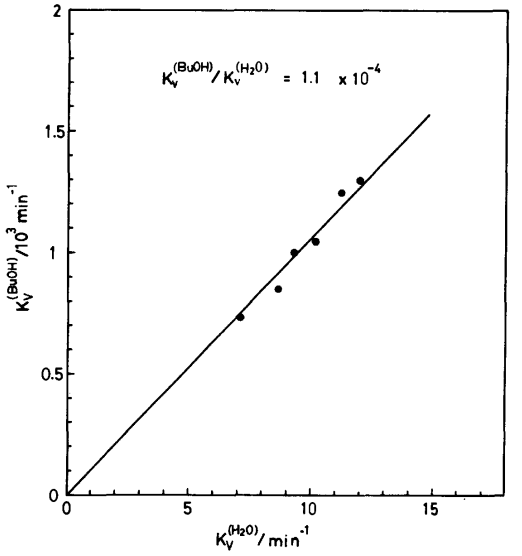

Fig. 4. Relationship between $K_v^{(BuOH)}$ and $K_v^{(H_2O)}$ at 298 K.

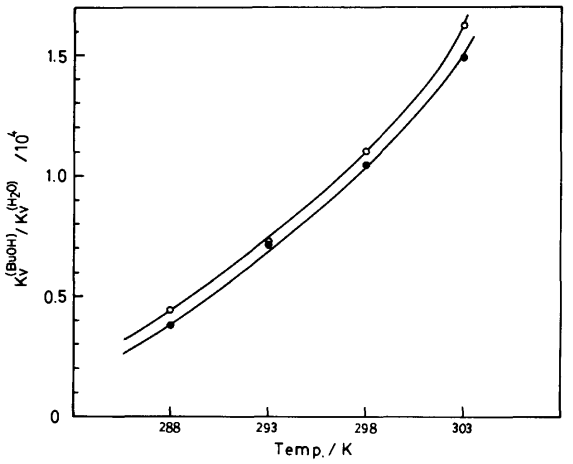

Fig. 5. Effect of temperature on $K_v^{(BuOH)}/K_v^{(H_2O)}$. 1-Butanol concentration: 0.05 mol dm^{-3}, ●: measured, ○: estimated.

in the gas phase, supporting the suggestion of Mackay and Leinonen.[11] Therefore, it is concluded that most of the resistance to these mass-transfer rates lies in the gas-phase boundary layer; thus, the ratio can be theoretically estimated from Eq. 3 since the resistance in the aqueous phase can be neglected.

$$K_v^{(1)}/K_v^{(H_2O)} = (H^{(1)}/RT)k_G^{(1)}a/k_G^{(H_2O)}a = (H^{(1)}/RT)(D_G^{(1)}/D_G^{(H_2O)})^n \quad (3)$$

where k_G is the mass-transfer coefficient in the gas phase; a is the interfacial contact area per liquid volume which corresponds to the reciprocal of the depth of water;[3] D_G is the diffusivity in the gas phase; R is the gas constant; and T is the absolute temperature. The value of n is suggested to be 1 and 2/3 according to the classical theory of the two-film mass-transfer model[17] and the analogy of Chilton and Colburn[18,19] ((Sherwood numbers)$\propto$(Schmidt numbers)$^{1/3}$), respectively. Experimentally, the values of n so far reported are in the range from 0.5 to 1.[20] Using Eq. 3, the ratio $K_v^{(BuOH)}/K_v^{(H_2O)}$ is estimated to be 1.2×10^{-4} for n=1 or 2.0×10^{-4} for n=0.5 at 298 K. In Fig. 5, the estimated ratios were obtained for n=1 in the temperature range 288 to 303 K. The diffusivities in the gas phase in Eq. 3 were calculated from the equation of Fuller *et al.*,[21] suggesting that the diffusivity is proportional to $T^{1.75}$. The good agreement of the measured values with the estimated values indicated that the estimated values for n=1 were better than those for n=0.5.

Table 1. The values of $K_v^{(1)}/K_v^{(H_2O)}$ measured and estimated, and of $D_G^{(1)}$ at 298 K

Tracer (i)	$D_G^{(1)}$/cm^2 s^{-1}	$K_v^{(1)}/K_v^{(H_2O)}\times10^4$	
		Measured	Estimated (n=1—0.5)
1-Butanol	0.0899	1.1±0.2	1.2—2.0
1-Pentanol	0.0807	1.6±0.2	1.3—2.3
1-Hexanol	0.0739	2.0±0.2	1.6—2.9
1-Heptanol	0.0684	1.9±0.2	1.8—3.4

Table 1 shows the measured and estimated ratios, $K_v^{(j)}/K_v^{(H_2O)}$, for 1-pentanol, 1-hexanol, and 1-heptanol with 1-butanol at 298 K. These results indicate the effective estimation of Eq. 3 in the n value range from 0.5 to 1. Therefore, Eq. 3 would give an "order of magnitude" estimation for the volatility of low-Henry's constant contaminants such as the pesticides. Table 2 shows the volatilization-rate constants, $K_{v(ocean)}^{(i)}$, and half-lives, $\tau^{(i)}$, of low- and high-Henry's constant contaminants in the ocean. The mass-transfer rates between the ocean and the atomosphere were reviewed in terms of the gas- and liquid-phase mass-transfer coefficients by Liss and Slater.[22] They suggested that the values of the gas- and liquid-phase mass-transfer coefficients were typically 30 m/h ($=k_{G(ocean)}^{(H_2O)}$) for water and 0.2 m/h ($=k_{L(ocean)}^{(O_2)}$) for oxygen, respectively. Hence, the relations of $K_{v(ocean)}^{(H_2O)}=k_{G(ocean)}^{(H_2O)}/L$ and $K_{v(ocean)}^{(O_2)}=k_{L(ocean)}^{(O_2)}/L$ in the ocean are held for the volatilization and reaeration rate constants, respectively, where L is the water depth. In Table 2, the volatilization-rate constant of the contaminant (i) in the ocean, $K_{v(ocean)}^{(i)}$, is estimated from Eq. 4 as the water depth L=1 m.

$$K_{v(ocean)}^{(1)} = K_{v(ocean)}^{(J)} \times (K_v^{(1)}/K_v^{(J)}) \quad (4)$$

where j refers to water (H_2O) or oxygen (O_2). While, the half-life of the contaminant in the ocean, $\tau^{(i)}$, is given by Eq. 5.

$$\tau^{(1)} = 0.693/K_{v(ocean)}^{(1)} \quad (5)$$

The values of $K_v^{(i)}/K_v^{(H_2O)}$ for DDT, dieldrin, α-HCH (α-hexachloro-cyclohexane), and DBP (dibutyl phthalate) in Table 2 were calculated from Eq. 3 using $H^{(i)}$ from the EPA compilation,[10] whereas the values of $K_v^{(i)}/K_v^{(O_2)}$ were experimentally obtained by Smith *et al.*[3] and Okouchi *et al.*[2] The volatilization rate of low-Henry's constant contaminants was very slow, compared with that of high-Henry's constant contaminants. However, the worldwide atmospheric distribution of pesticides such as DDT clearly indicates that the volatilization of pesticides from

Table 2. The volatilization rate constant, $K_{v(ocean)}^{(1)}$, and half-lives, $\tau^{(1)}$, of low- and high-Henry's constant contaminants in the ocean at 293—295 K as L=1 m

	Contaminant (i)	$H^{(1)}$/m^3 Pa mol^{-1}	$K_v^{(1)}/K_v^{(H_2O)}$	$K_v^{(1)}/K_v^{(O_2)}$	$K_{v(ocean)}^{(1)}$/h^{-1}	$\tau^{(1)}$/h
low-Henry's constant $H^{(1)}<2$	DDT	0.36 —1.6	2.5×10^{-5}—1.1×10^{-4}		7.4×10^{-4}—3.3×10^{-3}	936—211
	Dieldrin	0.049—0.76	3.6×10^{-6}—5.6×10^{-5}		1.1×10^{-4}—1.7×10^{-3}	6383—412
	α-HCH[a]	0.46 —0.78	4.2×10^{-5}—7.0×10^{-5}		1.2×10^{-3}—2.1×10^{-3}	556—328
	DBP[b]	0.16	1.2×10^{-5}		3.7×10^{-4}	1852
	(1-Butanol)	0.49	7.2×10^{-5}		2.2×10^{-3}	321
high-Henry's constant $H^{(1)}>400$	benzene	445		0.56	0.11	6.2
	tetrachloromethane	2300		0.63	0.13	5.5
	mercury	992		0.94	0.19	3.7

a) α-Hexachlorocyclohexane, b) Dibutyl phthalate.

aquatic systems or soils (or both) is an important process because of their toxicities and persistences. The ratio, $K_v^{(i)}/K_v^{(H_2O)}$, suggested in this work would be used to estimate the volatilization rate of low-Henry's constant contaminants ($H \leq 2$ m^3 Pa/mol) from environmental water bodies and wastewater treatment facilities to the atmosphere.

References

1) P. V. Roberts and P. G. Dandliker, *Environ. Sci. Technol.*, **17**, 484 (1983).

2) S. Okouchi, S. Sasaki, and Y. Harano, *Bull. Chem. Soc. Jpn.*, **57**, 338 (1984).

3) J. H. Smith, D. C. Bomberger Jr., and D. L. Haynes, *Environ. Sci. Technol.*, **14**, 1332 (1980).

4) C. Matter-Müller, W. Gujer, and W. Giger, *Water Res.*, **15**, 1271 (1981).

5) S. Kyosai, *Jpn. J. Water Pollut. Res.*, **4**, 205 (1981).

6) E. S. Tsivoglou, R. L. O'connel, C. M. Walter, P. J. Godsil, and G. S. Logsdon, *J. Water Pollut. Control Fed.*, **37**, 1343 (1965).

7) R. E. Rathbun and D. Y. Tai, *Water Res.*, **15**, 243 (1981).

8) D. F. Paris, W. C. Steen, and G. L. Baughman, *Chemosphere*, **4**, 319 (1978).

9) E. Atlas, R. Foster, and C. S. Giam, *Environ. Sci. Technol.*, **16**, 283 (1982).

10) J. H. Smith, W. R. Maybey, N. Bohonos, B. R. Holt, S. S. Lee, T. W. Chou, D. C. Bomberger, and T. Mill, *EPA-600/7-77-113* (1977).

11) D. Mackay and P. J. Leinonen, *Environ. Sci. Technol.*, **9**, 1178 (1975).

12) F. Acree, Jr., M. Beroza, and M. C. Bowman, *J. Agric. Food Chem.*, **11**, 278 (1963).

13) R. M. Slater and D. J. Spedding, *Arch. Environ. Contam. Toxicol.*, **10**, 25 (1981).

14) M. Callahan, M. Slimak, N. Gabel, I. May, C. Fowler, R. Freed, P. Jennings, R. Durfee, F. Whitmore, B. Maestri, W. Mabey, B. Holt, and C. Gould, *EPA-440/4-79-029* a and b (1979).

15) C. T. Chiou, V. H. Freed, L. J. Peters, and R. L. Kohnert, *Environ. International*, **3**, 231 (1980).

16) D. Mackay and T. K. Yuen, *Water Pollut. Res. J. Canada*, **15**, 83 (1980).

17) W. K. Lewis and W. G. Whitman, *Ind. Eng. Chem.*, **16**, 1215 (1924).

18) T. H. Chilton and A. P. Colburn, *Ind. Eng. Chem.*, **26**, 1183 (1934).

19) K. Onda, H. Takeuchi, and Y. Okumoto, *J. Chem. Eng. Jpn.*, **1**, 56 (1968).

20) K. Onda, "Gas Kyushu," Kagakukogyosha Inc., Tokyo (1972) p.97.

21) E. N. Fuller, K. Ensley, and J. C. Giddings, *Ind. Eng. Chem.*, **58**, 19 (1966).

22) P. S. Liss and P. G. Slater, *Nature*, **247**, 181 (1974).

A Temperature Dependence Study of ^{35}Cl NQR Frequencies in Dimethylammonium Hexachlorostannate(IV), Hexachlorotellurate(IV), and Hexachloroplatinate(IV)

Keizo HORIUCHI, Hiroyuki ISHIDA, and Daiyu NAKAMURA*
Department of Chemistry, Faculty of Science, Nagoya University, Chikusa-ku, Nagoya 464
(Received February 14, 1985)

The temperature dependence of ^{35}Cl NQR frequencies was observed for $[(CH_3)_2NH_2]_2SnCl_6$, $[(CH_3)_2NH_2]_2TeCl_6$, and $[(CH_3)_2NH_2]_2PtCl_6$. Two ^{35}Cl NQR frequencies were recorded for the tin complex between 77 and *ca.* 260 K, the intensity ratio of which was 2:1 for the high- to the low-frequency line. An unusual temperature variation of both frequencies attributable to the motion of the cation was observed, and the existence of a phase transition was suggested. For the tellurium complex, the NQR frequencies were observed below *ca.* 240 K. At higher temperatures, two signals having the same intensity ratio as that of the tin complex were detected as expected from the isomorphous relation between both complexes proved at room temperature. A phase transition was newly located for this complex at 98 K in addition to another one at 171 K previously reported. The intermediate phase yielded three broad signals having equal intensity, whereas four broad lines could be detected in the low-temperature phase where more than four lines may be expected by referring to the temperature-dependence curves of the NQR lines.

Recently, we studied the differential thermal analysis (DTA) of dimethylammonium (hereafter abbreviated as diMA) hexachlorotellurate(IV) and found a phase transition at 169 K.[1] Knop *et al.*[2] reported the occurrence of a phase transition in $(diMA)_2SnCl_6$ at 100 K from the study of IR absorptions. Dillon *et al.*[3] revealed a phase transition at 253 K in $(diMA)_2SnBr_6$ isomorphous with $(diMA)_2SnCl_6$ from the temperature dependence study of ^{79}Br NQR frequencies. For these hexachloro complexes, we also studied the ^1H NMR spin-lattice relaxation time, T_1, and the second moment of ^1H NMR absorptions at various temperatures in a fairly wide range of temperature.[1] This reveals the occurrence of the usual C_3 reorientation of the methyl groups of the cation and the 180° flip motion of the whole cation about its twofold pseudo-symmetry axis. However, no anomaly indicating the existence of phase transition was observed from these NMR measurements of both complexes.

Since NQR frequencies are very sensitive to a change in the structure of ionic crystals involving resonant nuclei, the NQR spectroscopy is a powerful means for the detection of phase transition and also for the precise location of the transition temperature, T_{tr}. The present investigation of the temperature dependence of ^{35}Cl NQR frequencies in $(diMA)_2SnCl_6$, $(diMA)_2TeCl_6$, and $(diMA)_2PtCl_6$ has been undertaken in order to confirm the existence of phase transitions for the former two complexes and to clarify the participation of the cationic motions in the temperature dependence of the ^{35}Cl NQR frequencies of these complexes.

Experimental

A modified Dean-type superregenerative spectrometer[4] was employed for the observation of chlorine NQR frequencies. The rf coil of the spectrometer including the sample sealed in a glass ampoule was placed in a Dewar vessel filled with petroleum ether. The sample temperature wanted was obtained by adding Dry-Ice or liquid nitrogen to petroleum ether. A chromel-alumel thermocouple was used for the determination of temperature. The sample temperature determined was estimated to be accurate within ±1 K. A homemade apparatus was employed for the experiments of DTA.[5] Copper-constantan thermocouples were used for the detection of heat anomalies and also for the determination of the sample temperature which was measured to be accurate within ±1 K.

The samples, $(diMA)_2SnCl_6$ and $(diMA)_2TeCl_6$, prepared for the previous NMR experiments were used for the present investigation. The platinum complex was synthesized in a method similar to that used in the preparation of $(diMA)_2SnCl_6$[1] from hexachloroplatinic acid and dimethylammonium chloride. Found: Cl, 42.55; N, 5.61; C, 9.63; H, 3.25%. Calcd for $[(CH_3)_2NH_2]_2PtCl_6$: Cl, 42.55; N, 5.60; C, 9.61; H, 3.23%.

Results

$[(CH_3)_2NH_2]_2SnCl_6$. The temperature variation of ^{35}Cl NQR frequencies observed for this complex is shown in Fig. 1. The resonance frequencies determined at various temperatures are given in Table 1 along with those of the other complexes.

At 196 K (Dry-Ice temperature), two ^{35}Cl NQR frequencies which were confirmed by observing the corresponding ^{37}Cl NQR signals were recorded. The high-frequency ($S/N \approx 100$) line was about twice as strong as that of the low-frequency one. With increasing temperature, the resonance frequency of the two lines decreased smoothly and the intensity of both lines became weak above *ca.* 250 K until they disappeared in the noise level at *ca.* 270 K, although the weak low-frequency line faded out at a slightly lower temperature. The DTA experiments carried

TABLE 1. ^{35}Cl NQR FREQUENCIES OBSERVED AT VARIOUS TEMPERATURES IN $[(CH_3)_2NH_2]_2SnCl_6$, $[(CH_3)_2NH_2]_2TeCl_6$, AND $[(CH_3)_2NH_2]_2PtCl_6$*

T/K	ν/MHz		
	$[SnCl_6]^{2-}$	$[TeCl_6]^{2-}$	$[PtCl_6]^{2-}$
77	16.762±0.005	16.44 ±0.02	26.86 ±0.01
	16.060±0.005	16.22 ±0.02	26.629±0.005
		16.13 ±0.02	
		15.90 ±0.02	
102	16.669±0.005	16.22 ±0.02 (100K)	26.829±0.008 (100K)
	16.110±0.005	16.04 ±0.02 (100K)	26.607±0.005 (100K)
		15.92 ±0.02 (100K)	
150	16.600±0.003	16.11 ±0.02	26.754±0.005
	16.120±0.003	16.01 ±0.02	26.537±0.005
		15.89 ±0.02	
170	16.576±0.003	16.02 ±0.01 (171K)	26.725±0.005
	16.109±0.003	15.88 ±0.01 (171K)	26.507±0.005
196	16.547±0.003	15.996±0.005	26.685±0.005
	16.089±0.003	15.865±0.005	26.467±0.005
220	16.524±0.003	15.969±0.005 (229K)	26.650±0.005
	16.065±0.003	15.834±0.008 (229K)	26.423±0.005
258	16.486±0.005		26.566±0.005 (273K)
	16.027±0.008		26.33 ±0.01 (273K)

* Two lines observed for this complex may be assigned to different crystalline modifications.

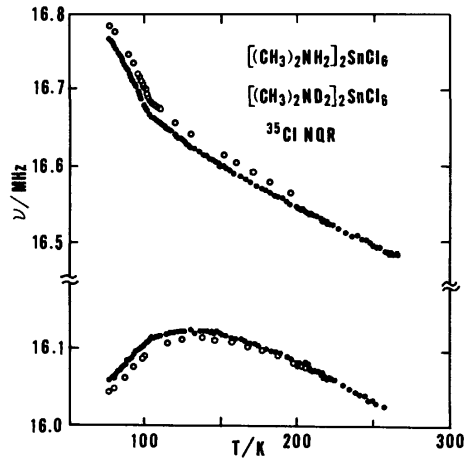

Fig. 1. Temperature dependences of ^{35}Cl NQR frequencies in dimethylammonium hexachlorostannate(IV). Dots and Circls indicate the resonance frequencies of $[(CH_3)_2NH_2]_2SnCl_6$ and $[(CH_3)_2ND_2]_2SnCl_6$, respectively.

out previously showed no heat anomaly up to 420 K.[1]

From the X-ray analysis of this complex,[2,6] it is known that the all complex anions in the crystal are crystallographically equivalent and there exist two nonequivalent chlorine atoms in the anion, *i.e.* two axially elongated chlorine atoms and four equatorial ones. Accordingly, the high- and low-frequency lines, respectively, can be unequivocally assigned to the equatorial and axial chlorine atoms of the hexachlorostannate(IV) anion by referring to the intensity ratio of the observed signals. It is quite reasonable that the axial chlorine atoms having a Sn–Cl bond longer than that of the equatorial ones yield a lower NQR frequency at a given temperature, because chlorine atoms having a longer metal-ligand bond is expected to be more ionic and to give a lower-frequency NQR line.

When the temperature decreased from 196 K, both lines of $(diMA)_2SnCl_6$ decreased their intensity gradually although the intensity ratio remained unchanged. The high-frequency line increased its frequency almost linearly with decreasing temperature down to 102 K, where the temperature coefficient, $d\nu/dT$, was changed discontinuously. Below this temperature, the absolute value of $d\nu/dT$ became larger as can be seen in Fig. 1. On the other hand, the low-frequency line exhibits quite unusual temperature variation. When the temperature increased from 77 K, the resonance frequency of the line increased almost linearly and fairly steeply up to *ca.* 100 K, indicating that the line has an unusual positive temperature coefficient. Above *ca.* 100 K, the temperature gradient of the line became discontinuously gentle and the ν *vs.* T curve yielded a broad maximum around 140 K. With increasing the temperature furthermore, the frequency of the line decreased monotonously.

Knop *et al.*[2] studied the temperature variation of the IR spectra of $(diMA)_2SnCl_6$ and concluded the

occurrence of a phase transition near 100 K by observing the splitting of the N–H stretching band of the NHD^+ group into a doublet below 100 K. They attributed the splitting of the IR band to the appearance of nonequivalent NH hydrogen atoms in the $(diMA)_2SnCl_6$ crystal. The present NQR investigation revealed a discontinuous change at 102 K in the gradient of both ν *vs.* T curves observed. This strongly suggests the existence of a higher-order phase transition in this crystal although no heat anomaly could be detected near 100 K on the DTA measurements repeatedly and carefully carried out.

To obtain further information about the phase transition suggested above, we prepared a partially deuterated analog, $[(CH_3)_2ND_2]_2SnCl_6$, and observed the temperature dependence of ^{35}Cl NQR frequencies. The results are also shown in Fig. 1. The temperature dependence curves obtained are very similar to those of the undeuterated analog. The curve of the high-frequency line shifts by *ca.* 20 kHz to the high-frequency side by *N*-deuteration whereas the curve of the low-frequency line moves to the low-frequency side by *N*-deuteration although the separation of the two curves increases gradually with decreasing temperature.

$[(CH_3)_2NH_2]_2TeCl_6$. The temperature dependence of ^{35}Cl NQR frequencies observed for this complex is exhibited in Fig. 2.

At 196 K, two fairly sharp ^{35}Cl NQR frequencies were observed having the intensity ratio approximately equal to 2:1 for the high- to the low-frequency line ($S/N\approx8$). With increasing temperature, the resonance frequency of both lines lowered almost linearly and the high- and low-frequency lines disappeared in the noise level at *ca.* 240 and 230 K, respectively. The disagreement of the fade-out temperatures is thought as arising from the unequal intensity of both lines. With increasing temperature, each line gradually weakened from the temperature which was lower than each fade-out temperature by *ca.* 10 K. These results are very similar to those of $(diMA)_2SnCl_6$. This is a reasonable consequence because $(diMA)_2TeCl_6$ is isomorphous with $(diMA)_2SnCl_6$ as confirmed already by X-ray powder patterns taken at room temperature.[1] No heat anomaly, of course, was detected above 196 K for $(diMA)_2TeCl_6$ in the DTA experiments performed previously.

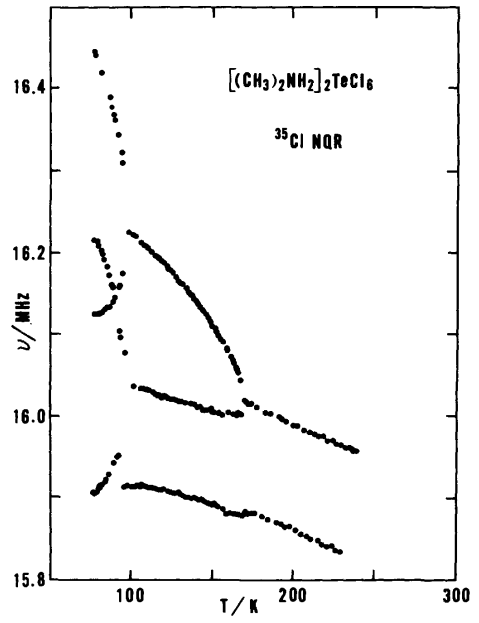

Fig. 2. Temperature dependences of ^{35}Cl NQR frequencies in $[(CH_3)_2NH_2]_2TeCl_6$.

When the temperature decreased from 196 K, the high-frequency line gradually broadened and suddenly disappeared at 171 K and two broad new lines having equal intensity ($S/N\approx3$) appeared at a slightly lower temperature. This indicates the existence of a phase transition as revealed previously.[1] The two new frequencies were observed above and below the resonance frequency of the high-frequency line of the high-temperature phase observed immediately above 171 K. The frequency of the broad high-frequency line newly recorded increased fairly sharply with decreasing temperature down to 98 K, where the signal disappeared. The broad low-frequency line increased its frequency almost linearly with decreasing temperature showing a mild gradient and also disappeared at 98 K. The low-frequency line of the high-temperature phase lowered its frequency slightly and discontinuously at 171 K and increased its frequency gently with decreasing temperature down to 98 K where the signal also disappeared. In the temperature range between 98 and 171 K, the lowest-frequency signal was also broad and the signal intensity was almost unchanged immediately above and below 171 K. Accordingly, three resonance lines having nearly the same intensity were observed in this temperature range. With increasing temperature, the same process of the temperature dependence of ^{35}Cl NQR frequencies could be followed exactly for this complex, indicating that the previously reported T_{tr}[1] of 169 K should be revised as 171 K.

At 77 K, four ^{35}Cl NQR frequencies having nearly equal intensity ($S/N\approx4$) to each other could be clearly observed. A very weak ($S/N\approx2$) and also very broad signal could be barely recorded near 15.95 MHz. However, the temperature dependence of this line could not be determined partly because this signal was too weak and broad to be measured accurately and partly because this line and another strong line with many side bands overlapped each other with increasing temperature. Two of the four lines lowered their frequencies very steeply with increasing temperature whereas the remaining two

lines showed unusual positive temperature coefficients. The four lines disappeared just below 98 K, at which temperature three fairly strong signals appeared.

From the above observation of the temperature dependence of ^{35}Cl NQR frequencies, one can conclude that $(diMA)_2TeCl_6$ undergoes structural phase transitions at 98 and 171 K and two and three crystallographically nonequivalent chlorine atoms exist in the high and intermediate phases, respectively. The two and three nonequivalent chlorine atoms can be assigned to the single $[TeCl_6]^{2-}$ ion in the crystal by comparing these results with those of $(diMA)_2SnCl_6$ and by referring to the fact that the doubly strong line of the high-temperature phase is split into two with equal intensity. In the low-temperature phase, there exist at least five nonequivalent chlorine atoms. To confirm the existence of the phase transition at 98 K, we undertook the experiments of DTA. However, no heat anomaly could be observed. This may be due to the low sensitivity of our apparatus at lower temperatures and also possibly due to the small heat anomaly of this phase transition.

$[(CH_3)_2NH_2]_2PtCl_6$. At 77 K, two ^{35}Cl NQR frequencies were observed for this complex. The high-frequency line was moderately strong and also broad whereas the low-frequency line was weak and fairly sharp. With increasing temperature, the resonance frequency of both lines decreased almost linearly although the low-frequency curve was very slightly convex. The high-frequency line became gradually sharp and weak with increasing temperature, although it could be clearly observed even at room temperature. On the other hand, the low-frequency line decreased its intensity until it disappeared below room temperature. At 196 K, the intensity ratio of the high- to the low-frequency line was approximately 7:1.

Discussion

According to the X-ray analysis recently carried out,[2,6] $(diMA)_2SnCl_6$ forms orthorhombic crystals belonging to the space group Pnnm with Z=2. The structure consists of parallel sheets of almost regular $[SnCl_6]^{2-}$ octahedra held together by hydrogen bonds formed between cationic NH_2^+ groups and chlorine atoms. Each NH_2^+ group is symmetrically H-bonded to the two nearest neighbor complex anions in a sheet and each complex anion is the recipient of H-bonds from four cations. Each N-H vector lies nearly along the pseudo-threefold axis of the anion but it deviates in such a way that the N-H···Cl H-bonds are described as asymmetrically trifurcated or close to out-of-plane bifurcated. Short H-bonds having the distance of 2.6 Å are formed between N-H hydrogen and equatorial chlorine atoms which have a shorter Sn-Cl bond distance, while the axial chlorine atoms form longer H-bonds (3.0 Å). Accordingly, each chlorine atom has N-H···Cl type H-bonds, the hydrogen atom of which exists nearly on the plane including the chlorine atom and perpendicular to the Sn-Cl bond axis.

The present NQR results completely agree with the above crystal structure especially in the features that the tin complex yields two ^{35}Cl NQR lines attributable to two nonequivalent chlorine atoms in the single anion and that the high- and low-frequency lines are assignable to the equatorial and axial chlorine atoms, respectively. This assignment is compatible with the foregoing Sn-Cl bond distance discussion.

By referring to the above X-ray results, the unusual temperature dependence of the ^{35}Cl NQR frequencies observed particularly for the low-frequency line and the phase transition suggested can be explained as follows.[7] Let an Sn-Cl bond axis be the z axis of the chlorine atom. Then, two hydrogen atoms forming H-bonds with the chlorine atom lie nearly along the x- and y-axes of the chlorine atom. This suggests that the p_x and p_y electrons of the chlorine atom are polarized and that the population of these electrons decreases to some extent. This results in a decrease in the ^{35}Cl NQR frequency.[7-9]

Here, we assume that the H···Cl distances involving the equatorial and the axial chlorine atoms are longer and shorter, respectively, at 77 K than the corresponding values determined at room temperature. This is achieved by widening the H-N-H angle which is reported to be 84° at room temperature although this value is exceptionally small. With increasing temperature, the equilibrium position of the hydrogen atoms moves to that determined at room temperature through the excitation of unharmonic deformation vibrations of NH_2^+ groups. This may result in an increase and a sharp decrease in the ^{35}Cl NQR frequencies of the low- and high-frequency lines, respectively. In this phase, two slightly nonequivalent NH groups, as pointed out its existence by Knop *et al.*[2] from the IR study of the stretching vibration of partially deuterated NHD^+ groups in the cation, can be allowed to exist in the crystal without changing the number of nonequivalent chlorine atoms in each complex anion. At 102 K, the slightly nonequivalent NH groups become equivalent forming symmetrical NH_2^+ groups in the crystal. However, the equilibrium positions of the H atoms are still near those of the low-temperature phase. With increasing temperature furthermore, the equilibrium positions move slightly and gradually to those determined at room temperature. The high-frequency line of the partially deuterated analog $[(CH_3)_2ND_2]_2SnCl_6$ also shows a discontinuous change in the temperature coefficient

of ^{35}Cl NQR frequencies near 102 K. This provides strong evidence for the existence of the phase transition suggested.

The NQR results of the high-temperature phase of $(diMA)_2TeCl_6$ can be explained along the same line as those obtained for $(diMA)_2SnCl_6$ at higher temperatures. In the intermediate phase, three broad NQR lines were observed suggesting the existence of strong dipolar interactions through N-H···Cl type H-bonding and/or the presence of some slight disorder in the position of CH_3 groups. In the low-temperature phase, more than four crystallographically nonequivalent chlorine atoms which presumably belong to the same complex anion exist, suggesting the presence of nonequivalent cations in the crystal in agreement with the results of our previous ^1H T_1 study.[1]

For $(diMA)_2PtCl_6$, two ^{35}Cl NQR lines having signal intensity greatly different from each other were observed. According to Ries,[10] this complex shows polymorphism and crystallizes in two morphologically different forms. In fact, the complex prepared in the present investigation yielded complicated X-ray powder patterns which are completely different from those of $(diMA)_2SnCl_6$ and $(diMA)_2TeCl_6$. The elementary analysis of the complex prepared exhibits perfect agreement with the theoretical value for $(diMA)_2PtCl_6$. Therefore, the two lines observed can be assigned to two different crystal forms. Although both forms have the same point-group symmetry D_{2h}, one form is easily crystallized with the bigger abundance ratio. Accordingly, the high-frequency line may be attributed to this crystalline form. No further discussion can be made of this complex because of the above ambiguity in the crystals prepared.

The ^{35}Cl NQR frequencies of $(diMA)_2SnCl_6$ and $(diMA)_2TeCl_6$ disappear in the noise level around 270 and 240 K, respectively. Each signal loses its intensity fairly quickly from the temperature lower by *ca.* 15 K than each fade-out temperature. The characteristic appearance of these temperature dependence curves below each fade-out temperature is that each ν *vs.* T curve decreases almost linearly with increasing temperature.

The fade-out phenomenon of NQR signals is usually interpreted in terms of a large fluctuation of the electric field gradient (EFG) produced at resonant nuclei by appropriate molecular motions such as molecular reorientation and molecular self-diffusion.[11] Brown *et al.*[12] observed the nuclear quadrupole relaxation time T_1 in $CaSnCl_6 \cdot 6H_2O$ and found a fairly sharp decrease in T_1 above 250 K, which was attributed to the reorientational motions of the complex anions. However, the ^{35}Cl NQR frequency could be observed up to 390 K. This suggests that the reorientational motion of the anions does not affect drastically the EFG of the chlorine atoms. Furthermore, the reorientation of octahedral hexachloro complex anions in various K_2PtCl_6 type complexes including $(NH_4)_2MCl_6$ is known usually to start far above room temperature.[13–15] Therefore, the fade-out of ^{35}Cl NQR signals in $(diMA)_2SnCl_6$ and $(diMA)_2TeCl_6$ which was observed below room temperature may not be explained by the fluctuation of EFG due to the motion of the complex anions.

From our ^1H NMR measurements previously carried out,[1] the 180° flip motion of the whole cation about its twofold pseudo-symmetry axis accompanying a large amplitude libration or small angle reorientation of the cation was detected above *ca.* 300 and 260 K for $(diMA)_2SnCl_6$ and $(diMA)_2TeCl_6$, respectively. These motions of the cations are expected to generate a large fluctuation of EFG produced at the chlorine nuclei of these complex anions, because the cation has two nonequivalent CH_3 groups and each chlorine atom has two H-bonded hydrogen atoms carrying a partial positive charge. The 180° flip motion of the cation results in a positional disorder of the CH_3 groups and the slow motion of NH_2^+ hydrogen atoms will disturb EFG at the chlorine nuclei and broaden the NQR signals. Therefore, one can conclude that the disappearance of the ^{35}Cl NQR signals of these complexes below room temperature is solely attributable to the motion of the cation as a whole.

References

1) H. Ishida, R. Ikeda, and D. Nakamura, *Ber. Bunsenges. Phys. Chem.*, **88**, 546 (1984).
2) O. Knop, T. S. Cameron, M. A. James, and M. Falk, *Can. J. Chem.*, **61**, 1620 (1983).
3) K. B. Dillon, J. Halfpenny, and A. Marshall, *J. Chem. Soc., Dalton Trans.*, **1983**, 1091.
4) D. Nakamura, Y. Kurita, K. Ito, and M. Kubo, *J. Am. Chem. Soc.*, **82**, 5783 (1960).
5) Y. Kume, R. Ikeda, and D. Nakamura, *J. Magn. Reson.*, **33**, 331 (1979).
6) M. H. B. Ghozlen, A. Daoud, and J. W. Bats, *Acta Crystallogr., Sect. B*, **37**, 1415 (1981).
7) D. Nakamura, R. Ikeda, and M. Kubo, *Coord. Chem. Rev.*, **17**, 281 (1975).
8) A. Sasane, T. Matsuo, D. Nakamura, and M. Kubo, *Bull. Chem. Soc. Jpn.*, **43**, 1908 (1970); *J. Magn. Reson.*, **4**, 257 (1971).
9) C. W. Fryer and J. A. S. Smith, *J. Chem. Soc. A*, **1970**, 1029.
10) A. Ries, *Z. Kristallogr.*, **36**, 321 (1902).
11) H. Chihara and N. Nakamura, *Adv. Nucl. Quad. Reson.*, **4**, 1 (1980).
12) R. J. C. Brown, B. K. Hunter, M. Mackowiak, and S. Segel, *J. Magn. Reson.*, **50**, 218 (1982).
13) K. R. Jeffrey and R. L. Armstrong, *Phys. Rev.*, **174**, 359 (1968).
14) R. L. Armstrong and H. M. van Driel, *Adv. Nucl. Quad. Reson.*, **2**, 179 (1975).
15) C. Dimitropoulos and J. Pelzl, *J. Mol. Struct.*, **58**, 107 (1980).

 © 1985 The Chemical Society of Japan Bull. Chem. Soc. Jpn., 58, 2595—2599 (1985)

Hydrophobic Indexes for Various Monosaccharides

Koichiro MIYAJIMA,* Katsunosuke MACHIDA, and Masayuki NAKAGAKI
Faculty of Pharmaceutical Sciences, Kyoto University Yoshida Shimoadachi-cho, Sakyo-ku, Kyoto 606
(Received February 21, 1985)

The hydrophobic and the hydrophilic surface areas of seven kinds of monosaccharide molecules were calculated by using Hermann's method. The hydrophobic indexes (Index A and Index B) which are defined as the ratio of the hydrophobic and the hydrophilic surface areas of the molecule are clearly correlated with the partition coefficient of monosaccharide between polystyrene gel and water, and the free energy change of transfer of monosaccharide from water to 1-butanol, indicating that the fraction of the hydrophobic surface area plays an important role in the interaction of monosaccharides and hydrophobic solutes in water.

Sugar has so far been regarded as a typical hydrophilic nonelectrolyte like urea. Generally sugars have nearly the same numbers of CH groups as OH groups in a molecule, and the hydration behavior of monosaccharide has been discussed in terms of the orientation of OH groups of hexopyranose ring.[1]

Recently several evidences have been revealed on the hydrophobic character of saccharides. Various saccharides are partitioned to polystyrene gel from aqueous phase.[2-4] The partition coefficients obtained from the gel chromatography using polystyrene gel as a stationary phase are different from each other irrespective of the same molecular formula and the same configuration (Cl), *i.e.* D-glucose, D-galactose, and D-mannose. The partition coefficients increase with the concentration of structure making salts such as NaCl, and decrease with increase of the concentration of structure breaking salt, NaSCN.[3] Inversely, cyclohexane is adsorbed by Sephadex gel, which is the polymer of D-glucose.[5]

On the other hand, the condensed ring compounds of D-glucose, such as cyclodextrins, include the hydrophobic solute in their cavities and the inner wall of the cavity has been regarded as hydrophobic.[6]

These experimental results seem to indicate that the saccharide molecule has the hydrophobic character even if it is considerably weak, because the interactions mentioned above may be hydrophobic.

In order to confirm that the nature of interactions mentioned above are hydrophobic, we investigated the correlation between the partition coefficients[3] and the surface area ratio of hydrophobic and hydrophilic groups for various monosaccharides molecules. For the partitioning of saccharide to polystyrene gel phase from aqueous phase may be mainly based on the adsorption of saccharide molecules onto the phenyl groups of polystyrene through hydrophobic interaction and the hydrophobic character of saccharides may possibly originate from the hydrophobic surface formed by the CH and CH_2 groups of monosaccharide molecules.[3,4] From these viewpoints, we calculated the hydrophobic and hydrophilic surface areas of seven kinds of monosaccharide molecules, on the assumption that the hydrophobic surface area is the area occupied by CH and CH_2 groups at a distance of 1.4 Å above the atom surface. Combining this area with the total surface area, the hydrophilic surface area is also obtained. Good correlations between the surface area ratio of hydrophobic and hydrophilic groups and the partition coefficients or the free energy of transfer were obtained.

Experimental

Calculation of Surface Area: Surface area of monosaccharides was calculated basically by the computer program QCPE 225 MOLAREA developed by Hermann.[7] The atomic coordinates mainly obtained from the X-ray data except for ribofuranose were used in the calculation. For the furanose-type saccharides, furanose ring was assumed to be planar and the atomic coordinates were obtained from usual bond lengths and bond angles. The van der Waals radii were used as the radii of the atoms. The surface area at a distance of 1.4 Å above the spherical atom surface was calculated on the assumption that the radius of water molecule is 1.4 Å. Since the OH groups of monosaccharide molecule rotate around the C-O axis, the OH group was approximated to the sphere with the radius of 1.72 Å.

Definition of Hydrophobic Area: Total hydrophobic surface area was defined as the area occupied by CH and CH_2 groups of monosaccharide. The hydrophilic surface area is the area occupied by OH and -O- groups and corresponds to the difference between total surface area and hydrophobic surface area.

Monosaccharide molecule is approximated to a disk which has two surfaces. The two surfaces of monosaccharide molecule are in general not equivalent in their hydrophobic areas, the one is richer in CH and CH_2 groups than the other.

For the calculation of the hydrophobic surface area of CH-rich surface (specified hydrophobic surface area), we first selected the CH and CH_2-rich surface from the molecular model and specified hydrophobic surface area occupied by the specified carbon and hydrogen atoms was calculated under the following conditions.

1) For the β-axial CH and CH_2 groups, the specified hydrophobic surface area is equal to the calculated area.

2) For the α-axial and α-equatorial CH and CH_2 groups, the specified hydrophobic surface area is zero.

3) For β-equatorial CH and CH_2 groups, the specified hydrophobic surface area is half the calculated area.

4) The specified hydrophobic surface area of monosaccharide molecule is the sum of the area obtained from 1) and 3).

For the calculation of the surface area of ribofuranose, we assumed that the five membered ring of furanose is planar. Therefore, every OH group attached to furanose ring belongs to either α- or β- type. In this case, the specified hydrophobic surface area of β-CH or CH_2 group was assumed to be the calculated area and that of α-CH or CH_2 group zero. The same criterion was applied to the calculation of the specified hydrophobic surface area of 2-deoxy-D-ribofuranose. Definition of the hydrophobic index: As an expression of hydrophobicity of a compound, the value of hydrophile-lipophile balance(HLB) is frequently used in the physical chemistry of surfactants. HLB value is originally the mass ratio of the hydrophilic and the lipophilic groups. In the similar manner, we defined the hydrophobic index (Index) as the surface area ratio instead of the mass ratio, because aldohexopyranoses, *i.e.* glucose, galactose and mannose, have the same mass ratio of hydrophobic and hydrophilic groups in this treatment.

The hydrophobicity of α- and β-anomers of monosaccharide A, index A_α and A_β, are defined by Eqs. 1 and 2, respectively. The index of monosaccharide A is the sum of indexes of each anomer.

$$\text{Index } A_\alpha = \frac{\text{Total hydrophobic surface area } (\alpha)}{\text{Total hydrophilic surface area } (\alpha)} \times \alpha\text{-anomer } \% \quad (1)$$

$$\text{Index } A_\beta = \frac{\text{Total hydrophobic surface area } (\beta)}{\text{Total hydrophilic surface area } (\beta)} \times \beta\text{-anomer } \% \quad (2)$$

$$\text{Index A} = \text{Index } A_\alpha + \text{Index } A_\beta \quad (3)$$

Since D-ribose and 2-D-deoxyribose have six and four isomers, respectively, indexes of these saccharides were calculated by the extention of the above treatment.

The indexes B_α and B_β were calculated by the similar equations to those of index A_α and A_β using the specified hydrophobic surface area instead of total hydrophobic surface area. Index B was defined as the sum of index B_α and B_β.

Results and Discussion

The results are shown in Tables 1 and 2. Funasaki *et al.*[8] correlated the hydrophobic surface area with hydrophobic interaction for oligoethylene glycol diethers and diesters. First we investigated the correlation between the average total hydrophobic surface area (=Σ hydrophobic surface area×anomer fraction) and the partition coefficients of monosaccharides (K_{av}) obtained from the polystyrene gel-water chromatography by Janado.[3] The magnitude of K_{av} increases in the order galactose<glucose<mannose<arabinose<xylose<ribose<deoxyribose. However the magnitude of the average total hydrophobic surface area calculated from the data of Table 1 lies in the order xylose<arabinose<glucose<mannose<galactose<ribose<deoxyribose, which is quite different from the order of magnitude of K_{av}.

On the other hand, the mangitude of average specified hydrophobic surface area (=Σ specified hydrophobic surface area×anomer fraction) lies in the order arabinose<xylose<mannose<galactose<glucose<ribose<deoxyribose. This order is also different from that of K_{av}. These results would be reasonable, because the hydrophobicity of the molecule depends on both the sizes of hydrophobic and the hydrophilic groups of the molecule as seen in the HLB values of the surfactants. It is reasonable to assume as a first approximation that the strength of hydrophobicity and hydrophilicity of a saccharide molecule depends on the dimensions of the surface area of hydrophobic and hydrophilic groups, respectively, because the hydrophilic groups are mainly OH groups except an ether oxygen group and hydrophobic groups are aliphatic CH or CH_2 groups.

Based on this idea, we calculated the hydrophobic index A (Index A) as shown in Table 1. From the definition of index, the larger the index is the stronger the hydrophobicity. Therefore, the order of hydrophobicity lies in the order, glucose<galactose<mannose<xylose<arabinose<ribose<deoxyribose. The reversing of the order is observed at glucose-galactose and arabinose-xylose as compared with the order of K_{av}. The dependences of K_{av} and log K_{av} on index A are shown in Figs. 1 and 2, respectively. Almost a linear relation is observed between index A and K_{av}. But a nonlinear relation is obtained between index A and log K_{av}. However index A increases with K_{av}. The relation between index A and the relative free energy of transfer of monosaccharide from water to 1-butanol, ΔG^{tr}[4] (galactose as a standard), is shown in Fig. 3. The negative value of ΔG^{tr} increases nonlinearly with index A. From Figs. 2 and 3, free energy of interaction of monosaccharide with hydrophobic compound is correlated nonlinearly with index A, because RT log K_{av} (R: the gas constant, T: absolute temperature) gives the energy dimension.

Based on the idea that the CH-rich surface interacts with hydrophobic solute, we calculated the index B by using the specified hydrophobic surface area instead of the total hydrophobic surface area. Therefore the index B refers to the preferential interaction of the CH-rich surface and hydrophobic solute. As seen in Table 2, index B lies in the order galactose<glucose<arabinose<mannose<xylose<ribose<deoxyribose. As compared with the order of K_{av}, the position of mannose is replaced by arabinose.

Table 1. Indexes A of various monosaccharides

Compounds	Conformation	Position of OH 12345	Anomer %	Total hydrophobic area (A^2)	Total hydrophilic area (A^2)	Index A
α-D-Glucose	C1 (G–G)	aeeee	36	97.1	243.3	38.7
β-D-Glucose	C1 (G–G)	eeeee	64	95.1	250.5	
α-D-Galactose	C1 (G–T)	aeeae	36	100.6	238.8	40.6
β-D-Galactose	C1 (G–T)	eeeae	64	98.1	247.0	
α-D-Mannose	C1 (G–G)	aaeee	68	97.1	231.4	42.0
β-D-Mannose	C1 (G–G)	eaeee	32	101.1	240.8	
α-D-Arabinose	1C	eeaa	63	100.7	193.4	48.1
β-D-Arabinose	1C	aeaa	34	93.3	206.9	
α-D-Xylose	C1	aeee	33	94.8	206.3	44.1
β-D-Xylose	C1	eeee	67	92.8	213.5	
α-D-Ribopyranose	1C	eaea	20	101.9	193.6	
α-D-Ribopyranose	C1	aeae		105.2	189.9	
β-D-Ribopyranose	1C	aaea	56	94.5	207.2	51.9
β-D-Ribopyranose	C1	eeae		109.2	189.3	
α-D-Ribofuranose	Plane	$\alpha\alpha\alpha\beta$	6	105.8	203.0	
β-D-Ribofuranose	Plane	$\beta\alpha\alpha\beta$	18	95.2	215.3	
2-Deoxy-α-D-ribopyranose	1C	e ea	70	130.7	152.0	
2-Deoxy-β-D-ribopyranose	1C	a ea		119.8	170.2	75.7
2-Deoxy-α-D-ribofuranose	Plane	α $\alpha\beta$	30	123.9	176.3	
2-Deoxy-β-D-ribofuranose	Plane	β $\alpha\beta$		122.6	176.3	

G: Gauch, T: Trans, a: axial, e: equatorial.

Table 2. Indexes B of various monosaccharides

Compounds	Specified hydrocarbon atoms	Specified hydrophobic area (A^2)	Index B
α-D-Glucose	3*, 5, (1/2·6)	46.3	20.9
β-D-Glucose	1, 3, 5, (1/2·6)	57.3	
α-D-Galactose	3, (1/2·4), 5, (1/4·6)	36.2	20.2
β-D-Galactose	1, 3, (1/2·4), 5, (1/4·6)	56.6	
α-D-Mannose	(1/2·2), 3, 5, (1/2·6)	44.0	21.8
β-D-Mannose	1, (1/2·2), 3, 5, (1/2·6)	67.5	
α-D-Arabinose	1, (1/2·4), (1/2·5)	46.2	21.7
β-D-Arabinose	(1/2·1), 2, (1/2·3), (1/4·5)	39.4	
α-D-Xylose	(1/2·1), 2, 4, (1/4·5)	48.5	22.3
β-D-Xylose	1, 3, (1/2·5)	45.7	
α-D-Ribopyranose (1C)	1, (1/2·2), 3, (1/2·4), (1/2·5)	69.4	26.7
α-D-Ribopyranose (C1)	(1/2·1), 2, (1/2·3), 4, (1/4·5)	59.9	
β-D-Ribopyranose (1C)	(1/2·2), 3, (1/2·4), (1/2·5)	48.8	
β-D-Ribopyranose (C1)	2, (1/2·3), 4, (1/4·5)	43.2	
α-D-Ribofuranose	1, 2, 3, (1/2·5)	68.8	
β-D-Ribofuranose	2, 3, (1/2·5)	52.7	
2-Deoxy-α-D-ribopyranose	1, (1/4·2), 3, (1/2·4), (1/2·5)	77.1	38.3
2-Deoxy-β-D-ribopyranose	(1/4·2), 3, (1/2·4), (1/2·5)	53.43	
2-Deoxy-α-D-ribofuranose	1, (1/2·2), 3, (1/2·5)	67.1	
2-Deoxy-β-D-ribofuranose	(1/2·2), 3, (1/2·5)	45.5	

*: Integer means the position of carbon atom.

As shown in Fig. 4, an almost linear relation is obtained between index B and K_{av}. The order of K_{av} is better correlated to that of index B than that of index A. As shown in Figs. 5 and 6, index B is nonlinearly correlated with log K_{av} and ΔG^{tr}.

We cannot judge from the above results which index is more closely correlated to the thermodynamic data. Judging from the fact that monosaccharide molecule rotates at considerably fast rate in aqueous solution, index A may be more plausible than index B.

The partition coefficients of monosaccharides between active charcoal and water[9] were not correlated to these indexes, indicating that the negatively charged surface of active charcoal may

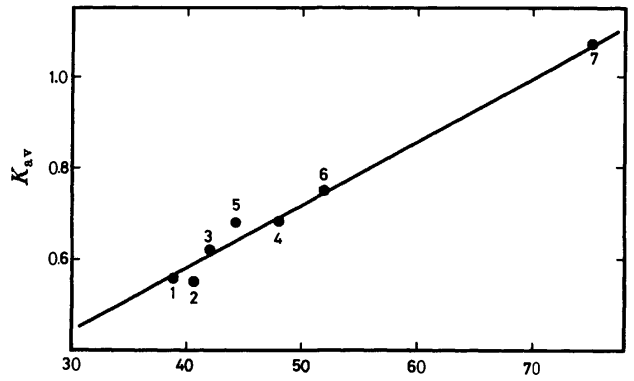

Fig. 1. Relation between Index A and K_{av}.
1: glucose, 2: galactose, 3: mannose, 4:arabinose, 5: xylose, 6: ribose, 7: deoxyribose.

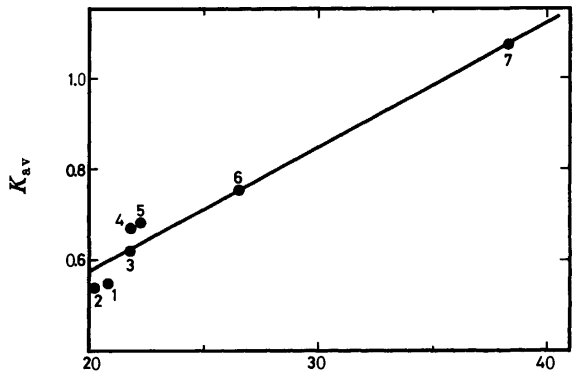

Fig. 4. Relation between Index B and K_{av}.
Symbols: see Fig. 1.

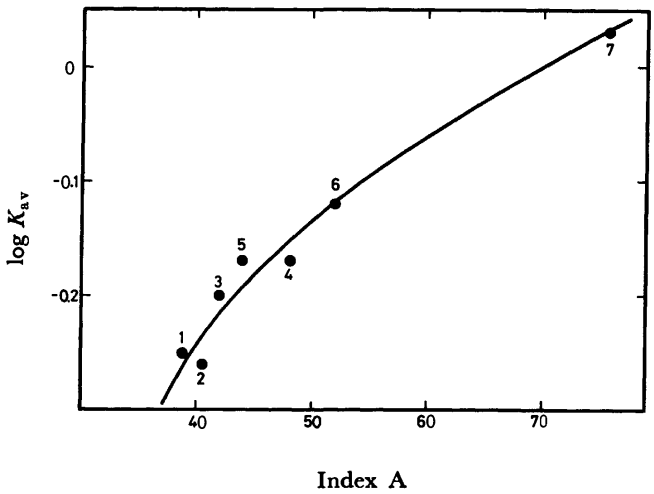

Fig. 2. Relation between Index A and log K_{av}.
Symbols: see Fig. 1.

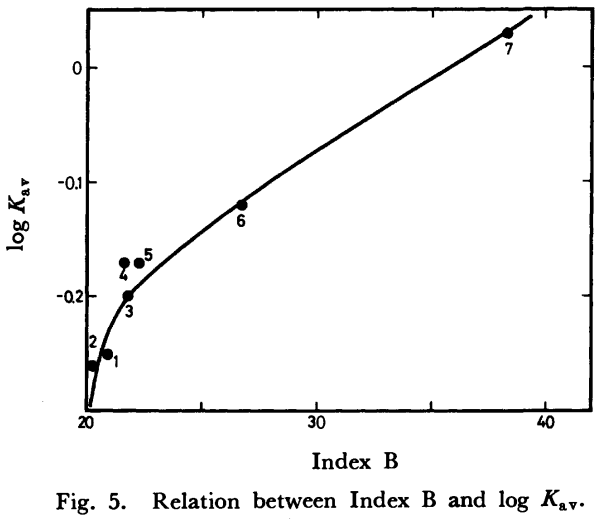

Fig. 5. Relation between Index B and log K_{av}.
Symbols: see Fig. 1.

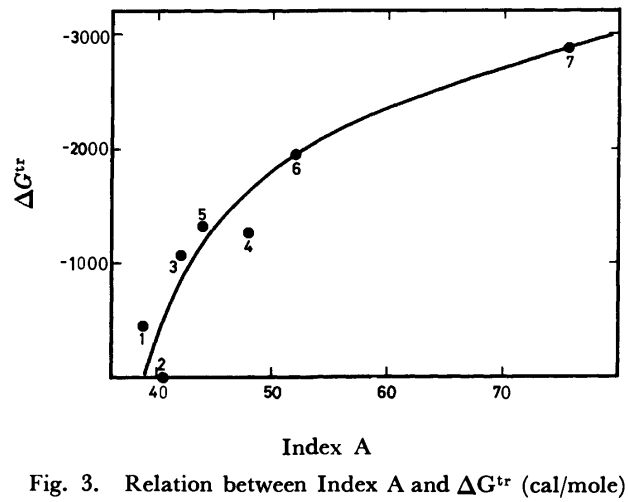

Fig. 3. Relation between Index A and ΔG^{tr} (cal/mole) (1 cal $=4.184$J).
Symbols: see Fig. 1.

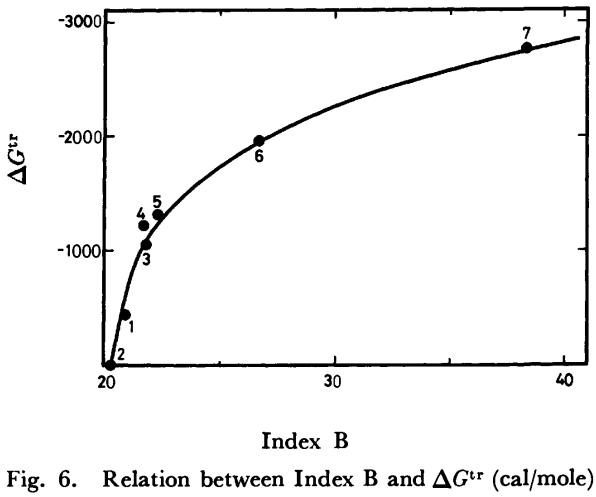

Fig. 6. Relation between Index B and ΔG^{tr} (cal/mole).
Symbols: see Fig. 1.

influence the interaction of monosaccharide molecule with charcoal surface.

An important problem of this treatment is related to the evaluation of hydrophilicity of the monosaccharide molecule, that is, the validity of the relation of hydrophilicity and the hydrophilic surface area. The hydrophilic character of saccharide molecule comes from the hydrogen bonding of OH groups with water molecules, which is stabilized by the suitable orientation of OH group of monosaccharide molecule. Water molecules form tridymite-like structure in liquid state.[1] Based on the special hydration model originally proposed by Kabayama and Patterson,[10] an equatorial OH group of pyranose ring is more favorable than an axial OH group on the formation of hydrogen bonding with water molecule in aqueous solution. In this calculation, the hydrophilic surface area occupied by equatorial OH group is larger than that of axial OH group at anomer carbon atom. But this relation does not always hold at another carbon atoms. Therefore, we cannot comment whether the difference of orientation of OH group reflects the surface area of hydrophilic group of monosaccharide at the present stage. We did not take into account the presence of monosaccharide of straight chain form throughout the discussion, because of its low amount in aqueous solution of equilibrium state.

In conclusion, it was revealed that the fraction of hydrophobic surface area is primarily important factor on the interaction of monosaccharides with hydrophobic compounds in water.

The authors express their sincere gratitude to Dr. T. Taga for his useful discussion of the conformation of monosaccharides and also to Dr. M. Janado for the presentation of thermodynamic data and fruitful discussion.

References

1) K. Miyajima, M. Sawada, and M. Nakagaki, *Bull. Chem. Soc. Jpn.*, **56**, 1620, 1954, 2905 (1983).
2) M. Janado, *Kagaku to Seibutsu*, **22**, 29 (1983).
3) M. Janado, "Aqueous Size-Exclusion Chromatography," ed by P. L. Dubin, Elsevier Amsterdam (1985) Chapter 2.
4) M. Janado, and Y. Yano, *J. Soln. Chem.* Accepted (1985).
5) N. V. B. Marsden, *Naturwissenschaften*, **64**, 148 (1977).
6) J. Szejtli, "Cyclodextrin and Their Inclusion Complexes," Akademiai Kiado, Budapest (1982) p. 102.
7) R. B. Hermann, *J. Phys. Chem.*, **76**, 2754 (1972).
8) N. Funasaki, S. Hada, S. Neya, and K. Machida, *J. Phys. Chem.*, to be published.
9) I. Abe and M. Kitagawa, *Carbon*, **21**, 189 (1983).
10) M. A. Kabayama and D. Patterson, *Can. J. Chem.*, **36**, 563 (1958).

 © 1985 The Chemical Society of Japan Bull. Chem. Soc. Jpn., 58, 2600—2607 (1985)

Free Radicals Produced from the Derivatives of Pyrylium Salts in Solution by Photoillumination

Shigeya Niizuma,*,† Nobuyoshi Sato,† Hiroki Kawata,† Yoshizo Suzuki,††
Takashi Toda,††† and Hiroshi Kokubun††††
†*College of Humanities and Social Sciences, Iwate University, Ueda, Morioka 020*
††*Faculty of Education, Iwate University, Ueda, Morioka 020*
†††*Department of Industrial Chemistry, Faculty of Engineering, Utsunomiya University, Ishii-machi, Utsunomiya 321*
††††*Department of Chemistry, Faculty of Science, Tohoku University, Aoba, Aramaki, Sendai 980*
(Received March 13, 1985)

The photoreactions of 2,4,6-triphenyl- (TPP), 2-*t*-butyl-4,6-diphenylpyrylium (2BDPP) and 2,4,6-triphenylthiopyrylium (TPTP) salts in tetrahydrofuran (THF) and/or 1,2-dimethoxyethane were investigated. Photoproducts were identified to be pyranyl radicals on the basis of photochemical behavior and ESR spectra. Quantum yields of one-electron reduction reactions of TPP, 2BDPP, and TPTP were obtained to be 0.21, 0.047, and 0.53, respectively. The hf coupling constants of protons in the radicals were determined by simulation. The photoillumination of TPP in THF at low temperatures revealed that a certain intermediate radical species was involved in this one-electron photoreduction.

Pyrylium salts are present as natural products in pigments named anthocyanin. They have a six-membered ring containing an oxygen atom of the oxonium type. Thus, the ring has a benzenoid structure and has almost the same stability as that of aromatic rings. The compound which has a sulfur atom instead of an oxygen is called a thiopyrylium salt. As the pyrylium ring has a positive charge, it exhibits a high reactivity to nucleophilic reagents. Further, it is expected that the salt can be easily reduced to neutral radical, which may be stable in a rather nonpolar media.

Among several kinds of derivatives of pyrylium and thiopyrylium tetrafluoroborate, 2,4,6-triphenyl- (TPP), 2-*t*-butyl-4,6-diphenylpyrylium (2BDPP) and 2,4,6-triphenylthiopyrylium (TPTP) salts were found to be subject to a one-electron photoreduction with high quantum yields. They can be converted into stable radical species in such nonpolar solvents as tetrahydrofuran (THF) and 1,2-dimethoxyethane (DME). Fundamental data concerning a photoreaction by steady light illumination at room temperature, the behavior of radicals produced by a short period of illumination at low temperatures and the results on an ESR spectra analysis of the photoproduct radicals are reported.

Experimental

Materials. All the pyrylium salts used have the form of tetrafluoroborate and were synthesized by the ordinary method.[1] 4,4′-Bi(2,4,6-triphenyl-4*H*-pyran-4-yl) (BTPP) was synthesized by reducing a TPP salt with zinc in a mixture of acetic acid–benzene–water after Panov *et al.*[2] THF and DME as solvents were distilled immediately after a few hours of refluxing on metallic sodium and then stocked on a sodium–potassium alloy in an ampoule connected to a vacuum line. Potassium trisoxalato ferrate (III) for the chemical actinometer was newly synthesized by the usual way before use.

Procedures. The device for illuminating the steady light and following the reaction is the same one as reported previously.[3] The light source was a Toshiba high-pressure mercury lamp USH-100UV with a suitable filter system (Toshiba UV-D36C and SL-1A for 365 nm, and Toshiba C-39B and L-42/Y-43 for 436 nm illumination). The light intensity was measured with a potassium trisoxalato ferrate (III) actinometer at each wavelength.[4] The electronic absorption spectra were taken with a Hitachi 228-type double-beam spectrophotometer. ESR spectra were recorded with a JEOL PE-1X-type ESR spectrometer. The simulation of ESR spectra was performed with the use of an NEC PC-9801 microcomputer and on-line Watanabe WX-4675 plotter. ENDOR spectra were taken with a Varian E-1700 ENDOR spectrometer.

Results and Discussion

General Aspects of Photoreactions and Identification of Photoproducts. The absorption spectrum of a TPP salt in THF is shown in Fig. 1-a. The solution was yellowish green and the absorption maxima were located at 278, 363, and 409 nm. When a solution was illuminated with 436-nm light, the spectrum changed with some isosbestic points and the color changed to pink. The photoproduct (which had absorption maxima at 515 and 555 nm in THF) was found to be a radical species since the solution exhibited a strong ESR signal. When the solution was kept in the dark, the absorption of the starting substance was gradually recovered and at the same time the pink color faded and the ESR signal diminished. By the introduction of air into the pink solution, a quarter of the absorption of the starting substance was recovered. The recovered product was again converted into the pink species and exhibited an ESR signal upon illumination. This indicates

that the pyrylium skeleton was retained in the photoproduct molecule. The reactant emitted blue fluorescence[5] in THF and DME but the photoproduct had no emission. The introduction of air into the photoproduct solution caused the emission.

On the basis of the electronic absorption spectrum, the photochemical behavior (mentioned above) and the results of an ESR analysis (see below), the photoproduct of which the electronic spectrum is given by the line (----) in Fig. 1-a is safely identified to be a neutral radical species, or pyranyl, which was formed by one-electron reduction of the pyrylium salt. The reductant is considered to be the solvent.

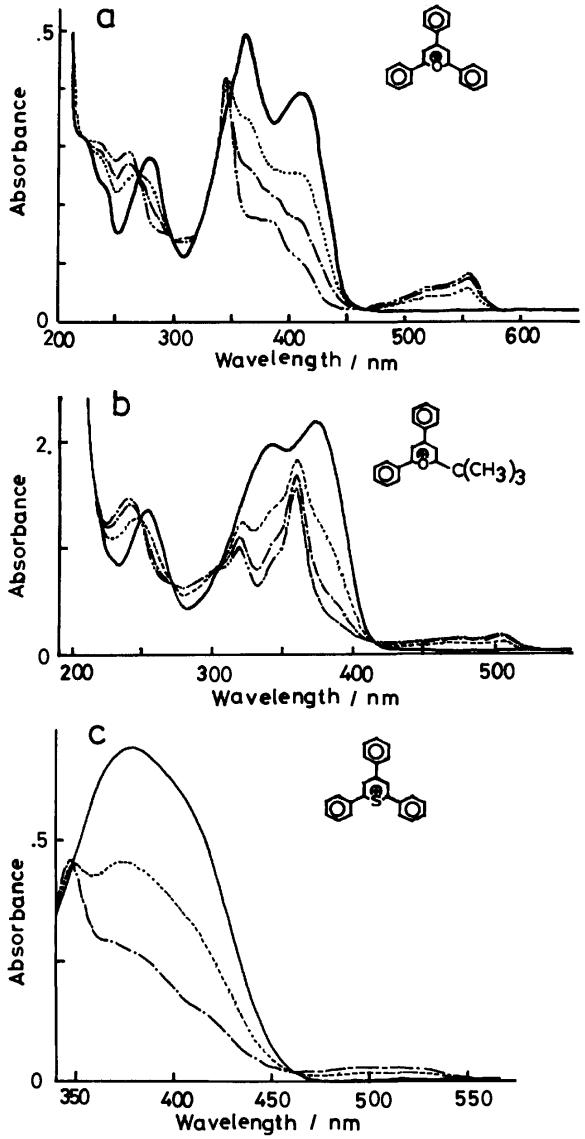

Fig. 1. Absorption spectra in THF and thier change with photoillumination a) of 436 nm light for 0 s(——), 30 s(·····), 1 min(– – –) and 3 min(– – – –), b) of 365 nm light for 0 s(——), 5 min(·····), 11 min (– – –) and 20 min(– – – –) and c) of 436 nm light for 0 s (——), 40 s(·····), and 2 min(– – –).

The spectral change of 2BDPP and TPTP salts upon illumination is shown in Figs. 1-b and c, respectively. Again, the photoproducts exhibited strong ESR signals, indicating that they were neutral radicals. Their electronic spectra are represented by the line (– – – –) in Fig. 1-b and the line (– – –) in Fig. 1-c, respectively.

Reaction Kinetics by Steady Light Illumination. The quantum yields of the photoreactions of the three salts mentioned above were examined as follows: The solutions were illuminated by an exciting light and the intensities of transmitted light were measured with a phototube-amplifier system. As the reaction rate is considered to be proportional to the amount of absorbed light, equation (1) holds.[3]

$$\ln (e^{2.303\varepsilon cd} - 1) = \text{const} - 2.303 \times 10^3 \phi \varepsilon I_0 t \qquad (1)$$

Here, ε, c, d, I_0, and t denote the extinction coefficient of the solute at the observing wavelength, the concentration of the solution, the optical-path length, the incident-light intensity and the time, respectively. ϕ represents the quantum yield of the reaction and is calculated from the slope of the straight line obtained by plotting $\ln(e^{2.303\varepsilon cd}-1)$ against t. ϕ values are listed in Table 1 as well as the ε values used for their calculation. The correction of ϕ for the inner filter effect was carried out in the case that the absorption wavelength of the photoproduct overlapped with that of the excitation wavelength. In Table 1, data on the 4-*t*-butyl-2,6-diphenylpyrylium (4BDPP) salt are added for comparison. The quantum yield for molecules with a higher symmetry tends to be higher. The fact that a higher quantum yield is observed when the ring O atom was replaced by an S atom is in line with the fact that the rate of a one-electron reduction of phenyl(thioxanthone) by Cr^{2+} ion is larger than that of phenyl xanthone.[6]

The effect of the light intensity on the reaction rate was examined about TPP and 4BDPP salts. A linear relation between them was obtained for both salts.

Table 1. Quantum yield of photoreduction ϕ and ε value in THF

Compound		TPP	2BDPP	4BDPP[a)]	TPTP
ε[b)]	365 nm	24500	20300	13300	23400
	436 nm	7690		830	8560
ϕ	365 nm[c)]	0.11[d)]	0.047[d)]		
	436 nm[c)]	0.21[e)]		0.23[e)]	0.53[d)]

a) Irreversible photoreaction. b) In 10^{-3} mol^{-1} cm^2. c) Irradiation wavelength. d) The value obtained by the correction of inner filter effect. e) The reaction rate was proportional to light intensity.

Thus, the photoreaction proceeds with a one-photon process.

An effect of the excitation wavelength on the quantum yield of pyrylium consumption was found to exist in the case of a TPP salt. The quantum yield for 365 nm illumination was about half that for 436 nm illumination, as given in Table 1. The spectral change with 365 nm illumination shows the occurrence of a decomposition reaction of pyrylium ring.

ESR Spectra of Photoproducts. The ESR spectrum of the neutral radical produced by the photoillumination of TPP salts and its temperature dependence are shown in Fig. 2. Simulated spectra are also given in the same figure. All the spectra at different temperatures could be simulated by using a single set of proton hf coupling constants. The spectrum at −10 °C had the smallest linewidth, 48 mG (1 G=10^{-4} T). It increased both at higher and lower temperatures. This implies that the main factor which contributes to the ESR linewidth switches at this temperature. It might represent, for example, a predomination of the spin-rotational interaction (T/η dependence) at the higher-temperature region and of an anisotropy of the Zeeman interaction between the spin and the external magnetic field (η/T dependence) at the lower region. The coupling constants determined by simulation are listed in Table 2 along with those from an ENDOR measurement. The unpaired spin density in the table was calculated using McLachlan's method based on a simple LCAO-MC method. Parameters used in the calculation are also given in the table. From the relation between the hf coupling constants *vs.* the absolute value of the spin densities, 37 G was obtained as McConnell's Q value. Such a large Q value was reported for *o*-semiquinones.[7] Q values for positive ions of aromatic hydrocarbons were also reported to be 36 G.[8] The cited values of the hf coupling constants in the table were those obtained from the radicals produced by zinc powder or other metal reduction in cyclohexane[9,10] and were in good accord with ours.

The ESR spectra of the photochemically produced radical from a 2BDPP salt in THF and their simulation are given in Fig. 3. Although a

Table 2. Coupling constants of pyranyl radicals

Radical and numbering	Position	Number of proton	hf coupling constants (G)				
			ESR			ENDOR	Calculation (Q=37G)
			23—20 °C	a)	b)	−40 °C	c)
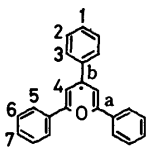	1	1	2.52	2.52	2.40	2.53	2.29
	2	2	0.80	0.84	0.83	0.78	0.85
	3	2	2.10	2.10	2.17	2.24	2.18
	4	2	1.68	1.68	1.66	1.57	1.74
	5	4	1.38	1.26	1.23	1.36	1.29
	6	4	0.42	0.42	0.41	0.41	0.49
	7	2	1.26	1.26	1.26	1.22	1.34
			23 °C	−30 °C	−50 °C	−30 °C	d)
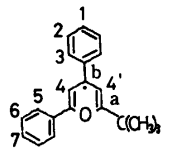	1	1	2.40	2.40	2.72	2.45	2.60
	2	2	0.84	0.82	0.82	0.84	0.96
	3	2	2.04	1.94	1.64	1.96	2.39
	4	1	3.22	3.08	3.26	2.80	2.74
	4'	1	0.84	0.80	0.82	0.84	0.96
	5	2	1.52	1.62	1.64	1.52	1.53
	6	2	0.50	0.54	0.54	0.50	0.61
	7	1	1.52	1.62	1.64	1.71	1.64
			23 °C	−9 °C	−20 °C	10 °C	e)
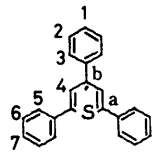	1	1	1.90	1.88	1.88	2.10	1.87
	2	2	0.72	0.70	0.70	0.70	0.71
	3	2	2.52	2.50	2.48	2.46	1.72
	4	2	1.32	1.30	1.28	1.14	1.56
	5	4	0.72	0.72	0.72	0.70	1.17
	6	4	0.44	0.46	0.46	0.36	0.46
	7	2	1.18	1.18	1.18	1.14	1.27

a) *cf.* Ref. 9 (see text). b) *cf.* Ref. 10 (see text). c) $\lambda=1.2$, $\alpha_0=\alpha_c+2.0\beta$, $\beta_a=0.743\beta$ and $\beta_b=0.883\beta$. d) $\lambda=1.2$, $\alpha_0=\alpha_c+2.0\beta$, $\beta_a=0.743\beta$, $\beta_b=0.883\beta$, and $\alpha_2=\alpha_c-0.17\beta$. e) $\lambda=1.2$, $\alpha_s=\alpha_c+1.7\beta$, $\beta_a=0.707\beta$, and $\beta_b=0.766\beta$. Here, α_i is a Coulomb integral of atom i and β is a resonance integral of carbon–carbon bond.

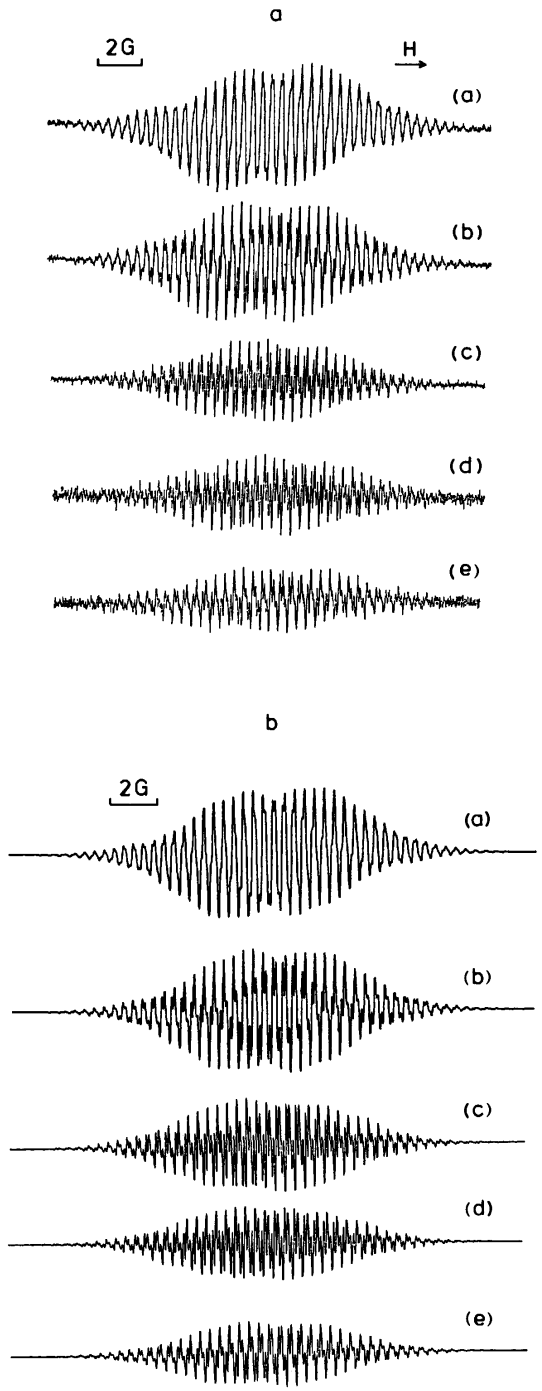

Fig. 2. a: ESR spectra of the radical produced from TPP by the irradiation of 436 nm for 4 min at 23 °C (a) in THF and at 23 °C (b), 0 °C (c), −10 °C (d), and −20 °C (e) in DME. b: Simulated spectra. The linewidths (ΔH_{msl}) used in simulation are 110 mG (a), 80 mG (b), 53 mG (c), 48 mG (d), and 64 mG (e).

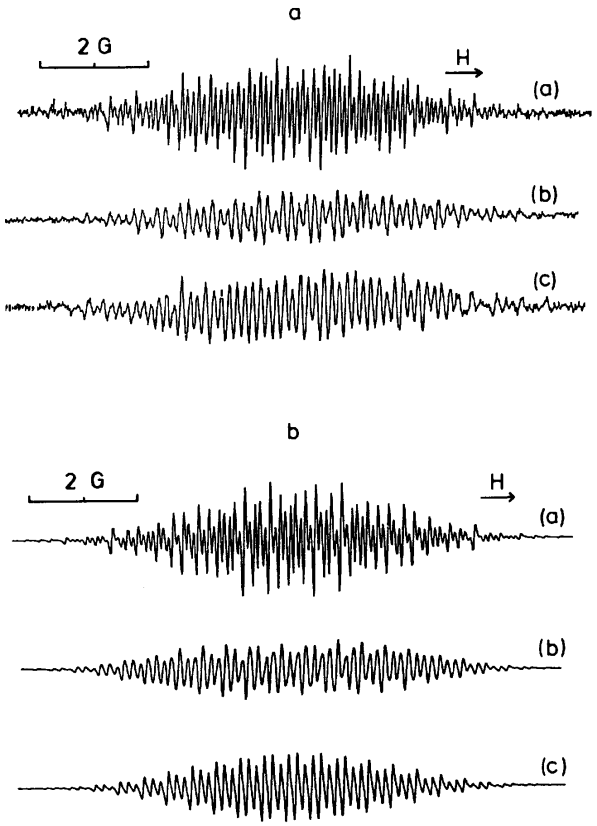

Fig. 3. a: ESR spectra of the radical produced from 2BDPP by the irradiation of 365 nm light for 4 min in THF at 25 °C (a), −30 °C (b), and −50 °C (c). b: Simulated spectra. Marks (a)—(c) correspond to those in ESR spectra.

remarkable change in the spectral shape with temperature change was observed, the simulation parameters were not appreciably different. A slight change in the rotation energy of the *t*-butyl group with temperature may lead to a slight change in the angles between the pyran ring and the two phenyl planes. This may cause a small change in the spin distribution in the molecule.

Figure 4 shows ESR spectra and their simulation for a 2,4,6-triphenyl-4*H*-thiopyran-4-yl radical. A slight variation in the hf coupling constants with temperature may be attributed to a variation in the rotation angle of the three phenyl groups to the thiopyryl ring.

The hf coupling constants of the three radical species were examined by ENDOR. The results coincided with those by the ESR method within the experimental errors and are given in Table 2. Thus, the electronic and steric structures of these radicals were very stable against a temperature change.

The Behavior of Radical at Low Temperatures. The ESR signal intensity of the photochemically produced radical from TPP in THF decreased reversibly with decreasing temperature. This may be due to the occurrence of the following dimerization equilibrium which has been reported for a chemically produced BTPP;[2]

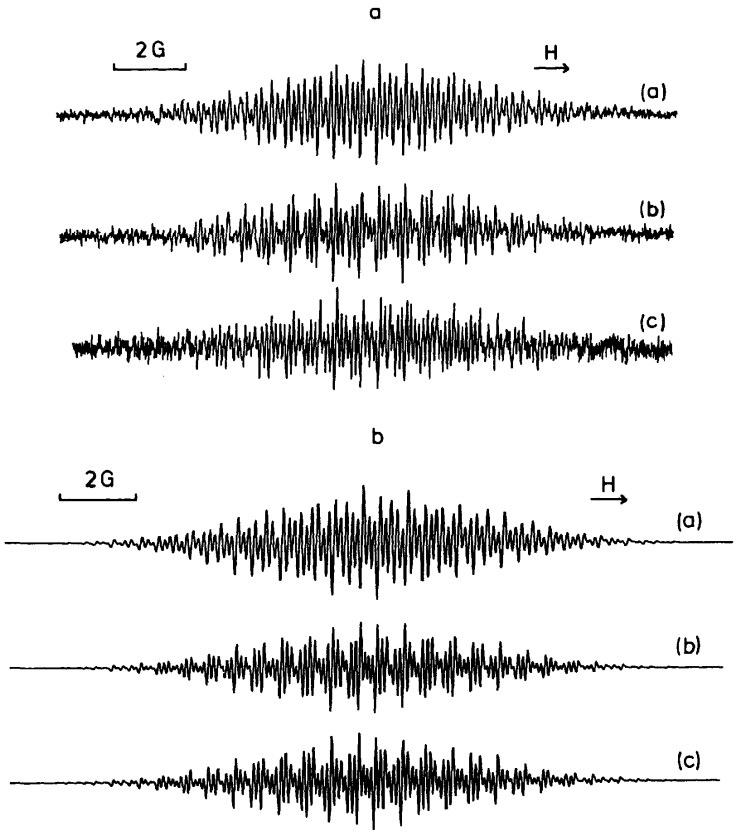

Fig. 4. a: ESR spectra of the radical produced from TPTP by the irradiation of 365 nm light for 4 min in DME at 23 °C (a), −9 °C (b), and −20 °C (c). b: Simulated spectra. Marks (a)—(c) correspond to those in ESR spectra.

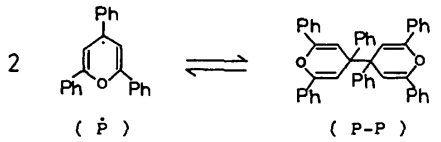

(-Ph=phenyl group)

If we estimate the signal intensity at an infinite temperature, I_∞, by extrapolation, the relative dissociation constant, K_d', can be calculated by Eq. 2;

$$K_d' = \frac{I^2}{I_\infty - I} \tag{2}$$

Here I is the signal inteinsity at temperature T. The plot of logalithm of K_d' against the reciprocal of the absolute temperature was found to be linear over a range from 10 to −60 °C, as shown in Fig. 5. From the slope of this straight line, the enthalpy of dissociation was obtained to be 43.1 kJ mol^{-1}. This value is in good atreement with 44.4 kJ mol^{-1} which we also obtained by the electronic absorption method for a system of chemically produced BTPP (P-P) in THF.

It was confirmed that chemically produced BTPP was quite stable against illumination. It is noteworthy that BTPP is partially converted into pyranyl radical only by thermal process.

Photoillumination at Low Temperature. It seems to be interesting to know whether a radical is formed by photoillumination at low temperatures or not. Indeed a radical was formed by a 436-nm illumination of the TPP salt in THF, even at low temperatures (−40—−100 °C). With an illumination time as short as three or four seconds, the ESR signal at a fixed magnetic field rose up first abruptly, attained a photostationary state and then started to decay immediately after the illumination terminated. It was difficult to observe the hf structure of its ESR signal even during photoillumination because of line broadening. At temperatures higher than −70 °C, the decay curve approached asymptotically not to zero level but to a constant level. We examined this phenomenon at ten-degree intervals between −30—−70 °C. The higher the temperature was, the higher this constant level was. A typical example is shown in Fig. 6. These stable signals showed the same hf pattern as those given in Fig. 2-a at room temperature. The decay rate increased as the temperature rose. The decay curve was successfully analyzed by a first-order reaction-rate equation. On

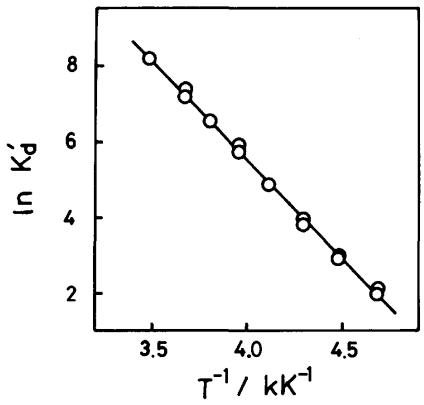

Fig. 5. The temperature dependence of the relative dissociation constant of photochemically produced BTPP in THF.

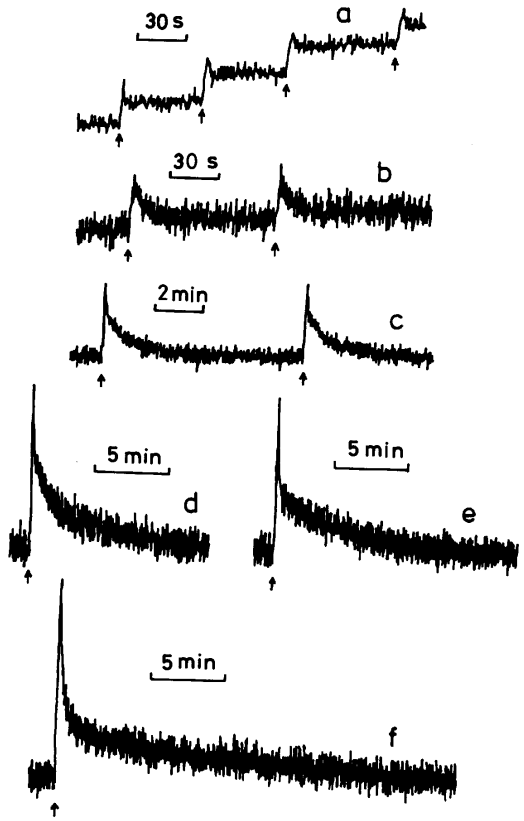

Fig. 6. The time profile of ESR signal intensity at the fixed magnetic field at −30 °C (a), −50 °C (b), −70 °C (c), −80 °C (d), −90 °C (e), and −100 °C (f). 3 to 4 second illumination of 436 nm light was performed at the time point of arrow mark.

the other hand, no permanent formation of the radical was observed at temperatures lower than −70 °C. Between −80—−100 °C, the decay curves were found to comprise two exponential decays, fast and slow ones, as shown in Fig. 6.

This phenomenon may be explained by the following simple scheme;

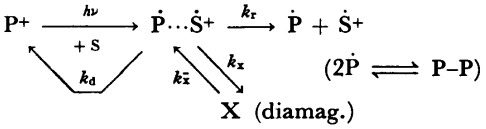

where P^+ is the TPP cation and S is the solvent molecule, which serves as an electron donor. As no similar reaction was observed in DME, the counter ion, BF_4^-, can not be the electron donor. We propose the very loosely complexed radical pair, $\dot{P}\cdots\dot{S}^+$, as an unstable species which showed a first-order decay at all the temperatures studied. This species may be trapped in a solvent cage with some lifetime. To explain the two-step decay at lower temperatures, a certain diamagnetic species X was postulated to be in equilibrium with the radical pair. It might be a spin-paired complex or a compound between pyrylium cation and THF molecule. Processes k_x and $k_{\bar{x}}$ express the faster decay and processes k_d and k_r the solwer one. At temperatures higher than −70 °C, k_x and $k_{\bar{x}}$ are so large that the faster decay does not appear explicitly. Below −70 °C, k_r becomes practically zero and the $\dot{P}\cdots\dot{S}^+$ species are considered to relax through process k_d into the original P^+ and S.

Since there is no reliable data regarding k_r for an analysis, we hereafter treat only decay at temperatures lower than −70 °C. If we neglect the process k_d at the initial stage of decay, $[\dot{P}\cdots\dot{S}^+]_0=[\dot{P}\cdots\dot{S}^+]+[X]$ holds. Starting with the first-order decay equation, $-d[\dot{P}\cdots\dot{S}^+]/dt=k_x[\dot{P}\cdots\dot{S}^+]-k_{\bar{x}}[X]$, we readily obtain Eq. 3.

$$\ln\left(\frac{[\dot{P}\cdots\dot{S}^+]}{[\dot{P}\cdots\dot{S}^+]_0}-\frac{k_{\bar{x}}\cdot}{k_x+k_{\bar{x}}}\right)=-(k_x+k_{\bar{x}})t+\text{const} \qquad (3)$$

Here, $[\dot{P}\cdots\dot{S}^+]$ is the radical concentration and $[P\cdots S^+]_0$ is the same quantity immediately after the light is turned off. In the later stage of a decay, the equilibrium $\dot{P}\cdots\dot{S}^+\rightleftharpoons X$ is considered to be achieved. Then, the decay curve can be represented by Eq. 4.

$$[P\cdots S^+]=[P\cdots S^+]_e\exp(-k_d t) \qquad (4)$$

Here, $[\dot{P}\cdots\dot{S}^+]_e$ is the radical concentration just after equilibrium is achieved. Plots of Eqs. 3 and 4 at various temperatures are shown in Fig. 7-a and b where ESR signal intensities, $(SI)_i$, were used instead of radical concentrations, $[\dot{P}\cdots\dot{S}^+]_i$. The equilibrium constant $K_x=k_x/k_{\bar{x}}$ is represented by $[\dot{P}\cdots\dot{S}^+]_e/([\dot{P}\cdots\dot{S}^+]_0-[\dot{P}\cdots\dot{S}^+]_e)$. k_x and $k_{\bar{x}}$ values were calculated separately from the slope of the lines in Fig. 7-a and the K_x values. They are listed in Table 3.

The Arrhenius plots of k_x, $k_{\bar{x}}$, and k_d are given in Fig. 8-a and b. The activation energies for the processes k_x, $k_{\bar{x}}$, and k_d were calculated (from the

TABLE 3. KINETIC PARAMETERS

Temperature °C	Decay constant (s^{-1})			Equilibrium constant
	k_x	$k_{\bar{x}}$	$k_d \times 10^3$	K_x a)
−80	0.140	0.127	5.00	1.19
−85	0.130	0.095	2.87	1.35
−90	0.109	0.065	3.44	1.69
−95	0.088	0.039	2.00	2.23
−100	0.066	0.021	1.15	3.16

a) $K_x = \dfrac{[\dot{P}\cdots\dot{S}^+]_e}{[\dot{P}\cdots\dot{S}^+]_0 - [\dot{P}\cdots\dot{S}^+]_e}$

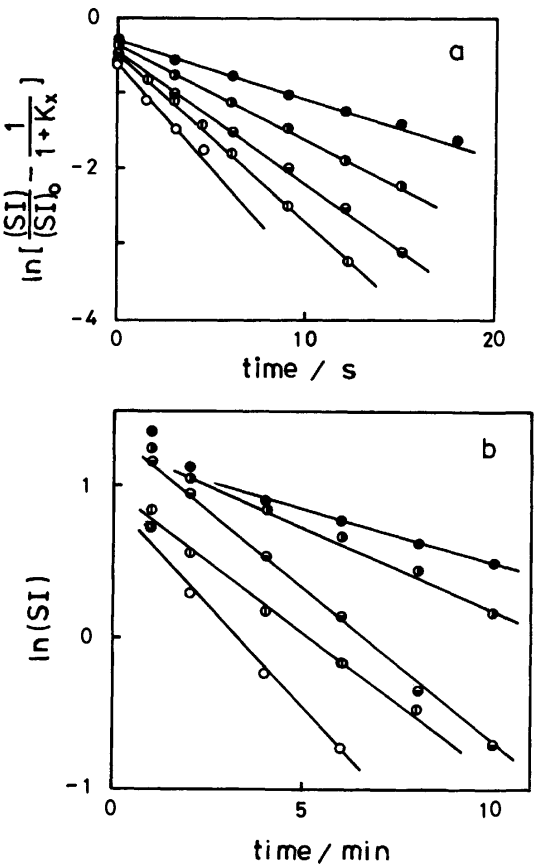

Fig. 7. The analysis of ESR signal decay by the rate equation of the first order reaction at various temperatures.
a: The faster decay, b: The slower decay
○: −80 °C, ◑: −85 °C, ◒: −90 °C, ◑: −95 °C, ●: −100 °C

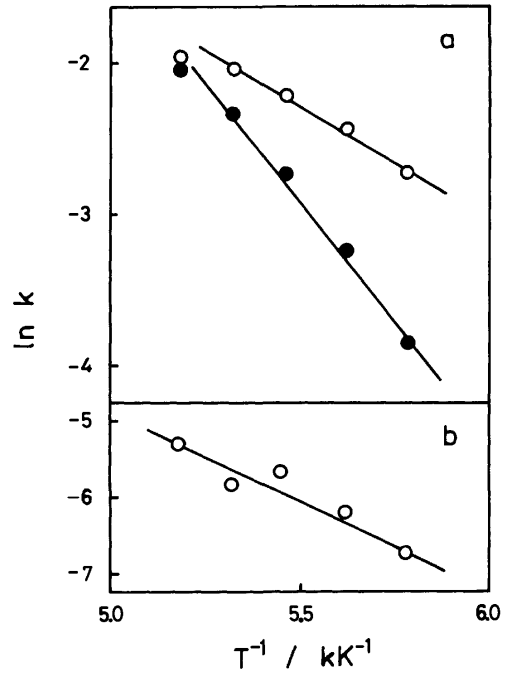

Fig. 8. The Arrhenius plot of k_x (a, ○), $k_{\bar{x}}$ (a, ●), and k_d (b).

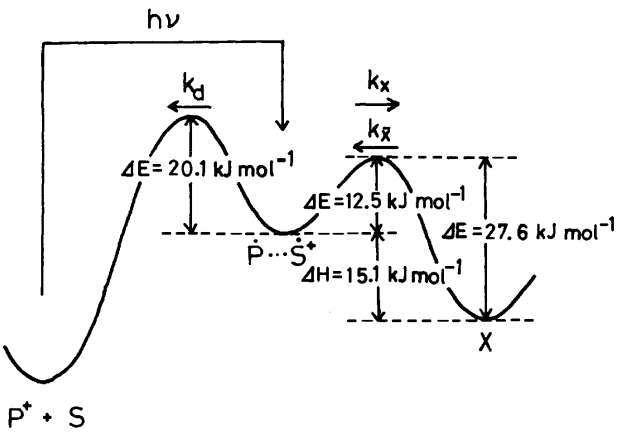

Fig. 9. Potential energy diagram among three systems; $P^+ + S$, $\dot{P}\cdots\dot{S}^+$ and X.
ΔE: Activation energy, ΔH: Enthalpy change.

slope of the lines in the figures) to be 12.5, 27.6, and 20.1 k J mol^{-1}, respectively. The enthalpy change of the reaction $\dot{P}\cdots\dot{S}^+ \rightarrow X$ was calculated to be −15.1 kJ mol^{-1}, the difference between the activation energies for the k_x and $k_{\bar{x}}$ processes. This quantity was also estimated from the temperature dependence of K_x (Table 3) to be −15.5 kJ mol^{-1}. This is in good

agreement with the above mentioned value.

A potential-energy diagram concerning the three systems is depicted in Fig. 9. In view of the relatively high activation energy, a certain modification of the molecular structure (for example, the transfer of a hydrogen atom) might be involved in the process k_x. Thus, it is also plausible that the back reaction to the original P^+ and S occurs from $\dot{P}\cdots\dot{S}^+$, which is formed only by an electron transfer.

The authors wish to thank Professor Masamoto Iwaizumi of Tohoku University for his help in taking ENDOR spectra. One of authors (S.N.) is indebted to the Japan Association of Chemistry for financial support.

References

1) K. Dimroth and K. H. Wolt, "Newer Methods of Preparative Organic Chemistry," ed by W. Foerst, Academic Press., New York (1964), Vol. III, pp 357—423.

A. T. Balaban *et al.*, "Pyrylium salts: Synthesis, Reactions and Physical properties (Advances in Heterocyclic Chemistry, Supplement 2)," ed by A. R. Katritzky, Academic Press., New York (1982), Chapter II.

2) V. B. Panov, M. V. Nekholoshev, and O. Yu. Okhlobystin, *Dokl. Akad. Nauk SSSR*, **243**, 372 (1978).

3) S. Kato, S. Minagawa, and M. Koizumi, This Bulletin, **34**, 1026 (1961); S. Niizuma and M. Koizumi, *ibid.*, **36**, 1692 (1963).

4) C. G. Hatchard and C. A. Parker, *Proc. Roy. Soc.*, **A235**, 518 (1956).

5) The fluorescence has the emission peak at 468 nm in acetonitrile (H. Kokubun and others, unpublished result.) No ESR signal was detected by photoillumination of acetonitrile solution in ESR cavity.

6) W. T. Bowie and M. R. Feldman, *J. Am. Chem. Soc.*, **99**, 4721 (1977).

7) G. Vincow and G. K. Fraenkel, *J. Chem. Phys.*, **34**, 1333 (1961).

8) I. C. Lewis and L. S. Singer, *J. Chem. Phys.*, **43**, 2721 (1965).

9) I. Degani, L. Lunazzi, and G. F. Pedulli, *Mol. Phys.*, **14**, 217 (1968).

10) K. Dimroth, *Top. Curr. Chem.*, **38**, 1 (1973).

Kinetic Studies of Solvent and Pressure Effects on Thermochromic Behavior of 6-Nitrospiropyran

Yoshimi Sueishi,* Masanobu Ohcho, and Norio Nishimura
Department of Chemistry, School of Science, Okayama University, Okayama 700
(Received March 13, 1985)

The thermal conversion of 6-nitrospiropyran from a merocyanine form to a spiro form was studied in various solvents and under high pressures. The rates of the thermal conversions were remarkably retarded in polar solvents, and a Kirkwood plot of the rate constants showed a large downward deviation as the solvent polarity increased. The rate constants (on a logarithmic scale) were linearly related to Kosower's *Z*-values. The values of the activation volumes were positive and divided into two groups: $\Delta V^{\neq} \approx 10$ cm^3 mol^{-1} (in nonpolar solvents) and $\Delta V^{\neq} \approx 20$ cm^3 mol^{-1} (in polar solvents). These findings suggest that for the reaction in polar solvents, specific interactions are operating and that the thermal conversion proceeds *via* a transition state which is much less polar than the initial state.

The photochromism and thermochromism of 1′,3′,3′-trimethyl-6-nitrospiro[2*H*-1-benzopyran-2,2′-indoline] (6-nitrospiropyran) have been recognized as the equilibrium between stable colorless and metastable colored forms (Scheme 1).[1]

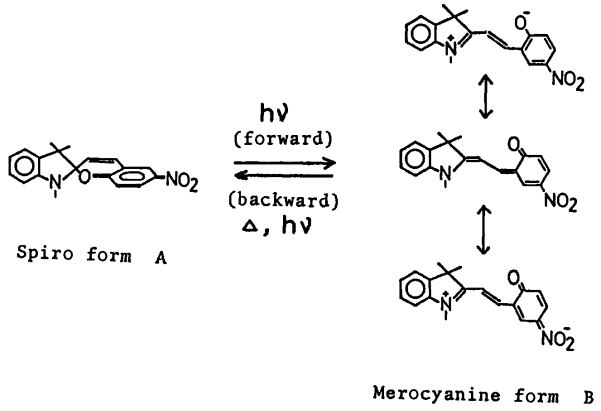

Scheme 1.

The absorption of light transforms the colorless form **A** having reciprocally orthogonal indoline and pyran rings into the colored form **B** having the structure of a merocyanine dye. This merocyanine form is considered as characterized by the coplanarity of the molecular skeleton. In the dark, form **B** thermally isomerizes to form **A**.[1] However, in spite of the fact that there have been some studies regarding the thermochromism of 6-nitrospiropyran, the mechanism of the thermal conversion (**B**→**A**) in relation to the polarity of the transition state has not been well established yet.

Very recently, we reported[2] that in the isomerization of 4-dimethylamino-4′-nitroazobenzene (NDAAB), the activation volumes ($\Delta V^{\neq} < 0$) tend to negatively increase with an increase in the solvent polarity. This trend regarding the pressure effect is just the reverse of that for some ionic reactions such as Menschutkin reactions.[3] We suggested, therefore, that this might be due to the dipole induced by polar solvents. Form **B** in Scheme 1 is electronically similar to *trans*-push-pull azobenzenes in the sense that the conjugation band shows remarkable shifts.[4] Therefore, it is of great interest to investigate the kinetic solvent effects of 6-nitrospiropyran and to compare these with those of push-pull azobenzenes such as NDAAB.

This work has been undertaken from such a point of view and a discussion regarding the electronic structure of the transition state is presented.

Experimental

Reagent. 1′,3′,3′-Trimethyl-6-nitrospiro[2*H*-1-benzopyran-2,2′-indoline] (6-nitrospiropyran) was purchased from Tokyo Chemical Industry Co. and was used as received; mp 179—180 °C (lit,[5] 179—180 °C).

Solvents. All the chemicals were of reagent grade. Hexane, cyclohexane, dioxane, and benzene were purified by drying over sodium wire and distillation. Chloroform, acetone, and acetonitrile were dried over calcium chloride, calcium sulfate, and calcium hydride, respectively, and distilled. *N*,*N*-Dimethylformamide (DMF) and dimethyl sulfoxide (DMSO) were dried over molecular sieves (Type 4A) and calcium hydride, respectively, and distilled under reduced pressure.

Apparatus and Procedure. The high-pressure techniques and procedures for kinetic measurements were the same as those described elsewhere.[2] The sample solution (*ca.* 10^{-4} mol dm^{-3}) was irradiated with a Toshiba H400-P mercury arc through an interference filter (Toshiba UV-D33D) to produce **B**. The thermal return was monitored by the change in the maximum absorption in the vicinity of 600 nm (**B**) by means of a Hitachi 139 spectrophotometer.

Results

The wavelengths at the maximum absorption of **B** of 6-nitrospiropyran and first-order rate constants in various solvents are given in Table 1, together with the activation parameters. The pressure dependence of the rate constants was treated by a quadratic equation (Eq. 1). The rate constants under high pressures and the activation volumes ($\Delta V^{\neq}$) at atmospheric pressure were estimated according to Eq. 2 and are given in Table 2.

Table 1. Rate constants and activation parameters for the thermal conversion of 6-nitrospiropyran (probable errors in parentheses)

	Solvent	Kosower's Z-values[a] / kJ mol^{-1}	λ_{max} / nm	$10^3\,k$/s^{-1} 20 °C	25 °C	30 °C	35 °C	40 °C	45 °C	Ea / kJ mol^{-1}	$\Delta S^*_{303\,K}$ / J K^{-1} mol^{-1}
1	Hexane	252	620, 565	28.1 (1.3)	47.7 (0.2)	78.4 (0.3)	130 (1)			76.4 (0.5)	−22.3 (1.6)
2	Cyclohexane	262	615, 585	20.8 (0.3)	37.6 (0.4)	73.1 (0.1)	105 (2)			83.0 (4.0)	−2.1 (13.2)
3	Dioxane	—	590	32.8 (0.1)	56.6 (0.4)	96.6 (0.1)	153 (1)			77.4 (0.8)	−17.6 (2.8)
4	Benzene	261	600	42.6 (0.1)	66.2 (1.8)	123 (1)	166 (1)			70.6 (3.9)	−38.6 (12.8)
5	Chloroform	264	580		21.9 (0.2)	40.0 (0.4)	79.1 (0.2)	137 (1)		95.9 (1.7)	36.6 (5.7)
6	Acetone	275	565		7.22 (0.04)	12.5 (0.2)	27.2 (0.1)	48.6 (0.2)		101 (4)	43.3 (11.7)
7	DMF	287	560		1.55 (0.07)	3.21 (0.02)	5.49 (0.02)	10.1 (0.1)		96.2 (2.3)	15.9 (7.7)
8	Acetonitrile	298	555		2.99 (0.09)	5.61 (0.02)	11.8 (0.1)	22.3 (0.1)		105 (2)	50.4 (6.7)
9	DMSO	298	550			0.997 (0.009)	1.92 (0.01)	3.56 (0.02)	6.53 (0.04)	101 (1)	21.2 (1.2)

a) Values taken from Ref. 18.

Table 2. Rate constants and activation volumes for the thermal conversion of 6-nitrospiropyran at 30 °C (probable errors in parentheses)

	Solvent	p/kg cm^{-2} [a]	$10^3\,k$/s^{-1} 1	100	200	400	800	1200	ΔV^* / cm^3 mol^{-1}
1	Hexane		78.4 (0.3)			64.6 (0.1)	58.5 (0.3)	53.1 (0.3)	12.8
2	Cyclohexane		73.1 (0.1)	69.9 (0.2)	68.4 (0.2)	63.2 (0.2)			9.4
3	Dioxane		96.6 (0.1)			84.1 (0.1)	71.2 (0.1)	62.4 (0.1)	9.8
4	Benzene		123(1)		118(3)	113(1)	110(1)		6.5
5	Chloroform		40.0 (0.4)			31.4 (0.1)	27.0 (0.1)	22.6 (0.4)	15.1
6	Acetone		12.5 (0.2)			9.61 (0.02)	7.33 (0.05)	5.88 (0.05)	19.5
7	DMF		3.21 (0.02)			2.45 (0.02)	2.06 (0.02)	1.72 (0.02)	17.5
8	Acetonitrile		5.61 (0.02)			4.18 (0.02)	3.17 (0.02)	2.60 (0.01)	21.2
9	DMSO		0.997 (0.009)			0.791 (0.010)	0.670 (0.002)	0.577 (0.003)	15.6

a) 1 kg cm^{-2} = 0.9807 × 10^5 Pa.

$$\ln k = a + bp + cp^2 \quad (1)$$

$$\Delta V^* = \left(\frac{\partial \ln k}{\partial p}\right)_{T,p=1} \approx -bRT \quad (2)$$

Discussion

Regarding the thermal conversion (**B**→**A**) of 6-nitrospiropyran, there are a few reports.[1] For example, Metras *et al.*[6] reported that the competitive ring-closure reaction takes place *via* either of the two conformational isomers. Meanwhile, Arnaud *et al.*[7] inferred the existence of four conformational isomers, and pointed out that a rapid equilibrium is established among them at room temperature and that the thermal conversion from **B** to **A** proceeds from one of them. A similar discussion has been presented by Tamagake *et al.*[8] who suggested eight possible conformational isomers. On the other hand, Flannery, Jr.[9] suggested that a rate-determining step (in polar solvents) is the dissociation of a dimer or of

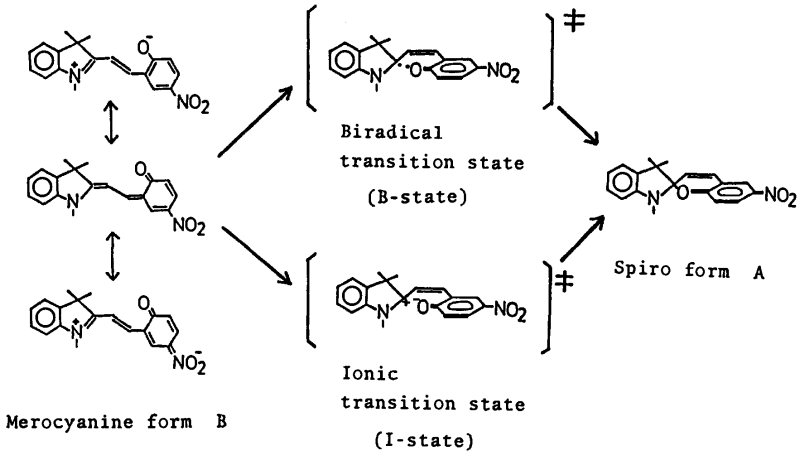

Scheme 2.

a solute-solvent complex.

As far as we examined the electronic spectrum and the time-dependence of its intensity in the dark, any evidence to support the above suggestions has not been found. The visible absorption spectra in alkanes consist of two bands (Table 1). From the temperature dependence of the intensities of these bands, Heiligman-Rim *et al.*[10] concluded that the bands could be ascribed to two different conformational isomers, not to the vibrational structure for a single species. In fact, the relative rate of the disappearance of these bands at any time was constant, indicating that a rapid equilibration between the two isomers had been attained before the ring-closure reaction (**B**→**A**) occured. Judging from the spectral shifts of merocyanine dyes,[11] the band in the vicinity of 620 nm in alkanes could be ascribed to the conformational isomer that dominantly exists in polar solvents (the structure has not been clarified yet). However, even if the reaction proceeds from one of the conformational isomers, there are two possible routes (Scheme 2): One involves the homolytic fission of the bond between the spiro C atom and the pyran oxygen to produce a biradical transition state (B-state) and the other involves a heterolytic fission to produce an ionic transition state (I-state). Since the thermal conversion from **B** to **A** is a Cyclization reaction, it is natural to assume these cyclic transition tates. In the transition state, the delocalization of the π-electrons, substantiated in form **B**, becomes impossible since the indoline and pyran parts of the molecule are reciprocally orthogonal. Accordingly, the I-state must be zwitterionic such as the products of the Menschutkin reaction.[3] In order to clarify which of these routes is more consistent with the experimental observations, we have examined the kinetic solvent and pressure effects regarding the thermal conversion.

Solvent Effects. Figure 1 shows an *Ea vs.* $\Delta S^{\neq}$ plot. Though *Ea* and $\Delta S^{\neq}$ do not necessarily line up in the order of the dielectric constants of the solvents and a scatter is observed, it could be said that the linear free energy relationship[12] roughly holds. If the reaction of this system proceeds by a competitive mechanism[6] and the mechanism continuously varies with solvent polarities,[9] the Ea-$\Delta S^{\neq}$ plot might be curved. From the plots, such an indication is not observed.

On the basis of the Kirkwood treatment,[13] the dielectric influence of solvents on the rate constants for unimolecular reactions is given by

$$\ln k = \ln k_0 + \frac{N}{RT}\left(\frac{\mu_{\neq}^2}{r_{\neq}^3} - \frac{\mu^2}{r^3}\right)\left(\frac{\varepsilon-1}{2\varepsilon+1}\right), \qquad (3)$$

where notations have their usual meanings. If the $(\mu_{\neq}^2/r_{\neq}^3 - \mu^2/r^3)$-term is independent of the solvent polarity, a linearity between ln k and $(\varepsilon-1)/(2\varepsilon+1)$ is expected and the slope can be regarded as a measure of the change in the dipole moment upon activation. As shown in Fig. 2, the linearity is poor. Very recently, a similar nonlinear behavior of the Kirkwood plot was reported by Asano and Okada[14] for the thermal *cis*-to-*trans* isomerization of NDAAB: The plot becomes nonlinear when the points for all polar solvents are included. Asano and Okada interpreted this in terms of a mechanism change from inversion to rotation. According to our view,[2] however, such a behavior is not due to the intervention of a competitive reaction but arises due to the neglect of the induced dipole in the polar solvents. The solvent-induced dipole moment is not involved in the Kirkwood treatment.

Recently, ^{1}H- and ^{13}C-NMR spectroscopy have been applied to the problem of the electronic structure of the molecules having a conjugation system. For instance, on the basis of the ^{1}H-NMR spectral shifts in various solvents, Mottaleb and Kader[15] interpreted their shifts as an indication of a solvent-induced change in the electronic structure. Moreover, in a

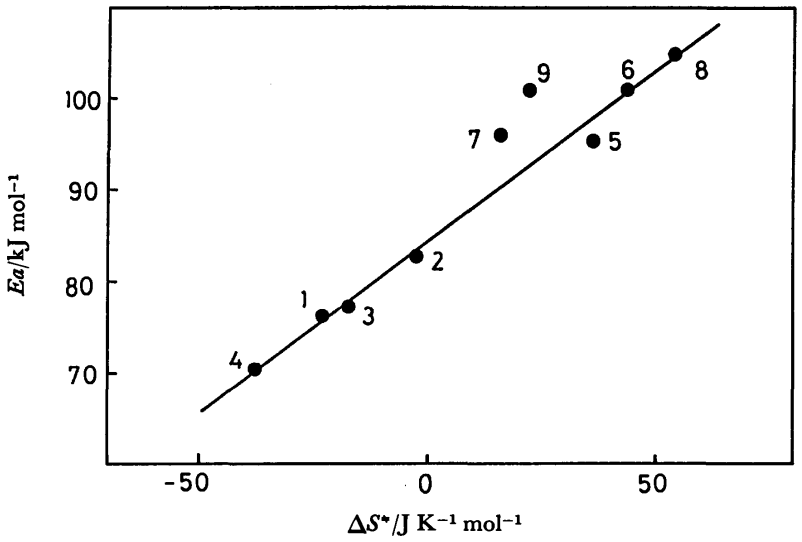

Fig. 1. Ea-ΔS^* relationship for the thermal conversion of 6-nitrospiropyran at 30 °C; correlation coefficient r 0.964.

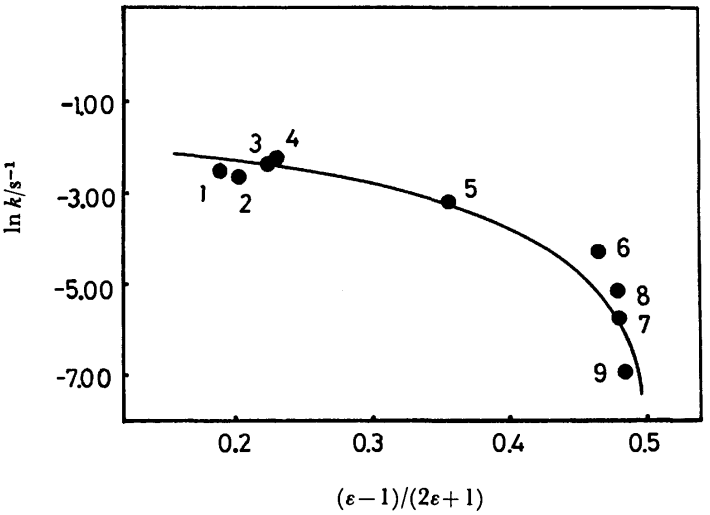

Fig. 2. The Kirkwood plot for the thermal conversion of 6-nitrospiropyran at 30 °C; correlation coefficient r −0.909.

theoretical investigation through the CNDO/S-CI method (including solvation for 4-[2-(1-methyl-4-pyridinio)ethenyl]phenolate which has a large π-electron system) Botrel *et al.*[16] showed a significant increase in the dipole moment with an increasing solvent polarity, and pointed out that it is important to take account of the change in the dipole moment induced by surrounding solvents. These are in accordance with our view.

In this connection, we considered that scales involving solute-solvent interactions at molecular levels would be better than a macroscopic dielectric constant in order to analyze the reaction-rate data. Whitten *et al.*[17] examined the relationship between the activation parameter $\Delta G^{\neq}$ of the thermal *cis*-to-*trans* isomerization of 4-diethylamino-4′-nitroazobenzene and the empirical scales (Koswer's Z-values, the Taft π^* parameter *etc.*), and have shown that they are linearly related (as a whole). We also have tentatively plotted ln k against Kosower's Z-values[18] (Fig. 3). Although a considerable scatter is observed (as in the case of azobenzenes shown in Ref. 17) the linearity is much improved over the Kirkwood plot. We could say, therefore, that for reactions where the change in the delocalization of π-electrons upon activation plays an important role, these empirical scales are better than the macroscopic ε-scale, although the choice of those scales is somewhat arbitrary.

In any case, the reaction rates were remarkably retarded in polar solvents (Table 1). If a biradical mechanism (Scheme 2) is assumed for the reaction, the transition state may be less polar than the initial one. This accounts for the above observations. On the contrary, if the reaction proceeds *via* the I-state,

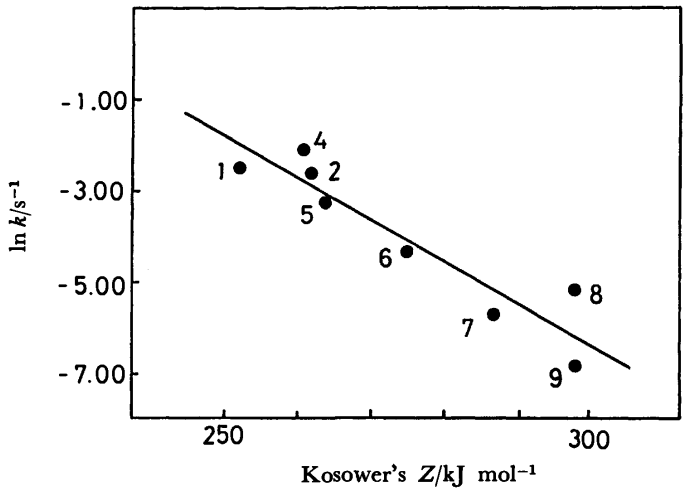

Fig. 3. $\ln k$ (at 30 °C) *vs.* Kosower's Z-values; correlation coefficient r −0.931.

an acceleration of the reaction rate is expected in analogy with the case of the Menschutkin reaction.[3] This is against the experimental observations.

Pressure Effects. The activation volume ($\Delta V^{\neq}$) is given (after differentiating Eq. 1 with respect to pressure) by,

$$\Delta V^{*} = \Delta V_0^{*} - N\left(\frac{\mu_{*}^{2}}{r_{*}^{3}} - \frac{\mu^{2}}{r^{3}}\right)\frac{3}{(2\varepsilon+1)^{2}}\left(\frac{\partial\varepsilon}{\partial p}\right)_T \quad (4)$$

where $\Delta V_0^{\neq}$ is the difference in the intrinsic volume of a reaction molecule between the initial and the transition states. The second term represents the change in volume due to solvation or electrostriction. In our case, if the thermal conversion (**B**→**A**) proceeds *via* the cyclic transition state, it may safely be considered that the change in the intrinsic volume ($\Delta V_0^{\neq}$) accompanying cyclization upon activation is similar to the activation volume of the Claisen rearrangement reaction,[19] which is considered not to involve a volume change due to electrostriction. The reported activation volumes are about −15 cm^3 mol^{-1} for the Claisen rearrangement reaction.[19] If the reaction proceeds *via* the zwitterionic transition state, solvent may be constricted upon activation, as exemplified by the Menschutkin reaction.[3] Accordingly, the value for the activation volume ($\Delta V^{\neq}$) is large and negative, as expected from Eq. 4. On the contrary, if the biradical mechanism is assumed for the reaction, a positive activation volume is expected due to the release of electrostricted solvent molecules, as Stwart and Weale[20] reported for the reverse Menschutkin reaction ($\Delta V^{\neq}$=45 cm^3 mol^{-1}). As can be seen in Table 2, the activation volumes obtained are all positive and divided roughly into two groups: $\Delta V^{\neq}\approx$10 cm^3 mol^{-1} (in nonpolar solvents) and $\Delta V^{\neq}\approx$20 cm^3 mol^{-1} (in polar solvents). Therefore, the biradical mechanism is more favorable than the ionic one.

On the assumptions of the biradical mechanism and $\Delta V_0^{\neq}\approx$−15 cm^3 mol^{-1}, the activation volume can be estimated according to Eq. 4. In benzene, by substituting the numerical values (μ=12.7 Debye,[21] $\mu_{\neq}\approx$0 Debye, r=4 Å (the distance between >N- and the nitro group), and $[3/(2\varepsilon+1)^2](\partial\varepsilon/\partial p)_T$=15×10^{-11} Pa^{-1} at 30 °C[22]) into Eq. 4, the change in volume due to desolvation is calculated to be 23 cm^3 mol^{-1}. Therefore, the total volume change ($\Delta V^{\neq}$) is calculated to be 8 cm^3 mol^{-1}. Similarly, the activation volume in hexane ($[3/(2\varepsilon+1)^2](\partial\varepsilon/\partial p)_T$=19.4×10^{-11} Pa^{-1} at 30 °C[22]) is estimated to be 14 cm^3 mol^{-1}. As may be seen in Table 2, these estimated values are approximately in accordance with the experimental ones. Similarly, the activation volume in acetone can be estimated as −7.7 cm^3 mol^{-1} ($[3/(2\varepsilon+1)^2](\partial\varepsilon/\partial p)_T$= 4.82×10^{-11} Pa^{-1} at 30 °C[22]). This value is extremely small compared with the observed one. The large discrepancy between the calculated and observed $\Delta V^{\neq}$-values in acetone may be ascribed to a change in the μ-term in Eq. 4 upon increasing the polarity of the solvent. In a previous section, we considered that the B-state is plausible and the extra dipole moment of form B with an ionic resonance structure is induced in polar solvents. The large positive $\Delta V^{\neq}$-value in acetone may be resposible for the increase in the dipole moment. The same trend has been observed for the thermal *cis*-to-*trans* isomerization of push-pull azobenzenes. The common situation is that a remarkable polarization through the delocalization of the π-electrons is considered to be substantiated both in the ground state (present case) and in the transition state (case of push-pull azobenzenes), and that the contribution of the polarized canonical resonance form is reinforced by polar solvents, in agreement with other evidence.[15,16] The large $\Delta V^{\neq}$-values in polar solvents can be qualitatively explained by this reasoning.

In conclusion, the kinetic solvent and pressure

effects are in favor of the biradical mechanism *via* the less-polar transition state for the thermal conversion (**B**→**A**) of 6-nitrospiropyran and against the ionic one *via* the polar transition state.

References

1) G. H. Brown, "Photochromism", Wiley, New York (1971) and references therein.

2) N. Nishimura, S. Kosako, and Y. Sueishi, *Bull. Chem. Soc. Jpn.*, **57**, 1617 (1984).

3) Y. Kondo, M. Uchida, and N. Tokura, *Bull. Chem. Soc. Jpn.*, **41**, 992 (1968) and references therein.

4) I. Shimizu, H. Kokado, and E. Inoue, *Kogyo Kagaku Zasshi*, **70**, 2344 (1970).

5) C. Balny and P. Douzou, *Mol. Photochem.*, **1** (2), 225 (1969).

6) T. C. Metras, M. Mosse, and C. Wippler, *J. Chim. Phys.*, **62**, 659 (1965).

7) J. Arnaud, C. Wippler, and F. Beaure D'Augeres, *J. Chim. Phys.*, **64**, 1165 (1967).

8) K. Tamagake, Y. Kohno, Y. Shiota, and Y. Fujita, *Nippon Kagaku Kaishi*, **1984**, 82.

9) J. B. Flannery, Jr, *J. Am. Chem. Soc.*, **90**, 5660 (1968).

10) R. Heiligman-Rim, Y. Hirshberg, and E. Fisher, *J. Phys. Chem.*, **66**, 2465, 2470 (1962).

11) A. Le Beuze, A. Botrel, A. Samat, P. Appriou, and R. Guglielmetti, *J. Chim. Phys.*, **75**, 255 (1978).

12) L. E. Leffler and E. Grunmald, "Rate and Equilibria of Organic Reaction," Wiley, New York (1963) and references therein.

13) J. Kirkwood, *J. Chem. Phys.*, **2**, 351 (1934).

14) T. Asano and T. Okada, *J. Org. Chem.*, **49**, 4389 (1984).

15) M. S. A. Abdel-Mottaleb and M. N. Abdel-Kader, *Indian J. Chem.*, **22B**, 1217 (1983).

16) A. Botrel, A. Le Beuze, P. Jacques, and H. Strub, *J. Chem. Soc., Faraday Trans. 2*, **80**, 1235 (1984).

17) K. S. Schanze, T. F. Mattox, and D. G. Whitten, *J. Org. Chem.*, **48**, 2808 (1983).

18) G. Irick and J. G. Pacifici, *Text. Res. J.*, **1972**, 391.

19) C. Walling and M. Naiman, *J. Am. Chem. Soc.*, **84**, 2628 (1962). E. Whally, *Adv. Phys. Org. Chem.*, **2**, 93 (1964).

20) J. M. Stewart and K. E. Weale, *Proc. Chem. Soc.*, 389 (1961).

21) D. Lapinenis-Grochowska, M. Kryszewski, and B. Nadolski, *J. Chem. Soc., Faraday Trans. 2*, **75**, 312 (1979).

22) H. Hartmann, A. Neunann, and G. Rinck, *Z. Phys. Chem.*, **44**, 204 (1965).

NQR Study of Phase Transitions in $SbCl_3 \cdot (C_6H_5)_2NH_2^+Cl^-$ and $2SbCl_3 \cdot C_6H_5OCH_3$

Hideta ISHIHARA,* Tsutomu OKUDA,† Koji YAMADA,† and Hisao NEGITA†
Department of Chemistry, Faculty of Education, Saga University, Honjo-machi, Saga 840
†*Department of Chemistry, Faculty of Science, Hiroshima University, Naka-ku, Hiroshima 730*
(Received March 29, 1985)

The temperature dependence of ^{35}Cl and $^{121,123}Sb$ NQR frequencies was measured in $SbCl_3 \cdot (C_6H_5)_2NH_2^+Cl^-$ between 77 and 300 K. A phase transition takes place at 108 K and ^{35}Cl NQR lines disappeared above about 275 K. Possible mechanisms of the phase transition and of the disappearance of ^{35}Cl NQR lines were suggested. The phase transition in $2SbCl_3 \cdot C_6H_5OCH_3$ was investigated by the NQR technique. The temperature dependence of the splitting of the $^{121}Sb(\nu_1)$ NQR lines in the low-temperature phase gave a critical exponent of $\beta=1/2$ near the transition point T_c. A Zeeman-effect experiment revealed that the crystals in both low- and high-temperature phases were monoclinic.

In the course of the study regarding the bond character in $SbCl_3$ molecular complexes[1,2] we have observed the phase transition and the disappearance of ^{35}Cl NQR lines in $SbCl_3 \cdot (C_6H_5)_2NH_2^+Cl^-$. A possible mechanism for the phase transition could be inferred on the basis of the crystal structure.[3] Kyuntsel' and Rosenberg reported a phase transition at 141 K in $2SbCl_3 \cdot C_6H_5OCH_3$ and suggested that the change of the relative position of $SbCl_3$ and methoxybenzene molecules took part in the phase transition.[4] We carried out a Zeeman-effect experiment on this compound in order to obtain information regarding the crystal structure.

Experimental

The compounds were prepared by melting and mixing $SbCl_3$ with diphenylammonium chloride and methoxybenzene in a molar ratio of 1:1 and 2:1, respectively. A single crystal of $2SbCl_3 \cdot C_6H_5OCH_3$ was prepared by the Bridgman method. NQR lines were displayed on an oscilloscope using a supperregenerative oscillator with the frequency modulation or recorded on a pen-recorder using an oscillator with the Zeeman modulation and a lock-in amplifier.

Results and Discussion

The results of the NQR measurement are listed in Table 1. The values for $2SbCl_3 \cdot C_6H_5OCH_3$ at 77 K are comparable to those already reported.[5]

$SbCl_3 \cdot (C_6H_5)_2NH_2^+Cl^-$. Figure 1 shows the temperature dependence of ^{35}Cl and $^{123}Sb(\nu_1)$ NQR frequencies between 77 and 300 K. The frequency-temperature curves of ^{35}Cl NQR lines showed a discontinuity at 108 K. The $^{121,123}Sb$ NQR lines were not observed below 108 K. We intended to search for the Sb NQR lines at 77 K between 6 and 48 MHz.

TABLE 1. NQR PARAMETERS FOR $SbCl_3 \cdot (C_6H_5)_2NH_2^+Cl^-$ AND $2SbCl_3 \cdot C_6H_5OCH_3$

Compound	T/K	Assignment		ν/MHz	
$SbCl_3 \cdot (C_6H_5)_2NH_2^+Cl^-$	77	^{35}Cl		20.39, 18.03, 17.32	
	109	^{123}Sb	ν_1[a]	29.96	$e^2Qq/h(^{121}Sb)=308.9$ MHz[b]
		^{121}Sb	ν_1	47.27	$\eta=0.136$
	263	^{35}Cl		19.91, 17.85, 17.10	
		^{123}Sb	ν_1	28.06	$e^2Qq/h(^{121}Sb)=294.4$ MHz[b]
		^{121}Sb	ν_1	44.85	$\eta=0.119$
$2SbCl_3 \cdot C_6H_5OCH_3$	77	^{35}Cl		20.82, 20.50, 20.42, 20.19, 19.14, 19.12	
		^{121}Sb	ν_1	63.12	$e^2Qq/h(^{121}Sb)=411.9$ MHz[c]
		^{121}Sb	ν_2[a]	123.09	$\eta=0.141$
		^{121}Sb	ν_1	61.19	$e^2Qq/h(^{121}Sb)=401.1$ MHz[c]
		^{121}Sb	ν_2	119.97	$\eta=0.125$
	R.T.[d]	^{35}Cl		19.81, 19.72, 18.80	
	298	^{121}Sb	ν_1	59.41	$e^2Qq/h(^{121}Sb)=389.1$ MHz[c]
		^{121}Sb	ν_2	116.38	$\eta=0.130$

a) ν_1 and ν_2 are frequencies corresponding to the transitions $\pm1/2 \leftrightarrow \pm3/2$ and $\pm3/2 \leftrightarrow \pm5/2$, respectively. b) The values of e^2Qq/h and η were derived from the frequency ratio of $\nu_1(^{121}Sb)/\nu_1(^{123}Sb)$. c) The values of e^2Qq/h and η were derived from the frequency ratio of ν_1/ν_2 for ^{121}Sb. d) R.T. signifies room temperature.

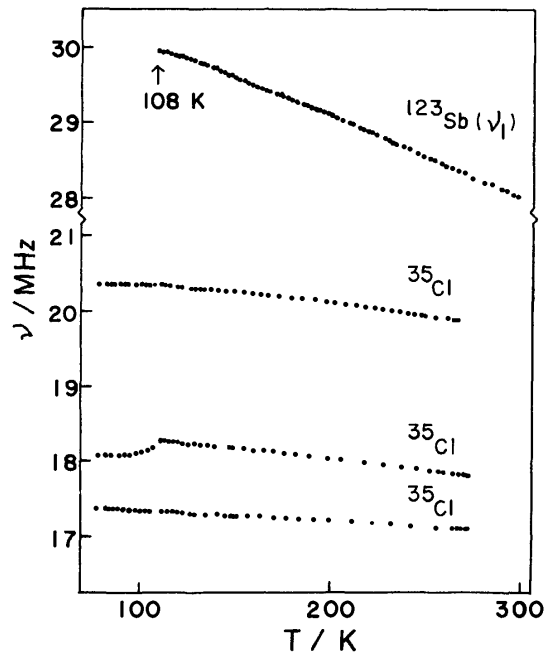

Fig. 1. Temperature dependence of $^{123}Sb(\nu_1)$ and ^{35}Cl NQR frequencies in $SbCl_3 \cdot (C_6H_5)NH_2{}^+Cl^-$.

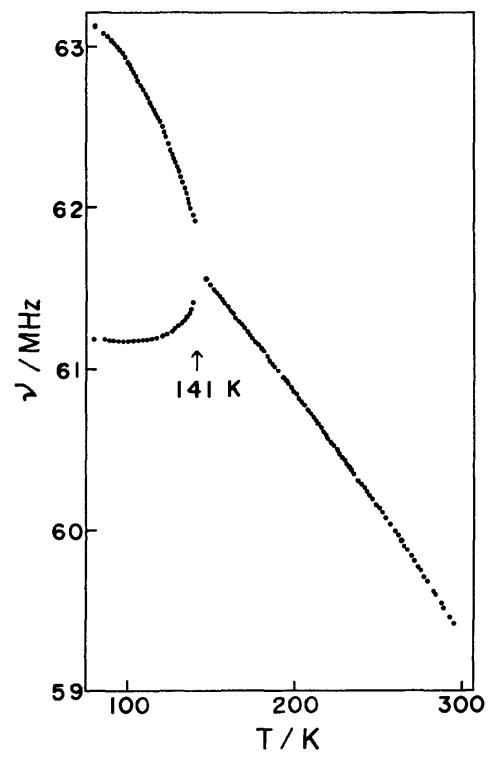

Fig. 2. Temperature dependence of $^{121}Sb(\nu_1)$ NQR frequencies in $2SbCl_3 \cdot C_6H_5OCH_3$.

One weak NQR line was recorded at 20.52 MHz and this line could not be assigned because the NQR line due to the corresponding isotope was not observed. One ^{35}Cl NQR line shows a greater frequency shift than the other two lines in the low-temperature phase. An assignment of the ^{35}Cl NQR lines to each chlorine atom in a crystal can be made on the basis of the relation between the Sb-Cl bond length and the ^{35}Cl NQR frequency,[2] *i.e.*, the NQR frequency generally decreases with an increasing bond length. Accordingly, this line is assigned to the chlorine atom in a position *trans* to the chloride ion situated at a distance of 3.130 Å from the Sb atom.[3] This chloride ion also forms a N-H···Cl^- hydrogen bond with the diphenylammonium cation.[3] We consider that in the low-temperature phase the N-H bond length becomes short and this results in the weakning of the H···Cl^- interaction and the approach of the chloride ion to the Sb atom. Therefore, below the transition point the coordination state about the Sb atom changes and then the Sb NQR frequencies change greatly. In addition, a ^{35}Cl NQR line due to a chlorine atom in the Sb-Cl bond *trans* to this chloride ion shows a decreased frequency since the Sb-Cl bond is weakened by the *trans* influence. This could be seen in some other $SbCl_3$ complexes.[1,2]

The ^{35}Cl NQR lines disappeared above about 275 K, but the Sb NQR lines were observed at room temperature. From the results of a ^1H NMR measurement, the second moment decreased from 9 G^2 at 270 K to 5 G^2 at 300 K. In addition, the thermal parameters of the carbon atoms in the diphenylammonium cation have large values according to an X-ray crystal-structure analysis.[3] These facts show that some motions of the cation take place at room temperature. We consider that these cation motions and/or the reorientation of the $SbCl_3$ molecule as is seen in $SbCl_3 \cdot C_8H_{10}$[2] cause the disappearance of the ^{35}Cl NQR lines. We could not observe the thermal anomaly around the transition point by a differential thermal analysis.

$2SbCl_3 \cdot C_6H_5OCH_3$. Figure 2 shows the temperature dependence of $^{121}Sb(\nu_1)$ NQR frequencies between 77 and 300 K. Below the transition point, the resonance line splits into two lines with equal intensity. The frequency difference Δ in the low-temperature phase serves as a measure of the order parameter.[6,7] It could be seen from the plot of Δ^2 as a function of temperature that Δ^2 was a linear function between 123 and 138 K. Then, the transition point T_c was obtained by a best-fit procedure and it gave T_c=141.3±0.8 K. Using this value, it was also possible to fit Δ to the function[6]

$$\Delta = D\varepsilon^{\beta}, \tag{1}$$

where $\varepsilon = |T_c - T|/T_c$ and β is the critical exponent. The values of D and β were obtained by the best fit of a log-log plot and it gave D=3.2±0.2 MHz and β=0.50±0.01 between $\varepsilon = 2.1\times10^{-2}$ and $\varepsilon = 1.2\times10^{-1}$. In

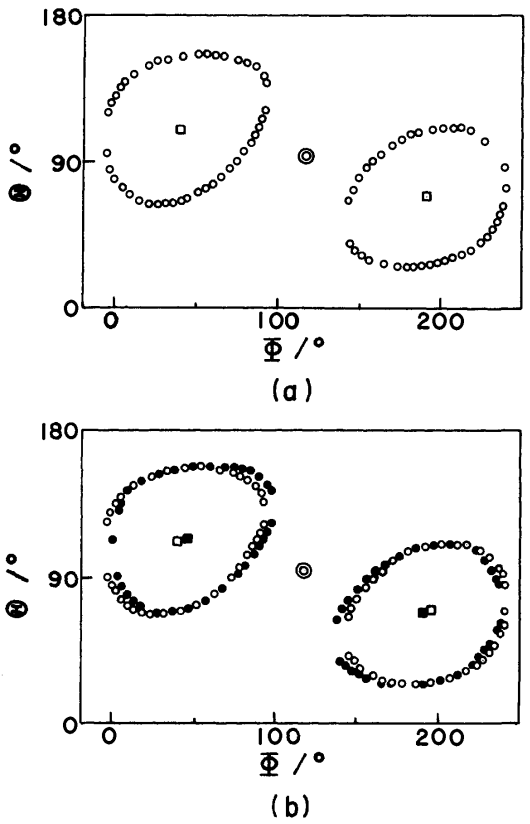

Fig. 3. Zero-splitting loci for $^{121}Sb(\nu_1)$ NQR lines in $2SbCl_3 \cdot C_6H_5OCH_3$.
(a) Zero-splitting loci at room temperature.
(b) Zero-splitting loci at liquid-nitrogen temperature, ● for the 63-MHz line and ○ for the 61-MHz line. ■ and □: principal z-axes of EFG tensors; ◎: two-fold axis.

addition, the average frequency of the two split lines in the low-temperature phase was not continuously connected with the extraporation of the high-temperature curve. These experimental results confirm that β=0.5. This value is consistent with what the usual molecular field theory predicts.[6,7]

Figure 3 shows the zero-splitting loci at room temperature and liquid-nitrogen temperature. The single crystal for the Zeeman experiment was not broken by repeated heating and cooling cycles through the transition point. The measured points were fitted to the equation of a quadratic cone by the least-squares method in order to obtain the direction of the principal axes of the electric field gradient (EFG) tensor and the asymmetry parameter η. The obtained values of η were 0.142±0.007 for the 63-MHz line and 0.130±0.003 for the 61-MHz line at liquid-nitrogen temperature and 0.138±0.005 for the line at room temperature, respectively. The polar coordinates (Φ, Θ) for the principal z-axes of the EFG tensors in both phases are listed in Table 2 with respect to an orthogonal-axis system fixed to a

Table 2. Polar coordinates of the principal z-axes of EFG tensors

Temperature	Resonance line	(Φ, Θ)/° [a]	
ca. 300 K		(39.0, 112.1)	(192.6, 70.2)
ca. 77 K	63-MHz	(42.1, 113.8)	(189.0, 69.4)
	61-MHz	(36.9, 111.8)	(194.3, 70.3)

a) The standard deviations of the directions of the magnetic field for zero-splitting from the leat-squares method are 0.2° at room temperature and 0.5° at liquid-nitrogen temperature.

crystal. The four zero-splitting loci which showed a Laue symmetry $2/m$ were obtained for each line in both phases. Only a pair of cones related to each other by the two-fold axis are represented in Fig. 3. The polar coordinates for the two-fold axis were obtained from the symmetry among the zero-splitting loci, *i.e.*, (117.7, 95.1) for the high-temperature phase and (117.6, 95.3) for the low-temperature phase. The Laue symmetry shows that the crystal in each phase belongs to a monoclinic system considering a number of ^{35}Cl and $^{121,123}Sb$ NQR lines. It is also apparent that two $SbCl_3$ molecules represented by the chemical formula are crystallographically equivalent in the high-temperature phase. We consider that the crystal in the high-temperature phase has two types of symmetry elements, *i.e.*, a two-fold screw axis and a center of symmetry by which two $SbCl_3$ molecules are related to each other and that the crystal loses its center of symmetry in the low-temperature phase. A phenomenon like this has been actually observed in $NH_4H(ClCH_2COO)_2$.[8] In addition, we suggest that the loss of the center of symmetry arises from the displacement of a methoxybenzene molecule. This suggestion could be derived from the results of an observation of the ^{35}Cl NQR lines.

In the 2:1 $SbCl_3$ molecular complexes with aromatic compounds, the lowest NQR line is generally assigned to the chlorine atom in the Sb–Cl bond perpendicular to the aromatic ring and the other chlorine atoms in the Sb–Cl bonds parallel to the ring give the higher NQR lines.[2] On the basis of the NQR frequencies for $2SbCl_3 \cdot C_6H_5OCH_3$ at room temperature, two resonance lines around 19 MHz were assigned to the chlorine atoms in the parallel Sb–Cl bonds and the line around 18 MHz to the one in the perpendicular Sb–Cl bond. Although each resonance line splits into two lines and, therefore, six resonance lines are observed in the low-temperature phase, we could distinguish three pairs of lines and also assigned them to individual lines in the high-temperature phase on the basis of the intensity ratio of the resonance lines for a single crystal. The magnitudes of the splittings at 77 K are 400 and 310 KHz for the chlorine atoms in the parallel Sb–Cl

bonds and 20 KHz for the one in the perpendicular Sb–Cl bond. The change of the crystal field which arises from the displacement of the methoxybenzene molecule must largely affect the chlorine atoms in the parallel Sb–Cl bonds near the ring. This is consistent with a suggestion by Kyuntsel' and Rosenberg.[4] For a more detailed discussion, a crystal-structure analysis is necessary. A differential thermal analysis shows that there is a small shift of the base line at the transition point and it is considered that a discontinuous change in the specific heat takes place.

References

1) T. Okuda, S. Gima, H. Ishihara, and H. Negita, *J. Mol. Struct.*, **81**, 261 (1982).

2) H. Ishihara, *J. Sci. Hiroshima Univ., Ser. A.* **45**, 319 (1981).

3) Von A. Lipka and D. Mootz, *Z. Anorg. Allg. Chem.*, **440**, 231 (1979).

4) I. A. Kyuntsel' and Yu. I. Rosenberg, *Teor. Eksp. Khim.*, **7**, 565 (1971).

5) V. S. Grechishkin and I. A. Kyuntsel', *Trudy ENI Permsk, State Univ.*, **12**, 9 (1966).

6) A. Zussman and A. Alexander, *J. Chem. Phys.*, **49**, 3792 (1968).

7) H. Chihara, N. Nakamura, and H. Okuma, *J. Phys. Soc. Jpn.*, **37**, 1385 (1974).

8) H. Chihara, A. Inaba, N. Nakamura, and T. Yamamoto, *J. Phys. Soc. Jpn.*, **35**, 1480 (1973).

Studies of Polystyrene-based Ion-exchange Fiber. III. A Novel Fiber-form Chelating Exchanger and Its Adsorption Properties for Heavy-metal Ions†

Toshio YOSHIOKA
Fibers Research Laboratories, Toray Industries, Inc., Sonoyama, Otsu 520
(Received May 4, 1985)

Fibrous chelating exchangers with $-N(CH_2COOH)_2$ and $-N(CH_2CH_2COOH)_2$ groups have been prepared for the first time by using a polystyrene–polypropylene composite fiber as the starting material. They have large surface areas per unit of weight and can be utilized in various forms. The properties of adsorbing Cu^{2+} are compared between these chelating fibers and an ordinary chelating resin. The former groups form more stable complexes with Cu^{2+} than the latter, probably because of their different chelating structure. The rate of the adsorption of Cu^{2+} to the fibers is dependent upon their water content and is from ten to fifty times as high as that to the resin. These results are explained by assuming that the diffusion within the exchangers is the major rate-controlling step in the adsorption process. The diffusion equation of isotopic ion exchange for a cylindrical endless fiber was solved in the case of ideal particle-diffusion control by modifying the method used for a spherical resin. The experimental data are interpreted in terms of their theoretical solutions. For practical application, the removal of Cu^{2+} and Mn^{2+} from various solutions was also carried out by using fixed-beds of these chelating fibers.

The preparation methods, fundamental characteristics, and acid-base catalytic properties of a polystyrene-based ion-exchange fiber (IONEX) have already been reported by the present author and his co-worker.[1,2] This ion-exchanger based on a polystyrene–polypropylene composite fiber has high mechanical strengths and can be used in various forms. The ion-exchange fiber also has two fundamental characteristics because of its larger surface areas; the ion exchange rate for metal ions is extremely high, and the capacity for adsorbing the macromolecular ionic substances is exceedingly large, compared with ordinary ion-exchange resins. Taking the latter characteristic into account, we have also studied the adsorption or immobilization to IONEX of biologically-active substances, such as enzyme, protein, and microorganism cell. These results have been published in preliminary reports.[3] Polystyrene is suitable for the addition not only of ionic groups, but also of various functional groups. The introduction of special functional groups to crosslinked polystyrene–polypropylene composite fibers is of especial interest. The quaternary phosphonium ions and crown ethers supported on the polystyrene–polypropylene composite fiber have been investigated as phase-transfer catalysts for numerous organic reactions by Tomoi and Kakiuchi.[4]

Recently selective chelating resins based on a styrene–divinylbenzene polymer have been intensively studied[5–8] and used for the separation, removal, and recovery of heavy-metal ions in the fields of waste-fluid treatment, the atomic-power industry, the food industry, and analytical chemistry. The use of chelating resins, however, has the disadvantage that the adsorption rate is very low because of their small ion dissociation in comparison with strong cation- and anion-exchange resins.[9–13] Although the adsorption rate is enhanced by using fine or crushed resins, the treatment of such resins becomes difficult.[11,13] It is also well-known that adsorption properties are affected by the physical structure of polymers supporting chelating groups.

In order to enhance the adsorption rate and to make the treatment easier, we have undertaken an investigation of fibrous chelating exchangers, which have large surface areas per unit of weight and which can be used in various forms. An iminodicarboxylic-acid-type chelating fiber has been prepared, for the first time, by using the polystyrene–polypropylene composite fiber as the starting material; it has then been used in the adsorption of Cu^{2+}.[14] In this paper the author would like to report on this chelating fiber and its ability to adsorb Cu^{2+}. The results of the adsorption rate will be discussed in terms of the kinetic theory of isotopic ion exchange for fiber systems, which is introduced in detail here. The results of removing Cu^{2+} and Mn^{2+} from various solutions by fixed-beds of the chelating fiber will also be described.

Experimental

Polystyrene–Polypropylene Composite Fiber. Forty-nine parts of polystyrene and 12 parts of polypropylene as the *sea* ingredient and 39 parts of polypropylene as the *island* ingredient were melt-spun at 255 °C into composite filaments with an *islands-in-a-sea* type sectional structure, as is shown in Fig. 1. The composite filaments were drawn five times as long as their original length in a conventional manner. The diameters of the *sea* and the *islands* of the resulting filaments were 20 and 3.1 μm respectively. Their tensile strength was 2.5 g d^{-1}.[14]

Crosslinked Polystyrene–Polypropylene Composite Fiber. Ten grams of the fiber were high-(or low-) crosslinked in 100 ml of a solution consisting of 5 wt% paraformaldehyde, 25 (45) wt% acetic acid, and 70 (50) wt% concd sulfuric acid

† A preliminary report of this work was presented in *Polym. Prepr. Jpn.*, **33**, 1615 (1984).

at 80 °C for 2 h.[14]

Iminodiacetic-acid(IDA)-type Chelating Fiber. Ten grams of the crosslinked fiber were acrylamidomethylated in a solution comprising 20 g of bis(acrylamidomethyl) ether, 200 ml of nitrobenzene, and 140 g of concd sulfuric acid at room temperature for 20 h. After being extracted with methanol, the fiber was treated in 450 ml of concd hydrochloric acid at 105 °C for 20 h; it was thus hydrolyzed into an aminomethylated fiber.[15] The IDA-type chelating IONEX was obtained by treating the aminomethylated fiber (10 g) with a solution consisting of 27 g of chloroacetic acid, 11 g of sodium hydroxide, 19 g of sodium carbonate, and 130 g of water at 100 °C for 8 h.[14] The structure of the IDA chelating group is shown in Fig. 2.

Iminodipropionic-acid(IDP)-type Chelating Fiber. Ten grams of the crosslinked fiber were chloromethylated in a solution comprising 100 ml of chloromethyl methyl ether and 10 ml of tin(IV) chloride at 30 °C for 1 h. Ten grams of the chloromethylated fiber were treated in a solution consisting of 160 g of *N, N, N″, N″*-tetrakis(2-cyanoethyl)diethylenetriamine and 350 ml of dioxane at 70 °C for 6 h. The IDP-type chelating IONEX was obtained by treating the fiber with 450 ml of concd hydrochloric acid at 60 °C for 6 h.[14,16] The structure of the IDP chelating group is also shown in Fig. 2.

Adsorption Capacity of Cu^{2+}. A chelating IONEX (0.25 g in the Na form) was added to 100 ml of a 0.013 M†† Cu^{2+} solution containing 0.5 M NaCl and a Clark Lubs buffer of pH 6.0, and then the mixture was strongly shaken at 20 °C for 24 h. The adsorption capacity of Cu^{2+} to the fiber was evaluated by measuring the concentration of Cu^{2+} in the solution before and after the adsorption treatment.

Water Content. A chelating IONEX in the Na form was immersed in a bath of deionized water at room temperature for a sufficient period of time to reach saturation. The fiber was then centrifugally dehydrated at 3000 r.p.m. for 5 min. Immediately thereafter, the wet weight (W) of the fiber was measured. The water content of the fiber was determined from the following equation:

$$\text{Water content} = (W - W_0)/W_0,$$

where W_0 is the absolutely dry weight of the fiber.

Chelating Resin and Measurements. The bead chelating resin (Diaion CR-10, IDA-type resin based on styrene-divinylbenzene copolymer) with a diameter of *ca.* 400 μm and a water content of 1.7 was obtained from the Mitsubishi Kasei Kogyo Co., Ltd. (Japan). The concentrations of Cu^{2+} and Mn^{2+} were determined by using an atomic absorption photometer.

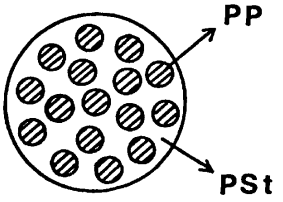

Fig. 1. Schematic cross section of composite fiber. Pst: Polystyrene, *sea* ingredient; PP: polypropylene, *island* ingredient.

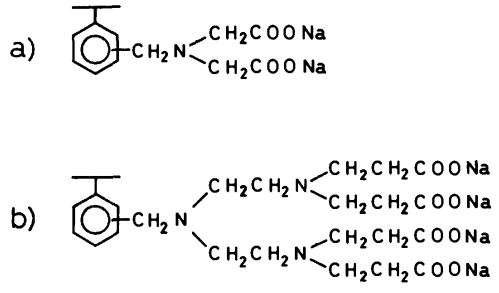

Fig. 2. Structures of the iminodicarboxylic-acid chelating groups. a) IDA-Na, b) IDP-Na.

†† 1 M=1 mol dm^{-3}.

Results and Discussion

Fibrous Chelating Exchanger. The process of preparing the chelating fiber is shown in Fig. 3. The chelating fiber in various forms, such as filament, cut fiber, knitted fabric, woven fabric, braid, felt, nonwoven fabric, chip, and paper, can be obtained by processing the polystyrene-polypropylene composite fiber before crosslinking reactions, as the fiber reinforced with polypropylene has high mechanical strengths. Figure 4 shows the polystyrene-poly-

Fig. 3. Process of preparing the polystyrene-based chelating fiber.

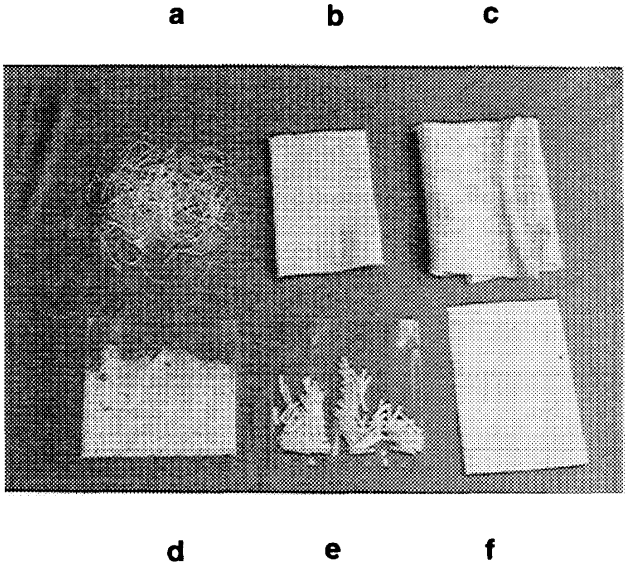

Fig. 4. Polystyrene-polypropylene composite fiber in various forms of filament (a), needle punched felt (b), knitted fabric (c), cut fiber (d), chip (e), and paper (f).

propylene composite fiber in the various forms. The characteristic data of the chelating IONEX are summarized in Table 1. The chelating filaments had a diameter of *ca.* 30 μm and exhibited a tensile strength of *ca.* 1.0 g d^{-1}. It was found that the low-crosslinked fibers have larger adsorption capacities and water contents than the high-crosslinked ones. The former result is explained by the fact that the amount of the aminomethyl or chloromethyl group introduced in the synthetic process is larger in the case of the low-crosslinked fiber because of its high reactivity.

Equilibrium Adsorption. The correlation between the adsorption capacity of Cu^{2+} and the pH in the solution for various chelating exchangers is shown in Fig. 5. The IDA-type fiber exhibits the same pH dependence as the CR-10 resin. The half-pH, where the adsorption capacity becomes half of pH 5.2, is 1.7. On the other hand, the IDP-type fiber exhibits a different pH dependence from the IDA-type; here, the half-pH is 2.9. These results indicate that the IDA type forms more stable complexes with Cu^{2+} than the IDP type.[7] This fact can be explained by assuming that the former coordinates to Cu^{2+} by forming five-members rings while the latter does so by forming six-members rings.

Adsorption Rate Ion exchange between the Na form of a chelating exchanger (0.25 g) and a 0.013 M Cu^{2+} solution containing 0.5 M NaCl and a Clark Lubs buffer of pH 6.0 (100 ml) was examined. Figure 6 displays the fractional attainment of the equilibrium as a function of the time. The fibers do not require ten minutes to attain 50% of equilibrium, whereas the resin requires more than one hour. Besides, the exchange rate becomes higher as the water content of the fibers increases, that is, as the degree of crosslinking is lowered. This means that the diffusion within the exchangers is the major rate-controlling step in the adsorption process. The plots of t_R/t_F *vs.* the water content of the fibers is given in Fig. 7, where t_R and t_F are the half-times of ion exchange for the resin and the fiber respectively. It can be seen from Fig. 7 that the exchange rate of the fiber is forty times higher than that of the resin when

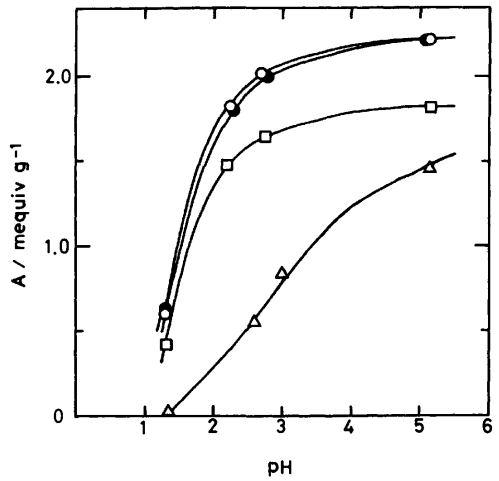

Fig. 5. Effect of pH in solution on adsorption capacity of Cu^{2+}. Adsorption to Na form of chelating exchanger (0.25 g) was carried out with 100 ml of 0.013 M Cu^{2+} solution containing 0.5 M NaCl and Clark Lubs buffer (20 °C, 24 h).
○: IONEX No. 1, □: IONEX No. 2, △: IONEX No. 4, ●: Diaion CR-10.

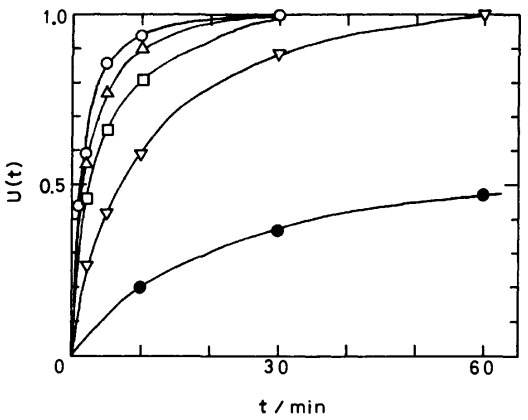

Fig. 6. Fractional attainment of equilibrium as a function of time. Ion exchange between Na form of chelating exchanger (0.25 g) and 0.013 M Cu^{2+} solution containing 0.5 M NaCl and Clark Lubs buffer of pH 6.0 (100 ml).
○: IONEX No. 1, □: IONEX No. 2, △: IONEX No. 4, ▽: IONEX No. 5, ●: Diaion CR-10.

Table 1. Characteristic data of chelating IONEX

No.	Chelating group	Fiber form[a]	Degree of crosslinking	Capacity[b] / mequiv g^{-1}	Water[c] content
1	IDA-Na	filament	low	2.2	2.6
2		filament	high	1.8	1.4
3		felt	high	1.8	—
4	IDP-Na	filament	low	1.5	1.7
5		filament	high	1.4	1.0

a) Diameter and composition of original fiber: 20 μm, *Sea*(PSt//PP)/*Islands*(PP) = (49//12)/39. b) Adsorption capacity for Cu^{2+}. c) $(W-W_0)/W_0$. W: wet weight, W_0: dry weight.

the fiber has the same water content (1.7) as the resin and that the exchange rate is independent of the structure of the chelating groups because of the diffusion control.

Theoretical Considerations. The theoretical solution of ion exchange[1,6,9] in a simple system (isotopic exchange) can be applied to our experimental results as a first-order approximation. We solve the diffusion equation in the case of an endless fiber with a radius of r_f and a length of l ($l \gg r_f$) by modifying the method used for a spherical resin.[1] The diffusion equation for the fiber systems in the case of an ideal particle-diffusion control is given by:

$$\frac{\partial \bar{C}_A}{\partial t} = \bar{D}_f\left(\frac{\partial^2 \bar{C}_A}{\partial r^2} + \frac{1}{r}\frac{\partial \bar{C}_A}{\partial r}\right), \tag{1}$$

where r is the radial coordinate of the fiber; t, the time; $\bar{C}_A$, the concentration of the A ion at r and t, and $\bar{D}_f$, the interdiffusion coefficient in the fiber. Hereafter, quantities with bars will refer to the interior of the fiber. A schematic drawing of the fiber systems is shown in Fig. 8. The general solution of Eq. 1 can be described as follows:

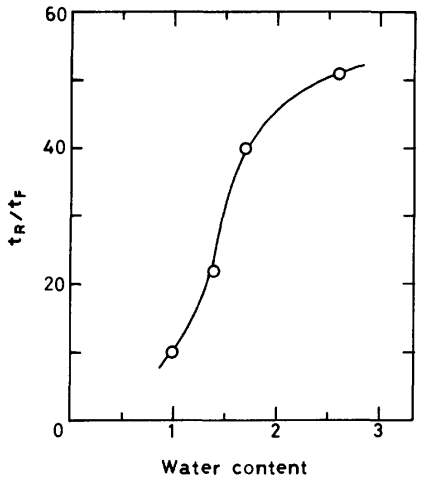

Fig. 7. t_R/t_F *vs.* water content of chelating IONEX. t_R: The half-time of ion exchange with Diaion CR-10, t_F: the half-time of ion exchange with chelating IONEX.

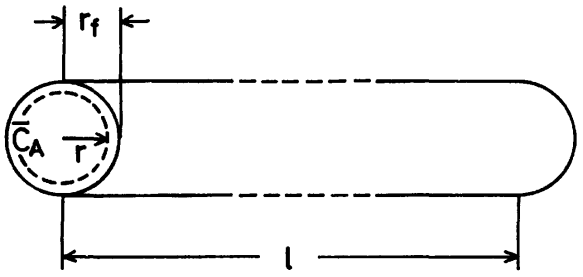

Fig. 8. Schematic drawing of fiber systems (Eq. 1).

$$\bar{C}_A = \sum_{n=1}^{\infty} A_n J_0(a_n r) \exp(-\bar{D}_f a_n^2 t), \tag{2}$$

where A_n is derived as:

$$A_n = \frac{2}{x_0^2[J_{i+1}(a_n x_0)]^2}\int_0^{x_0} x J_i(a_n x) f(x)\mathrm{d}x,$$

when $f(x)=\sum_{n=1}^{\infty} A_n J_i(a_n x)$ and $J_i(a_n x_0)=0$, in which $J_i(x)$ is the ith-order Bessel function.

The simple initial conditions are assumed to be:

$$\begin{aligned} &r > r_f,\ t = 0 && \bar{C}_A(r) = 0, \\ &0 \leqq r \leqq r_f,\ t=0 && \bar{C}_A(r) = \bar{C}_A{}^0 = \text{const.} \end{aligned} \tag{3}$$

Secondly we assume that the concentrations at the fiber surface are the same as in the bulk solution. The infinite solution volume condition is then postulated as:

$$r = r_f,\ t > 0 \qquad \bar{C}_A(t) = 0. \tag{4}$$

The conditions of Eqs. 3 and 4 give, respectively:

$$\bar{C}_A{}^0 = \sum_{n=1}^{\infty} A_n J_0(a_n r), \tag{5}$$

$$J_0(a_n r_f) = 0. \tag{6}$$

The A_n coefficients can, therefore, be determined from Eqs. 5 and 6 as follows:

$$\begin{aligned} A_n &= \frac{2}{r_f^2[J_1(a_n r_f)]^2}\int_0^{r_f} \bar{C}_A{}^0 r J_0(a_n r)\mathrm{d}r \\ &= \frac{2\bar{C}_A{}^0}{a_n r_f J_1(a_n r_f)}. \end{aligned} \tag{7}$$

The fractional attainment of the equilibrium, $U(t)$, is obtained from the integration of the solution $\bar{C}_A(r,t)$ throughout the fiber as:

$$U(t) = 1 - \frac{\int_0^{r_f} 2\pi r l \bar{C}_A \mathrm{d}r}{\pi r_f^2 l \bar{C}_A{}^0}. \tag{8}$$

By substituting Eqs. 2 and 7, Eq. 8 is finally reduced to:

$$\begin{aligned} U(t) &= 1 - \sum_{n=1}^{\infty}\frac{4}{a_n^2 r_f^2}\exp(-\bar{D}_f a_n^2 t) \\ &= 1 - \sum_{n=1}^{\infty}\frac{4}{x_n^2}\exp\left(-\frac{\bar{D}_f x_n^2 t}{r_f^2}\right), \end{aligned} \tag{9}$$

where the x_n quantities are the roots of the equation $J_0(x)=0$, as was preliminarily described in Ref. 1. From this equation, $U(t)$ is found to depend only on the magnitude of the dimensionless time parameter, $\bar{D}_f t/r_f^2$, which is plotted in Fig. 9 as a function of the parameter. The numerical values are tabulated in Table 2. The half-time of ion exchange is also

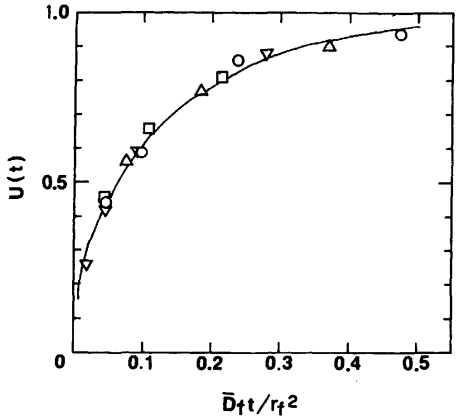

Fig. 9. Fractional attainment of equilibrium as a function of $\bar{D}_f t/r_f^2$. The solid line represents the theoretical curve for particle-diffusion controlled isotopic exchange in the case of cylindrical endless fiber (Eq. 9). Experimental points are plotted by use of empirical $\bar{D}_f$ obtained from Eq. 13. The notations for the points are used in the same meanings as Fig. 6.

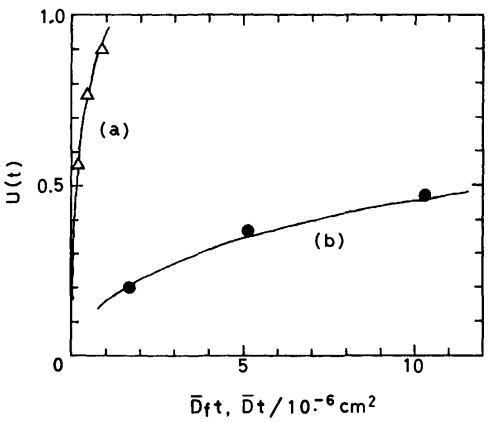

Fig. 10. Fractional attainment of equilibrium as a function of $\bar{D}_f t$ and $\bar{D}t$. The solid lines represent the theoretical curves for particle-diffusion controlled isotopic exchange. (a) Fiber with r_f=0.0015 cm and l=4.74 cm (Eq. 9), and (b) resin with r_0=0.02 cm (Eq. 11). Experimental points are plotted by use of empirical $\bar{D}_f$ and $\bar{D}$ obtained from Eqs. 13 and 14 respectively. The notations for the points are used in the same meanings as Fig. 6.

Table 2. Numerical values of

$$U(\tau) = 1 - \sum_{n=1}^{\infty} \frac{4}{x_n^2} \exp(-x_n^2\tau) \quad \text{(Eq. 9)}$$

τ	$U(\tau)$	τ	$U(\tau)$	τ	$U(\tau)$
0.005	0.155	0.05	0.452	0.20	0.782
0.01	0.215	0.06	0.489	0.25	0.837
0.02	0.299	0.08	0.553	0.30	0.878
0.03	0.360	0.10	0.606	0.40	0.932
0.04	0.410	0.15	0.708	0.50	0.962

readily derived from Eq. 9 as follows:

$$t_F = 0.065 r_f^2/\bar{D}_f. \tag{10}$$

The fractional attainment of the equilibrium, $U(t)$, within a spherical resin with a radius of r_0 has been described in the case of ideal particle-diffusion control by the following equation:

$$U(t) = 1 - \sum_{n=1}^{\infty} \frac{6}{X_n^2} \exp\left(-\frac{\bar{D}X_n^2 t}{r_0^2}\right) = 1 - \frac{6}{\pi^2} \sum_{n=1}^{\infty} \frac{1}{n^2} \exp\left(-\frac{\bar{D}\pi^2 n^2 t}{r_0^2}\right), \tag{11}$$

where $\bar{D}$ is the interdiffusion coefficient in the resin and where the quantities $X_n=\pi n$, the roots of the equation $J_{1/2}(x)=0$. The half-time of ion exchange has been calculated from Eq. 11 as follows:

$$t_R = 0.030 r_0^2/\bar{D} \tag{12}$$

The equations derived for the fractional attainments and the half-times do not involve $\bar{C}_A$ and remain unchanged under our experimental conditions.[6] Now, let us theoretically compare the ion-exchange rate of our fibers with that of the CR-10 resin, assuming that no polymer for the reinforcement in our fibers exists. The volume of the resin with r_0=0.02 cm corresponds to that of the fiber with r_f=0.0015 cm and l=4.74 cm. The theoretical $U(t)$ for the fiber and resin can be plotted as a function of the time parameter ($\bar{D}_f t$ and $\bar{D}t$) in Fig. 10 by using Eqs. 9 and 11 respectively. The half-times of ion exchange can also be obtained from Eqs. 10 and 12 respectively as:

$$t_F = 1.46 \times 10^{-9}/\bar{D}_f \tag{13}$$

$$t_R = 120 \times 10^{-9}/\bar{D}. \tag{14}$$

The ratio of the half-time of the resin to that of the fiber can be calculated to be 82 from Eqs. 13 and 14, as $\bar{D}_f=\bar{D}$ can be expected when the water contents are the same, that is, when there are the same degrees of crosslinking. The ratio obtained from the experimental data is, however, 40, about half the calculated ratio. This discrepancy can be interpreted on the assumption that the interdiffusion coefficients in our fibers are lowered because the polymer for reinforcement disturbs the diffusion of ions. The apparent $\bar{D}_f$ values for the fibers with the water contents of 1.0, 1.4, 1.7, and 2.6 can be directly evaluated from Eq. 13 to be 0.35, 0.80, 1.39, and 1.78×10^{-9} cm^2 s^{-1} respectively by using the half-times obtained from the experimental curves. Similarly, the apparent $\bar{D}$ value for the resin with the water content of 1.7 can be evaluated to be 2.86×10^{-9} cm^2 s^{-1} from Eq. 14. In Fig. 9, the experimental $U(t)$–$\bar{D}_f t/r_f^2$ data obtained by the use of these empirical interdiffusion coefficients are given, together with the theoretical curve. The experimental $U(t)$–$\bar{D}_f t$ and $-\bar{D}t$ data

obtained by the use of $\bar{D}_f=1.39\times10^{-9}$ cm^2 s^{-1} and $\bar{D}=2.86\times10^{-9}$ cm^2 s^{-1} are also compared with the theoretical curves in Fig. 10. Although the interpretation does not include direct comparisons of the observed rates with the results of calculations based on independent measurements, the experimental results are in fairly good agreement with the theoretical curves.

Practical Applications

Removal of Cu^{2+} from a Solution by Fix-bed Methods. A 830 mg dm^{-3} Cu^{2+} solution containing 0.5 M NaCl was passed through a column packed with a chelating exchanger at a space velocity (S. V.) of 10 h^{-1}. The breakthrough curves of the filamentary IONEX No. 4 and Diaion CR-10 columns are given in Fig. 11. The ion leaks through the resin column in the early stage, while the fiber column represents the breakthrough curve of a roughly *S* form. From this curve, the band length and utilization of the ion exchange can be evaluated to be 7.8 cm and 0.71 respectively. The band length for the resin column is estimated to be more than 30 cm. These results show that the utilization of the fiber is high, since the band length is short because of its rapid adsorption properties, even if the Cu^{2+} concentration is high.

The breakthrough volume of a cylindrical module made of the felt IONEX No. 3 was examined by using a feed solution of 100 mg dm^{-3} Cu^{2+} and compared with those of the felt IONEX No. 3 and filamentary IONEX No. 2 columns. The felt column is superior to the others, as is shown in Fig. 12. The breakthrough volume of the module, which has seventy times as large a filtrating area as the felt column, is 30% lower than that of the felt column. From the observation of the module colored with Cu^{2+}, it was found that some of its parts are not utilized because of an irregular flow. The breakthrough volume of the module is, however, almost equal to that of the filamentary column. It can be concluded that the cylindrical module is a suitable one for a rapid fluid treatment since it has a large filtrating area and a low pressure drop.

Removal of Mn^{2+} from a Solution by Fix-bed Methods. A 100 mg dm^{-3} Mn^{2+} solution containing 0.5 M NaCl was passed through columns of various chelating exchangers. The results are shown in Fig. 13. The breakthrough volume of the felt column is superior to that of the filamentary column, as was found in the case of Cu^{2+}. The minimum Mn^{2+} concentrations in the effluent for the resin columns are 0.2 mg dm^{-3} at S. V. 20 h^{-1} and 0.1 mg dm^{-3} at S. V. 10 h^{-1}, while those for the fiber columns are below 0.02 mg dm^{-3} at S. V. 20 h^{-1}.

Next, a 137.5 mg dm^{-3} Mn^{2+} solution containing 30 wt/vol% lysine was passed through the felt and resin columns at various space velocities. Figure 14 presents the space velocity dependence of the breakthrough volume. The minimum concentrations for the resin and felt columns are 0.05 mg dm^{-3} and below 0.02 mg dm^{-3} respectively at S. V. 5 h^{-1}. In the case of the resin column, the breakthrough volume decreases rapidly as the space velocity is raised, and the ion leak takes place in the early stage at S. V. 20 h^{-1}. On the other hand, even at S. V. 80 h^{-1}, the felt column gives 72% as large a

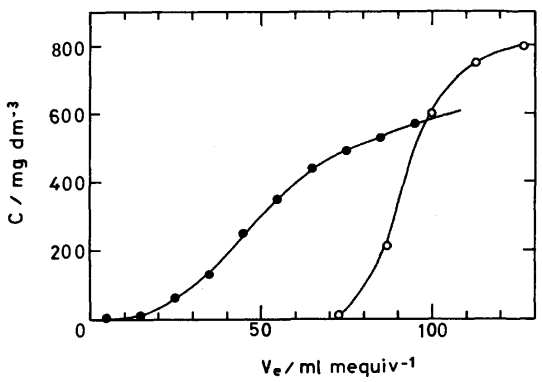

Fig. 11. Concentration of Cu^{2+} in effluent *vs.* effluent volume.
Feed solution, 830 mg dm^{-3} (0.013 M) Cu^{2+} solution containing 0.5 M NaCl and Clark Lubs buffer of pH 6.0; bed volume, 10 ml (1 cm × 13 cm); packed weight of chelating exchanger in Na form, 2.5 g; flow rate, 100 ml h^{-1} (S.V. 10 h^{-1}).
○: Filamentary IONEX No. 4, ●: Diaion CR-10.

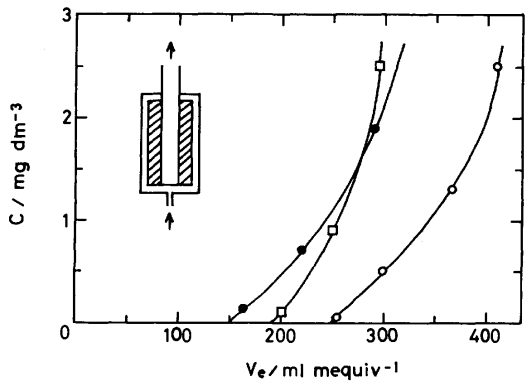

Fig. 12. Concentration of Cu^{2+} in effluent *vs.* effluent volume.
Removal of Cu^{2+} by using fixed-bed of chelating felt IONEX in H form. Feed solution, 100 mg dm^{-3} Cu^{2+} solution (pH 4.0); flow rate, S. V. 40 h^{-1}.
○: Felt IONEX No. 3 (1.1 g) in 5 ml (1.8 cm × 2 cm), □: felt IONEX No. 3 of cylindrical module (55 g) in 340 ml (inner diameter, 2.5 cm; outer diameter, 6.5 cm; height, 12 cm., see above side view), ●: filamentary IONEX No. 2 (1.25 g) in 5 ml (1 cm × 6.5 cm).

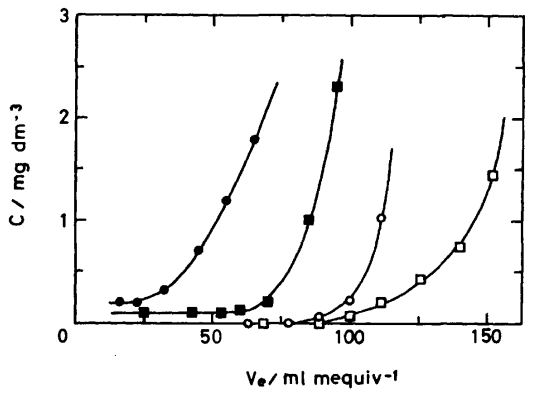

Fig. 13. Concentration of Mn^{2+} in effluent *vs.* effluent volume.
Removal of Mn^{2+} by using fixed-bed of chelating exchanger in H form. Feed solution, 100 mg dm^{-3} containing 0.5 M NaCl and Clark Lubs buffer (pH 6.0).
○: Filamentary IONEX No. 2 (1.25 g) in 5 ml (1 cm × 6.5 cm), S. V. 20 h^{-1}, □: felt IONEX No. 3 (1.1 g) in 5 ml (1.8 cm × 2 cm), S. V. 20 h^{-1}, ●: Diaion CR-10 (4.5 g) in 10 ml (1 cm × 13 cm), S. V. 20 h^{-1}, ■: Diaion CR-10 (9 g) in 20 ml (1 cm × 26 cm), S. V. 10 h^{-1}.

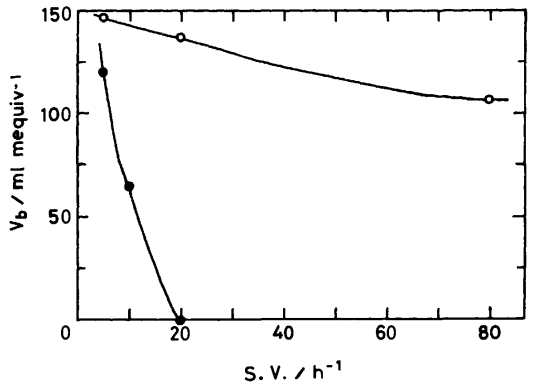

Fig. 14. Space velocity dependence of breakthrough volume in removal of Mn^{2+} from highly concentrated lysine solution. Breakthrough point, 1 mg dm^{-3} as Mn^{2+} in effluent; feed solution, 137.5 mg dm^{-3} Mn^{2+} solution containing 30 wt/vol% lysine (pH 5.4).
○: Lysine form of felt IONEX No. 3 (1.1 g) in 5 ml (1.8 cm × 2 cm), ●: lysine form of Diaion CR-10 (2.5 g) in 10 ml (1 cm × 13 cm).

breakthrough volume as at S. V. 5 h^{-1}, and its minimum concentration is still below 0.02 mg dm^{-3}. These results indicate that the chelating fiber can be utilized in various fields which require a rapid treatment or a high removal ratio, since it has such a high adsorption rate.

Conclusion

1. A fibrous chelating exchanger based on polystyrene has been prepared by using an *islands-in-a-sea* type composite fiber as the starting material. This fibrous chelating exchanger can be used in various forms because of its high mechanical strength.

2. This chelating fiber has from ten to forty times as high an adsorption rate for Cu^{2+} as the ordinary chelating resin. These results are interpreted in terms of the rate laws of ion exchange for the limiting case of ideal particle-diffusion control in a simple system.

3. A column packed with this chelating fiber has excellent removal properties for heavy-metal ions. A cylindrical module made of felt is a suitable one for a rapid fluid treatment.

The author is grateful to Professor Noboru Hirota and Dr. Hiroaki Ohya-Nishiguchi of Kyoto University for their kind advice and valuable discussions. He would also like to express his appreciation to Dr. Masaharu Shimamura for his helpful advice and illuminating discussions. He is also deeply indebted to Dr. Tatsuro Kawaguchi, Mr. Michihiko Tanaka, and Dr. Masaki Nishino for their continuous encouragement throughout this work. He is also much obliged to Mr. Kazuo Teramoto for his advice on the chemical treatments and to Mr. Seiichi Yoshikawa and other collaborators for the preparation of the composite fibers. The author also wishes to thank Toray Industries, Inc., for making this study possible.

References

1) T. Yoshioka and M. Shimamura, *Bull. Chem. Soc. Jpn.*, **56**, 3726 (1983).
2) T. Yoshioka and M. Shimamura, *Bull. Chem. Soc. Jpn.*, **57**, 334 (1984).
3) T. Yoshioka and M. Shimamura, *Polym. Prepr. Jpn.*, **32**, 1851, 1855 (1983).
4) M. Tomoi and H. Kakiuchi, *Makromol. Chem., Rapid Commun.* **5**, 685 (1984).
5) M. Okawara, Y. Komeda, and E. Imoto, *Kobunshi Kagaku*, **17**, 30 (1960).
6) F. Helfferich, "Ion Exchange," McGraw-Hill, New York (1962), pp. 45—47, pp. 259—266.
7) G. Kühn and W. Hoyer, *Makromol. Chem.*, **108**, 84 (1967).
8) E. Blasius and B. Brozio, "Chelates in Analytical Chemistry," ed by H. A. Flaschka and A. J. Barnard, Jr., Marcel Dekker, New York (1967), p. 49.
9) G. E. Boyd, A. W. Adamson, and L. S. Myers, Jr., *J. Am. Chem. Soc.*, **69**, 2836 (1947).
10) R. Turse and W. Rieman, *J. Phys. Chem.*, **65**, 1821 (1961).
11) C. Heitner-Wirguin and G. Markovits, *J. Phys. Chem.*, **67**, 2263 (1963).
12) A. Schwarz, J. A. Marinsky, and K. S. Spiegler, *J. Phys. Chem.*, **68**, 918 (1964).
13) A. Varon and W. Rieman, *J. Phys. Chem.*, **68**, 2716 (1964).

14) T. Yoshioka, K. Teramoto, and M. Shimamura, Japanese Laid-open Patent 120985 (1977); *Chem. Abstr.*, **88**, 122184a (1978).
15) T. Miyoshi, K. Teramoto, and M. Shimamura, Japanese Laid-open Patent 137293 (1978); *Chem. Abstr.*, **90**, 122697m (1979).
16) T. Aya, K. Chiba, and Z. Izumi, Japanese Laid-open Patent 80387 (1975); *Chem. Abstr.*, **84**, 136617y (1976).

 © 1985 The Chemical Society of Japan Bull. Chem. Soc. Jpn., 58, 2626—2633 (1985)

Kinetics of the Transfer of Picrate Ion at the Water/Nitrobenzene Interface

Toshiyuki OSAKAI, Tadaaki KAKUTANI, and Mitsugi SENDA*
Department of Agricultural Chemistry, Faculty of Agriculture, Kyoto University, Sakyo-ku, Kyoto 606
(Received February 12, 1985)

Kinetics of the transfer of picrate (Pic^-) ion at the interface between an aqueous solution of lithium chloride (LiCl) and a nitrobenzene solution of tetrabutylammonium tetraphenylborate (TBATPB) has been studied by phase-selective a.c. polarography with a two-electrode cell system. By assuming Butler-Volmer type equations for the rate constants, the kinetic parameters of the Pic^--ion transfer have been determined at various concentrations of LiCl (0.02—1.0 mol dm^{-3}) and TBATPB (0.05—0.17 mol dm^{-3}). The rate constants virtually do not change with the electrolyte concentrations. Frumkin correction for the double-layer effect of the rate constants has been examined. The result seems to indicate that the observed potential dependence of the rate constants obtained in moderately concentrated electrolyte solutions may reflect the real potential dependence of the rate constants.

In a previous paper[1] we have shown that the phase-selective a.c. polarographic method is useful for accurate measurement of the rate of ion (tetramethylammonium ion) transfer at the interface between two immiscible electrolyte solutions (water/nitrobenzene interface). In this study, we have applied this technique to determine the rate constants of the transfer of picrate (Pic^-) ion at the interface between an aqueous solution of lithium chloride (LiCl) and a nitrobenzene solution of tetrabutylammonium tetraphenylborate (TBATPB).

Dependence of the rate constants of ion transfer on the potential difference across the interface between two immiscible electrolyte solutions has been a subject of theoretical[2,3] and experimental[4-7] studies; with tetraalkylammonium ions at water/nitrobenzene[4] and water/1,2-dichloroethane[5] interfaces, and with cesium ion[6] and choline and acetylcholine ions[7] at the water/nitrobenzene interface. According to Samec *et al.*,[6,7] the observed potential dependence of the rate constants for the transfer of cesium, choline, and acetylcholine ions arises largely from the effect of the potential on the concentration of the transferred ions at the reaction planes, which are supposed to be located at the outer Helmholtz planes (OHP's) on each side of the interface. In this study we have determined the rate constants of the Pic^--ion transfer at the interface between aqueous and nitrobenzene solutions containing various concentrations of LiCl (0.02—1.0 mol dm^{-3}) and TBATPB (0.05—0.17 mol dm^{-3}), respectively. The observed rate constants were corrected for the double-layer effect (so called Frumkin correction) using the capacity data and the Gouy-Chapman theory. The results indicate that the formalism of Frumkin correction with the reaction planes being located at the OHP's to obtain the "true" rate constants is probably not valid for the Pic^--ion transfer across the water/nitrobenzene interface.

Experimental

The electrochemical cell employed in this study is represented by

	I	II		
Ag | AgCl	0.1 mol dm^{-3} TBACl (W)	x mol dm^{-3} TBATPB (N)		
	III			
	y mol dm^{-3} LiCl, c mol dm^{-3} LiPic (W)	AgCl	Ag,	(A)

where (W) and (N) stand for the aqueous and the nitrobenzene phases, respectively. The interface between phases II and III is the test interface at which the Pic^--ion transfer takes place. The left-hand reference electrode Ag/AgCl/0.1 mol dm^{-3} TBACl(W) was connected to the nitrobenzene phase (II) through sintered glass.[1] The potential drop across the interface between phases I and II is determined by the distribution potential of TBA^+ ion in the two phases.[8,9] In electrochemical measurements, a two-electrode cell system[1] was used. The solution resistance between the two reference electrodes, R_u, was measured with a laboratory-made linear bridge[1] with a 10 kHz a.c. generator and the ohmic drop due to R_u was compensated for by positive feedback.[1] The observed values of R_u were in the range between 0.96 and 3.27 kΩ. The details of electrochemical measurements have been described elsewhere.[1] The electrolytic cell was thermostated at 25±0.1 °C.

Lithium picrate (LiPic) was prepared by the reported method.[10] The other chemicals and the preparation of electrolyte solutions have been described elsewhere.[1]

Results

In the following, the potential E applied to Cell A is defined by the potential of the right-hand reference

electrode, E_{right}, referred to the potential of the left-hand reference electrode, E_{left}, that is, $E=E_{right}-E_{left}$. The flow of the positive charge from the aqueous to the nitrobenzene phase is taken as the positive current.

Cyclic Voltammetry. Cyclic voltammograms for the Pic^--ion transfer at the interface between aqueous solution of LiCl and nitrobenzene solution of TBATPB at various concentrations of the electrolytes as listed in Tables 1—3 were recorded at the voltage scan rate of 5 mV s^{-1}. At all concentrations used, well-defined reversible cyclic voltammograms were obtained at the scan rate of 5 mV s^{-1} (Fig. 1). The peak separation was 63±2 mV being close to the theoretical value of 60 mV for the reversible cyclic voltammogram. The midpoint potential, E_{mid}, which is considered to be equal to the reversible half-wave potential, agreed with the summit potential, E_s, of the admittance curves in a.c. polarography (see Figs. 2 and 3 and Tables 1—3) within the experimental errors (±4 mV). Figure 2 shows the dependence of E_{mid} and E_s on the logarithm of the mean activity of LiCl, $a^{\pm,w}_{LiCl}$, in the aqueous solution (phase III in Cell A). The experimental points in Fig. 2 lie on a straight line with the slope of −58 mV which is close to $-2.30RT/F$=−59 mV at 25 °C. Similarly, the change of E_{mid} and E_s with the change of TBATPB concentration was close to −59 mV per decade (Table 3). These results indicate that the ion-pair formation of Pic^--ion with Li^+ and TBA^+ ions is negligibly small in the concentration range studied (see Discussion).

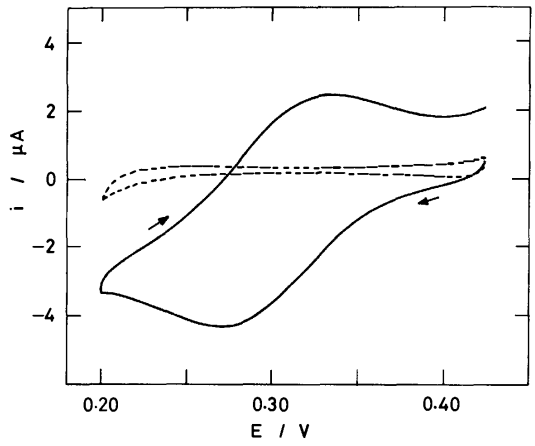

Fig. 1. A cyclic voltammogram for the transfer of 0.5 10^{-3} mol dm^{-3} Pic^- ion from a 0.1 mol dm^{-3} LiCl aqueous solution to a 0.1 mol dm^{-3} TBATPB nitrobenzene solution at the voltage scan rate of 5 mV s^{-1}. Dashed line shows a cyclic voltammogram in the absence of Pic^- ion.

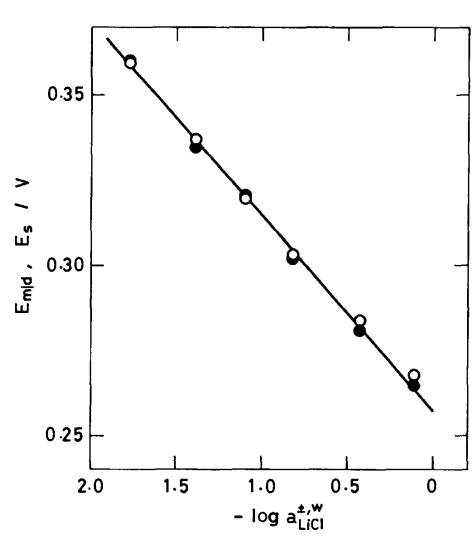

Fig. 2. Dependence of the midpoint potential (○) and the summit potential (●) on the logarithm of mean activity of LiCl in the aqueous phase when the concentration of TBATPB is 0.1 mol dm^{-3}. The slope of the straight line is −58 mV.

A.c. Polarography. In a.c. polarography, a small a.c. voltage (usually 5 mV peak to peak) was superimposed on the d.c. applied potential E_{dc} (usually at the scan rate of 5 mV s^{-1}), and the real (Y'_t) and the imaginary (Y''_t) components of the admittance, $Y_t=Y'_t+jY''_t$($j=(-1)^{-1/2}$), of the test interface in Cell A were measured at seven frequencies from 10 to 100 Hz. Curves a in Fig. 3 show representative plots of Y'_t and Y''_t against E_{dc}. Also plotted in Fig. 3 (curves b) are the real (Y'_B) and the imaginary (Y''_B) components of the admittance of the base aqueous solution/base nitrobenzene solution interface, $Y_B=Y'_B+jY''_B$. Thus, the ion-transfer admittance, $Y_F=Y'_F+jY''_F$, is determined by subtraction of Y_B from Y_t[1]:

$$Y'_F = Y'_t - Y'_B, \quad (1)$$

$$Y''_F = Y''_t - Y''_B. \quad (2)$$

Y'_F and Y''_F are plotted against E_{dc} in Fig. 3 (curves c). The summit potentials of the Y'_F and Y''_F *vs.* E_{dc} curves coincided with each other and were virtually equal to the corresponding reversibe half-wave potentials obtained from cyclic voltammetry, irrespective of the frequency, the Pic^--ion concentration, and the supporting-electrolyte concentrations. The summit potentials are summarized in Tables 1—3.

From the ion-transfer admittance, the ion-transfer impedance, Z_F, which is expressed by a series combination of resistance (r_s) and capacitance (c_s), *i.e.* $Z_F=r_s-j(1/\omega c_s)$, was calculated:

$$r_s = Y'_F/(Y'^2_F+Y''^2_F), \quad (3)$$

$$1/\omega c_s = Y''_F/(Y'^2_F+Y''^2_F), \quad (4)$$

where ω is the angular frequency of the a.c. signal

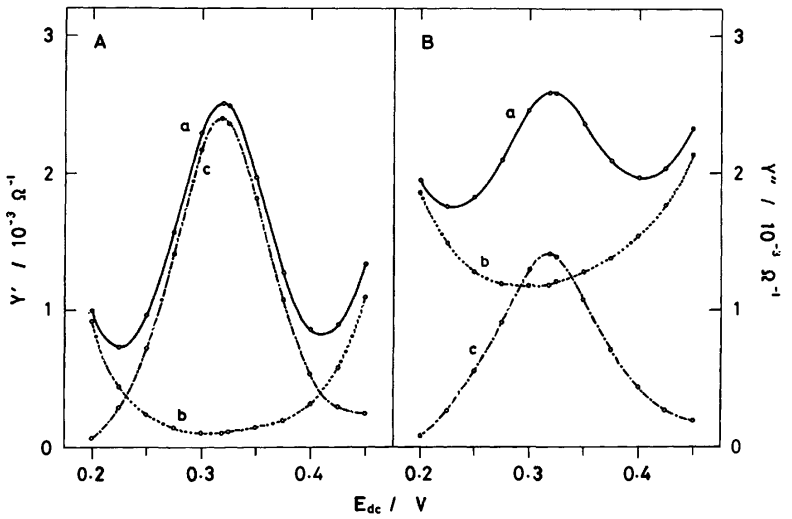

Fig. 3. Real (A) and imaginary (B) components of the admittance of the interface between a 0.1 mol dm^{-3} LiCl aqueous solution and a 0.1 mol dm^{-3} TBATPB nitrobenzene solution, at f=50 Hz, in the presence (a) and absence (b) of 0.5×10^{-3} mol dm^{-3} Pic$^-$ ion in the aqueous phase. Curve c shows the ion-transfer admittance, Y_F' and Y_F'', for the Pic$^-$ ion transfer corrected for the base admittance.

($\omega=2\pi f$, f being the frequency).

Determination of the Kinetic Parameters. For the sake of simplicity, we assume a linear kinetic equation:

$$I = I(E, C^W, C^N) = zFA[\vec{k}(E)C^W - \overleftarrow{k}(E)C^N], \quad (5)$$

for the ion-transfer current I, which is a function of the potential, E, and the surface concentrations of the transferred ion in the aqueous and nitrobenzene phases, C^W and C^N, respectively. Here, z is the ionic valence of the transferred ion ($z=-1$ for Pic$^-$ ion), F the Faraday constant, A the surface area of the interface, and $\vec{k}(E)$ and $\overleftarrow{k}(E)$ are the rate constants of ion transfer from the aqueous to the nitrobenzene phase and from the nitrobenzene to the aqueous phase, respectively, both being considered to be functions of the potential E. On the basis of the information obtained by cyclic voltammetry, we assume that the mass transfer of the ion is due to semi-infinite linear diffusion and that the ion-transfer reaction at the interface is d.c. reversible at the d.c. voltage scan rate of 5 mV s^{-1}, that is, the Nernst equation is valid for the mean surface concentrations or the d.c. components of the surface concentration of the transferred ion in both sides of the interface, $\overline{C}^W$ and $\overline{C}^N$:

$$E_{dc} = E^{\oplus} + (RT/zF)\ln(\overline{C}^N/\overline{C}^W), \quad (6)$$

where $E^{\ominus}$ is the standard ion-transfer potential (with respect to the reference electrodes in Cell A), R the gas constant, and T the absolute temperature. We also assume that the ion-pair formation of the transferred ion is negligibly small in both phases.

On the above assumptions, the ion-transfer impedance can be expressed, by analogy with the faradaic impedance theory of electrode reaction, by[1]

$$r_s = (\sigma/\omega^{1/2})[1+(2\omega)^{1/2}\lambda^{-1}], \quad (7)$$

$$1/\omega c_s = \sigma/\omega^{1/2}, \quad (8)$$

with

$$\sigma = \frac{4RT\cosh^2(\xi/2)}{z^2F^2A(2D^W)^{1/2}C^{W,\circ}}, \quad (9)$$

$$\lambda = \frac{\vec{k}}{(D^W)^{1/2}} + \frac{\overleftarrow{k}}{(D^N)^{1/2}}, \quad (10)$$

$$\xi = zF(E_{dc}-E^r_{1/4})/RT, \quad (11)$$

$$E^r_{1/4} = E^{\oplus} + (RT/zF)\ln(D^W/D^N)^{1/2}, \quad (12)$$

where $\vec{k}$ and $\overleftarrow{k}$ are the ion-transfer rate constants defined by $\vec{k}=\vec{k}(E=E_{dc})$ and $\overleftarrow{k}=\overleftarrow{k}(E=E_{dc})$ (see Eq. 5), respectively, and D^W and D^N are the diffusion coefficients of the transferred ion in the aqueous and nitrobenzene phases, respectively; $C^{W,\circ}$ is the bulk concentration of the ion in the aqueous phase (the bulk concentration in the nitrobenzene phase is assumed to be zero). When the ion-transfer reaction is d.c. reversible, we have $k\overline{C}^W=k\overline{C}^N$ from Eq 5. Using Eqs. 6, 11, and 12, we then have $\vec{k}=(D^W/D^N)^{1/2}\overleftarrow{k}\exp(\xi)$. Consequently, Eq. 10 can be rewritten as

$$\ln[\vec{k}/(D^W)^{1/2}] = \ln[\lambda/(1+\exp(-\xi))], \quad (13)$$

or

$$\ln[\overleftarrow{k}/(D^N)^{1/2}] = \ln[\lambda/(1+\exp(\xi))]. \quad (14)$$

Here λ can be obtained by Eqs. 7 and 8 as

$$\lambda = (2\omega)^{1/2}/(r_s c_s \omega - 1). \quad (15)$$

Thus these relationships enable us to determine the ion-transfer rate constants from the ion-transfer impedance.

We assume Butler-Volmer type equations for the potential dependence of the rate constants:

$$\vec{k} = k_s \exp[\vec{\alpha} z F(E_{dc} - E^{\bullet})/RT], \quad (16)$$

$$\overleftarrow{k} = k_s \exp[-\overleftarrow{\alpha} z F(E_{dc} - E^{\bullet})/RT], \quad (17)$$

where k_s is the standard rate constant, $\vec{\alpha}$ and $\overleftarrow{\alpha}$ ($\vec{\alpha} + \overleftarrow{\alpha} = 1$) are the transfer coefficients. Then, using Eqs. 10—12, Eqs. 13 and 14 can be rewritten as

$$\ln[\vec{k}/(D^W)^{1/2}] = \ln \Lambda + \vec{\alpha}\xi, \quad (18)$$

$$\ln[\overleftarrow{k}/(D^N)^{1/2}] = \ln \Lambda - \overleftarrow{\alpha}\xi, \quad (19)$$

with

$$\Lambda = k_s \left(\frac{1}{(D^W)^{1/2}}\right)^{\overleftarrow{\alpha}} \left(\frac{1}{(D^N)^{1/2}}\right)^{\vec{\alpha}}. \quad (20)$$

In Fig. 4, r_s and $1/\omega c_s$ at the summit potential are plotted against $\omega^{-1/2}$ for x=0.1 mol dm^{-3}, y=0.1 mol dm^{-3}, and c=0.5×10^{-3} mol dm^{-3} in Cell A. According to Eqs. 7 and 8, both plots gave straight lines with a common slope giving the diffusion coefficient of Pic$^-$ ion in the aqueous phase, D^W_{Pic}=8.8×10^{-6} cm^2 s^{-1} by Eqs. 9 and 11. For all compositions of the solution measured in this study (Tables 1—3) similar linear plots were obtained for the ion-transfer impedance in the d.c. potential range of $|E_{dc} - E_s| < 80$ mV. The D^W_{Pic} values obtained at various compositions of the solutions are summarized in Tables 1—3.

The potential dependence of the rate constants

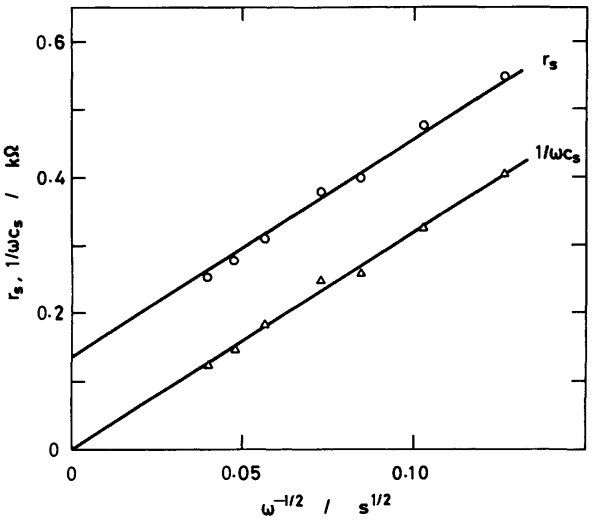

Fig. 4. Plot of the real (r_s) and imaginary ($1/\omega c_s$) components of ion-transfer impedance at the summit potential against $\omega^{-1/2}$ for the transfer of 0.5×10^{-3} Pic$^-$ ion at the interface between a 0.1 mol dm^{-3} LiCl aqueous solution and a 0.1 mol dm^{-3} TBATPB nitrobenzene solution.

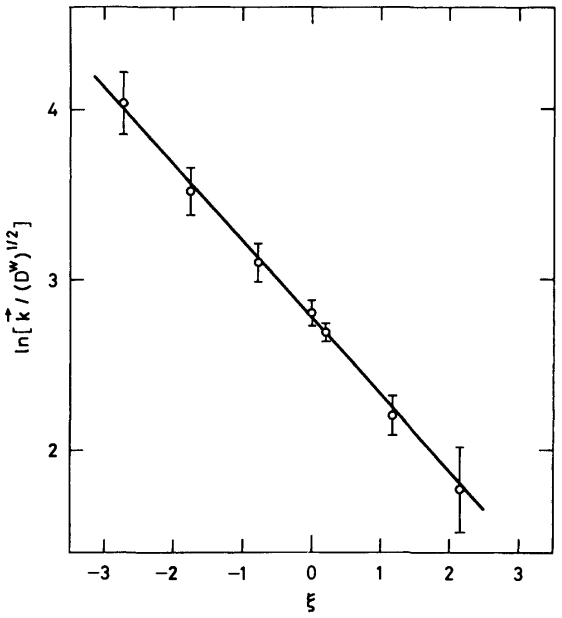

Fig. 5. Plot of $\ln[\vec{k}/(D^W)^{1/2}]$ *vs.* $\xi(=zF(E_{dc} - E^r_{1/2})/RT)$ for the transfer of 0.5×10^{-3} mol dm^{-3} Pic$^-$ ion at the interface between a 0.1 mol dm^{-3} LiCl aqueous solution and a 0.1 mol dm^{-3} TBATPB nitrobenzene solution. Vertical bars indicate the standard deviations.

Table 1. Kinetic parameters of Pic$^-$-ion transfer at the interface between a 0.1 mol dm^{-3} LiCl aqueous solution and a 0.1 mol dm^{-3} TBATPB nitrobenzene solution, determined at various concentrations of Pic$^-$ ion in the aqueous phase

C^W_{Pic} / 10^{-3} mol dm^{-3}	E_s / mV	ln Λ	k_s / 10^{-2} cm s^{-1}	$\vec{\alpha}$	D^W_{Pic} / 10^{-6} cm^2 s^{-1}
0.30	319	2.86±0.04	3.9	0.61±0.05	8.0
0.50	320	2.77±0.04	3.7	0.45±0.04	8.8
0.75	320	2.85±0.06	3.8	0.57±0.04	7.7
1.00	319	2.68±0.09	3.2	0.56±0.05	7.3
average	320	2.79±0.06	3.7±0.3	0.55±0.05	8.0±0.6

were analysed using Eqs. 13—15. A typical plot of $\ln[\vec{k}/(D^{W})^{1/2}]$ against ξ for $x=0.1$ mol dm^{-3}, $y=0.1$ mol dm^{-3}, and $c=0.5\times10^{-3}$ mol dm^{-3} in Cell A is shown in Fig. 5. Similar linear plots were obtained for all compositions of the solutions examined in this study. By fitting the $\ln[\vec{k}/(D^{W})^{1/2}]$ *vs.* ξ plot to Eq. 18, Λ and $\vec{\alpha}$ were determined. Then k_s was determined from Λ using Eq. 20 with $D^{W}_{Pic}=7.46\times10^{-6}$ cm^2 s^{-1} and $D^{N}_{Pic}=D^{W}_{Pic}/2.07$[11]$=3.60\times10^{-6}$ cm^2 s^{-1}. The kinetic parameters of Pic$^-$-ion transfer obtained at various Pic$^-$-ion concentrations at the interface between 0.1 mol dm^{-3} LiCl aqueous solution and 0.1 mol dm^{-3} TBATPB nitrobenzene solution are shown in Table 1. Also, the kinetic parameters of Pic$^-$-ion transfer obtained at various concentrations of LiCl in the aqueous solution and TBATPB in the nitrobenzene solution are shown in Tables 2 and 3.

Discussion

The cyclic voltammetric measurements show that the Pic$^-$-ion transfer at the water/nitrobenzene interface is d.c. reversible (nernstian) at the scan rate of 5 mV s^{-1}. This experimental finding ensures the validity of the Nernst equation for the mean surface concentration (Eq. 6) in a.c. polarography with the d.c. voltage scan rate of 5 mV s^{-1}. The d.c. reversibility of Pic$^-$-ion transfer at the water/nitrobenzene interface has been described also by Homolka and Marečcek.[12] Thus the mid-point potential, E_{mid}, can be equated to the reversible half-wave potential, $E^{I}_{1/2}$, which is related to the standard ion-transfer potential, $E^{\ominus}$, by Eq. 12. The standard ion-transfer potential of Pic$^-$-ion $E^{\ominus}_{Pic}$, observed with Cell A is expressed by

$$E^{\ominus}_{Pic} = \Delta\phi^{\ominus}_{Pic} + \Delta E^{A}_{ref}, \tag{21}$$

where $\Delta\phi^{\ominus}_{Pic}$ is the standard ion-transfer potential of Pic$^-$ ion at the water/nitrobenzene interface, and ΔE^{A}_{ref} is the constant determined solely by the left- and right-hand reference electrodes in Cell A. In the present case the left- and right-hand reference electrodes are reversible to TBA$^+$ and Cl$^-$ ions, respectively, and ΔE^{A}_{ref} is given as a function of the activities of TBA$^+$ and Cl$^-$ ions, a^{N}_{TBA} and a^{W}_{Cl}, in the nitrobenzene (II) and aqueous (III) solutions, respectively, by

$$\Delta E^{A}_{ref} = \text{constant} - (2.30RT/F)\log(a^{N}_{TBA}a^{W}_{Cl}). \tag{22}$$

Furthermore, if the ion-pair formation of Pic$^-$-ion with Li$^+$ and TBA$^+$ ions is appreciable, $\Delta\phi^{\ominus}_{Pic}$ in Eq. 21 should be replaced by $\Delta\phi^{\ominus'}_{Pic}$:

$$\Delta\phi^{\ominus'}_{Pic} = \Delta\phi^{\ominus}_{Pic} + \frac{RT}{F}\ln\frac{1+K^{N}_{LiPic}K^{N/W,\Delta\phi}_{Li}a^{W}_{Li}+K^{N}_{TBAPic}a^{N}_{TBA}}{1+K^{W}_{LiPic}a^{W}_{Li}+K^{W}_{TBAPic}(K^{N/W,\Delta\phi}_{TBA})^{-1}a^{N}_{TBA}}, \tag{23}$$

where K^{α}_{LiPic} and K^{α}_{TBAPic} (α=N and W) are the association constants of the ion pairs Li$^+$Pic$^-$ and TBA$^+$Pic$^-$ in the α phases, respectively, whereas $K^{N/W,\Delta\phi}_{TBA}$ and $K^{N/W,\Delta\phi}_{Li}$ are the ionic distribution co-

Table 2. Kinetic parameters of Pic$^-$-ion transfer[a] at the interface between a nitrobenzene solution of 0.1 mol dm^{-3} TBATPB and an aqueous solution of 0.02 to 1.0 mol dm^{-3} LiCl

C^{W}_{LiCl} / mol dm^{-3}	E_s / mV	ln Λ	k_s / 10^{-2} cm s^{-1}	$\vec{\alpha}$	D^{W}_{Pic} / 10^{-6} cm^2 s^{-1}
0.02	360	2.86±0.07	4.0	0.45±0.06	6.3
0.05	335	2.80±0.07	3.8	0.50±0.08	8.3
0.10	320	2.77±0.04	3.7	0.45±0.04	8.8
0.20	302	2.80±0.03	3.7	0.50±0.04	7.5
0.50	281	2.66±0.04	3.1	0.65±0.05	6.5
1.00	265	2.82±0.06	3.5	0.74±0.09	6.2

a) Determined at 0.50×10^{-3} mol dm^{-3} Pic$^-$ ion in the aqueous phase.

Table 3. Kinetic parameters of Pic$^-$-ion transfer[a] at the interface between an aqueous solution of 0.1 mol dm^{-3} LiCl and a nitrobenzene solution of 0.05 to 0.17 mol dm^{-3} TBATPB

C^{N}_{TBATPB} / mol dm^{-3}	E_s / mV	ln Λ	k_s / 10^{-2} cm s^{-1}	$\vec{\alpha}$	D^{W}_{Pic} / 10^{-6} cm^2 s^{-1}
0.05	333	2.76±0.08	3.5	0.60±0.06	7.1
0.10	320	2.77±0.04	3.7	0.45±0.04	8.8
0.17	310	2.64±0.03	3.2	0.49±0.02	8.5

a) Determined at 0.50×10^{-3} mol dm^{-3} Pic$^-$ ion in the aqueous phase.

efficients of TBA^+ and Li^+ ions, respectively, between nitrobenzene and water when the interfacial potential difference is $\Delta\phi$, and are given by

$$K_j^{N/W,\Delta\phi} = \exp[z_jF(\Delta\phi-\Delta\phi_j^*)/RT], \quad j = Li^+ \text{ and } TBA^+ \text{ and } z_j = +1. \tag{24}$$

The change in the effective diffusion coefficients caused by the ion-pair formation in this case hardly affects the $E_{1/2}^t$ values (see Eq. 12). The experimental results (Fig. 2 and Tables 2 and 3) show that the change of $E_{1/2}^t$ ($\approx E_{Pic}^{\circ}$) with Cl^- or TBA^+ activity is close to $-2.30RT/F = -59$ mV per decade, indicating that the variation in $\Delta\phi_{Pic}^{\circ\prime}$ with Li^+ and TBA^+ activities is negligibly small. Therefore the ion-pair formation of Pic^--ion with Li^+ and TBA^+ ions should be negligible in the concentration range of the electrolytes used in this study.

The plot of $\ln[\vec{k}/(D^W)^{1/2}]$ against ξ for the Pic^--ion transfer generally gave a straight line (Fig. 5). This is in contrast to the tetramethylammonium-ion transfer, in which the plot gave an appreciably upward convex curve (see Fig. 12 in Ref. 1). Thus we applied the Butler-Volmer type equations (Eqs. 16 and 17) to the rate constants of Pic^--ion transfer to determine the kinetic parameters Λ, k_s, and $\vec{\alpha}$. The results are summarized in Tables 1—3. Table 1 shows that the observed kinetic parameters are hardly dependent on Pic^--ion concentration in the range from 0.3×10^{-3} to 1.0×10^{-3} mol dm^{-3} indicating the validity of assuming the linear kinetic equation for the ion transfer (Eq. 5). As seen in Tables 2 and 3, the kinetic parameters, except the transfer coefficients, were virtually independent of the concentrations of LiCl and TBATPB in the aqueous and nitrobenzene solutions, respectively.

The electrical double layer of the interface between aqueous solution of LiCl and nitrobenzene solution of TBATPB consists of the inner layer which is sandwiched by the two diffuse double layers on the aqueous and nitrobenzene solution sides.[13] Accordingly, when an ion is transferred from one solvent to the other, the ion is transferred through the three layers, *i.e.* the diffuse double layer in one phase, the inner layer, and the other diffuse double layer in the other in series. The effect of the potential of the diffuse double layer on the concentrations of transferred ion at the reaction planes where the transfer of ion from one solvent to the other will take place can be expressed, in the first approximation, by the Frumkin equation for the double-layer correction:

$$C_2^W = C^W \exp[zF(\phi^W-\phi_2^W)/RT], \tag{25}$$

$$C_2^N = C^N \exp[zF(\phi^O-\phi_2^O)/RT], \tag{26}$$

where C_2^α (α=W or N) is the concentration of the transferred ion at the reaction plane on the aqueous (α=W) or nitrobenzene (α=N) solution side and C^α (α=W or N) is the surface concentration, *i.e.* the concentration of the transferred ion just outside the diffuse double layer. ϕ^W and ϕ^O are the inner potentials in the bulk of the aqueous and nitrobenzene solutions, respectively, and ϕ_2^W and ϕ_2^O are the potentials of the reaction planes on the respective solution sides. Consequently, Eq. 5 can be rewritten as

$$I = zFA(\vec{k}_{corr}C_2^W - \overleftarrow{k}_{corr}C_2^N), \tag{27}$$

with

$$\vec{k}_{corr} = \vec{k}\exp[-zF(\phi^W-\phi_2^W)/RT], \tag{28}$$

$$\overleftarrow{k}_{corr} = \overleftarrow{k}\exp[-zF(\phi^O-\phi_2^O)/RT], \tag{29}$$

where $\vec{k}_{corr}$ and $\overleftarrow{k}_{corr}$ are the "true" rate constants or the rate constants for the ion-transfer reaction taking place from the reaction plane on one solvent side to the reaction plane on the other. Upon assuming that the reaction planes are located on the OHP's on each solution side, the values of $\phi^W-\phi_2^W$ and $\phi^O-\phi_2^O$ can be calculated (in the absence of specific adsorption) by the Gouy-Chapman theory by knowing the surface charge density which was calculated from the double-

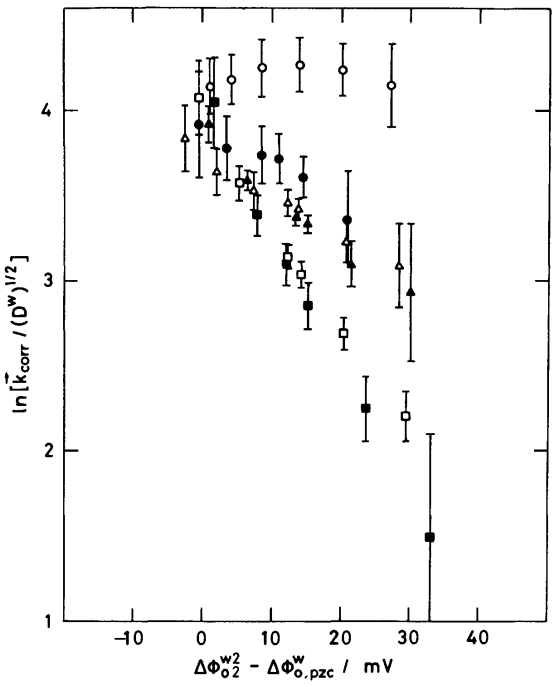

Fig. 6. Plot of $\ln[\vec{k}_{corr}/(D^W)^{1/2}]$ *vs.* $\Delta\phi_{o2}^{W2}-\Delta\phi_{o,pzc}^{W}$ for the Pic^--ion transfer at the interface between a nitrobenzene solution of 0.1 mol dm^{-3} TBATPB and an aqueous solution of (○) 0.02, (●) 0.05, (△) 0.10, (▲) 0.20, (□) 0.50, and (■) 1.0 mol dm^{-3} LiCl. Vertical bars indicate the standard deviations.

layer capacity data[14] and the potential of zero charge (pzc) data.[13] In Fig. 6, the values of $\ln[\vec{k}_{corr}/(D^W)^{1/2}]$ thus obtained for various concentrations of LiCl in the aqueous solution are plotted against the potential drop across the inner layer, $\Delta\phi_{O2}^{W2}=\phi_2^W-\phi_2^O$, referred to the potential drop across the inner layer at the pzc, $\Delta\phi_{O,pzc}^{W}=\phi_{pzc}^{W}-\phi_{pzc}^{O}$.[14] It has been shown[13,14] that the inner layer capacity of the interface between an aqueous solution of LiCl and a nitrobenzene solution of TBATPB depends only on the surface charge density (or the inner layer potential difference) and not on the concentration of LiCl in the aqueous solution. Therefore it is expected that the corrected rate constants obtained at various LiCl concentrations lie on a single curve representing the dependence of $\vec{k}_{corr}$ on $\Delta\phi_{O2}^{W2}$. In contrast to this expectation, the $\ln[\vec{k}_{corr}/(D^W)^{1/2}]$ *vs.* $\Delta\phi_{O2}^{W2}-\Delta\phi_{O,pzc}^{W}$ plots varies considerably with the concentration of LiCl in the aqueous solution (Fig. 6). Considerable variation of the $\ln[\overleftarrow{k}_{corr}/(D^N)^{1/2}]$ *vs.* $\Delta\phi_{O2}^{W2}-\Delta\phi_{O,pzc}^{W}$ plots with the change of TBATPB concentration in the nitrobenzene solution was also found for the corrected rate constants obtained at various TBATPB concentrations (data not shown). These results (Fig. 6) suggest that the formalism of Frumkin correction based on the assumption that the reaction planes are located on the OHP's on respective solution sides is not valid for this case, especially in moderately concentrated supporting electrolyte solutions.

In the above discussion, the potentials of OHP's were estimated by the basic Gouy-Chapman theory. Modifications of the basic Gouy-Chapman theory have been described.[16] In view of the smallness of the surface charge density (less than 4 μC cm^{-2}) and the moderate concentration of the electrolytes (less than 0.20 mol dm^{-3} except in a few extreme cases), however, we may conclude that the error caused by applying the basic Gouy-Chapman theory to the present system is probably small.

In the above discussion it is also assumed that the ion-pair formation of Pic$^-$ ion is negligible which is in harmony with the d.c. voltammetric data on Pic$^-$ ion. Available data on the ion-pair formation of Pic$^-$ ion in water and nitrobenzene are limited. However, according to Poonia *et al.*[15] $K_{LiPic}^{W}=12.8$, which suggests that the ion-pair formation of Pic$^-$ ion would be appreciable in concentrated LiCl aqueous solution. Accordingly, it is worth while discussing the possible effect of the ion-pair formation on the kinetic parameters of the ion transfer at the water/nitrobenzene interface. If the rate constants of the association and dissociation of the ion-pair are sufficiently large (*e.g.*(the first order rate constant)/$\omega \gg 1$), the a.c. faradaic impedance theory predicts that $\vec{k}$ and $\overleftarrow{k}$ in Eqs. 10, 13, 14 and the following equations should be replaced, respectively, by

$$\vec{k}' = \frac{\vec{k}}{1+K_{LiPic}^{W}a_{Li}^{W}+K_{TBAPic}^{W}(K_{TBA}^{N/W},\Delta\phi)^{-1}a_{TBA}^{N}} \tag{30}$$

and

$$\overleftarrow{k}' = \frac{\overleftarrow{k}}{1+K_{LiPic}^{N}K_{Li}^{N/W},\Delta\phi a_{Li}^{W}+K_{TBAPic}^{W}a_{TBA}^{N}}. \tag{31}$$

Thus, the $\ln[\vec{k}_{corr}/(D^W)^{1/2}]$ *vs.* $\Delta\phi_{O2}^{W2}-\Delta\phi_{O,pzc}^{W}$ plots, such as those in Fig. 6 should be also corrected by Eq. 30. However, it is clear that such a correction will not modify the scattered plots to align them on a single curve. Therefore we may conclude that the ion-pair formation of Pic$^-$ ion with TBA$^+$ and/or Li$^+$ ion, if any, would not seriously affect the above discussion.

The ion transfer from one solvent to the other should consist of desolvation of one solvent and resolvation with the other and could take place in the reaction layer of a certain thickness, possibly extending beyond the inner layer into the diffuse double layers (or even beyond the diffuse double layers in concentrated electrolyte solutions). The Frumkin correction, if any, should be applied to the concentrations of the transferred ion at the reaction planes which are supposed to be located distant from the OHP's toward the bulk of respective solutions. Samec and his coworkers, using relatively dilute LiCl solutions (0.05 and 0.01 mol dm^{-3}), found that the corrected rate constants of the transfer of Cs$^+$ [6] and choline and acetylcholine ions[7] at the aqueous solution of LiCl/nitrobenzene solution of TBATPB interface change little with the potential across the interface. This result led these authors to conclude that the observed potential dependence of the "apparent" rate constants arises largely from the effect of the porential on the concentration of the transferred ions at the reaction planes which are located at the OHP's. Actually, the potential dependence of the "corrected" rate constants in 0.02 mol dm^{-3} LiCl aqueous solution was relatively small (see Fig. 6). However, as discussed above, the strong potential dependence of the "corrected" rate constants of Pic$^-$-ion transfer observed in moderately concentrated electrolyte solutions seems to indicate that the observed potential dependence may reflect the real potantial dependence of the Pic$^-$-ion transfer rate constants at the water/nitrobenzene interface.

References

1) T. Osakai, T. Kakutani, and M. Senda, *Bull. Chem. Soc. Jpn.*, **57**, 370 (1984).

2) Z. Samec, *J. Electroanal. Chem. Interfacial Electrochem.*, **99**, 197 (1979).

3) O. R. Melroy and R. P. Buck, *J. Electroanal. Chem. Interfacial Electrochem.*, **136**, 19 (1982).

4) B. d'Epenoux, P. Seta, G. Amblard, and C. Gavach, *J. Electroanal. Chem. Interfacial Electrochem.*, **99**, 77 (1979).
5) Z. Koczorowski and G. Geblewicz, *J. Electroanal. Chem. Interfacial Electrochem.*, **139**, 177 (1982).
6) Z. Samec, V. Mareček, J. Weber, and D. Homolka, *J. Electroanal. Chem. Interfacial Electrochem.*, **126**, 105 (1981).
7) Z. Samec, V. Mareček, and D, Homolka, *J. Electroanal. Chem. Interfacial Electrochem.*, **158**, 25 (1983).
8) T. Kakutani, T. Osakai, and M. Senda, *Bull. Chem. Soc. Jpn.*, **56**, 991 (1983).
9) M. Senda, T. Kakutani, and T. Osakai, *Denki Kagaku*, **49**, 322 (1981).
10) I. M. Kolthoff, *Can. J. Chem.*, **59**, 1548 (1981).
11) T. Osakai, T. Kakutani, Y. Nishiwaki, and M. Senda, *Bunseki Kagaku*, **32**, E81 (1983).
12) D. Homolka and V. Mareček, *J. Electroanal. Chem. Interfacial Electrochem.*, **112**, 91 (1980).
13) T. Kakiuchi and M. Senda, *Bull. Chem. Soc. Jpn.*, **56**, 1753 (1983).
14) T. Osakai, T. Kakutani, T. Kakiuchi, and M. Senda, unpublished results.
15) N. S. Poonia, S. K. Sarad, A. Jayakumar, and G. C. Kumar, *J. Inorg. Chem.*, **41**, 1759 (1979).
16) For a review, see a) J. O'M Bockris and A. K. N. Reddy, "Modern Electrochemistry," Plenum Press, Vol. 2, New York (1970), pp. 623—843; b) R. Reeves, "Comprehensive Treatise of Electrochemistry," ed by J. O'M Bockris, B. E. Conway, and E. Yeager, Plenum Press, Vol. 1, New York (1980) pp. 83—134.

Photoelectrochemical Behavior of p-Type Boron Phosphide Photoelectrode in Acidic Solution

Ju-seong LEE,† Akira FUJISHIMA,* Kenichi HONDA,†† and Yukinobu KUMASHIRO†††
†Department of Industrial Chemistry, College of Engineering, Hanyang University, Seoul 133, Korea
*Department of Synthetic Chemistry, Faculty of Engineering, The University of Tokyo, Bunkyo-ku, Tokyo 113
††Division of Molecular Science, Kyoto University, Sakyo-ku, Kyoto 606
†††Electrotechnical Laboratory, Sakura-mura, Ibaraki 305
(Received February 20, 1985)

The photoelectrochemical behavior of p-type boron phosphide (p-BP) in acidic solution was investigated. The p-BP photocathode was stable in sulfuric acid solution under irradiation, and the band gap deduced from the photocurrent action spectrum in acidic solution was 2.0 eV. The gas evolved from p-BP photocathode was hydrogen which was obtained with a current efficiency of *ca.* 100%. The photocurrent was markedly increased by suitable ruthenium treatment of the BP. A photoelectrochemical cell (PEC), Pt(H_2)/0.5 M H_2SO_4(1 M=1 mol dm^{-3})//0.5 M H_2SO_4/p-BP, was shown to have an open-circuit photovoltage of 0.45 V and a fill factor of 0.25.

The photoassisted electrolysis of water using semiconductor electrodes has been studied extensively in the last few years.[1-7] One of the major requirements in any practical application is that the semiconductor be stable. Because it is very difficult to find intrinsically stable materials, considerable effort has been expended on electrode modifications to improve stability and charge transfer properties. Some of the methods employed or suggested includes the use of stabilizing redox couples in the electrolyte,[8-10] overcoating of unstable semiconductors with noble metals,[11] stable semiconductors,[12,13] and conductive polymers.[14-18]

Although much work has been done on semiconductors, hardly any has been reported on boron phosphide (BP) behavior after Ginley *et al.*[13] reported that BP stabilized n-Si, n-GaAs photoanodes, and after Grantham's patent[19]. In this paper, we report the attainment of quite stable photocurrents resulting in hydrogen production that were obtained from a p-BP electrode in acidic solution. Also, we report a detailed study of the effects of ruthenium treatment of a p-BP electrode surface.

Experimental

A BP single crystal was prepared by a flux method[20] under high pressure either at 10 or 18 atms. The BP crystal was etched for 10 min in fused sodium hydroxide at 420 °C and then washed with distilled water. After an ohmic contact was made with an indium-gallium alloy, a copper wire was connected with silver paste, and then all surfaces except one side were covered with an epoxy resin.

The same cell was used for photoelectrolysis and for measurement of current-potential curves. This cell consisted of two compartments separated by a cation

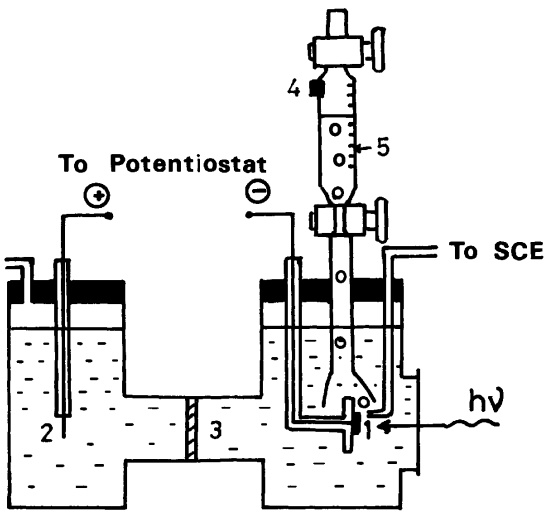

Fig. 1. Schematic of p-BP photoelectrolysis apparatus.
1: BP photoelectrode, 2: Pt counter electrode, 3: Cation exchange membrane separator, 4: Rubber stopper, 5: 2 ml calibrated burette.

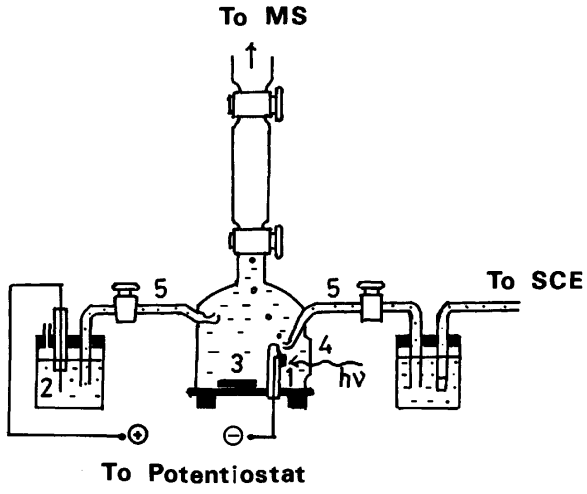

Fig. 2. Schematic of photoelectrolysis cell for mass spectrometric analyses.
1: BP photoelectrode, 2: Pt counter electrode, 3: Magnetic stirring bar, 4: Window for incident light, 5: Salt bridge.

exchange membrane (Selemion CMV, Asahi Chem. Co.) and a 2 ml burette in the catholyte chamber, as shown in Fig. 1. The volumes of catholyte and anolyte chamber were 100 and 80 ml, respectively. Another cell was used for mass spectrometric analysis, the volume of the catholyte of which was 1 ml, as shown in Fig. 2. These cells were equipped with the p-BP working electrode (av. surface area≈0.12 cm^2), a platinum wire counter electrode (dia. 1.0 mm × length 10 mm), and a saturated calomel electrode (SCE) as a reference electrode.

The light source was a 500W xenon lamp (Ushio Electric Inc.), and the light path included an infrared cut filter and quartz lens. Current-potential curves were taken by using a potentiostat/galvanostat system (Hokuto Denko Co.) in cojunction with an X–Y recorder. The hydrogen evolved was analyzed by means of a gas chromatograph (Hitachi model 163) and mass spectrometer (Ulvac YTP-150). The packing material of the column was molecular sieve 5A and the carrier gas for the gas chromatography was argon gas. Scanning electron microscopic and surface analyses were performed by means of a scanning electron microscope (Hitachi type S 550), X-ray detector (Kevex Co. type 7000-75), and a computer system (DEC Co. PDP 11/34). Ruthenium was applied to the BP surface by dipping the BP into ruthenium chloride solution [0.5—10% $RuCl_3$–methanolic solution (CH_3OH:H_2O=1:1)] and irradiating with 500W xenon lamp.

All chemicals were of reagent grade. Before all experiments, the electrolytic solutions were purged with nitrogen gas for more than 30 min.

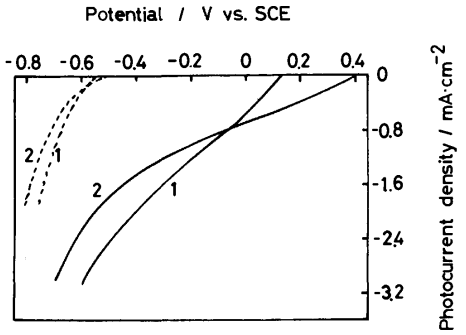

Fig. 3. Effect of irradiation on preparation pressure of BP on the current-potential curves for etched p-BP electrode in 0.5 M H_2SO_4 solution.
Dotted lines; In dark, Solid lines; Under irradiation, 1: 10 atm, 2: 18 atm.

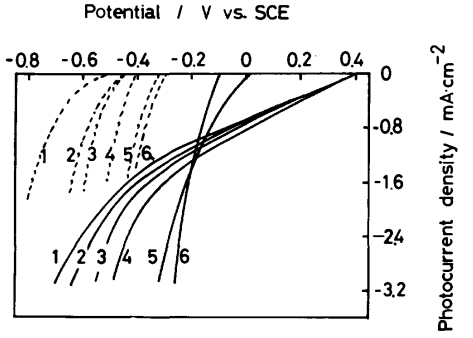

Fig. 4. Effect of ruthenium concentration on the current-potential curves for Ru-treated p-BP (18 atm) electrode in 0.5 M H_2SO_4 solution.
1: Bare etched BP. Nos. 2, 3, 4, 5, and 6 were treated with 1, 3, 5, 8, and 10% $RuCl_3$ solution on etched BP, respectively.
Dotted and solid lines have same meaning as in Fig. 3.

Results and Discussion

Current-potential Characteristics. The effect of irradiation on the current-potential curves for an etched p-BP photocathode in 0.5M H_2SO_4 is shown in Fig. 3 for samples prepared at 10 and 18 atm pressure. The photocurrent was shifted about 0.9V in the anodic direction compared to the dark current value. Since the optical to electrical conversion efficiency was reported to be increased by applying ruthenium on semiconductor surfaces[21,22] we determined the effect of ruthenium concentration on the photocurrent-potential curves for the BP treated with ruthenium(III) chloride in 0.5M H_2SO_4, shown in Fig. 4. Increasing the concentration of ruthenium(III) chloride solution increased the photocurrent. In the case of treating the BP surface with concentrated ruthenium chloride solution or of long-term irradiation of the BP surface in diluted ruthenium solution, the photocurrent was markedly shifted in the cathodic direction. This phenomenon of cathodic shift can be explained by a decrease of characterization of semiconductor to be covered with ruthenium metal or ruthenium oxide.

Dependence of Photocurrent on Wavelength and the Stability of a BP Cathode. The wavelength dependence of the photocurrent for p-BP prepared under 18 atm pressure is shown in Fig. 5. The quantum yield was calculated by dividing the photocurrent at a certain wavelength by the number of photons incident on the BP electrode. The threshold of the photocurrent response was about

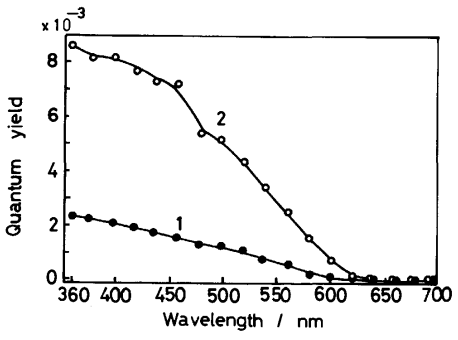

Fig. 5. Action spectrum of p-BP (18 atm).
Applied potential; −0.45 V *vs.* SCE.
1: Bare etched BP, 2: BP etched and treated with 3% $RuCl_3$ solution.

Table 1. Electrolysis results of p-BP (18 atm) cathode untreated and with a $RuCl_3$ methanolic solution (Electrolyte: 0.5 M H_2SO_4)

Set Pot. (V *vs.* SCE)	3% $RuCl_3$	Quantity of Electricity (Coulombs)	Electrolysis Time (min)	Av. Current Density (mA cm^{-2})	Hydrogen Gas Obtained (ml) BP	Pt	Current Efficiency (%) BP/Pt
−0.6	Untreated	5.2	440	2.4	0.55	0.62	88.7
−0.6	Treated	5.2	365	2.9	0.62	0.62	100.0
−1.0	Untreated	10.0	140	14.4	1.20	1.25	96.0
−1.0	Treated	10.0	67	30.1	1.25	1.25	100.0

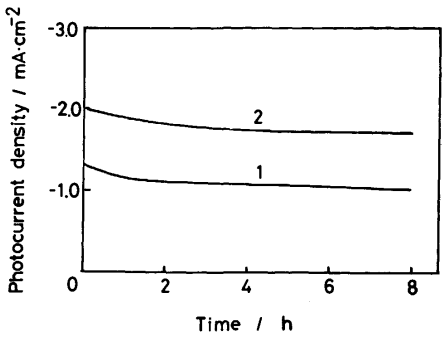

Fig. 6. Time dependence of photocurrent density at BP (18 atm) photocathode in 0.5 M H_2SO_4 solution. Applied potential; −0.4 V *vs.* SCE, Conditions of Nos. 1 and 2 were the same as in Fig. 5.

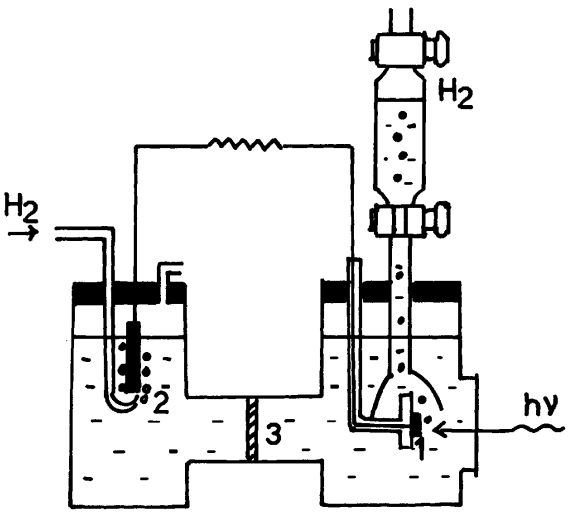

Fig. 7. Schematic diagram of PEC cell.
1: BP photoelectrode, 2: Platinized platinum electrode, 3: Cation exchange membrane.

600 nm (2.0 eV), in agreement with the direct band gap calculation. As is evident from Fig. 5, the p-BP photocathode will respond to sunlight of wavelength shorter than 600 nm.

Figure 6 shows the photocurrent-irradiation time profile for a p-BP photocathode with and without a ruthenium treatment. As shown for a cell where the photocathode process was according to hydrogen evolution, there was no evidence that the photocathode deteriorated.

Hydrogen Evolution. The hydrogen evolution produced by the BP and the Ru-treated BP photocathodes during electrolysis was determined by measuring the quantity of electricity under constant set potential, and the results are shown in Table 1. For the purpose of calculating the current efficiency, the volume of gas evolved from the BP photoelectrolytic cell of Fig. 1 was compared with the volume of hydrogen evolved from the cathode of the Pt cathode/Pt anode electrolytic cell in 0.5M H_2SO_4. These two cells were connected in series with each other. The results in Table 1 show that the photoreaction on the BP photocathode in an acidic solution produced hydrogen, and the current efficiency of the process was almost 100% by comparison with the Pt cathode.

p-BP/H_2SO_4 Photoelectrochemical (PEC) Cell.

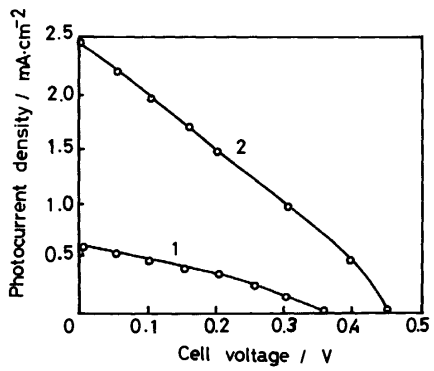

Fig. 8. Photocurrent-photovoltage characteristic of the cell Pt(H_2)/0.5 M H_2SO_4//0.5 M H_2SO_4/p-BP (1 atm). Irradiation source; 500 W xenon lamp.
1: Bare etched BP, 2: BP etched and treated with 3% $RuCl_3$ solution.

A PEC cell was made by connecting the p-BP semiconductor to a counter electrode by means of a variable resistive load in the external circuit. Schematic diagram of PEC cell is shown in Fig. 7. Figure 8 shows the power characteristic in the acidic

solution obtained with and without ruthenium treatment on the BP electrode using light from a 500W xenon lamp. From curve 2 in Fig. 8, we estimate that the open circuit photovoltage was 0.45 V, the short-circuit photocurrent density was 2.4 mA cm^{-2}, and the fill factor was 0.25. The overall conversion efficiency of optical to electrical energy for the PEC photovoltaic cell was much increased by the ruthenium treated BP but it was still low with respect to the case of InP.

Examination of Surface State of BP. The surfaces of different BP specimens after etching and treating with ruthenium were observed by scanning electron micrographs. It was found that the p-BP surface without etching had a very smooth surface while the surface of etched p-BP had many blisters. The surface of etched BP, which had been treated by dipping in methonolic ruthenium(III) chloride solution for 1 min, washing with water, and irradiating for 1 min with the 500W xenon lamp, observed the white and black areas by the scanning electron microscope.

Analytical results of X-ray fluoresence of the average area have indicated, for example, that weight percents of each component were Si 3.09%, P 87.97%, and Ru 8.94%, where Si was surface impurities on the BP semiconductor. The amount of ruthenium was greater in the white areas than the black areas. Therefore, the surface layer was not a homogeneous coating, but rather there were islands of ruthenium on the BP. By dipping the BP in the ruthenium solution for 5 min a thick ruthenium covered the BP surface, not only in the white areas but also in the black areas. The thicker, homogeneous ruthenium layer on the p-BP is undesirable because the deposited ruthenium would absorb and reflect photons before they could reach the semiconductor, thereby decreasing the cell efficiency. Therefore, it is necessary that the surface treatment is carried out with a suitable concentration of ruthenium and treatment time.

Conclusion

The p-BP photocathode has a good wavelength response (E_g=2.0 eV), and is stable in an acidic solution under irradiation. The gas evolved from this BP photocathode under irradiation was hydrogen which was produced with a current efficiency of about 100%. The photocurrent was markedly increased by a suitable surface ruthenium treatment of the BP.

The overall conversion efficiency of optical to electrical energy for the PEC photovoltaic cell was low, that was, the open-circuit photovoltage was 0.45V, the short-circuit photocurrent density was 2.4 mA cm^{-2}, and the fill factor was 0.25. Therefore, to make a more practical device it is necessary to improve this conversion efficiency.

References

1) A. Fujishima and K. Honda, *Nature*, **238**, 37 (1972).
2) H. Gerischer, *J. Electroanal. Chem.*, **58**, 263 (1975).
3) K. L. Hardee and A. J. Bard, *J. Electrochem. Soc.*, **123**, 1024 (1976); **124**, 215 (1977).
4) A. J. Nozik, *Ann. Rev. Phys. Chem.*, **29**, 189 (1978).
5) M. S. Wrighton, *Acc. Chem. Res.*, **12**, 303 (1979).
6) F. F. Fan, B. L. Wheeler, A. J. Bard, and R. N. Noufi, *J. Electrochem. Soc.*, **104**, 2031 (1982).
7) J. H. Kennedy and M. Anderman, *J. Electrochem, Soc.*, **130**, 848 (1983).
8) T. Inoue, T. Watanabe, A. Fujishima, and K. Honda, *Bull. Chem. Soc., Jpn.*, **52**, 1243 (1979).
9) A. B. Bocarsly, D. C. Bookbinder, R. N. Doiney, N. S. Lewis, and M. S. Wrighton, *J. Am. Chem. Soc.*, **102**, 3683 (1980).
10) A. Heller, H. J. Lowerenz, and B. Miller, *J. Am. Chem. Soc.*, **103**, 200 (1980).
11) Y. Nakato, S. Tonomura, and H. Tsubomura, *Ber. Bunsenges. Phys. Chem.*, **80**, 1002, 1289 (1976).
12) H. Morisaki, T. Watanabe, M. Iwase, and K. Yazawa, *Appl. Phys. Lett.*, **29**, 338 (1976).
13) D. S. Ginley, R. J. Baughman, and M. A. Butler, *J. Electrochem. Soc.*, **130**, 1999 (1983).
14) J. Prejza, I, Lundstrom, and T. Skotheim, *J. Electrochem. Soc.*, **129**, 1685 (1982).
15) R. A. Bull, F. F. Fan, and A. J. Bard, *J. Electrochem. Soc.*, **129**, 1009 (1982).
16) G. Cooper, R. Noufi, A. J. Frank, and A. J. Nozik, *Nature*, **295**, 578 (1982).
17) R. A. Simon, A. J. Ricco, and M. S. Wrighton, *J. Am. Chem. Soc.*, **104**, 2031 (1982).
18) T. Osa, *Denki Kagaku*, **49**, 380 (1981).
19) D. H. Grantham, U.S. Patent 4227977 (1980).
20) Y. Kumashiro, T. Yao, and S. Gonda, *J. Crystal Growth*, **70**, (1985), in press.
21) B. A. Parkinson, A. Heller, and B. Miller, *J. Electrochem. Soc.*, **126**, 954 (1979).
22) W. D. Johnston, Jr, H. J. Leamy, B. A. Parkinson, A. Heller, and B. Miller, *J. Electrochem. Soc.*, **127**, 90 (1980).

 © 1985 The Chemical Society of Japan Bull. Chem. Soc. Jpn., 58, 2638—2640 (1985)

Surface Treatment of *meso*-Carbon Microbeads by Oxygen Plasma

Masaaki SUGIURA, Kunio ESUMI,* Kenjiro MEGURO, and Hidemasa HONDA
Department of Applied Chemistry, Institute of Colloid and Interface Science, Science University of Tokyo, Kagurazaka, Shinjuku-ku, Tokyo 162
(Received March 23, 1985)

A surface treatment of *meso*-carbon microbeads was carried out using an oxygen plasma to improve the wettability in aqueous solution. The surface acidity of *meso*-carbon microbeads increased with treating time and the pH of the aqueous dispersion shifted to lower values. The zeta potential varied with treating time from a positive to a negative value. Further, the turbidity behavior of aqueous dispersion with treating time was similar to that of surface acidity. From these results, it was found that the surfaces of *meso*-carbon microbeads were oxidized by oxygen plasma, resulting in an enhancement of wettability of *meso*-carbon microbeads in an aqueous solution.

It is well known[1] that a mesophase transformation takes place in graphitizable organic materials (such as pitches) during pyrolysis at temperatures between 350 and 500 °C. During the heat treatment of pitches, mesophase spherule is formed due to an accumulation of oriented polycondensed aromatic hydrocarbons. The mesophase spherules that separated as quinoline insolubles from the mesophase pitches are called *meso*-carbon microbeads.

These do not melt or fuse upon a heat treatment and do not dissolve at room temperature in organic solvents such as quinoline, pyridine and benzene. From the chemical reactivity,[2] the pore structure,[3] the adsorption-desorption isotherms, and the heat-of-immersion,[4] of the *meso*-carbon microbeads, it has been recognized that the constituent unit of *meso*-carbon microbeads is a micelle composed of the molecules and that the micelles lie perpendicular to a pole of the sphere, as in the Taylor model.[5] The exteriors of *meso*-carbon microbeads melt in a medium of polynuclear aromatic hydrocarbons or pitch materials during a heat treatment. The *meso*-carbon microbeads in liquids similar to pitch under heat treatment behave in a similar manner as mesophase spherules produced in pitch during a heating.

In polycyclic aromatics, the reactivity of the edge carbon atoms at the periphery is very high, as is well known. Therefore, the surfaces of *meso*-carbon microbeads are interesting from the view point of the surface chemistry of solids. Hagiwara *et al.*[6] examined the possibility of using *meso*-carbon microbeads as a chromatographic filler. They confirmed that benzene derivatives could be separated using *meso*-carbon microbeads treated with a Friedel-Crafts reaction. When *meso*-carbon microbeads are used in an aqueous solution, there is a wetting problem since *meso*-carbon microbeads exhibit hydrophobic properties.

Recently, as one method for surface treatment, a plasma treatment[7] has become attractive, probably due to it being a dry process at low temperatures with a relatively low-pressure gas.

In this work, changes in the surface properties of *meso*-carbon microbeads upon a treatment of oxygen plasma were examined by measuring the surface acidity, surface charge, turbidity, and pH of *meso*-carbon microbeads in an aqueous solution.

Experimental

Materials. *Meso*-carbon microbeads were obtained through a separation from heat-treated quinoline soluble coal-tar pitch. The physical properties of the obtained *meso*-carbon microbeads were as follows: quinoline insoluble, 92.3%; benzene insoluble, 97.0%; volatile matter, 17.3%; ash, 0.3%; C/H=2.314; diameter, 2-15 μm.

Procedure. About 3 grams of *meso*-carbon microbeads were charged into a reactant vessel, followed by degassing down to 1.5 Torr. Then, oxygen gas was flowed at a rate of 100 ml/min into the vessel while evacuated *meso*-carbon microbeads were being treated with an oxygen plasma under various high-frequency powers and treating times. The pressure during the treatment was kept at about 3 Torr†. The high-frequency power used in this study was 25, 50, and 100 W, and the treating times were 1, 2, 3, and 4 h, respectively.

Measurements. About 0.1 grams of *meso*-carbon microbeads were put into 50 ml of deionized water, boiled for 15 min, then allowed to stand for 2 d. The, thus obtained, suspension's pH was measured with a pH meter (Denki Kagaku Keiki Co. Ltd.).

The zeta potential of the suspension used for the pH measurement was determined by an electrophoresis apparatus (Laser-Zee Model 500, Pen Kem.).

About 0.1 grams of *meso*-carbon microbeads were put into a sedimentation tube and 30 ml of deionized water was added. Then the solution was dispersed by supersonic waves for half an hour and the turbidity of the dispersion was measured after 1 d of standing.

The acidity of surface functional groups of *meso*-carbon microbeads was determined by a titration method which was the same as that Boehm[8] used. About 1 gram of *meso*-carbon microbeads and a 50-ml aqueous solution of 50 ml ($NaHCO_3$, Na_2CO_3, NaOH, and $NaOC_2H_5$) of 0.05

† 1 Torr=133.322 Pa.

to 0.1 M†† were placed in an Erlenmeyer flask. After shaking for 1 d at 25 °C, it was allowed to stand for 4 d; then, after centrifuging, 20 ml of the supernatant solution was titrated with 0.1 M HCl. At the same time, a blank test was carried out. From the difference in the titrations, the acidity of *meso*-carbon microbeads was evaluated.

Results and Discussion

The *meso*-carbon microbeads were treated with the oxygen plasma under conditions such as high-frequency power (25, 50, and 100 W) and an oxygen-flow rate of 100 ml min^{-1}. The plasma-treated samples were used for measuring the turbidity in an aqueous solution. The result is given in Fig. 1. The turbidity of the samples increased with an increased treating time. A maximum value appeared at 3 h; then, it decreased slightly for three different high-frequency powers. Further, the turbidity of the treated *meso*-carbon microbeads decreased upon increasing the high-frequency power. Thus, from the turbidity results, it is apparent that the *meso*-carbon microbeads become wettable in an aqueous solution upon treatment with an oxygen plasma.

To elucidate the surface charge of *meso*-carbon microbeads treated with the oxygen plasma, the zeta potential of treated samples in an aqueous solution was measured. At the same time, the pH of the dispersion was also measured. As shown in Fig. 2, the zeta potential of the untreated sample was positive. After the plasma treatment, the zeta potential became negative and reached a constant value after 1 h. It should be noted that the magnitude of zeta potential of the sample treated with the oxygen plasma increased upon decreasing the high-frequency power. From the facts that the pH of the aqueous dispersion of the plasma-treated samples was at around 5—4.5 and their zeta potential values were negative, the surface functional groups formed by the oxygen plasma treatment were acidic groups. Indeed, Ihara *et al.*[9] examined the surface functional groups of carbon black treated with oxygen plasma and they found that these groups were carboxyl, phenolic, and carbonyl groups and the concentrations of these groups varied with the

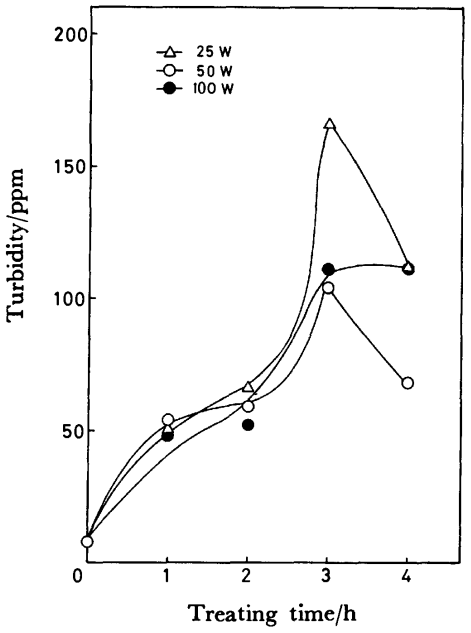

Fig. 1. The turbidity of aqueous dispersion of *meso*-carbon microbeads treated with oxygen plasma under various conditions.

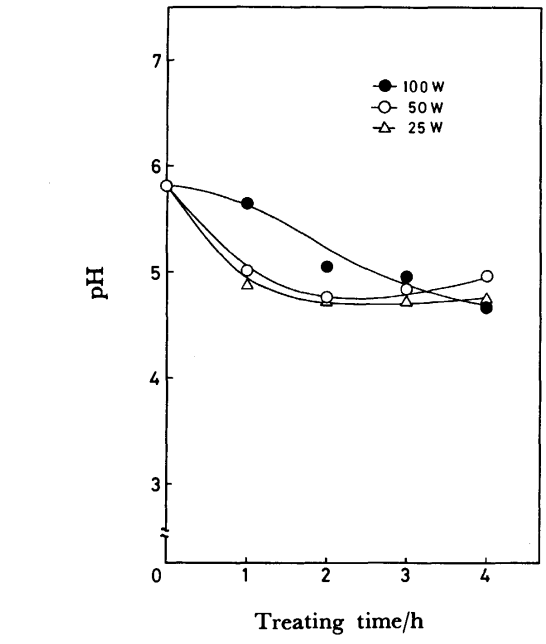

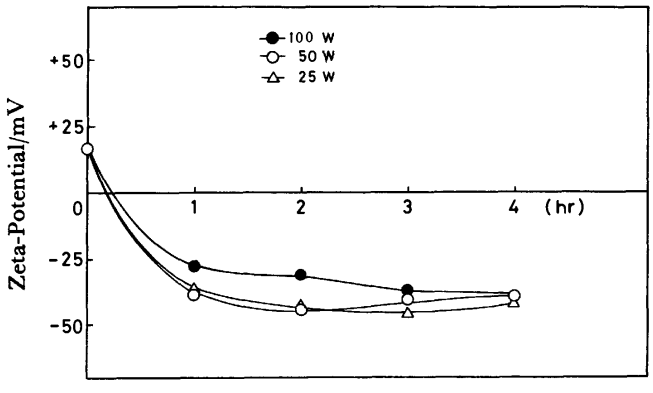

Fig. 2. The zeta potential and pH of aqueous dispersion of *meso*-carbon microbeads treated with oxygen plasma under various conditions.

1 M=1 mol dm^{-3}.

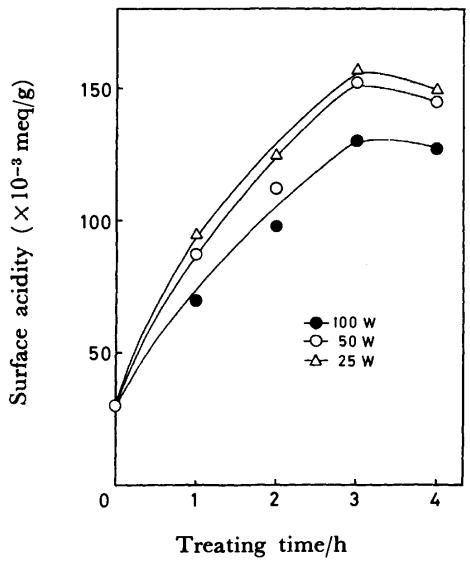

Fig. 3. The change in concentrations of surface functional groups as a function of treating time under various high-frequency powers.

Table 1. Concentrations of surface functional grours by oxygen plasma

Frequency power (W)	Treating time (h)	$\times 10^{-3}$ meg/g			
		Carboxyl	Phenolic	Carbonyl	Total
Untreated		5	12.5	12.5	30
25	1	60	15	20	95
	2	65	57.5	0	125
	3	70	70	17.5	157.5
	4	95	55	0	150
50	1	42.5	20	25	87
	2	82.5	15	15	112.5
	3	87.5	37.5	27.5	152.5
	4	65	0	67.2	132.2
100	1	30	40	0	70
	2	50	45	0	95
	3	100	30	0	130
	4	62.5	30	35	127.5

high-frequency power and treating time. In this work, the concentrations of surface functional groups were also determined by titration. The results are shown in Table 1 and Fig. 3. These functional groups(-COOH, -OH, C=O) were formed by the oxidation of *meso*-carbon microbeads as the oxygen plasma and the concentrations of these groups increased with the treating time, reached a maximum and then decreased. At each treating time, the order in the total concentrations of these groups was as follows: 25 W>50 W>100 W. This decrement in the total concentration of functional groups with longer treating times is probably due to a burn-off of the functional groups by a further oxygen plasma. Accordingly, in order to attain a maximum concentration of functional groups, a proper condition should be selected. It is noteworthy that even after the oxygen-plasma treatment, the surface area of the *meso*-carbon microbeads determined by nitrogen gas adsorption changed only a little compared with that for an untreated sample.

Compared with carbon black,[9] the *meso*-carbon microbeads were less oxidized due to the oxygen plasma. A maximum concentration of functional groups for *meso*-carbon microbeads was obtained at a treating time of 3 h. However, the concentrations of functional groups for carbon black[9] increased linearly with the treating time.

From the above results, it is concluded that the surfaces of *meso*-carbon microbeads become oxidized through the oxygen plasma, resulting in the formation of surface functional groups such as -COOH, -OH. Also, the wettability of *meso*-carbon microbeads treated with oxygen plasma in an aqueous solution is improved. Therefore, it is anticipated that the adsorption capacity for water-soluble materials would be enhanced upon using the *meso*-carbon microbeads treated with an oxygen plasma as the adsorbent.

References

1) H. Honda, *Mol. Cryst. Liq. Cryst.*, **94**, 97 (1983).
2) Y. Yamada, H. Honda, K. Fukuda, and S. Oi, *J. Fuel Soc. Jpn*, **55**, 704 (1976).
3) Y. Yamada, K. Takei, S. Hagiwara, and H. Honda, Preprint of 6th Annual Meeting of Carbon Soc. Japan, (1979) p. 6.
4) S. Hagiwara, Y. Yamada, H. Takahashi, and H. Honda, Preprint of 7th Annual Meeting of Carbon Soc. Japan, (1980) p. 70.
5) J. D. Brooks and G. H. Taylor, "Chemistry and Physics of Carbon," ed by P. L. Walker, Mercel Dekker, N. Y., 4, (1968) p. 243.
6) S. Hagiwara, Y. Yamada, H. Takahashi, and H. Honda, Preprint of 34th Discussion on Colloid and Interface Chemistry of Japan, (1981) p. 72.
7) J. R. Hollahan and A. T. Bell, "Techniques and Applications of Plasma Chemistry," John-Wiley and Sons, (1974).
8) H. P. Boehm, *Angew. Chem. Ieternat. Edit.*, **5**, 533 (1966).
9) T. Ihara, S. Ito, T. Kuwahara, and M. Kiboku, *Japan Soc. of Colour Material*, **54**, 531 (1981); **55**, 20 (1982).

 © 1985 The Chemical Society of Japan Bull. Chem. Soc. Jpn., 58, 2641—2647 (1985)

Electrochemical Behavior of Dibutyltin(IV) Compounds and Their Determination at ppb Levels by Differential Pulse Anodic Stripping Voltammetry

Hideki KITAMURA,* Akiyoshi SUGIMAE, and Masao NAKAMOTO
Environmental Pollution Control Center, Osaka Prefectural Government, 1-3-62 Nakamichi, Higashinari-ku, Osaka 537
(Received September 14, 1984)

The electrochemical behavior of dibutyltin(IV) compounds (Bu_2SnX_2) (X=chloride, laurate (L), and 6-methylheptyl maleate (MHM)) in 50% (v/v) and 80% (v/v) ethanol-water media (apparent pH 7.3) containing 0.002% Triton X-100 has been investigated by polarography and cyclic voltammetry. It has been found that Bu_2SnX_2 gives a two-electron transfer step at about −0.8 V *vs.* SCE, which consists of very close two one-electron steps, and a two-electron step at about −1.4 V in both media. Over the potential range of either side of the first reduction wave, both Bu_2SnX_2 and their reduction products are significantly adsorbed on the surface of a mercury electrode in 50% (v/v) ethanol, but not in 80% (v/v) ethanol. The adsorbed reduction products are readily re-oxidized at the mercury electrode in 50% ethanol. The re-oxidation peak was successfully utilized for the determination of traces of Bu_2SnCl_2 by means of the differential pulse anodic stripping voltammetry (DPASV) over the concentration range of 3—50 ppb (μg dm^{-3}) at the deposition time of 60 s. The DPASV behavior of Bu_2SnX_2 (X=chloride, L, MHM, and 1-dodecanethiolate) has been investigated in a 50% ethanol medium in detail. Further, a procedure has been developed for determining Bu_2SnX_2 in natural water down to ppb levels.

In recent years, organotin compounds attained rapidly commercial importance. Dibutyltin compounds are widely used as stabilizers for PVC plastics and as the control of helminthic and protozoal infections in poultry.[1] Various methods have been proposed for the determination of organotin compounds, *e.g.* atomic absorption spectrophotometry,[2,3] and fluorometry.[4] As the organotin compounds are reduced at a dropping mercury electrode (DME), this offers the possibility of direct determination.[5–14] Triphenyltin chloride (Ph_3SnCl)[5] and tributyltin compounds[6] are strongly adsorbed onto the electrode surface when reduced at the mercury electrode to the corresponding radicals. This property has been utilized for the determination of traces of Ph_3SnCl and tributyltin compounds by anodic stripping voltammetry (ASV).[5,7,8] Polarographic behavior of dialkyl- and diaryltin(IV) compounds (R_2SnX_2)(R= methyl, ethyl, butyl, phenyl, and X=anion) was also investigated in acids, ethanol-water, *etc.*[9–14] Fleet and Fouzder[11] showed that dibutyltin compounds (Bu_2SnX_2)(X=laurate (L) and maleate (M)) in the 80% (v/v) ethanol-water medium (pH 7.0) gave three reduction waves and proposed the following mechanism.

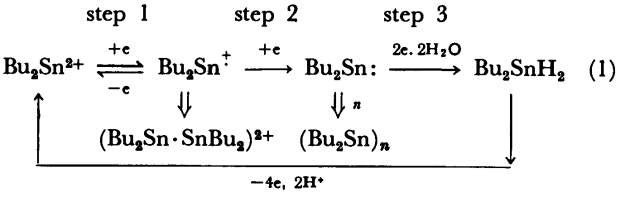

In this mechanism they, however, claimed that no adsorption of both depolarizers and their reduction products occurred at the surface of a mercury electrode. Morris[9] studied the polarographic behavior of diethyltin compounds (Et_2SnX_2) in aqueous acid solutions and claimed that a reversible two-electron step distorted by the formation of insoluble polymer products $(Et_2Sn)_n$ was observed on the electrode surface. We have investigated the polarographic behavior of Bu_2SnCl_2 in the 50% (v/v) ethanol-water medium (pH 7.3) containing 0.002% Triton X-100, a surface-active agent, as a maximum suppressor. Contrary to the previous work by Fleet and Fouzder[11] described above, significant adsorption has been found of both depolarizer and its reduction product(s) onto the mercury electrode, and the adsorbed reduction product(s) is readily re-oxidized. These findings has been successfully utilized for the determination of traces of Bu_2SnCl_2 by differential pulse anodic stripping voltammetry (DPASV) which is one of the most sensitive electrochemical techniques for trace analysis. Meanwhile there have been few reports on the ASV of dibutyltin compounds.

In this paper, we present a more detailed electrochemical behavior of Bu_2SnX_2 (X=chloride, L, and 6-methylheptyl maleate (MHM)) at the mercury electrode in the same medium as described above, primarily with the aim of developing a more sensitive method, *i.e.* DPASV, of Bu_2SnX_2 (X=chloride, L, MHM, and 1-dodecanethiolate (DT)).

Experimental

Materials. The following tin compounds were used in this study: Bu_2SnCl_2, Ph_3SnCl (Tokyo Kasei Kogyo, Tokyo, Japan), Bu_2SnL_2, Bu_2SnMHM_2, Bu_2SnDT_2, $(Bu_3Sn)_2O$ (ICN Pharmaceuticals, Inc., Life Sci. Group, Plainview, N. Y., USA). The purities of these compounds were higher than 95%. The stock solutions of tin compounds were prepared by dissolving them in 99.5%

ethanol (Wako Pure Chem., Osaka, Japan; Pesticide Analytical Grade). All reagents were analytical reagent grade. The cation-exchange resin for column chromatography (Amberlite CG-120, chromatographic grade, 200 mesh) was pre-washed in the usual manner, and conditioned with ethanol.[22]

Apparatus. Normal, reverse and differential pulse polarograms and cyclic voltammograms were measured on a Yanagimoto Voltammetric Analyzer (model P-1000) using a three-electrode cell. Throughout this study an aqueous saturated calomel electrode (SCE) and a spiral platinum electrode were used as a reference electrode and as a counter electrode, respectively. Cyclic voltammograms were measured with a hanging mercury drop electrode (HMDE) (Metrohm, Type EA290, electrode surface area 1.39±0.03 mm^2).

For DPASV, Yanagimoto Voltammetric Analyzer (P-1000) was used to supply both the applied potential for the pre-electrolysis and the voltage sweep for the stripping process. During pre-electrolysis the solution was constantly stirred by a Metrohm model E549 magnetic stirrer. The working electrode used was the same HMDE as that used in the measurement of cyclic voltammograms. The polarographic cell employed was Princeton Applied Research model K64.

The apparent pH values of ethanolic solutions were measured with a Hitachi pH meter molel F-7AD.

Procedure. Working solutions for all voltammetry were made up in constant ionic strength buffer medium (0.1 M in acetic acid and ammonia) at apparent pH 7.3. Unless otherwise stated, the solutions contained 50% ethanol and 0.002% Triton X-100.[5,9,11] Solutions were deoxygenated with a steam of purified nitrogen gas for 10 min prior to measurement, which was presaturated with ethanol–water (1:1) vapor.

For DPASV, after deaeration of the solution, a drop at the HMDE was formed and a constant voltage (−1.0 V for Bu_2SnX_2 and Ph_3SnCl, and −1.3 V for $(Bu_3Sn)_2O$) was applied for a given interval (60 s). The deposition proceeded in a stirred solution. After a quiescent period of 10 s, the electrode was polarized from the deposition potential to more positive values and the stripping peak was recorded. For every measurement the solution was deoxygenated for 2 min and a new drop was formed at the HMDE.

Results and Discussion

General Voltammetric Behavior. In order to develop a sensitive method for determining Bu_2SnX_2 (X=chloride, L, MHM, and DT), its voltammetric behavior, especially Bu_2SnCl_2, was investigated. Since Bu_2SnDT_2 is sparingly soluble in 50% (v/v) ethanol–water medium, it was not investigated.

Normal pulse polarograms (NPP) for Bu_2SnCl_2 in 50% (v/v) and 80% (v/v) ethanol–water media (apparent pH 7.3) are shown in Fig. 1. In both media, Bu_2SnCl_2 gives three reduction waves (I—III).[11] At 1×10^{-4} M (1 M=1 mol dm^{-3}) of Bu_2SnCl_2 in 50% ethanol, distortion is present at more negative potentials than −1.0 V (Fig. 1, curve 1), where the waves appear to split into several steps[9] which were ascertained from cyclic voltammetry. Compared with the respective potentials of three reduction waves of Bu_2SnX_2 (X=L and M) at −0.8, −1.0, and −1.4 V *vs.* SCE according to Scheme (1),[11] the first wave (I) in both media is probably attributed to a two-overlapped wave corresponding to the first and second steps, *i.e.* the formation of Bu_2Sn: which is polymerized to $(Bu_2Sn)_n$.[11] This is also confirmed by the fact that in tast polarography of Bu_2SnCl_2 the limiting current of the first wave (I) in 50% ethanol is the same as that in 80% ethanol. Further, the second wave (II) is probably due to a two-electron reduction of Bu_2Sn: to the hydride Bu_2SnH_2 (third step in Scheme 1).

There is significant adsorption of both Bu_2SnX_2 (X=chloride, L, and MHM) and their reduction products in 50% ethanol, as demonstrated by the appearance of a maximum at the first wave in normal[15] and reverse pulse polarograms, and the depression of electrocapillary curves of Bu_2SnX_2 at both sides of the maximum (Fig. 1). On the other hand, the first wave is accompanied with no maximum in 80% ethanol, indicating that there is no adsorption of the depolarizers and their reduction products in 80% ethanol, as was observed by Fleet and

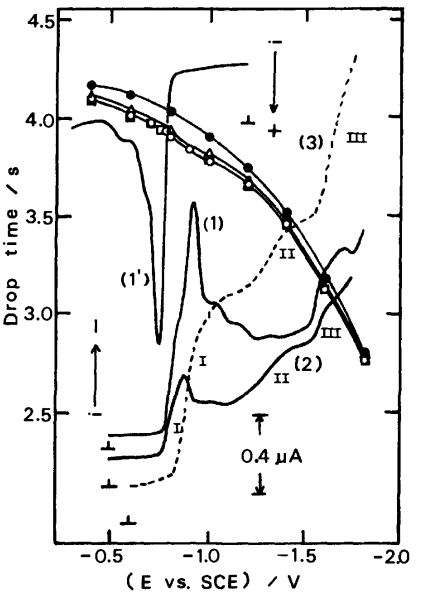

Fig. 1. Normal pulse and reverse pulse polarograms (NPP and RPP) of Bu_2SnCl_2 and electrocapillary curves (ECC) of Bu_2SnX_2 in the 0.1 M acetic acid–0.1 M ammonia buffer solution (pH 7.3) containing 0.002% Triton X-100.
Conditions of NPP and RPP: Ethanol, (1)(1')(2) 50% (v/v) and (3) 80% (v/v); $[Bu_2SnCl_2]$=(1)(1')(3) 1×10^{-4} M, (2) 4×10^{-5} M; (Initial potential *vs.* SCE) /V=(1)(2) −0.5, (1') −1.2, (3) −0.6. Conditions of ECC: Ethanol, 50% (v/v); $[Bu_2SnX_2]$=-●- 0 M, -○- 1×10^{-4} M Bu_2SnCl_2, -□- 1×10^{-4} M Bu_2SnL_2, -△- 1×10^{-4} M Bu_2SnMHM_2.

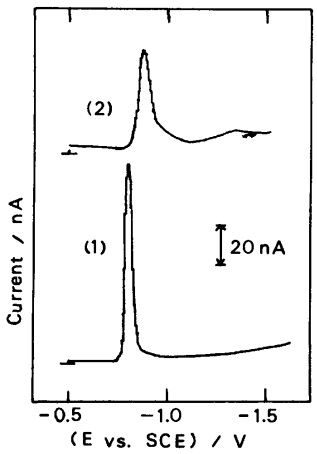

Fig. 2. Differential pulse polarograms (DPP) of 1×10^{-4} M Bu_2SnCl_2 solutions in 50% (v/v) and 80% (v/v) ethanol. Ethanol, (1) 50% (v/v) and (2) 80% (v/v), Conditions: modulation amplitude, 5 mV; pulse repetition time, 1 s; scan rate, 5 mV s^{-1}.

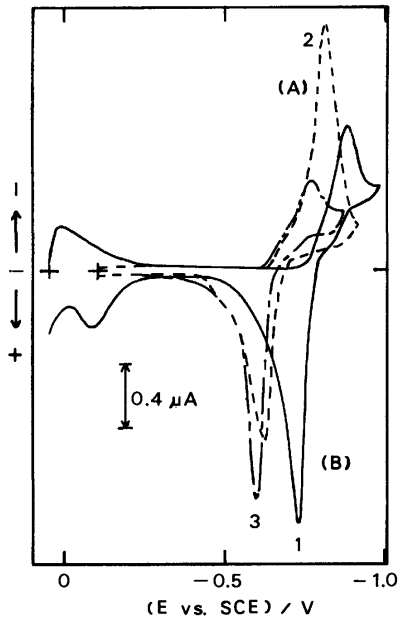

Fig. 3. Cyclic voltammograms of Bu_2SnX_2 in 50% (v/v) ethanol-water medium. (1) 1×10^{-4} M Bu_2SnCl_2, (2) 7×10^{-5} M Bu_2SnL_2, (3) 1×10^{-4} M Bu_2SnMHM_2; Starting potential, (1) +0.05 V, (2)(3) −0.1 V; scan rate, 200 mV s^{-1}.

Fouzder.[11]

Differential pulse polarograms (DPP) of Bu_2SnCl_2 show one distinct peak in both 80 and 50% ethanol-water media as shown in Fig. 2. A similar DPP was obtained for Bu_2SnL_2 in 50% ethanol. The peak in 50% ethanol (curve 1) is narrower and higher than that in 80% ethanol (curve 2) at the same concentration (1×10^{-4} M) of Bu_2SnCl_2. The half-widths ($W_{1/2}$) of Bu_2SnCl_2 in 50 and 80% ethanol and

Table 1. Peak potentials of dibutyltin compounds for cyclic voltammograms

Compounds (Bu_2SnX_2)	$E_{p,c}$ [a] (V)	$E_{p,a}$ [b] (V)
Bu_2SnCl_2	−0.90	−0.72
Bu_2SnL_2	−0.83	−0.65
Bu_2SnMHM_2	−0.77	−0.60

Conditions of cyclic voltammograms are the same as those in Fig. 3.
a) Peak potential of the cathodic peak. b) Peak potential of the anodic peak.

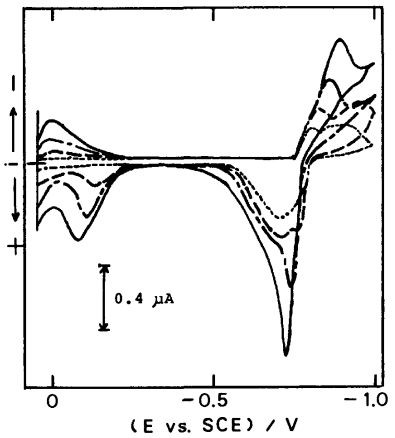

Fig. 4. Effect of scan rate on cyclic voltammograms of Bu_2SnCl_2. $[Bu_2SnCl_2] = 1 \times 10^{-4}$ M; scan rate/mV s^{-1} = ---- 20, —— 50, ---- 100, —— 200.

Bu_2SnL_2[11] in 80% ethanol without surface-active agents at the modulation amplitude (ΔE) of 50 mV are 57, 88, and 90 mV, respectively. The smaller $W_{1/2}$ in 50% ethanol than those in 80% ethanol probably depends partially on the adsorption of the depolarizer and its reduction product(s) in 50% ethanol.

Cyclic voltammograms of Bu_2SnX_2 (X=chloride, L, and MHM) in 50% ethanol are shown in Fig. 3, and the peak potentials on the forward and reverse scans are also shown in Table 1. Peaks (A) for Bu_2SnX_2 occur on the forward or cathodic scan corresponding to the reduction of Bu_2SnX_2. Peaks (B) for Bu_2SnX_2 on the reverse or anodic scan are observed corresponding to the re-oxidation or "stripping" of the products of (A) from the electrode.[16] This finding suggests that the reduction products of Bu_2SnX_2 accumulated on the electrode are readily re-oxidized. The current-voltage curve for the re-oxidation or "stripping" can be utilized for the determination of traces of Bu_2SnX_2 by ASV.

In cyclic voltammetry, scan rate is probably most important experimental parameter for studying the adsorption of reactants or products at the electrode.[17] The dependence of the scan rate on the cyclic voltammetric curve for 1×10^{-4} M Bu_2SnCl_2 in 50%

ethanol is shown in Fig. 4. At the relatively lower scan rate, two cathodic and two corresponding anodic peaks were observed, one of the latter being a shoulder. As the scan rate increases, the respective cathodic and anodic peak currents increase. With further increase of the scan rate above 100 mV s^{-1}, the cathodic and anodic peaks are reduced to one peak, and respective peak currents increase. This cyclic voltammetric behavior described above is analogous to the case, where the reduction product is strongly adsorbed on the stationary electrode,[17] as demonstrated by pulse polarography and electrocapillary curves.

Fleet and Fouzder[11] stated that in Scheme (1) Bu_2Sn^+ ion radical is stable in 80% (v/v) ethanol, but is unstable in <50% (v/v) ethanol as is shown by disappearance of the second wave in 50% ethanol. However, various electrochemical behavior of Bu_2SnX_2 as described above probably indicates that the first and second steps in Scheme (1) proceed at the very close potentials in 50% ethanol, and the reduction products are significantly adsorbed at the mercury electrode. The cause of this difference between both studies is not clear, but is presumably due to the presence or absence of Triton X-100 in ethanolic solutions.

DPASV. Since the voltammetric studies described above suggest the possibility of determining Bu_2SnX_2 by ASV in 50% ethanol, the detailed DPASV behavior of Bu_2SnX_2 (X=chloride, L, MHM, and DT), especially that of Bu_2SnCl_2, was investigated in 50% ethanol in order to develop a more sensitive method, and the DPASV behavior of Bu_2SnX_2 was partly compared to those of tributyltin compounds and Ph_3SnCl.

Typical differential pulse anodic stripping voltammograms for Bu_2SnCl_2, $(Bu_3Sn)_2O$, and Ph_3SnCl obtained in 50% ethanol are shown in Fig. 5. Similar voltammograms were obtained for the other Bu_2SnX_2 in question. The half-widths for the stripping peaks of Bu_2SnCl_2, $(Bu_3Sn)_2O$, and Ph_3SnCl are 30, 107 and 95 mV, respectively.

The variation of the stripping peak current with the mass concentration of Bu_2SnCl_2 was examined. The peak current rises linearly with the concentration of Bu_2SnCl_2 in the range of 3 to 50 ppb (1 ppb=1 μg dm^{-3}) at the deposition time of 60 s. It is to be stressed here that this linear range is a function

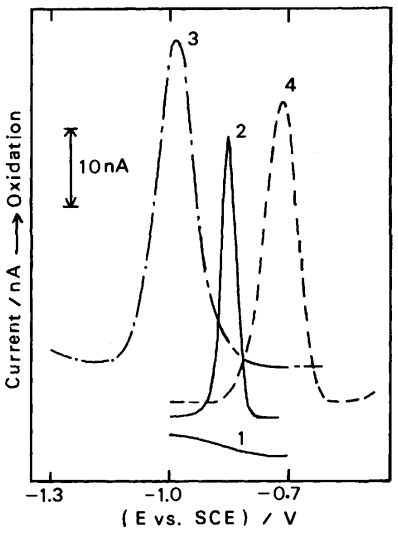

Fig. 5. Typical differential pulse anodic stripping voltammograms of Bu_2SnCl_2, Ph_3SnCl, and $(Bu_3Sn)_2O$ in 50% (v/v) ethanol–water medium of the same composition as in Fig. 1. Pulse repetition time, 0.1 s; modulation amplitude, 50 mV; scan rate 20 mV s^{-1}; deposition potential, (1) −1.0 V, (2) −1.0 V, (3) −1.3 V, and (4) −1.0 V; deposition time, 60 s (stirred); equilibration period, 10 s (unstirred). $[Bu_2SnCl_2]$/ppb=(1) 0 (blank), (2) 24.9; $[(Bu_3Sn)_2O]$/ppb=(3) 129; $[Ph_3SnCl]$/ppb=(4) 115.

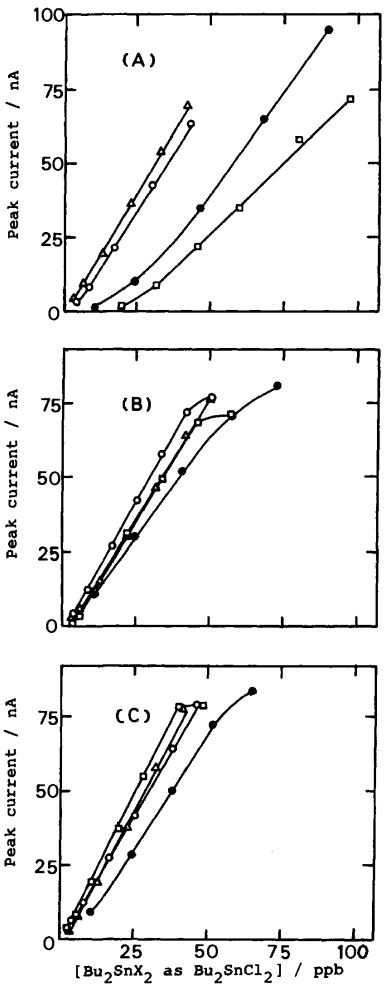

Fig. 6. Effect of potassium chloride on calibration curves of Bu_2SnX_2 in 50% (v/v) ethanol–water medium. [KCl]/M=(A) 0, (B) 0.1, and (C) 0.5, Species of Bu_2SnX_2; -○- Bu_2SnCl_2, -△- Bu_2SnDT_2, -●- Bu_2SnMHM_2, -□- Bu_2SnL_2.

of deposition time, stirring rate, *etc.*, and is not always valid under various conditions. Further, the rise is smaller than the linear value up to 70 ppb and the decrease occurs gradually again. This behavior is expected when a film of insulating material is formed as the reduction product.[9] Beyond a certain critical concentration, at which point the electrode is completely covered with the film, the stripping peak current increases slowly, if at all, with increasing depolarizer concentration. These findings indicate that, in the DPASV steps, the reduction of Bu_2SnCl_2 and the re-oxidation of its reduction product(s), which is only stabilized by the adsorption onto the mercury electrode,[9,11] should occur on the electrode surface.

The lower limits of detection of Bu_2SnCl_2, $(Bu_3Sn)_2O$, and Ph_3SnCl are 3, 2.5, and 7 ppb, respectively. The relative standard deviation at 8.4 ppb of Bu_2SnCl_2 (eight runs) was 3.1%.

The comparison of calibration curves of the respective Bu_2SnX_2 is of interest in connection with its chemical property. Each Bu_2SnX_2 in 50% ethanol–water medium gives a different calibration curve and further each calibration curve varies with the concentration of potassium chloride added in 50% ethanol–water medium (Fig. 6), where all concentrations of Bu_2SnX_2 are represented as that of Bu_2SnCl_2. Without potassium chloride (Fig. 6 A), the slopes of calibration curves giving straight lines increase in the following order: $Bu_2SnL_2 < Bu_2SnMHM_2 < Bu_2SnCl_2 — Bu_2SnDT_2$. Moreover, the intercepts at zero peak current of these straight lines decrease in the above order. These findings indicate that the DPASV steps of Bu_2SnX_2 occur readily in the above order. With increasing concentration of potassium chloride, the calibration curves of Bu_2SnL_2 and Bu_2SnMHM_2 approach gradually to that of Bu_2SnCl_2, but the calibration curve of Bu_2SnMHM_2 does not overlap even at 0.5 M potassium chloride. It was also observed that the stripping peak potential (E_p) of Bu_2SnMHM_2 is more positive than those of others in a medium without potassium chloride, and E_p of Bu_2SnMHM_2 approaches to those of others with increasing concentration of potassium chloride. These facts indicate that L and MHM of Bu_2SnX_2 are gradually replaced by chloride, and the replacement of MHM by chloride is not so easy as L. Further, the different DPASV behavior of Bu_2SnMHM_2 from others is probably ascribed to the effect of an olefinic double bond of Bu_2SnMHM_2.[11] On the other hand, the fact that the calibration curve of Bu_2SnDT_2 is very close to that of Bu_2SnCl_2 even in a medium without potassium chloride is presumably attributed to a strong and stable adsorption of Bu_2SnDT_2 and its reduction product(s) at the HMDE. This may be the result of the interaction between mercury and sulfur, as was observed for dioctyltin bis(mercaptoacetate) in 80% ethanol.[12] From the results described above, the bond between tin atom and X in Bu_2SnX_2 seems to possess a covalent property enhancing in the reverse order as mentioned above.

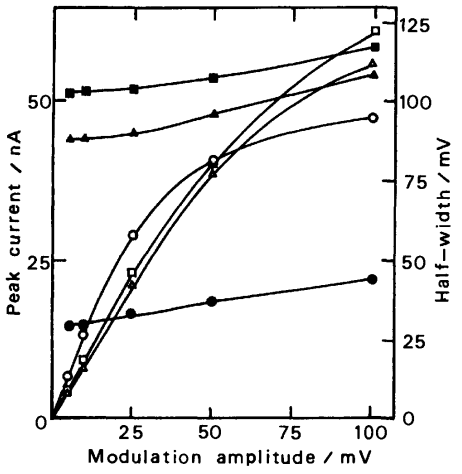

Fig. 7. Effects of modulation amplitude on peak current and half-width. -○-, -●- [Bu_2SnCl_2] = 25.2 ppb; -△-, -▲- [Ph_3SnCl] = 115 ppb; -□-, -■- [$(Bu_3Sn)_2O$] = 129 ppb. Peak current, -○-, -△-, -□-; half-width, -●-, -▲-, -■-.

Optimization of Instrumental Parameters: The effects of various instrumental parameters on the stripping peak current are shown below.

The effects of the ΔE on the peak current and the $W_{1/2}$ for Bu_2SnCl_2, $(Bu_3Sn)_2O$, and Ph_3SnCl are shown in Fig. 7. The peak currents of these compounds are proportional to the ΔE up to 25 mV. The $W_{1/2}$ for these compounds also increase with an increase in ΔE. These findings are generally observed in DPASV.[18–20] On the grounds of sensitivity and selectivity the modulation amplitude of 50 mV was chosen for this study.

The peak current is proportional to the deposition time up to 2 min. Hence, the deposition time of 1 min was chosen throughout this study.

The effect of the scan rate on the peak current of Bu_2SnCl_2 was examined over the scan rate of 5 to 100 mV s^{-1}. The peak current increased steeply with increasing scan rate in the range of 5—20 mV s^{-1} and increased gradually above 20 mV s^{-1}.

The plots of the deposition potential (E_{dep}) *vs.* peak current for Bu_2SnCl_2, $(Bu_3Sn)_2O$, and Ph_3SnCl are shown in Fig. 8. The plots for the other Bu_2SnX_2 were similar to that of Bu_2SnCl_2. The maximum peak current for each compound was observed in the narrow range. When deposited at −1.0 V, Bu_2SnCl_2 is co-deposited considerably with Ph_3SnCl, but scarcely with $(Bu_3Sn)_2O$.

Several DPASV behavior of Bu_3SnCl was also investigated and the DPASV behavior obtained for Bu_3SnCl was the same as that of $(Bu_3Sn)_2O$ described above.

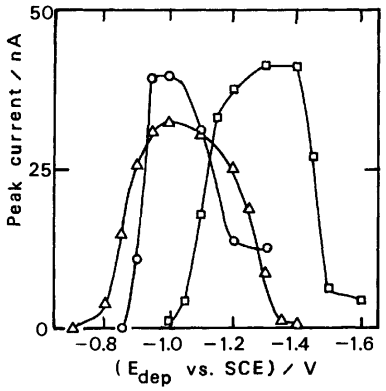

Fig. 8. Effect of deposition potential on peak current.
-○- $[Bu_2SnCl_2]=25.2$ ppb; -△- $[Ph_3SnCl]=100$ ppb;
-□- $[(Bu_3Sn)_2O]=129$ ppb.

On the grounds of the results described above, the instrumental parameters were chosen for the conditions shown in Fig. 5.

Stability of Stripping Peak Current of Bu_2SnX_2: Fleet and Fouzder[11] claimed that Bu_2Sn^+ ion radical is unstable in <50% (v/v) ethanol as described above. However, each stripping peak current of Bu_2SnX_2 in 50% ethanol was constant over the standing time at least up to 180 min under the stream of nitrogen gas.

Effect of Coexisting Substances: As can be seen in Fig. 6, the peak current of Bu_2SnCl_2 increased slightly with increasing concentration of potassium chloride added in 50% ethanol-water medium.

The effects of Ph_3SnCl and Bu_3SnCl on the determination of Bu_2SnCl_2 was also examined. As described above, Bu_2SnCl_2 is co-deposited with Ph_3SnCl, but scarcely with Bu_3SnCl when deposited at −1.0 V (Fig. 8). The presence of Ph_3SnCl in the concentration above 4 ppb depressed the peak current of Bu_2SnCl_2 (25.2 ppb). The presence of Bu_3SnCl at *ca.* 30 ppb scarcely affected the peak current of Bu_2SnCl_2 (25.2 ppb).

Determination of Bu_2SnX_2. On the basis of the above detailed study, an analytical method for the determination of Bu_2SnX_2 in natural water was developed. The proposed method involves extraction[21] and cleaning up by chromatography on a cation-exchange resin[22] in order to avoid interferences from heavy metals and organic materials in the measurement of DPASV.

To 250 ml of natural water was added 10 grams of sodium chloride (except for sea water) and 2 ml of hydrochloric acid (36%), and then Bu_2SnX_2 was extracted twice with 25 ml of 50% ethyl acetate-hexane. The extract was dried over anhydrous sodium sulfate, concentrated to about 5 ml by use of Kuderna-Danish concentrator and then evaporated to near dryness under the stream of nitrogen gas. The concentrate was dissolved in 10 ml of ethanol. The ethanolic solution was passed through a cation-exchange resin column (2×5 cm). After washing the column with 20 ml of ethanol and 10 ml of 5% (v/v) water-ethanol, Bu_2SnCl_2 was eluted with 13 ml of 5% (v/v) hydrochloric acid-ethanol. During extraction and cleaning up by chromatography, Bu_2SnX_2 will be converted to Bu_2SnCl_2. The eluate was neutralized to approximately pH 7.0 with ammonia and acetic acid. After adding buffer (pH 7.0) and Triton X-100 the solution was diluted to 25 ml with water, whereupon the final concentration of ethanol became 50% (v/v). Then, Bu_2SnCl_2 was determined by DPASV by use of the standard addition method.

Recovery tests of Bu_2SnCl_2 (1 μg) from river water and sea water were carried out, and the recovery percentages were 67 and 91%, respectively. The lower recovery percentage from river water is probably ascribed to the lower extractability of Bu_2SnCl_2 due to the absence of ions such as bromide.[23]

We wish to express our hearty thanks to Professor Toyokichi Kitagawa and Dr. Akio Ichimura of the Faculty of Science, Osaka City University for their helpful discussion and encouragement. We also wish to thank Mr. Yoshio Kuge of the Environmental Pollution Control Center, Osaka Prefectural Government for his encouragement, and Yanagimoto Mfg. Co. Ltd. for lending a polarographic instrument.

This study is partially supported by the Environmental Agency.

References

1) R. Ōgawara *et al. Kagaku No Ryoiki*, **18**, 1033 (1964).
2) V. F. Hodge, S. L. Seidel, and E. D. Goldberg, *Anal. Chem.*, **51**, 1256 (1979).
3) K. L. Jewett and F. E. Brinckman, *J. Chromatogr. Sci.*, **19**, 583 (1981).
4) Y. Arakawa and O. Wada, *Anal. Chem.*, **55**, 1901 (1983).
5) M. D. Booth and B. Fleet, *Anal. Chem.*, **42**, 825 (1970).
6) B. Fleet and N. B. Fouzder, *J. Electroanal. Chem.*, **63**, 59 (1975).
7) P. Kenis and A. Zirino, *Anal. Chim. Acta*, **149**, 157 (1983).
8) M. D. Booth, M. J. D. Brand, and B. Fleet, *Talanta*, **17**, 1059 (1970).
9) M. D. Morris, *Anal. Chem.*, **39**, 476 (1967).
10) M. D. Morris, *J. Electroanal. Chem.*, **16**, 569 (1968).
11) B. Fleet and N. B. Fouzder, *J. Electroanal. Chem.*, **63**, 69 (1975).
12) B. Fleet and N. B. Fouzder, *J. Electroanal. Chem.*, **63**, 79 (1975).
13) R. E. Dessy, W. Kitching, and T. Chivers, *J. Am. Chem. Soc.*, **88**, 453 (1966).
14) H. Kitamura, Y. Yamada, and M. Nakamoto, *Chem. Lett.*, 837 (**1984**).
15) G. C. Barker and J. A. Bolzan, *Z. Anal. Chem.*, **216**, 215 (1966).
16) A. M. Bond and I. D. Heritage, *Anal. Chem.*, **56**, 1222 (1984).

17) R. H. Wopschall and I. Shain, *Anal. Chem.*, **39**, 1514 (1967).
18) A. Saito and S. Himeno, *Nippon Kagaku Kaishi*, **10**, 1909 (1973).
19) E. P. Parry and R. A. Osteryoung, *Anal. Chem.*, **13**, 1634 (1965).
20) W. Lund and D. Onshus, *Anal. Chim. Acta*, **86**, 109 (1976).
21) H. Iwai, O. Wada, and Y. Arakawa, *J. Anal. Toxicology*, **5**, 300 (1981).
22) A. Williams, *Analyst*, **98**, 233 (1973).
23) H. A. Meinema, T. B. Wiersma, G. V. Hann, and E. C. Gevers, *Environ. Sci. Technol.*, **12**, 288 (1978).

A Nuclear Magnetic Resonance Study of the Exchange Reaction of Dimethyl Sulfoxide in Pentakis(dimethyl sulfoxide)oxovanadium(IV) Ions

Kiyoshi KAYA, Yasuhisa IKEDA, and Hiroshi FUKUTOMI*
Research Laboratory for Nuclear Reactors, Tokyo Institute of Technology, O-okayama, Meguro-ku, Tokyo 152
(Received March 19, 1985)

The dmso exchange reaction in $[VO(dmso)_5]^{2+}$ has been studied in the mixture of CD_3NO_2 and DMSO by means of ^1H NMR. The exchange rate is independent of the free DMSO concentration and the kinetic parameters are as follows: $k_{ex}(25\,^\circ C)=1.76\times10^3\ s^{-1}$, $\Delta H^*=60.1\pm4.3$ kJ mol^{-1}, and $\Delta S^*=18.5\pm12.9$ JK^{-1} mol^{-1}.

Ligand-exchange reactions in several oxovanadium (IV) complexes have been studied by using the NMR line-broadening method,[1-4] but the mechanisms for these reactions have not been proposed in detail. On the other hand, Lincoln[5] has shown that the plot of ΔH^* *vs.* ΔS^* for ligand-exchange reactions in oxovanadium(IV) complexes is linear and consistent with that for the ligand-exchange reactions in various uranyl(VI) complexes in which the reactions proceed dissociatively. Such an isokinetic relationship suggests that the reactivity of oxovanadium(IV) ions is very similar to that of uranyl(VI) ions, and that the ligand-exchange reactions in oxovanadium(IV) complexes seem to proceed dissociatively. However, the associative mechanism has been proposed for some complex-formation reactions in oxovanadium(IV) ions.[6-8] From this point of view, further studies for the ligand-exchange reactions in oxovanadium(IV) complexes are necessary to understand the mechanisms in detail. This paper reports the exchange of dmso (dimethyl sulfoxide) in the $[VO(dmso)_5]^{2+}$ ion. This reaction has already been studied by Angerman and Jordan with the NMR line-broadening method,[3] but no accurate kinetic parameters have been determined, because the slow exchange region, where the relaxation time is controlled by the chemical exchange rate,[9] was not observed in the temperature range above the freezing point of DMSO. In the present study, CD_3NO_2 was used as a diluent in order to extend the lower limit of temperature range. As a result, it became possible to observe the slow exchange region and to determine the kinetic parameters.

Experimental

The $[VO(dmso)_5](ClO_4)_2$ complex was synthesized by the same method as described in a previous paper.[10] Anal. Calcd for $[VO(dmso)_5](ClO_4)_2$: C, 18.30; H, 4.61; S, 24.42. Found: C, 18.28; H, 4.56; S, 24.38. Dimethyl sulfoxide (Wako Pure Chemical Ind. Ltd.) was distilled *in vacuo*, followed by distillation with 3A molecular sieves (Wako), and stored over 3A molecular sieves. Nitromethane-d_3 (CD_3NO_2, Merck 99%), which was used as a diluent and an NMR lock reagent, was dried over 3A molecular sieves. The UV and visible spectra of the $[VO(dmso)_5]^{2+}$ ion in DMSO and in the mixture of CD_3NO_2 and DMSO were measured on a Shimadzu UV-210A double-beam spectrophotometer. Sample solutions for NMR measurements were prepared by weighing $[VO(dmso)_5](ClO_4)_2$, DMSO, and CD_3NO_2 in a 1 cm^3 volumetric flask and were placed in NMR sample tubes and sealed under vacuum. All samples were prepared in a glove-box filled with dried nitrogen. ^1H NMR spectra of bulk DMSO were measured at 100 MHz on a JEOL JNM-FX 100 FT-NMR spectrometer equipped with a JNM-VT-3B temperature controller. Typical spectral settings are as follows: data points, 8K; spectral width, 1000 Hz; pulse width, 14 μs; pulse delay time, 2.5 s; number of scan, 4.

Results and Discussion

The absorption spectrum of the $[VO(dmso)_5]^{2+}$ ion in DMSO was measured, and the two absorption bands at 820 and 690 nm were assigned to the $^2B_2\rightarrow{}^2E(I)$ and $^2B_2\rightarrow{}^2B_1$ (10 Dq) transitions, respectively, from the molecular orbital diagram of Ballhausen and Gray.[11] Based on this assignment, Dq is calculated to be 1450 cm^{-1} and is consistent with that obtained by Angerman and Jordan.[3] The absorption spectrum of the $[VO(dmso)_5]^{2+}$ ion in the mixture of CD_3NO_2 and DMSO was compatible with that in DMSO. This fact indicates that the $[VO(dmso)_5]^{2+}$ ion has the same solvation structure in both solvents, DMSO and the mixture of CD_3NO_2 and DMSO.

On the basis of the spectrophotometric results, the dmso exchange in the $[VO(dmso)_5]^{2+}$ ion was measured in the mixture of CD_3NO_2 and DMSO by using the NMR line-broadening method. The line-width and chemical shift of the methyl proton signal of bulk DMSO in the presence and absence of the $[VO(dmso)_5]^{2+}$ ion were measured by varying temperature from −45 to 70 °C. In this temperature range, the line-width of methyl proton signal of DMSO changed with temperature, while no change was observed in chemical shift of the corresponding signal. In this case, the transverse relaxation time (T_2) is expressed as follows:[9]

$$\frac{1}{T_2}=\frac{1-p_m}{p_m}\left(\frac{1}{T_{2p}}-\frac{1}{T_{2a}}\right)=\frac{1}{T_{2m}+\tau_m}+\frac{1}{T_{2o}}, \quad (1)$$

where T_{2p} and T_{2a} are the transverse relaxation times of nuclei in the bulk solvent in the presence and absence of the paramagnetic metal ion, respectively, and are related with the full line-width ($\Delta\nu$) at half-height as $1/T_{2p}=\pi\Delta\nu_p$ and $1/T_{2a}=\pi\Delta\nu_a$, p_m is the ratio of the concentration of solvent bound to the paramagnetic metal ion to the concentration of free solvent, τ_m is the solvent exchange lifetime, T_{2m} is the transverse relaxation time of the coordinated solvent, and T_{2o} is the relaxation time of solvent outside the first-coordination sphere of the paramagnetic metal ion. The ralationship between τ_m and the first-order rate constant (k_{ex}) with temperature is as follows:

$$1/\tau_m = k_{ex} = (kT/h)\exp(-\Delta H^*/RT)\exp(\Delta S^*/R), \quad (2)$$

and the temperature dependence of T_{2m} and T_{2o} is assumed to be given by Eqs. 3 and 4, respectively.[12]

$$\frac{1}{T_{2m}} = C_m \exp\left(\frac{E_m}{RT}\right) \quad (3)$$

$$\frac{1}{T_{2o}} = C_o \exp\left(\frac{E_o}{RT}\right) \quad (4)$$

The values of T_2 were calculated based on the equatorial coordination number of four and from the assumption that the dmso exchange in the axial site is very faster than that in the equatorial site,[2,3] and hence only the dmso exchange in the equatorial site contributes to the line-broadening in the present temperature range. Figure 1 shows the typical plot of $\ln(1/T_2)$ *vs.* the reciprocal temperature. This figure indicates that T_2 is controlled by T_{2m}, τ_m, and T_{2o} successively as the temperature decreases, and that the above assumption is reasonable. If the dmso exchange in the axial site is not much faster than that in the equatorial site in the present temperature range, the value of $1/T_2$ should decrease again in the low temperature range as observed in the dmf (*N*,*N*-dimethylformamide) exchange in $[VO(dmf)_5]^{2+}$ ions.[4] Kinetic parameters were determined by a nonlinear least-squares fit of $1/T_2$ data to the equation obtained by substitution of Eqs. 2, 3, and 4 into Eq. 1. Kinetic parameters for solutions with various compositions were determined by the same manner and are listed in Table 1. The table shows that the exchange rate is independent of the concentration of DMSO and the ΔS^* values are positive. These results suggest that the dmso exchange in the equatorial site of the $[VO(dmso)_5]^{2+}$ ion proceeds through either the D or I_d mechanism. On the other hand, the activation volume (ΔV^*) for the dmso exchange reaction was determined to be $-5.3\pm0.4\,cm^3\,mol^{-1}$ in our recent study,[10] and suggested that the reaction proceeded associatively. Since the ΔS^* value is in conflict with the ΔV^* value, it is difficult to infer the mechanism of dmso exchange reaction. However, the A mechanism is excluded because the rate of dmso exchange is independent of [DMSO]. Furthermore, the D mechanism also seems to be unlikely from the following reasons. It was proposed that the solvent exchange reactions proceeding through the D mechanism have the positive ΔV^* value, because no net change occurs before and after the exchange reaction, so that negligible solvational change is expected and the observed ΔV^* value reflects the intrinsic volume change.[13,14] In addition, it was suggested that the

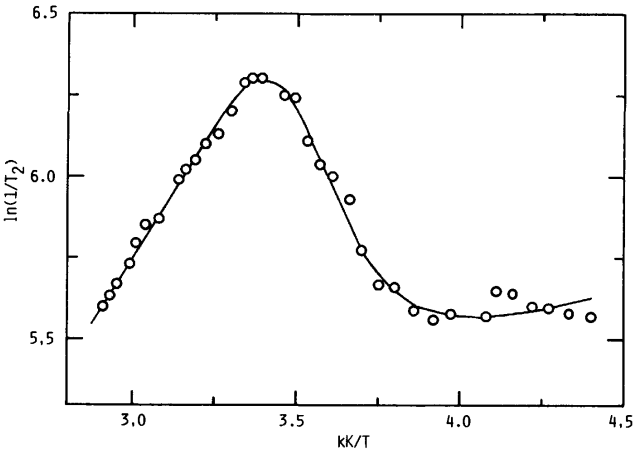

Fig. 1. A plot of $\ln(1/T_2)$ *vs.* $1/T$ for the exchange of dmso in $[VO(dmso)_5]^{2+}$. $[VO(dmso)_5^{2+}]=8.52\times10^{-3}$ mol kg^{-1}, [DMSO]$=1.21$ mol kg^{-1} and $[CD_3NO_2]=14.1$ mol kg^{-1}.

Table 1. Solution compositions and kinetic parameters for the exchange of dmso in $[VO(dmso)_5]^{2+}$

Solution	$[VO(dmso)_5^{2+}]$ / 10^{-3} mol kg^{-1}	[DMSO] / mol kg^{-1}	$[CD_3NO_2]$ / mol kg^{-1}	k_{ex}(25 °C) / 10^3 s^{-1}	ΔH^* / kJ mol^{-1}	ΔS^* / J K^{-1} mol^{-1}	S.D.[a]
i	10.0	0.314	15.9	1.51	66.5	39.1	0.05
ii	9.86	0.557	15.6	1.32	61.5	21.2	0.05
iii	9.71	0.716	15.4	2.51	56.9	11.1	0.07
iv	8.52	1.21	14.1	1.32	61.5	21.2	0.04
v	9.74	1.62	14.2	2.13	54.0	0.0	0.06

a) Standard deviation (S.D.) of nonlinear least-squares fit of $1/T_2$ data to the equation obtained by substitution of Eqs. 2, 3, and 4 into Eq. 1. S.D.$=\sqrt{\Sigma\{(Y_e-Y_c)^2/(n-1)\}}$, where Y_e and Y_c are the experimental and calculated values of $1/T_2$, respectively, and n is the number of experimental points.

ΔS^* value does not necessarily reflect the activated state owing to the contribution of the solvent rearrangement around the metal complexes, especially in mixed solvents.[15]

In the I mechanism, the exchange process in the equatorial site is expressed as follows:

$$[VO(dmso)_5]^{2+} + DMSO^* \overset{K_{os}}{\rightleftharpoons} [VO(dmso)_4(dmso)_{ax}]^{2+}\cdots DMSO^*$$
$$\xrightarrow[\text{slow}]{k_I} [VO(dmso)_3(dmso^*)(dmso)_{ax}]^{2+}\cdots DMSO$$
$$\xrightarrow[\text{fast}]{} [VO(dmso)_3(dmso^*)(dmso)_{ax}]^{2+} + DMSO,$$

where an asterisk is used to denote the exchanging species, $(dmso)_{ax}$ represents the coordinated dmso to the axial site, K_{os} is the formation constant of the outer-sphere complex, $[VO(dmso)_4(dmso)_{ax}]^{2+}\cdots DMSO^*$, and k_I is the dmso interchange rate constant between the dmso molecules in the equatorial sites and those in the second-coordination sphere above the triangular faces of the octahedral $[VO(dmso)_5]^{2+}$ ion[7,16] or the rate constant for a process involving intramolecular rearrangement of the coordinated dmso from the axial to the equatorial sites in $[VO(dmso)_4(dmso)_{ax}]^{2+}$.[17,18] For this mechanism, k_{ex} is given by

$$k_{ex} = k_I K_{os}[DMSO]/(1+K_{os}[DMSO]). \quad (5)$$

If $K_{os}[DMSO] \gg 1$, Eq. 5 can be simplified as $k_{ex}=k_I$ and gives the independence of the exchange rate from the DMSO concentration. In the present study, it is suggested that DMSO molecules may preferentially solvate around the $[VO(dmso)_5]^{2+}$ ion from the spectrophotometric results. This preferential solvation is due to the fact that the basity of DMSO is larger than that of CD_3NO_2 on the basis of Gutmann's donor number (DN).[19] In a previous paper[20] dealing with the dmso exchange of $UO_2(acac)_2dmso$ in CD_2Cl_2, the K_{os} value for the formation of $UO_2(acac)_2dmso\cdots DMSO$ was found to be *ca.* 5 M^{-1}(M=mol dm^{-3}). The K_{os} value for the present study is expected to be larger than 5 M^{-1} in spite of the fact that the dielectric constant of CD_3NO_2(35.94) is larger than that of CD_2Cl_2(8.93), because the positively charged $[VO(dmso)_5]^{2+}$ ion has a stronger affinity for DMSO than does the neutral $UO_2(acac)_2dmso$ complex. Therefore, it seems reasonable to consider that the condition, $K_{os}[DMSO] \gg 1$, is satisfied in the present study, and that the dmso exchange proceeds through the I mechanism. Especially, the I_a mechanism seems more likely because of the negative ΔV^* value. Nishizawa and Saito have proposed that the rate constant for the intramolecular rearrangement from the axial to the equatorial site is$\simeq 10^3$ s^{-1} at 25 °C. Since this value is comparable to the value for k_{ex}(1.8×10^3 s^{-1} at 25 °C) in our study, the possibility exists that the k_I pathway might be the intramolecular rearrangement proposed by Nishizawa and Saito.

The kinetic parameters for the present and previous studies on the ligand-exchange reactions in oxovanadium(IV) complexes are summarized in Table 2. For the ligand-exchange reactions in oxovanadium(IV) complexes with the ligands coordinated through oxygen, the values of exchange rate constants are almost identical with each other within a factor of 23, and the differences in ΔH^* value are also small in spite of the large differences in basicity and size of ligands. These facts suggest that the ligand-exchange reactions in oxovanadium(IV) complexes may not proceed dissociatively because the ligand basicity is one of the dominant kinetic factors in the dissociative process. On the other hand, Caldin and Bennetto proposed that the substitution reactions proceeding dissociatively exhibit an isokinetic relationship between ΔH^* and ΔS^* values.[15] Figure 2 shows the plot of ΔH^* *vs.* ΔS^* for the ligand exchange reactions in the equatorial site of oxovanadium(IV) complexes and reveals that the isokinetic

TABLE 2. KINETIC PARAMETERS FOR LIGAND EXCHANGE REACTIONS IN $[VO(L)_5]^{2+}$

L[a]	k_{ex}(25 °C)[b] / s^{-1}	ΔH^* / kJ mol^{-1}	ΔS^* / J K^{-1} mol^{-1}	Ref.
H_2O	7.4×10^2 (eq)	55.6	−6.3	1
	$\sim10^{11}$ (ax)			1
	5.0×10^2 (eq)	57.3	−2.4	2
CH_3OH	3.3×10^2 (eq)	50.4	−5.5	3
CH_3CN	2.9×10^3 (eq)	29.6	−84	3
dmf	2.0×10^2 (eq)	54.8± 2.5	−17.2± 7.5	4
	4.6×10^4 (ax)	64.0±10.5	58.2±37.7	4
dma	4.7×10^3 (eq)	42.3± 2.1	−33.1± 6.7	4
dmso	1.8×10^3 (eq)	60.1± 4.3	18.5±12.9	This work

a) dmf=*N*,*N*-dimethylformamide, and dma=*N*,*N*-dimethylacetamide. b) (eq) and (ax) denote the ligand exchange reactions in the equatorial and axial sites in $[VO(L)_5]^{2+}$, respectively.

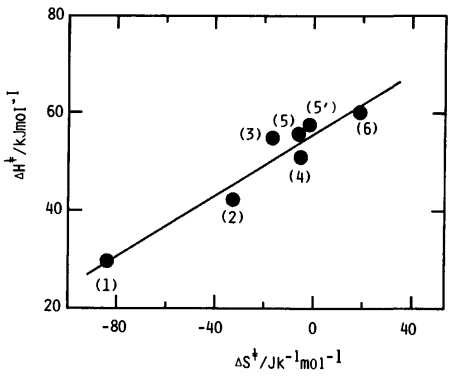

Fig. 2. A plot of $\Delta H^{\ddagger}$ *vs.* $\Delta S^{\ddagger}$ for the ligand exchange reactions in $[VO(L)_5]^{2+}$. L=CH_3CN (1), dma (2), dmf (3), CH_3OH (4), H_2O (5 and 5'), and dmso (6).

relationship is satisfied. Hence, if the proposal by Caldin and Bennetto is acceptable, the possibility still remains, in which the ligand-exchange reactions in oxovanadium(IV) complexes proceed dissociatively. Further studies for the activation volume and anation reactions in oxovanadium(IV) complexes are necessary to clarify the mechanism of the ligand exchange in the present complex.

References

1) J. Reuben and D. Fiat, *Inorg. Chem.*, **6**, 579 (1967).
2) K. Wuthrich and R. E. Connick, *Inorg. Chem.*, **6**, 583 (1967).
3) N. S. Angerman and R. B. Jordan, *Inorg. Chem.*, **8**, 65, (1969).
4) G. A. Miller and R. E. D. McClung, *J. Chem. Phys.*, **58**, 4358 (1969).
5) S. F. Lincoln, *Pure Appl. Chem.*, **51**, 2059 (1979).
6) H. Tomiyasu, S. Ito, and S. Tagami, *Bull. Chem. Soc. Jpn.*, **47**, 2843 (1974).
7) H. Tomiyasu and G. Gordon, *Inorg. Chem.*, **15**, 870 (1976).
8) O. Yokoyama, H. Tomiyasu, and G. Gordon, *Inorg. Chem.*, **21**, 1136 (1982).
9) T. J. Swift and R. E. Connick, *J. Chem. Phys.*, **37**, 307 (1962).
10) M. Harada, Y. Ikeda, H. Tomiyasu, and H. Fukutomi, *Chem. Lett.* **1984**, 1195.
11) C. J. Ballhausen and H. B. Gray, *Inorg. Chem.*, **1**, 111 (1962).
12) L. Rusnak and R. B. Jordan, *Inorg. Chem.*, **11**, 196 (1972).
13) D. R. Stranks, *Pure Appl. Chem.*, **38**, 303 (1974).
14) F. K. Meyer, K. E. Newman, and A. E. Merbach, *J. Am. Chem. Soc.*, **101**, 5588 (1979).
15) E. F. Caldin and H. P. Bennetto, *J. Soln. Chem.*, **2**, 217 (1973).
16) K. Wuthrich and R. E. Connick, *Inorg. Chem.*, **7**, 1377 (1968).
17) M. Nishizawa and K. Saito, *Inorg. Chem.*, **17**, 3676 (1978).
18) M. Nishizawa and K. Saito, *Inorg. Chem.*, **19**, 2284 (1980).
19) V. Gutmann and R. Schmid, *Coord. Chem. Rev.*, **12**, 263 (1974).
20) Y. Ikeda, H. Tomiyasu, and H. Fukutomi, *Bull. Chem. Soc. Jpn.*, **56**, 1060 (1983).

Hydrophobic Vitamin B_{12}. IV. Addition Reactions of Alcohols to Olefins as Catalyzed by Hydrophobic Vitamin B_{12} Derivatives†

Yukito MURAKAMI* and Yoshio HISAEDA
Department of Organic Synthesis, Faculty of Engineering, Kyushu University, Hakozaki, Higashi-ku, Fukuoka 812
(Received March 26, 1985)

Addition reactions of alcohols to olefins were catalyzed by hydrophobic vitamin B_{12} derivatives under aerobic irradiation conditions at the room temperature range. Ethyl vinyl ether, 1-pentene, and cyclohexene were adopted as olefins, while heptamethyl methylaquacobyrinate perchlorate and heptamethyl cyanoaquacobyrinate perchlorate were used as the starting complexes. Heptamethyl cobyrinate, which was generated from heptamethyl methylaquacobyrinate perchlorate by aerobic photolysis, is an appropriate catalyst for investigation of the reaction mechanism because the alkylated complex having the cobalt–carbon σ-bond, the reaction intermediate, has a long lifetime sufficient for its identification in the dark. On the other hand, heptamethyl cyanocobyrinate, which was derived from heptamethyl cyanoaquacobyrinate, is superior to heptamethyl cobyrinate as the catalyst for the addition reaction. The reaction proceeds *via* light-promoted decomposition of the alkylated complex, and the catalyst is regenerated upon autoxidation by air. These hydrophobic vitamin B_{12} derivatives are particularly effective homogeneous catalysts for the addition of an alcohol to an electron-rich olefin. Plausible reaction schemes for the catalytic cycle have been presented on the basis of experimental findings.

Recently, reactions of olefins catalyzed by vitamin B_{12} and its model complexes have been studied rather extensively,[1] but most of these studies deal with reduction of substrates as caused by the nucleophilic reactivity of the univalent cobalt species. On the other hand, the electrophilic reactivity of the tervalent cobalt species toward olefins has been scarcely examined. In this regard, Dolphin *et al.* reported that bromo(pyridine)cobaloxime and hydroxocobalamin undergo reaction with an electron-rich olefin such as ethyl vinyl ether in the presence of an alcohol to afford the corresponding alkylated complex, having the cobalt–carbon σ-bond, with the acetal moiety as the axial ligand under anaerobic conditions in the dark.[2] Cobalamin and cobaloxime are not efficient catalysts for the reaction in the light of the following observations: (i) the reaction between the catalyst and ethyl vinyl ether proceeds extremely slowly; (ii) an electron-rich olefin such as ethyl vinyl ether undergoes reaction, while other ordinary olefins such as ethylene, 2-methyl-1-butene, 2-ethyl-1-butene, 3,3-dimethyl-1-butene, and ethyl acrylate are unreactive. In addition, cobalamin is soluble in water, methanol, and ethanol, which exercise large solvation effects, while apolar organic solvents can not be used as reaction media because of insolubility of the complex.

We have been dealing with hydrophobic vitamin B_{12} derivatives which have ester groups in place of the peripheral amide moieties of the naturally occurring vitamin B_{12}.[3] These modified cobalt complexes are readily soluble in a wide range of organic solvents and expected to be utilized as homogeneous catalysts in such media. In this regard, we have carried out in this work the reactions of an electron-rich olefin, ethyl vinyl ether, and ordinary olefins, 1-pentene and cyclohexene, with alcohols, methanol and ethanol, in the presence of either heptamethyl methylaquacobyrinate perchlorate, $[(CH_3)(H_2O)Cob(III)7C_1ester]ClO_4$, or heptamethyl cyanoaquacobyrinate perchlorate, $[(CN)(H_2O)Cob(III)7C_1ester]ClO_4$, as the catalyst under aerobic irradiation conditions. The catalytic schemes are to be discussed on the basis of experimental findings obtained under various conditions.

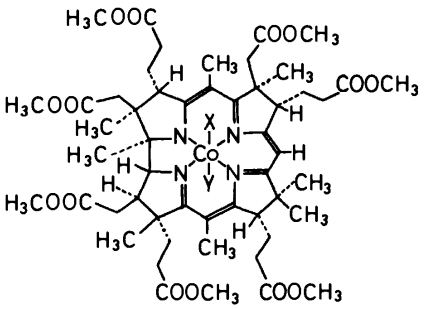

X=CN, Y=CN : $(CN)_2Cob(III)7C_1ester$
X=CH_3, Y=H_2O : $[(CH_3)(H_2O)Cob(III)7C_1ester]^+$
X=CN, Y=H_2O : $[(CN)(H_2O)Cob(III)7C_1ester]^+$
X=ROH, Y=ROH : $[(ROH)_2Cob(III)7C_1ester]^{2+}$
(R=alkyl and/or H)

Experimental

Materials. Cyanocobalamin was purchased from Nakarai Chemicals and used without further purification. Heptamethyl dicyanocobyrinate, $(CN)_2Cob(III)7C_1ester$, was derived from cyanocobalamin after the method of Werthemann *et al.*[4] Preparation of heptamethyl cobyrinate perchlorate, $[Cob(II)7C_1ester]ClO_4$, has been described previously.[3a] Ethyl vinyl ether, 1-pentene, cyclohexene, acrylonitrile, methanol, ethanol, and dichloromethane were purified and dried according to the standard procedures[5] and confirmed to be sufficiently pure by GLC.

† Contribution No. 770 from this Department.

Heptamethyl Cyanoaquacobyrinate Perchlorate, [(CN)(H$_2$O)-Cob(III)7C$_1$ester]ClO$_4$. $(CN)_2$Cob(III)7C$_1$ester (50 mg, 4.6×10^{-5} mol) was dissolved in 40 mL of dichloromethane, and the resulting purple solution was treated with 25 mL of 30% aqueous perchloric acid at room temperature. The orange dichloromethane layer was separated from the acidic aqueous layer and washed with distilled water. After being dried over sodium sulfate, the orange layer was evaporated to dryness *in vacuo* at room temperature. The residue was reprecipitated from benzene upon addition of hexane to afford fine red crystals: yield 50 mg (92%); UV_{max} (C_6H_6) 325 (ε 1.79×10^4), 356 (2.75×10^4), 406 (0.79×10^4), 490 (1.15×10^4), and 520 nm (0.91×10^4); IR (KBr) 2150 (C≡N), 1730 (ester C=O), and 1100 and 620 cm^{-1} (ClO_4^-).

Found: C, 53.75; H, 6.40; N, 6.03. Calcd for $C_{53}H_{75}ClCoN_5O_{19}$: C, 53.92; H, 6.40; N, 5.93.

Heptamethyl Methylaquacobyrinate Perchlorate, [(CH$_3$)(H$_2$O)-Cob(III)7C$_1$ester]ClO$_4$. [Cob(II)7C$_1$ester]ClO$_4$ (50 mg, 4.4×10^{-5} mol) was mixed with 600 mg of zinc powder dispersed in 30 mL of acetic acid, and the mixture was stirred for 10 min at room temperature under nitrogen atmosphere. All the following treatments were performed under subdued light. After the mixture turned dark green, it was stirred for 5 min upon addition of 1.0 g of methyl iodide. The residual zinc powder was removed by filtration, and 50 mL of 15%(w/w) aqueous sodium perchlorate was added to the filtrate. The reaction mixture was extracted with dichloromethane (50 mL×3), and the extract was washed with 5%(w/w) aqueous sodium hydrogencarbonate (50 mL) and distilled water (50 mL). After being dried over sodium sulfate, the yellow dichloromethane solution was evaporated to dryness *in vacuo* at room temperature. The residue was reprecipitated from benzene upon addition of hexane to afford brown powder: yield 43 mg (84%); UV_{max} (CH_2Cl_2) 264 (ε 2.14×10^4), 305 (2.36×10^4), 373 (0.85×10^4), and 457 nm (1.03×10^4); CD (CH_3OH) 260 ($\Delta\varepsilon$ −18.6), 323 (+13.7), 356 (−1.71), 378 (+1.38), 462 (−4.82), 508 (+2.87), and 550 nm (+1.69); IR (KBr) 1730 (ester C=O), and 1100 and 620 cm^{-1} (ClO_4^-); ^{1}H-NMR (CD_3OD, TMS) δ=−0.18 (3H, s, CH_3-Co), 1.02, 1.14, 1.40, 1.45, 1.62, 1.80, 2.35, and 2.40 (24H, each s, CH_3), 3.65 (21H, m, CO_2CH_3), and 6.65 (1H, s, H at C-10).

Found: C, 54.49; H, 6.61; N, 4.96. Calcd for $C_{53}H_{78}ClCoN_4O_{19}$: C, 54.43; H, 6.72; N, 4.80.

Although both Coα- and Coβ-methyl isomers are generally expected to be formed, the methylated complex prepared by the present method is regarded as the Coβ-methyl isomer in the light of UV, CD, and ^{1}H-NMR data.[6]

Spectroscopic Measurements. Electronic absorption spectra were recorded on a Hitachi 340 or a Hitachi 220A spectrophotometer. ^{1}H-NMR spectra were taken on a Hitachi R-24B spectrometer. ESR spectra were obtained with a JEOL JES-ME-3 X-band spectrometer equipped with a 100-kHz field modulation unit; a standard MgO/Mn^{II} sample calibrated with a NMR magnetometer was employed for calibration of the magnetic field.

Kinetic Measurements. Pseudo-first-order rate constants for the alkylation of heptamethyl cobyrinate, [(ROH)$_2$Cob(III)7C$_1$ester]$^{2+}$ (R=H and/or CH_3), with ethyl vinyl ether and methanol in dichloromethane were determined spectrophotometrically. A mixture of [(CH_3)-(H_2O)Cob(III)7C$_1$ester]ClO_4 (5.0×10^{-5} mol dm^{-3}), ethyl vinyl ether, methanol, and dichloromethane was placed in a spectrophotometric cell of 1-cm path length which was thermostated at 21.5±0.1 °C. The solution was irradiated with a conventional 500-W tungsten lamp from a distance of 20 cm for 1 min. [(CH_3)(H_2O)Cob(III)7C$_1$ester]ClO_4 was converted completely into [(ROH)$_2$Cob(III)7C$_1$ester]$^{2+}$ upon aerobic irradiation. Then, the complex thus formed was subjected to alkylation in the dark. Under the present experimental conditions, clear isosbestic points were observed in the course of alkylation along with absorbance decay of the 335-nm band which is characteristic of the dicationic cobalt complex. All the kinetic runs provided linear correlations for plots of $\ln(OD_t-OD_\infty)$ *vs.* time, where OD_t and OD_∞ stand for optical densities at time t and after completion of the reaction, respectively.

Catalytic Reactions. [(CN)(H_2O)Cob(III)7C$_1$ester]-ClO_4 was dissolved in a solution composed of ethyl vinyl ether and ethanol, and the mixture was placed in a Pyrex ampule (ϕ 20 mm). The reaction mixture was stirred and irradiated with a conventional 500-W tungsten lamp from a distance of 10 cm at 20±1 °C. As for the reaction carried out in the dark, the ampule was covered with aluminum foil. After an appropriate time interval, the reaction mixture was distilled *in vacuo* at room temperature and analyzed by means of GLC on a Shimadzu GC-4C apparatus with helium as a carrier gas. Identification of the reaction products was performed by coinjection of the distilled fraction with authentic samples into columns of Polyethylene Glycol 600, Silicone DC-550, and Silicone SE-30. A turnover number for the catalyst was calculated after correction for the blank reaction, if any, in the absence of the catalyst.

Results and Discussion

Reactions with [(CH$_3$)(H$_2$O)Cob(III)7C$_1$ester]ClO$_4$. When [(CH_3)(H_2O)Cob(III)7C$_1$ester]ClO_4 dissolved in a solution of ethyl vinyl ether and methanol was irradiated with the visible light for a short period of time under aerobic conditions, the complex was transformed into [(ROH)$_2$Cob(III)7C$_1$ester]$^{2+}$ which shows absorption maxima at 335, 490, and 510 nm (Fig. 1).[7] Then, the mixture was allowed to stand in the dark to afford an alkylated complex having the cobalt–carbon bond, which shows absorption maxima at 303 and 464 nm (Fig. 2); clear isosbestic points being observed along the progress of the reaction. When the starting complex was replaced with another alkylated complex such as [(C_2H_5)(H_2O)Cob-(III)7C$_1$ester]ClO_4 or [((CH_3O)$_2$$CHCH_2$)($H_2O$)Cob-(III)7C$_1$ester]$ClO_4$, the spectral changes identical with those shown in Figs. 1 and 2 were observed. Irradiation of [(CH_3)(H_2O)Cob(III)7C$_1$ester]ClO_4 with the visible light in methanol without ethyl vinyl ether under aerobic conditions resulted in the formation of [(ROH)$_2$Cob(III)7C$_1$ester]$^{2+}$, which was then converted into [Cob(II)7C$_1$ester]$^+$ in the dark, showing absorption maxima at 317 and 470 nm (Fig. 3). On the other hand, the anaerobic photolysis of [(CH_3)(H_2O)Cob(III)7C$_1$ester]ClO_4 in a solution of

ethyl vinyl ether and methanol gave [Cob(II)-7C$_1$ester]$^+$ as shown in Fig. 4, and the alkylated complex was not detected in a short period of time while the solution was allowed to stand further in the dark.

The ^{1}H-NMR spectra for [(CH$_3$)(H$_2$O)Cob(III)-7C$_1$ester]ClO$_4$ and the alkylated complex, which was obtained under the conditions described above, are shown in Fig. 5. The spectrum for the latter does not show the proton signal at $\delta=-0.18$ attributable to the cobalt-bound methyl group and is consistent with the structural formula, [((C$_2$H$_5$O)(CH$_3$O)CHCH$_2$)(H$_2$O)-Cob(III)7C$_1$ester]$^+$.

In the light of the above observations, [(CH$_3$)(H$_2$O)-Cob(III)7C$_1$ester]ClO$_4$ is apparently converted into [(ROH)$_2$Cob(III)7C$_1$ester]$^{2+}$ by the aerobic photolysis, and the latter complex undergoes alkylation with

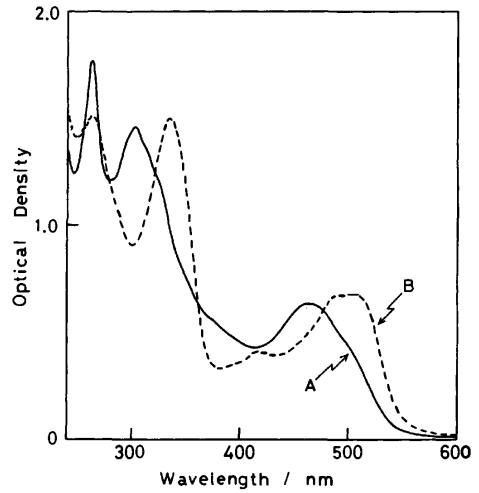

Fig. 1. Electronic spectra for the aerobic photolysis of [(CH$_3$)(H$_2$O)Cob(III)7C$_1$ester]ClO$_4$ in ethyl vinyl ether–methanol (1 : 1 v/v) at 21.5±0.1 °C: A, [(CH$_3$)-(H$_2$O)Cob(III)7C$_1$ester]ClO$_4$ (7.6×10^{-5} mol dm^{-3})before photolysis; B, irradiation with a 500-W tungsten lamp from a distance of 30 cm for 5 min to afford [(ROH)$_2$Cob(III)7C$_1$ester]$^{2+}$.

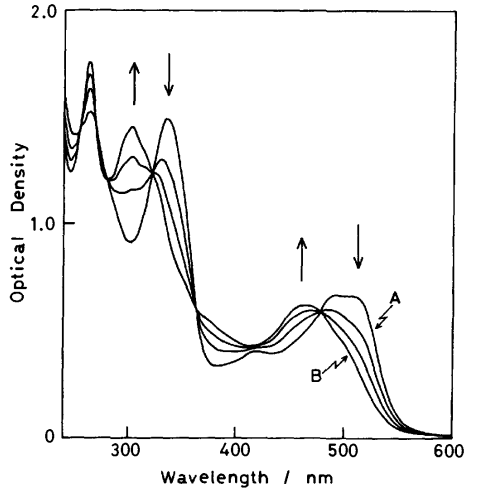

Fig. 2. Spectral change for formation of the cobalt–carbon bond derived from the aerobic photolysis product in the dark at 21.5±0.1 °C. Trends of spectral change with time are shown by arrows: A, the aerobic photolysis product, [(ROH)$_2$Cob(III)7C$_1$ester]$^{2+}$; B, the final product, [(C$_2$H$_5$O)(CH$_3$O)CHCH$_2$-Cob-(III)7C$_1$ester]$^+$. As for the amounts of reacting species, see Fig. 1.

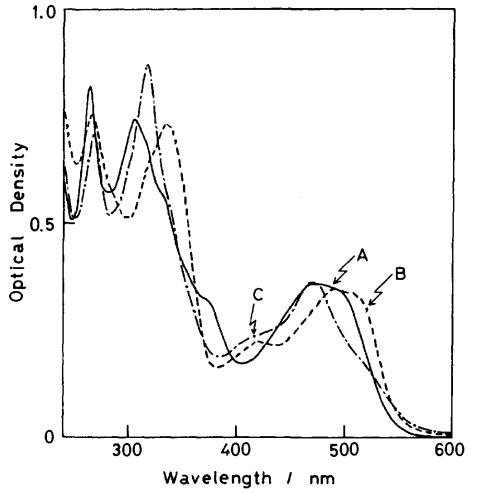

Fig. 3. Electronic spectra for the aerobic photolysis of [(CH$_3$)(H$_2$O)Cob(III)7C$_1$ester]ClO$_4$ in methanol at 21.5±0.1 °C: A, [(CH$_3$)(H$_2$O)Cob(III)7C$_1$ester]-ClO$_4$ (3.7×10^{-5} mol dm^{-3}) before photolysis; B, irradiated with a 500-W tungsten lamp from a distance of 30 cm for 5 min to afford [(ROH)$_2$Cob(III)7C$_1$-ester]$^{2+}$; C, on standing in the dark for 3 h after irradiation to afford [Cob(II)7C$_1$ester]$^+$.

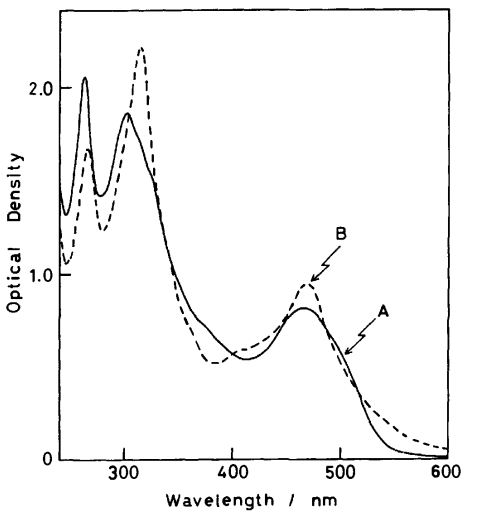

Fig. 4. Electronic spectra for the anaerobic photolysis of [(CH$_3$)(H$_2$O)Cob(III)7C$_1$ester]ClO$_4$ in ethyl vinyl ether–methanol (1 : 1 v/v) under argon atmosphere at 21.5±0.1 °C: A, [(CH$_3$)(H$_2$O)Cob(III)7C$_1$ester]-ClO$_4$ (8.66×10^{-5} mol dm^{-3}) before photolysis; B, irradiated with a 500-W tungsten lamp from a distance of 30 cm for 3 h to afford [Cob(II)7C$_1$ester]$^+$.

ethyl vinyl ether and methanol in the dark. Pseudo-first-order rate constants for the alkylation in various solutions were evaluated on the basis of spectral change typically shown in Fig. 2 and summarized in Table 1. The alkylation rate was found to increase as the concentration of ethyl vinyl ether was increased on one hand and to be reduced as the quantity of methanol was increased on the other. This result indicates that the reaction rate is controlled by the complex formation (*vide infra*) between ethyl vinyl ether and $[(ROH)_2Cob(III)7C_1ester]^{2+}$, which is enhanced as the solvent polarity is reduced: solvent polarity parmeters ($E_T(30)$) methanol, 55.5; dichloromethane, 41.1; ethyl vinyl ether, 35.1 kcal mol^{-1}.[8]

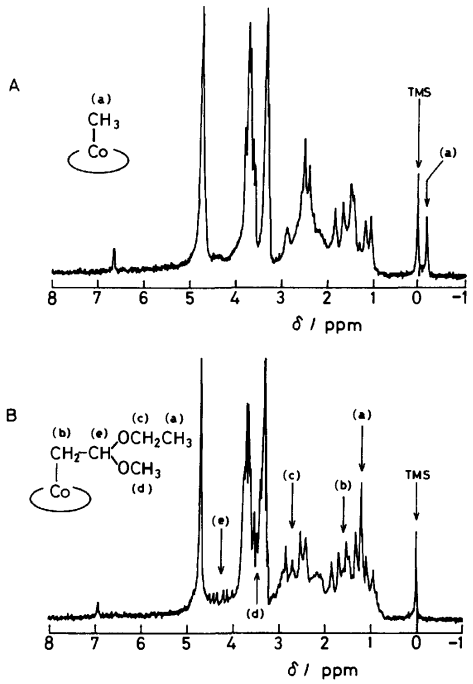

Fig. 5. ^{1}H-NMR (60 MHz) spectra of alkylated hydrophobic vitamin B_{12}'s in CD_3OD: A, $[(CH_3)(H_2O)$-$Cob(III)7C_1ester]ClO_4$; B, $[(CH_3)(H_2O)Cob(III)7C_1$-$ester]ClO_4$ (20 mg) in ethyl vinyl ether–methanol (1 : 1 v/v, 10 mL) being irradiated with a 500-W tungsten lamp from a distance of 30 cm for 3 h, allowed to stand in the dark for 24 h, and evaporated to dryness *in vacuo*.

Table 1. Pseudo-first-order rate constants for alkylation of hydrophobic vitamin B_{12}[a] at 21.5±0.1 °C under aerobic conditions in the dark

Entry	Medium (mL)			$k_{obsd} \times 10^5/s^{-1}$	k_{rel}[c]
	CH_3OH	EVE[b]	CH_2Cl_2		
1	0.75	0.50	1.75	3.41	1.00
2	0.75	0.60	1.65	5.49	1.61
3	0.75	0.70	1.55	7.17	2.10
4	0.75	0.75	1.50	7.85	2.30
5	0.75	0.80	1.45	9.10	2.67
6	0.75	0.90	1.35	12.6	3.70
7	0.75	1.00	1.25	15.5	4.55
8	0.50	0.75	1.75	9.08	2.66
9	1.00	0.75	1.25	2.88	0.84
10	1.50	1.50	0	9.35	2.74
11	1.00	2.00	0	17.1	5.01
12	0.75	2.25	0	24.9	7.30

a) $[(ROH)_2Cob(III)7C_1ester]^{2+}$ (R=H and/or CH_3), 5.0×10^{-5} mol dm^{-3}. b) Ethyl vinyl ether. c) Relative rate; k_{obsd} for entry 1 as a reference.

Reactions with [(CN)(H₂O)Cob(III)7C₁ester]ClO₄. When $[(CN)(H_2O)Cob(III)7C_1ester]ClO_4$ dissolved in a solution of ethyl vinyl ether and methanol was irradiated with the visible light under aerobic conditions and subsequently allowed to stand in the dark, the electronic spectrum did not undergo significant change; different from the spectral behavior of $[(CH_3)(H_2O)Cob(III)7C_1ester]ClO_4$ under comparable conditions. This does not mean, however, that the reaction does not take place. $[(CN)(H_2O)Cob$-$(III)7C_1ester]ClO_4$ shows no ESR signal in a solution of ethyl vinyl ether and methanol before irradiation (Fig. 6A), but characteristic signals due to the Co^{II} species[3a] were detected upon irradiation with the visible light under anaerobic conditions (Fig. 6B).

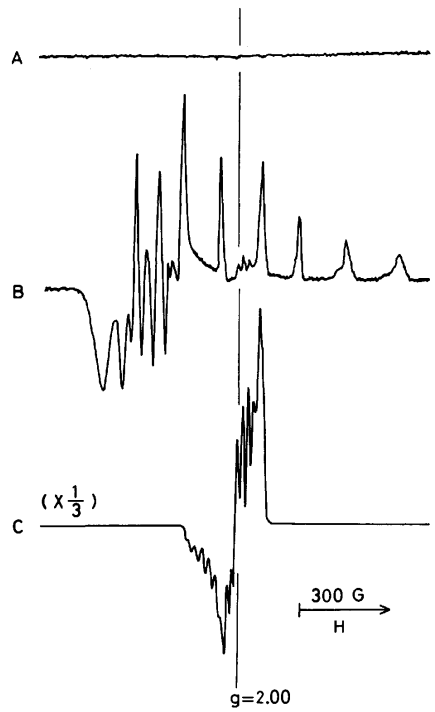

Fig. 6. ESR spectra for the following samples at 77 K: A, $[(CN)(H_2O)Cob(III)7C_1ester]ClO_4$ (2.7×10^{-3} mol dm^{-3}) in ethyl vinyl ether–methanol (3 : 1 v/v) in the dark under anaerobic conditions; B, sample A being irradiated with a 300-W tungsten lamp from a distance of 20 cm for 2 h at room temperature under anaerobic conditions; C, sample B being exposed to the open air.

Since such an ESR spectral change caused by the irradiation was insignificant for the cyanoaqua complex dissolved in diethyl ether and methanol under anaerobic conditions, a photosensitive alkylated complex was undoubtedly produced by the reaction of the complex with ethyl vinyl ether and methanol. Immediately after the reaction system was exposed to the open air, the ESR signals characteristic of the Co^{II} species were replaced with the ones due to the superoxo complex Co^{III}–O_2^-, the unpaired spin density being largely localized at the coordinated O_2^- group,[9] as shown in Fig. 6C. Since the superoxo complex was eventually converted into the original cyano complex[10] under irradiation conditions as confirmed by ESR and electronic spectroscopy, the Co^{II} species generated by the photolysis was readily oxidized to afford the Co^{III} species *via* formation of the superoxo complex under aerobic conditions.

The axial ligation constant (K) for [(CN)(H_2O)Cob(III)7C$_1$ester]ClO_4 with ethyl vinyl ether in dichloromethane was evaluated according to the method described previously;[3a] log K=−2. Even though the ligation constant was not evaluated because of its much smaller value in a polar medium used in the present reaction, such complex formation must take place so that the olefin is activated prior to the attack by methanol.

It is now clear that the alkylated complex is produced as the reaction intermediate in the course of the reaction with [(CN)(H_2O)Cob(III)7C$_1$ester]ClO_4 as the starting catalyst in a manner as observed for the reaction with [(CH_3)(H_2O)Cob(III)7C$_1$ester]ClO_4 (*vide supra*). In the light of the observation by electronic spectroscopy, the alkylated complex derived from [(CN)(ROH)Cob(III)7C$_1$ester]ClO_4 is decomposed by the trans effect provided by the axial cyano ligand much more readily than the one derived from [(ROH)$_2$Cob(III)7C$_1$ester]$^{2+}$.

When ethyl vinyl ether was used as an olefin, any oxygenation product was not detected by GLC. However, small amounts of cyclohexene oxide and 2-cyclohexen-1-ol (the total quantity, *ca.* 10 mole% of an amount of the alcohol adduct of cyclohexene produced) were obtained under the conditions described below by the reaction of cyclohexene with the superoxo complex. This result provides another evidence for the formation of the superoxo complex.

Catalytic Reactions and Turnover Behavior. The addition of an alcohol to ethyl vinyl ether took place by the catalysis of either [(ROH)$_2$Cob(III)-7C$_1$ester]$^{2+}$ or [(CN)(ROH)Cob(III)7C$_1$ester]$^+$ under aerobic irradiation conditions. Acetaldehyde ethyl methyl acetal and acetaldehyde diethyl acetal were the major products when methanol and ethanol were used, respectively. When a mixture of ethyl vinyl ether (1.9 g, 2.6×10^{-2} mol), ethanol (0.39 g, 8.6×10^{-3} mol), and [(CH_3)(H_2O)Cob(III)7C$_1$ester]ClO_4 (3.0 mg, 2.6×10^{-6} mol) was irradiated aerobically at 20±1 °C for 50 h with a 500-W tungsten lamp from a distance of 30 cm, acetaldehyde diethyl acetal was obtained in a yield, 10±2 times as much as the molar quantity of the hydrophobic vitamin B_{12} (refer to Eq. 1). In the

$$CH_2{=}CH{-}OC_2H_5 \xrightarrow[\substack{[(CH_3)(H_2O)Cob(III)7C_1ester]ClO_4 \\ \text{or} \\ [(CN)(H_2O)Cob(III)7C_1ester]ClO_4}]{C_2H_5OH,\ O_2,\ h\nu} CH_3{-}CH(OC_2H_5)_2 + CH_3CHO \quad (1)$$

course of the reaction, both alkylated and alkyl-free complexes, [((C$_2$H$_5$O)$_2$CHCH$_2$)(ROH)Cob(III)7C$_1$-ester]$^+$ and [(ROH)$_2$Cob(III)7C$_1$ester]$^{2+}$, respectively, were observed by means of electronic spectroscopy.

In the case that [(CN)(H_2O)Cob(III)7C$_1$ester]ClO_4 was used in place of the methylaqua complex otherwise under the same conditions, acetaldehyde diethyl acetal was obtained in a yield, 60±10 times as much as the molar quantity of the catalyst. This result indicates that the cyano complex is superior to the cyano-free complex as the catalyst for addition of an alcohol to the olefin. Time courses for the formation of acetaldehyde diethyl acetal as catalyzed by the former complex at 20±1 °C under aerobic conditions are shown in Fig. 7. The formation of the acetal was detected to a minor extent in the dark because the alkylated complex is thermally de-

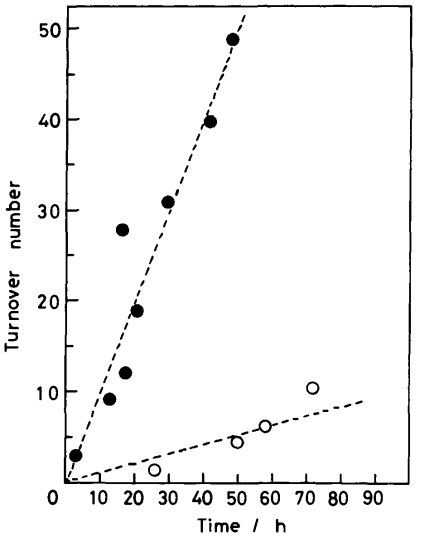

Fig. 7. Time courses for formation of acetaldehyde diethyl acetal as catalyzed by [(CN)(H_2O)Cob(III)-7C$_1$ester]ClO_4 under aerobic conditions at 20±1 °C. Composition of the initial reaction mixture: [(CN)-(H_2O)Cob(III)7C$_1$ester]ClO_4, 6.0 mg (5.1×10^{-6} mol); ethyl vinyl ether, 2.5 mL (1.9 g, 2.6×10^{-2} mol); ethanol, 0.50 mL (0.39 g, 8.6×10^{-3} mol). Turnover numbers for [(CN)(H_2O)Cob(III)7C$_1$ester]ClO_4 were calculated after correction for the blank reaction in the absence of the catalyst: ●, irradiated with a 500-W tungsten lamp from a distance of 10 cm; ○, in the dark.

composed by the trans effect originated from the axial cyano ligand. The acetal products, obtained by the reactions with C_2D_5OD and C_2H_5OD as alcohol components, were identified by NMR spectroscopy. A mixture of [(CN)(H_2O)Cob(III)7C_1ester]ClO_4 (10 mg, 8.5×10^{-6} mol), ethyl vinyl ether (2.25 g, 3.1×10^{-2} mol), and a deuterated ethanol (C_2H_5OD or C_2D_5OD, 0.48 g) was irradiated for 200 h, and the products were recovered in a manner as described in the experimental section. The major products were $CH_2DCH(OC_2H_5)(OC_2D_5)$ and $CH_3CH(OC_2H_5)_2$ when C_2D_5OD and C_2H_5OD were used, respectively; splitting patterns of the CH signal at δ=4.7 being a triplet and a quartet, respectively. This clearly indicates that the hydrogen atom is abstracted from the ethyl group of ethanol.

Judging from the spectral measurements and the product analyses, the catalytic reactions with the use of [(CH_3)(H_2O)Cob(III)7C_1ester]ClO_4 and [(CN)(H_2O)-Cob(III)7C_1ester]ClO_4 plausibly proceed *via* reaction cycles shown in Schemes 1 and 2, respectively. When the former complex is used as the starting one for example, the complex is first converted into the methyl-free complex by the aerobic photolysis. Ethyl vinyl ether, which is activated upon complex formation with the methyl-free complex in the second place, is subjected to the nucleophilic attack of an alcohol to afford an alkylated complex as the intermediate. The alkylated complex is then decomposed by the visible light to give the Co^{II} species and an acetal. [$(ROH)_2$Cob(III)7C_1ester]$^{2+}$ is regenerated by autoxidation of the Co^{II} species *via* formation of the superoxo-Co^{III} complex under aerobic conditions (see Scheme 1). It needs to be noted that the present reaction sequence is apparently similar to that of the coenzyme B_{12}-dependent enzymatic reaction, in which an alkylated complex is repeatedly produced and a product is obtained upon homolytic cleavage of the cobalt-carbon bond.[11]

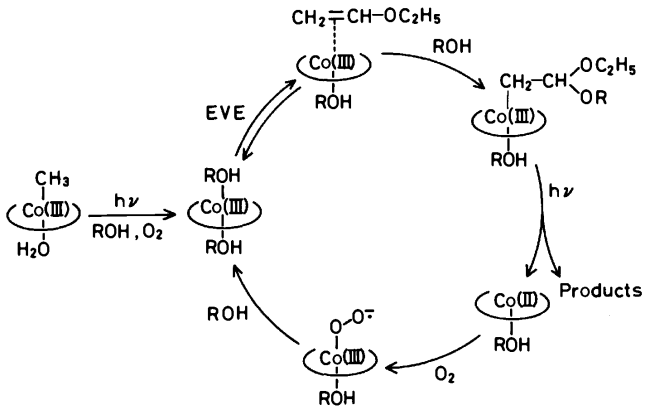

Scheme 1.

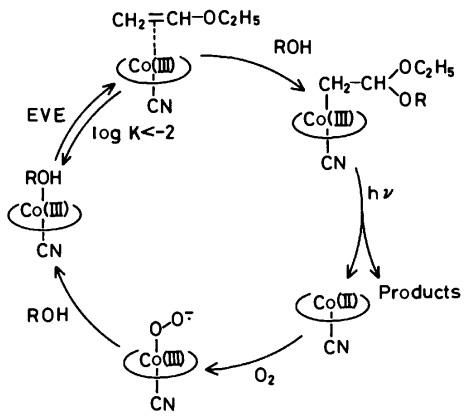

Scheme 2.

In order to make further clarification on the catalytic performance of the hydrophobic vitamin B_{12}, other olefins were also used in place of ethyl vinyl ether. Firstly, 1-pentene was used as a typical straight-chain olefin. The methyl-free Co^{III} complex, generated by the aerobic photolysis of [(CH_3)-(H_2O)Cob(III)7C_1ester]ClO_4 in 1-pentene and methanol, was transformed into the corresponding alkylated complex in the dark along with the spectral change similar to that shown in Fig. 2. However, the alkylation rate is extremely slow (*ca.* 1/50 of the rate with ethyl vinyl ether), while the alkylated complex is quite photo-labile and readily decomposed even under room light. When a mixture of 1-pentene (0.96 g, 1.4×10^{-2} mol), ethanol (1.2 g, 2.6×10^{-2} mol), and [(CN)(H_2O)Cob(III)7C_1ester]ClO_4 (3.9 mg, 3.3×10^{-6} mol) was irradiated at 20±1 °C for 150 h with a 500-W tungsten lamp from a distance of 10 cm under aerobic conditions, ethyl pentyl ether and ethyl 1-methylbutyl ether were obtained in the following yields; 15±5 and *ca.* 2 times, respectively, as much as the molar quantity of the hydrophobic vitamin B_{12} (refer to Eq. 2). Meanwhile, the reaction with

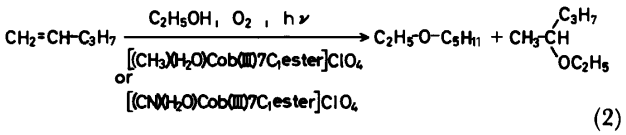

(2)

[(CH_3)(H_2O)Cob(III)7C_1ester]ClO_4 in place of the cyanoaqua complex otherwise under the same conditions afforded the former and latter ethers in the following respective yields; 3±1 and *ca.* 0.5 times as much as the molar quantity of the catalyst.

Secondly, cyclohexene was employed as a typical cyclic olefin. A mixture of cyclohexene (1.2 g, 1.5×10^{-2} mol), ethanol (1.2 g, 2.6×10^{-2} mol), and [(CN)(H_2O)Cob(III)7C_1ester]ClO_4 (9.7 mg, 8.2×10^{-6} mol) was irradiated at 20±1 °C for 150 h with a 500-W tungsten lamp from a distance of 10 cm under aerobic conditions, and cyclohexyl ethyl ether was obtained in a yield, 2±1 times as much as the molar quantity of the catalyst (refer to Eq. 3). The

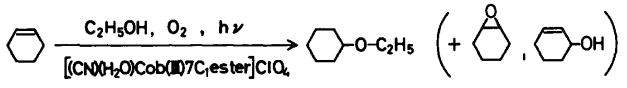

(3)

extremely low reactivity of cyclohexene may be partly attributed to a significant steric hindrance between the olefin and the catalyst against the formation of the corresponding complex.

Thirdly, acrylonitrile was used as a typical electron-deficient olefin. $[(ROH)_2Cob(III)7C_1ester]^{2+}$ was slowly converted into $[Cob(II)7C_1ester]^+$ in acrylonitrile and methanol under aerobic conditions in the dark without forming the corresponding alkylated complex. When a mixture of acrylonitrile (2.0 g, 3.8×10^{-2} mol), ethanol (0.39 g, 8.6×10^{-3} mol), and $[(CN)(H_2O)Cob(III)7C_1ester]ClO_4$ (10 mg, 8.5×10^{-6} mol) was aerobically irradiated for 100 h under conditions identical with those described above, any ethanol adduct (*e.g.*, 3-ethoxypropionitrile or 2-ethoxypropionitrile) was not detected by GLC.

In conclusion, it became apparent that the hydrophobic vitamin B_{12} catalyzes the nucleophilic attack of an alcohol on an olefin under mild conditions, aerobic irradiation with the visible light at the room temperature range. As for the substrate selectivity, an electron-rich olefin is more reactive with the present catalysts than ordinary olefins. $[(ROH)_2Cob(III)7C_1ester]^{2+}$ is an appropriate catalyst for investigation of the reaction mechanism because the alkylated intermediate complex has a long lifetime enough for its identification in the dark. On the other hand, $[(CN)(ROH)Cob(III)7C_1ester]^+$ is superior to the cyano-free Co^{III} complex as the catalyst for the addition reaction due to the trans effect exercised by the axial cyano ligand for the cleavage of the cobalt-carbon bond.

References

1) See for example: a) T. S. Wan and A. Fischli, *Helv. Chim. Acta*, **67**, 1883 (1984); b) R. Scheffold and R. Orlinski, *J. Am. Chem. Soc.*, **105**, 7200 (1983); c) R. Scheffold, G. Rytz, and L. Walder, "Modern Synthetic Methods," ed by R. Scheffold, John Wiley, New York (1983), Vol. 3, pp. 355—440.

2) a) R. B. Silverman and D. Dolphin, *J. Am. Chem. Soc.*, **95**, 1686 (1973); b) R. B. Silverman and D. Dolphin, *ibid.*, **96**, 7094 (1974); c) R. B. Silverman and D. Dolphin, *ibid.*, **98**, 4626 (1976).

3) a) Y. Murakami, Y. Hisaeda, and A. Kajihara, *Bull. Chem. Soc. Jpn.*, **56**, 3642 (1983); b) Y. Murakami, Y. Hisaeda, A. Kajihara, and T. Ohno, *ibid.*, **57**, 405 (1984); c) Y. Murakami, Y. Hisaeda, and T. Ohno, *ibid.*, **57**, 2091 (1984); d) Y. Murakami, Y. Hisaeda, and T. Ozaki, *Chem. Lett.*, **1985**, 473. e) Y. Murakami, Y. Hisaeda, T. Ohno, and T. Ozaki, *ibid.*, **1985**, 477.

4) L. Werthemann, R. Keese, and A. Eschenmoser, unpublished results; see L. Werthemann, Dissertation, ETH Zürich (Nr. 4097), Juris Druck & Verlag, Zürich (1968).

5) J. A. Riddick and W. B. Bunger, "Organic Solvents," Wiley-Interscience, New York (1970).

6) a) B. Kräutler and C. Caderas, *Helv. Chim. Acta*, **67**, 1891 (1984); b) M. Moskophidis, *Z. Naturforsch.*, **36C**, 497 (1981).

7) Either $[(CH_3OH)(H_2O)Cob(III)7C_1ester]^{2+}$ or $[(CH_3OH)_2Cob(III)7C_1ester]^{2+}$ is likely produced under irradiation conditions in the presence of a large excess of methanol. Since these complexes were not isolated for identification, we can not specify the structure at present.

8) The $E_T(30)$ value for ethyl vinyl ether was evaluated by electronic spectroscopy with dicyano(8,12-diethyl-1,2,3,7,-13,17,18,19-octamethyltetradehydrocorrinato)cobalt(III) as a probe. See: Y. Murakami, Y. Aoyama, and S. Nakanishi, *Inorg. Nucl. Chem. Lett.*, **12**, 809 (1976). As for $E_T(30)$, see: C. Reichardt, "Solvent Effects in Organic Chemistry," Verlag Chemie, Weinheim (1979).

9) a) A. V. Zelewsky, *Helv. Chim. Acta*, **55**, 2941 (1972); b) J. H. Bayston, N. K. King, F. D. Looney, and M. E. Winfield, *J. Am. Chem. Soc.*, **91**, 2775 (1969).

10) $[(CN)(H_2O)Cob(III)7C_1ester]^+$ is most likely converted into $[(CN)(ROH)Cob(III)7C_1ester]^+$ (R=alkyl) in the presence of a large excess of an alcohol after the initial reaction cycle without showing any significant change in spectral behavior.

11) B. T. Golding, "B_{12}," ed by D. Dolphin, John Wiley, New York (1982), Vol. 1, Chap. 15.

 © 1985 The Chemical Society of Japan Bull. Chem. Soc. Jpn., 58, 2659—2663 (1985)

Preparation of Michael Adducts of Isobutyraldehyde and Acetylenecarboxylic Esters *via* *N*-Isobutylidene-*t*-butylamine

Shingo MIYAJIMA* and Kunio ITO

Department of Applied Chemistry, Faculty of Engineering, Toyo University, Kawagoe, Saitama 350

(Received March 16, 1985)

N-Isobutylidene-*t*-butylamine reacted with methyl propiolate or dimethyl acetylenedicarboxylate to afford the Michael adducts predominantly. The adducts were converted to the corresponding formyl esters.

No Michael addition of isobutyraldehyde to acetylenecarboxylic esters has been reported, presumably because both the aldehyde and the acetylenes[1] undergo self-condensation in the presence of a strong base catalyst. The enamines derived from isobutyraldehyde react with electrophilic olefins to give 1,2- or 1,4-cycloaddition products,[2] which on hydrolytic ring opening yield Michael adducts. With acetylenecarboxylic esters, spontaneous rearrangement of initially formed cyclobutenes takes place and leads to dienamino esters.[3] Schiff's bases of α,α-disubstituted acetaldehydes are excellent complementary reagents to the enamines for the Michael addition to electrophilic olefins.[2a,4] With acetylenecarboxylic esters, however, only the formation of compounds resulting from *N*-alkenylation has been reported;[5] *N*-isobutylidenemethylamine, for example, reacts with two equivalents of dimethyl acetylenedicarboxylate to give a dihydropyridine derivative, a product of the reaction classified by Huisgen and Herbig[6] as a 1,4-dipolar cycloaddition.

We have investigated the reaction of *N*-isobutylidene-*t*-butylamine (**1**) with methyl propiolate (**2a**) or dimethyl acetylenedicarboxylate (**2b**) and found that the *t*-butyl group effectively prevents *N*-alkenylation, allowing the Michael addition to take place predominantly.

A solution of **2a** in tetrahydrofuran (THF) was gradually added to a stirred solution of **1** in THF heated at a bath temperature of 80 °C, and the heating was continued for an additional period of time. Fractional distillation afforded three isomeric products, the Michael adducts **3a** and **4a** and the enamino ester **5a**, in 45, 17, and 12% yields,

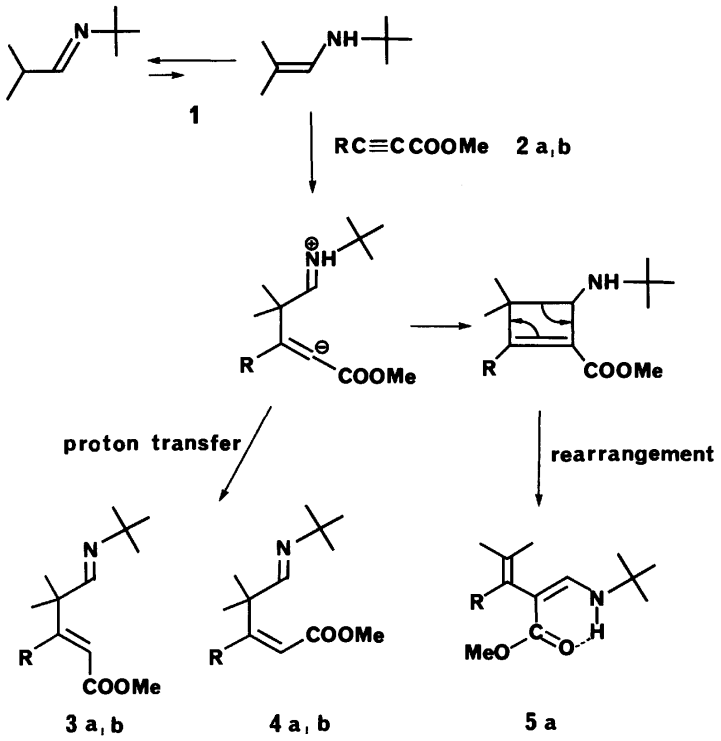

Fig. 1.

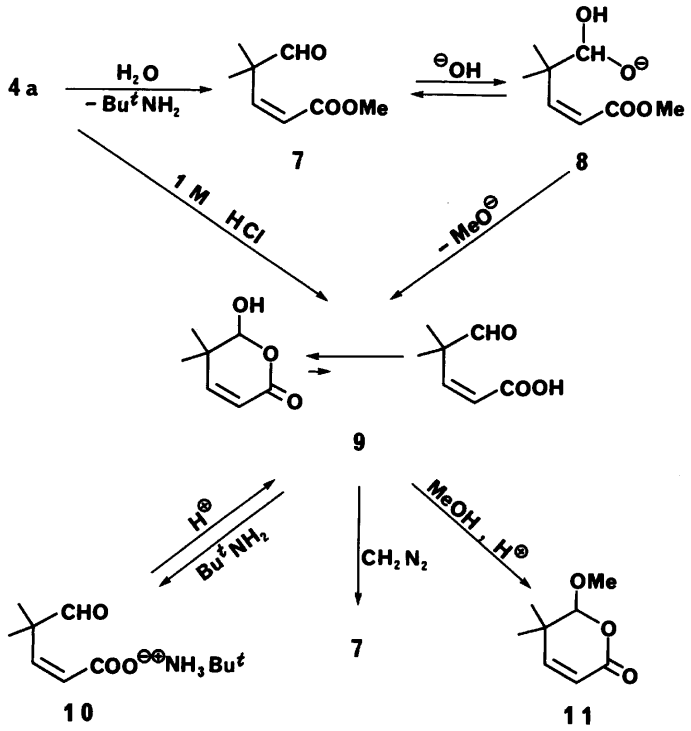
4a
H_2O
$-Bu^tNH_2$
CHO
COOMe
7
$^{\ominus}OH$
OH
CH
$O^{\ominus}$
COOMe
8
1 M HCl
$-MeO^{\ominus}$
OH
O
O
CHO
COOH
9
$H^{\oplus}$
Bu^tNH_2
CH_2N_2
$MeOH, H^{\oplus}$
CHO
$COO^{\ominus\oplus}NH_3Bu^t$
10
7
OMe
O
O
11

Fig. 2.

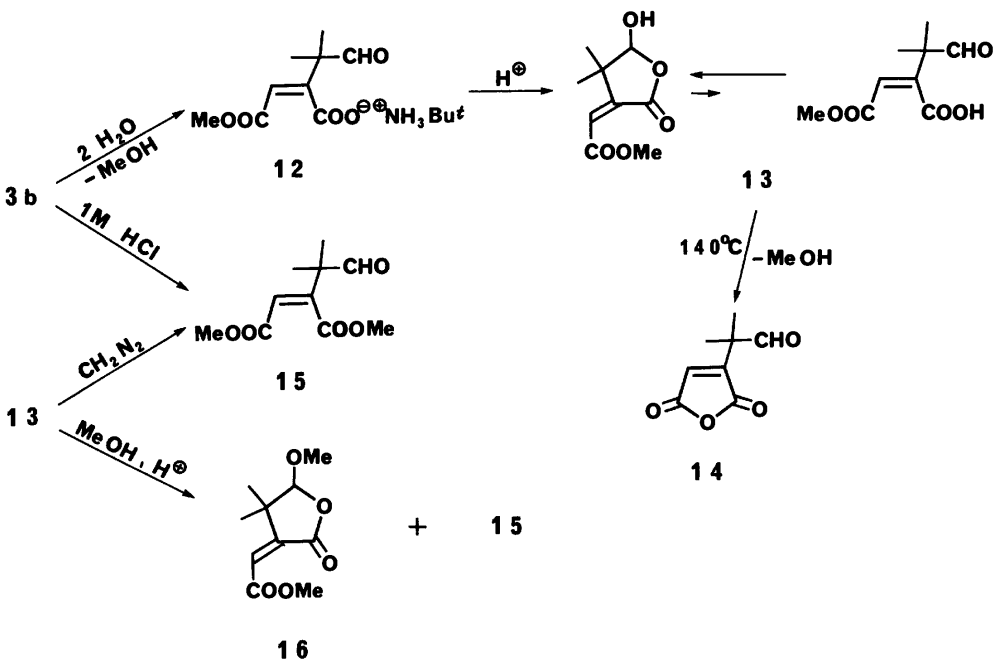
3b
$2\ H_2O$
$-MeOH$
CHO
MeOOC
$COO^{\ominus\oplus}NH_3Bu^t$
12
$H^{\oplus}$
OH
O
O
COOMe
13
CHO
MeOOC
COOH
1M HCl
CHO
MeOOC
COOMe
15
CH_2N_2
13
$MeOH, H^{\oplus}$
OMe
O
O
COOMe
16
+ 15
140°C
$-MeOH$
CHO
O
O
O
14

Fig. 3.

respectively (Fig. 1). These isomers were identified by their IR and ^{1}H NMR spectra and elemental analyses.

Reaction of **1** with **2b** was carried out in a similar manner. Distillation gave a mixture of the Michael adducts **3b** and **4b**, as judged by its ^{1}H NMR spectrum. When the mixture was heated at 160 °C for 2 h, isomerization took place and **3b** was obtained in 82% overall yield after distillation. The configuration of **3b** was further ascertained by its conversion to the maleic anhydride derivative **14**.

Apparently, the tautomeric enamine in equilibrium with the Schiff's base acts as a reacting species,[7] although the imino form is the only detectable form. The presumed pathways leading to the products are shown in Fig. 1.

The (*E*)-Michael adduct **3a**, on treatment with 1 M (1 M=1 mol dm^{-3}) HCl at room temperature, gave methyl (*E*)-4,4-dimethyl-5-oxo-2-pentenoate (**6**) in 94% yield.

The (*Z*)-adduct **4a**, on the other hand, was much less reactive under similar reaction conditions and both the imino and ester groups were slowly hydrolyzed to form the hydroxy lactone **9** (Fig. 2). Interestingly, when **4a** was stirred with water (50 times the weight of **4a**) at room temperature for 20 min, it went into solution and gave the carboxylate **10**. This rapid hydrolysis of the ester group of **4a** under such mild conditions can be explained in terms of intramolecular participation of the anion of the *gem*-diol in hydrolysis of **8**. The resulting hydroxy lactone **9**, which is in tautomeric equilibrium with the chain form,[8] combines with the initially liberated *t*-butylamine to afford **10**. Compound **9** was regenerated by acidification (85% yield based on **4a**).

When **9** was allowed to react with diazomethane, the (*Z*)-formyl ester **7** was obtained in 86% yield. Treatment of **9** with methanol containing H_2SO_4, on the other hand, gave the thermodynamically stabler[9] methoxy lactone **11** in a yield of 68%.

Similarly to **4a**, **3b** on treatment with water afforded the carboxylate **12**, which on acidification gave the hydroxy lactone **13** in 90% yield (Fig. 3). The formyl diester **15** was obtained by hydrolysis of **3b** with 1 M HCl in 79% yield. Alternatively, treatment of **13** with diazomethane gave a 92% yield of **15**. With methanol containing H_2SO_4 **13** yielded the methoxy lactone **16** (64%) along with a small amount of **15** (6%).

Experimental

Melting and boiling points are uncorrected. GLPC analyses were carried out with a Hitachi 163 instrument using an SE-30 or a PEG-20 M column. IR spectra were recorded on a Hitachi 285 or 260-50 spectrometer; absorptions are given in cm^{-1} in what follows. ^{1}H NMR data were obtained with a Hitachi R-24B spectrometer; chemical shifts are reported in δ relative to TMS or DSS and coupling constants (J) in Hz in what follows. Microanalyses were performed at the Microanalysis Laboratory, Department of Chemistry, Faculty of Science, the University of Tokyo. The Schiff's base **1** was prepared according to the procedure of Tiollais.[10] Compound **2a** was obtained by the method of Ingold[11] using commercial potassium hydrogen acetylenedicarboxylate as a starting material. **2b** of commercial grade was used without further purification. THF was dried with 4A Molecular Sieve.

Reaction of 1 with 2a. To a stirred solution of **1** (63.6 g, 0.500 mol) in THF (60 ml) heated at a bath temperature of 80 °C was added a solution of **2a** (46.2 g, 0.550 mol) in THF (50 ml) over a period of 1 h. Stirring and heating were continued for an additional 10 h. Removal of the solvent *in vacuo* and distillation of the residue gave an isomeric mixture of methyl (*E*)-(**3a**), methyl (*Z*)-5-(*t*-butylimino)-4,4-dimethyl-2-pentenoate (**4a**), and methyl 2-(*t*-butylaminomethylene)-4-methyl-3-pentenoate (**5a**) in a ratio of 61:23:16 (determined by GLPC): bp 56.0—92.0 °C/0.90 mmHg (1 mmHg=133.322 Pa); 87.9 g (83% based on **1**). Each isomer was isolated by redistillation through a 50 cm spinning band column; 47.5 g (45%) of **3a**, 18.0 g (17%) of **4a**, and 12.6 g (12%) of **5a** were obtained.

3a: bp 70.0—72.0 °C/0.90 mmHg; IR (neat) 1724 (C=O), 1670 (C=N), 1645 (C=C), and 977 ($^{H}\!>\!C\!=\!C\!<^{H}$); ^{1}H NMR ($CDCl_3$) 1.15 (s, 9H, $C(CH_3)_3$), 1.23 (s, 6H, $C(CH_3)_2$), 3.71 (s, 3H, CO_2CH_3), 5.76 (d, J=16, 1H, CH=C<u>H</u>CO_2Me), 7.00 (d, J=16, 1H, C<u>H</u>=CHCO_2Me), and 7.44 (s, 1H, CH=N). Found: C, 68.50; H, 10.18; N, 6.60%. Calcd for $C_{12}H_{21}NO_2$: C, 68.21; H, 10.02; N, 6.63%.

4a: bp 56.5—57.5 °C/0.90 mmHg; IR (neat) 1727 (C=O), 1663 (C=N), and 1637 (C=C); ^{1}H NMR ($CDCl_3$) 1.12 (s, 9H, $C(CH_3)_3$), 1.31 (s, 6H, $C(CH_3)_2$), 3.62 (s, 3H, CO_2CH_3), 5.77 (d, J=12, 1H, CH=C<u>H</u>CO_2Me), 6.28 (d, J=12, 1H, C<u>H</u>=CHCO_2Me), and 7.63 (s, 1H, CH=N). Found: C, 68.44; H, 9.78; N, 6.68%. Calcd for $C_{12}H_{21}NO_2$: C, 68.21; H, 10.02; N, 6.63%.

5a: bp 87.0—90.0 °C/0.90 mmHg; IR (neat) 3285 (NH), 1665 (C=O), and 1604 (C=C); ^{1}H NMR ($CDCl_3$) 1.28 (s, 9H, $C(CH_3)_3$), 1.68 (d, J=1.5, 3H, $C(CH_3)_2$), 1.76 (d, J=1.5, 3H, $C(CH_3)_2$), 3.63 (s, 3H, CO_2CH_3), 5.81 (m, 1H, C<u>H</u>=$C(CH_3)_2$), 6.76 (d, J=14, 1H, =C<u>H</u>NH), and 8.23 (br d, J=14, 1H, NH). Addition of CD_3OD containing a trace of HCl resulted in loss of the signal at 8.23 and collapse of the signal at 6.76 to a singlet. Found: C, 68.04; H, 10.15; N, 6.56%. Calcd for $C_{12}H_{21}NO_2$: C, 68.21; H, 10.02; N, 6.63%.

Reaction of 1 with 2b. To a stirred solution of **1** (127.2 g, 1.00 mol) in THF (260 ml) heated at a bath temperature of 70 °C was added a solution of **2b** (142.1 g, 1.00 mol) in THF (280 ml) during 1 h. Stirring and heating were continued for an additional 1 h. The solvent was removed *in vacuo* and the residue was distilled to give 222.7 g of the main fraction boiling at 107.0—111.0 °C (0.60 mmHg). GLPC on an SE-30 or a PEG-20 M column showed virtually a single peak. ^{1}H NMR analysis, however, indicated a mixture of the geometrical isomers, dimethyl [2-(*t*-butylimino)-1,1-dimethylethyl]maleate (**3b**) and dimethyl [2-(*t*-butylimino)-1,1-dimethylethyl]fumarate

(**4b**), in a ratio of *ca.* 70:30; besides the signals due to **3b**, which will be shown below, those attributable to **4b** were observed: 1.11 (s, 9H, $C(CH_3)_3$), 1.40 (s, 6H, $C(CH_3)_2$), 3.73 (s, 3H, CO_2CH_3), 3.81 (s, 3H, CO_2CH_3), 6.49 (s, 1H, C=CH), and 7.58 (s, 1H, CH=N).

The mixture was heated at 160 °C for 2 h and distillation gave 219.7 g (82% based on **1**) of **3b**: bp 88.5—89.0 °C/0.15 mmHg; IR (neat) 1732 (C=O), 1655 (C=N), and 1639 (C=C); ^{1}H NMR ($CDCl_3$) 1.16 (s, 9H, $C(CH_3)_3$), 1.30 (s, 6H, $C(CH_3)_2$), 3.73 (s, 3H, CO_2CH_3), 3.81 (s, 3H, CO_2CH_3), 5.86 (s, 1H, C=CH), and 7.51 (s, 1H, CH=N). Found: C, 62.34; H, 8.90; N, 5.05%. Calcd for $C_{14}H_{23}NO_4$: C, 62.43; H, 8.61; N, 5.20%.

Methyl (E)-4,4-Dimethyl-5-oxo-2-pentenoate (6). A mixture of **3a** (30.0 g, 0.142 mol) and 1 M HCl (220 ml) was stirred for 1 h at room temperature. The reaction mixture was extracted with ether (3×150 ml). The ethereal extract was washed with aq $NaHCO_3$, dried (Na_2SO_4), concentrated, and distilled, giving 20.9 g (94%) of **6**: bp 64.5—65.0 °C/0.75 mmHg; IR (neat) 1725 (C=O), 1650 (C=C), and 982 ($H>C=C<H$); ^{1}H NMR ($CDCl_3$) 1.26 (s, 6H, $C(CH_3)_2$), 3.71 (s, 3H, CO_2CH_3), 5.88 (d, J=16, 1H, CH=C<u>H</u>CO_2Me), 6.91 (d, J=16, 1H, C<u>H</u>=CHCO_2Me), and 9.41 (s, 1H, CHO). Found: C, 61.46; H, 7.90%. Calcd for $C_8H_{12}O_3$: C, 61.52; H, 7.74%. 2,4-Dinitrophenylhydrazone, mp 124.0—124.4 °C (from methanol). Found: C, 50.18; H, 4.64; N, 16.83%. Calcd for $C_{14}H_{16}N_4O_6$: C, 50.00; H, 4.80; N, 16.66%.

6-Hydroxy-5,5-dimethyl-5,6-dihydro-2H-pyran-2-one (9). The (*Z*)-imino ester **4a** (12.7 g, 0.0601 mol) was stirred with water (640 ml) at room temperature. After 20 min, it went into solution. The solution was washed with ether (100 ml) and concentrated with a rotary evaporator below 55 °C *in vacuo* until some crystals began to separate out. To the residue, 4 M HCl (18 ml) was added, and the resulting solution was extracted with ether (3×50 ml). The ethereal extract was dried (Na_2SO_4) and evaporated, leaving 7.22 g (85%) of **9**[12] as a crystalline solid, mp 62.0—64.0 °C. A sample was recrystallized from ether–hexane for analysis: mp 65.0—65.8 °C; IR (KBr) 3270 (OH) and 1670 (C=O); ^{1}H NMR ($CDCl_3$) 1.17 (s, 6H, $C(CH_3)_2$), 5.38 (d, J=1, 1H, CH), 5.81 (br s, 1H, OH, caused to disappear by adding D_2O), 5.88 (d, J=9.5, 1H, CH=C<u>H</u>CO), and 6.59 (dd, J=9.5, 1, 1H, C<u>H</u>=CHCO). (Found: C, 59.29; H, 7.38%)

t-Butylammonium (Z)-4,4-Dimethyl-5-oxo-2-pentenoate (10). A mixture of **4a** (18.5 mg) and D_2O (0.93 ml) was shaken at room temperature for 20 min. The ^{1}H NMR spectrum of the resulting solution was identical with that of **10** prepared as follows.

t-Butylamine (0.397 g, 5.43 mmol) was added dropwise to a solution of **9** (0.712 g, 5.01 mmol) in water (1.0 ml). The reaction mixture was cooled, and the precipitated crystals were collected and dried with KOH pellets *in vacuo* (0.785 g, 73%): mp 111.5—113.0 °C; IR (KBr) 3000—2800 ($\overset{+}{N}H_3$), 1726 (C=O), 1637 (C=C), 1540 ($\overset{+}{N}H_3$), and 1416 (COO^-); ^{1}H NMR (D_2O) 1.20 (s, 6H, $C(CH_3)_2$), 1.34 (s, 9H, $C(CH_3)_3$), 5.82 (d, J=12, 1H, CH=C<u>H</u>COO^-), 5.85 (d, J=12, 1H, C<u>H</u>=CHCOO^-), and 9.23 (s, 1H, CHO). Found: C, 61.51; H, 9.83; N, 6.49%. Calcd for $C_{11}H_{21}NO_3$: C, 61.37; H, 9.83; N, 6.51%.

Acid-catalyzed Hydrolysis of 4a. To 86.5 mg (0.409 mmol) of **4a** was added 0.60 ml of 1 M HCl in D_2O. The ^{1}H NMR spectrum of the resulting iminium salt showed signals at 1.46 (s, 9H, $C(CH_3)_3$), 1.55 (s, 6H, $C(CH_3)_2$), 3.76 (s, 3H, CO_2CH_3), 6.12 (d, J=12, 1H, CH=C<u>H</u>CO_2Me), 6.57 (d, J=12, 1H, C<u>H</u>=CHCO_2Me), and 8.72 (s, 1H, CH=$\overset{+}{N}$H). With the salt kept standing at room temperature for 1 d, the peak areas of the CO_2CH_3 protons and the CH=$\overset{+}{N}$H proton decreased to 25 and 24% of their initial areas, respectively, relative to the total area of the olefinic protons. After 2 d, the spectrum indicated the completion of reaction, *i.e.*, an approximately equimolar mixture of **9**, CH_3OD, and *t*-butylammonium chloride.

Methyl (Z)-4,4-Dimethyl-5-oxo-2-pentenoate (7). Diazomethane was fed into a stirred solution of **9** (5.80 g, 40.8 mmol) in ether (100 ml) with N_2 as a carrier gas until a yellow color persisted for several min. An air condenser was attached and the solution was refluxed to remove the excess of diazomethane. Evaporation and distillation gave 5.45 g (86%) of **7**:[12] bp 49.0—49.3 °C/0.80 mmHg; IR (neat) 1722 (C=O) and 1637 (C=C); ^{1}H NMR ($CDCl_3$) 1.30 (s, 6H, $C(CH_3)_2$), 3.67 (s, 3H, CO_2CH_3), 5.93 (d, J=12, 1H, CH=C<u>H</u>CO_2Me), 6.18 (d, J=12, 1H, C<u>H</u>=CHCO_2Me), and 9.46 (s, 1H, CHO). (Found: C, 61.32; H, 7.97%) 2,4-Dinitrophenylhydrazone, mp 119.8—120.2 °C (from methanol). Found: C, 50.16; H, 4.65; N, 16.53%. Calcd for $C_{14}H_{16}N_4O_6$: C, 50.00; H, 4.80; N, 16.66%.

6-Methoxy-5,5-dimethyl-5,6-dihydro-2H-pyran-2-one (11). A solution of **9** (2.00 g, 14.1 mmol) in methanol (40 ml) containing concd H_2SO_4 (0.078 g) was allowed to stand at room temperature for 3 h. The solution was poured into satd aq NaCl (120 ml) and the mixture was extracted with ether (3×60 ml). The ethereal extract was dried (Na_2SO_4), concentrated, and distilled to afford 1.49 g (68%) of **11**: bp 71.0—72.0 °C/1.0 mmHg; IR (neat) 1723 (C=O); ^{1}H NMR ($CDCl_3$) 1.11 (s, 3H, CCH_3), 1.18 (s, 3H, CCH_3), 3.54 (s, 3H, CO_2CH_3), 4.85 (d, J=1, 1H, CH), 5.86 (d, J=9.5, 1H, CH=C<u>H</u>CO), and 6.53 (dd, J=9.5, 1, 1H, C<u>H</u>=CHCO). Found: C, 61.28; H, 7.88%. Calcd for $C_8H_{12}O_3$: C, 61.52; H, 7.74%.

Methyl (Z)-5-Hydroxy-4,4-dimethyl-2-oxotetrahydrofuran-$\Delta^{3,\alpha}$-acetate (13). A mixture of **3b** (80.8 g, 0.300 mol) and water (4000 ml) was stirred at room temperature for 2.5 h. The resulting solution was washed with ether (2×400 ml) and concentrated on a rotary evaporator below 55 °C *in vacuo* until some crystals began to separate out. To the residue was added 80 ml of 4 M HCl, and the resulting solution was extracted with ether (3×150 ml). The ethereal extract was dried (Na_2SO_4) and evaporated, leaving 54.3 g (90%) of **13** as a crystalline solid; mp 71.0—75.0 °C. A sample was recrystallized from ether–hexane for analysis: mp 77.1—77.5 °C; IR (KBr) 3295 (OH), 1775, 1710 (C=O), and 1670 (C=C); ^{1}H NMR ($CDCl_3$) 1.25 (s, 6H, $C(CH_3)_2$), 3.82 (s, 3H, CO_2CH_3), 5.60 (s, 1H, CH), 5.72 (br s, 1H, OH, caused to disappear by adding D_2O), and 6.25 (s, 1H, C=CH). Found: C, 54.24; H, 6.26%. Calcd for $C_9H_{12}O_5$: C, 54.00; H, 6.04%.

t-Butylammonium (Z)-2-(1,1-Dimethyl-2-oxoethyl)-3-methoxycarbonylacrylate (12). A mixture of **3b** (28.0 mg) and D_2O (1.40 ml) was stirred at room temperature for 2.5 h. The ^{1}H NMR spectrum of the resulting solution was identical with that of **12** prepared as follows.

To a suspension of **13** (0.807 g, 4.03 mmol) in water (1.0 ml) warmed to 50 °C was added *t*-butylamine (0.298 g,

4.07 mmol). The resulting solution was cooled, and the precipitated crystals were collected and dried with KOH pellets *in vacuo* (0.548 g, 50%): mp 113.5—114.5 °C; IR (KBr) 3000—2800 ($\overset{+}{N}H_3$), 1720 (C=O), 1634 (C=C), 1540 ($\overset{+}{N}H_3$), and 1400 (COO^-); ^{1}H NMR (D_2O) 1.25 (s, 6H, $C(CH_3)_2$), 1.36 (s, 9H, $C(CH_3)_3$), 3.70 (s, 3H, CO_2CH_3), 5.69 (s, 1H, C=CH), and 9.33 (s, 1H, CHO). Found: C, 57.29; H, 8.77; N, 5.07%. Calcd for $C_{13}H_{23}NO_5$: C, 57.13; H, 8.48; N, 5.12%.

(1,1-Dimethyl-2-oxoethyl)maleic Anhydride (14). Compound **13** (40.0 g, 0.200 mol) was heated at 140 °C for 2 h under reduced pressure (20 mmHg). Distillation afforded 32.7 g (97%) of **14**: bp 103.0—106.0 °C/0.25 mmHg; mp 31.0—31.9 °C; IR (KBr) 1835, 1766, 1716 (C=O), and 1628 (C=C); ^{1}H NMR ($CDCl_3$) 1.51 (s, 6H, $C(CH_3)_2$), 6.76 (s, 1H, C=CH), and 9.50 (s, 1H, CHO). Found: C, 57.21; H, 4.78%. Calcd for $C_8H_8O_4$: C, 57.14; H, 4.80%.

Dimethyl (1,1-Dimethyl-2-oxoethyl)maleate (15).

Acidcatalyzed Hydrolysis of 3b: A mixture of **3b** (40.0 g, 0.149 mol) and 1 M HCl (300 ml) was stirred at room temperature for 10 min. Ether (200 ml) was added and stirring was continued for an additional 2 h. The ether layer was separated and the aq layer was extracted with ether (3×150 ml). The combined extracts were washed with a small amount of water, dried (Na_2SO_4), concentrated, and distilled, giving 25.0 g (79%) of **15**: bp 100.0—101.0 °C/0.50 mmHg; IR (neat) 1735, 1725 (C=O), and 1641 (C=C); ^{1}H NMR ($CDCl_3$) 1.28 (s, 6H, $C(CH_3)_2$), 3.70 (s, 3H, CO_2CH_3), 3.79 (s, 3H, CO_2CH_3), 5.91 (s, 1H, C=CH), and 9.38 (s, 1H, CHO). Found: C, 56.08; H, 6.88%. Calcd for $C_{10}H_{14}O_5$: C, 56.07; H, 6.59%. 2,4-Dinitrophenylhydrazone, mp 145.9—146.1 °C (from methanol). Found: C, 48.71; H, 4.47; N, 14.31%. Calcd for $C_{16}H_{18}N_4O_8$: C, 48.73; H, 4.60; N, 14.21%.

Formyl Diester 15 from 13: Treatment of **13** (16.0 g, 79.9 mmol) in ether (200 ml) with diazomethane and working up in the same manner as employed in the preparation of **7** yielded 15.8 g (92%) of a material boiling at 102.0—103.5 °C (0.65 mmHg), whose IR and ^{1}H NMR spectra were identical with those of **15** prepared as described above.

Methyl (Z)-5-Methoxy-4,4-dimethyl-2-oxotetrahydrofuran-$\Delta^{3,\alpha}$-acetate (16). A solution of **13** (3.01 g, 15.0 mmol) in methanol (60 ml) containing concd H_2SO_4 (0.11 g) was allowed to stand at room temperature for 4 h. The solution was poured into 180 ml of satd aq NaCl and the mixture was extracted with ether (2×90 ml). The ethereal extract was dried (Na_2SO_4), concentrated, and distilled with a 15 cm concentric column, giving 0.20 g (6%) of **15** (bp 99.0—101.5 °C/0.50 mmHg) and 2.05 g (64%) of **16** (bp 109.0—110.0 °C/0.50 mmHg, mp 68.0—69.6 °C). A sample of **16** was recrystallized from hexane-CCl_4 for analysis: mp 70.6—71.3 °C; IR (KBr) 1761, 1728 (C=O), and 1672 (C=C); ^{1}H NMR (CCl_4) 1.19 (s, 3H, CCH_3), 1.22 (s, 3H, CCH_3), 3.48 (s, 3H, OCH_3), 3.73 (s, 3H, CO_2CH_3), 4.95 (s, 1H, CH), and 6.08 (s, 1H, C=CH). Found: C, 56.02; H, 6.68%. Calcd for $C_{10}H_{14}O_5$: C, 56.07; H, 6.59%.

The authors thank Messrs. Hirofumi Yasuda and Kazuhiro Tatsuo for their experimental assistance.

References

1) R. M. Acheson and N. F. Elmore, "Advances in Heterocyclic Chemistry," ed by A. R. Katritzky and A. J. Boulton, Academic Press, New York (1978), Vol. 23, p. 263.

2) a) K. C. Brannock, A. Bell, R. D. Burpitt, and C. A. Kelly, *J. Org. Chem.*, **29**, 801 (1964); b) I. Fleming and M. H. Karger, *J. Chem. Soc., C*, **1967**, 226.

3) a) K. C. Brannock, R. D. Burpitt, V. W. Goodlett, and J. G. Thweatt, *J. Org. Chem.*, **28**, 1464 (1963); b) **29**, 818 (1964).

4) a) K. Ito, S. Miyajima, and K. Nakabayashi, *Yuki Gosei Kagaku Kyokai Shi*, **36**, 1058 (1978); b) M. Pfau, J. Ughetto-Monfrin, and D. Joulain, *Bull. Soc. Chim. Fr., Pt. 2*, **1979**, 627.

5) A. de Savignac and A. Lattes, *Bull. Soc. Chim. Fr.*, **1970**, 4476.

6) R. Huisgen and K. Herbig, *Justus Liebigs Ann. Chem.*, **688**, 98 (1965).

7) a) B. de Jeso and J. C. Pommer, *J. Chem. Soc., Chem. Commun.*, **1977**, 565; b) *J. Organomet. Chem.*, **137**, 23 (1977).

8) For a review of ring-chain tautomerism, see P. R. Jones, *Chem. Rev.*, **63**, 461 (1963).

9) The (Z)-formyl ester **7** dissolved in methanol containing H_2SO_4 or NaOMe as a catalyst was almost completely isomerized to the methoxy lactone **11**.

10) R. Tiollais, *Bull. Soc. Chim. Fr.*, **1947**, 708.

11) E. H. Ingold, *J. Chem. Soc.*, **127**, 1199 (1925).

12) A. A. Frimer, P. Gilinsky-Sharon, and G. Aljadeff, *Tetrahedron Lett.*, **23**, 1301 (1982).

Decompositions of Tropone Tosylhydrazone Sodium Salt in the Presence of Cyclopentadienone Derivatives. [4+2]-Type Cycloaddition Reactions of Cycloheptatrienylidene or 1,2,4,6-Cycloheptatetraene with Cyclopentadienone Derivatives

Katsuhiro SAITO* and Hiraku ISHIHARA
Department of Chemistry, Nagoya Institute of Technology, Gokiso-cho, Showa-ku, Nagoya 466
(Received April 19, 1985)

Tropone tosylhydrazone sodium salt, the precursor of the cyclic conjugated carbene (cycloheptatrienylidene), was decomposed in the presence of various cyclopentadienone derivatives to give endo- and exo-[4+2]-type adducts and benzotropylidene derivatives. The product ratios between the endo-[4+2]-type adducts and the exo-[4+2]-type adducts are considered to suggest that these addition reactions proceed *via* a cyclic conjugated allene (1,2,4,6-cycloheptatetraene), which is a valence-bond isomer of cycloheptatrienylidene. Upon heating, the [4+2]-type adducts gave the benzotropylidene derivatives *via* decarbonylation reactions followed by 1,5-hydrogen shifts.

Recently, medium-sized ring-conjugated allenes are attracting the attention of chemists from the viewpoint of the addition reactions and the molecular rearrangements of the allenes.[1] Allenes are twisted molecules with rectlinear three-carbon atoms. Consequently, medium-sized ring allenes are considered to have a considerable amount of strain energy. It is known that three-membered ring-cyclic carbenes, cyclopropylidenes, rearrange to allenes *via* ring-opening processes.[2]

Cycloheptatrienylidene (**2**), which is generated by the thermolysis of a tropone tosylhydrazone sodium salt (**1**) (accompanied by nitrogen gas and sodium *p*-toluenesulfinate (**3**)), is known to be a nucleophilic singlet carbene because of a contribution of the 6 π-electrons aromatic structure (**2b**).[3] Actually, **2**, preferentially reacts with electron-deficient double bonds,[3c] and adds to maleonitrile and fumalonitrile with stereospecificity.[3d]

Recently, a possibility of an isomerization of the carbene (2) and a medium-sized ring-conjugated allene, 1,2,4,6-cycloheptatetraene (4), was pointed out and a number of reports have been published concerning this isomerization.[3,4]

As a part of our research on the reactivity of **2**,[3f] we studied addition reactions of **2** with various cyclopentadienone derivatives and obtained a result which suggests that **2** is rearranged to 4. Here we wish to report on this result.

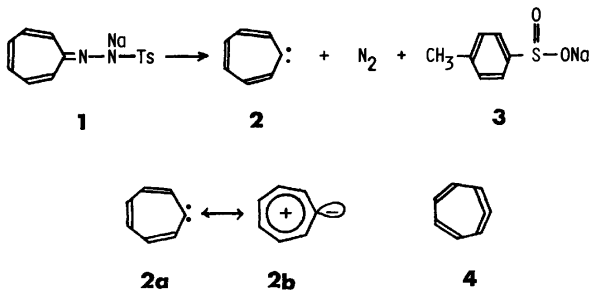

Fig. 1.

Results and Discussion

When tropone tosylhydrazone sodium salt (**1**) was allowed to decompose in anhydrous diglyme at 95 °C for 3 h in the presence of 2 mole equivalents of 2,5-dimethyl-3,4-diphenylcyclopentadienone (**5**), an endo-[4+2]-type adduct (**6**), exo-[4+2]-type adduct (**7**), and a benzotropylidene derivative (**8**) were afforded in 16, 2, and 9% yields, respectively. Under similar conditions, **1** was allowed to decompose in the presence of tetracyclone (**9**) to give an exo-[4+2]-type adduct (**10**) and two kinds of benzotropylidene derivatives (**11** and **12**)[3c] in 8, 6, and 10% yields, respectively. The same type of reaction of **1** with phencyclone (**13**) afforded an endo-[4+2]-type adduct (**14**) in a 17% yield. The analogous reaction of **1** with a cyclopentadienone derivative (**15**) gave a benzo-tropylidene derivative (**16**) in a 24% yield.

The endo- and exo-[4+2]-type adducts (**6** and **7**) gave the benzotropylidene derivative (**8**) in 79 and 80% yields upon heating at 105 °C for 180 h and 120 h, respectively. No interconversion between **6** and **7** was observed. The two kinds of benzotropylidene derivatives **11** and **12** were afforded by pyrolysis of exo-[4+2]-type adduct (**10**) at 100 °C for 80 h in 17 and 69% yields, respectively. On the other hand, upon heating at 100 °C for 2h, endo-[4+2]-type adduct (**14**) rearranged in a 80% yield to exo-[4+2]-type adduct (**17**), which gave a benzotropylidene derivative (**18**) in a 85% yield upon heating at 150 °C for 100 h. Considering this thermal isomerization of **14** to **17**, it seems not to be unreasonable to think that the exo-[4+2]-type adduct (**10**) is afforded by a thermal isomerization of the initially formed endo-[4+2]-type adduct, which corresponds to the endo-[4+2]-type adduct **6**.

The structures of the products were determined on

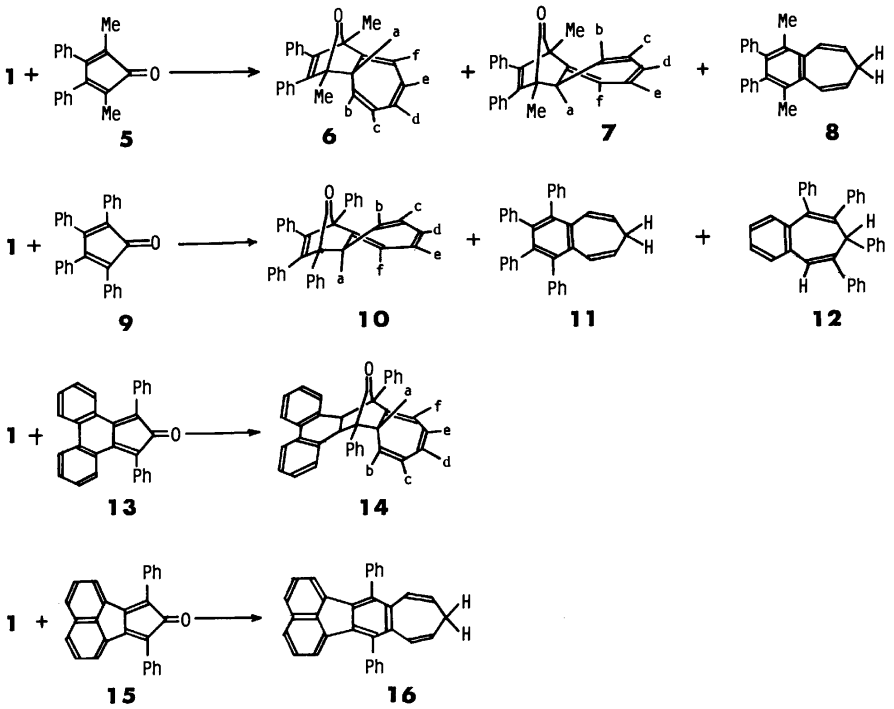

Fig. 2.

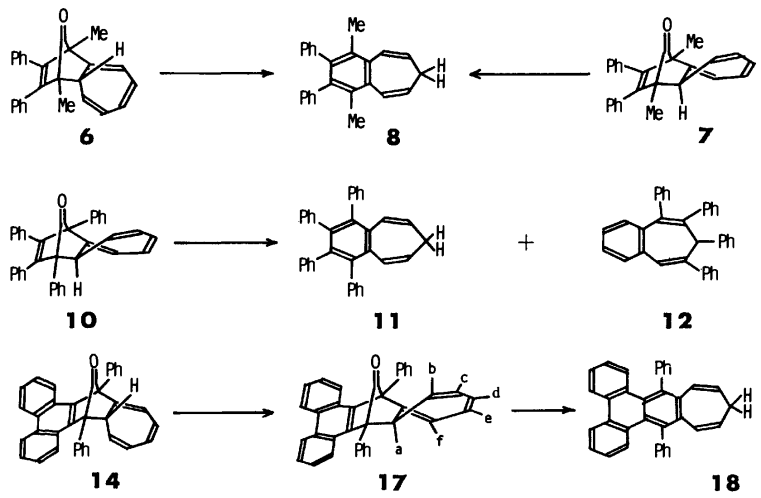

Fig. 3.

Table. NMR Data of the [4+2]-type adducts

Adducts		Chemical shifts (δ, ppm) in $CDCl_3$						Coupling constants (Hz)	
		H_a (d)	H_b (dd)	H_c (m)	H_d, H_e, H_f (m)	Me (s)	Ph (m)	J_{ab}	J_{ac}
Endo	6	3.12	4.91		6.1—6.7 (4H)	1.30, 1.48	7.0—7.5 (10H)	4	10
	14	4.35	4.73	5.70	6.3—6.7 (3H)		7.0—8.7 (18H)	4	10
	20[3f)]	3.68	4.75	5.85	6.1—6.5 (3H)		7.0—7.8 (14H)	4	10
Exo	7	2.30	5.21		6.2—6.9 (4H)		7.0—7.5 (10H)	4	10
	10	2.63	5.12		6.2—6.8 (4H)		7.0—7.8 (20H)	4	10
	17	2.30	5.43		6.2—6.9 (4H)		7.0—8.7 (18H)	4	10
	21[3f)]	2.60	5.15	6.05	6.3—6.7 (3H)		7.0—7.8 (14H)	4	10
	22[3f)]	2.46	4.63	5.86	6.2—6.5 (3H)		7.0—7.5 (8H)	4	10

the basis of their physical properties and confirmed by comparisons of these properties to those of the analogous compounds, such as **19**, **20**, and **21**.[3f,5,6] The stereochemistries of the endo- and exo-[4+2]-type adducts were determined by comparisons of the chemical shifts of the methine protons (H_a) of the adducts to those of the corresponding methine protons (H_a) of the endo-compound (**19**), exo-compound (**20**), and the compound **21**, whose methine proton corresponds to the methine proton of the exo-[4+2]-type adducts. The NMR signal of the methine proton (H_a) of **14** appears at a low field (4.35 ppm) compairing to that of **6** (3.12 ppm) because of a paramagnetic anisotropic effect of the phenyl group attached to the carbon atom adjacent to the carbon atom bearing the methine proton (H_a). The benzo-tropylidene derivatives **11** and **12** are compounds from the literature.[3e]

The formation mechanism of the [4+2]-type adducts (**6**, **7**, **10**, and **14**) via the carbene, cycloheptatrienylidene (**2**), requires a multistep reaction through the tropylium cation intermediate (**22**) (Path A). According to the Dreiding model there is no obvious difference between the steric repulsions in the formations of the endo-[4+2]-type adducts (**6** and **14**) and the exo-[4+2]-type adducts (**7** and **10**) from the corresponding intermediates (**22**). The fairly large difference between the yields of the endo-[4+2]-type adduct (**6**, 16%) and the exo-[4+2]-type adduct (**7**, 2%), and the preferential formation of the endo-[4+2]-type adduct (**14**, 17%) would suggest that the reaction does not proceed via the intermediate (**22**).[7]

The major formation of the endo-[4+2]-type adducts, which contain no less strain energies than those of the exo-[4+2]-type adducts suggests the contribution of a stabilization effect of a secondary orbital interaction in the transition state of Diels-Alder type addition reaction *via* the allene, 1,2,4,6-cycloheptatetraene (**4**) (Path B).[8] Cyclopentadienone derivatives are well known to be reactive enophiles in Diels-Alder type addition reactions.[5d,9] Oda has reported that a cyclic conjugated allene derivative reacted with an enophile, diphenylisobenzofuran, to give endo- and exo-[4+2]-type adducts in a yield ratio of 5:1, though without defining the stereochemistry of the adducts.[10]

As mentioned above, it is hard to conclude whether cycloheptatrienylidene (**2**) or 1,2,4,6-cycloheptatetraene (**4**) is involved in the reactions, but the allene mechanism (Path B), which indicates the isomerization of **2** to **4** seems to be plausible.

The benzotropylidene derivative (**8**, **11**, **16**, and **18**) are considered to be formed by the thermally allowed 1,5-hydrogen shift[7] of the intermediate (**23**), which is afforded by a decarbonylation reactions of the corresponding [4+2]-type adducts (**6**, **7**, **10**, and **17**).

Experimental

All the melting points are uncorrected. Mass, UV, and IR spectra were measured with the Hitachi M-52, Hitachi 220A, and DS 701 G spectrometers, respectively. NMR spectra were measured with a Hitachi R-20B or a Varian XL 200 spectrometers with tetramethylsilane as an internal standard. Wako gel C-200 and Wako gel B-5F were used for column and thin-layer chromatography, respectively. Diglyme was dried over Molecular Sieves 3A 1/16.

Reaction of 1 with 5. A mixture of **1** (23.84 g, 80 mmol), dimer of **5** (41.60 g, 160 mmol), and anhydrous diglyme (400 ml) was heated at 95 °C for 3 h. After evolution of nitrogen gas had ceased (1800 ml, *ca.* 100%), the gray powder of **3** (14.30 g, *ca.* 100%) was removed by filtration. The filtrate was extracted with ether, washed with water and brine, and dried over anhydrous sodium sulfate. After filtration, the solvent was removed on a rotary evaporator to give a mixture of crystals and an oil, which was chromatographed on silica gel to yield colorless crystals of **8** (2.45 g, 9%) by pet ether–benzene 9:1, colorless crystals of **6** (4.50 g, 16%) by pet ether–benzene 8:2, a colorless oil of **7** (0.64 g, 2%) by pet ether–benzene 7:3, and crystals of recovered dimer of **5** (3.91 g) by pet ether–benzene 3:7. The crystals of **6** and **8** were purified by

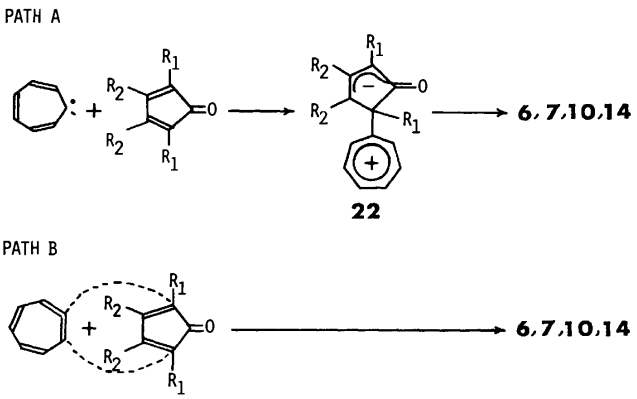

Fig. 5.

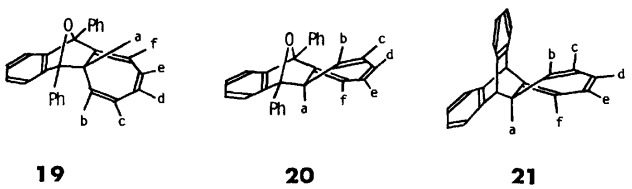

Fig. 4.

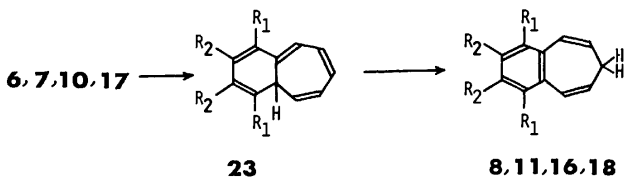

Fig. 6.

recrystallization from benzene and ethanol, respectively, and the oil of **7** was purified by thin-layer chromatography on silica gel using pet ether-benzene 9:1 as a developing solvent (R_f=0.61). **6**: Mp; 158—159 °C. Found: C, 89.37; H, 6.55%. Calcd for $C_{26}H_{22}O$: C, 89.11; H, 6.33%. Mass *m/z* (rel intensity): 350 (M^+, 4), 323 (50), 308 (100), 246 (10). UV (EtOH): 260 nm (log ε, 4.27). IR (KBr): 3030, 1780, 1600 cm^{-1}. **7**: Found: C, 88.08; H, 6.25%. Calcd for $C_{26}H_{22}O$: C, 89.11; H, 6.33%. Mass *m/z* (rel intensity): 350 (M^+, 11), 307 (100), 229 (11), 215 (6). UV (EtOH): 257 nm (log ε, 4.24). IR (neat): 3030, 1780, 1600 cm^{-1}. **8**: Mp 223—224 °C. Found: C, 92.90; H, 6.73%. Calcd for $C_{25}H_{22}$: C, 93.12; H, 6.88%. Mass *m/z* (rel intensity): 322 (M^+, 28), 321 (100), 308 (52), 293 (9). UV (EtOH): 253 nm (log ε, 4.36). IR (KBr): 3030, 1600 cm^{-1}. NMR ($CDCl_3$) δ (ppm)=2.12 (s, 6H), 2.32 (t, 2H, *J*=7 Hz), 6.02 (m, 2H), 6.51 (m, 2H), 7.0—7.5 (m, 10H).

Reaction of 1 with 9. A mixture of **1** (23.84 g, 80 mmol), **9** (51.52 g, 160 mmol) and anhydrous diglyme (400 ml) was heated at 95 °C for 3 h to evolve nitrogen gas (1800 ml, *ca.* 100%). After separation of the gray powder of **3** (14.30 g, *ca.* 100%) by filtration, the filtrate was treated as usual to give a mixture of crystals and an oil. The crystals of recovered **9** (37.11 g) were separated by filtration, and the filtrate was chromatographed on silica gel to yield colorless crystals of **12** (3.46 g, 10%), **11** (1.97 g, 6%), and **10** (2.34 g, 8%), in this order by pet ether-benzene 8:2. The crystals of **10** were further purified by recrystallization from benzene. **10**: Mp 190—191 °C. Found: C, 90.92; H, 5.41%. Calcd for $C_{36}H_{26}O$: C, 91.11; H, 5.52%. Mass *m/z* (rel intensity): 446 (M^+, 100), 369 (20), 291 (21). UV (EtOH): 253 nm (log ε, 4.18). IR (KBr): 3030, 1790, 1600 cm^{-1}.

Reaction of 1 with 13. A mixture of **1** (8.88 g, 30 mmol), **13**, (22.92 g, 60 mmol) and anhydrous diglyme (150 ml) was heated at 95 °C for 2 h to evolve nitrogen gas (600 ml, 90%). After separation of the gray powder of **3** (4.65 g, 87%) by filtration, the filtrate was treated as usual to yield a mixture of crystals and an oil. The crystals of recovered **13** (19.56 g) were separated by filtration and the filtrate was chromatographed on silica gel to give colorless crystals of **14** (2.41 g, 17%) by pet ether-benzene 5:5. The crystals of **14** were further purified by recrystallization from ethyl acetate. **14**: Mp 216—217 °C. Found: C, 91.21; H, 5.06%. Calcd for $C_{36}H_{24}O$: C, 91.27; H, 5.25%. Mass *m/z* (rel intensity): 472 (M^+, 20), 444 (100), 377 (25), 353 (15). UV (EtOH): 257 nm (log ε, 4.57). IR (KBr): 3030, 1785, 1600 cm^{-1}.

Reaction of 1 with 15. A mixture of **1** (8.88 g, 30 mmol), **15** (21.26 g, 60 mmol) and anhydrous diglyme (150 ml) was heated at 95 °C for 2 h to evolve nitrogen gas (650 ml, 97%). After separation of the gray powder of **3** (5.07 g, 95%) by filtration, the filtrate was treated as usual to give a mixture of crystals and an oil. The crystals of recovered **15** (19.89 g) were separated by filtration and the filtrate was chromatographed on silica gel to yield colorless crystals of **16** (1.57 g, 24%) by pet ether-benzene 1:1. Recrystallization from ethyl acetate gave pure crystals of **16**. **16**: Mp 254—256 °C. Found: C, 94.37; H, 5.03%. Calcd for $C_{33}H_{22}$: C, 94.70; H, 5.30%. Mass *m/z* (rel intensity): 418 (M^+, 100), 341 (22), 326 (18). UV (EtOH): 247 nm (log ε, 4.28). IR (KBr): 3030, 1600 cm^{-1}. NMR ($CDCl_3$) δ (ppm)=2.40(t, 2H, *J*=7 Hz), 5.81 (m, 2H), 6.43 (m, 2H), 7.1—7.9 (m, 16H).

Thermal Reaction of 6 to Form 8. A solution of **6** (760 mg) in toluene (7.5 ml) was heated at 105 °C for 180 h. After evaporation of the solvent on a rotary evaporator, the residue was thin-layer chromatographed on silica gel using pet ether-benzene 8:2 as a developing solvent to give colorless crystals of **8** (550 mg, 79%, R_f=0.78).

Thermal Reaction of 7 to Form 8. A solution of **7** (50 mg) in toluene (1 ml) was heated at 105 °C for 120 h. After evaporation of the solvent, the residue was thin-layer chromatographed on silica gel using pet ether-benzene 8:2 as a developing solvent to give a colorless crystals of **8** (40 mg, 80%).

Thermal Reaction of 10 to Form 11 and 12. A solution of **10** (128 mg) in toluene (3 ml) was heated at 100 °C for 80 h. After evaporation of the solvent, the residue was thin-layer chromatographed on silica gel using pet ether-benzene 8:2 as a developing solvent to give colorless crystals of **12** (90 mg, 69%, R_f=0.81) and colorless crystals of **11** (27 mg, 17%, R_f=0.68).

Thermal Isomerization of 14 to 17. A solution of **14** (40 mg) in deuteriochloroform (0.5 ml) was heated at 100 °C for 2 h in a sealed ampoul. After evaporation of the solvent, the residue was thin-layer chromatographed on silica gel using pet ether-benzene 7:3 as a developing solvent to give a colorless oil of **17** (32 mg, 80%, R_f=0.53). In spite of repeated purification by thin-layer chromatography on silica gel, the analytically pure sample of **17** could not be obtained. **17**: Mass *m/z* (rel intensity): 472 (M^+, 21), 444 (100), 377 (33), 353 (33). UV (EtOH): 254 nm (log ε, 4.50). IR (neat): 3030, 1790, 1605 cm^{-1}.

Thermal Reaction of 17 to Form 18. A solution of **17** (200 mg) in chloroform (5 ml) was heated at 150 °C for 100 h in a sealed ampoul. After evaporation of the solvent, the residue was thin-layer chromatographed on silica gel using pet ether-benzene 1:1 as a developing solvent to give a colorless oil of **18** (170 mg, 85%, R_f=0.83). **18**: Found: C, 94.38; H, 5.43%. Calcd for $C_{35}H_{24}$: C, 94.56; H, 5.44%. Mass *m/z* (rel intensity): 444 (M^+, 100), 367 (46), 352 (18). UV (EtOH): 293 nm (log ε, 4.05). IR (neat): 3030, 1600 cm^{-1}. NMR ($CDCl_3$) δ (ppm)=2.41 (t, 2H, *J*=7 Hz), 5.73 (m, 2H), 6.42 (m, 2H), 7.0—7.9 (m, 18H).

The authors are indebted to Professor Toshio Mukai of Tohoku University for his fruitfull suggestions.

References

1) O. L. Chapman and J. P. L. Loux, *J. Am. Chem. Soc.*, **100**, 1978 (1978); M. Balci and M. Harmandar, *Tetrahedron Lett.*, **25**, 237 (1984); J. Roser and W. Eberbach, *ibid.*, **25**, 2455 (1984); R. H. Paeker and W. M. Jones, *ibid.*, **25**, 1245 (1984); O. L. Chapman and U. E. Tsou, *J. Am. Chem. Soc.*, **106**, 7974 (1984); W. S. Trahanovsky and M. E. Scribner, *ibid.*, **106**, 7976 (1984).

2) W. von E. Doering and P. M. Laflamme. *Tetrahedron*, **2**, 75 (1964); O. L. Chapman, P. W. Wajtkowski, W. Adam, O. Rodriguez, and R. Rucktaschel, *J. Am. Chem. Soc.*, **94**, 1365 (1972); F. T. Bond and D. E. Bradway, *ibid.*, **87**, 4977 (1965); W. M. Jones and D. L. Klause, *ibid.*, **93**, 551 (1971).

3) a) W. M. Jones and C. L. Ennis, *ibid.*, **91**, 6391 (1969);

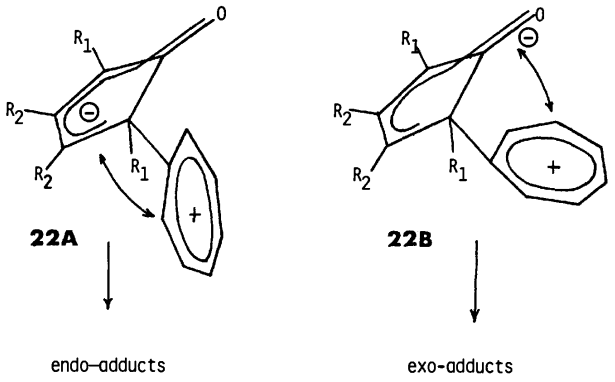

Fig. 7.

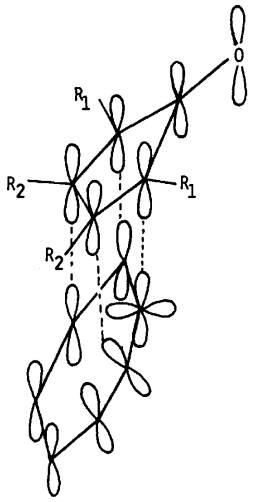

Fig. 8.

b) T. Mukai, T. Nakazawa, and K. Isobe, *Tetrahedron Lett.*, **1968**, 565; c) L. W. Christensen, E. E. Waali, and W. M. Jones, *J. Am. Chem. Soc.*, **94**, 2118 (1972); d) W. M. Jones, B. N. Hamon, R. C. Joins, and C. L. Ennis., *Tetrahedron Lett.*, **1969**, 3909; e) T. Mitsuhashi and W. M. Jones, *J. Chem. Soc., Chem. Commun.*, **1974**, 103; f) K. Saito, Y. Omura, and T. Mukai, *Chem. Lett.*, **1980**, 349.

4) K. Untch, International Symposium on the Chemistry of Non-Benzenoid Aromatic Compounds, Sendai, Japan, 1970; C. Mayor and W. M. Jones, *Tetrahedron Lett.*, **1977**, 3855; J. W. Harris and W. M. Jones, *J. Am. Chem. Soc.*, **104**, 7329 (1982).

5) a) C. H. Jutz, I. Rommel, I. Lengyel, and J. Feeney, *Tetrahedron*, **22**, 1809 (1966); b) A. S. Kende, *Tetrahedron Lett.*, **1967**, 2661; c) T. Toda, K. Saito, and T. Mukai, *ibid*, 1972, 1981; d) T. Sasaki, K. Kanematsu, H. Hayakawa, and M. Sugiura, *J. Am. Chem. Soc.*, **97**, 355 (1975).

6) T. Mitsuhashi and W. M. Jones have proposed the intermediate corresponding to **10** or its exo-isomer in the reaction of **1** with tetracyclones, though without isolation of them.[3e] We are indebted to Dr. Tsutomu Mitsuhashi of Tokyo University for his Fruitfull suggestions.

7) The preferential formation of the endo-adduct can not be explained by the charge interaction between the anion on the cyclopentadienone moiety and the cation on the cycloheptatriene moiety because of the following reason.[11] Both of the intermediates for the endo- (**22A**) and the exo-adduct (**22B**) are considered to feel almost the same amounts of charge interactions; *i.e.*, the former feels the interaction between the anion mainly on the five-membered ring part of the cyclopentadienone moiety and the cation on the seven-membered ring moiety, on the other hand, the latter feels the interaction between the anion on the carbonyl part of the cyclopentadienone moiety and the cation on the seven-membered ring moiety.

8) The secondary orbital interaction in the transition state is considered to be as shown below. R. B. Woodward and R. Hoffmann, *Angew. Chem., Int. Ed. Engl.*, **8**, 781 (1969); K. Saito, Y. Omura, and T. Mukai, *Bull. Chem. Soc. Jpn.*, **58**, 0000 (1985).

9) K. N. Houk, *Tetrahedron Lett.*, **1970**, 2621; L. A. Paquette, *J. Chem. Soc., Chem. Commun.*, **1971**, 1076; M. Yasuda, K. Harano, and K. Kanematsu, *J. Am. Chem. Soc.*, **103**, 3120 (1981).

10) M. Oda, Y. Ito, and Y. Kitahara, *Tetrahedron Lett.*, **1975**, 2587.

11) The possibility of the charge interaction was suggested by a referee. We are indebted to the referee for this suggestion.

 © 1985 The Chemical Society of Japan Bull. Chem. Soc. Jpn., 58, 2669—2672 (1985)

Hydroxylation of Aliphatic Compounds with *m*-Chloroperbenzoic Acid. Synthesis of Hydroxylated Vitamin K_1 Analogues

Motoo Tori, Masakazu Sono, and Yoshinori Asakawa*
Faculty of Pharmaceutical Sciences, Tokushima Bunri University, Yamashiro-cho, Tokushima 770
(Received April 30, 1985)

Pristane and 1,5,9,13-tetramethyltetradecyl acetate were treated with *m*-chloroperbenzoic acid in chloroform under reflux to afford hydroxylated derivatives, respectively. The products, 13- and 9-hydroxy-1,5,9,13-tetramethyltetradecyl acetates, were converted to hydroxylated vitamin K_1 analogues *via* the corresponding hydroxyphytols.

We have been studying the biotransformation of terpenoids in rabbits.[1] Compounds administered to mammals are often hydroxylated prior to excretion, a process which is related to detoxification.[2] We are interested in *in vitro* reactions which simulate this biological phenomenon. In 1979 Müller and Schneider reported that alicyclic compounds could be hydroxylated using *m*-chloroperbenzoic acid (*m*-CPBA).[3] Recently we have applied this reaction to dammarane,[4] lupane,[5] and friedelane[5] triterpenoids and have demonstrated the formation of tertiary and secondary alcohols. As a continuation of this work we have investigated the reactions of pristane and phytane derivatives with *m*CPBA and have applied the products of the reaction to the synthesis of vitamin K analogues.

Pristane (**1**) was treated with *m*CPBA in refluxing chloroform for 22 h, after which work-up and chromatography over silica-gel afforded two monohydric tertiary alcohols. ^{1}H NMR spectroscopy indicated that whilst the less polar alcohol, **2** (43% yield[6])[7] [IR 3350 cm^{-1}, δ=72.8 (s)] possessed only one tertiary methyl group [δ=1.15 (3H, s)], the more polar product, **3** (36% yield[6]) [IR 3350 cm^{-1}, δ=71.1 (s)][8] contained a 1-hydroxy-1-methylethyl group [δ=1.21 (6H, s)]. These observations led to structures **2** and **3**, 2,6,10,14-tetramethyl-6-pentadecanol (**2**) and 2,6,10,14-tetramethyl-2-pentadecanol (**3**), respectively. Further support for these structures was furnished by mass spectroscopy. The major peaks in the mass spectrum of **2** occurred at *m/z* 199 and 129 and resulted from bond fission α to the hydroxyl group (Fig. 1). An analogous fragmentation gave rise to the predominant ion with *m/z* 59 in the spectrum of **3**. As the tertiary alcohols are formed in relatively good yield, we examined the reactions of phytane derivatives with *m*CPBA.

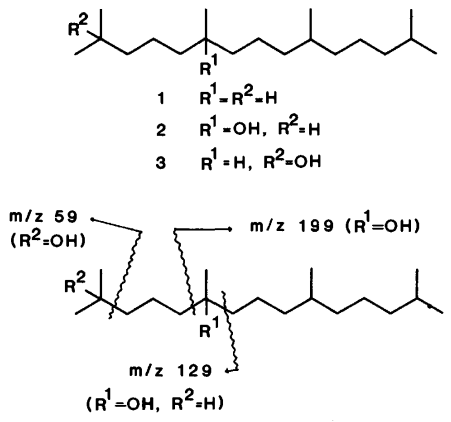

Fig. 1.

Since *m*CPBA reacts with the double bond of phytol (**4**), it was first of all necessary to protect the olefin. However, a simple protecting group was unavailable and we therefore planned to remove the allylic alcohol by ozonolysis; regeneration would be effected by a Wittig reaction at a later stage. The resulting ketone should be more readily protected.

Ozonolysis of phytol (**4**) in methanol at −18 °C followed by zinc/acetic acid reduction gave 6,10,14-trimethyl-2-pentadecanone (**5**)[8,9] in 91% yield after chromatographic purification over silica-gel. When the ethylene acetal of **5** was treated with *m*CPBA in $CHCl_3$ under reflux, many spots on TLC were observed due to the lability of the acetal to the acid formed in the reaction mixture. Therefore, the ketone **5** was reduced by $NaBH_4$ in MeOH followed by acetylation to **6**.[7] The acetate (**6**)[7] was then treated with *m*CPBA in $CHCl_3$ under reflux for 24 h to afford two hydroxylated derivatives after column chromatography over silica-gel. The spectral data of the less polar product (**7**)[7] [IR 3430, 1730, and 1240 cm^{-1}; *m/z* 243; δ=1.15 (3H, s), 1.20 (3H, d, *J*=6.4 Hz), 2.02 (3H, s), and 4.89 (1H, m)] indicated that **7** was 9-hydroxy-1,5,9,13-tetramethyltetradecyl acetate and those of the more polar product (**8**)[7] [IR 3420, 1730, and 1240 cm^{-1}; *m/z* 59; δ=1.21 (6H, s), 2.03 (3H, s), and 4.89 (1H, m)] suggested that **8** was 13-hydroxy-1,5,9,13-tetramethyltetradecyl acetate. The fact that 5-position was not hydroxylated is presumably due to the electrophilic nature of the reagent as described by Deno and Messer.[10] The hydroxy acetates, **7** and **8**, were hydrolyzed by methanolic KOH followed by Jones oxidation to give the corresponding hydroxy ketones, **9**[7] [IR 3450 and 1715 cm^{-1}; *m/z* 199; δ=1.16 (3H, s) and 2.13 (3H, s)] and **10** [IR 3430 and 1715 cm^{-1}; *m/z* 59; δ=1.21 (6H, s) and 2.14 (3H, s)], respectively. The ketone **9** was

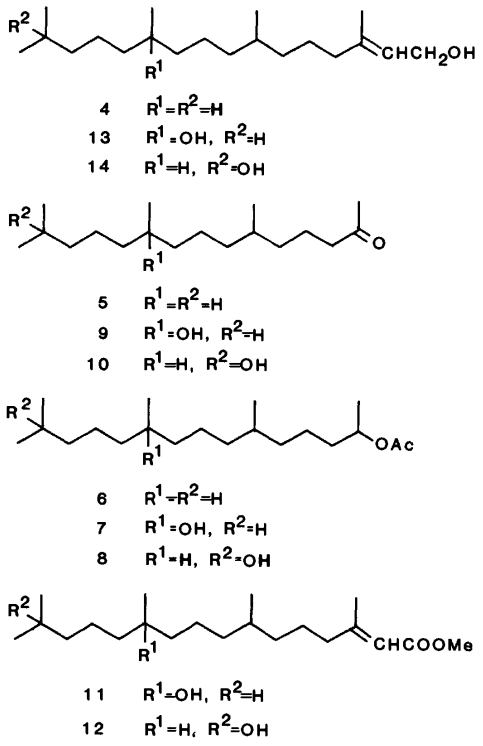

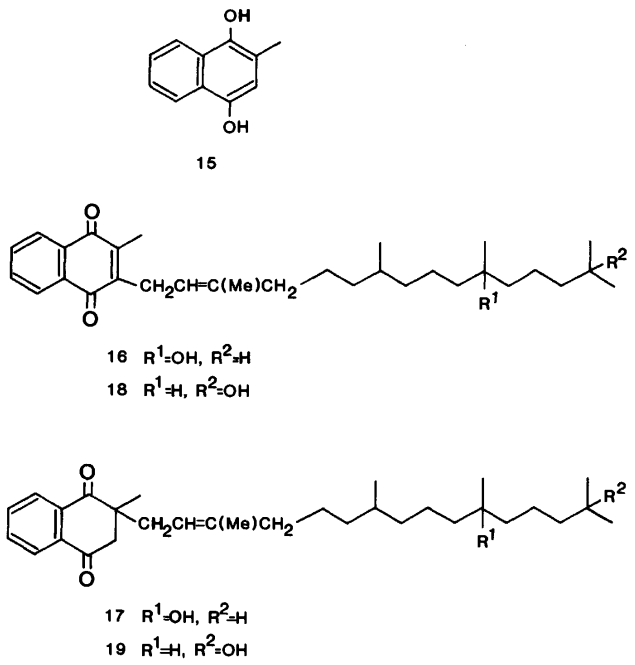

allowed to react with the anion prepared from methyl dimethoxyphosphorylacetate with sodium hydride in dry 1,2-dimethoxyethane at rt to yield methyl 11-hydroxy-3,7,11,15-tetramethyl-2-hexadecenoate (**11**)[7] [IR 3410, 1720, and 1645 cm^{-1}; *m/z* 322 $(M-18)^+$; δ=5.66 (bs)] in 49% yield after chromatographic purification. Methyl 15-hydroxy-3,7,11,15-tetramethyl-2-hexadecenoate (**12**) [IR 3400, 1715, and 1645 cm^{-1}; *m/z* 322 $(M-18)^+$ and 59; δ=5.67 (bs)] was prepared in the same manner in 64% yield. Although analysis by GC showed that **11** and **12** were *ca.* 1:1 mixtures of the geometric isomers, further separation was not attempted. Reduction of the methyl esters, **11** and **12**, using $LiAlH_4$ in dry ether gave the desired hydroxylated phytol derivatives, **13**[7] [IR 3310 cm^{-1}; *m/z* 294 $(M-18)^+$; δ=5.40 (m)] and **14** [IR 3330 cm^{-1}; *m/z* 294 $(M-18)^+$ and 59; δ=5.40 (m)], respectively. The structures were fully characterized by IR, NMR, and mass spectra.

The chemistry of vitamin K has been studied extensively[11] and synthesis[11] and biological studies[12] of its derivatives are still undertaken. Several works[12] on the preparation and estimation of hydroxylated vitamin K_1 derivatives have been reported, although the compounds are less active than vitamin K_1 itself. As a demonstration of the synthetic utility of the compounds obtained here, we next carried out the reaction of 2-methyl-1,4-naphthalenediol with the hydroxyphytols.

A mixture of the diol **13** and 2-methyl-1,4-naphthalenediol (**15**) in dioxane was treated with $KHSO_4$ at 40—50 °C for 4 h followed by Ag_2O oxidation. After the usual work-up, the residue was separated by prep TLC (AcOEt–PhH 1:4) to afford the desired 11′-hydroxyvitamin K_1 (**16**)[7] [IR 3580—3250, 1650, and 1610 cm^{-1}; *m/z* 466 (M^+); δ=5.00 (m)] in 17% yield in addition to the by-product, 2-methyl-2-(11-hydroxy-3,7,11,15-tetramethyl-2-hexadecenyl)-2,3-dihydro-1,4-naphthoquinone (**17**)[7] [IR 3580—3310 cm^{-1}; *m/z* 453 $(M-15)^+$; δ=5.03 (m)] in 18% yield. The diol (**14**) was next subjected to a condensation reaction with **15** and oxidation (Ag_2O) in the same manner to yield 15′-hydroxyvitamin K_1 (**18**) [IR 3580—3280 cm^{-1}; *m/z* 466 (M^+), 225 (base peak), and 59; δ=5.00 (m)] in 19% yield and 2-methyl-2-(15-hydroxy-3,7,11,15-tetramethyl-2-hexadecenyl)-2,3-dihydro-1,4-naphthoquinone (**19**) [IR 3580—3300 cm^{-1}; *m/z* 468 (M^+), 174 (base peak), and 59; δ=5.04 (m)] in 20% yield. The structures are consistent with the spectral data. In these reactions dehydration of the newly attached hydroxyl groups was not observed.

In conclusion, we have carried out the hydroxylation of the aliphatic compounds, pristane (**1**) and 1,5,9,13-tetramethyltetradecyl acetate (**6**) using *m*CPBA. In both cases hydroxylation occurred at the tertiary positions. Furthermore we have applied the products to the synthesis of vitamin K analogues. Although the biological activity of these analogues is still undetermined, the methodology may be applicable to other classes of natural products.

Experimental

General Procedures. Infrared (IR) spectra were recorded on a Shimadzu IR-408 infrared spectrometer.

Mass spectra were measured using a Shimadzu LKB-9000B, JEOL D-300, or JEOL HX-100 mass spectrometer operating at 70 eV. GC/MS was operated using PEG-20M (15%) or OV-17 (5%) columns (2 m each) with increasing temperature program (from 80 °C—220 °C, rate: 5 °C/min). ^{1}H and ^{13}C NMR spectra were measured in $CDCl_3$ using a JEOL JNM GX-400 (400 MHz for ^{1}H and 100 MHz for ^{13}C) spectrometer. High performance liquid chromatography (HPLC) analysis was determined on a JASCO liquid chromatograph model TRI ROTAR-V. Analytical and preparative thin layer chromatographies (TLC) were carried out on Kieselgel $60F_{254}$ 0.25 mm and 0.5 mm, respectively. Column chromatography was carried out on Kieselgel 60 (70—230 mesh, Merck).

Reactions of each substrate with *m*-chloroperbenzoic acid (*m*CPBA) were performed by addition of *m*CPBA (1—2 equiv) into a solution of the substrate in chloroform (*ca.* 35 mg/mL) and heating under reflux for 20—30 h. Successive washing of the reaction mixture with aq Na_2SO_3, aq $NaHCO_3$, and brine and evaporation of solvents after drying with $MgSO_4$ gave a residue.

Reaction of Pristane (1) with m*CPBA.* Pristane (**1**; 1.0 g) was treated with *m*CPBA (964 mg) in $CHCl_3$ (30 ml) under reflux for 22 h to afford a residue (1.3 g) after work-up. The residue was subjected to column chromatography on silica gel (120 g). Elution with 20% hexane–AcOEt gave 2,6,10,14-tetramethyl-6-pentadecanol (**2**) (289 mg) as an oil: Found: *m/z* 269.2844. Calcd for $C_{18}H_{37}O$: M 269.2844; IR (film) 3350 cm^{-1}; ^{1}H NMR δ=0.86 (3H, d, J=6.6 Hz), 0.87 (6H, d, J=6.6 Hz), 0.88 (6H, d, J=6.8 Hz), and 1.15 (3H, s); MS *m/z* 269 $(M-15)^+$, 199, 129, 111, 69, and 43; ^{13}C NMR δ=19.7 (q), 21.3 (t), 21.7 (t), 22.6 (3×q), 22.7 (q), 24.8 (t), 27.0 (q), 27.9 (d), 28.0 (d), 32.7 (d), 37.3 (t), 37.7 (t), 39.3 (t), 39.6 (t), 42.1 (t), 42.2 (t), and 72.8 (s); and 2,6,10,14-tetramethyl-2-pentadecanol (**3**)[8] (240 mg) as an oil: IR (film) 3350 cm^{-1}; ^{1}H NMR δ=0.85 (3H, d, J=6.3 Hz), 0.86 (3H, d, J=6.4 Hz), 0.87 (6H, d, J=6.6 Hz), and 1.21 (6H, s); MS *m/z* 269 $(M-15)^+$ and 59; ^{13}C NMR δ=19.7 (q), 19.7 (q), 21.8 (t), 22.6 (q), 22.7 (q), 24.5 (t), 24.8 (t), 28.0 (d), 29.2 (2×q), 32.8 (2×d), 37.3 (t), 37.4 (2×t), 37.6 (t), 39.4 (t) 44.3 (t), and 71.1 (s).

Preparation of 6,10,14-Trimethyl-2-pentadecanone (5). Ozone was bubbled through a solution of phytol (**4**; 679 mg) in MeOH (20 mL) at −18 °C for 20 min. Acetic acid (5 mL) was added and the solution was treated with Zn (*ca.* 10 mg) to afford 6,10,14-trimethyl-2-pentadecanone (**5**; 563 mg).[8,9]

Acetalization of 6,10,14-Trimethyl-2-pentadecanone (5). A mixture of the ketone (**5**; 184 mg), ethylene glycol (110 mg), *p*-toluenesulfonic acid (25 mg), and benzene (30 mL) was heated using a Dean-Stark water separator for 5 h yielding the ethylene acetal (55 mg) after work up and prep TLC: ^{1}H NMR δ=0.83—0.87 (m), 1.32 (s), 1.57 (s), and 3.94, (m); MS *m/z* 297 $(M-15)^+$, 87, and 43.

Preparation of 1,5,9,13-Tetramethyltetradecyl Acetate (6). A solution of the ketone (**5**; 2.1 g) in MeOH (10 mL) was treated with $NaBH_4$ (390 mg) at rt for 12 h to afford 6,10,14-trimethyl-2-pentadecanol, which was directly treated with Ac_2O in Py yielding 1,5,9,13-tetramethyltetradecyl acetate (**6**; 2 g) as an oil after usual work-up: Found: *m/z* 252.2787 $(M-CH_3COOH)^+$. Calcd for $C_{18}H_{36}$: M 252.2815; IR (film) 1730 and 1240 cm^{-1}; ^{1}H NMR δ=0.84 (6H, d, J=6.6 Hz), 0.87 (6H, d, J=6.6 Hz), 1.20 (3H, d, J=6.3 Hz), 2.03 (3H, s), and 4.89 (1H, m); MS *m/z* 252 $(M-CH_3COOH)^+$, 126, and 97.

Reaction of 1,5,9,13-Tetramethyltetradecyl Acetate (6) with m*CPBA.* A mixture of the acetate (**6**; 3.2 g), *m*CPBA (2.8 g), and $CHCl_3$ (90 mL) was heated under reflux for 24 h. Work-up and column chromatography (elution with hexane–AcOEt) gave 9-hydroxy-1,5,9,13-tetramethyltetradecyl acetate (**7**; 280 mg): oil; Found: *m/z* 310.2873 $(M-H_2O)^+$. Calcd for $C_{20}H_{38}O_2$: M 310.2872; IR (film) 3430, 1730, and 1240 cm^{-1}; ^{1}H NMR δ=0.86 (3H, d, J=6.6 Hz), 0.88 (6H, d, J=6.8 Hz), 1.15 (3H, s), and 1.20 (3H, d, J=6.4 Hz); MS *m/z* 268 $(M-CH_3COOH)^+$, 253, 243, 129, 69, and 43: and 13-hydroxy-1,5,9,13-tetramethyltetradecyl acetate (**8**) (350 mg): oil; Found: *m/z* 313.2790 $(M-CH_3)^+$. Calcd for $C_{19}H_{37}O_3$: M 313.2743; IR (film) 3420, 1730, and 1240 cm^{-1}; ^{1}H NMR δ=0.85 (3H, d, J=6.4 Hz), 0.86 (3H, d, J=6.6 Hz), 1.21 (6H, s), 2.03 (3H, s), and 4.89 (1H, m); MS *m/z* 253, 210, 59, and 43.

Preparation of 10-Hydroxy-6,10,14-trimethyl-2-pentadecanone (9). 9-Hydroxy-1,5,9,13-tetramethyltetradecyl acetate (**7**; 170 mg) was treated with 5% KOH–MeOH at rt for 12 h to yield 10-hydroxy-6,10,14-trimethyl-2-pentadecanol (148 mg), which was oxidized with Jones reagent (4 drops) to 10-hydroxy-6,10,14-trimethyl-2-pentadecanone (**9**; 105 mg) after purification by column chromatography on silica gel (15 g): oil; Found: *m/z* 302.3016 $(M+NH_4)^+$. Calcd for $C_{18}H_{40}O_2N$: M 302.3059; IR (film) 3450 and 1715 cm^{-1}; ^{1}H NMR δ=0.87 (3H, d, J=6.6 Hz), 0.88 (6H, d, J=6.6 Hz), 1.16 (3H, s), 2.13 (3H, s), and 2.41 (2H, t, J=7.6 Hz); MS *m/z* 269 $(M-CH_3)^+$, 199, 181, 69, and 43. ^{13}C NMR δ=19.3 (q), 21.1 (t), 21.2 (t), 21.5 (t), 22.5 (2×q), 26.8 (q), 27.7 (d), 29.6 (q), 32.4 (d), 36.2 (t), 37.3 (t), 39.4 (t), 41.9 (2×t), 43.9 (t), 72.5 (s), and 209.1 (s).

Preparation of 14-Hydroxy-6,10,14-trimethyl-2-pentadecanone (10). 13-Hydroxy-1,5,9,13-tetramethyltetradecyl acetate (**8**; 215 mg) was hydrolyzed and oxidized successively as before to afford 14-hydroxy-6,10,14-trimethyl-2-pentadecanone (**10**; 100 mg) as an oil: Found: *m/z* 302.3010 $(M+NH_4)^+$. Calcd for $C_{18}H_{40}O_2N$: M 302.3059; IR (film) 3430 and 1715 cm^{-1}; ^{1}H NMR δ=0.86 (6H, d, J=6.6 Hz), 1.21 (6H, s), 2.14 (3H, s), and 2.41 (2H, t, J=7.6 Hz); MS *m/z* 269 $(M-CH_3)^+$, 59, and 43; ^{13}C NMR δ=19.5 (q), 19.7 (q), 21.4 (t), 21.7 (t), 24.3 (t), 29.2 (2×q), 29.8 (q), 32.6 (d), 32.7 (d), 36.4 (t), 37.1 (t), 37.3 (t), 37.5 (t), 44.1 (t), 44.2 (t), 71.0 (s), and 209.4 (s).

Preparation of Methyl 11-Hydroxy-3,7,11,15-tetramethyl-2-hexadecenoate (11). To a stirred mixture of sodium hydride (58 mg) and methyl dimethoxyphosphorylacetate (143 mg) in dry DME (3 mL) was added a solution of 10-hydroxy-6,10,14-trimethyl-2-pentadecanone (**9**; 105 mg) in dry DME (2 mL) at rt under an Ar atmosphere. The reaction mixture was stirred overnight. Work-up as usual and column chromatography afforded recovered **9** (30 mg) and methyl 11-hydroxy-3,7,11,15-tetramethyl-2-hexadecenoate (**11**; 62 mg): oil; Found: *m/z* 327.2866 $(M-H_2O)^+$. Calcd for $C_{21}H_{38}O_2$; M 322.2871; IR (film) 3410, 1720, and 1645 cm^{-1}; ^{1}H NMR δ=0.86—0.89 (9H, m), 1.15 (3H, s), 1.88 (d, J=1.2 Hz), 2.15 (d, J=1.2 Hz), 3.67 (s), 3.68 (s), and 5.66 (bs); MS *m/z* 322 $(M-H_2O)^+$, 223, 114, and 69.

Preparation of Methyl 15-Hydroxy-3,7,11,15-tetramethyl-2-hexadecenoate (12). 14-Hydroxy-6,10,14-trimethyl-2-

pentadecanone (**10**; 101 mg) was reacted with the phosphonate reagent as before to afford the starting **10** (34 mg) and methyl 15-hydroxy-3,7,11,15-tetramethyl-2-hexadecenoate (**12**; 77 mg): oil; Found: *m/z* 322.2864 $(M-H_2O)^+$. Calcd for $C_{21}H_{38}O_2$: M 322.2870; IR (film) 3400, 1715, and 1645 cm^{-1}; ^1H NMR δ=0.85—0.89 (6H, m), 1.21 (6H, s), 1.88 (d, *J*=1.2 Hz), 2.15 (d, *J*=1.2 Hz), 3.67 (s), 3.68 (s), and 5.67 (bs); MS *m/z* 332, 293, 114, and 59.

*Preparation of 3,7,11,15-Tetramethyl-2-hexadecene-1,11-diol (**13**).* To a stirred solution of methyl 11-hydroxy-3,7,11,15-tetramethyl-2-hexadecenoate (**11**; 26 mg) in dry Et_2O (2 mL) was added $LiAlH_4$ (*ca.* 10 mg) at rt. After 2 h, the reaction mixture was worked up as usual to afford 3,7,11,15-tetramethyl-2-hexadecene-1,11-diol (**13**; 23 mg): oil; Found: *m/z* 330.3362 $(M+NH_4)^+$. Calcd for $C_{20}H_{44}O_2N$: M 330.3372; IR (film) 3310 cm^{-1}; ^1H NMR δ=0.84—0.89 (9H, m), 1.15 (3H, s), 1.66 (s), 1.73 (s), 1.97—2.06 (m), 4.11—4.15 (m), and 5.40 (m); MS *m/z* 294 $(M-H_2O)^+$, 276, 209, 191, 69, 55, and 43.

*Preparation of 3,7,11,15-Tetramethyl-2-hexadecene-1,15-diol (**14**).* Methyl 15-hydroxy-3,7,11,15-tetramethyl-2-hexadecenoate (**12**; 17 mg) was reduced with $LiAlH_4$ (*ca.* 10 mg) in dry Et_2O (2 mL) as before to give 3,7,11,15-tetramethyl-2-hexadecene-1,15-diol (**14**; 16 mg): oil; Found: *m/z* 330.3373 $(M+NH_4)^+$ (CI-MS). Calcd for $C_{20}H_{44}O_2N$: M 330.3372; IR (film) 3330 cm^{-1}; ^1H NMR δ=0.84—0.89 (m), 1.21 (s), 1.66 (s), 1.73 (s), 1.99 (m), 4.13 (m), and 5.40 (m); MS *m/z* 294 $(M-H_2O)^+$, 276, 191, 69, and 59.

*Preparation of 11′-Hydroxyvitamin K_1 (**16**).* A mixture of 3,7,11,15-tetramethyl-2-hexadecene-1,11-diol (**13**; 11 mg), 2-methyl-1,4-naphthalenediol (64 mg), $KHSO_4$ (42 mg), and dioxane (0.3 mL) was heated at 40—50 °C under Ar for 4 h and worked up as usual. After stirring with Ag_2O in dry Et_2O at rt, prep TLC afforded 11′-hydroxyvitamin K_1 (**16**; 3 mg): oil; Found: *m/z* 466.3400. Calcd for $C_{31}H_{46}O_3$: M 466.3445; IR ($CHCl_3$) 3580—3250, 1650, 1610, 1590, and 1455 cm^{-1}; ^1H NMR δ=0.82—0.90 (m), 1.14 (s), 1.16 (s), 2.19 (s), 3.37 (d, *J*=6.9 Hz), 5.00 (m), 7.68—7.70 (m), and 8.07—8.09 (m); MS *m/z* 466 (M^+), 448, 225, 69, 55, and 43: ^{13}C NMR δ=185.5 (s), 184.6 (s), and 72.9 (s): and 2-methyl-2-(11-hydroxy-3,7,11,15-tetramethyl-2-hexadecenyl)-2,3-dihydro-1,4-naphthoquinone (**17**; 3 mg): oil; Found: *m/z* 453.3356 $(M-CH_3)^+$. Calcd for $C_{30}H_{45}O_3$: M 453.3366; IR ($CHCl_3$) 3580—3310, 1690, 1590, and 1455 cm^{-1}, ^1H NMR δ=0.82—0.88 (m), 1.15 (s), 1.16 (s), 1.29 (s), 1.48 (s), 1.87—1.89 (m), 2.28—2.45 (m), 2.82—3.05 (m), 5.03 (m), 7.71—7.76 (m), and 8.00—8.09 (m); MS *m/z* 453 $(M-CH_3)^+$, 451, 383, 174, 69, 55, and 43.

*Preparation of 15′-Hydroxyvitamin K_1 (**18**).* 3,7,11,15-Tetramethyl-2-haxadecene-1,15-diol (**14**; 11 mg) was allowed to react with 2-methyl-1,4-naphthalenediol (63 mg) in dioxane (0.5 mL) using $KHSO_4$ (26 mg) as before to give 15′-hydroxyvitamin K_1 (**18**; 3 mg): oil; Found: *m/z* 466.3452. Calcd for $C_{31}H_{46}O_3$: M 466.3447; IR ($CHCl_3$) 3580—3280, 1650, 1610, 1590, and 1455 cm^{-1}; ^1H NMR δ=0.81—0.88 (m), 1.21 (s), 1.68 (s), 1.77 (s), 2.19 (s), 3.37 (d, *J*=6.8 Hz), 5.00 (m), and 7.68—7.70 (m); MS *m/z* 466 (M^+), 448, 433, 408, 225, 59, and 43; ^{13}C NMR δ=185.5 (s), 184.6 (s), and 71.1 (s): and 2-methyl-2-(15-hydroxy-3,7,11,15-tetramethyl-2-hexadecenyl)-2,3-dihydro-1,4-naphthoquinone (**19**; 4 mg): oil; Found: *m/z* 453.3379 $(M-CH_3)^+$. Calcd for $C_{30}H_{45}O_3$: M 453.3369; IR ($CHCl_3$) 3580—3300, 1690, 1590, 1455, and 1370 cm^{-1}; ^1H NMR δ=0.81—0.87 (m), 1.21 (s), 1.29 (s), 1.48 (s), 1.88 (m), 2.29—2.45 (m), 2.82—3.04 (m), 5.04 (m), 7.72—7.74 (m), and 8.02—8.08 (m); MS *m/z* 468 (M^+), 453, 451, 174, 69, 59, and 43.

We thank Dr. Hiroshi Hirota, The University of Tokyo, for measuring the high resolution mass spectra and Dr. Leslie J. Harrison for reading the manuscript prior to submission. This work is supported in part by a Grant-in-Aid for Cancer Research from the Ministry of Health and Welfare.

References

1) T. Ishida, Y. Asakawa, M. Okano, and T. Aratani, *J. Pharm. Sci.*, **68**, 928 (1979); T. Ishida, Y. Asakawa, T. Takemoto, and T. Aratani, *ibid.*, **70**, 406 (1981); Y. Asakawa, Z. Taira, T. Takemoto, T. Ishida, M. Kido, and Y. Ichikawa, *ibid.*, **70**, 710 (1981); T. Ishida, Y. Asakawa, and T. Takemoto, *ibid.*, **71**, 965 (1982).

2) T. S. Santhanakrishnan, *Tetrahedron*, **40**, 3597 (1985).

3) W. Müller and H. -J. Schneider, *Angew. Chem., Int. Ed. Engl.*, **18**, 407 (1979).

4) M. Tori, R. Matsuda, and Y. Asakawa, *Tetrahedron Lett.*, **26**, 227 (1985).

5) M. Tori, R. Matsuda, and Y. Asakawa, *Chem. Lett.*, **1985**, 167.

6) Yields shown are isolation yields based on consumed starting materials.

7) This is a mixture of diastereoisomers whose separation has not been attempted.

8) von H. Mayer, P. Schudel, R. Ruegg, and O. Ishler, *Helv. Chim. Acta*, **46**, 963 (1963).

9) von M. Schmid, F. Gerber, and G. Hirth, *Helv. Chim. Acta*, **65**, 684 (1982).

10) N. C. Deno and L. A. Messer, *J. Chem. Soc., Chem. Commun.*, **1976**, 1051.

11) L. F. Fieser, *J. Am. Chem. Soc.*, **61**, 3467 (1939); R. Hirschmann, R. Miller, and N. L, Wendler, *ibid.*, **76**, 4592 (1954); L. M. Jackman, R. Ruegg, G. Ryser, C. von Planta, U. Gloor, H. Mayer, P. Schudel, M. Kofler, and O. Ishler, *Helv. Chim. Acta*, **48**, 1332 (1965); K. Sato, S. Inoue, and K. Saito, *J. Chem. Soc. Perkin I*, **1973**, 2289; Y. Masaki, K. Hashimoto, and K. Kaji, *Chem. Pharm. Bull.*, **32**, 3959 (1984); and references cited therein.

12) J. Weichet, L. Blaha, J. Hodrova, B. Kakac, and V. Trcka, *Coll. Czech. Chem. Commun.*, **31**, 3607 (1966); C. F. Allen, H. Franke, and O. Hirayama, *Biochem. Biophys. Res. Commun.*, **26**, 562 (1976); D. R. Threlfall, *Biochim. Biophys. Acta*, **280**, 472 (1972); H. Weiser and A. W. Kormann, *Internat. J. Vit. Nutr. Res.*, **53**, 143 (1982); and references cited therein.

 © 1985 The Chemical Society of Japan Bull. Chem. Soc. Jpn., 58, 2673—2679 (1985)

Constituents of Seeds of *Brucea javanica*. Structures of New Bitter Principles, Yadanziolides A, B, C, Yadanziosides F, I, J, and L.[1,2]

Shin YOSHIMURA, Toshiro SAKAKI, Masami ISHIBASHI, Takahiko TSUYUKI,*
Takeyoshi TAKAHASHI,* and Tadashi HONDA†

Department of Chemistry, Faculty of Science, The University of Tokyo, Hongo Bunkyo-ku, Tokyo 113
†*Suntory Institute for Biomedical Research, 1-1, Wakayamadai, Shimamotocho, Mishimagun, Osaka 618*

(Received April 16, 1985)

Three new quassinoids and four new quassinoid glycosides were isolated from water-soluble fraction of methanol extract of seeds of *Brucea javanica* (L.) MERR, known as "Ya-dan-zi" in Chinese folklore and their structures were determined by spectral and chemical means. Yadanziosides F, I, J, and L were demonstrated to have antileukemic activity.

Quassinoids, bitter principles of Simaroubaceous plants have been extensively investigated from the interest in antileukemic activity and structure determination,[3] and some of them have been shown to exhibit useful biological activities.[4] In connection with our studies on bitter principles of *Picrasma ailanthoides* PLANCHON and *Ailanthus altissima* SWINGLE,[5] constituents of seeds of *Brucea javanica* (L.) MERR were examined and several new bitter principles were reported.[1,2] Seeds of *B. javanica* are known as "Ya-dan-zi" in Chinese folklore and have been used as a Chinese medicine for cancer. The main active compounds of the plant have been extensively investigated by Polonsky,[6] Geissman,[7] and Lee.[8] We examined minor components in the polar fraction. This paper deals with isolation and structure elucidation of new bitter quassinoids, yadanziolides A, B, and C (**1**, **2**, and **3**) and bitter quassinoid glycosides, yadanziosides F, I, J, and L (**4**, **5**, **6**, and **7**).

The methanol extract of defatted seeds of *B. javanica* was partitioned between dichloromethane and water. The aqueous layer was separated by silica-gel column chromatography eluted with a lower layer of chloroform–methanol–water. Each fraction was further purified by gel chromatography on Toyopearl HW-40S eluted with methanol and then a reversed phase chromatography on Lobar column Lichroprep RP-8 eluted with methanol–water. These isolation procedures afforded several new bitter principles together with known compounds, bruceosides A (**8**), B (**9**),[8] bruceins D (**10**), E (**11**),[8,9] and F (**12**).[10]

Yadanziolide A (**1**; *ca.* 0.01% yield) crystallized from methanol as colorless needles, mp 283—285 °C (decomp) and $[\alpha]_D^{28}$ −10.5° (pyridine). Elemental analysis indicates the formula $C_{20}H_{26}O_{10}$. The IR and UV spectra showed the presence of hydroxyl(s), a δ-lactone and an α,β-unsaturated carbonyl groups. Comparison of ^{1}H and ^{13}C NMR spectra of **1** with those of brucein F (**12**)[10] could lead to the structure (**1**) for yadanziolide A, which is a conjugated ketone corresponding to an oxidation product of brucein F (**12**). Brucein F (**12**) was treated with manganese dioxide in *N,N*-dimethylformamide to give the oxidation product, which was identical with **1** in respect to mp, IR, ^{1}H NMR, and TLC. Thus the structure of yadanziolide A (**1**) was determined to be 13β,20-epoxy-1β,11β,12α,14,15β,21-hexahydroxypicras-3-ene-2,16-dione.

When treated with acetic anhydride in pyridine at room temperature for 48 h, **1** give a tetraacetyl derivative (**13**), mp 202—203 °C. The ^{1}H NMR spectrum of **13** indicates that **13** is 1,12,15,21-tetra-*O*-acetylyadanziolide A.

Yadanziolide B (**2**; *ca.* 0.002% yield), mp 279—282 °C (decomp), was shown by elemental analysis to have the molecular formula, $C_{20}H_{26}O_{11}$, which possesses one more oxygen atom than **1**. The IR and UV spectra showed the presence of hydroxyl(s), a δ-lactone, and an α,β-unsaturated carbonyl groups. In the 400 MHz ^{1}H NMR and COSY spectra, all protons were assigned unambiguously (Table 1). A doublet signal at δ 5.70 (J=1.5 Hz) due to H-7 and a double-doublet signal at δ 4.24 (J=11.5 Hz) due to H-6 are shifted to a lower field than those of yadanziolide A (**1**). These observations suggest that the structure of yadanziolide B (**2**) is 6-hydroxy-substituted yadanziolide A (**1**). The coupling constants, $J_{5,6}$=11.5 Hz and $J_{6,7}$=1.5 Hz, suggest a trans-relationship between H-6 and an α(axial)-proton on C-5, and therefore the hydroxyl group on C-6 was determined to be in 6α(equatorial)-configuration. This assignment is firmly established by the fact that the NOE was observed between H-6 and $C_{(10)}$-CH_3 in the NOESY spectrum.

Yadanziolide B (**2**) was acetylated with acetic anhydride in pyridine to afford a pentaacetate (**14**), mp 278—283 °C (decomp). The ^{1}H NMR spectrum showed two methyl signals at δ 1.52 (s, 10-CH_3) and 2.03 (br s, 4-CH_3) together with signals due to acetoxyl groups at δ 1.96 (3H, s), 2.09 (6H, s), and 2.22 (6H, s). Thus the structure of yadanziolide B (**2**) was concluded to be 13β,20-epoxy-1β,6α,11β,12α,14,

15β,21-heptahydroxypicras-3-ene-2,16-dione.

Yadanziolide C (**3**; *ca.* 0.001% yield) crystallized from methanol–diethyl ether as colorless prisms, mp 292—297 °C (decomp). The elemental analysis indicates the molecular formula, $C_{20}H_{26}O_9$, which is the same as that of brucein D (**10**).[8,9] The IR and UV spectra showed the presence of hydroxyl(s), a δ-lactone, and an α,β-unsaturated carbonyl groups. The ^{1}H NMR spectrum revealed that the signals of H-1, H-5, and H-9 of yadanziolide C (**3**) shifted to a lower field than those of brucein D (**10**; see Table 2). Comparison of ^{13}C NMR spectra showed that the signals of C-5 and C-9 of **3** (δ 37.7 and 38.3, respectively) shifted to a higher field than those of **10** (δ 43.6 and 45.8, respectively).

When treated with acetic anhydride in pyridine at room temperature for 1 week, **3** gave 1,15-di-*O*-acetyl derivative (**15**; 35% yield) and 1,12,15-tri-*O*-acetyl derivative (**16**; 52% yield). Under the same conditions, brucein D (**10**) gave 1,12,15-tri-*O*-acetyl derivative in 96% yield.

These evidences suggest that the configuration of C-1, C-5, or C-9 might be defferent from that of brucein D (**10**). The extensive double resonance experiments at 400 MHz led to an unambiguous assignment of all protons for **3** (Table 2). Two broad doublet signals due to H-1 and H-12 were assigned as follows. Two signals at δ 4.46 and δ 4.66 were changed into broad singlets on addition of D_2O. Irradiation at δ 1.63 due to $C_{(10)}$-CH_3 resulted in a slight sharpening of the broad doublet at δ 4.66, while the signal at δ 4.46 remained unchanged. Therefore, the broad doublet signals at δ 4.66 and δ 4.46 are assigned to H-1 and H-12, respectively.

The coupling constants, $J_{5,6\alpha}$=3 Hz and $J_{5,6\beta}$=13.5 Hz, being the same as those of other picrasane derivatives, the proton at C-5 was determined to be in α(axial)-configuration.

The configurations at $C_{(1)}$-H and $C_{(9)}$-H were determined by differential NOE measurement. On saturation of the signal due to $C_{(10)}$-CH_3, increases in area of signals due to $C_{(1)}$-H and one of $C_{(20)}$-H_2 were observed, while an increase in area of the signal due to $C_{(9)}$-H was not detected, indicating $C_{(1\beta)}$-H and $C_{(9\alpha)}$-H orientations.

Thus the structure of yadanziolide C (**3**) was established to be 13β,20-epoxy-1α,11β,12α,14,15β-pentahydroxypicras-3-ene-2,16-dione, which corresponds to 1-epibrucein D.

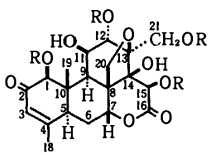

1 R=H

13 R=Ac

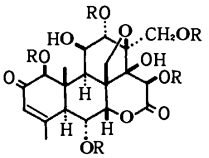

2 R=H

14 R=Ac

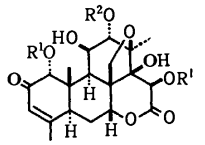

3 R^1-R^2-H

15 R^1-Ac, R^2-H

16 R^1-R^2-Ac

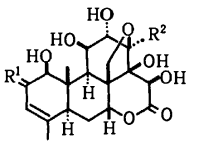

10 R^1=O, R^2-CH_3

11 R^1=α-OH, β-H, R^2-CH_3

12 R^1=α-OH, β-H; R^2-CH_2OH

Table 1. ^{1}H NMR Spectra of Yadanziolides A (**1**) and B (**2**) in C_5D_5N

		1[a]		**2**[b]	
		δ	*J*/Hz	δ	*J*/Hz
1-H		4.32 s [d]		4.35 s [d]	
3-H		6.10 br s		6.22 br s	
5-H		3.06 br d	12	3.39 br d	11.5
6-H	(6α-H)	2.31 dd	14, 3	4.24 dd	11.5, 1.5
	(6β-H)	c)			
7-H		5.44 br s		5.70 br s	
9-H		2.89 d	5	3.00 br s	
11-H		5.33 d	5	5.48 br s	
12-H		4.71 s [d]		4.79 s [d]	
15-H		6.06 s		6.21 s	
20-H		4.29 d	8	4.42 d	7
20-H′		5.00 d	8	5.06 d	7
21-H		4.63 d	12	4.71 d	11.5
21-H′		5.03 d	12	5.08 d	11.5
4-CH_3		1.75 br s		2.51 br s	
10-CH_3		1.43 s		1.62 s	

a) Measured at 90 MHz. b) Measured at 400 MHz. c) Not assignable. d) The assignments of these signals described in Ref. 1 were found to be revised.

Yadanzioside F (**4**; *ca.* 0.03% yield), a bitter glycoside, mp 202—207 °C, showed the presence of a secondary methyl, a tertiary methyl, an acetoxyl, and a methoxycarbonyl groups in 90 MHz ^{1}H NMR spectrum. The ^{13}C NMR spectrum and a peak observed at *m/z* 643 in the secondary ion mass spectrometry (SIMS) suggested the molecular formula, $C_{29}H_{38}O_{16}$, for **4**, which was supported by the following observations. In the EI mass spectrum, an abundant fragment ion at *m/z* 480 (M^+—162) indicated the presence of a hexose moiety. Yadanzioside F (**4**) was hydrolyzed with β-glucosidase to give brucein B (**17**).[10,11] Since a doublet signal due to $C_{(4)}$-CH_3 of the aglycone part of **4** was observed at δ 1.15 (*J*=5 Hz), it is indicated that the brucein B moiety isomerizes into a 3-keto-1-ene structure and the glycoside linkage is formed through an oxygen atom on C-2. The structure of yadanzioside F (**4**) was therefore formulated as 2-*O*-(β-D-glucosyl)brucein B.

Table 2. ^{1}H NMR Spectra of Yadanziolide C (**3**) and Brucein D (**10**) in C_5D_5N

	3[a]		**10**[b]	
	δ	J/Hz	δ	J/Hz
1-H	4.66 d	3	4.30 s [d]	
3-H	6.09 br s		6.10 br s	
5-H	3.60 br d	13.5	3.05 br d	13
6α-H	2.38 ddd	13.5, 3, 3	2.30 dt	14, 2
6β-H	1.72 ddd	13.5, 13.5, 3	c)	
7-H	5.52 t	3	5.47 t	2
9-H	3.62 d	5.5	2.84 d	5
11-H	4.97 t	5.5	5.37 d	5
12-H	4.46 d	3	4.52 s [d]	
15-H	6.03 s		6.04 s	
20-H	4.39 d	7.5	4.20 d	8
20-H′	5.01 d	7.5	4.91 d	8
4-CH_3	1.71 br s		1.74 br s	
10-CH_3	1.63 s		1.46 s	
13-CH_3	2.05 s		2.07 s	
-OH	5.50 d	5.5		
	7.05 s			
	7.53 d	3		
	7.66 br s			
	8.23 d	3		

a) Measured at 400 MHz. b) Measured at 90 MHz. c) Not assignable. d) The assignments of these signals described in Ref. 1 were found to be revised.

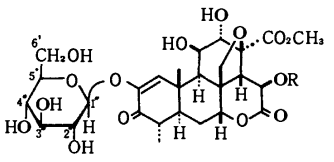

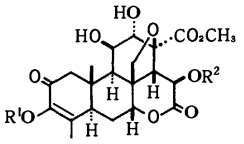

4 R=$COCH_3$

5 R^1=β-Glc, R^2=$COCH_3$

6 R=

7 R^1=β-Glc, R^2= 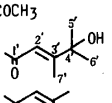

8 R=

9 R^1=β-Glc, R^2=

17 R^1=H, R^2=$COCH_3$

18 R^1=H, R^2=

19 R^1=H, R^2= 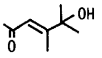

Yadanzioside I (**5**; *ca.* 0.02% yield) crystallized from ethanol as colorless needles, mp 287—290 °C (decomp). The molecular formula, $C_{29}H_{38}O_{16}$, was inferred by a peak at m/z 643 in the SIMS together with the ^{13}C NMR spectrum and hydrolysis with β-glucosidase giving brucein B (**17**). In the ^{1}H NMR spectrum, the $C_{(4)}$-CH_3 was observed at δ 2.04 as a singlet. In ^{13}C NMR spectrum, glycosylation shifts (see Table 3) of the signals due to C-3 and C-4 were observed, respectively, indicating that D-glucose is attached at C-3 of the aglycone. Thus the structure of yadanzioside I (**5**) was determined to be 3-*O*-(β-D-glucosyl)brucein B.

Yadanzioside J (**6**; *ca.* 0.002% yield), mp 198—202 °C, was suggested to have a molecular formula, $C_{32}H_{44}O_{17}$ by SIMS and ^{13}C NMR spectrum. The IR and UV spectra showed the presence of hydroxyl(s), a δ-lactone, and an α,β-unsaturated carbonyl groups. In the ^{1}H NMR spectrum, a doublet signal due to $C_{(4)}$-CH_3 of the aglycone part was observed at δ 1.16 (J=6.6 Hz), and a doublet signal due to the anomeric proton of the sugar part was observed at δ 5.35 (J=7.3 Hz). In the ^{13}C NMR spectrum, all of carbons were assigned (see Table 3). These indicate that the structure of **6** must be a 2-β-D-glucoside like bruceoside A or yadanzioside F and the aglycone must be 15-*O*-(3-hydroxy-3-methylbutanoyl)bruceolide.

On hydrolysis with 1.5 M sulfuric acid (1 M=1 mol dm^{-3})-methanol (1:2), **6** gave the aglycone (**18**) and D-glucose. The latter was identified as its trimethylsilyl derivative by GLC. The aglycone (**18**) was shown to have the molecular formula, $C_{26}H_{34}O_{12}$ by high-resolution mass spectrum. By comparison of the ^{1}H and ^{13}C NMR spectra with those of known bruceolides, the signals δ 1,34 (6H, s) and 2.43 (2H, s) in the ^{1}H NMR, and δ 170.7s, 48.6t, 69.2s, 29.8s, and 29.9s in the ^{13}C NMR (see Table 3) were well assigned to 3-hydroxy-3-methylbutanoate moiety. Thus the structure of **18** was determined to be 15-*O*-(3-hydroxy-3-methylbutanoyl)bruceolide, which is corresponding to 3′-hydroxybrucein A. From these evidences, the structure (**6**) is proposed for yadanzioside J.

Yadanzioside L (**7**; *ca.* 0.01% yield), mp 199—204 °C, was suggested to have a molecular formula, $C_{34}H_{46}O_{17}$, by a peak observed at m/z 727 in the SIMS and the ^{13}C NMR spectrum. On hydrolysis with 1.5 M sulfuric acid-methanol, **7** afford brucein C (**19**)[6,11,12] and D-glucose. The former was identified in respect to mp, IR, and ^{1}H NMR, and the latter was identified as its trimethylsilyl derivative by GLC examination. Glycosylation shifts of the signals due to C-3 and C-4 were observed in ^{13}C NMR, respectively, (see Table 3) which implies that D-glucose is attached at C-3 of the aglycone. An anomeric proton was observed at δ 5.40 as a doublet (J=7 Hz) in the ^{1}H NMR spectrum. Thus the structure of yadanzioside L (**7**) was determined to be 3-*O*-(β-D-glucosyl)-brucein C.

Yadanziosides F (**4**), I (**5**), J (**6**), and L (**7**) were demonstrated to have *in vivo* antileukemic activity against the murine P-388 lymphocytic leukemia at same strength as bruceoside A (**8**).

Experimental

General Procedures. All melting points were measured

Table 3. ^{13}C NMR Spectra of Yadanziosides F (**4**), I (**5**), J (**6**), L (**7**), bruceins B (**17**),[15] C (**19**),[15] and 15-*O*-(3-hydroxy-3-methylbutanoyl)-bruceolide (**18**)

No. of Carbon	**4**[a]	**5**[a]	**6**[a]	**7**[a]	**17**[b]	**19**[c]	**18**[a]
1	129.5 d	51.0 t	129.5 d	51.1 t	48.7	47.8	50.1 t
2	148.8 s	193.6 s	148.9 s	193.6 s	192.9	193.0	193.0 s
3	194.5 s	146.8 s [d]	194.5 s	146.6 s [d]	144.1	144.3	146.0 s
4	43.9 d	148.0 s [d]	43.8 d	147.9 s [d]	128.3	129.4	128.2 s
5	40.6 d	43.4 d	40.7 d	43.4 d	39.9	41.1	41.4 d
6	30.0 t	29.3 t	30.0 t	29.4 t	28.7	29.1	29.6 t
7	83.6 d	83.5 d	83.6 d	83.4 d	82.8	83.2	83.8 d
8	46.6 s	46.0 s	46.8 s	46.0 s	44.7	45.5	46.3 s
9	41.4 d	42.1 d	41.4 d	42.1 d	40.4	41.6	42.4 d
10	39.6 s	40.8 s	39.6 s	40.8 s	40.9	41.1	42.5 d
11	73.4 d	72.9 d	73.5 d	73.0 d	71.4	71.2	73.1 d
12	76.1 d	76.0 d	76.0 d	76.0 d	74.7	75.4	75.8 d
13	82.7 s	82.7 s	82.7 s	82.7 s	81.4	81.6	82.8 s
14	50.5 d	50.3 d	50.5 d	50.5 d	48.7	49.7	50.4 d
15	68.8 d	68.7 d	68.7 d	68.3 d	67.3	66.7	68.6 d
16	168.0 s	168.0 s	168.1 s	168.2 s	167.0	168.0	168.1 s
18	12.6 q	15.3 q	12.5 q	15.3 q	13.3	13.1	13.4 q
19	18.0 q	15.8 q	17.9 q	15.9 q	15.0	15.2	15.7 q
20	73.7 t	73.5 t	73.7 t	73.6 t	72.3	73.6	73.7 t
21	171.3 s	171.3 s	171.2 s	171.2 s	169.9	168.0	171.3 s
OMe	52.3 q	52.4 q	52.4 q	52.4 q	52.3	52.7	52.4 q
1′	169.7 s	169.8 s	170.7 s	166.4 s	168.7	165.9	170.7 s
2′	20.6 q	20.6 q	48.6 t	112.8 d	20.4	111.5	48.6 t
3′			69.2 s	168.2 s		171.3	69.2 s
4′			29.7 q	73.2 s		73.6	29.8 q
5′			29.8 q	28.9 q		27.9	29.9 q
6′				28.9 q		27.9	
7′				15.5 q		15.2	
1″	102.0 d	104.8 d	102.1 d	104.9 d			
2″	74.7 d	75.9 d	74.7 d	75.9 d			
3″	78.8 d [e]	78.5 d [e]	78.8 d [e]	78.6 d [e]			
4″	71.3 d	71.5 d	71.4 d	71.6 d			
5″	78.5 d [e]	78.3 d [e]	78.5 d [e]	78.4 d [e]			
6″	62.4 t	62.8 t	62.4 t	62.9 t			

a) Measured in C_5D_5N at 22.5 MHz. b) Measured in $(CD_3)_2SO$. c) Measured in $CDCl_3$. d, e) Signals within any vertical column may be reversed.

on a Mel-temp capillary melting point apparatus (Laboratory Devices) and uncorrected. Optical rotations were determined on a JASCO polarimeter DIP-181. Infrared (IR) spectra were measured on a Hitachi 260-30 spectrometer. Ultraviolet absorption (UV) spectra were measured on a Hitachi 340 spectrometer. Low and high resolution mass spectra (MS and HRMS, respectively) were run on a JEOL JMS-D300 mass spectrometer operating at 70 eV and secondary ion mass spectra (SIMS) on a Hitachi M-80 mass spectrometer. Proton nuclear magnetic resonance (^1H NMR) spectra (90 MHz) were taken using a Varian EM390 and carbon-13 nuclear magnetic resonance (^{13}C NMR) spectra (22.5 MHz) JEOL FX 90Q. Measurement of ^1H NMR spectra at 400 MHz was carried out on a JNM GX 400 (JEOL) spectrometer. Chemical shifts were expressed in δ-value (ppm downfield from tetramethylsilane as an internal standard) and coupling constants in Hz. Thin-layer chromatography (TLC) was carried out on Kieselgel 60 GF_{254} or Kieselgel 60 HF_{254} silasiert coated in 0.25 mm or on TLC plates Kieselgel 60/Kieselgur F_{254} (E. Merck). Wakogel C-200 (Wako), TSK-gel Toyopearl HW-40S (Toyo Soda), or Lobar column Lichroprep RP-8 size B (E. Merck) was used for column chromatography. Commercialized β-glucosidase available from Sigma Chemical Company was used.

Plant Material. Seeds of *Brucea javanica* (L.) Merr as Chinese medicine, "Ya-dan-zi", were ground to afford 60 kg of materials.

Extraction and Separation. Seeds (60 kg) were defatted with haxane (*ca.* 100 l) twice, and then extracted with methanol (*ca.* 100 l) twice. The extract was concentrated to give a syrup, to which the same volume of water was added, and defatted with hexane (*ca.* 7 l) four times. The aqueous layer was extracted five times with dichloromethane. The aqueous layer, on evaporation, gave a bitter residue (*ca.* 1 kg). A part of the residue (53 g) was absorbed on silica gel

(60 g), placed on a top of a silica-gel (1.2 kg) column, and eluted with a lower layer of chloroform-methanol-water (50:12:3; *ca.* 9 l, 65:35:10; *ca.* 9 l, 50:50:18; *ca.* 12 l), and 40 fractions (each 700 ml) were collected (Column A).

The each fraction was further separated by the following procedures.

Procedure A: Gel chromatography using Toyopearl HW-40S (2.4×100 cm). Elution was performed with methanol, and fractions (each 10 g) were collected by an automatic fraction collector. Flow rate was about 0.2 ml/min.

Procedure B: Reversed phase chromatography using Lobar column Lichroprep RP-8 size B. Elution was performed with methanol-water, and fractions were collected by an automatic fraction collector. Flow rate was about 1 ml/min. The ratio in volume of methanol-water is given in each chromatographic procedure.

Fractions 8 and 9 (1.02 g) of Column A were combined and separated by Procedure A. Fractions 44—52 (730 mg; Fraction A) and fractions 59—65 (Fraction B; 149 mg) were combined respectively on the basis of TLC examination. Recrystallization of Fraction B from methanol gave brucein D (**10**).

Fractions 10 and 11 (1.24 g) of Column A were combined together and separated by Procedure A. On the basis of TLC, fractions 32—36 (467 mg; Fraction C), fractions 37—41 (193 mg; Fraction D), fractions 42—49 (193 mg; Fraction E), and fractions 50—55 (241 mg; Fraction F) were combined, respectively.

Fraction A and Fraction C were combined and separated by Procedure B (methanol-water, 1:1). Fractions 13—25 (790 mg) were combined and identified to be bruceoside A (**8**).[7] Fractions 26—35 (138 mg) were combined and evaporated to give yadanzioside A (**20**).[2]

Fraction D was separated by Procedure B (methanol-water, 3:7). Fractions 18—23 and fractions 24—45 were identified to be yadanziolide C (**3**; 20 mg) and yadanzioside F (**4**; 58 mg), respectively.

Fraction E was recrystallized from methanol to give brucein D (**10**; 150 mg).

Fraction 12 and 13 (1.63 g) of Column A were separated by Procedure A. Fractions 38—47 (1.18 g; Fraction G) and fractions 52—57 (243 mg; Fraction H) were collected.

Fraction G was separated by Procedure B (methanol-water, 1:1). Fractions 17—23 were combined to give yadanziolide C (**3**; 59 mg). Fractions 24—36 (960 mg) were combined and further separated by Procedure B (methanol-water, 3:7). Fractions 24—51 were combined and evaporated to give yadanzioside F (**4**; 534 mg), and fractions 52—80 were combined and identified to be bruceoside B (**9**; 85 mg).[8]

Fraction F and Fraction H were combined and recrystallized from methanol to afford yadanziolide A (**1**; 410 mg).

Fractions 14 and 15 (1.98 g) of Column A were separated by Procedure A. Fractions 38—47 (1.57 g) were further sepatated by Procedure B (methanol-water, 3:7). Fractions 24—45 (419 mg) were ascertained to be a mixture of yadanzioside F (**4**), brucein E (**11**), and yadanzioside D (**21**)[2] by TLC examination (Kieselgel 60 HF_{254} silasiert, methanol-water, 4:6). Fractions 46—90 (761 mg) were also identified to be a mixture of yadanzioside D (**21**) and bruceoside B (**9**).

Fraction 16 of Column A was crystallized from methanol to give crystalline brucein E (**11**; 1.2 g). The mother liquor (1.16 g) was separated by Procedure A. Fractions 33—38 (372 mg; Fraction I) and fractions 39—43 (353 mg; Fraction J) were combined, respectively. Fraction I was further separated by Procedure B (methanol-water, 3:7). Fractions 44—46 were combined to give yadanzioside J (**6**; 50 mg) and fractions 47—53 were identified to be yadanzioside C (**22**; 200 mg). Fraction J was also separated by Procedure B (methanol-water, 3:7). Fractions 15—23 were combined to give yadanzioside I (**5** 178 mg) and fractions 24—50 were combined and evaporated to give brucein E (**11**; 150 mg).

Fractions 17 and 18 of Column A were crystallized from methanol to give crystalline brucein E (**11**; 450 mg). The mother liquor (2.7 g) was separated by Procedure A. Fractions 35—40 (935 mg; Fraction K), fractions 41—48 (526 mg; Fraction L) and fractions 52—56 (71 mg; Fraction M) were combined, respectively, on the basis of TLC examination. Fraction K was separated by Procedure B (methanol-water, 3:7). Yadanzioside **I** (**5**; 79 mg) was given from fractions 16—21, brucein E (**11**; 273 mg) from fractions 22—42, and yadanzioside L (**7**; 192 mg) from fractions 43—56. Fraction L was separated by Procedure B (methanol-water, 3:7). Fractions 15—23 were combined to give yadanzioside I (**5**; 178 mg) and fractions 24—50 gave brucein E (**11**; 220 mg).

Fractions 19 and 20 (2.36 g) of Column A were separated by Procedure A. Fractions 43—50 (880 mg; Fraction N) and fractions 51—70 (220 mg; Fraction O) were combined, respectively. Fraction N was crystallized from methanol to give brucein F (**12**).[10] Fraction M and Fraction O were combined and separated by procedure B (methanol-water, 1:1) to give yadanziolide B (**2**; 70 mg) from fractions 12—15.

Yadanziolide A (1). Colorless needles crystallized from methanol, mp 283—285 °C (decomn); $[\alpha]_D^{28}$ −10.5° (*c* 1.7, pyridine); IR (KBr) 3430, 1700, 1645, 1620, and 1025 cm^{-1}; UV (methanol) 240 nm (ε 9300); ^1H NMR (Table 1); ^{13}C NMR (C_5D_5N, 22.5 MHz) δ=11.5q, 22.2q, 28.0t, 43.6d, 45.7d, 48.6s, 50.7s, 64.7t, 70.6t, 70.7d, 75.4d, 78.3d, 79.1d, 83.0d, 83.8s, 84.6s, 124.9d, 163.5s, 174.9s, and 198.4s; MS (EI) *m/z* (%) 426 (M^+; 0.4), 408 (2), 390 (34), 372 (16), 151 (100), and 135 (88); Found: C, 56.04; H, 6.16%. Calcd for $C_{20}H_{26}O_{10}$: C, 56.33; H, 6.15%.

Oxidation of Brucein F (12) with Manganese Dioxide. A solution of brucein F (**12**; 52.6 mg) in *N,N*-dimethylformamide (10 ml) was treated with manganese dioxide (1 g, prepared by Attenburrow's procedure[13]) for 24 h at room temperature. After the usual work-up, the reaction mixture was separated by silica-gel column chromatography (C-200, 12 g) eluted with a lower layer of chloroform-methanol-water (50:12:3). The oxidation product, yadanziolide A (**1**; 9.2 mg) was identified by mp, IR, ^1H NMR, and TLC, and the starting material, brucein F (**12**; 11 mg) was recovered.

1,12,15,21-Tetra-O-acetylyadanziolide A (13). Yadanziolide A (**1**; 25 mg) was acetylated with acetic anhydride (1.5 ml) in pyridine (1.5 ml) at room temperature for 64 h. Addition of methanol and the usual work-up afforded a reaction mixture, which was purified by silica-gel column chromatography (C-200, 10 g) eluted with dichloromethane-ethyl acetate (2:1) to give 1,12,15,21-tetra-*O*-acetylyadanzi-

olide A (**13**; 34 mg), mp 202—203 °C (colorless prisms crystallized from methanol–diethyl ether); IR (KBr) 3430, 1750, 1685, 1630, 1380, 1245, and 1055 cm^{-1}; UV (ethanol) 239 nm (ε 9000); ^1H NMR ($CDCl_3$ 90 MHz) δ=1.38 (3H, s, 10-CH_3), 1.97 (6H, s, 4-CH_3 and OAc), 2.09 (3H, s, OAc), 2.18 (3H, s, OAc), 2.34 (1H, d, J=5 Hz, 9-H), 3.04 (1H, br d, J=11 Hz, 5-H), 4.00 (1H, d, J=5 Hz, 11-H), 4.02, 4.68 (each 1H, d, J=8 Hz, 20-H), 4.30, 4.49 (each 1H, d, J=13 Hz, 21-H), 5.04 (1H, s, 12-H), 5.16 (1H, br s, 7-H), 5.40 (1H, s, 1-H), 6.02 (1H, br s, 3-H), and 6.09 (1H, s, 15-H); MS (EI) m/z (%) 594 (M^+, 1), 576 (0.6), 552 (2), 534 (10), 492 (10), 474 (22), 432 (100), 267 (25), 151 f(25), 135 (26), and 60 (28); Found: m/z 594.1953. Calcd for $C_{28}H_{34}O_{14}$: M, 594.1948.

Yadanziolide A Monohydrate. Colorless prisms crystallized from aqueous methanol, mp 310—314 °C (decomp), IR (KBr) 3540, 3440, 1750, 1665, 1625, 1160, and 1075 cm^{-1}; Found: C, 53.78; H, 6.38%. Calcd for $C_{20}H_{26}O_{10}\cdot H_2O$: C, 54.05; H, 6.34%.

Yadanziolide B (2). Colorless needles crystallized from ethanol–diethyl ether, mp 279—282 °C (decomp); $[\alpha]_D^{23}$ +83° (c 4.3, methanol); IR (KBr) 3500, 3360, 1710, 1645, 1630 (sh), 1255, 1125, and 1070 cm^{-1}; UV (methanol) 244 nm (ε 10000); ^1H NMR (Table 1); ^{13}C NMR (C_5D_5N, 22.5 MHz) δ=12.5q, 27.1q, 44.6d, 49.2d, 51.1s, 51.2s, 64.6t, 68.2d, 70.0t, 70.9d, 75.5d, 78.6d, 83.3d, 83.8s, 83.8d, 84.3s, 126.9d, 166.4s, 174.7s, and 198.2s; MS (EI) m/z (%) 442 (M^+, 0.8), 424 (12), 406 (28), 388 (10), 378 (36), 360 (12), and 111 (100); Found: C, 54.11; H, 5.77%. Calcd for $C_{20}H_{26}O_{11}$: C, 54.30; H, 5.92%.

1,6,12,15,21-Penta-O-acetylyadanziolide B (14). Yadanziolide B (**2**; 27 mg) was acetylated with acetic anhydride (1.5 ml) in pyridine (1.5 ml) at room temperature for 5 d. The usual work-up and silica-gel column chromatography (dichloromethane–ethyl acetate, 2:1) yielded, after crystallization from methanol–diethyl ether, a pentaacetate (**14**; 28 mg), as colorless needless, mp 278—283 °C (decomp); IR (KBr) 3460, 1740, 1680, 1640, 1375, 1240, and 1030 cm^{-1}; UV (ethanol) 239 nm (ε 10000); ^1H NMR ($CDCl_3$, 90 MHz) δ=1.52 (3H, s, 10-CH_3), 1.96 (3H, s, OAc), 2.03 (3H, br s, 4-CH_3, 2.09 (6H, s, OAc), 2.22 (6H, s, OAc), 2.37 (1H, d, J=6 Hz, 9-H), 3.10 (1H, br d, J=11 Hz, 5-H),4.07 (1H, d, J=6 Hz, 11-H), 4.15, 4.70 (each 1H, d, J=8 Hz, 20-H), 4.27, 4.50 (each 1H, d, J=12 Hz, 21-H), 5.03 (1H, s, 12-H), 5.08 (1H, dd, J=11, 2 Hz, 6-H), 5.10 (1H, d, J=2 Hz, 7-H), 5.45 (1H, s, 1-H), 6.07 (1H, br s, 3-H), and 6.12 (1H, s, 15-H); MS (EI) m/z (%) 652 (M^+, 0.8), 634 (0.8), 610 (1.2), 592 (6), 567 (8), 550 (14), 532 (13), 490 (22), 472 (10), 430 (18), and 60 (100); Found: m/z 652.2031. Calcd for $C_{30}H_{36}O_{16}$: M, 652.2004.

Yadanziolide C (3). Colorless prisms crystallized from methanol–diethyl ether, mp 292—297 °C (decomp); $[\alpha]_D^{23}$ +29° (c 1.2, MeOH); IR (KBr) 3575, 3550, 3500, 3420, 1705, 1675, 1620, 1160, and 1060 cm^{-1}; UV (methanol) 244 nm (ε 11000); ^1H NMR (Table 2); ^{13}C NMR (C_5D_5N, 22.5 MHz) δ=15.0q, 19.5q, 22.0q, 28.0t, 37.7d, 38.3d, 44.6s, 49.7s, 70.5d, 70.5t, 73.2d, 76.2d, 79.7d, 82.0s, 82.6s, 85.5s, 125.0d, 161.6s, 174.9s, and 198.4s; MS (EI) m/z (%) 410 (M^+, 4), 392 (64), 374 (32), 151 (60), and 135 (100); Found: C, 58.27; H, 6.36%. Calcd for $C_{20}H_{26}O_9$: C, 58.53; H, 6.39%.

Acetylation of Yadanziolide C (3). Yadanziolide C (**3**; 21 mg) was treated with acetic anhydride (1 ml) and pyridine (1 ml) at room temperature for 1 week. After the usual work-up, the reaction mixture was separated by silica-gel column chromatography (C-200, 10 g) eluted with dichloromethane–ethyl acetate (2:1) to give the diacetate (**15**; 8.8 mg) and the triacetate (**16**; 14.2 mg). 1,15-Di-*O*-acetylyadanziolide C (**15**): mp 299—303 °C (colorles prisms from methanol–diethyl ether); IR (KBr) 3600, 3500, 1740, 1725, 1660, 1620, 1235, and 1075 cm^{-1}; UV (methanol) 246 nm (ε 10000); ^1H NMR ($CDCl_3$, 90 MHz) δ=1.37 (3H, s, 10-CH_3), 1.47 (3H, s, 13-CH_3), 1.97 (3H, br s, 4-CH_3), 2.14 (3H, s, OAc), 2.21 (3H, s, OAc), 2.42 (1H, br d, J=12 Hz, 6α-H), 2.50 (1H, 9-H), 3.11 (1H, br d, J=12 Hz, 5-H), 3.9—4.1 (3H, 11-H, 12-H, and 20-H), 4.51 (1H, d, J=8 Hz, 20-H′), 5.10 (1H, br s, 7-H), 5.15 (1H, s, 1-H), 5.92 (1H, br s, 3-H), and 6.40 (1H, s, 15-H); MS (EI) m/z (%) 494 (M^+, 0.4), 476 (0.8), 434 (3), 416 (3), 392 (2), 374 (15), 356 (5), 135 (100), and 60 (100); Found: m/z 494.1776. Calcd for $C_{24}H_{30}O_{11}$: M, 494.1787. 1,12,15-Tri-*O*-acetylyadanziolide C (**16**): mp 183—188 °C (powder); IR (KBr) 3450, 1750, 1680, 1640, 1380, 1235, 1070, and 1040 cm^{-1}; UV (methanol) 246 nm (ε 10000); ^1H NMR ($CDCl_3$, 90 MHz) δ=1.30 (3H, s, 10-CH_3), 1.41 (3H, s, 13-CH_3), 1.97 (3H, br s, 4-CH_3), 2.00 (3H, s, OAc), 2.11 (3H, s, OAc), 2.23 (3H, s, OAc), 2.45 (1H, br d, J=12 Hz, 6α-H), 3.05 (1H, br d, J=12 Hz, 5-H), 3.97, 4.55 (each 1H, d, J=8 Hz, 20-H), 4.10 (1H, d, J=5 Hz, 11-H), 4.89 (1H, d, J=1.5 Hz, 12-H), 5.18 (1H, br s, 7-H), 5.27 (1H, s, 1-H), 5.95 (1H, br s, 3-H), and 6.13 (1H, s, 15-H); MS (EI) m/z (%), 536 (M^+, 2), 494 (3), 476 (5), 458 (1), and 135 (100); Found: m/z 536.1917. Calcd for $C_{26}H_{32}O_{12}$: M, 536.1894.

Yadanzioside F (4). Amorphous solid, mp 202—207 °C; $[\alpha]_D^{23}$ +10° (c 4.1, ethanol); IR (KBr) 3450, 1740, 1680, 1630, and 1065 cm^{-1}; UV (ethanol) 256 nm (ε 6500); ^1H NMR (C_5D_5N, 90 MHz) δ=1.15 (3H, s, J=5 Hz, 4-CH_3), 1.63 (3H, s, 10-CH_3), 2.10 (3H, s, 15-OAc), 3.81 (3H, s, $COOCH_3$), 6.76 (1H, d, J=13 Hz, 15-H), and 7.22 (1H, s, 1-H); ^{13}C NMR (Table 3); MS (SIMS) 643 (MH^+), 481, and 439; Found m/z 480.1614. Calcd for $C_{23}H_{28}O_{11}$ (M−$C_6H_{10}O_5$): m/z 480.1629.

Enzymatic Hydrolysis of Yadanzioside F (4). A mixture of yadanzioside F (**4**; 143 mg) and β-glucosidase (41 mg) in water (10 ml) was allowed to stand for 2 weeks at 37 °C. Methanol (5 ml) was added and the mixture was heated at boiling-water temperature for 10 min. After being cooled, the mixture was filtered and the filtrate was evaporated *in vacuo*. The residue was separated by silica-gel column chromatography (chloroform–methanol, 9:1) to yield a pure compound (**17**; 37 mg). The physical and spectral data of **17** (IR, ^1H NMR, MS) are in agreement with literature[11] for brucein B (**17**). Found: m/z 480.1618. (M−$C_6H_{10}O_5$): m/z 480.1629.

Yadanzioside I (5). Colorless needles crystallized from ethanol, mp 287—290 °C (decomp); $[\alpha]_D^{28}$ −21° (c 1.0, methanol); IR (KBr) 3450, 1755, 1650, 1620 (sh), and 1065 cm^{-1}; UV (ethanol) 254 nm (ε 9700); ^1H NMR (C_5D_5N, 90 MHz) δ=1.69 (3H, s, 10-CH_3), 2.04 (3H, s, 4-CH_3), 2.10 (3H, s, 15-OAc), 3.81 (3H, s, $COOCH_3$), and 6.80 (1H, d, J=13 Hz, 15-H); ^{13}C NMR (Table 3); MS (SIMS) m/z 643 (MH^+) and 481; Found: m/z 480.1646. Calcd for $C_{23}H_{28}O_{11}$ (M—$C_6H_{10}O_5$): m/z 480.1629.

Enzymatic Hydrolysis of Yadanzioside I (5). A mixture of yadanzioside I (47 mg) and β-glucosidase (23 mg) in water (5 ml) was treated by the same procedure

as before. Brucein B (**17**; 11 mg) was isolated and identified as the sole aglycone.

Yadanzioside J (6). Amorphous solid, mp 198—202 °C; $[\alpha]_D^{22}$ −6.4° (*c* 2.8, methanol); IR (KBr) 3430, 1740, 1680, 1640, and 1075 cm^{-1}; UV (methanol) 254 nm (ε 8000); ^1H NMR (C_5D_5N, 400 MHz) δ=1.16 (3H, d, *J*=6.6 Hz, 4-CH_3), 1.61 (6H, s, 3′-CH_3×2), 1,64 (3H, s, 10-CH_3), 2.01 (1H, br d, *J*=15.0 Hz, 5-H), 2.52 (1H, d, *J*=5.1 Hz, 9-H), 2.88, 2.94 (each 1H, d, *J*=13.7 Hz, 2′-H), 3.80 (3H, s, $COOCH_3$), 3.90, 5.07 (each 1H, d, *J*=7.7 Hz, 20-H), 4.48 (1H, br d, *J*=10.3 Hz, 6″-H), 4.94 (1H, br s, 11-H), 5.13 (1H, br s, 12-H), 5.18 (1H, br s, 7-H), 5.35 (1H, d, *J*=7.3 Hz, 1″-H), and 7.27 (1H, s, 1-H); ^{13}C NMR (Table 3); MS (SIMS) *m/z* 701 (MH^+), 683, 539, 521, and 439; Found: *m/z* 538.2068. Calcd for $C_{26}H_{34}O_{12}$ (M−$C_6H_{10}O_5$): *m/z* 538.2051.

Acid Hydrolysis of Yadanzioside J (5). A solution of **5** (42 mg) in 1.5 M sulfuric acid-methanol (1:2, 6 ml) was refluxed for 5 h. The reaction mixture was concentrated *in vacuo* and extracted with dichloromethane four times. The combined dichloromethane layers were dried over anhydrous magnesium sulfate and evaporated under reduced pressure to give a product (21 mg) which was separated by silica-gel column chromatography (C-200, 10 g) eluted with methanol–chloroform (1:9) to give a pure compound (20 mg). This compound crystallized from methanol–diethyl ether to afford 15-*O*-(3-hydroxy-3-methylbutanoyl)-bruceolide (**18**) as colorless prisms: mp 251—254 °C (decomp); $[\alpha]_D^{19}$ +13° (*c* 1.4, methanol); IR (KBr) 3575, 3460, 1745, 1730, 1675, 1650, 1195, 1150, and 1070 cm^{-1}; UV (methanol) 278 nm (ε 8000); ^1H NMR ($CDCl_3$, 90 MHz) δ=1.34 (6H, s, 3′-CH_3×2), 1.39 (3H, s, 10-CH_3), 1.84 (3H, d, *J*=2 Hz, 4-CH_3), 2.40, 2.95 (each 1H, d, *J*=18 Hz, 1-H), 2.43 (2H, s, 2′-H_2), 3.13 (1H, d, *J*=13 Hz, 14-H), 3.75, 4.73 (each 1H, d, *J*=7 Hz, 20-H), 3.82 (3H, s, $COOCH_3$), 4.23 (2H, br s, 11-H and 12-H), 5.77 (1H, br s, 7-H), and 6.38 (1H, d, *J*=13 Hz, 15-H); ^{13}C NMR (Table 3); MS (EI) *m/z* (%) 538 (M^+, 1.5), 520 (12), 480 (26), 438 (50), 420 (20), 402 (20), 392 (28), 297 (46), 151 (74), and 83 (100); Found: *m/z* 538.2048. Calcd for $C_{23}H_{34}O_{12}$: M, 538.2051.

The aqueous layer, obtained from the acid hydrolysis of **5**, was passed through a short column of anion-exchange resin (Amberlite IRA-400, hydroxide form) and the eluate was evaporated under reduced pressure to give a residue which was identified as D-glucose (as trimethylsilyl derivative) by gas-liquid chromatography.

Yadanzioside L (7). Colorless needles crystallized from methanol–diethyl ether, mp 199—204 °C; $[\alpha]_D^{26}$ −0.7° (*c* 6.2, methanol); IR (KBr) 3420, 1735, 1640, and 1060 cm^{-1}; UV (methanol) 220 nm (ε 14000) and 254 nm (ε 9000); ^1H NMR (C_5D_5N, 90 MHz) δ=1.43 (6H, s, 4′-CH_3×2), 1.69 (3H, s, 3′-CH_3) 2.03 (3H, s, 4-CH_3), 2.38 (3H, s, 10-CH_3), 3.0—3.3 (2H, 1-H, and 14-H), 3.71 (3H, s, $COOCH_3$), 5.40 (1H, d, *J*=7 Hz, anomeric-H), 6.70 (1H, s, 2′-H), and 6.85 (1H,d, *J*=13 Hz, 15-H); ^{13}C NMR (Table 3); MS (SIMS) *m/z* 727 (MH^+) and 565; Found *m/z* 564.2182. Calcd for $C_{28}H_{36}O_{12}$ (M−$C_6H_{10}O_5$): *m/z* 564.2205.

Acid Hydrolysis of Yadanzioside L (7). The same treatment of a solution of **7** (94 mg) in 1.5 M sulfuric acid–methanol (1:2, 10 ml) as that described above led to the isolation of an aglycone (**19**; 47 mg). The physical and spectral data of **19** are in agreement with those[11] for brucein C (**19**). Found: *m/z* 564.2230. Calcd for $C_{28}H_{36}O_{12}$: M, 564.2205.

D-Glucose was also identified from aqueous layer by the same procedure described above.

The authors wish to thank Mr. Kazuhiro Matsushita of JEOL Co. Ltd. for the measurement of 400 MHz ^1H NMR spectra. They also thank Mr. Hideo Naoki of Suntory Institute for Bioorganic Research for the measurement of SIMS.

References

1) S. Yoshimura, T. Sakaki, M. Ishibashi, T. Tsuyuki, T. Takahashi, K. Matsushita, and T. Honda, *Chem. Pharm. Bull.*, **32**, 4698 (1984).

2) T. Sakaki, S. Yoshimura, M. Ishibashi, T. Tsuyuki, T. Takahashi, T. Honda, and T. Nakanishi, *Chem. Pharm. Bull.*, **32**, 4702 (1984).

3) J. Polonsky, *Fortschr. Chem. Org. Naturst.*, **30**, 101 (1973).

4) I. H. Hall, Y. F. Liou, K. H. Lee, S. G. Chaney, and W. Willingham, Jr., *J. Pharm. Sci.*, **72**, 626 (1983); C. Moretti, J. Polonsky, M. Vuilhorgne, and T. Prangé, *Tetrahedron Lett.*, **23**, 647 (1982) and references cited therein.

5) M. Ishibashi, S. Yoshimura, T. Tsuyuki T. Takahashi, A. Itai, and Y. Iitaka, *Bull. Chem. Soc. Jpn.*, **57**, 2885 (1984); S. Yoshimura, M. Ishibashi, T. Tsuyuki, T. Takahashi, and K. Matsushita, *Bull. Chem. Soc. Jpn.*, **57**, 2496 (1984) and references cited therein.

6) J. Polonsky, Z. Baskévitch, A. Gaudemer, and B. C. Das, *Experientia*, **23**, 424 (1967).

7) K. Y. Sim, J. J. Sims, and T. A. Geissman, *J. Org. Chem.*, **33**, 429 (1968).

8) K. H. Lee, Y. Imakura, Y. Sumida, R. -Y. Wu, and I. H. Hall, *J. Org. Chem.*, **44**, 2180 (1979).

9) J. Polonsky, Z. Baskévitch, M. B. Das, and J. Müller, *C. R. Acad. Sci., Ser. C*, **267**, 1346 (1968).

10) J. Polonsky, Z. Baskévitch, and J. Müller, *C. R. Acad. Sci., Ser. C*, **268**, 1392 (1969).

11) J. D. Phillipson and F. A. Darwish, *Planta Med.*, **41**, 209 (1981).

12) J. Polonsky, J. Varenne, T. Prangé and C. Pascard, *Tetrahedron Lett.*, **21**, 1853 (1980).

13) J. Attenburrow, A. F. B. Cameron, J. H. Chapman, R. M. Evans, B. A. Hems, A. B. A. Jensen, and T. Walker, *J. Chem. Soc.*, **1952**, 1094.

14) J. Polonsky and Z. Baskévitch, *J. Org. Chem.*, **40**, 2499 (1975).

Structures of New Quassinoid Glycosides, Yadanziosides A, B, C, D, E, G, H, and New Quassinoids, Dehydrobrusatol and Dehydrobruceantinol from *Brucea javanica* (L.) MERR[1)]

Toshiro SAKAKI, Shin YOSHIMURA, Masami ISHIBASHI, Takahiko TSUYUKI,*
Takeyoshi TAKAHASHI,* Tadashi HONDA,† and Toshihiro NAKANISHI†
Department of Chemistry, Faculty of Science, The University of Tokyo, Hongo, Bunkyo-ku, Tokyo 113
†*Suntory Institute for Biomedical Research, 1-1, Wakayamadai, Shimamotocho, Mishimagun, Osaka 618*
(Received April 16, 1985)

Quassinoid glycosides, yadanziosides A, B, C, D, E, G, and H, and two quassinoids, dehydrobrusatol and dehydrobruceantinol were isolated from seeds of *Brucea javanica*, and their structures were determined. These glycosides showed bitter taste and were demonstrated to have antileukemic activity.

In the preceding paper,[2)] the structure determination of three new quassinoids, yadanziolides A, B, and C, isolated from "Ya-dan-zi", seeds of *Brucea javanica* (L.) MERR was reported. As a continuation of studies on bitter principles of "Ya-dan-zi", quassinoid glycosides were examined, since our preliminary examination revealed the presence of many glycosides in the polar fraction of the methanol extract. Three quassinoid glycosides, bruceoside-A and -B[3)] and bruceantinoside A[4)] have been isolated from the same source as antileukemic constituents.

The methanol extract was subjected to separation to give seven new glycosides, yadanziosides A (**2**; 0.01%), B (**3**; 0.002%), C (**4**; 0.001%), D (**5**; 0.001%), E (**6**; 0.002%), G (**7**; 0.01%), and H (**8**; 0.001%), and two new quassinoids, dehydrobrusatol (**9**; 0.0002%) and dehydrobruceantinol (**10**; 0.0001%) together with brusatol(**1**),[5)] dehydrobrucein-A,[6)] brucein D,[7)] brucein E,[7)] bruceoside-A,[3)] bruceoside-B,[3)] bruceantinoside A,[4)] yadanziolide A,[2)] and yadanzioside F.[2)]

Yadanzioside B (**3**), mp 189—195 °C, showed a peak at *m/z* 707 due to $[M+Na]^+$ in SIMS, from which the molecular formula, $C_{32}H_{44}O_{16}$, was deduced. Its IR and UV spectra showed the presence of hydroxyl, δ-lactone, and conjugated enone moieties. An appearance of a peak at *m/z* 522.2082 ($[M-C_6H_{10}O_5]^+$) in the EI-high-resolution mass spectrum and the presence of a doublet signal (J=7.3 Hz) at δ 5.46 due to an anomeric proton in the ^{1}H NMR spectrum suggested that **3** should be a β-D-glucopyranoside. ^{1}H and ^{13}C NMR spectra (Tables 1 and 2) of **3** revealed that the aglycone must be brucein A (**11**)[6,8)] and glycosylation shifts of signals due to C-3 and C-4 were Δδ +1.9 and +18.1 ppm,[9,10)] respectively, in ^{13}C NMR spectra of **3** and **11**, leading to the structure assignment of yadanzioside B as 3-*O*-(β-D-glucopyranosyl)brucein A (**3**).

This assignment was supported by hydrolysis of **3**; treatment with 1.5 M (1 M=1 mol dm^{-3}) sulfuric acid afforded brucein A (**11**) and hydrolysis with hydrogen chloride in methanol yielded methyl D-glucoside, which was identified as its trimethylsilyl derivative by GLC.

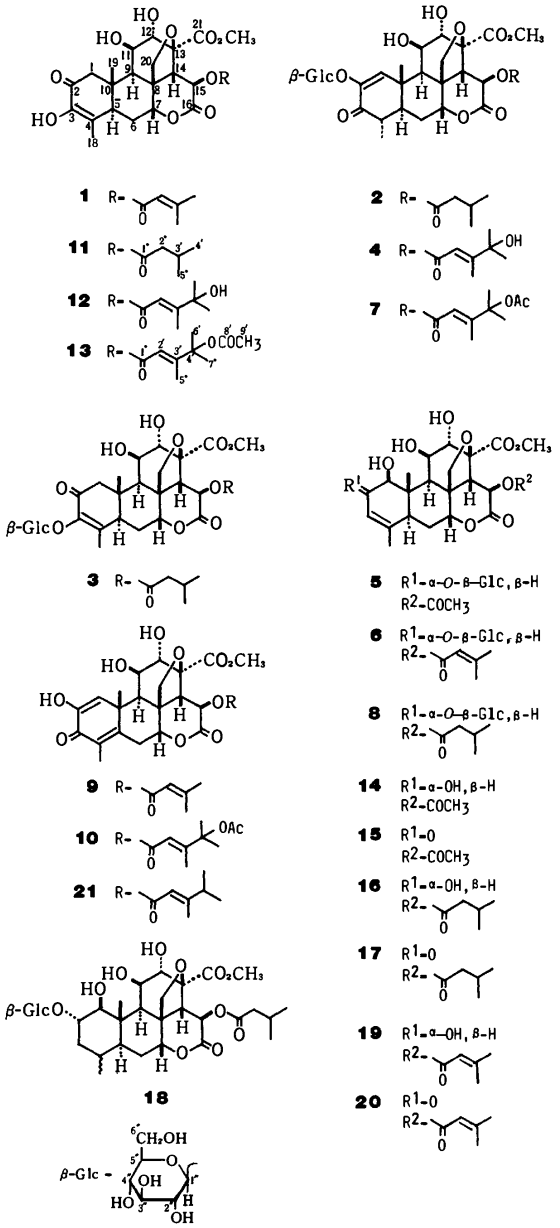

Carbon numbers of picrasane skeleton refer to those described in Chemical Abstracts and numbers of carbon atoms in the side-chain at C-15 are given conventionally.

Yadanzioside A (**2**), mp 200—204 °C, was shown to be a glucoside with the same molecular formula as that of **3** by SIMS. On hydrolysis with β-glucosidase, **2** afforded brucein A (**11**) as the major aglycone. The ^{1}H NMR spectrum of **2** showed the presence of a doublet signal (J=6 Hz) due to $C_{(4)}$-CH_3 at δ 1.13. This fact implies the brucein A moiety isomerizes into a 3-keto-1-ene structure, which forms the β-D-glucoside linkage through an oxygen atom on C-2 of the aglycone. The configuration of the $C_{(4)}$-CH_3 of **2** was assigned as β-equatorial on the basis of the structural similarity to bruceoside-A.[3] Thus the structure of yadanzioside A was determined to be 2-*O*-(β-D-glucosyl)brucein A (**2**).

Yadanzioside C (**4**), mp 204—209 °C, gave a peak at m/z 749 due to $[M+Na]^+$ in the SIMS, which corresponds to the molecular formula $C_{34}H_{46}O_{17}$ and a peak at m/z 564.2230 ($[M-C_6H_{10}O_5]^+$) in the EI-high-resolution mass spectrum. Acid hydrolysis of **3** with 1.5 M sulfuric acid in methanol gave brucein C (**12**)[6,8,11] as the aglycone. On treatment with hydrogen chloride in methanol yielded methyl D-glucoside. The ^{1}H NMR spectrum of **4** showed a doublet signal (J=7.0 Hz) at δ 5.37 due to an anomeric proton and a doublet signal (J=6.7 Hz) due to $C_{(4)}$-CH_3 at δ 1.19. These observations led to the structure, 2-*O*-(β-D-glucopyranosyl)brucein C (**4**) for yadanzioside C.

Yadanzioside G (**7**), mp 180—185 °C, showed the presence of three tertiary methyl groups, one secondary methyl, one olefinic methyl, one acetoxyl, and one methoxycarbonyl groups in the ^{1}H NMR spectrum. The molecular formula, $C_{36}H_{48}O_{18}$, was suggested by a peak at m/z 791 due to $[M+Na]^+$ in the SIMS. On hydrolysis with β-glucosidase, **7** afforded bruceantinol (**13**).[6,11] A doublet signal (J=6 Hz) due to $C_{(4)}$-CH_3 at δ 1.17 indicates the sugar moiety in yadanzioside G (**7**) was linked to C-2 of bruceantinol (**13**). Therefore, the structure of yadanzioside G is formulated as 2-*O*-(β-D-glucopyranosyl)bruceantinol (**7**).

Yadanzioside D (**5**), mp 207—212 °C, exhibited the IR-absorption bands due to hydroxyl and δ-lactone moieties, but no UV-absorption maximum characteristic of a conjugated enone moiety. In the EI-mass spectrum of **5**, a peak at m/z 480 derived from an aglycone was observed and the ^{1}H NMR spectrum suggests the presence of an acetoxyl group. Yadanzioside D (**5**) was hydrolyzed with β-glucosidase to yield the aglycone (**14**), whose molecular formula, $C_{23}H_{30}O_{11}$, was given by the high-resolution mass spectrum. The structure of **14** was determined by oxidation with manganese dioxide in *N*,*N*-dimethylformamide (DMF) leading to isobrucein B (**15**).[12,13] In the ^{1}H NMR spectrum of **14**, the signal due to $C_{(1)}$-H appeared at δ 4.01 as a doublet and its coupling constant between $C_{(1)}$-H and $C_{(2)}$-H was 8 Hz. A glycosylation shift (Δδ +11.0 ppm) due to

Table 1. ^{1}H NMR Spectra[a] of yadanziosides (**2**—**8**), **9**, **10**, and **13**.

	2[b]	**3**[c]	**4**[c]	**5**[b]	**6**[b]	**7**[b]	**8**[b]	**9**[d]	**10**[d]	**13**[e]
1-H	7.22 s	3.25 d (16.2)	7.29 s	f)	f)	7.25 s	f)	6.56 s	6.56 s	f)
2-H	—	—	—	4.45 m	4.42 m	—	4.42 m	—	—	—
3-H	—	—	—	5.72 brs	5.69 brs	—	5.69 brs	—	—	—
15-H	6.84 d (13)	6.9 br	6.9 br	6.78 d (12)	6.76 d (13)	6.81 d (13)	6.82 d (13)	f)	f)	6.23 d (13)
$C_{(4)}$-Me	1.13 d (6)	2.04 d (1.2)	1.19 d (6.7)	1.43 brs	1.43 brs	1.17 d (6)	1.42 brs	2.03 s	2.04 s	1.86 d (2)
$C_{(10)}$-Me	1.61 s	1.71 s	1.63 s	1.43 brs	1.43 brs	1.64 s	1.42 brs	1.66 s	1.66 s	1.41 s
CO_2Me	3.84 s	3.84 s	3.73 s	3.77 s	3.72 s	3.89 s	3.79 s	3.78 s	3.81 s	3.81 s
2′-H	f)	f)	6.77 d (1.2)	—	5.82 brs	6.06 s	f)	5.60 brs	5.74 d (1.2)	5.75 s
3′-H	0.96 d (6)	0.95 d (6.7)	2.40 brs	—	1.67 s	2.26 s	0.94 d (6)	2.16 d (1.2)	2.11 d (1.2)	2.14 d
	0.99 d (6)	0.98 d (6.7)		—	2.14 s		0.97 d (6)	1.91 d (1.2)		
4′-H	—	—	1.41 s	—	—	1.42 s	—	—	1.50 s	1.55 s
			1.42 s			1.46 s			1.52 s	1.55 s
4′-OAc	—	—	—	—	—	1.95 s	—	—	2.01 s	2.03 s
Anomeric-H	f)	5.46 (7.3)	5.37 d (7.0)	4.93 d (8)	4.94 d (6)	f)	f)	—	—	—

a) Coupling constants in Hz in parentheses. b) Measured at 90 MHz in C_5D_5N. c) Measures at 400 MHz in C_5D_5N. d) Measured at 400 MHz in $CDCl_3$. e) Measured at 90 MHz in $CDCl_3$. f) Not measured.

Table 2. ^{13}C NMR Spectra (22.5 MHz, C_5D_5N) of yadanziosides (YS's) and some their aglycones

No. of carbon	YSA(2)	YSB(3)	YSC(4)	YSD(5)	YSE(6)	YSG(7)	YSH(8)	9[a]	10[b]	11	14	16	19
1	129.6 d	51.1 t	129.3 d	84.9 d	84.8 d	129.7 d	84.9 d	122.3 d	121.9 d	50.1 t	84.5	84.5	84.3
2	148.8 s	193.6 s	149.2 s	84.3 d	84.2 d	148.8 s	84.3 d	145.8 s	145.8 s	192.2 s	73.3	73.3	73.3
3	194.6 s	147.9 s [c]	194.5 s	124.3 d	124.3 d	194.7 s	124.3 d	180.9 s	180.9 s	146.0 s	126.5	126.5	126.5
4	43.8 d	146.2 s [c]	43.8 d	135.8 s	135.9 s	43.9 d	135.8 s	130.8 s	130.9 s	128.1 s	135.8	135.8	135.8
5	40.6 d	43.3 d	40.5 d	43.1 d [c]	43.1 d [c]	40.4 d	43.1 d	156.8 s	156.3 s	42.4 d	43.4[c]	43.4	43.4[c]
6	30.0 t	29.3 t	30.0 t	28.3 t	28.3 t	30.1 t	28.3 t	32.5 t	32.4 t	29.6 t	28.6	28.6	28.7
7	83.5 d	83.5 d	83.5 d	81.2 d	81.2 d	83.5 d	81.2 d	83.9 d	83.7 d	83.7 d	82.3	82.3	82.4
8	46.6 s	46.1 s	46.7 s	46.7 s [d]	46.7 s [d]	46.6 s	46.7 s [c]	45.9 s	45.8 s	46.2 s	46.8[d]	46.9[c]	46.8[d]
9	41.3 d	42.2 d	41.4 d	43.0 d [c]	42.9 d [c]	41.4 d	43.1 d	41.4 d	41.4 d	42.4 d	43.3[c]	43.4	43.3[c]
10	39.5 s	40.8 s	39.7 s	44.4 s [d]	44.4 s [d]	39.6 s	44.4 s [c]	43.3 s	43.2 s	41.4 s	44.6[d]	44.6[c]	44.7[d]
11	73.4 d	73.1 d	73.6 d	75.5 d [e]	75.6[e]	73.4 d	75.5 d [d]	73.5 d [c]	75.9 d [c]	73.1 d	75.8	75.6[d]	75.8[e]
12	75.9 d	76.0 d [d]	76.1 d	75.6 d [e]	75.7[e]	76.0 d	75.7 d [d]	75.9 d [c]	77.2 d [c]	75.8 d	75.8	75.9[d]	75.9[e]
13	82.6 s	82.7 s	82.6 s	82.5 s	82.5 s	82.6 s	82.5 s	81.7 s	81.6 s	82.8 s	82.6	82.6	82.6
14	50.4 d	50.6 d	50.3 d	50.6 d	50.6 d	50.2 d	50.8 d	51.0 d	51	50.7 d	50.4	50.7	50.4
15	68.4 d	68.4 d	68.4 d	68.8 d	68.2 d	68.7 d	68.4 d	66.1 d	66.1 d	68.4 d	68.9	68.6	68.4
16	168.1 s	168.1 s	168.2 s [c]	168.0 s	168.2 s	168.0 s	168.2 s	166.5 s	166.1 s	168.1 s	168.0	168.2	168.3
18	12.5 q	15.3 q	12.6 q	20.7 q	20.8 q	12.5 q	20.7 q	10.9 q	11.9 q	13.4 q	20.9	20.9	21.0
19	17.9 q	15.8 q	18.0 q	12.1 q	12.1 q	18.0 q	12.1 q	23.6 q	23.7 q	15.7 q	12.3	12.3	12.4
20	73.1 t	73.6 t	73.8 t	74.1 t	74.1 t	73.7 t	74.1 t	73.2 t	73.4 t	73.8 t	74.1	74.1	74.1
21	171.1 s [c]	171.6 s [e]	171.2 s	171.5 s	171.4 s	171.7 s	171.6 s	171.5 s	171.5 s	171.6 s	171.6	171.7	171.5
OMe	52.3 q	52.4 q	52.4 q	52.2 q	52.2 q	52.6 q	52.2 q	53.0 q	53.4 q	52.3 q	52.3	52.3	52.2
1′	171.6 s [c]	171.2 s [e]	166.5 s	169.7 s	165.3 s	165.7 s	171.4 s	164.6 s	165.5 s [d]	171.3 s	169.7	171.5	165.4
2′	43.3 t	43.3 t	112.9 d	20.6 q	116.0 d	113.7 d	43.3 t	114.3 d	111.8 d	43.3 t	20.6	43.4	116.1
3′	25.8 d	25.9 d	168.3 s [c]		158.2 s	169.5 s	25.8 d	160.6 s	169.6 s	25.9 d		25.9	158.1
4′	22.4 q	22.4 q	73.2 s		27.0 q	82.3 s	22.5 q	27.5 q	82.2 s	22.4 q		22.5	27.0
5′	22.5 q	22.5 q	15.6 q		20.2 q	14.5 q	22.4 q	20.6 q	14.5 q	22.5 q		22.5	20.2
6′			28.9 q			26.4 q			26.3 q				
7′			28.9 q			25.8 q			26.0 q				
8′						163.3 s			164.7 s [d]				
9′						21.4 q			21.6 q				
1″	102.0 d	104.9 d	102.0 d	107.0 d	106.9 d	102.0 d	107.0 d						
2″	74.5 d	75.7 d [d]	74.7 d	76.1 d	76.0 d	74.6 d	76.1 d						
3″	78.7 d [d]	78.6 d [f]	79.0 d [d]	78.7 d [f]	78.6 d [f]	78.8 d [d]	78.7 d [e]						
4″	71.3 d	71.6 d	71.3 d	71.7 d	71.6 d	71.4 d	71.6 d						
5″	78.3 d [d]	78.4 d [f]	78.6 d [d]	78.6 d [f]	78.5 d [f]	78.4 d [d]	78.6 d [e]						
6″	62.3 t	62.8 t	62.4 t	62.8 t	62.7 t	62.4 t	62.8 t						

a) Measured in $CDCl_3$ at 22.5 MHz. b) Measured in $CDCl_3$ at 100 MHz. c) The assignments of these signals may be reversed in each column. d), e), and f) are the same as c).

C-2 was observed in the ^{13}C NMR spectra of **5** and **14**. These observations suggest that the configuration of $C_{(2)}$-OH of **14** is α-equatorial and the glycoside linkage forms through the C-2 oxygen atom, leading to the structure, 2-β-D-glucoside of the allylic alcohol (**14**) derived from isobrucein B (**15**) for yadanzioside D (**5**).

Yadanzioside H (**8**), mp 180—185 °C, showed a peak at *m/z* 709 due to $[M+Na]^+$ in the SIMS, indicating the molecular formula, $C_{32}H_{46}O_{16}$, and was hydrolyzed with β-glucosidase to give an aglycone (**16**). The aglycone (**16**) showed a similar ^1H NMR spectrum to that of **14**, except for the presence of an isopropyl group (δ 0.94 and 0.97, each d, J=6 Hz) instead of the acetyl group (δ 2.09, s) for **14**. Therefore, the structure (**16**) was deduced for the aglycone and the proposed structure was confirmed by oxidation with manganese dioxide yielding isobrucein A (**17**).[14]

In the ^{13}C NMR spectra of **8** and **16**, a glycosylation shift ($\Delta\delta$ +11.0 ppm) was observed at C-2, indicating the structure of yadanzioside H (**8**) should be assigned as a 2β-D-glucoside of the aglycone (**16**) derived from isobrucein A (**17**).

On hydrogenation, yadanzioside H (**8**) yielded a dihydro derivative (**18**), $C_{32}H_{48}O_{16}$, as the sole product judging from ^{13}C NMR, although the configuration of $C_{(4)}$-CH_3 could not be assigned.

Yadanzioside E (**6**), mp 190—195 °C, was inferred to be a 2′,3′-dehydro derivative of yadanzioside H (**8**) from the following observations. The molecular formula, $C_{32}H_{44}O_{16}$, was determined by the peak at *m/z* 707 due to $[M+Na]^+$ in the SIMS and the presence of $(CH_3)_2C$=CH- grouping (δ 1.67 (3H, s), 2.14 (3H, s), and 5.82 (1H, brs)) was revealed by the ^1H NMR spectrum.

On hydrolysis with β-glycosidase, yadanzioside E (**6**) afforded an aglycone (**19**), the ^1H NMR spectrum being compatible with the proposed structure. The aglycone (**19**) was oxidized with manganese dioxide in DMF to give a keto alcohol (**20**). The molecular formula, $C_{26}H_{32}O_{11}$, of **20** was determined by high-resolution mass spectrum and the presence of the $(CH_3)_2C$=CH- grouping was confirmed by a peak at *m/z* 83 characteristic of $[(CH_3)_2C=CH-C^+=O]$ together with ^1H NMR spectrum. Thus the structure of yadanzioside E (**6**) was proposed to be a 2β-D-glucoside of the aglycone (**19**). The proposed structure was firmly established as follows. Yadanzioside E (**6**) was hydrogenated over 10% palladium on carbon in ethanol to give a tetrahydro derivative, which was completely identical with the dihydro derivative (**18**) obtained from yadanzioside H (**8**).

Prior to yadanziosides, a fraction containing new quassinoids was eluted from the silica-gel column chromatography of the filtrate obtained by the separation of brusatol (**1**) (*loc. cit.*). The fraction was further subjected to separation by silica-gel column chromatography and then by reversed-phase preparative TLC to give new quassinoids, dehydrobrusatol (**9**) and dehydrobruceantinol (**10**).

Dehydrobrusatol (**9**), mp 157—160 °C, gave the molecular formula, $C_{26}H_{30}O_{11}$, in EI-high-resolution mass spectrum, which is two hydrogen atoms less than that of brusatol (**1**). The mass spectrum also showed prominent peaks at *m/z* 436 ($[M-82]^+$), and *m/z* 83, which indicate the presence of $(CH_3)_2C$=CH-CO- grouping. Dehydrobrusatol (**9**) exhibited the UV absorption maximum at 256 nm, which shifted to 340 and 262 nm on addition of alkali. This behavior is characteristic of dehydro-type quassinoids, such as dehydrobruceantin (**21**),[12] which shows the UV maxima at 259 and 225 nm and the former absorption shifts to 340 and 263 nm on addition of alkali. The ^1H NMR spectrum of **9** is similar to that of dehydrobruceantin (**21**) except for the side chain. These observations led to the structure (**9**) for dehydrobrusatol and the structure was supported by chemical transformation; brusatol (**1**) was treated with 2,3-dichloro-5,6-dicyano-*p*-benzoquinone (DDQ) in boiling benzene to give a dehydro product in 64% yield, which was identical with dehydrobrusatol (**9**).

Dehydrobruceantinol (**10**), mp 152—154 °C, showed the peak at *m/z* 627 due to $[M+Na]^+$ in the SIMS, which corresponds to the molecular formula, $C_{30}H_{36}O_{13}$. The EI-high-resolution mass spectrum gave a dehydration peak at *m/z* 586.2064. The ^1H NMR spectrum of **10** measured at 400 MHz was given in Table 1. Comparison with dehydrobrusatol (**9**) as to the skeletal structure and with bruceantinol (**13**) as to the side chain led to the construction of the structure (**10**) for dehydrobruceantinol.

Yadanziosides A, B, C, D, E, and G showed antileukemic activities against the murine P388 lymphocytic leukemia at a 10 mg/kg dose level and their ILS values[15] were 7.1, 4.1, 2.0, 9.2, 7.1, and 4.1%, respectively. These activities were found to be slightly stronger than that (ILS value; 2.0%) of bruceoside A.

Experimental[16]

Extraction and Separation. Pulverized seeds (60 kg) of *B. javanica* were defatted with hexane (100 l) twice and then extracted with methanol (100 l) twice. The methanol extract was concentrated *in vacuo* to give a syrup, to which the equal volume of water was added. The aqueous solution was completely defatted with hexane (7 l) three times and extracted with dichloromethane five times. The organic layer was concentrated to give a residue, which was dissolved in methanol kept at *ca.* 60 °C. The methanolic solution was allowed to stand at room temperature to afford brusatol (**1**) as crystals, which was filtered off. The filtrate was evaporated to give an oily residue (160 g), a part (36 g) of which was separated by the following procedures.

Column A. The oily residue (36 g) was subjected to separation by silica-gel (575 g) column chromatography.

Elution (each fraction 1 l) with PhH–AcOEt (2:1) gave fractions 1—7, PhH–AcOEt (1:1) fractions 8—16, AcOEt fractions 17—22, and AcOEt–MeOH fractions 23—32. Fraction 20 afforded brucein D (736 mg).

Column **B**. The fraction 9 of Column **A** yielded brusatol (**1**; 4.1 g) as crystals on standing, which was filtered off. The mother liquor, on evaporation, gave a residue (980 mg), which was chromatographed on silica gel (150 g) eluted with 5% MeOH in $CHCl_3$ (each fraction 30 ml). The fraction 20 (56 mg) was further separated by preparative TLC (RP-2, developed with H_2O–MeOH (6:4) twice) to give dehydrobrusatol (**9**; 13.6 mg), dehydrobrucein A (7.5 mg), and dehydrobruceantinol (**10**; 5.5 mg).

Column **C**. The fractions 23 and 24 of Column **A** were combined and evaporated to afford a residue (17.6 g), a part (10.7 g) of which was chromatographed on silica gel (865 g). Low layers of the following solvent-ratios of $CHCl_3$–MeOH–H_2O were used for elution (each fraction 400 ml): fractions 1—6; 25:4:1, fractions 7—10; 20:4:1, and fractions 11—24; 16:4:1.

Column **D**. The fractions 12 and 13 (1.5 g) of Column C were subjected to separation by a Lobar column (RP-8) eluted with MeOH–H_2O (4:6) and a total of 142 fractions (each 10 g) were collected. Fractions 30—63 gave bruceoside A (792 mg). Yadanziosides A (**2**; 151 mg) and G (**7**; 300 mg) were obtained from fractions 75—86 and 88—111, respectively. Fractions 113—125 afforded bruceantinoside A (24 mg).

Column **E**. The fraction 14 (932 mg) of Column C was purified by partition chromatography on silicic acid (400 g) absorbed with water (270 ml). Elution (each fraction 250 ml) was performed with 0, 3, 6,···24% EtOH in $CHCl_3$ (each 1 l).

Column **F**. The fractions 16 and 17 of Column **E** were combined (524 mg) and chromatographed using a Lobar column (RP-8). Elution was carried out with MeOH–H_2O and 28 fractions (each 10 g) were collected.

Column **G**. The fractions 17—24 (291 mg) of Column **F** were chromatographed on Toyopearl HW-40S eluted with MeOH (each 10 g). Fractions 37—39 (207 mg) were further purified by silica-gel (30 g) column chromatography eluted with a low layer of $CHCl_3$–MeOH–H_2O (16:4:1) to give yadanzioside E (**6**; 123 mg).

Column **H**. The fractions 25—28 (47 mg) of Column **F** were chromatographed using Toyopearl HW-40S. Elution with MeOH afforded yadanzioside H (**8**; 32 mg).

Column **I**. The fractions 16 (958 mg) of Column C was subjected to separation by partition chromatography on silicic acid (400 g) absorbed with water (270 ml). Elution (each 250 ml) was performed with 0, 3, 6, 9,···24% EtOH in $CHCl_3$ (each 1 l). Fractions 26—29 and 32—34 afforded yadanzioside D (**5**; 68 mg) and brucein E (35 mg), respectively.

Column **J**. The fractions 17—20 (681 mg) of Column **I** were chromatographed on a Lobar column (RP-8). Elution with MeOH–H_2O (1:1, each fraction 10 g) afforded bruceoside B (147 mg) from fractions 11—13. Fractions 18 and 19 were combined (62 mg) and further purified using Toyopearl HW-40S eluted with MeOH to give yadanzioside B (**3**; 52 mg).

Column **K**. The fractions 22—24 (128 mg) of Column **I** were chromatographed using Toyopearl HW-40S. Elution with MeOH afforded yadanzioside C (**4**; 86 mg).

Yadanzioside B (3). Amorphous solid, mp 189—195 °C (decomp), $[\alpha]_D^{26}$ −8.1° (*c* 0.84, EtOH); IR (KBr) 3425, 1735, 1635, and 1050 cm^{-1}; UV (ethanol) 255 nm (ε 8300); MS (SIMS) *m/z* 707 ($[M+Na]^+$), 523, and 439; High-resolution MS (EI) *m/z* 522.2082. Calcd for $C_{26}H_{34}O_{11}$ ($M-C_6H_{10}O_5$): *m/z* 522.2099.

Acid Hydrolysis of 3. Yadanzioside B (**3**; 36 mg) was treated with 1.5 M sulfuric acid (7 ml) and methanol (7 ml) at reflux temperature for 5 h. The usual work-up gave brucein A (**11**; 6 mg).

A solution of **3** (>1 mg) in a mixture of acetyl chloride (0.05 ml) and dry methanol (0.5 ml) was refluxed for 16 h. The reaction mixture was concentrated *in vacuo* to yield methyl D-glucoside, which was treated with trimethylsilyl chloride (10 μl) in pyridine (50 μl) and hexamethyldisilazane (5 μl). The trimethylsilylated product was identified by GLC retention time (9.4 min) by comparison with an authentic sample.

Yadanzioside A (2). Amorphous solid, mp 200—204 °C (decomp): $[\alpha]_D^{26}$ +3° (*c* 1.8, ethanol); IR (KBr) *ca.* 3400, 1740, 1675, 1625, and 1040 cm^{-1}; UV (ethanol) 256 nm (ε 5900); MS (SIMS) *m/z* 707 ($[M+Na]^+$), 523, 439, 421, and 403; High-resolution MS (EI) *m/z* 522.2127. Calcd for $C_{26}H_{34}O_{11}$ ($M-C_6H_{10}O_5$): *m/z* 522.2099.

Enzymatic Hydrolysis of 2. A mixture of yadanzioside A (**2**; 43 mg) and β-glucosidase (23 mg, Product of Sigma Chemical Company) in water (5 ml) was kept 2 weeks at 37 °C. The mixture was added to ethanol and heated at 80 °C for 10 min. After being cooled, the mixture was filtered and the filtrate was evaporated to dryness *in vacuo*. The residue was subjected to purification by column chromatography (C-200, 10 g) eluted with 10% MeOH in $CHCl_3$ to yield brucein A (**11**; 13 mg) as the aglycone and the starting material (20 mg). The aglycone, brucein A, was completely identical with an authentic sample.

Yadanzioside C (4). Amorphous solid, mp 204—209 °C (decomp); $[\alpha]_D^{26}$ +20° (*c* 0.92, ethanol); IR (KBr) 3445, 1740, 1680, 1640, and 1070 cm^{-1}; UV (ethanol) 221 nm (ε 14800) and 254 nm (ε 7800); MS (SIMS) *m/z* 749 ($[M+Na]^+$), 709, 673, 565, 547, 521, 439, 185, and 127; High-resolution MS (EI) *m/z* 564.2230. Calcd for $C_{28}H_{36}O_{12}$ ($M-C_6H_{10}O_5$): *m/z* 564.2207.

Acid Hydrolysis of 4. A solution of yadanzioside C (**4**; 38 mg) in 1.5 M sulfuric acid (10 ml) and methanol (10 ml) was refluxed for 5 h. The usual work-up gave brucein C (**12**; 13 mg), which was identical with an authentic sample.

A solution of **4** (>1 mg) in a mixture of dry methanol (0.5 ml) and acetyl chloride (0.05 ml) was refluxed for 16 h and the usual work-up afforded methyl D-glucoside.

Yadanzioside G (7). Amorphous solid, mp 180—185 °C (decomp); $[\alpha]_D^{22}$ +19° (*c* 1.2, ethanol); IR (KBr) 3450, 1740, 1685, 1645, 1075, 1050, and 1025 cm^{-1}; UV (ethanol) 222 nm (ε 16000) and 253 nm (ε 7800); MS (SIMS) *m/z* 791 ($[M+Na]^+$), 547, 127, and 109; High-resolution MS (EI) *m/z* 546.2103. Calcd for $C_{28}H_{34}O_{11}$ ($M-C_6H_{10}O_5-C_2H_4O_2$): *m/z* 546.2101.

Enzymatic Hydrolysis of 7. A solution of **7** (66 mg) and β-glucosidase (23 mg) in water (8 ml) was kept at 37 °C for 2 weeks and worked up as before to give bruceantinol

(**13**; 14 mg) and the starting material (31 mg).

Yadanzioside D (5). Amorphous soilid, mp 207—212 °C (decomp); $[\alpha]_D^{20}$ +38° (*c* 0.98, ethanol); IR (KBr) 3430, 1745, 1640, 1065, and 1040 cm^{-1}; MS (EI) *m/z* (%) 480 (0.8), 464 (1.5), 446 (1.4), 438 (1), 169 (27), 73 (100), 60 (72), and 57 (72); High-resolution MS (EI) *m/z* 480.1610. Calcd for $C_{23}H_{28}O_{11}$ ($M-C_6H_{12}O_5$): *m/z* 480.1630.

Enzymatic Hydrolysis of 5. Yadanzioside D (**5**; 29 mg) was hydrolyzed with β-glucosidase (10 mg) for 2 weeks at 37 °C to give an aglycone (**14**; 8 mg) and the starting material (**5**; 7 mg). **14**: mp 218—219 °C (from acetone-hexane); $[\alpha]_D^{26}$ +16° (*c* 0.63, pyridine); IR (KBr) 3450, 1745, 1640, 1060, and 1035 cm^{-1}; ^1H NMR (pyr-d_5, 90 MHz) δ=1.52 (3H, s; 10-Me), 1.55 (3H, brs; 4-Me), 2.09 (3H, s; 15-OAc), 2.60 (2H. br; 5- and 9-H), 3.78 (3H, s; CO_2Me), 3.85 (1H, d, *J*=8 Hz; 20-H), 3.90 (1H, br; 14-H), 4.01 (1H, d, *J*=8 Hz; 1-H), 4.50 (1H, m; 2-H),4.91 (1H, t-like; 7-H), 5.05 (1H, br; 12-H), 5.20 (1H, d, *J*=7 Hz; 20-H), 5.50 (1H, d, *J*=6 Hz; 11-H), 5.71 (1H, br; 3-H), and 6.76 (1H, d, *J*=13 Hz; 15-H); MS (EI) *m/z* (%) 482 (M^+; 2), 464 (6), 446 (8), 422 (5), 404 (7), 60 (100), and 57 (80); High-resolution MS (EI) *m/z* 482.1764. Calcd for $C_{23}H_{30}O_{11}$: *m/z* 482.1786.

Oxidation of 14 with Manganese Dioxide. The aglycone (**14**; 7 mg) was stirred with manganese dioxide (115 mg, preheated at 110 °C) in DMF (3 ml) for 6 h. The reaction mixture was filtered and the residue was washed with methanol. The filtrate and washings were combined and evaporated. The residue was purified by column chromatography on silica gel (C-200, 3 g). Elution with chloroform-methanol-water (16:4:1) gave isobrucein B (**15**; 5 mg), which was identified by comparison with an authentic specimen.

Yadanzioside H (8). Amorphous solid, mp 180—185 °C (decomp); $[\alpha]_D^{24}$ +33° (*c* 1.03, ethanol); IR (KBr) 3450, 1750, 1640, 1065, and 1040 cm^{-1}; MS (SIMS) *m/z* 709 ($[M+Na]^+$), 523, 507, and 439; MS (EI) *m/z* (%) 522 (0.6), 506 (0.6), 488 (2.7), 474 (2.2), 456 (3.8), 438 (4.2), 169 (26), 85 (59), and 57 (100); High-resolution MS (EI) *m/z* 522.2091. Calcd for $C_{26}H_{34}O_{11}$ ($M-C_6H_{12}O_5$): *m/z* 522.2099.

Enzymatic Hydrolysis of 8. Yadanzioside H (**8**; 43 mg) was hydrolyzed with β-glucosidase (15 mg) in water (5 ml) at 37 °C for 2 weeks to give an aglycone (**16**; 15 mg) and the starting material (**8**; 17 mg). **16**: mp 162—165 °C (from acetone-hexane); IR (KBr) 3455, 1750, 1640, 1060, and 1040 cm^{-1}; $[\alpha]_D^{26}$ +10° (*c* 1.0, pyridine); ^1H NMR (pyr-d_5, 90 MHz) δ=0.94 and 0.97 (each 3H, d, *J*=7 Hz; 3′-Me), 1.52 (3H, s; 10-Me), 1.53 (3H, brs; 4-Me), 2.60 (2H, br; 5- and 9-H), 3.80 (3H, s; CO_2Me), 3.85 (1H, d, *J*=8 Hz; 20-H), 3.98 (1H, d, *J*=7 Hz; 1-H), 4.50 (1H, m; 2-H), 4.87 (1H, brs; 7-H), 5.05 (1H, br; 12-H), 5.19 (1H, d, *J*=8 Hz; 20-H), 5.48 (1H, brd, *J*=5 Hz; 11-H), 5.70 (1H, br; 3-H), and 6.82 (1H, d, *J*=13 Hz; 15-H); MS (EI) *m/z* (%) 524 (M^+; 0.1), 506 (1), 85 (60), and 57 (100); Found: *m/z* 524.2279. Calcd for $C_{26}H_{36}O_{11}$: M, 524.2257.

Oxidation of 16 with Manganese Dioxide. The aglycone (**16**; 14 mg) was treated with manganese dioxide (230 mg) in DMF (4 ml) for 6 h. The same work-up as before afforded isobrucein A (**17**; 3 mg), which was identical with an authentic sample.

Hydrogenation of Yadanzioside H (8). A solution of yadanzioside H (**8**; 20 mg) in ethanol (3 ml) was hydrogenated in the presence of 10% palladium on carbon (10 mg) for 10 h. The usual work-up and separation by silica-gel chromatography afforded a dihydro derivative (**18**; 18 mg), mp 201—205 °C (from acetone-hexane); ^1H NMR (pyr-d_5, 90 MHz) δ=0.65 (3H, brs; 4-Me), 0.94 and 0.96 (each 3H, d, *J*=7; 3′-Me), 2.31 (2H, s; 2′-H), 3.80 (3H, s; CO_2Me), and 6.84 (1H, d, *J*=13 Hz; 15-H); ^{13}C NMR (pyr-d_5, 22.5 MHz) δ=12.9, 19.5, 22.5, 22.5, 25.8, 28.7, 29.2, 41.5, 43.4, 44.1, 44.6, 45.9, 46.9, 50.7, 52.3, 62.8, 68.4, 71.6, 73.6, 75.7, 75.9, 76.0, 78.6, 78.7, 82.4, 82.5, 83.5, 84.2, 106.9, 168.3, 171.5, and 171.6; MS (EI) *m/z* (%) 526 (0.2), 508 (0.6), 490 (0.7), 476 (0.7), 442 (0.6), 424 (1.5), 407 (1.7), 406 (2.4), 392 (1.9), 388 (1.6), 376 (1.5), 374 (1.5), 358 (1.6), 348 (2.4), 318 (2.8), 126 (17), 85 (50), 73 (24), 69 (32), 60 (100), and 57 (72).

Yadanzioside E (6). Amorphous solid, mp 190—195 °C (decomp); $[\alpha]_D^{23}$ +59° (*c* 1.6, ethanol); IR (KBr) 3450, 1740, 1645, 1080, 1060, and 1040 cm^{-1}; MS (SIMS) *m/z* 707 ($[M+Na]^+$), 519, 505, and 439; High-resolution MS (EI) *m/z* 520.1928. Calcd for $C_{26}H_{32}O_{11}$ ($M-C_6H_{12}O_5$): *m/z* 520.1943.

Enzymatic Hydrolysis of 6. Yadanzioside E (**6**; 39 mg) in water (5 ml) was enzymatically hydrolyzed with β-glucosidase (17 mg) at 37 °C for 2 weeks. The usual work-up and separation afforded an aglycone (**19**; 18 mg), mp 162—164 °C (from acetone-hexane); IR (KBr) 3450, 1740, 1645, 1055, and 1035 cm^{-1}; ^1H NMR (pyr-d_5, 90 MHz) δ=1.54 (6H, brs; 4- and 10-Me), 1.66 and 2.14 (each 3H, s; 3′-Me), 2.60 (2H, br; 5- and 9-H), 3.74 (3H, s; CO_2Me), 4.02 (1H, d, *J*=8 Hz; 1-H), 4.50 (1H, m; 2-H), 4.94 (1H, br; 7-H), 5.08 (1H, br: 12-H), 5.21 (1H, d, *J*=8 Hz; 20-H), 5.51 (1H, m; 11-H), 5.71 (1H, br; 3-H), 5.80 (1H, brs; 2′-H), and 6.75 (1H, d, *J*=13 Hz; 15-H); MS (EI) *m/z* (%) 522 (M^+; 0.1), 504 (0.4), 486 (3), and 83 (100); Found: *m/z* 522.2108. Calcd for $C_{26}H_{34}O_{11}$: M, 522.2102.

Oxidation of 19 with Manganese Dioxide. Oxidation of the aglycone (**19**; 15 mg) with manganese dioxide (245 mg) in DMF (3 ml) for 6 h gave a keto alcohol (**20**; 3 mg) after purification by silica-gel (5 g) column chromatography eluted with 10% MeOH in $CHCl_3$ **20**: Amorphous, mp 162—164 °C (from acetone-hexane); IR (KBr) 3460, 1750, 1675, 1660, 1085, 1065, and 1040 cm^{-1}; UV (ethanol) 222 nm (ε 17600); ^1H NMR ($CDCl_3$, 90 MHz) δ=1.19 (3H, s; 10-Me), 1.94 (3H, d, *J*=1 Hz; 3′-Me), 1.96 (3H, s; 4-Me), 2.19 (3H, brs; 3′-Me), 3.78 (3H, s; CO_2Me), 4.16 (1H, s; 1-H or 12-H), 4.29 (1H, brs; 12-H or 1-H), 4.77 (1H, br; 7-H), 4.82 (1H, d, *J*=6 Hz; 20-H), 5.64 (1H, brs; 2′-H), 6.12 (1H, brs; 3-H), and 6.23 (1H, d, *J*=14 Hz; 15-H); MS (EI) *m/z* (%) 520 (M^+; 0.7), 502 (1.5), and 83 (100); Found: *m/z* 520.1968. Calcd for $C_{26}H_{32}O_{11}$: M, 520.1943.

Hydrogenation of Yadanzioside E (6). Yadanzioside E (**6**; 46 mg) in ethanol (6 ml) was hydrogenated in the presence of 10% palladium on carbon (30 mg) for 4 h. The reaction product was worked up as usual to give a tetrahydro derivative (46 mg). The physical and spectral data were completely identical with those of **18**, obtained by the hydrogenation of yadanzioside H (**8**).

Dehydrobrusatol (9). Amorphous solid, mp 157—160 °C (from acetone-hexane); $[\alpha]_D^{22}$ +57° (*c* 1.4, ethanol); IR (KBr) 3440, 1740, 1635, 1140, 1080, and 1060 cm^{-1}; UV (ethanol) 256 nm (ε 7500); (ethanol+KOH) 340 nm and 262 nm; MS (EI) *m/z* (%) 518 (M^+; 1), 436 (>0.1), and 83 (100); Found: *m/z* 518.1784. Calcd for $C_{26}H_{30}O_{11}$: M, 518.1787.

Dehydrogenation of Brusatol (1). A solution of brusatol (**1**; 20 mg) in benzene (2 ml) was refluxed with DDQ (12 mg) for 6 h under nitrogen atmosphere. The reaction product was subjected to separation by silica-gel column chromatography. Elution with 3% 2-propanol in dichloromethane gave crude dehydrobrusatol (**9**; 16 mg), which was further chromatographed on silica gel. Elution with 1% methanol in chloroform afforded dehydrobrusatol (**9**; 13 mg), whose physical and spectral data were identical with those of the natural dehydrobrusatol (**9**).

Dehydrobruceantinol (10). Amorphous solid, mp 152—154 °C (from acetone-hexane); $[\alpha]_D^{22}$ +39° (*c* 0.45, ethanol); IR (KBr) 3445, 1740, 1635, 1260, 1165, and 1060 cm^{-1}; UV (ethanol) 255 nm (ε 8400); (ethanol+KOH) 336—340, 262, and 229 nm; MS (SIMS) *m/z* 627([M+Na]$^+$) and 567; High-resolution MS (EI) *m/z* 586.2064 and *m/z* 526.1866. Calcd for $C_{30}H_{34}O_{12}$ (M−H_2O): *m/z* 586.2051 and $C_{28}H_{30}O_{10}$ (M−H_2O−AcOH): *m/z* 526.1839, respectively.

The authors wish to thank Mr. Hideo Naoki of Suntory Institute for Bioorganic Research for measurement of SIMS.

References

1) T. Sakaki, S. Yoshimura, M. Ishibashi, T. Tsuyuki, T. Takahashi, T. Honda, and T. Nakanishi, *Chem. Pharm. Bull.*, **32**, 4702 (1984).

2) S. Yoshimura, T. Sakaki, M. Ishibashi, T. Tsuyuki, T. Takahashi, and T. Honda, *Bull. Chem. Soc. Jpn.*, **58**, 2673 (1985).

3) K. -H. Lee, Y. Imakura, Y. Sumida, R. -Y. Wu, and I. H. Hall, *J. Org. Chem.*, **44**, 2180 (1979).

4) M. Okano, K. -H. Lee, and I. H. Hall, *Lloydia*, **44**, 470 (1981).

5) K. Y. Sim, J. J. Sims, and T. A. Geissman, *J. Org. Chem.*, **33**, 429 (1968).

6) J. D. Phillipson and F. A. Darwish, *Planta Med.*, **41**, 209 (1981).

7) J. Polonsky, Z. Baskévitch, M. B. Das, and Müller, *C. R. Acad. Sci. Ser. C*, **267**, 1346 (1968).

8) J. Polonsky, Z. Baskévitch, A. Gaudemer, and B. C. Das, *Experientia*, **23**, 424 (1967).

9) J. Polonsky and Z. Baskévitch, *J. Org. Chem.*, **40**, 2499 (1975).

10) Glycosylation-shift values described in the preliminary report[1] should be reversed.

11) J. Polonsky, J. Varenne, T. Prangé, and C. Pascard, *Tetrahedron Lett.*, **21**, 1853 (1980).

12) S. M. Kupchan, R. W. Britton, J. A. Lacadie, M. F. Ziegler, and C. W. Siegel, *J. Org. Chem.*, **40**, 648 (1975).

13) C. Moretti, J. Polonsky, M. Vuilhorgne, and T. Prangé, *Tetrahedron Lett.*, **23**, 647 (1982).

14) J. Polonsky, Z. Baskévitch-Varon, and T. Sévenet, *Experientia*, **31**, 1113 (1975).

15) $\mathrm{LIS}(\%) = \left(\frac{\text{Mean life span (day) of sample}}{\text{Mean life span (day) of control}} - 1\right) \times 100$

16) General procedures are the same as those described in the preceding paper.[2]

 © 1985 The Chemical Society of Japan Bull. Chem. Soc. Jpn., 58, 2687—2696 (1985)

Boron Trifluoride Etherate-catalyzed Backbone Rearrangement of 13β,18β-Epoxybaccharan-3β-yl Acetate. A Sequential Migration of Two Methyl Groups and a Hydride in Biogenetic Direction[1)]

Shinya OHTA, Motoo TORI, Koji SUEMURA, Tomomi IROKAWA, Yoshihiko MORIYAMA,†
Takahiko TSUYUKI,* Takeyoshi TAKAHASHI,* Akiko ITAI,†† and Yoichi IITAKA††
Department of Chemistry, Faculty of Science, The University of Tokyo, Hongo, Bunkyo-ku, Tokyo 113
††*Faculty of Pharmaceutical Sciences, The University of Tokyo, Hongo, Bunkyo-ku, Tokyo 113*
†*Institute of Chemistry, Kyoto Prefectual University of Medicine, Taishogun, Kita-ku, Kyoto 603*
(Received May 24, 1985)

13β,18β-Epoxybaccharan-3β-yl acetate was treated with boron trifluoride etherate in acetic anhydride to afford a complex mixture, in which a formation of backbone rearrangement products, *D*:*C*-friedobacchar-9(11)-en- and -7-en-3β-yl acetates together with 3β-acetoxy-*D*-friedo-13,18-secobacchar-13-en-18-ylidene diacetate was observed. The *D*:*C*-friedobacchar-9(11)-ene derivative is the first example of the backbone rearrangement product formed by a sequential migration of two methyl groups and a hydride towards the biogenetic direction in baccharene-shionene series.

In biogenetic processes of triterpenes, some proceed enzymatically in direction to produce thermodynamically unstable products.[2)] A biogenesis of friedelin from oleanene-type precursor is known as a typical example of such energetically unfavorable processes.

Owing to the greater thermodynamic stability of the oleanene skeleton, most of the chemically-induced backbone rearrangement in oleanene-friedelene series proceed in the opposite direction from the biogenesis. On treatment with acid, for example, fridel-3-ene affords an equilibrium mixture of olean-13(18)-ene and 18α-olean-12-ene.[2)] Besides oleanene-friedelene series, the reactions of ursene-, lupene-, and baccharene-type triterpenes with acid do not give friedo-type triterpenes which would be produced by the biogenetic-like backbone rearrangement. However, it is possible to bring about the energetically unfavorable rearrangement in the biogenetic direction by combination with a free-energy releasing reaction which provides the thermodynamic driving force. Corey *et al.*[3)] reported backbone rearrangements of oleanene derivatives in the biogenetic direction under oxidative conditions. Paryzek[4)] and Baddeley *et al.*[5)] described the acid-catalyzed reaction of 9(11)-epoxylanostane derivatives in order to effect $C_{10}\rightarrow C_9$ methyl rearrangement. In these reactions, however, only one methyl group shifted towards biogenetic-like direction. Occurrence of a sequential multigroup rearrangement has never been observed so far.

The thermodynamic stability of baccharane skeleton was demonstrated by the following evidence. Treatment of bacchar-13(18)-en-3β-yl acetate (**1**)[6)] with hydrogen chloride in chloroform was found to yield a 1:1 mixture of bacchar-12-en-3β-yl acetate (**2**) and the starting material (**1**) by GLC examination; no skeletal rearrangement occurred. On the other hand, it has been shown that shiona-3,21-diene (**3**) is rearranged on treatment with boron trifluoride etherate ($BF_3\cdot OEt_2$) to give *D*:*C*-friedobaccharа-9(11),21-diene (**4**) and bacchara-12,21-diene (**5**),[7)] Therefore the baccharane skeleton was proved to be thermodynamically the most stable skeleton in the baccharene-shionene series.

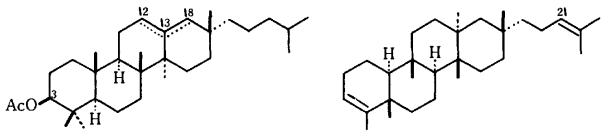

1 13(18)-ene
2 12-ene

3

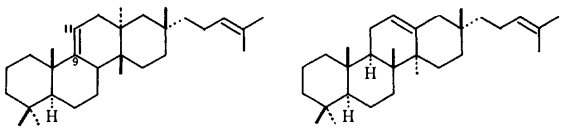

4

5

Paryzek[4b)] recommended the use of acetic anhydride as a solvent in a $BF_3\cdot OEt_2$-catalyzed backbone rearrangement, because BF_3–Ac_2O system is expected to be a useful reagent in which efficient skeletal rearrangements induced by an epoxide cleavage may proceed. Therefore, backbone rearrangement of 13β,18β-epoxybaccharan-3β-yl acetate (**6b**) in acetic anhydride was first examined.

13β,18β-Epoxybaccharan-3β-yl acetate (**6b**) was prepared by epoxidation of bacchar-13(18)-en-3β-yl acetate (**1**)[6,8)] with *m*-chloroperbenzoic acid (MCPBA). The epoxidation product was a mixture of α- and β-epoxides (**6a** and **6b**) in a ratio of 1:9, which was separated by silica-gel column chromatography. The

configuration of the epoxy ring was easily assignable from the ^{1}H NMR spectra.

13β,18β-Epoxybaccharan-3β-yl acetate (**6b**) was treated with $BF_3 \cdot OEt_2$ in acetic anhydride at 0 °C. The reaction product was separated by silica-gel column chromatography into three fractions, **A**, **B**, and **C**.

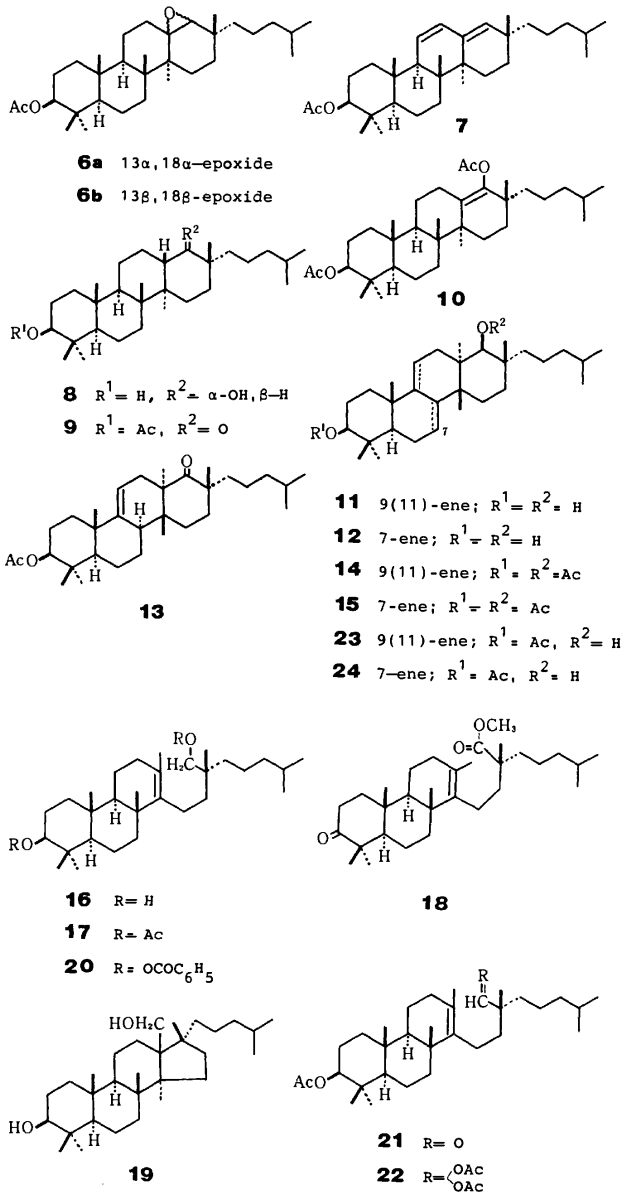

The fraction **A** was found to be bacchara-11,13(18)-dien-3β-yl acetate (**7**)[6] from the spectral data. The fraction **B** and **C** were shown to be mixtures by ^{1}H NMR spectral measurement, but each could not be separated by silica-gel column chromatography. The fraction **B** gave complicated signals appearing at δ 2.03, 2.07 (each *ca.* 3H, s), 4.45 (1H, dd), 4.90 and 4.92 (total *ca.* 0.7H, each s), and *ca.* 5.3 (*ca.* 0.5H, m). The fraction **C** showed complex signals appearing at δ 2.04, 2.06, 2.09, and 2.20 (each s), 3.35 (0.3—0.4H, m), *ca.* 4.45 (1H, m), 4.87 (0.3—0.4H, s), *ca.* 5.3 (0.1—0.2H, m), 6.69 and 6.71 (total *ca.* 0.4H, each s). On treatment with lithium aluminium hydride, the fraction **B** could be separated into three compounds, $\mathbf{B_1}$, $\mathbf{B_2}$, and $\mathbf{B_3}$ and the fraction **C** three compounds, $\mathbf{C_1}$, $\mathbf{C_2}$, and $\mathbf{C_3}$ by silica-gel column chromatography, respectively.

The compound $\mathbf{B_1}$ was identical with an authentic baccharane-3β,18α-diol (**8**).[8] Therefore the initial rearranged product is deduced to be bacchar-13(18)-ene-3β,18-diyl diacetate (**10**), which was formed directly by abstraction of the hydrogen or *via* 18-oxobaccharan-3β-yl acetate (**9**)[9] followed by acetylation under the reaction conditions (Scheme 1 [**A**]-*b*). The formation of **9** was supported by the rearrangement of **6b** in benzene (*vide infra*).

The compound $\mathbf{B_2}$, $C_{30}H_{52}O_2$, was a diol with a trisubstituted double bond, which was proved from the presence of a multiplet signal due to an olefinic proton at δ 5.38 in the ^{1}H NMR spectrum and characteristic fragment ion peaks at *m/z* 259 and *m/z* 247 in the mass spectrum. Comparison with olefinic signals of friedo-type triterpenes (see Table 1) revealed that the olefinic proton observed at δ 5.38 is corresponding to that of either 7-ene, 9(11)-ene, or 14-ene. A formation of the fragment ions at *m/z* 259 and *m/z* 247 is indicative of the presence of either 7-ene, 8-ene, or 9(11)-ene.[13] From these observations, the compound $\mathbf{B_2}$ was inferred to be either *D:C*-friedobacchar-9(11)-ene-3β,18β-diol (**11**) or a 7-ene isomer (**12**). On acetylation followed by oxidation, the compound $\mathbf{B_2}$ afforded a keto acetate (**13**), which showed a multiplet signal due to the olefinic proton at δ 5.38 in the ^{1}H NMR spectrum and fragment ion peaks at *m/z* 343 and *m/z* 344 in the mass spectrum. However, since further information concerning the exact position of the double bond could not be obtained from the spectral inspection for compound $\mathbf{B_2}$ and its derivative (**13**), X-ray single crystal analysis was carried out for the keto acetate (**13**). The crystals of **13** belong to a monoclinic, space group $P2_1$, and the lattice parameters are a=17.273(9), b=11.981(5), and c=7.323(3) Å, β=99.13(3)°, and D_c=1.08 g·cm^{-3} with two molecules in a unit cell. Intensity data were measured on a Philips PW1100 automatic four-circle diffractometer using monochromated Cu $K\alpha$ radiation. A total of 2349 non-zero, independent reflections with $3° \leq \theta \leq 78°$ were obtained by 2θ—θ scanning mode. The structure was solved by the direct method using MULTAN program and was refined by the block-diagonal least-squares method. All hydrogen atoms were located on a difference electron density map. The final R value was 0.056 assuming the anisotropic temperature factors for non-hydrogen atoms and the isotropic ones for the hydrogen atoms. The final atomic coordinates are listed in Table 2 and bond lengths and bond angles

are listed in Tables 3 and 4.[14] Figure 1 is a computer-generated perspective drawing of the molecule of the keto acetate (**13**).

Thus the structure of the keto acetate was determined to be 18-oxo-*D*:*C*-friedobacchar-9(11)-en-3β-yl aceteate (**13**) and therefore the compound **B**$_2$ is formulated as *D*:*C*-friedobacchar-9(11)ene-3β,18β-diol (**11**). This conclusion implies that the reaction product obtained by the backbone rearrangement of **6b** was *D*:*C*-friedobacchar-9(11)-ene-3β,18β-diyl diacetate (**14**).

The compound **B**$_3$, $C_{30}H_{52}O_2$, was shown to be a double-bond isomer of **B**$_2$ from the spectral data; it showed a multiplet signal at δ 5.35 in the ^{1}H NMR spectrum and fragment ion peaks at *m/z* 259 and *m/z* 247 in the mass spectrum. These spectral data lead to the conclusion that the compound **B**$_3$ is formulated as *D*:*C*-friedobacchar-7-ene-3β,18β-diol (**12**) and therefore the rearranged product is *D*:*C*-friedobacchar-7-ene-3β,18β-diyl diacetate (**15**).

The compound **C**$_1$ (**16**) showed the molecular formula, $C_{30}H_{54}O_2$ by the high-resolution mass spectrum and the ^{1}H NMR spectrum revealed the presence of two hydroxyl groups; one is secondary (δ 3.17, 1H, dd) and the other primary (δ 3.36, 2H, s). Since no signal due to unsaturation was observed in the ^{1}H NMR spectrum, the compound **C**$_1$ was inferred to be either a tetracyclic saturated diol or a tricyclic diol with a tetrasubstituted double bond. On acetylation, the compound **C**$_1$ afforded a diacetate (**17**), $C_{34}H_{58}O_4$, whose ^{1}H NMR spectrum showed the presence of an acetoxymethyl group (δ 3.82, 2H, s and δ 2.04, 3H, s) together with a secondary acetoxyl group (δ 4.46, 1H, dd and δ 2.04, 3H, s).

The presence of the hydroxymethyl group in the compound **C**$_1$ was confirmed by the following chemical conversion. The compound **C**$_1$ was oxidized with Jones reagent to give a keto carboxylic acid, which, without purification, was treated with diazomethane. The reaction product (**18**) showed the molecular ion at *m/z* 472 ($C_{31}H_{52}O_3$) and the presence of $COOCH_3$ group (δ 3.67, 3H,s; 1730 cm^{-1}) together with a carbonyl group (1705 cm^{-1}). From these evidence and mechanistic consideration, the structure of the compound **C**$_1$ was inferred first to be 17(18→13)*abeo*-baccharane-3β,18-diol (**19**). However, this structure assignment was found to be erroneous by X-ray diffraction analysis of the dibenzoate (**20**). Crystals of the dibenzoate (**20**) belong to orthorhombic, space group $P2_12_12_1$, and the lattice parameters are a=17.071(5), b=21.191(6), and c=10.870(3) Å and D_c=1.10 g·cm^{-3}. Four molecules are contained in the unit cell. Intensity data were measured by the same procedure as before and a total of 3173 non-zero, independent reflections with $3°\leq\theta\leq78°$ were obtained by 2θ—θ scanning mode. The structure was solved and refined by the same procedure as before. The final R value was 0.066

Table 1. δ-Values of olefinic protons of friedo-type triterpenes

Compound	δ-Value	Lit,
Bacchar-5-en-3β-ol	5.62 m (6-H)	10)
Alnus-5-en-3β-ol	5.63 dd (6-H)	11)
D:*C*-Friedobacchar-7-en-3β-ol	5.39 q (7-H)	10)
D:*C*-Friedobacchara-7,21-diene	5.362 ddd (7-H)	7)
D:*C*-Friedobacchara-9(11),21-diene	5.301 ddd (11-H)	7)
Tarolupenyl acetate	5.325 ddd (15-H)	12)
Tarolupeol	5.333 ddd (15-H)	12)

Table 2. Atomic positional parameters (×10^4) and isotropic temperature factors (×10^2) for non-hydrogen atoms of keto acetate (**13**) with estimated standard deviations in parentheses

Atom	x	y	z	B_{eq}[a]
C(1)	590(3)	−943(0)	10815(6)	618(8)
C(2)	1456(3)	−952(5)	11475(6)	708(9)
C(3)	1807(2)	−2000(4)	10830(6)	600(8)
C(4)	1702(2)	−2108(4)	8733(6)	548(7)
C(5)	807(2)	−1994(4)	8021(5)	475(6)
C(6)	586(2)	−2167(4)	5912(6)	591(8)
C(7)	−255(3)	−2021(5)	5208(6)	721(10)
C(8)	−797(2)	−1951(4)	6597(5)	471(6)
C(9)	−512(2)	−1163(3)	8115(5)	466(6)
C(10)	371(2)	−978(4)	8660(5)	501(7)
C(11)	−1036(3)	−598(4)	9003(6)	589(8)
C(12)	−1898(3)	−687(4)	8528(6)	579(8)
C(13)	−2158(2)	−1773(4)	7477(5)	452(6)
C(14)	−1669(2)	−1897(4)	5858(5)	460(6)
C(15)	−1951(2)	−2945(4)	4736(6)	545(7)
C(16)	−2824(3)	−2873(5)	3921(7)	691(9)
C(17)	−3386(2)	−2619(4)	5287(6)	594(8)
C(18)	−3013(3)	−1755(4)	6740(6)	577(8)
C(19)	1984(3)	−3280(4)	8251(7)	658(9)
C(20)	2229(3)	−1253(5)	7917(7)	666(9)
C(21)	577(3)	150(4)	7813(7)	707(9)
C(22)	−1977(3)	−2732(4)	8911(6)	556(7)
C(23)	−1829(3)	−857(5)	4558(7)	674(9)
C(24)	−4145(3)	−2099(6)	4240(9)	897(12)
C(25)	−3579(3)	−3713(5)	6245(7)	695(9)
C(26)	−4076(3)	−3601(5)	7750(7)	731(10)
C(27)	−4259(3)	−4742(6)	8528(9)	878(12)
C(28)	−4741(4)	−4679(6)	10085(10)	1003(15)
C(29)	−5574(4)	−4292(7)	9445(13)	1167(19)
C(30)	−4728(4)	−5836(9)	11003(12)	1378(21)
C(31)	2840(3)	−2645(5)	13137(6)	639(8)
C(32)	3698(3)	−2659(7)	13763(9)	1056(14)
O(1)	2631(2)	−2066(3)	11580(4)	747(6)
O(2)	2369(2)	−3109(3)	13897(5)	803(7)
O(3)	−3442(2)	−1099(3)	7345(5)	819(7)

a) $B_{eq}=8\pi^2(u_1^2+u_2^2+u_3^2)/3$.

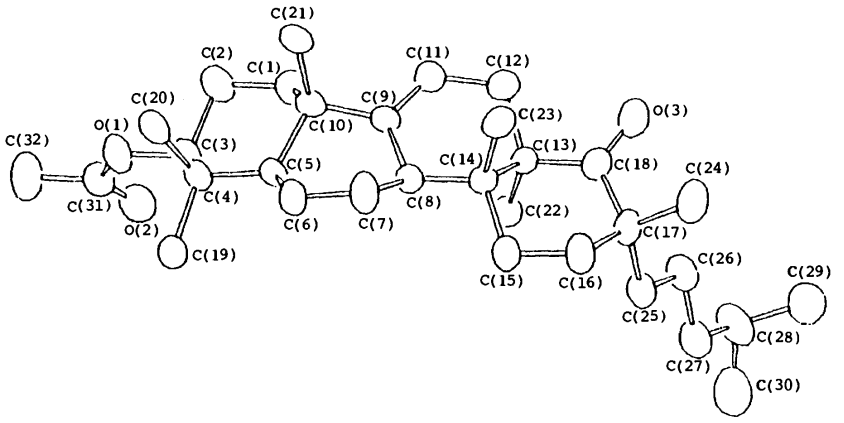

Fig. 1. Perspective view of 18-oxo-*D* : *C*-friedobacchar-9(11)-en-3β-yl acetate (**13**).

assuming the anisotropic temperature factors for non-hydrogen atoms and the isotropic ones for hydrogen atoms. The final atomic coordinates are listed in Table 5 and bond lengths and bond angles are listed in Tables 6 and 7.[14] Figure 2 is a computer-generated perspective drawing of the molecule of the dibenzoate (**20**), the structure being formulated as *D*-friedo-13,18-secobacchar-13-ene-3β, 18-diyl dibenzoate (**20**). Therefore, it is concluded that the initial rearranged product had been 3β-acetoxy-*D*-friedo-13,18-secobacchar-13-en-18-al (**21**), which was converted into its acylal (**22**) in the reaction conditions. This conclusion is supported by the presence of a singlet signal due to the acylal proton at δ 6.71 or δ 6.69 in the ^{1}H NMR spectrum of the fraction **C** (*loc. cit.*).

Table 3. Bond lengths (*l*/Å) of keto acetate (**13**) with estimated standard deviations in parentheses

Atom 1	Atom 2	Length	Atom 1	Atom 2	Length
C(1)	-C(2)	1.497(6)	C(13)	-C(14)	1.568(6)
C(1)	-C(10)	1.564(6)	C(13)	-C(18)	1.490(6)
C(2)	-C(3)	1.503(8)	C(13)	-C(22)	1.555(6)
C(3)	-C(4)	1.523(6)	C(14)	-C(15)	1.537(6)
C(3)	-O(1)	1.444(5)	C(14)	-C(23)	1.566(7)
C(4)	-C(5)	1.557(5)	C(15)	-C(16)	1.533(6)
C(4)	-C(19)	1.545(7)	C(16)	-C(17)	1.531(7)
C(4)	-C(20)	1.552(7)	C(17)	-C(18)	1.549(7)
C(5)	-C(6)	1.544(6)	C(17)	-C(24)	1.541(7)
C(5)	-C(10)	1.544(6)	C(17)	-C(25)	1.548(8)
C(6)	-C(7)	1.473(6)	C(18)	-O(3)	1.212(6)
C(7)	-C(8)	1.489(6)	C(25)	-C(26)	1.506(8)
C(8)	-C(9)	1.481(6)	C(26)	-C(27)	1.533(9)
C(8)	-C(14)	1.519(5)	C(27)	-C(28)	1.516(10)
C(9)	-C(10)	1.530(6)	C(28)	-C(29)	1.515(9)
C(9)	-C(11)	1.373(7)	C(28)	-C(30)	1.539(13)
C(10)	-C(21)	1.551(7)	C(31)	-C(32)	1.479(7)
C(11)	-C(12)	1.479(6)	C(31)	-O(1)	1.334(6)
C(12)	-C(13)	1.542(6)	C(31)	-O(2)	1.194(6)

The compound **C$_3$** showed a molecular ion peak at *m/z* 488, which indicates an increment corresponding to a substituent, CH_3-CH(OH)-, compared with those of the olefinic diols **B$_2$** (**11**) and **B$_3$** (**12**). Therefore, the initial reaction product of the backbone rearrangement was deduced to possess an additional acetyl group. It is conceivable that the olefin, such as **14** or **15**, which had been produced by the rearrangement was subjected to acetylation, because the rearrangement conditions could bring about Friedel-Crafts reaction. However, further investigation on the structure of **C$_3$** could not carried out because of a paucity of the material.

Since the compound **C$_2$** was found to be a complex mixture of compounds derived from acetylated products by the ^{1}H NMR spectrum, this fraction was not further examined.

On treatment with $BF_3 \cdot OEt_2$ in acetic anhydride, 13β,18β-epoxybaccharan-3β-yl acetate (**6b**) has been shown to afford backbone rearrangement products, *D*:*C*-friedobacchar-9(11)- and -7-ene-3β,18β-diyl diacetates (**14** and **15**), 3β-acetoxy-*D*-friedo-13,18-secobacchar-13-en-18-ylidene diacetate (**22**), and many unidentified acetylated products. Formation of these reaction products can be reasonably explained by the reaction pathway depicted as in Scheme 1. The epoxide ring of **6b** was cleaved by the attack of $BF_3 \cdot Et_2O$ to give a carbonium ion [**A**] at C-13. Deprotonations, *a* and *b*, would produce **7** and **10**, respectively, while a consecutive 1,2-methyl migration (pathways *c* and *d*) would yield a carbonium ion [**C**] at C-8, which affords **15** and **14** by deprotonation and 1,2-hydride shift (*f*) followed by deprotonation, respectively. The formation of *D*:*C*-friedobacchar-9(11)-ene derivative (**14**) is thus demonstrated by a sequential shift of 14α-Me, 8β-Me, and 9α-H of the baccharane skeleton to 13α-Me, 14β-Me, and 8α-H, respectively. It is noteworthy that the formation of

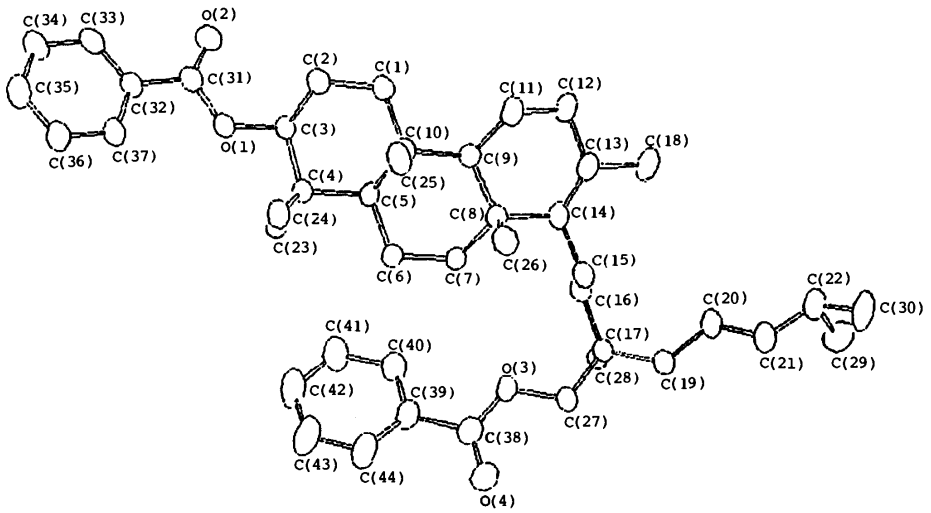

Fig. 2. Perspective view of *D*-friedo-13,18-secobacchar-13-ene-3β,18-diyl dibenzoate (**20**).

TABLE 4. BOND ANGLES (ϕ/°) OF KETO ACETATE (**13**) WITH ESTIMATED STANDARD DEVIATIONS IN PARENTHESES

Atom 1	Atom 2	Atom 3	Angle	Atom 1	Atom 2	Atom 3	Angle
C(2)	-C(1)	-C(10)	113.3 (3)	C(14)	-C(13)	-C(22)	111.4 (3)
C(3)	-C(2)	-C(1)	109.7 (4)	C(12)	-C(13)	-C(18)	111.2 (3)
C(4)	-C(3)	-C(2)	113.5 (4)	C(12)	-C(13)	-C(22)	106.0 (3)
C(4)	-C(3)	-O(1)	109.3 (4)	C(18)	-C(13)	-C(22)	109.7 (3)
C(2)	-C(3)	-O(1)	110.4 (4)	C(15)	-C(14)	-C(8)	111.7 (3)
C(5)	-C(4)	-C(3)	106.5 (3)	C(15)	-C(14)	-C(13)	108.5 (3)
C(5)	-C(4)	-C(19)	109.5 (4)	C(15)	-C(14)	-C(23)	108.3 (3)
C(5)	-C(4)	-C(20)	115.2 (4)	C(8)	-C(14)	-C(13)	111.0 (3)
C(3)	-C(4)	-C(19)	108.4 (4)	C(8)	-C(14)	-C(23)	108.7 (3)
C(3)	-C(4)	-C(20)	110.4 (4)	C(13)	-C(14)	-C(23)	108.6 (3)
C(19)	-C(4)	-C(20)	106.7 (4)	C(16)	-C(15)	-C(14)	111.8 (4)
C(6)	-C(5)	-C(4)	113.5 (3)	C(17)	-C(16)	-C(15)	116.3 (4)
C(6)	-C(5)	-C(10)	110.7 (3)	C(18)	-C(17)	-C(16)	110.1 (4)
C(4)	-C(5)	-C(10)	118.3 (3)	C(18)	-C(17)	-C(24)	107.5 (4)
C(7)	-C(6)	-C(5)	114.1 (4)	C(18)	-C(17)	-C(25)	110.5 (4)
C(8)	-C(7)	-C(6)	117.3 (4)	C(16)	-C(17)	-C(24)	109.4 (4)
C(9)	-C(8)	-C(7)	112.3 (4)	C(16)	-C(17)	-C(25)	109.4 (4)
C(9)	-C(8)	-C(14)	115.6 (3)	C(24)	-C(17)	-C(25)	109.9 (4)
C(7)	-C(8)	-C(14)	117.0 (4)	O(3)	-C(18)	-C(13)	120.4 (4)
C(10)	-C(9)	-C(8)	119.1 (3)	O(3)	-C(18)	-C(17)	118.2 (4)
C(10)	-C(9)	-C(11)	120.6 (4)	C(13)	-C(18)	-C(17)	121.3 (4)
C(8)	-C(9)	-C(11)	120.3 (4)	C(26)	-C(25)	-C(17)	116.4 (4)
C(21)	-C(10)	-C(1)	110.2 (3)	C(27)	-C(26)	-C(25)	111.6 (5)
C(21)	-C(10)	-C(5)	114.3 (4)	C(28)	-C(27)	-C(26)	113.9 (5)
C(21)	-C(10)	-C(9)	107.8 (4)	C(29)	-C(28)	-C(27)	113.0 (6)
C(1)	-C(10)	-C(5)	106.0 (3)	C(29)	-C(28)	-C(30)	111.0 (6)
C(1)	-C(10)	-C(9)	109.8 (3)	C(27)	-C(28)	-C(30)	108.2 (6)
C(5)	-C(10)	-C(9)	108.7 (3)	C(32)	-C(31)	-O(1)	113.2 (5)
C(12)	-C(11)	-C(9)	124.6 (4)	C(32)	-C(31)	-O(2)	125.0 (5)
C(13)	-C(12)	-C(11)	112.4 (4)	O(1)	-C(31)	-O(2)	121.8 (5)
C(14)	-C(13)	-C(12)	108.0 (3)	C(3)	-O(1)	-C(31)	118.1 (4)
C(14)	-C(13)	-C(18)	110.5 (3)				

14 and **15** is the first example of the energetically unfavorable rearrangement of triterpenes involving a sequential shift of the multigroup.

Table 5. Atomic positional parameters ($\times 10$)^4 and isotropic temperature factors ($\times 10^2$) for non-hydrogen atoms of dibenzoate (**20**) with estimated standard deviations in parentheses

Atom	x	y	z	B_{eq}[a]
C(1)	5734(2)	5565(2)	36(4)	501(6)
C(2)	6619(2)	5650(2)	−175(4)	538(7)
C(3)	7077(2)	5174(2)	583(4)	466(6)
C(4)	6843(2)	4483(2)	398(4)	459(6)
C(5)	5928(2)	4433(2)	494(4)	406(5)
C(6)	5620(2)	3760(2)	358(4)	497(6)
C(7)	4764(2)	3716(2)	770(4)	473(6)
C(8)	4217(2)	4163(2)	39(4)	445(6)
C(9)	4576(2)	4832(2)	139(4)	437(6)
C(10)	5447(2)	4906(2)	−291(4)	433(6)
C(11)	4007(2)	5323(2)	−412(5)	588(8)
C(12)	3271(3)	5335(2)	381(6)	708(9)
C(13)	2976(2)	4696(2)	769(5)	597(8)
C(14)	3385(2)	4165(2)	622(4)	480(6)
C(15)	3037(2)	3529(2)	949(4)	510(7)
C(16)	3075(2)	3358(2)	2307(4)	455(6)
C(17)	2779(2)	2696(2)	2668(4)	464(6)
C(18)	2167(3)	4722(3)	1327(7)	908(12)
C(19)	1950(2)	2558(2)	2177(5)	553(7)
C(20)	1297(3)	2967(2)	2627(5)	650(9)
C(21)	521(3)	2810(3)	1949(6)	796(11)
C(22)	−167(3)	3172(3)	2369(7)	772(11)
C(23)	7168(3)	4231(2)	−823(5)	678(9)
C(24)	7207(3)	4106(2)	1470(5)	651(8)
C(25)	5525(3)	4824(3)	−1695(4)	632(8)
C(26)	4104(3)	3912(2)	−1283(5)	626(8)
C(27)	3283(2)	2171(2)	2119(5)	526(7)
C(28)	2810(3)	2644(2)	4084(5)	582(7)
C(29)	−512(6)	2804(4)	3521(11)	1491(23)
C(30)	−866(4)	3083(4)	1515(9)	1350(19)
C(31)	8336(2)	5700(2)	592(4)	481(6)
C(32)	9153(2)	5644(2)	118(4)	467(6)
C(33)	9683(3)	6115(2)	431(5)	634(8)
C(34)	10453(3)	6073(3)	−3(6)	770(10)
C(35)	10683(3)	5577(3)	−746(6)	756(10)
C(36)	10152(3)	5120(3)	−1046(6)	720(9)
C(37)	9387(3)	5150(2)	−613(5)	597(8)
C(38)	4600(3)	1840(2)	2125(5)	585(7)
C(39)	5430(3)	2030(2)	2394(5)	596(8)
C(40)	5611(3)	2540(3)	3105(5)	661(9)
C(41)	6392(3)	2689(3)	3331(6)	813(11)
C(42)	6974(3)	2329(4)	2843(6)	893(12)
C(43)	6810(3)	1826(4)	2127(6)	929(13)
C(44)	6025(3)	1660(3)	1872(6)	838(11)
O(1)	7903(1)	5208(1)	253(3)	533(4)
O(2)	8100(2)	6130(1)	1204(3)	629(5)
O(3)	4096(1)	2289(1)	2432(3)	556(5)
O(4)	4410(2)	1349(2)	1680(5)	892(8)

a) $B_{eq}=8\pi^2(u_1^2+u_2^2+u_3^2)/3$.

The formation of seco-acylal (**22**) is interpreted in terms of mechanism involving 1,2-alkyl migration (*c*) followed by a bond fission (*e*). These skeletal rearrangements appear often in sesquiterpene oxides such as β-patchoulene oxide[15] or cyperene oxide,[16] and they also encounter in triterpene epoxides; for example 18,19-epoxylupane derivatives are transformed into 18,19-seco-lup-13(18)-ene (=baccha-r-13(18)-ene) derivatives on treatment with $BF_3\cdot OEt_2$.[17]

In this rearrangement reaction, a formation of Friedel-Crafts type acetylation products was observed, and these products caused the complication in the separation procedure. Then the backbone rearrangement reaction was examined in benzene.

13β,18β-Epoxybaccharan-3β-yl acetate (**6b**) was treated with $BF_3\cdot OEt_2$ in benzene at room temperature for 30 min. The reaction product was separated into five compounds by silica-gel chromatography.

The first-eluted compound was shown to be bacchara-11,13(18)-dien-3β-yl acetate (**7**). The second compound was also a known 18-oxobaccharan-3β-yl acetate (**9**),[9] which was identified with an authentic sample prepared by acetylation of 18-oxobaccharan-3β-ol.[8]

The third compound showing a singlet signal at δ 9.45 (1H) in the ^{1}H NMR spectrum, was inferred to

Table 6. Bond lengths (l/Å) of dibenzoate (**20**) with estimated standard deviations in parentheses

Atom 1	Atom 2	Length	Atom 1	Atom 2	Length
C(1)	-C(2)	1.539(6)	C(17)	-C(27)	1.527(6)
C(1)	-C(10)	1.523(6)	C(17)	-C(28)	1.545(7)
C(2)	-C(3)	1.519(6)	C(19)	-C(20)	1.494(6)
C(3)	-C(4)	1.531(6)	C(20)	-C(21)	1.551(7)
C(3)	-O(1)	1.457(4)	C(21)	-C(22)	1.476(8)
C(4)	-C(5)	1.569(5)	C(22)	-C(29)	1.588(13)
C(4)	-C(23)	1.535(7)	C(22)	-C(30)	1.524(10)
C(4)	-C(24)	1.544(7)	C(27)	-O(3)	1.450(5)
C(5)	-C(6)	1.528(5)	C(31)	-C(32)	1.491(6)
C(5)	-C(10)	1.551(5)	C(31)	-O(1)	1.330(5)
C(6)	-C(7)	1.531(5)	C(31)	-O(2)	1.198(5)
C(7)	-C(8)	1.548(6)	C(32)	-C(33)	1.390(6)
C(8)	-C(9)	1.548(6)	C(32)	-C(37)	1.373(6)
C(8)	-C(14)	1.557(5)	C(33)	-C(34)	1.401(7)
C(8)	-C(26)	1.544(6)	C(34)	-C(35)	1.382(8)
C(9)	-C(10)	1.567(5)	C(35)	-C(36)	1.366(8)
C(9)	-C(11)	1.544(6)	C(36)	-C(37)	1.390(7)
C(10)	-C(25)	1.542(6)	C(38)	-C(39)	1.502(6)
C(11)	-C(12)	1.525(7)	C(38)	-O(3)	1.327(5)
C(12)	-C(13)	1.506(7)	C(38)	-O(4)	1.193(6)
C(13)	-C(14)	1.332(6)	C(39)	-C(40)	1.364(7)
C(13)	-C(18)	1.509(7)	C(39)	-C(44)	1.403(8)
C(14)	-C(15)	1.515(6)	C(40)	-C(41)	1.392(7)
C(15)	-C(16)	1.521(6)	C(41)	-C(42)	1.360(9)
C(16)	-C(17)	1.543(6)	C(42)	-C(43)	1.350(10)
C(17)	-C(19)	1.541(6)	C(43)	-C(44)	1.413(8)

Table 7. Bond angles (ϕ/°) of dibenzoate (**20**) with estimated standard deviations in parentheses

Atom 1	Atom 2	Atom 3	Angle	Atom 1	Atom 2	Atom 3	Aangle
C(2)	-C(1)	-C(10)	112.9 (3)	C(16)	-C(15)	-C(14)	114.9 (3)
C(3)	-C(2)	-C(1)	110.4 (3)	C(17)	-C(16)	-C(15)	116.7 (3)
C(4)	-C(3)	-C(2)	115.4 (3)	C(19)	-C(17)	-C(16)	112.7 (3)
C(4)	-C(3)	-O(1)	105.4 (3)	C(19)	-C(17)	-C(27)	104.1 (3)
C(2)	-C(3)	-O(1)	109.4 (3)	C(19)	-C(17)	-C(28)	111.3 (3)
C(5)	-C(4)	-C(3)	108.4 (3)	C(16)	-C(17)	-C(27)	112.2 (3)
C(5)	-C(4)	-C(23)	113.2 (3)	C(16)	-C(17)	-C(28)	107.9 (3)
C(5)	-C(4)	-C(24)	108.4 (3)	C(27)	-C(17)	-C(28)	108.6 (3)
C(3)	-C(4)	-C(23)	110.7 (3)	C(20)	-C(19)	-C(17)	117.5 (4)
C(3)	-C(4)	-C(24)	106.9 (3)	C(21)	-C(20)	-C(19)	111.0 (4)
C(23)	-C(4)	-C(24)	109.1 (4)	C(22)	-C(21)	-C(20)	114.9 (5)
C(6)	-C(5)	-C(4)	113.6 (3)	C(29)	-C(22)	-C(21)	106.4 (6)
C(6)	-C(5)	-C(10)	111.5 (3)	C(29)	-C(22)	-C(30)	97.4 (6)
C(4)	-C(5)	-C(10)	116.6 (3)	C(21)	-C(22)	-C(30)	111.8 (6)
C(7)	-C(6)	-C(5)	111.0 (3)	O(3)	-C(27)	-C(17)	108.7 (3)
C(8)	-C(7)	-C(6)	112.8 (3)	C(32)	-C(31)	-O(1)	111.2 (3)
C(9)	-C(8)	-C(7)	106.6 (3)	C(32)	-C(31)	-O(2)	124.5 (4)
C(9)	-C(8)	-C(14)	109.2 (3)	O(1)	-C(31)	-O(2)	124.3 (4)
C(9)	-C(8)	-C(26)	115.5 (3)	C(33)	-C(32)	-C(31)	117.8 (4)
C(7)	-C(8)	-C(14)	110.1 (3)	C(33)	-C(32)	-C(37)	120.0 (4)
C(7)	-C(8)	-C(26)	110.0 (3)	C(31)	-C(32)	-C(37)	122.2 (4)
C(14)	-C(8)	-C(26)	105.4 (3)	C(34)	-C(33)	-C(32)	118.9 (5)
C(10)	-C(9)	-C(8)	116.5 (3)	C(35)	-C(34)	-C(33)	120.8 (5)
C(10)	-C(9)	-C(11)	114.4 (3)	C(36)	-C(35)	-C(34)	119.3 (5)
C(8)	-C(9)	-C(11)	110.0 (3)	C(37)	-C(36)	-C(35)	120.7 (5)
C(25)	-C(10)	-C(1)	107.8 (3)	C(32)	-C(37)	-C(36)	120.3 (4)
C(25)	-C(10)	-C(5)	115.2 (3)	C(39)	-C(38)	-O(3)	111.7 (4)
C(25)	-C(10)	-C(9)	111.5 (3)	C(39)	-C(38)	-O(4)	124.8 (5)
C(1)	-C(10)	-C(5)	107.1 (3)	O(3)	-C(38)	-O(4)	123.5 (5)
C(1)	-C(10)	-C(9)	109.1 (3)	C(40)	-C(39)	-C(38)	122.5 (4)
C(5)	-C(10)	-C(9)	106.0 (3)	C(40)	-C(39)	-C(44)	120.5 (5)
C(12)	-C(11)	-C(9)	108.1 (4)	C(38)	-C(39)	-C(44)	117.0 (5)
C(13)	-C(12)	-C(11)	114.7 (4)	C(41)	-C(40)	-C(39)	119.8 (5)
C(14)	-C(13)	-C(12)	123.4 (4)	C(42)	-C(41)	-C(40)	120.2 (6)
C(14)	-C(13)	-C(18)	123.9 (5)	C(43)	-C(42)	-C(41)	121.1 (6)
C(12)	-C(13)	-C(18)	112.6 (4)	C(44)	-C(43)	-C(42)	120.5 (6)
C(15)	-C(14)	-C(8)	116.7 (3)	C(39)	-C(44)	-C(43)	117.9 (5)
C(15)	-C(14)	-C(13)	121.2 (4)	C(3)	-O(1)	-C(31)	120.5 (3)
C(8)	-C(14)	-C(13)	122.0 (4)	C(27)	-O(3)	-C(38)	116.0 (3)

be an aldehyde (**21**) with the secobaccharene skeleton, the structure of which was confirmed by chemical conversion into *D*-friedo-13,18-secobacchar-13-ene-3β,18-diol (**16**) by lithium aluminium hydride-reduction. Therefore, the structure of the third compound was determined to be 3β-acetoxy-*D*-friedo-13,18-secobacchar-13-en-18-al (**21**).

The fourth compound (δ 3.33 (1H, s), 4.46 (1H, dd), and 5.35 (1H, m); *m/z* 486, 301, and 289) and the fifth compound (δ 3.34 (1H, s), 4.47 (1H, dd), and 5.31 (1H, m); *m/z* 486, 301, and 289) were suggested to be 18β-hydroxy-*D*:*C*-friedobacchar-9(11)- and -7-en-3β-yl acetates (**23** and **24**), respectively from the spectral data. These compounds were found to be identical with those obtained by acetylation of the corresponding diols (**11** and **12**), respectively.

Previously we reported that the $BF_3 \cdot OEt_2$-catalyzed backbone rearrangement of 3,4-epoxytriterpenes in solvents with low nucleophilicity proceeds up to C, D, or E ring to give 12-, 18-, or 19-ene derivative, while the rearrangement in solvents with high nucleophilicity, such as diethyl ether or tetrahydrofuran, is interupted in early stage to afford *D*:*A*- or *D*:*B*-friedo type triterpenes preferentially.[10,11,18-20] In order to examine the migratory aptitude, the epoxide (**6b**) was treated with $BF_3 \cdot OEt_2$ in various solvents and the results were summarized in Table 8.

In backbone rearrangement reactions in the

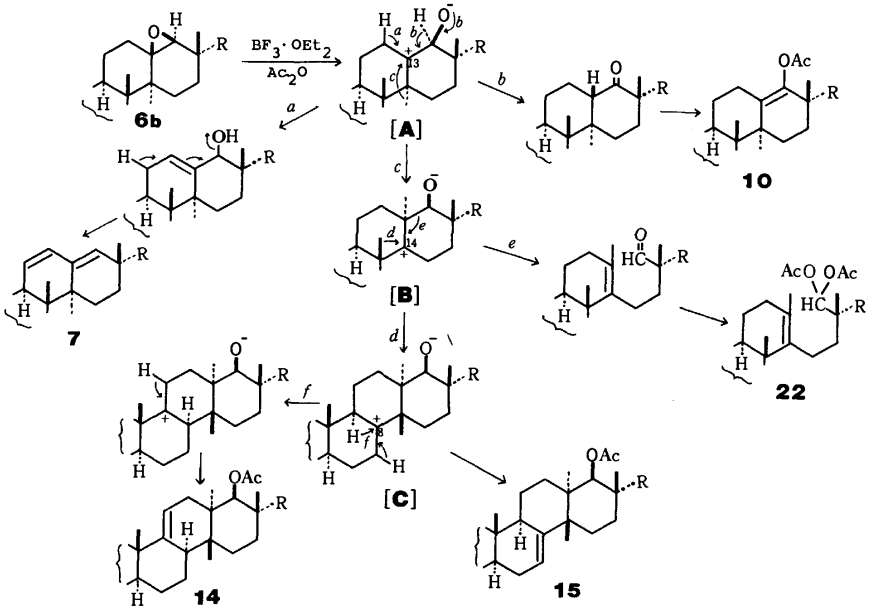

Scheme 1.

Table 8. Relative amount ratios of products in the reaction of 13β,18β-epoxide (**6b**) with $BF_3 \cdot OEt_2$ at room temperature

Solvent	Reaction time (min)	diene (**7**)	18-one (**9**)	18-al (**21**)	9(11)-ene (**23**)	**7**-ene (**24**)
Hexane[a)]	30	25	15	10	30	20
Benzene[b)]	30	50	17	7	16	10
Dichloromethane[a)]	30	55	15	10	15	5
Acetonitrile[a)]	30	60	10	5	15	10
Diethyl ether[b)]	60	60	15	6	3	10
Tetrahydrofuran[a)]	180	80	Trace	Trace	10	Trace
Acetic anhydride[b)]	120	14	31[c)]	15[c)]	31[c)]	9[c)]

a) Determined by GLC. b) Calculated from isolated yield. c) The reaction products are the corresponding acetates or acylal.

energetically unfavorable direction, it is anticipated that the effects of the nucleophilicity of the solvents on the degree of the rearrangement were larger than in energetically favorable rearrangements. In fact, the table showed that relative yields of thermodynamically unfavorable products (**23** and **24**) increased in hexane and benzene, while they decreased in diethyl ether and tetrahydrofuran. Furthermore, it is also proved that acetic anhydride is a useful solvent which enables the effective backbone rearrangement.

Experimental

General Procedures. Melting points were measured on a Mel-temp capillary melting point apparatus (Laboratory Devices) and are uncorrected. IR spectra were measured with a Hitachi 260-30 spectrometer, mass spectra with a JMS-D300 (JEOL) mass spectrometer at 70 eV with a direct inlet system, and ^1H NMR spectra with a Varian EM-390 (90 MHz) spectrometer. Chemical shifts are expressed in δ (ppm downfield from TMS as an internal standard) and coupling constants in Hz. GLC analysis was carried out on a Shimadzu Gas Chromatograph GC-6A equipped with a hydrogen-flame ionization detector. Thin-layer chromatography was carried out on Kieselgel 60 GF_{254} (E. Merck) coated in 0.25 mm-thickness (for analytical) and in 0.5 mm-thickness (for preparative). Wakogel C-200 (Wako) was used for silica-gel column chromatography.

Treatment of Bacchar-13(18)-en-3β-yl Acetate (1) with Hydrogen Chloride. A solution of bacchar-13(18)-en-3β-yl acetate (**1**; 27.8 mg) in chloroform (30 ml) was saturated with dry hydrogen chloride and the solution was stirred for 22 h at room temperature. After the usual work-up, the reaction product was examined by GLC (column: Dexsil-300GC, temperature: 270—300 °C (5 °C/min), N_2: 60 ml/min) and was shown to be a 1:1 mixture of 13(18)-ene (**1**) and 12-ene (**2**). The retention times were 9.3 and 11.3 min for **1** and **2**, respectively.

Epoxyidation of Bacchar-13(18)-en-3β-yl Acetate (1). Bacchar-13(18)-en-3β-yl acetate (**1**; 114 mg) was dissolved in dichloromethane (5 ml) and the solution was stirred with

MCPBA (110 mg) and sodium hydrogencarbonate (300 mg) at room temperature. The reaction product was treated with a sodium hydrogensulfite solution, worked-up usually, and was subjected to separation by column chromatography on silica gel (120 g). Elution with hexane–ether (96:4) gave 13α,18α-epoxide (**6a**; 10 mg) and 13β,18β-epoxide (**6b**; 95 mg). **6a**: mp 182—183 °C (from $CHCl_3$–MeOH); IR (KBr) 1735 and 1255 cm^{-1}; ^1H NMR ($CDCl_3$) δ=2.0 (3H, s, Ac), 2.3 (1H, s, 18β-H), and 4.5 (1H, m, 3α-H); MS *m/z* (%) 486 (M^+; 63), 468 (21), and 383 (100); Found: *m/z* 486.4020. Calcd for $C_{32}H_{54}O_3$: M, 486.4071. **6b**: mp 130.5—131.5 °C (from $CHCl_3$–MeOH); IR (KBr) 1740 and 1255 cm^{-1}; ^1H NMR ($CDCl_3$) δ=2.0 (3H, s, Ac), 2.65 (1H, s, 18α-H), and 4.5 (1H, m, 3α-H); MS *m/z* (%) 486 (M^+, 35), 468 (92), 383 (100); Found: *m/z* 486.4046. Calcd for $C_{32}H_{54}O_3$; M, 486.4071.

Backbone Rearrangement of 13β,18β-Epoxybaccharan-3β-yl Acetate (6b) in Acetic Anhydride. 13β,18β-Epoxybaccharan-3β-yl acetate (**6b**; 230 mg) was dissolved in freshly distilled acetic anhydride (50 ml). To the solution kept at 0 °C, $BF_3 \cdot OEt_2$ (0.2 ml) was added and the stirring was continued for 2 h. The reaction product was then poured into a cold mixture of a saturated sodium hydrogencarbonate solution (50 ml) and ether (200 ml) with vigorous stirring and the ethereal layer was separated. The aqueous layer was extracted with ether and the ethereal extract was combined with the ether layer, washed with brine, and dried over sodium sulfate. The organic extract, after evaporation, was dissolved in hexane and the solution was charged on a column of silica gel (25 g) covered with Florisil (2 g). Elution was performed with 5% ethyl acetate in hexane and 19 fractions (each 50 ml) were collected. Fractions 4 and 5, fractions 6—10, and fractions 14—19 afforded, on evaporation, fractions **A** (20 mg), **B** (115 mg), and C (80 mg), respectively.

The fraction **A** was identical with an authentic baccharа-11,13(18)-dien-3β-yl acetate (**7**)[6] in every respect.

Hydrolysis and Separation of Fraction B. The fraction **B** (115 mg), dissolved in tetrahydrofuran (THF) (15 ml), was heated with lithium aluminium hydride (LAH) (25 mg) at reflux for 30 min. The reaction product was worked up as usual and subjected to separation by column chromatography on silica gel (10 g). Elution with 10% ethyl acetate in hexane gave a mixture (*ca.* 100 mg) of compound B_1 (**8**) and compound B_2 (**11**) (fractions 15—18, each 20 ml) and compound B_3 (**12**; 11.5 mg, fractions 19—22). The mixture was subjected to further separation by column chromatography on silica gel (5 g) and eluted with hexane–dichloromethane–ethyl acetate (20:20:1) to afford **8** (42 mg) and **11** (42 mg). Baccharane-3β,18α-diol (**8**): mp 164—167 °C (from Et_2O–MeOH); IR (Nujol) 3500 and 3350 cm^{-1}; ^1H NMR ($CDCl_3$) δ=3.2 (1H, m) and 3.25 (1H, br s); MS *m/z* 446 (M^+), 428, 410, and 95 (base peak); Found: *m/z* 446.4190. Calcd for $C_{30}H_{54}O_2$: M, 446.4123. *D:C*-Friedobacchar-9(11)-ene-3β,18β-diol (**11**): mp *ca.* 202 °C (decomp) (from MeOH); IR (Nujol) 3450—3400 cm^{-1}. ^1H NMR ($CDCl_3$) δ=3.21 (1H, dd, *J*=10 and 6 Hz; $C_{(3\alpha)}$-H), 3.38 (1H, s; $C_{(18\alpha)}$-H), and 5.38 (1H, m; $C_{(11)}$-H); MS *m/z* 444 (M^+), 429, 411, 408, 393 (base peak), 259, 247, 241, and 229; Found: *m/z* 444.3959. Calcd for $C_{30}H_{52}O_2$: M, 444.3967. *D:C*-Friedobacchar-7-ene-3β,18β-diol (**12**): mp 230—233 °C (from MeOH); IR (film) 3430 cm^{-1}; ^1H NMR ($CDCl_3$) δ=3.24 (1H, dd, *J*=9 and 6 Hz; $C_{(3\alpha)}$-H), 3.34 (1H, s; $C_{(18\alpha)}$-H, and 5.35 (1H, m; $C_{(7)}$-H); MS *m/z* 444 (M^+), 429, 426, 411, 408, 393, 383, 259 (base peak), 247, 241, and 229.

Hydrolysis and Separation of Fraction C. The fraction C (80 mg) was dissolved in THF (10 ml) and treated with LAH (20 mg) at reflux temperature for 30 min. The reaction product was worked up as before to afford an oily residue (70 mg), which was subjected to separation by column chromatography on silica gel (4 g). Elution with 10% ethyl acetate in hexane gave compound C_1 (**16**; 20 mg), 20% ethyl acetate in hexane a mixture C_2 (25 mg), and 33% ethyl acetate in hexane compound C_3 (16 mg), respectively.

Compound C_1, *D*-friedo-13,18-secobacchar-13-ene-3β,18-diol (**16**): mp 99—103 °C (from MeOH); IR (Nujol) 3450 cm^{-1}; ^1H NMR ($CDCl_3$) δ=1.55 (3H, s; $C_{(13)}$-CH_3), 3.17 (1H, dd, *J*=9 and 6 Hz; $C_{(3\alpha)}$-H) and 3.36 (2H, s, CH_2-OH); MS *m/z* 446 (M^+), 431, 428, 413, 275 (base peak), and 257; Found: *m/z* 446.4088. Calcd for $C_{30}H_{54}O_2$: M, 446.4121.

Since the compound C_2 was found to be a complex mixture of compounds derived from acetylated rearranged products, further examination was not carried out.

Compound C_3: IR (Nujol) 3380 cm^{-1}; ^1H NMR ($CDCl_3$) δ=3.23 (1H, dd, *J*=10 and 6 Hz; $C_{(3\alpha)}$-H), 3.32 (1H, s; $C_{(18\alpha)}$-H), and 4.20 (1H, m; -CH(OH)CH_3); MS *m/z* 488 (M^+), 443, 429, 425, 407, 397, and 223.

*18-Oxo-*D:C*-friedobacchar-9(11)-en-3β-yl Acetate (13).* *D:C*-Friedobacchar-9(11)-ene-3β,18β-diol (**11**; 43 mg) was treated with acetic anhydride and pyridine at room temperature overnight to afford a diacetate (**14**; 6.5 mg) and a monoacetate (**23**; 30 mg). Diacetate (**14**): mp 179.5—181 °C (from MeOH); IR (Nujol) 1745, 1735, and 1245 cm^{-1}. ^1H NMR ($CDCl_3$) δ=2.02 and 2.06 (each 3H, s; OAc), 4.50 (1H, m; $C_{(3\alpha)}$-H), 4.90 (1H, s; $C_{(18\alpha)}$-H), and 5.35 (1H, m; $C_{(11)}$-H); MS *m/z* 528 (M^+), 513, 468 (base peak), 453, 393, 301, and 241; Found: *m/z* 528.4124. Calcd for $C_{34}H_{56}O_4$. Monoacetate (**23**): mp 244—248 °C (from $CHCl_3$–MeOH), IR (Nujol) 3550 and 1740 cm^{-1}. ^1H NMR ($CDCl_3$) δ=3.33 (1H, s; $C_{(18\alpha)}$-H), 4.46 (1H, dd, *J*=9 and 6 Hz; $C_{(3\alpha)}$-H), and 5.35 (1H, m; $C_{(11)}$-H); MS *m/z* 486 (M^+), 471, 453, 426, 411, 393, 383, 301 (base peak), 289, 241, and 229; Found: *m/z* 486.4028. Calcd for $C_{32}H_{54}O_3$: M, 486.4073.

The monoacetate (**23**; 29 mg) in acetone (10 ml) was oxidized with Jones reagent (0.05 ml) at 0 °C for 20 min. The usual work-up and crystallization from chloroform–methanol gave a keto acetate (**13**; 9 mg), mp 115.5—117.5 °C; IR (film) 1740, 1692, and 1245 cm^{-1}; ^1H NMR ($CDCl_3$) δ=2.05 (3H, s; OAc), 4.47 (1H, dd, *J*=10 and 6 Hz; $C_{(3\alpha)}$-H), and 5.38 (1H, m; $C_{(11)}$-H); MS *m/z* 484 (M^+), 469, 409, 400, 344, and 343 (base peak); Found: *m/z* 484.3919. Calcd for $C_{32}H_{52}O_3$: M, 484.3917.

D-*Friedo-13,18-secobacchar-13-ene-3β,18-diyl Diacetate (17).* Acetylation of a diol (**16**) by the usual procedure gave a diacetate (**17**) as an oily material, IR (film) 1745 and 1250 cm^{-1}; ^1H NMR ($CDCl_3$) δ=1.53 (3H, s; $C_{(13)}$-CH_3), 2.04 (6H, s; 2×OAc), 3.82 (2H, s; -CH_2-OAc), and 4.46 (1H, dd, *J*=9 and 6 Hz; $C_{(3\alpha)}$-H); MS *m/z* 530 (M^+), 470, 455, 395, 317 (base peak), and 257; Found: *m/z* 530.4261. Calcd for $C_{34}H_{58}O_4$: M, 530.4333.

D-*Friedo-13,18-secobacchar-13-ene-3β,18-diyl Dibenzoate (20).* A diol (**16**; 5 mg) was treated with benzoyl chloride and pyridine at room temperature for 6 h. The usual work-up and crystallization from chloroform–methanol gave a dibenzoate (**20**; 2.5 mg), mp 135.5—137.5 °C; IR (film) 1715,

1280, 1120, and 720 cm^{-1}; ^1H NMR ($CDCl_3$) δ=1.53 (3H, s; $C_{(13)}$-CH_3), 4.07 (2H, brs; CH_2-OBz) 4.63 (1H, dd, J=9 and 6 Hz; $C_{(3\alpha)}$-H), and 7.9—8.1 (10H; aromatic protons); MS m/z 532 ($M-C_6H_5COOH)^+$, 517, 489, 410 ($M-2\times C_6H_5COOH)^+$, 395, 257, and 57 (base peak); High resolution MS m/z 532.4278. Calcd for $C_{37}H_{56}O_2$ ($M-C_6H_5COOH$): m/z 532.4278.

Methyl 3-Oxo-D-friedo-13,18-secobacchar-13-en-18-oate (18). A solution of a diol (**16**; 10 mg) in acetone was treated with an excess of Jones reagent. After addition of isopropyl alcohol, the reaction mixture was filtered through a column of Florisil. The filtrate gave, on evaporation, a keto carboxylic acid, which was dissolved in ether and methylated with diazomethane. The reaction product was purified by column chromatography on silica gel, eluted with 10% ethyl acetate in hexane to afford a keto methyl ester (**18**; 5 mg), IR (film) 1730 and 1705 cm^{-1}; ^1H NMR ($CDCl_3$) δ=1.53 (3H, s; $C_{(13)}$-CH_3), 2.35—2.6 (2H; $C_{(2)}$-H_2) and 3.67 (3H, s; -$COOCH_3$); MS m/z 472 (M^+), 440, 412, 384, 343, 315, 291, and 69 (base peak).

Backbone Rearrangement of 13β,18β-Epoxybaccharan-3β-yl Acetate (6b) in Benzene. A solution of 13β,18β-epoxide (**6b**; 115 mg) in dry benzene (5 ml) was treated with $BF_3\cdot OEt_2$ (0.02 ml) at room temperature for 30 min with stirring. The reaction product was worked up as before and separated by column chromatography on silica gel (4 g). Bacchara-11,13(18)-dien-3β-yl acetate (**7**; 58.5 mg) was eluted with 3% ethyl acetate in hexane. Elution with 5% ethyl acetate in hexane gave 18-oxobaccharan-3β-yl acetate (**9**; 18.8 mg) and an aldehyde (**21**; 7.3 mg), and elution with 10% ethyl acetate in hexane gave 18β-hydroxy-*D:C*-friedobacchar-9(11)-en-3β-yl acetate (**23**; 17.8 mg) and its 7-ene isomer (**24**; 11.5 mg). 18-Oxobaccharan-3β-yl acetate (**9**):[9] mp 184.5—186 °C (from $CHCl_3$-MeOH); IR (Nujol) 1725, 1700, and 1245 cm^{-1}; ^1H NMR ($CDCl_3$) δ=2.67 (1H, m; $C_{(17)}$-H) and 4.47 (1H, dd, J=10 and 6 Hz; $C_{(3\alpha)}$-H); MS m/z 486 (M^+), 468, 426, 411, 408, and 402; Found: m/z 486.4111. Calcd for $C_{32}H_{54}O_3$: M, 486.4073. Aldehyde (**21**): ^1H NMR ($CDCl_3$) δ=1.52 (3H, s; $C_{(13)}$-CH_3), 2.03 (3H, s; $C_{(3\beta)}$-OAc), 4.46 (1H, dd, J=9 and 6 Hz; $C_{(3\alpha)}$-H), and 9.45 (1H, s; $C_{(17)}$-CHO). The aldehyde (**21**; 5 mg) was converted into a diol (**16**) by reduction with LAH (5 mg). 18β-Hydroxy-*D:C*-friedobacchar-9(11)-en-3β-yl acetate (**23**): mp 244—248 °C (from $CHCl_3$-MeOH); IR (Nujol) 3350 and 1740 cm^{-1}; ^1H NMR ($CDCl_3$) δ=2.0 (3H, s; $C_{(3\beta)}$-OAc), 3.33 (1H, s, $C_{(18\alpha)}$-H), 4.46 (1H, dd, J=9 and 6 Hz; $C_{(3\alpha)}$-H), and 5.35 (1H, m; $C_{(11)}$-H); MS m/z 486 (M^+), 471, 453, 426, 411, 393, 383, 301, 289, 241 (base peak), and 229; Found: m/z 486.4028. Calcd for $C_{32}H_{54}O_3$: M, 486.4073. 18β-Hydroxy-*D:C*-friedobacchar-7-en-3β-yl acetate (**24**): mp 77—78 °C (from MeOH); IR (Nujol) 3550, 1725, and 1245 cm^{-1}; ^1H NMR ($CDCl_3$) δ=2.03 (3H, s; $C_{(3\beta)}$-OAc), 3.34 (1H, s; $C_{(18\alpha)}$-H), 4.47 (1H, m; $C_{(3\alpha)}$-H), and 5.31 (1H, m; $C_{(7)}$-H); MS m/z 486 (M^+), 471, 411, 301, 289, 241, and 229; Found: m/z 486.4084. Calcd for $C_{32}H_{54}O_3$: M, 486.4073.

Acetylation of Diols (11 and 12). Diols (**11** and **12**) were acetylated with acetic anhydride and pyridine at room temperature to afford acetates (**23** and **24**), respectively, which were identifid by ^1H NMR, MS, and TLC.

Backbone Rearrangement of 13β,18β-Epoxybaccharan-3β-yl Acetate (6b) in Diethyl Ether and in Other Solvents. 13β, 18β-Epoxide (**6b**; 30 mg) was treated with $BF_3\cdot OEt_2$ in diethyl ether and the usual work-up and separation by chromatography gave a diene (**7**; 18 mg), a ketone (**9**; 4.5 mg), an aldehyde (**21**; 1 mg), 9(11)-en (**23**; 1 mg), and 7-ene (**24**; 3 mg).

A small amount of 13β,18β-epoxide (**6b**) was treated with $BF_3\cdot OEt_2$ in hexane, dichloromethane, acetonitrile, and THF, respectively, and each reaction product, after the usual work-up, was examined by GLC (column: Dexsil-300GC, temperature: 240—290 °C (5 °C/min)). The relative yields of products were given in Table 8 and their retention times were 9.0, 10.6, 13.5, 14.1, and 14.9 min for **7**, **21**, **24**, **9**, and **23**, respectively.

References

1) A preliminary account of this report: K. Suemura, T. Irokawa, M. Tori, S. Ohta, Y. Moriyama, T. Tsuyuki, T. Takahashi, A. Itai, and Y. Iitaka, *Chem. Lett.*, **1982**, 1617.

2) *e.g.* R. M. Coates, *Fortschr. Chem. Org. Naturst.*, **33**, 74 (1976).

3) I. Agata, E. J. Corey, A. G. Hortmann, J. Klein, S. Proskow, and J. J. Ursprung, *J. Org. Chem.*, **30**, 1698 (1965).

4) a) Z. Paryzek, *J. Chem. Soc., Perkin Trans., 1*, **1979**, 1222; b) *Tetrahedron Lett.*, **1976**, 4761.

5) G. V. Baddeley, H. J. Samaan, J. H. Simes, and T. H. Ai, *J. Chem. Soc., Perkin Trans., 1*, **1979**, 7.

6) L. Cattel, L. Delprino, and A. Dietsch, *Gazz. Chim. Ital.*, **109**, 705 (1979).

7) K. Masuda, K. Shiojima, and H. Ageta, *Chem. Pharm. Bull.*, **31**, 2530 (1983).

8) S. Ohta, M. Tori, T. Tsuyuki, and T. Takahashi, *Bull. Chem. Soc. Jpn.*, **56**, 2187 (1983).

9) E. Suokas and T. Hase, *Acta Chem. Scand.*, **25**, 2359 (1971).

10) K. Tachibana, M. Tori, Y. Moriyama, T. Tsuyuki, and T. Takahashi, *Bull. Chem. Soc. Jpn.*, **50**, 1552 (1977).

11) M. Tori, T. Torii, K. Tachibana, S. Yamada, T. Tsuyuki, and T. Takahashi, *Bull. Chem. Soc. Jpn.*, **50**, 469 (1977).

12) H. Ageta, K. Shiojima, K. Masuda, and T. Lin, *Tetrahedron Lett.*, **1981**, 2289.

13) H. Budzikiewicz, J. M. Wilson, and C. Djerassi, *J. Am. Chem. Soc*, **85**, 3688 (1963).

14) The complete F_o—F_c data, anisotropic thermal parameters for non-hydrogen atoms, atomic positional parameters and isotropic thermal parameters for hydrogen atoms, and bond lengths and bond angles containing hydrogen atoms are deposited as Document Nos. 8544 and 8545 for **13** and **20**, respectively, at the Office of the Editor of Bull. Chem. Soc. Jpn.

15) L. Bang, I. G. Guest, and G. Ourisson, *Tetrahedron Lett.*, **1972**, 2089.

16) L. Bang and G. Ourisson, *Tetrahedron Lett.*, **1969**, 3761; *Tetrahedron*, **29**, 2097 (1973).

17) E. Suokas and T. Hase, *Acta Chim. Scand., B* **31**, 231 and 633 (1977).

18) M. Tori, T. Tsuyuki, and T. Takahashi, *Bull. Chem. Soc. Jpn.*, **50**, 3381 (1977).

19) S. Yamada, S. Yamada, K. Tachibana, Y. Moriyama, Y. Tanahashi, T. Tsuyuki, and T. Takahashi, *Bull. Chem. Soc. Jpn.*, **49**, 1134 (1976).

20) Y. Yokoyama, Y. Moriyama, T. Tsuyuki, and T. Takahashi, *Bull. Chem. Soc. Jpn.*, **54**, 234 (1981).

X-Ray Photoelectron Spectra of Halogen-bridged One-dimensional Pd^{II}–Pd^{IV} Mixed-valence Complexes, $[Pd(en)_2][PdX_2(en)_2](ClO_4)_4$

Masahiro YAMASHITA,* Ichiro MURASE, and Isao IKEMOTO†

Laboratory of Chemistry, College of General Education, Kyushu University, Ropponmatsu, Fukuoka 810

†*Department of Chemistry, Faculty of Science, Tokyo Metropolitan University, Setagaya-ku 158*

(Received March 2, 1985)

Synopsis. X-Ray photoelectron spectra of $[Pd^{II}(en)_2][Pd^{IV}X_2(en)_2](ClO_4)_4$ (en=ethylenediamine, X=Cl and Br) were measured. The difference in the binding energies of Pd3d between Pd^{II} and Pd^{IV} in the bromo-bridged complex is smaller than that in the chloro-bridged complex. This result is consistent with those of the crystal structures, electrical conductivities, and electronic spectra previously reported.

Recently halogen-bridged one-dimensional M^{II}–M^{IV} mixed-valence complexes of Pt, Pd, and Ni have attracted much interest from the various viewpoints of the chemistry and physics of low-dimensional compounds.[1,2] In these complexes, the four-coordinate M^{II} and six-coordinate M^{IV} are stacked alternately with bridging halogens as shown below.[3-5] In the Pt complexes, it has been pointed out

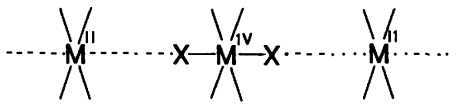

that the ratio between the Pt^{IV}–X and Pt^{II}...X distances increases consecutively and approaches unity on going from the chloro to the iodo homologs, suggesting that the difference between the oxidation states of Pt^{II} and Pt^{IV} decreases in the order of Cl>Br>I. This was clearly verified by the X-ray photoelectron spectra and XANES.[6,7] These results coincide with those of the electrical conductivities, and electronic and emission spectra.[8,9] On the other hand, to our knowledge, X-ray photoelectron spectral studies on the Pd^{II}–Pd^{IV} mixed-valence complexes are few. In this study, the X-ray photoelectron spectra of the Pd^{II}–Pd^{IV} mixed-valence complexes, $[Pd(en)_2][PdX_2(en)_2](ClO_4)_4$ (X=Cl and Br) have been measured in order to evaluate the oxidation states of Pd atoms in the mixed-valence complexes. The results are compared with those of the crystal structures,[10,11] electronic spectra,[9] and electrical conductivities.[8]

Experimental

The Pd^{II}–Pd^{IV} mixed-valence complexes, $[Pd(en)_2][PdX_2(en)_2](ClO_4)_4$ (X=Cl and Br) were prepared by the method previously reported.[12]

The X-ray photoelectron spectra were obtained with a Mg-$K\alpha$ exciting irradiation on a SHIMADZU ESCA 750. The spectrometer was calibrated by using Cls (285.0 eV).

Results and Discussion

Figure 1 shows the X-ray photoelectron spectra of $Pd3d_{5/2}$ and $Pd3d_{3/2}$ for the $[Pd(en)_2][PdX_2(en)_2](ClO_4)_4$. These compounds were very susceptible to X-ray irradiation damage and thereby the spectra changed gradually with time during the measurements as has been experienced in the Ni^{II}–Ni^{IV} mixed-valence complexes.[13,14] Therefore, the spectral measurements were carried out as quick as possible at a lower voltage.

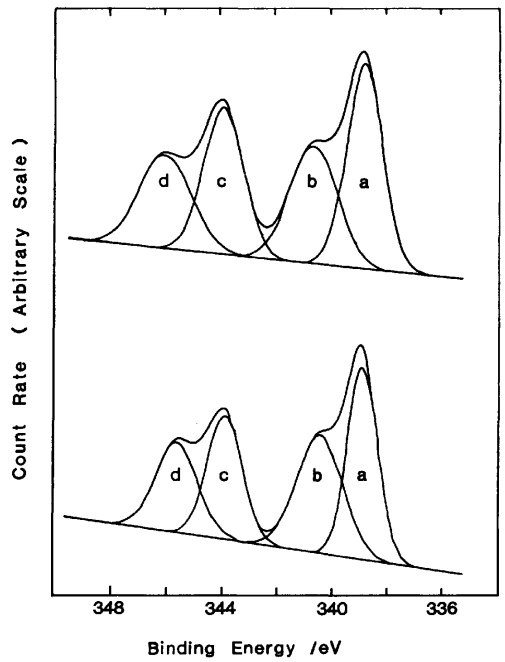

Fig. 1. X-Ray photoelectron spectra of $[Pd(en)_2][PdX_2(en)_2](ClO_4)_4$.
Top and bottom spectra are X=Cl and Br, respectively. Each spectrum is resolved into four components by simulation. a: $Pd^{II}3d_{5/2}$, b: $Pd^{IV}3d_{5/2}$, c: $Pd^{II}3d_{3/2}$, d: $Pd^{IV}3d_{3/2}$.

For the Pd^{II}–Pd^{IV} mixed-valence complexes, the spectra should be interpreted as a superposition of four bands, *i.e.*, $3d_{5/2}$ and $3d_{3/2}$ of Pd^{II} and Pd^{IV}. We have resolved the observed spectra into the Pd^{II} and Pd^{IV} components by the computer simulation. Although the intensities of Pd^{II} and Pd^{IV} components are assumed to be essentially the same as each other, the intensity of Pd^{IV} component is a little smaller than that of the Pd^{II} one. This is probably due to X-ray irradiation damage. Moreover, the intensity of the resolved Pd^{IV} spectra decreased, whereas that of the Pd^{II} spectra increased with time of X-ray irradiation. Since the spectral intensity corresponds to the number of species, it can be said from the observation that the decrease of the Pd^{IV} species were

Table 1. Results of Pd3d binding energies, distance ratios, conductivity measurements, and peak positions of absorption spectra of $[Pd(en)_2][PdX_2(en)_2](ClO_4)_4$

X	$3d_{5/2}$		$3d_{3/2}$		R[a]	$\sigma_{r.t.}$[b]	ΔE[b]	$h\nu_{max}$[c]
	Pd^{II}	Pd^{IV}	Pd^{II}	Pd^{IV}		$\Omega^{-1}\,cm^{-1}$	eV	eV
Cl	338.75	340.64	343.94	346.04	0.77	2.0×10^{-12}	0.81	2.05
Br	338.94	340.54	344.09	345.79	0.86	1.2×10^{-8}	0.49	1.22

a) Refs. 10 and 11. b) Ref. 8. c) Ref. 9.

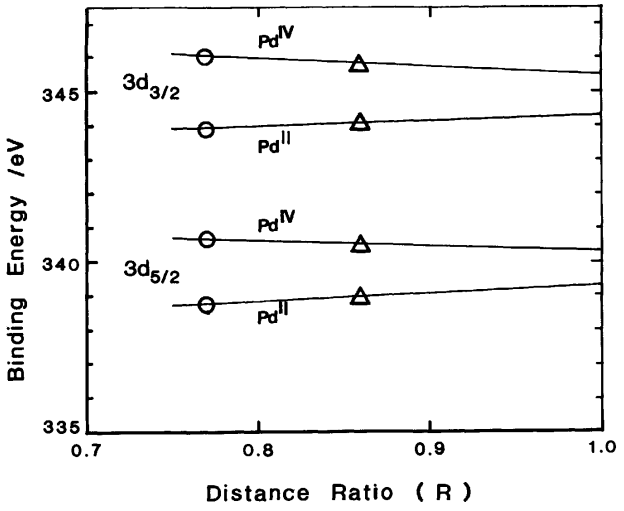

Fig. 2. Correlation between distance ratios and binding energies.
○: $[Pd(en)_2][PdCl_2(en)_2](ClO_4)_4$, △: $[Pd(en)_2][PdBr_2(en)_2](ClO_4)_4$.

roughly equal to the increase of the Pd^{II} species. This indicates that the Pd^{IV} state is decomposed to produce the Pd^{II} state. Quite a similar spectral change due to X-ray irradiation has been observed in the Ni^{II}–Ni^{IV} mixed-valence complexes.[13,14]

As the bridging halogen shifts from Cl to Br, the $Pd^{IV}3d$ binding energies become lower while those of the Pd^{II} become higher. The difference in the binding energies of $Pd3d_{5/2}$ between Pd^{II} and Pd^{IV} in the bromo-bridged complex (1.6 eV) is smaller than that in the chloro-bridged complex (1.9 eV). This result is essentially consistent with that of the crystal structures, that is, the ratio (R) between the Pd^{IV}–X and Pd^{II}...X distances in the bromo-bridged complex (0.86) is larger than that in the chloro-bridged complex (0.77) as listed in Table 1.[10,11] Therefore, we can estimate roughly the Pd^{III} binding energy as shown in Fig. 2 by the extrapolation procedure to R=1 in the correlation between the binding energies and the distance ratios.

Since the difference between the oxidation states of the Pd^{II} and Pd^{IV} in the bromo-bridged complex is smaller than that in the chloro-bridged complex as shown in the X-ray photoelectron spectra, the wave number of the intervalence charge transfer from Pd^{II} to Pd^{II} along the chain is lower in the bromo-bridged complex than in the chloro-bridged complex.[9] In the same way, the activation energy in the electrical conductivity, which is mainly concerned with the oxidation states of Pd^{II} and Pd^{IV}, is smaller in the bromo-bridged complex than in the chloro-bridged complex.[8]

References

1) J. S. Miller and A. J. Epstein, *Prog. Inorg. Chem.*, **20**, 1 (1976).
2) H. J. Keller, "Extended Linear Chain Compounds," ed by J. S. Miller, Plenum Press, New York (1982), Vol. 1, p. 357.
3) H. Endres, H. J. Keller, R. Martin, H. N. Gung, and U. Treagar, *Acta Crystallogr., Sect. B*, **35**, 1885 (1979).
4) M. Tanaka, I. Tsujikawa, K. Toriumi, and T. Ito, *Acta Crystallogr., Sect. B*, **38**, 2793 (1982).
5) M. Yamashita, H. Ito, K. Toriumi, and T. Ito, *Inorg. Chem.*, **22**, 1566 (1983).
6) M. Yamashita, N. Matsumoto, and S. Kida, *Inorg. Chim. Acta*, **31**, L381 (1978).
7) H. Tanino, H. Oyanagi, M. Yamashita, and K. Kobayashi, *Solid State Commun.*, **53**, 953 (1985).
8) R, Aoki, Y. Hamaue, S. Kida, M. Yamashita, T. Takemura, Y. Furuta, and A. Kawamori, *Mol. Cryst. Liq. Cryst.*, **81**, 301 (1982).
9) Y. Wada, T. Mitani, M. Yamashita, and T. Koda, *J. Phys. Soc. Jpn.*, **54**, 3143 (1985).
10) A. L. Beauchamp, D. Layek, and T. Theophanides, *Acta Crystallogr., Sect. B*, **38**, 1158 (1982).
11) M. Yamashita, K. Toriumi, and T. Ito, *Acta Crystallogr., Sect. C*, in press.
12) N. Matsumoto, M. Yamashita, and S. Kida, *Bull. Chem. Soc. Jpn.*, **51**, 2334 (1978).
13) M. Yamashita and T. Ito, *Inorg. Chim. Acta*, **87**, L5 (1984).
14) M. Yamashita, I. Murase, I. Ikemoto, and T. Ito, *Chem. Lett.*, **1985**, 1133.

Reaction Volume for the OH^- Addition to Hexafluoroacetylacetonate Ligand on Co^{III} Complex

Yoichi KITAMURA

Department of Chemistry, Faculty of Science, Ehime University, Matsuyama, Ehime 790

(Received March 14, 1985)

Synopsis. For the title reaction in water: $L_4Co(hfac)^z+OH^-=L_4Co(hfacOH)^{z-1}$, reaction volumes ($\Delta V°$) at infinite dilution were obtained at 25 °C, where A_4 is $(NH_3)_4$, $(en)_2$, α-trien, β-trien, $f(N)$-*i*-dtma, α-edda, β-edda, and Hhfac stands for hexafluoroacetylacetone. The resulting $\Delta V°$ values supported the addition of OH^- to $CoA_4(hfac)^z$.

In our recent report, a unique character was clarified for the reaction between an OH^- ion and a Co^{III} complex containing a hfac ligand in water.[1] That is, the color of a $CoL_4(hfac)^z$ complex changes rapidly and reversibly upon a pH change of the solution.

This phenomenon can be explained by a shift in the following equilibrium:[1,2]

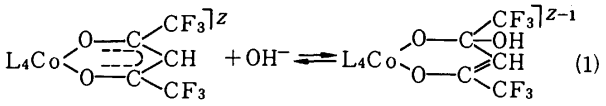

(1)

In another work, $\Delta V°$ was obtained for 19 acid-base reactions of an octahedral complex:[3]

$$MA^z + OH^- = MB^{z-1} + H_2O \quad (2)$$

In Reaction 2, MA^z is an octahedral transition-metal (Pt^{IV}, Rh^{III}, Co^{III}) complex with ligand A=H_2O, NH_3, and $C_2O_4H^-$; MB^{z-1} is the corresponding conjugate base complex with ligand B=OH^-, NH_2^-, and $C_2O_4^{2-}$, where the charge (z) on the reactant ranges from -2 to 4. The $\Delta V°$'s at 25 °C for these reactions can be summarized as:

$$\Delta V° = (-2.5\pm0.2)\Delta Z^2 + (14.5\pm0.8)\ \mathrm{cm^3\ mol^{-1}}, \quad (3)$$

where ΔZ^2=(charge of the product complex)^2−(charge of the reactant complex)^2=1−2z, and the first term in Eq. 3 corresponds to the electrostatic volume contribution due to the interaction with solvent and the second to the intrinsic volume of ions.

Interest has been developed here regarding whether the distinct difference between Reactions 1 and 2 is reflected in their reaction volumes. Thus, in the present work, $\Delta V°$ of Reaction 1 has been obtained dilatometrically for seven $CoL_4(hfac)^z$ complexes. Their magnitudes are discussed in relation to Eq. 3.

Experimental

The respective complex (perchlorate) was obtained and identified in a previous work.[1]

Dilatometry was carried out using a Carlsberg dilatometer as described before.[3] 15 cm^3 of an aqueous complex solution was mixed with 3 cm^3 of NaOH and the resulting volume change (Δv_{exptl}) was observed. Generally, two runs were performed at one condition. The correction term (Δv_{corr}) for the change in the ionic strength upon mixing was calculated as before.[3] $\Delta V°$ has been calculated from $\Delta v_o=\Delta v_{exptl}-\Delta v_{corr}$, where the degree of the completion of the neutralization process (R%) has been taken into account.

Results and Discussion

The dilatometric results and the reaction volume obtained, therefrom, are summarized in Tables 1 and 2. The experimental $\Delta V°$'s range from moderately positive to moderately negative. Thus, the main contribution to $\Delta V°$ may be ascribed to the solvational change around the complex during Reaction 1.[4]

The $\Delta V(3)$ in Table 2 is the reaction volume calculated upon inserting the relevant value of ΔZ^2 into Eq. 3. The value definitely differs from the corresponding experimental $\Delta V°$. On the other hand, assuming that the difference in the electrostriction volume for $CoL_4(hfacOH)^{z-1}$ and $CoL_4(hfac)^z$ equals (-2.5 ± 0.2) $cm^3\ mol^{-1}$, the volume change of Reaction 1 can be predicted as follows by the use of

Table 1. Dilatometric results at 25 °C

Complex[a]	C[b]/mM	NaOH/mM	$\Delta v_{exptl}/\mu l$	$\Delta v_{corr}/\mu l$	R%
$[Co(NH_3)_4hfac](ClO_4)_2$	10	50	1.55, 1.63	−0.14	100
		100	1.39	−0.20	100
$[Co(en)_2hfac](ClO_4)_2$	10	50	1.44, 1.50	−0.14	100
		100	1.41, 1.42	−0.20	100
α-$[Co(trien)hfac](ClO_4)_2$	10	50	1.14, 1.25	−0.14	100
β-$[Co(trien)hfac](ClO_4)_2$	9.5	47.5	1.49, 1.42	−0.13	100
$f(N)$-$[Co(i\text{-}dtma)hfac](ClO_4)$	7.5	37.5	0.20, 0.09	−0.04	100
α-Co(edda)hfac	4.0	20	−0.53, −0.43	−0.01	94
β-Co(edda)hfac	3.0	15	−0.19, −0.17	−0.01	98

a) Trien=triethylenetetramine, *i*-dtma=*N*,*N*-bis(2-aminoethyl)glycinate, edda=ethylenediamine-*N*,*N*′-diacetate.
b) Complex concentration.

Table 2. Volume change ($cm^3\ mol^{-1}$) for the reaction of $CoL_4(hfac)^z$ with OH^- ion in water at 25 °C

Complex	ΔZ^2	Experimental	Calculated	
		$\Delta V°$	$\Delta V(3)$	$\Delta V(4)$
$Co(NH_3)_4hfac^{2+}$	−3	11.2±0.4	22.0±1.4	6.1±2.6
$Co(en)_2hfac^{2+}$	−3	10.7±0.1	22.0±1.4	6.1±2.6
α-Co(trien)hfac^{2+}	−3	8.9±0.4	22.0±1.4	6.1±2.6
β-Co(trien)hfac^{2+}	−3	11.1±0.3	22.0±1.4	6.1±2.6
f(*N*)-Co(*i*-dtma)hfac$^+$	−1	1.6±0.5	17.0±1.0	1.1±2.2
α-Co(edda)hfac	1	−8.3±0.9	12.0±1.0	−3.9±2.2
β-Co(edda)hfac	1	−3.9±0.3	12.0±1.0	−3.9±2.2

$\overline{V}(OH^-)=1.4\pm2\ cm^3\ mol^{-1}$:[5]

$$\Delta V° = (-2.5\pm0.2)\Delta Z^2 - (1.4\pm2)\ cm^3\ mol^{-1} \quad (4)$$

The experimental $\Delta V°$'s agree fairly well with those $\Delta V(4)$ calculated using Eq. 4. Thus, the magnitudes of the experimental $\Delta V°$'s reinforce the suggestion that the origin of the rapid and reversible color change of the $CoL_4(hfac)^z$ solution is not a deprotonation from $CoL_4(hfac)^z$ but an addition of OH^- to $CoL_4(hfac)^z$. It should be noted that measurements regarding the reaction volume could, thus, become relevant tools for discriminating a reaction type.

Alternatively, a linear correlation between the experimental $\Delta V°$ and the ΔZ^2 can be obtained by a least-squares method:

$$\Delta V° = (-4.2\pm0.4)\Delta Z^2 - (2.1\pm0.8)\ cm^3\ mol^{-1} \quad (5)$$

The intercepts of Eqs. 4 and 5 coincide well, whereas the ΔZ^2 coefficients somewhat differ. According to the Drude-Nernst equation regarding electrostriction, the ΔZ^2 coefficient is inversely proportional to the assumed common ionic radius (r) of the reactant and the product.[6] Since a ΔZ^2 coefficient of $-2.5\ cm^3\ mol^{-1}$ corresponds to r=1.7 Å, that ($-4.2\ cm^3\ mol^{-1}$) of Eq. 5 corresponds to r=1.0 Å.[3] Although small, the thus-derived r is not so far from reality since the coordination bond lengths are 2.0—2.5 Å. Also, the effective charge may be fairly concentrated towards the center of the complex ion.[3] Consequently, the charge dependence of $\Delta V°$ can be consistently understood by using the Drude-Nernst equation regarding electrostriction.

The author wishes to thank Mr. Ryuichi Kume, a graduate student of Ehime University, for his co-operative work regarding the preliminary experiment.

References

1) S. Aygen, Y. Kitamura, K. Kuroda, R. Kume, H. Kelm and R. van Eldik, *Inorg. Chem.*, **24**, 423 (1985).
2) Y. Kitamura and R. van Eldik, *Transition Met. Chem.*, **9**, 257 (1984).
3) Y. Kitamura and R. van Eldik, *Ber. Bunsenges. Phys. Chem.*, **88**, 418 (1984).
4) T. Asano and W. J. le Noble, *Chem. Rev.*, **78**, 407 (1978).
5) F. J. Millero, "Water and Aqueous Solutions: Structure, Thermodynamics and Transport Processes," ed by R. A. Horne, Wiley-Interscience: London, Chapter 13 (1972).
6) P. Drude and W. Nernst, *Z. Phys. Chem.*, **15**, 79 (1894).

A Raman Study of Aqueous KOH Solution in Glassy State

Hitoshi KANNO* and Jiro HIRAISHI†
Department of Chemistry, Meisei University, Hino, Tokyo 191
†*National Chemical Laboratory for Industry, 1-1 Higashi, Yatabe, Tsukubagun, Ibaraki 305*
(Received April 1, 1985)

Synopsis. Raman spectra of an aqueous KOH solution were measured in the OH stretching region and in the low frequency region (<700 cm^{-1}). Contrary to the results reported by Sharma and Kashyap,[5] only one Raman band specific to an aqueous KOH solution was observed at ≈285 cm^{-1} in the low frequency Raman spectrum.

Raman spectra of aqueous alkali hydroxide solutions have been investigated in the OH stretching frequency region by a large number of workers.[1-3] One of the notable characteristics of the OH stretching Raman spectrum is the existence of the sharp peak at 3620 cm^{-1}. This is due to the stretching vibrations of the OH^- ions in the solution.

On the other hand, it seems that there have been only two Raman studies[4,5] on the low frequency region of alkali hydroxide solutions. Sharma and Kashyap[5] observed two new bands in the low frequency Raman spectra for aqueous NaOH and KOH solutions, in addition to the two restricted translational Raman bands at ≈60 and ≈170 cm^{-1} which are common to all aqueous solutions.[4,6] However, Walrafen,[4] who measured Raman spectra of many aqueous electrolyte solutions including LiOH, NaOH, and KOH solutions, didn't mention about the new band(s) in his low frequency Raman spectra for the LiOH, NaOH, and KOH solutions.

We have recently shown that vitrification of an aqueous solution reduces the Rayleigh scattering wing in a Raman spectrum of the solution, thus permitting unequivocal detection and characterization of weak Raman bands near the exciting line.[7] Therefore, it would be interesting to see the Raman spectrum of aqueous alkali hydroxide solution in the glassy state to clarify the discrepancy of the two reports. We here report a Raman study of glassy aqueous KOH solution.

The sample solutions were prepared by dissolving the commercially obtained KOH pellets (Wako chemicals, guaranteed grade) into distilled water. Raman measurements were essentially the same as previously reported.[7] The concentration of alkali hydroxide solution was determined by titration using Methyl Orange as an indicator against a standardized 0.1 M HCl (1 M=1 mol dm^{-3}) solution. Here the KOH concentration was denoted by R (=moles of water/moles of KOH).

The obtained Raman spectra for both liquid and glassy states of a KOH solution (R=3.9) are shown in Fig. 1. Contrary to the results by Sharma and Kashyap,[5] we see only one Raman peak specific to the KOH solution in the low frequency Raman spectrum. Judging from the Raman spectra reported by Sharma and Kashyap, they devided the single broad Raman envelope into two components: One at 292 cm^{-1} and the other at 332 cm^{-1}. Depolarization measurements indicate that the band at ≈285 cm^{-1} is polarized. It must be pointed out that Raman spectra for glassy NaOH (or NaOD) solutions also gave similar results: single peak at ≈285 cm^{-1} for a $NaOH-H_2O$ solution and at ≈283 cm^{-1} for a $NaOD-D_2O$ solution (intensity is concentration dependent).[8] The two restricted translational Raman

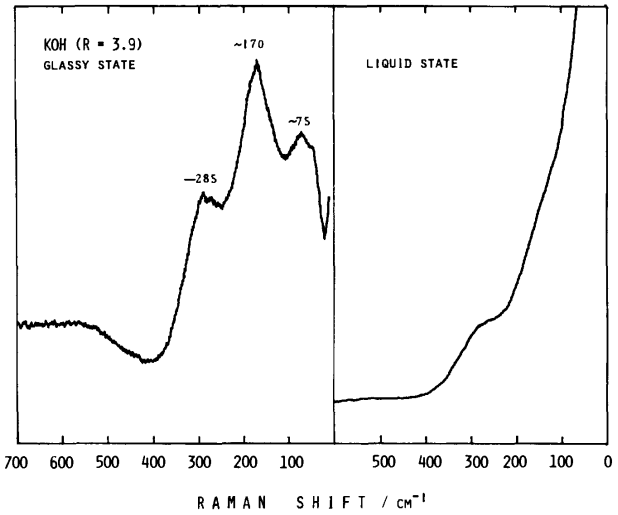

Fig. 1. Raman spectra of aqueous KOH solution (R= 3.9) in low frequency region (10~700 cm^{-1} for the glassy state, 70~600 cm^{-1} for the liquid state).

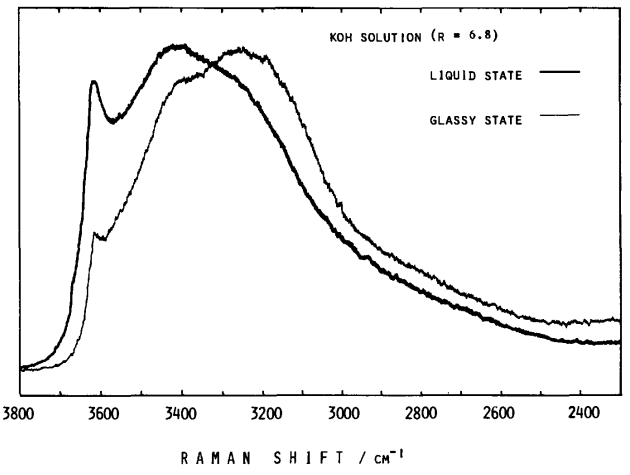

Fig. 2. Raman spectra in the OH stretching vibrational region of aqueous KOH solution (R=6.8).
Thick curve : liquid state at room temperature; thin curve: glassy state at liquid nitrogen temperature.

peaks at ≈170 and ≈75 cm^{-1} are usually assigned to the stretching ($\nu_{OH..O}$) and bending ($\delta_{OH...O}$) vibrations of the hydrogen-bonds between water molecules (and water molecules and anions).[4,6] As the peak at ≈285 cm^{-1} increases in intensity with increasing KOH concentrations and it is observed only in aqueous solutions of alkali hydroxides and ammonia, we come to conclude that it is due to the stretching vibrations of hydrogen-bonds between water molecules and OH^- ions. The fact that its frequency virtually remains unchanged with KOH concentrations also supports the assignment.

The OH stretching Raman spectra for both liquid and glassy states are shown in Fig. 2. It is observed that the relative intensity of the peak at ≈3620 cm^{-1} decreases from a liquid state to a glassy state. This arises from the decrease in ionisation of KOH at low temperatures. The most characteristic feature of the OH stretching Raman spectrum is the continuity of the spectrum down to about 2200 cm^{-1}. A similar continuum is observed in a Raman spectrum of an acid solution.[8-10] It is to be noted that the OH stretching Raman spectrum terminates at about 2900 cm^{-1} in most aqueous electrolyte solutions.[11]

The hydrogen-bonds between oxonium ions and water molecules are very strong.[12,13] Pernoll *et al.*[9] attributed the continua observed in acid solutions to the large polarizability of the hydrogen-bonds caused by protons in the hydrated oxonium ions. A similar interpretation can be invoked to explain the continuum for the KOH solution. Here the OH^- ions play the same role as oxonium ions do in an acid solution. In an aqueous acid solution, protons move around very quickly among water molecules so that each H_3O^+ ion is short-lived scarcely enough to vibrate as a distinct species.[14,15] These rapid proton movements shift and split the energy levels of the OH stretching vibrations, resulting in the continuous distribution of the OH stretching vibrations to lower frequency region.

An interesting point is that the continuum rather increases in intensity in the glassy KOH solution when the intensities are compared by making the peak heights of both states (liquid and glassy states) equal. This is mainly due to the increase in hydrogen-bond strength going from a liquid state to a glassy state, as revealed by the shift of the spectrum peak to a lower frequency side. The intensity increase in the frequency region of 3100—3300 cm^{-1} is a clear indication that strongly hydrogen-bonded structure is recovered to some extent in the glassy state. Liquid water has a strong peak near 3200 cm^{-1} whose intensity grows as the temperature approaches the freezing point of water and this feature is ascribed to the increase of strongly hydrogen-bonded water molecules in the liquid with temperature decrease.[17] The fact that amorphous solid water and polycrystalline ice, where all water molecules are strongly coupled with hydrogen-bonds, have the strongest peak at ≈3100 cm^{-1}[18,19] also substantiates the above interpretation.

This work was in part assisted by a Grant-in-Aid for Scientific Research from the Ministry of Education, Science, and Culture.

References

1) W. R. Busing and D. F. Hornig, *J. Phys. Chem.*, **65**, 286 (1961).
2) G. Zundel, "Hydration and Intermolecular Interactions," Academic Press, New York (1969), pp. 169—172.
3) V. Mazzacurati, M. Nardone, and G. Signorelli, *Chem. Phys.*, **17**, 227 (1976).
4) G. E. Walrafen, *J. Chem. Phys.*, **40**, 3249 (1964).
5) S. K. Sharma and S. C. Kashyap, *J. Inorg. Nucl. Chem.*, **34**, 3623 (1972).
6) G. E. Walrafen, "Water, a Comprehensive Treatise," ed by F. Franks, Plenum Press, New York (1972), Vol. 1, Chap. 5.
7) H. Kanno and J. Hiraishi, *Chem. Phys. Lett.*, **68**, 46 (1979); *J. Raman Spectroscopy*, **9**, 85 (1980); **12**, 224 (1982).
8) H. Kanno and J. Hiraishi, unpublished data.
9) a) G. Zundel and H. Metzger, *Z. Physik. Chem. (Frankfurt)*, **58**, 225 (1968); b) I. Pernoll, U. Maier, R. Janoschek, and G. Zundel, *J. Chem. Soc., Faraday Trans. 2*, **71**, 201 (1975).
10) P. A. Giguεrre, C. Martel, and S. Turrell, *Chem. Phys. Lett.*, **56**, 231 (1978).
11) G. E. Walrafen, *J. Chem. Phys.*, **55**, 768 (1971).
12) P. A. Giguεrre and J. G. Guillot, *J. Phys. Chem.*, **86**, 3231 (1982).
13) H. G. Lee, Y. Matsumoto, T. Yamaguchi, and H. Ohtaki, *Bull. Chem. Soc. Jpn.*, **56**, 443 (1983).
14) T. Ackermann, *Z. Physik. Chem.(Frankfurt)*, **27**, 253 (1961); *ibid.*, **41**, 113 (1964).
15) R. A. M. O'Ferral, G. W. Koepple, and A. J. Kresga, *J. Am. Chem. Soc.*, **93**, 1 (1971).
16) H. Kanno and J. Hiraishi, *Chem. Phys. Lett.*, **107**, 438 (1984).
17) J. R. Sherer, M. K. Go, and S. Kint, *J. Phys. Chem.*, **77**, 2108 (1973); **78**, 1304 (1974).
18) S. A. Rice, *Topics Current Chem.*, **60**, 109 (1975).
19) T. C. Sivakumar, S. A. Rice, and M. G. Sceats, *J. Chem. Phys.*, **69**, 3468 (1978).

On the Assignment of Band II in the Electronic Spectrum of $[Ni(H_2O)_6]^{2+}$

Hisao Ito and Kozo Sone*

Chemical Laboratory, College of General Education, Tokushima University, Minami-josanjima-cho, Tokushima 770

**Department of Chemistry, Faculty of Science, Ochanomizu University, Otsuka, Bunkyo-ku, Tokyo 112*

(Received April 10, 1985)

Synopsis. $[Ni(H_2O)_6]^{2+}$ shows two absorption maxima in the red part of the visible spectrum. The one with the lower frequency has been assigned to the $^3A_{2g}\rightarrow{}^3T_{1g}(F)$ transition, and the other to the spin-forbidden $^3A_{2g}\rightarrow{}^1E_g$ transition. A closer comparison with related spectral data, however, makes the reverse assignment more reasonable.

As is well known, high-spin octahedral Ni(II) complexes show three d-d bands in their electronic spectra if there is no other absorption (CT and/or ligand band(s)) covering some of them. These bands are denoted by I, II, and III (in the order of increasing frequency) and are assigned to transitions $^3A_{2g}\rightarrow{}^3T_{2g}(F)$, $^3A_{2g}\rightarrow{}^3T_{1g}(F)$, and $^3A_{2g}\rightarrow{}^3T_{1g}(P)$, respectively, within the $3d^8$ electronic system. The spectra of $[Ni(NH_3)_6]^{2+}$ and $[Ni(en)_3]^{2+}$ are typical examples of this spectral pattern. The spectrum of $[Ni(H_2O)_6]^{2+}$ is also very similar to these. However, its band II, which appears in the red part of the visible spectrum, is apparently composed of two maxima, *i.e.*, band IIa at 416 THz[1](721 nm) and band IIb at 457 THz(656 nm). The latter is somewhat weaker than the former.[2]

In 1950, Sone collected a number of spectral data regarding octahedral Ni(II) complexes and found that there is a reasonably good linear relationship between the frequencies of bands II and III. He also pointed out that this relation holds well in the case of $[Ni(H_2O)_6]^{2+}$, if its band IIb (and not band IIa which is apparently stronger) is identified with the band II of other complexes.[3]

In 1956, Ito measured the electronic spectra of many octahedral Ni(II) complexes with special care, and discovered that, in most cases, there is a very weak absorption band at the lower-frequency side of their band II. This band appears as a weak shoulder (or merely as a slight inflection) which often is scarcely discernible. Its position and intensity could be determined only by analyzing the whole spectrum into Gaussian-type components, which Ito carefully carried out. This band can now be assigned to the spin-forbidden $^3A_{2g}\rightarrow{}^1E_g$ transition which, according to the Tanabe-Sugano diagram, is expected to appear in the vicinity of band II. It should naturally be very weak. Figure 1 shows an example of such an analysis.[4,5]

Ito also studied the numerical relations among the ν_{max} values of the three bands, which he refined by the above-mentioned analyses. He found that a linear relationship which is similar to that found by Sone approximately holds between any two of the three ν_{max} values. These are denoted by ν_I, ν_{II}, and ν_{III}, respectively.[6] He also found another relation, $(\nu_{II})^2=\nu_I\nu_{III}$, which holds as well. He confirmed that band IIb of $[Ni(H_2O)_6]^{2+}$ satisfies these rules much better than band IIa. This shows again that the former should be taken as band II of this complex.[4]

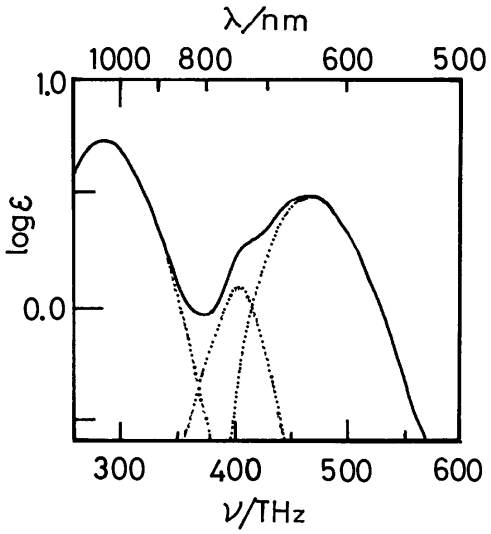

Fig. 1. Analysis of band II of $[Ni(gly)(H_2O)_4]^+$(gly= glycinate ion) in aqueous solution into two Gaussian-type components. After Ref. 4).

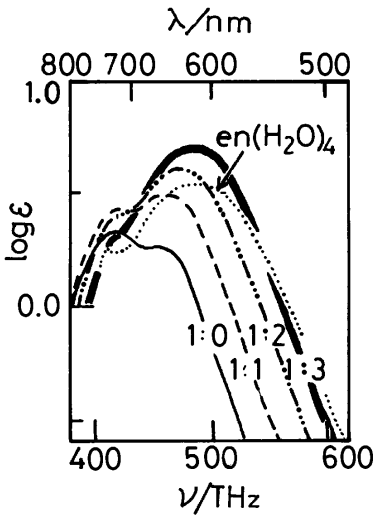

Fig. 2. Change of the absorption spectrum of $[Ni(H_2O)_6]^{2+}$ caused by the addition of NH_3. $C_{Ni^{2+}}$: 0.2 mol dm^{-3}, $C_{NH_4^+}$ (added as NH_4NO_3): 6 mol dm^{-3} The ratio Ni^{2+}: NH_3 is given on each curve. The spectrum of $[Ni(en)(H_2O)_4]^{2+}$ is also shown.

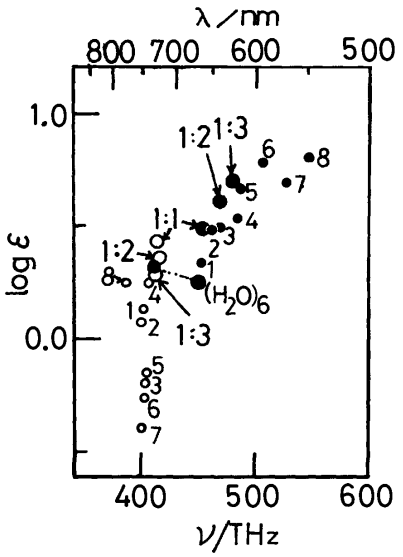

Fig. 3. The positions and intensities of band II (●) and spin-forbidden band (○) of various octahedral Ni(II) complexes in aqueous solution. Nonaqueous ligands in the coordination spheres of these complexes are: 1, asp(−I); 2, gly; 3, asp(−II); 4, en: 5, 2gly; 6, $5NH_3$; 7, $6NH_3$; 8, 3en. (asp(−I) and asp(−II) mean aspartate ions of charge −1 and −2, respectively). Apparent values taken from the curves 1 : 1 to 1 : 3 of Fig. 2 are also plotted. The points for bands IIa and IIb of $[Ni(H_2O)_6]^{2+}$ are shown by (●----●). For further details, *cf.* Refs. 4) and 10).

In spite of these early findings, later investigators generally identified band IIa of this complex with band II itself, and band IIb with the spin-forbidden band superposed on it, as may seem upon first glance.[7] There was also another explanation which denies the intervention of a spin-forbidden transition and ascribes the appearance of the two maxima to spin-orbit coupling.[8]

Recently, Ito examined the spectral data of aqueous solutions containing $[Ni(H_2O)_6]^{2+}$, NH_3, and various anions (ClO_4^-, NO_3^-, and Cl^-). Some of his curves are shown in Fig. 2. Here, one can see that, in going from a solution of $[Ni(H_2O)_6]^{2+}$ to those of Ni(II) ammine complexes, band IIa remains nearly at the same position. However, band IIb moves steadily in conformity with the spectrochemical series. This seems to be an indication that the former is the spin-forbidden band since, according to the Tanabe-Sugano diagram, its frequency should be quite insensitive to the variation in the ligand field strength. Band IIb should, thus, be identified with band II of other complexes, as was formerly pointed out by himself and Sone. A comparison with the curve of $[Ni(en)(H_2O)_4]^{2+}$, which is also shown in the same Figure, makes this view still more convincing.

On the basis of these findings, the earlier data of Ito[4] were reexamined, and the values of ν_{II} and ν_{sf} (*i.e.*, the frequency of the spin-forbidden band) of various Ni(II) complexes obtained by his curve analyses were plotted against their intensities (log ε), as shown in Fig. 3. It is now evident that the points for ν_{II} and those for ν_{sf} collect around two distinct curves. The former depend notably on the nature of the ligands and obey the spectrochemical series. However, the latter are nearly independent of the ligands, as expected from the Tanabe-Sugano diagram. Moreover, it can be observed, in general, that with the decrease of the frequency difference between band II and the spin-forbidden band, the intensity difference between them also tends to diminish (*i.e.*, band II tends to become weaker, and the spin-forbidden band stronger). This can be ascribed to an increased mixing of the nature of these transitions which occurs in the same direction.

The positions and intensities of bands IIa and IIb of $[Ni(H_2O)_6]^{2+}$, which were also refined by curve analyses, are plotted in Fig. 3. Now, it is easy to see that band IIa is better correlated with the spin-forbidden band of other complexes, and band IIb with their band II. Here, however, the two bands are so close that an exceptionally strong mixing takes place, making the former band quite spin-allowed and the latter somewhat spin-forbidden. Thus, they show a characteristic reversal of their intensities. In such a case, it may be reasonable to take the weighted mean (or center of gravity) of the two bands and assume it to be the ν_{II} of the system which should be used when the Tanabe-Sugano diagram and related formulas are applied to these data. Nephelauxetic parameters (B and β) of reasonable magnitude can be estimated in this way.[9]

Thanks of the authors are due to Prof. Hideo Yamatera for his valuable comments regarding this work.

References

1) In this paper, the positions of the bands are shown in frequencies (THz=10^{12} s^{-1}) and not in wave numbers, to be consistent with the former publications of Sone[3] and Ito[4] where 10^{13} s^{-1} was used as their units.

2) For an elementary explanation of these spectra, *cf.*, *e.g.*, F. A. Cotton and G. Wilkinson, "Advanced Inorganic Chemistry," 4th ed., Wiley, New York (1980), p. 786.

3) K. Sone, *Nippon Kagaku Zasshi*, **71**, 270 (1950).

4) H. Ito, *Nippon Kagaku Zasshi*, **77**, 1383 (1956).

5) Y. Tanabe and S. Sugano, *J. Phys. Soc. Jpn.*, **9**, 753, 766 (1954).

6) $\nu_{II}=1.467\,\nu_I+5.49$; $\nu_{III}=0.940\,\nu_{II}+34.84$; $\nu_{III}=1.418\,\nu_I+38.85$.

7) O. G. Holmes and D. S. McClure, *J. Chem. Phys.*, **26**, 1686 (1957); C. K. Jφrgensen, *Acta Chem. Scand.*, **9**, 1362 (1955).

8) A. D. Liehr and C. J. Ballhausen, *Ann. Phys.*, **6**, 134 (1959); *Mol. Phys.*, **2**, 123 (1959).

9) *Cf.* A. B. P. Lever, "Inorganic Electronic Spectroscopy," Elsevier, Amsterdam (1968), p. 216.

10) For more spectral data which support the view expressed in the present paper, and experimental technique employed to get them, *cf.* H. Ito, *J. Sci. Univ. Tokushima*, **18**, 15 (1985).

Isomers of the (2,4-Pentanedionato)bis(*N*-phenylethylenediamine)cobalt(III) Ion

Yue OUYANG,† Masaaki KOJIMA, and Junnosuke FUJITA*
Department of Chemistry, Faculty of Science, Nagoya University, Chikusa-ku, Nagoya 464
(Received May 1, 1985)

Synopsis. By reaction of $[Co(acac)_2(Ph\text{-}en)]^+$ (acac=2,4-pentanedionate ion, Ph-en=*N*-phenylethylenediamine) with Ph-en in methanol in the presence of active charcoal, three racemic pairs of diastereomers, *Δ(SS)Λ(RR)*-, *Δ(SR)Λ(RS)*-, and *Δ(RR)Λ(SS)-trans(N*-Ph,*N*-Ph)-$[Co(acac)(Ph\text{-}en)_2]^{2+}$ were obtained. The isomers epimerize in water, methanol, and ethanol to give an equilibrium mixture of the isomers.

Cobalt(III) complexes with *N*-phenyl-substituted amines are usually unstable because of both steric and electronic reasons.[1] However, in a previous paper,[2] we reported that such amines form stable cobalt(III) complexes with two acac (acac=2,4-pentanedionate ion) ligands.

In this paper, we report the preparation and characterization of $[Co(acac)(Ph\text{-}en)_2]^{2+}$ (Ph-en=*N*-phenylethylenediamine) where only one acac ligand is contained.

Experimental

Three Isomers of trans(N-*Ph*,N-*Ph*)-$[Co(acac)(Ph\text{-}en)_2]^{2+}$. To a methanol solution (150 cm^3) of $[Co(acac)_2(Ph\text{-}en)]ClO_4$[2] (3.0 g, 5.4 mmol) were added active charcoal (0.5 g), acetic acid (1 cm^3) and a methanol solution (10 cm^3) of Ph-en (1.6 g, 11.6 mmol). The mixture was stirred for 6 d at room temperature and then filtered. The purple filtrate was diluted with 0.01 mol dm^{-3} HCl (2 dm^3) and applied on a column (ϕ4.5 cm×30 cm) of SP-Sephadex C-25. By elution with 0.3 mol dm^{-3} NaCl–0.04 mol dm^{-3} HCl, the column showed five bands; purple, red, brown, green, and brown in the order of elution. The fastest-moving purple band contained unreacted $[Co(acac)_2(Ph\text{-}en)]^+$, and the slowest-moving brown band a mixture of highly-charged species. Sodium perchlorate was added to the eluate containing the green band (G) and the mixture was cooled to yield a green precipitate. It was collected by filtration, washed with cold water, and air dried. Yield (isomer G: *Δ(SS)Λ(RR)*): 0.14 g (4%). Found: C, 39.73; H, 4.91; N, 8.63%. Calcd for $C_{21}H_{31}N_4Cl_2CoO_{10}$=$[Co(acac)(Ph\text{-}en)_2](ClO_4)_2$: C, 40.08; H, 4.97; N, 8.90%. From each of the brown (B) and the red (R) eluates, the perchlorate of the complex was obtained by the same method as that for isomer G. Each product was dissolved in acetone–0.1 mol dm^{-3} HCl, and the acetone was slowly evaporated to yield crystals. Yield (isomer B: *Δ(SR)Λ(RS)*): 0.61 g (18%). Found: C, 39.99; H, 4.96; N, 8.73%. Calcd for $C_{21}H_{31}N_4Cl_2CoO_{10}$=$[Co(acac)(Ph\text{-}en)_2](ClO_4)_2$: C, 40.08; H, 4.97; N, 8.90%. Yield (isomer R, *Δ(RR)Λ(SS)*): 0.021 g (0.6%). Found: C, 38.78; H, 5.10; N, 8.61%. Calcd for $C_{21}H_{33}N_4Cl_2CoO_{11}$=$[Co(acac)(Ph\text{-}en)_2](ClO_4)_2\cdot H_2O$: C, 38.96; H, 5.14; N, 8.66%.

Isomer Distribution at Equilibrium. Each isomer (*ca.* 0.1 g) was dissolved in water, methanol, or ethanol (5 cm^3) at 20 °C. Portions of the reaction mixture were withdrawn at timed intervals, diluted with 0.1 mol dm^{-3} HCl, and the absorption spectra were measured. The experiments were carried out until the mixture attained equilibrium and no change in the spectra was observed. The equilibrated reaction mixture was diluted with 0.04 mol dm^{-3} HCl (30 cm^3), and the solution was subjected to column chromatography on SP-Sephadex C-25 (column: ϕ 0.9 cm×25 cm; eluent: 0.3 mol dm^{-3} NaCl–0.04 mol dm^{-3} HCl) in order to examine the distribution of the isomers.

Measurements. Absorption spectra in dil $HClO_4$ solutions (pH *ca.* 1.2) were recorded on a Hitachi 323 or a JASCO 610B spectrophotometer and ^1H NMR spectra in acetone-d_6 solutions on a JEOL PMX 60 spectrometer using TMS as an internal reference.

Results and Discussion

The $[Co(acac)(Ph\text{-}en)_2]^{2+}$ complex was prepared from $[Co(acac)_2(Ph\text{-}en)]ClO_4$ and Ph-en in methanol in the presence of active charcoal. The complex was separated into three isomers (G, B, and R) by column chromatography on SP-Sephadex C-25. In the course of the separation, the complex was found to isomerize in water to give an equilibrium mixture of the three isomers. In order to avoid the isomerization, the aqueous solutions were kept acidic (pH<1.5). When isomer G is dissolved in water, the color of the solution changes from green to greenish brown, and the solution attained equilibrium in *ca.* 10 min. The rate is dependent upon pH; the lower the pH, the slower the reaction. The isomer distribution at equilibrium at 20 °C was analyzed by column chromatographic technique, the ratio being isomer R:isomer B:isomer G=5:78:17. The runs starting from any isomer gave the same result within the experimental error (*ca.* ±3%). The isomerization was also observed for methanol and ethanol solutions, and the isomer distributions at equilibrium were the same as that for the aqueous solution. In methanol the complex attained equilibrium in *ca.* 10 min. However, in 0.8 mol dm^{-3} *p*-toluenesulfonic acid–methanol, the isomers showed no detectable change in the absorption spectra over 40 h at room temperature. A rate of inversion at coordinated secondary amine nitrogen (M-NHR^1R^2; R^1,R^2: alkyl substituent) is known to be proportional to hydroxide ion concentration.[3,4] Recemization (inversion at N-CH_3) of *trans,trans*-$[Co(NO_2)_2(CH_3NHCH_2CH_2NH_2)_2]^+$ in methanol has been reported to obey a rate law of the form R=[complex]·$[CH_3O^-]$.[5] Thus the isomerization of the present complex is suggested to be epimerization caused by inversion at the chiral nitrogen atoms remaining the geometrical configuration of the donor atoms unchanged.

† Present address: Department of Chemistry, University of Hainan, Hainan Island, Kwantung Province, The People's Republic of China.

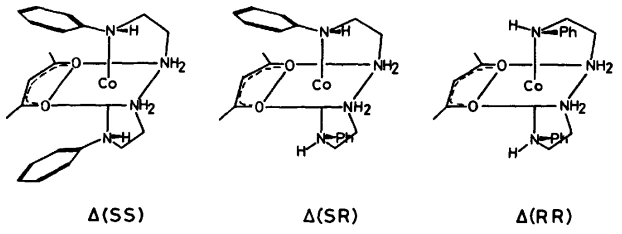

Fig. 1. Schematic structures of the three isomers of *Δ-trans(N*-Ph,*N*-Ph)-$[Co(acac)(Ph\text{-}en)_2]^{2+}$.

The $[Co(acac)(Ph\text{-}en)_2]^{2+}$ ion has three possible geometrical isomers with respect to the arrangement of two *N*-Ph groups. When the presence of three asymmetric centers, one at the cobalt atom and the others at the asymmetric nitrogen atoms, are taken into consideration, the number of isomers increases to ten racemic pairs. However, some of the isomers can be ruled out for steric reasons. Examination of molecular models indicates that only the *trans*(*N*-Ph,*N*-Ph) configuration can form three stable racemic pairs of diastereomers (Fig. 1). The structures of three isomers obtained in this study were assigned on the basis of the ^1H NMR and absorption spectra. In the *Δ(SS)Λ(RR)* configuration, the two phenyl groups are placed over and under the acac chelate ring and the methine proton will be strongly shielded by the phenyl groups. The resonance at a high field, δ=4.18 of isomer G can be assigned to the shielded methine proton, and the isomer is assigned to the *Δ(SS)Λ(RR)* configuration. Isomer R which exhibits the methine proton signal at a low field (δ=6.10) is assigned to the *Δ(RR)Λ(SS)* configuration in which the acac ligand is not shielded by the phenyl groups. The signal of methyl protons of isomer G (δ=1.77) is also observed at a higher field than that of isomer R (δ=2.13). Isomer B gives two methyl singlets (δ=1.88 and 1.90) and the methine singlet (δ=5.21) in the region between the corresponding signals of isomers G and R. Thus isomer B is assigned to the *Δ(SR)Λ(RS)* configuration where only one of the phenyl groups is placed over the acac chelate ring.

Figure 2 shows absorption spectra of the three isomers. All the isomers show the first absorption band, $^1A_{1g}\rightarrow{}^1T_{1g}$ (O_h) in the region of 16900 to 17950 cm^{-1} (isomer G: 16900 (2.71), isomer B: 17570 (2.56), isomer R: 17950 (2.54) in cm^{-1} (log ε)). The second absorption band, $^1A_{1g}\rightarrow{}^1T_{2g}$ (O_h) is almost hidden by strong charge-transfer bands. These first absorption bands are shifted largely to lower energy and become more intense compared to that of $[Co(acac)(NH_2CH_2CH_2NH_2)_2]^{2+}$ (20100 cm^{-1}, log ε=2.14).[6] Similar differences in absorption spectra are observed between $[Co(acac)_2(Ph\text{-}en)]^+$ and $[Co(acac)_2(NH_2CH_2CH_2NH_2)]^+$.[2] For the $[Co(acac)_2(Ph\text{-}en)]^+$[2] and $[Co(acac)_2(PhNHCH_2CH_2NH\cdot Ph)]^+$[7]

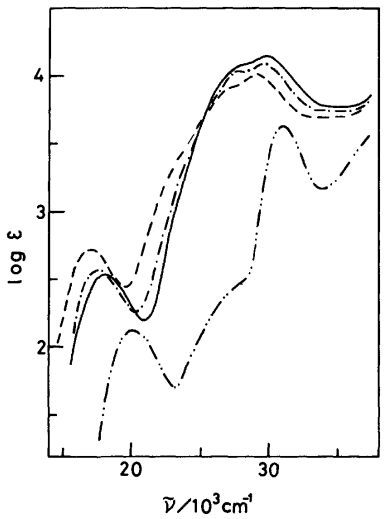

Fig. 2. Absorption spectra of isomer G *(Δ(SS)Λ-(RR))* (– –), isomer B *(Δ(SR)Λ(RS))* (–·–), and isomer R *(Δ(RR)Λ(SS))* (——) of $[Co(acac)(Ph\text{-}en)_2]^{2+}$ in dil $HClO_4$ (pH *ca.* 1.2) and of $[Co(acac)(NH_2CH_2CH_2NH_2)_2]^{2+}$ (–··–) in water.

complexes, the isomer in which the phenyl group is placed over an acac chelate ring has been observed to exhibit the first absorption band at lower energy than those of the other isomers. These observations in absorption spectra lead to the assignments that isomers G, R, and B have the *Δ(SS)Λ(RR)*, *Δ(RR)-Λ(SS)*, and *Δ(SR)Λ(RS)* configurations, respectively. These assignments are in accord with those obtained on the basis of ^1H NMR spectra.

As stated previously, the complex in solution exists in three isomers R (*Δ(RR)Λ(SS)*), B (*Δ(SR)Λ(RS)*), and G (*Δ(SS)Λ(RR)*) in the molar ratio of 5:78:17, respectively at equilibrium (20 °C). The most abundant is isomer B where only one of the phenyl groups is placed over the acac chelate ring. It is not clear whether the interaction between the phenyl and pseudoaromatic acac groups is attractive or repulsive.

References

1) M. Zehnder and H. Löliger, *Helv. Chim. Acta*, **63**, 754 (1980).
2) Y. Ouyang, M. Kojima, and J. Fujita, *Bull. Chem. Soc. Jpn.*, **57**, 3574 (1984).
3) B. Halpern, A. M. Sargeson, and K. R. Turnbull, *J. Am. Chem. Soc.*, **88**, 4630 (1966).
4) W. G. Jackson and A. M. Sargeson, "Rearrangements in Ground and Excited States," ed by P. de Mayo, Academic Press, New York (1980), Vol. 2, p. 273.
5) D. A. Buckingham, L. G. Marzilli, and A. M. Sargeson, *J. Am. Chem. Soc.*, **90**, 6028 (1968).
6) L. J. Boucher, *Inorg. Chim. Acta*, **6**, 29 (1972).
7) Y. Ouyang, M. Kojima, and J. Fujita, unpublished data.

Electron Transfer Initiated Replacement of Bromo and Methoxyl Groups with Aryliminodi-, Arylamino-, and Arylthiomagnesium Reagents

Masao Ōkubo,* Yasuhiro Nakagawa, Masatoshi Yoshida, and Hidenobu Yanase
Department of Chemistry, Faculty of Science and Engineering, Saga University, Honjō-machi, Saga 840
(Received November 8, 1984)

Synopsis. The replacement of bromo and methoxyl groups of fluorenone, *N*-(9-fluorenylidene)aniline, and α-benzylideneacetophenone with ArSMgBr(***S***), ArNHMgBr(***NH***), and ArN(MgBr)$_2$(***N***) were examined. The distribution of products obtained in the reactions with the reagents including ArMgBr(***C***) and ArOMgBr(***O***) were explained in terms of relative electron-donating abilities of reagents: ***C*>*S*>*NH*>*N*>*O***.

Grignard(ArMgBr, ***C***) and aryliminodimagnesium(ArN(MgBr)$_2$, aryl-IDMg, ***N***) reagents react with polar double bonds in the manners of addition and condensation, respectively.[1-4] However, the electron transfer from reagent to substrate is common to the reactions of ***C*** and ***N***, and the distribution of products is explained qualitatively in terms of the combination of relative electron-donating and -accepting abilities(EDA and EAA) of reactants.[5] The lower EDA of reagent ***N*** than that of ***C*** suggested on the basis of product distribution[5] was established by polarographic measurement of oxidation peak potentials.[6]

The study was thus extended to the electron transfer initiated replacement of 1-bromo substituent on fluorenone and *N*-(9-fluorenylidene)aniline[7,8] as well as that of methoxyl group on the benzylic position of α-benzylideneacetophenone[2] in the reaction with not only ***C*** and ***N*** but also with arylamino-, arylthio-, and aryloxymagnesium reagents (***NH***, ***S***, and ***O***). The product distribution will be explained in terms of relative EDA of the five magnesium reagents.

Results and Discussion

A set of reactions examined in order to convert 1-bromofluorenone (**1**) into *N*-(1-arylthio-9-fluorenylidene)aniline (**4**) and related reactions using ***C***,[7] ***N***,[7] ***S***, and ***O*** are shown in Scheme 1. Another set of reactions examined are the replacement reactions of methoxyl group of α-(α-methoxybenzylidene)acetophenone(**6a—6d**)[9] by the treatment with ***N***, ***NH***, and ***S*** shown in Scheme 2. The yields of normal and abnormal products are summarized in Table 1 (Runs A—E).

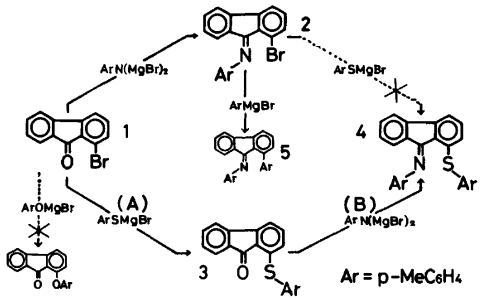

Scheme 1.

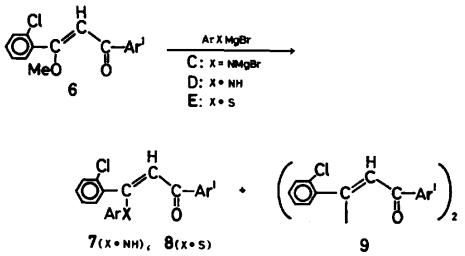

Scheme 2.

In Runs A, B, and E, the involvement of electron transfer is indicated explicitly by the formation of abnormal products due to typical radical processes: hydrogen abstraction from solvent (Run A), oxidative dimerization of reagent (Runs B_1 and B_2), reductive dimerization of substrate (Runs E_1—E_5), and radical recombination (Run A). On the treatment of **6** with ***N*** and ***NH*** having *para*- and *meta*-substituents (Runs C_1, C_2, D_1, and D_3), normal product **7** is formed in excellent yields. Abnormal product **9b**, however, is formed when the reagents have 2,6-dimethyl groups, which favor the demethoxylation followed by dimerization over the replacement (Runs C_3 and D_4) because the electron transfer is suppressed slightly and the process for the formation of **7** greatly. The latently involved electron transfer in the reactions of benzophenone with ***C*** and ***N*** is revealed similarly by use of *o*-Me-substituted reagents.[1,3] The reactivity of magnesium reagents must thus be estimated on the basis of their EDA instead of nucleophilicity.

The variation of yields of normal and abnormal products in the reactions of the same type of substrates with the different reagents is interpreted as follows. Imine **2** reacts with ***C***[7] but not with ***S*** (Scheme 1) because EDA of ***S*** is lower than that of ***C***. In the reaction with **6** (Scheme 2), ***S*** gives almost exclusively the abnormal product **9c** (Run E_1) while ***NH*** gives excellent yields of normal products **7a** and **7d** (Runs D_1 and D_3): The results are ascribed to the distinctly high EDA of ***S*** responsible for vigorous electron transfer compared with the medium EDA of ***NH*** for the mild and latent electron transfer. The low yield of **7a** obtained by use of a small excess of ***NH*** in Run D_2, in comparison with the good result of Run D_1, suggests the possibility that one mol of ***NH*** is consumed for electron transfer and another mol for product formation. Attempted variation of conditions of the reaction with ***S*** was not satisfactorily effective for improvement of the yield of **8** (Runs E_2—E_5). The substrates **1** and **6b** were recovered unchanged from the mixtures with ***O***: The red-brown coloration of the mixtures with ***O*** as well as that of ***S*** with **2** indicates that σ-complexes are formed (*vide infra*) but

Table 1. Products in the reactions of magnesium reagents *S*, *NH*, and *N* with Substrates **1**, **3**, and **6a—6d**

Run	Substrate[a]		Reagent[a,b]		Products[c]			
					(normal)		(abnormal)	
	No.	$Ar^1=R^1Ph$	Type	Ar=RPh	No.	Yield/%	No.	Yield/%
A	**1**	—	***S***	*p*-Me	**3**	92	2-ArS-THF[d]	38
B_1	**3**	—	***N***	*p*-Me	**4**	31	$(ArN=)_2$[e]	3
B_2	**3**	—	***N***	*p*-Me	**4**	84	$(ArN=)_2$[e]	8
C_1	**6a**	H	***N***	*p*-Me	$\mathbf{7a}^{Me}$	85	—	—
C_2	**6d**	DMB[f]	***N***	*p*-Me	$\mathbf{7d}^{Me}$	88	—	—
C_3	**6b**	*p*-Me	***N***	TM[g]	**7b**	39	**9b**	58
D_1	**6a**	H	***NH***	*m*-MeO	$\mathbf{7a}^{MeO}$	92	—	—
D_2	**6a**	H	***NH***	*m*-MeO	$\mathbf{7a}^{MeO}$	30	—	—
D_3	**6d**	DMB[f]	***NH***	*m*-MeO	$\mathbf{7d}^{MeO}$	96	—	—
D_4	**6b**	*p*-Me	***NH***	TM[g]	**7b**	33	**9b**	66
E_1	**6c**	*p*-MeO	***S***	*p*-Me	**8c**	trace	**9c**	90
E_2	**6c**	*p*-MeO	***S***	*p*-Me	**8c**	25	**9c**	65
E_3	**6c**	*p*-MeO	***S***	*p*-Me	**8c**	9	**9c**	85
E_4	**6b**	*p*-Me	***S***	*p*-Me	**8b**	14	**9b**	75
E_5	**6b**	*p*-Me	***S***	*p*-Me	**8b**	31	**9b**	60

a) The substituents R^1 of **6a—6d** and R of reagents are given. b) The abbreviations of reagents are given in the text. Molar equivalent amount of reagents and addition manner are given in Experimental. c) Yields based on the substrates used. d) *p*-Methylphenyl 2-oxolanyl sulfide. e) 4,4'-Dimethylazobenzene. f) 2,6-Dimethyl-4-*t*-butyl. g) 2,4,6-Trimethyl.

the electron transfer is impossible because of much lower EDA's compared with the respective EAA's. Taking the polarographically determined order (***C>NH>N***)[6] into account, all the results of the reactions of Schemes 1 and 2 are interpretable in terms of the relative EDA: ArMgBr>ArSMgBr>ArNHMgBr>$ArN(MgBr)_2$>ArOMgBr.

Since magnesium has strong affinity for oxygen, the reactions are initiated with the coordination of carbonyl oxygen to Mg atom of reagent. The rate-determining nature of *σ-complex formation* in the condensation of ***N*** with diaryl ketones was proposed on the basis of the fact that electron-repelling substituents of substrate favor the product formation.[3,5] In contrast, the rate-determining nature of *electron transfer* in the reaction of ***C*** with benzophenones established by thermochemical measurement[10] was confirmed by the acceleration of ketyl formation by electron-attracting substituent of substrate.[1,11] Accordingly, the rate-determining process of the reactions with ***C***, ***S***, ***NH***, and ***N*** is localized on one of the two essentially common initial processes; subsequent ones for the product formation are not rate-determining. The dependence of product distribution on the EDA's of different types of reagent is reasonable.

The simple concept will be helpful in utilizing variuos types of magnesium reagents, and is expected to be quantified.

Experimental

The substrates **1** and **2** were prepared previously.[7] The solutions of reagents ***S***, ***NH***, ***N***, and ***O*** were prepared by the addition of calculated amount of benzenethiol, aniline, and phenol to the EtMgBr solution in tetrahydrofuran (THF).[7]

In the typical Runs, substrate(3.23 mmol) dissolved in THF(15 ml) was mixed with the THF solution(30 ml) of given amount of reagent. Molar equivalent amounts of reagents used in individual runs are: 1.5(D_2), 2.0(B_1), 2.2(E_2, E_4, and E_5), 3.0(A, C_3, D_1, D_3, D_4, E_1, and E_4), 4.0(C_1 and C_3), and 5.0(B_2). In Runs A—D and E_1, the substrates were added in normal manner at once at 0 °C(A, B_1, and B_2), at once at room temperature(C_1—C_3 and D_1—D_4), and over the period of 5 min at −78 °C(E_1). In Runs E_2—E_5, the reagent ***S*** was added in reverse manner at −78 °C over the period of 20 min(E_2, E_4, and E_5) and 60 min(E_3).

The mixtures were neated at 55 °C for 3 h (A—D) and 1 h (E). No reaction took place on the treatment of **2** with ***S*** and **1**(or **6b**) with ***O*** even by use of 8.0 mol of reagents.

The products mixtures were chromatographed on silica gel (Wako Gel, C-200 and C-300). All the ^1H-NMR spectra and elemental analyses of products were satisfactory.

The authors wish to thank Mr. Mitsunao Tokisada for the study of the reactions of runs C_3 and D_4.

References

1) M. Ōkubo, *Bull. Chem. Soc. Jpn.*, **48**, 2057 (1975).
2) M. Ōkubo, *Bull. Chem. Soc. Jpn.*, **50**, 2379 (1977).
3) M. Ōkubo and S. Ueda, *Bull. Chem. Soc. Jpn.*, **53**, 281 (1980); M. Ōkubo, S. Hayashi, M. Matsunaga, and Y. Uematsu, *Bull. Chem. Soc. Jpn.*, **54**, 2337 (1981).
4) M. Ōkubo, T. Takahashi, and K. Koga, *Bull. Chem. Soc. Jpn.*, **56**, 199 (1983).
5) M. Ōkubo, M. Yoshida, K. Horinouchi, H. Nishida, and Y, Fukuyama, *Bull. Chem. Soc. Jpn.*, **56**, 1196 (1983).
6) M. Ōkubo, T. Tsutsumi, A. Ichimura, and T. Kitagawa, *Bull. Chem. Soc. Jpn.*, **57**, 2679 (1984).
7) M. Ōkubo and Y. Uematsu, *Bull. Chem. Soc. Jpn.*, **55**, 1121 (1982).
8) P. S. Ayscough and R. Wilson, *J. Chem. Soc.*, **1963**, 5412.
9) C. Bickel, *J. Am. Chem. Soc.*, **68**, 865 (1946); **69**, 73 (1947).
10) T. Holm, *Acta Chem. Scand., Ser. B* **28**, 809 (1974).
11) M. Ōkubo, *Bull. Chem. Soc. Jpn.*, submitted.

Ultrasounds in Synthetic Reactions. III. Reduction of Organic Halides with Nickel(II) Chloride-Zinc-Water[1)]

Junzo YAMASHITA,* Yoshio INOUE, Takashi KONDO, and Harukichi HASHIMOTO
Department of Applied Chemistry, Faculty of Engineering, Tohoku University, Aramaki-Aoba, Sendai 980
(Received March 29, 1985)

Synopsis. The reductive dehalogenation of aryl chlorides as well as other organic halides was facilitated with nickel(II) chloride-zinc-water in hexamethylphosphoric triamide irradiated with ultrasound.

There are a number of methods for the reduction of alkyl or aryl halides using transition metals.[2)] But aryl chlorides are rather resistant to the reduction. It is known that low valent nickel complexes *in situ* generated from nickel(II) salt-zinc powder-triphenylphosphine(TPP) in *N,N*-dimethylformamide(DMF) are able to oxidatively add a large number of organic halides to yield coupling products.[3,4)] The reduction of aryl halides also proceeds with a similar reagent: zinc-water-a catalytic amount of nickel(II) chloride-TPP-sodium iodide in DMF.[5)] But the work-up procedure is frequently troublesome due to the presence of TPP. Recently Takagi and Hayama[6)] reported that the Ullmann type coupling reaction could be effectively achieved by means of *in situ*-generated nickel(0) species in hexamethylphosphoric triamide(HMPA) without TPP.

We wish to report a convenient method for the reduction of aryl halides, especially aryl chlorides, under mild conditions; aryl halides, zinc, water, nickel(II) chloride, and sodium iodide are sonicated in HMPA to yield the dehalogenated products. Ultrasound-irradiation is known to accelerate a variety of organic reactions, particularly those involving metals.[1,7)]

Experimental

Materials and Analysis. HMPA was dried over Molecular Sieves 5A, distilled under nitrogen *in vacuo*, and stored over Molecular Sieves 5A. All other reagents were used as obtained commercially. Reaction products were identified by the comparison of retention times in GLC and mass spectra (JEOL D 300 mass spectrometer) with those of the authentic samples. The yields of products were determined by GLC (Shimadzu GC 3AH using a Silicone GE SE-52 20 wt% on Chromosorb W AW, or FFAP 10 wt% on Chromosorb W AW DMCS column).

General Procedures for Reduction Reactions. To a 50 cm^3 3-necked flask, which contained 0.98 g(15 mmol) of zinc powder, 1.30 g(10 mmol) of nickel chloride, and 0.90 g(6 mmol) of chlorobenzene, 0.3 cm^3(16.7 mmol) of water, 0.200 g of toluene(an internal standard for GLC analysis) and 15 cm^3 of HMPA were added under nitrogen atmosphere and the mixture was irradiated with ultrasound(53 W, 41 kHz) at 60 °C. The yields of products were determined by GLC.

Results and Discussion

The reactions of aryl halides with zinc, nickel chloride, water and sodium iodide were carried out in HMPA at 60 °C under ultrasound-irradiation.

$$\text{R–X} \xrightarrow[\text{H}_2\text{O, NaI, HMPA, 60 °C}]{\text{NiCl}_2\text{, Zn, Ultrasound}} \text{R–H}$$

Several reaction parameters were examined and the results are shown in Table 1. The ease of reduction of halobenzenes decreased in the order: iodobenzene>bromobenzene>chlorobenzene(runs 1,2, and 4), which is consistent with the proposed oxidative addition mechanism.[4,5,6,8)] Iodobenzene and bromobenzene gave a small amount of the coupling product, biphenyl, whereas chlorobenzene and other aryl chlorides afforded only a trace amount of the coupling byproducts. Iodobenzene could be reduced without the coupling byproduct when cobalt(II) acetate or iron(II) sulfate was used instead of nickel(II) chloride(runs 12 and 13). The higher selectivity in the reduction compared with that using TPP[5)] is favorable as a synthetic method. The increasing amount of sodium iodide and nickel chloride increased the yield(runs 3—7). The role of sodium iodide is not clear, but it may promote the reduction of nickel chloride by zinc[4,5)] and/or the reduction of an arylnickel intermediate.[6)] The yield decreased when the reduction was carried out in DMF. The reduction was not observed in tetrahydro-

Table 1. Effect of various reaction parameters on the reaction of halobenzenes[a)]

Run	Ph-X	$NiCl_2$/mmol	NaI/mmol	Reaction time/h	Yield of PhH/%
1	Ph-I	10	6	0.5	87[g)]
2	Ph-Br	10	6	1	91[h)]
3	Ph-Cl	10	0	2	64
4	Ph-Cl	10	6	2	81
5	Ph-Cl	10	12	2	93
6	Ph-Cl	5	6	2	54
7	Ph-Cl	7.5	6	2	69
8	Ph-Br	5	6	4	81
9	Ph-Br[b)]	5	6	4	64
10	Ph-Br[c)]	5	6	4	56
11	Ph-Br[d)]	5	6	4	0
12	Ph-I[e)]		8	4	93
13	Ph-I[f)]		6	4	92

a) Reaction conditions: Ph-X, 5 mmol; Zn, 15 mmol; H_2O, 0.3 cm^3; HMPA 15 cm^3; 60 °C under sonication. b) Solvent: DMF 15 cm^3. c) Solvent: THF 13 cm^3 and HMPA 2 cm^3. d) Solvent: THF 15 cm^3. e) $Co(OOCCH_3)_2$(7.5 mmol) instead of $NiCl_2$. f) $Fe_2(SO_4)_3$(2.5 mmol) instead of $NiCl_2$. g) Biphenyl yield, 13%. h) Biphenyl yield, 7%.

Table 2. Reduction of various organic halides[a)]

Run	Organic halide	$NiCl_2$ mmol	NaI mmol	Reaction time/h	Yield %
14	C_6H_5Cl	10	6	4	95
15	*p*-MeC_6H_4Cl	15	6	3	100
16	*p*-$MeOC_6H_4Cl$	15	6	3	86
17	*p*-$HOCH_2C_6H_4Cl$	10	6	1	15
18	*p*-NCC_6H_4Cl	10	6	1	22
19	1-$C_{10}H_7Cl$[b)]	10	6	8	100
20	$C_6H_5CH_2Cl$	10	6	1	47[c)]
21	*n*-$C_7H_{15}Cl$	10	6	1	85
22	$C_6H_{11}Br$[d)]	10	6	1	82

a) See Table 1 for reaction conditions. b) 1-Chloronaphthalene. c) The yield of bibenzyl was 50%. d) Bromocyclohexane.

furan(THF), but proceeded by the addition of a small amount of HMPA to THF(runs 10 and 11). Although the reaction proceeded with ordinary stirring, the ultrasonic irradiation could increase the rate of reaction by 20—50%.

The reduction of various aryl chlorides as well as alkyl halides proceeded smoothly in rather short reaction time to give the reduction products in very high yields with the exception of *p*-chlorobenzyl alcohol and *p*-chlorobenzonitrile, where the reaction stopped within an hour and the starting materials were recovered. These results are shown in Table 2.

In conclusion, the present method is a very convenient procedure for the reduction of organic halides, especially aryl chlorides.

A part of this work was presented at the Joint Regional Meeting of Chem. Soc. Jpn. and Associated Societies of Tohoku Region, Yonezawa, October 5 (1984), Abstr. No. 1B16.

References

1) The previous report, J. Yamashita, Y. Inoue, T. Kondo, and H. Hashimoto, *Bull. Chem. Soc. Jpn.*, **57**, 2335 (1984).

2) M. Hudlicky, "Reductions in Organic Chemistry," Ellis Horwood Ltd., Chichester(1984), pp. 63—69; M. Tashiro, and K. Nakayama, *J. Chem. Soc., Perkin Trans. 1*, **1983**, 2315; S. T. Lin and J. A. Roth, *J. Org. Chem.*, **44**, 308 (1979); M. Tashiro, A. Iwasaki, and K. Nakayama, *J. Org. Chem.*, **43**, 196 (1978).

3) A. S. Kende, L. S. Liebeskind, and D. M. Braitsch, *Tetrahedron Lett.*, **1975**, 3375.

4) M. Zembayashi, K. Tamao, J. Yoshida, and M. Kumada, *Tetrahedron Lett.*, **1977**, 4089.

5) I. Colon, *J. Org. Chem.*, **47**, 2622 (1982).

6) K. Takagi, N. Hayama, and S. Inokawa, *Bull. Chem. Soc. Jpn.*, **53**, 3691 (1980).

7) O. Repic and S. Vogt, *Tetrahedron Lett.*, **23**, 2729 (1982); B. -H. Han and P. Boudjouk, *Organometallics*, **2**, 269 (1983); K. S. Suslick and R. E. Johnson, *J. Am. Chem. Soc.*, **106**, 6856 (1984) and references cited therein.

8) M. F. Semmelhack, P. Helquist, L. D. Jones, L. Keller, L. Mendelson, L. S. Ryono, J. G. Smith, and R. D. Stauffer, *J. Am. Chem. Soc.*, **103**, 6460 (1981).

Decarboxylative Photoaddition of 3-Butenoate Anion to 1-Methyl-2-phenyl-1-pyrrolinium Perchlorate *via* Electron-transfer Reaction

Yoshiaki KURAUCHI, Kazuya OHGA,* Hideo NOBUHARA, and Shigeru MORITA†

Department of Environmental Chemistry and Engineering, Faculty of Engineering, Oita University, Dannoharu, Oita 870-11

(Received April 11, 1985)

Synopsis. The photolysis of 1-methyl-2-phenyl-1-pyrrolinium perchlorate (**1**) with a 3-butenoate anion in an aqueous solution efficiently gives a 2-allylpyrrolidine adduct. Mechanistic studies demonstrate that the photoreaction is induced by a one-electron transfer from 3-butenoate to the singlet excited-state of **1**.

Photoinduced electron-transfer reactions of systems containing iminium cation chromophores have been extensively investigated in recent years with synthetic[1] and biological[2] interests. Mariano *et al.*[3-6] have elucidated mechanistic details regarding photoreactions of pyrrolinium cations with a variety of electron donors such as olefins, allylsilanes, allenes, and arenes. In these, electron transfers to the excited singlet states of the cations take place to give 2-pyrrolidinyl radicals. Cation radical intermediates derived from the electron donors are transformed into neutral radicals by nucleophilic capture, deprotonation or desilylation followed by radical coupling with the pyrrolidinyl radicals leading to the production of photoadducts. In this note, we show that when a 3-butenoate anion is used as an electron donor in an aqueous solution, an allylic photoaddition to 1-methyl-2-phenyl-1-pyrrolinium perchlorate (**1**) occurs to give 1-methyl-2-phenyl-2-(2-propenyl)pyrrolidine (**2**) similar to a reaction in allylsilane systems.[4]

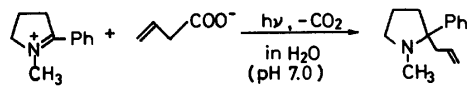

1 **2**

Results and Discussion

1 was irradiated in an aqueous solution whose pH was adjusted to 7.0 with NaOH and contained 0.388 M (1 M=1 mol dm^{-3}) 3-butenoic acid to afford **2**. This was isolated after extraction with chloroform and was distilled under a reduced pressure in a 67.9% yield. The identification of **2** was made by a direct comparison of the ^{1}H NMR and IR spectra with those of an authentic sample[4] prepared by the photoaddition of 3-(trimethylsilyl)propene to **1**. No dark reaction to produce **2** was observed and the fluorescence and absorption spectra of **1** in aqueous solutions containing the acid revealed the absence of an excited- and ground-state complex formation. When the solution pH was not neutralized and, thus, the carboxylic acid existed predominantly in an undissociated form, the yield of **2** was reduced to about one-fortieth. This suggested that the adduct was mainly produced by a photoreaction with the carboxylate anionic form.

One of the requirements for the feasibility of an electron-transfer-initiated photoaddition in the olefin-pyrrolinium cation pairs is an efficient quenching of the fluorescences of the cations by olefins.[3,4] Certainly, the rate constant (k_q=(3.08±0.08)×10^9 M^{-1} s^{-1}) of the fluorescence quenching of 2-phenyl-1-pyrrolinium perchlorate by the undissociated form in acetonitrile (obtained from the slope of a linear Stern-Volmer plot) was comparable to those for methyl 3-methyl-2-butenoate (3.7×10^9)[3] and 3-(trimethylsilyl)propene (5.25×10^9 M^{-1} s^{-1})[4] which are able to undergo photoaddition. Furthermore, it should be noted that quenching of the fluorescence of **1** by the anionic form ($k_q\tau$=3.00±0.06 M^{-1})[7] in an aqueous solution was more efficient than that by the excellent olefin quencher, the undissociated form ($k_q\tau$=1.84±0.03 M^{-1}). Thus, the allylic photoaddition described above seems to be induced not only by an electron transfer from the vinyl group of the 3-butenoate anion to the singlet excited state of **1** (^{1}**1***), but also by an electron transfer from the carboxylato group (Scheme 1). In fact, an acetate anion quenched the fluorescence of **1**,[8] though the $k_q\tau$ value (1.14±0.07 M^{-1}) was no more than *ca.* one-third the value for the butenoate and no more than *ca.* one-half the value for the butenoic free acid. The calculated free-energy change (−1.1 eV)[9] using estimated one-electron oxidation potentials of carboxylates[10] and the reduction potential (−0.95 V *vs.* SCE in an aqueous solution) and singlet energy (3.9 eV) of **1** also suggests that a one-electron transfer from the carboxylato group should be energetically feasible.

The steady-state analysis of a sequence, analogous to that for the allylsilane systems,[4] shown in Scheme 1, gives $\phi_a^{-1}=\alpha_a^{-1}+(\alpha_a k_q\tau[\text{3-butenoate}])^{-1}$, where ϕ_a and α_a represent the quatum yield of the formation of **2** and the limiting ([3-butenoate]→∞)ϕ_a, respectively. The ratio of the intercept to slope from a linear plot of ϕ_a^{-1} *vs.* [3-butenoate]$^{-1}$ shown in Fig. 1 was 2.6±0.5 M^{-1} and closely agreed with the $k_q\tau$ value (3.00 M^{-1}) obtained from fluorescence quenching. This agreement of mathematically equivalent quantities obtained independently of one another suggests that the fluorescence quenching and photoaddition are kinetically coupled and, thus, that the photoaddition proceeds *via* the singlet excited state of **1**. In addition, the reciprocal of the intercept, α_a (0.33) and

† Present address: Oita Prefecture Advanced Technology Department Research Institute, Nakahanda, Oita 879-76.

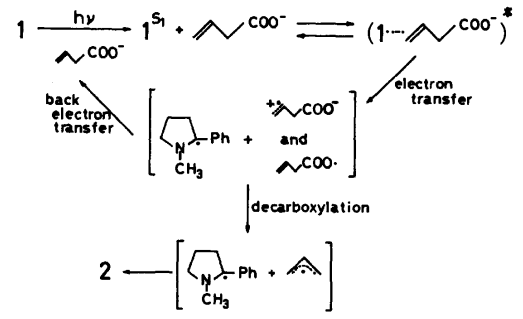

Scheme 1.

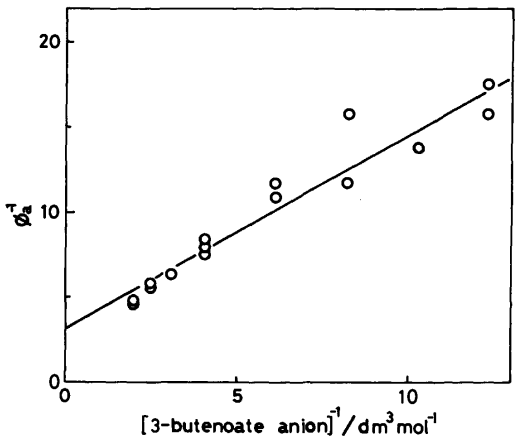

Fig. 1. Double reciprocal plot of the quantum yield for formation of **2** *vs.* the concentration of 3-butenoate anion.

the ratio (0.69) of ϕ_a (0.22±0.02) to the quantum yield for the disappearance of 1 (ϕ_{dis}=0.32±0.03) obtained at [3-butenoate] of 0.5 M had larger values than those regarding the photoaddition of 3-(trimethylsilyl)-propene (α_a=0.02 and ϕ_a/ϕ_{dis}=0.5).[4] This indicates a higher efficiency of the adduct formation with a 3-butenoate anion.

Experimental

The ^{1}H NMR, UV, and IR spectra were recorded on a Hitachi R-24B, a Shimadzu UV 202, and a Hitachi 285, respectively. The fluorescence emission was measured using a Shimadzu RF-510 spectrometer. **1** was prepared and purified according to a method from the literature:[7b] mp 117.5—119.0 °C (uncorrected). 3-Butenoic acid was commercially available and distilled *in vacuo* just before use.

Photolysis of 1 with 3-Butenoate Anion. In an aqueous solution (200 cm^3) containing 3-butenoic acid (6.67 g, 0.0776 mol) adjusted to pH 7.0 with NaOH, **1** (401 mg, 1.54 mmol) was dissolved and irradiated for 60 min. The irradiation was carried out using a 400-W high-pressure mercury lamp (Riko-Sha UVL-400HA) equipped with a Pyrex water-jacket under an atmosphere of argon. The photolysate was acidified (pH 1) with HCl and then concentrated to 5 cm^3 *in vacuo*. The acidic solution was made basic (pH 10) with NaOH, saturated with NaCl, and extracted with three 20-cm^3 portions of chloroform. The extract was dried over anhydrous Na_2SO_4 and then concentrated *in vacuo*. The resulting oily residue was purified by distillation under a reduced pressure to give 213 mg (67.9% yield) of a clear oily product **2**.

Fluorescence Quenching Experiments. The relative intensities of the fluorescence at 380 nm of **1** (1×10^{-3} M) were measured at 25±1 °C. The excitation wavelength was 305 nm and concentrations of the quenchers were in the 0.1—0.5 M ranges.

Quantum Yields. Quantum yields were measured using a linear optical-bench system equipped with a 500-W super-high-pressure mercury lamp (Ushio USH-500D) at 25±1 °C. The 280-nm band (1.54×10^{14} quanta s^{-1}) isolated with a monochrometer (Jarrel Ash JE-25E) was used to irradiate an argon-purged aqueous solution (pH 6.0, [**1**]=1.00×10^{-3} M, [3-butenoate]=0.5 M). Product analyses were performed by GLC (Shimadzu GC-3BF, 5% PEG 20M) for reaction mixtures worked up as in the preparative run. Biphenyl was used as an internal standard. The degrees of the disappearance of **1** were determined from the decrease of the absorbance at the λ_{max} of 258 nm. The conversions were not more than 10%. The relative quantum yields for the formation of **2** at different concentrations of 3-butenoate were obtained at 25±1 °C using a merry-go-round apparatus at the center of which was the 400-W high-pressure mercury lamp employed in the preparative run.

The authors wish to thank Professor Patrick S. Mariano of the University of Maryland for his helpful comments.

References

1) For example, F. T. Chiu, J. W. Ullrich, and P. S. Mariano, *J. Org. Chem.*, **49**, 228 (1984).

2) For example, U. Ott, R. Traber, P. Hemmerich, and H. E. A. Kramer, *Photochem. Photobiol.*, **40**, 309 (1984).

3) P. S. Mariano, *Acc. Chem. Res.*, **16**, 130 (1983) and references therein.

4) K. Ohga, U. C. Yoon, and P. S. Mariano, *J. Org. Chem.*, **49**, 213 (1984); K. Ohga and P. S. Mariano, *J. Am. Chem. Soc.*, **104**, 618 (1982).

5) K. Somekawa, K. Haddaway, P. S. Mariano, and J. A. Tossell, *J. Am. Chem. Soc.*, **106**, 3060 (1984).

6) A. J. Y. Lan, S. L. Quillen, R. O. Heuckeroth, and P. S. Mariano, *J. Am. Chem. Soc.*, **106**, 6439 (1984).

7) a) Fluorescence parameters of **1** in acetonitrile are little affected by the addition of water.[7b] Accordingly, the k_q value is estimated bo be *ca.* 3×10^9 M^{-1} s^{-1}, near the diffusion-controlled limit (6×10^9 M^{-1} s^{-1}), using τ(1 ns)[4] of **1** in acetonitrile; b) P. S. Mariano, J. Stavinoha, and E. Bay, *Tetrahedron*, **37**, 3385 (1981).

8) Acetic acid can not serve as a quencher for the fluorescence.

9) D. Rehm and A. Weller, *Isr. J. Chem.*, **8**, 259 (1970).

10) a) The critical potential of acetate (1.9 V *vs.* SCE)[10b] was employed since it was difficult to observe the anodic waves of the butenoate and acetate in aqueous solutions; b) L. Eberson, "Carboxylic Acids," in "Organic Electrochemistry," ed by M. M. Baizer, Marcel Dekker, New York (1973), Chap. XIII.

Preferred Conformation of 1-Phenyl-2-propanol. *Ab initio* and Molecular Mechanics Calculations with Geometry Optimization

Kazuhisa ABE,* Minoru HIROTA, and Keiji MOROKUMA†
Department of Applied Chemistry, Faculty of Engineering, Yokohama National University, Hodogaya-ku, Yokohama 240
†*Institute for Molecular Science, Myodaiji, Okazaki 444*
(Received April 19, 1985)

Synopsis. The most stable conformation of 1-phenyl-2-propanol, optimized by *ab initio* and molecular mechanics (MM2) calculations, is a phenyl-methyl anti and phenyl-OH gauche conformation with an intramolecular OH-π hydrogen bond.

Weak interactions such as OH-π hydrogen bond,[1] CH-π interaction,[2] and van der Waals interaction[3] often play an important role in determining conformations of various organic molecules. We have reported recently the stereochemistry of $C_6H_5CH_2XR$-type compounds (X=CHOH, C=O, S=O; R=CH_3, C_2H_5, *i*-C_3H_7, *t*-C_4H_9) by use of molecular mechanics (MMI) and pointed out the importance of the nonbonded weak interaction.[4] In order to understand the nature of these weak interactions in detail, we studied in this letter conformations of 1-phenyl-2-propanol with *ab initio* molecular orbital as well as molecular mechanics calculations.

Methods

We used the programs Gaussian 80[5] for *ab initio* calculation and MM2[6] for molecular mechanics calculation. The geometries of conformers were optimized with the Hartree-Fock method with the STO-3G basis set. It took about 5 h in CPU time to reach one of the local energy minima of 1-phenyl-2-propanol. At the STO-3G geometries, the energies and electron distributions were recalculated with the 4-31G basis set. Comparing with STO-3G calculations, 4-31G calculations give more reliable results about energy difference of isomers. In the case of geometry optimization by MM2, the required CPU time for this molecule was about 10—20 s.

Results and Discussion

The *ab initio* calculation showed that the most stable conformer was a phenyl-methyl anti and phenyl-OH gauche type with an intramolecular OH-π hydrogen bond (Table 1). The OH-π hydrogen bond energy was estimated to be 2.20 kcal† mol^{-1} from the energy difference between conformers **B** and **C**. From the temperature dependent IR measurement on 1-phenyl-2-propanol($\bar{\nu}_{OH}$(free)=3626 cm^{-1}, $\bar{\nu}_{OH\text{-}\pi}$= 3604 cm^{-1}), we determined experimentally this energy to be 1.0 kcal mol^{-1}. The *ab initio* calculation overestimates the hydrogen-bond interaction in this case. From the dihedral angle H(6)-C(1)-C(4)-C(9), we found that the benzene ring was twisted around the C(4)-C(1) bond in **A** and **D** conformers so as to avert the steric congestion between methyl and

TABLE 1. RELATIVE ENERGIES, OPTIMIZED GEOMETRIES, VIBRATIONAL FREQUENCY AND ELECTRON DISTRIBUTION OF 1-PHENYL-2-PROPANOL

Conformation	**A**	**B**	**C**	**D**
E/kcal mol^{-1}	−0.64	0.0[a]	−2.20	+0.38
R_{OH}/Å	0.991	0.990	0.990	0.993
C-O-H/deg	104.01	104.07	104.07	104.09
W[b](4-1-2-15)/deg	−60.92	−177.50	−178.09	60.0
W(6-1-4-9)	41.10	32.66	33.25	24.26
Population				
C=(Ph)[c]	6.167	6.159	6.171	6.161
H(OH)	0.608	0.605	0.596	0.605
O	8.730	8.724	8.736	8.725
O-H	0.253	0.254	0.249	0.254
OH-Ph(×10^2)[d]	−0.029	−0.016	1.62	−0.021
CH_3-Ph(×10^3)[e]	4.79	−0.33	−0.29	7.44
$\bar{\nu}_{OH}$/cm^{-1}	4240	4240	4240	4240
Scaled	3600	3600	3600	3600

a) The total energy is −422.05271 hartree with the 4-31G basis set at a STO-3G optimized geometry. b) Dihedral angle. c) Averaged value of the population on the carbon atoms in the benzene ring. d) Sum of the OH proton-carbon overlap population over 6 carbon atoms of the benzene ring. e) Sum of the CH_3 proton-carbon overlap population over 3 CH_3 protons and 6 benzene-ring carbon atoms.

† 1 cal_{th}=4.184 J.

phenyl groups. In conformers **A** and **D**, these dihedral angles change from the normal angle(30°) to 41° and 24°, respectively.

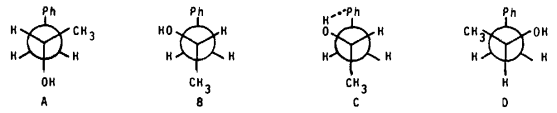

The population analysis reveals the evidence for the intramolecular OH-π hydrogen bond as follows:

1) In conformer **C** (dihedral angle C(1)-C(2)-O(3)-H(8): −59.73°) there is a small positive sum of populations (1.62×10^{-2}) between the OH proton and the carbon atoms of the benzene ring, indicating a bonding interaction. In the other conformers, in which these dihedral angles are nearly 180° and OH proton cannot interact with benzene ring, the sums are all negative.

2) The overlap population of the OH bond in **C** (0.249) is the smallest among the conformers, indicating that the OH bond of **C** is the weakest. But the OH stretching frequencies estimated from the calculated diagonal force constant at the STO-3G level are essentially identical among these conformers (4220 cm^{-1}, which gives 3600 cm^{-1} when scaled with a factor 1.17).[7] This may be due to the neglect of off-diagonal elements.

3) Conformer **C** has the smallest atomic population on the OH proton (0.596) and the largest average atomic population on the carbon atoms of the benzene ring (6.171). These values also support the presence of OH-π interaction.

From the optimized geometry of OH-π intramolecularly hydrogen bonded form (Fig. 1) we find the fact that the OH proton(8) is interacting equally with two carbon atoms (C(4), C(9)) of the benzene nucleus and is located above the surface with an OH(8)···C(4) or C(9) distance of 2.60 Å. Ōki and Iwamura[8] reported that the OH proton and the benzene nucleus were interacting in the same form as found above based on the IR experiments on similar 2-phenylethanol.

The geometry optimized MM2 calculation revealed the same preferred conformation. The optimized geometries of conformers are quite similar to those from *ab initio* calculations. The energy difference between **B** and **C** (−0.228 kcal mol^{-1}) is thought to correspond to intramolecular OH-π hydrogen bond energy. Careful examination of the steric energy components of **B** and **C** conformers clearly indicates that the dipole energy term mainly contributes to the stabilization of OH-π hydrogen bonded form. But the hydrogen-bond energy is rather small in comparison with the experimental value (1.0 kcal mol^{-1}). Therefore the present MM2 calculation is not adequate for studying the hydrogen bond system. It is necessary to add an extra energy term corresponding to the delocalization contribution of hydrogen bond to steric energy from MM2 in order to evaluate the hydrogen bond and steric energy correctly.

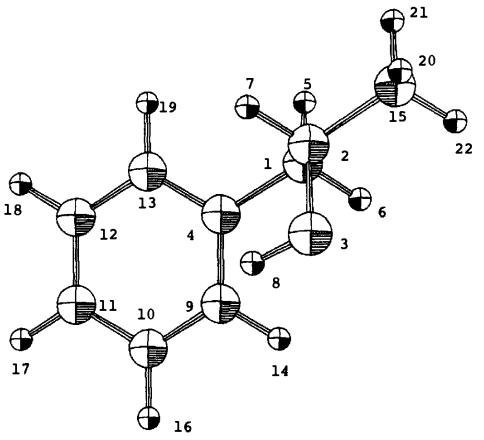

Fig. 1. Optimized Geometry of Conformer **C**.

As to the CH-π interaction, we cannot show a definitive evidence at this calculation level that CH_3 protons and the benzene nucleus are interacting. Some results may be taken to give the qualitative evidences of the CH-π interaction. In the conformer **A** and **D**, in which CH-π interaction is possible, a small positive overlap population is found (4.79×10^{-3} and 7.44×10^{-3}, respectively). This small positive bond population suggests a very small attractive interaction between CH_3 and π-electrons of the benzene ring. This suggests the presence of a delocalizative interaction between CH_3 and benzene ring. In addition, MM2 calculation estimates a considerably large attractive van der Waals interaction(−0.45 kcal mol^{-1}) between CH_3 and the benzene nucleus in conformer **A**. In other conformers, this interaction energy (CH_3-Ph) is about 0.1 kcal mol^{-1} smaller than that of **A**.

References

1) K. Morokuma and G. Wipff, *Chem. Phys. Lett.*, **74**, 400 (1980); J. Sicher, M. Cherest, Y. Gault, and H. Felkin, *Collect. Czech. Chem. Commun.* **27**, 2907 (1962).

2) Y. Kodama, K. Nishihata, M. Nishio, and Y. Iitaka, *J. Chem. Soc. Perkin Trans. 2*, **1976**, 1490.

3) R. E. Carter and P. Stilbs, *J. Am. Chem. Soc.*, **98**, 7515 (1976); B. Aurivillius and R. E. Carter, *J. Chem. Soc., Perkin Trans. 2*, **1978**, 1033.

4) M. Hirota, T. Sekiya, K. Abe, H. Tashiro, M. Karatsu, M. Nishio, and E. Osawa, *Tetrahedron*, **39**, 3091 (1983).

5) The *ab initio* calculations were performed by use of the Gaussian 80 (QCPE 13) program at the Institute for Molecular Science. With this program we can make an *ab initio* calculation of some molecules with the number of Contracted Gaussian Type Orbitals (CGTO) below 127. In the case of 4-31G calculations of 1-phenyl-2-propanol, the number of CGTO is 114.

6) QCPE 395, N. L. Allinger, *J. Am. Chem. Soc.*, **99**, 8127 (1977).

7) P. Pulay, "Modern Theoretical Chemistry," ed by H. F. Schaefer, Plenum Press, New York, (1978) Vol. 4, P. 153.

8) M. Ōki and H. Iwamura, *Bull. Chem. Soc. Jpn.*, **32**, 1135 (1959).

Improved Catalytic Activity of Cyclopentadienylcobalt in the Preparation of Pyridines from Acetylenes and Nitriles

Yasuo WAKATSUKI* and Hiroshi YAMAZAKI
The Institute of Physical and Chemical Research, Wako, Saitama 351
(Received April 22, 1985)

Synopsis. The catalytic activity of cyclopentadienylcobalt increases greatly upon introducing a methoxycarbonyl group into the cyclopentadienyl ring, and by carring out the reaction with a vigorous exclusion of oxygen. Among the precursors we have examined, the most active one was [Co(Cp^z)(cot)] (Cp^z=methoxycarbonyl-substituted cyclopentadienyl; cot=cyclooctatetraene) which can generate the active species at 100 °C.

In 1973, we reported that the cyclopentadienylcobalt (CpCo) species catalyzed cyclocotrimerization of alkynes with the C≡N triple bond of nitriles to give substituted pyridines (Eq. 1).[1]

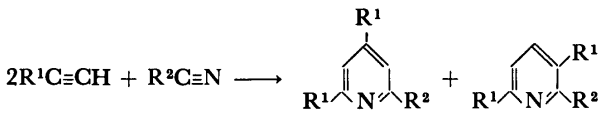

$2R^1C{\equiv}CH + R^2C{\equiv}N \longrightarrow$ (substituted pyridine) + (substituted pyridine)

R^1=H, alkyl, aryl: R^2=alkyl, aryl (1)

The "CpCo" species can be generated from several precursors such as CpCo(diene),[2] Cp_2Co,[3] and $CpCo(CO)_2$.[4] Entry into the catalytic cycle is also possible by starting from cobaltacyclopentadiene complexes.[1] The mechanism of Reaction 1 (involving the metallacycle intermediate) has been fairly well understood.[5]

The catalytic activity of cobalt, in terms of pyridine moles produced per g-atom Co, has been reported to be 190,[1] 200,[4] and 400.[6] Recently, Bönnemann and coworkers have used η^6-borinato in place of the Cp ligand, thereby improving the catalytic activity to *ca.* 2100 for the cooligomerization of HC≡CH with CH_2=CHCN.[7]

We have found that the catalytic activity of cobalt with the easily available η^5-Cp ligand can be greatly enhanced by (1) the exclusion of oxygen, (2) introduction of a CO_2Me group to the Cp ligand, and (3) lowering the reaction temperature. The test reaction that we employed was the cotrimerization of methylacetylene with acetonitrile (R^1=R^2=Me in Reaction 1). In order to check the maximum activity of the catalyst, we carried out the reaction in the presence of a large amount of the reactant so that the conversions would not exceed 80%. When all three of the above conditions are satisfied, the catalytic activity reaches as high as *ca.* 4000 moles of trimethylpyridine per g-atom Co.

The effect of oxygen on the reaction is shown in Fig.1. When the reaction mixture is carefully degassed by use of a vacuum line, even the conventional CpCo(**1**,**5**-cod) exhibits high catalytic activity (*ca.* 2200 at 130 °C). However, its activity drops sharply when an increasing amount of oxygen is added to the system. A (η^5-$C_5H_4CO_2Me$)Co (abbreviated as Cp^zCo) analogue has a higher

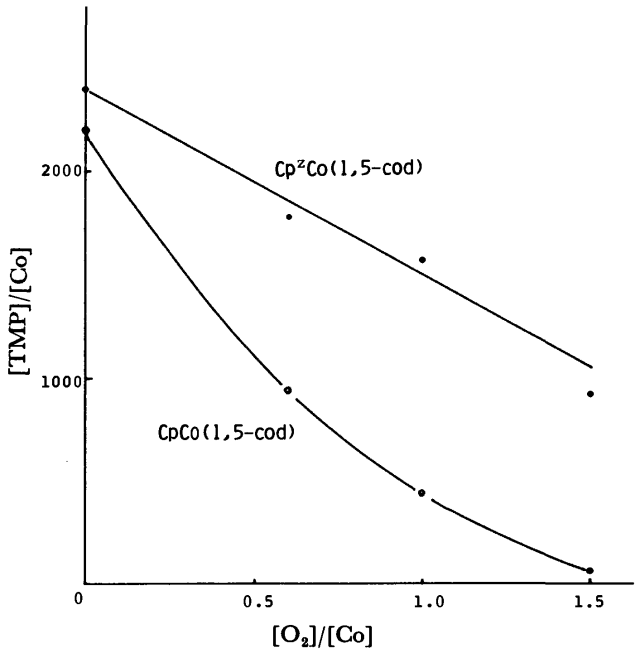

Fig. 1. Higher resistance of the Cp^zCo system towards deactivation by added oxygen.
[TMP]: amount of obtained trimethylpyridine, [Co]: amount of the catalyst used.
Reaction condition: 130 °C, 16 h.

resistance toward oxygen, and still maintains a reasonable catalytic activity (950) even in the presence of an excess amount of oxygen.

The other advantage of using Cp^zCo(**1**,**5**-cod) is that the reaction is much faster than for the case of the parent CpCo(**1**,**5**-cod), as evidenced by the time-conversion curves (A and B) in Fig. 2. A part of this phenomena must arise from an easier release of the **1**,**5**-cod ligand from Cp^zCo(**1**,**5**-cod) than from CpCo(**1**,**5**-cod), *i.e.* a faster generation of the active species in the former system. We have measured the reaction rate for the exchange of the complexed and free diene: Cp^zCo(**1**,**5**-cod) was found to release the diene 10-times faster than CpCo(**1**,**5**-cod) in an acetonitrile solution.

When the reaction temperature was lowered from 130 to 100 °C, the catalytic activity by use of Cp^zCo(**1**,**5**-cod) markedly increased while the reaction rate decreased (curve C). The reaction rate at this lower temperature can be improved by employing cyclooctatetraene (cot), an easier leaving ligand, instead of **1**,**5**-cod (curve D). In contrast, the catalytic activity of CpCo saturates at around 2000, even when CpCo(cot) is used as the precursor and the reaction is carried out at 100 °C (curve E). The difference observed in curves D and E implies that the Cp^zCo system either has a higher reactivity regarding

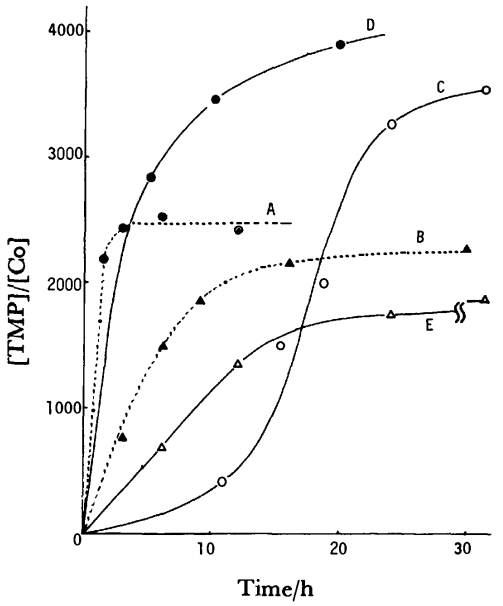

Fig. 2. Comparison of catalytic activity of CpCo and Cp^2Co systems.
[TMP]: amount of obtained trimethylpyridine, [Co]: amount of the catalyst used.
A: Cp Co(**1,5**-cod) 130 °C, B: CpCo(**1,5**-cod) 130 °C, C: Cp Co(**1,5**-cod) 100 °C, D: Cp^2Co(cot) 100 °C, E: CpCo(cot) 100 °C.

cooligomerization or a higher resistance to deactivation than the parent CpCo system.

Experimental

Column chromatography was carried out using Sumitomo alumina KCG-30 under a nitogen atmosphere. GLC analyses were performed at 110 °C on a Shimadzu GC-8A equipped with a 0.3×300-cm glass column packed with 15% PEG-20M on Uniport-HP. Tetradecane was used as an inner reference to determine the amount of each product.

(η^5-Methoxycarbonylcyclopentadienyl)(η^4-1,5-cyclooctadiene)-cobalt(Cp^2Co(1,5-cod)): Sodium methoxycarbonylcyclopentadienide was prepared, according to a method from the literature,[8] (from sodium cyclopentadienide (7 mmol in 4 ml THF) and dimethyl carbonate (1 ml) by heating at reflux temperature for 1 h). Under a nitrogen atmosphere and at room temperature, the cyclopentadienide solution was transferred all at once into a flask (100 ml) containing a benzene solution (20 ml) of chlorotris(triphenylphosphine)cobalt (4.4 g, 5 mmol) and **1,5**-cyclooctadiene (2 ml). The flask was stoppered and vigorously shaken. A dark-red color immediately developed. The reaction mixture was allowed to stand overnight and was then filtered through a short column of alumina (25×25 mm) by the aid of additional benzene (10 ml). The filtrate was concentrated to *ca.* 10 ml and after the addition of hexane (20 ml), it was kept at room temperature overnight. Colorless crystals were formed and discarded, and the solution was chromatographed on alumina (deactivated by addition of 5% of H_2O, 25×200 mm). The column was washed with hexane and then with a 4/1 mixture of hexane/benzene. An orange-red band was eluted by a 1/1 mixture of hexane/benzene. The eluate was concentrated almost to dryness. The residue was dissolved in hexane (5 ml) and was kept in a refrigerator overnight to yield orange-brown crystals of the title compound. They were recrystallized from hexane; yield: 0.78 g (54%); mp 86—87 °C.

$C_{15}H_{19}O_2Co$	Calcd	C 62.07	H 6.60
(290.25)	Found	62.13	6.59

IR (Nujil): ν=1720, 1700 cm^{-1} (ester). ^{1}H-NMR ($CDCl_3$/TMS_{int}): δ=1.6, 2.4, 3.6 (C_8H_{12}); 3.95 (CH_3); 4.40, 5.03 (C_5H_4) ppm.

(η^5-Methoxycarbonylcyclopentadienyl)(η^4-cyclooctatetraene)-cobalt(Cp^2Co(cot)): This compound can be prepared in the same manner as above, using cyclooctatetraene (1 ml) in place of cyclooctadiene. Red-brown crystals; yield: 0.46 g (32%); mp 67—68 °C.

$C_{15}H_{15}O_2Co$	Calcd	C 62.95	H 5.28
(286.22)	Found	62.84	5.25

IR (Nujol): ν=1720, 1700 cm^{-1} (ester). ^{1}H-NMR (CD_2Cl_2): δ=3.64 (=CH–, coordinated); 3.90 (CH_3); 4.55, 5.11 (C_5H_4); 5.56 (=CH–, uncoordinated).

Cotrimerization of Methylacetylene with Acetonitrile: Crystals of Cp^2Co(cot) (28.6 mg) were dissolved in benzene (40 ml) under argon (this solution can be stored in a refrigerator for several months without any decomposition). A portion of this solution (1 ml) was transferred by syringe to an ampule. The ampule was connected to a vacuum line. The solution was degassed by three freeze-pump-thaw cycles. In another ampule containing benzene (1.5 ml) and acetonitrile (2.5 ml), methylacetylene (*ca.* 1.3 g) was condensed by bubbling through the gas at 0 °C. The second ampule was attached to a vacuum line and the mixture was degassed by three cycles of freeze-pump-thaw. Finally it was distilled into the first ampule containing the cobalt complex. The ampule was sealed and heated to 100 °C for 20 h. Unreacted reactants and the solvent were evaporated under a reduced pressure (25 mmHg (1 mmHg=133.322 Pa)) and the oily residue (1.43 g) was subjected to an GLC analysis. The products were 1,3,5-trimethylbenzene (0.30 mmol), 1,2,4-trimethylbenzene (1.69 mmol), 2,4,6-trimethylpyridine (5.12 mmol), and 2,3,6-trimethylpyridine (4.65 mmol). Trimethylpyridine was isolated upon extracting it from an ethereal solution of the residue using an 18% HCl aquous solution. After neutralization with KOH, the pyridine was again extracted with ether. Drying of the solution with Na_2SO_4 and evaporation of the ether under a reduced pressure gave a colorless oil (1.04 g) which was a 51/46 mixture of 2,4,6- and 2,3,6-trimethylpyridine. Other runs can be performed similarly.

References

1) Y. Wakatsuki and H. Yamazaki, *Tetrahedron Lett.* **1973**, 3383.
2) H. Bönnemann, W. Brijoux, R. Brinkmann, W. Meurers, and R. Mynott, *J. Organomet. Chem.*, **272**, 231 (1984) and references therein.
3) Y. Wakatsuki and H. Yamazaki, *Synthesis*, **1976**, 26.
4) K. P. C. Vollhardt and A. Naimann, *Angew. Chem.* **89**, 758 (1977); *Angew. Chem. Int. Ed. Eng.* **16**, 708 (1977).
5) Y. Wakatsuki and H. Yamazaki, *J. Chem. Soc., Dalton Trans.*, **1978**, 1278.
6) W. Brijoux, in PhD Dissertation, University of Dortmund (1979).
7) H. Bönnemann, W. Brijoux, R. Brinkmann, and W. Meurers, *Helv. Chim. Acta*, **67**, 1616 (1984).
8) W. P. Hart, D. W. Macomber, and M. D. Rausch. *J. Am. Chem. Soc.*, **102**, 1196 (1980).

Reaction of Carbon Dioxide with 1-Phenylaziridine Catalyzed by Organo-antimony and -tin Compounds

Haruo MATSUDA, Akira NINAGAWA,* and Hiroshi HASEGAWA
Department of Applied Chemistry, Faculty of Engineering, Osaka University, Yamadaoka, Suita, Osaka 565
(Received April 23, 1985)

Synopsis. The reactions of carbon dioxide(CO_2) with 1-phenylaziridine(**1**) to afford 3-phenyl-2-oxazolidone(**2**) were carried out in the presence of organo-antimony and -tin compounds as catalysts. Tetraphenylstibonium bromide(Ph_4SbBr) and triphenyltin bromide(Ph_3SnBr) were found to be active catalysts. The use of a polar aprotic solvent, such as a HMPA, provided optimal reaction conditions.

In our previous papers,[1] we reported that organometallic compounds of group IVA, VA, and VIA are effective catalysts for the cycloaddition reaction of CO_2 to oxiranes to afford the corresponding cyclic carbonates. However, little is known about the catalysts for the syntheses of 2-oxazolidones from the reactions of CO_2 with aziridines, except for the ammonium salts[2] and iodine[3] which are effective catalysts for the reactions of CO_2 with 1-substituted phenylaziridines and 2-methylaziridine, respectively. In this study, we found that Ph_4SbBr and Ph_3SnBr were also effective catalysts for the synthesis of **2** from the reaction of CO_2 with **1**.

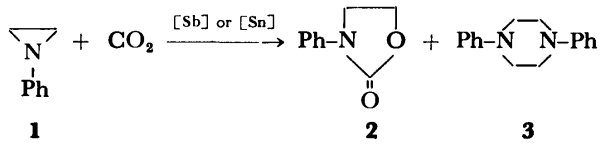

1 **2** **3**

Results and Discussion

The reactions of CO_2 with **1** were carried out in the presence of organo-antimony and -tin compounds. As shown in Table 1, in the case of Ph_4SbBr, **2** and 1,4-diphenylpiperazine(**3**) were obtained in 86 and 9% yields, respectively, whereas other antimony compounds show low selectivity. On the other hands, with Ph_3SnBr, **3** was obtained as a main product. On the basis of the above results, the reactions catalyzed by Ph_4SbBr and Ph_3SnBr were carried out under various conditions to survey the optimal conditions.

The yield of **2** in the reaction catalyzed by Ph_4SbBr at 80 °C increases linearly with an increase in reaction time, whereas, that of **3** increases during the first 10 min and then does not increase. In the case of Ph_3SnBr, the yields of **2** and **3** increase with an increase in the reaction time. To check the effect of reaction temperature, the reactions were carried out at temperatures from 40 °C up to 120 °C. In the case of Ph_4SbBr, **2** was selectively obtained above 60 °C. On the other hand, Ph_3SnBr did not show catalytic activity up to 60 °C, but the yields of **2** and **3** increased at higher temperature above 80 °C. In order to improve the catalytic activity of Ph_4SbBr and Ph_3SnBr, the reactions were carried out in solvents of different polarities as shown in Table 2. The solvent effect is very clear. The use of polar aprotic solvents such as HMPA and DMSO gave **2** in high yields, whereas the nonpolar solvents such as benzene and hexane gave poorer results.

Table 1. Catalytic activities of the organometallic compounds in the reaction of CO_2 with **1**[a]

Catalyst	Yield/%[b]	
	2	**3**
Ph_4SbCl	7	19
Ph_4SbBr	86	9
Ph_3SbBr_2	63	30
Ph_3SbO	0	trace
Me_3SbCl_2	trace	8
Me_3SbBr_2	18	45
Me_3SbI_2	4	45
Ph_3SnCl	0	0
Ph_3SnBr	23	47
n-Bu_3SnBr	11	18
n-Bu_2SnBr_2	15	44
None	0	0

a) **1**: 30 mmol, CO_2: 50 kg/cm², Catalyst: 0.5 mmol, Temp: 80 °C, Time: 6 h. b) Yields are of isolated products obtained after column chromatography.

Table 2. Effect of solvent on the reactions of CO_2 with **1** in the presence of Ph_4SbBr and Ph_3SnBr at 80 °C[a]

Catalyst	Solvent	μ(D)[d]	Yield/%[e]	
			2	**3**
Ph_4SbBr[b]	HMPA	5.37	93	0
	DMSO	4.3	85	Trace
	DMF	3.82	75	Trace
	Acetonitrile	3.37	53	4
	THF	1.75	21	3
	Dioxane	0.45	20	0
	Hexane	0.085	20	6
	Benzene	0	17	2
Ph_3SnBr[c]	HMPA		76	Trace
	DMF		25	15
	THF		0	Trace
	Hexane		0	Trace

a) **1**: 10 mmol, CO_2: 50 kg/cm², Catalyst: 0.5 mmol, Solvent: 2 ml. b) 1 h. c) 3 h. d) Ref. 9. e) Yields were determined by GC.

Experimental

Materials. The organometallic compounds, Ph_3SbBr_2,[1c] Ph_4SbBr,[1c] Ph_4SbCl,[4] Me_3SbCl_2,[5] Me_3SbBr_2,[5] Me_3SbI_2,[5] Ph_3SbO,[6] Ph_3SnCl,[1d] Ph_3SnBr,[1d] n-Bu_3SnBr,[7] n-Bu_2SnBr_2[7] were prepared by the reported methods and checked by elemental analysis. 1-Phenylaziridine was prepared from 2-anilinoethanol.[8] The solvents were used after rectification.

Reaction Procedure. A mixture of 3.64 cm^3 (30 mmol) of **1** and 0.257 g (0.5 mmol) of Ph_3SbBr_2 was placed into a 50 cm^3 stainless steel autoclave. CO_2 was then introduced at a pressure of *ca.* 50 atmospheres (58.8 bar). The reaction was carried out for 6 h at 80 °C. After completion of the reaction, CO_2 was allowed to escape from the autoclave and the product was separated by column chromatography on silica gel (Wako-gel C-200; chloroform as an eluent). **3** was obtained from the first fraction and **2** from the second fraction. These were recrystallized from ethanol to give pure products. **2**; 2.7 g (yield 55%), mp 115—117 °C (lit,[9] 117—119 °C). **3**; 0.9 g (yield 25%), mp 166—169 °C (lit,[10] 163—164 °C).

Analytical gas chromatography(GC) was performed on a Shimadzu GC-3BT gas chromatograph by the use of Silicone OV-1 as packing.

This work was supported by the Grant-in-Aid for the Scientific Research No. 58470067 from the Ministry of Education, Science and Culture.

References

1) a) H. Matsuda, A. Ninagawa, R. Nomura, and T. Tsuchida, *Chem. Lett.*, **1979**, 573; b) H. Matsuda, A. Ninagawa, and R. Nomura, *ibid.*, **1979**, 1261; c) R. Nomura, A. Ninagawa, and H. Matsuda, *J. Org. Chem.*, **45**, 3735 (1980); d) R. Nomura, M. Kimura, S. Teshima, A. Ninagawa, and H. Matsuda, *Bull. Chem. Soc. Jpn.*, **55**, 3200 (1982).

2) A. P. Sineokov, F. N. Gladysheve, and V. S. Etlis, *Kim. Geterotsikl. Soedin.*, **1970**, 611: *Chem. Abstr.*, **73**, 66351d (1970).

3) a) K. Soga, S. Hosoda, H. Nakamura, and S. Ikeda, *J. Chem. Soc., Chem. Commun.*, **1976**, 617; b) K. Soga, S. Hosoda, and S. Ikeda, *Nippon Kagaku Kaishi*, **1978**, 246.

4) H. H. Willard, L. R. Perkins, and F. F. Blicke, *J. Am. Chem. Soc.*, **70**, 737 (1948).

5) H. Hibbert, *Ber. Deut. Chem. Ges.*, **39**, 160 (1906).

6) D. L. Venezky, C. W. Sink, B. A. Nevett, and W. F. Fortescue, *J. Organomet. Chem.*, **35**, 131 (1972).

7) H. Matsuda and S. Matsuda, *Kogyo Kagaku Zasshi*, **63**, 1960 (1960).

8) a) W. M. Pearlman, *J. Am. Chem. Soc.*, **70**, 871 (1948); b) H. W. Heine, B. L. Kapur, and C. S. Mitch, *ibid.*, **76**, 1173 (1954).

9) J. A. Riddick and W. B. Bunger, "Organic Solvents," in "Techniques of Chemistry," 3rd ed, ed by A. Weissberger, Wiley-Interscience, New York, (1970).

10) M. E. Dyen and D. Swern, *Chem. Rev.*, **67**, 197 (1967).

11) H. W. Heine, B. L. Kapur, and C. S. Mitch, *J. Am. Chem. Soc.*, **76**, 1173 (1954).

Synthesis of Ketazines from Dinitrogen Coordinated to Tungsten†

Masanobu HIDAI,* Masa-aki KURANO, and Yasushi MIZOBE
Engineering Research Institute, Faculty of Engineering, The University of Tokyo, Yayoi, Bunkyo-ku, Tokyo 113
(Received April 24, 1985)

Synopsis. When treated with a methanol/acetone mixture at 50 °C, the complex *trans*-$[W(N_2)_2(PPh_2Me)_4]$ gives acetone azine in moderate yield, although the yield is slightly lower than that from *cis*-$[W(N_2)_2(PMe_2Ph)_4]$. Under UV irradiation, these dinitrogen complexes produce acetone azine even at room temperature.

Direct synthesis of organonitrogen compounds from molecular nitrogen and a relatively cheap organic feedstock is an attractive field in the chemistry of nitrogen fixation. We have already reported that one dinitrogen ligand in the complex *cis*-$[W(N_2)_2(PMe_2Ph)_4]$ (**1**) is converted mainly to ammonia by reaction with alcohols at 50 °C, whereas ketazines are produced in good yields when complex **1** is treated with alcohol/ketone mixtures (ROH/$R^1R^2C{=}O$) at 50 °C.[1] The ligating dinitrogen is first protonated by alcohols to give intermediate complexes $[W(OR)_2(NNH_2)(PMe_2Ph)_3]$. In the presence of ketones, the intermediate complexes are more amenable to the condensation with ketones[2] than to the protonation at the terminal nitrogen atom. The resulting diazoalkane complexes $[W(OR)_2(NN{=}CR^1R^2)(PMe_2Ph)_3]$ react with alcohols to liberate hydrazones ($H_2NN{=}CR^1R^2$), which further condense with ketones to form ketazines as the final products. Thus, 0.88 mol of acetone azine per W atom is formed by treating complex **1** with a methanol/acetone mixture. The yield is further improved up to 0.94 mol/W atom by the addition of base to the system. Since acetone azine is easily converted to hydrazine by hydrolysis, this reaction is considered as a potential method for the synthesis of hydrazine from dinitrogen. In this paper, we wish to describe the application of this reaction system to a series of tungsten and molybdenum dinitrogen complexes $[M(N_2)_2(PR_3)_4]$ (M=W or Mo; PR_3=tertiary phosphines).

Results and Discussion

Investigations of the reactions of a series of tungsten and molybdenum dinitrogen complexes $[M(N_2)_2(PR_3)_4]$ with alcohol/ketone mixtures have disclosed that, in addition to complex **1**, *trans*-$[W(N_2)_2(PPh_2Me)_4]$ (**2**) also gives acetone azine in moderate yield by reaction with methanol/acetone mixtures at 50 °C. However, none of the other dinitrogen complexes *cis*-$[Mo(N_2)_2(PMe_2Ph)_4]$, *trans*-$[M(N_2)_2(dpe)_2]$, *trans*-$[M(N_2)(^nPrCN)(dpe)_2]$ and *trans*-$[W(N_2)_2(dpe)(PPh_2Me)_2]$(M=W or Mo; dpe=$Ph_2PCH_2CH_2PPh_2$) produces acetone azine under similar conditions.

In Table 1 is shown the yield of acetone azine obtained by treatment of complex **2** with methanol/acetone mixtures. It is to be noted that use of a methanol/acetone mixture with the volume ratio 4:1 gives only a trace amount of the azine from complex **2**, although the azine is formed in high yield from complex **1** under similar conditions. This is only because complex **2** is scarcely soluble in the mixed solvent. Therefore, if toluene or THF is added to this system to dissolve complex **2**, the yield of the azine is remarkably improved. A great difference of complex **2** from complex **1** is observed in the effect of base addition to the reaction system. For complex **1**, the yield of the azine is improved almost up to 1 mol/W atom in the presence of KOH or NaOMe.[1] However, for complex **2**, addition of base strongly supresses the formation of the azine.

The mechanism for formation of the azine from complex **2** may be essentially the same as that from complex **1** (*vide supra*). Actually, the hydrido-hydrazido(2-) complex $[WCl_3H(NNH_2)(PPh_2Me)_2]$, which is derived from complex **2** and HCl in CH_2Cl_2, reacts with methanol/acetone mixtures at 50 °C to produce acetone azine in moderate yield (0.31 mol/W atom). The azine is probably formed *via* a diazoalkane complex derived from the condensation of the hydrazido(2-) complex with acetone. Details of the condensation of hydrido-hydrazido(2-) complexes with carbonyl compounds will be reported separately.[3]

Formation of ketazines from ligating dinitrogen in complexes **1** and **2** by treatment with alcohol/ketone mixtures does not proceed at room temperature but only at an elevated temperature (50 °C). However, under irradiation by mercury lamp, the complexes give ketazines very smoothly at room temperature, although the yields of ketazines are lower than those in the reactions at 50 °C and ethanol or 2-propanol does not work as the proton source instead of methanol. Addition of NaOMe slightly increases the yield of acetone azine (Table 2). In the UV irradiated reaction, a suspension of the reaction mixture gradually turns to a dark solution within about 3 h. The yields of ketazines are no longer increased after 4 h.

Experimental

All manipurations were carried out under dinitrogen using standard Schlenk tube techniques. Complexes *cis*-$[W(N_2)_2(PMe_2Ph)_4]$,[4] *trans*-$[W(N_2)_2(PPh_2Me)_4]$,[5] and $[WCl_3H(NNH_2)(PPh_2Me)_2]$[5] were prepared according to the published methods.

Reactions of Complex 2 with Methanol/Acetone Mixtures.

† Preparation and Properties of Molybdenum and Tungsten Dinitrogen Complexes. 22.

Table 1. Formation of acetone azine from *trans*-$[W(N_2)_2(PPh_2Me)_4]$ (**2**)[a]

Run	System				Yield
	Methanol ml	Acetone ml	Solvent ml	NaOMe mol/W atom	mol/W atom
1	5	5	—	—	0.62
2	5	5	—	—	0.74[b,c]
3	8	2	—	—	Tr.
4	2	1	Toluene, 3	—	0.64[b]
5	5	5	—	4	0
6	2	1	THF, 3	—	0.24[b]
7	2	1	THF, 3	4	0.05[b]

a) Complex **2**, 100 mg; Reaction time, 18 h; Reaction temperature, 50 °C. b) The yield of N_2H_4 after base distillation of the reaction mixture. c) 0.20 mol NH_3/W atom was also formed.

Table 2. Formation of ketazines from *cis*-$[W(N_2)_2(PMe_2Ph)_4]$ (**1**) and *trans*-$[W(N_2)_2(PPh_2Me)_4]$ (**2**) under UV irradiation[a]

Complex[b]	System			Yield of Ketazines
	Alcohol ml	Ketone ml	NaOMe mol/W atom	mol/W atom
1	MeOH, 4	Acetone, 1	—	0.46
1	MeOH, 4	Acetone, 1	4	0.66
1	MeOH, 4	Diethyl ketone, 1	—	0.40
1	EtOH, 4	Acetone, 1	—	Tr.
2	MeOH, 4	Acetone, 4	—	0.17

a) Reaction temperature, r.t.; Reaction time, 4 h. b) Complex **1**, 150 mg; Complex **2**, 100 mg.

In a typical run, complex **2** (*ca.* 100 mg) was suspended in a methanol (5 ml)/acetone (5 ml) mixture under dinitrogen and stirred for 18 h at 50 °C. The orange-red suspension was gradually converted into a dark blue solution. Acetone azine produced (0.62 mol/W atom) was quantitatively analyzed by an Ohkura Model 103 Gas Chromatograph equipped with a 5 mm×2 m stainless steel column packed with PEG 6000. When methanol/acetone/toluene and methanol/acetone/THF mixtures were used, the yield of the azine was determined by measuring the amount of hydrazine obtained by base distillation of the reaction mixture.

Reaction of Complex 2 with Methanol/Acetone/NaOMe Mixtures. Complex **2** was treated with a methanol (5 ml)/acetone (5 ml) mixture in the presence of NaOMe (4 mol/W atom) for 18 h at 50 °C. A considerable amount of unreacted complex **2** was recovered from the mixture and formation of acetone azine was not observed. When THF (3 ml) was added to a methanol (2 ml)/acetone (1 ml) mixture to dissolve complex **2**, acetone azine was formed in low yield (0.05 mol/W atom), which is much lower than that without NaOMe (0.24 mol/W atom).

Reactions of Complexes 1 and 2 with Alcohol/Ketone Mixtures under UV Irradiation. Complex **1** or **2** (100—130 mg) charged in a quartz Schlenk tube was suspended in an alcohol/ketone mixture and irradiated by Ushio 500 W mercury lamp. The reaction temperature was kept at room temperature by cooling with a fan. Acetone azine and diethyl ketone azine were analyzed by GLC as described above.

The financial support of this research by the Ministry of Education, Science and Culture of Japan (Grant-in-Aid for Developmental Scientific Research 58850181) is greatly appreciated.

References

1) A. Watakabe, T. Takahashi, D.-M. Jin, I. Yokotake, Y. Uchida, and M. Hidai, *J. Organomet. Chem.*, **254**, 75 (1983).

2) P. C. Bevan, J. Chatt, M. Hidai, and G. J. Leigh, *J, Organomet. Chem.*, **160**, 165 (1978).

3) M. Hidai, A. Takahashi, T. Takahashi, S. Aramaki, Y. Uchida, and Y. Mizobe, unpublished results.

4) J. Chatt, G. A. Heath, and R. L. Richards, *J. Chem. Soc., Dalton Trans.*, **1974**, 2074.

5) J. Chatt, A. J. Pearman, and R. L. Richards, *J. Chem. Soc., Dalton Trans.*, **1977**, 2139.

Direct *N*-Allylation of Amides with 2-Allylisourea Catalyzed by Palladium(0)

Yoshio INOUE,* Masaaki TAGUCHI, and Harukichi HASHIMOTO
Department of Applied Chemistry, Faculty of Engineering, Tohoku University, Aoba, Aramaki, Sendai 980
(Received April 24, 1985)

Synopsis. Direct *N*-allylation of amides catalyzed by palladium(0) complexes took place under neutral conditions by the use of 2-allylisourea as the allylating agent.

Direct alkylation of amides using reagents such as alkyl halides or sulfonates under neutral conditions generally leads to a mixture of *O*- and *N*-alkylated product. In order to obtain pure *N*-substituted amides, it is usually necessary to generate the amide anion by the use of strong base such as sodium amide or sodium hydride before treatment with alkylating agent.[1] Recently, it was informed that alumina coated with potassium fluoride was effective in promoting *N*-alkylation of amides.[2] The alkylation of amides with alcohols in the presence of ruthenium catalyst has also been reported.[3] Very lately, palladium-catalyzed reaction of allylic substrates with sodium *p*-toluenesulfonamide was shown to afford *N*-allylic derivatives.[4] In a previous paper,[5] we have reported the palladium-catalyzed direct α-allylation of ketones with 2-allyl-1,3-dicyclohexylisourea (**1**), obtained from the reaction of allyl alcohol with dicyclohexylcarbodiimide.[6] Herein we report a novel direct *N*-allylation of amide with **1** under neutral conditions.

The *N*-allylation of amides was performed generally as follows: A solution of **1** (1 eq.), an amide (1 eq.), [Pd(dba)$_2$](2 mol%)[dba=dibenzylideneacetone], and dppe (2 mol%)[dppe=$Ph_2PCH_2CH_2PPh_2$] in dry *N*,*N*-dimethylformamide (DMF) was stirred at 60—100 °C for 1—2 h under nitrogen atmosphere. Usually the progress of the reaction was conveniently monitored

$$CH_2{=}CHCH_2OH + CyN{=}C{=}NCy \longrightarrow CH_2{=}CHCH_2OC(NCy)NHCy$$

1

$$RCNH_2 + \mathbf{1} \xrightarrow[-(NHCy)_2CO]{Pd(0)} RCNH(CH_2CH{=}CH_2) + RCN(CH_2CH{=}CH_2)_2$$

(cy=cyclohexyl)

by the deposition of 1,3-dicyclohexylurea formed. The occurrence of *N*-allylation over *O*-allylation was confirmed spectroscopically by comparing with an authentic sample. Use of [Pd(PPh$_3$)$_3$] complex as the catalyst instead of [Pd(dba)$_2$]-dppe did not give rise to the product. Results are given in Table 1. Various amides were allylated in moderate to good yields. For primary amides, mono- and diallylation took place. The sulfur counterpart of acetanilide, *i.e.*, thioacetanilide, was selectively *S*-allylated. Toluenesulfonamide (*o*- and *p*-) could be readily *N*-allylated at 25 °C by this method. In this case, exclusive diallylation occurred.

$$CH_3CONHPh + R^1OC(NCy)NHCy \xrightarrow[100\,^\circ C,\ 1\ h,\ DMF]{[Pd(dba)_2]\text{-dppe}} CH_3CONR^2Ph$$

Table 1. Allylation of amide[a]

Amide	Reaction temp/°C	Reaction time/h	Product	Yield[b]/%
CH_3CONH_2	60	2	CH_3CONHR	45[c]
			CH_3CONR_2	37[c]
$PhCONH_2$	60	1	PhCONHR	27
			$PhCONR_2$	48
$CH_3CONHPh$	100	1	$CH_3CONRPh$	67
$CH_3CSNHPh$	25	0.25	$CH_3(RS)C{=}NPh$	60
$CH_2{=}C(CH_3)CONH_2$	60	2	$CH_2{=}C(CH_3)CONHR$	20
			$CH_2{=}C(CH_3)CONR_2$	40
2-Pyrrolidone	60	1	*N*-Allylpyrrolidone	86[c]
Caprolactam	60	1	*N*-Allylcaprolactam	87[c]
o-$CH_3C_6H_4SO_2NH_2$	25	1	o-$CH_3C_6H_4SO_2NR_2$	62
p-$CH_3C_6H_4SO_2NH_2$	25	1	p-$CH_3C_6H_4SO_2NR_2$	65

a) 2-Allylisourea (5 mmol), amide (5 mmol), [Pd(dba)$_2$] (2 mol%), dppe (2 mol%), DMF (10 cm^3); R=allyl. b) Isolated yield, based on 2-allylisourea. c) GLC yield.

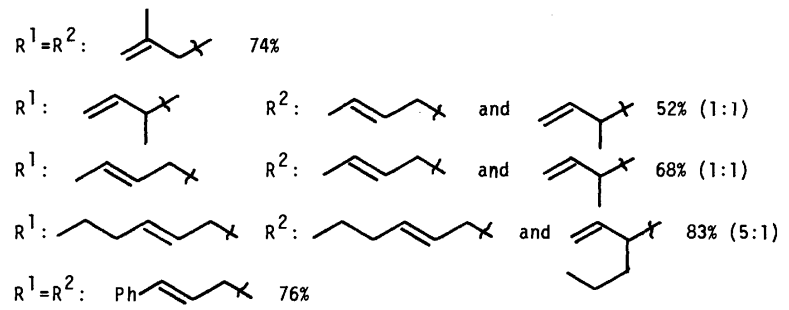

The reaction of several 2-allylic-substituted isoureas with acetanilide was also investigated. For the allylic system bearing a bulky substituent, the less substituted end tended to react preferentially. Unfortunately, a γ,γ-disubstituted allyl derivative, *i.e.*, 2-prenylisourea, did not undergo the reaction. 1-Methyl-2-propenyl- and 2-butenylisourea realized the same composition of the possible two products. This may indicate that both reactions proceed *via* a same intermediate.[7] Although the mechanism of the reaction is not so clear, we propose a tentative pathway *via* (π-allyl)palladium intermediate **2**, which is derived from oxidative addition of 2-allylisourea **1** to palladium(0). The isourea anion thus formed is supposed to be basic enough to abstract an amide proton to afford imidate intermediate **3**. Then reductive coupling gives the observed product.

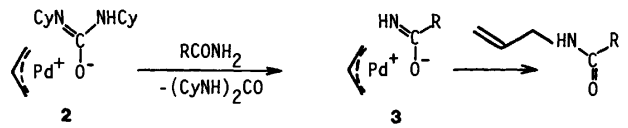

2 **3**

Experimental

Preparation of 2-Allylic-substituted Isoureas. They were prepred from allylic alcohols and dicyclohexylcarbodiimide in the presence of a catalytic amount of cuprous chloride according to the published method.[6]

Allylation of Amides. An amide (5 mmol) was allowed to react with 2-allyl-1,3-dicyclohexylisourea (5 mmol) in dry DMF (10 cm^3) in the presence of [Pd(dba)$_2$](0.1 mmol) and dppe (0.1 mmol) under the conditions cited in Table 1. After the reaction was complete, water was added to the mixture. The product was extracted with ether and purified by column chromatography on silica gel. Certain samples for spectroscopic analyses were obtained by preparative GLC. They were denoted by asterisk(*) in the following.

Allyl N-*Phenylthioacetimidate*: An oil. IR (neat) 1628, 1127, 980, 910, 770, and 695 cm^{-1}; ^{1}H NMR ($CDCl_3$) δ=1.84 (s, 3H), 3.61 (d, 2H), 4.81—5.32 (m, 2H), 5.51—6.22 (m, 1H), and 6.25—7.28 (m, 5H); MS (70 eV) *m/z* 191 (M^+), 176, 118, 85, 83, and 77.

N-*(2-Methyl-2-propenyl)acetanilide*: An oil. IR (neat) 1660, 1380, 1275, 900, and 700 cm^{-1}; ^{1}H NMR ($CDCl_3$) δ=1.74 (s, 3H), 1.80 (s, 3H), 4.29 (s, 2H), 4.71 (s, 1H), 4.82 (s, 1H), and 7.06—7.65 (m, 5H); MS (70 eV) *m/z* 189 (M^+), 174, 147, 146, 132, and 106.

N-*(2-Butenyl)acetanilide**: An oil. IR (CCl_4) 1660, 1370, 970, and 698 cm^{-1}; ^{1}H NMR ($CDCl_3$) δ=1.60 and 1.71 (tentatively assigned to (*Z*)- and (*E*)-CH_3C=C, respectively, d, 3H (1:2)), 1.82 (s, 3H), 4.06—4.30 (m 2H), 5.28—5.58 (m, 2H), and 6.94—7.48 (m, 5H) MS (70 eV) *m/z* 189 (M^+) 146, 132, and 93.

N-*(1-Methyl-2-propenyl)acetanilide**: An oil. IR (neat) 1660, 1495, 1385, 1000, and 920 cm^{-1}; ^{1}H NMR ($CDCl_3$) δ=1.12 (d, 3H) 1.79 (s, 3H), 4.84—5.00 (m, 1H), 5.08—5.22 (m, 1H), 5.23—6.12 (m, 2H), and 6.86—7.50 (m, 5H); MS (70 eV) *m/z* 189 (M^+), 174, 146, 132, and 93.

N-*(2-Hexenyl)acetanilide*: An oil. IR (neat) 1660, 1387, 1265, 960, and 695 cm^{-1}; ^{1}H NMR ($CDCl_3$) δ=0.80 (t, 3H), 1.00—1.60 (m, 2H), 1.80 (s, 3H), 1.80—2.15 (m, 2H), 4.25 (d, 2H), 5.35—5.60 (m, 2H), and 7.13—7.55 (m, 5H); MS (70 eV) *m/z* 217 (M^+), 174, 146, 132, and 93.

N-*(1-Propyl-2-propenyl)acetanilide**: An oil. IR (CCl_4) 1660, 1495, 1380, 995, and 925 cm^{-1}; ^{1}H NMR ($CDCl_3$) δ=0.90 (t, 3H), 1.16—1.58 (m, 4H), 1.74 (s, 3H), 4.84—5.92 (m, 4H), and 7.02—7.58 (m, 5H); MS (70 eV) *m/z* 217 (M^+), 174, 133, 132, and 93.

N-*Cinnamylacetanilide*: An oil. IR (neat) 1625, 1432, 1406, 1250, 962, and 692 cm^{-1}; ^{1}H NMR ($CDCl_3$) δ=1.76 (s, 3H), 4.35 (d, 2H), 6.13—6.37 (m, 2H), and 6.90—7.42 (m, 10H); MS (70 eV) *m/z* 251 (M^+), 208, 160, 117, and 115.

References

1) B. C. Challis and J. A. Challis, "Comprehensive Organic Chemistry," ed by I. O. Sutherland, Pergamon Press, Oxford (1979), Vol. 2, p. 957.

2) J. Yamawaki, T. Ando, and T. Hanafusa, *Chem. Lett.*, **1981**, 1143.

3) Y. Watanabe, T. Ohta, and Y. Tsuji, *Bull. Chem. Soc. Jpn.*, **56**, 2647 (1983).

4) S. E. Bystrom, R. Aslanian, and J.-E. Bäckvall, *Tetrahedron Lett.*, **26**, 1749 (1985).

5) Y. Inoue, M. Toyofuku, and H. Hashimoto, *Chem. Lett.*, **1984**, 1227.

6) E. Vowinkel and I. Büthe, *Chem. Ber.*, **107**, 1353 (1974).

7) In order to obtain stereochemical information on this reaction, we prepared an optically active 2-allylic-substituted isourea derived from *l-cis*-carveol,[8] and submitted to the reaction with acetanilide. However the only product isolated was a triene, 2-methyl-5-isopropenyl-1,3-cyclohexadiene. Exclusive 1,4-elmination took place.

8) R. H. Reitsema, *J. Am. Chem. Soc.*, **75**, 1996 (1953).

Structure Determination of a New Bitter Principle, Shinjulactone L, from *Ailanthus altissima*

Masami ISHIBASHI, Takahiko TSUYUKI,* and Takeyoshi TAKAHASHI*
Department of Chemistry, Faculty of Science, The University of Tokyo, Hongo, Bunkyo-ku, Tokyo 113
(Received May 30, 1985)

Synopsis. A new quassinoid, shinjulactone L, was isolated from *Ailanthus altissima* SWINGLE and the structure was determined to be 12β-acetoxy-2α-hydroxypicrasane-1,11,16-trione by spectral and chemical means.

In previous papers we have reported the isolation and structure elucidation of several quassinoids[1-5] and quassinoid glycosides[6] from *Ailanthus altissima* SWINGLE (Shinju or Niwaurushi in Japanese). Further investigation on bitter principles of the plant led to the isolation of a new quassinoid, shinjulactone L (**1**) from the root bark of this plant.

Shinjulactone L (**1**) crystallized from acetone–benzene as colorless prisms, mp 261—262 °C. High-resolution mass spectrum indicated the molecular formula, $C_{22}H_{30}O_7$. The ^1H and ^{13}C NMR spectra showed the presence of two secondary methyl, two tertiary methyl, two isolated carbonyl, one lactone, and one acetoxyl groups. Since six of seven oxygen atoms were thus characterized, the remaining one oxygen atom was ascribed to a hydroxyl group, the presence of which was supported by the IR absorption band at 3450 cm^{-1}.

The ^1H NMR spectrum of shinjulactone L (**1**) was very similar to that of shinjulactone H (**2**)[3] except for the presence of a signal due to an acetoxyl group and a lower field resonance of a doublet (δ 5.12) which is ascribed to a proton attached to an acetoxyl-bearing carbon atom. In the ^1H NMR of **1** a signal due to a proton attached to a hydroxyl-bearing carbon atom was observed at δ 4.70 as double-double doublets, which are very similar to the signal due to $C_{(2)}$–H (δ 4.77 ddd) observed in ^1H NMR of **2** (see Table 1). This fact suggests that the structure of the A ring of shinjulactone L (**1**) is the same as that of shinjulactone H (**2**). The presence of a carbonyl group at C-11 position and the acetoxyl group at C-12β position in the C ring was also clarified by the ^1H NMR spectrum of **1**; $C_{(9)}$–H appeared at δ 2.93 as a singlet signal and a large coupling constant (J=12.5 Hz) of the doublet signal due to $C_{(12)}$–H was observed. As a result of discussions developed above, the structure of shinjulactone L (**1**) was proposed to be 12-*O*-acetylshinjulactone H, which was finally confirmed by chemical conversion as follows. Shinjulactone L (**1**) was acetylated with acetic anhydride and pyridine to give a diacetate (**3**), which was completely identical with the diacetate (**3**) derived from shinjulactone H (**2**). Thus the structure of shinjulactone L (**1**) was determined to be 12β-acetoxy-2α-hydroxypicrasane-1,11,16-trione. This structure had been previously proposed for acetylamarolide by Casinovi *et al.*[7] but the structure of acetylamarolide was later revised to **4**.[8]

TABLE 1. ^1H NMR SPECTRA OF SHINJULACTONES L AND H (**1** AND **2**)[a]

	1[b]		**2**[c],[3]	
	δ	J	δ	J
2-H	4.70 ddd	11.5, 7, 5	4.77 ddd	12, 7.5, 4.5
7-H	4.29 t	2.5	4.31 dd	3, 2.5
9-H	2.93 s		2.94 s	
12-H	5.12 d	12.5	4.01 dd	11, 3
4-Me	0.94 d	6.5	0.95 d	6.5
8-Me	1.18 s [d]		1.13 s [e]	
10-Me	1.56 s [d]		1.58 s [e]	
13-Me	1.09 d	7.5	1.20 d	7
2-OH	3.84 d	5	3.43 d	4.5
12-OH	—		3.53 d	3
12-OAc	2.20 s		—	

a) δ and J values are expressed in ppm and Hz, respectively. b) Measured at 90 MHz in $CDCl_3$. c) Measured at 400 MHz in $CDCl_3$. d) Signals may be reversed. e) Signals may be reversed.

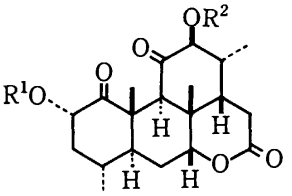

1 R^1=H, R^2=Ac
2 R^1=R^2=H
3 R^1=R^2=Ac

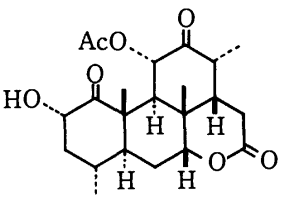

4

Experimental[9]

Materials and Isolation of Shinjulactone L (1). Root bark of *A. altissima* was collected at the Botanical Gardens, Faculty of Science, The University of Tokyo in August 1982. The isolation procedures are the same as described in the preceding paper.[5] The fraction containing amarolide 11-acetate (**4**)[7,8] mainly was further separated by silica-gel column chromatography eluted with ethyl acetate–chloroform (1:2) to afford shinjulactone L (**1**; *ca.* 0.0005% yield).

Shinjulactone L (1). Colorless prisms from acetone–benzene, mp 261—262 °C; $[\alpha]_D^{26}$ −41° (*c* 0.65, $CHCl_3$); IR (KBr) 3450, 1745, 1730, and 1230 cm^{-1}; ^1H NMR (Table 1); ^{13}C NMR ($CDCl_3$) δ=15.0q, 15.1q, 18.3q, 20.5q, 23.6q, 26.6t, 27.4t, 27.8d, 35.6d, 38.6s, 45.3d, 46.5t, 46.9d, 47.3d, 48.8s, 69.9d, 77.6d, 81.8d, 168.9s, 169.8s, 201.5s, and 212.4s; MS *m/z* (%) 406 (M^+; 19), 378 (13), 364 (18), 362 (19), 346 (100),

303 (36), and 206 (57); Found: *m/z* 406.1979. Calcd for $C_{22}H_{30}O_7$: M, 406.1990.

Acetylation of Shinjulactone L (1). Shinjulactone L (**1**; *ca.* 10 mg) was acetylated with acetic anhydride (2 ml) in pyridine (2 ml) at room temperature for 18 h. After addition of methanol and evaporation, the reaction mixture was purified by silica-gel column chromatography eluted with 15% acetone-benzene to afford 2-*O*-acetylshinjulactone L (**3**; 10 mg), which was identified with 2,12-di-*O*-acetylshinjulactone H (**3**) by TLC, ^{1}H NMR, IR, and mass spectra.

The authors wish to express their thanks to Mr. Eiichi Ishii of the Botanical Gardens for collection of the roots of *A. altissima.*

References

1) M. Ishibashi, T. Tsuyuki, T. Murae, H. Hirota, T. Takahashi, A. Itai, and Y. Iitaka, *Bull. Chem. Soc. Jpn.*, **56**, 3683 (1983).

2) H. Naora, M. Ishibashi, T. Furuno, T. Tsuyuki, T. Murae, H. Hirota, T. Takahashi, A. Itai, and Y. Iitaka, *Bull. Chem. Soc. Jpn.*, **56**, 3694 (1983).

3) M. Ishibashi, S. Yoshimura, T. Tsuyuki, T. Takahashi, and K. Matsushita, *Bull. Chem. Soc. Jpn.*, **57**, 2013 (1984).

4) T. Furuno, M. Ishibashi, H. Naora, T. Murae, H. Hirota, T. Tsuyuki, T. Takahashi, A. Itai, and Y. Iitaka, *Bull. Chem. Soc. Jpn.*, **57**, 2484 (1984).

5) M. Ishibashi, S. Yoshimura, T. Tsuyuki, T. Takahashi, A. Itai, and Y. Iitaka, *Bull. Chem. Soc. Jpn.*, **57**, 2885 (1984).

6) S. Yoshimura, M. Ishibashi, T. Tsuyuki, T. Takahashi, and K. Matsushita, *Bull. Chem. Soc. Jpn.*, **57**, 2496 (1984).

7) C. G. Casinovi, V. Bellavita, G. Grandolini, and P. Ceccherelli, *Tetrahedron Lett.*, **1965**, 2273.

8) W. Stöcklin, M. Stefanović, T. A. Geissman, and C. G. Casinovi, *Tetrahedron Lett.*, **1970**, 2399.

9) General procedures are the same as described in the preceding paper.[5]

Synthetic Photochemistry. XXXII.[1] Structures of By-products Formed in the Photocycloaddition of Myrcene to Methyl 2,4-Dioxoalkanoates

Hitoshi TAKESHITA,* Kei KOMIYAMA,† and Koya OKAISHI†

Research Institute of Industrial Science, 86, Kyushu University, Kasuga-koen, Kasuga, Fukuoka 816

†*Graduate School of Engineering Sciences, 39, Kyushu University, Kasuga-koen, Kasuga, Fukuoka 816*

(Received April 2, 1985)

Synopsis. Structures of the by-products formed in the photocycloaddition of myrcene to methyl 2,4-dioxohexanoate and 2,4-dioxopentanoate were elucidated. They were shown to be formed by a 1,5-hydrogen shift of the intermediate (2+2)π adducts of conjugated dienes.

In the course of the photocycloaddition studies regarding myrcene (**1**), a conjugated monoterpene diene, to methyl 2,4-dioxopentanoate (**2**)[1] and to methyl 2,4-dioxohexanoate (**3**),[2] we have isolated a hitherto unknown mode of by-products which were derived from the protoadducts (**A** and **B**) of the (2+2)π adducts (**C**—**F**). This paper will describe the determination of their structures.

The reaction of **1** with **2** afforded a minor product (**4**) in a 20% yields when irradiation was performed between 0 and 5 °C. Since the photocycloaddition of **2** with olefins gives preparatively useful 1,5-diketones in good yields with a highly *regio*-selective fashion, an investigation of such by-product formation should be important. The molecular-weight determination of **4** by the mass spectrum[3] was confirmed to be a 1:1-adduct; *m/z*, 280 (M^+). Among its fragment ions, the acetyl group (*m/z*, 43), the base peak, and another prominent peak due to $C_{10}H_{16}$-moiety (*m/z*, 136) were suggestive. An alternative possibility of $C_9H_{12}O$ for the latter peak was eliminated by the appearance of the same fragment in the mass spectrum of a similar product (**5**) derived from **1** and **3**. In addition, another strong peak due to C_5H_9-ion (*m/z*, 69) ascribable to a 3-methyl-2-butenyl (prenyl) fragment appeared in both the spectra of **4** and **5**. Therefore, they are composed of two moieties, an intact C_{10}-framework of myrcene and the dioxoalkanoate group, linked with one C–C bond.

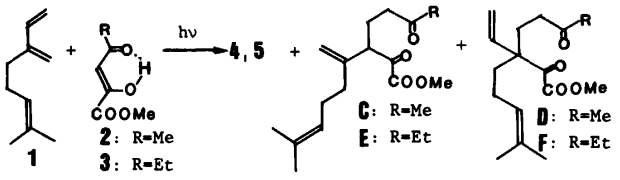

Scheme 1.

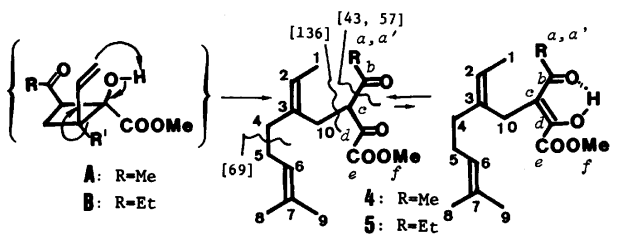

Scheme 2.

The NMR spectra[4] of **4** and **5**, respectively, exhibited not only the presence of acyl groups together with an oxalyl group [δ=2.20(3H, s) for **4** and 1.02(3H, t, J=7 Hz) and 3.83(2H, q, J=7 Hz) for **5**], but also signals ascribable to three methyl groups on the sp^2-carbons. It is certain that the signals for the two methyls are ascribable to the original isopropylidene moiety of **1**, and the third methyl signals (d, J=7 Hz), whose spin-coupling was confirmed respectively by double irradiation experiments, indicated the formation of an ethylidene group from the vinyl group in **1** (Scheme 2). Other than those mentioned, the NMR spectra of **4** and **5** resembled each other. This indicated that their structural relationships and structures could be discussed on the same ground. The NMR spectrum of **4** showed a pair of signals, 2.58(2H, d, J=7 Hz) and 4.25(1H, t, J=7 Hz), which were ascribable to the $R_2C{=}CR{-}CH_2{-}CH(CO)_2$-group. The methine signal disappeared upon a brief treatment with deuterium oxide. At the same time, the methylene signal at 2.58 changed to a singlet. As expected, the integration of the methine, the methylene, and the methoxy methyl signals were weaker than other signals; therefore, although the iron(III) chloride test was negative (as ordinary monoalkylated β-diketone), **4** should be an equilibrated keto-enol mixture. The methylene signal at 3.27 and the methyl signal at 3.84 should be attributable to the enolic tautomer. Due to this tautomerism, the ^{13}C-NMR spectrum of **4** was quite complicated, but its spectrum could, nevertheless, be analyzed with the aid of the assignment for myrcene and citronellol (Table 1). Its spectrum disclosed three carbonyl carbons, four olefinic carbons, and another ten aliphatic carbons.

Consequently, the structure of **4** could be expressed (as shown) and the other product **5** is the propionyl homolog.

The structures of **4** and **5** suggest that their formation involves a formal *retro*-Prins reaction, that is a 1,5-hydrogen shift from the *proto*-(2+2)π-adducts (**A** and **B**) to the 2-alkanoylcyclobutanols.

The yield of **4** or **5** was improved when the irradiation was carried out at low temperatures. Between 0 and 5 °C, the yield of **4** was 22%, but at an elevated temperature (25—30 °C),[5] its formation was suppressed and became practically undetectable. On the other hand, when irradiation was carried out at −35 °C, the yield of **4** was 28%. Furthermore, yields of **4** were as low as 4.8% when the irradiation was stopped immediately after a complete consumption of the starting material. Therefore, **4** and **5** are

Table 1. The ^{13}C NMR spectra of **4** and **5** (δ in $CDCl_3$)

No.	(**2**) [a]	Keto forms		Enol forms	
		4	**5**	**4**	**5**
1	(115.5)	13.3	13.2	13.3	13.2
2	(139.0)	120.2	119.9	122.6	122.4
3	(135.9)	134.8	134.6	136.4	136.6
4	(30.8)	30.6	30.6	27.7	27.8
5	(24.5)	25.6	26.2	26.6	26.5
6	(124.4)	123.9	124.0	123.6	123.5
7	(131.0)	131.5	131.0	131.8	131.6
8	(17.1)	17.6	17.5	17.6	17.5
9	(25.1)	26.6	26.9	14.9	25.4
10	(112.6)	26.8	16.9	36.2	37.0
a		25.6	7.3	25.6	8.1
a'			34.6		36.2
b		203.9	206.2	200.0	204.4
c		59.8	58.9	109.2	109.0
d		189.1	188.9	171.8	168.9
e		163.0	163.3	160.7	160.7
f		52.8	53.2	53.2	53.0

a) This column is included as a reference.

photochemical-reaction products from the metastable *proto*-photoadducts, **A** and **B**.

The intramolecular nature of the hydrogen shift is obvious due to its occurrence in the aprotic solvent.

In the case of the photochemical reaction of **1** with 2-methyl-1,3-butadiene (isoprene, **6**),[6] none of the *retro*-Prins product were detected. The IR spectral monitoring of the reaction suggested that the *proto*-adducts from **2** and **6** are quickly dealdolized at that temperature.

In conclusion, from the required geometry for the formation of **4** or **5**, the cycloaddition of **2** or **3** has been established to proceed *via* a geometry in which the hydroxyl and the vinyl group are *cis*. The retention of the ground-state geometry of **2**, a six-membered chelation structure, has already been proven by a chemical-structure determination of the (4+2)π-adducts of **2** with cyclopentadiene.[7]

Experimental

Photocycloaddition of 1 to 2. An EtOAc solution (20 cm^3) of **1** (300 cm^3) and **2** (500 mg) was irradiated by means of a 400-W high-pressure mercury lamp through a Pyrex glass filter between 0 and 5 °C under a nitrogen atmosphere for 8 h. Any excess **1** was then collected by distillation *in vacuo*, and the residue was chromatographed on a silica-gel column. From the least polar fractions eluted by hexane–AcOEt (9:1), a colorless oil was obtained as a mixture of three compound.[1] Subsequently, the mixture was rechromatographed on a prepacked silica-gel column by use of a System 500 apparatus, Nippon Waters, Co., to give **C**,[1] **D**,[1] and **4**, a colorless oil, 215 mg (22%) [Found: C, 68.58; H, 8.67%; M$^+$, 280.1675. Calcd for $C_{16}H_{24}O_4$: C, 68.54; H, 8.63%; M$^+$, 280.1675. ^1H NMR δ=1.59(3H, s), 1.63(3H, d, J=7 Hz), 1.67(3H, s), 2.0(4H, m), 2.20(3H, s), 2.30(3H, s)*,[8] 2.57(1H, d, J=8 Hz, s by add. D_2O), 3.21(2H, s), 3.81(3H, s)*, 3.84(3H, s), 4.36(1H, t, J=8 Hz), 5.00(1H, br. s), 5.36(1H, q, J=7 Hz). IR ν: 1740, 1720, 1220 cm^{-1}].

Photocycloaddition of 1 to 3. A neat mixture of **1** (25 cm^3) and **3** (500 mg) were placed in a cylindrical vessel and irradiated by means of a high-pressure mercury lamp between 0 and 5 °C for 8 h. The mixture was then distilled *in vacuo* to recover **1**, and the residue was chromatographed on a silica-gel column to give a crude photoadduct mixture.[2] Repeated chromatography of the fractions by high-pressure liquid chromatography (HPLC) on Micro-polasil with hexane–AcOEt (95:5) afforded **E**,[2] **F**,[2] and **5**, a colorless oil, 21 mg (2%) [Found: C, 69.58; H, 8.67; M$^+$, 294.1836. Calcd for $C_{17}H_{26}O_4$: C, 69.36; H, 8.90%; M$^+$, 294.1831. ^1H NMR δ=1.06(3H, t), 1.58(6H, s), 1.62(3H, d, J=7 Hz), 1.99(4H, m), 2.58(2H, d, J=7 Hz), 2.59(2H, q, J=7 Hz), 3.27(2H, s)*,[8] 3.83(3H, s)*, 3.85(3H, s), 4.25(1H, t, J=7 Hz), 5.05(1H, m), 5.35(1H, q, J=7 Hz). IR ν: 1740, 1720, 1225 cm^{-1}], from the least polar fractions.

Photocycloaddition of 1 to 2 at Low Temperature. When a neat mixture of **1** (2.5 cm^3) and **2** (50 mg) was externally irradiated between −35 and −30 °C, after 1 h the mixture showed a formation of **4** in 4.8% yield together with **C** and **D**, in 52.4% and 42.8% yields, according to a gas-liquid chromatographic (GLC) analysis. When the irradiation was continued for another 3 h, the mixture was shown to be **C** (45%), **D** (27%), and **4** (28%), using a GLC analysis. The repeated HPLC separation of the mixture on Micro-polasil with hexane–AcOEt (95:5) furnished analytical samples of **C** (24 mg), **D** (14 mg), and **4** (19 mg).

Photocycloaddition of to 2 between 25 and 35 °C. When the same mixture of **1** (2.5 cm^3) and **2** (50 mg) was similarly irradiated between 25 and 35 °C for 2 h, the mixture became negative to the coloration with $FeCl_3$. The HPLC of a mixture on Micro-polasil with hexane–AcOEt (95:5) gave only **C** (17 mg) and **D** (33 mg).

Photochemical Reaction of 1 with 6 at Low Temperature. Attempted Preparation of the Photochemical Ene Reaction Product. An anhydrous EtOAc solution (30 cm^3) of **2** (250 mg) and **6** (*ca.* 2 g) was irradiated by means of a high-pressure mercury lamp for 6 h at −30 °C. After the evaporation of the volatile materils *in vacuo*, the residue was chromatographed on a silica-gel column to give only two previously characterized normal photoadducts.[7]

References

1) Part XXXI: K. Okaishi, T. Hatsui, and H. Takeshita, *Kyushu Daigaku Sogo Rikogaku Kenkyuka Hokoku*, **7**, 21 (1985).

2) H. Takeshita and K. Komiyama, *Kyushu Daigaku Seisan Kagaku Kenkyusho Hokoku*, **73**, 25 (1982).

3) The mass spectra were measured by an OlSG-2Model Spectrometer, JEOL..

4) The NMR spectra were measured by an FX 100 Model spectrometer, JEOL, in $CDCl_3$ solutions throughout, and the chemical shifts were expressed in δ units from the internal Me_4Si.

5) The temperature was obtained by cooling with the running tap water in the summer.

6) H. Takeshita, T. Hatsui, and T. Masuda, *Kyushu Daigaku Sogo Rikogaku Kenkyuka Hokoku*, **1**, 35 (1978); H. Takeshita, T. Hatsui, N. Kato, T. Masuda, and H. Tagoshi, *Chem. Lett.*, **1982**, 1037.

7) H. Takeshita, A. Mori, and Y. Toyonaga, *Bull. Chem. Soc., Jpn.*, **48**, 307 (1975).

8) The asterisked signals were those of the enolic isomers of **4** and **5**. Enol contents in $CDCl_3$ were *ca.* 20% for both **4** and **5**.

Gas Chromatography-Mass Spectrometry of *N*-Trifluoroacetyl Trimethylsilyl Esters of Some Iminodicarboxylic Acids

Katsuhiro KAWASHIRO,* Shiro MORIMOTO, and Hideyuki YOSHIDA
Department of Chemical Engineering, Faculty of Engineering, Tokushima University, Minamijosanjima, Tokushima 770
(Received April 15, 1985)

Synopsis. The simultaneous *N*-trifluoroacetylation and *O*-trimethylsilylation of some iminodicarboxylic acids were studied by the use of a mixture of α,α,α,α′,α′,α′-hexafluoro-*N*-methyldiacetamide and *N*,*O*-bis(trimethylsilyl)trifluoroacetamide, as a derivatizing reagent. The resulting *N*-trifluoroacetyl trimethylsilyl ester derivatives gave rather complicated mass spectra with molecular (M^+) and M−15 (loss of CH_3) ions upon electron impact at 20 eV.

Previously we reported EI mass spectra of *N*-trifluoroacetyl (TFA) butyl ester[1] and *N*-trimethylsilyl (TMS) TMS ester[2] derivatives of some iminodicarboxylic acids (IDCAs). It has been shown that the TMS derivatives had advantages over the *N*-TFA butyl ester derivatives in terms of the simplicity of preparation and the easily recognizable mass spectra containing both molecular (M^+) and M−15 (loss of CH_3) ions. The major drawback of the TMS derivatives is incomplete trimethylsilylation (formation of both di- and tri-TMS) due to the steric hindrance of *N*-substituent groups. This may be overcome by introducing a TFA group to the imino nitrogen instead of the TMS group, which is less bulky and also a good *N*-masking group for amino acid esters for gas chromatography. Although two groups[3-6] have reported the preparation of *N*-TFA TMS derivatives of some common amino acids, a convenient single-step derivatization has not been established yet.

We were interested in fast and convenient preparation of *N*-TFA di-TMS esters of some IDCAs on a small scale for gas chromatography-mass spectrometry (GC–MS). This paper deals with a single-step preparation of such volatile derivatives, and also with their mass spectra upon electron impact at 20 eV. The IDCAs include iminodiacetic acid (**1**), 2- and 3-(carboxymethylamino)propionic acids (**2** and **3**), and 2,2′-, 2,3′-, and 3,3′-iminodipropionic acids (**4**—**6**).

Results and Discussion

When a suspension of **3** (50 μmol) in a mixture of

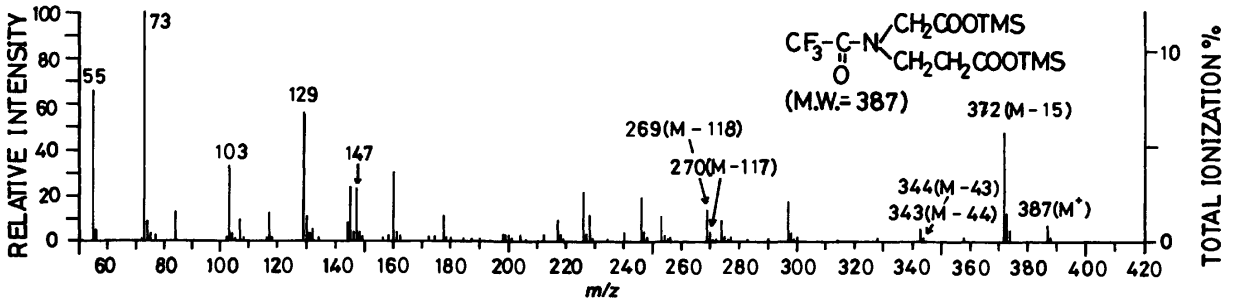

Fig. 1. Mass spectrum of *N*-TFA di-TMS ester of **3**.

Table 1. Some selected ions of *N*-TFA di-TMS esters of **1**—**6**

Parent IDCA	*m/z*[a]										
	M^+	M−15	M−43	M−44	M−117	M−118	M−131	M−189	M−207	Others	
1	373 (3)	358 (24)	330 (1)	329 (4)	256 (1)	255 (3)	—	—	—	147 (44)	73 (100)
2	387 (1)	372 (24)	344 (2)	343 (8)	270 (22)	—	—	198 (6)	180 (34)	147 (33)	73 (100)
3	387 (7)	372 (48)	344 (2)	343 (5)	270 (4)	269 (14)	256 (2)	198 (3)	180 (2)	73 (100)	55 (65)
4[b]	401 (1)	386 (37)	358 (2)	357 (4)	284 (27)	283 (1)	—	212 (99)	194 (50)	166 (52)	73 (100)
5	401 (1)	386 (22)	—	357 (1)	284 (32)	283 (1)	—	212 (14)	194 (100)	73 (53)	55 (69)
6	401 (3)	386 (30)	358 (1)	—	284 (8)	283 (33)	270 (2)	212 (4)	194 (13)	129 (86)	55 (100)

a) Values in parentheses indicate relative intensity. b) A first GC peak.

equal volumes (0.20 ml) of α,α,α,α′,α′,α′-hexafluoro-*N*-methyldiacetamide (*N*-methyl-bis(trifluoroacetamide), MBTFA)[7], *N*,*O*-bis(trimethylsilyl)trifluoroacetamide (BSTFA), and acetonitrile was heated at 100 °C for 30 min, a clear solution was obtained. GC analysis showed a single peak, which was determined to be *N*-TFA di-TMS ester of **3** by GC-MS (Fig. 1). Similarly, the other IDCAs except for **4**, gave the corresponding *N*-TFA di-TMS esters on the single-step derivatization (at 100 °C for 30 min). As a typical example, the time course of derivatization of **1** at 100 °C was studied by GC. The peak area ratio of *N*-TFA di-TMS ester of **1** to an internal standard (phenanthrene) became constant after reaction time of 20 min. Although small amounts of both di- and tri-TMS derivatives were present at an early stage of the derivatization (10 min), these two disappeared completely after reaction time of 20 min. These findings indicate that **1** can be converted in a high yield into the *N*-TFA di-TMS ester under the conditions (at 100 °C for 30 min).

In the instance of **4**, however, the derivatization became complicated and gave a mixture of the corresponding *N*-TFA di-TMS ester, TMS derivatives (both di- and tri-), and an unknown by-product[8] under the conditions (at 100 °C for 30 min).

The *N*-TFA di-TMS esters exhibited sharp and symmetrical GC peaks on a packed column. There were no indications of their adsorption on solid supports because of the presence of the stable *N*-TFA group. Retention times of the *N*-TFA di-TMS esters are generally intermediate between those of the corresponding di- and tri-TMS derivatives.[2]

Figure 1 presents the mass spectrum of *N*-TFA di-TMS ester of **3**, as a typical example. Some selected ions for **1**—**6** are listed in Table 1. Both M^+ and M−15 ions characteristic of TMS derivatives are seen for **1**—**6**. These spectra were more complex than those of the corresponding di- and tri-TMS derivatives.[2]

α,α′-IDCAs (**1**, **2**, and **4**) are generally characterized by M−43 (CH_3+CO), M−44 (CO_2), M−117 (COOTMS), M−189 (COOTMS+CH_2=Si(CH_3)$_2$), and M−207 (COOTMS+CH_2=Si(CH_3)$_2$+H_2O). The M−189 and M−207 were absent for **1**. The *N*-TFA group may play an important role for the formation of the M−44 because this ion was not observed for the corresponding TMS derivatives.[2] The M−44 ion[9] can be explained by migration of a TMS group to the carbonyl oxygen of the *N*-TFA group and subsequent elimination of a neutral species CO_2 from the rearranged M^+ ion. Analogous fragmentations are known for *N*-acylglycine TMS esters.[10] The amine fragment, M−117, which constituted a base peak for the corresponding TMS derivatives (both di- and tri-)[2] becomes less abundant.

On the other hand, β,β′-IDCA (**6**) is characterized by a complex spectrum with M−43, M−117, M−118 (COOTMS+H), M−131 (CH_2COOTMS), and M−207. In addition, M−69 (CF_3) and M−97 (CF_3CO) were observed for **6**. The M−44 characteristic of α,α′-IDCAs is not seen in this instance. The structurally most important amine fragment, M−131, which constituted a base peak for the corresponding tri-TMS derivative,[2] becomes far less abundant.

Compound **3** exhibits a complicated spectrum in which both ions characteristic of α,α′- and β,β′-IDCAs are present (Fig. 1). In contrast to **3**, **5** exhibited a similar spectrum to the corresponding α,α′-IDCA, **4**. These facts indicate that either of the fragmentation characteristics of α,α′- or β,β′-IDCAs can take place predominantly depending on the structures of α,β′-IDCAs.

Experimental

Materials. MBTFA was obtained from Gasukuro Kogyo Co. Ltd. BSTFA, acetonitrile, and the IDCAs were the same as previously reported.[2]

Derivatization. About 50 μmol of each IDCA was weighed into a 1 ml mini screw vial (Maruemu MV-1). Acetonitrile (0.20 ml), MBTFA (0.20 ml), and BSTFA (0.20 ml) were added to the vial. It was closed tight with a silicone cap and then heated at 100 °C for different durations in a constant-temperature air bath (Yamato Drying-Oven, DX-58).

GC. GC was carried out with a Hitachi 163 gas chromatograph equipped with a flame ionization detector and a glass column (3 mmϕ×1 m) packed with 1.5% OV-101 on Chromosorb G HP (100/120 mesh) (Shimadzu). The temperature was programmed linearly from 100 °C (5 min hold) to 230 °C at a rate of 5 °C min^{-1}. Nitrogen was the carrier gas flowing at 30 ml min^{-1}. Retention times of the *N*-TFA di-TMS esters: **1** 11.5 min, **2** 12.3 min, **3** 14.0 min, **4** 11.8 and 12.8 min, **5** 14.8 min, **6** 17.4 min. Retention time of phenanthrene: 17.0 min.

GC-MS. GC-MS was carried out with a JEOL JMS-D 300 mass spectrometer connected with a JGC-20 KP gas chromatograph, and mass spectra upon electron impact at 20 eV were obtained. The GC-MS conditions were the same as previously reported.[1]

References

1) K. Kawashiro, S. Morimoto, and H. Yoshida, *Bull. Chem. Soc. Jpn.*, **57**, 1097 (1984).
2) K. Kawashiro, S. Morimoto, and H. Yoshida, *Bull. Chem. Soc. Jpn.*, **57**, 2871 (1984).
3) H. R. Kricheldorf and M. Fehrle, *Synthesis*, **6**, 420 (1974).
4) M. Schwarz and G. Michael, *J. Chromatogr.*, **118**, 101 (1976).
5) G. Michael, *J. Chromatogr.*, **188**, 251 (1980).
6) G. Michael, *J. Chromatogr.*, **196**, 160 (1980).
7) M. Donike, *J. Chromatogr.*, **78**, 273 (1973).
8) Although low-resolution mass spectrum of the by-product (M^+, *m/z* 496) was obtained, its structure could not be determined in the present study.
9) The identity of the M−44 (CO_2) was confirmed for **3** by a high-resolution mass measurement. Found: *m/z* 343.1235. Calcd for $C_{12}H_{24}NO_3F_3Si_2$: M−CO_2, 343.1248.
10) P. V. Fennessey and S. S. Tjoa, *Org. Mass Spectrom.*, **15**, 202 (1980).

Solvent Effects on Absorption Spectra of Substituted Azobenzenes

Yoshimi SUEISHI,* Mari ASANO, Shunzo YAMAMOTO, and Norio NISHIMURA
Department of Chemistry, School of Science, Okayama University, Okayama 700
(Received April 17, 1985)

Synopsis. McRae's formula including the quadratic term was applied to an analysis of absorption spectra of substituted azobenzenes in various solvents. It has been suggested that the interaction between the solvent dipole and the solvent-induced solute dipole plays an important role.

Recently, we have reported[1] that the absorption maximum of *trans*-4-dimethylamino-4′-nitroazobenzene (NDAAB) and the rate of its thermal cis-to-trans isomerization are quite sensitive to solvent polarities. Influences of dipole interactions on absorption frequencies were investigated theoretically by Ooshika[2] and McRae.[3] Irick, Jr. and Pacifici[4] and Misono *et al.*[5] applied McRae's formula to absorption spectra of substituted azobenzenes. However, they neglected the quadratic Stark term which represents the contribution of the interaction between the permanent dipole of solvent molecules and the solute dipole thereby induced. Indeed, in the case of less polar solutes such as azulene, the term was reported[6] as negligibly small. McRae[3] suggested, however, that if both solute and solvent are highly polar, the Stark term would make an important contribution.

We reported[1] that solute-solvent interactions such as the dipole-induced dipole one might be operative in very polar solvents for thermal isomerization reactions of NDAAB and 4,4′-bis(diethylamino)azobenzene (BDEAAB). Thereupon, we have examined the Stark term in the McRae equation by using NDAAB and BDEAAB.

Experimental

The reagent grade solvents were used as supplied. The preparation of azobenzenes was described elsewhere.[1]

The absorption spectra were measured with a Hitachi 228 spectrophotometer. For BDEAAB, the separation of absorption spectra was made according to an attached program.

Results and Discussion

The frequencies at the absorption maxima of *trans*-NDAAB and *trans*-BDEAAB in various solvents are given in Table 1. In the case of *trans*-BDEAAB, the absorption spectra consist of three bands which are considered to arise from a normal vibrational structure, and the separation of the spectra was successful by taking their fourth-order derivative (Fig. 1). In Table 1, the lowest-frequencies (0-0 band) in various solvents are listed. As shown in Table 1, ν_{obsd} of BDEAAB is also sensitive to solvent polarity as with NDAAB. It is noteworthy that bis-BDEAAB exhibits more remarkable solvent effects on the absorption spectra than 4-dimethylaminoazo-

Table 1. Observed and calculated absorption frequencies of NDAAB and BDEAAB in various solvents and ν_{gas}, $(AL+B)$, C, and F values

		NDAAB		BDEAAB	
		ν_{obsd}/cm^{-1}	ν_{calcd}/cm^{-1}	ν_{obsd}/cm^{-1}	ν_{calcd}/cm^{-1}
1	Hexane	22624	22793	21882	21996
2	Heptane	22624	22650	21739	21878
3	Cyclohexane	22371	22244	21692	21540
4	Methylcyclohexane	22422	22278	21786	21566
5	CCl_4	22026	21871	21322	21245
6	Toluene	21459	21515	20964	20953
7	Benzene	21413	21508	20747	20930
8	Diethyl ether	22026	22341	21368	21854
9	Chlorobenzene	20747	20614	20576	20411
10	4-Methyl-2-pentanone	21097	21035	20833	20869
11	Cyclohexanone	20576	20373	20790	20323
12	Ethyl benzoate	20747	20719	20534	20513
13	Propionitrile	20833	20917	20534	20792
14	Acetonitrile	20877	21008	20661	20872
15	DMSO	19920	19820	20080	19876
	ν_{gas}/cm^{-1}	28544		26789	
	$-(AL+B)/cm^{-1}$	30877		25729	
	$-C/cm^{-1}$	1712		485	
	$-F/cm^{-1}$	1809		2115	
	S.D.[a]$/cm^{-1}$	71		136	

a) Standard deviation of the difference between the calculated and observed values in various solvents.

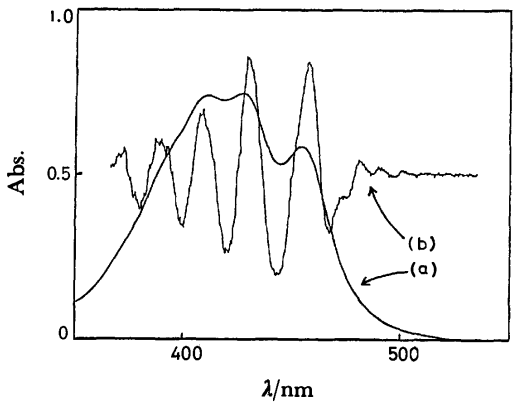

Fig. 1. Absorption spectrum of BDEAAB in hexane (a) and its fourth-order derivative (b).

benzene (DAAB).[1]

McRae[3] proposed a general expression for frequency shifts which arise from dipole interactions:

$$\Delta\nu = (AL+B)\left(\frac{n^2-1}{2n^2+1}\right) + C\left(\frac{D-1}{D+2}-\frac{n^2-1}{n^2+2}\right) + F\left(\frac{D-1}{D+2}-\frac{n^2-1}{n^2+2}\right)^2, \quad (1)$$

where $\Delta\nu$ is the difference between absorption frequencies in solution and in gas phase ($\nu_{obsd}-\nu_{gas}$). Other notations are the same as McRae's.

If the contribution of the F-term which comes from solvent dipole-solute induced dipole interaction is sufficiently small to be neglected for polar solvents, as Irick, Jr. and Pacifici[4] reported, a linear relation between $\{\Delta\nu-(AL+B)[(n^2-1)/(2n^2+1)]\}$ and $\{[(D-1)/(D+2)]-[(n^2-1)/(n^2+2)]\}$ is expected. However, as shown in Fig. 2, the upward curvature is obtained when the points for very polar solvents are included. Therefore, we have treated our data by the quadratic regression equation, and the estimated C- and F-values are given in Table 1.

It is noted that the absolute C-value of BDEAAB is considerably small compared with that of NDAAB. This can naturally be understood since the dipole moment of 4,4'-disubstituted *trans*-azobenzenes such as BDEAAB in ground state must be nearly zero. Both of the absolute F-values are considerably large compared with those reported by Robertson *et al.*[6] (*e.g.*, $|F|=12$ cm^{-1} for ^1L_b of naphthalene and $|F|=200$ cm^{-1} for ^1B_b of naphthacene). This is considered as a good indication of the change in the solute dipole moment induced by solvents. Very recently, solvent-induced changes in electronic structures of molecules having conjugation systems have been investigated with the help of ^{1}H NMR absorption spectra.[7] Moreover, Betrel *et al.*[8] have made a theoretical investigation using the CNDO/SCI method

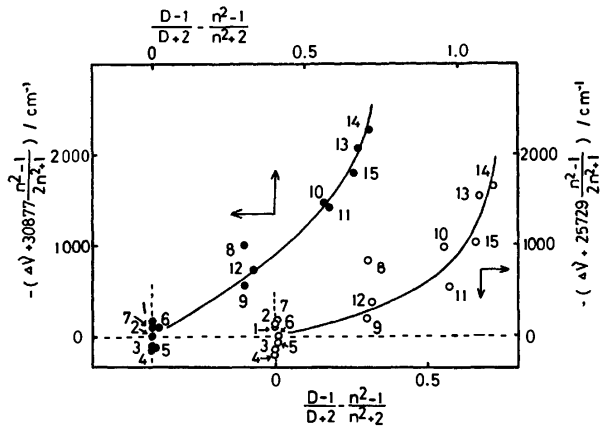

Fig. 2. Relation between $\{\Delta\nu-(AL+B)[(n^2-1)/(2n^2+1)]\}$ and $\{[(D-1)/(D+2)]-[(n^2-1)/(n^2+2)]\}$; ●: NDAAB, ○: BDEAAB. Key is shown in Table 1.

including solvation on the problem of electronic structure. They suggested a significant increase in the solute dipole moment with increasing solvent polarity. This is in accordance with the above results.

In Table 1, the ν-values calculated by using the estimated constants are also given. The standard deviation for the linear plot of ν_{calcd} against ν_{obsd} is much improved compared with the reported one (S. D. 203 cm^{-1}).[4]

Recently, we have shown that rate constants for the isomerization of NDAAB derivatives were well correlated with the absorption maxima of their *trans*-isomers, and suggested that specific solute-solvent interactions might give rise to a polarization of solute molecules enhanced by surrounding polar solvent molecules upon activation. It has been shown that the quadratic term in Eq. 1 plays an important role for the spectral shifts of the push-pull and push-push azobenzenes by polar solvents. Therefore, the present work supports our previous view just mentioned above.

References

1) N. Nishimura, S. Kosako, and Y. Sueishi, *Bull, Chem. Soc. Jpn.*, **57**, 1617 (1984).
2) Ooshika, *J. Phys. Soc. Jpn.*, **9**, 594 (1954).
3) E. G. McRae, *J. Phys. Chem.*, **61**, 562 (1957).
4) G. Irick, Jr. and J. G. Pacifici, *Text. Res. J.*, **1972**, 391.
5) T. Misono, Y. Yatabe, Y. Nagao, and Y. Abe, *Nippon Kagaku Kaishi*, **3**, 452 (1984).
6) W. W. Robertson, A. D. King, and O. E. Weigang, Jr., *J. Chem. Phys.*, **35**, 464 (1961).
7) M. S. A. Abdel-Mottaleb and M. N. Abdel-Kader, *Indian, J. Chem.*, **22B**, 1217 (1983).
8) A. Betrel, A. Le Beuze, P. Jacques, and H. Strub, *J. Chem. Soc., Faraday Trans. 2*, **80**, 1234 (1984).

^{79}Br and ^{127}I Nuclear Quadrupole Resonance of Mixed Valency Compounds Ga_2X_4(X=Br, I)

Tsutomu OKUDA,* Hiroshi HAMAMOTO, Hideta ISHIHARA, and Hisao NEGITA
Department of Chemistry, Faculty of Science, Hiroshima University, Higashisenda-machi, Naka-ku, Hiroshima 730
(Received January 14, 1985)

Synopsis. ^{79}Br and ^{127}I nuclear quadrupole resonances(NQR) were observed in α-Ga_2Br_4, β-Ga_2Br_4, and Ga_2I_4 at various temperatures. Resonance lines disappeared at 353, 335, and 448 K for α-, β-Ga_2Br_4, and Ga_2I_4 respectively. The wide separation of the ^{127}I resonance lines in Ga_2I_4 may be attributed to the interaction between the Ga^+ ions and the I atoms.

The X-ray crystal analysis has shown that Ga_2Cl_4 is a mixed valency compound with the ionic structure of $Ga^+(GaCl_4)^-$, that the Ga atom is tetrahedrally coordinated by four Cl atoms, and that the Ga^+ ion is surrounded by eight Cl atoms.[1] The Raman spectrum has revealed that Ga_2Br_4 fused at about 453 K also has the ionic structure of $Ga^+(GaBr_4)^-$.[2] Corbett and Hershaft have reported that Ga_2Br_4 exists in two crystalline forms, with melting points of 426 and 437.5 K.[3] Recently, X-ray crystal analysis has shown that Ga_2I_4 has an ionic structure similar to Ga_2Cl_4.[4]

In the present study, we observed the NQR of Ga_2X_4(X=Br, I) and examined the phase transitions and interionic interaction. The NQR of α-Ga_2Br_4 has already been investigated by Deeg and Weiss.[5]

Experimental

Ga_2Br_4 was prepared by heating equimolar amounts of Ga and $HgBr_2$ in a glass reaction tube.[6] The α-form was obtained by gradually cooling the mixture from 426 K, and the β-form, by cooling it rapidly from 438 K. Ga_2I_4 was prepared by heating equimolar amounts of Ga anf HgI_2 at 484 K in a glass tube. In each case, the compound was purified by eliminating Hg as a by-product.

NQR was measured by using superregenerative oscillators with Zeeman modulation. The temperature of the sample was determined with the aid of a copper-constantan thermocouple.

Results and Discussion

Table 1 shows the observed NQR frequencies of Ga_2X_4(X=Br, I). The ^{79}Br resonance frequencies of α-Ga_2Br_4 are in good agreement with those reported by Deeg and Weiss.[5] Two ^{79}Br resonance lines were also observed for β-Ga_2Br_4. The two lines of the β-form are widely separated, whereas those of the α-form are close to each other. The wide separation of the resonance lines suggests that the shape of the $GaBr_4^-$ ion is a distorted tetrahedron. In the case of Ga_2Cl_4, a contraction in volume has been reported by Fedrov and Lovetskaya when the α-form is transformed to the β-form.[7] This causes the intermolecular distances to shorten. Therefore, the influence of the crystal field on the electric field gradients becomes large, and the resonance lines result in a wide separation or multiple split. A similar relation can be expected to hold for Ga_2Br_4.

As the temperature was raised from 77 K, all the resonance lines in α- and β-Ga_2Br_4 decreased gradually in frequency, but the curves of the frequency *vs.* the temperature in the α-form crossed at about room temperature. The resonance lines disappeared at 353 and 335 K for the α- and β-forms respectively. When the temperature of each sample was brought back from the temperature of the line-disappearance to room temperature, however, no resonance lines could be observed. However, when each sample was once melted and then cooled to room temperature, its resonance lines could again be observed. Our differential thermal analysis measurements showed that, with an increase in the temperature from room temperature, one peak was recorded near 370 K for the α-form and two peaks were recorded near 355 and 390 K for the β-form.

TABLE 1. NQR PARAMETERS IN Ga_2X_4(X=Br, I) AT 293 K

Compound	Nucleus	Frequency/MHz[a]		η/%	$\frac{e^2Qq/h}{\text{MHz}}$
		$\nu_1(\pm1/2\leftrightarrow\pm3/2)$	$\nu_2(\pm3/2\leftrightarrow\pm5/2)$		
α-Ga_2Br_4	^{79}Br	128.85	—	—	—
	^{79}Br	128.92	—	—	—
β-Ga_2Br_4	^{79}Br	128.44	—	—	—
	^{79}Br	122.59	—	—	—
Ga_2I_4	^{127}I	113.65	227.09	2.62	757.08
	^{127}I	131.94	262.14	7.16	874.71
	^{127}I	134.27	262.61	13.24	878.46
	^{127}I	163.71	280.90	36.64	960.13

a) The experimental errors are within ±0.02 MHz for ^{79}Br and ^{127}I.

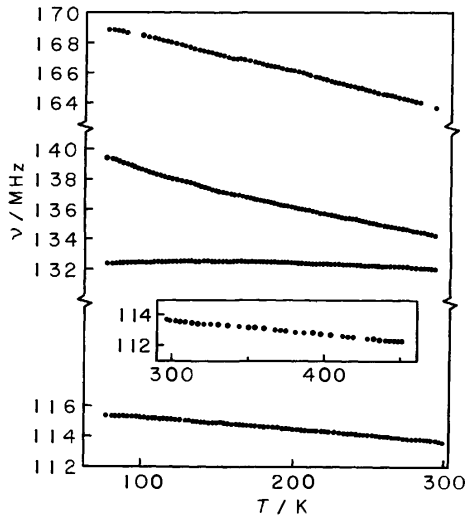

Fig. 1. Temperature dependence of ν_1 NQR frequencies of ^{127}I in Ga_2I_4.

Therefore, it seems likely that the disappearance of the resonance lines is due to the phase transition.

The eight ^{127}I resonance lines listed in Table 1 were observed for Ga_2I_4. There is an ambiguity in pairing the ^{127}I resonance lines because the pairing of these lines was done in the order of frequency. The other combination gives slightly different values for the asymmetry parameter, η, and the quadrupole coupling constant, e^2Qq/h. The four $\nu_1(\pm 1/2 \leftrightarrow \pm 3/2)$ lines of ^{127}I are so widely separated that the small distortion in the shape of the GaI_4^- ion can not be attributed to the line separation.

According to the X-ray analysis by Gerlach *et al.*,[3] the Ga–I bond lengths are 2.537(5), 2.541(4), 2.541(4), and 2.608(4)Å, and all I–Ga–I angles are within 3.1° of the tetrahedral angle. The shape of the GaI_4^- ion slightly distorted from a regular tetrahedron; therefore, the distortion of the shape of the anion can not be reasonable as the cause of the line separation. The I···I distances in the GaI_4^- ion range from 4.121 to 4.266 Å, and the I···I distances between GaI_4^- ions are equal to the sum of the van der Waals radii.[3] Accordingly, the I···I distances can not cause the resonance lines to separate widely. One Ga^+ ion is surrounded by eight I atoms at distances ranging from 3.281 to 3.820 Å, and the number of Ga^+ ions with which a given I atom interacts differs with each crystallographically nonequivalent I atom.[3] Therefore, the wide separation of the resonance lines is ascribable mainly to the Ga^+···I interaction.

Figure 1 shows the temperature dependence of the ν_1 NQR frequencies of ^{127}I in Ga_2I_4. All the resonance lines decreased in frequency with the increase in the temperature. The slopes of the curve for the higher two resonance lines are large, while those of the rest are small. In the temperature region above room temperature, the temperature dependence was observed only for the lowest resonance line, as is shown in Fig. 1. As the temperature was raised, the resonance line decreased monotonously in its frequency. The intensity of the resonance line became gradually small from about 400 K and disappeared at 451 K. When the temperature was brought back to room temperature, the resonance lines could be observed again.

References

1) G. Garton and H. M. Powell, *J. Inorg. Nucl. Chem.*, **4**, 84 (1957).

2) L. A. Woodward, N. N. Greenwood, J. R. Hall, and I. J. Worrall, *J. Chem. Soc.*, **1958**, 1505.

3) J. D. Corbett and A. Hershaft, *J. Am. Chem. Soc.*, **80**, 1530 (1958).

4) G. Gerlach, W. Hönle, and A. Simon, *Z. Anorg. Allg. Chem.*, **486**, 7 (1982).

5) T. Deeg and A. Weiss, *Ber. Bunsenges. Phys. Chem.*, **79**, 497 (1975).

6) R. C. Carlston, E. Griswold, and J. Kleinberg, *J. Am. Chem. Soc.*, **80**, 1532 (1958).

7) P. I. Fedrov and G. A. Lovetskaya, *Russ. J. Inorg. Chem.*, **13**, 1730 (1968).

The Magnetic Properties of the Copper(II) Complexes with ω-Amino Carboxylic Acids

Shuji EMORI,* Toshihiko NOGUCHI, and Yoneichiro MUTO
Department of Chemistry, Faculty of Science and Engineering, Saga University, Honjo-machi, Saga 840
(Received March 19, 1985)

Synopsis. Compounds of formula $CuX_2(OOC(CH_2)_m NH_3)_2 \cdot nH_2O$ (m=2—5 and X=Cl or Br) and $CuX_{3/2}(OOCCH_2NH_3)$ (X=Cl or Br) have been prepared and characterized by means of magnetic susceptibility and IR spectroscopy measurements. The correlation of their magnetic moments with the pK_a values of their parent carboxylic acids is discussed.

In general, α- and β-amino carboxylic acids form metal chelates in which the amino nitrogen and carboxylate oxygen atoms act as donors. However, a recent X-ray study[1] of the complex formed by the reaction between copper(II) chloride and glycine, has shown that ammonio acetate coordinates to the metal ion *via* a carboxyl group and that copper(II) acetate-type dimer units are created. This suggests that not only *N*-protected amino carboxylic acids, such as *N*-acetylglycine,[2] *N*-tosylglycine[3] and hippuric acid,[4] but amino carboxylic acids can act generally as simple carboxylic acids. The resultant copper(II) compounds seem to be appropriate to investigate the effect of the NH_3^+ group on their magnetic properties. Thus, we tried to isolate the copper(II) compounds from the acidic solutions with various ω-amino carboxylic acids.

A compound with a stoichiometry of $CuCl_2(OOC(CH_2)_mNH_3)_2 \cdot nH_2O$, where m=2—5, was precipitated in green crystals when a slight excess of amino carboxylic acid and a small amount of a 2 mol dm^{-3} HCl solution were added to a warm solution (*ca.* 40 °C) of copper(II) chloride. Then, the mixture was allowed to stand in a refrigerator overnight. The corresponding bromide salt was also obtained in a similar way. Fresh samples of the obtained compounds mostly contain water molecules (IR band at *ca.* 3450 cm^{-1}). The water was gradually lost when stored under anhydrous conditions. The corresponding glycine compound, $CuCl_2(OOCCH_2NH_3)_2 \cdot 2H_2O$, was also isolated by Castillo and Ramirez,[5] but its magnetic moment (μ_{eff}=1.81 BM at 22 °C) and IR data indicate that the compound has a monomeric structure. Since two isomers of the analogous chromium(II) bromide compound, $CrBr_2(OOCCH_2NH_3)_2 \cdot 2H_2O$, were isolated by Herzog *et al.*,[6,7] we attempted to isolate the isomeric form of $CuCl_2(OOCCH_2NH_3)_2 \cdot 2H_2O$. The mixed valence compound $CuCl_{3/2}(OOCCH_2NH_3)$, however, was isolated[1] as dark-green crystals instead of the expected isomer. This compound can be obtained more efficiently by reacting glycine with an acidic aqueous solution including equimolar amounts of copper(I) and copper(II) chlorides and allowing the solution to stand in a refrigerator overnight. The corresponding bromide salt is also obtained in a similar way.

The magnetic moments of the present compounds (Table 1) were evaluated per copper(II) ion from their susceptibilities observed at room temperature and the relevant Pascal constants.[8] The magnetic susceptibilities of the chloride salts were measured from liquid nitrogen up to room temperature (Fig. 1) and agreed well with the theoretical equation for the

TABLE 1. ANALYTICAL DATA AND EFFECTIVE MAGNETIC MOMENTS AT 20 °C

Compounds	Found (Calcd) (%)					μ_{eff}/BM
	Cu	X	C	H	N	
$CuCl_{3/2}(OOCCH_2NH_3)$	33.02 (33.13)	27.70 (27.73)	12.41 (12.52)	2.66 (2.63)	7.26 (7.30)	1.36
$CuBr_{3/2}(OOCCH_2NH_3)$	24.73 (24.59)	46.32 (46.37)	9.15 (9.30)	1.84 (1.95)	5.36 (5.42)	1.31
$CuCl_2(OOCCH_2CH_2NH_3)_2 \cdot H_2O$	19.18 (19.22)	21.67 (21.44)	21.71 (21.80)	4.86 (4.88)	8.44 (8.47)	1.35
$CuBr_2(OOCCH_2CH_2NH_3)_2 \cdot H_2O$	15.28 (15.15)	37.90 (38.09)	17.07 (17.18)	3.85 (3.88)	6.68 (6.68)	1.35
$CuCl_2(OOCCH_2CH_2CH_2NH_3)_2 \cdot 3/2H_2O$	17.38 (17.28)	19.40 (19.28)	26.42 (26.13)	5.82 (5.76)	7.70 (7.62)	1.33
$CuBr_2(OOCCH_2CH_2CH_2NH_3)_2 \cdot 1/2H_2O$	14.56 (14.49)	36.55 (36.44)	21.40 (21.91)	4.35 (4.37)	6.26 (6.39)	1.33
$CuCl_2(OOCCH_2CH_2CH_2CH_2NH_3)_2 \cdot 2H_2O$	15.85 (15.70)	18.15 (17.52)	29.45 (29.67)	6.42 (6.47)	6.87 (6.92)	1.33
$CuBr_2(OOCCH_2CH_2CH_2CH_2NH_3)_2$	14.00 (13.89)	35.22 (34.92)	26.01 (26.25)	4.88 (4.85)	6.10 (6.12)	1.28
$CuCl_2(OOCCH_2CH_2CH_2CH_2CH_2NH_3)_2 \cdot 2H_2O$	14.70 (14.68)	16.42 (16.38)	33.00 (33.30)	6.97 (6.99)	6.45 (6.47)	1.32
$CuBr_2(OOCCH_2CH_2CH_2CH_2CH_2NH_3)_2 \cdot 2H_2O$	12.15 (12.18)	30.55 (30.63)	27.48 (27.63)	5.61 (5.80)	5.37 (5.37)	1.29

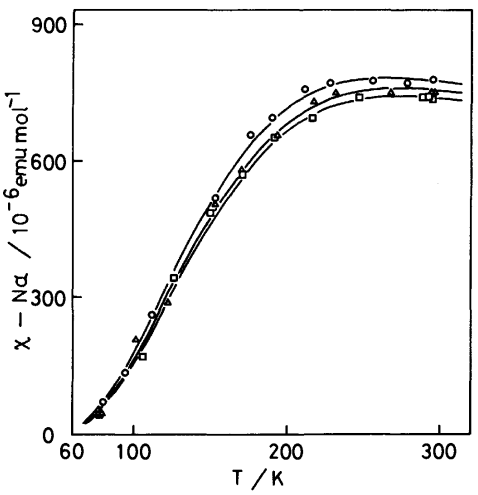

Fig. 1. Magnetic susceptibilities of the copper(II) chloride compounds with 3-aminopropionic (○), 4-aminobutyric (△) and 6-aminohexanoic (□) acids. The solid curve represents the Bleaney-Bowers equation.

susceptibility of binuclear copper(II) compounds (Bleaney-Bowers equation[9]), using the following parameters: g=2.18 and $2J$=−315 cm^{-1}, g=2.15 and $2J$=−320 cm^{-1}, and g=2.15 and $2J$=−324 cm^{-1} for the compounds with 3-aminopropionic(β-alanine), 4-aminobutyric and 6-aminohexanoic acids, respectively, and $N\alpha$=60×10^{-6} emu mol^{-1} (1 emu mol^{-1}=4π×10^{-6} m^3 mol^{-1}). IR spectra of the solid complexes show the bands near 1520 and 1580 cm^{-1} connected with NH_3^+ deformations[10] in addition to the characteristic bands in the range 1430—1450 and 1600—1660 cm^{-1} connected with symmetric and unsymmetric stretching vibrations of the carboxyl groups.[11] The obtained results show clear evidence for the presence of a dinuclear subunit, which contains four zwitterionic amino carboxylic acids bound with the copper(II) ions *via* carboxyl group like copper(II) acetate monohydrate. The axial positions seem to be occupied by halide ions, because there exists a slight difference in the magnetic moments between the chloride and bromide salts. It is consistent with the fact that the magnetic moments of the anhydrous compounds are not greatly different from those of the hydrated compounds, water being probably involved in hydrogen bonding in the packing of the molecules.

It has already been pointed out that the magnetic superexchange interaction in the dimeric carboxylates is related to the donor-acceptor character of bridging and axial ligands.[12] Although this relationship does not take into account the effect of the metal-ligand bond or steric effects in the axial ligand coordination, it has been supported experimentally[13,14] and shown to be consistent with the results of molecular orbital analyses of the bridged dimeric structure.[15] In this series of bridging ligands, the pK_a value varies from 2.36 for glycine to 3.53, 4.03, 4.27, and 4.43 for 3-aminopropionic, 4-aminobutyric, 5-aminovaleric and 6-aminohexanoic acids, respectively.[16] From Table 1, it can be seen that, except for the glycine compounds, the trend that magnetic moments in the series of the same halide salts increase as the acid strength of the ammonio carboxylic acids (pK_{a_1}) becomes stronger. This trend is consistent with the variation of singlet-triplet separation values(−2J) determined for a series of chloride salts. X-Ray and magnetic susceptibility studies of the glycine compound $CuCl_{3/2}(OOCCH_2NH_3)$ have shown that this polymeric compound is composed of cupric dimeric subunits with an exchange integral $2J$=−385 cm^{-1}.[1] Although this strong antiferromagnetic interaction was explained by the presence of an electrophilic NH_3^+ group,[1] a large number of magnetic data for copper(II) halogenoacetates[17] have shown that the σ-electron attracting effect produces a comparative decreasing magnetic interaction. The disobedience of the general trend suggests that the strong interaction in the glycine compound is attributable to steric effects or the coordination of the axial chlorine to a copper(I) ion. The fact that the magnetic moments of the chloride salts are higher than those of bromide salts indicates that the antiferromagnetic interaction in dimeric copper(II) carboxylate adducts tends to become stronger as the basicity of the added axial ligands becomes weaker.[18]

References

1) T. Glowiak and H. Kozlowski, *Inorg. Chim. Acta*, **46**, L65 (1980).
2) K. E. Hyde, P. L. Bocko, D. Martynec, G. F. Kokoszka, and M. Lynch, *J. Inorg. Nucl. Chem.*, **39**, 703 (1977).
3) L. Antolini, L. Menabue, G. C. Pellacani, G. B. Gavioli, G. Grandi, L. P. Battaglio, A. B. Corradi, and G. Marcotrigiano, *J. Chem. Soc., Dalton Trans.*, **1984**, 1687.
4) P. Sharrock, C. H. Thibaudeau, and A. Caille, *Inorg. Chem.*, **18**, 510 (1979).
5) M. Castillo and E. Ramirez, *Transition Met. Chem.*, **9**, 268 (1984).
6) S. Herzog and H. Aul, *Z. Chem.*, **6**, 382 (1966).
7) S. Herzog and W. Kalies, *Z. Anorg. Allg. Chem.*, **351**, 237 (1967).
8) G. Foex, "Constants Sélectionées, Diamagnétisme et Paramagnétisme," Masson, Paris (1957).
9) J. Lewis, Y. C. Lin, L. K. Royston, and R. C. Thomson, *J. Chem. Soc.*, **1965**, 428.
10) L. J. Bellamy, "The Infrared Spectra of Complex Molecules," 3rd ed., Chapman and Hall, London (1975).
11) S. Yamada, H. R. Nakamura, and R. Tsuchida, *Bull. Chem. Soc. Jpn.*, **31**, 303 (1958).
12) M. Kato, H. B. Jonnasen, and J. C. Fanning, *Chem. Rev.*, **64**, 99 (1964).
13) R. W. Jotham, S. F. A. Kettle, and J. A. Marks, *J. Chem. Soc., Dalton Trans.*, **1972**, 428.
14) J. Mrozinski and E. Heyduk, *J. Coord. Chem.*, **13**, 291 (1984).
15) P. J. Hey, J. C. Yhibeault, and R. Hoffmann, *J. Am. Chem. Soc.*, **97**, 4884 (1975).
16) A. Albert and E. P. Serjearnt, "Ionization Constants of Acids and Bases," Methuen Co., London (1962).
17) M. Melnik, *Coord. Chem. Rev.*, **36**, 1 (1981).
18) Y. Muto, T. Tokii, K. Chijiwa, and M. Kato, *Bull. Chem. Soc. Jpn.*, **57**, 1008 (1984).

Synthesis of Guanidino-1,3,5-triazines Using DMF

Kokoro Iio* and Eiichi Ichikawa†
Industrial Products Research Institute, Yatabe-machi Higashi, Tsukuba-gun, Ibaraki 305
†*Faculty of Engineering, Tokyo Institute of Technology, Ookayama, Meguro-ku, Tokyo 152*
(Received March 12, 1985)

Synopsis. 2,4,6-Triguanidino-1,3,5-triazine and 2,4,6-tris(3-methylguanidino)-1,3,5-triazine were synthesized in 42 and 52% yields, respectively, by the cyclotrimerization of cyanoguanidine and 1-methyl-3-cyanoguanidine using DMF as a solvent in the presence of hydrogen chloride. 1-Phenyl-3-cyanoguanidine, 1,2-dimethyl-3-cyanoguanidine, and 2-imidazolidinylidenecyanamide, however, were cyclodimerized to the corresponding guanidino-1,3,5-triazines in a similar manner.

Our previous papers[1–3] described that 2,4-diamino-6-guanidino-1,3,5-triazine (**1**), 2-amino-4,6-diguanidino-1,3,5-triazine (**2**) and 1-amidino-2,4,6-triguanidino-dihydro-1,3,5-triazine (**3**) were prepared by a reaction of cyanoguanidine using phenol or pyridine–nitrobenzene as a solvent in the presence of hydrogen chloride. Especially 2,4,6-triguanidino-1,3,5-triazine (**4**) was not formed directly through the above reaction, but was produced quantitatively upon an elimination reaction of cyanamide from **3** in an alkaline solution.

In this paper, we wish to report a convenient method of synthesizing **4** by the cyclotrimerization of cyanoguanidine using DMF as a solvent, together with the reaction of substituted cyanoguanidines in DMF.

The reaction of cyanoguanidine in the presence of equimolar hydrogen chloride in DMF gave **4** and **1** in 42 and 8% yields, respectively. However, **2**, **3** and cyanamide were not detected in this reaction, and **3** did not release cyanamide under the conditions of this reaction. These results suggest that **4** was formed by the cyclotrimerization of cyanoguanidine.

The reaction was extended to substituted cyanoguanidines. Consequently, 2,4,6-tris(3-methylguanidino)-1,3,5-triazine (**5**) was obtained in 52% yield by the cyclotrimerization of 1-methyl-3-cyanoguanidine. The structure of **5** was established by its acid hydrolysis, which gave cyanuric acid and methylguanidine in 69 and 58% yields, respectively. The reaction of 1-phenyl-3-cyanoguanidine, however, did not afford the expected 2,4,6-tris(3-phenylguanidino)-1,3,5-triazine, and provided only the normal type of 3-phenylguanidino-1,3,5-triazines,[3] which was 2-amino-4-anilino-6-(3-phenylguanidino)-1,3,5-triazine (**6**) by the cyclodimerization of the starting material, in 21% yield. **6** was confirmed with an authentic sample.[3] In a similar manner, 1,2-dimethyl-3-cyanoguanidine and 2-imidazolidinylidenecyanamide were also cyclodimerized and deposited 1-methyl-2-methylamino-4-imino-6-(2,3-dimethylguanidino)-1,4-dihydro-1,3,5-triazine (**7**) and 2-amino-4-(4,5-dihydro-1*H*-imidazol-2-ylamino)-6,7-dihydroimidazo[1,2-*a*][1,3,5]triazine (**8**) from the DMF solution in 41 and 67% yields, respectively. **7** and **8** were also obtained in a phenol solvent in 81 and 71% yields, respectively, upon a treatment of the solution.[3] The structure of **7** was established by an elemental analysis, the mass spectrum and acid hydrolysis. This gave 1-methyl-1,3,5-triazine-2,4,6(1*H*,3*H*,5*H*)-trione, 1,3-dimethylguanidine, methylamine and ammonia. The structure of **8** was also established by an elemental analysis, its mass spectrum and acid hydrolysis, giving 6,7-dihydroimidazo[1,2-*a*][1,3,5]triazine-2,4-diol (**9**), 4,5-dihydro-1*H*-imidazol-2-amine and ammonia. These results suggest that the cyclotrimerization of cyanoguanidines using DMF has a limitation.

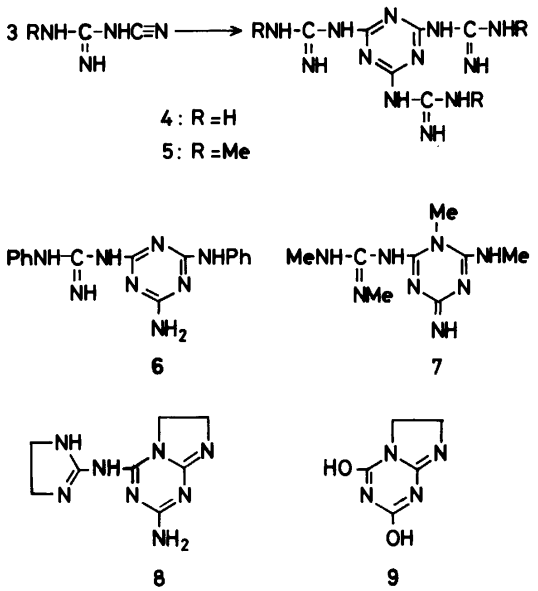

Experimental

2,4,6-Triguanidino-1,3,5-triazine (4). Hydrogen chloride (8.75 g, 0.24 mol) was introduced into a stirred solution of cyanoguanidine (16.81 g, 0.20 mol) in 155 ml of DMF at room temperature. The solution was stirred at 80 °C for 110 min and then evaporated under reduced pressure. 2-Propanol was added to the oily residue and the resulting precipitate was collected by filtration. The precipitate was dissolved in water. After removing the insoluble material, the solution was adjusted to pH 13.6 with an aqueous sodium hydroxide solution. Then, the precipitate, the free state of **4**, was filtered off and washed with water. The yield was 0.69 g (3%). After the filtrate was made acidic with 6 mol dm^{-3} of nitric acid, the precipitate, **4** nitrate (8.51 g, 29%), was filtered off. The filtrate was concentrated to yield **1** nitrate (6.12 g, 21%) and the nitrate of the mixture. The mixture was separated to **1** (0.54 g, 1%; insoluble to the aqueous ammonia solution) and amidinourea (2.28 g, 3%; insoluble to the acetic acid solution) as the picrates. The filtrate of 2-propanol solution was concentrated to yield

amidinourea (6.53 g, 10%) and guanidine (3.51 g, 6%) as the picrates.

In a similar manner, a cyanoguanidine–acetone adduct (hydrochloride)[4] used as a starting material gave **4** (42%) and **1** (8%) at 80 °C after 30 min, or gave **4** (40%) and **1** (1%) at room temperature after 5 d.

2,4,6-Tris(3-methylguanidino)-1,3,5-triazine (5). Hydrogen chloride (3.65 g, 0.1 mol) was introduced into a stirred solution of 1-methyl-3-cyanoguanidine[5] (9.81 g, 0.1 mol) in 70 ml of DMF below 10 °C. The solution was stirred at 80 °C for 3 h. After cooling, a precipitate was filtered off and washed with 2-butanone. The yield of **5** was 7.31 g, (52%). Recrystallization from a dilute hydrochloric acid provided pure **5** as the hydrochloride: mp 313 °C; Found: C, 25.39; H, 5.28; N, 39.39; Cl, 24.82%. Calcd for $C_9H_{18}N_{12}\cdot 3HCl\cdot H_2O$: C, 25.63; H, 5.50; N, 39.86; Cl, 25.22%. IR (KBr) 810 cm^{-1} (1,3,5-triazine ring). Recrystallization from a dilute nitric acid provided pure **5** as the nitrate: mp 265.5 °C (dec). Found: C, 21.63; H, 4.51, N. 42.25%. Calcd for $C_9H_{18}N_{12}\cdot 3HNO_3\cdot H_2O$; C, 21.56; H, 4.62; N, 41.91%. IR (KBr) 810 cm^{-1} (1,3,5-triazine ring).

2-Amino-4-anilino-6-(3-phenylguanidino)-1,3,5-triazine (6). Hydrogen chloride (18.60 g, 0.51 mol) was introduced into a stirred solution of 1-phenyl-3-cyanoguanidine[6] (80.09 g, 0.50 mol) in 386 ml of DMF at room temperature. The solution was stirred at 80 °C for 3 h, and then concentrated under reduced pressure to give *N*-(phenylamidino)urea as the picrate (76.58 g, 38%). After filtering off, the filtrate was extracted with water, and then the oily residue was dissolved in acetone. The acetone solution was evaporated to dryness and the residue was recrystallized from methanol to give 9.47 g (10%) of **6** as the hydrochloride.[3] The extracted solution was made alkaline with ammonia, and the resulting precipitate was recrystallized from a dilute nitric acid to give 11.29 g (11%) of **6** as the nitrate.[3]

1-Methyl-2-methylamino-4-imino-6-(2,3-dimethylguanidino)-1,4-dihydro-1,3,5-triazine (7). In a similar manner as for the preparation of **5**, **7** was obtained from 1,2-dimethyl-3-cyanoguanidine.[5] The yield was 41%. Recrystallization from water provided pure **7** as the hydrochloride: mp 245—246 °C; IR (KBr) 780 cm^{-1} (1,3,5-triazine ring). Found: C, 30.30; H, 7.00; N, 36.32; Cl, 11.90%. Calcd for $C_8H_{16}N_8\cdot HCl\cdot 3H_2O$: C, 30.53; H, 7.36; N, 35.60; Cl, 11.26%. MS Found: *m/z* 244. Calcd for $C_8H_{16}N_8$: M, 244.

2-Amino-4-(4,5-dihydro-1H-imidazol-2-ylamino)-6,7-dihydroimidazo[1,2-a][1,3,5]triazine (8). In a similar manner, **8** was obtained from 2-imidazolidinylidenecyanamide[7] in 64% yield. Recrystallization from 0.5 mol dm^{-3} of hydrochloric acid provided pure **8** as the hydrochloride: mp 337 °C. IR (KBr) 780 cm^{-1} (1,3,5-triazine ring). Found: C, 34.88; H, 5.35; N, 41.42; Cl, 13.11%. Calcd for $C_8H_{12}N_8\cdot HCl\cdot H_2O$: C, 34.98; H, 5.49; N, 40.79; Cl, 12.91%. MS Found: *m/z* 220. Calcd for $C_8H_{12}N_8$: M, 220.

Acid Hydrolysis. By the same procedure described in our previous paper,[8] **5** was refluxed in 6 mol dm^{-3} of hydrochloric acid for 133 h and gave unreacted **5** (6%), cyanuric acid (69%), methylguanidine as the picrate (58%). Ammonia was detected in the solution.

In a similar manner, **7** was refluxed for 10 h and gave 1-methyl-1,3,5-triazine-2,4,6(1*H*,3*H*,5*H*)-trione[9] (15%. mp 285—286 °C; MS *m/z* 143), 1,3-dimethylguanidine (96%) and methylamine (4%). Ammonia was also detected in the solution.

In a similar manner, **8** was refluxed for 48 h and gave 4,5-dihydro-1*H*-imidazol-2-amine[10] (77%) and **9**[11,12] (70%). Ammonia was also detected in the solution. By a Hinsberg test, **9** was confirmed to be the tertiary amine. Recrystallization from a dilute hydrochloric acid provided pure **9** as the hydrochloride: mp 302 °C (dec). (Found: C, 28.32; H, 4.34; N, 27.07; Cl, 16.63%. **9**: MS *m/z* 154).

References

1) S. Bando, E. Ichikawa, and K. Odo, *Yuki Gosei Kagaku Kyokai Shi*, **28**, 521 (1970).

2) S. Bando, E. Ichikawa, and K. Odo, *Yuki Gosei Kagaku Kyokai Shi*, **31**, 584 (1973).

3) S. Bando, E. Ichikawa, and K. Odo, *Yuki Gosei Kagaku Kyokai Shi*, **34**, 566 (1976).

4) M. Yamada, E. Ichikawa, and K. Odo, *Yuki Gosei Kagaku Kyokai Shi*, **21**, 946 (1963).

5) T. Suyama and K. Odo, *Yuki Gosei Kagaku Kyokai Shi*, **29**, 65 (1971).

6) K. Odo, E. Ichikawa, K. Takanoyama, T. Hirae, and T. Otsuka, *Yuki Gosei Kagaku Kyokai Shi*, **30**, 167 (1972).

7) C. M. Baltzer, C. G. McCartz, *J. Org. Chem.*, **38**, 155 (1973).

8) K. Iio and E. Ichikawa, *Bull. Chem. Soc. Jpn.*, **57**, 2009 (1984).

9) E. Fisher and F. Frank, *Chem. Ber.*, **30**, 2604, (1897); W. J. Close, *J. Am. Chem. Soc.*, **75**, 3617 (1953).

10) M. P. Pierron, *Ann. Chim. (Paris)*, [9], **11**, 361 (1919).

11) F. C. Schaefer, *J. Am. Chem. Soc.*, **77**, 5922 (1955).

12) R. Hinkens, R. Promel, and R. H. Martin, *Helv. Chim. Acta*, **44**, 299 (1961).

A Through Space/Bond Interaction Analysis on the Shape of Band Structure of Polynitrilomethylidyne

Yuriko Aoki, Akira Imamura,* and Hiroyuki Teramae
Department of Chemistry, Faculty of Science, Hiroshima University, Hiroshima 730
Department of Hydrocarbon Chemistry, Faculty of Engineering, Kyoto University, Kyoto 606
(Received February 1, 1985)

The concept of the through space/bond interaction presented by Hoffmann *et al.* was extended to study electronic states of polymers. The band shape of lone pair orbitals was investigated by truncating converged Fock matrices and overlap integrals except for the terms corresponding to the through bond and particular through space interactions. This method was used by applying the *ab initio* tight-binding crystal orbital method to three isomers of one-dimensional polynitrilomethylidyne, for which the dependences of the lone pair orbital energy on the wave number vector differ significantly from one another. The band shape of the lone pair orbital is related intimately to the interaction with H atoms. The effect of each through space interaction on the band shape of the lone pair orbital may be reasonably interpreted in terms of the symmetry of crystal orbitals. This method seems expedient for analyzing qualitatively lone pair bands of various polymers at the *ab initio* level.

The concept of the through space/bond interaction introduced by Hoffmann *et al.* in 1968 has made a great contribution to the evaluation of the size of interaction between lone pair orbitals.[1] The through bond interaction can be quantitatively analyzed in more detail by using localized molecular orbitals transformed from canonical molecular orbitals. In the present article, an application of this through space/bond concept to one-dimensional polymer systems by using atomic orbitals was attempted in expectation of characterizing electronic states of various polymers.

In recent years a number of theoretical studies on conjugated organic polymers have been reported. We chose polynitrilomethylidyne, which possesses conjugated carbon–nitrogen double bonds, as a model polymer system for test calculation on the through space/bond interaction. This polymer has recently been synthesized, and it was found that the conductivity σ_{300K} was up to $10^{-10}\ \Omega^{-1}\mathrm{cm}^{-1}$ in spite of the possession of an even number of electrons in the unit cell.[2,3] For this reason polynitrilomethylidyne has been the object of several theoretical studies. Polynitrilomethylidyne is composed of trans-zigzag, trans-cisoid, and cis-transoid forms as shown in Fig. 1. For the trans-zigzag form, Karpfen[4,5] carried out an optimization of the geometry at the Hartree-Fock *ab initio* double zeta level by assuming that the unit cell of an infinite polymer consists of a single HCN molecule. Furthermore, the force constant, band structure, and density of state were investigated in comparison with those for polyacetylene in the literature.[6] Kertesz and co-workers[7,8] applied the restricted and unrestricted Hartree-Fock methods to studying the alternating and nonalternating structures of the trans-zigzag $(-HCN-)_x$ linear chains. Bredas *et al.*[9,10] calculated the ionization potential, band width, and band gap for the trans-zigzag polynitrilomethylidyne by using the valence effective Hamiltonian technique. For the hydrogen-bonded hydrogen cyanide polymer chain, *ab initio* studies based on crystallographic data[11,12] were previously reported in comparison with HCN molecules or their aggregates.[13,14] On the other hand, the trans-cisoid and cis-transoid forms have only rarely been studied in detail from the theoretical point of view.

In this study, *ab initio* calculations were performed on the three isomers of polynitrilomethylidyne, and by using the matrix elements obtained the through space/bond method was applied to analyzing the lone pair bands. The purpose of this study was to investigate the applicability of this method by examining the influence of the interaction between atomic orbitals on the shape of lone pair bands.

Method

The *ab initio* crystal orbital method used in this study is based on the general SCF tight-binding LCAO formalism[15] corresponding essentially to Roothaan's Hartree-Fock equation for molecules,[16] taking into account all neighbor interactions and overlap integrals. The outline of this theory is described below. A delocalized wave function of a single electron in the periodic potential of a one-dimensional crystal is represented as a linear combination of Bloch basis orbitals $\phi_i^k(r)$, which are written as periodic combinations of n atomic orbitals χ_r:

$$\phi_i^k(r_1) = (2N+1)^{-1/2}\sum_{m=-N}^{+N}\sum_{r=1}^{n}\exp(ikR_m)C_{ir}(k)\chi_r(r_1-R_m), \quad (1)$$

where k denotes a wave number vector in the first Brillouin zone, i an energy band, and i the imaginary number or the square root of -1. The term $\chi_r(r_1-R_m)$ stands for an atomic orbital localized in the m-th cell at $R_m(m=0, \pm1, \pm2, \cdots\cdots, \pm N)$, and $2N+1$ is the number of elementary cells. Applying the well known non-relativistic Hamiltonian

$$H = \sum_{\mu}\left\{-\frac{1}{2}\Delta_\mu + V(\mu)\right\} + \sum_{\mu>\nu}\frac{1}{r_{\mu\nu}} \quad (2)$$

to the antisymmetrized product of the one-electronic wave function Eq. 1 and using the orthonormality condition

$$\langle\phi_i^k(r_1)|\phi_j^k(r_1)\rangle = \delta_{ij}, \quad (3)$$

we obtain the total electronic energy as

$$E = 2\sum_{i}^{\text{occ}} H_{ii} + \sum_{i}^{\text{occ}}\sum_{j}^{\text{occ}} (2J_{ij} - K_{ij}) \tag{4}$$

where

$$H_{ij} = \int \phi_i(1)\left\{-\frac{1}{2}\Delta_1 + V(1)\right\}\phi_j(1)\,d\tau_1,$$

$$J_{ij} = \iint \phi_i(1)\,\phi_j(2)\frac{1}{r_{ij}}\phi_i(1)\phi_j(2)\,d\tau_1 d\tau_2,$$

$$K_{ij} = \iint \phi_i(1)\,\phi_j(2)\frac{1}{r_{ij}}\phi_j(1)\phi_i(2)\,d\tau_1 d\tau_2,$$

Substituting the crystal orbital Eq. 1 into Eq. 3 and using the periodic boundary condition, we obtain the corresponding total electronic energy per unit cell as

$$E = 2\sum_{i}^{\text{occ}}\sum_{k=0}^{2\pi}\sum_{r}\sum_{s} C_{ir}^{*}(k)C_{is}(k)\sum_{m=-M}^{+M}\exp(\mathbf{i}kR_m)I_{rs}^{0m}(R_m)$$
$$+ \sum_{i}^{\text{occ}}\sum_{k=0}^{2\pi}\sum_{m}\sum_{h}\sum_{l}\sum_{r}\sum_{s}\sum_{t}\sum_{u} P_{tu}^{hl}C_{ir}^{*}(k)C_{is}(k)\exp(\mathbf{i}kR_m)$$
$$\times\left\{2\left\langle {}^{0m}_{rs}\middle|{}^{hl}_{tu}\right\rangle - \left\langle {}^{0h}_{rt}\middle|{}^{ml}_{su}\right\rangle\right\}, \tag{5}$$

where M denotes the number of cells included in the summation, and

$$I_{rs}^{0m}(R_m) = \langle\chi_r(r_1)|h(1)|\chi_s(r_1-R_m)\rangle,$$

$$P_{tu}^{hl} = (2N+1)^{-1}\sum_{k'=0}^{2\pi}\sum_{j=1}^{\text{occ}}\exp\{\mathbf{i}k'(R_l-R_h)\}C_{jt}^{*}(k')C_{ju}(k'),$$

$$\left\langle {}^{0\,m}_{r\,s}\middle|{}^{h\,l}_{t\,u}\right\rangle = \langle\chi_r(r_1)\chi_s(r_1-R_m)|r_{12}^{-1}|\chi_t(r_2-R_h)\chi_u(r_2-R_l)\rangle,$$

These last three equations correspond to the one-electron core integral, the density matrix, and the two-electron integral, respectively. Symbols r, s, t, and u denote the atomic orbitals in the elementary cells characterized by symbols 0, m, h, and l, respectively. Putting the overlap integral between the r-th atomic orbital in the central cell and the s-th atomic orbital in the m-th cell as

$$S_{rs}^{0m}(R_m) = \langle\chi_r(r_1)|\chi_s(r_1-R_m)\rangle \tag{6}$$

and applying the Ritz variation method to the Eq. 5, we can obtain the eigenvalue problem

$$\sum_{s}\sum_{m=-M}^{+M}\exp(\mathbf{i}kR_m)[F_{rs}^{0m}(R_m) - S_{rs}^{0m}(R_m)E_t(k)]C_{is}(k) = 0, \tag{7}$$
$$(k=0,\ \cdots,\ 2\pi)$$

where F_{rs}^{0m} is the Fock matrix element between the r-th atomic orbital in the central segment and the s-th atomic orbital in the m-th cell and is given by

$$F_{rs}^{0m}(R_m) = I_{rs}^{0m}(R_m)$$
$$+ \sum_{h}\sum_{l}\sum_{t}\sum_{u} P_{tu}^{hl}\left\{2\left\langle {}^{0\,m}_{r\,s}\middle|{}^{h\,l}_{t\,u}\right\rangle - \left\langle {}^{0h}_{rt}\middle|{}^{m\,l}_{su}\right\rangle\right\}. \tag{8}$$

If the expression for the Fock matrix element between Bloch orbitals $F_{rs}(k)$ and that for the corresponding overlap integral $S_{rs}(k)$ are defined as

$$F_{rs}(k) = \sum_{m=-M}^{+M}\exp(\mathbf{i}kR_m)F_{rs}^{0m}(R_m), \tag{9}$$

$$S_{rs}(k) = \sum_{m=-M}^{+M}\exp(\mathbf{i}kR_m)S_{rs}^{0m}(R_m), \tag{10}$$

then the eigenvalue problem for a given value of k in the first Brillouin zone is obtained as

$$\sum_{s}F_{rs}(k)C_{is}(k) = \sum_{s}S_{rs}(k)C_{is}(k)E_i(k). \tag{11}$$

As a result the secular equation to be solved is given by

$$|F_{rs}(k) - S_{rs}(k)E_i(k)| = 0. \tag{12}$$

Based on this theory, the Polymer Gaussian 74 program has been extensively developed by Suhai[6] within the Hartree Fock scheme. *Ab initio* calculations were performed on three typical isomers of the polynitrilomethylidyne one-dimensional model polymer by using this program with an STO-3G basis set. The k-points in half the Brillouin zone were used, and the convergence criterion of 10^{-6} for the difference of density matrix elements was adopted. Twice the magnitude of the lattice vector was taken as a translational vector corresponding to the unit cell shown in Fig. 1, and the contribution up to the seventh neighbor interaction in core resonance integrals and two- electron integrals was taken into consideration. The influence of lattice sum truncation on computed total energy and energy bands for the three forms of polynitrilomethylidyne were investigated. The geometries used here are the same as those described in Refs. 17 and 18 for the CNDO/2 method.

The natural development of this study was the introduction of the through bond/space concept into polymer systems. Analysis of band shapes must be possible by neglecting Fock matrix elements and overlap integrals between particular

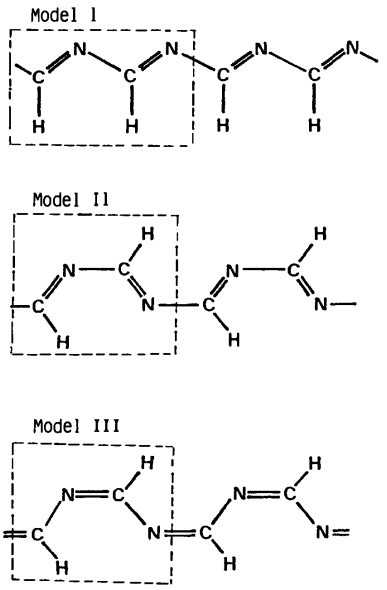

Fig. 1. Structures of the isomers of polynitrilomethylidyne: trans-zigzag (Model I), trans-cisoid (Model II) and cis-transoid (Model-III). The unit cells are surrounded with broken lines.

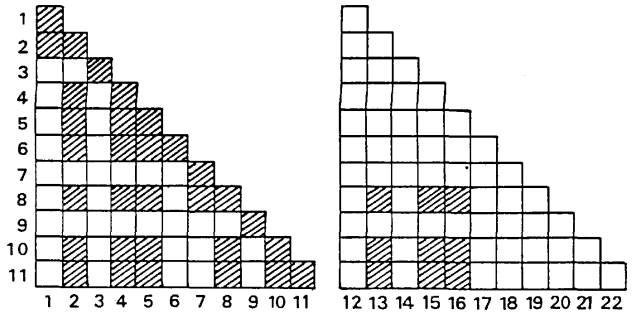

Fig. 2. Through bond interaction elements: (a) terms within a single HCN unit. (b) terms between nearest neighboring two single HCN units. 1—5: 1s, 2s, $2p_x$, $2p_y$, $2p_z$ orbitals on C atom; 6: 1s orbital on H atom; 7—11: 1s, 2s, $2p_x$, $2p_y$, $2p_z$ orbitals on N atom; 12—16: 1s, 2s, $2p_x$, $2p_y$, $2p_z$ orbitals on the neighboring C atom; 17: 1s orbital on the neighboring H atom; 18—22: 1s, 2s, $2p_x$, $2p_y$, $2p_z$ orbitals on the neighboring N atom. This polymer is on the y—z plane.

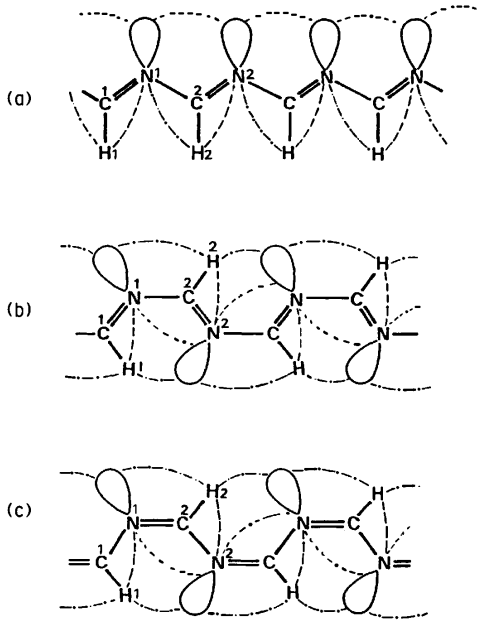

Fig. 3. The main through space components used in this analysis.
····· N1-N2 interaction, ------ N1-H1 and N2-H2 interaction, -·-·-· N1-H2 and N2-H1 interaction.
(a) Model I, (b) Model II, (c) Model III.

atomic orbitals. Then all Fock matrix elements and overlap integrals were classified into two kinds of interaction patterns. One type is those terms relating to the through bond interactions which include the Fock matrices given by Eq. 9 and overlap integrals given by Eq. 10 for diagonal elements and those between the 1s and 2s orbitals belonging to the same atom and between valence orbitals belonging to the nearest neighboring atoms. Here, valence orbitals mean the 2s, $2p_x$, $2p_y$, and $2p_z$ orbitals on the C and N atoms and the 1s orbitals on the H atoms. The matrix elements of the through bond interaction in the secular equation Eq. 12 for polynitrilomethylidyne are shown in Fig. 2(a) for the terms within a single HCN unit and in Fig. 2(b) for the terms between two single nearest neighbor HCN units. These elements were included for all cases of analyses. The other type is the through space interactions which include the terms except those for the through bond interaction, that is, those between particular valence orbitals belonging to different atoms. In this study three kinds of through space interactions shown in Fig. 3 were selected for the analysis of the lone pair bands. The procedure for the actual calculation was as follows:

1. The Fock matrix elements and the overlap integrals converged by usual *ab initio* calculations were stored.
2. Of the elements obtained in step 1, the through bond elements shown in Figs. 2(a) and (b), and only significant elements in the through space interactions were explicitly taken into account; the other elements were left out.
3. By using the new matrix elements retained in step 2, the eigenvalue problem given by Eq. 11 for each wave number vector was solved only once without further iterations.

The Gaussian 74 program was modified for the above-mentioned procedure. The relationship between band shapes and crystal orbitals for each through space interaction can be investigated by using the eigenvectors and energies obtained in step 3. The change in energy bands caused by increasing through space components between selected pairs of atomic orbitals, revealed a trend quantitatively consistent to the full interaction. In this process, the most significant through space interaction was found by comparing changes of band shapes.

Results and Discussion

The finite neighbor approximation is a difficult problem in the evaluation of multi-center integrals because even Fock matrix elements obtained with wrong cutoff conditions give artificially stable energy states. Suhai has reported that total energies are strongly dependent upon the number of neighbors included, and that the sphere of elementary cells within which Fock matrix elements have to be calculated is determined only by the magnitude of exchange integrals. His study for polyacetylene demonstrated that

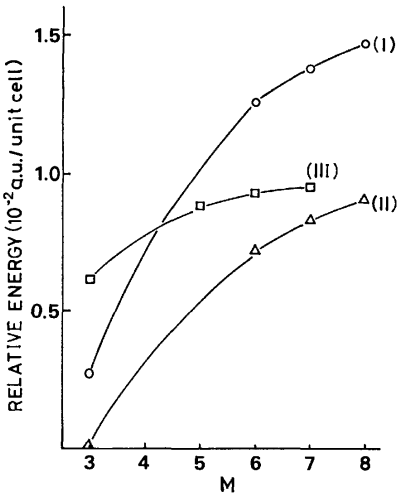

Fig. 4. Relative total energy per $\{HCN\}_2$ unit as function of the number (M) of interacting $\{HCN\}_2$ neighbors in three models of polynitrilomethylidyne Model I, Model II, and Model III.

limiting converged energies were obtained finally by taking into consideration up to the 28th neighboring C_2H_2 unit. In order to obtain some insight into convergency properties of the three forms of polynitrilomethylidyne, *ab initio* calculations were carried out for each case which includes the lattice summation up to each of the third to eighth neighbor interactions. Figure 4 shows that the third neighbor approximation is insufficient to obtain converged energy values. The total energy difference converges to a certain extent with up to eight neighbor lattice summations, but the effect of lattice truncation does not completely disappear. We did not determine for polynitrilomethylidyne how far interactions in the two-electron integrals should be taken into consideration to reach the correct limiting value, because it was not the purpose of this study.

The band structures and densities of state obtained by

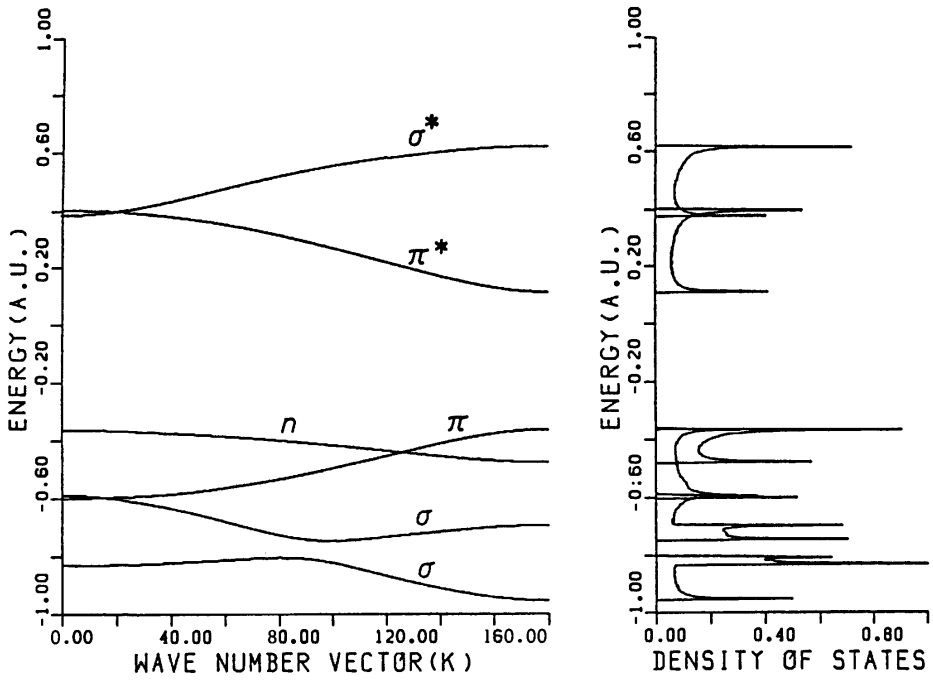

Fig. 5. Band structure and density of states of trans-zigzag polynitrilomethylidyne.

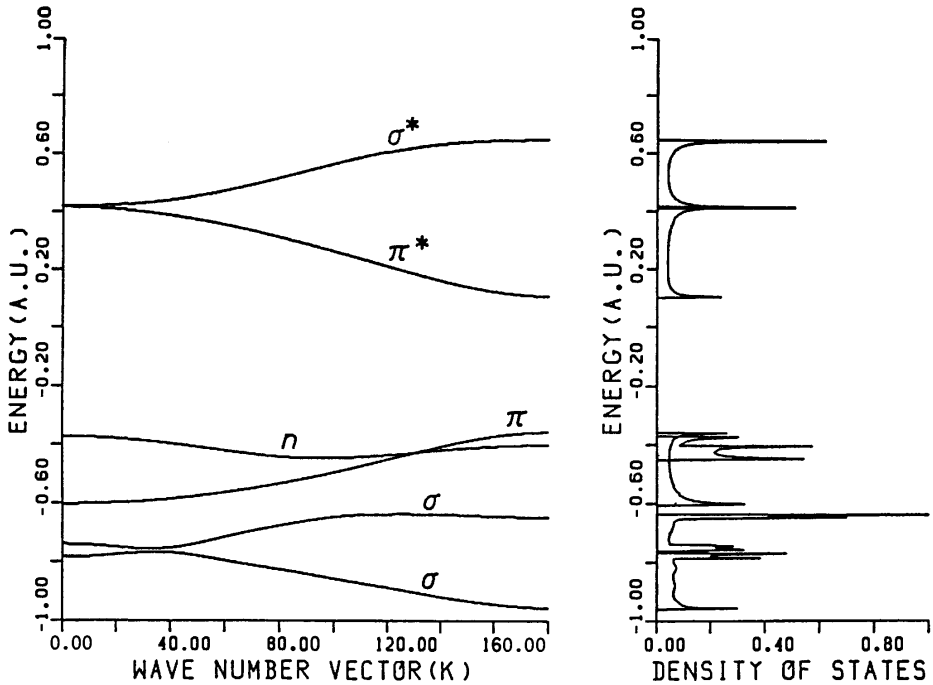

Fig. 6. Band structure and density of states of trans-cisoid polynitrilomethylidyne.

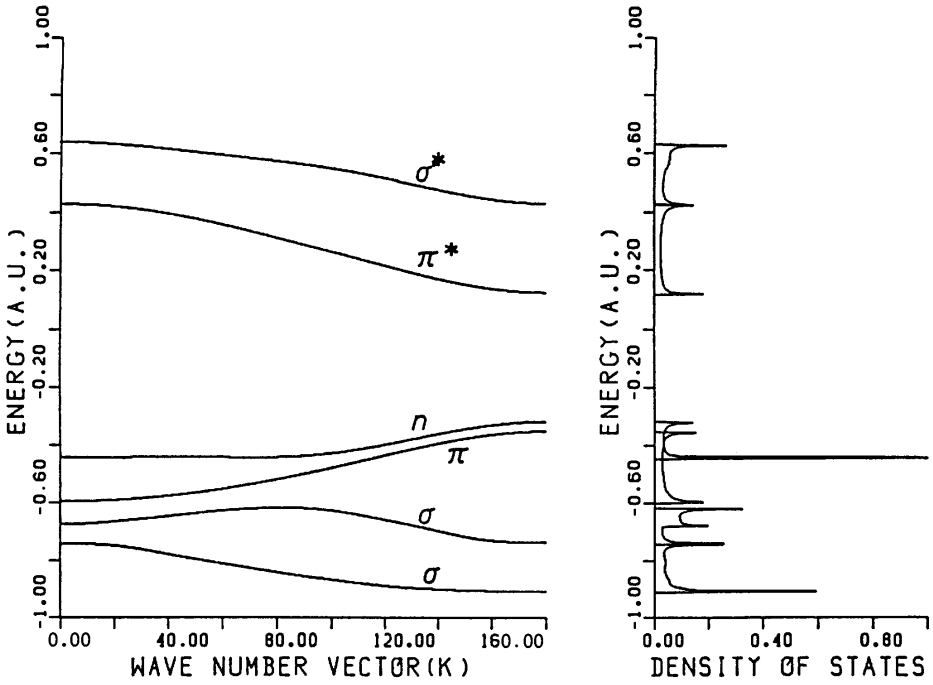

Fig. 7. Band structure and density of states of cis-transoid polynitrilomethylidyne.

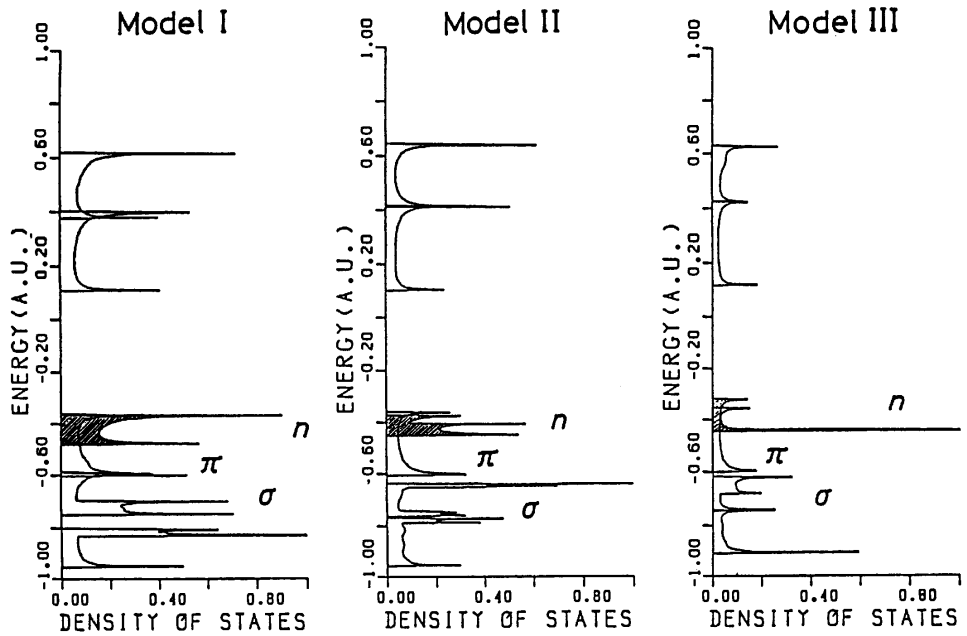

Fig. 8. Density of states for three models of polynitrilomethylidyne.

including up to the seventh neighbors are shown in Figs. 5—7 for the three forms of polynitrilomethylidyne. These polymers are insulators because the band gaps between the valence and conduction bands are as much as 12.0—12.5 eV. The energy bands obtained by these *ab initio* calculations with the STO-3G basis set indicate that the bands are correspondingly similar for the three isomers, but that the lone pair bands on the N atoms differ from one another significantly. In particular, it is noteworthy that there are three peaks in the density of state for the lone pair band of the trans-cisoid form in contrast to the other two forms, as can be seen in Fig. 8. The magnitudes of the energies for all the wave number vectors at the seventh neighbor level are larger for the three forms by about 0.01 au than those at the third neighbor level, but no effect on the band shape is caused by the increase in number of included neighbors. Therefore, the effect of the more distant neighbors on the interaction pattern between orbitals may be neglected without leading to serious errors. So the lone pair bands of the three forms were analyzed by the through space/bond method based on the matrix

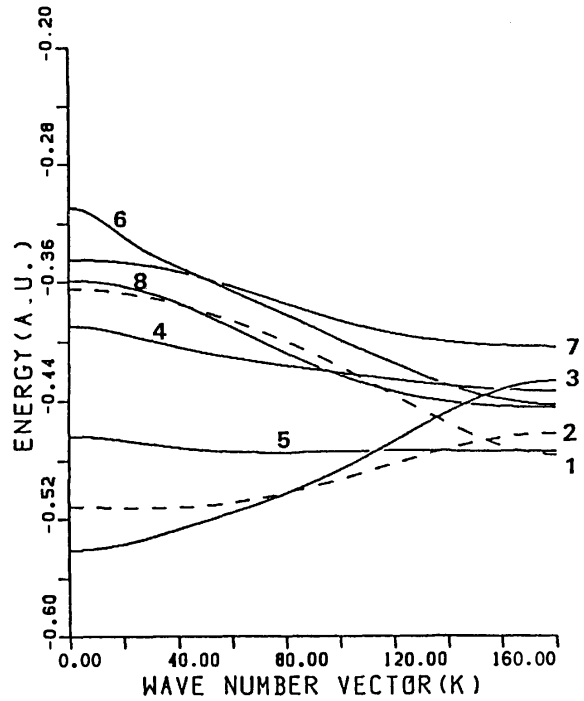

Fig. 9. The change in energy band of the lone pair orbital by analysis of the through space/bond method for Model I. 1. Full interaction, 2. Through bond interaction. The interactions 3—8 are shown added to 2. 3. N1-N2 interaction, 4. N1-H1 and N2-H2 interaction, 5. N1-H2 and N2-H1 interaction, 6. 4+5, 7. 3+4+5 and C(valence orbitals)-N(1s orbital).

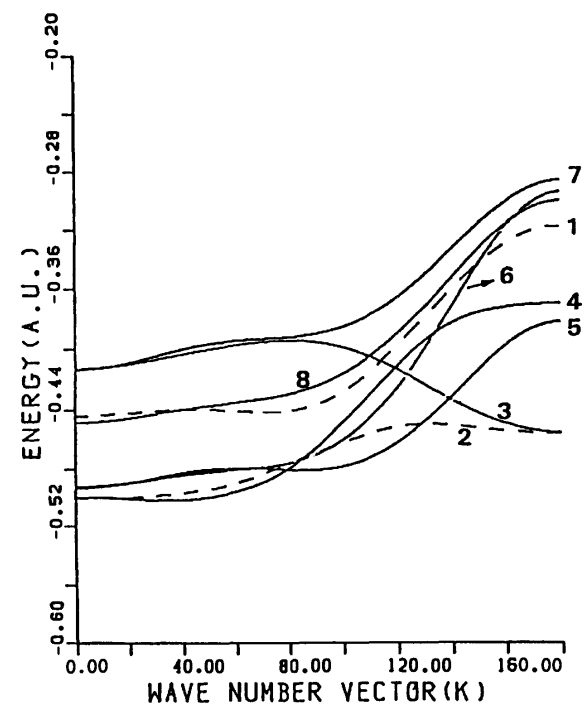

Fig. 11. The change in energy band of the lone pair orbital by analysis of the through space/bond method for Model III. The notations used in this figure are the same as those in Fig. 9.

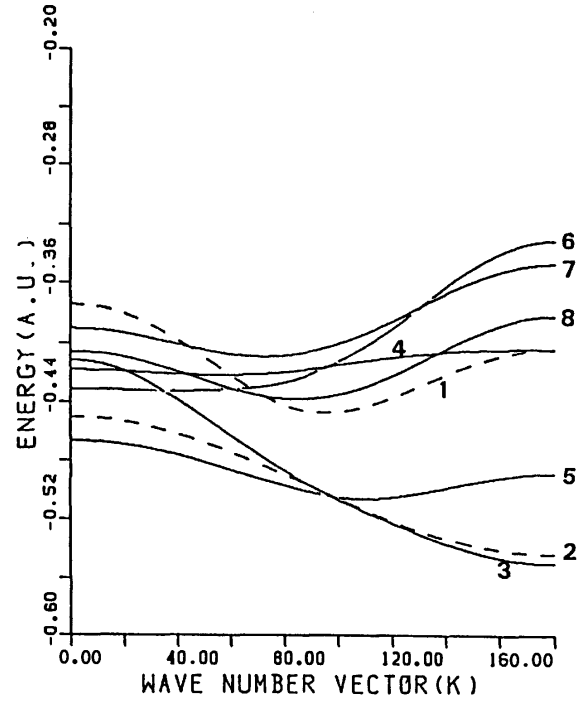

Fig. 10. The change in energy band of the lone pair orbital by analysis of the through space/bond method for Model II. The notations used in this figure are the same as those in Fig. 9.

elements obtained by including up to the third neighbors, in order to clarify which interaction between the atomic orbitals is most important.

The lone pair bands obtained by this through space/bond analysis are shown in Figs. 9—11 for trans-zigzag, trans-cisoid, and cis-transoid forms, respectively. The broken curve 1 refers to the full interaction including all the interactions between atomic orbitals, and the broken curve 2 to the pure through bond interaction including only the matrix elements between valence orbitals on two directly bonded atoms as shown in Fig. 2. We chose the six interactions denoted by 3—8 in Figs. 9—11 as the through space interactions to be added to the pure through bond interaction. In interactions 3—7 only the interactions between valence orbitals are included. The effect of each through space interaction on the lone pair band is discussed below for the three forms of polynitrilomethylidyne in terms of the symmetry or the phase of crystal orbitals. In crystal orbitals the range k=0°—90° belongs to the symmetric band within a unit cell and the range k=90°—180° to the antisymmetric band. The crystal orbitals at k=0° and 180° are schematically shown in Fig. 12. Furthermore, the crystal orbitals at k=0° and 180° are symmetric with respect to those of the nearest neighboring unit cells. Therefore, the crystal orbitals at k=0° are symmetric within a unit cell and symmetric to the nearest neighboring unit cells, whereas the crystal orbitals at k=180° are antisymmetric within a unit cell and symmetric to the nearest neighboring unit cells.

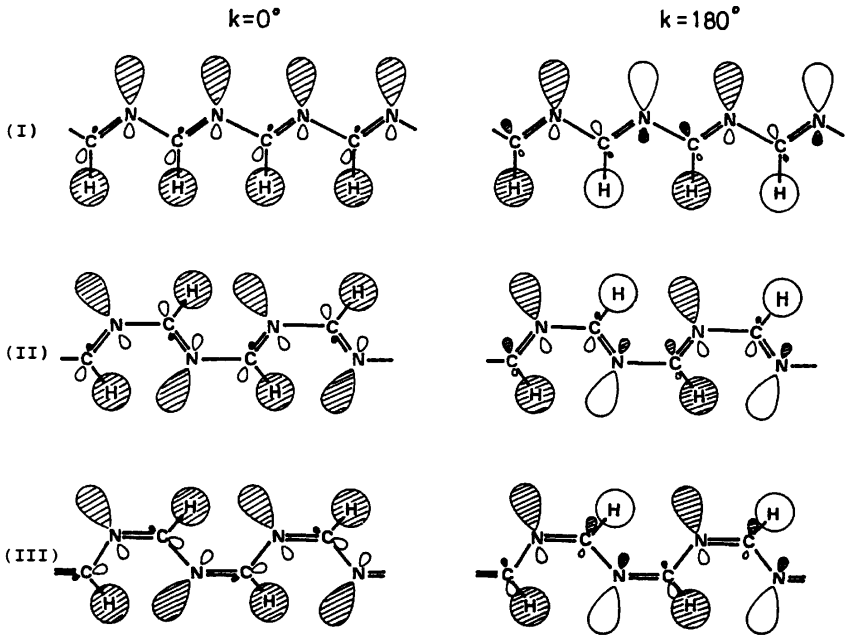

Fig. 12. Schematic representation of the magnitude of the coefficients of the atomic orbitals in the crystal orbitals in the through bond interaction for the three models of polynitrilomethylidine. Shaded areas represent positive lobes; unshaded negative.

Model I. When interaction 3 between orbitals on the neighboring N atoms (see Fig. 3) was added to the through bond interaction, the energy of the MO was lowered by 0.03 au at $k=0°$ and raised by 0.04 au at $k=180°$. As shown in the schematic orbitals (Fig. 12(I)), the lone pair orbitals belonging to N1 and N2 are symmetric at $k=0°$ and antisymmetric at $k=180°$ within a unit cell and symmetric with respect to the nearest neighboring unit cells at both the k-points; that is, all the overlap integrals between the nearest neighboring lone pair orbitals are positive at $k=0°$ and negative at $k=180°$. Therefore, it should be expected that the MO is stabilized at $k=0°$ and destabilized at $k=180°$ due to interaction 3, since the positive overlap implies bonding and the negative one anti-bonding. By interaction 4 between the lone pair orbital on N1 and the 1s orbital on H1 as well as on N2 and H2 (see Figs. 3 and 12), the MO is raised by 0.12 au in energy at $k=0°$ and by 0.03 au at $k=180°$ relative to the pure through bond interaction 2. It seems that this change relates to the antibonding properties between the orbitals on N1 and H1 or N2 and H2, because the enlarged lone pair orbital on the N atom and the 1s orbital on the H atom are out-of-phase within a single HCN molecule at all the k-points. By interaction 5 between the lone pair orbital on N1 and the 1s orbital on H2 or on N2 and H1, the MO is raised by 0.05 au in energy at $k=0°$ and lowered by 0.015 au at $k=180°$. This can be considered to be caused by the negative overlap between the lone pair orbital on N1 and the 1s orbital on H2 at $k=0°$ and the positive overlap at $k=180°$ in all the unit cells. The greater destabilization in interaction 4 than that in interaction 5 at $k=0°$ may be due to the shorter distance in interaction 4 between the N and H atoms. By interaction 6 which consists of interactions 4 and 5, the band shape is made roughly similar to that for the full interaction 1. The additivity rule holds approximately for the through bond interaction because the energy gain in interaction 6 relative to the through bond interaction 2 corresponds nearly to the sum of the increases from interactions 4 and 5 at all the k-points. By interaction 7 which is equal to the interaction 6 having the interaction between the lone pair orbitals on the neighboring N atoms added, the MO is lowered by 0.03 au in energy at $k=0°$ and raised by 0.04 au at $k=180°$. Interaction 6 is to interaction 7 what the pure through bond interaction 2 is to interaction 3. Finally by interaction 8 which is equal to interaction 7 having the interaction between the 1s orbital on the N atom and the valence orbitals (2s, $2p_x$, $2p_y$, and $2p_z$) on the C atom added, the band shape is in approximate agreement with the full interaction 1 except near $k=180°$. It was found that the effect of the interaction between the 1s orbital of N and the valence orbitals of C should not be neglected since the lone pair band is stabilized to some extent by this interaction. In conclusion, it was ascertained that interaction 6 between the lone pair orbital and the H atoms belonging to both neighboring C atoms dominates the through space interaction.

Model II. In this structure which is planar and possesses a screw axis symmetry in a unit cell, the interaction between the lone pair orbital and the 1s orbital on the H atom would be expected to be the main through space interaction, judging from the positions

of the atoms around the lone pair orbital. Similar reasoning as has been developed for the trans-zigzag form can be applied to the trans-cisoid form. By interaction 3, the MO is raised by 0.04 au in energy at $k=0°$ and is lowered by 0.01 au at $k=180°$ relative to the through bond interaction 2. As shown in the schematic orbitals (Fig. 12(II)), the overlap between the neighboring lone pair orbitals possesses antibonding properties at $k=0°$ and bonding properties at $k=180°$ over all the unit cells, since the enlarged lone pair orbitals within a unit cell are out-of-phase at $k=0°$—90° and in-phase at $k=90°$—180°. This is probably the reason for the destabilization in energy at $k=0°$ and the stabilization at $k=180°$. By interaction 4 (see Figs. 3 and 10), the MO is raised by 0.03 au in energy at $k=0°$ and by 0.14 au energy at $k=180°$. As in the trans-zigzag form, this behavior is considered to relate to the antibonding properties between the lone pair orbital on N1 and the 1 s orbital on H1 or on N2 and H2, because the lone pair orbital and the 1 s orbital on the H atom are out-of-phase within a single HCN molecule. By interaction 5, the energy level is lowered by 0.1 or 0.2 au in energy at $k=0°$ and raised by 0.05 au at $k=180°$. This may be due to the positive overlap at $k=0°$ and the negative overlap at $k=180°$ between the 1 s orbital on H1 and the lone pair orbital on N2, as can be seen from the phase of the MO. Because of this through space interaction, the band shape becomes closely similar to that for the full interaction 1, aside from the values of energy. Interaction 6, equal to the interaction 5 with interaction 4 added, has the same effect as the through bond interaction 2 has on interaction 4, that is, the MO is raised by 0.04 au in energy at $k=0°$ and by 0.16 au at $k=180°$ By interaction 7, for which interaction 3 between the nearest neighboring lone pair orbitals has been added to interaction 6, the MO is raised by 0.04 au in energy at $k=0°$ and lowered by 0.02 au at $k=180°$. As in the trans-zigzag form, the additivity rule approximately holds for interactions 3 and 6 in the through bond interaction 7. By interaction 8, the band shape is allowed to have a more consistent trend toward that for the full interaction 1. It was found that the 1 s orbital on N has a considerable contribution to the stabilization of the lone pair band in a similar manner as it has in the trans-zigzag form. The result that interaction 5 is the most important through space interaction in determining the band shape of the lone pair orbital in this trans-cisoid form, may be expected from the structure of the polymer.

Model III. By interaction 3, the energy level relative to that for interaction 2 is raised by as much as 0.09 au at $k=0°$, in contrast with little change at $k=180°$. As shown in the schematic orbitals (Fig. 12(III)), this behavior can be considered to be caused by the larger magnitude of the negative overlap at $k=0°$ than that of the positive overlap at $k=180°$ between the nearest neighboring lone pair orbitals. Otherwise, considering the shape of the wave function obtained, there may be a possibility that the difference in shape between the crystal orbitals on the C atoms is related to this behavior through a second order effect arising from this through space perturbation. By interaction 4, the MO is raised by 0.09 au at $k=180°$ due to the expected large negative overlap (see Figs. 3 and 12). On the other hand, no effect can be seen at $k=0°$, in contrast with the case of the trans-cisoid form. By interaction 5, the MO is raised by 0.01 au at $k=0°$ and by 0.075 au at $k=180°$. The destabilization at $k=180°$ can be considered to be caused by the large negative overlap, but this explanation seems inapplicable at $k=0°$. The band shape at all the k-points closely resembles that for the full interaction as with the trans-cisoid form, aside from the magnitude of energy. By interaction 6, which is equal to interaction 5 having interaction 4 added, the MO is raised by 0.09 au at $k=180°$ but not changed at $k=0°$. The additivity rule holds almost exactly since the energy gain in interaction 6 over the through bond interaction 2 corresponds to the sum of those in interactions 4 and 5 at all the k-points. By interaction 7, the MO is raised by 0.08 au at $k=0°$ and 0.01 au at $k=180°$ relative to that for interaction 6, and the additivity rule holds approximately. By interaction 8, the band shape is made still more similar to that for the full interaction as in models I and II. The result is that interaction 5 is the most important through space interaction as in the case of the trans-cisoid form. On the other hand, the energy level near $k=0°$ is hardly affected by the through space interaction between the lone pair orbitals and the 1 s orbitals on the H atoms, in contrast with the case of the trans-cisoid form. The differences between the trans-cisoid and cis-transoid forms with respect to the k-dependence of the lone pair band due to each through space interaction may result from the difference in the second order contribution of the through space perturbation. With respect to this point, more quantitative analysis is required for more detailed comparison.

Summary of the Results for Models I, II, and III. Although k-dependences of energy levels vary from model to model, they can reasonably be interpreted on the basis of the schematic orbitals shown in Fig. 12. For interaction 3, model I leads to a dependence different from those given by models II and III, in conformity with their differences in molecular structure. Of the various interactions adopted, the most important one for the determination of the curve shape is interaction 6 (composed of interactions 5 and 6) for model I and interaction 5 for models II and III. This consequence is in accord with the molecular structures of models I, II, and III. For all models I—III, interaction 8 gives curve shapes similar to those of the full interaction; that is, the interaction between the 1s orbital on the N atom and the valence orbitals on the C atom lowers the energy levels at all points of k, leading to the similar shapes. Finally, it should also be pointed out that the addi-

tivity rule for these interactions was found to hold approximately for all the three models.

Conclusion

In this paper we have developed a method for applying the through space/bond interaction to polymer systems at the *ab initio* level. As a result of applying this method to three isomers of polynitrilomethylidyne, it has been found that the interaction between the lone pair orbital and the H atoms bonded to both the neighboring C atoms governs the band shape of the lone pair orbital for the trans-zigzag form, and that the interaction between the lone pair orbital and the opposite H atoms belonging to the neighboring unit cell is most important for the trans-cisoid and cis-transoid forms. It is essentially desirable that energies of the through space interaction between pairs of localized crystal orbitals should be evaluated quantitatively. Therefore, this paper involves some obscurity in the definition of the through bond interaction because this analysis is based on atomic orbitals. However, qualitatively reasonable results on the relationship between the inter-orbital interaction pattern and the band shape have been obtained in spite of the omission of the troublesome transformation from atomic to localized orbitals. The results presented here have proved this method to be useful with the advantage of simplicity and convenience for rough estimation of the interaction between orbitals for various polymers possessing lone pair orbitals.

This work was supported in part by a Grant-in-Aid for Scientific Research from the Ministry of Education, Science and Culture. The numerical calculations were performed on the HITAC M-200H computer systems at the Information Center of Hiroshima University and the Computer Center of the Institute for Molecular Science. The authors are grateful to Dr. D. Munch for critically reading and correcting the manuscript for this paper.

References

1) R. Hoffmann, A. Imamura, and W. J. Hehre, *J. Am. Chem. Soc.*, **90**, 1499 (1968).
2) D. Wohrle, *Tetrahedron Lett.*, **22**, 1969 (1971).
3) D. Wohrle, *Makromol. Chem.*, **175**, 1751 (1974).
4) A. Karpfen, *Chem. Phys. Lett.*, **64**, 299 (1979).
5) A. Karpfen, "Lecture notes in physics series, No. 113. Recent advances in the quantum theory of polymers," ed by J. M. Andre, J. L. Bredas, J. Delhalle, J. Ladik, G. Leroy, and C. Moser, Springer, Berlin, (1980), p. 137.
6) S. Suhai, *J. Chem. Phys.*, **73**, 3843 (1980).
7) M. Kertesz, J. Koller, and A. Azman, *Int. J. Quantum Chem.*, **18**, 645 (1980).
8) M. Kertesz, J. Koller, and A. Azman, *Chem. Phys. Lett.*, **69**, 225 (1980).
9) J. L. Bredas, R. R. Chance, R. Silbey, G. Nocolas, and P. Durant, *J. Chem. Phys.*, **75**, 2455 (1981).
10) J. L. Bredas, B. Themans, and J. M. Andre, *J. Chem. Phys.*, **78**, 6137 (1983).
11) W. J. Dulmage and W. N. Lipscomb. *Acta Crystallogr.*, **4**, 330 (1951).
12) A. I. M. Rae, *Mol. Phys.*, **16**, 257 (1969).
13) M. Kertesz, J. Koller, and A. Azman, *Chem. Phys. Lett.*, **41**, 146 (1976).
14) A. Karpfen, *Chem. Phys.*, **79**, 211 (1983).
15) G. Del Re, J. Ladik, and G. Biczo, *Phys. Rev.*, **155**, 997 (1967).
16) C. C. J. Roothaan, *Revs. Mod. Phys.*, **23**, 69 (1951).
17) M. Ohsaku, H. Murata, and A. Imamura, *Eur. Polym. J.*, **17**, 327 (1981).
18) M. Ohsaku, T. Sasaki, H. Murata, and A. Imamura, *Eur. Polym. J.*, **17**, 913 (1981).

Conductometric and Potentiometric Studies of the Association of α-Cyclodextrin with Ionic Surfactants and Their Homologs

Iwao SATAKE,* Tadashi IKENOUE, Tokuro TAKESHITA,
Katumitu HAYAKAWA, and Tamaki MAEDA
Department of Chemistry, Faculty of Science, Kagoshima University, Korimoto, Kagoshima 890
(Received April 11, 1985)

The conductometric determination was made of the association constants of α-cyclodextrin (αCD) with ionic surfactants and their homologs. For 1-alkanesulfonate ions with carbon atoms (n) of 5—12, the association constant was found to increase regularly with n and become abruptly constant at $n=10$. The association constants for sodium 1-dodecanesulfonate, dodecylammonium chloride, dodecyltrimethylammonium chloride, and 1-dodecylpyridinium chloride were all similar in their magnitude. The effect of complexation on the micellar properties of sodium dodecyl sulfate and dodecyltrimethylammonium chloride were also studied potentiometrically by determining the counterion activities. In both cases, the critical micelle concentration increased regularly, while the degree of counterion association to the micelle decreased almost linearly with increasing αCD concentrations. It was suggested that the αCD–surfactant ion complex is solubilized in the hydrophilic surface region of surfactant micelle to give rise to a decrease in the surface charge density.

Cyclodextrins have been well known to form inclusion compounds with a variety of small molecules by several kinds of driving forces.[1] In the complexation of bulky hydrophobic molecule such as 1-adamantanecarboxylate, the hydrophobic interaction has been found to play an important role.[2] It is thus interesting to study the interactions of cyclodextrins with the surfactant ion which has an ionic head group as well as a large hydrocarbon chain of varying hydrophobicity. In this connection, Okubo *et al.*[3] made the conductometric study of the complexations of α- and β-cyclodextrins (αCD and βCD) with sodium dodecyl sulfate (SDS) and hexadecyltrimethylammonium bromide (CTAB) in water and mixed solvents. They found that in all cases an apparent critical micelle concentration increases regularly with increasing cyclodextrin concentration. In conformity with the difference of the hydrophobicities of the surfactant ion and cyclodextrin, the association constant, K, was found to increase in the order of SDS–αCD<SDS–βCD <CTAB–αCD<CTAB–βCD. They also pointed out that the decrease in K in mixed solvents comes partly from the decrease in hydrophobic attractive interaction between cyclodextrin and surfactant ion.

These observations prompted us to study the cyclodextrin–surfactant ion interactions both from thermodynamic and colloid chemical standpoints. In this paper is described the conductometric determination of the association constants of α-cyclodextrin with various ionic surfactants and their homologs. The potentiometric study was also undertaken to obtain information about the effect of complexation on the micellar properties of sodium dodecyl sulfate and dodecyltrimethylammonium chloride.

Experimental

Materials. Sodium dodecyl sulfate (SDS, Nakarai Chemicals Ltd.) and 1-dodecylpyridinium chloride (DPC, Tokyo Kasei Kogyo Co. Ltd.) were dissolved in hot ethanol and refluxed with active carbon for 10 h, respectively. After cooling the filtrate, the precipitate was further recrystallized twice from ethanol. The purification of dodecyltrimethylammonium chloride (DTAC, Tokyo Kasei Kogyo Co. Ltd.) was the same as that described above, except that acetone was used. Dodecylammonium chloride (DAC) was prepared from dodecylamine (purity>99%, Nakarai Chemicals Ltd.).[4] Sodium *p*-dodecylbenzenesulfonate (SDBS, purity>99%, Wako Pure Chemical Industry Co. Ltd.), sodium 1-alkanesulfonates with carbon atoms (n) of 5—8, 11, and 12 (Tokyo Kasei Kogyo Co. Ltd., guaranteed grade), and α-cyclodextrin (αCD, purity>98%, Seikagaku Kogyo Co. Ltd.) were used without further purifications. Sodium 1-alkanesulfonates with n of 9 and 10 were synthesized from the alkyl bromides purified by vacuum distillation.[5]

Conductivity Measurements. The conductivity was measured with an accuracy of ±0.1 μS by using a TOA Electronics Ltd. Conductivity Meter model CM-50AT. The cell constant of the conductivity cell was estimated to be 1.005 cm^{-1} at 25 °C. In order to remove trace amounts of conducting impurities, the aqueous solution of αCD was passed through the mixed ion bed (Bio-Rad AG501-X8). The concentration of αCD was determined gravimetrically by drying aliquots of the stock solution over phosphorus pentaoxide under reduced pressure and estimating the water content of the resulting powder from elementary analysis. The conductivity was measured as a function of αCD concentration, C_h, at a constant amphiphile concentration of around 2.5 mmol dm^{-3}.

Electromotive Force Measurements. The counterion activities in SDS and DTAC solutions were measured at 25 °C by using a TOKO Ion Electrode type 1100 Na^+ and a chloride ion selective ceramic electrode, National IE-510103, respectively. The electromotive forces (EMF) of the following cells were measured with an accuracy of ±0.1 mV by using a Corning Digital 112 Research pH Meter.

Sodium ion electrode (or Chloride ion electrode)|
Sample solution|1 mol dm^{-3} NH_4NO_3 Agar bridge|
Reference electrode (Ag–AgCl)

Prior to the measurements with surfactant solutions, these electrodes were calibrated with a sodium chloride solution of known activity.[6] In both cases, the electrode showed an ideal response of 59.2 mV per decade change in measuring ion activity in the concentration range between 5×10^{-3} and 0.1 mol dm^{-3}. The counterion activity was determined as a

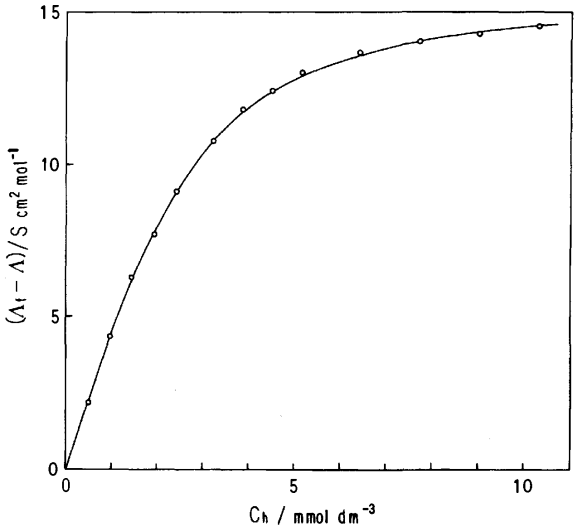

Fig. 1. Plots of $\Lambda_f - \Lambda$ *vs.* αCD concentration (C_h) for sodium 1-nonanesulfonate solution at 25 °C. C= 2.496 mmol dm^{-3}.
O, observed; solid line, calculated from Eq. 4 with K=1.49×10^3 dm^3 mol^{-1} and $\lambda_f - \lambda_a$=15.8 S cm^2 mol^{-1}.

function of the surfactant concentration, C, under the conditions where the molar ratio of αCD to surfactant, R (=C_h/C), was kept constant.

Results and Discussion

Association Constant. Figure 1 shows the typical plots of $\Lambda_f - \Lambda$ *vs.* αCD concentration for sodium 1-nonanesulfonate at 25 °C, where Λ_f and Λ represent the equivalent conductivity in the absence and presence of αCD respectively. It has been found that neither Na^+ nor Cl^- interacts appreciably with αCD.[7] Thus the successive decrease in Λ can reasonably be ascribed to the increase in the concentration of the associated 1-nonanesulfonate ion which has considerably smaller ionic equivalent conductivity than that of unassociated one. Similar results were also obtained for all of the amphiphiles studied.

In dilute electrolyte solution, which is the case for the present experiments, the activity coefficient ratio of associated and unassociated ions can safely be set equal to unity. Moreover, the activity coefficient of αCD is negligible under our experimental conditions.[8] Therefore, assuming a 1:1 reaction scheme,[3]

$$R^{\pm} + \alpha CD \rightleftharpoons \alpha CD \cdot R^{\pm}, \quad (1)$$

the association constant, K, can be written as

$$K = f/(1-f)(C_h - fC), \quad (2)$$

where $R^{\pm}$ refers to the amphiphilic ion and f to the fraction of $R^{\pm}$ associated with αCD, respectively. If we denote the ionic equivalent conductivities of $R^{\pm}$ and αCD·$R^{\pm}$ by λ_f and λ_a, we may write

$$\Lambda_f - \Lambda = f(\lambda_f - \lambda_a). \quad (3)$$

The use of Eqs. 2 and 3 for the evaluation of K requires a knowledge of λ_a. Unfortunately, however, the value of λ_a is somewhat difficult to estimate, since Λ decreases slightly but continuously even at higher αCD concentrations (see Fig. 1). This is especially true for 1-alkanesulfonate ion with shorter alkyl chain length. It follows immediately from Eqs. 2 and 3 that

$$\Lambda_f - \Lambda = \frac{\lambda_f - \lambda_a}{2KC}[K(C+C_h) + 1 - \sqrt{\{K(C+C_h)+1\}^2 - 4K^2CC_h}]. \quad (4)$$

Table 1. The conductometric and thermodynamic parameters of αCD–amphiphile systems

Amphiphile	C	Temp	Λ_f	$\lambda_f - \lambda_a$	K	$-\Delta G^\circ$
	mmol dm^{-3}	°C	S cm^2 mol^{-1}	S cm^2 mol^{-1}	dm^3 mol^{-1}	kJ mol^{-1}
$C_nH_{2n+1}SO_3Na$						
n=5	2.485	25	76.9	19.6	1.57×10^2	22.5
n=6	2.503	10	50.7	11.6	5.38×10^2	25.6
	2.526	25	74.2	17.9	3.79×10^2	24.7[a]
	2.503	40	99.5	24.1	2.81×10^2	23.9
n=7	2.552	10	50.2	11.6	8.70×10^2	26.7
	3.143	25	73.3	16.7	6.76×10^2	26.1[b]
	2.552	40	98.4	21.6	5.59×10^2	25.7
n=8	2.540	25	72.9	16.3	1.08×10^3	27.3
n=9	2.496	25	71.5	15.8	1.49×10^3	28.1
n=10	2.500	25	71.3	14.5	2.02×10^3	28.8
n=11	2.520	25	69.9	13.8	2.07×10^3	28.9
n=12	2.503	25	69.8	13.1	2.14×10^3	29.0
SDS	2.687	25	69.0	14.5	1.12×10^3	27.4
SDBS	0.869	25	67.5	8.2	5.73×10^3	31.4
DAC	2.544	25	99.1	14.9	2.27×10^3	29.1
DTAC	2.536	25	98.8	13.1	2.48×10^3	29.3
DPC	2.712	25	91.1	11.5	2.80×10^3	30.1

a) ΔH°=−15.8 kJ mol^{-1}, ΔS°=29.9 J K^{-1} mol^{-1}.
b) ΔH°=−10.7 kJ mol^{-1}, ΔS°=51.7 J K^{-1} mol^{-1}.

On the basis of Eq. 4, therefore, the values of K and $\lambda_f-\lambda_a$ were all evaluated from the plots of $\Lambda_f-\Lambda$ *vs.* C_h by using the non-linear least squares method (Gauss-Newton algorithm). The results are summarized in Table 1 together with the standard free energy change of complex formation, ΔG°, estimated from K_x (=55.5 K). The solid line in Fig. 1 shows the calculated conductivity curve from Eq. 4 with parameters thus determined for sodium 1-nonanesulfonate. The agreement between experimental and calculated curves is quite satisfactory over whole range of C_h, indicating the validity of a 1:1 reaction scheme. Similar agreements were also observed for all amphiphiles studied.

The most remarkable feature of Table 1 is the regular increase in K with the number of carbon atoms (n) and the leveling-off phenomenon above n=10 for 1-alkanesulfonate ions. The corresponding chain length dependence of ΔG° is shown in Fig. 2. These results suggest that αCD cavity accomodates succesively the methylene groups of hydrocarbon tail presumably by hydrophobic interaction. It is worth noting here that αCD molecule can accommodate at most 5 methylene groups of a fully extended alkyl chain in its hydrophobic cavity of 0.67 nm[9] long. According to the geometric consideration, therefore, the leveling-off phenomenon of K or ΔG° appears to occur at $n\approx6$ even if we take into account the fact that the methylene group closest to the ionic head group shows little or no hydrophobicity.[10] As is clearly shown in Fig. 2, however, this is not the case for the present result. In an inclusion process of long hydrocarbon chain, it seems thus highly probable that the additional 4 methylene groups can still interact with other part of αCD molecule than hydrophobic cavity, presumably with the lateral hydrophilic surfaces. A similar interaction was reported by Komiyama and Bender[2] for a complexation of bulky 1-adamantanecarboxylate with αCD. In this case, the complexation was found not only to accompany large positive entropy change but to occur in such a way that the guest molecule sits on top of the cavity. In Table 1 are also given the standard enthalpy and entropy changes estimated for 1-hexane- and 1-heptanesulfonate ions from temperature dependence of K_x. In the case of 1-hexanesulfonate ion, the contribution of enthalpy term to ΔG° is larger than that of entropy term ($-T\Delta S^\circ$), while the reverse is found for 1-heptanesulfonate ion. Although the detailed mechanism remains unclear, the observed decrease in the magnitude of ΔH° and the drastic increase in ΔS° for 1-heptanesulfonate ion are supposed to arise partly from the partial breakdown of the water structure around OH groups due to the penetration of hydrocarbon tail into lateral hydrophilic surface and partly from the change in the water structure around hydrocarbon tail associated with the transfer process from bulk phase to hydrophilic surface region.

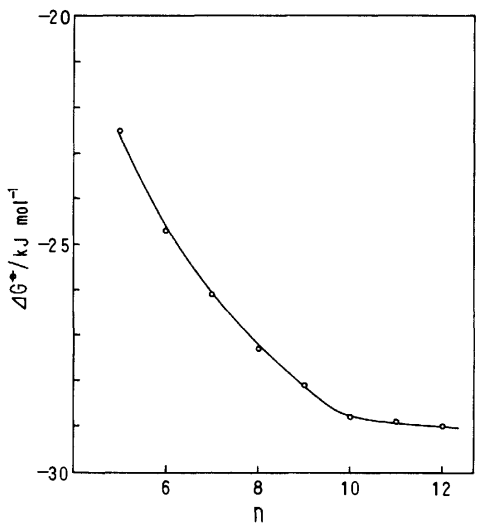

Fig. 2. The chain length dependence of ΔG° for sodium 1-alkanesulfonate at 25 °C.

The inspection of Table 1 also reveals another interesting feature that the association constants for surfactants with dodecyl chain, *i. e.*, sodium 1-dodecanesulfonate, DAC, DTAC, and DPC, are all similar in their magnitude in spite of the differences in the chemical and electrical properties of ionic head group. This fact suggests that the interaction between ionic head group and αCD molecule plays a minor role in the inclusion process of surfactant ion. An exceptional increase in K for SDBS can reasonably be ascribed to the presence of the additional aromatic ring, since a number of aromatic compounds have been found to interact strongly with αCD.[1] It should be noted that the value of K for sodium 1-dodecanesulfonate is about twice as large as that for SDS. In micelle formation of SDS, the extra oxygen atom in the sulfate group has been known to behave as an extra CH_2 group.[11] The presence of this anomalous oxygen atom may be responsible for the observed decrease in K for SDS.

Micellar Properties. In the complexation of the surfactant ion, the resulting complex is still supposed to behave like an amphiphilic ion with apparently shorter chain length. One might thus expect that the addition of αCD to surfactant solutions would affect not only the critical micelle concentration (cmc, C_o) but the micellar properties such as the degree (β) of counterion association to the micelle. Thus, we made the potentiometric determinations of β in solutions of SDS and DTAC in the presence of αCD. Figure 3 shows the typical semilogarithmic plots of the EMF (E_-) of the chloride ion electrode *vs.* DTAC concentration at varying values of R. The break point in this figure corresponds to the cmc at a given value of R. Similar behaviors were also observed for SDS solutions. In Fig. 4 are plotted the critical micelle concentrations thus determined for DTAC and SDS as a function of R. It should be noted that the cmc

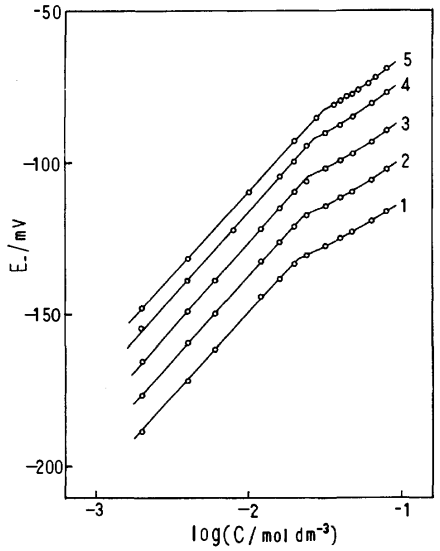

Fig. 3. The semilogarithmic plots of E_- *vs.* C for DTAC solution at 25°C. 1, $R=0$; 2, $R=0.091$; 3, $R=0.185$; 4, $R=0.275$; 5, $R=0.366$. The curves 2, 3, 4, and 5 are displaced upward by 10, 20, 30, and 40 mV, respectively.

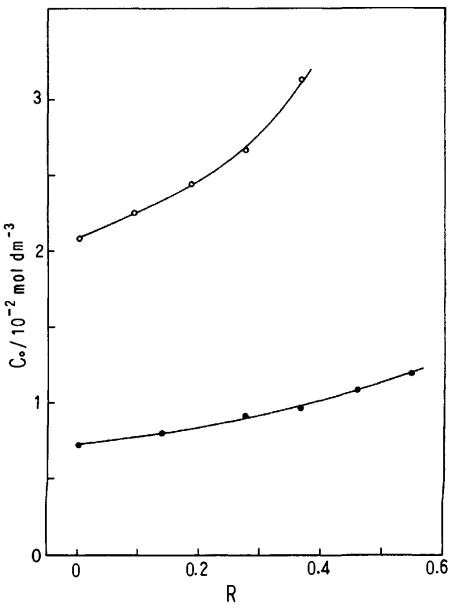

Fig. 4. Plots of C_0 *vs.* R at 25°C. ●, SDS; ○, DTAC.

becomes progressively higher as R increases and eventually disappears at R larger than 0.4 for DTAC and 0.6 for SDS respectively. Okubo *et al.*[3] assumed implicitly that the increase in an apparent cmc comes only from the increase in the concentration of the associated surfactant ion, *i.e.*, the concentration (C_m) of the monomeric surfactant ion available for the micellization process remains constant even in the presence of cyclodextrins. From the thermodynamical standpoint, however, other factors than that described above, *e.g.* the effect of the electrical potential at the micellar surface (ψ_s) on C_m can not be ignored even at the cmc,

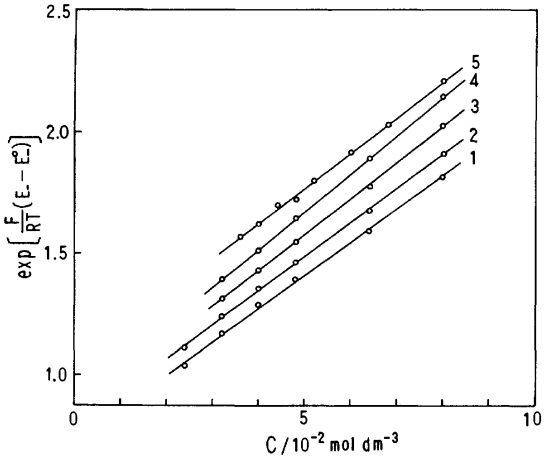

Fig. 5. Plots of the right-hand side of Eq. 6 *vs.* C for DTAC solution at 25°C. 1, $R=0$; 2, $R=0.091$; 3, $R=0.185$; 4, $R=0.275$; 5, $R=0.366$. The straight lines 2, 3, 4, and 5 are displaced upward by 0.1, 0.2, 0.3, and 0.5, respectively.

since an increase in the cmc is necessarily accompanied by the regular decrease in the magnitude of ψ_s by virtue of the increase in total counterion concentration. In fact the value of C_m calculated from Eq. 2 with K in Table 1 is not constant but decreases appreciably as R increases. For example with SDS, the value of C_m at the cmc decreases down to 6.20×10^{-3} mol dm^{-3} at $R=0.548$ (*cf.* $C_m=7.18\times10^{-3}$ mol dm^{-3} at $R=0$). If the associated surfactant ions are solubilized in the hydrophilic surface region of the micelle, the resulting depression in surface charge density will play an additional role in determining the value of ψ_s.

The EMF of the chloride ion electrode can be described as

$$E_- = E^{\circ}_- + (RT/F)\ln a_-, \tag{5}$$

where E°_- refers to the standard electrode potential and a_- to the chloride ion activity; other symbols have their usual meanings. Denoting the values of E_- and a_- at the cmc by E°_- and a°_- respectively, we immediately have

$$a_-/a^{\circ}_- = \exp\,[(F/RT)(E_- - E^{\circ}_-)]. \tag{6}$$

Figure 5 shows the plots of the right-hand side of Eq. 6 *vs.* DTAC concentration at higher concentrations than cmc. In agreement with the results[12-15] reported for counterion activities in various ionic surfactant solutions without host molecule, the chloride ion activity increases linearly with increasing DTAC concentration regardless of the value of R. This is also the case for SDS solutions containing αCD. These results allow us to estimate the degree of counterion association to the micellle at the cmc, β_o, as a function of R. If we denote the total intermicellar concentration of the associated and unassociated surfactant ions in bulk phase by C_b, and the counterion activity

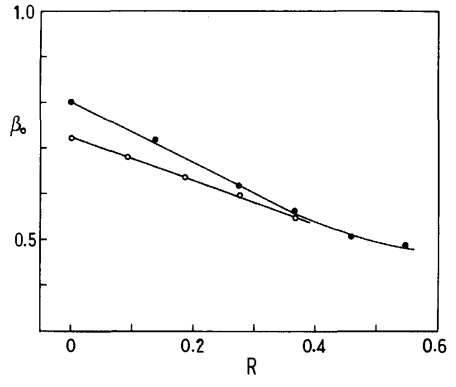

Fig. 6. Plots of β_o *vs.* R at 25 °C. ●, SDS; ○, DTAC.

coefficient by γ_-, Eq. 6 can be rewritten as

$$a_-/a^\circ_- = \gamma_-[C_b+(1-\beta)(C-C_b)]/\gamma^\circ_- C_o. \quad (7)$$

In solution of ionic surfactant alone, it is usually assumed that the values of γ_-, β, and C_b which in such case represents the concentration of the monomeric surfactant ion remain constant in the concentration range above cmc.[12-14,16] Because of the complications arising from the presence of the associated surfactant ions, it is somewhat doubtful whether the same assumption can be applicable for the present systems. Apart from the concentration dependences of γ_-, β, and C_b, however, we can easily estimate the value of β_o from the slope of the straight line in Fig. 5, since the changes in these parameters can safely be ignored at least in quite narrow concentration range above cmc. The results are shown in Fig. 6. An important feature of Fig. 6 is the regular decrease in β_o with respect to R. In their theoretical study of the counterion condensation on charged planar surface, Engström and Wennerström[17] have derived the following expression for the fraction, P_c, of counterions bound to the surface region of thickness Δ which is the order of the diameter of a hydrated counterion.

$$P_c = 1 - [1-(\sigma Ze\Delta/2\varepsilon_r\varepsilon_o kT)]^{-1} \quad (8)$$

Here, σ is the surface charge density, Ze the charge of the counterion, ε_r the relative permittivity, and ε_o the permittivity of a vacuum, respectively. In view of the fact that most of the micellar properties of ionic surfactant solutions can be interpreted in terms of the lamellar model,[18] P_c in Eq. 8 is supposed to be closely related to β_o. This in turn suggests that the observed decrease in β_o arises virtually from a decrease in the magnitude of surface charge density. It seems therefore most likely that the surfactant ion associated with bulky cyclodextrin molecule is solubilized in the hydrophilic surface region of surfactant micelle to give rise to a decrease in surface charge density.

As mentioned previously, the break point in EMF *vs.* log C plots became undetectable at R higher than 0.4 for DTAC and 0.6 for SDS, respectively. Therefore, the limiting value of β_o appears to correspond to the critical surface charge density, σ_{crit}, below which the counterion fixation no longer takes place. For example with SDS, the tentative estimation based on Eq. 8 with Δ=0.45 nm[6] leads to σ_{crit} of one unit charge per 2.1 nm^2 at R=0.548. On account of the definite size of the micellar aggregate, however, the actual value of σ_{crit} will probably be larger than that estimated above.

The present work was supported by a Grant-in-Aid for Scientific Research No. 59540269 from the Ministry of Education, Science and Culture.

References

1) M. L. Bender and M. Komiyama, "Cyclodextrin Chemistry," Springer-Verlag, Berlin (1978); W. Saenger, *Angew. Chem. Int. Ed. Engl.*, **19**, 344 (1980).
2) M. Komiyama and M. L. Bender, *J. Am. Chem. Soc.*, **100**, 2259 (1978).
3) T. Okubo, H. Kitano, and N. Ise, *J. Phys. Chem.*, **80**, 2661 (1976).
4) I. M. Kolthoff and W. Strickes, *J. Phys. Colloid Chem.*, **52**, 915 (1948).
5) S. Zuffanti, *J. Am. Chem. Soc.*, **62**, 1044 (1940).
6) J. Kielland, *J. Am. Chem. Soc.*, **59**, 1675 (1937).
7) E. A. Lewis and L. D. Hansen, *J. Chem. Soc., Perkin Trans. 2*, **1973**, 2081.
8) K. Miyajima, M. Sawada, and M. Nakagaki, *Bull. Chem. Soc. Jpn.*, **56**, 3556 (1983).
9) W. J. James, D. French, and R. E. Rundle, *Acta Crystallogr.*, **12**, 385 (1959).
10) C. Tanford, "The Hydrophobic Effect: Formation of Micelles and Biological Membranes," 2nd ed., John Wiley & Sons, New York (1980), p. 14.
11) Ref. 10) p. 68.
12) C. Botré, V. L. Crescenzi, and A. Male, *J. Phys. Chem.*, **63**, 650 (1959).
13) L. Shedlovsky, C. W. Jacob, and M. B. Epstein, *J. Phys. Chem.*, **67**, 2075 (1963).
14) I. Satake, T. Tahara, and R. Matuura, *Bull. Chem. Soc. Jpn.*, **42**, 319 (1969).
15) P. Stenius and P. Ekwall, *Acta Chem. Scand.*, **21**, 1643 (1967).
16) A. Yamauchi, T. Kunisaki, T. Minematsu, Y. Tomokiyo, T. Yamaguchi, and H. Kimizuka, *Bull. Chem. Soc. Jpn.*, **51**, 2791 (1978).
17) S. Engström and H. Wennerström, *J. Phys. Chem.*, **82**, 2711 (1978).
18) K. Shinoda, T. Nakagawa, B. Tamamushi, and T. Isemura, "Colloidal Surfactants," Academic Press, New York (1963), Chap. 1.

 © 1985 The Chemical Society of Japan Bull. Chem. Soc. Jpn., 58, 2751—2755 (1985)

Oxidation of Triose Reductone by Oxidizing Inorganic Radicals Generated by Pulse Radiolysis

Hideo Horii,* Yasuo Abe, and Setsuo Taniguchi
Radiation Center of Osaka Prefecture, Shinke-cho, Sakai 593
(Received April 22, 1985)

Triose reductone (2,3-dihydroxy-2-propenal) was oxidized by $Cl_2^{\cdot-}$, $Br_2^{\cdot-}$, $I_2^{\cdot-}$, $(SCN)_2^{\cdot-}$, and $N_3^{\cdot}$ to produce a triose reductone radical which had an absorption maximum at 398 nm, ε=5500 $M^{-1}cm^{-1}$ (1 M=1 mol dm^{-3}) and decayed by second-order kinetics. The rate constants for the reactions of triose reductone with these oxidizing inorganic radicals were obtained. The pK_a of this radical was found to be 1.4.

Triose reductone (2,3-dihydroxy-2-propenal) was first synthesized by the decomposition of glucose in an alkaline aqueous solution and its structure was determined to be CH(OH)=C(OH)CHO by H. von Euler and C. Martius.[1] A very important characteristic of "reductone" is the strong reducing ability which is due to its enediol group, -C(OH)=C(OH)-.[2] Euler *et al.*[3] proposed that triose reductone has a double five-membered ring. Obata *et al.*[4] provided experimental proof for this by NMR and mass spectra of triose reductone and presumed the following two formulas in D_2O, $(CD_3)_2CO$, DMSO solution.

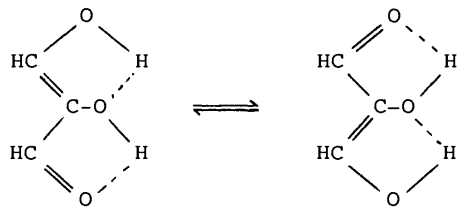

Well-known reductones, L-ascorbic acid,[5-7] adrenaline,[8] and dopamine[9] which play significant roles in biological systems, have been studied by pulse radiolysis. Thus, the oxidation of the reductones have been shown to proceed through the intermediate radicals. Furthermore, it is important and interesting to clarify the oxidation mechanisms of other enediol compounds. Triose reductone is yielded in biological systems[1,10-12] and in the process of browning reaction.[13] Also, it reacts with amino compounds to yield anil compounds[2] or causes a DNA-breaking action in the presence of Cu^{2+}.[14] The enzymatic oxidation of triose reductone has been reported to produce a free radical in the ESR study.[15] It is useful to study the oxidation mechanism of triose reductone, as it is one of the most simple reductones. We have studied the oxidations of triose reductone using oxygen and hydrogen peroxide,[16] a peroxodisulfate ion,[17] and a hexacyanoferrate(III) ion,[18] kinetically. It was found in our previous paper[19] that triose reductone is oxidized by $(SCN)_2^{\cdot-}$ and $Br_2^{\cdot-}$ to yield a one-electron oxidized radical. In this paper we studied oxidations of triose reductone by oxidizing species $Cl_2^{\cdot-}$, $I_2^{\cdot-}$, $N_3\cdot$ including $(SCN)_2^{\cdot-}$, and $Br_2^{\cdot-}$ [19] kinetically and disclosed the reaction mechanisms.

Experimental

Pulse irradiation was accomplished using the 18 Mev linac (High Voltage Engineering Co.) of the Radiation Center of Osaka Prefecture at room temperature (about 20 °C). Pulses of 10-MeV electrons of 0.5—2 μs duration were diffused by an aluminum plate (0.5—3 mm thick) for regulating the pulse dose. The dose of a pulse was monitored by the current which was collected on a brass plate located directly behind the irradiation cell. The 1.5-cm long irradiation vessel was made of thermal quartz for light path windows. The sample solution was refreshed from a Pyrex stock bottle after each pulse-irradiation by a magnetic valve under gas (N_2O or Ar) pressure. All solutions were prepared from triply distilled water. Dinitrogen monoxide (Showa Denko Co., High Purity, upper limit of O_2 content: 10 ppm) was used after the deaeration of solutions by argon (Osaka Sanso Co., Instrument Argon). The solutions were bubbled before irradiation for ≈60 min with Ar and N_2O which converts the hydrated electron into the OH radical. Triose reductone was prepared and purified by the method of Euler and Martius.[1] All other chemicals used were of analytical reagent grade. The light of a 500 W Xe lamp (Ushio Denki Co.) was focused on the irradiation cell and was detected by a photomultiplier (1P28, Hamamatsu TV) after passing through a grating monochromator (Nikon, G-250). The signals were recorded by a personal computer (YHP Co., 9815A) through a transient recorder (Riken Denshi Co., TCH-1000) and analyzed.[20] Dosimetry was performed with N_2O-saturated 0.01 M KSCN solutions taking the value of G(OH) and $\varepsilon_{472\,nm}$ for $(SCN)_2^{\cdot-}$ as 6.13 and 7580 $M^{-1}cm^{-1}$.[21] The pH of the solution was generally adjusted by an addition of appropriate amounts of $HClO_4$ or NaOH.

Results and Discussion

Rate Constants for the Oxidations of Triose Reductone with Inorganic Radicals. The rate constants for the oxidation of triose reductone with $(SCN)_2^{\cdot-}$, $Cl_2^{\cdot-}$, $Br_2^{\cdot-}$, and $I_2^{\cdot-}$ were measured by following the exponential decay of each absorbance (472, 340, 340, and 380 nm) as a function of the substrate concentration. The rate constant, in the case of $N_3\cdot$, was measured by following the first-order decay and growth of the absorbance due to triose reductone at 310 nm and the triose reductone radical at 400 nm, respectively. The rate constants were identical with each other regarding both decay and growth within experimental errors. The rate constants

Table 1. Rate constants in $M^{-1}s^{-1}$ for the reactions of triose reductone and ascorbic acid with inorganic oxidizing radicals

Oxidant	$k(TRH_2)$	$k(TRH^-)$	$k(AH_2)$[a]	$k(AH^-)$[a]
$Cl_2^-\cdot$	1.1×10^9		6.8×10^8	
$N_3\cdot$		4.0×10^9		
$Br_2^-\cdot$	2.2×10^8	1.8×10^9	1.1×10^8	1.1×10^9
$(SCN)_2^-\cdot$	2.7×10^7	9.0×10^8	1.0×10^7	6.0×10^8
$I_2^-\cdot$	$\leqq1\times10^6$	3.4×10^8	5×10^6 $\leqq6\times10^5$[b]	1.4×10^8

TRH_2: Triose reductone. TRH^-: Monoanion of triose reductone AH_2: Ascorbic acid. AH^-: Monoanion of ascorbic acid. a) Ref. 5. b) This study, at pH 2.

Table 2. One-electron reduction potentials of inorganic radicals

inorganic radical	E^0(V)
$Cl_2^-\cdot$	2.3
$N_3\cdot$	1.93
$Br_2^-\cdot$	1.7
$(SCN)_2^-\cdot$	1.25
$I_2^-\cdot$	1.0

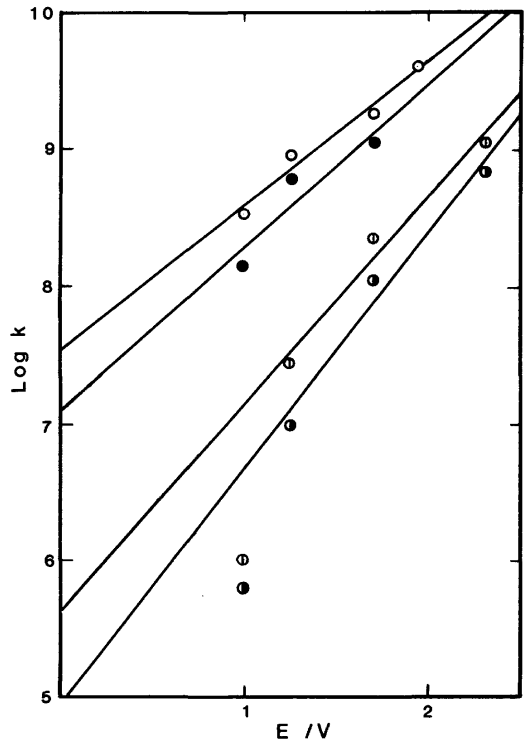

Fig. 1. Dependence of k (rate constant) on the reduction potential of inorganic radicals.
TRH_2 (Φ), TRH^- (○), AH_2 (◑), AH^- (●).

of both dissociated and undissociated forms are summarized in Table 1. For the sake of a comparison, the data of L-ascorbic acid[5] are also listed in Table 1. The reactivities of triose reductone with these oxidizing species are in the order of $Cl_2^-\cdot > N_3\cdot > Br_2^-\cdot > (SCN)_2^-\cdot > I_2^-\cdot$, similar to ascorbic acid. One-electron reduction potentials[22] of the oxidizing species (Table 2) explain the reactivity order well. The rate constants for oxidation are larger in triose reductone than in ascorbic acid, except that of $I_2^-\cdot$ with undissociated ascorbic acid quoted from a reference.[5] We found from the decay of $I_2^-\cdot$ at 410 nm that the reaction rate constant of $I_2^-\cdot$ with ascorbic acid was smaller than 6×10^5 M^{-1} s^{-1}. The latter value seems more reasonable from the relation mentioned above. The stronger reducing power of triose reductone in comparison with ascorbic acid was also shown in the reductions of peroxodisulfate[17,23] and hexacyanoferrate(III).[18,24] The dependences of log k (k: rate constants for oxidation by inorganic radicals) on the reduction potential (E (ev)) in both triose reductone and ascorbic acid are presented in Fig. 1. They are almost linear except for reactions of $I_2^-\cdot$ with undissociated triose reductone and ascorbic acid. This result shows that the electron-transfer reactions that occur in these systems are as predicted from the Marcus theory.[25] Triose reductone has two dissociation constants[16] ($pK_1=5.0$, $pK_2=13.0$). Therefore, the reaction scheme can be described as follows.

$$H_2O \rightsquigarrow e_{aq}^-, H, OH, H_2O_2, H_2 \quad (1)$$

$$N_2O + e_{aq}^- \xrightarrow{H_2O} OH + OH^- + N_2 \quad (2)$$

$$X^- + OH \longrightarrow X\cdot + OH^- \quad (3)$$
(X=SCN, Cl, Br, I)

$$X^- + X\cdot \longrightarrow X_2^-\cdot \quad (4)$$

$$N_3^- + OH \longrightarrow N_3\cdot + OH^- \quad (5)$$

$$TRH_2 \overset{K_1}{\rightleftharpoons} TRH^- + H^+ \overset{K_2}{\rightleftharpoons} TR^{2-} + 2H^+ \quad (6)$$

$$TRH_2 \text{ (or } TRH^-) + X_2^-\cdot \longrightarrow TRH\cdot \text{ (or } TR^{-}\cdot) + 2X^- \quad (7)$$

$$TRH_2 \text{ (or } TRH^-) + N_3\cdot \longrightarrow TRH\cdot \text{ (or } TR^{-}\cdot) + N_3^- \quad (8)$$

Absorption Spectra. Triose reductone is oxidized with $X_2^-\cdot$ (X=SCN, Cl, Br, I) or $N_3\cdot$ radicals to generate transient species, as mentioned above. The absorption spectra observed in these systems (Fig. 2) are identical with each other within experimental errors. The absorption spectrum (Fig. 2) almost completely disappears upon the addition of 0.2 M *t*-BuOH which scavenges OH radicals. The result supports the idea that transient absorption is produced by a reaction of triose reductone with the inorganic radicals. The absorption spectrum shows a quite symmetrical (Gaussian-type) band with a maximum at 398 nm and a width at half-maximum of 71 nm. The absorption coefficient at 398 nm is 5500 $M^{-1}cm^{-1}$. The solid line in Fig. 2 represents the simulated Gaussian-curve with the deviation of 32 nm, and fits well with a observed ab-

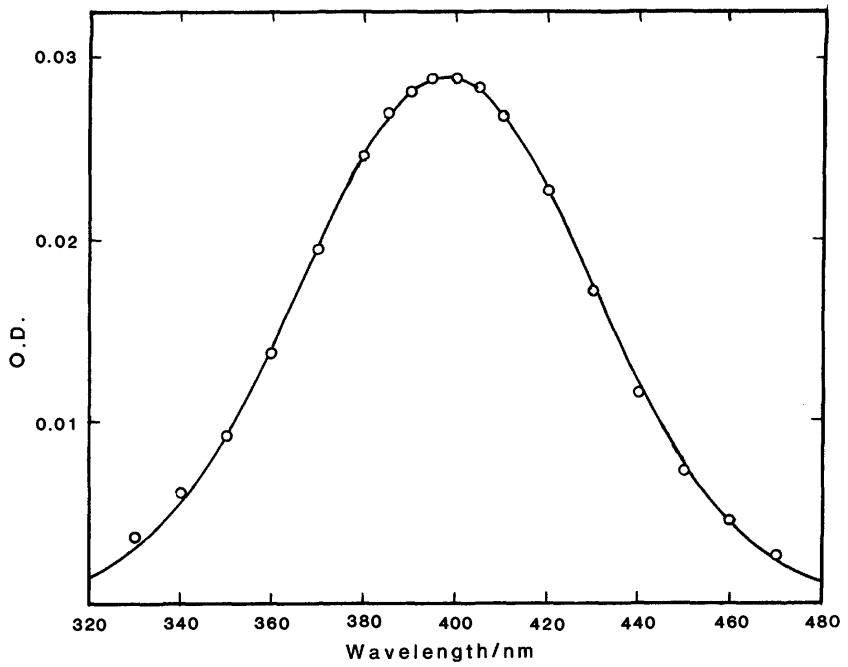

Fig. 2. Transient absorption spectrum produced by pulse irradiation of N_2O saturated 3×10^{-4} M triose reductone solution. Average dose, 536 rad; 20 mM KSCN, KBr, NaN_3; pH 9.6.

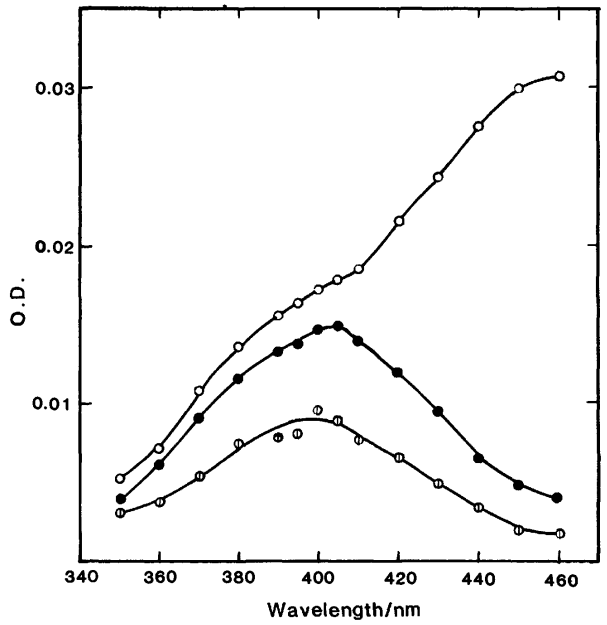

Fig. 3. Time change of transient spectrum produced by $(SCN)_2^-$ at pH 3.2. N_2O saturated 3×10^{-4}M triose reductone, 20 mM KSCN; Average dose, 536 rad; 0(○), 200(●), 900(◑), μs after the pulse.

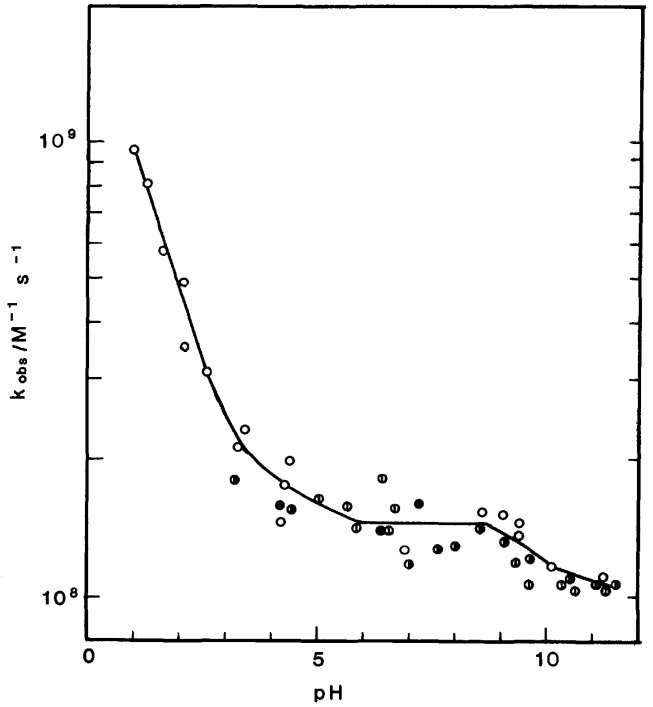

Fig. 4. Dependence of decay rate constants of the triose reductone radical corrected for ionic strength on pH. N_2O saturated solution of 2×10^{-4}, 3×10^{-4} M triose reductone; 10, 20 mM KBr (○); 5, 20 mM KSCN (◑); 5, 10, 20 mM NaN_3 (◑); 3, 20 mM KI (●).

sorption data. The ascorbic acid radical also has a very symmetric-type band with a maximum at 360 nm and a half-maximum width of 50 nm.[26] Figure 3 shows the time-changes of the transient absorption spectrum produced by $(SCN)_2^-$ radicals at pH 3.2. It indicates that the $(SCN)_2^-$ radical (λ_{max}=472 nm) is gradually converted into the triose reductone radical (reaction 7), since the rate constant for the reaction $TRH_2+(SCN)_2^-$ is rather small (2.7×10^7 $M^{-1}s^{-1}$) in comparison with that for dissociated triose reductone (9.0×10^8 $M^{-1}s^{-1}$).

Rate of Radical Decay. Triose reductone radicals including both TRH· and TR^{-}· (*vide infra*) decay by

second-order kinetics over a wide pH range (pH 1—11.5). Figure 4 shows the relationship between the second-order rate constants for the decay of the radical (TRH· and/or TR^{-}·) and the pHs of solutions, where the rate constants were corrected for ionic strength. The rate constant decreases slightly from pH 9 to 12.5 and is almost constant in the range of pH 6—9 and increases steeply from pH 4 to pH 1. The change of the rate constant around pH 10 is not at present understandable. The dependence of the decay rate of the radical on pH is probably due to H^+ as well as the ascorbate radical[5] and the decay rate may be affected by the dissociation of the radical below pH 2.5, whose pK_a is 1.4 as shown later. But, the hydrated electron reacts with H^+ competitively with N_2O to yield the H radical below pH ≈2.5. Also the transient species produced by the reaction of triose reductone with the H radical might affect the apparent rate constants. Hence, the decay mechanism of the radical is complicated below pH ≈2.5. The rate of a reaction between two ions is dependent on the ionic strength (μ), as given approximately[27] by

$$\log k/k_0 = Z_A Z_B(1.02\mu^{1/2})/(1+\mu^{1/2}) = Z_A Z_B m \qquad (I)$$

where k_0 is the value of k at zero ionic strength, and Z_A, Z_B are the charges of two ions, and μ is the total ionic strength. The effect of the ionic strength on the decay rate of the triose reductone radical was studied at pH 8.0, where the radical is presumed to be dissociated from the pK_a (1.4) as shown later, using sodium sulfate to vary μ. The results are shown in Fig. 5, where the observed values of log k are plotted as a function of m. The slope of the line in Fig. 5 is about 0.7. Hence, the oxidized intermediate can be assigned to the anion radical TR^{-}·

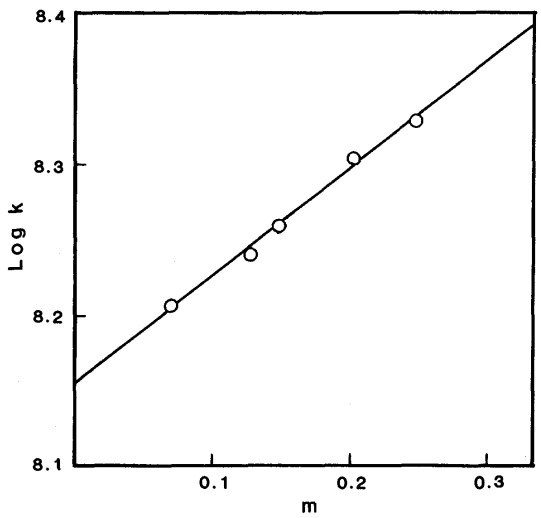

Fig. 5. Effect of ionic strength on decay rate of the triose reductone radical.
N_2O saturated solution of 3×10^{-4} M triose reductone; 5 mM KSCN; pH 8.0.

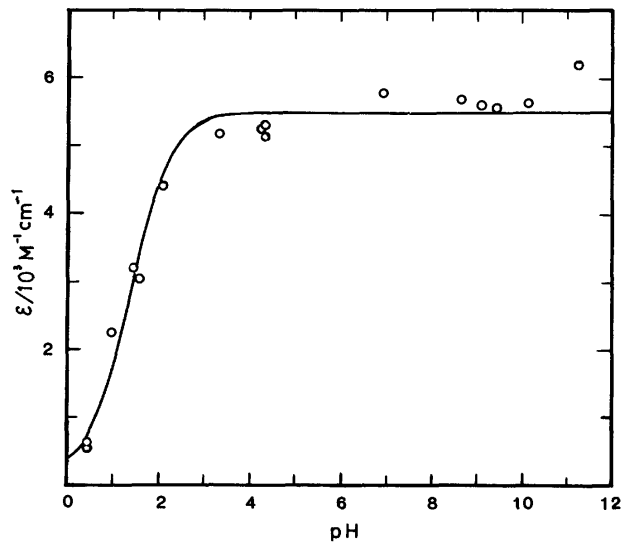

Fig. 6. Dependence of molar extinction coefficient (ε) of the triose reductone radical on pH. N_2O saturated solutions of 3×10^{-4} M triose reductone; 10, 20 mM KBr.

pK_a of the Triose Reductone Radical. The molar extinction coefficients (ε) of triose reductone radical determined at 400 nm as a function of pH are shown in Fig. 6. Below pH 3 the hydrated electron (e^-_{aq}) reacts with proton (H^+) to produce the H radical. But, the transient species which is produced by the reaction of triose reductone with the H radical has only a small extinction coefficient ($\varepsilon_{400\,nm}$=300). The extinction coefficient was obtained in the system of 1 mM TRH_2, 0.2 M *t*-BuOH, at pH 1. The numerical values of ε were corrected for the H^+ effect, as H^+ reacts with e^-_{aq} to yield the H radical. The smooth line in Fig. 6 was computed by assuming that the pH dependence of the extinction coefficient results from the acid dissociation process, using $\varepsilon^{TRH\cdot}_{400\,nm}$=200 $M^{-1}cm^{-1}$, $\varepsilon^{TR^{-}\cdot}_{400\,nm}$= 5500 $M^{-1}cm^{-1}$. The acid dissociation constant giving the best fit to the data is pK_a=1.4. In the γ-ray radiolysis of 5 mM KBr, 26 μM TRH_2, N_2O saturated solution at pH 8.5, G(-TRH_2) (the consumption G value of TRH_2) was obtained as about 3. As $G(Br_2^{-}\cdot)$ is 6.1 in the system above, the triose reductone radical is presumed to decay by disproportionation mechanism in the same way as the ascorbic acid radical.[5] Consequently, the triose reductone radical decays according to the following scheme.

$$TRH\cdot \overset{pK_a=1.4}{\rightleftharpoons} TR^{-}\cdot + H^+ \qquad (9)$$

$$TR^{-}\cdot + TR^{-}\cdot \xrightarrow{H^+} TRH_2 \text{ (or } TRH^-) + TR \qquad (10)$$

However, it is not clear in this study whether the triose reductone radical is in equilibrium with a dimer similar to the ascorbic acid radical,[7] as follows.

$$TR^{-}\cdot + TR^{-}\cdot \rightleftharpoons TR_2^{2-} \qquad (11)$$

Table 3. Dissociation constants for triose reductone, ascorbic acid, and their radicals

	Triose reductone	Ascorbic acid
pK_1	5.0	4.3[a]
pK_2	13.0	11.6[a]
Radical		
pK_a	1.4	−0.45[b]

a) Ref. 31. b) Ref. 28.

Fessenden, Schuler, and co-workers[28,29] showed by an ESR study that the ascorbic acid radical has a structure with an unpaired electron spread over a highly conjugated tricarbonyl system with a pK_a of −0.45. Therefore, the triose reductone radical ($TR^{-\cdot}$) probably has the following conjugated structure, as it has a similar enediol group with a carbonyl group as well ascorbic acid. In the molecular orbital calculation

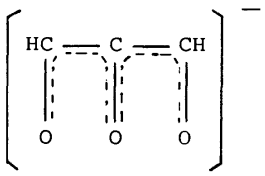

study[30] of triose reductone, the result also shows that the radical is in a resonated anion form, while the spin density is localized somewhat on the central oxygen atom.

The dissociation constants of ascorbic acid, triose reductone, and their radicals are summarized in Table 3. In each case, pK_a of triose reductone and its radical is larger than that of ascorbic acid and ascorbate radical. Namely, it shows that ascorbic acid and its radical are stronger acids than those of triose reductone, respectively. The dissociation constants of the reductone radicals are greater by a factor of over 10^3 than that of the respective reductones. This fact shows that these reductone radicals are far more acidic than the corresponding reductone.

The authors wish to thank the members of the linac group for operating the linac.

References

1) H. von Euler and C. Martius, *Liebigs. Ann. Chem.*, **505**, 73 (1933).
2) D. Nomura and H. Omura, "Chemistry of Reductone," Uchida Rokakuho Publishing Co., Ltd., Tokyo, (1969).
3) H. von. Euler and H. Hasselquist, *Arkiv. Kemi.*, **26A**, Nr. 25 (1948).
4) H. Obata and T. Tokuyama, *Nippon Kagaku Zasshi*, **91**, 1098 (1970).
5) M. Schöneshöfer, *Z. Naturforsh.*, **27b**, 649 (1972).
6) B. H. J. Bielski, D. A. Comstock, and R. A. Bowen, *J. Am. Chem. Soc.*, **93**, 5624 (1971).
7) B. H. J. Bielski, A. O. Allen, and H. A. Schwarz, *J. Am. Chem. Soc.*, **103**, 3516 (1981).
8) W. Bors, M. Saran, C. Michel, E. Lengfelder, C. Fuchs, and R. Spöttl, *Int. J. Radiat. Biol.*, **28**, 353 (1975).
9) H. W. Richter and W. H. Waddell, *J. Am. Chem. Soc.*, **105**, 5434 (1983).
10) G. Hesse and H. Schildknecht, *Angew. Chemie.*, **68**, 75 (1956).
11) S. Adachi, *Nippon Nôgeikagaku Kaishi*, **30**, 713 (1956).
12) H. von Euler and E. Klussmann, *Z. Physiol. Chem.*, **217**, 167 (1933).
13) J. E. Hodge, *J. Agr. Food Chem.*, **1**, 928 (1953).
14) K. Shinohara, M. So, M. Nonaka, K. Nishiyama, H. Murakami, and H. Omura, *J. Nutr. Sci. Vitaminol.*, **29**, 481 (1983).
15) I. Yamazaki and L. H. Piette, *Biochim. Biophys. Acta*, **77**, 47 (1963).
16) Y. Abe, H. Horii, S. Taniguchi, K. Kamai, and M. Takagi, *Bull. Chem. Soc. Jpn.*, **56**, 467 (1983).
17) Y. Abe, H. Horii, and S. Taniguchi, *Bull. Chem. Soc. Jpn.*, **57**, 222 (1984).
18) Y. Abe, T. Dohmaru, H. Horii, and S. Taniguchi, *Can. J. Chem.*, **63**, 1005 (1985).
19) H. Horii, Y. Abe, S. Taniguchi, S. Maeda, and T. Watanabe, *Chem. Lett.*, **1983**, 1313.
20) H. Horii, S. Fujita, T. Mori, and S. Taniguchi, *Radiat. Phys. Chem.*, **19**, 231 (1982).
21) R. H. Schuler, L. K. Patterson, E. Janata, *J. Phys. Chem.*, **84**, 2089 (1980).
22) J. Butler, E. J. Land and A. J. Swallow, *Radiat. Phys. Chem.*, **23**, 265 (1984).
23) M. Kimura, A. Kobayashi, and K. Boku, *Bull. Chem. Soc. Jpn.*, **55**, 2068 (1982).
24) U. S. Mehrotra, M. C. Agrawal, and S. P. Mushran, *J. Phys. Chem.*, **73**, 1996 (1969).
25) R. A. Marcus, *J. Chem. Phys.*, **43**, 3477 (1965).
26) R. H. Schuler, *Radiat. Res.*, **69**, 417 (1977).
27) R. E. Weston, H. A. Schwarz, "Chemical Kinetics," Prentice-Hall, Inc., Englewood Cliffs, N. J., 169 (1972).
28) G. P. Laroff, R. W. Fessenden, and R. H. Schuler, *J. Am. Chem. Soc.*, **94**, 9062 (1972).
29) R. W. Fessenden and N. C. Verma, *Biophys. J.*, **24**, 93 (1978).
30) Y. Abe, H. Horii, S. Taniguchi, S. Yamabe, and T. Minato, 50th National Meeting of the Chemical Society of Japan, Tokyo, April 1985, Abstr., No. 1U36.
31) E. Schauenstein, *Monatsh. Chem.*, **79**, 495 (1948).

Electronic Structure and Lattice Distortion of Benzene Anion

Minoru KIMURA,† Hiroyuki KAWABE, Kiyoshi NISHIKAWA, and Shigeyuki AONO*
†*Department of Physics, Faculty of Science, Kanazawa University, Marunouchi, Kanazawa 920*
Department of Chemistry, Faculty of Science, Kanazawa University, Marunouchi, Kanazawa 920
(Received April 27, 1985)

Electronic structure, especially the charge density or the spin density of the benzene anion (exactly dihydrophenylide ion) is investigated by the Hubbard Hamiltonian with vibronic interaction. Two limiting cases, *i.e.*, $I/\beta \ll 1$ and $I/\beta \gg 1$ (I is the electron repulsion on site, β the absolute value of transfer integral.) are analytically examined. For whole range of this ratio, the numerical calculation has been performed. The actual system falls into the latter case, where the electron correlation produces a strong effect on the spin density distribution.

The benzene molecule is a typical subject for theories of electronic states of molecules, while the benzene anion is of interest also from physical viewpoints. In the molecular orbital theory, the benzene molecule has the unoccupied doubly degenerate orbitals. The odd electron of the benzene anion, therefore, would equally populate on these degenerate levels.

If the vibronic coupling exists, the degenerate levels are strongly coupled through an interaction with a certain mode of the vibration, and then the degeneracy is removed to lead to a distorted ground state, *i.e.*, the so-called Jahn-Teller effect arises. Almost all the studies have been made along the above-mentioned simple picture.[1-6] Even in the elaborated work,[4] the electronic state was considered within a single-particle picture for the odd electron, which neglects the role of electron repulsion.

Recently similar problems have been studied in solid state physics, *e.g.*, the study of various ordered phases in the infinite chain molecule.[7] In this decade the so-called many-body technique employed in these investigations are getting familiar also in quantum chemistry. One of the great advantages of the many-body thoery lies in making the investigating procedure systematic and pictorial. In the present work, we employ this method to study the distorted nonuniform ground state in the benzene anion, taking into account the most dominant part of the electron interaction.

Model Hamiltonian and One-electron Theory

Let us consider the system to be described by the P.P.P. Hamiltonian with terms which is responsible for lattice distortion,

$$H = \sum_{r,\sigma}\alpha_r n_{r\sigma} - \sum_{r,\sigma}(\beta_{r,r+1}a^+_{r\sigma}a_{r+1\sigma}+\text{h.c.}) + \frac{1}{2}\sum_{r,s,\sigma} I_{r,s}n_{r\sigma}n_{s-\sigma} + \frac{1}{2}M\Omega^2\sum_r Q_r^2, \quad (1)$$

where α_r is the Coulomb integral of the site r, $\beta_{r,s}$ is the resonance integral and $I_{r,s}$ the electron–electron interaction constant. The last term of Eq. 1 represents the elastic energy due to the distortion Q_r of the site r from its C_6-symmetric configuration. It includes the compressional energy of σ electrons. In the undistorted symmetric configuration, α_r and $\beta_{r,s}$ are uniform. Therefore, so long as Q_r is small, they are expanded in Q_r and can be written as

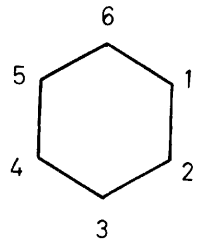

Fig. 1. Site numbers for the benzene anion.

$$a_r = \alpha_0 + gQ_r + \frac{1}{2}\Delta\alpha(\delta_{r,3}+\delta_{r,6}), \quad (2)$$

$$\beta_{r,r\pm1} = \beta + g'Q_r, \quad (3)$$

where g and g' are the expansion coefficients. The last term of Eq. 2 represents the perturbation arising from the interaction with solvent which may be added, say, at the sites r=3 and 6 (Fig. 1), which reduces the molecular symmetry from C_6 to C_2. It will be time-dependent in view of thermal motion of solvent molecules. However, if we assume that it is sufficiently slow as compared to motion of the phase of the distortion, we can consider it as a static perturbation. As will be shown below, its effect is to pin up the phase of the distortion at the particular site so as to minimize the total energy.

Equation 3 has been used to study the bond-alternation in polyene (for example the model of Su, Schriefer and Heeger in considering polyacetylene[7]), while Eq. 2 was considered by Holstein[8] to study the polaron in molecular chains. The second terms of Eqs. 2 and 3 both contribute to the change of the energy of the electrons due to the distortion. However, in the present study, they yield essentially the same physical effect except for the difference of the phases of distortion, so that we shall take only the change of α_r of Eq. 2 into account, and consider

$$\beta_{r,r\pm1} = \beta \quad (4)$$

as a constant.

The electron–electron interaction plays an important role in the electron distribution, which was not

considered in the early works.[1-7] However, the full consideration of electron interaction in Eq. 1 is so complex as to preclude physical pictures, therefore we shall consider only the on-site repulsion $I_{r,r}=I$ in order to examine the essential features qualitatively.[9-11]

Then, the Hamiltonian to be considered becomes

$$H = H_0 + H_{\rm int} + H_{\rm L}, \tag{5}$$

$$H_0 = -\beta\sum_{r,\sigma}(a^+_{r\sigma}a_{r+1\sigma}+\text{h.c.}), \tag{6}$$

$$H_{\rm int} = g\sum_{r,\sigma}Q_r n_{r\sigma} + \frac{1}{2}I\sum_{r,\sigma}n_{r\sigma}n_{r-\sigma} + \frac{1}{2}\Delta\alpha\sum_{r,\sigma}n_{r\sigma}(\delta_{r,3}+\delta_{r,6}), \tag{7}$$

$$H_{\rm L} = \frac{1}{2}M\Omega^2\sum_r Q_r^2. \tag{8}$$

Now, let us outline the one-electron theory of Jahn-Teller distortion. The molecular orbitals given by H_0 have LCAO coefficients at the atomic site r as given by,

$$C_{r,k_n} = 1/\sqrt{6}\,e^{ik_n r}, \tag{9}$$

where the periodic boundary condition for k_n imposes that

$$k_n = \frac{\pi}{3}n \quad (n=0, \pm1, \pm2, 3), \tag{10}$$

and the one-electron spectrum is given by

$$\varepsilon_n = -2\beta\cos k_n. \tag{11}$$

In the neutral benzene, the orbitals $n=0$ and ±1 are occupied. The odd electron in the benzene anion may occupy either one of the orbitals with $n=+2$ or -2, so that the state of the anion is doubly degenerate (the spin of the odd electron is fixed). Therefore, any perturbation which has the component of C_2-symmetry will remove this degeneracy, even if it may be considerably small. Indeed, if the electron-electron interaction is neglected for a time, the first order perturbation theory gives the splitting of ε_2 as

$$\tilde{\varepsilon}_\pm = \varepsilon_2 \pm \Delta. \tag{12}$$

We express the distortion of C_2-mode, which couples with the orbitals $n=\pm2$, as

$$Q_r = \frac{1}{6}Q(e^{ik_2 r+i\varphi}+e^{-ik_2 r-i\varphi}), \tag{13}$$

where Q and φ are the amplitude and the phase of distortion, respectively. Then, Δ is given by

$$\Delta = \frac{1}{6}\{(\Delta\alpha)^2 - gQ\Delta\alpha\cos\varphi + g^2Q^2\}^{1/2}. \tag{14}$$

The odd electron must occupy the level $\tilde{\varepsilon}_-$, so that the energy change caused by the distortion is

$$W = -\Delta + \frac{1}{6}M\Omega^2Q^2. \tag{15}$$

Equation 15 plays the role of adiabatic potential for the system. The ground state configuration is obtained by minimizing W with respect to Q and φ, and as optimum values we obtain

$$\varphi_0 = 0 \text{ or } \pi, \tag{16}$$

according to $\Delta\alpha<0$ or >0, respectively, and

$$Q_0 = g/(2M\Omega^2). \tag{17}$$

The minimum of W is negative, so that the Jahn-Teller distortion is stabilized. The odd electron distribution becomes nonuniform as given by

$$\Delta n_r = \frac{1}{6}(1\mp\cos\frac{2\pi}{3}r), \tag{18}$$

where the sign $\mp$ corresponds to $\Delta\alpha\gtrless0$. Within this approach the spin density distribution is the same as Eq. 18 apart from the factor 1/2 (Fig. 2). Equation 18 is the same as obtained by Hobey and McLachlan.[3]

Green's Function Theory

In benzene the electron repulsion is not considered to be small and the one-electron theory considering only the degenerate orbitals with $n=\pm2$ is too simple to explain the real system. We must consider all the seven electrons together in the framework of the many-body theory, even within the Hartree-Fock scheme. For this purpose it is convenient to introduce the Green's function defined by

$$G^\sigma_{r,s}(t) = -i\langle T[a_{r\sigma}(t)a^+_{s\sigma}(0)]\rangle. \tag{19}$$

Transforming the atomic orbitals into the molecular orbitals, Eq. 19 becomes

$$G^\sigma_{r,s}(t) = \frac{1}{6}\sum_{p,q}G^\sigma_{p,q}(t)e^{ipr-iqs}, \tag{20}$$

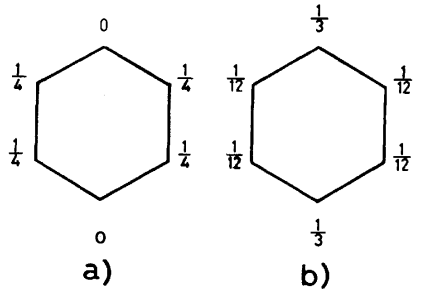

Fig. 2. The electron density distribution in the one-electron theory. a) $\Delta\alpha>0$, b) $\Delta\alpha<0$.

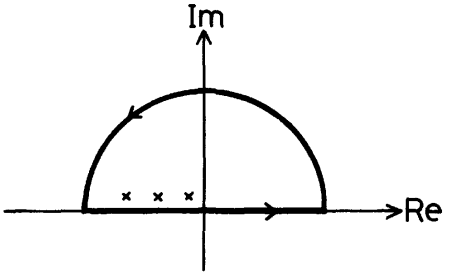

Fig. 3. Closed contour for Eq. 25. The crosses represent the singular points of the Green's function. The contour of integration in the complex plane is the real axis from $-\infty$ to ∞ and the semicircle of the upper half plane.

where

$$G^{\sigma}_{p,q}(t) = -i\langle T[a_{p\sigma}(t)a^{+}_{q\sigma}(0)]\rangle. \tag{21}$$

The Fourier transform of the Green's function is defined as

$$G^{\sigma}_{p,q}(t) = \int_{-\infty}^{\infty}\frac{d\varepsilon}{2\pi}G^{\sigma}_{p,q}(\varepsilon)e^{-i\varepsilon t}. \tag{22}$$

It can be expected that the special role played by the C_2-mode of distortion remains important so long as the electron repulsion is not too strong and we thus consider that the dominant components of the Green's function $G^{\sigma}_{p,q}(t)$ are those for $q=p$, $p\pm k$, where we denote as $k\equiv k_2=2\pi/3$, and the other components can be neglected. The electron distribution is then

$$n_{r\sigma} = n_{\sigma} + \sum_{p}(\langle a^{+}_{p+k\sigma}a_{p\sigma}\rangle e^{-ikr}+\text{c.c.}). \tag{23}$$

The first term of Eq. 23 is the uniform part of the density of the electron

$$n_{\sigma} = \frac{1}{N}\sum_{p}\langle a^{+}_{p\sigma}a_{p\sigma}\rangle = \begin{cases}4/6 \text{ for spin up}\\ 3/6 \text{ for spin down.}\end{cases} \tag{24}$$

The second term of Eq. 23 represents the non-uniform distribution. It is expressed by the Green's function as

$$\begin{aligned}\langle a^{+}_{p+k\sigma}a_{p\sigma}\rangle &= \frac{1}{i}\lim_{t\to 0-}G^{\sigma}_{p,p+k}(t)\\ &= \int_{-\infty}^{\infty}\frac{d\varepsilon}{2\pi i}G^{\sigma}_{p,p+k}(\varepsilon)e^{-i\varepsilon 0^{+}}.\end{aligned} \tag{25}$$

The ε-integral of Eq. 25 is estimated by closing the contour on the upper half plane as in Fig. 3 to be

$$\langle a^{+}_{p+k\sigma}a_{p\sigma}\rangle = \sum_{i\in\text{occ}}\text{residue of } G^{\sigma}_{p,p+k}(\varepsilon_i), \tag{26}$$

where ε_i is the i-th pole of the Green's function. The total energy can be expressed also by the Green's function as (see Appendix for details)

$$\begin{aligned}E = \frac{1}{2}\sum_{p,\sigma}\int\frac{d\varepsilon}{2\pi i}[&(\varepsilon+n_{-\sigma}I+\varepsilon_p)G^{\sigma}_{p,p}(\varepsilon)\\ &+\frac{1}{6}(gQe^{i\varphi}+\Delta\alpha)G^{\sigma}_{p,p+k}(\varepsilon)\\ &+\frac{1}{6}(gQe^{-i\varphi}+\Delta\alpha)G^{\sigma}_{p,p-k}(\varepsilon)].\end{aligned} \tag{27}$$

Equation 27 can be estimated by the sum of the residue of the occupied levels as expressed by Eq. 26.

Now, the equation of motion for the Green's function leads to[12]

$$\begin{aligned}i\frac{\partial}{\partial t}G^{\sigma}_{r,s}(t) = &\delta_{r,s}\delta(t)\\ &+\{gQ_r+\frac{1}{2}\Delta\alpha(\delta_{r,3}+\delta_{r,6})\}G^{\sigma}_{r,s}(t)\\ &-\beta\{G^{\sigma}_{r+1,s}(t)-G^{\sigma}_{r-1,s}(t)\}\\ &+I\Gamma^{\sigma}_{r,s}(t),\end{aligned} \tag{28}$$

where

$$\Gamma^{\sigma}_{r,s}(t) = -i\langle T[n_{r-\sigma}(t)a_{r\sigma}(t)a^{+}_{s\sigma}(0)]\rangle \tag{29}$$

is the higher order Green's function. Within the Hartree-Fock scheme $\Gamma^{\sigma}_{r,s}$ is approximated by decoupling as

$$\Gamma^{\sigma}_{r,s}(t) = n_{r-\sigma}G^{\sigma}_{r,s}(t). \tag{30}$$

Then, in the molecular orbital representation the equation becomes

$$\begin{aligned}(\varepsilon-\varepsilon_p-In_{-\sigma})G^{\sigma}_{p,q}(\varepsilon) - C_{\sigma}G^{\sigma}_{p+k,q}(\varepsilon)\\ - C^{*}_{\sigma}G^{\sigma}_{p-k,q}(\varepsilon) = \delta_{p,q},\end{aligned} \tag{31}$$

where

$$C_{\sigma} = \frac{1}{6}(gQe^{-i\varphi}+\Delta\alpha+D_{-\sigma}), \tag{32}$$

and

$$D_{\sigma} = I\sum_{p}\langle a^{+}_{p+k\sigma}a_{p\sigma}\rangle \tag{33}$$

is determined by Eq. 25. It is easily shown that the total energy is minimized when C_{σ} and D_{σ} are real and $\varphi=0$ or π. The system as expressed by Eq. 31 is separated into two sets of equations as illustrated in Fig. 4. Then, the equations for $G_{p,p}$ and $G_{p,p\pm k}$ are expressed as

$$\begin{bmatrix}\varepsilon-\omega_{2,\sigma} & -C_{\sigma} & -C_{\sigma}\\ -C_{\sigma} & \varepsilon-\omega_{0,\sigma} & -C_{\sigma}\\ -C_{\sigma} & -C_{\sigma} & \varepsilon-\omega_{2,\sigma}\end{bmatrix}\begin{bmatrix}G^{\sigma}_{2,q}\\ G^{\sigma}_{0,q}\\ G^{\sigma}_{-2,q}\end{bmatrix} = \begin{bmatrix}\delta_{2,q}\\ \delta_{0,q}\\ \delta_{-2,q}\end{bmatrix}, \tag{34}$$

$$\begin{bmatrix}\varepsilon-\omega_{1,\sigma} & -C_{\sigma} & -C_{\sigma}\\ -C_{\sigma} & \varepsilon-\omega_{3,\sigma} & -C_{\sigma}\\ -C_{\sigma} & -C_{\sigma} & \varepsilon-\omega_{1,\sigma}\end{bmatrix}\begin{bmatrix}G^{\sigma}_{1,q}\\ G^{\sigma}_{3,q}\\ G^{\sigma}_{-1,q}\end{bmatrix} = \begin{bmatrix}\delta_{1,q}\\ \delta_{3,q}\\ \delta_{-1,q}\end{bmatrix}, \tag{35}$$

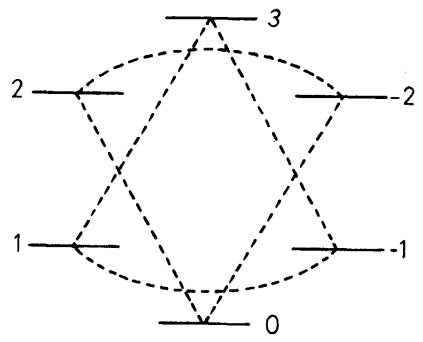

Fig. 4. The coupling of the orbitals in Eqs. 34, 35 by dashed lines.

where

$$\omega_{i,\sigma} = \varepsilon_i + n_{-\sigma}I. \tag{36}$$

The one-electron energies given by the eigenvalues of Eqs. 34 and 35 are expressed as

$$\tilde{\varepsilon}_i^\sigma = \tilde{\omega}_i^\sigma + n_{-\sigma}I, \tag{37}$$

where

$$\begin{aligned}
\tilde{\omega}_1^\sigma &= \frac{1}{2}(-\beta+C_\sigma-\gamma_+^\sigma),\\
\tilde{\omega}_2^\sigma &= -\beta - C_\sigma,\\
\tilde{\omega}_3^\sigma &= \frac{1}{2}(\beta+C_\sigma-\gamma_-^\sigma),\\
\tilde{\omega}_4^\sigma &= \beta - C_\sigma,\\
\tilde{\omega}_5^\sigma &= \frac{1}{2}(-\beta+C_\sigma+\gamma_+^\sigma),\\
\tilde{\omega}_6^\sigma &= \frac{1}{2}(\beta+C_\sigma+\gamma_-^\sigma),\\
\gamma_\pm^\sigma &= 3\sqrt{\beta^2 \pm (2/3)\beta C_\sigma + C_\sigma^2}.
\end{aligned} \tag{38}$$

Then, Green's functions are solved as

$$\begin{aligned}
G_{0,0}^\sigma(\varepsilon) &= \frac{\varepsilon-\tilde{\omega}_2^\sigma-C_\sigma}{Det_2^\sigma(\varepsilon)},\\
G_{1,1}^\sigma(\varepsilon) &= G_{-1,-1}^\sigma(\varepsilon) = \frac{1}{2}\left\{\frac{\varepsilon-\tilde{\omega}_3^\sigma}{Det_1^\sigma(\varepsilon)}+\frac{1}{\varepsilon-\tilde{\varepsilon}_2^\sigma}\right\},\\
G_{2,2}^\sigma(\varepsilon) &= G_{-2,-2}^\sigma(\varepsilon) = \frac{1}{2}\left\{\frac{\varepsilon-\tilde{\omega}_0^\sigma}{Det_2^\sigma(\varepsilon)}+\frac{1}{\varepsilon-\tilde{\varepsilon}_4^\sigma}\right\},\\
G_{3,3}^\sigma(\varepsilon) &= \frac{\varepsilon-\tilde{\omega}_1^\sigma-C_\sigma}{Det_1^\sigma(\varepsilon)},
\end{aligned} \tag{39}$$

and

$$\begin{aligned}
G_{-1,1}^\sigma(\varepsilon) &= G_{1,-1}^\sigma(\varepsilon) = \frac{1}{2}\left\{\frac{\varepsilon-\tilde{\omega}_3^\sigma}{Det_1^\sigma(\varepsilon)}-\frac{1}{\varepsilon-\tilde{\varepsilon}_2^\sigma}\right\},\\
G_{-2,2}^\sigma(\varepsilon) &= G_{2,-2}^\sigma(\varepsilon) = \frac{1}{2}\left\{\frac{\varepsilon-\tilde{\omega}_0^\sigma}{Det_2^\sigma(\varepsilon)}-\frac{1}{\varepsilon-\tilde{\varepsilon}_4^\sigma}\right\},\\
G_{3,1}^\sigma(\varepsilon) &= G_{1,3}^\sigma(\varepsilon) = G_{3,-1}^\sigma(\varepsilon) = G_{-1,3}^\sigma(\varepsilon) = \frac{C_\sigma}{Det_1^\sigma(\varepsilon)},\\
G_{0,2}^\sigma(\varepsilon) &= G_{2,0}^\sigma(\varepsilon) = G_{0,-2}^\sigma(\varepsilon) = G_{-2,0}^\sigma(\varepsilon) = \frac{C_\sigma}{Det_2^\sigma(\varepsilon)},
\end{aligned} \tag{40}$$

Table 1. The self-consistent solutions for the weak repulsion

	$\Delta\alpha>0$	$\Delta\alpha<0$
$D+$	$-1/2I$	$1/2I$
$D-$	0	0
$C+$	$1/6(gQ+\Delta\alpha)$	$-1/6(gQ+\lvert\Delta\alpha\rvert)$
$C-$	$-I/12+1/6(gQ+\Delta\alpha)$	$I/12-1/6(gQ+\lvert\Delta\alpha\rvert)$
Δn_r	$1/6(1-\cos 2\pi/3r)$	$1/6(1+\cos 2\pi/3r)$
S_r	$1/12(1-\cos 2\pi/3r)$	$1/12(1+\cos 2\pi/3r)$
φ	0	π

Δn_r is the distribution of the excess charge normalized as $\sum\Delta n_r=1$. S_r is the spin distribution.

where

$$\begin{aligned}
Det_1^\sigma(\varepsilon) &= (\varepsilon-\tilde{\varepsilon}_3^\sigma)(\varepsilon-\tilde{\varepsilon}_6^\sigma),\\
Det_2^\sigma(\varepsilon) &= (\varepsilon-\tilde{\varepsilon}_5^\sigma)(\varepsilon-\tilde{\varepsilon}_1^\sigma).
\end{aligned} \tag{41}$$

Analytic Solutions in Limiting Cases

The Green's functions, which is dependent on the potential C_σ, must be solved self-consistently with Eqs. 32 and 33. The equations are solved numerically as shown in the next section. Here we give the analytic solutions for two limiting cases of the weak and strong repulsion, as follows.

1. Weak repulsion $\beta \gg |C_\sigma|$ $(I \ll \beta)$

In this case the essential features of the one-electron theory described above are remain unchanged. The occupied levels are in ascending order

$$\begin{aligned}
&\omega_1^+, \omega_2^+, \omega_3^+, \omega_4^+, \omega_1^-, \omega_2^-, \omega_3^- \quad \text{for } \Delta\alpha > 0\\
&\omega_1^+, \omega_3^+, \omega_2^+, \omega_5^+, \omega_1^-, \omega_3^-, \omega_2^- \quad \text{for } \Delta\alpha < 0.
\end{aligned} \tag{42}$$

The self-consistent solution in the leading order in I/β are listed in Table 1. The real and small parameter of expansion is $|C_\sigma|/\beta$, but not I/β. The former is small as far as I is not too large even if it exceeds β, as will be demonstrated numerically.

The energy gain of the distortion is given by

$$\begin{aligned}
\Delta E &= E - E_0\\
&= -\frac{1}{6}(gQ+|\Delta\alpha|) + \frac{M}{6}\Omega^2Q^2,
\end{aligned} \tag{43}$$

where E_0 is the H. F. energy of undistorted configuration of the benzene anion,

$$E_0 = -7\beta + I. \tag{44}$$

The magnitude of Q for the equilibrium configuration is determined by the minimization of Eq. 43 as

$$Q_0 = g/(2M\Omega^2). \tag{45}$$

Equations 43 and 45 agree with the results in the one-electron theory.

2. Strong repulsion $\beta \ll |C_\sigma|$ $(I \gg \beta)$

The occupied levels are the same as Eq. 42. The

TABLE 2. TWO CLASSES OF THE SELF-CONSISTENT SOLUTIONS FOR THE STRONG REPULSION, ONE STABLE (A) AND ONE UNSTABLE (B)

	A (stable)	B (unstable)
$D+$	$-2I$	I
$D-$	$3/2I$	$-3/2I$
$C+$	$I/4+1/6(gQ+\Delta\alpha)$	$-I/4+1/6(gQ+\lvert\Delta\alpha\rvert)$
$C-$	$-I/3+1/6(gQ+\Delta\alpha)$	$I/6+1/6(gQ+\lvert\Delta\alpha\rvert)$
Δn_r	$1/6(1-\cos 2\pi/3r)$	$1/6(1-\cos 2\pi/3r)$
S_r	$1/12(1-7\cos 2\pi/3r)$	$1/12(1+5\cos 2\pi/3r)$
φ	0	0

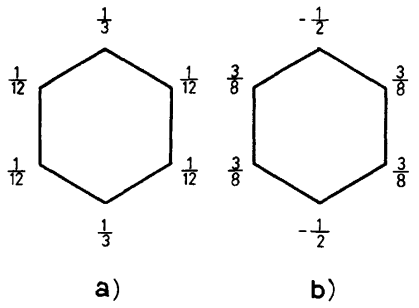

Fig. 5. a) Excess charge distribution, b) Spin distribution.

solutions are given in Table 2. In this case two classes of self-consistent solutions A and B are possible. The energy gain of A and B are, respectively

$$\Delta E_A = I + \beta - \frac{1}{6}(gQ+\Delta\alpha) + \frac{M}{6}\Omega^2Q^2, \quad (46)$$

$$\Delta E_B = -\frac{1}{2}I + \beta - \frac{1}{6}(gQ+\Delta\alpha) + \frac{M}{6}\Omega^2Q^2. \quad (47)$$

As long as $I \gg \beta$, the energy of A is lower than that of B irrespective of the sign of $\Delta\alpha$, so that A is the stable configuration. The minimum of Eq. 46 gives Q_0 as the same as Eq. 45. The distributions of the excess charge and spin are illustrated in Fig. 5. The effect of the electron-repulsion is drastic. The odd electron polarizes the electrons at the levels of $n=0, \pm 1$ which already exist in the neutral benzene, and leads to the negative spin density at sites 3 and 6.

Numerical Results

For the whole range of I, the numerical analysis is performed. We give values of the parameters as follows.

$$\Delta\alpha = 0.01,$$
$$g = 0.04,$$
$$Q = 0.02.$$

The sign of $\Delta\alpha$ represents the electrophilicity or the nucleophilicity of the solvent. The absolute value of $\Delta\alpha$ and g can be selected rather arbitrarily, because they affect hardly on the results. Q is the value that lets the total energy minimize on $I=3$ (this value of I would probably correspond to the electron correlation for the benzene molecule.).

The results are shown in Figs. 6—10. All the resultant values for $I \geqq 15$ are very close to the analytic solutions given in the previous section. The I dependence of C_σ, D_σ/I and that of energy E are represented in Figs. 6 and 7, respectively. As illustrated in figures, two classes of self-consistent solutions, one stable and one unstable, exist as mentioned before. The solid and dashed curves correspond to the stable solution A and the unstable one B, respectively. The orbital patterns corresponding to the two classes of solutions for $I=3$ and 12 are illustrsted in Fig. 8. It is easy to see that the patterns for unstable solution does not give the proper ground state.

Figure 9 shows the behavior of the charge density and the spin density *versus* I. In this figure the solid and dashed curves correspond to the values on sites 1 and 6, respectively.

Figure 10 represents the relation between the total energy E and the displacement Q, and shows the stabilization of energy due to the Jahn-Teller effect. On calculating the total energy, we assigned the value of 4.12 for the parameter $M\Omega^2$ which is calculated from

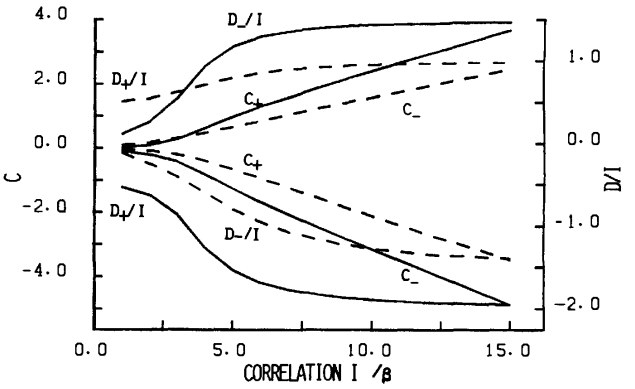

Fig. 6. C_σ and D_σ/I *vs.* I. I is represented in the unit $\beta=1$. We give values of the parameters as follows: $\Delta\alpha=0.01$, $g=0.04$, $Q=0.02$. The solid and dashed curves correspond to the stable and unstable solutions, respectively.

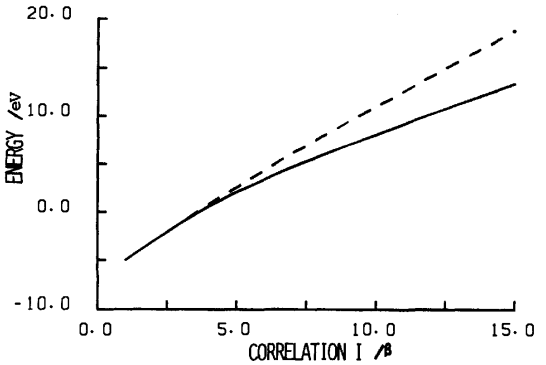

Fig. 7. E *vs.* I. All parameters and curves are the same as Fig. 6.

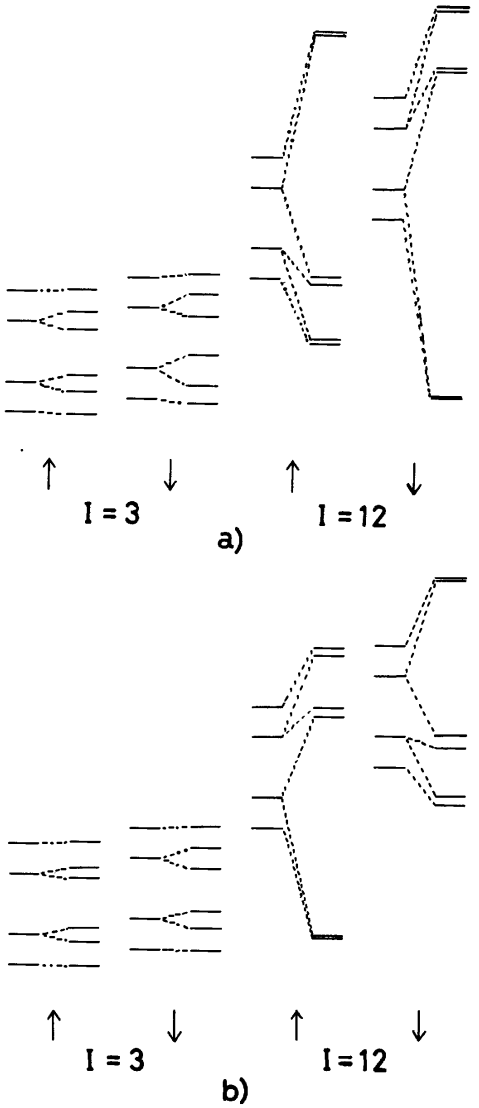

Fig. 8. The orbital patterns for the undistorted and distorted cases with $I=3$ and 12 are compared. a) Orbital patterns for stable solution, b) For unstable one. The up and down arrows represent the up and down spin orbitals, respectively. All parameters are the same as Fig. 6.

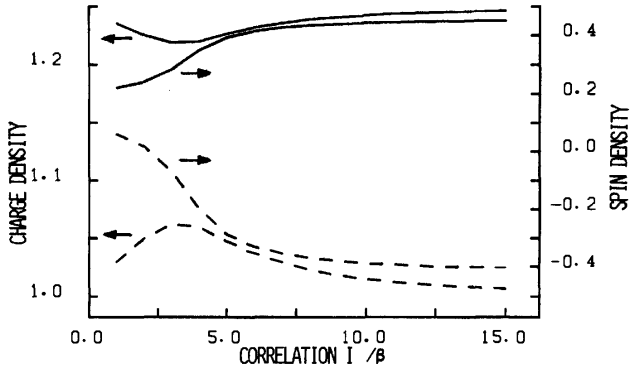

Fig. 9. The charge density and the spin density *vs.* I. The solid and dashed curves correspond to the densities for the case of the stable solution on sites 1 and 6, respectively. All parameters are the same as Fig. 6.

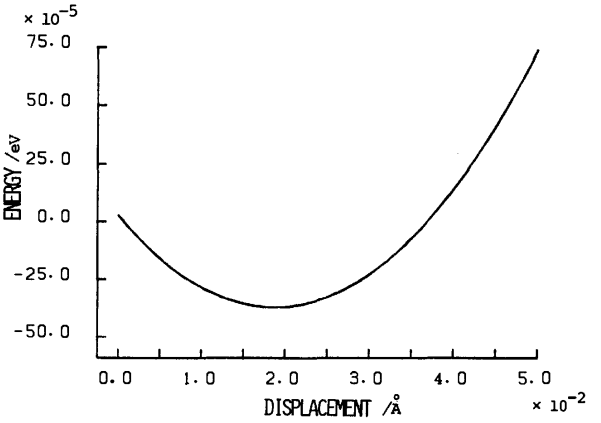

Fig. 10. The energy gain due to the distortion Q. The energy is expressed in eV and Q in Å. $\Delta\alpha=0.01$, $g=0.04$, $I=3$, $M\Omega^2=4.12$.

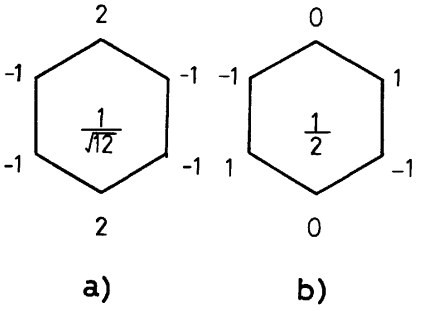

Fig. 11. The wave functions of unoccupied and degenerate levels of benzene. The numbers inside the rings are normalization factor.

the force constant of the E_g^+ vibronic mode of the benzene molecule.[13] The energy is minimized at $Q=0.02$ Å.

Concluding Remarks

We have analyzed the Jahn-Teller distortion of the benzene anion on the basis of the modified P.P.P. models. As far as the repulsion is weak, our results confirm the simple theory considering only the odd electron of the anion.[3] But if the repulsion becomes strong, *i.e.*, $I/\beta>15$ the effect of other π electrons becomes significant. This effect appears more remarkably on the distribution of the spin than that of the charge. The discrepancy between the distributions of the spin and charge originates from the exchange interaction between the π electrons which is not considered in the single electron theory.

We wish to stress a few points. Look at Fig. 11 which displays the amplitude of the unoccupied, degenerate wave functions with $n=\pm2$ of benzene. The odd electron of the benzene anion is equally distributed on these two states. However, this picture is only for pictorial understanding and each pattern of the charge density distribution given by a) or b) in Fig. 11 is of less meaning by itself, but the mean of them would correspond to usual experimental observations. This

aspect holds even if the vibronic interaction is introduced in Eq. 7 to remove the degeneracy, since the phase of the electron distribution remains still arbitrary.

The external perturbation which reduces the molecular symmetry from C_6 to C_2 and fixes the phase φ is given by the last term of Eq. 7. Let this perturbation work during a characteristic time τ. So long as τ is large enough compared with the time scale during which the position determining experimental observation can be made, the states indicated in Fig. 11 a) and b), and the similar ones in Fig. 5 become meaningfull. The curious distributions of the odd electron density or the spin density shown in Fig. 5 are to be understood as an event taking place in the characteristic time τ. In other words, we may imagine that during this time the solvent molecules are located near the positions 3 and 6. If τ is quite small, we would observe time averaged uniform distributions for the charge and spin densities. Such consideration plays an important role in the analysis of the observed ESR spectra of this ion.[14]

Finally we stress that the negative spin densities at sites 3 and 6 induced by the strong electron interaction are interesting, because it makes an excellent contrast to the case of the single electron theories.

Appendix

In this appendix we derive Eq. 27 for the total energy.[15] First, the Hamiltonian (Eqs. 5—7) are re-written as

$$H_{el} = H_1 + H_2, \tag{48}$$

where

$$H_1 = -\beta\sum_{r,\sigma}(a^+_{r\sigma}a_{r+1\sigma}+\text{h.c.}) + \frac{1}{2}\Delta\alpha\sum_{r,\sigma}n_{r\sigma}(\delta_{r,3}+\delta_{r,6}) + g\sum_{r,\sigma}Q_r n_{r\sigma}, \tag{49}$$

$$H_2 = \frac{1}{2}I\sum_{r,\sigma}n_{r\sigma}n_{r-\sigma}. \tag{50}$$

The expectation value of H_1 is expressed as

$$\langle H_1\rangle = -i[-\beta\sum_{r,\sigma}\{G^{\sigma}_{r+1,r}(t)+G^{\sigma}_{r-1,r}(t)\} + \sum_{r,\sigma}(gQ_r+\frac{1}{2}\Delta\alpha(\delta_{r,3}+\delta_{r,6})G^{\sigma}_{r,r}(t)]_{t\to 0^-}. \tag{51}$$

The expectation value of H_2 is written as

$$\langle H_2\rangle = \frac{1}{2}I\sum_{r,\sigma}\langle a^+_{r\sigma}a^+_{r-\sigma}a_{r-\sigma}a_{r\sigma}\rangle. \tag{52}$$

Comparing Eq. 52 with Eqs. 28 and 29, we obtain

$$\langle H_2\rangle = -\frac{i}{2}\sum_{r,\sigma}[(i\frac{\partial}{\partial t}-gQ_r-\Delta\alpha\delta_{r,6})G^{\sigma}_{r,r}(t) + \beta\{G^{\sigma}_{r+1,r}(t) + G^{\sigma}_{r-1,r}(t)\}]_{t\to 0^-}. \tag{53}$$

Adding Eqs. 51, 53, and the elastic energy Eq. 8, we obtain Eq. 27.

References

1) A. D. Liehr, *Z. Phys. Chem.*, **9**, 338 (1956).
2) L. C. Snyder, *J. Chem. Phys.*, **33**, 619 (1960).
3) W. D. Hobey and A. D. McLachlan, *J. Chem. Phys.*, **33**, 1695 (1960).
4) H. M. McConnel and A. D. McLachlan, *J. Chem. Phys.*, **34**, 1 (1961).
5) M. Kimura, K. Nishikawa, and S. Aono, *Bull. Chem. Soc. Jpn.*, **54**, 3619 (1981).
6) K. Nishikawa, M. Kimura, and S. Aono, *Bull. Chem. Soc. Jpn.*, **54**, 3624 (1981).
7) W. P. Su, J. R. Schriefer, and A. J. Heeger, *Phys. Rev.*, **B34**, 2099 (1980).
8) T. Holstein, *Ann. Phys.*, **8**, 325 (1959).
9) S. Kivelson and D. E. Heim, *Phys. Rev.*, **B26**, 4278 (1982).
10) Y. Toyozawa, *J. Phys. Soc. Jpn.*, **50**, 1861 (1981).
11) K. Nasu and Y. Toyozawa, *J. Phys. Soc. Jpn.*, **51**, 2098 (1982).
12) J. Hubbard, *Proc. Roy. Soc.*; **A276**, 238 (1963).
13) S. Mizushima and T. Shimanouchi, "Infrared Absorption and Raman Effect," Kyoritsu publishing, Tokyo, (1985).
14) M. G. Townsent and S. I. Weissman, *J. Chem. Phys.*, **32**, 309 (1960).
15) A. L. Fetter and J. D. Walecka, "Quantum Theory of Many-Particle Systems," McGraw-Hill, New York, (1971).

 © 1985 The Chemical Society of Japan Bull. Chem. Soc. Jpn., 58, 2763—2768 (1985)

ESR Spectra of Benzene Anion

Minoru KIMURA,† Hiroyuki KAWABE, Kiyoshi NISHIKAWA, and Shigeyuki AONO*
†*Department of Physics, Faculty of Science, Kanazawa University, Marunouchi, Kanazawa 920*
Department of Chemistry, Faculty of Science, Kanazawa University, Marunouchi, Kanazawa 920
(Received April 27, 1985)

Based on the spin density calculated in our previous paper,[1] the ESR spectra of the benzene anion (exactly the dihydrophenylide ion) are analyzed by the Bloch equation. A hyperfine spectrum broader than those of usual aromatic radicals attributes to the chemical exchange process that the ion in question surrounded by solvent molecules undergoes a rotational motion characterized by the time τ which is the life time of chemical exchange. The line shape for each hyperfine spectrum is given in terms of $1/T_2$ and τ under the condition of $\tau/T_2 \ll 1$.

It is an old story that, in the liquid state, the ESR spectra of the benzene anion were considerably broader[2] than those of usual aromatic radicals with less symmetric character as naphthalene anion (dihydronaphthylide ion). The similar phenomena have been observed in coronene and triphenylene,[2] which suggest that the unusual broad lines may be associated with the Jahn-Teller distortion. The normal states of those ions would be orbitally degenerate if the original symmetries of the parent molecules were retained. If the vibronic interaction is introduced to this system, the orbital degeneracy will be removed and the lattice distortion should arise (the Jahn-Teller effect). McConnell and McLachlan[3] have studied this in such a way that the electronic part is based on the Hückel approximation and the vibronic part is considerably elaborated. In our previous paper,[1] we have investigated the same problem by the Hubbard Hamiltonian with the vibronic interaction (including the dominant part of electron correlation). Both results agree with each other in the limitting case of the electron correlation being negligible. However, the latter demonstrates the important effect of the electron correlation which causes the negative spin densities at opposing corners of the benzene anion. In the second half of their paper,[3] McConnell and McLachlan discussed about the broad lines from the view points of chemical exchange briefly and only qualitatively. The main purpose of the present paper is to analyze the line shape in more detail, using the Bloch equation with chemical exchange.

A deutrium substitution of a hydrogen has been used in order to lift experimentally the orbital degeneracy. In this way, the complicated but sometimes well resolved spectra have been observed not only for the benzene anion[4] but also for more complicated radicals.[5] We consider that these observations partly support the chemical exchange mechanism with the reduction of symmetry due to the Jahn-Teller distortion for the unusual broad line.

Line Shape Analysis of Bloch Equation with Chemical Exchange

Let us consider the Bloch equation for some conformation X which appears during the chemical exchange process,[6]

$$\frac{dG_X}{dt} + \eta_X G_X = -i\omega_1 M_0, \tag{1}$$

where

$$G_X = u_X + iv_X,$$
$$\eta_X = \frac{1}{T_2} - i(\Delta\omega + \omega_X), \tag{2}$$

and u and v are the in-phase and out-of-phase magnetization. The latter being responsible for the absorption process, we are interested in the imaginary part of G. And $\omega_1 = \gamma_e H_1$, γ_e is the gyromagnetic ratio of electron, H_1 is the magnitude of the applied microwave field, assuming no saturation, $M_0 \approx M_z$, M_z is the static magnetization along the direction of the external field, T_2 is the transverse relaxation time without taking into account of chemical exchange, ω_X is the hyperfine shift due to proton, $\Delta\omega = \omega_0 - \omega$ with $\omega_0 = \gamma_e H_0$, H_0 is the intensity of the external field along the z-axis and ω is the frequency.

Equation 1 gives the result,

$$G_X(t) = -\frac{i\omega_1 M_0}{\eta_X}\{1 - \exp(-\eta_X t)\} + G_X^0 \exp(-\eta_X t), \tag{3}$$

where

$$G_X^0 = G_X(t=0). \tag{4}$$

Assuming the characteristic time τ_X for the conformation X, we have the time average of $G_X(t)$ as,

$$\bar{G}_X = \frac{1}{\tau_X}\int_0^\infty G_X(t) \exp(-t/\tau_X) dt$$
$$= -\frac{i\omega_1 M_0}{1+\eta_X \tau_X} + \frac{G_X^0}{1+\eta_X \tau_X}. \tag{5}$$

In order to relate $\bar{G}_X$ with the observation we have to average over all possible values of G_X^0. The value of G_X^0 depends on the immediate past of the system. If the molecular conformation changes to the conformation X from the conformations I's with the probabilities ρ_I's, it follows that

$$\langle G_X^0 \rangle = \sum_I{}' \rho_I \langle \bar{G}_I \rangle, \tag{6}$$

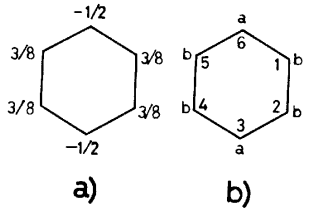

Fig. 1. Spin distribution in the benzene anion. a): Strong correlation limit, b): General case. The numbers indicate the site.

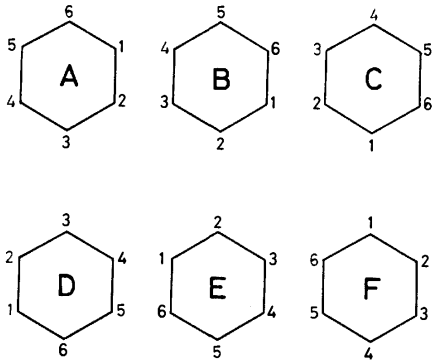

Fig. 2. Various orientations of the benzene anion. The conformations *A*—*F* appear with the rotational motion of anion. The numbers indicate the sites and the spin densities are *a* at the sites 3 and 6, and *b* at the other sites.

but the summation with a prime is restricted to the immediate past conformations for *X*. From Eqs. 5 and 6 we get the following relation,

$$\langle\bar{G}_X\rangle = -\frac{i\omega_1 M_0}{1+\eta_X\tau_X} + \frac{1}{1+\eta_X\tau_X}\sum_I{}'\rho_I\langle\bar{G}_I\rangle. \tag{7}$$

This procedure of incorporating the second term corresponds to including chemical exchange. The actual observation can be interpreted from

$$\langle G\rangle = \sum_X P_X\langle\bar{G}_X\rangle, \tag{8}$$

where P_x is the existing probability of conformation *X* and the summation is over the all possible conformations.

Physical Model

In our previous paper,[1] we obtained for the benzene anion the state in which the spin distribution is shown in Fig. 1a (the strong correlation limit) and in Fig. 1b (general case). As was stressed there, these are the cases that the anion is fixed for a characteristic time τ by the solvent effect. We assume that the anion rotates from time to time to take various orientations as shown in Fig. 2 and each conformation has the same characteristic time τ and the same probability of existance, namely, $P_x=1/6$.

Look at the conformation A in Fig. 2. The immediate past history of this conformation should be either B or F, each of which changes into A with the same probability 1/2. Therefore. Eq. 7 becomes

$$\langle\bar{G}_A\rangle = -\frac{i\omega_1 M_0\tau}{1+\eta_A\tau} + \frac{\langle\bar{G}_B\rangle+\langle\bar{G}_F\rangle}{2(1+\eta_A\tau)}, \tag{9}$$

which is abbreviated as

$$g_A + c_A(g_B+g_F) = d_A \tag{10}$$

where

$$g_A = \langle\bar{G}_A\rangle,$$
$$c_A = -\frac{1}{2(1+\eta_A\tau)},$$
$$d_A = -\frac{i\omega_1 M_0\tau}{1+\eta_A\tau}. \tag{11}$$

For the other conformations similar equations hold. They are altogether written in matrix form as

$$\begin{bmatrix} g_A \\ g_B \\ g_C \\ g_D \\ g_E \\ g_F \end{bmatrix} = \begin{bmatrix} 1 & c_A & 0 & 0 & 0 & c_A \\ c_B & 1 & c_B & 0 & 0 & 0 \\ 0 & c_C & 1 & c_C & 0 & 0 \\ 0 & 0 & c_D & 1 & c_D & 0 \\ 0 & 0 & 0 & c_E & 1 & c_E \\ c_F & 0 & 0 & 0 & c_F & 1 \end{bmatrix}^{-1} \begin{bmatrix} d_A \\ d_B \\ d_C \\ d_D \\ d_E \\ d_F \end{bmatrix}, \tag{12}$$

and $\langle G\rangle$ related to the actual observation can be obtained by

$$\langle G\rangle = \frac{1}{6}\sum_X g_X. \tag{13}$$

From Eqs. 12 and 13 we obtain

$$\langle G\rangle = \frac{1}{6}\frac{1}{\det}\sum_X d_X F_X, \tag{14}$$

where

$$\det = \begin{vmatrix} 1 & c_A & 0 & 0 & 0 & c_A \\ c_B & 1 & c_B & 0 & 0 & 0 \\ 0 & c_C & 1 & c_C & 0 & 0 \\ 0 & 0 & c_D & 1 & c_D & 0 \\ 0 & 0 & 0 & c_E & 1 & c_E \\ c_F & 0 & 0 & 0 & c_F & 1 \end{vmatrix},$$

$$F_A = 1 - c_B - c_F - c_C c_D - c_D c_E + c_B(c_D c_E + c_E c_F) + c_F(c_B c_C + c_C c_D) + c_B c_C c_D c_E - c_E c_F(c_B c_C - c_C c_D) - 2c_B c_C c_D c_E c_F. \tag{15}$$

In obtaining F_B—F_F, we need only the cyclic permutation of suffixes in the second formula in Eq. 15, step by step.

Now we turn to evaluate the hyperfine shifts.

(1) I_Z=3: Every protons have the up spin.

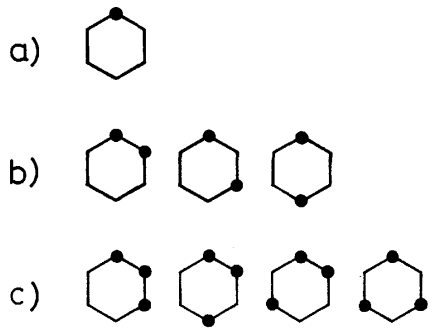

Fig. 3. Irreducible patterns. The solid circles indicate the sites to which the protons with down spin link.
a): For $I_z=2$, b): For $I_z=1$, c): For $I_z=0$.

In this case, every conformations designated by A—F in Fig. 2 have the same proton hyperfine shift. *i.e.*,

$$\omega_A = \omega_B = \omega_C = \omega_D = \omega_E = \omega_F = 2a + 4b \quad [1],$$

where we omit the multiplicative constant, Q ($\approx$23 G, 1 G=10^{-4} T), for simplicity, a is the spin density at the sites 3 and 6, b at the other sites and the number in the square bracket indicates the degeneracy number.

(2) $I_Z=2$: One of the six protons has the down spin.

This case is displayed by the irreducible pattern shown in Fig. 3a. Combining this with the patterns shown in Fig. 2, we obtain

$$\omega_A = \omega_D = 4b,$$
$$\omega_B = \omega_C = \omega_E = \omega_F = 2a + 2b \quad [6].$$

(3) $I_Z=1$: Two of the six protons have the down spin.

This case is classified into three subcases as displayed by the irreducible patterns shown in Fig. 3b. The hyperfine shift will be calculated for each,

$$\text{(3a)} \quad \omega_A = \omega_B = \omega_D = \omega_E = 2b,$$
$$\omega_C = \omega_F = 2a \quad [6],$$
$$\text{(3b)} \quad \omega_A = \omega_C = \omega_D = \omega_F = 2b,$$
$$\omega_B = \omega_E = 2a \quad [6].$$
$$\text{(3c)} \quad \omega_B = \omega_C = \omega_E = \omega_F = 2a,$$
$$\omega_A = \omega_D = -2a + 2b \quad [6].$$

(4) $I_Z=0$: A half of the six protons have the down spin.

This case has four subcases which are displayed in Fig. 3c. The hyperfine shift is expressed as follows

$$\text{(4a)} \quad \omega_A = \omega_B = \omega_C = \omega_D = \omega_E = \omega_F = 0 \quad [6],$$
$$\text{(4b)} \quad \omega_A = \omega_D = -2a + 2b,$$
$$\omega_B = \omega_E = 0,$$
$$\omega_C = \omega_F = 2a - 2b \quad [6],$$
$$\text{(4c)} \quad \omega_A = \omega_D = 0,$$
$$\omega_B = \omega_E = -2a + 2b,$$
$$\omega_C = \omega_F = 2a - 2b \quad [6],$$
$$\text{(4d)} \quad \omega_A = \omega_B = \omega_C = \omega_D = \omega_E = \omega_F = 0 \quad [2].$$

Line Shape

In order to obtain the line shape for every hyperfine components, it is convenient to re-classify the above mentioned cases as follows.

Group 1: $\omega_A=\omega_B=\omega_C=\omega_D=\omega_E=\omega_F$.

This group consists of the three cases (1), (4a), and (4d). We calculate $\langle G\rangle$ by Eq. 14, and obtain

$$\langle G\rangle = \frac{d}{(1+2c)}, \tag{16}$$

where we used the relation

$$c = c_A = c_B = c_C = c_D = c_E = c_F,$$
$$d = d_A = d_B = d_C = d_D = d_E = d_F. \tag{17}$$

Substituting Eqs. 1 and 11 into Eq. 16, we have

$$\langle G\rangle = \frac{1}{(1/T_2)^2+(\Delta\omega+\omega_A)^2}\left\{-\omega_1 M_0 \Delta\omega + i\omega_1 M_0 \frac{1}{T_2}\right\}, \tag{18}$$

of which the imaginary part is

$$v = \frac{\omega_1 M_0/T_2}{(1/T_2)^2+(\Delta\omega+\omega_A)^2}. \tag{19}$$

Thus we get a Lorentzian line shape with the resonance frequency $\Delta\omega$, the peak height v_{peak} and the natural width $\Delta\omega_{1/2}$ given by

$$\Delta\omega = -\omega_A,$$
$$v_{peak} = \omega_1 M_0 T_2,$$
$$\Delta\omega_{1/2} = \frac{1}{T_2}. \tag{20}$$

Group 2: $\omega_A=\omega_D$, $\omega_B=\omega_C=\omega_E=\omega_F$.

This group consists of the two cases (2) and (3c). In the present case we have

$$\langle G\rangle = \frac{1}{6}\left\{\frac{2d_A(1-c_B)+4d_B(1-c_A)}{1-2c_Ac_B+c_B}\right\}. \tag{21}$$

Thus

$$v = \frac{-\omega_1 M_0\{1/T_2+4/27\cdot(\omega_A-\omega_B)^2\tau\}}{\{1/T_2-2/3\cdot(\Delta\omega+\omega_A)(\Delta\omega+\omega_B)\tau\}^2+\{\Delta\omega+1/3\cdot(\omega_A+2\omega_B)\}^2}. \tag{22}$$

In getting this result, we have assumed $\tau/T_2 \ll 1$, since $\tau\approx10^{-10}$ s[7] and for free radicals in solution the natural width of resonance lines is typically $\approx$0.1 G,[8] which is correspond to $T_2\approx10^{-6}$ s.

We proceed further by carrying out an approximate calculation. Obviously we have a resonance line around $\Delta\omega=-\omega_A$ where v takes the value given by

$$v_{\text{peak}} = -\omega_1 M_0 \left[\frac{1/T_2 + 4/27 \cdot (\omega_A - \omega_B)^2 \tau}{(1/T_2)^2 + 4/9 \cdot (\omega_A - \omega_B)^2} \right]. \quad (23)$$

Noting that $\omega_A - \omega_B \approx 10^7\ \text{s}^{-1}$, $\tau(\omega_A - \omega_B) \approx 10^{-3}$ and $\tau/T_2 \approx 10^{-4}$, we have $v_{\text{peak}} \fallingdotseq -\omega_1 M_0/(3/\tau)$. The corresponding half width being $3/\tau$, we add this to the natural width $1/T_2$ to obtain

$$v_{\text{peak}} = \frac{-\omega_1 M_0}{3/\tau + 1/T_2},$$
$$\Delta\omega_{1/2} = \frac{3}{\tau} + \frac{1}{T_2}. \quad (24)$$

In the same way, we obtain the corresponding expressions for another resonance at $\Delta\omega = -\omega_B$

$$v_{\text{peak}} = \frac{-\omega_1 M_0}{3/4\tau + 1/T_2},$$
$$\Delta\omega_{1/2} = \frac{3}{4\tau} + \frac{1}{T_2}. \quad (25)$$

and for the one at $\Delta\omega = -(\omega_A + 2\omega_B)/3$,

$$v_{\text{peak}} = \frac{-\omega_1 M_0}{4/27 \cdot (\omega_A - \omega_B)^2 \tau + 1/T_2},$$
$$\Delta\omega_{1/2} = \frac{4}{27}(\omega_A - \omega_B)^2 \tau + \frac{1}{T_2}. \quad (26)$$

Group 3: $\omega_B = \omega_E$, $\omega_A = \omega_C = \omega_D = \omega_F$.

This group consists of the single case (3b). Various lines belonging to this group can be described by interchanging suffixes A and B of Eqs. 24—26, that is,

$$\Delta\omega = -\omega_B,$$
$$v_{\text{peak}} = \frac{-\omega_1 M_0}{3/\tau + 1/T_2},$$
$$\Delta\omega_{1/2} = \frac{3}{\tau} + \frac{1}{T_2}, \quad (27)$$

and

$$\Delta\omega = -\omega_A,$$
$$v_{\text{peak}} = \frac{-\omega_1 M_0}{3/4\tau + 1/T_2},$$
$$\Delta\omega_{1/2} = \frac{3}{4\tau} + \frac{1}{T_2}, \quad (28)$$

and

$$\Delta\omega = -\frac{1}{3}(\omega_B + 2\omega_A),$$
$$v_{\text{peak}} = \frac{-\omega_1 M_0}{4/27 \cdot (\omega_B - \omega_A)^2 \tau + 1/T_2},$$
$$\Delta\omega_{1/2} = \frac{4}{27}(\omega_B - \omega_A)^2 \tau + \frac{1}{T_2}. \quad (29)$$

Group 4: $\omega_C = \omega_F$, $\omega_A = \omega_B = \omega_D = \omega_E$.

This group also consists of the single case (3a). In this case, replacing B in the equations obtained in Group 3 by C, we obtain

$$\Delta\omega = -\omega_C,$$
$$v_{\text{peak}} = \frac{-\omega_1 M_0}{3/\tau + 1/T_2},$$
$$\Delta\omega_{1/2} = \frac{3}{\tau} + \frac{1}{T_2}, \quad (30)$$

and

$$\Delta\omega = -\omega_A,$$
$$v_{\text{peak}} = \frac{-\omega_1 M_0}{3/4\tau + 1/T_2},$$
$$\Delta\omega_{1/2} = \frac{3}{4\tau} + \frac{1}{T_2}, \quad (31)$$

and

$$\Delta\omega = -\frac{1}{3}(\omega_C + 2\omega_A),$$
$$v_{\text{peak}} = \frac{-\omega_1 M_0}{4/27 \cdot (\omega_C - \omega_A)^2 \tau + 1/T_2},$$
$$\Delta\omega_{1/2} = \frac{4}{27}(\omega_C - \omega_A)^2 \tau + \frac{1}{T_2}. \quad (32)$$

Group 5: $\omega_A = \omega_D$, $\omega_B = \omega_E$, $\omega_C = \omega_F$.

This group consists of the two cases (4b) and (4c). In a similar way as used in the previous cases, we obtain

$$\langle G \rangle = \frac{1}{3} \frac{[d_A(1 - c_B - c_C + c_B c_C) + d_B(1 - c_C - c_A + c_C c_A) + d_C(1 - c_A - c_B + c_A c_B)]}{(1 - c_A c_B - c_B c_C - c_C c_A + 2 c_A c_B c_C)}. \quad (33)$$

Thus

$$v = \frac{-\omega_1 M_0 [1/T_2 + 4\tau/9 \cdot W(\Delta\omega)]}{[1/T_2 + 4\tau/9 \cdot X^2(\Delta\omega)]^2 + 1/9 \cdot Y^2(\Delta\omega)}, \quad (34)$$

where

$$X^2(\Delta\omega) = \Delta_A\Delta_B + \Delta_B\Delta_C + \Delta_C\Delta_A,$$
$$Y(\Delta\omega) = \Delta_A + \Delta_B + \Delta_C, \quad (35)$$

with the abbreviations of, for example,

$$\Delta_A = \Delta\omega + \omega_A,$$
$$W(\Delta\omega) = X^2(\Delta\omega) - \frac{1}{3}Y^2(\Delta\omega)$$
$$= \Delta_A\Delta_B + \Delta_B\Delta_C + \Delta_C\Delta_A - \frac{1}{3}(\Delta_A + \Delta_B + \Delta_C)^2. \quad (36)$$

Resonance lines will appear at the frequencies obtained from $X^2(\Delta\omega) = 0$ and $Y^2(\Delta\omega) = 0$.

In the latter case, the situation is rather simple and we obtain

$$\Delta\omega = -\frac{1}{3}(\omega_A + \omega_B + \omega_C),$$
$$v_{\text{peak}} = \frac{-\omega_1 M_0}{1/T_2 + 4\tau/9 \cdot W(\Delta\omega)},$$

$$\Delta\omega_{1/2} = \frac{1}{T_2} + \frac{4\tau}{9} W(\Delta\omega). \tag{37}$$

In the former, we begin with solving $X^2(\Delta\omega)=0$ and obtain two solutions,

$$\begin{aligned}\Delta\omega &= \omega_+ \text{ and } \omega_- \\ &= -(\omega_A+\omega_B+\omega_C) \\ &\quad \pm \sqrt{(\omega_A+\omega_B+\omega_C)^2 - 1/3\cdot(\omega_A\omega_B+\omega_B\omega_C+\omega_C\omega_A)}.\end{aligned} \tag{38}$$

At $\Delta\omega=\omega_+$ for example, we have

$$v_{\text{peak}} = \frac{-\omega_1 M_0[1/T_2+4\tau/9\cdot W(\omega_+)]}{(1/T_2)^2+1/9\cdot Y^2(\omega_+)}. \tag{39}$$

Employing the approximate procedure to obtain Eq. 24, we get

$$\begin{aligned}&\Delta\omega = \omega_k \quad (k \text{ is } + \text{ or } -.), \\ &v_{\text{peak}} = \frac{-\omega_1 M_0}{Y^2(\omega_k)/[4\tau W(\omega_k)]+1/T_2}, \\ &\Delta\omega_{1/2} = \frac{Y^2(\omega_k)}{4\tau W(\omega_k)} + \frac{1}{T_2}.\end{aligned} \tag{40}$$

We should like to emphasize that there are three kinds of lines from the view point of the τ dependence. The first one has the peak height which is independent of τ, as given in Eq. 20, the second one is given by Eqs. 26, 29, 32, and 37, roughly speaking, v_{peak} is inversely proportional to τ and the third one is given by Eqs. 24, 25, 27, 28, 30, 31, and 40, v_{peak} is inversely proportional to τ^{-1}, namely proportional to τ. Let us consider the usual (high temperature) case. Although the value of τ becomes smaller and smaller with increasing temperature, the line shape of the first one is temperature independent, while in the second one the line shape is determined mainly by $1/T_2$ and the third one disappears.

Numerical Analysis and Discussions

In order to help our understanding, we deal with the high temperature limit. *i.e.*, $\tau=0$. In this case, the resonance lines of which peak heights are independent of τ and are inversely proportional to τ will appear. From Eqs. 19 and 26 we can see $\Delta\omega=1/T_2$ and $v_{\text{peak}}=-\omega_1 M_0 T_2$ by putting $\tau=0$. Therefore, the peak heights are determined by the number of degeneracy. In Table 1 the groups in the previous section, the resonance frequencies and the degeneracy numbers are listed. Obviously the peak heights for each resonance line are described by the binomical coefficients and the resonance frequencies are equally spaced. Note that as seen from Fig. 1b 2a+4b is the total spin density. Therefore, in the high temperature limit the spaces are independent of the spin density distribution.

For various values of τ, we can simulate the line shapes as shown in Figs. 4 and 5. We can see how the

Table 1. The states of nuclear spin and hyperfine coupling constant

Group	I_z	$-\omega_R/Q$[a)]	D[a)]
1	3	$2a+4b$	1
	0	0	6
	0	0	2
2	2	$2/3(2a+4b)$	6
	2	$1/3(2a+4b)$	3
3	1	$1/3(2a+4b)$	6
4	1	$1/3(2a+4b)$	6
5	0	0	6
	0	0	6

a) ω_R is the resonance frequency, Q is the constant which relate the spin density to the hyperfine splitting, so ω_R/Q is the resonance frequency in Q unit and D is the number of degeneracy.

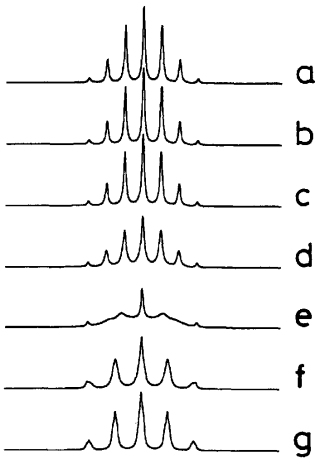

Fig. 4. Line shapes. $T_2=1.0\times10^{-6}$ s, $a=0.24$, $b=0.005$. a): $\tau=1.0\times10^{-12}$ s, b): $\tau=1.0\times10^{-11}$ s, c): $\tau=1.0\times10^{-10}$ s, d): $\tau=1.0\times10^{-9}$ s, e): $\tau=1.0\times10^{-8}$ s, f): $\tau=1.0\times10^{-7}$ s, g): $\tau=1.0\times10^{-6}$ s.

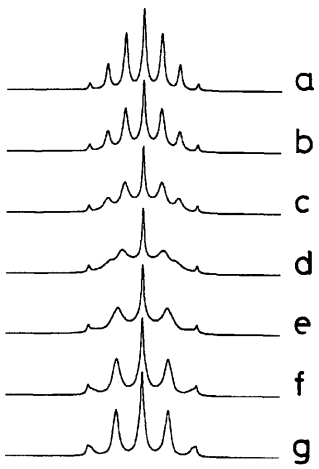

Fig. 5. The qualitative change of line shapes. $T_2=1.0\times10^{-6}$ s, $a=0.24$, $b=0.005$. a): $\tau=1.25\times10^{-9}$ s, b): $\tau=2.5\times10^{-9}$ s, c): $\tau=5.0\times10^{-9}$ s, d): $\tau=1.0\times10^{-8}$ s, e): $\tau=2.0\times10^{-8}$ s, f): $\tau=4.0\times10^{-8}$ s, g): $\tau=8.0\times10^{-8}$ s.

line shapes change as the values of τ are increased: The different behaviors of three type of lines as mentioned in the last part of the previous section are discernible. Under the condition of $\tau/T_2 \ll 1$ (the cases Figs. 4a—d), the lines whose intensities are proportional to τ hardly appear. This should correspond to the actual experiment.[2] The extremely narrow lines with $\tau=10^{-12}$ s in Fig. 4a are such ones as observed in the aromatic anions of the less symmetry, *e.g.*, naphthalene anion. The lines in Fig. 4c or Fig. 4d which correspond to $\tau=10^{-10}$ or 10^{-9} s, respectively, have considerable likeliness with the observed ones. We can guess that the benzene anion tumbles in this time scale in solution.

As τ gets larger, the lines which are neglected in the case of $\tau \fallingdotseq 0$ are seen. This makes the line structure complicated and results in the apparent broad lines as seen in Figs. 4e—g. Note that in computer simulation line shapes are directly described without the condition of $\tau/T_2 \ll 1$. From Figs. 4f and 4g, we can see patterns which are qualitatively different from Figs. 4a—e. The last three cases have not been observed in experiments yet. The transient patterns in this change are shown in Fig. 5. Here we can observe that the second line from the edge is gradually disappearing.

References

1) M. Kimura, H. Kawabe, K. Nishikawa, and S. Aono, *Bull. Chem. Soc. Jpn.*, **58**, 2756 (1985).
2) M. G. Townsent and S. I. Weissman, *J, Chem. Phys.*, **32**, 309 (1960).
3) H. M. McConnell and A. D. McLachlan, *J. Chem. Phys.*, **34**, 1 (1961).
4) R. G. Lawler, J. R. Bolton, G. K. Fraenkel, and T. H. Brown, *J. Am. Chem. Soc.*, **86**, 520 (1964).
5) K. Mukai, T. Mishima, and K. Ishizu, *J. Chem. Phys.*, **66**, 1680 (1977).
6) A. Carrington, *Mol. Phys.*, **5**, 425 (1962).
7) S. Aono and I. Ohno, *Kogyo. Kagaku. Zassi*, **68**, 1530 (1965).
8) J. E. Wertz and J. R. Bolton, "ELECTRON SPIN RESONANCE," McGraw-Hill, New York, (1972).

 © 1985 The Chemical Society of Japan Bull. Chem. Soc. Jpn., 58, 2769—2772 (1985)

CIDEP Study of 1,4-Naphthosemiquinone in Alcohols

Shigeya NIIZUMA,*,† Nobuyoshi SATO,† Hiroki KAWATA,† Osamu MURAKAMI,††
Akihiko KANEMOTO,†† and Hiroshi KOKUBUN††
†*College of Humanities and Social Sciences, Iwate University, Ueda, Morioka 020*
††*Department of Chemistry, Faculty of Science, Tohoku University, Aoba, Aramaki, Sendai 980*
(Received May 2, 1985)

A Chemically Induced Dynamic Electron Polarization (CIDEP) signal of 1,4-naphthosemiquinone (NQH·) was examined by intermittent-light irradiation to a system of 1,4-naphthoquinone (NQ) and phenol (PhOH) in toluene–2-propanol (2:3), toluene–ethanol (2:3), and neat 2-propanol. The enhancement factors of the initial polarization and the F-pair polarization of the systems were determined separately. From the unusual pattern of a time profile of the ESR signal with a CIDEP phenomenon observed on the photoirradiated NQ–PhOH system in ethanol, it is concluded that in ethanol the photoexcited NQ first abstracts a hydrogen to give NQH·, then NQH· releases a proton to form NQ^-.

Quinones are important compounds in biochemistry, especielly as a component of an acceptor or a carrier of electrons in an electron-transport system in photosynthesis. The photochemistry of quinones in alcohols has been extensively investigated. The primary process has been generally considered to be that of hydrogen abstraction from a solvent by photoexcited quinones. But, the anionic mechanism for the photoreduction of *p*-benzoquinone to the hydronquinone was proposed by Yoshida *et al.*[1] They also reported that when 1,4-naphthoquinone (NQ) in ethanol is photoirradiated, the ESR signal of two types of radicals, *i.e.* semiquinone anion (NQ^-) and semiquinone neutral radical (NQH·), are observed at the same time.[2] Each of these radicals is known to exhibit strong signals due to Chemically Induced Dynamic Electron Polarization (CIDEP) by selecting the conditions of their formation.[3–5]

In a previous paper,[6] we treated a system of duroquinone and phenol (PhOH) in neat 2-propanol or in various organic solvents mixed with 2-propanol and detected the CIDEP signal of durosemiquinone (using a sector system and the usual ESR spectometer with a 100 kHz field modulation). In this paper, we report on a separate determination of the initial polarization (V^I) and the F-pair polarization (V^F) of NQH· which is produced photochemically from NQ and PhOH in a mixed solvent of alcohols and toluene and in neat 2-propanol. We also report on the reaction mechanism of the photoreduction of NQ with PhOH in alcohols (ethanol and 2-propanol) by taking advantage of a CIDEP phenomenon observed on its semiquinone.

Experimentals

Materials. NQ (Nakarai Chemical Co., G. R. grade) was refined by a sublimation method after being recrystallized from methanol. PhOH, ethanol and 2-propanol (Wako Junyaku, G. R. grade) were used without further purification.

Procedures. The concentrations of NQ and PhOH in alcohols were fixed to 0.05 (or sometimes 0.08) and 2.0 mol dm^{-3}, respectively. The temperature upon irradiation was −40 °C. The CIDEP observation system was almost the same as that used in a previous paper[6] except that a Boxcar integrator (NF Model BX-531 with PB-10 Sampling unit) online with a microcomputer (NEC PC-8001) and a plotter (Watanabe Model WX-4675) were used instead of a minicomputer (JEOL EC-6) and the recorder used in the previous study, respectively. The electronic absorption spectra were taken with a Hitachi 228 double-beam spectrophotometer.

Results and Discussion

Aspects of Absorption Spectra. In order to observe the outline of the photoreaction of NQ in alcohols, the absorption spectra of the systems and their change upon irradiation were observed. A typical example is shown in Fig. 1-a. The difference spectrum (spectrum (4)) obtained from the spectrum (1) (0.05 mol dm^{-3} NQ and 2.0 mol dm^{-3} PhOH in 2-propanol) and (2) (0.05 mol dm^{-3} NQ in 2-propanol) has a new peak at 360 nm. This indicates that an interaction takes place between NQ and PhOH in their ground states. When the light from a high-pressure mercury lamp was irradiated without a filter, the absorption spectrum of the 2-propanol solution containing NQ and PhOH changed with isosbestic points at 346 and 402 nm. Except for the unknown weak band appearing at 420—430 nm, the general feature of the spectral change reflected a decrease of NQ, accompanied with an increase of dihydronaphthoquinone or naphthalenediol (NQH_2), as shown in Fig. 1-b.

ESR Spectra and Its Time Profile. Some examples of the observed ESR spectra are shown in Fig. 2. When 2-propanol was used as a solvent, only the NQH· signal was observed in the photostationary state in cases with or without PhOH. When ethanol was used, the NQ^- signal was detected overlapping that of NQH·. Especially, in the system containing PhOH, the NQ^- signal predominated. The hf coupling constants of protons were determined to be 0.324 mT (2H) and 0.064 mT (4H) for NQ^- and 0.701 mT (1H) and 0.174 mT (3H) for NQH·. These values are consistent with those in the literatures[2,7] within the error limit. The time profile of the ESR signal was observed at magnetic fields fixed at several points along the resonance line. Typical examples are given in Fig. 3 for a NQ

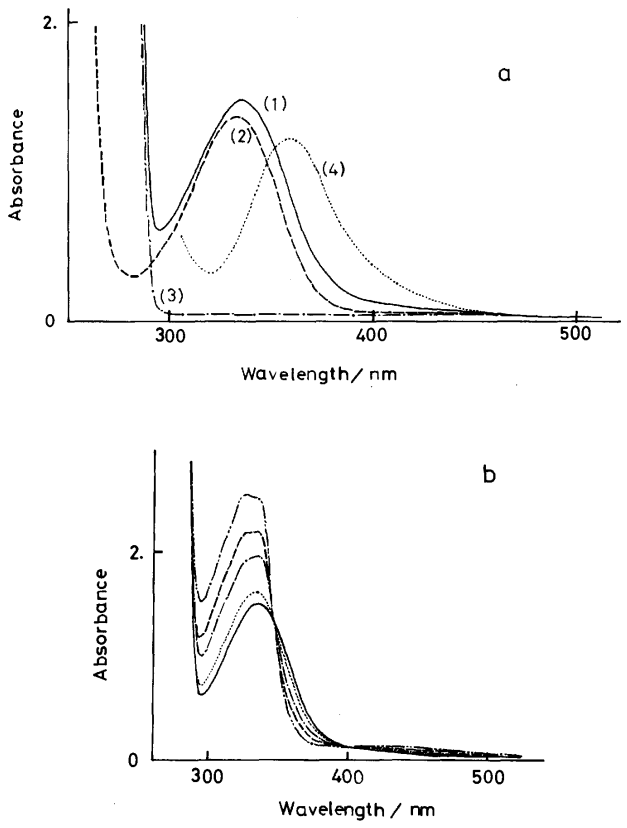

Fig. 1-a. Absorption spectra of CIDEP observation systems.
(1) 0.05 mol dm^{-3} NQ and 2.0 mol dm^{-3} PhOH, (2) 0.05 mol dm^{-3} NQ, and (3) 2.0 mol dm^{-3} PhOH in 2-propanol and (4) the difference between spectra (1) and (2) (the ordinate; $\times$ 1/5).
b. Spectral change with photoirradiation: before irradiation (——), 10 min (·····), 50 min (—·—), 100 min (– – –), and 220 min (– – –) irradiation of 2-propanol solution containing 0.05 mol dm^{-3} NQ and 2.0 mol dm^{-3} PhOH by 100 W highpressure mercury lamp without filter.

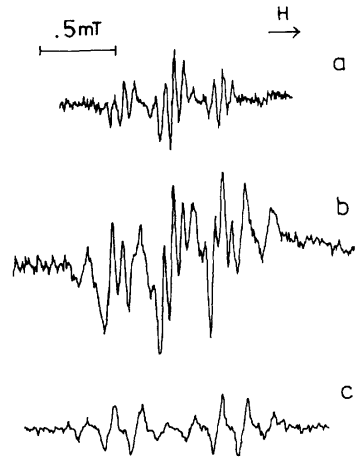

Fig. 2. ESR spectra observed in the photostationary state of the systems a: NQ+PhOH in ethanol at −40 °C, b: NQ in ethanol at −80 °C and c: NQ in 2-propanol at −40 °C.

and PhOH system in a toluene–2-propanol (2:3) mixed solvent. The fixed position of the magnetic field is pointed out by the arrows above the ESR spectrum in the figure. Since we chose 0.2 mT (or sometimes 0.08 mT) as the field-modulation width, the spectrum of NQH· formed a doublet of quartet with a broad linewidth and that of NQ^- also became a broad triplet. At the end of the light-ON period, a steady state condition regarding radical concentration was achieved. The zero level of the signal intensity was determined by an analysis of the decay curve.[8]

The Enhancement Factor for NQH· Radical.
Three kinds of solvent systems, *i.e.* toluene–2-propanol (2:3), toluene–ethanol (2:3) and neat 2-propanol systems, were used for the determination of the enhancement factors V^I and V^F. It is noteworthy that no NQ^- signal was detected in the solvent systems containing toluene. V^I and V^F were calculated as follows.[8] First, I and I_0 were taken from the pettern in the figure as the difference between the zero level and level e, and that between the zero level and level a, respectively. The dimensionless quantity V' was defined to be $(I-I_0)/I_0$. This is represented as Eq. 1 by using V^I (net effect) and V^F (multiplet effect),

$$V' \equiv \frac{I-I_0}{I_0} = \frac{V^I}{1+V^F} \tag{1}$$

As the signal of NQH· radical had no hf line at the center of the spectrum, V^I and V^F were obtainied by using Eq. 2.

$$\left.\begin{aligned} V^I &= 2\left(\frac{1}{V'(n)} - \frac{1}{V'(n')}\right)^{-1} \\ \bar{V}^F(n) &= \frac{\dfrac{1}{V'(n)} - \dfrac{1}{V'(n')}}{\dfrac{1}{V'(n)} + \dfrac{1}{V'(n')}} \end{aligned}\right\} \tag{2}$$

Here, n and n' are the numbers assigned to a pair of hf lines at the symmetric and mutually opposite positions to the center of the spectrum. $V'(n)$ is the value of V' at line n. $\bar{V}^F(n)$ is the mean value of $|V^F(n)|$ and $|V^F(n')|$, and was derived on the condition that $V^F(n) = -V^F(n')$. The time profile was observed at eight field points, each of which corresponded to the maximum or the minimum of hf lines 2, 3, 3′, and 2′, in Fig. 3. The velue of V' was found to be larger at higher field lines. This indicates the presence of a contribution from E/A type F-pair polarization in addition to initial polarization. By the method mentioned above, V^I and V^F values were separately estimated for three solvent systems containing 2.0 mol dm^{-3} PhOH, as listed in Table 1. These values are, however, the apparent enhancement factors. In order to obtain V^I values which can be compared with the values for other solvent systems, the corrections for the radical halflife $t_{1/2}$ and for the spin-lattice relaxation time of the radical T_1 must be made.[9,10] $t_{1/2}$ was evaluated from an

analysis of the decay curve after light-OFF in Fig. 3.[8] As T_1 was considered to be independent of a solvent, $\bar{V}^I_{av}$ $t_{1/2}$ values were calculated and were found to be in good agreement among three solvent systems (see Table 1). When toluene is mixed with the solvent, the viscosity decreases. Consequently, the radical lifetime $t_{1/2}$ becomes shorter. The fact results in an observation of the larger V' (Table 1). Further the intrinsic $\bar{V}^I_{av}t_{1/2}$ value was determined in a toluene-2-propanol system to be 7.1 ms by extrapolating the concentration of PhOH to infinite,[9] as shown in Fig. 4. If we borrow a T_1 value of $\approx$10 μs from the data by Frydkjear and Muus,[5] the intrinsic enhancement factor V^{∞}_{int} is calculated to be -7.1×10^2. According to the Eq. 14 of the previous paper,[6] (DK+3EI)$=-0.3\,cm^{-1}$ is obtained. Here, D and E are zero-field splitting constants, and K and I are parameters showing anisotropy of $S_1\rightarrow T_n$ intersystem crossing rate. (S_1: the excited singlet state, T_n: the n'th excited triplet state). Although the value is based on many assumptions, it seems to be reasonable and be in good agreement with the date obtained by Murai *et al.*[11] They estimated the D and E of the 1,4-naphthoquinone triplet state to be −0.330 and $0.019\,cm^{-1}$, respectively, by observing the time-resolved ESR spectrum of the triplet state in glassy matrices at 77 K. The longitudinal relaxation time $^3T_1$ of the triplet NQ was estimated to be 13 ns from the slope of the plot in Fig. 4, using the value of k_q (the NQ triplet quenching rate constant by PhOH)$=0.58\times10^8$ $mol^{-1}\,dm^3\,s^{-1}$.[12]

V^F values are given in Table 1 as the form of the ratios of $\bar{V}^F/\bar{V}^I_{av}$ to exclude the effect of the exciting light intensity. The ratio of $\bar{V}^F_2/\bar{V}^F_3$ is a little larger than the theoretical one based on the radical pair mechanism[13] ($\approx$1.3 by rough estimation) but is reasonable in comparison with the literature.[5]

Mechanism of Photoreduction in Ethanol. The broad triplet line obtained by the use of the modulation of 0.2 mT was assigned to the signal of a NQ^- radical. To take the time profiles, the magnetic field was fixed at a minimum and a maximum signal points of each resonance line of the derivative curve. All six patterns that were recorded were unusual when we assumed the presence of only one radical species. Among them, two most unusual patterns concerning the central resonance line are shown in Fig. 5. At the field point (1) in Fig. 5-a, the absorption of the photostationary signal is represented by the downward one. If the emission of NQ^- occurs immediately after irradiation, the signal level should move upwards. In addition to this, runs both during light-ON and after light-OFF were not simple. These unusual facts can be understood by considering that in this system, first NQH· is formed and it changes to NQ^- during the time scale of the measurement. The following is an explanation for the observation: the *g*-value of NQ^- is a little larger than

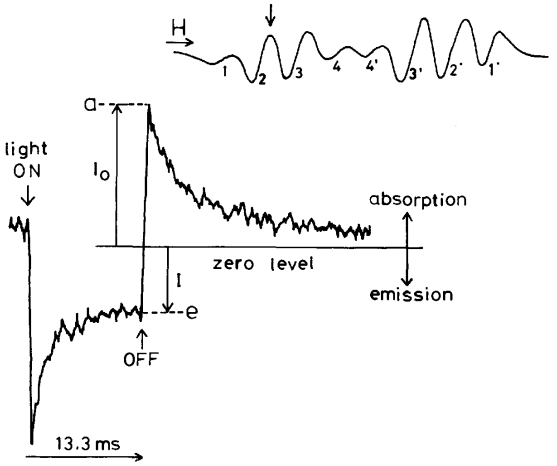

Fig. 3. Time profile of ESR signal intensity observed on NQ and PhOH system in toluene-2-propanol (2:3) mixed solvent.

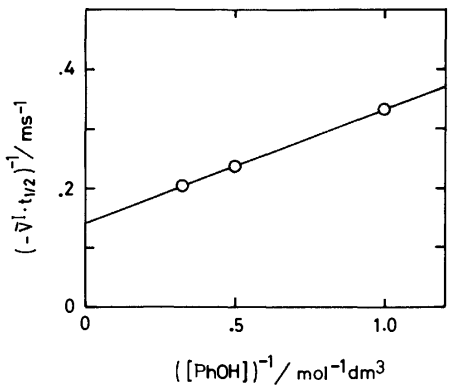

Fig. 4. Effect of PhOH concentration on $\bar{V}^I$ $t_{1/2}$ of NQH· in toluene-2-propanol (2:3) mixed solvent at −40 °C.

Table 1. Enhancement factors for NQH· radical[a]

Solvent	$\bar{V}_2^I$	$\bar{V}_3^I$	$\bar{V}_{av}$[b]	$\bar{V}_2^F/\lvert\bar{V}_{av}^I\rvert$	$\bar{V}_3^F/\lvert\bar{V}_{av}^I\rvert$	$t_{1/2}$/ms	$\bar{V}_{av}^I\cdot t$/ms
Toluene-*i*-PrOH(2:3)	−1.49	−1.50	−1.50	−0.055	−0.022	2.8	−4.2
Toluene-EtOH(2:3)	−1.69	−1.73	−1.71	−0.068	−0.012	2.4	−4.1
i-PrOH	—	—	−0.96	≈0	≈0	4.4	−4.2

a) The system of [NQ]$=0.05\,mol\,dm^{-3}$ and [PhOH]$=2.0\,mol\,dm^{-3}$. b) The avearage of $\bar{V}_2^I$ and $\bar{V}_3^I$. Subscripts 2 and 3 indicate the magnetic field position depicted in Fig. 3.

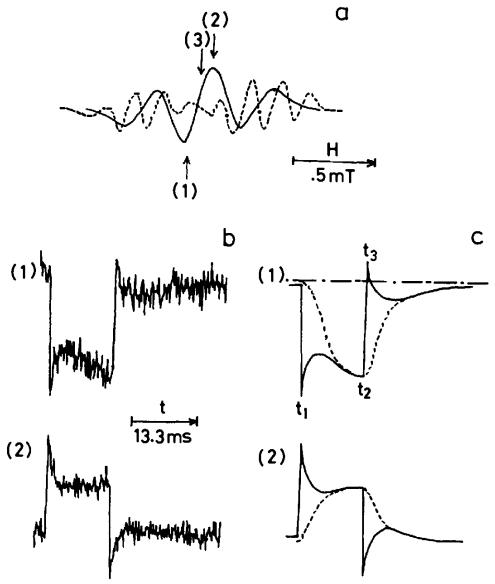

Fig. 5. Time profile observed on NQ and PhOH system in ethanol.
a: The overlapping relation between ESR spectrum of NQ· radical (——) and that of NQH· radical (·····).
The arrows numbered (1)—(3) are the fixed tion of the magnetic field.
b: The unusual time profiles. The numbers (1) and (2) correspond to those in a.
c: The time profiles extracted from the runs (1) and (2) in b.

that of NQH·; thus, their spectra overlap with each other as shown in Fig. 5-a. The feature of the run was extracted and is depicted in Fig. 5-c. At time t_1, almost all radical species present were the polarized naphthosemiquinone, NQH·*. Thus, this level is only a reflection of the amount of NQH·*. At t_2, the signal level comprizes those from NQH·*, NQH· (in thermal equilibrium) and NQ^- (in thermal equilibrium, produced from NQH·). At t_3, the level is the sum of those of NQH· and NQ^-, both in thermal equilibrium. Thus, the following relation holds for these levels:

$$\text{level}(t_2) - \text{level}(t_1) = \text{level}(t_3) \quad (3)$$

The zero level of this run is determined by Eq. 3, as shown by the horizontal line in the figure. Further, we can infer the time dependence of the formation and disappearance of NQ^- qualitatively. It may be given by the broken line in the figure, if we assume that $V'(\text{NQH}\cdot)=-1$ and the signal intensity ratio of NQH· to NQ^- at t_2 is -1. The circumstances are the same as with those mentioned above in the case of the field position (2), except that the level movement is upside-down (Fig. 5-c).

In order to make clear that NQ^- exhibited no CIDEP signal, we carefully chose a field position where NQH· had a zero signal intensity ((3) in Fig. 5-a) and examined the time profile there. The run had much noise but no CIDEP signal appeared. There was some time-lag before a riseup of the signal and the shape of the signal-decay after light-OFF was also unusual. The facts may support the idea that NQ^- is not formed initially but second in the reaction sequence. Thus, it is concluded that in ethanol photoexcited NQ abstracts a hydrogen atom from PhOH first and changes to NQH··. Then NQH· promptly releases a proton to convert to NQ^-. This is the reason why the NQ^- signal is observed with continuous light irradiation and no CIDEP signal for NQ^- is detected in ethanol. In 2-propanol, NQH· does not release a proton. The difference in the behavior of NQH· might be attributed to the slight difference in the dielectric constants of the two alcohols. The idea is consistent with the fact that no NQ^- signal appeared in a toluene–ethanol system. NQ^- may be more stabilized in a polar media than NQH··. This conclusion is in contrast to that of Wong,[4] who also observed a CIDEP signal of NQH· produced photochemically in 2-propanol or 2-butanol. In his case, the reductant was a solvent. By the addition of pyridine to the solution, NQH· changed to NQ^-, which exhibited no CIDEP signal.

References

1) S. Noda, T. Doba. T. Mizuta, M. Miura, and H. Yoshida, *J. Chem. Soc., Perkin Trans, 2*, **1980**, 61.
2) H. Yoshida, K.Hayashi, and T. Werashina, *Bull. Chem. Soc. Jpn.*, **45**, 3515 (1972); H. Yoshida, J. Sohma, and T. Warashina, *ibid.*, **47**, 1396 (1974).
3) S. K. Wong, D. A. Hutchison, and J. K. S. Wan, *Can. J. Chem.*, **52**, 251 (1974).
4) S. K. Wong, *J. Am. Chem. Soc.*, **100**, 5488 (1978).
5) S. Frydkjear and L. T. Muus, *Chem. Phys.*, **51**, 335 (1980).
6) A. Kanemoto, S. Niizuma, S. Konishi, and H. Kokubun, *Bull. Chem. Soc. Jpn.*, **56**, 46 (1983).
7) P. B. Ayscough and R. C. Sealy, *J. Chem. Soc., Perkin Trans. 2*, **1973**, 543.
8) The procedure is described in detail at the section of "Analysis of the Time Profile" in our previous paper.[6]
9) J. K. S. Wan and A. J. Elliot, *Acc. Chem. Res.*, **10**, 161 (1977).
10) R. W. Fessenden, *J. Chem. Phys.*, **58**, 2489 (1973).
11) H. Murai, M. Minami, T. Hayashi, and Y. I'Haya, *Chem. Phys.*, **93** (2), 333 (1985).
12) A. J. Elliot and J. K. S. Wan, *J. Phys. Chem.*, **82**, 444 (1978).
13) F. J. Adrian, "Chemically Induced Magnetic Polarization," ed by L. T. Muus, P. W. Atkins, K. A. McLauchlan, and J. B. Pedersen, D. Reidel Pub. Co., Holland (1977), Chapter V.

 © 1985 The Chemical Society of Japan Bull. Chem. Soc. Jpn., 58, 2773—2777 (1985)

Stopped-flow Studies on Binding of Cu^{2+} Ion to Human Serum Albumin

Naohisa KURE, Thoru NAKATSUKA, Takayuki SANO,* and Tatsuya YASUNAGA
Department of Materials Science, Faculty of Science, Hiroshima University, Naka-ku, Higashisenda-machi, Hiroshima 730
(Received May 11, 1985)

Both static and kinetic investigations have been carried out regarding the interaction between Cu^{2+} and human serum albumin (HSA). The static experiment, using a UV spectrophotometric technique, shows the presence of one primary binding site and other weaker binding sites at pH 5.2. The kinetic experiment, using stopped-flow apparatus, revealed a reaction process on the order of several seconds and a rapid absorbance change within the dead-time of the apparatus. These results are discussed from the viewpoint of the substitution effect of the second residue of the N-terminal position in the protein with reference to the previously reported results for a Cu^{2+}–bovine serum albumin (BSA) system.

The bindig of the Cu^{2+} ion to bovine serum albumin (BSA) and/or human serum albumin (HSA) has been widely studied. Extensive investigations by Peters,[1-5] Breslow,[6] Gurd,[5,7] and Sarker[8-10] revealed that a specific binding site of Cu^{2+} is located at the N-terminal sequence of both albumins (Asp-Thr-His- for BSA and Asp-Ala-His- for HSA), and that the chelation of a Cu^{2+} ion formed at this site involves coordination by α-amino, imidazolyl, and two peptide nitrogens in the neutral pH range. Different types of bound species were also evident at low pH from visible and circular dichroism spectroscopies.[2,6,10] In previous studies of the kinetics of a Cu^{2+}–BSA system,[11] we revealed that one low-pH type complex is also formed at the N-terminal sequence of BSA in competition with a chelation complex. This present report is concerned with a further kinetic study on the binding of a Cu^{2+} ion to serum albumin by using HSA from the viewpoint of the substitution effects of alanin for threonin at the second residue of the N-terminal position in serum albumin.

Experimental

Materials. Human serum albumin (essentially fatty acid-free) was purchased from Sigma Chem. Co. and fractionated on a Sephadex G-150 column to obtain a monomeric form. The concentration of the HSA monomer was determined spectrophotometrically.[12] Solutions of Cu^{2+} ions were produced by direct weighing of anhydrous $CuSO_4$. The pH values of solutions were adjusted by H_2SO_4 and/or KOH, and no pH buffer was added. All measurements were made in a 1-mM† solution of K_2SO_4. Analyticalgrade reagents were used throughout.

Equilibrium Dialysis. The extent of binding was measured using the equilibrium dialysis technique with a dialysis cell (Sanko Plastics Co. type 5044-05) having ten separate chambers. After 70 to 80 h of dialysis at 25 °C, concentration of Cu^{2+} in the dialyzed solutions were determined with a Perkin-Elmer Model 5000 atomic absorption spectrophotometer. The detection limit of this method for the Cu^{2+} concentration was 1.5×10^{-7} M. The pH values of the dialyzed solutions were 5.02±0.07.

Spectrophotometry. The difference spectra of HSA solutions in the presence and absence of Cu^{2+} ions were measured in the ultraviolet region using a Union Giken SM 401 spectrophotometer at 25±0.2 °C.

Stopped-flow Experiments. The kinetic measurements were carried out using a Union Giken Stopped-flow spectrophotometer RA 401. The dead-time of the apparatus is 5 ms. For the case of very small signal amplitudes, its relaxation time was obtained by signal averaging 2—10 measurements using the averaging capabilities of a wave-memory apparatus. All kinetic measurements were made at 25±0.2 °C.

† 1 M=1 mol dm^{-3}.

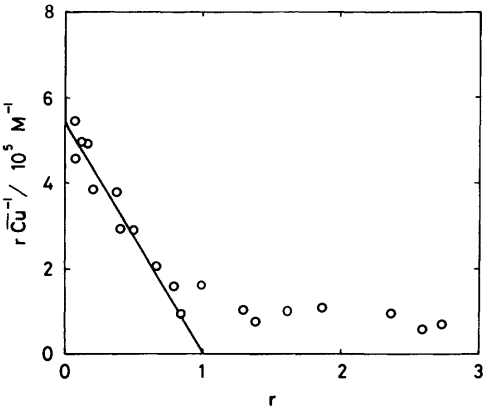

Fig. 1. Scatchard plot of the binding of Cu^{2+} ion to HSA in 1 mM K_2SO_4 solution at pH 5.02±0.07 and 25±0.2 °C. The slope of the solid line yields $K_p=(5.3\pm0.5)\times10^5$ M^{-1} for the binding constant of the primary site.

Results

Static Measurements. Figure 1 illustrates a Scatchard plot of the binding of the Cu^{2+} ion to HSA monomer obtained by an equilibrium dialysis technique at pH 5.02±0.07. The shape of the isotherm clearly demonstrates the presence of one primary binding site with high affinity and number of secondary sites with low affinities. From the slope of this isotherm in the range of $r<1$ (r is binding ratio of bound Cu^{2+} to protein), the binding constant for the primary site was estimated to be $K_p=(5.3\pm0.5)\times10^5$ M^{-1}; where subscript p refers to the value for the primary site.

The binding of Cu^{2+} to HSA was also examined spectrophotometrically at pH 5.0 by monitoring the absorbance change at a wave length 255 nm which is specific to a charge-transfer transition from amino,

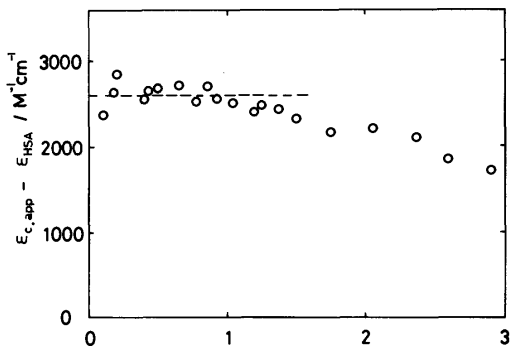

Fig. 2. A plot of $\varepsilon_{c,app}-\varepsilon_{HSA}$ *vs.* binding ratio r. The data were obtained from the spectrophotometric titration of HSA (2.0×10^{-5} M) solutions with various amounts of Cu^{2+} ions at 255 nm, pH 5.0±0.02, and 25±0.2°C.

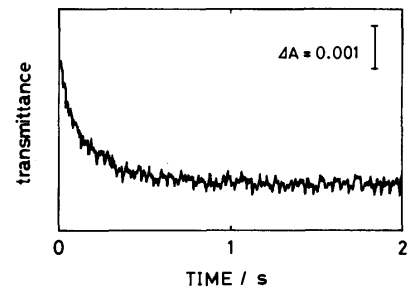

Fig. 3. A typical oscillographic trace of the stopped-flow experiments of the reaction between Cu^{2+} ion (4.0×10^{-6} M) and HSA (2.0×10^{-5} M) monitored by the change in the transmittance intensity (increasing upward) at 255 nm, pH 4.6 and 25±0.2°C in 1 mM K_2SO_4 solution. The magnitude of the absorbance change is indicated by the bar in the upper right-hand corner.

carboxylato, imidazolyl groups, and ionized peptide nitrogens to bound Cu^{2+}.[11] Since the contribution from the free Cu^{2+} ion to the absorbance is negligibly small at the present wave length of 255 nm, the observed change in absorbance (ΔA^{255}) may be written as

$$\Delta A^{255}/\text{cm} = (\varepsilon_{c,app}-\varepsilon_{HSA})\cdot\bar{C}, \qquad (1)$$

where ε_{HSA}, $\varepsilon_{c,app}$, and $\bar{C}$ denote the molar extinction coefficient of HSA at 255 nm, the apparent molar extinction coefficient of the complex and its equilibrium concentration, respectively. The variation of $\varepsilon_{c,app}-\varepsilon_{HSA}$, which is given by calculating $\Delta A^{255}/\bar{C}$ using the binding data obtained above, was represented as a function of the binding ratio r in Fig. 2. The constancy of the value of $(\varepsilon_{c,app}-\varepsilon_{HSA})$ up to an r value of unity gives further evidence for the presence of one primary site. Since the highest affinity site on HSA for the Cu^{2+} ion has been identified to be the three N-terminal peptides (Asp-Ala-His),[8-10] the primary site found in the present study is most likely attributable to this sequence. The apparent molar extinction coefficient of the complex formed at this site ($\varepsilon_{c,app}$) was estimated to be 22100 $M^{-1}cm^{-1}$ by using a value of 19500 $M^{-1}cm^{-1}$ for ε_{HSA}.

Kinetic Measurements. In order to detect a reaction between the Cu^{2+} ion and the primary site of HSA, stopped-flow experiments were carried out at a small *M/P* (metal to protein ratio) of 0.2 by using a change in the absorbance at 255 nm. As shown in Fig. 3, a single relaxation process was observed in the sec range under various pH and concentration values. Other reaction processes were not discernible within the time resolution of the apparatus (5 ms—100 s). The spectra of the solutions after mixing were quite stable over a period of 2 d.

The reciprocal relaxation time (τ^{-1}) was determined by a semilogarithmic plot of the reaction curve near the equilibrium point. The pH and concentration dependences of the obtained τ^{-1} are represented in Figs.

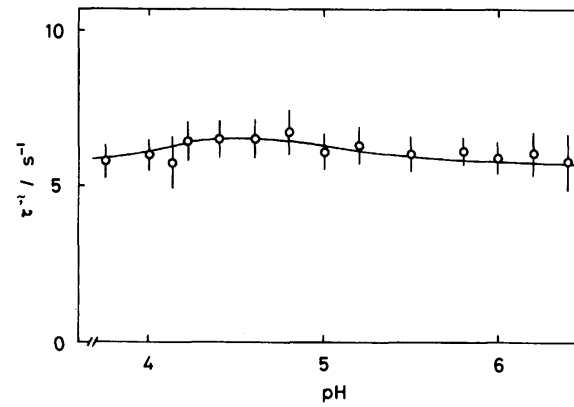

Fig. 4. The pH dependence of τ^{-1} at a fixed concentrations of Cu^{2+} (4.0×10^{-6} M) and HSA (2.0×10^{-5} M).

4 and 5, respectively. The behaviors for τ^{-1} (shown in these figures) are quite similar to a previous observation in a Cu^{2+}–BSA system,[11] but the present τ^{-1} is several times larger.

On the other hand, the absorbance changes (ΔA_{SF}) at 255 nm (estimated directly from the reaction traces observed by the stopped-flow measurements) are represented as a function of pH in Fig. 6, together with the total absorbance changes (ΔA_{total}) measured during static spectrophotometrical experiments at the same wavelength. Disagreement between ΔA_{SF} and ΔA_{total} implies the presence of at least one more reaction process within the dead-time of the stopped-flow apparatus accompanied by the absorbance changes (ΔA_{DT}) corresponding to the difference between ΔA_{total} and ΔA_{SF}. As judged from the pH dependence of ΔA_{DT} and ΔA_{SF}, a complex formed within the dead-time of the apparatus predominates above pH 5.5, and the other complex yielded by the observed reaction process around pH 4.5. These features in the complexation of Cu^{2+} ion with HSA are also quite similar to those previously observed for a Cu^{2+}–BSA system.[11]

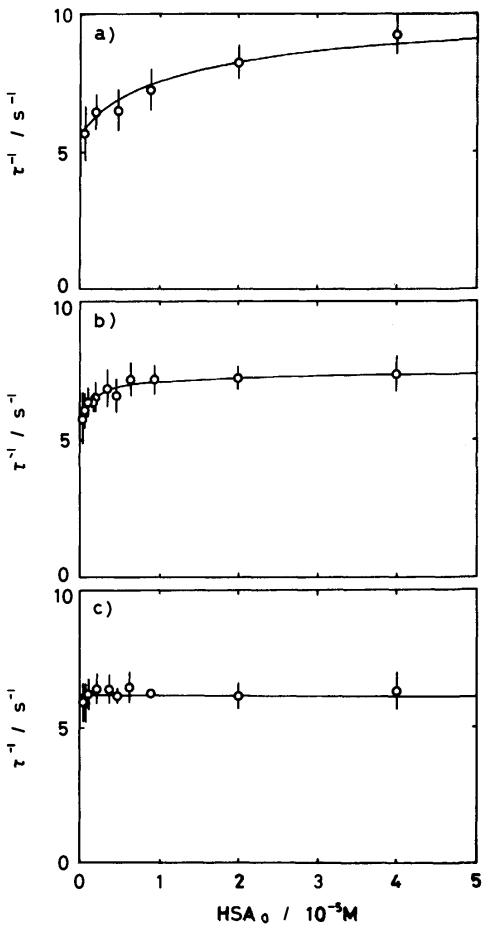

Fig. 5. The variation of τ^{-1} with the total concentration of HSA (HSA_0) at a fixed M/P of 0.2: (a), pH 4.2; (b), pH 4.6; (c), pH 5.2.

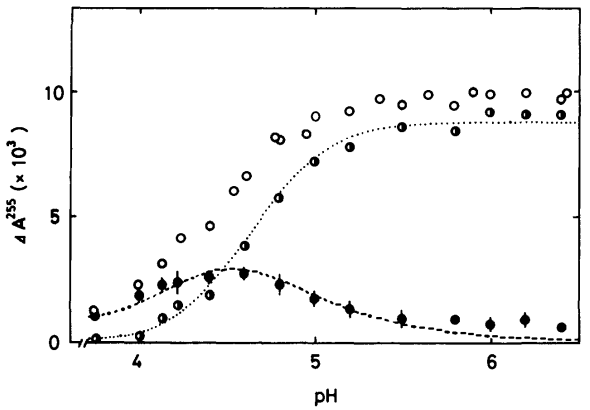

Fig. 6. The pH dependence of absorbance changes at 255 nm due to the reaction between Cu^{2+} (4.0×10^{-6} M) and HSA (2.0×10^{-5} M): ○, the total absorbance change (ΔA_{total}) measured spectrophotometrically; ●, the absorbance change (ΔA_{SF}) observed by stopped-flow method; ○, the absorbance change within the dead-time of the stopped-flow apparatus (ΔA_{DT}) determined from $\Delta A_{total}-\Delta A_{SF}$ at each pH value.

Examination of Reaction Mechanism. Looking for close simillarities regarding the kinetic behaviors for Cu^{2+}–BSA and Cu^{2+}–HSA systems, the following reaction mechanism is proposed for the binding of a Cu^{2+} ion to the three N-terminal peptides of BSA. This is also being applied to the present system.

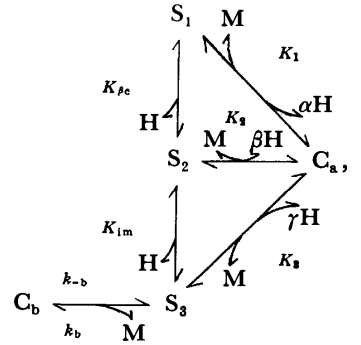

(I)

with

$$K_b = \frac{k_b}{k_{-b}}, \tag{2}$$

K_i (i=1, 2, 3, b), k_i (i=b, -b), H, M, C_a, and C_b denote binding constants, rate constants, protons, free Cu^{2+} ions, complex formed from the rapid reaction, and the other complex formed during the observed reaction, respectively. α, β, and γ are the number of protons released in each step and S_i (i=1, 2, 3) refers to the possible protonated states of the three N-terminal peptides of HSA, defined as S_1: Asp(protonated β-carboxyl)-Ala-His(protonated imidazolyl), S_2: Asp(deprotonated β-carboxyl)-Ala-His(protonated imidazolyl), S_3: Asp(deprotonated β-carboxyl)-Ala-His(deprotonated imidazolyl). The equilibria among these states are characterized by two acid dissociation constants of $K_{\beta c}$ (for β-carboxyl group) and K_{im} (for imidazolyl group), since the α-amino group of the terminal aspartyl residue (pK_a=7.73[10]) is almost acidic under the present pH conditions of 3.7—6.4. The values of $K_{\beta c}$ and K_{im} were calculated using pK_a values (2.98 for β-carboxyl group and 6.55 for imidazolyl group) obtained from titration studies of a synthetic tripeptide of HSA primary site by Iyer *et al.*[10]

Firstly, the observed absorbance changes (ΔA_{DT}) within the dead-time of the apparatus were analyzed on the basis of the rapid equilibria represented in the right-hand side of Mechanism I. The cyclic nature of the scheme requires

$$K_1 = K_{\beta c}K_2 = K_{\beta c}K_{Im}K_3, \tag{3}$$

$$\alpha = \beta + 1 = \gamma + 2. \tag{4}$$

By use of the molar extinction coefficients, ε of C_a and HSA, the equation of a net absorbance change resulting from the formation of C_a is given by

$$\Delta A_{DT}/\text{cm} = (\varepsilon_{C_a}-\varepsilon_{HSA})\cdot\bar{C}_{a,r}, \tag{5}$$

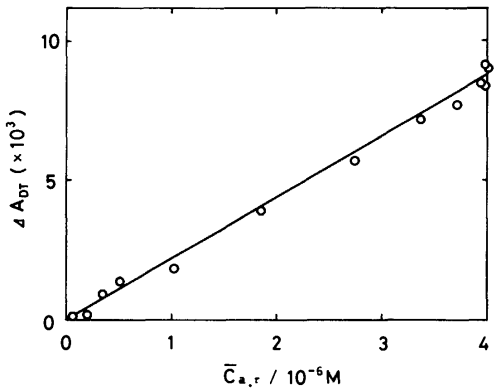

Fig. 7. A plot of ΔA_{DT} *vs.* $\bar{C}_{a,r}$ calculated for $\gamma=1$ and $K_3=105$.

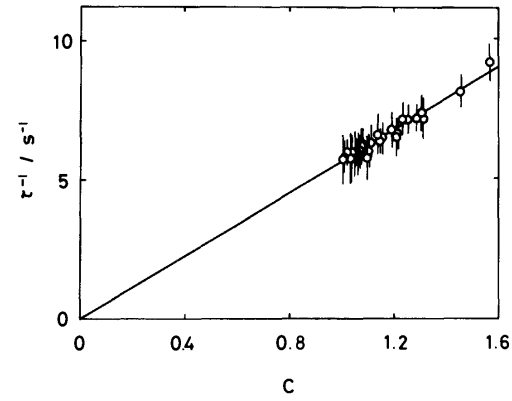

Fig. 8. A plot of τ^{-1} obtained at various pH and concentrations *vs.* the concentration term in Eq. 9, designated by C in this figure and calculated for $K_b=1.9\times10^{-6}\,M^{-1}$.

with

$$\bar{C}_{a,r}=\frac{1}{2A}\{A(M_0+S_0)+B-\sqrt{A^2(M_0-S_0)+2AB(M_0+S_0)+B^2}\}, \quad (6)$$

$$A=K_1/\bar{H}_r^{r+2}, \quad (7)$$

$$B=1+K_{\beta c}/\bar{H}_r+K_{\beta c}K_{1m}/\bar{H}_r^2, \quad (8)$$

where the bar with subscripts r and 0 refer to the equilibrium concentration after rapid equilibria and the total concentration of each species, respectively. In the present analyses, the equilibrium proton concentrations were approximated by the final concentrations since pH changes in solutions after mixing were within ±0.03 of the initial pH values. As shown in Fig. 7, a plot of experimental values of ΔA_{DT} *vs.* $\bar{C}_{a,r}$ calculated using $\gamma=1$ and $K_3=105\pm8$ gives an excellent straight line through the origin. From the slope of this line, the value of ε_{C_a} was estimated to be 21700 $M^{-1}cm^{-1}$. As can be seen from Fig. 6, data regarding ΔA_{DT} fall on the theoretical curve (dotted line) calculated from Eqs. 5—8 while using this value. This demonstrates the plausibility of a reaction scheme involving a rapid equilibria.

Subsequently, the reaction given by the left-hand side of the proposed mechanism was examined on the basis of data for both τ^{-1} and ΔA_{SF} obtained from the present stopped-flow measurements. By coupling with a rapid equilibria, the equations for τ^{-1} and ΔA_{SF} in the present process can be written as

$$\tau^{-1}=k_{-b}\left[K_b\frac{\bar{S}_3(F-K_3\bar{M}/\bar{H})}{F(1+K_3\bar{S}_3/\bar{H})}+\frac{\bar{M}}{F}+1\right], \quad (9)$$

with

$$F=(1+\bar{H}/K_{\beta c})(\bar{H}+K_3\bar{S})/K_{1m}+K_3(\bar{M}+\bar{S}_3)/\bar{H}+1, \quad (10)$$

and

$$\Delta A_{SF}/cm=(\varepsilon_{C_a}-\varepsilon_{HSA})(\bar{C}_a-\bar{C}_{a,r})+(\varepsilon_{C_b}-\varepsilon_{BSA})C_b, \quad (11)$$

respectively. The overbar and ε_{C_b} denote the equilibrium concentration of each reacting species and the molar extinction coefficient of C_b, respectively. The concentration term in brackets in Eq. 9 was calculated for various values of K_b. As shown in Fig. 8, a plot of τ^{-1} obtained at various pH values and concentrations *vs.* the concentration term calculated by using $K_b=1.9\times10^6\,M^{-1}$ gives a good proportionality through the origin. From the slope of this line, k_{-b} was determined to be 5.1 s^{-1} and k_b was calculated to be $9.7\times10\ M^{-1}s^{-1}$. All the data of τ^{-1} fall on the theoretical curves calculated using these values, as can be seen from Figs. 4 and 5. Furthermore, the theoretical curve of ΔA_{SF}, drawn with a dashed line in Fig. 6, was calculated from Eq. 11 by using $\varepsilon_{C_b}=24000\ M^{-1}cm^{-1}$ and gives a good fit with the data at each pH value. This good agreement between the theoretical curves and the experimental data confirms the validity of Mechanism I.

The apparent association constant K_{app}, defined as $(C_a+C_b)/(\bar{S}_1+\bar{S}_2+\bar{S}_3)\cdot M$, and the apparent molar extinction coefficient $\varepsilon_{c,app}$ can be calculated from the following relations:

$$K_{app}=\frac{K_1/\bar{H}+K_{\beta c}K_{1m}K_b/\bar{H}^2}{1+K_{\beta c}/\bar{H}+K_{\beta c}K_{1m}\bar{H}^2}, \quad (12)$$

and

$$\varepsilon_{c,app}=\frac{\varepsilon_{C_a}\bar{C}_a+\varepsilon_{C_b}\bar{C}_b}{\bar{C}_a+\bar{C}_b}. \quad (13)$$

Calculations using these equations yield $K_{app}=3.1\times10^5\ M^{-1}$ and $\varepsilon_{c,app}=22200\ M^{-1}cm^{-1}$ for pH 5.0. Good agreement with the values ($K_p=5.3\times10^5\,M^{-1}$ and $\varepsilon_{c,app}=22100\ M^{-1}cm^{-1}$) obtained statically also strongly supports the present assignments.

Discussion

Both the static and kinetic studies in the present

TABLE 1. STOICHIOMETRIC AND KINETIC CONSTANTS FOR BINDING OF Cu^{2+} TO SERUM ALBUMIN AT 25 °C AND MOLAR EXTINCTION COEFFICIENTS OF COMPLEXES AT 255 nm

Source	γ[c]	K_3[d]	K_b	k_b	k_{-b}	$\varepsilon_{C_a}(\Delta\varepsilon_{C_a})$	$\varepsilon_{C_b}(\Delta\varepsilon_{C_b})$
			$10^6\,M^{-1}$	$10^6\,M^{-1}s^{-1}$	s^{-1}	$M^{-1}cm^{-1}$	$M^{-1}cm^{-1}$
HSA[a]	1	105±8	1.9±0.3	9.7±1.8	5.1±0.3	21700 (2200)	24000 (4500)
BSA[b]	1	60±10	3.9±0.8	5.2±1.3	1.3±0.1	23700 (2300)	26200 (4800)

a) This work. b) Previous work.[11] c) Values of α and β can be calculated from Eq. 3. d) Values of K_1 and K_2 can be calculated from Eq. 4.

work clearly showed that two types of Cu^{2+} complexs (C_a and C_b) are formed at the three N-terminal peptides of HSA (Asp-Ala-His) by the same mechanism proposed for the binding of a Cu^{2+} ion to BSA terminal peptides (Asp-Thr-His-). In previous work regarding a Cu^{2+}-BSA system,[11] we revealed that C_a is a chelated complex with a square-planar configuration involving α-amino, imidazolyl and two peptide nitrogens. This was originally proposed by Peters and Blumenstock.[2] We also proposed that C_b is a low-pH type complex with a ring structure made by coordinations with imidazolyl nitrogen and β-carboxylato oxygen. In order to see the substitition effect on the complexation, the stoichiometric constants, kinetic constants, and the molar extinction coefficients of the complexes were determined for both albumins and are summarized in Table 1. The molar extinction coefficients in this table involve the absorption of the albumin molecule itself (at 255 nm), which arises mainly from the aromatic groups in the protein. Thus, the net changes in the molar extinction coefficients due to complexation ($\Delta\varepsilon_{C_a}$ and $\Delta\varepsilon_{C_b}$) were estimated by the substraction of ε_{HSA} or ε_{BSA} from the corresponding ε_{C_a} and ε_{C_b}, and are given within parentheses in Table 1. Good agreement between the obtained values for HSA ($\Delta\varepsilon_{C_a}$=2200, $\Delta\varepsilon_{C_b}$=4500) and those for BSA ($\Delta\varepsilon_{C_a}$=2300, $\Delta\varepsilon_{C_b}$=4800) confirm the formation of the same types of complexes at the terminal sites of both albumins. However, the equilibrium and rate constants are somewhat different for each albumin beyond the experimental uncertainties. Especially, the value of k_{-b} obtained for BSA ($1.3\,s^{-1}$) is about one-fourth of that for HSA ($5.1\,s^{-1}$). This result can be explained on the basis of the ring structure of C_b. The construction of molecular models for this complex showed that the side chain of the second residue (α-hydroxyethyl group for BSA, methyl group for HSA) is always outside of the peptide ring. In such a configuration, a bulky and hydrophilic 1-hydroxyethyl group would not only interfere with the binding of a peptide chain to the outside, but would participate in the ordering of water molecules around the complex. These functions of this group are most likely responsible for the stabilization of an already formed ring structure of C_b. This is consistent with the observed k_{-b} reduction for a BSA system.

Finally, it is worth noting that the complexation of Cu^{2+} with the N-terminal site of albumin can be easily understood without any consideration of the N-F transition of albumin occurring in the range of pH 3.5—4.5. This is presumably because the N-terminal domain of albumin is maintained in a compact form through the N-F transition, in contrast to the disordered C-terminal domain.[13]

References

1) T. Peters, Jr., *Biochim. Biophys. Acta*, **39**, 546 (1960).
2) T. Peters, Jr. and F. A. Blumenstock, *J. Biol. Chem.*, **242**, 1574 (1967).
3) T. Peters, Jr. and C. Hawn, *J. Biol. Chem.*, **243**, 1566 (1967).
4) R. A. Bradshaw and T. Peters, Jr., *J. Biol. Chem.*, **244**, 5582 (1969).
5) W. T. Shearer, R. A. Bradshaw, F. R. N. Gurd., and T. Peters, Jr., *J. Biol. Chem.*, **242**, 5451 (1967).
6) E. Breslow, *J. Biol. Chem.*, **239**, 3252 (1964).
7) R. A. Bradshaw, W. T. Shearer, and F. R. N. Gurd, *J. Biol. Chem.*, **243**, 3817 (1968).
8) S. Law and B. Sarkar, *J. Biol. Chem.*, **246**, 5938 (1971).
9) S. Law, T. P. A. Kruck, and B. Sarkar, *J. Biol. Chem.*, **249**, 5878 (1974).
10) K. S. Iyer, S. Law, S. H. Laurie, and B. Sarkar, *Biochem. J.*, **169**, 61 (1978).
11) N. Kure, H. Nakatsuji, T. Sano, and T. Yasunaga, *Bull. Chem. Soc. Jpn.*, **57**, 2712 (1984).
12) F. B. Edwards, R. B. Rombauer, and B. J. Campbell, *Biochem. Biophys. Acta*, **194**, 234 (1969).
13) H. Terada and K. Miyake, *Kolloid-Z. Z. Polymer*, **251**, 139 (1973).

Volume Changes and Equilibrium Constants for Protonation of $[M(edta)]^{2-}$

Kouzou YOSHITANI
Faculty of General Education, Gifu University, Yanagido, Gifu 501-11
(Received February 27, 1985)

The volume changes and the equilibrium constants for the first protonation of $[Co(edta)]^{2-}$, $[Ni(edta)]^{2-}$, and $[Cu(edta)]^{2-}$ (H_4edta=ethylenediaminetetraacetic acid) have been determined from density and pH measurements at 25 °C. In the case of $[Cu(edta)]^{2-}$, a second protonation is assumed to successively occur. The volume change and the equilibrium constant for the second protonation have been estimated. The volume changes for the first protonation of Co(II)-, Ni(II)-, and Cu(II)-edta chelates were small and positive (3.5, 3.3, and 4.8 $cm^3\,mol^{-1}$, respectively) and that for the second protonation of a Cu(II)-edta chelate was larger than the first one (8 $cm^3\,mol^{-1}$).

Although the structures of a number of metal-edta chelates in the solid state have been established by X-ray studies,[1] their structures in aqueous solutions are still not so clear. Much attention has been given to determining their structures using a variety of experimental techniques.[2-5] Recently, the partial molal volumes and volume changes for the complex formation of $[M(edta)]^{2-}$ have been determined and useful information about solution structures of the edta-chelates has been obtained.[6]

In this study, the volume changes and the equilibrium constants for the protonation of $[M(edta)]^{2-}$ (M= Co(II), Ni(II), and Cu(II)) are determined and discussed in relation to their structures in neutral and acidic solutions.

Experimental

The edta-chelates, $Na_2[Co(edta)]\cdot 3.5H_2O$, $Na_2[Ni(edta)]\cdot 3H_2O$, and $Na_2[Cu(edta)]\cdot 3H_2O$, were as previously used.[6] The metal chelates were dried *in vacuo* for one week at 110 °C before use. The concentrations of the metal chelate electrolytes were determined by weight. $HClO_4$ was obtained from Nakarai Chemicals, Ltd. and was used as received. All the solutions were prepared with distilled and deionized water. The specific conductivity was less than $2\times10^{-7}\ \Omega^{-1}\,cm^{-1}$. The densities were measured with a digital density meter (Shibayama Scientific Co., Ltd. Model SSD-200). Details of the measurements have been described elsewhere.[7] The pH values of the solutions were determined with a digital pH meter (TOA Electronics Ltd. Model HM-15A), which was calibrated by using standard buffer solutions (Merck). The temperature of the water bath was controlled to 25.00±0.002°C.

Results and Discussion

The aqueous solutions of edta-chelates (*ca.* 0.02 mol dm^{-3}) were mixed with the $HClO_4$ solutions (*ca.* 0.02 mol dm^{-3}). The volume changes on the first protonation, ΔV_1, for eqilibrium, $MY^{2-}+H^+=MHY^-$, have been determined from the equation:

$$\Delta V_{mix}=\frac{1000d}{w_1+w_2}\left(\frac{w_1+w_2}{d}-\frac{w_1}{d_1}-\frac{w_2}{d_2}\right)=\alpha[M]\Delta V_1, \quad (1)$$

where ΔV_{mix} is the volume change of mixing per 1 dm^3 of the mixed solution, w_1, w_2 and d_1, d_2 are the weights and densities of the edta-chelates and the $HClO_4$ solutions before mixing, d is the density of the mixed solution, [M] is the total molar concentration of the edta-chelates in the mixed solution, $[M]=[MY^{2-}]+[MHY^-]$, and α is the degree of the protonation, ($\alpha=[MHY^-]/([MY^{2-}]+[MHY^-])$), respectively. No correction for the volume change of the dilution was made, which was assumed to be within the experimental error. The α value can be calculated from the pH value of the mixed solution by a successive iteration as follows. First, the activity coefficients of the ions are assumed to be unity and an approximate α value is obtained from the equation:

$$\alpha=([A]-[H^+])/[M], \quad (2)$$

where [A] is the total molar concentration of H^+ and MHY^- in the mixed solution, $[A]=[H^+]+[MHY^-]$, and can be calculated from the initial concentration of the $HClO_4$ solution. By using this estimated α value, the ionic strength and the activity coefficients of the ions according to the Davies' equation[8] are obtained. A more accurate α can then be obtained from the pH value, the activity coefficient of H^+ and Eq. 2. The iteration process is repeated until the consistent α value is obtained. The thermodynamic equilibrium constant for the first protonation of MY^{2-} can be calculated from the obtained consistent α value and activity coefficients:

$$K_1^\circ=\frac{\alpha[M]y_1}{[H^+]y_1(1-\alpha)[M]y_2}, \quad (3)$$

where y_1 and y_2 are the molar activity coefficients of the monovalent and divalent ions, respectively. In Table 1, the total concentrations, [M] and [A], pH, $\log K_1^\circ$ and ΔV_1 are listed. In these mixed solutions, the metal chelate ions are considered to be stably present from their stability constants[9] and the pH values of the mixed solutions. The constant $\log K_1^\circ$ and ΔV_1 values are obtained for $[Co(edta)]^{2-}$ ($\log K_1^\circ=3.55\pm0.01$ $mol^{-1}\,dm^3$, $\Delta V_1=3.5\pm0.2$ $cm^3\,mol^{-1}$) and for $[Ni(edta)]^{2-}$ ($\log K_1^\circ=3.53\pm0.01$ $mol^{-1}\,dm^3$, $\Delta V_1=3.3\pm0.3$ $cm^3\,mol^{-1}$). However, the $\log K_1^\circ$ values for $[Cu(edta)]^{2-}$ increase with decreasing the pH values of the mixed solutions.

TABLE 1. THE VALUES OF THE EQUILIBRIUM CONSTANTS AND THE VOLUME CHANGES FOR THE FIRST PROTONATION OF $[M(edta)]^{2-}$

[M] / mol dm^{-3}	[A] / mol dm^{-3}	pH	log K_1°	ΔV_1 / cm^3 mol^{-1}
		$[Co(edta)]^{2-}$		
0.01426	0.005849	3.513	3.55	3.6
0.01330	0.006837	3.363	3.55	3.5
0.01246	0.008795	3.224	3.55	3.5
0.01226	0.007901	3.193	3.56	3.7
0.01196	0.008208	3.138	3.56	3.1
0.01139	0.008795	3.033	3.56	3.7
		$[Ni(edta)]^{2-}$		
0.01397	0.006833	3.382	3.54	3.4
0.01396	0.006837	3.379	3.53	3.2
0.01309	0.007690	3.243	3.53	3.0
0.01258	0.008190	3.158	3.53	3.5
0.01226	0.008507	3.105	3.53	2.9
0.01196	0.008793	3.049	3.53	3.4
0.01164	0.009109	2.993	3.53	3.2
0.01117	0.009573	2.902	3.53	3.8
		$[Cu(edta)]^{2-}$		
0.01532	0.005133	3.618	3.53	
0.01460	0.005854	3.520	3.54	
0.01362	0.006832	3.385	3.56	
0.01226	0.008199	3.202	3.61	
0.01167	0.008791	3.120	3.65	
0.01136	0.009097	3.078	3.68	
0.01114	0.009318	3.074	3.71	
0.01022	0.010245	2.908	3.90	
0.009359	0.01117	2.766		
0.009147	0.01138	2.735		
0.009080	0.01139	2.735		
0.008230	0.01229	2.592		
0.007917	0.01261	2.544		

This indicates that the second protonation occurs successively. Therefore, the first and second protonations for $[Cu(edta)]^{2-}$ in these mixed solutions are considered:

$$MY^{2-} + H^+ = MHY^-, \qquad K_1° = [MHY^-]/[MY^{2-}][H^+]y_2, \tag{4}$$

$$MHY^- + H^+ = MH_2Y, \qquad K_2° = [MH_2Y]/[MHY^-][H^+]y_1^2. \tag{5}$$

The total molar concentrations are defined by:

$$[M] = [MY^{2-}] + [MHY^-] + [MH_2Y], \tag{6}$$

$$[A] = [H^+] + [MHY^-] + 2[MH_2Y]. \tag{7}$$

Combining Eqs. 4—7 gives:

$$\frac{[A]-[H^+]}{\{2[M]-([A]-[H^+])\}[H^+]^2y_1^2y_2} = \frac{[M]-([A]-[H^+])}{\{2[M]-([A]-[H^+])\}[H^+]y_1^2}K_1° + K_1°K_2°. \tag{8}$$

A plot of the values of the left-hand side of Eq. 8 against the corresponding values for the coefficients of K_1° enables both K_1° and K_2° to be obtained. The required

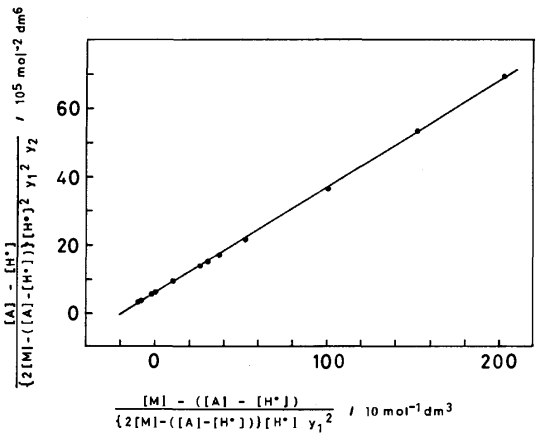

Fig. 1. The best fitted plot of Eq. 8.

values of $[H^+]$, y_1 and y_2 are obtained by similar successive iterations as before. The best fitted plot of Eq. 8 is obtained by four iterations and is shown in Fig. 1. Thus, K_1° and K_2° values for the first and second protonations are evaluated from Fig. 1 by a least squares-method ($\log K_1° = 3.49 \pm 0.01$ mol^{-1} dm^3 and $\log K_2° = 2.26 \pm 0.01$ mol^{-1} dm^3, respectively). The volume changes for the first and the second protonation for $[Cu(edta)]^{2-}$, ΔV_1 and ΔV_2, are calculated using the equation:

$$\Delta V_{mix} = [M]\{\alpha_1\Delta V_1 + \alpha_2(\Delta V_1 + \Delta V_2)\}, \tag{9}$$

where α_1 and α_2 are the fractions of $CuHY^-$ and CuH_2Y, respectively, and can be estimated from the obtained values for K_1° and K_2°. The values of ΔV_1 and ΔV_2 are 4.8 ± 0.2 cm^3 mol^{-1} and 8 ± 1 cm^3 mol^{-1}, respectively.

The estimated values for $\log K$ ($K = [MHY^-]/[MY^{2-}][H^+]$) of $[Co(edta)]^{2-}$, $[Ni(edta)]^{2-}$, $[Cu(edta)]^{2-}$ at the 0.1 mol dm^{-3} ionic strength (3.10, 3.08, and 3.04 mol^{-1} dm^3, respectively) are in good agreement with the literature values (3.0, 3.2, and 3.0 mol^{-1} dm^3, respectively).[9]

It is well known that the first and second protonations to a free $edta^{4-}$ ion take place at the nitrogen atoms.[10,11] However, spectrophotometric studies indicate that the first protonation to stable edta-chelate ions takes place at the oxygen atom in the carboxylate group of the ligand.[12,13] Then, the monoprotonated edta-chelate, in which edta acts as a pentadentate ligand, one carboxyl group is free and the water molecule occupies the sixth coordination site, is expressed as $[M(edtaH)(H_2O)]^-$. The volume changes for the first protonation, ΔV_1, of the edta-chelates of Co(II), Ni(II), and Cu(II) (3.5, 3.3, and 4.8 cm^3 mol^{-1}, respectively) are considerably smaller than that for the protonation of the simple acetate ion, which is reported to be 11.3 cm^3 mol^{-1}.[14] The same has been found for the entropy changes for the protonation of these edta-chelates:[15] They are considerably smaller than that for the protonation of H_2edta^{2-}, which relates to the protonation of the carboxylate group in the free ligand.[15] This may

be explained by the fact that the first protonation reaction of the edta-chelate involves the substitution reaction of the coordinated carboxylate group by a water molecule prior to actual protonation. The protonation of the free carboxylate group of the edta chelate is accompanied by a positive volume change. However, the substitution reaction may be considered to be accompained by a negative volume change due to the electrostriction of the coordinated water molecule and due to the localized charge of the free carboxylate group.

It has been proposed that, in neutral solutions of these edta chelates, there are dynamic equilibria between the dominant sexidentate form and the quinquedentate form, the latter having a water molecule and a free carboxylate group.[3-5] The amount of the dominant sexidentate form has been estimated by a NMR study as 81, 67, and 62% for Co(II)-, Ni(II)-, and Cu(II)-edta chelate, respectively.[5] The volume change from the sexidentate form to the quinquedentate form for the Co(II)-edta chelate has been estimated to be -4.9 $cm^3 mol^{-1}$ from an ultrasonic study.[4] If this value is assumed to be independent of the central metal cation, the volume changes due to the protonation of the free carboxylate group of the edta chelate are calculated to be 7.5, 6.6, and 7.8 $cm^3 mol^{-1}$ for Co(II)-, Ni(II)-, and Cu(II)-edta chelates, respectively. These values are smaller than that of the volume change for the protonation of the acetate anion (11.3 $cm^3 mol^{-1}$). However, they are comparable in magnitude with that of the formate anion (8.5 $cm^3 mol^{-1}$).[4] Taking into account the difference that one is a simple carboxylate anion and the other is a complex ion, the ΔV_1 values seem to be reasonable.

For simple dibasic carboxylate anions, such as the malonate and the oxalate ions, the volume changes for the first and second protonation, ΔV_1 and ΔV_2, are in the order, $\Delta V_1 > \Delta V_2$,[16] which is expected from simple electrostatic theory such as the Drude-Nernst formulation.[17] The differences between ΔV_1 and ΔV_2 diminish when the two charged centers are sufficiently separeted.[16] However, the ΔV_1 and ΔV_2 obtained for the Cu(II)-edta chelate are in a reverse order. If the second protonation of the Cu(II)-edta chelate takes place at the free carboxylate group in the same manner as the first one, the ΔV_2 should be smaller than that of the ΔV_1, or at least the same magnitude. In the solid state, the diprotonated Cu(II)-edta has a tetragonally distorted structure with a free carboxyl arm and a water molecule occupying the sixth coordination site and two elongated bonds of metal-nitrogen and metal-oxygen of the carboxylate.[18] The second protonation has been assummed to take place at the uncoordinated oxygen atom in the longer bonded carboxylate group.[18] If the diprotonated Cu(II)-edta in the solution has a similar structure to that in the the solid state, the smaller ΔV_1 compared to ΔV_2 for the Cu(II)-edta may be understandable.

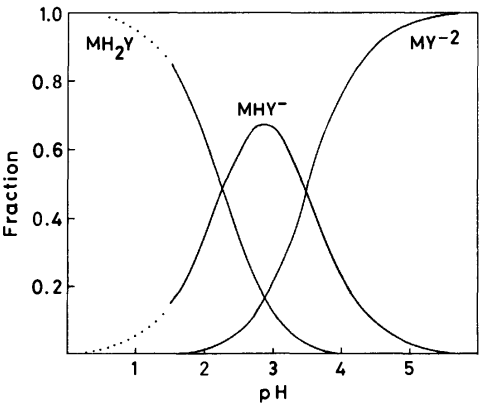

Fig. 2. Distribution of the Cu(II)-edta chelate species as a function of pH.

Although the equilibrium constants for the first protonation of the stable edta-chelate ions have been determined by spectrophotometric studies[3,19] or the by-product of the determination of the stability constants of the edta-chelates, a study of the second protonation is thought to be difficult because of the low solubility of the diprotonated edta-chelate. In this study, the concentrations of the Cu(II)-edta chelate in the mixed solutions were sufficiently low (0.015—0.008 mol dm^{-3}) and precise pH measurements have enabled us to determine the equilibrium constants for the second protonation of Cu(II)-edta chelate. In Fig. 2, the fractions of three species of the Cu(II)-edta chelate at the acidic medium are shown. The monoprotonated Cu(II)-edta chelate starts to form at around pH 5, and the maximum in the fraction is attained at around pH 3 with a fraction of 0.6. The diprotonated Cu(II)-edta chelate begins to form at around pH 4 and the monoprotonated and diprotonated species are present in an equimolar condition around at pH 2.3.

The author wishes to thank Professor Yuroku Yamamoto and Dr. Manabu Yamamoto of Hiroshima University for their helpful discussions.

References

1) R. H. Nuttall and D. M. Stalker, *Talanta*, **24**, 355 (1977).

2) A. A. McConnell, R. H. Nuttall, and D. M. Stalker, *Talanta*, **25**, 425 (1978).

3) W. C. E. Higginson and B. Samuel, *J. Chem. Soc. (A)*, **1970**, 1579.

4) S. Harada, Y. Funaki, and T. Yasunaga, *J. Am. Chem. Soc.*, **102**, 136 (1980); Y. Funaki, S. Harada, K. Okumiya, and T. Yasunaga, *ibid*, **104**, 5325 (1982).

5) J. Oakes and E. G. Smith, *J. Chem. Soc., Faraday Trans. 2*, **77**, 299 (1981); J. Oakes and E. G. Smith, *J. Chem. Soc., Faraday Trans. 1*, **79**, 543 (1983).

6) K. Yoshitani, *Bull. Chem. Soc. Jpn.*, **58**, 1646 (1985).

7) K. Yoshitani, M. Yamamoto, and Y. Yamamoto, *Bull. Chem. Soc. Jpn.*, **56**, 1978 (1983).

8) C. W. Davies, *J. Chem. Soc.*, **1938**, 2093.

9) A. E. Martell and R. M. Smith, "Critical Stability Constants," Plenum Press, New York (1974), Vol. 1, pp. 206—207.
10) K. Nakamoto, Y. Morimoto, and A. E. Martell, *J. Am. Chem. Soc.*, **85**, 309 (1963).
11) D. Chapman, D. R. Lloyd, and R. H. Prince, *J. Chem. Soc.*, **1963**, 3645.
12) D. T. Sawyer and J. T. Tackett, *J. Am. Chem. Soc.*, **85**, 2390 (1963).
13) K. Krishnan and R. H. Plane, *J. Am. Chem. Soc.*, **90**, 3195 (1968).
14) H. Hoiland, *J. Chem. Soc., Faraday Trans. 1*, **70**, 1180 (1974).
15) A. P. Brunetti, G. H. Nancollas, and P. N. Smith, *J. Am. Chem. Soc.*, **91**, 4680 (1969).
16) H. Hoiland, *J. Chem. Soc., Faraday Trans. 1*, **71**, 797 (1975).
17) P. Drude and W. Nernst, *Z. Physik. Chem. (Frankfurt)*, **15**, 79 (1894).
18) F. S. Stephens, *J. Chem. Soc. (A)*, **1969**, 1723.
19) T. R. Bhat and M. Krishnamurthy, *J. Inorg. Nucl. Chem.*, **25**, 1147 (1963).

The Synthesis, and the Crystal and Molecular Structure of [Diaquatetrakis-(thiocyanato)cobalt(II)mercury(II)]-*N,N*-Dimethylacetamide (1/2), $CoHg(SCN)_4(H_2O)_2 \cdot 2\{CH_3CON(CH_3)_2\}$

Hisashi KINOSHITA,* Mamoru SHIMOI,† Akira OUCHI,† and Shoichi SATO††

Department of Chemistry, Faculty of Liberal Arts, Shizuoka University, Ohya, Shizuoka 422

†*Department of Chemistry, College of Arts and Sciences, The University of Tokyo, Komaba, Meguro-ku, Tokyo 153*

††*The Institute for Solid State Physics, The University of Tokyo, Roppongi-7, Minato-ku, Tokyo 106*

(Received April 22, 1985)

The new complex indicated in the title was synthesized and its crystal and molecular structures were determined by the use of a single-crystal X-ray diffraction method. The crystal is tetragonal, with the space group $P\bar{4}$, and the cell constants are $a=12.124(5)$ and $c=7.985(2)$ Å. The structure was solved using the heavy-atom method, and the final R value was 0.039. Two kinds of crystallographically independent mercury atoms in the unit cell are tetra-coordinated and they are in the tetrahedral geometry, where four sulfur atoms of the thiocyanate ions are ligated, respectively. The cobalt atom is hexa-coordinated, and is in an octahedral geometry, where four nitrogen atoms of the thiocyanate ions are coordinated equatorially, and two water oxygen atoms axially. Thiocyanate ions span mercury and cobalt atoms to form two-dimensional networks parallel to the (001) plane. The planar polymeric complexes are linked to the c-axis direction, through hydrogen bonds between coordinated water molecules and *N,N*-dimethylacetamide.

The tetrakis(thiocyanato)cobalt(II)mercury(II), $CoHg(SCN)_4$ (**1**), has a so called "diamond-like" three-dimensional polymeric structure,[1] and to study such complexes is attractive. Some of the Lewis-base adducts of **1** were synthesized,[2,3] and the structure of some adducts, $CoHg(SCN)_4L_2$ (where L=pyridine (**2**),[4] *N,N*-dimethylformamide (**3**),[5] and triphenylphosphine (**4**)[6]), as well as $CoHg(SCN)_4(tu)_4$ (**5**) (where tu=thiourea)[7] were already elucidated. Complexes **2** and **3** have a three-dimensional polymeric structure, where both of the base ligands are coordinated as an unidentate, taking *trans* positions in **2** and *cis* positions in **3**. Compex **4** has a one-dimensional "ladder-like" structure, where each dimer ring is linked to their neighbors on both sides by a pair of weak Hg–S bonds, respectively. Complex **5** consists of discrete anionic and cationic complexes, $[Hg(tu)_4]^{2+}$ and $[Co(SCN)_4]^{2-}$, and no bridging exists between them.

In this research we could obtain a new type Lewis-base adduct, indicated in the title (**6**), which includes two moles of water and two moles of *N,N*-dimethylacetamide (DMA) per one mole of the core complex **1**. The cobalt(II) atom in this complex was expected to be in an octahedral configuration since the complex is reddish-brown in color. However, no more details regarding its structure were clarified by the spectroscopic method. Although the structure of the *N,N*-dimethylformamide adduct, **3**, was already known, this complex has not only DMA molecules but also water molecules. It is of the $CoHg(SCN)_4L_2L'_2$ type. Consequently, we have determined its structure using an X-ray diffraction technique with its single crystal.

Experimental

Synthesis of Diaquatetrakis(thiocyanato)cobalt(II)mercury(II)-DMA (1/2) 6. To a finely powdered **1** (1.00 g, 2.0 mmol), was added about 10 cm^3 of a mixed solvent of DMA and water (1:1=v/v). This mixture was warmed and stirred until **1** was dissolved. The solution, which was reddish violet in color, was left standing at about 15 °C over night. The deposited crystals were separated, washed with mixed solvent and water and dried by pressing between filter paper sheets. The yield was 1.28 g (85—91%). The crystals used for the X-ray structure analysis were obtained from a more dilute solution of the mixed solvent after being left standing for several days. Anal. Found: Co, 8.35; C, 20.41; H, 3.19; N, 12.26%. Calcd for $CoHgC_{12}H_{22}N_6O_4S_4$: Co, 8.39; C, 20.53; H, 3.16; N, 11.97%.

Intensity-data Collection. A parallelepiped crystal with the dimensions of 0.28×0.22×0.11 mm^3 along the unit cell axes was used for the intensity measurement. Crystallographic data are: $CoHgC_{12}H_{22}N_6O_4S_4$, F.W.=702.13, tetragonal, space group $P\bar{4}$, $Z=4$, $a=12.124(5)$, $c=7.958(2)$ Å, $U=1169.4(8)$ Å^3, $D_m=1.99(3)$, $D_x=1.99$ Mg m^{-3}, μ(Mo $K\alpha$)=7.80 mm^{-1}. Reflections within a range of $3°<2\theta<70°$ were collected on a Rigaku Denki AFC-6A automated four circle X-ray diffractometer, with graphite-monochromated Mo $K\alpha$ radiation. The ω—2θ scan technique was employed (scan speed, 4° min^{-1} in 2θ; scan width, $\Delta\omega=1.05+0.5\tan\theta$°). The crystal was stable during the measurement process. Of the 5597 reflections measured in a quartant of the reciprocal space, 1081 independent reflections with $|F_o|>3\sigma(|F_o|)$ were used for the structure determination. The intensities were corrected for the Lorentz and polarization factors as well as for the absorption. The latter correction was made using numerical Gaussian integration.[8]

Structure Determination. The structure was solved by the heavy-atom method. The positions of the mercury(II) and cobalt(II) atoms were deduced from a three-dimensional Patterson map, while the other non-hydrogen atoms were located by means of succesive Fourier syntheses. Their positions and thermal parameters (firstly isotropic and finally anisotropic) were refined by a block-diagonal least squares method. At the final refinement step, shifts of all the parameters were less than $\sigma/3$'s. The final R value[9] (applying anisotropic temperature parameters) was 0.039. The R value was 0.041 for the structure with an inverse chirality. We carried also out a refinement using an alternate space group P4, where two kinds of cobalt atoms are on four-fold axes and mercury atoms lie on two-fold axes. However, the $CoHg(SCN)_4$ skeleton was almost equivalent to that of $P\bar{4}$. The main difference lies in the orientation of the DMA mole-

cules. As unreasonably short contacts occured between the DMA molecules in this ordered structure, an orientational disorder of the DMA molecules was introduced into the refinement. This disorder shows favor to a hydrogen-bond formation regarding all coordinated water molecules. The refinement converged R=0.065 and no improvement was attained in the R value. From these points, the space group P4 is thought to be less probable.

Although the space group P4/m is also possible, it was apparent that an adoption of this group implies that no ordered arrangement could be realized for almost all the atoms. Consequently, the space group was considered unacceptable.

All the calculations were carried out on a HITAC M-280H computer at the Computer Center of the University of Tokyo using the local version of the UNICS program system.[10] The atomic-scattering factors were taken from the tables.[11]

Other Measurements. The magnetic moment of the solid sample was measured at 20 °C using a Gouy balance. The infrared absorption spectra were obtained by means of a JASCO A202 grating infrared spectrophotometer using Nujol and hexachloro-1,3-butadiene mull. The visible diffuse reflectance spectrum of the solid complex was measured by means of a Hitachi 124 spectrophotometer using MgO as the reference.

Results and Discussion

The final atomic parameters of the non-hydrogen atoms are listed in Table 1, while the selected bond lengths, bond angles, and some of the short interatomic distances that were assumed to be hydrogen bonds are tabulated in Table 2.[12] In Figs 1 and 2, perspective drawings of the complex around a mercury atom Hg (1), and that around a cobalt atom, together with the hydrogen-bond bridging between the neighboring cobalt atoms along the c-axis, respectively, are given. The numbering scheme is also shown in the figures. The geometry atound the Hg (2) atom is nearly the same that around the Hg(1) atom. The projection of the structure along the c-axis is shown in Fig. 3.

Table 1. Final atomic coordinates ($\times 10^4$) and equivalent isotropic temperature factors of non-hydrogen atoms, with estimated standard deviations in parentheses

Atom	x	y	z	B_{eq}/Å^2 [a]
Hg(1)	0	0	0	2.48
Hg(2)	5000	5000	0	2.48
Co	5000	0	487(2)	1.95
O(W1)	5000	0	3154(13)	3.12
O(W2)	5000	0	−2154(14)	3.78
S(1)	1370(3)	1259(3)	−1447(6)	3.85
S(2)	3860(4)	3724(3)	1798(6)	4.88
N(1)	534(8)	3390(7)	−591(16)	2.87
N(2)	4469(8)	1708(8)	637(16)	3.09
C(1)	910(8)	2509(7)	−925(14)	1.91
C(2)	4307(9)	2547(8)	1051(19)	2.81
C(11)	3685(15)	2981(13)	6730(25)	5.51
C(12)	3309(9)	2107(12)	5565(19)	3.40
C(13)	1980(15)	1375(14)	3606(26)	5.64
C(14)	1764(14)	3248(15)	4756(27)	6.16
N(11)	2399(9)	2224(11)	4689(21)	4.09
O(11)	3800(8)	1129(9)	5418(12)	4.18

a) The isotropic temperature factors were computed using the following expression: $B_{eq}=4/3(B_{11}a^2+B_{22}b^2+B_{33}c^2)$. The B_{ij}'s are defined by: $\exp[-(h^2B_{11}+k^2B_{22}+l^2B_{33}+2hlB_{13}+2hkB_{12}+2klB_{23})]$.

Table 2. Selected bond lengths and bond angles, with estimated standard deviations in parentheses

Bond length	l/Å	Bond length	l/Å
Hg(1)-S(1)	2.533(4)	Hg(2)-S(2)	2.520
Co-N(2)	2.171(10)	Co-N(1^{ii})	2.058(9)
Co-O(W1)	2.123(10)	Co-O(W2)	2.101(11)
N(1)-C(1)	1.191(13)	C(1)-S(1)	1.668(10)
N(2)-C(2)	1.088(15)	C(2)-S(2)	1.639(12)
O(W1)···O(11)	2.690(13)	O(W2)···O(11^{iii})	2.779(14)
C(12)-O(11)	1.332(17)	C(12)-N(11)	1.313(19)
C(11)-C(12)	1.48(3)	C(13)-N(11)	1.44(3)
C(14)-N(11)	1.46(2)		

Bond angle	ϕ/°	Bond angle	ϕ/°
S(1)-Hg(1)-S(1^{i})	125.92(12)	S(1)-Hg(1)-S(1^{ii})	101.93(11)
S(2)-Hg(2)-S(2^{vi})	108.81(14)	S(2)-Hg(2)-S(2^{vii})	110.80(15)
N(1^{ii})-Co-N(1^{vi})	175.4(4)	N(2)-Co-N(2^{v})	173.7(4)
N(2)-Co-N(1^{vi})	88.8(4)	N(2)-Co-N(1^{ii})	90.9(4)
N(2)-Co-O(W1)	86.9(4)	N(2)-Co-O(W2)	93.2(4)
N(1^{ii})-Co-O(W1)	87.7(4)	Hg(1)-S(1)-C(1)	102.4(4)
Hg(2)-S(2)-C(2)	98.5(5)	S(1)-C(1)-N(1)	176.8(9)
S(2)-C(2)-N(2)	170.0(12)	Co-N(2)-C(2)	164.2(10)
Co-N(1^{ii})-C(1^{ii})	168.4(8)	C(11)-C(12)-O(11)	123.7(13)
C(11)-C(12)-N(11)	121.0(14)	O(11)-C(12)-N(11)	115.2(13)
C(12)-N(11)-C(13)	122.6(13)	C(12)-N(11)-C(14)	121.0(14)
C(13)-N(11)-C(14)	116.4(14)		
O(W1)···O(11)···O(W2^{iv})	86.1(4)		
O(11)···O(W1)···O(11^{v})	95.9(5)		
O(11)···O(W2^{iv})···O(11^{v})	91.9(5)		

Key to the symmetry operations: i, $-x$, $-y$, z; ii, y, $-x$, $-z$; iii, 1.0$-x$, $-y$, $-1.0+z$; iv, x, y, 1.0+z; v, 1.0$-x$, $-y$, z; vi, 1.0$-y$, x, $-z$; vii, 1.0$-x$, 1.0$-y$, z.

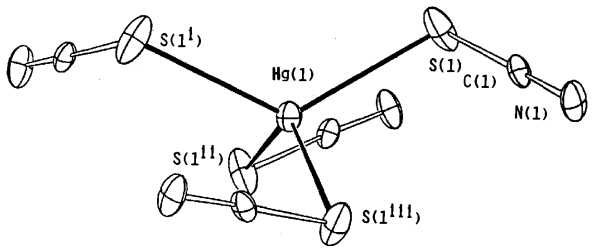

Fig. 1. A perspective drawing of the complex around a mercury(II) atom (Hg(I)), with the numbering scheme.

Each mercury atom is coordinated tetrahedrally to four thiocyanate ions, and lies on a four-fold improper rotation axis. The tetrahedron around Hg (2) is almost regular. However, that around Hg (1) is a little deformed. The Hg-S bond lengths are normal and are nearly equal to the sum of both the atomic radii, r_{Hg}=1.48 and r_S=1.04 Å.[13a] The angles Hg-S-C, 102.4(4) and 98.5(5)°, are a little larger than those in related complexes such as **1**, **2**, and **3**.

The cobalt atom is hexa-coordinated and is in a octahedral geometry, where four nitrogen atoms of

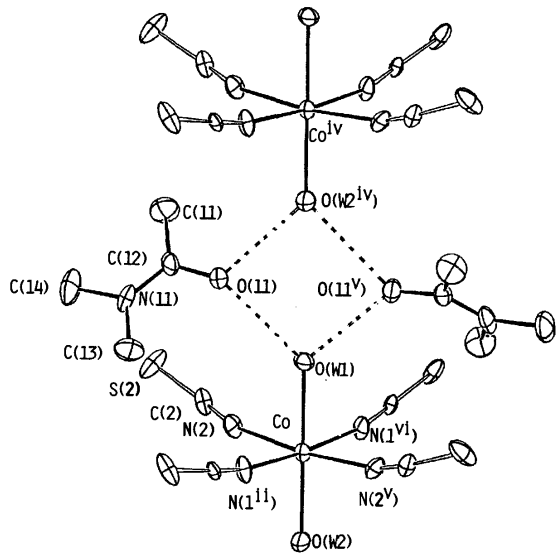

Fig. 2. A perspective drawing of the complex around a cobalt(II) atom and the hydrogen-bond bridging to the next metal atom, with the numbering scheme.

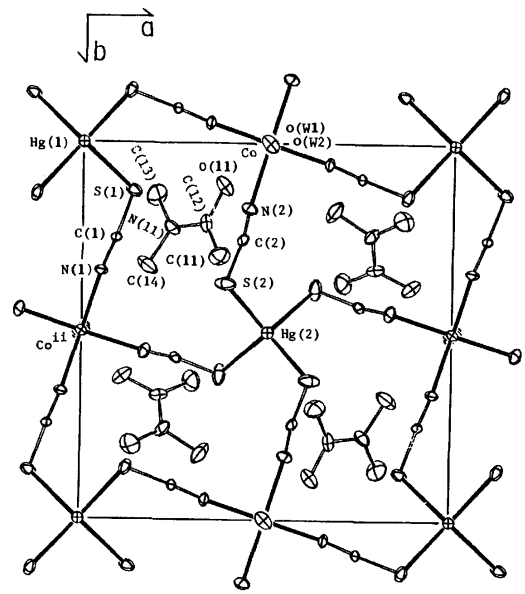

Fig. 3. The crystal packing diagram of the complex.

the thiocyanate ions are ligated equatorially and two water oxygen atoms axially along the c-axis directions. The cobalt atom as well as two oxygen atoms lie on the two-fold axis. All Co-N and Co-O bond lengths are normal, considering the respective atomic radii: r_{Co}=1.32, r_N=0.70, and r_O=0.66 Å.[13a]

The Co-N-C angles are 164.2(10) and 168.4(8)°, and are far from linear. In many isothiocyanato complexes, the M-N-C angles are approximately 180°; and in some related compounds such as **1** and **3**, the angles are not much different from 180°.[1,5] However, more deformed angles in this complex are found in **2** and **4** (about 165°).[4,6] Therefore, the angles in this complex are not exceptional. The N-C-S angles, 176.8(9) and 170.0(12)°, are a little less than 180°. Such a deformation was scarcely found in the common thiocyanato complexes, including **1**—**4**. In Cd(ben)$(SCN)_2$ (where ben=bis(2-aminoethyl)amine) the angles are 167.8(9) and 170.8(10)°,[14] and in $Hg(SCN)_2[(C_6H_5)_3P]$ one of them is 164.2°.[15] Therefore, the relatively large deviations of the bond angles in this complex are thought to be due to a crystal packing effect. Consequently, the bridgings in this complex may be deformed and stressed.

As shown in Table 2, the bond lengths and angles of the DMA molecule are normal except for C(12)-O(11). The length 1.332(17) Å is longer than the values observed in the carbonyl group of common organic compounds, 1.20—1.22 Å.[16] This fact is probably due to hydrogen bondings which are described later. The bond length (C(12)-N(11), 1.313(19) Å) almost corresponds with Pauling's double-bonding C=N distance, 1.29 Å.[13b] Such a short C-N bond is also found in many amide molecules.

The crystal consists of layers parallel to the (001) plane. In a layer, the cobalt atoms slightly deviate (by 0.387 Å) above or below the plane on which the mercury atoms are situated. The cobalt and mercury atoms are bridged by thiocyanate ions to form a two-dimensional network. No bridging ligand exists between the network. The cobalt atoms are linked along the [001] direction through hydrogen bonds between the coordinated water and the DMA oxygen atoms; the hydrogen bonds are shown in Fig. 2. The angles, $O(11)\cdots O(W1)\cdots O(11^V)$ and $O(11)\cdots O(W2^{IV})\cdots O(11^V)$ are 95.9(5) and 91.9(5)°, which are smaller than the H-O-H angles of water molecule, 104.5°.

When **6** in a powder state was kept in an organic solvent such as benzene or acetone at 15°C, it turned blue in color within one day. The residual solid found to be **1**. Thus, the DMA and water molecules in **6** could be easily removed. From this, the bonds of the additional molecules, DMA and water, in **6** are thought not to be stable.

The infrared absorption spectra of complex **6**, as well as **1** and DMA were measured and compared with each other. Some of the results are shown in Table 3. The corresponding absorption maximum wave numbers of the main peaks of the free DMA, such as 1508, 1400, 1265, 1190, 1018, and 592 cm^{-1}, are also found in the spectrum of **6**. As shown in the table, the ν(C=O) peaks of **6** are red shifted by 40 cm^{-1}, probably due to the strong hydrogen bonds to the oxygen atom of DMA in **6**. The peaks concerned with the thiocyanate ion appear almost at the same region in the spectra of **1** and **6**, as shown in the table. The ν(O-H)peaks of **6** appear at 3360 and 3250 cm^{-1}, which are near to those of the ν_1 and ν_3 peaks of free water in the solid state (3400 and 3220 cm^{-1}).[17] Therefore, the splitting is likely to be due to the strong hydrogen bonds of the water molecules in **6**.

The magnetic moment of **6** is about 4.83 BM (1 BM=9.274078(36)$\times 10^{-24}$ JT^{-1}) at 20°C. Its visible

Table 3. Infrared absorption spectral data of **1**, **6**, and DNA (in ν/CM^{-1})

6	1	DMA	Tentative assignment
3360(s) 3250(s)			ν(OH)
2970(m) 2930(m)		2940(s)	ν(CH)
2150(s)	2150(s)		ν(CN)
1648(m)			δ(HOH)
1600(s)		1640(s)	ν(CO)
720(s)	720(s)		ν(CS)
462(m)	470(s)		δ(SCN)
440(m)	447(s)		

1, $CoHg(SCN)_4$; 6, $CoHg(SCN)_4(H_2O)_2 \cdot 2DMA$; DMA, *N*,*N*-dimethylacetamide.

reflectance spectrum shows the main peak of the d-d band at 517 nm with an intense shoulder at about 485 nm. These values are almost the same as those of the related adducts, such as **2** or **3**.[2] These facts are explained by the octahedral geometry around the cobalt atom in this complex as shown by the result of the X-ray structure analysis mentioned above.

References

1) J. W. Jeffery and K. M. Rose, *Acta Crystallogr., Sect B*, **24**, 653 (1968).

2) R. Makhija, L. Pazdernik, and R. Rivest, *Can. J. Chem.*, **51**, 438 (1973).

3) P. P. Singh, *Coord. Chem. Rev.*, **32**, 33 (1980).

4) A. L. Beauchamp, L. Pazdernik, and R. Rivest, *Acta Crystallogr., Sect B*, **32**, 650 (1976).

5) M. R. Udupa and B. Krebs, *Inorg. Chim. Acta*, **42**, 37 (1980).

6) H. Kinoshita, M. Shimoi, and A. Ouchi, *Bull. Chem. Soc. Jpn.*, **58**, 1304 (1985).

7) A. Korczynski and M. A. Porai-Koshits, *Rocz. Khim.*, **39**, 1567 (1965).

8) W. R. Busing and H. A. Levy, *Acta Crystallogr.*, **10**, 180 (1957).

9) $R=\sum||F_o|-|F_c||/\sum|F_o|$.

10) "The Universal Crystallographic Computation Program-System (UNICS)," ed by T. Sakurai, Crystallographic Society of Japan, Tokyo (1967).

11) "International Tables for X-ray Crystallography," Kynoch Press, Birmingham (1974) Vol. IV, pp. 72, 150.

12) The final thermal parameters and the final F_o-F_c table are deposited as Document No. 8542 at the office of the Editor of the *Bull. Chem. Soc. Jpn.*

13) L. Pauling, "The Nature of the Chemical Bonds," 3rd ed, Cornell Univ. Press, N. Y. (1960), a) pp. 246, 249, b) 228, 230.

14) M. Cannas, G. Carta, A. Cristini, and G. Marongin, *Inorg. Chem.*, **16**, 228 (1977).

15) R. Makhija, R. Rivest, and A. L. Beauchamp, *Can. J. Chem.*, **57**, 2555 (1979).

16) W. J. le Noble, "Highlights of Organic Chemistry," Marcel Dekker, N. Y. (1974), p. 26.

17) K. Nakamoto, "Infrared and Raman Spectra of Inorganic and Coordination Compounds," 3rd ed, Wiley-Interscience, N. Y. (1978), p. 119.

Structure of Ni(II)- and Zn(II)-Glycinato Complexes in Aqueous Solution Determined by EXAFS Spectroscopy

Kazuhiko Ozutsumi, Toshio Yamaguchi, Hitoshi Ohtaki,* Kazuyuki Tohji,† and Yasuo Udagawa†
Department of Electronic Chemistry, Tokyo Institute of Technology at Nagatsuta, Nagatsuta-cho 4259, Midori-ku, Yokohama 227
†Institute for Molecular Science, Myodaiji, Okazaki 444
(Received May 18, 1985)

The EXAFS spectroscopy has been used to determine the structure of the bis(glycinato) complexes of nickel(II) and zinc(II) ions of low solubility (0.1—0.3 mol dm^{-3}) in aqueous solution. The structural parameters were evaluated by the least-squares analysis both in the reciprocal and in the real spaces on the basis of various standard samples of known structures. Analysis of the EXAFS spectra of aqueous solutions containing the bis(glycinato) complexes of nickel(II) and zinc(II) ions has revealed that both complexes have two additional water molecules bound to the central metal ions to complete the octahedral structure. The structure of the nickel(II) complex is similar both in crystals and in solution, whereas the bis(glycinato)zinc(II) in solution is coordinated with two water molecules instead of two neighboring glycinato carbonyl oxygen atoms in the solid state.

X-Ray and neutron diffraction techniques have long been used in the investigations of the structure of metal complexes in solution.[1,2] In recent years the EXAFS (extended X-ray absorption fine structure) spectroscopy has been proved to be successful for studies of the short-range order of atoms in solution.[3–5] From both diffraction and EXAFS methods can be obtained structural information related to the radial distribution of atom pairs in a system; the number of neighboring atoms around a central atom, the interatomic distance between them and its root-mean-square deviation. However, there are some differences in the nature of information to be obtained from both methods. EXAFS data bear on the near-neighbor environment of an X-ray absorbing atom only, while scatterings of all atom pairs with different distances are detected by conventional diffraction techniques. Since the contribution of the structures of the solvent and solvated anions to the total diffraction pattern is very large particularly in dilute solutions, structural information on metal complexes may sometimes be hidden by it. The difficulity may be overcome by increasing the concentration of metal ions and by selecting an appropriate counter anion, however. The diffraction method thus has a limited use in the case of dilute solutions. In the EXAFS spectra, on the contrary, the contribution from the solvent structure is absent and the interaction of the nearest neighbors with an absorbing atom is most emphasized, and hence the EXAFS method may be the most suitable for structural determination of metal complexes of low concentration in solution.

According to the single-electron and single-scattering theory of the EXAFS,[6–8] it is essential in structural analysis to evaluate the backscattering amplitude of the scatterer and the phase shifts due to the absorber and scatterers. The method of estimation of these parameter values, as well as data reduction procedures, differs in different groups and laboratories. It seems ambiguous to what extent different treatments and analyses of EXAFS spectra affect the final structure data to be obtained. The first aim of the present study is, therefore, to examine uncertainties in structural data obtained by the EXAFS method. To this aim, EXAFS oscillations are extracted by using two different programs. The phase-shifts and the backscattering amplitudes are estimated either from Teo-Lee's values[9] based on pseudo *ab initio* calculations or from the EXAFS spectra of standard references of known structure. Least-squares fitting calculations are then made both in the reciprocal and in the real spaces on the basis of the various standard references.

The structure of the mono- and tris(glycinato) complexes of nickel(II),[10] copper(II),[11] and zinc(II)[12] ions in aqueous solutions has been determined by means of X-ray diffraction. However, the structure of the relevant bis(glycinato) complexes in solution is not determinable by the conventional X-ray analysis due to their low solubility in water (less than 0.3 mol dm^{-3}). The second aim is, therefore, to determine the structure of the bis(glycinato) complexes of nickel(II) and zinc(II) in solution by the EXAFS method. The solubility of the bis(glycinato)copper(II) complex in water was too low (≈0.025 mol dm^{-3}) to determine the structure of the complex even by the present transmission mode EXAFS experiment.

Experimental

EXAFS Measurements. EXAFS spectra were measured on a laboratory X-ray absorption spectrometer consisting of a Johansson cut bent crystal (Ge(220)), a rotating anode generator (Rigaku Ru-200) and a fast solid-state detector. Details of the spectrometer have been described elsewhere.[13]

Samples measured were aqueous solutions containing the $[M(gly)_3]^-$ (1 mol dm^{-3}) or $[M(gly)_2]$ (0.1—0.3 mol dm^{-3}) (M= Ni(II), Zn(II), and gly=glycinate ion) complex as a main species, which were prepared in the same way as previously described.[10,12] Crystalline samples of the bis(glycinato) complexes of both metals, the structure of which has been investigated by an X-ray diffraction method,[15,16] were also measured for comparison. Aqueous metal nitrate solutions (1 mol dm^{-3}) containing haxaaqua ions and crystalline

Table 1. Samples for EXAFS measurements

Sample	Species	Mole ratio C_{gly}/C_M	C_M/mol dm^{-3}
Powder A	NiO	0	—
Solution B	$[Ni(OH_2)_6]^{2+}$	0	1.023
Solution C	$[Ni(gly)_3]^-$	3.94	1.000
Solution D	$[Ni(gly)_2]$	2.00	0.1225
Powder E	$[Ni(gly)_2(OH_2)_2]$	2.00	—
Powder F	ZnO	0	—
Solution G	$[Zn(OH_2)_6]^{2+}$	0	1.004
Solution H	$[Zn(gly)_3]^-$	5.09	1.245
Solution I	$[Zn(gly)_2]$	2.00	0.2919
Powder J	$[Zn(gly)_2]\cdot H_2O$	2.00	—

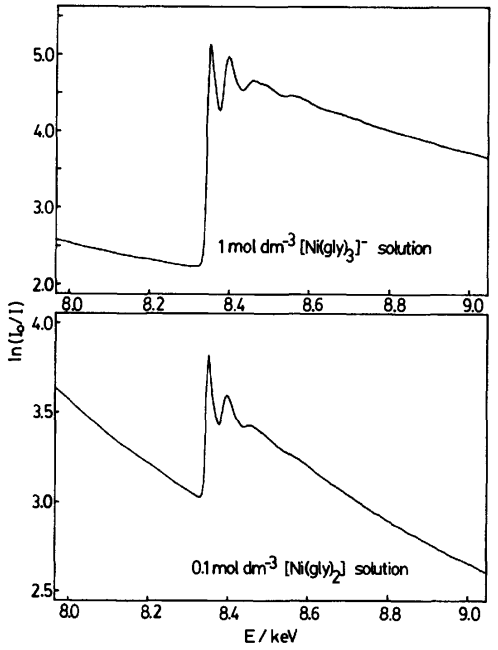

Fig. 1. The absorption spectra for the solutions containing the $[Ni(gly)_3]^-$ (upper part) and $[Ni(gly)_2]$ (lower part) complexes.

powders of the metal oxides were measured as structure standards.[14,17] Details of the samples are summarized in Table 1.

The solution samples were held between thin Mylar windows by the use of a spacer with an adequate thickness to obtain an effective jump at the absorption edge (μx=1—2 with the absorption coefficient μ and the sample thickness x). The powder samples were mixed and ground with boron nitride to dilute the sample, and finally pressed to thin pellets.

The absorbance μx is given as $\ln(I_0/I)$, where I and I_0 are the X-ray intensities with and without a sample, respectively. The intensities I_0 and I were measured at the same time by a partially transmitting ion chamber and an SSD, respectively. The data collection time for covering the required energy region was approximately 10 h and more than 1×10^7 counts of I_0 were obtained at each data point. Measurements were repeated at least twice in order to examine the reproducibility of the results.

An example of the absorption spectra for the solution samples containing high and low concentrations of main species ($[Ni(gly)_3]^-$ and $[Ni(gly)_2]$ complexes) is depicted in Fig. 1.

Data Reduction Procedure. The EXAFS data were analyzed by two different programs, *i.e.* ours (program I) and the one used in the Xerox Palo Alto Laboratory (program II).

Program I. Background absorption other than that for the K edge of an absorption atom of interest was evaluated by least-squares fitting Victoreen's formula[19] to the preedge and was subtracted from the total absorption by extrapolation. The smooth K-shell absorption μ_0 due to an isolated atom was estimated by fitting a smooth curve to the observed absorption spectrum using a cubic spline function.[20] Two or three knots over the whole region were enough to give a good approximation for μ_0.

The modulation $\chi(k)$ was extracted and normalized by the following equation;

$$\chi(k) = \{\mu(k)-\mu_0(k)\}/\mu_0(k) \quad (1)$$

where k is the photoelectron wave vector ejected and is given as $\sqrt{2m(E-E_0)/\hbar^2}$. E denotes the energy of the incident X-rays and E_0 is the binding energy of a K-shell electron.

Program II. Details of the data treatments are referred to the literature.[18] Background absorption was approximated with a function of $A+B\cdot E^{-p}$, where A, B, and p were empirical parameters which were determined by a least-squares fit to the absorption data below the K-edge of interest. In practice, p is found to be between 1 and 3, consistent with Victoreen's formula used in program I. The EXAFS pattern was extracted by assuming a 6th-order polynomial function for the smooth K-shell absorption μ_0.

The $k\cdot\chi(k)$ values obtained by both programs are compared in Fig. 2. As seen in Fig. 2, an approximation of μ_0 by either program I or II is equally good for the extraction of $\chi(k)$. The oscillation of the EXAFS data weighted by k^n was converted by the Fourier transformation into the radial distribution in the r-space as

$$\phi(r) = \sqrt{(1/2\pi)}\int_{k_{min}}^{k_{max}} k^n\cdot\chi(k)\cdot W(k)\cdot\exp(-2ikr)dk. \quad (2)$$

Here $W(k)$ is the window function to reduce ripples due to the truncation effect. The window functions employed in programs I and II were, respectively, of the Hanning type[21] and of Gaussian type. The resulting $\phi(r)$ values obtained with n=2 by using program I are shown in Fig. 3.

Least-squares Calculation. The structure parameters (interatomic distances, mean square displacements and coordination numbers) were obtained by comparing the observed EXAFS spectra and the model function given by the single scattering theory[6-8,22] as,

$$\chi(k)_{calcd} = \sum_j\{n_j/(k\cdot r_j^2)\}\exp(-2\sigma_j^2k^2)B_jF_j(\pi,k) \times\sin(2kr_j+\alpha_j(k)), \quad (3)$$

where $F_j(\pi,k)$ is the backscattering amplitude from each of n_j scatterers j at distance r_j from the X-ray absorbing atom. σ_j^2 is the mean square displacement of the equilibrium distance r_j and B_j is the amplitude reduction factor related to inelastic losses at the absorbing atom due to the many-body effect.[22] $\alpha_j(k)$ is the total scattering phase shift experienced by the photoelectron.

The observed spectra can be compared with the theoretical ones by a least-squares procedure in either r- or k-space. The

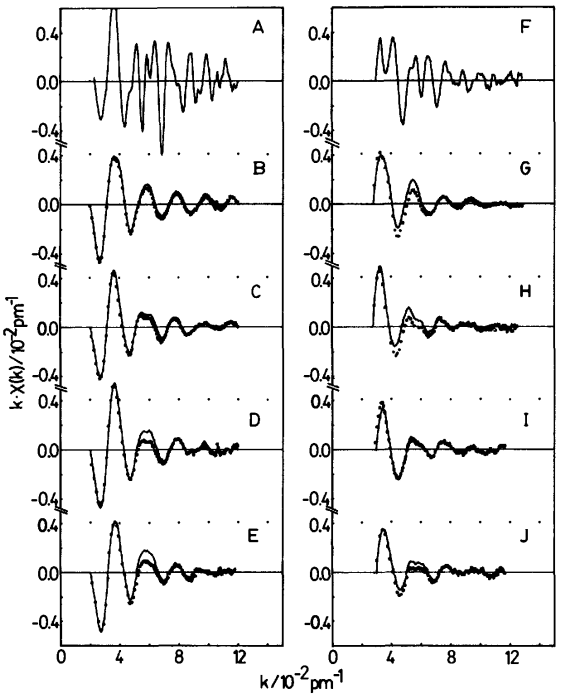

Fig. 2. The EXAFS spectra for the samples measured. The solid lines and the dots were obtained, respectively, by the cubic spline fits (program I) and the 6th-order polynomial fits (program II). A: NiO powder, B: $[Ni(OH_2)_6]^{2+}$ in solution, C: $[Ni(gly)_3]^-$ in solution, D: $[Ni(gly)_2]$ in solution, E: $[Ni(gly)_2(OH_2)_2]$ powder, F: ZnO powder, G: $[Zn(OH_2)_6]^{2+}$ in solution, H: $[Zn(gly)_3]^-$ in solution, I: $[Zn(gly)_2]$ in solution and J: $[Zn(gly)_2]\cdot H_2O$ powder.

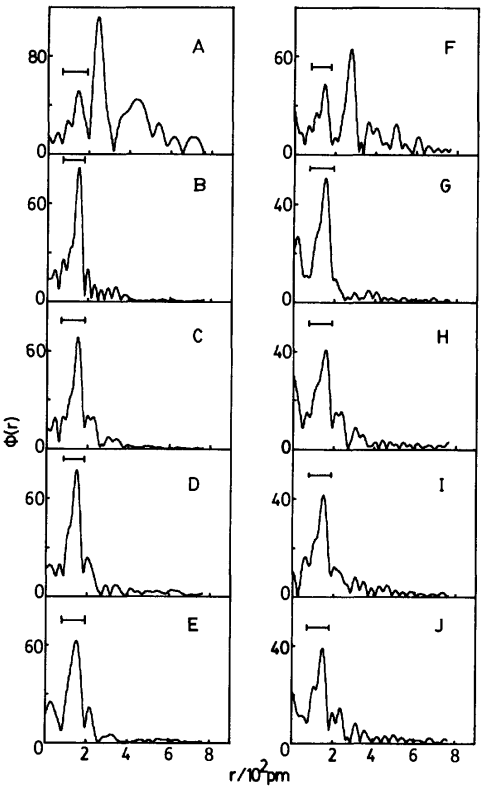

Fig. 3. The Fourier transform $\phi(r)$ of the EXAFS spectra shown in Fig. 1, uncorrected for the phase shifts. The bars indicate the r-range of the inverse Fourier transform shown in Fig. 4 (dots).

latter procedure needs an additional Fourier backfiltering of the peak of interest in the $\phi(r)$ curve. Theoretically both analyses in the k- or r-space should give equivalent results.

We examined least-squares calculations both in the r- and k-spaces.

Analysis in the k-*Space (program I).* A curve fitting procedure in the k-space was applied to the Fourier filtered $k^2\cdot\chi(k)_{obsd}$ values to minimize the error-square sum U_1,

$$U_1 = \sum_{k_{min}}^{k_{max}} k^4(\chi(k)_{obsd}-\chi(k)_{calcd})^2. \quad (4)$$

The values of $F_j(\pi,k)$ and $\alpha_j(k)$ for $\chi(k)$ in Eq. 3 were quoted from the tables reported by Teo and Lee.[9] The values are given against the absolute k-values and thus an improper evaluation of E_0 should result in a systematic distortion of the k-scale and affect the interatomic distances to be determined. Furthermore, the theoretical values of the backscattering amplitudes $F_j(\pi,k)$ are usually larger by *ca.* 50% than those observed,[23] which sometimes give unreasonable bond lengths between an X-ray absorbing central atom and its neighboring ones and the coordination numbers. In this procedure the parameters E_0 and B were estimated from the standard samples of known structure (here we employed the $[M(OH_2)_6]^{2+}$ and MO (M^{2+}=Ni^{2+} and Zn^{2+})) and then they were used as constant values in the course of the analysis of the EXAFS spectra of unknown samples, while r, σ, and n were refined as variables.

Analysis in the r-*Space (program II).* The analysis of the first peak in the r-space followed the procedure, the details of which have been described elsewhere.[18] The E_0 values were fixed to the values estimated in the previous section. The essential formulae are described below.

The $\phi(r)$ values can be expressed by the convolution of two functions as

$$\phi_j(r) = \sum_j \int_0^\infty \frac{dr'}{r'^2} p_{ij}(r')\xi_{ij}(r-r'). \quad (5)$$

$p_{ij}(r)$ is the pair correlation function and ξ_{ij} is the peak function which contains the information on the electron scattering process such as the backscattering amplitude, photoelectron phase-shift and so on. The pair correlation function was assumed to be a Gaussian expressed by

$$p_{ij}(r) = n_j/\sqrt{(2\pi\sigma_j^2)}\ \exp\left[-(r-r_j)^2/2\sigma_j^2\right]. \quad (6)$$

The peak function ξ_{ij} including the phase-shifts and the backscattering amplitudes can be empirically extracted from the $\phi(r)$ values of the standard references of known structure according to Eqs. 5 and 6. Since the ξ_{ij} is insensitive to crystal structure, local bonding, *etc.*,[18] the ξ_{ij} values thus evaluated were adopted in the structure analysis of unknown samples. The model function $\phi_m(r)$ for unknown samples was calculated by using Eq. 5 with the ξ_{ij} values.

The curve fits were carried out by comparing the real (Re) and the imaginary (Im) parts of the $\phi(r)$ with $\phi_m(r)$ values to minimize the error-square sum U_2,

$$U_2 = (2N)^{-1}\sum^N \{\mathrm{Re}(\phi-\phi_m)^2/[(\mathrm{Re}\phi)^2+\{\mathrm{Re}(d\phi/dr)\}^2] + \mathrm{Im}(\phi-\phi_m)^2/[(\mathrm{Im}\phi)^2+\{\mathrm{Im}(d\phi/dr)\}^2]\}. \quad (7)$$

In the course of the calculation, parameters of the radial shift Δr, additional broadening $\Delta\sigma$ and coordination number n were allowed to vary as independent variables. The bond length of the structural references was fixed at the values established from the X-ray diffraction method.

Raman Spectroscopic Measurement. Raman spectra for the bis(glycinato)zinc(II) complex in the solid and solution states were measured with a JEOL laser Raman spectrometer JRS-S1 with the use of the 514.5 nm excited line of Ar^+ laser.

Results and Discussion

Selection of Structure Standards. In order to examine the applicability of the structural standard to the structure analysis of complexes in solution, we examined the spectra of crystalline powder of metal oxides and aqueous metal nitrate solutions containing hexaaqua $[M(OH_2)_6]^{2+}$ ions, the structure of both species having been known.[14,17] The EXAFS spectra $k\cdot\chi(k)$ and the Fourier-transformed function $\phi(r)$ for the structure references are shown in Figs. 2 (A, B, F, and G) and 3 (A, B, F, and G), respectively. In the course of the least-squares fits in the k-space (program I) for the M–O signature within the crystalline metal oxides and within the $[M(OH_2)_6]^{2+}$ in the solutios, parameters E_0, B, and σ were all allowed to vary simultaneously, while the coordination number n was fixed at the known value (6 for NiO, 4 for ZnO and 6 for the aquanickel(II) and -zinc(II) ions). The values for the central atom phase-shift of atom M and those for the backscattering phase-shift and amplitude of atom O were taken from the theoretical values by Teo and Lee. The M–O distance r, which has been determined by the X-ray diffraction method,[14,17] was also allowed to vary in order to check the reproducibility of the value. The results are given in Table 2. The values of E_0 thus estimated agreed with each other in the standard substances of a given metal and seemed reasonable because the interatomic distances converged to the literature values.[14,17] However, the B values obtained for the metal oxides were smaller by a factor of 1.2—1.5 than those for the aqueous solutions. This leads to 20—50% larger coordination number when we use the metal oxides as a standard for the analysis of unknown samples than one uses the solution standard, although the bond length determined may be independent of the selection of the references. Agreements between experimental and calculated $k^2\cdot\chi(k)$ curves are shown in Fig. 4 (A, B, F, and G).

Least-squares fits in the r-space, in which the $\phi(r)$ peak due to the M–O bonds within the $[M(OH_2)_6]^{2+}$ ions were compared with those of the M–O bonds in the metal oxides as the standard, gave larger coordination number than the correct value of six, whereas the bond lengths obtained were in good agreement with those determined by the X-ray diffraction method.

Thus, we concluded that the metal nitrate solutions were more suitable structural references for the solution samples than the metal oxides, even though both of them have the same coordination atoms at the similar distance.

Table 2. Comparison of E_0 and B values obtained by the least-squares fits from different standard materials. Standard deviations are given in parentheses

Material	E_0/eV	10^3B	r/pm	σ/pm	$r_{X\text{-ray}}$/pm
$Ni(NO_3)_2$ solution	8349(1)	393(3)	202(1)	1.4(5)	204[a]
NiO powder	8348(1)	258(6)	208(1)	3.1(6)	208[b]
$Zn(NO_3)_2$ solution	9674(1)	406(3)	207(1)	6.5(3)	208[a]
ZnO powder	9675(1)	353(5)	196(1)	3.8(4)	194—197[b]

a) Ref. 14. b) Ref. 17.

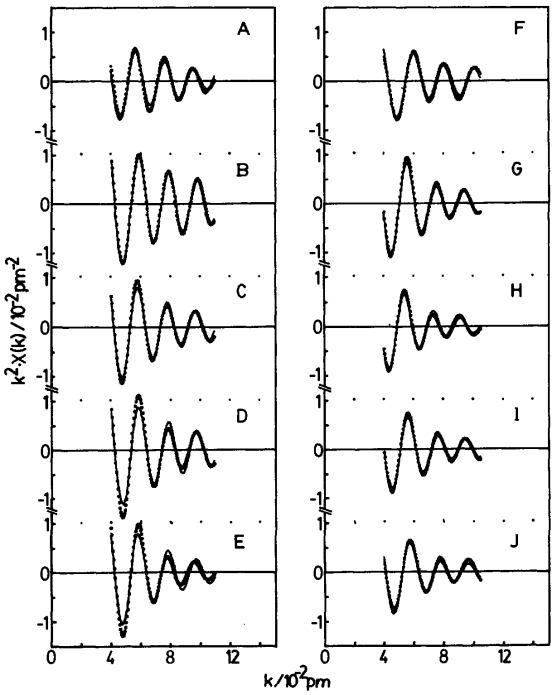

Fig. 4. The Fourier filtered $k^2\cdot\chi(k)$ curves of the main peak depicted in Fig. 3. The dotted and solid lines represent, respectively, the observed and calculated values by using parameter values in Tables 3 and 4.

In the course of the analysis of the EXAFS spectra of glycinato complexes by adopting the phase-shifts empirically evaluated, they should be evaluated from compounds of well established structure including M–O and M–N bonds. However, since phase shifts can be well approximated to be the same for atoms having similar number of electrons,[24] the phase-shift of the backscattering atom N (sometimes even atom C) was assumed to be the same as that of atom O, which was evaluated from the $[M(OH_2)_6]^{2+}$ ions.

Ni(II) Complexes. The $k\cdot\chi(k)$ curves and the $\phi(r)$ values of the solution samples containing the tris- and bis(glycinato) complexes and the crystalline powders of the bis(glycinato) complex are depicted in Figs. 2 (C, D, and E) and 3 (C, D, and E), respectively.

Table 3. Results of the curve fits for the nickel (II)-glycinato complexes with distance r and root-mean-square displacement σ. $\Delta\sigma$ denotes the difference between the sample and the standard $[Ni(OH_2)_6]^{2+}$. Standard deviations are given in parentheses

Complex	Scatterer	Program I		Program II		X-ray
		r/pm	σ/pm	r/pm	$\Delta\sigma$/pm	
$[Ni(OH_2)_6]^{2+}$(aq)	O	202(1)	1.4(5)	204[b]	—	204[c]
$[Ni(gly)_3]^-$(aq)	O or N	205(1)	5.5(1)	209	6.4	
	O	201(1)	1.4[a]	204	0.0	203[d]
	N	210(1)	1.4[a]	212	8.0	214[d]
$[Ni(gly)_2(OH_2)_2]$(aq)	O or N	204(1)	3.7(3)	204	3.4	
$[Ni(gly)_2(OH_2)_2]$(c)	O or N	204(1)	4.7(4)	205	4.7	210[e] (2×Ni−OH_2)
						206[e] (2×Ni−O)
						208[e] (2×Ni−N)

a) The values were kept constant during the calculation. b) Employed as a standard from Ref. 14. c) Ref. 14. d) Ref. 10. e) Ref. 15.

A small but significant shoulder at about 6×10^{-2} pm^{-1} appearing in the $k\cdot\chi(k)$ curves of samples C, D, and E, which has not been observed in solution B, indicated that there should be at least two interactions with different distances contributing to the EXAFS oscillations.

In the $\phi(r)$ curve for sample solution C containing the tris(glycinato)nickelate(II) complex as the predominant species, two peaks were observed at about 150 and 220 pm. The first peak at 150 pm was ascribable to the first neighbor Ni-O and Ni-N pairs within the $[Ni(gly)_3]^-$ complex. The small and slightly split second peak at 220 pm was not significantly affected by different estimations of the smooth background μ_0 and the selections of k_{min} and k_{max} values for the Fourier transformation, and hence it indicated a significant signature. The peak might be assignable to the next nearest neighbor Ni···C distance within the tris(glycinato) complexes, although the peak might also contain a spurious one due to the truncation effect of the Fourier transform.

Firstly, the predominant peak at 150 pm, indicated by a bar in the figure, was analyzed by using the least-squares method in the k-space for the Fourier filtered $k^2\cdot\chi(k)$ values. Theoretical values by Teo and Lee[9] were used for the phase-shifts and the backscattering functions in combination with program I. The coordination number was fixed to the known value (n=6). The model of only one backscatterer (O or N) gave a satisfactory agreement between the calculated and observed $k^2\cdot\chi(k)$ values with the bond length of 205 pm and the σ value of 5.5 pm. However, the σ value estimated from this model was about four times larger than that (1.4 pm) obtained for the Ni-O bond within the reference $[Ni(OH_2)_6]^{2+}$ ion (see Table 3). The σ value thus obtained for the Ni-O and Ni-N bonds within the $[Ni(gly)_3]^-$ complex seemed unreasonably large, because the temperature factors for the Ni-O and Ni-N bonds within the complex were virtually the same as that of the Ni-OH_2 bond within the $[Ni(OH_2)_6]^{2+}$ complex.[10,14] Therefore, we assumed that the σ values of the both Ni-O and Ni-N were the same as the value of the standard hexaaqua complex (σ=1.4 pm) and allowed the lengths of the both Ni-O and Ni-N bonds to vary independently. As a result, the least-squares calculation converged to two different lengths of the Ni-O (201 pm) and Ni-N (210 pm) bonds, independent of the initial value inserted for the lengths of the two bonds (Table 3).

A similar consideration was examined in the data analysis in the r-space. The first peak at 150 pm was directly analyzed in the r-space by using program II by assuming one and two Gaussian models, the peak due to the Ni-O bonds within the $[Ni(OH_2)_6]^{2+}$ being employed as the standard. The results are given in Table 3.

As seen in Table 3, both calculations for the data in the k- and r-spaces gave similar results that under the assumption of one kind of the bond length the Ni-O and Ni-N distances were 205—209 pm, while the Ni-O and Ni-N bond lengths were 201—204 and 210—212 pm, respectively, under the assumption of two different lengths for the Ni-O and Ni-N bonds. The difference in calculations between two programs I and II was less than 3 pm, which was compared with the difference in the standard Ni-O distance estimated by the different programs for the $[Ni(OH_2)_6]^{2+}$ ion.

The analysis of the first peak both in the k- and r-spaces thus gives almost the same results and thus errors caused by a Fourier backfiltering are within experimental errors. In addition, the choice of either theoretical or empirical values for the phase-shifts and backscattering amplitudes does not significantly affect the result as long as suitable standard samples are adopted in order to obtain reasonable E_0 and B values. We can recommend to employ the $[Ni(OH_2)_6]^{2+}$ complex in solution as the standard rather than NiO in the course of the structural analysis of the $[Ni(gly)_3]^-$ in solution, because the former standard gives a better B value leading to more reasonable coordination number of the complexes in solution.

The present EXAFS analysis by using both programs I and II gave the results consistent with those from X-ray diffraction.[10]

The analysis of the second peak at 220 pm was not possible because it was too small to apply the curve-fit

TABLE 4. RESULTS OF THE CURVE FITS FOR THE ZINC(II)-GLYCINATO COMPLEXES WITH DISTANCE r AND ROOT-MEAN-SQUARE DISPLACEMENT σ. $\Delta\sigma$ DENOTES THE DIFFERENCE BETWEEN THE SAMPLE AND THE STANDARD $[Zn(OH_2)_6]^{2+}$. STANDARD DEVIATIONS ARE GIVEN IN PARENTHESES

Complex	Scatterer	Program I		Program II		X-ray
		r/pm	σ/pm	r/pm	$\Delta\sigma$/pm	
$[Zn(OH_2)_6]^{2+}$(aq)	O	207(1)	6.5(3)	208[b]	—	208[c]
$[Zn(gly)_3]^-$(aq)	O or N	213(1)	6.8(1)	214	7.7	
	O	213(1)	6.5[a]	210	0.2	212[d]
	N	213(1)	6.5[a]	219	8.9	212[d]
$[Zn(gly)_2(OH_2)_2]$(aq)	O or N	207(1)	6.6(2)	208	5.5	
$[Zn(gly)_2]\cdot H_2O$(c)	O or N	203(1)	7.0(3)	204	8.7	

a) The values were kept constant during the calculation. b) Employed as a standard from Ref. 14. c) Ref. 14. d) Ref. 12.

procedure, although we could approximately estimate the Ni···C distance to be about 280 pm from the peak position after the correction for the phase-shift, which reasonably agreed with the literature value determined by means of solution X-ray diffraction (290 pm).[10]

The same analytical procedure was applied to the solution and powder samples of the bis(glycinato)nickel(II) complex. The amplitude of the first peak in the Fourier transform was similar in both samples (Fig. 3, D and E) and hence the curve-fits gave very similar results (Table 3), which implied that the environment of the Ni(II) ions should be very similar in both states. Therefore, the bis(glycinato)nickel(II) in the aqueous solution was expected to have a six-coordination with two additional water molecules to complete the octahedral configuration as in the crystalline state.[12] A mean value (208 pm) of the distances found in the X-ray crystallographic investigation[15] was slightly longer than the value found by the EXAFS measurement (204 pm for the average bond length), but the difference was almost within uncertainties of the latter.

Zinc(II) Complexes. The $k\cdot\chi(k)$ and $\phi(r)$ values of the solution samples containing the tris- and bis(glycinato) complexes and of the bis(glycinato)-zinc(II) complex in powder are shown in Figs. 2 and 3 (H, I, and J). The predominant first peak at 150 pm in Fig. 3 (H, I, and J) are due to the first neighbor Zn-O and Zn-N bonds within the glycinato complexes.

The structure of the Zn(II)-glycinato complexes was analyzed in the same manner as decribed in the previous section for the nickel(II) complexes. For solution H containing the $[Zn(gly)_3]^-$ complex as a predominant species, the least-squares calculations for the first peak at 150 pm in the $\phi(r)$ curve (Fig. 3H) were performed both in the k- and r-spaces with two models with the same length for the Zn-O and Zn-N bonds and with the different lengths of the two bonds. Both model calculations gave the similar results (see Table 4). The interatomic distances thus determined are consistent with those reported in an X-ray diffraction study.[12]

The structure of the bis(glycinato)zinc(II) complex in the solid state was reported to be apically distorted octahedral with additional two carbonyl oxygen atoms within the glycinate ions coordinated to adjacent Zn-(II) ions,[16] although the complete structural analysis was not yet achieved. Bis-complexes of zinc(II) ion with various bidentate ligands are known to have the tetrahedral structure. However, as is seen in Fig. 3 (I and J) the amplitude of the first peak for both solution and powder samples is very similar, which indicates a similar coordination number for the bis-complex in both states. The curve fit analysis in the k-space for the first peak in Fig. 3I gave the coordination number of nearly six independent of the initial value at the least-squares approach. Thus, it was concluded that the bis(glycinato)zinc(II) complex has an octahedral structure with two additional water molecules in aqueous solution.

The mean bond distance (203 pm) for the powder sample seemed to be slightly shorter than that found in the solution (207 pm). This trend was not observed in the case of the bis(glycinato)nickel(II) complexes.

In Raman spectral measurements of the Zn-N stretching frequency in the bis(glycinato)zinc(II) complex the band observed at $(467\pm5)\,cm^{-1}$ in the crystal shifted to $(434\pm5)\,cm^{-1}$ in the aqueous solution. The shift of the Zn-N stretching frequency by *ca.* $33\,cm^{-1}$ found in the present study has also been reported by Krishnan and Plane,[23] which suggested lengthening of the Zn-N bond in the solution state. The longer Zn-N bond in solution than in crystal found in the present EXAFS study may correspond to the shift of the Zn-N stretching frequency toward the lower frequency side in the Raman spectra in solution. The weakening of the Zn-N bond (and probably in the Zn-O bond, too) of the bis(glycinato)zinc(II) complex in solution compared with that in crystal may be caused by a stronger electron donation from coordinated water molecules in the bis-complex in solution than that from carbonyl oxygen atoms in the solid state.

This work was supported by the Joint Studies Program (1983—1984) of the Institute for Molecular Science and by the Grant-in-Aid for Scientific Reseach No. 57470054 from the Ministry of Education, Science and Culture. The authors (T. Y. and H. O.) thank Dr. J. B. Boyce (Xerox Palo Alto Reseach Centers) for his kind help in using their computer program and his valuable

discussion. A part of the calculations was carried out at the Institute for Molecular Science in Okazaki.

References

1) H. Ohtaki, *Rev. Inorg. Chem.*, **4**, 103 (1982).
2) J. E. Enderby and G. W. Neilson., *Rep. Prog. Phys.*, **44**, 38 (1981).
3) D. R. Sandstrom, B. R. Stults, and R. B. Greegor, "Structural Evidence for Solutions from EXAFS Measurements," in "EXAFS Spectroscopy," ed by B.-K. Teo and D. C. Joy, Plenum Press, New York (1981), Chap. 9, pp. 139—157.
4) T. Yamaguchi, O. Lindqvist, J. B. Boyce, and T. Claeson, "EXAFS, X-Ray and Neutron Diffraction of Electrolyte Solutions," in "EXAFS and Near Edge Structure III," ed by K. O. Hodgson, B. Hedman, and J. E. Penner-Hahn, Springer-Verlag, Berlin (1984), pp. 417—419.
5) M. Sano, T. Maruo, and H. Yamatera, *Bull. Chem. Soc. Jpn.*, **57**, 2757 (1984).
6) D. E. Sayers, E. A. Stern, and F. W. Lytle, *Phys. Rev. Lett.*, **27**, 1204 (1971).
7) E. A. Stern, *Phys. Rev. B*, **10**, 3027 (1974).
8) E. A. Stern, D. E. Sayers, and F. W. Lytle, *Phys. Rev. B*, **11**, 4836 (1975).
9) B.-K. Teo and P. A. Lee, *J. Am. Chem. Soc.*, **101**, 2815 (1979).
10) K. Ozutsumi and H. Ohtaki, *Bull. Chem. Soc. Jpn.*, **56**, 3635 (1983).
11) K. Ozutsumi and H. Ohtaki, *Bull. Chem. Soc. Jpn.*, **57**, 2605 (1984).
12) K. Ozutsumi and H. Ohtaki, *Bull. Chem. Soc. Jpn.*, **58**, 1651 (1985).
13) K. Tohji, Y. Udagawa, T. Kawasaki, and K. Masuda, *Rev. Sci. Instrum.*, **54**, 1482 (1983).
14) H. Ohtaki, T. Yamaguchi, and M. Maeda, *Bull. Chem. Soc. Jpn.*, **49**, 701 (1976).
15) H. C. Freeman and J. M. Guss, *Acta Crystallogr., Sect. B*, **24**, 1133 (1968).
16) B. W. Low, F. L. Hirshfeld, and F. M. Richards, *J. Am. Chem. Soc.*, **81**, 4412 (1959).
17) R. W. G. Wyckoff, "Crystal Structures," Interscience, New York (1964), Vol. 1.
18) J. B. Boyce, T. M. Hayes, and J. C. Mikkelsen, Jr., *Phys. Rev., B*, **23**, 2876 (1981).
19) "International Tables for X-Ray Crystallography," Kynoch Press, Vol. III, p. 161.
20) P. A. Lee, P. H. Citrin, P. Eisenberger, and B. M. Kincaid, *Rev. Mod. Phys.*, **53**, 769 (1981).
21) F. J. Harris, *Proc. IEEE*, **66**, 51 (1978).
22) B. Lengeler and P. Eisenberger, *Phys. Rev., B*, **21**, 4507 (1980).
23) J. J. Rehr, E. A. Stern, R. L. Martin, and E. R. Davidson, *Phys. Rev., B*, **17**, 560 (1978).
24) T. Yamaguchi, O. Lindqvist, J. B. Boyce, and T. Claeson, *Acta Chem., Scand., Ser., A*, **38**, 423 (1984).
25) K. Krishnan and R. A. Plane, *Inorg. Chem.*, **6**, 55 (1967).

Preparation and Stereochemistry of Cobalt(III) Complexes Containing 1,1,10,10-Tetraphenyl-4,7-diaza-1,10-diphosphadecane or 2,11-Dimethyl-5,8-diaza-2,11-diphosphadodecane, $R_2PCH_2CH_2NHCH_2CH_2NHCH_2CH_2PR_2$ ($R=C_6H_5$ or CH_3)

Masamichi ATOH, Kazuo KASHIWABARA, and Junnosuke FUJITA*
Department of Chemistry, Faculty of Science, Nagoya University, Chikusa-ku, Nagoya 464
(Received May 23, 1985)

New quadridentate phosphine ligands, 1,1,10,10-tetraphenyl-4,7-diaza-1,10-diphosphadecane (pp-PNNP) and 2,11-dimethyl-5,8-diaza-2,11-diphosphadodecane (mm-PNNP), were prepared from $(ClCH_2CH_2NHCH_2-)_2 \cdot 2HCl$ and $NaPR_2$ ($R=C_6H_5$, CH_3) and purified through their Ni(II) complexes. Seven new cobalt(III) complexes containing the phosphine ligand were prepared: $[CoX_2(pp\text{- or }mm\text{-}PNNP)]^{n+}$ ($X_2=(Cl)_2$, $(NCS)_2$, $C_5H_7O_2^-$(2,4-pentanedionate ion), and CO_3^{2-}). Four complexes of $[CoX_2(pp\text{- or }mm\text{-}PNNP)]^+$ (X=Cl, NCS) afforded only a trans(X,X) isomer, and $[Co(acac)(pp\text{- or }mm\text{-}PNNP)]^{2+}$ and $[Co(CO_3)(pp\text{-}PNNP)]^+$ complexes yielded a cisβ isomer. The geometrical structures were assigned on the basis of the NMR and visible-ultraviolet absorption spectra.

As an extension of the studies on cobalt(III)-phosphine complexes, we have prepared quadridentate phosphine ligands, $R_2PCH_2CH_2NHCH_2CH_2NHCH_2CH_2PR_2$ ($R=C_6H_5$ or CH_3) which have a set of PNNP donor atoms, and their cobalt(III) complexes. The skeleton of the ligand is an intermediate one of $NH_2CH_2CH_2NHCH_2CH_2NHCH_2CH_2NH_2$ (trien) and $(C_6H_5)_2PCH_2CH_2P(C_6H_5)CH_2CH_2P(C_6H_5)CH_2CH_2P(C_6H_5)_2$ (tetraphos). The $[CoCl_2(trien)]^+$ complex forms all possible geometrical isomers, trans, cisα, and cisβ,[1] while the $[CoX_2(tetraphos)]^+$ (X=Cl, Br) complexes[2] yield only the cisβ isomer. It is of interest to examine the stereoselectivity for complexes containing the above intermediate ligand. An analogous ligand, $(C_6H_5)_2PCH_2CH_2N(CH_3)CH_2CH_2N(CH_3)CH_2CH_2P(C_6H_5)_2$, and its cobalt(II) and nickel(II) complexes have been prepared by Sacconi and Dei,[3] but there has been no report on the cobalt(III) complexes containing such a quadridentate PNNP-type ligand.

The following abbreviations are used for the ligands: $(C_6H_5)_2PCH_2CH_2NHCH_2CH_2NHCH_2CH_2P(C_6H_5)_2$=pp-PNNP and $(CH_3)_2PCH_2CH_2NHCH_2CH_2NHCH_2CH_2P(CH_3)_2$=mm-PNNP.

Experimental

The phosphine ligands were prepared and handled under an atmosphere of nitrogen until they formed cobalt(III) complexes. All solvents used for the preparation were deoxygenated by bubbling nitrogen for 20 min immediately before use. Tetramethyldiphosphine,[4] diphenylphosphine,[5] and $(ClCH_2CH_2NHCH_2-)_2 \cdot 2HCl$[6] were prepared according to the literature methods. Absorption and ^{13}C NMR specta were recorded on a Hitachi 323 spectrophotometer and a Jeol JNM-GX 400 spectrometer, respectively.

Preparation of Ligands. 1,1,10,10-Tetraphenyl-4,7-diaza-1,10-diphosphadecane (pp-PNNP). To liquid ammonia (300 cm^3) containing metallic sodium (1.84 g, 80 mmol) in a 500 cm^3 three-necked round bottom flask with a mechanical stirrer and an ammonia gas inlet was added dropwise diphenylphosphine (14.89 g, 80 mmol) over 5 min with stirring at −78 °C. On stirring for 1 h the color of the solution changed from deep blue to orange. To the orange solution was added $(ClCH_2CH_2NHCH_2-)_2 \cdot 2HCl$ (5.16 g, 20 mmol) in small portions with stirring. Stirring was continued for 1 h, giving a colorless solution. After liquid ammonia had been evaporated, water (50 cm^3) and then diethyl ether (100 cm^3) were added to the residue with stirring. The ethereal layer separated from the aqueous layer was dried over $MgSO_4$ (*ca.* 5 g) overnight. A viscous liquid (8.5 g) was obtained by removing the solvent and unreacted diphenylphosphine by vacuum distillation. The liquid was mixed with a methanol solution (*ca.* 40 cm^3) of $Ni(ClO_4)_2 \cdot 6H_2O$ (10 g, 27 mmol) with stirring, affording immediately a yellow precipitate. It was filtered and dissolved in hot methanol (600 cm^3), and then the solution was filtered. The filtrate was stored in a refrigerator overnight to yield yellow crystals, which were filtered, washed with water and then diethyl ether, and air-dried. Yield: 7.35 g. The filtrate was concentrated to 150 cm^3 and stored in a refrigerator to give additional crystals (0.8 g). Total yield: 8.15 g. Found: C, 47.78; H, 4.44; N, 3.63%. Calcd for $C_{30}H_{36}N_2O_9P_2Cl_2Ni$=[Ni(pp-PNNP)]$(ClO_4)_2 \cdot H_2O$: C, 47.40; H, 4.47; N, 3.68%. The nickel complex is soluble in methanol, ethanol, and CH_2Cl_2, but not in water.

[Ni(pp-PNNP)]$(ClO_4)_2 \cdot H_2O$ (8.15 g, 10.7 mmol) and KCN (14 g, 210 mmol) were stirred in a mixture of CH_2Cl_2 (30 cm^3) and water (100 cm^3) for 20 min, and then benzene (100 cm^3) was added to the mixture. The organic layer was separated from water, dried over $MgSO_4$ (*ca.* 3 g), and evaporated under reduced pressure to yield a viscous liquid, which solidified on standing. Yield: 4.7 g. mp 59 °C. Found: C, 71.54; H, 7.02; N, 5.40%. Calcd for $C_{30}H_{36}N_2OP_2$=pp-PNNP$\cdot H_2O$: C, 71.70; H, 7.22; N, 5.57%.

2,11-Dimethyl-5,8-diaza-2,11-diphosphadodecane (mm-PNNP). To liquid ammonia (150 cm^3) containing metallic sodium (1.90 g, 83 mmol) in a 300 cm^3 three-necked flask was added dropwise tetramethyldiphosphine (5.05 g, 41 mmol) with stirring at −78 °C. The solution was stirred for 1 h. To the resulting orange solution was added $(ClCH_2CH_2NHCH_2-)_2 \cdot 2HCl$ (5.33 g, 21 mmol) in small portions with stirring. After stirring for 1 h, liquid ammonia was evaporated, and then water (50 cm^3) and diethyl ether (40 cm^3) were added to the residue with stirring. The ethereal layer was separated from the aqueous layer and dried over $MgSO_4$ (*ca.* 3 g) overnight.

The solvent and unreacted dimethylphosphine were removed by vacuum distillation. The colorless oily product (2.5 g) thus obtained was used for preparing cobalt(III) complexes without further purification because of a small amount. The ligand can be purified *via* the Nickel(II) complex in the same manner as for pp-PNNP.

Preparation of Complexes. trans*(Cl,Cl)-[CoCl$_2$(pp-PNNP)]ClO$_4$·H$_2$O.* To a methanol solution (20 cm^3) of Co(ClO$_4$)$_2$·6H$_2$O (830 mg, 2.27 mmol) was added pp-PNNP (1.10 g, 2.27 mmol) with stirring, affording orange crystals. Methanol was removed under vacuum, and the residue was dissolved in CH_2Cl_2. Chlorine gas was bubbled into the CH_2Cl_2 solution for 10 min, and then nitrogen gas for 20 min to remove excess Cl_2. To the resulting green solution was added methanol (20 cm^3), and the solution was evaporated to a small volume under reduced pressure, yielding a green precipitate (the solution should not be evporated to dryness since perchlorates of complexes are potentially explosive in a solid state). Additional methanol (250 cm^3) was added to the concentrate. The mixture was warmed at 70 °C for 10 min and then mixed with $NaClO_4 \cdot H_2O$ (20 g) in methanol (20 cm^3). On cooling green crystals were obtained, filtered, washed with water and then diethyl ether, and air-dried. Yield: 1.0 g. Found: C, 49.31; H, 4.95; N, 3.80%. Calcd for $C_{30}H_{36}N_2O_5P_2Cl_3Co$: C, 49.23; H, 4.96; N, 3.83%. The complex is soluble in methanol, CH_2Cl_2, and $CHCl_3$, but not in water and diethyl ether.

trans*(Cl,Cl)-[CoCl$_2$(mm-PNNP)]ClO$_4$.* To *cis*-[CoCl$_2$(en)$_2$]Cl[7] (en=ethylenediamine) (3.5 g, 12 mmol) in a mixture of water (10 cm^3) and methanol (30 cm^3) was added mm-PNNP (1.12 g, 4.75 mmol) with stirring. The solution was stirred for 3 h at room temperature and filtered to remove [Co(en)$_3$]Cl$_3$ precipitated. The filtrate was warmed with concd HCl (4 cm^3) at 60 °C for 1 h, and then evaporated to dryness under reduced pressure. The residue was dissolved in water (200 cm^3), and the solution was applied on a column (ϕ7 cm×15 cm) of SP-Sephadex C-25 (Na^+ form). By elution with 0.05 mol dm^{-3} HCl, a blue eluate was obtained, a red brown band remaining on the top of the column. The blue eluate was evaporated to dryness under reduced pressure, and the blue product was extracted with ethanol. The extract was evaporated again to dryness under reduced pressure, and the residue was mixed with $NaClO_4 \cdot H_2O$ (2.0 g) in water (10 cm^3), yielding blue crystals, which were filtered, washed with water and then diethyl ether, and air-dried. Yield: 282 mg. Found: C, 25.89; H, 5.94; N, 6.00%. Calcd for $C_{10}H_{26}N_2O_4P_2Cl_3Co$: C, 25.80; H, 5.63; N, 6.02%. The complex is soluble in methanol and acetone, slightly in water, but not in diethyl ether, $CHCl_3$, and CH_2Cl_2.

cis*β-[Co(acac)(pp-PNNP)](ClO$_4$)$_2$·H$_2$O.* A methanol solution (50 cm^3) containing *trans*(Cl,Cl)-[CoCl$_2$(pp-PNNP)]ClO$_4$·H$_2$O (150 mg, 0.21 mmol) and Li(acac) (60 mg, 0.57 mmol) was stirred for 20 min at room temperature. The resulting orange-red solution was diluted with water (200 cm^3), and the solution was applied on a column (ϕ3.5 cm×70 cm) of SP-Sephadex C-25. By elution with 0.2 mol dm^{-3} NaCl, two very small orange bands and a large red one were eluted successively. The eluate of the large red band was collected and concentrated to 40 cm^3 under reduced pressure. On addition of $NaClO_4 \cdot H_2O$ the concentrate gave a red precipitate, which was filtered, washed with a small amount of water, and air-dried. Yield: 47 mg. Found: C, 48.69; H, 4.83; N, 3.27%. Calcd for $C_{35}H_{43}N_2O_{11}P_2Cl_2Co$: C, 48.91; H, 5.04; N, 3.26%. The complex is soluble in water, methanol, and CH_2Cl_2, but not in diethyl ether.

cis*β-[Co(acac)(mm-PNNP)](ClO$_4$)$_2$·H$_2$O.* A mixture of [Co(acac)$_3$][8] (870 mg, 2.44 mmol) and mm-PNNP (580 mg, 2.45 mmol) in methanol (100 cm^3) was stirred at room temperature for 3 h. To the resulting solution was added water (200 cm^3), and then unreacted mm-PNNP and [Co(acac)$_3$] were extracted with diethyl ether three times (50 cm^3 ×3). The aqueous layer was diluted with water to 1 dm^3, and the solution was applied on a column (ϕ3.5 cm×10 cm) of SP-Sephadex C-25. After complexes with the +1 charge contained in the adsorbed product had been eluted with 0.05 mol dm^{-3} NaCl, those with the +2 charge were eluted with 0.2 mol dm^{-3} NaCl. The orange eluate collected was evaporated to dryness under reduced pressure, and the orange product was extracted with ethanol (70 cm^3). The extract was diluted with water (200 cm^3) and rechromatographed with a column (ϕ3.5 cm×100 cm) of SP-Sephadex C-25 and an eluent of 0.2 mol dm^{-3} NaCl. The column showed a very small violet and a large red band. The eluate of the red band was concentrated to 50 cm^3 under reduced pressure. The concentrate was mixed with $NaClO_4 \cdot H_2O$ (3 g) to yield an orange-red precipitate, which was recrystallized from hot water (60 °C), giving red crystals. Yield: 505 mg. Found: C, 29.55; H, 5.42; N, 4.55%. Calcd for $C_{15}H_{35}N_2O_{11}P_2Cl_2Co$: C, 29.48; H, 5.77; N, 4.58%. The complex is soluble in water, methanol, and acetone, but not in $CHCl_3$, CH_2Cl_2, and diethyl ether.

cis*β-[Co(CO$_3$)(pp-PNNP)]Cl·NaCl·H$_2$O.* To a methanol solution (100 cm^3) of *trans*(Cl,Cl)-[CoCl$_2$(pp-PNNP)]ClO$_4$·H$_2$O (500 mg, 0.68 mmol) were added $(NH_4)_2CO_3$ (200 mg, 2.08 mmol) and active charcoal (100 mg). The mixture was stirred for 8 h at room temperature, and then filtered. The filtrate was diluted with water (1 dm^3), and the solution was applied on a column (ϕ3.5 cm×40 cm) of SP-Sephadex C-25. The adsorbed product was eluted with 0.05 mol dm^{-3} NaCl. The eluate of the first main red band was collected and concentratred to 30 cm^3 under reduced pressure. The concentrate was mixed with NaCl (*ca.* 10 g) and stored in a refrigerator to yield red crystals, which were filtered, washed with a small amount of water and then diethyl ether, and air-dried. Yield: 74 mg. Found: C, 52.15; H, 4.92; N, 3.55%. Calcd for $C_{31}H_{36}N_2O_4P_2Cl_2CoNa$: C, 52.05; H, 5.07; N, 3.92%. An additional amount of the complex was obtained as the perchlorate by adding excess $NaClO_4 \cdot H_2O$ to the filtrate. Yield: 53 mg. Found: C, 52.52; H, 4.64; N, 3.79%. Calcd for $C_{31}H_{34}N_2P_2O_7ClCo$=[Co(CO$_3$)(pp-PNNP)](ClO$_4$): C, 52.97; H, 4.87; N, 3.99%. Both the chloride and perclorate are soluble in water, methanol, and CH_2Cl_2, but not in diethyl ether.

trans*(NCS,NCS)-[Co(NCS)$_2$(pp-PNNP)]Cl·4H$_2$O.* A methanol solution (20 cm^3) containing *trans*(Cl,Cl)-[CoCl$_2$(pp-PNNP)]ClO$_4$·H$_2$O (100 mg, 0.14 mmol) and KNCS (70 mg, 0.7 mmol) was stirred at 50 °C for 30 min. The resulting red solution was diluted with a mixture of water (50 cm^3) and methanol (30 cm^3), and the solution was applied on a column (ϕ3.5 cm×50 cm) of SP-Sephadex C-25. By elution with a 0.05 mol dm^{-3} NaCl methanol–water (1:3) solution, the eluate of the first red band was collected. The complex in the eluate was extracted with chloroform two times (30 cm^3×2), and the extract was evaporated to dryness under reduced pressure. The residue was dissolved again in methanol (5 cm^3), and the solution was mixed with NaCl (2 g) in water (20 cm^3), giving a red precipitate. Red crystals

were obtained by dissolving the precipitate in a mixture of methanol and water (1:1) and by evaporating the solution slowly at room temperature. Yield: 23 mg. Found: C, 50.35; H, 5.32; N, 7.63%. Calcd for $C_{32}H_{42}N_4O_4P_2S_2ClCo$: C, 50.10; H, 5.51; N, 7.30%. The complex is soluble in methanol, acetone, $CHCl_3$, and CH_2Cl_2, but not in water and diethyl ether.

trans(NCS,NCS)-[Co(NCS)$_2$(mm-PNNP)]Cl·1/2(NaCl)·H$_2$O. A methanol solution (50 cm^3) containing *trans*(Cl,Cl)-[$CoCl_2$(mm-PNNP)]ClO_4 (140 mg, 0.30 mmol) and KNCS (140 mg, 1.44 mmol) was stirred at 60 °C for 40 min. The resulting red solution was diluted with water (1 dm^3), and applied on a column (ϕ3.5 cm×50 cm) of SP-Sephadex C-25. By elution with 0.05 mol dm^{-3} NaCl, orange and blue bands were obtained. The eluate of the orange band was collected and evaporated to dryness under reduced pressure, and the complex was extracted from the residue with ethanol (100 cm^3). The extract was evaporated to dryness under reduced pressure, and the residue was again dissolved in water (5 cm^3). The solution was mixed with NaCl (1.5 g) at 50 °C, and stored in a refrigerator to yield red crystals, which were filtered, washed with a small amount of cold water, and air-dried. Yield 71 mg. Found: C, 29.21; H, 5.64; N, 11.46%. Calcd for $C_{12}H_{28}N_4OP_2S_2Cl_{1.5}Na_{0.5}Co$: C, 29.17; H, 5.71; N, 11.34%. The complex is soluble in water, methanol, and ethanol, but not in diethyl ether and $CHCl_3$.

Results and Discussion

Preparation. Multidentate ligands containing both nitrogen and phosphorus donor atoms have been usually prepared by reaction of ω-chloroalkylamines with phosphides.[9] Sacconi and Dei[3] prepared a linear-quadridentate ligand, $(C_6H_5)_2PCH_2CH_2N(CH_3)CH_2$-$CH_2N(CH_3)CH_2CH_2P(C_6H_5)_2$ which has a set of PNNP donor atoms, from $(ClCH_2CH_2N(CH_3)CH_2-)_2\cdot 2HCl$ and $KP(C_6H_5)_2\cdot$(dioxane)$_2$. We have prepared pp-PNNP and mm-PNNP by a similar method using $NaP(C_6H_5)_2$ and $NaP(CH_3)_2$, respectively, generated from $PH(C_6H_5)_2$ or $(CH_3)_2PP(CH_3)_2$ and metallic sodium in liquid ammonia. These quadridentate ligands were not purified by vacuum distillation because of a high boiling point. The purification was achieved through their Ni(II) complexes. Pure pp-PNNP solidified on standing at room temperature, whereas mm-PNNP remained oily. Yields of the ligands seemed to depend largely on the purity of reactants and the presence of moisture. The pp-PNNP ligand was also prepared from (2-aminoethyl)diphenylphosphine(edpp) and 1,2-dibromoethane, but the separation of the ligand from unreacted edpp was somewhat troublesome. In the air pp-PNNP is rather stable, but mm-PNNP is readily oxidized.

The $[CoCl_2(pp\text{-}PNNP)]^+$ complex was prepared by oxidizing the Co(II)–pp-PNNP complex with chlorine in a moderate yield. However, the corresponding mm-PNNP complex was not obtained by this method, but done by reaction of the ligand with $[CoCl_2(en)_2]^+$ in a fairly poor yield. The oxidizing method by chlorine is not effective either for a trialkylphosphine complex, *trans*(Cl,Cl)-$[CoCl_2(edmp)_2]^+$ (edmp=(2-aminoethyl)-dimethylphosphine),[10] although the corresponding (2-aminoethyl)diphenylphosphine(edpp) complex is obtained easily by this method.[11] Green $[CoCl_2(pp\text{-}PNNP)](ClO_4)\cdot H_2O$ was used for preparing other complexes of $[CoX_2(pp\text{-}PNNP)]^{n+}$ (X=NCS$^-$, X$_2$=CO$_3^{2-}$, and acac). Although several geometrical isomers are possible for the pp-PNNP complex, only one isomer was formed for each complex as confirmed by column chromatography and ^{13}C NMR spectra. On the contrary, the corresponding NCS$^-$ and acac complexes of edpp, $[CoX_2(edpp)_2]^{n+}$, form two geometrical isomers, trans(NCS, NCS)cis(P,P) and cis(NCS,NCS)trans(P,P),[12] and trans-(P,P) and trans(P,N),[11] respectively, by similar reactions with $[CoCl_2(edpp)_2]^+$. The mm-PNNP complexes also yielded only one isomer. The $[Co(NCS)_2(mm\text{-}PNNP)]^+$ complex was obtained by the reaction of $[CoCl_2(mm\text{-}PNNP)]^+$ with KNCS in a 48% yield. The reaction between $[CoCl_2(mm\text{-}PNNP)]^+$ and Li(acac) yielded $[Co(acac)(mm\text{-}PNNP)]^{2+}$ in a poor yield (7%), but that between mm-PNNP and $[Co(acac)_3]$ gave the complex in a better yield (36%). This is quite in contrast to the reactions of pp-PNNP with $[Co(acac)_3]$ and of $[CoCl_2(pp\text{-}PNNP)]^+$ with Li(acac) resulting in 8 and 27% yields, respectively. Synthetic methods for Co(III)–phosphine complexes should be designed carefully by considering the kind of phosphine ligands.[13] The reaction between $[CoCl_2(mm\text{-}PNNP)]^+$ and $(NH_4)_2CO_3$ at room temperature scarcely proceeded, and decomposition occurred at a higher temperature. The reaction of $[CoCl_2(mm\text{-}PNNP)]$ with a large excess of $(NH_4)_2CO_3$ gave a trace amount of an orange complex assignable to $[CoCO_3(mm\text{-}PNNP)]^+$. However, it was not isolated because of a extremely low yield. Attempts to prepare [Co(en)(pp-PNNP or mm-PNNP)]$^{3+}$ from the dichloro complex and en were all unsuccessful.

Stereochemistry. There are three possible geometrical isomers for X=Cl$^-$ and NCS$^-$, and two for X$_2$=CO$_3^{2-}$ and acac in the $[CoX_2(PNNP)]$-type complex. The geometrical structures were assigned on the basis of the NMR and ligand field absorption spectra. The ^{13}C NMR and absorption spectral data are summarized in Tables 1 and 2, respectively.

The ^{13}C NMR spectra of $[CoX_2(pp\text{- or mm-}PNNP)]^+$ (X=Cl$^-$ and NCS$^-$) indicate the complexes to be either the trans or cisα isomer which have C_2 symmetry (Fig. 1). Each of these complexes shows two kinds of phenyl or methyl signals (Table 1). Since both trans and cisα isomers are chiral (the trans isomer having chiral nitrogen donor atoms), the two phenyl or methyl groups on a phosphorus atom are diastereomeric to each other, and should be magnetically unequivalent. Thus geometrical structures of the complexes can not be assigned unequivocally from the NMR spectra. In Fig. 2 are compared the absorption spectra of $[CoCl_2(pp\text{- or mm-}PNNP)]^+$ and $[Co(NCS)_2(pp\text{-}PNNP)]^+$ with those of the corresponding bis(edpp) and bis(edmp) complexes. Molecular structures of $[CoCl_2(edpp)_2]^+$ and

Table 1. ^{13}C NMR spectral data, δ/ppm[a] (J/Hz[b])

Complexes (solvent)	acac			PNNP						
	CH_3	CH	CO	P-CH_3	P-CH_2	N-CH_2[c]	N-CH_2[d]	P-C_1	*o*-P	*m*-P	*p*-P
$[CoCl_2(pp\text{-}PNNP)]^+$ (CD_3OD)	—	—	—	—	36.66t(28)	49.90s	54.11s	131.13t(46) 135.21t(31)	135.18t(13) 135.63t(8)	129.16t(9) 129.30t(10)	132.02s 132.10s
$[Co(NCS)_2(pp\text{-}PNNP)]^+$ (CD_3OD)	—	—	—	—	34.54t(28)	49.98s	55.36s	136.06t(46) e)	134.27t(9) 134.72t(8)	130.43t(10) 130.74t(10)	133.08s 132.98s
$[CoCl_2(mm\text{-}PNNP)]^+$ (CD_3OD)	—	—	—	13.04t(35) 13.16t(32)	36.38t(28)	47.84s	53.83s	—	—	—	—
$[Co(NCS)_2(mm\text{-}PNNP)]^+$ (D_2O)	—	—	—	12.35t(32) 13.23t(31)	36.16t(31)	48.18s	54.53s	—	—	—	—
$[Co(acac)(pp\text{-}PNNP)]^{2+}$ (D_2O)	26.93s 27.61d(5)	101.38s	189.95s 192.11s	—	28.97d(29) 30.15d(29)	48.19s 48.36s	51.36s 51.91s	121.02d(43) 127.70d(45)	131.41d(7) 131.94d(7)	129.83d(12) 129.98d(11)	132.20s 132.77s
$[CoCO_3(pp\text{-}PNNP)]^+$ (CD_3OD)	—	—	—	—	29.43d(28) 33.40d(32)	f) 49.84s	52.38s 53.23s	125.70d(43) 127.52d(44)	132.43d(8) 133.05d(8)	130.31(9) 130.50d(11)	132.32s 133.13s
$[Co(acac)(mm\text{-}PNNP)]^{2+}$ (D_2O)	26.82s 27.61d(5)	100.52s	190.97s 192.12s	8.93d(34) 9.35d(34) 11.13d(28) 12.66d(31)	31.54d(28) 33.45d(28)	46.90s 47.02s	50.53s 50.62s	—	—	—	—

a) Internal reference: TMS and dioxane for CD_3OD and D_2O solutions, respectively. b) The J values for triplet signals are given by the width between the outer peaks. c) P-C-C-N. d) N-C-C-N. e) Overlapped with other peaks. f) Overlapped with solvent peaks.

Table 2. Absorption spectral data. (Solvent: CH_3OH, at 298K)

Complexes	$\nu_{max}/10^3\,cm^{-1}$ ($\log\varepsilon$)		
trans(Cl,Cl)-$[CoCl_2(pp\text{-}PNNP)]^+$	16.25(2.08), 31.4(4.21),	21.5(2.4)*, 39.0(4.1)*,	26.5(3.5)*, 44.5(4.5)*
trans(NCS,NCS)-$[Co(NCS)_2(pp\text{-}PNNP)]^+$	18.62(2.63),	25.5(3.8)*,	32.47(4.19)
trans(Cl,Cl)-$[CoCl_2(mm\text{-}PNNP)]^+$	16.95(2.19), 37.59(4.26),	24.5(2.3)*, 40.0(4.22)*	29.59(3.48)
trans(NCS,NCS)-$[Co(NCS)_2(mm\text{-}PNNP)]^+$	20.16(2.95), 40.57(4.23)	28.37(3.49),	32.10(3.67),
cisβ-$[Co(acac)(pp\text{-}PNNP)]^{2+}$	19.50(2.90), 45.0(4.58)*	29.0(3.9)*,	31.75(4.39),
cisβ-$[Co(CO_3)(pp\text{-}PNNP)]^+$	19.72(2.68),	25(2.6)*,	32.15(4.35)
cisβ-$[Co(acac)(mm\text{-}PNNP)]^{2+}$	20(2.54)*, 39.5(4.38)	22.75(2.68),	29.5(3.40)*

* Shoulder absorption.

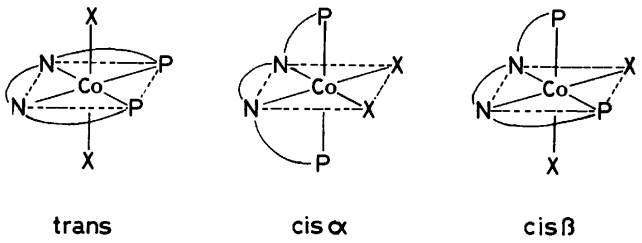

Fig. 1. Geometrical isomers of the $[CoX_2(PNNP)]$-type complex.

$[Co(NCS)_2(edpp)_2]^+$ given in Fig. 2 have been determined to trans(Cl,Cl)cis(P,P)[10] and trans(NCS,NCS)-cis(P,P),[12] respectively, by X-ray analysis, and that of $[CoCl_2(edmp)_2]^+$ assigned to trans(Cl,Cl)cis(P,P) by comparing the absorption spectrum with those of the corresponding isomers of edpp and ebpp ((2-aminoethyl)butylphenylphosphine) complexes.[10] From a comparison of these spectra, $[CoCl_2(pp\text{- and mm-}PNNP)]^+$ and $[Co(NCS)_2(pp\text{-}PNNP)]^+$ can be assigned to the trans isomer. The spectrum of $[Co(NCS)_2(mm\text{-}PNNP)]^+$ is somewhat different from that of $[Co(NCS)_2(pp\text{-}PNNP)]^+$. However, the mm-PNNP complex shows a very similar ^{13}C NMR spectrum to that of $[CoCl_2(mm\text{-}PNNP)]^+$, indicating the trans isomer.

The *trans*(X,X)-$[CoX_2(pp\text{- or mm-}PNNP)]^+$ complex can have two diastereomers, racemic (*RR* and *SS*) and meso (*RS*) forms for the chiral nitrogen donor atoms. Both the NMR spectra and column chromatograms indicate that each of the trans isomers yielded only one of these two diastereomers selectively. When the complexes are the racemic form, the structures can be assigned by optical resolution. However, attempts to resolve the complexes by column chromatography using Sephadex LH-20 or SP-Sephadex C-25 were unsuccessful. The ^{13}C NMR spectra of $[Co(NCS)_2(pp\text{- or mm-}PNNP)]^+$ indicate that the two NCS^- groups are magnetically equivalent, although the observed signals (pp-PNNP: 143.25 ppm, mm-PNNP: 144.72 ppm) were very weak. Thus the complexes can be assigned to the racemic form (C_2 symmetry), since the two NCS^- groups in the meso form (C_s symmetry) should be magnetically unequivalent.

The ^{13}C NMR spectra of $[Co(acac)(pp\text{- or mm-}PNNP)]^{2+}$ and $[Co(CO_3)(pp\text{-}PNNP)]^+$ clearly indicate that the complexes are the cisβ isomer which has only C_1 symmetry (Table 1). The arrangement of donor atoms in the cisβ isomer is the same as that in trans(P,N) isomers of the corresponding edpp and edmp complexes. In the ^{13}C NMR spectra of [Co-

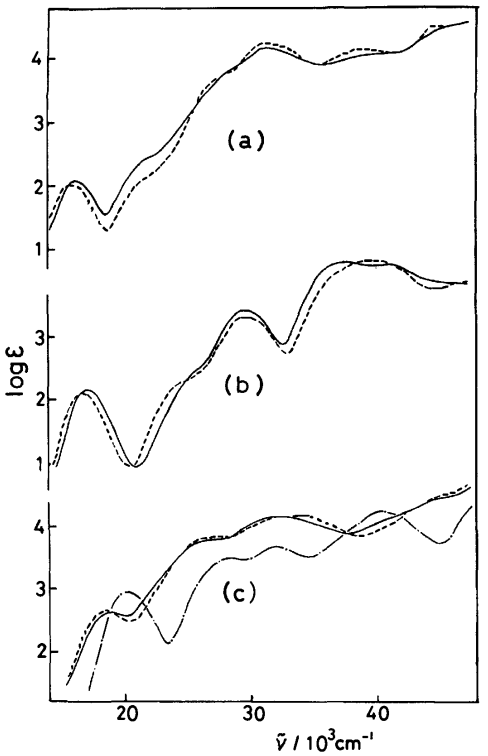

Fig. 2. Absorption spectra of trans(X,X) complexes. (a): *trans*-[$CoCl_2$(pp-PNNP)]$^+$ (——) and *trans*(Cl,Cl),*cis*(P,P)-[$CoCl_2$(edpp)$_2$]$^+$ (------), (b): *trans*-[$CoCl_2$(mm-PNNP)]$^+$ (——) and *trans*(Cl,Cl), *cis*(P,P)-[$CoCl_2$(edmp)$_2$]$^+$ (------), (c): *trans*-[Co(NCS)$_2$(pp-PNNP)]$^+$ (——), *trans*(NCS,NCS), *cis*(P,P)-[Co(NCS)$_2$(edpp)$_2$]$^+$ (------), and *trans*-[Co(NCS)$_2$(mm-PNNP)]$^+$ (—·—·—).

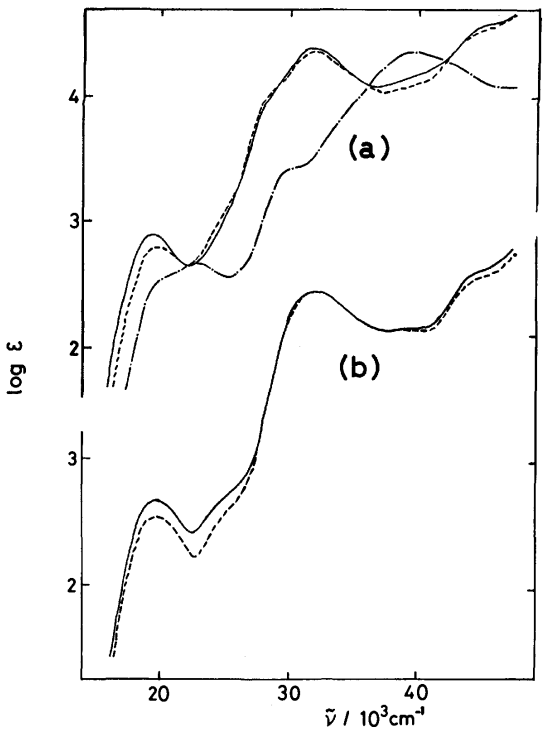

Fig. 3. Absorption spectra of *cisβ*-[Co(O-O)(PNNP)]-type Complexes. (a): *cisβ*-[Co(acac)(pp-PNNP)]$^{2+}$ (——), *trans*(P,N)-[Co(acac)(edpp)$_2$]$^{2+}$ (------), and *cisβ*-[Co(acac)(mm-PNNP)]$^{2+}$ (—·—·—), (b): *cisβ*-[Co(CO_3)(pp-PNNP)]$^+$ (——) and *trans*(P,N)-[Co(CO_3)(edpp)$_2$]$^+$ (------).

(acac)(pp- or mm-PNNP)]$^{2+}$, one of two methyl groups of acac which resonates at a lower magnetic field exhibits a coupling with the phosphorus atom trans to the oxygen donor atom of acac. The same coupling has been observed for the *trans*(P,N)-[Co(acac)-(edpp)$_2$]$^{2+}$.[11]

The absorption spectra of [Co(acac or CO_3)(pp-PNNP)]$^{n+}$ also resemble remarkably those of respective *trans*(P,N)-[Co(acac or CO_3)(edpp)$_2$]$^{n+}$. (Fig. 3) The absorption spectral pattern of [Co(acac)(pp- and mm-PNNP)]$^{2+}$ are different from each other over the whole region. The pp-PNNP complex shows the single first absorption band at 19500 cm^{-1}, and the pattern is also similar to that of [Co(acac)(en)(dppe)]$^{2+}$(dppe=1,2-bis-(diphenylphosphino)ethane).[11] On the other hand, the mm-PNNP complex exhibits a peak at 22750 cm^{-1} and a shoulder at *ca.* 20000 cm^{-1} in the first absorption region, and the pattern of which is quite similar to that of [Co(acac)(en)(dmpe)]$^{2+}$ (dmpe=1,2-bis(dimethylphosphino)ethane).[14] The ligand field strengths of mm-PNNP and dmpe may be much stronger than those of pp-PNNP and edpp to cause a splitting of the first absorption band of the complex.

The authors wish to thank the Ministry of Education for Scientific Research Grant-in-Aid Nos. 58470032 and 60470046.

References

1) A. M. Sargeson and G. H. Searle, *Inorg. Chem.*, **6**, 787 (1967).
2) A. L. Hale, H. C. Jewiss, and W. Levason, *Inorg. Chim. Acta.*, **97**, 85 (1985).
3) L. Sacconi and A. Dei, *J. Coord. Chem.*, **1**, 229 (1971).
4) H. Neibergall and B. Langefeld, *Chem. Ber.*, **95**, 64 (1962).
5) L. Horner, P. Beck, and H. Hoffmann, *Chem. Ber.*, **92**, 2092 (1959).
6) L. Valgha, L. Toldy, Ö. Fehér, and S. Lendrai, *J. Chem. Soc.*, **1957**, 805.
7) *Inorg. Synth.*, Vol. II, p. 223.
8) *Inorg. Synth.*, Vol. V, p. 188.
9) C. A. McAuliffe and W. Levason, "Phosphine, Arsine, and Stibine Complexes of Transition Elements," Elsevier, Amsterdam (1979).
10) I. Kinoshita, Y. Yokota, K. Matsumoto, S. Ooi, K. Kashiwabara, and J. Fujita, *Bull. Chem. Soc. Jpn.*, **56**, 1067 (1983).
11) M. Atoh, I. Kinoshita, K. Kashiwabara, and J. Fujita, *Bull. Chem. Soc. Jpn.*, **55**, 3179 (1982).
12) M. Atoh, K. Kashiwabara, H. Ito, T. Ito, and J. Fujita, *Bull. Chem. Soc. Jpn.*, **57**, 3139 (1984).
13) I. Kinoshita, K. Kashiwabara, J. Fujita, K. Matsumoto, and S. Ooi, *Bull. Chem. Soc. Jpn.*, **54**, 2683 (1981).
14) T. Ohishi, K. Kashiwabara, and J. Fujita, *Bull. Chem. Soc. Jpn.*, **56**, 3441 (1983).

Reduction of Aryl Halides and *N*-Hydroxy Nitrogen Compounds in Fast Atom Bombardment Mass Spectrometry

Takemichi NAKAMURA,* Hidemi NAGAKI, and Takeshi KINOSHITA
Analytical and Metabolic Research Laboratories, Sankyo Co., Ltd., 2-58, Hiromachi 1-Chome, Shinagawa-ku, Tokyo 140
(Received April 13, 1985)

Aromatic halogenated compounds and *N*-hydroxy nitrogen compounds were reduced to dehalogenated and deoxy analogs, respectively, in the fast atom bombardment ion source of a mass spectrometer. The reaction was found to occur in the liquid phase on exposure to a neutral fast atom beam.

Fast atom bombardment mass spectrometry (FAB/MS) and mass spectrometry mass spectrometry (MS/MS)[1,2] are very useful tools for characterizing polar or nonvolatile organic compounds.[3,4] In connection with a study on the FAB/MS of naturally occurring chlorinated peptide antibiotics (*e.g.* vancomycin[5,6]), we found that ions which might be assigned to quasi-molecular ions of the original compounds and those of mono-dechlorinated analogs were observed at the same time. These dechlorinated species seemed to exist regardless of the purity of the original samples. So this phenomenon was considered to be attributable to reduction of the corresponding chlorinated compounds. To confirm the assumption, halogenated model compounds were examined. Furthermore, several *N*-hydroxy nitrogen compounds were also tested for reduction under FAB measurement conditions.

Results and Discussion

The FAB spectrum of *p*-chlorophenylalanine (**1**) is shown in Fig. 1. A protonated molecular ion (*m/z* 200) was observed in the spectrum. Surprisingly, a

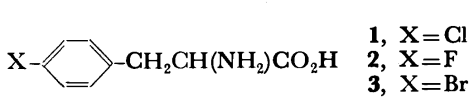

1, X=Cl
2, X=F
3, X=Br

non-chlorine-containing ion (*m/z* 166) corresponding to MH^+ of phenylalanine was also recorded at a notable relative intensity (23% of the sum of *m/z* 200 and 202). This ion (*m/z* 166) can not be derived from

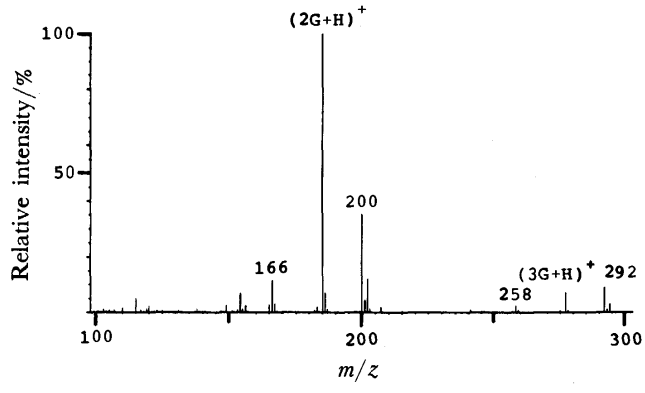

Fig. 1. Positive ion FAB spectrum of **1**. Glycerol is represented by G. The ions at *m/z* 258 and 292 are glycerol adducts of *m/z* 166 and 200, respectively.

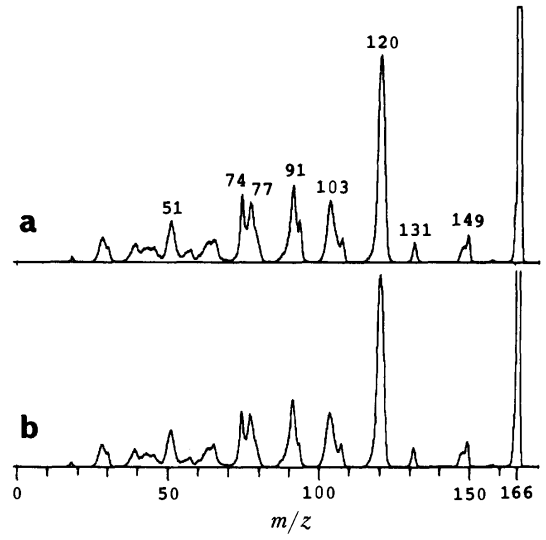

Fig. 2. CAD spectra of (a) *m/z* 166 in the FAB spectrum of **1** and (b) protonated molecular ion of phenylalanine yielded by FAB ionization. The precursor ions were resolved at high resolution (10,000).

MH^+ of **1** (*m/z* 200) since mass difference between these ions (34 u) is smaller than mass number of chlorine. The structure of the ion at *m/z* 166 was determined to be the same as that of MH^+ of phenylalanine, because the collisionally activated dissociation (CAD) spectra of both ions were identical (Fig. 2).

The relative abundance of *m/z* 166 was dependent on the kinetic energy of the neutral fast atom beam (16, 23, and 26% for 4, 6, and 8 keV, respectively) and increased over the period of irradiation (Fig. 3). These results suggest that the ion at *m/z* 166 was formed by bombardment of the fast atom beam at the surface of the sample solution.

The FAB spectra of *p*-fluorophenylalanine (**2**) and *p*-bromophenylalanine (**3**) also showed identical ions (*m/z* 166). The relative abundances of the ions at *m/z* 166 were 3.3% to *m/z* 186 and 51% to the sum of *m/z* 244 and 246, respectively. It seemed that the carbon–halogen bond strength directly reflected the amount of the reduced species.

Very recently, similar results on halogenated nucleosides have been reported by McCloskey *et al.*[7] They proposed the process that the halogen atoms on aromatic rings were replaced by hydrogen atoms of

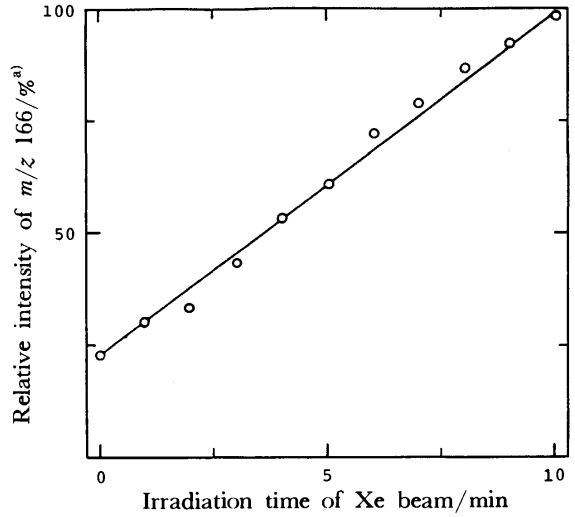

Fig. 3. Relationship between irradiation time and relative abundances of m/z 166 in FAB spectra of **1**. a) Calculated based on the sum of m/z 200 and 202.

glycerol molecules *via* radical intermediates based on deuterium labeling experiments. In present MS/MS studies, on the other hand, the structure of reduced products of **1**—**3** have been confirmed directly.

Such reductions occur not only in the case of halogenated compounds. Other examples were found in the case of *N*-hydroxy nitrogen compounds, namely, benzohydroxamic acid (**4**), 1-hydroxybenzotriazole (**5**), and *N*-hydroxysuccinimide (**6**).

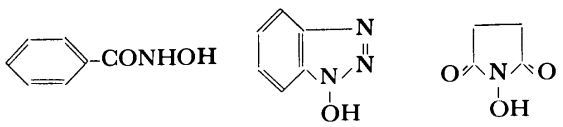

4 **5** **6**

The FAB spectrum of **4** (Fig. 4) exhibits MH^+ of **4** (m/z 138) and $MH^+ - 16$ (m/z 122, 60% of m/z 138). The ion at m/z 122 was not derived from MH^+ (m/z 138), because the metastable ion (MI) spectrum and CAD spectrum of MH^+ did not show any peak at m/z 122. The CAD spectrum of m/z 122 is identical to that of MH^+ of benzamide (Fig. 5). These results indicate that **4** was reduced to benzamide during the measurement of the FAB spectrum.

Similar phenomena were observed in the cases of **5** and **6**. The FAB spectra of **5** and **6** showed m/z 120 ($MH^+ - 16$, 51% of MH^+) and m/z 100 ($MH^+ - 16$, 31% of MH^+), respectively. The MS/MS experiments revealed that the ions ($MH^+ - 16$) were not derived from MH^+ but were identical to MH^+ of the corresponding reduced products in each case.

Since trace amounts of reduced products were recovered from the sample matrix solutions after FAB measurement of compounds **1**, **3**, **4**, and **5**, it was determined that the reactions occurred in the liquid

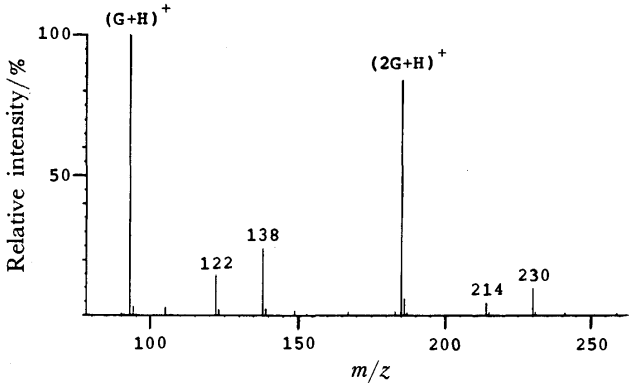

Fig. 4. Positive ion FAB spectrum of **4**. Glycerol is represented by G. The ions at m/z 214 and 230 are glycerol adducts of m/z 122 and 138, respectively.

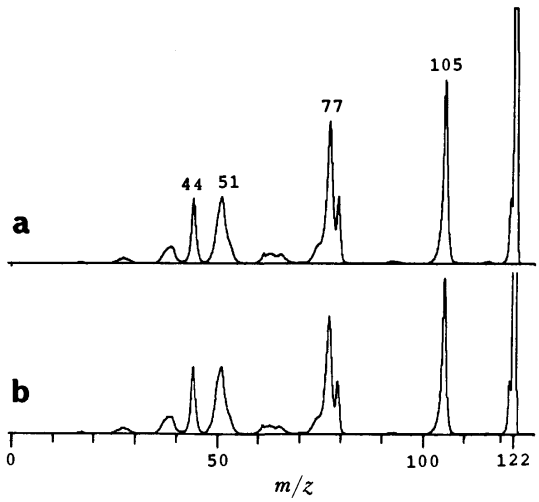

Fig. 5. CAD spectra of (a) m/z 122 in the FAB spectrum of **4** and (b) protonated molecular ion of benzamide yielded by FAB ionization. The precursor ions were resolved at high resolution (10,000).

phase as a result of bombardment by fast atoms, at least in part. Accumulation and time dependence of the relative intensities of MH^+ of the reduced products were not observed in previous work.[7] This disagreement may be caused by some differences of experimental conditions, *e.g.*, sample concentration, density of neutral atom beams, sputtering efficiency of sample molecules, and pressure of ion sources.

The results presented in this paper indicate that it is difficult to determine the purity or quantity of the above types of compounds by FAB/MS. However, in the cases that the purity of the samples has been established on the basis of other data, the phenomena described above are very useful for characterization of these compounds.

Experimental

Materials. All compounds were obtained from commercial sources: **1**, **2**, **4**, **5**, and **6**, Tokyo Kasei Kogyo Co.; **3** and glycerol (99.5%), Aldrich Chemical Co. They were

used without further purification. Compounds **1**—**6** were examined by GC/MS as trimethylsilyl derivatives (for **4**—**6**) or *N*-trifluoroacetyl trimethylsilyl esters (for **1**—**3**). Dehalogenated analogs of **1**—**3** or *N*-deoxy analogs of **4**—**6** could not be detected in each case (the limits of detection were 0.25% for dehalogenated analogs and 1% for deoxy analogs). Xenon (99.998%) was purchased from Showa Denko Co.

Apparatus and Procedures. All FAB mass spectra and MS/MS (MI and CAD) spectra were obtained using a JEOL JMS-HX100 mass spectrometer, which consists of a conventional geometry high resolution mass spectrometer followed by a second electrostatic analyzer (ESA-2). The kinetic energy of the xenon fast atom beam was made up to 6 keV unless otherwise stated.

The methanolic or aqueous ethanolic solutions of 10μg samples were mixed with glycerol (1 μl), then applied on stainless steel probe tips and introduced into a FAB ion source through a vacuum lock. Scanning of the magnetic field and irradiation of a fast atom beam were started at the same time and FAB spectra were recorded.

The MI and CAD spectra were obtained with the ESA-2 scanning. Collisionally activated dissociation experiments were performed at a high collision energy (5 keV).[2] Chemically pure argon was used as a neutral target gas introduced into the collision cell placed between the magnetic field and the ESA-2.

Sample solutions were recovered after irradiation by a fast atom beam (*ca.* 30 min) and examined by TLC.

References

1) F. W. McLafferty, *Science*, **214**, 280 (1981).
2) R. G. Cooks, and G. L. Glish, *Chem. Eng. News*, **59** (Nov. 30), 40 (1981).
3) T. Nakamura, H. Nagaki, and T. Kinoshita, *Ann. Rep. Sankyo Res. Lab.*, **36**, 178 (1984).
4) T. Kinoshita, H. Nagaki, M. Nakajima, and M. Inukai, *Mass Spectroscopy*, **32**, 169 (1984).
5) C. M. Harris, H. Kopecka, and T. M. Harris, *J. Am. Chem. Soc.*, **105**, 6915 (1983).
6) M. Barber, R. S. Bordoli, R. D. Sedgwick, and A. N. Tyler, *Anal. Chem. Symp. Ser.*, **12**, 129 (1983).
7) S. K. Sethi, C. C. Nelson, and J. A. McCloskey, *Anal. Chem.*, **56**, 1975 (1984).

Reactions of Enolic Biotin Models

Hiroki KONDO,* Katsuhito MIURA, Eiji SEKI, and Junzo SUNAMOTO
Department of Industrial Chemistry, Faculty of Engineering, Nagasaki University, Nagasaki 852
(Received April 27, 1985)

In order to delineate the mechanism of biotin-dependent carboxylation reactions, the following model experiments have been carried out. In reactions of carbonate derivatives such as methyl chloroformate with 2-ethoxy-2-imidazoline (**1**), a putative enolic biotin model, or 2-imidazolidinone (**2**), the former showed a much higher reactivity to provide the methoxycarbonylated **1** (**3**). Reactions of **3** with benzenethiolate, cyclohexylamine and carbanions have also been investigated as a model of transcarboxylation from *N*-carboxybiotin to an acceptor substrate. Only carbanions attack the carbonyl carbon of **3**, leading to rupture of the C–O bond, but not of the N–C bond. A net "carboxyl" transfer was effected with 1-methoxycarbonylimidazole (**9**) as a donor substrate. Implications of these results in biotin catalysis are discussed.

Biotin is the coenzyme involved in the synthesis of long-chain fatty acids in biological systems.[1-3] This enzymatic carboxylation takes place in two discrete steps as shown in Eqs. 1a and 1b. Biotin-dependent carboxylation reactions are interesting from a synthetic as well as a biochemical point of view. Despite efforts it has been unsuccessful to duplicate biotin-mediated carboxylation in nonenzymatic systems. One of the major reasons for this lies in the poor reactivity of the ureido nitrogen of biotin upon which carboxylation occurs.[4] Enzymes appear to overcome this problem by utilizing the free energy released upon hydrolysis of ATP to activate one or more of the reactants (Eq. 1a). Several hypotheses have been proposed to account in chemical terms for the role of ATP in biotin carboxylation. One of the attractive hypotheses claims that ATP might phosphorylate the ureido oxygen of biotin to generate an enolic structure (**5**).[5] This mechanism attracted considerable attention in recent years,[6-8] though rigorous structural proof of the thermodynamically unstable **5** has not been provided. In this article we attempted to assess the reactivity of a stable model compound of putative **5** toward several carbonate derivatives. Furthermore, model carboxyl-transfer reactions from a methoxycarbonylated biotin model to an acceptor substrate have also been investigated.

$$\text{E-Biotin} + HCO_3^- + \text{ATP} \rightleftharpoons \text{E-Biotin-}CO_2^- + \text{ADP} + \text{Pi} \quad (1a)$$

$$\text{E-Biotin-}CO_2^- + \text{RH} \rightleftharpoons \text{E-Biotin} + RCO_2H \quad (1b)$$

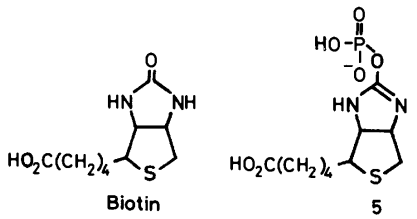

Results

Reactions of 1 and 2 with Carbonate Derivatives.

We have chosen 2-ethoxy-2-imidazoline (**1**) as a model for the enolic form of biotin and compared its reactivity with that of the keto model compound (**2**) toward several carbonate derivatives, methyl chloroformate, methoxycarbonyl dimethyl phosphate (MDP), and methyl *p*-nitrophenyl carbonate (MPNC). The reactions were routinely followed by ^1H NMR or HPLC, but the products were isolated, where necessary, for identification by a comparison with the authentic specimen. A reaction of **2** with methyl chloroformate gives **4** (Scheme 1), but a large excess of reagent and

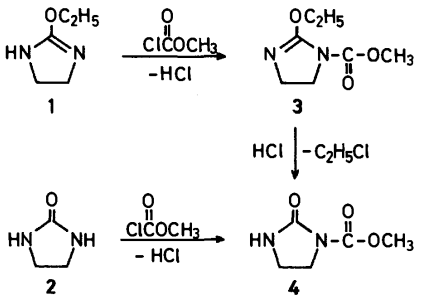

Scheme 1.

refluxing (≈60 °C) of the reaction mixture for several hours are usually needed to drive the reaction to completion. On the other hand, a mild condition (one equiv of methyl chloroformate and room temperature) is sufficient to methoxycarbonylate **1** with methyl chloroformate, thus demonstrating that **1** is by far the more reactive than **2** toward this reagent. Conversely, treatment of **1** with methyl chloroformate under the condition adopted for **2** (see above) gave **4** in quantitative yield. It was later found that **4** was produced *via* **3** as stated above and that because of its acid lability **3** is transformed into **4** by the hydrochloric acid generated in the preceeding reaction (Scheme 1).[9]

In addition to methyl chloroformate both MDP and MPNC are able to methoxycarbonylate **1** under mild conditions. Thus treatment of **1** with one equiv of MDP or MPNC at room temperature yielded **3** in excellent yield. MDP possesses potentially two sites for nucleophilic attack,[10] but the reaction with **1** took place solely on the carbon. No conversion of **3** into **4** was observed

TABLE 1. REACTION OF 1 WITH CARBONATE DERIVATIVES AT 25 °C. THE EXTENT OF REACTION WAS EVALUATED BY INTEGRATING THE ^{1}H NMR SIGNAL INTENSITIES.

Reagent[a]	[Reagent]/[1]	Solvent	Conversion/%	
			6 min	32 min
$ClCO_2CH_3$	1.0	$CDCl_3$	100	—
MDP	1.1	$CDCl_3$	75±5	100
MPNC	1.0	DMSO-d_6	40±5	80±5

a) MDP, methoxycarbonyl dimethyl phosphate; MNPC, methyl *p*-nitrophenyl carbonate.

when the reaction mixture of **1** and MDP or MPNC was refluxed in chloroform for 30 min, because the acids liberated in these reactions, dimethyl hydrogenphosphate and *p*-nitrophenol, are not acidic enough to bring about such a transformation.[9] The rates of methoxycarbonylation of **1** by these reagents are compared in Table 1. No reaction took place between **2** and MDP or MPNC even after 2 d in refluxing chloroform. This indicates that these two reagents are not electrophilic enough to methoxycarbonylate **2** and that there is a sharp difference between **1** and **2** in the reactivity toward carbonate carbonyls. The difference is too large to allow comparison of the reactivity of both compounds directly on the same scale.

Reactions of 3 and 4 with Nucleophiles. Reactions of **3**, **4**, and related compounds with sulfur and nitrogen bases as well as carbanions have been studied as a model of carboxyl transfer reactions (Eq. 1b). Similar reactions of **3** and **4** with hydroxide ions in water have already been reported.[11] A sample of **3** or **4** was allowed to react with 2 equiv of sodium benzenethiolate in DMSO-d_6 and the progress of reaction was followed by ^{13}C NMR. As has been reported previously,[12] compound **4** reacts with benzenethiolate at room temperature (≈20 °C) to provide methyl phenyl sulfide and **2**. The half time of the reaction was estimated as 30 min. By reference to the similar reaction of hydroxide ions in water,[11] the reaction was presumed to follow the sequence given in Scheme 2.[12] Unlike in the saponification in water, however, compound **7** has never been detected by ^{13}C NMR during the reaction in the present system, indicating that decarboxylation of **7** is fast compared to the demethylation step. The reaction of **3** follows the identical pathway, albeit at a decreased rate. The half time was estimated to be ≈25 min at 66 °C. The nucleophilic attack of benzenethiolate on the methyl carbon of **3** is the rate-determining step and the reaction products obtained were exclusively methyl phenyl sulfide and **1**. The lability of the intermediates (**6** and **7**) hampered comparison of the rates of their decarboxylation.

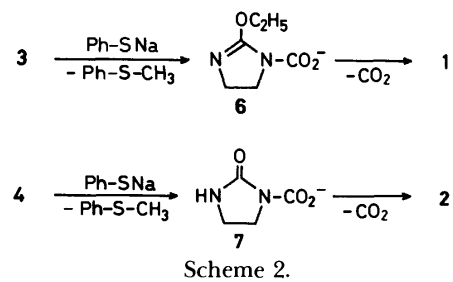

Scheme 2.

A reaction of **3** with cyclohexylamine afforded 1-methoxycarbonyl-2-cyclohexylaminoimidazolidine quantitatively (isolated yield 75%). In contrast, the attack of secondary or tertiary amines on the compound carrying an extra methyl group on 3-N of **3** takes place on the ethyl carbon, not on the 2-position.[7] The presence of a positive charge on the 3-N in the latter substrate appears to be responsible for this difference. Because of the charge the molecule is rendered electron-deficient, thus making the ethyl migration to a nucleophile possible. Compound **4** followed a similar pathway to that for **3** in the reaction with primary amines; initial nucleophilic attack on the ureido carbonyl provided a ring-opened product of substrate.[12]

A reaction of **3** with 3 molar equiv of phenylmagnesium bromide was carried out in THF at 0 °C for 10 h. The reaction mixture was worked up as usual. Inspection of the products by ^{1}H NMR in CCl_4 with CH_2Cl_2 as the internal standard revealed that following compounds had been obtained: 1-benzoyl-2-ethoxy-2-imidazoline (**8**) 52%, benzophenone 6%, triphenylmethanol 11%, and unreacted **3** 14%. This mode of product distribution is consistent with a sequence of reactions shown in Scheme 3. Initial attack of the Grignard reagent on the carbonyl carbon of **3** is followed by scission of the C–O bond, but not of the N–C bond. The product (**8**) undergoes further reactions with phenylmagnesium bromide to give benzophenone and triphenylmethanol. The possibility of an alternative pathway by way of methyl benzoate is ruled out, because the ester, if produced, could have survived under the present reaction conditions (see below). Analogous results were obtained for the reaction of **4** with phenylmagnesium bromide,[13] indicating that the electronic structure of the electrophilic center is not different significantly between the two compounds.

The above results suggest that net carboxyl transfer might be achieved if the basicity of the pertinent nitrogen is lowered. Hence 1-methoxycarbonylimidazole (**9**) was chosen as a donor substrate. Reaction of **9** with phenylmagnesium bromide, indeed, provided methyl benzoate (Scheme 3). For example, a reaction of **9** with 2 molar equiv of phenylmagnesium bromide yielded the following products: methyl benzoate 51%, benzophenone 1%, triphenylmethanol 5%, and unreacted **9** 8%. This result clearly indicates that the N–C bond cleavage or "the carboxyl" transfer has taken place. An alternative pathway that produces 1-benzoylimidazole as the initial product may also be envisioned, because the latter two products can be generated from either methyl benzoate or 1-benzoylimidazole. Furthermore, only 65% of the substrate initially present were identi-

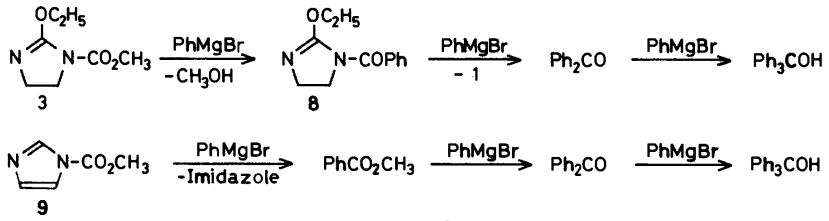

Scheme 3.

fied as above and the rest might be, at least in part, accounted for by 1-benzoylimidazole, which may be lost during work-up due to its water lability. Nevertheless, the methyl benzoate pathway is the main one, since the ester was obtained as the major product at least in one instance (above).

Discussion

From the results presented above, two main conclusions have been drawn. First, the stable enolic biotin model (**1**) possesses a much higher nucleophilicity than the corresponding keto model (**2**) toward a carbonyl carbon of the carbonate derivatives (a hydrogencarbonate surrogate). A similar behavior of both models was reported briefly for the hydrolytic reaction of carboxylic esters in water.[14] Also consistent with these is the observation that whereas 3-methyl-2-imidazolidinone was unable to add to the carbonyl carbon of a carbamate, the corresponding enol could.[15] All these phenomena may be rationalized in terms of a difference in the basicity of the pertinent nitrogen of the two compounds: The pK_a for the conjugate acid of **1** is $\approx$9[14] while the corresponding value for **2** ≈ -1.[16] Taken together, it is suggested that the ultimate function of ATP in the first partial reaction of carboxylation (Eq. 1a) is to enhance basicity and hence nucleophilicity of the nitrogen of biotin in question through phosphorylation of the ureido carbonyl.

It is, however, noted that despite suggestions for the participation of *O*-phosphono enolic structure (**5**) in biotin catalysis, its existence has not been proven in an explicit manner. The enolic structure of biotin in its unphosphorylated form is predicted theoretically to be unstable.[17] It is also pointed out that an alternative explanation may be invoked for the role of ATP, *e.g.*, phosphorylation of hydrogencarbonate, another substrate in the carboxylation of biotin (Eq. 1a).[18] The resulting mixed anhydride is expected to exhibit a higher reactivity than hydrogencarbonate. In fact, this mode of activation of a carboxyl group by ATP is rather general in synthase reactions in which an amide or ester bond is formed concomitant with ATP hydrolysis.[19]

Secondly, it was found that compound **3** undergoes reaction with various nucleophiles in a way quite analogous to that for compound **4**,[12] demonstrating that the electronic structure around the reaction center is not different significantly between the two. Compounds **3** and **4** have several potential sites for nucleophilic attack (Scheme 4), of which sites b and c are present in the *N*-carboxybiotin intermediate as well.

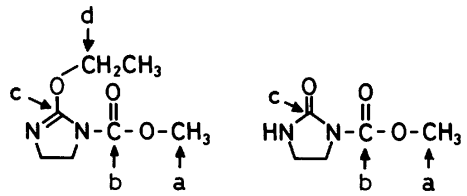

Scheme 4.

As noted above and previously,[7,11,12] oxygen and sulfur nucleophiles attack site a and nitrogen nucleophiles attack mostly site c. Only carbanions attack site b, an observation reminiscent of the fact that the enzymatic carboxyl transfer takes place on the ("active") carbon in most cases.[1-3] The initial addition of a carbanion to the ester carbonyl (site b) of **3** and **4** is followed by scission of the C-O bond. A "carboxyl" transfer was effected by employing 1-methoxycarbonylimidazole (**9**) as the donor substrate. The lower basicity of the imidazole nitrogen to which the methoxycarbonyl group is linked appears to be responsible for this difference; the pK_a of imidazole being $\approx$14,[20] while that of urea 25—33.[21] This implies that the N-C bond cleavage becomes feasible where the basicity of the pertinent nitrogen is low enough to make it a good leaving group. This result might be of value in relation to the mechanism of the enzymatic carboxyl transfer. As shown above, the carboxyl carbon bonded to the ureido nitrogen is a poor electrophile. To achieve transfer of the carboxyl group, one might have to enhance the electrophilicity of the carboxyl carbon and/or the nucleophilicity of the carboxyl-acceptor substrate. One way of doing this would be the electrophilic catalysis. For example, protonation or metal coordination to the ureido ring should bring about an electronic shift from the carboxyl group,[22,23] thereby facilitating nucleophilic attack of the incoming nucleophile on that site (Scheme 4). To corraborate this hypothesis further work is being continued in this laboratory.

Experimental

Materials. Common chemicals including 2-imidazolidinone (**2**, ethyleneurea) were obtained from commercial sources. The following compounds were prepared by the

literature methods specified; 2-ethoxy-2-imidazoline (**1**),[24] 1-methoxycarbonyl-2-ethoxy-2-imidazoline (**3**),[25] 1-methoxycarbonyl-2-imidazolidinone (**4**),[4] 1-methoxycarbonylimidazole,[26] methoxycarbonyl dimethyl phosphate.[27] 1-Benzoyl-2-ethoxy-2-imidazoline (**8**) was prepared by reaction of 1-benzoyl-2-imidazolidinone with triethyloxonium tetrafluoroborate. The crude product was purified by column chromatography on silica gel with acetonitrile as an eluant and by recrystallization from hexane, mp 46—48 °C. IR (KBr) 1673 (C=O), 1648 cm^{-1} (C=N). NMR (CCl_4): δ=0.84 (t, 3H, $-CH_3$), 3.52 (t, 2H, $-CH_2-$), 3.93 (t, 2H, $-CH_2-$), 4.01 (q, 2H, $-CH_2-CH_3$), 7.10—7.28 (m, 5H, $-C_6H_5$). Found: C, 66.27; H, 6.45; N, 12.92%. Calcd for $C_{12}H_{14}N_2O_2$: C, 66.03; H, 6.46; N, 12.83%.

Apparatus. Electronic and infrared absorption spectra were determined on a Hitachi 124 and Jasco A-100 spectrophotometer, respectively. ^1H NMR spectra were taken on a Jeol JNM-MH-100 spectrometer. Chemical shifts are expressed in parts per million relative to internal TMS. ^{13}C NMR spectra were determined on a Jeol JNM-FX-90Q spectrometer operating at 22.5 MHz. Typical experimental parameters were the following: spectral width of 5000 Hz with acquisition of 8 K data points, 10-μs pulse, and a recovery time of 3s. Mass spectra were determined with a Jeol JMS-DX 300 mass spectrometer. High-performance liquid chromatography (HPLC) was run on a Toyo Soda HLC 802 UR with Merck LiChrospher Si-100 as the stationary phase (4×300 mm) and chloroform–methanol (98:2 by vol.) as the eluant. When run at a flow rate ≈1.0 ml/min following retention times (min) were obtained MPNC 2.7, methyl chloroformate 3.2, **1** 3.8, **3** 4.7, *p*-nitrophenol 6.2, **4** 8.2.

Reaction of 1 with MPNC. A mixture of 120 mg (1.03 mmol) of **1** and 220 mg (1.12 mmol) of MPNC in 20 ml of $CHCl_3$ was refluxed for 12 h. The solvent was removed *in vacuo* and the residue was purified by column chromatography on silica gel (1.6×22 cm) with acetonitrile as an eluant in 62% yield, mp 67.5—70.0 °C (lit,[25] 67—70 °C).

Reaction of 3 with Cyclohexylamine. A sample of **3** (50 mg, 0.29 mmol) and cyclohexylamine (70 μl, 0.58 mmol) were allowed to react in chloroform at 60 °C for 24 h. Evaporation of the solvent *in vacuo* left an oil, to which was added hydrochloric acid equimolar to **3**. The product obtained as a hydrochloride in 75% yield was recrystallized from ethanol, mp 142—145 °C. R_f 0.59 ($CHCl_3$). IR(KBr) 1728 cm^{-1} (C=O). MS *m/z* 225.14715 (M^+). Calcd for $C_{11}H_{19}N_3O_2$ as free base: 225.14761.

Reaction of 9 with Phenylmagnesium Bromide. To a THF solution (12 ml) of phenylmagnesium bromide (24.6 mmol) was added a THF solution (40 ml) of **9** (1.68 g, 13.3 mmol) at 0 °C. The mixture was stirred for 10 h. The reaction was terminated by the addition of 10 ml of water and the solid formed was removed by filtration. The filtrate was extracted with ether (3×10 ml) and chloroform (3×10 ml). The combined extracts were dried over $MgSO_4$. Evaporation of the solvents left an oil, which was dissolved in carbon tetrachloride together with 846 μl (13.3 mmol) of dichloromethane for submission to NMR measurements.

The authors are grateful to prof. A. Marquet for informing them of her unpublished results and for helpful discussions. They also thank Drs. K. Sakata and N. Nishino for determining mass spectra. This work was supported by a Grant-in-Aid for Special Project Research 57102007 from the Ministry of Education, Science and Culture.

References

1) J. Moss and M. D. Lane, *Adv. Enzymol.*, **35**, 321 (1971).
2) H. G. Wood and R. E. Barden, *Ann. Rev. Biochem.*, **46**, 385 (1977).
3) S. Numa and T. Tanabe, "Fatty Acid Metabolism and its Regulation," ed by S. Numa, Elsevier, Amsterdam (1984), Chap. 1.
4) M. Caplow, *J. Am. Chem. Soc.*, **87**, 5774 (1965).
5) J. Retey and F. Lynen, *Biochem. Z.*, **342**, 256 (1965).
6) R. Kluger and P. D. Adawadkar, *J. Am. Chem. Soc.*, **98**, 3741 (1976).
7) M. J. Cravey and H. Kohn, *J. Am. Chem. Soc.*, **102**, 3928 (1980).
8) C. Blonski, M-B. Gasc, A. Klaebe, J-J. Perie, R. Roques, J. P. Declercq, and G. Germain, *J. Chem. Soc., Perkin Trans. 2*, **1982**, 7.
9) H. Kondo, K. Miura, and J. Sunamoto, *Bull. Chem. Soc. Jpn.*, **55**, 3347 (1982).
10) A. J. Lambie, *Tetrahedron Lett.*, **1966**, 3709.
11) H. Kondo, K. Miura, and J. Sunamoto, *Tetrahedron Lett.*, **23**, 659 (1982).
12) N. Matsumura, Y. Yagyu, H. Kawai, Y. Otsuji, and E. Imoto, *Nippon Kagaku Kaishi*, **1977**, 362.
13) N. Matsumura, K. Matsukawa, Y. Sakaguchi, and H. Inoue, *Bull. Chem. Soc. Jpn.*, **55**, 1667 (1982).
14) A. F. Hegarty, T. C. Bruice, and S. J. Benkovic, *J. Chem. Soc., Chem. Commun.*, **1969**, 1173.
15) C. M. Visser and R. M. Kellogg, *Bioorg. Chem.*, **6**, 79 (1977).
16) M. Caplow, *Biochemistry*, **8**, 2656 (1969).
17) G. M. Maggiora, *J. Theor. Biol.*, **43**, 51 (1974).
18) Y. Kaziro, L. F. Hass, P. D. Boyer, and S. Ochoa, *J. Biol. Chem.*, **237**, 1460 (1962).
19) C. Walsh, "Enzymatic Reaction Mechanisms," Freeman, San Francisco (1979), Chap. 5.
20) G. Yagil, *Tetrahedron*, **23**, 2855 (1967).
21) A. H. Corwin and J. D. Reinheimer, *J. Am. Chem. Soc.*, **73**, 1184 (1951).
22) H. Kondo, D. Horiguchi, S. Ikeda, J. Sunamoto, and K. Tsujii, *J. Org. Chem.*, **44**, 4430 (1979).
23) H. Kondo, K. Miura, S. Uno, and J. Sunamoto, *J. Inorg. Biochem.*, **21**, 93 (1984).
24) G. I. Poos, J. Kleis, and C. K. Cain, *J. Org. Chem.*, **24**, 645 (1959).
25) H. Kohn, M. J. Cravey, J. H. Arceneaux, R. L. Cravey, and M. R. Willcott, III, *J. Org. Chem.*, **42**, 941 (1977).
26) S. Iwasaki, *Helv. Chim. Acta*, **59**, 2738 (1976).
27) A. A. Shamshurin, O. E. Krivoshchekova, and M. Z. Krimer, *Zh. Obsch. Khim.*, **35**, 1877 (1965).

Chemical Synthesis of a Heat-stable Enterotoxin of *Yersinia enterocolitica*

Shoko YOSHIMURA and Yasutsugu SHIMONISHI*
Institute for Protein Research, Osaka University, Yamada-oka 3-2, Suita, Osaka 565
(Received May 23, 1985)

A peptide with the amino acid sequence Ser-Ser-Asp-Trp-Asp-Cys-Cys-Asp-Val-Cys-Cys-Asn-Pro-Ala-Cys-Ala-Gly-Cys of heat-stable enterotoxin (ST) produced by *Yersinia enterocolitica* was synthesized by a conventional method. The synthetic peptide was found to be identical with the corresponding natural peptide by chemical and physicochemical criteria, thus establishing the amino acid sequence of an ST of *Yersinia enterocolitica*.

Low-molecular-weight heat-stable enterotoxins (ST's) responsible for acute diarrhea in man and domestic animals are produced by several enteric bacteria such as enterotoxigenic *Escherichia coli* [1] and *Yersinia enterocolitica* [2,3]. The ST's isolated from these two kinds of bacteria have similar biological properties and their toxicities are neutralized by both homologous and heterologous anti-sera against these ST's [4]. These facts imply the similarity of at least the biologically and immunologically active structures of these ST's. Recently, we purified six molecular species of the enterotoxin to homogeneity from the culture supernatant of *Y. enterocolitica* by high-performance liquid chromatography and determined their amino acid sequences [5,6], as shown in Fig. 1. The sequence of the 13 amino acid residues in the C-terminal portion except for Asp and Val at positions 20 and 21, respectively, was identical with those of ST's produced by enterotoxigenic *E. coli* from the near-N-terminal Cys residue to the Cys residue at the 2nd position from the C-terminus, which were previously determined [7—10] and are shown in Fig. 1. These findings provided evidence that ST's of *Y. enterocolitica* and enterotoxigenic *E. coli* have common biological and immunological properties. However, the N-terminal sequences of the ST's isolated from these bacteria were quite different. These results raised the question of whether the divergence in the N-terminal portions reflects solely mutation in the transposon gene encoding ST [11] or a difference of the biological and physicochemical properties of the ST's. Therefore, it seemed interesting to examine the effect of the N-terminal sequence on various properties of these ST's.

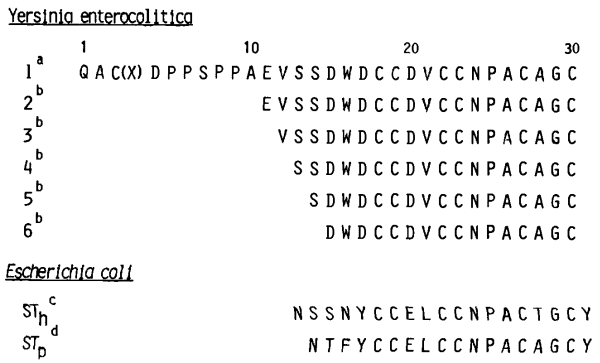

Fig. 1. Amino acid sequences of ST's of *Y. enterocolitica* and enterotoxigenic *E. coli*: a) cited from Ref. 5, b) from Ref. 6, c) from Ref. 7, and d) from Ref. 8—10.

In this work, we synthesized peptide 4 in Fig. 1, which consists of 18 amino acid residues from Ser at position 13 from the N-terminus to the C-terminal Cys, and compared the chemical and physicochemical properties of the synthetic peptide with those of natural peptide 4. This study also forms part of an investigation of the structure-activity relationship of heat-stable enterotoxins of *Y. enterocolitica* and enterotoxigenic *E. coli*, which will be reported in a subsequent paper [12].

Experimental

The general and analytical methods used were described in the preceding paper [13,14]. All chemicals used for preparative experiments were of reagent grade, those used for analysis were of guaranteed grade and solvents were distilled before use. The general procedure for purification of a product from a reaction mixture was as follows: The precipitate formed in the reaction mixture was filtered off and the filtrate was concentrated to a syrup or solid. The syrup or solid was dissolved in AcOEt and washed successively with 0.1 M† HCl, 5% aq $NaHCO_3$, and water. The washed solution was dried over anhydrous Na_2SO_4 and concentrated to dryness. In general, the concentration of solution was carried out under reduced pressure. Aminopeptidase M was purchased from the Protein Research Foundation (Minoh, Osaka). The HPLC apparatus consisted of a Hitachi 655 Liquid Chromatograph equipped with a multi-wave UV monitor, type 635M (Tokyo). YMC-ODS resin (S-5) was obtained from Yamamura Chemical Laboratories Co. (Kyoto) and was packed in our laboratory into columns of 4×250 mm and 8×300 mm for analytical and preparative experiments, respectively. The abbreviations used in this paper are those recommended by the IUPAC-IUB [*J. Biol. Chem.*, **247**, 977 (1972)]. Additional abbreviations are: MBzl, *p*-methylbenzyl; TFA, trifluoroacetic acid; DMF, *N,N*-dimethylformamide; TEA, triethylamine; DMSO, dimethyl sulfoxide.

Boc-Gly-Cys(MBzl)-OBzl (Ia). H-Cys(MBzl)-OBzl·Tos-OH (10.4 g, 33 mmol) was dissolved in CH_2Cl_2 (300 ml) and cooled to 0°C. The chilled solution was mixed with TEA (4.6 ml, 33 mmol) and Boc-Gly-OH (5.3 g, 30 mmol) with

† 1 M=1 mol dm^{-3}.

stirring. The solution was then mixed with DCC (6.8 g, 33 mmol) at below −20 °C and stirred at the same temperature for 1 h and at room temperature overnight. The syrup separated from the reaction mixture was crystallized from a mixture of $CHCl_3$, ether, and hexane, wt 9.6 g (67.3%), mp 55—56 °C, $[\alpha]_D^{20}$ −28.2° (*c* 1.0, DMF).

Found: C, 63.49; H, 7.11; N, 6.14; S, 6.91%. Calcd for $C_{25}H_{32}O_5N_2S$: C, 63.54; H, 6.83; N, 5.93; S, 6.77%.

*Boc-Cys(MBzl)-Ala-OMe (**Ib**).* Boc-Cys(MBzl)-OH·DCHA (15.2 g, 30 mmol) was dissolved with H-Ala-OMe·HCl (4.2 g, 30 mmol) in CH_2Cl_2 (150 ml), cooled below −20 °C and mixed with DCC (6.9 g, 33 mmol). The solution was stirred at below −20 °C for 1 h and at room temperature for 2.5 h. The syrup obtained from the reaction mixture was crystallized from ether and hexane; wt 10.3 g (83.7%), mp 87—88 °C, $[\alpha]_D^{20}$ −35.2° (*c* 1.0, DMF).

Found: C, 58.50; H, 7.49; N, 6.75; S, 7.68%. Calcd for $C_{20}H_{30}O_5N_2S$: C, 58.52; H, 7.37; N, 6.83; S, 7.80%.

*Boc-Cys(MBzl)-Ala-N_2H_3 (**Ic**).* Compound **Ib** (8.2 g, 20 mmol) was dissolved in MeOH (150 ml) and mixed with 100% hydrazine hydrate (30 ml). The solution was stirred at room temperature for 1 h and concentrated to a solid. The solid was recrystallized from MeOH and ether; wt 7.9 g (96.3%), mp 136—137 °C, $[\alpha]_D^{20}$ −14.0° (*c* 1.0, DMF).

Found: C, 55.42; H, 7.42; N, 13.60; S, 7.89%. Calcd for $C_{19}H_{30}N_4O_4S$: C, 55.60; H, 7.37; N, 13.65; S, 7.80%.

*Boc-Cys(MBzl)-Ala-Gly-Gys(MBzl)-OBzl (**I**).* Compound **Ia** (2.36 g, 5.0 mmol) was dissolved in TFA (10 ml) and stirred at room temperature for 30 min. The solution was concentrated to a syrup. Meanwhile, compound **Ic** (2.26 g, 5.5 mmol) was dissolved in DMF (20 ml) and cooled below −20 °C. The solution was stirred with 6.72 M HCl in dioxane (3.5 ml) and isopentyl nitrite (0.78 ml, 6 mmol) at the same temperature for 30 min, and then mixed with a solution of the above syrup in DMF (20 ml) and TEA (3.3 ml) and stirred at 0 °C for 1 h. The solid isolated from the reaction mixture was crystallized from a mixture of MeOH, ether, and hexane; wt 3.0 g (80.0%), mp 144—145 °C, $[\alpha]_D^{20}$ −20.3° (*c* 1.0, DMF).

Found : C, 62.08; H, 6.75; N, 7.40; S, 8.66%. Calcd for $C_{39}H_{50}O_7N_4S_2$: C, 62.38; H, 6.71; N, 7.46; S, 8.52%.

*Boc-Cys(MBzl)-Cys(MBzl)-Asn-Pro-Ala-Cys(MBzl)-Ala-Gly-Cys(MBzl)-OBzl (**II**).* Compound **I** (2.63 g, 3.5 mmol) was dissolved in TFA (10 ml) and stirred at room temperature for 30 min. The solution was concentrated to a syrup, which was triturated in ether. Meanwhile, Boc-Cys(MBzl)-Cys(MBzl)-Asn-Pro-Ala-N_2H_3 [14] (3.32 g, 4.0 mmol) was dissolved in DMF (15 ml) and cooled below −20 °C. The chilled solution was mixed with 6.72 M HCl in dioxane (2.6 ml) and isopentyl nitrite (0.59 ml, 4.5 mmol). The mixture was stirred at below −20 °C for 30 min, and then with a solution of the above solid in DMF (15 ml) and TEA (3 ml) at 0 °C for 4 d. The product separated from the reaction mixture was recrystallized from EtOH and ether; wt 5.0 g (98.5%), mp 179—180 °C, $[\alpha]_D^{20}$ −78.4° (*c* 1.0, DMF).

Found: C, 60.16; H, 6.65; N, 9.58; S, 8.78%. Calcd for $C_{73}H_{94}O_{13}N_{10}S_4$: C, 60.57; H, 6.55; N, 9.68; S, 8.84%.

*Boc-Cys(MBzl)-Cys(MBzl)-Asp(OBu^t)-Val-OMe (**IIIa**).* Z-Asp(OBu^t)-OH·DCHA (5.05 g, 10 mmol) and H-Val-OMe·HCl (1.68 g, 10 mmol) were dissolved in CH_2Cl_2 (50 ml) and cooled to −20 °C. The chilled solution was stirred with DCC (2.3 g, 11 mmol) at the same temperature for 1 h and at room temperature for 3 h. The syrup isolated from the reaction mixture was dissolved in MeOH (200 ml) and hydrogenated over 5% palladium-charcoal in the presence of 1 equiv of HCl at room temperature for 3 h. The catalyst was filtered off and the filtrate was concentrated to a syrup. Meanwhile, Boc-Cys(MBzl)-Cys(MBzl)-N_2H_3 [14] (6.0 g, 11 mmol) was dissolved in DMF (15 ml), cooled below −20 °C and stirred with 6.72 M HCl in dioxane (2.62 ml) and isopentyl nitrite (1.56 ml, 12 mmol) for 30 min. The solution was mixed with a solution of the above syrup in DMF (15 ml) and TEA (3.86 ml) and stirred at 0 °C for 3 d. The syrup isolated from the reaction mixture was solidified to an amorphous powder in ether and hexane; wt 8.16 g (100%).

*Boc-Cys(MBzl)-Cys(MBzl)-Asp(OBu^t)-Val-N_2H_3 (**III**).* Compound **IIIa** (8.16 g, 10 mmol) was dissolved in MeOH (200 ml) and cooled to 0 °C. The solution was mixed with 100% hydrazine hydrate, stirred at room temperature for 2 h and then concentrated to a solid. The solid was recrystallized from EtOH; wt 5.8 g (71.6%), mp 184—185 °C, $[\alpha]_D^{20}$ −35.4° (*c* 1.0, DMF).

Found: C, 57.82; H, 7.32; N, 10.57; S, 7.80%. Calcd for $C_{40}H_{60}O_8N_6S_2 \cdot 1/2H_2O$: C, 58.16; H, 7.44; N, 10.18; S, 7.75%.

*Boc-Cys(MBzl)-Cys(MBzl)-Asp(OBu^t)-Val-Cys(MBzl)-Cys-(MBzl)-Asn-Pro-Ala-Cys(MBzl)-Ala-Gly-Cys(MBzl)-OBzl (**IV**).* Compound **II** (2.17 g, 1.5 mmol) was dissolved in TFA (10 ml) and stirred at room temperature for 30 min. The solution was concentrated to a syrup, which was solidified in ether. Meanwhile, compound **III** (1.47 g, 1.8 mmol) was dissolved in DMF (8 ml) and cooled below −20 °C. The solution was stirred with 6.72 M HCl in dioxane (1.4 ml) and isopentyl nitrite (0.26 ml, 2.0 mmol) at −20 °C for 30 min and then mixed with a solution of the above solid in DMSO (5 ml) and TEA (1.53 ml). The mixture was stirred at 0 °C for 5 d in a refrigerator and then concentrated to a syrup, which was triturated in ice water. The solid was recrystallized from DMF and EtOH; wt 2.7 g (83.1%), mp 222 °C (dec), $[\alpha]_D^{20}$ −64.6° (*c* 0.5, DMSO).

Found: C, 60.43; H, 6.81; N, 9.18; S, 9.06%. Calcd for $C_{108}H_{142}O_{19}N_{14}S_6$: C, 60.83; H, 6.71; N, 9.20; S, 9.00%.

*Boc-Asp(OBu^t)-Cys(MBzl)-Cys(MBzl)-Asp-Val-Cys(MBzl)-Cys(MBzl)-Asn-Pro-Ala-Cys(MBzl)-Ala-Gly-Cys(MBzl)-OBzl (**V**).* Compound **IV** (2.13 g, 1.0 mmol) was dissolved in TFA (10 ml), stirred at room temperature for 2 h and concentrated to a syrup, which was triturated in ether. The solid was dissolved in a mixture of DMF (5 ml) and DMSO (5 ml), cooled to 0 °C and mixted with TEA (0.28 ml) and a solution of Boc-Asp(OBu^t)-ONSu (0.53 g, 1.5 ml) in 1-methyl-2-pyridone (5 ml). The solution was stirred at room temperature for 1 d and concentrated to a semisolid, which was collected with AcOEt and ether. The solid was recrystallized from EtOH; wt 1.9 g (84.8%), mp 219—220 °C (dec), $[\alpha]_D^{20}$ −63.4° (*c* 0.5, DMSO).

Found: C, 59.57; H, 6.46; N, 9.27; S, 8.42%. Calcd for $C_{112}H_{147}O_{22}N_{15}S_6$: C, 59.85; H, 6.59; N, 9.35; S, 8.54%.

*Z-Asp(OBu^t)-Trp-OMe (**VIa**).* Z-Asp(OBu^t)-OH·DCHA (10.1 g, 20 mmol) and H-Trp-OMe·HCl (5.09 g, 20 mmol) were dissolved in CH_2Cl_2 (200 ml), cooled below −10 °C and mixed with a solution of DCC (4.54 g, 22 mmol) in CH_2Cl_2 (50 ml). The mixture was stirred at room temperature overnight. The resulting precipitate was filtered off and the filtrate was concentrated to a syrup. The syrup was purified as described above and triturated in hexane; wt 10.5 g (100%), mp 55—56 °C, $[\alpha]_D^{20}$ +2.8° (*c* 1.0, DMF).

Found: C, 64.04; H, 6.41; N, 7.95%. Calcd for $C_{28}H_{33}O_7N_3$:

C, 64.23; H, 6.35; N, 8.03%.

*Boc-Ser-Ser-OMe (**VIb**).* Boc-Ser-N_2H_3 (2.20 g, 10 mmol) was dissolved in DMF (30 ml), cooled below −20 °C and mixed with 6.72 M HCl in dioxane (5.24 ml) and isopentyl nitrite (1.43 ml, 11 mmol). The solution was stirred at −20 °C for 30 min, and then mixed with H-Ser-OMe·HCl (1.56 g, 10 mmol) and TEA (6.3 ml). The mixture was stirred at 0 °C for 2 d in a refrigerator. The precipitate formed was filtered off and the filtrate was concentrated to a syrup. The syrup was washed with ether and hexane and crystalllized from a mixture of AcOEt, ether, and hexane; wt 3.0 g (98.0%), mp 62—64 °C.

Found: C, 46.92; H, 7.20; N, 9.34%. Calcd for $C_{12}H_{22}O_7N_2$: C, 47.05; H, 7.24; N, 9.15%.

*Boc-Ser-Ser-N_2H_3 (**VIc**).* Compound **VIb** (3.0 g, 9.8 mmol) was dissolved in MeOH (150 ml), cooled below 0 °C and mixed with 100% hydrazine hydrate (20 ml). The mixture was stirred at room temperature for 2 h and then concentrated to a solid. The solid was recrystallized from MeOH and ether; wt 2.9 g (94.8%), mp 146—147 °C, $[\alpha]_D^{20}$ +3.8° (*c* 1.0, DMF).

Found: C, 38.42; H, 7.61; N, 16.94%. Calcd for $C_{11}H_{12}O_6N_4 \cdot 2H_2O$: C, 38.59; H, 7.64; N, 16.37%.

*Boc-Ser-Ser-Asp(OBu^t)-Trp-OMe (**VId**).* Compound **VIa** (2.62 g, 5.0 mmol) was dissolved in MeOH (100 ml) and hydrogenated over 5% palladium-charcoal in the presence of 1 eq of HCl at room temperature for 1.5 h. The catalyst was filtered off and the filtrate was concentrated to a syrup. Meanwhile, compound **VIc** (1.84 g, 6.0 mmol) was dissolved in DMF (20 ml) and cooled below −20 °C. The chilled solution was stirred with 6.72 M HCl in dioxane (3.5 ml) and isopentyl nitrite (0.91 ml, 7.0 mmol) at the same temperature for 30 min, and then with a solution of the above syrup in DMF (20 ml) and TEA (4.0 ml) at 0 °C for 1 d. The resulting precipitate was filtered off and the filtrate was concentrated to a syrup. The syrup was purified as described above and triturated in ether and hexane; wt 2.45 g (73.8 %).

*Boc-Ser-Ser-Asp(OBu^t)-Trp-N_2H_3 (**VI**).* Compound **VId** (1.2 g, 1.8 mmol) was dissolved in MeOH (40 ml), cooled to 0 °C and mixed with 100% hydrazine hydrate (4 ml). The solution was stirred at room temperature for 2.5 h and concentrated to a syrup. The syrup was triturated in ether and reprecipitated from EtOH and ether; wt 0.99 g (82.5 %), mp 166—168 °C, $[\alpha]_D^{20}$ −13.4° (*c* 1.0, DMF).

Found: C, 50.31; H, 6.83; N, 17.81%. Calcd for $C_{30}H_{45}O_{10}N_7 \cdot N_2H_4 \cdot H_2O$: C, 50.48; H, 7.19; N, 17.67%.

*Boc-Ser-Ser-Asp(OBu^t)-Trp-Asp-Cys(MBzl)-Cys(MBzl)-Asp-Val-Cys(MBzl)-Cys(MBzl)-Asn-Pro-Ala-Cys(MBzl)-Ala-Gly-Cys(MBzl)-OBzl (**VII**).* Compound **V** (1.12 g, 0.5 mmol) was dissolved in TFA (10 ml) and stirred at room temperature for 2 h. The solution was concentrated to a syrup, which was solidified in ether. Meanwhile, compound **VI** (0.40 g, 0.6 mmol) was dissolved in DMF (4 ml) and cooled below −20 °C. The solution was mixed with 6.72 M HCl in dioxane (0.7 ml) and isopentyl nitrite (0.1 ml, 0.7 mmol), stirred at the same temperature for 30 min, and mixed with a solution of the above solid in 1-methyl-2-pyridone (6 ml) and TEA (0.87 ml). The mixture was stirred at 0 °C for 5 d in a refrigerator. The resulting precipitate was filtered off and the filtrate was concentrated to a solid, which was recrystallized from DMF and EtOH; wt 0.68 g (50.0%), mp 207—208 °C, $[\alpha]_D^{20}$ −62.0° (*c* 0.35, DMSO). Amino acid ratio in the acid hydrolysate: Asp, 3.45 (3); Ser, 1.42 (2); Pro, 0.94 (1); Gly, 1.02 (1); Ala, 2.00 (2); Cys, not determined; Val, 0.66 (1); Trp, 0.58 (1).

Found: C, 57.64; H, 6.10; N, 10.22; S, 7.23%. Calcd for $C_{133}H_{172}O_{30}N_{20}S_6 \cdot 2H_2O$: C, 57.90; H, 6.32; N, 10.15; S, 6.96%.

Removal of Protecting Groups and Air Oxidation. Compound **VII** (68 mg, 25 μmol) was mixed with anisole (0.2 ml) and treated with anhydrous liquid hydrogen fluoride (4 ml) at 0 °C for 1 h [15]. The hydrogen fluoride was removed by evaporation under reduced pressure and the residue was dissolved in 99% formic acid (1.5 ml). The solution was washed twice with hexane and diluted with water to 500 ml. The solution was adjusted to pH 8.0 by adding aqueous ammonia and stood at room temperature for 3 d with occasional stirring. Then it was adjusted to pH *ca.* 7.0 with acetic acid and lyophilized. The residue was purified by high-performance liquid chromatography, as described below.

High-performance Liquid Chromatography (HPLC). The HPLC column was equilibrated with 10% acetonitrile in 0.05% trifluoroacetic acid and after injection of the sample, was developed with a linear-gradient of 10—40% acetonitrile with increase in acetonitrile concentration of 1%/min at a flow rate of 1 ml min^{-1}. Eluates were monitored simultaneously for absorbance at 220 and 280 nm using a double-wavelength flow-through spectrophotometer.

Aminopeptidase M Digestion. Synthetic or natural peptide 4 (60 μg) was dissolved in 0.01 M pyridinium acetate buffer (pH 7.0) (100 μl) and digested with aminopeptidase M (5 μg) at 38 °C for 20 h. The reaction was stopped by addition of acetic acid. The solution was applied to a reversed-phase column of HPLC and the adsorbed material was eluted as described above.

Edman-degradation. Synthetic peptide was degraded by the Edman method, as described previously [16]. The degraded product was analyzed by HPLC, as described above.

Heat Stability. The synthetic peptide was dissolved at a concentration of 200 μg ml^{-1} in 0.01 M phosphate buffered saline (pH 7.2). The solution was sealed in capillary tubes and heated for a given period at the required temperature. Then the solution was cooled in an ice-bath and analyzed by HPLC, as described above.

Results and Discussion

Synthesis. The protected linear peptide **VII** consisting of 18 amino acid residues from Ser at position 13 from the N-terminus to the C-terminal Cys was synthesized by a similar procedure to that used for the synthesis of a heat-stable enterotoxin of enterotoxigenic *E. coli* [13], as shown in Fig. 2. All protecting groups were removed with anhydrous liquid hydrogen fluoride [15], and the resulting free linear peptide was air-oxidized in a dilute solution (5×10^{-5} M) until no free mercapto groups could be detected. The air-oxidized product had the HPLC profile shown in Fig. 3A on a reversed-phase column. The fraction shown by a vertical bar was most toxic and was eluted at the same retention time as natural peptide 4, as shown in Fig. 3B. The separated fraction was confirmed to be pure by repeated HPLC, as shown in Fig. 3C. The yield of the purified peptide was about 2.8% on the basis of the protected peptide **VII**. This low yield was considered to be due to various side-reactions

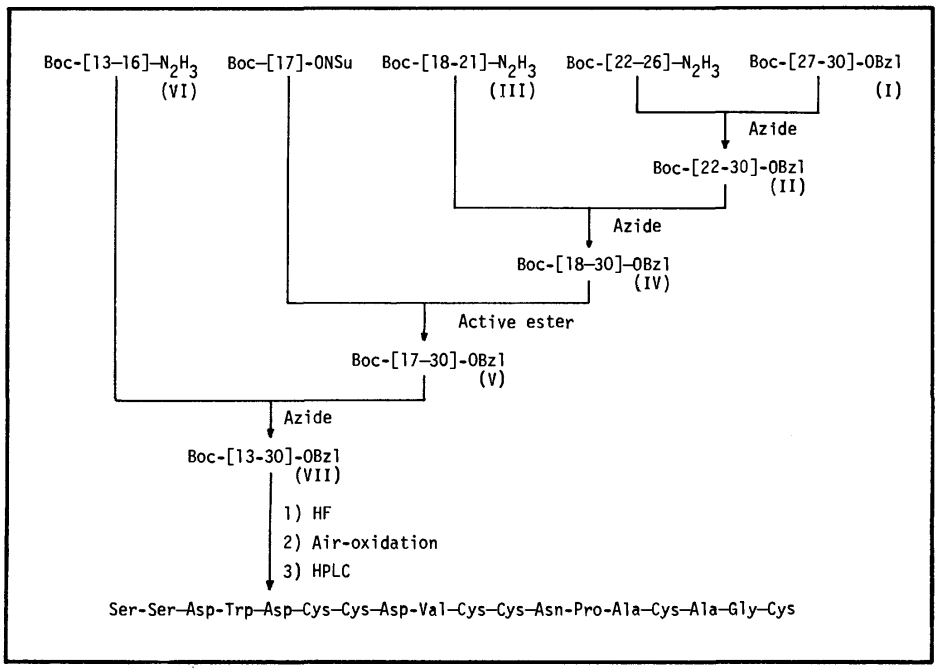

Fig. 2. Scheme for synthesis of a heat-stable enterotoxin of *Y. enterocolitica*.

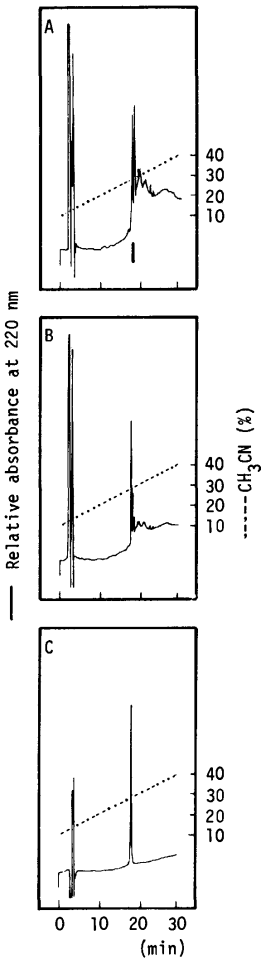

Fig. 3. HPLC profiles on a reversed-phase column (YMC-ODS S-5, 4×250 mm) of A) a deprotected, air-oxidized solution of synthetic peptide, B) a mixture of A) and natural peptide 4, and C) purified synthetic peptide.

during deprotection and air oxidation of the protected peptide **VII**, as shown in Fig. 3A. The amino acid composition and mass value of the purified synthetic peptide were identical with those of natural peptide 4, as shown in Table 1. The toxicity of this synthetic peptide was in the same order as that of natural peptide 4 in a fluid accumulation test in suckling mice [17]. The biological and immunological properties of the synthetic peptide and its shorter peptides will be described elsewhere [12].

Identification of the Synthetic Peptide with the Natural Peptide. To confirm that the synthetic peptide had the same structure as the natural peptide 4, we treated both with aminopeptidase M and compared the digests by HPLC, as shown in Fig. 4. The digest of the synthetic peptide was eluted later than that of the original peptide (Fig. 4B), but had the same retention time as natural peptide 6 lacking the two N-terminal amino acid residues of natural peptide 4 (Fig. 4C). The digest of natural peptide 4 was also eluted in the same position as natural peptide 6 and the digest of the synthetic peptide (not shown). The peak fraction in Fig. 4A was isolated and subjected to amino acid analysis and FAB mass spectrometry, as described in Table 1. Results indicated that the N-terminal Ser-Ser sequence of the synthetic peptide was removed by treatment with aminopeptidase M yielding natural peptide 6.

Then, we subjected the synthetic peptide to one step of Edman degradation. The degraded peptide was eluted at the same retention time on HPLC as natural peptide 5 and had the same amino acid composition and mass value as those of natural peptide 5, as shown in Fig. 5 and Table 1, respectively. Namely, removal of

TABLE 1. AMINO ACID COMPOSITIONS AND MASS VALUES OF SYNTHETIC PEPTIDES AND DEGRADED PEPTIDES AND THEIR COMPARISON WITH THOSE OF NATURAL PEPTIDES[a]

	Synthetic peptide			Natural peptide[b]		
	4	APase digest	Edman degraded	4	6	5
Asp	3.90 (4)	3.83 (4)	3.95 (4)	4.05 (4)	4.23 (4)	3.98 (4)
Thr				0.02	0.07	0.02
Ser	1.82 (2)		1.02 (1)	1.92 (2)	0.23	1.09 (1)
Glu				0.10	0.30	0.10
Gly	0.96 (1)	1.04 (1)	1.01 (1)	0.98 (1)	1.06 (1)	1.02 (1)
Ala	2 (2)	2 (2)	2 (2)	2 (2)	2 (2)	2 (2)
1/2Cys	4.25 (6)	4.74 (6)	4.83 (6)	4.75 (6)	4.76 (6)	4.83 (6)
Val	0.70 (1)	0.69 (1)	0.76 (1)	0.74 (1)	0.83 (1)	0.76 (1)
Met				0.03	0.05	0.02
Ile				0.03	0.09	0.03
Leu				0.02	0.09	0.03
Tyr				0.02	0.03	0.01
Phe				0.02	0.07	—
Lys				0.03	0.07	0.06
His				—	0.03	0.01
Trp	0.51 (1)	0.89 (1)	0.83 (1)	0.95 (1)	0.96 (1)	0.90 (1)
Arg				0.02	0.04	0.03
Pro	1.09 (1)	0.96 (1)	1.09 (1)	1.05 (1)	1.21 (1)	1.04 (1)
$[M+H]^+$	1845.5	1671.4	1757.9	1845.4	1671.4	1758.6

a) Values were calculated as mol/mol of Ala; numbers in parentheses indicate nearest integer values. b) Cited from Ref. 6.

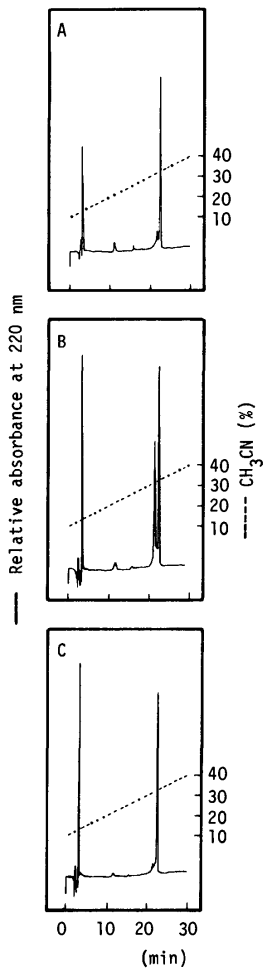

Fig. 4. HPLC profiles on a reversed-phase column (YMC-ODS S-5, 4×250 mm) of A) the aminopeptidase M digest of synthetic peptide, B) a mixture of A) and the undigested synthetic peptide, and C) a mixture of A) and natural peptide 6.

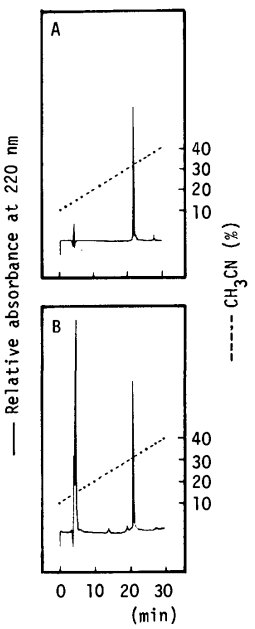

Fig. 5. HPLC profiles on a reversed-phase column (YMC-ODS S-5, 4×250 mm) of A) the synthetic peptide after one step of Edman degradation and B) a mixture of A) and the natural peptide 5.

the N-terminal Ser residue from the synthetic peptide resulted in formation of a peptide identical with natural peptide 5. These results clearly indicate that the synthetic peptide had the same primary and secondary structures as those of natural peptide 4.

Heat Stability. A crude ST isolated from *Y. enterocolitica* has been reported to be more heat-resistant than ST of enterotoxigenic *E. coli*, when assayed in suckling mouse [18]. However, the temperature stability of ST of *Y. enterocolitica* has not yet

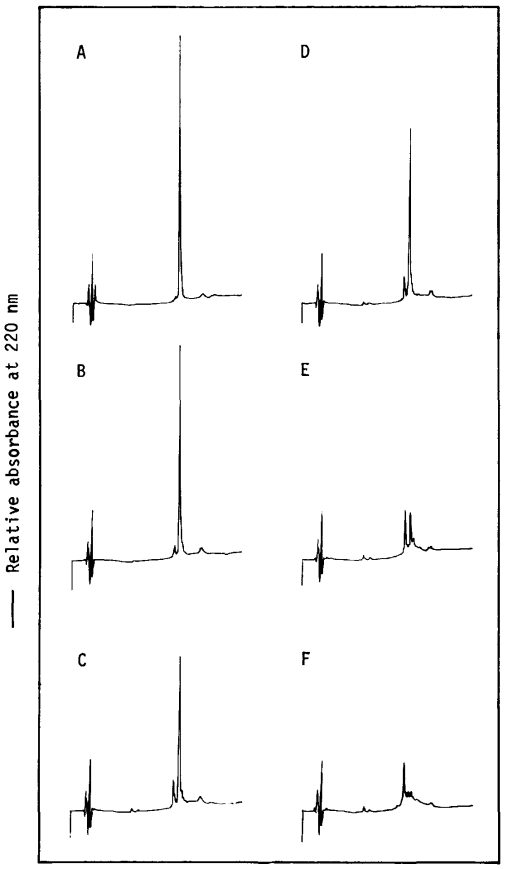

Fig. 6. HPLC profiles on a reversed-phase column (YMC-ODS S-5, 4×250 mm) of heat-treated synthetic peptide: (left column) A) after 10 min at 100 °C, B) after 30 min at 100 °C, C) after 60 min at 100 °C; (right column) D) after 10 min at 120 °C, E) after 30 min at 120 °C, and F) after 60 min at 120 °C.

been examined quantitatively, because purified ST could not be obtained. Since we obtain pure synthetic ST of *Y. enterocolitica* in the present study, we examined its heat stability by the same method as that used for testing the heat stability of ST of enterotoxigenic *E. coli* by HPLC [19]. The stabilities of the natural and synthetic ST's could not be compared, because the natural toxin could be isolated only in minute quantity [6]. Figure 6 illustrates the HPLC profiles of the synthetic toxin after heating at 100 °C and 120 °C for various periods. When the synthetic ST was heated at 100 °C for 30 min, its peak area on HPLC was reduced only to about 75% of that of the untreated ST, while ST of enterotoxigenic *E. coli* was destroyed significantly under the same conditions [19]. Furthermore, after heating at 100 °C for 60 min or at 120 °C for 10 min, about two-thirds of the original peak remained unchanged and the biological activity remained almost unchanged. These results support a previous qualitative experiment [18] which showed that ST of *Y. enterocolitica* was highly heat-resistant, showing no reduction of enterotoxigenic activity after heating for 30 min at 100 °C or 120 °C. This stability of ST of *Y. enterocolitica* was comparable to that of shorter analogues of ST of enterotoxigenic *E. coli*, which consist of 13 and 14 amino acid residues from near the N-terminal Cys residue to the Cys residue at position 2 from the C-terminus and the C-terminal Tyr residue [19,20], respectively. This high heat stability of ST of *Y. enterocolitica* may be due to the difference of its N-terminal sequence from that of enterotoxigenic *E. coli* or the presence of Asp-Val in place of Glu-Leu in ST of enterotoxigenic *E. coli*. We are now examining the relation of the thermodynamic stability and the biological activity.

We are indebted to Dr. S. Hara, Department of Chemistry, College of Science, Osaka University, for amino acid analyses. This work was supported in part by Grants-in-Aid for Scientific Research, No. 58122002 and 59340034 (to Y. S.) from the Ministry of Education, Science and Culture of Japan.

References

1) H. W. Smith and C. L. Gyles, *J. Med. Microbiol.*, **3**, 387 (1970).
2) J. Delmore, L. Michel, C. Martineau, and L. Lafleur, *Can. Med. Assoc. J.*, **11**, 281 (1974).
3) S. Kohl, J. A. Jacobson, and A. Nahmias, *J. Pediatr.*, **89**, 77 (1977).
4) K. Okamoto, A. Miyama, T. Takeda, Y. Takeda, and T. Miwatani, *FEMS Microbiol. Lett.*, **16**, 85 (1983).
5) T. Takao, N. Tominaga, Y. Shimonishi, S. Hara, T. Inoue, and A. Miyama, *Biochem. Biophys. Res. Commun.*, **125**, 845 (1984).
6) T. Takao, N. Tominaga, S. Yoshimura, Y. Shimonishi, S. Hara, T. Inoue, and A. Miyama, *Eur. J. Biochem.*, in press (1985).
7) S. Aimoto, T. Takao, Y. Shimonishi, S. Hara, T. Takeda, Y. Takeda, and T. Miwatani, *Eur. J. Biochem.*, **129**, 257 (1982).
8) T. Takao, T. Hitouji, S. Aimoto, Y. Shimonishi, S. Hara, T. Takeda, Y. Takeda, and T. Miwatani, *FEBS Lett.*, **152**, 1 (1983).
9) C. Lazure, N. G. Seidah, M. Chretien, R. Lallier, and S. St-Pierre, *Can. J. Biochem. Cell Biol.*, **61**, 287 (1983).
10) B. Ronnberg, T. Wadstrom, and H. Jornvall, *FEBS Lett.*, **153**, 183 (1983).
11) M. So, F. Heffron, and B. J. McCarthy, *Nature (London)*, **277**, 453 (1979).
12) S. Yoshimura, Y. Hidaka, Y. Shimonishi, S. Hara, T. Takeda, T. Miwatani, and Y. Takeda, in preparation.
13) S. Yoshimura, M. Miki, H. Ikemura, S. Aimoto, Y. Shimonishi, T. Takeda, Y. Takeda, and T. Miwatani, *Bull. Chem. Soc. Jpn.*, **57**, 125 (1984).
14) H. Ikemura, S. Yoshimura, S. Aimoto, Y. Shimonishi, S. Hara, T. Takeda, Y. Takeda, and T. Miwatani, *Bull. Chem. Soc. Jpn.*, **57**, 2543 (1984).
15) S. Sakakibara, Y. Shimonishi, Y. Kishida, M. Okada, and H. Sugihara, *Bull. Chem. Soc. Jpn.*, **40**, 2164 (1967).
16) S. Yoshimura, T. Takao, H. Ikemura, S. Aimoto, Y. Shimonishi, S. Hara, T. Takeda, Y. Takeda, and T. Miwatani, *Bull. Chem. Soc. Jpn.*, **57**, 1381 (1984).
17) Y. Takeda, T. Takeda, T. Yano, K. Yamamoto, and

T. Miwatani, *Infect. Immun.*, **25**, 978 (1979).
18) J. M. Boyce, D. J. Evans, Jr., D. G. Evans, and H. L. DuPont, *Infect. Immun.*, **25**, 532 (1979).
19) S. Aimoto, H. Watanabe, H. Ikemura, Y. Shimonishi, T. Takeda, Y. Takeda, and T. Miwatani, *Biochem. Biophys. Res. Commun.*, **112**, 320 (1983).
20) S. Yoshimura, H. Ikemura, H. Watanabe, S. Aimoto, Y. Shimonishi, S. Hara, T. Takeda, T. Miwatani, and Y. Takeda, *FEBS Lett.*, **181**, 138 (1985).

A Convenient Synthesis of 6-Hydroxy-7,9-bis(*p*-methoxybenzyl)-5-methylene-2-oxa-7,9-diazabicyclo[4.2.2]decane-8,10-dione

Masanori YAMAURA, Tsuneji SUZUKI, Hironobu HASHIMOTO, Juji YOSHIMURA,* and Chung-gi SHIN†
Laboratory of Chemistry for Natural Products, Faculty of Science, Tokyo Institute of Technology, Midori-ku, Yokohama 227
†*Laboratory of Organic Chemistry, Faculty of Technology, Kanagawa University, Kanagawa-ku, Yokohama 221*
(Received January 5, 1985)

The title compound, the key intermediate for a total synthesis of bicyclomycin, was synthesized from *N,N'*-diacetyl anhydroglycine through twelve steps. The three-carbon branch for the construction of the bicyclic skeleton was introduced to the 2,5-piperazinedione ring as an alkylidene substituent, and then the olefinic function was converted into a diol function. The formation of bicyclic ring was achieved by treatment with *N*-bromosuccinimide followed by the intramoleculer substitution of the primary hydroxyl group in the side chain, and finally the secondary hydroxyl group was converted to the methylene function by an improved Peterson reaction.

Bicyclomycin (**1**) produced by *Streptomyces sapporonensis*[1] and *S. Aizunensis*[2] from leucine and isoleucine[3] is a member of the large class of naturally occurring 2,5-piperazinediones (PDO) with an unusual structure.[4] Several synthetic efforts have been made for **1**, and both racemic[5] and optically active **1**[6,7] were recently synthesized.

Two strategies have been selected for synthesis of **1**, that is, the introduction of a carbon chain, which is necessary for the bicyclic bridge, before (path A)[8] or after formation of PDO ring (paths B and C). However, no report which reached the final goal through path A has appeared because the reaction steps are rather complicated. In the path B,[9] the substituent X for activation of C-3 and C-6 was used for both the introduction of methylene-branched four-carbon unit and cyclization into the bicyclic key intermediate (a), and it was converted into **1** by the aldol condensation with methyl-branched four-carbon unit (b).[5,6] In our previous communication,[10] the olefinic function of an alkylidene-PDO was oxidized stereoselectively to a diol function (c: Y=OH, Z=H_2), then cyclized by the treatment with *N*-bromosuccinimide (NBS), and finally the secondary hydroxyl group was converted into the methylene group to yield the title compound. This paper describes detailed data of the communication.

Results and Discussion

First of all, three different synthetic routes of 3-benzyloxypropanal (**2**) which is the three-carbon unit for the construction of bicyclic ring were examined. In the first route, the reaction of benzyl alcohol with 3 equivalents of 3-chloro-1,1-diethoxypropane[11] gave 3-benzyloxy-1,1-diethoxypropane in 71% yield, acidic hydrolysis of which gave **2** in 97% yield (route A). In the second one, oxidation of 3-benzyloxy-1-propanol[12] with chromium trioxide and pyridine gave **2** in 72% yield (route B). In the last one, partial hydrolysis of 4-benzyloxy-1,2-*O*-isopropylidene-1,2-butanediol[13] and oxidation of the product with lead tetraacetate gave **2** in 90% overall yield (route C). This route was the most convenient for large scale preparation of **2**.

Then, condensation of *N,N'*-diacetylanhydroglycine with **2** in *N,N*-dimethylformamide (DMF) in the presence of equimolar potassium *t*-butoxide[14] gave only one isomer of 1-acetyl-3-(3-benzyloxypropylidene)-PDO (**3**) in 82% yield, whose configuration was deduced to be *Z* from the fact that its *N*-acetylation with acetic anhydride did not proceed.[15] Oxidation with lead tetraacetate[16] and *m*-chloroperbenzoic acid[8d] which were successful in the case of 3-benzylidene-1,4-dialkyl-PDO and 3-alkylidene-1,4-dialkyl-PDO could

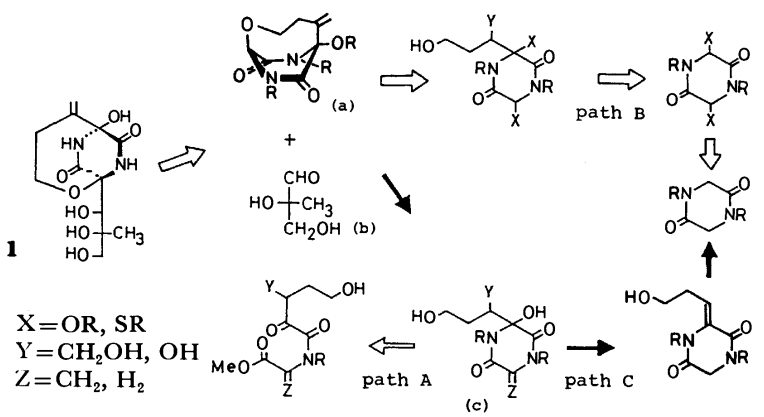

Scheme 1. Retro-synthesis of bicyclomycin

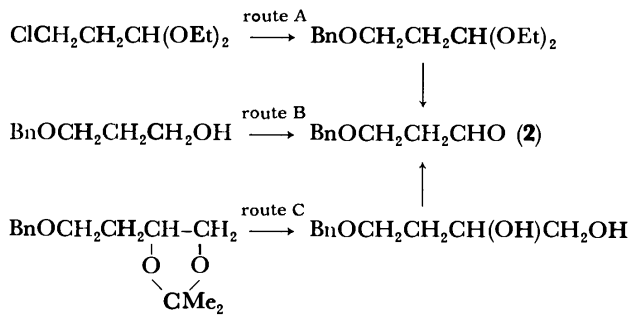

Scheme 2. Syntheses of 3-benzyloxypropanal (**2**)

not be applied to **3**, probably due to the electron-withdrawing effect of *N*-acetyl group. Reaction of **3** with osmium tetraoxide and sodium chlorate[17a] gave the corresponding diol (**6**) in 58% yield, but, the use of *N*-methylmorpholine-*N*-oxide[17b] or hydrogen peroxide[17c] as the cooxidant gave poor results. An osmium oxidation of 3-(3-benzyloxypropylidene)-1,4-bis(*p*-methoxybenzyl)-PDO (**5**) which was prepared from **3** *via* *N*-deacetylated product (**4**) in 72% overall yield, gave **7** in 46% yield, in which a partial oxidative *N*-de(*p*-methoxybenzyl)ation was deduced by the formation of *p*-anisaldehyde.

Isopropylidenation of the diol function in **6** with 2-methoxypropene–pyridinium *p*-toluenesulfonate in acetone gave the desired product (**9a**) and its 3-epimer (**9b**) in 95 and 2% yield, respectively. In this reaction, the suspended **6** dissolved by addition of a small amount of acetone within 5 min and then **9a** deposited from the reaction mixture. In a similar way, **7** was converted into the *O*-isopropylidene derivative (**12**) in 94% yield. However, the isopropylidenation of **6** with 2,2-dimethoxypropane–*p*-toluenesulfonic acid gave a 1:2 mixture of **9a** and partial *O*-methylation product (**8**) in 94% yield. The formation of **8** indicates the acid-catalyzed substitution of the tertiary hydroxyl group of **6** with methanol liberated by acetal exchange. On the other hand, the reaction of **6** with acetone-anhydrous copper(II) sulfate and acetone–acid (*p*-toluenesulfonic acid or sulfuric acid) gave negative and complex results, respectively.

On the other hand, mono(*p*-methoxybenzyl)ation of deacetylated derivative (**10**), which was obtained quantitatively by treatment of **9a** with hydrazine, with equimolar sodium hydride and *p*-methoxybenzyl bromide gave **11** in 87% yield. A further *p*-methoxybenzylation of **11** gave **12** in 76% yield, together with a enol ether (**18**: 11%). When *p*-methoxybenzyl chloride instead of the bromide is used, a 1:1 mixture of **12** and **18** was formed. The yield of one step synthesis of **12** from **10** was 62%. Hydrogenolysis of **9a** in methanol in the presence of palladium–carbon gave the *O*-debenzylated product (**13**) in 75% yield. This conversion could be also achieved by treatment of **9a** with equimolar NBS to afford **13** and *O*-benzoylated by-product (**14**) in 92 and 6% yields, respectively. A similar reduction of **11** or **18** and **12** gave the same **15** and **16** in quantitative yields, respectively. Compound **16** was also obtained from **15** by successive *p*-methoxybenzylation (**17**) and hydrogenolysis.

Cyclization of **16** in chloroform with 1.1 equimolar NBS[8b] and excess barium carbonate at room temperature for 4 d gave the corresponding bicyclic derivative (**19**) in 86% yield. The use of 2 equimolar NBS gave **19** in only 11% yield, due to the oxidation of *p*-methoxybenzyl groups. The same reaction without barium carbonate for 24 h gave **19**, the corresponding spiro cyclic compound (**21**), starting material (**16**) in 12, 63, and 7% yields, respectively. However, a similar reaction of **15** for 24 h in the presence of barium carbonate gave the corresponding bicyclic (**20**), spiro (**22**), and recovered **16** in 30, 16, and 42% yields, respectively. The structures of spiro derivatives, **21** and **22**, were proved by conversion into acetates, **23a**,

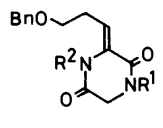

3: R^1=Ac, R^2=H
4: R^1=R^2=H
5: R^1=R^2=MBn

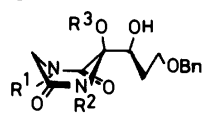

6: R^1=Ac, R^2=R^3=H
7: R^1=R^2=MBn, R^3=H
8: R^1=Ac, R^2=H, R^3=Me

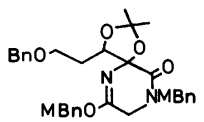

18

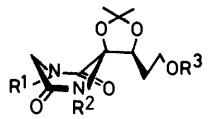

9a: R^1=Ac, R^2=H, R^3=Bn
9b: 3-epimer of **9a**
10: R^1=R^2=H, R^3=Bn
11: R^1=MBn, R^2=H, R^3=Bn
12: R^1=R^2=MBn, R^3=Bn
13: R^1=Ac, R^2=R^3=H
14: R^1=Ac, R^2=H, R^3=Bz
15: R^1=MBn, R^2=R^3=H
16: R^1=R^2=MBn, R^3=H
17: R^1=R^2=R^3=MBn

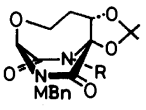

19: R=MBn
20: R=H

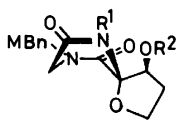

21: R^1=MBn, R^2=H
22: R^1=R^2=H
23a: R^1=MBn, R^2=Ac
23b: 5-epimer of **23a**
24: R^1=H, R^2=Ac

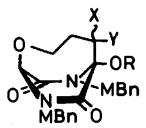

29: R=X=H, Y=OH
30: R=H, X, Y=O
31: R=H, X=OH, Y=CH_2TMS
32: R=H, X, Y=CH_2
33: R=TBS, X, Y=CH_2

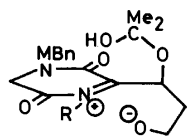

25

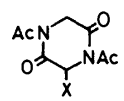

26: X=Br
27: X=OAc
28: X=SAc

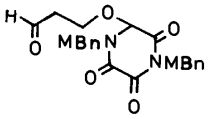

34

23b, and **24**, respectively. Compounds **23a** and **23b** were an epimeric pair of spiro configuration. The formation of spiro derivatives accompanied with *O*-deisopropylidenation may be the acid-assisted formation of iminium (**25**) or imino intermediate. An attempted similar reaction of **13** did not proceed and the starting material was recovered, probably due to electron-withdrawing effect of *N*-acetyl group. Considering that the reaction of *N,N'*-diacetylanhydroglycine with equimolar NBS and successive treatment of the unstable monobromo derivative (**26**) with sodium acetate or potassium thioacetate gave the corresponding 2-substituted PDO (**27** and **28**) in 71 and 68% yields, respectively, the difference in the reactivity between **13** and *N,N'*-diacetylanhydroglycine may be attributed to the absence and presence of a resonance system in the PDO-ring.

Then, the treatment of **19** with a 1:1 mixture of 2 M (M=mol dm^{-3}) hydrochloric acid and tetrahydrofuran (THF) at 40 °C for 24 h gave the corresponding *O*-deisopropylidenated product (**29**) in 83% yield. The reaction with 70% acetic acid at an elevated temperature or with trifluoroacetic acid at room temperature gave a complex result. The selective oxidation of the secondary hydroxyl group of **29** with dimethyl sulfoxide-oxalyl dichloride[18] gave the desired 5-oxo compound (**30**) in 91% yield, while oxidation with pyridinium chlorochromate gave an undesired ring-cleavaged compound **34** in 61% yield. Direct conversion of carbonyl function of **30** into methylene group with the Witting reagent $Ph_3P{=}CH_2$, methylenedimagnesium dibromide,[19] and Tabbe reagent $Cp_2TiCH_2AlClMe_2$[20] could not be performed. Therefore, an improved Peterson reaction as stepwise conversion was used for this purpose. Addition of trimethylsilylmethylmagnesium chloride to **30** gave the addition product (**31**) in 52% yield, as a 4:1 mixture of diastereomers. However, the next elimination reaction did not proceed under the usual conditions,[21] and barely the treatment with 0.08 M sulfuric acid in THF at room temperature for 3 d gave the methylene derivative (**32**) in 48% yield. Because an activation method by introduction of *O*-sulfonyl or halogen function[21] can not be used in this case, the elimination was accomplished by treatment of 5,6-ditrifluoroacetate of **31** with tetrabutylammonium fluoride followed by removal of the remaining trifluoroacetyl group at *O*-6 to give **32** in 81% yield. Treatment of **32** with *t*-butyldimethylsilyl triflate[22] gave the corresponding 6-*O*-protected derivative (**33**) in 80% yield.

^{1}H NMR data of 6-substituted PDO, spiro cyclic and bicyclic derivatives, and ^{13}C NMR data of 6-substituted PDO are summarized in Tables 1—4, respectively.

Among *O*-isopropylidene derivatives (Table 1), the chemical shift of H-1' protons of **9a** is lower than that of **9b** by 0.78 ppm. This phenomenon indicates that the carbonyl group in PDO ring and H-1' of **9a** are in *cis*-relation in regard with the isopropylidene ring. It is interesting that the difference in the chemical shift of two methyl protons of isopropylidene group in 4-(*p*-methoxybenzyl)-PDO (**12**, **16**, and **17**) is commonly 0.22 ppm, whereas those in others are within 0.07 ppm. These facts support that the mono(*p*-methoxybenzyl)-ation of **10** occurred selectively at the farer nitrogen from oxolane-ring to give 1-substituted product (**11**). The lower chemical shift of methylene protons of *O*-(*p*-methoxybenzyl) group and singlet signal of methyl protons of isopropylidene group in **18** prove the enol ether structure. Some of above-mentioned observations are also supported from ^{13}C NMR data (Table 4). In a comparison of ^{13}C NMR chemical shifts for **9a** and **9b** the larger differences were observed for C-1' and acetyl carbon. The lower field shift of C-3 and C-1' in 4-substituted derivatives (**12** and **16**) may be due to the anisotropic effect of the 4-(*p*-methoxybenzyl) group. In the case of **18**, the enolated carbonyl carbon shifted markedly to the upper field, whereas C-6 resonates in slightly higher field.

Spiro cyclic (Table 2) and bicyclic derivatives (Table 3) can be easily distinguished from the appearance of an AB-quartet of H-8a and H-8b and of a singlet of H-1, respectively, and the large coupling of the former is characteristic to H-6 of original PDO-ring. The absence and the presence of isopropylidene protons also support their structures. Moreover, it is characteristic that one of methylene protons at C-3 of the bicyclic derivatives resonated at extraordinary higher field than the other proton at C-3 as well as the corresponding methylene protons of spiro cyclic derivatives, which indicates the diamagnetic anisotropy in the perpendicular direction of the PDO-ring.

In the cases of **23a** and **23b**, a larger difference was observed in the chemical shift of H-4 protons, indicating that H-4 and carbonyl group in PDO-ring of **23a** are in *cis*-relation in regard with the five-membered ring. The configuration of **24** is probably similar to that of **23a**. The presence of sp^2 C-5 carbon in **30** and **33** in clearly shown by ^{13}C NMR (see Experimental).

Experimental

General. Melting points were determined with a Mel-Temp apparatus or with a Yanagimoto micro melting-point apparatus, and were not corrected. IR spectra (cm^{-1}) were recorded with a Hitachi EPI-G2 grating spectrometer. ^{1}H and ^{13}C NMR spectra were recorded with a JEOL JMN PS-100 and a JEOL FX-90Q spectrometers, respectively, in $CDCl_3$ with tetramethylsilane as the internal standard, unless otherwise noted. Column chromatography was performed on Wakogel C-200 or C-300.

Preparation of 3-Benzyloxypropanal (2). a) A mixture of 3-chloro-1,1-diethoxypropane (257 g, 1.54 mol), benzyl alcohol (55.5 g, 0.513 mol), sodium hydroxide (103 g, 2.57 mol), and tetrabutylammonium hydrogensulfate (17.4 g, 0.051 mol) in saturated sodium chloride (410 cm^3) was vigorously stirred at 60 °C for 12 h and then at 100 °C for 48 h, poured into ice-water, and extracted with benzene. The usual processing of

TABLE 1. ^{1}H NMR DATA OF 6-SUBSTITUTED 2,5-PIPERAZINEDIONE DERIVATIVES

Compound	H-6a ($J_{6a,6b}$)	H-6b	H-1′ ($J_{1',2'}$)	H-2′	H-3′ ($J_{2',3'}$)	CMe_2	Others
3	—4.36s—		6.32t (8.0)	2.6—2.3m	3.59t (5.2)	—	9.30bs(NH), 7.23s(Ph), 4.52s(CH_2 in Bn), 2.59s(Ac)
5	—3.82s—		6.29t (7.5)	2.51dt	3.54t (7.0)	—	7.28s(Ph), 7.18d, 6.90d, 6.98d and 6.71d(8H, *J*=8.0 Hz, 2×MBn), 4.86s, 4.51s and 4.46s(3×CH_2 in Bn and MBn), 3.72s and 3.71s (2×OMe)
6	4.50d (17.8)	4.22d	4.4—4.1m	2.0—1.5m	3.66t (5.0)	—	7.70bs(NH), 7.36s(Ph), 4.77bs and 2.55bs(2×OH), 4.49s(CH_2 in Bn), 2.54s(Ac)
7	4.21d (17.5)	3.64d	4.44t (7.5)	2.2—1.5m	3.9—3.5m	—	7.28s(Ph), 7.32d, 7.09d and 6.74d(8H, *J*=8.5 Hz, 2×MBn), 5.04bs and 1.96bs(2×OH), 4.75d, 4.31d and 4.4—3.5m(*J*=14.0 Hz, 2×CH_2 in MBn), 4.46s (CH_2 in Bn), 3.73s(6H, 2×OMe)
8	—4.38s—		4.17dd (8.0,4.0)	2.1—1.7m	3.9—3.4m	—	7.31s(Ph), 7.14s(NH), 4.51s(CH_2 in Bn), 3.37s (OMe), 2.62s(Ac), 2.21bs(OH)
9a	4.46d (18.0)	4.04d	5.00t (6.4)	2.2—1.9m	3.8—3.5m	1.49s 1.44s	7.40s(NH), 7.29s(Ph), 4.51d and 4.37d(*J*=12.0 Hz, CH_2 in Bn) 2.48s(Ac)
9b	4.36d (18.5)	4.06d	4.22 (6.0)	2.4—2.1m	3.8—3.4m	1.50s	7.82s(NH), 7.26s(Ph), 4.43s(CH_2 in Bn), 2.49s(Ac)
10[a]	3.94d (18.0)	3.54d	4.88 (6.5)	2.1—1.8m	3.7—3.5m	1.49s 1.47s	7.40s(Ph), 7.40bs and 6.44bs(2×NH), 4.46s(CH_2 in Bn)
11	3.92d (18.0)	3.62d	5.04t (6.4)	1.96ddt	3.62dd (2.4,6.4)	1.42s	7.80s(NH), 7.41s(Ph), 7.16d and 6.89d(4H, *J*=8.0 Hz, MBn) 4.47s(CH_2 in Bn), 4.65d and 4.10d(*J*=14.4 Hz, CH_2 in MBn)
12	—3.83s—		4.80t (6.6)	1.82dt	3.62t (6.0)	1.75s 1.53s	7.40s(Ph), 7.29d, 6.85d, 7.21d and 6.85d(8H, *J*=8.5 Hz, 2×MBn), 4.88d, 4.46d, 4.56d and 4.42d(*J*= 15.6 and 14.0 Hz, 2×CH_2 in MBn), 4.46s(CH_2 in Bn), 3.78s(2×OMe).
13	4.74d (18.8)	4.10d	5.01t (7.2)	2.2—1.9m	3.9—3.7m	1.54s 1.48s	7.68bs(NH), 2.28bs(OH), 2.62s(Ac)
14	4.69d (18.0)	4.04d	5.05t (7.0)	2.3—2.0m	4.28t (6.0)	1.49s 1.42s	8.05—7.8m(2H, Bz), 7.6—7.0m(4H, NH and Bz), 2.46s(Ac)
15	3.97d (18.0)	3.80d	5.01t (6.8)	2.1—1.7m	3.73t (6.0)	1.46s	8.07s(NH), 7.10d and 6.84d(4H, *J*=8.0 Hz, MBn), 4.56d and 4.52d (*J*=14.0 Hz, CH_2 in MBn), 3.79s (OMe), 2.88bs(OH)
16	—3.86s—		4.74t (5.6)	2.2—1.6m	3.9—3.6m	1.73s 1.52s	7.26d, 6.82d, 7.18d and 6.77d(8H, *J*=8.0 Hz, 2×MBn), 4.87d, 4.42d, 4.74d and 4.37d(*J*=14.5 and 14.5 Hz, 2×CH_2 in MBn) 3.78s and 3.75s(2×OMe), 2.25bs(OH)
17	—3.82s—		4.72t (7.0)	1.9—1.6m	3.54t (6.0)	1.73s 1.51s	7.26d, 6.86d, 7.20d, 6.78d, 7.12d and 6.78d(12H, *J*=8.5 Hz, 3×MBn), 4.82d, 4.40d, 4.52d and 4.31d(*J* =14.5 and 14.0 Hz, 2×CH_2 in NMBn), 4.36s(CH_2 in OMBn), 3.75s(9H, 3×OMe)
18[b]	3.86d (18.4)	3.56d	4.90t (6.5)	2.0—1.6m	3.57dd (6.2,2.5)	1.57s	7.37s(Ph), 7.36d, 6.94d, 7.20d and 6.88d(8H, *J*=8.5 Hz, 2×MBn), 5.16s(CH_2 in OMBn), 4.44s (CH_2 in Bn), 4.68d and 4.24d(*J*=13.8 Hz, CH_2 in NMBn), 3.83s and 3.80s(2×OMe)

a) Measured in DMSO-d_6. b) The same numbering of carbon skeleton as those of PDO derivative is used.

TABLE 2. ^{1}H NMR DATA OF SPIRO CYCLIC DERIVATIVES

Compound	H-8a ($J_{A,B}$)	H-8b	H-4 ($J_{3a,4}$)	H-3a	H-3b ($J_{3b,4}$)	H-2 ($J_{3a,3b}$)	Others
23a	3.92d (18.0)	3.69d	5.50dd (7.0)	2.60m (6.0)	2.20m (12.0)	4.6—4.2m	7.34d, 6.85d, 7.20d, and 6.81d(8H, *J*=8.5 Hz, 2×MBn), 4.79d, 4.09d, 4.61d and 4.49d(*J*=14.0 and 14.5 Hz, 2×CH_2 in MBn), 3.77s and 3.72s (2×OMe), 2.08s(Ac)
23b	3.98d (18.5)	3.76d	5.05t (7.5)	2.5—2.2dt		4.6—4.2m	2.27d, 6.85d, 7.22d, and 6.82d(8H, *J*=8.0 Hz, 2×MBn), 4.95d, 4.13d, 4.63d and 4.41d(*J*= 14.5 Hz, 2×CH_2 in MBn), 3.82s (2×OMe), 1.79s (Ac)
24	3.98d (18.0)	3.77d	5.72dd (7.0)	3.0—2.5m (4.2)	2.3—1.9m	4.2—3.8m	7.23d and 6.91d(4H, *J*=8.0 Hz, MBn), 6.9bs (NH), 4.59d and 4.56d(*J*=14.0 Hz, CH_2 in MBn), 3.81s(OMe), 2.11s(Ac)

TABLE 3. ^{1}H NMR DATA OF BICYCLIC DERIVATIVES

Compound	H-1	H-5 ($J_{5,4a}$)	H-4a,b ($J_{5,4b}$)	H-3a ($J_{3a,4}$)	H-3b ($J_{3a,3b}$) ($J_{3b,4}$)	Others
19	5.19s	4.18dd (10.8)	2.4—1.6m (3.8)	4.02ddd (1.4,8.0)	3.31ddd (13.5) (9.0,1.4)	7.25d, 6.82d, 7.25d and 6.80d(8H, J=8.0 Hz, 2×MBn), 4.93d, 4.30d 4.84d and 4.30d(J=14.0 Hz, 2×CH_2 in MBn), 3.79s and 3.76s (2×OMe), 1.72s and 1.66s(2×CMe)
20	5.09s	4.13dd (10.4)	2.4—1.8m (5.0)	3.98ddd (2.0,6.0)	3.31ddd (14.0) (9.0,1.8)	7.26d and 6.82d(4H, J=8.4 Hz, MBn), 6.9bs(NH), 4.87d and 4.18d(J=14.2 Hz, CH_2 in MBn), 3.80s (OMe), 1.56s (2×CMe)
29	5.20s	4.1—3.6m	2.4—1.5m	4.1—3.6m	3.21dd (13.8) (9.6)	7.26d, 6.78d, 7.26d and 6.74d(8H, J=8.0 Hz, 2×MBn), 5.19bs(OH) 4.90d, 4.51d, 4.82d and 4.30d(J=14.0 Hz, 2×CH_2 in MBn), 3.80s and 3.78s(2×OMe)
30	5.40s	—	2.3—2.1m	3.9—3.6m	3.19ddd (13.5) (7.0,4.0)	7.26d, 6.79d, 7.17d and 6.70d (8H, J=8.0 Hz 2×MBn), 5.34bs(OH) 5.04d, 4.36d, 4.90d and 4.19d(J=13.6 and 14.2 Hz, 2×CH_2 in MBn) 3.82s and 3.77s(2×OMe)
32	5.24s	—	2.3—2.1m	3.9—3.7m	3.4—3.1m	7.36d, 6.84d, 7.28s and 6.76d(8H, J=8.0 Hz, 2×MBn), 5.59s and 5.08s(olefinic), 5.00bs(OH), 4.90d, 4.20d, 4.61d and 4.43d(J=14.0 and 14.5 Hz, 2×CH_2 in MBn), 3.81s and 3.78s(2×OMe)
33	5.15s	—	2.4—1.6m	3.8—3.5m	3.4—3.2m	7.26d, 6.73d, 7.22d and 6.84d(8H, J=8.5 Hz, 2×MBn), 5.55s and 5.03s(olefinic), 5.15d, 3.97d, 4.77 and 4.61d (J=14.0 Hz, 2×CH_2 in MBn), 3.81s and 3.77s(2×OMe), 0.92s, 0.42s and 0.15s(TBS)

TABLE 4. ^{13}C NMR DATA OF 6-SUBSTITUTED 2,5-PIPERAZINEDIONE DERIVATIVES

Compound	C-6	C-3	C-3′	C-2′	C-1′	C-2 and 5	Others
9a[a]	46.3t	88.7s	72.6t	28.5t	78.7d	165.4s, 167.1s	172.0s and 28.5q(Ac), 139.0s, 129.0d, 128.0d and 127.9d(aromatic), 110.8s, 27.5q and 26.0q(Ip), 67.3t(OCH_2)
9b[a]	46.3t	89.5s	72.9t	29.4t	80.8d	166.1s, 166.5s	172.2s, 26.9q(Ac), 138.9s, 129.0d and 128.3d (aromatic), 111.0s and 27.4q(Ip) 67.3t (OCH_2)
11	48.6t	87.2s	72.8t	28.8t	78.9d	162.2s, 167.1s	159.4s, 138.1s, 129.8d, 128.4d, 127.4d, 126.9s and 114.2d(aromatic), 110.3s, 27.9q and 25.2q(Ip), 66.8t(OCH_2), 55.2q(OMe) 49.2t (NCH_2)
12	47.0t	93.2s	73.1t	29.8t	82.5d	163.3s, 164.5s	159.4s, 158.4s, 137.9s, 129.8d, 129.1s, 128.7d, 128.4d, 127.7d, 127.6d, 126.7s, 114.3d and 113.5d(aromatic), 111.9s, 26.1q and 25.1q(Ip) 66.9t(OCH_2), 55.1q(2×OMe) 49.4t and 48.5t (2×NCH_2)
16	47.0t	93.2s	59.6t	31.6t	83.0d	163.4s, 164.5s	159.4s, 158.3s, 129.8d, 129.0s, 128.6d, 126.6s, 114.2d and 113.4d(aromatic), 112.0s, 26.0q and 25.1q(Ip), 55.1q and 55.0q(2×OMe) 49.5t, 48.5t(2×NCH_2)
18[c]	45.5t	89.5s	73.0t	29.3t	80.7d	164.8s, 159.2s[b]	159.7s[b], 159.5s[b], 138.5s, 130.2d, 129.9d, 128.4d, 128.3s, 127.6d, 127.4s, 114.3d and 114.0d(aromatic), 110.5s, 28.5q and 26.1q(Ip), 67.7t(2×OCH_2) 55.3q (2×OMe), 49.2t(NCH_2)

a) Measured in DMSO-d_6. b) The Assignment may be exchanged. c) The same numbering of carbon skeleton as those of PDO derivative is used.

the extract gave a crude oil which was purified by distillation to give colorless oily 3-benzyloxy-1,1-diethoxypropane (86.2 g, 71%). Bp 118—120 °C/11 Torr[†]; ^{1}H NMR: δ=7.72 (s, 5H, Ph), 4.69 (t, 1H, $J_{1,2}$=6.0 Hz, H-1), 4.49 (s, 2H, CH_2Ph), 3.85—3.3 (m, 6H, H-3 and 2×OCH_2 in Et) 1.93 (dt, 2H, $J_{2,3}$=6.0 Hz, H-2), 1.19 (t, 6H, J=7.5 Hz, 2× Me in Et). A solution of the above oil (30.0 g, 126 mmol) in acetone (60 cm^3) and 1 M hydrochloric acid (60 cm^3) was stirred at room temperature for 3 h, evaporated to a half volume, and extracted with chloroform. The usual processing of the extract and distillation of the product gave **2** (20.0 g, 97%). Bp 71—74 °C/1.3 Torr, IR: 1720 (C=O), ^{1}H NMR: δ=9.72 (t, 1H, $J_{1,2}$=2.0 Hz, H-1), 7.32 (s, 5H, Ph), 4.52 (s, 2H, CH_2Ph), 3.78 (t, 2H, $J_{2,3}$=6.0 Hz, H-3), 2.56 (dt, 2H, H-2).

Found: C, 73.09; H, 7.20%. Calcd for $C_{10}H_{12}O_2$: C, 73.14; H, 7.34%.

b) A mixed solution of chromium trioxide (55.0 g, 550 mmol) and pyridine (90 cm^3) in dry dichloromethane (1.1 dm^3) was vigorously stirred at room temperature for 30 min, 3-benzyloxy-1-butanol (15.2 g, 92.0 mmol) was added dropwise to it, then stirred for 2 h, and filtered. After the usual

[†] 1 Torr≈133.322 Pa.

work-up, the rough product was passed through a short silica-gel column, and purified by distillation to give **2** (10.9 g, 72%).

c) A mixed solution of 4-benzyloxy-1,2-*O*-isopropylidene-1,2-butanediol (112 g, 0.474 mol) in dioxane (400 cm^3) and 1 M hydrochloric acid (400 cm^3) was kept at room temperature for 12 h, poured into ice-water, and then extracted with dichloromethane. The usual processing of the extract gave a crude syrupy 4-benzyloxy-1,2-butanediol. ^1H NMR: δ=7.33 (s, 5H, Ph), 4.52 (s, 2H, CH_2Ph), 4.2—3.4 (m, 5H, H-1, 2, and 4), 3.2 and 2.6 (each bs, 2H, 2×OH), 1.9—1.6 (m, 2 H, H-3). To a solution of the above syrup in benzene (900 cm^3) was added lead tetraacetate (280 g, 0.576 mol) with stirring, the mixture was kept for 12 h at room temperature, and then filtered. The filtrate was poured into water and extracted with ethyl acetate. The usual processing of the extract and distillation of the oily product gave colorless **2** (69.8 g, 90%).

1-Acetyl-3-(3-benzyloxypropylidene)-2,5-piperazinedione (3). To a solution of 1,4-diacetyl-PDO (20.0 g, 101 mmol) and **2** (21.5 g, 131 mmol) in *N,N*-dimethylformamide (DMF, 80 cm^3) was added dropwise a solution of potassium *t*-butoxide (11.8 g, 106 mmol) in *t*-butyl alcohol (212 cm^3) at 0 °C with stirring, and the mixture was kept at 0 °C for 2 h and at room temperature for 12 h, neutralized with acetic acid and poured into ice-water. The crystals formed were filtered and recrystallized from ethanol-ether to give **3** (25.0 g, 82%) as prisms. Mp 119 °C; IR: 3180 (NH), 1715 (Ac), 1680 (amide), 1640 (C=C).

Found: C, 63.85; H, 5.83; N, 9.27%. Calcd for $C_{16}H_{18}N_2O_4$: C, 63.56; H, 6.00; N, 9.27%.

*3-(3-Benzyloxypropylidene)-1,4-bis-(*p*-methoxybenzyl)-2,5-piperazinedione (5).* To a solution of **3** (5.0 g, 16.6 mmol) in DMF (20 cm^3) was added 70% hydrazine hydrate (2.37 g, 33.2 mmol) at 0 °C, and the mixture was kept at 0 °C for 3 h, poured into ice-water. The *N*-deacetylated product (**4**) deposited (4.32 g) was filtered and dried. To a suspension of sodium hydride in DMF was added dropwise a solution of **4** in DMF (50 cm^3) at 0 °C with stirring, and after 2 h, *p*-methoxybenzyl bromide (7.67 g, 38.2 mmol) was further added dropwise. The reaction mixture was stirred for 2 h at 0 °C and for 12 h at room temperature, neutralized with acetic acid, poured into ice-water, and then extracted with ethyl acetate. The usual work-up of the extract gave a crude syrup, which was purifield on a silica-gel column (hexane-ethyl acetate 7:3) to give colorless syrupy **5** (5.97 g, 72%).

Found: C, 71.72; H, 6.58; N, 5.52%. Calcd for $C_{30}H_{32}N_2O_5$: C, 71.98; H, 6.44; N, 5.60%.

Oxidation of 3 and 5 with Osmium Tetraoxide. To a solution of **3** (7.40 g, 24.5 mmol) in dioxane (120 cm^3) was added a solution of sodium chlorate (10.4 g, 98.0 mmol) in water (30 cm^3) and osmium tetraoxide (62 mg, 0.24 mmol) with stirring. After 3 days at room temperature, the reaction mixture was evaporated to a half volume, poured into water, and then extracted with chloroform. The usual work-up of the extract gave a crude syrup, which was crystallized from ethyl acetate-ether to give 1-acetyl-3-(3-benzyloxy-1-hydroxypropyl)-3-hydroxy-PDO (**6**) as colorless prisms. Purification of the residue obtained from the filtrate on a silica-gel column (dichloromethane-acetone 4:1) gave the second crops of **6** as a monohydrate. Total yield of **6** was 5.04 g (58%). Mp 92 °C, IR: 3250 (OH, NH), 1735 (Ac), 1710, and 1680 (amide).

Found: C, 54.10; H, 6.41; N, 7.75%. Calcd for $C_{16}H_{20}N_2O_6 \cdot H_2O$: C, 54.23; H, 6.26; N, 7.91%.

A similar oxidation of **5** (380 mg, 0.759 mmol) gave a crude syrup, which was crystallized from acetone-ether to give 3-(3-benzyloxy-1-hydroxypropyl)-3-hydroxy-1,4-bis(*p*-methoxybenzyl)-PDO (**7**) as colorless prisms in 46% (187 mg) yield. Mp 140—141 °C; IR: 3450 (OH), 1665 (amide).

Found: C, 66.92; H, 6.48; N, 5.27%. Calcd for $C_{30}H_{34}N_2O_7$: C, 67.40; H, 6.41, N, 5.24%.

Isopropylidenation of 6 and 7. Method A: To a suspension of dried **6** (3.90 g, 11.6 mmol) in acetone (16 cm^3) was added 2-methoxypropene (9.6 cm^3) and catalytic amount of pyridinium *p*-toluenesulfonate with stirring. Compound **6** once dissolved within 5 min and new precipitate deposited after 15 min. After keeping the mixture for 24 h at room temperature, the precipitate was filtered and recrystallized from chloroform-ether to give 1-acetyl-3-(3-benzyloxy-1-hydroxy propyl)-3-hydroxy-3,1′-*O*-isopropylidene-PDO (**9a**) as colorless prisms. The residue from the filtrate was purified on a silica-gel column (chloroform-acetone 9:1) to give **9a** and its 3-epimer (**9b**).

9a: yield, 4.15 g (95%). Mp 151 °C, IR: 3200 (NH), 1730sh (Ac), 1710, and 1685 (amide).

9b: yield, 92 mg (2.1%), mp 138—140 °C (prisms from chloroform-ether).

Found for **9a**: C, 60.52; H, 6.42; N, 7.23%, and for **9b**: C, 60.73; H, 6.51; N, 7.30%. Calcd for $C_{19}H_{24}N_2O_6$: C, 60.62; H, 6.43; N, 7.44%.

Method B: To a solution of **6** (500 mg, 1.45 mmol) in acetone (20 cm^3) was added 2,2-dimethoxypropane (1 cm^3) and catalytic amount of *p*-toluenesulfonic acid with stirring at room temperature. After 12 h, the reaction mixture was neutralized with pyridine, and evaporated. The residue was separated on a silice-gel column (chloroform-acetone 9:1) to give **9a** (169 mg, 31%) and syrupy 1-acetyl-3-(3-benzyloxy-1-hydroxypropyl)-3-methoxy-PDO (**8**: 343 mg, 63%).

Found: C, 58.06; H, 6.21; N, 7.89%. Calcd for $C_{17}H_{22}N_2O_6$: C, 58.27; H, 6.33; N, 8.00%.

A similar treatment of **7** (3.90 g, 7.30 mmol) by the method A, and purification of the product on a silica-gel column (hexane-ethyl acetate 4:1) gave 3-(3-benzyloxy-1-hydroxypropyl)-3-hydroxy-3,1′-*O*-isopropyridene-1,4-bis(*p*-methoxybenzyl)-PDO (**12**: 3.92 g, 94%). Mp 131 °C (prisms from ether-hexane).

Found: C, 68.68; H, 6.69; N, 4.84%. Calcd for $C_{33}H_{38}N_2O_7$: C, 68.97; H, 6.67; N, 4.88%.

3-(3-Benzyloxy-1-hydroxypropyl)-3-hydroxy-3,1′-O-isopropylidene-2,5-piperazinedione (10). A solution of **9a** (530 mg, 1.41 mmol) in DMF (5 cm^3) and 70% hydrazine (0.20 cm^3) was stirred at 0 °C for 3 h, and poured into ice-water. The precipitate deposited was filtered and recrystallized from methanol-ether to give **10** (470 mg, 99%) as colorless needles of mp 164 °C.

Found: C, 60.86; H, 6.54; N, 8.25%. Calcd for $C_{17}H_{22}N_2O_5$: C, 61.06; H, 6.63; N, 8.38%.

p-*Methoxybenzylation of 10, 11, and 15.* The reaction procedure is exemplified by the preparation of 3-(3-benzyloxy-1-hydroxypropyl)-3-hydroxy-3,1′-*O*-isopropylidene-1-(*p*-methoxybenzyl)-PDO (**11**). To a suspension of 50% sodium hydride (316 mg, 6.58 mmol) in DMF (50 cm^3) was added dropwise a solution of **10** (2.0 g, 5.98 mmol) in DMF (20 cm^3) at 0 °C with stirring. After keeping the conditions for 1 h, *p*-methoxybenzyl bromide (1.44 g, 7.16 mmol) was further added. The mixture was stirred at 0 °C for 2 h and then

at room temperature for 12 h, neutralized with acetic acid, poured into ice-water, and extracted with ethyl acetate. The usual work-up of the extract gave crude crystals, which were recrystallized from ethanol–ether to give **11** as colorless prisms. The residue from the filtrate was separated on a silica-gel column (hexane–ethyl acetate 7:3) to give **11** and **12** (242 mg, 7.0%). **11**: yield, 2.35 g (87%). Mp 131 °C, IR: 3190 (NH), 1690 (amide).

Found: C, 65.98; H, 6.75; N, 5.88%. Calcd for $C_{25}H_{30}N_2O_6$: C, 66.06; H, 6.65; H, 6.16%.

A repeating similar reaction of **11** (410 mg, 0.903 mmol), and separation of products on a silica-gel column (hexane–ethyl acetate 4:1) gave **12** (392 mg, 76%) and 3-(3-benzyloxy-1-hydroxypropyl)-3-hydroxy-3,1′-*O*-isopropylidene-1-(*p*-methoxybenzyl)-5-(*p*-methoxybenzyloxy)-3,6-dihydro-2(1*H*)-pyrazinone (**18**: 58 mg, 11%) as a colorless syrup.

Found: C, 68.81; H, 6.84; N, 4.73%. Calcd for $C_{33}H_{38}N_2O_7$: C, 68.97; H, 6.67; N, 4.88%.

One-step reaction of **10** (2.0 g, 5.98 mmol) with 2 equimolar sodium hydride and *p*-methoxybenzyl bromide gave **12** (2.13 g, 62%) and **18** (441 mg, 13%). A similar reaction of **15** (623 mg, 1.71 mmol) with 2 equimolar reagents gave syrupy 3-hydroxy-3-[1-hydroxypropyl-3-(*p*-methoxybenzyloxy)]-3,1′-*O*-isopropylidene-1,4-bis(*p*-methoxybenzyl)-PDO (**17**) in 57% (568 mg) yield.

Found: C, 67.42; H, 6.64; N, 4.47%. Calcd for $C_{34}H_{40}N_2O_8$: C, 67.53; H, 6.67; N, 4.63%.

Hydrogenolysis of O-*Benzyl Group of* **9a**, **11**, *and* **12**. The reaction procedure is exemplified by the preparation of 3-(1,3-dihydroxypropyl)-3-hydroxy-3,1′-*O*-isopropylidene-1,4-bis(*p*-methoxybenzyl)-PDO (**16**). A solution of **12** (74 m, 0.13 mmol) in ethanol (50 cm³) was catalytically hydrogenated with 10% palladium–carbon (30 mg) at room temperature for 24 h. The usual processing of the reaction mixture gave **16** (62 mg, 98%) which was crystallized from ether–hexane. Mp 159 °C (prisms), IR: 3500 (OH), 1670 (amide).

Found: C, 64.21; H, 6.61; N, 5.70%. Calcd for $C_{26}H_{32}N_2O_7$: C, 64.45; H, 6.61; N, 5.78%.

A similar hydrogenolysis of **11** (1.16 g, 2.56 mmol) gave 3-(1,3-dihydroxypropyl)-3-hydroxy-3,1,-*O*-isopropylidene-1-(*p*-methoxybenzyl)-PDO (**15**) in quantitative (930 mg) yield. Mp 180 °C (prisms from ethanol–ether), IR: 3450 (OH), 3220 (NH), 1680 (amide).

Found: C, 59.48; H, 6.48; N, 7.53%. Calcd for $C_{18}H_{24}N_2O_6$: C, 59.33; H, 6.64; N, 7.69%.

Compounds **15** and **16** were also obtained from **18** (83 mg, 0.144 mmol) and **17** (96 mg, 0.165 mmol) in 92% (48 mg) and 99% (79 mg) yields, respectively. 1-Acetyl-3-(1,3-dihydroxypropyl)-3-hydroxy-3,1′-*O*-isopropylidene-PDO (**13**) was obtained from **9a** (0.500 g, 1.33 mmol) in 75% (286 mg) yield. Mp 194—195 °C (prisms from ethanol–ether).

Found: C, 50.21; H, 6.29; N, 9.65%. Calcd for $C_{12}H_{18}N_2O_6$: C, 50.35; H, 6.34; N, 9.79%.

Oxidative Removal of O-*Benzyl Group of* **9a** *with* N-*Bromosuccinimide*. A mixed suspension of **9a** (100 mg, 0.266 mmol) in chloroform (40 cm³), trilead(II) dicarbonate dihydroxide (1 g) and NBS (57 mg, 0.32 mmol) was vigorously stirred at room temperature for 24 h, and then filtered. The filtrate was treated by usual procedure and the products were separated on a silica-gel column (benzene–ethyl acetate 5:2) to give **13** (66 mg, 92%) and 1-acetyl-3-(3-benzoyloxyl-1-hydroxypropyl)-3-hydroxy-3,1′-*O*-isopropylidene-PDO (**14**: 6 mg, 6%) as a colorless hard syrup.

Found: C, 58.33; H, 5.71; N, 7.08%. Calcd for $C_{19}H_{22}N_2O_7$: C, 58.45; H, 5.68; N, 7.18%.

Cyclization of **15** *and* **16** *with* N-*Bromosuccinimide*. The reaction procedure is exemplified by the preparation of 5,6-dihydroxy-5,6-*O*-isopropylidene-7,9-bis(*p*-methoxybenzyl)-2-oxa-7,9-diazabicyclo[4.2.2]decane-8,10-dione (**19**). A suspension of **16** (97 mg, 0.20 mmol), barium carbonate (1.0 g) and powdered 4 A molecular sieves (1 g) in dry chloroform (10 cm³) was vigorously stirred at room temperature for 12 h, NBS (39.2 mg, 0.22 mmol) was added to it, and the resulting mixture was further stirred for 72 h, then filtered. The filtrate was poured into saturated sodium hydrogencarbonate and extracted with chloroform. The usual work-up of the extract gave a crude syrup, which was purified on a silica-gel column (hexane–ethyl acetate 7:3) to give **19** (83 mg, 86%). Mp 130 °C (prisms from ether–hexane); IR: 1705, 1685 (amide). ^{13}C NMR: δ=166.6s and 164.5s (C-8,10), 159.3s, 158.4s, 130.0d, 129.0d, 128.8d, 126.8s, 114.0d, and 113.4d (aromatic), 113.0s, 25.4q and 24.2q (Ip), 91.5s (C-6), 86.6d and 82.3d (C-1,5), 60.8t (C-3), 54.9q (2×OMe), 48.0t and 45.9t (2×NCH_2), 28.2t (C-4).

Found: C, 64.38; H, 6.28; N, 5.76%. Calcd for $C_{26}H_{30}N_2O_7$: C, 64.71; H, 6.27; N, 5.81%.

A similar cyclization of **16** (97 mg, 0.20 mmol) in chloroform (10 cm³) without barium carbonate and molecular sieves at room temperature for 24 h gave **19** (12 mg, 12%) and 4-hydroxy-6,9-bis(*p*-methoxybenzyl)-1-oxa-6,9-diazaspiro[4.5]-decane-7,10-dione (**21**: 54 mg, 63%). The usual acetylation of **21** in pyridine with acetic anhydride, and purification of the product on a silica-gel column (hexane–ethyl acetate 2:3) gave the 4-acetate (**23a**: 46 mg, 41%, mp 171 °C, prisms from ethanol–ether) and it's 5-epimer (**23b**, 48 mg, 44%) as colorless syrup.

^{13}C NMR for **23a**: δ=170.0s and 20.2q (Ac), 166.2s and 163.9s (C-7, 10), 159.2s, 158.5s, 129.7s, 126.6s, 129.5d, 114.1d, and 113.3d (aromatic), 93.2s (C-5), 77.7d (C-4), 67.1t (C-2), 55.0q (2×OMe), 48.8t and 48.7t (NCH_2×2), 46.8t (C-8), 31.1t (C-3), and for **23b**: δ=169.5s, and 20.3q (Ac), 164.1s (C-7, 10), 159.5s, 158.5s, 129.7s, 129.5s, 126.6s, 114.1d, and 113.3d (aromatic), 93.3s (C-5), 78.3d (C-4), 68.6t (C-2), 55.2q, 55.1q (2×OMe), 49.1t (2×NCH_2), 44.5t (C-8), 29.6t (C-3).

Found for **23a**: C, 63.93; H, 6.10; N, 5.85%, and for **23b**: C, 64.13; H, 6.16; N, 5.73%. Calcd for $C_{25}H_{28}N_2O_7$: C, 64.09; H, 6.02; N, 5.98%.

A similar cyclization of **15** (182 mg, 0.499 mmol) in chloroform (10 cm³) without molecular sieves at room temperature gave 5,6-dihydroxy-5,6-*O*-isopropylidene-9-(*p*-methoxybenzyl)-2-oxa-7,9-diazabicyclo[4.2.2]decane-8,10-dione (**20**: 54 mg, 30%) and 4-hydroxy-9-(*p*-methoxybenzyl)-1-oxa-6,9-diazasprio[4.5]decane-7,10-dione (**22**: 24 mg, 16%). **20**: mp 181—182 °C (prisms from chloroform–ether), IR: 3200 (NH), 1695 (amide).

Found; C, 59.23; H, 6.04; N, 7.73%. Calcd for $C_{18}H_{22}N_2O_6$: C, 59.66; H, 6.12; N, 7.73%.

The usual acetylation of **22** (30 mg, 0.098 mmol) in pyridine with acetic anhydride, and purification of the product on a preparative TLC (hexane–acetone 1:1) gave 4-acetoxy-9-(*p*-methoxybenzyl)-1-oxa-6,9-diazaspiro[4,5]decane-7,10-dione (**24**: 14 mg, 41%). Mp 148 °C (prisms from ethanol–ether), IR: 3220 (NH), 1735 (Ac), 1690, and 1670 (amide).

Found: C, 58.46; H, 5.72; N, 7.85%. Calcd for $C_{17}H_{20}N_2O_6$:

C, 58.61; H, 5.79; N, 8.04%.

3-Acetoxy- (**27**) *and 3-Acetylthio-1,4-diacetyl-2,5-piperazinediones* (**28**). A solution of NBS (94 mg, 0.53 mmol) and *N,N'*-diacetylanhydroglycine (100 mg, 0.51 mmol) in chloroform (10 cm^3) was stirred at room temperature for 12 h, poured into saturated sodium hydrogencarbonate, and extracted with chloroform. The usual processing of the extract gave crude syrupy monobromo derivative (**26**). IR: 1730 (Ac), 1720, and 1710 (amide); ^1H NMR: δ=6.85 (s, 1H, H-3), 5.22 and 4.27 (ABq, 2H, J=17.5 Hz, H-6), 2.62 (s, 6H, Ac×2). When this reaction was performed in the presence of potassium acetate (742 mg, 7.6 mmol), 3-acetoxy derivative (**27**) was obtained as a colorless hard syrup after purification on a silica-gel column with benzene–ethyl acetate (7:3). Yield, 91 mg (71%), IR: 1740 and 1730 (Ac), 1710 and 1700 (amide). ^1H NMR: δ=7.22 (s, 1H, H-3), 5.10 and 4.25 (ABq, 2H, J=18.0 Hz, H-6), 2.59 (s, 6H, 2×NAc), 2.13 (s, 3H, OAc).

Found: C, 46.80; H, 4.82; N, 10.99%. Calcd for $C_{10}H_{12}N_2O_6$: C, 46.88; H, 4.72; N, 10.93%.

The reaction in the presence of potassium thioacetate instead of potassium acetate as above, and the product was purified on a silica-gel column (benzene–ethyl acetate 7:3) to give **28** as a colorless hard syrup in 68% yield. IR: 1740 and 1720 (Ac), 1710 and 1700 (amide); ^1H NMR: δ=6.60 (s, 1H, H-3), 5.13 and 4.26 (ABq, 2 H, J=18.0 Hz, H-6), 2.61 (s, 6H, 2× NAc), 2.45 (s, 3H, SAc).

Found: C, 44.23; H, 4.41; N, 10.24%. Calcd for $C_{10}H_{12}N_2O_5S$: C, 44.11; H, 4.44; N, 10.29%.

*5,6-Dihydroxy-7,9-bis(*p*-methoxybenzyl)-2-oxa-7,9-diazabicyclo[4.2.2]decane-8,10-dione* (**29**). A solution of **19** (51.0 mg, 0.106 mmol) and 2 M hydrochloric acid (2 cm^3) in tetrahydrofuran (THF, 5 cm^3) was heated at 50 °C, for 24 h, poured into saturated sodium hydrogencarbonate, and extracted with dichloromethane. The usual processing of the extract gave a crude syrup, which was purified on a flash column (hexane–ethyl acetate 3:2) to give **29** (40.5 mg, 83%) as a colorless syrup. Mp 154—155 °C (prisms from ethanol–ether), IR: 3450(OH), 1675 (amide), ^{13}C NMR (DMSO): δ= 169.9s and 163.9s, (C-8,10), 159.7s, 158.6s, 131.6s, 130.8d, 129.3d, 128.6s, 114.8d, and 114.1d, (aromatic), 86.9s (C-6), 83.1d (C-1), 78.3d (C-5), 60.1t (C-3), 55.9q (2×OMe), 47.9t and 46.9t (2×NCH_2), 30.5t (C-4).

Found: C, 59.98; H, 5.71; N, 5.85%. Calcd for $C_{23}H_{26}N_2O_7 \cdot H_2O$: C, 59.99; H; 6.13; N, 6.08%.

*6-Hydroxy-7,9-bis(*p*-methoxybenzyl)-2-oxa-7,9-diazabicyclo[4.2.2]decane-5,8,10-trione* (**30**). A solution of oxalyl dichloride (0.115 cm^3, 1.35 mmol) in dichloromethane (5 cm^3) and dimethyl sulfoxide (DMSO, 0.5 cm^3) in dichloromethane (2 cm^3) were mixed with vigorous stirring at −78 °C for 5 min, then a solution of dried **29** (270 mg, 0.611 mmol) in DMSO (2.5 cm^3) and dichloromethane (2 cm^3) was added dropwise to the mixture. The reaction mixture was stirred for 20 min at −78 °C, then a solution of triethylamine (0.511 cm^3, 3.66 mmol) in dichloromethane (1 cm^3) was further added to it, and stirred for 5 min. The temperature being raised to 0 °C, the reaction mixture was poured into saturated ammonium chloride, and extracted with dichloromethane. The usual processing of the extract gave a crude syrup, which was purified on a flash column (hexane–ethyl acetate 4:1) to give **30** (246 mg, 91%) as crystals. Mp 138 °C (prisms from ether–hexane), IR: 3360 (OH), 1730 (C=O), 1680 (amide), ^{13}C NMR: δ=202.6s (C-5), 164.2s and 161.7s, (C-8,10), 159.7s, 159.5s, 131.7d, 130.4d, 126.1s, 125.8s, 114.3d, and 113.8d (aromatic), 86.4s (C-6), 83.0d (C-1), 57.9t (C-3), 55.2q and 55.1q (2×OMe), 48.5t and 43.8t (2×NCH_2), 40.3t (C-4).

Found: C, 53.09; H, 5.54; N, 6.17%. Calcd for $C_{23}H_{24}N_2O_7$: C, 62.72; H, 5.49; N, 6.36%.

*6-(2-Formylethoxy)-1,4-bis(*p*-methoxybenzyl)-2,3,5-piperazinetrione* (**34**). To a solution of **29** (12.0 mg, 0.027 mmol) in dichloromethane (1 cm^3) was added sodium acetate (4.8 mg, 0.059 mmol) and pyridinium chlorochromate (11.6 mg, 0.054 mmol) with vigorous stirring at room temperature. After stirring for 24 h, the mixture was poured into water, and extracted with dichloromethane. The usual processing of the extract gave a crude product, which was purified on preparative TLC (ether) to give **34** (7.2 mg, 61%) as a colorless syrup. ^1H NMR: δ=9.59 (t, 1H, $J_{3',4'}$=1.5 Hz, CHO), 7.29, 6.84, 7.24, and 6.78 (each d, 8H, J=8.5 Hz, MBn×2), 5.17 and 4.17 (ABq, 2H, J=13.5 Hz, CH_2 in MBn), 4.89 (s, 2H, CH_2 in MBn), 4.85 (s, 1H, H-6), 3.9—3.7 (m, 2H, H-2'), 3.81 and 3.88 (each s, 6H, 2×OMe), 2.63 (dt, 2H, $J_{2',3'}$=6.0 Hz, H-3').

Found: C, 62.93; H, 5.52; N, 6.20%. Calcd for $C_{23}H_{24}N_2O_7$: C, 62.72; H, 5.49; N, 6.36%.

*6-Hydroxy-7,9-bis(*p*-methoxybenzyl)-5-methylene-2-oxa-7,9-diazabicyclo[4.2.2]decane-8,10-dione* (**32**). To a mixture of magnesium (49.7 mg, 2.05 mmol) and trimethylsilylmethyl chloride (418 mg, 1.05 mmol) in dry ether (10 cm^3) was added catalytic amount of iodine with vigorous stirring at 40 °C. After the stirring was continued for 30 min, the mixture was diluted with dry ether (120 cm^3), cooled to −30 °C, and a solution of **29** (300 mg, 0.682 mmol) in THF (10 cm^3) was further added dropwise to it. The reaction mixture was stirred at −30 °C for 4 h, poured into saturated ammonium chloride, and extracted with chloroform. The usual processing of the extract gave a crude syrup, which was purified on a flash column (hexane–ethyl acetate 7:3) to give colorless syrupy 5,6-dihydroxy-7,9-bis(*p*-methoxybenzyl)-5-trimethylsilylmethyl-2-oxa-7,9-diazabicyclo[4.2.2]decane-8,10-dione (**31**: 192 mg, 52%) as a mixture of 5-epimers. To a solution of **31** (192 mg, 0.354 mmol) in dichloromethane (6 cm^3) was added 4-dimethylaminopyridine (864 mg, 7.08 mmol) and trifluoroacetic anhydride (743 mg, 3.54 mmol) with vigorous stirring at room temperature. After stirring was continued for 1 h, a solution of tetrabutylammonium chloride (1.48 g, 5.32 mg) in acetonitrile (30 cm^3) and potassium fluoride (616 mg, 10.6 mmol) was further added, and the mixture was heated at 40 °C for 12 h, then *O*-detrifluoroacetylated by addition of methanol (5 cm^3), poured into saturated ammonium chloride, and extracted with chloroform. The usual processing of the extract gave a crude syrup, which was purified on a flash column (hexane–ethyl acetate 4:1) to give colorless syrupy **32** (125 mg, 81%).

Found: C, 65.82; H, 6.11; N, 6.28%. Calcd for $C_{24}H_{26}N_2O_6$: C, 65.74; H, 5.98; N, 6.39%.

Another method for the elimination reaction was accomplished as follows: a solution of **31** (14.0 mg, 0.0267 mmol) in 0.08 M sulfuric acid in THF (0.5 cm^3) was permitted to stand for 12 h at room temperature, poured into saturated sodium hydrogencarbonate, and extracted with chloroform. The usual processing of the extract gave a crude syrup, which was purified on a flash column (hexane–ethyl acetate 7:3) to give **32** (5.6 mg, 48%).

*6-(t-Butyldimethylsilyloxy)-1,9-bis(*p*-methoxybenzyl)-5-methylene-2-oxa-7,9-diazabicyclo[4.2.2]decane-8,10-dione* (**33**).
To a solution of **32** (10.0 mg, 0.0228 mmol) in dichloromethane (1 cm^3) was added 2,6-lutidine (12.2 mg, 0.114 mmol)

and 0.1 M *t*-butyldimethylsilyl triflate (0.342 cm^3, 0.0342 mmol) solution in dichloromethane with vigorous stirring at room temperature. The mixture was stirred for 12 h, poured into saturated ammonium chloride, and extracted with ethyl acetate. The extract was washed successively with 0.1 M hydrochloric acid, saturated sodium hydrogencarbonate, and saturated sodium chloride, dried over anhydrous magnesium sulfate, and then evaporated. The residue was purified on a flash column (hexane–ethyl acetate 4:1) to give **33** (10.1 mg, 80.2%) as a colorless hard syrup. ^{13}C NMR: δ=167.7s and 163.4s (C-8,10), 159.4s, 158.9s, 130.7d, 130.3d, 128.0s, 126.7s, 114.4d, and 113.3d, (aromatic), 148.6s and 118.0t (olefinic), 87.9s (C-6), 81.5d (C-1), 63.8t (C-3), 55.3q and 55.2q (2×OMe), 47.2t and 44.0t (NCH_2X2), 35.7t (C-4).

Found: C, 65.41; H, 7.28; N, 5.03%. Calcd for $C_{30}H_{40}N_2O_6Si$: C, 65.20; H, 7.30; N, 5.07%.

References

1) T. Miyoshi, N, Miyairi, H. Aoki, M. Kohsaka, H. Sakai, and H. Imanaka, *J. Antibiot.*, **25**, 569 (1972).

2) S. Miyamura, N. Ogasawara, H. Otsuka, S. Miwayama, H. Tanaka, T. Take, T. Uchiyama, H. Ochiai, K. Abe, K. Koizumi, K. Asao, K. Matsuki, and T. Hoshino, *J. Antibiot.*, **25**, 610 (1972).

3) T. Miyoshi, M. Iseki, T. Konomi, and H. Imanaka, *J. Antibiot.*, **33**, 480, 488 (1980).

4) T. Kamiya, S. Maeno, M. Hashimoto, and Y. Mine, *J. Antibiot.*, **25**, 576 (1972); Y. Tokuma, S. Koda, T. Miyoshi, and Y. Morimoto, *Bull. Chem. Soc. Jpn.*, **47**, 18 (1974); H. Maag, J. F. Blount, D. L. Coffen, T. V. Steppe, and F. Wong, *J. Am. Chem. Soc.*, **100**, 6786 (1978).

5) S. Nakatsuka, K. Yamada, K. Yoshida, O. Osano, Y. Murakami, and T. Goto, *Tetrahedron Lett.*, **24**, 5627 (1983); S. Nakatsuka and T. Goto, *Heterocycles*, **21**, 61 (1984).

6) R. M. Williams, R. W. Armstrong, and J.-S. Dung, *J. Am. Chem. Soc.*, **106**, 5748 (1984).

7) J. Yoshimura, M. Yamaura, T. Suzuki, and H. Hashimoto, *Chem. Lett.*, **1984**, 2157.

8) a) L. V. Dunkerton and R. M. Ahmed, *Tetrahedron Lett.*, **21**, 1803 (1980); b) C. Shin, Y. Sato, and J. Yoshimura, *ibid.*, **22**, 2401 (1981); c) T. Fukuyama, B. D. Robins, and R. A. Sachleben, *ibid.*, **22**, 4155 (1981); d) J. H. Hoare and P. Yates, *J. Chem. Soc., Chem. Commun.*, **1981**, 1126; e) P. Yates and J. H. Hoare, *Can. J. Chem.*, **61**, 519, 1397 (1983).

9) R. M. Williams, *Tetrahedron Lett.*, **22**, 2341 (1981); R. M. Williams, O. P. Anderson, R. W. Armstrong, J. Josey, H. Meyers, and C. Eriksson, *J. Am. Chem. Soc.*, **104**, 6092 (1982); R. M. Williams, J.-S. Dung, J. Josey, R. M. Armstrong, and H. Meyers, *ibid.*, **105**, 3214 (1983); S. Nakatsuka, K. Yoshida, and T. Goto, *Tetrahedron Lett.*, **22**, 2009 (1981); A. Sera, K. Itoh, H. Yamada, and R. Aoki, *Heterocycles*, **22**, 713 (1984).

10) M. Yamaura, T. Suzuki, H. Hashimoto, J. Yoshimura, and C. Shin, *Chem. Lett.*, **1984**, 1547.

11) T. Wakamiya, K. Konishi, H. Chaki, T. Teshima, and T. Shiba, *Heterocycles*, **15**, 999 (1981); H. H. Freedman and R. A. Dubois, *Tetrahedron Lett.*, **1975**, 3251.

12) C. L. Butler, A. G. Renfrew, and M. Clapp, *J. Am. Chem. Soc.*, **60**, 1472 (1938).

13) M. Majewski, D. L. J. Clive, and P. C. Anderson, *Tetrahedron Lett.*, **25**, 2101 (1984).

14) C. Gallina and A. Liberatori, *Tetrahedron Lett.*, **1973**, 1135; *Tetrahedron*, **30**, 667 (1974).

15) C. Shin, H. Hayakawa, K. Mikami, and J. Yoshimura, *Tetrahedron Lett.*, **1977**, 863; C. Shin, H. Hayakawa, H. Kato, K. Mikami, and J. Yoshimura, *J. Chem. Soc., Perkin Trans. 1*, **1980**, 419.

16) A. Mikillop and M. E. Ford, *Tetrahedron*, **30**, 2467 (1974).

17) a) J. Y. Savoie and D. Brassard, *Can. J. Chem.*, **49**, 3515 (1971); b) V. Van Rheenen, R. C. Kelly, and D. Y. Cha, *Tetrahedron Lett.*, **1976**, 1973; c) J. F. Eastham, G. B. Miles, and C. A. Krauth, *J. Am. Chem. Soc.*, **81**, 3114 (1959).

18) A. J. Mancuso, S.-L. Huang, and D. Swern, *J. Org. Chem.*, **43**, 2480 (1978); A. J. Mancuso and D. Swern, *Synthesis*, 1981, 165.

19) F. Bertini, P. Grasselli, and G. Zubiani, *Tetrahedron*, **26**, 1281 (1970); J. Yoshimura, K. Sato, H. Wakai, and M. Funabashi, *Bull. Chem. Soc. Jpn.*, **49**, 1169 (1976).

20) F. U. Tebbe, G. W. Parshall, and G. S. Reddy, *J. Am. Chem. Soc.*, **100**, 3611 (1978).

21) P. F. Hudrlik and D. Peterson, *J. Am. Chem. Soc.*, **97**, 1464 (1975).

Benzofuran Derivatives. II. Synthesis of 2,3-Dihydrobenzofurans from Ethyl 2-Acylphenoxyacetates

Tsuneo SUZUKI
Nippon Dental University, Niigata, 1-8, Hamaura-cho, Niigata 951
(Received January 24, 1985)

Ethyl 3-alkyl-3-hydroxy-5-nitro-2,3-dihydro-2-benzofurancarboxylates were obtained from the reaction of ethyl 2-acyl-4-nitrophenoxyacetates with potassium hydroxide in dry dioxane. The relative ratios of the *cis* and *trans* isomers with respect to C-2 and C-3 stereochemistry varied according to the structure of the acyl group. When the acyl group was acetyl, propionyl, or isobutyryl group, the *cis* isomers (2-alkoxycarbonyl groups and 3-hydroxyl groups are *cis*) were exclusively obtained in high yields. On the other hand, a nearly equimolecular amount of the *cis* and *trans* isomers was obtained from the reaction of 2-formyl derivatives under the same conditions.

A number of 2,3-dihydrobenzofuran derivatives have been synthesized from the reaction of salicylaldehydes with ethyl α-bromophenylacetates[1] or by its modified reactions.[2,3] The stereochemistry of the *cis* and *trans* isomers of 2,3-dihydrobenzofurans was determined by ^{1}H NMR spectra and chemical reactions.[2,4]

In the previous paper,[5] it was suggested that the *cis* and *trans* isomers of 3-alkyl-3-hydroxy-2,3-dihydro-2-benzofurancarboxylate ions were important intermediates for the production of benzofurans and 2-benzofurancarboxylic acids in the Rössing reaction of 4-substituted 2-acylphenoxyacetic acids.[6] However, such intermediates were not obtained at that time. In this paper, the author reports the syntheses and the stereochemistry of *cis*- and *trans*-2,3-dihydrobenzofurans obtained by the base-catalyzed intramolecular cyclization reaction of ethyl 2-acyl-4-nitrophenoxyacetates (the *cis* isomer is shown by an *cis* relationship between C-2 alkoxycarbonyl groups or carboxyl groups and C-3 hydroxyl groups).[7]

Results and Discussion

The syntheses of ethyl esters **1c** and **1d** were carried out according to the reported method.[5] Ethyl esters **1a** and **1b** were prepared by esterification of the corresponding carboxylic acids.

When esters **1a—d** were refluxed with three equivalents of potassium hydroxide in dry dioxane, 2,3-dihydrobenzofurans (**2a—d** and **3a,b**), ethyl 2-benzofurancarboxylates (**4a—d**), 2-benzofurancarboxylic acids (**5a—d**), and 2,3-dihydro-2-benzofurancarboxylic acids (**6b, d**) were obtained, respectively. The isolated yields of compounds **2—6** are summarized in Table 1. In the case of esters **1b—d**, 2,3-dihydrobenzofurans (**2b** and **3b**, **2c**, and **2d**) were obtained in high yields (65—70%), whereas ester **1a** afforded 2,3-dihydrobenzofurans (**2a** and **3a**) in a poor yield (8%). The spectral data of **2a,b** and **3a,b** are listed in Table 2.

A mixture of the two isomers **2a** and **3a** (3:2 mole ratio) was produced by the treatment of **1a** with base. The structural assignments of the two isomers are as follows. The ^{1}H NMR spectrum of the major component **2a** showed the C-2 methine proton signal at δ 5.26 (d, J=6.8 Hz) and that of the minor component **3a** gave the C-2 methine proton signal at δ 5.17 (d, J= 3.3 Hz). In general, the coupling constants due to C-2 and C-3 protons of 2,3-disubstituted 2,3-dihydrobenzofurans are $J_{cis} > J_{trans}$[8] as predicted by the Karplus equation.[9] The ^{1}H NMR signal of the C-2 proton of **3a** was located about δ 0.1 upfield from that of the C-2 proton of **2a** by the anisotropic effect of C-3 hydroxyl groups.[10] Additionally, a large nuclear Overhauser effect (15%) was observed between C_2–H and C_3–H in the major product **2a**, whereas a small effect (8%) in the minor product **3a** as shown in Table 3.[11,12] A large NOE is measured when the irradiation proton and the measured proton have *cis*-configura-

TABLE 1. THE REACTION OF ETHYL 2-ACYL-4-NITROPHENOXYACETATES (**1a—d**) WITH POTASSIUM HYDROXIDE IN DRY DIOXANE[a]

Starting Materials **1** (R)	Recovery of **1**/%	Isolated Yields of Products/%				Total Yields/%
		2 and **3** (**2**:**3**[b])	**4**	**5**[c]	**6**[c]	
1a (H)	62	8 (3:2)	1	0.5		71.5
1b (CH_3)	5	70 (16:1)	8	1	3	87
1c (CH_2CH_3)	2	67 (1:0)	10	2		81
1d ($CH(CH_3)_2$)	0	65 (1:0)	5	4	18	92

a) Esters **1a—d** were refluxed with potassium hydroxide in a 1:3 mole ratio in 30 ml of dry dioxane for 1 h. b) The ratios of the two isomers were determined by ^{1}H NMR analyses on the products **2** and **3** separated by silica-gel column chromatography. The isomerization of the two isomers was not recognized during chromatography. c) Acids **4** and **5** were analysed as the corresponding methyl esters.

Table 2. Physical data of 2,3-dihydrobenzofurans (**2a,b** and **3a,b**)

Compounds	R	^{1}H NMR[a,b] C_2-H	C_3-R
2a	H	5.26 (d) ($J_{2H,3H}$=6.8 Hz)	5.62 (t)
3a	H	5.17 (d) ($J_{2H,3H}$=3.3 Hz)	5.56 (dd)
2b[c]	CH_3	4.99 (s)	1.88 (s)
3b[c]	CH_3	5.18 (s)	1.65 (s)

a) The chemical shifts in ppm down field from internal TMS in $CDCl_3$. b) Carefully argon degassed solution of **2a,b** and **3a,b** were used for the measurement. c) The structure of **2b** and **3b** were not assigned by IR measurements in $CHCl_3$ or $CDCl_3$.

Table 3. The NOE values (%) for 2,3-dihydrobenzofurans (**2a—d** and **3a,b**)

Compounds	Observed Signal [Irradiated Signal] NOE/%
2a	C_2-H [C_3-H] 15
3a	C_2-H [C_3-H] 8
2b	C_2-H [C_3-CH_3] 34
3b	C_2-H [C_3-CH_3] 15
2c	C_2-H [C_3-CH_2-] 8; C_2-H [C_3-C-CH_3] 17
2d	C_2-H [C_3-CH-] 5; C_2-H [C_3-C-CH_3[a]] 15; C_2-H [C_3-C-CH_3[b]] 12

The gas dissolved in solution was removed by bubbling with argon. a) The chemical shift of the methyl proton is δ 0.90. b) The chemical shift of the methyl proton is δ 1.08.

tions.[11] All these results suggest that the major product **2a** is *cis*, and the minor product **3a** is *trans*.

The ethyl ester **1b** afforded a mixture of the two isomers **2b** and **3b** in a 16:1 mole ratio. The chemical shift of the C-2 methine proton of **3b** is located about δ 0.2 downfield from that of the methine proton of **2b** by the anisotropic effect of C-3 methyl group.[8c,13] A large NOE (34%) was observed between C_2-H and C_3-Me in the product **2b**, whereas a small NOE (15%) was obtained in the product **3b**.[11,12] Thus, the major component **2b** was assigned to the *cis* isomer and the minor component **3b** to the *trans* isomer.

Ethyl esters **1c** and **1d** afforded the corresponding 2,3-dihydrobenzofurans **2c** and **2d** in high yields, respectively. Only one component of two isomers was detected with ^{1}H NMR measurement of the products. Similarly, the structure of **2c** and **2d** was concluded to be *cis* from the NOE measurement as described for the *cis* isomers **2a** and **2b**. An acid **6d** was assigned to *cis* stereochemistry by methylation followed by comparison with an authentic sample **8d** obtained from the reaction of methyl ester **7d** with potassium hydroxide.

As shown in Table 1, the relative ratios of the two isomers were varied according to the structure of the acyl group. In the case of **1b—d**, the exclusive production of the *cis* isomers **2b—d** is explained by the steric repulsion of the ethoxycarbonyl group and the methyl, ethyl, or isopropyl group at the cyclization step. On the other hand, in the case of **1a**, compounds **2a** and **3a** were obtained in a nearly equimolecular ratio because the steric repulsion between the ethoxycarbonyl group and hydrogen atom is small.

2,3-Dihydrobenzofurans **2b** and **3b** were treated with potassium hydroxide in dry dioxane to elucidate the reaction mechanism, respectively. The results are listed in Table 4.

In the case of the *cis* isomer **2b**, products **4b, 5b,** and **6b** were obtained in 9, 2, and 13% yields, respectively. A mixture of the two isomers **2b** and **3b** (70%; **2b**:**3b**=14:1) were recovered. On the other hand, in the case of the *trans* isomer **3b**, compounds **4b** and **5b** were produced in 71 and 15% yields, respectively. A mixture of compounds **2b** and **3b** (14%; **2b**:**3b**=2:1) was recovered. The structure of the acid **6b** was assigned to the *cis*-configuration by methylation followed by comparison with an authentic sample **8b**, prepared later, in which a NOE (33%) of C-2 methine proton was observed by the irradiation of C-3 methyl proton. These results showed that isomerization between the two isomers took place and the *cis* isomer

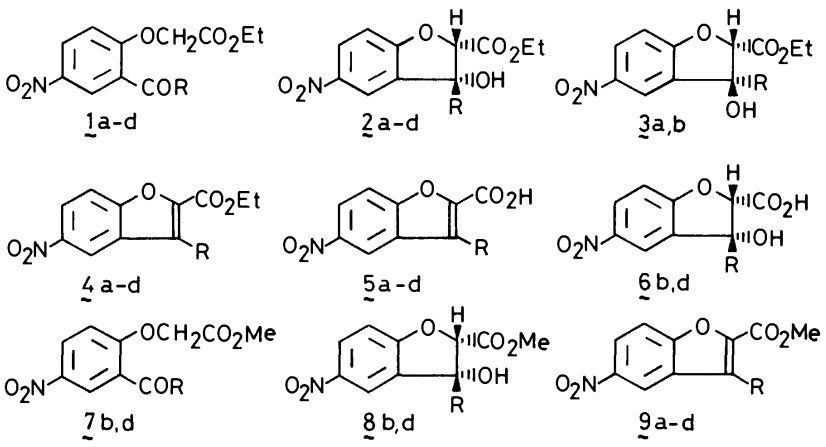

TABLE 4. THE REACTION OF 2,3-DIHYDROBENZOFURANS (**2b** AND **3b**) WITH POTASSIUM HYDROXIDE IN DRY DIOXANE

Starting Materials	Recovery of **2** and **3**/%(**2**:**3**[a])	Isolated Yields of Products/%			Total Yields/%
		4	**5**[b]	**6**[b]	
2b	70 (14:1)	9	2	13	94
3b	14 (2:1)	71	15		100

a) The ratios of the two isomers were determined by ^{1}H NMR measurement. b) Acids **4** and **5** were analysed as the corresponding methyl esters.

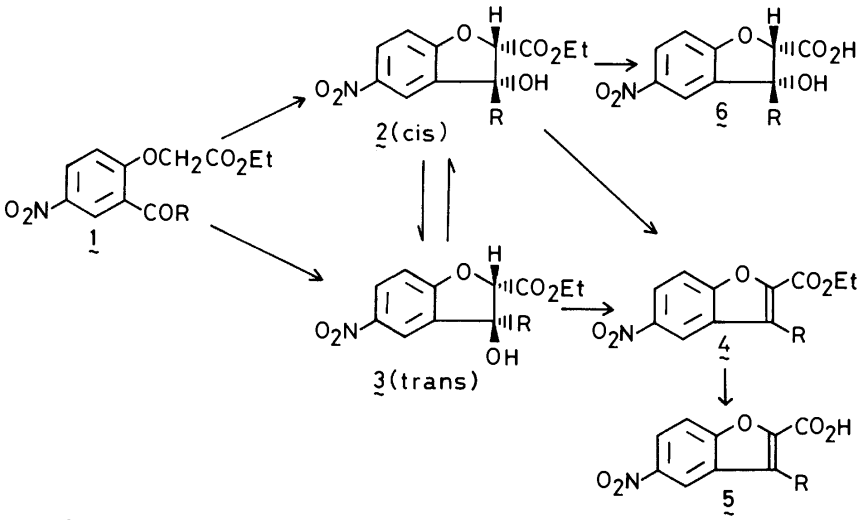

Scheme 1. The reaction pathways for the production of 2,3-dihydrobenzofurans (**2** and **3**) and related compounds (**4**, **5**, and **6**).

2b was more stable than the *trans* isomer **3b** as the steric repulsion between the ethoxycarbonyl group and the methyl group in **2b** was smaller than that in **3b**;[8a] compound **3b** was more prone to dehydration than the *cis* isomer **2b** because the *trans* isomer **3b** was sterically less hindered to the approach of the base.

As shown in Scheme 1, the ester **4b** must be obtained mainly from the *cis* isomer **2b** in the reaction of the ester **1b** and base because the product composition of **4b** and **5b** from the ester **1b** was similar to that of products from **2b**, though the *trans* isomer **3b** afforded the ester **4b** in a high yield.

Experimental

All the melting points are uncorrected. The infrared absorption spectra (IR) were determined on a JASCO IRA-2 spectrometer. The nuclear magnetic resonance spectra (^{1}H) and nuclear Overhauser effects were determined at 90 MHz on a JEOL JNM-FX 90Q FT NMR spectrometer, using tetramethylsilane as an internal standard. Analytical and preparative HPLC were carried out with a YANACO Liquid Chromatograph L-4000 W apparatus equipped with a UV detector. A Yanapak ODS-T column (4 mm×25 cm) was used. The solvent system of 18—20% acetonitrile and 0.05 M (1 M=1 mol dm^{-3}) potassium dihydrogenphosphate buffer (pH=3.1) (vol/vol) was used as eluent. Wakogel C-200 (Wako) was used for column chromatography. Dry dioxane was prepared by the method of Fieser.[14] Unless otherwise stated, anhydrous sodium sulfate was employed as the drying agent.

A General Procedure for the Reaction of Ethyl 2-Acyl-4-nitrophenoxyacetates (1a—d) with Potassium Hydroxide in a 1:3 Mole Ratio. A typical procedure will be described for the reaction of **1b**. A mixture of **1b** (300 mg, 1.12 mmol), potassium hydroxide powder (191 mg, 3.40 mmol), and dry dioxane (30 ml) was refluxed for 1 h. After cooling, insoluble materials in the reaction mixture were removed by filtration. The residue obtained upon evaporation of the dioxane was dissolved in benzene and insoluble materials were filtered. After evaporation of the benzene, the residue (254 mg) was chromatographed on silica gel (30 g). The first fraction eluted with benzene gave 23 mg (8%) of **4b** as crystals. The second fraction eluted with benzene–ether (30:1) gave 15 mg (5%) of **1b** as crystals. The third fraction eluted with benzene–ether (20:3) gave 210 mg (70%) of a mixture of **2b** and **3b** as crystals. The relative ratio of **2b** and **3b** (16:1) was determined by ^{1}H NMR spectroscopy.

The insoluble materials obtained above were combined and dissolved in water and acidified with 6 M hydrochloric acid. The resulting acids were extracted with ether and methylated with diazomethane. The residue (40 mg) obtained upon evaporation of the ether was chromatographed on silica gel (15 g). The first fraction eluted with benzene gave the methyl ester of **5b** (3 mg, 1%) as colorless crystals, which were identified by comparison with an authentic sample of **9b** obtained later. The second fraction eluted with benzene–ether (20:3) gave the methyl ester of **6b** (9 mg, 3%) as crystals. This was identified by comparison with an authentic sample **8b** obtained from the reaction of **7b** with potassium hydroxide.

The results of the reaction of esters **1a**, **1c**, and **1d** with potassium hydroxide in dry dioxane are listed in Table 1. Methyl esters of **5a**, **5c**, **5d**, and **6d** were identified by comparison with authentic samples **9a**, **9c**, **9d**, and **8d** obtain-

ed later.

2c: Colorless crystals from benzene, mp 108—110 °C. IR(KBr): ν_{max} 3420 (OH) and 1735 cm^{-1} (CO_2). Found: C, 55.29; H, 5.35%. Calcd for $C_{13}H_{15}NO_6$: C, 55.51; H, 5.38%.

2d: Colorless plates from hexane-benzene, mp 106—107 °C. IR(KBr): ν_{max} 3432 (OH) and 1739 cm^{-1} (CO_2). Found: C, 56.80; H, 5.72%. Calcd for $C_{14}H_{17}NO_6$: C, 56.95; H, 5.80%.

4a: Colorless prisms from benzene, mp 152—153 °C. IR(KBr): ν_{max} 1729 cm^{-1}(CO_2). Found: C, 56.21; H, 3.86%. Calcd for $C_{11}H_9NO_5$: C, 56.17; H, 3.85%.

4b: Colorless short needles from hexane-benzene, mp 146.0—147.5 °C. IR(KBr): ν_{max} 1700 cm^{-1} (CO_2). Found: C, 57.87; H, 4.53%. Calcd for $C_{12}H_{11}NO_5$: C, 57.83; H, 4.44%.

4c: Colorless short needles from benzene, mp 110.5—111.0 °C. IR(KBr): ν_{max} 1722 cm^{-1} (CO_2). Found: C, 59.61; H, 5.07%. Calcd for $C_{13}H_{13}NO_5$: C, 59.31; H, 4.98%.

4d: Colorless short needles from benzene-hexane, mp 103.5—106.0 °C. IR (KBr): ν_{max} 1719 and 1707 cm^{-1} (CO_2). Found; C, 60.38; H, 5.36; N, 5.20%. Calcd for $C_{14}H_{15}NO_5$: C, 60.65; H, 5.45; N, 5.05%.

Separation and Identification of cis- *and* trans-*2,3-Dihydrobenzofurans (**2a, b** and **3a, b**).*

*Ethyl Esters **2a** and **3a**.* The *cis* isomer **2a** was obtained by fractional crystallization of the mixture of **2a** and **3a** (5:2 mole ratio) from benzene-ether followed by ether. The *trans* isomer **3a** was separated from the mixture of two isomers by using an HPLC and purified by recrystallization of the crude compound **3a**.

2a: Colorless plates from benzene-hexane, mp 134—135 °C.[15] IR(KBr): ν_{max} 3540 (OH) and 1727 cm^{-1} (CO_2). Found: C, 52.07; H, 4.33; N, 5.38%. Calcd for $C_{11}H_{11}NO_6$: C, 52.17; H, 4.38; N, 5.53%.

3a: Colorless short needles from benzene-hexane, mp 96—97 °C.[15] IR(KBr): ν_{max} 3440 (OH) and 1728 cm^{-1} (CO_2). Found: C, 52.33; H, 4.38; N, 5.35%. Calcd for $C_{11}H_{11}NO_6$: C, 52.17; H, 4.38; N, 5.53%.

*Ethyl Esters **2b** and **3b**.* The *cis* isomer **2b** was obtained by fractional crystallization of the mixture of **2b** and **3b** (14:1 mole ratio) from benzene. The *trans* isomer **3b** was obtained by column chromatography of the residue obtained by concentration of the mother liquor on silica gel and eluted with benzene-ether (30:1).

2b: Colorless plates, mp 156.0—157.5 °C. IR(KBr): ν_{max} 3440 (OH) and 1740 cm^{-1} (CO_2). Found: C, 53.67; H, 4.85%. Calcd for $C_{12}H_{13}NO_6$: C, 53.93; H, 4.90%.

3b: Crystals, mp 52.5—54.0 °C. IR(KBr): ν_{max} 3430 (OH) and 1725 cm^{-1} (CO_2). Found: C, 54.00; H, 5.02; N, 5.21%. Calcd for $C_{12}H_{13}NO_6$: C, 53.93; H, 4.90; N, 5.24%.

*The Reaction of 2,3-Dihydrobenzofurans (**2b** and **3b**) with Potassium Hydroxide.* A typical procedure will be described for the reaction of **2b**. A mixture of **2b** (100 mg, 0.37 mmol), potassium hydroxide powder (63 mg, 1.12 mmol), and dry dioxane (10 ml) was refluxed for 1 h. The reaction mixture was worked up as described for the reaction of **1b** with potassium hydroxide. From the residue obtained upon evaporation of benzene, ethyl ester **4b** (8 mg) was obtained in 9% yield. Seventy percent of a mixture of **2b** and **3b** (70 mg, 14:1 mole ratio) was recovered. Methyl esters of **5b** (2 mg) and **6b** (12 mg) were obtained by methylation in 2 and 13% yields, respectively. The result of the reaction of **3b** with potassium hydroxide in dry dioxane is listed in Table 4.

*Preparation of Materials (**1a—d, 7b, 7d, 8b, 8d,** and **9a—d**).* Compounds **1c** and **1d** were prepared according to the reported method.[5] Ethyl ester **1a** was prepared from 2-formyl-4-nitrophenoxyacetic acid[5] by heating with ethanol and sulfuric acid. Similarly, ethyl ester **1b** was prepared from 2-acetyl-4-nitrophenoxyacetic acid[5] obtained by nitration[16] of 2-acetylphenoxyacetic acid.[17] Compound **1b** was identified by comparison with an authentic sample obtained by the reported method.[5] Methyl esters **7b** and **7d** were obtained from the corresponding phenoxyacetic acids[5] by methylation with diazomethane, respectively. In the same manner as has been described for **2b**, 2,3-dihydrobenzofurans **8b** and **8d** were obtained from the corresponding methyl esters **7b** and **7d**, respectively. Methyl esters **9a—d** were prepared by methylation of acids **5a**[18] and **5b—d**[5] with diazomethane, respectively.

1a: Colorless short needles from ethanol, mp 91—93 °C. Found: C, 52.40; H, 4.38%. Calcd for $C_{11}H_{11}NO_6$; C, 52.17; H, 4.38%.

7b: Colorless short needles from methanol, mp 105.0—106.5 °C. Found: C, 52.16; H, 4.29%. Calcd for $C_{11}H_{11}NO_6$: C, 52.17; H, 4.38%.

7d: Yellow crystals from hexane-ether, mp 57.0—57.8 °C. Found: C, 55.32; H, 5.35; N, 4.89%. Calcd for $C_{13}H_{15}NO_6$: C, 55.51; H, 5.38; N, 4.98%.

8b: Colorless short needles from benzene, mp 133.0—134.0 °C. IR (KBr): ν_{max} 3415 (OH) and 1750 cm^{-1} (CO_2). Found: C, 52.09; H, 4.38; N, 5.40%. Calcd for $C_{11}H_{11}NO_6$: C, 52.17; H, 4.38; N, 5.53%.

8d: Pale yellow prisms from ether-hexane, mp 96.0—97.5 °C(bp 156 °C at 2 Torr; 1 Torr=133.322 Pa). IR(KBr): ν_{max} 3420 (OH) and 1748 cm^{-1}(CO_2). Found: C, 55.54; H, 5.32%. Calcd for $C_{13}H_{15}NO_6$: C, 55.51; H, 5.38%.

9a: Colorless short needles from benzene, mp 163.5—164.5 °C. Found: C, 54.32; H, 3.14%. Calcd for $C_{10}H_7NO_5$: C, 54.32; H, 3.19%.

9b: Colorless short needles from methanol, mp 147.0—148.5 °C. Found: C, 56.29; H, 3.98%. Calcd for $C_{11}H_9NO_5$: C, 56.17; H, 3.85%.

9c: Colorless plates from benzene-hexane, mp 120—121 °C. Found: C, 58.06; H, 4.52%. Calcd for $C_{12}H_{11}NO_5$: C, 57.83; H, 4.44%.

9d: Colorless short needles from benzene-hexane, mp 110 °C. Found: C, 59.19: H, 4.96%. Calcd for $C_{13}H_{13}NO_5$: C, 59.31; H, 4.98%.

The Nuclear Overhauser Effect Measurement. The solution (calcd 5% wt/vol) was filtered and carefully degassed by argon. A small amount of tetramethylsilane was used as an internal standard. The irradiation power of the second radio frequency field was checked by using a standard sample of 4% 3-hydroxy-4-methoxybenzaldehyde-[$^2H_1$]chloroform solution (wt/vol) as the NOE (20%) of C-5 hydrogen atom was observed by the irradiation of C-4 methoxyl group. The homogated decoupling technique was employed in the measurement (at least three measurements were made).

The author is grateful to Mr. Yoshiaki Matsuda for the elemental analyses and to Mr. Naohiro Hiratsuka for the nuclear magnetic resonance analyses.

References

1) S. Kawai, T. Nakamura, and N. Sugiyama, *Proc. Imp. Acad.* (Tokyo), **15**, 45 (1939); S. Kawai, T. Nakamura, and M.

Yoshida, *Ber.*, **73B**, 581 (1940); A. F. Wagner, U. S. Patent 2892847 (1959); *Chem. Abstr.*, **54**, 570d (1960); E. Ceratti, *Ann. Sci. Univ. Besancon Chim.* [3], No 1. 79 (1963); *Chem. Abstr.*, **61**, 1465f (1964); A. S. Angeloni and M. Tramontini, *Ann. Chem.* (Rome)., **55**, 1028 (1965); *Chem. Abstr.*, **64**, 5028g (1966); K. Schofield, R. S. Ward, and A. M. Choudhurg, *J. Chem. Soc., C*, **1971**, 2834.

2) M. Ghelardoni, V. Pestellini, and C. Musante, *Gazz. Chim. Ital.*, **99**, 1273 (1969); *Chem. Abstr.*, **73**, 24801v (1970).

3) G. N. Walker and R. T. Smith, *J. Org. Chem.*, **36**, 305 (1971).

4) S. P. Pappas, B. C. Pappas, and J. E. Blackwell, Jr., *J. Org. Chem.*, **32**, 3066 (1967).

5) T. Suzuki, T. Horaguchi, T. Shimizu, and T. Abe, *Bull. Chem. Soc. Jpn.*, **56**, 2767 (1983) and references cited therein.

6) A. Rössing, *Ber.*, **17**, 2998 (1884).

7) T. Horaguchi, H. Narita, and T. Suzuki, *Bull. Chem. Soc. Jpn.*, **56**, 184 (1983).

8) a) D. P. Brust, D. S. Tarbell, S. M. Hecht, E. C. Hayward, and L. D. Colebrook, *J. Org. Chem.*, **31**, 2192 (1966); b) E. C. Hayward, D. S. Tarbell, and L. D. Colebrook, *ibid.*, **33**, 399 (1968); c) M. P. Mertes and L. J. Powers, *ibid.*, **36**, 1805 (1971); d) S. P. Pappas, R. D. Zehr, and J. E. Alexander, *J. Heterocycl. Chem.*, **7**, 1215 (1970); e) L. H. Zalkow, E. Keinan, S. Steindel, A. R. Kalyanarman, and J. A. Bertrand, *Tetrahedron Lett.*, **1972**, 2873.

9) M. Karplus, *J. Am. Chem. Soc.*, **85**, 2870 (1963).

10) A C-2 methine proton of *cis* isomer of 5-bromo-2-isopropyl-3-hydroxy-2,3-dihydrobenzofuran appeared at δ 3.99, while a corresponding methine proton of *trans* isomer appeared at δ 3.96. See, for an example, L. H. Zalkow and M. Ghosal, *J. Org. Chem.*, **34**, 1646 (1969). These authors originally assigned the two isomers incorrectly. Later work has corrected this error; see a lit, 8e.

11) R. A. Bell and J. K. Saunders, "Topics in Stereochemistry," ed by N. L. Allinger and E. L. Eliel, John Wiley & Sons, New York (1973), Vol. 7, P. 1 and references cited therein.

12) M. Gordon, W. C. Howell, C. H. Jackson, and J. B. Stothers, *Can. J. Chem.*, **49**, 143 (1971); R. D. G. Cooper, P. V. DeMarco, J. C. Cheng, and N. D. Jones, *J. Am. Chem. Soc.*, **91**, 1408 (1969).

13) The C-3 methine proton of *cis* 3-acetoxy-2-methyl-5-nitro-2,3-dihydrobenzofuran appeared at δ 6.25, on the other hand the C-3 methine proton of *trans* isomer appeared at δ 5.94. See, for an example, lit 8c. The chemical shift of C-2 hydrogen atom of *cis* isomer of methyl 3,6-dimethyl-5-hydroxy-2,3-dihydro-2-benzofurancarboxylate is located δ 0.52 down field from the corresponding C-2 hydrogen atom of *trans* isomer. See, for an example, T. Kozuka, *Bull. Chem. Soc. Jpn.*, **55**, 2415 (1982).

14) L. F. Fieser, "Experiments in Organic Chemistry," 3rd ed, D. C. Heath and Company, Boston (1955), p. 284.

15) The melting points were determined on Shimazu MM-2 micro melting point determination apparatus.

16) W. A. Jacobs and M. Heidelbelger, *J. Am. Chem. Soc.*, **39**, 2188 (1917).

17) G. Rosseels, J. Matteazzi, M. Clarlet, and M. Prost, *Ing. Chem.* (Brusseles), **53**, 37 (1971); *Chem. Abstr.*, **77**, 5258q (1972).

18) H. Erlenmeyer, M. Grubenmann, and H. Bloch, *Helv. Chim. Acta*, **31**, 75 (1948).

Surface Behaviors of Nucleic Acid Base-Containing Lipids in Monolayer and Bilayer Systems

Hiromi KITANO* and Helmut RINGSDORF†
Department of Polymer Chemistry, Kyoto University, Kyoto 606
†*Institute of Organic Chemistry, Mainz University, Mainz, West Germany*
(Received Feburary 12, 1985)

Three kinds of nucleic acid base-containing lipids were synthesized and the surface behaviors of these compounds in monolayer and bilayer systems were examined. In the monolayer systems, the addition of a complementary nucleoside to a subphase solution extended the monolayer much more efficiently than that of other nucleosides because of hydrogen bonding between a pair of complementary bases. In the monolayer and bilayer systems, the photodimerization reaction of a thymine ring was confirmed by the change in the surface pressure of the monolayer and the decrease in absorbance and the broadening of the phase-transition peak in the DSC curve of the liposome solution.

Mutual recognition of complementary nucleic acid bases is a fairly essential factor for the reproduction and generation of cells. To mimic these phenomena, many researchers have introduced nucleic acid bases into soluble polymers, polymer gels and micelles.[1-3] Considering the fact that replication of DNA occurs in cells, it is worthwhile to examine the mutual recognition of nucleic acid bases in model cell systems. In this project we studied the mutual recognition of nucleic acid bases in monolayer and bilayer systems which resembled membrane systems. Nucleic acid bases with lipophilic groups are also very interesting as both drug delivery systems and drugs themselves. Researchers have observed various remarkable effects of lipophilic nucleotides as anti-tumor reagents,[4a-c] and it is worthwhile to obtain basic information about the properties of nucleic acid base derivatives with long alkyl chains.

Experimantal

Materials. Three kinds of amphiphiles with nucleic acid bases (Ad(I), Ad(II), and Thy(I)) were synthesized (Scheme 1).

a) Ad(I). 9-(2-Chloroethyl)adenine was synthesized by the method of Ueda *et al.*[5,6] Dioctadecylamine (Fluka, three times recrystallized from acetone before use) (0.625 g, 1.2 mmol) and 0.12 g (0.607 mmol) of 9-(2-chloroethyl)-adenine were dissolved in 1-butanol (50 cm³) and the solution was refluxed for 5 d. After evaporating the solvent, an oily mixture was purified by silica-gel column chromatography using ethanol as an eluent. The eluate was evaporated and the oily product was precipitated in cold acetonitrile (Ad(I) 67 mg, 14.2% yield). Found; C, 69.45; H, 11.72; N, 10.40. Calcd for $C_{43}H_{83}N_6Cl$; C, 71.82; H, 11.55; N, 11.69.

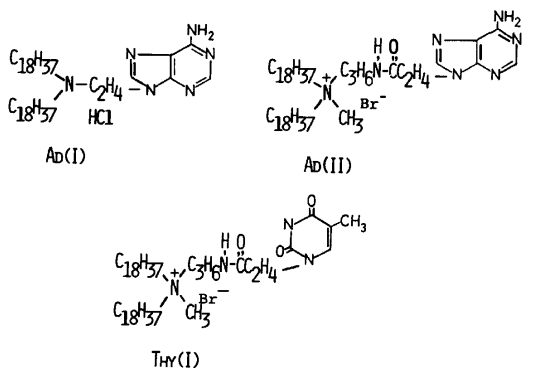

Scheme 1. Chemical structures of nucleic acid base-containig lipids examined here.

b) Ad(II). A *p*-Nitrophenyl ester of 9-(2-carboxyethyl)adenine was synthesized by the same method of Overberger and Inaki.[7] (3-Aminopropyl)methyldioctadecylammonium bromide hydrochloride[8] (1.22 g, 1.72 mmol) and 0.548 g (1.5 mmol) of 9-(2-carboxyethyl)adenine *p*-nitrophenyl ester were dissolved in 50 cm³ of a dichloromethane-*N*,*N*-dimethylformamide mixture (4:1) and 0.5 cm³ (3.59 mmol) of triethylamine was added. The mixture was continuously stirred for 2 d at room temperature. After evaporating the solvent, an oily yellow mixture was purified using silica-gel column chromatography with ethanol as an eluent. Just after the yellow colored *p*-nitrophenol flowed out of the column, the eluent was changed to $CHCl_3$–methanol (2:1). After the addition of a few drops of concd HBr, the collected eluate was evaporated and the oily product was precipitated in cold acetonitrile (HBr salt of Ad(II) 0.573 g, 40.5% yield). Found; C, 60.38; H, 9.83; N, 10.24. Calcd for $C_{48}H_{93}N_7OBr_2$; C, 61.06; H, 9.93; N, 10.38.

c) Thy(I). One g (1.41 mmol) of (3-aminopropyl)-methyldioctadecylammonium bromide hydrochloride[8] and 0.5 g (1.57 mmol) of 1-(2-carboxyethyl)thymine *p*-nitrophenyl ester[7] were reacted using a similar method for Ad(II) (Thy(I) 0.412 g, 34.2% yield). Found; C, 66.85; H, 11.02; N, 6.50. Calcd for $C_{48}H_{93}N_4O_3Br$; C, 67.49; H, 10.97; N, 6.56.

Monolayer Measurements. Surface-pressure measurements were carried out using a Wilhelmy system connected to a Commodore PET 4032 microprocessor with a floppy-disc memory system. The volume of the subphase solution was about 200 cm³. Millipore water was used for the preparation of a subphase solution. The temperature of the subphase was maintained by circulating water using a Lauda K4R water bath.

Bilayer Structure Formation. The necessary amount of nucleic acid base-containing amphiphile was suspended in distilled water using a vortex mixer. The solution was ultrasonicated using a Branson sonifier (Model B15P, 200 W 20 kHz) at 60 °C for 5 min. The liposome that was obtained was negatively stained using a 2(w/v)% ammonium molybdate solution on a carbon-evaporated copper mesh (10 nm thickness on G200 mesh, Polaron Equipment Ltd., Watford, England)

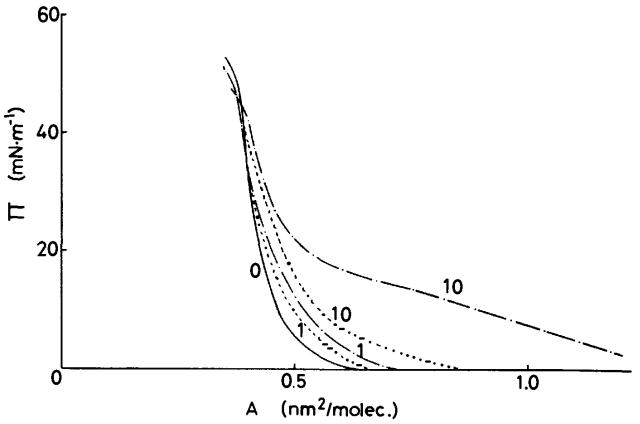

Fig. 1. Effects of nucleosides on the monolayer of Ad(I) at 10°C in mmol dm^{-3}.
—·—·—, in the presence of thymidine, ----, in the presence of adenosine.

for measurements using a JEM-100U electron microscope (Nihon Denshi, Tokyo, Japan).

UV Measurements. To observe any decrease in the absorption of the Thy(I) liposome solution due to photodimerization, a Beckman spectrophotometer (Model DU-6) was used.

UV Irradiation. To examine the photodimerization reaction of a Thy(I) liposome solution, a 200-V mercury lamp (Oriel) was used at 100 mA. The sample solution (10 mg cm^{-3}) was poured into a quarz cuvette (1×1×4 cm) and was placed at the distance of 20 cm from the light source at room temperature. The surface behavior of the Thy(I) monolayer was also observed before and after UV-irradiation. During a photo-reaction involving the monolayer of Thy(I) for 45 min (at 14°C), the surface tension of the monolayer was automatically maintained at 30 mN m^{-1}.

DSC Measurements. Phase transition behaviors of the Ad(II)- and Thy(I)-liposomes were observed using a Perkin Elmer DSC-2C. The volumes and concentration of samples in DSC alminium cells were 70×10^{-6} dm^3 and 10 mg cm^{-3}, respectively. The temperature was increased at a rate of 2.5°C min^{-1}.

Results and Discussion

A. Monolayer System. At first, we observed the surface behavior of the nucleic acid-base-containing amphiphiles in the monolayer system. Figure 1 shows the effects of adenosine and thymidine on the Ad(I) monolayer. Upon an addition of thymidine to the subphase, the monolayer expanded extraordinarily. However, an addition of adenosine induced a relatively smaller expansion. The smaller increase in the surface area in the Ad(I)–adenosine system can be attributed to a hydrophobic base-stacking effect since purine rings of adenosine and adenine are more hydrophobic than a pyrimidine ring of thymine. On the contrary, the larger expansion effects observed for an Ad(I)–thymidine system is due to the hydrogen-bonding-induced complementary base pairs between thymine and adenine rings. By the addition of 0.01 M (1 M=1 mol dm^{-3}) or 0.1 M of HCl to the subphase solution, the expanding effect of thymidine became much smaller because of a protonation of the amino group of Ad(I). This is consistent with the hydrogen-bonding effect regarding the thymidine–adenine ring interaction. Similar tendencies were also observed in the Ad(II)- and Thy(I)-monolayer systems. The surface area of the Thy(I) monolayer was, for example, 0.78 nm^2 molecule^{-1} at 15 mN m^{-1}. In the presence of 1 mM of adenosine, the surface area of the Thy(I) monolayer was increased by 0.24 nm^2 molecule^{-1}, whereas a smaller increase (0.10 nm^2 molecule^{-1}) was observed in the presence of 1 mM of thymidine.

The UV irradiation of the Thy(I) monolayer at 30 mN m^{-1} (densely packed conditions) for 45 min increased the surface area (surface area at 40 mN m^{-1}; from 0.54 nm^2 molecule^{-1} to 0.62 nm^2 molecule^{-1}). Though the amount of the reaction product was too small for a confirmation, the photodimerization of the thymine moiety of Thy(I) probably occured. In the case of the photodimerization of an amphiphilic cinnamic acid derivative in the monolayer system, a slight decrease in the surface area was observed.[9] In this case, the cinnamic acid moiety existed in the lipophilic region. On the contrary, the thymine moiety of Thy(I) existed near the ammonium head group. These differences might be the reason for the different tendencies regarding the photodimerization.

Bilayer System. Upon ultrasonication, suspended solutions of both Ad(II) and Thy(I) turned opaque and the diameters of the liposomes formed were estimated to be 60—300 nm (widely distributed) from electron micrographs. The bilayer structures of these solutions were confirmed by a small-angle X-ray scattering method (SAXS) using a Kratky U-slit system with a position-sensitive-proportional counter (Rigaku Denki, Tokyo, Japan).[10] In plots of the relative intensities *vs.* the scattering vectors of the Thy(I) solution, for example, a sharp peak at 4.3—4.2 nm, which reflects the thickness of the bilayer of Thy(I), was clearly observed (using a CPK model, the length of the octadecyl chain of a stretched Thy(I) molecule was estimated to be about 2.1 nm). The phase-transition temperatures of these liposome solutions were quite similar (Ad(II), 42.1°C, Thy(I), 42.5°C) with each other. This was probably due to a similar structure regarding the lipophilic parts.

Upon UV irradiation of the Thy(I)-liposome solution, a decrease in absorbance at 270 nm could be observed and attributed to the photodimerization of the thymine moiety (Fig. 2). This was because upon dimerization the thymine ring loses its aromaticity. There was no recovery of absorption at 270 nm after heating at 60°C for 10 min. This excludes the probability of a hydration of the thymine moiety during the UV irradiation. From electron micrographs and SAXS measurements, the liposome structure was observed to be maintained both before and after UV

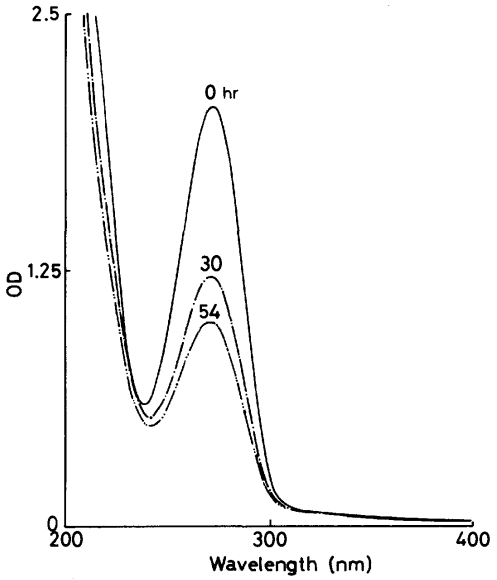

Fig. 2. Effect of uv irradiation on the absorbance of Thy(I)-liposome solution. [Thy(I)]=0.2 mmol dm^{-3}.

irradiation. Dimerization of Thy(I) was also confirmed by gel-permeation chromatography. After UV irradiation, a Thy(I) liposome solution was lyophilized and the obtained powder was dissolved in dichloromethane and carried on a Pharmacia Sephadex LH-20 column (2×20 cm). It was then eluted using dichloromethane. Elution of dimeric compounds from a column was observed using a Shodex SE-11 refractometer and the conversion of the dimerization reaction was estimated to be 50% after UV irradiation for 54 h. We tried to evaluate the structure of the dimerization product using ^{13}C NMR. However, the conversion of the reaction was so low and the amount of product was so small that it was very difficult to resolve the ^{13}C NMR spectra. At present we consider that a head-to-head and cis form dimerization is most probable from the molecular structure of Thy(I). The rate of the observed dimerization was much smaller than the polymer solution system.[11] This was probably because the long distance between thymine moieties was unfavorable for realizing dimerization (the distance between thymine moieties must be shorter than 0.4—0.5 nm for photodimerization).[12] Due to the bulkiness of the head group of the liposome-forming molecule, such a tight packing might be difficult. The unfavorable turbidity of the liposome solution and the lack of a cooperative action of the neighboring thymine ring might also be possible reasons for the slow dimerization reaction observed. After dimerization, the peak of a Thy(I)-liposome solution in DSC measurements was observed to be broader than that of the starting Thy(I)-liposome solution (peak width at half height; 3.7 °C→6.8 °C). This is probably because of the heterogenicity of the partially dimerized membrane surface. Upon mixing Ad(II) and Thy(I) liposome solutions, no large change in the DSC profiles was observed compared to those of Ad(II)- and Thy(I)-liposome solutions. This is probably because of the electrostatic repulsive forces between the cationic liposome particles. After incubating the mixed liposome solution at 350 K for 8 h, the peak was observed to be much broader than the starting solution (peak width at half height; 3.7 °C→7.1 °C) and the transition temperature shifted to a lower region by 2.3 °C during the slow fusion of these Ad(II)- and Thy(I)-liposomes and the following base-base interaction in the same liposome particle.

In conclusion, a mutual recognition of complementary nucleic acid bases could be observed in a monolayer system. A dimerization reaction involving thymine derivatives could also be observed in these systems. Especially in the liposome system, a clear decrease in the absorption of the thymine ring was observed. Further systematic studies of various kinds of nucleic acid base-containing lipids are presently in progress.

We wish to thank Professor Norio Ise, Kyoto University, for his helpful suggestions and Mr. Hideki Matsuoka, Kyoto University, for technical assistance. We also thank Dr. Hirokazu Hasegawa, Kyoto University, for taking electron micrographs of liposomes. H. K. thanks the Alexander von Humboldt Foundation, Bonn, and the Naito Memorial Science Foundation, Tokyo, for their fellowships.

References

1) J. Pitha, M. Akashi, and M. Draminski, in "Biomedical Polymers: Polymeric Materials and Pharmaceuticals for Biomedical Use" (E. P. Goldberg and A. Nakajima, Eds.) pp. 271—297 Academic Press, New York 1980.

2) K. Takemoto and Y. Inaki, *Adv. Polym. Sci.*, **41**, 1 (1981).

3) T. Okubo and N. Ise, *Adv. Polym. Sci.*, **25**, 135 (1977).

4) a) M. MacCoss, E. K. Ryu, I. Hong-Chung, and T. Matsushita, Proc. Int. Round Table Nucleosides Nucleotides Their Biol. Appl., 4th pp. 255—263, Antwerp 1981; b) A. F. Rosenthal and L. A. Vargas, *J. Chem. Soc., Chem.Commun.*, **1981**, 976; c) F. Ramirez, S. B. Mandal, and J. F. Marecek, *Synthesis*, **1982**, 402; *J. Am. Chem. Soc.*, **104**, 5483 (1982).

5) N. Ueda, K. Kondo, M. Kono, K. Takemoto, and M. Imoto, *Makromol. Chem.*, **120**, 13 (1968).

6) J. H. Lister and G. M. Timmis, *J. Chem. Soc.*, **1960**, 327.

7) C. G. Overberger and Y. Inaki, *J. Polym. Sci., Polym. Chem.*, **17**, 1739 (1979).

8) H. Kitano and H. Ringsdorf, publication in preparation.

9) T. Teng, H. Koch, and H. Ringsdorf, publication in preparation.

10) N. Ise, T. Okubo, S. Kunugi, H. Matsuoka, K. Yamamoto, and Y. Ishii, *J. Chem. Phys.*, **81**, 3294 (1984).

11) Y. Suda, Y. Inaki, and K. Takemoto, *J. Polym. Sci., Polym. Chem.*, **21**, 2813 (1983).

12) "Photochemistry and Photobiology of Nucleic Acids" (S. Y. Wang, Ed.) Academic Press, New York 1976.

Ozonolysis of 3-Methyl-1-phenyl-4-phenylazo-5-pyrazolone

Masaki MATSUI,* Akihiro KONDA, and Katsuyoshi SHIBATA
Department of Industrial Chemistry, Faculty of Engineering, Gifu University, Yanagido, Gifu 501-11
(Received March 18, 1985)

In chlorinated solvents, 3-methyl-1-phenyl-4-phenylazo-5-pyrazolone (**1**) easily reacts with ozone to give benzene (**2**), phenol (**3**), chlorobenzene (**4**), *o*-chlorophenol (**5**), biphenyl (**6**), and 3-methyl-1-phenyl-2-pyrazoline-4,5-dione (**7**). The formation of these products is explained by an electrophilic ozone attack on the hydrazone tautomer **1'**.

It is of interest to study the reaction of coloring matter with ozone in view of an ozone treatment of dye wastewater and the ozone fading of dyes.

The authors have reported a series of ozonization reactions of dyes and their model compounds.[1)]

We discuss here the ozonolysis of 3-methyl-1-phenyl-4-phenylazo-5-pyrazolone, a model compound of azo-pyrazolone dyes.

Experimental

Instruments. Ozone was generated by a Nihon Ozon 0-1-2 type ozonizer. Melting points were measured with a Yanagimoto micro melting-point apparatus. Gas chromatography was performed on Shimadzu 4CPF and Ohkura 802 gas chromatographs. IR, UV, NMR, and MS spectra were obtained with Hitachi EPI-S2, Hitachi EPS-3T, JEOL JUM-GX 270, and Hitachi M-52 spectrometers, respectively.

Materials. 3-Methyl-1-phenyl-4-phenylazo-5-pyrazolone (**1**) was synthesized by a diazotization-coupling method and recrystallized from ethanol; mp 157°C (lit,[2)] 155°C). 4-Arylazo-3-methyl-1-phenyl-5-pyrazolones were also synthesized by the same procedure. Benzene (**2**), phenol (**3**), chlorobenzene (**4**), *o*-chlorophenol (**5**), and biphenyl (**6**) were pure grades which were available commercially. 3-Methyl-1-phenyl-2-pyrazoline-4,5-dione (**7**) was isolated from the reaction mixture by glc using a Silicone OV-1 column; mp 118°C (lit,[3)] 119°C). The purity of materials was confirmed by gas chromatography.

Ozonolysis Reaction. Ozonolysis was carried out with an ozone-nitrogen mixture (ozone: 0.39—1.10 mmol, nitrogen: 200 ml min^{-1}) on 1 mmol of substrate in 50 ml of solvent at 0°C. The reaction mixture was allowed to stand for 40 min and was treated with dimethyl sulfide. The disappearence of peroxide activity was confirmed by a KI test. The products were analyzed by gas chromatography using 2% OV-1, 2% FFAP, and Gaskuropak 54 columns. Product identification was made by comparing the mass spectra with those of authentic samples. Product determination was also made by gas chromatography.

Calculation of Rate Constant. Ozonolysis was carried out with an ozone-oxygen mixture (ozone: 0.15 mmol min^{-1}, oxygen 200 ml min^{-1}) on 0.5 mmol of substrate in 200 ml of chloroform at 0°C. The reaction was followed by measuring the absorption maximum (395 nm) every 1 min. The reaction was then applied to pseudo first-order kinetics, shown in Eq. 1.

$$\ln S_0/S_t = k_x(\text{obsd}) \times t, \quad (1)$$

where S_0 is an initial concentration of substrate, S_t is the concentration after ozonolysis reaction for t min, and k_x (obsd) is a pseudo first-order rate constant. The treatment gave a good relation and the rate constant was calculated. The obtained rate constant was then corrected for the existence ratio of the hydrazone tautomer, as shown in Eq. 2.

$$k_x(\text{corr}) = \frac{k_x(\text{obsd})}{R_{\text{Hydrazone}}} \times 100, \quad (2)$$

where k_x (corr) is a pseudo first-order rate constant corrected, and $R_{\text{Hydrazone}}$ is an existence ratio (%) of the hydrazone tautomer in chloroform. The result is shown in Table 1.

Table 1. Pseudo first-order rate constants on the ozonization of 4-(substituted phenylazo)-3-methyl-1-phenyl-5-pyrazolones[a)]

Substituent	k_X(obsd) / min^{-1}	Existence ratio of hydrazone tautomer[b)] / %	k_X(corr) / min^{-1}	log k_X(corr)/k_H(corr)
4-OCH_3	1.75	97	1.80	0.269
4-CH_3	1.45	96	1.51	0.192
3-CH_3	0.95	96	0.99	0.009
H	0.92	95	0.97	0
3-OCH_3	0.78	91	0.86	−0.052
4-Cl	0.71	87	0.82	−0.073
4-$COCH_3$	0.36	86	0.42	−0.363
4-NO_2	0.30	85	0.35	−0.442

a) Ozonization was carried out with an ozone-oxygen mixture (ozone: 0.15 mmol min^{-1}, oxygen: 200 ml min^{-1}) on 0.5 mmol of substrate in 200 ml of chloroform at 0°C. b) The existence ratio was determined by the ^{1}H NMR analysis.

TABLE 2. OZONOLYSIS OF 3-METHYL-1-PHENYL-4-PHENYLAZO-5-PYRAZOLONE[a)]

Run	Sol	Ozone introduced	Conv	Yield[b)]/%				Reactivity[c)]	Dissolved[d)] ozone	Hydrazone[e)] form	Viscosity[f)]
		mmol	%	2	3	4	7		mmol dm^{-1}	%	cp
1	$CHCl_3$	0.39	25	70	16	7	77	0.64	3.6	95	0.701
2	$CHCl_3$	0.71	45	54	7	5	30	0.63	3.6	95	0.701
3	CH_2Cl_2	0.74	54	54	6	10	14	0.73	3.7	98	0.537
4	CCl_4	1.10	50	—	5	22	26	0.45	4.7	87	0.734

a) The reaction was carried out with an ozone–nitrogen mixture (nitrogen: 200 ml min^{-1}) on 1.0 mmol of 3-methyl-4-phenylazo-5-pyrazolone in 50 ml of solvent at 0°C. Trace amounts of *o*-chlorophenol (**5**) and biphenyl (**6**) were also detected in each case. b) Yield was based on the substrate reacted with ozone. c) Reactivity was based on **1** (reacted)/ozone(introduced). d) Dissolved ozone was determined by iodometric titration. e) The ratio was based on the ^{1}H NMR analysis. f) η Value at 0°C.

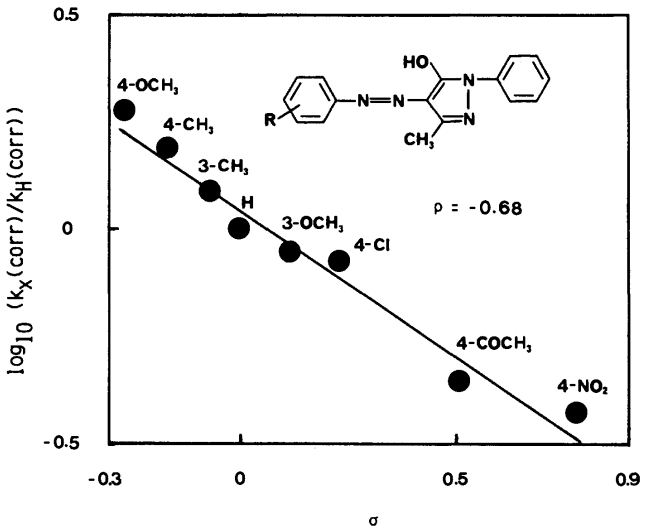

Fig. 1. Hammett's plot for the ozonolysis of 4-arylazo-3-methyl-1-phenyl-5-pyrazolones.
The reaction was carried out with an ozone-oxygen mixture on 0.5 mmol of substrate in 200 ml of chloroform at 0°C.

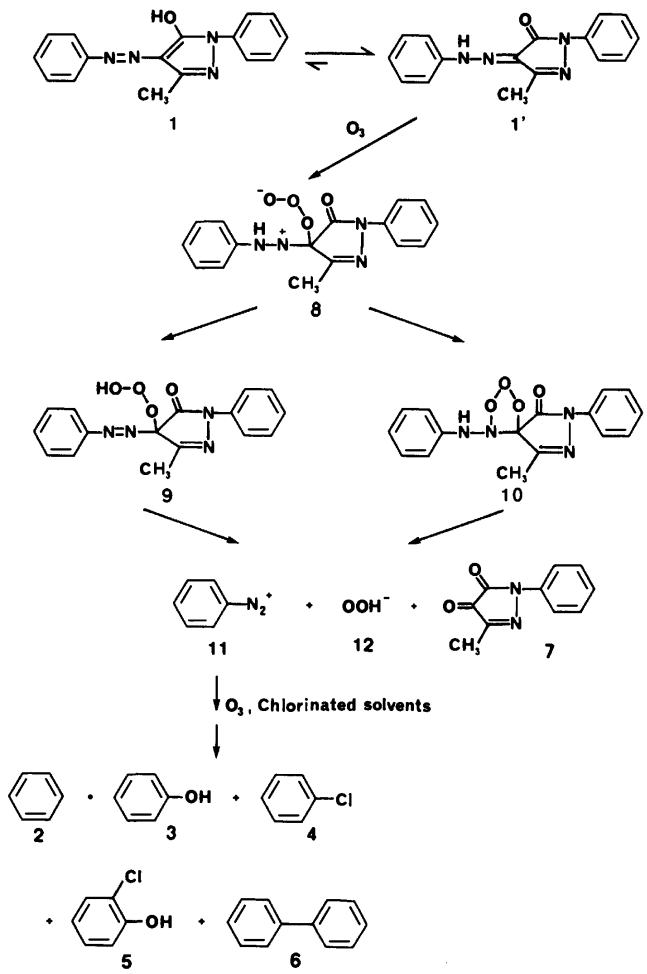

Scheme 1.

Results and Discussion

When 3-methyl-1-phenyl-4-phenylazo-5-pyrazolone (**1**) was ozonized in chloroform, benzene (**2**), phenol (**3**), chlorobenzene (**4**), *o*-chlorophenol (**5**), biphenyl (**6**), and 3-methyl-1-phenyl-2-pyrazoline-4,5-dione (**7**), were detected in the reaction mixture. The formation of trace amounts of hygroscopic compounds were also observed. The result is shown in Table 2. The reactivity of **1** with ozone in carbon tetrachloride was smaller than in the other solvents. The possible factors controlling the rate are the viscosity of the solvent, the amount of dissolved ozone, and the ratio of the hydrazone tautomer. The amount of dissolved ozone in each solvent was then measured by iodometric titration. Generally, *o*-hydroxy azo compounds exist as equiribrium mixture of azo-hydrazone tautomers. In 1963, Jones *et al.* determined the structure of the hydrazone tautomer of **1** as the quinone hydrazone form **1'**.[4)] The IR and ^{1}H NMR spectra showed a presence of the NH and C=O groups (IR: 3400 (weak, ν_{NH}) and 1655 ($\nu_{C=O}$) cm^{-1} and ^{1}H NMR δ=13.70 (br. s)), suggesting that the hydrazone tautomer is predominant. The ratio of **1'** in each solvent was then calculated from an ^{1}H NMR analysis. Under the reaction conditions, the reactivity of **1** with ozone seems to depend on both the ratio of the hydrazone tautomer and the viscosity of the solvent. The reactivity increased with an increasing ratio of the hydrazone tautomer **1'** and a decreasing viscosity of the solvent.

The effect of a substituent on the ozonolysis reaction

of **1** was investigated. Since treatment by pseudo first-order kinetics gave a good relation, the rate constant was calculated in the same way. On the other hand, the effect of a substituent on the azo-hydrazone tautomeric equiribrium of *o*-hydroxy azo compounds has been reported.[5] As shown in Table 1, an existence ratio of 4-(substituted phenylazo)-3-methyl-1-phenyl-5-pyrazolones was in the following order of substituent, 4-OCH_3>3-CH_3,4-CH_3>H>3-OCH_3>4-Cl>4-$COCH_3$>4-NO_2. This is consistent with that of the electron-donative ability of the substituent. Then, the rates of the ozonolysis reactions of 4-(substituted phenylazo)-3-methyl-1-phenyl-5-pyrazolones were corrected for the existence ratio of the hydrazone tautomer. The results are shown in Table 1. The plots of the logarithms of the relative rates k(corr) thus obtained against Hammett's σ constants gave a straight line whose slope was found to be $\rho=-0.68$ ($r=-0.98$). The result is shown in Fig. 1. The negative value of ρ appears consistent with the electrophilicity of ozone.

The probable ozonolysis mechanism is shown in Scheme 1. Ozone electrophilically attacks the hydrazone tautomer **1'** to give a primary ozonide **9** and/or the hydrotrioxide **10** *via* **8**. These unstable intermediates could not be isolated. They cleave to benzenediazonium ion (**11**), hydroperoxide ion (**12**), and 3-methyl-1-phenyl-2-pyrazoline-4,5-dione (**7**). When the ozonolysis reaction was carried out in the presence of 2-naphthol, 1-phenylazo-2-naphthol was detected, suggesting the formation of **11** during the reaction. The diazonium ion **11** is converted into benzene (**2**), phenol (**3**), chlorobenzene (**4**), *o*-chlorophenol (**5**), biphenyl (**6**), and nitrogen gas in the chlorinated solvent. From the results that when 2-naphthol was added to the hygroscopic compound formed during the ozonolysis reaction of **1**, 1-phenylazo-2-naphthol was detected, and that the hygroscopic compound showed the presence of chlorine ions by a Beilstein test, it was concluded that benzenediazonium chloride is at least one of the components of the hygroscopic material.

References

1) M. Matsui, H. Nakabayashi, K. Shibata, and Y. Takase, *Bull. Chem. Soc. Jpn.*, **57**, 3312 (1984).

2) F. A. Snavery, W. C. Fernelius, and B. P. Block, *J. Am. Chem. Soc.*, **79**, 1028 (1957).

3) F. A. Snavery and F. A. Suydam, *J. Org. Chem.*, **24**, 2039 (1959).

4) R. Jones, A. J. Ryan, S. Sternhell, and S. E. Wright, *Tetrahedron*, **19**, 1497 (1963).

5) V. Bekárek, J. Dobáš, J. Socha, P. Vetešník, and M. Večeřa, *Collect. Czech. Chem. Commun.*, **35**, 1406 (1970).

The Carbon-13 NMR Spectra and Electronic Structure of 3*H*-Phenoxazin-3-ones

Kan-ichi HASEGAWA* and Yoshio UENO†

Department of Natural Science, Nagoya University of Arts, Shikatsu-cho, Nishikasugai-gun, Aichi 481
†*Department of Industrial Chemistry, Nagoya Institute of Technology, Gokiso-cho, Showa-ku, Nagoya 466*

(Received March 27, 1985)

The ^{13}C NMR chemical shifts of 3*H*-phenoxazin-3-one (**1**) and eighteen of its derivatives are reported. The chemical shifts of **1** can be explained in terms of a successive polarization of the π-conjugated framework by an electron-withdrawing carbonyl group and a π-donating ether oxygen. The principal factor solution for the chemical shifts of the 2-substituted 3*H*-phenoxazin-3-ones suggests that the first and the second factors collectively controlling the 2-substituent effect are electronic and steric effects, respectively. A dual substituent parameter analysis elucidated the transmission modes of the polar and resonance effects of the 2-substituents, and that the first and the fourth factor loadings multiplied by the corresponding standard deviation of the chemical shifts correlate with the CNDO/2 substituent-induced σ and π charge densities.

Phenoxazin-3-ones and their imine analogues are the chromophores in a number of synthetic dyestuffs such as oxazine dyes and redox indicators.[1] As is well known, 3*H*-phenoxazin-3-one (**1**) is the chromophore part of the actinomycins produced by a Streptomyces species of soil bacteria and the initial step of the bonding between actinomycin D and DNA to inhibit RNA synthesis is considered to be the intercalation of a phenoxazin-3-one ring system between the guanine-cytosine base pairs.[2]

There have been few investigations of the electronic properties of 3*H*-phenoxazin-3-ones,[3] although many papers have been devoted to their syntheses and analyses of their IR,[4,5] UV,[4] and ^1H NMR spectra[6] in connection with advanced dye and medical chemistry. Pashkevich *et al.* have studied the annelation effect of a benzene ring on the electronic structure of all possible mono- and diannelated derivatives of **1** by means of the Hückel MO method and found a satisfactory correlation between the experimental and calculated energies of the $\pi \rightarrow \pi^*$ transitions.[3]

^{13}C NMR is a very powerful analytical tool to study the electronic structure of a carbon skeleton and the nature of bonding. In a previous paper, we reported the ^{13}C NMR chemical shifts of 3*H*-phenothiazin-3-one and eleven of its methyl derivatives.[7] In this paper, we extend the ^{13}C NMR chemical shifts of **1** and its derivatives, including the 2-substituents, and elucidate the transmission pattern of an electronic substituent effect by means of both Taft's dual substituent parameter (DSP) treatment[8] and the principal factor method.[9]

Experimental

Materials. The syntheses of **1**[10] and its 2-amino- (**4**),[10] 2-acetamido- (**7**),[10] 2-anilino- (**8**),[11] 2-hydroxy- (**10**),[12] 7-methoxy- (**13**),[13] 7-ethoxy- (**14**),[14] 7-acetoxy- (**15**),[14] 2-amino-1,9-dimethyl- (**18**),[5] and 2-amino-4,6-dimethyl- (**19**)[5] derivatives were performed according to the usual methods. 2-Methyl- (**2**),[15] 2-ethyl- (**3**),[15] 2-methylamino- (**5**),[16] 2-ethylamino-(**6**),[16] 2-(*N*-methylanilino)- (**9**),[17] 4-methyl- (**11**),[15] 2,4-dimethyl- (**16**),[15] and 2,4-diethyl-3*H*-phenoxazin-3-ones (**17**)[15] were prepared as described in previous papers. *N*-Phenyl-*p*-benzoquinone monoimine (**20**) was prepared according to the method of Uemura and Abe.[18] All the compounds were purified by TLC and column chromatography and checked by means of their IR and ^1H NMR spectra. Their spectral and physical properties were in agreement with available data from the literature. 4-Ethyl-3*H*-phenoxazin-3-one (**12**) was synthesized as in the case of **11**; mp 150—151 °C. Anal. Found: C, 74.42; H, 4.78; N, 5.91%. Calcd for $C_{14}H_{11}NO_2$: C, 74.65; H, 4.92; N, 6.22%.

Procedures. The ^{13}C NMR spectra were recorded on a Varian XL-200 Fourier-transform spectrometer at room temperature at 50.3 MHz using 10-mm sample tubes and a deuterium lock. Samples were prepared in a $CDCl_3$ solvent with tetramethylsilane as an internal reference except for **10** in dimethyl-d_6 sulfoxide. In the case of the dimethyl sulfoxide solvent, the ^{13}C NMR data were converted on the basis of 39.5 ppm of the dimethyl sulfoxide reference peak. A linear least-squares analysis for Taft's DSP equation was carried out by means of the Gauss-Newton method. The values of substituent constants, such as σ_I, σ_R^0, σ_R^{BA}, σ_R^+, F, and R for the electronic effect on the 2-substituents, were taken from Refs. 8c and 19. The values of the substituent constants not found in the literature were estimated from the known values of the corresponding σ_m, σ_p^{BA}, σ_p^+, and σ_p^0 by using the equations $\sigma_I = 1.5\sigma_m - 0.5\sigma_p$ and $\sigma_R^A = \sigma_p^A - \sigma_I$ where suffix A stands for 0, BA or +. The values of the Inamoto-Masuda group electronegativity χ and the inductive scale ι not found in Ref. 20 are as follows: $NHCH_3$, 3.031, 2.496; NHC_2H_5, 3.032, 2.496; NHC_6H_5, 3.034, 2.498; $NCH_3C_6H_5$, 3.016, 2.486.[21] Melting points were determined on a Yanagimoto micromelting apparatus and are uncorrected.

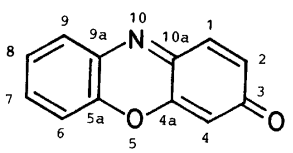

Fig. 1. Numbering of **1**.

Theoretical

CNDO/2 calculations[22] were carried out as in a previous paper.[7] The planar geometry of **1** was determined from the X-ray data[2] of actinomycin D obtained by means of a light-atom analysis and transferred to its

TABLE 1. ^{13}C NMR CHEMICAL SHIFTS OF 3*H*-PHENOXAZIN-3-ONES[a)]

Substituent	Chemical shift, δ												
	C-1	C-2	C-3	C-4	C-4a	C-5a	C-6	C-7	C-8	C-9	C-9a	C-10a	Others
Nil(**1**)	135.2	134.8	186.4	107.0	149.7	148.8	116.2	132.8	125.5	130.5	133.4	144.0	
2-Me(**2**)	132.1	[144.4]	186.2	106.5	149.3	149.0	116.1	131.3	125.3	130.1	133.5	143.8	16.5(Me)
2-Et(**3**)	130.1	[149.6]	185.9	106.7	149.2	149.1	116.1	132.0	125.2	129.7	133.5	143.8	22.6(CH_2), 12.2(Me)
2-NH_2(**4**)	100.9	[151.0]	178.9	104.2	148.7	146.0	116.1	129.6	125.3	128.8	133.7	142.8	
2-NHMe(**5**)	96.1	[150.0]	180.3	103.9	148.5	146.8	116.0	128.9	125.3	128.4	134.1	142.6	29.3(Me)
2-NHEt(**6**)	96.1	[149.9]	180.3	103.9	148.5	145.7	115.9	128.8	125.2	128.4	134.1	142.6	37.4(CH_2), 13.7(Me)
2-NHAc(**7**)	113.9	[149.4]	179.7	104.1	149.1	147.9	116.1	131.8	125.7	130.1	134.0	143.3	24.9(Me), 169.2(CO)
2-NHPh(**8**)	112.7	[149.8]	180.3	104.0	148.7	146.5	116.1	129.7	125.5	128.8	134.2	142.8	146.5(C_i), 121.6(C_o), 129.6(C_m), 124.6(C_p)
2-NMePh(**9**)	110.0	[149.3]	181.7	106.5	148.9	148.6	116.0	129.8	125.1	128.8	133.9	142.8	148.5(C_i), 124.3(C_o), 129.4(C_m), 125.4(C_p), 42.8(Me)
2-OH(**10**)	103.1	[155.6]	185.1	104.0	149.2	147.3	115.7	127.0	125.0	126.8	134.1	141.5	
4-Me(**11**)	134.7	134.0	185.9	[116.7]	145.8	148.5	116.1	132.4	125.1	130.2	133.3	143.8	9.7(Me)
4-Et(**12**)	134.9	134.0	185.3	[121.4]	145.3	149.5	116.1	132.2	125.1	130.2	133.4	144.5	15.7(CH_2), 12.7(Me)
7-OMe(**13**)	134.7	134.2	186.3	106.7	149.9	148.2	100.1	[163.7]	113.7	131.6	128.4	145.6	56.2(Me)
7-OEt(**14**)	134.7	134.2	186.4	106.7	149.9	145.7[b)]	100.5	[163.1]	114.0	131.6	128.3	145.5[b)]	64.7(CH_2), 14.6(Me)
7-OAc(**15**)	135.2	134.8	186.3	107.3	149.3	148.4	109.7	[153.5]	119.2	131.2	131.3	144.4	21.1(Me), 168.5(CO)
2,4-Me_2(**16**)	131.6	[143.6][b)]	185.8	[115.0]	145.5	149.0	116.0	130.6	124.9	129.9	133.3	144.3[b)]	16.8(2-Me), 7.8(4-Me)
2,4-Et_2(**17**)	129.8	[149.0]	185.0	[120.9]	145.0[b)]	149.4	116.0	131.5	124.9	129.0	133.4	144.4[b)]	22.9(2-CH_2), 16.0(4-CH_2), 12.8(4-Me), 12.1(2-Me)
2-NH_2-1,9-Me_2(**18**)	[113.4]	[143.2]	180.1	102.8	149.4	142.8[b)]	113.4	129.0	125.9	[138.3]	132.3	142.6[b)]	9.5(1-Me), 16.8(9-Me)
2-NH_2-4,6-Me_2(**19**)	100.2	[148.3]	177.9	[114.9]	145.2	147.9	[125.4]	130.7	124.3	126.4	134.3	142.7	14.9(6-Me), 7.7(4-Me)
N-Ph-*p*-QI(**20**)[c)]	141.7	132.7	187.3	128.0	133.4	120.5	129.0	126.1	129.0	120.5	149.4	157.2	
Δδ(PXZ—PTZ)[d)]	−4.7	−0.1	3.8	−12.6	13.9	25.0	−8.9	1.5	−2.7	−3.5	−5.7	−2.1	

a) Square brackets denote the positions of substituted carbons. b) Similar values may be interchanged. c) *N*-Phenyl-*p*-benzoquinone monoimine numbered as for **1**. d) Chemical shift difference between **1** and 3*H*-phenothiazin-3-one.

derivatives. The atomic coordinates of substituents were computed from known data regarding the corresponding bond lengths and bond angles.[23)] The CNDO/2 calculations of **4** shows that the pyramidal structure of an amino group, where one of the NH bonds is coplanar with the quinonoid ring and turns toward the CO group, is more stable than the planar structure. Therefore, CNDO/2 calculations of the 2-amino derivatives were carried out for the pyramidal structure. The geometry of *N*-phenyl-*p*-benzoquinone monoimine was estimated using the data of *N*-chloro-*p*-benzoquinone monoimine described in a preceding paper[7)] and assuming a torsional angle of 30° between the phenyl and quinonoid rings.

Results and Discussion

*^{13}C Chemical Shifts of 3*H*-Phenoxazin-3-one.* The ^{13}C chemical shifts of 3*H*-phenoxazin-3-ones are listed in Table 1. Their chemical shifts can be assigned on the basis of those of 3*H*-phenothiazin-3-ones[7)] and phenyl vinyl ether,[24)] and the estimation from the substituent-induced chemical shifts (SCS) of the corresponding group on benzenes and olefins.[25)] The replacement of the bridged S atom of 3*H*-phenothiazin-3-one by an O atom resulted in downfield shifts of C-3, C-4a, C-5a, and C-7, and upfield shifts of the other carbons, *i.e.*, a symmetrical change in the sign of the SCS toward the N–O axis.

The signal at δ 186.4 for the carbonyl carbon of **1** appeared at a lower field (by 3.8 ppm) than that of 3*H*-phenothiazin-3-one, but higher (by 0.9 ppm) than that of **20**. A similar result has been observed regarding the difference (4.2 ppm) of the chemical shifts of the carbonyl carbons between 3-ethylthio-5,6-dimethyl- and 3-ethoxy-2-cyclohexenones.[19b)] The remarkably high shielding of C-4 of **1** suggests a resonance of the vinyl ether type, *i.e.*, a strong π-polarization of the olefinic double bond by the ether oxygen. The high shielding of C-6 and C-8 is ascribed to the increased $2p_\pi$ electron densities because of the ortho and para positions with respect to the ether oxygen. The values of the upfield shifts of C-4, C-6, C-8, and C-9a caused by the oxygen substitution of 3*H*-phenothiazin-3-one were lower than those of the corresponding carbons between the phenyl vinyl ether and the phenyl vinyl sulfide.[24)] From the chemical shifts of C-1, C-3, and C-9, the partial positive charge of the carbonyl carbon of **1** seems to be less delocalized than that of the 3*H*-phenothiazin-3-one.

It is considered that **20** may serve as a reference compound to elucidate the relative abilities of O and S atoms interposed between two conjugated rings to transmit electronic effects. However, the finding that the ^{13}C chemical shifts of **20** are similar to those of the corresponding carbons of aniline[25)] and *N*-chloro-*p*-benzoquinone monoimine[7)] suggests a remarkably twisted structure between the phenyl and the quinonoid rings of **20** owing to a steric hindrance. Therefore, it is reasonable that the introduction of the bridged oxygen on **20** resulted in an SCS similar to or a little more than those of vinyl ether toward benzene

TABLE 2. THE FACTOR SCORES OF THE 2-SUBSTITUENTS OBTAINED BY THE PRINCIPAL FACTOR METHOD

Substituent	F_I	F_{II}	F_{III}	F_{IV}
H	1.830	−0.087	0.345	−2.063
Me	1.176	−0.619	−0.496	0.236
Et	1.032	−0.726	−0.478	1.495
NH_2	−0.546	0.694	−1.207	−0.396
NHMe	−0.880	0.431	−0.509	−0.030
NHEt	−1.050	0.386	−0.993	−0.824
NHAc	0.297	1.664	1.873	0.965
NHPh	−0.455	0.953	0.530	−0.117
NMePh	−0.089	−0.654	−0.643	1.206
OH	−1.314	−2.040	1.581	−0.468

for the ortho and the ipso carbons but the remarkable downfield shift for the meta carbon. C-10a moves to a higher field by 13.2 ppm relative to the imino carbon of **20**; the considerable upfield shift may be explained in terms of the nature of the oxazine ring rather than the substituent effect on the quinone imine.

Substituent Effect. To evaluate the factors controlling the chemical shifts of all the carbons of the 2-substituted phenoxazin-3-ones and their contributions, data analyses of the chemical shifts of **1—10** were performed using the principal factor method.[9] In the factor analysis, the chemical shift (or SCS) data matrix was transformed into a standard score matrix composed of 10×12 elements using Eq. 1:

$$z_{ij} = (\delta_{ij} - \bar{\delta}_j)/\sigma_j \quad (1)$$

where z_{ij} and δ_{ij} are the elements of the standard score matrix and the original chemical shift (or SCS) data matrix for the carbon j on substituent i, respectively; $\bar{\delta}_j$ and σ_j are mean and the standard deviations of variable j, respectively. The factor-loading and score matrices were derived from the correlation matrix, between the variables, whose diagonal elements are equal to communality by maximizing the sum of the squared loadings of the first factor (F_I). Thus,

$$z_{ij} = \sum_{m=1}^{M} f_{im} a_{jm} \quad (2)$$

where a_{jm} is the m th factor loading for variable j and f_{im} the m th factor score for substituent i, equivalent to the substituent constant. M indicates the upper limit of m and is equal to the number of positive eigenvalues obtained by the diagonalization of the correlation matrix, 11 in this case. From Eqs. 1 and 2

$$\delta_{ij} = \sum_{m=1}^{M} f_{im} a_{jm} \sigma_j + \bar{\delta}_j. \quad (3)$$

Table 2 shows the factor scores of the 2-substituents of 3*H*-phenoxazin-3-ones calculated by the principal-factor method. None of the factor score series obtained were found to be parallel to a single known substituent parameter. From the correlation of the factor scores with various substituent scales, the following multiparameter equations were found to be statistically sufficient to interpret F_I—F_{IV}.[26]

$$F_I = -2.55\Delta\iota + 0.67\sigma_R^+ + 1.76 \quad (r=0.985, n=7) \quad (4)$$

$$F_{II} = -21.89(C_2\text{-X}) + 23.25B_3 - 4.65B_3^2 + 4.89 \quad (r=0.967, n=8) \quad (5)$$

$$F_{III} = 12.24\sigma_I + 5.95\sigma_R^0 + 0.36B_4' - 0.17 \quad (r=0.975, n=7) \quad (6)$$

$$F_{IV}[27] = 29.27\Delta\iota + 3.92\sigma_R^+ - 0.79B_2 - 4.91N - 1.30 \quad (r=0.973, n=7) \quad (7)$$

where C_2–X represents the atomic distance[23] between C-2 and the substituent X, and B_2, B_3, and B_4' stand for the STERIMOL parameters[28] of the substituent. B_4' cooperates with B_1 as the wide scale of the substituent and corresponds to B_4 except for B_2 in the cases of the NH_2 and $NHCOCH_3$ groups. N in Eq. 7 denotes the number of lone-pair electrons of the central atom of substituent X.

As Eqs. 4 and 5 suggest, the F_I and F_{II} terms are associated with the electronic and the steric effects of the substituents, respectively. The F_{III} and the F_{IV} scales seem to depend not only on the electronic effect, but also on the steric effect, provided that F_{IV} can also be explained mainly in terms of the STERIMOL B_2 parameter as well as the electronic substituent parameter.[27]

Table 3 lists the factor loadings of the carbons along with the average and standard-deviation values of the chemical shifts. The above four factors account for 96% of the variability in the chemical-shift data matrix. The chemical shifts for C-1 induced by the 2-substituents can be explained mainly in terms of the first factor, *i.e.*, only the electronic parameter. As the contribution of the first factor (for the chemical shifts of all the carbons of the 2-substituted 3*H*-phenoxazin-3-ones) is only 67.4%, two or three factors including the steric factors are, in general, necessary to accurately evaluate the substituent effects that affect the chemical shifts for the other carbons; in particular, for the SCS of C-2, F_I and F_{IV} are taken into consideration.

As the product of the factor loading and the standard deviation of the chemical shifts shows, the first factor has a maximum effect on the chemical shift of C-1 and its electronic variation is transmitted to the alternative carbons (C-3, and C-9, C-5a, and C-7) which are the benzenoid ortho and para carbons relative to the N atom. The attenuation factors are 13, 7, 7, and 12%, respectively. Although F_I, F_{III}, and F_{IV} are associated with the resonance effect of the 2-substituents, the sign of the factor loading of the first factor coincides with that of the corresponding transmission coefficient of the resonance effect in Taft's DSP treatment because of

TABLE 3. THE FACTOR LOADINGS OF 2-SUBSTITUTED 3H-PHENOXAZIN-3-ONES OBTAINED BY THE PRINCIPAL FACTOR METHOD[a)]

Position	Factor loading				Main factor[b)]	$\bar{\delta}$[c)]	$\overline{SCS}$[d)]	S.D.[e)]	I×S.D.	II×S.D.
	I	II	III	IV						
C-1	0.951	−0.178	0.127	0.038	I	113.02	−22.21	14.05	13.36	−2.50
C-2	−0.822	−0.122	0.093	0.482	I, IV	148.37	13.59	5.20	−4.27	−0.63
C-3	0.623	−0.727	0.131	−0.119	I, II	182.47	−3.88	2.86	1.78	−2.08
C-4	0.843	−0.407	−0.224	0.117	I, II	105.06	−1.90	1.30	1.10	−0.53
C-4a	0.796	−0.391	0.389	−0.160	I, II, III	148.98	−0.73	0.37	0.29	−0.14
C-5a	0.801	−0.404	0.176	0.341	I, II, IV	147.58	−1.21	1.24	0.99	−0.50
C-6	0.812	0.558	−0.100	0.024	I, II	116.03	−0.16	0.12	0.10	0.07
C-7	0.939	0.303	0.018	0.099	I	130.18	−2.65	1.70	1.60	0.52
C-8	0.422	0.822	0.378	−0.014	I, II, III	125.31	−0.17	0.19	0.08	0.16
C-9	0.894	0.425	−0.047	0.072	I, II	129.05	−1.42	1.04	0.93	0.44
C-9a	−0.858	0.241	0.298	0.070	I	133.86	0.45	0.29	−0.25	0.07
C-10a	0.935	0.258	−0.198	0.086	I	142.98	−0.98	0.71	0.66	0.18
Factor contributions/%	67.4	20.4	4.7	3.6	2.1(V)[f)]		1.1(VI)[g)]			

a) Along with the product of the factor loading and the standard deviation of the ^{13}C chemical shifts. b) The contribution of the factor loading clearing the lower limit (a_{if}^2>0.10) is important. c) The average of the chemical shift. d) The average of the SCS. e) The standard deviation of the chemical shift. f) The fifth factor contribution. g) The sixth factor contribution.

the high contribution (*vide infra*). In the factor loading of the second factor having a steric character, the sign for almost all the quinonoid carbons is opposite to that for most benzenoid carbons. It is reasonable that the second factor causes the relatively large changes in the chemical shifts of C-1 and C-3.

Plots of the chemical shifts of C-2 versus the Inamoto-Masuda group electronegativities χ of the 2-substituents (**1**, **4**—**10**) excluding alkyl group afforded the excellent correlation;

$$\delta = 16.25\chi + 100.37 \quad (r=0.985,\ n=8) \tag{8}$$

This finding reinforces such an explanation that the contributions of the σ_R^+ terms in F_I and F_{IV} mainly controlling the SCS of C-2 offset each other by multiplicating their factor loadings.[29] The C_α or C_{ipso} SCS of monosubstituted methanes,[30,31] ethanes,[30] and benzenes[30,31] have also been reported to be proportional to the group electronegativity of the substituent.

Taft's DSP analysis is convenient for a simple interpretation of substituent effects in terms of the relative proportions of field/inductive and resonance effects shown by Eq. 9.

$$\delta = \rho_I\sigma_I + \rho_R\sigma_R + \delta_0 \tag{9}$$

where δ and δ_0 indicate the ^{13}C chemical shift of the carbon of interest and the intercept of the DSP equation respectively. ρ_I and ρ_R represent the transmission coefficients of the field/inductive and the resonance effects, respectively.

Although the pairs of substituent parameters giving the best correlation with the chemical shifts depend on the positions of the carbons, the chemical shifts of C-1 correlate very well with all of the substituent constants used for the DSP equation. As Eq. 7 shows, the behavior of the alkyl groups for C-2 appears to be different from that of the other 2-substituents in terms of an orbital-repulsion effect due to the absence of lone-pair electrons. The ρ values were obtained by applying Eq. 9 to the chemical shifts of **1** and six 2-substituted analogues (**2**, **3**, **4**, **7**, **8**, and **10**).

The polar and resonance effects will be discussed on the basis of both the ρ_I—ρ_R^0 values which are well applied to other compounds and the ρ_I—ρ_R^+ values having generally high correlation coefficients for the quinonoid carbons. Table 4 shows the ρ values for all the carbons of 2-substituted 3*H*-phenoxazin-3-ones. The resonance effect of the 2-substituents is most strongly transmitted to C-1; the magnitude (ρ_R^0= 70.73) for the resonance effect is similar to those (ρ_R^0= 63.03 and 75.54 respectively) for the effects in 3-substituted 2-cyclohexenes[32] and 2-substituted 1,4-naphthoquinoes.[33] The resonance effect of C-1 is transmitted to the alternant carbons, C-3 and C-4a, with attenuation factors of 20—22% and 2—3%, respectively. The magnitude of the reverse resonance effect of C-2 is 46—53% as high as that for the normal resonance effect of C-1. Those attenuation ratios are somewhat high relative to the values estimated by the first factor because not only the first factor but also the third and the fourth factors contribute to the resonance effect. The ρ_R^+ values of the benzenoid meta carbons, C-6 and C-8, relative to the N atom are almost zero.

It is reasonable from the resonance of the α,β-unsaturated ketone or imine between C-4a and C-3 or N that the ρ_R^+ value of C-4a is positive; the presence of an enone resonance between C-3 and C-4a is supported by indications that the signs of factor loadings from F_I to F_{IV} for C-4a are equal to those for C-3.

There are several main factors such as classical σ-inductive, π-inductive, direct through-space field, and

TABLE 4. CORRELATIONS OF THE ^{13}C CHEMICAL SHIFTS OF 3*H*-PHENOXAZIN-3-ONES WITH SUBSTITUENT CONSTANTS[a]

Symbol[b]	C-1	C-2[c]	C-3[d]	C-4	C-4a	C-5a	C-6	C-7	C-8[d]	C-9	C-9a	C-10a
ρ_I	−18.38	19.33	−11.63	−3.56	1.15	2.14	−0.29	−0.14	1.68	−0.38	1.13	−1.83
ρ_R^0	70.73	−32.44	14.44	5.42	2.11	7.53	0.40	9.31	0.59	5.11	−0.72	3.22
δ_0	136.12	136.40	186.43	106.74	149.53	149.38	116.18	132.77	125.44	130.49	133.52	144.01
r	0.993	0.940	0.966	0.921	0.858	0.904	0.659	0.813	0.899	0.737	0.749	0.854
f	0.120	0.341	0.260	0.390	0.514	0.427	0.752	0.582	0.437	0.676	0.663	0.520
ρ_I	−31.06	28.54	−12.44	−3.82	0.89	1.30	−0.42	−1.85	1.47	−1.51	0.95	−2.42
ρ_R^+	17.32	−9.17	3.87	1.58	0.56	2.02	0.08	2.16	0.09	1.18	−0.29	0.78
δ_0	134.82	134.91	186.37	106.79	149.52	149.35	116.16	132.53	125.40	130.35	133.46	143.94
r	0.989	0.980	0.998	0.975	0.916	0.965	0.620	0.786	0.829	0.710	0.832	0.851
f	0.147	0.200	0.068	0.224	0.402	0.262	0.784	0.619	0.560	0.704	0.555	0.526

a) Calculated from the seven point data set of the chemical shifts of **1**—**4**, **7**,**8**, and **10** except for C-2, C-3, and C-8. b) The symbols of ρ_I, ρ_R^0, and ρ_R^+ indicate the transmission coefficients having connections with σ_I, σ_R^0, and σ_R^+ respectively; δ_0 and r represent the intercept and the correlation coefficient for the DSP equation. f=S. D./R. M. S. c) Alkyl groups were excluded from the correlation. d) Calculated from the data with the hydroxyl group excluded.

TABLE 5. CNDO/2 π AND TOTAL ELECTRON DENSITIES OF 3*H*-PHENOXAZIN-3-ONES

Substituent		C-1	C-2	C-3	C-4	C-4a	C-5a	C-6	C-7	C-8	C-9	C-9a	C-10a
Nil(**1**)		3.9959	4.0454	3.7474	4.1354	3.8122	3.8332	4.0504	3.9692	4.0097	3.9943	3.9552	3.9348
	π	0.9800	1.0008	0.8578	1.1332	0.9263	0.9509	1.0569	0.9648	1.0306	0.9779	1.0468	1.0073
2-Me(**2**)		4.0249	3.9988	3.7540	4.1387	3.8117	3.8365	4.0494	3.9721	4.0087	3.9973	3.9529	3.9312
	π	1.0253	0.9632	0.8615	1.1372	0.9222	0.9558	1.0557	0.9697	1.0292	0.9823	1.0418	0.9969
2-Et(**3**)		4.0306	3.9991	3.7549	4.1389	3.8117	3.8372	4.0491	3.9727	4.0084	3.9979	3.9523	3.9296
	π	1.0349	0.9564	0.8624	1.1380	0.9215	0.9570	1.0553	0.9708	1.0288	0.9832	1.0407	0.9948
2-NH_2(**4**)		4.0659	3.9155	3.7671	4.1386	3.8115	3.8403	4.0480	3.9751	4.0072	4.0001	3.9501	3.9214
	π	1.0764	0.9398	0.8632	1.1434	0.9172	0.9620	1.0538	0.9749	1.0270	0.9870	1.0365	0.9871
2-NHMe(**5**)		4.0928	3.8879	3.7672	4.1396	3.8107	3.8443	4.0464	3.9786	4.0059	4.0041	3.9473	3.9131
	π	1.1225	0.9308	0.8656	1.1484	0.9123	0.9684	1.0519	0.9809	1.0252	0.9927	1.0308	0.9763
2-NHEt(**6**)		4.0723	3.9123	3.7684	4.1387	3.8117	3.8413	4.0477	3.9760	4.0069	4.0011	3.9493	3.9199
	π	1.0871	0.9287	0.8645	1.1441	0.9167	0.9635	1.0534	0.9764	1.0266	0.9884	1.0350	0.9843
2-OH(**10**)		4.0793	3.8553	3.7762	4.1376	3.8105	3.8400	4.0475	3.9743	4.0070	3.9995	3.9504	3.9185
	π	1.0915	0.9389	0.8645	1.1476	0.9140	0.9624	1.0535	0.9737	1.0266	0.9860	1.0375	0.9889
4-Me(**11**)		3.9955	4.0481	3.7557	4.0802	3.8392	3.8341	4.0508	3.9708	4.0096	3.9961	3.9534	3.9317
	π	0.9776	1.0039	0.8637	1.0957	0.9646	0.9516	1.0573	0.9673	1.0305	0.9803	1.0438	1.0001
4-Et(**12**)		3.9954	4.0478	3.7564	4.0798	3.8437	3.8340	4.0505	3.9709	4.0096	3.9970	3.9539	3.9296
	π	0.9770	1.0046	0.8645	1.0887	0.9734	0.9515	1.0572	0.9677	1.0306	0.9811	1.0438	0.9984
7-OMe(**13**)		3.9926	4.0512	3.7459	4.1378	3.8104	3.8111	4.1094	3.7848	4.0780	3.9707	3.9814	3.9468
	π	0.9760	1.0101	0.8550	1.1363	0.9264	0.9220	1.1219	0.9098	1.0971	0.9466	1.0883	1.0288
7-OEt(**14**)		3.9922	4.0521	3.7456	4.1390	3.8101	3.8107	4.1200	3.7860	4.0685	3.9707	3.9827	3.9483
	π	0.9753	1.0115	0.8544	1.1381	0.9257	0.9196	1.1288	0.9064	1.0919	0.9475	1.0904	1.0314
7-OAc(**15**)		3.9954	4.0400	3.7295	4.1273	3.8133	3.8177	4.0861	3.7858	4.0200	3.9802	3.9531	3.9242
	π	0.9830	0.9945	0.8824	1.1212	0.9357	0.9409	1.0910	1.0015	1.0478	0.9700	1.0418	0.9920
2,4-Me_2(**16**)		4.0244	4.0016	3.7624	4.0837	3.8384	3.8372	4.0498	3.9735	4.0086	3.9989	3.9512	3.9282
	π	1.0228	0.9665	0.8676	1.0999	0.9602	0.9563	1.0560	0.9719	1.0291	0.9845	1.0390	0.9902
2-NH_2-1,9-Me_2(**18**)		4.0192	3.9408	3.7670	4.1401	3.8130	3.8333	4.0595	3.9671	4.0279	3.9553	3.9702	3.9361
	π	1.0401	0.9800	0.8603	1.1438	0.9188	0.9479	1.0717	0.9585	1.0552	0.9513	1.0657	1.0048
2-NH_2-4,6-Me_2(**19**)		4.0658	3.9172	3.7749	4.0837	3.8372	3.8590	4.0020	3.9961	4.0014	4.0123	3.9454	3.9170
	π	1.0742	0.9422	0.8689	1.1075	0.9538	0.9876	1.0204	1.0036	1.0150	1.0054	1.0252	0.9788
N-Ph-*p*-QI(**20**)[a]		3.9867	4.0408	3.7672	4.0442	4.0034	4.0174	3.9921	3.9975	3.9893	4.0138	3.8998	3.9024

a) *N*-Phenyl-*p*-benzoquinone monoimine numbered as for **1**.

orbital repulsion effects which contribute to ρ_I.[34] In the case of the σ-inductive effect, the σ electron-deficient state of the carbon of interest induced by a σ-acceptor substituent decreases rapidly with an increasing number of intervening bonds between the substituent and the carbon.

The signs of the ρ_I values shown in Table 4 are consistent with those of the π-charge densities induced by the 2-substituents, except for the cases of C-6 and C-10a. Therefore, it is concluded that the main factors determining the ρ_I values, except for those of the carbon which is linked directly to the substituent, originate from π-inductive/field and orbital-repulsion effects rather than from a σ-inductive effect. A part of these polar effects spread along the π framework in the same manner as the resonance effect but with the different

attenuation ratios; the observed negative or positive ρ_I values in Table 4 suggest that the polar effect of the 2-substituents such as NH_2 and OH groups cooperates with the corresponding resonance effect in upfield or downfield shifts of all the carbons other than C-4a, C-5a, and C-8, respectively. The absolute ρ_I values for the quinonoid carbons indicate the lowering of the polar effect on going from C-2 to C-4a in the clockwise direction as well as the anticlockwise one of C-1→C-4a.

The ρ_I value (−6.11) for C-2 of 3-substituted 2-cyclohexenones[32] is much less negative than that (−18.38) for C-1 of **1**. The π electron density of the substituted carbon of the former is decreased by the π acceptor carbonyl group. The lesser polar effect for the olefinic β carbon may be ascribed to the lesser orbital repulsion responsible for the more decreased π electron density of the substituted carbon.

Judging from the SCS of 2-methyl, 4-methyl, and 2,4-dimethyl groups, the SCS values for all the carbons of 3*H*-phenoxazin-3-ones do not alter greatly in comparison with those of 3*H*-phenothiazin-3-ones. It is shown from the comparison between mono- and disubstituted analogues of methyl and ethyl groups on the 2- and 4-positions that an additivity relationship can be applied for 3*H*-phenoxazin-3-ones as well as for 3*H*-phenothiazin-3-ones.

Electronic Structure of 3H-Phenoxazin-3-ones. As Taft's DSP analysis for 3*H*-phenoxazin-3-ones shows, problems may arise during attempts to rationalize the ^{13}C chemical shifts on the basis of either π or the total electron densities alone. Table 5 lists the CNDO/2 π and total electron densities of 3*H*-phenoxazin-3-ones for the planar structure of their backbones. The ^{13}C chemical shifts gave a better correlation with the dual parameter system (r=0.940) composed of the π and σ electron densities than the π (r=0.908) or total electron density (r=0.919).

$$\delta = -100.29\sigma - 225.12\pi + 656.96 \quad (r=0.940,\ n=180) \quad (10)$$

Using INDO π and σ electron densities, the value of the correlation coefficient, r, for the chemical shifts of all the carbons of **1** is enhanced to be 0.955.[35] As Eq. 10 shows, the ^{13}C chemical shifts are much more sensitive to the π electron densities than the σ electron densities.

Figure 2 shows the CNDO/2 charge densities for **1** and the substituent-induced charge densities for **2**, **4**, and **11**. The π charge densities of all the carbons of **1** show alternative polarizations due to the presence of the electron-withdrawing carbonyl group and the π electron-donating ether oxygen. The CNDO/2 σ charge densities of their carbons of **1** indicate the partial positive charges on the carbons bonded to the heteroatoms and the lesser positive charges on C-6 and C-8. C-2 has the highest σ electron density among the twelve carbons of **1**.

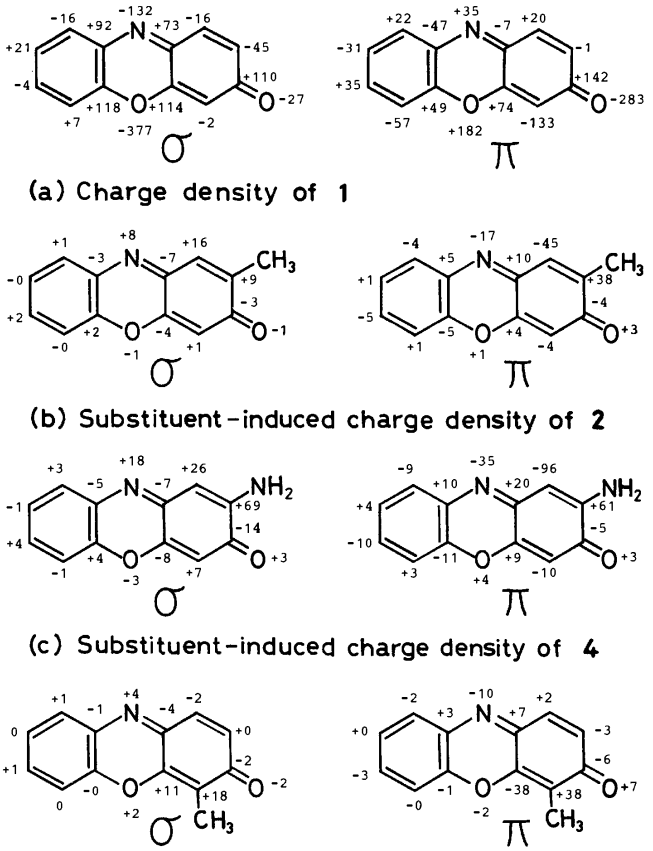

Fig. 2. CNDO/2 σ and π charge densities of **1** and substituent-induced σ and π charge densities. The values shown should be divided by 1000 to obtain electron charge units.

The delocalization of the lone-pair or pseudo-π electrons of the 2-substituent resulted in the increased π electron densities at C-1, C-3, C-5a, C-7, and C-9. The negative substituent-induced π charge density of C-4 suggests the polarization of the C-4–C-4a bond by the ether oxygen. The upfield shift of C-10a by the 2-substituent, contrary to the estimation from the CNDO/2 calculations, may be explained in terms of an enimine resonance between C-4 and C-10a.

From the correlation of the CNDO/2 π or σ charge density induced by the 2-substituents such as methyl, ethyl, amino, and hydroxyl groups with the parameters obtained by the principal factor method, Eq. 11 holds for all substituents with r=0.94—0.99;

$$10^4\Delta q_i = \mathrm{A}a_{i_1}\sigma_i + \mathrm{B}a_{i_4}\sigma_i + \mathrm{C} \quad (11)$$

where Δq_i indicates the substituent-induced CNDO/2 π or σ charge density of the carbon i and A, B, and C are constants; a_{ij} and σ_i stand for the j th factor loading and the standard deviation of the chemical shifts for the carbon i shown in Table 3, respectively.

Table 6 lists the values of these constants for the 2-substituents. In the case of the π-electron system, A and

TABLE 6. THE CORRELATION OF THE SUBSTITUENT-INDUCED CNDO/2 π OR σ CHARGE DENSITIES OF 2-SUBSTITUTED 3H-PHENOXAZIN-3-ONES WITH THE FACTORS OBTAINED BY PRINCIPAL FACTOR METHOD[a)]

Substituent	π-Electron system				σ-Electron system			
	A	B	C	r	A	B	C	r
2-Me(**2**)	−39.36	65.30	28.19	0.973	11.35	64.83	−22.62	0.940
2-Et(**3**)	−47.54	75.01	33.96	0.973	15.34	45.89	−25.14	0.935
2-NH_2(**4**)	−80.92	68.92	60.90	0.973	10.40	307.61	−40.53	0.987
2-OH(**10**)	−91.85	51.78	66.87	0.978	2.59	527.20	−43.41	0.991

a) The constants of A, B, and C are equal to those in Eq. 11; r denotes correlation coefficient.

C become negatively and positively larger, respectively, with an increasing group-electronegativity of the 2-substituents. In the case of the σ-electron system, as σ_I of the 2-substituents increases, A decreases while B becomes larger; the more the group electronegativity of the 2-substituents increases, the more C increases negatively. The F_I—F_{IV} pair rather than the F_I—F_{II} or F_I—F_{III} pair gave a better correlation with the σ-electron densities as well as the π-electron densities. The $a_i\sigma_i$ terms can be replaced by the transmission coefficients, obtained by a DSP treatment, with little change of r for the π-electron system but with a considerable lowering of r for σ-electron system.

In the case of **11**, the substituent-induced partial charges distribute in contrast with the polarization of **1** except for those of C-1 and C-4a for the σ system and those of C-1 and C-2 for the π system. The partial charges of C-4a is dispersed by the enone and the enimine resonances.

From a comparison of **2**, **11**, **16**, and the corresponding 3*H*-phenothiazin-3-ones, the significant difference for the relative abilities of the O and the S atoms to transmit the electronic effect of substituents was not observed because the π-electron transfer between the benzenoid and the quinonoid rings was carried out chiefly through the N atom.

The present work was supported by a Grant-in-Aid for Scientific Research No. 59550570 from the Ministry of Education, Science and Culture. Thanks are due to the Computer Center of the Institute for Molecular Science for its assistance in the CNDO/2 calculations.

References

1) J. K. Landquist, "Six-membered Ring Systems," in "Comprehensive Organic Chemistry, Vol. 4, Heterocyclic Compounds," ed by P. G. Sammes, Pergamon Press, Oxford (1979).

2) S. C. Jain and H. M. Sobell, *J. Mol. Biol.*, **68**, 1 (1972).

3) K. I. Pashkevich, G. B. Afanas'eva, E. G. Kovalev, and I. Ya. Postovskii, *Khim. Geterostsikl. Soedin.*, No. 10, 1316 (1970).

4) H. Musso and H. Matthies, *Chem. Ber.*, **90**, 1814 (1957).

5) J. F. Corbett, *Spectrochemica Acta*, **21**, 1411 (1965).

6) H. Achenbach and J. Worth, *Chem. Ber.*, **110**, 12 (1977).

7) K. Hasegawa and Y. Ueno, *Bull. Chem. Soc. Jpn.*, **57**, 510 (1984); the values of the chemical shifts for C-1 and C-10a of 1,2,4-trimethyl-3*H*-phenothiazin-3-one (**12**) in Table 1 in p. 511 must be interchanged: δ_{C-1}=142.5, δ_{C-10a}=145.8.

8) a) R. W. Taft, *J. Phys. Chem.*, **64**, 1805 (1960); b) P. R. Wells, S. Ehrenson, and R. W. Taft, *Prog. Phys. Org. Chem.*, **6**, 147 (1968); c) S. Ehrenson, R. T. C. Brownlee, and R. W. Taft, *ibid.*, **10**, 1 (1973).

9) For example, a) A. L. Comrey, "A first course in factor analysis," Academic Press (1973); b) S. Shiba, "Factor Analysis (in Jap.)," second ed., Univ. Tokyo Pub. (1979).

10) B. A. K. Chibber, A. Balasubramanian, and T. Viswanatha, *Can. J. Biochem.*, **51**, 204 (1973).

11) G. B. Afanas'eve, I. Ya. Pastovskii, and T. S. Viktorova, *Khim. Geterostsikl. Soedin.*, No. 9, 1200 (1978).

12) G. W. K. Cavill, P. S. Clezy, and F. B. Whitfield, *Tetrahedron*, **12**, 139 (1961).

13) K. H. Meyer and W. E. Elbers, *Chem. Ber.*, **54**, 337 (1921).

14) R. Nietzki, A. Dietze, and H. Mäckler, *Chem. Ber.*, **22**, 3020 (1889).

15) Y. Ueno, *J. Heterocyclic Chem.*, **19**, 1579 (1982).

16) Y. Ueno, *Liebigs. Ann. Chem.*, **161** (1983).

17) Y. Ueno, *Pharmazie*, **38**, 626 (1983).

18) T. Uemura and M. Abe, *Bull. Chem. Soc. Jpn.*, **12**, 59 (1937).

19) a) R. T. C. Brownlee, D. G. Cameron, R. D. Topson, A. R. Katritzky, and A. F. Pozharsky, *J. Chem. Soc., Perkin Trans.*, **2**, 247 (1974); b) G. R. Bedford and P. J. Taylor, *Org. Magn. Reson.*, **9**, 49 (1977); c) C. Hansch, A. Leo, S. H. Unger, K.-H. Kim, D. Nikaitani, and E. J. Lien, *J. Med. Chem.*, **16**, 1207 (1973); d) C. Hansch, S. D. Rockwell, P. Y. C. Jow, A. Leo, and E. E. Steller, *ibid.*, **20**, 304 (1977); e) N. Inamoto, "Chemical Seminor 10, Hammett Rules-structure and reactivity (in Jap.)," Maruzen (1983).

20) a) N. Inamoto and S. Masuda, *Chem. Lett.*, **1982**, 1003; b) N. Inamoto and S. Masuda, *ibid.*, **1982**, 1007.

21) N. Inamoto, private communication.

22) J. A. Pople and D. L. Beveridge, "Approximate Molecular Orbital Theory," McGraw-Hill, New York, N. Y. (1970); J. A. Pople and G. A. Segal, *J. Chem. Phys.*, **44**, 3289 (1966).

23) L. E. Sutton, "Table of Interatomic Distances," Special Publications No. 11 and 18, ed by the Chemical Society, London (1958) and (1965).

24) W. F. Reynolds and R. A. McClelland, *Can. J. Chem.*, **55**, 536 (1977).

25) a) J. B. Stothers, "Carbon-13 NMR Spectroscopy," Academic Press, New York (1972); b) F. W. Wehrli and T. Wirthlin, "Introduction of Carbon-13 NMR Spectra," Heyden & Son, London (1978); c) G. C. Levy, R. L. Lichter, and G. L. Nelson, "Carbon-13 Nuclear Magnetic Spectroscopy," second ed., John Wiley & Sons, New York (1980).

26) Obtained from either the seven point data set of H, CH_3, C_2H_5, NH_2, $NHCOCH_3$, NHC_6H_5, and OH groups or eight point data set composed of the seven and NHC_2H_5 groups.

27) a) $F_{IV}=22.70\Delta\iota+1.13\sigma_R^+-3.72N-2.06$ ($r=0.949$, $n=7$); b) $F_{IV}=3.44\sigma_I+4.38\sigma_R^0+6.57B_1-8.59$ ($r=0.948$, $n=7$); c) $F_{IV}=14.16B_2-3.01B_2^2-0.80B_2^3-12.33$ ($r=0.942$, $n=8$).

28) A. Verloop, W. Hoogenstraaten, and J. Tipker, "Drug Design," Vol. VII, E. J. Ariëns, Academic Press, New York (1976).

29) From Eq. 4 and Ref. 27a, $0.482F_{IV}-0.822F_I=13.04\Delta\iota-0.01\sigma_R^+-1.74N-2.44$.

30) H. Spiesecke and W. G. Schneider, *J. Chem. Phys.*, **35**, 731 (1961).

31) N. Inamoto, S. Masuda, K. Tokumaru, K. Tori, M. Yoshida, and Y. Yoshimura, *Tetrahedron Lett.*, 3711 (1976).

32) Calculated for the six point data set (H, Ph, OEt, and NBu_2 in Table 1 in Ref. 19b, Me from *Can. J. Chem.*, **43**, 596 (1965), and NMe_2 from *Org. Magn. Reson.*, **5**, 456 (1965)); C-1: $\delta=4.71\sigma_I+6.15\sigma_R^0+198.85$ ($r=0.947$), $\delta=2.43\sigma_I+1.71\sigma_R^+ + 198.72$ ($r=0.907$); C-2: $\delta=-6.11\sigma_I+63.03\sigma_R^0+132.94$ ($r=0.988$), $\delta=-28.18\sigma_I+18.06\sigma_R^+ +131.95$ ($r=0.979$); C-3: $\delta=43.96\sigma_I-17.74\ \sigma_R^0+154.98$ ($r=0.880$), $\delta=51.37\sigma_I-4.55\sigma_R^+ + 155.62$ ($r=0.856$).

33) G. Höfle, *Tetrahedron*, **33**, 1963 (1977); C-1: $\delta=-14.22\sigma_I+1.80\sigma_R^0+184.61$ ($r=0.9997$), $\delta=-14.37\sigma_I+0.75\sigma_R^+ + 184.61$ ($r=0.9997$); C-2: $\delta=-4.12\sigma_I-48.33\sigma_R^0+140.68$ ($r=0.907$), $\delta=-5.34\sigma_I-21.79\sigma_R^+ +140.27$ ($r=0.985$); C-3: $\delta=15.24\sigma_I+5.54\sigma_R^0+140.94$ ($r=0.933$), $\delta=12.15\sigma_I+32.94\sigma_R^+ + 141.23$ ($r=0.984$), for the five point data set (H, OMe, OAc, Cl, and Me from *Tetrahedron Lett.*, 619 (1976)). For the σ_R^+ system, the OAc group was excluded because of its unknown value.

34) W. F. Reynolds, *Prog. Phys. Org. Chem.*, **14**, 165 (1982).

35) $\delta=-79.55\sigma-212.76\pi+582.55$ ($r=0.955$, $n=12$).

Intermolecular Bromine Transfer of 2-Amino-7-bromotropone Derivatives Catalyzed by Strong Acid[1)]

Hidetsugu WAKABAYASHI,* Sumio ISHIKAWA, Harue OKAI,† and Tetsuo NOZOE†
Department of Chemistry, Faculty of Science, Josai University, Sakado, Saitama 350-02
†*Tokyo Research Laboratories, Kao Corporation, 1-3 Bunka, Sumida-ku, Tokyo 131*
(Received April 17, 1985)

Upon heating acetic acid containg a trace amount of concd sulfuric acid at 120 °C under nitrogen, 2-bromo-7-(2-hydroxyanilino)tropone (**1a**) gave 6-bromocyclohepta[*b*][1,4]benzoxazine (**2a**) as the main product and cyclohepta[*b*][1,4]benzoxazine, its 6,8-dibromo derivative and trace amounts of other mono-, di-, and tribromo compounds. This reaction became much more complex in the presence of oxygen. A similar bromine transfer was observed for 2-bromo-7-(dimethylamino)-, 7-(2-hydroxy-5-methylanilino)-, and 7-(2-methoxyanilino)tropone although the cite of the intermolecular bromine transfer depended upon the structures of the substrates and the reaction conditions. In contrast, **2a** and 2-amino-5-bromotropone derivatives were completely stable towards the strong acid. Possible reaction pathways for this bromine transfer reaction are discussed.

We previously reported that 2-bromo-7-(2-hydroxyanilino)tropone (**1a**) afforded an almost quantitative yield of 6-bromocyclohepta[*b*][1,4]benzoxazine (**2a**) upon heating at 120 °C in acetic acid containing a trace amount of concd sulfuric acid.[2)] However, upon repeating the preparation of **2a** and carefully separating the reaction products by chromatography, we isolated unexpected and interesting by-products. The structures of these compounds are reported in this paper together with a mechanistic study regarding the unique bromine transfer involved in the formation of these compounds. This can be regarded as another example of our frequent observation[3)] that a subtle change of reaction conditions causes a considerable alteration of product ratios.

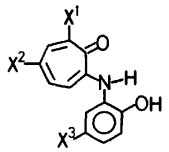

1	X^1	X^2	X^3
a	Br	H	H
b	H	H	H
c	Br	Br	H
d	H	Br	H
e	Br	H	Me
f	H	H	Me
g	Br	Br	Me

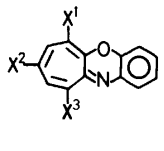

2	X^1	X^2	X^3
a	Br	H	H
b	H	H	H
c	Br	Br	H
d	H	Br	H
e	Br	H	Br
f	Br	Br	Br
g	Cl	H	H

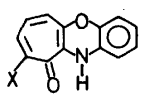

3a : X=H
3b : X=Br

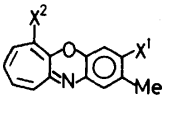

4a : X^1=H, X^2=Br
4b : X^1=X^2=H
4c : X^1=X^2=Br

Results and Discussion

When **1a** was heated at 120 °C for 2 h in acetic acid containing a trace amount of concd sulfuric acid, a detailed observation using HPLC showed that the reaction mixture contained, besides the main product **2a**, a large number of simultaneously formed by-products. The separation of these reaction products using silica-gel centrifugal chromatography afforded **2a**[2)] (55% yield), the parent cyclohepta[*b*][1,4]benzoxazine[2)] (**2b**, brown needles, 4% yield), the 6,8-dibromo derivative (**2c**, brown needles, 10% yield), cyclohepta[*b*][1,4]benzoxazin-10(11*H*)-one[4)] (**3a**, red needles, 3% yield), and its 9-bromo derivative (**3b**, red needles, 11% yield) as well as unreacted starting material (**1a**, 14% yield) and small proportions of 8-bromo (**2d**), 6,10-dibromo (**2e**), and 6,8,10-tribromo compound (**2f**). Furthermore, it was confirmed that 2-aminotropone derivatives **1b** and **1c** were also present in small quantities. Structures of these products were established either on the basis of their spectral data (see Experimental section) or by separate syntheses.

When conducted under nitrogen, the above reaction yielded **2a** (71%), **2b** (7.4%), and **2c** (6.8%) along with trace amounts of **2d**—**f**, but no oxo derivatives, **3a** and **3b**. As compound **3a** was produced from **2b** upon exposure to air for a long period or upon airation at 120 °C in acetic acid, **3a** was apparently a secondary, autoxidation product of **2b**. On the other hand, compound **3b** was formed from **1a** by oxygenation at 120 °C in acetic acid, suggesting that **3b** was most likely produced by the autoxidation of the cyclic tautomer, as shown in Scheme 1.

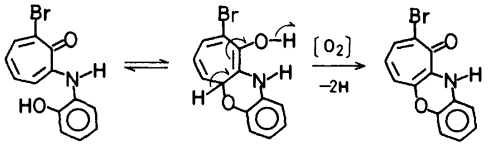

1a 3b

Scheme 1.

A similar acidic treatment of 2-bromo-7-(2-hydroxy-5-methylanilino)tropone (**1e**) under nitrogen resulted in a ring-closure to give **4a**[5)] (66% yield), the bromine-free compound (**4b**, 6.4% yield), and the 3,6-dibromo-2-methyl derivative (**4c**, 6.4% yield). The structures were based on their spectral data; the ABCX signal pattern

of the four protons on the seven-membered ring of **4c** in the ^{1}H NMR closely resembles those of **2a**. Thus, the cite of the second bromine atom on the benzene ring [at C-3 based on the small J value (<1 Hz) between the remaining two ring-proton signals] was established. It was confirmed that the 6-bromocyclohepta[*b*][1,4]benzoxazines **2a** and **4a** were completely stable under these conditions.

These results suggested that a bromine migration reaction under strongly acidic conditions had taken place at the stage of the anilinotropones (**1a**, **1e**) prior to the ring-closure. Indeed, when the methyl ether (**5a**)[2] that was prevented from cyclizing to the benzoxazine was subjected under the same conditions, 2-(2-methoxyanilino)tropone (**5b**)[6] and its dibromo derivative (**5c**) were obtained.

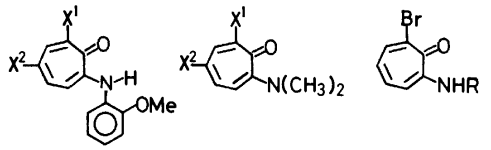

5	X^1	X^2
a	Br	H
b	H	H
c	Br	Br
d	H	Br

6	X^1	X^2
a	Br	H
b	H	H
c	Br	Br
d	H	Br

7a: R=H
7b: R=Me

Then, in order to examine the role of the arylamino group in this bromine-transfer reaction, 2-bromo-7-(dimethylamino)tropone (**6a**) was similarly treated with concd sulfuric acid-acetic acid at 120°C. The reaction was followed by time-dependent HPLC, which clearly showed the simultaneous formation of three main products. A spectroscopic analysis, as well as a comparison with the authentic specimens prepared separately, clarified the structures of these compounds to be bromine-free 2-(dimethylamino)tropone (**6b**),[7] its 5,7-dibromo (**6c**), and 5-bromo derivative (**6d**). Treatment of 2-amino- and 2-(methylamino)-7-bromotropone (**7a,b**)[8] with the same mixed acid afforded a similar type of products derived by the apparent disproportionation reaction.

The use of perchloric acid or phosphoric acid (instead of concd sulfuric acid) in acetic acid for the ring-closure of **1a** also caused a bromine transfer, but yields of products **2b** and **2c** became considerably lower. The use of concd hydrochloric acid afforded 6-chloro compound (**2g**) besides **2a**—c; **2g** was confirmed to be produced from the 6-bromo compound (**2a**) (but not from the ring-opened precursor **1a**) by the halogen-exchange reaction. It should be noted that, when **1a** was heated at 120°C under nitrogen in acetic acid containing concd hydrobromic acid, 8-bromocyclohepta[*b*][1,4]benzoxazine (**2d**) became the main product (47% yield) instead of **2a** (3% yield) or **2b**,c (8% yield each).

The fact that the described acid-catalyzed bromine migration takes place only when the bromine atom is situated at C-7** of the 2-aminotropone form (**I**), suggests the following probable reaction pathways (Scheme 2).

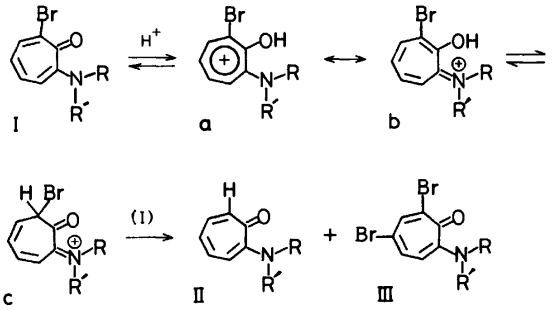

Scheme 2.

The 2-(arylamino)- and 2-(dimethylamino)-7-bromotropone (**1a** and **6a**) give their protonated tropylium species (**a**). It was stabilized as an iminium form (**b**) and existed in equilibrium with the tautomeric keto form (c). The latter presumably reacts as an electrophilic reagent towards the unprotonated substrate (**I**), resulting in a transfer of the bromine atom to give 2-aminotropones (**II**) and the 5,7-dibromo derivatives **III** in a manner analogous to a disproportionation reaction. The reactive intermediate c is most likely to undergo electrophilic bromination at a position having the highest nucleophilicity in the molecule **I**.[9] This gives rise to a dibromo product in which, in some cases, the second bromine atom is on the benzene ring (*e.g.*, **4c**). The formation of a larger proportion of the 8-bromo compound **2d** from **1a** upon heating in HBr-AcOH could be explained by the transformation of the intermediate c (Scheme 2) to **II**, assisted by the bromide anion. This liberated a certain quantity of bromine atoms. Subsequently, this resulted in bromination at the 5-position of 2-aminotropones (**II**), followed by an acid-catalyzed ring-closure to afford **2d**. This pathway is supported by the fact that **1b** gave only **2b** under the same conditions.

Although the exact mechanisms of this unusual substitution and the ring-closure involving an interesting intermolecular bromine shift are currently under a detailed investigation, the present experimental results clearly demonstrate a further example of the diversity of chemical reactions and the intricate character of troponoid compounds.

Experimental

Melting points are uncorrected. The IR and electronic spectra were taken on a Shimadzu IR-450 and a Shimadzu UV-202 spectrometer, respectively. The UV spectra in acid and alkali were taken after adding a few drops of 3 M HCl or 3 M NaOH (1 M=1 mol dm^{-3}) to a sample solution. The

**2-Amino-5-bromotropones are stable under these acidic condition.

NMR spectra were measured in $CDCl_3$ (unless otherwise specified) on a JEOL JNM-PS/PFT (100 MHz) and a JEOL JNM-GX270 (270 MHz) spectrometer using TMS as an internal standard. The mass spectra were taken on a JEOL JMS-DX300 mass spectrometer and a Shimadzu LKB 9000 GC-mass spectrometer at 75 eV. The HPLC was carried out with Hitachi gel #3011 with MeOH–hexane (9:1) as a solvent. The centrifugal chromatography was performed with a Hitachi CLC-5 instrument in a Fuji silica-gel layer (KT-2151, 5-mm thick) using benzene as an eluant.

Reaction of 2-Bromo-7-(2-hydroxyanilino)tropone (1a).

A. Under Aerobic Conditions: A trace amount of concd sulfuric acid was added to a solution of **1a** (700 mg) in acetic acid (8 ml). The mixture was heated at 120 °C for 2 h and evaporated *in vacuo*. The residue was neutralized with aqueous $NaHCO_3$ and extracted with benzene. The combined extracts were washed with water, dried (Na_2SO_4), and concentrated *in vacuo*. The residual solid was chromatographed centrifugally in a layer of silica gel with benzene as the eluant, giving **2a**[2] (360 mg, 55% yield), **2b**[2] (20 mg, 4% yield), **2c** (see below, 85 mg, 10% yield), **3a**[4] (15 mg, 3%), **3b** (see below, 75 mg, 11%), **2d** (see below, 5 mg, 0.8%), **2e** (see below, <1%), and **2f** (see below, <1%). The starting material **1a** (≃100 mg, 14%) containing a small proportion of **1b**,[2] and **1c** (see below) were recovered by eluating the silica-gel layer with MeOH.

B. Under Nitrogen. A solution of **1a** (393 mg) in acetic acid (4 ml) containing a trace amount of concd sulfuric acid was heated under nitrogen at 120 °C for 2 h, followed by the same work-up procedures as above, giving **2a** (262 mg, 71%), **2b** (19.5 mg, 7.4%), **2c** (32.5 mg, 6.8%), and **2d—f** (6 mg, <2%), along with **1a** containing **1b** and **1c** (50 mg, 13%).

2,4-Dibromo-7-(2-hydroxyanilino)tropone (1c). A mixture of 2,4-dibromo-7-methoxytropone[10] (500 mg, 1.70 mmol) and *o*-aminophenol (287 mg, 2.63 mmol) in 1-butanol was heated at 120 °C for 2 h. After cooling, the precipitates were filtered off and recrystallized from methanol to give 565 mg (90%) of **1c** [2,4-dibromo-7-methoxytropone (30 mg, 6%) was recovered from the filtrate]: yellow needles; mp 198—199 °C; UV λ_{max} (MeOH) 264 (log ε, 4.20), 359 (3.89), and 438 nm (4.00); IR (KBr) 3400 (OH), 3350 (NH), and 1588 cm^{-1} (C=O); ^1H NMR (100 MHz) δ=8.65 (1H, bs, NH), 8.42 (1H, d, $J_{3,5}$=2.0 Hz, H-3), 7.50 (1H, dd, $J_{5,6}$=11.2 Hz, H-5), 7.0—7.2 (4 H, m, H-3′, 4′, 5′, 6′), and 6.59 (1H, d, H-6).

Found: C, 42.10; H, 2.49; N, 3.78%; M^+, 373. Calcd for $C_{13}H_9NO_2Br_2$: C, 42.08; H, 2.48; N, 3.78%; M, 373.

6,8-Dibromocyclohepta[b][1,4]benzoxazine (2c). A solution of **1c** (161 mg) in acetic acid (5 ml) containing a trace amount of concd sulfuric acid was heated at 120 °C for 1.5 h under nitrogen, followed by the same procedures as those described for **1a**. The residual solid was recrystallized from benzene to give 132 mg (86%) of **2c**: brown needles; mp 165—166 °C; UV λ_{max}(MeOH) 262 (log ε, 4.47), 306 (3.66), and 415 nm (3.86); IR (KBr) 3080 (CH) and 1637 cm^{-1} (C=N); ^1H NMR (270 MHz) δ=6.8—6.9 (3H, m, H-1, 2, 3), 6.79 (1H, d, $J_{7,9}$=2.2 Hz, H-7), 6.60 (1H, m, H-4), 6.19 (1H, dd, $J_{9,10}$=12.9 Hz, H-9), and 5.89 (1H, d, H-10), ($CDCl_3$+CF_3COOD) δ=8.00 (1H, d, $J_{7,9}$=2.2 Hz, H-7), 7.44 (1H, dd, $J_{9,10}$=11.9 Hz, H-9), 7.05 (1H, td, J=8.0 and 1.5 Hz, H-2 or 3), 6.96 (1H, td, J=8.0 and 1.5 Hz, H-3 or 2), 6.70—6.85 (2H, m, H-1, 4), and 6.75 (1H, d, H-10).

Found: C, 44.43; H, 2.13; N, 3.77%; M^+, 355. Calcd for $C_{13}H_7NOBr_2$: C, 44.23; H, 2.00; N, 3.97%; M, 355.

9-Bromocyclohepta[b][1,4]benzoxazin-10(11H)-one (3b): Red needles (from benzene); mp 223—224 °C; UV λ_{max} (MeOH) 240 (log ε, 4.22), 270 (4.08), 294 (4.04), 330 (3.80), and 500 nm (3.79); IR (KBr) 3300 (NH) and 1574 cm^{-1} (C=O); ^1H NMR (270 MHz) δ=7.79 (1H, dd, $J_{6,8}$=1.0 and $J_{7,8}$=9.5 Hz, H-8), 6.79 (1H, dd, $J_{6,7}$=11.1 Hz, H-6), 6.5—6.8 (4H, m, H-1, 2, 3, 4), and 6.42 (1H, dd, H-7).

Found: C, 53.55; H, 2.83; N, 4.91%; M^+, 291. Calcd for $C_{13}H_8NO_2Br$: C, 53.82; H, 2.78; N, 4.83%; M, 291.

8-Bromocyclohepta[b][1,4]benzoxazine (2d): Red brown needles (from benzene); mp 163—164 °C; UV λ_{max} (MeOH) 262 (log ε, 4.43), 271 (4.35), 298 (3.93), and 414 (4.12), (MeOH+3 M HCl) 265 (log ε, 4.43), 273 (4.35), 325 (3.95), and 447 nm (4.06); IR (KBr) 1580 cm^{-1} (C=N); ^1H NMR (270 MHz) δ=6.7—6.8 (3H, m, H-1, 2, 3), 6.38 (1H, m, H-4), 6.24 (1H, dd, $J_{7,9}$=2.0 and $J_{6,7}$=10.2 Hz, H-7), 6.21 (1H, dd, $J_{9,10}$=13.2 Hz, H-9), 5.84 (1H, d, H-10), and 5.12 (1H, d, H-6).

Found: C, 56.92; H, 3.22; N, 5.13%; M^+, 275. Calcd for $C_{13}H_8NOBr$: C, 56.96; H, 2.94; N, 5.11%; M, 275.

6,10-Dibromocyclohepta[b][1,4]benzoxazine (2e): Red brown solid; UV λ_{max} (MeOH) 261, 270, 313, and 414 nm, (MeOH+3 M HCl) 268, 273, 325, 448, and 480 nm; M^+, 355.

6,8,10-Tribromocyclohepta[b][1,4]benzoxazine (2f): Red brown solid; UV λ_{max} (MeOH) 238, 263, 271, 400, 416, and 445 nm, (MeOH+3 M HCl) 258, 309, and 393 nm; M^+, 435.

Reaction of 2-Bromo-7-(2-hydroxy-4-methylanilino)tropone (1e). A similar treatment (to that for **1a**) of **1e** (500 mg) with acetic acid (10 ml) containing a trace amount of concd sulfuric acid at 120 °C for 1.5 h under nitrogen gave **4a**[5] (310 mg, 66%), **4b** (see below, 22 mg, 6.4%), and **4c** (see below, 38 mg, 6.4%), besides the recovered **1e** (100 mg, 20%) containing **1f** and **1g** (<2% each).

2-Methylcyclohepta[b][1,4]benzoxazine (4b). A mixture of 2-chlorotropone (370 mg, 2.63 mmol) and 2-amino-4-methylphenol (486 mg, 3.95 mmol) in acetic acid (5 ml) was heated at 120 °C for 3 h, followed by the same work-up procedures as for **1a**. This gave 280 mg (51%) of **4b**: red brown needles (from benzene); mp 86—87 °C; UV λ_{max} (MeOH) 256 (log ε, 4.28), 264 (4.35), 273 (4.31), 305 (3.73), and 415 nm (4.01), (MeOH+3 M HCl) 226 (log ε, 4.38), 268 (4.38), 275 (4.40), 326 (3.88), and 440 (3.98); IR (KBr) 2930 (CH) and 1600 cm^{-1} (C=N); ^1H NMR (270 MHz) δ=6.61 (1 H, d, $J_{1,3}$=2 Hz, H-1), 6.55 (1H, dd, $J_{3,4}$=8 Hz, H-3), 6.28 (1H, d, H-4), 6.16 (2H, m, H-9, 10), 5.99 (1H, ddd, $J_{7,8}$=10.7, $J_{6,7}$=9.4, and $J_{7,9}$=1.5 Hz, H-7), 5.79 (1H, td, $J_{8,10}$=3.9 and $J_{8,9}$=10.7 Hz, H-8), 5.46 (1H, d, H-6), and 2.12 (3H, s, CH_3).

Found: M^+, 209.0813. Calcd for $C_{14}H_{11}NO$: M, 209.0840.

3,6-Dibromo-2-methylcyclohepta[b][1,4]benzoxazine (4c): Red brown needles (from benzene); mp 121—122 °C; UV λ_{max} (MeOH) 232 (log ε, 4.20), 268 (4.28), 275 (4.25), 305 (3.83), and 415 nm (3.94), (MeOH+3 M HCl) 235 (log ε, 4.18), 275 (4.25), 281 (4.26), 325 (3.84), and 450 nm (3.83); IR (KBr) 1631 cm^{-1} (C=N); ^1H NMR (100 MHz) δ=6.80 (1H, s, H-4), 6.72 (1H, s, H-1), 6.39 (1H, td, $J_{7,9}$=0.5 and $J_{7,8}$=11.7 Hz, H-7), 6.05 (2H, m, H-9, 10), 5.58 (1H, $J_{8,9}$=4.4 Hz, H-8), and 2.20 (3H, s, CH_3).

Found: M^+, 364.9059, 366.9056, and 368.9024 (1:2:1). Calcd for $C_{14}H_9NOBr_2$: M, 364.9051, 366.9032, and 368.9012.

2,4-Dibromo-7-(2-methoxyanilino)tropone (5c). A suspension of **1c** (80 mg) in ether was treated with an excess of ethereal diazomethane. After allowing it to stand for 1 d, the solvent was evaporated *in vacuo* and the residual solid was chromatographed in a short column of alumina with ether as an eluant, giving 80 mg (96%) of **5c**: yellow needless (from

methanol); mp 165—166°C; UV λ_{max} (MeOH) 264 (log ε, 4.18), 359 (3.95), and 438 nm (4.17); IR (KBr) 3250 (NH) and 1584 cm^{-1} (C=O); ^1H NMR (100 MHz, CD_3OD) δ=8.51 (1H, d, $J_{3,5}$=2.0 Hz, H-3), 7.57 (1H, dd, $J_{5,6}$=11.2 Hz, H-5), 7.1—7.4 (4H, m, H-3′, 4′, 5′, 6′), 6.91 (1H, d, H-6), and 3.88 (3H, s, CH_3).

Found: C, 43.70; H, 2.80; N, 3.64%; M^+, 387. Calcd for $C_{14}H_{11}NO_2Br_2$: C, 43.67; H, 2.88; N, 3.64%; M, 387.

*2-Bromo-7-(dimethylamino)tropone (**6a**).* A solution of 2-bromo-7-methoxytropone[11] (230 mg) and an excess of 40% aqueous dimethylamine in ethanol (5 ml) was heated at 70°C for 4 h. The solvent was evaporated *in vacuo* and the crude product was chromatographed in a column of silica gel with benzene–methanol (50:1) and recrystallized from methanol, giving 196 mg (80%) of **6a**, besides the recovered staring material (30 mg, 13%): yellow needles (from methanol); mp 93—94°C; UV λ_{max} (MeOH) 264 (log ε, 4.31), 358 (4.14), and 437 nm (4.05), (MeOH+3 M HCl) 255 (log ε, 4.27), 273 (4.10), 324 (3.80), 356 (4.01), and 437 nm (3.81); IR (KBr) 1580 cm^{-1} (C=O); ^1H NMR (270 MHz) δ= 7.93 (1H, d, $J_{3,4}$=9.5 Hz, H-3), 7.07 (1H, dd, $J_{5,6}$=10.2 and $J_{4,5}$=10.5 Hz, H-5), 6.52 (1H, d, H-6), 6.33 (1H, dd, H-4), and 3.14 (6H, s, $2CH_3$).

*2,4-Dibromo-7-(dimethylamino)tropone (**6c**).* Procedures similar to those for **6a** were followed. 2,4-Dibromo-7-methoxytropone (50 mg) afforded 35 mg (67%) of **6c** after purification by HPLC and recrystallization from methanol (10 mg of the starting material was recovered): yellow needles (from methanol); mp 96—97°C; UV λ_{max} (MeOH) 270 (log ε, 4.22), 356 (4.04), 369 (4.14), 443 (3.87), and 461 (3.86); IR (KBr) 1580 cm^{-1} (C=O); ^1H NMR (270 MHz) δ=8.16 (1H, d, $J_{3,5}$=2.2 Hz, H-3), 7.33 (1H, dd, $J_{5,6}$=11.7 Hz, H-5), 6.24 (1H, d, H-6), and 3.13 (6H, s, $2CH_3$).

*5-Bromo-2-(dimethylamino)tropone (**6d**).* 5-Bromo-2-methoxytropone[8] (270 mg) was similarly treated with an excess of 40% dimethylamine, giving 270 mg (94%) of **6d** after purification by chromatography in a column of silica gel with 50:1 benzene–MeOH: yellow oil; UV λ_{max} (MeOH) 257 (log ε, 4.23), 361 (4.18), and 430 nm (3.88), (MeOH+3 M HCl) 252 (log ε, 4.24), 364 (3.93), and 388 nm (3.92); IR (neat) 1590 cm^{-1} (C=O); ^1H NMR (270 MHz) δ=7.30 (1H, dd, $J_{3,4}$=11.2 and $J_{4,6}$=2.2 Hz, H-4), 7.26 (1H, dd, $J_{6,7}$=12.7 Hz, H-6), 6.70 (1H, d, H-7), 6.21 (1H, d, H-3), and 3.09 (6H, s, $2CH_3$).

*2-Bromo-7-(methylamino)tropone (**7b**).* A mixture of 7-bromo-2-methoxytropone (144 mg, 0.67 mmol), methylamine hydrochloride (184 mg, 2.72 mmol), and sodium hydride (48 mg, 2.0 mmol) in ethanol (3 ml) was heated at 80°C for 20 h. After cooling, the precipitates were filtered off and recrystallized from ethanol (removing NaCl by filtration), giving 133 mg (93%) of **7b**: yellow plates; mp 169—170°C; UV λ_{max} (MeOH) 250 (log ε, 4.27), 258 (4.36), 277 (3.81), 332 (3.95), 342 (4.06), 398 (3.89), and 420 nm (4.12); IR (KBr) 3280 (NH) and 1585 cm^{-1} (C=O); ^1H NMR (270 MHz) δ=8.14 (1H, dd, $J_{3,4}$=10.1 and $J_{3,5}$=1.0 Hz, H-3), 7.64 (1H, bs, NH), 7.33 (1H, td, $J_{4,5}$=$J_{5,6}$=10.1 Hz, H-5), 6.58 (1H, dd, $J_{4,6}$=1.0 Hz, H-6), 6.52 (1H, td, H-4), and 3.09 (3H, s, CH_3).

*Reaction of 2-Bromo-7-(2-hydroxyanilino)tropone (**1a**) Catalyzed by concd Hydrochloric Acid.* A similar treatment of **1a** (100 mg, 0.34 mmol) with acetic acid (5 ml) containing a trace amount of concd hydrochloric acid at 120°C for 4 h under nitrogen gave **2g** (see below, 20 mg, 25%), **2a** (27 mg, 29%), **2b** (4 mg, 6%), and **2c** (6 mg, 5%), besides the recovered **1a** (30 mg, 30%).

*6-Chlorocyclohepta[b][1,4]benzoxazine (**2g**)*: Brown needles (from benzene); mp 96—97°C; UV λ_{max} (MeOH) 224 (log ε, 4.21), 260 (4.29), 267 (4.26), 296 (3.77), and 413 nm (3.98), (MeOH+3 M HCl) 228 (log ε, 4.25), 264 (4.23), 270 (4.23), 324 (3.83), 425 (3.87), and 458 nm (3.81); IR (KBr) 1625 cm^{-1} (C=N); ^1H NMR (270 MHz) δ=6.87 (1H, m, $J_{2,3}$=$J_{3,4}$=7.8 and $J_{1,3}$=1.5 Hz, H-3), 6.86 (1H, m, $J_{1,2}$=7.8 Hz, H-1), 6.82 (1H, m, H-2), 6.59 (1H, dd, H-4), 6.18 (1H, d, $J_{7,8}$=11.8 Hz, H-7), 6.14 (1H, d, $J_{9,10}$=12.8 Hz, H-10), 6.08 (1H, dd, $J_{8,9}$=7.5 Hz, H-9), and 5.69 (1H, dd, H-8).

Found: M^+, 229.0301 and 231.0150 (3:1). Calcd for $C_{13}H_8NOCl$: M, 229.0294 and 231.0264.

*Reaction of 2-Bromo-7-(2-hydroxyanilino)tropone (**1a**) Catalyzed by Concd Hydrobromic Acid.* A similar treatment of **1a** (500 mg, 1.71 mmol) with acetic acid (10 ml) containing a trace amount of concd hydrobromic acid at 120°C for 4 h under nitrogen gave **2d** (220 mg, 47%), **2a** (15 mg, 3%), **2b** (28 mg, 8%), and **2c** (50 mg, 8%), besides the recovered **1a** (80 mg, 16%).

We thank Professors K. Takase (Tohoku Univ.) and H. Yamamoto (Okayama Univ.) for their helpful discussions.

References

1) Presented at the 43th National Meeting of the Chemical Society of Japan, Tokyo, April 1981, Abstr., No. 1H40.

2) T. Nozoe, T. someya, and H. Okai, *Bull. Chem. Soc. Jpn.*, **52**, 1156 (1979).

3) T. Nozoe, *Pure Appl. Chem.*, **54**, 975 (1982).

4) T. Someya, H. Okai, H. Wakabayashi, and T. Nozoe, *Bull. Chem. Soc. Jpn.*, **56**, 2756 (1983).

5) T. Nozoe, H. Okai, H. Wakabayashi, and S. Ishikawa, *Chem. Lett.*, **1984**, 1147.

6) T. Nozoe, H. Okai, and T. Someya, *Bull. Chem. Soc. Jpn.*, **51**, 2185 (1978).

7) T. Nozoe, S. Seto, H. Takeda, S. Morosawa, and K. Matsumoto, *Sci. Repts. Tohoku Univ.*, I, **36**, 126 (1952).

8) T. Nozoe, S. Seto, H. Takeda, S. Morosawa, and K. Matsumoto, *Proc. Japan Acad.*, **27**, 556 (1951).

9) Reaction indexes (f_r^E) for electrophilic reactions of **7a** by the HMO method: C-1 (0.126), C-2 (0.0026), C-3 (0.139), C-4 (0.002), C-5 (0.150), C-6 (0.006), C-7 (0.132).

10) M. Yasunami, Y. Sasagawa, and K. Takase., *Chem. Lett.*, **1980**, 205.

11) T.Nozoe, Y. Kitahara, K. Yamane, and A. Yoshikoshi, *Proc. Japan Acad.*, **27**, 18 (1951).

Electronic and Steric Effects of Alkyl Group on Denitrosation of 3-Alkyl-1-methyl-1-nitrosothioureas

Masayoshi Isobe
Department of Chemistry, Saitama Medical School, 981 Kawakado, Moroyama, Iruma-gun, Saitama 350-04
(Received April 23, 1985)

A series of 3-alkyl-1-methyl-1-nitrosothioureas with R=CH_3, C_2H_5, *cyclo*-C_6H_{11} (**3**), $(CH_3)_2CH$ (**4**), $C_2H_5(CH_3)CH$, and $(CH_3)_3C$ were synthesized and their rates of acid catalyzed (pH<6.5) denitrosation measured. According to rate measurements in CH_3COOD-D_2O, the kinetic isotope effect $k_H:k_D$ is 1.25 for **4**. Except **3**, a linear plot of log k_R/k_{Me} for the denitrosation of $RNHCSN(NO)CH_3$ *vs.* σ^* provides $\rho^*=-0.98$ ($r=-0.997$). The significant factor affecting the rate-determining step of the denitrosation of these *N*-nitrosothioureas at pH 4.6 is the electronic effect of the substituent at the N_3 position.

Carcinogenic nitrosamines are caused to result from reaction of a dietary or endogenous nitrite with ingested amines.[1] However, nitrite *in vivo* is not the only possible origin of nitroso compounds. Certain aromatic nitrosamines[2,3] and many aliphatic nitrosamines[4] act as nitrosating agents toward naturally occurring amines under acidic conditions. In aqueous acid solutions, nucleophiles usually attack the protonated form of nitrosamine in the rate-determining step,[5] but when strongly electron-withdrawing groups are present in nitrosamine, proton transfer to nitrosamine is believed to be rate-limiting. The latter situation arises in reactions of *N*-nitroso amides[6-9] and *N*-nitroso sulfonamide.[10] Besides the above *N*-nitroso compounds 3-cyclohexyl-1-methyl-1-nitrosothiourea was also found to be protonated in the rate-determining step in denitrosation.[11]

On the other hand, reactions of thiourea (or alkylthiourea) with nitrous acid[12] or *N*-methyl-*N*-nitrosoaniline[13] have been investigated, with a conclusion that *S*-nitrosation occurs to form the intermediate $(NH_2)_2C=\overset{+}{S}-N=O$, which is capable of acting directly as a nitrosating agent. Synthesis and decomposition of a series of *N*-nitrosothioureas have recently been studied with an anticipation that isothiocyanate released from them should be less reactive toward proteins than isocyanate, and the formation mechanism and conformation of *N*-nitrosothioureas and stereoelectronic control of their aqueous decomposition have been revealed by Lown and Chauhan,[14] but no effect of substituents at N_3 on the denitrosation has been examined. In relation to isothiocyanates it should be noted that some isothiocyanates have exhibited antitumor properties in their own right.[15] Therefore, it is interesting and necessary for understanding the mechanism of denitrosation to study the effect of substituents at the N_3 position of 3-alkyl-1-methyl-1-nitrosothioureas quantitatively and evaluate their trans-

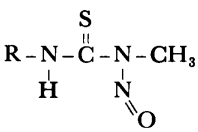

1 R=CH_3
2 R=C_2H_5
3 R=*cyclo*-C_6H_{11}
4 R=$(CH_3)_2CH$
5 R=$C_2H_5(CH_3)CH$
6 R=$(CH_3)_3C$

Table 1. Decomposition product from 3-alkyl-1-methyl-1-nitrosothioureas under acidic conditions[a]

Nitroso-thiourea	3-Alkyl-1-methyl-thiourea/%	3-Alkyl-1-methyl-urea/%
1	80[b]	—
3	66	17[c]
4	38	11[c]
6	24	40
6(N_2)[d]	22.4	4.5[c]
6(N_2, $NaNO_2$)[e]	37	37[c]

a) Acetate buffer (pH 4.6), 0.05 M, and μ=0.2 (NaCl). b) Acetate buffer (pH 5.0), 0.05 M, and μ=0.2 (NaCl). c) From NMR analysis; not isolated yield. d) Under nitrogen atmosphere. e) With sodium nitrite under nitrogen atmosphere.

nitrosating abilities from a chemical viewpoint. In this research the denitrosation of a series of *N*-methyl-*N*-nitrosothioureas having various substituents at the N_3 position has been studied under acidic conditions.

Results and Discussion

Decomposition of **3** and **4** in acetate buffer (pH 4.6) produced predominantly 3-cyclohexyl-1-methylthiourea (**3a**) (66%) and 3-isopropyl-1-methylthiourea (**4a**) (38%), respectively, and that of **1** in acetate buffer (pH 5.0) produced 1,3-dimethylthiourea (**1a**) (80%). These results suggest that in the decomposition of **1**, **3**, or **4** under these acidic conditions the protonated *N*-nitrosothioureas are led markedly to the unimolecular excision of the NO^+ group or the denitrosation by the attack of nucleophile. Decomposition of **6** in acetate buffer (pH 4.6) produced a mixture of 3-*t*-butyl-1-methylthiourea (**6a**) and 3-*t*-butyl-1-methylurea (**6b**) in a ratio of **6a**:**6b**=37:63, which implies formation of protonated *N*-nitrosothiourea and *S*-nitrosoisothiourea, followed by unimolecular denitrosation or nucleophilic attack leading to thiourea or urea derivative (Scheme 1). The results are summarized in Table 1. The formation of these products is different from that of products (urea, nitrosourea, and propyl isothiocyanate) from 1,3-dipropyl-1-nitrosothiourea under acidic conditions (acetone:1 M HCl=5:1)(1 M=1 mol dm^{-3}) studied by Lown and Chauhan.[14]

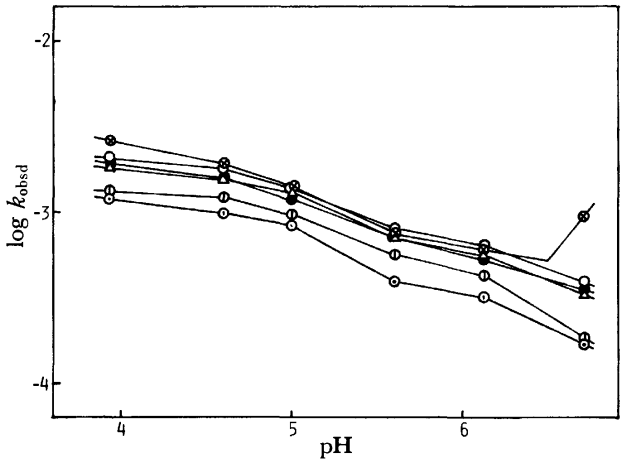

Fig. 1. pH-Rate profiles for decomposition of **1** — **6** at 36.9°C, pH 3.90—5.60 (acetate buffer), pH 6.12 (imidazole buffer), and pH 6.70 (Tris buffer), 0.05 M, μ=0.2 (NaCl), **1** (⊙), **2** (Φ), **3** (○), **4** (△), **5** (●), and **6** (⊗).

Table 2. Test for catalysis by nucleophile in the denitrosation of **4** at pH 4.6[a]

Added Nucleophile	$10^3k_0/s^{-1}$[b]
0	1.37±0.01
0.176 M NaCl	1.56±0.03
0.176 M NaBr	1.71±0.02
1.05 M NaBr	1.61±0.01
0.176 M NaSCN	1.63±0.03
1.05 M NaSCN	1.56±0.01
0.176 M NaI	1.70±0.02
0.176 M NaN_3	1.72±0.04

a) [**4**]=8.28×10^{-5} M in acetate buffer at 36.9°C. b) The errors are given by deviation from average of two runs.

pH-log k_{obsd} plots (pH 3.9—6.7) for the decomposition of compounds **1—6** are shown in Fig. 1. As shown in Fig. 1, decomposition rate constants for **1—6** decrease with increase in pH (pH<6.5), which indicates that all of them are subject to acid catalysis[11] and that the reactivity follows the sequence **6>3>5>4>2>1** at pH 4.6. The pH-rate profile for the decomposition of **6** shows an inverted-bell curve around pH 6.5, exhibiting the highest reactivity in this series above pH 6.5. The rate constant for the denitrosation of **4** at pH 4.6 is almost unaffected by the presence of nucleophile Br^- or SCN^-, as shown by the data in Table 2. This feature contrasts with the denitrosation of nitrosamine previously studied[5] but resembles the pattern of denitrosation for *N*-nitroso amide[9] and *N*-nitroso sulfonamide.[10]

To evaluate the solvent deuterium isotope effect, the rate of denitrosation at 36.9°C was measured in CH_3COOD-D_2O. Results obtained at the same buffer ratio ([HA(DA)]/[A^-]=1.04, 0.05 M, μ=0.2) revealed that the denitrosation of **4** is slower in CH_3COOD-D_2O than in CH_3COOH-H_2O by a factor of 1.25 (Table 3). This feature argues against fast pre-equilibrium formation of the protonated form of *N*-nitrosothiourea, and rather suggests that the proton transfer is rate-limiting. The above results resemble those of *N*-nitroso amide (k_H/k_D=1.9 or 1.3)[6,8] and nitroso sulfonamide (k_H/k_D=1.5)[10] rather than those of nitrosamine (k_H/k_D=*ca.* 0.5—0.6).[16,17]

Table 3. Solvent deuterium isotope effect[a] in the denitrosation of **4**

$10^3k_H/s^{-1}$	1.56±0.03[b]
$10^3k_D/s^{-1}$	1.24±0.01
k_H/k_D	1.25

a) [HA(DA)]/[A^-]=1.04 (A=CH_3COO), [**4**]=8.28×10^{-5} M, and μ=0.2 (NaCl) at 36.9°C. b) The errors are given by deviation from average of two runs.

Scheme 1 is a probable outline mechanism for the denitrosation presented as capable of explaining the observations. The initial *N*-protonation of *N*-nitroso-

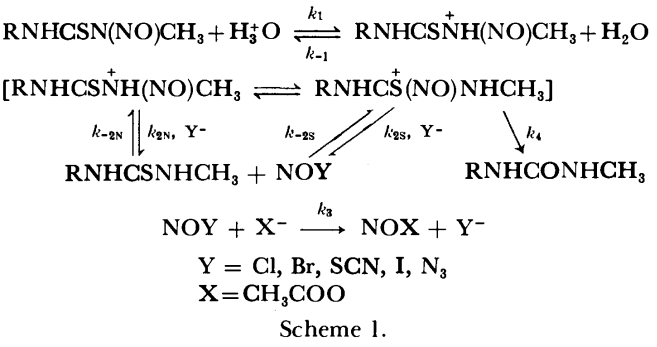

Scheme 1.

thiourea is written as a one-stage process for simplicity and *O*-protonation is not considered. The rate constant k_2 is composed of k_{2N} and k_{2S}. The step k_{-2}(*i.e.*, $k_{-2N}+k_{-2S}$) is negligible in the presence of excess X^-. The general expression of rate constant derived from Scheme 1

$$k_0 = k_1k_2[H_3^+O][Y^-]/(k_{-1}+k_2[Y^-]) \quad (1)$$

is simplified to two limiting forms

$$k_0 = k_1k_2[H_3^+O][Y^-]/k_{-1}, \quad (2)$$

$$k_0 = k_1[H_3^+O], \quad (3)$$

which correspond to different reaction patterns based on the inequalities $k_{-1} \gg k_2[Y^-]$ and $k_{-1} \ll k_2[Y^-]$, respectively. The catalysis by Y^- is in effect caused to disappear only if $k_{-1} \ll k_2[Y^-]$, with a result that Eq. 1 reduces to $k_0=k_1[H_3^+O]$, which is the form observed in this work.

In order to know electronic and steric effects of substituents at N_3 on denitrosation, Taft's Eq.[18]

$$\log k_R/k_{Me} = \rho^*\sigma^* + \delta Es \quad (4)$$

was applied to the data at pH 4.6 in Fig. 1. The ρ^* and δ values computed by using the least squares

method are −0.70 and −0.048, respectively. A plot of log $k_R/k_{Me}-\rho^*\sigma^*$ against *Es* gave an inferior correlation coefficient (r=−0.529) (Fig. 2). This indicates that the steric effect of substituent R is small for the transition state of protonation of these compounds **1—6**. Therefore, to know the electronic effect of substituents at the N_3 position on the protonation, log k_R/k_{Me} values from the data at pH 4.6 in Fig. 1 are plotted against σ^* into Fig. 3. The points for R=CH_3, C_2H_5, $(CH_3)_2CH$, $C_2H_5(CH_3)CH$, and $(CH_3)_3C$ provide a linear relationship (slope ρ^*=−0.98, r=−0.997) as given by

$$\log k_R/k_{Me} = \rho^*\sigma^* = -0.98\sigma^*. \quad (5)$$

This indicates that the denitrosation is influenced mainly by the electronic effect of substituents at the N_3 position. The more the substituent at N_3 releases electrons and increases the electron density at the N_1 position, the more the protonation on N_1 is facilitated.[19] The above result supports that the protonation on the N_1 nitrogen atom is the rate-determining step in the denitrosation of **1—6**. The positive deviation for R=*cyclo*-C_6H_{11}, which becomes pronounced at higher temperatures (36.9°C) at pH 5.0 (Table 4), may be due to inversion of the cyclohexyl group which permits the favorable conformation for the protonation on the N_1 position. This electronic effect (ρ^*=−0.98) of substituent R on the denitrosation is much smaller than that on alkaline hydrolyses of alkyl nitrite (ρ^*=2.67).[20]

In the denitrosation process of **6** (Scheme 1), the increase in electron density at the N_1 nitrogen atom by the electron-releasing effect of the *t*-butyl group may facilitate the protonation on the N_1 nitrogen atom to form a protonated intermediate. For **6**, the transition state to form a protonated *N*-nitroso or *S*-nitroso intermediate must be stabilized, by the electron-releasing effect of the *t*-butyl group, more than for **1**, **3**,

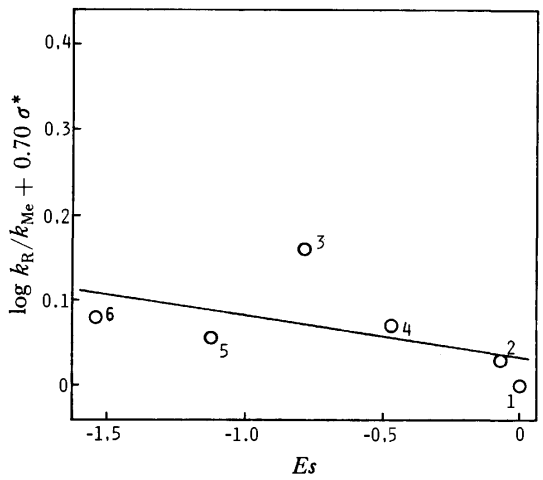

Fig. 2. Plot of log k_R/k_{Me}+0.70σ^* for the denitrosation of the $RNHCSN(NO)CH_3$ in acetate buffer (pH 4.6) against Taft's Es values, δ=−0.048 (r=−0.529).

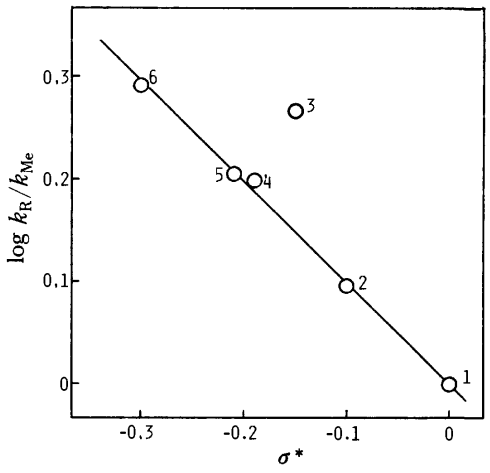

Fig. 3. Plot of log k_R/k_{Me} *vs.* σ^* for the denitrosation of the $RNHCSN(NO)CH_3$ series (pH 4.6). ρ^*=−0.98 (r=−0.997) for the R=CH_3, C_2H_5, $(CH_3)_2CH$, $C_2H_5(CH_3)CH$, and $(CH_3)_3C$.

Table 4. Kinetic data for denitrosation of 3-alkyl-1-methyl-1-nitrosothioureas

Nitrosothiourea[a]	Temp/°C	$10^4k_0/s^{-1}$[b]	ΔH^*/kJ mol^{-1}	ΔS^*/J mol^{-1}K^{-1}
1	17.0	1.05±0.02		
	25.0	2.50±0.03		
	36.9	8.32±0.02	75.3	−61.5
3	17.0	1.84±0.02		
	25.0	4.01±0.04		
	36.9	14.21±0.04	76.6	−52.3
4	17.0	1.80±0.02		
	25.0	3.97±0.03		
	36.9	12.98±0.02	72.8	−65.7
5	17.0	1.82±0.01		
	25.0	4.03±0.01		
	36.9	11.85±0.74	67.3	−83.7
6	17.0	2.26±0.01		
	25.0	5.03±0.02		
	36.9	14.27±0.18	65.7	−87.4

a) 8.28×10^{-5} M, acetate buffer (pH 5.0), 0.05 M, and μ=0.2 (NaCl). b) The errors are given by deviation from average of two runs.

and **4** so as to result in a larger increase of solvation, which may in turn lead to a larger decrease (21.7—35.1 $J\,mol^{-1}K^{-1}$) in the activation entropy of **6** than those of the others (**1**, **3**, and **4**) (Table 4). In nitrosation of thiourea (EtNHCSNHEt) by an equimolar amount of $NaNO_2$ and 0.5 M HCl in acetone at −10°C, the *S*-nitroso intermediate leads to urea *via* elimination of HSNO and addition of water to the carbodiimide thus formed.[14] But the decomposition of **6** in this acetate buffer solution (pH 4.6) at 37°C in the absence of oxygen (under nitrogen atmosphere) produced **6b** in one fifth amount of **6a**. This distribution of products suggests that the existence of oxygen greatly influences the production of **6b**.[21] Williams[13] has reported that the reaction of thiourea with *N*-methyl-*N*-nitrosoaniline in acid solution in the absence of oxygen forms no Fischer-Hepp rearrangement products but merely the denitrosation product *N*-methylaniline, which suggests that the nitrous acid can be regenerated using oxygen dissolved in the solution according to

$$2NO + O_2 = 2NO_2$$
$$NO_2 + NO = N_2O_3$$
$$N_2O_3 + H_2O = 2HNO_2$$

Scheme 2.

In fact, the decomposition of **6** in acetate buffer (pH 4.6) containing sodium nitrite under nitrogen atmosphere produced a mixture of **6a** and **6b** in a ratio of **6a**:**6b**=1:1 (Table 1). Therefore, the protonated intermediate of **6** is attacked mainly by the nitrous acid formed from oxygen to produce **6b** with no production of carbodiimide followed by addition of water.

These results lead to a conclusion that the electronic effect of substituents at the N_3 position has a predominant effect on the protonation on the N_1 nitrogen atom. It is probable that the denitrosation in this system (**1**—**6**) is not greatly affected by the steric factor of substituent R lying remote from the nitroso group. In this series, acid catalysis is a prerequisite for the denitrosation process different from hydrolysis of alkyl nitrite under neutral conditions[22] and the rate constants of denitrosation of these *N*-nitrosothioureas are in good correlation to σ^* values with one exception, which indicates that the values may be useful as an index of transnitrosating abilities of *N*-nitrosothioureas.

Experimental

Melting points were determined on a Yamato MP-21 melting point apparatus and are uncorrected. IR spectra were recorded on a Shimadzu IR-400 spectrophotometer and ^1H NMR spectra were recorded with a Hitachi R-24 instrument. Microanalyses were performed in the Microanalytical Laboratory of the Institute of Physical and Chemical Research, Wako-shi.

Materials. Ethylamine, *t*-butylamine, and methyl isothiocyanate were obtained from Wako Pure Chemical Co., and cyclohexylamine, isopropylamine, and *s*-butylamine from Tokyo Kasei Co.

General Method for the Preparation of N-Nitrosothioureas. 3-Alkyl-1-methylthiourea were synthesized through reaction of the corresponding alkylamines and methyl isothiocyanate. A dilute solution of HCl (0.07 M, 20 ml) was added dropwise for 20 min to a suspension of 3-alkyl-1-methylthiourea (2.0—6.0 mmol) and sodium nitrite (2.0—6.0 mmol) in CH_2Cl_2 (20 ml) with stirring and cooling (0°C) under a nitrogen atmosphere, and the mixture was stirred with cooling (0°C) for additional 40 min by following the method of Lown and Chauhan.[14] After the reaction was over, the organic layer was taken out, washed with water, dried ($MgSO_4$), and subjected to evaporation to afford crude *N*-nitrosothioureas **1**—**6**, which were purified except **2** by either crystallization from pentane or by chromatography over silica gel.

1,3-Dimethyl-1-nitrosothiourea (1): mp 46—47°C (lit,[14] mp 46°C).

3-Isopropyl-1-methyl-1-nitrosothiourea (4) (56%): An oil, IR (neat) 3340 (NH), 2990, 1505, 1405 (N=O), 1175 (C=S), and 1020 cm^{-1}; NMR ($CDCl_3$) δ=1.36 (6H, d, J=6.0 Hz, $C(CH_3)_2$), 3.46 (3H, s, N-CH_3), 4.67 (1H, q, J=6.4 Hz, $C\underline{H}Me_2$), and 8.26 (1H, br s, NH). Found: C, 37.32; H, 6.89; N, 26.12; S, 19.94. Calcd fo $C_5H_{11}N_3OS$: C, 37.25; H, 6.88; N, 26.06; S, 19.89.

3-s-Butyl-1-methyl-1-nitrosothiourea (5) (51%): An oil; IR (neat) 3330 (NH), 2980, 1505, 1405 (N=O), 1170 (C=S), and 1010 cm^{-1}; NMR ($CDCl_3$) δ=0.98 (3H, t, J=6.8 Hz, $CH_2C\underline{H}_3$), 1.30 (3H, d, J=6.0 Hz, $CHC\underline{H}_3$), 1.68 (2H, q, $C\underline{H}_2CH_3$), 3.48 (3H, s, N-CH_3), 4.85—4.25 (1H, m, $C\underline{H}(CH_3)C_2H_5$), and 8.40 (1H, br s, NH). Found: C, 41.10; H. 7.43; N, 24.16; S, 18.32. Calcd for $C_6H_{13}N_3OS$: C, 41.12; H, 7.48; N 23.98; S, 18.30.

3-t-Buthyl-1-methyl-1-nitrosothiourea (6) (69%): An oil; IR (neat) 3375 (NH), 2980, 1520, 1500, 1420 (N=O), 1200, 1160, and 935 cm^{-1}; NMR ($CDCl_3$) δ=1.59 (9H, s, $C(CH_3)_3$), 3.43 (3H, s, N-CH_3), 8.55 (1H, br s, NH). Found: C, 41.07; H, 7.46; N, 23.92; S, 18.39. Calcd for $C_6H_{13}N_3OS$: C, 41.12; H, 7.48; N, 23.98; S, 18.30.

Kinetic Measurements. The kinetic method was the same as described previously.[11] Reactions were monitored spectrophotometrically by following the disappearance of the absorption maximum at 266—270 nm with a Shimadzu UV 200 spectrophotometer. The reaction followed pseudo first-order kinetics; infinity readings were obtained after 8—10 half lives. The value of the pH of buffer was determined with a Toa Denpa HM-5A pH meter. A mixture of 3-ethyl-1-methyl-1-nitrosothiourea (**2**) and 3-methyl-1-ethyl-1-nitrosothiourea (**2′**) was obtained from nitrosation of 3-ethyl-1-methylthiourea and its separation by column chromatography (silica gel) with 30% ether-hexane as eluent failed of success after successive two trials. Therefore the rate constant of **2** was obtained from kinetic measurements on both the first fraction (**2**:**2′**=68:32) and the last fraction (**2**:**2′**=23:77) separated by column chromatography. Estimated values in acetate buffer (pH 4.6, 36.9°C) are as follows: $k=1.22\times10^{-3}\,s^{-1}$ for **2** and $k=2.08\times10^{-3}\,s^{-1}$ for **2′**; NMR ($CDCl_3$) for **2** δ=1.37 (3H, t, J=7.2 Hz, $CH_2C\underline{H}_3$), 3.46 (3H, s, N-CH_3), 3.56—4.02 (2H, m, $C\underline{H}_2CH_3$), and 8.58 (1H, br s, NH) and for **2′** δ=1.04 (3H, t, J=7.0 Hz, $CH_2C\underline{H}_3$), 3.26 (3H, d, J=5.0 Hz, N-CH_3), 4.24 (2H, q, J=7.2 Hz, $C\underline{H}_2CH_3$), and 8.52 (1H, br s, NH). The first fraction (**2**:**2′**=68:32): an oil. Found; C, 33.08; H, 6.21; N, 27.88; S, 21.44. Calcd

for $C_4H_9N_3OS$: C, 32.64; H, 6.16; N, 28.55; S, 21.78.

Product Analyses. A solution of **1** (15 mg, 0.144 mmol) in 3 ml of MeOH was added to 100 ml of acetate buffer solution (pH 5.0, 0.05 M, μ=0.2 with NaCl) and stirred for 2 h and 50 min at 37 °C. After cooling, the contents were neutralized with 0.1 M NaOH and saturated with NaCl and extracted with chloroform (40 ml×3) and the combined extracts were washed with saturated NaCl solution, dried ($MgSO_4$), and evaporated to give 1,3-dimethylthiourea (9 mg, 80%): mp 62—63 °C; NMR ($CDCl_3$) δ=2.99 (6H, d, J=4.8 Hz, CH_3) and 6.30 (2H, br s, NH). **3** (50 mg, 0.248 mmol) in acetate buffer solution (pH 4.6) for 1 h at 37 °C was allowed to produce 3-cyclohexyl-1-methylthiourea (**3a**) and 3-cyclohexyl-1-methylurea (**3b**) (white solids, 34.7 mg, 83%, **3a**:**3b**=80:20 from NMR spectrum) by following a similar procedure as described above. **3a**: mp 163—164 °C; NMR ($CDCl_3$) δ=1.00—2.20 (10H, m, CH_2), 2.94 (3H, d, J=5.2 Hz, N-CH_3), 3.55—4.00 (1H, m, CH-N), 5.66 (1H, br s, NH), and 5.90 (1H, br s, NH). **4** (16 mg, 0.099 mmol) in acetate buffer solution (pH 4.6) for 1 h at 37 °C produced mainly 3-isopropyl-1-methylthiourea (**4a**) together with 3-isopropyl-1-methylurea (**4b**) (9.3 mg, 50%, **4a**:**4b**=78:22 from NMR spectrum). **4a**: NMR ($CDCl_3$) δ=1.21 (6H, d, J=6.6 Hz, $C(CH_3)_2$), 2.96 (3H, d, J=4.8 Hz, N-CH_3), 4.24 (1H, o, 7.0 Hz, $C\underline{H}(CH_3)_2$), 5.90 (1H, br s, NH), and 6.26 (1H, br s, NH). **6** (100 mg, 0.571 mmol) in acetate buffer solution (pH 4.6) for 1 h at 37 °C through a similar course as described above produced a mixture of white solids (**6x** and 3-*t*-butyl-1-methylurea (**6b**), 49 mg, 64%, **6x**:**6b**=37:63 from NMR spectrum). **6b** was isolated by recrystallization from hexane-acetone; **6x** was not isolated from the mixture but its IR and NMR spectra were in accord with those of **6a**. **6b**: mp 134—135 °C; IR (KBr) 3390 (NH), 3330 (NH), 1625 (C=O), 1560, 1360, 1275, and 1215 cm^{-1}; NMR ($CDCl_3$) δ=1.30 (9H, s, $C(CH_3)_3$), 2.65 (3H, d, J=4.8 Hz, N-CH_3), 5.01 (1H, br s, NH), and 5.21 (1H, br s, NH); UV λ_{max}^{MeOH} 245 (ε 170) and 206 nm (1940). Found: C, 55.29; H, 10.95; N, 21.38. Calcd for $C_6H_{14}N_2O$: C, 55.35; H, 10.84; N, 21.52. **6x**=**6a**: NMR ($CDCl_3$) δ=1.42 (9H, s, $C(CH_3)_3$), 3.02 (3H, d, J=4.8 Hz, N-CH_3), 6.14 (2H, br s, NH); UV λ_{max}^{MeOH} 245 (ε 11600) and 212 nm (9300). **6** (51 mg, 0.291 mmol) in acetate buffer solution (pH 4.6) for 1 h at 37 °C under nitrogen atmosphere produced a mixture of white solids (**6a** and **6b**, 11 mg, 27%, **6a**:**6b**=83:17 from NMR spectrum). **6** (51 mg, 0.291 mmol) in acetate buffer solution (pH 4.6) containing sodium nitrite (20 mg, 0.291 mmol) for 1 h at 37 °C under nitrogen atmosphere produced a mixture of white solids (**6a** and **6b**, 30 mg, 74%, **6a**:**6b**=50:50 from NMR spectrum).

The author wishes to thank Professor Kazuo Nagamatsu and Dr. Kazuyuki Yano at Saitama Medical School for their helpful comments and useful discussions. This work was supported in part by a Grant-in-Aid for Scientific Research No. 57771470 from the Ministry of Education, Science, and Culture.

References

1) W. Lijinsky, H. W. Taylor, C. Snyder, and P. Nettesheim, *Nature (London)*, 244, 176 (1973).
2) H. Sieper, *Chem. Ber.*, **100**, 1646 (1967).
3) B. C. Challis and M. R. Osborne, *J. Chem. Soc., Chem. Commun.*, **1972**, 518.
4) S. S. Singer, G. M. Singer, and B. B. Cole, *J. Org. Chem.*, **45**, 4931 (1980).
5) I. D. Biggs and D. L. H. Williams, *J. Chem. Soc., Perkin Trans. 2*, **1975**, 107.
6) C. N. Berry and B. C. Challis, *J. Chem. Soc., Perkin Trans. 2*, **1974**, 1638.
7) B. C. Challis and S. P. Jones, *J. Chem. Soc., Perkin Trans. 2*, **1975**, 153.
8) J. K. Snyder and L. M. Stock, *J. Org. Chem.*, **45**, 1990 (1980).
9) G. Hallett and D. L. H. Williams, *J. Chem. Soc., Perkin Trans. 2*, **1980**, 1372.
10) D. L. H. Williams, *J. Chem. Soc., Perkin Trans. 2*, **1976**, 1838.
11) M. Isobe, *Bull. Chem. Soc. Jpn.*, **57**, 601 (1984).
12) K. Al-Mallah, P. Collings, and G. Stedman, *J. Chem. Soc., Dalton Trans.*, **1974**, 2469; P. Collings, K. Al-Mallah, and G. Stedman, *J. Chem. Soc., Perkin Trans. 2*, **1975**, 1734.
13) D. L. H. Williams, *J. Chem. Soc., Perkin Trans. 2*, **1977**, 128.
14) J. W. Lown and S. M. S. Chauhan, *J. Org. Chem.*, **48**, 507, 513, 3901 (1983).
15) L. W. Wattenberg, *Cancer Res.*, **41**, 2991 (1981).
16) T. D. B. Morgan and D. L. H. Williams, *J. Chem. Soc., Perkin Trans. 2*, **1972**, 74.
17) J. T. Thompson and D. L. H. Williams, *J. Chem. Soc., Perkin Trans. 2*, **1977**, 1932.
18) W. A. Pavelich and R. W. Taft, Jr., *J. Am. Chem. Soc.*, **79**, 4935 (1957).
19) ^{15}N Chemical shifts (δ) of various *N*-nitrosothioureas including **1** and **3** have been investigated by Lown and Chauhan[14] (**1**: N_3H (δ=98.5), $>N_1$ (273.7); **3**: N_3H (δ=141.9), $>N_1$ (273.6)) and the progressive effect of the increase in bulk of the N_3 substituent in the *N*-nitrosothioureas on the preferred conformations has also been examined by them, with a suggestion that the NH proton becomes less accessible for interacting with the solvent.[14] These results support that the protonation on the N_1 position is much more facilitated in the *N*-nitrosothiourea which has a strongly electron-releasing and bulkier substituent at the N_3.
20) S. Oae, N. Asai, and K. Fujimori, *J. Chem. Soc., Parkin Trans. 2*, **1978**, 571.
21) M. Isobe, *Chem. Lett.*, **1985**, 65.
22) M. P. Doyle, J. W. Terpstra, R. A. Pickering, and D. M. LePoire, *J. Org. Chem.*, **48**, 3379 (1983).

 © 1985 The Chemical Society of Japan Bull. Chem. Soc. Jpn., 58, 2849—2854 (1985)

α,β-Epoxy Sulfoxides as Useful Intermediates in Organic Synthesis. II.[1] A Novel Synthesis of α-Sulfenylated Ketones and α-Sulfenylated Aldehydes from α,β-Epoxy Sulfoxides

Tsuyoshi SATOH, Takumi KUMAGAWA, and Koji YAMAKAWA*

Faculty of Pharmaceutical Sciences, Science University of Tokyo, Ichigaya-funagawara-machi, Shinjuku-ku, Tokyo 162

(Received April 26, 1985)

Treatment of α,β-epoxy sulfoxides, prepared from 1-chloroalkyl phenyl sulfoxides and carbonyl compounds, with various kinds of alkane- or arenethiolates afforded α-sulfenylated ketones in good yields. This method also offered a novel procedure for a synthesis of α-sulfenylated aldehydes.

Since the pioneering work of Trost and others, it is recognized that α-sulfenylated carbonyl compounds, including α-sulfinylated and α-sulfonylated carbonyl compounds, are useful and versatile compounds in synthetic organic chemistry.[2] The synthetic methods of α-sulfenylated carbonyl compounds are classified into two categories. One is the S_N2 displacement of α-halo ketones with alkanethiolates[3] and the other is the sulfenylation of carbanions (ketone enolate anions) with dialkyl disulfides or other electrophilic sulfenylating reagents.[4] These methods are widely used in the synthesis of α-sulfenylated carbonyl compounds but they have some drawbacks. The former method is useful only when regio-selectively halogenated carbonyl compounds are easily available. The latter has four fundamental problems. The first is a regioselectivity. Especially when simple unsymmetrical ketones are sulfenylated; it is very difficult to obtain regioselectively sulfenylated ketones exclusively by this method. The second one is the feasibility for bis-sulfenylation. The third one is the availability of dialkyl disulfide or other electrophilic sulfenylating reagents. The last one is the applicability of these methods to a synthesis of α-sulfenylated aldehydes.

In previous papers,[1,5] we have reported a method for the preparation of dialkyl ketones, aldehydes, and α-sulfenylated ketones from α,β-epoxy sulfoxides. In this paper we describe, in detail, a simple and useful method for a synthesis of α-sulfenylated ketones and α-sulfenylated aldehydes through the reaction of α,β-epoxy sulfoxides (**4**) with sodium alkanethiolates or sodium arenethiolates according to Scheme 1.

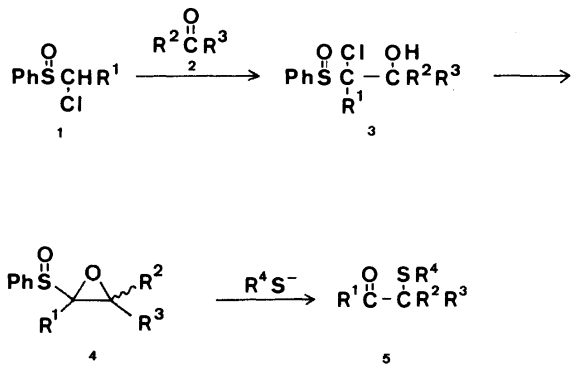

Scheme 1.

Results and Discussion

α,β-Epoxy sulfoxides (**4**) were initially reported by Durst in 1969.[6] They are easily prepared from chloromethyl phenyl sulfoxide (**1**; R^1=H) or 1-chloroalkyl phenyl sulfoxides (**1**; R^1=alkyl)[7] and carbonyl compounds (**2**) *via* chlorohydrins (**3**) in good overall yields. A few synthetic methods have already been reported[8] by using α,β-epoxy sulfoxides (**4**) but these interesting compounds have scarcely been used in organic synthesis. We have found that the β carbon of α,β-epoxy sulfoxides is highly reactive to various kinds of thiolates to afford α-sulfenylated ketones in good to excellent yields.[5]

The results of the reaction of α,β-epoxy sulfoxides (**4a—i**) with sodium benzenethiolate are summarized in Table 1. As shown in Table 1, various kinds of α-phenylsulfenylated ketones (**5a—i**) were synthesized through this method in good yields. More notable is the regiochemistry of the products. Treatment of 3,4-epoxy-3-phenylsulfinylnonane (**4a**) and 2,3-epoxy-3-phenylsulfinylnonane (**4b**) with two equivalents of sodium benzenethiolate in ethanol gave 4-phenylthio-3-nonanone (**5a**) and 2-phenylthio-3-nonanone (**5b**) in 87 and 80% yields, respectively, without any contamination by their regioisomers as shown in Table 1. Similarly, the epoxy sulfoxides (**4c**) and (**4d**) afforded single phenylsulfenylated ketones (**5c**) and (**5d**) in good yields without their regioisomers. As described above, the sulfenylation of ketones through the reaction of ketone enolate anions with electrophilic sulfenylating reagents possess a big problem, that is, the regioselectivity. Actually, the sulfenylation of 3-nonanone (**6**) and 1-phenyl-2-butanone (**7**) according to Trost's procedure[4e] gave a mixture of **5a** and **5b** (ratio 3:4),[9] a mixture of **5c** and **5d** (ratio 16:1)[9] in moderate

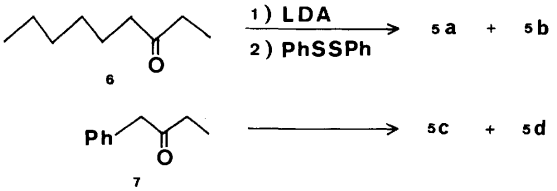

Scheme 2.

TABLE 1. SYNTHESIS OF α-PHENYLTHIO KETONES FROM α,β-EPOXY SULFOXIDES (4) AND SODIUM BENZENETHIOLATE

	α,β-Epoxy sulfoxide (4) R_1	R_2	R_3	PhSNa equiv.	Conditions	Ketone 5	Yield[a] %
4a	CH_3CH_2	$CH_3(CH_2)_4$	H	2	r.t. 45 min	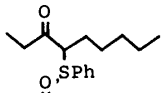	5a 87
4b	$CH_3(CH_2)_5$	CH_3	H	2	0°C, 30 min	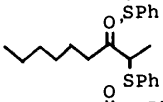	5b 80
4c	CH_3CH_2	Ph	H	2	r.t. 1 h	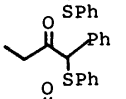	5c 74
4d	$PhCH_2$	CH_3	H	3	0°C, 2.5 h	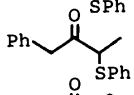	5d[1] 92
4e	$CH_3(CH_2)_5$	$-(CH_2)_5-$		7	reflux 2.5 h	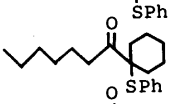	5e 96
4f	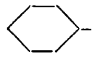	$CH_3(CH_2)_4$	H	3	0°C, 6 h	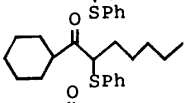	5f 93
4g	CH_3CH_2	CH_3	CH_3	7	50°C, 2.5 h	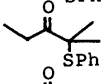	5g 91
4h	$PhCH_2$	CH_3	CH_3	7	r.t. 3 h	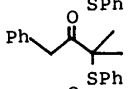	5h 91
4i	$(CH_3)_2CH$	$-(CH_2)_2-C(O)(O)-(CH_2)_2-$		10	reflux 24 h	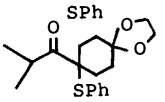	5i 66 (92)[b]

a) Isolated yields after silica-gel column chromatography. b) Calculated from consumed starting material.

yields as shown in Scheme 2. Both sulfenylated ketones **5a** and **5b**, **5c** and **5d** have the same R_f values on silica-gel thin-layer chromatography and they are hardly separable by the usual techniques. From these results, it can be understood that the present method is one of the best ways for the preparation of relatively simple sulfenylated ketones. The synthesis of α-phenylsulfenylated ketones (**5e**) and (**5f**) is another example of the preparation of regioselectively sulfenylated isomers.

Attention should be called to the reaction of **4d** and **4h** with sodium benzenethiolate. Treatment of **4d** with three equivalents of sodium benzenethiolate in ethanol at room temperature for 20 min gave the desired **5d** and bis-sulfenylated ketone (**8**) in 47 and 52% yields, respectively. Similary, treatment of **4h** with three equivalents of sodium benzenethiolate at room temperature for 6 h gave a sulfenylated ketone (**5h**) and a bis-sulfenylated ketone (**9**) in 54 and 30% yields, respectively. The formation of these bis-sulfenylated ketones may be interpreted as shown in Scheme 3. The reaction of **4d** and **4h** with sodium benzenethiolate gives α-sulfenylated ketones **5d** and **5h** along with sodium benzenesulfenate. This sulfenate oxidizes thiophenol to give diphenyl disulfide. On the other hand, the hydrogen on the benzyl carbon of **5d** and **5h**

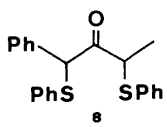
8

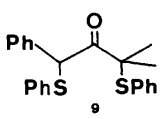
9

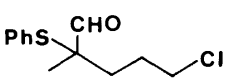
10

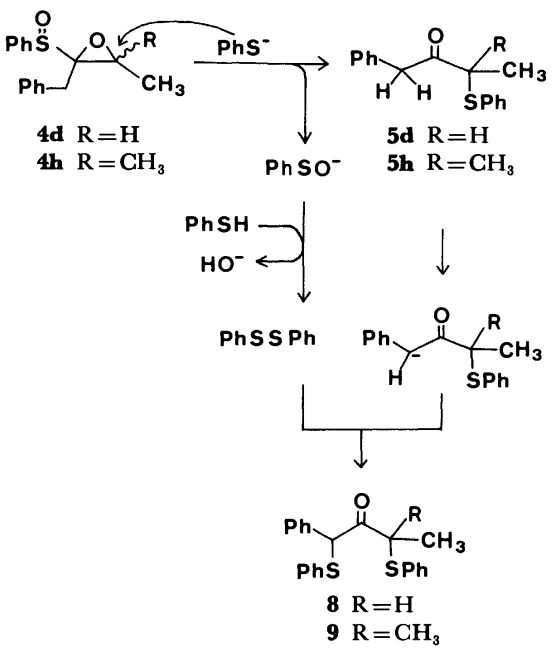

Scheme 3.

Table 2. Synthesis of α-sulfenylated ketones from α,β-epoxy sulfoxides (4) and thiolates other than benzenethiolate

	α,β-Epoxy sulfoxide (4) R1	R2	R3	Thiolate equiv.	Conditions	Ketone 5		Yield[a] %
4c	CH_3CH_2	Ph	H	$CH_3(CH_2)_3SNa$ (10)	0°C, 2h	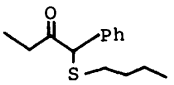	5j	73
4c	CH_3CH_2	Ph	H	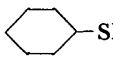 (10)	r.t. 30min	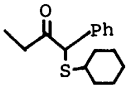	5k	73
4c	CH_3CH_2	Ph	H	$HO(CH_2)_2SNa$ (10)	0°C, 30min	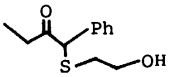	5l	53
4c	CH_3CH_2	Ph	H	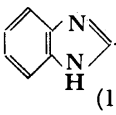 (10)	r.t. 20min	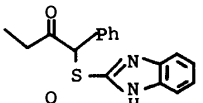	5m	82
4d	$PhCH_2$	CH_3	H	$NaOCOCH_2SNa$ (5)	r.t. 20min	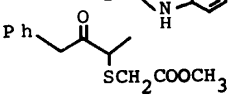	5n	95[b]

a) Isolated yields after silica-gel column chromatography. b) Isolated as a methyl ester.

Table 3. Synthesis of α-phenylthio aldehydes from α,β-epoxy sulfoxides (4) and sodium benzenethiolate

	α,β-Epoxy sulfoxide (4)	PhSNa equiv.	Conditions	Aldehyde 5		Yield[a] %
4k	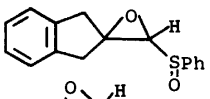	2	r.t. 40min	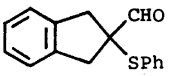	5o	83
4l	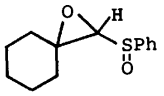	2	40°C, 2h	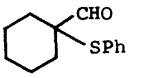	5p	79
4m	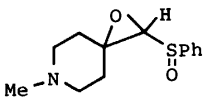	2	r.t. 4h	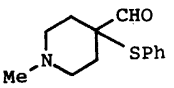	5q	55
4n	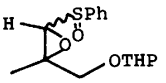	2	r.t. 1h	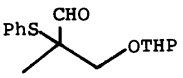	5r	64
4o	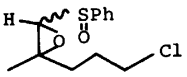	5	40°C, 1h	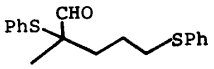	5s	59

a) Isolated yields after silica-gel column chromatography.

(these hydrogens are very acidic because of adjacent carbonyl group and phenyl ring) is deprotonated by sodium benzenethiolate giving a carbanion, which attacks the diphenyl disulfide[10] to afford the bis-sulfenylated ketones (**8**) and (**9**). The formation of these bis-sulfenylated ketones were simply prevented by using a large excess of benzenethiolate at a lower reaction temperature as shown in Table 1.

The present method also permits thiolates other than benzenethiolate to be easily introduced at the β-carbon of α,β-epoxy sulfoxides (**4**) to afford α-sulfenylated carbonyl compounds in good yields under very mild conditions, as is shown in Table 2. As mentioned above, only limited numbers of dialkyl or diaryl disulfides, or electrophilic sulfenylating reagents are available, these sulfenylated ketones in Table 2 (**5j**—n) are not easily obtained by the reaction of ketone enolate anions with electrophilic sulfenylating reagents. To prevent the formation of by-products, such as phenylsulfenylated compounds[11] or products deriving from the desired sulfenylated ketones, excess (five to ten-fold excess) thiolate and low temperature (0°C to room temperature) were found to be suitable for obtaining the desired α-sulfenylated ketones.

As mentioned above, direct sulfenylation of aldehydes through the reaction of enolate anion of aldehyde with sulfenylating reagents is difficult and no good methods have been reported to make α-sulfenylated aldehydes. From the equation in Scheme 1, one would expect that the reaction of **4** having hydrogen as R^1 with thiolates may give α-sulenylated aldehydes (**5**; R^1=H).

The α,β-epoxy sulfoxide (**4k**), prepared from 2-indanone and chloromethyl phenyl sulfoxide in good overall yield, on treatment with two equivalents of sodium benzenethiolate in ethanol at room temperature for 40 min gave α-phenylsulfenylated aldehyde (**5o**) in 83% yield. Other results are summarized in Table 3. All the epoxy sulfoxides in Table 3 reacted with sodium benzenethiolate under mild conditions to afford the desired aldehydes in moderate to good yields. When **4o** was treated with benzenethiolate under room temperature, some chloro aldehyde (**10**) was obtained along with **5s**. This implies that the rate of opening of the epoxide of **4o** by thiolate is slightly faster than that of the substitution of chloro substituent.

In conclusion a novel and versatile procedure for a synthesis of α-sulfenylated ketones and α-sulfenylated aldehydes has been developed from chloromethyl phenyl sulfoxide and carbonyl compounds through the reaction of α,β-epoxy sulfoxides with various kinds of thiolates. The commercial availability of starting materials and ease of handling, mildness of the reaction conditions, and high yields of the products, the present method offers a simple and useful approach to a synthesis of relatively simple α-sulfenylated carbonyl compounds.

Experimental

General. All melting points and boiling points are uncorrected. A Shibata GTO-250 glass tube oven was used for bulb-to-bulb distillation and boiling points are given as the temperature of the heating bath. The isomeric ratio of the products was determined by gas-liquid phase chromatography (GLC) using a Shimadzu GC-6AM (OV-101, 20 m) instrument. Infrared (IR) spectra were measured directly on an NaCl plate or in KBr disks with a Hitachi 215 spectrometer. ^{1}H-NMR spectra were measured in $CDCl_3$ solution with a JEOL FX-100 pulse Fourier-transform spectrometer using Me_4Si as an internal standard. Electron impact mass spectra (MS) were obtained on a Hitachi M-80 double focusing spectrometer at 70 eV by direct insertion. For TLC analysis throughout this work, Merck precoated TLC plates (Kieselgel 60 F_{254}, 0.25 mm) were used. Silica gel BW-127 ZH (Fuji-Davison) containing 2% fluorescence 254 and quartz column were used for column chromatography and the products having UV absorption were detected by UV irradiation. In experiments requiring dry solvent, THF was distilled from benzophenone ketyl; ethanol was dried by sodium metal and distilled.

General Procedure for the Preparation of α,β-Epoxy Sulfoxides (4): A synthesis of 3,4-epoxy-3-phenylsulfinylnonanone (**4a**) is described. To a solution of lithium diisopropylamide (3 mmol) in dry THF (8 ml) at −60 °C under N_2 was added a solution of 1-chloropropyl phenyl sulfoxide[7] (2.5 mmol) in 2 ml of dry THF dropwise with stirring and the solution was stirred for 15 min. Hexanal (3.75 mmol) was added to the reaction mixture through a syringe and the reaction was immediately quenched by aq NH_4Cl. The whole was extracted with ether–benzene and the organic layer was washed with sat. aq NH_4Cl. After the usual work-up, the crude products were purified by silica-gel column chromatography to give chlorohydrins (**3a-L**)[12] and (**3a-P**).[12] **3a-L** (30% yield): Colorless oil; IR (neat): 3250 (OH), 1030, 1020 (SO) cm^{-1}; NMR: δ=0.83 (3H, t, *J*=6.5 Hz), 1.36 (3H, t, *J*=7 Hz), 1.9—2.5, 2.5—3.0 (each 1H, m), 3.80 (1H, m), 7.4—7.9 (5H, m); MS *m/z* (%): 126 ([M−$C_9H_{17}ClO$]$^+$, 100), 105 (15), 78(31). **3a-P** (37% yield): Colorless oil; IR (neat): 3380 (OH), 1080, 1040 (SO) cm^{-1}; NMR: δ=0.89 (3H, t, *J*=6.5 Hz), 1.19 (3H, t, *J*=7 Hz), 2.10 (2H, m), 3.74 (1H, dd, *J*=9, 2 Hz), 7.4—7.8 (5H, m); MS *m/z* (%): 126 ([M−$C_9H_{17}ClO$]$^+$, 100), 105(78), 78(31).

To a solution of **3a-L** (1 mmol) in 12 ml of MeOH was added 30% aq KOH (2.5 ml) dropwise with stirring and the mixture was stirred at room temperature for 1 h. The reaction mixture was neutralized by NH_4Cl and the MeOH was evaporated. The residue was extracted with benzene and the organic layer washed with sat. aq NH_4Cl. After the usual work-up, the product was purified by silica-gel column chromatography to afford 89% yield of **4a-L**.[13] Colorless oil; IR (neat): 1090, 1055 (SO) cm^{-1}; NMR: δ=0.82 (3H, t, *J*=7 Hz), 0.88 (3H, t, *J*=6.5 Hz), 3.64 (1H, t, *J*=6 Hz), 7.4—7.8 (5H, m); MS m/z (%): 266 (M$^+$, trace), 126(10), 77(10), 57(100); Found: *m/z* 266.1321. Calcd for $C_{15}H_{22}O_2S$: M, 266.1338. The epoxy sulfoxide (**4a-P**)[13] was synthesized from **3a-P** as similar procedure described above in 90% yield as a colorless oil. IR (neat): 1090, 1050 (SO) cm^{-1}; NMR: δ=0.70 (3H, t, *J*=7 Hz), 0.94 (3H, t, *J*=6.5 Hz), 3.25 (1H, t, *J*=6 Hz), 7.4—7.7 (5H, m); MS *m/z* (%): 266 (M$^+$, trace), 126(8), 77(6), 57(100); Found: *m/z* 266.1333. Calcd for $C_{15}H_{22}O_2S$: M, 266.1339.

1,2-Epoxy-1-phenyl-2-phenylsulfinylbutane (4c). Chlorohydrin **3c-L** (45% yield): Colorless prisms; mp 140—142 °C; IR (KBr): 3210 (OH), 1035 (SO) cm^{-1}; NMR: δ=1.29 (3H, t, *J*=7 Hz), 2.02 (1H, dq, *J*=15, 7 Hz), 2.97 (1H, dq, *J*=15, 7 Hz), 4.93 (1H, s), 7.23 (5H, s), 7.5—8.0 (5H, m); MS *m/z* (%): 309 ([M+1]$^+$, trace), 126(100), 105(40), 91(47); Found: C, 62.45; H, 5.52; Cl, 11.65; S, 10.44%. Calcd for $C_{16}H_{17}ClO_2S$: C, 62.23; H, 5.55; Cl, 11.48; S, 10.38%. **3c-P** (52% yield): Colorless prisms; mp 110 °C (dec); IR (KBr): 3370 (OH), 1035 (SO) cm^{-1}; NMR: δ=0.94 (3H, t, *J*=7 Hz), 1.3—2.3 (2H, m), 5.31 (1H, s), 7.2—7.9 (10H, m); MS *m/z* (%): 182(11), 147(27), 126(100), 105(38); Found: C, 62.30; H, 5.49; Cl, 11.62; S, 10.58%. Calcd for $C_{16}H_{17}ClO_2S$: C, 62.23; H, 5.55, Cl, 11.48; S, 10.38%. Epoxy sulfoxide **4c-L** (99% yield): Colorless oil; IR (neat): 1045, (SO) cm^{-1}; NMR: δ=0.76 (3H, t, *J*=7 Hz), 1.1—2.0 (2H, m), 4.77 (1H, s), 7.1—7.9 (10H, m); MS *m/z* (%): 272 (M$^+$, 0.6), 147 ([M−PhSO]$^+$, 47), 91(100); Found *m/z* 272.0846. Calcd for $C_{16}H_{16}O_2S$: M, 272.0869. **4c-P** (99% yield): Colorless oil; IR (neat): 1045 (SO) cm^{-1}; NMR: δ=0.85 (3H, t, *J*=7 Hz), 1.4—1.8 (1H, m), 2.37 (1H, sextet, *J*=7 Hz), 4.42 (1H, s), 7.2—7.8 (10H, m); MS *m/z* (%): 272 (M$^+$, trace), 147 ([M−PhSO]$^+$, 35), 91(100); Found *m/z* 272.0909. Calcd for $C_{16}H_{16}O_2S$: M, 272.0870.

1,2-Epoxy-1-cyclohexyl-1-phenylsulfinylheptane (4f). Chlorohydrin **3f-L** (46% yield): IR (neat): 3375 (OH), 1040 (SO) cm^{-1}; NMR: δ=0.80 (3H, t, *J*=6 Hz), 3.95 (1H, t, *J*=6 Hz), 7.4—7.9 (5H, m). **3f-P** (47% yield): Colorless oil; IR (neat): 3410 (OH), 1085, 1060, 1030, (SO) cm^{-1}; NMR: δ=0.89 (3H, t, *J*=6 Hz), 3.70 (1H, bd, *J*=8 Hz), 7.3—7.8 (5H, m). Epoxy sulfoxide **4f-L** (85% yield): Colorless oil; IR (neat): 1095, 1060 (SO) cm^{-1}; NMR: δ=0.91 (3H, t, *J*=7 Hz), 3.55 (1H, dd, *J*=7, 5 Hz), 7.4—7.7 (5H, m); MS *m/z* (%): 320 (M$^+$, 0.3), 304 (0.7), 195 ([M−PhSO]$^+$, 8), 126(7), 111(24),

83(100); Found: *m/z* 320.1829. Calcd for $C_{19}H_{28}O_2S$: M, 320.1809. **4f-P** (93% yield): Colorless oil; IR (neat): 1090, 1050 (SO) cm^{-1}; NMR: δ=0.95 (3H, t, *J*=6 Hz), 3.26 (1H, t, *J*=6 Hz), 7.4—7.8 (5H, m).

2,3-Epoxy-2-methyl-3-phenylsulfinylpentane (4g). Chlorohydrin **3g** (99% yield): Colorless prisms; mp 76—77 °C; IR (KBr): 3350 (OH), 1035 (SO) cm^{-1}; NMR: δ=0.93 (3H, t, *J*=7 Hz), 1.43, 1.67 (each 3H, s), 1.99 (2H, m), 7.3—7.8 (5H, m); MS *m/z* (%): 162 ([M−$C_6H_{11}ClO$]$^+$, 86), 78 (32), 43 (100); Found: C, 55.10; H, 7.31; Cl, 13.67; S, 12.33%. Calcd for $C_{12}H_{17}ClO_2S$: C, 55.27; H, 6.57; Cl, 13.59; S, 12.30%. Epoxy sulfoxide **4g** (75% yield): Colorless oil; IR (neat): 1075, 1040 (SO) cm^{-1}; NMR:δ=0.50 (3H, t, *J*=7 Hz), 1.41, 1.83 (5H, m); MS *m/z* (%): 224 (M$^+$, trace), 126(48), 99 ([M−PhSO]$^+$, 79), 43 (100).

α,β-Epoxy Sulfoxide (4m). Chlorohydrin **3m** (85% yield): Colorless prisms; mp 165 °C (dec); IR (KBr): 3400 (OH), 1085, 1040 (SO) cm^{-1}; MS *m/z* (%): 287 (M$^+$, 0.4), 272 ([M−CH_3]$^+$, 40), 270(99), 126(58), 70(83), 42(100). Epoxy sulfoxide **4m** (95% yield): Colorless oil; IR (neat): 1090, 1050 (SO) cm^{-1}; NMR: δ=2.37 (3H, s), 4.76 (1H, s), 7.5—7.8 (5H, m); MS *m/z* (%): 251 (M$^+$, 1.8), 234(46), 126(32), 96(26), 83 (100); Found: *m/z* 251.1003. Calcd for $C_{13}H_{17}NO_2S$: M, 251.0979.

1,2-Epoxy-5-chloro-2-methyl-1-phenylsulfinylpentane (4o). Chlorohydrin **3o** (97% yield): Diastereomeric mixture; colorless needles; mp 138—145 °C; IR (KBr): 3360 (OH), 1045 (SO) cm^{-1}; MS *m/z* (%): 126 ([M−$C_6H_{10}Cl_2O$]$^+$, 100), 78(37), 43(50). Epoxy sulfoxide **4o** (12% yield): Colorless oil; IR (neat): 1085, 1045 (SO) cm^{-1}; NMR: δ=1.44 (3H, s), 3.72 (1H, s), 4.04 (1H, t, *J*=6 Hz), 7.5—7.9 (5H, m); MS *m/z* (%): 258 (M$^+$, 0.1), 133 ([M−PhSO]$^+$, 41), 126(100); Found: *m/z* 258.0457. Calcd for $C_{12}H_{15}ClO_2S$: M, 258.0479.

All other α,β-epoxy sulfoxides (**4**) are reported in Ref. 1.

General Procedure for the Preparation of α-Sulfenylated Ketones and α-Sulfenylated Aldehydes: A synthesis of 4-phenylthio-3-nonanone (**5a**) is described. To 2 ml of dry EtOH NaH (60% oil suspension; 20 mg; 0.5 matom) was added followed by thiophenol (52 μl; 0.5 mmol) at 0 °C under N_2 atmosphere. A solution of 3,4-epoxy-3-phenylsulfinylnonane (**4a**) (68 mg; 0.25 mmol) in 0.5 ml of EtOH was added to the benzenethiolate solution and the reaction mixture was stirred at room temperature under N_2 atmosphere for 45 min. The reaction mixture was neutralized by adding NH_4Cl and the EtOH evaporated. The residue was extracted with benzene and the organic layer was washed with sat. aq NH_4Cl, dried and concentrated. The crude product was purified by silica-gel column chromatography to afford 54.5 mg (87%) of 4-phenylthio-3-nonanone (**5a**) as a colorless oil. IR (neat): 1705 (CO) cm^{-1}; NMR: δ=0.88 (3H, t, *J*=7 Hz), 1.03 (3H, t, *J*=7 Hz), 3.58, 3.59 (each 1H, q, *J*=7 Hz), 3.63 (1H, t, *J*=7 Hz), 7.1—7.5 (5H, m); MS *m/z* (%): 250 (M$^+$, 24), 193 ([M−C_2H_5CO]$^+$, 100), 123(73), 109(18), 83(29); Found: *m/z* 250.1384. Calcd for $C_{15}H_{22}OS$: M, 250.1389.

2-Phenylthio-3-nonanone (5b). Colorless oil; IR (neat): 1710 (CO) cm^{-1}; NMR: δ=0.87 (3H, t, *J*=7 Hz), 1.40 (3H, d, *J*=7 Hz), 2.60 (2H, m), 3.76 (1H, q, *J*=7 Hz), 7.1—7.4 (5H, m); MS *m/z* (%): 250 (M$^+$, 10), 137 ([M−$C_6H_{13}CO$]$^+$, 100), 109 (16); Found: *m/z* 250.1363. Calcd for $C_{15}H_{22}OS$: M, 250.1389.

1-Phenyl-1-phenylthio-2-butanone (5c). Colorless prisms; mp 35—36 °C (sublimation); IR (neat): 1710 (CO) cm^{-1}; NMR: δ=0.98 (3H, t, *J*=7 Hz), 2.44, 2.64 (each 1H, dq, *J*=18, 7 Hz), 4.95 (1H, s), 7.1—7.4 (10H, m); MS *m/z* (%): 256 (M$^+$, 5), 200 (16), 199 ([M−C_2H_5CO]$^+$, 100), 165 (10), 91(16); Found: *m/z* 256.0907. Calcd for $C_{16}H_{16}OS$: M, 256.0920.

1-Phenyl-1,3-bis(phenylthio)-2-butanone (8). Diastereomeric mixture; colorless oil; IR (neat): 1720 (CO) cm^{-1}; NMR: δ=1.26, 1.30 (each d, *J*=7 Hz), 3.71, 3.94 (each q, *J*=7 Hz), 5.32, 5.46 (each s), 7.0—7.5 (m); MS *m/z* (%): 364 (M$^+$, 9), 255 ([M−PhS]$^+$, 14), 227 (11), 199 ([M−C_9H_9OS]$^+$, 100).

1-(1-Phenylthiocyclohexyl)-1-heptanone (5e). Colorless oil; IR (neat): 1705 (CO) cm^{-1}; NMR: δ=0.90 (3H, t, *J*=7 Hz), 2.74 (2H, t, *J*=7 Hz), 7.26 (5H, s); MS *m/z* (%): 304 (M$^+$, 2), 191 ([M−$C_7H_{13}O$]$^+$, 100); Found: *m/z* 304.1839. Calcd for $C_{19}H_{28}OS$: 304.1858.

1-Cyclohexyl-2-phenylthio-1-heptanone (5f). Colorless oil; IR (neat): 1710 (CO) cm^{-1}; NMR: δ=0.87 (3H, t, *J*=7 Hz), 2.68 (1H, m), 3.68 (1H, dd, *J*=8, 7 Hz), 7.1—7.4 (5H, m); MS *m/z* (%): 304 (M$^+$, 13), 193 ([M−$C_7H_{11}O$]$^+$, 100), 123 (38); Found: *m/z* 304.1857. Calcd for $C_{19}H_{28}OS$: M, 304.1859.

2-Methyl-2-phenylthio-3-pentanone (5g). Colorless oil; IR (neat): 1695 (CO) cm^{-1}; NMR: δ=1.10 (3H, t, *J*=7 Hz), 1.41 (6H, s), 2.79 (2H, q, *J*=7 Hz), 7.27 (5H, s); MS *m/z* (%): 208 (M$^+$, 7), 191 (3), 151 ([M−C_2H_5CO]$^+$, 100), 109 (13); Found: *m/z* 208.0911. Calcd for $C_{12}H_{16}OS$: M, 208.0920.

3-Methyl-1-phenyl-3-phenylthio-2-butanone (5h). Colorless oil; IR (neat): 1715 (CO) cm^{-1}; NMR: δ=1.44 (6H, s), 4.07 (2H, s), 7.1—7.3 (10H, m); MS *m/z* (%): 270 (M$^+$, 4), 151 ([M−$PhCH_2CO$]$^+$, 100); Found: *m/z* 270.1083. Calcd for $C_{17}H_{18}OS$: M, 270.1078.

3-Methyl-1-phenyl-1,3-bis(phenylthio)-2-butanone (9). Colorless crystals; mp 97—98 °C; IR (KBr): 1695 (CO) cm^{-1}; NMR: δ=1.25, 1.42 (each 3H, s), 5.60 (1H, s), 7.0—7.4 (15H, m); MS *m/z* (%): 378 (M$^+$, 4), 269(5), 199(36), 151 ([M−$C_{14}H_{11}OS$]$^+$, 100); Found: *m/z* 378.1084. Calcd for $C_{23}H_{22}OS_2$: M, 378.1111.

2-Methyl-1-(4,4-ethylenedioxy-1-phenylthiocyclohexyl)-1-propanone (5i). Colorless oil; IR (neat): 1700 (CO) cm^{-1}; NMR: δ=1.20 (6H, d, *J*=7 Hz), 3.40 (1H, septet, *J*=7 Hz), 3.92 (4H, bs), 7.26 (5H, bs); MS *m/z* (%): 320 (M$^+$, 4), 249 ([M−C_4H_7O]$^+$, 90), 205(8), 187(26), 99(100); Found: *m/z* 320.1457. Calcd for $C_{18}H_{24}O_3S$: M, 320.1444.

1-Butylthio-1-phenyl-2-butanone (5j). Colorless oil; IR (neat): 1715 (CO) cm^{-1}; NMR: δ=0.87 (3H, t, *J*=7 Hz), 1.00 (3H, t, *J*=7 Hz), 2.3—2.7 (4H, m), 4.61 (1H, s), 7.1—7.4 (5H, m); MS *m/z* (%): 236 (M$^+$, 2), 199(11), 179 ([M−C_2H_5CO]$^+$, 100), 123(43), 91(38); Found: *m/z* 236.1214. Calcd for $C_{14}H_{20}OS$: M, 236.1233.

1-Cyclohexylthio-1-phenyl-2-butanone (5k). Colorless oil; bp 170 °C/ 5 mmHg[†]; IR (neat): 1720 (CO) cm^{-1}; NMR : δ=0.99 (3H, t, *J*=7 Hz), 2.4—2.8 (3H, m), 4.68 (1H, s), 7.1—7.4 (5H, m); MS *m/z* (%): 262 (M$^+$, 1), 205 ([M−C_2H_5CO]$^+$, 69), 199(4), 123(100); Found: *m/z* 262.1387. Calcd for $C_{16}H_{22}OS$: M, 262.1390.

1-(2-Hydroxyethylthio)-1-phenyl-2-butanone (5l). Colorless oil; IR (neat): 3400 (OH), 1710 (CO) cm^{-1}; NMR: δ= 1.01 (3H, t, *J*=7 Hz), 2.3—2.7 (2H, m), 2.63 (2H, t, *J*=6 Hz), 3.67 (2H, bt, *J*=6 Hz), 4.73 (1H, s), 7.32 (5H, bs); MS *m/z* (%): 224 (M$^+$, 1), 167 ([M−C_2H_5CO]$^+$, 100), 150(10), 123 (12), 91 (54); Found: *m/z* 224.0861. Calcd for $C_{12}H_{16}O_2S$: M, 224.0870.

1-(Benzimidazol-2-ylthio)-1-phenyl-2-butanone (5m). Colorless powder; mp 141—142 °C; IR (KBr): 1725 (CO)

[†] 1 mmHg≈133.322 Pa.

cm^{-1}; NMR: δ=0.99, 1.12 (each t, J=7 Hz), 2.0—2.7 (2H, m), 5.34, 5.84 (each s), 6.9—7.8 (m); The complexity of the signals is thought to be due to the restricted rotation of the imidazolylthio group; MS m/z (%): 296 (M^+, 33), 240 (100), 239 ([M−C_2H_5CO]$^+$, 56), 207 (40); Found: C, 68.89; H, 5.35; N, 9.42; S, 10.83%; M^+ 296.0987. Calcd for $C_{17}H_{16}N_2OS$: C, 68.89; H, 5.44; N, 9.45; S, 10.82%; M, 296.0983.

3-Methoxycarbonylmethylthio-1-phenyl-2-butanone (5n). Colorless oil; IR (neat): 1745, 1715 (CO) cm^{-1}; NMR: δ= 1.39 (3H, d, J=7 Hz), 3.18 (2H, s), 3.61 (1H, q, J=7 Hz), 3.69 (3H, s), 3.91, 3.96 (each 1H, d, J=15 Hz), 7.23 (5H, m); MS m/z (%): 252 (M^+, 20), 193 ([M−$C_2H_3O_2$]$^+$, 3), 133 ([M−$PhCH_2CO$]$^+$, 78), 91 (100); Found: m/z 252.0791. Calcd for $C_{13}H_{16}O_3S$: M, 252.0818.

2-Phenylthio-2-indancarbaldehyde (5o). Colorless oil; IR (neat); 2725 (CHO), 1730, 1725 (CO) cm^{-1}; NMR: δ=3.13, 3.47 (each 2H, d, J=16 Hz), 7.21 (4H, s), 7.2—7.5 (5H, m), 9.57 (1H, s); MS m/z (%): 220 (M^+, 17), 191 ([M−CHO]$^+$, 81), 123 (28), 110 (40), 109 (26), 81 (100).

1-Phenylthio-1-cyclohexanecarbaldehyde (5p). Colorless oil; IR (neat): 2720 (CHO), 1720 (CO) cm^{-1}; NMR: δ=1.1— 2.0 (10H, m), 7.1—7.5 (5H, m), 9.29 (1H, s); MS m/z (%): 254 (M^+, 13), 225 ([M−CHO]$^+$, 33), 145 ([M−PhS]$^+$, 27), 116 (49), 115 (100).

4-Formyl-N-methyl-4-phenylthiopiperidine (5q). Colorless oil; IR (neat): 1710 (CO) cm^{-1}; NMR: δ=1.8—2.3 (6H, m), 2.29 (3H, s), 2.6—2.9 (2H, m), 7.2—7.5 (5H, m), 9.30 (1H, s); MS m/z (%): 235 (M^+, 11), 207 ([M−CO]$^+$, 17), 174 (3), 126 ([M−PhS]$^+$, 79), 109(13), 96(44), 83(100); Found: m/z 235.1020. Calcd for $C_{13}H_{17}NOS$: M, 235.1030.

2-Methyl-2-phenylthio-3-tetrahydropyranyloxypropanal (5r). Diastereomeric mixture; colorless oil; IR (neat): 1730 (CO), 1020 (COC) cm^{-1}; NMR: δ=1.34, 1.38 (each s), 3.49, 3.64, 3.93, 4.05 (each d, J=10 Hz), 4.62 (1H, bs), 7.2—7.6 (m), 9.46, 9.47 (each s); MS m/z (%): 280 (M^+, 2), 179 ([M− THPO]$^+$, 8), 166(51), 140(34), 109(29), 85(100).

2-Methyl-2,5-bis(phenylthio)pentanal (5s). Colorless oil; IR (neat): 2720 (CHO), 1720 (CO) cm^{-1}; NMR: δ=1.24 (3H, s), 2.93 (2H, t, J=7 Hz), 7.1—7.4 (10H, m), 9.35 (1H, s); MS m/z (%) 316 (M^+, 30), 287 ([M−CHO]$^+$, 8), 207 ([M−PhS]$^+$, 39), 177(64), 150(42), 123(58), 109(100); Found: m/z 316.0943. Calcd for $C_{18}H_{20}OS_2$: M, 316.0954.

The authors are grateful to Dr. S. Saito, Tanabe Seiyaku Co., for elemental analysis and Miss Sawabe, Mrs. Yamatani, and Miss Khim of this laboratory for NMR and mass spectral measurements. This work was supported in part by a Grant-in-Aid for Scientific Research No. 59771658 from the Ministry of Education, Science and Culture.

References

1) Part I: T. Satoh, Y. Kaneko, T. Izawa, K. Sakata, and K. Yamakawa, *Bull. Chem. Soc. Jpn.*, **58**, 1983 (1985).

2) B. M. Trost, *Chem. Rev.*, **78**, 363 (1978).

3) P. A. Gassman, T. J. van Bergen, D. P. Gilbert, and B. W. Cue, Jr, *J. Am. Chem. Soc.*, **96**, 5495 (1974); B. M. Trost and A. J. Bridges, *ibid.*, **98**, 5017 (1976); R. A. Murphy, Jr, and M. P. Cava, *Tetrahedron Lett.*, **25**, 803 (1984).

4) a) J. A. Barltrop and K. J. Morgan, *J. Chem. Soc.*, **1960**, 4486; b) H. J. Monteiro, *J. Org. Chem.*, **42**, 2324 (1977); c) N. Kharasch, H. L. Wehrmeister, and H. Tigermann, *J. Am. Chem. Soc.*, **69**, 1612 (1947); d) D. Seebach and M. Teschner, *Tetrahedron Lett.*, **1973**, 5113; e) B. M. Trost, T. N. Salzmann, and K. Hiroi, *J. Am. Chem. Soc.*, **98**, 4887 (1976); f) B. M. Trost and G. S. Massiot, *J. Am. Chem. Soc.*, **99**, 4405 (1977); g) M. L. Quesada and R. H. Schlessinger, *J. Org. Chem.*, **43**, 346 (1978).

5) T. Satoh, Y. Kaneko, T. Kumagawa, T. Izawa, K. Sakata, and K. Yamakawa, *Chem. Lett.*, **1984**, 1957.

6) T. Durst, *J. Am. Chem. Soc.*, **91**, 1034 (1969).

7) K. M. More and J. Wemple, *J. Org. Chem.*, **43**, 2713 (1978).

8) a) D. F. Tavares, R. E. Estep, and M. Blezard, *Tetrahedron Lett.*, **1970**, 2373; b) V. Reutrakul and W. Kanghae, *ibid.*, **1977**, 1377; c) D. F. Taber and B. P. Gunn, *J. Org. Chem.*, **44**, 450 (1979); d) T. Durst, K-C. Tin, F. de Reinach-Hirtzbach, J. M. Decesare, and M. D. Ryan, *Can. J. Chem.*, **57**, 258 (1979).

9) The ratio of the products was determined by GLC and NMR spectral measurements.

10) B. M. Trost and J. H. Rigby, *Tetrahedron Lett.*, **1978**, 1667.

11) When this reaction was carried out with less than three equivalents of alkane- or arenethiolate, some amounts of α-phenylthio ketone was observed. The source of benzenethiolate is thought to be the liberated benzenesulfenate from α,β-epoxy sulfoxide.[1]

12) The diastereomers of the chlorohydrin (**3**) are expressed as **L** or **P**, in which **3-L** is the chlorohydrin having large R_f value (less polar chlorohydrin).

13) The diastereomers of the α,β-epoxy sulfoxide (**4**) are expressed as **L** or **P**. **4-L** and **4-P** are epoxy sulfoxides derived from the chlorohydrins **3-L** and **3-P**, respectively.

Preparation and Thermolysis of *N*-Ammonioamidates Containing Hydroxyl Group in Acyl Moiety

Araki MASUYAMA, Kikuo TSUCHIYA, and Mitsuo OKAHARA*
Department of Applied Chemistry, Faculty of Engineering, Osaka University, Yamadaoka 2-1, Suita, Osaka 565
(Received May 2, 1985)

The title *N*-ammonioamidates (aminimides) were prepared in satisfactory yields from lactones or α-hydroxy carboxylates. By the thermolysis of these aminimides in mesitylene, some types of urethane compounds were formed, depending on the structure of the aminimide and on the concentration of the solutions.

N-Ammonioamidates (aminimides) have been studied on the application to surfactants,[1,2] phase transfer catalysts,[3] and ion carriers in membrane transport systems.[4] As it is well known that they readily rearrange to isocyanates upon heating,[5] aminimides are considered as precursors of urethane or urea derivatives since isocyanates are convertible into urethane or urea compounds through a reaction with alcohols or amines.

On the other hand, the segmented-polyether-urethane polymer has recently been utilized as a "biomedical polymer material" for artificial hearts and artificial blood vessels.[6,7] Investigations of a new precursor of this type of urethane have been developed. As one of them, the preparation of a so-called "AB type" urethane-precursor which contains both a hydroxyl- and a functional group convertible into isocyanate in the same molecule have been reported.[8,9] But these are only a few studies regarding aminimide as an "AB type" precursor.[10,11]

We have previously reported the synthesis of urethane-type crown ethers by a thermolytic reaction of aminimides containing an α-hydroxyoligo(ethylenoxy) group.[12] In the present paper, the preparations and properties of aminimides with a hydroxyl group in an acyl moiety from commercially available lactones or α-hydroxy carboxylates are described. Futhermore, the effects of the structure of aminimide and the solution concentration on the types of urethane compounds that were formed by thermolyses of aminimides in mesitylene are discussed.

Results and Discussion

Aminimides (**4**) were prepared from lactones (**1**) or α-hydroxy carboxylates (**2**) by the following two methods (Scheme 1).

(A) Hydrazinium Iodide Method. Aminimides were obtained by a one-step reaction between **1** and *N,N,N*-trimethylhydrazinium iodide (**3**), which was formed in quantitative yield from *N,N*-dimethylhydrazine and methyl iodide, in *t*-butyl alcohol in the presence of potassium *t*-butoxide.[13]

(B) Hydrazine Method. This method consisted of two-steps reactions. The preparation of acylhydrazines (**6**) from **1** or **2** and excess hydrazine hydrate (80%) (**5**) followed by a reaction with a large excess of methyl iodide (more than six folds to **1**) in methanol in the presence of potassium carbonate yielded aminimides.

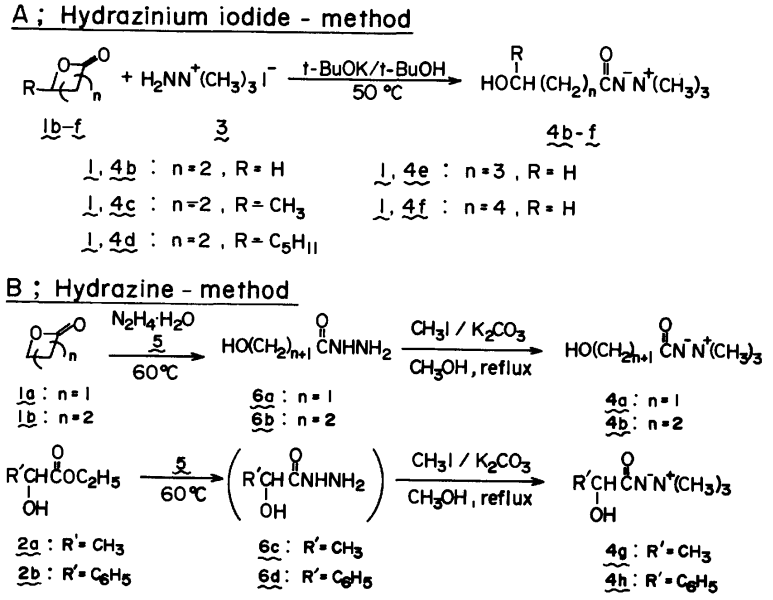

Scheme 1.

Table 1. Yield and melting point of aminimides (**4**)

Aminimide	Method[a)]	Yield[b,c)] %	Mp θ_m/°C
4a	B	75 (53)	125—126
4b	A	80 (62)	107—108
4b	B	82	
4c	A	93 (69)	92—94
4d	A	85 (63)	86—88
4e	A	94 (61)	95—96
4f	A	85 (68)	116—117
4g	B	86 (55)	108—109
4h	B	81 (59)	140(dec)

a) A; Hydrazinium iodide method, B; Hydrazine method. b) Crude yields based on **1** or **2**. c) Values in parentheses are yields after recrystallization.

After reactions involving both methods, crude products of aminimides were separated by extraction with dichloromethane and pure compounds were obtained by recrystallization from acetone or ethyl acetate. The isolated products were characterized by spectral and elemental analyses (Tables 4 and 5). The yields and melting points of **4** are listed on Table 1. Differences in the yields of *N*-trimethylammonio-4-hydroxybutanamidate (**4b**) from 4-butanolide (**1b**) were not observed between both methods, and **4b** was obtained in good yield (above 80%) by each method. However, in the hydrazinium iodide-method, aminimides were hardly obtained from 3-propanolide (**1a**) and α-hydroxy carboxylates (**2**). The hydrazine-method has some advantages: Using an inexpensive hydrazine hydrate (**5**) instead of *N,N,N*-trimethylhydrazinium iodide and being applicable to both lactones and α-hydroxy carboxylates. Intermediates, 3-hydroxypropanohydrazide (**6a**) and 4-hydroxybutanohydrazide (**6b**), obtained from **1a** and **1b**, respectively, were isolated by recrystallization from ethanol and identified by spectral analyses (Table 4). However, there was no difference in yield when crude acylhydrazine was used in a following reaction without further purification.

The thermolysis of prepared aminimides (**4a**—h) was carried out in mesitylene as an inert and high-boiling-point solvent. The aminimide was stirred at 160°C in mesitylene under a nitrogen atmosphere until the carbonyl absorption in the IR spectrum shifted to about 1700 cm^{-1} due to the formation of a urethane bond. The solvent was evaporated off and the residue (solid or semisolid) was extracted with chloroform to separate the soluble and insoluble portions (insoluble one; Fraction 3). The chloroform-soluble portion was further separated into the distillate (Fraction 1) and the residue (Fraction 2) by distillation at 120°C/2.7 Pa using a Kugelrohr apparatus.

The thermolysis was carried out in both dilute (1.00 g of aminimide/100 ml of mesitylene) and concentrated (1.00 g of aminimide/10 ml of mesitylene) conditions. The yields of reaction products and the weight percentage of each fraction are shown in Table 2.

In the thermolyses of **4a—f**, the distillates (Fraction 1) were white solids which showed one peak in GLC. Also, needle-like crystals were obtained by recrystallization from ethyl acetate. From their spectral data and elemental analyses, these fractions were identified as cyclic urethanes (**7a—f**). These compounds may be formed by the intramolecular addition of a hydroxyl group to an isocyanato group which was introduced by a thermolytic rearrangement of the aminimides. The properties and an elemental analysis of **7a—f** are shown in Tables 3 and 5.

The residual compounds in the distillation (Frac-

Table 2. Thermolysis of aminimides (**4a—h**)

Run	Aminimide	Reaction system[a)]	Reaction time/h	Yield[b)] g	Fraction ratio/wt % Fr.1[c)]	Fr.2[d,e)]	Fr.3[f)]
1	**4a**	Dilute	6	0.57	≃100	Trace	0
2	**4a**	Concd	3	0.55	40	55 (157)	5
3	**4b**	Dilute	2	0.55	≃100	Trace	0
4	**4b**	Concd	3	0.52	30	65 (255)	5
5	**4c**	Dilute	3	0.65	≃100	Trace	0
6	**4c**	Concd	3	0.60	70	27 (270)	3
7	**4d**	Dilute	3	0.68	≃100	Trace	0
8	**4d**	Concd	3	0.69	55	45 (242)	0
9	**4e**	Dilute	3	0.56	32	38 (416)	30
10	**4e**	Concd	3	0.51	0	15 (425)	85
11	**4f**	Dilute	3	0.57	10	65 (555)	25
12	**4f**	Concd	3	0.54	0	10 (520)	90
13	**4g**	Dilute	5	0.61	37	18 (271)	45
14	**4g**	Concd	5	0.59	0	21 (285)	79
15	**4h**	Dilute	5	0.70	31	28 (354)	41
16	**4h**	Concd	5	0.68	0	17 (339)	83

a) Dilute system: 1.00 g (**4**)/100 ml (mesitylene); concd system: 1.00 g (**4**)/10 ml (mesitylene). b) Yield of the residue after removal of mesitylene. c) The distillate of chloroform-soluble portion using a Kugelrohr apparatus (120°C/2.7 Pa). d) The residue of chloroform-soluble portion by Kugelrohr-distillation. e) Values in parentheses are number-averaged molecular weights ($\overline{Mn}$) measured by a VPO in a chloroform at 25°C. f) The chloroform-insoluble portion.

Table 3. Characterization of cyclic urethanes (**7a—f**)

Compound	Starting aminimide	Mp θ_m/°C	IR (KBr pellet) ν/cm^{-1}	^{1}H NMR ($CDCl_3$) δ	MS (70 eV) *m/z*(rel. intensity)
7a	**4a**	88—89	3370, 1730	3.62(t, 2H), 4.44(t, 2H), 6.55(s, 1H)	87(M^+, 100), 59(49), 42(23), 28(43)
7b	**4b**	83—84	3275, 1690	1.96(q, 2H), 3.35(t, 2H), 4.30(t, 2H), 6.6—7.2(br, 1H)	101(M^+, 100), 56(39), 33(16), 29(23), 28(77)
7c	**4c**	98—99	3260, 1720	1.38(d, 3H), 1.75(m, 2H), 3.35(q, 2H), 4.41(m, 1H), 6.88(s, 1H)	115(M^+, 40), 71(21), 56(45), 43(66), 42(70), 30(100), 28(99)
7d	**4d**	102—103	3265, 1700	0.88(t, 3H), 1.1—2.1(m, 10H), 3.35(m, 2H), 4.25(m, 1H), 6.75(s, 1H)	171(M^+, 1), 100(88), 82(23), 74(41), 55(69), 43(30), 30(100)
7e	**4e**	61—62	3345, 1710	1.6—2.0(m, 4H), 3.15(q, 2H), 4.16(t, 2H), 6.47(s, 1H)	115(M^+, 77), 70(11), 56(21), 42(100), 30(60)
7f	**4f**	75—76	3350, 1700	1.5—2.0(m, 6H), 3.30(m, 2H), 4.20(t, 2H), 6.05(s, 1H)	129(M^+, 11), 68(40), 56(99), 43(82), 30(100)

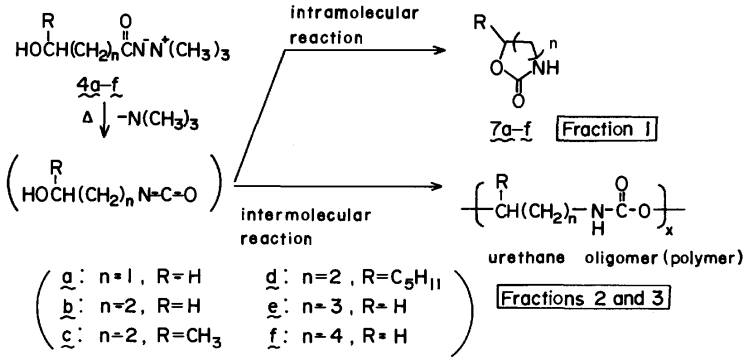

Scheme 2.

tion 2) were semisolids which showed some peaks for longer retention times than that of the corresponding Fraction 1 in GLC. But their IR spectra and both the chemical shifts and integral ratios in their ^{1}H NMR were similar to those of the corresponding Fraction 1. Their molecular weights were determined by a VPO method (Table 2) and they were considered as the urethane oligomers with low molecular weights which might be formed by the intermolecular reaction between hydroxyl and isocyanato groups. It is probable that Fraction 2 was for the most part cyclic oligomers since their molecular weights were not so large and the existence of expected terminal groups in linear structures were not observed in the ^{1}H NMR spectra.

The chloroform-insoluble matter (Fraction 3) was a white or pale-brown solid and showed the same IR spectra as the corresponding Fraction 2. Thus, Fraction 3 could be considered as a linear or cyclic urethane polymer with a higher molecular weight than Fraction 2. However, their molecular weights and ^{1}H NMR spectra were not measured since they were only slightly soluble in water, alcohols, tetrachloromethane or other organic solvents.

The mechanism of the formation of the urethane compounds mentioned above is shown in Scheme 2.

In the thermolyses of α-hydroxyl type aminimides (**4g,h**), Fraction 1 was obtained as a pale-yellow liquid which showed some peaks in GLC and absorption peaks at 1830 and 1760 cm^{-1}, besides 1710 cm^{-1} in IR spectra. But the formation of compound **7**- type cyclic urethane was not detected by mass spectra. Additionally, their ^{1}H NMR spectra were complicated, so that their ingredients could not be identified. The IR spectra of Fraction 2 was similar to that of Fraction 1. Fraction 3 was a white solid which showed a strong absorption peak at 1740 cm^{-1}.

As shown in Table 2, the formation ratios of cyclic urethanes (**7**), urethane oligomers with low molecular weights, and urethane polymers was considerably affected by both the chain length (defined as the number of carbons between carbonyl and hydroxyl group of **4**) and the concentration of the solution. In the case of dilute conditions, five-membered (**7a**) and six-membered rings (**7b—d**) of cyclic urethanes were quantitatively formed from **4a** (chain length=2) and **4b—d** (chain length=3), respectively, and the formation of oligomer and polymer was not observed

(Table 2. Runs 1, 3, 5, and 7). On the other hand, oligomers were mainly obtained in the thermolysis of **4e** and **4f**. It seems reasonable that an intermolecular reaction took place prior to an intramolecular reaction in which a seven- (**7e**) or eight-membered ring (**7f**) compound was formed (Runs 9 and 11). In concentrated conditions, oligomer was also formed in a reaction of **4a—d** (Runs 2, 4, 6, and 8) and a polymer was obtained (for the most part) in the case of **4e** and **4f** (Runs 10 and 12).

Experimental

The ^{1}H NMR and IR spectra were taken on a JEOL JNM-PS-100 spectrometer and a Hitachi 260 spectrometer, respectively. The mass spectra were measured with a Hitachi RMU-6E mass spectrometer at an ionization potential of 70 eV. The GLC analyses were performed on a Shimadzu gas chromatograph GC-4CPT using a 1 m×3 mm column packed with 10% Silicone OV-1 on Uniport KS. The number-averaged molecular weight was measured with a Hitachi Perkin Elemer 115-type vapor-pressure osmometer in a chloroform solution at 25 °C. The starting materials were the commercial products of analytical reagent grade. Their purities were checked by GLC and IR, and they were purified by distillation when necessary. *N,N,N*-Trimethylhydrazinium iodide (**3**) was obtained as a white solid by the interaction of equivalent *N,N*-dimethylhydrazine and methyl iodide in diethyl ether at 20 °C and used without further purification. Mesitylene was distilled under a reduced pressure before use.

Preparation of N-*Trimethylammonio-4-hydroxybutanamidate (4b) by the Hydrazinium Iodide Method.* Potassium metal (4.7 g, 0.12 mol) was dissolved in 300 ml of *t*-butyl alcohol, and then **3** (20.2 g, 0.10 mol) and 4-butanolide (**1b**, 8.6 g, 0.10 mol) were slowly added, in turn, to the solution. After 5 h of stirring at 50 °C and subsequent neutralization by hydrochloric acid (to pH 8.0), the reaction mixture was filtered. The precipitate was washed with dichloromethane, and the solvent was removed from a combined solution of filterate and washings. The solid-liquid extraction of the residue with dichloromethane several times was followed by the filteration and evaporation of the extracts. This afforded 12.8 g of crude aminimide, as white solids (80%). The pure **4b** was obtained by recrystallization from acetone as fine white needles (9.9 g, 62%). Crude aminimide showed a similar IR spectrum as the corresponding pure one. Using a similar procedure, *N*-(trimethylammonio)hydroxyalkanamidates (**4c—5**) were also obtained (Table 1).

Preparation of N-*Trimethylammonio-3-hydroxypropanamidate (4a) by the Hydrazine Method.* A mixture of 3-propanolide (**1a**, 7.2 g, 0.10 mol) and hydrazine hydrate (80%) (9.4 g, 0.15 mol) was stirred at 60 °C for 5 h. After evaporation of the unreacted hydrazine, methyl iodide (85.2 g, 0.60 mol) was dropped into the suspension of the crude 3-hydroxypropanohydrazide (**6a**, 10.9 g, about 0.1 mol) and potassium carbonate (27.6 g, 0.20 mol) in 300 ml of methanol at 20 °C. The reaction mixture was stirred for 8 h at reflux temperature, and then an insoluble solid was separated by filtration. Excess methyl iodide and the solvent of the

Table 4. Characterization of aminimides (**4**) and acylhydrazines (**6**)

Compound	IR (KBr pellet)	^{1}H NMR ($CDCl_3$)	MS (70 eV)
	ν/cm^{-1}	δ	*m/z* (rel. intensity)
4a	3200, 1580	2.21(t, 2H), 3.33(s, 9H), 3.72(t, 2H), 4.7(br, 1H)	146(M^+, 3), 101(14), 59(100), 58(47)
4b	3300, 1580	1.77(m, 2H), 2.25(t, 2H), 3.35(s, 9H), 3.65(t, 2H), 5.4—5.9(br, 1H)	160(M^+, 2), 116(27), 101(39), 59(100), 58(62)
4c	3350, 1580	1.16(d, 3H), 1.65(m, 2H), 2.25(m, 2H), 3.37(s, 9H), 3.80(m, 1H), 5.5(br, 1H)	174(M^+, 3), 116(18), 101(36), 59(100), 58(56)
4d	3350, 1580	0.87(t, 3H), 1.1—1.6(m, 8H), 1.70(m, 2H), 2.28(m, 2H), 3.36(s, 9H), 3.70(m, 1H), 4.6—5.8(br, 1H)	230(M^+, 2), 159(42), 116(24), 101(40), 59(100), 58(71)
4e	3350, 1580	1.4—1.9(m, 4H), 2.06(t, 2H), 3.38(s, 9H), 3.60(t, 2H), 4.3(s, 1H)	174(M^+, 1), 116(14), 101(39), 59(100), 58(61)
4f	3300, 1580	1.2—1.8(m, 6H), 2.05(t, 2H), 3.40(s, 9H), 3.62(t+s, 2H+1H)	188(M^+, 2), 116(28), 101(34), 59(100), 58(54)
4g	3300, 1600	1.29(d, 3H), 3.40(s, 9H), 3.7—4.1(br, 1H), 4.00(q, 1H)	146(M^+, 1), 101(42), 59(100), 58(74)
4h	3330, 1600	3.22(s, 9H), 4.63(s+s, 1H+1H), 7.1—7.6(m, 5H)	149(M^+—59, 3), 106(66), 101(16), 77(72), 59(58), 58(100)
6a[a]	3300, 1630	2.16(t, 2H), 3.58(t, 2H), 4.6(br, 3H), 8—10(br, 1H)	104(M^+, 1) 73(20), 43(28), 32(100)
6b[b]	3300, 1640	1.63(m, 2H), 2.02(m, 2H), 3.40(t, 2H), 4.15(s, 2H), 4.47(t, 1H), 8.9(s, 1H)	118(M^+, 3), 87(10), 43(14), 32(100)

a) Mp; 95—97 °C. b) Mp; 94—96 °C.

TABLE 5. ELEMENTAL ANALYSIS OF AMINIMIDES (**4**) AND CYCLIC URETHANES (**7**)

Compound	Molecular formula	Found (Calcd)/%		
		H	C	N
4a	$C_6H_{14}N_2O_2$	9.61 (9.65)	49.25 (49.30)	19.12 (19.16)
4b	$C_7H_{16}N_2O_2$	9.94 (10.07)	52.39 (52.48)	17.23 (17.48)
4c	$C_8H_{18}N_2O_2$	10.35 (10.41)	55.01 (55.15)	15.99 (16.08)
4d	$C_{12}H_{26}N_2O_2$	11.27 (11.38)	62.33 (62.57)	12.04 (12.16)
4e	$C_8H_{18}N_2O_2$	10.32 (10.41)	55.21 (55.15)	15.91 (16.08)
4f	$C_9H_{20}N_2O_2$	10.61 (10.71)	57.53 (57.42)	14.85 (14.88)
4g	$C_6H_{14}N_2O_2$	9.55 (9.65)	49.54 (49.30)	19.32 (19.16)
4h	$C_{11}H_{16}N_2O_2$	7.75 (7.74)	63.42 (63.44)	13.37 (13.45)
7a	$C_3H_5NO_2$	5.85 (5.79)	41.51 (41.38)	16.08 (16.09)
7b	$C_4H_7NO_2$	6.96 (6.98)	47.23 (47.52)	13.80 (13.85)
7c	$C_5H_9NO_2$	7.88 (7.88)	52.10 (52.16)	12.10 (12.17)
7d	$C_9H_{17}NO_2$	9.97 (10.01)	63.00 (63.13)	8.20 (8.18)
7e	$C_5H_9NO_2$	7.95 (7.88)	52.22 (52.16)	12.14 (12.17)
7f	$C_6H_{11}NO_2$	8.59 (8.58)	55.62 (55.80)	10.85 (10.84)

filtrate were evaporated off. The residue was extracted with acetone several times followed by filtration and evaporation of the extracts. This afforded 11.0 g of crude aminimide as white solids (75%). The pure **4a** was obtained by recrystallization from acetone as fine white needles (7.7 g, 53%). Using a similar procedure, aminimides (**4b**, **4g**, and **4h**) were also obtained (Table 1). A characterization of the aminimides (**4a**—**h**) and the isolated acylhydrazines (**6a** and **6b**) (recrystallization from ethanol) was accomplished by a standard method (Table 4). The elemental analysis of **4a**—**h** is shown in Table 5.

Thermolysis of 4a under Dilute Conditions. Dry mesitylene (100 ml) was heated at 160 °C in a 200-ml separable reaction flask under a nitrogen atmosphere. After the addition of **4a** (1.00 g, 6.84 mmol) to hot mesitylene, the solution was stirred until the absorption peak (based on the carbonyl group in the IR spectrum of aliquot) completely shifted to about 1700 cm^{-1} (6 h). Then, the solvent was evaporated off and the residue (0.57 g, solid), which was entirely dissolved in chloroform and showed one main peak in GLC, was distilled using a Kugelrohr apparatus (120 °C/2.7 Pa) to give 0.55 g of 2-oxazolidinone (**7a**) as fine white needles (92% yield based on **4a**). A very small amount of residue was observed. The thermolysis and work-up of the thermolytic products of **4b**—**d** under dilute conditions were undertaken in the same way as above since the crude product in each case was also wholly dissolved in chloroform. Perhydro-1,3-oxazin-2-one (**7b**, 86%), 6-methylperhydro-1,3-oxazin-2-one (**7c**, 95%), and 6-pentylperhydro-1,3-oxazin-2-one (**7d**, 90%) were obtained from **4b**, **4c**, and **4d**, respectively.

Thermolysis of 4e under Dilute Conditions. A solution of **4e** (1.00 g, 5.74 mmol) in dry mesitylene (100 ml) was heated as described above. The solvent was evaporated off and the residue (0.56 g, semisolid) was extracted with chloroform (100 ml) and filtered. The insoluble solid was washed with chloroform and dried *in vacuo* (pale brown; 0.17 g after drying). The chloroform extracts were combined, the solvent was evaporated off, and the residue (0.39 g) was distilled using the Kugelrohr apparatus at 120 °C/2.7 Pa to separate a distillate (0.18 g) as fine white needles and a residue (0.21 g) as a pale-brown solid. The distillate was identified as perhydro-1,3-oxazepin-2-one (**7e**, 27% yield based on **4e**). Perhydro-1,3-oxazocin-2-one (**7f**, 0.06 g, 8% yield based on **4f**) as a distillate, 0.37 g of a residue, and a 0.14 g of chloroform-insoluble solid were obtained from **4f** using a similar procedure.

The elemental analysis of **7a**—**f** is shown in Table 5.

Thermolysis of 4a under Concentrated Conditions. A solution of **4a** (1.00 g, 6.84 mmol) in dry mesitylene (10 ml) in a 50-ml separable reaction flask was heated at 160 °C for 3 h with stirring under a nitrogen atmosphere. The work-up of the reaction product was performed in the same way as the case of the thermolysis of **4e** under dilute conditions. Cyclic urethane (**7a**, 0.22 g, 37% yield based on **4a**) as a distillate, a 0.31 g of residue, and a 0.02 g of chloroform-insoluble solid were afforded. A thermolysis of aminimides (**4b**—**f**) under concentrated conditions was carried out using a similar procedure.

The results of thermolytic reactions, including α-hydroxyl type aminimides (**4g**,**h**), are presented in Table 2.

References

1) E. Kameyama, S. Inokuma, A. Akagawa, and T. Kuwamura, *Nippon Kagaku Kaishi*, **1974**, 1789.

2) I. Ikeda, N. Hirata, S. Komori, and M. Okahara, *Nippon Kagaku Kaishi*, **1975**, 135.

3) S. Inokuma, E. Kameyama, and T. Kuwamura, *Yukagaku Zasshi*, **32**, 332 (1983).

4) S. Tsuchiya, Y. Yamada, and M. Seno, *J. Chem. Soc., Chem. Commun.*, **1983**, 995.

5) W. J. McKillip, E. A. Sedor, B. M. Culbertson, and S. Wawzonek, *Chem. Rev.*, **73**, 255 (1973).

6) E. W. Merrill, V. Sa Da Costa, E. W. Salzman, D. Brier-Russel, L. Kuchner, D. F. Waugh, G. Trudel, III, S. Stopper, and V. Vitale, *Adv. Chem. Ser.*, **199**, 95 (1982).

7) M. Szycher and V. L. Poirier, *Ind. Eng. Chem. Prod. Res. Dev.*, **22**, 588 (1983).

8) J. F. Kinstle and L. E. Sepulveda, *J. Polym. Sci., Polym. Lett. Ed.*, **15**, 467 (1977).

9) N. D. Ghatge and J. Y. Jadhav, *J. Polym. Sci., Polym. Lett. Ed.*, **21**, 1941 (1983).

10) D. Aelony and W. J. McKillip, *J. Heterocycl. Chem.*, **9**, 923 (1972).

11) A. C. Mehta, D. O. Rickter, H. S. Kolesinski, and L. D. Taylor, *J. Polym. Sci., Polym. Chem. Ed.*, **21**, 1159 (1983).

12) A. Masuyama, Y. Nakamura, T. Iwasaki, and M. Okahara, *Synth. Commun.*, **15**, 521 (1985).

13) W. J. McKillip and R. C. Slagel, *Can. J. Chem.*, **45**, 2619 (1967).

The Structure of Cellulose Produced by *Acetobacter xylinum* in the Presence of a Fluorescent Brightener. The Influence of Concentration of a Brightener in the Medium on the Structure of Cellulose

Akira KAI* and Hitoshi KITAMURA†
Department of Industrial Chemistry, Faculty of Technology, Tokyo Metropolitan University, Fukazawa, Setagaya-ku, Tokyo 158
(Received May 13, 1985)

The influence of the concentration of a brightener on the structure of cellulose from an *Acetobacter* culture in the presence of a fluorescent brightener was examined. At a brightener concentration above 0.05 wt%, the X-ray diffraction diagram of cellulose from an incubated medium was observed. Except for the intensity of the diffraction corresponding to the (020) plane of cellulose I, the intensity of diffraction of the (110) plane became very weak and diffraction of the ($1\bar{1}0$) plane disappeared. A new diffraction, not corresponding to cellulose I or II, occurred inside. The position of each diffraction pattern was constant and independent of the concentration of the brightener. As the brightener concentration of the medium became lower, in the X-ray diagram of the dyed cellulose that was produced, the diffraction intensity of both the ($1\bar{1}0$) and (110) planes of cellulose I increased, and a new diffraction pattern gradually disappeared. In the case of an extraction of dyed cellulose from an incubated medium with a brightener (above 0.05 wt%), the same result was obtained. The above results suggest that the monomolecular layer of a brightener is included between the ($1\bar{1}0$) planes of the produced cellulose.

Acetobacter xylinum (A. xylinum) extrudes cellulose in an amorphous state from a cell.[1-3] However, it inevitably continues to form cellulose I crystals. Therefore, it is essential to determine the structure of the nascent cellulose in order to elucidate the biogenesis of a bacterial cellulose microfibril.

Brown *et al.* reported that when *A. xylinum* is cultured in the presence of a fluorescent brightener having a strong affinity toward cellulose, the morphology of the produced cellulose changes.[2] We found that the X-ray diffraction diagram of the specimen obtained from the incubated medium with a fluorescent brightener shows the characteristic diffraction patterns of a cellulose-brightener complex.[4,5] However, when the brightener was extracted from the complex, the diffraction patterns of cellulose I occurred in its X-ray diagram.[4] These facts showed that an examination of the structure of the dyed cellulose produced in the presence of a brightener is very essential in order to elucidate the structure of the nascent cellulose produced by *A. xylinum*.

In this paper, the influence of the brightener concentration of the medium on the structure of cellulose obtained from incubation in the presence of a fluorescent brightener was examined.

Experimental

Cultures of Cells and Preparations of the Samples for X-ray Photographing. Previously described methods were employed.[3]

Culture of A. xylinum (IFO 13693) in the Presence of a Fluorescent Brightener: 60 ml of a cellulose-free cell suspension[3] (pH 7.0) was added to 140 ml of a complex medium with a fluorescent brightener (Nippon Kayaku, Kayaphor FB conc: 4,4′-bis[4-anilino-6-bis(2-hydroxyethyl)amino-1,3,5-triazin-2-ylamino]-2,2′-stilbenedisulfonic acid) of various concentration (ranging from 10^{-4} to 10^{-1} wt%) and was then incubated for 24 h at 28 °C.

Preparations of the Samples: The collected cellulose was washed with a weak aqueous alkali solution several times, and from this the following samples were prepared after further treatment. T-1: the cellulose was washed with a 70 vol% aqueous ethanol solution several times to remove the free brightener at room temperature. T-2: the aqueous ethanol washed cellulose was extracted by boiling in a solution of 70 vol% aqueous ethanol for 18 h (aqueous ethanol was exchanged for fresh one every 3 h). T-3: the ethanol extracted cellulose was refined in a boiling 1 wt% aqueous NaOH solution for 10 h under a N_2 atmosphere.

X-Ray Photographing: Each sample was compressed to an isotropic disk with a diameter of 1.5 mm and a thickness of about 1 mm. X-ray diffraction diagrams of the samples were made with a flat-film camera (with the X-ray beam perpendicular to a flat surface of the disks) with Ni filtered Cu $K\alpha$ radiation (35 kV, 15 mA, time of exposure: about 35 min) at a specimen film distance of 50 mm. A Rigaku Denki made Rota-Unit RU-3v was used for photographing.

Results and Discussion

In the X-ray diffraction diagram of the sample (after a rejection of any free brightener from the incubated medium at a brightener concentration greater than 0.05 wt%) except for the intensity of the diffraction corresponding to the (020) plane of cellulose I, the diffraction intensity of the (110) plane becomes very weak and the diffraction of the ($1\bar{1}0$) plane disappears (Fig. 1b, 1c). A new diffraction which does not correspond to cellulose I or II occurred inside. As the concentration of the brightener in the medium became lower, the diffraction intensity of both the ($1\bar{1}0$) and (110) planes of cellulose I increased. On the contrary, a new diffraction pattern disappeared gradually. In the case of the medium with a brightener of less than about 0.001 wt%, the intensity of each

† Present address: Yakult Honsha Co. Ltd., Higashisinbashi, Minato-ku, Tokyo 105.

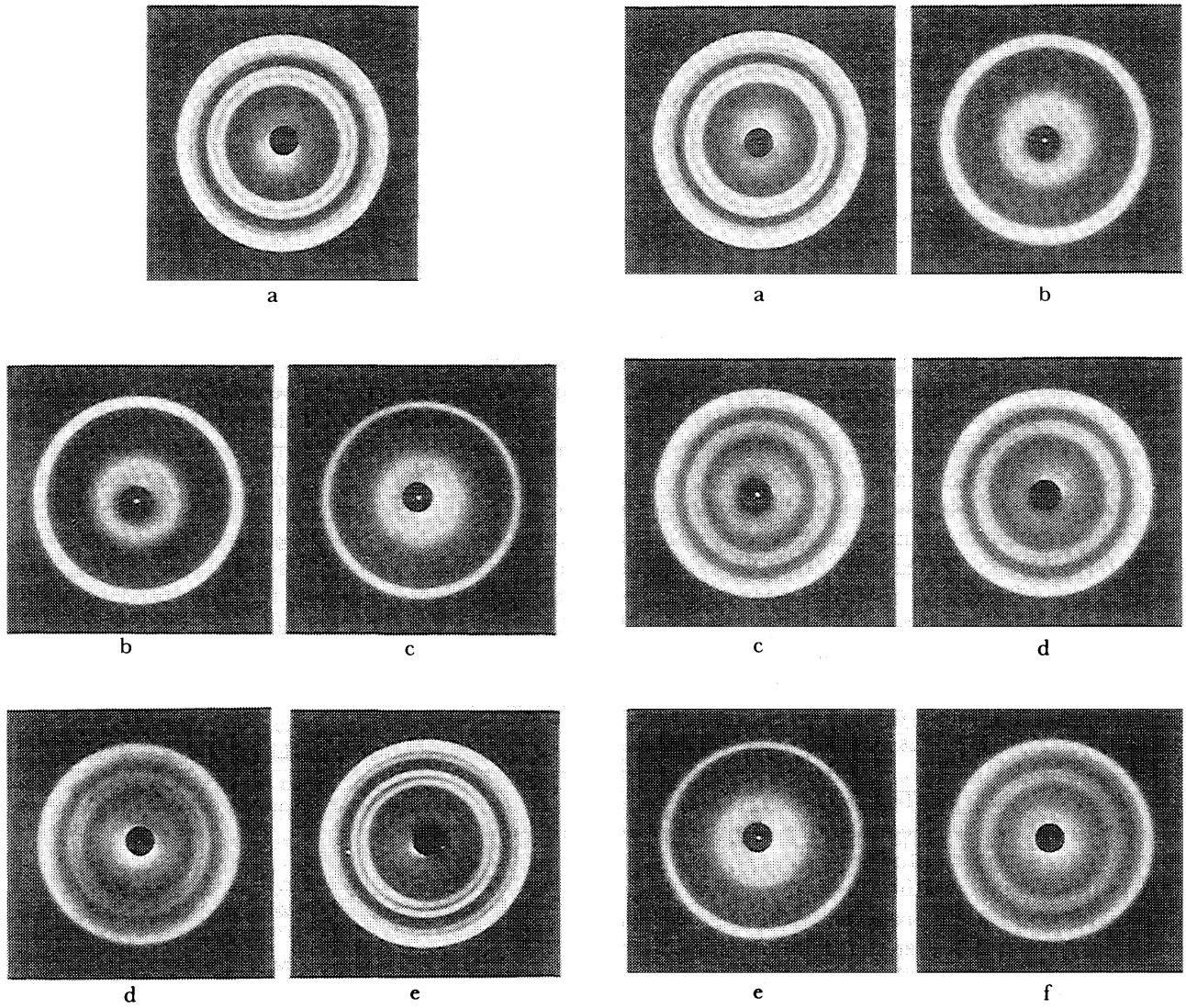

Fig. 1. X-Ray diffraction diagrams of samples, after rejection of the free brightener, obtained from the *Acetobacter* culture in the presence of a fluorescent brightener of various concentrations.
The brightener concentration of the medium (wt%); a: 0 (Cellulose I sample), b: 0.1, c: 0.05, d: 0.01, e: a little under 0.001.

diffraction of the cellulose was almost the same that of cellulose I (Fig. 1).

Brown *et al.* reported that for concentrations of a brightener greater than 0.1 mM (0.0086 wt%), the brightener disrupts the assembly of crystalline cellulose I microfibrils and their integration into a composite ribbon by a stoichiometric binding to glucose residues of newly-polymerized glucan chains.[6] The minimum concentration, at that the morphological change of cellulose takes place, generally corresponds to the result from the X-ray test on the complex in this study.

On the other hand, in the case of an extraction of the cellulose-brightener complex obtained from an incubated medium with a brightener above 0.05 wt%, the same result was found as in the case of lowering

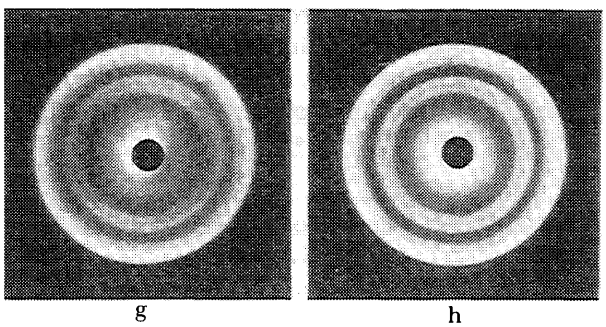

Fig. 2. Change in the X-ray diffraction diagram of the dyed cellulose with extraction.
a: Cellulose I sample, b: T-1-treated sample, which was obtained from the medium with a brightener of 0.1 wt%. c: T-2-treated sample b, d: T-3-treated sample c, e: T-1-treated sample, which was obtained from the medium with a brightener of 0.05 wt%. f: T-3-treated sample e, g: T-1-treated sample, which was obtained from the medium with a brightener of 0.01 wt%. h: T-3-treated sample g.

the brightener concentration of the medium. When the complex was treated with methods T-2 and T-3, in

its X-ray diagram the intensity of each diffraction of cellulose I increased as removing a brightener from it. The intensity of a new diffraction pattern gradually became weaker (Fig. 2). However, the intensities of the diffractions of each sample differed with the brightener concentration of the medium.

We reported previously, from a calculation regarding an X-ray diagram of the cellulose-brightener complex obtained from the incubated medium with a brightener of 0.1 wt%, that a new diffraction corresponds to $(1\bar{1}0)$ plane of the complex, and that a brightener is included between the $(1\bar{1}0)$ planes.[5] Therefore, the spacing of the $(1\bar{1}0)$ plane of the complex becomes 7.4 Å broader than that of cellulose I. The spacing of the $(1\bar{1}0)$ plane of the complex was unchanged even if the amount of the brightener in a complex differed. This fact suggests that a monomolecular layer of a brightener is included between the $(1\bar{1}0)$ planes of the complex. In the sample obtained from the incubated medium with a brightener of above 0.05 wt% (as its X-ray diagram was unchanged), the surfaces of cellulose sheets (corresponding to the $(1\bar{1}0)$ plane of the complex) capable of being dyed seemed to be saturated by a brightener. As the given concentration of a brightener in the medium becomes lower, the surfaces of cellulose sheets become dotted with the brightener. Therefore, it is suggested that the intensity of the diffraction of the $(1\bar{1}0)$ plane of cellulose I increased for the possibility of an increased mutual binding of the cellulose sheet.

Brown *et al.* suggested from the observation of the morphology of cellulose produced in the presence of a fluorescent brightener that the cellulose chains are extruded from a bacterial cell to be in the form of sheets corresponding to the (020) plane of cellulose I, and that the cellulose sheet is formed by hydrogen bonding of cellulose chains.[6] Therefore, they suggested that a fluorescent brightener is included between the (020) planes. However, the fact, that both the intensity and the spacing of the diffraction pattern corresponding to the (020) plane of cellulose I are scarcely changed even with the amount of brightener in a sample, suggests that their theory is inadequate.

The fact that the spacing of the $(1\bar{1}0)$ plane of the cellulose produced in the presence of a fluorescent brightener widens with a definite value and that the spacing of the (020) plane is unchanged independent of the concentration of a brightener, indicates that cellulose chains in the form of a monomolecular layer corresponding to the $(1\bar{1}0)$ plane of cellulose I are extruded from a cell. The behavior of the nascent cellulose toward a fluorescent brightener shows that between the cellulose sheets, the medium components are included. This view is equivalent to that obtained from an examination of the behavior of the nascent cellulose toward sodium tungstophosphate.[3] It is well known that the spacing of the $(1\bar{1}0)$ plane widens preferentially when natural cellulose is exposed either to intracrystalline swelling reagents (such as sodium hydroxide and potassium acetate) or to chemical substitution reactions (such as acetylation and nitration).[7] A cellulose sheet corresponding to the $(1\bar{1}0)$ plane may be an elementary unit of natural cellulose.

References

1) J. R. Colvin and G. G. Leppard, *Can. J. Microbiol.*, **23**, 701 (1977).

2) C. H. Haigler, R. M. Brown, and M. Benziman, *Science*, **210**, 903 (1980).

3) A. Kai and J. Kogusuri, *Nippon Kagaku Kaishi*, **1982**, 148. A. Kai, *Bull. Chem. Soc. Jpn.*, **57**, 836, 2816 (1984).

4) A. Kai, *Makromol. Chem., Rapid Commun.*, **5**, 307 (1984).

5) A. Kai, *Makromol. Chem., Rapid Commun.*, **5**, 653 (1984).

6) R. M. Brown, C. H. Haigler, J. Suttie, A. R. White, E. Roberts, C. Smith, T. Itoh, and K. Cooper, *Appl. Polym. Symp.*, **37**, 33 (1983).

7) M. Takai, Y. Tsuta, J. Hayashi, and S. Watanabe, *Polym. J.*, **7**, 157 (1975).

 © 1985 The Chemical Society of Japan Bull. Chem. Soc. Jpn., 58, 2863—2869 (1985)

Photochemical Electron-transfer Reactions of Biphenyl-2,2′-dicarboximide and Naphthalene-1,8-dicarboximide with Olefin. Dependence of the Reaction Course on the Structure of the Aromatic Imide[1)]

Yasuo KUBO,* Takeo ARAKI, and Kazuhiro MARUYAMA†

Department of Chemistry, Faculty of Science, Shimane University, Matsue, Shimane 690

†*Department of Chemistry, Faculty of Science, Kyoto University, Kyoto 606*

(Received May 16, 1985)

Photoreactions of *N*-methylbiphenyl-2,2′-dicarboximide and *N*-ethylnaphthalene-1,8-dicarboximide (**2**) with 1,1-diphenylethylene (**3**) in methanol gave methanol-incorporated 1 : 1 : 1-adduct (**7**) and 2,2-diphenylethyl methyl ether (**6**), an anti-Markovnikov adduct of methanol to **3**. The ratio of the two types of products largely depends on the structure of the aromatic imides. Probably the spin densities of the radical anions of the aromatic imides seem to play an important role to determine the reaction courses after the photochemical electron-transfer process. Similar results were obtained in the photoreaction of *N*-(2-phenylallyl) aromatic imides; elimination induced by methanol-incorporation *vs. anti*-Markovnikov addition of methanol. Photoreactions of *N*-(*trans*-3-phenylallyl) aromatic imides in methanol gave methanol-incorporated *O*-cyclized products (**20** and **27**) and *C*-cyclized products (**21** and **28**). A tentative mechanism for the *O*-cyclization is proposed; *i.e.*, intramolecular electron transfer followed by *anti*-Markovnikov addition of methanol to the radical cation of the double bond moiety, nucleophilic attack of the aromatic imide radical anion moiety, secondary electron-transfer, and then polar addition of methanol.

Recently, photoreactions involving electron-transfer process have received much attention from synthetic and mechanistic aspects in organic photochemistry.[2)] Numerous photo-reactions between electron-donor (D) and electron-acceptor (A) molecules have been studied in view of ion radical intermediate.[3)] For example, nucleophiles such as methanol can add to photochemically generated cation radicals of olefins.[4)] However, factors which control the reaction courses after the photochemical electron-transfer between D and A molecules, seem to be not always clear. Little systematic investigation has been known in this field.

In the course of studies on the photochemistry of imides,[5)] we and other groups have found in the photoreactions of phthalimide-olefin systems a variety of alcohol(solvent)-incorporated intermolecular addition[6)] and intramolecular cyclization products,[7)] which seem to occur *via* electron-transfer process. However, the imides employed in the previous investigations have been confined to phthalimides, and little information has been reported on the effects of arene structures of arenedicarboximides (aromatic imides).[8)] Our studies have been focused on the effects of extended π-conjugation system in the arene structure.[9)]

Here we report the results of intermolecular photoreactions of *N*-methylbiphenyl-2,2′-dicarboximide (**1**) and *N*-ethylnaphthalene-1,8-dicarboximide (**2**) with 1,1-diphenylethylene (**3**), and intramolecular photoreactions of *N*-(2- and 3-phenylallyl)biphenyl-2,2′- and naphthalene-1,8-dicarboximides in methanol, comparing with those of the phthalimide derivatives. The results indicate that the structure of the aromatic imide play an important role to determine the reaction courses after the photochemical electron-transfer process.

Results

Intermolecular Photoreactions of Aromatic Imides with 3 in Methanol. Photoreaction of *N*-methylphthalimide (**4**) (9.9 mM, 1 mM = 1×10^{-3} mol dm^{-3}) with **3** (12 mM) under N_2 for 5 h gave methanol-incorporated adduct (**5**) (44%) and 2,2-diphenylethyl methyl ether (**6**) (12% based on used **4**) together with recovered **4** (36%) (Eq. 1) as previously reported.[6a,d)] Irradiation of **1**

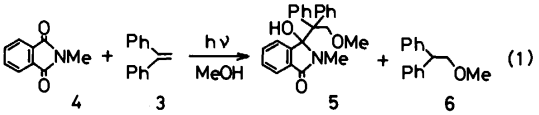

(1)

and **3** in similar conditions gave **7** (31%) and **6** (44%) together with recovered **1** (58%) (Eq. 2). The product

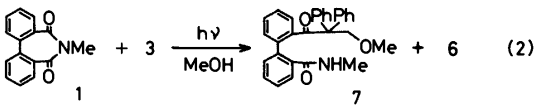

(2)

(**7**) is probably derived from a primary adduct (**8**) by 1,3-hydrogen migration which is the familiar reaction in the imide photochemistry (Eq. 3).[10)] Irradiation

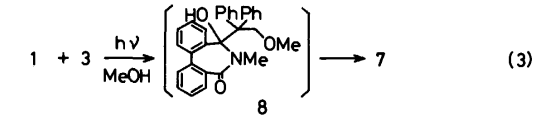

(3)

of **2** and **3** in similar conditions gave **6** (70%) together with recovered **2** (93%) (Eq. 4). In Eq. 4, **2** acts as a

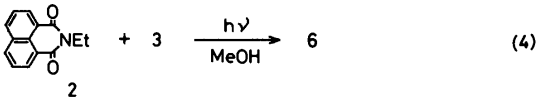

(4)

typical electron-transfer photosensitizer for the *anti*-Markovnikov addition of methanol to **3**.[4] The results of the intermolecular reaction show that the yields of the methanol-incorporated adducts (**5** and **7**) decreases, and at the same time the yield of **6** increases, with extension of the conjugated aromatic π-system of the aromatic imide.

Intramolecular Photoreactions of N-(2-Phenylallyl) Aromatic Imides in Methanol. Photoreaction of *N*-(2-phenylallyl)phthalimide (**9**) (0.6 mM) in methanol was reported to give methanol-incorporated elimination products, phthalimide (**10**) (30%) and 3-methoxy-2-phenyl-1-propene (**11**) (30%) (Eq. 5).[7a]

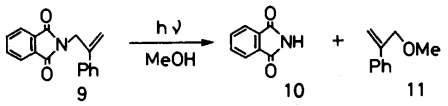

9 10 11 (5)

Irradiation of *N*-(2-phenylallyl)biphenyl-2,2′-dicarboximide (**12**) (0.4 mM) in methanol similarly gave biphenyl-2,2′-dicarboximide (**13**) (25%) and **11** (25%) (Eq. 6). Irradiation of *N*-(2-phenylallyl)naphtha-

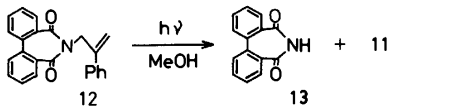

12 13 (6)

lene-1,8-dicarboximide (**14**) (0.5 mM) in methanol gave an *anti*-Markovnikov adduct of methanol (**15**) (27%), naphthalene-1,8-dicarboximide (**16**) (20%), and **11** (22%) (Eq. 7). Thus, the electron-transfer photo-

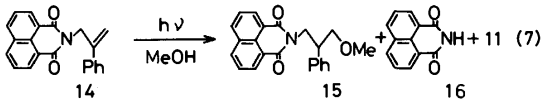

14 15 16 (7)

sensitized addition of methanol was observed only in the reaction of **14** which had the most extended aromatic π-system.

Intramolecular Photoreactions of N-(trans-3-Phenylallyl) Aromatic Imides in Methanol. Photoreaction of *N*-(*trans*-3-phenylallyl)phthalimide (**17**) (5 mM) in methanol was reported to give methanol-incorporated *C*-cyclized products [**18a** (68%) and **18b** (17%)] (Eq. 8).[7a,e]

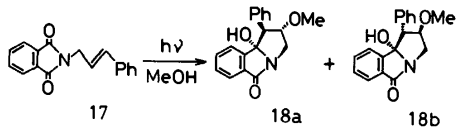

17 18a 18b (8)

Irradiation of *N*-(*trans*-3-phenylallyl)biphenyl-2,2′-dicarboximide (**19**) (3.3 mM) in methanol gave a mixture of two groups of products; *i.e.*, two stereoisomers of methanol-incorporated *O*-cyclized products [**20a** (30%) and **20b** (5%)], and two stereoisomers of methanol-incorporated *C*-cyclized products [**21a** (21%) and **21b** (17%)] (Eq. 9). The isomers were isolated by

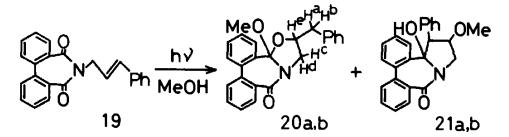

19 20a,b 21a,b (9)

chromatography.

The structures of **20a** and **20b** were assigned on the basis of the spectral data and chemical manipulations outlined below. Combination of the ^{1}H and ^{13}CNMR multiplicity and chemical shifts, and the IR data gave rise to at least four characteristic common features in the structures of **20a** and **20b**. Namely, (i) one amide group [**20a**: IR-1640 cm^{-1}: ^{13}C NMR δ=165.1 (s), **20b**: IR-1628 cm^{-1}: ^{13}C NMR δ=165.1 (s)], but no hydroxyl group (IR), is present. (ii) The benzyl moiety is directly bonded to a ring system and characterized by having the triplet carbon [**20a**: δ=39.6 (t), **20b**: δ=39.3 (t)], and the nonequivalent methylene protons (H^a and H^b). (iii) One quaternary carbon atom [**20a**: δ=108.8 (s), **20b**: δ=109.5 (s)] corresponds reasonably to the acetal carbon [arom-*C*(OMe)(O-)N] adjacent to an aromatic system. (iv) Protons in the methoxyl group [**20a**: δ=2.83 (s), **20b**: δ=2.90 (s)] are strongly shielded by the biphenyl group.

As expected from the acetal structures, **20a** and **20b** were found to be highly sensitive to acid. Thus, on treatment with hydrochloric acid in chloroform, both of pure **20a** and **20b** were converted to an equilibrium mixture of **20a**:**20b**=0.63:1, probably *via* a stable tertiary carbonium ion intermediate. In addition, treatment of a mixture of **20a** and **20b** (6:1) with hydrochloric acid in acetonitrile-water (4/1 volume ratio) followed by acetylation with acetic anhydride and pyridine gave an imide (**22**) (70%) (Eq. 10).

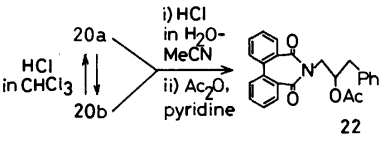

22 (10)

The structures of **21a** and **21b** were deduced from the similarity of the spectral data to those of **18a** and **18b**.[7a] As expected, an elimination product (**23**) was formed quantitatively from each of **21a** and **21b** upon treatment with hydrochloric acid in chloroform (Eq. 11).

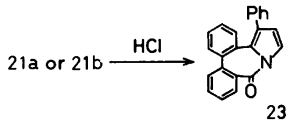

23 (11)

Photoreaction of **19** (3.3 mM) in 50 ml of methanol-d_1 (>99%) was carried out to examine the deuterium incorporation in **21a**. The ^{1}H NMR spectrum of the isolated **21a** showed that the integration of H^a and H^b signals was reduced to 55±5% compared with those of

the other signals, although the ratio of the integration of H^a to that of H^b could not be determined because of the considerable overlapping of these signals. The result indicates almost quantitative one-deuterium incorporation at the benzylic position (H^a and H^b) of **21a**.

Irradiation of *N*-(*trans*-3-phenylallyl)naphthalene-1,8-dicarboximide (**24**) (3.5 mM) in methanol followed by chromatographic (SiO_2) separation gave **25** (58%) and **26** (trace) (Scheme 1). That the products **25** and

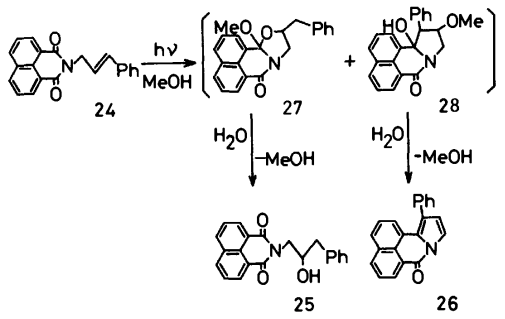

Scheme 1.

26 were not observed in the reaction mixture immediately after the photolysis suggested the isolated products were derived from primary products during the separation. The primary products could not be obtained probably due to their instability. However, the primary photoproducts are presumed to be methanol-incorporated *O*-cyclized products (**27**) for **25**, and methanol-incorporated *C*-cyclized products (**28**) for **26**, respectively, in view of the results obtained in the photolysis of **19**.

Triplet Photosensitization of 19. The photocyclization of **19** (styryl moiety, E_T=59.8 kcal mol^{-1})[11] was not sensitized by benzophenone (E_T=69.2 kcal mol^{-1})[12] as a triplet sensitizer. The benzophenone sensitization in methanol gave only an equilibrium mixture of **19** and the *cis* isomer (0.4:0.6). The result seems to indicate that the photocyclization of **19** directly occurs from the singlet excited state of the aromatic imide moiety.

Discussion

Mechanism on the Intermolecular Photoreactions of Aromatic Imides with 3 and Intramolecular Photoreactions of N-(2-Phenylallyl) Aromatic Imides. Photoreaction of *N*-methylnaphthalene-1,8-dicarboximide and **3** in benzene, a nonpolar solvent, was reported to give a cyclobutane.[9a] In benzene no photoreaction of **1** and **3** was observed even on the prolonged irradiation. However, in methanol the distinct mode of photoreactions was observed as described above.

A reasonable mechanism for the intermolecular photoreactions of **1**, **2**, and **4** with **3** is shown in Scheme 2, where **1**, **2**, and **4** are denoted as **29**. The singlet excited state of the imides readily undergoes

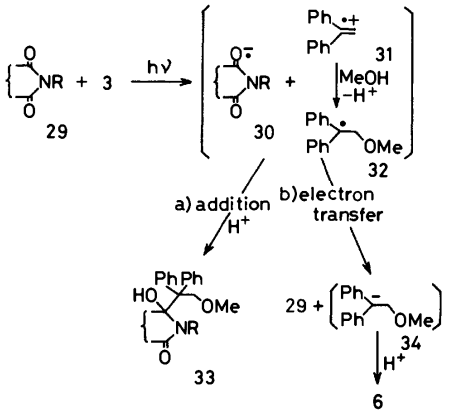

Scheme 2.

one-electron reduction through interaction with the electron-rich olefin **3** to give **30** and **31**. The cation radicals **31** are captured by methanol to give **32**. Whether the methanol-incorporated addition to the imide carbonyl group or the *anti*-Markovnikov addition of methanol to **3** predominates is controlled at this stage by the relative rate of bond formation between **30** and **32** to generate the coupling products **33** (path a) *vs.* electron-transfer from **30** to **32** to produce an alkyl anion (**34**) (path b). The results of photoreaction of **1**, **2**, and **4** with **3** suggest the path b is more efficient than the path a in the photoreaction of imide which has the more extended aromatic π-system.

A mechanism for the intramolecular photoreactions of **9**, **12**, and **14** is shown in Scheme 3, where **9**,

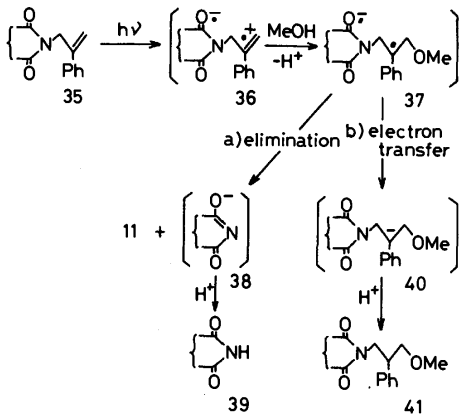

Scheme 3.

12, and **14** are denoted as **35**. Whether the elimination induced by methanol-incorporation or the *anti*-Markovnikov addition of methanol to the olefinic moiety predominates is also controlled by the relative rate of bond cleavage of the 1,4-biradical (**37**) to generate the elimination products (**11** and **39**) (path a) *vs.* the intramolecular electron transfer within **37** to produce an alkyl anion (**40**). The results suggest that the path b can compete with the path a only in the photoreaction of imide **14** which has the most extended aromatic π-system.

The alternative of the path a or the path b in the both photoreactions might be due to the ability of the radical anion of the imide moiety to serve as a reducing agent in reduction of the alkyl radical moiety in path b.[13] The relative reduction potentials of the imide moiety can be used to estimate the energetics and, thus, the rate for the electron transfer processes. However, the one-electron reduction potential of phthalimide (**10**) ($E_{1/2}=-1.47$ V)[14] is somewhat lower than that of naphthalene-1,8-dicarboximide (**16**) ($E_{1/2}=-1.25$ V).[14] Thus, the electron-transfer from the radical anion of naphthalene-1,8-dicarboximide moiety to the alkyl radical moiety (path b) would be expected to be less competitive with the path a than for the case of the corresponding phthalimide moiety, inconsistently with the results.

The alternative of the path a or the path b may be due to the ability of the radical anion of the imide moiety to serve as a radical reactant with the alkyl radical moiety in path a. In the case the relative spin densities of the radical anion of imide moieties can be used to estimate the rate for the radical reaction processes. In accord with the results, the calculated spin density (McLachlan method) at the carbonyl carbon of the radical anion of **10** (0.174) was reported to be considerably larger than that of **16** (0.067).[14] Consequently, whether the reaction proceeds by the path a or the path b seems to mainly depend on the ability of the radical anion of the imide moiety to serve as a radical reactant with the alkyl radical moiety in path a, which is reflected in the relative spin densities of the radical anion of the aromatic imide.

Mechanism on the Intramolecular Photoreactions of N-(trans-*3-Phenylallyl) Aromatic Imides.* The two types of products, *O*-cyclized and *C*-cyclized products, were obtained in the photoreaction of **19** and **24**. Especially, the *O*-cyclization seems to be novel in the photochemistry of the carbonyl compounds.

A possible mechanistic scheme for the intramolecular photo-reaction of **17**, **19**, and **24** is shown in Scheme 4, where **17**, **19**, and **24** are denoted as **42**. The initial step is photoinduced intramolecular electron-transfer from the electron-donating double bond to the excited imide moiety to form an intermediate (**43**), in analogy with the cases of the other systems. Successive anti-Markovnikov addition of methanol to the radical cation moiety results in the formation of **44**. The divergent behavior of these systems stems from the variable reactivity of the intermediate (**44**). From the intermediate, intramolecular coupling (cyclization) of the aromatic imide radical anion moiety and alkyl radical moiety (**44**→**45**), followed by protonation (**45**→**46**), gives *C*-cyclized products (**46**).[7a] Alternatively, intramolecular nucleophilic attack of the aromatic imide radical anion moiety accompanying elimination of methoxide ion (**44**→**47**), followed by intramolecular electron transfer (**47**→**48**) and polar addition of methanol (**48**→**49**), results in

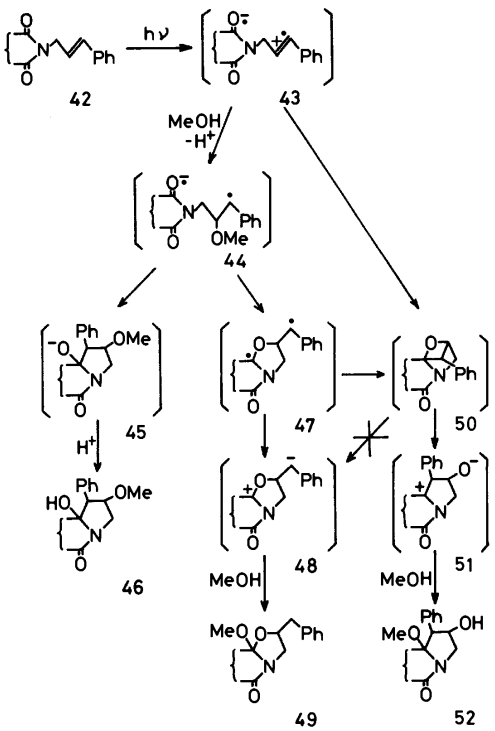

Scheme 4.

the formation of the *O*-cyclized products (**49**). One deuterium incorporation at the benzylic position of **21a** in the photoreaction in methanol-d_1 supports the presence of the zwitter-ionic precursor (**48**). Whether the intramolecular coupling (radical reaction) (**44**→**45**) or the nucleophilic attack (**44**→**47**) predominates seems to depend on the ability of the radical anion of the imide moiety to serve as a radical reactant with the alkyl radical moiety, which is reflected in the relative spin densities of the radical anion of the aromatic imide, in analogy with the cases of the intermolecular photoreaction and the intramolecular photo-reaction of *N*-(2-phenylallyl) aromatic imides.

Another mechanism for the *O*-cyclization of **42**, involving intramolecular oxetane formation might be considered, as the oxetane formation was sometimes reported in photoreactions of aromatic imides and olefins.[9b,15] However, heterolytic cleavage of the oxetane (**50**) derived from **43** or **47** was expected to occur at the C–O bond to give the more stable zwitter ion (**51**), rather than at the C–C bond of the oxetane ring to give **48**. Thus, the mechanism involving the oxetane formation could not rationalize the observed structures of the products. Furthermore, the expected methanol-adduct (**52**) from **51** was not observed in the photoreaction.

In conclusion, this work demonstrates that the structure of the aromatic imide (electron acceptor) play an important role to determine the reaction course after the photochemical electron transfer between the aromatic imide and the olefin (electron donor). These results are also of interest in terms of the effect of the geometrical situation between the acceptor and the

donor on the reaction course after the electron-transfer process.

Experimental

The mps were measured by a Yanagimoto micromelting point apparatus, and are uncorrected. ^{1}H NMR spectra were determined on a JEOL JNM-MH-100 spectrometer in $CDCl_3$ solution. IR spectra were obtained with a Hitachi 260-50 spectrophotometer. Mass spectra were measured on a JEOL JMS-DX-300 apparatus. Microanalyses were performed on a Yanagimoto CHN corder MT-2. UV irradiation was carried out with an Eikosha PIH 300-W high-pressure Hg-lamp through Pyrex filter under N_2 at ambient temperature. Column chromatography was done on Wakogel C-200 (silica gel, 74—149 μ). HPLC analyses were performed on a Hitachi 635 A apparatus.

Materials. *N*-Methylbiphenyl-2,2′-dicarboximide (**1**) and *N*-ethylnaphthalene-1,8-dicarboximide (**2**)[16] were prepared by the reaction of the corresponding anhydride and amine.

1: Mp 167—169 °C; ^{1}H NMR δ=3.51 (s, 3H, NMe), 7.4—8.0 (m, 8H, Arom H); IR (KBr) 1695 (imide), 1658 (imide), 1606, 1352, 1322, 740 cm^{-1}. Found: C, 75.89; H, 4.82; N, 5.96%. Calcd for $C_{15}H_{11}NO_2$: C, 75.93; H, 4.67; N, 5.90%.

The imides (**12**, **14**, **19**, and **24**) were prepared by the reaction of the corresponding imide and halide in an analogous manner as described in the preparation of *N*-alkenylphthalimides.[7a]

N-(2-Phenylallyl)biphenyl-2,2′-dicarboximide (12): From the reaction of **13** and 3-bromo-2-phenyl-1-propene,[17] 60% based on the bromide; mp 95—97 °C (from ethanol): ^{1}H NMR δ=5.01 (s, 1H, C=CH_2), 5.11 (s, 2H, NCH_2), 5.29 (s, 1H, C=CH_2), 7.2—8.0 (m, 13H, arom H); IR (KBr) 1688 (imide), 1640 (imide), 1358, 1238, 736 cm^{-1}. Found: C, 81.50; H, 5.20; N, 4.08%. Calcd for $C_{23}H_{17}NO_2$: C, 81.39; H, 5.05; N, 4.13%.

N-(2-Phenylallyl)naphthalene-1,8-dicarboximide (14): From the reaction of **16** and 3-bromo-2-phenyl-1-propene, 53% based on the bromide; mp 181—183 °C (from ethanol); ^{1}H NMR δ=4.97 (s, 1H, C=CH_2), 5.19 (s, 2H, NCH_2), 5.32 (s, 1H, C=CH_2), 7.2—7.7 (m, 5H, Ph), 7.74 (t, 2H, arom H), 8.23 (d, 2H, arom H), 8.63 (d, 2H, arom H); IR (KBr) 1698 (imide), 1658 (imide), 1348, 1236, 782 cm^{-1}. Found: C 80.58; H, 4.96; N, 4.50%. Calcd for $C_{21}H_{15}NO_2$: C, 80.49; H, 4.83; N, 4.47%.

N-(trans-3-Phenylallyl)biphenyl-2,2′-dicarboximide (19): From the reaction of **13** and cinnamyl chloride,[18] 80% based on the chloride; mp 155—157 °C (from ethanol); ^{1}H NMR δ=4.81 (d, *J*=6 Hz, 2H, NCH_2), 6.28 (dt, *J*=6, 16 Hz, 1H, CH_2CH=C), 6.66 (d, *J*=16 Hz, 1H, PhC*H*=C), 7.1—8.0 (m, 13H, arom H); IR (KBr) 1702 (imide), 1662 (imide), 1340, 1328, 746 cm^{-1}. Found: C, 81.63; H, 5.26; N, 4.16%. Calcd for $C_{23}H_{17}NO_2$: C, 81.39; H, 5.05; N, 4.13%.

N-(trans-3-Phenylallyl)naphthalene-1,8-dicarboximide (24): From the reaction of **16** and cinnamyl chloride, 75% based on the chloride; mp 149—151 °C (from ethanol); ^{1}H NMR δ=4.93 (d, *J*=6 Hz, 2H, NCH_2), 6.37 (dt, *J*=6, 16 Hz, 1H, CH_2CH=C), 6.76 (d, *J*=16 Hz, 1H, PhC*H*=C), 7.0—7.5 (m, 5H, Ph), 7.72 (t, 2H, arom H), 8.18 (d, 2H, arom H), 8.58 (d, 2H, arom H); IR (KBr) 1704 (imide), 1670 (imide), 1388, 1340, 1242, 786 cm^{-1}. Found: C, 80.27; H, 5.02; N, 4.41%. Calcd for $C_{21}H_{15}NO_2$: C, 80.49; H, 4.83; N, 4.47%.

1,1-Diphenylethylene (**3**) was a commercial sample from Tokyo Chemical Industry.

Intermolecular Photoreactions of Aromatic Imides with 3. Solutions of aromatic imide (**1** and **2**) (9.9 mM) and **3** (12 mM) in 20 cm^3 of methanol were irradiated for 5 h. After evaporation of the solvent, the residue was subjected to chromatography to give the products. 2,2-Diphenylethyl methyl ether (**6**) was identical with a sample prepared by irradiation of *p*-dicyanobenzene, **3**, and phenanthrene (sensitizer) in methanol.[4a] On the other hand, the irradiated methanol solutions were analyzed by HPLC and ^{1}H NMR measurements with an internal standard to determine the yields of the products.

N-Methyl-2′-(2,2-diphenyl-3-methoxy-1-oxopropyl)biphenyl-2-carboxamide (7): Mp 156—158 °C; ^{1}H NMR δ=2.49 (d, *J*=4 Hz, 3H, NH*Me*, these signals were changed to s by shaking with D_2O), 3.14 (s, 3H, OMe), 4.23 and 4.37 (ABq, *J*=19 Hz, 2H, CH_2OMe), 6.9—7.9 (m, 19H, arom H+NH); IR (KBr) 3370 (NH), 1672 (amide and ketone), 1542, 1232, 758, 702 cm^{-1}. Found: C, 80.31; H, 6.00; N, 3.15%; M$^+$, 449. Calcd for $C_{30}H_{27}NO_3$: C, 80.15; H, 6.05; N, 3.12%; M, 449.

Intramolecular Photoreactions of N-(2-Phenylallyl) Aromatic Imides. Solutions of *N*-(2-phenylallyl) aromatic imides (**12** and **14**) in 400 cm^3 of methanol were irradiated for 5 h. After evaporation of the solvent, the residue was subjected to chromatography to give the products. 3-Methoxy-2-phenyl-1-propene (**11**) was identical with an authentic sample.[19] Biphenyl-2,2′-dicarboximide (**13**) was identical with an authentic sample.[20] Naphthalene-1,8-dicarboximide (**16**) was also identical with a commercial sample from Nakarai Chemical Industry. On the other hand, the irradiated methanol solutions were analyzed by HPLC and ^{1}H NMR measurements with an internal standard to determine the yields of the products.

N-(3-Methoxy-2-phenylpropyl)naphthalene-1,8-dicarboximide (15): Mp 115—117 °C; ^{1}H NMR δ=3.21 (s, 3H, OMe), 3.5—3.8 [m, 3H, PhC(*H*)CH_2OMe], 4.36 (dd, *J*=7, 12 Hz, 1H, NCH_2), 4.58 (dd, *J*=6, 12 Hz, 1H, NCH_2), 7.1—7.5 (m, 5H, Ph), 7.71 (t, 2H, arom H), 8.17 (d, 2H, arom H), 8.57 (d, 2H, arom H); IR (KBr) 1709 (imide), 1678 (imide), 1602, 1354, 1248, 802 cm^{-1}. Found: C, 76.41; H, 5.81; N, 3.97% M$^+$, 345. Calcd for $C_{22}H_{19}NO_3$: C, 76.50; H, 5.55; N, 4.06%; M, 345.

Intramolecular Photo-reaction of 19. A solution of **19** in 400 cm^3 of methanol was irradiated for 5 h. After evaporation of the solvent, the residue was subjected to chromatography to give the products. On the other hand, the irradiated methanol solution was analyzed by HPLC and ^{1}H NMR measurement with an internal standard to determine the yields of the products.

6-Benzyl-4b-methoxy-6,7-dihydro-4bH,9H-dibenz-[3′,4′:5′,6′]-azepino[2,1-b]oxazol-9-one Isomer A (20a): Mp 156—158 °C; ^{1}H NMR δ=2.83 (s, 3H, OMe), 2.95 (dd, *J*=6.1, 13.5 Hz, 1H, H^a), 3.27 (dd, *J*=6.4, 13.5 Hz, 1H, H^b), 3.42 (dd, *J*=9.6, 11.2 Hz, 1H, H^c), 4.19 (dd, *J*=5.9, 11.2 Hz, 1H, H^d), 4.5—5.0 (m, 1H, H^e), 7.1—8.1 (m, 13H, arom H); ^{13}C NMR δ=39.6 (t, CH_2Ph), 50.8 (q, OMe), 50.9 (t, NCH_2), 76.1 (d, OCH), 108.8 [s, Ph*C*(OMe)(O–)N], 125.1, 126.9, 127.7, 128.2, 128.4, 128.6, 129.2, 129.5, 129.7, 129.8, 129.9, 130.3, 130.9, 132.9, 135.7, 136.4, 137.3, 137.6 (18C, arom C), 165.1 (amide); IR (KBr) 1640 (amide), 1455, 1408, 1079, 1045, 742 cm^{-1}. Found: C, 77.62; H, 5.97; N, 3.68% M$^+$, 371. Calcd for $C_{24}H_{21}NO_3$: C, 77.60; H, 5.70; N, 3.77%; M, 371.

Isomer B (20b): Mp 150—152 °C; ^{1}H NMR δ=2.90 (s, 3H, OMe), 3.06 (dd, *J*=6.6, 13.9 Hz, 1H, H^a), 3.27 (dd, *J*=6.0, 13.9 Hz, 1H, H^b), 3.57 (dd, *J*=9.2, 11.0 Hz, 1H, H^c), 4.03 (dd, *J*=5.9, 11.0 Hz, 1H, H^d), 4.3—4.7 (m, 1H, H^e), 7.1—8.1 (m,

13H, arom H); ^{13}C NMR δ=39.3 (t, CH_2Ph), 49.7 (q, OMe), 50.5 (t, NCH_2), 75.6 (d, OCH), 109.5 [s, Ph*C*(OMe)(O-)N], 123.0, 125.2, 127.0, 127.5, 128.0, 128.5, 128.7, 128.9, 129.2, 129.5, 129.9, 130.7, 131.4, 131.8, 136.0, 136.2, 138.0, 138.4 (18C, arom C), 165.1 (amide); IR (KBr) 1628 (amide), 1458, 1419, 1122, 742 cm^{-1}. Found: C, 77.86; H, 5.91; N, 3.82%; M$^+$, 371. Calcd for $C_{24}H_{21}NO_3$: C, 77.60; H, 5.70; N, 3.77% M, 371.

4b-Hydroxy-6-methoxy-5-phenyl-4b,5,6,7-tetrahydro-9H-dibenzo[c,e]pyrrolo[1,2-a]azepin-9-one Isomer A (21a): Mp 191—192.5 °C; ^{1}H NMR δ=3.51 (s, 3H, OMe), 3.86 (dd, J=4, 13 Hz, 1H), 4.2 (br s, 1H, OH), 4.24 (dd, J=7, 13 Hz, 1H), 4.28 (d, J=3 Hz, 1H), 4.2—4.5 (m, 1H), 6.9—7.0 (m, 2H, arom H), 7.1—7.6 (m, 9H, arom H), 7.9—8.1 (m, 1H, arom H); IR (KBr) 3280 (OH), 1640 (amide), 1460, 1420, 1130, 755, 713 cm^{-1}. Found: C, 77.46; H, 5.62; N, 3.80%; M$^+$, 371. Calcd for $C_{24}H_{21}NO_3$: C, 77.60; H, 5.70; N, 3.77%; M, 371.

Isomer B (21b): Mp 213—215 °C; ^{1}H NMR δ=2.8 (br s, 1H, OH), 3.26 (s, 3H, OMe), 3.34 (d, J=10 Hz, 1H), 4.2—4.4 (m, 1H), 4.5—4.7 (m, 1H), 7.1—8.0 (m, 13H, arom H); IR (KBr) 3280 (OH), 1610 (amide), 1455, 1416, 1108, 743, 708 cm^{-1}. Found: C, 77.87; H, 5.50; N, 3.85%; M$^+$, 371. Calcd for $C_{24}H_{21}NO_3$: C, 77.60; H, 5.70; N, 3.77%; M, 371.

Acid Isomerization and Degradation of 20a and 20b. To a solution of 30 mg of **20a** in 10 cm^3 of chloroform was added a few drops of hydrochloric acid. After 1 d, the solution was washed with water and dried. Then, after evaporation of the solvent, the residue was examined by measurement of ^{1}H NMR spectrum with an internal standard to contain a mixture of **20a** and **20b** (the isomer ratio was 0.63:1, the total yield was 78%). A similar result was obtained starting from 15 mg of **20b**.

To a solution of 30 mg of a mixture of **20a** and **20b** (6:1) in 30 cm^3 of acetonitrile-water (4/1 volume ratio) added a few drops of hydrochloric acid. After 1 d, the solvent was evaporated and the residue was subjected to chromatography to give an alcohol. ^{1}H NMR spectrum of the alcohol could not be obtained due to the low solubility in $CDCl_3$. Thus, the alcohol was converted to its acetate (**22**) (70% based on **20a**+**20b**) by acetic anhydride and pyridine.

N-(2-Acetoxy-3-phenylpropyl)biphenyl-2,2'-dicarboximide (22): Mp 117—120 °C; ^{1}H NMR δ=2.44 (s, 3H, OAc), 2.7—2.8 (m, 2H, CH_2Ph), 3.51 (dd, J=6, 14 Hz, 1H, NCH_2), 4.34 (dd, J=3, 14 Hz, 1H, NCH_2), 5.5—5.7 (m, 1H, CHOAc), 6.9—7.7 (m, 12H, arom H), 8.2 (dd, J=2, 7 Hz, 1H, arom H); IR (KBr) 1740 (ester), 1700 (imide), 1655 (imide), 1338, 1242, 1035, 744 cm^{-1}. Found: C, 74.91; H, 5.59; N, 3.48%; M$^+$, 399. Calcd for $C_{25}H_{21}NO_4$: C, 75.17; H, 5.30; N, 3.51%; M, 399.

Acid Degradation of 21a and 21b. To a solution of 30 mg of **21a** in 10 cm^3 of chloroform was added a few drops of hydrochloric acid. After 1 d, the solution was washed with water and dried. Then, after evaporation of the solvent, chromatography of the residue gave 22 mg (85%) of **23**. A similar result was obtained starting from 30 mg of **21b** (yield 76%).

5-Phenyl-9H-dibenzo[c,e]pyrrolo[1,2-a]azepin-9-one (23): Mp 169—171.5 °C; ^{1}H NMR δ=6.58 (d, J=3 Hz, 1H), 7.0—7.9 (m, 13H, arom H), 8.07 (d, 1H, arom H); IR (KBr) 1708 (amide), 1364, 1340, 704, 753 cm^{-1}. Found: C, 86.13; H, 4.62; N, 4.36%; M$^+$, 321. Calcd for $C_{23}H_{15}NO$: C, 85.96; H, 4.71; N, 4.36%; M, 321.

Intramolecular Photoreaction of 24. A solution of **24** in 400 cm^3 of methanol was irradiated for 5 h. After evaporation of the solvent, the residue was subjected to chromatography to give **25** and **26**. The primary photoproducts could not be obtained probably due to the instability on the separation. Chromatography on aluminium oxide also gave **25** and **26**. The ^{1}H NMR spectrum of the irradiation mixture revealed that the **25** and **26** were not the primary products, and the primary products showed mainly two methoxy singlets at δ=2.84 and 3.02 (intensity ratio 4:1).

N-(2-Hydroxy-3-phenylpropyl)naphthalene-1,8-dicarboximide (25): Mp 148—150 °C; ^{1}H NMR δ=2.5—2.7 (br s, 1H, OH), 2.8—3.0 (m, 2H, CH_2Ph), 4.2—4.4 (m, 3H, NCH_2CH OH), 7.1—7.4 (m, 5H, Ph), 7.67 (t, 2H, arom H), 8.14 (d, 2H, arom H), 8.51 (d, 2H, arom H); IR (KBr) 3500 (OH), 1702 (imide), 1644 (imide), 1592, 1236, 782 cm^{-1}. Found: C 76.10; H, 4.99; N, 4.31%; M$^+$, 331. Calcd for $C_{21}H_{17}NO_3$: C, 76.12; H, 5.17; N, 4.23%; M, 331. Its acetate: mp 117—120 °C; ^{1}H NMR δ=1.81 (s, 3H, OAc), 3.02 (d, J=7 Hz, 2H, CH_2Ph), 4.23 (dd, J=3, 13 Hz, 1H, NCH_2), 4.59 (dd, J=9, 13 Hz, 1H, NCH_2), 5.6—5.8 (m, 1H, CHOAc), 7.0—7.4 (m, 5H, Ph), 7.67 (t, 2H, arom H), 8.14 (d, 2H, arom H), 8.53 (d, 2H, arom H); IR (KBr) 1732 (ester), 1703 (imide), 1672 (imide), 1596, 1341, 1243, 786 cm^{-1}. Found: C, 73.84; H, 5.29; N, 3.72%; M$^+$, 373. Calcd for $C_{23}H_{19}NO_4$: C, 73.98; H, 5.13; N, 3.75%; M, 373.

11-Phenyl-7H-benzo[de]pyrrolo[2,1-a]isoquinolin-7-one (26): Mp 171—173 °C; ^{1}H NMR δ=6.49 (d, J=4 Hz, 1H), 7.1—8.0 (m, 10H, arom H), 8.13 (d, J=7 Hz, 1H, arom H), 8.69 (d, J=7 Hz, 1H, arom H); IR (KBr) 1715 (amide), 1590, 1321, 785 cm^{-1}. Found: C, 85.47; H, 4.30; N, 4.77%; M$^+$, 295. Calcd for $C_{21}H_{13}NO$: C, 85.40; H, 4.44; N, 4.74%; M, 295.

Triplet Photosensitization of 19. The photoreaction of **19** (3.3 mM) in the presence of benzophenone (30 mM) was carried out with light of >340 nm (filter: Pyrex and aq 5,7-dimethyl-1,4-diazacyclohepta-4,7-dienium perchlorate[21]) in methanol. The irradiated methanol solution was analyzed by HPLC with an internal standard to determine the yields of the products. The *cis* isomer of **19** was obtained by the repeated recrystallization (ethanol) of the irradiated mixture.

N-(cis-3-Phenylallyl)biphenyl-2,2'-dicarboximide: Mp 136—138 °C; ^{1}H NMR δ=4.98 (dd, J=2, 7 Hz, 2H, NCH_2), 5.65 (dt, J=7, 12 Hz, 1H, NCH_2CH=C), 6.58 (dt, J=2, 12 Hz, 1H, C=CHPh), 7.2—8.0 (m, 13H, arom H); IR (KBr) 1692 (imide), 1658 (imide), 1360, 1342, 1318, 738 cm^{-1}. Found: C, 81.11; H, 5.10; N, 4.05%. Calcd for $C_{23}H_{17}NO_2$: C, 81.39; H, 5.05; N, 4.13%.

The authors wish to express their thanks to Mrs. Yukimi Kinuta and Mr. Tetsufumi Misawa for their experimental assistance. The present work was partially supported by a Grant-in-Aid for Scientific Research No. 574199 from the Ministry of Education, Science and Culture.

References

1) Y. Kubo, T. Araki, and K. Maruyama, Symposium on Photochemistry, Kanazawa, October 1982, Abstr., No IA213.

2) P. S. Mariano, *Acc. Chem. Res.*, **16**, 130 (1983); S. L. Mattes and S. Farid, *ibid.*, **15**, 80 (1980); R. S. Caldwell and D. Creed, *ibid.*, **13**, 45 (1980); F. D. Lewis, *ibid.*, **12**, 152 (1979).

3) K. Mizuno, M. Ishii, and Y. Otsuji, *J. Am. Chem. Soc.*, **103**, 5570 (1981); D. S. Steichen and C. S. Foote, *ibid.*, **103**, 1855 (1981); D. R. Arnold, R. M. Borg, and A. Albini, *J. Chem.*

Soc., Chem. Commun., **1981**, 138.

4) a) T. Majima, C. Pac, A. Nakasone, and H. Sakurai, *J. Am. Chem. Soc.*, **103**, 4499 (1981); b) V. R. Rao and S. S. Hixson, *ibid.*, **101**, 6458 (1979); c) A. J. Maroulis and D. R. Arnold, *Synthesis*, **1979**, 819; d) A. J. Maroulis, Y. Shigemitsu, and D. R. Arnold, *J. Am. Chem. Soc.*, **100**, 535 (1978).

5) For reviews see: P. H. Mazzocchi, "Organic Photochemistry," ed by A. Padwa, Marcel Dekker, New York (1981), Vol. 5, p. 421; Y. Kanaoka, *Acc. Chem. Res.*, **11**, 407 (1978).

6) a) K. Maruyama and Y. Kubo, *J. Org. Chem.*, **51**, 1426 (1985); b) P. H. Mazzocchi and F. Khachik, *Tetrahedron Lett.*, **22**, 4189 (1981); c) P. H. Mazzocchi, S. Minamikawa, and P. Wilson, *ibid.*, **1978**, 4361; d) K. Maruyama and Y. Kubo, *Chem. Lett.*, **1978**, 851.

7) a) K. Maruyama and Y. Kubo, *J. Org. Chem.*, **46**, 3612 (1981); b) H. Hayashi, S. Nagakura, Y. Kubo, and K. Maruyama, *Chem. Phys. Lett.*, **72**, 291, (1980); c) M. Machida, K. Oda, K. Maruyama, Y. Kubo, and Y. Kanaoka, *Heterocycles*, **14**, 779 (1980); d) K. Maruyama, and Y. Kubo, *J. Am. Chem. Soc.*, **100**, 7772 (1978); e) K. Maruyama, Y. Kubo, M. Machida, K. Oda, Y. Kanaoka, and K. Fukuyama, *J. Org. Chem.*, **43**, 2303 (1978).

8) P. H. Mazzocchi, C. Somich, and C. Ammon, *Tetrahedron Lett.*, **25**, 3551 (1984).

9) a) Y. Kubo, T. Araki, and K. Maruyama, *Chem. Lett.*, **1984**, 1909; b) Y. Kubo, S. Tojo, M. Suto, R. Toda, and T. Araki, *ibid.*, **1984**, 2075.

10) Y. Kanaoka, Y. Migita, K. Koyama, Y. Sato, H. Nakai, and T. Mizoguchi, *Tetrahedron Lett.*, **1973**, 1193; P. H. Mazzocchi, M. J. Bowen, and N. K. Narian, *J. Am. Chem. Soc.*, **99**, 7063 (1977).

11) D. O. Cowan and A. A. Baum, *J. Am. Chem. Soc.*, **92**, 2153 (1970).

12) S. L. Murov, "Handbook of Photochemistry," Marcel Dekker, New York, (1973), p. 3.

13) J. L. Stavinoha and P. S. Mariano, *J. Am. Chem. Soc.*, **103**, 3136 (1981).

14) R. E. Sioda and W. S. Koski, *J. Am. Chem. Soc.*, **89**, 475 (1967).

15) M. Machida, H. Takeuchi, and Y. Kanaoka, *Tetrahedron Lett.*, **23**, 4981 (1982); P. H. Mazzocchi, L. Klingler, M. Edwards, P. Wilson, and D. Shook, *ibid.*, **24**, 143 (1983).

16) Jaubert, *Ber.*, **28**, 362 (1895) ("Beilsteins Handbuch der Organischen Chemie," **21**, p. 527).

17) J. S. McConaghy, Jr. and W. Lwowski, *J. Am. Chem. Soc.*, **89**, 2357 (1967).

18) T. Posner, *Ber.*, **26**, 1858 (1893).

19) M. G. Baldwin and S. F. Reed, Jr., *J. Polym. Sci., Polym. Chem. Ed.*, **6**, 2627 (1968).

20) H. W. Underwood, Jr. and L. A. Clough, *J. Am. Chem. Soc.*, **51**, 583 (1929).

21) K. Kasha, *J. Opt. Soc. Am.*, **38**, 929 (1948).

Interaction of Hydrophobic Cyclic Dipeptides and Acylbenzenes as Studied by Fluorescent Quenching

Toshiro Ootubo, Shunsaku Kimura, and Yukio Imanishi*
Department of Polymer Chemistry, Kyoto University, Yoshida Honmachi, Sakyo-ku, Kyoto 606
(Received May 24, 1985)

The effect of the hydrophobic interaction on the association in aqueous media of tyrosine-containing cyclic dipeptides and 1-acyl-4-bromobenzenes having various lengths of acyl chain was investigated by quenching of the fluorescence of the former compounds by the latters. In ethanol, the change of fluorescence intensity (I_0/I) was linearly related to the quencher concentration according to the Stern-Volmer's plot, which was attributed to a dynamic quenching. In this case, structures of fluorophores and quenchers did not affect the quenching constant. However, in a buffer solution, I_0/I was linearly related to the quencher concentration according to the Perrin's plot, which was attributed to a static quenching. Perrin's quenching constants depended on the structure of fluorophores and quenchers. In some cases, a quencher molecule was bound to a fluorophore by hydrophobic interaction in a favorable arrangement for fluorescent quenching. In aqueous solution, fluorophores and quenchers formed comparatively large aggregates with nonspecific arrangement for fluorescent quenching. In this case, Perrin's quenching constants were independent of the nature of quenchers and related with the size of formed aggregates.

Recognition of substrates by enzymes and of agonists by receptors is very important as the beginning step of physiological responses. Hydrophobic and electrostatic interactions are particularly important in biological host-guest interactions. However, the contribution of the hydrophobic interaction has not quantitatively been investigated.[1] Cyclic peptides provide a useful model system for the study of the hydrophobic interaction in the enzyme-mimetic reaction, because the possible conformations of cyclic peptides are very restricted due to the cyclic structure.[2] Histidine-containing cyclic dipeptides have been investigated for the hydrolytic catalyst.[3-8] Tanihara, *et al.* showed that a substrate was bound to a cyclic peptide by hydrophobic interaction and the rate of the hydrolysis of the substrate was enhanced because of a favorable orientation of the bound substrate toward a catalytic group of the cyclic dipeptide.[9] However, since the observed reaction rate constant is a function of either the substrate binding or the intramolecular attack by a catalytic group, the hydrophobic effect on the binding step was not estimated in a quantitative way.

In the present investigation cyclic dipeptides, which consist of a tyrosine and an aliphatic amino acid, were synthesized and their interactions with 1-acyl-4-bromobenzenes having various lengths of acyl chain were investigated by the fluorescence quenching measurement. The interaction between them in aqueous media was believed to occur by hydrophobic forces. A quenching of tyrosine fluorescence by the bromobenzene moiety of the substrate is not affected by the orientation of functional groups in the associate, so that the interactions involved in the binding step can be characterized in a more quantitative way.

Experimental

Cyclic dipeptides, *cyclo*(D-Ala-CM-L-Tyr) (F(D-Ala)), *cyclo*(L-Leu-CM-L-Tyr) (F(L-Leu)), and *cyclo*(D-Leu-CM-L-Tyr) (F(D-Leu)), were synthesized according to the method reported by Kopple, *et al.*,[10] in which CM represents a carboxymethyl group introduced to the hydroxyl group of tyrosine to increase the water-solubility of cyclic dipeptides.

Quenchers, 1-acyl-4-bromobenzenes, used in the present investigation were $CH_3(CH_2)_nCOC_6H_4Br$(p) (n=0 (Q_1), 2 (Q_3), and 4 (Q_5)) and $HOOC(CH_2)_nCOC_6H_4Br$(p) (n=4 (Q_5^-) and 8 (Q_9^-)). Q_1, Q_3, and Q_5 were synthesized from bromobenzene and corresponding acyl chlorides using $AlCl_3$ as a catalyst, and Q_5^- and Q_9^- were synthesized by the hy-

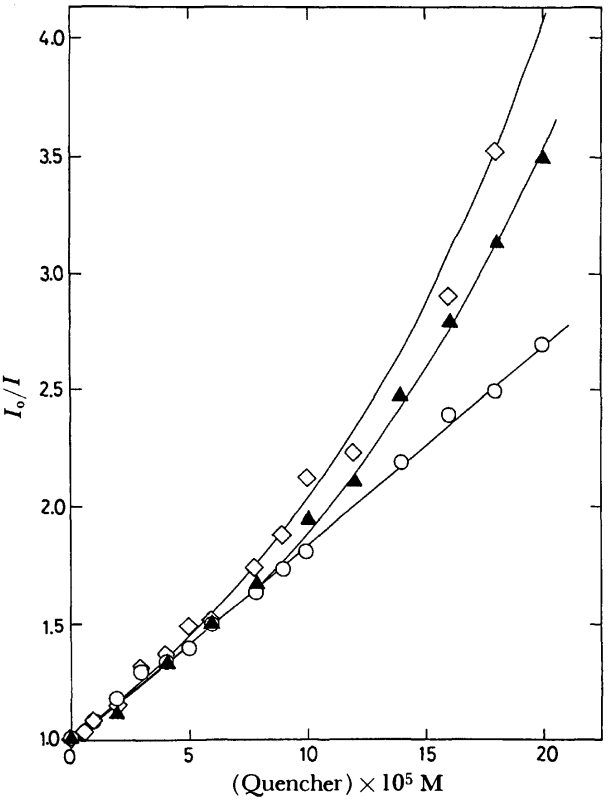

Fig. 1. Stern-Volmer's plot of the change of fluorescence intensity of F(L-Leu) with the addition of Q_5 in 20% dioxane/H_2O (◇), 20% dioxane/buffer (▲), and ethanol (○).

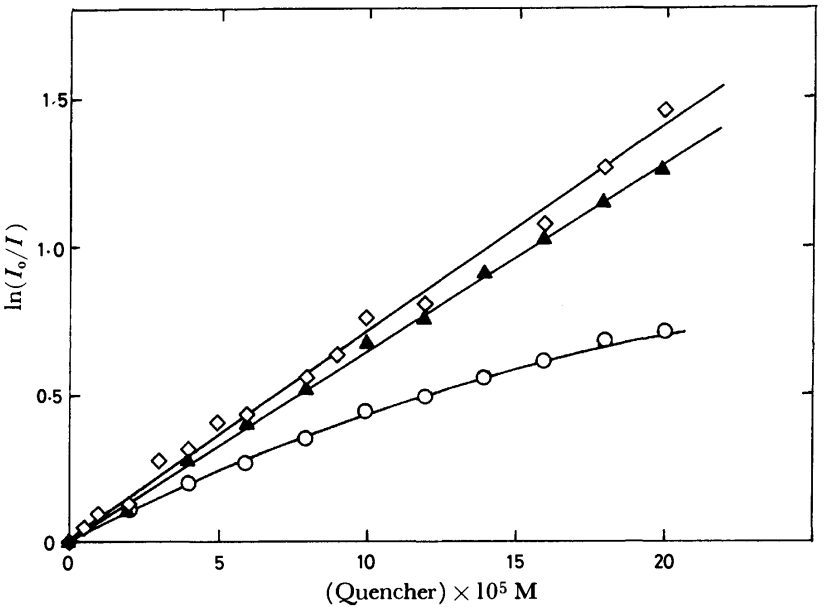

Fig. 2. Perrin's plot of the change of fluorescence intensity of F(L-Leu) with the addition of Q_5 in 20% dioxane/H_2O (◇), 20% dioxane/buffer (▲), and ethanol (○).

drolysis of the reaction product between bromobenzene and monoethyl ester chloride of the corresponding diacid catalyzed by $AlCl_3$. All of the synthesized compounds were identified by IR, ^1H NMR, and elementary analysis.

Fluorescence measurements were carried out on a Hitachi MPF-4 spectrofluorometer at 50 °C. Excitation wavelengths were 277 and 278 nm in ethanol and aqueous solution, respectively. The concentration of fluorophore was 1×10^{-5} M (1 M=1 mol dm^{-3}). The quencher was added with an aliquot of ethanol solution (2×10^{-2} M). Buffer solution was prepared from tris(hydroxymethyl)aminomethane (pH 7.5, 10 mM).

Results and Discussion

Solvent Effect on the Interaction between Cyclic Dipeptides and Quenchers. The change of the fluorescence intensity of a fluorophore F(L-Leu) with the addition of a quencher Q_5 was determined and is shown in Fig. 1 in the form of the Stern-Volmer's plot. In ethanol, I_0/I (the fluorescence intensity without the quencher relative to that with the quencher) is linearly related to the quencher concentration. Therefore, the fluorophore is quenched by the quencher in diffusion-controlled collisions, which is a dynamic quenching.[11] On the other hand, in aqueous solution the plot between I_0/I and the quencher concentration gave a concave curve. However, Perrin's plot of I_0/I against the quencher concentration showed a linear relation in aqueous solution throughout this range of quencher concentration, whereas it led to a convex curve for quenching in ethanol solution (Fig. 2). Therefore, in aqueous solution, fluorophores and quenchers should form aggregates due to the hydrophobic interaction, which is a static quenching.[12]

The efficiency of quenching decreased in the order

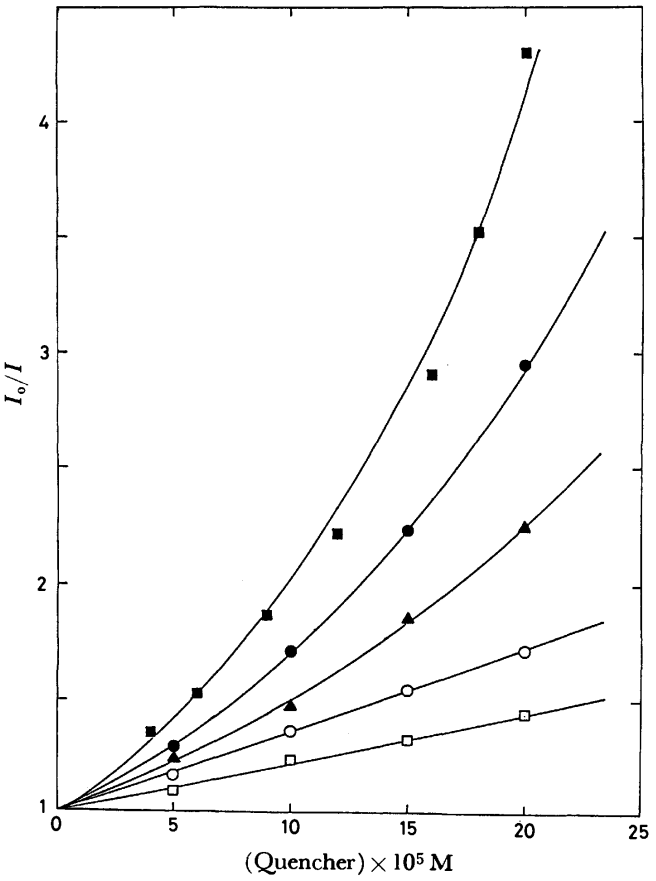

Fig. 3. Stern-Volmer's plot of the change of fluorescence intensity of F(L-Leu) with the addition of Q_5 in 20% dioxane/H_2O (■), 40% dioxane/H_2O (●), 60% dioxane/H_2O (▲), 80% dioxane/H_2O (○), and dioxane (□).

Table 1. Stern-Volmer's quenching constants ($k_Q \times 10^3\,M^{-1}$) in ethanol

Quencher	*Cyclo*(L-Leu-CM-L-Tyr)	*Cyclo*(D-Leu-CM-L-Tyr)	*Cyclo*(D-Ala-CM-L-Tyr)
$CH_3COC_6H_4Br(p)$	5.35	5.28	5.26
$CH_3(CH_2)_2COC_6H_4Br(p)$	5.31	5.19	5.28
$CH_3(CH_2)_4COC_6H_4Br(p)$	5.24	5.33	5.37

Table 2. Perrin's quenching constants ($k_Q \times 10^3\,M^{-1}$) in 20% dioxane/buffer

Quencher	*Cyclo*(L-Leu-CM-L-Tyr)	*Cyclo*(D-Leu-CM-L-Tyr)	*Cyclo*(D-Ala-CM-L-Tyr)
$CH_3COC_6H_4Br(p)$	6.14	6.00	5.77
$CH_3(CH_2)_4COC_6H_4Br(p)$	6.27	6.22	5.72
$HOOC(CH_2)_4COC_6H_4Br(p)$	5.94	5.72	5.69
$HOOC(CH_2)_8COC_6H_4Br(p)$	6.03	6.18	5.71

that 20% dioxane/H_2O>20% dioxane/buffer>ethanol. The influence of the solvent composition on the quenching of the fluorescence of F(L-Leu) by Q_5 was examined (Fig. 3). When the dioxane content was more than 80%, straight lines of the Stern-Volmer's plot was obtained. On the other hand, when the dioxane content was less than 80%, concave curves of the Stern-Volmer's plot were obtained. These results support the explanations for Figs. 1 and 2 that hydrophobic interactions are involved in the quenching process in aqueous solution.

Quenching in Ethanol. Stern-Volmer's quenching constants in ethanol were determined from the slope of the Stern-Volmer's plot and are summarized in Table 1. In all combinations of fluorophores and quenchers, a linear relation was obtained between I_0/I and the quencher concentration, and the quenching constants were almost the same for all combinations. Therefore, it is concluded that the fluorescence is quenched by the diffusion-controlled collision with a quencher, and that the structure of fluorophores and quenchers does not affect the quenching constant.

Quenching in 20% Dioxane/Buffer.

Perrin's quenching constants in 20% dioxane/buffer were determined from the slope of the Perrin's plot and are summarized in Table 2. In the case of F(D-Ala) the quenching constants by Q_1 and Q_5 or $Q_{\bar{5}}$ and $Q_{\bar{9}}$ were almost the same without the dependence on the length of acyl chain of the quencher. On the other hand, in the cases of F(L-Leu) and F(D-Leu) the quenching constants with Q_5 were larger than those with Q_1, and the quenching constants with $Q_{\bar{9}}$ were larger than those with $Q_{\bar{5}}$. These results can be explained by the difference of hydrophobic interactions between the cyclic dipeptides and the quenchers. The isobutyl substituent of F(L-Leu) or F(D-Leu) is hydrophobic enough to represent the difference of interaction due to different lengths of acyl chain. However, the methyl substituent of F(D-Ala) is not hydrophobic enough to represent different degrees of interaction.

When Q_1 and Q_5 were used as quenchers, the quenching constants decreased in the order that F(L-Leu)>F(D-Leu)>F(D-Ala). The same order was also found in the case of $Q_{\bar{5}}$ as a quencher. However, the quenching constant of F(D-Leu) with $Q_{\bar{9}}$ was larger than that of F(L-Leu). This is also shown in Fig. 4, which shows the change of Perrin's quenching constant as a function of the composition of F(D-Leu)/F(L-Leu) mixture. These results suggest that the orientation of F(D-Leu) with respect to $Q_{\bar{9}}$ might be specific as a result of the hydrophobic interaction between the long acyl chain of $Q_{\bar{9}}$ and the isobutyl substituent of F(D-Leu). In this case the bromobenzene moiety of the quencher could come close to the tyrosine residue. This consideration agrees with the result that *cyclo*(D-Leu-L-His) was a more efficient catalyst than *cyclo*(L-Leu-L-His) in the hydrolysis of *p*-nitrophenyl laurate and decanoate.[6,8] The efficient hydrolysis by *cyclo*(D-Leu-L-His) was explained in terms of the hydrophobic substrate bound by the hydrophobic interaction with isobutyl substituent of the cyclic dipeptide to a sterically favorable position for the intramolecular nucleophilic attack by the imidazolyl substituent.

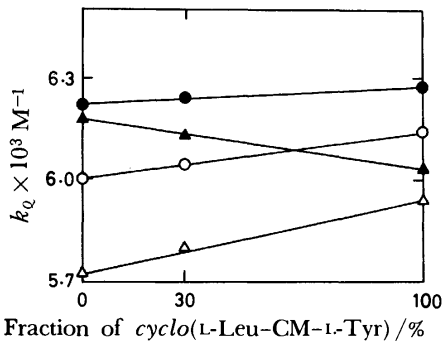

Fig. 4. Perrin's quenching constants of F(L-Leu), F(D-Leu), and their 3/7 mixture with the addition of Q_1 (○), Q_5 (●), $Q_{\bar{5}}$ (△), and $Q_{\bar{9}}$ (▲) in 20% dioxane/buffer.

Perrin's quenching constant of F(D-Leu) or F(L-Leu) with Q_5 was larger than that with $Q_{\bar{5}}$. The association of the fluorophore with $Q_{\bar{5}}$ might be weaker than that with Q_5 due to the electrostatic repulsion between the negative charges of the fluorophore and $Q_{\bar{5}}$.

TABLE 3. Perrin's QUENCHING CONSTANTS ($k_Q \times 10^3\ M^{-1}$) IN 20% DIOXANE/H_2O

Quencher	*Cyclo*(L-Leu-CM-L-Tyr)	*Cyclo*(D-Leu-CM-L-Tyr)	*Cyclo*(D-Ala-CM-L-Tyr)
$CH_3COC_6H_4Br$(p)	7.00	6.32	6.04
$CH_3(CH_2)_2COC_6H_4Br$(p)	6.99	6.34	6.06
$CH_3(CH_2)_4COC_6H_4Br$(p)	7.01	6.34	6.07

TABLE 4. COUPLING CONSTANTS (Hz) OF $C^{\alpha}H$ AND $C^{\beta}H$ PROTONS, THE FRACTION OF SIDE CHAIN CONFORMERS (%), AND CHEMICAL SHIFTS (ppm) OF $C^{\alpha}H$ OF CYCLIC DIPEPTIDES

	Tyr residue				The other residue		
	$J_{\alpha-\beta}$		U/%	F/%	$C^{\alpha}H$	$C^{\alpha}H$	Solvent
Cyclo(L-Leu-CM-L-Tyr)	4.15	5.34	39.3	60.7	4.22	3.51	C_2D_5OD
	3.92	4.88	31.8	68.2	4.49	3.85	D_2O (pH=7.5)
Cyclo(D-Leu-CM-L-Tyr)	4.19	4.63	32.6	67.4	4.28	2.94	C_2D_5OD
	3.96	4.64	30.9	69.1	4.63	3.33	D_2O (pH=7.5)
Cyclo(D-Ala-CM-L-Tyr)	3.67	4.88	30.6	69.4	4.17	2.85	C_2D_5OD
	3.86	4.68	30.3	69.7	4.49	3.22	D_2O (pH=7.5)

Quenching in 20% Dioxane/H_2O. Perrin's quenching constants in 20% dioxane/H_2O were determined by the same method as employed in the preceding section, and are shown in Table 3. The quenching constants decreased in the order that F(L-Leu)> F(D-Leu)>F(D-Ala), and this order was obtained with any kinds of quenchers examined. Furthermore, the quenching constants are independent of the length of acyl chain of quenchers, indicating the absence of any specific interactions. Carboxyl groups do not completely dissociate under experimental conditions, and a large aggregate of cyclic dipeptides and quenchers might be formed by hydrophobic interaction. The aggregate is not expected to take any defined structure, which might be the reason for the absence of specific interaction in quenching process.

Different quenching constants between F(L-Leu) and F(D-Leu) should be attributable to different orientations of the side chains in the cyclic dipeptides, which were investigated by the H-C^{α}-C^{β}-H coupling constants ($J_{\alpha-\beta}$) of NMR spectra. The aromatic group can take either a folded form (F) or two unfolded forms (U). In the folded form, the aromatic group protrudes over the plane of the cyclic dipeptide. The fractions were calculated according to Pachler's equation[13] and are shown in Table 4. The predominant conformation was found to be the folded form for all cyclic dipeptides, and the solvent effect on the conformation was not remarkable. Another evidence for the aromatic group stacking over the 2,5-piperazinedione ring is obtained from the chemical shifts of $C^{\alpha}H$. The chemical shifts of $C^{\alpha}H$ of the Tyr residue and the other residue are shown in Table 4. The chemical shifts of Ala-$C^{\alpha}H$ of F(D-Ala) and Leu-$C^{\alpha}H$ of F(D-Leu) were found to shift to a higher magnetic field compared with 3.96 ppm for Leu-$C^{\alpha}H$ of *cyclo*(D-Leu-L-Leu) and 3.92 ppm for Leu-$C^{\alpha}H$ of *cyclo*(L-Leu-L-Leu), which do not contain an aromatic amino acid, in CD_3OD, and 3.51 ppm for Leu-$C^{\alpha}H$ of F(L-Leu) in C_2D_5OD. This observation may be explained in terms that in the cases of F(D-Ala) and F(D-Leu), $C^{\alpha}H$ of the Ala or Leu residue and the aromatic group of Tyr residue stick out on the same side of the cyclic skeleton, and that the aromatic group protrudes over the $C^{\alpha}H$, that is, indicating a folded structure. The folded conformations are depicted in Fig. 5, which may explain a larger quenching constant of F(L-Leu) than F(D-Leu). Since the molecular size of F(L-Leu) is more compact than that of F(D-Leu), the former is expected to form a larger hydrophobic aggregate than the latter, which, in turn, makes Perrin's active sphere overlap with each other and increases the ability of quencher apparently.

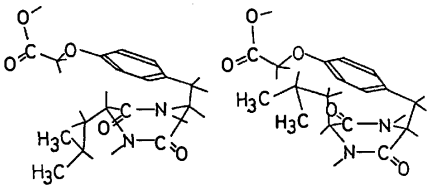

cyclo(D-Leu-CM-L-Tyr) *cyclo*(L-Leu-CM-L-Tyr)

Fig. 5 The folded conformations of F(D-Leu) and F(L-Leu).

In the case of the cyclic peptide, the specific interaction could be realized under the suitable combination of the hydrophobic and electrostatic interaction with the substrate.

References

1) W. P. Jencks, "Catalysis in Chemistry and Enzymology," McGraw-Hill, New York, (1969).

2) Y. Imanishi, *Adv. Polym. Sci.*, **20**, 1 (1976).

3) J. C. Sheehan and D. N. McGregar, *J. Am. Chem. Soc.*, **84**, 3000 (1962).

4) K. D. Kopple, R. R. Jarabak, and P. L. Bhatia, *Biochemistry*, **2**, 958 (1963).

5) Y. Murakami, A. Nakano, K. Matsumoto, and K.

Iwamoto, *Bull. Chem. Soc. Jpn.*, **51**, 2690 (1978).
6) Y. Imanishi, M. Tanihara, T. Sugihara, and T. Higashimura, *Biopolymers*, **16**, 2203 (1977).
7) K. Kawaguchi, M. Tanihara, and Y. Imanishi, *Polym. J.*, **15**, 97 (1983).
8) Y. Masuda, M. Tanihara, Y. Imanishi, and T. Higashimura, *Bull. Chem. Soc. Jpn.*, **58**, 497 (1985).
9) M. Tanihara, Y. Imanishi, and T. Higashimura, *Biopolymers*, **16**, 2217 (1977).
10) K. D. Kopple and H. G. Ghazarian, *J. Org. Chem.*, **33**, 862 (1968).
11) O. Stern and M. Volmer, *Physik. Z.*, **2**, 183 (1919).
12) F. Perrin, *Compt. Rend.*, **178**, 1978 (1924).
13) K. Pachler, *Spectrochim. Acta*, **20**, 581 (1964).

 © 1985 The Chemical Society of Japan Bull. Chem. Soc. Jpn., 58, 2875—2881 (1985)

Mechanism of the Direct and Triplet-sensitized Photolysis of *N*-(1-Naphthoyl)-*O*-(*p*-toluoyl)-*N*-phenylhydroxylamine

Tadamitsu SAKURAI,* Hidenori SUKEGAWA, and Hiroyasu INOUE
Department of Applied Chemistry, Faculty of Technology, Kanagawa University, Kanagawa-ku, Yokohama 221
(Received May 29, 1985)

Quantum yields (Φ) were determined for benzophenone-sensitized and direct photolysis of the title hydroxylamine (NT). Analysis of linear Stern-Volmer plots of the reciprocal of Φ against the reciprocal of NT concentration reveals that the sensitized decomposition of NT takes place *via* its first triplet excited state (T_1) produced by triplet-triplet energy transfer from benzophenone to NT. The fact that the quantum yields for the direct photolysis are independent of NT concentration indicates no occurrence of both self-quenching and induced decomposition of NT by the photochemically generated radicals. Closer examination of the micellar and solvent viscosity effects on the quantum yields for the direct photolysis with 313-nm light shows the existence of at least two spin-correlated (singlet) radical pairs: One is a contact radical pair whose recombination eventually yields 1,3-toluoyloxyl-migrated product and the other a solvent-separated radical pair from which 1,5-toluoyloxyl-migrated product is derived in competition with diffusive escape from the solvent or micelle cage. Exclusive occurrence of the direct photolysis from the first singlet excited state (S_1) was explained on the basis of the large energy gap between S_1 and T_1 (31 kcal mol^{-1}) which is likely to make intersystem crossing from S_1 to T_1 very inefficient.

We have discussed qualitatively the mechanism of direct and triplet-sensitized photolysis of *N,O*-diacyl-*N*-phenylhydroxylamines on the basis of the chemical yields of photoproducts, and concluded that photoreactions under direct irradiations proceed exclusively through the singlet excited state affording 1,3- and 1,5-aroyloxyl-migrated products ("in-cage" products) along with the fragmentation products ("out-of-cage" products).[1] On the other hand, triplet-sensitized photolysis gives only the fragmentation products. These intriguing effects of spin multiplicity of the excited states that is responsible for the reaction on the product distribution gave an impetus to more quantitative investigation on the photolysis of *N,O*-diacylhydroxylamines. It has been also one of the important problems encountered in our previous work whether or not the "in-cage" products come from the reaction that takes place within the identical solvent cage. Thus the title hydroxylamine (NT) was chosen for the present study and quantum yields for the direct and sensitized photolysis of NT were determined in order to solve this problem and then shed more light on the mechanism of the photolysis under conditions where geminate radicals with different spin multiplicity are produced.

Results

Quenching of the Phosphorescence of Benzophenone by NT. To ensure the occurrence of triplet-triplet energy transfer from benzophenone (the first singlet excitation energy, E_{S_1}=74.4; the first triplet excitation energy, E_{T_1}=69.2 kcal mol^{-1}; 1 kcal=4.18 kJ)[2] to NT (E_{S_1}=90, E_{T_1}=59 kcal mol^{-1}),[1] phosphorescence quenching experiments were conducted under argon at room temperature (24±1 °C). This energy transfer can be clearly seen in the efficient quenching of sensitizer's emission that follows linear Stern-Volmer relationships with the slopes ($k_t\tau_T$ where k_t and τ_T are the rate constant for triplet energy transfer and the lifetime of triplet benzophenone without NT, respectively) of 1600 M^{-1} (1 M^{-1}=1 dm^3 mol^{-1}) in 1,2-dichloroethane and 2500 M^{-1} in acetonitrile (Fig. 1). These $k_t\tau_T$ values are collected in Table 1. From the reported lifetimes of triplet benzophenone in the absence of any quencher (τ_T=14 μs in carbon tetrachloride[3] and 26 μs in acetonitrile[4]), we obtain k_t=1.1×10^8 and 0.96×10^8 M^{-1}s^{-1} in 1,2-dichloroethane and acetonitrile, respectively. Under the present experimental conditions neither fluorescence nor phosphorescence of NT could be detected.

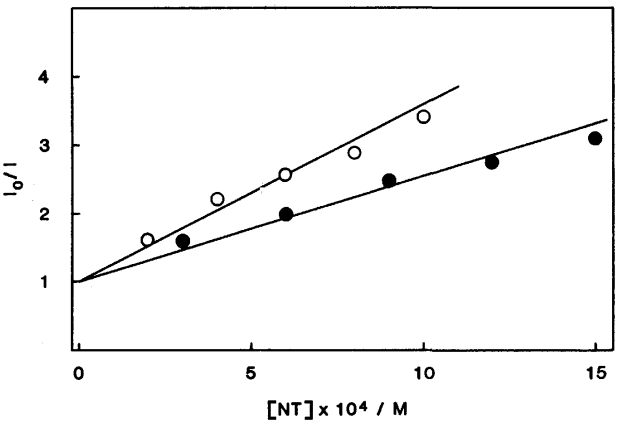

Fig. 1. Stern-Volmer plots of quenching of benzophenone (0.03 M) phosphorescence by NT in acetonitrile (○) and 1,2-dichloroethane (●) under argon at room temperature (24±1 °C). Excitation wavelength=366 nm. I and I_0 refer to the phosphorescence intensity of benzophenone with and without NT, respectively.

Quantum Yields for Triplet-sensitized Photolysis. As expected, irradiation of an N_2-saturated solution of NT (1.00—6.60 mM, 1 mM=10^{-3} mol dm^{-3}) in the presence of benzophenone (0.03 M) with 366-nm light led to only the fragmentation products **4—6**, as determined by HPLC analysis. Even trace amounts of

Table 1. Quantum yields for the triplet-sensitized photolysis of NT (1.00—6.60 mM) by benzophenone (0.03 M) at 23±2°C

1 M=1 mol dm^{-3}

Solvent	Φ_{lim}[a]			Φ_6[b]	Φ_2[c]	Φ_3[c]	k_d/k_r	$k_t\tau_T$[d]	$k_t\tau_T$[e]
	$\Phi_{-NT,lim}$	$\Phi_{4,lim}$	$\Phi_{5,lim}$					M^{-1}	M^{-1}
CH_2ClCH_2Cl	0.820	0.570	0.244	0.36	≈0	≈0	0.22	2700[f]	
								740[g]	
								1400[h]	
								mean 1600	1600
CH_3CN	0.578	0.088	0.077	0.30	≈0	≈0	0.73	5500[f]	
								1300[g]	
								1600[h]	
								mean 2800	2500

a) $\Phi_{-NT,lim}$, $\Phi_{4,lim}$, and $\Phi_{5,lim}$ are the limiting quantum yields (Φ_{lim}), *i.e.*, the quantum yields extrapolated to the infinite concentration of NT, for disappearance of NT and formation of **4** and **5**, respectively. b) Quantum yield for formation of **6** (GLC analysis) determined for 6.60 mM NT. c) Φ_2 and Φ_3 represent quantum yields for appearance of **2** and **3**, respectively. d) From quantum yield measurements. e) From quenching of sensitizer's phosphorescence by NT. f) From linear plot of $1/\Phi_{-NT}$ *vs.* 1/[NT]. g) From linear plot of $1/\Phi_5$ *vs.* 1/[NT]. h) From linear plot of $1/\Phi_4$ *vs.* 1/[NT].

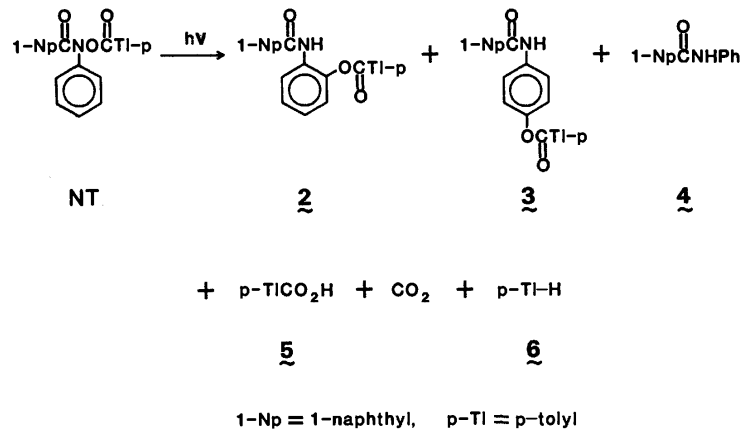

the rearrangement products **2** and **3** could not be detected in this benzophenone-sensitized photolysis. The quantum yields (Φ) for the disappearance of NT and for the appearance of the products were determined by using a potassium trioxalatoferrate(III) actinometer. The large values of quantum yields indicate very efficient sensitized decomposition to take place (Table 1).

Control experiments demonstrate that no photolysis of NT occurs without the sensitizer and that the photoproducts **4**—**6** undergo negligible sensitized decomposition. One can see, however, some unknown HPLC peaks on the chromatograms in both solvents, which may be responsible for a little poor mass balance of the sensitized photolysis. No attempt to separate and identify these unknown products was made because this inevitable side reaction appears to make no serious trouble in discussing the reaction mechanism based on the quantum yields of the photoproducts in which we are interested. In addition, HPLC analysis of a 1,2-dichloroethane or an acetonitrile solution of benzophenone before and after the irradiation reveals that hydrogen abstraction from the solvent by the benzophenone triplet takes place to a negligible extent during the irradiation with 366-nm light.

If the triplet-sensitized reaction of NT with benzophenone (B) proceeds according to Scheme 1 in which Φ_{isc} refers to the quantum yield of intersystem crossing and is known to be unity, we expect a linear relation between $1/\Phi$ and 1/[NT] under the steady-state approximation as evident from Eqs. 1—3 even though reactions giving unknown products are taken into consideration. From the linear Stern-Volmer plots of $1/\Phi_{-NT}$,

$$1/\Phi_{-NT} = (1+k_d/k_r)(1+1/k_t\tau_T[NT]) \quad (1)$$

$$1/\Phi_4 = (1+k_d/k_r)(1+k_u^N/k_4)(1+1/k_t\tau_T[NT]) \quad (2)$$

$$1/\Phi_5 = (1+k_d/k_r)(1+(k_6+k_u^T)/k_5)(1+1/k_t\tau_T[NT]) \quad (3)$$

$1/\Phi_4$, and $1/\Phi_5$ *vs.* 1/[NT] (Fig. 2), we obtain the limiting quantum yields (Φ_{lim}) for both the disappearance of NT and the formation of **4** and **5**, which are collected in Table 1. The intercept/slope ratios of these linear plots give the $k_t\tau_T$ values, while the values of k_d/k_r can be estimated by using Eq. 1.

Quantum Yields for Direct Photolysis. In order

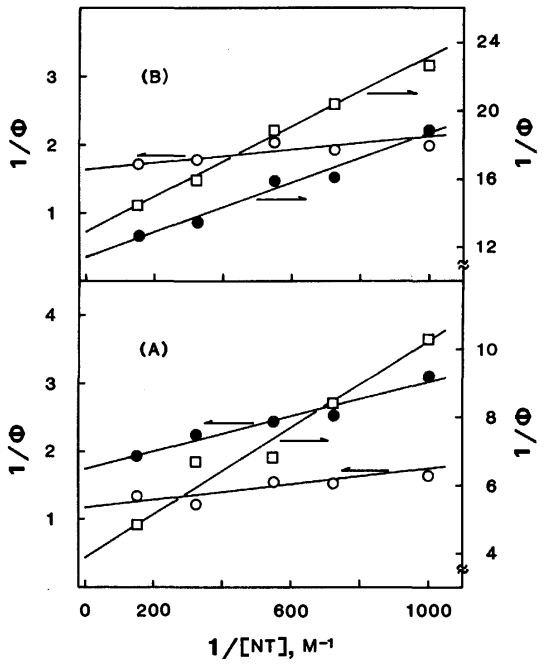

Fig. 2. Stern-Volmer plots of $1/\Phi_{-NT}$ (○), $1/\Phi_4$ (●), and $1/\Phi_5$ (□) *vs.* 1/[NT] for benzophenone (0.03 M)-sensitized photolysis with 366-nm light in 1,2-dichloroethane (A) and in acetonitrile (B).

to minimize undesired secondary photodecompositions of the products **2**—**5**, quantum yields for the direct photolysis with 313-nm light were determined at low conversions (5—10%) of starting NT. From Table 2 we see that the mass balance of the photolysis is fairly good. Direct irradiations of **2**—**5** indicate their very slight decomposition (less than 5%) to take place under conditions in which quantum yields shown in Table 2 were estimated.

Effects of solvents and hexadecyltrimethylammonium chloride (HTAC) micelle on the quantum yields for the disappearance of NT and for the formation of **2**—**5** were examined and results obtained are summarized in Table 2. In addition, quantum yield measurements were made on a 1,2-dichloroethane solution of NT whose initial concentration varied from 1.00×10^{-3} to 6.60×10^{-3} M (Fig. 3).

Discussion

Triplet Sensitization. The observation of a linear plot of $1/\Phi$ against the reciprocal of NT concentration is in accord with our suggested scheme for the sensitized photolysis (Scheme 1). Involvement of the benzophenone triplet in this sensitization is clearly seen in the finding that the $k_t\tau_T$ values (2500 M^{-1} in acetonitrile and 1600 M^{-1} in 1,2-dichloroethane), determined from the phosphorescence quenching experiments, are in satisfactory agreement with the average values of $k_t\tau_T$ (2800 M^{-1} in acetonitrile and 1600 M^{-1} in 1,2-dichloroethane), obtained from the linear plots of $1/\Phi$ *vs.* 1/[NT]. Because the rates of hydrogen abstraction from various compounds by the benzophenone triplet has been known to lie in the range 10^3—10^5 $M^{-1}s^{-1}$,[10] the estimated k_t values (0.96×10^8 and 1.1×10^8 $M^{-1}s^{-1}$ in acetonitrile and 1,2-dichloroethane, respectively) also show that benzophenone acts merely as an agent for energy transfer during the reaction, accompanying its negligible decomposition, and thus that NT undergoes sensitized decomposition

	process (rate constant)
$B(S_0) \xrightarrow{h\nu} B^*(S_1) \xrightarrow{\Phi_{isc}=1} B^*(T_1)$	absorption and intersysten crossing
$B^*(T_1) \xrightarrow{k_d^B = 1/\tau_T} B(S_0)$	deactivation to the ground state (k_d^B)
$B^*(T_1) + NT(S_0) \xrightarrow{k_t} B(S_0) + NT^*(T_1)$	energy transfer (k_t)
$NT^*(T_1) \xrightarrow{k_d} NT(S_0)$	deactivation (k_d)
$NT^*(T_1) \xrightarrow{k_r} N\bullet + T\bullet$	homolysis of the N–O bond (k_r)
$N\bullet \xrightarrow{k_4}$ 1-naphthanilide (4)	hydrogen abstraction (k_4)
$N\bullet \xrightarrow{k_u^N}$ unknown product(s)	side reaction(s) (k_u^N)
$T\bullet \xrightarrow{k_5}$ p-toluic acid (5)	hydrogen abstraction (k_5)
$T\bullet \xrightarrow{k_6}$ toluene (6)	decarboxylation and hydrogen abstraction (k_6)
$T\bullet \xrightarrow{k_u^T}$ unknown product(s)	side reaction(s) (k_u^T)

N• = 1-NpC(O)NPh•, T• = p-TlC(O)•

Scheme 1.

TABLE 2. QUANTUM YIELDS FOR THE DIRECT PHOTOLYSIS OF NT WITH 313-nm LIGHT AT 28±3°C

Solvent[a] (η)[b]	Dielectric constant	Φ_{-NT}	Φ_2	Φ_3	Φ_4	Φ_5
CH_3CN (0.326)[c]	37.5[c]	0.150±0.030	0.044±0.005	0.032±0.005	0.012±0.002[d]	0.041±0.005
CH_2ClCH_2Cl (0.730)[c]	10.36[c]	0.140±0.022	0.048±0.007	0.029±0.005	0.044±0.004	0.045±0.008
Sulfolane (10.286)[c]	43.3[c]	0.104±0.020	0.061±0.003	0.013±0.001	0.011±0.001	0.015±0.002
HTAC(0.1 M) (18)[e]	18[f]	0.127±0.040	0.094±0.015	0.016±0.001	≈0	≈0

a) [NT]=5.00×10^{-3} M in organic solvents and 3.00×10^{-3} M in HTAC micelle. The critical micelle concentration of HTAC has been reported to be 1.5×10^{-3} M.[5] b) Viscosity in centipoise (cP) at 30°C. c) Ref. 6. d) This decrease in Φ_4 in acetonitrile is due to side reactions of the amido radical taking place in competition with its hydrogen abstraction giving **4** as previously discussed.[1] e) The intramicellar viscosity of HTAC has been estimated to be ≤21 cP at 20°C[7] and 18 cP at 30°C.[8] f) Ref. 9.

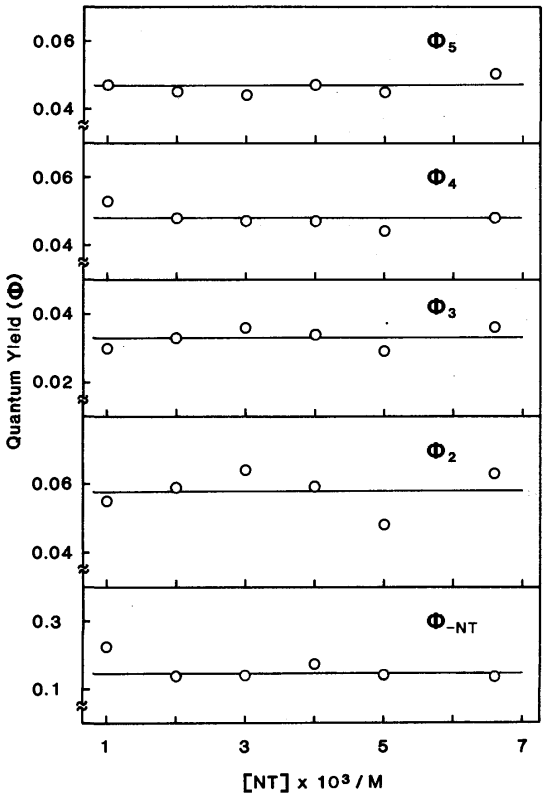

Fig. 3. Quantum yields for the direct photolysis with 313-nm light as a function of NT concentration in 1,2-dichloroethane.

through triplet-triplet energy transfer from the sensitizer to NT.

On the other hand, our values of k_d/k_r require that the resulting NT triplet dissipates its energy in part without dissociating into the amido and aroyloxyl radicals. Comparison of these values in two solvents used establishes higher reactivity of the NT triplet in 1,2-dichloroethane than in acetonitrile. We can also estimate the values of k_u^N/k_4 and k_u^T/k_5 from Eqs. 2 and 3 with these k_d/k_r values: k_u^N/k_4=6 in acetonitrile and 0.4 in 1,2-dichloroethane; k_u^T/k_5=2 in the former and 0.6 in the latter on assuming $k_6/k_5=\Phi_6/\Phi_5$. The values of k_u^N/k_4 and k_u^T/k_5 thus evaluated show that a complicated fragmentation of the triplet-derived radicals takes place in acetonitrile, while hydrogen abstraction and decarboxylation constitute a major fragmentation process in 1,2-dichloroethane.

Similar decreased efficiency of geminate recombination of radical pairs has been observed in the triplet-sensitized photodecompositions of peroxides,[11] azo compounds,[12] and allyl phenyl ether.[13] The most reasonable explanation for these observations was that there is a barrier to recombination of a caged radical pair produced as a triplet because spin inversion of a triplet radical pair must precede its coupling in the cage. The presence of the barrier results in preferential diffusive separation of radicals from the cage. This concept of triplet→singlet spin inversion in a radical pair has been critically scrutinized and then verified to have a wide applicability to reactions of spin-correlated radical pairs.[14] No formation of **2** and **3** in our triplet-sensitized photolysis of NT can be nicely explained in terms of the idea mentioned above. An illustration of the sensitized photolysis of NT appears in Scheme

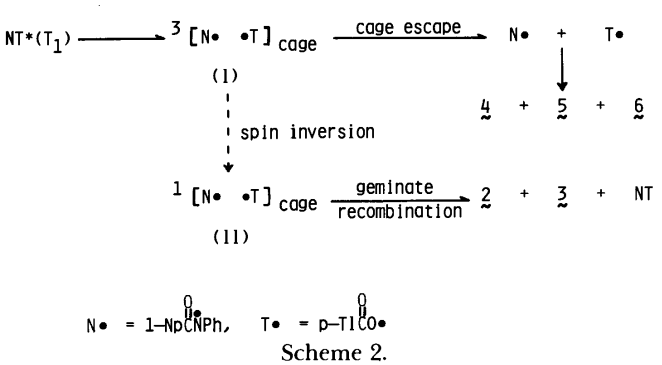

Scheme 2.

2. The observation that Φ_2 and Φ_3 are negligibly small compared to Φ_4, Φ_5, and Φ_6 suggests that in our system the rate of spin inversion from the triplet pair (I) to the singlet pair (II) should be slow enough to allow the exclusive escape of the radical pair from the cage.

Direct Irradiation. Our previous results of the direct photolysis of NT that occurs through the singlet excited state provided us some interesting problems to be solved:[1] (1) Is there self-quenching or induced decomposition of starting NT brought about by radicals produced? and (2) Are the rearrangement products **2** and **3** derived from recombination within the identical solvent cage?

Figure 3 shows that neither Φ_{-NT} nor Φ_{2-5} varies over the concentration range of NT investigated, allowing us to conclude that no starting NT meets with self-quenching and induced decomposition under conditions examined.

To answer the next question, we have studied solvent effects on the quantum yields for the photolysis with 313-nm light. It was suggested in the previous work[1] that the chemical yields of **2**, **3**, and **5** are not sensitive to both the polarity of solvents of comparable viscosity and the ease with which hydrogen atoms of solvents are abstracted by the photochemically generated toluoyloxyl radical, whereas the yield of **4** is very sensitive to this ease of solvents. Despite the secondary hydrogens of sulfolane and HTAC are very likely to be much more reactive toward hydrogen abstraction by free radicals compared with the primary hydrogens of acetonitrile,[15] the quantum yields of the fragmentation products (especially Φ_5) are much smaller in sulfolane and HTAC than in acetonitrile, indicating that the quantum yields shown in Table 2 correlate neither with the solvent polarity nor with the reactivity of a solvent hydrogen atom. This finding provides further support for the suggestion mentioned above. Thus the quantum yields for the direct photolysis seem to nicely correlate with the solvent viscosity although the slightly smaller value of Φ_5 in acetonitrile than that in 1,2-dichloroethane indicates that the reactivity of solvents toward hydrogen abstraction also plays a some but minor role in determining the relative extent of "out-of-cage" and "in-cage" reactions. The facts that decarboxylation of the toluoyloxyl radical giving eventually toluene is a minor process in the direct photolysis and that a complicated fragmentation of the amido radical occurs in relatively inert solvents toward hydrogen abstraction allow us to use Φ_5 rather than Φ_4 as a measure of the extent of "out-of-cage" reaction. These considerations force us to discuss solvent effects on Φ_{-NT}, Φ_2, and Φ_5 solely from the standpoint of micellar and solvent viscosity effects on the efficiency of geminate recombination of radical pairs.

On the other hand, micelles are known to become a good device for causing an efficient cage reaction of radical pair produced photochemically or thermally.[14] The photolysis in aqueous HTAC micelle is, therefore, expected to significantly reduce the rate of escape of the radical pair from the micelle cage, causing more efficient geminate recombination and hence leading to a decrease in Φ_{-NT} and Φ_5 and an increase in Φ_2 and Φ_3. An increase in the solvent viscosity will exert similar but less remarkable effects on these quantum yields.

Micellar effects on Φ_{-NT}, Φ_2, and Φ_5 are consistent with this expectation. However, a decrease in Φ_3 was observed in the photolysis in HTAC micelles. Almost no formation of the fragmentation products **4** and **5** is interpreted to mean that the recombination of the radical pair formed in the micelle is much faster than the exit of these hydrophobic radicals from the micelle. As expected the increased viscosity effects on the efficiency of geminate recombination are less remarkable compared to micellar effects on this efficiency, though both effects are similar, supporting the view that the hydrophobic micelle aggregate serves as a cage for causing more efficient cage reaction than that in homogeneous sulfolane solution whose macroscopic viscosity is comparable to the intramicellar microviscosity of HTAC.

Different dependence of Φ_2 and Φ_3 upon reaction environments indicates the existence of at least two spin-correlated radical pairs as originally inferred by Noyes:[16] One is a contact radical pair (III) whose recombination eventually yields 1,3-rearrangement product **2** and the other a solvent-separated radical pair (IV) from which 1,5-rearrangement product **3** is derived in competition with regeneration of (III) and diffusive escape out of the solvent or micelle cage as shown in Scheme 3.

According to Scheme 3, an increase in the solvent viscosity should impede primary cage reaction to a negligible extent whereas secondary cage and fragmentation reactions are suppressed to different extent by increasing the solvent viscosity.[17] Furthermore, this suppression of secondary cage and fragmentation reactions will result in an increase in Φ_2 and a decrease in Φ_{-NT}. These are consistent with the results obtained. The finding that the solubilized probe can move about within the micelle offers a good explanation for the formation of **3** in the photolysis in the micelle.[18] In micellar system hydrocarbon chain of the micelle-forming surfactant may serve as a solvent. Because the triplet radical pair generated selectively from the first triplet excited state (T_1) of NT results in the appearance of the cage coupling products **2** and **3** in a negligible quantum yield, the spin multiplicity of two caged radical pairs (III) and (IV) must be singlet. Exclusive occurrence of the direct photolysis from the first singlet excited state (S_1) should be due to the much slower rate of intersystem crossing relative to the rate of reaction which arises from S_1, namely, $k_{isc} \ll k_r^{S_1}$ in Scheme 3. In view of the fact that a large singlet-triplet energy gap reduces Franck-Condon factor,[19] it is reasonable to believe that the large energy gap between S_1 and T_1 for NT (ΔE_{ST}= 31 kcal mol^{-1}) renders the rate of intersystem crossing from S_1 to T_1 considerably slow.

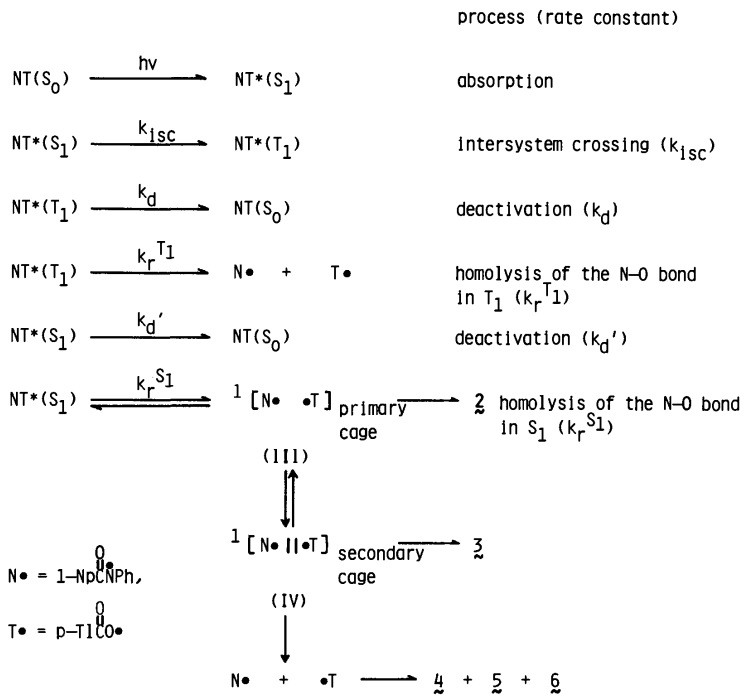

Scheme 3.

Experimental

General Methods. HPLC analysis of the photoproducts was performed on a Hitachi 638-50 high-performance liquid chromatography apparatus with a 2.6×500-mm ODS (Hitachi gel #3050) column. Linear calibration curves for each compound, prepared under the same analytical conditions, were employed to quantify both disappearance of starting material and appearance of the products. GLC analysis was carried out on a Hitachi 663-50 gas chromatograph using 2-m column packed with 10% Silicone SE-30 on Uniport B (60/80 mesh, Gasukuro Kogyo Inc.). Phosphorescence of benzophenone with and without quencher was measured under argon with a Shimadzu RF-500 spectrophotofluorimeter. UV spectra were taken on a Shimadzu UV-210A spectrophotometer.

Materials and Solvents. *N*-(1-Naphthoyl)-*O*-(*p*-toluoyl)-*N*-phenylhydroxylamine (NT) and authentic compounds for the photoproducts **2**—**5** were prepared and purified according to the same procedure as previously described.[1] 1,2-Dichloroethane (spectrograde from Dojin Chemical Co.) and Sulfolane (Merck, Uvasol) were used without further purification. The same method as before[1] was employed to get highly-purified acetonitrile. Acetonitrile and water (HPLC grade from Wako Pure Chemical Industries, Ltd.) were used as received for HPLC analysis. Pure benzophenone was obtained by repeated recrystallization from aqueous ethanol. Hexadecyltrimethylammonium chloride (HTAC, Wako) was recrystallized twice from acetone–methanol and dried *in vacuo* at room temperature.

Quantum Yield Determinations. Quantum yields were determined according to the method of Hatchard and Parker[20] which employs a potassium trioxalatoferrate(III) actinometer solution. A 450 W high pressure Hg lamp was used as the light source from which 313-nm light for direct irradiation was isolated by means of a potassium chromate (0.002 M) in a 1% aqueous solution of potassium carbonate and Corning 7-54 filters. The 366-nm light from the same Hg lamp was selected with Corning 0-52, Corning 7-37, and Toshiba IRA-25S glass filters.

In the sensitized reaction, more than 99% of the incident light was absorbed by benzophenone because molar absorption coefficients of NT and benzophenone at 366 nm are 2.6 and 50 ($M^{-1}cm^{-1}$) in acetonitrile, respectively, and 3.1 and 58 ($M^{-1}cm^{-1}$) in 1,2-dichloroethane, respectively, at room temperature. All the quantum yields for the direct and sensitized photolysis are average of more than three determinations. Quantum yields for the photolysis in HTAC micelles were determined in the same manner as that used for homogeneous solutions.

On the other hand, the solubility of NT in water could not be determined accurately owing to turbidity of the solution. However, the saturated water solution gave no signs of the absorption of NT so that NT concentration in water should be less than 10^{-6} M. On solubilization of NT in HTAC micelles by ultrasonic dispersal the solution became clear and showed no turbidity. The possibility of hydrolysis of NT in this micellar solution before and after the photolysis can be ruled out because HPLC analysis of the micellar solution indicated no formation of *p*-toluic acid and *N*-(1-naphthoyl)-*N*-phenylhydroxylamine.

References

1) T. Sakurai, S. Yamada, and H. Inoue, *Chem. Lett.*, **1983**, 975; T. Sakurai, H. Yamamoto, S. Yamada, and H. Inoue, *Bull. Chem. Soc. Jpn.*, **58**, 1174 (1985).

2) S. L. Murov, "Handbook of Photochemistry," Marcel Dekker, New York, N. Y. (1973), p. 3.

3) M. W. Wolf, R. E. Brown, and L. A. Singer, *J. Am. Chem. Soc.*, **99**, 526 (1977). We assumed that τ_T in carbon tetrachloride nearly equals τ_T in 1,2-dichloroethane.

4) T. Arai, T. Wakabayashi, H. Sakuragi, and K. Tokumaru, *Chem. Lett.*, **1985**, 279.

5) J. A. Cella, D. N. Eggenberger, D. R. Noel, L. A. Harriman, and H. J. Harwood, *J. Am. Chem. Soc.*, **74**, 2061 (1952).

6) J. A. Riddick and W. B. Bunger, "Organic Solvents," in "Techniques of Chemistry," 3rd ed, ed by A. Weissberger, Wiley-Interscience, New York, N. Y. (1970), Vol. 2, p. 399 (CH_3CN), p. 355 (CH_2ClCH_2Cl), and p. 467 (sulfolane).

7) J. Emert, C. Behrens, and M. Goldenberg, *J. Am. Chem. Soc.*, **101**, 771 (1979).

8) N. J. Turro, M. Aikawa, and A. Yekta, *J. Am. Chem. Soc.*, **101**, 772 (1979).

9) K. Kalyanasundaram and J. K. Thomas, *J. Am. Chem. Soc.*, **99**, 2039 (1977).

10) C. Walling and M. J. Gibian, *J. Am. Chem. Soc.*, **87**, 3361 (1965).

11) C. Walling and M. J. Gibian, *J. Am. Chem. Soc.*, **87**, 3413 (1965); K. Tokumaru, A. Ohshiba, T. Nakata, H. Sakuragi, and T. Mishima, *Chem. Lett.*, **1974**, 571.

12) J. R. Fox and G. S. Hammond, *J. Am. Chem. Soc.*, **86**, 4031 (1964); P. D. Bartlett and N. A. Porter, *ibid.*, **90**, 5317 (1968).

13) N. Shimamura and A. Sugimori, *Bull. Chem. Soc. Jpn.*, **44**, 281 (1971).

14) N. J. Turro, B. Kraeutler, and D. R. Anderson, *J. Am. Chem. Soc.*, **101**, 7435 (1979); N. J. Turro and B. Kraeutler, *Acc. Chem. Res.*, **13**, 369 (1980); N. J. Turro and G. C. Weed, *J. Am. Chem. Soc.*, **105**, 1861 (1983); P. Herve, F. Nome, and J. H. Fendler, *ibid.*, **106**, 8291 (1984).

15) K. U. Ingold, "Free Radicals," ed by J. K. Kochi, Wiley-Interscience, New York, N. Y. (1973), Vol. 1, p. 74; J. K. Kochi, *ibid.*, Vol. 2, p. 689.

16) R. M. Noyes, *J. Am. Chem. Soc.*, **77**, 2042 (1955).

17) We felt that temperature effects on the quantum yields for the rearrangement and fragmentation reactions allow us to discuss this point in more detail. However, temperature dependence of these quantum yields in a given solvent provided us no information of value concerning the mechanism of photorearrangements because side reactions that begin to occur at temperatures above *ca.* 40°C lowers the accuracy of the estimated quantum yields.

18) M. Almgren, E. Grieser, and J. K. Thomas, *J. Am. Chem. Soc.*, **101**, 279 (1979) and references cited therein.

19) N. J. Turro, "Modern Molecular Photochemistry," W. A. Benjamin, Menlo Park, California (1978), p. 185.

20) C. G. Hatchard and C. A. Parker, *Proc. R. Soc. London, Ser. A*, **235**, 518 (1956).

The Wittig-type Reaction of O=C-, C=C-, and N=C-Substituted Methylenetriphenylphosphoranes with *N*-Sulfinyl-*p*-toluenesulfonamide. An Intramolecular 1,3-Dipolar Cyclization of Imidoyl-conjugated Thione *S*-Imides

Takao SAITO, Michio NAKANE, Toshihiko WATANABE, Shinichi MOTOKI,*
Kimiko KOBAYASHI,† and Tosio SAKURAI*,†
Department of Chemistry, Faculty of Science, Science University of Tokyo, Kagurazaka, Shinjuku-ku, Tokyo 162
†*The Institute of Physical and Chemical Research, Hirosawa, Wako, Saitama 351-01*
(Received May 23, 1985)

The Wittig-type reactions of *N*-sulfinyl-*p*-toluenesulfonamide with (1) O=C-, (2) C=C-, and (3) N=C-conjugated phosphorus ylides were investigated. In the reaction with (1), *N*-sulfinyl-*p*-toluenesulfonamide reacted at both the ylide and the carbonyl moiety to form TsN=C-conjugated thione *S*-imide, which underwent intramolecular 1,3-dipolar cycloaddition of the CSN group with the aromatic C=C bond of the tosyl group giving a structurally unique spiro-fused tricyclic adduct. The structure of the adduct was determined by means of X-ray diffraction. In the reactions with (2) and (3), 1-azadiene and sulfobetaines were obtained instead of the expected conjugated thione *S*-imides.

We recently reported the first synthesis of α,β-unsaturated (conjugated) thione *S*-imides by the reaction of 3-aminopropene-1-thiones with chloramine salts.[1] The imides showed an interesting chemical property namely that they cyclize reversibly to thiazoline compounds depending on the solvent.

In view of continued interest in conjugated thiocumulenes, we have attempted the synthesis of O=C-, C=C-, and N=C-conjugated thione *S*-imides by the Wittig-type reaction of *N*-sulfinylamines with the corresponding phosphorus ylides. This method is conceivable because of our previous successful preparation of fluorenethione *S*-tosylimides by this Wittig-type reaction.[2]

In the previous paper[2] we reported that (benzoylphenylmethylene)triphenylphosphorane **1a** reacted with *N*-sulfinyl-*p*-toluenesulfonamide (**2**) to form the imidoyl-conjugated thione *S*-tosylimide **3a**, which subsequently underwent an intramolecular 1,5-dipolar cyclization giving a 1,2,3-thiadiazoline compound **4a**. However, reinvestigation of the reaction products in a series of the reactions applying ^{13}C NMR and X-ray diffraction analysis reveals that we were previously misled by the spectral features. This paper deals with new and unexpected results including a revised structure (**5**).

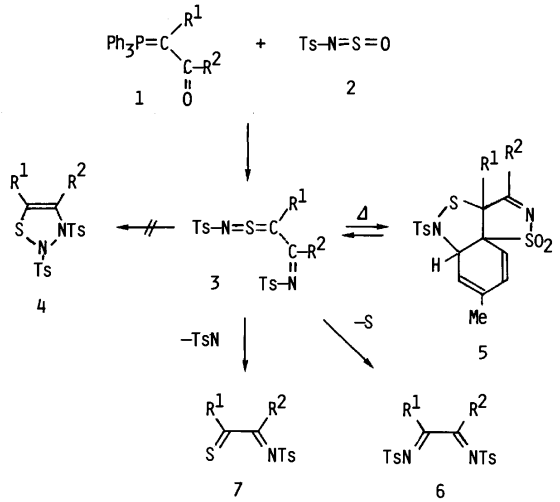

	R^1	R^2
a	Ph	Ph
b	Ph	p-MeC_6H_4
c	Ph	p-$MeOC_6H_4$
d	Ph	p-ClC_6H_4
e	p-MeC_6H_4	Ph
f	p-MeC_6H_4	p-MeC_6H_4
g	p-$MeOC_6H_4$	Ph
h	p-$MeOC_6H_4$	p-MeC_6H_4

Scheme 1.

TABLE 1. REACTION OF (ACYLARYLMETHYLENE)TRIPHENYLPHOSPHORANES (**1**) WITH *N*-SULFINYL-*p*-TOLUENESULFONAMIDE (**2**)

	R^1	R^2	Reaction time/h	Yield/% **5**	Yield/% **6**	Mp, θ_m/°C **5**	Mp, θ_m/°C **6**
a	Ph	Ph	16	40	12	186—187	200—201
b	Ph	p-MeC_6H_4	16	42	9	189—190	195—196
c	Ph	p-$MeOC_6H_4$	18	57	6	193—194	196—197
d	Ph	p-ClC_6H_4	9	34	16	184—185	70—72
e	p-MeC_6H_4	Ph	14	28	7	193—194	196—197
f	p-MeC_6H_4	p-MeC_6H_4	12	21	6	189—192	220—223
g	p-$MeOC_6H_4$	Ph	20	20	13	170—171	196—197
h	p-$MeOC_6H_4$	p-MeC_6H_4	17	25	9	166—167	178—179

TABLE 2. MASS SPECTRAL FRAGMENTATION PATTERNS OF **3** AND **5** (m/z)/%

	3b	**3c**	**5a**	**5b**	**5c**
M^+	562(0)	578(vw)	548(vw)	562(vw)	578(0)
M^+-TsH	406(5)	422(7)	392(4)	406(vw)	422(3)
R^2CNTs^+	272(11)	288(7)	258(9)	272(5)	288(6)
M^+-2Ts	252(15)	268(29)	238(15)	252(11)	268(24)
$M^+-2Ts-N$	238(vw)	254(29)	224(9)	238(9)	254(30)
R^1CSN^+	135(21)	135(23)	135(23)	135(18)	135(27)
R^1CS^+	121(76)	121(52)	121(9)	121(62)	121(10)
	5d	**5e**	**5f**	**5g**	**5h**
M^+	582(0)	562(vw)	576(vw)	578(0)	592(0)
M^+-Ts	426(vw)	406(5)	420(3)	422(23)	436(22)
R^2CNTs^+	292(2)	258(7)	272(3)	258(vw)	272(vw)
M^+-2Ts	272(vw)	252(18)	266(18)	268(41)	282(46)
$M^+-2Ts-N$	258(5)	238(9)	252(4)	254(10)	268(4)
R^1CSN^+	135(25)	149(13)	149(31)	165(21)	165(64)
R^1CS^+	121(10)	135(77)	135(16)	151(69)	151(19)

vw: very weak Tol^+ 91(100%) in all cases.

Results and Discussion

In refluxing benzene (acylarylmethylene)triphenylphosphoranes **1** reacted with *N*-sulfinyl-*p*-toluenesulfonamide (**2**) at the both functional sites, namely the ylide and the acyl moietiy, yielding compounds **5**—**7** (Scheme 1, Table 1).[3] The structures of **5a**, **b**, and **5d**—**h** were confirmed by comparisons of the spectroscopic data (IR, MS, ^1H, and ^{13}CNMR) with those of **5c**, of which the structure was proved by means of the X-ray diffraction analysis (*vide infra*). The reaction mixture was colored orange at the first stage of the reaction, and ultimately turned greenish blue.[4] Although the orange substances are rather labile, they could be isolated in the case of the reactions of **1b**, c when performed at room temperature or below, and were identified as the N=C-conjugated thione *S*-imides **3b**, c on the basis of the spectral analyses and the reactions described below (Scheme 3).

The thione *S*-imides **3b**,c exhibited characteristic absorption bands of νCSN at 990 cm^{-1} and of νC=NTs at 1550 cm^{-1} in the IR spectra. In the mass spectra of **3** and **5**, almost the same fragmentation patterns were observed (Table 2). This indicates the reversible transformation between **3** and **5**, *e.g.* for **3c** and **5c**, as shown in Scheme 2. Although molecular ion peaks and their desulfurized fragment peaks $\mathbf{6}^{\cdot+}$ were hardly detected (E.I. at 70 eV), the peaks [M^+ −TsH] are very indicative of these unique cycloadducts **5**, because facile elimination of TsH can be envisaged from **5** rather than from **3**. The ^1H NMR spectra of **3b**, c were in good agreement with the proposed structures. The assignments are given in Experimental Section. The geometrical isomerism of **3**, if present, about the bent CSN and C=NTs moieties was not determined. The geometrical rigidity is probably lost to a considerable extent by contribution of a 1,5-dipolar structure due to the conjugation. In the

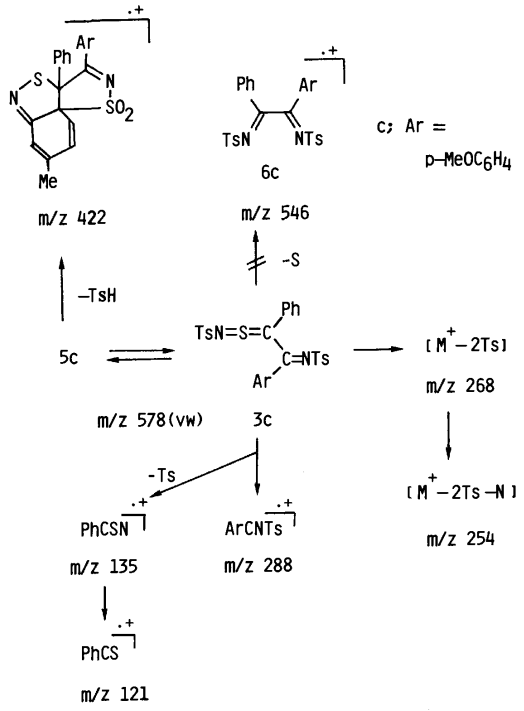

Scheme 2.

^{13}CNMR spectra of **3b**,c, the cumulene and imine carbons resonated at a low field of δ=167.2 and 176.3 for **3b**, and 166.3 and 176.6 for **3c**, respectively.

As expected, heating of the isolated imides **3b**, c in benzene gave **5b**, c and **6b**, c along with small amounts of **7b**, c. Interestingly, heating (>~110 °C) of **5c** in xylene gave reversion to **3c**, suggesting the existence of equilibrium between **3** and **5** at a higher temperature. This retro-cyclization is also observed during the reactions of **3c** and **5c** with triphenylphosphine; the reactions of both **3c** and **5c** with triphenylphosphine produced **7c**, **8**, **9**, and **10c** (Scheme 3). There is no doubt that in both reactions the products (**7**—**10**) are formed from **3c** by nucleophilic attack of triphenylphosphine at the CSN moiety. It should be

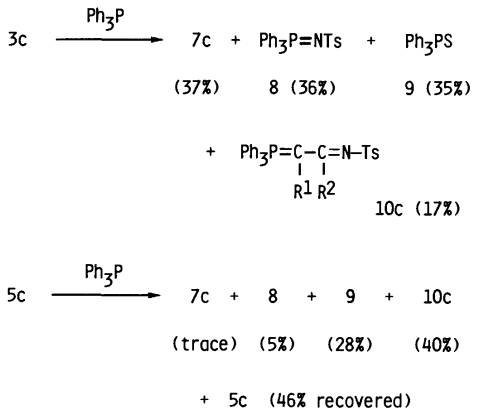

Scheme 3.

noted that the reaction of **3c** was facile even at low temperature (5—8°C) while that of **5c** took place only at higher temperature (>~70°C) which is required for the retro-cyclization to **3c**.

The reaction of C=C-conjugated phosphorus ylide **11a** with **2** yielded a 1-azadiene **14**, which might be formed from the conjugated thione *S*-imide **13** by sulfur extrusion *via* a thiaziridine ring[5] (Scheme 4).

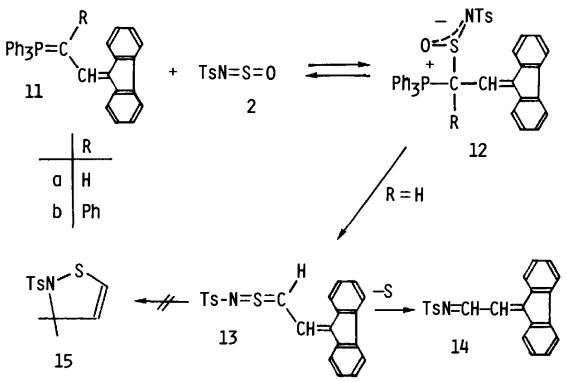

Scheme 4.

Neither **13** nor its 1,5-dipolar cyclization product (**15**) was obtained. On the other hand, the reaction of **11b** with **2** stopped at the stage of the betaine **12** under the same reaction conditions, but an isolation of **12** failed.

Treatment of **16** having a N=C in conjugation with the ylide function with **2** formed a hygroscopic betaine **17** which was ultimately hydrolyzed to give a betaine of sulfur dioxide, **18** (Scheme 5). Treatment of the betaine **18a** with potassium *t*-butoxide led to reconversion to the starting ylide (**16a**). The betaine **18** was also obtained by bubbling sulfur dioxide into a solution of the ylide **16** (Table 3). From the betaines **17** and **18** the corresponding conjugated thione *S*-imides **19** and *S*-oxide **20**,[6] respectively, could not be obtained.

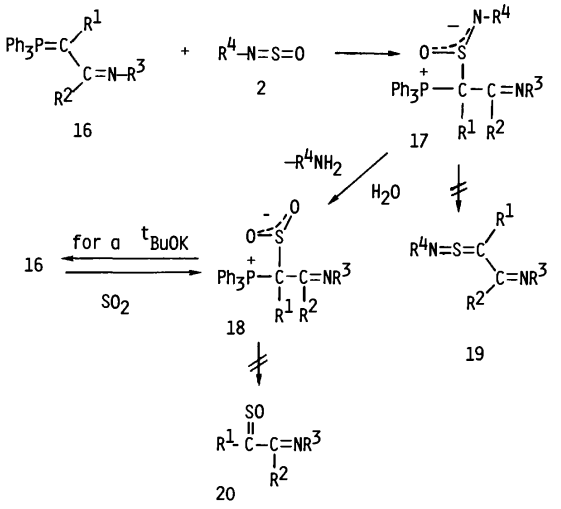

Scheme 5.

The present results of these Wittig-type reactions reveal that this methodology is promising to prepare conjugated thione *S*-imides, although a limited number of substituents leads a completion of the reaction and stabilizes these conjugated thione *S*-imides sufficiently.

Structure Determination of **5**.

4,5-Diaryl-10-methyl-7-tosyl-2,6-dithia-3,7-diazatricyclo-[6.4.0.0^{1,5}]dodeca-3,9,11-triene 2,2-Dioxides (**5**). In the ^{13}C NMR spectra of **5**, single-frequency off-resonance decoupling (SFORD) measurements showed signals of the tertiary and two quaternary carbons assigned to the carbons at C(8), C(5), and C(1), respectively (Table 4). This unambiguously excludes the structure **4**. In the ^{1}H NMR spectra H(8), H(9), CH_3(10), H(11), and H(12) protons exhibited plural couplings similar to those of 2-methyl-1,3-cyclohexadiene bicyclo compounds.[7] The assignments of the signals are compiled in Table 5.

X-Ray Diffraction. X-Ray diffraction data were collected on a Rigaku AFC automated four-circle diffractometer. The crystal data, details of experimental conditions, and the structure analysis procedures are listed in Table 6. Atomic parameters are given in Table 7. The atomic scattering factors and *f'*, *f''* values were taken from International Tables for X-Ray Crystallograpy.[8] The calculations were carried out on a FACOM M-380 computer using the UNICS-III[9] and ORTEP[10] programs. A stereoscopic drawing of the molecule is shown in Fig. 1, and the selected

TABLE 3. REACTION OF YLIDE **16** WITH **2** AND SULFUR DIOXIDE

2, 16—20	R^1	R^2	R^3	R^4	Reagent	Yield/% 18a	18b
a	H	Ph	Ph	Ph	**2a**	53	48
b	Ph	$PhCH_2$	Mes	Ts	**2b**	54	9
					SO_2	93	61

Table 4. ^{13}C NMR spectral data of **5** (δ, TMS, $CDCl_3$)[a]

5	C(1)	C(4)	C(5)	C(8)	CH_3(10)	CH_3(Ts)
a	86.20	175.57	b)	68.56	21.05	21.64
b	86.16	175.57	b)	68.56	21.10	21.73
c	86.20	163.93	77.19	68.61	21.10	21.73
d	86.30	174.74	75.87	68.61	21.10	21.69
f	86.06	175.82	75.58	68.46	21.05	21.69
g	85.91	175.87	75.58	68.42	21.10	21.64
h	85.86	175.87	75.43	68.37	21.10	21.69

a) **5e** is sparingly soluble in $CDCl_3$ or DMSO-d_6. b) Superimposed on the peak of the solvent ($CDCl_3$).

Table 5. ^1H NMR spectral data of **5** (δ, TMS, $CDCl_3$)[a]

5	H(8)	H(9)	H(11)	H(12)	CH_3(10)	CH_3(Ts)	Ar-H	Others
a	5.60 br,m	6.25 br,m	5.89(dd) J_9=1.0 J_{12}=8	4.92(d) J_{11}=8	1.85(dd) J_7=1.5 J_8=1.5	2.40(s)	6.6—7.7 (m)	—
b	5.52 br,m	6.18 br,m	5.84(dd) J_9=1.0 J_{12}=11	4.87(d) J_{11}=11	1.85(dd) J_7=1.5 J_8=1.5	2.40(s)	6.6—7.6 (m)	2.36(s) (CH_3)
c	5.54 br,m	6.18 br,m	5.84(dd) J_9=1.0 J_{12}=10	4.86(d) J_{11}=10	1.86(dd) J_7=1.5 J_8=1.5	2.42(s)	6.6—7.7 (m)	3.84(s) (OCH_3)
d	5.49 br,m	6.20 br,m	5.86(dd) J_9=1.0 J_{12}=10	4.88(d) J_{11}=10	1.86(dd) J_7=1.5 J_8=1.5	2.42(s)	6.7—7.6 (m)	—
f	5.52 br,m	6.32 br,m	5.83(dd) J_9=1.5 J_{12}=10	4.88(d) J_{11}=10	1.86(dd) J_7=1.5 J_8=1.5	2.40(s)	6.5—7.6 (m)	2.28(s) 2.36(s) ($2CH_3$)
g	5.54 br,m	6.18 br,m	5.87(dd) J_9=1.0 J_{12}=10	4.90(d) J_{11}=10	1.87(dd) J_7=1.5 J_8=1.5	2.41(s)	6.6—7.6 (m)	3.76(s) (OCH_3)
h	5.52 br,m	6.16 br,m	5.86(dd) J_9=1.0 J_{12}=10	4.88(d) J_{11}=10	1.86(dd) J_7=1.5 J_8=1.5	2.40(s)	6.7—7.7 (m)	2.38(s) 3.74(s) (CH_3,OCH_3)

a) **5e** is sparingly soluble in $CDCl_3$ or DMSO-d_6.

bond lengths and angles are given in Figs. 2 and 3. The reaction of **3** to **5** occurs through the bond formation between C(1) and C(3), and N(2) and C(4), which results the three fused rings system A, B, C. The torsion angles within these rings are shown in Fig. 4. The isothiazolidine ring B is considerably deformed. The distance C(1)-C(3), 1.587 Å, is longer than the ordinary single bond distance 1.54 Å. The six-membered ring C takes half chair form. The dihedral angles among the mean planes A, B, C are 74.8(1), 71.6(1), and 80.9(1)° for A-B, B-C, and C-A, respectively.

Complete F_o—F_c data, hydrogen atomic parameters and anisotropic thermal parameters are deposited as Document No. 8549 at the Office of the Editor of *Bull. Chem. Soc. Jpn.*

Experimental

All melting points are uncorrected. IR spectra were measured on a Hitachi Model 260-10 spectrometer. ^1H and ^{13}C NMR spectra were recorded on a JEOL JNM-FX 100 spectrometer in $CDCl_3$ solution using tetramethylsilane as an internal standard (^1H; at 100 MHz, ^{13}C; at 25.05 MHz). Mass spectra were recorded on a Hitachi double focusing mass spectrometer RMU-7M, operating at an ioninzing potential of 70 eV. Elemental analyses were performed using a Yanaco Model MT-3 CHN corder.

N-Sulfinylamines (**2**),[11] the conjugated ylides **1**,[12] **11a**,[13] **16**[14] were prepared by the methods reported in the literature. Ylide **11b** was newly synthesized by the modified method.[13]

11b: Deep red cubes, mp 197—198 °C. IR(KBr) 1540 and 1440 cm^{-1}. MS *m/z* 528 (2%, M^+). Found: C, 88.70; H, 5.51%. Calcd for $C_{39}H_{29}P$: C,88.61; H, 5.53%.

[*A*] *General Procedure for the Reaction of (Acylarylmethylene) triphenylphosphorane (1) with* N-*Sulfinyl*-p-*toluenesulfonamide (2).* A solution of **2** (6.6 mmol) in dry benzene (10 cm^3) was added dropwise to a benzene solution (50 cm^3) of **1** (3.0 mmol) with stirring at room temperature, and then the reaction mixture was heated under reflux for 9—20h until the orange color of **3** disappeared. Removal of the solvent and column chromatography (silica gel, benzene) of the residue gave **5** and **6** (Table 1). When **5** was contaminated with a small amount of blue **7**, the crude **5** was washed with diethyl ether-hexane and recrystallized from chloroform-hexane to give analytically pure **5** as colorless crystals.

4,5-Diaryl-10-methyl-7-tosyl-2,6-dithia-3,7-diazatricyclo[6.4.0.0^{1,5}]-dodeca-3,9,11-triene 2,2-Dioxide (5). **5a**: IR(KBr) 1555 (C=N), 1345, 1165 (SO_2) cm^{-1}. Found: C, 61.38; H, 4.17; N,

TABLE 6. CRYSTAL DATA, DETAILS OF EXPERIMENTAL CONDITIONS AND STRUCTURE ANALYSIS PROCEDURES FOR X-RAY DIFFRACTION OF **5c**

Crystal Data	
Formula	$C_{29}H_{26}N_2O_5S_3$
Crystal color	Colorless
shape	Prismatic
size(mm)	0.34×0.34×0.31
Crystal system	Orthorhombic
Space group	$P2_12_12_1$
Unit cell dimensions a(Å)	13.268(3)
b(Å)	19.738(2)
c(Å)	10.245(2)
Unit cell volume U(Å^3)	2683(1)
Z	4
μ(mm^{-1})	0.306
F(000)	1208
Experimental[a]	
Radiation and wavelength λ(Å)	Mo $K\alpha$, 0.71073(graphite monochromatized)
Scan speed ω (deg/min)	4
Max. 2θ(deg)	55
Range of hkl	h=0—17, k=0—25, l=0—13
Temperature of measurement(K)	296
Criterion for observed reflections	$\|F_o\|>3\sigma(\|F_o\|)$
No. of unique reflections	2674
Structure analysis	
Method	The direct method using MULTAN78[15]
Method of refinement	The block-diagonal least-squares
Magnitudes in LS refinement	$\|F\|$
Weight	Unit weight for all reflections
Temperature factors	Anisotropic temperature factors for all non-hydrogen atoms
No. of refined parameters	457
Method of locating and refining H-atoms	Difference Fourier syntheses
Final values of R	0.034
$R\omega$	0.034
S	0.047
Ratio of max. LS shift to error	0.39(H-atom)
Max. and min. height in final diff. Fourier (eÅ^{-3})	0.23, −0.20

a) Deterioration correction was made but not for absorption.

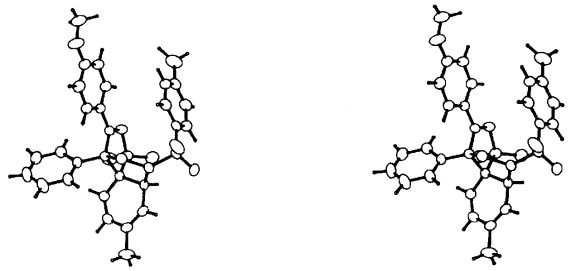

Fig. 1. Stereoscopic view of **5c**.

TABLE 7. ATOMIC PARAMETERS

Positional parameters are multiplied by 10^5. Thermal parameters are given by the equivalent temperature factors.

Atom	X	Y	Z	B_{eq}/Å^2
S(1)	31220(6)	13524(5)	55971 (9)	2.6
S(2)	2951(6)	20066(5)	61583 (9)	2.4
S(3)	5188(7)	8977(5)	80654 (9)	3.1
O(1)	38610(19)	15233(15)	46422(29)	3.8
O(2)	32409(20)	7361(13)	63179(30)	3.7
O(3)	18311(23)	48006(14)	92159(31)	4.4
O(4)	6093(26)	1817(14)	79153(29)	4.6
O(5)	−3652(20)	11965(18)	86088(27)	4.5
N(1)	30449(21)	19996(15)	66282(28)	2.6
N(2)	5912(23)	11971(15)	65606(28)	2.6
C(1)	18426(24)	14073(17)	48777(32)	2.1
C(2)	22828(24)	23781(17)	63792(33)	2.1
C(3)	15213(23)	21440(17)	53390(33)	2.1
C(4)	11477(24)	8615(17)	54998(33)	2.2
C(5)	4139(26)	5431(16)	45605(38)	2.6
C(6)	5332(28)	5493(17)	32778(37)	2.8
C(7)	13794(30)	9260(20)	27264(35)	3.0
C(8)	19670(28)	13257(19)	34246(34)	2.7
C(9)	21609(23)	30213(17)	71014(33)	2.2
C(10)	28771(26)	31907(18)	80359(38)	2.7
C(11)	28025(27)	37808(18)	87691(37)	2.9
C(12)	19915(29)	42129(18)	85585(37)	2.9
C(13)	12723(27)	40565(19)	76182(40)	3.0
C(14)	13477(26)	34678(17)	69031(37)	2.6
C(15)	26027(40)	50324(24)	100957(49)	4.4
C(16)	14373(25)	26463(17)	42021(33)	2.2
C(17)	5652(27)	27041(19)	34687(36)	2.8
C(18)	5229(30)	31426(22)	24213(39)	3.6
C(19)	13552(34)	35237(21)	20885(40)	3.7
C(20)	22272(32)	34671(20)	28066(41)	3.5
C(21)	22685(26)	30317(20)	38618(38)	2.9
C(22)	15527(26)	11914(18)	89754(34)	2.5
C(23)	15071(29)	18265(19)	95604(38)	3.1
C(24)	23388(32)	20593(19)	102303(37)	3.2
C(25)	32041(30)	16718(20)	103492(37)	3.1
C(26)	32181(30)	10284(20)	97786(39)	3.3
C(27)	24022(30)	7845(19)	90855(38)	3.1
C(28)	40950(33)	19467(30)	110968(49)	5.3
C(29)	−1553(31)	1966(24)	23457(46)	4.1

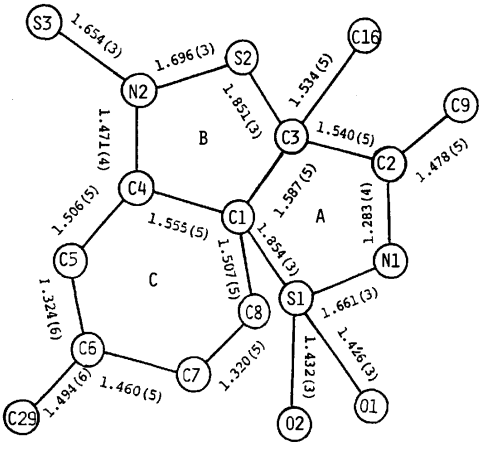

Fig. 2. Selected bond lengths (l/Å) within tricyclic system A,B, and C.

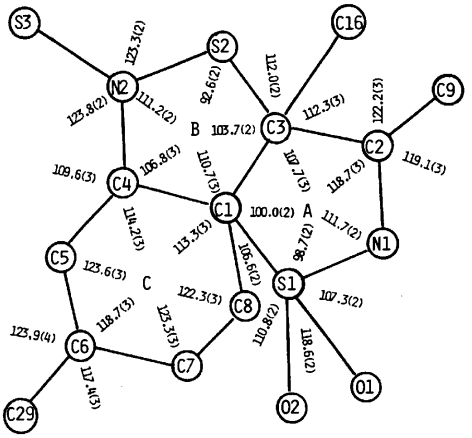

S1–C1–C4	109.9(2)
C3-C1-C8	114.9(3)
O1–S1–C1	110.1(2)
O2-S1–N1	109.4(2)
S2-C3–C2	107.9(2)
C1–C3–C16	112.7(3)

Fig. 3. Selected bond angles (ϕ/°) within tricyclic system A,B, and C.

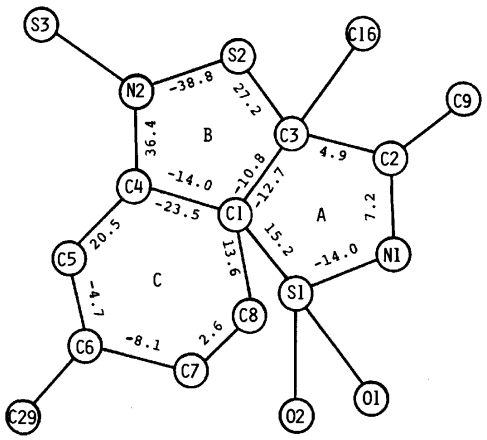

Fig. 4. Torsion angles (θ°).

5.12; S, 17.31%. Calcd for $C_{28}H_{24}N_2O_4S_3$: C, 61.29; H, 4.41; N, 5.11; S, 17.53%.

5b: IR(KBr) 1550 (C=N), 1350, and 1160 (SO_2) cm^{-1}. Found: C, 61.96; H, 4.70; N, 4.91; S, 17.06%. Calcd for $C_{29}H_{26}N_2O_4S_3$: C, 61.90; H, 4.66; N, 4.98; S, 17.09%.

5c: IR(KBr) 1550 (C=N), 1350, and 1165 (SO_2) cm^{-1}. Found: C, 60.21; H, 4.50; N, 4.81; S, 16.92%. Calcd for $C_{29}H_{26}N_2O_5S_3$: C, 60.19; H, 4.53, N, 4.84; S, 16.62%.

5d: IR(KBr) 1550 (C=N), 1350, and 1160 (SO_2) cm^{-1}. Found: C, 57.70; H, 4.01; N, 4.79%. Calcd for $C_{28}H_{23}N_2O_4S_3Cl$: C, 57.67; H, 3.98; N, 4.80%.

5e: IR(KBr) 1560 (C=N), 1345, and 1160 (SO_2) cm^{-1}. Found: C, 62.01; H, 4.65; N, 4.99%. Calcd for $C_{29}H_{26}N_2O_4S_3$: C, 61.90; H, 4.66; N, 4.98%.

5f: IR(KBr) 1550 (C=N), 1340, and 1160 (SO_2) cm^{-1}. Found: C, 62.50; H, 4.88; N, 4.85%. Calcd for $C_{30}H_{28}N_2O_4S_3$: C, 62.48;H, 4.89; N, 4.86%.

5g: IR(KBr) 1560 (C=N), 1350, and 1160 (SO_2) cm^{-1}. Found: C, 60.20; H, 4.51; N, 4.84%. Calcd for $C_{29}H_{26}N_2O_5S_3$: C, 60.19;H, 4.53;N, 4.84%.

5h: IR(KBr) 1550 (C=N), 1340, and 1165 (SO_2) cm^{-1}. Found: C, 60.81;H, 4.77; N, 4.73%. Calcd for $C_{30}H_{28}N_2O_5S_3$: C, 60.79; H, 4.76; N, 4.73%.

1,2-Diaryl-N,N′-ditosyl-1,2-ethanediimine (6). ***6a***: IR (KBr) 1560 cm^{-1} (C=N). ^1H NMR ($CDCl_3$) δ=2.38 (s, 6H, $2CH_3$(Ts)), 7.19—7.85 (m, 18H, Ar-H). ^{13}C NMR ($CDCl_3$) δ=172.75 (C=N), 21.64 (CH_3(Ts)). MS (70eV) *m/z* 516 (vw, M^+), 258 (20%, PhC=NTs·+), 91 (100, *p*-Tol·+).

6b, *e*: IR(KBr) 1590 and 1560 cm^{-1} (C=N). ^1H NMR δ= 2.35 (s, 3H, CH_3), 2.38 (s, 6H, $2CH_3$(Ts)), 7.10—7.90 (m, 17H, Ar-H). ^{13}C NMR δ=172.94, 172.51 (C=N), 21.83 (CH_3), 21.64 (CH_3(Ts)). MS *m/z* 530 (vw, M^+) 272 (17, *p*-TolC=NTs·+), 258 (6, PhC=NTs·+), 91 (100, *p*-Tol·+).

6c, *g*: IR(KBr) 1590 and 1555 cm^{-1} (C=N). ^1H NMR δ= 2.43 (s, 6H, $2CH_3$(Ts)), 3.83 (s, 3H, OCH_3), 6.8—8.0 (m, 17H, Ar-H). ^{13}C NMR δ=173.04, 171.53 (C=N), 55.60 (OCH_3), 21.64 (CH_3(Ts)). MS *m/z* 546 (vw, M^+), 288 (27, *p*-$CH_3OC_6H_4C$=NTs·+), 258 (4, PhC=NTs·+), 91 (100, *p*-Tol·+).

6d: IR(KBr) 1585 and 1555 cm^{-1} (C=N). ^1H NMR 2.42 (s, 6H, $2CH_3$ (Ts)), 7.2—7.9 (m, 17H, Ar-H). ^{13}C NMR 172.16, 171.48 (C=N), 21.64 (s, 6H, $2CH_3$(Ts)). MS *m/z* 550 (vw, M^+), 292 (5, *p*-ClC_6H_4C=NTs·+), 258 (11, PhC=NTs·+), 91 (100, *p*-Tol·+).

6f: IR(KBr) 1550 cm^{-1} (C=N). ^1H NMR 2.36 (s, 6H, $2CH_3$), 2.40 (s, 6H, $2CH_3$(Ts)), 7.10—7.88 (m, 16H, Ar-H). ^{13}C NMR 172.70 (C=N), 21.83(CH_3), 21.64 (CH_3(Ts)). MS *m/z* 544 (vw, M^+), 272 (18, *p*-TolC=NTs·+), 91 (100, *p*-Tol·+).

6h: IR(KBr) 1585 and 1550 cm^{-1} (C=N). ^1H NMR 2.34 (s, CH_3), 2.37 (s, 6H, $2CH_3$(Ts)), 3.76 (s, 3H, OCH_3), 6.66—7.90 (m, 16H, Ar-H). ^{13}C NMR 172.79, 171.73 (C=N), 55.55 (OCH_3), 21.74 (CH_3), 21.59 (CH_3(Ts)). MS *m/z* 560 (vw, M^+), 288 (22, *p*-CH_3OC=NTs·+), 272 (8, *p*-TolC=NTs·+), 91 (100, *p*-Tol·+).

1-Phenyl-2-(p-methoxyphenyl)-2-tosylimino-1-ethanethione (7c): Blue oil, IR(neat) 1535 (C=N), 1315, and 1150 (SO_2) cm^{-1}. ^1H NMR ($CDCl_3$) 2.35 (s, 3H, CH_3(Ts)), 3.70 (s, 3H, OCH_3), 6.7—8.0 (m, 12H, Ar-H). ^{13}C NMR ($CDCl_3$) 235.52 (C=S), 175.94 (C=N), 55.49 (OCH_3), 21.50 (CH_3(Ts)). MS *m/z* 409 (2%, M^+), 288 (3, M^+—PhCS), 254 (56, M^+—Ts), 121 (100, PhCS·+).

1-p-Tolyl-2-phenyl-2-tosylimino-1-ethanethione (7e): Blue oil, IR (neat) 1560 (C=N), 1330 and 1160 (SO_2) cm^{-1}. ^1H NMR ($CDCl_3$) 2.35 (s, 3H, CH_3), 2.39 (s, 3H, CH_3(Ts)), 7.1—7.9 (m, 13H, Ar-H). ^{13}C NMR ($CDCl_3$) 233.35 (C=S), 176.18 (C=N), 21.96 (s, CH_3), 21.55 (s, CH_3(Ts)). MS *m/z* 393 (3, M^+), 238 (10, M^+—Ts), 135 (100, *p*-TolCS·+).

[*B*] *Isolation of 1,2-Diaryl-2-tosylimino-1-ethanethione S-Tosylimides **3b**, c.* To a solution of **2** (3.0 mmol) in benzene (50 cm^3) was added dropwise a solution of **1** (6.6 mmol) in benzene (10 cm^3) with stirring at 10—15 °C. The reaction mixture was stirred for 5—10h at room temperature until the materials were consumed (TLC). Evaporation of the solvent without heating and column chromatography (silica gel, 1/50 ethyl acetate/benzene) of the residue gave **3** as orange-red oil in 70—79% yields. The isolated thione *S*-imides **3b**,c (2 mmol) were heated at reflux in 50 cm^3 of benzene for 16—18 h. The work-up as described in the procedure A gave **5b** (40% yield) and **6b** (5% yield) or **5c** (40%) and **6c** (2%) along with **7b**,**c** (trace).

3b: IR($CHCl_3$) 1550 (C=N), and 990 (CSN) cm^{-1}. ^1H NMR ($CDCl_3$) δ=2.37 (s, 6H, $2CH_3$), 2.42 (s, 3H, CH_3), 7.06—7.86 (m, 17H, Ar-H). ^{13}C NMR ($CDCl_3$) δ=176.28 (C=N), 167.22 (CSN), 146.26—125.06, 21.74, 21.54, and 21.35 (CH_3).

3c: IR(KBr) 1550 (C=N), and 990 (CSN) cm^{-1}. ^1H NMR ($CDCl_3$) δ=2.30 (s, 3H, CH_3), 2.36 (s, 3H, CH_3), 3.74 (s, 3H, OCH_3), 6.62—7.78 (m, 17H, Ar-H). ^{13}C NMR ($CDCl_3$) δ= 176.60 (C=N), 166.27 (CSN), 165.15—114.66, 55.60 (OCH_3), 21.49 (CH_3), 21.25 (CH_3).

[*C*] *Thermolysis of 5c.* When the adduct **5c** (1.6 mmol) was heated at 112°C in xylene (75 cm^3)-benzene (35 cm^3), orange-colored **3c** appeared and was identified by TLC. After heating for 28 h, the usual work-up and column chromatography of the reaction mixture gave **6c** (19% yield), **7c** (2% yield) and an unidentified colorless oil.

[*D*] *Reaction of 3c with Triphenylphosphine.* To a benzene solution (40 cm^3) of **3c** (2.0 mmol) was added a benzene solution (10 cm^3) of triphenylphosphine (2.1 mmol) in a cold bath. After stirring at room temperature for 12 h, removal of the solvent and column chromatography (silica gel, benzene→ethyl acetate) of the residue gave 0.3 g of **7c** (37% yield), 0.31 g of **8** (36%), 0.20 g of **9** (35%), and 0.22 g of **10c** (17%).

10c: Colorless crystals, mp 248—251°C. IR(KBr) 1610, 1440, 1390, 1140, and 1090 cm^{-1}. ^1H NMR ($CDCl_3$) δ=2.21 (s, 3H, CH_3(Ts)), 3.62 (s, 3H, OCH_3), 6.5—7.6 (m, 28H, Ar-H). ^{13}C NMR ($CDCl_3$) δ=171.36 (d, J_{C-P}=7.3 Hz, C=N), 82.48 (d, J_{C-P}=101.3 Hz, C=P), 54.87 (OCH_3), 21.20 (CH_3(Ts)). MS *m/z* 639 (9, M^+), 484 (34, M^+—Ts), 262 (4, PPh_3), 222 (100, M^+—Ts-PPh_3).

[*E*] *Reaction of 5c with Triphenylphosphine.* To a solution of **5c** (1.2 mmol) in chloroform (5 cm^3) was added a benzene solution (35 cm^3) of an equimolar amount of triphenylphosphine. The reaction mixture was heated at reflux for 22 h. After cooling to room temperature, the precipitate (partial **5c**) was filtered. The work-up of the filtrate in the same manner as described in the procedure D gave **7c** (trace), **8** (5%), **9** (28%), **10c** (40%), *p*-toluenesulfonamide, and 46% (total)-recovered **5c**.

[*F*] *Reaction of C=C-conjugated Ylides 11 with N-Sulfinyl-p-toluenesulfonamide (2).* To a partial suspension of **11b** (1.24 g, 2.74 mmol) in benzene (30 cm^3) was added a benzene solution (20 cm^3) of **2** (0.71 g, 3.3 mmol) at temperatures of 10—15°C. The resulted reaction mixture was warmed for 10 min until the solution turned clear. The solvent was evaporated and the residue was recrystallized from dichloromethane-diethyl ether to give **14** in a 45% yield.

14: Yellow needles, mp 204—205°C. IR(KBr) 1600 and 1560 (C=N) cm^{-1}. ^1H NMR ($CDCl_3$) δ=2.44 (s, 3H, CH_3(Ts)), 7.06 (d, *J*=10 Hz, 1H, =CH-), 7.12—7.96 (m, 12H, Ar-H), 9.68 (d, *J*=10 Hz, 1H, -CH=N-). MS *m/z* 359 (4, M^+), 204 (100, M^+—Ts), 91 (24, Tol^+). Found: C, 73.55; H, 4.81; N, 3.92%. Calcd for $C_{22}H_{17}O_2NS$: C, 73.51; H, 4.77; N, 3.90%.

[G] *Reaction of N=C-conjugated Ylides 16 with N-Sulfinylamines (2) and Sulfur Dioxide.* To a benzene solution (25 cm^3) of **16** (4.55 mmol) was added dropwise a benzene solution (10 cm^3) of **2** (4.51 mmol) at temperatures of about 10°C. The orange suspension turned to a clear solution. The reaction mixture was very hygroscopic. On standing in the air it hydrolyzes to form white crystals **18**, which were filtered off and washed with benzene.

18a: White needles, mp 133—135°C (dec). IR(KBr) 1570 (C=N), 1440 (P-C), and 1260 (SO_2) cm^{-1}. MS *m/z* 455 (58, M^+—SO_2), 378 (12, M^+—SO_2-Ph), 262 (100, Ph_3P).

18b: White needles, mp 252—254°C. IR(KBr) 1660 (C=N), 1445 (P-C), and 1265 (SO_2) cm^{-1}. MS *m/z* 587 (36, M^+—SO_2), 496 (100, M^+—SO_2-CH_2Ph), 262 (30, Ph_3P). Dry sulfur dioxide gas was bubbled into a benzene solution (20 cm^3) of **16** (2.0 mmol). After 2h orange suspension turned to a white suspension. The precipitate was collected by filtration to give **18a, b**, which were identical with the products obtained above.

[*H*] *Conversion of 18a to 16a by Base.* A suspended mixture of **18a** (0.52 g, 1.0 mmol) and potassium *t*-butoxide (0.62 g, 2.0 mmol) in benzene (20 cm^3) was stirred for 3 h. Removal of the solvent and extraction of the residue by chloroform gave **16a** in an 89% yield (recrystallized from chloroform-petroleum ether).

The authors wish to express their thanks to Professor Binne Zwanenburg of University of Nijmegen for his helpful discussions and revising manuscript.

References

1) T. Saito, N. Shibahara, and S. Motoki, *Tetrahedron Lett.*, **24**, 4435 (1983).
2) T. Saito and S. Motoki, *J. Org. Chem.*, **42**, 3922 (1977).
3) Even in the reactions of equimolar amounts of **1** and **2**, there was no difference of the products (**5**—**7**) but decreases in yields of **5** and **6**.
4) The blue substances were **7**, though only **7c,e** were identified spectroscopically. The first isolation of this type of a compound, 1,2-diphenyl-2-tosylimino-1-ethanethione (**7a**), has been reported very recently; U. Zoller, *J. Org. Chem.*, **50**, 1107 (1985).
5) S. Tamagaki, K. Sakaki, and S. Oae, *Bull. Chem. Soc. Jpn.*, **46**, 2608 (1973).
6) B. Zwanenburg, *Recl. Trav. Chim. Pays-Bas*, **101**, 1 (1982).
7) W. Brügel, "Handbook of NMR Spectral Parameters," Heydon & Son, London (1979), Vol. 1, p. 138.
8) "International Tables for X-Ray Crystallography," Kynoch Press, Birmingham, (1974) Vol. IV.
9) T. Sakurai and K. Kobayashi, *Rikagaku Kenkyusho Hokoku*, **55**, 69 (1979).
10) C. K. Johnson, ORTEP. "Oak Ridge Thermal Ellipsoid Plot Plogram," ORNL-3794, Oak Ridge National Laboratory, Oak Ridge, TN (1965).
11) G. Kresze and W. Wucherpfennig, *Angew. Chem., Int. Ed. Engl.*, **6**, 149 (1967).
12) H. Bestmann and B. Arnason, *Chem. Ber.*, **95**, 1513 (1962).
13) H. Fischer and H. Fischer, *Chem. Ber.*, **99**, 658 (1966).
14) H. Yoshida, T. Ogata, and S. Inokawa, *Bull. Chem. Soc. Jpn.*, **50**, 3315 (1977); R. Huisgen and J. Wulff, *Tetrahedron Lett.*, **1967**, 917.
15) P. Main, S. E. Hull, L. Lessinger, G. Germain, J.-P. Declercq, and M. M. Woolfson, "MULTAN. A Program for the Automatic Solution of Crystal Structures from X-Ray Diffraction Data," Univ. of York, England, and Louvain, Belgium (1978).

Optical Resolution of β-Hydroxynorvaline

Masaki YAMADA† and Kenji OKAWA*
Department of Chemistry, Faculty of Science, Kwansei Gakuin University, Nishinomiya 662
(Received June 14, 1985)

β-Hydroxy-DL-norvaline(HyNva) was successfully separated into its diastereoisomers by fractional crystallization from 2-propanol as *p*-toluenesulfonic acid(TsOH) salts. The two racemic diastereoisomers were resolved into four stereoisomers by Vogler's method, using diastereomers of the *N*-benzyloxycarbonyl DL-amino acid and L-tyrosine hydrazide.

β-Hydroxy-DL-norvaline (HyNva) is very useful as a threonine analogue[1] and is needed as a starting material in the synthesis of Actinomycin D analogues. However, optical resolution of the four isomers of HyNva had not been achieved. In the present study, we attempted to separate and optically resolve HyNva into its four stereoisomers.

HyNva was prepared by the condensation reaction of copper(II) glycinate with propionaldehyde, by a method originally proposed by Akabori, Okawa.[2] This method usually gives a mixture of two diastereoisomers, which is difficult to separate. Y. Ariyoshi *et al.*[3] did report separating HyNva into diastereoisomers, but the reagents used were not accessible. In the present study, we found that the *erythro*- and *threo*-forms of HyNva could be easily isolated as the TsOH salts by partial recrystallization from 2-propanol. The configurational assignment of HyNva was done by paper chromatography[4] and 60 MHz ^{1}H-NMR spectroscopy in aqueous solutions.[3] The ratio of the *erythro*- and *threo*-forms of synthetic HyNva was found to be 40:60 by HPLC analysis.[5]

Optical resolution of the two racemic compounds was attempted. First, enzymatic reaction was tried for the *threo*-form, but *N*-acetyl-HyNva(DL-*threo*) could not be resolved using aminoacylase in aqueous solution (pH=6.8). Using Vogler's method,[6] we were able to resolve the DL-*threo* (**Ia**) and DL-*erythro* (**Ib**) forms using the diastereomers of the *N*-benzyloxycarbonyl DL-amino acid (**III**) (**IV**) and L-tyrosine hydrazide. (Fig. 1).

Four stereoisomers were obtained and reduced by catalytic hydrogenation to obtain free HyNva (**Ia$_1$**) (**Ia$_2$**) (**Ib$_1$**) (**Ib$_2$**). The melting points and specific rotations of these isomers are summarized in Table 1.

The configuration of the α-carbon atom was elucidated by optical rotatory dispersion (ORD) spectroscopy in hydrochloric acid solutions (pH=1).[7] The ORD spectra of **Ia$_2$** and **Ib$_2$** exhibited a positive Cotton effect (positive absorption peaks at 225 nm), showing

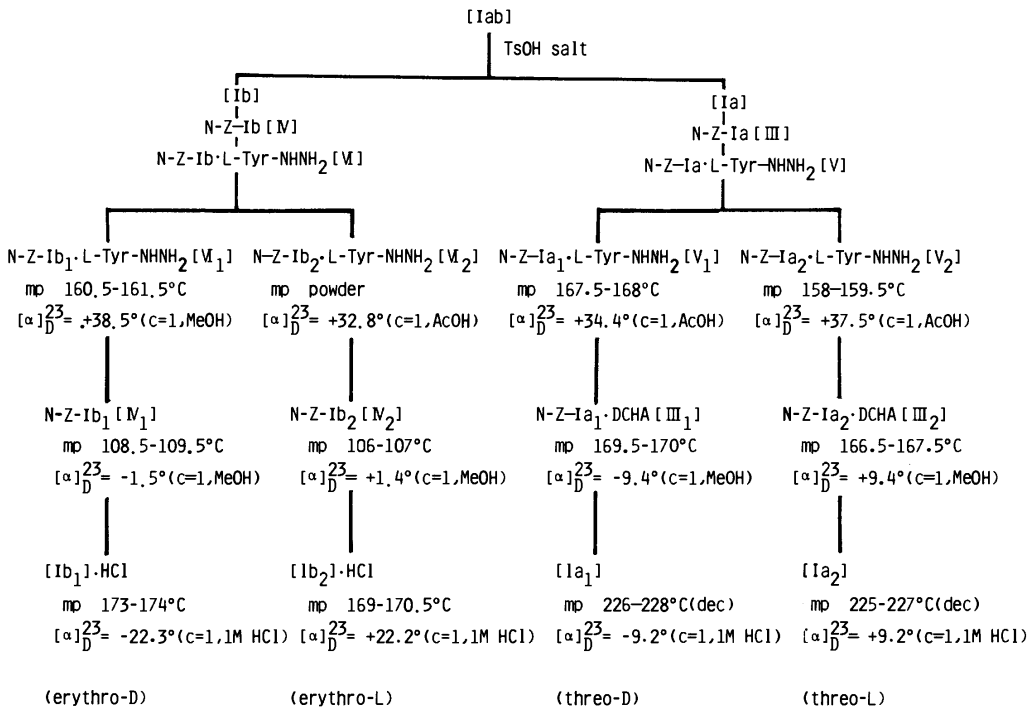

Fig. 1.

†Present address: Organic Chemistry Research Laboratory of Tanabe Seiyaku Co., Ltd., 2-2-50, Kawagishi, Toda 335.

TABLE 1. MELTING POINTS AND SPECIFIC ROTATION DATA

Form			Mp θ_m/°C	$[\alpha]_D^{23}$ °(c=1, 1M HCl)
threo	**Ia**$_1$	D	226—228(dec)	−9.2
	Ia$_2$	L	225—227(dec)	+9.2
erythro*	**Ib**$_1$	D	173—174	−22.3
	Ib$_2$	L	169—170.5	+22.2

*Hydrochloride.

these compounds to be of the L-form. **Ia**$_1$ and **Ib**$_1$ displayed a negative Cotton effect (negative absorption peak at 225 nm), which showed that they were of the D-form.

Experimental

β-Hydroxynorvaline (Iab). **Iab** was prepared by the glycine-copper method in 44% yield, mp 197—198°C (dec) Found: C, 44.91; H, 8.33; N, 10.46%. Calcd for $C_5H_{11}O_3N$: C, 45.10; H. 8.33; N, 10.52%.

Separation of Diastereomers. A suspension of **Iab** (7.4 g, 5.6 mmol) in methanol (100 ml) was added to a methanol solution of TsOH (10.7 g, 5.6 mmol) and the solvent was removed *in vacuo*. Crystals of **Iab** TsOH salt were obtained in *ca.* 100% yield and subjected to fractional crystallization from hot 2-propanol. The first crystals of **Ib** TsOH salt (6.4 g, 35%) were removed by filtration and **Ia** TsOH salt (6.5 g, 36%) was obtained from the filtrate. Both of amino acid TsOH salts were decomposed with the pyridine-methanol solution, and recrystallization from hot water gave **Ia** [mp 215—217°C(dec)] and **Ib** [mp 241—242°C(dec)] in quantitative yields.

N-Benzyloxycarbonyl-Ia (III). **III** was prepared from **Ia** and benzyloxycarbonyl chloride by the usual method in 85% yield as a syrup.

L-Tyrosine Hydrazide Salt of III (V). L-Tyrosine hydrazide (26.3 g, 0.14 mol) was added to a solution of **III** (36 g, 0.14 mol) in methanol (250 ml), and the solution was warmed at 65°C. After removal of the insoluble material, the solution was concentrated, and addition of tetrahydrofuran gave **V** in quantitative yield (62 g).

Resolution of Racemic III. A solution of **V** (62 g, 0.14 mol) in methanol (200 ml) was warmed at 65°C. The first crop (**V**$_1$) of **V** crystallized on cooling (18.5 g, 72%). $[\alpha]_D^{23}$=+34.4° (c 1.0, AcOH), mp 167.5—168°C. The mother solution was concentrated and the remaining crystals were dissolved in methanol (100 ml). This solution was left at room temperature for 24 h, and a second crop (**V**$_2$) of **V** was obtained (17 g, 64%). $[\alpha]_D^{23}$=+37.3° (c 1.0, AcOH), mp 158—159.5°C. From the mother solution of **V**$_2$, racemic **V** was obtained (8.5 g). Found: **V**$_1$ C, 57.01; H, 6.60; N, 12.09%. **V**$_2$ C, 57.35; H, 6.56; N, 12.12%. Calcd for $C_{22}H_{30}N_4O_7$: C, 57.13; H, 6.54; N, 12.11%.

III$_1$ was obtained from **V**$_1$ by treatment with 3 M[††] hydrochloric acid and purified as the dicyclohexylamine (DCHA) salt. mp 169.5—170°C, $[\alpha]_D^{23}$=−9.4° (c 1.0, MeOH). The DCHA salt of **III**$_2$ was obtained from **V**$_2$ in the same way. mp 166.5—167.5°C, $[\alpha]_D^{23}$=+9.4° (c 1.0, MeOH). Found: **III**$_1$ C, 67.18; H, 8.92; N, 6.29% **III**$_2$ C, 66.75; H, 8.92; N, 6.40%. Calcd for $C_{25}H_{40}O_5N_2$: C, 66.90; H. 8.99; N, 6.24%.

β-Hydroxynorvaline Ia$_1$, *Ia*$_2$. The mixture of **III**$_1$, palladium black and hydrochloric acid was stirred for 3 h at room temperature under bubbling with hydrogen gas. After removal of the catalyst, the solution was neutralized and concentrated under reduced pressure, giving **Ia**$_1$. Mp 226—228°C (dec), $[\alpha]_D^{23}$=−9.2° (c 1.0, 1 M HCl) **Ia**$_2$ was obtained by the catalytic hydrogenation described above. mp 225—227°C (dec), $[\alpha]_D^{23}$=+9.2°(c 1.0, 1 M HCl). Found: **Ia**$_1$ C, 45.10; H, 8.33; N, 10.52% **Ia**$_2$ C, 44.93; H, 7.99; N, 10.50%. Calcd for $C_5H_{11}O_3N$: C, 44.73; H, 8.30; N, 10.66%.

β-Hydroxynorvaline Ib$_1$, *Ib*$_2$. The *erythro*-form of HyNva (**Ib** series) was obtained like the *threo*-form of HyNva (**Ia** series) and **Ib**$_1$, **Ib**$_2$ were also obtained.

[Ib$_1$]·HCl $[\alpha]_D^{23}$=−22.3° (c 1.0, 1 M HCl), mp 173—174°C, [Ib$_2$]·HCl $[\alpha]_D^{23}$=+22.2° (c 1.0, 1 M HCl), mp 169—170.5°C, Found: [Ib$_1$]·HCl C, 35.04; H, 6.90; N, 8.13; Cl, 21.11%, [Ib$_2$]·HCl C, 34.87; H, 6.97; N, 8.28; Cl, 19.60%. Calcd for $C_5H_{12}O_3HCl$: C, 35.41; H, 7.13; N, 8.26; Cl, 20.90%.

The authors wish to thank Dr. T. Yamada, Konan University, for the HPLC analytical data; Dr. M. Fujino, Takeda Chemical Industries, Ltd., for the ORD spectra data; and Miss T. Higashino and Miss N. Okinaka for their assistance with the experimental work.

References

1) I. Shiio, R. Miyajima, and S. Nakanori, *J. Biochem.*, **68**, 859 (1970).
2) M. Sato, K. Okawa, and S. Akabori, *Bull. Chem. Soc. Jpn.*, **30**, 937 (1957).
3) Y. Ariyoshi and N. Sato, *Bull. Chem. Soc. Jpn.*, **44**, 3435 (1971).
4) K. Schaw and S. Fox, *J. Am. Chem. Soc.*, **75**, 3421 (1953).
5) T. Yamada, unpublished data.
6) K. Vogler and P. Lanz, *Helv. Chim. Acta.*, **49**, 1348 (1966).
7) J. C. Craig and S. K. Roy, *Tetrahedron*, **1965**, 391.

[††] 1M=1 mol dm^{-3}.

 © 1985 The Chemical Society of Japan Bull. Chem. Soc. Jpn., 58, 2891—2899 (1985)

Reactions of NH Radicals. IV. Photolysis of HN_3 in the Presence of CH_4 at 313 nm

Sukeya KODAMA*

Department of Applied Chemistry, College of Engineering, University of Osaka Prefecture, Sakai, Osaka 591

(Received September 5, 1983)

The photolysis of HN_3 vapor in the presence of CH_4 was studied at 313 nm, 30 °C, and a low light intensity. The reaction products were N_2, H_2, NH_4N_3, $CH_3NH_2 \cdot HN_3$, and CH_3N_3. CH_3 radicals were also detected as intermediates. The quantum yields of these products were measured as a function of the CH_4 and HN_3 pressures. The following mechanisms for the main reactions were proposed: $HN_3+h\nu(313\,nm) \rightarrow N_2+NH(a^1\Delta)$; $NH(a^1\Delta)+HN_3 \rightarrow 2N_2+2H$(2a); $NH(a^1\Delta)+HN_3 \rightarrow N_3+NH_2$ (2b); $NH(a^1\Delta)+HN_3 \rightarrow N_2+N_2H_2^*$ (2c); $NH(a^1\Delta)+CH_4 \rightarrow CH_3NH_2^*$ (3); $NH(a^1\Delta)+CH_4 \rightarrow NH(X^3\Sigma^-)+CH_4$ (4); $CH_3NH_2^* \rightarrow H+CH_2NH_2$ or CH_3NH (5); $CH_3NH_2^* \rightarrow CH_3+NH_2$ (6). The rate-constant ratios at 30°C were: $k_3/k_2=0.175$; $k_4/k_2=0.177$; $k_6/k_5=0.133$. The collisional deactivation of $CH_3NH_2^*$ was not found in the total pressure range, from 6.4 to 24.3 kPa.

The photolysis of HN_3 in the presence of Xe,[1] C_2H_6,[2] and C_2H_4[3] at 313 nm has been studied previously, and the following facts were found: HN_3 is a useful source for the first excited singlet, NH ($a^1\Delta$); ethylamine is produced by the insertion of NH ($a^1\Delta$) into a C–H bond of C_2H_6, and the reactions of NH ($a^1\Delta$) with HN_3 and C_2H_4 having the π bond are much faster than that with C_2H_6 consisting of only the σ bond.

On the reactions of $NH(a^1\Delta)$ with C_2H_6, the collisional deactivation by C_2H_6 from $NH(a^1\Delta)$ to $NH(X^3\Sigma^-)$ was also found.[2] Therefore, it is of interest to compare these reactions between saturated hydrocarbons for the insertion and collisional deactivation reactions. In this work, methane, which is the simplest hydrocarbon, was chosen as the reactant.

On the reactions of NH with CH_4, Miller[4] has found N_2, H_2, and NH_4N_3 as the main products, with HCN and C_2H_6 as minor products, in the photolysis of HN_3 with CH_4. However, the formation of $CH_3NH_2 \cdot HN_3$ could not be found in the mass-spectrometric analysis. Cornell *et al.*[5] have studied the flash and steady photolyses of $HN_3(DN_3)$ with hydrocarbons including methane. They have found that the principal nitrogen-containing products are HCN and alkanenitriles in the steady state photolysis. Richardson and Setser[6] have studied the thermal decomposition of HN_3 in the presence of CH_4 and other hydrocarbons over the temperature range of 285—470°C. They have found N_2, NH_3, and a nonvolatile polymer as the products in the HN_3 and CH_4 system. However, the formations of H_2, CH_3NH_2, and N_2H_4 were negative in the mass-spectrometric and gas-liquid chromatographic analyses. Thus, they have concluded that the pyrolysis of HN_3 is not a good source of NH.

It appears to be significant to compare the insertion efficiencies of $NH(a^1\Delta)$ into C–H bonds of simple saturated hydrocarbons, the collisional spin-relaxation efficiencies of $NH(a^1\Delta)$ by such hydrocarbons, and the unimolecular decomposition rates of the alkylamines formed by the insertion reactions. From such a standpoint, the reaction mechanism and rates of the photolysis of HN_3 in the presence of CH_4 were investigated in this work to continue the study with C_2H_6.[2]

Experimental

The methane, obtained from the Takachiho Chemical Co., was 99.8% pure. It was purified each time before use by condensation and evacuation at −196°C and the temperature of solid nitrogen (about −220°C). The preparation and purification of HN_3, like the apparatus and procedure used for the reaction, were the same as those described previously.[1,2] All the runs in this work were carried out at 313 nm and 30°C. The light intensity was reduced with a screen to suppress any radical–radical reactions. The irradiation time was 90 min, and the degree of conversion of HN_3 was less than 4% for all the runs.

The reaction products were N_2, H_2, NH_4N_3, $CH_3NH_2 \cdot HN_3$, and CH_3N_3. The formation of CH_3N_3, passing through a Dry Ice–acetone trap, was found by gas-chromatographic analysis using a Silicone SE-30 column.[3] No HCN was detected by the pyridine-pyrazolone method.[7]

In order to inspect the radical intermediates, the products of the photolysis of HN_3 with CH_4 and NO were analysed by gas chromatography using an 1-m column of Silicone SE-30 at room temperature. Similarly, the products of the photolysis of $CH_3N_2CH_3$ with NO or NO_2 were also analysed gas-chromatographically where the same conditions. The retention times of the two peaks of the former products were in accord with those of the latter products. This suggests the formation of CH_3 radicals as intermediates.

For the identification of NH_4N_3 and $CH_3NH_2 \cdot HN_3$, the volatile, white products trapped at the temperature of Dry Ice–acetone were analyzed by means of a mass spectrometer (Hitachi RMU6E); the spectrum is shown in Fig. 1. The peaks of m/z=17, 18, 30, 31, 42, 43, and 57 correspond to NH_3^+, NH_4^+, $CH_2NH_2^+$ or CH_3NH^+, $CH_3NH_2^+$, N_3^+, HN_3^+, and $CH_3N_3^+$ respectively. However, the parent peaks of NH_4N_3 (m/z=60) and $CH_3NH_2 \cdot HN_3$ (m/z=74) were not found, although a low ionizing voltage of 15 V was applied. On the other hand, the volatile, white products were introduced into a solid-sodium-hydroxide column to remove the HN_3.[2] A mass spectrum of the HN_3-removed products at the ionizing voltage of 17 V is shown in Fig. 2. The peaks of m/z=17 and 31 indicate the molecular ions of NH_3 and CH_3NH_2 respectively. Thus, the formation of $CH_3NH_2 \cdot HN_3$ and NH_4N_3 was verified.

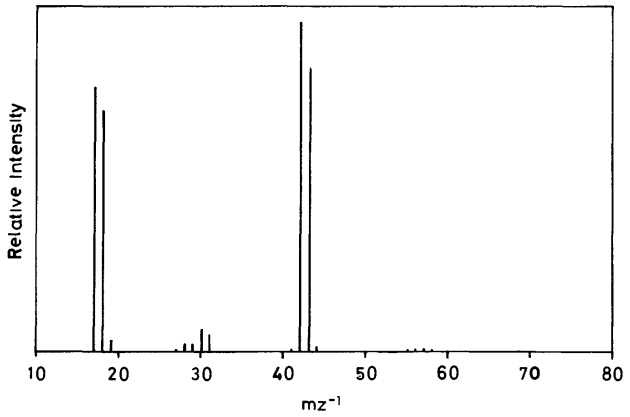

Fig. 1. Mass spectrum of the products trapped at the Dry Ice-acetone temperature. The ionizing voltage is 15 V.

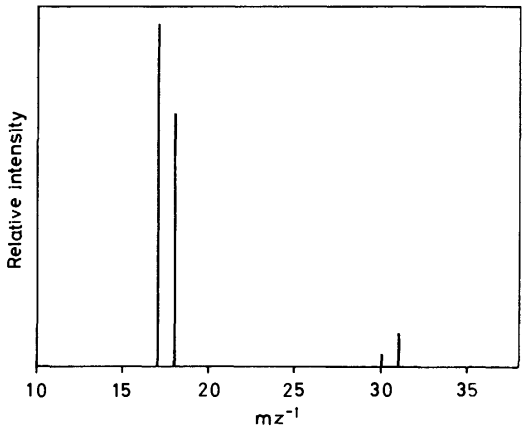

Fig. 2. Mass spectrum of the substances removed HN_3 from the products trapped at the Dry Ice-acetone temperature. The ionizing voltage is 17 V.

The HN_3-removed products were also subjected to gas-chromatographic analysis at 10°C using a 2-m column of KOH(5%)-paraffin liquid(20%) coated on Chromosorb WAW. The formation of CH_3NH_2 was thus confirmed. However, little CH_3NH_2 was formed in the presence of a small amount of NO.

On the quantitative analyses of N_2, H_2, NH_4N_3, and $CH_3NH_2 \cdot HN_3$, the reaction products were separated at the temperatures of solid nitrogen and Dry Ice-acetone. The gases passing through the trap at −220°C are N_2, H_2, and a part of the CH_4 used as the reactant. The separation of H_2 from the mixture was carried out using a silica-gel column at −196°C.[1] The separation of N_2 and CH_4 was achieved by gas chromatography using a 5A molecular-sieve column.[2]

NH_4N_3 and $CH_3NH_2 \cdot HN_3$, condensed at the temperature of Dry Ice-acetone, were introduced into a CuO column at about 550°C. The amounts of N_2, NO, N_2O, and CO_2 formed as combustion products were determined by the method described previously.[2] The amounts of $CH_3NH_2 \cdot HN_3$ and NH_4N_3 can be calculated from those equations: $[CH_3NH_2 \cdot HN_3]=[CO_2]$ and $[NH_4N_3]=([N_2]+[N_2O])/2+[NO]/4-[CO_2]$.

The quantum yields of the reaction products were determined using HN_3 as an actinometer.[1]

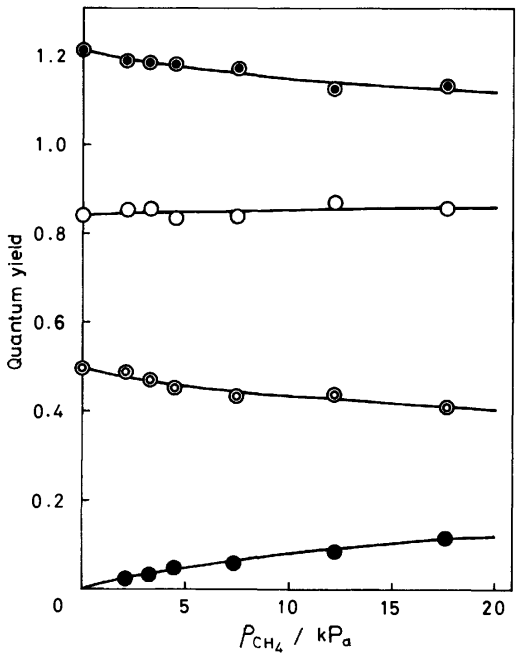

Fig. 3. Results of the photolysis of HN_3 of 6.67 kPa, measured as a function of CH_4 pressure at 313 nm, 30°C, and the low absorbed light intensity of 4.45×10^{14} quanta s^{-1}. ⊙, $\phi_{N_2}/4$; ○, $\phi_{NH_4N_3}$; ◎, ϕ_{H_2}; ●, $\phi_{CH_3NH_2 \cdot HN_3}$.

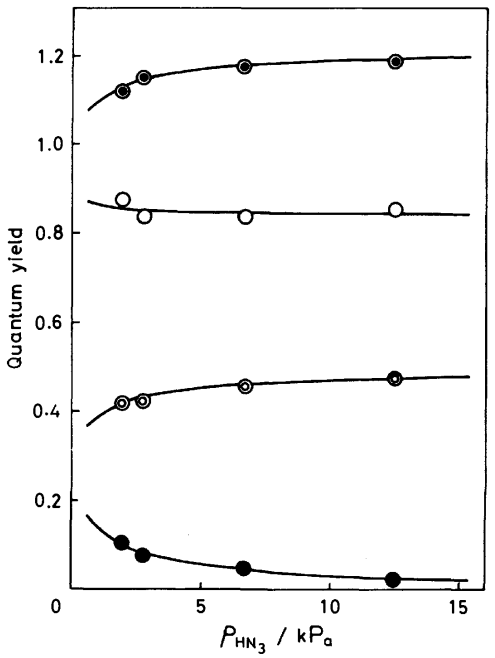

Fig. 4. Results of the photolysis measured as a function of HN_3 pressure at 4.44 kPa of CH_4, 30°C, 313 nm, and the incident light intensity of 3.83×10^{15} quanta s^{-1}. ⊙, $\phi_{N_2}/4$; ○, $\phi_{NH_4N_3}$; ◎, ϕ_{H_2}; ●, $\phi_{CH_3NH_2 \cdot HN_3}$.

Results

The results of the photolysis of HN_3 of 6.67 kPa, measured as a function of the CH_4 pressure at 313

nm and at 30°C, and the absorbed-light intensity of 4.45×10^{14} quanta s^{-1} are shown in Fig. 3. It may be seen in Fig. 3 that ϕ_{N_2} and ϕ_{H_2} decrease, but $\phi_{CH_3NH_2\cdot HN_3}$ and $\phi_{NH_4N_3}$ increase, as the CH_4 pressure increases.

Figure 4 shows the results of the photolysis measured as a function of the HN_3 pressure at 4.44 kPa of CH_4, 30°C, 313 nm, and at the incident-light intensity of 3.83×10^{15} quanta s^{-1}. In Fig. 4, it is found that ϕ_{N_2} and ϕ_{H_2} increase, but $\phi_{NH_4N_3}$ and $\phi_{CH_3NH_2\cdot HN_3}$ decrease, with an increase in the HN_3 pressure.

Discussion

Reaction Mechanism. On the basis of the experimental results in this work and in the light of the results achieved by previous investigators, the following reaction mechanism is postulated for the photolysis of HN_3 vapor in the presence of CH_4, where A and M denote HN_3 and CH_4 molecules respectively:

$$A + h\nu(313\,nm) \longrightarrow N_2 + NH(a^1\Delta) \quad (1)$$

$$NH(a^1\Delta) + A \longrightarrow 2N_2 + 2H \quad (2a)$$

$$NH(a^1\Delta) + A \longrightarrow N_3 + NH_2 \quad (2b)$$

$$NH(a^1\Delta) + A \longrightarrow N_2 + N_2H_2^* \quad (2c)$$

$$NH(a^1\Delta) + M \longrightarrow CH_3NH_2^* \quad (3)$$

$$NH(a^1\Delta) + M \longrightarrow NH(X^3\textstyle\sum^-) + M \quad (4)$$

$$CH_3NH_2^* \longrightarrow H + CNH_4 \quad (5)$$

$$CH_3NH_2^* \longrightarrow CH_3 + NH_2 \quad (6)$$

$$CNH_4 + A \longrightarrow CH_3NH_2 + N_3 \quad (7)$$

$$CNH_4 + A \longrightarrow CH_3N_3 + NH_2 \quad (8)$$

$$CH_3 + A \longrightarrow CH_4 + N_3 \quad (9)$$

$$CH_3NH_2 + A \longrightarrow CH_3NH_2\cdot HN_3. \quad (10)$$

The succeeding reactions for species consisting of only nitrogen and hydrogen atoms are as follows:[1] $NH(X^3\textstyle\sum^-)+A\rightarrow H_2+2N_2$ (11); $NH(X^3\textstyle\sum^-)+A\rightarrow NH_2+N_3$ (12); $H+A\rightarrow H_2+N_3$ (13); $H+A\rightarrow NH_2+N_2$ (14); $N_2H_2^*\rightarrow N_2H_2^{**}$ (15); $N_2H_2^*+A\rightarrow N_2+H_2+A$ (16); $N_2H_2^*+A\rightarrow NH_3+2N_2$ (17); $N_2H_2^{**}+A\rightarrow NH_3+2N_2$ (18); $NH_2+A\rightarrow NH_3+N_3$ (19); $NH_3+A\rightarrow NH_4N_3$ (20); $N_3+A\rightarrow N_3\cdot A$ (21); $2N_3\cdot A\rightarrow 3N_2+2A$ (22).

Since the formation of methylamine has been confirmed by the mass-spectrometric and gas-chromatographic measurements, it is clear that the first excited singlet, NH($a^1\Delta$), formed by the photolysis of HN_3 at 313 nm[1] reacts to give methylamine by insertion into a C–H bond of CH_4, just as in the case where the formation of $C_2H_5NH_2$ was found in the photolysis of HN_3 with C_2H_6.[2] Reaction 4 is a collisional spin-relaxation process by CH_4 from NH($a^1\Delta$) to NH($X^3\textstyle\sum^-$), as was found for Xe[1] and C_2H_6.[2]

Since the enthalpy change of Reaction 3 is −459.8 kJ mol^{-1}, Reactions 5 and 6 are energetically possible. The unimolecular decompositions of CH_3NH_2* to give $2H_2$+HCN, CH_2+NH_3, and H_2+CH_2=NH are also energetically possible. However, these reactions can probably be excluded for the following reasons: No HCN was detected; the formation of C_2H_6 by the insertion reaction, $CH_2+CH_4\rightarrow C_2H_6$, was not observed, and the detachment of H_2 from CH_3NH_2* by the molecular mechanism was not found in the reaction kinetics to be discussed later. Reactions other than those described above are not energetically possible for the unimolecular decompositions of CH_3NH_2*, judging from the standard heats of formation listed in Table 1.

For the CNH_4 formed by Reaction 5, two structures of CH_2NH_2 and CH_3NH are possible. Hadley and Volman[8] have found, by means of the ESR method, that the major radical formed by the photolysis of methylamine in a solid matrix at 184.9 nm is CH_3NH. Hatano *et al.*[9] have also found, by a ESR study that CH_3NH is preferentially formed in the photolysis, by the use of low-pressure mercury lamp, of methylamine adsorbed on the surface of the porous Vycor glass at 77 K. On the photolyses of CD_3NH_2 vapor at 184.9, 147.0, and 123.6 nm, the formations of both CD_2NH_2 and CD_3NH are considerable, judging from the amounts of H_2, HD, and D_2 formed in the absence and the presence of C_2D_4[10] or NO and O_2.[11] Fukui *et al.*[12] have observed that the production of CH_2NH_2 from methylamine is less than that of CH_3NH upon the electron impact, while the peak of $CD_2NH_2^+$ was much higher than that of CD_3NH^+ in the mass spectrum of CD_3NH_2. On the other hand, according to simple estimations made by the RRK theory,[13] the greater part of the CH_3NH_2* can be expected to decompose to give CH_2NH_2, because the bond-dissociation energy of CH_3NH–H is 19.7 kJ mol^{-1}, higher than that of H–CH_2NH_2.[14] Judging from the results cited above, it seems that both CH_2NH_2 and CH_3NH radicals are formed in Reaction 5.

Reaction 6 is supported by the fact that CH_3 radicals were detected as intermediates. The collisional deactivation of CH_3NH_2* by a third body is negative, because $\phi_{CH_3NH_2\cdot HN_3}$ depends on the concentration ratio $[CH_4]/[HN_3]$, but is independent of the total pressure of CH_4 and HN_3, as will be discussed later. Reaction 7 means that CH_3NH_2 is formed by the hydrogen abstraction of CNH_4 (CH_2NH_2 and CH_3NH) from HN_3. The idea of the existence of CNH_4 radicals is supported by the fact that the formation of CH_3NH_2 is suppressed in the presence of NO. In the same way as has been discussed previously for the succeeding reactions of CH_2NH_2 radicals,[2] Reaction

TABLE 1. STANDARD HEATS OF FORMATION

Species	$\Delta H^\circ_{f,298}$ / kJ mol^{-1}	Ref.	Species	$\Delta H^\circ_{f,298}$ / kJ mol^{-1}	Ref.
H	218.0	a	CH_3	146.9	f
$N(^4S_{3/2})$	474.1	a	CH_4	−74.8	f
$N(^2D_{5/2})$	703.7	a	CN	418.4	f
$NH(X^3\Sigma^-)$	352.2	a	HCN	130.5	f
$NH(a^1\Delta)$	506.6	a	HNC	482.4	g
$NH_2(\tilde{X}^2B_1)$	171.5	a	CH=NH	312	h
NH_3	−46.0	a	CH_2=N	260	i
HN_3	299.8	a	CH_2=NH	94.6	f
$C(^3P_o)$	715.0	b	CH_2NH_2	154.8	j
$C(^1D_2)$	837.0	b,c	CH_3NH	174.5	k
CH	594.1	b	CH_3NH_2	−28.0	f
$CH_2(\tilde{X}^3\Sigma_g^-)$	384.5	d	CH_3N_3	280.3	f
$CH_2(\tilde{a}^1A_1)$	<481	d,e	CH_3-N=CH_2	72.4	f

a: Ref. 1. b: J.A. Kerr, *Chem. Rev.*, **66**, 465 (1966). c: C.E. Moore, "Atomic Energy Levels," Vol. I. National Bureau of Standards, Washington (1949); "Selected Tables of Atomic Spectra," NSRDS-NBS 3, National Bureau of Standards, Washington (1965~). d: W.A. Chupka and C. Lifshitz, *J. Chem. Phys.*, **48**, 1109 (1968). e: G. Herzberg, "Electronic Spectra of Polyatomic Molecules," Van Nostrand, New York (1966). f: Ref. 2. g: Ref. 14a. h: Estimated by assuming that the enthalpy change of the CH_2=NH→H+CH=NH reaction is 435 kJ mol^{-1}. i: Estimated by assuming that the enthalpy change of the CH_3-N=CH_2→CH_3+N=CH_2 reaction is 335 kJ mol^{-1}. j: Ref. 14e. k: Ref. 14b.

8 was introduced for the following reasons: the reaction is energetically possible, and CH_3N_3 was found, but no products other than those described above could be detected.

The possibility of the formation of CH_3NH_2 by means of the cross-combination reaction $CH_3+NH_2\rightarrow CH_3NH_2$ can be excluded, because no C_2H_6 or N_2H_4 (m/z=32) was found to be formed by the self-dimerization reactions of the CH_3 and NH_2 radicals. Miller[4] has found the formation of small amounts of C_2H_6 and HCN in the photolysis of HN_3 with CH_4. The formation of HCN was also observed in the photolysis of HN_3 with C_2H_6 at high light intensities.[2] It seems that these products are formed by these reactions: $2CH_3\rightarrow C_2H_6$ and $CNH_4+N_3\rightarrow HCN+N_2+NH_3$. However, these reactions are negative in the present work, because the photolysis was carried out at a low light intensity and no C_2H_6 and HCN could be detected.

Reaction 9 is a hydrogen-abstraction reaction by CH_3 radicals from HN_3. Konar and Darwent[15] have reported k_9 to be 1.48×10^{-16} cm^{3}molecule^{-1}s^{-1} at 25°C. Creak *et al.*[16] have reported that the specific rate of a hydrogen abstraction reaction by CH_3 radicals from CH_4 is $10^{-11.78}\exp[-62.34(\text{kJ mol}^{-1})/RT]$ cm^3 molecule^{-1}s^{-1}. From both data, it is found that the hydrogen-abstraction reaction from HN_3 is 7.6×10^6 times faster than that from CH_4 at 25°C. On the other hand, Bras and Combourieu[17] have found that the rate constant for the reactions of hydrogen atoms with HN_3 is $10^{-10.60}\exp[-19.25(\text{kJ mol}^{-1})/RT]$ cm^3 molecule^{-1}s^{-1}. Kurylo and Timmons[18] have reported that the specific rate of a hydrogen-abstraction reaction by hydrogen atoms from CH_4 is $10^{-9.94}\exp[-49.37(\text{kJ mol}^{-1})/RT]$ cm^{3}molecule^{-1}s^{-1}. From both results, it is found that the reactions of hydrogen atoms with HN_3, Reactions 13 and 14, is 3.4×10^4 times faster than that with CH_4 at 30°C.

Judging from these results, it seems that the reactions of CH_4 with the CH_3, $NH(X^3\Sigma^-)$, H, NH_2, and N_3 radicals are negligible, and that these radicals disappear upon such reactions with reactive HN_3 as Reactions 9, 11 to 14, 19, 21, and 22. Reactions 10, 15 to 18, and 20 have been discussed previously[1,2] and so are omitted here.

Reaction Kinetics. The following reaction kinetics were formulated to confirm the mechanism of Reactions 1 to 22 and to obtain the rate-constant ratios.

On the quantum yield of $CH_3NH_2\cdot HN_3$, this equation:

$$\frac{1}{\phi_{CH_3NH_2\cdot HN_3}} = \frac{k_5+k_6}{k_5}\frac{k_7+k_8}{k_7}\left(\frac{k_3+k_4}{k_3}+\frac{k_2}{k_3}\frac{[HN_3]}{[CH_4]}\right) \quad \text{(I)}$$

can be derived, where:

$$k_2 = k_{2a} + k_{2b} + k_{2c}.$$

The plot of $1/\phi_{CH_3NH_2\cdot HN_3}$ *vs.* $[HN_3]/[CH_4]$ is shown in Fig. 5.

On the formations of H_2 and $CH_3NH_2\cdot HN_3$, Eq. II can be derived:

$$\frac{\phi_{H_2}}{\phi_{CH_3NH_2\cdot HN_3}} = \frac{k_7+k_8}{k_7}\left(\frac{k_4}{k_3}\frac{k_5+k_6}{k_5}\frac{k_{11}}{k_{11}+k_{12}}+\frac{k_{13}}{k_{13}+k_{14}}\right) + \frac{k_5+k_6}{k_5}\frac{k_7+k_8}{k_7}\left(\frac{2k_{2a}}{k_3}\frac{k_{13}}{k_{13}+k_{14}} + \frac{k_{2c}}{k_3}\frac{k_{16}}{k_{16}+k_{17}+k_{15}/[HN_3]}\right)\frac{[HN_3]}{[CH_4]} \quad \text{(II)}$$

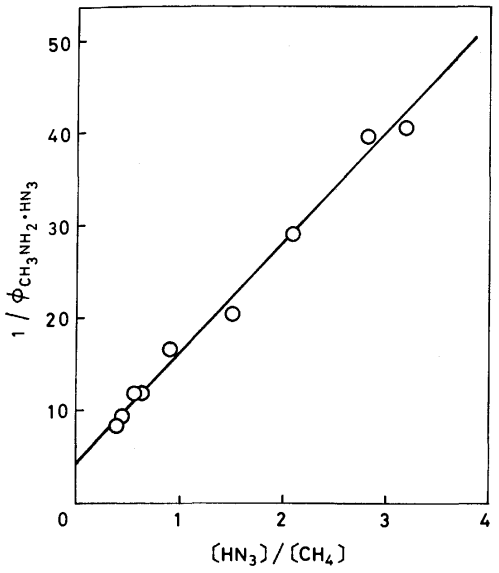

Fig. 5. Plot of $1/\phi_{CH_3NH_2\cdot HN_3}$ *vs.* $[HN_3]/[CH_4]$.

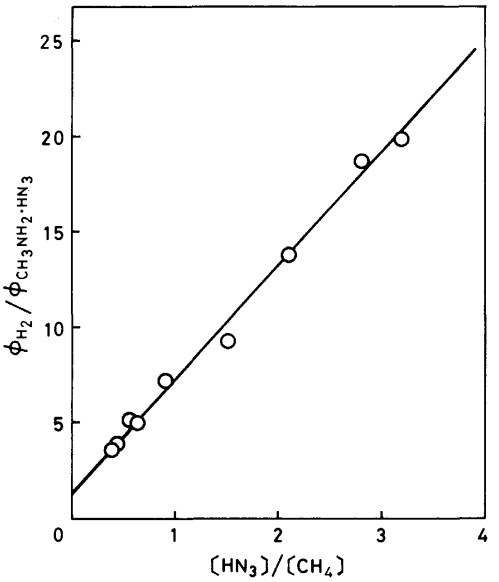

Fig. 6. Plot of $\phi_{H_2}/\phi_{CH_3NH_2\cdot HN_3}$ against $[HN_3]/[CH_4]$.

The plot of $\phi_{H_2}/\phi_{CH_3NH_2\cdot HN_3}$ *vs.* $[HN_3]/[CH_4]$ is shown in Fig. 6.

Equation III can be derived for the formations of N_2, H_2, and $CH_3NH_2\cdot HN_3$:

$$\frac{\phi_{N_2}+\phi_{H_2}}{\phi_{CH_3NH_2\cdot HN_3}} = \frac{k_7+k_8}{k_7}\left(1+4\frac{k_3+k_4}{k_3}\frac{k_5+k_6}{k_5}\right) + 4\frac{k_2+k_{2a}}{k_3}\frac{k_5+k_6}{k_5}\frac{k_7+k_8}{k_7}\frac{[HN_3]}{[CH_4]} \quad \text{(III)}$$

The plot of $(\phi_{N_2}+\phi_{H_2})/\phi_{CH_3NH_2\cdot HN_3}$ *vs.* $[HN_3]/[CH_4]$ is shown in Fig. 7.

By using the values obtained previously[1] of $k_{2a}/k_2=0.336$, $k_{2c}/k_2=0.414$, $k_{12}/k_{11}=3.22$, $k_{14}/k_{13}=1.15$, $k_{15}/k_{16}=2.27\times10^{-7}$ mol cm^{-3}, and $k_{17}/k_{16}=1.19$, the

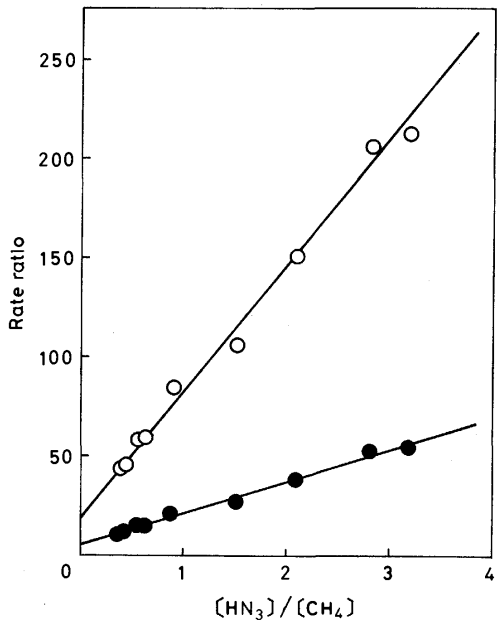

Fig. 7. Plots of $(\phi_{N_2}+\phi_{H_2})/\phi_{CH_3NH_2\cdot HN_3}$ (○) and $(\phi_{NH_4N_3}+\phi_{H_2})/\phi_{CH_3NH_2\cdot HN_3}$ (●) *vs.* $[HN_3]/[CH_4]$. The lower straight line was calculated from Eq. IV using the known rate constant ratios.

values of $k_3/k_2=0.175$, $k_4/k_2=0.177$, $k_6/k_5=0.133$, and $k_8/k_7=0.85$ can be obtained from the intercepts and the slopes in Figs. 5, 6, and 7. As to the value of k_8/k_7, a value similar to that for CH_2NH_2 radicals[2] was obtained.

In order to verify the rate-constant ratios obtained above, Eq. IV was derived for the formations of NH_4N_3, H_2, and $CH_3NH_2\cdot HN_3$:

$$\frac{\phi_{NH_4N_3}+\phi_{H_2}}{\phi_{CH_3NH_2\cdot HN_3}} = \frac{k_3+k_4}{k_3}\frac{k_5+k_6}{k_5}\frac{k_7+k_8}{k_7}+\frac{k_8}{k_7} + \frac{k_2+k_{2a}}{k_3}\frac{k_5+k_6}{k_5}\frac{k_7+k_8}{k_7}\frac{[HN_3]}{[CH_4]} \quad \text{(IV)}$$

The plot of $(\phi_{NH_4N_3}+\phi_{H_2})/\phi_{CH_3NH_2\cdot HN_3}$ *vs.* $[HN_3]/[CH_4]$ is also shown in Fig. 7. The values calculated from Eq. IV using the rate-constant ratios obtained above are shown by the lower straight line in Fig. 7. Fig. 7 shows that the straight line accords well with the experimental values.

Comparisons of Rate Constants. Chao *et al.*[19] have studied the decomposition rate of the chemically activated CH_3NH_2 which was formed by the reaction of NH_3 with the $^1CH_2$ produced by the photolysis of CH_2N_2. They have found that the specific rate of the unimolecular decomposition is 1.7×10^{10} s^{-1} for the photolysis at 435.8 nm and 2.3×10^{10} s^{-1} at 366 nm. The half-lifes for $C_2H_5NH_2$*[2] and n-$C_3H_7NH_2$*[20] were evaluated from these unimolecular decomposition rates. The half-life for CH_3NH_2* in this work was also calculated using the RRKM theory, as will be discussed below. These hallf-lifes are shown in Table 2. Here, the half-life (τ) was calculated from the

TABLE 2. HALF-LIFE AND DECOMPOSITION MODE OF CHEMICALLY ACTIVATED ALKYLAMINES

Alkylamine	Half life(τ) / s	Fraction by radical mechanism (R_r)	Fraction of R-CH_2NH_2 bond fission ($R_{R\text{-}CH_2NH_2}$)
CH_3NH_2[a]	$\approx 7.7\times10^{-12}$[e]	1.00	0.88[j]
CH_3NH_2[b]	4.1×10^{-11}[f], 3.0×10^{-11}[g]		
$C_2H_5NH_2$[c]	6.8×10^{-11}	0.96[h]	1.00
n-$C_3H_7NH_2$[d]	1.78×10^{-10}	0.28[i]	0.96[k]

a) This work. b) Ref. 19. c) Ref. 2. d) Ref. 20. e) From the RRKM calculation by the Gorin model. f) CH_2N_2 was photodecomposed at 435.8 nm. g) CH_2N_2 was photolyzed at 366 nm. h) The residual fraction is due to the $C_2H_5NH_2^* \rightarrow CH_3CN+2H_2$ reaction. i) The residual is caused by these reactions; n-$C_3H_7NH_2^* \rightarrow CH_4+C_2H_5N$, $C_2H_4+CH_3NH_2$, $C_2H_6+CH_2NH$, $H_2+C_3H_7N$, and $C_3H_6+NH_3$. j) This is the maximum value, because the CH_3NH-H bond fission may also be possible. The residual is due to $CH_3NH_2^* \rightarrow CH_3+NH_2$. k) This value was estimated from these relations: the formation ratio of n-$C_3H_7NH_2$ to i-$C_3H_7NH_2$ is 1.55; the decomposition rate to give C_2H_5 radicals from both n- and i-$C_3H_7NH_2^*$ is 1.39 times faster than the rate to give CH_3 radicals, and the half-life of n-$C_3H_7NH_2^*$ is almost the same as that of i-$C_3H_7NH_2^*$. The residual fraction is due to n-$C_3H_7NH_2^* \rightarrow CH_3+CH_2CH_2NH_2$.

$\tau=\ln 2/\sum_i k_i$ relation, where k_i is the specific rate of i-th unimolecular decomposition. It can be seen in Table 2 that the half-life increases with an increase in the carbon number of alkylamines and with a decrease in the total internal energy in the $CH_3NH_2^*$ molecules, as will be discussed below.

The ratio of the sum of the rates of decomposition caused by the radical mechanism to the sum of all the decomposition rates, R_r, is also shown in Table 2. The ratio for decompositions by the molecular mechanism increases with an increase in the carbon number of alkylamines. This may be because the chance for the formation of three- and four-center transition states, resulting in decompositions by the molecular mechanism, increases with an increase in the molecular complexity.

The ratio of the R-CH_2NH_2 bond fission rate to the sum of all single-bond fission rates by the radical mechanism, $R_{R-CH_2NH_2}$, is also shown in Table 2, where R means H for CH_3NH_2, CH_3 for $C_2H_5NH_2$, and C_2H_5 for n-$C_3H_7NH_2$. It is found that the ratio for the R-CH_2NH_2 bond fission is very high on these amines. Meanwhile, no C–N bond fission was observed on the unimolecular decomposition of $C_2H_5NH_2^*$,[2] although the C–N bond dissociation energy is 20.2 kJ mol^{-1} lower than that of the C–C bond. Similarly, hardly no C–N bond fission was found on the unimolecular decomposition of n-$C_3H_7NH_2^*$,[20] and the probability of the CH_3–$CH_2CH_2NH_2$ bond fission was also found to be very small. Such a high R-CH_2NH_2 bond fission efficiency may be because the CH_2NH_2 group of the activated complex which produces the R-CH_2NH_2 bond rupture is stabilized by the interaction of an unpaired electron of the C atom with nonbonding electrons of the N atom in the next position.[21]

Although the R-CH_2NH_2 bond fission proceeds with a high efficiency, the $k_5>k_6$ relation can not be explained in terms of the enthalpy, for the $CH_3NH_2 \rightarrow H+CH_2NH_2$ reaction is 54.4 kJ mol^{-1} more endothermic than the $CH_3NH_2 \rightarrow CH_3+NH_2(\tilde{X}^2B_1)$ reaction.

On the other hand, Kassab *et al.*[22] have computed the potential surface on the decomposition of CH_3NH_2 using *ab initio* methods; they have suggested this reaction:

$$CH_3NH_2 \longrightarrow CH_3 + NH_2(\tilde{A}^2A_1) \qquad (6)$$

for the decomposition of $CH_3NH_2(A')$ in the ground state, as well as where the $NH_3 \rightarrow H+NH_2(\tilde{A}^2A_1)$ reaction can be anticipated for the decomposition of ammonia in the ground state[23] from the correlation by symmetry.[24] Provided that the electronic state of NH_2 formed by Reaction 6 is $\tilde{A}^2A_1$, Reaction 6 becomes 68.2 kJ mol^{-1} more endothermic than Reaction 5. In this case, the $k_5>k_6$ relation is explainable.

As for the $HN_3+NH(a^1\Delta) \rightarrow N_3+NH_2(\tilde{A}^2A_1)$ reaction, of the same kind as Reaction 6, the formation of $NH_2(\tilde{A}^2A_1)$ has been observed by McDonald *et al.*[25] and Piper *et al.*[26] Kajimoto *et al.*[27] have also observed the emission of $NH_2(\tilde{A}^2A_1)$ formed by a similar reaction, $HN_3+H \rightarrow N_2+NH_2(\tilde{A}^2A_1)$. The formation of $NH_2(\tilde{A}^2A_1)$ by Reaction 6 is also supported by the fact that hardly no C–N bond rupture was found in the unimolecular decompositions of $C_2H_5NH_2^*$[2] and $C_3H_7NH_2^*$.[20]

In order to examine the adequacy of Reaction 6 bring about $NH_2(\tilde{A}^2A_1)$ and to obtain the absolute value of k_6, calculation by means of the RRKM theory was carried out. The specific rate calculated by means of the RRKM theory for the unimolecular decompositions of chemically activated molecules, k_E, is given by this equation:[28]

$$k_E = \frac{q_r^* q_{1r}^*}{q_r} \frac{\Gamma(s)}{\Gamma(s^*+r^*/2+1)} \frac{\prod_{i=1}^{s} h\nu_i}{h\prod_{i=1}^{s^*} h\nu_i^* (kT)^{r^*/2}} \times \frac{[E^*+a^*E_z^*]^{s^*+r^*/2}}{[E^*+E_0+aE_z]^{s-1}} \qquad (V)$$

Here, s, s^*, and r^* indicate the numbers of degrees of freedom for the vibrations of the molecule, and for the

vibrations and internal free rotations of the activated complex, respectively.

In the case of a single-bond fission, the activated complex should be very loose because of the critical state, and it must have the same structure as that for the radical recombination which is a reverse reaction. Thus, the Gorin model[29] was used in this case, assuming that the activated complex is an associated form of the CH_3 radical (planar, D_{3h}) and the $NH_2(\tilde{A}\,^2A_1(\Pi))$ radical (linear, $D_{\infty h}$). According to this "loosest" model, s, s^*, and r^* become 15, 10, and 5 respectively.

q_r and q_{ir}^* are the partition functions for the rotation of the molecule and the internal free rotation of the complex. By the Gorin model, the partition function for the rotation of the complex, q_r^*, can be expressed by this equation:[30]

$$q_r^* = \frac{8\pi^2 I(2/3)\mu kT}{\sigma h^2}\left(\frac{2A}{kT}\right)^{1/3} \qquad \text{(VI)}$$

Since both CH_3 and NH_2 groups are nonpolar, the attractive potential constant in the Lennard-Jones 12-6 intermolecular potential, A, can be calculated from the Slater and Kirkwood equation[3,31] for the dispersion term. The polarizabilities of the CH_3 and NH_2 groups were estimated to be 2.24 and 1.78×10^{-30} m^3 from the atomic polarizabilities of 1.039(C), 0.905(N), and $0.401(H)\times10^{-30}$ m^3. The number of outer-shell electrons is 7 for both CH_3 and NH_2 groups. The σ in Eq. VI is unity in this case.

The internal energy change of Reaction 6 at 0 K, E_o, was estimated to be 460.8 kJ mol^{-1} from the standard enthalpy change of 469.0 kJ mol^{-1}. The vibrational wave numbers ($\bar{\nu}_i$)[32] and the moments of inertia[19] for the CH_3NH_2 molecule and the vibrational wave numbers ($\bar{\nu}_i^*$)[33-35] and the moments of inertia for the complex are shown in Table 3. The last term in Eq. V was calculated from the relations derived by Rabinovitch *et al.*[36] The values of k_6 at 303 K, measured as a function of the excess energy (E^*) in the activated complex, are shown in Fig. 8.

On the photolysis of HN_3 at 313 nm, an excess energy of 177.9 kJ mol^{-1} is released and then distributed to N_2 and NH($a^1\Delta$) as fragments. Since the distribution fraction of the energy to NH($a^1\Delta$) is unclear, it was assumed that slightly less than one half of the excess energy is divided to NH($a^1\Delta$). Then, the total internal energy in CH_3NH_2* formed by Reaction 3 becomes about 540 kJ mol^{-1}. Since E_o is 460.8 kJ mol^{-1}, E^* becomes about 79 kJ mol^{-1}. The value of k_6 corresponding to this energy is 1.05×10^{10} s^{-1} as may be seen in Fig. 8. From $k_6/k_5=0.133$, $k_5=7.9\times10^{10}$ s^{-1} is obtained. Thus, the half-life of CH_3NH_2* obtained from $\tau=\ln 2/(k_5+k_6)$ becomes 7.7×10^{-12} s.

RRKM calculations by the methods described above were also carried out for the decomposition rates of the CH_3NH_2* formed under the reaction conditions

Table 3. Models for the unimolecular decomposition of CH_3NH_2

	Molecule		Complex	
Wavenumber cm^{-1}	3424	1430	3162(2)[a]	
	3360	1424	3044(1)[a]	
	2985	1195	1396(2)[a]	
	2962	1130	607(1)[b]	
	2820	1044	3440(1)[c]	
	1623	780	3325(1)[d]	
	1485	264	633(2)[d]	
	1474			
Moment of inertia 10^{-47} kg m^2	38.4		5.85[e]	3.34[f]
	36.5		2.92[e]	3.34[f]
	7.8		2.92[e]	

a) Ref. 33. b) Ref. 34. c) Estimated value for the antisymmetric stretching vibration of $NH_2(\tilde{A}\,^2A_1(II))$. d) Ref. 35. e) Ref. 24, p. 609. Calculated from r_o(C-H)= 1.079 Å for $CH_3(\tilde{X}\,^2A_2'', D_{3h})$. f) Ref. 35. Calculated from r_o(N-H)=1.004 Å for $NH_2(\tilde{A}\,^2A_1(II))$.

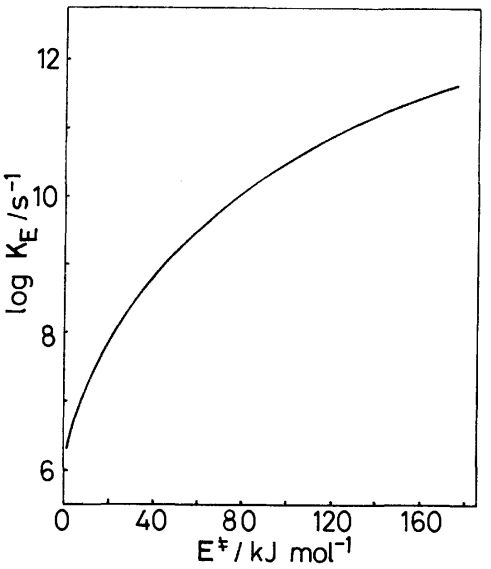

Fig. 8. Specific rate of Reaction 6 by the RRKM calculation, measured as a function of the excess energy.

performed by Chao *et al.*;[19] the calculated values were found to be consistent with their experimental values. The low E^* was the reason that the decomposition rates observed by them are slow as compared with that in this work.

On the other hand, the specific rate for the collisional deactivation of CH_3NH_2* by a third body(Q), k_z, can be calculated from the Lennard-Jones collision frequency as described previously.[2] The values of σ and ε/k used in the calculation are 4.30 and 500 for CH_3NH_2,[37] 3.82 and 137 for CH_4,[38] and 3.98 Å and 240 K for HN_3[2] respectively. The highest total pressure in the present work is 24.27 kPa (P_{HN_3}=6.67 and P_{CH_4}=17.60 kPa). In this case, the rate ratio of the collisional deactivation to the unimolecular decompositions of CH_3NH_2*, $k_z[Q]/(k_5+k_6)$, becomes 0.038. This result is consistent with the experimental finding that the collisional

Table 4. Relative fractions for the unimolecular decompositions of the chemically and photochemically activated methylamine

Wavelength	Excitation energy	Relative fraction/%		
nm	kJ mol^{-1}	$H+CNH_4$	H_2+CNH_3	CH_3+NH_2
Chemically activated[a]	≈540[e]	88.3	0	11.7
244—194[b]	490—617	91.3	0[f]	8.7
184.9[c]	647	89.1	7.4	3.5
147[d]	814	68	19	13
147[c]	814	56.4	38.7	4.9
123.6[c]	968	55.6	37.9	6.5

a) This work. b) Ref. 39. c) Ref. 11. d) Ref. 10. e) Estimated from the enthalpy change. f) The formation amount of H_2 converges to zero with an increase in the pressure of O_2 as a scavenger.

deactivation of CH_3NH_2* could not be found within the limits of experimental accuracy. It thus appears that the calculated values of k_5, k_6, and τ obtained above are reasonable.

On the photolysis of CH_3NH_2 vapor, the primary processes are, in general, given by this mechanis:[10,11,39]

$$CH_3NH_2 + h\nu \begin{cases} \nearrow H + CNH_4 \\ \longrightarrow H_2 + CNH_3 \\ \searrow CH_3 + NH_2, \end{cases}$$

except for the decompositions of $CH_3NH_2+h\nu$(123.6 nm)→CH_4+NH($c^1\Pi$) and others in very-short-wavelength systems.[40] Provided that the succeeding reactions for H atoms and CH_3 radicals are H+RH→H_2+R, CH_3+RH→CH_4+R, and $2CH_3$→C_2H_6, the relative fractions for three photodissociation processes can be calculated by means of the following simplified relations: $[H_2-H_2(scav)]/[H_2+CH_4+2C_2H_6]$ for $H+CNH_4$; $[H_2(scav)]/[H_2+CH_4+2C_2H_6]$ for H_2+CNH_3; $[CH_4+2C_2H_6]/[H_2+CH_4+2C_2H_6]$ for CH_3+NH_2. Here, $[H_2(scav)]$ indicates the amount of H_2 formed in the presence of a scavenger such as O_2 and NO. The relative fractions are shown in Table 4, together with the fractions for the umimolecular decompositions of CH_3NH_2* formed by Reaction 3.

Table 4 shows that the relative fractions for the chemically activated CH_3NH_2* are very similar to those for the photochemically activated CH_3NH_2* at 244 to 194 nm, and that the fraction for the formation of H_2 by the molecular mechanism increases with an increase in the excitation energy. It is also found that the fraction for $H+CNH_4$ is always larger than the fraction for CH_3+NH_2. Regarding this trend, Kassab *et al.*[22] have found, from theoretical considerations, that the potential barrier resulting in the CH_3–NH_2 bond rupture is higher than that for the CH_3NH–H bond rupture on the photodissociation of the lowest excited singlet, CH_3NH_2.

On the efficiencies of the reactions of NH($a^1\Delta$) with saturated hydrocarbons, the rate-constant ratio of the insertion reaction of NH($a^1\Delta$) into a C–H bond to the reactions of NH($a^1\Delta$) with HN_3 is 0.175 (k_3/k_2) for CH_4 and 0.334 for C_2H_6.[2] The low efficiency for CH_4 may be due to the facts that the number of C–H bonds of CH_4 is less than that of C_2H_6 and that the C–H bond-dissociation energy of CH_4 is higher than that of C_2H_6. The rate-constant ratio of the collisional spin relaxation of NH($a^1\Delta$) to Reaction 2 is 0.177 (k_4/k_2) for CH_4, and 0.217 for C_2H_6.[2] The difference may be because the collisional spin-relaxation efficiency depends on the molecular complexity, that is, the number of atoms constituting a saturated hydrocarbon molecule. More details will be presented in a later work.[20]

Summary. The reaction efficiencies of NH($a^1\Delta$) with CH_4 and the unimolecular decomposition rates of the CH_3NH_2* formed by the insertion were investigated. The insertion efficiency of NH($a^1\Delta$) into a C–H bond of CH_4 was 0.52 as compared with that of C_2H_6. This difference appears to be caused by the higher C–H bond dissociation energy and the lower C–H bond number than those for C_2H_6. The collisional deactivation efficiency of NH($a^1\Delta$) to NH($X^3\Sigma^-$) by CH_4 was 0.82 of that by C_2H_6. The unimolecular decomposition, CH_3NH_2*→H+CNH_4 (5), was 7.5 times faster than the CH_3NH_2*→CH_3+NH_2 (6) decomposition, although the C–H or N–H bond dissociation energy is higher than that of the C–N bond. However, this is explainable provided that the electronic state of NH_2 formed by Reaction 6 is $\tilde{A}^2A_1$. From the RRKM calculation by the Gorin model, $k_5 \approx 7.9\times10^{10}$ s^{-1}, $k_6 \approx 1.05\times10^{10}$ s^{-1}, and τ (half-life of CH_3NH_2*)$\approx 7.7\times10^{-12}$ s were estimated. These results are in accord with the experimental result that the collisional deactivation of CH_3NH_2* was not observed in the total pressure range lower than 24.3 kPa.

I would like to thank Mr. Jun Fukuchi for his cooperation.

References

1) S. Kodama, *Bull. Chem. Soc. Jpn.*, **56**, 2348 (1983).
2) S. Kodama, *Bull. Chem. Soc. Jpn.*, **56**, 2355 (1983).
3) S. Kodama, *Bull. Chem. Soc. Jpn.*, **56**, 2363 (1983).
4) E. D. Miller, Ph. D. Dissertation, Catholic University of America, Washington, D. C., 1961.
5) D. W. Cornell, R. S. Berry, and W. Lwowski, *J. Am. Chem. Soc.*, **88**, 544 (1966).
6) W. C. Richardson and D. W. Setser, *Can. J. Chem.*, **47**,

2725 (1969).
7) J. M. Kruse and M. G. Mellon, *Anal. Chem.*, **25**, 446 (1953).
8) S. G. Hadley and D. H. Volman, *J. Am. Chem. Soc.*, **89**, 1053 (1967).
9) K. Hatano, N. Shimamoto, T. Katsu, and Y. Fujita, *Bull. Chem. Soc. Jpn.*, **47**, 4 (1974).
10) J. J. Magenheimer, R. E. Varnerin, and R. B. Timmons, *J. Phys. Chem.*, **73**, 3904 (1969).
11) E. P. Gardner and J. R. McNesby, *J. Phys. Chem.*, **86**, 2646 (1982).
12) K. Fukui, I. Fujita, and K. Kuwata, *Bull. Chem. Soc. Jpn.*, **45**, 2278 (1972).
13) By assuming D(H-CH_2NH_2)=400.8, D(CH_3NH-H)= 420.5 kJ mol^{-1}, $s-1=8$, and the same frequency (ν) for both decompositions, the formation ratio of CH_2NH_2 to CH_3NH becomes 26 for E^*=459.8 as the standard enthalpy change of Reaction 3 and 3.4 for E^*=540 kJ mol^{-1}, as will be discussed later, from the calculations of the RRK rate expression $k_d=\nu(1-D/E^*)^{s-1}$.
14) a) S. W. Benson, "Thermochemical Kinetics," Wiley, New York, 1968; b) S. W. Benson and H. E. O'Neal, "Kinetic Data on Gas Phase Unimolecular Reactions," NSRDS-NBS-21, National Bureau of Standards Reference Data System, U. S. Department of Commerce (1970); c) D. M. Golden, R. K. Solly, N. A. Gac, and S. W. Benson, *J. Am. Chem. Soc.*, **94**, 363 (1972); d) A. A. Zavitsas, *ibid.*, **94**, 2779 (1972); e) D. K. S. Sharma and J. L. Franklin, *ibid.*, **95**, 6562 (1973); f) "Handbook of Chemistry and Physics," 55th ed, ed by R. C. Weast, Chemical Rubber Co. Press, Cleveland, Ohio (1974—1975); g) R. T. Sanderson, *J. Am. Chem. Soc.*, **97**, 1367 (1975).
15) R. S. Konar and B. DeB. Darwent, *Can. J. Chem.*, **48**, 2280 (1970).
16) G. A. Creak, F. S. Dainton, and K. J. Ivin, *Trans. Faraday Soc.*, **58**, 326 (1962).
17) G. Le Bras and J. Combourieu, *Int. J. Chem. Kinet.*, **5**, 559 (1973).
18) M. J. Kurylo and R. B. Timmons, *J. Chem. Phys.*, **50**, 5076 (1969).
19) K. J. Chao, C. L. Lin, M. Hsu, and S. Y. Ho, *J. Phys. Chem.*, **83**, 1241 (1979).
20) S. Kodama, *Bull. Chem. Soc. Jpn.*, **58**, 2900 (1985).
21) J. M. Howell and P. Jφrgensen, *J. Am. Chem. Soc.*, **95**, 2813 (1973).
22) E. Kassab, J. T. Gleghorn, and E. M. Evleth, *J. Am. Chem. Soc.*, **105**, 1746 (1983).
23) A. E. Douglas, *Disc. Faraday Soc.*, **35**, 158 (1963).
24) G. Herzberg, "Molecular Spectra and Molecular Structure. III. Electronic Spectra and Electronic Structure of Polyatomic Molecules," Van Nostrand Reinhold Co., New York (1966), p. 460.
25) J. R. McDonald, R. G. Miller, and A. P. Baronavski, *Chem. Phys. Lett.*, **51**, 57 (1977).
26) L. G. Piper, R. H. Krech, and R. L. Taylor, *J. Chem. Phys.*, **73**, 791 (1980).
27) O. Kajimoto, T. Kawajiri, and T. Fueno, *Chem. Phys. Lett.*, **76**, 315 (1980).
28) R. A. Marcus, *J. Chem. Phys.*, **20**, 355, 359 (1952); G. Z. Whitten and R. S. Rabinovitch, *ibid.*, **41**, 1883 (1964).
29) E. Gorin, *Acta Physicochim. URSS*, **9**, 681 (1938); E. Gorin, W. Kauzmann, J. Walter, and H. Eyring, *J. Chem. Phys.*, **7**, 633 (1939).
30) E. V. Waage and B. S. Rabinovitch, *Chem. Rev.*, **70**, 377 (1970).
31) J. C. Slater and J. G. Kirkwood, *Phys. Rev.*, **37**, 682 (1931); J. G. Kirkwood, *Physik. Z.*, **33**, 57 (1932).
32) A. Y. Hirakawa, M. Tsuboi, and T. Shimanouchi, *J. Chem. Phys.*, **57**, 1236 (1972).
33) A. Snlson, *J. Phys. Chem.*, **74**, 537 (1970).
34) L. Y. Tan, A. M. Winer, and G. C. Pimentel, *J. Chem. Phys.*, **57**, 4028 (1972).
35) Ref. 24, p. 584.
36) G. Z. Whitten and B. S. Rabinovitch, *J. Chem. Phys.*, **38**, 2466 (1963); D. C. Tardy and B. S. Rabinovitch, *ibid.*, **48**, 1427 (1968).
37) Estimated from the values of σ and ε/k for the NH_3, CH_3OH, CH_3Cl, C_2H_4, and C_2H_6 molecules.
38) J. O. Hirschfelder, R. B. Bird, and E. L. Spotz, *J. Chem. Phys.*, **16**, 968 (1948).
39) J. V. Michael and W. A. Noyes, *J. Am. Chem. Soc.*, **85**, 1228 (1963).
40) M. Kawasaki and I. Tanaka, *J. Phys. Chem.*, **78**, 1784 (1974).

Reactions of NH Radicals. V. Photolysis of HN_3 in the Presence of C_3H_8 at 313 nm

Sukeya KODAMA*

Department of Applied Chemistry, College of Engineering, University of Osaka Prefecture, Sakai, Osaka 591

(Received September 5 , 1983)

The photolysis of HN_3 vapor in the presence of C_3H_8 was studied at 313 nm and 30 °C. The main products were N_2, H_2, CH_4, C_2H_6, C_3H_6, NH_4N_3, $CH_3NH_2 \cdot HN_3$, $C_2H_5NH_2 \cdot HN_3$, and *n*- and *i*-$C_3H_7NH_2 \cdot HN_3$. The quantum yields of these products were measured as a function of the pressure of HN_3 or C_3H_8. The following mechanisms for the main reactions was proposed: $HN_3+h\nu(313\text{ nm}) \rightarrow N_2+NH(a^1\Delta)$; $NH(a^1\Delta)+HN_3 \rightarrow 2N_2+2H$, NH_2+N_3, and $N_2+N_2H_2^*$ (2); $NH(a^1\Delta)+C_3H_8 \rightarrow C_3H_7NH_2^*$(*n*- and *i*-propylamine) (3); $NH(a^1\Delta)+C_3H_8 \rightarrow NH(X^3\Sigma^-)+C_3H_8$ (4); $C_3H_7NH_2^* \rightarrow CH_3+C_2H_4NH_2$ (5); $CH_4+C_2H_4NH$ (6), $C_2H_4+CH_3NH_2$ (7), $C_2H_5+CH_2NH_2$ (8), $C_2H_6+CH_2NH$ (9), $H_2+C_3H_6NH$ (10), and $NH_3+C_3H_6$ (11); $C_3H_7NH_2^*+HN_3 \rightarrow C_3H_7NH_2+HN_3$ (12); $C_3H_7NH_2^*+C_3H_8 \rightarrow C_3H_7NH_2+C_3H_8$ (13). The rate constant ratios are: $k_3/k_2=1.28$; $k_4/k_2=0.262$; $k_6/k_5=0.109$; $k_7/k_5=0.050$; $k_8/k_5=1.39$; $k_9/k_5=0.040$; $k_{10}/k_5=1.20$; $k_{11}/k_5=4.72$; $k_{12}/k_5=666$ dm^3 mol^{-1}; $k_{13}/k_5=860$ dm^3 mol^{-1}. The formation ratio of *n*-$C_3H_7NH_2$/*i*-$C_3H_7NH_2$ was 1.55, regardless of the total pressure. The half-life of 1.78×10^{-10} s for $C_3H_7NH_2^*$ was obtained by using the collision theory. The relative and absolute rate constants were compared for the reactions of $NH(a^1\Delta)$ with CH_4, C_2H_6, and C_3H_8; it was found that the relative yield for the insertion of $NH(a^1\Delta)$ into a C–H bond increases with a decrease in the C–H bond dissociation energy.

The reactions of $NH(a^1\Delta)$ with HN_3,[1] Xe,[1] C_2H_6,[2] C_2H_4,[3] and CH_4[4] have been studied previously. It was found that HN_3 is a useful source for the first excited singlet $NH(a^1\Delta)$ and that $NH(a^1\Delta)$ reacts to give amine by insertion into a C–H bond, such as CH_3NH_2 from CH_4[4] and $C_2H_5NH_2$ from C_2H_6.[2] It is of interest to compare the relative reactivities for the reactions of $NH(a^1\Delta)$ with simple saturated hydrocarbons, such as CH_4, C_2H_6, C_3H_8, and *i*-C_4H_{10}, and to compare the relative efficiencies of the insertion per C–H bond for primary, secondary, and tertiary C–H bonds.

For the reactions of NH with saturated hydrocarbons, Miller[5] has studied the photolysis of HN_3 in the presence of CH_4, C_3H_8, *n*-C_4H_{10}, *i*-C_4H_{10}, and $(CH_3)_4C$, and measured the amines formed by the reactions of NH with these hydrocarbons. He has found that the amine yield increases in this order: C_3H_8<*n*-C_4H_{10}<*i*-C_4H_{10}<$(CH_3)_4C$. Back *et al.* have studied the flash photolysis of HNCO in the presence of C_3H_8[6] and the steady photolysis of HNCO with C_2H_6, C_3H_8, and $(CH_3)_4C$ at 51 °C.[7] They have found that the yield of CO was reduced to about one-third of its value in pure HNCO, the yield of N_2 was reduced close to zero, and the yield of H_2 was markedly enhanced in the presence of parafins. However, no amines could be detected. Thus, they suggested the decomposition of the vibrationally excited amines formed by insertion reactions. Richardson and Setser[8] have studied the thermal decomposition of HN_3 in the presence of CH_4, C_2H_6, and C_3H_8. However, no evidence was found for the reaction of NH with these hydrocarbons in the temperature range from 285 to 470 °C. Konar *et al.*[9] have investigated the photolysis of HN_3 in the presence of C_2H_6 and *i*-C_4H_{10} at 214 nm and room temperature, and showed that the formation rates of N_2 and H_2 decrease with an increase in the hydrocarbon pressure.

Recently, Tsunashima *et al.*[10] have studied the photolysis of HN_3 in liquid ethane, propane, and isobutane at the Dry Ice–methanol temperature, they have found the formation of ethylamine from C_2H_6, propyl- and isopropylamine from C_3H_8, and of butyl- and *t*-butylamine from *i*-C_4H_{10}. They have also estimated that the relative efficiencies of the insertion of ^{1}NH into primary, secondary, and tertiary C–H bonds are 1.0, 1.9, and 2.3 respectively. Hamada *et al.*[11] have studied the photolysis of HN_3 in liquid cyclopropane and in binary solutions of ethane and cyclopropane at the Dry Ice–methanol temperature, and reported that the insertion rate of $NH(a^1\Delta)$ into a C–H bond of cyclopropane is 1.05 times faster than that of ethane.

Kajimoto and Fueno[12] have studied the photolysis of HN_3 with C_2H_6 in the gas phase at 254 nm. From the pressure dependences of the yields of the insertion product($C_2H_5NH_2$) and the fragmentation products (CH_3 and C_2H_5), they have found that the branching ratios for three pathways of the insertion of $NH(a^1\Delta)$ into a C–H bond of C_2H_6, the hydrogen abstraction from C_2H_6 by $NH(a^1\Delta)$, and the electronic quenching of $NH(a^1\Delta)$ to $NH(X^3\Sigma^-)$ were 0.6, 0.1, and 0.3 respectively. Kondo *et al.*[13] have studied the effects of the reactions of $NH(a^1\Delta)$ with C_3H_8 on the photolysis of HN_3 at 254 nm, and determined that the relative secondary/primary C–H bond reactivity per bond is 1.5 for the insertion and 7.5 for the abstraction, results based on the pressure dependence of the yields of the insertion products (*n*-$C_3H_7NH_2$ and *i*-$C_3H_7NH_2$) and the fragmentation products (C_2H_5, *n*-C_3H_7, and *i*-C_3H_7).

In order to compare the specific rates for the insertion of $NH(a^1\Delta)$ into C–H bonds of simple saturated hydrocarbons, the collisional deactivations of $NH(a^1\Delta)$ to $NH(X^3\Sigma^-)$ by the hydrocarbons, and the unimolecular decomposition of the alkylamines formed by the insertion, the photolysis of HN_3 in the presence of C_3H_8 was investigated in this work, a continuation of our earlier studies with C_2H_6[2] and CH_4.[4]

Experimental

The propane obtained from the Takachiho Chemical Co. was 99.8% pure. It was purified each time before use by means of condensation and evacuation at the temperature of liquid nitrogen. The preparation and purification of HN_3, and the apparatus and procedure for the reaction, were the same as have been described previously.[1,2] All the runs in this work were carried out at 313 nm and 30 °C. The light intensity was reduced by screens to eliminate radical-radical reactions. The irradiation time was usually 90 min, and the degree of conversion of HN_3 was below 3 per cent.

The detected reaction products were N_2, H_2, CH_4, C_2H_4, C_2H_6, C_3H_6, CH_3N_3, NH_4N_3, $CH_3NH_2 \cdot HN_3$, $C_2H_5NH_2 \cdot HN_3$, and n- and i-$C_3H_7NH_2 \cdot HN_3$. No HCN was detected in the analysis by the pyridine-pyrazolone method.[14]

In order to inspect the radical intermediates, the products formed by the photolysis of HN_3 with C_3H_8 and NO at 313 nm were analysed gas chromatographically by the use of a Silicone SE-30 1-m column at room temperature. The retention times of these products (RNO_x) were then compared with those of the products formed on the photolyses of $CH_3N_2CH_3$, $C_2H_5COC_2H_5$, $(i\text{-}C_3H_7)_2CO$, and n-$C_3H_7COCH_3$ with NO, in the same gas chromatographic conditions. From the comparisons, the formations of CH_3 and C_2H_5 radicals as intermediates were confirmed, but few n-C_3H_7 or i-C_3H_7 radicals were found. The photolysis of HN_3 with C_3H_8 and NO at 254 nm was also carried out in order to inspect the effect of the wavelength. Thus, the large two peaks for i-C_3H_7 radicals, together with the peaks for the CH_3, C_2H_5, and n-C_3H_7 radicals, were found. The results at 254 nm are in accord with the results of Kondo *et al.*,[13] except that they did not detect any CH_3 radicals.

For the identification of the nitrogen-containing products, white volatile products condensed at the Dry Ice-acetone temperature were introduced into a solid sodium hydroxide column in order to remove the HN_3 from the white volatile products.[2,10] A mass spectrum of the HN_3-removed products at the ionizing voltage of 15 V is shown in Fig. 1. The mass spectra of the n- and i-$C_3H_7NH_2$ samples were also observed at the ionizing voltage of 15 V. In the spectra, the large peaks of m/z=30 ($CH_2NH_2^+$) for n-$C_3H_7NH_2$ and of m/z=44 ($CH_3CHNH_2^+$) for i-$C_3H_7NH_2$ were found, together with the parent-molecule-ion ($C_3H_7NH_2^+$) peak and its protonated-ion ($C_3H_7NH_3^+$) peak.

The product peaks of m/z=17, 18, 31, 32, 45, 46, 59, and 60 in Fig. 1 correspond to NH_3^+, NH_4^+, $CH_3NH_2^+$, $CH_3NH_3^+$, $C_2H_5NH_2^+$, $C_2H_5NH_3^+$, $C_3H_7NH_2^+$, and $C_3H_7NH_3^+$ respectively. The large peak of m/z=30 ($CH_2NH_2^+$) seems to arise from the electron-impact reactions of $CH_3NH_2 \rightarrow H+CH_2NH_2^+ + e^-$, as found in the mass spectrum of CH_3NH_2,[2,4,15] and of n-$C_3H_7NH_2 \rightarrow C_2H_5+CH_2NH_2^+ + e^-$, as observed in the spectrum of the n-$C_3H_7NH_2$ sample. Similarly, the large peak of m/z=44 may be due to the electron-impact reactions of $C_2H_5NH_2 \rightarrow H+C_2H_4NH_2^+ + e^-$ and i-$C_3H_7NH_2 \rightarrow CH_3+CH_3CHNH_2^+ + e^-$. The peak of m/z=58 may result from the $C_3H_7NH_2 \rightarrow H+C_3H_6NH_2^+ + e^-$ reaction.

For the quantitative analyses of the reaction products, first, these products were separated at the temperature of solid nitrogen (about −220 °C), −160 °C, and the Dry Ice-acetone temperature. Quantitative separations of N_2, H_2, and CH_4 passing through a trap at −220 °C were carried out by the procedures described previously.[2] C_2H_4, C_2H_6, and a part of the unconverted C_3H_8, condensed at −220 °C, were collected into a Toepler gauge, and the total volume was determined. The separations of C_2H_4, C_2H_6, and C_3H_8 were carried out by gas chromatography using a silica-gel column (2 m) at 60 °C.

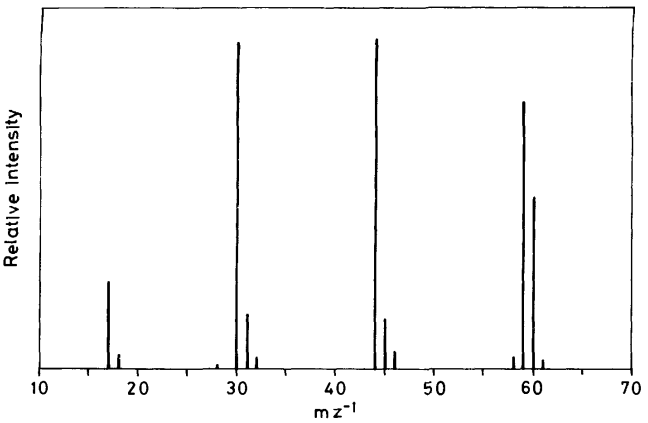

Fig. 1. Mass spectrum of the substances removed HN_3 from the white volatile products trapped at the Dry Ice-acetone temperature. The ionizing voltage is 15 V.

NH_4N_3 and the salts of amines with HN_3, condensed at the Dry Ice-acetone temperature, were introduced into a CuO column at about 550 °C. The amounts of N_2, NO, N_2O, and CO_2 produced as the combustion products were determined by a previously described method.[2] The total amount of nitrogen atoms, (N), is given by $(N)=2N_2+2N_2O+NO$. The total amount of carbon atoms in the products is identical with the amount of carbon dioxide formed by the combustion, (CO_2).

In order to determine the relative yields of CH_3NH_2, $C_2H_5NH_2$, i-$C_3H_7NH_2$, and n-$C_3H_7NH_2$, the HN_3-removed products were also analysed by means of gas chromatography at 10 °C using a 2-m columun of KOH (5%)-paraffin liquid (20%) coated on Chromosorb WAW.[16] The retention times of CH_3NH_2, $C_2H_5NH_2$, and i-$C_3H_7NH_2$ relative to n-$C_3H_7NH_2$ are 0,23, 0.36, and 0.56 respectively.

The quantum yields of the products were determined using HN_3 as an actinometer.[1]

Results

The photolysis of HN_3 of 6.7 kPa at 4.0 kPa of C_3H_8 was carried out as a function of the absorbed-light intensity in the range from 4.5 to 18.8×10^{14} quanta s^{-1}. The results, shown in Fig. 2, show that ϕ_{H_2} and ϕ_{CH_4} are independent of the light intensity, while ϕ_{N_2}, $\phi_{(N)}$, and $\phi_{(CO_2)}$ increase slightly with a decrease in the light intensity, but all the quantum yields converge to a constant value as the light intensity decreases.

The results for the photolysis of HN_3 of 6.7 kPa, measured as a function of the C_3H_8 pressure at the low absorbed-light intensity of 4.5×10^{14} quanta s^{-1}, are shown in Fig. 3. It may be seen in Fig. 3 that ϕ_{N_2} and ϕ_{H_2} decrease, $\phi_{(CO_2)}$ and $\phi_{(N)}$ increase, and ϕ_{CH_4}, $\phi_{C_2H_4}$, and

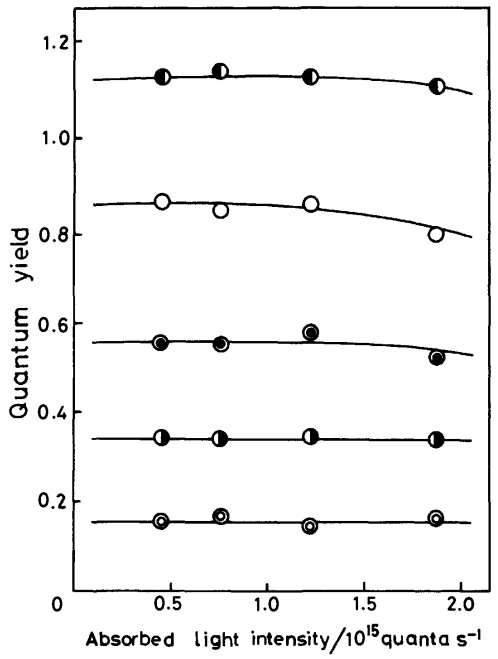

Fig. 2. Results for the photolysis of HN_3 of 6.7 kPa, measured as a function of the absorbed light intensity at 313 nm, 30 °C, and 4.0 kPa of C_3H_8. ◐, $\phi_{N_2}/3$; ○, $\phi_{(N)}/4$; ⊙, $\phi_{(CO_2)}$; ◑, ϕ_{H_2}; ◎, $4\phi_{CH_4}$.

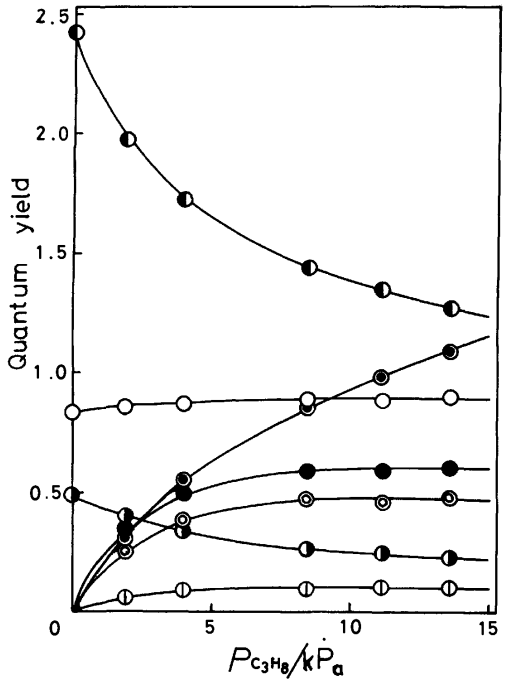

Fig. 3. Results of the photolysis of HN_3 of 6.7 kPa, measured as a function of C_3H_8 pressure at 313 nm, 30 °C, and the low absorbed light intensity of 4.5×10^{14} quanta s^{-1}. ◐, $\phi_{N_2}/2$; ⊙, $\phi_{(CO_2)}$; ○, $\phi_{(N)}/4$; ◑, ϕ_{H_2}; ◎, $10\phi_{CH_4}$; ●, $10\phi_{C_2H_6}$; ⊕, $50\phi_{C_2H_4}$.

$\phi_{C_2H_6}$ decrease *via* a maximum value at about 10 kPa as the C_3H_8 pressure increases.

Figure 4 shows the results of the photolysis measured as a function of the HN_3 pressure at 4.0 kPa of

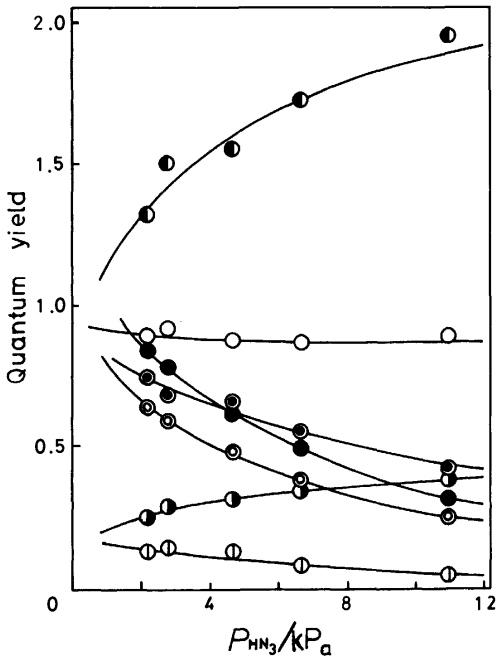

Fig. 4. Results of the photolysis measured as a function of HN_3 pressure at 4.0 kPa of C_3H_8, 30 °C, 313 nm, and the low incident light intensity of 3.9×10^{15} quanta s^{-1}. ◐, $\phi_{N_2}/2$; ⊙, $\phi_{(CO_2)}$; ○, $\phi_{(N)}/4$; ◑, ϕ_{H_2}; ◎, $10\phi_{CH_4}$; ●, $10\phi_{C_2H_6}$; ⊕, $50\phi_{C_2H_4}$.

C_3H_8 and the low incident-light intensity of 3.9×10^{15} quanta s^{-1}. In Fig. 4, it is found that ϕ_{N_2} and ϕ_{H_2} increase, but $\phi_{(N)}$, $\phi_{(CO_2)}$, ϕ_{CH_4}, $\phi_{C_2H_4}$, and $\phi_{C_2H_6}$ decrease, with an increase in the HN_3 pressure.

On the photolysis of HN_3 of 6.7 kPa with C_3H_8 of 4.0 kPa and NO of 0.47 kPa at the absorbed-light intensity of 4.5×10^{14} quanta s^{-1}, the ϕ_{CH_4}, $\phi_{C_2H_6}$, and $\phi_{C_2H_4}$ values were 0.00374 (1/10.2 of that without NO), 0.00138 (1/35.6 of that without NO), and 0.00172 (the same as that without NO) respectively.

The amines obtained under the same experimental conditions as those in Figs. 3 and 4 were analysed by means of gas chromatography. Table 1 shows the yields of CH_3NH_2, $C_2H_5NH_2$, and n-$C_3H_7NH_2$ relative to that of i-$C_3H_7NH_2$. It may be seen in Table 1 that CH_3NH_2/i-$C_3H_7NH_2$ and $C_2H_5NH_2/i$-$C_3H_7NH_2$ decrease with an increase in the C_3H_8 or HN_3 pressure, while n-$C_3H_7NH_2/i$-$C_3H_7NH_2$ is constant regardless of the total pressure and the concentration ratio $[HN_3]/[C_3H_8]$.

Discussion

Reaction Mechanism. On the basis of the present experimental results and in the light of the results achieved by previous investigations,[1-4] the following reaction mechanism was postulated for the photolysis of HN_3 in the presence of C_3H_8, where A and P denote HN_3 and C_3H_8 molecules:

$$A + h\nu(313\,nm) \longrightarrow N_2 + NH(a^1\Delta) \quad (1)$$

Table 1. Relative yields of amines

P_{HN_3}	$P_{C_3H_8}$	CH_3NH_2	$C_2H_5NH_2$	n-$C_3H_7NH_2$
kPa	kPa	i-$C_3H_7NH_2$	i-$C_3H_7NH_2$	i-$C_3H_7NH_2$
6.7	1.9	1.05	1.19	1.67
6.7	4.0	0.48	0.71	1.48
6.7	8.4	0.38	0.52	1.56
6.7	13.6		0.41	1.52
6.7	17.1	0.28	0.35	1.44
2.3	4.0		1.04	1.50
2.8	4.0	0.57	0.88	1.59
4.7	4.0		0.86	1.58
11.1	4.0	0.53	0.65	1.61

$$NH(a^1\Delta) + A \longrightarrow 2N_2 + 2H \quad (2a)$$

$$NH(a^1\Delta) + A \longrightarrow NH_2 + N_3 \quad (2b)$$

$$NH(a^1\Delta) + A \longrightarrow N_2 + N_2H_2^* \quad (2c)$$

$$NH(a^1\Delta) + P \longrightarrow C_3H_7NH_2^* \quad (3)$$

$$NH(a^1\Delta) + P \longrightarrow NH(X^3\Sigma^-) + P \quad (4)$$

$$C_3H_7NH_2^* \longrightarrow CH_3 + C_2H_4NH_2 \quad (5)$$

$$C_3H_7NH_2^* \longrightarrow CH_4 + C_2H_4NH \quad (6)$$

$$C_3H_7NH_2^* \longrightarrow C_2H_4 + CH_3NH_2 \quad (7)$$

$$C_3H_7NH_2^* \longrightarrow C_2H_5 + CH_2NH_2 \quad (8)$$

$$C_3H_7NH_2^* \longrightarrow C_2H_6 + CH_2NH \quad (9)$$

$$C_3H_7NH_2^* \longrightarrow H_2 + C_3H_6NH \quad (10)$$

$$C_3H_7NH_2^* \longrightarrow NH_3 + C_3H_6 \quad (11)$$

$$C_3H_7NH_2^* + A \longrightarrow C_3H_7NH_2 + A \quad (12)$$

$$C_3H_7NH_2^* + P \longrightarrow C_3H_7NH_2 + P \quad (13)$$

$$CH_2NH_2 + A \longrightarrow CH_3NH_2 + N_3 \quad (14)$$

$$CH_2NH_2 + A \longrightarrow CH_3N_3 + NH_2 \quad (15)$$

$$H + A \longrightarrow H_2 + N_3 \quad (16)$$

$$H + A \longrightarrow NH_2 + N_2 \quad (17)$$

$$H + P \longrightarrow H_2 + C_3H_7 \quad (18)$$

$$R_1\ (R_1=CH_3, C_2H_5, C_3H_7, C_2H_4NH_2) + A \longrightarrow R_1H + N_3 \quad (19)$$

$$R_2NH_2\ (R_2=CH_3, C_2H_5, C_3H_7) + A \longrightarrow R_2NH_2\cdot HN_3 \quad (20)$$

$$R_3NH\ (R_3=CH_2, C_2H_4, C_3H_6) + A \longrightarrow R_3NH\cdot HN_3. \quad (21)$$

The succeeding reactions for species consisting of only nitrogen and hydrogen atoms are as follows:[1] $NH(X^3\Sigma^-)+A\rightarrow H_2+2N_2$ (22); $NH(X^3\Sigma^-)+A\rightarrow NH_2+N_3$ (23); $N_2H_2^*\rightarrow N_2H_2^{**}$ (24); $N_2H_2^*+A\rightarrow N_2+H_2+A$ (25); $N_2H_2^*+A\rightarrow NH_3+2N_2$ (26); $N_2H_2^{**}+A\rightarrow NH_3+2N_2$ (27); $NH_2+A\rightarrow NH_3+N_3$ (28); $NH_3+A\rightarrow NH_4N_3$ (29); $N_3+A\rightarrow N_3\cdot A$ (30); $2N_3\cdot A\rightarrow 3N_2+2A$ (31).

Since the formation of propyl- and isopropylamines has been confirmed by the gas-chromatographic and mass-spectrometric measurements, it is clear that the first excited singlet, NH($a^1\Delta$), formed by the photolysis of HN_3 at 313 nm[1] reacts to give propylamine upon insertion into a C–H bond of C_3H_8. The $C_3H_7NH_2^*$ formed by Reaction 3 implies vibrationally excited propylamine and isopropylamine, because both insertions into primary and secondary C–H bonds for C_3H_8 are possible.[10,11]

On the reactions of NH($a^1\Delta$) with C_3H_8 as a saturated hydrocarbon, a possible process other than the insertion is the collisional deactivation by C_3H_8 to NH($X^3\Sigma^-$). The collisional spin-relaxation process, Reaction 4, was also found for Xe,[1] CH_4,[4] and C_2H_6.[2] Kondo *et al.*[13] have proposed a hydrogen-abstraction reaction: $NH(a^1\Delta)+C_3H_8\rightarrow n$-$C_3H_7$ or i-$C_3H_7+NH_2$, from C_3H_8 by NH($a^1\Delta$) upon photolysis at 254 nm. However, this reaction can be disregarded in the present work at 313 nm, because hardly no n-C_3H_7 or i-C_3H_7 radicals were formed. A non-abstraction mechanism is also supported by the fact that the intercept of the plot of NH_3/N_2 *vs.* $[HN_3]/[C_3H_8]$ is zero on the photolysis of HN_3 in liquid propane at from 250 to 320 nm.[10]

Reactions 5 and 8 show the unimolecular decompositions of $C_3H_7NH_2^*$ by the radical mechanism; they were established by the facts that CH_3 and C_2H_5 radicals were detected as intermediates and that ϕ_{CH_4} and $\phi_{C_2H_6}$ were reduced drastically in the presence of NO. The formations of CH_4, C_2H_4, and C_2H_6 from $C_3H_7NH_2^*$ by the molecular mechanism are represented by Reactions 6, 7, and 9; they are explainable by the facts that they are formed even in the presence of NO.

On the photolysis in the presence of NO, no drastical decrease for ϕ_{H_2} was observed. This suggests the formation of H_2 by a molecular mechanism such as

Reaction 10. Reaction 11 is supported by the fact that C_3H_6 was formed even in the presence of NO. Kondo *et al.*[13] have presented two fragmentation reactions, n-$C_3H_7NH_2^* \rightarrow n$-$C_3H_7+NH_2$ and i-$C_3H_7NH_2^* \rightarrow i$-$C_3H_7+NH_2$, in the photolysis at 254 nm. However, the fragmentations seem to be negligible in the photolysis at 313 nm, because scarcely no n-C_3H_7 or i-C_3H_7 radicals were detected. Reactions 12 and 13 are the collisional deactivation processes of $C_3H_7NH_2^*$ by HN_3 and C_3H_8 to give stable propyl- and isopropylamines, as was found for $C_2H_5NH_2^*$.[2]

Reaction 15 was introduced to explain the facts that the formation of CH_3N_3 was found and that the formation ratio $CH_3NH_2/C_2H_5NH_2$ is considerably less than $\phi_{C_2H_6}/\phi_{CH_4}$, although the yields of Reactions 6, 7, and 9 are very small as compared with those of Reactions 5 and 8. Reactions 14 and 15 were also found in the photolysis of HN_3 with C_2H_6.[2] Reaction 18 was introduced because the H atoms formed by Reaction 2a, exothermic with 370 kJ mol^{-1}, are in a "hot" state, and also because the rate of hydrogen abstraction from C_3H_8 by H atoms is much faster than that for C_2H_6.[17]

Reaction 19 is the hydrogen-abstraction reaction by CH_3, C_2H_5, C_3H_7, and $C_2H_4NH_2$ radicals from HN_3. Reaction 20 was supported by the experimental fact that basic amines (R_2NH_2) react with acidic HN_3 in the vapor phase to give the azide salts ($R_2NH_2 \cdot HN_3$) as a white volatile powder.[2]

Because of the unstable products, the chemical structures of the CH_2NH, C_2H_4NH, and C_3H_6NH formed by the molecular mechanisms of Reactions 6, 9, and 10 are not clear. However, these products (R_3NH) may have a basic imino or amino group, and they may be stabilized by forming the azide salts ($R_3NH \cdot HN_3$) with acidic HN_3, as in Reaction 21. The reactions other than those mentioned above have been discussed previously[1] and so are omitted here.

Reaction Kinetics. The reaction kinetics were carried out in order to confirm the mechanisms of Reactions 1 to 31, and in order to obtain the rate-constant ratios for these reactions. Since the formation ratio, n-$C_3H_7NH_2/i$-$C_3H_7NH_2$, is independent of the total pressure, as may be seen in Table 1, the ratio of collisional deactivation to unimolecular decomposition for n-$C_3H_7NH_2^*$ may be said to be the same as that for i-$C_3H_7NH_2^*$. Therefore, it is possible to treat the reaction kinetics for n-$C_3H_7NH_2^*$ and i-$C_3H_7NH_2^*$ collectively.

Regarding the formations of CH_4, C_2H_6, and C_2H_4, Eqs. I and II can be derived:

$$\phi_{C_2H_6}/\phi_{CH_4} = (k_8+k_9)/(k_5+k_6) \qquad \text{(I)}$$

$$\phi_{C_2H_4}/\phi_{CH_4} = k_7/(k_5+k_6) \qquad \text{(II)}$$

Plots of $\phi_{C_2H_6}/\phi_{CH_4}$ and $\phi_{C_2H_4}/\phi_{CH_4}$ *vs.* $[HN_3]/[C_3H_8]$ are shown in Fig. 5; both ratios are constant regardless of the $[HN_3]/[C_3H_8]$ ratio and the total pressure.

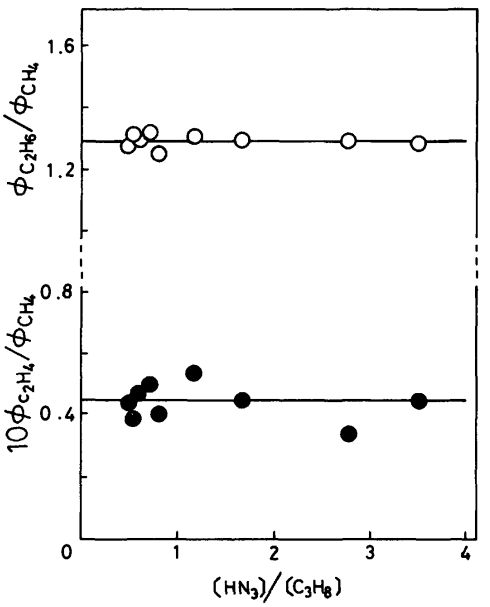

Fig. 5. Plots of $\phi_{C_2H_6}/\phi_{CH_4}$ (○) and $10\phi_{C_2H_4}/\phi_{CH_4}$ (●) *vs.* $[HN_3]/[C_3H_8]$.

When the quantum yields of CH_4 and C_2H_6 in the presence of NO, $\phi_{CH_4}(NO)$ and $\phi_{C_2H_6}(NO)$, are compared with those without NO, these relations:

$$\phi_{CH_4}(NO)/\phi_{CH_4} = k_6/(k_5+k_6) = 0.098 \qquad \text{(III)}$$

$$\phi_{C_2H_6}(NO)/\phi_{C_2H_6} = k_9/(k_8+k_9) = 0.028 \qquad \text{(IV)}$$

are obtained. From the values in Fig. 5 and Eqs. III and IV, k_6/k_5=0.109, k_7/k_5=0.050, k_8/k_5=1.39, and k_9/k_5=0.040 can be derived.

For the formations of CH_4 and (CO_2), Eq. V can be derived:

$$\frac{\phi_{(CO_2)}}{\phi_{CH_4}} = 2 + \frac{k_7+k_8k_{14}/(k_{14}+k_{15})+k_9+3k_{10}}{k_5+k_6} + \frac{3k_{12}[HN_3]}{k_5+k_6} + \frac{3k_{13}[C_3H_8]}{k_5+k_6} \qquad \text{(V)}$$

Plots of $\phi_{(CO_2)}/\phi_{CH_4}$ *vs.* P_{HN_3} or $P_{C_3H_8}$ are shown in Fig. 6. By using the k_{15}/k_{14}=0.852 obtained previously,[2] k_{10}/k_5=1.20, k_{12}/k_5=666 dm^3 mol^{-1}, and k_{13}/k_5=860 dm^3 mol^{-1} can be obtained from the intercepts and the slopes in Fig. 6.

Equation VI can be derived for the formations of N_2, H_2, (N), and CH_4:

$$\frac{\phi_{(N)}+3\phi_{H_2}-\phi_{N_2}}{3\phi_{CH_4}} = \frac{k_6+k_7+k_9+2k_{10}+k_{11}}{k_5+k_6} + \frac{k_{13}[M]}{k_5+k_6}, \qquad \text{(VI)}$$

where:

$$[M] = [C_3H_8] + (k_{12}/k_{13})[HN_3].$$

A plot of $(\phi_{(N)}+3\phi_{H_2}-\phi_{N_2})/3\phi_{CH_4}$ *vs.* P_M is shown in Fig. 7; k_{11}/k_5=4.72 was obtained from the intercept.

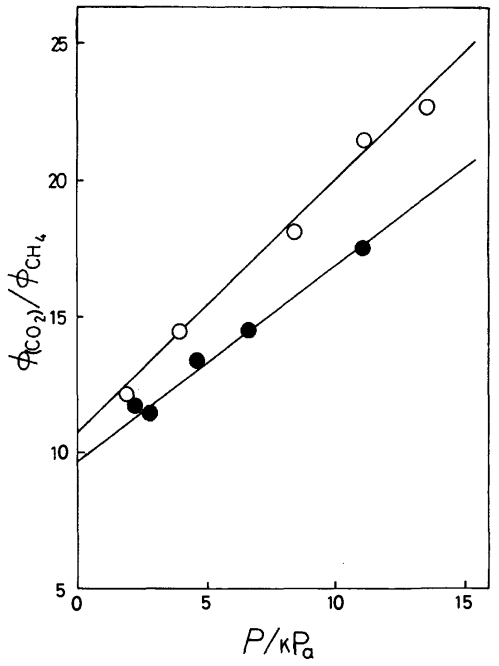

Fig. 6. Pressure dependences of $\phi_{(CO_2)}/\phi_{CH_4}$. ○, Measured as a function of C_3H_8 pressure at 6.7 kPa of HN_3; ●, measured as a function of HN_3 pressure at 4.0 kPa of C_3H_8.

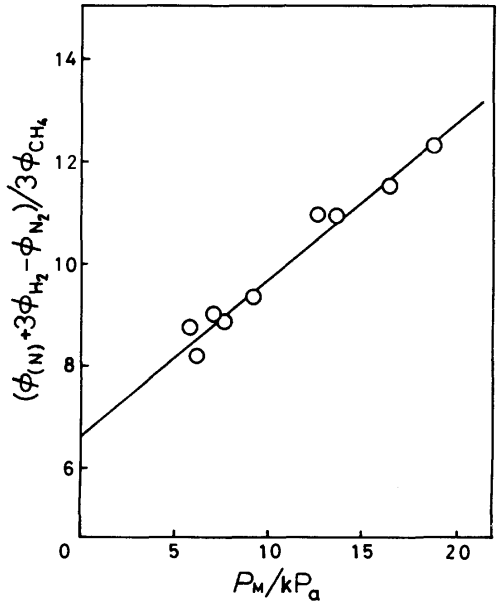

Fig. 7. Plot of $(\phi_{(N)}+3\phi_{H_2}-\phi_{N_2})/3\phi_{CH_4}$ *vs.* P_M.

Regarding the formation of amines, Eqs. VII and VIII can be derived:

$$\frac{CH_3NH_2}{C_2H_5NH_2} = \frac{k_7}{k_5} + \frac{k_8}{k_5}\frac{k_{14}}{k_{14}+k_{15}} \qquad \text{(VII)}$$

$$\frac{n\text{-}C_3H_7NH_2+i\text{-}C_3H_7NH_2}{C_2H_5NH_2} = \frac{k_{13}}{k_5}[M] \qquad \text{(VIII)}$$

Plots of $CH_3NH_2/C_2H_5NH_2$, (n-$C_3H_7NH_2$+i-$C_3H_7NH_2$)/$C_2H_5NH_2$, and n-$C_3H_7NH_2$/i-$C_3H_7NH_2$ *vs.* P_M are shown in Fig. 8. It may be found in Fig. 8 that the formation ratios of $CH_3NH_2/C_2H_5NH_2$ and n-$C_3H_7NH_2$/i-$C_3H_7NH_2$ are constant, regardless of the P_M, and that the (n-$C_3H_7NH_2$+i-$C_3H_7NH_2$)/$C_2H_5NH_2$ formation ratio is proportionate to P_M. The average value of the n-$C_3H_7NH_2$/i-$C_3H_7NH_2$ formation ratio was 1.55. The average value of $CH_3NH_2/C_2H_5NH_2$ is in accord with the value calculated using k_7/k_5=0.050, k_8/k_5=1.39, and k_{15}/k_{14}=0.852. The value of k_{13}/k_5 obtained from the slope in Fig. 8 is also consistent with those obtained from Figs. 6 and 7.

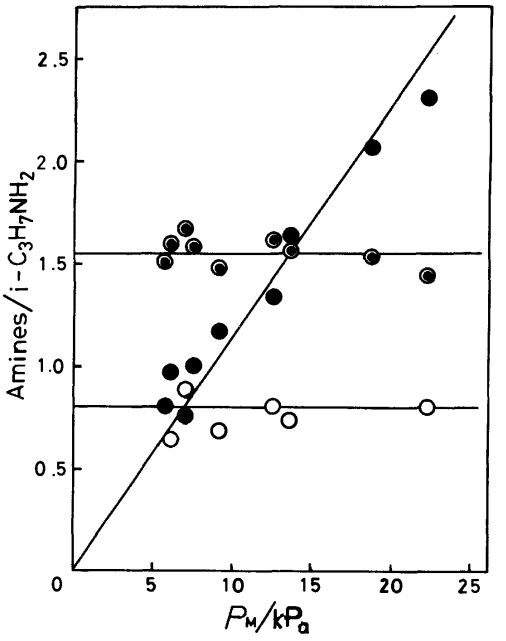

Fig. 8. Pressure dependences of $CH_3NH_2/C_2H_5NH_2$ (○), n-$C_3H_7NH_2$/i-$C_3H_7NH_2$ (⊙), and (n-$C_3H_7NH_2$+i-$C_3H_7NH_2$)/$3C_2H_5NH_2$ (●).

Regarding the formation of N_2, H_2, (N), and CH_4, Eqs. IX and X can be derived:

$$\left(\frac{\phi_{H_2}+\phi_{(N)}/4}{\phi_{CH_4}} - \frac{k_{10}}{k_5+k_6}\right)\Big/\alpha = 1 + \frac{k_4}{k_3} + \frac{k_2+k_{2a}}{k_3}\frac{[HN_3]}{[C_3H_8]} \qquad \text{(IX)}$$

$$\left(\frac{\phi_{N_2}+\phi_{H_2}}{\phi_{CH_4}} - \frac{3k_5+3k_8+k_{10}}{k_5+k_6}\right)\Big/4\alpha = \frac{1}{4} + \frac{k_4}{k_3} + \frac{k_2+k_{2a}}{k_3}\frac{[HN_3]}{[C_3H_8]}, \qquad \text{(X)}$$

where:

$$k_2 = k_{2a} + k_{2b} + k_{2c}$$

and:

$$\alpha = \frac{k_5+k_6+k_7+k_8+k_9+k_{10}+k_{11}+k_{12}[HN_3]+k_{13}[C_3H_8]}{k_5+k_6}.$$

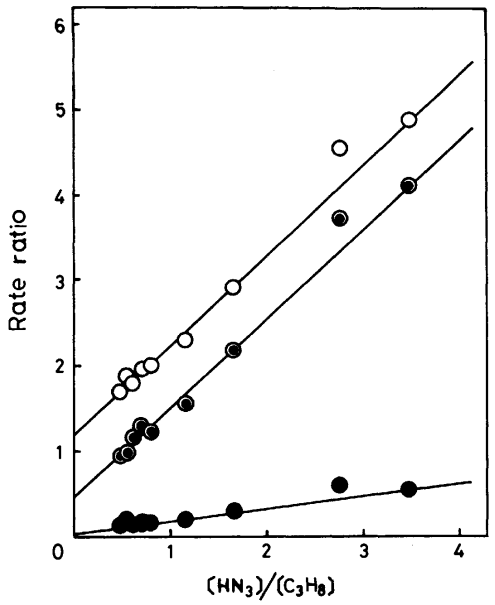

Fig. 9. Plots of the rate ratios *vs.* $[HN_3]/[C_3H_8]$. ○, $[(\phi_{H_2}+\phi_{(N)}/4)/\phi_{CH_4}-k_{10}/(k_5+k_6)]/\alpha$; ⊙, $[(\phi_{N_2}+\phi_{H_2})/\phi_{CH_4}-(3k_5+3k_8+k_{10})/(k_5+k_6)]/4\alpha$; ●, $[\phi_{H_2}/\phi_{CH_4}-k_{10}/(k_5+k_6)]/\alpha-\beta$.

Plots of $[(\phi_{H_2}+\phi_{(N)}/4)/\phi_{CH_4}-k_{10}/(k_5+k_6)]/\alpha$ and $[(\phi_{N_2}+\phi_{H_2})/\phi_{CH_4}-(3k_5+3k_8+k_{10})/(k_5+k_6)]/4\alpha$ *vs.* $[HN_3]/[C_3H_8]$ are shown in Fig. 9. From the intercept and the slope for Eq. IX and the $k_{2a}/k_2=0.336$ obtained previously,[1] $k_3/k_2=1.28$ and $k_4/k_2=0.262$ were obtained. The same values were also obtained for Eq. X.

For the formations of H_2 and CH_4, Eq. XI can be derived:

$$\left(\frac{\phi_{H_2}}{\phi_{CH_4}}-\frac{k_{10}}{k_5+k_6}\right)\Big/\alpha-\beta=\frac{k_4}{k_3}\frac{k_{22}}{k_{22}+k_{23}}+\frac{k_{2c}}{k_3}\frac{k_{25}}{k_{24}/[HN_3]+k_{25}+k_{26}}\frac{[HN_3]}{[C_3H_8]}, \quad \text{(XI)}$$

where:

$$\beta=\frac{2k_{2a}}{k_3}\frac{k_{16}[HN_3]+k_{18}[C_3H_8]}{(k_{16}+k_{17})[HN_3]+k_{18}[C_3H_8]}\frac{[HN_3]}{[C_3H_8]}.$$

A plot of $[\phi_{H_2}/\phi_{CH_4}-k_{10}/(k_5+k_6)]/\alpha-\beta$ against $[HN_3]/[C_3H_8]$ is also shown in Fig. 9. The solid circles denote the values of $[\phi_{H_2}/\phi_{CH_4}-k_{10}/(k_5+k_6)]/\alpha-\beta$ calculated using the experimental values of ϕ_{H_2}/ϕ_{CH_4}. The lowest straight line represents the calculated values for the right side of Eq. XI. In these calculations, the values obtained above and the values obtained previously[1] of $k_{2a}/k_2=0.336$, $k_{2c}/k_2=0.414$, $k_{17}/k_{16}=1.15$, $k_{23}/k_{22}=3.22$, $k_{24}/k_{25}=2.27\times10^{-4}$ mol dm^{-3}, and $k_{26}/k_{25}=1.19$ were used. As is shown in Fig. 9, the best fit for the experimental and calculated values was obtained when $k_{18}/k_{16}=0.51$.

Comparisons of Rate Constants. The specific rates of Reactions 12 and 13 can be estimated from these equations:

Table 2. Calculated values of k_z and k_5 at 30°C

M	σ_M	$\varepsilon_{M\text{-}M}/k$	k_z	$k_5(\eta=1)$
	Å	K	10^{14} cm^3 mol^{-1} s^{-1}	10^8 s^{-1}
HN_3	3.96[a]	240[a]	3.08	4.63
C_3H_8	4.84[b]	300[b]	3.90	4.53

a) Ref. 2. b) Ref. 19.

$$k_{12}=(\eta k_z)_{HN_3} \quad \text{(XII)}$$

$$k_{13}=(\eta k_z)_{C_3H_8}. \quad \text{(XIII)}$$

Here, k_z is the collision number of $C_3H_7NH_2$* per second and η is the collisional stabilization efficiency. The values of k_z can be calculated by means of the Lennard-Jones collision frequency:

$$k_z=N_A\sigma_{B\text{-}M}^2(8\pi kT/\mu_{B\text{-}M})^{1/2}\Omega_{B\text{-}M}^{(2,2)*}, \quad \text{(XIV)}$$

as has been described previously.[2] The values of $\Omega_{B\text{-}M}^{(2,2)*}$ can conveniently be tabulated[18] as a function of $kT/\varepsilon_{B\text{-}M}$ with the Lennard-Jones well depth, $\varepsilon_{B\text{-}M}=(\varepsilon_{B\text{-}B}\varepsilon_{M\text{-}M})^{1/2}$. The $\sigma_{B\text{-}M}$ is given by $\sigma_{B\text{-}M}=(\sigma_B+\sigma_M)/2$.

Assuming that the σ_B and $\varepsilon_{B\text{-}B}/k$ values of *n*-$C_3H_7NH_2$ are the same as those of *i*-$C_3H_7NH_2$, the values of $\sigma_B=5.04$ Å and $\varepsilon_{B\text{-}B}/k=380$ K for both propyl- and isopropylamines were estimated in the light of those for *n*-C_4H_{10},[19] *i*-C_4H_{10},[20] *n*-C_3H_7OH,[21] and $(CH_3)_2N$-NH_2.[22] The calculated values of k_z at 30°C are shown in Table 2. The $(k_z)_{C_3H_8}/(k_z)_{HN_3}$ ratio is almost equal to the experimentally obtained ratio, $(k_{13}/k_5)/(k_{12}/k_5)$. This means that the $C_3H_7NH_2$* is deactivated with every collision ($\eta=1$), just as in the collisional deactivations by CO_2, HN_3, and C_2H_6 of $C_2H_5NH_2$*.[2] In the photolysis of HN_3 in liquid C_3H_8 at the Dry Ice–methanol temperature, no decomposition products of $C_3H_7NH_2$* formed by the insertion could be found.[10] The main reason for this may be that the concentration of deactivator molecules is about 3500 times higher than that in the present system.

The absolute value of k_5 can be estimated from:

$$k_5=(\eta k_z)_{C_3H_8}/(k_{13}/k_5)_{obsd}. \quad \text{(XV)}$$

It was estimated to be 4.53×10^8 s^{-1} from the calculated value of k_z for C_3H_8, the observed value of k_{13}/k_5, and $\eta=1$. Similarly, the absolute value of k_5 obtained from k_z for HN_3, the observed value of k_{12}/k_5, and $\eta=1$ was 4.63×10^8 s^{-1}, as is shown in Table 2. From the average value of $k_5=4.58\times10^8$ s^{-1} and the rate-constant ratios of k_6/k_5 and others, the absolute values of k_6, k_7, k_8, k_9, k_{10}, and k_{11} were estimated to be 0.50, 0.23, 6.4, 0.18, 5.5, and 21.6×10^8 s^{-1} respectively. On the other hand, the rate-constant of the unimolecular decomposition of $C_2H_5NH_2$* formed by the reaction of $NH(a^1\Delta)$ with C_2H_6 was 9.8×10^9 s^{-1} for $C_2H_5NH_2^* \rightarrow CH_3+CH_2NH_2$ and 3.7×10^8 s^{-1} for $C_2H_5NH_2^* \rightarrow CH_3CN+2H_2$.[2]

TABLE 3. RELATIVE REACTIVITIES FOR THE REACTIONS OF NH($a^1\Delta$) WITH X AT 30°C

X	k_r/k_2	k_d/k_2	$(k_r+k_d)/k_2$	k_d/k_r
HN_3[a]	1.000	0	1.000	0
Xe[a]	0	0.187	0.187	—
C_2H_4[b]	1.637	0	1.637	0
CH_4[c]	0.175	0.177	0.352	1.011
C_2H_6[d]	0.334	0.217	0.551	0.650
C_3H_8[e]	1.279	0.262	1.541	0.205

a) Ref. 1. b) Ref. 3. c) Ref. 4. d) Ref. 2. e) This work.

The half-life of $C_3H_7NH_2$* obtained from the $\tau=\ln 2/(k_5+k_6+k_7+k_8+k_9+k_{10}+k_{11})$ relation is 1.78×10^{-10} s. On the other hand, the half-life of $C_2H_5NH_2$* is 6.8×10^{-11} s.[2] Thus, the half-life of $C_3H_7NH_2$* is 2.6 times longer than that of $C_2H_5NH_2$*. This trend is reasonable, because the rate of unimolecular decomposition decreases with an increase in the internal degree of freedom of the activated molecule.[23]

When the reactions of NH($a^1\Delta$) with a reactant (X) are represented by these general expressions:

$$NH(a^1\Delta) + X \longrightarrow \text{Products} \qquad k_r$$

$$NH(a^1\Delta) + X \longrightarrow NH(X^3\Sigma^-) + X, \quad k_d$$

the values of k_r/k_2, k_d/k_2, $(k_r+k_d)/k_2$, and k_d/k_r for C_3H_8 are shown in Table 3 together with those obtained previously.[1-4] It may be seen in Table 3 that k_r/k_2, k_d/k_2, and $(k_r+k_d)/k_2$ increase, but k_d/k_r decreases, with an increase in the carbon number in a saturated hydrocarbon molecule. Meanwhile, the k_r/k_2 ratio of the saturated hydrocarbons consisting of only the σ bond is, in general, low as compared with that of C_2H_4 having the π bond.

The values of $(k_r+k_d)/k_2$, $((k_r+k_d)/k_2)_{rel}$, $k_r/(k_r+k_d)$, and $(k_r/k_2)_{rel}$ for saturated hydrocarbons are shown in Table 4, where $((k_r+k_d)/k_2)_{rel}$ and $(k_r/k_2)_{rel}$ indicate the values of $(k_r+k_d)/k_2$ and k_r/k_2 relative to those of C_2H_6. It may be seen in Table 4 that the values of $((k_r+k_d)/k_2)_{rel}$, $k_r/(k_r+k_d)$, and $(k_r/k_2)_{rel}$ for our works are similar to those obtained by Tsunashima *et al.*[10] and by Kajimoto *et al.*[12,13] However, the values of $(k_r+k_d)/k_2$ obtained in the liquid phase by Tsunashima *et al.*[10] are much less than those in our works. The main reason for the large discrepancy seems to be due to the difference in phase (vapor and liquid), as has been discussed previously.[2] The values of $(k_r+k_d)/k_2$ obtained at 254 nm by Kajimoto *et al.*[12,13] are also small as compared with our values. This dissimilarity may be due to the effect of the wavelength.

The formation ratio of n-$C_3H_7NH_2$/i-$C_3H_7NH_2$ was 1.55, regardless of the total pressure. This ratio means that the insertion rate of NH($a^1\Delta$) into a secondary C–H bond of C_3H_8 is 1.94 times faster than that into a primary C–H bond. This value is well consistent with the value of 1.9 obtained by Tsunashima *et al.*[10] Kondo *et al.*[13] have obtained the insertion efficiency ratio of 1.5 in the photolysis at 254 nm. Tsunashima *et al.*[10] have also found that the insertion efficiency into a tertiary C–H bond of isobutane is 2.3 times higher than that for a primary C–H bond. In general, the insertion efficiency per C–H bond, ζ_i(C–H), can be represented by this equation:

$$\zeta_i(\text{C–H}) = f_i(k_r/k_2)_{obsd}/F, \qquad \text{(XVI)}$$

where $F=n_pf_p+n_sf_s+n_tf_t$. Here, n_p, n_s, and n_t indicate the number of primary, secondary, and tertiary C–H bonds respectively in a saturated hydrocarbon molecule. Similarly f_p, f_s, and f_t denote the relative efficiencies for the insertions into primary, secondary, and tertiary C–H bonds respectively. f_i means f_p, f_s, or f_t. If f_p is fixed as a basis, then f_p becomes unity.

The values of f_i, F, $(k_r/k_2)_{obsd}$, and ζ_i(C–H) are shown in Table 5, together with the ratio of the ζ_i(C–H) of X to the ζ_i(C–H) of CH_4, $\zeta_i(\text{C–H})_X/\zeta_p(\text{C–H})_{CH_4}$. The bond-dissociation energies of these C–H bonds, D_i(C–H), are also listed in Table 5. These bond-dissociation energies were calculated assuming that the standard heats of the formation of CH_4, C_2H_6, C_3H_8, i-C_4H_{10}, c-C_3H_6, H, CH_3, C_2H_5, n-C_3H_7, i-C_3H_7, i-C_4H_9, t-C_4H_9, and c-C_3H_5 were −74.9, −84.7, −103.8, −134.5, 53.3, 218.0, 145.2,[24] 117.2,[25] 87.9,[26] 73.6,[27] 58.6,[27] 35.1,[28] and 255.2[27] kJ mol^{-1} respectively. The plot of $\zeta_i(\text{C–H})_X/\zeta_p(\text{C–H})_{CH_4}$ *vs.* D_i(C–H) is shown in Fig. 10; it shows that $\zeta_i(\text{C–H})_X/\zeta_p(\text{C–H})_{CH_4}$ increases with a decrease in D_i(C–H), especially in the range lower than 420 kJ mol^{-1}. From the results shown in Fig. 10, it may be possible to predict the over-all insertion efficiency for reactions of NH($a^1\Delta$) with saturated hy-

TABLE 4. COMPARISONS OF $(k_r+k_d)/k_2$, $k_r/(k_r+k_d)$, AND k_r/k_2

X	$\frac{k_r+k_d}{k_2}$	$\left(\frac{k_r+k_d}{k_2}\right)_{rel}$	$\frac{k_r}{k_r+k_d}$	$\left(\frac{k_r}{k_2}\right)_{rel}$
CH_4	0.352[a]	0.64[a]	0.497[a]	0.524[a]
C_2H_6	0.551[a] 0.0093[b] 0.13[c]	1.00 1.00 1.00	0.606[a] 0.86[b] 0.7[c]	1.00 1.00 1.00
C_3H_8	1.54[a] 0.026[b] 0.45[c]	2.80[a] 2.78[b] 3.46[c]	0.830[a] 0.79[b] 0.95[c]	3.83[a] 2.6[b] 4.7[c]
i-C_4H_{10}	0.033[b]	3.58[b]	0.75[b]	3.1[b]
c-C_3H_6				1.05[d]

a) Refs. 2 and 4, and this work. b) Ref. 10. $(k_r+k_d)/k_2$ was calculated from their values of $k_r/(k_r+k_d)$ and k_2/k_r. c) Refs. 12 and 13. Included in k_r the specific rate of the abstraction reaction, NH($a^1\Delta$)+C_2H_6→NH_2+C_2H_5 or NH($a^1\Delta$)+C_3H_8→NH_2+C_3H_7. d) Ref. 11.

TABLE 5. INSERTION EFFICIENCIES PER C-H BOND

X	Type of C-H bond[a]	f_i	F	$\left(\frac{k_r}{k_2}\right)_{obsd}$	ζ_i(C-H)	$\frac{\zeta_i(C\text{-}H)_X}{\zeta_p(C\text{-}H)_{CH_4}}$	D_i(C-H)[b] kJ mol^{-1}
CH_4	p	1	4	0.175[f]	0.0438	1.000	438.0
C_2H_6	p	1	6	0.334[g]	0.0557	1.272	419.8
C_3H_8	p	1	9.87	1.279[c]	0.1296	2.959	409.7
	s	1.94[c]			0.2508	5.727	395.5
c-C_3H_6	s	1[d]	6	0.351[h]	0.0585	1.337	419.9
i-C_4H_{10}	p	1	11.3	1.525[i]	0.1350	3.082	411.1
	t	2.3[e]			0.3104	7.088	387.6

a) p, s, and t denote the primary, secondary, and tertiary C-H bonds respectively. b) Calculated from the standard heats of the formation of hydrocarbons, H, and radicals; see text. c) This work. d) f_i was regarded as unity, because cycropropane has the secondary hydrogen alone. e) Ref. 10. f) Ref. 4. g) Ref. 2. h) Calculated from $(k_r(C_2H_6)/k_2)_{obsd}$=0.334 (Ref. 2) and $(k_r(c\text{-}C_3H_6)/k_r(C_2H_6))_{obsd}$=1.05 (Ref. 11). i) The value of 1.525 (0.334×3.83×3.1/2.6) was estimated from the data of $(k_r(C_2H_6)/k_2)_{obsd}$=0.334 (Ref. 2), $(k_r(C_3H_8)/k_2)_{rel}$=3.83 (Table 4), $(k_r(i\text{-}C_4H_{10})/k_2)_{rel}$= 3.1 (Ref. 10), and $(k_r(C_3H_8)/k_2)_{rel}$=2.6 (Ref. 10).

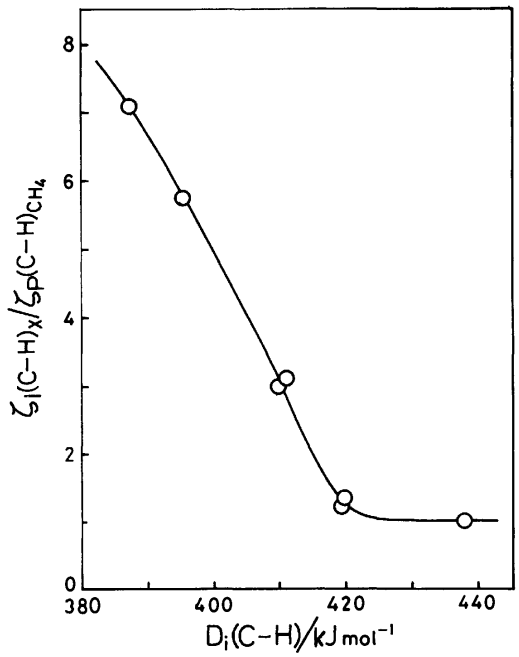

Fig. 10. Plot of $\zeta_i(C\text{-}H)_X/\zeta_p(C\text{-}H)_{CH_4}$ *vs.* $D_i(C\text{-}H)$.

drocarbons.

The absolute value of k_2 which was observed by Piper, Krech, and Taylor,[29] k_2(PKT), is 1.084×10^{14} cm^3 mol^{-1} s^{-1}. If this value is applied, the absolute rate-constant for the over-all quenching of NH($a^1\Delta$) by X, k_q(X), can be calculated by this equation:

$$k_q(X) = \frac{(k_r+k_d)_X}{k_2}k_2(PKT). \quad \text{(XVII)}$$

The values of k_q(X) calculated from $(k_r+k_d)_X/k_2$ in Table 3 and k_2(PKT) are shown in Table 6 ; the Table shows that k_q(X) increases with an increase in the carbon number in a X molecule.

On the other hand, the maximum rate-constant of the bimolecular reaction in the gas phase, k_b, can be calculated by this equation:[30]

$$k_b = \frac{2\Gamma(1-2/s)N_A}{\sigma}\left(\frac{2\pi kT}{\mu}\right)^{1/2}\left[\frac{(s-2)A}{2kT}\right]^{2/s}, \quad \text{(XVIII)}$$

when the intermolecular attractive potential, u, is expressed by $u=-A/r^s$. The attractive potential constant, A, can be calculated from the dispersion term reported by Slater and Kirkwood[31] and the induction term for NH and X:

$$A = \frac{3he\alpha_{NH}\alpha_X}{4\pi m_0^{1/2}[(\alpha/N_e)_{NH}^{1/2}+(\alpha/N_e)_X^{1/2}]} + \alpha_X\mu_D(NH)^2, \quad \text{(XIX)}$$

as has been described previously.[3] The values of k_b calculated using s=6, $\Gamma(2/3)$=1.354, σ=1, T=303 K, $\alpha_{NH}=1.38\times10^{-24}$ cm^3,[32] μ_D(NH)=1.627 debye,[33] and N_e(NH)=6 are shown in Table 6, together with $k_q(X)/k_b$. It may be found in Table 6 that k_b increases slightly with an increase in the carbon number in X, while $k_q(X)/k_b$ increases considerably from 1/10 for CH_4 to 1/2.6 for C_3H_8.

The absolute and relative quenching rates of C(2^1D_2),[34,35] O(2^1D_2),[36-38] S(3^1D_2),[39,40] and CH_2 ($^1A_1$)[41,42] by CH_4, C_2H_6, C_3H_8, and others have been observed widely. These over-all quenching-rate constants are shown in Table 7, together with those for

TABLE 6. COMPARISONS OF k_q(X), k_b, AND $k_q(X)/k_b$ AT 303 K

X	k_q(X) 10^{14} cm^3 mol^{-1} s^{-1}	α 10^{-24} cm^3	N_e	A 10^{-67} J cm^6	k_b 10^{14} cm^3 mol^{-1} s^{-1}	$k_q(X)/k_b$
CH_4	0.382	2.60[a]	8	92.9	3.83	0.0997
C_2H_6	0.597	4.48[b]	14	160.7	4.05	0.148
C_3H_8	1.671	6.35[b]	20	228.2	4.30	0.389

a) Ref. 18b, p. 950. b) P. Sliwinski, *Z. Phys. Chem. (Frankfurt am Main)*, **63**, 263 (1969).

TABLE 7. COMPARISONS OF THE OVER-ALL QUENCHING-RATE CONSTANTS AT ABOUT 300 K

Quencher	Quenching-rate constant/10^{-11} cm^3 molecule^{-1} s^{-1}				
	C(2^1D_2)	O(2^1D_2)	S(3^1D_2)	NH($a^1\Delta$)	$CH_2(^1A_2)$
HN_3				18[a]	
Xe	11[a]	7.2[a]	4.0[a]	3.4[a]	1.6[h]
C_2H_4	37[a]	35.6[a]	25[a]	29.5[a]	15.0[i]
CH_4	21.0[b]	14.0[c]	8.6[e]	6.3[f]	7.0[i]
C_2H_6		26.0[a]	4.3[a]	9.9[a]	19.0[i]
C_3H_8		33.3[d]		27.8[g]	24.0[i]

a) Ref. 3. b) Ref. 35. c) Ref. 38. d) Estimated from $k_q^{O(^1D)}(C_2H_6)=26.0\times10^{-11}$ cm^3 molecule^{-1} s^{-1} and $k_q^{O(^1D)}(C_3H_8)/k_q^{O(^1D)}(C_2H_6)=1.28$ (Ref. 37). e) Ref. 39. f) Ref. 4. g) This work. h) Ref. 41. i) Ref. 42.

NH($a^1\Delta$). Table 7 shows that the absolute quenching rates of NH($a^1\Delta$) by Xe, C_2H_4, CH_4, C_2H_6, and C_3H_8 are very similar to those of C($^1D_2$), O($^1D_2$), S($^1D_2$), and $CH_2(^1A_1)$, which are isoelectronic with NH($a^1\Delta$).

Summary. From the formation ratio of the *n*-$C_3H_7NH_2$ and *i*-$C_3H_7NH_2$ produced in the photolysis of HN_3 at 313 nm and 30 °C in the presence of C_3H_8, the insertion efficiency of NH($a^1\Delta$) into a secondary C–H bond of C_3H_8 was found to be 1.94 times higher than that of a primary C–H bond. The relative insertion efficiencies per C–H bond were 1.00 for CH_4, 1.27 for C_2H_6, 2.96(p) and 5.73(s) for C_3H_8, 1.34 for *c*-C_3H_6, and 3.08(p) and 7.09(t) for *i*-C_4H_{10}, judging from comparisons of the present and previous results.[2,4,10,11] Here, p, s, and t indicate the primary, secondary, and tertiary C–H bonds. The insertion efficiency per C–H bond increases with a decrease in the C–H bond dissociation energy. The insertion-rate constants, as estimated from the absolute reaction rate of NH($a^1\Delta$) with HN_3,[29] were 1.90, 3.62, and 13.9×10^{13} cm^3 mol^{-1}s^{-1} for CH_4, C_2H_6, and C_3H_8 respectively. The over-all quenching-rate constants of NH($a^1\Delta$) by CH_4, C_2H_6, C_3H_8, C_2H_4,[3] and Xe[1] were, respectively, 3.82, 5.97, 16.7, 17.7, and 2.03×10^{13} cm^{3}mol^{-1}s^{-1}; they were found to be very similar to those of C($^1D_2$), O($^1D_2$), S($^1D_2$), and $CH_2(^1A_1)$, which are isoelectronic with NH($a^1\Delta$).

The author is grateful to Mr. Jun Fukuchi for his cooperation.

References

1) S. Kodama, *Bull. Chem. Soc. Jpn.*, **56**, 2348 (1983).
2) S. Kodama, *Bull. Chem. Soc. Jpn.*, **56**, 2355 (1983).
3) S. Kodama, *Bull. Chem. Soc. Jpn.*, **56**, 2363 (1983).
4) S. Kodama, *Bull. Chem. Soc. Jpn.*, **58**, 2891 (1985).
5) E. D. Miller, Ph. D. Dissertation, Catholic University of America, Washington, D. C., 1961.
6) R. A. Back, *J. Chem. Phys.*, **40**, 3493 (1964).
7) J. L. Brash and R. A. Back, *Can. J. Chem.*, **43**, 1778 (1965).
8) W. C. Richardson and D. W. Setser, *Can. J. Chem.*, **47**, 2725 (1969).
9) R. S. Konar, S. Matsumoto, and B. DEB. Darwent, *Trans. Faraday Soc.*, **67**, 1698 (1971).
10) S. Tsunashima, J. Hamada, M. Hotta, and S. Sato, *Bull, Chem. Soc. Jpn.*, **53**, 2443 (1980).
11) J. Hamada, S. Tsunashima, and S. Sato, *Bull. Chem. Soc. Jpn.*, **55**, 1739 (1982).
12) O. Kajimoto and T. Fueno, *Chem. Phys. Lett.*, **80**, 484 (1981).
13) O. Kondo, J. Miyata, O. Kajimoto, and T. Fueno, *Chem. Phys. Lett.*, **88**, 424 (1982).
14) J. M. Kruse and M. G. Mellon, *Anal. Chem.*, **25**, 446 (1953).
15) K. Fukui, I. Fujita, and K. Kuwata, *Bull. Chem. Soc. Jpn.*, **45**, 2278 (1972).
16) A. T. James, *Biochem. J.*, **52**, 242 (1952); A. T. James and A. J. P. Martin, *Analyst*, **77**, 915 (1952).
17) W. E. Jones, S. D. MacKnight, and L. Teng, *Chem. Rev.*, **73**, 407 (1973). The hydrogen-abstraction rate by H atoms from C_3H_8 is about ten times faster than that from C_2H_6 at 30 °C.
18) a) J. O. Hirschfelder, R. B. Bird, and E. L. Spotz, *J. Chem. Phys.*, **16**, 968 (1948); b) J. O. Hirschfelder, C. F. Curtiss, and R. B. Bird, "Molecular Theory of Gases and Liquids," Wiley (1954), p. 1126.
19) L. S. Tee, S. Gotoh, and W. E. Stwart, *Ind. Eng. Chem., Fundam.* **5**, 356 (1966).
20) Ref. 18b, p. 1112.
21) J. Roberts, *Brit. Chem. Eng.*, **8**, 753 (1963).
22) E. Wilhelm and R. Battino, *J. Chem. Phys.*, **55**, 4012 (1971).
23) B. S. Rabinovitch and D. W. Setser, *Adv. Photochem.*, **3**, 1 (1964).
24) P. Warneck, *Z. Naturforsch., Teil A*, **26**, 2047 (1971).
25) A. L. Castelhano, P. R. Marriott, and D. Griller, *J. Am. Chem. Soc.*, **103**, 4262 (1981).
26) F. P. Lossing and G. P. Semeluk, *Can. J. Chem.*, **48**, 955 (1970).
27) J. A. Kerr, *Chem. Rev.*, **66**, 465 (1966).
28) M. Rossi and D. M. Golden, *Int. J. Chem. Kinet.*, **11**, 969 (1979).
29) L. G. Piper, R. H. Krech, and R. L. Taylor, *J. Chem. Phys.*, **73**, 791 (1980).
30) K. Yang and T. Ree, *J. Chem. Phys.*, **35**, 588 (1961).
31) J. C. Slater and J. G. Kirkwood, *Phys. Rev.*, **37**, 682 (1931); J. G. Kirkwood, *Physik. Z.*, **33**, 57 (1932).
32) Estimated by assuming the atomic polarizabilities of 0.401×10^{-24} cm^3 for H and 0.975×10^{-24} cm^3 for N.
33) P. E. Cade and W. M. Huo, *J. Chem. Phys.*, **45**, 1063 (1966).
34) D. Husain and L. J. Kirsch, *Trans. Faraday Soc.*, **67**,

2886 (1971).
35) D. Husain and L. J. Kirsch, *Trans. Faraday Soc.*, **67**, 3166 (1971).
36) W. B. DeMore, *J. Phys. Chem.*, **73**, 391 (1969); R. J. Cvetanović, *Can. J. Chem.*, **52**, 1452 (1974); G. E. Streit, C. J. Howard, A. L. Schmeltekopf, J. A. Davidson, and H. I. Schiff, *J. Chem. Phys.*, **65**, 4761 (1976); J. A. Davidson, H. I. Schiff, T. J. Brown, G. E. Streit, and C. J. Howard, *ibid.*, **69**, 1213 (1978).
37) I. S. Fletcher and D. Husain, *Can. J. Chem.*, **54**, 1765 (1976).
38) J. A. Davidson, H. I. Schiff, G. E. Streit, J. R. McAfee, A. L. Schmeltekopf, and C. J. Howard, *J. Chem. Phys.*, **67**, 5021 (1977).
39) H. E. Gunning and O. P. Strausz, *Adv. Photochem.*, **4**, 143 (1966); P. Fowles, M. deSorgo, A. J. Yarwood, O. P. Strausz, and H. E. Gunning, *J. Am. Chem. Soc.*, **89**, 1352 (1967).
40) D. L. Little, A. Dalgleish, and R. J. Donovan, *Discuss. Faraday Soc.*, **53**, 211 (1972).
41) M. N. R. Ashfold, M. A. Fullstone, G. Hancock, and G. W. Ketley, *Chem. Phys.*, **55**, 245 (1981).
42) A. O. Langford, H. Petek, and C. B. Moore, *J. Chem. Phys.*, **78**, 6650 (1983).

 © 1985 The Chemical Society of Japan Bull. Chem. Soc. Jpn., 58, 2911—2916 (1985)

Shock-tube Studies of N_2O Decomposition and N_2O-H_2 Reaction

Yoshiaki HIDAKA,* Hirokazu TAKUMA,† and Masao SUGA†

Advanced Instrumentation Center for Chemical Analysis, Ehime University, Bunkyo-chō, Matsuyama 790

†*Department of Chemistry, Faculty of Science, Ehime University, Bunkyo-chō, Matsuyama 790*

(Received February 6, 1985)

N_2O decomposition and N_2O-H_2 reaction were studied behind incident and reflected shock waves in the temperature range 1450—2200 K and pressure range 0.6—3.5 atm using both single-pulse and time-resolve techniques. A computer-simulation study was performed to determine the rate-constant expressions of important elementary reactions. Computer calculations showed that the values of the rate constant for $N_2O+O \xrightarrow{k_2} N_2+O_2$ and $N_2O+O \xrightarrow{k_3} NO+NO$ (cited in current papers) are too low. The rate-constant expressions were found to be $k_2=7.0\times10^{14}\exp(-28\,\text{kcal}/RT)$ cm^3 mol^{-1} s^{-1} and $k_3=5.6\times10^{14}\exp(-28\,\text{kcal}/RT)$ cm^3 mol^{-1} s^{-1}. The rate constant expression for $N_2O+H \xrightarrow{k_4} N_2+OH$, was found to be $k_4=1.5\times10^{14}\exp(-15\,\text{kcal}/RT)$ cm^3 mol^{-1} s^{-1}.

The decomposition of N_2O and the reaction of N_2O-H_2 have been extensively studied at high temperatures (above 1000 K) by many workers.[1-18] Previous experimental studies have shown that an initiation step in both the N_2O decomposition and the N_2O-H_2 reaction is the breaking of the nitrogen-oxygen bond.

$$N_2O + M \xrightarrow{k_1} N_2 + O + M. \quad (1)$$

The values of k_1 reported are in agreement within a factor of approximately 2 to 3. However, the reported activation energies (E_1's) scatter between 61 and 40 kcal/mol. Even in recent years, Sulzmann *et al.*,[18] Endo *et al.*,[17] Dean *et al.*[16] and Roth and Just[15] have reported E_1=56, 57.6, 51.7, and 61 kcal/mol, respectively. The oxygen atoms generated by reaction (1) react with N_2O or H_2 as follows,

$$N_2O + O \xrightarrow{k_2} N_2 + O_2, \quad (2)$$

$$N_2O + O \xrightarrow{k_3} NO + NO, \quad (3)$$

$$H_2 + O \xrightarrow{k_7} OH + H. \quad (7)$$

Values of the rate constants published for reactions (2) and (3) are widespread. The reported ratios of k_3/k_2 separate almost into two groups over the same temperature range; one is k_3/k_2=0.9—1.2,[5,6,8,13,18] other is k_3/k_2=0.3—0.5.[3,10] The reported values of the rate constant of reaction (4) are also scattered.

$$N_2O + H \xrightarrow{k_4} N_2 + OH. \quad (4)$$

In this study, we wish to report the rate constants k_1, k_2, k_3, and k_4, with which we can interpret both the N_2O decomposition and the N_2O-H_2 reaction over the temperature range 1450—2200 K.

Experimental

The apparatus and procedures have already been described in detail,[19,20] so only a brief description is given here. Infrared emission through two 0.8 mm slits and an interference filter (λ_{max}=4.68 μm, half-width=0.1 μm) was observed with a Fujitsu IV-200C4 InSb detector to study the time variation of the N_2O concentration. In runs using reflected shock waves, reacted gas mixtures were introduced to a pre-evacuated container made of Aluminum (25 cc in volume) through a valve near an end-plate after about 20 s from the infrared-emission measurements. The reacted mixtures were analyzed on a mass spectrometer (Nihondensi-JMS-01SG-2). In the analysis, the isotope ^{36}Ar (0.34%), which was included in ^{40}Ar, was used as a reference material. Since the concentration of ^{36}Ar was comparable to NO and O_2 concentrations produced in our experiment, it was possible to accurately determine these concentrations. The energy of the ionizing electron beam was 12 eV. The use of such a relatively low voltage has a major advantage. The formation of fragment ions was almost completely eliminated, thus simplifying the interpretation of the mass spectra. A measurement of absolute concentrations is possible using relative sensitivity factors. These factors were determined under conditions as close as possible to those used in the determination of the product concentration during the N_2O decomposition and the N_2O-H_2 reaction. The analyzed peaks of the reacted gases were of mass numbers, 44, 32, and 30, corresponding to N_2O, O_2, and NO, respectively. No peak was found at a mass number of 46 (NO_2). In the determination of the O_2 concentration, the background signal at a mass number of 32 was substracted from the O_2 signal.

Data interpretation was achieved by computer simulation. The computer calculations[20,21] and the effective heating time used[20] were essentially the same as described previously. The temperature of the reaction system increases as the reaction progressed because the decomposition of N_2O and N_2O-H_2 reaction are exothermic. This temperature change might affect the N_2O emission intensity greatly. Hence, simulations of time-variations were carried out with programs that considered the dependence of the emission-intensity on temperature.

The compositions of employed reaction mixtures were as follows: (A) 2.0% N_2O, 98.0% Ar; (B) 2.0% N_2O, 1.0% H_2, 97.0% Ar; (C) 1.0% N_2O, 0.5% H_2, 98.5% Ar; (D) 0.5% N_2O, 1.0% H_2, 98.5% Ar. The N_2O decomposition with mixture (A) and N_2O-H_2 reaction with mixtures (B)—(D) were studied behind incident (1500 K$<T_2<$2200 K, 0.6 atm$<P_2<$1.1 atm) and reflected (1500 K$<T_5<$2100 K, 2.0 atm$<$

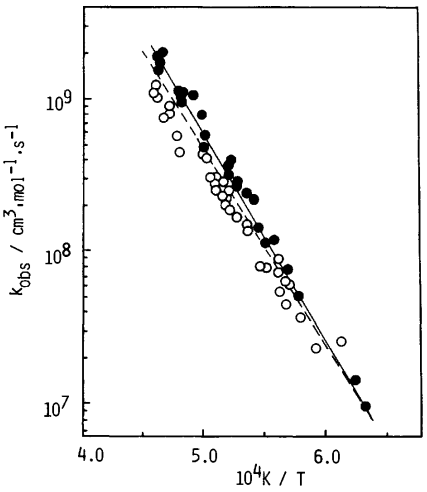

Fig. 1. Arrhenius plot showing comparison of the present results with data of other works.
●: Observed behind incident shock waves with mixture (A); ○: Observed behind reflected shock waves with mixture (A); ——: $2k_1$ reported by Roth and Just; ------: $2k_1$ observed by Olschewski *et al.* and Endo *et al.*.

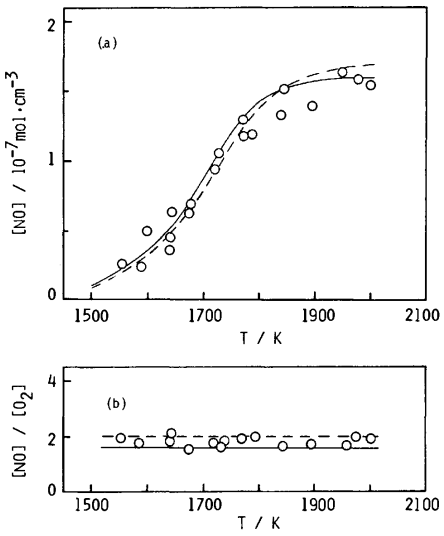

Fig. 2. Relationship between $[N_2O]$ or $[NO]/[O_2]$ and temperature.
○: Observed with mixture (A); ——: computed with Table 1; ------: computed with the mechanism and rate constant expressions reported by Baulch *et al.*.

P_5<3.5 atm) shock waves with both single-pulse and time-resolve techniques. H_2 and Ar, specified to be 99.9 and 99.99% pure, respectively, were obtained from commercial cylinders and were used without further purification. The N_2O gas obtained from a commercial cylinder was purified by trap-to-trap distillations. The purity (99.9% or higher) was confirmed by a gas-chromatographic analysis.[19]

Results and Discussion

The time variation of the N_2O concentration at 4.68 μm was observed behind incident and reflected shock waves with mixture (A). The observed rate constant, k_{obsd}, for N_2O decomposition was calculated from the intial slope (within 20 μs) of the time variation. The values of $k_{obsd}=2.6\times10^{15}\exp(-60.7\,\text{kcal}/RT)$ $cm^3 mol^{-1}s^{-1}$ obtained with incident shock waves are in good agreement with the values of the $2k_1$ reported by Roth and Just,[15] and are similar to the $2k_1$ reported by Olschewski *et al.*[4] and Endo *et al.*[17] as shown in Fig. 1. The values of $k_{obsd}=6.24\times10^{14}\exp(-56.9\,\text{kcal}/RT)$ $cm^3 mol^{-1}s^{-1}$ obtained with reflected shock waves, however, are slightly lower than those obtained with incident shock waves. The deviation between the two is larger at high temperatures than at low temperatures. This shows that the initial temperatures (within 20 μs) behind reflected shock waves are somewhat lower than those calculated from incident shock speeds. The real gas temperatures at the reflected shock front are considered to be 70±40 K lower than those calculated. This finding is consistent with that reported by Tsuchiya and Kuratani.[25] This phenomenon has also been reported by several workers,[22-25] who showed that the pressure and temperature slowly increased with time after the arival of reflected shock waves. The average temperature during the reaction time (about 1000 μs) was also shown to be comparable to the temperature calculated from the incident shock speed.[25] The temperature under our experimental condition, however, should be examined, since the temperature parameter is very important in calculating the rate constants. Since the mechanism and rate constant expressions of the H_2-O_2 reaction are known very well, it is possible to check the average temperature behind reflected shock waves by comparing the observed results with the calculated ones. By using the same method as mentioned in a previous paper,[21] the temperatures behind reflected shock waves were examined. The average temperature during 100—1200 μs was shown to be almost the same as that

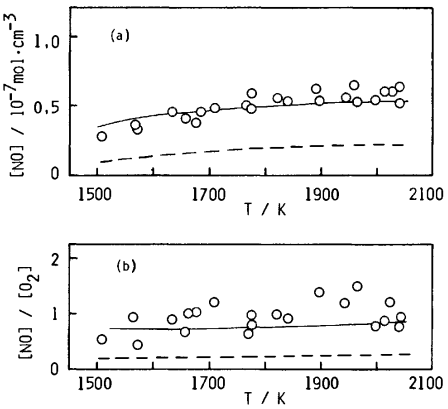

Fig. 3. Realtionship of [NO] or $[NO]/[O_2]$ and temperature.
○: Observed with mixture (B); ——: computed with Table 1; ------: computed with the mechanism and rate constant expressions reported by Baulch *et al.*.

TABLE 1. ELEMENTARY REACTIONS AND RATE CONSTANT EXPRESSIONS[a)]

	Reaction	A	n	E	Ref.[b)]
1	$N_2O+M=N_2+O+M$	1.4×10^{15}	0.0	61200	15
2	$N_2O+O=N_2+O_2$	7.0×10^{14}	0.0	28000	This work
3	$N_2O+O=NO+NO$	5.6×10^{14}	0.0	28000	This work
4	$N_2O+H=N_2+OH$	1.5×10^{14}	0.0	15000	This work
5	$H_2+M=H+H+M$	2.2×10^{12}	0.5	92600	
6	$O_2+M=O+O+M$	1.8×10^{11}	0.5	95700	
7	$H_2+O=OH+H$	2.2×10^{14}	0.0	13700	
8	$H_2+OH=H_2O+H$	5.2×10^{13}	0.0	6500	
9	$O_2+H=OH+O$	1.2×10^{17}	−0.9	16630	
10	$O_2+H+M=HO_2+M$	2.5×10^{15}	0.0	0	
11	$HO_2+H=OH+OH$	2.5×10^{14}	0.0	1900	
12	$HO_2+OH=H_2O+O_2$	5.0×10^{13}	0.0	1000	
13	$OH+OH=H_2O+O$	5.5×10^{13}	0.0	7000	
14	$OH+H+M=H_2O+M$	7.5×10^{23}	−2.6	0	

a) Rate constants in the form, $AT^n\exp(-E/RT)$, in cm, mol, cal, and K units. b) The reference for reactions 5—14 is Ref. 20.

calculated from the incident shock speed. Hence, the temperature T calculated from incident shock speeds was employed for the analysis of quenched reactant and product concentrations. The product distribution was determined by analyzing the product concentration on a mass spectrometer. The relationships of [NO] and [NO]/[O_2] *vs.* T with mixture (A) are shown in Figs. 2(a) and (b), respectively. The ratio [NO]/[O_2] is about 2 over the temperature range 1600—2000 K. This also shows $k_2/k_3\fallingdotseq1$. This result is in agreement with those of Gutman *et al.*,[5] Borisov,[6] Barton and Dove,[8] Dean,[13] and Sulzmann *et al.*[18] The relationships [NO] and [NO]/[O_2] *vs.* T with mixture (B) are shown in Figs. 3(a) and (b), respectively. In mixture (A), [NO] and [NO]/[O_2] observed at each temperature can be interpreted using the mechanism and rate-constant expressions recommended by Baulch *et al.*[26] However, the results calculated with Table 1 are better than those. While, in mixture (B),[NO] and [NO]/[O_2] observed at each temperature are bigger than those obtained by using their mechanism and rate constant expressions as shown in Figs. 3(a) and (b). The findings show that the values of k_2 and k_3 are too small to interpret these. When $k_2=7.0\times10^{14}\exp(-28\,\mathrm{kcal}/RT)$ $\mathrm{cm^3\,mol^{-1}\,s^{-1}}$ and $k_3=5.6\times10^{14}\exp(-28\,\mathrm{kcal}/RT)$ $\mathrm{cm^3\,mol^{-1}\,s^{-1}}$ are employed, the computed results are in good agreement with those measured as may be shown in Figs. 3(a) and (b). Our k_2 and k_3 values are about six, four, six and nineteen times those recommended by Baulch *et al.*[26] and recently reported Monat *et al.*,[14] Sulzmann *et al.*[18] and Dean *et al.*,[16] respectively, as may be shown in Fig. 4. While our values of k_2 and k_3 are found (Fig. 4) to be similar to and about one half of those reported by Lin and Bauer[27] and Henrici and Bauer,[7] respectively. Henrici and Bauer evaluated the k_3 value from a study with a N_2O–H_2 mixture and reported that the k_2 and k_3 values estimated in the study of N_2O decomposition were too low to account for the rate of formation of NO in the shock-heated reaction of N_2O with H_2. It is found that the values of k_2 and k_3

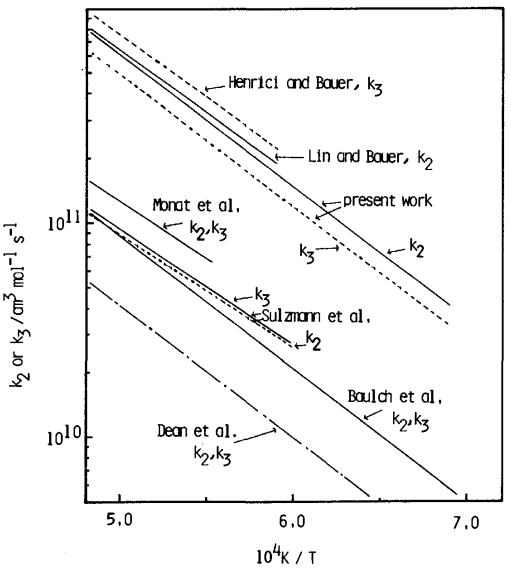

Fig. 4. Comparison of our k_2 or k_3 value with those reported in recent years. —·—: Extraporated value of Dean *et al.*.

reported in the study of N_2O decomposition are fairly smaller than those estimated with the N_2O–H_2 mixture.

The values of k_2 and k_3 reported by several workers except for Henrici and Bauer[7] and Lin and Bauer[27] have been estimated from results regarding the N_2O decomposition: The rate constants were obtained from measurements of the N_2O or NO concentration. When values between Dean's value[16] and ours are used as the rate constants of k_2 and k_3, the product concentrations calculated for the N_2O decomposition scarcely vary as may be seen in Figs. 2(a) and 2(b). The values of k_2 and k_3 between these are found to be insensitive regarding N_2O decomposition. If the values of k_2 and k_3 were estimated from the study of N_2O decomposition, one might always find smaller values for k_2 and k_3 than the real values. Thus, it is difficult to estimate relieable values of k_2 and k_3 from the study of N_2O decomposition. However, in the N_2O–H_2 reaction, the values of k_2 and k_3 are sensitive to

TABLE 2. ELEMENTARY REACTION AND RATE CONSTANT EXPRESSIONS

Reaction	A	n	E
$NO+OH=NO_2+H$	1.0×10^{14}	0.0	1200
$NO+N_2O=NO_2+N_2$	2.0×10^{14}	0.0	50000
$NO+O_2=NO_2+O$	1.0×10^{12}	0.0	45000
$H+NO+M=HNO+M$	3.1×10^{15}	0.0	−7000
$OH+HNO=NO+H_2O$	8.5×10^{13}	0.0	0
$H+NO_2=NO+OH$	5.4×10^{14}	0.0	1740
$N_2O+H=NO+NH$	1.0×10^{11}	0.0	30000
$NO_2+M=NO+O+M$	1.0×10^{16}	0.0	65000

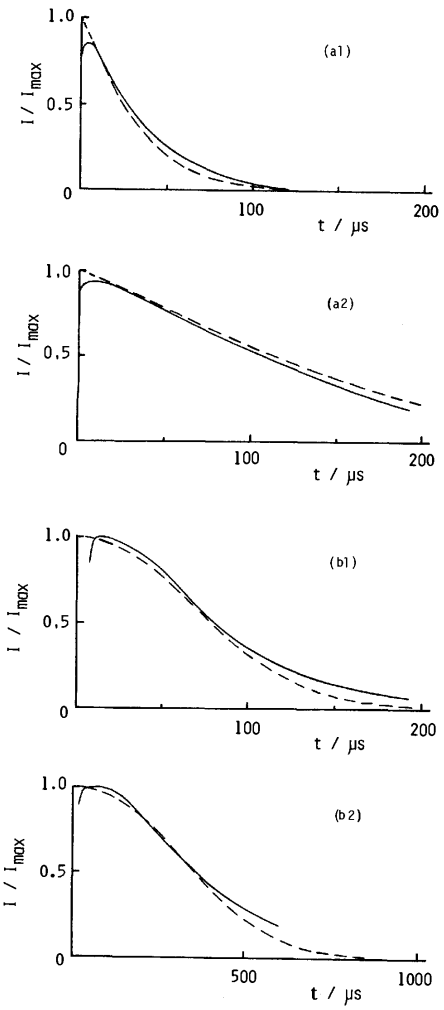

Fig. 5. Comparison of N_2O profiles computed using Table 1 with observed emissions. The broken and solid lines show values computed with Table 1 and observed, respectively.
(a1) Mixture (A), T_2=2151 K; (a2) mixture (A), T_2=1923 K; (b1) mixture (D), T_5=1774 K; (b2) mixture (D), T_5=1559 K.

product concentrations. In the N_2O–H_2 reaction, therefore, we can estimate relieable values for k_2 and k_3. Using these values, one can also interpret the results in the N_2O decomposition well, as shown in Fig. 2(a) and 2(b), Fig. 5(a) and Fig. 6(a).

The k_2 and k_3 expressions may be accurate to within ±20% under our experimental conditions. Systematic errors in the instrumentation and kinetic model may contribute this much again. We therefore, suggest that our k_2 and k_3 expressions are probably accurate to within ±50%.

Reaction (4) is also important for the interpretation of the H_2–N_2O reaction. The value of the rate constant k_4 strongly influences the N_2O consumption. When the expression $k_4=1.5\times10^{14}\exp(-15\,\mathrm{kcal}/RT)$ $\mathrm{cm^3\,mol^{-1}\,s^{-1}}$ was employed, the calculated results were in good agreement with the observed ones. This value is about one half of that reported by Fenimore and Jones[1] and is about twice that reported by Dixon-Lewis and Williams[28] or by Baulch *et al.*[26] The value of k_4 is also considered to be probably accurate to within ±50%.

Several reactions for the production and consumption of NO have been reported. They are shown in Table 2. The calculations with mechanism including reactions of Table 2 were carried out and the influence of these reactions on the NO concentration produced was examined. These reactions were found to be unimportant under our experimental conditions.

A comparison of the observed emission profiles with the computed N_2O profiles with mixtures (A) and (D) is shown in Figs. 5(a1)—(b2). In both the N_2O decomposition and the H_2–N_2O reaction, the curves calculated with Table 1 are in good agreement with the observed ones within experimental accuracy. t_{80}, t_{50}, and t_{20} were defined as the elapsed times between the shock arrival and the 80, 50, and 20% consumptions of the maximum $[N_2O]$, respectively. τ was also defined as the elapsed time between the shock arrival and the onset of the rapid decrease in the N_2O concentration.[29] Plots of τ, t_{80}, and t_{50} or t_{20} *vs.* $1/T$ for mixtures (A),(B), and (D) are shown in Figs. 6(a)—(c). The calculted τ, t_{80}, t_{50}, and t_{20} are in good agreement with experimental ones.

Henrici and Bauer[7] have measured the concentration profiles of OH in the reaction of H_2 with N_2O over the temperature range 1700—2600 K and over a total density 0.7×10^{-5}—1.4×10^{-5} mol $\mathrm{cm^{-3}}$. These are similar to our experimental conditions. Hence, we selected their results in order to check the OH concentration in the modeling. A comparison of calculated $[OH]_{max}/P_1$ with $[OH]_{max}/P_1$ measured by Henrich and Bauer[7] is shown in Fig. 7. The values computed using Table 1 explain their results well, as shown in Fig. 7. Hence, the values of k_2 and k_3, which are about six times those recommended by Baulch *et al.*,[26] are considered to be appropriate for an interpretation of the OH concentration in the N_2O–H_2 reaction.

Conclusion

N_2O decomposition and N_2O–H_2 reactions were studied behind incident and reflected shock waves in

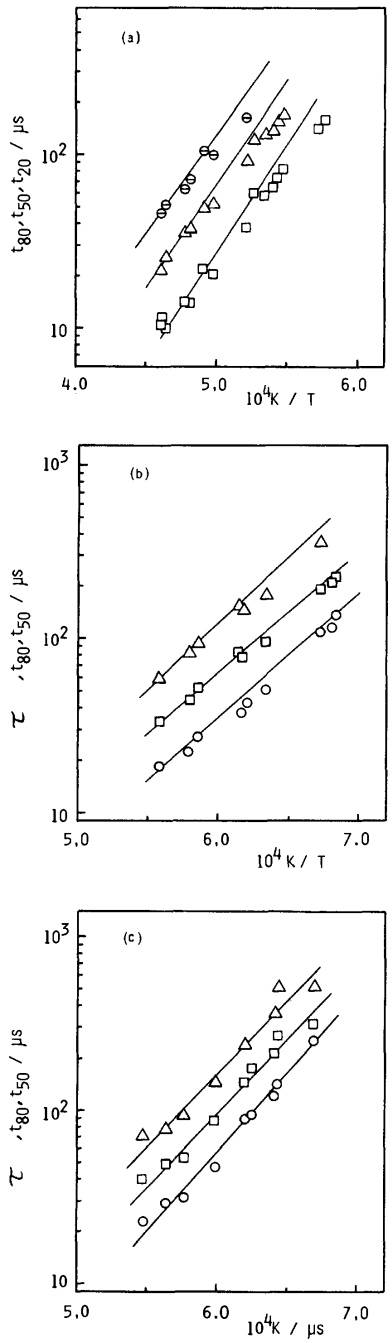

Fig. 6. Comparison of log t_{80}, log t_{50}, and log τ or log t_{20} computed using Table 1 with observed ones. The observed values at t_{20}, t_{50}, t_{80}, and τ are shown with symbols ⊖, △, □, and ○, respectively.
(a) results for mixture (A) behind incident shock waves; (b) results for mixture (B) behind incident shock waves; (c) results for mixture (D) behind reflected shock waves.

the temperature range 1450—2200 K with both single-pulse and time-resolve techniques. Our results support the value reported by Roth and Just[15] as the k_1 value. The rate constant expressions $k_2=7.0\times10^{14}$ exp(−28kcal/RT) $cm^3mol^{-1}s^{-1}$, $k_3=5.6\times10^{14}$ exp(−28 kcal/RT) $cm^3mol^{-1}s^{-1}$ and $k_4=1.5\times10^{14}$ exp(−15 kcal/RT) $cm^3mol^{-1}s^{-1}$ for reactions $N_2O+O\rightarrow N_2+O_2$,

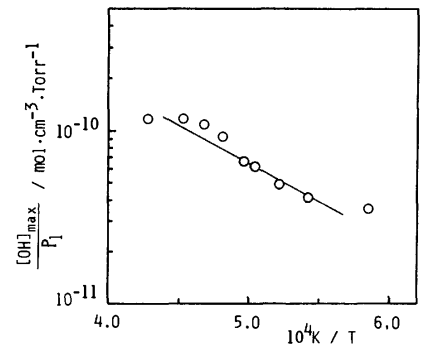

Fig. 7. Comparison of $[OH]_{max}/P_1$ calculated using Table 1 with $[OH]_{max}/P_1$ measured by Henrich and Bauer.
○: Observed by Henrich and Bauer; ——: computed with Table 1.

$N_2O+O\rightarrow NO+NO$ and $N_2O+H\rightarrow N_2+OH$ were derived, respectively.

References

1) C. P. Fenimore and G. W. Jones, *Symp. (Int.) Combust. Proc. 8th*, 1962, 127 (1963).
2) E. S. Fishburne and R. Edse, *J. Chem. Phys.*, **41**, 1297 (1964); **44**, 515 (1966).
3) W. Jost, K. W. Michel, J. Troe, and H. G. Wagner, *Z. Naturforsch*, **19a**, 59 (1964).
4) H. A. Olschewski, J. Troe, and H. G. Wagner, *Ber. Bunsenges. Phys. Chem.*, **70**, 450 (1966).
5) D. Gutman, R. L. Belford, A. J. Hay, and R. Pancirov, *J. Phys. Chem.*, **70**, 1793 (1966).
6) A. A. Borisov, *Kinetika i Kataliz*, **9**, 482 (1968).
7) H. Henrici and S. H. Bauer, *J. Chem. Phys.*, **50**, 1333 (1969).
8) S. C. Barton and J. E. Dove, *Can. J. Chem.*, **47**, 521 (1969).
9) D. Milks and R. A. Matula, *Sym. (Int.) Combust. Proc., 14th*, 1972, 83 (1973).
10) W. H. Lipkea, D. Milks, and R. A. Matula, *Combust. Sci. and Technol.*, **6**, 257 (1973).
11) J. E. Dove, W. S. Nip, and H. Teitelbaum, *Symp. (Int.) Combust. Proc. 15th*, 1974, 903 (1975).
12) E. A. Albers, K. Hoyermann, H. Schacke, K. J. Schmatjko, H. G. Wagner, and J. Wolfrum, *Symp. (Int.) Combust. Proc. 15th*, 1974, 765 (1975).
13) A. M. Dean, *Int. J. Chem. Kinet.*, **8**, 459 (1976).
14) J. P. Monat, R. K. Hanson, and C. H. Kruger, *Combust. Sci. and Technol.*, **16**, 21 (1977).
15) P. Roth and T. Just, *Ber. Bunsenges. Phys. Chem.*, **81**, 572 (1977).
16) A. M. Dean, D. C. Steiner, and E. E. Wang, *Combust. Flame*, **32**, 73 (1978).
17) H. Endo, K. Glanzer, and J. Troe, *J. Phys. Chem.*, **83**, 2083 (1979).
18) K. G. P. Sulzmann, J. M. Kline, and S. S. Penner, *Symp. (Int.) Shock Tube and Waves, Proc.* **12th**, 1979, 465 (1980).
19) Y. Hidaka, T. Chimori, S. Shiba, and M. Suga, *Chem. Phys. Lett.*, **111**, 181 (1984).
20) Y. Hidaka, S. Shiba, H. Takuma, and M. Suga, *Int. J.*

Chem. Kinet., **17**, 441 (1985).
21) Y. Hidaka, S. Takahashi, H. Kawano, M. Suga, and W. C. Gardiner, Jr., *J. Phys. Chem.*, **86**, 1429 (1982).
22) R. A. Strehlow and A. Cohen, *J. Chem. Phys.*, **30**, 257 (1959).
23) G. B. Skinner, *J. Chem. Phys.*, **31**, 268 (1959).
24) T. A. Brabbs, S. A. Zlatarich, and F. E. Belles, *J. Chem. Phys.*, **33**, 307 (1960).
25) S. Tsuchiya and K. Kuratani, *J. Chem. Phys.*, **42**, 2986 (1965).
26) D. L. Baulch, D. D. Drysdale, D. G. Horne, and A. C. Lloyd, "Evaluated Kinetic Data for High Temperature Reactions," Vol. 2, Butterworths, 1973.
27) M. C. Lin and S. H. Bauer, *J. Chem. Phys.*, **50**, 3377 (1969).
28) G. Dixon-Lewis and D. J. Williams, "Gas Phase Combust." ed by C. H. Bamford and C. F. H. Tipper, Elsevier 1977.
29) Y. Hidaka, Y. Tanaka, H. Kawano, and M. Suga, *Mass Spectroscopy*, **29**, 191 (1981).

 © 1985 The Chemical Society of Japan Bull. Chem. Soc. Jpn., 58, 2917—2922 (1985)

Pressure and Temperature Effects on Conformational Equilibria between Rotational Isomers. II. Isobutyl and *s*-Butyl Halides in Hexane and Methanol

Hiroyasu NOMURA* and Shinobu KODA

Department of Chemical Engineering, School of Engineering, Nagoya University, Chikusa-ku, Nagoya 464

(Received March 22, 1985)

The conformational changes in isobutyl halides (*i*-BuX) and *s*-butyl halides (*s*-BuX) in hexane and methanol have been analyzed by Raman spectroscopy as a function of temperature and pressure. The enthalpy and volume differences in the conformational changes from P_C (*trans*) to P_H (*gauche*) of *i*-BuX and from S_{HH}(*trans*) to $S_{HH'}$(*gauche* I) and to S_{CH}(*gauche* II) of *s*-BuX in the dissolved state have been obtained. The enthalpy and volume differences, ΔH and ΔV, of all the conformational changes depended on the solvents and the concentration in solution. In the solution of hexane, the ΔH ($P_C \rightarrow P_H$) of *i*-BuCl and *i*-BuBr both increased with a decrease in the concentration of *i*-BuX. The ΔV ($P_C \rightarrow P_H$) of *i*-BuCl increased with an increase in the contents of the solvents, hexane, but that of *i*-BuBr decreased. The concentration dependences of ΔH and ΔV were discussed on the basis of the intermolecular interactions. The relation between ΔH and ΔV was also discussed on the basis of thermodynamic consideration.

In our previous papers,[1,2] the conformational changes in some halogenoalkanes, such as 1,2-dihalogenoethane and butyl halides, in the pure liquid state have been analyzed by Raman spectroscopy as a function of temperature and pressure. The enthalpy and volume differences in the rotational isomers of these halogenoalkanes have been obtained.

In the dissolved state, it is well known that the enthalpy differences in the conformers are strongly related to some physical properties of the solvents, such as the dielectric constant and specific solute-solvent interactions in solutions.[3-5] It is also expected that the volume difference in the conformers in solution will depend on the solvent. There have been a few papers concerning this subject.[6,7] However, as their measurements were fragmentary and not systematic, they have not been sufficient to elucidate the solvent effects of the volume difference between the rotational isomers of a molecule.

In this paper, we will report the enthalpy and volume differences of the conformers of 1-halogeno-2-methylpropane and 2-halogenobutane (hereafter abbreviated as *i*-BuX and *s*-BuX; X=halogene) in hexane and methanol as obtained by Raman spectroscopy. These solvents, hexane and methanol, were chosen for the following reasons: (i) the dielectric constant of hexane is smaller than those of the halogenoalkanes investigated here, while that of methanol is larger, and (ii) hexane is an inert solvent for the halogenoalkanes, but the solvent methanol can be expected to interact with the halogenoalkanes.

We discussed the solvent effects and the concentration dependences of the enthalpy and volume differences of *i*-BuX and *s*-BuX in hexane and methanol. The relation between ΔH and ΔV was also discussed.

Experimental

The characteristic bands of the X-sensitive modes of each halogenoalkane have been well investigated and assigned to the rotational isomers.[8-13] The structures of the isomers concerned here are illustrated in Fig. 1, where their characteristic vibrational frequencies used are also given.

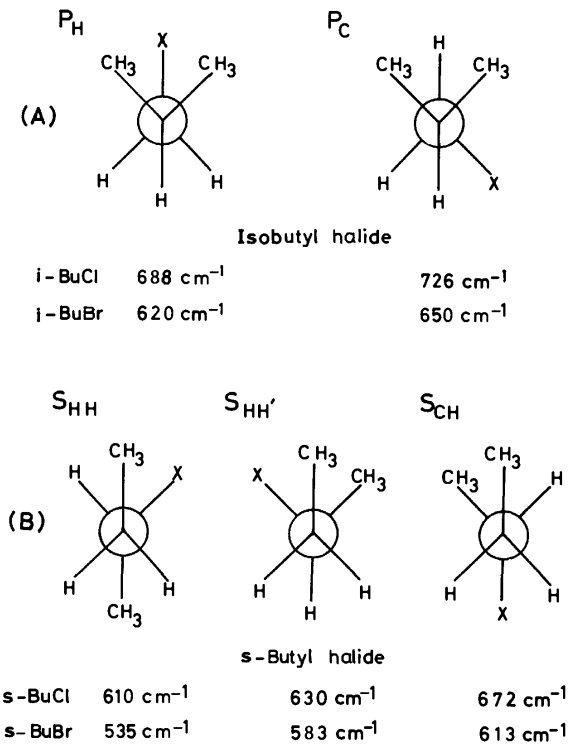

Fig. 1. Rotational isomers for butyl halides and the vibrational frequency of the C-X stretching mode, where X denotes Cl or Br.

Samples: The chemicals (commercial products) were purified by fractional distillation under reduced pressure. The solvents, hexane and methanol, were spectro-grade reagents (Nakarai Chemicals, Ltd.) and were used without further purification.

Raman Spectroscopy: The Raman spectra under high pressure were recorded using a laser Raman spectrometer, JEOL-Ul (manufactured by Japan Electron Optical Laboratory Co., Ltd.) and an argon-ion laser (NEC Co., Ltd.).

The pressure was measured by means of a Heise precision Bourdon-type gauge. The temperature dependence of the Raman spectra was measured at the atmospheric pressure, using a variable-temperature cell of the Harney-Miller type. The detailed experimental procedure and the data analysis have been described elsewhere.[1,2] The accuracy of the integrated intensities is within 3%.

Compressibility and Density Measurements: The densities of the solutions were measured by a pycnometer (20 cm^3) at temperatures from 15 to 30°C. The adiabatic compressibility was determined from the density and the sound velocity data using the Laplace equation. The sound velocity measurements of the solutions were carried out using an ultrasonic interferometer operating at a constant frequency of 5.000 MHz.

Results

For the samples investigated here, the Raman frequency of the X-sensitive stretching vibrational modes of each conformer did not change in the solutions of hexane and methanol, and it was independent of the temperature and pressure changes in the temperature and pressure ranges concerning in this work.

The equilibrium constant, K, of the conformational equilibrium, A⇌B, can be expressed as:[3]

$$K = \frac{n_B}{n_A} = \frac{I_B \Omega_A}{I_A \Omega_B} \tag{1}$$

where n is the number of molecules, I is the Raman intensity, and Ω is the absolute scattering cross-section. The suffixes A and B refer to the conformers. Assuming that the Ω_A/Ω_B ratio is independent of the temperature and pressure changes in the whole range of measurements, we can estimate the enthalpy and volume differences between the two conformers on the basis of Arrhenius and van't Hoff equations;

$$\Delta H = -R\left[\frac{\partial \ln [I_A/I_B]}{\partial [1/T]}\right] \tag{2}$$

$$\Delta V = -RT\left[\frac{\partial \ln [I_A/I_B]}{\partial P}\right] \tag{3}$$

As an illustration of typical data, Figs. 2 and 3 show $\ln[I_{PH}/I_{PC}]$ *vs.* $1/T$ and P plots for *i*-BuCl in hexane at 40 and 80 mol% of the *i*-BuCl solute. The enthalpy and volume differences, ΔH and ΔV, are estimated, respectively, from the slopes in Figs. 2 and 3. The values thus obtained are summarized in Tables 1 and 2, along with the data of these samples in the neat state previously.[2] For comparison, the enthalpy differences of these compounds in the gaseous state are also shown in Table 1.

As may be seen in Table 1 and 2, strong solvent and concentration dependences of ΔH and ΔV were observed. Especially in the case of *i*-BuBr, the ΔH in the neat state showed a negative value, −0.7±0.1 kJ mol^{-1}. It seems unreasonable, but the ΔH of *i*-BuBr

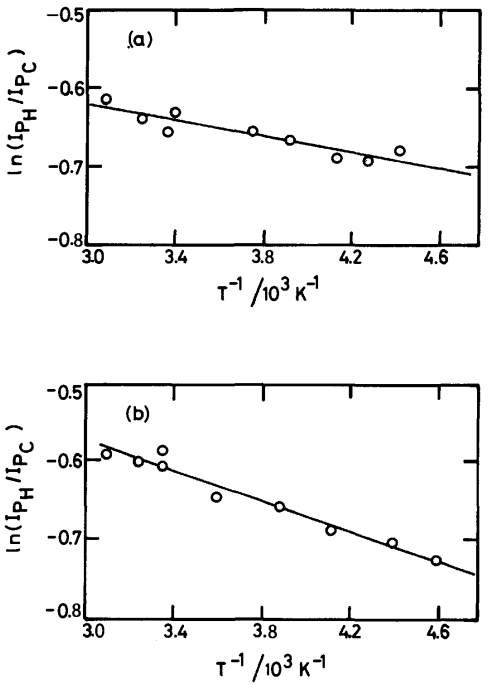

Fig. 2. Relationships between the logarithmic ratio of integrated intensities and temperature. (a) 80 mol% of *i*-BuCl in hexane. (b) 40 mol% of *i*-BuCl in hexane.

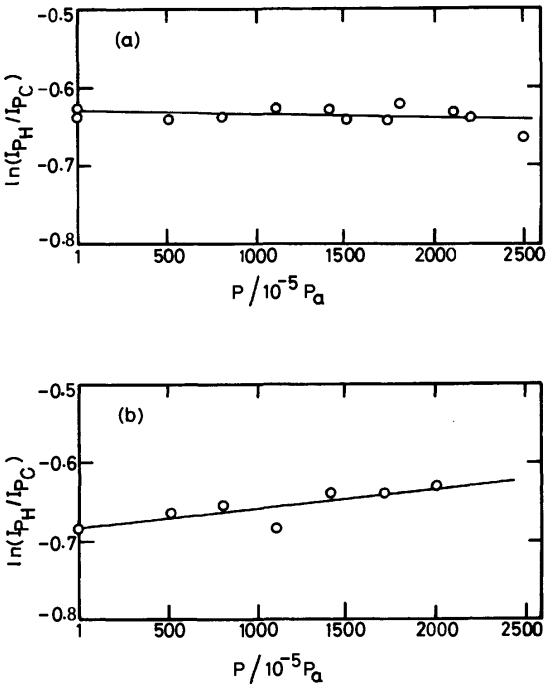

Fig. 3. Relationships between the logarithmic ratio of integarated intensities and pressure. (a) 80 mol% of *i*-BuCl in hexane. (b) 40 mol% of *i*-BuCl in hexane.

increased with a decrease in the contents of *i*-BuBr in solutions. Moreover, the positive volume difference of *i*-BuCl also decreased with an increase in the contents of hexane and changed to a negative value, −0.6₂±

Table 1. Conformational enthalpy differences, ΔH (kJ mol^{-1}) in hexane and methanol

	Neat[a]	In hexane			In methanol	Gas
		80 mol%	60 mol%	40 mol%	40 mol%	
i-BuCl						$0.6_1\pm0.4$
$P_C\rightarrow P_H$	0.0	$0.4_5\pm0.05$	$0.5_9\pm0.08$	$0.7_7\pm0.04$	$0.2_9\pm0.07$	$0.9_6\pm0.08$[b]
i-BuBr						
$P_C\rightarrow P_H$	-0.7 ± 0.1	$-0.1_9\pm0.04$	$-0.1_0\pm0.04$	$0.0_3\pm0.03$	$-0.2_5\pm0.06$	1.25 ± 1.3[b]
s-BuCl						
$S_{HH}\rightarrow S_{HH'}$	2.3 ± 0.4			2.3 ± 0.2	1.3 ± 0.1	
$S_{HH}\rightarrow S_{CH}$	2.5 ± 0.4			2.1 ± 0.1	1.9 ± 0.07	
s-BuBr						
$S_{HH}\rightarrow S_{HH'}$	2.7 ± 0.4			2.9 ± 0.2	3.0 ± 0.1	2.3 ± 0.2
$S_{HH}\rightarrow S_{CH}$	3.0 ± 0.4			2.5 ± 0.1	2.9 ± 0.1	1.5 ± 0.2

a) Ref. 2). b) Ref. 13).

Table 2. Conformational volume differences, ΔV (cm^3 mol^{-1}) in hexane and methanol

	Neat[a]	In hexane			In methanol
		80 mol%	60 mol%	40 mol%	40 mol%
i-BuCl					
$P_C\rightarrow P_H$	0.5 ± 0.1	$0.1_3\pm0.07$	$-0.3_9\pm0.07$	$-0.6_2\pm0.0_4$	$-0.4_6\pm0.04$
i-BuBr					
$P_C\rightarrow P_H$	-0.7 ± 0.2	$-0.7_9\pm0.08$	$-0.2_5\pm0.04$	$-0.5_3\pm0.04$	$-0.6_9\pm0.03$
s-BuCl					
$S_{HH}\rightarrow S_{HH'}$	-1.4 ± 0.4			$-1.8_0\pm0.2$	$-0.1_3\pm0.2$
$S_{HH}\rightarrow S_{CH}$	-0.8 ± 0.3			$-0.5_4\pm0.2$	0.0 ± 0.06
s-BuBr					
$S_{HH}\rightarrow S_{HH'}$	2.0 ± 0.4			$-1.4_5\pm0.2$	$0.8_2\pm0.2$
$S_{HH}+S_{CH}$	0.6 ± 0.2			$-0.9_1\pm0.1$	$0.1_8\pm0.2$

a) Ref. 2.

0.0_4 cm^3 mol^{-1} at the 40 mol% of *i*-BuCl.

For *s*-BuCl and *s*-BuBr, the enthalpy changes from S_{HH} to $S_{HH'}$ are nearly equal to those from S_{HH} to S_{CH} in the liquid and dissolved states. Therefore, the potential energies of the conformers, $S_{HH'}$ and S_{CH}, may be almost the same. The values of ΔH of *s*-BuBr in hexane and methanol are comparable to those in the gaseous state. This indicates that the intermolecular contribution to ΔH is small. In the cases of *s*-BuCl and *s*-BuBr, the signs of the ΔV of $S_{HH}\rightarrow S_{HH'}$ and $S_{HH}\rightarrow S_{CH}$ in hexane are both negative, but in methanol they are positive for *s*-BuBr and negative for *s*-BuCl. The signs of the ΔV of these conformational changes of *s*-BuCl and *s*-BuBr in methanol are the same as in the neat state. These results indicate that molecules of *s*-butyl halides in the neat state as well as those placed in methanol are in a strongly interacting field, as a result of the high dielectric constants of the media surrounding the central *s*-butyl halides. The absolute values of the volume changes caused by the $S_{HH}\rightarrow S_{HH'}$ transformation are about two or three times larger than those of $S_{HH}\rightarrow S_{CH}$, although the energy differences in the corresponding conformational changes are nearly equal in the two solutions.

Discussion

The origin of the enthalpy and volume differences, ΔH and ΔV, between the rotational isomers in solution can be divided into two factors. One is caused by the intermolecular interaction, and the other, by the intramolecular character. The solvent and concentration dependences of both ΔH and ΔV indicate that the intermolecular effects are predominant.

The changes in the intrinsic volume of each conformer were often estimated and compared with those obtained experimentally.[6,14] The intrinsic volume differences between the rotational isomers were calculated by the Bondi's method.[15] The results and van der Waals volumes are summarized in Table 3. The calculated volume changes are one or two orders of magnitude smaller than those obtained experimentally, but for *s*-BuCl and *s*-BuBr the order of the volume change of $S_{HH}\rightarrow S_{HH'}$ and $S_{HH}\rightarrow S_{CH}$ agrees with the experimental one.

The concentration dependences of the volume differences between the two conformers of *i*-BuCl and *i*-BuBr are shown in Fig. 4 as a function of the contents of the solute in hexane solutions. The concentration dependences are quite different for *i*-BuCl and *i*-BuBr. For *i*-BuCl, the volume difference, ΔV, decreased with an increase in the contents of hexane in solutions, but for *i*-BuBr, ΔV increased. As is shown in Fig. 4, the ΔV values of those two compounds seem to level off to a constant value at higher contents of hexane in solutions. On the other hand, the volume changes

TABLE 3. CALCULATION OF VOLUME DIFFERNCE AND VAN DER WAALS VOLUME BY BONDI METHOD ($cm^3\ mol^{-1}$)

	Volume differences	van der Waals volume
i-BuCl		
$P_C \rightarrow P_H$	0.04	56.37
i-BuBr		
$P_C \rightarrow P_H$	0.05	58.47
s-BuCl		
$S_{HH} \rightarrow S_{HH'}$	0.03	56.37
$S_{HH} \rightarrow S_{CH}$	0	
s-BuBr		
$S_{HH} \rightarrow S_{HH'}$	0.12	58.47
$S_{HH} \rightarrow S_{CH}$	0.08	

The following parameters were used in the calculation:

Radii (Å)	Bond lengths (l/Å)		Bond angles (ϕ/°)
r(H)=1.20	C-H	1.10	C-C-C 112.2°
r(C)=1.70	C-C	1.53	C-C-H 110.4°
r(Cl)=1.77	C-Cl	1.77	C-C-Cl 110.0°
r(Br)=1.84	C-Br	1.95	C-C-Br 111.0°
			Cl-C-H 106.6°
			Br-C-H 105.4°

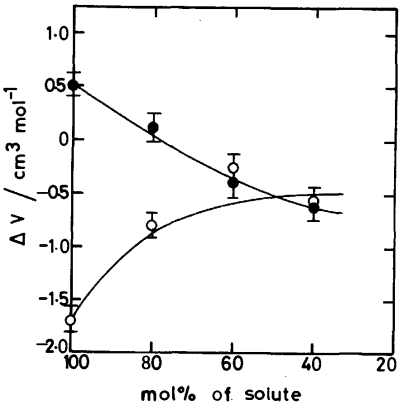

Fig. 4. Concentration dependence of ΔV of isobutyl halides in hexane. ●; *i*-BuCl ○; *i*-BuBr.

upon conformational change in the gaseous state are zero as is shown in Table 1. Therefore, ΔV becomes powerful measure of the changes in the packing of molecules in the liquid and dissolved states.

As may be seen in Table 1, the conformational enthalpy differences in *i*-BuCl and *i*-BuBr in hexane increase with an increase in the contents of hexane in solutions. In the neat state, such strong intermolecular interactions as dipole-dipole interactions are working. These strong intermolecular interactions will be reduced by the addition in solutions of hexane, which is an ineart solvent. Therefore, the enthalpy differences in these compounds increase with an increase in the concentration of hexane in solutions, and they tend to approach those in the gaseous state. The enthalpy difference in the gaseous state, ΔH_{gas}, corresponds to that of the intramolecular one. As a result, the enthalpy difference, $\Delta = \Delta H_{liq} - \Delta H_{gas}$, is a measure of the intermolecular interaction of the molecules in the liquid and dissolved states.

The enthalpy difference, $\Delta = \Delta H_{liq} - \Delta H_{gas}$, can be

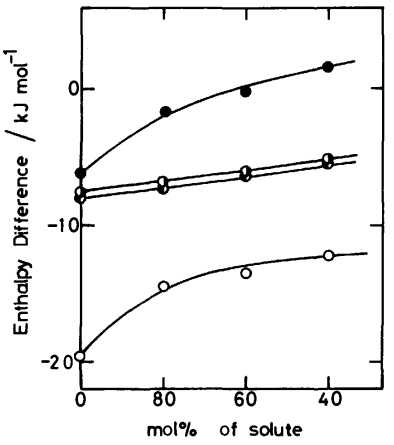

Fig. 5. Concentration dependence of enthalpy differences of isobutyl halides in hexane. $\Delta(=\Delta H_{liq} - \Delta H_{gas})$ of *i*-BuCl (●) and *i*-BuBr (○), obtained by the spectroscopic method. $\Delta H'$ of *i*-BuCl (○) and *i*-BuBr (○), calculated from Eq. 4.

estimated by the procedure proposed by Mizushima *et al.*,[16] using the reaction-field theory of Onsager:[17]

$$\Delta H' = \frac{\varepsilon - 1}{2\varepsilon + 1}\left[\left(\frac{\mu}{a^3}\right)_g - \left(\frac{\mu}{a^3}\right)_t\right] \quad (4)$$

where ε is the dielectric constant of the solvent and where μ and a are the dipole moment and the radius of the cavity of each conformer. The suffixes t and g refer to the states of *trans* and *gauche* respectively. The dipole moments of each conformer of the *i*-BuCl and *i*-BuBr were estimated by the method proposed by Miyagawa.[18] The radius of the cavity of these compounds was assumed to be the van der Waals radius of each conformer, whose value is indicated in Table 3. This assumption has been used by many investigators.[3,16] This dielectric constants of *i*-BuCl, *i*-BuBr, hexane, and methanol are found in the literature.[19] However, the dielectric constants of the solutions investigated here were not available; they were estimated using the following additivity rule of the molar polarization, $[p]$:

$$[p] = x_1[p_1] + x_2[p_2], \quad [p] = \frac{\varepsilon + 1}{\varepsilon - 2}\frac{M}{\rho}$$

where x_i refers to the mole fraction of the mixtures. The calculated values of the enthalpy difference, $\Delta H'$, are shown in Fig. 5, where the experimental values of $\Delta = \Delta H_{liq} - \Delta H_{gas}$ are also plotted. As may be seen in Fig. 5, the values of $\Delta H'$ increase with an increase in the contents of hexane in solutions. This trend well explains the experimental results, but the absolute numerical values of $\Delta H'$ are in very poor agreement with those obtained by experiments. This discrepancy between $\Delta H'$ and $\Delta(=\Delta H_{liq} - \Delta H_{gas})$ must be due to the poor estimation of the cavity radius, a, and the dipole moment, μ, of each conformer.

Equation 4 is the result of the first approximation, in which induced dipole moments were not taken into account. Besides, Eq. 4 involves only the long-range force; it does not take into account the short-range effects, especially the local packing effect of molecules. These short-range effects are all reflected in the term of the radius of the cavity. The estimation of the radius of the cavity of the rotational isomers is very important, but at present a precise estimation is very difficult.

Devauer and Lascombe[20] have thermodynamically related the enthalpy difference, Δ, to the volume change associated with the conformational change in liquids as following:

$$\Delta = \Delta H_{liq} - \Delta H_{gas} = RT^2\left(\frac{\partial f}{\partial T}\right)_V + \Delta V_{liq}\frac{\alpha T}{\beta_T} \quad (6)$$

where α and β_T are the expansion coefficient and compressibility respectively where f is $\ln[K/K_0]$, where K is the equilibrium constant for the liquid and/or dissolved state, K_0, that for gaseous state, and the other symbols have their usual meaning.

The thermodynamic parameters, α and β_T, of Eq. 6 for hexane solutions of *i*-BuCl and *i*-BuBr were determined as follows. The thermal expansion coefficient, α, was determined directly by the data of the temperature dependence of the density in solutions. The isothermal compressibility was calculated from the thermodynamic relation:

$$\beta_T = \beta_s + \frac{T\alpha^2 V}{C_p} \quad (7)$$

where the adiabatic compressibility, β_s, was determined with the aid of the Laplace equation, ($\beta_s = 1/(\rho u^2)$), from the data of density, ρ, and sound velocity, u, in solutions. The heat capacity of hexane and methanol was found in the literature,[19] but the halogenoalkanes investigated here no data were available. Therefore, the value for butyl chloride, 9.9 J/g.*K*.,[21] was adopted for the halogenoalkanes concerned in this work. The C_p's in solutions were estimated by assuming this relation

$$C_p = x_1 C_{p,1} + x_2 C_{p,2} \quad (8)$$

The values of $RT^2(\partial f/\partial T)_V$ thus obtained are summarized in Table 4. The values of $RT^2(\partial f/\partial T)_V$ are comparable in order with the values of Δ and $\Delta V_{liq}\alpha T/\beta_T$. Thermodynamically, the $RT^2\,(\partial f/\partial T)_V$ term corresponds to the internal energy difference between the liquid and gaseous states. The internal energy difference cannot be neglected in Eq. 6.

At this stage, it is difficult to calculate the physical properties concerning volume by statistical mechanical method. However, information about the internal energy of the solution is obtainable by the theoretical calculation on the basis of statistical mechanics and/or a computer-simulation experiment. The internal energy of the binary solution is calculated by the following equation:[22]

Table 4. The values of $RT^2(\partial f/\partial T)_V$ (kJ mol^{-1}) in Eq. 6.

		Hexane			Methanol
		80 mol%	60 mol%	40 mol%	40 mol%
i-BuCl					
$P_C \rightarrow P_H$	-0.7_6	-0.2_0	0.0_7	0.0_3	-0.1_8
i-BuBr					
$P_C \rightarrow P_H$	-1.4_1	-1.2_1	-1.2_8	-1.0_8	-1.2_9
s-BuBr					
$S_{HH} \rightarrow S_{HH}'$	0.2_3			0.9_5	0.9_5
$S_{HH} \rightarrow S_{CH}$	1.3_0			1.2_5	1.4_0

$$E = \frac{3}{2}NkT + \frac{2N^2}{V}\left[x_1^2\int_0^\infty u_{11}(r)g_{11}(r)r^2dr + 2x_1x_2\int_0^\infty u_{12}(r)g_{12}(r)r^2dr + x_2^2\int_0^\infty u_{22}(r)g_{22}(r)r^2dr\right]$$

$$x_1 = \frac{N_1}{N},\quad x_2 = \frac{N_2}{N},\quad N_1 + N_2 = N \quad (9)$$

where u_{ij} is the pair potential for molecules of i and j and g_{ij}, the radial distribution function. As may be seen in the equation, the short-range effects are involved in the term of the radial distribution function of each pair. We are now trying to calculate the internal energy using the theory of the reference interaction site model (RISM), which was proposed by Chandler *et al.*[23] We want to compare the calculated value with the experimental results obtained here.

The authors would like to express their appreciation to Prof. Teizo Kitagawa of the Institute for Molecular Science for permission to use the high-pressure apparatus. This work was financially supported in part by a Grant-in-Aid for Scientific Research from the Ministry of Education. (No. 59540259).

References

1) H. Nomura, K. Murasawa, N. Ito , F. Iida, and Y. Udagawa, *Bull. Chem. Soc. Jpn.*, **57**, 3321 (1984).
2) H. Nomura, Y. Udagawa, and K. Murasawa, *J. Mol. Struct.*, **126**, 229 (1985).
3) T. Fujiyama and M. Kakimoto, *Bull. Chem. Soc. Jpn.*, **49**, 2346 (1976).
4) M. Hayashi, *Nippon Kagaku Zasshi*, **78**, 536 (1957).
5) K. R. Crook and E. Wyn-Jones, *J. Chem. Phys.*, **50**, 3446 (1969).
6) Y. Taniguchi, H. Takaya, P. T. T. Wong, and E. Whalley, *J. Chem. Phys.*, **75**, 4815 (1981).
7) Y. Taniguchi, *J. Mol. Struct.*, **126**, 241 (1985).
8) J. J. Shipman, V. L. Folt, and S. Krimm, *Spectrochim. Acta.*, **18**, 1603 (1962).
9) F. F. Bently, N. T. McDevitt, and A. L. Rozek, *Spectrochim. Acta.*, **20**, 105 (1964).
10) P. N. Gates, E. F. Mooney, and H. A. Willis *Spectrochim. Acta.*, **23A**, 2043 (1967).
11) G. A. Crowder and Mohammad-Reza Jalilian,

Spectrochim. Acta., **34A**, 707 (1978).
12) G. A. Crowder and Way-Yu Lin, *J. Mol. Struct.*, **64**, 193 (1980).
13) E. Wyn-Jones and W. J. Orville-Thomas, *Trans. Faraday Soc.*, **64**, 2907 (1968).
14) D. J. Gradiner and R. W. Jackson, *J. Chem. Soc., Chem. Commun.*, **79**, 159 (1981).
15) A. Bondi, "Physical Properties of Molecular Crystals, Liquids, and Glasses" John Wiley & Sons, New York (1968).
16) S. Mizushima, "Structure of Molecules and Internal Rotation," Acad. Press, New York (1954), p. 42.
17) L. Onsager. *J. Am. Chem. Soc.*, **58**, 1486 (1936).
18) I. Miyagawa, *Nippon Kagaku Zasshi.*, **75**, 1057 (1954).
19) "Kagaku Binran" ed by Chem. Soc. Jpn., Maruzen (1984).
20) J. Devaure and J. Lascombe, *Nouva Chim.*, **3**, 579 (1979).
21) "International Critical Tables," McGraw-Hill, New York Vol. 5 (1928).
22) T. Boublik, I. Nozbeda and K. Hlavaty, "Statistical Thermodynamics of Simple Liquids and Their Mixtures," Elsevier Sci. Publishing (1980).
23) H. C. Anderson and D. Chandler, *J. Chem. Phys.*, **57**, 1918, 1930 (1972).

Assignment of Conjugate Double Bond Systems Produced in Heated PVA Film by Absorption and Excitation Spectra

Kazunori MARUYAMA, Hiroshi AKAHOSHI, Michio KOBAYASHI, and Yoshié TANIZAKI*
Department of Materials Science and Technology, Technological University of Nagaoka, Nagaoka, Niigata 949-54
(Received May 4, 1985)

Absorption, emission and excitation spectra of heat-treated PVA film have been interpreted as corresponding to mixtures of $-(CH=CH)_n-$ and $-(CH=CH)_n-CO-$, which are distinguishable from each other according to whether spectrum is accompanied with fine structures or not. The former shows fine structures and has had n determined to be 2—14 by analysis of peak locations on the basis of linearity for Lewis-Calvin's plot. For the latter, n has been determined to be 1—7, and Lewis-Calvin's plot between the wavelength of band maximum and n also shows a good linearity.

There are a number of reports concerning electronic spectra of heat-treated poly(vinyl alcohol) [PVA].[1] A somewhat troublesome problem for the analysis of spectra is that thermally decomposed products of PVA are mixtures of many different polymers and that it is not possible to extract each component for analysis.

Absorption spectra of a heat-treated PVA film are very much influenced by heating temperature, heating time, and impurities contained. The coloration of PVA by heat is promoted by various compounds such as sulfuric acid, hydrochloric acid, phosphoric acid,[2] and sodium acetate.[3] Actually, commercial PVA powder, which contains about 0.5 wt% sodium acetate produced by alkaline saponification, will get colored easily by heating.

PVA is a polymer composed of a main chain of C–C bond with an OH group attached. Therefore, the final pyrolytic product should be graphite. In the initial stage of heating, however, we can focus our concern on products of two types of polyenes and polyenones. In fact, electronic spectra of PVA films which underwent various treatments including heating as in this study, were explainable merely in terms of formation of conjugate doulble bonds by dehydration and dehydrogenation, nor their spectral data gave any positive suggestion for severance of the main chain of polymer. Accordingly, all kinds of π electron systems to be formed along the framework of the chain must be restricted to the two types mentioned above. Fortunately, electronic spectra of the two types are distinguishable from each other according to whether spectrum is accompanied with fine structures or not. Furthermore, a judgement on the kinds of polyenes with fine structures can be made by analysis of peak locations and their intervals. On the other hand, the kinds of polyenones which show band spectra should be distinguishable on the basis of the correlation between the wavelength of band maximum and the number n of conjugate double bonds, because the difference of adjacent band maxima is equivalent to the difference between n and $n+1$, *i.e.*, $-CH=CH-$. Practically, the authors have presupposed tacitly the above considerations and have pointed out the existence of polyenes $-(CH=CH)_n-$ and polyenones $-(CH=CH)_n-CO-$ with $n=2—5$ and 2—3, respectively.[4]

In the present study as a continuation, the authors will analyze the correlation between absorption and the number of conjugate double bonds, assuming that fine structures are due to polyenes, whereas bands are due to polyenones (to be called polyene-carbonyl in this paper).

Experimental

PVA used was a commercial one (Koso Chemical Co., Ltd.), of which the average polymerization degree was 1400 and alkaline saponification was 99—100%. PVA poweder of 10—30 g was dissolved in distilled water of 200 cm^3 at 90 °C, and the solution was poured on a horizontal glass plate (30×30 cm). After it was dried at room temperature in 10 d, a PVA film about 100—300 μm thick was obtained. This film was kept for 2 h at 80 °C and put into use as the original film to be called PVA-1.

The PVA film was digested in a mixed solution of 0.1 M (1 M=1 mol dm^{-3}) $NaBH_4$ and 0.1 M NaOH for 1 d to reduce carbonyl group, and was washed with 0.05 M HCl solution and then with distilled water. In addition, it was digested in the following solutions separately and was dried at room temperature: the film digested in CH_3COONa solution is called PVA-2; in HCl solution, PVA-3; in H_2SO_4 solution, PVA-4; in H_3PO_4 solution, PVA-5.

Heat treatment of sample film was carried out with a sample being fixed on a metal holder in order to avoid wrinkling by heating. A sample film was set in a heating compartment and heated up to the desired temperature at a rate of 10 °C min^{-1} in a 0.5 dm^3 min^{-1} flow of nitrogen.

Absorption spectra were measured with a Shimadzu UV-360 spectrophotometer, and emission and excitation spectra with a Shimadzu RF-502 spectrophotometer. Fluorescence spectra were measured from the front side of film with an incident angle of 35° in the region 260—650 nm.

Results

PVA-1. The film of PVA-1 itself is colorless and its spectrum shown as Fig. 1(a)-1 has two weak absorption bands at 280 and 330 nm, which are already assigned to $-(CH=H)_2-CO-$ and $-(CH=CH)_3-CO-$, respectively.[5] When the PVA-1 film is heated,

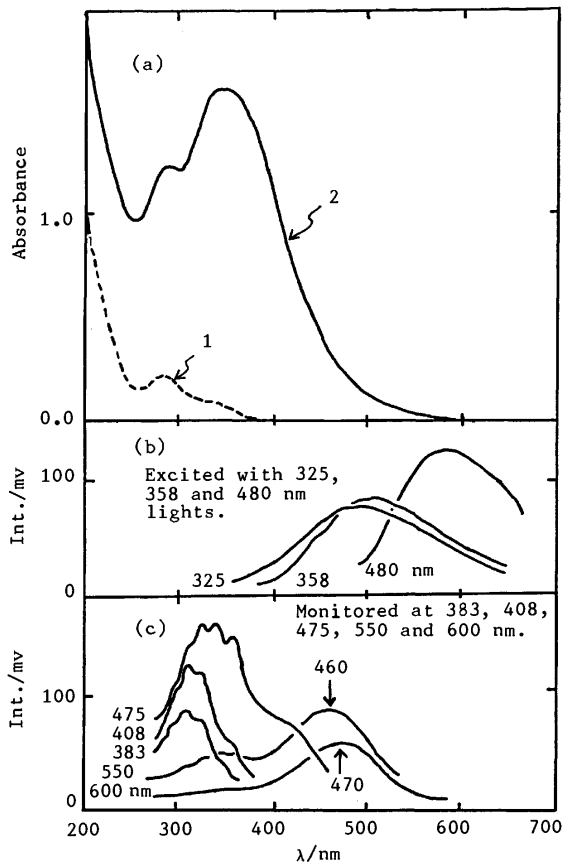

Fig. 1. Absorption (a), emission (b) and excitation spectra (c) of heat-treated PVA-1 film at 175 °C. Film thickness: 290 μm. (a)-1: Before heating, (a)-2: after heating.

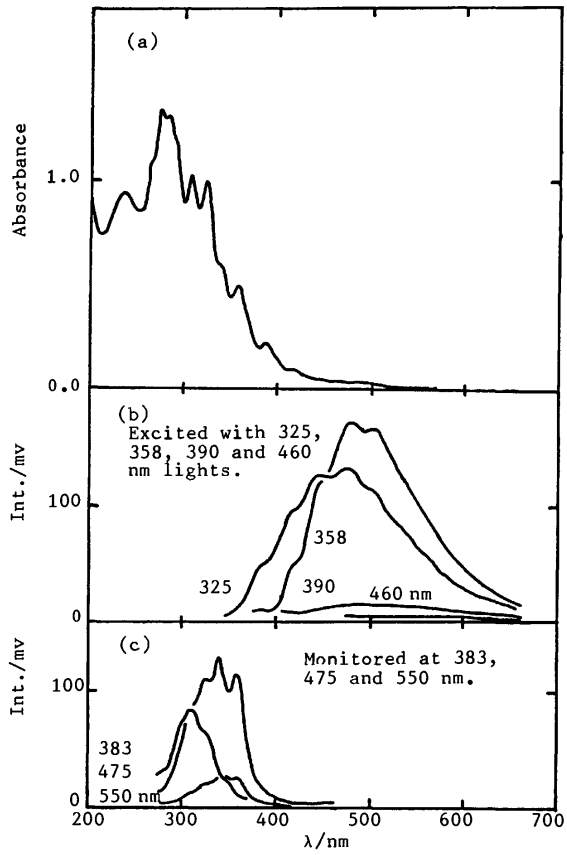

Fig. 2. Absorption (a), emission (b) and excitation spectra (c) after digestion of heated PVA-1 film (Fig. 1(a)-2) in 0.1 M NaOH-$BaBH_4$ mixed solution.

it becomes pale yellow and shows the spectrum of Fig. 1(a)-2 which has two strong bands at 280 and 340 nm. The spectral change from Fig. 1(a)-1 to (a)-2 is as follows: the 280 nm band grows without changing its maximum wavelength and the 330 nm band grows up to the 340 nm band. This indicates that the band maximum of triene-carbonyl is at 340 nm rather than at 330 nm.

Figures 1(b) and 1(c) show emission and excitation spectra for the absorption of Fig. 1(a)-2, respectively. For the emission spectra, it is noticed that the broad band at about 590 nm due to excitation by 480 nm light is most intense, in spite of the fact that the absorption intensity at 480 nm is weaker than those at the other excitation wavelengths. In the excitation spectra of Fig. 1(c), the peaks of the fine structures are at the same wavelengths as those of tetraene and pentaene assigned previously.[4] Therefore, the absorptions by these polyenes should be contained in the absorption spectrum of Fig. 1(a)-2, though any fine structures are not observable. In the excitation spectra, the other broad bands without fine structures appear at 460 and 470 nm. These bands changed their maximum wavelengths depending on monitor wavelengths, which indicates that respective bands consist of two overlapped bands.

The heat-treated PVA-1 film turned almost colorless in the aqueous solution of $NaBH_4$ in 1 d. Its absorption, emission, and excitation srectra are shown in Figs. 2(a), (b), and (c), respectively. By the treatment with $NaBH_4$, the 280 and 340 nm bands of Fig. 1(a)-2 are caused to disappear and instead a fine structure is caused to reveal itself as shown in Fig. 2(a). This change indicates that diene-carbonyl (280 nm band) and triene-carbonyl (340 nm) become diene and triene, respectively, as a result of reduction of the carbonyl group by $NaBH_4$, and that the other polyene-carbonyls (longer wavelengths) are reduced to the corresponding polyenes such as tetraene, pentaene, *etc.*

In the emission spectra of Fig. 2(b), any bands similar to the intense band at about 590 nm in Fig. 1(b) could not be observed. This may be due to too weak an absorption intensity (Fig. 2(a)) at the excitation wavelength (460 nm). In the excitation spectra of Fig. 2(c), such intense bands as shown at 460 nm in Fig. 1(c) are lacking completely for the monitor at 550 nm in spite of the sufficient intensity of emission (see Fig. 2(b)).

PVA-2. Figure 3(a)-1 shows the absorption spectrum for the purified PVA film called PVA-2.

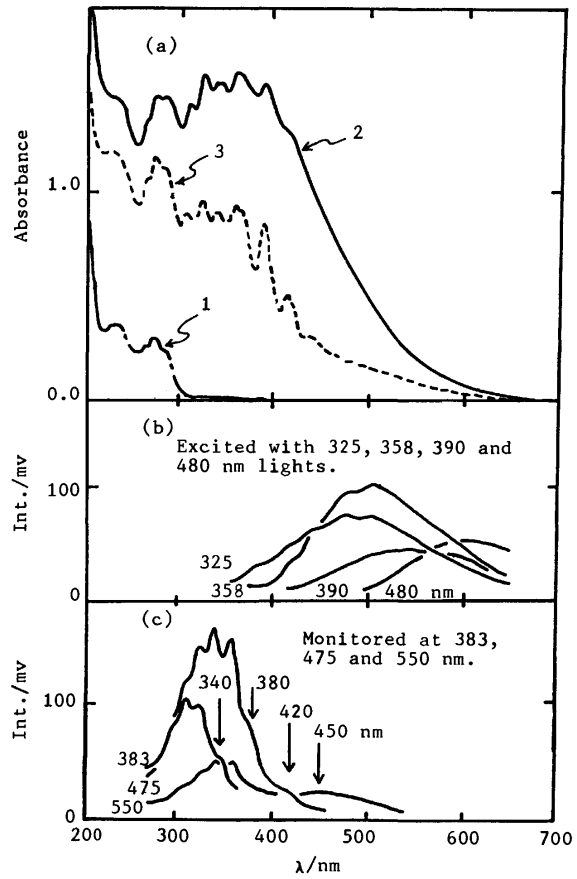

Fig. 3. Absorption (a), emission (b) and excitation spectra (c) of heated PVA-2 film at 175°C. Film thickness: 290 μm. (a)-1: Before heating, this is doubled spectrum in absorption, (a)-2: after heating, (a)-3: after digestion of heated PVA-2 film ((a)-2) in 0.1 M NaOH-$NaBH_4$ mixed solution.

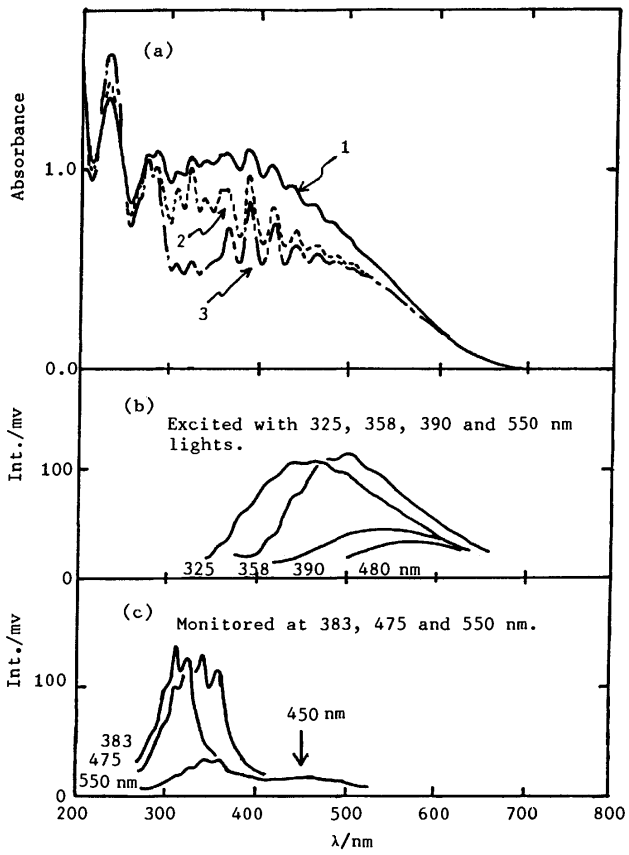

Fig. 4. Absorption (a), emission (b) and excitation spectra (c) of heated PVA-3 film at 120°C. Film thickness: 120 μm. (a)-1: After heating, (a)-2 and (a)-3: after digestion of heated PVA-3 film ((a)-1) for 1 day and further 3 days, respectively, in 0.1 M NaOH-$NaBH_4$ mixed solution.

There are two bands with maxima at 234 and 273 nm, and in both sides of each band faint fine structures are recognized. The spectral change from Fig. 1(a)-1 to 3(a)-1 shows that by purification diene-carbonyl (280 nm) changes to diene (234 nm) and triene-carbonyl (340 nm) to triene (273 nm).

Figures 3(a)-2, (b), and (c) show, respectively, the absorption, emission and excitation spectra of a brown film of heated PVA-2. The wavelengths of the peaks and shoulders of the fine structure in Fig. 3(a)-2 coincide well with those of the corresponding peaks appearing in Fig. 2(a). The emission spectra of Fig. 3(b) and the excitation spectra of Fig. 3(c) are similar in character to those of Figs. 1(b) and (c), respectively: the broad emission band at about 590 nm due to the excitation at 480 nm, and the excitation bands at 420 (shoulder) and 450 nm by the monitor at 475 and 550 nm, respectively. All the wavelengths of the peaks of the fine structures of Fig. 3(c) coincide with those of some peaks in Figs. 1(c) and 2(c).

Figure 3(a)-3 shows the absorption spectrum for the case when the heated PVA-2 film was reduced by $NaBH_4$. The emission and excitation spectra, which are not inserted here, did not show any emission (590 nm) or excitation bands (420—470 nm) in the longer wavelength region, in common with the cases of Figs. 2(b) and (c).

PVA-3 and PVA-4. When the films of PVA-3 and PVA-4 were heated, they got colored red. Both the red films showed similar absorption, emission, and excitation spectra. Therefore, only the case of PVA-3 is presented here in Fig. 4.

The emission and excitation spectra obtained for the absorption of Fig. 4(a)-1 are in Figs. 4(b) and (c), respectively, which resemble those of Figs. 3(b) and (c), respectively.

In the absorption spectra of Fig. 4(a), the fine structures continue over a longer wavelength region than those of the other samples. Figure 4(a)-1 shows the absorption spectrum of the heated PVA-3 film, and Figs. 4(a)-2 and -3 show the spectra after the treatment by $NaBH_4$, *i.e.*, 1 d digestion for the former and 3 d for the latter in 0.1 M NaOH-$NaBH_4$ mixed solution. By the 1 d digestion, the absorption intensity of Fig. 4(a)-1 is decreased in the range about 300—600 nm and the fine structure is sharpened (Fig. 4(a)-2). Further digestion causes the intensity to decrease further,

especially for the peaks at 310 and 325 nm (to be assigned to tetraene) and at 342 and 358 nm (to pentaene) (Fig. 4(a)-3). On the other hand, the 234 nm band of diene increases during the digestion. The change from Fig. 4(a)-1 to (a)-3 by the $NaBH_4$ treatment indicates that the conversion of long polyenes to diene and momoene is effected by the reduction, and that tetraene and pentaene are especially easier to be reduced.

PVA-5. When the PVA-5 film was heated, it turned yellowish brown. The absorption spectrum of this colored film is similar to that of Fig. 3(a)-3. The excitation spectra, however, show only the peaks of tetraene and pentaene lacking the broad band, in spite of the condition of heating temperature being similar with the heated PVA-2 film (Fig. 3(c)).

Discussion

Assignment of Peaks of Fine Structures. (a) Absorption Spectra: In our experiment, the peak wavelengths of fine structures revealed in the spectra of the treated PVA films almost coincide with one another regardless of any sorts of treatments upon PVA films. The peak wavelengths range from 226 to 540 nm. Of the peaks, those in the region 226—358 nm have been assigned to the 0←0, 1←0, and 2←0 transitions of polyenes $-(CH=CH)_n-$ with n=2—5.[4] Moreover, the peaks for each transition have resulted in a linear relation with respect to Lewis-Calvin's plot,[6] *i.e.*, the relationship between λ^2 (λ is peak wavelength) and n.[4]

In Fig. 5, λ^2 of the rest peaks over n=5 are plotted in white circles on the extended 0←0 line for n=2—5, except the solid circle at n=6 which is assigned to 1←0 (366 nm). The white circles fall on a line broken at the position n=9. However, if we shift horizontally the white circles by a unit of n to the right, the respective circles will fall into the extended straight line of the 1←0 transition as shown by the solid circles.

Sondheimer *et al.*[7] have plotted the relationship between λ^2 and n for the free polyenes $H-(CH=CH)_n-H$ (n=3—8 and 10). According to their plot, a linear relation is obtained while n is small, but the points for n=8 and 10 turn downwards off the line. As is likewise presupposed from the absorption spectra of polyacetylenes,[8] the value of λ^2 shows a tendency to approach a certain value as n increases. It is a matter of common knowledge that λ^2 of conjugate systems in the same series approaches a certain value for larger numbers of n, but the limits of n for which λ^2 changes linearly are not always definite.

As shown in Fig. 5, if all the peaks (white circles) are assigned to the 0←0 transitions, the limits of straight line would become equal to n=9, and if assigned to the 1←0 transitions, even the point for n=14 would be put on a straight line. Though it cannot definitely be answered which is true, the latter assignment may be considered to be right for the following reason.

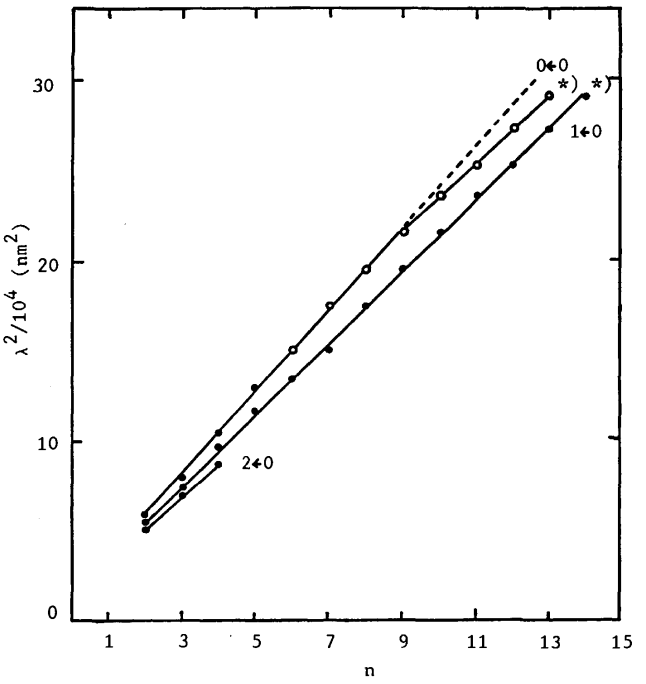

Fig. 5 Relationship of λ^2 *vs.* n for polyenes in heated PVA films. *) (539 nm) to be observed only when PVA film is uni-axially stretched before heating.

TABLE 1. ASSIGNMENT OF ABSORPTION PEAKS OF $-(CH=CH)_n-$ PRODUCED IN HEATED PVA FILM

n	Wavelength/nm		
	0←0	1←0	2←0
2	242	234	226
3	285	273	262
4	325	310	295
5	358	342	
6		366	
7		390	
8		418	
9		442	
10		465	
11		486	
12		503	
13		523	
14		540[a)]	

a) Observed when PVA film is uni-axially stretched before heating.

In the present experiment, a mixture of π electron systems of the polyene type is observed. In such mixtures, peaks of a system of conjugation number n may be influenced by the overlapping effect in the n+1 system, in such a way that the 0←0 peak is influenced more than the 1←0 and 2←0 peaks. At the same time, the 2←0 peak may be overlapped by the 0←0 peak of the n−1 system. And moreover, the intensity of the 2←0 peak is generally weaker than those of the 0←0 and 1←0 peaks. For this reason, the 1←0 peak is very liable

TABLE 2. ASSIGNMENT OF ABSORPTION AND EXCITATION BANDS OF POLYENE-CARBONYLS $-(CH=CH)_n-CO-$ PRODUCED IN HEATED PVA FILMS

Assigned n and wavelength		Observed wavelength/nm				
n	nm	Fig. 1(a)	Fig. 1(c)	Fig. 2(c)	Fig. 3(c)	Fig. 4(c)
2	280	280				
3	340	340	340[a)]	350[a)]	340[a)]	
4	380			380[a)]	380[a)]	
5	420		420[a)]		420[a)]	
6	450		460		450	450
7	480		470			

a) Shoulder.

to be observed because of its least influence from other systems.

In Fig. 5, the linearity of the plot of 1←0 peaks is of remarkably long-range. At the present stage, we cannot explain the reason for the long-range linearity. However, a fact that the observed π electron system is formed locally within a very long C-C bond chain, may make a cause of the fact that the linear region extends to larger n's than in the case of free molecule.

Based on the above considerations, let us assume that all the observed peaks over n=5 are assigned to the 1←0 transitions, and we may obtain the assignment given in Table 1.

(b) Excitation Srectra: The absorption spectra of the heated PVA films shown in Figs. 1—4 are considerably different from one another, but in their excitation spectra only the fine structures of tetraene and pentaene are commonly observed and none of the other polyenes. The reason why any fine structures for n larger than 5 (pentaene) could not be observed, may be that the produced amount of polyenes is too small to be detected. We thus heated enough PVA-3 film till it turned deep reddish black. Nevertheless, its excitation spectra did show only the peaks of tetraene and pentaene, and again no peaks of the other polyenes. This result indicates that the fluorescence efficiency of the other polyenes is very small. In fact, D'Amico *et al.*[9] have shown that the efficiency is markedly decreased in going from tetraene to hexaene molecule. They have estimated that the fluorescence quantum yield of hexaene molecule is at most 1/50 that of tetraene, and predicted that longer conjugate polyene molecules show no fluorescence. Hence, our result supports their prediction positively.

Assignment of Absorption Bands of Polyene-Carbonyls. Let us regard the absorption bands without fine structures as those of the polyene-carbonyls of the type $-(CH=CH)_n-CO-$, types of $-(CH=CH)_n-CO-(CH=CH)_m-$ and others being neglected because the chance of their formation is considered to be small. All such bands and shoulders observed here are collected in the column headed "Observed wavelength" of Table 2.

The 280 and 340 nm bands in Table 2 (the column headed "Fig. 1(a)") have already been assigned to diene-carbonyl (n=2) and triene-carbonyl (n=3), respectively.[5] Since the minimum difference with $-(CH=CH)_n-CO-$ is one double bond -CH=CH-, the change in wavelength of the band maxima for successive n's ought to be step-like. In the case of polyenes $-(CH=CH)_n-$ (Table 1), for instance, the peak-intervals in the same kind of transitions are about 30—40 nm for the smaller n's. With this taken into consideration, with Table 2, it is reasonabe to assign the 380 and 420 nm shoulders to n=4 and 5 of $-(CH=CH)_n-CO-$, respectively.

As pointed out in the "Results" section, either of the 460 and 470 nm bands in Table 2 (the column headed "Fig. 1(c)") consist of two subbands. By supposing the main component of the 460 nm band is identical with the 450 nm band of the columns headed "Fig. 3(c)" and "Fig. 4(c)" in Table 2, the shift by overlapped band is estimated to be 10 nm. Therefore, if the 10 nm shift by overlapped band (train of 450 nm band) is expected for the 470 nm band, the wavelength of the main band can be estimated to be 480 nm.

According to the above consideration, the bands and shoulders regarded as the absorptions of polyene-carbonyls are all assigned as shown in the first and second columns of Table 2.

In the above we have found that the 1←0 peaks of polyenes furnish a linearity of Lewis-Calvin's plot in a wide range of n. Since the polyene-carbonyls assigned in Table 2 have the structure in which a C=O bond is joined to polyene at the terminal, the shift of the band maximum for successive n's of $-(CH=CH)_n-CO-$ is dependent upon the increase in number of -CH=CH- bonds. Therefore, a linearity of Lewis-Calvin's plot is also expected for the band maxima of polyene-carbonyls. The plot is shown by solid circles in Fig. 6, which meets our expectation. The white circles in Fig. 6 are of the same plot for $CH_3-(CH=CH)_n-CHO$, for which are used the band maxima reported by Blout and Fields.[10] Evidently, the Lewis-Calvin's plot is curved for the case of free molecule. The difference (Fig. 6) between $-(CH=CH)_n-CO-$ and $CH_3-(CH=CH)_n-CHO$ may be due to the same sequence as the case between $-(CH=CH)_n-$ (Fig. 5) and the corresponding free molecule.

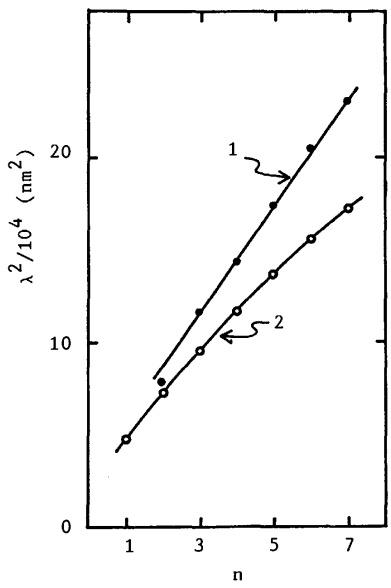

Fig. 6. Relationship of λ^2 *vs.* n for polyene-carbonyls in the heated PVA films. 1: This study, 2: cited from Ref. 10.

Das and Becker[11] have reported that the polyene-aldehydes CH_3-$(CH{=}CH)_n$-CHO of n=2—5 do not show fluorescence at room temperature but emit weak or moderately strong fluorescence at 77 K. In connection with their study, we point out that the solid PVA substrate film has a nature characterestic of a glassy solvent, though well known empirically. This is because, in our experiment, the fluoresence from polyene-carbonyls of n=3—7 could be detected, even at room temperature.

References

1) C. A. Finch, "Poly Vinyl Alcohol," John Wiley & Sons New York (1973), p. 477.
2) L. Drechsel and P. Goerlich, *Infrared Phys.*, **3**, 229 (1963).
3) K. E. Perepelkin and O. O. Borodina, *Sov. Plast.*, (2), **1968**, 17.
4) K. Maruyama, H. Akahoshi, M. Kobayashi, and Y. Tanizaki, *Chem. Lett.*, **1983**, 1863.
5) K. Yamaguchi, M. Amagasa, S. Kinumaki, and T. Takahashi, a paper presented at the Annual Meeting of High Polymer Chemistry, Tokyo, June 1-2, 1956.
6) G. N. Lewis and M. Calvin, *Chem. Rev.*, **25**, 237 (1937).
7) F. Sondheimer, D. A. Ben-Efrain, and R. Molovsky, *J. Am. Chem. Soc.*, **83**, 1675 (1961).
8) I. Harada, M. Tasumi, H. Shirakawa, and S. Ikeda, *Chem. Lett.*, **1978**, 1411.
9) K. L. D'Amico, C. Manos, and R. L. Christensen, *J. Am. Chem. Soc.*, **102**, 1777 (1980).
10) E. R. Blout and M. Fields, *J. Am. Chem. Soc.*, **70**, 189 (1948).
11) P. K. Das and R. S. Becker, *J. Phys. Chem.*, **86**, 921 (1982).

 © 1985 The Chemical Society of Japan Bull. Chem. Soc. Jpn., 58, 2929—2934 (1985)

The Pressure Effect on Conductances of KCl in Ethanol-Water Mixtures at 25 °C

Masakatsu UENO,* Noriaki TSUCHIHASHI, and Kiyoshi SHIMIZU
Department of Applied Chemistry, Faculty of Engineering, Doshisha University, Karasuma Imadegawa, Kamigyo-ku, Kyoto 602
(Received May 17, 1985)

The molar conductances of KCl in 5, 10, 15, 20, and 30 mol% ethanol–water mixtures were measured in the dilute concentration range of (2—8)×10^{-4} M (1 M=1 mol dm^{-3}) at 25 °C up to 1500 kgf cm^{-2} (1 kgf cm^{-2}=0.9807×10^5 Pa). The Fuoss-Onsager conductance equation for unassociated electrolytes was used to determine the limiting molar conductance, $\Lambda°$, of KCl in 5 and 10 mol% of ethanol. In 15, 20, and 30 mol% of ethanol, where the ionic association takes place, the Shedlovsky equation was employed to obtain $\Lambda°$ and the association constant K_A of KCl. The limiting ionic molar conductances of the K^+ and Cl^- ions were determined by combining $\Lambda°$ with the limiting transference number for KCl. The Walden products of both K^+ and Cl^- ions decrease with an increase in the pressure in 5 mol% of ethanol, but in 15 mol% of ethanol and above they increase with an increase in the pressure. These facts indicate that the breaking effect of these ions appears prominently in about 5 mol% of ethanol.

Studies of the electrolytic conductance in binary solvent systems of alcohols and water are of interest because such systems are useful in elucidating not only the effect of a change in the dielectric constant on the association of electrolytes into ion pairs, but also the influence of the solvent structure on the limiting ionic conductances.

In previous papers,[1,2] we reported the pressure and temperature effects on the transference numbers for KCl in ethanol–water mixtures. Here we wish to present data on the electrolytic conductances of KCl in the same solvent systems at high pressures at 25 °C, and to discuss the variation in the ionic Walden products with the ethanol content and the pressure.

Experimental

Chemicals and Solutions. The chemicals used were the same as those described in the previous paper.[1] All the solutions of potassium chloride KCl were prepared by weight. A proper quantity of the stock solution (2×10^{-3} M KCl aqueous solution) was weighed into a dry weighing bottle of about 150 cm^3 and then diluted gravimetrically with conductivity water and ethanol in order to yield the desired composition of the solvent and concentration of the solution. The concentrations of the solutions in M were determined by assuming that the densities of dilute KCl solutions were equal to that of the solvent.

Apparatus. The high-pressure system for the conductance measurement is illustrated in Fig. 1. Pressure generated by means of a hand pump was measured to ±3 kgf cm^{-2} by means of a calibrated Bourdon gauge (Nagano Keiki Seisakusho, Ltd.). The temperature of the oil bath in which a pressure vessel was immersed was kept constant at (25±0.03) °C. The conductance cell installed in the pressure vessel was made by modifying a hypodermic syringe (capacity, 10 cm^3); the oil pressure was transmitted to the solution through a glass piston of the syringe.

Unplatinized electrodes were used for all the measurements, since the resistances of solutions decreased monotonously with the time when lightly platinized electrodes were employed. In order to eliminate electrode polarization errors caused by using unplatinized electrodes, the resistances of solutions were measured at 0.2, 0.5, 1, 2, and 5 kHz by means of a sine wave oscillator (Model 361B), a conductance bridge (Model 362B), and a standard resistor (Model 363B) manufactured by Fuso Seisakusho, Ltd. The measured resistances were found to be linear functions of the reciprocal of the frequency, f, except for 0.2 kHz, and to increase with a decrease in the frequency, as is typical of electrode polarization. The extrapolated value at $1/f$=0 was assumed to be the correct value. The cell constants at atmospheric pressure, as determined by this method from the conductances of 5×10^{-4}, 1×10^{-3}, and 1×10^{-2} M KCl aqueous solutions,[3] agreed within ±0.03%, which indicates that electrode polarization errors are eliminated. The cell constant thus determined was 0.3860 cm^{-1}, and it was assumed to be invariant with the pressure.

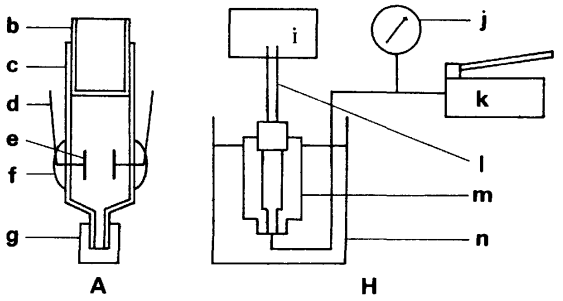

Fig. 1. High-pressure system for the conductance measurement.
A: Conductance cell of a syringe type, b: glass piston, c: glass cylinder, d: platinum lead, e: platinum electrode, f: Araldite, g: Teflon cap; H: pressure-generating system, i: conductance bridge, j: Bourdon-type pressure gauge, k: hand pump, l: leading wire, m: high-pressure vessel, n: oil bath.

Results

The physical properties of the various solvent mixtures, the density, ρ,[4] the viscosity, η,[4,5] and the dielectric constant, ε,[6] at high pressures and at 25 °C used in the data analysis are from the literature; they are summarized in Table 1, where the ρ,[7] η,[8] and ε[9] values of water are also included. Table 2 shows the

TABLE 1. PROPERTIES OF ETHANOL–WATER MIXTURES AT HIGH PRESSURES AT 25 °C

P/kgf cm^{-2}	ρ/g cm^{-3}	ε	η/cP
	Water		
1	0.9970	78.5	0.8937
500	1.0181	80.2	0.8865
1000	1.0372	81.9	0.8897
1500	1.0546	83.5	0.9034
	5 mol% of ethanol		
1	0.9772	71.7	1.426
500	0.9951	73.3	1.396
1000	1.0133	74.9	1.386
1500	1.0300	76.2	1.392
	10 mol% of ethanol		
1	0.9626	66.1	1.973
500	0.9816	67.8	1.996
1000	0.9991	69.3	2.035
1500	1.0142	70.7	2.065
	15 mol% of ethanol		
1	0.9486	60.6	2.310
500	0.9687	62.3	2.460
1000	0.9863	63.8	2.585
1500	1.0025	65.2	2.683
	20 mol% of ethanol		
1	0.9336	55.8	2.453
500	0.9539	57.5	2.663
1000	0.9717	59.1	2.880
1500	0.9877	60.5	3.080
	30 mol% of ethanol		
1	0.9043	47.7	2.467
500	0.9232	49.4	2.800
1000	0.9418	50.8	3.157
1500	0.9590	52.2	3.510

molar conductances, Λ, of KCl in ethanol–water mixtures at 25 °C as a function of the pressure, P. The molar conductances were reproducible within±0.1%.

The limiting molar conductances, Λ°, of KCl in 5 and 10 mol% of ethanol were obtained by analyzing the conductance data with the aid of the Fuoss-Onsager conductance equation for unassociated electrolytes:[10,11]

$$\Lambda = \Lambda^\circ - Sc^{1/2} + Ec \log c + Jc, \tag{1}$$

where c is the molar concentration (M) and where S, E, and J are the parameters in Eq. 1; S is the Onsager limiting slope, the form of E is $(E_1\Lambda^\circ - 2E_2)$, in which both E_1 and E_2 depend only upon solvent properties, and J is a function of the ion-size parameter, $\mathring{a}$. However, in 15 mol% of ethanol and above, the data analysis obtained by the use of Eq. 1 gives a very low value of $\mathring{a}$, which means that KCl is slightly associated in these mixtures. Thus, the Shedlovsky equation:[12]

$$1/\Lambda S(z) = 1/\Lambda^\circ + K_A c\Lambda S(z) f_\pm^2/\Lambda^{\circ 2}, \tag{2}$$

where:

$$S(z) = \{z/2 + [1 + (z/2)^2]^{1/2}\}^2, \tag{3}$$

$$z = [8.204 \times 10^5 \Lambda^\circ/(\varepsilon T)^{3/2} + 82.50/\eta(\varepsilon T)^{1/2}] \times (c\Lambda/\Lambda^{\circ 3})^{1/2}, \tag{4}$$

TABLE 2. MOLAR CONDUCTANCES Λ/S cm^2 mol^{-1} OF KCl IN COMPRESSED ETHANOL–WATER MIXTURES AT VARIOUS CONCENTRATIONS AT 25 °C

P/kgf cm^{-2}	c[a]/10^{-4} M					
	2.000	3.000	4.000	5.000	6.000	8.000
			5 mol% of ethanol			
1	102.3$_7$	102.1$_5$	101.9$_5$	101.7$_5$	101.5$_8$	101.4$_1$
500	102.6$_5$	102.5$_5$	102.2$_5$	102.1$_3$	101.9$_0$	101.7$_3$
1000	102.3$_8$	102.2$_5$	102.0$_5$	101.9$_0$	101.7$_3$	101.5$_1$
1500	101.6$_3$	101.5$_5$	101.3$_5$	101.2$_0$	100.9$_7$	100.7$_3$
			10 mol% of ethanol			
1	76.7$_7$	76.5$_8$	76.4$_2$	76.3$_1$	76.1$_7$	75.9$_7$
500	75.3$_8$	75.1$_8$	75.0$_5$	74.8$_6$	74.7$_7$	74.6$_2$
1000	74.1$_7$	73.9$_8$	73.8$_5$	73.7$_0$	73.5$_5$	73.4$_5$
1500	72.9$_3$	72.7$_8$	72.7$_1$	72.5$_5$	72.3$_7$	72.2$_4$
			15 mol% of ethanol			
1	64.4$_0$	64.1$_0$	63.8$_0$	63.6$_0$	63.4$_0$	63.1$_5$
500	61.2$_0$	60.9$_0$	60.7$_0$	60.5$_0$	60.3$_0$	60.0$_5$
1000	58.5$_0$	58.3$_0$	58.1$_0$	57.9$_0$	57.7$_0$	57.4$_8$
1500	56.1$_0$	55.8$_0$	55.6$_0$	55.4$_5$	55.3$_0$	55.1$_0$
			20 mol% of ethanol			
1	57.0$_0$	56.6$_0$	56.3$_5$	56.1$_5$	55.9$_0$	55.7$_0$
500	52.9$_0$	52.6$_0$	52.4$_0$	52.2$_0$	52.0$_0$	51.7$_5$
1000	49.5$_0$	49.2$_0$	49.0$_0$	48.8$_0$	48.6$_5$	48.4$_5$
1500	46.4$_0$	46.2$_0$	46.0$_0$	45.8$_5$	45.7$_0$	45.5$_0$
			30 mol% of ethanol			
1	49.1$_0$	48.8$_0$	48.5$_5$	48.3$_0$	48.0$_5$	47.8$_0$
500	44.7$_0$	44.4$_0$	44.2$_0$	44.0$_0$	43.8$_0$	43.5$_8$
1000	40.7$_0$	40.4$_0$	40.2$_0$	40.0$_5$	39.9$_0$	39.7$_0$
1500	37.0$_5$	36.8$_0$	36.6$_0$	36.5$_0$	36.3$_5$	36.2$_0$

a) Concentrations at atmospheric pressure.

Table 3. Values of $\Lambda°$/S cm^2 mol^{-1}, $t_+°$, $\lambda_\pm°$/S cm^2 mol^{-1}, $\mathring{a}$/Å, and K_A/mol^{-1} dm^3 in ethanol–water mixtures as a function of the pressure at 25 °C

P/kgf cm^{-2}	$\Lambda°$	$t_+°$	$\lambda_+°$	$\lambda_-°$	$\mathring{a}$	K_A
			Water			
1	149.9$_1$	0.490$_6$	73.5$_5$	76.3$_6$	1.$_5$	
500	151.7$_7$	0.486$_6$	73.8$_5$	77.9$_2$	1.$_8$	
1000	152.2$_2$	0.481$_8$	73.3$_4$	78.8$_8$	2.$_6$	
1500	151.4$_2$	0.479$_5$	72.6$_1$	78.8$_1$	5.$_8$	
			5 mol% of ethanol			
1	103.3$_2$	0.502$_4$	51.9$_1$	51.4$_1$	1.$_1$	
500	103.6$_5$	0.498$_4$	51.6$_6$	51.9$_9$	1.$_1$	
1000	103.3$_5$	0.495$_3$	51.1$_9$	52.1$_6$	3.$_2$	
1500	102.6$_5$	0.492$_2$	50.5$_2$	52.1$_3$	1.$_1$	
			10 mol% of ethanol			
1	77.5$_2$	0.505$_7$	39.2$_0$	38.3$_2$	1.$_2$	
500	76.1$_0$	0.503$_2$	38.2$_9$	37.8$_1$	1.$_2$	
1000	74.8$_7$	0.501$_9$	37.5$_8$	37.2$_9$	1.$_3$	
1500	73.6$_5$	0.500$_1$	36.8$_3$	36.8$_2$	1.$_2$	
			15 mol% of ethanol			
1	65.2$_4$	0.504$_9$	32.9$_4$	32.3$_0$		18.$_2$
500	61.9$_8$	0.503$_2$	31.1$_9$	30.7$_9$		16.$_5$
1000	59.2$_6$	0.502$_2$	29.7$_6$	29.5$_0$		15.$_0$
1500	56.7$_5$	0.501$_3$	28.4$_5$	28.3$_0$		13.$_9$
			20 mol% of ethanol			
1	57.8$_1$	0.500$_4$	28.9$_3$	28.8$_8$		22.$_4$
500	53.6$_7$	0.499$_2$	26.7$_9$	26.8$_8$		20.$_4$
1000	50.1$_7$	0.498$_5$	25.0$_1$	25.1$_6$		19.$_2$
1500	47.0$_4$	0.498$_0$	23.4$_3$	23.6$_1$		16.$_3$
			30 mol% of ethanol			
1	50.0$_4$	0.486$_6$	24.3$_5$	25.6$_9$		26.$_8$
500	45.4$_8$	0.487$_7$	22.1$_8$	23.3$_0$		23.$_1$
1000	41.3$_5$	0.488$_3$	20.1$_9$	21.1$_6$		22.$_2$
1500	37.6$_2$	0.489$_6$	18.4$_2$	19.2$_0$		18.$_4$

and:

$$-\ln f_\pm^2 = 3.649\times10^6[c\Lambda S(z)/\Lambda°]^{1/2}/(\varepsilon T)^{3/2} \quad (5)$$

was employed to obtain $\Lambda°$ and the association constant, K_A, from Λ in 15 mol% of ethanol and above; here, $f_\pm$ and T are the mean activity coefficient by the Debye-Hückel limiting law and the absolute temperature respectively. The values of $\Lambda°$, $\mathring{a}$, and K_A thus obtained are listed in Table 3, together with those of $\Lambda°$ and $\mathring{a}$ in water, which were obtained by recalculating the data in Ref. 13 with the aid of Eq. 1. The present values of $\Lambda°$ at atmospheric pressure are in good agreement with the more accurate ones[14] within ±0.2%. No high-pressure data are available for comparison in these systems, however. As is shown in Table 3, $\Lambda°$ decreases with an increase in the ethanol content at each pressure and with an increase in the pressure in each solvent except for 5 mol% of ethanol, where the $\Lambda°$-*vs.*-pressure curve has a slight maximum, as in the case of water.

The limiting ionic molar conductances, $\lambda_i°$, of the K^+ and Cl^- ions listed in Table 3 were determined by combining $\Lambda°$ with the limiting cation-transference number, $t_+°$, for KCl as follows:

$$\lambda_+° = \Lambda° t_+°, \quad (6)$$

$$\lambda_-° = \Lambda° - \lambda_+°. \quad (7)$$

The limiting cation-transference numbers shown in Table 3 were obtained using the Kay-Dye equation:[15]

$$t_+° = t_+ + [(0.5-t_+)/\Lambda°]\Delta\Lambda_e, \quad (8)$$

where t_+ is the cation-transference number at the molar concentration c and where $\Delta\Lambda_e$ is the electrophoretic contribution to conductance, expressed by the Fuoss-Onsager conductance equation:[10]

$$\Delta\Lambda_e = \beta c^{1/2}/(1+\kappa'\mathring{a}), \quad (9)$$

$$\beta = 82.50/\eta(\varepsilon T)^{1/2}, \quad (10)$$

$$\kappa' = 50.3c^{1/2}/(\varepsilon T)^{1/2}, \quad (11)$$

where $\mathring{a}$ is the ion-size parameter in Å. The values of η and ε are given in Table 1, $\Lambda°$ is determined in this work, and the value of t_+ in 0.02 M KCl solution is taken from Ref. 1; the value of $\mathring{a}$ taken from Ref. 16, *i.e.*, 3.08 Å, is assumed to be independent of the solvent composition and the pressure. It should be noted that the ionic association has no direct effect on the transference number, since it is the ratio of the conductance of the ion to that of the salt, and that the value of $t_+°$ is little affected by the use of a nominal

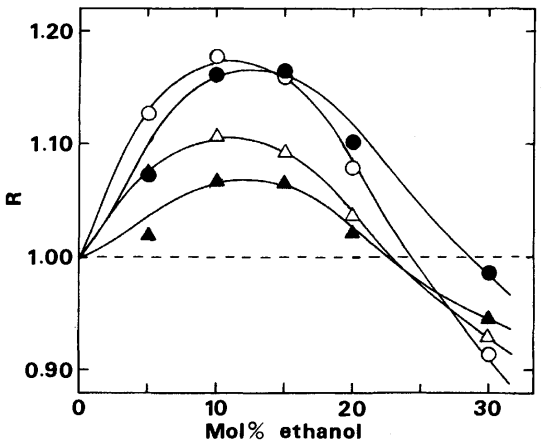

Fig. 2. Ionic Walden products normalized to their values in water as a function of mol% of ethanol. ○: 1 atm, ●: 1500 kgf cm^{-2} for the K^+ ion, and △: 1 atm, ▲: 1500 kgf cm^{-2} for the Cl^- ion.

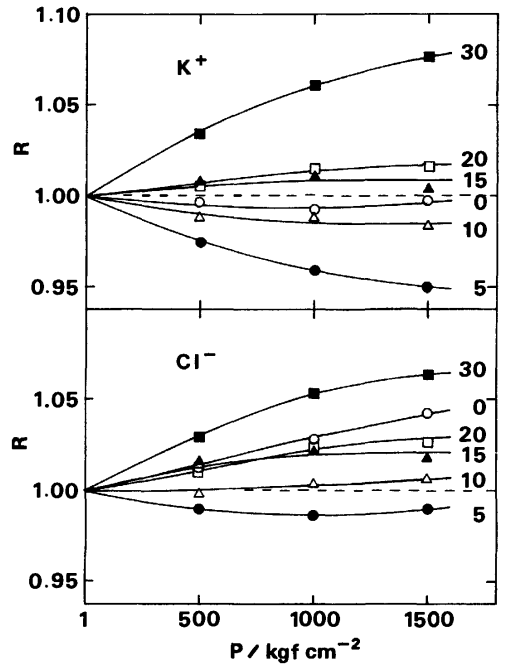

Fig. 3. Ionic Walden products normalized to their values at 1 atm as a function of the pressure. Mol% of ethanol is shown in the plot.

concentration (0.02 M) instead of a real concentration in Eqs. 9 and 11, since the ionic association is slight, the concentration of the solution is low enough, and the value of t_+ is close to 0.5 in our case.

The pressure dependence of $\lambda_i°$ in the various solvent mixtures agrees qualitatively with that of the fluidity of the solvent mixtures, $1/\eta$, except in the case of 5 mol% of ethanol, where $\lambda_+°$ decreases monotonously with an increase in the pressure, though $1/\eta$ has a maximum at about 900 kgf cm^{-2}.

Figures 2 and 3 show the variation in the ionic Walden products, $\lambda_i°\eta$, with the ethanol content and the pressure respectively. The ionic Walden products initially increase with the ethanol content up to about 10 mol% of ethanol and then decrease at each pressure studied. As is shown in Fig. 3, the pressure coefficient of the Walden product of the K^+ ion at atmospheric pressure is negative for water, 5, and 10 mol% of ethanol, is most negative for 5 mol% of ethanol, and becomes positive for 15 mol% of ethanol and above, while that of the Cl^- ion is negative for only 5 mol% of ethanol.

The association constant, K_A, increases with the ethanol content and decreases with the pressure, as is shown in Table 3. This trend coincides with the change in the dielectric constant of the solvent. The volume change on the ionic association, $\Delta\overline{V}°$, was estimated by means of the equation:[17]

$$\Delta\overline{V}° = -RT(\partial \ln K_A/\partial P)_T - RT\beta_s, \quad (12)$$

where β_s is the compressibility of the solvent and R is the gas constant. The values obtained at atmospheric pressure are 3.5, 4.0, and 4.8 cm^3 mol^{-1} for 15, 20, and 30 mol% of ethanol respectively.

Discussion

It is convenient to express the ionic Walden product as a sum of terms:[18]

$$\lambda_i°\eta = (\lambda_i°\eta)_{CS} + (\lambda_i°\eta)_{CE}, \quad (13)$$

where the charged-sphere contribution, $(\lambda_i°\eta)_{CS}$, is written as:

$$(1/\lambda_i°\eta)_{CS} = (1/\lambda_i°\eta)_{IS} + (1/\lambda_i°\eta)_{DR}. \quad (14)$$

Here, the term IS gives the contribution to the conductance to be expected from inert spheres, while the term subscripted DR gives the contribution to the conductance resulting from charging the spheres and is identified as a solvent dipole relaxation effect. The last term, subscripted CE, is a term that contains the effects resulting from changes in the solvent in the vicinity of an ion.

If we use, as the charged-sphere contribution, the Zwanzig dielectric friction theory,[19] which is based on a continuum model for the solvent, the ionic Walden product is expressed as:

$$\lambda_i°\eta = eF/[A_s\pi r_i + A_z\phi r_i^{-3}], \quad (15)$$

where ϕ is given by:

$$\phi = e^2(\tau/\eta)[(\varepsilon-\varepsilon_\infty)/\varepsilon(2\varepsilon+1)], \quad (16)$$

with A_s=6 and A_z=3/8 for complete sticking, and A_s=4 and A_z=3/4 for complete slipping. Here, e, F, r_i, τ, and ε_∞ are the protonic charge, the Faraday constant, the radius of an ion, the solvent dielectric relaxation time, and the infinite-frequency dielectric constant

respectively. Equation 15 predicts that the increase in ϕ will lead to a decrease in the ionic Walden product if r_i is taken to be the crystallographic radius of the ion and does not change with the solvent composition and the pressure. At atmospheric pressure, ϕ is shown to increase with the ethanol content by using the values of τ,[20] η, and ε of water, 20 and 30 mol% of ethanol, and on the assumption that ε_∞ is equal to that of water.[21] Therefore, the Zwanzig equation cannot explain the initial increase in the ionic Walden products with the ethanol content, as was pointed out by Kay *et al.*[22] However, the decrease in the ionic Walden products with the ethanol content in the range of (20—30) mol% of ethanol is qualitatively in agreement with the experimental results shown in Fig. 2.

Here, let us consider the pressure dependence of the ionic Walden products in each solvent. The pressure dependence of ϕ is expressed as follows:

$$\frac{1}{\phi}\left(\frac{\partial\phi}{\partial P}\right)_T = \left[\frac{-2\varepsilon(\varepsilon-2\varepsilon_\infty)+\varepsilon_\infty}{\varepsilon(\varepsilon-\varepsilon_\infty)(2\varepsilon+1)}\right]\left(\frac{\partial\varepsilon}{\partial P}\right)_T + \frac{1}{\tau}\left(\frac{\partial\tau}{\partial P}\right)_T - \frac{1}{\eta}\left(\frac{\partial\eta}{\partial P}\right)_T. \quad (17)$$

The first term on the right-hand side of Eq. 17 is negative for all the solvent mixtures studied, because ε increases with an increase in the pressure, as is shown in Table 1, and ε_∞ can be expected to be very small compared with ε. Although there is no available data on τ at high pressures in ethanol–water mixtures, τ is anticipated to decrease with an increase in the pressure, by analogy with the case of water.[23] The decrease in the τ of water with the pressure is attributed to the bending of hydrogen bonds between water molecules caused by pressure. Therefore, the second term can also be expected to be negative. The third term, except in the cases of water and 5 mol% of ethanol, is negative, since η increases with an increase in the pressure, as is shown in Table 1. Thus, ϕ decreases with an increase in the pressure in 10 mol% of ethanol and above. In the cases of water and 5 mol% of ethanol, η initially decreases with an increase in the pressure. However, this contribution to $(1/\phi)(\partial\phi/\partial P)_T$ is comparable with that of the first term, and the two contributions cancel each other out; in the case of water, the contribution of the second term is about twice as large as those of the first and third terms. Therefore, ϕ decreases with the pressure even in water and 5 mol% of ethanol. The Zwanzig equation predicts that the ionic Walden product will increase with the pressure. This prediction agrees with the experimental results in 15 mol% of ethanol and above, as is shown in Fig. 3. However, the pressure coefficients of the Walden product of the K^+ ion in water, 5, and 10 mol% of ethanol and that of the Cl^- ion in 5 mol% of ethanol, *i.e.*, in the water-rich region, do not agree with the predictions of the theory.

In the water-rich region, the water structure is more strengthened than that in water by the addition of a small amount of ethanol.[24] Thus, in this region the second term on the right-hand side of Eq. 13, $(\lambda_i^\circ\eta)_{CE}$, must be taken into consideration. If the effective viscosity in the vicinity of an ion is less than the bulk viscosity of a solvent, the ion obtains excess mobility. An increase in the pressure will cause the water structure to weaken by bending the hydrogen bonds between water molecules. Thus, the excess mobility will decrease with an increase in the pressure. This effect brings about the decrease in the ionic Walden product with an increase in the pressure. For the K^+ ion, this can be seen in water, 5, and 10 mol% of ethanol; it is most prominent in 5 mol% of ethanol. The Cl^- ion is also classified as a breaking ion. However, the Walden product in water increases with an increase in the pressure. The assumption that this is based on the contribution of the dielectric friction is curious, because the contribution of the dielectric friction to the conductance may be expected to be less for the Cl^- ion than for the K^+ ion, since the crystallographic radius of a Cl^- ion is larger than that of a K^+ ion.[25] Therefore, the specific interaction between the Cl^- ion and water molecules must be considered. The interaction between the Cl^- ion and water molecules includes the contribution of hydrogen bonds.[26] If the pressure weakens the hydrogen bonds, the Cl^- ion will obtain excess mobility. This effect may be gradually reduced by adding ethanol to water, thus enhancing the basicity of the solvent mixtures,[27] and the decrease in the Walden product of the Cl^- ion in 5 mol% of ethanol with the pressure may be attributed to the structure-breaking effect of the Cl^- ion, since the water structure is most strengthened in this region.

References

1) M. Ueno, S. I, and K. Shimizu, *Bull. Chem. Soc. Jpn.*, **56**, 846 (1983).

2) M. Ueno, S. I, and K. Shimizu, *Bull. Chem. Soc. Jpn.*, **58**, 1225 (1985).

3) G. C. Benson and A. R. Gordon, *J. Chem. Phys.*, **13**, 473 (1945).

4) M. Yusa, G. P. Mathur, and R. A. Stager, *J. Chem. Eng. Data*, **22**, 32 (1977).

5) The viscosities of 5 mol% of ethanol at high pressures have been estimated by smoothing the data of Ref. 4.

6) T. Moriyoshi, T. Ishii, and S. Takahashi, 20th High Press. Conf. Jpn., 1979, Abstr., p. 199; T. Moriyoshi, private communication.

7) C. T. Chen, R. A. Fine, and F. J. Millero, *J. Chem. Phys.*, **66**, 2142 (1977).

8) J. B. Cappi, Ph. D. Thesis, London University, 1964; K. E. Bett and J. B. Cappi, *Nature*, **207**, 620 (1965).

9) K. R. Srinivasan and R. L. Kay, *J. Chem. Phys.*, **60**, 3645 (1974).

10) R. M. Fuoss and F. Accascina, "Electrolytic Conductance," Interscience Pub., New York (1959), Chap. 15.

11) P. C. Carman, *J. Phys. Chem.*, **74**, 1653 (1970).

12) T. Shedlovsky, *J. Franklin Inst.*, **225**, 739 (1938); R. M. Fuoss and T. Shedlovsky, *J. Am. Chem. Soc.*, **71**, 1496 (1949).
13) K. Shimizu and N. Tsuchihashi, *Rev. Phys. Chem. Jpn.*, **49**, 18 (1979).
14) R. L. Kay and T. L. Broadwater, *J. Solution Chem.*, **5**, 57 (1976); J. L. Hawes and R. L. Kay, *J. Phys. Chem.*, **69**, 2420 (1965).
15) R. L. Kay and J. L. Dye, *Proc. Natl. Acad. Sci. U. S. A.*, **49**, 5 (1963).
16) C. G. Swain and D. F. Evans, *J. Am. Chem. Soc.*, **88**, 386 (1966).
17) S. D. Hamann, "Physico-Chemical Effects of Pressure," Butterworths Scientific Pub., London (1957), Chap. 8.
18) R. L. Kay, "Water. A Comprehensive Treatise," ed by F. Franks, Plenum Press, New York (1973), Vol. 3, Chap. 4.
19) R. Zwanzig, *J. Chem. Phys.*, **52**, 3625 (1970).
20) D. E. Buck, *U. S. Govt. Res. Develop. Rept.*, **40**, 59 (1965).
21) J. B. Hasted, "Water. A Comprehensive Treatise," ed by F. Franks, Plenum Press, New York (1972), Vol. 1, Chap. 7.
22) R. L. Kay, G. P. Cunningham, and D. F. Evans, "Hydrogen-Bonded Solvent Systems," ed by A. K. Convington and P. Jones, Taylor and Francis, Ltd., London (1968), pp. 249—260.
23) R. Pottel and E. Asselborn, *Ber. Bunsenges. Phys. Chem.*, **83**, 29 (1979).
24) F. Franks and D. J. G. Ives, *Quart. Rev. London*, **20**, 1 (1966).
25) L. Pauling, "The Nature of the Chemical Bond," 3rd ed, Cornell University, New York (1960), Chap. 13.
26) M. Nakahara, K. Shimizu, and J. Osugi, *Nippon Kagaku Zasshi*, **92**, 785 (1971).
27) D. Feakins, "Physico-Chemical Processes in Mixed Aqueous Solvents," ed by F. Franks, Heinemann Education Books, Ltd., London (1967), pp. 71—99.

Mechanism of Resonant Two-photon Transitions *via* Repulsive Intermediate States. Experimental and Theoretical Studies on I_2 Vapor

Jun SHIRAISHI, Yuichi FUJIMURA,* Takeshi NAKAJIMA, Masahiro KAWASAKI,*,† Kazuo KASATANI,† Hiroyasu SATO,† and Ikuzo TANAKA*,††

Department of Chemistry, Faculty of Science, Tohoku University, Sendai 980

†*Chemistry Department of Resources, Mie University, Kamihama-cho, Tsu 514*

††*Department of Chemistry, Tokyo Institute of Technology, Ohokayama, Meguro, Tokyo 152*

(Received May 27, 1985)

Mechanisms of resonant two-photon transitions *via* repulsive intermediate states are experimentally and theoretically studied. Polarization ratios, $\Omega=\sigma_{\infty}/\sigma_{11}$ (where σ_{∞} and σ_{11} are the cross section of the two-photon transitions obtained by the circularly polarized light and that by the linearly polarized light, respectively) of the two-photon excitation of iodine vapor have been measured in the wavelength range of 420—510 nm. An expression for the polarization ratio for the two-photon absorption in which both simultaneous and sequential processes take place has been presented. The polarization ratios calculated by using the δ-function approximation for the repulsive intermediate states as a function of the laser frequency for the iodine molecule system explain qualitatively the experimental result. This indicates that both the simultaneous and the sequential process take place in the frequency region measured.

Multi-photon spectroscopy has made a great contribution to clarifying structures of electronically excited states of molecules and the dynamical processes taking place in these states.[1] Most of papers so far reported were concerned with resonant multi-photon transitions *via* bound intermediate states. Resonant multi-photon transitions *via* repulsive intermediate states such as bound-free-bound or bound-free-free transition can be induced with production of fragments. These types of the multi-photon transition can be observed in iodine and halogen substituted compounds *etc.*[2,3] At present mechanisms of the multi-photon transitions involving repulsive intermediate states are not well known. It is interesting to investigate which is dominant, simultaneous or sequential process. The latter is induced by elastic collisions between molecules and perturbers.

One of the methods for identifying the mechanisms of the multi-photon transitions is to measure the polarization ratio Ω defined by ratio of the transition probability obtained by using circularly polarized light to that obtained by using parallel linearly polarized light. Kasatani *et al.*[4] have observed two- and three-photon transitions of I_2 *via* the repulsive intermediate states in gases. From the polarization measurement of the fluorescence excitation spectra, they have found that even though the I_2 molecule excited in the energy region beyond the attractive potential of the B state, the photon absorption proceeds *via* the real repulsive intermediate states. Another method is to analyze the vibronic structure appearing in the spectra.

The purpose of this paper is to investigate the mechanisms of resonant two-photon transitions *via* repulsive intermediate states from both experimental and theoretical points of view. We first report polarization ratios of two-photon fluorescence excitation spectra of gaseous I_2 in the laser wavelength range of 420—510 nm. Secondly effects of the repulsive intermediate states on the resonant two-photon absorption (TPA) probability are theoretically studied. Neglecting effects of molecular rotations, and assuming the molecules to be randomly oriented, we derive expressions for the transition probabilities of the simultaneous and sequential TPA processes. In the Born-Oppenheimer and Condon approximations, these expressions are divided into two terms. One involves electronic transition matrix elements relevant to the two-photon transitions with laser intensity. This term depends on the polarization of photon for the simultaneous TPA process. The other term is a line shape function which characterizes the vibronic intensity distribution. Expressions for the line shape functions for the simultaneous process and sequential one are derived by using the δ-function approximation to the repulsive intermediate states and the displaced harmonic oscillator approximation to the initial and final states. In deriving the expressions for the line shape functions, two cases can be considered, depending on the dimensionless potential displacement Δ between the initial and final states: one is the weak coupling case in which $\Delta \leq 1$, and the other is the strong coupling case which is characterized by a large potential displacement. Ion pair states in I_2 can be taken as belonging to the latter case. In this paper, we derive an expression for the line shape function of the TPA process of I_2 in the strong coupling case. Finally the frequency dependence of the polarization ratio is evaluated and is compared with that observed for the gaseous I_2 molecule.

Experimental

The Polarization Measurements of I_2 Vapor. Iodine vapor in a quartz cell at 90°C was excited by visible light from an N_2 laser pumped dye laser (Molectron UV-24 and DL-14) in the wavelength range of 420—510 nm. The laser intensity was $\lesssim$1 mj/pulse of a few nanoseconds. The

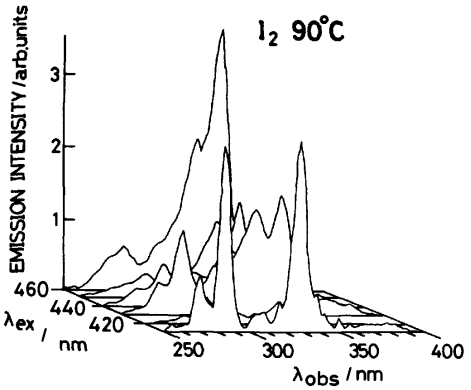

Fig. 1. Fluorescence spectra taken at various excitation wavelengths of I_2 vapor at 90°C.

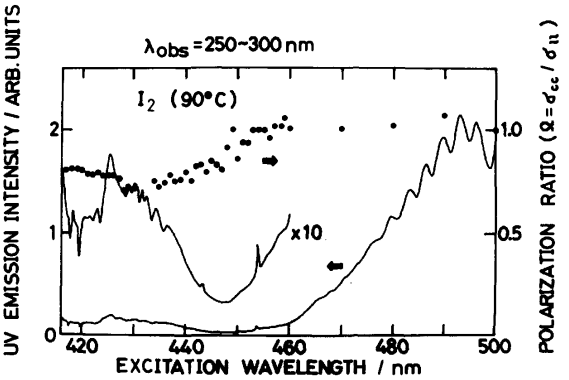

Fig. 2. Fluorescence excitation spectra (solid curves) and polarization ratios (points) of I_2 vapor at 90°C.

band width was around 0.4 cm^{-1}. The ultraviolet emission from iodine molecules was observed at right angles to the focused laser beam with a monochromator (or a filter), a telescope and a photomultiplier (Hamamatsu Photonics R-166 UH or 1P28). In order to measure the effect of the polarization of laser light on the two-photon absorptivity, the laser beam was passed through a rotatable double Fresnel rhomb followed by a single Fresnel rhomb. This optical arrangement provides linearly or circularly polarized light without changing the optical pass and intensity of the laser beam. At the lower vapor pressure, the polarization ratio could not be quantitatively measured because of low *S/N* ratios.

By the excitation of iodine vapor at $\lambda_{ex} \geq 498.9$ nm *i.e.*, below the dissociation limit of the B (0_u^+) state, the UV emission was observed at 385, 342, 320, 287, and 270 nm as reported previously.[4] When the energy of laser light was above the dissociation limit $\lambda_{ex} < 498.9$ nm, the UV emission was still observed at various wavelengths as shown in Fig. 1. When the UV emission intensity was measured as a function of excitation wavelength, the intensity decreased drastically at $\lambda_{ex} < 498.9$ nm with unfocused laser light. The excitation spectra were detected for two UV wavelength regions, one with an interference filter centered at 320 nm, and the other with a broad band pass filter (240—330 nm). UV excitation spectra taken by these two methods were essentially the same. The decrease in UV intensity is caused by the decrease in the number density of the intermediate B 0_u^+ state for two-photon absorption process,

$$I_2 + \hbar\omega_R \longrightarrow I_2^*(B\,0_u^+),$$

$$I_2^*(B\,0_u^+) + \hbar\omega_R \longrightarrow I_2^{**}.$$

Same sharp decrease in the excitation spectra at $\lambda_{ex} < 498.9$ nm has been reported when iodine vapor was irradiated by the visible laser light from a flash lamp pumped dye laser, the peak power of which was weaker than the N_2 laser pumped dye laser by a factor of ≈200. This drastic intensity change at $\lambda < 498.9$ nm, however, was not observed when the laser light was focused by a lens (f=30 mm). This is probably because the pumping rate to the upper state(s) by the focused laser light is comparable to the dissociation rate of the intermediate state.

The influence of the incident light polarization (circular or linear) on the rate of the photon absorption process was investigated at various laser wavelengths. The results for benzene were in good agreement with those obtained by Friedrich and McClain.[5] The polarization ratios for iodine vapor were measured by observing the UV emission with the UV band pass filter as shown in Fig. 2. They were found to be essentially unity in the laser wavelength range of 450—510 nm where iodine molecules absorb visible light in the transition from the ground states to the dissociative states B (0_u^+) and 1_u. Below 450 nm, one-photon absorption diminishes. When the laser wavelength became less than 450 nm, the transition probabilities or UV emission decreased and the polarization ratios began to deviate from unity as shown in Fig. 2. This deviation indicates that the contribution of two-photon absorption *via* the real dissociative state becomes less important and that *via* virtual states becomes important. The interaction time between photons and dissociative state becomes shorter with increasing the photon energy because the dissociative lifetime is classically a function of the incident photon energy. At the shorter wavelength region observed the polarization ratio became less than 1.0. This transition corresponds to $\Delta\Omega=0$, or $0_g^+ - X0_g^+$ two-photon transition *via* virtual states.[6] In the following sections we shall discuss theoretically both two-photon transition probabilities through a dissociative state and polarization ratios in more detail.

Theoretical

Transition Probabilities of Resonant TPA via Repulsive Intermediate States. We consider a resonant two-photon absorption (TPA) *via* repulsive intermediate states as shown in Fig. 3. The two-photon transition probability from vibronic state a to n, $W_{a\to n}(\omega_R)$ can be approximately expressed in terms of the simultaneous transition probability $W_{a\to n}^{sim}(\omega_R)$ and the sequential one $W_{a\to m}^{seq}(\omega_R)$ as

$$W_{a\to n}(\omega_R) \simeq W_{a\to n}^{sim}(\omega_R) + W_{a\to n}^{seq}(\omega_R), \quad (1)$$

where we have assumed that molecules absorb identical two-photons with frequency ω_R and polarization vector $\vec{\lambda}$, and mixed terms have been omitted though these may make a significant contribution

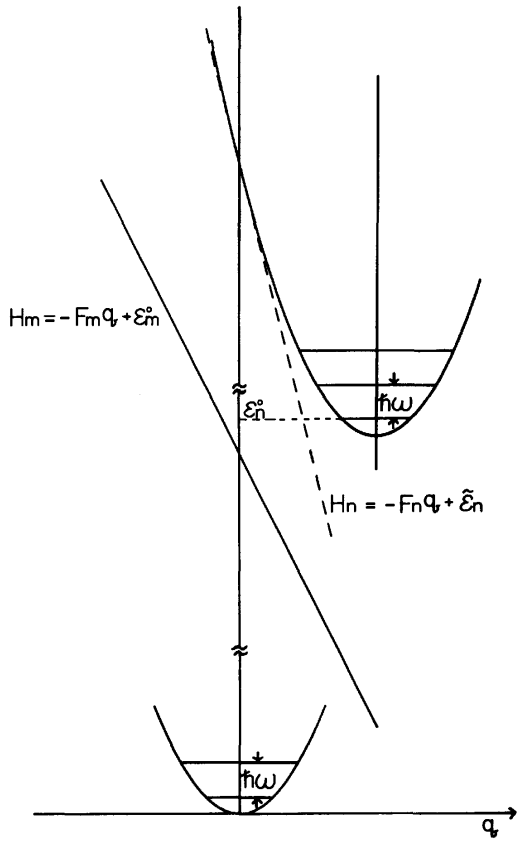

Fig. 3. Model potentials for TPA in the strong coupling case. Potentials of the initial and final states are expressed in terms of displaced harmonic ones with frequency ω and a large displacement Δ. Potential of the intermediate state is approximated by a linear one.

in some cases.[7] General forms for the transition probabilities have already been given elsewhere.[7] In the Born-Oppenheimer approximation in which wave functions can be expressed as a product of electronic (Φ) and vibrational (θ) ones, and in the Condon approximation, we can separate the simultaneous transition probability into two terms, a polarization dependent term P_λ and a line shape function $L(\omega_R)$:[8-12]

$$W^{sim}_{a\to n}(\omega_R) = P^{sim}_\lambda L^{sim}(\omega_R), \tag{2}$$

where

$$P^{sim}_\lambda = \langle\langle |\vec{H}'_{nm}\cdot\vec{\lambda}\,\vec{H}'_{ma}\cdot\vec{\lambda}|^2\rangle\rangle, \tag{3}$$

$$L^{sim}(\omega_R) = \frac{2}{\hbar^4}\mathrm{Re}\sum_a\sum_n \frac{\rho_{aa}}{i\omega_{na}+\Gamma_{na}} \times \left|\int d\omega_m \frac{\langle\theta_n|\theta_m\rangle\langle\theta_m|\theta_a\rangle}{i\omega_{ma}+\Gamma_{ma}}\right|^2, \tag{4}$$

where summations are carried out over the vibronic states of the a and n electronic states. In Eq. 3, double bracket $\ll\cdots\gg$ denotes averaging over orientations of the molecules, and $\vec{H}'_{nm}=\langle\Phi^0_n|\vec{H}'|\Phi^0_m\rangle$ is the matrix element of the molecule-photon interaction Hamiltonian. In Eq. 4, ρ_{aa} represents the population in the initial state, $\omega_{na}=\omega_n-\omega_a-2\omega_R$, $\omega_{ma}=\omega_m-\omega_a-\omega_R$ in which ω_n, ω_m, and ω_a denote molecular eigenfrequencies of the relevant states, and Γ, dephasing constant between two states, for example, is given by

$$\Gamma_{ma} = \frac{1}{2}(\Gamma_{mm}+\Gamma_{aa})+\Gamma^{(d)}_{ma}, \tag{5}$$

in which Γ_{mm} is the population decay constant of state m, and $\Gamma^{(d)}_{ma}$ the pure dephasing constant.[7,13,14]

Assuming the sequential process to be induced by intermolecular interactions between molecules and heat bath, we can express the two-photon transition probability in the similar way,

$$W^{seq}_{a\to n}(\omega_R) = P^{seq}L^{seq}(\omega_R), \tag{6}$$

where

$$P^{seq} = \langle\langle|\vec{H}'_{nm}\cdot\vec{\lambda}|^2\rangle\rangle\langle\langle\vec{H}'_{ma}\cdot\vec{\lambda}|^2\rangle\rangle \propto |\vec{H}'_{nm}|^2|\vec{H}'_{ma}|^2, \tag{7}$$

which is independent of polarization, and $L^{seq}(\omega_R)$, the line shape function for the sequential TPA is given as

$$L^{seq}(\Omega_R) = \frac{2}{\hbar^4}\mathrm{Re}\sum_a\rho_{aa}\sum_n\int d\omega_m\int d\omega_k(\Gamma_{ma}-\Gamma_{mk}+\Gamma_{ak}) \times \frac{\langle\theta_a|\theta_m\rangle\langle\theta_m|\theta_n\rangle\langle\theta_n|\theta_k\rangle\langle\theta_k|\theta_a\rangle}{(i\omega_{mn}+\Gamma_{mn})(i\omega_{ak}+\Gamma_{ak})(i\omega_{ma}+\Gamma_{ma})(i\omega_{mk}+\Gamma_{mk})}. \tag{8}$$

In order to evaluate ω_R-dependence of the transition probability of resonant TPA *via* repulsive intermediate states, we now derive expressions for the line shape functions $L^{sim}(\omega_R)$ and $L^{seq}(\omega_R)$ by using one dimensional model shown in Fig. 3.

Nuclear potentials of the initial a and final n electronic states are assumed to be characterized by displaced harmonic potentials with displacement Δ: The corresponding Hamiltonians $\hat{H}_a$ and $\hat{H}_n$ are expressed in the forms,

$$\hat{H}_a = \frac{\hbar\omega}{2}(\hat{p}^2+q^2), \tag{9a}$$

and

$$\hat{H}_n = \frac{\hbar\omega}{2}\{\hat{p}^2+(q-\Delta)^2\} + \varepsilon^0_n, \tag{9b}$$

where q and $\hat{p}$ are the dimensionless nuclear coordinate and the conjugated momentum, respectively. ω represents the frequency of the vibrational mode.

Vibronic Hamiltonian of repulsive intermediate states is assumed to be given by

$$\hat{H}_m = \frac{\hbar\omega}{2}\hat{p}^2 - F_m q + \varepsilon^0_m, \tag{10}$$

with $F_m>0$. We shall consider the line shape function

of the simultaneous TPA *via* repulsive intermediate states in the strong coupling case.

a) Simultaneous TPA: Applying the generating function method[15] to Eq. 4, we obtain

$$L^{\mathrm{sim}}(\omega_{\mathrm{R}}) = \frac{2}{\hbar^4}\int_{-\infty}^{\infty}\mathrm{d}t\int_0^{\infty}\mathrm{d}\tau\int_0^{\infty}\mathrm{d}\tau' \exp\left[-\Gamma_{na}|t| - \Gamma_{ma}(\tau+\tau') - 2i\omega_{\mathrm{R}}t - i\omega_{\mathrm{R}}(\tau'-\tau)\right]G(\tau,\tau',t), \quad (11)$$

where $G(\tau,\tau',t)$, generating function for the simultaneous TPA, is given as

$$G(\tau,\tau',t) = \sum_a \langle\theta_a|\rho_{aa}\exp\left[-\mathrm{i}\hat{H}_a(t+\tau'-\tau)/\hbar\right] \times \exp\left[\mathrm{i}\hat{H}_m\tau'/\hbar\right]\exp\left[\mathrm{i}\hat{H}_m t/\hbar\right] \times \exp\left[-\mathrm{i}\hat{H}_m\tau/\hbar\right]|\theta_a\rangle. \quad (12)$$

For simplicity we assume the vibrational mode of molecules to be in the low temperature limit. A temperature dependent line shape function can be derived by using the Boson operator technique.[16] In order to derive an expression for the line shape function within the δ-function approximation, we neglect the nuclear kinetic energy in the Hamiltonian for the repulsive intermediate states. In this approximation we obtain a line shape function as

$$L^{\mathrm{sim}}(\omega_{\mathrm{R}}) = \frac{2}{\hbar^4}\int_{-\infty}^{\infty}\mathrm{d}t\int_0^{\infty}\mathrm{d}\tau\int_0^{\infty}\mathrm{d}\tau' \exp\left[\mathrm{i}(\tilde{\varepsilon}_n/\hbar-\omega/2-2\omega_{\mathrm{R}})t - \Gamma_{na}|t| - (F_m\tau'-F_m\tau+F_n t)^2/4\hbar^2 + \mathrm{i}(\varepsilon_m^0/\hbar-\omega/2-\omega_{\mathrm{R}})\tau' - \mathrm{i}(\varepsilon_m^0/\hbar-\omega/2-\omega_{\mathrm{R}})\tau - (\tau+\tau')\Gamma_{ma}\right], \quad (13)$$

where quantum number dependences of Γ have been neglected. A brief derivation of Eq. 13 is given in Appendix A. In the case in which condition $\hbar\Gamma_{na}<F_n$ is satisfied, we can neglect effects of the dephasing constant Γ_{na} in Eq. 13. In this case after integration over t in Eq. 13 we obtain

$$L^{\mathrm{sim}}(\omega_{\mathrm{R}}) = \frac{4\sqrt{\pi}}{\hbar^3 F_n}\exp\left[-\left(\frac{\tilde{\varepsilon}_n-\hbar\omega/2-2\hbar\omega_{\mathrm{R}}}{F_n}\right)^2\right] \times\left|\int_0^{\infty}\mathrm{d}\tau\exp\left[-\mathrm{i}\left\{\varepsilon_m^0/\hbar-\omega/2-\omega_{\mathrm{R}} - (\tilde{\varepsilon}_n/\hbar-\omega/2-2\omega_{\mathrm{R}})\frac{F_m}{F_n}\right\}-\Gamma_{ma}\tau\right]\right|^2. \quad (14)$$

Integration over τ in Eq. 14 yields an analytical expression for the simultaneous TPA in the strong coupling case as,

$$L^{\mathrm{sim}}(\omega_{\mathrm{R}}) = \frac{4\sqrt{\pi}}{\hbar^3 F_n}\exp\left[-\left(\frac{\tilde{\varepsilon}_n-\hbar\omega/2-2\hbar\omega_{\mathrm{R}}}{F_n}\right)^2\right] \times\frac{r^2}{\{\tilde{\varepsilon}_n/\hbar-\omega/2-r(\varepsilon_m^0-\omega/2)-(2-r)\omega_{\mathrm{R}}\}^2+r^2\Gamma_{ma}^2}, \quad (15)$$

with $r=F_n/F_m$. The first term in Eq. 15 is equivalent to the band shape function for the one-photon bound-free transition with optical frequency $2\omega_{\mathrm{R}}$. In the usual case in which $F_n>\Gamma_{ma}r/|2-r|$, the band shape for the simultaneous TPA process is dominated by the second term in Eq. 15. This indicates that the maximum of the band locates at $\{\tilde{\varepsilon}_n/\hbar-\omega/2-r(\varepsilon_m^0-\omega/2)\}/(2-r)$ with the effective width $\Gamma_{ma}r/|2-r|$. The same expression for the line shape function as Eq. 15 can be derived if the vibronic Hamiltonian of the final state is assumed to be expressed in terms of a linear potential, $\hat{H}_n=-F_nq+\tilde{\varepsilon}_n$, in stead of using the approximation expansion Eq. A. 9.

b) Sequential TPA: The line shape function for the sequential TPA in the strong coupling case takes the form

$$L^{\mathrm{seq}}(\omega_{\mathrm{R}}) = \frac{2}{\hbar^4}\mathrm{Re}\sum_a\rho_{aa}\int\mathrm{d}\omega_n\int\mathrm{d}\omega_m\int\mathrm{d}\omega_k(\Gamma_{ma}-\Gamma_{mk}+\Gamma_{ak}) \times\frac{\langle\theta_a|\theta_m\rangle\langle\theta_m|\theta_n\rangle\langle\theta_n|\theta_k\rangle\langle\theta_k|\theta_a\rangle}{(\mathrm{i}\omega_{mn}+\Gamma_{mn})(\mathrm{i}\omega_{ak}+\Gamma_{ak})(\mathrm{i}\omega_{ma}+\Gamma_{ma})(\mathrm{i}\omega_{mk}+\Gamma_{mk})}. \quad (16)$$

For the strong coupling case, the linear potential approximation can be adopted both to the intermediate and final state potentials, and the overlap integral between the two states can be expressed as

$$\langle\theta_m|\theta_n\rangle = (F_nF_m)^{-1/2}\delta(q_m-q_n). \quad (17)$$

Applying Eq. 17 into Eq. 16 and integrating over the frequencies ω_n and ω_k, we obtain

$$L^{\mathrm{seq}}(\omega_{\mathrm{R}}) = \frac{2}{\hbar^4}\int_{-\infty}^{\infty}\mathrm{d}q_m\frac{(2\Gamma_{ma}-\Gamma_{mm})\Gamma_{mn}}{\Gamma_{mm}} \times\frac{1}{[\{(\tilde{\varepsilon}_n-F_nq_m)/\hbar-(\varepsilon_m^0-F_mq_m)/\hbar-\omega_{\mathrm{R}}\}^2+\Gamma_{mn}^2]} \times\frac{|\theta_a(q_m)|^2}{[\{(\varepsilon_m^0-F_mq_m-\hbar\omega/2)/\hbar-\omega_{\mathrm{R}}\}^2+\Gamma_{ma}^2]}, \quad (18)$$

where we have restricted ourselves to the TPA in the low temperature limit. In the case in which $F_m\gg\hbar\Gamma_{ma}$ is satisfied, the integrand in Eq. 18 involves the δ-function in the limit $\hbar\Gamma_{ma}/F_m\to0$. In this case the integration over q_m can be performed as

$$L^{\mathrm{seq}}(\omega_{\mathrm{R}}) = \frac{2\pi}{\hbar^3}\frac{(2\Gamma_{ma}-\Gamma_{mm})\Gamma_{mn}}{F_m\Gamma_{mm}\Gamma_{ma}} \times\frac{\exp\left[-\left(\frac{\varepsilon_m^0-\hbar\omega/2-\hbar\omega_{\mathrm{R}}}{F_m}\right)^2\right]}{\{\varepsilon_n^0/\hbar-\omega/2-2\omega_{\mathrm{R}}-r(\tilde{\varepsilon}_n/\hbar-\omega/2-\omega_{\mathrm{R}})\}^2+\Gamma_{mn}^2}. \quad (19)$$

From Eq. 19, we can see that the peak of the band for the sequential TPA process locates at the same frequency as that for the simultaneous process, and its effective width is given by $\Gamma_{mn}/|2-r|$.

Polarization Ratio of the Resonant TPA of I_2 Vapor. We consider the polarization ratio for the TPA in the presence of both simultaneous and sequential processes at the same time. In this case, the polarization ratio $\Omega(\omega_{\mathrm{R}})$ can be defined as

$$\Omega(\omega_{\mathrm{R}}) = \frac{W_{a\to n}^{\rightrightarrows}(\omega_{\mathrm{R}})}{W_{a\to n}^{\uparrow\uparrow}(\omega_{\mathrm{R}})} = \frac{P_{\rightrightarrows}^{\mathrm{sim}}L^{\mathrm{sim}}(\omega_{\mathrm{R}})+P^{\mathrm{seq}}L^{\mathrm{seq}}(\omega_{\mathrm{R}})}{P_{\uparrow\uparrow}^{\mathrm{sim}}L^{\mathrm{sim}}(\omega_{\mathrm{R}})+P^{\mathrm{seq}}L^{\mathrm{seq}}(\omega_{\mathrm{R}})}. \quad (20)$$

The polarization dependence of the simultaneous TPA

has been studied by McClain,[10] Monson and McClain,[9] Nascimento,[11] and Bray and Hochstrasser[12] included rotational effects. In order to calculate the polarization ratio, the values of $P_{\lambda}^{sim}/P^{seq}$ must be determined. Averaging the P_{λ}^{sim} of Eq. 3 over the orientation of the molecule, we obtain

$$P_{\uparrow\uparrow}^{sim} = \frac{1}{15}[3\{(M_{na}^{xx})^2+(M_{na}^{yy})^2+(M_{na}^{zz})^2\} + 4\{(M_{na}^{xy})^2+(M_{na}^{xz})^2+(M_{na}^{yz})^2\} + 2\{M_{na}^{xx}M_{na}^{yy}+M_{na}^{xx}M_{na}^{zz}+M_{na}^{yy}M_{na}^{zz}\}], \quad (21)$$

for the linearly polarized light, and

$$P_{\infty}^{sim} = \frac{1}{30}[4\{(M_{na}^{xx})^2+(M_{na}^{yy})^2+(M_{na}^{zz})^2\} + 12\{(M_{na}^{xy})^2+(M_{na}^{xz})^2+(M_{na}^{yz})^2\} - 4\{M_{na}^{xx}M_{na}^{yy}+M_{na}^{xx}M_{na}^{zz}+M_{na}^{yy}M_{na}^{zz}\}], \quad (22)$$

for the circularly polarized light, where M_{na} the two-photon electronic transition matrix element, for example, is given by

$$M_{na}^{xy} = \langle \Phi_n^0|x|\Phi_m^0\rangle\langle\Phi_m^0|y|\Phi_a^0\rangle. \quad (23)$$

In the similar way the P^{seq} given by Eq. 7 is written as

$$P^{seq} = \frac{1}{9}\{(H_{nm}^{x})^2+(H_{nm}^{y})^2+(H_{nm}^{z})^2\} \times \{(H_{ma}^{x})^2+(H_{ma}^{y})^2+(H_{ma}^{z})^2\}, \quad (24)$$

where, for example,

$$H_{nm}^{x} = \langle \Phi_n^0|x|\Phi_m^0\rangle. \quad (25)$$

From Eq. 24 we can see that the two-photon transition matrix element of the sequential process is independent of the polarization of light.

For the resonance TPA of I_2, the final state which is dipole allowed belongs to a Σ_g^+ or Π_g state in the optical frequency range reported in this paper. We consider the following two cases.

$$\text{(i)}\quad \Sigma_g^+ \text{ or } \Pi_{0g} \xleftarrow{x,\,y} \Pi_{1u} \xleftarrow{x,\,y} \Sigma_g^+.$$

By using $M_{na}^{xx}=M_{na}^{yy}$ in Eqs. 21 and 22, we obtain $P_{11}^{sim}=(8/15)(M_{na}^{xx})^2$ and $P_{\infty}^{sim}=(2/15)(M_{na}^{xx})^2$. Similary from Eq. 24 we obtain $P^{seq}=(4/9)(M_{na}^{xx})^2$. Using these expressions for the electronic matrix elements, we can express Eq. 20 in terms of the line shape functions as

$$\Omega(\omega_R) = \frac{3L^{sim}(\omega_R)+10L^{seq}(\omega_R)}{12L^{sim}(\omega_R)+10L^{seq}(\omega_R)}. \quad (26)$$

It should be noted that the polarization ratio $\Omega(\omega_R)$ is dependent only on the value of $L^{sim}(\omega_R)/L^{seq}(\omega_R)$ and independent of the position of the peak of the line shape functions for the simultaneous and sequential processes. In cases in which effects of elastic collisions can be neglected, and the simultaneous process dominates the TPA process, the polarization ratio is then independent of laser frequency ω_R and $\Omega(\omega_R)=0.25$. In other extreme cases in which sequential process is dominant, we obtain $\Omega(\omega_R)=1$.

$$\text{(ii)}\quad \Pi_{1g} \text{ or } \Pi_{2g} \xleftarrow{z} \Pi_{1u} \xleftarrow{x,\,y} \Sigma_g^+.$$

Substituting $M_{na}^{xz}=M_{na}^{yz}$ into Eqs. 21 and 22, we obtain $P_{11}^{sim}=(8/15)(M_{na}^{xz})^2$ and $P_{\infty}^{sim}=(12/15)(M_{na}^{xz})^2$. Similary we obtain $P^{seq}=2/9(M_{na}^{xz})^2$. From these relations, the polarization ratio is expressed as

$$\Omega(\omega_R) = \frac{18L^{sim}(\omega_R)+5L^{seq}(\omega_R)}{12L^{sim}(\omega_R)+5L^{seq}(\omega_R)}. \quad (27)$$

In cases in which effects of elastic collisions can be neglected, we obtain $\Omega(\omega_R)=1.5$. In other extreme cases in which sequential process is dominant, on the other hand, we obtain $\Omega(\omega_R)=1$. In the real system in which collisional dephasings take place and both simultaneous and sequential processes make a contribution to the TPA, we can see that the polarization ratio depends on the laser frequency used.

Discussion

It has experimentally been shown that the two-photon absorption process above the dissociation limit of the B state may occur before the excited iodines dissociate or during the dissociation process,

$$I_2 \xrightarrow{\hbar\omega_R} I_2^* \xrightarrow{\hbar\omega_R} I_2^{**}.$$

The dissociation rate is estimated to be faster than $10^{-12}\,s^{-1}$ from the results of photofragment spectroscopy,[17] and the pumping rate to I_2^{**} from the dissociative state must be comparable to it. Concerning the pumping process above the dissociation limit of the B state, the following recombination mechanism is another plausible one,

$$I_2 + \hbar\omega_R\ (<498.9\text{ nm}) \longrightarrow 2I,$$

$$I + I \xrightarrow{M} I_2^*\ (B\,0_u^+),$$

$$I_2^*\ (B\,0_u^+) + \hbar\omega_R \longrightarrow I_2^{**},$$

where M is an iodine parent molecule as a third body. If this is the case, both UV emission intensity and VIS emission intensity originating from bound levels of the B state increase with the pressure of the third body, M. When the pressure of I_2 increased from 0.2 Torr to 27 Torr (1 Torr=133.322 Pa) by changing the cell temperature from 20 °C to 90 °C, the VIS emission was still undetectable but the UV emission intensity increased ten-fold for irradiation at $\lambda_{ex}<498.9$ nm.

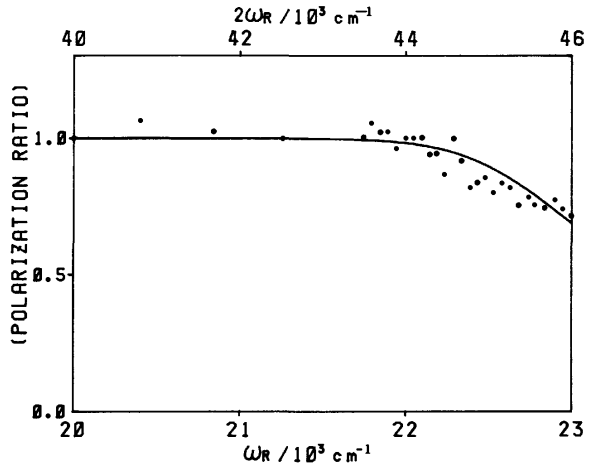

Fig. 4 The calculated polarization ratios for I_2 vapor. Points represent the experimental results (see Fig. 2). The molecular parameters used are ω=215 cm^{-1}, $\varepsilon_m^0/\hbar$=20300 cm^{-1}, $\tilde{\varepsilon}_n/\hbar$=48000 cm^{-1}, Γ_{ma}=5 cm^{-1}, Γ_{mn}=3 cm^{-1}, Γ_{mm}=4 cm^{-1}, $F_m/\hbar$=3200 cm^{-1}, and $F_n/\hbar$=2000 cm^{-1}.

Thus, the recombination mechanism should be excluded from the two-photon absorption process.

Expressions for the transition probabilities and the polarization ratio of TPA *via* repulsive intermediate states have been derived within the Born-Oppenheimer adiabatic approximation and the Condon approximation. It has been shown that abilities of the simultaneous and sequential TPA processes are dominated by two factors. One is the electronic transition matrix elements with polarization of photons. For the simultaneous process, this factor depends on the polarization of photons, and for the sequential process, on the other hand, it is independent of the polarization. The other factor is a line shape function representing the vibronic intensity distribution of the TPA spectra.

We are now in a position to calculate the polarization ratio for the resonant TPA of I_2. The nuclear potential of the ground state is assumed to be harmonic with a frequency ω=215 cm^{-1}; its equilibrium point is located at 2.66 Å. Analytical forms of the repulsive potential energy curve of the $^1\Pi_{1u}$ state have been proposed by Tellinghuisen,[18] and Williams *et al.*[19] In this calculation, we adopt $\varepsilon_m(q)=-3200q+20300$ (in cm^{-1} units), which is very close to the expression derived to reproduce the potential energy and its slope at the equilibrium nuclear position in the ground state.[14] The nuclear potential of the final state is not well known to our knowledge. A large equibibrium nuclear distance compared with that of the ground state is predicted. It will, therefore, be a good approximation to regard the TPA of the I_2 system as the strong coupling case. In Fig. 4 the Σ_g^+or $\Pi_{0g}\leftarrow\Pi_{1u}\leftarrow\Sigma_g^+$transition is considered; the polarization ratios calculated by using Eq. 22 are shown. The parameter used are $\tilde{\varepsilon}_n/\hbar$=48000 cm^{-1}, Γ_{ma}=5 cm^{-1}, Γ_{mn}=3 cm^{-1} and Γ_{mm}=4 cm^{-1}. These dephasing and damping constants have been assumed to be independent of ω_R, which should be valid in a restricted frequency range near the resonant region. Figure 4 shows that the polarization ratio is a decrease function with a constant value near the resonance as increasing the laser frequency. This indicates that the simultaneous process increases in its contribution to the resonant TPA process. For the comparison, the observed ratios are indicated by points. We can see that there is a good correlation between the observed and calculated polarization ratios. Thus, the polarization behavior measured can qualitatively be explained in terms of the gradual increase in the contribution of the simultaneous process.

In this paper it is assumed that the sequential process is induced by an elastic interaction between the molecules and heat bath from the basis of the pressure effect appeared in the UV emission intensity obtained by the puming process above the dissociation limit of the B state though the quantitative investigation of the pressure effect has not been reported. Dissociation processes of I_2 play an important role in the resonant multiphoton transition especially *via* the repulsive Franck-Condon state because in this state the magnitude of the dissociation rate constant is in the ps order which is much larger than that of the pure dephasing constant.[20] The dissociation rate constant is a function of the laser frequency. As the laser frequency increases, the rate constant increases with its magnitude comparable to that of the pure dephasing constant which is reflected in the pressure effect observed above the dissociation threshold.

We have neglected rotation of I_2 in the analysis of the polarization ratio for the resonant TPA. Polarization is destroyed by M-changing collisions when time of rotation is comparable or faster than the interaction time between photons and molecule. In this case rotational effects on the polarization dependence of the TPA have to be taken into account.[12] For the TPA *via* the dissociative intermediate states, the rotational effects can safely be neglected because the interaction time between photons and the dissociative state is much shorter than time of the rotation.

Finally it would be worth to mention that the theoretical treatment developed in this paper can be easily applied to resonance Raman scattering from molecules with repulsive resonant states.[21] The expression for the cross section for the resonance Raman scattering is obtained from that of the transition probability of the simultaneous TPA process by specifying both incident and emitted photons and by letting $\Delta\rightarrow 0$.

To summarize, experimental and theoretical studies have been carried out in order to clarify the mechanism of the resonant two-photon transition involving repulsive intermediate states. It has been shown from the polarization ratios measurement of the gaseous I_2 molecules that the sequential process makes a significant contribution even in a laser frequency range

belonging to the repulsive states. Both simultaneous and sequential two-photon transitions take place below the wavelength around 450 nm, which has qualitatively been explained by using the expression for the polarization ratio derived though the expression has been derived by using a simple model.

Appendix A. Derivation of Eq. 13

In this Appendix, we shall present a derivation of Eq. 13 on the basis of the Boson operator algebra. From Eq. 12, the generating function in the low temperature limits can be expressed as

$$G(\tau, \tau', t) = \langle 0|\exp(i\hat{H}_m\tau'/\hbar)\exp(i\hat{H}_n t/\hbar)\exp(i\hat{H}_m\tau/\hbar) \times \exp[-i\hat{H}_a(t-\tau+\tau')/\hbar]|0\rangle, \quad (A.1)$$

where $|0\rangle$ denotes the vibrational eigenket in the zeroth state of the ground electronic state. In terms of the Boson operators $\hat{b}$, $\hat{b}^\dagger$ which satisfy $[\hat{b}, \hat{b}^\dagger]=1$, the vibronic Hamiltonians related to TPA are given as

$$\hat{H}_a = \hbar\omega\left(\hat{b}^\dagger\hat{b} + \frac{1}{2}\right), \quad (A.2)$$

$$\hat{H}_m = -\frac{F_m}{\sqrt{2}}(\hat{b}+\hat{b}^\dagger) + \varepsilon_m^0, \quad (A.3)$$

and

$$\hat{H}_n = \hat{H}_a - \hbar\omega\Delta(\hat{b}+\hat{b}^\dagger) + \frac{\hbar\omega\Delta^2}{2} + \varepsilon_n^0. \quad (A.4)$$

In deriving Eq. A.3, the nuclear kinetic energy term has been omitted. This is equivalent to the delta function approximation for the repulsive state.

Using the expression,

$$\exp(i\hat{H}_n t/\hbar) = \exp\left[i\varepsilon_n^0 t/\hbar + \frac{\Delta^2}{2}\{\exp(i\omega t)-1\}\right] \times \exp(i\hat{H}_a t/\hbar)\exp[-\lambda(t)\hat{b}^\dagger]\exp[\lambda^*(t)\hat{b}], \quad (A.5)$$

where $\lambda(t)=(\Delta/\sqrt{2})[1-\exp(-i\omega t)]$, Eq. A.1 is rewritten as

$$G(\tau, \tau', t) = \exp\left[i\varepsilon_n^0 t/\hbar + \frac{\Delta^2}{2}\{\exp(i\omega t)-1\} + i\tau'(\varepsilon_a^0 - \hbar\omega/2)/\hbar - i\tau(\varepsilon_a^0 - \hbar\omega/2)/\hbar\right]U(\tau, \tau', t), \quad (A.6)$$

where

$$U(\tau, \tau', t) = \langle 0|\exp[-i\tau' F_m(\hat{b}+\hat{b}^\dagger)/\sqrt{2}\hbar]\exp[it\omega\hat{b}^\dagger\hat{b}] \times \exp[-\lambda(t)\hat{b}]\exp[\lambda^*(t)\hat{b}]\exp[i\tau F_m(\hat{b}+\hat{b}^\dagger)/\hbar]. \quad (A.7)$$

Utilizing the Boson operator algebra, Eq. A.7 is expressed as

$$U(\tau, \tau', t) = \exp\left[-F_m^2(\tau^2+\tau'^2)/4\hbar^2 + F_m^2\tau\tau'\exp(it\omega)/2\hbar^2 - iF_m\tau'\lambda^*(t)/\sqrt{2}\hbar + iF_m\tau\lambda^*(t)/\sqrt{2}\hbar\right]. \quad (A.8)$$

We expand $(\Delta/\sqrt{2})\exp(i\omega t)$ in Eq. A.6 to second order of t:

$$\frac{\Delta}{\sqrt{2}}\exp(i\omega t) \simeq \frac{\Delta}{\sqrt{2}}\left(1 + i\omega t - \frac{\omega^2 t^2}{2}\right). \quad (A.9)$$

Substitution of Eqs. A.8 and A.9 into Eq. A.6 results in

$$G(\tau, \tau', t) = \exp[i(\bar{\varepsilon}/\hbar - \omega/2)t + i(\varepsilon_m^0/\hbar - \omega/2)\tau' - i(\varepsilon_m^0/\hbar - \omega/2)\tau - (F_m\tau' - F_m\tau + F_n t)^2/4\hbar^2], \quad (A.10)$$

where $\bar{\varepsilon}_n=\varepsilon_n^0+\hbar\omega\Delta^2/2$, and $F_n=\Delta\omega$. Substituting Eq. A.10 into 11, we obtain the desired expression:

$$L^{sim}(\omega_R) = \frac{2}{\hbar^4}\int_{-\infty}^{\infty}dt\int_0^{\infty}d\tau\int_0^{\infty}d\tau'\exp[i(\bar{\varepsilon}_n/\hbar - \omega/2 - 2\omega_R)t - \Gamma_{na}|t| - (F_m\tau' - F_m\tau + F_n t)^2/4\hbar^2 + i(\varepsilon_m^0/\hbar - \omega/2 - \omega_R)\tau' - i(\varepsilon_m^0/\hbar - \omega/2 - \omega_R)\tau - (\tau+\tau')\Gamma_{ma}]. \quad (A.11)$$

References

1) S. H. Lin, Y. Fujimura, H. J. Neusser, and E. W. Schlag, "Multiphoton Spectroscopy of Molecules," Academic Press, New York (1984).

2) J. Danon, H. Zacharias, H. Rottke, and K. H. Welge, *J. Chem. Phys.*, **76**, 2399 (1982).

3) A. Gedanken, M. B. Robin, and Y. Yafet, *J. Chem. Phys.*, **76**, 4798 (1982).

4) K. Kasatani, Y. Tanaka, K. Shibuya, M. Kawasaki, K. Obi, H. Sato, and I. Tanaka, *J. Chem. Phys.*, **74**, 895 (1981).

5) D. M. Friedrich and W. M. McClain, *Chem. Phys. Lett.*, **32**, 541 (1975).

6) W. M. McClain and R. A. Harris, "Excited States," ed by E. C. Lim, Academic Press, New York, (1978) Vol. 3, p. 1.

7) Y. Fujimura and S. H. Lin, *J. Chem. Phys.*, **74**, 3726 (1981).

8) D. M. Friedrich and W. M. McClain, *Ann. Rev. Phys. Chem.*, **31**, 559 (1980).

9) P. R. Monson and W. M. McClain, *J. Chem. Phys.*, **53**, 29 (1970).

10) W. M. McClain, *J. Chem. Phys.*, **55**, 2789 (1971).

11) M. A. C. Nascimento, *Chem. Phys.*, **74**, 51 (1983).

12) R. G. Bray and R. M. Hochstrasser, *Mol. Phys.*, **31**, 1199 (1976).

13) K. E. Jones and A. H. Zewail, "Advances in Laser Chemistry," ed by A. H. Zewail, Springer, Berlin, (1978) p. 196, M. J. Burns, W. K. Liu, and A. H. Zewail, "Spectroscopy and Excitation Dynamics of Condensed Molecular System," ed by V. M. Agranovich and R. M. Hochstrasser, North-Holland, (1983) p. 301.

14) Y. Fujimura, T. Nakajima, M. Kawasaki, H. Sato, and I. Tanaka, *J. Phys. Chem.*, **87**, 2277 (1983).

15) Y. Fujimura and S. H. Lin, *J. Chem. Phys.*, **70**, 247 (1979).

16) Y. Fujimura and S. H. Lin, *J. Chem. Phys.*, **71**, 3733 (1979).

17) R. Sander and K. Wilson, *J. Chem. Phys.*, **63**, 4242 (1975).

18) J. Tellinghuisen, *J. Chem. Phys.*, **57**, 2397 (1972).

19) P. F. Williams, A. Fernández, and D. L. Rousseau, *Chem. Phys. Lett.*, **47**, 150 (1977).

20) To our knowledge, the magnitude of the pure electronic dephasing constant relevant to the transition

between the dissociative and bound states of I_2 has not been reported. The magnitude of the dephasing constant between the bound ($B^3\Pi_{0^+u}$) and bound ($^1\Sigma_g^+$) states has been measured by Brewer and Kano (R. G. Brewer and S. S. Kano, "Laser-Induced Processes in Molecules," ed by K. L. Kompa and S. D. Smith, Springer-Verlag, Berlin, (1979) p. 54). From the view point of the large potential energy change between the dissociative and bound states it is deduced that the magnitude of the pure dephasing constant relevant to the transition between the dissociative and bound states is larger than that reported by Brewer and Kano. See also Ref. 14.

21) P. Baierl and W. Kiefer, *J. Chem. Phys.*, **77**, 1693 (1982).

 © 1985 The Chemical Society of Japan Bull. Chem. Soc. Jpn., 58, 2943—2946 (1985)

The Crystal and Molecular Structure of 2,3,6,8,9-Pentaphenyl-1-thia-6-azaspiro[4.4]nona-2,8-diene-4,7-dione

Noritake YASUOKA,† Yasushi KAI, and Nobutami KASAI*
Department of Applied Chemistry, Faculty of Engineering, Osaka University, Yamadaoka, Suita, Osaka 565
(Received June 3, 1985)

The title compound crystallizes in monoclinic form, space group $P2_1/c$ with $a=20.810(1)$, $b=16.000(1)$, $c=18.131(1)$ Å, $\beta=107.77(1)°$, $Z=8$. The structure was established by the direct method and refined including all hydrogen atoms by the blockdiagonal least-squares procedure, $R=0.062$ for 4609 observed reflections. The heterocyclic spiran skeletons in two independent molecules have the same structure; however, four phenyl rings out of five take different conformations to the hetero rings to which they attached.

Very recently, T. Agawa and co-workers obtained heterocyclic spiran as a result of a metal carbonyl-promoted tandem cycloaddition to the sulfur-containing heterocumulenes.[1] Equimolar amounts of phenyl isothiocyanate (**1**), diphenylcyclopropenone (**2**), and tetracarbonylnickel(0) were reacted in DMF at 65—70°C to give the new heterocyclic spirans (**4** and **5**) in addition to the pyrroline (**3**). In relation with this

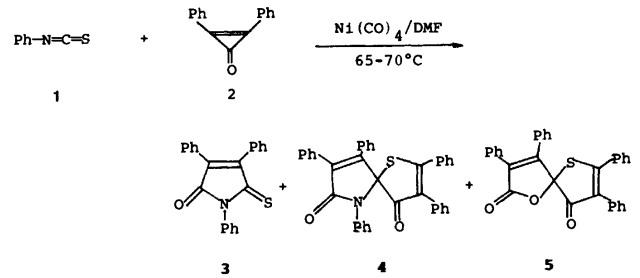

study, the molecular structure of **4** has been determined by means of X-ray diffraction in order to obtain informations on the exact syructure.

Experimental

Crystal Data. $C_{37}H_{25}NO_2S$, M 547.7, monoclinic, space group $P2_1/c$, $a=20.810(2)$, $b=16.000(1)$, $c=18.131(1)$ Å, $\beta=107.77(1)°$, $V=5748.7(6)$ Å^3, $D_c=1.266$ g cm^{-3} for $Z=8$, μ(Cu $K\alpha$)=12.3 cm^{-1}.

The integrated intensities were measured on a Rigaku four-circle diffractometer using nickel-filtered Cu $K\alpha$ radiation. The θ—2θ scan technique was employed at a 2θ rate of 4° min^{-1} and the scan width was $\Delta 2\theta=(2.0+0.3\tan\theta)°$. Backgrounds were measured for 7.5 s at both ends of a scan. Four standard reflections measured after every 60 reflections to monitor the stability and orientation of the crystal showed no significant decay throughout the data collection. Lorentz and polarization corrections were made but the absorption correction was ignored.

Structure Solution and Refinement

As the space group is $P2_1/c$ and $Z=8$, an asymmetric unit contains two independent molecules.

The structure was solved by the direct method (*MULTAN*).[2] Non-hydrogen atoms of the two crystallographically independent molecules were located on the E map with the highest figure of merit. The refinement was carried out anisotropically by the block-diagonal least-squares procedure (*HBLS* V),[3] the function minimized being $\sum\omega(\Delta F)^2$. Hydrogen atoms were located on the difference Fourier map, all of which were included in the refinement with isotropic temperature factors. Finally the R index converged to 0.062 for 4609 observed reflections. The weighting scheme used at the final cycle of the refinement was $\omega=\{\sigma^2(F_o)-0.0280|F_o|+0.0049|F_o|^2\}^{-1}$, where σ is the standard deviation obtained from the counting statistics. The final atomic coordinates with equivalent isotropic temperature factors[4] are listed in Table 1.†† Atomic scattering factors for non-hydrogen atoms were taken from the International Tables for X-Ray Crystallography,[5] and those for hydrogen atoms from Stewart, Davidson and Simpson.[6]

Results and Discussion

A perspective view (*ORTEP*)[7] of the two crystallographically independent molecules (A and B molecules) are depicted in Fig. 1. The molecules have 1-thia-6-azaspiro[4.4]nona-2,8-diene-4,7-dione skeleton (abbreviated as spiran skelton hereafter) as expected by the spectral data.[1] The present molecule is probably the first example of the spiro[4.4]nonane structure with two mixed heteroatoms (N and S) next to the spiro carbon determined by means of X-ray diffraction, whereas dioxa and dithia analogues have been reported, hitherto.[8] Bond lengths and bond angles in the spiran skeletons are given in Table 2. As seen in Fig. 1 and Table 2, the spiran skeltons in the A and B molecules have the same structure. The corresponding bond lengths and bond angles in the two molecules are all equal within the limits of errors. Of the four C=O bond lengths, the C(4)=O(41) bonds[1.148(5) and 1.165

†Present address: Himeji Institute of Technology, Shosha, Himeji, Hyogo 671-22.

††Tables of anisotropic thermal parameters, atomic coordinates of hydrogen atoms, bond lengths and bond angles in benzene rings, and observed and calculated structure factors are kept at the Chemical Society of Japan, Document No. 8546.

TABLE 1. FINAL ATOMIC COORDINATES OF NON-HYDROGEN ATOMS WITH ESTIMATED STANDARD DEVIATIONS IN PARENTHESES

Atom	x	y	z	B_{eq}/Å^2 [4]	Atom	x	y	z	B_{eq}/Å^2 [4]
S(1A)	0.52313(6)	0.39893(8)	0.94428(8)	4.80	S(1B)	0.97608(6)	0.59330(7)	0.53152(7)	3.76
C(2A)	0.5615(2)	0.3002(3)	0.9438(3)	3.5	C(2B)	0.9330(2)	0.6842(3)	0.5440(3)	3.0
C(3A)	0.5226(2)	0.2326(3)	0.9431(3)	3.5	C(3B)	0.9635(2)	0.7579(3)	0.5410(3)	3.2
C(4A)	0.4532(2)	0.2538(3)	0.9387(3)	4.0	C(4B)	1.0299(2)	0.7484(3)	0.5291(3)	3.3
C(5A)	0.4463(2)	0.3488(3)	0.9534(3)	3.9	C(5B)	1.0429(2)	0.6547(3)	0.5119(3)	3.2
N(6A)	0.3860(2)	0.3878(2)	0.9045(2)	3.8	N(6B)	1.1101(2)	0.6238(2)	0.5516(2)	3.4
C(7A)	0.3452(2)	0.4162(3)	0.9462(3)	4.0	C(7B)	1.1454(2)	0.6058(3)	0.4994(3)	3.7
C(8A)	0.3800(2)	0.3973(3)	1.0287(3)	3.6	C(8B)	1.0998(2)	0.6273(3)	0.4216(3)	3.3
C(9A)	0.4387(2)	0.3583(3)	1.0347(3)	3.8	C(9B)	1.0402(2)	0.6524(3)	0.4267(3)	3.5
O(41A)	0.4080(2)	0.2098(2)	0.9303(2)	5.2	O(41B)	1.0695(2)	0.8003(2)	0.5301(2)	4.3
O(71A)	0.2909(2)	0.4500(2)	0.9175(2)	5.6	O(71B)	1.2023(2)	0.5785(2)	0.5167(2)	4.7
C(21A)	0.6322(2)	0.3033(3)	0.9431(3)	3.8	C(21B)	0.8668(2)	0.6689(3)	0.5563(3)	3.2
C(22A)	0.6568(3)	0.2420(3)	0.9045(3)	4.8	C(22B)	0.8578(2)	0.5993(3)	0.5976(3)	4.1
C(23A)	0.7228(3)	0.2466(4)	0.9021(4)	6.6	C(23B)	0.7962(3)	0.5856(3)	0.6104(3)	5.0
C(24A)	0.7643(3)	0.3119(4)	0.9399(4)	8.1	C(24B)	0.7439(3)	0.6398(3)	0.5825(3)	5.1
C(25A)	0.7400(3)	0.3729(4)	0.9780(4)	6.8	C(25B)	0.7517(3)	0.7083(3)	0.5401(3)	5.4
C(26A)	0.6744(3)	0.3691(3)	0.9793(3)	5.1	C(26B)	0.8123(3)	0.7224(3)	0.5253(3)	4.8
C(31A)	0.5445(2)	0.1445(3)	0.9509(3)	3.9	C(31B)	0.9411(2)	0.8424(3)	0.5547(3)	3.1
C(32A)	0.5093(3)	0.0853(3)	0.8989(3)	5.9	C(32B)	0.9373(3)	0.9058(3)	0.5004(3)	4.3
C(33A)	0.5294(3)	0.0016(4)	0.9093(4)	7.2	C(33B)	0.9187(3)	0.9861(3)	0.5136(3)	5.2
C(34A)	0.5826(3)	−0.0223(4)	0.9685(4)	7.4	C(34B)	0.9030(3)	1.0046(3)	0.5788(3)	5.2
C(35A)	0.6176(3)	0.0354(4)	1.0205(3)	7.2	C(35B)	0.9052(3)	0.9432(3)	0.6323(3)	5.8
C(36A)	0.5984(3)	0.1191(3)	1.0131(3)	5.6	C(36B)	0.9247(3)	0.8625(3)	0.6210(3)	4.8
C(61A)	0.3669(2)	0.3902(3)	0.8213(3)	4.2	C(61B)	1.1357(2)	0.6136(3)	0.6336(3)	3.6
C(62A)	0.3816(3)	0.4610(3)	0.7858(3)	5.8	C(62B)	1.1824(3)	0.5522(3)	0.6644(3)	5.3
C(63A)	0.3596(3)	0.4655(4)	0.7044(3)	7.2	C(63B)	1.2093(3)	0.5443(4)	0.7440(3)	6.5
C(64A)	0.3238(3)	0.4020(4)	0.6618(3)	7.7	C(64B)	1.1890(3)	0.5951(4)	0.7925(3)	6.2
C(65A)	0.3094(3)	0.3302(4)	0.6975(3)	7.2	C(65B)	1.1406(3)	0.6546(4)	0.7627(3)	6.1
C(66A)	0.3313(3)	0.3250(4)	0.7784(3)	5.8	C(66B)	1.1133(3)	0.6644(3)	0.6817(3)	5.3
C(81A)	0.3502(3)	0.4188(3)	1.0903(3)	4.2	C(81B)	1.1224(3)	0.6199(3)	0.3515(3)	4.2
C(82A)	0.2817(3)	0.4099(3)	1.0778(3)	5.2	C(82B)	1.0788(3)	0.5924(4)	0.2818(3)	5.8
C(83A)	0.2534(3)	0.4269(4)	1.1364(3)	7.1	C(83B)	1.1019(3)	0.5861(4)	0.2172(3)	7.8
C(84A)	0.2944(3)	0.4539(4)	1.2078(3)	8.7	C(84B)	1.1667(3)	0.6077(4)	0.2221(4)	8.7
C(85A)	0.3624(3)	0.4650(4)	1.2201(3)	8.1	C(85B)	1.2097(3)	0.6350(4)	0.2898(4)	8.0
C(86A)	0.3910(3)	0.4475(4)	1.1626(3)	5.9	C(86B)	1.1890(3)	0.6419(4)	0.3571(3)	5.8
C(91A)	0.4842(3)	0.3144(3)	1.1017(3)	4.3	C(91B)	0.9812(2)	0.6875(3)	0.3677(3)	3.9
C(92A)	0.4565(3)	0.2551(3)	1.1383(3)	5.9	C(92B)	0.9836(3)	0.7675(3)	0.3419(3)	5.5
C(93A)	0.4979(3)	0.2060(4)	1.1992(3)	7.6	C(93B)	0.9247(3)	0.8038(4)	0.2901(3)	7.6
C(94A)	0.5657(3)	0.2177(4)	1.2214(4)	7.9	C(94B)	0.8668(3)	0.7579(4)	0.2649(3)	7.6
C(95A)	0.5946(3)	0.2763(4)	1.1881(4)	8.0	C(95B)	0.8641(3)	0.6770(4)	0.2880(3)	6.8
C(96A)	0.5535(3)	0.3263(4)	1.1267(3)	5.9	C(96B)	0.9210(3)	0.6421(4)	0.3405(3)	5.2

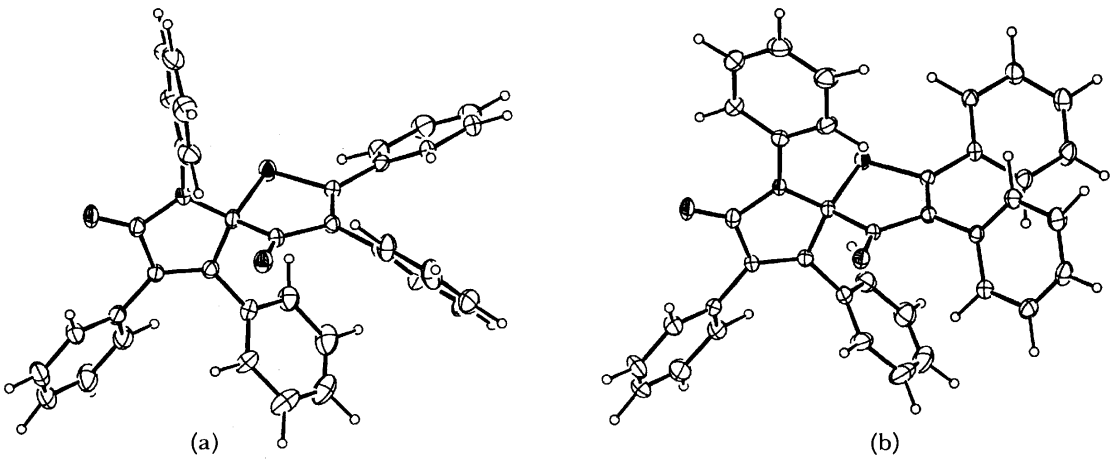

Fig. 1. A perspective view[7] of two independent molecules of **4**. (a) A molecule, (b) B molecule. Non-hydrogen atoms are drawn as thermal ellipsoids with 20% probability level, and hydrogen atoms as spheres with B=1.0 Å^2.

TABLE 2. BOND LENGTHS AND BOND ANGLES IN 1-THIA-6-AZASPIRO[4.4]NONA-2,8-DIENE-4,7-DIONE SKELETON IN **4** WITH ESTIMATED STANDARD DEVIATIONS IN PARENTHESES

	Molecule			Molecule	
	A	B		A	B
Bond lengths[l/Å]					
S(1)-C(2)	1.771(4)	1.758(4)	S(1)-C(5)	1.841(5)	1.824(5)
N(6)-C(5)	1.440(6)	1.450(5)	N(6)-C(7)	1.375(5)	1.392(5)
C(2)-C(3)	1.349(6)	1.348(6)	C(8)-C(9)	1.346(6)	1.335(6)
C(3)-C(4)	1.461(6)	1.470(6)	C(7)-C(8)	1.481(6)	1.481(6)
C(4)-C(5)	1.557(6)	1.571(6)	C(5)-C(9)	1.537(6)	1.530(6)
C(4)-O(41)	1.148(5)	1.165(5)	C(7)-O(71)	1.218(5)	1.211(5)
Bond angles[ϕ/°]					
C(5)-S(1)-C(2)	90.9(2)	91.6(2)	S(1)-C(2)-C(3)	116.4(4)	117.0(3)
S(1)-C(2)-C(21)	115.0(3)	114.6(3)	C(3)-C(2)-C(21)	128.6(4)	128.4(4)
C(2)-C(3)-C(4)	113.3(4)	113.0(4)	C(2)-C(3)-C(31)	126.7(4)	128.1(4)
C(4)-C(3)-C(31)	119.9(4)	118.6(4)	C(3)-C(4)-C(5)	111.0(4)	110.7(4)
C(3)-C(4)-O(41)	128.4(5)	128.0(4)	C(5)-C(4)-O(41)	120.5(4)	121.3(4)
S(1)-C(5)-C(4)	106.4(3)	106.8(3)	S(1)-C(5)-N(6)	111.9(3)	113.4(3)
S(1)-C(5)-C(9)	113.0(3)	112.9(3)	C(4)-C(5)-N(6)	115.2(4)	115.2(4)
C(4)-C(5)-C(9)	107.6(4)	105.5(4)	N(6)-C(5)-C(9)	102.8(4)	103.0(4)
C(5)-N(6)-C(7)	111.9(4)	111.2(4)	C(5)-N(6)-C(61)	124.6(4)	123.5(4)
C(7)-N(6)-C(61)	123.3(4)	125.2(4)	N(6)-C(7)-C(8)	107.2(4)	106.4(4)
N(6)-C(7)-O(71)	124.1(4)	125.1(4)	C(8)-C(7)-O(71)	128.8(4)	128.4(4)
C(7)-C(8)-C(9)	109.1(4)	110.0(4)	C(7)-C(8)-C(81)	121.9(4)	121.3(4)
C(9)-C(8)-C(81)	129.0(4)	128.7(4)	C(5)-C(9)-C(8)	109.1(4)	109.2(4)
C(5)-C(9)-C(91)	121.0(4)	119.3(4)	C(8)-C(9)-C(91)	128.9(4)	130.7(4)

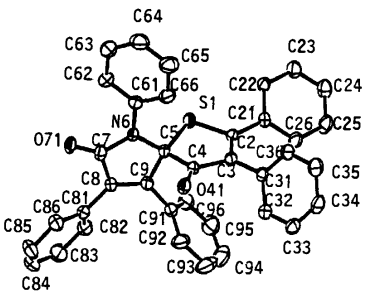

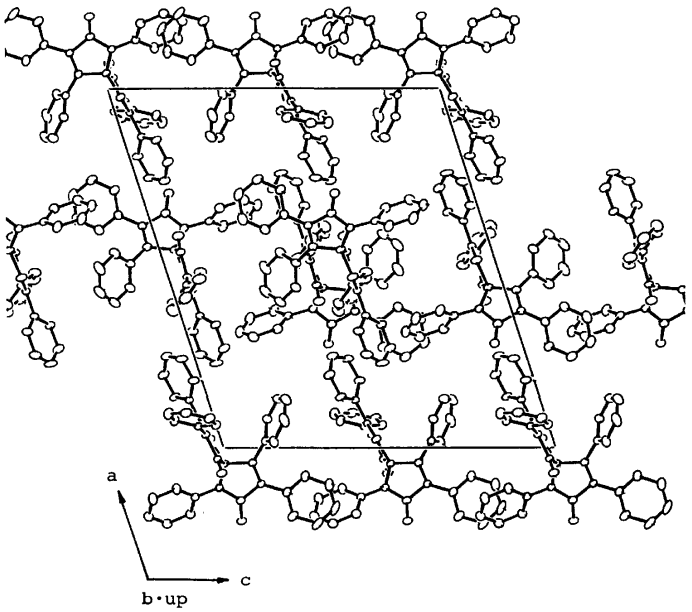

Fig. 2. Crystal structure projected down along the b axis.[7]

(5) Å] are much shorter than the C(7)=O(71)[1.218(5) and 1.211(5) Å].

Among the bond angles around the spiro carbon atom, the S(1)-C(5)-C(9), S(1)-C(5)-N(6) and C(4)-C(5)-N(6) angles are larger, whereas the other angles are smaller, than the tetrahedral angle. At the C(5) atom the dihedral angle between the plane defined by the S(1), C(4), and C(5) and that formed by the C(5), N(6), and C(9) atoms in the A molecule is 86.7°, and that in the B 86.4°. Both of them are slightly smaller than 90°. For both molecules the heterocyclic ring defined by the S(1), C(2), C(3), C(4), and C(5) atoms (heterocycle 1) and those made by the C(5), N(6), C(7), C(8), and C(9) atoms (heterocycle 2) are all approximately planar. In each molecule the planarity of the heterocycle 1 is slightly better than that of the heterocycle 2. The dihedral angles between these rings are 84.6 and 85.3° in the A and B molecules, respectively.

All the benzene rings attached to the heterocycles have normal structure, C-C(av)=1.383 Å and C-C-C(av)=120°. In each molecule most of them take different conformations to the hetero rings to which they attached except the phenyl group defined by the carbon atoms from C(81) to C(86). These benzene rings make equal dihedral angles [38.2 and 39.2°] to the heterocycle 2 in the A and B molecules.

Crystal Structure. The packing of molecules in the crystal is drawm in Fig. 2. The closest intermolecular atomic contact is 3.345(8) Å between the C(94A)(x, y, z) and C(22A)(x, 0.5−y, 0.5+z) atoms. Other short contacts are observed between the A and B molecules, C(63B)(x, y, z)···O(71A)=3.436(6) and C(64B)(x, y, z)···O(71A)=3.477(6) Å.

Computations were done mainly on a NEAC 2200-500 computer at the Computation Center, Osaka University. At the final stage an ACOS 850 computer was used at the Crystallographic Research Center, Institute for Protein Research, Osaka University.

The authors wish to express their deep thanks to Professor Toshio Agawa and coworkers of Osaka University for crystals and helpful discussion.

References

1) Y. Ohshiro, H. Nanimoto, H. Tanaka, M. Komatsu, T. Agawa, M. Yasuoka, Y. Kai, and N. Kasai, *Tetrahedron Lett.*, **26**, 3015 (1985).

2) G. Germain, P. Main, and M. M. Woolfson, *Acta Crystallogr., Sect. A*, **27**, 368 (1971).

3) T. Ashida, *HBLS* V, "The Universal Crystallographic Computing System-Osaka," The Computation Center, Osaka Univ., 1973 p. 55.

4) W. C. Hamilton, *Acta Crystallogr.*, **12**, 609 (1959).

5) International Tables for X-Ray Crystallography, Vol. IV, Kynoch Press, Birmingham (1974), p. 71.

6) R. F. Stewart, E. R. Davidson, and W. T. Simpson, *J. Chem. Phys.* **42**, 3175 (1965).

7) C. K. Johnson, *ORTEP* II, Report ORNL-5138, Oak Ridge National Laboratory, Tennessee (1976).

8) a) H. Nozaki, M. Hiroi, D. Takaoka, and M. Nakayama, *J. Chem. Soc., Chem. Commun.*, **1983**, 1107; b) G. Ege, K. Glibert, F. W. Nader, *Chem. Ber.*, **114**, 1074 (1981); c) V. Zabel, *Eur. Cryst. Meeting*, **1976**, 255; d) H. Irie, N. Masaki, K. Ohno, K. Osaki, T. Taga, and S. Uyeo, *J. Chem. Soc., Chem. Commun.*, **1970**, 1066.

Motion of CF_3 Groups and Phase Transition in $[Cu_4(CF_3COO)_4]\cdot 2C_6H_6$ as Studied by ^1H and ^{19}F NMR Techniques

Atsushi KUBO, Ryuichi IKEDA, Jose Antonio SAMPEDRO,†
Motomichi INOUE,† and Daiyu NAKAMURA*
Department of Chemistry, Faculty of Science, Nagoya University, Chikusa, Nagoya 464
†*CIPM, Universidad de Sonora, Hermosillo, Sonora, Mexico*
(Received June 10, 1985)

The temperature variation of ^1H and ^{19}F nuclear spin-lattice relaxation times T_1 in $[Cu_4(CF_3COO)_4]\cdot 2C_6H_6$ was observed at different resonance frequencies. From the NMR experiments, it was found that this complex undergoes a first order phase transition at 130 K, which was confirmed by DTA measurements. In the room-temperature phase, ^1H gave normal exponential magnetization recovery curves and $\log T_1$ linearly decreased with increasing $10^3\,T^{-1}$ whereas ^{19}F gave nonexponential magnetization recovery curves, from which long- and short-T_1 components could be derived. This indicates that the C_3 reorientation of CF_3 groups about their respective symmetry axis is responsible for ^{19}F T_1 and for ^1H T_1 as well through ^1H–^{19}F cross relaxation. This was confirmed from the coincidence of the $\log T_1$ *vs.* 10^3T^{-1} curve of the long component and that of ^1H T_1. A very small activation energy of 5.5 kJ mol^{-1} was obtained for the CF_3 reorientation. For the low-temperature phase, both ^1H and ^{19}F yielded nonexponential magnetization decay curves.

Recently, some Cu(I) complexes having capability to absorb and desorb CO, olefins, aromatic molecules *etc.* attract much attention from their usability as a carrier or a separator of those molecules.[1,2] Among these complexes, copper(I) trifluoroacetate is of interest in the formation of a fairly stable complex, $[Cu_4(CF_3COO)_4]\cdot 2C_6H_6$ by absorbing benzene vapor. It is so stable that we can investigate its solid state properties fairly in detail.[1,3,4]

According to Rodesiler and Amma,[3] this complex crystallizes in a monoclinic system $P2_1/n$ with $Z=4$. The structure can be described as a planar lozenge of four Cu atoms which are held together by bridging trifluoroacetate groups. Each CO_2^- group is approximately perpendicular to the Cu_4 plane but adjacent CO_2^- groups are on the opposite side of the plane. Two benzene molecules, between which the Cu_4 unit is placed, face each other. Although the Cu–C (in benzene) distances are longer than those determined in similar complexes,[5,6] all C atoms in each benzene ring having large thermal parameter are fairly definitely located. However, it is strange enough that no positional data of F atoms could be determined in their X-ray study. This suggests the presence of some disorder in the orientation of CF_3 groups and/or the occurrence of nearly free rotation of the groups. To clarify this point, the present investigation has been undertaken.

Experimental

Copper(I) trifluoroacetate synthesized by the method reported in literature[1] was purified by sublimation *in vacuo* at 140 °C. The compound was dissolved in benzene and the solvent was removed by vacuum distillation. The compound desorbs and adsorbs benzene molecules rather freely. The curve of the adsorption isotherm shows a plateau at 5 mmHg (1 mmHg=133.322 Pa) benzene vapor pressure, where the composition is determined as $[Cu_4(CF_3COO)_4]\cdot 2C_6H_6$. At higher benzene vapor pressure, the compound adsorbs additional benzene molecules physically giving $[Cu_4(CF_3COO)_4]\cdot nC_6H_6$ ($n>2$). Therefore, the number of "coordinated" benzene molecules was regulated by adjusting the equilibrium vapor pressure of benzene at 5 mmHg. The sample thus prepared was sealed in glass ampoules and employed for NMR and differential thermal analysis (DTA) measurements.

Two homemade pulsed NMR spectrometers[7,8] were employed for the determination of ^1H and ^{19}F nuclear spin-lattice relaxation times (T_1) at various temperatures using a conventional π-τ-$\pi/2$ pulse sequence. The experiments of DTA were carried out by means of a homemade apparatus.[9] Temperatures were determined by use of a copper-constantan thermocouple and were estimated to be accurate within ±1 K.

Results and Discussion

The $\log T_1$ values of ^1H observed at 20 and 45.500 MHz plotted against $10^3\,T^{-1}$ for $[Cu_4(CF_3COO)_4]\cdot 2C_6H_6$ are shown in Fig. 1. Figure 2 shows a similar plot for the ^1H and ^{19}F nuclei determined at 45.500 and 42.804 MHz, respectively, under the same strength of applied magnetic field.

At room temperature, ^1H T_1 determined at 20 MHz yielded a fairly large value of *ca.* 30 s. With decreasing temperature, $\log T_1$ decreased linearly against 10^3-T^{-1} down to *ca.* 100 K, below which temperature the magnetization recovery curves became suddenly nonexponential and yielded long- and short-T_1 components as given in Fig. 1. The $\log T_1$ value determined at 45.500 MHz decreased with decreasing temperature along the same line as that obtained at 20 MHz down to *ca.* 100 K. Below this temperature, nonexponential magnetization recovery curves were also detected. The foregoing observation suggests the occurrence of phase transition.

To confirm this point, we carried out the experiments of DTA below room temperature. When the sample was cooled, an exothermic anomaly appeared at *ca.* 100 K, while an endothermic peak was recorded at 130 K with increasing the temperature from *ca.*

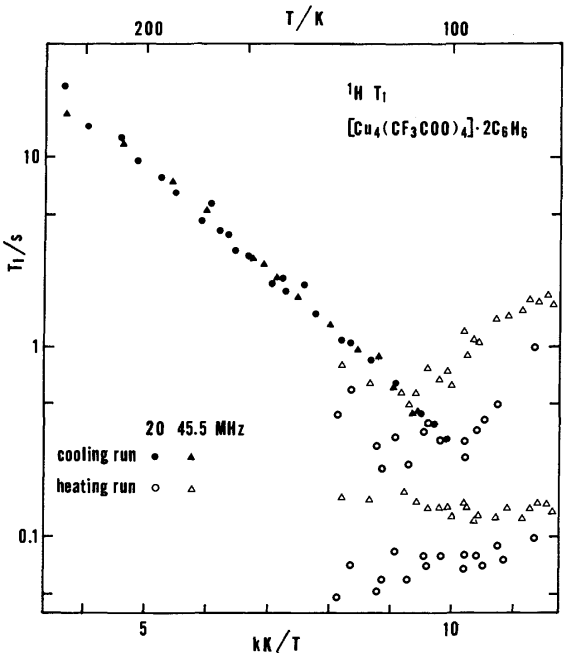

Fig. 1. Temperature dependences of ^{1}H T_1 in $[Cu_4(CF_3COO)_4]\cdot 2C_6H_6$ observed at 20 (●) and 45.500 (▲) MHz for the high-temperature phase and its supercooled one. For the low-temperature phase, long- and short-T_1 components observed with increasing temperature at the resonance frequencies of 20 (○) and 45.500 (△) MHz are plotted.

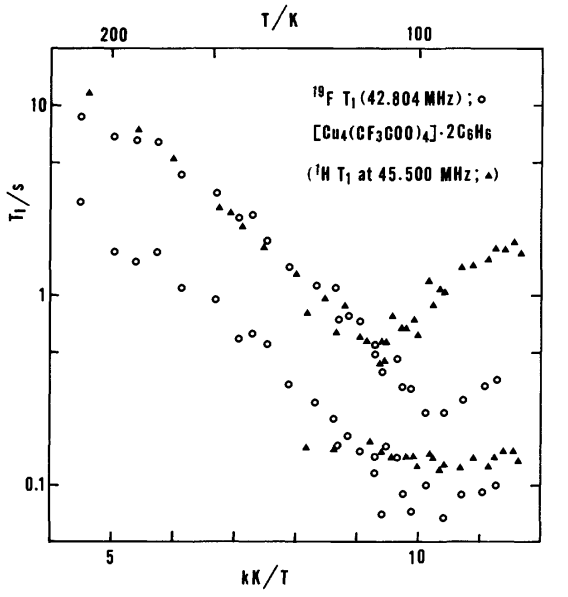

Fig. 2. Temperature dependences of ^{19}F T_1 in the complex observed at 42.804 MHz. The long- and short-T_1 components indicated by circles (○) observed for both phases are shown. Almost the same values were obtained for both cooling and heating runs. ^{1}H T_1 values determined at 45.500 MHz indicated by ▲ are shown for comparison.

80 K, showing the occurrence of thermal hysteresis. Accordingly, one can conclude that $[Cu_4(CF_3COO)_4]\cdot 2C_6H_6$ crystals undergo a first order phase transition at 130 K.

This complex contains ^{1}H and ^{19}F nuclei both of which have large magnetic moments and, therefore, it is expected that the T_1 values of both nuclei are governed by the motional process of benzene molecules and/or CF_3 groups through the mechanism of cross relaxation between them.[10] In solid benzene, the C_6 reorientation about the symmetry axis of the molecule is known to be activated near 100 K,[11] while Punkkinen *et al.* reported that CF_3 groups in solid CF_3COOAg perform the C_3 reorientation about their symmetry axis with the activation energy, E_a of 25 kJ mol^{-1}.[12] To obtain more detailed information about the motional process responsible for the ^{1}H T_1 values observed above, the T_1 measurements were performed on ^{19}F nuclei at the resonance frequency of 42.804 MHz. This frequency was selected so that the magnetic field where ^{19}F nuclei resonate at the above frequency was the same as that employed for the foregoing ^{1}H experiments.

It is characteristic for this complex that the magnetization of ^{19}F nuclei exhibits nonexponential recovery in both high- and low-temperature phases. The ^{19}F T_1 values of the former phase clearly belong to the hot side of the T_1 minimum because $\log T_1$ decreases linearly against $10^3\,T^{-1}$ down to *ca.* 100 K. The magnetization recovery curves observed could be explained as arising from two long- and short-T_1 components. It is interesting to note that both components yielded no discernible discontinuity at both transformation temperatures (T_{tr}) from high- to low-temperature phase on the cooling run and also from low- to high-temperature phase on the heating run. The $\log T_1$ *vs.* $10^3\,T^{-1}$ curve of the long component of ^{19}F T_1 in the high-temperature phase coincided with that of the ^{1}H T_1 as shown in Fig. 2. This indicates that the cross relaxation is operative between ^{1}H and ^{19}F nuclei and the same motional process governs the T_1 of both nuclei.

The existence of the short-T_1 component for the high-temperature phase in addition to the long one suggests that the motion responsible for the relaxation process of both nuclei is that of CF_3 groups, possibly the C_3 reorientation of the groups. The appearance of the nonexponential recovery curves for ^{19}F nuclear magnetization in the temperature region above its T_1 minimum can be interpreted in terms of cross correlation of ^{19}F–^{19}F dipolar interactions within a CF_3 group performing rapid reorientation about its C_3 axis. The nonexponential magnetization recovery curves explainable by the cross correlation have been found for ^{1}H T_1 in CH_3 groups of various organic compounds containing the group[13,14] and also for ^{19}F T_1 in CF_3COOAg.[12]

To confirm the C_3 reorientation of CF_3 groups activated in the present complex, we estimated the 2nd moment, M_2 of ^{19}F NMR from the analysis of free induction decay (FID) signals observed at 120 and 90 K. The FID curves $M_x(t)$ observed were as-

sumed to be expressed as a function of time, t by[15]

$$M_x(t) = M_x(0) \exp(-a^2t^2/2). \quad (1)$$

Here, a is a parameter determining the width of the Gaussian function. From this equation, M_2 can be given as

$$M_2 = a^2. \quad (2)$$

Least-squares-fitting calculation of Eq. 1 to the observed FID curves by use of SALS[16] at the Computation Center of Nagoya University afforded the approximate M_2 values of 1.9 and 2.3 G^2 (1 G=10^{-4} T) at 120 and 90 K, respectively.

The rigid lattice M_2 value of isolated CF_3 groups can be calculated as 7.3 G^2 by use of the geometrical parameters of a CF_3 group determined for CF_3COOAg crystals.[17] When isolated CF_3 groups perform the rapid C_3 reorientation, M_2 reduces the value to 1.8 G^2. In the present crystals, the ^{19}F M_2 value for the CF_3 group performing the C_3 reorientation is expected to become larger due to ^{19}F–^{19}F and ^{19}F–^1H dipolar interactions with ^{19}F in neighboring CF_3 groups and ^1H in neighboring benzene molecules, respectively. Accordingly, the above M_2 values estimated from FID observed indicate that the CF_3 groups perform the C_3 reorientation rapidly enough in the NMR time scale even at 90 K.

Figure 1 shows that ^{19}F T_1 detected by the spin-lattice relaxation of ^1H nuclei through cross relaxation between ^{19}F and ^1H in the high-temperature phase gives the same $\log T_1$ *vs.* 10^3 T^{-1} curve for the two different applied magnetic fields. This indicates that the observed ^{19}F T_1 can be interpreted in terms of usual dipolar interactions expressed by[18]

$$T_1^{-1} = C[\tau/(1+\omega^2\tau^2)+4\tau/(1+4\omega^2\tau^2)], \quad (3)$$

where C, τ, and ω denote the motional constant for the CF_3 groups, the correlation time of the C_3 reorientation of the group, and the angular resonance frequency, respectively. Here, we assume an Arrhenius relationship between τ and the activation energy E_a, for the motional process as

$$\tau = \tau_0 \exp(E_a/kT), \quad (4)$$

where τ_0 denotes the correlation time at the limit of infinite temperature. From the gradient of the $\log T_1$ *vs.* 10^3 T^{-1} curves obtained for both ^1H T_1 and ^{19}F T_1 in the room-temperature phase, one can evaluate E_a for the C_3 reorientation of the CF_3 groups using Eqs. 3,4 as 5.5 kJ mol^{-1}.

The obtained E_a value is very small as compared with that of 25 kJ mol^{-1} reported for the same motional mode in CF_3COOAg crystals.[12] Therefore, one can conclude that the CF_3 groups in the present complex are nearly free to rotate in the crystal. This is compatible with the result of X-ray analysis[3] which was incapable of locating the positions of the F atoms, although there still remains a possibility that the CF_3 groups are statistically disordered and undergo C_3 reorientation almost freely. The C_6 reorientation of benzene molecules in this crystal could not be detected for the present investigation possibly because the motion may be so rapid that it gives very short correlation time at least in the room-temperature phase.

For the low-temperature phase, nonexponential magnetization recovery curves were observed for both ^1H and ^{19}F nuclei. This may be due to the dipolar cross relaxation between ^{19}F and ^1H nuclei because they are usually observed on the low-temperature side of T_1 minima when cross relaxation between heteronuclei is effectively operative.[19,20] The T_1 values of both nuclei obtained for the low-temperature phase mostly belong to the cold side of T_1 minima. No further discussion for the results of T_1 measurements in this phase may be made because no structural data can be available.

It is noteworthy, however, that the ^{19}F T_1 value of both components changes almost smoothly with changing temperature across T_{tr} on both heating and cooling runs whereas the ^1H T_1 value changes drastically at T_{tr}. When the temperature was lowered, ^1H $\log T_1$ decreased linearly against 10^3 T^{-1} to *ca.* 100 K, where two T_1 values appeared suddenly. With increasing temperature in the low-temperature phase, two ^1H T_1 values were obtained up to 130 K, above which temperature the single ^1H T_1 of the high-temperature phase appeared. These facts suggest that the phase transition of this complex affects the motional state of the benzene molecules more strongly than that of the CF_3 groups.

References

1) N. Yanagihara, J. A. Sampedro, R. Casillas, Q. Fernando, and T. Ogura, *Inorg. Chem.*, **21**, 475 (1982).

2) M. Pasquali, C. Floriani, G. Venturi, A. Gaetani-Manfredotti, and A. Chiesi-Villa, *J. Am. Chem. Soc.*, **104**, 4092 (1982).

3) P. F. Rodesiler and E. L. Amma, *J. Chem. Soc., Chem. Commun.*, **1974**, 599.

4) P. F. Rodesiler and E. L. Amma, *J. Inorg. Nucl. Chem.*, **39**, 1227 (1977).

5) R. W. Turner and E. L. Amma, *J. Am. Chem. Soc.*, **88**, 1877 (1966).

6) M. B. Dines and P. H. Bird, *J. Chem. Soc., Chem. Commun.*, **1973**, 12.

7) L. S. Prabhumirashi, R. Ikeda, and D. Nakamura, *Ber. Bunsenges. Phys. Chem.*, **85**, 1142 (1981).

8) S. Gima, Y. Furukawa, R. Ikeda, and D. Nakamura, *J. Mol. Struct.*, **111**, 189 (1983).

9) Y. Kume, R. Ikeda, and D. Nakamura, *J. Magn. Reson.*, **33**, 331 (1979).

10) M. Goldman, "Spin Temperature and Nuclear Magnetic Resonance in Solids," Oxford Univ. Press, London, 1970, p. 178.

11) E. R. Andrew and R. G. Eades, *Proc. Roy. Soc.*, **A218**,

537 (1953).
12) M. Punkkinen, L. P. Ingman, D. G. Taylor, and P. S. Allen, *J. Phys. C*, **8**, 2159 (1975).
13) R. L. Hilt and P. S. Hubbard, *Phys. Rev.*, **134**, 392 (1964).
14) R. A. Wind, S. Emid, D. J. Ligthelm, J. F. J. M. Pourquié, and J. Smidt, *Bull. Magn. Reson.*, **6**, 71 (1984).
15) A. Abragam, "The Principle of Nuclear Magnetism," Oxford Univ. Press, London, 1961, p. 115.
16) T. Nakagawa and Y. Koyanagi, Program Library in the Computation Center of Nagoya Univ., Code No. 466.
17) R. G. Griffin, J. D. Ellett, Jr., M. Mehring, J. G. Bullitt, and J. S. Waugh, *J. Chem. Phys.*, **57**, 2147 (1972).
18) N. Bloembergen, F. M. Purcell, and R. V. Pound. *Phys. Rev.*, **73**, 679 (1948).
19) D. E. O'Reilly, E. M. Peterson, and T. Tang, *Phys. Rev.*, **160**, 333 (1967).
20) Y. Furukawa and H. Kiriyama, *Bull. Chem. Soc. Jpn.*, **51**, 3438 (1978).

 © 1985 The Chemical Society of Japan Bull. Chem. Soc. Jpn., 58, 2951—2954 (1985)

Zn^{II}-bearing Green Rust II and Its Spontaneous Transformation into Zn^{II}-bearing Ferrite in Aqueous Solution

Yutaka TAMAURA

Department of Chemistry, Tokyo Institute of Technology, Ookayama, Meguro-ku, Tokyo 152

(Received January 16, 1985)

When solutions containing Fe^{II}, Zn^{II}, and SO_4^{2-} ions were oxidized by a mixed gas of air and nitrogen at pH 6.7 (25 °C), a Zn^{II}-bearing green rust II (GR-II), which is a uniform crystalline precipitate with a definite chemical composition, was formed. The mol ratio of Zn^{II}/Fe^{II} in the Zn^{II}-bearing GR-II increased linearly with an increase in the Zn^{II}/Fe^{II} mol ratio in the reaction solution. The distribution coeffient of Zn^{II} between the solid (Zn^{II}-bearing GR-II) and the solution phase is 3.3 times higher than that of Fe^{II}. The Zn^{II}-bearing GR-II was spontaneously transformed into Zn^{II}-bearing ferrite. In this reaction, Zn^{2+} ions in the Zn^{II}-bearing GR-II are preferentially incorporated into the ferrites.

Green rusts (hexagonal crystal), which are composed of Fe^{II}, Fe^{III}, and sulphate or halogenide ions are formed in the course of the atmospheric rusting of iron or mild steel, or in the course of the oxidation reaction of an $Fe(OH)_2$ suspension.[1-3] X-ray crystallographic study of the green rusts has been reported by Bernal *et al.*[1] In the previous paper,[4] we examined the synthesis of a pure green rust II having a definite chemical composition, $(Fe^{3+})_1(Fe^{2+})_2(SO_4^{2-})$-$(OH^-)_{5-2n}(O^{2-})_n$. This green rust II is obtained as a crystalline precipitate from a solution containing Fe^{II} and sulphate ions by air oxidation at pH 6.8 and 25 °C. In this reaction, one mol Fe^{III} ion, formed by the oxidation, combines with two mols of Fe^{II} and one mol of sulphate ions, to form the green rust II. Thus, this is a coprecipitation reaction of the metal ions forming a definite crystalline precipitate. In the present paper, we have studied the coprecipitation reaction of Zn^{II} ions into the green rust II (formation of the Zn^{II}-bearing GR-II). This paper also describes the spontaneous transformation of the Zn^{II}-bearing GR-II into the Zn^{II}-bearing ferrite. Generally, GR-II is considered to be transformed into ferrites only by an oxidation reaction.[4] The spontaneous transformation means that GR-II is transformed into ferrites without oxidation.

Experimental

Chemicals. All chemicals were of analytical grade, and distilled water was used for the preparation of chemical solutions. NaOH solutions were prepared by dissolving NaOH in distilled water through which nitrogen gas had been passed to remove dissolved oxygen.

Apparatus. The reaction vessel described in the previous paper[4] was used.

Chemical Analysis. The Fe^{II} and Fe_{total} contents were determined by the 2,2′-bipyridyl method[5] after dissolving the sample in HCl (1:1). The Zn^{II} content was analyzed by atomic absorption. The SO_4^{2-} content was determined by X-ray fluorescence (Toshiba X-ray Spectrometer Model AFV 777) from the intensity of sulfur in a $BaSO_4$ precipitate collected on a glass fiber filter (Toyo Roshi GA 100 type).

Synthesis of the Zn^{II}-bearing GR-II. A solution [0.7 dm³, $FeSO_4 \cdot 7H_2O$ (2.5—10.0 g), $ZnSO_4 \cdot 7H_2O$ (0—2.5 g), and Na_2SO_4(25 g)] was oxidized with a mixed gas of air and nitrogen [air/N_2=1:1 (1 atm), flow rate; 3.0 dm³ min^{-1}] at pH 6.7±0.05 and 25 °C. During the oxidation, an alkaline solution (0.10 mol dm^{-3}) was added to maintain a pH of 6.7. After 40 min, nitrogen gas was passed through in place of the mixed gas, and the reaction vessel was cooled in a water bath chilled with ice. The greenish precipitates formed were collected by centrifugation under a nitrogen atmosphere, washed with distilled water freed from oxygen (4 °C), and suspended in distilled water (4 °C). The Zn^{II}-bearing GR-II is stable under a nitrogen atmosphere at temperatures below 4 °C.

For the measurement of the metal ions in the Zn^{II}-bearing GR-II in the course of the air oxidation, 0.005 dm³ of the reaction suspension was transferred under a nitrogen atmosphere to a 0.05 dm³ centrifuging tube chilled in ice water. After centrifuging under a nitrogen atmosphere at 3000 r.p.m for 5 min, the precipitate was washed with cold distilled water freed from oxygen, and the contents of the Fe^{III}, Fe^{II}, and Zn^{II} ions were determined.

Spontaneous Transformation Reaction of the Zn^{II}-bearing GR-II. The suspension of the Zn^{II}-bearing GR-II (0.05 dm³, 25 °C) was transferred into 0.4 dm³ of distilled water freed from oxygen (the temperature of the distilled water had been adjusted to get 70 °C after the mixing). The pH of the reaction suspension was adjusted to 10.5 by adding NaOH solution during the reaction. After allowing the reaction suspension to stand at 70 °C under a nitrogen atmosphere for 12 h, the product was isolated by transferring 0.2 dm³ of the reaction suspension to 0.1 dm³ of an oxygen-free acetate buffer solution (pH 4.1, 0.05 mol dm^{-3}) to dissolve the metal ions released during the transformation reaction. The product was collected by centrifugation under a nitrogen atmosphere, washed with oxygen-free water and acetone, successively, and dried under a nitrogen atmosphere. The dried product was examined by X-ray diffractometry. The chemical composition was determined after dissolving it in HCl solution (1:1).

Results and Discussion

Formation of the Zn^{II}-bearing GR-II. When the solutions containing Fe^{II}, Zn^{II}, and SO_4^{2-} ions (the Zn^{II}/Fe^{II} mol ratio =0—1.0) were oxidized by a mixed gas of air and nitrogen at pH 6.7 (25 °C), the clear solutions became turbid, and greenish precipitates were formed. The amount of the precipitates in-

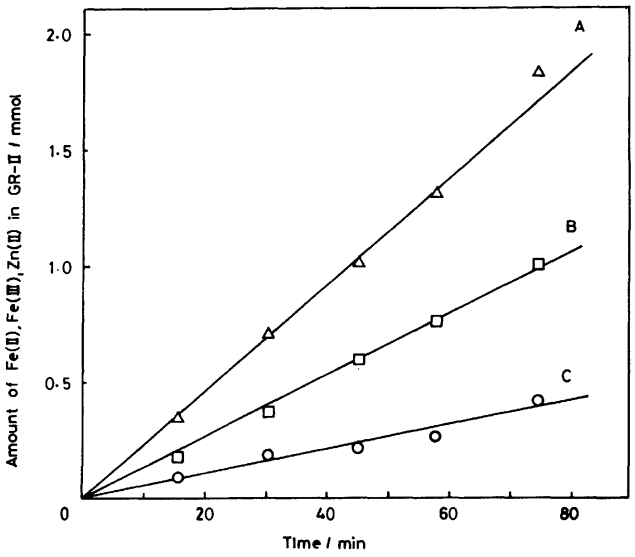

Fig. 1 Time variation of the amounts of Fe^{II}- (Curve A), Fe^{III}(B), and Zn^{II}(C) in the Zn^{II}-bearing GR-II formed during the oxidation reaction. The Zn^{II}/Fe^{II} mol ratio in the initial solution was 0.091.

creased with the oxidation time. Chemical analysis showed that the precipitates contained Fe^{III}, Fe^{II}, and Zn^{II} ions. As shown in Fig. 1, the amount of each metal ion coprecipitated as the greenish precipitates increased linearly with the oxidation time. This shows that the mol fractions of the metal ions in the precipitate are constant; a precipitate with a definite chemical composition was formed. The same results were obtained for the different mol ratios of Zn^{II}/Fe^{II} in the reaction solutions. In the following experiments, we used the greenish precipitates obtained at 40 min of the oxidation time. The X-ray diffraction pattern of the precipitate obtained at 40 min of the oxidation time corresponded to that of the green rust II.[1] In the IR spectrum, strong bands of SO_4^{2-} ion ($1100\,cm^{-1}$) appeared. These results show that Fe^{III} ions formed by the oxidation combine with the Fe^{II}, Zn^{II}, and SO_4^{2-} ions, and form the green rust II, which contains Zn^{II} ions.

The metal mol fraction of Zn^{II} in the Zn^{II}-bearing GR-II increased with an increase in the mol ratio of $Zn^{II}/(Zn^{II}+Fe^{II})$ in the initial solution, as shown by Curve A in Fig. 2. Contrarily, the mol fraction of Fe^{II} decreased (Curve C). However, the mol fraction of Fe^{III} (Curve B) remained nearly constant. The mol ratios of $(Zn^{II}+Fe^{II})/Fe^{III}$ in the Zn^{II}-bearing GR-II (the ratios of the bivalent to trivalent metal ions) are nearly equal to 2:1, which corresponds to the mol ratio of bivalent to trivalent metal ions in the green rust II having no Zn^{II} ions. This suggests that the Fe^{II} ions in the green rust II are preferentially replaced by the Zn^{II} ion. Chemical analysis showed that the chemical composition of the Zn^{II}-bearing GR-II was expressed by $(Zn^{2+})_x(Fe^{2+})_{2-x}(Fe^{3+})(SO_4^{2-})(OH^-)_5$.

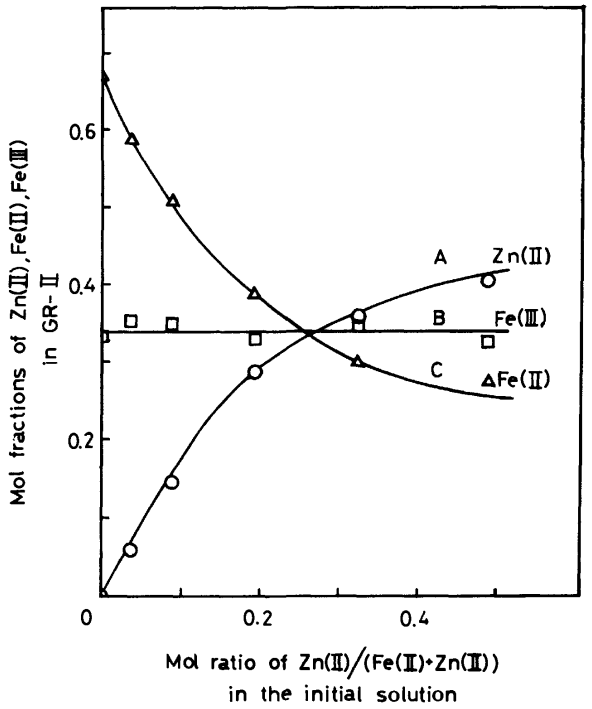

Fig. 2. The relationship between the mol fractions of metal ions (Zn^{II}; Curve A, Fe^{III}; B, and Fe^{II}; C) in the Zn^{II}-bearing GR-II and the mol ratio of $Zn^{II}/(Zn^{II}+Fe^{II})$ in the initial reaction solution. The Zn^{II}-bearing GR-II was obtained at 40 min of the oxidation time.

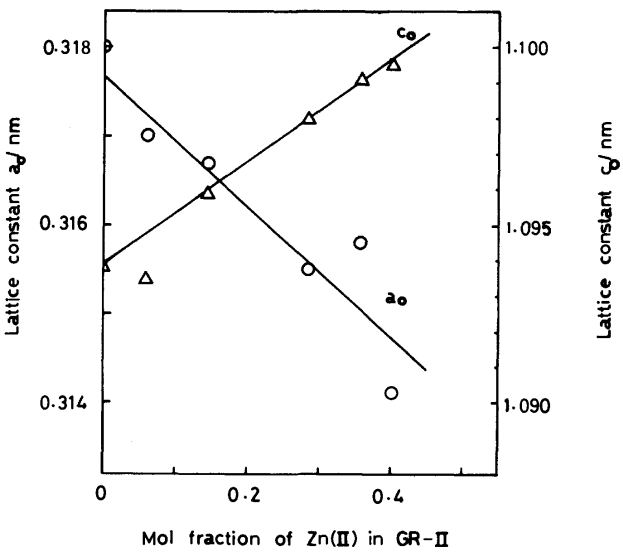

Fig. 3. The relationship between the lattice constants (a_o and c_o) and the mol fraction of Zn^{II} in the Zn^{II} bearing GR-II.

Figure 3 shows the relationship between the lattice constants and the Zn^{II} content in the Zn^{II}-bearing GR-II. As can be seen here, the lattice constant of c_o increased with an increase in the Zn^{II} content, but that of a_o decreased. Since the ion radius of Zn^{2+} is larger than that of Fe^{2+}, it is considered that the Fe^{II} ions arraied along c_o axis in the green rust II are

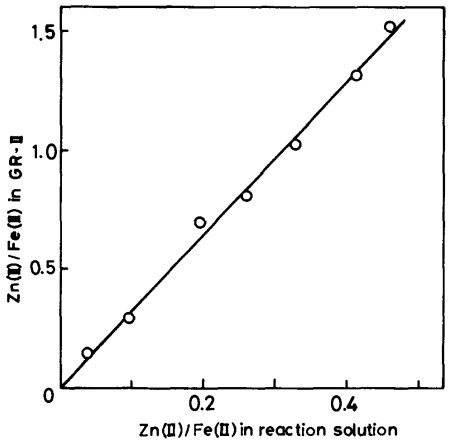

Fig. 4. The relationship between the Zn^{II}/Fe^{II} mol ratio (R_{grn}) in the Zn^{II}-bearing GR-II and those of the Zn^{II}/Fe^{II} mol ratio (R_{sol}) in the initial reaction solution.

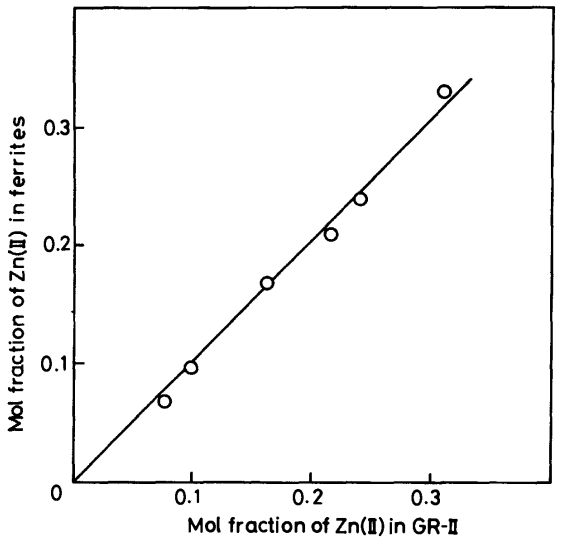

Fig. 5. The relationship between the mol fraction of the Zn^{II} in the Zn^{II}-bearing GR-II and that in the Zn^{II}-bearing ferrites formed by the spontaneous transformation reaction.

preferentially replaced by the Zn^{II} ions.

Figure 4 shows the relationship between the Zn^{II}/Fe^{II} mol ratio (R_{grn}) in the Zn^{II}-bearing GR-II and those of the Zn^{II}/Fe^{II} mol ratio (R_{sol}) in the initial reaction solution. As can be seen here, R_{grn} linearly increases with an increase in R_{sol}. The distribution coefficients of the partitioned ions (D_f and D_z for Fe^{II} and Zn^{II}, respectively) in solid (Zn^{II}-bearing GR-II) and solution phases are given by

$$D_f = [Fe^{II}_{grn}]/[Fe^{II}_{sol}] \quad (1)$$

$$D_z = [Zn^{II}_{grn}]/[Zn^{II}_{sol}]. \quad (2)$$

From these equations, we obtain

$$R_{grn} = \left(\frac{D_z}{D_f}\right)\frac{[Zn^{II}_{sol}]}{[Fe^{II}_{sol}]}. \quad (3)$$

After 40 min of oxidation time, about 8—10 mol% of the metal ions in the reaction solution was consumed with the formation of the Zn^{II}-bearing GR-II. As a first approximation, the concentrations of the Zn^{II} and Fe^{II} ions in the initial solution are substituted for $[Zn^{II}_{sol}]$ and $[Fe^{II}_{sol}]$ in Eq. 3, then

$$R_{grn} \simeq \left(\frac{D_z}{D_f}\right)R_{sol}. \quad (4)$$

Since the linear relationship in Fig. 4 is considered to be represented by Eq. 4, the slope of the line in Fig. 4 gives the value of D_z/D_f. This value suggests that the distribution coeffient of Zn^{II} between the solid (Zn^{II}-bearing GR-II) and the solution phases is 3.3 times higher than that of Fe^{II}. In general, the term "distribution coefficient" is adopted for the phenomena where substances are distributed between two phases without any chemical reactions. In the precipitation reaction studied here, the metal ions of Fe^{II} and Zn^{II} in the solution phase are transferred into the solid phase accompanying the chemical reactions; the physical meaning of D_z and D_f in Eqs. 1—4 are different from the general meaning of the distribution coeffient.

Spontaneous Transformation of the Zn^{II}-bearing GR-II into Zn-bearing Ferrites. X-Ray diffractometry showed that the product obtained by allowing the suspension of the Zn^{II}-bearing GR-II to stand under a nitrogen atmosphere at 70 °C was a spinel compound. The chemical composition of the product corresponded to a Zn^{II}-bearing ferrite.

Electron microscopic observation showed that the hexagonal particles characteristic of the GR-II changed to spherical or cubic particles characteristic of ferrites. In the IR spectrum of the product, only bands corresponding to the ferrite appeared (strong band at 570 cm^{-1}). Thus, the Zn^{II}-bearing GR-II is spontaneously transformed into the Zn^{II}-bearing ferrite.

The Zn^{II} content in the ferrites increased with an increase in the Zn^{II}-bearing GR-II. Figure 5 shows the relationship between the mol fraction of the Zn^{II} ion $[Zn^{II}/(Zn^{II}+Fe^{II}+Fe^{III})]$ in the ferrites and that in the Zn^{II}-bearing GR-II. As can be seen here, the mol fractions of the Zn^{II} in the ferrites are equal to that in the Zn^{II}-bearing GR-II. This suggests that the spontaneous transformation reaction is represented by

$$2(Zn^{2+})_x(Fe^{2+})_{2-x}(Fe^{3+})(SO_4^{2-})(OH^-)_5 + 2H^+ \longrightarrow (Zn_x^{2+}, Fe^{2+}_{1-x})(Fe^{3+})_2O_4 + xZn^{2+} + (3-x)Fe^{2+} + 2SO_4^{2-} + 6H_2O. \quad (5)$$

The mol ratio of Zn^{2+}/Fe^{2+} in the Zn^{II}-bearing GR-II $[x/(2-x)]$ is smaller than that in the ferrite $[x/(1-x)]$, suggesting that the Zn^{2+} ions in the Zn^{II}-bearing GR-II

are preferentially incorporated into the ferrites in the spontaneous transformation reaction.

References

1) J. D. Bernal, D. R. Dasgupta, and A. L. Mackay, *Clay Min. Bull.*, **4**, 15 (1959).
2) T. Misawa, T. Kyuno, W. Suetaka, and S. Shimodaira, *Corros. Sci.*, **11**, 35 (1971).
3) M. Kiyama, *Bull. Chem. Soc. Jpn.*, **47**, 1646 (1974).
4) Y. Tamaura, T. Yoshida, and T. Katsura, *Bull. Chem. Soc. Jpn.*, **57**, 2411 (1984).
5) I. Iwasaki, T. Katsura, T. Ozawa, M. Mashima, H. Haramura, and B. Iwasaki, *Bull. Volc. Soc. Jpn., Ser.* **2**, **5**, 75 (1960).

Studies of the Hydrous Niobium(V) Oxide Ion Exchanger. II. Affinity for Various Cations

Yasushi INOUE,* Hiromichi YAMAZAKI, Kazushi OKADA, and Kazuhiko MORITA
Department of Nuclear Engineering, Faculty of Engineering, Tohoku University, Aramaki, Sendai 980
(Received February 13, 1985)

In order to elucidate the fundamental properties of hydrous niobium(V) oxide as a cation exchanger, the stoichiometry of cation exchange and the selectivity for various cations were studied. As the reversibility and the equivalent exchange between the cations were confirmed, this material showed an ideal cation-exchange reaction. The affinity series for alkali metal ions and alkaline earth metal ions were $Cs^+ \gg K^+ \gg Li^+$ and $Ba^{2+} \gg Sr^{2+} \geqq Ca^{2+} > Mg^{2+}$ respectively; the values decreased in the order of the increase in the hydrated ionic radii of the cations. For transition metal ions, the distribution coefficients had a strong correlation with the first hydrolysis constants of the cations and/or the first stability constants of their acetato complexes. Based on this finding, the transition metal ions are considered to be adsorbed on the exchanger by a bond partially covalent in character, rather than by a pure ionic bond. The pH-dependency of the distribution coefficients of the cations was discussed in terms of the effects of the dissociation of the exchange sites on the overall ion-exchange equilibrium.

Through a comprehensive study of preparing the hydrous niobium(V) oxide ion exchanger, a recommended procedure for synthesizing the exchanger was established, as has been reported previously.[1] The method has the merits of simplicity and good reproducibility. The exchanger thus prepared is a semitransparent, amorphous solid which is hard enough to be used for column operation; it can be converted to the pure H^+ form by conditioning it with a 0.1 mol dm^{-3} HCl solution. The material has the cation-exchange capacity of 2.3 mmol Na^+ g^{-1} (at pH 10) and possesses at least two kinds of weakly dissociable ion-exchange sites. Its stability against various chemicals and during storage was also investigated, as has been described in the foregoing report.[1]

Abe and Ito reported that the exchanger exhibited only a cation-exchange property,[2] but Sukharov *et al.* reported anion exchange with $Cr_2O_7^{2-}$.[3] However, a systematic study has not been made of exchange reactions on hydrous niobium(V) oxide. In the present investigation, the distribution coefficients of various cations were determined as a function of the pH in order to study the ion-exchange mechanism.

Experimental

Reagents and Apparatus. The niobium(V) chloride, of the highest purity grade, was obtained from the Mitsuwa Kagaku Yakuhin Kaisha, Ltd. All the other reagents used were of the highest purity grade and were obtained from Wako Pure Chemical Industries, Ltd., or E. Merck AG. A well-type NaI(Tl) scintillation counter (Fuji Denki Model NHS-2) was employed for the measurement of the γ-radioactivity. All the other apparatuses were the same as those described previously.[1]

Preparation of the Exchanger. Synthetic method No. 4 was chosen from the various methods of preparation described in the preceeding paper: Twenty-five grams of niobium(V) chloride were dissolved in 50 cm^3 of a concentrated hydrochloric acid, followed by dilution to 1 dm^3 with distilled water. The solution was hydrolyzed thermally by boiling it for 2 h in a 3-dm^3, round-bottomed flask equipped with a reflux condenser. The precipitate thus formed was washed with distilled water until no chloride ion was detected in the filtrate. Then the precipitate was air-dried at room temperature. The dried product was then immersed in distilled water to break it down into fine particles. The granules were dried again at room temperature. Particles larger than desired, if any, were ground in a porcelain mortar and sieved to obtain the required particle sizes. The exchanger of a desired particle size(−100 +200 mesh) was converted to the H^+ form by treating it with a 0.1 mol dm^{-3} HCl solution by the procedure described previously.[1] Finally, the exchanger was air-dried and stored in a desiccator containing a saturated NH_4Cl solution (relative humidity, 79% at 25 °C). The exchanger had a composition of $Nb_2O_5 \cdot 5.3H_2O$ and an ion-exchange capacity of *ca.* 1.5 mmol Na^+ g^{-1} at pH 8, where an inflection point was observed in the titration curve of the material.

Distribution Coefficients. The distribution coefficients, K_d, were determined in the following way, unless otherwise noted.

A 0.30-g portion of the exchanger in the H^+ form was immersed in 18 cm^3 of the solution with a suitable pH value, adjusted by using a desired combination of 0.11 mol dm^{-3} NaCl and 0.11 mol dm^{-3} HCl or 0.11 mol dm^{-3} NaOH, for 2 d, at room temperature. A 2-cm^3 portion of the solution containing each metal ion was mixed with the above solution to make the concentration of the cation 1×10^{-4} mol dm^{-3} and the ionic strength 0.10 mol dm^{-3}. The mixture was then allowed to stand until the concentration of the cation in the supernatant solution became constant (about 2 to 9 d). The pH and the concentration of the cation in the supernatant solution were then measured. The K_d value, expressed in cm^3 g^{-1}, was calculated in the usual manner.

The metal ions were added as their chlorides, except Fe^{3+}, Th^{4+}, and UO_2^{2+}, for which the corresponding nitrates were used. The analyses of Cs, Sr, Ba, Mn, Fe, Co, Sc, Y, Ce, Eu, Np, and Am were carried out radiometrically using ^{137}Cs, ^{85}Sr, ^{133}Ba, ^{54}Mn, ^{59}Fe, ^{60}Co, ^{45}Sc, ^{88}Y, ^{144}Ce, ^{152}Eu, ^{239}Np, and ^{241}Am respectively as tracers. Their radioactive purities were confirmed by means of γ-ray spectrometry. The ^{239}Np tracer was prepared by milking it from ^{243}Am by the method of Sill.[4] The oxidation state of neptunium at a tracer concentration was adjusted by the method of Inoue and Tochiyama.[5] The Th^{4+} and the UO_2^{2+} were analyzed

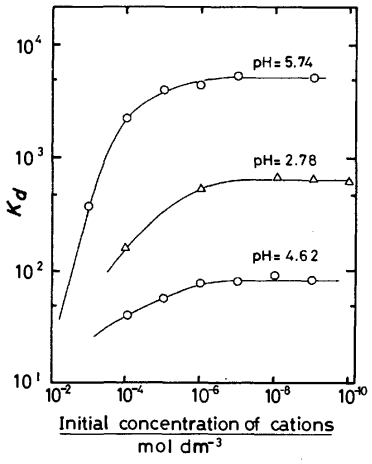

Fig. 1. Effect of the concentration of cations on their distribution coefficients.
○: Co^{2+}, △: Sc^{3+}.

spectrophotometrically using arsenazo III[6] and 2-(5-Bromo-2-pyridylazo)-5-(diethylamino)phenol[7] respectively as coloring reagents, while the concentrations of the other cations were determined by means of atomic-absorption spectrophotometry.

Ion-exchange Stoichiometry. The exchanger in the H^+ form was immersed in an alkaline solution of sodium ions, of a suitable concentration (ionic strength=0.016 mol dm^{-3}), for 2 d at room temperature, with intermittent shaking. This was followed by chemical analysis, and the ratio of the amount of sodium ions taken up in the exchanger to that of the hydrogen ions released from the exchanger was evaluated from the difference between the initial and final concentrations of the respective ions present in the solution. The Na^+ was converted to pure chloride and was indirectly determined by titrating the Cl^-. The OH^- and CO_3^{2-} were determined by differential titration.

Results and Discussion

The Dependency of K_d Values on the Concentration of the Cations. Figure 1 shows the K_d values for Co^{2+} and Sc^{3+} as a function of their initial concentrations at constant pH values. The K_d values were nearly constant in the concentration region lower than 10^{-8} mol dm^{-3}, wherefrom they decreased with an increase in the concentration. The concentration-dependency of the K_d values may be ascribed to the limited amount of cation-exchange sites in the pH region adopted in the present experiment, since the uptake of Na^+ on the exchanger commences at about pH 4.[1] Because of this observation, a strict comparison of the selectivity for various cations should be made at a concentration lower than 10^{-8} mol dm^{-3}. However, it is very difficult to set up the above situation because of the limits of analytical sensitivities for some cations. Thus, an initial concentration of 1×10^{-4} mol dm^{-3} was used mainly for the comparison of the K_d values of various cations.

Stoichiometry and Reversibility of the Exchange Reaction. Table 1 presents the results concerning the stoichiometry of the exchange reaction between H^+ on the exchanger and Na^+ in the solution. The equivalent ratio of the H^+ released to the Na^+ sorbed was unity, within the limits of experimental error (Table 1). Figure 2 shows the results concerning the reversibility of the ion-exchange reaction between Eu^{3+} and H^+. After the determination of the K_d values at several pH values (A, B in the figure), a small amount of a HCl solution (less than 0.5% in volume) was added to the supernatant solution to lower the pH. This new solution was then allowed to stand until a new equilibrium had been attained, and then the K_d values were measured again (A′, B′ in the fugure). The points A and B shifted to A′ and B′ respectively as a result of the change of the pH in the solutions. Since A′ and B′ fall on the same straight line as A and B, the exchange reaction between Eu^{3+} and H^+ is considered to be reversible. From the stoichiometry and the reversibility of the ion-exchange reaction, the hydrous niobium(V) oxide shows an ideal cation-exchange reaction.

Selectivity for Cations. Figure 3 shows the pH-dependency of the K_d values for the representative elements. The orders of selectivity for alkali metal ions: $Cs^+ \gg K^+ \gg Li^+$, and for alkaline earth metal

Table 1. Verification of equivalence of exchange between Na^+ and H^+

Ionic strength	(I) Na^+ uptaken	(II) H^+ released	Stoichiometry
mol dm^{-3}	mequiv g^{-1}	mequiv g^{-1}	(I)/(II)
0.016 (OH^-/Cl^-=0.25)[a]	1.77±0.06	1.76±0.03	1.01±0.04

a) : Molar ratio.
Conditions; Exchanger: 0.31 g, Solution: 300 cm^3, Duration of immersion: 2 d at room temperature.

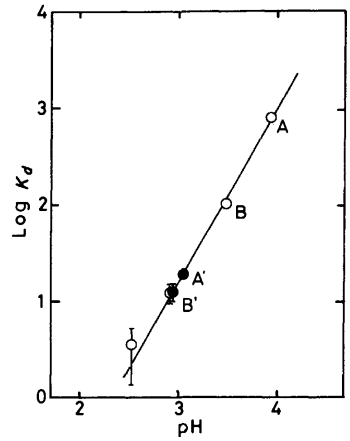

Fig. 2. Reversibility of the exchange reaction between Eu^{3+} and H^+.
Conditions; Ionic strength: 0.10 mol dm^{-3}(NaCl-HCl) at room temperature, Initial concentration of Eu^{3+}: 1×10^{-4} mol dm^{-3}.

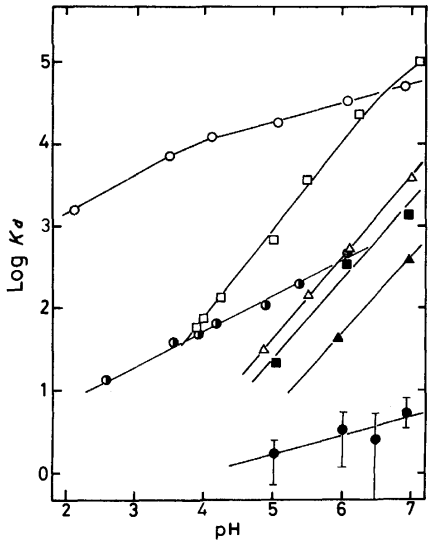

Fig. 3. Log K_d for some metal ions as a function of pH. Conditions; Ionic strength: 0.10 mol dm^{-3} (HCl-NaCl-NaOH) at room temperature, Initial concentration of cation: 1×10^{-4} mol dm^{-3}. Cation; ●: Li^+, ◑: K^+, ○: Cs^+, ▲: Mg^{2+}, ■: Ca^{2+}, △: Sr^{2+}, □: Ba^{2+}.

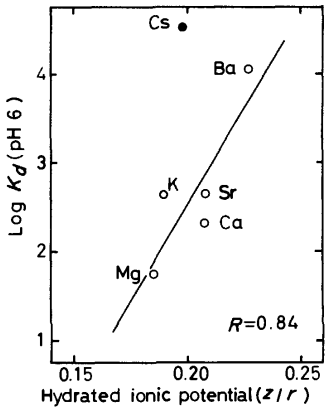

Fig. 4. Relation between log K_d and hydrated ionic potential of cation.
Hydrated ionic potential=z/r; z: Charge of cation, r: Hydrated ionic radius.[8] R: Correlation coefficient (except Cs^+).

ions: $Ba^{2+} \gg Sr^{2+} \geqq Ca^{2+} > Mg^{2+}$, are similar to that of strongly acidic ion-exchange resin, in which the selectivity coefficients for ions with the same ionic charge increase with a decrease in the hydrated ionic radii of the cations. This may be due to the increase in the strength of the electrostatic interaction between the hydrated cations and the fixed anionic groups. Such interaction must be closely related to the ionic potential of hydrated cations (hydrated ionic potential). In fact, the log K_d value at pH 6 for these cations closely correlates to their hydrated ionic potentials (the correlation coefficient was 0.84), as is shown in Fig. 4. Here, the hydrated ionic radii were those reported by Wiklander.[8] The selectivity for Cs^+, however, was markedly high, in spite of the smaller

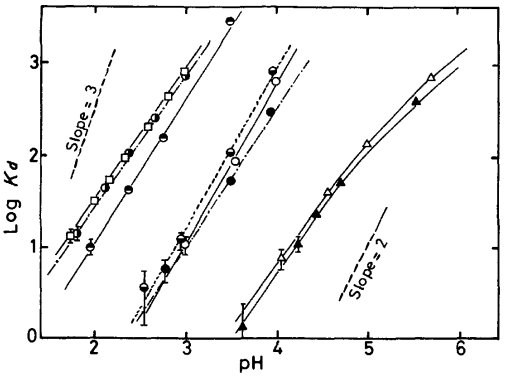

Fig. 5. Log K_d for some metal ions as a function of pH. Conditions; Ionic strength: 0.10 mol dm^{-3} (HCl-NaCl-NaOH) at room temperature, Initial concentration of cation: 1×10^{-4} mol dm^{-3}. Cation; □: UO_2^{2+}, ◑: Fe^{3+}, ◓: Sc^{3+}, ●: Y^{3+}, ◒: Eu^{3+}, ○: Ce^{3+}, △: Co^{2+}, ▲: Mn^{2+}.

hydrated ionic potential.

Figure 5 shows that the pH-dependency of the K_d values for bi- and tervalent transition metal ions was: $UO_2^{2+} \geqq Fe^{3+} > Sc^{3+} \gg Eu^{3+} \geqq Ce^{3+} \geqq Y^{3+} \gg Co^{2+} \geqq Mn^{2+}$. By comparing the figure with Fig. 3, the affinity for bivalent transition metal ions (except UO_2^{2+}) may be seen to be similar to that for alkaline earth metal ions. Furthermore, the affinity of the exchanger for tervalent cations is, on the whole, much greater than that for bivalent cations. Hence, the electrostatic force may be an important factor in deciding the selectivity of the hydrous niobium(V) oxide. This affinity series, however, is the exact reverse of what would be expected from the selectivity for alkali- and alkaline earth metal ions. Figure 6 shows the results for some actinoid ions. The Am(III) ion appears to have an affinity similar to those of other transition metal ions with the same charge. The actinyl species, such as NpO_2^+, NpO_2^{2+} and UO_2^{2+}, had, however, higher K_d values than those to be expected from their charges; the affinity for those species was greater than, or similar to, that for tervalent transition metal ions. This finding cannot be explained only in terms of the electrostatic interaction between the hydrated ions and the anionic sites in the exchanger.

In order to understand the important factors affecting the selectivity for the transition metal ions, the K_d values for the metal ions at pH 3 were compared with their ionic potentials, their first hydrolysis constants,[9] and the first stability constants of their acetato complexes.[11] The results are shown in Table 2. Here, the ionic radii used were those obtained by using crystals in which the ion had the coordination number of 6[10] and the log K_d values which could not be obtained by the experiment were those estimated from the extrapolation of the log K_d *vs.* pH plot in Fig. 5. This table indicates that the K_d values correlate more strongly with the stability constants (R=0.96) and the hydrolysis constants (R=0.91) than with the ionic potential

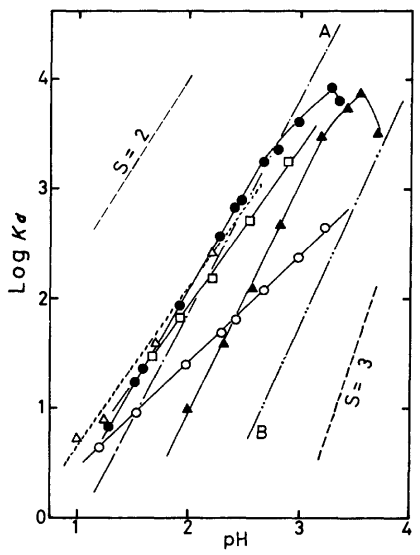

Fig. 6. Log K_d for some actinoid ions as a function of pH. Conditions; Ionic strength: 0.10 mol dm^{-3} ($HClO_4$-$NaClO_4$), Temperature: 40±3°C. Concentration of cations; △: Th(IV) 1.8×10^{-5} mol dm^{-3}, □: U(VI) 1.3×10^{-5} mol dm^{-3}, ○: Np(V) tracer S= 0.97, ●: Np(VI) tracer in 4×10^{-4} mol dm^{-4} $KMnO_4$ S=1.8, ▲: Am(III) tracer S=2.1, A: Sc^{3+} tracer, B: Y^{3+} tracer. S: Slope.

Table 2. Interaction between exchanging cations and exchange sites

Metal ion	log K_d(at pH 3)	A[1]	B[2]	C[3]
UO_2^{2+}	3.66	—	2.61	−5.8
Fe^{3+}	3.62	4.35	3.36	−2.19
Sc^{3+}	3.40	3.39	—	−4.3
Eu^{3+}	2.10	2.76	2.13	−7.8
Ce^{3+}	1.90	2.61	1.91	−8.3
Y^{3+}	1.73	2.88	1.68	−7.7
Co^{2+}	0.14	2.53	1.10	−9.65
Mn^{2+}	0.02	2.46	0.8	−10.59
		R=0.83	R=0.96	R=0.91

1) A=z/r: Ionic potential; z=Change of cation, r=Ionic radius(coordination number (6)).[10] 2) B=log K_{11} (CH_3COO^-): First stability constant(equilibrium quotient at 25°C and ionic strength 0.1).[11] 3) C=log K_{11} (OH^-): First hydrolysis constant.[9]
R=Correlation coefficient.

(R=0.83). Therefore, we can conclude that, in the ion-exchange reactions for transition metal ions, the formation of a covalent bond between the anionic sites in the exchanger and metal ions is a factor in determining the selectivity of the exchanger, along with the remote coulombic interaction.

Selectivity for Cations in Tracer Concentrations. The cation-exchange reaction is expressed as a combination of the following two reactions:

$$HR \rightleftharpoons H^+ + R^-, \tag{1}$$

$$nR^- + M^{n+} \rightleftharpoons R_nM, \tag{2}$$

where R^- denotes the dissociated form of the exchanger, and M^{n+} the exchanging cations. The equilibrium constants for these reactions can be written as:

$$K_a = \frac{a_H\bar{a}_R}{\bar{a}_{HR}} = \frac{a_H\bar{m}_R\bar{\gamma}_R}{\bar{m}_{HR}\bar{\gamma}_{HR}}, \tag{3}$$

$$K = \frac{\bar{a}_{R_nM}}{\bar{a}_R{}^n a_M} = \frac{\bar{m}_{R_nM}\bar{\gamma}_{R_nM}}{\bar{m}_R{}^n\bar{\gamma}_R{}^n m_M\gamma_M}, \tag{4}$$

where a represents the activity; m, the concentration and γ, the activity coefficient. A bar refers to the exchanger phase. (For the sake of simplicity, the charge of the species is omitted in these expressions.)

From the material balance,

$$\bar{m}_R + \bar{m}_{HR} + n\,\bar{m}_{R_nM} = E \tag{5}$$

E is the total ion-exchange capacity. If the concentration of the exchanging cation, M^{n+}, is negligibly small,

$$\bar{m}_R + \bar{m}_{HR} = E \tag{5'}$$

holds.

From Eqs. 3 through 5′, distribution coefficients of M^{n+} can be written as:

$$K_d = \frac{KK_a{}^n\bar{\gamma}_{HR}{}^n\gamma_M}{\bar{\gamma}_{R_nM}} \cdot \frac{E^n}{\left[1+\frac{K_a\bar{\gamma}_{HR}}{a_H\bar{\gamma}_R}\right]^n} \cdot \frac{1}{a_H{}^n}. \tag{6}$$

If the pH of the solution is very low, Eq. 6 can be simplified to:

$$\log K_d = \text{constant} + n\text{pH}, \tag{7}$$

while in highly alkaline solutions:

$$\log K_d = \text{constant}. \tag{8}$$

As has been reported previously,[1] the exchanger commences the uptake of Na^+ at around pH 4, and it increases in its ion-exchange capacity for Na^+ with pH. Consequently, at the tracer concentration, the plot of log K_d *vs.* pH will show a straight line with a slope of n in the pH range lower than around 4. The deviation of the results in Figs. 5 and 6 from Eq. 7 may be ascribed to the strong dependency of the K_d values on the concentration of cations (Fig. 1), but it cannot be explained only from this reason, because the slope of the straight line was not appreciably affected by the concentration, as is evident from the results on Sr^{2+} (Fig. 7). Figure 7 also shows that the K_d value for Sr^{2+} is independent of the pH values in the pH region higher than 8; this agrees with Eq. 8. As is shown in Figs 6 and 8, for uni- and bi-charged cations, the straight lines have approximately the same slopes (Co^{2+}: 1.7, NpO_2^+: 0.97, NpO_2^{2+}: 1.8), as would be predicted from Eq. 7, while the ter-valent cations show slopes (Y^{3+}: 2.3, Sc^{3+}: 1.8, Am^{3+}:

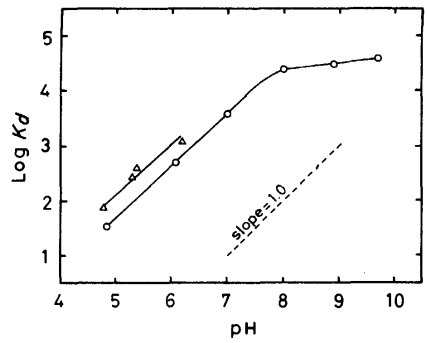

Fig. 7. Effect of the concentration of Sr^{2+} on the pH-dependency of the K_d values.
Ionic strength: 0.10 mol dm^{-3} (NaCl-NaOH) at room temperature, Initial concentration of Sr^{2+}/mol dm^{-3}; ○: 1×10^{-4}, △: 1×10^{-8}.

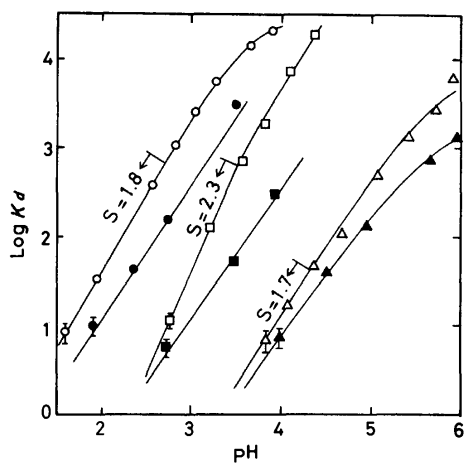

Fig. 8. Effect of the concentration of Co^{2+}, Y^{3+}, and Sc^{3+} on the K_d values.
Ionic strength: 0.10 mol dm^{-3} (HCl-NaCl-NaOH) at room temperature, Initial concentration of cations/mol dm^{-3}, Co^{2+}; ▲: 1×10^{-4}, △: 1×10^{-8}, Y^{3+}; ■: 1×10^{-4}, □: 1×10^{-10}, Sc^{3+}; ●: 1×10^{-4}, ○: 1×10^{-10}.

2.1) smaller than those to be expected from Eq. 7 in spite having the conditions which satisfy this equation. This contradiction may be solved by considering that the charge in the exchanger is not balanced only by these reactions, (1) and (2). The first explanation can be based on the Donnan exclusion principle, which claims that the electrolytes with counter ions (in this case, cations) of a higher charge will be more easily introduced in the exchanger than those of a lower charge, if the co-ions (anions) have the same charge. As the exchanger is mainly in the undissociated form in the pH range lower than 4, the chloride ions can easily diffuse into the exchanger by means of Donnan adsorption. Accordingly, the lowering of the slope of the straight lines will be more pronounced for tervalent than for uni- and bivalent cations. The second explanation is that the charge in the exchanger, instead of the H^+, will be balanced by the release of Na^+ which is trapped in an exchanger phase surrounded by a solution with a high Na^+-concentration, even in a solution with a low pH.

In any case, further investigation must be carried out before the cation-exchange mechanism can be unambiguously understood.

References

1) Y. Inoue, H. Yamazaki and Y. Kimura, *Bull. Chem. Soc. Jpn.*, submitted for publication.
2) M. Abe and T. Ito, *Nippon Kagaku Zasshi*, **86**, 1259 (1965).
3) V. V. Sakharov, N. E. Ivanova, S. S. Korovin, and M. A. Zakharov, *Russ. J. Inorg. Chem.*, **19**, 313 (1974).
4) C. W. Sill, *Anal Chem.*, **38**, 802 (1966).
5) Y. Inoue and O. Tochiyama, *J. Inorg Nucl. Chem.*, **39**, 1443 (1977).
6) H. Onishi, *Analyst*, **12**, 1153 (1963).
7) D. A. Johnson and T. M. Florence, *Anal. Chim. Acta*, **53**, 73 (1971); *Talanta*, **22**, 253 (1975).
8) L. Wiklander, *Ann. Royal Agr. Coll. Sweden*, **14**, 1 (1946).
9) C. F. Baes, Jr., and R. E. Mesmer, "The Hydrolysis of Cations," John Wiley and Sons, New York (1976).
10) R. D. Shannon and C. T. Prewitt, *Acta Crystallogr.*, **B 25**, 925 (1969); **A 32**, 751 (1976).
11) A. E. Martell and R. M. Smith, "Critical Stability Constants, Volume 3: Other Organic Ligands," Plenum Press, New York (1977), p. 3.

Adsorption and Orientation of Isomeric Phthalic Acids on Alumina Surface Observed by Inelastic Electron Tunneling Spectroscopy

Morihide HIGO,* Sinichi MIZUTARU, and Satuo KAMATA
Faculty of Engineering, Kagoshima University, Korimoto, Kagoshima 890
(Received April 20, 1985)

The vibrational spectra of phthalic, isophthalic and terephthalic acid adsorbed onto the alumina surface have been measured by using inelastic electron tunneling spectroscopy. The tunneling spectra of these acids were obtained by liquid-phase doping with water or various alcohol solutions. The detailed assignments for these spectra are given, together with a comparison of their infrared and Raman spectra. It has been found that both phthalic and isophthalic acid are adsorbed onto the alumina surface mainly as the dicarboxylate ions. However, a comparison between the tunneling spectra of terephthalic and *p*-acetylbenzoic acid shows that terephthalic acid is adsorbed predominantly as the monocarboxylate ion onto the surface when doped with alcohol solutions. Hydrogen bonding is observed among the adsorbed hydrogen terephthalate ions. These results show a difference in their orientation and different probabilities of chemical interaction between the alumina surface and the carboxyl groups of the adsorbed isomeric phthalic acids.

A great deal of interest has been paid to a new technique for investigating the adsorbed species on metal surfaces. The vibrational spectra of such species should give important information on their structure and the adsorption mechanism. Inelastic electron tunneling spectroscopy (IETS), discovered in 1966 by Jaklevic and Lambe,[1] reveals the vibrational spectrum of adsorbed species on the oxide surface of a metal-oxide-metal tunneling junction at cryogenic temperatures, as is shown in Fig. 1. Several authors[2-7] have reviewed the principle, apparatus and application; they have demonstrated the potential of IETS.

When a dc-bias voltage is applied across the junction, electrons can tunnel from one electrode through the oxide into the opposite electrode. A vibrational mode of frequency, ν, appears as a peak in the second derivative of the characteristic current-voltage (I-V) function of the junction, d^2I/dV^2, at a voltage of $V=h\nu/e$, where h is Planck's constant and e is the electron charge. Both infrared and Raman-active vibrational modes appear in the IET spectrum. The useful spectral range extends from 400 to 4000 cm^{-1} and includes all molecular vibrations. The high sensitivity and resolution of IETS enable us to measure the detailed spectrum of a fraction of a monolayer of adsorbed species. In general, the oscillating dipole moment perpendicular to the oxide surface couples to tunneling electrons more strongly than that parallel to the surface. Thus, IETS may be expected to be a powerful analytical technique for investigating the chemical interaction and the structure of molecules adsorbed onto the oxide surfaces.

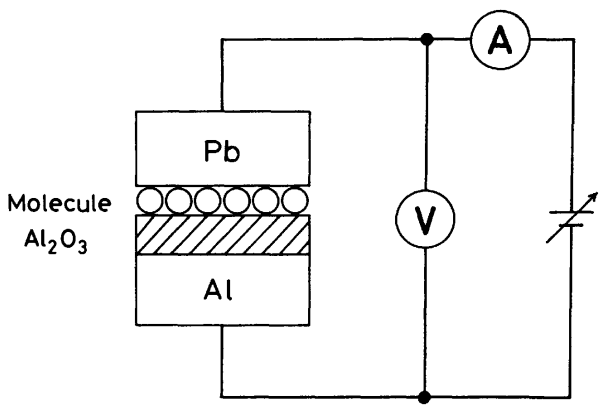

Fig. 1. Schematic representation of the tunneling junction.

The tunneling spectra of benzoic acid,[8] phenol,[9] and benzenesulfonic acid[10] have been measured and indicated their structures on the oxide surfaces. These molecules are found to be adsorbed onto the alumina as anions. The tunneling spectrum of benzaldehyde shows that this molecule reacts with alumina to give the adsorbed benzoate ion.[3,11] In the cases of molecules with two functional groups, however, not so many studies have been carried out. Lewis *et al.*[12] have observed the tunneling spectra of the isomers of catechol, *i.e.*, *o*-, *m*-, and *p*-$C_6H_4(OH)_2$, on Al_2O_3. They found that both catechol and resorcinol are adsorbed as dianions, whereas hydroquinone is adsorbed predominantly as a monoanion. Oxley *et al.*[13] have previously reported that the isomeric phthalic acids are adsorbed onto Al_2O_3 as benzenedicarboxylate ions. Monjushiro *et al.*[14] have studied the adsorption of some *o*-substituted benzoic acids onto Al_2O_3.

The vibrational spectra of isomeric phthalic acids[15] and their ions[16] were measured by means of infrared and Raman spectroscopy. Detailed diagrams for the atom motions involved in these modes can be found in the book by Varsányi.[17] A comparison between these spectra and the tunneling spectra gives valuable information on these molecules adsorbed onto Al_2O_3. Since alumina is widely used as a catalyst or catalyst support,[18] it is important to know the orientation and structure of adsorbed species in order to understand the reaction mechanism on the catalyst. The isomeric phthalic acids have two carboxyl groups. Their structure on the alumina surface can easily be clarified by examining the characteristic C=O group. In our previous paper,[19] it has been shown that terephthalic acid is adsorbed predominantly as the monocarbox-

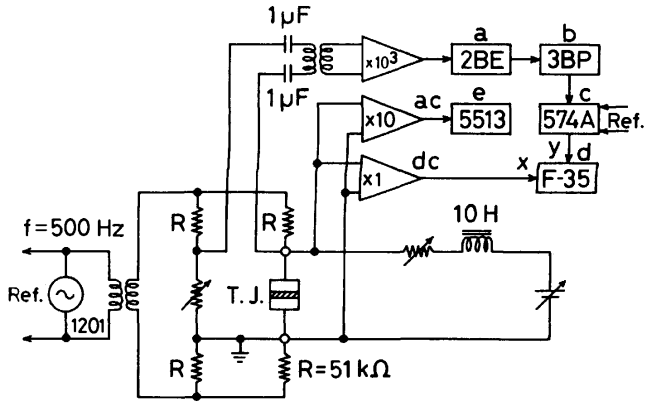

Fig. 2. Schematic diagram of the circuit. One arm of the bridge contains the tunneling junction (T. J.). a) notch filter b) bandpass filter c) lock-in amplifier d) X-Y recorder e) oscilloscope.

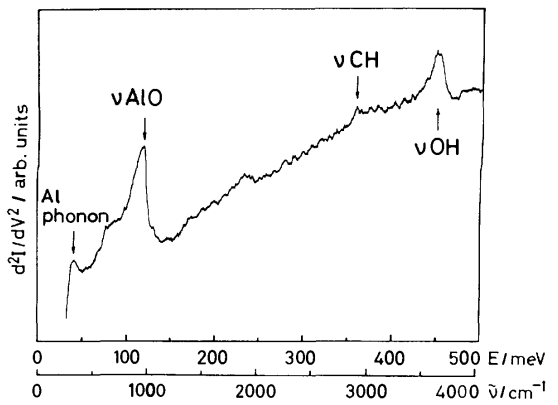

Fig. 3. Tunneling spectrum of the undoped Al-Al_2O_3-Pb junction made by an oxygen glow discharge. Junction resistance: 63 Ω; modulation voltage: 4 mVpp; time constant of the lock-in amplifier: 30 s; trace time: 109 min.

ylate ion onto the alumina surface when doped with alcohol solutions. In this paper, we will consider the tunneling spectra of phthalic, isophthalic, and terephthalic acid, together with their detailed assignments. The structure of these molecules on the alumina surface is clarified. The chemical interaction between the carboxyl groups and the surface is also discussed.

Experimental

The method of junction preparation involves evaporation and oxidation techniques in a liquid nitrogen-trapped diffusion-pumped bell jar. Aluminium (99.999%, Mituwa Chemicals) was evaporated from a molybdenum boat on a clean glass slide (13×37×1 mm) to form three strips (1 mm wide) at a pressure of 10^{-5} Torr (1 Torr=133.322 Pa). The strips were oxidized by exposure to pure oxygen (99.8%, 1 atom) or in an oxygen-dc glow discharge (400—800 V, 30 mTorr, 5 mA, 10—60 s) in the bell jar.[20]

The slide was removed from the vacuum system, dipped into a solution containing the sample molecules, and left for about 3 min to complete the adsorption. The phthalic, isophthalic, and terephthalic acid (Kanto Chemicals) were purified by recrystallization from water. Guaranteed-reagent grade methanol, ethanol and 1-propanol, and distilled water were used as the solvents.

The slide was returned to the vacuum system, and the junctions (1×1 mm area) were completed with an evaporated Pb (99.999%, Wako Chemicals) cross strip (1 mm wide). The resistance of the junction was measured with a digital multimeter (Kikusui 1502). The operations mentioned above were done in a class 10000 clean room (Airtech Japan AER-233C). The slide was mounted in a sample holder and preliminarily cooled with liquid nitrogen at 77 K. Silver paint and solder were used for attaching the leads to the junctions. The sample holder was then inserted into a liquid helium Dewar (Osaka Sanso Hi·CRIC-10), where the junctions were cooled at 4.2 K.

The tunneling spectrum was obtained by measuring the second derivative of the tunneling current through the junction at the liquid helium temperature. A diagram of the circuit is shown in Fig. 2. A 500 Hz ac modulation signal of 2.0—4.0 mV peak-to-peak from a low-distortion oscillator (NF E-1201) and a slowly varying dc voltage from a bias supply were applied to the junction. The aluminium electrode was negatively biased with respect to the Pb electrode. The modulation signal through an amplifier (LM 308H) was monitored with an oscilloscope (Kikusui 5513). The second harmonic signal was differentially amplified (LM 308AH) and detected with a lock-in amplifier (NF LI-574A), with a notch filter (NF 2BE) and a bandpass filter (NF 3BP), preceded by the bridge circuit developed by Adler and Jackson.[21] The bridge circuit achieved an ac rejection of 50 dB. The output of the lock-in amplifier was then applied to the y axis of an x-y recorder (Rikendenki F-35). The dc voltage across the junction was applied through a buffer amplifier (LM 308H) to the x axis. Acceptable resistances for the junctions were in the range of 30—3000 Ω, while matched resistances were in the range of 50—500 Ω.

Results

Performance Test of the Apparatus and Procedures. The tunneling spectrum of an undoped Al-Al_2O_3-Pb junction made by an oxygen glow discharge is shown in Fig. 3. There is a smoothly varying background due to the change in the elastic conductance as the bias voltage is increased. The features and the peak positions of the spectrum agree well with those previously reported.[1-7,22,23] The peaks at about 300 and 940 cm^{-1} are due to the aluminium phonon and the vibrational mode of the aluminium oxide respectively.[22,23] The broad peak at about 3600 cm^{-1} arises from the stretching vibration of the surface hydroxyl species. The OH bending mode appears at about 700 cm^{-1} as the shoulder of the strong peak at 940 cm^{-1}. The weak and broad structure at 1300—1900 cm^{-1} is caused by both the second harmonics of the bending mode of OH and the vibrational mode of AlO.[22] Recently, Gauthier *et al.*[23] have proposed other assignments: the structure near 1900 cm^{-1} and the shoulder at about 700 cm^{-1} are caused by the vibrational and bending mode of an aluminium hydride located near the Al-

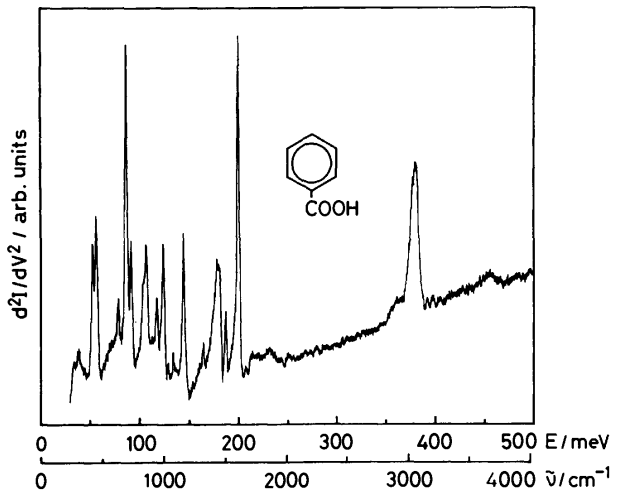

Fig. 4. Tunneling spectrum of benzoic acid doped with a methanol solution of 1.0 mg/ml. Junction resistance: 81 Ω; modulation voltage: 3 mVpp; time constant: 10 s; trace time: 154 min.

Al_2O_3 interface respectively. The peak of the OH bending mode is involved in the strong peak at 940 cm^{-1}.[23] The small peak at around 2900 cm^{-1} is due to the CH stretching mode of a hydrocarbon contamination; its very weak intensity shows that the contamination of the junction is negligible.

The tunneling spectra of benzoic acid have shown that benzoic acid is adsorbed onto the alumina surface as benzoate ion.[8,13] Tunneling spectroscopy shows that benzaldehyde reacts with Al_2O_3 and is also adsorbed as benzoate ion onto the surface.[3,11] Because of the clear features of its spectrum and the detailed assignment, the benzoate ion is a good sample for examining our apparatus and procedures.

The tunneling spectrum of benzoic acid is shown in Fig. 4. The junction was made by liquid doping with a methanol solution of 1.0 mg/ml. The spectrum was measured with a 10-s time constant of the lock-in amplifier and a 2.5-h trace time. In order to obtain a spectrum of good quality, a long trace time should be taken; it is important to spend six time constants per resolution element of the spectrum. Hansma[7] has shown that, if traces are swept faster than these times, shifts in peaks are observed. At 4.2 K, the top lead electrode is superconducting and a correction of −1 meV (−8 cm^{-1}) for the energy gap should be made to measure peak positions accurately.[24] The top lead electrode also causes the peak shifts due to the image dipole effect. The peak of the vibrational mode of the adsorbed hydroxyl species on the surface has a large shift. However, it has been shown that the shifts are less than of the order of 0.5 meV (4 cm^{-1}) for the peaks of the benzoate ion on Al_2O_3.[24] Oxley *et al.*[13] suggested that peaks may shift because of parasitic resistances of electrodes and connection leads when two-point probe measurements are carried out.

The resolution of the tunneling spectrum depends on two broadening contributions: modulation voltage broadening and thermal broadening. The tunneling spectrum in Fig. 4 was measured with a modulation voltage of 3 mV peak-to-peak at 4.2 K. The resolution was estimated to be 2.5 meV (20 cm^{-1}) by measuring the narrowest peak width in the spectrum. The peak positions of the spectrum are in good agreement with those of the spectra reported previously[3,8,11,13] as is shown in Table 1. The accuracy of the peak position of our spectrum is estimated to be ±0.5 meV (±4 cm^{-1}). These results show that our apparatus and procedures are suitable for the accurate measurement of a tunneling spectrum.

Table 1. Vibrational frequencies (cm^{-1}) for benzoate ions adsorbed onto Al_2O_3 measured by IETS

This work	Oxley *et al.*[a]	Walmsley *et al.*[b]	Hansma[c]	Korman and Coleman[d]
3058 s		3051	3065 m	
3036 sh		3021	3025 m	
2997 sh		2990		
2895 w b			2888 w	
1598 vs	1602 s	1601	1597 vs	1607
1565 sh	1576 sh	1576		1559
	1550 sh			
1487 m	1497 m	1492	1491 m	1500
1448 sh	1451 sh	1447	1450 sh	1453
1426 s	1430 s	1428	1433 m	1437
1309 m	1308 w	1312		1319
		1178		
1154 s	1157 s	1154	1153 m	1161
		1097		
1073 w	1073 w	1070	1068 vw	1072
1026 w	1025 w	1026	1021 vw	1030
987 s	987 s	987	988 m	994
936 m	936 m	938	936 m	940
	885 w			
843 s	850 s	848	847 m	853
825 sh	824 m	823	823 m	827
720 m	722 m	722	723 m	728
684 vs	686 s	687	686 s	690
616 m	618 m	617	617 m	621
434 s	437 s	440	440 m	440
406 s	402 s	404	406 m	407
301 m			307 w	

vs=very strong, s=strong, m=medium, w=weak, vw=very weak, sh=shoulder, b=broad. a) Ref. 13. b) Ref. 11. c) Ref. 3. d) Ref. 8.

Spectra and Peak Assignments for Isomeric Phthalic Acids. The tunneling spectra of phthalic, isophthalic, and terephthalic acid doped from an ethanol solution of 0.5 mg/ml are shown in Fig. 5. For the sake of comparison, the tunneling spectrum of the ethanol solvent is also shown in the same figure. Evans and Weinberg[25] have reported that ethanol is adsorbed as ethoxide ion onto the alumina surface at room temperature. However, the weak peak intensity in the tunneling spectrum of ethanol shown in Fig. 5 indicates almost no contribution from this solvent to the tunneling spectra of isomeric phthalic acids. The tunneling spectra of methanol and 1-propanol have been measured; it has been found that their peak

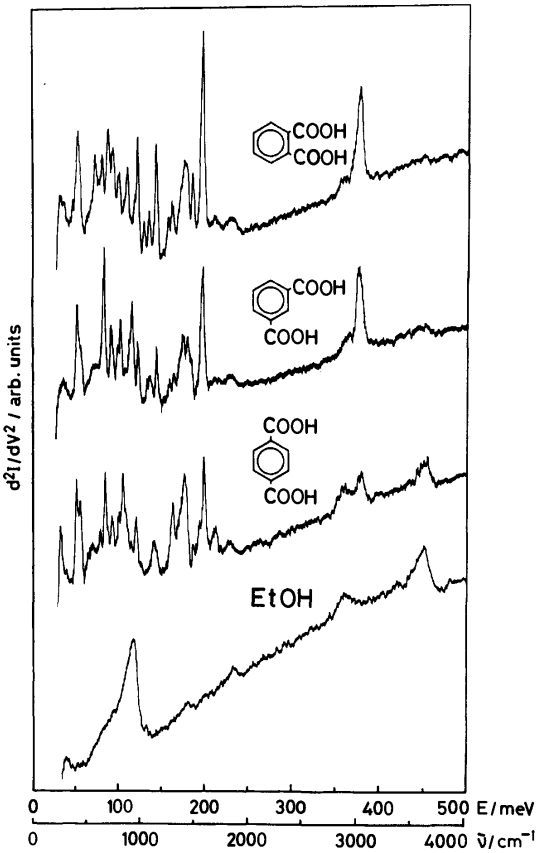

Fig. 5. Tunneling spectra of phthalic, isophthalic and terephthalic acid doped with an ethanol solution of 0.5 mg/ml. Junction resistances: 42—78 Ω; modulation voltage: 3 mVpp; time constant: 10 s; trace times: 145—200 min.

intensity is also weak enough to be neglected. Because the tunneling spectrum reveals both infrared and Raman-active vibrational modes, useful information on the adsorbed molecule is obtained by comparing the tunneling spectrum with its infrared and Raman spectrum.

Phthalic Acid: The tunneling spectrum of phthalic acid has a very weak C=O peak at 1704 cm^{-1}. The weak and broad peak at 3596 cm^{-1} is due to the vibrational mode of the surface OH species, as has been mentioned before. Instead, the tunneling spectrum has a strong symmetric stretching, a medium wagging, and a strong rocking mode of the COO^- groups at 1422, 644, and 422 cm^{-1} respectively. When a carboxylic acid is adsorbed onto the alumina surface as a carboxylate ion, the asymmetric vibrational mode of the COO^- group shares a change in the dipole moment parallel to the surface. The peak intensity of this vibrational mode in the tunneling spectrum is weak because of the orientational selection rule.[8,11] The peak of the asymmetric stretching mode of the COO^- groups of the phthalate ion is considered to be involved in the very strong peak at 1588 cm^{-1}. There is no peak corresponding to the scissoring mode of the COO^- groups. The tunneling spectra of phthalic acid doped with solutions of water, methanol, and 1-propanol

Table 2. Vibrational frequencies (cm^{-1}) and mode assignments for phthalic acid on Al_2O_3 measured by IETS

IETS	Phthalate Ion[a] Infrared	Raman	Assignment
3596 w b			νOH (surface)
3037 s	3025 vw	3025 vw	νCH (20b)
2894 w b			(contamination)
1704 vw			νC=O
1588 vs	1584 s	1582 w	νCC (8a)
1486 m	1478 m	1479 w	νCC (19b)
1422 s b	1418 vs	1420 s	$\nu_s COO^-$
1296 m	1287 w	1288 w	βCH (3)
1260 w	1259 w	1260 w	νCX (7a)
1149 s	1145 w	1146 m	βCH (15)
1081 m	1082 m	1082 vw	βCH (9b)
1035 m	1035 m	1041 s	βCH (18b)
980 s	980 w		γCH (5)
957 sh	956 w		γCH (10a)
881 m	882 w	895 vw	γCH (10b)
802 m	825 s	826 s	νCC (1)
744 m	753 s		γCH (11)
702 m	694 s		γCC (4)
644 m	649 s	654 s	$\gamma_s COO^-$
582 m	579 m	589 vw	βCC (6b)
422 s	423 s	423 m	$\beta_{as} COO^-$
374 sh			?
285 w			Al phonon
259 m		262 w	βCX (9a)

a) Ref. 16.

are identical with that doped with an ethanol solution. The spectrum is also independent of the acid concentration (0.1—1.0 mg/ml). These results show that phthalic acid reacts with Al_2O_3 by loosing the protons of the COOH groups and is adsorbed onto the surface as the benzenedicarboxylate ion.

The peak assignments for the tunneling spectrum are shown in Table 2, together with those for the vibrational modes of the ion obtained by means of infrared and Raman spectroscopy.[16] In this table, stretching vibrations are denoted by ν, in-plane bending modes are designated by β, and out-of-plane bending vibrations perpendicular to the plane, by γ. The symmetric or asymmetric vibration is indicated by the subscript of s or as respectively. Of the bending modes of the COO^- group, β_s designates the scissoring vibration, β_{as} denotes the rocking, and γ_s, the wagging mode. In parenthesis is shown the Wilson number for the normal vibration of the benzene ring.[16,17]

The COO^- groups of the phthalate ion are assumed to be rotated 33° with respect to the plane of the aromatic ring.[16] The phthalate ion has C_s symmetry and 42 normal vibrations, which are classified as 30 ring vibrations and 12 vibrations of the substituents. These modes are both infrared and Raman-active.[16] The ring vibrations are divided into 21 in-plane and 9 out-of-plane vibrations.[17]

Isophthalic Acid: A detailed analysis of the tunneling spectrum and a comparison with the infrared and Raman spectrum show that isophthalic acid is also

Table 3. Vibrational frequencies (cm^{-1}) and mode assignments for isophthalic acid on Al_2O_3 measured by IETS

IETS	Isophthalate Ion[a] Infrared	Raman	Assignment
3621 w b			νOH (surface)
3038 s	3033 vw		νCH (7a)
2888 w b			(contamination)
1684 vw			νC=O
1587 s	1584 sh	1585 m	νCC (8b)
1467 sh	1477 m		νCC (19b)
1441 s	1429 m	1437 s	νCC (19a)
1402 s b	1391 m	1405 s	ν_sCOO$^-$
1311 w	1315 sh		νCC (14)
1281 vw	1262 w		βCH (3)
1151 m	1157 vw	1159 m	βCH (9b)
1088 w	1085 w	1083 w	βCH (18b)
1061 vw	1069 m	1074 vw	βCH (18a)
980 m	980 w		γCH (5)
930 s	932 w		νCX (7b)
824 m	818 m	820 s	νCC (1)
801 sh			?
737 m	733 s		β_sCOO$^-$
672 s	674 w		γCC (4)
582 w b	553 w	555 vw	βCC (6b)
440 sh			?
418 s	401 m	402 vw	β_{as}COO$^-$
294 m b			Al phonon

a) Ref. 16.

adsorbed onto the alumina surface as the benzenedicarboxylate ion. The tunneling spectrum is independent of the solvent used (water, methanol, ethanol, and 1-propanol) and the acid concentration (0.1—1.0 mg/ml). The peak assignments are shown in Table 3, together with those for the vibrational modes of the ion. The tunneling spectrum has a strong ν_s, a medium β_s, and a strong β_{as} COO$^-$ peak at 1402, 737, and 418 cm^{-1} respectively. The ν_{as}COO$^-$ peak is considered to be involved in the strong peak at 1587 cm^{-1}, as in the case of phthalic acid. There is no peak corresponding to the γ_sCOO$^-$ mode.

The isophthalate ion has 42 normal vibrations with C_{2v} symmetry. These vibrations are both infrared and Raman-active, and are classified as 30 ring vibrations and 12 vibrations of the substituents, as in the case of the phthalate ion.[16]

Terephthalic Acid: The tunneling spectrum of terephthalic acid has a medium νOH (3623 cm^{-1}) and a medium νC=O (1699 cm^{-1}) peak. The strong peak at 1423 cm^{-1} is due to the βOH and/or the ν_sCOO$^-$ mode. The peaks at 867, 619, and 436 cm^{-1} are caused by β_s, γ_s, and β_{as} of the COO group for the acid and/or the COO$^-$ group for the ion. The spectrum has a very weak ν_{as}COO$^-$ peak at 1550 cm^{-1}. This finding that the tunneling spectrum of terephthalic acid has the C=O peak and the COO$^-$ peaks indicates the presence of the monocarboxylate ion on the alumina surface. The peak assignments are shown in Table 4 with those for the vibrational modes of terephthalic acid[15] and its ion.[16]

Terephthalic acid and the terephthalate ion with a D_{2h} point group have 48 and 42 normal vibrations respectively. Of these vibrations, 30 are due to ring vibrations. In the case of these molecules, the mutual-exclusion principle holds and a vibrational mode with

Table 4. Vibrational frequencies (cm^{-1}) and mode assignments for terephthalic acid on Al_2O_3 measured by IETS

IETS	Terephthalic Acid[a] Infrared	Raman	Terephthalate Ion[b] Infrared	Raman	Assignment
3623 m b					νOH
3042 m	3066 w			3062 w	νCH (20b, 7b)
2873 w b					(contamination)
1699 m	1682 s b	1632 vs			νC=O
1594 s		1615 s		1597 sh	νCC (8b)
1550 sh			1575 s b	1549 w	ν_{as}COO$^-$
1493 w	1575 m		1497 m		νCC (19a)
1423 s b	1422 s	1452 m	1380 s b	1413 vs	βOH, ν_sCOO$^-$
1302 m	1315 w		1311 w		νCX (13)
1136 m		1126 s		1127 s	βCH (9a)
1003 vw	1018 m		1012 m		βCH (18a)
963 m	997 w			968	γCH (17a)
916 vw				910	γCH (10b)
867 sh	881 m		882 m		β_sCOO, β_sCOO$^-$
839 s		835 s		857 s	νCC (1)
797 vw		804 m			βCH-βCX (18b-15)
736 m	734 s		745 s		βCC (12)
677 s		675 m		707 w	γCC (4)
619 w		635 s	620 w	633 m	γ_sCOO, γ_sCOO$^-$
540 w b	525 m				γCC (16b)
436 s	449 m		449 m		β_{as}COO, β_{as}COO$^-$
400 s			412 w	412 vw	γ_{as}COO$^-$+γCH (5)
298 sh		287 m		277 vw	βCX (9b), Al phonon
242 m		272 s		252 m	γCX (5)

a) Ref. 15. b) Ref. 16.

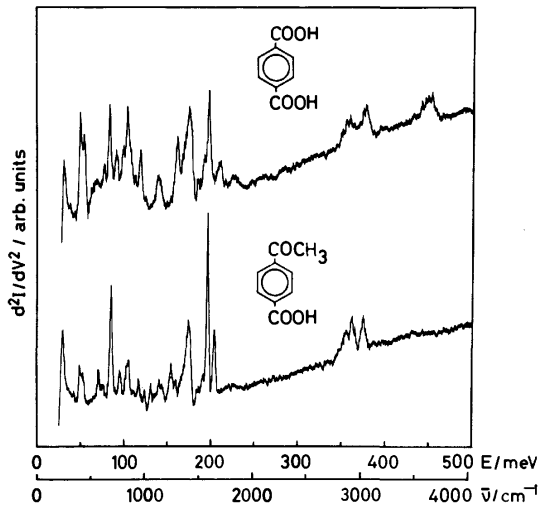

Fig. 6. Tunneling spectrum of *p*-acetylbenzoic acid doped with an ethanol solution of 0.5 mg/ml. Junction resistance: 376 Ω; modulation voltage: 3 mVpp; time constant: 10 s; trace time: 152 min. Tunneling spectrum of terephthalic acid is also shown for a comparison. The relative intensity of the C=O peak of terephthalic acid is similar to that of *p*-acetylbenzoic acid.

a symmetry species appears either in the infrared or Raman spectrum.[15,16] In Table 4, however, this principle is neglected for reasons of simplicity.

Discussion

Comparison of Tunneling Spectrum of Terephthalic and p-*Acetylbenzoic Acid.* Most peaks in the tunneling spectra of isomeric phthalic acids can be clearly identified, and their peak positions agree closely with those of the infrared and Raman spectra. This indicates that the phthalate ions on Al_2O_3 are not strongly perturbed by adsorption. However, these tunneling spectra show a difference in the chemical interaction between the COOH group and the alumina surface. It is found that both phthalic and isophthalic acid react with Al_2O_3 by loosing the protons of two COOH groups and are adsorbed onto the surface as benzenedicarboxylate ions. On the other hand, the tunneling spectrum of terephthalic acid clearly shows the unreacting COOH group, thus indicating the presence of the monocarboxylate ion on the surface. It seems that terephthalic acid is adsorbed onto Al_2O_3 as both the monoanion and the dianion.

The tunneling spectrum of *p*-acetylbenzoic acid (Aldrich Chemicals) is shown in Fig. 6, with that of terephthalic acid. The spectrum of *p*-acetylbenzoic acid has a strong νC=O (1663 cm^{-1}) and νCOO^- (1418 cm^{-1}) peak, showing that this molecule is adsorbed onto Al_2O_3 as the monocarboxylate ion.[26] The relative intensities of the νC=O to the νCOO^- peaks in both the tunneling spectra of terephthalic and *p*-acetylbenzoic acid are similar to each other. This similarity indicates that terephthalic acid is adsorbed predominantly as the monocarboxylate ion onto the Al_2O_3 such as *p*-acetylbenzoic acid.

Oxley *et al.*[13] have previously measured the tunneling spectra of terephthalic acid doped with solutions of both water and ethanol onto Al_2O_3 formed by an oxygen glow discharge. Their spectra, however, have no C=O peak, and they concluded that terephthalic acid is adsorbed onto the surface as the dicarboxylate ion. We examined the experimental conditions in detail and found that the tunneling spectra of terephthalic acid doped with a solution of 1-propanol or methanol onto Al_2O_3 formed by both exposure to oxygen and a glow discharge also have the C=O peak. The relative intensity of the C=O peak is almost independent of the acid concentration (0.01—1.5 mg/ml); this shows saturation coverage. In the case of a methanol solution, however, the relative intensity is somewhat weak. The spectrum from an aqueous solution has the very weak C=O peak. This finding may suggest that terephthalic acid is adsorbed as the dicarboxylate ion when doped with an aqueous solution. It is found that the tunneling spectrum of terephthalic acid strongly depends on the solvent used. Thus, judging from the results of a comparison between the tunneling spectra of terephthalic and *p*-acetylbenzoic acid, we conclude that terephthalic acid is adsorbed predominantly as the monocarboxylate ion onto the alumina surface at almost saturation coverage when doped with either ethanol or 1-propanol solution.

The tunneling spectrum of *p*-acetylbenzoic acid has no νOH peak, but it has the sharp and clear νC=O peak. It seems that the C=O group interacts with neither the adsorbed *p*-acetylbenzoic acid nor the alumina surface. On the other hand, the spectrum of terephthalic acid has the broad νOH and νC=O peak. Judging from the asymmetric tailing of the OH peak and the broadness of the C=O peak, hydrogen bonding seems to be present. Two types of hydrogen bonding seem to be important: hydrogen bonding among the adsorbed hydrogen terephthalate ions and hydrogen bonding between the hydroxylated alumina surface. Because terephthalic acid is adsorbed with its benzene ring nearly perpendicular to the surface at saturation coverage, as will be discussed later, and because it has the unreacting COOH group at the para position, hydrogen bonding among the adsorbed hydrogen terephthalate ions seems to be more important. A similar result has been obtained in the case of diphenol in IETS;[12] both catechol and resorcinol are adsorbed predominantly onto the alumina surface as diphenolate ions, while hydroquinone is adsorbed mainly as the monophenolate ion and extensive hydrogen bonding is observed.

Adsorption and Orientation of Isomeric Phthalic Acids. The adsorption mechanism and orientation of the isomeric phthalic acids on the alumina surface were

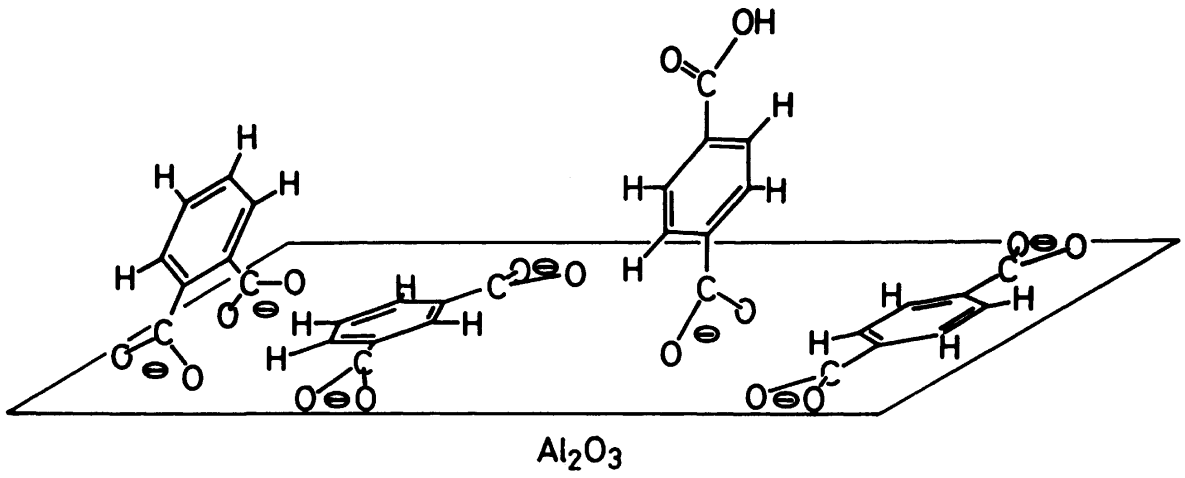

Fig. 7. Schematic representation of the adsorbed isomeric phthalic acids on Al_2O_3. Their dissociation constants in water are also shown.

studied by using a molecular model. A schematic representation of these acids on Al_2O_3 is shown in Fig. 7, with their dissociation constants in water. The isomeric phthalic acids have two carboxyl groups and they dissociate stepwise in water. For phthalic acid, the first dissociation constant is larger and the second is smaller than the others. Thus, phthalic acid may be expected to be adsorbed mainly as the monocarboxylate ion, if a similar tendency in the difference of dissociation constants holds in alcohol solutions. However, the tunneling spectra show that the structures of these acids adsorbed onto the surface are not explained by their dissociation constants; both phthalic and isophthalic acid are adsorbed mainly as dicarboxylate ions, while terephthalic acid is adsorbed predominantly as monocarboxylate ion. This finding indicates a difference in the geometry of the interaction between the alumina surface and the COOH groups of the adsorbed isomeric phthalic acids.

In the cases of phthalic and isophthalic acid, when they are adsorbed at one of the COOH groups, the other groups seem to be very close to the surface. Thus, the COOH group dissociates more easily than would be expected from their second dissociation constants. The tunneling spectra of these acids are independent of the solvent and their concentrations. These acids are considered to be adsorbed at saturation coverage. It seems that the benzene ring of the phthalate ion has a relatively large angle with respect to the surface, even if the COO^- groups are rotated, since the carbon and hydrogen atoms of the ring are not expected to interact with the alumina surface. On the other hand, because of the molecular model, the ring of the isophthalate ion is considered to be nearly parallel to the surface. The close agreement of the peak positions of the benzene ring of the tunneling spectrum of the isophthalate ion with those of the infrared and Raman spectrum shows that the ring has almost no interaction with the surface. A comparison of the tunneling spectra of the two acids indicates that the peak intensity of the out-of-plane and in-plane ring vibrational modes are comparable: Vibrations 4, 11, 10b, 5 (out-of-plane) and 6b, 1 (in-plane) for phthalic acid, and Vibrations 4, 5 (out-of-plane) and 1, 7b (in-plane) for isophthalic acid. This finding is unexpected in view of the orientational selection rule.

Kirtley and Hall[27] have calculated the peak intensity of the tunneling spectrum of the methanesulfonate ion adsorbed onto Al_2O_3 by using a transfer Hamiltonian theory. They have found that the calculated peak intensity depends strongly on the distance of the dipole from the Pb electrode; the orientational selection rule is favorable for a mode vibrating perpendicular to the surface when molecules are situated close to the interface. However, this rule does not hold for molecules deep within the insulator. Though no such calculation has been done for isomeric phthalic acids, it seems that the result of Kirtley and Hall is applicable qualitatively to the benzenedicarboxylate ions. Because the benzene rings of adsorbed phthalate and isophthalate ion are at some distance from the interface of the Pb electrode, the orientational selection rule is not expected to hold strictly. These results suggest that care must be taken to use the selection rule in discussing the orientation of the adsorbed species in tunneling spectroscopy.

In the case of terephthalic acid, since the molecule has the COOH groups at the para position, the molecule must fall and become parallel to the surface in order to be adsorbed as the dicarboxylate ion. If this process takes a longer time than the first process of

adsorption, many molecules will remain on the surface as monocarboxylate ions. The tunneling spectra doped with various alcohol solutions are independent of their concentrations and indicate saturation coverage. Langan and Hansma[28] have measured the surface concentration of the adsorbed benzoate ion on Al_2O_3. They have reported that this molecule occupies an area of 15 Å^2 at saturation coverage. This area is almost equal to that calculated from the diameter of the benzene ring (5 Å). According to this result, the adsorbed hydrogen terephthalate ion is also considered to occupy the same area of the surface and thus can not fall at saturation coverage. Therefore, the terephthalic acid remains on the surface as the monocarboxylate ion. The observed hydrogen bonding also supports the predominance of the hydrogen terephthalate ion on the surface.

Concluding Remarks. The detailed analysis of the vibrational spectra of the isomeric phthalic acids adsorbed onto Al_2O_3 from alcohol solutions makes it possible to clarify the difference in chemical interaction between the COOH group and the surface. This difference is caused by their orientations and the different probabilities of chemical interaction between the COOH group and the surface. These results suggest the importance of the orientation of adsorbed species for their reactivity and selectivity on an alumina catalyst. Inelastic electron tunneling spectroscopy is a useful analytical tool for investigating the adsorbed species on the oxide surface and their chemical interaction with it.

The authors wish to thank Professor Dr. Hirochika Enokiya of the Faculty of Science for his help in preparing liquid helium for our use. The authors also wish to thank Dr. Siegfried Ewert of Technische Hochschule Aachen (Fed. Rep. of Germany) for his valuable comments. The present study was partially supported by a Grant-in-Aid for Scientific Reserch No. 59750622 from the Ministry of Education, Science and Culture.

References

1) R. C. Jaklevic and J. Lambe, *Phys. Rev. Lett.*, **17**, 1139 (1966); *Phys. Rev.*, **165**, 821 (1968).
2) R. G. Keil, T. P. Graham, and K. P. Roenker, *Appl. Spectrosc.*, **30**, 1 (1976).
3) P. K. Hansma, *Phys. Rep.*, **C30**, 145 (1977).
4) W. H. Weinberg, *Ann. Rev. Phys. Chem.*, **29**, 115 (1978).
5) T. Wolfram, "Inelastic Electron Tunneling Spectroscopy," Springer-Verlag, Berlin Heidelberg New York (1978).
6) S. Ewert, *Appl. Phys.*, **A26**, 63 (1981).
7) P. K. Hansma, "Tunneling Spectroscopy," Plenum, New York (1982).
8) C. S. Korman and R. V. Coleman, *Phys. Rev.*, **B15**, 1877 (1977).
9) I. W. N. McMorris, N. M. D. Brown, and D. G. Walmsley, *J. Chem. Phys.*, **66**, 3952 (1977).
10) J. T. Hall and P. K. Hansma, *Surf. Sci.*, **71**, 1 (1978).
11) D. G. Walmsley, W. J. Nelson, N. M. D. Brown, and R. B. Floyd, *Appl. Surf. Sci.*, **5**, 107 (1980).
12) B. F. Lewis, W. M. Bowser, J. L. Horn, T. Luu, and W. H. Weinberg, *J. Vac. Sci. Technol.*, **11**, 262 (1974); W. H. Weinberg, W. M. Bowser, and B. F. Lewis, *Japan J. Appl. Phys. Suppl.* **2**, Pt. 2, 863 (1974).
13) D. P. Oxley, A. J. Bowles, C. C. Horley, A. J. Langley, R. G. Pritchard, and D. L. Tunnicliffe, *Surf. Interface Anal.*, **2**, 31 (1980).
14) H. Monjushiro, K. Murata, and S. Ikeda, *Bull. Chem. Soc. Jpn.*, **57**, 2428 (1984).
15) J. F. Arenas and J. I. Marcos, *Spectrochim. Acta, Part A*, **36**, 1075 (1980).
16) J. F. Arenas and J. I. Marcos, *Spectrochim. Acta, Part A*, **35**, 355 (1979).
17) G. Varsányi, "Assignments for Vibrational Spectra of Seven Hundred Benzene Derivatives," Adam Hilger, London (1974).
18) G. H. Posner, *Angew. Chem., Int. Ed. Engl.*, **17**, 487 (1978).
19) S. Kamata and M. Higo, *Chem. Lett.*, **1984**, 2017.
20) J. L. Miles and P. H. Smith, *J. Electrochem. Soc.*, **110**, 1240 (1963).
21) J. G. Adler and J. E. Jackson, *Rev. Sci. Instrum.*, **37**, 1049 (1966).
22) W. M. Bowser and W. H. Weinberg, *Surf. Sci.*, **64**, 377 (1977).
23) G. Gauthier, S. de Cheveigné, J. Klein, and M. Belin. *Phys. Rev.*, **B29**, 1748 (1984).
24) J. Kirtley and P. K. Hansma, *Phys. Rev.*, **B13**, 2910 (1976).
25) H. E. Evans and W. H. Weinberg, *J. Chem. Phys.*, **71**, 1537 (1979).
26) C. S. Korman, J. C. Lau, A. M. Johnson, and R. V. Coleman, *Phys. Rev.*, **B19**, 994 (1979).
27) J. Kirtley and J. T. Hall, *Phys. Rev.*, **B22**, 848 (1980).
28) J. D. Langan and P. K. Hansma, *Surf. Sci.*, **52**, 211 (1975).

Syntheses and Crystal and Molecular Structure of [Hexaaquabis-(2-naphthalenesulfonato)lanthanoid(III)] 2-Naphthalenesulfonate Trihydrate, $[Ln(C_{10}H_7SO_3)_2(H_2O)_6](C_{10}H_7SO_3)\cdot 3H_2O$ (Ln=Pr, Nd, Sm, Eu, Gd, Dy, Er, and Yb)

Yoshiyuki OHKI,† Yasuo SUZUKI,† Masao NAKAMURA, Mamoru SHIMOI, and Akira OUCHI*
Department of Chemistry, College of Arts and Sciences, The University of Tokyo, Komaba, Meguro-ku, Tokyo 153
†*Department of Industrial Chemistry, Faculty of Engineering, Meiji University, Higashi-Mita, Tama-ku, Kawasaki, Kanagawa 214*
(Received April 26, 1985)

Eight isomorphous 2-naphthalenesulfonato complexes of lanthanoids(III) (Pr, Nd, Sm, Eu, Gd, Dy, Er, and Yb) were synthesized, and the structures of five of them were determined by the single-crystal X-ray-diffraction method. They are monoclinic, with the space group of $P2_1$; the cell constants of the Pr^{III} complex, for example, were $a=18.228(8)$, $b=7.498(4)$, $c=14.177(9)$ Å, $\beta=107.75(4)°$, $Z=2$, and its final R value was 0.043. The unit-cell size of the complex decreases with the increase in the atomic number of the metal atom. The central metal atom is in a square-antiprism geometry and is octa-coordinated with two unidentate 2-naphthalenesulfonato ligands and six water-oxygen atoms. Nonligated oxygen atoms of the sulfonato ions form hydrogen-bonds with the coordinated and lattice water molecules to form a double-layered network along the ab-plane. All the naphthalene rings stand together to form hydrophobic sheets between the hydrogen-bonding networks.

It has already been reported by several authors that the carboxylato or the oxoacid-anionic ligands are coordinated to the metal atoms in a variety of ways, especially in their lanthanoid complexes. In the cases of carboxylato ligands, they act not only as unidentate, but also as bidentate chelating or bridging ligands.[1-5] In the case of the sulfato complexes, the ligands act as bridging ligands or as the chelating bidentate.[6,7] Therefore, it is very interesting to examine the coordination geometry of some sulfonates of lanthanoid(III). The structure of the lanthanoid(III) ethyl sulfate enneahydrates has already been clarified.[8,9] In their crystals, not the ethyl sulfate ions but nine water molecules are ligated to the central metal atom, and the sulfate anions as well as the water molecules, including the coordinated ones, are linked by the network of hydrogen bonds.

This time, we have succeeded in obtaining the title complexes in the crystalline state. Therefore, we have tried to determine their structures by the single-crystal X-ray-diffraction method: not only the structure of one complex, but also a series of isomorphous ones were investigated comparatively, especially with regard to the changes resulting from the increase in the atomic number of the central metal atom.

Experimental

Synthesis of [Hexaaquabis(2-naphthalenesulfonato)praseodymium(III)] 2-Naphthalenesulfonate Trihydrate. Praseodymium(III) chloride hexahydrate (1.0 g, 2.8 mmol) and sodium 2-naphthalenesulfonate (2.1 g, 9.1 mmol) were dissolved in about 20 cm^3 of a warmed ethanol-water mixed solvent (2:1=v/v), after with the solution was stirred and filtered while it was hot. When the filtrate has cooled, the complex was deposited, and the product was collected and washed by the mixed solvent, ethanol, and diethyl ether, in that order. The yield was 1.5 g on the average (1.6 mmol, 58%). The neodymium, samarium, europium, gadolinium, dysprosium, erbium, and ytterbium complexes were also obtained in almost the same way; the yields were about 60% on the average. The complexes thus obtained could be recrystallized from the ethanol-water (2:1=v/v) mixed solvent. The crystals used for the single-crystal X-ray-diffraction method were those deposited from the 2-propanol-water (2:1=v/v) mixed solvent solution, which had been left standing in open vessels over a silica-gel desiccator at the ambient temperature. Attempts to obtain the lanthanum(III) and cerium(III) complexes using the same operation were not successful, probably because the stable forms of their complexes are different from those of the heavier lanthanoids. The europium(III) complex is colorless, implying that there is no charge-transfer band such as is observed in some *O,O'*-dialkyl dithiophosphates of the metal.[10] Anal. ($MC_{30}H_{39}O_{48}S_3$) M, C, H. (M=Pr, Nd, Sm, Eu, Gd, Dy, Er, and Yb).

Single-crystal X-Ray Analyses. All of these complexes were found to be isostructural from their X-ray powder patterns; the structures of five complexes (M=Pr, Eu, Gd, Er, and Yb) were determined by the single-crystal X-ray-diffraction method. They are monoclinic, space group $P2_1$, $Z=2$; their other crystallographic data are shown in Table 1, together with some experimental conditions and the final R values, obtained by applying the anisotropic thermal parameters to all the non-hydrogen atoms.[11]

The reflections in the ranges shown in Table 1 were collected on a Rigaku AFC-6A automated four-circle X-ray diffractometer with graphite-monochromated Mo$K\alpha$ radiation (the scan speed was 4°min^{-1}), the ω—2θ scan technique being employed; the scan widths were $(1.03+0.5\tan\theta)°$ for the praseodymium, europium, and ytterbium complexes, $(1.05+0.5\tan\theta)°$ for the samarium complex, and $(1.37+0.5\tan\theta)°$ for the erbium complex. The intensities were corrected for Lorentz and polarization factors, but not for absorption and extinction. Reflections with $|F_o|>3\sigma(|F_o|)$ were used for refinements.

Structure Determination. The structure of the praseodymium(III) complex was solved by the heavy-atom

TABLE 1. CRYSTALLOGRAPHIC DATA OF THE $[M(C_{10}H_7SO_3)_2(H_2O)_6](C_{10}H_7SO_3)\cdot 3H_2O$ COMPLEXES

M=	Pr	Eu	Gd	Er	Yb
F.W.	924.7	935.7	941.1	951.1	956.9
$a(l/Å)$	18.228(8)	18.148(9)	18.150(13)	18.095(4)	18.069(7)
$b(l/Å)$	7.498(4)	7.467(3)	7.465(3)	7.439(2)	7.427(3)
$c(l/Å)$	14.177(10)	14.096(8)	14.084(9)	14.033(7)	13.993(14)
$\beta(\phi/°)$	107.75(4)	107.73(5)	107.82(7)	107.78(3)	107.83(5)
$V(v/Å^3)$	1845.5(19)	1819.4(17)	1816.8(20)	1798.6(11)	1787.8(21)
$D_m(d/Mg\,m^{-3})$	1.65(3)	1.73(3)	1.71(3)	1.75(3)	1.77(3)
$D_x(d/Mg\,m^{-3})$	1.66	1.71	1.72	1.76	1.78
μ(Mo $K\alpha$)(n/mm^{-1})	1.57	1.98	2.13	2.67	3.01
Number of reflections measured	5811	4537	5712	5662	5626
Reflection used for the calculation	4993	3823	5413	5011	4887
Measured range ($\phi/°$)	3—60	3—55	3—60	3—60	3—60
R	0.043	0.054	0.033	0.043	0.043
R value with inverse chirality	0.045	0.055	0.037	0.047	0.045
Size of the crystal used (v/mm^3)	0.25×0.20× 0.08	0.21×0.23× 0.10	0.28×0.25× 0.15	0.25×0.25× 0.12	0.25×0.25× 0.10

method. The positions of the metal and some sulfur atoms were deduced from the three-dimensional Patterson map. The positional and thermal parameters were refined successively by the repeated block-diagonal least-squares method and by the Fourier syntheses.

At the end, all the non-hydrogen atoms were found. The positions of the naphthalene hydrogen atoms were calculated by assuming the C-H bond-length to be 1.08 Å; their B_{iso}'s were assumed to be 6.0. The parameters of the hydrogen atoms were fixed in the refinement.

The structures of the other isomorphous complexes were solved by starting with the parameters of the praseodymium(III) complex. As the crystals have no center of symmetry, refinements using inverse chirality were also carried out. For each complex, we adopted the chirality which gave a lower R-value; the respective final R-values for the alternate chirality are also shown in Table 1. According to our selection, europium and gadolinium complexes can be expected to have the structure opposite to that of the other three.

All the calculations were carried out on a HITAC M-280H apparatus at the Computer Center of The University of Tokyo, using the local version of the UNICS program.[12] The atomic-scattering factors were taken from Ref. 13.

Other Measurements. The X-ray powder patterns of these complexes were obtained by the use of a diffractometer, Model DX-GO-F JEOL, using Cu $K\alpha$ radiation in the range from 4° to 30° in 2θ. Their infrared absorption spectra were obtained by means of a JASCO A-202 grating infrared spectrophotometer, using Nujol and hexachloro-1,3-butadiene mull.

Results and Discussion

The final atomic parameters of the complexes are listed in Table 2 (1—5), while some bond lengths and angles as well as some interatomic distances, which are thought to be the hydrogen-bonding ones, are tabulated in Table 3.[14] A perspective drawing of the praseodymium(III) complex around the central

TABLE 2. FINAL ATOMIC COORDINATES (×10^4), WITH ESTIMATED STANDARD DEVIATIONS IN PARENTHESES, AND THEIR EQUIVALENT ISOTROPIC TEMPERATURE FACTORS (B_{eq}/Å^2)

1) [Hexaaquabis(2-naphthalenesulfonato) praseodymium(III)] 2-Naphthalenesulfonate Trihydrate

Atom	x	y	z	B_{eq}/Å^2[a]
Pr	7227.9(2)	7500	5049.1(2)	1.8_1
S(1)	6068(1)	4470(3)	3160(1)	2.3_9
S(2)	6991(1)	11019(3)	6814(1)	2.4_4
S(3)	9585(1)	5042(3)	3319(1)	2.6_0
O(1)	6764(3)	5484(8)	3692(4)	3.0_8
O(2)	6109(3)	2659(13)	3545(4)	3.5_7
O(3)	5370(3)	5391(9)	3151(4)	3.2_6
O(4)	6808(3)	9463(8)	6158(4)	3.0_8
O(5)	6359(3)	12293(11)	6553(4)	3.4_4
O(6)	7724(3)	11837(8)	6853(4)	3.3_5
O(7)	8816(3)	4495(9)	3302(4)	3.6_7
O(8)	9877(4)	6553(10)	3939(4)	4.7_5
O(9)	10129(3)	3568(9)	3568(5)	4.3_6
O(W1)	8279(3)	7218(12)	4271(4)	4.3_7
O(W2)	8380(3)	8967(8)	6171(4)	3.2_5
O(W3)	7992(3)	4974(8)	5923(4)	3.5_9
O(W4)	5891(3)	8408(8)	4147(4)	3.1_3
O(W5)	7314(3)	10344(9)	4231(5)	4.3_1
O(W6)	6388(3)	5662(8)	5762(4)	3.7_7
O(W7)	4821(3)	6361(9)	5350(4)	3.9_1
O(W8)	9495(4)	4928(10)	6199(7)	6.2_2
O(W9)	8797(4)	11130(10)	4270(5)	4.9_0
C(1)	5473(4)	4865(11)	1169(6)	2.5_6
C(2)	6068(4)	4315(10)	1933(5)	2.2_2
C(3)	6754(4)	3524(11)	1776(5)	2.6_3
C(4)	6773(4)	3335(12)	824(6)	2.9_3
C(5)	6135(4)	3862(10)	0(5)	2.3_6
C(6)	6138(5)	3633(12)	−987(6)	3.2_9
C(7)	5518(5)	4089(12)	−1761(6)	3.3_5
C(8)	4854(5)	4847(13)	−1580(6)	3.3_8
C(9)	4845(5)	5107(12)	−637(6)	3.1_4
C(10)	5484(4)	4643(10)	186(5)	2.3_2
C(11)	7731(4)	10557(11)	8767(6)	2.7_3
C(12)	7074(4)	10194(10)	8001(5)	2.4_5
C(13)	6458(4)	9178(12)	8126(6)	2.9_8
C(14)	6502(4)	8583(12)	9046(6)	3.0_4
C(15)	7141(4)	8962(11)	9885(5)	2.9_1

Table 2. (Continued)

1) [Hexaaquabis(2-naphthalenesulfonato) praseodymium(III)] 2-Naphthalenesulfonate Trihydrate

Atom	x	y	z	B_{eq}/Å$^{2a)}$
C(16)	7181(6)	8424(13)	10846(6)	4.2$_1$
C(17)	7812(7)	8864(16)	11636(7)	5.2$_2$
C(18)	8426(5)	9847(16)	11497(6)	4.6$_5$
C(19)	8413(5)	10361(14)	10576(6)	3.8$_1$
C(20)	7770(4)	9964(11)	9738(5)	2.8$_3$
C(21)	8903(4)	5247(11)	1333(5)	2.7$_4$
C(22)	9531(4)	5688(10)	2105(5)	2.4$_1$
C(23)	10147(4)	6702(11)	1949(6)	2.9$_6$
C(24)	10117(4)	7159(11)	1029(6)	3.2$_6$
C(25)	9489(4)	6717(11)	199(6)	3.0$_2$
C(26)	9449(5)	7194(14)	−771(6)	4.1$_0$
C(27)	8829(7)	6700(15)	−1561(7)	5.1$_2$
C(28)	8221(6)	5742(15)	−1401(7)	4.3$_1$
C(29)	8230(5)	5287(13)	−470(6)	3.6$_5$
C(30)	8871(4)	5733(11)	354(5)	2.7$_6$

2) [Hexaaquabis(2-naphthalenesulfonato) europium(III)] 2-Naphthalenesulfonate Trihydrate

Atom	x	y	z	B_{eq}/Å$^{2a)}$
Eu	2772.4(4)	2500	4957.7(5)	1.5$_9$
S(1)	3919(2)	5538(5)	6820(3)	2.0$_7$
S(2)	3008(2)	−992(5)	3212(3)	2.1$_4$
S(3)	415(2)	4991(6)	6671(3)	2.4$_2$
O(1)	3228(6)	4479(16)	6307(8)	2.6$_6$
O(2)	3879(7)	7401(30)	6417(8)	3.6$_7$
O(3)	4635(6)	4656(18)	6823(8)	3.0$_9$
O(4)	3193(7)	608(16)	3868(7)	2.7$_5$
O(5)	3648(6)	−2234(22)	3467(7)	2.9$_3$
O(6)	2259(7)	−1793(16)	3202(8)	3.2$_1$
O(7)	1193(6)	5514(17)	6679(8)	2.9$_9$
O(8)	114(9)	3454(20)	6040(9)	5.0$_9$
O(9)	−131(7)	6466(19)	6397(10)	3.9$_0$
O(W1)	1750(6)	2828(22)	5735(8)	3.5$_5$
O(W2)	1632(6)	1071(17)	3857(8)	2.8$_9$
O(W3)	2024(6)	5061(17)	4102(9)	3.1$_4$
O(W4)	4094(6)	1646(16)	5829(8)	2.6$_8$
O(W5)	2696(8)	−239(18)	5771(10)	4.2$_6$
O(W6)	3586(6)	4299(15)	4276(8)	2.7$_6$
O(W7)	5168(6)	3687(18)	4650(9)	3.4$_5$
O(W8)	524(8)	5124(20)	3848(13)	5.5$_4$
O(W9)	1222(7)	−1074(21)	5731(10)	4.5$_1$
C(1)	4524(9)	5123(21)	8800(11)	2.0$_5$
C(2)	3905(8)	5692(20)	8062(10)	1.8$_5$
C(3)	3244(9)	6494(23)	8214(11)	2.4$_8$
C(4)	3231(9)	6715(24)	9163(12)	2.5$_8$
C(5)	3863(8)	6144(22)	9994(11)	2.2$_2$
C(6)	3859(10)	6411(23)	10994(12)	2.7$_8$
C(7)	4483(10)	5903(26)	11780(12)	3.1$_3$
C(8)	5135(10)	5180(25)	11607(12)	3.0$_6$
C(9)	5170(10)	4935(22)	10635(12)	2.8$_3$
C(10)	4509(9)	5408(21)	9810(12)	2.2$_1$
C(11)	2273(9)	−522(22)	1256(11)	2.3$_6$
C(12)	2915(8)	−161(21)	2024(10)	1.9$_0$
C(13)	3533(9)	822(24)	1895(12)	2.5$_0$
C(14)	3508(10)	1454(24)	949(12)	3.0$_7$
C(15)	2862(9)	1079(24)	115(12)	2.8$_2$
C(16)	2818(12)	1630(30)	−859(13)	4.1$_7$
C(17)	2206(12)	1105(31)	−1638(14)	4.3$_1$
C(18)	1578(11)	163(31)	−1513(13)	3.9$_9$
C(19)	1561(13)	−345(31)	−545(14)	4.7$_5$
C(20)	2215(9)	54(21)	278(12)	2.5$_5$
C(21)	1094(9)	4747(22)	8665(11)	2.3$_8$
C(22)	474(8)	4292(22)	7887(11)	2.1$_8$

2) [Hexaaquabis(2-naphthalenesulfonato) europium(III)] 2-Naphthalenesulfonate Trihydrate

Atom	x	y	z	B_{eq}/Å$^{2a)}$
C(23)	−158(9)	3362(23)	8049(12)	2.7$_2$
C(24)	−118(9)	2875(23)	8964(12)	3.0$_1$
C(25)	496(9)	3278(22)	9822(11)	2.4$_3$
C(26)	578(10)	2860(20)	10789(12)	3.1$_6$
C(27)	1204(13)	3326(28)	11565(13)	4.4$_9$
C(28)	1756(12)	4234(28)	11438(13)	3.9$_5$
C(29)	1793(10)	4744(25)	10467(13)	3.1$_3$
C(30)	1137(10)	4328(22)	9639(11)	2.6$_0$

3) [Hexaaquabis(2-naphthalenesulfonato) gadolinium(III)] 2-Naphthalenesulfonate Trihydrate

Atom	x	y	z	B_{eq}/Å$^{2a)}$
Gd	2773.3(1)	2500	4959.8(1)	1.6$_0$
S(1)	3917(1)	5528(2)	6815(1)	2.1$_3$
S(2)	3003(1)	−996(2)	3219(1)	2.1$_7$
S(3)	420(1)	4979(2)	6665(1)	2.3$_8$
O(1)	3224(2)	4483(6)	6295(3)	2.6$_3$
O(2)	3867(3)	7345(9)	6417(3)	3.3$_4$
O(3)	4630(2)	4645(7)	6824(3)	2.8$_0$
O(4)	3185(2)	570(6)	3885(3)	2.7$_6$
O(5)	3641(2)	−2264(8)	3486(3)	3.1$_7$
O(6)	2262(3)	−1818(6)	3178(3)	2.9$_5$
O(7)	1190(2)	5540(7)	6693(3)	3.1$_5$
O(8)	134(3)	3442(8)	6040(3)	4.3$_5$
O(9)	−135(3)	6432(7)	6400(4)	4.0$_0$
O(W1)	1750(2)	2820(8)	5724(3)	3.6$_9$
O(W2)	1640(2)	1108(7)	3863(3)	2.7$_6$
O(W3)	2024(2)	4973(7)	4107(4)	3.2$_7$
O(W4)	4076(2)	1612(6)	5828(3)	2.7$_9$
O(W5)	2689(3)	−251(7)	5778(4)	3.9$_7$
O(W6)	3587(2)	4298(6)	4261(4)	3.1$_6$
O(W7)	5163(3)	3663(8)	4640(4)	3.7$_2$
O(W8)	513(3)	5091(8)	3816(5)	5.5$_8$
O(W9)	1213(3)	−1064(8)	5742(4)	4.4$_3$
C(1)	4516(3)	5143(8)	8815(4)	2.2$_4$
C(2)	3902(3)	5698(8)	8057(4)	2.1$_5$
C(3)	3238(3)	6469(9)	8217(4)	2.4$_4$
C(4)	3221(3)	6690(9)	9173(4)	2.7$_4$
C(5)	3860(3)	6150(8)	10003(4)	2.3$_6$
C(6)	3869(4)	6387(10)	10997(5)	2.9$_6$
C(7)	4486(4)	5913(11)	11766(5)	3.4$_5$
C(8)	5149(4)	5177(10)	11584(5)	3.2$_7$
C(9)	5157(4)	4891(9)	10635(4)	2.7$_7$
C(10)	4513(3)	5377(8)	9812(4)	2.1$_5$
C(11)	2271(3)	−528(8)	1250(4)	2.3$_7$
C(12)	2920(3)	−164(8)	2021(4)	2.1$_1$
C(13)	3545(3)	830(9)	1900(4)	2.6$_3$
C(14)	3497(4)	1437(9)	965(5)	2.9$_9$
C(15)	2858(4)	1044(9)	137(4)	2.7$_0$
C(16)	2814(5)	1591(11)	−852(5)	4.0$_6$
C(17)	2191(5)	1133(13)	−1642(5)	4.6$_9$
C(18)	1560(5)	166(13)	−1497(5)	4.4$_6$
C(19)	1586(4)	−359(11)	−557(5)	3.6$_9$
C(20)	2234(3)	61(9)	277(4)	2.5$_7$
C(21)	1094(3)	4780(8)	8661(4)	2.5$_5$
C(22)	465(3)	4319(8)	7884(4)	2.2$_9$
C(23)	−148(3)	3332(9)	8036(5)	2.7$_2$
C(24)	−125(3)	2840(9)	8977(5)	3.0$_3$
C(25)	511(4)	3304(9)	9811(4)	2.7$_7$
C(26)	556(4)	2829(10)	10800(5)	3.5$_0$
C(27)	1168(5)	3325(11)	11579(5)	4.3$_2$
C(28)	1791(4)	4268(12)	11425(5)	3.8$_1$
C(29)	1776(4)	4736(11)	10482(5)	3.4$_7$
C(30)	1127(3)	4288(8)	9647(4)	2.5$_3$

TABLE 2. (Continued)

4) [Hexaaquabis(2-naphthalenesulfonato) erbium(III)] 2-Naphthalenesulfonate Trihydrate

Atom	x	y	z	B_{eq}/Å$^{2a)}$
Er	7226.3(2)	7500	5031.8(2)	1.48
S(1)	6092(1)	4479(3)	3203(2)	1.99
S(2)	6998(1)	10986(3)	6755(2)	2.05
S(3)	9579(1)	5013(4)	3342(2)	2.22
O(1)	6787(4)	5548(11)	3730(5)	2.57
O(2)	6145(4)	2671(16)	3602(5)	3.14
O(3)	5383(4)	5350(11)	3205(5)	2.77
O(4)	6823(4)	9410(10)	6095(5)	2.55
O(5)	6361(4)	12267(12)	6486(5)	2.95
O(6)	7735(4)	11810(10)	6783(5)	2.88
O(7)	8810(4)	4437(11)	3322(5)	3.06
O(8)	9858(6)	6570(12)	3961(6)	4.52
O(9)	10144(4)	3553(11)	3615(6)	3.63
O(W1)	8230(4)	7171(11)	4294(5)	3.20
O(W2)	8344(4)	8844(10)	6122(5)	2.52
O(W3)	7962(4)	5055(10)	5849(6)	3.01
O(W4)	5941(4)	8411(10)	4161(4)	2.36
O(W5)	7308(4)	10191(11)	4220(6)	3.58
O(W6)	6432(4)	5748(10)	5742(5)	2.84
O(W7)	4847(4)	6334(12)	5366(6)	3.67
O(W8)	9471(4)	4912(12)	6170(8)	4.81
O(W9)	8784(5)	11017(13)	4267(6)	4.26
C(1)	5492(5)	4854(13)	1200(6)	1.97
C(2)	6107(5)	4304(13)	1959(6)	2.07
C(3)	6770(5)	3522(14)	1792(7)	2.38
C(4)	6785(5)	3308(14)	841(7)	2.50
C(5)	6140(5)	3854(12)	5(6)	2.02
C(6)	6141(6)	3614(15)	−1002(7)	2.81
C(7)	5517(7)	4072(16)	−1776(7)	3.11
C(8)	4852(6)	4800(16)	−1597(7)	3.09
C(9)	4840(6)	5089(15)	−647(7)	2.73
C(10)	5492(5)	4633(12)	199(7)	2.02
C(11)	7731(5)	10514(14)	8738(7)	2.39
C(12)	7085(5)	10152(13)	7953(6)	1.92
C(13)	6456(5)	9152(14)	8081(7)	2.33
C(14)	6495(6)	8560(14)	9017(8)	2.86
C(15)	7147(6)	8961(15)	9865(7)	2.59
C(16)	7192(7)	8398(16)	10842(8)	3.65
C(17)	7806(8)	8871(18)	11641(8)	4.06
C(18)	8441(7)	9842(20)	11495(8)	4.04
C(19)	8425(6)	10358(17)	10557(8)	3.18
C(20)	7773(5)	9946(14)	9716(7)	2.37
C(21)	8904(5)	5224(14)	1333(7)	2.33
C(22)	9534(5)	5668(13)	2122(7)	2.18
C(23)	10157(5)	6664(15)	1962(7)	2.63
C(24)	10128(5)	7161(12)	1031(8)	2.72
C(25)	9494(5)	6692(14)	189(7)	2.42
C(26)	9452(6)	7193(16)	−796(8)	3.32
C(27)	8830(8)	6683(18)	−1596(8)	4.02
C(28)	8206(7)	5722(19)	−1430(8)	3.63
C(29)	8220(6)	5267(16)	−483(7)	3.13
C(30)	8872(5)	5696(13)	350(6)	2.07

5) [Hexaaquabis(2-naphthalenesulfonato) ytterbium(III)] 2-Naphthalenesulfonate Trihydrate

Atom	x	y	z	B_{eq}/Å$^{2a)}$
Yb	7726.4(2)	7500	5028.4(2)	1.65
S(1)	6098(1)	4500(3)	3212(2)	2.21
S(2)	7000(1)	11003(3)	6743(2)	2.23
S(3)	9579(1)	5028(3)	3349(2)	2.44
O(1)	6786(3)	5571(10)	3734(5)	2.80
O(2)	6155(4)	2672(17)	3618(5)	3.56
O(3)	5383(3)	5375(10)	3199(5)	2.88
O(4)	6822(4)	9439(9)	6082(4)	2.75
O(5)	6362(4)	12271(12)	6472(5)	3.18
O(6)	7738(4)	11830(9)	6790(5)	3.15
O(7)	8809(4)	4460(11)	3317(5)	3.17
O(8)	9863(5)	6563(12)	3968(5)	4.79
O(9)	10143(4)	3595(11)	3623(6)	3.95
O(W1)	8229(4)	7180(9)	4274(5)	2.95
O(W2)	8332(3)	8867(9)	6097(5)	2.62
O(W3)	7960(4)	5113(9)	5857(5)	3.18
O(W4)	5954(3)	8413(9)	4180(4)	2.50
O(W5)	7311(4)	10197(10)	4207(6)	3.64
O(W6)	6435(4)	5768(9)	5723(5)	3.15
O(W7)	4849(4)	6362(11)	5363(5)	3.65
O(W8)	9471(4)	4912(12)	6158(7)	4.96
O(W9)	8773(4)	11059(12)	4255(6)	4.44
C(1)	5493(5)	4877(12)	1192(7)	2.34
C(2)	6105(5)	4354(12)	1965(6)	2.05
C(3)	6778(5)	3562(13)	1794(7)	2.56
C(4)	6788(5)	3328(14)	828(7)	2.87
C(5)	6142(5)	3867(12)	6(6)	2.18
C(6)	6140(6)	3613(15)	−1001(7)	3.19
C(7)	5509(6)	4113(15)	−1773(7)	3.29
C(8)	4848(6)	4838(15)	−1592(7)	3.40
C(9)	4837(6)	5130(14)	−636(7)	2.90
C(10)	5493(5)	4642(12)	193(6)	2.14
C(11)	7724(5)	10546(13)	8724(7)	2.29
C(12)	7084(5)	10173(12)	7957(6)	1.95
C(13)	6451(5)	9158(14)	8073(7)	2.47
C(14)	6499(5)	8568(14)	9011(7)	2.98
C(15)	7141(5)	8974(13)	9856(7)	2.71
C(16)	7184(6)	8452(16)	10855(8)	3.79
C(17)	7818(7)	8882(18)	11645(7)	4.37
C(18)	8450(7)	9864(18)	11500(8)	4.15
C(19)	8421(6)	10387(15)	10550(8)	3.49
C(20)	7771(5)	9964(13)	9705(7)	2.51
C(21)	8901(5)	5224(13)	1340(7)	2.59
C(22)	9530(5)	5677(12)	2121(7)	2.18
C(23)	10158(5)	6690(13)	1975(7)	2.61
C(24)	10129(5)	7184(12)	1023(7)	2.79
C(25)	9491(5)	6721(13)	190(7)	2.63
C(26)	9454(6)	7185(14)	−807(7)	3.49
C(27)	8836(8)	6722(17)	−1587(8)	4.30
C(28)	8206(7)	5756(18)	−1434(8)	3.92
C(29)	8222(6)	5293(15)	−484(8)	3.53
C(30)	8867(5)	5715(13)	350(7)	2.57

a) The equivalent isotropic temperature factors were computed using the following expression: $B_{eq}=4/3(B_{11}a^2+B_{22}b^2+B_{33}c^2+B_{13}ac\cos\beta)$. The B_{ij}'s are defined by: $\exp[-(h^2B_{11}+k^2B_{22}+l^2B_{33}+2klB_{23}+2hlB_{13}+2hkB_{12})]$.

metal atom, as well as the numbering scheme, is shown in Fig. 1. The crystal packing diagram is shown in Fig. 2, and the linkages between the complex molecules, in Fig. 3, schematically.

The central metal atom is octa-coordinated and is in a deformed square-antiprism geometry, where two oxygen atoms of the respective 2-naphthalenesulfonato ligand, as well as six water-oxygen atoms, are ligated. The naphthyl group of the ligand is large and is, moreover, non-polar compared with the polar moiety around the central metal atoms. Therefore, two coor-

Table 3. Selected bond lengths and bond angles of the $[M(C_{10}H_7SO_3)_2(H_2O)_6](C_{10}H_7SO_3)\cdot 3H_2O$ complexes

M=	Pr	Eu	Gd	Er	Yb
Bond length	(l/Å)	(l/Å)	(l/Å)	(l/Å)	(l/Å)
M-O(1)	2.389(10)	2.351(19)	2.335(8)	2.278(12)	2.255(12)
M-O(4)	2.441(10)	2.38(2)	2.370(8)	2.333(13)	2.332(12)
M-O(W1)	2.495(13)	2.44(3)	2.427(10)	2.362(13)	2.372(12)
M-O(W2)	2.472(7)	2.424(14)	2.399(5)	2.355(8)	2.329(8)
M-O(W3)	2.452(7)	2.441(14)	2.388(6)	2.338(8)	2.303(8)
M-O(W4)	2.477(5)	2.424(11)	2.400(5)	2.372(7)	2.342(6)
M-O(W5)	2.455(10)	2.369(19)	2.383(8)	2.330(12)	2.338(11)
M-O(W6)	2.492(10)	2.403(18)	2.416(7)	2.373(12)	2.344(11)
Av. of M-O(Wn)[a]	2.474(10)	2.416(20)	2.402(8)	2.355(11)	2.338(10)
Av. of all M-O[b]	2.459(10)	2.403(24)	2.390(8)	2.343(12)	2.327(11)
M-O calcd.[c]	2.476	2.416	2.403	2.354	2.335
S(1)-O(1)	1.475(6)	1.473(12)	1.470(5)	1.480(8)	1.468(7)
S(1)-O(2)	1.456(12)	1.50(3)	1.460(8)	1.499(15)	1.463(15)
S(1)-O(3)	1.444(7)	1.456(15)	1.449(5)	1.439(9)	1.441(8)
S(2)-O(4)	1.465(9)	1.486(18)	1.471(7)	1.467(11)	1.458(10)
S(2)-O(5)	1.455(7)	1.443(14)	1.454(5)	1.454(8)	1.447(8)
S(2)-O(6)	1.456(7)	1.482(15)	1.463(5)	1.457(9)	1.450(8)
S(3)-O(7)	1.454(7)	1.461(15)	1.448(6)	1.449(9)	1.441(8)
S(3)-O(8)	1.433(10)	1.45(2)	1.443(8)	1.443(13)	1.429(12)
S(3)-O(9)	1.455(7)	1.453(14)	1.449(5)	1.460(5)	1.442(8)
Av. of coord. S-O[d]	1.470(8)	1.480(15)	1.471(6)	1.474(10)	1.463(9)
Av. of all S-O[e]	1.455(9)	1.467(19)	1.456(6)	1.455(11)	1.449(10)
O(7)···O(W1)[f]	2.798(17)	2.76(3)	2.804(12)	2.824(18)	2.798(16)
O(W7)···O(W4^{ii})[f]	2.767(12)	2.77(2)	2.782(9)	2.789(14)	2.807(13)
O(9)···O(W2^{iv})[f]	2.646(8)	2.654(18)	2.652(7)	2.655(11)	2.669(10)
O(W8)···O(8^{iv})[f]	2.809(11)	2.77(2)	2.797(9)	2.797(14)	2.792(13)
O(W5)···O(2^{vi})[f]	2.735(10)	2.71(2)	2.725(8)	2.734(12)	2.714(12)
O(W9)···O(7^{vi})[f]	2.878(14)	2.89(3)	2.873(11)	2.876(17)	2.857(16)
Bond angle	(ϕ/°)	(ϕ/°)	(ϕ/°)	(ϕ/°)	(ϕ/°)
M-O(1)-S(1)	140.9(7)	140.6(14)	140.7(5)	141.2(9)	141.3(9)
M-O(4)-S(2)	146.4(6)	145.5(12)	146.8(5)	147.2(7)	147.3(7)
M-O(W1)···O(7)	135.2(4)	136.9(8)	136.7(3)	137.3(4)	137.3(4)
M-O(W5)···O(2^{vi})[f]	124.0(4)	124.5(8)	124.6(3)	125.3(5)	124.7(5)
M-O(W2)···O(9^{v})[f]	132.4(5)	132.8(9)	133.9(4)	134.4(6)	134.9(5)

a) The average of M-O(Wn)(n=1—6), where the oxygen atom are ligated to the metal atom. b) The average of the bond lengths between the central metal atom and all the ligated oxygen atoms around it. c) The sum of the metal (tripositive, octacoordinated) and the oxygen (dinegative, dicoordinated) ionic radii proposed by Shannon.[15] d) The average of the S(1)-O(1) and S(2)-O(4), where both the oxygen atoms are ligated. e) The average of all nine S-O bond lengths of the sulfonate ions in the complex. f) Keys to the symmetric operations: ii, 1.0−x, −0.5+y, 1.0−z; iv, 2.0−x, −0.5+y, 1.0−z; v, 2.0−x, 0.5+y, 1.0−z; vi, x, 1.0+y, z for the Pr, Er and Yb comolexes, and the corresponding ones for the Eu and Gd complexes, which have the opposite structure.

dinated sulfonato ligands, and consequently the ligated O(1) and O(4) atoms, take the positions around the metal atom the most separated from each other.

As is shown in Table 3, the M-O distances to the ligated sulfonato oxygen atoms are shorter than those to the ligated water-oxygen atoms. The latter distances almost exactly agree with the sum of the respective metal (M^{3+}, in octa-coodination) and oxygen (O^{2-}, in di-coordination) ionic radii reported by Shannon.[15] On the other hand, as the former M-O bond lengths are shorter than the respective sums, the bondings can be expected to be stronger than the common M-O bonds of the lanthanoid complexes. Although the M-O(1) bond length is clearly shorter than the sum, even in the heavy lanthanoid complexes, the differeces between the M-O(4) bond length and the sum of the ionic radii are not very large, especially in the erbium and ytterbium complexes. In the case of the tetraacetato complexes of lanthanoids (M=La···Sm), the weakest M-O bond length in the complex was found to increase with the decrease in the atomic number of the central metal atom because of the loss of its coordination space around the metal atom, while the other M-O bond lengths decrease depending on the decrease in the metal atomic radius caused by the lanthanoid contraction.[3] In this case, the same tendency was recognized: the M-O(1) bond length, which is supposed to be stronger than M-O(4), is always shorter than the metal-aqueous oxygen-atom bond lengths, while the weaker M-O(4) bond is weakened to almost the same extent as the metal-water oxygen-atom ones when the atomic number of the central metal atom increases.

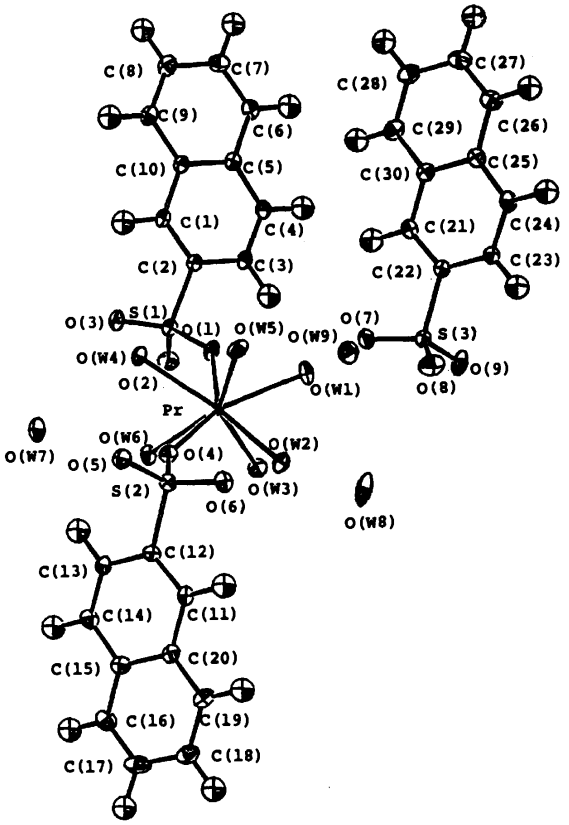

Fig. 1. A perspective drawing of the praseodymium (III) complex with the numbering scheme.

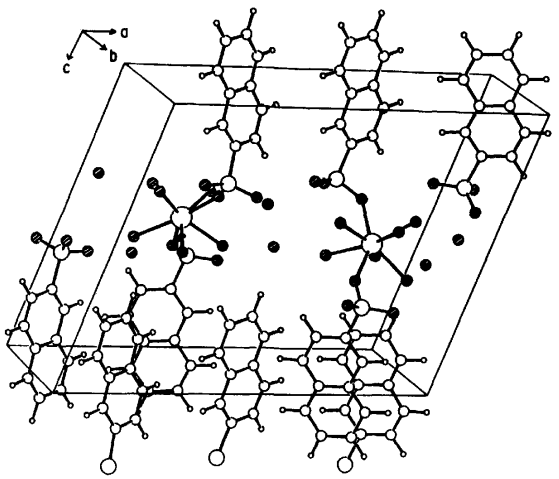

Fig. 2. Crystal packing diagram of the praseodymium(III) complex.

The planarity of the square of the square-antiprism geometry around the metal atom including O(1) is not so exact as that containing O(4). The deformation is caused by the M–O(1) bond, which is stronger than the M–O(4) bonding.

As is shown in Fig. 2, the crystal is composed of alternate layers of hydrophilic and hydrophobic groups parallel to the ab plane. The metal atoms are almost on the plane (0 0 2), and the oxygen atoms are coordinated from both sides of the plane. The oxygen atoms on each side form a hydrogen-bonding network; although there are some hydrogen bondings between the two networks, there are not many.

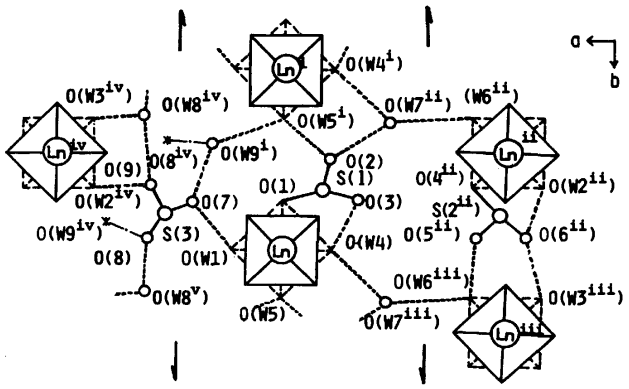

Fig. 3. The schematic presentation of the bridgings between the lanthanoid(III) complex molecules. The network shown in the figure is that in the layer lower than the metal atom plane. As the two-fold screw axes exist, which are shown in the figure, the same type of the linkage-network exists also in the upper layer. Keys to the symmetric operations: i, x, $-1.0+y$, z; ii, $1.0-x$, $-0.5+y$, $1.0-z$; iii, $1.0-x$, $0.5+y$, $1.0-z$; iv, $2.0-x$, $-0.5+y$, $1.0-z$; v, $2.0-x$, $0.5+y$, $1.0-z$.

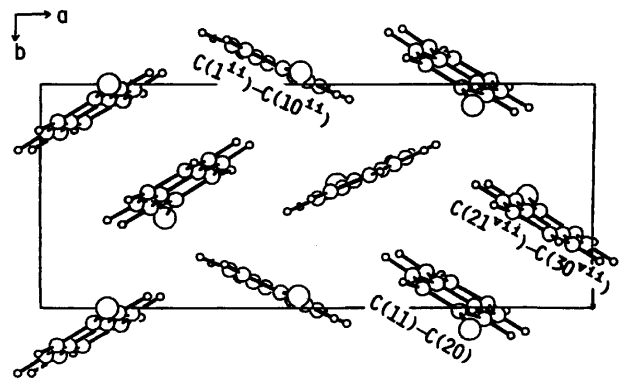

Fig. 4. Packing projection of the naphthalene rings together with the sulfonato sulfur atoms of the anions on the (0 0 1) plane. Keys to the symmetry operations: ii, $1.0-x$, $-0.5+y$, $1.0-z$; vii, x, y, $1.0+z$.

Figure 4 shows the packing of the naphthalene rings projected on the ab plane. They stand almost perpendicular to the ab plane. The angles between the ab plane and the C(1)–C(10), C(11)–C(20), and C(21)–C(30) rings are 89.1, 81.6, and 84.3° respectively in the praseodymium(III) complex. There is a tendency for these angles to become larger with the decrease in the unit-cell volumes. The C(11)–C(20) ring is almost parallel to the C(21)–C(30) ring, and when the former ring is projected on the latter plane, about 33% of the area overlaps. In the case of the praseodymium(III) complex, the distance between these rings is from 3.387 to 3.619 Å, which is almost the same as the thickness of the aromatic molecules;[16] however, the distance decreases with the decrease in

Table 4. The interfacial distances (l/Å) and the angles (ϕ/°) to the 001 plane of the sulfonato naphthalene rings

M=	Pr	Eu	Gd	Er	Yb
Interfacial min.	3.387	3.360	3.374	3.380	3.370
distances[a] max.	3.619	3.581	3.608	3.575	3.561
Angles of planes[b]					
C(1)-C(10)	89.09	89.18	89.27	89.35	89.52
C(11)-C(20)	81.59	82.02	81.85	82.02	82.06
C(21)-C(30)	84.33	84.25	84.41	84.28	84.25

a) The respective maximum and minimum interfacial distances between the naphthalene rings, C(11)-C(20) and C(21^{vii})-C(30^{vii}),[b,c] which are almost parallel to each other. b) Respective naphthalene rings are shown by the included carbon atoms. c) Key to the symmetric operation: vii x, y, 1.0+z.

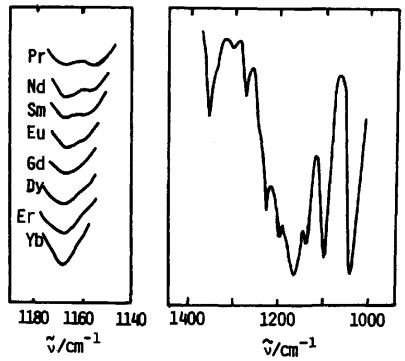

Fig. 5. Infrared absorption spectra of the complexes in the ν(S=O) region. Right; the spectrum of the gadolinium(III) complex in the region. Left; the peak of ν(S=O) of the complexes (the name of the central metal atoms are shown in the figure).

the unit-cell parameters because of the lanthanoid contraction of the central metal ion. The interfacial distances and the angles to the ab plane of the naphthalene rings are shown in Table 4. Thus, the naphthalene rings are packed quite closely to form a hydrophobic layer between hydrophilic layers.

The infrared spectrum of the ν(S=O) region of the gadolinium(III) complex is shown in Fig. 5; the general features of the spectra of the other complexes are almost the same throughout the region from 400 to 4000 cm^{-1}. A slight difference between them was, however, found in those of the peaks at about 1100 cm^{-1}; the peak at 1100 cm^{-1} is identified as one of the ν(S=O) peak of the sulfonato group.[17] The peak of the praseodymium(III) complex split into two; 1167 and 1156 cm^{-1}. The latter peak is weakened when the atomic number of the central metal atom increases; in the case of the ytterbium(III) complex, only a slight shoulder was observed at the lower-wave-number side of the 1167 cm^{-1} peak.

The authors wish to thank the Shin-Etsu Chemical Ind. Co., Ltd., for presenting the highly pure lanthanoid oxides.

References

1) G. G. Sadikov, G. A. Kukina, and M. A. Porai-Koshits, *Zh. Strukt. Khim.*, **8**, 551 (1967).
2) M. C. Favas, D. L. Kepert, B. W. Skelton, and H. White, *J. Chem. Soc., Dalton Trans.*, **1980**, 454.
3) H. Sawase, Y. Koizumi, Y. Suzuki, M. Shimoi, and A. Ouchi, *Bull. Chem. Soc. Jpn.*, **57**, 2730 (1984).
4) Y. Koizumi, H. Sawase, Y. Suzuki, T. Takeuchi, M. Shimoi, and A. Ouchi, *Bull. Chem. Soc. Jpn.*, **57**, 1809 (1984).
5) R. C. Mehrotra and R. Bohra, "Metal Carboxylates," Acad. Press, New York (1983), p. 11.
6) L. A. Aslanov, V. B. Rybakov, V. M. Ionov, M. A. Porai-Koshits, and V. I. Ivanov, *Dokl. Akad. Nauk. SSSR*, **204**, 1122 (1972).
7) B. Eriksson, L. O. Larsson, L. Niinistö, and U. Skoglund, *Inorg. Chem.*, **13**, 290 (1974).
8) J. Albertsson and I. Elding, *Acta Crystallogr., Sect. B*, **33**, 1460 (1977).
9) R. W. Broach and J. M. William, *Acta Crystallogr., Sect. B*, **35**, 2317 (1979).
10) R. Nakamura, K. Nagai, M. Shimoi, and A. Ouchi, *Bull. Chem. Soc. Jpn.*, **57**, 2919 (1984).
11) $R=\sum||F_o|-|F_c||/\sum|F_o|$.
12) "Universal Crystallographic Computation Program System (UNICS)," ed by T. Sakurai, Crystallographic Society of Japan, Tokyo (1967).
13) "International Tables for X-Ray Crystallography," Kynoch Press, Birmingham (1974), Vol. IV, pp. 72, 150.
14) The positions of the hydrogen atoms, the final thermal parameters, and the final F_o—F_c tables are deposited as Document No. 8543 at the Office of the Editor of the *Bull. Chem. Soc. Jpn.*
15) R. D. Shannon, *Acta Crystallogr., Sect. A*, **32**, 751 (1976).
16) L. Pauling, "The Nature of the Chemical Bonds," 3rd ed, Cornell Univ. Press, N. Y. (1960), p. 260.
17) L. J. Bellamy, "The Infrared Spectra of Complex Molecules," Chapman and Hall, London, U. K. (1978), p. 407.

 © 1985 The Chemical Society of Japan Bull. Chem. Soc. Jpn., 58, 2975—2980 (1985)

Conductometric Study of Cobalt(II), Nickel(II), Copper(II), and Zinc(II) Perchlorates in Methanol–Ethylene Glycol Mixtures

Hidekazu DOE* and Toyokichi KITAGAWA

Department of Chemistry, Faculty of Science, Osaka City University, Sumiyoshi-ku, Osaka 558

(Received April 30, 1985)

The ionic association constants of $M(ClO_4)_2$ (M=Co, Ni, Cu, Zn) were determined by conductometric measurements in methanol–ethylene glycol mixtures of 100, 80, 60, 40, 20, and 0 wt% methanol compositions at 5, 15, 25, 35, and 45 °C. The conductometric data were analyzed using a modified Fuoss and Edelson method. The association constant of an ion pair $M^{2+}ClO_4^-$, K_{1A}, was studied and thermodynamic functions, ΔH_{1A}° and ΔS_{1A}°, for that association were determined at 25 °C. Free-energy changes, ΔG_{1A}° ($=-RT\ln K_{1A}$), at 25 °C which slowly decreased with an increase in the ethylene glycol content in a solvent, are in good agreement with estimates from Fuoss' theory regarding ionic association. Values of both ΔH_{1A}° and ΔS_{1A}° were positive in many systems: *i.e.*, unfavorable enthalpy and favorable entropy changes, and those were obtained near to estimates from the Fuoss' theory in pure methanol, 100 wt%. However, there have been a few systems with a negative ΔH_{1A}° (Co, Ni, and Zn at 40 and 20 wt%, and Co at 0 wt%), contrary to theoretical expectations. These results are discussed from the standpoint of a changing solvation between M^{2+} and $MClO_4^+$. In all the solvents, moreover, the ΔH_{1A}° and ΔS_{1A}° values have been in a sequence according to Co<Ni<Cu>Zn. The results of limiting molar conductances, Λ_0, are discussed regarding Walden products.

Many problems concerning ionic solvation have been attracting the attention of chemists in various fields.[1] After taking some interest in the ionic associations between divalent metal cations and a perchlorate anion, we previously[2] made a study of various $M(ClO_4)_2$'s in methanol. In that study, conductometric data were treated using the Fuoss and Edelson method in which an ion-activity coefficient of M^{2+}, y_{2+}, was calculated using the Debye-Hückel second approximation in a manner different from the original paper. There, the Debye-Hückel limiting equation was used.[3] According to our calculation, the ionic association constant of $M^{2+}ClO_4^-$, K_{1A}, is about 10% less for the second approximation than for the limiting equation. The Fuoss and Edelson method was also established on the basis of the Onsager limiting equation. As done in the y_{2+}-calculation, it would therefore be more desirable to treat conductance data using an approximation involving the factor $1+\kappa a$ for moderate concentrations[4] than the Onsager limiting equation. Thus, using such a modified Fuoss and Edelson method, we have made a study of the ionic associations of Co(II), Ni(II), Cu(II), and Zn(II) perchlorates in methanol–ethylene glycol (EG) mixtures.

Both methanol and EG are amphiprotic nonaqueous solvents, but they are typical ionic media like water. The molecular volume of EG, which has a molecular structure that combines two methanol molecules, is less than twice that of methanol. The viscosity of EG is much larger than that of methanol. Their dielectric constants are also different from each other. Of course, methanol and EG resemble each other relatively, regarding their chemical properties as solvents. Therefore, research concerning their mixtures should yield good information concerning various solvent effects due to differences in physical properties: viscosity, dielectric constant, molecular volume, compressibility, *etc.*

Experimental

Materials. The preparation and purification of $M(ClO_4)_2\cdot 6H_2O$ salts were described previously.[2] Methanol and EG were dried over 3A molecular sieves and distilled fractionally. EG was distilled under a reduced pressure of 25 mmHg.† The electric conductivities of the purified methanol and EG were 1.5×10^{-7} and 1.6×10^{-8} S cm^{-1} at 25 °C, and the water contents were 0.023 and 0.024 wt%, respectively. The mixed solvents were prepared by weighing each solvent to an accuracy of $<\pm0.05$%. All reagents were special grade materials (Wako).

Physical Properties of Solvents. The densities of solvents at 25 °C were determined using a vibrating densimeter (Model 01D, Sodev Inc., Sherbrooke, Canada), with chlorobenzene and methylcyclohexane as standards.[5] The accuracy of the measurements was $\pm2\times10^{-5}$ g cm^{-3}. The densities of pure methanol and EG at other temperatures were calculated using $v=v_0(1+\alpha_1 t+\alpha_2 t^2+\alpha_3 t^3)$, where v and v_0 are the volumes of the solvents at t and 0 °C, respectively. The α's are the thermal-expansion coefficients (α_1, α_2, and α_3 are 1.1342×10^{-3}, 1.3635×10^{-6}, and 0.8741×10^{-8} for methanol, and 0.5657×10^{-3}, 1.7074×10^{-6}, and 0.293×10^{-8} for EG, respectively).[6] Densities of the mixtures at temperatures other than 25 °C were also calculated based on the densities of pure solvents at corresponding temperatures and volume change rates of mixing. Then, it was assumed that the rates at 25 °C, which can be calculated based on densities of the mixtures at 25 °C, are equal to those at the other temperatures. The results are shown in Table 1.

Using an Ostwald viscometer, viscosities were measured in the usual way. Water was used as a standard substance.[7] The viscosity results are summarized in Table 2.

Measurements of dielectric constants were carried out by a resonance method at a frequency of 1 MHz. Constants for the standard methanol are cited from Albright and Gosting.[8] The results are shown in Table 3.

Temperatures were controlled within an accuracy and

† 1 mmHg≈133.322 Pa.

Table 1. Densities (g cm^{-3}) of methanol–ethylene glycol mixtures at 278.15—318.15 K

wt% Methanol	278.15 K	288.15 K	298.15 K[a)]	308.15 K	318.15 K
100	0.8050	0.7958	0.78656	0.7772	0.7677
80	0.8606	0.8515	0.84226	0.8329	0.8234
60	0.9200	0.9111	0.90207	0.8929	0.8834
40	0.9835	0.9751	0.96639	0.9575	0.9484
20	1.0514	1.0436	1.03560	1.0273	1.0187
0	1.1237	1.1170	1.10996	1.1026	1.0949

a) Measured with the accuracy of $<\pm 2\times10^{-5}$ g cm^{-3}.

Table 2. Viscosities (cP: 1 cP=10^{-3} kgm^{-1} s^{-1}) of methanol–ethylene glycol mixtures at 278.15—318.15 K

wt% Methanol	278.15 K	288.15 K	298.15 K	308.15 K	318.15 K
100	0.7261	0.6244	0.5422	0.4742	0.4174
80	1.268	1.047	0.8746	0.7399	0.6339
60	2.371	1.865	1.499	1.223	1.016
40	5.098	3.756	2.853	2.222	1.768
20	13.08	8.782	6.213	4.530	3.433
0	43.48	26.10	16.74	11.27	7.929

These values involve the errors of at least ±0.14—0.28% caused by the accuracy of temperature.

Table 3. Dielectric constants of methanol–ethylene glycol mixtures at 278.15—318.15 K

wt% Methanol	278.15 K	288.15 K	298.15 K	308.15 K	318.15 K
100	36.88	34.70	32.66	30.74	28.92
80	38.30	36.20	34.05	32.06	30.22
60	39.84	37.70	35.49	33.53	31.69
40	41.37	39.14	36.88	34.75	32.92
20	43.25	40.93	38.58	36.42	34.53
0	45.52	43.01	40.57	38.35	36.37

These values involve the errors of at least ±0.04% caused by the accuracy of temperature.

precision of ±0.01 and ±0.0005 °C for density, ±0.05 and ±0.01 °C for viscosity, and ±0.05 and ±0.02 °C for the dielectric constant measurements, respectively.

Electric Conductances. The measurements were carried out with a Yanagimoto Model MY-8 conductivity outfit and a type C cell, which had a cell constant of 0.3801± 0.0006. This represents a mean value calibrated at 5, 15, 25, 35, and 45 °C with potassium chloride (Aldrich, 99.999% reagent).[9] All temperatures were controlled with an accuracy of $<\pm0.1$ °C using a Sharp TE-12K thermoelectric circulating system. The ClO_4^- concentrations, c, of the measured solutions were in the range of 1.5—20×10^{-4} M (M=mol dm^{-3}). When, therefore, a hexahydrated $M(ClO_4)_2$ solution of $c=2\times10^{-3}$ M was prepared, water of about 0.014 wt% was added to the solvents, inherently containing water of 0.023—0.024 wt%. However, this increase in water probably did not much affect our results and are negligible in comparison with other experimental errors. The measured solutions were prepared in an air-conditioned room (about 25 °C) and their molar concentrations were taken as those at 25.0 °C. Molarities at other temperatures were corrected using the densities of the corresponding temperatures.

Data Treatment

Conductometric data were treated using a modified Fuoss and Edelson method. According to the original method,[3] only the ionic equilibrium was considered:

$$M^{2+} + ClO_4^- \rightleftharpoons MClO_4^+ \quad (K_{1A}) \tag{1}$$

Then they derived the following equation based on the Onsager limiting law:

$$\Lambda F = \Lambda_0 - XK_{1A}/\Lambda_0 \tag{2}$$

where

$$X = cy_{2+}\Lambda F(\Lambda F - \Lambda_0/2)$$
$$F = \{(1-\delta c^{1/2})^{-1} + (\Lambda_0-\lambda_0)/2\Lambda\}/\{1+(\Lambda_0-\lambda_0)/2\Lambda_0\}$$

where Λ and Λ_0 are the molar and the limiting molar conductances of $1/2\,M(ClO_4)_2$, respectively. λ_0 and c are the limiting molar conductance of ClO_4^- and the total concentration of ClO_4^-, respectively. The symbol δ is Onsager's slope divided by Λ_0. In previous papers,[2,10] the ion activity coefficient of M^{2+}, y_{2+}, was calculated using the Debye-Hückel second approximation (Eq.3) with an ion-size parameter, a, of 6 Å:[2]

$$\log y = -Az_i^2 I^{1/2}/(1+BaI^{1/2}) \tag{3}$$

The Fuoss and Edelson function, F (in Eq. 2), has been calculated by us using Eq. 4 in which $\delta c^{1/2}/(1+BaI^{1/2})$ is used instead of $\delta c^{1/2}$:

$$F = [\{1-\delta c^{1/2}/(1+BaI^{1/2})\}^{-1} + (\Lambda_0-\lambda_0)/2\Lambda]/\{1+(\Lambda_0-\lambda_0)/2\Lambda_0\} \tag{4}$$

I indicates the ionic strength: $I=1.5\times c$.

λ_0 is 70.1 Scm^2 mol^{-1} in methanol at 25.0 °C.[11] Since, however, we had no data regarding the λ_0's at other conditions, solvents and temperatures, we calculated them on the basis of a value of 70.1. Briefly speaking, they were determined proportionally to mean Λ_0 values of $Co(ClO_4)_2$, $Ni(ClO_4)_2$, and $Zn(ClO_4)_2$ at the respective conditions. The evaluation procedure of λ_0 and the thermodynamic functions, $\Delta H_{1A}^\ominus$ and $\Delta S_{1A}^\ominus$, have been described in more detail elsewhere.[2]

Results and Discussion

Limiting Molar Conductances. The result of limiting molar conductances (Table 4) will be scrutinized *via* the Walden product, $\Lambda_0\eta$. Plots of the $\Lambda_0\eta$ of $Zn(ClO_4)_2$ are shown in Fig. 1 as functions of the wt% composition of methanol. As shown in this figure, there are three characteristics of the $\Lambda_0\eta$'s for all the $M(ClO_4)_2$'s. 1) $\Lambda_0\eta$ increases upon going from

TABLE 4. LIMITING MOLAR CONDUCTANCES ($S\,cm^2\,mol^{-1}$) OF $1/2\,M(ClO_4)_2$ AND ClO_4^- IN METHANOL–ETHYLENE GLYCOL MIXTURES AT 278.15—318.15 K

wt% Methanol	278.15 K	288.15 K	298.15 K	308.15 K	318.15 K
			$Co(ClO_4)_2$		
100	98.6±0.13	114.0±0.10	130.7±0.14	149.0±0.10	169.3±0.22
80	64.4±0.09	77.0±0.10	90.5±0.09	105.5±0.12	122.2±0.20
60	38.0±0.07	47.5±0.08	57.9±0.09	69.6±0.12	82.8±0.17
40	19.72±0.02	26.24±0.03	33.7±0.05	42.4±0.08	52.4±0.12
20	8.27±0.02	12.03±0.03	16.65±0.04	22.3±0.07	28.9±0.09
0	2.605±0.002	4.314±0.003	6.61±0.006	9.68±0.01	13.60±0.02
			$Ni(ClO_4)_2$		
100	99.2±0.13	114.7±0.08	131.5±0.12	150.0±0.16	170.6±0.17
80	64.13±0.03	76.9±0.05	90.6±0.07	106.0±0.10	123.0±0.14
60	39.3±0.05	49.2±0.05	60.2±0.09	72.7±0.10	86.7±0.17
40	20.13±0.04	26.8±0.06	34.5±0.07	43.4±0.10	53.7±0.13
20	8.43±0.01	12.26±0.02	17.01±0.03	22.80±0.04	29.7±0.06
0	2.69±0.005	4.48±0.008	6.89±0.014	10.10±0.02	14.19±0.02
			$Cu(ClO_4)_2$		
100	97.6±0.16	113.2±0.20	130.1±0.23	149.4±0.31	171.4±0.45
80	63.2±0.12	75.8±0.15	89.6±0.18	105.3±0.21	123.0±0.21
60	37.2±0.07	46.8±0.09	57.4±0.12	69.5±0.16	83.2±0.30
40	19.37±0.04	25.93±0.04	33.5±0.06	42.4±0.07	52.7±0.10
20	8.29±0.02	12.15±0.03	16.9±0.05	22.9±0.05	30.2±0.06
0	2.666±0.004	4.43±0.007	6.85±0.010	10.12±0.014	14.36±0.02
			$Zn(ClO_4)_2$		
100	95.9±0.09	110.9±0.11	127.1±0.13	145.0±0.16	164.5±0.19
80	62.7±0.15	75.1±0.17	88.4±0.22	103.2±0.27	119.6±0.31
60	36.9±0.06	46.1±0.08	56.3±0.09	67.9±0.10	81.0±0.12
40	19.45±0.03	25.85±0.04	33.2±0.05	41.7±0.07	51.3±0.11
20	8.30±0.01	12.08±0.02	16.72±0.03	22.39±0.04	29.14±0.04
0	2.637±0.004	4.38±0.005	6.74±0.008	9.88±0.012	13.90±0.02
			ClO_4^- [a]		
100	52.9	61.2	70.1 [b]	80.1	90.9
80	34.5	41.3	48.6	56.8	65.8
60	20.7	26.0	31.7	38.3	45.6
40	10.7	14.3	18.3	23.1	28.4
20	4.51	6.57	9.09	12.2	15.9
0	1.43	2.38	3.66	5.37	7.54

a) Calculated according to the procedure in the text. b) Ref. 11.

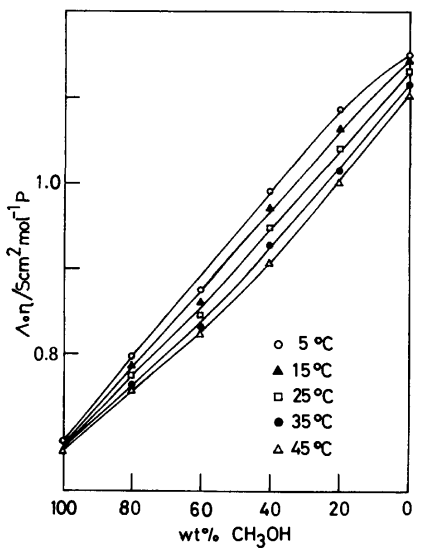

Fig. 1. The plots of Walden products of $Zn(ClO_4)_2$ against wt% of methanol at various temperatures.

methanol to EG; from 100 to 0 wt%, ($\Lambda_o\eta$'s of EG are about 1.6 times as large as those of methanol). 2) $\Lambda_o\eta$'s of all the systems except Cu in methanol decrease with an increase in temperature: negative temperature coefficients of $\Lambda_o\eta$. 3) The negative temperature coefficient (characteristic 2) is most significant at 40 wt% (in the 40 wt% mixture, $\Lambda_o\eta$'s at 5 °C are 1.06—1.09 times as large as those at 45 °C). Molar ionic conductances of these divalent metal ions are larger than those of hydrophilic structure-making ions like Li^+ and Na^+ in methanol. Probably the primary solvation shells of the M^{2+}'s are relatively firm and considerably structured in methanol.[2] We think the same situation can also be established in EG. Therefore, the M^{2+} must move with only the primary solvation shell in the solvents and the effect of the secondary solvation appears to be very small. The size of the primary solvated ion is expected to be smaller in EG than in methanol because of the high solvating power of EG.[12] Thus, this is probably a cause of

Table 5. Ionic association constants, K_{1A} (M^{-1}), of $M(ClO_4)_2$ in methanol–ethylene glycol mixtures at 278.15-318.15 K

wt% Methanol	278.15 K	288.15 K	298.15 K	308.15 K	318.15 K
			$Co(ClO_4)_2$		
100	151±7	167±4	194±6	225±4	264±8
80	153±6	160±6	166±5	174±6	193±8
60	117±8	117±8	114±7	117±8	123±10
40	92±5	85±6	78±6	75±7	78±10
20	79±7	70±8	64±9	53±12	50±12
0	61±2	64±3	55±3	54±4	52±5
			$Ni(ClO_4)_2$		
100	131±3	147±4	170±5	202±6	245±6
80	126±2	138±4	152±4	170±5	194±7
60	110±5	118±4	124±6	138±6	155±9
40	89±9	87±10	80±9	76±10	83±11
20	80±6	71±5	69±7	68±6	66±8
0	63±7	83±7	87±9	86±8	85±7
			$Cu(ClO_4)_2$		
100	143±7	166±8	201±9	257±11	336±15
80	126±8	141±9	160±9	191±9	229±9
60	86±7	95±8	107±8	124±9	137±16
40	51±7	58±6	64±7	69±7	79±8
20	54±8	56±9	63±9	77±8	99±7
0	64±5	69±6	77±5	87±5	100±6
			$Zn(ClO_4)_2$		
100	109±5	120±5	144±6	173±6	203±7
80	119±10	129±11	138±12	154±13	171±13
60	89±6	88±7	87±7	91±6	102±6
40	88±6	82±6	79±6	71±6	63±8
20	93±7	83±7	76±6	69±8	67±6
0	69±5	77±4	80±4	79±4	81±4

characteristic 1. In a previous work regarding methanol systems, a brief description concerning negative temperature coefficients was made using the thermal expansion of a solvated ion.[2] However, these coefficients are too negative in EG-rich solvents to be explained in terms of thermal expansion. According to a well known structure effect,[13] ClO_4^- (a typical structure-breaking ion) can exhibit a large negative temperature coefficient for the Walden product in EG-rich solvents, if EG is a highly structured solvent in comparison with methanol. If so, this could also be applied to an explanation of characteristic 1.

On the other hand, we think that the large negative temperature coefficients of $\Lambda_o\eta$ in EG-rich solvents might be closely related to the density, the molecular volume, and/or the compressibility of the solvents. Methanol has a larger molecular volume for its molecular structure (*cf.* introduction) and has a much higher compressibility than EG. That is to say, methanol is expected to have loose interactions and wide spaces among methanol molecules in comparison with EG. Hence, it appears that a change in the size of a solvated ion exerts a larger influence on $\Lambda_o\eta$ in dense EG than in methanol. In connection with an explanation of characteristic 1, it may be further inferred that the primary solvated M^{2+}, which moves as a single kinetic unit, exhibits a structure-breaking effect in dense and viscous (probably highly structured) EG. As shown in the density data (Table 1), mixed solvents of methanol-EG have negative excess volumes of mixing. The maximum volume decrease occurs at 40 wt%. Analogically, this may be a cause of the characteristic 3. As another cause of characteristic 3, we think that the sizes of solvated ions in the mixtures increase with a temperature increase because the proportion of methanol and EG molecules in the sheath of solvation (and/or the structure of the sheath) varies with temperature.

Ionic Association Constants. The results of K_{1A} are summarized in Table 5. Before a discussion regarding them, it is necessary to describe the difference between the previous[2] and the present results for pure methanol: in the previous study we took no account of the $1+\kappa a$ term in the conductance equation. Because the $1+\kappa a$ term has been introduced in the conductance equation of the present study (Eq. 4), the present K_{1A}'s have become larger than the previous ones though there are no changes in the order of magnitude of K_{1A}. The present values are 1.84 ($Co(ClO_4)_2$ at 45 °C) −2.45 ($Zn(ClO_4)_2$ at 5 °C) times larger than previous ones. These ratios seem to be larger, the smaller K_{1A} is, and to be smaller, the higher the temperature is. Similar results were obtained for K_{1A} of alkaline-earth metal perchlorates. Some of these have been reported elsewhere.[14]

The K_{1A} values (Table 5) will be discussed *via* the

TABLE 6. THERMODYNAMIC FUNCTIONS OF IONIC ASSOCIATION OF $M^{2+}ClO_4^-$ AT 298.15 K

wt% Methanol	Co	Ni	Cu	Zn	Fuoss[a]
			ΔH_{1A}°(kJ/mol)		
100	10.7±0.7	11.7±0.6	16.1±1.1	12.1±1.0	11.6
80	4.1±1.0	8.0±0.6	11.2±1.2	6.7±1.9	10.6
60	0.9±1.6	6.3±1.1	9.1±2.2	2.6±1.6	9.4
40	−3.3±2.2	−1.9±2.8	7.7±2.6	−6.0±2.3	9.1
20	−8.8±4.1	−2.8±2.2	11.6±2.9	−6.0±2.0	8.4
0	−4.3±1.7	4.2±2.3	8.2±1.6	2.4±1.4	7.8
			ΔS_{1A}° (J/(K mol))		
100	79±2	82±2	98±4	82±3	81
80	56±3	69±2	80±4	64±7	76
60	43±6	62±4	69±7	46±5	70
40	25±7	30±9	60±9	16±8	68
20	5±14	26±7	73±10	16±7	63
0	20±6	51±8	64±5	44±5	59
			ΔG_{1A}° (kJ/mol)		
100	−13.1±0.04	−12.7±0.07	−13.1±0.10	−12.3±0.10	−12.7
80	−12.7±0.08	−12.5±0.07	−12.6±0.14	−12.2±0.21	−12.1
60	−11.7±0.16	−12.0±0.13	−11.6±0.19	−11.1±0.19	−11.5
40	−10.8±0.19	−10.9±0.29	−10.3±0.26	−10.8±0.19	−11.1
20	−10.3±0.37	−10.5±0.23	−10.3±0.36	−10.7±0.20	−10.5
0	−9.9±0.13	−11.1±0.24	−10.8±0.16	−10.9±0.13	−9.9

a) Calculated by Fuoss' theory at a distance of closest approach of 6 Å.[15]

influences of the following three variables: metal element, solvent composition, and temperature. Regarding the influences from different metal elements, there are few remarkable characteristics. According to a discussion in a previous paper,[2] these metal ions make relatively firm primary solvation shells in methanol, probably much more in EG. Therefore, it is thought that specific properties of the metal ions hardly appear in the K_{1A} values. We have to get more information concerning ionic association in order to understand the small and vague variations in K_{1A}.

The K_{1A} values tend to decrease with an increase in the EG content of the solvent; the tendency is the stronger the higher the temperature is. It is sure that such a decrease in K_{1A} is partly due to an increase in the dielectric constants of EG-rich solvents. If, however, this decrease is observed more carefully, it is found that the K_{1A} values decrease sharply up to 40 wt%, but slightly and irregularly between 40 and 0 wt% for all the salts. This can not be interpreted by the increase in dielectric constants. However, it might be explained by a view that a change in the composition and/or structure of the M^{2+} solvation shell caused by the ionic association depresses the stabilization of ion pairs M^{2+}(solvated)ClO_4^- in mixed solvents.

The temperature influence, according to the results of ΔH_{1A}° at 25 °C (Table 6), is complicated, but interesting. Curves of $\ln K_{1A}$ plotted as a function of T^{-1}, $d(\ln K_{1A})/d(T^{-1})=-\Delta H_{1A}^\circ/R$, have various shapes in the present systems. Though there are some interesting characteristics regarding the shapes of these lines, we have too little information to discuss them here. The results of ΔS_{1A}° and ΔG_{1A}° at 25 °C are also summarized in Table 6, and their values are compared with theoretical values calculated using Fuoss' theory concerning ionic association with at the distance of closest approach (6 Å).[15] The previous results for methanol (the previous K_{1A}'s were smaller than the present ones) are compared with values calculated for a distance of 7.4 Å. This is an estimation for an ion pair $M(CH_3OH)_6^{2+}ClO_4^-$ perfectly separated by a primary solvation shell of M^{2+}.[2]

According to the results of ΔH_{1A}° (Table 6), only $Cu(ClO_4)_2$ has a tendency different from the other $M(ClO_4)_2$. The ΔH_{1A}°'s of $Cu(ClO_4)_2$ (except in pure methanol) are in good agreement with the theoretical values if their errors are considered. On the other hand, the ΔH_{1A}°'s of $M(ClO_4)_2$ (except $Cu(ClO_4)_2$) have common characteristics. ΔH_{1A}°'s at 100 wt% are in good agreement with theoretical values. These rapidly decrease with an increase in the EG content of the solvent until 40—20 wt% (where the composition goes to 0 wt%: pure EG, those get to increase reversely). It is especially noteworthy that the ΔH_{1A}° values at 40—20 wt% are negative (the electrostatic theory of ionic association never gives a negative value to ΔH_{1A}°).[2] If the positive value of ΔH_{1A}° (and/or the positive value of ΔS_{1A}°) is explained by the fact that a solvation of M^{2+} is weakened by the ion pairing of $M^{2+}ClO_4^-$, the small ΔH_{1A}°, including the negative one, (and the small ΔS_{1A}°) in EG rich solvents will probably mean that the degree of the weakening of the M^{2+} solvation is small because of the high solvating power of EG. The very small values of ΔH_{1A}° at 40—20 wt% may also be explained by the view that the enthalpic instabilization of a M^{2+} solvation attended by $M^{2+}ClO_4^-$ ion pairing is depressed due to the change in the com-

position and/or the structure of the solvation shell (simultaneously an entropic stabilization is depressed considerably). On the other hand, the positive ΔH_{1A}° of Cu probably has some relation to a Jahn-Teller distortion of its solvation shell,[2] though we can not present a detailed discussion now.

As mentioned in the discussion regarding K_{1A}, the ΔG_{1A}° values of all the $M(ClO_4)_2$ are similar to each other, and are in good agreement with the theoretical values. That is to say, because ΔS_{1A}° mutually complements ΔH_{1A}° for ΔG_{1A}°, the results of ΔS_{1A}° will also support the above discussion for the results of ΔH_{1A}°. Moreover, it is very interesting that the values of both ΔH_{1A}° and ΔS_{1A}° have been in the sequence of Co<Ni<Cu>Zn in all the solvents. In order to understand this, it will be necessary to make further investigations.

In conclusion, the primary solvated M^{2+} moves as a single kinetic unit and the secondary solvation only gives small effects on the Walden products of M^{2+} in the solvents. The size of the primary solvated M^{2+} will be smaller in EG-rich solvents than in methanol because of the high solvating power of EG. In EG-rich solvents, furthermore, the primary solvated M^{2+} may be rather a structure breaker. Thus, the Walden products of $M(ClO_4)_2$ probably result in the large values for EG-rich solvents. A strong solvation of M^{2+} with EG also causes a small ΔH_{1A}°. We thus suggest that the $\Delta H_{1A}^{\circ}/\Delta G_{1A}^{\circ}$ ratio increases with an increase in the solvating power of a solvent. In mixed solvents, especially in 40 or 20 wt%, it seems that the composition and/or structure of the solvation shell of M^{2+} varies with temperature and/or with the ionic association. If so, such a variation in the solvation shell must cause the large negative temperature coefficients of the Walden products, and must cause the small ΔH_{1A}° and ΔS_{1A}° (and also maybe the slightly small ΔG_{1A}° as a result of complementarity between ΔH_{1A}° and ΔS_{1A}°). The negative temperature coefficients of the Walden products may also result from the fact that ClO_4^- is a structure-breaking ion.

We thank Dr. Reiji Tanaka of Osaka City University for his very kind help and advice in the measurements of the physical properties of solvent. The present study has been partially supported by a Grant-in-Aid for Scientific Research from the Ministry of Education, Science and Culture.

References

1) J. O' M. Bockris and A. K. M. Reddy, "Modern Electrochemistry," Plenum Press, New York (1970), Vol. 1, Chap. 2—4; J. E. Desnoyers and C. Jolicoeur, "Ionic Solvation," in "Comprehensive Treatise of Electrochemistry," ed by B. E. Conway, J. O' M. Bockris, and E. Yeager, Plenum Press, New York (1983), Vol. 5, Chap. 1.

2) H. Doe, T. Kitagawa, and K. Sasabe, *J. Phys. Chem.*, **88**, 3341 (1984).

3) R. M. Fuoss and D. Edelson, *J. Am. Chem. Soc.*, **73**, 269 (1951).

4) R. A. Robinson and R. H. Stokes, "Electrolyte Solutions," Butterworths, London (1955), p. 169.

5) R. Tanaka, *Netsusokutei*, **6**, 2 (1979).

6) "Kagaku-binran (Kiso-hen)," 2nd ed by The Chemical Society of Japan, Maruzen, Tokyo (1975), p. 687.

7) A. Korosi and B. K. Fabuss, *Anal. Chem.*, **40**, 157 (1968).

8) P. S. Albright and u. L. J. Gosting, *J. Am. Chem. Soc.*, **68**, 1061 (1946).

9) H. C. Parker and E. W. Parker, *J. Am. Chem. Soc.*, **46**, 312 (1924).

10) H. Doe, A. Shibagaki and T. Kitagawa, *Inorg. Chem.*, **22**, 1639 (1983); H. Doe and T. Kitagawa, *ibid.*, **21**, 2272 (1982); H. Doe, M. Matsui, and T. Shigematsu, *Bull. Inst. Chem. Res., Kyoto Univ.*, **58**, 154 (1980).

11) B. E. Conway, "Electrochemical Data," Elsevier, Amsterdam (1952).

12) K. Burger, "Solvation, Ionic and Complex Formation Reactions in Non-Aqueous Solvents; Experimental Methods for Their Investigation (Studies in Analytical Chemistry; 6)," Elsevier, Amsterdam (1983).

13) R. L. Kay, "Ionic Transport in Water and Mixed Aqueous Solvents," in "Water," ed by F. Franks, Plenum Press, New York (1973), Vol. 3, Chap. 4; R. L. Kay and D. F. Evans, *J. Phys. Chem.*, **70**, 2325 (1966).

14) H. Doe, A. Matsuda, and T. Kitagawa, *Bunseki Kagaku*, **33**, E511 (1984).

15) R. M. Fuoss, *J. Am. Chem. Soc.*, **80**, 5059 (1958).

Spectrophotometric and Polarimetric Investigations on Complex Formation between Copper(II) and Cyclodextrins in an Alkaline Solution

Yoshihisa MATSUI* and Kohji KINUGAWA
Department of Agricultural Chemistry, Shimane University, Nishikawatsu, Matsue 690
(Received May 10, 1985)

Copper(II) forms a 1:1 complex (CuCD), as well as a 2:1 complex (Cu_2CD), with cyclodextrin (CD) in an alkaline solution. An equilibrium constant (K_{dsp}) for the disproportionation reaction of Cuα-CD to $Cu_2\alpha$-CD and α-CD was determined by spectrophotometry and polarimetry to be *ca.* 17 in 1.0 mol dm^{-3} NaOH at 25 °C. The K_{dsp} value gradually decreased with increasing NaOH concentration. A ligand-exchange reaction of Cu_2CD with ethylenediaminetetraacetic acid (EDTA) to give Cu(edta)$^{2-}$ and CD was also examined by means of spectrophotometry and polarimetry. The equilibrium constants (K_{lex}) for the ligand-exchange reaction was evaluated to be *ca.* 2.1 for an α-CD system and *ca.* 1.2 for a β-CD system in 1.0 mol dm^{-3} NaOH at 25 °C. The K_{lex} value decreased rapidly with increasing NaOH concentration. The role of OH^- in the complexation of Cu(II) with CD is discussed on the basis of these results.

Cyclodextrins (CD) are cyclic oligomers composed of six (α-CD), seven (β-CD), or more α-D-glucopyranose units linked 1→4 as in amylose. It has been revealed that copper(II) forms a 2:1 complex (Cu_2CD) with CD in an alkaline solution.[1,2] Although the structure of the complex has not fully been elucidated, it has been suggested that the two pairs of C2 and C3′ secondary hydroxyl groups of contiguous glucose units of CD are cross-linked by the $Cu(OH^-)_2$ Cu or $Cu(OH^-)(O^{2-})$ Cu ion bridge.[2] The complex not only binds an organic substrate within the cavity of CD but also markedly affects the reaction rate of the substrate in a similar manner as metalloenzymes.[3]

In the course of a study on Cu_2CD, we found that Cu(II) forms a 1:1 complex (CuCD) with CD, as well as a 2:1 complex, especially when the CD concentration is much higher than the Cu(II) concentration. The present work was undertaken to examine the complexation of Cu(II) with CD in more detail by means of spectrophotometry and polarimetry. Furthermore, a ligand-exchange reaction of Cu_2CD with ethylenediaminetetraacetic acid (EDTA) was examined in order to obtain further insight into the thermodynamic stability of Cu_2CD.

Experimental

Materials. The α- and β-CD's and copper sulfate were commericially available and were recrystallized from water. The disodium salt of EDTA of a reagent grade was used without further purification.

Apparatus. Absorption spectra were recorded using a Hitachi Model 220 spectrophotometer. Polarimetric measurements were carried out with a Union Giken Model PM-101 polarimeter.

Spectrophotometry and Polarimetry of Complexation between Cu(II) and CD. Changes in absorbance and optical rotation of an alkaline CD solution with an addition of Cu(II) were followed by means of a spectrophotometer and a polarimeter at 25 °C. A typical run was as follows: Two kinds of aqueous NaOH solutions were prepared, *i.e.*, 100 mmol dm^{-3} CD solutions containing no (Soln A) and 100 mmol dm^{-3} (Soln B) $CuSO_4$. The concentration of NaOH was adjusted to 1.0, 1.5, 2.0, or 2.5 mol dm^{-3}. Two cm^3 portions of Soln A were pipetted into a pair of 1-cm quartz cells for spectrophotometry. The cells were maintained at 25 °C by means of jackets through which water was circulated from a constant-temperature bath. After the absorption spectrum of the control solution was recorded by scanning from 800 to 370 nm, 0.025 cm^3 portions of Soln B were consecutively added to a sample cell. For each addition of Soln B, the absorption spectrum of the resulting solution was recorded. The change of absorbance (*Abs*) at λ=685 nm, where *Abs* reaches close to a maximum, was used for an analysis of the data. Changes in the optical rotation (*P*) of Soln A upon consecutive additions of Soln B were similarly followed at λ=405 nm, where the resulting solution showed only a slight absorption of light.

Determination of Equilibrium Constants for the Disproportionation Reaction of CuCD to Cu_2CD and CD. The value of *Abs* at 685nm for an alkaline CD solution increased with an increase in the total concentration (*a*) of Cu(II). Then, molar absorbance (*Abs/a*) for Cu(II) was plotted against the ratio (*R*) of *a* to the total concentration (*b*) of CD (Figs. 1 and 2). If Cu(II) forms only a single CD complex such as Cu_2CD as had been suggested previously,[1] the value of *Abs/a* should be constant for any *R* value. However, the observed *Abs/a* value increased with an increasing *R* value. For a Cu-α-CD system, all the plots obtained were virtually fitted to a curved line, irrespective of the *b* value. On the other hand, the *Abs/a* value for a Cu-β-CD system changed not only with a change in *R* but also with a change in *b*. It was postulated that Cu(II) forms a 1:1 complex (CuCD) with CD as well as a 2:1 complex (Cu_2CD) at small *R* values. Then, the transformation of CuCD to Cu_2CD with an increase in *R* is represented by a disproportionation reaction as follows:

$$2CuCD = Cu_2CD + CD. \quad (1)$$

The equilibrium constant (K_{dsp}) for the disproportionation reaction is represented by

$$K_{dsp} = yz/x^2, \quad (2)$$

where *x*, *y*, and *z* are the equilibrium concentrations of CuCD, Cu_2CD, and CD respectively. The concentration of uncomplexed Cu(II) is neglected, since it may be very low in such an alkaline solution. Then,

$$a = x + 2y \quad (3)$$

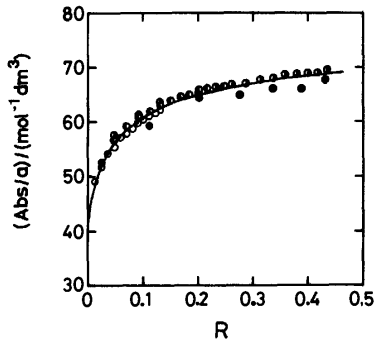

Fig. 1. Plots of Abs/a at λ=685 nm *vs.* R for a Cu-α-CD system in 1.5 mol dm^{-3} NaOH at 25 °C. [α-CD]=10 (●), 25 (◑), 50 (◐), and 100 (○) mmol dm^{-3}.

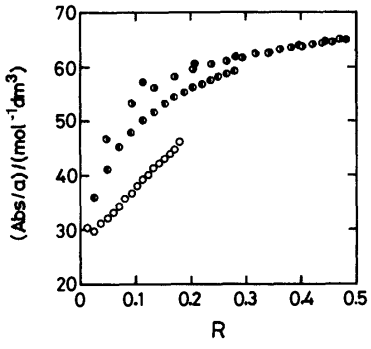

Fig. 2. Plots of Abs/a at λ=685 nm *vs.* R for a Cu-β-CD system in 1.5 mol dm^{-3} NaOH at 25 °C. [β-CD]=10 (●), 25 (◑), 50 (◐), and 100 (○) mmol dm^{-3}.

and

$$b = x + y + z. \tag{4}$$

Substitution of Eqs. 3 and 4 into Eq. 2 yields

$$x = ad \tag{5}$$

and

$$y = a(1-d)/2, \tag{6}$$

where

$$d = \frac{[R(2-R)(4K_{dsp}-1)+1]^{1/2}-1}{R(4K_{dsp}-1)}. \tag{7}$$

The total absorbance due to the Cu(II) complexes is given by

$$Abs = \varepsilon_1 x + \varepsilon_2 y, \tag{8}$$

where ε_1 and ε_2 are the molar absorption coefficients of CuCD and Cu_2CD, respectively. Upon introducing Eqs. 5 and 6 to Eq. 8, the following is derived:

$$Abs/a = \varepsilon_1 d + \varepsilon_2(1-d)/2. \tag{9}$$

Since d is only a function of R (Eq. 7), Abs/a is also dependent on R alone. This deduction agrees with the observed results for a α-CD system as shown in Fig. 1. In a Cu-β-CD system, the Abs/a value at a constant R value decreased with increasing b (Fig. 2). This suggests that some reaction other than the disproportionation of CuCD to Cu_2CD and CD occurs at high CD concentrations. However, no reasonable reaction mechanism can be offered to explain the observation at the present stage of investigation.

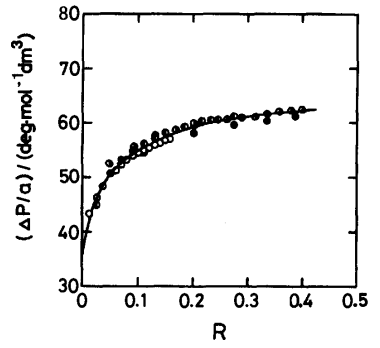

Fig. 3. Plots of $\Delta P/a$ at λ=405 nm *vs.* R for a Cu-α-CD system in 1.5 mol dm^{-3} NaOH at 25 °C. [α-CD]=10 (●), 25 (◑), 50 (◐), and 100 (○) mmol dm^{-3}.

In the case of polarimetry, the P value for Soln A decreased with an increasing a value. Figure 3 illustrates the plots of $\Delta P/a$ *vs.* R for a Cu-α-CD system, where ΔP is the difference (P_0-P) between optical rotations in the absence (P_0) and in the presence (P) of Cu(II). The plots were also virtually fitted to a curved line, irrespective of b. If the molar optical rotations of CD, CuCD, and Cu_2CD are denoted by f_0, f_1, and f_2 respectively, P_0 and P are given by

$$P_0 = f_0 b \tag{10}$$

and

$$P = f_0 z + f_1 x + f_2 y. \tag{11}$$

From Eqs. 4, 10, and 11, the following is derived:

$$\Delta P = \Delta f_1 x + \Delta f_2 y, \tag{12}$$

where $\Delta f_1 = f_0 - f_1$ and $\Delta f_2 = f_0 - f_2$. Upon introducing Eqs. 5 and 6 to Eq. 12, we obtain

$$\Delta P/a = \Delta f_1 d + \Delta f_2(1-d)/2. \tag{13}$$

This equation is very similar to Eq. 9, and $\Delta P/a$ is also dependent on d or R alone, as was shown in Fig. 3. The K_{dsp} values, as well as the values of ε_1 and ε_2 or Δf_1 and Δf_2, for Cu-α-CD systems at various NaOH concentrations were estimated by analyzing the relationships between Abs/a or $\Delta P/a$ and R by the least-squares curve-fitting method with a microcomputer. In a Cu-β-CD system, the $\Delta P/a$ value was dependent not only on R but also on b in a similar manner as the Abs/a value. Thus, no numerical analysis was attempted.

Spectrophotometry and Polarimetry of Ligand-exchange Reaction between Cu_2CD and EDTA. Changes in the absorbance and optical rotation of an alkaline Cu_2CD solution upon an addition of EDTA were followed using a spec-

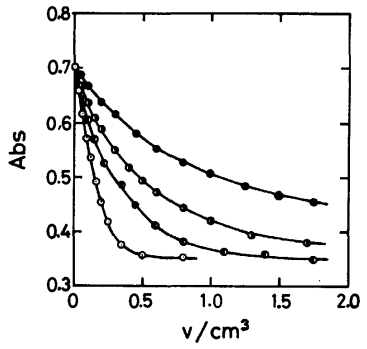

Fig. 4. Plots of *Abs vs. v* for a Cu_2 α-CD-EDTA system in 0.5 (○), 1.0 (◐), 1.5 (◑), and 2.0 (●) mmol dm^{-3} NaOH at 25 °C.

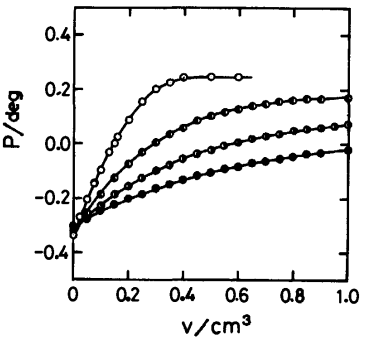

Fig. 5. Plots of ΔP *vs. v* for a Cu_2 α-CD-EDTA system in 0.5 (○), 1.0 (◐), 1.5 (◑), and 2.0 (●) mmol dm^{-3} NaOH at 25 °C.

trophotometer and a polarimeter at 25 °C. A typical run was as follows: Two kinds of aqueous solutions of NaOH at a given concentration (0.5, 1.0, 1.5, 2.0, or 2.5 mol dm^{-3} NaOH) were prepared, *i.e.*, (Soln A) an alkaline solution containing 10 mmol dm^{-3} CD and 10 mmol dm^{-3} $CuSO_4$, and (Soln B) an alkaline solution containing 100 mmol dm^{-3} EDTA and 10 mmol dm^{-3} $CuSO_4$. A portion (2.0 cm^3) of Soln A was pipetted into a sample cell, and absorption spectrum was recorded. Then, 0.025 to 0.30 cm^3 potions Soln B were consecutively added to a sample cell. For each addition of Soln B, the absorption spectrum of the resulting solution was recorded. Changes in absorbance (*Abs*) at 685 nm were used for an analysis of the data. Changes in optical rotation (*P*) of Soln A upon consecutive additions of Soln B were similarly followed at λ=405 nm.

Determination of Equilibrium Constant for the Ligand-exchange Reaction of Cu_2CD with EDTA. The value of *Abs* at 685 nm for Soln A decreased with an addition of Soln B. Figure 4 shows plots of *Abs vs. v*, where *v* is the cumulative volume (cm^3) of Soln B added to 2 cm^3 of Soln A. On the other hand, the value of *P* at 405 nm for Soln A increased with an addition of Soln B (Fig. 5). It was postulated that Cu_2CD in Soln A reacts with EDTA in Soln B to give $Cu(edta)^{2-}$ and CD (Eq. 14).

$$Cu_2CD + 2edta^{4-} = 2Cu(edta)^{2-} + CD \qquad (14)$$

The molar absorbance of Cu_2CD at 685 nm is more than double that of $Cu(edta)^{2-}$; thus, the *Abs* value for Soln A decreases upon an addition of Soln B. Both EDTA and CD are optically inert at 685 nm. The molar optical rotation of Cu_2CD at 405 nm is smaller than that of CD. Therefore, the *P* value for Soln A increases with an addition of Soln B. Both EDTA and $Cu(edta)^{2-}$ are polarimetrically inert at 405 nm.

An equilibrium constant (K_{lex}) for a ligand-exchange reaction expressed by Eq. 14 is given by

$$K_{lex} = w^2z/(yu^2), \qquad (15)$$

where *u*, *w*, *y*, and *z* are the equilibrium concentrations of EDTA, $Cu(edta)^{2-}$, Cu_2CD, and CD respectively. Let *a*, *b*, and *c* be the total concentrations of Cu, CD, and EDTA respectively,

$$a = 2y + w, \qquad (16)$$

$$b = y + z, \qquad (17)$$

and

$$c = u + w. \qquad (18)$$

From Eqs. 15 to 18, we obtain

$$(1+K_{lex})w^3 - [(a+2c)K_{lex}+a-2b]w^2 + cK_{lex}(2a+c)w - ac^2K_{lex} = 0. \qquad (19)$$

If the value of K_{lex} is given, it is possible to determine the *w* value by solving Eq. 19 under conditions where *w* is a positive real number and is smaller than *a* and *c*. When *w* is thus determined, the values of *y* and *z* are calculated by $y=(a-w)/2$ and $z=b-y$. Then, the observed *Abs* and *P* values are given by

$$Abs = \varepsilon_1 w + \varepsilon_2 y \qquad (20)$$

and

$$P = f_0 z + f_2 y, \qquad (21)$$

where ε_1 and ε_2 are the molar absorption coefficients at λ=685 nm for $Cu(edta)^{2-}$ and Cu_2CD respectively, and f_0 and f_2, the molar optical rotations at λ=405 nm for CD and Cu_2CD respectively. Although it is possible to determine directly the values of ε_1, ε_2, f_0, and f_2 by spectrophotometric and polarimetric measurements of solutions containing individual complexes, these quantities as well as K_{lex} were estimated by analyzing relationships between *Abs* or *P* and *v* (the cumulative volume of Soln B added to 2 cm^3 of Soln A) by use of the least-squares curve-fitting method with a FACOM M-140F computer at Shimane University. The values of ε_1 and ε_2, thus estimated, virtually agreed with those directly determined. However, the values of f_0 and f_2 did not always agree. Therefore, the value of f_0 was fixed in the analytical computation to be 32.8 deg cm^{-1} mol^{-1} dm^3 for α-CD and 41.4 deg cm^{-1} mol^{-1} dm^3 for β-CD, which were experimentally determined. This calculation improvement gave reasonable f_2 and K_{lex} values for both α- and β-CD systems.

Results and Discussion

Table 1 shows the K_{dsp} values as well as the molar

Table 1. Parameters for the disproportionation reaction of Cuα-CD to Cu_2 α-CD and α-CD at 25 °C

[NaOH]	Spectrophotometry			Polarimetry		
	ε_1	ε_2	K_{dsp}	Δf_1	Δf_2	K_{dsp}
mol dm^{-3}	cm^{-1} mol^{-1} dm^3	cm^{-1} mol^{-1} dm^3		deg cm^{-1} mol^{-1} dm^3	deg cm^{-1} mol^{-1} dm^3	
1.0	36	157	17.0	34	142	17.3
1.5	42	155	11.0	36	142	12.3
2.0	42	156	10.2	36	144	7.5
2.5	41	151	7.3	33	142	6.6

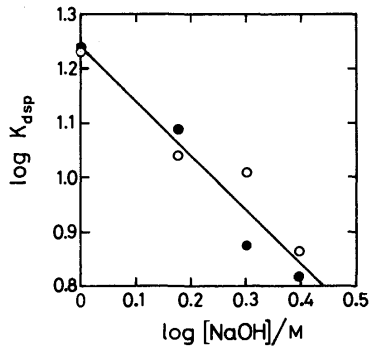

Fig. 6. Plots of log K_{dsp} *vs.* log [NaOH] for a Cu_2-α-CD system at 25 °C. The K_{dsp} values were determined by spectrophotometry (○) and polarimetry (●). 1 M = 1 mmol dm^{-3}.

absorption coefficients (ε_1 and ε_2) and the differences (Δf_1 and Δf_2) in molar optical rotation determined for a Cu-α-CD system by a least-squares analysis of the spectrophotometric and polarimetric data in Figs. 1 and 3. The K_{dsp} values estimated by the two methods agreed fairly well with each other at every NaOH concentration, and decreased with increasing NaOH concentration. The ε_1, ε_2, Δf_1, and Δf_2 values were virtually constant, irrespective of the NaOH concentration. The average values were $\varepsilon_1 = 40 \pm 2$ cm^{-1} mol^{-1} dm^3, $\varepsilon_2 = 154 \pm 2$ cm^{-1} mol^{-1} dm^3, $\Delta f_1 = 35 \pm 1$ deg cm^{-1} mol^{-1} dm^3, and $\Delta f_2 = 143 \pm 1$ deg cm^{-1} mol^{-1} dm^3. The molar optical rotation (f_0) of α-CD at $\lambda = 405$ nm was determined to be 32.8 deg cm^{-1} mol^{-1} dm^3, so that the molar optical rotations (f_1 and f_2) of Cuα-CD and $Cu_2\alpha$-CD were evaluated to be -2 ± 1 and -110 ± 1 deg cm^{-1} mol^{-1} dm^3, respectively.

Figure 6 shows a plot of log K_{dsp} *vs.* log [NaOH]. The plot is virtually linear, and the correlation analysis with the least-squares method gave Eq. 22.

$$\log K_{dsp} = 1.24 - 0.99 \log [\mathrm{NaOH}]; \quad n = 8,\ r = -0.969 \quad (22)$$

In this equation, n is the number of data and r, a correlation coefficient. The slope of the plot is *ca.* -1.0, which shows that the disproportionation reaction of Cuα-CD to $Cu_2\alpha$-CD and CD is accompanied by the release of 1 mole of OH$^-$. Thus, the stoichiometry for the disproportionation reaction is represented by

$$2[Cu(AH_2)(OH)_2]^{2-} \rightleftharpoons [Cu_2(A)(OH)_2]^{2-} + AH_3^- + OH^- + H_2O, \quad (23)$$

where AH_4 refers to α-CD. It is reasonable to consider that one of the hydroxyl groups of α-CD dissociates in such a strongly alkaline solution to give an alkoxide anion (AH_3^-), since the pK_a value for α-CD is 12.332 at 25 °C.[4]

Tables 2 and 3 show the K_{lex}, ε_1, ε_2, f_0, and f_2 values determined for the ligand-exchange reactions of $Cu_2\alpha$-CD and $Cu_2\beta$-CD respectively with EDTA by the least-squares analyses of spectrophotometric and polarimetric data. The K_{lex} values estimated by the two methods agreed well with each other at every NaOH concentration, and they decreased rapidly with an increasing concentration of NaOH. The values of ε_1, ε_2, and f_2 were virtually constant, irrespective of the NaOH concentration. The average values were $\varepsilon_1 = 32 \pm 1$ cm^{-1} mol^{-1} dm^3, $\varepsilon_2 = 135 \pm 2$ cm^{-1} mol^{-1} dm^3, and $f_2 = -97 \pm 2$ deg cm^{-1} mol^{-1} dm^3 for a α-CD system and $\varepsilon_1 = 32 \pm 1$ cm^{-1} mol^{-1} dm^3, $\varepsilon_2 = 132 \pm 1$ cm^{-1} mol^{-1} dm^3, and $f_2 = -85 \pm 2$ deg cm^{-1} mol^{-1} dm^3 for a β-CD system. The f_2 value, thus estimated for a α-CD system, is in fair agreement with the corresponding value estimated above from the disproportionation reaction.

Figure 7 shows plots of log K_{lex} *vs.* log [NaOH] for both α- and β-CD systems. The correlation analysis with the least-squares method gave Eq. 24 for a α-CD system and Eq. 25 for a β-CD system.

$$\log K_{lex} = 0.38 - 4.54 \log [\mathrm{NaOH}]; \quad n = 10,\ r = -0.995 \quad (24)$$

$$\log K_{lex} = 0.08 - 4.17 \log [\mathrm{NaOH}]; \quad n = 10,\ r = -0.995 \quad (25)$$

The slopes of the plots are *ca.* 4—5. These results suggest that the stoichiometry of the ligand-exchange reaction is mostly expressed by

$$[Cu_2(A)(OH)_2]^{2-} + 2\mathrm{edta}^{4-} + 3H_2O \rightleftharpoons 2[Cu(\mathrm{edta})]^{2-} + AH_3^- + 5OH^-. \quad (26)$$

According to Gorelova, *et al.*,[5] [Cu(edta)]$^{2-}$ reacts with OH$^-$ to afford [Cu(edta)(OH)]$^{3-}$ in an alkaline solution. Then, it is possible that a part of [Cu(edta)]$^{2-}$ in Eq. 26 is converted to [Cu(edta)(OH)]$^{3-}$

TABLE 2. PARAMETERS FOR THE LIGAND-EXCHANGE REACTION OF $Cu_2\alpha$-CD WITH EDTA AT 25°C

[NaOH]	Spectrophotometry			Polarimetry		
	ε_1	ε_2	K_{lex}	f_0	f_2	K_{lex}
mol dm^{-3}	cm^{-1} mol^{-1} dm^3	cm^{-1} mol^{-1} dm^3		deg cm^{-1} mol^{-1} dm^3	deg cm^{-1} mol^{-1} dm^3	
0.5	35	138	72.8	32.8	−100	48.0
1.0	34	137	2.03	32.8	−102	2.22
1.5	32	138	0.368	32.8	−97	0.427
2.0	29	132	0.0616	32.8	−94	0.127
2.5	29	130	0.0322	32.8	−90	0.0562

TABLE 3. PARAMETERS FOR THE LIGAND-EXCHANGE REACTION OF $Cu_2\beta$-CD WITH EDTA AT 25°C

[NaOH]	Spectrophotometry			Polarimetry		
	ε_1	ε_2	K_{lex}	f_0	f_2	K_{lex}
mol dm^{-3}	cm^{-1} mol^{-1} dm^3	cm^{-1} mol^{-1} dm^3		deg cm^{-1} mol^{-1} dm^3	deg cm^{-1} mol^{-1} dm^3	
0.5	34	132	26.5	41.4	−86	21.2
1.0	34	133	1.26	41.4	−89	1.14
1.5	30	132	0.131	41.4	−86	0.226
2.0	31	131	0.0576	41.4	−84	0.0774
2.5	30	131	0.0257	41.4	−79	0.0397

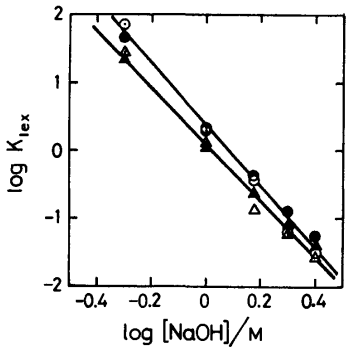

Fig. 7. Plots of log K_{lex} *vs.* log[NaOH] for Cu_2 α-CD-EDTA (○ and ●) and $Cu_2\beta$-CD-EDTA (△ and ▲) systems at 25°C. The K_{lex} values were determined by spectrophotometry (○ and △) and polarimetry (● and ▲). 1 M=1 mol dm^{-3}.

with the consumption of one mole of OH^-. This may be a reason why the slopes of the plots in Fig. 7 are less than 5.

Brunetti, *et al.*[6] have determined the log K value for a reaction represented by Eq. 27 to be 18.87.

$$Cu^{2+} + edta^{4-} \rightleftharpoons [Cu(edta)]^{2-} \quad (27)$$

By combining Eq. 27 with Eq. 26, we obtain

$$2Cu^{2+} + AH_3^- + 5OH^- \rightleftharpoons [Cu_2(A)(OH)_2]^{2-} + 3H_2O. \quad (28)$$

The log K value for this reaction was calculated to be 37.41 for a α-CD system and 37.66 for a β-CD system at [NaOH]=1.0 mol dm^{-3}. Furthermore, we obtain from Eqs. 23 and 28

$$Cu^{2+} + AH_3^- + 3OH^- \rightleftharpoons [Cu(AH_2)(OH)_2]^{2-} + H_2O. \quad (29)$$

The log K value for this reaction was calculated to be 18.09 for a α-CD system at [NaOH]=1.0 mol dm^{-3}. These results indicate that both of Cuα-CD and $Cu_2\alpha$-CD are very stable in 1.0 mol dm^{-3} NaOH, although they are unstable in a neutral aqueous solution.

It has been suggested in a previous paper[2] that the structure of a $Cu_2\beta$-CD complex is $[Cu_2(A)(OH)(O)]^{3-}$ rather than $[Cu_2(A)(OH)_2]^{2-}$. If this suggestion is valid, the stoichiometry of the ligand-exchange reaction for a β-CD system should be expressed by

$$[Cu_2(A)(OH)(O)]^{3-} + 2edta^{4-} + 4H_2O \rightleftharpoons 2[Cu(edta)]^{2-} + AH_3^- + 6OH^-, \quad (30)$$

instead of Eq. 26. Then, the slope of the plot of log K_{lex} *vs.* log [NaOH] should be equal to −6 for a β-CD system. However, the slope experimentally determined was −4.17. It is not clear why this discrepancy was brought about. It is possible to consider that the alkoxide ion (AH_3^-) of β-CD dissociates further into a divalent anion (AH_2^{-2}) in an solution higher in alkaline concentration than 1 mol dm^{-3}. The formation of AH_2^{2-}, together with the formation of $[Cu(edta)(OH)]^{3-}$, would consume OH^-, resulting in a decrease in the slope of the log K_{lex} *vs.* log [NaOH] plot. Although this explanation is plausible, there is no clear evidence supporting it at the present time. A more detailed examination is currently under way for a β-CD system.

References

1) Y. Matsui, T. Kurita, and Y. Date, *Bull. Chem. Soc.*

Jpn., **45**, 3229 (1972).
2) Y. Matsui, T. Kurita, M. Yagi, T. Okayama, K. Mochida, and Y. Date, *Bull. Chem. Soc. Jpn.*, **48**, 2187 (1975).
3) Y. Matsui and D. Suemitsu, *Bull. Chem. Soc. Jpn.*, **58**, 1658 (1985).
4) R. I. Gelb, L. M. Schwartz, and D. A. Laufer, *Bioorg. Chem.*, **11**, 274 (1982).
5) R. I. Gorelova, V. A. Babich, and I. P. Gorelov, *Zh. Neorg. Khim.*, **16**, 1873 (1971).
6) A. P. Brunetti, G. H. Nancollas, and P. N. Smith, *J. Am. Chem. Soc.*, **91**, 4680 (1969).

ESR Studies on Salicylaldehyde Schiff Base Complexes of Copper(II). I. Bis(*N*-cyclohexyl- and *N*-cycloheptyl-salicylideneaminato)copper(II) Complexes and Their Derivatives in Polycrystals

Akira TAKEUCHI, Shoichiro YAMADA, and Hiroshi YOKOI†,*
Institute of Chemistry, College of General Education, Osaka University, Toyonaka, Osaka 560
†*Chemical Research Institute of Non-aqueous Solutions, Tohoku University, Sendai 980*
(Received May 11, 1985)

Twelve of the title complexes including color isomers show powder ESR spectra of various line shapes. These complexes are a novel series of copper(II) complexes which have very weak intermolecular spin-exchange interactions in crystals. Brown complexes and most green complexes show monomer and dimer ESR spectra, respectively. It is demonstrated by ESR measurements that the above green complexes are transformed into the brown ones only by grinding those green crystals finely and forcefully with agate mortar and pestle.

There have been many works showing that metal(II) complexes with bidentate *N*-substituted salicylideneamines (I) (abbreviated as M(X-sal-R)$_2$) have various configurations, depending upon R and X.[1-3] These

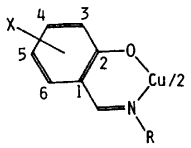

I

complexes often show color isomerism. This kind of studies about the copper(II) complexes can also be carried out by the ESR method in new and interesting aspects. The purpose of this paper is to report powder ESR results for twelve of the complexes, in connection with their structures and properties in crystals. In this work, the complexes with R=cyclohexyl, 3,3,5-trimethylcyclohexyl, and cycloheptyl (abbreviated as Ch, Me$_3$Ch, and Cp, respectively) have been dealt with.

Experimental

All the salicylaldehyde Schiff base complexes of copper(II) were prepared according to the literature,[4] using commercially available reagents. Color isomers for some of the complexes were obtained as previously reported.[5] Twelve complexes prepared in this work are as follows: green Cu(H-sal-Ch)$_2$, brown Cu(H-sal-Ch)$_2$, green Cu(5-Cl-sal-Ch)$_2$, brown Cu(5-Cl-sal-Ch)$_2$, brown Cu(5-Br-sal-Ch)$_2$, green Cu(5-NO$_2$-sal-Ch)$_2$, greenish brown Cu(H-sal-Me$_3$Ch)$_2$, brown Cu(3-MeO-sal-Me$_3$Ch)$_2$, olive brown Cu(5,6-benzo-sal-Ch)$_2$, brown Cu(H-sal-Cp)$_2$, green Cu(5-Cl-sal-Cp)$_2$, and green Cu(5-Br-sal-Cp)$_2$, where Cu(5,6-benzo-sal-Ch)$_2$ denotes bis(*N*-cyclohexyl-2-hydroxy-1-naphthylmethyleneaminato)-copper(II).

X-Band ESR spectra for the above complexes in polycrystals were measured at room temperature and at the temperature of liquid nitrogen with a Varian E-4 ESR spectrometer. Sample powders for ESR measurements were obtained by grinding crystals of the complexes with agate mortar and pestle.

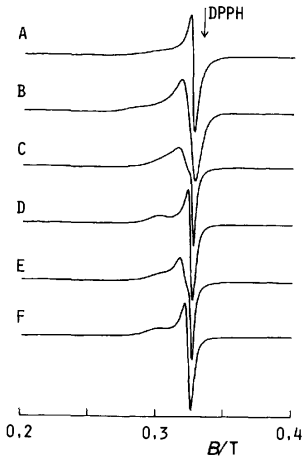

Fig. 1. Powder ESR spectra (X-band; room temperature); A, brown Cu(H-sal-Ch)$_2$; B, brown Cu(H-sal-Me$_3$Ch)$_2$; C, brown Cu(H-sal-Cp)$_2$; D, brown Cu(5-Cl-sal-Ch)$_2$; E, brown Cu(5-Br-sal-Ch)$_2$; F, green Cu(5-NO$_2$-sal-Ch)$_2$.

Results and Discussion

Powder ESR Spectra. The powder ESR spectra of the present complexes at room temperature have a wide variety of line shapes, as shown in Figs. 1—5. These spectra had almost no temperature dependence.

Figure 1 shows the powder ESR spectra of five brown or brownish complexes and green Cu(5-NO$_2$-sal-Ch)$_2$. These spectra appear within a comparatively narrow field range 0.26—0.35 T, and are of a common spectral type for polycrystals of monomeric copper(II) complexes,[6] except that the spectra are very broad in line shape. Brown Cu(H-sal-Ch)$_2$, one of the complexes in Fig. 1, really has one monomeric molecule in the unit cell, as determined by X-ray structural analysis;[7] interestingly, this complex has planar coordination. The spectra in Fig. 1 are so broad in line shape that g anisotropies are barely observed. This line broadening is probably due to insufficient spin-exchange narrowing toward the coalescense of four copper hyperfine lines to a single line, meaning that intermolecular spin-exchange interaction energies (J)

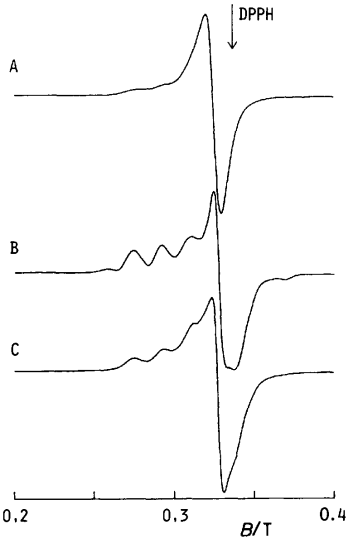

Fig. 2. Powder ESR spectra (X-band; room temperature); A, brown Cu(3-MeO-sal-Me_3Ch)$_2$; B, olive brown Cu(5,6-benzo-sal-Ch)$_2$ (softly and coarsely ground powder); C, olive brown Cu(5,6-benzo-sal-Ch)$_2$ (forcefully and finely ground powder).

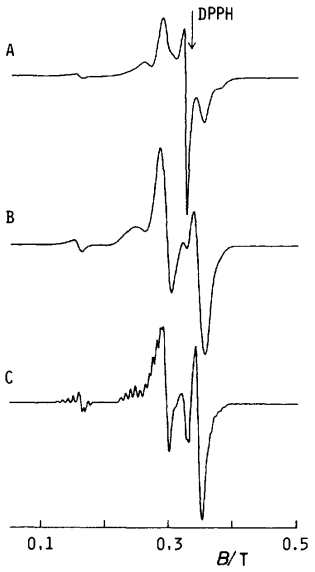

Fig. 3. Powder ESR spectra (X-band; room temperature) and frozen solution ESR spectrum (X-band; 77 K): A, green Cu(H-sal-Ch)$_2$; B, green Cu(5-Br-sal-Cp)$_2$; C, Cu(5-Br-sal-Ch)$_2$ in toluene (almost saturated).

are as small as the order of 0.1 cm^{-1},[8] On the other hand, in Fig. 2, hyperfine structures are clearly observed in the low-field spectral part. This fact indicates that the complexes of Fig. 2 are monomeric in the crystals with $|J| \lesssim 0.02$ cm^{-1}. The existence of such complexes in this series supports the above interpretation of the line broadening in Fig. 1. In Fig. 2(B), extra weak ESR signals at both sides of the monomer signal are clearly observed, but are of obscure origin at present. Further discussion on Fig. 2 (B) and (C) will be given later.

The powder ESR spectra in Fig. 3, whose signals occur over a much wider field range, are quite different in line shape from those in Figs. 1 and 2. The most remarkable feature of Fig. 3(A) and (B) is the appearance of weak half-field signals around 0.15 T. This spectral pattern is typical of triplet-state copper(II) dimers, as evidenced by the fact that Fig. 3(B) is almost identical in line shape with the frozen-solution spectrum of Cu(5-Br-sal-Ch)$_2$ shown in Fig. 3(C), which can be analyzed as a typical dimer spectrum by computer simulation;[9] detailed analyses of this kind of spectra with such well-resolved hyperfine structures as shown in Fig. 3(C) will be given in the next paper in this series of work.[10] Figure 3(B) is of the spectral type accompanying no spin-exchange narrowing effect of hyperfine lines, indicating that the inter-dimer spin-exchange interaction of green Cu(5-Br-sal-Cp)$_2$ is as extremely weak as $|J| \lesssim 0.01$ cm^{-1}. The powder ESR spectra of green Cu(5-Cl-sal-Cp)$_2$ and green Cu(5-Cl-sal-Ch)$_2$ were similar to Fig. 3(A) and (B), respectively. The peak positions of Fig. 3(A) in the range 0.2—0.4 T slightly shifts toward the center, compared with those of Fig. 3(B). This means that the $|J|$ value of the former system is a little larger than that of the latter one. All the copper(II) complexes in this work have thus been found to be a novel series of sample systems which have very weak intermolecular spin-exchange interactions in crystals, suggesting that bulky cyclohexyl and related groups may have some steric effect in breaking easy spin-exchange pathways in crystals. As has been estimated above, green Cu(H-sal-Ch)$_2$ exists as dimers in crystals. This is really consistent with the structural result obtained by X-ray analysis,[11] where monomeric halves in the dimer fundamentally have a flattened tetrahedral coordination. This work has revealed that all the complexes which show dimer ESR spectra are green ones, while brown or brownish complexes show monomer spectra; green Cu(5-NO_2-sal-Ch)$_2$ forms an exception, but this might result from some effect of the strong electron-withdrawing group of 5-NO_2.

Easy Transformation of Crystal Forms. We have found that some complexes in this study show different powder ESR spectra, according to how finely and forcefully their crystals are ground into powder with agate mortar and pestle, as exemplified in Figs. 2, 4, and 5; this will hereafter be called grinding effect. Figure 4 demonstrates this effect for green Cu(H-sal-Ch)$_2$; its softly and coarsely ground powder shows Fig. 4(A), and, by further grinding the powder finely and forcefully, the spectrum changes to Fig. 4(B), in which a sharp absorption near 0.32 T remarkably increases in intensity relatively to other signals. It is interesting to note that this sharp signal completely agrees with Fig. 1(A) for its brown complex, indicating that polycrystals of green Cu(H-sal-Ch)$_2$ are transformed into those of the brown form by the grinding

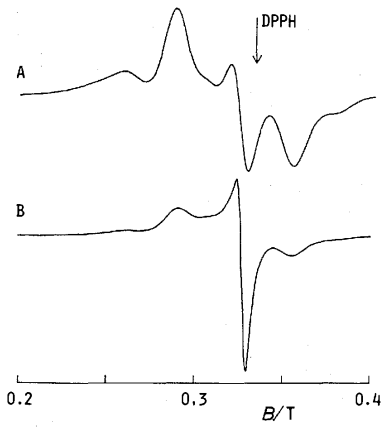

Fig. 4. Powder ESR spectra of green Cu(H-sal-Ch)$_2$ (X-band; room temperature): A, softly and coarsely ground powder; B, forcefully and finely ground powder.

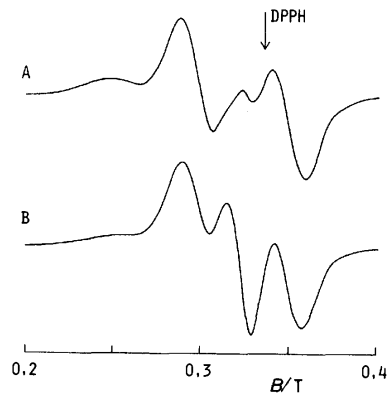

Fig. 5. Powder ESR spectra of green Cu(5-Cl-sal-Ch)$_2$ (X-band; room temperature): A, softly and coarsely ground powder; B, forcefully and finely ground powder.

effect. Roughly speaking, the grinding effect may be resolved into stress and frictional heat effects. Although heating the brown complex at 165—175 °C is known to yield the green one,[1,12] the brown complex showed no grinding effect. This fact suggests that the grinding effect is not always frictional heat effect, but may essentially be stress effect. The presumption that the brown form is favored by stress or pressure is also supported by the fact that the brown form of Cu(H-sal-Ch)$_2$ is slightly higher in density than the green one.[11] From a molecular-level point of view, the observation of the above grinding effect surprisingly means that a drastic molecular rearrangement from dimers to monomers, accompanied by molecular conformational changes, can take place easily in crystals without their melting.

Figure 5 shows another example of grinding effect for green Cu(5-Cl-sal-Ch)$_2$. Similarly, the green complex was transformed into the brown one by grinding effect. Green Cu(5-Cl-sal-Cp)$_2$ and green Cu(5-Br-sal-Cp)$_2$ showed spectral changes similar to those in Figs. 4 and 5, respectively, by grinding effect. A different spectral change due to the effect was also observed for olive brown Cu(5,6-benzo-sal-Ch)$_2$, as shown in Fig. 2. In this case, the grinding effect weakens the intensities of signals at both sides of the monomer's one, and slightly changes the monomer spectrum itself, suggesting that this complex possibly has two slightly different crystal forms. Judging from all these observations on the grinding effect, it is said that we must be careful of the possibility of the effect in any experiment where the grinding operation of crystals is needed.

References

1) S. Yamada and A. Takeuchi, *Coord. Chem. Rev.*, **43**, 187 (1982).

2) S. Yamada, *Coord. Chem. Rev.*, **1**, 415 (1966); S. Yamada, "Novel in Coordination Chemistry," ed by B. J. Trzebiatowska and M. Rudolph, Polish Acad. Sci. (1974), p. 189.

3) R. H. Holm, G. W. Everett, Jr., and A. Chakravorty, *Prog. Inorg. Chem.*, **7**, 83 (1966); R. H. Holm and M. J. O'Connor, *ibid.*, **14**, 241 (1971).

4) P. Pfeiffer and H. Glaser, *J. Prakt. Chem.*, **153**, 265 (1939).

5) A. Takeuchi and S. Yamada, *Rev. Roum. Chim.*, **22**, 781 (1977).

6) B. J. Hathaway and D. E. Billing, *Coord. Chem. Rev.*, **5**, 143 (1970); H. Yokoi, M. Sai, T. Isobe, and S. Ohsawa, *Bull. Chem. Soc. Jpn.*, **45**, 2189 (1972); H. Yokoi, *ibid.*, **47**, 639 (1974).

7) H. Tamura, K. Ogawa, A. Takeuchi, and S. Yamada, *Chem. Lett.*, **1977**, 889.

8) H. Abe, K. Ono, I. Hayashi, J. Shimada, and K. Iwanaga, *J. Phys. Soc. Jpn.*, **9**, 814 (1954); H. Abe and K. Ono, *ibid.*, **11**, 947 (1956); K. Ono and M. Ohtsuka, *ibid.*, **13**, 206 (1958); A. Abragam and B. Bleaney, "Electron Paramagnetic Resonance of Transition Ions," Clarendon Press, Oxford (1970), p. 527.

9) M. Chikira and T. Isobe, *Bull. Chem. Soc. Jpn.*, **45**, 3006 (1972); H. Yokoi and M. Chikira, *J. Chem. Soc., Dalton Trans.*, **1975**, 2101; T. D. Smith and J. R. Pilbrow, *Coord. Chem. Rev.*, **13**, 173 (1974).

10) H. Yokoi, A. Takeuchi, and S. Yamada, *Bull. Chem. Soc. Jpn.*, **58**, 2990 (1985).

11) H. Tamura, K. Ogawa, A. Takeuchi, and S. Yamada, *Bull. Chem. Soc. Jpn.*, **52**, 3522 (1979).

12) I. Masuda, unpublished data.

ESR Studies on Salicylaldehyde Schiff Base Complexes of Copper(II). II.[1] Bis(*N*-cyclohexyl- and *N*-cycloheptyl-salicylideneaminato)copper(II) Complexes and Their Derivatives in Solutions

Hiroshi YOKOI,* Akira TAKEUCHI,† and Shoichiro YAMADA†
Chemical Research Institute of Non-aqueous Solutions, Tohoku University, Sendai 980
†*Institute of Chemistry, College of General Education, Osaka University, Toyonaka, Osaka 560*
(Received May 11, 1985)

Ten of the title complexes in frozen toluene solutions and occasionally in other solutions have been studied by the ESR method. Most of the complexes showed both monomer and dimer ESR spectra simultaneously, and the equilibrium constant for 2 monomer ⇆ dimer has been determined by analyzing the concentration dependence of the intensity ratios of dimer and monomer ESR signals. The results indicate that the equilibrium constants of the complexes are dependent in a marked but subtle way, not upon the bulkiness of *N*-substituents, but upon both kind and position of the substituents introduced into the ligand benzene rings, and that the equilibrium constants are solvent-dependent. All the observed dimer ESR spectra were similar to each other, and computer simulation analysis of the spectra has revealed that the dimers formed in toluene have the same structures as that in green crystals of bis(*N*-cyclohexylsalicylideneaminato)copper(II). On the other hand, monomers of the title complexes have been found to show various degrees of tetrahedral distortion in the coordination geometry.

The title complexes (I) (abbreviated as Cu(X-sal-R)$_2$†) have various conformations, depending upon R

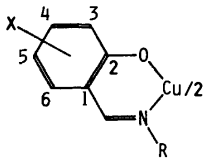

I

and X, and show color isomerism.[2–4] X-Ray structural analyses and ESR studies have confirmed that these complexes are monomeric or dimeric in crystals.[1,5,6] Coordination chemistry of these complexes in solutions is now of great interest. We report here ESR results of these complexes in solutions, especially in toluene, with the intention of elucidating their structures and properties.

Experimental

The same sample complexes as in the previous work were used here.[1] X-Band ESR spectra were measured for the complexes in solutions at the temperature of liquid nitrogen and at room temperature, with a Varian E-4 ESR spectrometer. Commercial Nakarai's "spectrograde" solvents were used without further purification. The solubilities of the complexes in toluene at room temperature were determined spectrophotometrically.

Results and Discussion

Monomeric Complexes. Most of the present complexes in frozen toluene solutions simultaneously showed both monomer and dimer ESR spectra superimposed on each other. In these solutions, monomers and dimers are in equilibrium, since the intensity ratio of dimer and monomer ESR signals for any of the complexes increases with its concentration,[7–9] as exemplified by Fig. 1. On the other hand, Cu(H-sal-Cp)$_2$ and Cu(3-MeO-sal-Ch)$_2$ at any concentration did not show dimer ESR spectra at all, but monomer spectra alone, as shown in Fig. 2; Cu(H-sal-*t*-Bu)$_2$ is just the same in this respect.[10,11] Figure 2(C) is the monomer ESR spectrum of Cu(H-sal-Ch)$_2$. Its line shape was invariant at any low concentration, but is slightly different from those of the other two spectra

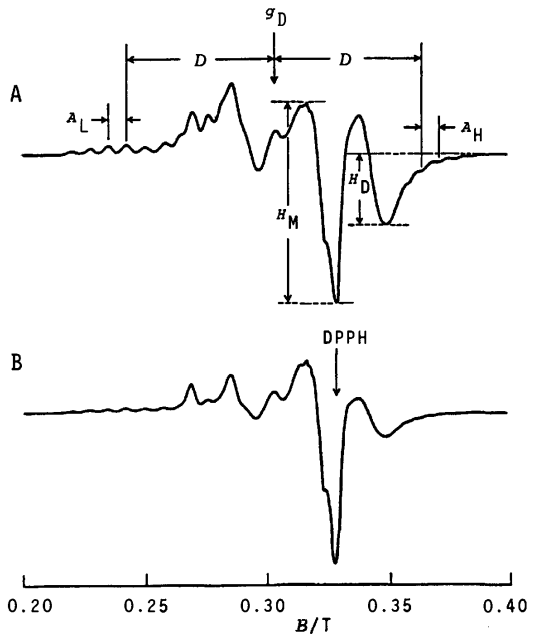

Fig. 1. X-Band ESR spectra of Cu(5-Br-sal-Cp)$_2$ in toluene at 77 K: A, 2.5×10^{-3} M; B, 5.0×10^{-4} M. The parameters of g_D, D, A_L, A_H, H_D, and H_M are defined in A (see text as to the meanings of these parameters).

†The abbreviations of substituents used in this work are as follows: Ch, cyclohexyl; Me$_3$Ch, 3,3,5-trimethylcyclohexyl; Cp, cycloheptyl; Me, methyl; MeO, methoxyl; *i*-Pr, isopropyl; *t*-Bu, *t*-butyl.

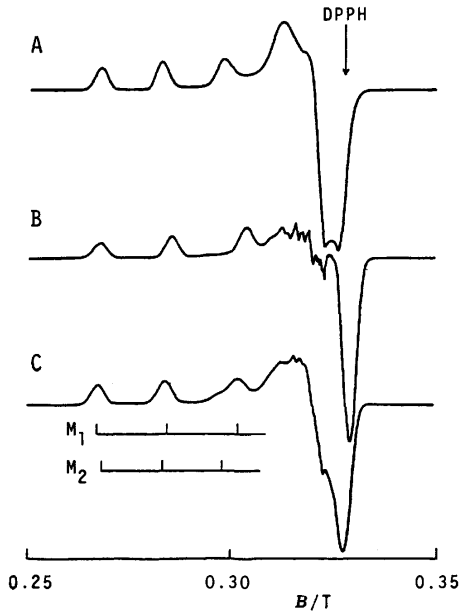

Fig. 2. X-Band ESR spectra of the monomeric Cu(X-sal-R)$_2$ complexes in toluene at 77 K: A, Cu(H-sal-Cp)$_2$, 2.5×10^{-3} M; B, Cu(3-MeO-sal-Ch)$_2$, 2.5×10^{-3} M; C, Cu(H-sal-Ch)$_2$, 5.0×10^{-4} M. In C, the low field spectral part is analyzed as due to two different monomeric species, M_1 and M_2.

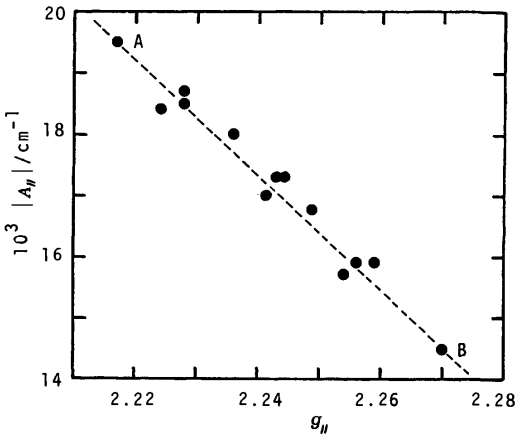

Fig. 3. Plot of $A_{\parallel}$ against $g_{\parallel}$ for the monomeric Cu(X-sal-R)$_2$ complexes; A and B, plots for Cu(H-sal-Me)$_2$ and Cu(H-sal-*t*-Bu)$_2$, respectively; the other plots, from Table 1.

in Fig. 2 at the low field part. These observations are quite similar to those of Cu(H-sal-*i*-Pr)$_2$,[11] showing that there are two different monomeric species for Cu(H-sal-Ch)$_2$ in toluene.

Table 1 summarizes the $g_{\parallel}$ and $A_{\parallel}$ values determined for all the monomeric complexes in frozen toluene solutions, together with the g_0 and A_0 values in fluid toluene solutions at room temperature. A series of Cu(H-sal-R)$_2$ are known to show various degrees of tetrahedral distortion in the coordination geometry, depending upon the bulkiness of R;[11,12] for instance, the dihedral angles between two chelate rings for Cu(H-sal-Me)$_2$ and Cu(H-sal-*t*-Bu)$_2$ in crystals are 0 and 62°, respectively, and the latter is the largest of the structures reported so far.[13] A linear relationship between $g_{\parallel}$ and $A_{\parallel}$ has been demonstrated for these complexes, as shown in Fig. 3 by a dotted straight line drawn through the data of Cu(H-sal-Me)$_2$ and Cu(H-sal-*t*-Bu)$_2$.[12] Plots of the $g_{\parallel}$ and $A_{\parallel}$ values from Table 1 have also been found to fall on the same straight line (Fig. 3), indicating that the present monomeric complexes in toluene show various degrees of the tetrahedral distortion ranging from almost null to that of Cu(H-sal-*t*-Bu)$_2$, in spite of the fact that Ch, Cp, and their derivatives are almost the same in bulkiness.

Dimer Formation Constants. Undoubtedly, a monomer (M)-dimer (D) equilibirum, $2M \rightleftharpoons D$, is established in the solution systems for which both monomer and dimer ESR spectra are simultaneously observed, as has been confirmed so far.[7-9] The value of $R=H_D/H_M \propto [D]/[M]$ can be directly obtained from each spectrum, where H_D and H_M are the peak heights of any specific dimer and monomer ESR signals,

Table 1. Monomer ESR parameters[a]

Cu(X-sal-R)$_2$ X	R	$g_{\parallel}$	$10^4\,\lvert A_{\parallel}\rvert$ / cm^{-1}	g_0	$10^4\,\lvert A_0\rvert$ / cm^{-1}
H	Ch[b]	2.236	180	2.119	66
		2.254	157		
5-Cl	Ch	2.241	170	2.119	67
5-Br	Ch	2.243	173	2.119	64
5-NO_2	Ch	2.252	167	2.120	67
H	Me_3Ch	2.228	185	2.117	67
3-MeO	Me_3Ch	2.224	184	2.115	68
5,6-benzo	Ch	2.228	187	2.114	68
H	Cp	2.256	159	2.119	66
5-Cl	Cp	2.259	159	2.116	62
5-Br	Cp	2.244	173	2.119	65

a) The $g_{\parallel}$ and $A_{\parallel}$ values were determined from frozen toluene solution ESR spectra at 77 K, and the g_0 and A_0 values, from fluid toluene solution ESR spectra at room temperature. b) Two different species were identified.

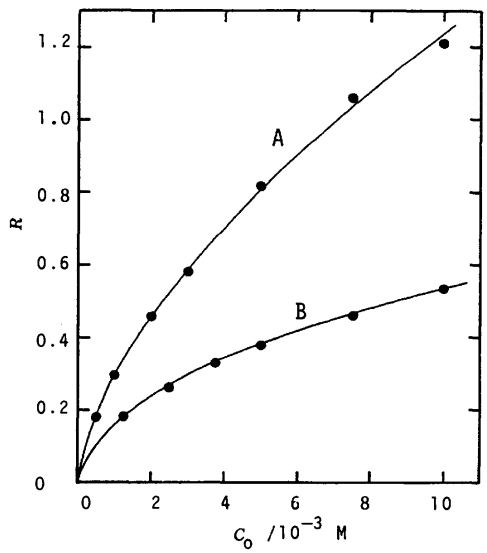

Fig. 4. Relationship between R and C_0 for Cu(5-Br-sal-Ch)$_2$ (A) and Cu(5-Cl-sal-Ch)$_2$ (B): (●), experimental; (——), calculated (see text).

respectively. Then, R is expressed as

$$R = (\sqrt{8KC_0+1}-1)/P$$

where K is the equilibrium or dimer formation constant, P the proportionality constant and C_0 the total concentration. K and P can be determined by fitting the above equation to experimental plots of R against C_0. The observation was made by quickly freezing a toluene solution in liquid nitrogen, using quartz sample tubes of the same size. The equilibrium constant obtained, therefore, is considered to be pertinent for a temperature somewhat lower than the freezing point of toluene. Throughout this work, the monomer and dimer ESR signals used for the determination of H_M and H_D respectively were selected as shown in Fig. 1. All the K, P, R, and C_0 values, together with the solubilities of the complexes in toluene, are listed in Table 2. Two examples of experimental plots of R against C_0 and their fitting curves are given in Fig. 4 for illustration.

As to the dimerization ability of the present complexes, much is elucidated from Table 2. Cu(H-sal-Cp)$_2$ has no dimerization ability, but its 5-halogeno derivatives have. Similarly, the 5-halogeno derivatives of Cu(H-sal-Ch)$_2$ dimerize much more easily than the parent complex. Cu(H-sal-Me$_3$Ch)$_2$ can dimerize a little more easily than Cu(H-sal-Ch)$_2$, but these complexes are roughly comparable in the K value to Cu(H-sal-Me)$_2$.[9] These facts indicate that the apparent bulkiness of N-substituents is not an important factor in the dimerization, except for N-t-Bu; not only Cu(H-sal-t-Bu)$_2$ but also its 5-halogeno and 5-NO$_2$ derivatives were found to have no dimerization ability. The intrinsic nature of the present dimerization, however, is so subtle that, for the 5-Cl and 5-Br derivatives of Cu(H-sal-Ch)$_2$, the former has a much larger K value than the latter, while, for those of Cu(H-sal-Cp)$_2$, the reverse is observed. It is noteworthy that drastic changes of K from 75 to 8.5×10^3 and 1.4×10^5 M^{-1} are brought about only by the introduction of 5-Cl and 5-NO$_2$ respectively into Cu(H-sal-Ch)$_2$. Similar enhancing effects of the nitro group on the dimerization ability of other kinds of planar complexes have been reported so far.[9,10] The K values of Cu(H-sal-Me)$_2$ and of its 5-Me, 5-Br, and 5-MeO derivatives were determined to be 2.4×10^2, 1.8×10^2, 2.3×10^3, and 2.1×10^3 M^{-1}, respectively;[8] clearly, the latter two are larger than the former two. The NO$_2$ and MeO substituents are representative π-electron-withdrawing and donating groups, respectively, and the halogeno substituents are also typical functional groups with remarkable substituent effects. From these facts it is clear that such influential groups as halogens, NO$_2$, and MeO at the 5-position have a common substituent effect of enhancing the present dimerization ability

Table 2. Values[a] of K, P, and R and solubility[b]

Cu(X-sal-R)$_2$		K	P	$R(10^3C_0)$[c]	Solubility
X	R	M^{-1}		M	M
H	Ch	75	38	0.068(20.00); 0.057(15.00); 0.043(10.00); 0.026(5.00); 0.016(2.50)	0.039
5-Cl	Ch	8,500	47.0	0.535(10.00); 0.460(7.50); 0.380(5.00); 0.331(3.75); 0.260(2.50); 0.180(1.25)	0.042
5-Br	Ch	800	5.82	1.210(10.00); 1.050(7.50); 0.814(5.00); 0.585(3.00); 0.458(2.00); 0.296(1.00); 0.180(0.50)	0.018
5-NO$_2$	Ch	140,000	1,200	0.017(0.40); 0.015(0.30); 0.012(0.20)	0.00048
H	Me$_3$Ch	105	67	0.100(68.8); 0.083(51.6); 0.065(34.4); 0.045(17.2); 0.027(8.6)	0.20
3-MeO	Me$_3$Ch	0			>0.75
5,6-benzo	Ch	140	34	0.032(2.98); 0.024(1.99); 0.013(1.00)	0.0047
H	Cp	0			0.13
5-Cl	Cp	44	55	0.052(40.0); 0.044(30.0); 0.034(20.0); 0.020(10.0)	0.094
5-Br	Cp	2,400	16.6	0.541(5.12); 0.490(4.26); 0.434(3.41); 0.373(2.56); 0.291(1.71); 0.191(0.85); 0.125(0.43)	0.029

a) See text as to the definition of K, P, and R. b) Solubility in toluene at room temperature. c) $R(C_0)$ expresses the observed R value at the total concentration of C_0.

Table 3. Dimer ESR parameters[a)]

Cu(X-sal-R)$_2$ X	R	Medium[b)]	g_D	10^3D	10^3A_L	10^3A_H
				cm^{-1}		
H	Ch	Toluene	2.172	62.4	7.6	6.6
		Polycrystal	2.11	61		
5-Cl	Ch	Toluene	2.172	61.4	7.8	7.0
		Polycrystal	2.16	62	7.6	
5-Br	Ch	Toluene	2.168	61.3	7.6	6.6
5-NO_2	Ch	Toluene	2.201	58.1	8.0	5
H	Me_3Ch	Toluene	2.172	59.1	7.8	6.6
5,6-benzo	Ch	Toluene	2.169	58.6	8.6	6.7
5-Cl	Cp	Toluene	2.168	61.2	7.6	6.6
5-Br	Cp	Toluene	2.172	61.7	7.6	6.8
		Polycrystal	2.15	62	8	
Calcd[c)]			2.169	62.0	8.0	6.6

a) See text (Fig. 1) as to the definition of dimer ESR parameters. b) Medium at 77 K. c) Values derived from the computer simulation spectrum (Fig. 5(A)), which was calculated with the following parameters, assuming a parallel planar dimer: $g_{\parallel}$=2.245, $g_{\perp}$=2.050, $A_{\parallel}$=0.0087 cm^{-1}, $A_{\perp}$=0.0015 cm^{-1}, r=3.67 Å, ξ=37°, ΔH_1=2.5 mT, ΔH_2=2.2 mT (ΔH_1, ΔM=1 spectral line width).

markedly. On the other hand, Cu(3-MeO-sal-Me_3Ch)$_2$ has no dimerization ability, as well as Cu(3-MeO-sal-Me)$_2$;[8)] furthermore, the K value of Cu(3-Me-sal-Me)$_2$ is smaller than that of Cu(H-sal-Me)$_2$,[8)] suggesting the possibility that 3-substituents depress the dimerization. Cu(5,6-benzo-sal-Ch)$_2$ dimerizes about twice more easily than Cu(H-sal-Ch)$_2$, suggesting that the enlargement of ligand π-electron systems may be a favorable factor in this dimerization, in conformity with the general belief that stacking interaction between planar molecules with π-electron systems is stronger, as the π-electron sytems are larger. In conclusion, there are remarkable substituent effects on the present dimerization ability, but further work is needed to analyze the dimerization ability in more detail.

Interestingly, Table 2 indicates that there is a tendency for the K value to increase with a decrease in the solubility. This seems to be qualitatively understandable from the generality that the solubility is lower, as the intermolecular interaction is stronger.

Dimeric Structures. The present dimer ESR spectral features can be described by the dimer ESR parameters, g_D, D, A_L, and A_H, which are defined in Fig. 1. Table 3 summarizes all these parameter values determined from frozen toluene solution spectra, together with those from several powder spectra.[1)] Inspection of this table indicates that all the dimers are essentially similar in structure, becasue their dimer ESR parameters are almost similar to each other. These dimer ESR spectra can be analyzed by the computer simulation method, assuming a parallel planar dimer with the distance (r) of 3.67 Å between the two copper atoms and the angle (ξ) of 37° between the $g_{\parallel}$ axis and the copper–copper axis, as has been applied previously;[14,15)] the simulation spectrum thus obtained is shown in Fig. 5(A), which approximately reproduces the observed spectrum of Cu(5-Br-sal-Ch)$_2$ (Fig. 5(B)). The dimer ESR parameters determined from this simulation spectrum are in good agreement with the observed ones, as shown in Table 3.

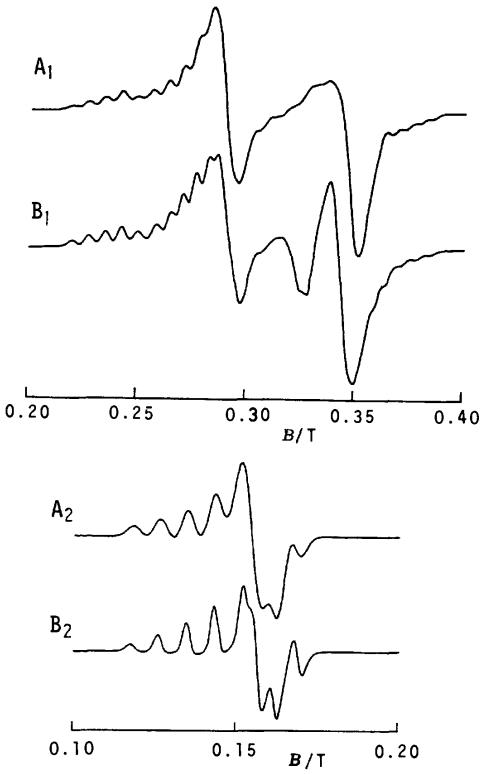

Fig. 5. Comparison between simulated and experimental dimer ESR spectra; A_1 and A_2, simulation spectra, calculated with the parameters of $g_{\parallel}$=2.245, $g_{\perp}$=2.050, $A_{\parallel}$=0.0087 cm^{-1}, $A_{\perp}$=0.0015 cm^{-1}, r=3.67 Å, ξ=37°, ΔH_1=2.5 mT, ΔH_2=2.2 mT, ν=9.23 GHz (the suffixes 1 and 2 correspond to ΔM=1 and 2 spectra, respectively; ΔH, line width; see text as to details of the computer simulation); B_1 and B_2, observed spectra for Cu(5-Br-sal-Ch)$_2$ in almost saturated toluene solutions at 77 K.

Interestingly, an X-ray crystal structure determina-

tion of green Cu(H-sal-Ch)$_2$ has revealed that the molecules exist as dimers of an approximately parallel planar type with r=3.38 Å and ξ=36°; actually, the monomeric halves of the dimers do not have a planar coordination geometry, but a somewhat tetrahedrally-distorted one with a dihedral angle of about 30°.[6] These r and ξ values are in fair agreement with those estimated above by the computer simulation method, in consideration of a point-dipole approximation used in the simulation in which the r value is generally estimated to be several % larger than the actual one.[16] Now, it is reasonably concluded that all the dimers formed in toluene have the same structures as that in green Cu(H-sal-Ch)$_2$ crystals.[††]

Solvent Effects of Dimerization. The dimer formation constants of the present complexes are remarkably solvent-dependent, as is usual with many other analogous systems.[15,18] The R values of Cu(5-Br-sal-Ch)$_2$ at 0.0050 M (1 M=1 mol dm^{-3}) in the mixtures of 4 parts of toluene and 1 part of pyridine, *N*,*N*-dimethylformamide (DMF), dichloromethane, methanol, and dimethyl sulfoxide (DMSO) were changed into 0, 6, 20, 38, and 98% of that in pure toluene, respectively. Interestingly, DMSO has almost no effects on the dimer formation, while DMF remarkably depresses it, in spite of both solvents being nearly equal in the basicity or donicity.[19] It seems likely that the above difference between DMSO and DMF is attributed to the presence of a π-system in the DMF molecule, because the so-called π-π interaction is considered as an important driving force for the dimerization of complexes with π-ligands; depressing effects of DMF on this kind of dimerization will be discussed elsewhere in more detail. Pyridine completely inhibits the dimerization by its strongly coordinating ability, the resultant complexes probably being sterically difficult of dimerization. It is to be noted that dichloromethane and methanol also have depressing effects on the dimerization. The solubility of Cu(5-Br-sal-Ch)$_2$ in methylcyclohexane, the saturated hydrocarbon of toluene, is remarkably low, compared with that in toluene. Accordingly, the dimer formation constant in methylcyclohexane was apparently larger than that in toluene, in agreement with the expectation discussed above.

[††] As seen in Table 3, green Cu(H-sal-Ch)$_2$ in polycrystals is somewhat different in the g_D value from others, but this might be a result of intricate magnetic interaction among dimers in the crystals.[1,17]

References

1) Part I: A. Takeuchi, S. Yamada, and H. Yokoi, *Bull. Chem. Soc. Jpn.*, **58**, 2987 (1985).

2) S. Yamada and A. Takeuchi, *Coord. Chem. Rev.*, **43**, 187 (1982).

3) S. Yamada, *Coord. Chem. Rev.*, **1**, 415 (1966); S. Yamada, "Novel in Coordination Chemistry," ed by B. J. Trzebiatowska and M. Rudolph, Polish Acad. Sci. (1974), p. 189.

4) R. H. Holm, G. W. Everett, Jr., and A. Chakravorty, *Prog. Inorg. Chem.*, **7**, 83 (1966); R. H. Holm and M. J. O'Connor, *ibid.*, **14**, 241 (1971).

5) H. Tamura, K. Ogawa, A. Takeuchi, and S. Yamada, *Chem. Lett.*, **1977**, 889.

6) H. Tamura, K. Ogawa, A. Takeuchi, and S. Yamada, *Bull. Chem. Soc. Jpn.*, **52**, 3522 (1979).

7) H. Yokoi and T. Isobe, *Bull. Chem. Soc. Jpn.*, **44**, 1446 (1971); *ibid.*, **46**, 447 (1973).

8) M. Chikira, H. Yokoi, and T. Isobe, *Bull. Chem. Soc. Jpn.*, **47**, 2208 (1974).

9) M. Chikira, H. Kon, R. A. Hawley, and K. M. Smith, *J. Chem. Soc., Dalton Trans.*, **1979**, 246.

10) M. Chikira and T. Isobe, *Bull. Chem. Soc. Jpn.*, **48**, 2052 (1975).

11) H. Yokoi, *Bull. Chem. Soc. Jpn.*, **47**, 3037 (1974).

12) H. Yokoi and A. W. Addison, *Inorg. Chem.*, **16**, 1341 (1977).

13) E. C. Lingafelter, G. L. Simmons, and B. Morosin, *Acta Crystallogr.*, **14**, 1222 (1961); D. Hall, S. V. Sheat, and T. N. Waters, *J. Chem. Soc. (A)*, **1968**, 460; T. P. Cheeseman, D. Hall, and T. N. Waters, *ibid.*, **1966**, 685.

14) M. Chikira and T. Isobe, *Bull. Chem. Soc. Jpn.*, **45**, 3006 (1972).

15) H. Yokoi and M. Chikira, *J. Chem. Soc., Dalton Trans.*, **1975**, 2101.

16) M. Chikira and H. Yokoi, *Bull. Chem. Soc. Jpn.*, **50**, 3232 (1977).

17) H. Yokoi and M. Chikira, *J. Am. Chem. Soc.*, **97**, 3975 (1975).

18) H. Yokoi, *Bull. Chem. Soc. Jpn.*, **47**, 497 (1974).

19) W. B. Jensen, *Chem. Rev.*, **78**, 1 (1978).

Physicochemical Speciation of Trace Elements in River Water by Means of Ultrafiltration

Yoshiyuki TANIZAKI,* Masao YAMAZAKI, and Sumiko NAGATSUKA
Tokyo Metropolitan Isotope Research Center, Fukazawa, Setagaya-ku, Tokyo 158
(Received May 21, 1985)

Ultrafiltration and Millipore filtration techniques have been used in the speciation of trace elements in Tama River water. The size distribution was clarified for 32 elements by means of neutron-activation analysis in order to discuss their chemical or physical forms. Alkali and alkaline-earth elements were primarily found in the dissolved-size fraction (<0.45 μm). Their dissolved species were mostly distributed in the smallest-molecular-weight fraction (<MW 500), although the alkaline-earth elements were also recognized to a significant extent (20—30%) in the middle-molecular-weight fraction (MW 10^4—500). Transition elements were principally associated with the suspended-size fraction (>0.45 μm) in the upper reaches of the river, but in the lower reaches they were chiefly fractionated as the dissolved species, with the exception of Sc and Fe. The dissolved V and Mn were distributed in the smallest-molecular-weight fraction, while the Co, Ni, and Zn were divided between two smaller-molecular-weight fractions (MW 10^4—500 and <MW 500). Light rare-earth elements were mostly associated with suspended materials. Heavier rare-earth elements were, on the contrary, mainly found in the dissolved-size fraction, while their dissolved species were concentrated in the middle-molecular-weight fraction. The dissolved species for As, Se, Sb, and W were divided into two smaller-molecular-weight fractions, although As, Se, and W were predominantly found in the middle-molecular-weight fraction and Sb was mainly detected in the smallest-molecular-weight fraction. Aluminium and Ag were mainly associated with suspended materials. Furthermore, the dissolved Al was mostly distributed in the smallest-molecular-weight fraction, while the Ag was concentrated in the largest-molecular-weight fraction (>MW 10^4).

Trace elements in natural water are found in various physical or chemical forms, such as simple ions, ion pairs, organic or inorganic complexes, and metal ions sorbed onto particulates or colloids. The determination of thier chemical species is of great importance not only in order to substantiate their geochemical behavior in natural water, but also in order to estimate their utilities and toxicities towards aquatic organisms. A variety of physicochemical separation techniques have been used in the study of trace-element characterizations in natural water.[1-3] The size-separation methods, such as filtration,[4-7] ultrafiltration,[8-11] gel filtration, and dialysis[12,13] are used the most commonly because of their simplicities. However, no one has yet applied the size-separation techniques to a systematic analysis of multi-elements. In a previous paper,[14] we ourselves reported on the physicochemical speciation of 31 elements in Tama River water, using a combination of the Millipore filtration (MF) technique and neutron-activation analysis (NAA). However, it was not possible to separate perfectly trace elements between "colloidals" and "true solutions," for the smallest pore size of commercially available Millipore filter is 0.025 μm, even though the boundary in size between the above two states probably lies in the range of 0.01—0.001 μm.[1,2,15] The ultrafiltration (UF) technique is extensively used to separate dissolved compounds into various molecular-weight ranges using a variety of membrane filters. In this paper, we tried to separate 32 elements and 6 major components dissolved in Tama River water into several molecular-weight fractions by utilizing the UF technique in order to estimate their chemical species.

Experimental

Water Samples. The river water samples were collected from three stations of the Tama River, Hamura (Station A), Kinuta (B), and Denenchofu (C). The sampling stations are shown in Fig. 1. The Hamura site lies near prime agricultural land, while the Kinuta and Denenchofu sites lie near industrial/urban stretches. Thirty liters of each water sample was placed in a clean Pyrex glass bottle and then immediately pre-filtrated using a Millipore filter with pore size of 8 μm in order to remove large particles. Another five liters of the water sample was taken as the original material in a polyethylene bottle without any filtration, it was then acidified immediately with 30 ml of nitric acid (Super Special Grade). The water qualities at the time of sampling are listed in Table 1 for the three stations.

Filtration. The pre-filtrated water samples were divided into six 5-liter portions. Two portions of the filtrate were used for the MF experiment, and the other four portions were used for the UF experiment. The sample from the Hamura site was not, however, submitted to the UF experiment.

(A) Millipore filtration. An all-glass Millipore apparatus and two kinds of Type HA Millipore filters, with a diameter of 142 mm and with average pore sizes of 0.45 and 0.05 μm, were used for the MF experiment. The procedures have been described in detail in the previous paper.[14]

(B) Ultrafiltration. A Model UHP-150 ultrafiltration cell (Toyo Roshi Corp.) and four kinds of ultrafilters, UK-200 (molecular-weight cut-off 2×10^5), UK-10 (10^4), UH-1 (1000), and UH-05 (500), with diameter of 150 mm, were employed for the UF experiment. The decontamination and washing of each filter were done by soaking them successively in a sodium hydroxide solution (1 mol dm^{-3}) for 1 d and a sodium hydrogencarbonate solution, followed by passing 5 liters of redistilled water through the filter under the pure-

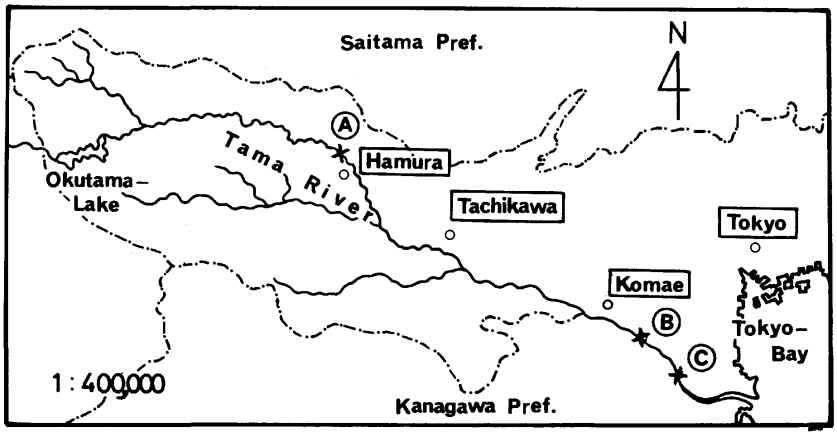

Fig. 1. Sampling locality.

TABLE 1. WATER QUALITY OF THE TAMA RIVER AT THE TIME OF SAMPLING

Parameter	River-water sample		
	A	B	C
Sampling station	Hamura	Kinuta	Denenchofu
Date	1/11/82	31/10/83	12/12/83
Water temp/°C	14.7	13.9	9.3
pH	8.2	7.0	6.9
Conductivity/$\mu S\,cm^{-1}$	80	246	275
ER[a]/$mg\,l^{-1}$	101	273	348
SiO_2/$mg\,l^{-1}$	25	21	20
4.3 Bx./$mequiv\,l^{-1}$	0.71	1.16	1.64
SO_4^{2-}/$mg\,l^{-1}$	13.2	30.7	52.8
Cl^-/$mg\,l^{-1}$	1.6	26.9	41.6
TOC[b]/$mg\,l^{-1}$	0.55	1.79	4.06

a) Amount of evaporated residue. b) Total organic carbon.

nitrogen gas pressure. Four portions of pre-filtrated samples were filtered using the four kinds of ultrafilters, one by one. The filtration was carried out under stirring and under nitrogengas pressures of 2—4.5 atm according to the molecularweight cut-off of the filters. The resulting four filtrates were transferred to a clean 5-liter polyethylene bottle and then acidified with 30 ml of the nitric acid in order to prevent any adsorption of trace elements on the walls of the bottles.

Neutron-activation Analysis. The procedures for the NAA experiment, the preparation of the neutron-irradiation samples, the neutron irradiation, and the gamma-ray counting were reported in detail in our previous papers.[14,16,17]

Analysis of Major Components. The concentration of silica (SiO_2) in the river water was determined by colorimetry using ammonium molybdate, while the sulfate (SO_4^{2-}) concentration was measured by turbidimetry using a barium chloride-gelatin solution. The alkalinity (4.3 Bx) was titrated with sulfuric acid (0.01 $mol\,dm^{-3}$) in the presence of a Bromocresol Green (BCG) indicator. The concentration of chloride ions (Cl^-) was measured by Mohl's method. The determination of the total organic carbon (TOC) concentration was performed by utilizing a TOC analyzer (Shimazu Model 10A).

Results and Discussion

The concentrations of the 32 elements were determined for the six filtrates resulting from the MF and UF experiments and for the original (non-filtrated) water sample by means of NAA. The statistical errors based on the gamma-ray counting were 5—30% for Ag, Ba, Ce, Cr, Eu, Ho, K, Fe, La, Mg, Se, Tb, Tm, and U, and less than 5% for the other 18 elements.

The trace-element concentrations in the pre-filtrated water sample and the residual water in the ultrafiltration cell were also determined in order to calculate the mass balance of the trace elements during the UF experiment. The results show that the loss due to adsorption was 20—50% for Fe, Ag, U, La, Ce, Sm, Eu, and Tb. For the other elements, the loss or contamination was less than 10%.

The size distributions in diameter (μm) and in the molecular-weight ranges were calculated for the 32 elements and 6 major components by means of the scheme shown in Fig. 2. The results were classified by size into two fractions, F (>0.45 μm) and F (<0.45 μm); furthermore, in the later fraction, they were classified into three molecular-weight fractions, F (>MW 10^4), F (MW 10^4—500), and F (<MW 500). The results are shown in Tables 2—8.

As a general rule, chemical constituents with a size smaller than 0.45 μm are defined as "dissolved," while those with a size larger than 0.45 μm are clas-

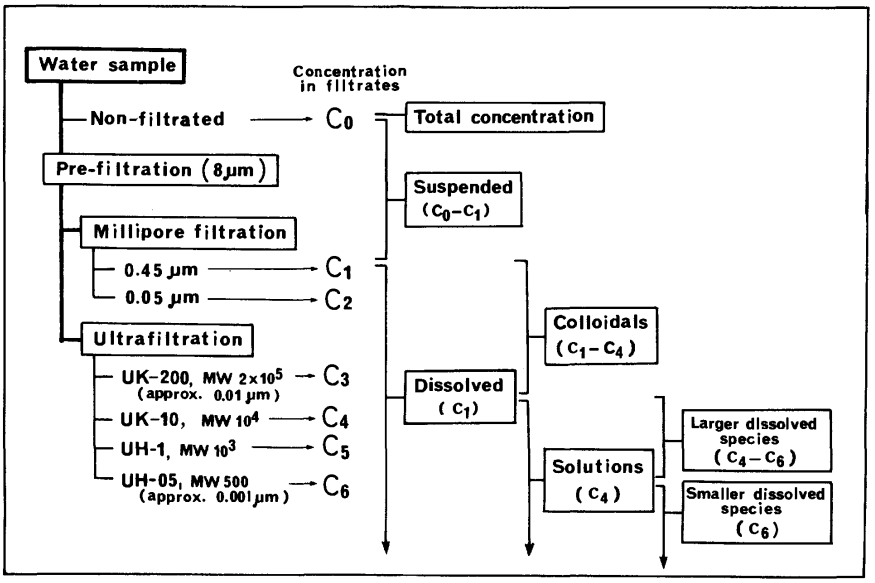

Fig. 2. Scheme for speciation of trace elements in river water by size fractionation techniques.

TABLE 2. FRACTIONATION RESULTS OF MAJOR COMPONENTS IN THE RIVER WATER

Component	Sampling station	Total content	Millipore filtration		Ultrafiltration of dissolved species		
			>0.45μm (suspended)	<0.45μm (dissolved)	>MW 10^4 (colloidals)	MW 10^4—500 (larger dissolved species)	<MW 500 (smaller dissolved species)
ER (mg/l)	A	101	2(2.0)	99(98.0)	—	—	—
	B	273	12(4.4)	261(95.6)	0(0)	44(16.9)	217(83.1)
	C	348	16(4.6)	332(95.4)	4(1.2)	60(18.1)	268(80.7)
SiO_2 (mg/l)	A	25.3	—	—	—	—	—
	B	20.6	0(0)	20.6(100)	0(0)	1.8(8.7)	18.8(91.3)
	C	20.4	0(0)	20.4(100)	0(0)	2.1(10.3)	18.3(89.7)
4.3Bx (meq/l)	A	0.71	0(0)	0.71(100)	—	—	—
	B	1.16	0(0)	1.16(100)	0(0)	0.21(18.1)	0.95(81.9)
	C	1.64	0.03(1.8)	1.61(98.2)	0(0)	0.25(15.5)	1.36(84.5)
SO_4^{2-} (mg/l)	A	13.2	0(0)	13.2(100)	—	—	—
	B	30.7	2.4(7.8)	28.3(92.2)	0.9(3.2)	16.4(57.9)	11.0(38.9)
	C	52.8	0(0)	52.8(100)	0(0)	28.8(54.5)	24.0(45.5)
Cl^- (mg/l)	A	1.6	0(0)	1.6(100)	—	—	—
	B	26.9	0(0)	26.9(100)	0(0)	0.4(1.5)	26.5(98.5)
	C	41.6	0(0)	41.6(100)	0(0)	0.6(1.4)	41.0(98.6)
TOC (mg/l)	A	0.55	0.23(41.8)	0.32(58.2)	—	—	—
	B	1.79	0.25(14.0)	1.54(86.0)	0.35(22.7)	1.01(65.6)	0.18(11.7)
	C	4.06	0.39(9.6)	3.67(90.4)	1.18(32.1)	1.97(53.7)	0.52(14.2)

The values in parenthesis are the percentages of each fraction.

sified as "particulate" or "suspended." The "dissolved" constituents need not be in a true solution, but can include "colloidals."[3] In this paper, it is assumed that the constituents with a size larger than molecular weight 10^4 (>MW 10^4) are "colloidals," while those with a size smaller than molecular weight 10^4 are "true solution," according to the method reported by Steinnes.[2] Furthermore, the constituents with molecular weights ranging from 10^4 to 500 (MW 10^4—500) are defined as larger dissolved species, while those passing through the ultrafilter with a molecular-weight cut-off of 500 (<MW 500) are classified as smaller dissolved species. The larger dissolved species included organic complexes, polyhydroxo complexes, *etc.*, while the smaller dissolved species are made up of free ions, ion pairs, *etc.*[2]

Major Components (ER, SiO_2, 4.3 Bx, SO_4^{2-}, Cl^-, and TOC). The total contents of all the major components except for SiO_2 were higher in the lower reaches (Stations B and C) of the Tama River than those in the upper reaches (Station A), as can be seen in Table 2. Especially, the high enrichments in Cl^- and TOC concentrations for Stations B and C indicate that the lower reaches of the river are greatly influenced by anthropogeneous pollution. This is proved too by the enrichments of the other com-

TABLE 3. FRACTIONATION RESULTS OF ALKALI ELEMENTS IN THE RIVER WATER

Element	Sampling station	Total content	Millipore filtration		Ultrafiltration of dissolved species		
			>0.45μm	<0.45μm	>MW 10^4	MW 10^4—500	<MW 500
Na (mg/l)	A	3.4	0(0)	3.4(100)	—	—	—
	B	23.3	0(0)	23.3(100)	0.5(2.1)	1.3(5.6)	21.5(92.3)
	C	37.1	0(0)	37.1(100)	1.0(2.7)	3.3(8.9)	32.8(88.4)
K (mg/l)	A	1.0	0(0)	1.0(100)	—	—	—
	B	4.0	0(0)	4.0(100)	0(0)	0.3(7.5)	3.7(92.5)
	C	6.3	0(0)	6.3(100)	0(0)	0.8(12.7)	5.5(87.3)
Rb (μg/l)	A	1.62	0.75(46.3)	0.87(53.7)	—	—	—
	B	2.19	0.12(5.5)	2.07(94.5)	0.12(5.8)	0.14(6.8)	1.81(87.4)
	C	4.29	0(0)	4.29(100)	0.09(2.1)	0.26(6.1)	3.94(91.8)
Cs (μg/l)	A	0.097	0.081(83.5)	0.016(16.5)	—	—	—
	B	0.033	0.017(51.5)	0.016(48.5)	0.002(12.5)	0(0)	0.014(87.5)
	C	0.053	0.008(15.1)	0.045(84.9)	0.003(6.7)	0.002(4.4)	0.040(88.9)

TABLE 4. FRACTIONATION RESULTS OF ALKALINE-EARTH ELEMENTS IN THE RIVER WATER

Element	Sampling station	Total content	Millipore filtration		Ultrafiltration of dissolved species		
			>0.45μm	<0.45μm	>MW 10^4	MW 10^4—500	<MW 500
Mg (mg/l)	A	1.0	0(0)	1.0(100)	—	—	—
	B	5.1	0(0)	5.1(100)	0.8(15.7)	1.1(21.6)	3.2(62.7)
	C	6.1	0(0)	6.1(100)	0.4(6.6)	1.4(22.9)	4.3(70.5)
Ca (mg/l)	A	14.9	0(0)	14.9(100)	—	—	—
	B	21.2	0(0)	21.2(100)	4.2(19.8)	3.6(17.0)	13.4(63.2)
	C	25.8	0(0)	25.8(100)	2.2(8.5)	7.2(27.9)	16.4(63.6)
Sr (μg/l)	A	58	0(0)	58(100)	—	—	—
	B	124	0(0)	124(100)	2(1.6)	35(28.2)	87(70.2)
	C	159	0(0)	159(100)	5(3.2)	53(33.3)	101(63.5)
Ba (μg/l)	A	8.1	3.8(46.9)	4.3(53.1)	—	—	—
	B	11.6	1.3(11.2)	10.3(88.8)	0.6(5.8)	2.4(23.3)	7.3(70.9)
	C	16.1	2.3(14.3)	13.8(85.7)	1.0(7.3)	3.8(27.5)	9.0(65.2)

ponents, such as Na, Mg, and heavy metals, which will be discussed later.

The major components were mostly fractionated as dissolved species (<0.45 μm), although 42, 14, and 10% of TOC for Stations A, B, and C respectively were associated with suspended materials (>0.45 μm). Most (81—99%) of the dissolved species for evaporated residue (ER), SiO_2, 4.3 Bx, and Cl^- was found in the smallest-molecular-weight fraction (<MW 500). Consequently, these four components are mainly present in the water as smaller dissolved species. The dissolved SO_4^{2-}, on the other hand, was chiefly divided between two smaller-molecular-weight fractions (MW 10^4—500 and <MW 500). This indicates that SO_4^{2-} is present in the water not only as simple ions, but also as larger molecules. The dissolved TOC was mainly distributed in the middle-molecular-weight fraction (MW 10^4—500), although 23—32% of the TOC was also found in the largest-molecular-weight fraction (>MW 10^4). Organic materials occurring in natural water have a very heterogeneous composition. The bulk of these natural organics is made up of fulvic and humic acids which have molecular-weight ranges of roughly 10^2—10^4 and 10^4—10^6 respectively, although their structures are generally poorly known and the above values are not to be regarded as definitive in any way.[2] These fulvic and humic acids contribute greatly to the dissolution of trace elements.[9,13,18,19]

Alkali and Alkaline-earth Elements (Na, K, Rb, Cs, Mg, Ca, Sr, and Ba). The total concentrations of Na, K, and Mg in the lower reaches of the river were higher than those in the upper reaches by a factor of 4—12, as can be seen in Tables 3 and 4. No significant differences in the total concentrations for Rb, Ca, Sr, and Ba could be found among the three sampling stations, even though they were also given in the higher values to some extent (about 2 times) for the lower reaches. On the other hand, higher Cs concentration was observed in the upper reaches.

Almost all the Na, K, and Rb was fractionated as dissolved species (<0.45 μm), although 46% of the Rb at Station A was distributed in the suspended-size fraction (>0.45 μm). Cesium was mainly associated with suspended materials at Station A. At Station C, on the contrary, it was predominantly found in the dissolved-size fraction. The Cs at Station B was divided between two fractions. Most (87—92%) of the dissolved alkali-metal elements were distributed in the smallest-molecular-weight fraction (<MW 500). It is well known that alkali-metal elements are dissolved in natural water as univalent cations. The

TABLE 5. FRACTIONATION RESULTS OF TRANSITION ELEMENTS IN THE RIVER WATER

Element	Sampling station	Total content	Millipore filtration		Ultrafiltration of dissolved species		
			>0.45μm	<0.45μm	>MW 10^4	MW 10^4—500	<MW 500
Sc (μg/l)	A	0.095	0.092(96.8)	0.003(3.2)	—	—	—
	B	0.068	0.055(80.9)	0.013(19.1)	0.001(7.7)	0.011(84.6)	0.001(7.7)
	C	0.044	0.028(63.6)	0.016(36.4)	0.002(12.5)	0.012(75.0)	0.002(12.5)
V (μg/l)	A	1.22	0.55(45.1)	0.67(54.9)	—	—	—
	B	1.51	0.20(13.2)	1.31(86.8)	0.08(6.1)	0.16(12.2)	1.07(81.7)
	C	3.35	0.42(12.5)	2.93(87.5)	0.28(9.6)	0.42(14.3)	2.23(76.1)
Cr (μg/l)	A	0.370	0.240(64.9)	0.130(35.1)	—	—	—
	B	0.331	0.200(60.4)	0.131(39.6)	0.026(19.9)	0.056(42.7)	0.049(37.4)
	C	0.416	0.145(34.9)	0.271(65.1)	0.096(35.4)	0.101(37.3)	0.074(27.3)
Mn (μg/l)	A	9.6	8.5(88.5)	1.1(11.5)	—	—	—
	B	37.6	14.0(37.2)	23.6(62.8)	1.4(5.9)	8.0(33.9)	14.2(60.2)
	C	76.5	3.9(5.1)	72.6(94.9)	7.8(10.7)	15.1(20.8)	49.7(68.5)
Fe (μg/l)	A	349	344(98.6)	5(1.4)	—	—	—
	B	177	164(92.7)	13(7.3)	9(69.2)	3(23.1)	1(7.7)
	C	289	234(81.0)	55(19.0)	46(83.6)	6(10.9)	3(5.5)
Co (μg/l)	A	0.127	0.106(83.5)	0.021(16.5)	—	—	—
	B	0.236	0.068(28.8)	0.168(71.2)	0.006(3.6)	0.091(54.2)	0.071(42.2)
	C	0.433	0.029(6.7)	0.404(93.3)	0.033(8.2)	0.241(59.6)	0.130(32.2)
Ni (μg/l)	A	0.85	0(0)	0.85(100)	—	—	—
	B	3.39	0(0)	3.39(100)	0.17(5.0)	1.85(54.6)	1.37(40.4)
	C	7.19	0(0)	7.19(100)	0(0)	4.85(67.5)	2.34(32.5)
Zn (μg/l)	A	2.52	1.81(71.8)	0.71(28.2)	—	—	—
	B	6.88	3.00(43.6)	3.88(56.4)	0.24(6.2)	1.72(44.3)	1.92(49.5)
	C	10.2	1.61(15.8)	8.59(84.2)	2.11(24.6)	2.44(28.4)	4.04(47.0)

fractionation results are in fair agreement with this knowledge.

The Mg, Ca, and Sr were completely fractionated as dissolved species. For Ba, 47% in the upper reaches and 11—14% in the lower reaches were associated with suspended materials. Although the dissolved alkaline-earth elements were chiefly classified in the smallest-molecular-weight fraction, like the alkali-metal elements, considerable amounts (30—37%) of them were also found in two larger-molecular-weight fractions (>MW 10^4 and MW 10^4—500). This shows that a large portion (63—70%) of the alkaline-earth elements are dissolved in the river water as simple bivalent cations, while the remainder are present as complexes or colloids with a larger molecular weight.

Transition Elements (Sc, V, Cr, Mn, Fe, Co, Ni, and Zn). The total concentrations of Sc and Fe in the upper reaches (Station A) were higher than those in the lower reaches (Stations B and C). On the other hand, higher concentrations of V, Mn, Co, Ni, and Zn were observed for the lower reaches, as is shown in Table 5. This indicates that the Sc and Fe in the river water are mainly derived from rocks or their efflorescences in the drainage basin, while the other five heavy metals are chiefly supplied by anthropogeneous sources.[14]

The transition elements in the upper reaches were generally associated with the suspended-size fraction (>0.45 μm), except for Ni. In the lower reaches, however, they were mainly fractionated as dissolved species (<0.45 μm), although 64% of the Sc and 81% of the Fe were still recognized in the suspended-size fraction even at Station C. Exceptionally, Ni was found in the dissolved-size fraction from all the sampling stations. Large portions of the dissolved V and Mn (76—82% and 60—68% respectively) were distributed in the smallest-molecular-weight fraction (<MW 500). Therefore, V and Mn are mainly dissolved in the river water as inorganic ions, such as $VO_2(OH)_3^{2-}$, Mn^{2+} or their simple compounds.[20] A considerable part (21—34%) of the Mn was also found in the middle-molecular-weight fraction (MW 10^4—500), so that the possibility of the occurrence of a Mn-organic complex cannot be neglected. Although the majority of the Sc and Fe was associated with suspended materials, as has been stated above, the remaining, dissolved portions of these elements were mostly distributed in the middle- and the largest-molecular-weight fractions respectively. Only 5—12% of these could be detected in the smallest-molecular-weight fraction. This shows that the chief dissolved species of Sc is a larger complex such as polyhydroxide, while Fe is present in the colloidal state.[21] The dissolved Co, Ni, and Zn were mainly divided into two smaller-molecular-weight fractions (MW 10^4—500 and <MW 500), though a considerable part (25%) of the Zn from Station C was found in the largest-molecular-weight fraction (>MW 10^4). Therefore, these three elements may be expected to be present in the river water not only as bivalent cations (M^{2+}), but also as complexes with naturally occurring organic ligands. On the other hand, Cr was divided into three molecular-weight fractions. Consequently, the dissolved Cr in the river water is composed of a sexivalent ion (CrO_4^{2-}), an inorganic

TABLE 6. FRACTIONATION RESULTS OF RARE-EARTH ELEMENTS IN THE RIVER WATER

Element	Sampling station	Total content	Millipore filtration		Ultrafiltration of dissolved species		
			>0.45μm	<0.45μm	>MW 10^4	MW 10^4—500	<MW 500
La (ng/l)	A	193	179(92.7)	14(7.3)	—	—	—
	B	140	128(91.4)	12(8.6)	4(33.3)	6(50.0)	2(16.7)
	C	97	70(72.2)	27(27.8)	21(77.8)	4(14.8)	2(7.4)
Ce (ng/l)	A	575	541(94.1)	34(5.9)	—	—	—
	B	174	150(86.2)	24(13.8)	2(8.3)	13(54.2)	9(37.5)
	C	122	83(68.0)	39(32.0)	20(51.3)	11(28.2)	8(20.5)
Sm (ng/l)	A	36.2	33.9(93.6)	2.3(6.4)	—	—	—
	B	21.7	19.8(91.2)	1.9(8.8)	0.6(31.6)	1.0(52.6)	0.3(15.8)
	C	16.0	12.0(75.0)	4.0(25.0)	1.2(30.0)	2.2(55.0)	0.6(15.0)
Eu (ng/l)	A	9.55	9.15(95.8)	0.40(4.2)	—	—	—
	B	5.71	5.09(89.1)	0.62(10.9)	0.25(40.3)	0.28(45.2)	0.09(14.5)
	C	3.50	2.79(79.7)	0.71(20.3)	0.45(63.4)	0.21(29.6)	0.05(7.0)
Tb (ng/l)	A	ND	—	—	—	—	—
	B	1.86	1.41(75.8)	0.45(24.2)	0.04(8.9)	0.33(73.3)	0.08(17.8)
	C	7.16	2.00(27.9)	5.16(72.1)	1.50(29.1)	3.38(65.5)	0.28(5.4)
Ho (ng/l)	A	ND	—	—	—	—	—
	B	—	—	—	—	—	—
	C	9.40	1.89(20.1)	7.51(79.9)	1.51(20.1)	5.42(72.2)	0.58(7.7)
Tm (ng/l)	A	ND	—	—	—	—	—
	B	7.57	3.07(40.6)	4.50(59.4)	—	—	—
	C	30.2	4.9(16.2)	25.3(83.8)	2.8(11.1)	19.8(78.3)	2.7(10.6)
Yb (ng/l)	A	ND	—	—	—	—	—
	B	34.5	8.2(23.8)	26.3(76.2)	4.6(17.5)	19.0(72.2)	2.7(10.3)
	C	68.9	6.5(9.4)	62.4(90.6)	7.7(12.3)	50.3(80.6)	4.4(7.1)
Lu (ng/l)	A	ND	—	—	—	—	—
	B	7.05	0.83(11.8)	6.22(88.2)	0.68(10.9)	5.11(82.2)	0.43(6.9)
	C	27.5	2.8(10.2)	24.7(89.8)	3.0(12.1)	20.2(81.8)	1.5(6.1)

or organic complex, and inorganic Cr(III), which is quantitative co-precipitated on colloidal iron(III) hydroxide.[22]

Rare-earth Elements (REEs; La, Ce, Sm, Eu, Tb, Ho, Tm, Yb, and Lu). The total concentrations of such light REEs as La, Ce, Sm, and Eu in the upper reaches (Station A) were higher than those in the lower reaches (Stations B and C). For such heavier REEs as Tb, Ho, Tm, Yb, and Lu, on the contrary, higher concentrations were observed in the lower reaches, as is shown in Table 6.

The light REEs were mostly found in the suspended-size fraction (>0.45 μm), even though a considerable part (20—32%) of these elements at Station C was fractionated as dissolved species (<0.45 μm). On the other hand, heavier REEs in the lower reaches were mainly distributed in the dissolved-size fraction, although, at Station B, 76% of the Tb and 41% of the Tm were still associated with suspended materials. In the upper reaches, these elements could not be detected. The dissolved light REEs were mainly divided between two larger-molecular-weight fractions (>MW 10^4 and MW 10^4—500). On the other hand, the heavier REEs were chiefly (65—82%) distributed in the middle-molecular-weight fraction (MW 10^4—500). These findings suggest that the REEs in the river water are primarily derived from rocks or their efflorescences, and then that heavier REEs are dissolved by forming complexes in the lower reaches of the river, where the water has an abundance of complexing ligands, such as natural organics and anions. In the upper reaches, with a poor TOC concentration, they cannot be detected. Light REEs tend to co-precipitate with iron(III) hydroxide,[14] so that they are still associated with suspended materials or colloids.

Others (As, Se, Sb, W, Al, Ag, and U). The total concentrations of Al and U in the upper reaches were considerably higher than those in the lower reaches, as is shown in Table 8. This indicates that these elements are derived from rocks in the drainage basin in a manner similar to Fe, Sc, Cs, and light REEs. On the contrary, a higher Ag concentration was observed in the lower reaches, where the river water was greatly polluted by artificial sources. In the upper reaches, Ag was not detected. There were no large differences in the total concentrations of As, Se, Sb, and W among the three sampling stations, as can be seen in Table 7.

Almost all the As, Se, Sb, and W was distributed in the dissolved-size fraction (<0.45 μm). The dissolved species of these elements were mainly divided into two smaller-molecular-weight fractions (MW 10^4—500 and <MW 500), although As, Se, and W were predominantly found in the middle-molecular-weight fraction, while Sb was more concentrated in the smallest-molecular-weight fraction. It is well known that these four elements tend to form oxoanions, such as $HAsO_4^{2-}$, SeO_3^{2-}, $Sb(OH)_6^-$, and WO_4^{2-}, in natural water, as do V or Cr. However, the fractionation

TABLE 7. FRACTIONATION RESULTS OF ARSENIC, SELENIUM, ANTIMONY, AND TUNGSTEN IN THE RIVER WATER

Element	Sampling station	Total content	Millipore filtration		Ultrafiltration of dissolved species		
			>0.45μm	<0.45μm	>MW 10^4	MW 10^4—500	<MW 500
As (μg/l)	A	0.610	0(0)	0.610(100)	—	—	—
	B	0.754	0.035(4.6)	0.719(95.4)	0.036(5.0)	0.426(59.3)	0.257(35.7)
	C	0.535	0(0)	0.535(100)	0.088(16.4)	0.256(47.9)	0.191(35.7)
Se (μg/l)	A	0.086	0(0)	0.086(100)	—	—	—
	B	0.091	0.005(5.5)	0.086(94.5)	0.008(9.3)	0.063(73.3)	0.015(17.4)
	C	0.128	0.016(12.5)	0.112(87.5)	0.023(20.5)	0.061(54.5)	0.028(25.0)
Sb (μg/l)	A	0.176	0(0)	0.176(100)	—	—	—
	B	0.264	0(0)	0.264(100)	0.021(8.0)	0.059(22.3)	0.184(69.7)
	C	0.258	0(0)	0.258(100)	0.019(7.4)	0.089(34.5)	0.150(58.1)
W (μg/l)	A	0.072	0(0)	0.072(100)	—	—	—
	B	0.098	0(0)	0.098(100)	0.006(6.1)	0.058(59.2)	0.034(34.7)
	C	0.067	0(0)	0.067(100)	0.008(11.9)	0.042(62.7)	0.017(25.4)

TABLE 8. FRACTIONATION RESULTS OF ALUMINIUM, SILVER, AND URANIUM IN THE RIVER WATER

Element	Sampling station	Total content	Millipore filtration		Ultrafiltration of dissolved species		
			>0.45μm	<0.45μm	>MW 10^4	MW 10^4—500	<MW 500
Al (μg/l)	A	603	524(86.9)	79(13.1)	—	—	—
	B	263	196(74.5)	67(25.5)	0(0)	1(1.5)	66(98.5)
	C	229	127(55.5)	102(44.5)	9(8.8)	1(1.0)	92(90.2)
Ag (μg/l)	A	ND	—	—	—	—	—
	B	0.069	0.053(76.8)	0.016(23.2)	0.012(75.0)	0.002(12.5)	0.002(12.5)
	C	0.126	0.069(54.8)	0.057(45.2)	0.049(85.9)	0.003(5.3)	0.005(8.8)
U (μg/l)	A	0.058	0.012(20.7)	0.046(79.3)	—	—	—
	B	0.022	0.005(22.7)	0.017(77.3)	0.004(23.5)	0.011(64.7)	0.002(11.8)
	C	0.025	0.003(12.0)	0.022(88.0)	0.005(22.7)	0.014(63.7)	0.003(13.6)

results show that As, Se, and W are present in the river water as such larger dissolved compounds as organic complexes,[23] in preference to those simple oxoanions.

Aluminium was, in the upper reaches, mainly distributed in the suspended-size fraction, while in the lower reaches it was fractionated as dissolved species to a considerable extent (25—44%). For Ag, 77% in Station B and 55% in Station C were associated with suspended materials. Most (77—88%) of the U was found in the dissolved-size fraction at all the sampling stations. The dissolved Al, Ag, and U were predominantly found in the smallest-, the largest-, and the middle-molecular-weight fractions respectively. This indicates that the dissolved Al exists as simple inorganic ions, and that the Ag is chiefly associated with colloidal materials, while the U can be expected to be present in the form of an uranil complex.

Conclusions

Using the UF technique and the NAA method, it was possible to obtain some knowledge about the dissolved species of trace elements existing in Tama River water. Alkali and alkaline-earth elements, Al, V, Mn, and Sb, dissolved in the river water were predominantly present as simple ions or their small molecule compounds, although a considerable part (20—30%) of the alkaline-earth elements, Mn, and Sb were also dissolved as complexes with larger-molecular-weight sizes. The dissolved Co, Ni, Zn, and As were mainly divided into the smallest- and middle-molecular-weight fractions, so that their chief dissolved species were probably both simple ions and complexes. The dissolved Sc, heavier REEs, Se, W, and U were mainly present by forming complexes. On the other hand, Fe, Ag, and some light REEs dissolved in the river water were primarily associated with colloidal materials.

Several tedious problems, however, still remain to be examined concerning the UF technique, much as with the MF technique.[14] For example, the pore diameter of the filter may show considerable variation, so that a precise separation of trace elements is difficult. Furthermore, a clogging of the filter pores, contamination from the filtering apparatus and the filter themselves, and losses due to adsorption on the filter are more insidious problems in the UF experiment. Further consideration in greater detail will be necessary to minimize analytical errors.

References

1) C. E. Batley, "Trace Element Speciation in Surface Water and its Ecological Implications," ed by Gary G. Leppard, Plenum Press, New York and London (1983), p. 17.

2) E. Steinnes, "Trace Element Speciation in Surface Water and its Ecological Implications," ed by Gary G. Leppard, Plenum Press, New York and London, (1983), p. 37.

3) S. J. De Mora and R. M. Harrison, *Water Res.*, **17**, 723 (1983).
4) V. C. Kennedy and G. W. Zellweger, *Water Resour. Res.*, **10**, 785 (1974).
5) R. Wagemann and G. J. Brunskill, *Int. J. Environ. Anal. Chem.*, **4**, 75 (1975).
6) D. P. H. Laxen and I. M. Chandler, *Anal. Chem.*, **54**, 1350 (1982).
7) D. P. H. Laxen and R. M. Harrison, *Water Res.*, **17**, 71 (1983).
8) R. G. Smith, Jr., *Anal. Chem.*, **48**, 74 (1976).
9) P. Benes, E. T. Gjessing, and E. Steinnes, *Water Res.*, **10**, 711 (1976).
10) M. R. Hoffmann, E. C. Yost, S. J. Eisenreich, and W. J. Maier, *Environ. Sci. Technol.*, **15**, 655 (1981).
11) J. P. Giesy Jr., G. J. Leversee, and D. R. Williams, *Water Res.*, **11**, 1013 (1977).
12) P. Benes and E. Steinnes, *Water Res.*, **8**, 947 (1974).
13) R. D. Guy and C. L. Chakrabarti, *Can. J. Chem.*, **54**, 2600 (1976).
14) Y.Tanizaki, M.Yamazaki, and S.Nagatsuka, *Bull. Chem. Soc. Jpn.*, **57**, 1545 (1984).
15) B. Mason, "Principles of Geochemistry," Third ed., John Wiley and Sons, New York (1966), Chap. 6.
16) S. Nagatsuka and Y. Tanizaki, *Radioisotopes*, **23**, 693 (1974).
17) Y.Tanizaki and S.Nagatsuka, *Bull. Chem. Soc. Jpn.*, **56**, 619 (1983).
18) C. Steelink, *J. Chem. Educ.*, **54**, 599 (1977).
19) E. R. Sholkovitz and D. Copland, *Geochim. Cosmochim. Acta*, **45**, 181 (1981).
20) R. M. Garrels and C. L. Christ, "Solutions, Minerals, and Equilibria," Harper and Row, New York (1965), Chap. 4.
21) J. Rodier, "Analysis of Water," English translation by IPST staff, Wiley, New York (1975), p. 310.
22) R. Fukai and D. Vas, *J. Oceanog. Soc. Jpn.*, **23**, 298 (1967).
23) K. Takayanagi and G. T. F. Wong, *Geochim. Cosmochim. Acta*, **49**, 539 (1985).

Preparation and Characterization of Cobalt(III) Complexes Containing $(CH_3)_2As(CH_2)_nAs(CH_3)_2$ (n=2, 3)

Katsumi IWATA, Masaaki KOJIMA, and Junnosuke FUJITA*
Department of Chemistry, Faculty of Science, Nagoya University, Chikusa-ku, Nagoya 464
(Received June 12, 1985)

Twelve new complexes, *trans*-$[CoX_2(dmae \text{ or } dmap)_2]^+$ (X=Cl, Br, I; dmae=1,2-bis(dimethylarsino)ethane, dmap=1,3-bis(dimethylarsino)propane), *cis*-$[CoX_2(dmap)_2]^+$ (X=Cl, Br), $[Co(CO_3)(dmae \text{ or } dmap)_2]^+$, and $[Co(acac)_{3-n}(dmap)_n]^{n+}$($n$=0, 1, 2; acac=2,4-pentanedionate ion) were prepared and characterized. From a comparison of the $^1A_{1g} \rightarrow {}^1E_g$ (D_{4h}) d-d absorption bands of analogous *trans*-dichloro complexes of phosphines and amines, the order of spectrochemical series for the group 5B elements was suggested to be P > As > N. Largely reduced interelectronic repulsions between the crystal field levels were observed for the carbonato complexes. Isomerization of *cis*-$[CoCl_2(dmap)_2]^+$ to the trans isomer was studied in methanol in the temperature range of 20.1—49.9 °C. The rate has a first-order dependence on the complex concentration. The rate constant at 54.9 °C, calculated from the $\Delta H^{\neq}$ (115.2 kJ mol^{-1}) and $\Delta S^{\neq}$ (53.8 J mol^{-1} K^{-1}) values, is 10^3 times as large as that reported for *cis*-$[CoCl_2(diars)_2]^+$ (diars=*o*-phenylenebis(dimethylarsine)) at the same temperature.

According to Pearson's HSAB model,[1] a cobalt(III) ion which belongs to a hard acid prefers a hard base such as ammonia or water to a soft base such as arsine ligands in complex formation. However, several arsine ligands such as *o*-phenylenebis(dimethylarsine) (diars)[2-6] and *cis*-bis(dimethylarsino)ethylene[7] have been reported to form stable cobalt(III) complexes. All the cobalt(III)–arsine complexes reported so far involve an unsaturated group which shows strong absorption bands in the ultraviolet region and sometimes makes band assignments of the complexes difficult.

In this paper we report the preparation and absorption spectra of cobalt(III) complexes containing a saturated arsine chelate, 1,2-bis(dimethylarsino)ethane (dmae) and 1,3-bis(dimethylarsino)propane (dmap). The paper also describes isomerization of *cis*-$[CoCl_2(dmap)_2]^+$ to the trans isomer in methanol.

Experimental

The arsine ligands, dmae and dmap were handled under a nitrogen atmosphere until they formed air-stable cobalt(III) complexes. Tetrahydrofuran was dried with sodium and deoxygenated by distillation in a stream of nitrogen.

1,2-Bis(dimethylarsino)ethane, dmae. This compound was prepared by the method of Sommer[8] from $(CH_3)_2AsSAs(CH_3)_2$, metallic sodium, and 1,2-dibromoethane in liquid ammonia. Yield: *ca.* 2%. The compound was not purified by fractional distillation because of the very low yield. Tetramethyldiarsine which was the most abundant by-product was removed by evaporation under reduced pressure, and the residue was used to prepare *trans*-$[CoCl_2(dmae)_2]ClO_4$ (*vide infra*).

1,3-Bis(dimethylarsino)propane, dmap. This compound was prepared by the method of Sommer[8] with a slight modification. A tetrahydrofuran solution (500 cm^3) of sodium dimethylarsenide (0.2 mol) was prepared by the method of Phillips and Vis[9] from sodium (10.3 g, 0.45 mol) and iododimethylarsine[10] (47.9 g, 0.207 mol). To this solution was added 1,3-dibromopropane (21.0 g, 0.104 mol) at 0 °C with stirring. Water (50 cm^3) was added to the resulting white suspension, and then tetrahydrofuran was evaporated under reduced pressure. The residue was shaken with diethyl ether to extract the diarsine. The ethereal layer was separated and dried with anhydrous calcium chloride. The desiccant was filtered off, the ether evaporated, and the residue was distilled at 86—90 °C and 2670 Pa to give a colorless liquid. Yield: 11.3 g (43%). ^{1}H NMR ($CDCl_3$) δ=0.93 (12H, s, $AsCH_3$), 1.26 (2H, m, β-CH_2), and 1.55 (4H, t, $AsCH_2$).

trans-[CoCl$_2$(dmae)$_2$]ClO$_4$. To an ethanol solution (20 cm^3) of $CoCl_2 \cdot 6H_2O$ (0.96 g, 4.0 mmol) was added an ethanol solution (10 cm^3) of dmae prepared from 13.4 g of $(CH_3)_2AsSAs(CH_3)_2$ and 10.5 g of $BrCH_2CH_2Br$ in the manner described above. Air was bubbled through the resulting green solution for 90 min, and then 1 mol dm^{-3} HCl (27 cm^3) was added, a dark green solution being yielded. The ethanol was evaporated under reduced pressure and to the concentrate was added $NaClO_4$ (0.42 g). A green solid which precipitated was collected by filtration, washed successively with 1 mol dm^{-3} $HClO_4$, methanol, ethanol, methanol–diethyl ether (1:10), and diethyl ether, and dried *in vacuo*. Yield: 0.39 g. Found: C, 20.73; H, 4.42%. Calcd for $C_{12}H_{32}As_4Cl_3CoO_4$: C, 20.43; H, 4.57%. ^{1}H NMR (CD_2Cl_2) δ=1.63 (24H, s, $AsCH_3$) and 2.43 (8H, s, $AsCH_2$). The complex is soluble in water and ethanol.

trans-[CoBr$_2$(dmae)$_2$]ClO$_4$. This complex was prepared from *trans*-$[CoCl_2(dmae)_2]ClO_4$ and KBr by metathesis. To a methanol solution (10 cm^3) of *trans*-$[CoCl_2(dmae)_2]ClO_4$ (0.100 g, 0.14 mmol) was added an aqueous solution (5 cm^3) of KBr (1.0 g, 8 mmol). The mixture was stirred overnight at 40 °C, and then evaporated to dryness under reduced pressure. The residue was extracted with dichloromethane (10 cm^3). The extract was mixed successively with methanol (10 cm^3), water (3 cm^3), and 70% $HClO_4$ (0.5 cm^3), and the solvent was evaporated slowly at room temperature to give a yellow-green precipitate. The product seemed to be impure, since the ^{1}H NMR spectrum in CD_2Cl_2 showed two singlets attributable to the As-methyl protons at 1.73 and 2.09 ppm. The pure complex was obtained by repeated recrystallization from dichloromethane–methanol–70% $HClO_4$ by the method as above until the signal at 2.09 ppm disappeared completely. Yield: 0.06 g (53%). Found: C, 18.63; H, 4.10%. Calcd for $C_{12}H_{32}As_4Br_2ClCoO_4$: C, 18.15; H, 4.06%. ^{1}H NMR (CD_2Cl_2) δ=1.73 (24H, s, $AsCH_3$) and 2.46 (8H, s, $AsCH_2$).

trans-[CoI$_2$(dmae)$_2$]ClO$_4$. This complex was prepared from *trans*-$[CoCl_2(dmae)_2]ClO_4$ and NaI by metathesis. To an ethanol solution (10 cm^3) of *trans*-$[CoCl_2(dmae)_2]ClO_4$ (0.053 g, 0.075 mmol) was added an excess of NaI (0.35 g, 2.3 mmol), the color of the solution changing from green to

brown. The solution was refluxed for 10 min, and to the resulting reddish brown solution was added an aqueous solution (5 cm^3) of $NaClO_4$ (0.50 g). The mixture was evaporated to *ca.* 5 cm^3 to yield reddish brown plates or needles, which were collected by filtration, washed successively with water, ethanol–diethyl ether (1:5), and diethyl ether. Yield: 0.050 g (75%). Found: C, 16.43; H, 3.55%. Calcd for $C_{12}H_{32}As_4ClCoI_2O_4$: C, 16.22; H, 3.63%. ^1H NMR (CD_3CN) δ=1.99 (24H, s, $AsCH_3$) and 2.51 (8H, s, $AsCH_2$).

[Co(CO$_3$)(dmae)$_2$]ClO$_4$·2NaClO$_4$. To a hot methanol solution (3 cm^3) of *trans*-[$CoCl_2$(dmae)$_2$]ClO_4 (0.223 g, 0.31 mmol) were added Li_2CO_3 (0.20 g, 2.7 mmol) and water (5 cm^3). The mixture was heated on a water-bath for 15 min, and then allowed to cool to room temperature. The resulting orange reaction mixture was filtered to remove remaining *trans*-[$CoCl_2$(dmae)$_2$]ClO_4 and Li_2CO_3. The filtrate was mixed with a saturated aqueous solution (2 cm^3) of $NaClO_4$, and the volume of the solution was reduced to *ca.* 5 cm^3 under reduced pressure. The concentrate was stored in a refrigerator to give an orange precipitate. The precipitate was collected by filtration, extracted with methanol, and the extract was mixed with a saturated aqueous solution (2 cm^3) of $NaClO_4$. By evaporating the methanol, the desired complex was obtained as orange plates. They were collected by filtration, washed with methanol–diethyl ether (1:5) and then diethyl ether. Yield: 0.107 g (36%). Found: C, 16.65; H, 3.43%. Calcd for $C_{13}H_{32}As_4Cl_3CoNa_2O_{15}$: C, 16.62; H, 3.43%. ^1H NMR (D_2O) δ=1.46 (6H, s, $AsCH_3$), 1.51 (6H, s, $AsCH_3$), 1.57 (6H, s, $AsCH_3$), 1.89 (6H, s, $AsCH_3$), and 2.3—2.7 (8H, m, $-CH_2-$).

trans-*[CoCl$_2$(dmap)$_2$]Cl·H$_2$O.* To an ethanol solution (20 cm^3) of $CoCl_2·6H_2O$ (1.23 g, 5.2 mmol) was added an ethanol solution (10 cm^3) of dmap (2.6 g, 10.3 mmol). The color of the solution changed from blue to dark green and a precipitate was formed. By adding concd HCl (4 cm^3) the precipitate was dissolved. Air was bubbled through the solution for 1 h, and then water (40 cm^3) was added. The ethanol was evaporated under reduced pressure to give a green precipitate. After cooling the mixture overnight in a refrigerator, the precipitate was collected by filtration and washed successively with 1 mol dm^{-3} HCl, ethanol–diethyl ether (1:10), and diethyl ether. Yield: 3.0 g (84%). Found: C, 24.13; H, 5.51%. Calcd for $C_{14}H_{38}As_4Cl_3CoO$: C, 24.46; H, 5.57%. The presence of water of crystallization was suggested from the IR spectrum. The complex is soluble in water, ethanol, acetonitrile, and dichloromethane.

trans-*[CoCl$_2$(dmap)$_2$]ClO$_4$.* This complex was obtained by adding 70% $HClO_4$ (0.1 cm^3) to a methanol solution (5 cm^3) of the chloride (0.30 g, 0.44 mmol). Diethyl ether (15 cm^3) was added to ensure the precipitation of the perchlorate. The green precipitate was collected by filtration and washed successively with 1 mol dm^{-3} $HClO_4$, methanol–diethyl ether (1:3), and diethyl ether. Yield: 0.30 g (94%). Found: C, 22.96; H, 4.95%. Calcd for $C_{14}H_{36}As_4Cl_3CoO_4$: C, 22.93; H, 4.95%. ^1H NMR (CD_2Cl_2) δ=1.52 (24H, s, $AsCH_3$) and 1.9—2.9 (12H, m, $-CH_2-$). The complex is soluble in ethanol, acetonitrile, and dichloromethane, but insoluble in water.

trans-*[CoBr$_2$(dmap)$_2$]ClO$_4$.* To an ethanol solution (10 cm^3) of $CoBr_2·6H_2O$ (0.23 g, 0.70 mmol) were added an ethanol solution (5 cm^3) of dmap (0.35 g, 1.4 mmol), and concd HBr (1 cm^3). Air was bubbled into the solution for 30 min, and then 5 mol dm^{-3} $HClO_4$ (5 cm^3) was added. Yellow-green flocculent crystals formed were collected by filtration and washed succesively with 1 mol dm^{-3} $HClO_4$, cold methanol, and diethyl ether. Yield: 0.51 g (90%). Found: C, 20.49; H, 4.46%. Calcd for $C_{14}H_{36}As_4Br_2ClCoO_4$: C, 20.45; H, 4.41%. ^1H NMR (CD_2Cl_2) δ=1.62 (24H, s, $AsCH_3$) and 2.0—2.6 (12H, m, $-CH_2-$).

[Co(CO$_3$)(dmap)$_2$]ClO$_4$·2NaClO$_4$·CH$_3$OH. This complex was prepared by a method similar to that for [Co(CO_3)(dmae)$_2$]ClO_4·2$NaClO_4$. To a hot methanol solution (3 cm^3) of *trans*-[$CoCl_2$(dmap)$_2$]Cl·H_2O (0.47 g, 0.68 mmol) were added Li_2CO_3 (0.20 g, 2.7 mmol) and water (3 cm^3). The mixture was heated on a water-bath for 15 min, the color of the solution changing from green to dark red. The methanol was removed under reduced pressure at 40 °C, and to the concentrate was added a saturated aqueous solution (1 cm^3) of $NaClO_4$. The mixture was cooled at 0 °C, mixed with 5 mol dm^{-3} $HClO_4$ in order to decompose residual Li_2CO_3, and then filtered to remove remaining *trans*-[$CoCl_2$(dmap)$_2$]-ClO_4. To the concentrate was added dichloromethane (5 cm^3), and the mixture was stirred for a while to form a red precipitate. A saturated solution (5 cm^3) of $NaClO_4$ was added, and the mixture was allowed to stand at 5 °C overnight. The red precipitate was collected by filtration and washed successively with cold water, cold methanol, dichloromethane, and diethyl ether. Yield: 0.21 g (31%). Found: C, 19.22; H, 4.03%. Calcd for $C_{16}H_{40}As_4CoCl_3Na_2O_{16}$: C, 19.18; H, 4.06%. The presence of 1 mol of methanol of crystallization was confirmed by the ^1H NMR spectrum. The complex is soluble in water, methanol, and acetonitrile, but insoluble in dichloromethane.

cis-*[CoCl$_2$(dmap)$_2$]ClO$_4$.* To a cold (*ca.* 0 °C), stirred suspension of the carbonato complex (0.50 g, 0.50 mmol) in water (10 cm^3) was added dropwise cold (*ca.* 0 °C) 6 mol dm^{-3} HCl (20 cm^3). The resulting purple solution was filtered, to the filtrate was added $NaClO_4$ (5 g), and the mixture was stored in a refrigerator for 3 h. Purple crystals which precipitated were collected by filtration and washed successively with water, ethanol, dichloromethane–diethyl ether (1:1), and diethyl ether. Yield: 0.32 g (87%). Found: C, 22.95; H, 4.89%. Calcd for $C_{14}H_{36}As_4Cl_3CoO_4$: C, 22.93; H, 4.95%. ^1H NMR (CD_2Cl_2) δ=1.48 (6H, s, $AsCH_3$), 1.56 (6H, s, $AsCH_3$), 1.59 (6H, s, $AsCH_3$), 1.66 (6H, s, $AsCH_3$), and 1.9—2.5 (12H, m, $-CH_2-$). The complex was not recrystallized, since it is liable to isomerization in solution to give the trans isomer (*vide infra*). However, the ^1H NMR spectrum of the complex prepared as above shows no signal attributable to the trans isomer.

cis-*[CoBr$_2$(dmap)$_2$]ClO$_4$.* This complex was obtained as dark violet crystals from the carbonato complex by a method similar to that for the corresponding dichloro complex using HBr instead of HCl. Yield: 68%. Found: C, 20.48; H, 4.48%. Calcd for $C_{14}H_{36}As_4Br_2ClCoO_4$: C, 20.46; H, 4.41%. ^1H NMR (CD_2Cl_2) δ=1.54 (6H, s, $AsCH_3$), 1.62 (6H, s, $AsCH_3$), 1.65 (6H, s, $AsCH_3$), 1.88 (6H, s, $AsCH_3$), and 2.0—2.5 (12H, m, $-CH_2-$).

trans-*[CoI$_2$(dmap)$_2$]ClO$_4$.* To a solution (12 cm^3) of the carbonato complex (0.10 g, 0.10 mmol) in water–acetonitrile (1:5) were added NaI (0.30 g, 2 mmol) and 5 mol dm^{-3} $HClO_4$ (4 cm^3). The mixture was stirred for 30 min, and then evaporated to a small volume under reduced pressure to form dark red plates. They were collected by filtration, washed successively with water, cold methanol, and diethyl ether, and dried *in vacuo*. Yield: 0.083 g (91%). Found: C, 18.41; H, 3.99%. Calcd for $C_{14}H_{36}As_4ClCoI_2O_4$: C, 18.35; H, 3.96%.

^1H NMR (CD_2Cl_2) δ=1.80 (24H, s, $AsCH_3$) and 2.0—2.5 (12H, m, $-CH_2-$). This complex is soluble in dichloromethane and acetonitrile, but insoluble in ethanol and water.

[Co(acac)(dmap)$_2$](ClO$_4$)$_2$·H$_2$O (acac=2,4-pentanedionate ion). To a warm solution (5 cm^3) of *trans*-[$CoCl_2$(dmap)$_2$]-ClO_4 (0.21 g, 0.29 mmol) in methanol was added an aqueous solution (10 cm^3) of lithium 2,4-pentanedionate (0.05 g, 0.47 mmol). The mixture was heated at 70 °C for 3 h. The resulting red solution was diluted with water (100 cm^3) and applied on a column (ϕ4.5 cm×22 cm) of SP-Sephadex C-25 (Na^+ form). On elution with 0.1 mol dm^{-3} $NaClO_4$, three bands developed; purple ([Co(acac)$_2$(dmap)]$^+$, small amount), yellow-green (*trans*-[$CoCl_2$(dmap)$_2$]$^+$, small amount), and red ([Co(acac)(dmap)$_2$]$^{2+}$, large amount) in the order of elution. The eluate containing the slowest-moving red band was collected and evaporated to *ca.* 20 cm^3 under reduced pressure. The concentrate was stored in a refrigerator to form a red precipitate. It was collected by filtration and washed successively with cold 1 mol dm^{-3} $HClO_4$, methanol–diethyl ether (1:3), and diethyl ether. Yield: 0.14 g (57%). Found: C, 25.57; H, 4.85%. Calcd for $C_{19}H_{45}As_4Cl_2CoO_{11}$: C, 25.96; H, 5.16%. ^1H NMR (CD_3NO_2) δ=1.56 (6H, s, $AsCH_3$), 1.60 (12H, s, $AsCH_3$), 1.69 (6H, s, $AsCH_3$), 1.9—2.5 (12H, m, $-CH_2-$), 2.19 (6H, s, CCH_3), and 5.89 (1H, s, $-CH-$). ^{13}C NMR (CD_3NO_2) δ=7.3 (q), 7.5 (q), 10.2 (q), 13.8 (q), 21.2 (t), 27.1 (q), 27.7 (t), 27.8 (t), and 102.3 (d). The complex is soluble in water and methanol, and slightly soluble in ethanol.

[Co(acac)$_2$(dmap)]ClO$_4$. To a methanol solution (10 cm^3) of [Co(acac)$_3$] (0.50 g, 1.4 mmol) were added an ethanol solution (10 cm^3) of dmap (0.10 g, 0.4 mmol) and active charcoal (0.10 g). The mixture was stirred for 2 d at room temperature and then filtered. The purple filtrate was diluted with water (20 cm^3), and the unreacted arsine ligand was extracted with petroleum ether. The aqueous phase was diluted with water (100 cm^3) and applied on a column (ϕ4.5 cm×10 cm) of SP-Sephadex C-25 (Na^+ form). The column was washed with water to remove remaining [Co(acac)$_3$]. By elution with 0.05 mol dm^{-3} NaCl, a purple ([Co(acac)$_2$-(dmap)]$^+$) and a red (a mixture of [Co(acac)(dmap)$_2$]$^{2+}$ and [$Co(H_2O)_6$]$^{2+}$) band developed in this order. The eluate containing the main purple band was collected and evaporated to a small volume under reduced pressure. To the concentrate was added $NaClO_4$ (0.2 g), and the complex was extracted with dichloromethane. The extract was washed with water, and mixed with a small amount of ethanol. The mixture was evaporated to a small volume, and to the concentrate was added diethyl ether. A purple precipitate was collected by filtration and washed successively with water, methanol–diethyl ether (1:5), and diethyl ether. Yield: 0.22 g (92%). Found: C, 33.57; H, 5.41%. Calcd for $C_{17}H_{32}As_2ClCoO_8$: C, 33.55; H, 5.30%. ^1H NMR (CD_2Cl_2) δ=1.23 (6H, s, $AsCH_3$), 1.43 (6H, s, $AsCH_3$), 1.7—2.2 (m, $-CH_2-$), 1.84 (6H, s, CCH_3), 2.19 (6H, s, CCH_3), and 5.48 (2H, s, $-CH-$). ^{13}C NMR (CD_2Cl_2) δ=4.9 (q), 5.6 (q), 20.6 (t), 22.9 (t), 26.6 (q), 27.3 (q), and 98.9 (d). The complex is soluble in ethanol and dichloromethane, but insoluble in water.

Measurements. Absorption spectra were obtained using a Hitachi 323 or a JASCO 610B spectrophotometer. ^1H NMR spectra were recorded on a JEOL PMX-60 or a JEOL FX 100 spectrometer, and ^{13}C NMR spectra on a JEOL FX 100 spectrometer.

Kinetics. Rates of isomerization of *cis*-[$CoCl_2$(dmap)$_2$]-ClO_4 to the trans isomer in methanol were followed by measuring the change in absorbance at 535 nm in the temperature range of 20.1—49.9 °C. The complex concentrations were *ca.* 1.3×10^{-3} mol dm^{-3}. The temperature of the solutions was kept constant within ±0.1 °C by use of a temperature-controlled circulating bath, Yamato-Komatsu CET-24W. In each kinetic run, the plot of $\ln(A_t-A_\infty)$ *vs.* time gave a straight line at least four half-lives, where A_t and A_∞ denote the absorbance at time t and at infinite time at 535 nm, respectively. The slope gave the first-order rate constant of isomerization, k, and Eyring treatment of $\log(k/T)$ *vs.* T^{-1} yielded the activation parameters.

Results and Discussion

Preparation and Characterization of the Complexes. Because of the very poor yield of the dmae ligand, most of the study has been done on the dmap complexes, although five-membered dmae chelate complexes would be more fundamental.

A *trans*-[$CoCl_2$(chelate)$_2$]$^+$ complex is known to be a good starting material for preparing various bis-(chelate)cobalt(III) complexes. The two chloride ions in the *trans*-[$CoCl_2$(dmae)$_2$]$^+$ and *trans*-[$CoCl_2$-(dmap)$_2$]$^+$ complexes are also easily replaced by such ligands as a carbonate and a 2,4-pentanedionate ion. Both *trans*-dichloro complexes were prepared in good yield by air-oxidation of a mixture of cobalt(II) chloride hexahydrate and the corresponding arsine ligand in ethanol, and by treating with hydrochloric acid. The trans configuration was suggested by green in color characteristic of a trans (Cl, Cl) configuration and confirmed by the ^1H NMR spectra. The *trans*-dichloro complexes give only one resonance attributable to the As–methyl protons. Since the puckering of the chelate rings will be rapid on the NMR time scale, four methyl groups in the trans isomer should be in equivalent environment. On the other hand, the purple [$CoCl_2$(dmap)$_2$]$^+$ complex prepared by treating [$Co(CO_3)$(dmap)$_2$]$^+$ with hydrochloric acid at *ca.* 0 °C exhibits four resonances in the As–methyl region (1.2—2.0 ppm) and is assigned to the cis isomer. The configurations of the dibromo and diiodo complexes were also assigned on the basis of the NMR and absorption spectra (*vide infra*). The *trans*-[$CoBr_2$(dmae)$_2$]$^+$ complex was prepared by reaction between *trans*-[$CoCl_2$(dmae)$_2$]$^+$ and potassium bromide in methanol. The complex thus yielded was necessary to recrystallize several times to purify; the most abundant impurity contained in the crude product may be the *trans*-bromochloro complex. In order to avoid contamination by the mixed halogeno complex, *trans*-[$CoBr_2$(dmap)$_2$]$^+$ was prepared by a method similar to that for the *trans*-dichloro complex using cobalt(II) bromide hexahydrate and hydrobromic acid instead of cobalt(II) chloride hexahydrate and hydrochloric acid. The *cis*-[$CoBr_2$(dmap)$_2$]$^+$ complex was prepared by a method similar to that for the corresponding *cis*-dichloro complex from [$Co(CO_3)$(dmap)$_2$]$^+$ and

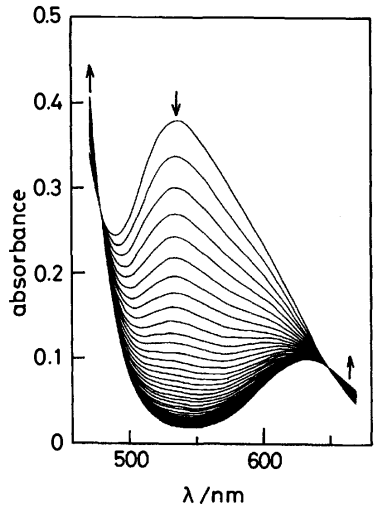

Fig. 1. Change in absorption spectrum of *cis*-[$CoCl_2(dmap)_2$]ClO_4 in methanol at 30.3 °C (recorded intervals: 30 min). Trends of spectral changes with time are shown by arrows.

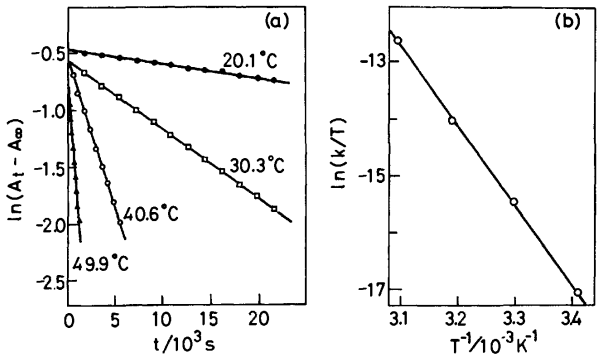

Fig. 2. (a) Plots of $\ln(A_t - A_\infty)$ against time at 20.1, 30.3, 40.6, and 49.9 °C and (b) Eyring treatment of $\ln(k/T)$ against T^{-1}.

hydrobromic acid.

Both *cis*-dichloro and dibromo complexes isomerize in solution to the trans isomer. Figure 1 shows the change in absorption spectrum at intervals during the isomerization of *cis*-[$CoCl_2(dmap)_2$]ClO_4 in methanol at 30.3 °C. Two isosbestic points were found at 649 and 478 nm in all the experiments (20.1—49.9 °C). The final spectrum was identical with that of a freshly prepared solution of *trans*-[$CoCl_2(dmap)_2$]ClO_4. When the experiment was carried out in deuterated methanol, the final ^1H NMR spectrum of the solution showed only signals attributable to the trans isomer. These results indicate that the cis isomer isomerizes to the trans isomer. Rates of the isomerization were followed by measuring the change in absorbance at 535 nm (Experimental, Fig. 2, and Tables 1 and 2). The rate constant 1.97×10^{-3} s^{-1} at 54.9 °C calculated from the ΔH^* and ΔS^* values is larger by a factor of 10^3 than that of *cis*-[$CoCl_2(diars)_2$]$^+$ at the same temperature (1.63×10^{-6} s^{-1}).[11,12] The isomerization of the dmap complex was also studied in the presence of 150 times molar amounts of lithium chloride. The first-order dependence in the complex concentration was maintained, the rates being decreased a little (Table 1).

TABLE 1. RATE CONSTANTS FOR ISOMERIZATION OF *cis*-[$CoCl_2(dmap)_2$]$^+$ IN METHANOL

t/°C	k/s^{-1}
20.1	$(1.18\pm0.01)\times10^{-5}$
30.3	$(5.92\pm0.02)\times10^{-5}$
40.6	$(2.61\pm0.01)\times10^{-4}$
49.9	$(1.04\pm0.01)\times10^{-3}$
20.2[a]	$(1.03\pm0.01)\times10^{-5}$
30.3[a]	$(4.89\pm0.01)\times10^{-5}$
40.6[a]	$(2.32\pm0.01)\times10^{-4}$
49.8[a]	$(8.61\pm0.02)\times10^{-4}$

a) Lithium chloride added (0.195 mol dm^{-3}).

TABLE 2. THERMODYNAMIC PARAMETERS FOR ISOMERIZATION OF THE COMPLEXES

complex	ΔH^*/ kJ mol^{-1}	ΔS^*/ J mol^{-1} K^{-1}	$\Delta G^*_{25°C}$/ kJ mol^{-1}
cis-[$CoCl_2(dmap)_2$]$^+$	115.2±0.7	53.8±2.3	99.2±1.5
cis-[$CoCl_2(dmpp)_2$]$^+$[a]	106.4±0.9	2.1±2.9	105.8±1.7

a) From Ref. 13.

Table 2 compares the activation parameters of isomerization for *cis*-[$CoCl_2(dmap)_2$]$^+$ with those for the analogous phosphine complex, *cis*-[$CoCl_2(dmpp)_2$]$^+$ (dmpp=1,3-bis(dimethylphosphino)propane). Although the ΔH^* value for the dmap complex is larger than that for the dmpp complex, the former complex isomerizes faster than the latter one at 25 °C because of the large positive activation entropy. If we assume that the two complexes isomerize *via* the same mechanism, the difference in rate may be explained by a steric factor; differences in bond distance, Co–E and E–C (E=As, P), should cause different steric interactions around the E–CH_3 groups. More data are needed to discuss in detail.

The reaction of [$Co(CO_3)(dmap)_2$]$^+$ with sodium iodide and perchloric acid yielded *trans*-[$CoI_2(dmap)_2$]$^+$, and no cis isomer was formed even the reaction was carried out at 0 °C. The *cis*-diiodo complex will be sterically unstable because of the interaction between the two large iodide ions and will isomerize very rapidly to the stable trans isomer. The *trans*-[$CoI_2(dmae)_2$]$^+$ complex was obtained easily from *trans*-[$CoCl_2(dmae)_2$]$^+$ and sodium iodide in ethanol by metathesis. The first diiodo-arsine complex, [$CoI_2(diars)_2$]$^+$ which was prepared by Nyholm[2] was once assigned as the cis isomer from the absorption spectrum,[14] but later assigned as the trans isomer from the ^1H NMR spectrum.[5]

The [$Co(acac)_2(dmap)$]$^+$ complex was prepared in high yield from [$Co(acac)_3$] and dmap in methanol–ethanol (1:1) in the presence of active charcoal. Although the reaction was carried out with an excess of

$[Co(acac)_3]$, the formation of $[Co(acac)(dmap)_2]^{2+}$ was observed in column chromatography. The result suggests that the dmap ligand has a strong affinity toward cobalt(III) in $[Co(acac)_3]$ and $[Co(acac)_2(dmap)]^+$. However, attempts to prepare $[Co(dmap)_3]^{3+}$ by the reaction of $[Co(acac)_3]$ or *trans*-$[CoCl_2(dmap)_2]^+$ with a large excess of dmap were all unsuccessful. Examination of molecular models indicates that $[Co(dmap)_3]^{3+}$ involves severe steric interactions among the ligands in any conformation of the six-membered chelate rings. Ohishi *et al.*[15] have suceeded in preparing $[Co(dmpe)_3]^{3+}$(dmpe=1,2-bis(dimethylphosphino)ethane) from *trans*-$[CoCl_2(dmpe)_2]^+$ and dmpe. We have not attempted to prepare the analogous arsine complex, $[Co(dmae)_3]^{3+}$, because of the very poor yield of dmae. A complex of the $[Co^{III}As_6]^{3+}$-type has been prepared for the diars ligand by Burstall and Nyholm.[3]

Absorption Spectra. Figure 3 shows the absorption spectra of *trans*-$[CoCl_2(As\text{-}As)_2]^+$ where As–As denotes dmae, dmap, and diars,[4] and Table 3 lists the spectral data. The structure of the diars complex has been determined by X-ray analysis.[16] Thus the dmae and dmap complexes which give spectra similar to that of the diars complex can be assigned to the trans isomer. This assignment is in accord with that given from the ^1H NMR spectra. All the dichloro complexes exhibit a low energy absorption band with intensities $\log\varepsilon$= 1.8—2.1, and the bands are assigned to the split component (I_a, $^1A_{1g}\rightarrow{}^1E_g$ (D_{4h})) of the first absorption band ($^1A_{1g}\rightarrow{}^1T_{1g}(O_h)$) from a comparison with the spectrum of *trans*-$[CoCl_2(en)_2]^+$ (Fig. 3, en=ethylenediamine).[17,18] The I_b ($^1A_{1g}\rightarrow{}^1A_{2g}$ (D_{4h})) component and the second d-d band are not observed by overlapping of the strong bands (25000—26000 cm^{-1}), which can be assigned as mainly the Co–As and Co–Cl charge-transfer bands.[19] The spectrochemical series for the arsine ligands is determined from examination of maximum positions of the I_a components: diars>dmae>dmap. For a series of *trans*-dichloro cobalt(III) complexes with analogous phosphine ligands a similar order has been reported: *o*-phenylenebis(dimethylphosphine)>dmpe> dmpp.[13] The trend that the d-d absorption bands shift to lower energies as the number of ring members of a chelate ligand increases from five to six has been observed for cobalt(III)–diamine complexes such as *trans*-$[CoCl_2(en)_2]^+$ (I_a: 16100 cm^{-1})[17,18] and *trans*-$[CoCl_2(tn)_2]^+$ (I_a: 15400 cm^{-1}, tn=trimethylenediamine).[20] In a series of *trans*-dichloro cobalt(III) complexes with a five-membered chelate, dmae, dmpe, and en, the energy of the I_a component decreases in the order, dmpe (17300 cm^{-1})[13]>dmae (16100 cm^{-1}) ~en (16100 cm^{-1}). Thus the spectrochemical series for the group 5B elements seems to be P>As~N. However, dmpe and dmae are a di(tertiary phosphine) and a di(tertiary arsine), respectively, while en is a di(primary amine). It is known that cobalt(III) complexes containing *N,N,N',N'*-tetramethylethylenediamine (Me_4-en), an

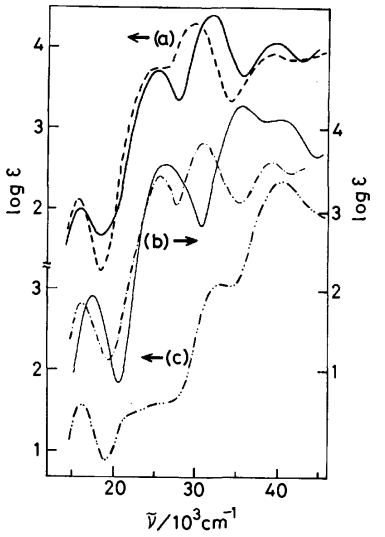

Fig. 3. Absorption spectra of (a) *trans*-$[CoCl_2(dmae)_2]^+$ (——) and *trans*-$[CoCl_2(dmap)_2]^+$ (---) in acetonitrile, (b) *trans*-$[CoCl_2(diars)_2]^+$ (—·—, from Ref. 4) and *trans*-$[CoCl_2(dmpe)_2]^+$ (——, from Ref. 13) in methanol, and (c) *trans*-$[CoCl_2(en)_2]^+$ (—··—) in methanol.

Table 3. Absorption spectral data

Complex	$\tilde{\nu}_{max}/10^3\,cm^{-1}$ ($\log(\varepsilon/cm^{-1}\,mol^{-1}\,dm^3)$)
trans-$[CoCl_2(dmae)_2]^{+a)}$	16.1(2.01) 25.3(3.73) 31.7(4.42) 39.4(4.07)
trans-$[CoBr_2(dmae)_2]^{+a)}$	15.3(1.94) 23.3(3.52) 30.8(4.29) 34.9(4.18) 42.6(4.13)
trans-$[CoI_2(dmae)_2]^{+a)}$	14.4(1.97) 18(sh, 2.84) 20.6(3.68) 30.1(4.24) 38.8(4.34) 40.0(4.01)
$[Co(CO_3)(dmae)_2]^{+b)}$	20.5(2.94) 24.5(2.80) 33.1(4.29)
trans-$[CoCl_2(dmap)_2]^{+a)}$	15.7(2.11) 25.0(3.77) 29.6(4.31) 39.1(3.94)
trans-$[CoBr_2(dmap)_2]^{+b)}$	15.0(2.09) 23.3(3.64) 28.7(4.24) 34.9(4.14) 40(sh, 3.95)
trans-$[CoI_2(dmap)_2]^{+a)}$	14.0(1.99) 17.5(sh, 2.86) 20.5(3.69) 29.9(4.13) 33.8(4.17) 40.1(4.08)
cis-$[CoCl_2(dmap)_2]^{+a)}$	17(sh, 2.60) 18.7(2.74) 22.5(sh, 3.01) 27.4(4.13) 31.9(4.11) 35(sh, 3.98) 40(sh, 3.97)
cis-$[CoBr_2(dmap)_2]^{+a)}$	16(sh, 2.57) 17.8(2.68) 25.5(sh, 3.89) 29.2(4.10) 33.8(4.11) 36.6(4.14)
$[Co(CO_3)(dmap)_2]^{+b)}$	20.1(3.01) 24.4(2.84) 30.9(4.38) 33(sh, 4.16) 35(sh, 4.02) 43(sh, 3.87)
$[Co(acac)_2(dmap)]^{+a)}$	17.5(sh, 2.59) 19.9(2.68) 32.3(4.07) 34.2(4.08) 44.4(3.98)
$[Co(acac)(dmap)_2]^{2+a)}$	19.5(3.16) 30(sh, 3.99) 34(sh, 4.48) 37.0(4.64)

Solvent, a): CH_3CN, b): CH_3OH.

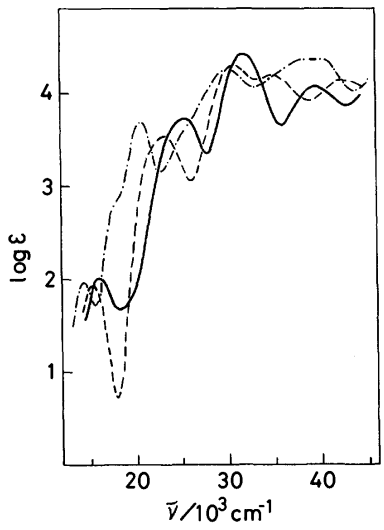

Fig. 4. Absorption spectra of *trans*-$[CoX_2(dmae)_2]^+$ in acetonitrile; X=Cl (——), Br (---), and I (—·—).

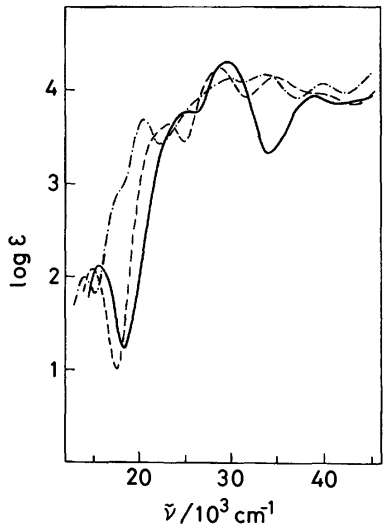

Fig. 5. Absorption spectra of *trans*-$[CoX_2(dmap)_2]^+$ in acetonitrile; X=Cl (——), Br (---), and I (—·—).

analogous ligand to dmpe and dmae, shift the d-d absorption bands to lower energy to a large extent compared with those of the corresponding en complexes (for example, $[Co(acac)_2(en)]^+$: 18450 cm^{-1}, $[Co(acac)_2(Me_4\text{-}en)]^+$: 16600 cm^{-1}).[21-23] Thus the appropriate order for the spectrochemical series would be dmpe (P)>dmae (As)>Me_4-en (N). A similar result (P>As) has been reported for $[PdCl_2\{NH_2CH_2CH_2E(n\text{-}C_4H_9)(C_6H_5)\}]$ (E=P, As).[24]

Figures 4 and 5 show the absorption spectra of *trans*-$[CoX_2(dmae)_2]^+$ and *trans*-$[CoX_2(dmap)_2]^+$ (X=Cl, Br, I), respectively. In either series, the energy of the I_a component decreases in the order Cl>Br>I. The diiodo complexes show a shoulder ($\log\varepsilon\approx2.8$) at *ca.* 18000 cm^{-1}. Such a shoulder is also observed for the analogous phosphine complex, *trans*-$[CoI_2(dmpe)_2]^+$,[13] however, the origin of the transition is unknown.

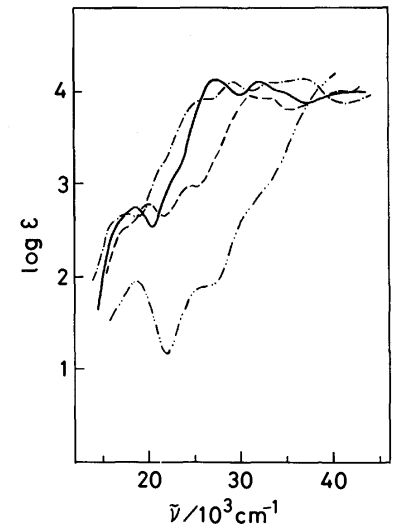

Fig. 6. Absorption spectra of *cis*-$[CoX_2(dmap)_2]^+$ in acetonitrile; X=Cl (——) and Br (—·—), *cis*-$[CoCl_2(diars)_2]^+$ (---, from Ref. 4) in ethanol, and *cis*-$[CoCl_2(en)_2]^+$ (—··—) in water.

The absorption spectra of *cis*-$[CoX_2(dmap)_2]^+$ (X=Cl, Br) are shown in Fig. 6 together with those of the diars and en complexes. The dichloro-dmap complex shows the first absorption band maximum at 18700 cm^{-1} with a shoulder at the low energy side (*ca.* 17000 cm^{-1}). The intensities of these bands are considerably higher than those of *cis*-$[CoCl_2(en)_2]^+$.[25] The large absorption coefficients are also observed for the d-d transitions of other *cis*-$[CoCl_2As_4]^+$-type complexes.[4,19,26,27] If the shoulder at *ca.* 22500 cm^{-1} in the spectrum of *cis*-$[CoCl_2(dmap)_2]^+$ is assigned as mainly the second absorption band, the dmap ligand will reduce largely the interelectronic repulsion of the central cobalt atom; the energy separation between the $^1T_{1g}$ and $^1T_{2g}$ manifolds is much smaller than that of *cis*-$[CoCl_2(en)_2]^+$[25] where the cobalt(III) ion is surrounded by hard donor atoms (Fig. 6). Such largely reduced interelectronic repulsion in a cobalt(III)-arsine complex is more clearly shown for $[Co(CO_3)(dmae)_2]^+$ and $[Co(CO_3)(dmap)_2]^+$; the energy differences (4000 and 4300 cm^{-1}, respectively) between the first and the second absorption bands are about half of that (8260 cm^{-1}) for $[Co(CO_3)(en)_2]^+$[28] (Fig. 7). Small energy differences between the first and the second absorption bands of cobalt(III) complexes have also been reported for phosphine complexes such as $[Co\{(CH_3)_2PCH_2CH_2NH_2\}_3]^{3+}$[29] and $[Co(dmpe)_3]^{3+}$.[15] The spectrum of *cis*-$[CoBr_2(dmap)_2]^+$ is similar to that of the corresponding dichloro complex except that the former is shifted to lower energy side compared to the latter.

Figure 8 shows the absorption spectra of a series of the $[Co(acac)_{3-n}(dmap)_n]^{n+}$($n$=0, 1, 2) complexes. The bands in the region of 16000 to 20000 cm^{-1}, which can be assigned to the first d-d absorption band, shift to higher energy and become more intense as the number

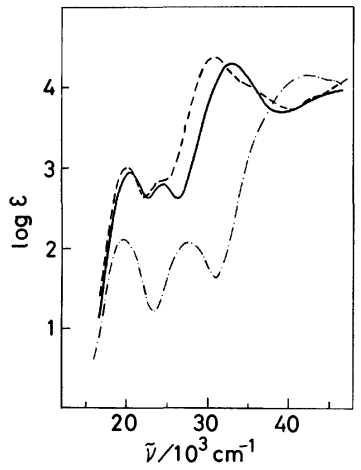

Fig. 7. Absorption spectra of $[Co(CO_3)(dmae)_2]^+$ (——) in methanol, $[Co(CO_3)(dmap)_2]^+$ (---) in methanol, and $[Co(CO_3)(en)_2]^+$ (---) in water.

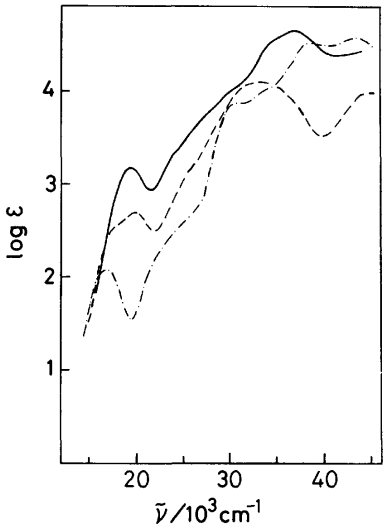

Fig. 8. Absorption spectra of $[Co(acac)_{3-n}(dmap)_n]^{n+}$ n=0 (—·—) in methanol and n=1 (---) and n=2 (——) in acetonitrile.

of dmap increases.

The present work was partially supported by a Grant-in-Aid for Scientific Research No. 58470032 from the Ministry of Education, Science and Culture.

References

1) R. G. Pearson, *J. Am. Chem. Soc.*, **85**, 3533 (1963); *J. Chem. Educ.*, **45**, 581 (1968).
2) R. S. Nyholm, *J. Chem. Soc.*, **1950**, 2071.
3) F. H. Burstall and R. S. Nyholm, *J. Chem. Soc.*, **1952**, 3570.
4) T. M. Dunn, R. S. Nyholm, and S. Yamada, *J. Chem. Soc.*, **1962**, 1564.
5) B. K. W. Baylis and J. C. Bailar, Jr., *Inorg. Chem.*, **9**, 641 (1970).
6) B. Bosnich, W. G. Jackson, and W. McLaren, *Inorg. Chem.*, **13**, 1133 (1974).
7) R. D. Feltham, H. G. Metzger, and W. Silverthorn, *Inorg. Chem.*, **7**, 2003 (1968).
8) K. Sommer, *Z. Anorg. Chem.*, **377**, 278 (1970).
9) J. R. Phillips and J. H. Vis, *Can. J. Chem.*, **45**, 676 (1967).
10) G. J. Burrows and E. E. Turner, *J. Chem. Soc.*, **1920**, 1373.
11) A. Peloso and M. L. Tobe, *J. Chem. Soc.*, **1964**, 5063.
12) A. Peloso and G. Dolcetti, *J. Chem. Soc., A*, **1969**, 1506.
13) T. Ohishi, Doctoral Thesis, Nagoya University, 1985.
14) S. Yamada, *Coord. Chem. Rev.*, **2**, 83 (1967).
15) T. Ohishi, K. Kashiwabara, and J. Fujita, *Chem. Lett.*, **1981**, 1371.
16) P. K. Bernstein, G. A. Rodley, R. Marsh, and H. B. Gray, *Inorg. Chem.*, **11**, 3040 (1972).
17) Y. Shimura and R. Tsuchida, *Bull. Chem. Soc. Jpn.*, **28**, 572 (1955).
18) M. Nakahara and M. Mitsuya, *Bull. Chem. Soc. Jpn.*, **45**, 2209 (1972).
19) B. Bosnich, W. G. Jackson, and S. B. Wild, *J. Am. Chem. Soc.*, **95**, 8269 (1973).
20) H. Kawaguchi, Y. Yano, and S. Kawaguchi, *Bull. Chem. Soc. Jpn.*, **42**, 136 (1969).
21) Y. Ouyang, M. Kojima, and J. Fujita, *Bull. Chem. Soc. Jpn.*, **57**, 3574 (1984).
22) R. J. York, W. D. Bonds, Jr., B. P. Costoradis, and R. D. Archer, *Inorg. Chem.*, **8**, 789 (1969).
23) K. Akamatsu and Y. Shimura, *Bull. Chem. Soc. Jpn.*, **51**, 2586 (1978).
24) Y. Shigetomi, M. Kojima, and J. Fujita, *Bull. Chem. Soc. Jpn.*, **58**, 258 (1985).
25) M. Linhard and M. Weigel, *Z. Anorg. Chem.*, **271**, 101 (1952).
26) R. D. Feltham and W. Silverthorn, *Inorg. Chem.*, **7**, 1154 (1968).
27) B. Bosnich, S. T. D. Lo, and E. A. Sullivan, *Inorg. Chem.*, **14**, 2305 (1975).
28) J. Springbφrg and C. E. Schäffer, *Inorg. Synth.*, **XIV**, 64 (1973).
29) I. Kinoshita, K. Kashiwabara, J. Fujita, K. Matsumoto, and S. Ooi, *Bull. Chem. Soc. Jpn.*, **54**, 2683 (1981).

Optical Energy Storage by Bilayer Electrodes, Polymerized Coordination Compounds of Ruthenium or Iron

Seiichi KANDA* and Royce W. MURRAY†

Department of Applied Chemistry, Faculty of Engineering, The University of Tokushima, Minamijosanjima, Tokushima 770

†*The Kenan Laboratory of Chemistry, University of North Carolina, Chapel Hill, North Carolina 27514, U.S.A*

(Received November 22, 1984)

Electrochemistry of bilayer electrodes has until now been investigated mainly in the dark. For the further development of the photoelectrochemistry of bilayer electrodes and its application to optical-energy storage, a polymer of *N*-[4-[2-(trimethoxysilyl)ethyl]benzyl]-*N'*-methyl-4,4'-bipyridinium dibromide ($BVSiBr_2$), a photoredox siloxane polymer, was employed as a photosensitive outer-layer, and bis(2,2'-bipyridine)bis(4-vinylpyridine)ruthenium(II) bis(hexafluorophosphate), $[Ru(bpy)_2(vpy)_2](PF_6)_2$, or tris(4-methyl-4'-viny-2,2'-bipyridine)iron(II) bis(hexafluorophosphate), $[Fe(vbpy)_3](PF_6)_2$ was electrochemically polymerized as the inner layer on the surface of an SnO_2 electrode. Direct and indirect photochemical reductions(trapping) of the outer layer siloxan polymer were attempted in the following ways: 1) the outer-layer, poly($BVSiBr_2$), was chemically trapped with a methylviologen radical, MV^+, produced photochemically in an illumination cell and transferred to the electrochemical cell, 2) the outer-layer was photochemically trapped by UV irradiation in the presence of photosensitive alcohols (*i*-PrOH and EtOH) and 3) by photochemical trapping with tris(2,2'-bipyridine)-ruthenium and triethanolamine. The lst and the 2nd methods yielded results expressed by cyclic voltammograms showing an accumulation of poly($BVSi^+$), that is, a storage of optical energy in the outer-layer. The result of the 3rd method was negative.

One of the authors (Murray) has presented a theory and an experimental demonstration of a "two-layer electrode" which comprises two electroactive layers on a conducting electrode.[1-3] These are physically discrete and are formed of electroactive materials (usually not a semiconductor) with different redox potentials. The essence of a two-layer or "bilayer" scheme is that an electron transfer between the conductor electrode and the outer electroactive layer is forced catalytically by an electron-transfer mediation through redox states of the inner electroactive layer.

When photoreductive or photooxidative materials are used as the outer-layer components, photochemically excited energy is stored within a specific range of the electrode potential, depending upon the redox potentials of the inner-layer compounds. The reduced or oxidized excited state of the outer layer has been named the "trapped state," and this phenomenon has potential use for solar energy storage cells. This paper presents a few examples of this type of electrode.

Experimental

Chemicals and Equipments. The organosilane monomer *N*-[4-[2-(trimethoxysilyl)ethyl]benzyl]-*N'*-methyl-4,4'-bipyridinium dibromide ($BVSiBr_2$) (**1**) was prepared as described in the literature.[2] Onto a deck-glass, SnO_2 films,

1 $(CH_3O)_3SiCH_2CH_2$– 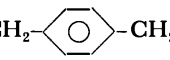 –CH_2–

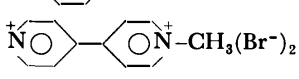 –$CH_3(Br^-)_2$

or inner films, a drop of a methanolic solution of $BVSiBr_2$ (*ca.* 8×10^{-3} mg in a 9 μL solution) was spread. A rapid methanol evaporation is recommended for producing a uniform film. For condensation polymerization, a hydrogen chloride vapor and warm moisted air were blown successibly on the monomer films, then stored in a vacuum oven for more than two hours. *N,N'*-dimethyl-4,4'-bipyridinium dichloride, methylviologen, ($MVCl_2$) hydrate, benzophenone and Et_4NClO_4 (TEAP) were reagent grade. The potentiostat and electrochemical cells were of conventional design and the SnO_2 electrodes were highly doped films on glass, as previously used.[2] Electrochemical potentials are with reference to a NaCl-saturated calomel electrode (SSCE). Before taking cyclic voltammograms, the electrolytic solution was flushed with N_2. An Hg lamp (Baush and Lomb 33-86-25-01) and a monochromator system were used for irradiations at 313 or 366 nm.

Electrochemical Polymerization of the Inner Films. The monomer complexes $[Ru(bpy)_2(vpy)_2]$ $(PF_6)_2$ (vpy=4-vinylpyridine) and $[Fe(vbpy)_3](PF_6)_2$(vbpy=4-methyl-4'-vinyl-2,2'-bipyridine) were prepared by a method from the literature by Mr. C. R. Leidner.[1] The electrochemical polymerization processes were carried out in a 2-mM** concentration of each complex in 0.1 M Et_4NClO_4/CH_3CN. The potentials applied to the electrode, SnO_2, in these solutions were cyclically swept between −0.8 and −1.8 volt *vs.* SSCE for about 20 min.[2] The coverages, Γ, of the insoluble polymers was determined electrochemically.

Results and Discussion

Photochemistry of $BVSi^{2+}$ Monomer. For a preliminary check of the photochemistry of a $BVSi^{2+}$ monomer solution, the following types of reductive solvents were used. The ratio of components CH_3OH, C_2H_5OH, *i*-C_3H_7OH, and CH_3CN in a mixed solvent A was 1:1:1:1 in volume, for solvent B 0.1:0:1:3; and for solvent C 0:1:0:4. Primes are used to designate solvents (A' and B') of which 4 mL were added to 5 mg of benzophenone. To purge the dissolved oxygen, nitrogen gas was bubbled into the solutions A, A',

** 1 M = 1 mol dm^{-3}.

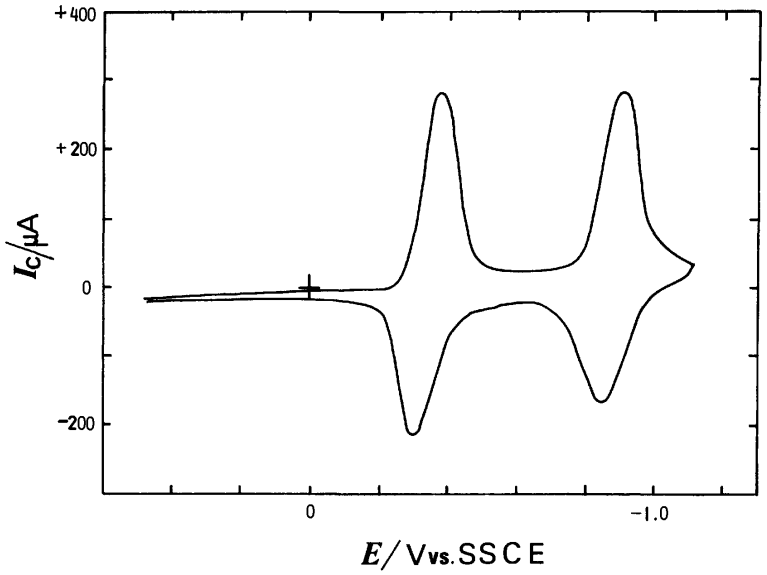

Fig. 1. Cyclic voltammetry of SnO_2/poly($BVSiBr_2$) layer electrode at 0.1 V/s in 0.1 M Et_4NClO_4/CH_3CN.

B and B′ of 2×10^{-4} M $BVSiBr_2$ for 20 min. The solutions were then irradiated at 313 and 366 nm. In solutions A and A′, a violet color emerged and increased in intensity for 50—60 min. It then slowly faded and after 3—4 h the solution became light yellow. In solutions B and B′ of $BVSiBr_2$ of the same concentration, the irradiation instantly made them intense violet; however the color tended to fade sooner than in the previous cases (solvents A and A′) with irradiation. To produce a more complete deoxygenation, a freeze-pump-thaw (FPT) method (4 or 5 cycles) was applied to solutions B′ and C. The $BVSiBr_2$ (2×10^{-4} M) in solution B′ exhibited a violet color even in the room light during the process of FPT. Then, the color faded away after one hour. Thereafter, no color appeared even upon irradiation with an intense light source.

$BVSi^{2+}$ (8×10^{-3} M) in solvent B′ exhibited intense violet upon Hg-lamp irradiation. By shaking the sealed Pyrex tube, the violet color quickly faded. This procedure was repeated more than ten times. The time needed for one cycle became longer and longer; finally, the blue-violet color faded away without further recovery. Upon Hg-lamp irradiation, 8×10^{-3} M $BVSi^{2+}$ in solvent C exhibited a blue color which was much weaker in intensity than in the previous case. Shaking the tube did not cause a weakening of the color and continuous irradiation caused the color to intensify to a certain degree. Fading was very slow and a recovery of the color was possible with UV irradiation.

Such nonpermanent colorations of a $BVSiBr_2$ monomer in several solvents indicate:

1) a photochemical generation of the $BVSi^{+}$ radical;

2) a more or less slow reoxidation of $BVSi^{+}$ to $BVSi^{2+}$ by some oxidants which probably exsist as impurities, even in the purified solutions by freeze-pump-thaw (FPT) method; and that

3) the mechanisms of the coloration are different, depending upon the solvent and/or the photoactive reductants.

Poly($BVSiBr_2$) Film on SnO_2 or Glass. The coverage of the polymer on the substrate can be first calculated from the concentration and the spread volume of the stock solution. This is shown to be $7—8\times10^{-9}$ mol/cm^2 upon assuming uniform films. Secondly the electrochemically determined coverage was calculated from the cathodic peaks on the cyclic voltammogram ($BVSi^{2+/1+/0}$) in CH_3CN (0.1 M TEAP), and the values obtained are 2.36, 3.9, 2.16, and 2.93×10^{-9} mol/cm^2 (average value $2.8\pm0.7\times10^{-9}$ mol/cm^2), as shown in Fig. 1. The difference in the coverages estimated by the above two methods (2.8/8=0.35) can be attributed to a nonuniformity of the film thickness and/or a partial polymerization which might have resulted in the dissolution of a monomer or oligomer of $BVSiBr_2$. The nonuniformity resulted in an underestimation of the coverage in the electrochemical determination.

Preliminary qualitative tests regarding solvents for the photochemical reduction of a poly ($BVSiBr_2$) film on a substrate were as follows. Solvent A dissolves films slowly under UV irradiation, and both the solution and the films became violet. This lasted for a while. In solvent B′, the irradiation caused changes in the colors of the films on both glass and SnO_2 to black or violet. These lasted for more than one month in vessels isolated from oxygen. The stability of the color of a polymer film which differs from the case of the monomer can be attributed to the insensitivity of polymeric solids towards oxidants in comparison with that of a monomer.

TABLE 1. COMPARISON OF AMOUNTS OF THE OUTER-LAYER POLY ($BVSi^{2+}$) AND THE EFFECTIVE AMOUNTS OF ($BVSi^{+}$) COMPONENTS ON THE INNER-LAYER $[Ru(bpy)_2(vpy)_2](PF_6)_2$ OR $[Fe(vbpy)_3](PF_6)_2$ IN THREE WAYS

Inner layer	$[Ru(bpy)_2(vpy)_2](PF_6)_2$ 5×10^{-8} mol cm^{-2}	$[Fe(vbpy)_3](PF_6)_2$ 8×10^{-9} mol cm^{-2}
$BVSi^{2+}$/mol cm^{-2} estimated From volume of soln.[a]	5×10^{-7}	1.5×10^{-8}
From untrap-curve after Electrochem-trapping[b]	6.2×10^{-8}	1.2×10^{-8}
From untrap-curve after Being trapped by $MV^{+\cdot}$ [b]	7.6×10^{-8}	1.0×10^{-8}

Scan rate: 20 mV/s. a) $BVSi^{2+}$ stock solution: 23 mg of the dibromide in 25 ml of ethanol. b) Effective value of poly($BVSi^{+}$) calculated by Eq. 1.

Chemical Trapping with Photochemically Produced MV^{+} Representative examples of a bilayer electrode for chemical trapping are as follows: 5×10^{-7} mol of $BVSi^{2+}$/5×10^{-8} mol of poly($[Ru(bpy)_2(vpy)_2](PF_6)_2$)/$SnO_2$ and 1.5×10^{-8} mol of $BVSi^{2+}$/8×10^{-9} mol of poly($[Fe(vbpy)_3](PF_6)_2$)/SnO_2. The amounts of $BVSi^{2+}$ were estimated from the spread volumes and the concentrations of the stock solutions, whereas those of inner complex films were evaluated from cyclic voltammograms. As shown in Table 1, the iron-polymer film was adjusted to be thinner than the ruthenium-polymer film, since the structure of poly-($[Fe(vbpy)_3](PF_6)_2$) is tighter and stabler than that of poly($[Ru(bpy)_2(vpy)_2](PF_6)_2$). When the inner film is not tight enough to separate the outer film from the electrode, a leak causes cathodic current peaks of the $BVSi^{2+}$ at the usual potentials of $BVSi^{2+/1+}$ and $BVS^{1+/0}$, that is, at -0.34 and -0.865 V *vs.* SSCE, respectively. For this reason, Ru-complex films were made to be about ten times as thick as Fe-complex films (in moles). In order to obtain precise amounts of trapped poly ($BVSi^{+\cdot}$) in the process of untrapping, the outer films, poly ($BVSi^{2+}$), were made to be more than twice that of the inner films (in moles).

Poly($BVSi^{2+}$) in outer films was reduced using photochemically reduced methylviologen (MV^{+}) as follows; 4×10^{-3} M of a $MVCl_2$ hydrate stock solution in a mixed solvent (1 mL, C_2H_5OH+9 mL, CH_3CN) was irradiated with an Hg lamp in a glass vial under nitrogen bubbling and an addition of 10 mg of benzophenone. One mL of the intense-blue solution produced photochemically within 5 min was transferred through Teflon tubing using the pressure of the nitrogen gas to the electrochemical cell where the bilayers on SnO_2 were set in 10 mL CH_3CN(TEAP). After holding it in the (MV^{2+}/MV^{+}) solution at an open circuit for 10 to 15 min, cyclic voltammograms of the Ru-complex bilayers were recorded between +0.5 and +2.0 V, and between +0.5 and +1.8 V for the Fe-complex bilayer.

As shown in Figs. 2A and 2B, the first anodic peaks are much larger than the cathodic peaks and the successive anodic peaks in the second and the third cycles. These differences are mainly attributed to the theoretically expected untrapping currents of the poly ($BVSi^{+}$). In these potential ranges, the oxidation of poly ($BVSi^{+}$, $BVSi^{0}$) in the outer films and Ru^{2+} in the inner films takes place, but poly ($BVSi^{2+}$) is not reduced (owing to the rule of the bilayer). The integrated values of anodic and cathodic currents during the 2nd and 3rd cycles are expected to be equal if the untrapping of poly ($BVSi^{+}$) is completed during the first anodic scan. However, it is apparent from Fig. 2A that even in the 2nd and 3rd cycles the equalities do not hold. As the voltammogram was taken in a solution which still contained MV^{+}, the untrapped $BVSi^{2+}$-unit would be trapped to form $BVSi^{+}$-unit again in the whole period of time. This causes the above-mentioned inequality between the integrated cathodic and anodic currents. This tendency is emphasized when the inner film is resistive for the transport of the charge which originates from the outer film, as is shown in the case of a Ru-complex inner film.

In order to avoid this ambiguity, based on a continuing trapping by MV^{+} in the calculation of the untrapping charge ($BVSi^{+}\rightarrow BVSi^{2+}$), the trapped bilayer electrodes were quickly washed with aceton and were untrapped in a methylviologen-free acetonitrile (TEAP) solution. For the bilayer with a Ru-complex, the results were calculated using

$$\int I_a dt - \int I_c dt = \int I_a(BVSi^{+\cdot}) dt. \quad (1)$$

These are shown in the 3rd row of Table 1. The expected equality on the 2nd and 3rd reverse processes was satisfactorily effected.

By scanning from -1.5 to +2.0 V *vs.* SSCE at 20 mVs^{-1} in CH_3CN (TEAP), the outer layer can be trapped (reduced) and untrapped electrochemically; by this method, an effective amount of the electrochemically reducible $BVSi^{2+}$ through the inner film (Ru-complex) under the experimental conditions was estimated and is shown in the 2nd row of the table. The values in the 2nd and 3rd rows are nearly equal, whereas that in the lst row (estimated from the volume of the solution) is very much different. This can presumably be attributed to an incomplete untrapping process due to the thickness of the inner film, which

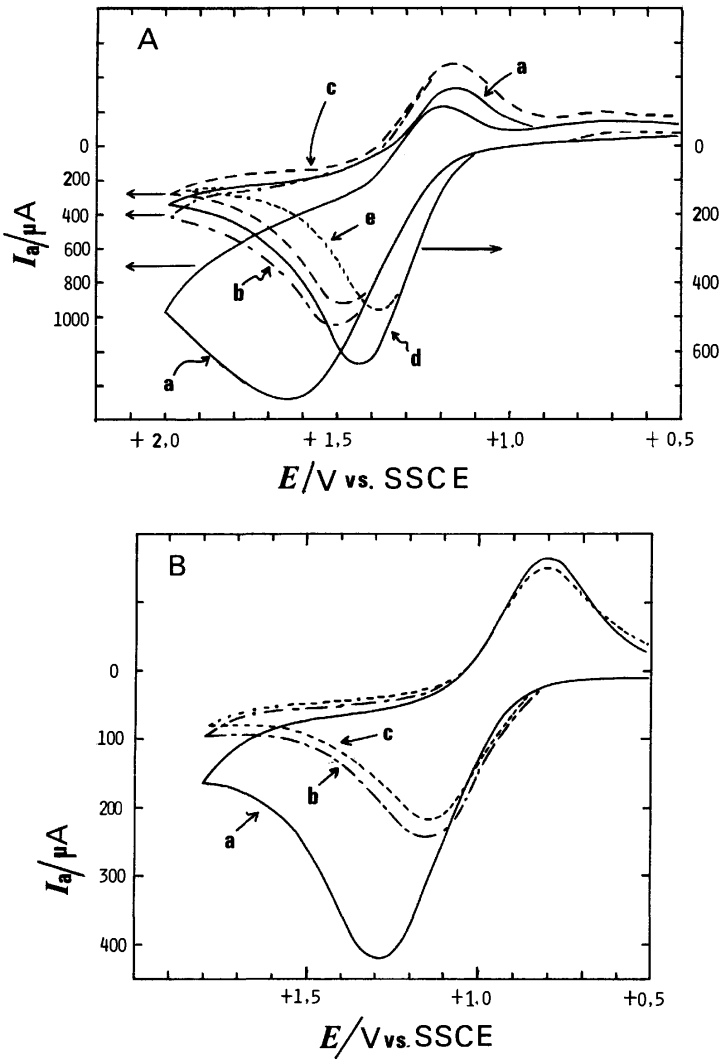

Fig. 2. Untrapping of outer-layer poly($BVSi^{+}$) trapped by MV^{+} in CH_3CN (0.1 M Et_4NClO_4). A) $[Ru(bpy)_2(vpy)_2](PF_6)_2$ inner layer, curve a: 1st scan at 100 mV/s after an exposure for 15 min to MV^{+}, b: 2nd scan at 100 mV/s immediately after the 1st scan, c: 4th scan at 100 mV/s immediately after the 3rd scan, d: 1st scan at 20 mV/s after an exposure for 13 min to MV^{+}, e: 2nd scan at 20 mV/s immediately after the 1st scan. B) $[Fe(vbpy)_3](PF_6)_2$ inner layer. curve a: 1st scan at 100 mV/s an exposure for 14 min to MV^{+}, b: 2nd scan at 100 mV/s immediately after the 1st scan, c: 3rd scan at 100 mV/s immediately after the 2nd scan.

causes the large electrical resistance. It also corresponds to the fact that the untrapped-charge value calculated with Eq. 1 for a fast scan rate (100 mVs^{-1}), is smaller than that for the above case (20 mVs^{-1}).

Contrary, in the case of an iron-complex inner film, the three values in the table were in fair agreement each other. This is probably because of a complete untrapping of outer film species due to the smooth transport of the charge through the inner/outer-film interface and the bulk of the inner film. Also the smoothness is consistent with the independence of the untrapped charge value using Eq. 1 for the scan rates. However, there is still a small discrepancy between the values in the 1st and those in the 3rd row. This is attributable to the nonuniformity of the thickness of the outer film, which might result in an incomplete untrapping in the thicker parts.

In all these speculations uncertainties regarding an evaluation of the electrode area and graphical integrations of cyclic voltammograms were inevitable. Upon considering this, any detailed discussion concerning these minor discrepancies are unnecessary.

Attempts of Photochemical Trapping of $[Ru(bpy)_2(vpy)_2](PF_6)_2$/Poly($BVSiBr_2$) by Direct Irradiation in The Presence of Alcohols or $[Ru(bpy)_3]$. In an electrolytic cell with a quartz window the bilayer elec-

TABLE 2. UNTRAPPING OF PHOTOCHEMICALLY TRAPPED POLY(BVSi^{+})/[Ru(bpy)$_2$(vpy)$_2$](PF$_6$)$_2$ BY ALCOHOLS UNDER UV IRRADIATION (366 nm)

Reductant added to 25 mL CH_3CN(TEAP)			amount/10^{-9} mol of oxidation between +0.5 and +1.8 V				$\gamma = \frac{Q_a^{(1)} - Q_a^{(2\text{ or }3)}}{Q_a^{(2\text{ or }3)}}$ %	
			Q_a		Q_c			
			trial A	trial B	trial A	trial B	trial A	trial B
1%	EtOH	1st[b]	11.5	11.6	9.3	10.0	25	33
		2nd	9.2	8.7	9.0	9.0		
1%	EtOH	1st	14.7	13.5	12.8	12.6	40	39
4%	*i*-PrOH	3rd	10.5	9.7				
1%	EtOH	1st	8.4		6.08		29	
4%	*i*-PrOH	3rd	6.5		6.45			
	$Bz_2C{=}O$[a]							
1%	EtOH [c]	1st	7.1		5.0		20	
4%	*i*-PrOH							
	$Bz_2C{=}O$[a]	3rd	5.9		5.0			

a) Benzophenone. b) Sequence of cycling between +0.5 and +1.8 V *vs.* SSCE. c) In dark.

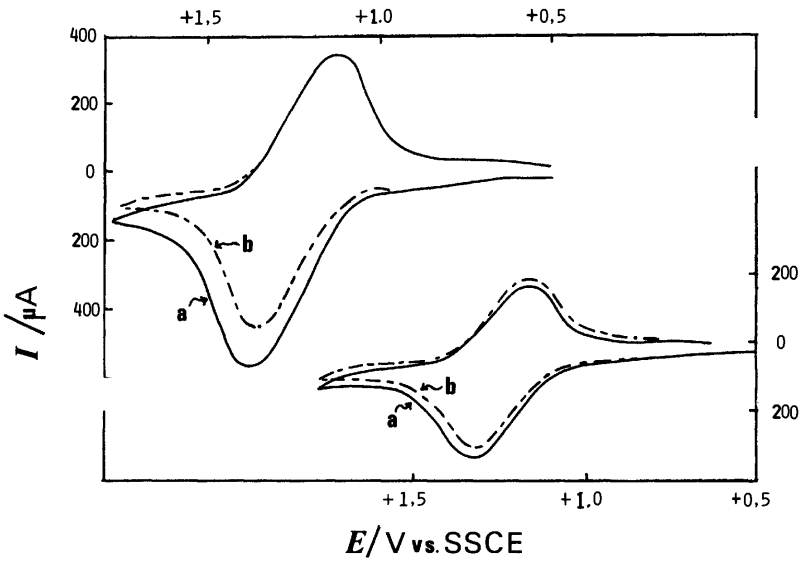

Fig. 3. Untrapping of poly(BVSiBr$_2$)/[Ru(bpy)$_2$(vpy)$_2$](PF$_6$)$_2$/SnO$_2$ after UV irradiation in 1% EtOH, 4% *i*-PrOH, and 95%CH_3 CN. Left: curve a: 1st scan after irradiation at 366 nm through quartz window for 25 min, b: 3rd scan immediately after twice successive scans; Right: curve a: 1st scan after 25 min N_2 flush in dark, b: 3rd scan.

trode was dipped in a 1% ethanol solution in CH_3CN (TEAP). The solution was then irradiated with 366 nm light from a xenon lamp with an UV cut filter (<350 nm) for 15 to 25 min. A cyclic voltammogram between +0.5 and +1.5 V *vs.* a AgCl/Ag electrode on the bilayer electrode suggested a gradual photodecomposition of the layers. Thus, the trapping and untrapping can be evaluated by

$$\gamma = (Q_a^{(1)} - Q_a^{(3)})/Q_a^{(3)}, \quad (2)$$

where graphically integrated electrical charge values, $Q_a^{(1)}$ and $Q_a^{(3)}$, stand for electrochemically oxidized amounts of poly (BVSi^{+}) in the lst cycle and the 3rd cycle, respectively. $Q_c^{(i)}$ (the *i*-th cathodically reduced amount) and $Q_a^{(i)}$ in several trials involving different solvents where 2-propanol (4%) and benzophenone (45 mg in 20 mL of solution) were successively added, are tabulated in Table 2 as well as γ values for each. As can be seen from the Table 2 and Fig. 3, ethanol and 2-propanol are effective in photochemical reductions; but, a further addition of benzophenone caused a simultaneous reduction of Q_a, Q_c, and γ. Irradiation with 366 nm light in the presence of benzophenone caused the photoactive substances in the bilayers to be decomposed, resulting in the disappearance of the cathodic and the anodic peaks.

Expecting a trapping of poly(BVSi^{2+}) in the outer film, the Ru-complex bilayer was immersed in a CH_3CN (TEAP) solution which contained a sensitizer 8×10^{-6} M [Ru(bpy)$_3$]$^{2+}$, and a sacrificial reductant, 4×10^{-5} M triethanolamine. It was then irradiated at 450 nm (200 Watt xenon lamp, monochromatized, with UV cut filter). No remarkable effect was ob-

served except a gradual decrease in the redox currents in the cyclic voltammogram.

Conclusion

Three types of photoenergy conversion to chemical energy and its storage have been attempted using bilayer electrodes which were composed of a poly ($BVSi^{2+}$) outer layer and an Fe- or Ru-complex inner layer:

1. The outer layers were trapped by MV^{+} (reductant) derived photochemically from MV^{2+},
2. The outer layers were photochemically trapped in the presence of ethanol and 2-propanol, and
3. Photochemically excited $[Ru(bpy)_3]^{2+}$ with a sacrificial reductant, *i.e.*, triethanolamine, was not reductive to the outer layer.

The results show that the stable radical, MV^{+}, and the alcohols which are permeable through the poly($BVSi^{2+}$) film, are effective for the outer film. However, the excited species of $[Ru(bpy)_3]^{2+}$, with a lifetime of about 10^{-6} s, is not effective in such a heterogeneous redox reaction.

This research was supported by the Japan Society for the Promotion of Science for the Cooperative Photoconversion and Photosynthesis Research Program. S. Kanda acknowledges the hospitality of Murrays' group and the valuable advice given by Prof. Whitten and Dr. Chandrasekaran during his visit in the last quarter of 1981. The assistance during these experiments provided by Mr. L. D. Margerum and Mr. C. R. Leidner is noteworthy.

References

1) H. D. Abruna, P. Denisevich, M. Umana, T. J. Meyer, and R. W. Murray, *J. Amer. Chem. Soc.*, **103**, 1 (1981).
2) P. Denisevich, K. W. Willman, and R. W. Murray, *J. Amer. Chem. Soc.*, **103**, 4727 (1981).
3) K. W. Willman and R. W. Murray, *J. Electroanal. Chem.*, **133**, 211 (1982).

Oxidation of Coals in Liquid Phases. VII. Oxidation of Oxygen-containing Model Compounds of Coal by Oxygen in Concentrated Sodium Hydroxide Solutions

Hirohide FURUYA, Ryoichi UWABE, Nobuyuki SUTOH, Akitsugu OKUWAKI,*
Akira AMANO, and Taijiro OKABE
Department of Applied Chemistry, Faculty of Engineering, Tohoku University, Aramaki, Sendai 980
(Received December 26, 1984)

Oxidation of 26 model compounds of low-ranked coal was performed to study the formation mechanisms of oxalic acid from coal. A mixture of 0.02 mol of the model compound, 4—60 g of NaOH, and 50 g of water was placed in a 300 cm^3 autoclave and oxidized at 523 K and P_{O_2}=5 MPa for 120 min. Acetic acid was produced from phenols within 15 min and oxidized selectively to oxalic acid. The yield ratio(yield of oxalic acid(%)/yield of CO_2 (%)) from most of the model compounds was higher than 1. These phenomena agreed well with those of low-ranked coal under the same oxidation conditions. The overall reaction rates, yields of oxalic acid, and yield ratios increased rapidly with an increasing concentration of NaOH as in the oxidation of coal. This behavior can be explained resonably well by an alkali-catalyzed oxidation mechanism regarding organic substances.

Oxalic acid is produced in high yields, 40—50%, on a carbon base during the oxidation of low-ranked coal by O_2 in concentrated NaOH solutions.[1] The mechanism of this reaction has been discussed.[2]

Oxidation of coal-model compounds by HNO_3[3] or by $KMnO_4$[3,4] has been carried out to elucidate the basic structure of coal, since it is very complicated. In this previous work, including $KMnO_4$ oxidation of lignite and peat,[5] the yield of oxalic acid was appreciably low. In the present study, 26 oxygen-containing model compounds were oxidized to investigate the formation mechanism of oxalic acid in high yield during the oxidation of coal by O_2 in concentrated NaOH solutions. The model compounds are classified as follows: (a) aliphatic carboxylic acids, (b) aromatic compounds such as phenols and carboxylic acids, and (c) alicyclic or heterocyclic compounds. Low-ranked coal contains these types of functional groups[2] and we may disclose what kinds of the functional groups in coal give oxalic acid in good yield during oxidation using these model compounds. The effect of the NaOH concentration on the oxidation of acetic acid, hydroxyacetic acid, 1,2-benzenediol, and 4-hydroxycinnamic acid is also examined, and the high selectivity in the formation of oxalic acid from acetic acid is explained in terms of the alkali-catalyzed oxidation mechanism.

Experimental

Reagents. Instead of free acid, the sodium salts of acetic acid, propionic acid, and butyric acid were used. The chemicals used were reagent grade except NaOH. Sodium hydroxide was the only guaranteed reagent and the amount of carbon contained in the NaOH as a carbonate was corrected in the calculation of the CO_2 yield for the model compounds.

Oxidation. A 240 cm^3 SUS 316 beaker was put in a 300-cm^3 autoclave fitted with a magnetic stirrer. A mixture 0.02-mol mixture of the model compound (0.03 mol only for acetic acid), 4-60 g of NaOH, and 50 g of water were placed in the beaker and heated to 523 K within 40—60 min after replacing the air with N_2. The O_2 partial pressure was kept at 5±0.2 MPa while stirring at 1200 min^{-1}. After a reaction time of 120 or 15 min, the autoclave was cooled and the reaction mixture was washed and diluted to 1 dm^3. Oxalate, carbonate, and the sodium salts of volatile acids contained in the solution were determined by a previously described methods.[2] In the present work, it was confirmed by a GC-MS analysis that the volatile acids were composed of acetic acid. For this reason, the yield of volatile acids was expressed as the yield of acetic acid.

Results and Discussion

Effect of Types of Model Compounds. The yields of oxalic acid, CO_2, and acetic acid and the yield ratios of oxalic acid to CO_2 are summarized in Table 1 for the oxidation of 26 model compounds for 120 min at 523 K. The numbers (from **1** to **9**) in the lefthand side of Table 1 correspond to each model compound in the following text.

Aliphatic Carboxylic Acids: The oxidation of acetic acid gave a 75% yield of oxalic acid, and the yield ratio (yield of oxalic acid(%)/yield of CO_2(%)) was very high. The overall yields of oxalic acid at 120 min for acetic acid, propionic acid, and butyric acid were larger than those of the aromatic carboxylic acids as shown in Table 1B; however, there was not a great difference in the overall yield (93—98%) among these monocarboxylic acids. The yield ratio for propionic acid was the smallest among the monocarboxylic acids. Clearly, this indicates that propionic acid gives CO_2 and a certain C_2 compound. If the C_2 compound is acetic acid or hydroxyacetic acid, the yield ratio must be 1.0 or 1.7, respectively, since the yield ratios for acetic acid and hydroxyacetic acid were 3.4 and 18.9 at 120 min. The yield ratio for adipic acid was high but the reaction rate was slower than those of the three monocarboxylic acids. This tendency was also noted in $KMnO_4$ oxidation of dicarboxylic acids.[4] Both the reaction rate and the yield ratio for hydroxyacetic acid were extremely high.

Phenols and Aromatic Carboxylic Acids: Phenol was easily cleaved and gave oxalic acid in good yield and

Table 1. Oxidation of model compounds for 120 minutes at 523 K and 25 mol NaOH/kg water

Compd. No.	Model Compd.	Product yield/% Oxalic acid	CO_2	Acetic acid	Yield ratio[b]
	A. Aliphatic carboxylic acid				
	Acetic acid	75.4	22.2	1.4[c]	3.4
	Propionic acid	54.6	41.7	0	1.3
	Butyric acid	61.6	29.9	1.5	2.1
	Adipic acid	32.8	13.3	19.4	2.5
	Hydroxyacetic acid	94.7	5.0	0	18.9
	Hydroxyacetic acid[a]	96.7	3.2	0	30.2
	B. Phenols and aromatic carboxylic acids				
	Phenol	51.6	29.9	17.8	1.7
	1,2-Benzenediol	54.1	26.5	12.3	2.1
	1,3-Benzenediol	57.8	31.5	12.3	2.1
	1,4-Benzenediol	53.4	33.9	8.2	1.6
1	4-s-Butylphenol	49.2	42.6	2.6	1.2
2	*p*-Hydroxyacetophenone	49.3	48.7	0.5	1.0
3	4-Hydroxycinnamic acid	30.1	22.9	34.7	1.3
4	2-Hydroxy-1-naphthalene-carbaldehyde	20.8	18.9	5.8	1.1
	Benzoic acid	34.3	20.4	2.5	1.7
	1,2-Benzenedicarboxylic acid	29.9	17.5	0.8	1.7
	1,3-Benzenedicarboxylic acid	36.9	21.0	1.3	1.8
	1,4-Benzenedicarboxylic acid	4.3	3.2	0.2	1.4
	1-Naphthalenecarboxylic acid	17.5	14.2	0.8	1.2
	2-Naphthalenecarboxylic acid	13.2	11.3	0	1.2
5	9-Anthracenecarboxylic acid	17.6	15.9	0	1.1
6	3-Phenylpropionionic acid	35.7	22.0	3.0	1.6
7	4-Methoxycinnamic acid	24.0	24.1	33.9	1.0
	C. Alicyclic and heterocyclic compounds				
	Cyclohexanol	14.5	29.1	1.4	0.5
8	1,2-Cyclohexanedicarboxylic acid	57.9	36.6	1.1	1.6
9	3-Cyclohexylpropionic acid	44.7	35.1	14.2	1.3
	Furfural	40.1	48.6	3.1	0.8

a) Reaction time 1 h. b) Yield of oxalic acid(%)/yield of CO_2. c) Unreacted acetic acid.

yield ratio. There was not a great difference in the results among phenol and dihydric phenols as shown in Table 1B. Yield ratios among dihydric phenols were of the order of 1,2-≃1,3->1,4-benzenediol.

If one of the hydrogens on a benzene ring of phenol was substituted by a saturated aliphatic side chain such as **1** and **2**, the yield ratios were lowered from 1.7 to 1.0—1.2. These values are close to the yield ratios for low-ranked coal.[1] This may be caused by an increasing formation of CO_2 by the oxidation of the side chain. Compound **3** was easily oxidized and yielded a large amount of acetic acid but both yields of oxalic acid and CO_2 were small. The yield ratio for **4** was 1.1, however, the reaction rate was small. The benzenecarboxylic acids were more stable than the phenols during the oxidation as shown in Table 1C. 1,4-Benzenedicarboxylic acid was especially stable. This is due to the extremely slow reaction rate, as it hardly dissolves into concentrated NaOH solutions.[6] Although the reaction rates for **4**, **5**, 1-naphthalenecarboxylic acid, and 2-naphthalenecarboxylic acid were very small, the yield ratios for these naphthalene- and anthracenecarboxylic acids were as high as 1.2. The yield ratios for phenol and benzenediols (1.6—2.1) were a little larger than those for benzoic acid and benzenedicarboxylic acids (1.4—1.8). This may be caused by the difference in the yield of acetic acid since acetic acid afforded 75% oxalic acid. The phenols yielded 8.2—17.2% acetic acid whereas the benzenecarboxylic acids yielded only 0.2—2.5% as shown in Table 1B and 1C. The fact that the yield ratios for the above four phenols and benzenecarboxylic acids were as high as 1.4—2.1 indicates that the aliphatic carboxylic acids of even carbon numbers are predominantly formed during the cleavage of both aromatic rings. Such aliphatic carboxylic acids produced oxalic acid more than the aliphatic carboxylic acids of odd carbon numbers. Acetic and butyric acids afforded 75.4 and 61.6% oxalic acid respectively, whereas, propionic acid 54.6%. Work is in progress to clarify the cleavage products.

Model compounds **3** and **7** yielded 30% of oxalic acid: close to that for 1,2- and 1,3-benzenedicarboxylic acids. The important characteristics of these compounds are that a large amount of acetic acid was produced and the reaction rates were also large.

Alicyclic and Heterocyclic Compounds Containing Oxygen: The reaction rate for cyclohexanol was slow

Table 2. Formation of acetic acid at 15 minutes oxidation

Model Compound	Product yield/% Oxalic acid	CO_2	Acetic acid	Yield ratio[b]
Propionic acid	5.2	5.2	87.3[a]	1.0
1,2-Benzenediol	28.8	12.7	28.9	2.3
1	16.6	9.3	29.5	1.8
2	4.0	5.9	13.9	0.7
3	8.1	3.8	29.1	2.2
7	8.5	2.8	4.6	1.8

a) Unreacted propionic acid. b) Yield of oxalic acid(%)/yield of CO_2(%).

and the yield ratio was the smallest. Model compounds **8** and **9** were oxidized more easily than the corresponding aromatic compounds, 1,2-benzenedicarboxylic acid and **6**, respectively. A furan ring was cleaved as easily as phenol, however, the yield ratio was small, 0.8.

Formation of Acetic Acid in the Initial Stage of Oxidation. The results of oxidation for 15 min are shown in Table 2 for propionic acid, 1,2-benzenediol, **1**, **2**, **3**, and **7**. The yield of acetic acid for **7** was the smallest after 15 min of oxidation. This shows the effect of substituents on the reactivity of aromatic rings. Model compound **3** with a phenolic hydroxyl group was easily oxidized to afford a large amount of acetic acid compared to **7** with a methoxyl group as shown in Table 2.

The model compounds, except **7**, yielded acetic acid in large amounts. This behavior agreed well with that of low-ranked coal which also afforded 20—25% of acetic acid at 15 min of oxidation.[1] 1,2-Benzenediol yielded 29% of acetic acid and 41% of oxalic acid and CO_2, respectively. Clearly, the aromatic rings activated by the substitution of the hydroxyl group were easily cleaved and yielded large amounts of oxalic acid. 1,2-Benzenediol was cleaved to afford muconic acid derivatives.[7] The mechanism in which three hydrogen atoms combine with one carbon atom to produce a methyl group in acetic acid under such strong oxidative conditions may be a disproportionation of the double bonds in these intermediates.

In spite of the fact that the sum of the yield of oxalic acid and the yields of CO_2 for **1** and **3** were 26 and 12%, respectively, the corresponding yields of acetic acid were about 30%. Consequently, not only the cleavage of the aromatic rings but also the cleavage of side chains *via* peroxide anions[8] contribute to the formation of acetic acid. An identification of the cleavage products is necessary for a detailed determination of the mechanism.

Mechanism of the Oxidation. Concentration Effects Regarding NaOH: Figures 1—4 show the effects of the NaOH concentration on the yields of oxalic acid, CO_2, and acetic acid during the oxidation (120 min) of acetic acid, hydroxyacetic acid, 1,2-benzenediol, and **3**. The important phenomena regarding the oxidation are shown in Fig. 1 for acetic acid and can be summarized as

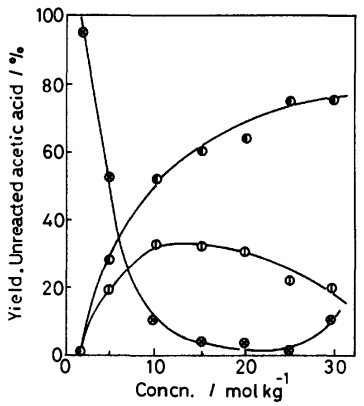

Fig. 1. Effect of NaOH concentration on the yields of oxalic acid, CO_2, and unreacted acetic acid in the oxidation of acetic acid: (◐) oxalic acid, (Φ) CO_2 (⊗) unreacted acetic acid.

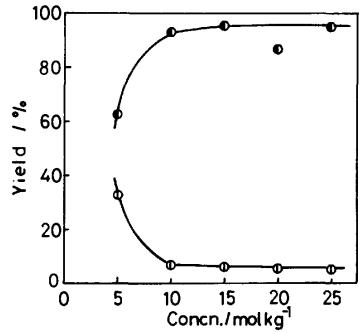

Fig. 2. Effect of NaOH concentration on the yields of oxalic acid and CO_2 in the oxidation of hydroxyacetic acid: (◐) oxalic acid, (Φ) CO_2.

follows:

I. Acetic acid was hardly oxidized at 2 mol kg^{-1}.

II. The reaction rate, yield of oxalic acid, and yield ratio increased rapidly upon increasing the NaOH concentration at 5—20 mol kg^{-1}.

III. The yield of CO_2 was held almost constant at 10—20 mol kg^{-1}.

IV. The reaction rate decreased at 20—30 mol kg^{-1} and the previously produced acetic acid remained.

The yield ratios for 1,2-benzenediol and **3** (Figs. 3 and 4) were lowered at concentrations of 20 mol kg^{-1} or higher; however, these yield ratios should

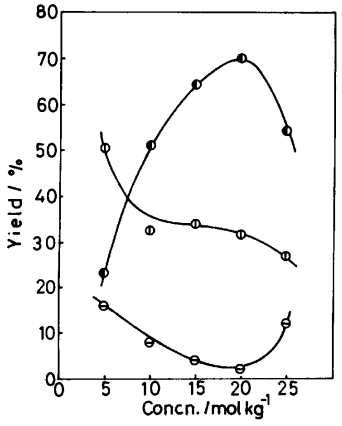

Fig. 3. Effect of NaOH concentration on the yields of oxalic acid, CO_2, and acetic acid in the oxidation of 1,2-benzenediol: (◐) oxalic acid, (Φ) CO_2, (⊖) acetic acid.

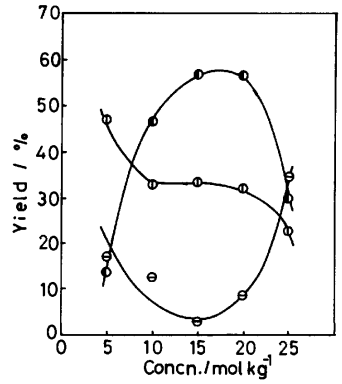

Fig. 4. Effect of NaOH concentration on the yields of oxalic acid, CO_2, and acetic acid in the oxidation of 4-hydroxycinnamic acid: (◐) oxalic acid, (Φ) CO_2, (⊖) acetic acid.

increase with longer reaction times (>120 min). The reason is that the large amount of acetic acid produced within 120 min produces selectively oxalic acid which increases the yield ratios with longer reaction times. The oxidation rates of oxalic acid are very small under such conditions.[2]

Mechanism: Scheme 1 shows a mechanism for the formation of oxalic acid and CO_2 from acetic acid. A carbanion is formed by the abstraction of a proton from the acetate ion with OH^- and yields an intermediate peroxide anion by the reaction with O_2. An oxalate ion may be produced by further abstraction of a proton and successive oxidation of the intermediate from which CO_2 may be formed competitively by the monomolecular cleavage of the C–C bond by a mechanism such as the epoxide mechanism or the Baeyer-Villiger mechanism.[9]

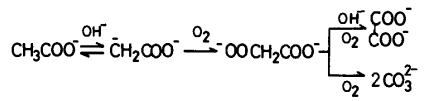

Scheme 1.

The above phenomena can essentially be explained by the following mechanism.

I. Equations 1 and 2 are the dissociation equilibrium in a NaOH–CH_3COONa solution at elevated tem-

$$CH_3COONa \longrightarrow CH_3COO^- + Na^+ \quad (1)$$

$$NaOH \rightleftharpoons OH^- + Na^+ \quad (2)$$

peratures. At 523 K, NaOH behaves as a weak electrolyte, as the pK_b is estimated to be 1.5.[10] Consequently, the concentration of OH^- is much smaller than the formal concentration of NaOH. In addition, the dissociation of NaOH is depressed by a common-ion effect of the Na^+ liberated from a complete dissociation of CH_3COONa (0.6 mol kg^{-1}). Thus, the reaction rate is very small because the equilibrium concentration of the carbanion is extremely low.

II. The formation of carbanion is promoted upon increasing the concentration of OH^- through the equilibrium. Thus, oxidation is accelerated. The yield of oxalic acid and the yield ratio increase with an increasing OH^- concentration. This is due to the effect of the abstraction of a proton by OH^- from the peroxide anion. This enhances the selective formation of oxalic acid in competitive reactions. On the other hand, the monomolecular cleavage of the C–C bond is not affected by the OH^- concentration.

III. The solubility of CH_3COONa decreases with an increasing concentration of NaOH. Such a tendency is observed in a great number of NaOH–sodium salt systems.[6] In contrast, the formation of the carbanion and the peroxide anion is promoted with an increasing NaOH concentration. In 10—20 mol kg^{-1} concentrations, these opposite effects compensate each other and the concentration of peroxide anions is kept almost constant. Thus, the yield of CO_2 *via* peroxide anions is held constant.

IV. In 20—30 mol kg^{-1} concentrations, the solubillity of CH_3COONa drops further and the concentration of the peroxide anion begins to fall. The rate-of-formation of oxalic acid drops, but the selectivity to form oxalic acid is relatively promoted. Thus, the yield ratio continues to increase, whereas, the overall reaction rate drops.

Based on this mechanism, the difference in the reactivities among several compounds can be explained in connection with the pK_a for the separation of hydrogen from the model compounds. The peroxide anions for acetic acid and hydroxyacetic acid may be $(^-OO)H_2CCOO^-$ and $OH(OO^-)HCCOO^-$, respectively. The value of pK_a for methylene hydrogen tends to be larger than that for methine hydrogen.[11] Thus, the reaction rate and yield ratio for hydroxyacetic acid are much larger than those for acetic acid. In the case of aliphatic monocarboxylic acids, the reactivities for acetic acid, propionic acid, and butyric acid were approximately equal. This may indicate that the reac-

tion takes place by the abstraction of hydrogen on the opposite carbon to the carboxyl carbon. Consequently, the reason for the low reactivity of adipic acid is that the opposite carbon is stabilized as a carboxyl carbon and no hydrogen is abstracted. The difference in the reactivities between 1,2-cyclohexanedicarboxylic acid and 1,2-benzenedicarboxylic acid or between **7** and **9** can be similarly explained.

Relationships between the Behavior of Model Compounds and That of Coal. The behavior of many model compounds and low-ranked coal such as Tempoku peat (C 54.7% daf), Yallourn coal (C 62.3% daf), and Nakayama coal (C 67.9% daf) agreed well with the formation of acetic acid and the high yield ratio of 1 or more.[1] This is because low-ranked coal contains a large amount of oxygen such as phenolic hydroxyl and carboxyl groups,[2] and the development of condensation of aromatic rings is inadequate. In contrast, a low yield ratio of 0.8 for high-ranked coal such as Goonyella coal (C 90.2% daf) and Miike coal (C 86.9% daf) was not obtained except with cyclohexanol and furfural. This is because most of the model compounds used were oxidized in an aqueous phase, and gas-phase oxidation of insoluble compounds did not take place as was observed in the oxidation of the high-ranked coal.[1] However, the reaction rate for the model compounds with fused aromatic rings such as **4**, 1-naphthalenecarboxylic acid, 2-naphthalenecarboxylic acid, and **9** were smaller than those for the model compounds with a benzene ring such as phenol, 1,2-benzenediol, benzoic acid, **6**, **7**, *etc.* Thus, regarding reaction rates, the behavior of model compounds with fused aromatic rings agreed with that of high-ranked coal.

The present work was partially supported by a Grant-in-Aid from the General Sekiyu Research Promotion Foundation.

References

1) A. Okuwaki, N. Sutoh, H. Furuya, A. Amano, and T. Okabe, *Ind. Eng. Chem. Prod. Res. Dev.*, **23**, 648 (1984).
2) N. Sutoh, H. Oikubo, A. Okuwaki, A. Amano, and T. Okabe, *Nippon Kagaku Kaishi* **1984**, 1418.
3) T. Yokokawa, Y. Watanabe, S. Kajiyama, and Y. Takegami, *Nenryo Kyokai Shi*, **39**, 590 (1960).
4) R. B. Randall, M. Benger, and C. M. Groocock, *Proc. R. Soc. London, Ser. A*, **165**, 432 (1938).
5) W. A. Bone, L. G. B. Parsons, R. H. Sapiro, and C. M. Groocock, *Proc. R. Soc. London, Ser. A*, **148**, 492 (1935).
6) H. Furuya, M. Kato, N. Sutoh, A. Okuwaki, and T. Okabe, *Nippon Kagaku Kaishi*, **1983**, 1488.
7) T. Matsuura, "Oxygen-Oxidation Reaction," Maruzen, Tokyo, (1977), p. 192.
8) J. Gierer, F. Imsgard, and I. Noren, *Acta Chem. Scand. B*, **31**, 561 (1977).
9) Y. Sawaki and C. S. Foote, *J. Am. Chem. Soc.*, **101**, 6292 (1979).
10) L. S. Walter, *Am. J. Sci.*, **261**, 151 (1963).
11) J. B. Hendrickson, D. J. Cram, and G. S. Hammond, "Organic Chemistry" 3rd. ed., McGraw-Hill Kohgakusha, Tokyo (1970), p. 304.

Near-infrared Photocurrent of a Zinc Oxide Electrode Covered with Silver Atoms

Hatsumi TANEMURA, Yoshiro YONEZAWA,* and Hiroshi HADA
Department of Industrial Chemistry, Faculty of Engineering, Kyoto University, Yoshida, Kyoto 606
(Received February 27, 1985)

Synopsis. A near-infrared photocurrent has been observed in a sintered ZnO electrode whose surface was covered with Ag atoms. The photocurrent became more evident when silver deposition was carried out with a relatively large charging current. The importance of H^+ reduction which competed with silver reduction is pointed out.

We have studied the electrochemistry of sintered zinc oxide (ZnO) electrodes to clarify the mechanism of the photoreduction of silver ions (Ag^+) at the surface of ZnO.[1] In the course of this research, it was noted that the ZnO surface suffered some changes in its physicochemical properties after the deposition of a considerable amount of Ag atoms. Kolb *et al.* have reported a near-infrared photocurrent regarding a ZnO single crystal electrode covered with a monolayer of Ag atoms.[2] It is worthwhile to examine the nature of the near-infrared photocurrent of ZnO electrodes in more detail.

A ZnO electrode was prepared from a ZnO powder, SASEX-4000, (Sakai Kagaku Co., Ltd.,) in the same manner as reported previously.[1] The surface area of the electrode was about 1 cm^2. The electrochemical cell contained a ZnO electrode, a platinum counter electrode, and a saturated KCl, Ag, AgCl reference electrode. The electrode potential in this Note referred to a saturated KCl, Ag, AgCl electrode. A Hokutodenko HA-104 potentiostat/galvanostat with an electronic picoammeter TR-8641 (Takeda Riken Co., Ltd.,) was used for the measurement of the photocurrent. As a light source, a 45-W tungsten-iodide lamp (Shimadzu Seisakusho Co., Ltd.,) was used in combination with a grating monochromator (Shimadzu Seisakusho Co., Ltd.,) and a glass filter, VR-67 (Toshiba Co., Ltd.,). The ratio of the number of incident photons was determined by means of a calibrated thermopile (Nihon Bunko Co., Ltd.,). The optical absorption spectrum of the electrolyte solution was taken into account in order to calibrate the number of incident photons at the electrode surface. The action spectrum of the photocurrent was corrected to a constant photon flux incident to the electrode surface at the wavelength, λ=700—1200 nm. All the measurements were carried out at the room temperature. Before the measurements, the ZnO surface was etched with 85% H_3PO_4 and washed in water. Dissolved oxygen in the electrolyte solution was purged by the introduction of high-purity nitrogen gas. We employed a galvanostatic method with a controlled charging current, i_{ch}, to deposit Ag atoms at the ZnO surface (electrochemical charging).

Cyclic current-voltage curves for the ZnO electrode were measured in the dark in 0.5 M KNO_3 (1 M=1 mol dm^{-3})(Fig. 1). On the cathodic scan, the current began to rise at about −0.7 V due to hydrogen evolution. When $AgClO_4$ was added to the solution, the

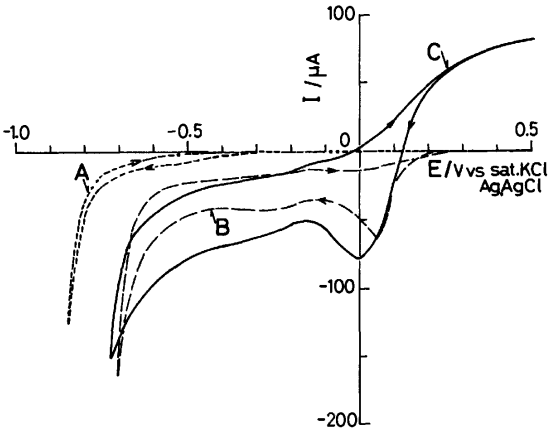

Fig. 1. Cyclic current (I)-voltage(E) curves of ZnO electrode.
Electrolyte: A: 0.5 M KNO_3 (———), B, C: 0.5 M KNO_3 and 10^{-3} M $AgClO_4$.
Curve B (— — — —) is obtained in the dark, curve C (———) by illumination with λ=365 nm light from 500 W xenon lamp. Scan rate is 20 mV s^{-1}.

Ag deposition was seen by a current rise of around +0.2 V on the cathodic scan. It was noticed that at the Ag-covered ZnO surface, hydrogen evolution commenced about 0.3 V earlier than at a bare electrode surface. Catalytic action of metal atoms at the semiconductor surface has been discussed by Kolb *et al.*[2] On the anodic scan, the photocurrent began to rise at *ca.* −0.2 V when the ZnO electrode in the electrolyte solution containing Ag^+ was illuminated with λ=365 nm light. The absence of a well-defined stripping peak of Ag indicates that photo-generated holes are consumed with the dissolution of ZnO.

We deposited the Ag atoms at the ZnO surface in an electrolyte solution composed of 0.5 M KNO_3 and 10^{-3} M $AgClO_4$. As the electrode potential during charging, E_{ch}, with i_{ch}=5 μA was about +0.2 V, a greater part of the charging current contributed to the reduction of Ag^+. The action spectra of the anodic photocurrent at +0.5 V are given in Fig. 2. The increase in the photocurrent, ΔI, being defined as the subtraction of the photocurrent before silver deposition, I_0, from that after silver deposition, I_{ch}, is also shown in Fig. 2. The dark anodic current was less than 1 nA at +0.5 V. The near-infrared photocurrent increased several times after charging the electrode by the quantity of electricity, Q_{ch}=6.0 mC. ΔI at λ=800—900 nm was about 2.5 nA. We next employed a relatively large i_{ch} of 200 μA. As E_{ch} was *ca.* −0.75 V, the reduction of both Ag^+ and H^+ was possible in view of Fig. 1. Some of the evolved hydrogen was absorbed inside of ZnO and silver layers. The action spectrum of the photocurrent (Fig. 3) shows that ΔI at λ=800—900 nm was *ca.* 30 nA for Q_{ch}=6.0 mC, which is about one order larger than ΔI of case C in Fig. 2. Figure 4 shows the

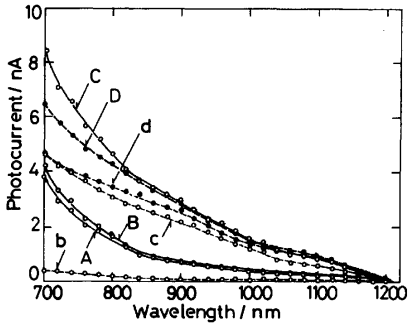

Fig. 2. Action spectra of anodic photocurrent of ZnO electrode.
Electrolyte: 0.5 M KNO_3 and 10^{-3}M $AgClO_4$, Electrode potential: +0.5 V.
A: Before charging, I_0, B: after electrochemical charging with i_{ch}=5 μA for 120 s (Q_{ch}=0.6 mC), I_{ch}, C: after electrochemical charging with i_{ch}=5 μA for 1200 s (Q_{ch}=6.0 mC), I_{ch}, D: after photochemical charging with λ=365 nm light (Q_{ch}=*ca.* 6.0 mC), I_{ch}.
The dashed lines b, c, and d denote the increase in photocurrent, $\Delta I=I_{ch}-I_0$, for B, C, and D, respectively. The magnitude of the photocurrent, D and d is reduced by one-half.

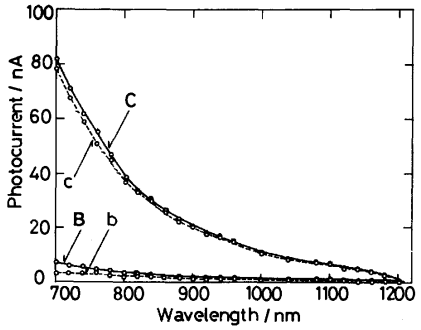

Fig. 3. Action spectra of anodic photocurrent of ZnO electrode.
Electrolyte, electrode potential: the same as in Fig. 2.
B: After electrochemical charging with i_{ch}=200 μA for 3 s (Q_{ch}=0.6 mC), I_{ch}, C: after electrochemical charging with i_{ch}=200 μA for 30 s (Q_{ch}=6.0 mC), I_{ch}.
The dashed lines b, c denote ΔI for B, C, respectively.

action spectrum after charging the electrode in a 0.5 M KNO_3 solution with i_{ch}=200 μA. The main electrode reaction was the reduction of H^+, as E_{ch} was *ca.* −0.9 V in this case. ΔI for Q_{ch}=6.0 mC was only about 0.1 nA at λ=800—900 nm. We then tried to superpose hydrogen on the silver layer. In the first place, the ZnO electrode was charged in the same electrolyte solution as in Fig. 2 with i_{ch}=5 μA for 1200 s (silver deposition). Then, the second charging was carried out in a 0.5 M KNO_3 solution with i_{ch}=200 μA for 30 s (hydrogen evolution). The action spectrum of the photocurrent after two-step deposition is added to Fig. 4. The magnitude of ΔI proved to be smaller than that of case C in Fig. 3: ΔI at λ=800—900 nm was *ca.* 2.5 nA.

Kolb *et al.* have ascribed the near-infrared photocurrent to an optical interfacial electron transfer between Ag adatoms and the ZnO electrode.[2] It has often been observed that extrinsic surface states are introduced to a semiconductor surface when some chemical species are adsorbed on it.[3] We could assume that electronic excitation from the surface states to the conduction band of ZnO is important as an additional mechanism of the near-infrared photocurrent of the ZnO electrode covered with Ag atoms. The enhanced photocurrent in Fig. 3 is probably due to a relatively large i_{ch}. It has been found that the current efficiency of Ag^+ reduction amounts to *ca.* 100% for an i_{ch} smaller than 20 μA and is less than 50% for an i_{ch} greater than 100 μA.[4] As the photocurrent of the electrode after the superposition of silver and hydrogen in Fig. 4 was not so large, we can state that extrinsic surface states responsible to the near-infrared photocurrent are introduced to the ZnO surface during the co-deposition of silver and hydrogen under relatively large i_{ch} conditions. As the distinct structure of the action spectra in Figs. 2—4 is blurred, it seems that occupied energy levels of the surface states are located in a diffuse manner within the forbidden energy band of ZnO.

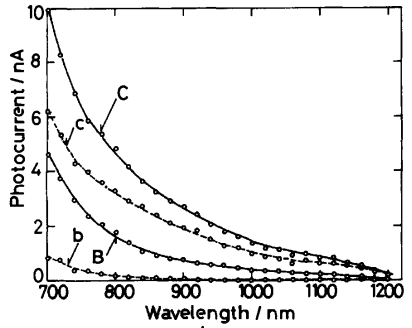

Fig. 4. Action spectra of anodic photocurrent of ZnO electrode.
Electrode potential: +0.5 V.
B: After electrochemical charging in 0.5 M KNO_3 with i_{ch}=200 μA for 30 s (Q_{ch}=6.0 mC), I_{ch}, C: after electrochemical charging firstly in 0.5 M KNO_3 and 10^{-3} M $AgClO_4$ with i_{ch}=5 μA for 1200 s (Q_{ch}=6.0 mC) and secondly in 0.5 M KNO_3 with i_{ch}=200 μA for 30 s (Q_{ch}=6.0 mC), I_{ch}.
The dashed lines, b, c denote ΔI for B, C, respectively.

We finally examined the possibility of the increase of near-infrared photocurrent as a result of the photodeposition of Ag atoms at the ZnO surface (photochemical charging). The ZnO electrode in a solution composed of 0.5 M KNO_3 and 10^{-3} M $AgClO_4$ was disconnected from the electric circuit and illuminated with λ=365 nm light from a 500 W xenon lamp.[1] After photochemical charging by Q_{ch}=*ca.* 6.0 mC, as estimated by a local-cell consideration,[1] the action spectrum of the near-infrared photocurrent was not so different from that obtained by electrochemical charging (Fig. 2). Therefore, the origin of the photocurrent is the same regarding both electrochemical and photochemical chargings.

References

1) H. Hada, H. Tanemura, and Y. Yonezawa, *Bull. Chem. Soc. Jpn.*, **51**, 3154 (1978).
2) D. M. Kolb, M. Przasnyski, and H. Gerischer, *Z. Phys. Chem., (N. F.)*, **93**, 1 (1974).
3) T. Wolfram and Ş. Ellialtıoğlu, in "Theory of Chemisorption," J. R. Smith ed., Springer-Verlag, Berlin Heidelberg New York (1980), p. 149.
4) H. Tanemura, Y. Yonezawa, and H. Hada, to be published.

Methods for Observing the Deformation of an Aqueous Paramagnetic Solution in a Magnetic Field

Takashi YASUOKA,* Tadahiko KIDOKORO, and Shunmei MITSUZAWA
Department of Chemistry, Faculty of Science, Tokai University, Kitakaname, Hiratsuka 259-12
(Received March 14, 1985)

Synopsis. Two methods have been worked out for the observation of the deformation of a paramagnetic aqueous solution in a magnetic field. The deformation was observed on: (1) a layer of a solution covered with a water-immiscible organic liquid and (2) a drop of the solution suspended in the liquid.

The paramagnetism of a solution of a heavy metal salt can be demonstrated by the deformation of the solution occurring in a magnetic field. If a test tube containing the solution is placed between the poles of an electromagnet, a distinct elevation of the surface takes places near the poles.[1] We have worked out two simple methods to magnify the deformation, so that a visual estimation of its magnitude is possible.

Our methods are based on the fact that the presence of a water-immiscible liquid in contact with the solution gives rise to an increase in the deformability of the solution in a magnetic field; this is a result of the reduction of the gravitational force acting on it. The experimental details are given below.

I. A JEOL JM-360 electromagnet (pole diam., 300 mm; pole distance, 60 mm, and maximum flux density, 1.4 tesla) was used. Three cm^3 of a paramagnetic salt solution (1 mol dm^{-3}) was poured into an acrylic plastic cell (10×60×60 mm) to a depth of 5 mm. Benzene was then added, forming an upper layer since the benzene and the solution do not mix with each other. The cell was then set between the poles of the electromagnet. The magnetic field was applied, and the resulting change in the form of the solution in the cell was photographed. Solutions of $CuCl_2$, $NiCl_2$ $CoCl_2$, and $FeCl_3$ were studied. Commercial reagents of a guaranteed grade were used without further purification.

Figure 1 shows the deformation of the layer of a $FeCl_3$ solution placed in magnetic fields of 0, 0.9, and 1.3 tesla. With an increase in the field intensity the solution is attracted towards the magnetic poles, finally splitting into two parts. The deformation of solutions of $CuCl_2$, $NiCl_2$, $CoCl_2$, and $FeCl_3$ in the field of 1.3 tesla is shown in Fig. 2. The change in the form of the solution layer in the magnetic field, as expressed by the difference in the height of the solution at its center and at its periphery, decreases in this order: $FeCl_3$, $CoCl_2$, $NiCl_2$, and $CuCl_2$. This is in line with the order of the number of unpaired electrons or Bohr magnetons in each metallic ion and enables a rough estimation of these numbers.

II. A straight-bar electromagnet (pole diam., 30 mm; maximum flux density, 0.18 tesla) was used. A single drop of a solution was suspended in a water-immiscible liquid with the same density as that of the drop, and its deformation in a magnetic field was observed. An acrylic cell (60×60×60 mm) containing the sample was set in contact with a pole of the magnet.

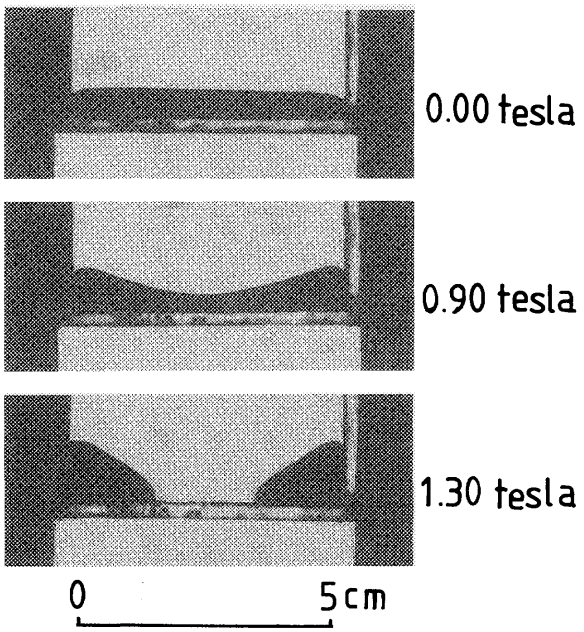

Fig. 1. Deformation of a $FeCl_3$ solutions in magnetic field.

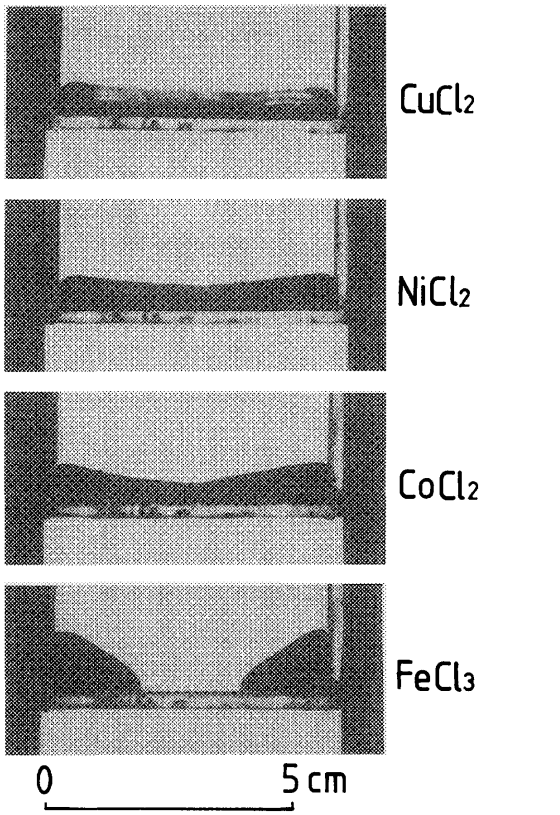

Fig. 2. Deformation of various solution in magnetic field of 1.3 tesla.

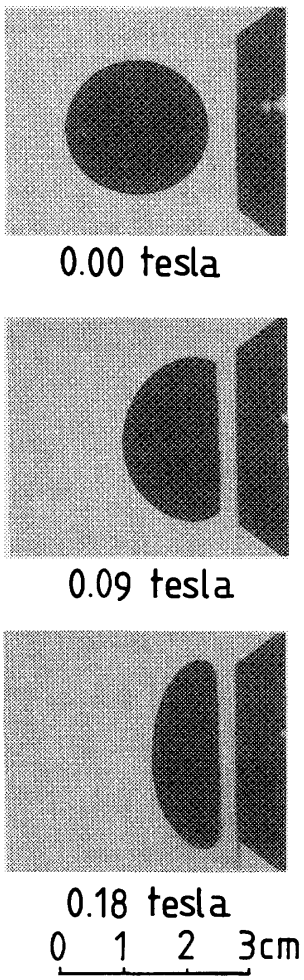

Fig. 3. Deformation of a drop of $FeCl_3$ solution in magnetic field.

The water-immiscible liquid of the desired density was prepared by adjusting the mixing ratio of benzene and carbon tetrachloride and was then poured into the cell. When 8 cm^3 of a $FeCl_3$ solution (3 mol dm^{-3}) was introduced into the liquid, it turned into a spherical drop. The deformation of the drop at 0, 0.9, and 0.18 tesla is shown in Fig. 3. The drop is spherical at 0 tesla, but it undergoes conspicuous deformation with an increase in the magnetic field. The deformation of the solution is far more marked in this case than in **I**.

These methods will be useful in demonstration experiments and also for a rough estimation of solution paramagnetism or magnetic-field strength.

The authors wish to thank Prof. Tsunetaka Sasaki for his kind interest in and suggestions for this work.

Reference

1) T. Katsurai, *Sci. Papers Inst. Phys. Chem. Reseach (Tokyo)*, **35**, 224 (1939), Fig. 25.

Concerning Bent Structures of Cumulenones

Hiroshi ICHIKAWA* and Yukiko EBISAWA
Hoshi College of Pharmacy, Shinagawa, Tokyo 142
(Received May 2, 1985)

Synopsis. The cause of the unusual bent structures of cumulenones has been studied by HF/6-31G and MP3/6-31G methods. It is concluded that participation of the lone pair electrons to the adjacent π-bond results in the deformed structures.

Cumulenones ($CH_2=(C)_n=0$, $n=0, 1, 2, \cdots$) are topic compounds in practical and theoretical respects. Practically, they are potential candidates for interstellar compounds as those discovered for $n=0$ and 1.[1] It is an urgent requirement to establish those structures in order to assign unidentified microwave spectra of unidentified intersteller molecules. The structures of cumulenones have also aroused considerable theoretical interest[2] since an unusual bent structure has been determined for $n=2$.[3] A question arises as to what causes the distortion on the structures of cumulenones. We have studied this problem and have reached a very plausible explanation.

Recently, Farnell and Radom[2a] reported that the theoretically most stable structures of propadienone and butatrienone are planar-bent and orthogonal-bent structures, respectively. Such distortions from a C_{2v} structure appear when the electron-correlation is included in the calculation. They also noted the results for the next members of the series, pentatetraenone ($CH_2(C)_4=0$) and hexapentaenone ($CH_2(C)_5=0$). Both of these molecules have been found to be bent even at the 4-31G[4] level.[2a] Thus, it seems that this bending of the carbon chain is a characteristic of cumulenones, alternating as a function of chain length between in-plane and out-of-plane structures.

There are two plausible reasons that can be considered from the organic chemistry of a carbonyl group, both of which are not well expressed in the Hartree-Fock theory. An oxygen atom has a larger electronegativity than a carbon atom. The withdrawal of a π-electron to the oxygen atom produces a cationic center on the carbon atom of the carbonyl group (**1**). Such a carbocation can interact with the β-carbon atom (C_3) in either a π (**2**) or σ (**3**) way. But, only the former interaction agrees with the observed bending direction.

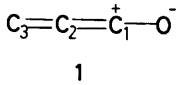

1

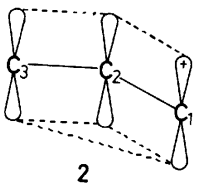

2

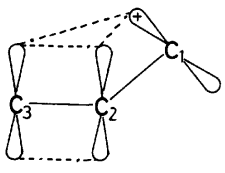

3

The alternating contribution of a carbonyl group represents a participation of one pair of the lone-pair electrons of the oxygen atom into an adjacent p-atomic orbital (AO) or a π-bond (**4**). This resonance concept has been proposed by Brown *et al.* to explain the bent structure of propadienone.[3b] Such a contribution is

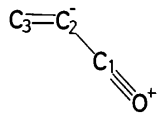

4

regarded as a minor one from the point of view of the organic chemistry of a molecule. However, it often appears in ion chemistry as an acyl cation (R-C≡O$^+$). If this contribution takes place, the hybridization of the α-carbon atom (C_2) may be changed toward sp^2. This also explains the observed bending characteristics of cumulenones. In order to determine which resonance structure contributes the most, we examined a series of cumulenyliums and cumulenides which are regarded as canonical structures of cumulenones.

Table 1 shows the relationship between the total energies and the bond angles of cumulenyliums and cumulenides (using the HF/6-31G[5] and MP3/6-31G method[6]). Optimization was carried out by HF/6-31G for all geometrical parameters except the fixed bond angle.[7] Table 2 shows the results of similar calculations regarding referential compounds. These can be compared with the ions listed in Table 1.

From Table 1, it can be seen that the most stable structure for cumulenylium has a C_{2v} symmetry. Therefore, it should be understood that a cationic interaction does not make a major contribution to the distortion of cumulenone. Tables 1 and 2 indicate that a distortion of the bond by 10 degrees requires, by Hartree-Fock theory, only *ca.* 1 kcal/mol for both neutral molecules and cumulenyliums (either in-plane or out-of-plane). The existence of carbocation seems to have nothing to do with the flexibility. The inclusion of electron correlation reduces up to the half of such energy. This shows that cumulenyl groups are easily bent, although they look rigid according to the structural expressions of organic chemistry.

The C_{2v} structures of cumulenides have higher total energies than those of specifically distorted structures. The optimized structures are largely deformed from the C_{2v} symmetry and all have the Cs structures. The bending direction alternates as the number of carbon atoms increases, in accordance with the direction in cumulenones. Therefore, it is strongly suggested that the cause of a bent structure in cumulenones can be attributed to the participation of the lone-pair electrons. This theory can also explain why cumulenones with longer chains are apt to be deformed

TABLE 1. RELATIONSHIP BETWEEN TOTAL ENERGIES AND BOND ANGLES IN CUMULENYLIUMS AND CUMULENIDES[a)]

	in-plane						out-of-plane					
	α	β	γ	HF/6-31G	MP2/6-31G	MP3/6-31G	α	β	γ	HF/6-31G	MP2/6-31G	MP3/6-31G
cation												
$H_2C{=}C{=}C{-}H$	(180.0)	180.0		−114.913119	−115.154736	−115.166638						
	(170.0)	182.8		1.0	0.4	0.5	(170.0)	179.9		0.7	0.2	0.2
	(160.0)	186.1		3.8	1.9	2.1	(160.0)	179.9		2.6	1.3	1.2
							(170.0)					
$H_2C{=}C{=}C{=}C{-}H$	(180.0)	180.0	180.0	−152.749069	−153.077903	−153.089299						
	(170.0)	180.0	179.9	0.7	0.2	0.0	(170.0)	182.1	180.0	1.0	−0.1	−0.1
	(160.0)	180.7	180.0	2.7	1.4	1.1	(160.0)	185.8	180.0	3.9	1.1	1.2
anion												
$H_2C{=}C{=}C{=}H$	(180.0)	(180.0)		−115.154770	−115.418316	−115.429553						
	(170.0)	183.2		1.3	0.9	0.9	(170.0)	237.4		−4.0	−6.1	−6.7
	(160.0)	186.6		5.0	3.7	3.7	(160.0)	238.0		−0.4	−4.5	−4.8
optimized structure							175.7	237.5		−115.162019	−115.427657	−115.440049
$H_2C{=}C{=}C{=}C{-}H$	(180.0)	(180.0)	(180.0)	−152.970564	−153.316692	−153.329619						
	(170.0)	179.1	244.4	−11.8	−10.3	−11.8	(170.0)	179.6	179.6	1.2	0.3	0.3
	(160.0)	180.8	242.6	−11.1	−11.1	−12.2	(160.0)	179.2	179.2	4.9	2.5	2.5
optimized structure	178.6	176.9	245.1	−152.989666	−153.332544	−153.348040						
$H_2C{=}C{=}C{=}C{-}H$	(170.0)	180.5	239.9	−11.5	−15.3	−14.8	(170.0)	182.3	(180.0)	1.1	0.3	0.2
	(160.0)	187.5	239.4	−9.0	−14.4	−13.7	(160.0)	185.2	(180.0)	4.4	2.8	2.6
optimized structure	174.3	178.4	240.3	−152.989374	−153.340916	−153.353018						

a) Values in parentheses are fixed bond angles. Other bond angles are optimized to the total energy with restriction of the fixed angles. Total energies are shown only for the optimized structures and the C_{2v} structures. Other energies are expressed by the differences from those for the C_{2v} structures in kcal/mol.

TABLE 2. RELATIONSHIP BETWEEN TOTAL ENERGIES AND BOND ANGLES IN NEUTRAL MOLECULES

	α	HF/6-31G	MP2/6-31G	MP3/6-31G
$CH_3{-}C{\equiv}C{-}H$	180.0	−115.823530	−116.090768	−116.103855
	170.0	1.1	0.4	0.5
	160.0	4.4	2.3	2.5
$CH_2{=}C{=}CH_2$	180.0	−115.821517	−116.081443	−116.102218
	170.0	1.1	0.8	0.8
	160.0	4.6	3.3	3.2
$CH_2{=}C{=}O$				
in-plane	180.0	−151.649119	−151.951174	−151.946052
	170.0	1.5	1.1	4.3
	160.0	5.9	4.6	7.8
out-of-plane	170.0	1.5	1.1	4.3
	160.0	6.2	4.6	7.7

more easily: the contribution of the resonance structure **4** forms a negative charge on C_2. It is unstable in a short chain since the negative charge cannot be well delocalized.

References

1) S. Green, *Annu. Rev. Phys. Chem.*, **92**, 103 (1981).

2) a) L. Farnell and L. Radom, *J. Am. Chem. Soc.*, **106**, 25 (1984); b) L. Farnell and L. Radom, *Chem. Phys. Lett.*, **91**, 373 (1982); c) A. Komornicki, C. E. Dykstra, M. A. Vincent, and L. Radom., *J. Am. Chem. Soc.*, **103**, 1652 (1981).

3) a) G. L. Blackman, R. D. Brown, R. F. C. Brown, and G. L. McMullen, *J. Mol. Spectry.*, **68**, 488 (1977); b) R. D. Brown, P. D. Godfrey, R. Champion, and D. McNaughton, *J. Am. Chem. Soc.*, **103**, 5711 (1981).

4) R. Ditchfield, W. J. Hehre, and J. A. Pople, *J. Chem. Phys.*, **54**, 724 (1971).

5) W. J. Hehre, R. Ditchfield, and J. A. Pople, *J. Chem. Phys.*, **56**, 2257 (1972).

6) The MP3/6-31G method represents that electron correlation is incorporated by the second and third-order Moller-Plesset perturbation theory (C. Moller and M. S. Plesset, *Phys. Rev.*, **46**, 618 (1934)) using MO's obtained by the 6-31G method.

7) We have used the GAUSSIAN-80H program (Hitac Version of GAUSSIAN-80 (QCPE 437, 1982)) at the Computer Center of the University of Tokyo.

Electrochemical Reduction Products of Carbon Dioxide at Some Metallic Electrodes in Nonaqueous Electrolytes

Kaname Ito,* Shoichiro Ikeda, Nobuhiro Yamauchi, Takaya Iida, and Takehiko Takagi
Department of Applied Chemistry, Nagoya Institute of Technology, Gokiso-cho, Showa-ku, Nagoya 466
(Received May 4, 1985)

Synopsis. Regarding the electrochemical reduction of carbon dioxide in nonaqueous electrolytes, it has been clarified that the main products are oxalic acid at a Pb electrode and carbon monoxide at Sn and In electrodes. In the case of a Zn electrode, substantial amounts of oxalic acid, glyoxylic acid and carbon monoxide have been produced.

According to previous papers,[1-3] the electrochemical reduction products of carbon dioxide dissolved in aqueous electrolytes under either ordinary or high pressures were mainly formic acids at electrodes of indium (In), lead (Pb), tin (Sn), zinc (Zn), and cadmium (Cd).

We have reported in another paper[4] that for nonaqueous electrolytes consisting of dimethyl sulfoxide (DMSO) and tetraalkylammonium salts, such as $(C_2H_5)_4NClO_4$ (TEAP), the main product is oxalic acid at a Pb electrode. It was suggested that carbon monoxide should probably form at In, Sn, and Zn electrodes.

Therefore, in the present paper a cyclic gas flow system for supplying CO_2 to an electolytic cell was employed in order to determine gaseous products on the electrochemical reduction of carbon dioxide at various metallic electrodes. This was investigated in nonaqueous electrolytes using propylene carbonate instead of DMSO. The effects of various electrode metals and electrlytic conditions on the products are described.

Experimental

An electolytic cell made of Teflon was designed for separating a cathode chamber from an anode chamber with an ion-exchange membrane, Nafion 315. This system was made gas tight. The cyclic gas flow system was designed to use a peristaltic mini-pump, a gas sampler and a manometer for supplying CO_2 gas to a cell. Gaseous products in the cyclic gas were determined as well as products at various electrolytes.

Working electrodes were prepared from solid-state metals such as Pb (purity 99.99%), Sn (99.999%), In (99.999%), and Zn (99.9999%). These have been employed as described in previous papers.[1-4] The reference electrode utilized in the present work consisted of a silver silver chloride electrode with a (0.01 M LiCl+0.1 M TEAP)(1 M=1 mol dm^{-3})/ propylen carbonate solution saturated with AgCl. The potentials given in the present paper are with respect to this Ag/AgCl reference electrode.

Since commercially obtained guaranteed reagent propylene carbonate possessed various impurities, it was purified using Jasinski and Kirkland's method.[5] The catholyte and the anolyte each utilized 10 ml of a 0.1 M TEAP/ propylen carbonate nonaqueous electrolyte prepared from the synthesized TEAP[3] and purified propylen carbonate. The water content of the electrolyte was determined by Karl Fischer's titration method[6] to be 320 ppm.

Electrolytic experiments for a determination of the reduction products of carbon dioxide were carried out using working-electrodes with surface areas of 2.47 to 7.20 cm^2. After an electrolyte within a cell was sufficiently saturated with CO_2 gas and the system was substituted by CO_2 gas, it was closed and the enclosed gas was made to flow at a rate of 0.9 cm^3 min^{-1} using a peristaltic pump. The electrolytic current was potentiostatically flowed at 100 or 200 C (coulombs). The products in the electrolytes were qualitatively and quantitatively determined by high-performance liquid

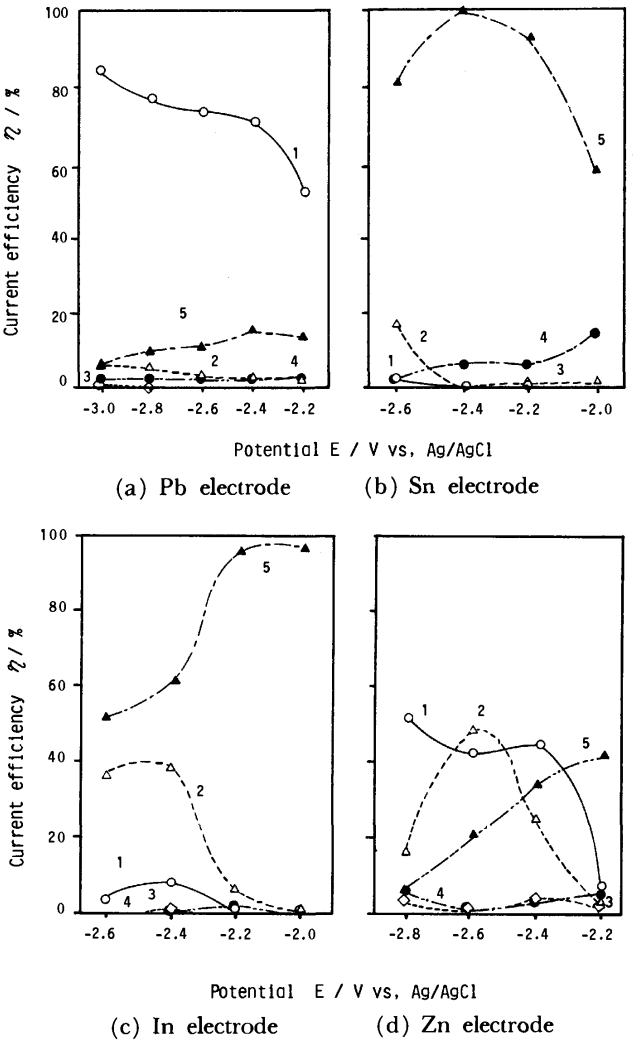

Fig. 1. Current efficiencies of electroreduction products of CO_2 in the cases of Pb(a), Sn(b), In(c), and Zn(d) electrodes.
Electrolyte: 0.1 M TEAP/propylen carbonate, Quantity of electricity passed: 100 C (a) or 200 C (b, c, d). Curve 1 (—○——): Oxalic acid, 2 (-△——): Glyoxylic acid, 3 (--◇---): Glycolic acid, 4 (-●----): Formic acid, 5 (—▲—·—): Carbon monoxide.

chromatgraphy. Gas chromatgraphy was used to determine the gaseous products in the cyclic gas. This equipment and the operating conditions were similar to that described in a previous paper.[4]

Results and Discussion

The electrochemical reduction products in both the electrolyte and the cyclic gas were determined. The obtained results are illustrated in Fig.1 as current efficiencies of products with respect to certain potentials (−2.0 to −3.0 V) for each electrode.

When a Pb electrode was employed, the main product was oxalic acid and the current efficiency increased to *ca.* 80% at −3.0 V, as shown in Fig. 1-(a). The efficiencies for formic, glyoxylic and glycolic acids were less than 5% in a potential range of −2.2 to −3.0 V, though 6 to 15% for carbon monoxide. On the other hand, when a Sn electrode was employed, the main product was carbon monoxide and its current efficiency increased to *ca.* 100% at −2.4 V, as shown in Fig. 1-(b). Other products had relatively lower efficiencies. In the case of an In electrode, as shown in Fig. 1-(c), the main product was also carbon monoxide at every potential measured; however, the current efficiencies, though *ca.* 95% in the potential range of −2.0 to −2.2 V, decreased to below 60% at potentials less than −2.4 V. Also, glyoxylic acid, instead of carbon monoxide, was produced with a current efficiency of *ca.* 40%. In the case of a Zn electrode, as shown in Fig. 1-(d), oxalic acid, glyoxylic acid and carbon monoxide were produced with substantial current efficiencies. According to these results, it has been experimentally comfirmed that carbon monoxide is the main product for Sn and In electrodes. This was not comfirmed in a previous paper.[4]

Consequently, although Saveant *et al.*[7] have reported that the production of oxalic acid by the electroreduction of carbon dioxide in a nonaqueous electrolyte was mainly dependent on the current densities from experimental results using only Pb and Hg electrodes, it may be concluded that the electroreduction products for carbon dioxide are primarily dependent on the electrode metals employed. Then, the main products are oxalic acid at a Pb electrode and carbon monoxide at Sn and In electrodes. Also, the current efficiencies regarding the products at each electrode are affected by the electrode potentials.

References

1) K. Ito, T. Murata, and S. Ikeda, *Bull. Nagoya Inst. Tech.*, **27**, 209 (1975).
2) K. Ito, S. Ikeda, and M. Okabe, *Denki Kagaku*, **48**, 247 (1980).
3) K. Ito, S. Ikeda, T. Iida, and H. Niwa, *Denki Kagaku*, **49**, 106 (1981).
4) K. Ito, S. Ikeda, T. Iida, and A. Nomura, *Denki Kagaku*, **50**, 463 (1982).
5) R. J. Jasinski and Kirkland, *Anal. Chem.*, **39**, 1663 (1967).
6) K. Muroi, *Bunseki*, **1979**, 74.
7) C. Amatore and J. M. Saveant, *J. Am. Chem. Soc.*, **103**, 5021 (1981).

A Set of Rate Constants for the Reactions of OH Radicals with Aromatic Hydrocarbons

Tomohiro OHTA* and Toshiro OHYAMA†
Department of Environmental Sciences, Tokyo Metropolitan Research Laboratory of Public Health, Hyakunincho, 3-Chome, Shinjuku-ku, Tokyo 160
†*Science University of Tokyo, Kagurazaka, Shinjuku-ku, Tokyo 162*
(Received May 10, 1985)

Synopsis. The rate constants for the reactions of OH radicals with seventeen aromatic hydrocarbons were determined at atmospheric pressure and room temperature from competitive reactions with hexane, using H_2O_2 as the OH-radical source. A useful trend was found in the structure-reactivity relationship.

Since aromatic hydrocarbons are important constituents of polluted urban air, and since they are believed to be consumed mainly by reactions with OH radicals, several papers have been published on the rate constants for the reactions of OH radicals with aromatic hydrocarbons.[1,2] Besides absolute rate constants determined by sophisticated techniques, relative rate constants determined by competitive reactions between aromatic hydrocarbons and a certain reference compound at atmospheric pressure and room temperature have been reported.[3,4] They used NO_x as a source of OH radicals, but we have proposed a different and simpler method to produce OH from the photolysis of hydrogen peroxide (H_2O_2, 90%) at 2537 A to obtain the rate constants for the reaction of OH with atmospheric elements of interest and have reported some empirical relationships between the reactivity towards OH and the structures of the olefins.[5,6] We here try to apply the method to aromatic hydrocarbons, using hexane as a reference compound, and propose a set of rate constants for the reactions of OH with a series of aromatic hydrocarbons; further, we try to find a useful trend in the reactivity-structure relationship.

The experimental procedure and data treatment were similar to those described in previous works.[5,6] Plots of $\ln([\text{aromatic}]_0/[\text{aromatic}]_t)$ against $\ln([\text{hexane}]_0/[\text{hexane}]_t)$ were on excellent straight lines for any compound; the slopes show the relative rate constants of aromatics to hexane. At least ten runs were carried out to determine the relative rate constants. The rate constants did not show any dependence on the variation in the initial concentrations of the reactants. Since methoxybenzene was photolyzed by the irradiation at 2537 A, methyl nitrite prepared by ourselves was used as another OH radical source by irradiating it in a mixture of reactants and oxygen at 360 nm.[7] No decomposition of other aromatics was observed because of short-time, weak irradiation.

A set of rate constants for the reactions of OH radicals with aromatic hydrocarbons is shown in Table 1, along with the literature data. The error limits in the table are the standard deviations for repeated runs. Most of the rate constants determined in this work showed fairy good agreement with literature values determined by completely different methods. For the compounds

TABLE 1. ROOM-TEMPERATURE RATE CONSTANTS FOR THE REACTIONS OF AROMATIC HYDROCARBONS WITH OH RADICALS

Aromatic	Rate constant		Reference[b]
	Relative to k_{hexane}	Absolute[a] $\times10^{-12}$ cm^3 molecule^{-1} s^{-1}	
Benzene	0.26±0.01	1.53±0.06	1.59±0.12[8], 1.24±0.12[9], 1.20±0.15[10], 1.21±0.09[11]
Toluene	1.08±0.03	6.37±0.08	6.11±0.40[8], 3.9±1.7[3], 5.78±0.58[9], 5.78±0.58[9], 6.40±0.64[10], 6.36±0.69[11]
Ethylbenzene	1.16±0.05	6.84±0.30	7.5±1.5[4], 7.95±0.50[12]
Isopropylbenezene	1.12±0.06	6.61±0.30	5.7±1.1[4], 7.79±0.50[12]
Propylbenzene	1.18±0.04	6.94±0.24	5.8±1.2[4], 5.86±0.50[12]
t-Butylbenzene	0.82±0.08	4.84±0.47	
O-Xylene	2.24±0.10	13.2±0.6	12.0±3.6[3], 15.3±1.5[9], 14.3±1.5[10], 12.4±1.2[10], 14.2±1.7[13]
2-Ethyltoluene	2.23±0.22	13.2±1.3	12.9±2.6[4]
M-Xylene	3.97±0.11	23.4±0.7	21.0±1.4[3], 23.6±2.4[9], 20.2±4.0[4], 24.0±2.5[10], 20.6±1.3[12]
3-Ethyltoluene	3.80±0.18	22.4±1.1	18.3±3.7[4]
P-Xylene	2.31±0.10	13.6±0.6	11.5±2.5[3], 12.2±1.2[9], 15.3±1.7[10], 10.5±1.0[12], 13.5±1.4[13]
4-Ethyltoluene	2.30±0.22	13.6±1.3	12.2±2.4[4]
1,2,3-Trimethylbenzene	5.30±0.73	31.3±4.3	21.3±4.5[3], 26.4±2.6[9], 33.3±4.5[10]
1,2,4-Trimethylbenzene	5.65±0.22	33.3±1.3	30.8±5.6[3], 33.5±3.4[9], 40.0±4.5[10]
1,3,5-Trimethylbenzene	6.94±0.94	40.9±5.6	62.4±7.5[10]
Fluorobenzene	0.16±0.02	0.87±0.03	
Methoxybenzene	2.52±0.10	14.9±0.6	19.6±2.4[14]

a) Absolute rate constants were derived using a rate constant for the reaction of OH with hexane of 5.9×10^{-12} cm^3 molecule^{-1} s^{-1}, the mean of three values in Ref. 1). b) Numbers in bracket indicate references.

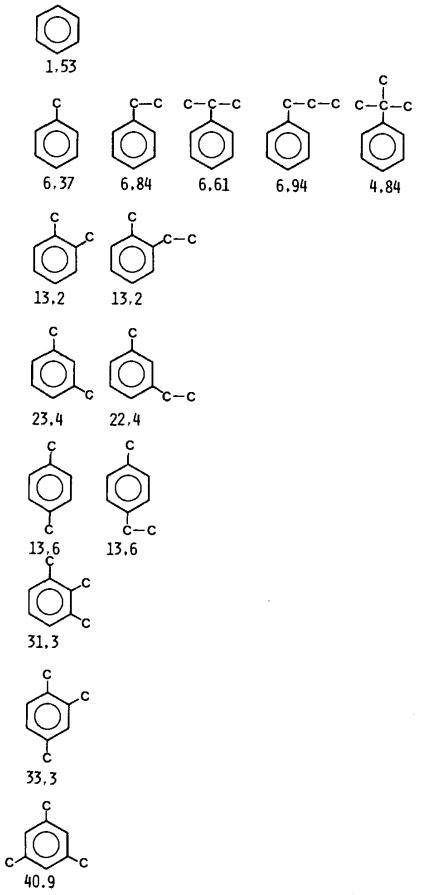

Fig. 1. Reactivity-structure relationship of aromatic hydrocarbons towards OH radicals. (all units in 10^{-12} cm^3 $molecule^{-1}$ s^{-1}).

whose literature values are diverse, our values generally agreed with the most recent values.

Since the set of rate constants for the series of aromatics was obtained under the same experimental conditions and using the same reference compound, it is possible for us to compare the rate constants one by one. Figure 1 shows the aromatic hydrocarbons classified by the positions and length of the substituents, along with the obtained rate constants in this work. It was confirmed that the OH-radical rate constants at room temperature increase as the degree of alkyl substitution increases, showing the same trend of degree and position of alkylation as in $O(^3P)$-atom reactions.[14] This implies that the major reaction path is the electrophilic addition of OH radicals to aromatic rings.

Furthermore, we notice that an empirical rule was derived from Fig. 1. The replacement of the methyl group on the aromatic ring by a longer alkyl chain (C_2, C_3) will not much affect the reactivity of methyl-substituted aromatics; the rate constants for aromatics on the same row in Fig. 1 are almost equal to each other except for *t*-butylbenzene in the row of toluene derivatives. There has been some uncertainty as to the branching ratio for the abstraction of methyl-H to the overall reaction in the reaction of toluene with OH radicals. The most recent work of Atkinson *et al.*[15] indicates that, at 300 K, the branching ratio is 0.08±0.03; however, the reported values have varied from 0.16,[10] 0.15±0.02,[16] to 0.1—0.02 (most probably 0.04).[11] The finding that toluene, ethylbenzene, isopropyl- and propylbenzenes have almost identical rate constants supports the lower value of the branching ratio of abstraction, because the loss of reactive methyl-H in toluene by replacement with methyl group (s) did not make the rate constant for unsubstituted toluene decrease significantly. *t*-Butylbenzene, apart from the four homologs, showed a smaller rate constant. The steric hindrance of the *t*-butyl group for the OH radical attack at the ortho position may explain it.

The trend found in this work is useful in getting an overall understanding of the reactivity of a series of aromatic hydrocarbons towards OH radicals and in evaluating the rate constants reported separately.

The authors wish to thank Professor Tanaka, Science University of Tokyo, for his valuable help.

References

1) R. Atkinson, K. R. Darnall, A. L. Lloyd, A. M. Winer, and J. N. Pitts, Jr., *Adv. Photochem.*, **11**, 375 (1979), and the references cited therein.
2) R. Atkinson and A. C. Lloyd, *J. Phys. Chem. Ref. Data*, **13**, 315 (1984).
3) G. J. Doyl, A. C. Lloyd, K. R. Darnall, A. M. Winer, and J. N. Pitts, Jr., *Environ. Sci. Technol.*, **9**, 237 (1975).
4) A. C. Lloyd, K. R. Darnall, A. M. Winer, and J. N. Pitts, Jr., *J. Phys. Chem.*, **80**, 789 (1976).
5) T. Ohta, *J. Phys. Chem.*, **87**, 1209 (1983).
6) T. Ohta, *Int. J. Chem. Kinet.*, **16**, 879 (1984).
7) T. Ohta, *Int. J. Chem. Kinet.*, **16**, 1495 (1984).
8) D. D. Davis, W. Bollinger, and S. Fisher, *J. Phys. Chem.*, **79**, 293 (1975).
9) D. A. Hansen, R. A. Atkinson, and J. N. Pitts, Jr., *J. Phys. Chem.*, **79**, 1763 (1975).
10) R. A. Perry, R. Atkinson, and J. N. Pitts, Jr., *J. Phys. Chem.*, **81**, 296 (1977).
11) F. P. Tully, A. R. Ravishankara, R. L. Thompson, J. M. Nicovich, R. C. Shah, N. M. Kreutter, and P. H. Wine, *J. Phys. Chem.*, **85**, 2262 (1981).
12) A. R. Ravishankara, S. Wagner, S. Fisher, G. Smith, R. Sciff, R. T. Watson, G. Tess, and D. D. Davis, *Int. J. Chem. Kinet.*, **10**, 783 (1978).
13) J. M. Nicovich, R. L. Thompson, and A. R. Ravishankara, *J. Phys. Chem.*, **85**, 2913 (1981).
14) J. T. Herron and R. E. Huie, *J. Phys. Chem. Ref. Data*, **2**, 467 (1973).
15) R. Atkinson, W. P. L. Carter, and A. M. Winer, *J. Phys. Chem.*, **87**, 1605 (1983).
16) R. A. Kenley, J. E. Davenport, and D. G. Hendry, *J. Phys. Chem.*, **85**, 2740 (1981).

Photoinduced Electron-transfer from Thiols to $[Ru(bpy)_3]^{2+}$ in Aqueous Solutions

Tokuji MIYASHITA and Minoru MATSUDA*
Chemical Research Institute of Nonaqueous Solutions, Tohoku University, Katahira 2-1-1, Sendai 980
(Received May 27, 1985)

Synopsis. The quenching of photoexcited $[Ru(bpy)_3]^{2+}$ by water-soluble thiols was studied by steady-state and time-resolved measurements. 2-Mercaptobenzoic acid and 4-mercaptopyridine which give the delocalized thiolate ions in water quenched $[Ru(bpy)_3]^{2+*}$ effectively, and $[Ru(bpy)_3]^{+}$ was formed by the quenching. No quenching occurred with cysteine and 2-mercaptoethanol.

Photoinduced electron-transfer with $[Ru(bpy)_3]^{2+}$ (bpy=2,2′-bipyridine) has been extensively investigated.[1] Previously, we reported that a photoexcited $[Ru(bpy)_3]^{2+}$ was quenched by benzenethiolate ion in nonaqueous solution (acetonitrile) and that $[Ru(bpy)_3]^{+}$ absorbing around 510 nm was formed in good yield.[2] The back electron-transfer reaction from $[Ru(bpy)_3]^{+}$ to PhS· was suppressed by the rapid dimerization reaction of thiyl radicals and $[Ru(bpy)_3]^{+}$ could exist with a relatively long lifetime in this system. The overall reaction can be expressed by Eq. 1 and the reverse process (the back electron-transfer reaction to disulfide) is slow.

$$2[Ru(bpy)_3]^{2+} + 2PhS^- \underset{\text{slow}}{\overset{h\nu}{\rightleftharpoons}} 2[Ru(bpy)_3]^{+} + PhSSPh \quad (1)$$

The application of this redox couple to photogalvanic cell was also reported.[3] Thermodynamically, $[Ru(bpy)_3]^{+}$ can reduce water to H_2.[4] In this letter we study the photoinduced electron-transfer from water-soluble thiols to $[Ru(bpy)_3]^{2+*}$ in order to search good redox couples used in aqueous solutions.

Experimental

$[Ru(bpy)_3]Cl_2 \cdot 6H_2O$ was synthesized according to published procedures.[5] Commercially available thiols were purified by recrystallization. The steady-state emission intensity was measured with Shimadzu RF 503A spectrofluorophotometer. Laser photolysis experiments for the lifetime quenching were carried out with a frequency-doubled Q-switched ruby laser system (347.1 nm pulse: 20 ns pulse width). The xenon-flash apparatus delivered a flash (10 μs pulse) with 112.5 joule was used for the detection of transient $[Ru(bpy)_3]^{+}$.

Results and Discussion

The quenching experiments of $[Ru(bpy)_3]^{2+*}$ by cysteine, 2-mercaptoethanol, 4-mercaptopyridine, and 2-mercaptobenzoic acid were carried out by steady-state measurement in deoxygenated solution. Cysteine and 2-mercaptoethanol did not quench the emission of $[Ru(bpy)_3]^{2+*}$ under a wide variation in pH (6-11; Borax buffer), whereas 2-mercaptobenzoic acid and 4-mercaptopyridine showed effective quenchings (Table 1). The Stern-Volmer plots for them are shown

TABLE 1. THE QUENCHING OF $[Ru(bpy)_3]^{2+*}$ BY WATER-SOLUBLE THIOLS

Thiols	pK_a	Quenching at pH>pK_a(−SH)
2-Mercaptobenzoic acid	3.0 (-COOH)	
	8.5 (-SH)	$k_q=1.7\times10^9$ dm^3 l^{-1} s^{-1}
4-Mercaptopyridine	10.6 (-SH)	$k_q=5\times10^7$ dm^3 l^{-1} s^{-1}
Cysteine	1.7 (-COOH)	
	8.3 (-SH)	No quenching
	10.8 (-NH_2)	
2-Mercaptoethanol	10 (-SH)	No quenching

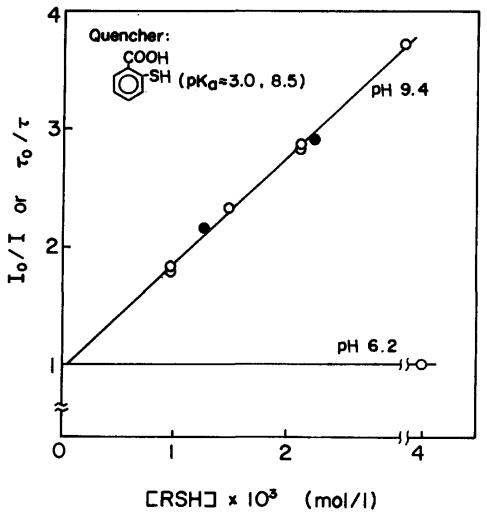

Fig. 1. Plots of I_0/I (○) and τ_0/τ (●) *vs.* [RSH] for quenching of $[Ru(bpy)_3]^{2+*}$ by 2-mercaptobenzoic acid.

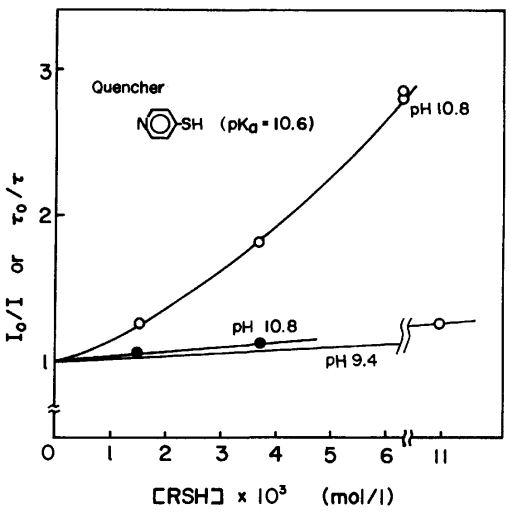

Fig. 2. Plots of I_0/I (○) and τ_0/τ (●) *vs.* [RSH] for quenching of $[Ru(bpy)_3]^{2+*}$ by 4-mercaptopyridine.

in Figs. 1 and 2. The quenchings are effective in pH region larger than their pK_a's. Apparently thiolate ion formed from the dissociation of -SH group is necessary for the quenching. The thiolate ions derived from 2-mercaptobenzoic acid and 4-mercaptopyridine are conjugated with aromatic moieties, and the delocalization is favorable to the orbital overlapping in electron-transfer process, resulting in the effective quenching.

The emission lifetimes were measured by exciting $[Ru(bpy)_3]^{2+}$ with a 347.1 nm-pulse (20 ns pulse width, ruby laser). The emission decays were single-exponential in the absence and the presence of quenchers, whose slopes varied with the concentration of the quencher. The plots of τ_0/τ *vs.* [RSH] were superimposed upon Figs. 1 and 2. The dynamic quenching rate constants for 2-mercaptobenzoic acid and 4-mercaptopyridine were obtained to be 1.7×10^9 (pH=9.4) and 5×10^7 $dm^3\,mol^{-1}\,s^{-1}$ (pH=10.8), respectively. As shown in Fig. 1, the slope of the plots of I_0/I *vs.* [RSH] was identical with that of the plots of τ_0/τ, suggesting that only dynamic quenching takes place and the quenching of $[Ru(bpy)_3]^{2+*}$ with *o*-sulfidobenzoate ion proceeds by the usual Stern-Volmer behavior. In contrast with this, the quenching by pyridinethiolate ion is almost static quenching (Fig. 2). Although the emission and the absorption spectra of $[Ru(bpy)_3]^{2+}$ were not changed in the presence of pyridinethiolate ion, somewhat association of $[Ru(bpy)_3]^{2+*}$ with the anion resulting in the static quenching seems to take place. The following xenon flash photolysis study is suggesting the association.

The formation of the transient species absorbing around 520 nm was detected by means of xenon flash photolysis of the aqueous solution (pH=9.4) containing $[Ru(bpy)_3]^{2+}$ and 2-mercaptobenzoic acid. The species can be assigned to $[Ru(bpy)_3]^{+}$ as shown elsewhere.[2,6] The decay profile is shown in Fig. 3. The decay obeyed good first-order kinetics with a rate constant $k=6.5\times10^3\,s^{-1}$, which implies that the back electron-transfer reaction was suppressed. It has been reported that when Eu(II) and aromatic amines were used as quenchers, the decays of $[Ru(bpy)_3]^{+}$ obeyed second-order kinetics with rate constants 2.7×10^7 and 10^7–10^{10} $dm^3\,mol^{-1}\,s^{-1}$, respectively.[7,8] On the other hand, the formation of $[Ru(bpy)_3]^{+}$ can not be detected in $[Ru(bpy)_3]^{2+}$-4-mercaptopyridine system. This may be caused by the rapid back electron-transfer in the static quenching pair.

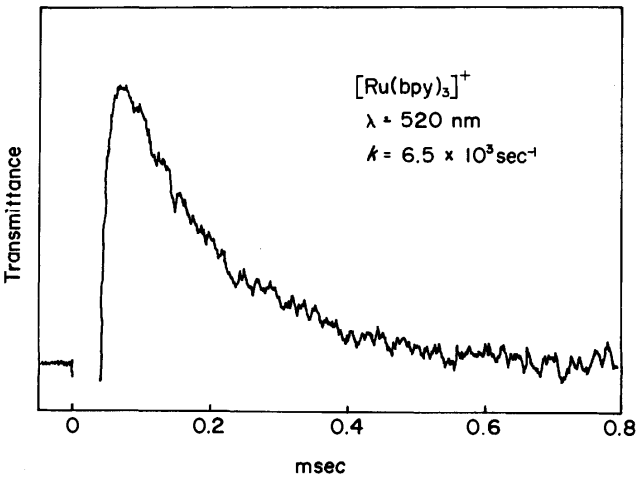

Fig. 3. Decay profile of transient absorption (λ= 520 nm) of $[Ru(bpy)_3]^{+}$ in aqueous solution (pH= 9.4; RSH: 2-mercaptobenzoic acid).

Steady-state irradiation on the buffer solution (pH=9.4) containing $[Ru(bpy)_3]^{2+}$, 2-mercaptobenzoic acid, and PtO_2 as preliminary experiments was carried out. H_2 evolution was confirmed by gas chromatography (Molecular sieves 5A, 60—80 mesh, 2 m, temp; 35 °C, carrier; N_2, TCD detector) though the yield is low.

References

1) V. Balzani, L. Maggi, M. F. Manfrin, F. Bolletta, and G. S. Laurence, *Coord. Chem. Rev.*, **15**, 321 (1975); T. Miyashita, T. Murakata, and M. Matsuda, *J. Phys. Chem.*, **87**, 4529 (1983).

2) T. Miyashita and M. Matsuda, *Bull. Chem. Soc. Jpn.*, **54**, 1740 (1981).

3) T. Miyashita and M. Matsuda, *J. Phys. Chem.*, **85**, 3122 (1981).

4) N. E. Tokel-Takvoryan, R. E. Hemingway, and A. J. Bard, *J. Am. Chem. Soc.*, **95**, 6582 (1973).

5) I. Fujita and H. Kobayashi, *Ber. Bunseges. Phys. Chem.*, **76**, 115 (1972); R. A. Palmer and T. S. Piper, *Inorg. Chem.*, **5**, 864 (1966).

6) J. H. Baxendale and M. Fiti, *J. Chem. Soc., Dalton Trans.*, **1972**, 1995.

7) C. Creutz and N. Sutin, *J. Am. Chem. Soc.*, **98**, 6384 (1976).

8) C. P. Anderson, D. J. Salmon, T. J. Meyer, and R. C. Young, *J. Am. Chem. Soc.*, **99**, 1980 (1977).

Equilibrium Solubilities of Benzene, Toluene, Ethylbenzene, and Propylbenzene in Silver Nitrate Solutions

Isao SANEMASA,* Seiji ARAKAWA, Cheng Yun PIAO, and Toshio DEGUCHI
Department of Chemistry, Faculty of Science, Kumamoto University, Kurokami 2-39-1, Kumamoto 860
(Received April 1, 1985)

Synopsis. By making use of the solute vapor, the equilibrium solubilities of benzene and three alkylbenzenes in $AgNO_3$ solutions have been measured. The complex formation constants of silver ions are estimated for each solute, and the results are compared with literature values.

It is well known that silver ions form complexes with a wide variety of organic compounds having C–C double bond(s). The formation constants for some aromatic hydrocarbons have been determined by measuring aqueous solubilities of the solutes in the presence of Ag^+ ions.[1-3]

We have reported a method of preparing aqueous solutions saturated with a solute such as aromatic hydrocarbons and iodine.[4,5] The technique involves introducing the solute vapor which is in equilibrium with a liquid or a solid solute, into water and circulating it in a closed system. Here we have applied the method to silver nitrate solutions to determine complex formation constants of Ag^+ with benzene and alkylbenzenes, and the results will be compared with the literature values.

Experimental

All the electrolytes and the nonelectrolytes used were of an analytical reagent grade. Deionized redistilled water was used to prepare silver nitrate solutions, an ionic strength of which was adjusted to 1.00 by adding a suitable amount of the KNO_3 stock solution. The concentration of Ag^+ in the $AgNO_3$ stock solution was determined in advance by the Fajans method. The experimental procedure and the apparatus employed in this work have been previously described in detail.[4] After the solubility equilibrium had been attained (*ca.* 10 min), definite portions of the aqueous phase were withdrawn, and the solute concentrations were determined by extraction with chloroform, followed by spectrophotometric measurements.

Results and Discussion

The complex formations of Ag^+ with aromatic hydrocarbons have been shown as follows:[1] $Ag^+ + \phi = Ag^+\cdot\phi^+$, K_1, and $Ag^+ + Ag\cdot\phi^+ = Ag_2\cdot\phi^{2+}$, K_2, where ϕ denotes hydrocarbon molecule, K_1 and K_2 being stepwise complexation constants. The total concentration of hydrocarbon, C_ϕ, and that of silver ions, C_{Ag}, present in the solution, are expressed as follows;

$$C_\phi = [\phi]_{eq}(1 + K_1[Ag^+]_{eq} + K_1K_2[Ag^+]_{eq}^2) \quad (1)$$

$$C_{Ag} = [Ag^+]_{eq}(1 + K_1[\Phi]_{eq} + 2K_1K_2[\Phi]_{eq}[Ag^+]_{eq}) \quad (2)$$

where the subscript means the equilibrium concentration. Let, in the absence and presence of Ag^+ ions, the hydrocarbon solubility in 1.00 mol dm^{-3} KNO_3 be S_o and S_{obsd}, respectively. Then, $[\phi]_{eq}$ and C_ϕ are equal to S_o and S_{obsd}, respectively, since the hydrocarbon molecules in the aqueous phase free from complexation with Ag^+ are also equilibrated with the solute in the vapor phase. The solubilities of hydrocarbons are small, and even K_1 which is larger than K_2, exhibits no more than a single figure for each hydrocarbon. Hence $[Ag^+]_{eq}$ can be made equal to C_{Ag}. Then, Eq. 1 becomes

$$S_{obsd}/S_0 = 1 + K_1C_{Ag} + K_1K_2C_{Ag}^2. \quad (3)$$

The results of the solubility measurements for each hydrocarbon in KNO_3 solutions containing Ag^+ ions up to 0.5 mol dm^{-3} are listed in Table 1. The K_1 and K_2 values have been determined with the aid of Eq. 3 by a curve-fitting method, and the results are summarized in Table 2 together with the literature values. The magnitude of our K_1 value is in the order of benzene<toluene>ethylbenzene>propylbenzene. It has been suggested that the K_1 value decreases due to a

TABLE 1. SOLUBILITIES OF BENZENE AND THE ALKYLBENZENES IN SILVER NITRATE SOLUTIONS AT 25°C[a]

C_{Ag}[b] / mol dm^{-3}	Solubilities of[c] Benzene / 10^{-2} mol dm^{-3}	Toluene / 10^{-3} mol dm^{-3}	Ethylbenzene / 10^{-3} mol dm^{-3}	Propylbenzene / 10^{-4} mol dm^{-3}
0	1.54(1.00)	3.43(1.00)	1.02(1.00)	2.39(1.00)
0.02	1.62(1.05)	3.60(1.05)	1.07(1.05)	
0.04	1.68(1.09)	3.81(1.11)	1.12(1.10)	
0.05				2.66(1.11)
0.06	1.75(1.14)	4.04(1.18)	1.18(1.16)	
0.08	1.82(1.18)	4.23(1.23)	1.24(1.22)	
0.10	1.89(1.23)	4.39(1.28)	1.29(1.27)	2.95(1.23)
0.15				3.35(1.40)
0.20	2.26(1.47)	5.46(1.59)	1.56(1.53)	3.60(1.51)
0.30	2.65(1.72)	6.51(1.90)	1.87(1.83)	4.46(1.87)
0.40	3.02(1.99)	7.79(2.27)	2.18(2.14)	5.30(2.22)
0.50	3.50(2.27)	9.30(2.71)	2.52(2.47)	6.43(2.69)

a) Ionic strength was adjusted with KNO_3 to be 1.00. b) The toltal concentration of silver ions present in the aqueous solution. c) The S_{obsd}/S_o ratio is indicated in the parentheses.

TABLE 2. COMPLEX FORMATION CONSTANTS OF SILVER IONS WITH BENZENE AND THE ALKYLBENZENES AT 25°C

Hydrocarbon	K_1/dm³ mol⁻¹		K_2/dm³ mol⁻¹	
	This work	Literature	This work	Literature
Benzene	2.30	2.41[a]	0.349	0.212[a]
Toluene	2.79	2.95[a]	0.675	0.214[a]
Ethylbenzene	2.57	2.7[b]	0.341	0.15[b]
Propylbenzene	2.16	2.9[b]	1.18	

a) Ref. 1. b) Ref. 3.

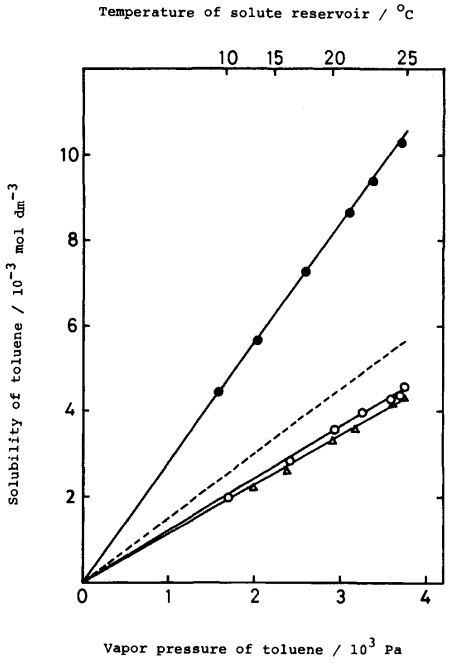

Fig. 1. Equilibrium solubilities of toluene in KNO_3 solutions at 25.00°C *vs.* vaper pressure.
Pure water (dotted line), 1.00 mol dm^{-3} KNO_3 (△), 0.0197 mol dm^{-3} $AgNO_3$ in 1.00 mol dm^{-3} KNO_3 (○), 0.492 mol dm^{-3} $AgNO_3$ in 1.00 mol dm^{-3} KNO_3 (●).

steric hindrance as the carbon number of a homologous series increases.[1,3,6] With this view, the K_1 value reported in the literature seems to be overestimated for propylbenzene. Our K_2 values are considerably larger than the literature ones, but there is no criterion to judge which is more adequate. In order to determine the K_2 values with a minimum uncertainty, the solubility measurements should be made under higher Ag^+ concentrations. Such conditions, however, cause another uncertainty. In general, the aqueous solubility of a nonelectrolyte depends not only on the concentration, but also on the type of an electrolyte present in the solution, which is referred to the salting (-out or -in) effect. This effect may differ with Ag^+ and K^+, the latter having been added to keep the ionic strength constant, and the difference is to be pronounced at higher Ag^+ concentrations. It should be noted that the literature K_2 values have been determined at relatively higher Ag^+ concentrations up to 1.000 mol dm^{-3}.[1,3]

The present method of preparing aqueous solutions saturated with solute vapor is useful to see whether the solubility obeys Henry's law or not.[4] The solubility of toluene vapor obeys Henry's law in KNO_3 solutions

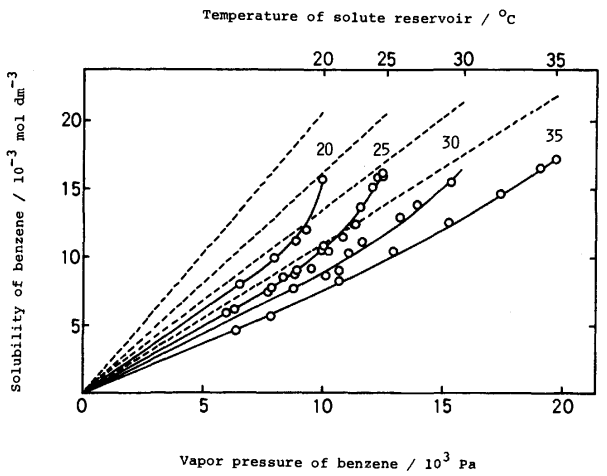

Fig. 2. Equilibrium solubilities of benzene in KNO_3 solutions *vs.* vapor pressure.
Pure water (dotted line), 1.00 mol dm^{-3} KNO_3 (solid line).
The figure near each line indicates the temperature of aqueous solution.

(Fig. 1). This is also the case for the other alkylbenzenes studied here. In sharp contrast, the solubility of benzene vapor has been found to deviate from the law (Fig. 2). Though the reason for the deviation observed for benzene is not clear at present time, a plausible interpretation is that benzene molecules dissolved in KNO_3 solutions associate with each other to dimerize. There have been reported two opposite observations in the literature, one supporting dimerization of benzene,[7] the other not.[8] If dimerization does occur due to hydrophobic interaction between benzene molecules in water,[7] the presence of electrolytes in the solution may be expected to promote dimerization owing to their hydration. It is to be noted that if benzene molecules dissolved in KNO_3 solutions exist as a dimer to an appreciable extent, the K_1 value for benzene determined by us and by others might have been underestimated. If we consider the steric effect to be a main factor as for alkylbenzenes, it seems likely that the K_1 of benzene is rather larger than that of toluene, though the larger K_1 value of toluene has been explained in terms of an inductive effect of the methyl substituent.[1]

References

1) L. J. Andrews and R. M. Keefer, *J. Am. Chem. Soc.*, **71**, 3644 (1949).
2) L. J. Andrews and R. M. Keefer. *J. Am. Chem. Soc.*, **72**, 3113 (1950).
3) L. J. Andrews and R. M. Keefer, *J. Am. Chem. Soc.*, **72**, 3054 (1950).
4) I. Sanemasa, M. Araki, T. Deguchi, and H. Nagai, *Bull. Chem. Soc. Jpn.*, **55**, 1054 (1982).
5) I. Sanemasa, T. Kobayashi, C. Y. Piao, and T. Deguchi, *Bull. Chem. Soc. Jpn.*, **67**, 1352 (1984).
6) M. A. Muhs and F. T. Weiss, *J. Am. Chem. Soc.*, **84**, 4697 (1962).
7) E. E. Tucker, E. H. Lane, and S. D. Christian, *J. Solution Chem.*, **10**, 1 (1981).
8) W. J. Green and H. S. Frank, *J. Solution Chem.*, **8**, 187 (1979).

The Crystal Structure of Ion-exchanged Mordenite

Masatoki ITO* and Yoshihiko SAITO*
Department of Chemistry, Faculty of Science and Technology, Keio University, Hiyoshi, Kohoku-ku, Yokohama 223
(Received April 1, 1985)

Synopsis. The crystal structure of hydrated mordenite, yielded at Hokiyadake, Nagano City, Japan, $Na_{1.4}Ca_{2.9}Al_{7.2}Si_{40.8}O_{96}\cdot nH_2O$, were refined to R=0.070 for 1526 observed reflections. Notable ordering of the aluminum positions of the aluminosilicate framework was observed.

Study of the location of aluminum atom in mordenite provides a basis for the interpretation of its catalytic properties. All structure determinations for mordenite so far reported have been done on a specimen from Challis Valley, Idaho.[1-2] The structure revealed the weak electron density peaks other than the Cmcm stacking. Here we report the structure of another mordenite obtained at Hokiyadake, Nagano City, Japan, which has a distinct ordering of aluminum atoms in the $AlSi_5O_{12}$ silicate framework. The calcium atoms populated as dominant cations in this mordenite.

Experimental

Single crystals of natural mordenite from Hokiyadake, Nagano City, Japan were ion-exchanged with 1 M HCl solution at room temperature for 24 h, yielding the composition, $Na_{1.4}Ca_{2.9}Al_{7.2}Si_{40.8}O_{96}\cdot nH_2O$ from atomic absorption and ICP spectrometry. A needle crystal with dimensions of 0.20×0.08×0.06 mm was used for the X-ray measurements. The crystal data are: $Na_{1.4}Ca_{2.9}Al_{7.2}Si_{40.8}O_{96}\cdot nH_2O$, orthorhombic, Cmcm, a=18.089(3), b=20.412(4), c=7.504(1) Å, U=2771(2) Å^3, d_m=1.80 g cm^{-3}, μ(Mo $K\alpha$)=7.88 cm^{-1}, λ(Mo $K\alpha$)=0.7107 Å. Intensity data were collected on a Rigaku AFC-5 automated four-circle diffractometer with graphite monochromator up to 2θ=60°. Cell parameters were refined by a least-squares method on the basis of 15 2θ values for Mo $K\alpha$ radiation (20°<2θ<40°). 1526 unique reflections with $|F_o|>3\sigma(|F_o|)$ were measured. No absorption correction was made. Cations and water molecules were located and the structures were refined by the alternating use of least-squares and Fourier methods, the UNICS-III computation program system[3] being employed. Final R value for the hydrated sample is 0.070 for 1526 observed reflections. In the final cycle $(\Delta/\sigma)_{max}$ was 0.2 for the x coordinate of O(6). No peaks higher than 0.35 e Å^{-3} were observed in the final difference density map. Complex neutral atom scattering factors from the International Tables for X-Ray Crystallography[4] were used. Table 1 gives the positional parameters for the silicate framework atoms and the cations.*

Results and Discussion

Interatomic distances and bond angles in the mordenite framework are listed in Table 2. The fundamental framework showed no stacking faults in contrast to the previous results reported by Mortier *et al.*[2] Chemical analysis showed that Ca^{2+} and also Na^+ remained in spite of prolonged ion-exchange by 1 M HCl (1 M=1 mol dm^{-3}) and that the former dominates by far over the latter. Therefore, extra framework electron densities were assigned to Ca^{2+}, Na^+, and orderly adsorbed water molecules. Ca^{2+} is located at the center of the six-membered rings, whereas the cation in the main channel is ascribed to Na^+ since the former

TABLE 1. POSITIONAL PARAMETERS (×10^4) AND EQUIVALENT ISOTROPIC TEMPERATURE FACTORS $B_{eq}=4/3\sum_i\sum_j\beta_{ij}a_ia_j$.[5]

	x	y	z	B_{eq}/Å^2
T1(AL)	2008(1)	4279(1)	5413(3)	0.9
T2(AL)	1959(1)	1915(1)	5461(3)	1.1
T3(AL)	873(1)	3854(1)	2500	0.8
T4(AL)	859(1)	2278(1)	2500	0.8
01	1250(3)	4188(3)	4322(9)	2.7
02	1230(3)	1945(3)	4241(9)	2.7
03	2642(4)	3774(3)	4835(10)	3.9
04	955(4)	3057(4)	2500	3.3
05	1674(4)	1964(5)	7500	3.2
06	1821(4)	4212(5)	7500	2.5
07	2346(5)	5000	5000	2.2
08	2500	2500	5000	4.5
09	0	4114(6)	2500	2.0
010	0	2051(6)	2500	1.9
CA	0	5000	0	3.9

TABLE 2. INTERATOMIC DISTANCES AND BOND ANGLES IN THE MORDENITE FRAMEWORK

T1-01	1.609(5)	03-T1-01	112.9(3)	T1-01-T3	144.9(3)
T1-03	1.616(6)	03-T1-06	111.1(4)	T2-02-T4	145.0(3)
T1-06	1.610(2)	03-T1-07	104.8(3)	T2-03-T1	157.5(6)
T1-07	1.625(3)	01-T1-06	107.9(3)	T4-04-T3	168.7(5)
		01-T1-07	109.6(3)	T2-05-T2	143.1(7)
mean	1.615 Å	06-T1-07	110.7(3)	T1-06-T1	153.1(6)
				T1-07-T1	135.6(7)
T2-02	1.606(5)	mean	109.5°	T2-08-T2	180.0(5)
T2-03	1.588(5)			T3-09-T3	145.0(6)
T2-05	1.610(3)	08-T2-02	110.5(2)	T4-010-T4	146.8(6)
T2-08	1.583(2)	08-T2-03	107.7(4)		
		08-T2-05	110.8(3)	mean	152.0°
mean	1.597 Å	03-T2-02	109.6(5)		
		03-T2-05	109.6(5)		
T3-01	1.664(5)	02-T2-05	106.4(3)		
T3-04	1.639(7)				
T3-09	1.656(4)	mean	109.0°		
mean	1.656 Å	01-T3-01	109.8(3)		
		04-T3-09	112.5(4)		
T4-02	1.620(5)	04-T3-01	111.4(2)		
T4-04	1.588(7)	09-T3-01	105.7(3)		
T4-010	1.616(3)				
		mean	109.4°		
mean	1.611 Å				
		02-T4-02	108.1(3)		
		04-T4-010	112.9(4)		
		04-T4-02	111.6(2)		
		010-T4-02	106.2(3)		
		mean	109.4°		

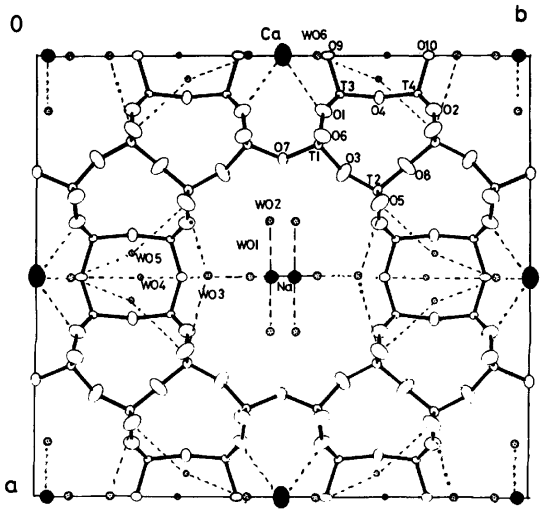

Fig. 1. The crystal structure viewed down along the c axis. WO stands for ordered water molecule.

electron density exceeded by far than the latter.

The T(Si or Al atoms)–O distance was influenced by the Si and Al contents and their positions in the framework. The overall mean T–O distance of 1.620 Å compares well with the typical values for the mordenite as shown in Table 2. The mean T3–O distance, 1.656 Å, is longer than the other T–O distances, which is suggestive of more probable accumulation of the aluminum atoms on the T3 site than on the remaining three. Figure 1 shows the crystal structure viewed down along the c axis. The Ca^{2+} at (0, 1/2, 0) was not exchanged by 1 M HCl. This is explained by the existence of ordered AlO_4^- tetrahedra at T3 site. The larger charge 2+ of Ca^{2+} rather than Na^+ could favor the charge compensation of AlO_4^-. The presence of the mirror plane (100) in Cmcm may lead to unfavorable charge distribution of the neighboring AlO_4^- tetrahedra. Thus, Al(T3) and adjacent symmetry related Al(T3′) atoms might be statistically disordered, and the space group Cmcm adopted in the present investigation represents a pseudo-symmetry.

The structure for dehydrated mordenite was also determined. The cell dimensions reduced to a= 17.941(4), b=20.276(6), c=7.482(2) Å by dehydrating a capillaried sample at 10^{-5} Torr and 350 °C for 48 h. During dehydration the Na^+ remaining in the center of the large channel, which occupied the two positions at random near the center, moved to the side wall of the main channel, and the T3-09-T3′ angle changed by up to 8.1° (1.4°) with mean change of 2.2°. The remarkable ring puckering of the framework skeletons reduced the symmetry from Cmcm to the lower space group.

The authors wish to thank Dr. A. Kato for supplying the mordenite sample.

References

1) W. M. Meier, *Zeit. fur Krist.* **115**, 439 (1961).
2) W. J. Mortier, J. J. Pluth, and J. V. Smith, *Mat. Res. Bull.* **10**, 1319 (1975), *ibid.*, **11**, 15 (1976); J. L. Schlenker, J. J. Pluth and J. V. Smith, *ibid.*, **14**, 751, 849, 961 (1979).
3) T. Sakurai and K. Kobayashi, *Rikagaku Kenkyusho Hokoku*, **55**, 69 (1979).
4) International Tables for X-Ray Crystallography Vol. IV., Kynoch Press, Birminghum, England (1974).
5) W. C. Hamilton, *Acta Crystallogr.* **12**, 609 (1959).

Stereoisomers of the Bis(1,10-phenanthroline){(1*R*,2*R*)-1,2-cyclohexanediamine}cobalt(III) Complex

Akira TATEHATA* and Shigeru NATSUME
Department of Chemistry, Faculty of Science, Shizuoka University, Ohya, Shizuoka 422
(Received May 1, 1985)

Synopsis. The diastereomers of $[Co(R\text{-chxn})(phen)_2]^{3+}$ (R-chxn=$(-)_{589}$-(1*R*,2*R*)-1,2-cyclohexanediamine, phen= 1,10-phenanthroline) were prepared and characterized by absorption, circular dichroism, and ^1H NMR spectra. The preference of Δ-isomer in the complex formation was observed and the degree of the stereoselectivity was greater than that of the corresponding $[Co(R\text{-pn})(phen)_2]^{3+}$ (pn= 1,2-propanediamine).

Stereoselectivity in the formation of the mixed ligand Co(III) complexes of the type $[Co(aa)(phen)_2]^{n+}$ has been investigated. No remarkable stereoselectivity between Λ and Δ isomers was observed for certain complexes containing a chiral α-hydroxy carboxylate ion such as (*R*,*R*)- or (*S*,*S*)-tartrate and (*S*)-malate ions,[1] whereas fairly high stereoselectivity was observed for this type of (*S*)-α-amino acidato[2] and (*S*)- or (*R*)-pn[3] complexes. We report here the preparation,characterization, and stereoselectivity in the formation of the diastereomers of $[Co(R\text{-chxn})(phen)_2]^{3+}$.

Experimental

1,2-Cyclohexanediamine, chxn, (Aldrich Chemical Co.) was separated into cis and trans isomers by the procedure of Kidani *et al.*[4] Optically active *R*-chxn was obtained by resolving *trans*-chxn according to the method of Galsbøl *et al.*[5]

Preparation and Separation of Isomers. A methanol solution (2.3 cm^3, 10% v/v) of *R*-chxn was added to a suspension of *cis*-$[CoCl_2(phen)_2]Cl\cdot 3H_2O$ (1.0 g, 1.7 mmol) in methanol (50 cm^3). The mixture was stirred for 3 h at 40 °C, and then diluted with water. This solution was passed through an SP-Sephadex column (φ2.7×40 cm), and the adsorbed complexes were eluted with a 0.3 mol dm^{-3} NaCl solution. Yellow ($[Co(phen)_3]^{3+}$), yellowish-orange($[Co(R\text{-chxn})(phen)_2]^{3+}$), and orange ($[Co(R\text{-chxn})_2(phen)]^{3+}$) bands were developed in this order. The effluent of the second band containing the desired complex was diluted with water and passed through an SP-Sephadex column (φ2.7×3 cm). The adsorbed complex was transferred to the top of another SP-Sephadex column (φ2.7×130 cm) and eluted with a 0.15 mol dm^{-3} $Na_2[Sb_2(d\text{-tart})_2]$ solution to separate the diastereomers. The eluted bands of diastereomers were collected, and to them the same procedure was followed as for the corresponding pn complex.[3] Two diastereomers were obtained as crystals of the perchlorate. Found for the Λ isomer: C, 40.92; H, 3.68; N, 9.66%. Calcd for $C_{30}H_{36}N_6Cl_3CoO_{15}$ (trihydrate): C, 40.67; H, 4.10; N, 9.49%. Found for the Δ isomer: C, 41.51; H, 3.79; N, 9.72%. Calcd for $C_{30}H_{34}N_6Cl_3CoO_{14}$(dihydrate): C, 41.52; H, 3.95; N, 9.68%.

Measurements. Absorption and CD spectra were obtained on a Shimadzu MPS-50L recording spectrophotometer and a JASCO J-20 spectropolarimeter, respectively. The CD magnitude was corrected by the use of that of *Λ*-$(+)_{589}$-$[Co(en)_3]I_3\cdot H_2O$. ^1H NMR spectra (90 MHz) were measured on a Varian EM-390 spectrometer in both D_2O and CD_3OD solutions using DDS (sodium 2,2-dimethyl-2-silapentane-5-sulfonate) and TMS(tetramethylsilane), respectively, as an internal standard reference.

Results and Discussion

The absorption and the CD spectra of $[Co(R\text{-chxn})(phen)_2]^{3+}$ are shown in Fig. 1, where their numerical data are also given. The absolute configurations of the isomers were assigned on the basis of the CD spectra in the regions of the first absortion band and the phenanthroline $\pi\cdot\pi^*$ transitions. The configurational and vicinal effect curves under the first absorption band estimated by the conventional method are shown in Fig. 2 together with the vicinal effect curve of the corresponding *R*-pn complex for comparison.[3] The vicinal effect curves of $[Co(R\text{-chxn})(phen)_2]^{3+}$ and $[Co(R\text{-pn})(phen)_2]^{3+}$ are quite similar to each other though the former slightly shifts to longer wavelengths, indicating that the chelate ring of *R*-pn has the same λ conformation as that of *R*-chxn fixed by the cyclohexane ring. ^1H NMR spectra of $[Co(R\text{-chxn})(phen)_2]^{3+}$ were at first measured in D_2O solution. Since the chemical shifts of H_{2a} and H_{3e} protons of the *R*-chxn coordinated in the Λ isomer were not distinct because of overlap with the methylene protons of DSS, the ^1H NMR spectra of the complexes were remeasured in CD_3OD solution. The signals of each proton of the cyclohexane ring have been assigned by the use of spin-decoupling technique and by reference to the corresponding proton signals of $[Co(R\text{-chxn})(CN)_4]^-$.[6] By measuring the midpoint of the multiplets, chemical shifts of the diastereomers of $[Co(R\text{-chxn})(phen)_2]^{3+}$

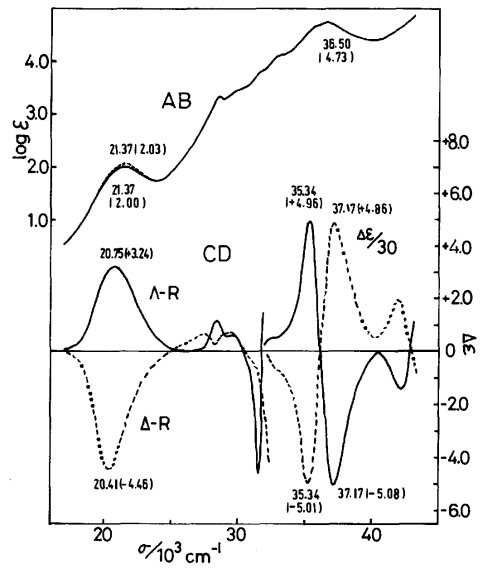

Fig. 1. Absorption and CD spectra of *Λ*-$(+)_{546}$-(——) and *Λ*-$(-)_{546}$-$[Co(R\text{-chxn})(phen)_2]^{3+}$ (----).

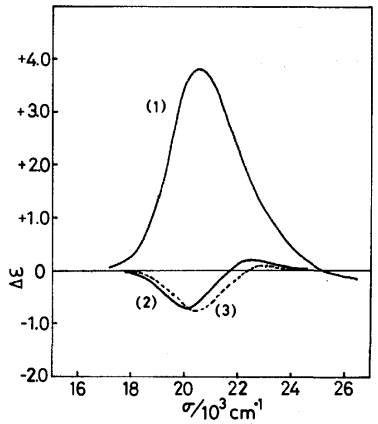

Fig. 2. Configurational effect (1) and vicinal effect (2) curves for Δ-[Co(*R*-chxn)(phen)$_2$]$^{3+}$ and vicinal effect curve (3) for Δ-[Co(*R*-pn)(phen)$_2$]$^{3+}$.

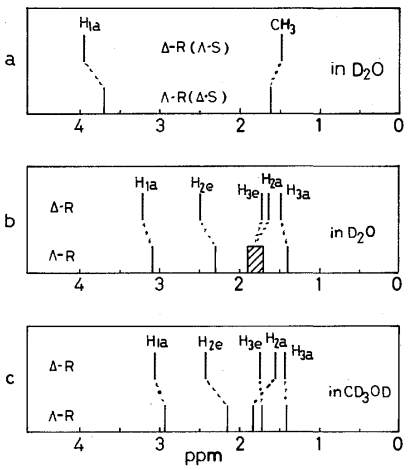

Fig. 3. The distribution of the chemical shifts of the *R*-pn of the [Co(*R*-pn)(phen)$_2$]$^{3+}$ in D_2O solution (a), and the *R*-chxn of the [Co(*R*-chxn)(phen)$_2$]$^{3+}$ in D_2O solution (b) and in CD_3OD solution (c). In each figure Δ-R isomer is shown at the upper part and Λ-R isomer at the lower part.

and [Co(*R*-pn)(phen)$_2$]$^{3+}$ are summerized in Fig. 3 with the assignment of the proton signals. The schematic structures and the numbering of protons of the *R*-chxn and *R*-pn complexes are shown in Fig. 4. There is a

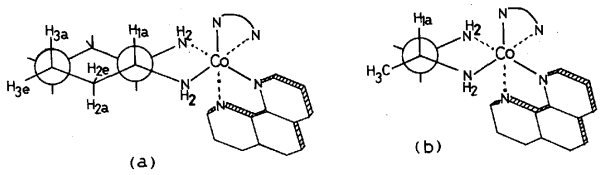

Fig. 4. Schematic structures of *R*-chxn moiety of Δ-[Co(*R*-chxn)(phen)$_2$]$^{3+}$ (a) and of *R*-pn moiety of Δ-[Co(*R*-pn)(phen)$_2$]$^{3+}$ (b) and their numbering of protons.

similar tendency between the spectra of the *R*-chxn complexes and those of the *R*-pn complexes owing to the ring-current effect of the aromatic phenanthroline ligand. The axial methine H_{1a} proton, the equatorial methylene H_{2e} proton, and axial and equatorial methylene H_{3a} and H_{3e} protons for the Δ-*R* chxn complex resonate at a lower field than the corresponding protons of the Λ-*R* chxn complex, as can be also seen for the axial methine H_{1a} proton of the Δ-*R* pn complex.[3] On the other hand, the signals due to the axial methylene H_{2a} proton of *R*-chxn complexes appear at a higher field by 0.28 ppm in the Δ isomer than in the Λ isomer, as observed for the methyl signals of the Δ-*R* pn complex. (Fig. 3) The diastereomeric ratio of the formation of [Co(*R*-chxn)(phen)$_2$]$^{3+}$ was Δ-*R*/Λ-*R*=5.9±0.2 in methanol at 40°C. Although the ring-current effect may play some role in causing the stereoselectivity, it is rather difficult to explain the favored diastereomer solely in terms of ring-current effect. This stereoselectivity may come mainly from a steric factor. Molecular models suggest a sterically less favored configuration for Λ-propellor owing to the serious repulsive interactions between H_{2a} and N–H protons of *R*-chxn and the α-proton of phenanthroline.

References

1) A. Tatehata, *Inorg. Chem.*, **15**, 2086 (1976); *ibid.*, **17**, 725 (1978).
2) A. Tatehata, *Inorg. Chem.*, **21**, 2496 (1982).
3) A. Tatehata and S. Natsume, *Bull. Chem. Soc. Jpn.*, **57**, 1419 (1984).
4) R. Saito and Y. Kidani, *Chem. Lett.*, **1976**, 123.
5) F. Galsbøl, P. Steenbøl, and B. S. Sørensen, *Acta Chem. Scand.*, **26**, 3605 (1972).
6) M. Goto, M. Takeshita, and T. Sakai, *Inorg. Chem.*, **17**, 314 (1978).

Preparation of $Cs_2ZrY(PO_4)_3$ and Related New Compounds

Akira ONO
National Institute for Research in Inorganic Materials, Namiki 1-1, Ibaraki, 305
(Received May 8, 1985)

Synopsis. New compounds have been prepared with the chemical formula $A_2ZrM(PO_4)_3$ with A=K, Rb or Cs and M=Y or In. X-Ray diffraction data can be indexed based on a cubic cell with a langbeinite-type structure. $CsTi_2(PO_4)_3$ could not be obtained but $CsTi_3P_5O_{19}$ was synthesized between 1100—1275 °C. It crystallized with a space group C2/c or Cc with $Z=4$.

Nasicon-type compounds have been studied in relation to sodium ion conductor.[1,2] However, recent studies regarding these substances have revealed the existence of a new structural family of low thermal-expansion materials.[3,4] These studies have been carried out mainly on sodium- or calcium-bearing Nasicon-type compounds; therfore, we have investigated potassium-, rubidium-, and caesium-bearing compounds. During this study, we obtained novel compounds, such as $K_2ZrY(PO_4)_3$, $K_2ZrIn(PO_4)_3$, $Rb_2ZrIn(PO_4)_3$, $Rb_2ZrY(PO_4)_3$, $Cs_2ZrY(PO_4)_3$, $Cs_2ZrIn(PO_4)_3$ and $CsTi_3P_5O_{19}$. This article reports on the preparation and properties of these compounds.

Experimental

Cs_2CO_3, Rb_2CO_3, TiO_2, ZrO_2, In_2O_3, Y_2O_3, KH_2PO_4, and $NH_4H_2PO_4$ were mixed in stoichiometric ratios in an agate mortar with ethyl alcohol and then dried in air. The mixtures were fired at 250 °C for 15 h and calcined at 600 °C for 2 h. The calcines were heated at 1100 °C for 5 min before sealing in a platinum tube of 6 mm in diameter. The sample in platinum capsules were heated at 950—1315 °C for 1—72 h, and then quenched in water.

The products were identified by optical microscopy and X-ray powder diffraction. Lattice constants were determined at room temperature with a Toshiba diffractometer, ADG-301, at a scanning rate of 0.25° 2θ per min. Powdered quartz or KCl was added as an internal standard.

Weissenberg and Precession photographs for a single crystal of $CsTi_3P_5O_{19}$ were obtained using Ni-filtered or unfiltered Cu $K\alpha$ radiation. The unit-cell dimensions of a single crystal were determined using an automatic four-circle X-ray diffractometer, Rigaku Denki Co., Ltd. with Mo $K\alpha$ radiation filtered with a graphite monochromator.

The chemical composition of $CsTi_3P_5O_{19}$ was analyzed using an electron-probe microanalyzer, JXA 5A. A single crystal of TiP_2O_7 was used as the standard for Ti and P.

Results and Discussion

$K_2ZrY(PO_4)_3$ and $K_2ZrIn(PO_4)_3$. These compounds were prepared below 1315 °C as isotropic granular aggregates. As shown in Table 1, X-ray patterns are similar to that of cubic $KTi_2(PO_4)_3$ with a langbeinite-type structure.[5] The lattice constant of $K_2ZrY(PO_4)_3$ is 1.0336 nm, and 1.0180 nm for $K_2ZrIn(PO_4)_3$. Solid solutions between rhombohedral $KZr_2(PO_4)_3$ and cubic $K_2ZrY(PO_4)_3$ or $K_2ZrIn(PO_4)_3$ were not produced judging from the lattice constants of the synthetic materials.

$Cs_2ZrY(PO_4)_3$ and $Cs_2ZrIn(PO_4)_3$. Single phases of isotropic crystals were prepared below 1315 °C

Table 1. X-Ray diffraction data

$K_2ZrY(PO_4)_3$			$CsTi_3P_5O_{19}$[a]		$CsTi_3P_5O_{19}$[b]		
hkl	*d*/nm	*I*	*d*/nm	*I*	*hkl*	*d*/nm	*I*
111	0.5972	13	0.753	14	020	0.830	9
210	0.4614	30	0.705	70	021	0.598	9
211	0.4226	20	0.608	12	130	0.493	15
300	0.3447	15	0.461	53	220	0.4541	15
310	0.3270	100	0.448	40	$11\bar{2}$	0.4146	50
311	0.3117	30	0.4287	47	131		
320	0.2866	13	0.4167	100	022	0.3830	9
321	0.2762	70	0.3931	15	041	0.3744	86
410	0.2507	8	0.3782	80	310	0.3531	66
411	0.2417	5	0.3656	65	$22\bar{2}$	0.3393	60
331	0.2373	5	0.3612	75	150	0.3195	9
421	0.2253	5	0.3525	14	$24\bar{1}$	0.3180	12
422	0.2109	20	0.3249	60	202	0.3114	14
430	0.2064	7	0.3217	50	311	0.3085	100
510	0.2029	20	0.3017	100	$15\bar{1}$	0.3030	28
511	0.1992	7	0.2960	40	$33\bar{1}$	0.2999	12
520	0.1921	19	0.2915	65	060	0.2769	25
521	0.1886	4	0.2769	50	331	0.2721	12
			0.2688	55	113	0.2618	11
			0.2615	20	313	0.2445	35
			0.2523	15	062	0.2320	14
			0.2458	10	263	0.1940	8

a) 1055 °C, b) 1115 °C.

from stoichiometric starting materials. The X-ray peaks could be indexed on the basis of a primitive isometric space lattice. The X-ray pattern was similar to that of K-bearing analogous compounds, but reflection peaks 111, 210, and 300 were very weak. The lattice constant of $Cs_2ZrY(PO_4)_3$ is 1.0471 nm and that of $Cs_2ZrIn(PO_4)_3$ is 1.0340 nm.

$Rb_2ZrY(PO_4)_3$ and $Rb_2ZrIn(PO_4)_3$. These compounds were prepared at 1115 °C for 24 h and these showed similar X-ray powder patterns. When these X-ray patterns were compared with those of K- and Cs-bearing analogous compounds, systematic changes were clearly observed. For example, the intensities of the 220 peaks increased with increasing sizes of the alkali metal atoms. On the other hand, the reverse was observed for the intensities of the 210 peaks. The lattice constant of $Rb_2ZrY(PO_4)_3$ is 1.0402 nm, and that of $Rb_2ZrIn(PO_4)_3$ is 1.0237 nm.

$CsTi_3P_5O_{19}$. Columnar crystal and glass were prepared by heating a stoichiometric mixture of $CsTi_2(PO_4)_3$ between 1100 and 1275 °C. The crystalline phase was formulated as $CsTi_3P_5O_{19}$ on the basis of a chemical analysis using an electron-probe microanalyzer. The single phase of $CsTi_3P_5O_{19}$ was obtained between 1100—1275 °C from a stoichiometric starting material. The X-ray powder pattern given in Table 1 was indexed on the basis of a monoclinic unit cell with a=1.0966 nm, b=1.6572 nm, c=0.8754 nm, β=100.11°. The density, measured by the method of Archimedes, was found to be 3.10 g cm^{-3}. This is in good agreement with the calculated value for four chemical formula units per cell.

The space-group of $CsTi_3P_5O_{19}$ was determined from the systematically missing reflections in the Weissenberg photographs. The single crystals were crystallized in a monoclinic symmetry with the following missing reflections: $h+k+l$: $h+k=2n$ (n: integer), $0kl$: $k=2n$, $h0l$: $l=2n$, $hk0$: $h+k=2n$, $h00$: $h=2n$ and $0k0$: $k=2n$. These extinctions indicate a space group of C2/c or Cc. Diffused streaks parallel to the a*-axis are present in an $h0l$ Precession photograph.

$CsTi_3P_5O_{19}$ melts incongruently at 1280 °C. TiP_2O_7 and glass are present in a product quenched from 1280 °C.

Crystalline materials prepared at 1055—1090 °C for 194 h showed the X-ray diffraction pattern given in Table 1. A single-crystal X-ray study of the low-temperature polymorph was impossible because of the small grain sizes. A chemical analysis using an electron-probe microanalyzer suggests that the Cs_2O contents of the crystals prepared from the starting materials with a $CsTi_3P_5O_{19}$ composition are consistent with that of $CsTi_3P_5O_{19}$; however, the Cs_2O contents of those prepared from starting materilas with a $CsTi_2(PO_4)_3$ composition were slightly higher than that of $CsTi_3P_5O_{19}$. We could not obtain $CsTi_2(PO_4)_3$ at any temperature, although analogous compounds such as $MTi_2(PO_4)_3$, M:Li, Na, K, Rb, or Tl, were crystallized in rhombohedral forms.[6]

The author thanks Dr. F. P. Okamura for instruction regarding X-ray methods for a single crystal.

References

1) H. Y-P. Hong, *Mater. Res. Bull.*, **11**, 173 (1976).
2) F. d'Yvoire, M. Pintard-Screpel, E. Brety, and M. de la Rochere, *Solid State Ionics*, **10**, 851 (1983).
3) R. Roy, D. K. Agrawal, J. Alamo, and R. A. Roy, *Mater. Res. Bull.*, **19**, 471 (1984).
4) G. E. Lenain, H. A. Mckinstry, S. Y. Limaye, and A. Woodward, *Mater. Res. Bull.*, **19**, 1451 (1984).
5) R. Masse, A. Drif, J-C. Guitel, and I. Tordjman, *Bull. Soc. Fr. Mineral. Cristallogr.*, **58**, 381 (1972).
6) M. R. Masse, *Bull. Soc. Fr. Mineral. Cristallogr.*, **93**, 500 (1970).

Anion-catalyzed Phase-transfer Catalysis. II. Effects of Anionic Tetrakis[3,5-bis(trifluoromethyl)phenyl]borate Catalyst in Phase-transfer-catalyzed Sulfonium Ylide Formation

Yasuichiro SHIRAKI,† Kazutaka ONITSUKA,† Keisuke TAKUMA, Takaaki SONODA, and Hiroshi KOBAYASHI*

Research Institute of Industrial Science, Kyushu University 86, Kasuga, Fukuoka 816
†Department of Molecular Science and Technology, Graduate School of Engineering Sciences, Kyushu University 39, Kasuga, Fukuoka 816

(Received December 12, 1984)

Synopsis. Tetrakis[3,5-bis(trifluoromethyl)phenyl]-borate (TFPB) ion as an anionic phase-transfer catalyst promoted the formation of oxirane from various carbonyl substrates and trimethylsulfonium chloride in a two-phase mixture of dichloromethane and concentrated aqueous sodium hydroxide.

Sulfonium methylide can be conveniently generated in a hydrophobic organic medium under phase-transfer catalytic (PTC) conditions by use of a cationic catalyst which functions to incorporate hydroxide ions into the hydrophobic organic medium.[1] An anionic catalyst might also be useful for the same purpose, where the catalyst would help to incorporate the sulfonium ions into the organic phase. We have developed a highly lipophilic tetrakis[3,5-bis(trifluoromethyl)phenyl]borate (TFPB) ion[2] as an anionic phase-transfer catalyst.[3] This note is to describe the catalytic behavior of TFPB toward the formation of sulfonium methylide in an aqueous-organic two-phase system.

Results and Discussion

In the formation of phenyloxirane from benzaldehyde and trimethylsulfonium iodide under PTC conditions (see Table 1) the addition of a TFPB catalyst caused the reaction rate to approximately double, but still it took 9.5 h for the reaction to attain a quantitative yield. A similar catalytic effect seemed likely in some ketone reactions, though it would not be effective enough for preparative use.

Reactions involving reactive trimethylsulfonium chloride[4,5] with various carbonyl substrates are also summarized in Table 1. Benzaldehyde was completely converted to phenyloxirane within half an hour, irrespective of the presence or absence of a TFPB catalyst. The yield of phenyloxirane was quantitative when catalyzed with TFPB, while the yield without the catalyst was somewhat lower.

Cyclohexanone, acetophenone, and benzophenone afforded corresponding oxirane products in quantitative yields within 4 h. Without a TFPB catalyst a reaction mixture of the former two ketones formed an emulsion and suffered some difficulties in product separation. The last ketone was less reactive and gave the oxirane in a lower yield (71%) without the catalyst.

The concentration of the aqueous alkali was required to be as high as 50 w/w% for a satisfactory yield of oxirane.[5]

An increasing amount of the TFPB catalyst correspondingly accelerated the reaction rate, but also caused a decreased conversion of benzaldehyde. When the reaction started with equimolar amounts of trimethylsulfonium iodide and benzaldehyde, the conversion of benzaldehyde stopped at a stage where approximately an equimolar amount of benzaldehyde remained with the TFPB catalyst; *e. g.* when 25 and 50 mol% of sodium TFPB were added, the reactions stopped within 1.7 and 1 h with 25 and 55% of the benzaldehyde remaining unreacted, respectively.[6]

When an equimolar amount of sodium TFPB was added to the sulfonium salt, neither oxirane formation nor a Cannizzaro reaction occurred, even under prolonged vigorous agitation. This indicated that a 1:1 binary ion pair of trimethylsulfonium and TFPB ions was so stable as not to yield the sulfonium methylide in the two-phase system.

TFPB salts were found to disperse in the form of aggregates in solution phases.[7] The particle sizes of aggregates varied with the counter cation and the solvent. Also the sizes of sodium TFPB particles were measured using a light-scattering method.[8] Aggregates of 200 and 20 molecules were found in water and dichloromethane, respectively. The catalytic behavior of TFPB in the present PTC system might have some connection with the aggregation of TFPB and related ionic species.

TABLE 1. YIELDS OF OXIRANES IN PTC REACTION OF SULFONIUM HALIDES

Halide	Reaction conditions[a]	Yield[b]/% (Reaction time/h)			
		PhCHO	cy-C_6H_{10}=O	PhMeC=O	Ph_2C=O
Cl	(A)	97 (0.5)	Quant. (4)	Quant. (4)	Quant. (4)
Cl	(B)	91 (0.5)	Quant. (3)	Quant. (4)	71 (4)
I	(A)	98 (9.5)[c]	24 (48)	23 (48)	8 (48)
I	(B)	59 (9.5)	13 (48)	12 (48)	7 (48)

a) Reaction conditions (A); catalyzed with sodium TFPB (10 mol%). (B); without the catalyst. b) By GLC analyses of the reaction mixture. c) The use of 40 and 25 w/w% aqueous alkali afforded the phenyloxirane in the yields of 70% (22-h reaction) and 10% (19-h reaction), respectively, under the similar conditions.

TFPB salts were also shown to cause a suppression of the Cannizzaro reaction of benzaldehyde. In a separate run without the sulfonium salt under similar two-phase conditions, the addition of sodium TFPB reduced the yield of benzyl alcohol in the Cannizzaro reaction of benzaldehyde to one forth of that without the catalyst. Trimethylsulfonium TFPB was also effective in retarding the Cannizzaro reaction, though to a somewhat smaller extent than the sodium salt.

Thus, the anionic TFPB catalyst appeared to function in a similar way as the cationic ones in promoting oxirane formation with trimethylsulfonium halides under PTC conditions.

Experimental

Reaction of a Carbonyl Compound with Trimethylsulfonium Halide under PTC Conditions. A mixture of trimethylsulfonium chloride[9] (2.4 mmol), the aldehyde or ketone (1.6 mmol), 50 w/w% aqueous sodium hydroxide (20 cm^3), dichloromethane (20 cm^3) and an internal standard for GLC analysis (biphenyl for the reactions of benzaldehyde and benzophenone and tetradecane for those of cyclohexanone and acetophenone) was stirred at 1000 rpm by a mechanical stirrer at room temperature in both the presence and absence of sodium TFPB (0.24 mmol, (10 mol%)). The reaction was followed by GLC analyses of aliquots from the dichloromethane layer with reference to an internal standard. Results are summarized in Table 1.

The reaction products were characterized as follows: 1-Oxaspiro[2.5]octane; a colorless oil, IR and ^{1}H-NMR spectral comparisons with that of the authentic specimen separately prepared:[10] 1-Methyl-1-phenyloxirane; a colorless oil, ^{1}H-NMR ($CDCl_3$, TMS): 1.648 (d, J_{CH_3-H}=0.74 Hz, 3H of CH_3), 2.689 (d.q., J_{H-H}=5.61 Hz, J_{H-CH_3}=0.74 Hz, 1H of CH_2), 2.871 (d, J_{H-H}=5.61 Hz, 1H of CH_2), and 7.275 (m, 5H). (lit[11]: 1.63 (s, CH_3), 2.58 and 2.77 (two d. J=6 Hz, CH_2), 7.27 (s, ArH)): 1,1-Diphenyloxirane; colorless solid melting at 54—56 °C (lit,[12] mp 55—56 °C). ^{1}H-NMR ($CDCl_3$, TMS): 3.250 (s, 2H of CH_2) and 7.314 (s, 10H of ArH). (lit[12] 3.14 (CH_2) and 7.36 (ArH)).

Reactions of trimethylsulfonium iodide were carried out under similar PTC conditions.

Cannizzaro Reaction of Benzaldehyde in a Two-phase System. A mixture of benzaldehyde (2.3 mmol) in dichloromethane (20 cm^3) and 50 w/w% aqueous sodium hydroxide (20 cm^3) was stirred in a similar manner with or without the addition of a 10 mol% TFPB salt. The reaction was followed by GLC in a similar manner. After a 23-h reaction without a TFPB salt, 40% of the benzaldehyde was converted to give benzyl alcohol in a 19% yield. With the addition of sodium TFPB and trimethylsulfonium TFPB, 23-h reactions converted 10 and 21% of the aldehyde to form benzyl alcohol in yields of 5 and 11%, respectively.

References

1) E. V. Dehmlow and S. S. Dehmlow, "Phase Transfer Catalysis," 2nd ed, Verlag Chemie, Weinheim (1983), pp. 194—199 and references cited therein.

2) H. Nishida, N. Takada, M. Yoshimura, T. Sonoda, and H. Kobayashi, *Bull. Chem. Soc. Jpn.*, **57**, 2600 (1984).

3) H. Iwamoto, T. Sonoda, and H. Kobayashi, *Tetrahedron Lett.*, **24**, 4703 (1983) and the references of the same authors cited therein.

4) C. M. Starks and C. Liotta, "Phase Transfer Catalysis. Principles and Techniques," Academic Press, New York (1978), pp. 18—20.

5) M. Rosenberger, W. Jackson, and G. Saucy, *Helv. chim. Acta*, **63**, 1665 (1980).

6) Reaction conditions; the sulfonium iodide (0.16 mmol) and benzaldehyde (0.16 mmol) in a two-phase mixture of dichloromethane (20 cm^3) and 50% aqueous sodium hydroxide (20 cm^3) at room temp.

7) Regarding the aggregation behaviors of TFPB salts, see also T. Takada, T. Sonoda, and H. Kobayashi, *Bunseki Kagaku*, **32**, E191 (1983).

8) The light-scattering measurement facilities were afforded by Professor Toyoki Kunitake in the Department of Organic Synthesis, Kyushu University, to whom the authors are grateful.

9) A. Brändström, "Preparative Ion Pair Extraction. An Introduction to Theory and Practice," Apotekarsocieteten/Hässle Lakemedel, Stockholm, (1976), p. 153. Trimethylsulfonium chloride for preparative use was conveniently prepared by treating aqueous trimethylsulfonium iodide with 0.3% chlorine water. Liberated iodine was removed by decantation and ether-extraction. The resulting aqueous solution was adjusted to pH 7—8 with sodium hydrogencarbonate and evaporated to dryness.

10) E. J. Corey and M. Chaykovsky, *Org. Synth.*, Coll. Vol. V, 755 (1973).

11) Y. Ogata, Y. Sawaki, and H. Shimizu, *J. Org. Chem.*, **43**, 162 (1978).

12) E. J. Corey and M. Chaykovsky, *J. Am. Chem. Soc.*, **87**, 1353 (1965).

The Crystal Structure of 3a,5,6a-Triphenyl-3,3a-dihydro-2*H*-furo[3,2-*b*]pyrrole-2,6(6a*H*)-dione

Shuntaro MATAKA, Kazuko UEHARA, Kazufumi TAKAHASHI, Masashi TASHIRO,* Kunitoshi YOSHIHIRA,† Kayoko KAWAZOE,†† Sadao SATO,†† and Chihiro TAMURA††

Research Institute of Industrial Science and Department of Molecular Science and Technology, Graduate School of Engineering Sciences, Kyushu University 86, 6-1, Kasuga-kohen, Kasuga, Fukuoka 816

†*National Institute of Hygienic Sciences, 1-18-1, Kamiyoga, Setagaya-ku, Tokyo 158*

††*Analytical and Metabolic Research Laboratories, Sankyo Co. Ltd., 1-2-58, Hiromachi, Shinagawa-ku, Tokyo 140*

(Received March 16, 1985)

Synopsis. The structure of 3a,5,6a-triphenyl-3,3a-dihydro-2*H*-furo[3,2-*b*]pyrrole-2,6(6a*H*)-dione in the crystalline state was determined by X-ray analysis. The crystals are monoclinic, space group P2/a, a=16.606(8), b=7.314(2), c=16.295(9)Å, β=111.67(4), z=4. The final R value was 0.067 for 2453 reflections.

Recently, we reported the formation of 3,3a-dihydro-2*H*-furo[3,2-*b*]pyrrole-2,6(6a*H*)-diones by the air-oxidation of the enamines which were formed by the condensation of 1,3-diketones with 3-aminopropanates.[1] In the IR spectra of this novel heterocycle, two carbonyl bands were characteristically observed at 1800—1790 and 1760—1755 cm^{-1}, respectively, measured as a KBr pellet. Of these, the one at the higher wave number is reasonably attributable to the carbonyl group of the cyclic ester, while the other seems unusual for the 1-pyrrolin-3-one carbonyl which is formally conjugated with the C=N bond.

In this context, the crystal structure of the titled compound (**1**) has been determined by X-ray analysis.

Results and Discussion

Crystal Data. $C_{24}H_{17}NO_3$, MW=367.4, monoclinic, space group P2/a, a=16.606(8), b=7.314(2), c=16.295(9) Å, β=111.67(4)°, Z=4, D_x=1.33 g cm^{-3}, μ(Cu K_α=1.5418Å)=0.67 mm^{-1}. The intensities of 2453 observable reflections with $F_o \geq 2\sigma F_0$ ($2\theta \leq 128°$) were collected on Rigaku AFC5 apparatus equipped with a rotating-anode X-ray generator and using a graphite monochromator. The structure was solved by direct methods using MULTAN[2] and refined by block-diagonal least-squares methods. All the H atoms were located in a difference Fourier map. Final cycles of least squares (non-hydrogen atoms anisotropic, H atoms isotropic) gave R=0.067 (R_w=0.071, w=1.0). The positional parameters for non-hydrogen atoms are listed in Table 1.[3]

A perspective drawing of the molecular structure is shown in Fig. 1, and the bond lengths and angles are listed in Tables 2 and 3, which are within usual values. The two carbonyl groups have almost the same bond lengths. The 1-pyrroline ring is planar within ±0.080(19)Å; the oxygen atom of the carbonyl group deviates by 0.254(19)Å from the plane and the torsion angle O(3)–C(5)–C(6)–N(1) is calculated to be 170.3(4)°. From the above results and the C(5)–C(6) bond length of 1.506(5)Å, it is suggested that there is less delocalization of electrons at the O=C–C=N moiety. The tetrahydrofuran ring is close to envelope conformation,

TABLE 1. FRACTIONAL ATOMIC COORDINATES (×10⁴) AND THERMAL PARAMETERS WITH ESTIMATED STANDARD DEVIATIONS IN PARENTHESES

Atom	x	y	z	B_{eq}/Å²
O(1)	3151(2)	1758(4)	6176(2)	2.38(7)
O(2)	3522(2)	4191(5)	5575(2)	3.60(9)
O(3)	3804(2)	−1173(4)	7586(2)	3.48(9)
N(1)	3577(2)	3363(4)	8071(2)	2.08(8)
C(1)	3191(2)	3616(6)	6062(2)	2.43(11)
C(2)	2774(3)	4613(6)	6609(3)	2.38(11)
C(3)	2747(2)	3192(5)	7292(2)	1.75(9)
C(4)	2808(2)	1311(5)	6857(2)	1.80(10)
C(5)	3591(2)	404(5)	7561(2)	2.15(10)
C(6)	4029(2)	1896(5)	8207(2)	2.01(10)
C(7)	1982(2)	3478(5)	7579(2)	2.06(10)
C(8)	2113(3)	3921(6)	8450(3)	3.15(12)
C(9)	1397(3)	4256(7)	8690(3)	4.49(16)
C(10)	569(3)	4104(7)	8081(3)	4.22(16)
C(11)	432(3)	3672(6)	7215(3)	3.64(14)
C(12)	1139(3)	3386(6)	6960(3)	2.72(12)
C(13)	2034(2)	73(5)	6500(2)	1.86(10)
C(14)	1631(3)	−261(7)	5609(3)	3.04(12)
C(15)	914(3)	−1438(8)	5315(3)	4.39(16)
C(16)	608(3)	−2245(7)	5909(4)	4.26(16)
C(17)	1014(3)	−1911(6)	6797(3)	3.82(14)
C(18)	1731(3)	−764(6)	7099(3)	2.85(12)
C(19)	4876(2)	1696(5)	8927(2)	2.02(10)
C(20)	5501(3)	532(6)	8847(3)	2.85(12)
C(21)	6311(3)	415(7)	9528(3)	3.41(13)
C(22)	6486(3)	1461(7)	10278(3)	3.39(13)
C(23)	5868(3)	2594(7)	10375(3)	3.08(12)
C(24)	5058(3)	2716(6)	9696(3)	2.56(11)

TABLE 2. BOND LENGTHS (l/Å) WITH ESTIMATED STANDARD DEVIATIONS IN PARENTHESES

Bond distance		l/Å	Bond distance		l/Å
O(1)	–C(1)	1.377(5)	C(8)	–C(9)	1.405(5)
O(1)	–C(4)	1.459(4)	C(9)	–C(10)	1.371(6)
O(2)	–C(1)	1.196(4)	C(10)	–C(11)	1.382(7)
O(3)	–C(5)	1.203(5)	C(11)	–C(12)	1.398(4)
N(1)	–C(3)	1.494(4)	C(13)	–C(14)	1.378(5)
N(1)	–C(6)	1.281(5)	C(13)	–C(18)	1.394(5)
C(1)	–C(2)	1.504(5)	C(14)	–C(15)	1.402(6)
C(2)	–C(3)	1.536(5)	C(15)	–C(16)	1.382(6)
C(3)	–C(4)	1.568(5)	C(16)	–C(17)	1.374(7)
C(3)	–C(7)	1.521(4)	C(17)	–C(18)	1.389(5)
C(4)	–C(5)	1.532(5)	C(19)	–C(20)	1.386(5)
C(4)	–C(13)	1.502(4)	C(19)	–C(24)	1.392(5)
C(5)	–C(6)	1.505(5)	C(20)	–C(21)	1.395(5)
C(6)	–C(19)	1.468(4)	C(21)	–C(22)	1.378(7)
C(7)	–C(8)	1.393(5)	C(22)	–C(23)	1.373(5)
C(7)	–C(12)	1.393(5)	C(23)	–C(24)	1.394(5)

Table 3. Bond angles (ϕ/°) with estimated standard deviations in parentheses

Bond angle			ϕ/°	Bond angle			ϕ/°
C(1)	-O(1)	-C(4)	112.1(2)	C(3)	-C(7)	-C(12)	120.1(2)
C(3)	-N(1)	-C(6)	112.0(3)	C(3)	-C(7)	-C(8)	120.7(2)
O(1)	-C(1)	-C(2)	110.0(2)	C(8)	-C(7)	-C(12)	119.1(2)
O(2)	-C(1)	-C(2)	130.4(8)	C(7)	-C(8)	-C(9)	119.6(3)
O(1)	-C(1)	-O(2)	119.6(5)	C(8)	-C(9)	-C(10)	120.7(4)
C(1)	-C(2)	-C(3)	104.2(3)	C(9)	-C(10)	-C(11)	120.0(2)
N(1)	-C(3)	-C(2)	107.2(2)	C(10)	-C(11)	-C(12)	119.9(3)
N(1)	-C(3)	-C(4)	105.4(2)	C(7)	-C(12)	-C(11)	120.5(3)
C(2)	-C(3)	-C(4)	104.0(1)	C(4)	-C(13)	-C(18)	118.2(2)
C(2)	-C(3)	-C(7)	112.4(3)	C(4)	-C(13)	-C(14)	121.9(3)
N(1)	-C(3)	-C(7)	109.9(2)	C(14)	-C(13)	-C(18)	119.9(4)
C(4)	-C(3)	-C(7)	117.4(3)	C(13)	-C(14)	-C(15)	119.3(3)
O(1)	-C(4)	-C(13)	111.1(2)	C(14)	-C(15)	-C(16)	120.5(4)
O(1)	-C(4)	-C(3)	104.8(3)	C(15)	-C(16)	-C(17)	119.9(5)
O(1)	-C(4)	-C(5)	101.8(1)	C(16)	-C(17)	-C(18)	120.2(4)
C(3)	-C(4)	-C(5)	102.7(2)	C(13)	-C(18)	-C(17)	120.1(3)
C(3)	-C(4)	-C(13)	121.0(2)	C(6)	-C(19)	-C(20)	121.0(3)
C(5)	-C(4)	-C(13)	113.4(4)	C(6)	-C(19)	-C(24)	119.4(3)
O(3)	-C(5)	-C(4)	126.7(4)	C(20)	-C(19)	-C(24)	119.5(2)
O(3)	-C(5)	-C(6)	127.7(3)	C(19)	-C(20)	-C(21)	119.9(4)
C(4)	-C(5)	-C(6)	105.5(3)	C(20)	-C(21)	-C(22)	119.8(4)
N(1)	-C(6)	-C(19)	123.3(5)	C(21)	-C(22)	-C(23)	121.0(3)
N(1)	-C(6)	-C(5)	112.7(2)	C(22)	-C(23)	-C(24)	119.4(4)
C(5)	-C(6)	-C(19)	124.0(5)	C(19)	-C(24)	-C(23)	120.3(4)

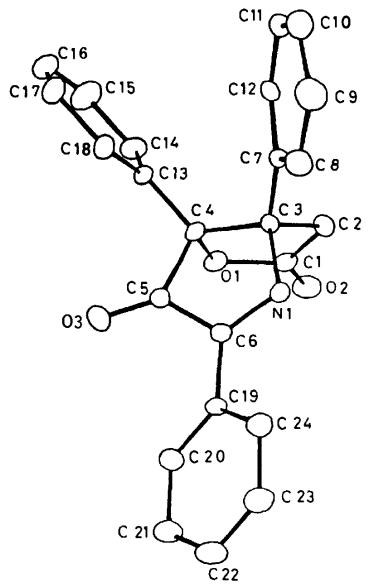

Fig. 1. A perspective drawing of **1**.

C(3) being 0.333(16)Å out of the least-squares plane formed by the other four atoms. The two heterocyclic rings are cis-fused to each other, and the dihedral angle of the rings is 104.1(2)°. The dihedral angle of the phenyl group on C(3) and C(4) is 45.1(2)°. The crystal structure is stabilized mainly by van der Waals forces; the shortest intermolecular distance is 3.128(4) A for O(2)···C(1) (1/2−x, y, 1−z).

References

1) S. Mataka, K. Uehara, K. Takahashi, M. Tashiro, K. Yoshihira, K. Kawazoe, S. Sato, and C. Tamura, *Synthesis*, **1984**, 663.

2) G. Germain, P. Main, and M. M. Woolfson, *Acta Cryst.*, **A27**, 368 (1971).

3) Thermal parameters for the non-hydrogen atoms, fractional coordinates and isotropic thermal parameters for hydrogen atoms, bond lengths involving hydrogen atoms, and observed and calculated structure factors are kept at the Chemical Society of Japan (Document No. 8536).

Thermal Decomposition of 2,2-Bis(*t*-butyldioxy)-3-methylbutane

Takeshi KOMAI* and Shuji SUYAMA
Chemicals and Explosives Research Laboratory, Nippon Oil & Fats Co., Taketoyo-cho, Chita-gun, Aichi 470-23
(Received April 1, 1985)

Synopsis. The activation parameters for decomposition of 2,2-bis(*t*-butyldioxy)-3-methylbutane (**2**) in diphenylmethane are ΔH^*=144.8 kJ mol^{-1} and ΔS^*=49.4 JK^{-1} mol^{-1}. The decomposition products of **2** are *t*-butyl alcohol, acetone, isopropyl methyl ketone and *t*-butyl peracetate. *t*-Butyl peracetate (**4**) is an intermediate which decomposes during reaction. This peroxide **2** decomposes with homolytic one-bond cleavage at one of the peroxide groups and the resulting 1-(*t*-butyldioxy)-1,2-dimethylpropoxyl radical (**3**) decomposes subsequently to *t*-butyldioxy or isopropyl groups with β-elimination.

A little report has been published on concerning the decomposition mechanism of peroxides with peroxyacetal structure. Dickey *et al.*[1] reported the thermal decomposition of 2,2-bis(*t*-butyldioxy)butane in cumene and dibutyl phthalate. Kinetic data indicate first order decomposition with an activation energy of 150.6 kJ mol^{-1}. They also obtained 92% of *t*-butyl alcohol per *t*-butoxyl radical as decomposition product. Mageli and co-workers[2] studied the thermal decomposition of butyl 4,4-bis(*t*-butyldioxy)valerate (**1**) in dodecane. As decomposition products they obtained acetone, *t*-butyl alcohol, butyl propionate and butyl levulinate. They proposed the decomposition mechanism of **1** based on some assumption. For example *t*-butyl peracetate (**4**) is proposed as one of the decomposition intermediates, but any amount of **4** was not detected in the decomposition products.

In the present paper, we have studied the thermal decomposition of 2,2-bis(*t*-butyldioxy)-3-methyl butane (**2**) in diphenylmethane.

Results and Discussion

The rates of thermal decomposition of **2** were obtained by the disappearance of **2** by GLPC. The results gave good first-order rate constants over two half reaction. When the peroxide concentration was varied over ten to forty-fold range, the variation in the rates was within the experimental error as shown in Table 1. Addition of *t*-butyl catechol as a radical trapper also did not change the rate significantly. These results rule out radical-induced homolysis reactions under the experimental conditions.

The thermal decomposition products of **2** in diphenylmethane were analyzed by GLPC and GLPC-MS techniques, being identified by comparison with the corresponding authentic samples. The liquid products of the decomposition at 110°C for 4 h are acetone, *t*-butyl alcohol, isopropyl methyl ketone, *t*-butyl peracetate and 1,1,2,2-tetraphenylethane. *t*-Butyl hydroperoxide was not detected. Decomposition products of 74 to 88 percent per the peroxide were obtained.

The dependence of these products on the reaction time is shown in Fig. 1. The decrease of **2** is compatible with the increase of the isopropyl methyl ketone (**5**) and **4**. However in the latter stage (after 12 h) the amount of consumed **2** does not agree with the sum of **4** and **5** because of consecutive decomposition of **4**.

The following scheme for the thermal decomposition of **2** explains the observed experimental data. The initial step is a homolytic one-bond cleavage to give a primary radical (**3**) rather than simultaneous fission of both peroxyl bonds as discussed below.

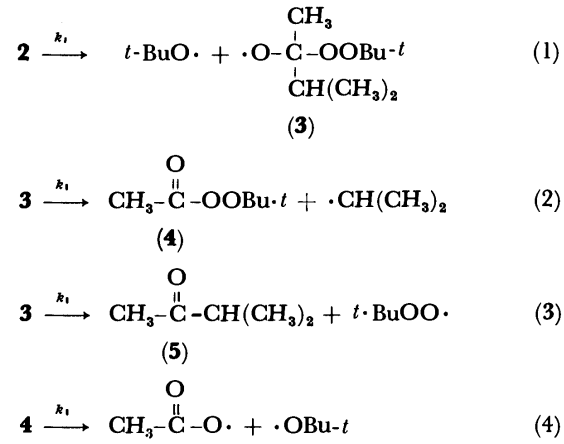

TABLE 1. RATE CONSTANTS AND ACTIVATION PARAMETERS FOR THE DECOMPOSITION OF 2,2-BIS(*t*-BUTYLDIOXY)-3-METHYLBUTANE IN Ph_2CH_2

Temp	Initial Concd	$k_d\times10^4$	Activation Parameters	
°C	M	s^{-1}	ΔH^* kJ mol^{-1}	ΔS^* JK^{-1} mol^{-1}
90	0.0952	0.108±0.006	141.6±2.0	48.6±5.2
100	0.0952	0.375±1.006		
110	0.0116	1.29±0.06		
110	0.0981	1.38±0.01		
110	0.100[a]	1.36±0.01		
110	0.196	1.33±0.01		
110	0.448	1.37±0.01		
120	0.0952	4.11±0.03		

a) 0.025 M of *t*-butyl catechol is present.

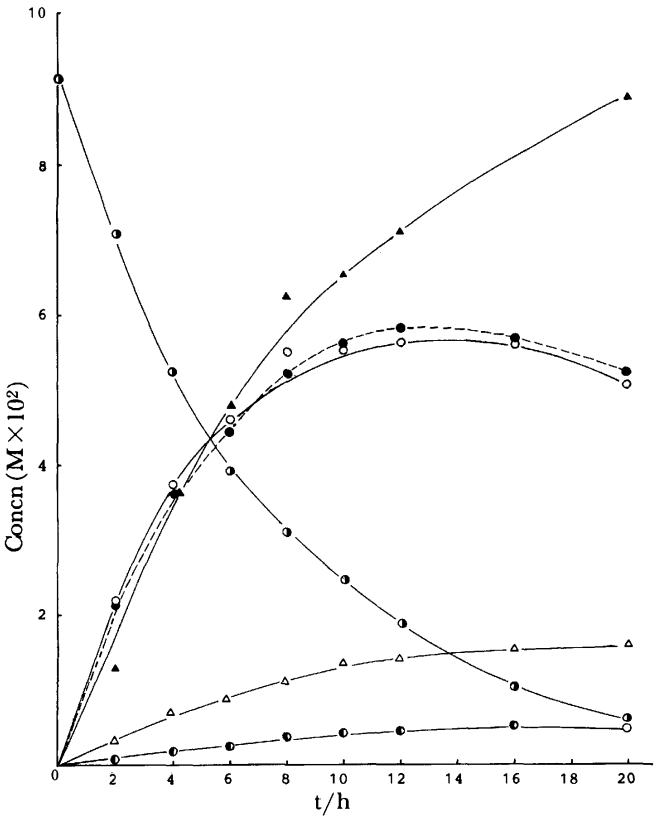

Fig. 1. Decomposition of **2** in Ph_2CH_2 at 100°C. ▲: *t*-BuOH, △: CH_3COCH_3, ◑: **2**, ◐: **5**, ○: **4**, Observed data. ●: **4**, Theoretical data calculated by Eq. 6 using $[\mathbf{2}]_0$=0.0915 M, $k_1=3.75\times10^{-5}\,s^{-1}$ and $k_4=1.23\times10^{-5}\,s^{-1}$.

The first reason is that the activation parameters for the decomposition of **2** are similar to those of di-*t*-butyl peroxide[3] ($\Delta H^{\neq}$=153.8 kJ mol^{-1}, $\Delta S^{\neq}$=48.1 JK^{-1} mol^{-1}), which shows homolytic cleavage of the peroxyl bond. The second reason is that *t*-butyl peracetate (**4**) is formed in the initial stage of the reaction. From Table 1 and Fig. 1, *t*-butyl peracetate is assumed to be more stable than the peroxyacetal (**2**). In fact, we obtained $1.23\times10^{-5}\,s^{-1}$ at 100°C and $4.19\times10^{-5}\,s^{-1}$ at 110°C as the first order rate constants for **4** in diphenylmethane. These values are 30 to 40 percent lower than those of **2**.

The formation of **5** is possible by several paths. One possibility is that **3** abstracts hydrogen atom from solvent and resulting half peroxyacetal decomposes to **5** and *t*-butyl hydroperoxide. However, this route is ruled out with following reason. Table 2 shows yields of **4** and **5** in several solvents at 90°C. From these results, it is seen that amounts of **5** per consumed **2** and ratio of **4**/**5** are not changed by the solvents, indicating that the hydrogen abstraction is unimportant. Another possibility, the elimination of *t*-butyl peroxyl radical, is reasonable. (Eq. 3). This type of reaction has been already proposed for the decomposition of α,α-bis(*t*-butyldioxy)toluene.[6]

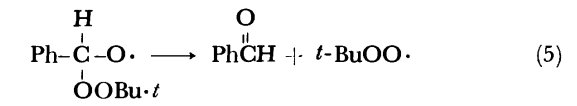

(5)

Table 2. Yields of isopropyl methyl ketone and *t*-butyl peracetate for the decomposition of **2** in several solvents at 90°C

Solvent	Consumed **2**	Product M mole		**4**/**5**
	M moles	**4**	**5**	
Ph_2CH_2	0.34	0.28	0.05	5.6
$CFCl_2$–$CFCl_2$	—[a]	0.17	0.03	5.7
t-BuOH	0.33	0.26	0.04	6.5
$PhC(CH_3)_3$	0.31	0.18	0.03	6.0

a) Not determined.

The methyl radical elimination from the radical **3** is unimportant, since the rate of the elimination of isopropyl radical is thousand order larger than that of methyl radical.[8]

Using equations (1),(2), and (3) and the steady-state assumption, the concentration of **4** is given by Eq. 5.

$$d[\mathbf{4}]/dt = \alpha k_1[\mathbf{2}] - k_4[\mathbf{4}] \quad (5)$$

where $\alpha = k_2/(k_2 + k_3)$,

Integration of Eq. 5 gives Eq. 6.

$$[\mathbf{4}] = k_1[\mathbf{2}]_0(e^{-k_4t} - e^{-\alpha k_1 t})/(\alpha k_1 - k_4) \quad (6)$$

Using $k_1=3.75\times10^{-5}\,s^{-1}$, $k_4=1.23\times10^{-5}\,s^{-1}$, and $[\mathbf{2}]_0$= 0.0915 M (1 M=1 mol dm^{-3}), the α value of 0.88 is obtained with simulation. The obtained curve is shown by the dotted line in Fig. 1. The elimination rate of *t*-butyldioxy radical from *t*-alkoxyl radical is about one-seventh of isopropyl radical.

Experimental

Materials. 2,2-Bis(*t*-butyldioxy)-3-methylbutane was prepared by the reaction of isopropyl methyl ketone with *t*-butyl hydroperoxide in the presence of 65% surfuric acid. The purity of this compound was determined by GLPC method was 98.9%: MS (70 eV) *m/z* (rel intensity) 159(2), 73(100), 59(28), and 43(44). IR(CCl_4) 2980, 2930, 2880, 1480, 1390, 1370, 1250, 1200, 1150, 1100, 1030 and 880 cm^{-1}. ^{1}H NMR ($CDCl_3$) δ=0.94 (6H, d, $CH(CH_3)_2$) δ=1.20 (21H, m, *t*-CH_3), δ=2.22 (1H, q, CH).

Analysis of Decomposition Products. Products were analyzed in comparison with an authentic sample by GLPC and GLPC-MS. GLPC analysis was performed on a Shimadzu GC-6A gas chromatograph with column of Silicone SE-30 on Shimalite W, 2m using undecane as an internal standard. The GLPC-MS analysis of the products was carried out with a JEOL JMS D300 mass spectrometer.

References

1) F. H. Dickey, J. H. Raley, F. F. Rust, R. S. Treseder, and W. E. Vaughan, *Ind. Eng. Chem.*, **41**, 1673 (1947).
2) S. W. Bukata, L. L. Zabrocki, M. F. Mclaughlin, J. R. Kolczynsky, and O. L. Mageli, *Ind. Eng. Chem., Prod. Res. Dev.*, **3**, 261 (1964).
3) J. H. Raley, F. F. Rust, and W. E. Vaughan, *J. Am. Chem. Soc.*, **70**, 1336 (1948).
4) P. D. Bartlett and R. R. Hiatt, *J. Am. Chem. Soc.*, **80**, 1398 (1958).
5) C. Walling and R. T. Clark, *J. Am. Chem. Soc.*, **96**, 4530 (1974).
6) Y-L. Fan and R. G. Shaw, *J. Chem. Soc.*, **1973**, 1803.
7) A. V. Tobolsky and R. B. Mescrobian, "Organic Peroxides," Interscience, New York, (1954), pp. 91—92.
8) D. G. Hoare and W. A. Waters, *J. Chem. Soc.*, **1964**, 2552.

CD Spectra of 2,4-Dinitrophenyl Derivatives of α-Amino Acids Having Polynuclear Aromatic Group in the Side Chain. Absolute Configuration of 3-(9-Anthryl)alanine

Masao KAWAI,* Taketoshi MATSUURA, Yasuo BUTSUGAN, Syun EGUSA,†
Masahiko SISIDO,†† and Yukio IMANISHI†

Department of Applied Chemistry, Nagoya Institute of Technology, Gokiso-cho, Showa-ku, Nagoya 466
†*Department of Polymer Chemistry, Kyoto University, Sakyo-ku, Kyoto 606*
††*Research Center for Medical Polymers and Biomaterials, Kyoto University, Sakyo-ku, Kyoto 606*

(Received April 20, 1985)

Synopsis. CD spectra of 2,4-dinitrophenyl (Dnp) derivatives of α-amino acids having polynuclear aromatic group in the side chain with L- and D-configuration showed negative and positive Cotton effect, respectively, around 400 nm in consistent with previously proposed Dnp-aromatic rule. Application of the rule revealed D-configuration of levorotatory 3-(9-anthryl)alanine, which was further confirmed by chiroptical comparison of the 2,4-dinitrophenyl derivative and its *p*-methoxyanilide.

CD spectra of 2,4-dinitrophenyl (Dnp) derivatives of L-α-amino acids having aromatic side chain exhibit characteristic negative Cotton effect around 400 nm.[1,2] A general rule named Dnp-aromatic rule was proposed as described in Fig. 1: *i.e.*, Dnp derivatives of general formula **1** and **1′**, having stereochemistry corresponding to aromatic α-amino acids with L- and D-configuration, show negative and positive Cotton effect, respectively, at the longest wavelength band of DnpNH chromophore.[2]

As examples of aromatic α-amino acids having polynuclear condensed aromatic group in the side chain, L-3-(1-naphthyl)alanine,[3] L-3-(2-naphthyl)alanine,[3] D-1-naphthylglycine,[4] D-2-naphthylglycine,[4] and D-3-(1-pyrenyl)alanine[5] were converted into the corresponding Dnp derivatives **2a—e**. As summarized in Table 1 all of these compounds exhibited intense Cotton effect around 400 nm, and in agreement with Dnp-aromatic rule the sign of the Cotton effect was negative and positive for the derivatives with L- and D-configuration, respectively. Thus Dnp-aromatic rule was shown to be valid for these polynuclear aromatic α-amino acid derivatives.

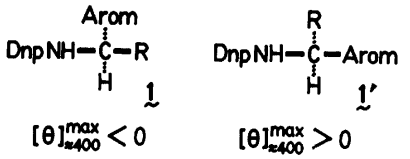

Fig. 1. Dnp-aromatic rule.
Arom implies an achiral group which contains an aromatic chromophore. R implies a nonaromatic group.

Optically active 3-(9-anthryl)alanine hydrochloride ($[\alpha]_D^{21}$ −43°, c 0.058, ethanol) was synthesized,[6] but its absolute configuration was not known yet. CD spectrum of Dnp derivative **3a** of the anthrylalanine exhibited an outstanding positive Cotton effect ([θ] +50800) at 414 nm, which indicated D-configuration of the amino acid.

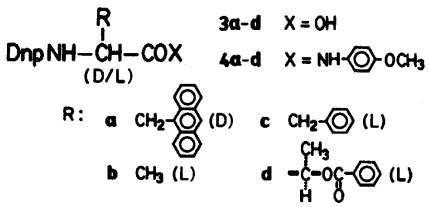

p-Methoxyanilides, such as **4b**, of Dnp-L-α-amino acids with nonaromatic side chain, which correspond to general formula **1′**, exhibit prominent Cotton effect around 400 nm.[2,7] Positive contribution of the anilide chromophore to $[\theta]_{\approx 400}^{max}$ value of Dnp-L-α-amino acids was also observed for the *p*-methoxyanilides, **4c** and **4d**, of Dnp-L-phenylalanine **3c**[1,2] and *N*-Dnp-*O*-benzoyl-L-threonine **3d**,[8] respectively (Table 2). The threonine derivative **3d** was known to exhibit positive Cotton effect at 403 nm,[9] in spite of L-configuration of the α-carbon, which is due to the presence of additional chiral center in the chromophore-bearing side chain.[8] Thus introduction of *p*-methoxyanilide group to Dnp-α-amino acids with L- and D-configuration was assumed to give positive and negative contribution, respectively, to the Cotton effect.

Magnitude of the positive Cotton effect of Dnp-(9-anthryl)alanine *p*-methoxyanilide **4a** is smaller than that of **3a** as shown in Table 2 indicating negative contribution of the anilide chromophore, which is consistent with above-assigned D-configuration of this amino acid residue.

TABLE 1. COTTON EFFECT AROUND 400 nm OF Dnp DERIVATIVES OF α-AMINO ACIDS HAVING POLYNUCLEAR AROMATIC GROUP IN THE SIDE CHAIN

	Formula	Configuration of α-carbon	Arom	R	$[\theta]^{max}(\lambda/nm)$
2a	**1**	L	(1-Naphthyl)methyl	CO_2H	−19300 (403)
2b	**1**	L	(2-Naphthyl)methyl	CO_2H	−17500 (403)
2c	**1′**	D	1-Naphthyl	CO_2H	+17100 (400)
2d	**1′**	D	2-Naphthyl	CO_2H	+25600 (396)
2e	**1′**	D	(1-Pyrenyl)methyl	CO_2H	+30800 (410)

TABLE 4. CD SPECTRAL DATA OF Dnp- AMINO ACIDS AND *p*-METHOXYANILIDES RECORDED IN METHANOL

Compd	Molecular ellipticity ($[\theta]\times10^{-3}$) and wavelength (λ/nm) in parentheses.[a]
2a	−19.3(403), 0(336), +5.4(316 sh), +9.5(297), +8.5(292), +9.3(285), 0(272), −12(250 sh), −116(223), −32(215)
2b	−17.5(403), 0(343), +6.3(318), 0(288), −6.9(263), 0(248), +69(229), 0(225), −160(220 sh)
2c	+17.1(400), 0(342), −6.0(310), −3.2(293), −5.8(260), 0(249), +13(235), 0(232), −232(220 sh)
2d	+25.6(396), 0(355), −18.4(330), −5.0(290), −286(230), 0(218), +32(215), 0(212)
2e	+30.8(410), 0(368), −68.8(341), −10.9(331), −13.5(328), 0(322), +8.8(319), +4.5(310 sh), 0(302), +5.4(288 sh), −33.9(276), −11.6(268), −13.0(265), −5(254 sh), −2(249), −214(240), −100(234 sh), −29(220)
3a	+50.8(414), 0(389), −13.7(382), −12.7(378), −22.8(368), 0(349), +17.3(329), 0(295), −2.4(289), 0(284), +141(260), 0(253), −97(228), 0(215)
4a	+34.3(418), 0(392), −22.3(381 sh), −27.5(368), 0(349), +24.2(327), +3.4(288), +65.8(265), 0(255), −77(242 sh), −95(226)
4c	+4.4(395), 0(371), −18.6(335), −4.6(290), −62(252), −26(223)
4d	+14.2(390), 0(354), −13.4(320), −5.4(290), −41(250 sh), −50(240), −16(224)

a) sh: Shoulder.

TABLE 2. COMPARISON OF $[\theta]^{max}$ VALUES AROUND 400 nm OF Dnp-α-AMINO ACIDS (**3a—d**) AND THEIR *p*-METHOXYANILIDES (**4a—d**)

	$[\theta]^{max}_{\approx400}$ of **3**	$[\theta]^{max}_{\approx400}$ of **4**	Contribution of the anilide	Configuration of α-carbon
a	+50800	+34300	−	D
b	+1600	+12900	+	L
c	−9100	+4400	+	L
d	+5000	+14200	+	L

TABLE 3. MELTING POINTS, SOLVENT OF CRYSTALLIZATION, AND MOLECULAR FORMULA OF Dnp-AMINO ACIDS AND *p*-METHOXYANILIDES

Compd	Mp θ_m/°C	Solvent of Crystallization	Formula[a]
2a	90—93	H_2O[b]	$C_{19}H_{15}N_3O_6\cdot1/4H_2O$
2b	196—198	$CHCl_3$	$C_{19}H_{15}N_3O_6\cdot3/4H_2O$
2c	133—138	Methanol-H_2O	$C_{18}H_{13}N_3O_6\cdot1/2H_2O$
2d	105—110	Methanol-H_2O	$C_{18}H_{13}N_3O_6\cdot1/2H_2O$
2e	211—215	Ethyl acetate	$C_{25}H_{17}N_3O_6\cdot CH_3CO_2C_2H_5$
3a	206—210	Ethyl acetate-Hexane	$C_{23}H_{17}N_3O_6$
4a	265—268	Acetone-Methanol	$C_{30}H_{24}N_4O_6$
4c	203—204	Benzene	$C_{22}H_{20}N_4O_6$
4d	139—141	Benzene	$C_{24}H_{22}N_4O_8$

a) Satisfactory analytical data (C, H, N ±0.35%) were obtained for the given formula. b) Precipitate from aquaous acidic solution.

Experimental

Dnp-amino acids were prepared from parent amino acids using 1-fluoro-2,4-dinitrobenzene and $NaHCO_3$ in ethanol-H_2O (2:1). *p*-Methoxyanilides, **4a** and **4c**, were synthesized from Dnp-amino acids, **3a** and **3c**, respectively, and *p*-anisidine using dicyclohexylcarbodiimide. *N*-Dnp-*O*-benzoyl-L-threonine *p*-methoxyanilide **4d** was prepared by benzoylation of Dnp-L-threonine *p*-methoxyanilide[2] with benzoyl chloride-pyridine.

Melting points were uncorrected and were listed in Table 3 along with solvents of recrystallization. CD spectra were recorded in methanol solutions at room temperature on a JASCO J-40C spectropolarimeter and were summarized in Table 4.

The authors are grateful to Kanegafuchi Chemical Industry Co. Ltd. for kind gift of naphthylglycines and to Dr. Ukon Nagai of Mitsubishi-Kasei Institute of Life Sciences for helpful discussions.

References

1) M. Kawai, U. Nagai, and M. Katsumi, *Tetrahedron Lett.*, **1975**, 2845.
2) M. Kawai, U. Nagai, M. Katsumi, and A. Tanaka, *Tetrahedron*, **34**, 3435 (1978).
3) M. Sisido, S. Egusa, and Y. Imanishi, *J. Am. Chem. Soc.*, **105**, 1041, 4077 (1983).
4) D-1- and D-2-Naphthylglycines were supplied by Kanegafuchi Chemical Industry Co. Ltd.
5) S. Egusa, M. Sisido, and Y. Imanishi, *Chem. Lett.*, **1983**, 1307; S. Egusa, M. Sisido, and Y. Imanishi, *Macromolecules*, **18**, 882 (1985).
6) S. Egusa, M. Sisido, and Y. Imanishi, to be published.
7) M. Kawai and U. Nagai, *Tetrahedron Lett.*, **1977**, 3889.
8) M. Kawai, U. Nagai, and A. Tanaka, *Bull. Chem. Soc. Jpn.*, **55**, 1213 (1982).
9) The $[\theta]$ values of **3d** were erroneously given in Table 1 of Ref. 8, which must be corrected as follows: $[\theta]_{403}$ +5000, $[\theta]_{350}$ 0, $[\theta]_{318}$ −1500, $[\theta]_{298}$ 0, $[\theta]_{266}$ +4600, $[\theta]_{244}$ 0, and $[\theta]_{222}$ −14800.

Photochemical Reaction of 1,4-Naphthoquinone Derivatives with Pyrrole Derivatives. Synthesis of 2-(2-Pyrrolyl)-1,4-naphthoquinone Derivatives

Kazuhiro MARUYAMA,* Tetsuo OTSUKI,† and Hitoshi TAMIAKI
Department of Chemistry, Faculty of Science, Kyoto University, Kyoto 606
(Received April 24, 1985)

Synopsis. Photochemical reaction of 2-bromo-1,4-naphthoquinone derivatives with pyrrole derivatives in benzene gave regioselectively 2-(2-pyrrolyl)-1,4-naphthoquinone derivatives. Photoinduced electron transfer process may be involved in the reaction.

Thermal reaction of *p*-benzoquinone with pyrrole derivatives has attracted much attention from the viewpoint of dye development,[1] but that of less reactive 1,4-naphthoquinone derivatives has never been investigated. In our previous papers[2] it was reported that photochemical reactions of 2,3-dichloro-1,4-naphthoquinone (**1j**) with furan and thiophene derivatives gave 2-chloro-3-(2-furyl)- and (2-thienyl)-1,4-naphthoquinone derivatives. In this paper, we shall describe photochemical reactions of 1,4-naphthoquinone derivatives **1** with pyrrole derivatives **2**. Some of the reactions afforded 2-(2-pyrrolyl)-1,4-naphthoquinone derivatives **3**, but others failed to give the similar products **3**. The success of the photoreaction to yield **3** depends upon the formation of the charge transfer (CT) complex of **1** with **2** in the ground state.

Results and Discussion

When a benzene solution of 2-bromo-3-methoxy-1,4-naphthoquinone (**1a**) and 1-methylpyrrole (**2a**) was irradiated by a high pressure mercury arc lamp, the yellow solution immediately turned to pale red. Upon only five minutes irradiation at room temperature, 57% of **1a** was consumed and 2-methoxy-3-(1-methyl-2-pyrrolyl)-1,4-naphthoquinone **3a** was isolated as a sole product after the purification of the reaction mixture by column chromatography.

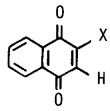

1f—i

1f; X = OCH_3
g; X = CH_3
h; X = H
i; X = Cl

2b—e

2b; R = H
c; R = C_2H_5
d; R = $CH_2C_6H_5$
e; R = $COCH_3$

The photochemical reactions of a variety of 1,4-naphthoquinone derivatives **1b—j** with **2a** were examined. The reactions of **1b—d** with **2a** gave **3b—d**, but those of **1e—j** with **2a** gave no similar compounds **3**. The pyrrole **2a** formed CT complexes with **1a—d**, h—j depending upon their reduction potentials $E_{1/2}$.[3] The formation of the CT complexes whose formation constants K reflect $E_{1/2}$ of **1** is an important requisition for the photochemical reaction. Moreover, the rather weak C–Br bond is necessary for the successful formation of **3**. The important contribution of the CT complex formation was further suggested by perturbing the pyrrole moiety. Pyrrole derivatives **2b—d** formed CT complexes with **1a**. Photoreactions of **1a** with **2b—d** gave 2-methoxy-3-(2-pyrrolyl)-1,4-naphthoquinone derivatives **3e—g**. Pyrrole derivative **2e** containing electron-withdrawing substituent formed no CT complex and induced no similar reaction. On the other hand, 1,2,5-trimethylpyrrole (**2f**) formed CT complex with **1a**. The photoreaction of **1a** with **2f**, however, gave no similar product because both the reactive α-positions of the pyrrole were blocked by methyl groups. The reaction of **1a** with 1-methylindole (**2g**) also gave similar products. In this case, the products were consisted of two isomers; *i.e.*, α-substituted **3h** (50%) and isomeric β-substituted **3i** (10%) (see Scheme 1). Any products photosubstituted on positions of fused benzene ring of **2g** were not obtained.

Table 1. Reaction of 2-bromo-1,4-naphthoquinone derivative **1a—e** with 1-methylpyrrole **2a**

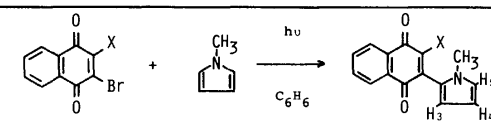

1a—e **2a** **3a—d**

X		$E_{1/2}$[a]/V	K[b]/dm³ mol⁻¹	Yield[c]/%
$N(CH_3)_2$	(**1e**)	−1.18	0	*[d]
CH_3	(**1b**)	−0.97	0.04	38 (**3b**)
OCH_3	(**1a**)	−0.92	0.09	64 (**3a**)
H	(**1c**)	−0.86	0.15	4 (**3c**)
Br	(**1d**)	−0.77	0.20	75 (**3d**)

a) Determined by cyclic voltammetry using Ag/0.01 mol dm⁻³ $AgClO_4$ (in CH_3CN) as a reference electrode. See Ref 4). b) Determined by UV technique at 22°C. See Ref 2). c) All yields were based on consumed **1**. d) The only product isolated was 2-bromo-3-methylamino-1,4-naphthoquinone which did not react with **2a**. See Ref. 5).

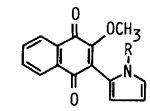

3e—g

3e; R = H
f; R = C_2H_5
g; R = $CH_2C_6H_5$

This reaction did not proceed by heat,[6] but only by light. The CT formation between two reactants seems to be prerequisite for the successful product formation as described above. In addition, it was reported that cyanide ion dominantly attacked α-position of cation radical of **2a** and attacked both α-position (85%) and β-position (15%) of cation radical of **2g**.[7] The photochemical reaction had the same regioselectivity. Judging from the above facts, the photo-

†Present address: Department of Chemistry, The Pennsylvania State University, The Schuylkill Campus, State Highway, Schuylkill Haven, PA 17972, U.S.A.

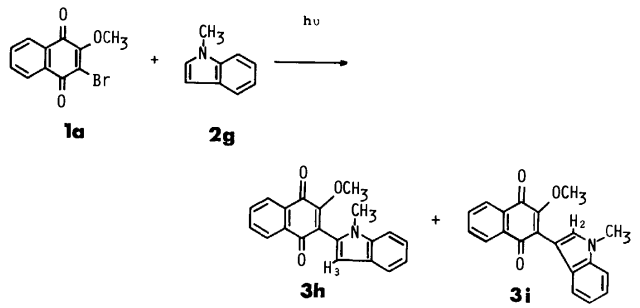

Scheme 1.

chemical reaction may include initial electron-transfer process from **2** to **1**.[8]

Experimental

General Procedure. A benzene solution (30 ml) of **1** (0.1 mmol) and 10 equivalents of **2** (1 mmol) was irradiated by a high pressure mercury arc lamp (300 W) through $CuSO_4$ aq solution filter under nitrogen atmosphere at room temperature. After irradiation for a suitable time[9] the starting quinone **1** and the photosubstituted product **3** were isolated by using column chromatography on silica gel with benzene as an eluent. All yields were based on consumed **1**.

Identification of the Products. *2-Methoxy-3-(1-methyl-2-pyrrolyl)-1,4-naphthoquinone* ***3a***: 64% yield; purple needles; mp 119—120 °C (from ethanol); UV (ethanol) 494.5 nm (ε 1800); IR (KBr) 1660 cm^{-1} (C=O); ^1H NMR ($CDCl_3$) δ=3.5 (3H, s), 3.75 (3H, s), 6.2—6.4 (2H, m, H_3 and H_4), 6.8—6.9 (1H, m, H_5), 7.7—7.9 (2H, m), and 8.1—8.3 (2H, m); ^{13}C NMR ($CDCl_3$) δ=35.00 (q), 60.59 (q), 108.51 (d, C-H_3), 113.78 (d, C-H_4), 121.66 (s), 121.99 (s), 124.50 (d, C-H_5), 126.29 (d), 126.61 (d), 131.33 (s), 131.98 (s), 133.44 (d), 134.09 (d), 157.89 (s), 181.28 (s), and 184.60 (s); MS *m/z* (rel intensity) 267 (M^+; 100), 252 (M^+-CH_3; 20), 238 (M^+-NCH_3; 10), 224 (30), 184 (8), 170 (17), 157 (14), 156 (45), and 142 (60); Found: C, 72.08; H, 4.92; N, 5.27%; *m/z* 267.0875. Calcd for $C_{16}H_{13}NO_3$: C, 71.90; H, 4.90; N, 5.24%; M, 267.0895.

2-Methyl-3-(1-methyl-2-pyrrolyl)-1,4-naphthoquinone ***3b***: 38% yield; red needles; mp 99.5—100.5 °C; Found: C, 76.24; H, 5.42; N, 5.52%; M^+, 251. Calcd for $C_{16}H_{13}NO_2$: C, 76.48; H, 5.21; N, 5.57%; M, 251.

2-(1-Methyl-2-pyrrolyl)-1,4-naphthoquinone ***3c***: 4% yield; red plates; mp 95—6 °C; Found: C, 76.11; H, 4.56; N, 5.87%; M^+, 237. Calcd for $C_{15}H_{11}NO_2$: C, 75.93; H, 4.67; N, 5.90%; M, 237.

2-Bromo-3-(1-methyl-2-pyrrolyl)-1,4-naphthoquinone ***3d***: 75% yield; purple needles; mp 156—8 °C; Found: C, 57.23; H, 3.25; N, 4.26; Br, 24.99%; M^+, 315 and 317. Calcd for $C_{15}H_{10}NO_2Br$: C, 56.99; H, 3.19; N, 4.43; Br, 25.27%; M, 315 and 317.

2-Methoxy-3-(2-pyrrolyl)-1,4-naphthoquinone ***3e***: 10% yield; purple needles; mp 115—9 °C; UV (ethanol) 521 nm (ε 4800); IR (KBr) 3400 cm^{-1} (NH); Found: C, 70.95; H, 4.37; N, 5.29%; M^+, 253. Calcd for $C_{15}H_{11}NO_3$: C, 71.14; H, 4.38; N, 5.53%; M, 253.

2-(1-Ethyl-2-pyrrolyl)-3-methoxy-1,4-naphthoquinone ***3f***: 60% yield; purple needles; mp 114—9 °C; Found: C, 72.35; H, 5.33; N, 4.81%; M^+, 281. Calcd for $C_{17}H_{15}NO_3$: C, 72.58; H, 5.37; N, 4.98%; M, 281.

2-(1-Benzyl-2-pyrrolyl)-3-methoxy-1,4-naphthoquinone **3g**: 50% yield; purple needles; mp 119—121 °C; Found: C,76.78; H, 4.88; N, 4.03; M^+, 343. Calcd for $C_{22}H_{17}NO_3$: C, 76.95; H, 4.99; N, 4.08%; M, 343.

2-Methoxy-3-(1-methyl-2-indolyl)-1,4-naphthoquinone ***3h***: 50% yield; red needles: mp 192—5 °C; UV (ethanol) 487 nm (ε 1200); ^1H NMR ($CDCl_3$) δ=6.6 (1H, m, H_3); Found: C, 75.45; H, 4.60; N, 4.32%; M^+, 317. Calcd for $C_{20}H_{15}NO_3$: C, 75.69; H, 4.76; N, 4.41%; M, 317.

2-Methoxy-3-(1-methyl-3-indolyl)-1,4-naphthoquinone ***3i***: 10% yield; purple needles; mp 131—5 °C; UV (ethanol) 513 nm (ε 2900); ^1H NMR ($CDCl_3$) δ=7.56 (1H, m, H_2); Found: C, 75.54; H, 4.79; N, 4.54%; M^+, 317. Calcd for $C_{20}H_{15}NO_3$: C, 75.69; H, 4.76; N, 4.41%; M, 317.

References

1) R. Mohläu and A. Redlich, *Ber.*, **44**, 3605 (1911); P. Pratesi, *Gazz. Chim. Ital.*, **66**, 215 (1936); E. Bullock, *Can. J. Chem.*, **36**, 1744 (1958); H. Fischer, A. Treibs, and E. Zancker, *Chem. Ber.*, **92**, 2026 (1959).

2) K. Maruyama and T. Otsuki, *Bull. Chem. Soc. Jpn.*, **50**, 3429 (1977); *Chem. Lett.*, **1977**, 851.

3) When **2a** was added to a benzene solution of **1a**, a new absorption band (λ_{max}=449 nm) appeared. The CT formation of **1e—g** with **2a** was not recognized.

4) K. Maruyama, T. Otsuki, and S. Tai, *J. Org. Chem.*, **50**, 52 (1985).

5) D. W. Cameron and R. G. F. Giles, *J. Chem. Soc. (C)*, **1968**, 1461.

6) Reaction of **1** with **2** gave no similar product even by refluxing in benzene under nitrogen atmosphere.

7) K. Yoshida, *J. Am. Chem. Soc.*, **101**, 2116 (1979).

8) The electron transfer may occur *via* the excitation of the CT complex of **1** with **2** or the formation of the encounter complex of photo-excited **1** with **2**. Then the formed ion radical pair or exciplex seemed to give **3** (see Ref. 4). Therefore, the reaction showed solvent effect; in polar solvents (acetonitrile, methanol) it gave no **3** but in nonpolar solvents (hexane, carbon tetrachloride, benzene) it gave **3**.

9) Irradiation time was 5 min for **3a**, **f**, **g**, 10 min for **3e**, **h**, i, 30 min for **3b**,**c**, and 10 h for **3d**.

X-Ray Crystal Structure of 9-Methyl-3-oxo-2-oxabicyclo[4.4.0]dec-4-ene-6,9-carbolactone. Revised Structure of Iodolactonization Product of 9-Methyl-3-oxo-2-oxabicyclo[4.4.0]deca-4,8-diene-6-carboxylic Acid

Mitsuru NAKAYAMA,* Junji KURAMOTO, Takanao MATSUI,† and James D. WHITE††

Department of Chemistry, Faculty of Science, Hiroshima University, Higashisenda-machi, Naka-ku, Hiroshima 730

†*Faculty of Engineering, Miyazaki University, Miyazaki 880*

††*Department of Chemistry, Oregon State University, Corvallis, Oregon 97331, U.S.A.*

(Received May 1, 1985)

Synopsis. The structure of the title compound, deiodo lactone compound, was determined by X-ray crystallographic analysis: The results lead to a revision of the previously proposed structure for iodolactonization product of 9-methyl-3-oxo-2-oxabicyclo[4.4.0]deca-4,8-diene-6-carboxylic acid.

Previously, we have reported that hydrolysis of the Diels-Alder adducts (**1a** and **1b**) of methyl 2-oxo-2*H*-pyran-5-carboxylate with isoprene to the corresponding acids, 9- and 8-methyl-3-oxo-2-oxabicyclo-[4.4.0]deca-4,8-diene-6-carboxylic acid (**2a** and **2b**), followed by iodolactonization, gave iodo lactones (**3a** and **3b**), respectively.[1] Since the proposed structure **3a** was inconsistent in some respects with a recent examination of the off-resonance ^{13}C-NMR spectrum, which showed doublet signal at δ 22.5 due to CH–I and singlet signal at δ 84.3 due to C–O,[2] the structure of the iodo lactone was reinvestigated in detail, resulting in a revision to 8-iodo-9-methyl-3-oxo-2-oxabicyclo-[4.4.0]dec-4-ene-6,9-carbolactone (**4**) from **3a**.[3] In addition, reduction of the iodo lactone with tributyltin hydride afforded the deiodonation product, whose structure was confirmed unambiguously to be 5,9-dioxatricyclo [6.2.2.0^{1,6}]dodecane compound (**5**) by X-ray crystallographic analysis. In this paper, we report on the crystal structure of **5** and the structural revision of iodolactonization product (**3a**→**4**).

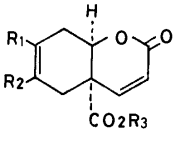

1a $R_1=R_3=Me$, $R_2=H$
1b $R_1=H$, $R_2=R_3=Me$
2a $R_1=Me$, $R_2=R_3=H$
2b $R_1=R_3=H$, $R_2=Me$

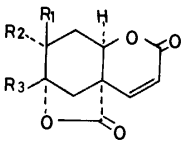

3a $R_1=I$, $R_2=Me$, $R_3=H$
3b $R_1=I$, $R_2=H$, $R_3=Me$

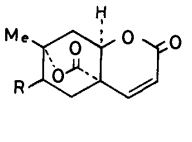

4 R = I
5 R = H
6 R = SePh

Experimental

9-Methyl-3-oxo-2-oxabicyclo[4.4.0]dec-4-ene-6,9-carbolactone (5). To a solution of 120 mg of iodo lactone **4**[1] in 5 ml of dry toluene was added 200 mg of tributyltin hydride (97%) with stirring at 5 °C under N_2. After stirring was continued for 7 h at 5 °C and then for 24 h at room temperature, methanol was added to the reaction mixture. The solvent was removed *in vacuo* at room temperature to give colorless oil which was chromatographed on silica gel using dichloromethane as eluent to afford 55 mg of **5**; colorless prisms, mp 97—99 °C recrystd from benzene–hexane; IR($CHCl_3$) 1760—1730 cm^{-1}; ^{1}H-NMR ($CDCl_3$) δ=1.46 (3H, s, C_9–CH_3), 1.72—2.66 (6H, m, 3X–CH_2–), 4.62 (1H, dd, J=4.8 and 9.6 Hz, C_1–H), 5.96 and 7.24 (each 1H, d, J=10.2 Hz, C_4– and C_5–H); MS m/z 208 (M^+); Found: C, 63.56; H, 5.81%. Calcd for $C_{11}H_{12}O_4$: C, 63.45; H, 5.81%.

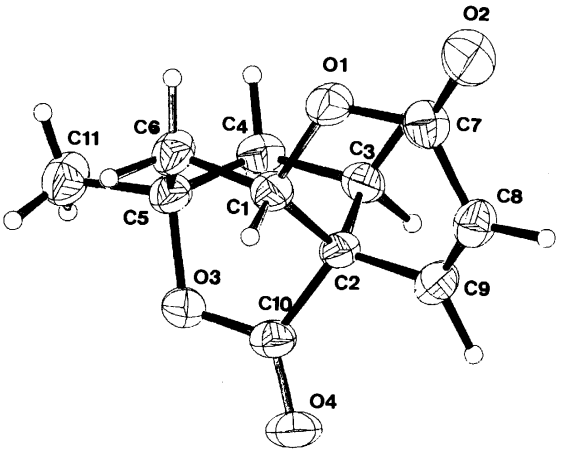

Fig. 1. Perspective view of the X molecule.

X-Ray Measurement. A colorless, single crystal with dimensions of about 0.4×0.4×0.4 mm^3 was used. The crystal data are as follows: $C_{11}H_{12}O_4$, mol wt 208.2, triclinic, space group $P\bar{1}$, a=7.601(1), b=11.179(1), c=12.147(1) Å, α=85.26(1), β=80.18(1), γ=80.57(1)°, Z=4, D_c=1.38 g cm^{-3}. The cell dimensions and diffraction intensities were measured on an automated, four-circle diffractometer with graphite-monochromated, Mo$K\alpha$ radiation (λ=0.7107 Å). The 2θ—ω scan technique was applied at a variable scan rate. Three standard reflections, measured at intervals of every 200 reflections, showed no significant decrease in intensities during the course of data collection. The intensities were corrected for the Lorentz and polarization factors, but not for the absorption or extinction effect. In the range of 2θ values up to 55°, 3707 unique structure factor magnitudes above the $3\sigma(F)$ level were selected for the structure determination.

Structure Determination

The structure was solved by direct method, MULTAN 78.[4] Tangent procedure was carried out using 220 $|E|$ values above 2.03. E-map revealed the locations of 24 non-hydrogen atoms. The rest 6 non-hydrogen atoms had been located in difference Fourier map. Some of hydrogen atoms had also been located in the above map and other hydrogen ones at calculated position. The structure refined by the block-diagonal least-squares method in UNICS III[5] program system with anisotropic temperature factor for non-hydrogen

TABLE 1. THE FINAL ATOMIC PARAMETERS AND ESTIMATED STANDARD DEVIATIONS[a)]

Atom	x	y	z	B_{eq}/Å^{2}[b)]
O(1)X	3530(3)	2819(2)	6232(2)	4.85
O(2)X	6230(4)	2267(2)	5293(2)	7.16
O(3)X	67(3)	5140(2)	8390(2)	4.51
O(4)X	1816(4)	6544(2)	7900(2)	5.85
C(1)X	2242(4)	3840(2)	6676(2)	4.00
C(2)X	3063(4)	4449(2)	7503(2)	3.72
C(3)X	3332(4)	3583(3)	8543(2)	4.23
C(4)X	1514(5)	3256(3)	9120(3)	4.63
C(5)X	61(4)	3809(3)	8441(3)	4.21
C(6)X	515(4)	3399(3)	7248(3)	4.70
C(7)X	5236(5)	3031(3)	5831(3)	4.99
C(8)X	5769(4)	4157(3)	6119(3)	4.78
C(9)X	4791(4)	4820(3)	6915(3)	4.58
C(10)X	1639(4)	5492(2)	7926(2)	4.18
C(11)X	−1822(5)	3652(3)	8994(3)	6.06
O(1)Y	2708(3)	2900(2)	2892(2)	5.80
O(2)Y	776(4)	3831(2)	4217(2)	6.79
O(3)Y	5243(3)	−325(2)	1518(2)	5.85
O(4)Y	2717(4)	−1089(2)	2053(2)	7.13
C(1)Y	3100(5)	1868(3)	2159(3)	5.11
C(2)Y	3082(4)	716(2)	2894(3)	4.26
C(3)Y	4576(5)	577(3)	3635(3)	5.65
C(4)Y	6389(6)	550(4)	2908(3)	6.51
C(5)Y	6178(5)	680(3)	1708(3)	5.11
C(6)Y	4984(5)	1852(3)	1426(3)	5.66
C(7)Y	1276(5)	2911(3)	3737(3)	5.41
C(8)Y	421(5)	1829(3)	3954(3)	6.02
C(9)Y	1268(5)	771(3)	3585(3)	6.23
C(10)Y	3611(5)	−321(3)	2134(3)	4.81
C(11)Y	7974(6)	522(4)	943(4)	8.45

a) The atomic coordinates are multiplied by 10^4. b) W.C. Hamilton, *Acta Crystallogr.*, **12**, 609 (1959).

atoms and isotropic ones for hydrogen atoms. The final R value was 0.071.[6)] Atomic scattering factors were taken from the International Tables for X-Ray Crystallography.[7)] The final atomic parameters are listed in Table 1. The two crystallographically independent molecules of **5**, X and Y, have the almost same geometries containing those absolute configurations.[6)] From the above results, the structure of **5** was shown to be 9-methyl-3-oxo-2-oxabicyclo-[4.4.0]dec-4-ene-6,9-carbolactone.

References

1) T. Matsui, T. Inoue, M. Nakayama, and J. D. White, *Bull. Chem. Soc. Jpn.*, **56**, 647 (1983).

2) Preliminary assignments of the ^{13}C-NMR spectra for these compounds are corrected as follows; **4**: δ=22.5 (C_8), 26.4 (C_9–CH_3), 33.9 and 35.5 (C_7 and/or C_{10}), 43.4 (C_6), 74.5 (C_1), 84.3 (C_9), 122.3 (C_4), 143.6 (C_5), 161.9 (C_3), 169.6 (–CO_2– of C_6); **3b**: δ=20.7 (C_9), 25.5 (C_8–CH_3), 36.1 and 37.9 (C_7 and/or C_{10}), 49.4 (C_6), 73.6 (C_1), 86.7 (C_8), 123.5 (C_4), 144.4 (C_5), 162.8 (C_3), 172.7 (–CO_2– of C_6).

3) More recently, Colvin and Brown reported that both iodo- and seleno-lactonization of acid (**2a**) gave the corresponding lactones (**4** and **6**); B. A. Brown and E. W. Colvin, *J. Chem. Soc., Chem. Commun.*, **1984**, 1514.

4) P. Main, S. E. Hull, L. Lessinger, G. Germain, J. P. Declercq, and M. M. Woolfson, 1978, "MULTAN 78, A System of Computer Programs for the Automatic Solution of Crystal Structures from X-Ray Diffraction Data," University of York, England.

5) T. Sakurai and K. Kobayashi, *Rikagaku Kenkyusho Hokoku*, **55**, 69 (1979).

6) The complete *Fo* and *Fc* data, a table of bond length, and a figure of the cell contents perpendicular to bc plane are deposited at the Office of the Editor of the Bulletin of the Chemical Society of Japan (Document No. 8548).

7) "International Tables for X-Ray Crystallography," The Kynoch Press, Birmingham (1974), Vol. IV.

Resolution of Alcohols as Esters by HPLC on (+)-Poly(triphenylmethyl methacrylate)[1]

Yoshio Okamoto,* Shiro Honda, Koichi Hatada, and Heimei Yuki†
Department of Chemistry, Faculty of Engineering Science, Osaka University, Toyonaka, Osaka 560
(Received May 2, 1985)

Synopsis. Various secondary alcohols were resolved as benzoates or 3,5-dichlorobenzoates by high-performance liquid chromatography on optically active (+)-poly(triphenylmethyl methacrylate). Almost completely resolved alcohols include 2-butanol, 2-pentanol, 2-octanol, 3-octanol, 1-phenylethanol, *cis*-2-methylcyclohexanol, *trans*- and *cis*-3-methyl-cyclohexanol, and tetrahydrofurfuryl alcohol.

A unique optically active polymer bearing a stable helical conformation, poly(triphenylmethyl methacrylate) (PTrMA),[2] has been widely used as a chiral stationary phase for high-performance liquid chromatography (HPLC) to resolve various racemic compounds.[3] The PTrMA usually resolves nonpolar compounds rather than polar ones under reversed-phase chromatographic conditions with a polar eluent like methanol. Thus, a direct resolution of alcohols was not effected but it was attained as esters and even 2-butanol was completely resolved in a form of 3,5-dichlorobenzoate. Usually, the resolution of simple aliphatic alcohols is not easy and is a time-consuming process.

Experimental

All esters used in this work were synthesized from racemic alcohols and acid chlorides. The preparations of (+)-PTrMA[4] and the packing material[3c,5] for HPLC were reported previously. The material was packed in a stainless steel column (25×0.46 (id) cm) by a slurry method. The resolution was accomplished with a JASCO TRIROTOR II chromatograph equipped with a JASCO UVIDEC-100-III UV detector at 15 °C, methanol being used as the eluent.

Results and Discussion

Figure 1 demonstrates the chromatograms of the resolution of *s*-butyl 3,5-dichlorobenzoate and 1-ethylhexyl benzoate on a (+)-PTrMA column. Both compounds were completely resolved. The resolution results are summarized in Table 1. In the resolution of 2-butanol and 2-pentanol, 3,5-dichlorobenzoates were better resolved than benzoates (Entries **1—4**). Separation factor (α) increased in the order of 2-octanol>2-pentanol>2-butanol (Entries **6**, **3**, and **1**). However, 3-methyl-2-butanol was not resolved even as 3,5-dichlorobenzoate (Entry **5**). 3-Octanol was resolved more efficiently than 2-octanol (Entries **6** and **7**). Simple primary alcohols were difficult to resolve (Entries **9** and **10**), although Yoshii and coworkers have reported that a racemic primary alcohol having a more bulky group is completely resolved as benzoate on a (+)-PTrMA column.[3h]

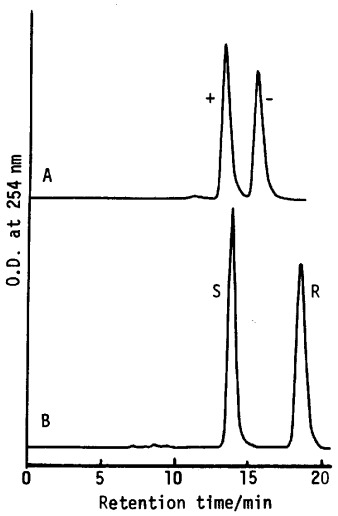

Fig. 1. Chromatograms of the resolution of *s*-butyl 3,5-dichlorobenzoate (A) and 1-ethylhexyl benzoate (B) on a (+)-PTrMA column. (Column: 25 cm×0.46 (id) cm, eluent: methanol (0.5 ml/min), 15 °C).

In the resolution of 1-phenylethanol, the benzoate was the most suitable ester (Entry **11**). Other esters showed rather broad peaks, which resulted in low resolution factors (R_s) as seen in Entries **12—15**. Several cyclic aliphatic alcohols were well resolved as benzoates (Entries **16—21**). *cis*- and *trans*-3-Methylcyclohexyl benzoates showed rather different capacity factors (k_1'), indicating that the separation of cis- and trans-isomers is possible as well as their resolution.

We have already reported that the resolution of dibenzoates of 2,4-pentanediol, *trans*-1,2- and *trans*-1,3-cyclohexanediol is also possible on (+)-PTrMA.[3b,c] These data indicate that the (+)-PTrMA column is useful for the resolution of various alcohols in the form of benzoate derivatives. Oi and Kitahara[6] reported the resolution of various alcohols as 3,5-dinitrophenylurethane derivatives on chiral columns consisting of chiral 1-(1-naphthyl)ethylamine and 2-(4-chlorophenyl)isovaleric acid; a hexane-1,2-dichloroethane mixture containing a small amount of ethanol was used as the eluent. A similar resolution has also been reported by Pirkle and Hyun.[7] The chiral recognition mechanism of our system seems different from such work in which a polar interaction plays an important role in chiral recognition. In our system, a nonpolar interaction or a π-π interaction is likely to be more important than the polar interaction.

This work was partly supported by the Grant-in-Aid for Developmental Scientific Research (58850188).

†Present address: Tezukayama-Gakuin Women's Junior College, Tezukayama, Sumiyoshi-ku, Osaka 558.

TABLE 1. RESOLUTION OF ESTERS (R_1R_2CH-$OCOR_3$) ON A (+)-PTrMA COLUMN[a]

Entry	Ester			k_1'[c]	α[d]	R_s[e]
	R_1	R_2	R_3[b]			
1	C_2H_5	CH_3	Ph	0.86(R)	~1	0
2	C_2H_5	CH_3	3,5-$Cl_2C_6H_3$	1.17(+)	1.36	1.47
3	*n*-C_3H_7	CH_3	Ph	0.94(R)	1.18	1.32
4	*n*-C_3H_7	CH_3	3,5-$Cl_2C_6H_3$	1.12(+)	1.40	1.56
5	i-C_3H_7	CH_3	3,5-$Cl_2C_6H_3$	1.35	1	0
6	*n*-C_6H_{13}	CH_3	Ph	0.89(S)	1.23	1.56
7	*n*-C_5H_{11}	C_2H_5	Ph	1.32(S)	1.60	4.44
8	CH_2=CH	CH_3	3,5-$Cl_2C_6H_3$	1.13	1.03	>0
9	$C_2H_5(CH_3)CH$	H	3,5-$Cl_2C_6H_3$	1.40	1	0
10	*n*-$C_3H_7(CH_3)CH$	H	3,5-$Cl_2C_6H_3$	1.49	1	0
11	Ph	CH_3	Ph	2.16(R)	2.42	6.19
12	Ph	CH_3	4-$NO_2C_6H_4$	1.04	1.22	0.81
13	Ph	CH_3	3,5-$(NO_2)_2C_6H_3$	0.67	1.18	0.65
14	Ph	CH_3	3,5-$Cl_2C_6H_3$	1.74	1.42	>0
15	Ph	CH_3	2-Naphthyl	2.39	1.55	1.28
16	Methyl		Ph	2.50	1.15	0.91
17	*cis*-2-Methylcyclohexyl		Ph	1.34	1.34	1.90
18	*cis*-3-Methylcyclohexyl		Ph	1.43	1.26	1.27
19	*trans*-3-Methylcyclohexyl		Ph	2.70	1.19	0.91
20	*trans*-2-Cyclohexylcyclohexyl		Ph	8.02	1.22	1.16
21	Tetrahydrofurfuryl		Ph	1.37	1.11	1.04

a) Chromatographic conditions are given in Fig. 1. b) 3,5-$Cl_2C_6H_3$=3,5-dichlorophenyl, 3,5-$(NO_2)_2C_6H_3$=3,5-dinitrophenyl. c) k_1' (capacity factor to the first-eluted enantiomer)=(retention time of the first-eluted enantiomer-dead time)/dead time. The sign in parenthesis is that of optical rotation at 365 nm or absoluted configuration. d) α(separation factor)=(capacity factor of the second-eluted enantiomer)/k_1'. e) Resolution factor=2×(difference of retention time of the second-and first-eluted enantiomers)/(sum of the band widths of the two enantiomer peaks).

References

1) Chromatographic Resolution 8. Part 7: Y. Okamoto, M. Kawashima, and K. Hatada, *J. Am. Chem. Soc.*, **106**, 5357 (1984).

2) a) Y. Okamoto, K. Suzuki, K. Ohta, K. Hatada, and H. Yuki, *J. Am. Chem. Soc.*, **101**, 4769 (1979); b) Y. Okamoto, K. Suzuki, and H. Yuki, *J. Polym. Sci. Polym. Chem. Ed.*, **18**, 3043 (1980).

3) a) H. Yuki, Y. Okamoto, and I. Okamoto, *J. Am. Chem. Soc.*, **102**, 6356 (1980); b) Y. Okamoto, I. Okamoto, and H. Yuki, *Chem. Lett.*, **1981**, 835; c) Y. Okamoto, S. Honda, I. Okamoto, H. Yuki, S. Murata, R. Noyori, and H. Takaya, *J. Am. Chem. Soc.*, **103**, 6971 (1981); d) M. Nakazaki, K. Yamamoto, and M. Maeda, *J. Org. Chem.*, **46**, 1985 (1981); e) R. Noyori, N. Sano, S. Murata, Y. Okamoto, H. Yuki, and I. Ito, *Tetrahedron Lett.*, **23**, 2669 (1982); f) Y. Kawada, H. Iwamura, Y. Okamoto, and H. Yuki, *ibid.*, **24**, 791 (1983); g) Y. Okamoto, S. Honda, E. Yashima, and H. Yuki, *Chem. Lett.*, **1983**, 1221; h) Y. Takeuchi, M. Furumura, and E. Yoshii, *Chem. Pharm. Bull.*, **31**, 3967 (1983); i) Y. Toya, S. Nakatsuka, and T. Goto, *Tetrahedron Lett.*, **24**, 5753 (1983); j) A. Tajiri, M. Fukuda, M. Hatano, T. Morita, and K. Takase, *Angew. Chem. Int. Ed. Engl.*, **22**, 870 (1983); k) Y. Okamoto, E. Yashima, K. Hatada, and K. Mislow, *J. Org. Chem.*, **49**, 557 (1984); l) Y. Okamoto, S. Honda, K. Hatada, I. Okamoto, Y. Toga, and S. Kobayashi, *Bull. Chem. Soc. Jpn.*, **59**, 1681 (1948); m) Y. Okamoto, S. Honda, H. Yuki, H. Nakamura, Y. Iitaka, and T. Nozoe, *Chem. Lett.*, **1984**, 1149; n) Y. Okamoto, E. Yashima, and K. Hatada, *J. Chem. Soc., Chem. Commun.*, **1984**, 1051; o) K. Yamamoto, H. Fukushima, Y. Okamoto, K. Hatada, and M. Nakazaki, *J. Chem. Soc. Chem. Commun.*, **1984**, 1111; p) K. Yamamoto, H. Fukushima, and M. Nakazaki, *ibid.*, **1984**, 1490; q) P. Salvadori, C. Rosini, and C. Bertucci, *J. Org. Chem.*, **49**, 5050 (1984); r) K. Yamamoto, T. Ueda, H. Yumioka, Y. Okamoto, and T. Yoshida, *Chem. Lett.*, **1984**, 1977; s) K. Meurer, A. Aigner, and F. Vögtle, *J. Inclusion Phen.*, **3**, 51 (1985); t) W. Kissener and F. Vögtle, *Angew. Chem. Int. Ed. Engl.*, **97**, (1985) **22**, 222 (1985).

4) Y. Okamoto, H. Shohi, and H. Yuki, *J. Polym. Sci. Polym. Lett. Ed.*, **21**, 601 (1983).

5) This type of a chiral column (Chiralpak-OT) is available from Daicel Chem. Ind. Ltd., Shinzaike, Himeji, Japan.

6) N. Oi and H. Kitahara, *J. Chromatogr.*, **265**, 117 (1983).

7) W. H. Pirkle and M. H. Hyun, *J. Org. Chem*, **49**, 3043 (1984).

Replacement of a Carbonyl Group of Camphor by an Oxygen Atom. Synthesis of 1,7,7-Trimethyl-2-oxabicyclo[2.2.1]heptane[1)]

Hiroshi SUGINOME* and Shinji YAMADA
Organic Synthesis Division, Department of Chemical Process Engineering, Faculty of Engineering, Hokkaido University, Sapporo 060
(Received May 10, 1985)

Synopsis. A four-step transformation of (+)-camphor into a hitherto undescribed 1,7,7-trimethyl-2-oxabicyclo[2.2.1]-heptane is described.

Only a limited number of the general methods for the synthesis of cyclic ethers have been available. We have recently reported a new and versatile method involving β-scission of alkoxyl radicals for transforming cyclic ketones into cyclic ethers with the original ring size and the transformation of number of steroidal ketones[2,3)] and adamantanone[3)] into the corresponding cyclic ethers has been achieved by this method.

In this paper we report the transformation of camphor, a representative bridged bicyclic ketone, into a hitherto undescribed 1,7,7-trimethyl-2-oxabicyclo-[2.2.1]heptane by this method[3)]. The results may demonstrate that the method can be applied to the preparation of bridged oxabicyclics and oxaterpenoids in general by the substitution of the carbonyl group of a variety of bridged bicyclic ketones, mono- and sesquiterpenoids. These bridged oxabicyclic compounds and oxaterpenoids may be of potential utility as the molecules having interesting biological as well as physical properties.

The Baeyer-Villiger oxidation of camphor has been well investigated.[4)] We have found that the oxidation of (+)-camphor (**1**) with *m*-chloroperbenzoic acid in dichloromethane gives 1,8,8-trimethyl-2-oxabicyclo-[3.2.1]-octan-3-one (**2**) as the major product together with 1,8,8-trimethyl-3-oxabicyclo[3.2.1]octan-3-one (**3**). The isolated yields of these isomeric lactones were 48 and 26% respectively. Reduction of **2** with diisobutylaluminium hydride (DIBAL) gave a 5.5:1 ratio of *endo* to *exo* lactols **4**. A similar reduction of **3** afforded a 5:1 ratio of *endo* and *exo* lactol **5** as judged by the ^{1}H NMR spectra. A mixture of lactols **4** in benzene was transformed into the corresponding hypoiodite with mercury(II) oxide and iodine in the presence of pyridine and then irradiated in an atmosphere of a nitrogen with a Pyrex-filtered light to give an oily iodo formate **6** in a 60% yield with an accompanying formation of lactone **2** (26%). The treatment of iodo formate **6** with methyllithium gave 1,7,7-trimethyl-2-oxabicyclo[2.2.1]heptane (**7**) in a 79% yield. On the other hand, a similar photolysis of the hypoiodite derived from a mixture of lactol **5** as above afforded an oily product **10** in a 60% yield together with lactone **3** (21%). High-resolution mass spectrometry indicated that it had the molecular formula $C_{10}H_{16}O_2$ and the IR, ^{1}H NMR and mass spectra indicated that it was (*R*)-4-formyloxymethyl-2,3,3-trimethylcyclopentene (**10**). It is apparently formed *via* the elimination of HI from the intermediate **9** generated from a carbon-centered radical **8** as outlined in the Scheme. The major parts of parent lactones **2** and **3** in these photolysis are formed by disproportionation of the alkoxyl radicals.

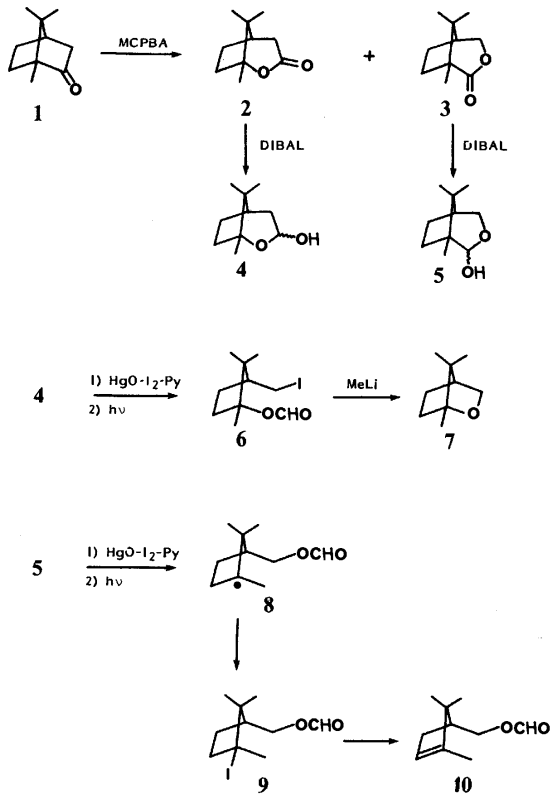

Scheme

Experimental

Mp's were determined with a Yanagimoto micro mp apparatus. IR spectra were determined for Nujol mulls, unless stated otherwise, with a Hitachi Model 285 infrared spectrophotometer. ^{1}H NMR spectra were determined with a JEOL PS200 high-resolution FT-NMR spectrometer (200 MHz) (solvent, $CDCl_3$, $SiMe_4$ as an internal reference). TLC was carried out on Merck Kiesel gel 60, PF254. The high- and low-resolution mass spectra were recorded with a JEOL JMS-D-300 spectrometer (70 eV) (Faculty of Agriculture of this university).

Baeyer-Villiger Oxidation of (+)-Camphor (1). To a solution of (+)-camphor (1 g) (Wako Pure Chemical Ind. Ltd.) in dichloromethane (20 ml) was added *m*-chloroperbenzoic acid (2.5 g) and *p*-toluenesulfonic acid (0.5 g). The solution was set aside for a week at room temperature while stirring. The solution was worked up in the usual way to give a mixture of two lactones. The product was subjected to column chromatography (Merck Kiesel gel 60, 70—230 mesh, 50 g). Elution with a 10:1 benzene–diethyl ether afforded first the starting camphor (**1**) (90 mg) and then lactone **3** (312 mg) and finally lactone **2** (542 mg).

Reduction of 1,8,8-Trimethyl-2-oxabicyclo[3.2.1]octan-3-one (2) with DIBAL. To a solution of the lactone **2** (359 mg) in dry toluene (50 ml) cooled at −78 °C, was added dropwise DIBAL in hexane (3 ml). The solution was stirred for 1.5 h at −78 °C and poured into iced water. After the solution was filtered, the filtrate was worked up by the usual method. A crude product (365 mg) was subjected to column chromatography (Merck Kiesel gel 60, 70—230 mesh). Elution with a 5:1 benzene–diethyl ether gave an amorphous solid (309 mg) which was a 1:5.5 mixture of *endo* and *exo* lactols **4**. (Found: M^+, 170. 1316. Calcd for $C_{10}H_{18}O_2$: 170. 1306); IR; 3370 (OH), 1120, 1061, 1012, 927, and 855 cm^{-1}; ^1H NMR δ=0.86 (3H, s, Me), 1.09 (3H, s, Me), 1.11 (3H, s, Me), 3.41 (1H, d, J=6.35 Hz, OH), 5.14 (0.86 H, m, CHOH of the *endo* isomer), and 5.28; (0.14 H, m, CHOH of the *exo* isomer); MS. *m/z* (rel. intensity), 170 (M^+, 0.6%), 152 (M^+-H_2O, 0.7), 124 (3.5), 109 (100), 67 (23.9), 55 (21.1) and 41 (38.8).

Reduction of 1,8,8-Trimethyl-3-oxabicyclo[3.2.1]octan-2-one (3) with DIBAL. To a solution of the lactone **3** (300 mg) in dry toluene (50 ml) cooled at −78 °C, was added dropwise DIBAL in hexane (2.5 ml). The solution was stirred for 3 h at −78 °C and poured into iced water. After the solution had been filtered, the filtrate was worked up by the usual method. A crude product (298 mg) was subjected to preparative TLC with a 5:1 benzene–diethyl ether to give a lactol **5** (250 mg). (Found: M^+ 170. 1334. Calcd for $C_{10}H_{18}O_2$: 170, 1307); IR 3380 (OH), 1086, and 1009 cm^{-1}; ^1H NMR δ=0.86, 0.90, and 1.07 (each 3H, each s, 1,8,8-Me of *endo* isomer), 0.87, 0.92, and 1.00 (each 3H, each s, 1,8,8-Me of *exo* isomer), 3.50 (1H, dd, J=11.23 and 2.46, 4-H of *endo* isomer), 4.07 (1H, d, J=11.23, 4-H of *endo* isomer), 4.89 (1H, d, J=6.33, 3H of *endo* isomer), 3.39 (1H, dd, J=10.74 and 2.93, 4-H of *exo* isomer), 4.23 (1H, d, J=10.74, 4-H of *exo* isomer), and 4.70 (1H, d, J= 2.93, 3H of *exo* isomer); MS *m/z* (rel. intensity), 170 (M^+, 0.6), 152 (M^+-H_2O, 0.7), 124 (3.5), 109 (100%).

Irradiation of the Hypoiodite of the Lactol 4 in the Presence of Mercury(II) Oxide and Iodine. To the lactol **4** (200 mg) in dry benzene (59 ml) containing pyridine (0.5 ml) was added mercury(II) oxide (598 mg) and iodine (598 mg). The solution in a Pyrex vessel was flushed with nitrogen and irradiated with a 100-W high pressure Hg arc for 1.5 h. The solution was filtered and the filtrate was worked up in the usual manner to give a crude oily product (285 mg). This product was subjected to preparative TLC to give a TLC more mobile fraction A (208 mg) and a TLC less mobile fraction B (52 mg). The oily fraction A was an iodo formate **6**. (Found: M^+, 296. 0311), Calcd for $C_{10}H_{17}IO_2$: 296. 0274; IR (neat) 1724 (CHO), and 1180 cm^{-1} (OCHO); ^1H NMR, δ=0.87 (3H, s, Me), 0.99 (3H, s, Me), 1.43 (3H, s, Me), 2.03—2.22 (4H, s, $-CH_2CH_2-$), 3.00 (1H, dd, J=10.74 and 9.28 Hz, one of CH_2I), 3.34 (1H, dd, J=9.28 and 3.24 Hz, one of CH_2I) and 8.02 (1H, s, OCHO); MS *m/z* (rel. intensity) 296 (M^+, 0.2%), 250 (M^+-OCH_2O, 1.5), 123 ($M^+-I-OCH_2O$, 100), 81 (14.3), 71 (12.7), 55 (18.7), and 43 (28.5). The fraction B was lactone **2**.

Irradiation of the Hypoiodite of the Lactol 5 in the Presence of Mercury(II) Oxide and Iodine. To the lactol **5** (188 mg) in dry benzene (55 ml) containing pyridine (0.5 ml) was added mercury(II) oxide (477 mg) and iodine (564 mg). The solution in a Pyrex vessel was irradiated for 70 min as in the case of the lactol **4**. The solution was worked up as usual. The crude product was subjected to preparative TLC to give a TLC more mobile fraction A (111 mg) and a TLC less mobile fraction B (39 mg). The fraction A was an oily formate **10**. (Found: M^+ 168. 1121. Calcd for $C_{10}H_{18}O_2$: IR (neat) 1726 (CHO), and 1169 cm^{-1} (OCHO); ^1H NMR, δ=0.87 (3H, s, Me), 1.08 (3H, s, Me), 1.60 (3H, br, s, C=C-Me), 1.91—2.41 (3H, m, $\rangle CH-CH_2-CH=C\langle$ 5.22 (1H, br, s, CH=C) and 8.08 (1H, s, OCHO), MS *m/z* 168 (M^+, 0.4%), 122 (M^+-OCH_2O, 10.9), 107 (100) and 91 (15.0). The fraction B was lactone **3**.

1,7,7-Trimethyl-2-oxabicyclo[2.1.1]heptane (7). A solution of the formate (65 mg) in THF (25 ml) was cooled at −78 °C by Dry Ice–methanol. To this solution was added dropwise methyllithium in diethyl ether [1 M (1 M=1 mol dm^{-3}) solution] (0.6 ml). After the solution had been stirred for 1 h at −78 °C, the temperature of the solution rose to room temperature. The solvent was removed by a rotary evaporator as much as possible and the concentrate was diluted with diethyl ether. The solution was washed with water and dried over anhydrous Na_2SO_4. After the removal of Na_2SO_4, the residual solution was concentrated. The yield of 2-oxabicyclo[2.1.1]heptane (**7**) determined by GLC was 79%. The pure 2-oxabicyclo[2.1.1]heptane (**7**), mp 34—37 °C, was isolated by preparative gas chromatography. (Found: M^+, 140. 1192. Calcd for $C_9H_{16}O$: 140. 1199); IR (neat) 1089, 1022, 975, and 930 cm^{-1}; ^1H NMR, δ=0.95, 0.99 and 1.11 (each 3H, each s, 1,7,7-Me), 3.45 (1H, d, J=7.33, *endo* 3-H), 3.87 (1H, m, *exo* 3-H).

References

1) Photoinduced Transformations. Part 81. Part 80. H. Suginome and S. Yamada, *Tetrahedron Lett.*, **26**, 3715 (1985).

2) H. Suginome and S. Yamada, *J. Org. Chem.*, **50**, 2489 (1985).

3) Preliminary Communication. H. Suginome and S. Yamada, *Tetrahedron Lett.*, **25**, 3995 (1984).

4) A. Baeyer and V. Villiger, *Chem. Ber.*, **32**, 3625 (1899); R. R. Sauers, *J. Amer. Chem. Soc.*, **81**, 925 (1959); R. R. Sauers and G. P. Ahearn, *ibid.*, **83**, 2759 (1961). For a review on a regioselectivity of the Baeyer-Villiger oxidation of bridged bicyclic ketones, see G. R. Krow, *Tetrahedron*, **37**, 2697 (1981).

Synthesis of Chiral 18-Crown-6 Derivatives and Dibenzocrown Ethers Incorporating *trans*-Tetrahydrofuran-2,5-diylbis(methylene) Units of Known Absolute Configuration

Koichiro NAEMURA,* Iwao EBASHI, and Atsushi MATSUDA
Department of Chemistry, Faculty of Engineering Science, Osaka University, Toyonaka, Osaka 560
(Received May 22, 1985)

Synopsis. By using (−)-*trans*-2,5-bis(hydroxymethyl)-tetrahydrofuran (**1**) of known absolute configuration as a chiral diethylene glycol unit, 18-crown-6 derivatives **8**, **9**, **12**, and dibenzocrown ethers **14**, **15** containing *trans*-tetrahydrofuran-2,5-diylbis(methylene) unit were prepared in enantiomerically pure forms. Their abilities to extract alkali metal picrates were investigated.

A variety of crown ethers incorporating 2,5-disubstituted tetrahydrofuranocycle have been prepared. Most of them, however, were composed of achiral *cis*-tetrahydrofuran-2,5-diylbis(methylene) unit. Stoddart[1] prepared chiral 18-crown-6 derivative possessing *trans*-tetrahydrofuran-2,5-diylbis(methylene) unit by using 2,5-anhydro-D-mannitol. In our preceding paper,[2] we reported the synthesis of some dibenzo-18-crown-6 derivatives **16**, **17**, and **18** containing two *trans*-tetrahydrofuran-2,5-diylbis(methylene) units as a chiral diethylene glycol fragment. Here we describe the preparation of chiral 18-crown-6 derivatives **8**, **9**, and **12** containing one, two, and three *trans*-tetrahydrofuran-2,5-diylbis(methylene) units and chiral dibenzocrown ethers **14** and **15** incorporating the same unit, and the solvent extraction of alkali metal picrates with these crown ethers. Stereoisomers of **8** and **12** containing *cis*-tetrahydrofuran-2,5-diylbis(methylene) units have been prepared by Cram.[3]

Condensation of (−)-**5**, obtained from (−)-(2*R*,5*R*)-2,5-bis(hydroxymethyl)tetrahydrofuran (**1**),[2] with tetraethylene glycol in THF and NaH provided a 42% yield of (−)-*trans*-tetrahydrofurano-18-crown-6 (**8**). Crown ether **9** composed of two tetrahydrofuranocycles was synthesized stepwise. Treatment of (−)-**5** with ethylene glycol mono(tetrahydropyranyl) ether in THF and NaH followed by acid hydrolysis gave (−)-**7** in 48% overall yield. The glycol **7** was condensed with (−)-**5** to provide a 12% yield of (−)-**9**. Crown ether **12** incorporating three tetrahydrofuranocycles was also prepared stepwise *via* the glycol **11**. Treatment of (−)-**1** with 1 equiv of 3,4-dihydro-2*H*-pyran gave (+)-**2**. Tosylation of (−)-**1** with 1 equiv of tosyl chloride gave the monotosylate **3** together with the ditosylate (−)-**5**, and tetrahydropyranylation of **3** provided (−)-**4**. Treatment of (+)-**2** with (−)-**4** and NaH gave (+)-**10**, hydrolysis of which afforded (−)-**11**. Condensation of (−)-**11** with (−)-**5** in DMSO–diethylene glycol dimethyl ether (diglyme) and NaH gave a 17% yield of (+)-**12**. Dibenzo-15-crown-5 derivative **14** and dibenzo-18-crown-6 derivative **15** were prepared *via* the common intermediate (+)-**13** which was obtained by condensation of (−)-**5** with pyrochatechol mono(tetrahydropyranyl) ether followed by acid hydrolysis. Treatment of (+)-**13** with ethylene glycol ditosylate in THF and KOBu^t provided a 30% yield of (−)-**14**, and (+)-**15** was prepared in 60% yield by condensation of (+)-**13** with diethylene glycol ditosylate. The cation-binding ability of crown ethers was assessed by solvent extraction of aqueous solution of alkali metal picrate with chloroform solution containing crown ether. The results are summerized in Table 1.

TABLE 1. EXTRACTION OF ALKALI METAL PICRATES[a]

Host	Extractability/%			
	Li^+	Na^+	K^+	Cs^+
8	3	5	54	24
9	2	4	53	22
12	2	3	48	19
18-crown-6	3	6	66	33
14	1	10	16	3
15	0	16	42	7
16	0	15	38	10
17	0	20	46	7
18	0	23	36	8
dibenzo-18-crown-6	0	3	35	7

a) The solvent extraction was carried out according to the procedure reported in our preceding paper.[4]

18-Crown-6 derivatives **8**,**9**, and **12** possess low extractabilities for alkali metal ions as compared with the parent 18-crown-6. The origin of the decrease in

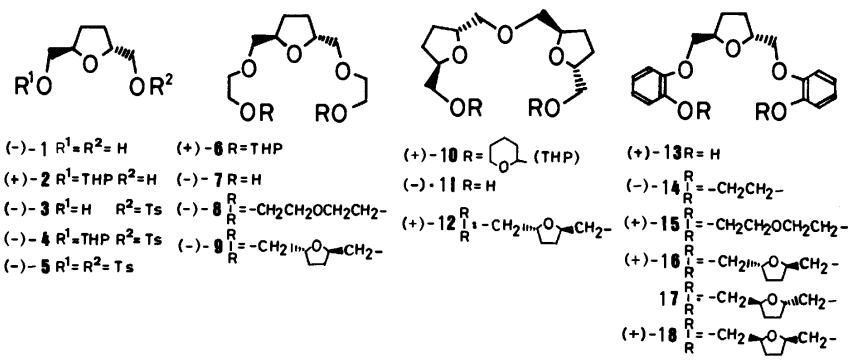

extractabilities may be attributed to the restricted conformation of crown ether ring, resulting from incorporation of the constrained *trans*-2,5-disubstituted tetrahydrofuran moiety into the 18-crown-6 constitution. On the other hand, rather high extractabilities of dibenzo-18-crown-6 derivatives **15—18** are probably ascribed to the increased basicity of tetrahydrofuran oxygen atoms over ordinary crown ether oxygen atoms.

Experimental

(+)-(2R,5R)-2-Hydroxymethyl-5-(2-tetrahydropyranyloxymethyl)tetrahydrofuran (2). Tetrahydrophyranylation of (−)-**1**[2] (4.50 g, 34.0 mmol) was carried out according to Parham's procedure[5] to give **2** (3.35 g, 46% yield), bp 120—125 °C (air-bath temp) (1 mmHg); $[\alpha]_{405}^{22}$ +3.8° (*c* 0.798, EtOH). Found: C, 59.90; H, 9.28%. Calcd for $C_{11}H_{20}O_4$: C, 61.09; H, 9.32%.

(−)-(2R,5R)-2-(2-Tetrahydropyranyloxymethyl)-5-(tosylmethyl)tetrahydrofuran (4). Tosylation[2] of (−)-**1** (2.68 g, 20.3 mmol) with tosyl chloride (3.86 g, 20.3 mmol) in pyridine followed by chromatography on alumina gave (−)-**5** (2.05 g), $[\alpha]_D^{22}$ −10.8°[2] and **3** (1.31 g). Tetrahydropylanylation[4] of **3** (1.31 g) followed by chromatography (benzene eluent) provided **4** (1.33 g, 18% overall yield) as a liquid, $[\alpha]_{405}^{25}$ −4.2° (*c* 0.811, EtOH); MS *m/z* 370 (M^+).

(−)-(5R,8R)-5,8-Epoxy-3,10-dioxadodecane-1,12-diol (7). A mixture of ethylene glycol mono(tetrahydropyranyl) ether (2.32 g, 15.9 mmol) and NaH (760 mg, 31.8 mmol) in 50 mL of DMSO–diglyme (1/3 volume ratio) was stirred at 30—35 °C for 2.5 h under N_2 and then to the mixture was added a solution of (−)-**5** (3.50 g, 7.94 mmol), $[\alpha]_D^{22}$ −10.8°, in 25 mL of the same solvent. The mixture was stirred at 50—55 °C for further 24 h under N_2. After a usual workup, chromatography on alumina (benzene) gave (+)-**6** (1.69 g), $[\alpha]_{405}^{23}$ +4.6° (*c* 0.917, EtOH), acid hydrolysis of which in MeOH and *p*-toluenesulfonic acid[2] provided (−)-**7** (830 mg, 48% overall yield) as a liquid, $[\alpha]_D^{24}$ −18.8° (*c* 0.894, $CHCl_3$); MS *m/z* 220 (M^+).

(−)-(15R,18R)-15,18-Epoxy-1,4,7,10,13-pentaoxacyclononadecane (8). To a boiling suspension of NaH (720 mg, 30.0 mmol) in dry THF (180 mL) was added a solution of (−)-**5** (4.00 g, 9.08 mmol) and tetraethylene glycol (1.76 g, 9.08 mmol) in dry THF (270 mL) over a 22 h period under N_2. The mixture was refluxed for further 48 h. After a usual workup, alumina chromatography ($CHCl_3$) provided (−)-**8** (1.11 g, 42% yield) as a liquid, $[\alpha]_D^{22}$ −8.7° (*c* 0.963, $CHCl_3$); MS *m/z* 290 (M^+); ^{1}H NMR ($CDCl_3$) δ=1.45—2.05 (4H, m), 3.40—3.55 (4H, m), 3.69 (16H, t), 4.10—4.35 (2H, m). Found: C, 57.65; H, 9.01%. Calcd for $C_{14}H_{26}O_6$: C, 57.91; H, 9.03%.

(−)-(6R,9R,16R,19R)-6,9:16,19-Diepoxy-1,4,11,14-tetraoxacycloeicosane (9). Condensation of (−)-**7** (830 mg, 3.77 mmol) with (−)-**5** (1.66 g, 3.77 mmol) in DMSO–diglyme and NaH followed by alumina chromatography ($CHCl_3$) gave (−)-**9** (159 mg, 12% yield) as a viscous liquid, $[\alpha]_D^{25}$ −16.4° (*c* 0.825, $CHCl_3$); MS *m/z* 316 (M^+). Found: C, 60.65; H, 8.89%. Calcd for $C_{16}H_{28}O_6$: C, 60.74; H, 8.92%.

(−)-(2R,5R,9R,12R)-2,5:9,12-Diepoxy-7-oxatridecane-1,13-diol (11). Condensation of (+)-**2** (730 mg, 3.38 mmol) with (−)-**4** (1.25 g, 3.38 mmol) in DMSO–diglyme and NaH gave **10** (1.04 g), $[\alpha]_{405}^{24}$ +2.4° (*c* 0.639, EtOH). Hydrolysis of **10** (1.04 g) in MeOH and *p*-toluenesulfonic acid followed by chromatography (ether–MeOH 9:1) provided **11** (520 mg, 62% overall yield) as a liquid, $[\alpha]_D^{20}$ −3.7°(*c* 0.369, EtOH); MS *m/z* 246 (M^+). Found: C, 58.30; H, 8.91%. Calcd for $C_{12}H_{22}O_5$: C, 58.51; H, 9.00%.

(+)-(3R,6R,10R,13R,17R,20R)-3,6:10,13:17,20-Triepoxy-1,8,15-trioxacyclohenicosane (12). Condensation of (−)-**11** (457 mg, 1.85 mmol) with (−)-**5** (817 mg, 1.85 mmol) in DMSO–diglyme and NaH followed by alumina chromatography ($CHCl_3$) gave (+)-**12** (108 mg, 17% yield) as a viscous liquid, $[\alpha]_{405}^{22}$ −9.9° (*c* 0.527, $CHCl_3$); ^{1}H NMR ($CDCl_3$) δ=1.5—2.1 (12H, m), 3.45 (12H, d, *J*=5 Hz), 4.0—4.4 (6H, m); MS *m/z* 342 (M^+). Found: C, 62.95; H, 8.84%. Calcd for $C_{18}H_{30}O_6$: C, 63.13; H, 8.83%.

(−)-(6R,9R)-2,3:12,13-Dibenzo-6,9-epoxy-1,4,11,14-tetraoxacyclohexadeca-2,12-diene (14). Condensation of (+)-**13**[2] (1.00 g, 3.16 mmol), $[\alpha]_D^{22}$ +17.0°, with ethylene glycol ditosylate (980 mg, 6.32 mmol) in dry THF and KOBu^t was carried out according to the procedure as described for **16**.[2] Chromatography on alumina (benzene) followed by recrystallization (hexane) provided (−)-**14** (322 mg, 30% yield), mp 107—108 °C; $[\alpha]_D^{20}$ −23.1° (*c* 0.755, $CHCl_3$); ^{1}H NMR ($CDCl_3$) δ=1.6—2.2 (4H, m), 4.0—4.2 (4H, m), 4.32 (4H, s), 4.60 (2H, br s), 6.90 (8H, s); MS *m/z* 342 (M^+). Found: C, 69.91; H, 6.49%. Calcd for $C_{20}H_{22}O_5$: C, 70.15; H, 6.48%.

(+)-(6R,9R)-2,3:12,13-Dibenzo-6,9-epoxy-1,4,11,14-pentaoxacyclononadeca-2,12-diene (15). A procedure similar to that for **16**[2] using (+)-**13** (1.50 g, 4.74 mmol) and diethylene glycol ditosylate (1.64 g, 3.95 mmol) gave (+)-**15** (1.11 g, 60% yield), mp 172—174 °C (hexane–benzene); $[\alpha]_D^{22}$ +7.0° (*c* 0.840, $CHCl_3$); ^{1}H NMR ($CDCl_3$) δ=1.75—2.40 (4H, m), 4.0—4.2 (12H, m), 4.60 (2H, br s), 6.82 (8H, s); MS *m/z* 386 (M^+). Found: C, 68.29; H, 6.64%. Calcd for $C_{22}H_{26}O_6$: C, 68.38; H, 6.78%.

References

1) J. A. Haslegrave, J. F. Stoddart, and D. J. Thompson, *Tetrahedron Lett.*, **1979**, 2279.

2) M. Nakazaki, K. Naemura, M. Makimura, A. Matsuda, T. Kawano, and Y. Ohta, *J. Org. Chem.*, **47**, 2429 (1982).

3) J. M. Timko, S. S. Moore, D. M. Walba, P. C. Hiberty, and D. J. Cram, *J. Am. Chem. Soc.*, **99**, 4207 (1977).

4) K. Naemura, I. Ebashi, and M. Nakazaki, *Bull. Chem. Soc. Jpn.*, **58**, 767 (1985).

5) W. E. Parham and E. L. Anderson, *J. Am. Chem. Soc.*, **70**, 4187 (1948).

Selective Synthesis of LPG from Synthesis Gas

Kaoru FUJIMOTO,* Hitoshi SAIMA, and Hiro-o TOMINAGA
Department of Synthetic Chemistry, Faculty of Engineering, The University of Tokyo, Bunkyo-ku, Hongo, Tokyo 113
(Received February 21, 1985)

Synopsis. C_2–C_4 paraffins were produced from synthesis gas with selectivities higher than 80% at 300 °C and 21 atm by utilizing hybrid catalysts composed of a methanol-synthesis catalyst and a Y-type zeolite. The diffusion of lower olefins within zeolite pores and their hydrogenation on a methanol-synthesis catalyst were found to be important factors in controlling selectivity.

Liquified Petroleum Gas (LPG) is important for both home and transportation fuels. It is mainly composed of propane and butanes which maintain a proper vapor pressure at the ambient temperature. Several attempts have been made to produce LPG from synthesis gas with a precipitated Fe–Mn–Cu catalyst,[1] a fused-iron catalyst[2] and a supported molybdenum catalyst.[3] Since the above mentioned catalysts belong to the category of a Fischer -Tropsch catalyst, the hydrocarbon distribution follow the Anderson-Schluz-Flory distribution. This means that a significantly high selectivity regarding methane is inevitable.

Recently, Chang *et al.* have reported that the synthesis-gas conversions with H-ZSM-5 loading oxides of Cr, Zn, and Al give ethane with selectivities as high as 83% at around 400 °C and 100 atm.[4] The present authors showed that hydrocarbon mixtures with markedly different distributions were produced from synthsis gas using hybrid catalysts composed of a methanol-synthesis catalyst and zeolite.[5,6,7]

In the present paper, unique hybrid catalyst systems which give LPG with excellent selectivities are reported.

Experimental

The zeolite used as one component of the hybrid catalysts was prepared by treating a high-silica Y-type zeolite (supplied by Shokubai Kasei Inc., $SiO_2/Al_2O=7.6$) with steam at 450 °C for 1 hr(St-DAY). Methanol-synthesis catalysts, used as other components, were 4 wt% Pd/SiO_2,[6] home-made Cu–Zn–Al mixed oxide prepared following a method described by Shimomura *et al.*[8] (Cu:Zn:Al=40:23:37 in atomic ratio) or a commercially available Cu-based low-pressure methanol-synthesis catalyst (BASF S3-85). The Pd/SiO_2 catalyst was activated by treating with flowing hydrogen at 450 °C for 2 h. The copper-based catalysts were activated by flowing hydrogen at 300 °C for 3 h. The details of the preparative method regarding the hybrid catalysts has been described elsewhere.[5,6]

The reaction apparatus and procedures for a synthesis-gas reaction and a product analysis are the same as those described before.[6]

Results and Discussion

As demonstrated in Fig. 1, the methanol conversion on St-DAY and of synthesis-gas conversion with a hybrid catalyst composed of Cu–Zn(A) and St-DAY give hydrocarbon mixtures with extremely different compositions. The methanol conversion gives C_1–C_6 aliphatics containing significant amounts of olefins, aromatic hydrocarbons composed of mostly penta- and hexamethyl-benzenes (not shown in the figure), and coke. On the other hand, the synthesis-gas conversion gives C_2, C_3, C_4, and C_5 paraffins, exclusively, with a complete lack in aromatic hydrocarbons and a small amount of coke (0.6%).

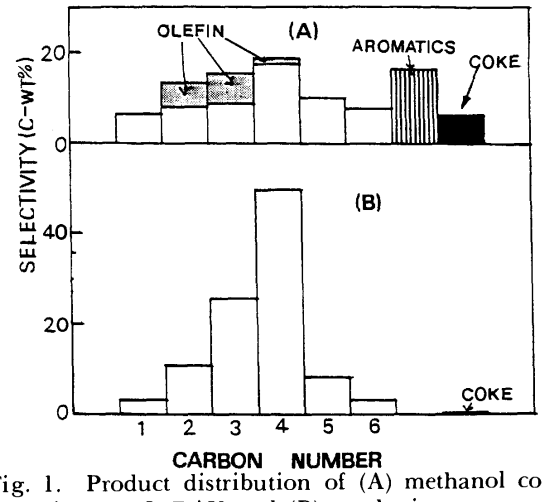

Fig. 1. Product distribution of (A) methanol conversion on St-DAY and (B) synthesis gas conversion on hybrid catalyst containing St-DAY.
(A): Methanol conversion on St-DAY only, 300 °C, 21 atm, 10% methanol in synthesis gas ($H_2/CO=2/1$), W/F=5g-cat h/mol, hydrocarbon yield= 97%, (B): Synthesis gas conversion on Cu-Zn(A)/St-DAY(1/1 weight ratio) 300 °C, 21 atm, $H_2/CO=2/1$, W/F= 10 g-cat h/mol, hydrocarbon yield=36.0%.

It has been known that methanol conversion with large-pore zeolite such as Y-type zeolite gives polymethylated benzenes as well as aliphatic hydrocarbons and coke because of its large pores. Thus, the new features of the products of synthesis-gas conversion with a hybrid catalyst, which are characterized by a lack of olefins, aromatics, and coke, should be attributed to some new catalytic effects caused by hybridization. This subject will be discussed later.

Table 1 shows the catalytic performances of 3 types of hybrid catalysts containing 3 different methanol-synthesis catalysts. It is apparent that all three catalysts give C_2–C_5 paraffins with selectivities higher than 90% and no aromatics while the hydrocarbon yield depends strongly on the catalyst. The distinction should be attributed to the activity of each methanol-synthesis catalyst since the first step of hydrocarbon formation in the present system is methanol formation. Although product patterns regarding the two hybrid catalysts containing Cu–Zn (A) and Cu–Zn (B) are quite similar, the pattern on the Pd/SiO_2 -based catalyst differs significantly from those on the former two catalysts. The latter one gives a product which is more rich in ethane and propane and is poorer in butanes. As discussed in more detail later, the most important reaction for controlling the product selectivity is the hydrogenation of the lower olefins which are inter-

TABLE 1. HYDROGENATION OF CARBON MONOXIDE WITH HYBRID CATALYSTS

Catalyst	Pd/SiO St-DAY[2]	Cu-Zn (A) St-DAY	Cu-Zn (B) St-DAY	Cu-Zn (A) St-DAY	Cu-Zn (A) St-DAY
Temperature (°C)	300	300	300	270	320
W/F (g-cat h/mol)	10.1	2.7	3.4	3.2	3.2
Product Yield (%/CO fed)					
Hydrocarbon	6.4	15.0	35.7	5.1	20.0
Methanol	tr.	0.3	1.0	0.1	0.4
Dimethyl ether	tr.	1.0	4.3	1.6	0.9
Carbon dioxide	2.0	3.7	30.7	6.0	18.5
(Methanol[a)])	(4.6)	(4.2)	(4.6)	(3.0)	(2.4)
Hydrocarbon distribution (carbon wt%)					
C_1	1.1	1.6	2.2	2.0	4.9
C_2	19.7	8.7	10.7	9.2	10.4
C_3	28.8	16.1	24.7	14.5	22.6
C_4	33.8	50.3	49.6	45.3	43.9
C_5	13.2	14.2	8.2	15.5	11.4
C_6^+	3.5	9.1	2.6	13.6	6.8
Pressure: 20 kg/cm², H_2/CO=2/1					

a) With methanol-synthesis catalyst only.

mediates from methanol to aromatics. Thus, it is assumed that the hydrogenation of the lower olefins, which terminates the carbon-chain growth, is more prominent for a Pd/SiO_2 based catalyst.

It should also be noted that the hydrocarbon yield in a synthesis-gas conversion with the hybrid catalyst exceeds the yield of methanol from synthesis gas with the methanol-synthesis catalyst alone under the same reaction condition. This fact could be interpreted to mean that while methanol fromation is controlled by thermodynamic equilibrium under the conditions adopted here, a quick conversion of methanol to hydrocarbon in situ by zeolite lowers the concentration, which enables a further conversion of synthesis gas beyond the thermodynamic limit of methanol formation. A clear tendancy of the product pattern to sift to the lighter side with increasing temperature is recognized, and is identical to that of methanol conversion on zeolites.

The drastic change in the product patterns from the methanol conversion system to the synthesis-gas conversion system should be attributed to some new reactions generated by the hybridization of the zeolite with the methanol catalyst. The change is most likely interpreted by the following scheme. As pointed out already,[6] the hydrogenation of lower olefins and the methylation by methanol of aromatic hydrocarbons are new and important reactions which control the product pattern of a hybrid catalyst system, as demonstrated in Fig. 2. The methanol produced on the methanol-synthesis catalyst moves to the zeolite surface to be converted to dimethyl ether and then to lower olefins.[9] Either dimethyl ether or olefins diffuse in the zeolite pores and some of them come out of the pores to the bulk gas phase. Olefins in the bulk-gas phase have a chance to be hydrogenated to lower paraffins, which terminate the carbon chain growth since methanol synthesis catalysts are active for olefin hydrogenation. When the zeolites with middle-size pores are used, aromatic hydrocarbons and coke are formed since olefins stay in the pores long enough to polymerize into aromatics due to their slow diffusion.[4,7] In the case where a large-pore zeolite (such as a Y-type zeolite) is used, almost all of lower olefins come out of the pores, without polymirizing into aromatics, and are hydrogenated to paraffins on the methanol synthesis catalyst because of the three-times higher diffusion rate in the zeolite pores than that for a middle-pore zeolite (mordenite).[10]

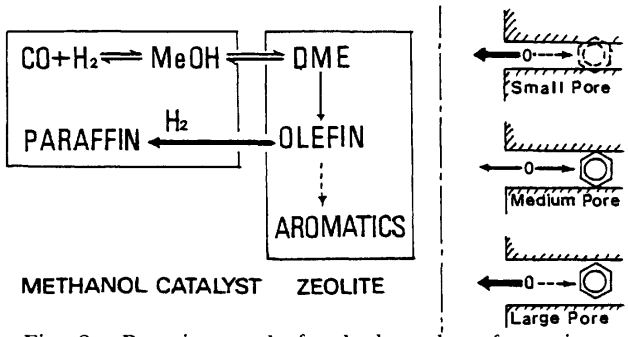

Fig. 2. Reaction path for hydrocarbon formation from synthesis gas on hybrid catalyst containing methanol synthesis catalyst and zeolite.

This work was financially supported by the Iwatani Foundation. This fact is greatly appreciated.

References

1) S. Kodama, K. Tarama, A. Mishima, K. Fujita, and M. Yasuda, *Kogyo Kagaku Zasshi*, **46**, 69 (1943).
2) J. C. Hoogendoorn, Preprint of "IGT Symposium" (1973).
3) C. B. Murchison, and D. A. Murdick, Hydrocarbon Processing, Jan. 160 (1981).
4) C. D. Chang, J. N. Miale, R. F. Socha, *J. Catal.*, **90**, 84 (1984).
5) K. Fujimoto, Y. Kudo, and H. Tominaga, Nippon *Kagaku Kaishi* **1982**, 206.
6) K. Fujimoto, Y. Kudo, and H. Tominaga, *J. Catal.*, **87**, 136 (1984).
7) H. Saima, K. Fujimoto, and H. Tominaga, *Bull. Chem. Soc. Jpn*, in press.
8) K. Shimomura, K. Ogawa, M. Oba, and Y. Kotera, *J. Catal.*, **52**, 191 (1978).
9) C. D. Chang and A. J. Silvestri, *J. Catal.*, **47** 249 (1977).
10) H. Saima, K. Fujimoto, and H. Tominaga unpublished data.

 © 1985 The Chemical Society of Japan Bull. Chem. Soc. Jpn., 58, 3061—3067 (1985)

Kinetic Study of the Decay of Chlorine Dioxide in Supercooled and Glassy Organic Solvents

Nobuaki OHTA*,† and Keiji KUWATA
Department of Chemistry, Faculty of Science, Osaka University, Toyonaka 560
(Received January 18, 1985)

Chlorine dioxide (ClO_2), which is a stable free radical, decayed in supercooled and glassy liquid 3-methylhexane (3MHX) and 3-methylpentane near their glass transition temperatures (T_g's). The decay of ClO_2, however, was not observed in toluene or 2-methyl-1-propanol. The kinetic analysis of the decay of ClO_2 in 3MHX is reasonably explained by its diffusional motion and dimer formation. The diffusion constants of ClO_2 in 3MHX at temperatures around T_g were estimated in the analysis.

Chlorine dioxide (ClO_2) is well-known to be a stable free redical at room temperature. It was found, however, that ClO_2 decayed in glassy and supercooled liquid 3-methylhexane near its glass transition temperature (T_g) and reappeared at temperatures higher than T_g by about 40 K. These observations have not previously been reported, hence there is a need to explain the mechanism responsible for this decay. The behavior of ClO_2 in some other organic glassy and supercooled liquids is also described.

Experimental

Chlorine dioxide was synthesized by dropping sulfuric acid into a mixture of potassium chlorate and oxalic acid, followed by a passage through an aqueous solution of sodium hydroxide and drying on phosphorus pentaoxide (P_2O_5). The product was further dried over P_2O_5 under vacuum and stored in a glass reservoir in a freezer to prevent decomposition.

3-Methylhexane and 3-methylpentane (99% purity) were purchased from Aldrich Chemicals Co. and heptane, toluene, and 2-methyl-1-propanol (ISB) were reagents of guaranteed grade from Wako Pure Chemicals. These materials were further purified by the methods recommended in the literature.[1] Purity of ISB was 99.54% and the impurities in the other materials were less than 0.01% on gas chromatographic analysis. The purified materials were dried under vacuum and stored in glass ampules. To avoid contamination from vacuum grease in storage, greaseless stopcock with Teflon plunges and ball joints with Teflon O-rings were used.

The purified solvent was degassed by several freeze-pump-thaw cycles and distilled into a calibrated measuring tube under vacuum. A desired amount of solvent was then distilled from the tube into a quartz tube for ESR measurement. Gaseous ClO_2 was taken from the reservoir to an ampule of known volume and introduced into the quartz tube by condensation. The amount of ClO_2 added to the solvent was determined from the volume of the ampule and the pressure of ClO_2. The vapor pressure of ClO_2 was estimated from the temperature of the reservoir. The sample solutions sealed in the ESR tubes were stored in a freezer to prevent loss of ClO_2.

ESR measurements were carried out using a home-built X-band spectrometer equipped with a cryostat using a stream of nitrogen as refrigerant. The cryostat was able to maintain a sample at any temperature from 79 K to 200 K within ±0.1 K for any desired period. The ESR spectrometer consisted of a homodyne-detection system with 450 kHz field modulation. The change in the sensitivity of the ESR measurement was monitored with manganese oxide doped in magnesium oxide.

Usually, the sample solution was kept at 200 K for 3 h to establish the saturation of ClO_2 into solvent, then vitrified by plunging in liquid nitrogen.[2] The glassy solution containing ClO_2 was immediately inserted in the sample became the same as that of the cryostat within 3 min after insertion of the sample.

Analysis of the decay of ClO_2 was carried out with a NEAC 2200/700-computer at Osaka University and a HITAC 8700-computer at Hiroshima University.

Results and Discussion

ESR of ClO_2 in glassy 3-methylhexane (3MHX) gave a pronounced anisotropic spectrum as shown in Fig. 1. When the sample solution was inserted in the cryostat at 97.0 K, the amplitude of the spectrum decreased with time as shown in Fig. 2. As the amplitude decreased, no change in the line shape was observed in the range of ±75 mT from the peak (2). Figure 3 shows the spectra for solutions at higher concentration than that of the solution whose spectrum is shown in Fig. 2 and at a different temperature. Although the difference of the ClO_2 concentration did not produce any remarkable spectral changes, the decay of the signal in the solution of higher concentration became more rapidly at 97.0 K. As the temperature of the solution was raised to 106.3 K, the ClO_2 signal was hardly observed as shown in Fig. 3(B). After the signal disappeared no precipitate was found in the solution. No ESR absorption due to a triplet-state molecule in the $g=4$ region was descernible even at a gain 200 times greater. On further heating a nearly isotropic

† Present address: Department of Applied Physics and Chemistry, Faculty of Engineering, Hiroshima University, Shitami, Saijyo-Cho, Higashi-Hiroshima 724.

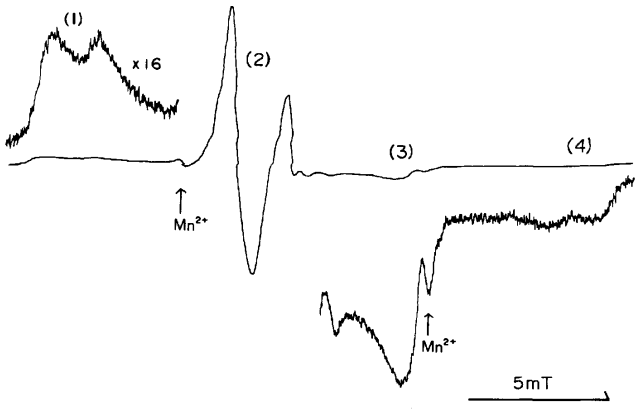

Fig. 1. The ESR spectrum of ClO_2 in 3MHX at 77 K. Peaks indicated by arrows are signals from Mn^{2+} in MgO for the field-calibration.

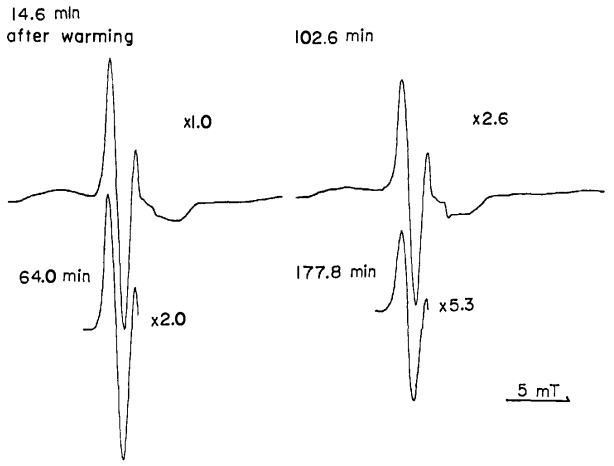

Fig. 2. The ESR spectra of ClO_2 in 3MHX containing ClO_2 of 4.5×10^{-3} mol dm^{-3} at 97.0 K.

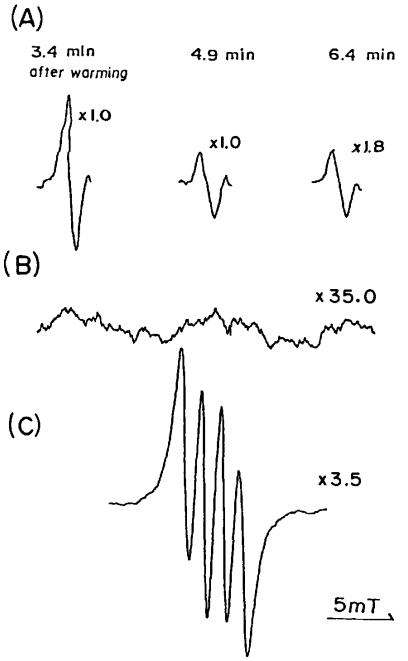

Fig. 3. The ESR spectra of ClO_2 in 3MHX containing ClO_2 of 1.8×10^{-2} mol dm^{-3} at various temperatures: 97.0 K (A), 106.3 K (B), and 131.6 K (C).

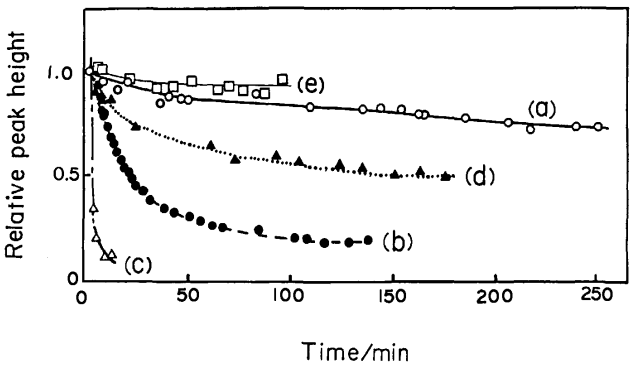

Fig. 4. The decay of peak (2) of Fig. 1 in 3MHX containing ClO_2 of 1.1×10^{-2} mol dm^{-3} at various temperatures: at 87.9 K (a), 96.2 K (b), 105.8 K (c), 115.7 K (d), and 125.3 K (e). The peak heights are normalized by the peak height of the first measurement.

spectrum of Fig. 3(C) for ClO_2 appeared at 131.6 K. As the solution was heated after vitrification and subsequent reinsertion in the cryostat at 97.0 K, the same results were obtained.

ClO_2 in 3-methylpentane (3MP) decayed near 80 K. The decay of ClO_2, however, was not observed in the supercooled and glassy liquids of toluene and 2-methyl-1-propanol (ISB) or in polycrystalline heptane at temperatures ranging from 79 K to about 200 K.

The decay of ClO_2 could be caused by the reaction of ClO_2 with impurities of the solvents and/or oxygen. On consideration of the high purities of the solvents and the use of degassed solutions, those reactions are not responsible for the decay. Besides ClO_2, chlorine monoxide and chlorine trioxide are paramagnetic. As their ESR spectra[3] differ from the spectra of ClO_2, the change of ClO_2 to the monoxide or the trioxide is not able to explain the results. No other phase transitions of 3MHX and of 3MP near their glass transition temperatures (88 K[4] and 77 K[5]), besides the glass transitions, have been reported as far as we know.

Figure 4 shows the decay of peak (2) in 3MHX at various temperatures near T_g. At 77 K, where 3MHX is in the glassy state, ClO_2 gradually decayed with a half life of one week. When the temperature was raised, the rate of decay increased between 77 K and 105 K, however, it decreased above 105 K.

Figure 5 shows the decay of ClO_2 at various

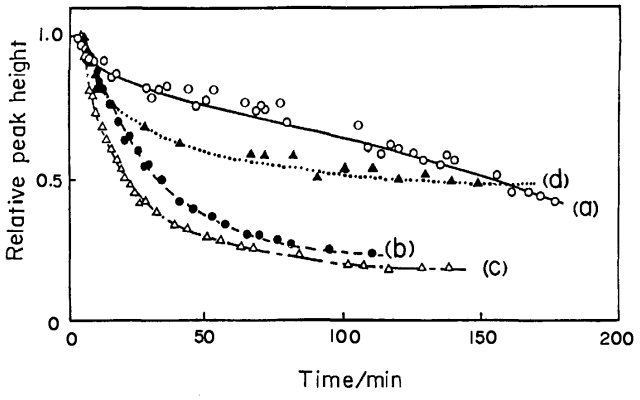

Fig. 5. Additive effect of ClO_2 on the decay of peak (2) of Fig. 1 in 3MHX at 96 K. The nominal concentration of ClO_2 are: 1.6×10^{-3} mol dm^{-3} (a), 5.5×10^{-3} (b), 1.1×10^{-2} (c), and 3.5×10^{-2} (d). The peak heights are normalized by the peak height of the first measurement.

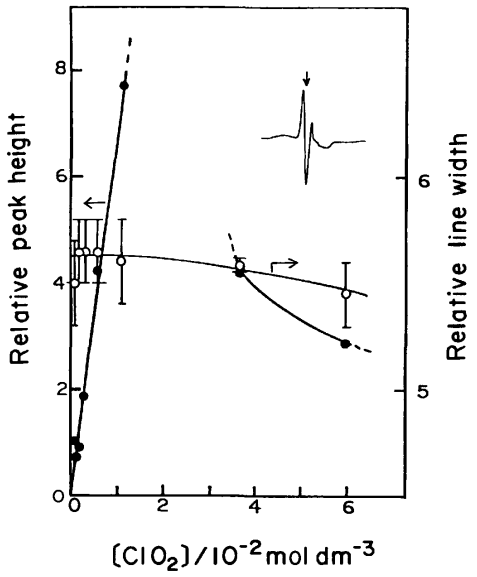

Fig. 6. Additive effect of ClO_2 on the heights and widths of peak (2) of Fig. 1 in 3MHX at 77 K.

nominal concentrations at 96.0 K. The concentrations were calculated from the added amounts of ClO_2 and the volume of the solvent at 77 K which was estimated from its density at 77 K.[6] The decay is faster with addition of ClO_2 until the concentration was increased at about 2×10^{-2} mol dm^{-3}. When the concentration is at 3.5×10^{-2} mol dm^{-3}, the decay slows down.

The plots of the widths and the heights of the peak (2) are shown in Fig. 6 against the nominal concentration of ClO_2 at 77 K. The peak widths seem to be effectively independent of the concentration. Assuming no change of ESR lineshape with the ClO_2 decay, the independence of the peak widths on the nominal concentration indicates that change of ClO_2 concentration can be related to the ESR peak-heights. The heights linearly increase with the addition of ClO_2 up to 1×10^{-2} mol dm^{-3}. In the range of the concentration, $(4—6)\times10^{-2}$ mol dm^{-3}, the peak heights gradually decrease with the addition of ClO_2. In this range the precipitation of ClO_2 was not observed. The decrease of the peak heights at high ClO_2 concentration will be discussed later.

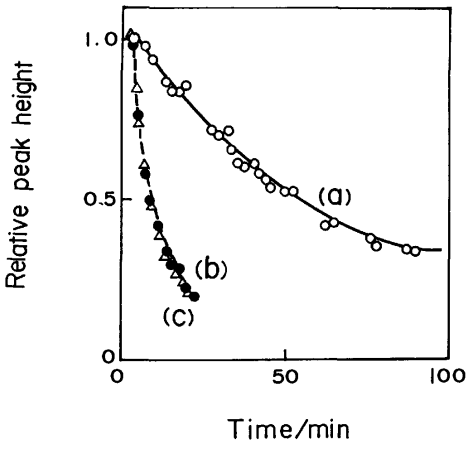

Fig. 7. The decay of peak (2) of Fig. 1 in 3MHX containing ClO_2 of 4.3×10^{-2} mol dm^{-3} at 105.9 K on various thermal treatments of the samples. Lines (a), ○; and (b), ●, are obtained after immediate inserition of the samples from 200 K and 77 K, respectively, into the cryostat of 105.9 K. After annealing for 1 d at 77 K, line (c), △, was obtained. The peak heights are normalized by the peak height of the first measurement.

Analysis of the Decay of ClO_2. Taking into consideration the above results, we assumed that the decay of ClO_2 in 3MHX is due to the formation of a diamagnetic dimer of ClO_2 ($[ClO_2]_2$) described in Eq. 1.

$$ClO_2 + ClO_2 \rightarrow [ClO_2]_2. \quad (1)$$

The dissociation of the dimer was considered in the explanation of the temperature dependence of the decay shown in Fig. 4. The diffusional motion of the ClO_2 molecule was also taken into consideration of the decay because of the high viscosity of 3MHX (about 10^{17} Pa s at T_g[7]).

Before analyses of the curves in Figs. 4 and 5 it is necessary to decide whether the initial distribution of ClO_2 is uniform or not.[8] Figure 7 shows the effects of various thermal treatments of the samples on the decay of the peak (2) of Fig. 1. The curves (a) and (b) were obtained after immediate insertion of the samples into the cryostat of 105 K from 200 K and 77 K, respectively. When the sample was inserted

into the cryostat of 105 K after annealing for 1 d at 77 K, the curve (c) was obtained. No uniform distribution of the ClO_2 molecules resulting from rapid cooling presumably accelerates the decay.

Waite obtained solutions of the kinetic equations of the diffusion-controlled bimolecular reaction A+B→AB with some boundary condition.[9] His theory has been applied and also extended to the analyses of the annealing of the radiation defects in the solid by several authors.[10] We applied Waite theory to the analysis of the decay of ClO_2 considering the reversibility of the reaction (Eq. 1).

According to his theory, the change in the ClO_2 concentration will be expressed by the change in the joint probability density $\rho_{ij}(t)$ between the ith reactant and the jth reactant at time t. As Waite demonstrated, the $\rho_{ij}(t)$ satisfies

$$D_i\nabla_i^2\rho_{ij}(t) + D_j\nabla_j^2\rho_{ij}(t) + f_{ij}(t)\rho_{ij}(t) = \partial_{ij}\rho(t)/\partial t, \quad (2)$$

where $f_{ij}(t)$ act as time-dependent chemical rate-of-raction coefficients. D_i and D_j are the diffusion constants of the ith and jth reactants, respectively; for the ClO_2 decay, $D_i=D_j=D$. The boundary conditions are given as

$$\rho_{ij}(t) = \rho_{eq} \quad \text{for } r \leqq R_0, \quad (3)$$

and

$$\rho_{ij}(t=0) - \rho_{eq} = N\exp[-r^2(\lambda R_0)^{-2}] \quad \text{for } r>R_0. \quad (4)$$

ρ_{eq} is the equilibrium joint probability, $r=|r_i-r_j|$, and R_0 is the radius of the capture sphere. N is a normalization constant and λ is a parameter to be determined from the experimental data. The boundary conditions show that at $r=R_0$ ClO_2 molecules over the equilibrium concentration (which may be propotional to solubility of ClO_2 in 3MHX) immediately react with the other molecules and the initial distribution of ClO_2 molecules is expressed by Eq. 4. Using the boundary conditions, we solved Eq. 2 and rewrote the solution in terms of the fraction of the decay ψ. The results are:

$$\begin{aligned} d\psi/dt = {} & 2\pi R_0^3 C_0'(\psi_{eq}-\psi)^2 z(1+2\pi^{-1/2}z^{-1}) \\ & + 2\pi R_0^3[2\pi^{-1/2}\exp(-\lambda^{-2})\lambda^4(z^2+\lambda^2)^{-2} \\ & + \{2\lambda^2(z^2+\lambda^2)^{-1} - 4\lambda^2(z_s+\lambda^2)^{-2}\} \\ & \times \lambda z(z^2+\lambda^2)^{-1/2}\exp\{-(z^2+\lambda^2)^{-1}\} \\ & \times \mathrm{erf}\{\lambda^{-1}z(z^2+\lambda^2)^{-1/2}\}](1-\phi_0)N \\ & \times \exp\left(\int_0^t f_{ii'}dt\right), \end{aligned} \quad (5)$$

where

$$\int_0^t f_{ii'}dt = -\int_0^z 4\pi R_0^3 C_0'(\psi_{eq}-\psi)(z+2\pi^{-1/2})dz, \quad (6)$$

$$\mathrm{erf}(x) = \int_x^\infty \pi^{-1/2}\exp(-\alpha^2)d\alpha, \quad (7)$$

$$\psi = (C_0'-C)/C_0', \quad (8)$$

and

$$z = (8Dt/R_0)^{1/2}. \quad (9)$$

C is the concentration of ClO_2 at time t and C_0' is the concentration of the first measurement. ψ_{eq} is the equilibrium fraction of the decay. For short times such that $8Dt \ll (\lambda R_0)^2$,

$$\psi - \psi_0 \simeq 8^{1/2}R_0^3 N\exp(-\lambda^{-2})(2Dt)^{1/2}, \quad (10)$$

where ψ_0 is the fraction of the decay at time $t=0$. Equation 10 indicates that at short times ψ is propotional to the square root of t. The Runge-Kutta technique was used in the computer-assisted evaluation of Eq. 5. The parameters taken in this calculation were ψ_0, ψ_{eq}, λ, R_0, and the initial slope of the plots of ψ *versus* $t^{1/2}$.

The best fits of ψ for the temperature dependence of the decay below 105 K (in Fig. 4) are shown in Fig. 8 as a function of $t^{1/2}$ with the experimental points of ψ. The results that at early stages ψ is propotional to $t^{1/2}$ agree with the expectations from Eq. 10. Table 1 summarizes some parameters used in those calculations. Decrease of R_0 with temperature is considered to indicate greater solvation of ClO_2. At a distance of λR_0 the probability density of other molecules around

TABLE 1. PARAMETERS USED FOR THE SIMULATION OF THE DECAY OF ClO_2 IN 3-METHYLHEXANE AT VARIOUS TEMPERATURES[a]

Parameter[b]	T/K			
	77.4	87.9	96.2	105.8
λ	1	2	2.5	4
$R_0/10^{-8}$ cm[c]	20	10	8	5
$\lambda R_0/10^{-8}$ cm	20	20	20	20
$D/10^{-13}$ cm^2 min^{-1}	5.9×10^{-6}	2.3×10^{-4}	6.0×10^{-2}	2.3

a) The nominal concentration of ClO_2 is 1.1×10^{-2} mol dm^{-3}. b) For definition see the text. c) 1 cm = 10^{-2} m.

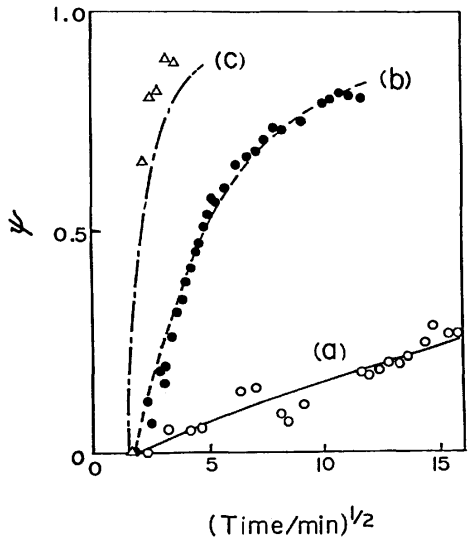

Fig. 8. The decay of ClO_2 in 3MHX containing ClO_2 of 1.1×10^{-2} mol dm^{-3} at various temperatures: 87.9 K (a), 96.2 K (b), and 105.8 K (c). The lines show the calculation by use of Eq. 5 in the text. The parameters used in these calculations are shown in Table 1.

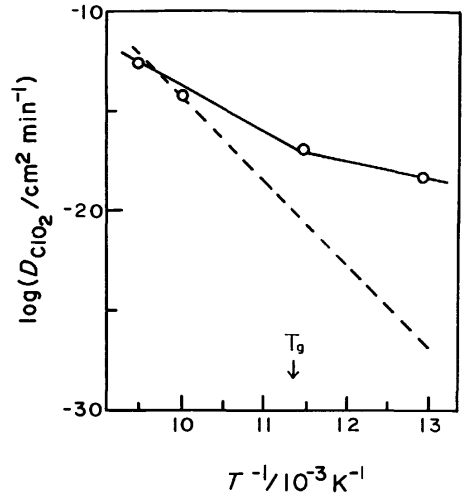

Fig. 9. The Arrhenius plots of diffusion constants of ClO_2 in 3MHX containing ClO_2 of 1.1×10^{-2} mol dm^{-3}. The open circles show the values of the constants shown in Table 1. The dashed line shows the calculation by use of Eq. 11.

one molecule has the maximum value. The constant value of λR_0 is to be expected since the sample solutions were always vitrified by plunging them into liquid nitrogen. Slower cooling of the solutions presumably produces sparse distribution of ClO_2 molecules, that is a large λR_0 value, and may retard the ClO_2 decay as shown in Fig. 7. The values of ψ_{eq} of the lines in Fig. 8 were greater than 0.98, but at $\psi_{eq}>0.975$ the calculated lines dis not change with the value of ψ_{eq}. From the estimated ψ_{eq}'s at various temperatures the change in the enthalpy of the formation of the ClO_2 dimer was estimated to be -17 KJ mol^{-1} at the lower limit. The reasonable fits of ψ for the temperature dependence over 105 K, however, were difficult to explain. As the solutions were heated to the proper temperature over 105 K, the ClO_2 molecules decayed at around 105 K. This situation probably made reasonable fits difficult.

Figure 9 shows Arrhenius plots of the diffusion constants (D's) of ClO_2. The dashed line is the plots of the diffusion constants (D_η's) calculated with Stokes-Einstein's relation given by

$$D_\eta = kT/6\pi\eta a. \quad (11)$$

Here k is the Boltzmann constant, T is the temperature, η is the viscosity, and a is the radius of the molecule. The values of η were taken from the reported values of Ling and Willard.[7] At temperatures around T_g the values of η were estimated by the extrapolation of the reported values. Below T_g the values of D are greater than those of D_η. Above T_g the values of D seem to be near those of D_η. The value of Arrhenius E factor of η was reported as 79 KJ mol^{-1},[7] while the value of D was estimated to be 68 KJ mol^{-1} above T_g.

The plots show that at T_g a translational motion of ClO_2 is accelerated. On the other hand the rotational correlation time of ClO_2 in 3MHX did not show any clear changes at T_g.[11] Seki *et al.*[12] studied the polymerization of vinyl acetate in the glassy state by differential thermal analyses and showed that it polymerizes at temperatures just above T_g, *i.e.* in the supercooled state. They considered that certain immobilized "motion freedom" in the glassy state melts at just above T_g and makes possible the rearrangement and the diffusion of reactant to occur at an appreciable rate. On considering their results and ours the immobilized freedom might be assigned to a translational motion of a molecule.

Figure 10 shows the calculation of the additive effect on the decay (Fig. 5) with the experimental points. The line (c) in Fig. 10 shows the calculation by the use of the initial concentration estimated from the peak height shown in Fig. 6. The calculations using the nominal concentration as the initial concentration failed to reproduce the experimental points. By the addition of ClO_2 the close pairs may convert into the diamagnetic dimers above a certain concentration of ClO_2 even at 77 K. The decrease of the ESR peak-height with addition of ClO_2 shown in Fig. 6 presumably results from the formation of the diamagnetic dimers. Some parameters used in those analyses are summarized in Table 2. In the table r^* is the mean separation of ClO_2 molecules when they uniformly distribute in 3MHX. As ClO_2 added, the

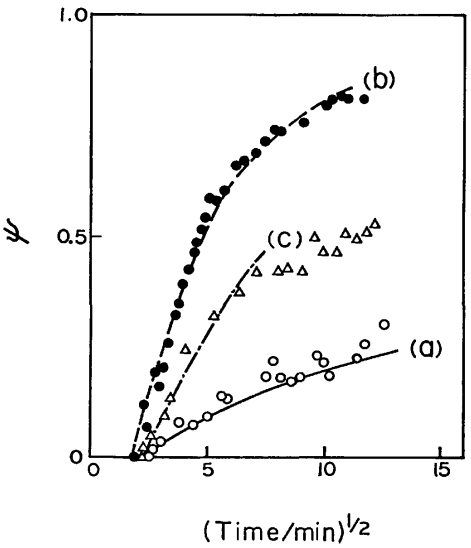

Fig. 10. Additive effect of ClO_2 on its decay in 3MHX at 96 K. The nominal concentration of ClO_2 are at 1.6×10^{-3} (a), 1.1×10^{-2} (b), and 3.5×10^{-2} (c) in units of mol dm^{-3}. The lines show the calculation by use of Eq. 5 in the text. The parameters used in these calculations are shown in Table 2.

TABLE 2. PARAMETERS USED FOR THE SIMULATION OF THE ADDITIVE EFFECT OF ClO_2 ON ITS DECAY IN 3-METHYLHEXANE AT 96 K

Parameter[a]	$[ClO_2]/10^{-3}$ mol dm^{-3}		
	1.6	11	35
λ	2	2.5	3.33
$R_0/10^{-8}$ cm	10	8	6
$\lambda R_0/10^{-8}$ cm	20	20	20
$D/10^{-15}$ cm^2 min^{-1}	0.11	6.0	5.6
$r^*/10^{-8}$ cm	100	53	36

a) For definition see the text.

values of r^* decrease, but, those of λR_0 are almost constant at 2×10^{-9} m. The difference of the diffusion constants at low and high concentrations may indicate some changes in the properties of the solvent induced by the addition of ClO_2.

As mentioned above, ClO_2 did not decay in supercooled and glassy liquids of toluene and ISB or in polycrystalline heptane. The well-resolved vibrational structure of the electronic absorption spectra of ClO_2 in liquid paraffins disappeared when a hydrogen-bonding solute was added.[13] Adams reported that the paramagnetic relaxation mechanisms of ClO_2 in hydrogen-bonding or electron-donating solvents, such as alcohols and aromatic hydrocarbons, were different from the mechanisms in paraffin solvents.[14] He considered that the difference was due to the ClO_2-solvent interaction which was stronger in hydrogen-bonding or electron-donating solvents than in paraffin solvents. On the basis of those studies no decay of ClO_2 in toluene and in ISB might be explained in consideration of the high activation energy arising from the ClO_2-solvent interactions. This speculation is not valid to explain why there is no decay of ClO_2 in heptane. This may result from the fact that heptane is in the polycrystalline state at the temperatures discussed in the present paper.

A few reports mentioned the formation of the ClO_2 dimer.[15,16] Norman and Porter reported that the electronic absorption spectra of ClO_2 in isopentane-methylcyclohexane rigid solutions were different from the spectra in the liquids.[15] They considered that the difference of the spectra was due to the formation of the ClO_2 dimer. Nielson and Woltz studied the infrared spectra of gaseous ClO_2.[16] They speculated that an absorption band at 1.9×10^4 m^{-1} was caused by the dimerization or higher ploymerization of ClO_2. Though those studies do not confirm the presence of a ClO_2 dimer, the reasonable fits of our kinetic analyses suggest that the presence of the ClO_2 dimer is a plausible explanation. To gain additional evidence for the ClO_2 dimer, a study of the optical absorption spectra of ClO_2 in 3MHX around T_g, and some theoretical calculations on the electronic states of ClO_2 and its dimer for assignment of the absorption bands are being planned.

We thank Professor Takahisa Ichikawa for financial assistance in the use of the computers of Hiroshima University.

References

1) J. A. Riddick and W. B. Bunger, "Organic Solvents," 3rd ed, Wiley-Interscience, New York (1970).

2) Cooling rates of a sample were at 2000 K min^{-1} and at 500 K min^{-1} in the temperature ranges, 185 K—150 K and 150 K—105 K, respectively. The average cooling rate was at about 600 K min^{-1}.

3) P. W. Atkins, J. A. Brivati, N. Keen, M. C. R. Symons, and P. A. Trevalion, *J. Chem. Soc.*, **1962**, 4785.

4) H. M. Huffman, G. S. Parks, and S. B. Thomas, *J. Am. Chem. Soc.*, **52**, 3241 (1930).

5) D. R. Douslin and H. M. Huffman, *J. Am. Chem. Soc.*, **68**, 1704 (1946).

6) L. Kevan, "Advances in Radiation Chemistry," ed by M. Burton and J. L. Magee, Wiley-Interscience, New York (1974), Vol. 4, pp 181—305.

7) A. C. Ling and J. E. Willard, *J. Phys. Chem.*, **72**, 3349 (1968).

8) "Reactions in Condensed Phases," ed by H. Eyring, in "Physical Chemistry An Advanced Treatise," ed by H. Eyring, D. Henderson, and W. Jost, Academic Press, New York (1975), Vol. VII.

9) T. R. Waite, *Phys. Rev.*, **107**, 463, 471 (1957); T. R. Waite, *J. Chem. Phys.*, **28**, 103 (1958).

10) B. Ya. Yurkov, *Fiz. Tuerd. Tela*, **3**, 3563 (1961)[*Sov. Phys. Solid State*, **3**, 2591 (1962); K. Dettman, *Phys. Status Solid*, **10**, 269 (1965); D. Peak and J. W. Corbett, *Phys. Rev.*, **B5**, 1226 (1972).
11) N. Ohta and K. Kuwata, *J. Chem. Phys.*, **82**, 3420 (1985).
12) K. Nakatsuka, K. Adachi, H. Suga, and S. Seki, *Polymer Lett.*, **B6**, 779 (1968).
13) P. W. Atkins, A. Horsfield, and M. C. R. Symons, *J. Chem. Soc.*, **1964**, 5220.
14) J. Q. Adams, *J. Chem. Phys.*, **45**, 4167 (1966).
15) I. Norman and G. Porter, *Proc. Roy. Soc.*, **A230**, 399 (1955).
16) A. H. Nielson and P. J. H. Woltz, *J. Chem. Phys.*, **20**, 1878 (1952).

The Theoretical Study of the Solvophobic Interaction

Masaharu OHBA and Kiyoshi ARAKAWA*
Research Institute of Applied Electricity, Hokkaido University, Sapporo 060
(Received February 2, 1985)

The relation between a solvophobic interaction (SI) and a solute-solute radial distribution function is discussed. The SI is defined as the difference between the indirect part of the solute-solute potential of the mean force in a solvent and that in a "homomorphic" solvent. It was calculated using the RHNC-like integral equation of RISM-1 for a dilute solution of hard spheres in a solvent composed of polar hard dumb-bells. The existence of a SI was comfirmed in a simple system. The SI in this system proved to have originated from the effect of a dipole-dipole interaction between solvent molecules making the excluded volume of the solute molecules small. It was found that the strength of a SI decreases with increasing temperature. It was also shown that Ben-Naim's measure [*J. Chem. Phys.*, **54**, 1387 (1971)] gives an incorrect conclusion with respect to the temperature dependence of the SI of this system because it includes an excess factor irrelevant to a SI.

Hydrophobic interactions have been investigated by many authors,[1-5] but from a microscopic point of view, their essential character is still not clear. Recently, molecular dynamical calculations were performed[6,7] and semiphenomenological theories were proposed on the basis of an integral equation for liquids.[8,9] However, no clear conclusions have been reached. Statistical mechanical studies from first principles are required in order to clarify the microscopic properties of the hydrophobic interactions, and then, an investigation on solvophobic interactions (SI) is expected to be fruitful as the first step for a thorough understanding of hydrophobic interactions.

There are two problems regarding a study of the SI. The first is how the SI is defined on the basis of statistical mechanics. Ben-Naim[10] related the SI to the potential of the mean force between two solute molecules. However, the potential of the mean force includes a contribution which has no direct connection with the SI, and in the definition of the SI it must be subtracted from the potential of the mean force. The second is to calculate the SI defined by statistical mechanics from first principles. To understand the fundamental aspects of the SI, we investigated the SI of a dilute solution of hard spheres in a polar solvent composed of dipolar hard dumb-bells using the RHNC-like integral equation of RISM-1.[11,12]

The Solvophobic Interaction and the Potential of the Mean Force

In this section, we consider the SI induced in a solution including nonpolar molecules in a solvent. For simplicity, consider the solute molecules to be spherical, and the interaction potential between two solute molecules $U_{AA}(r)$ to have no angular dependence. Hereafter, subscripts A and S denote the solute and the solvent species, respectively.

The potential of mean force between two solute molecules $W_{AA}(r)$ is defined by

$$W_{AA}(r) = -k_B T \ln g_{AA}(r), \tag{1}$$

where k_B is the Boltzmann constant, T the absolute temperature and $g_{AA}(r)$ the radial distribution function between two solute molecules. The physical meaning of $W_{AA}(r)$ is "the free energy change which is caused when two solute molecules move each other from an infinite separation to a distance r in a given solvent." The indirect part of $W_{AA}(r)$ is given by

$$w_{AA}(r) = W_{AA}(r) - U_{AA}(r) = -k_B T \ln y_{AA}(r), \tag{2}$$

where $y_{AA}(r)$ is the indirect pair correlation function between two solute molecules. $w_{AA}(r)$ is the effective potential between the two solute molecules induced by all the other molecules, and it is identical with Ben-Naim's $\delta A^{HI}(r)$.[10]

Here, we consider that the solvent-solvent interaction $U_{SS}(i_S, j_S)$ can be divided into two parts,[13]

$$U_{SS}(i_S, j_S) = U_{SS}^{(0)}(i_S, j_S) + U_{SS}^{(1)}(i_S, j_S). \tag{3}$$

$U_{SS}^{(0)}(i_S, j_S)$ is the hard-core potential including the dispersion force. $U_{SS}^{(1)}(i_S, j_S)$ is the interaction other than $U_{SS}^{(0)}(i_S, j_S)$, including the contribution of the dipole-dipole interaction, the hydrogen bond and others. i_S and j_S denote the positions and orientations of the i-th and the j-th solvent molecules, respectively. Then, we define $w_{AA}^{(0)}(r)$ as the indirect part of the potential of the mean force between two solute molecules in a homomorphic solvent in the same state as the solution, where a "homomorphic solvent" denotes a solvent composed of molecules whose intermolecular interaction is expressed as $U_{SS}^{(0)}(i_S, j_S)$. Since $w_{AA}^{(0)}(r)$ is the effective potential caused by the packing effect of molecules with a hard core in nonpolar solvents, it has no direct relation to the SI. It is equivalent to the indirect part of the potential of the mean force in liquids composed of nonpolar molecules. It must be subtracted from $w_{AA}(r)$. Here, we define $\delta w_{AA}(r)$ as follows,

$$\delta w_{AA}(r) = w_{AA}(r) - w_{AA}^{(0)}(r). \tag{4}$$

$\delta w_{AA}(r)$ is the effective potential between two solute molecules. This is the quantity which expresses the SI of a solution.

When the solute molecules are hard spheres, $w_{AA}(0)=-\Delta\mu_A$.[8,14] Here, $\Delta\mu_A$ is the chemical potential of solute molecules in a solution with respect to an ideal gas. Thus, we have

$$\delta w_{AA}(0) = \Delta\mu_A^{(0)} - \Delta\mu_A, \tag{5}$$

where $\Delta\mu_A^{(0)}$ is the chemical potential of the solute molecules in a homomorphic solvent. Equation 5 shows that $\delta w_{AA}(0)$ is the chemical potential change with respect to a transfer of the solute molecules from the solvent to the homomorphic solvent. Thus, Eq. 5 gives grounds for the fact that the chemical potential change with respect to the transfer of solutes from water to a hydrocarbon solvent is a good measure for the strength of the hydrophobic interaction.

In the following sections, we calculate $\delta w_{AA}(r)$ of the dilute solutions of hard spheres in a solvent composed of polar hard dumb-bells.[15]

The Application to the Dilute Solutions of Hard Spheres in Polar Solvents

The system considered is a dilute solution of nonpolar molecules in a polar solvent. Solute molecules are hard spheres with a diameter σ_{AA}. Solvent molecules are two fused hard spheres with the same diameter σ_{SS}, on whose center the charges $+q_S$ and $-q_S$ are sited. The bond length of a solvent molecule is l. An illustration of a molecule is shown in Fig. 1.

The total potential energy of the solution is assumed to be the sum of all pairs of intermolecular potentials. The intermolecular potential between the i-th molecule of type M and the j-th molecule of type M′ is given by

$$U_{MM'}(i_M, j_{M'}) = \sum_\alpha \sum_\gamma u_{\alpha M\gamma M'}(|r_{iM}^\alpha - r_{jM'}^\gamma|), \tag{6}$$

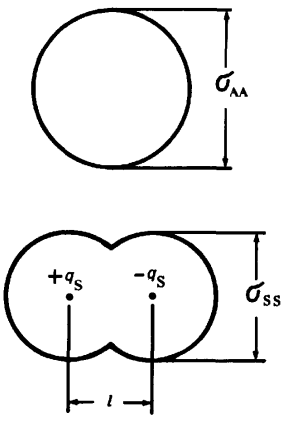

Fig. 1. The shapes of the solute molecule and the solvent molecule.

where $u_{\alpha M\gamma M'}(|r_{iM}^\alpha - r_{jM}^\gamma|)$ is the interaction potential between the α-th atom of the i-th molecule of type M (A or S) and the γ-th atom of the j-th molecule of type M′. r_{iM}^α is the position of the α-th atom of the i-th molecule of type M. The atom-atom interactions are given as

$$u_{\alpha S\gamma S}(r) = u_{SS}^{(0)}(r) + q_{\alpha S}q_{\gamma S}/4\pi\varepsilon_0 r, \tag{7}$$

$$u_{\alpha SA}(r) = u_{SA}^{(0)}(r), \tag{8}$$

$$u_{AA}(r) = u_{AA}^{(0)}(r), \tag{9}$$

$$u_{MM'}^{(0)}(r) = \begin{cases} \infty, & r<\sigma_{MM'} \\ 0, & r>\sigma_{MM'} \end{cases} \tag{10}$$

where we assume that $\sigma_{AS}=(\sigma_{AA}+\sigma_{SS})/2$. ε_0 is the dielectric constant of the vacuum. In this system, $U_{SS}^{(0)}(i_S, j_S)$ and $U_{SS}^{(1)}(i_S, j_S)$ in the previous section are given as

$$U_{SS}^{(0)}(i_S, j_S) = \sum_\alpha \sum_\gamma u_{SS}^{(0)}(|r_{iS}^\alpha - r_{jS}^\gamma|)$$

and

$$U_{SS}^{(1)}(i_S, j_S) = \sum_\alpha \sum_\gamma q_{\alpha S}q_{\gamma S}/4\pi\varepsilon_0|r_{iS}^\alpha - r_{jS}^\gamma|,$$

respectively.

Radial distribution functions and $\delta w_{AA}(r)$ were obtained by solving the RHNC-like integral equation of RISM-1,[11,12] and the procedures of the calculation are quite identical with those described in reference 12.

Results and Discussion

The present system is characterized by five parameters, as follows: the reduced number densities of solute molecules and solvent molecules $\rho_A^*=\rho_A\sigma_{AA}^3$ and $\rho_S^*=\rho_S d^3$, the reduced dipole moment of solvent molecules $\mu_S^*=(\mu_S^2/4\pi\varepsilon_0 k_B T d^3)^{1/2}$, the reduced bond length of solvent molecules $L^*=l/\sigma_{SS}$, and the ratio of σ_{AA} to σ_{SS} $\sigma_{AA}^*=\sigma_{AA}/\sigma_{SS}$. Here, ρ_A and ρ_S are the number densities of solute molecules and solvent molecules, respectively, $\mu_S=q_S l$ the magnitude of the dipole moment of solvent molecules, and d the diameter of a hard sphere whose volume is the same as a solvent molecule. It is given by the following equation

$$d^3 = \sigma_{SS}^3(1+3L^*/2-L^{*3}/2).$$

Because of symmetry, we have four types of atom-atom radial distribution functions, as follows; $g_{AA}(r)$, $g_{AS+}(r)=g_{S+A}(r)=g_{AS-}(r)=g_{S-A}(r)\equiv g_{AS}(r)$, $g_{S+S+}(r)=g_{S-S-}(r)$ and $g_{S+S-}(r)=g_{S-S+}(r)$.

The Structure of the Solution. The atom-atom radial distribution functions of the solution are shown in Figs. 2a—c. The broken curves indicate atom-atom radial distribution functions of the solution in a homomorphic solvent. Figure 2a shows

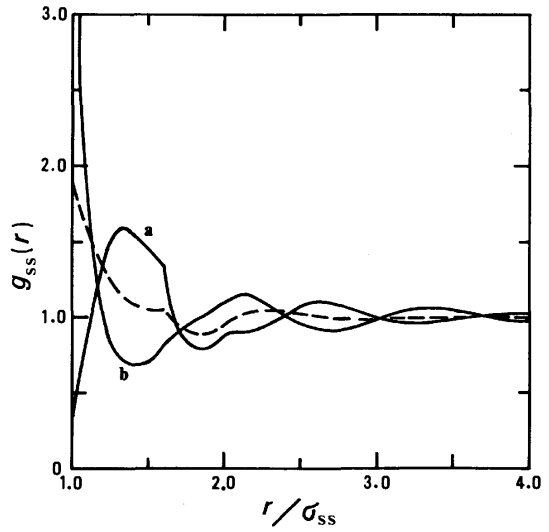

Fig. 2a. The solvent-solvent radial distribution functions for the solution at $\rho_A^*=0.001$, $\rho_S^*=0.8$, $\mu_S^*=3.0$, $L^*=0.6$ and $\sigma_{AA}^*=1.0$. a; $g_{S+S+}(r)$, b; $g_{S+S-}(r)$, ----; $g_{SS}^{(0)}(r)$.

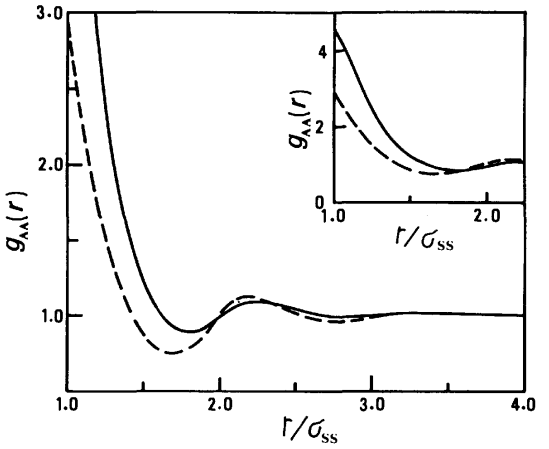

Fig. 2b. The solute-solute radial distribution functions for the same solution as Fig. 2a. ——; $g_{AA}(r)$, ----; $g_{AA}^{(0)}(r)$.

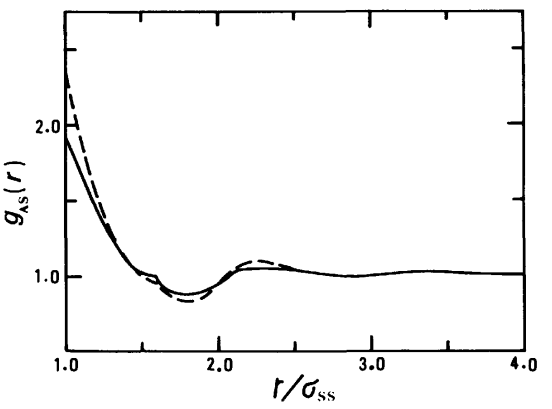

Fig. 2c. The solute-solvent radial distribution functions for the same solution as Fig. 2a. ——; $g_{AS}(r)$, ----; $g_{AS}^{(0)}(r)$.

that an orientational correlation between two solvent molecules exists over a considerably long-range region.[11] As seen in Fig. 2b, $g_{AA}(r)$ is larger than that in a homomorphic solvent at $r<2\sigma_{SS}$, and in Fig. 2c the contact value of $g_{AS}(r)$ is smaller than that in a homomorphic solvent. This result shows that the solvent molecules are atracted to each other by dipole-dipole interactions. Thus, the probability that solute molecules approach each other is enlarged. This confirms the presence of a solvophobic interaction in this system.

The Solvophobic Interaction. The potential of the mean force between two solute molecules and the solvophobic interaction $\delta w_{AA}(r)$ are shown in Fig. 3. These are calculated from the solute-solute radial distribution functions shown in Fig. 2b. $w_{AA}(r)$ and $w_{AA}^{(0)}(r)$ have maxima at $r\approx1.6\sigma_{AA}$ and have an oscilltory structure around the asymptotic value zero. $\delta w_{AA}(r)$ has a maximum at $r\approx2.1\sigma_{AA}$, but the maximum is very small. The value of $\delta w_{AA}(r)$ is negative at $r<r_{max}$ and nearly equal to zero at $r<r_{max}$, where r_{max} denotes the position of the first maximum of $\delta w_{AA}(r)$. This shows that the dipole-dipole

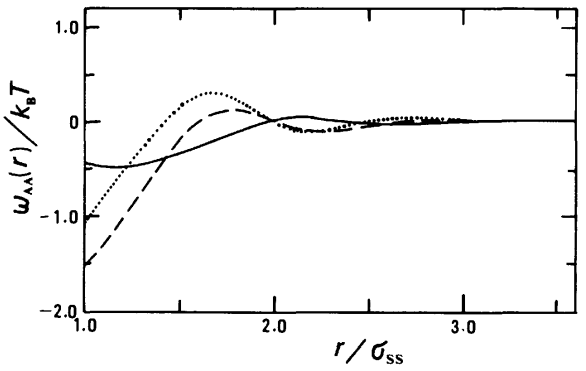

Fig. 3. The potential of mean force between two solute molecules for the same solution as Fig. 2. ——; $\delta w_{AA}(r)$, ----; $w_{AA}(r)$, ····; $w_{AA}^{(0)}(r)$.

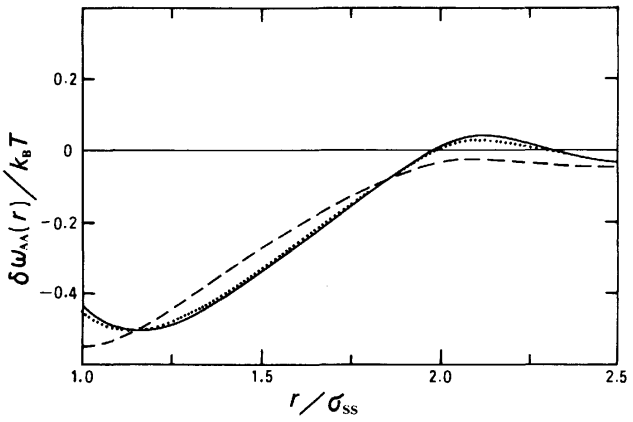

Fig. 4. The solvophobic interactions at $\rho_S^*=0.8$, $\mu_A^*=3.0$, $L^*=0.6$ and $\sigma_{AA}^*=1.0$. ——; $\rho_A^*=0.001$, ····; $\rho_A^*=0.01$, ----; $\rho_A^*=0.04$.

interaction between solvent molecules induces an apparent and effective attraction between the two solute molecules, that is, a solvophobic interaction. It is also shown that the SI is short ranged. $\delta w_{AA}(r)$ has a small minimum at $r \approx 1.2\sigma_{AA}$. The minimum is probably an artifact due to the approximation of the RHNC-like integral equation. $\delta w_{AA}(r)$ decreases with decreasing r near the contact distance.

The concentration dependence of $\delta w_{AA}(r)$ is shown in Fig. 4. $\delta w_{AA}(r)$ for $\rho_A^*=0.01$ is practically the same as that for $\rho_A^*=0.001$ and no appreciable difference between $\delta w_{AA}(r)$ for $\rho_A^*=0.001$ and that for more dilute solutions was found. This shows that $\rho w_{AA}(r)$ at $\rho_A^*=0.001$ can be safely regarded as that for a solution at infinite dilution. Figure 5 shows that the strength of the SI increases with increasing μ_S^* and the position of the maximum is unchanged. It is found from Fig. 6 that the bond length of solvent molecules has little effect on the SI when the dipole moment of solvent molecules is held constant.

Figures 7 and 8 show the effect of the size of solute molecules on the SI. Shapes of $g_{AS}(r)$ at $\sigma_{AA}^*=0.8$ and 1.6 are very similar (Fig. 7). This indicates that a change in the size of solute molecules has little effect on the solvent structure around the solute molecules. The magnitude of $|\delta w_{AA}(r)|$ at $r<r_{max}$ increases remarkably with an enlargement of the size of the solute molecules (Fig. 8), and the position of the maximum coincides with each other when the curves are plotted on the abscissa $(r-\sigma_{AA})/\sigma_{SS}$. It is found that the positions of the maximum of $\delta w_{AA}(r)$ of all systems shown in Figs. 3—6 and 8 are approximately expressed as $r_{max}=\sigma_{AA}+1.1\sigma_{SS}$, which is nearly equal to the diameter of the excluded volume of solute molecules $(\sigma_{AA}+\sigma_{SS})$. Thus, it is said that the SI is negligible when excluded volumes of two solute molecules do not overlap with each other and is attractive when the excluded volumes do overlap. Namely, the SI acts to make the total excluded volume of solute molecules small when the excluded volumes overlap. Then, taking account of the size dependence of $\delta w_{AA}(r)$ at $r<r_{max}$ (Fig. 8) together, it is concluded that the origin of the SI is the effect of the attractive dipole-dipole interaction between solvent molecules to make the excluded volume of solute

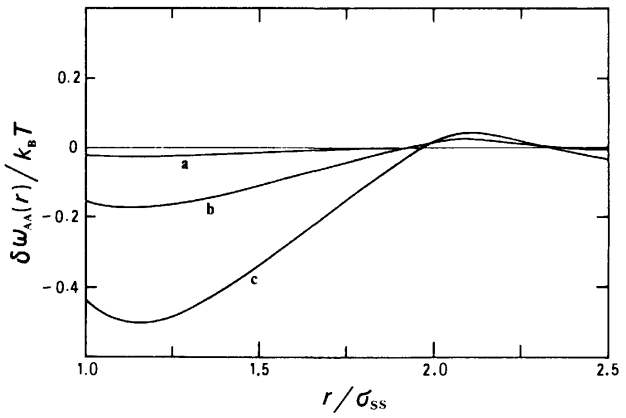

Fig. 5. The solvophobic interactions at $\rho_A^*=0.001$, $\rho_A^*=0.8$, $L^*=0.6$, and $\sigma_{AA}^*=1.0$. a; $\mu_S^*=1.0$, b; $\mu_S^*=2.0$, c; $\mu_S^*=3.0$.

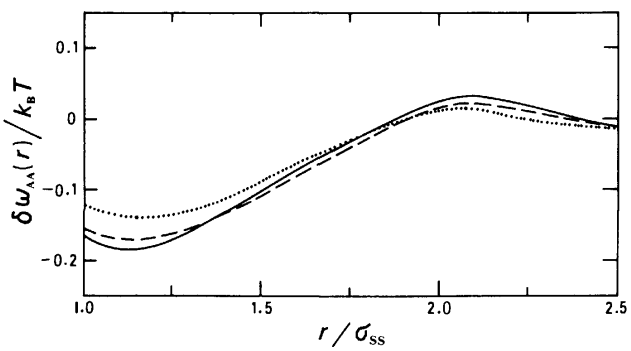

Fig. 6. The solvophobic interactions at $\rho_A^*=0.001$, $\rho_S^*=0.8$, $\mu_S^*=3.0$, and $\sigma_{AA}^*=1.0$. ——; $L^*=0.4$, ----; $L^*=0.6$, ;···· $L^*=0.8$.

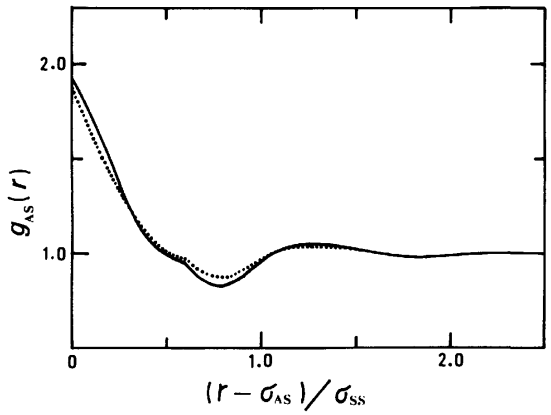

Fig. 7. The solute-solvent radial distribution functions at $\rho_A^*=0.001$, $\rho_S^*=0.8$, $\mu_S^*=3.0$, and $L^*=0.6$. ——; $\sigma_{AA}^*=1.6$, ----; $\sigma_{AA}^*=0.8$.

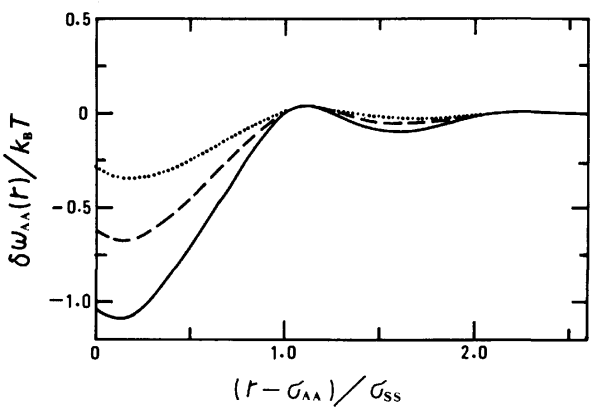

Fig. 8. The solvophobic interactions at $\rho_A^*=0.001$, $\rho_S^*=0.8$, $\mu_S^*=3.0$, and $L^*=0.6$. ——; $\sigma_{AA}^*=1.6$, ----; $\sigma_{AA}^*=1.2$, ····; $\sigma_{AA}^*=0.8$.

Table 1. The temperature dependence of the solvophobic interaction at $\rho_A^*=0.001$, $\rho_S^*=0.8$, $L^*=0.6$, and $\sigma_{AA}^*=1.0$

$1/ck_BT$[a)]	$cw_{AA}(\sigma_{AA})$	$cw_{AA}^{(0)}(\sigma_{AA})$	$c\delta w_{AA}(\sigma_{AA})$
9.00	−0.168	−0.119	−0.049
6.25	−0.216	−0.172	−0.044
4.00	−0.307	−0.269	−0.038
2.25	−0.509	−0.478	−0.031
1.00	−1.097	−1.077	−0.020
0.25	−4.316	−4.308	−0.008
0	—	—	0

a) $c=4\pi\varepsilon_0 d^3/\mu_S^2$.

molecules small. In this respect, the SI of this system is an energetic effect. A solvophobic solvation like the ice-berg as stated by Némethy and Sheraga[3] does not exist, or hardly contributes to the SI even if the solvophobic solvation exists. If the solvophobic solvation is the main source of the SI, the range of the SI must be longer than $(\sigma_{AA}+2\sigma_{SS})$ which is the shortest distance when the solvation cells of two solute molecules contact each other.

The temperature dependence of the SI is shown in the Table 1. It is noted that $w_{AA}(\sigma_{AA})$ is identical with $\delta A^{SI}(\sigma_{AA})=\Delta\mu_D-2\Delta\mu_M$, Ben-Naim's measure of the SI,[4,10] where $\Delta\mu_D$ and $\Delta\mu_M$ are the chemical potentials of the dimer and the monomer of the solute molecules in the solution, respectively. $|\delta w_{AA}(\sigma_{AA})|$ decreases with increasing temperature, which means that the strength of the SI of this system decreases as the temperature increases. On the other hand, $|w_{AA}(\sigma_{AA})|$ increases with increasing temperature. This is because $\ln y_{AA}^{(0)}(r)=-w_{AA}^{(0)}(r)/k_BT$ of this system does not depend on the temperature. $|w_{AA}^{(0)}(\sigma_{AA})|$ becomes larger in propotion to the temperature, and resultantly the increment of $|w_{AA}^{(0)}(\sigma_{AA})|$ exceeds the decrement of $|\delta w_{AA}(\sigma_{AA})|$. Thus, Ben-Naim's measure, $w_{AA}(\sigma_{AA})$, gives an incorrect conclusion with respect to the temperature dependence of the SI of this system, because its temperature dependence is dominated by that of $w_{AA}^{(0)}(r)$ which is essentially irrelevant to the SI.

Concluding Remarks

It was shown that the SI can be expressed by $\delta w_{AA}(r)=w_{AA}(r)-w_{AA}^{(0)}(r)$, and that Ben-Naim's measure of the SI, which is identical with $w_{AA}(r)$, gives an incorrect temperature dependence because it includes an excess term, like $w_{AA}^{(0)}(r)$ which is irrelevant to the SI.

$\delta w_{AA}(r)$ of dilute solutions of hard spheres in a polar hard dumb-bell solvent was calculated by means of an RHNC-like integral equation of RISM-1 in order to clarify the microscopic properties of the SI. It was shown from this calculation that (1) the dipole–dipole interaction between solvent molecules can cause the SI, (2) the SI in this system mainly originates from the effect of a dipole–dipole interaction between solvent molecules to make the excluded volume of solute molecules small, and (3) a solvophobic solvation like the ice-berg does not exist or hardly contributes to the SI of this system.

References

1) W. Kauzman, *Adv. Protein Chem.*, **14**, 1 (1959).
2) H. S. Frank and M. W. Evans, *J. Chem. Phys.*, **13**, 507 (1945).
3) G. Némethy and H. A. Scheraga, *J. Chem. Phys.*, **36**, 3382, 3401 (1962); *J. Phys. Chem.*, **66**, 1773 (1962).
4) A. Ben-Naim, "Hydrophobic Interactions," Plenum Press, New York (1980).
5) K. Arakawa, K. Tokiwano, N. Ohtomo, and H. Uedaira, *Bull. Chem. Soc. Jpn.*, **52**, 2483 (1979).
6) A. Geiger, A. Rahman, and F. H. Stillinger, *J. Chem. Phys.*, **70**, 263 (1979).
7) D. C. Rapaport and H. A. Scheraga, *J. Phys. Chem.*, **86**, 873 (1982).
8) L. R. Pratt and D. Chandler, *J. Chem. Phys.*, **67**, 3683 (1977); **73**, 3430 (1980).
9) A. Tani, *Mol. Phys.*, **48**, 1229 (1983); **51**, 161 (1984).
10) A. Ben-Naim, *J. Chem. Phys.*, **54**, 1387, 3696 (1971); **57**, 5257, 5266 (1972).
11) M. Ohba and K. Arakawa, *Bull. Chem. Soc. Jpn.*, **55**, 1387 (1982).
12) M. Ohba and K. Arakawa, *Bull. Chem. Soc. Jpn.*, **58**, 9 (1985).
13) In general, the intermolecular interaction is expressed as the sum of potentials of hard core repulsions, dispersion forces, dipole–dipole interactions and others. The interaction between nonpolar molecules consists of the first two factors. The occurrence of the SI is thus ascribed to the presence of the other facters ($U_{SS}^{(1)}(i_S, j_S)$ in Eq. 3).
14) E. Meeron and A. J. F. Siegert, *J. Chem. Phys.*, **48**, 3139 (1968).
15) In the following sections, calculations are carried out without dispersion forces in $U_{SS}^{(0)}(i_S, j_S)$. Inclusion of dispersion forces is supposed to cause no important changes to the conclusions of the present calculations.

 © 1985 The Chemical Society of Japan Bull. Chem. Soc. Jpn., 58, 3073—3075 (1985)

Yields of Solvated Electrons at 30 Picoseconds in Water and Alcohols

Takashi SUMIYOSHI, Kazunori TSUGARU, Tatsuya YAMADA, and Meiseki KATAYAMA*
Department of Atomic Science and Nuclear Engineering, Faculty of Engineering, Hokkaido University, Sapporo 060
(Received May 11, 1985)

Direct measurements of the yield of hydrated electrons in aqueous solutions and solvated electrons in alcohols were carried out using a stroboscopic picosecond pulse radiolysis system. The yield of solvated electrons was obtained by simultaneous consideration of the pulse shape and radiation doses. The yield at 30 ps after irradiation, $G(e^-_{aq})_{30ps}$, was determined to be 4.8±0.3 products per 100 eV as compared to the $G(e^-_{aq})_{100ns}$ of 2.7. Experimental values, including the present ones, are higher by 0.3 than the theoretical ones calculated using the spur diffusion model in the time period from 3×10^{-11} to 10^{-8} s. Nevertheless, both results show a quite similar time dependence, *i.e.*, fast decay of hydrated electrons in spur reactions. The *G*-values of solvated electrons at 30 ps were also determined in alcohols. The *G*-value of solvated electron is 3.4±0.3 in both methanol and ethanol, 2.0±0.3 in 1-propanol and 2.3±0.3 in ethylene glycol.

Hydrated electrons in aqueous solutions and solvated electrons in alcohols have been well known as one of the main products in radiation chemistry. Since the solvated electron reacts very rapidly in the spur in the time region from ps to ns, the experimental yield obtained depends on the time resolution of the apparatus. Radiation chemistry of aqueous solutions has been reasonably explained by the spur diffusion model.[1] This model was originally proposed by Samuel and Magee[2] and is now widely known in various forms. The model adequately explains the dependence of experimental molecular product yields with solute concentrations and also LET effects.[1,3] The initial yield of the hydrated electron before it escapes the spur is an extremely important parameter for the spur diffusion model. Calculations by Schwarz predict the initial yield of e^-_{aq} to be 4.78.[1] However, there is a substantial difference between the experimental *G*-values obtained in the time region 30—100 ps. Wolff *et al.*[4] reported $G(e^-_{aq})=4.0\pm0.2$ at 30 ps by measurements using a stroboscopic picosecond pulse radiolysis (SPR) system with a train of fine structure electron pulses. Recently Jonah *et al.*[5] reported $G(e^-_{aq})=4.6\pm0.2$ at 100 ps using a single picosecond electron pulse. This significant disagreement prompted us to measure the $G(e^-_{aq})$ at 30 ps.

The yields of solvated electrons in several alcohols were also measured.

Experimental

The experiment was carried out using an SPR system with a time resolution of about 30 ps and the radiation source of a 45 MeV electron pulse from the S-band LINAC at Hokkaido University.[6] The optical apparatus of the SPR system was basically the same as that designed by Bronskill *et al.*,[7] and the Čerenkov light produced in a 10 cm air path was used as an analyzing light. To obtain good linearity, the detection system was equipped with an amplifier (ORTEC 451) and A/D converter (NAIG 161) instead of a stretcher, a differential amplifier and an integrator.[7] The optical absorption signals of e^-_{aq} were observed at 633 nm in pure water and 0.5 M† $HClO_4$. The cell used had a 2 cm optical path length and two circular apertures of 3 mm at its front and rear. The pure water in 1 dm^3 reservoir was bubbled with pure argon before and during irradiation and circulated through the cell by a pump. The yield of e^-_{aq} at 30 ps was obtained by simulations considering the pulse shape and radiation doses. The shape of the macro pulse was measured by monitoring the Čerenkov light with a photomultiplier (HAMAMATSU TV R446UR) and a 500 MHz oscilloscope (TEXTRONIX 7904), and it could be approximated to a Gaussian with a half width of 11 ns. The dose was measured by the absorption signal of e^-_{aq} in pure water at 100 ns assuming $G(e^-_{aq})=2.7$.[8] The dose measurement was carried out by a conventional nanosecond pulse radiolysis technique using the SPR system, which allows a He-Ne laser (633 nm) to pass through the irradiation volume of the sample. The output of the photomultiplier was fed into a transient digitizer (IWATSU DM901) having the shortest resolvable time of 10 ns, and then displayed on an X-Y recorder. The observed dose was 4.3±0.3 krad/macro pulse as $\varepsilon_{633nm}=1.44\times10^4\ M^{-1}\ cm^{-1}$ for e^-_{aq}.[4] Aqueous solutions were prepared with triply distilled water. Alcohols were guaranteed reagents (Wako Junyaku) and were used without purifications.

Results and Discussion

Figure 1 shows the SPR signal of decay of e^-_{aq} observed at 633 nm in 0.5 M $HClO_4$. The dashed line and dotted line are computer simulated kinetic traces of e^-_{aq}. Since the observation time was limited up to 350 ps after each fine structure pulse, high acid concentrations were used to prevent the significant buildup of absorption signal from one fine structure pulse to the next.

The bimolecular rate constant for the scavenging reaction of e^-_{aq} has been measured as $(1.2\pm0.2)\times10^{10}\ M^{-1}\ s^{-1}$ for $[H^+_{aq}]$ from 0.5—5.0 M.[9] Therefore, the half lifetime of e^-_{aq}

† 1 M=1 mol dm^{-3}.

$$e^-_{aq} + H^+_{aq} \xrightarrow{k_2} H\cdot \quad (1)$$

in 0.5 M $HClO_4$ solutions is expected to be 120 ps. By this reason, the decay of e^-_{aq} during the pulse, which brought about a decrease in the initial step height by a factor of 0.88,[9] was taken into account, and correction for the density (1.03) of solutions was also made in the simulation.

The experimental kinetic trace of e^-_{aq} was best reproduced by adapting $G(e^-_{aq})_{30\,ps}=4.8$. A simulated trace with $G(e^-_{aq})_{30\,ps}=4.0$[4] is also shown in Fig. 1

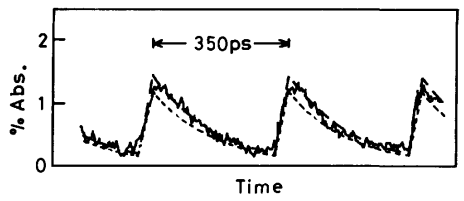

Fig. 1. The kinetic trace of e^-_{aq} observed at 633 nm in 0.5 M $HClO_4$. The dashed and dotted lines are simulated traces with $G(e^-_{aq})_{30ps}$ as 4.8 and 4.0 respectively. The dose was 4.3 krad/macro pulse and the half life time was 120 ps.

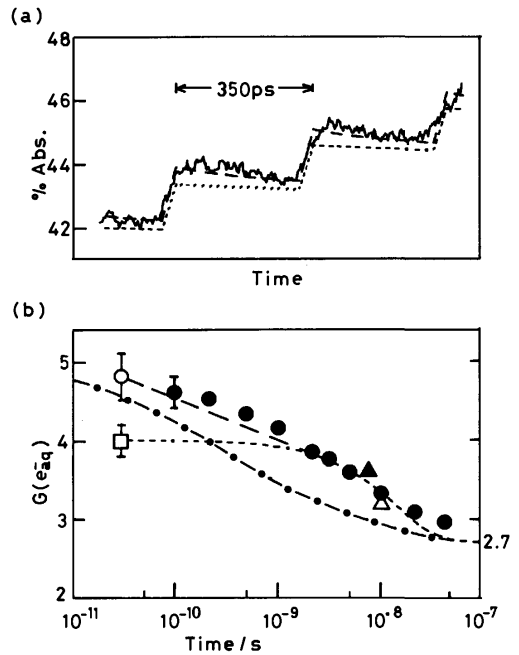

Fig. 2. (a) The kinetic trace of e^-_{aq} observed at 633 nm in pure water. The dashed and dotted lines are simulated traces with time dependences given in (b). (b) The time dependences of $G(e^-_{aq})$ in pure water. (○),[10] (□),[4] (●),[5] (▲),[13] and (△)[14] are experimental values.
(—·—·—) is the theoretical time dependence of $G(e^-_{aq})$ by Schwarz.[1]

(dotted line) for comparison. From several experimental results, we concluded that $G(e^-_{aq})_{30\,ps}=4.8\pm0.3$.[10]

The error of $G(e^-_{aq})_{30\,ps}$ depends directly on the error of radiation dose measurements, while it depends on the shape of the electron macro pulse only slightly. If the shorter pulse width of 10 ns was used to simulate instead of the 11 ns that was actually observed, the best fit was obtained with $G(e^-_{aq})_{30\,ps}=4.7\pm0.3$. It should be noted that the present experiments give a higher $G(e^-_{aq})_{30\,ps}$ value than that reported by Wolff *et al.*[4] irrespective of the similar experimental conditions; however, $G(e^-_{aq})$ values close to those of present studies have been suggested in some steady state studies.[11,12]

The solid line in Fig. 2a shows the kinetic trace of e^-_{aq} observed in pure water. The dashed line and the dotted line are computer simulated kinetic traces. In the case of pure water, the half lifetime of e^-_{aq} ($T_{1/2}>10$ ns) is much longer than the interval of fine structure pulses (350 ps). Therefore the observed step signals correspond to each fine structure pulse are superimposed on the level of absorption which is due to the buildup of the signals. To analyze the experimental data, two kinds of time dependence of $G(e^-_{aq})$ were considered. The dashed line in Fig. 2b is given by fitting to experimental data[4,5,13,14] which include the present experimental value, $G(e^-_{aq})_{30\,ps}=4.8$ and can be expressed by equations;

$$\begin{aligned} G(e^-_{aq}) &= -0.53\log t - 0.77 \\ &\text{for } 3\times10^{-11} < t < 2.7\times10^{-9}\,\text{s} \\ &= 1.3\exp(-t/1.4\times10^{-8}) + 2.7 \\ &\text{for } t > 2.7\times10^{-9}\,\text{s}. \end{aligned} \quad (2)$$

On the other hand, if we take the lower $G(e^-_{aq})$ value at 30 ps which had been reported by Wolff *et al.*[4] as 4.0, the time dependence of $G(e^-_{aq})$ which is shown by the dotted line in Fig. 2b can be given by

$$G(e^-_{aq}) = 1.3\exp(-t/1.4\times10^{-8}) + 2.7. \quad (3)$$

Corresponding simulation traces are shown in Fig. 2a and it is clear that the time dependence of $G(e^-_{aq})$ which contains $G(e^-_{aq})_{30ps}=4.8$ gives a satisfactory fitted trace.

In Fig. 2b, the typical theoretical time dependence of $G(e^-_{aq})$ calculated by Schwarz[1] is also shown for comparison. Experimental values, except one by Wolff *et al.*,[4] exhibit quite similar time dependence to the theoretical one, while they are higher by 0.3 than the theoretical one in the time period from 3×10^{-11} to 10^{-8} s. This may suggest that the spur diffusion model is not adequate in its present form.

Recently, Trumbore *et al.*[15] have improved the spur diffusion model and reported excellent agreement between calculated and experimental e^-_{aq} decay kinetics in pure water over a wide time range (10^{-11}—10^{-5} s).

Figire 3 shows the kinetic traces of decay of solvated

Table 1. Measured doses and other parameters used for kinetic simulations of the decay of solvated electrons in alcohols

	Methanol	Ethanol	1-Propanol	Ethylene glycol
Dose per macro pulse/krad	2.7	4.0	4.0	3.0
Wavelength/nm	630	700	700	580
Extinction coefficient/M^{-1} cm^{-1}	10200[16]	9300[16]	12800[17]	14000[17]
Half life time/ns	0.5	0.5	0.5	0.5
$G(e^-_{sol})_{30\ ps}$	3.4±0.3	3.4±0.3	2.0±0.3	2.3±0.3

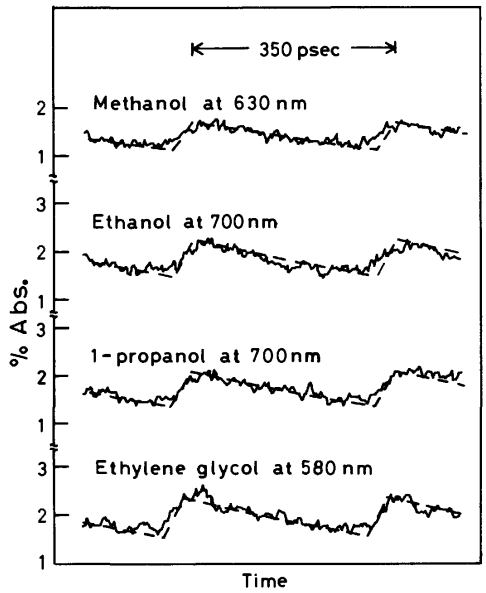

Fig. 3. Kinetic traces of solvated electrons in methanol (630 nm), ethanol (700 nm), 1-propanol (700 nm), and ethylene glycol (580 nm) in 0.10–0.15 M H_2SO_4 solutions. Dashed lines are simulated traces with parameters given in Table 1.

electrons in various alcohols at room temperature. Since in alcohols fast decaying infrared absorption was observed and attributed to the electrons in shallow traps,[18] 0.10—0.15 M H_2SO_4 was added to eliminate their contribution to the absorption of the normal solvated electron. The dashed lines are computer simulated kinetic traces which were calculated by adapting measured doses and other parameters given in Table 1. After several experimental runs, $G(e^-_{sol})_{30ps}$ values were determined to be 3.4±0.3 in both methanol and ethanol, 2.0±0.3 in 1-propanol and 2.3±0.3 in ethylene glycol.

It is expected that the radiolysis of alcohols should exhibit similar spur decay, but the spur diffusion model has not yet been applied to alcohols. The present $G(e^-_{sol})_{30ps}$ values should be useful in theoretical treatment of the spur model of alcohols.

The authors wish to acknowledge Dr. T. Enoto and Messrs. H. Tanida and K. Sato for their help in stabilizing and operating the LINAC.

References

1) H. A. Schwarz, *J. Phys. Chem.*, **73**, 1928 (1969).
2) A. H. Samuel and J. L. Magee, *J. Chem. Phys.*, **21**, 1080 (1953).
3) A. Appleby and J. L. Magee, *J. Phys. Chem.*, **73**, 1937 (1969).
4) R. K. Wolff, M. J. Bronskill, J. E. Aldrich, and J. W. Hunt, *J. Phys. Chem.*, **77**, 1350 (1973).
5) C. D. Jonah, M. S. Matheson, J. R. Miller, and E. J. Hart, *J. Phys. Chem.*, **80**, 1267 (1976).
6) T. Sumiyoshi, S. Sawamura, Y. Koshikawa, and M. Katayama, *Bull. Chem. Soc. Jpn.*, **55**, 2341 (1982).
7) M. J. Bronskill, W. B. Taylor, R. K. Wolff, and J. W. Hunt, *Rev. Sci. Instrum.*, **41**, 333 (1970).
8) E. J. Hart and M. Anbar, "The Hydrated Electron" Wiley-Interscience, New York (1970).
9) M. J. Bronskill, R. K. Wolff, and J. W. Hunt, *J. Chem. Phys.*, **53**, 4201 (1970).
10) T. Sumiyoshi and M. Katayama, *Chem. Lett.*, 1887 (1982).
11) T. I. Balkas, J. H. Fendler, and R. H. Schuler, *J. Phys. Chem.*, **74**, 4497 (1970).
12) W. H. Hamill, *J. Phys. Chem.*, **73**, 1341 (1969).
13) G. V. Buxton, *Proc. R. Soc. London, Ser. A*, **328**, 9 (1972).
14) J. K. Thomas and R. V. Bensasson, *J. Chem. Phys.*, **46**, 4147 (1967).
15) C. N. Trumbore, W. Youngblade, and D. R. Short, *J. Phys. Chem.*, **88**, 5057 (1984).
16) K. N. Jha, G. L. Bolton, and G. R. Freeman, *J. Phys. Chem.*, **76**, 3876 (1972).
17) M. C. Sauer, Jr., S. Arai, and L. M. Dorfman, *J. Chem. Phys.*, **42**, 708 (1965).
18) K. Y. Lam and J. W. Hunt, *J. Phys. Chem.*, **78**, 2414 (1974).

Collisional Deactivation of N(2^2P) Atoms by Simple Molecules

Hironobu UMEMOTO,* Koichiro SUGIYAMA, Shigeru TSUNASHIMA, and Shin SATO†
Department of Applied Physics, Tokyo Institute of Technology, Ookayama, Meguro-ku, Tokyo 152
†*Research Laboratory for Nuclear Reactors, Tokyo Institute of Technology, Ookayama, Meguro-ku, Tokyo 152*
(Received June 14, 1985)

Cross sections for the quenching of N(2^2P) by a variety of simple organic and inorganic compounds have been determined by using a pulse radiolysis-optical absorption technique. It was found that N(2^2P) is less reactive than N(2^2D) in every case, despite its higher energy. The quenching cross sections for unsaturated hydrocarbons were found to be about one tenth of that for gas kinetic collisions, while those for saturated hydrocarbons and most inorganic substances were much smaller. The quenching cross sections for alkane hydrocarbons increase with the number of C-H bonds, and show a minor dependence onC-H bond strengths.

In general, electronically excited-state atoms and molecules are more reactive than ground-state species. This is because the energies of these excited states are higher than those of the ground states, and more exit channels, both chemical and physical, are accessible. However, it is not necessarily true that the upper excited states are more reactive than the lower excited states. For example, the 2^1S_0 state of atomic oxygen is known to be generally less reactive than the lower excited state, O(2^1D_2).[1] The situation is also similar for the optically metastable states of atomic carbon and sulfur, the $^1S_0$ and $^1D_2$ states.[2,3]

The reactions of metastable excited nitrogen atoms have been given much attention since they are believed to be very long-lived in the upper atmosphere and play important roles in atmospheric and environmental chemistry. Pioneering work by Husain and his co-workers showed that the upper excited state, N($2^2P_{1/2,3/2}$), is also less reactive than the lower lying excited state, N($2^2D_{3/2,5/2}$), to some inorganic molecules.[4,5] However, no systematic work has been performed on the quenching of N(^2P) by organic molecules. In addition, some of the values obtained by Husain *et al.* have been questioned.[6] Therefore, we have measured the reaction rates of N(^2P) with simple organic and inorganic molecules and compared them with those of N(^2D).

Experimental

The experimental apparatus and the procedure were similar to those described elsewhere.[7,8] Briefly, 107±2 kPa of nitrogen gas containing a small amount of a quencher gas (< 3 Pa for efficient quenchers such as C_2H_4, <2.4 kPa for inefficient quenchers such as SF_6) was irradiated, through an aluminium foil (80 μm thick), with a pulsed electron beam generated by a Febetron 706 (Hewlett Packard Co.). Since the lifetimes of the charged and highly excited species are considered to be very short (<10 μs) compared with the time region in the present work (0.5—5 ms), only metastable atomic and molecular nitrogen, N(^2P, ^2D) and $N_2(A^3\Sigma_u^+)$, were important intermediates in the present system. Ground-state atomic nitrogen is very inert to most stable molecules.[7,9] The effect of metastable species other than N(^2P) will be discussed later. As has been discussed in a previous paper,[7] the concentration of N(^2P) is very small compared with that of the quenching gases, and it can be postulated that the reaction is pseudo-first-order and the rate constants can be determined by measuring the decay rates of N(^2P). The change in the concentration of N(^2P) atoms was measured by the absorption of atomic lines around 174 nm, which correspond to the $3^2P_J \leftarrow 2^2P_J$ transitions, derived from a cw microwave-powered discharge lamp with a flow of He and a trace amount of N_2. The linear relationship between the optical density and the atomic concentration has been checked in a previous study.[7] The reaction vessel was made of stainless steel and a pair of MgF_2 windows was attached to it, perpendicular to the path of the electron beam. Transmitted light at 174 nm was detected with a combination of a vuv monochromator (Shimadzu SGV-50) and a photomultiplier tube (Hamamatsu R976). Then, the signal was processed with a wave memory (NF Circuit Design Block Co. WM-852) and a computer (NEC PC-9801F) after amplification. In order to obtain a sufficient signal intensity, the slits of the monochromator were wide open (1 mm), and it was impossible to resolve the fine structures of the atomic lines. Therefore, the obtained rate constants in this work were those of the overall reactions of N($^2P_{1/2}$) and N($^2P_{3/2}$). Gas pressures were measured with a Wallace and Tiernan type pressure gauge (Nagano Keiki 62-075) and an MKS Baratron (220AHS-2A5-B-1). All experiments were performed at 295±3 K.

Research-grade N_2(Toyo Sanso), H_2 and D_2(both Takachiho Kako) were used after being passed through a furnace containing reduced copper chips at 590 K and a trap filled with molecular sieve 4A at 77 K. O_2(Nihon Sanso), CO(Takachiho Kako), and He(Suzuki Shokan) were used after having been passed through a cold trap at 77 K. Products of Takachiho Kako were used for Xe, CO_2, SF_6, CH_4, C_2H_6, *c*-C_3H_6, C_3H_8, *neo*-C_5H_{12}, C_2H_4, and C_2H_2. Sources and purities of fluoroethenes were the same as those reported previously.[8] Sources of other materials were: Showa Denko: N_2O, Matheson Gas Products: Cl_2, Tokyo Kasei: *n*- and *i*-C_4H_{10}, and Merck Frosst Canada: C_2D_6 and C_3D_8. All gases condensable at 77 K were purified by repeated trap-to-trap distillation using an appropriate slush bath. CH_4 was used after having been degassed at 77 K for a short time (*ca.* 30 s). Since a gas-chromatographic check showed that C_3D_8 contained a few percent of

C_3D_6, it was further purified by passing through a column of silica gel moistened with H_2SO_4. Isotopic purities of C_2D_6 and C_3D_8 were checked mass-spectroscopically. Their nominal isotopic purities (99.5%) were confirmed.

Results

In the presence of 107 kPa of N_2 without any quenchers, the decay rate of the N(²P) concentration was found to be $7.7\times10^2\ s^{-1}$ (average of 25 runs). Since the radiative lifetime of N(²P) is very long (12 s), there must be some deactivaion processes, even in this system. If this decay is due to the quenching by N_2, the corresponding bimolecular rate constant will be $18\ m^3\ mol^{-1}\ s^{-1}$; however this value should be regarded as the upper limit since there can be some deactivation contribution due to the walls. Although this cannot be a major process, since the decay rate increased with the increase in the N_2 pressure, this possibility cannot be completely ruled out. A diffusional loss from the optical path is not considered to make a contribution, since the decay rate for N(⁴S) measured by the absorption of resonance lines around 120 nm was much smaller. Quenching by ground-state atomic nitrogen, N(⁴S), must be a minor process since the atomic concentration was in the order of $3\times10^{-5}\ mol\ m^{-3}$,[7] and the bimolecular rate constant for the deactivation of N(²P) was measured to be less than $4\times10^5\ m^3\ mol^{-1}\ s^{-1}$.[6,10] It is considered that this quenching process is due mainly to a three-body recombination, but Taghipour and Brennen have showed that a two-body process is far more dominant below 1.3 kPa and that the termolecular rate constant is smaller than $7\times10^4\ m^6\ mol^{-2}\ s^{-1}$.[10] Quenching due to impurities in N_2 may also have a minor importance since it must be assumed that N_2 contained more than 10 ppm of O_2 or 1 ppm of unsaturated hydrocarbons in order to explain the present results by impurity quenching.

In the presence of quenchers, the decay rate increased linearly with the partial-pressure of the quencher. Figures 1 and 2 show the partial pressure dependence of the decay rates for several quenchers. From the least-squares slopes of such plots, the bimolecular quenching rate constants could be obtained. The results are summarized in Table 1, together with the results of other investigators. In this table, the rate constants have been converted to cross sections; $\sigma_Q=k_Q(8kT/\pi\mu)^{-1/2}$, where k_Q is the quenching rate constant, k is the Boltzmann constant, T is the absolute temperature, and μ is the reduced mass. The error limits are the standard deviations.

As for the effect of other active species, N(²D) does not play a significant part, since a large amount of N_2 quenches fairly rapidly. By employing the rate constant regarding the deactivation obtained in a previous work, the lifetime can be calculated to be

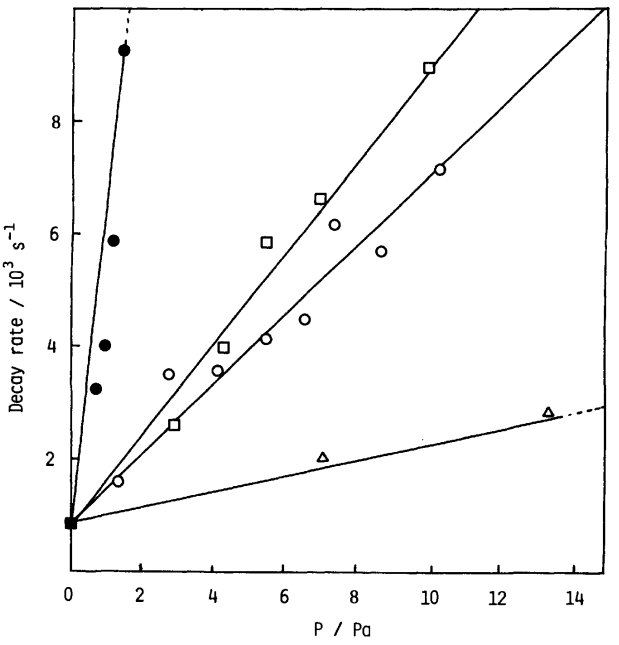

Fig. 1. The decay rates of N(²P) atoms as a function of the C_2H_2(●), *neo*-C_5H_{12}(□), O_2(○), or C_2H_6(△) pressure. As for C_2H_2 and C_2H_6, there are data points which are out of the range of this figure. The symbol ■ represents the average of 25 runs measured in the absence of any quenchers. This point was weighted by a factor of 5 in the calculations of the least squares slopes.

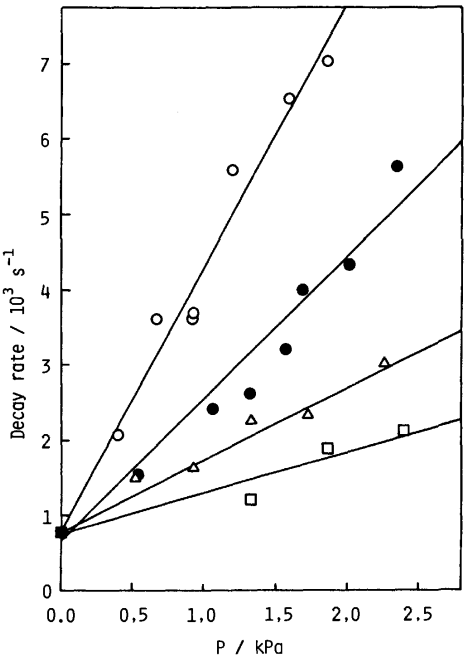

Fig. 2. The decay rates of N(²P) atoms as a function of the H_2(○), D_2(●), CO_2(△), or SF_6(□) pressure.

Table 1. Cross sections for the quenching of $N(2^2P)$

Quencher	Cross section/10^{-20} m^2	
	this work	literature values
Xe	$<6.2\times10^{-5}$	
N_2	$<5.0\times10^{-6}$	1×10^{-5} a)
		6×10^{-3} b)
		4.0×10^{-6} c)
H_2	$(7.6\pm0.3)\times10^{-4}$	1.0×10^{-4} a)
		$<4\times10^{-5}$ d)
D_2	$(5.5\pm0.3)\times10^{-4}$	
O_2	0.31 ± 0.02	0.32 a)
		≤0.2 d)
		0.44 e)
Cl_2	3.3 ± 0.4	3.0 f)
CO	$(7.9\pm0.9)\times10^{-4}$	0.11 a)
		$<9\times10^{-4}$ d)
H_2O	0.063 ± 0.007	
CO_2	$(5.1\pm0.2)\times10^{-4}$	1.4×10^{-4} a)
		1.8×10^{-4} d)
N_2O	$(8.7\pm0.7)\times10^{-3}$	7×10^{-3} a)
		3.3×10^{-3} d)
SF_6	$<3.5\times10^{-4}$	
CH_4	0.0085 ± 0.0005	
C_2H_6	0.066 ± 0.004	
C_2D_6	0.060 ± 0.005	
c-C_3H_6	0.25 ± 0.02	
C_3H_8	0.25 ± 0.02	
C_3D_8	0.34 ± 0.02	
n-C_4H_{10}	0.36 ± 0.02	
i-C_4H_{10}	0.47 ± 0.04	
neo-C_5H_{12}	0.46 ± 0.02	
C_2H_4	3.9 ± 0.3	3.4 c)
C_2H_3F	4.0 ± 0.4	
$CH_2=CF_2$	0.87 ± 0.04	
cis-CHF=CHF	4.2 ± 0.1	
C_2HF_3	3.2 ± 0.2	
C_2F_4	3.3 ± 0.2	
C_2H_2	2.8 ± 0.3	

a) Ref. 5. b) Ref. 11; Measured at 400 K. c) Ref. 7. d) Ref. 6. e) Ref. 12. f) Ref. 13.

3 μs under the present conditions.[7] The MgF_2 windows used in the experiments involving $N(^2P)$ were exposed to vacuum ultraviolet light for a long time, and did not transmit the resonance triplet lines around 120 nm. Therefore, $N(^4P)$ is not considered to be formed optically from $N(^4S)$. Then, the only active species which could disturb the present measurements would be $N_2(A^3\Sigma_u^+)$. Meyer *et al.* have shown that $N(^4S)$ quenches $N_2(A^3\Sigma_u^+)$ to produce $N(^2P)$.[14] The quenching-rate constant has been measured to be fairly large; $2-3\times10^7$ m^3 mol^{-1} s^{-1}.[14,15] If the quantum efficiency for the production of $N(^2P)$ is large, this reaction can become a cause of errors regarding the present measurements. However, if $N(^2P)$ is formed predominantly in this reaction, the initial concentration of $N(^2P)$ must strongly depend on the partial pressures of the added gases. For instance, the quenching rate of $N_2(A)$ by 1.2×10^{-3} mol m^{-3}(3 Pa) of ethene is two orders of magnitude larger than that by 3×10^{-5} mol m^{-3} of $N(^4S)$,[16] and the initial concentration of $N(^2P)$ in the presence of ethene should be much smaller than that in pure N_2. The present experimental results completely contradict this. The transmittance of 174-nm light shortly after irradiation was almost constant, around 75%, regardless of the pressure of the quencher. This strongly suggests that $N(^2P)$ is formed at the initial stage, probably from ionic species, and that the quantum yield for the production of $N(^2P)$ from $N_2(A)$ and $N(^4S)$ is low. For a further check, we also measured the decay rate of $N(^4S)$ in pure N_2, as well as the ratio of the initial concentration of $N(^2P)$ to that of $N(^4S)$. The ratio was estimated from measurements of the transmittance at 174 nm and at 120 nm, the resonance triplet lines of $N(^4S)$, and the known atomic-transition probabilities.[17] Because of a self-reversal phenomenon, the literature values of the transition probabilities are not good for estimating the relative concentrations, but they may be used in a first approximation. The result is that the ratio is 0.12, while the decay rate of $N(^4S)$ is about 10 s^{-1}. This means that, even if $N(^4S)$ which disappeared from the viewing zone was all converted to $N(^2P)$, there is only a 4% increase in the $N(^2P)$ concentration during a typical time range, 0.5 ms.

In the presence of hydrocarbons, $N_2(A^3\Sigma_u^+)$ is supposed to produce free radicals, since its energy is much higher than C–H bond energies. These free radicals must be very reactive with $N(^2P)$. In order to estimate their effect, we simulated the temporal profiles of the concentrations of the unstable species by the Runge Kutta method, assuming the following reaction mechanism:

$$N_2(A) + RH \rightarrow N_2 + R + H, \quad (1)$$

$$N(^2P) + RH \rightarrow \text{Products}, \quad (2)$$

$$N(^2P) + R \rightarrow \text{Products}, \quad (3)$$

$$N(^4S) + R \rightarrow \text{Products}, \quad (4)$$

$$R + R \rightarrow \text{Products}. \quad (5)$$

The values of the initial concentrations of $N_2(A)$, $N(^2P)$, and $N(^4S)$ were chosen to be 7×10^{-6}, 4×10^{-6}, and 3×10^{-5} mol m^{-3}, respectively. The concentration of $N_2(A)$ was estimated from theoretical calculations of the *G*-values.[18] The rate constants for Reactions 3—5 were assumed to be 2×10^8 m^3 mol^{-1} s^{-1}; *i.e.* those of every collision. The rate constants for the quenching of $N_2(A)$ by a variety of hydrocarbons have been reported by Maruta *et al.*,[16] but the branching ratios for the production of R are not

known. Then, we employed a very severe condition, that the ratios are unity. According to this simulation, the relative errors in the estimation of the rate constants of Reaction 2 were shown to be less than 9%. Therefore, this effect also seems minor.

Discussion

Quenching by Inorganic Compounds. As Table 1 shows, the agreement between the present results and the literature values is fairly good except for H_2, although the values obtained by Young and Dunn seem a little small in every case. The quenching cross section for N_2 obtained by Lin and Kaufman at 400 K is larger than the others by more than two orders of magnitude. Schofield has questioned this value,[2] but this may imply the presence of a large activation energy, more than 60 kJ/mol. The cross section for CO reported by Husain *et al.* seems too large and erroneous. As for H_2 the value of Husain *et al.* is smaller than the present one by a factor of 8, while that of Young and Dunn is still smaller. We think it is hard to explain this discrepancy by impurities in H_2. The possible contaminant in H_2 is O_2. If Husain's value is true, in order to explain the present result, it is necessary to assume that the H_2 that we used contained more than 0.5% of O_2, which sounds unrealistic. One possible explanation is that the rate constant is pressure dependent. Husain *et al.* and Young and Dunn conducted their experiments with total pressures below 6.7 kPa.[4,6] Ours were at 107 kPa. According to the recent work by Berman and Lin, the rate constant for $CH+H_2$ reaction changes by a factor of 6, between 3.3 and 80 kPa.[19] They also found a similar pressure dependence for the $CH+N_2$ reaction.[20] Quenching by D_2 is only slightly inefficient than that by H_2. If this difference between H_2 and D_2 is due to a change in the activation energies, that will be 0.8 kJ/mol, much smaller than the difference in the zero-point energies of H_2 and D_2. This small difference suggests that the vibrational energy of $H_2(D_2)$ is reserved at the transition state, or there is no large activation energy and the small quenching efficiency is due only to a symmetry restriction.

Table 2 shows a comparison of the cross sections for the quenching of N(^{2}P) and N(^{2}D). In every case, without an exception, the cross section of N(^{2}P) is smaller than that of N(^{2}D). The unreactive nature of N(^{2}P) to diatomic and linear triatomic molecules has been satisfactorily explained in terms of the concept of adiabatic correlation.[2,23] In the next section we would like to see if it is possible to extend this concept to nonlinear polyatomic molecules.

Concept of Adiabatic Correlation. An extension of the concept of adiabatic correlation to nonlinear polyatomic molecules has been proposed but has not been generally accepted.[24] It is true, strictly speaking, that correlation diagrams cannot be readily constructed for complex polyatomics. However, the inertness of the upper excited states of C, O, S, and N atoms to simple alkane hydrocarbons compared to their lower excited states implies the presence of some general rule. Table 3 gives a comparison of the ratios of the rate constants for the quenching of the upper and the lower excited states of O, S, N, and P atoms by H_2, CH_4, and C_2H_6. Although the values for CH_4 and C_2H_6 are smaller than those for H_2, they are all larger than unity. Sometimes, united-atoms concept is very useful, but it seems to be an oversimplification in the present

Table 2. Cross sections for the quenching of N(^{2}P, ^{2}D)

Quencher	$\sigma_Q/10^{-20}$ m^2	
	^{2}P	^{2}D
N_2	$<5.0\times10^{-6}$	0.002[a]
H_2	7.6×10^{-4}	0.18[b]
O_2	0.31	0.76[b]
Cl_2	3.3	4.9[c]
CO	7.9×10^{-4}	0.25[d]
NO	3.3[a]	4.3[a]
H_2O	0.063	28[e]
CO_2	5.1×10^{-4}	0.089[b]
N_2O	0.0087	0.39[b]
CH_4	0.0085	0.50[b]
C_2H_6	0.066	3.3[b]
C_3H_8	0.25	6.0[b]
n-C_4H_{10}	0.36	7.0[b]
neo-C_5H_{12}	0.46	6.3[b]
C_2H_4	3.9	4.5[a]
		10.1[b]
CH_2=CF_2	0.87	7.2[b]
C_2H_2	2.8	13.8[b]

a) Ref. 7. b) Ref. 21. c) Ref. 13. d) Ref. 5. e) Ref. 22.

Table 3. Ratios of the rate constants for the quenching of the upper and lower states of O, S, N, and P[a]

Quencher	Ratio of rate constants			
	O(^{1}D)/O(^{1}S)[b]	S(^{1}D)/S(^{1}S)[c]	N(^{2}D)/N(^{2}P)[d]	P(^{2}D)/P(^{2}P)[c]
H_2	5×10^5	2×10^4	2×10^2	10
CH_4	6×10^3	3×10^3	60	4
C_2H_6	3×10^2	3×10^2	50	2

a) Values for C atoms are not included because of the sparseness of the data. b) Ref. 1. c) Ref. 2. d) Table 2.

cases. For example, a united atom of CH_3 is F and CH_4 should be replaced by HF in this approximation. Meanwhile, it can easily be shown that $N(^2P_u)+HF(X^1\Sigma^+)$ correlates adiabatically to one of the energetically accessible states, $NH(a^1\Delta)+F(^2P_u)$ and it is impossible to explain the inertness of the upper state with this concept. On the other hand, it is possible to account for the large ratios shown in Table 3 for CH_4 by assuming that the reaction proceeds holding C_s or C_{3v} symmetry. For instance, if it is assumed that N atoms approach CH_4 along one of the three-fold axes of CH_4 and that the reaction proceeds on a surface with C_{3v} symmetry (end-on attack), or that they approach along one of the σ planes and reaction proceeds with C_s symmetry (side-on attack), the main features of the correlation diagram for $N+H_2$ would be applicable to the $N+CH_4$ system. A similar discussion might be possible for $N+C_2H_6$, although the symmetry restriction would be less rigorous.

Exit Channels in the Quenching by Hydrocarbons. Relatively efficient quenching by unsaturated hydrocarbons apparently results from interactions with π electrons. The initial step must be an addition reaction to the unsaturated bonds. This is followed by decomposition or stabilization. Fluorine substitution has minor effects on the rate constants except for $CH_2=CF_2$, in which case, the quenching cross section is 1/4 of those for other fluoroethenes.

As for reactions with saturated hydrocarbons, it should be noted that the cross sections divided by the number of the C-H bonds are almost constant from C_3H_8 to *neo*-C_5H_{12} as is shown in Table 4. It should also be pointed out that there is no large isotope effect between C_2H_6 and C_2D_6, and C_3H_8 and C_3D_8. In the reactions of $OH(X^2\Pi)$, $O(^3P)$, and $Hg(^3P)$, the cross sections are much smaller than those for gas kinetic collisions and increase with a decreasing C-H bond energy.[25-27] Meanwhile, the cross sections for $O(^1D)$, $CH(X^2\Pi)$, and $CH(A^2\Delta)$ show minor dependence on the C-H bond strength.[1,28,29] For example, the ratio of the cross section per C-H bond for the reaction of $OH(X^2\Pi)$ with *i*-C_4H_{10} to that with *neo*-C_5H_{12} at room temperature is 3.2, while that for $O(^1D)$ is 1.1.[1,25] Fairly large C-H *vs.* C-D isotope effect has also been observed in the reactions of OH and $Hg(^3P)$.[25,30] It has been considered that, in the cases of $OH(X^2\Pi)$, $O(^3P)$, and $Hg(^3P)$, the reactions proceed *via* H(D)-atom abstraction from the C-H(C-D) bonds; some theoretical interpretations have also been presented.[25,26,31,32] On the other hand, insertion reactions have been postulated to occur predominantly in the cases of $O(^1D)$ and CH radicals.[28,29,33] In other words, the rate constants for the abstraction reactions with energy barriers show great variation with the C-H bond strength, while those for insertion do not. Table 4 shows a comparison of the cross sections for the reactions of excited N atoms, $O(^1D)$, and CH radicals. Although the quenching efficiencies for N atoms are one or two orders of magnitude smaller than those for $O(^1D)$ and CH radicals, they show parallel behavior. This strongly suggests that the quenching of $N(^2D)$ and $N(^2P)$ cannot be characterized by an abstraction of H-atoms. The quenching of $N(^2D)$ to $N(^4S)$ is highly spin-forbidden and it is hard to consider that such a process proceeds so rapidly. Therefore, we conclude that insertion reactions are also dominant for $N(^2D)$. On the other hand, in the case of $N(^2P)$, deactivation to $N(^2D)$ is a spin-allowed process, although this may be non-adiabatic. The small cross sections for CH_4 and C_2H_6 may reflect the low efficiencies of nonadiabatic transitions or the presence of a steric hindrance, which has been postulated in the case of $Hg(^3P)$ quenching.[34] For a further discussion, information regarding the temperature dependence of the reaction rates, as well as the identification of the exit channels, would be useful.

References

1) K. Schofield, *J. Photochem.*, **9**, 55 (1978).
2) K. Schofield, *J. Phys. Chem. Ref. Data*, **8**, 723 (1979).
3) D. Husain and D.P. Newton, *J. Chem. Soc., Faraday Trans. 2*, **78**, 51 (1982).
4) D. Husain, L.J. Kirsch, and J.R. Wiesenfeld, *Faraday Disc. Chem. Soc.*, **53**, 201 (1972).

TABLE 4. CROSS SECTIONS FOR THE REACTIONS OF N, O, AND CH WITH ALKANES PER C-H BOND

Quencher	Cross section per C-H bond/10^{-20} m^2				
	$N(^2P)$[a]	$N(^2D)$[b]	$O(^1D)$[c]	$CH(X^2\Pi)$[d]	$CH(A^2\Delta)$[e]
CH_4	0.002	0.13	4.3	2.8	0.53
C_2H_6	0.01	0.55	6.8	5.3	2.2
C_3H_8	0.03	0.75	6.9	5.8	2.6
n-C_4H_{10}	0.04	0.70	7.2	6.2	3.1
i-C_4H_{10}	0.05		6.9		
neo-C_5H_{12}	0.04	0.53	6.3		

a) This work. b) Ref. 21. c) Ref. 1. d) Ref. 28. e) Ref. 29.

5) D. Husain, S.K. Mitra, and A.N. Young, *J. Chem. Soc., Faraday Trans. 2*, **10**, 1721 (1974).
6) R.A. Young and O.J. Dunn, *J. Chem. Phys.*, **63**, 1150 (1975).
7) K. Sugawara, Y. Ishikawa, and S. Sato, *Bull. Chem. Soc. Jpn.*, **53**, 3159 (1980).
8) H. Umemoto, K. Sugiyama, S. Tsunashima, and S. Sato, *Bull. Chem. Soc. Jpn.*, **58**, 1228 (1985).
9) J.V. Michael and J.H. Lee, *Chem. Phys. Lett.*, **51**, 303 (1977).
10) A. Taghipour and W. Brennen, *Chem. Phys.*, **37**, 363 (1979).
11) C.-L. Lin and F. Kaufman, *J. Chem. Phys.*, **55**, 3760 (1971).
12) M.P. Iannuzzi and F. Kaufman, *J. Chem. Phys.*, **73**, 4701 (1980).
13) M.P. Iannuzzi and F. Kaufman, *J. Am. Chem. Soc.*, **101**, 4002 (1979).
14) J.A. Meyer, D.W. Setser, and D.H. Stedman, *J. Phys. Chem.*, **74**, 2238 (1970).
15) P.H. Vidaud, R.P. Wayne, M. Yaron, and A. von Engel, *J. Chem. Soc., Faraday Trans. 2*, **72**, 1185 (1976); O.J. Dunn and R.A. Young, *Int. J. Chem. Kinet.*, **8**, 161 (1976).
16) H. Maruta, S. Tsunashima, and S. Sato, Abs. No. IA129, 25th Symposium on Photochemistry, Okayama, October 1984.
17) H. Okabe, "Photochemistry of Small Molecules," John Wiley and Sons, Inc., New York (1978), p. 369.
18) K. Okazaki and S. Sato, *Bull. Chem. Soc. Jpn.*, **48**, 3523 (1975).
19) M.R. Berman and M.C. Lin, *J. Chem. Phys.*, **81**, 5743 (1984).
20) M.R. Berman and M.C. Lin, *J. Phys. Chem.*, **87**, 3933 (1983).
21) B. Fell, I.V. Rivas, and D.L. McFadden, *J. Phys. Chem.*, **85**, 224 (1981).
22) T.G. Slanger and G. Black, *J. Chem. Phys.*, **64**, 4442 (1976).
23) R.J. Donovan and D. Husain, *Chem. Rev.*, **70**, 489 (1970).
24) R.J. Donovan, *Prog. React. Kinet.*, **10**, 253 (1979).
25) R. Atkinson, K.R. Darnall, A.C. Lloyd, A.M. Winer, and J.N. Pitts, Jr., *Adv. Photochem.*, **11**, 375 (1979).
26) R.E. Huie and J.T. Herron, *Prog. React. Kinet.*, **8**, 1 (1975).
27) R.A. Holroyd and G.W. Klein, *J. Phys. Chem.*, **67**, 2273 (1963).
28) M.R. Berman and M.C. Lin, *Chem. Phys.*, **82**, 435 (1983).
29) C.J. Nokes and R.J. Donovan, *Chem. Phys.*, **90**, 167 (1984).
30) M.G. Bellas, Y. Rousseau, O.P. Strausz, and H.E. Gunning, *J. Chem. Phys.*, **41**, 768 (1964); K. Yang. *J. Am. Chem. Soc.*, **89**, 5344 (1967).
31) A.C. Vikis and H.C. Moser, *J. Chem. Phys.*, **53**, 2333 (1970); H.E. Gunning, J.M. Campbell, H.S. Sandhu, and O.P. Strausz, *J. Am. Chem. Soc.*, **95**, 746 (1973); G.C. Marconi, G. Orlandi, and G. Poggi, *Chem. Phys. Lett.*, **40**, 88 (1976).
32) P. Andresen and A.C. Luntz, *J. Chem. Phys.*, **72**, 5842 (1980); A.C. Luntz and P. Andresen, *ibid.*, **72**, 5851 (1980).
33) H. Yamazaki and R.J. Cvetanović, *J. Chem. Phys.*, **41**, 3703 (1964); G. Paraskevopoulos and R.J. Cvetanović, *ibid.*, **50**, 590 (1969); G. Paraskevopoulos and R.J. Cvetanović, *ibid.*, **52**, 5821 (1970); A.C. Luntz, *ibid.*, **73**, 1143 (1980).
34) A.B. Callear and J.C. McGurk, *J. Chem. Soc., Faraday Trans. 2*, **69**, 97 (1973).

 © 1985 The Chemical Society of Japan Bull. Chem. Soc. Jpn., 58, 3082—3086 (1985)

Vapor Phase Carbonylation of Alkyl Chloroacetates

Kiyonori SHINODA* and Kensei YASUDA
Toyama Technical College, 13 Hongo, Toyama 939
(Received April 19, 1985)

The vapor-phase carbonylation of alkyl chloroacetates with rhodium trichloride supported on active carbon was carried out under various conditions. The reaction equation for the preparation of dialkyl malonate from alkyl chloroacetate in the presence of alcohol with carbon monoxide is given as:

$$CH_2ClCOOR + ROH + CO = CH_2(COOR)_2 + HCl$$

The carbonylation proceeded smoothly at 175 °C with an inert solvent as well as with an alkoxide anion donor, such as alcohol, ether, and an ester. The mechanism of the rhodium trichloride-catalyzed carbonylation is probably similar to that of methanol to acetic acid.

The carbonylations of alkyl chloroacetate with carbon monoxide in the presence of alcohol, catalyzed by cobalt carbonyl, have been known for a number of years.[1-7] At present, though, little is known about the vapor-phase carbonylation, since the volatility of metal carbonyl is unavoidable at high temperatures. Consequently, the reaction system has been held under elevated pressure to keep sufficient carbon monoxide in the liquid phase by the use of an autoclave.

Furthermore, alkaline reagents, such as amine,[1,2] sodium alkoxide,[3] alkali metal hydroxide,[4] sodium carbonate[5,6] and alkaline earth metal hydroxide[7], are necessary to remove hydrogen chloride from the reaction field in a large quantity in order to promote the carbonylation. It is said that the effect of the pH of a reaction system on the yield of dialkyl malonate is sensitive and that the exact control of reaction conditions is extremely important.

The present investigation was undertaken in order to examine the vapor-phase carbonylation of alkyl chloroacetate into dialkyl malonate under atmospheric pressure. In accordance with the above views, several searches were made for an effective catalyst and carrier for the carbonylation. Rhodium trichloride was more active when supported on a carrier of a relatively low activity, such as active carbon. Dimethyl malonate was obtained in a good yield in the vapor-phase carbonylation of methyl chloroacetate with rhodium trichloride supported on active carbon.[8] In particular, the present paper is concerned with several alkyl chloroacetates and with several different solvents such as the alkoxide-anion donor at the vapor-phase carbonylation catalyzed by rhodium trichloride supported on active carbon.

Experimental

Materials. The methyl chloroacetate, ethyl chloroacetate, and isopropyl chloroacetate (Tokyo Kasei Kogyo, K.K.) were of a reagent grade and were used without further purification. The active carbon, rhodium trichloride trihydrate, alcohols, ethers, esters, formaldehyde dimethyl acetal, acetic acid, and dichloromethane were purchased from the Wako Pure Chemicals Co. The active carbon was cylindrical in form, 7 mm in length and 4 mm in diameter.

Preparation of Catalyst. The solution was prepared by dissolving 1 g of rhodium trichloride trihydrate in 100 ml of alcohol or water. 10 g of active carbon was impregnated with this solution, and the solution was evaporated to dryness with the oven in the air.

Apparatus. A flow-type system was used.[9] A Pyrex reaction vessel, with a tube 40 cm in length and 2.6 cm in diameter, was heated in a vertical electric furnace. The evaporator, a glass tube, was placed in an electrically wound vertical furnace. The reaction temperature was measured with a Chromel-Alumel thermocouple in a thermowell placed in the catalyst bed.

General Procedure for the Carbonylation of Alkyl Chloroacetates. 11 g of the catalyst (1 g of rhodium trichloride trihydrate supported on 10 g of active carbon) was placed in the middle of the reactor, the bed being supported by necking the reactor tube. While the reaction temperature was regulated, carbon monoxide gas was passed over the catalyst. A mixture of alkyl chloroacetate and the solvent was prepared with the volume ratio of 1:5. Carbon monoxide gas was fed in at the rate of 0.25 mol/h, as measured with a flow meter. The mixture was then fed into the evaporator with a microfeeder at the rate of 20 ml/h in liquid and preheated to 150 °C, the vapor being passed to the reactor. Therefore, carbon monoxide gas was mixed with the vapor of alkyl chloroacetate and the solvent in the evaporator. The product gas stream entered a cooler and was condensed in a water-ice trap. The reaction products were analyzed by means of gas chromatography (PEG 6000, Porapak).

Carbonylation of Methyl Chloroacetate. Methyl chloroacetate was fed into the reactor at the rate of 0.038 mol/h, together with the solvent, and was carbonylated with carbon monoxide over the catalyst. The feed mole ratio of the solvent to methyl chloroacetate was made to vary with the changes in the molecular weight and density of the solvents, because the volume ratio of the solvent to methyl chloroacetate was kept constant. These values are given in Tables 1 and 2. The main reaction products were methyl acetate and dimethyl malonate. The side reaction products were the methyl methoxyacetate and methyl glycolate formed by the direct reaction of methyl chloroacetate with methanol and water. On the other

hand, methanol, formaldehyde dimethyl acetal, and methyl acetate reacted with methyl chloroacetate in an atmosphere of carbon monoxide to form dimethyl malonate and were converted at the same time into hydrogen chloride, chloromethyl ether, and acetyl chloride respectively. Since hydrogen chloride was not detected in the waste gas, the chloride ion in the liquid product was determined by the Volhard method. This was confirmed by titration with a standard solution of a base. Moreover, the effect of water on the product composition was investigated by varying the amount of water added to the methanol.

Carbonylation of Ethyl Chloroacetate. A mixture of ethyl chloroacetate and a solvent was fed into the reactor at the rate of 20 ml/h. Therefore, the feed rate of ethyl chloroacetate was 0.032 mol/h. Ethyl chloroacetate was carbonylated with carbon monoxide in the presence of ethanol, diethyl ether, or ethyl acetate into diethyl malonate. While diethyl ether was transformed into ethyl chloride, ethyl acetate was converted into acetyl chloride.

Carbonylation of Isopropyl Chloroacetate. The feed rate of isopropyl chloroacetate was 0.027 mol/h. The isopropyl chloroacetate was carbonylated in the presence of diisopropyl ether with carbon monoxide into diisopropyl malonate in a good yield, and diisopropyl ether was transformed into isopropyl chloride. Isopropyl chloroacetate reacted with isopropyl acetate to give diisopropyl malonate and acetyl chloride.

Results and Discussion

Carbonylation of Alkyl Chloroacetate in the Presence of Alcohol. Dialkyl malonates are important chemical intermediates for the fine chemicals and are manufactured in the form of various alkyl types.

Hence, the relation of the alkyl group to the reactivity was investigated at 150—175 °C. The product compositions for the carbonylation of methyl chloroacetate in the presence of methanol at 175 °C are given in Table 1. The chlorine liberated from methyl chloroacetate during carbonylation was recovered as hydrogen chloride. Several times as much hydrogen chloride was formed in the steady state as at the initial step of the reaction. It might be assumed that the desorption rate of hydrogen chloride from the surface of active carbon was faster than that of dimethyl malonate. The recovery of hydrogen chloride in the free form was 50—70%. It seemed that hydrogen chloride reacted partly with methanol on the surface of the catalyst at the reaction temperature, as methyl chloride was found in the effluent gas.

The reaction equation for the preparation of dimethyl malonate from methyl chloroacetate in the presence of methanol with carbon monoxide is given as:

$$CH_2ClCOOCH_3 + CH_3OH + CO = CH_2(COOCH_3)_2 + HCl \quad (1)$$

Figure 1 shows the effect of the water content in methanol upon the conversion of methyl chloroacetate into methyl acetate. The formation of methyl acetate increased with an increase in the water content. Methyl chloroacetate may be carbonylated, in the presence of water with carbon monoxide, into methyl hydrogen malonate. However, there was no detectable amount of methyl hydrogen malonate. It has been well-known that malonic acid and methyl hydrogen malonate are thermally unstable compounds. Therefore, methyl acetate might be formed by the thermal decomposition of methyl hydrogen malonate. The carbonylation of methyl chloroacetate catalyzed by rhodium trichloride supported on active carbon is a fairly selective reaction.

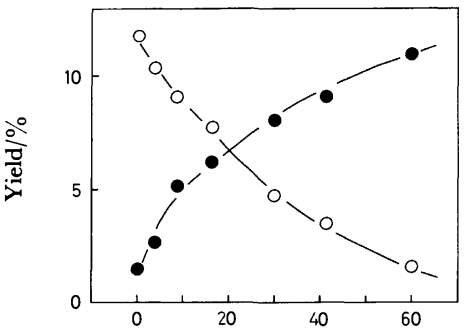

Fig. 1. Effect of the water content in methanol on the formation of methyl acetate at 175°C.
●: CH_3COOCH_3, ○: $CH_2(COOCH_3)_2$

Table 1. Product compositions for the carbonylation of methyl chloroacetate at 175 °C[a)]

Reaction time/h	Product composition/mol × 10^{-3}/h					
	CH_3COOCH_3	$CH_2(OCH_3)COOCH_3$	$CH_2ClCOOCH_3$	$CH_2(OH)COOCH_3$	$CH_2(COOCH_3)_2$	HCl
1	1.20	—	36.17	—	0.52	6.31
3	1.07	0.02	31.71	—	5.09	4.26
6	1.15	0.04	30.98	—	5.72	3.26
11	1.03	0.05	31.26	—	5.55	3.45
16	0.98	0.04	31.34	0.04	5.49	3.35
20	0.89	0.04	31.34	0.03	5.59	3.46

a) The feed mole ratio ($CH_3OH/CH_2ClCOOCH_3$) was 10.9.

Ethyl chloroacetate was carbonylated into diethyl malonate in the presence of ethanol with carbon monoxide on the rhodium trichloride catalyst, while diisopropyl malonate was formed from isopropyl chloroacetate and 2-propanol.

Figure 2 shows the effect of the reaction time on the conversion of alkyl chloroacetates into dialkyl malonates at 150 °C. All curves have a tendency to increase the conversion at the initial reaction step because of the adsorption of dialkyl malonate on active carbon. It has been reported that the elongation of the reaction time led to a decrease in the yield of dimethyl malonate at higher temperatures.[8] However, no indications of the deactivation of the catalyst were recognized at this temperature. It could be anticipated that the durability of catalytic activity was continued for a considerably long time at a moderate temperature. The yield of dialkyl malonate decreased with an increase in the bulkiness of the alkyl group. The carbonylation of alkyl chloroacetate with carbon monoxide in the presence of alcohol is a nucleophilic reaction. The nucleophilicity of higher alcohol is increased by the inductive effect of the alkyl group. The steric hindrance and inductive effect of the alkyl group compensated for each other. Consequently, it was thought that the conversion of ethyl chloroacetate into diethyl malonate was approximately equal to that of isopropyl chloroacetate.

Carbonylation of Alkyl Chloroacetate in the Presence of the Alkoxide Anion Donor. Alkyl chloroacetate was diluted with an inert solvent such as dichloromethane as well as with an ether and an ester as an alkoxide-anion donor. In addition, we tried to carbonylate methyl chloroacetate into dimethyl malonate when such diluents were not used. The method of carbonylation was identical to that described

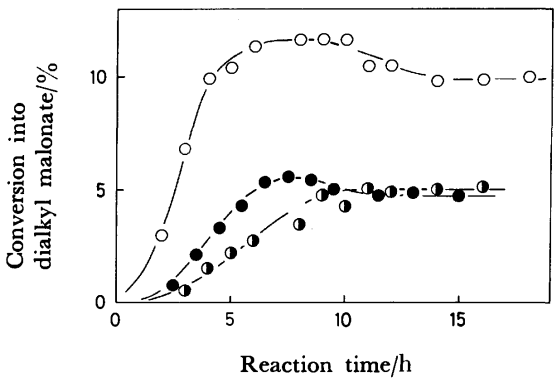

Fig. 2. Variation of catalytic activity with reaction time at 150 °C.
○: $CH_2(COOCH_3)_2$, ◑: $CH_2(COOC_2H_5)_2$, ●: $CH_2[COOCH(CH_3)_2]_2$
Mole ratio: $CH_3OH/CH_2ClCOOCH_3=10.9$, $C_2H_5OH/CH_2ClCOOC_2H_5=9.1$, $(CH_3)_2CHOH/CH_2ClCOOCH(CH_3)_2=8.2$

Table 2. Product compositions for the carbonylation of alkyl chloroacetates with various solvents at 175 °C

Starting material	Mole ratio (Solvent/$CH_2ClCOOR$)		Product composition/mol %	By-product/mol %
$CH_2ClCOOCH_3$[a]	—	1.5 CH_3COOCH_3,	90.5 $CH_2ClCOOCH_3$, 5.3 $CH_2(COOCH_3)_2$	2.7 $CH_2ClCOCl$
$CH_2ClCOOCH_3$-CH_2Cl_2	6.87	1.5 CH_3COOCH_3,	92.9 $CH_2ClCOOCH_3$, 3.4 $CH_2(COOCH_3)_2$	2.2 $CH_2ClCOCl$
$CH_2ClCOOCH_3$-$CH_2(OCH_3)_2$	4.97		97.4 $CH_2ClCOOCH_3$, 2.6 $CH_2(COOCH_3)_2$	5.3 CH_2ClOCH_3 +CH_3COOCH_3
$CH_2ClCOOCH_3$-CH_3COOCH_3	5.54		93.7 $CH_2ClCOOCH_3$, 6.3 $CH_2(COOCH_3)_2$	6.7 CH_3COCl
$CH_2ClCOOCH_3$-CH_3COOH	7.69	9.5 CH_3COOCH_3,	90.3 $CH_2ClCOOCH_3$, 0.2 $CH_2(COOCH_3)_2$	CH_3COCl
$CH_2ClCOOC_2H_5$-$C_2H_5OC_2H_5$	5.09	2.2 $CH_3COOC_2H_5$,	89.6 $CH_2ClCOOC_2H_5$, 8.2 $CH_2(COOC_2H_5)_2$	2.5 C_2H_5Cl
$CH_2ClCOOC_2H_5$-$CH_3COOC_2H_5$	5.40		94.2 $CH_2ClCOOC_2H_5$, 5.8 $CH_2(COOC_2H_5)_2$	8.2 CH_3COCl
$CH_2ClCOOCH(CH_3)_2$-$(CH_3)_2CHOCH(CH_3)_2$	4.45	0.4 $CH_3COOCH(CH_3)_2$,	87.3 $CH_2ClCOOCH(CH_3)_2$, 12.3 $CH_2[COOCH(CH_3)_2]_2$	4.3 $(CH_3)_2CHCl$
$CH_2ClCOOCH(CH_3)_2$-$CH_3COOCH(CH_3)_2$	5.35		94.6 $CH_2ClCOOCH(CH_3)_2$, 5.4 $CH_2[COOCH(CH_3)_2]_2$	2.0 CH_3COCl

a) The feed rate of $CH_2ClCOOCH_3$ was 0.057 mol/h.

previously in the case of alcohol. The experimental results obtained by the vapor-phase carbonylation of alkyl chloroacetate in the presence of various solvents at 175 °C are given in Table 2.

These results are particularly surprising in view of the fact that dimethyl malonate was formed with dichloromethane, which is an inert solvent, and in the absence of a solvent in the vapor-phase carbonylation. It was found that the reaction product contained a small quantity of dimethyl malonate, even when acetic acid was used. On the other hand, dimethyl malonate was obtained in a good yield by the use of methyl acetate instead of dichloromethane. When considered in connection with these experimental results, ester might act as the alkoxide-anion donor. The reason why the formation of dimethyl malonate in the absence of a solvent or in the presence of an inert solvent was found is as follows. Methyl chloroacetate itself has been shown to act as an anion donor. These reactions proceeded according to the following equation:

$$2CH_2ClCOOCH_3 + CO = CH_2(COOCH_3)_2 + CH_2ClCOCl \quad (2)$$

That is to say, the ester was transformed into acid chloride, which was then converted into acid with water and ester with alcohol. Similarly, ether, as the alkoxide-anion donor, reacted with alkyl chloroacetate and carbon monoxide to form alkyl chloride. When acetic acid was used as the starting material, methyl acetate was produced in a significant amount because of the decomposition of methyl hydrogen malonate. Many reports have been published on the mechanism of a rhodium complex-catalyzed carbonylation of methanol to acetic acid.[10-14] Rhodium compounds, in conjunction with various forms of iodide, can be used for the carbonylation of methanol to acetic acid, whereas no direct evidence has been provided as to the chloride forms with a variety of catalysts.

However, it can be assumed that rhodium trichloride acts as a catalyst or catalyst precursor, because the reaction system does not contain any type of iodide.

Taking these previous papers into account, the present reaction scheme may be illustrated as below:

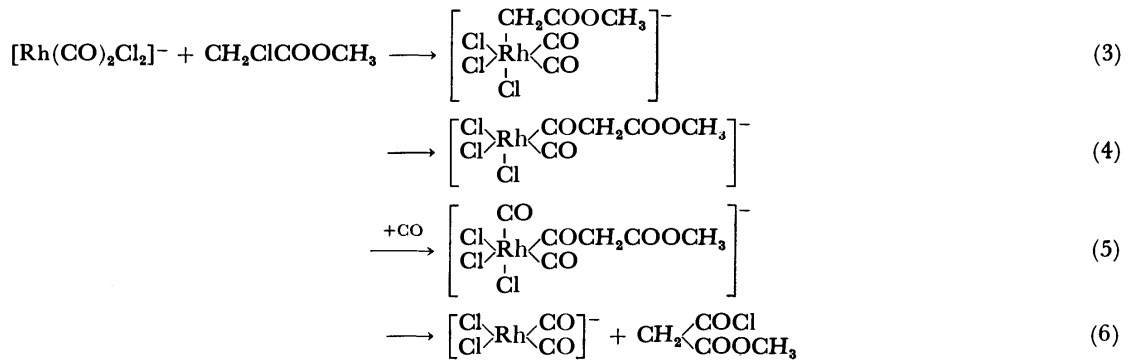

(3) (4) (5) (6)

Since the amount of dialkyl malonate remained unchanged upon the addition of water or alcohol, intermediary acid chloride probably plays an important role in the postulated step. On the basis of the experimental results, the pathways for the formation of dialkyl malonates can be given by the following equations:

$$ClCOCH_2COOR + ROH = CH_2(COOR)_2 + HCl \quad (7)$$
$$+ ROR = CH_2(COOR)_2 + RCl \quad (8)$$
$$+ CH_2(OR)_2 = CH_2(COOR)_2 + CH_2ClOR \quad (9)$$
$$+ CH_3COOR = CH_2(COOR)_2 + CH_3COCl \quad (10)$$
$$+ CH_2ClCOOR = CH_2(COOR)_2 + CH_2ClCOCl \quad (11)$$
$$+ CH_3COOH = [HOOCCH_2COOR] + CH_3COCl \quad (12)$$
$$+ H_2O = [HOOCCH_2COOR] + HCl \quad (13)$$

Methyl hydrogen malonate is unstable and may be decomposed into methyl acetate and carbon dioxide according to Eq. 14:

$$[HOOCCH_2COOR] = CH_3COOR + CO_2 \quad (14)$$

References

1) R. F. Heck and D. S. Breslow, *J. Am. Chem. Soc.*, **85**, 2779 (1963).

2) T. Suzuki, T. Matsuki, K. Kudo, and N. Sugita,

Nippon Kagaku Kaishi, **1983**, 1483.
3) Dynamit Nobel A.-G., *Ger. Offen.* 2524389 (1976).
4) Dynamit Nobel A.-G., *Ger. Offen.* 2603026 (1977).
5) Asahi Denka Kogyo K.K., *Jpn. Kokkai Tokkyo Koho* 78108918 (1978).
6) Denki Kagaku Kogyo K.K., *Jpn. Kokkai Tokkyo Koho* 8053241 (1980).
7) Dynamit Nobel A.-G., *Can. Patent* 1080251 (1980).
8) K. Shinoda and K. Yasuda, *Chem. Lett.*, **1985**, 9.
9) K. Shinoda, *Bull. Chem. Soc. Jpn.*, **47**, 2406 (1974).
10) F. E. Paulik and J. F. Roth, *Chem. Commun.*, **1968**, 1578.
11) K. Ohno and J. Tsuji, *J. Am. Chem. Soc.*, **90**, 99 (1968).
12) D. Forster, *J. Am. Chem. Soc.*, **98**, 846 (1976).
13) R. P. Lowry and A. Aguilo, *Hydrocarbon Process.*, **53**, (11) 103 (1974).
14) K. Masuda, H. Mitani, K. Oku, and Y. Yamazaki, *Nippon Kagaku Kaishi*, **1982**, 249.

 © 1985 The Chemical Society of Japan Bull. Chem. Soc. Jpn., 58, 3087—3091 (1985)

Synthesis of 5-*O*- and 6-*O*-Methyldihydrostreptomycin

Teruo KISHI, Tsutomu TSUCHIYA,* Naokazu KOGA, Yoshihiko KOBAYASHI, and Sumio UMEZAWA

Institute of Bioorganic Chemistry, 1614 Ida, Nakahara-ku, Kawasaki 211

(Received May 10, 1985)

5-*O*- and 6-*O*-Methyldihydrostreptomycin have been prepared from dihydrostreptomycin by a sequence of reactions involving methylation of a selectively protected derivative (**4**) with diazomethane in the presence of tin(II) chloride. The structures of the final products were confirmed by their ^{13}C-NMR spectra and the TACu method.

Streptomycin is inactivated by resistant bacteria[1,2,3] producing inactivating enzymes: AAD(3″) or APH(3″) which adenylylates or phosphorylates the 3″-hydroxyl group, and AAD(6) or APH(6) which adenylylates or phosphorylates the 6-hydroxyl group of streptomycin and dihydrostreptomycin† to give the corresponding *O*-adenylyl or *O*-phosphoryl compounds. To counteract the action of the enzymes AAD(3″) or APH(3″), 3″-deoxydihydrostreptomycin[4,5,6] and 3″-epidihydrostreptomycin[7,8] had been prepared. These compounds showed satisfactory activities against the resistant bacteria owing to the lack of the equatorial 3″-hydroxyl group to be modified. Another device for the enzymes AAD(6) or APH(6), however, was unsuccessful. Chemically prepared 6-deoxydihydrostreptomycin[9] showed only very weak antibacterial activity, suggesting that the 6-hydroxyl group plays an important role in the mechanism of antibacterial action. In connection with our interest in the structure-activity relationships, in this paper, we have described the synthesis of 5-*O*- and 6-*O*-methyldihydrostreptomycin (**9** and **10**). The former derivative (**9**) was prepared to determine the steric influence of the neighboring substituent on the 6-modifying mechanism.

Tris(N^G,N^G,*N*-benzyloxycarbonyl)dihydrostreptomycin (**1**),[10] the starting compound, was treated with *p*-tolualdehyde dimethyl acetal in the presence of acid catalyst under strictly dry conditions. Tris (N^G,N^G,*N*-benzyloxycarbonyl)-5,6:3′,3′a:4″,6″-tris(*O*-*p*-methylbenzylidene)dihydrostreptomycin (**2**) was obtained with slight accompanied mono-, di-, and overacetalated derivatives. Chromatographic separation gave the pure **2**. In this acetal-exchange reaction, formations of N^G,*O*-acetals such as 3,3′a:4″,6″-bis(*O*-*p*-methylbenzylidene)-N^G,*O*-(*p*-methylbenzylidene) derivatives bearing cyclic bridges between 1-N^G,2-*O*, 2-*O*,3-N^G, or 1-N^G,6-*O*, were also suspected. Formation of such type of compounds was found[11] in the reaction of 2-guanidino-1-cyclohexanols with 1,1-dimethoxycyclohexane (in *N*,*N*-dimethylformamide in the presence of *p*-toluenesulfonic acid). In the above case, however, they were successfully removed in the purification step.

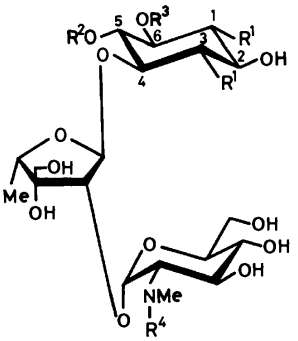

	R^1	R^2	R^3	R^4
DHSM	NHC(=NH)NH_2	H	H	H
1	NHC(=NZ)NH_2[19]	H	H	Z
9	NHC(=NH)NH_2	Me	H	H
10	NHC(=NH)NH_2	H	Me	H
11	NH_2	Me	H	H
12	NH_2	H	Me	H
13	NH_2	H	H	H

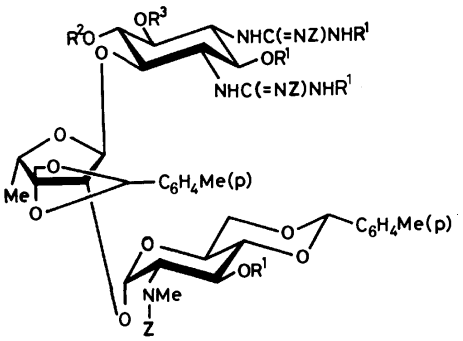

	R^1	R^2	R^3
2	H	$CHC_6H_4Me(p)$	
3	Ac	$CHC_6H_4Me(p)$	
4	Ac	H	H
5	Ac	Me	H
6	Ac	H	Me
7	H	Me	H
8	H	H	Me

Z = $C_6H_5CH_2OCO$-

† As the name dihydrostreptomycin has been widely used, we have used this trivial name.

Acetylation of **2** with acetic anhydride in pyridine gave the tetraacetate (**3**), the positions of the acetyl groups being estimated 1,3-N^G,N^G and 2,3″-*O*,*O*. Selective deacetalation of **3** in a medium containing acetic acid gave the corresponding 5,6-*O*-deacetalated derivative (**4**) in a moderate yield. Careful methylation of **4** with diazomethane in the presence[12] of tin(II) chloride gave a mixture of 5-*O* and 6-*O*-methyl derivatives (**5** and **6**), which, without purification, deacetylated (to give **7** and **8**). Treatment of the product mixture with sodium in liquid ammonia (to remove the *p*-methylbenzylidene and benzyloxycarbonyl groups) followed by repeated chromatography gave 5-*O*- and 6-*O*-methyldihydrostreptomycin (**9** and **10**).

The structures of the final products were determined by the ^{13}C-NMR spectra (Table 1). Since dihydrostreptomycin gave well-separated signals at pD≈6, the spectra of the minor (**9**) and the major (**10**) products were measured at the same pD. The ^{13}C signals of **9** and **10** except for C-5,6 were both readily assigned on the basis of comparison of the corresponding chemical shifts of dihydrostreptomycin.[13] The remaining resonances of the minor product (**9**) were those at δ 83.8 and 71.9, and of the major (**10**), at δ 73.7 and 82.5. Since C-5 and C-6 of dihydrostreptomycin resonated[13] at δ 74.2 and 72.4 at pD≈6, respectively, the signals at δ 71.9 of **9** and δ 73.7 of **10** were assigned to C-6 and C-5 of the respective compounds. The signals of 80′(δ) of **9** and **10** were, therefore, assigned to the resonances of C-5 and C-6 carrying the OMe groups of the respective compounds, the chemical shifts being typical[14] for the carbons carrying an ether group. Furthermore, as the results of the negative shift effect of *O*-methylation at the neighboring positions,[14] the signals of C-4 and C-6 of **9**, and C-1 and C-5 of **10** were respectively shifted upfield, compared to the chemical shifts of the corresponding carbons of dihydrostreptomycin. Thus, the major (**10**) and the minor (**9**) methylated products were determined 6-*O*- and 5-*O*-methyldihydrostreptomycin, respectively. These results, in turn, supported that **3** had 5,6-*O*- and not N^G,*O*-benzylidene structure, as already described.

Table 1. The ^{13}C chemical shifts[a] of **9**, **10** and dihydrostreptomycin dissolved in D_2O at pD 6[b]

Carbon	**9**	**10**	Dihydrostreptomycin[13]
C-1	59.6	58.7	59.8
C-2	71.4	71.3	71.5
C-3	59.4	59.1	59.1
C-4	76.0	77.9	78.7
C-5	83.8	73.7	74.2
C-6	71.9	82.5	72.4
C-1′	106.7	106.3	106.7
C-2′	84.4	85.2	84.9
C-3′	81.6	81.5	81.7
C-3′a	64.4	64.3	64.2
C-4′	79.0	78.8	78.5
C-5′	13.6	13.5	13.5
C-1″	94.1	94.6	94.4
C-2″	62.0	62.0	62.1
C-3″	70.3	70.3	70.3
C-4″	70.1	70.1	70.3
C-5″	73.6	73.6	73.6
C-6″	61.3	61.3	61.3
C(1)NH*C*(=NH)NH_2	159.0	158.8	159.2
C(3)NH*C*(=NH)NH_2	158.3	158.5	158.6
NCH_3	32.7	32.7	32.8
OCH_3	60.9	61.2	

a) In ppm downfield from TMS calculated as $\delta^{TMS} = \delta^{dioxane} + 67.4$ ppm. b) Adjusted by addition of DCl.

The structures of **9** and **10** were confirmed by the tetraamminecopper(II) (TACu)§ method[15,16] on their deamidino derivatives (Table 2). Deamidination of **9**, **10** and dihydrostreptomycin according to Polglase[17] gave the corresponding 1,3-diamino derivatives (**11**, **12**, and **13**[17]). 1,3-Di(deamidino)-5-*O*-methyldihydrostreptomycin (**11**) and **13** showed similar $\Delta[M]_{TACu}$ and $\Delta[M]_{TACu\text{-}NH_3}$ values owing to the lack of participation for complexing including the functional groups at C-5, although, in **11**, the proportion of the complexing like B (see Fig. 1) seemed to be slightly less than that in **13**, In 1,3-di(deamidino)-6-*O*-methyldihydrostreptomycin (**12**), the degree of the A-type complex in TACu solution was considered to be essentially the same with the complexings of the other compounds (**11** and **13**). However, after addition of ammonia, complexing could occur both at NH_2(1)-OH(2)(sign−) and OH(2)-NH_2(3)(sign+) competitively, thus showing the value as expected from the apparent complexing formed only at $NHCH_3$(2″)-OH(3″)(see Fig. 2).

The antibacterial spectra of **9** and **10** showed that they had only very slight activities, suggesting that

§ TACu can form complex only with a pair of vicinal amino and hydroxyl groups having relative special orientations of ≈60° dihedral angle and the $\Delta[M]_{TACu}$(= $[M]_{TACu} - [M]_{H_2O}$) shows a value of ±900°, the sign being decided by counterclockwise (positive) or clockwise (negative) orientation in the Newman projection of -(*NH*$_2$)CH-CH(*OH*)-. In the case of **13**, TACu forms complexes mainly at NHMe(2″)-OH(3″)(sign+) and NH_2(1)-OH(2)-(sign−) to give roughly cancelled value (+340[16]), and by slight addition of ammonia to the TACu solution,[16] the latter complex almost disappeared and, instead, two new complexes at OH(2)-NH_2(3)(sign+) and NH_2(1)-OH(6)-(sign+) appeared, to result in giving a large positive value of $\Delta[M]_{TACu\text{-}NH_3}$(+2530[16]). This phenomenon was interpreted by the assumption that TACu made complexes in streptamine portion of **13** in a state of equilibrium as depicted in Fig 1.[16]

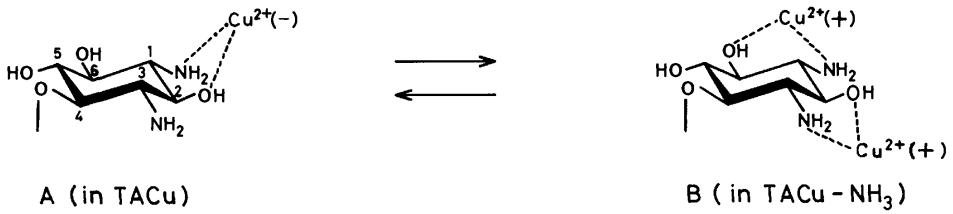

Fig. 1.

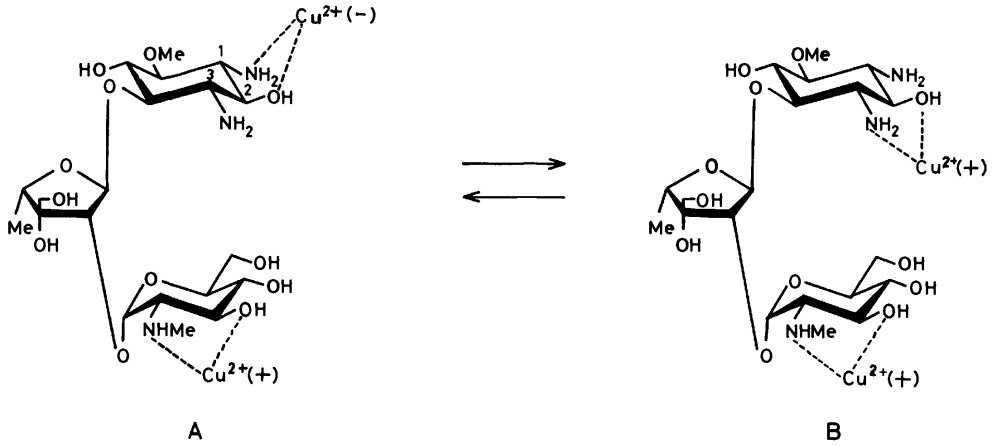

In TACu a mixture of 1,2-(type A, ≈73%) and 2,3-complexes(type B, ≈27%) was expected, and in TACu-NH_3, 1,2-(≈46%) and 2,3-complexes(≈54%).

Fig. 2.

Table 2. $\Delta[M]_{TACu}$ values of **11**, **12**, and **13**[17] before and after addition of ammonia

	$[M]_{H_2O}$	$[M]_{TACu}$[a]	$\Delta[M]_{TACu}$	$[M]_{TACu\text{-}NH_3}$[b]	$\Delta[M]_{TACu\text{-}NH_3}$
11	−1110	−760	+350	+920	+2030
12	−1410	−930	+480	−440	+970
13	−1260	−1000	+260	+1380	+2600

a) 0.01 mmol of each sample (as the hydrogencarbonate) was dissolved in 1.0 ml of 0.16 mmol TACu solution and the rotation of the solution was measured in 0.1 dm tube at 436 nm.[16] b) After measuring the $[M]_{TACu}$, 0.001 ml each of 15 mol dm^{-3} ammonium hydroxide solution was added to the solution (0.55 mol) and the rotation of the solution was again measured. The procedure was repeated until the rotation reached to a constant value.[16]

masking of the hydroxyl at C-5 or C-6 both greatly influences the binding of the antibiotic to the bacterial ribosome.

Experimental

General. ^{1}H-NMR spectra were recorded at 90 MHz with a Varian EM-390 spectrometer except for **9** and **10**, the spectra of which being recorded at 250 MHz in the FT mode with a Bruker WM 250 spectrometer. ^{13}C-NMR spectra were recorded in the FT mode with a Bruker WM 250 spectrometer operating at 62.5 MHz. Thin-Layer chromatography (TLC) was performed on Wakogel B5. For column chromatography, silica gel (Wakogel C-200) was used.

1,3,2″-Tris(N^G,N^G,N-*benzyloxycarbonyl*)-*5,6:3′,3′a:4″,6″-tris*(O-p-*methylbenzylidene*)*dihydrostreptomycin* (**2**). To a solution of **1** (6.0 g) in dry *N,N*-dimethylformamide (120 ml) were added *p*-tolualdehyde dimethyl acetal (24 ml) and molecular sieves 5A (6 g) and, after stirring for 30 min, was added anhydrous *p*-toluenesulfonic acid (3 g), and the mixture was stirred at 60 °C for 5 h under reduced pressure (≈15 Torr (1 Torr=133.322 Pa); to remove the methanol liberated). The solution was poured into a saturated aqueous sodium hydrogencarbonate solution (27 ml) and the precipitates were filtered off with aid of methanol. (If the addition of the reaction mixture to the alkaline solution is reversed, yield of **2** sometimes greatly decreased

owing to removal of the 5,6-acetal group.) The filtrates and washings combined were concentrated to give a syrup, that was extracted with chloroform. The organic solution was washed with saturated aqueous sodium chloride, dried (Na_2SO_4), and concentrated. Addition of hexane to the concentrate gave a solid (≈6 g). Purification of the solid by silica-gel column chromatography with benzene–ethanol–triethylamine (30:1:0.1) as the developer gave an amorphous solid of **2**, 3.18 g (41%), $[\alpha]_D^{25}$ −64° (*c* 1, chloroform). ^{1}H-NMR ($CDCl_3$) δ=1.2—1.4 [3H, CH_3(5′)], 2.3 (9H br s, 3C*H*$_3$C$_6$H$_4$–).

Found: C, 64.12; H, 6.01; N, 7.59%. Calcd for $C_{69}H_{77}N_7O_{18}$: C, 64.19; H, 6.01; N, 7.40%.

*1,3-Di-*N^G*-acetyl-2,3″-di-*O*-acetyl-1,3,2″-tris(*N^G,N^G,N*-benzyloxycarbonyl)-5,6:3′,3′a:4″,6″-*tris(O-p-*methylbenzylidene)dihydrostreptomycin (3).* A mixture of **2** (900 mg) and acetic anhydride (4.8 ml) in pyridine (13.5 ml) was kept at room temperature overnight. Pouring the solution into ice water (100 ml) gave precipitates, that was thoroughly washed with water, then dried to give a solid of **3**, 1.00 g (99%), TLC (benzene–ethanol=15:1): R_f=0.75 (*cf.* **2**: 0.2), $[\alpha]_D^{20}$ −37° (*c* 1, chloroform).

^{1}H-NMR ($CDCl_3$) δ=1.2—1.4 [3H, CH_3(5′)], 1.9—2.2 (12H, mainly 4 singlets with different strength, 4Ac), 2.4 (9H, s, 3C*H*$_3$C$_6$H$_4$–), 2.74 (3H, s, NCH_3).

Found: C, 63.06; H, 5.95; N, 6.46%. Calcd for $C_{77}H_{85}N_7O_{22}$; C, 63.32; H, 5.86; N, 6.71%.

*1,3-Di-*N^G*-acetyl-2,3″-di-*O*-acetyl-1,3,2″-tris(*N^G,N^G,N*-benzyloxycarbonyl)-3′,3′a:4″,6″-bis(*O-p-*methylbenzylidene)dihydrostreptomycin (4).* A solution of **3** (1062 mg) in a mixture of 1,4-dioxane (25 ml) and 50% aqueous acetic acid (25 ml) was allowed to stand at room temperature for 4 h. The solution was poured, with careful agitation, into water (100 ml) containing sodium hydrogencarbonate (20 g) and the mixture extracted with chloroform. The extract, after dried (Na_2SO_4), was concentrated to give a residue, that contained three products, on checking by TLC (benzene–ethanol=15:1), having R_f 0.25 (slight), 0.17 (**4**, major), and 0.12 (slight). Separation with silica-gel column chromatography with benzene–ethanol–triethylamine (30:1:0.05) gave a solid of **4**, 634 mg (64%), $[\alpha]_D^{20}$ −38° (*c* 1, chloroform).

^{1}H-NMR ($CDCl_3$) δ=≈1.3 [3H, CH_3(5′)], 1.9—2.2 (12H, mainly 3 peaks, including unresolved, small strength, 4Ac), 2.4 (6H s, 2C*H*$_3$C$_6$H$_4$–), 2.74 (3H br s, NCH_3).

Found: C, 60.77; H, 6.02; N, 7.06%. Calcd for $C_{69}H_{79}N_7O_{22}$: C, 61.01; H, 5.86; N, 7.22%.

Reaction of 4 with Diazomethane. To an ice-cold solution of **4** (240 mg) in methanol (2.7 ml) containing $SnCl_2 \cdot 2H_2O$ (8 mg, 0.2 mol equiv for **4**) was added diazomethane in ether[18] in small portions, and the reaction was monitored by TLC (benzene–ethanol=7:1). After 20 ml addition of the ether solution, the starting **4** (R_f= 0.37) almost disappeared and the products (**5**, **6**, R_f= 0.43) appeared. Concentration gave a residue, that was extracted with chloroform. The extract was washed thoroughly with water, dried (Na_2SO_4), and concentrated to give a solid (232 mg). The ^{1}H-NMR ($CDCl_3$) spectrum of the products gave a clear peak at δ=3.6 (OMe).

5-O- and 6-O-Methyldihydrostreptomycin (9 and 10). A crude mixture of **5** and **6** (220 mg) dissolved in methanol (22 ml) containing 15 M aqueous ammonia (0.44 ml)(1 M=1 mol dm^{-3}) was kept at room temperature for 1 h. Concentration gave a residue (190 mg), that was purified by silica-gel column chromatography with benzene–ethanol (15:1) to give a mixture of **7** and **8** (125 mg). In the ^{1}H-NMR spectrum, no peak was observed near δ=2 (Ac). A solution of the mixture (115 mg) in oxolane (1.5 ml) was gradually poured into a solution of sodium (≈60 mg) in liquid ammonia (15 ml) maintained at −60 °C, and the blue solution was kept at the temperature for 1.5 h. Addition of methanol until the color disappeared was followed by raising the temperature until 30 °C in order to evaporate the ammonia. The residue was then neutralized with 1 M aqueous hydrochloric acid and charged on a column of Amberlite CG 50 (NH_4^+ form, 20 ml). After washing the column with water, the products were eluted by aqueous ammonium carbonate solution (l→5%, the concentration was gradually changed) and the portion positive for biacetyl color test (indication for the presence of guanidino group) was collected and repeatedly concentrated with several additions of water to remove ammonium carbonate to give a solid (a mixture of **9** and **10**, 32 mg). The mixture was dissolved in 50% aqueous acetic acid (0.6 ml) and separated by column chromatography of microcrystalline cellulose powder (Avicel SF, 15 g, Funakoshi Co., Tokyo) with 1-butanol–pyridine–water–acetic acid (6:4:3:1). Fractions containing **9** and **10** were, respectively, concentrated, and the residue was purified by a column of Amberlite CG 50 (NH_4^+ form) with 5% aqueous ammonium carbonate. The fractions positive for biacetyl were repeatedly concentrated with several additions of water (to remove $(NH_4)_2CO_3$) to give, after drying, solids of **9**, 6.5 mg (5% based on **4**) and **10**, 18.5 mg (15% based on **4**), each as the carbonate.

9: $[\alpha]_D^{20}$ −79° (*c* 0.8, water).

^{1}H-NMR (D_2O, the hydrogencarbonate salt) δ=1.25 [3H d, *J*=7 Hz, CH_3(5′)], 2.43 (3H s, NCH_3), 2.62 (1H dd, H-2″), 3.33 (1H unresolved t, H-5) 3.62 (3H s, OCH_3), 3.83 (1H dd, *J*=4.8 and 12 Hz) and 3.92 (1H dd, *J*=2 and 12 Hz)(H-6,6′), 4.225 (1H d, H-2′), 4.27 (1H q, *J*=7 Hz, H-4′), 5.26 (1H d, H-1″), and 5.29 (1H d, H-1′); $J_{1',2'}$=1, $J_{1'',2''}$=3, and $J_{2'',3''}$=11 Hz.

^{1}H-NMR (D_2O+DCl; pD<1) δ=1.24 [3H d, CH_3(5′)], 2.89 (3H s, NCH_3), 3.32 (1H, H-5), 3.35 (1H dd, H-2″), 3.60 (3H s, OCH_3), 4.25 (1H q, H-4′), 4.305 (1H d, H-2′), 5.28 (1H d, H-1′), and 5.57 (1H d, H-1″); *J* values were the same with those of the hydrogencarbonate.

Found: C, 39.95; H, 6.67; N, 13.55%. Calcd for $C_{22}H_{43}N_{27}O_{12} \cdot 2H_2CO_3$: C, 39.94; H, 6.56; N, 13.59%.

10: $[\alpha]_D^{20}$ −88° (*c* 1, water).

^{1}H-NMR (D_2O, the hydrogencarbonate salt) δ=1.24 [3H d, *J*=7 Hz, CH_3(5′)], 2.41 (3H s, NCH_3), 2.61 (1H dd, H-2″), 3.24 (1H unresolved t, H-6), 3.59 (3H s, OCH_3), 3.83 (1H dd, *J*=4.8 and 12 Hz) and 3.93 (1H dd, *J*=2 and 12 Hz)(H-6,6′), 4.205 (1H d, H-2′), 4.30 (1H q, *J*=7 Hz, H-4′), 5.23 (1H d, H-1″), and 5.29 (1H d, H-1′); $J_{1',2'}$=1, $J_{1'',2''}$=3, and $J_{2'',3''}$=11 Hz.

^{1}H-NMR (D_2O+DCl, pD>1) δ=1.24 [3H d, CH_3(5′)], 2.90 (3H s, NCH_3), 3.25 (1H unresolved t, *J*=≈8 Hz, H-6), 3.36 (1H dd, H-2″), 3.60 (3H s, OCH_3), 4.30 (1H q, H-4′), 4.32 (1H d, H-2′), 5.31 (1H d, H-1′), and 5.58 (1H d, H-1″).

Found: C, 37.65; H, 6.52; N, 12.91%. Calcd for $C_{22}H_{43}N_{27}O_{12} \cdot 2H_2CO_3 \cdot 2H_2O$: C, 37.50; H, 6.84; N, 13.04%.

Alkaline Degradation[17] of 9, 10, and Dihydrostreptomycin. The hydrogencarbonate salts of **9**, **10**, and dihydostrepto-

mycin (20 mg each) were respectively treated in the same manner as reported[17] (1 ml of 90% saturated aqueous barium hydroxide, refluxing for 28 h), and the products were purified by a Dowex 1×2 (OH^- form) resin column with water to give chromatographycally homogeneous (TLC, with chloroform–ethanol-17% aqueous ammonia= 2:2:1), ninhydrin positive, diacetyl and Ehrlich negative, solids of **11** (16 mg#, R_f=0.52), **12** (15 mg#, R_f=0.65) and **13**[17] (16 mg, R_f=0.31).

We are grateful to Professor Hamao Umezawa of Institute of Microbial Chemistry for the discussions, support and encouragements.

References

1) H. Umezawa, *Adv. Carbohydr. Chem. Biochem.*, **30**, 183 (1974).
2) J. Davies, and S. O'Connor, *Ann. Rev. Microbiol.*, **32**, 469 (1978).
3) H. Umezawa and S. Kondo, "Aminoglycoside Antibiotics," ed by H. Umezawa and I. R. Hooper, Springer-Verlag, Berlin, Heidelberg, New York (1982) p. 267—292.
4) H. Sano, T. Tsuchiya, S. Kobayashi, M. Hamada, S. Umezawa, and H. Umezawa, *J. Antibiot.*, **29**, 978 (1976).
5) T. Usui, T. Tsuchiya, H. Umezawa, and S. Umezawa, *Bull. Chem. Soc. Jpn.*, **54**, 781 (1981).
6) S. Umezawa and T. Tsuchiya, "Aminoglycoside Antibiotics," ed by H. Umezawa and I. R. Hooper, Springer-Verlag, Berlin, Heidelberg, New York, (1982) p. 37—110.
7) T. Tsuchiya, S. Sakamoto, T. Yamasaki, S. Umezawa, and H. Umezawa, *J. Antibiot.*, **35**, 639 (1982).
8) T. Tsuchiya and T. Shitara, *Carbohydr. Res.*, **109**, 59 (1982).
9) T. Tsuchiya, T. Kishi, S. Kobayashi, Y. Kobayashi, S. Umezawa, and H. Umezawa, *Carbohydr. Res.*, **104**, 69 (1982).
10) T. Yamasaki, T. Tsuchiya, and S. Umezawa, *J. Antibiot.*, **31**, 1233 (1978).
11) Y. Takagi, O. Kawashima, T. Tsuchiya, H. Sano, and S. Umezawa, *Bull. Chem. Soc. Jpn.*, **49**, 3108 (1976).
12) M. Arimori and T. Kawasaki, *Chem. Pharm. Bull.*, **18**, 677 (1970).
13) M. H. Munro, R. M. Stroshane, and K. L. Rinehart, Jr., *J. Antibiot.*, **35**, 1331 (1982).
14) W. Voelter, E. Breitmaier, E. B. Rathbone, and A. M. Stephen, *Tetrahedron*, **29**, 3845 (1973) and references cited therein.
15) S. Umezawa, T. Tsuchiya, and K. Tatsuta, *Bull. Chem. Soc. Jpn.*, **39**, 1235 (1966).
16) T. Usui, T. Tsuchiya, and S. Umezawa, *J. Antibiot.*, **31**, 991 (1978).
17) W. J. Polglase, *J. Org. Chem.*, **27**, 1923 (1962).
18) T. J. de Boer and H. J. Backer, *Org. Synth.*, Coll. Vol. 4, 250 (1963).
19) H. Paulsen, P. Stadler, A. Banaszek, and F. Toedter, *Chem. Ber.*, **110**, 1908 (1977).

The elemental analyses fluctuated in every sample possibly on account of the difference of uptake of CO_2 from the air, but the data showed no much deviation from the values as the monocarbonate.

 © 1985 The Chemical Society of Japan Bull. Chem. Soc. Jpn., 58, 3092—3098 (1985)

The Reaction of *cyclo*-Triphosphate with L-α- or β-Alanine

Mitsutomo TSUHAKO,* Akemi NAKAJIMA, Tohru MIYAJIMA,† Shigeru OHASHI,†
Hiroyuki NARIAI,†† and Itaru MOTOOKA††
Kobe Women's College of Pharmacy, Kitamachi, Motoyama, Higashinada-ku, Kobe 658
†*Department of Chemistry, Faculty of Science, Kyushu University 33 Hakozaki, Higashi-ku, Fukuoka 812*
††*Department of Chemistry, Faculty of General Education, Kobe University, Tsurukabuto, Nada-ku, Kobe 657*
(Received May 22, 1985)

The reaction of sodium *cyclo*-triphosphate(P_{3m}) with L-α- or β-alanine in an aqueous solution was investigated using anion-exchange chromatography, ^{31}P-NMR spectroscopy, chemical analysis for phosphorus and alanine, IR spectroscopy, and thin-layer chromatography(TLC). 1) P_{3m} readily reacted with L-α-alanine at pH 10 and 12 to form two orthophosphate derivatives of α-alanine: *N*-(1-carboxyethyl)phosphoramidate(P_1-(*N*)ala) and 1,3,2-oxazaphospholidin-2-olate derivative(P_1-(*N,O*)ala) of five-membered ring structure. 2) Only triphosphate derivative, *N*-(2-carboxyethyl)triphosphoramidate(P_3-(*N*)ala), was obtained in the reaction of P_{3m} and β-alanine. 3) The total yield of P_1-(*N*)ala and P_1-(*N,O*)ala was about 75% when P_{3m} was allowed to react with α-alanine at a molar ratio of 1:3 and pH 12, while the yield of P_3-(*N*)ala was about 80% in the reaction of P_{3m} with β-alanine at a molar ratio of 1:1 and pH 12. 4) Oligopeptides such as L-alanylalanine(dimer) and L-alanylalanylalanine(trimer) were formed in the reaction of P_{3m} with α-alanine. 5) Under acidic conditions, P_3-(*N*)ala recyclized to the starting material P_{3m} and β-alanine. 6) The mechanism of the reaction of P_{3m} with α- or β-alanine is discussed.

Phosphorus pentaoxide, polyphosphoric acid, phosphoryl chloride,[1-3] and various organic phosphorus compounds[4-6] have been used as phosphorylating agents for organic and bioorganic compounds. Phosphorylation with these compounds, however, requires special and cumbersome techniques and is usually accompanied by the formation of considerable amounts of by-products.

Feldmann reported in 1965—1967 that phosphorylation of alkylamines,[7] phenols,[8] and alcohols[9] can be effected by the use of *cyclo*-triphosphate(P_{3m}). Following this, Rabinowitz[10-12] reported in 1969—1971 that amino acids (glycine and alanine) condense to form oligopeptides in the presence of polyphosphate or P_{3m}. These facts lead one to imagine that inorganic condensed phosphates such as polyphosphate and P_{3m} might have played an important role in the creation of proteins from amino acids in the prebiotic process which preceded the emergence of life on the earth.[11,13,14] However, little is known about the reaction products and mechanism of P_{3m} with amino acids. As a part of our developmental work on the application of P_{3m} as a phosphorylating agent, the present authors investigated the reaction of P_{3m} with L-α- or β-alanine under various conditions (molar ratio of alanine to P_{3m}, pH, and reaction time) in order to characterize the structure and yields of the reaction products as well as the reaction mechanism.

P_{3m} has many advantages over any other phosphorylating agents; it is a component of metaphosphate, which has been approved for safety as a food additive.[15] Furthermore it is very easy to handle and requires no special technique for phosphorylation. The present authors have already reported that P_{3m} is of great value as a phosphorylating agent for nucleosides.[16]

Experimental

Chemicals. Sodium *cyclo*-triphosphate hexahydrate, $Na_3P_3O_9 \cdot 6H_2O$, was prepared by the procedure described in the previous paper[17] and recrystallized three times from aqueous solution. Reagent-grade L-α- and β-alanine, and potassium acetyl phosphate (Rasa Industries Ltd.) were used without further purification. Unless otherwise stated, guaranteed grade reagents from Wako Chemical Industries Ltd., were used.

Reaction between cyclo-*Triphosphate with* L-α- *or* β-*Alanine.* In the reaction of P_{3m} with L-α-alanine, 50 cm^3 of 0.5 mol dm^{-3} aqueous sodium *cyclo*-triphosphate(P_{3m}) solution was mixed with 50 cm^3 of 0.5—1.5 mol dm^{-3} aqueous L-α-alanine solutions. The pH values of the mixed solutions were about 5.2—5.3. In the reaction of P_{3m} with β-alanine, on the other hand, 50 cm^3 of 0.5 mol dm^{-3} aqueous P_{3m} solution was mixed with 50 cm^3 of 0.5 mol dm^{-3} aqueous β-alanine solution, and the pH value of the mixed solution was about 6.1. These mixed solutions were then adjusted to the predetermined pH value(pH 12, 10, 7, or 4) by use of a sodium hydroxide solution or hydrochloric acid, and the reaction was allowed to stand at room temperatue. Since the pH of each mixed solution decreased as the reaction progressed, the solution was constantly adjusted to the predetermined pH by adding a sodium hydroxide solution.

^{31}P-NMR Measurement. A JEOL FT-NMR Spectrom eter (Model JNN-FX 100) operating at 40.25 MHz for ^{31}P was used. 85% orthophosphoric acid was used as a reference.

TLC Analysis. For analysis of L-α-alanine, L-alanylalanine(dimer), L-alanylalanylalanine(trimer), and β-alanine, TLC was used. A mixed solvent consisting of $CHCl_3$, CH_3OH, and 17% aqueous ammonia (2:2:1) was used, with silica gel plates (made by E. Merck Co. and Wako Chemical Industries Ltd.).

Anion-exchange chromatography, IR spectroscopy, and

the determination of phosphorus and α-alanine were carried out by the methods described in the previous paper.[18]

Results and Discussion

Reaction of cyclo-*Triphosphate with* L-α- *or* β-*Alanine.* After aqueous solutions of P_{3m} and L-α- or β-alanine were mixed, the mixtures were adjusted to a desired pH(12, 10, 7, or 4) with sodium hydroxide or hydrochloric acid, and then allowed to stand at room temperature. Reaction products obtained by the reaction of P_{3m} with α- or β-alanine were separated and determined by anion-exchange chromatography. Figures 1-a and b show the anion-exchange chromatograms of the reaction products of P_{3m} with α- or β-alanine at a molar ratio of 1:1, pH 12, and at room temperature. In the reaction of P_{3m} with α-alanine, two elution peaks of unknown compounds (designated as Compounds I and II) were observed between those of ortho-(P_1) and pyrophosphate(P_2). In the reaction between P_{3m} and β-alanine, on the other hand, a large peak of an unknown compound (Compound III) appeared at 1400 cm^3 of the effluent, other than the peaks of ortho-, pyro-, tri-(P_3), and tetraphosphate(P_4). As can be seen from Fig. 1-a and b, the formation of Compound I and P_2 was predominant in the P_{3m}-α-alanine system, whereas the predominant product in the P_{3m}-β-alanine system was Compound III, with P_1, P_2, P_3, and P_4 being formed only in very small quantities.

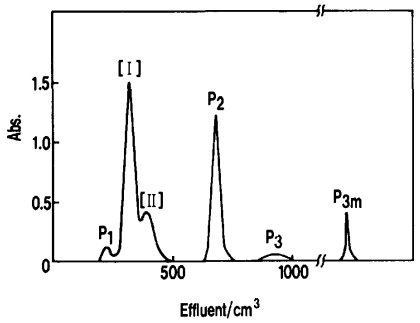

Fig. 1-a. Elution pattern of the reaction products of P_{3m} with L-α-alanine at pH 12.
P_{3m}: $CH_3CH(NH_2)COOH$=0.5 mol dm^{-3}: 1.5 mol dm^{-3}, room temp, after 3 d.

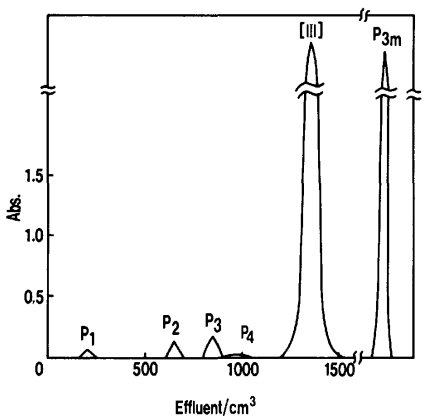

Fig. 1-b. Elution pattern of the reaction products of P_{3m} with β-alanine at pH 12
P_{3m}: $NH_2CH_2CH_2COOH$=0.5 mol dm^{-3}: 0.5 mol dm^{-3}, room temp, after 14 d.

Structures of Compounds I, II, and III. The molecular structures of Compounds I, II, and III were determined by means of chemical analysis, IR spectroscopy, and ^{31}P-NMR spectroscopy. In addition, the reaction of Compounds I, II, and III in an acidic solution was investigated in order to determine the structure.

Compound II was fractionated by anion-exchange chromatography according to the method described in the previous paper.[17] The amounts of phosphorus and α-alanine in Compound II were determined by chemical analysis and with an amino acid analyzer.[18] It was found that the ratio of phosphorus to α-alanine in Compound II is 1:0.96, showing that Compound II may be an orthophosphate derivative of α-alanine containing P_1 and α-alanine in the molar ratio of 1:1.

The IR spectrum of compound II is shown in Fig. 2. Characteristic absorptions that can be assigned to α-alanine were noticed at about 2850 ($\nu_{s\,CH_2}$), 1595 ($\nu_{C=O}$), 1450 (ν_{CH_2}), 1412 ($\nu_{C=O}$), and 1358 cm^{-1} (ν_{C-H}).[19] In addition, characteristic absorptions due to the P-O-C(↑) and P-N bonds(⇡) were observed at the vicinity of 1150 and 900 cm^{-1},[20,21] and 710 cm^{-1},[22-24] respectively. These results demonstrate that Compound II is a phosphate derivative of α-alanine having both P-O-C and P-N bonds in its molecule. For reference, the IR spectrum of the raw material, L-α-alanine, is also shown in Fig. 2-(1).

Figure 3 shows the ^{31}P-NMR spectra of the reaction products between P_{3m} and α-alanine. As can be seen in the ^{1}H-decoupling spectrum, singlet peaks corre-

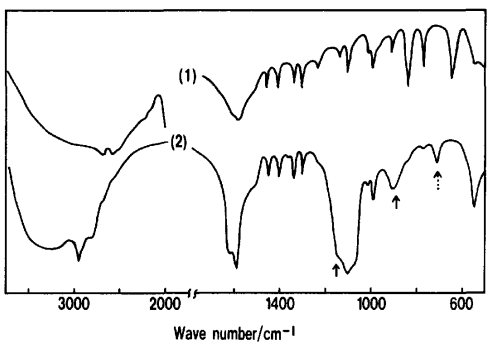

Fig. 2. IR spectra of L-α-alanine and product (II)
(1): L-α-alanine, (2): product (II)
↑: P-O-C bond, ⇡: P-N bond.

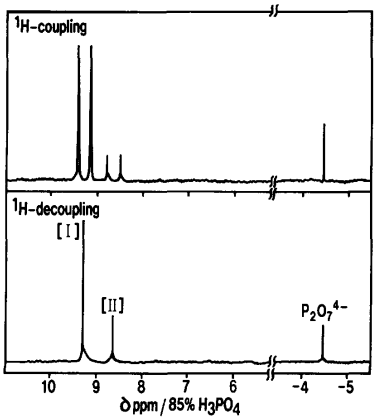

Fig. 3. ^{31}P-NMR spectra of the reaction products in the L-α-alanine—P_{3m} system
P_{3m}: L-α-alanine=0.5 mol dm^{-3}: 1.5 mol dm^{-3}
pH 12, room temp.

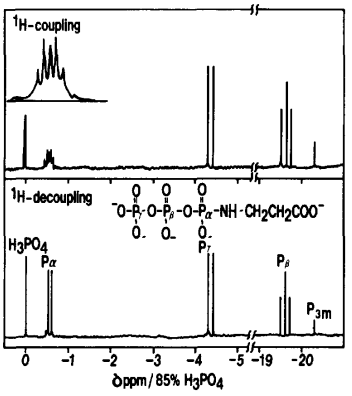

Fig. 4. ^{31}P-NMR spectra of the reaction products in the β-alanine—P_{3m} system
P_{3m}: β-alanine=0.5 mol dm^{-3}: 0.5 mol dm^{-3}
pH 12, room temp.

sponding to the two unknown compounds were observed at δ (chemical shift) 9.3 and 8.7 ppm. From the peak heights (amounts) of Compounds I and II on anion-exchange chromatogram (Fig. 1), peaks at δ 9.3 and 8.7 ppm were attributable to Compounds I and II, respectively. It was found from the ^{1}H-decoupling spectrum that these compounds are both orthophosphate derivatives of α-alanine. The fact that each singlet peak split into doublets due to ^{1}H-coupling suggests that Compounds I and II might be two of the following three compounds: *N*-(1-carboxyethyl)phosphoramidate(P_1-(*N*)ala) containing P-N bond in the molecule, $^{-}O-\overset{\overset{O}{\|}}{P}(O^-)-NHCH(CH_3)COO^-$, 2-aminopropionyl phosphate having P-O-C bond, $^{-}O-\overset{\overset{O}{\|}}{P}(O^-)-O-\overset{\overset{O}{\|}}{C}-CH(CH_3)-NH_2$, and 4-methyl-5-oxo-1,3,2-oxazaphospholidin-2-olate 2-oxide (P_1-(*N,O*)ala) of five-membered ring structure,

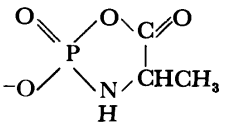

Since the proton on a nitrogen atom undergoes rapid exchange, the spin-spin coupling to phosphorus atom(P-N-H) has not been observed. Of these, the possibility of the formation of 2-aminopropionyl phosphate was excluded because no ^{1}H-coupling of phosphorus atom was observed in ^{31}P-NMR spectrum of authentic acetyl phosphate, $^{-}O-\overset{\overset{O}{\|}}{P}(O^-)-O-\overset{\overset{O}{\|}}{C}-CH_3$.

Therefore, the two unknown compounds could be P_1-(*N*)ala and P_1-(*N,O*)ala. It may thus be deduced that Compound II(δ 8.7 ppm) would be P_1-(*N,O*)ala, because its IR spectrum (Fig. 2) showed the presence of both P-O-C and P-N bonds in the molecule. On the other hand, when an aqueous solution of Compound II was acidified to pH 4, hydrolysis took place to give P_1 and α-alanine. Based on all the experimental results, Compound II was identified as an orthophosphate derivative of α-alanine, 1,3,2-oxazaphospholidin-2-olate derivative(P_1-(*N,O*)ala).

It was difficult to investigate the structure of Compound I by use of IR spectroscopy and chemical analysis, because this compound could not be isolated in a pure form by the chromatographic separation due to its unstability at neutral conditions. However, the result of ^{31}P-NMR spectrum (^{1}H-decoupling) shows that Compound I is an orthophosphate derivative of α-alanine. Since this readily undergoes hydrolysis under neutral and acidic conditions to form P_1 and α-alanine, it is expected that this compound contains P-N bond in its molecule. Based on these facts, we deduced that Compound I may probably be *N*-(1-carboxyethyl)-phosphoramidate(P_1-(*N*)ala).

Figure 4 shows the ^{31}P-NMR spectra of the reaction products of P_{3m} and β-alanine at a molar ratio of 1:1 and pH 12. By comparing with the ^{31}P-NMR spectra of triphosphoramidate in the literature,[25] Compound III was identified as a triphosphate derivative of β-alanine, *N*-(2-carboxyethyl)triphosphoramidate(P_3-(*N*)ala). In the ^{1}H-decoupling spectrum of Fig. 4, the doublets at δ −0.6 and −4.3 ppm were assigned to the end phosphorus atoms, P_α and P_γ, respectively, and the triplet at −19.6 ppm corresponded to the middle phosphorus atom, P_β. Each of the doublets of P_α should in principle split into triplets in ^{1}H-coupling by the influence of the two hydrogen atoms of $-NHCH_2COO^-$, but actually quintet was observed as a result of overlapping.

Table 1. Change of the amounts of phosphorus compounds due to pH

Compound / pH	P_1 (%)	P_2 (%)	P_3 (%)	[III] (%)	P_{3m} (%)
pH 12	0.8	0.6	0.6	69.3	28.6
pH 4	0.8	0.6	0.8	0.0	97.9
pH4-pH12	0.0	0.0	+0.2	−69.3	+69.3

The reaction solution containing a large amount of Compound III was divided into two portions, one being set at pH 12 and the other being controlled to pH 4 by adding dilute hydrochloric acid, and both samples were analyzed by anion-exchange chromatography. The results are shown in Table 1; the amounts of phosphorus compounds at pH 12 in top row, those at pH 4 in middle row, and the difference between the two pH levels in bottom row. Compound III formed in 69.3% yield at pH 12 disappeared completely at pH 4, regenerating the starting material P_{3m}. This result indicates that Compound III recylized to P_{3m} as shown in formula(1) under acidic conditions.

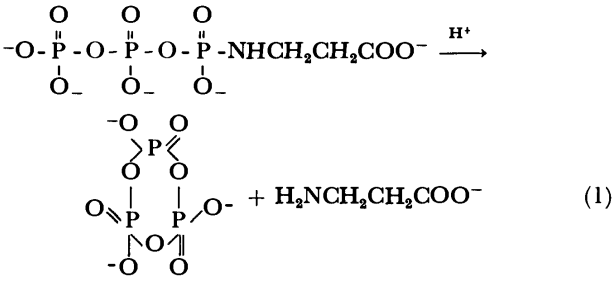

(1)

Quimby[25] and Feldmann[7] have reported in the study of the reaction of P_{3m} with ammonia or various alkylamines that amidotriphosphate or *N*-alkyltriphosphoramidate formed were readily recyclized to produce P_{3m} under acidic conditions.

Amounts of Compounds I, II, and III. Figure 5 shows the changes in the amounts of P_1, P_2, P_3, P_1-(*N*)ala, and P_1-(*N,O*)ala formed by the reaction of P_{3m} with α-alanine at a molar ratio of 1:1, pH 12 and at room temperature. As can be seen from Fig. 1-a, elution peaks of P_1-(*N*)ala and P_1-(*N,O*)ala overlapped with each other, so the amounts of these compounds are shown as total in Fig. 5. The total amount of P_1-(*N*)ala and P_1-(*N,O*)ala gradually increased with the passage of reaction time, reaching about 33.5% after 22 d. P_2 was formed in a considerable quantity at the initial stage of the reaction, while the amounts of P_1 and P_3 gradually increased as the reaction progressed.

Figure 6 shows the changes in the amounts of phosphates formed by the reaction of P_{3m} and α-

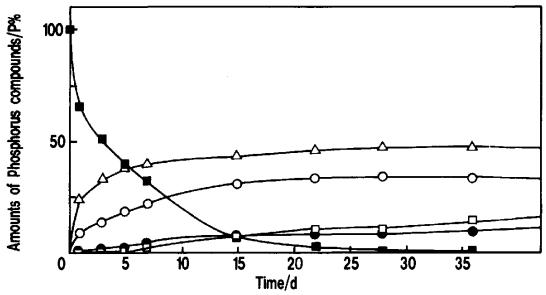

Fig. 5. Change of the amounts of phosphorus compounds in the reaction of P_{3m} with L-α-alanine at pH 12.
P_{3m}: L-α-alanine=0.5 mol dm^{-3}: 0.5 mol dm^{-3}
—○—: P_1-(N)ala+P_1-(N,O)ala, —●—: P_1, —△—: P_2, —□—: P_3, —■—: P_{3m}

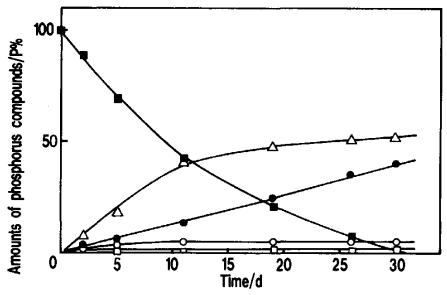

Fig. 6. Change of the amounts of phosphorus compounds in the reaction of P_{3m} with L-α-alanine at pH 10
P_{3m}: L-α-alanine=0.5 mol dm^{-3}: 0.5 mol dm^{-3}
—○—: P_1-(*N*)ala+P_1-(*N,O*)ala, —●—: P_1, —△—: P_2, —□—: P_3, —■—: P_{3m}.

alanine at a mixing ratio of 1:1 and pH 10. In this case, the total amount of P_1-(*N*)ala and P_1-(*N,O*)ala was about 6%, which was much lower than that at pH 12. The amount of P_1, on the other hand, increased linearly with the reaction time, amounting to about 39% after 30 d. The formation of P_1 was notable compared with the case of pH 12. No reaction took place between P_{3m} and α-alanine under neutral and acidic conditions. It is clear from these results that P_{3m} readily reacts with α-alanine under alkaline conditions and that the reactivity lowers with decreasing pH, until eventually no reaction occurs when the pH is lowered to 7.

Figure 7 shows the changes in the amounts of various phosphates when the reaction was carried out using 0.5 mol dm^{-3} P_{3m} and 1.5 mol dm^{-3} α-alanine (mixing ratio=1:3) at pH 12. As is apparent from Figs. 5 and 7, the reaction proceeded much faster at a mixing ratio of 1:3 than at that of 1:1. The total amounts of P_1-(*N*)ala and P_1-(*N,O*)ala formed at a reaction ratio of 1:3 were much greater than those formed at 1:1. P_1-(*N*)ala and P_1-(*N,O*)ala began to be formed immediately at the initial stage of the reaction, whose total amount reached about 65% after

3 d. After that, the amount continued to increase slowly until a nearly constant level of about 75% was reached. The slight decrease in the amount of P_2 after 2 d was due to the precipitation of crystals of tetrasodium pyrophosphate decahydrate, $Na_4P_2O_7 \cdot 10H_2O$, which were removed from the solution phase.

Figure 8 shows the changes in the amounts of phosphorus compounds formed by the reaction between P_{3m} and β-alanine (molar ratio=1:1) at pH 12 and room temperature. A rapid formation of P_3-(*N*)ala was observed. This amount reached about 54% in 10 d and increased slowly thereafter. The amount of P_3 increased linearly with the reaction time, which was presumably due to the hydrolysis of P_{3m}. Since P_1, P_2, and P_4 were formed in quite small quantities (about 1.3, 2.5, and 0.4%, respectively), they are not shown in Fig. 8. Such low yields of P_1 and P_2 provided further evidence that Compound III is a triphosphate derivative of β-alanine. The formation of P_4 when the reaction was continued for long periods is considered to be a result of a reaction of free P_1 with P_3-(*N*)ala having a P–N bond.[26]

Formation of Oligopeptides. The reaction products of P_{3m} with α- or β-alanine were analyzed by TLC to investigate the peptide bond formation of alanine in the reaction solutions. As can be seen in Fig. 9, which indicates, other than the spot of monomeric alanine, those of its dimer(L-alanylalanine) and trimer(L-alanylalanylalanine) in the reaction of P_{3m} with α-alanine were formed. On the other hand, no oligopeptide was formed in the reaction of P_{3m} with β-alanine.

Feldmann,[27] Paecht and Katchalsky,[28] and Koshland[29] reported that a compound having a

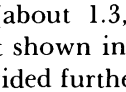

structure reacts with a free amino acid to form a peptide bond. Based on these results, the authors have postulated a reaction mechanism for the

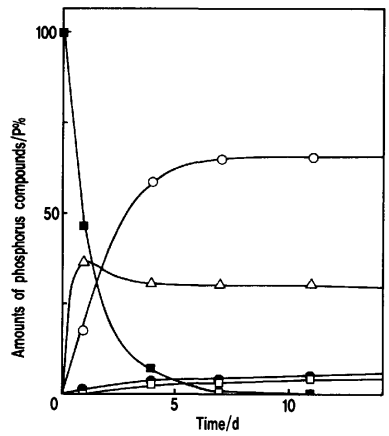

Fig. 7. Change of the amounts of phosphorus compounds in the reaction of P_{3m} with L-α-alanine at pH 12.
P_{3m}: L-α-alanine=0.5 mol dm^{-3}: 1.5 mol dm^{-3}
—○—: P_1-(*N*)ala+P_1-(*N,O*)ala, —●—: P_1, —△—: P_2, —□—: P_3, —■—: P_{3m}.

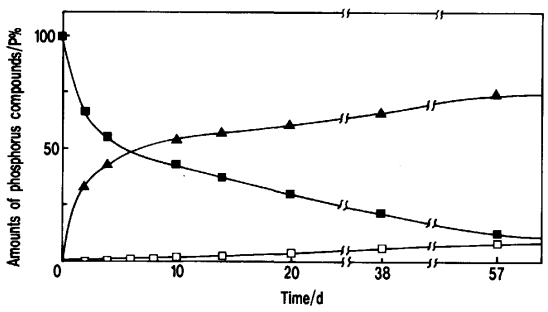

Fig. 8. Change of the amounts of phosphorus compounds in the reaction of P_{3m} with β-alanine at pH 12.
P_{3m}: β-alanine=0.5 mol dm^{-3}: 0.5 mol dm^{-3}
—▲—: P_3-(*N*)ala, —□—: P_3, —■—: P_{3m}.

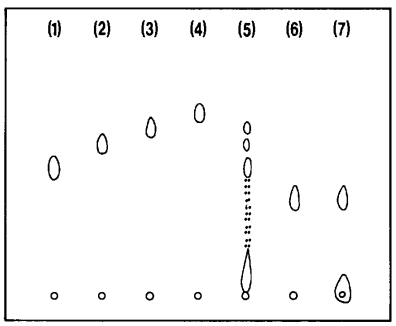

Fig. 9. Thin-layer chromatogram for the reaction products of P_{3m} with L-α-alanine or β-alanine.
(1): L-alanine (monomer), (2) L-alanine (dimer), (3): L-alanine (trimer), (4): L-alanine (tetramer), (5): 24 d after the reaction of P_{3m} with L-α-alanine, (6): β-alanine (monomer), (7): 14 d after the reaction of P_{3m} with β-alanine.

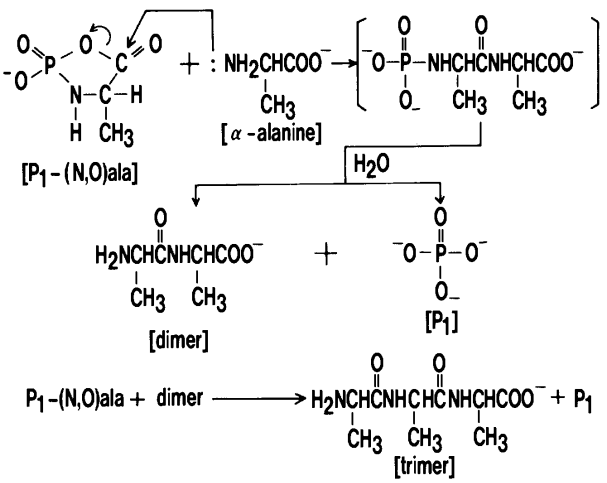

Fig. 10. Mechanism of formation of oligopeptides in the reaction of P_{3m} with L-α-alanine.

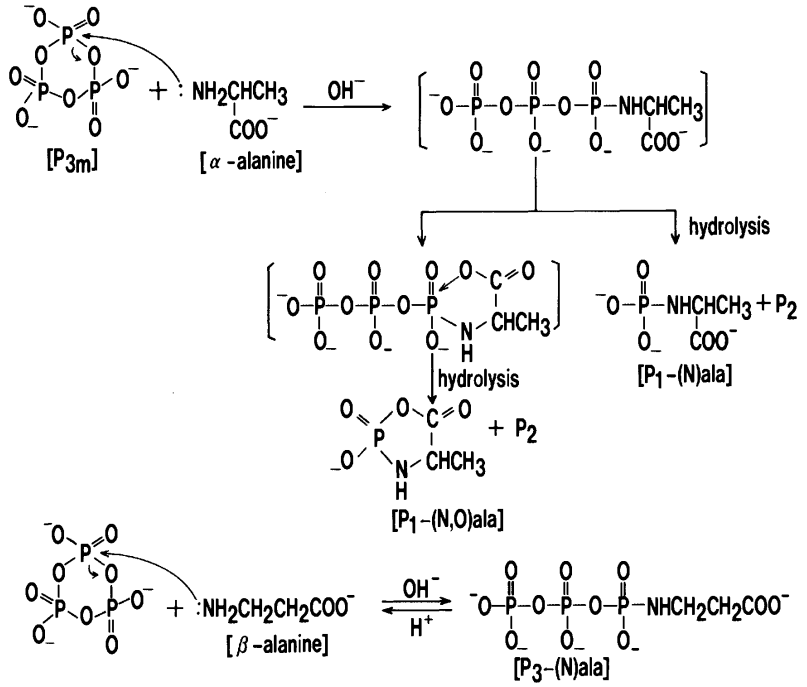

Fig. 11. Mechanism of the reaction of P_{3m} with L-α- alanine or β-alanine.

formation of the dimer and trimer of α-alanine as shown in Fig. 10. A nucleophilic attack by the amino group of free α-alanine on the carboxylate carbon atom of P_1-(*N*,*O*)ala, gives an orthophosphate derivative of alanylalanine as a reaction intermediate, which is unstable and readily undergoes hydrolysis to form alanylalanine and P_1. The dimer then reacts with P_1-(*N*,*O*)ala in a similar manner to afford the trimer. Tetramer and higher oligomers should also be formed through the same mechanism, which, however, could not be detected by TLC probably because of the small amounts present. Such oligopeptide formation has already been observed by our previous investigation on the reaction of P_{3m} with glycine.[18]

On the contrary, oligopeptides were not formed at all in the reaction of P_{3m} with β-alanine, showing that P_3-(*N*)ala formed in this reaction did not react with free β-alanine to produce its oligomers. It may be apparent from the foregoing that the five-membered ring compound, P_1-(*N*,*O*)ala, plays an important role in the formation of oligopeptides in the reaction of P_{3m} with alanine.

Mechanism of the Reaction of cyclo-*Triphosphate with α- or β-Alanine.* The mechanism of the reaction between P_{3m} and α- or β-alanine in alkaline solutions is shown in Fig. 11. In the reaction of P_{3m} with α-alanine, a nucleophilic attack by the amino group of α-alanine upon the phosphorus atom of P_{3m} causes a ring opening of the latter to form a triphosphate derivative of α-alanine having a P–N bond in the molecule as an intermediate. This intermediate, which is very unstable (as evidenced by the fact that it cannot be detected by either HPLC or anion-exchange chromatography), is considered to undergo hydrolysis through the following two routes: (1) an attack by the carboxyl group upon the phosphorus atom of the intermediate to form propionyl triphosphate with a five-membered ring structure, followed by hydrolysis into P_1-(*N*,*O*)ala and P_2, and (2) a direct hydrolysis of the intermediate to form P_1-(*N*)ala and P_2.

There is no possibility of a direct attack by the carboxyl group of α-alanine upon the phosphorus atom of P_{3m}, because no reaction takes place between CH_3COO^- and P_{3m} under the same conditions. In the reaction between P_{3m} and β-alanine, on the other hand, it is assumed that the ring opening of P_{3m} is caused by a nucleophilic attack of the amino group of β-alanine upon its phosphorus atom, producing P_3-(*N*)ala. This compound is stable in an alkaline solution, but readily recyclizes to P_{3m} under acidic conditions. Thus, the reaction of P_{3m} with β-alanine is reversible, depending on the pH.

The difference in the reaction mechanisms of *cyclo*-triphosphate with α- and β-alanine is outstanding, that is, the formation of a heterocyclic compound takes place with α-alanine but not with β-alanine. A further precise study is necessary in order to clarify any differences in the mechanisms.

We are indebted to Prof. Morifusa Eto and Dr. Eiichi Kuwano at Faculty of Agriculture in Kyushu University for the ^{31}P-NMR measurements.

References

1) R. H. Hall and H. G. Khorana, *J. Amer. Chem. Soc.*, **77**, 1871 (1955).
2) A. W. Schwartz and C. Ponnamperuma, *Nature*, **218**, 443 (1968).
3) M. Yoshikawa, T. Kato, and T. Takenishi, *Tetrahedron Lett.*, **1967**, 5065.
4) M. Ikehara, T. Ueda, and E. Ohtsuka, "Kakusan Yuki Kagaku," Kagaku Dojin (1979), p. 85.
5) M. Ikehara, *Tanpakushitsu Kakusan Khoso*, **6**, 615 (1961).
6) E. Ohtsuka, "Kagaku Sousetsu," Gatsukai Shutsupan Center (1985), No. 46, p. 209.
7) W. Feldmann, *Z. Chem.*, **1**, 26 (1965).
8) W. Feldmann, *Chem. Ber.*, **99**, 3251 (1966).
9) W. Feldmann, *Chem. Ber.*, **100**, 3850 (1967).
10) J. Rabinowitz, *Helv. Chim. Acta*, **52**, 2663 (1969); **53**, 1350 (1970); **54**, 1483 (1971).
11) J. Rabinowitz, *Nature*, **224**, 795 (1969).
12) N. M. Chung, R. Lohrmann, L. E. Orgel, and J. Rabinowitz, *Tetrahedron*, **27**, 1205 (1971).
13) J. Hulshof and C. Ponnamperuma, *Origins of Life*, **7**, 197 (1976).
14) Tanpakushitsu Shoreikai, "Tanpakushitsu," Tokyo Kagaku Dojin (1983), p. 121.
15) M. Ishidate(editor), "Shokuhin Tenkabutsu Koteisho Kaisetsusho," 4th ed., Hirokawa Shoten (1979), p. B-922.
16) M. Tsuhako, M. Fujimoto, S. Ohashi, H. Nariai, and I. Motooka, *Bull. Chem. Soc. Jpn.*, **57**, 3274 (1984).
17) M. Tsuhako, N. Fujita, A. Nakahama, T. Matsuo, M. Kobayashi, and S. Ohashi, *Bull. Chem. Soc. Jpn.*, **53**, 1968 (1980).
18) M. Tsuhako, S. Ohashi, H. Nariai, and I. Motooka, *Chem. Pharm. Bull.*, **30**, 3882 (1982).
19) M. Ishidate (editor), "Shokuhin Tenkabutsu Koteisho Kaisetsusho," 4th ed., Hirokawa Shoten (1979), p. B-47.
20) K. Nakanishi, "Infrared Absorption Spectrum," Nankodo (1970), p. 60.
21) D. E. C. Corbridge, in M. Grayson and E. J. Griffith (editors), "Topics in Phosphorus Chemistry," John Wiley and Sons, Inc., New York (1969), Vol. 6, p. 278.
22) D. E. C. Corbridge and E. J. Lowe, *J. Chem. Soc.*, **1954**, 493.
23) D. E. C. Corbridge, *J. Appl. Chem.*, **6**, 456 (1956).
24) E. Kobayashi, *Nippon Kagaku Kaishi*, **1972**, 38; **1973**, 1437.
25) O. T. Quimby and T. J. Flautt, *Z. Anorg. Allg. Chem.*, **296**, 220 (1958).
26) M. Tsuhako, A. Nakahama, S. Ohashi, H. Nariai,and I. Motooka, *Bull. Chem. Soc. Jpn.*, **56**, 1372 (1983).
27) W. Feldmann, *Z. Chem.*, **4**, 154 (1969).
28) M. Paecht and A. Katchalsky, *Biochim. Biophys. Acta*, **90**, 260 (1964).
29) D. E. Koshland, *J. Amer. Chem. Soc.*, **73**, 4103 (1951).

Synthesis and Properties of the [n](2,5)Pyridinophane Ring System[1)]

Tomoshige KOBAYASHI and Makoto NITTA*
Department of Chemistry, School of Science and Engineering, Waseda University, Shinjuku-ku, Tokyo 160
(Received June 6, 1985)

The synthesis and properties of a series of [n](2,5)pyridinophane derivatives (**13a—e**) (n=10, 8, 7, and 6) are described. These compounds are prepared in low yields by the [Mo(CO)$_6$]-induced cycloaddition reaction of 3-aryl-4,5-polymethylene-substituted isoxazoles (**11a—e**) with dimethyl acetylenedicarboxylate. The reaction pathways are suggested to involve the inclusion of the acetylenic ester across the C-4–C-5 bond of the N-complexed isoxazoles and the subsequent elimination of the oxygen atom from the resulting isoxazoline ring. The structures of **13a—e** are established on the basis of the ^{1}H-NMR, ^{13}C-NMR, and UV spectra. A significant strain for the pyridine ring in **13a—e** is reflected in the UV spectra. As the [n] decreases in **13—e**, there is a red shift in the absorption spectra. This feature is in good accordance with that observed in a series of [n]paracyclophane ring systems.

Much interest has been focussed on the chemistry of the cyclophanes.[2)] Especially, the [n]paracyclophane ring system (**1**)(n=6—12) has been one of the simplest models for clarifying the correlation of the aromaticity with the distortion of the benzene ring from planarity.[2)] The synthesis of "more bent" benzene ring than the previous example is though still an intriguing and challenging problem. The [n]paracyclophane ring system **1** has been synthesized for most values of [n], from 16 to 6.[2,3)] The [n]paracyclophane **1** (n=6), which has the smallest methylene chain known for this series, was first reported by Jones *et al.* in 1974.[3c)] However, it is only recently that new efficient routes to the [6]paracyclophane derivatives (**2**)[3g)] and (**3**),[3h)] both of which have substituents on the benzene ring, were developed. Their X-ray studies revealed that the benzene rings are highly deformed (*ca.* 20°) from planarity.[3g,h)]

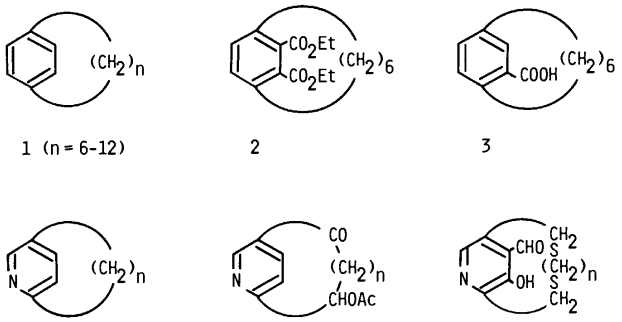

1 (n = 6-12) 2 3

4 (n = 8-12) 5 (n = 9, 10) 6 (n = 4, 5)

In contrast to these studies, only a few examples of the aza analogue, the [n](2,5)pyridinophane ring system, have been known. The first example of [n](2,5)pyridinophane (**4**) (n=8—12) appeared in 1968.[4)] The functionalization of **4** (n=9 and 10) leading to **5** has also been studied.[5)] With a view toward a model for vitamin B$_6$-dependent enzyme, the chemistry of [n](2,5)pyridinophane (**6**)(n=4 and 5) containing pyridoxal has also been studied.[6)] Thus, the smallest value of [n] for [n](2,5)pyridinophane known so far is [8].[4)]

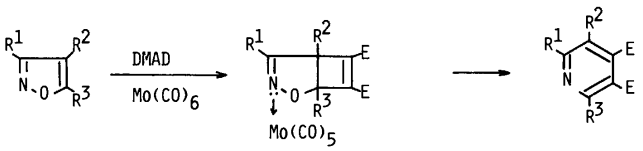

7 8 9

Scheme 1.

In our previous studies,[7)] [Mo(CO)$_6$] has been shown to effect a novel inclusion of the acetylenic ester across the C-4–C-5 bond of isoxazoles **7** and the subsequent elimination of an oxygen atom to give pyridine derivatives **9** *via* an intermediate **8** (Scheme 1). If this reaction is applicable to some 4,5-polymethylene-substituted isoxazoles (R^2-R^3=-(CH$_2$)$_n$- in **7**), [n](2,5)pyridinophanes can be expected as the products. We wish to describe here on the synthesis of [6](2,5)pyridinophane derivatives (**13d, e**), which might contain one of the most deformed pyridine rings, as well as a series of [10], [8], and [7] homologues, (**13a—c**).

Results and Discussion

The synthetic sequences of the [n](2,5)pyridinophane derivatives **13** are illustrated in Scheme 2. The syntheses of the desired 3-aryl-4,5-polymethylene-substituted isoxazoles (**12**) were achieved by method similar to that used in the preparation of ring-annelated isoxazoles.[8)] The 1,3-dipolar cycloaddition of benzonitrile oxide to 1-(1-pyrrolidinyl)-1-cycloalkenes (**10a—d**) afforded the corresponding cycloadducts, 4,5-polymethlene-subsituted 3-phenyl-5-(1-pyrrloidinyl)isoxazolines (**11a—d**). Similarly, the isoxazoline (**11e**) was obtained from the reaction of 4-chlorobenzonitrile oxide with **10d**. Compounds **11a, b** and **11d, e** were easily purified by recrystallization to give colorless crystals. On the other hand, oily **11c** decomposed on distillation [at *ca.* 120 °C (bath temp)/667 Pa]. Therefore, **11c** was purified by column chromatography on silica gel to give a

colorless oil and then submitted to the next step. On the acid-catalyzed elimination of the pyrrolidine, **11a—e** were converted to the desired 3-aryl-4,5-polymethylene-substituted isoxazoles (**12a—e**). The yields of the 2-isoxazolines **11a—e** and the isoxazoles **12a—e** are listed in Table 1. The structures of **11a—e** and the **12a—e** were unequivocally assigned on the basis of the physical data (see Experimental section). According to the procedure employed in our related studies,[7] the reaction of the isoxazoles **12** (1 mmol) with dimethyl acetylenedicarboxylate (DMAD, 2 mmol) in the presence of $[Mo(CO)_6]$ (1 mmol) afforded [*n*](2,5)pyridinophane derivatives (**13a—e**). Although the yields of **13a—e** are only 5—11% (Table 1), no other product is isolated except for hexamethyl benzenehexacarboxylate (*ca.* a 10% yield based on the DMAD used), which results from the $[Mo(CO)_6]$-induced trimerization of DMAD.[7]

The formation of **13a—e** can be best explained by the reaction pathways shown in Scheme 3.[7] The initial stage of this reaction would be the coordination of $[Mo(CO)_5]$ on the nitrogen atom of the isoxazole **12**, leading to **14**. In **14**, there may be a delocalization of the d-electron from the molybdenum atom to the π^* (LUMO) of the isoxazole moiety.[9] In the presence of DMAD, the C-5-atom of **14** may connect with DMAD to give **15**, the following cyclization would afford the propellane-type[3] intermediate **16**. The facile N-O bond cleavage of the 2-isoxazoline ring has been shown previously.[7,10] Thus, the intermediate **16** undergoes the cleavage of both N-O and C-4-C-5 bonds to give the complexed vinylnitrene **17**.[11] The cyclization of **17** to lead to **18**[7,12] and the subsequent decomplexation eliminating CO_2 and $[Mo(CO)_4]$ result in the formation of the [*n*](2,5)pyridinophane derivatives **13a—e**.

The structures of **13a—e** were determined on the basis of the elemental analyses and the mass, IR, ^{1}H-NMR, ^{13}C-NMR, and UV spectra (see Experimental section). Considering the ^{1}H-NMR spectra, several protons of the methylene chain appear at δ 0.60—0.95 (10H) for **13a**, at δ 0.10—2.10 (12H) for **13b**, at δ 0.20—2.20 (10H) for **13c**, at δ 0.45—0.98 (4H) for **13d**, and at δ 0.40—0.80 (4H) for **13e**. These protons located over the face of the corresponding pyridine ring. The shielding effect can be exactly attributed to the aromatic ring current of the pyridine ring. However, the degree of the shielding effect for the methylene chain in **13a** and **13b** seems to be smaller than that of [*n*](2,5)pyridinopane **4**.[4] In compound **4**, the high-field signals appear at δ 0.2—2.2 (16H) for **4** (n=10) and at δ −0.40—1.85 (12H) for **4** (n=8). Thus, it can be suggested the two methoxycarbonyl groups on the pyridine ring of **13** reduce the ring current. Furthermore, **13d** exhibits a signal at δ 3.30 (1H, J_{jem}=12.0 Hz, J_{vic}=6.0 Hz). The signal could be assigned to the H_α proton (Fig. 1), which is located in the deshielding region of the phenyl group. A similar characteristic is observed in **13e**. This fact suggests that the [6](2,5)pyridinophane derivatives

TABLE 1. YIELDS OF ISOXAZOLINES **11**, ISOXAZOLES **12**, AND [*n*](2,5)PYRIDINOPHANES **13**

			Yield/%		
	Ar	[*n*]	**11**	**12**	**13**
a	Ph	10	30	97	11
b	Ph	8	21	98	8
c	Ph	7	59	67	8
d	Ph	6	43	87	8
e	4-ClC_6H_4	6	56	57	5

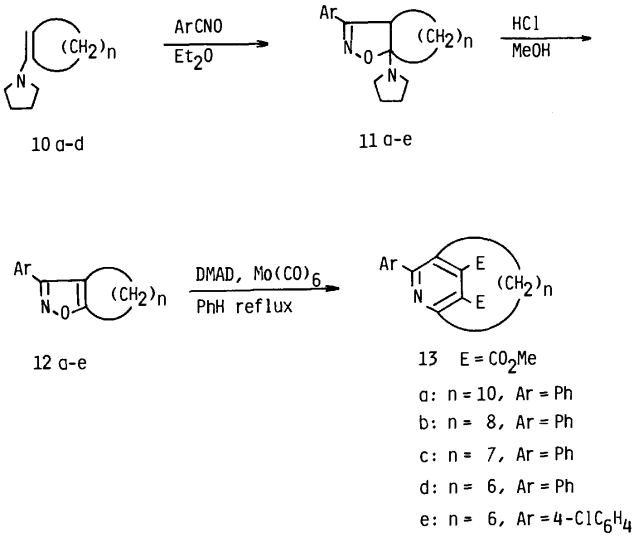

Scheme 2.

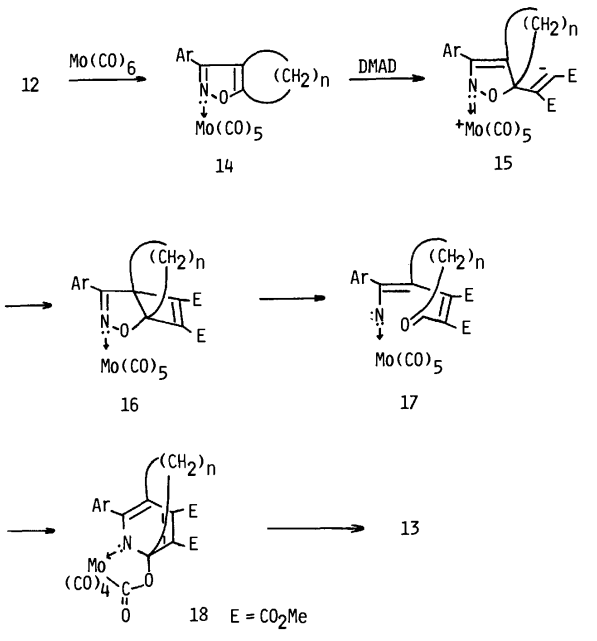

Scheme 3.

Table 2. UV Data of the [n](2, 5)pyridinophanes **13a—d**, **4**, and the [n]paracyclophanes **1**

[n]	λ_{max} (log ε) (nm)									
	13[a]			**4**[b]			**1**[c]			
—	**19**:[d]	—	252, (4.33)	305 (4.24)	—	—	**20**:[c]	—	214,	265
[10]	**13a**:	—	253, (4.01)	302 (4.03)	216, (3.83)	271 (3.53)		—	223,	268
[9]		—	—	—	218, (3.79)	273 (3.48)		—	224,	271
[8]	**13b**:	—	266, (4.02)	313 (3.93)	223, (3.79)	278 (3.49)		—	230,[e]	276[e]
[7]	**13c**:	230, (4.12)	273, (3.97)	322 (3.87)	—	—		216,	245,	283
[6]	**13d**:	249, (4.12)	285, (3.90)	342 (3.80)	—	—		212,	253,	296

a) This work; b) Ref. (4); c) Ref. (3c); d) Ref. (7); e) Ref. (3d).

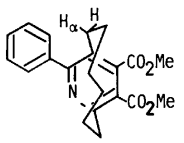

Fig. 1.

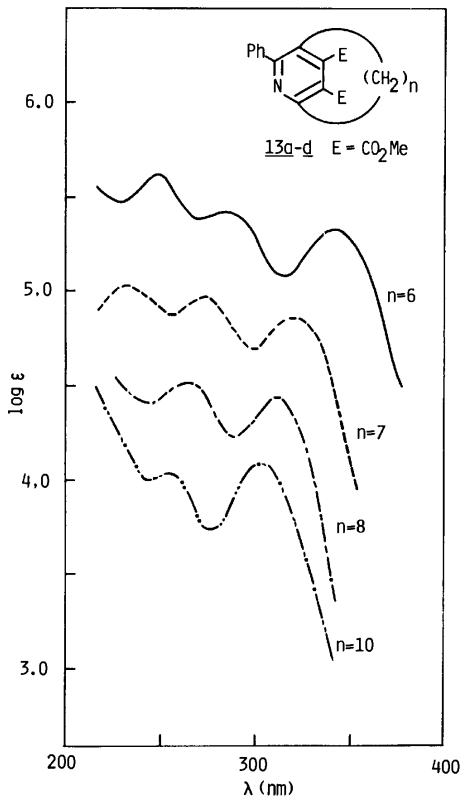

Fig. 2. UV spectra of the [n](2,5)pyridinophanes **13a—d** in absolute ethanol.
The curves are displayed upward successively by 0.5 log unit from the curve immediately below.

13d, **e** have rather rigid structures. The ^{13}C-NMR of the **13a—e** series are similar to each other, and the ring-current effect for the methylene chain seems to be negligibly small. The ring-current effect for the chemical shift of ^{13}C-NMR is not a predominant factor and often overwhelmed by a steric compression.[13]

The UV spectra of **13a—d** in ethanol are depicted in Fig. 2. The absorption maxima of [n](2,5)pyridinophane **13a—d**, **4**, and a series of [n]paracyclophane **1** along with the model compounds, 2-methyl-3,4-bis(methoxycarbonyl)-6-phenylpyridine (**19**)[7] and 1,4-diethylbenzene (**20**),[3c] are also summarized in Table 2. The significant ring strain of the [n](2,5)pyridinophane derivatives **13a—d** is reflected in the UV spectra. An increase in the red shift is observed for **13—d** as the value of [n] decreases. Since the absorption maximum of **13a** is very similar to that of **19**, **13a** seems to contain a planar and less-constrained pyridine ring. In contrast, the longest absorption maxima of **13d** and **13e**, both of which have the smallest value of [n] in the **13** series are exactly shifted to wavelength longer by 40 and 43 nm respectively as compared to **13a**. These features are in good agreement with those observed in the series of the [n]paracyclophanes **1**[3c,d] and the [n](2,5)pyridinophanes **4**.[4] Therefore, these can be no doubt that the [n](2,5)pyridinophanes **13d** and **13e** contain one of the most deformed pyridine ring thus far obtained.

Experimental

The IR spectra were recorded on a Shimadzu IR-400 spectrometer. The ^{1}H-NMR spectra were recorded on a Hitachi R-24 (60 MHz) spectrometer, and the chemical shifts are given in ppm (δ) relative to an internal $SiMe_4$ standard. The ^{13}C-NMR spectra were recorded on a JMN-FX90Q (22.5 MHz) spectrometer. The mass-spectral studies were conducted on a Shimadzu GCMS QP-1000 spectrom-

eter at 70 eV. All of the melting points are uncorrected. The solvents were dried and purified by the standard methods. The enamines, 1-(1-pyrrolidinyl)cyclododecene (**10a**),[14] 1-pyrrolidino-1-cyclodecene (**10b**),[14] 1-pyrrolidino-1-cyclononene (**10c**),[15] and 1-pyrrolidino-1-cyclooctene (**10d**),[15] were prepared by the method described in the literature. Benzohydroximoyl chloride and 4-chlorobenzohydroximoyl chloride were also obtained by the standard method.[16]

General Procedure for the Synthesis of 2-Isoxazolines ***11a—e.*** A solution of enamine **10** (30 mmol) and triethylamine (5 cm^3) in ether (200 cm^3) was cooled at 0 °C. To this solution we then slowly added a solution of benzohydroximoyl chloride (30 mmol) in ether (30 cm^3). The reaction mixture was stirred at 0 °C for 6 h, and then it was poured into water (100 cm^3). The ether layer was separated, washed with water, and dried over $MgSO_4$. The ether was removed *in vacuo* to give the 2-isoxazolines **11a—e**.

Compounds **11a**, **b**, **d**, and **11e** were purified by recrystallization to give colorless crystals. Compound **11c** was obtained as a colorless oil and decomposed on distillation [*ca.* 120 °C (bath temp)/667 Pa]. Therefore, **11c** was purified by column chromatography on silica gel using benzene as the eluent and submitted to the next step. The structures of **11a—e** were determined on the basis of the following physical data. For **11a**: mp 78—79 °C (from hexane); IR ($CHCl_3$), 2920, 1451, 1343, 1130 cm^{-1}; ^{1}H-NMR ($CDCl_3$) δ=1.20—2.45 (24H, m), 2.40—3.05 (4H, m), 3.10—3.55 (1H, m), 7.20—7.70 (5H, m). Found: C, 77.98; H, 9.75; N, 7.72%. Calcd for $C_{23}H_{34}N_2O$: C, 77.92; H, 9.67; N, 7.90%. For **11b**: mp 115—116 °C (from hexane); IR ($CHCl_3$), 2923, 1605, 1574, 1492, 1453, 1358, 1134 cm^{-1}; ^{1}H-NMR ($CDCl_3$) δ=1.10—2.50 (20H, m), 2.50—3.10 (4H, m), 3.12—3.41 (1H, m), 7.18—7.70 (5H, m). Found: C, 77.05; H, 8.99; N, 8.52%. Calcd for $C_{21}H_{30}N_2O$: C, 77.25; H, 9.26; N, 8.58%. For **11c**: colorless oil; IR ($CHCl_3$), 2923, 1605, 1574, 1492, 1453, 1358, 1132 cm^{-1}; ^{1}H-NMR ($CDCl_3$) δ=1.20—2.25 (18H, m), 2.25—3.00 (4H, m), 3.10—3.35 (1H, m), 7.20—7.80 (5H, m). For **11d**: mp 126—128 °C (from hexane); IR ($CHCl_3$), 2928, 2857, 1449, 1349, 1328, 1250 cm^{-1}; ^{1}H-NMR ($CDCl_3$), δ=1.40—2.40 (16H, m), 2.45—2.95 (4H, m), 3.10—3.35 (1H, m), 7.30—7.68 (5H, m). Found: C, 76.53; H, 8.85; N, 9.30%. Calcd for $C_{19}H_{26}N_2O$: C, 76.47; H, 8.78; N, 9.39%. For **11e**: mp 128—129 °C (from hexane); IR ($CHCl_3$), 2923, 2808, 1594, 1494, 1402, 1338, 1090, 1011 cm^{-1}; ^{1}H-NMR ($CDCl_3$), δ=1.10—2.40 (16H, m), 2.40—2.90 (4H, m), 3.10—3.30 (1H, m), 7.32 (2H, d, J=8.6 Hz), 7.60 (2H, d, J=8.6 Hz). Found: C, 68.41; H, 7.49; N, 8.42%. Calcd for $C_{19}H_{25}N_2OCl$: C, 68.56; H, 7.57; N. 8.42%.

General Procedure for the Synthesis of Isoxazoles ***12a—e.*** A solution of the 2-isoxazoline **11** (10 mmol) in methanol (25 cm^3) and concentrated HCl (45 cm^3) was refluxed for 1 h. The solution was then neutralized with aqueous NaOH and extracted with benzene. The benzene extract was washed with water and dried over Na_2SO_4. After the benzene had been evaporated, the residue was purified by recrystallization or distillation to give the isoxazoles **12a—e**. **12a**: mp 38—39 °C (from hexane); IR (CCl_4), 2915, 2865, 1620, 1468, 1445, 1410 cm^{-1}; ^{1}H-NMR ($CDCl_3$) δ=1.20—2.10 (16H, m), 2.50—3.00 (4H, m), 7.30—7.80 (5H, m); MS, *m/z* (rel intensity), 283 (M^+, 100). Found: C, 80.28; H, 8.79; N, 4.88%. Calcd for $C_{19}H_{25}NO$: C, 80.52; H, 8.89; N, 4.94%. **12b**: bp 128 °C/132 Pa; IR (film), 2923, 1618, 1582, 1473, 1447, 1414, 1335, 1273, 1131 cm^{-1}; ^{1}H-NMR ($CDCl_3$) δ=1.05—2.10 (12H, m), 2.45—3.00 (4H, m), 7.15—7.65 (5H, m); MS, *m/z* (rel intensity), 255 (M^+, 14), 77 (100). Found: C, 79.65; H, 8.38; N, 5.38%. Calcd for $C_{17}H_{21}NO$: C, 79.96; H, 8.29; N, 5.49%. **12c**: bp 120—125 °C/132 Pa; IR ($CHCl_3$), 2911, 1620, 1583, 1465, 1445, 1418, 1353, 1283, 1205 cm^{-1}; ^{1}H-NMR ($CDCl_3$) δ=1.18—2.05 (10H, m), 2.40—2.70 (2H, m), 2.73—3.00 (2H, m), 7.30—7.75 (5H, m); MS, *m/z* (rel intensity), 241 (M^+, 53), 77 (100). Found: C, 79.67; H, 7.78; N, 5.52%. Calcd for $C_{16}H_{19}NO$: C, 79.63; H, 7.94; N, 5.80%. **12d**: mp 54—55 °C (from hexane); IR ($CHCl_3$), 2932, 2857, 1594, 1584, 1449, 1418, 1351, 1261, 1126, 1071, 1010 cm^{-1}; ^{1}H-NMR ($CDCl_3$) δ=1.35—2.05 (8H, m), 2.40—2.75 (2H, m), 2.75—3.10 (2H, m), 7.22—7.70 (5H, m); MS *m/z* (rel intensity), 227 (M^+, 100). Found: C, 79.05; H, 7.69; N, 6.08%. Calcd for $C_{15}H_{17}NO$: C, 79.26; H, 7.54; N, 6.16%. **12e**: mp 97—98 °C (from hexane); IR ($CHCl_3$), 2941, 1620, 1441, 1143, 1081, 1020 cm^{-1}; ^{1}H-NMR ($CDCl_3$), δ=1.35—2.10 (8H, m), 2.40—2.75 (2H, m), 2.75—3.05 (2H, m), 7.40 (2H, d, J=9.0 Hz), 7.50 (2H, d, J=9.0 Hz); MS, *m/z* (rel intensity), 263 (M^+, 33), 261 (M^+, 100). Found: C, 68.72; H, 6.23; N, 5.47%. Calcd for $C_{15}H_{16}NOCl$: C, 68.83; H, 6.16; N, 5.35%.

General Procedure for the Synthesis of [n](2,5)Pyridinophanes ***13a—e.*** A solution of the isoxazole **12** (1 mmol), [$Mo(CO)_6$] (1 mmol), and DMAD (2 mmol) in benzene (10 cm^3) was refluxed for 24 h under dry-nitrogen atmosphere. After hexane (10 cm^3) was added to the reaction mixture, it was filtered through Celite to remove insoluble material. The filtrate was concentrated, and the resulting residue was separated by TLC on silica gel using benzene as the developer to give the [*n*](2,5)pyridinophane derivatives **13a—e** and hexamethyl benzenehexacarboxylate (*ca.* 10% yield in each case based on the DMAD used). The UV spectra of **13a—d** are displayed in Fig. 2, while absorption maxima are summarized in Table 3. **13a**: bp 150 °C (bath temp)/66 Pa; IR ($CHCl_3$), 1729 cm^{-1}; ^{1}H-NMR ($CDCl_3$) δ=0.60—0.95 (10H, m), 1.00—2.06 (6H, m), 2.83—3.35 (4H, m), 3.88 (3H, s), 3.90 (3H, s), 7.30—7.75 (5H, m); ^{13}C-NMR ($CDCl_3$) δ=24.4, 25.9, 26.5, 26.6, 27.2, 27.4, 27.6, 27.7, 28.2, 35.2 (methylene chain), 52.4 (methoxyl groups), 128.4, 128.7, 129.7, 139.8, 142.4, 158.4, 161.3, 167.1, 167.7 (aromatic rings and carbonyls); MS, *m/z* (rel intensity), 409 (M^+, 38), 350 (100). Found: C, 73.12; H, 7.42; N; 3.19%. Calcd for $C_{25}H_{31}NO_4$: C, 73.32; H, 7.63; N, 3.42%. **13b**: bp 145 °C (bath temp)/132 Pa; IR ($CHCl_3$), 1721 cm^{-1}; ^{1}H-NMR ($CDCl_3$) δ=0.10—2.10 (12H, m), 2.10—3.10 (3H, m), 3.30—3.60 (1H, m), 3.87 (3H, s), 3.91 (3H, s), 7.30—7.62 (3H, m), 7.69—7.98 (2H, m); ^{13}C-NMR ($CDCl_3$) δ=24.8, 25.3, 27.9, 28.8, 29.3, 30.1, 30.8, 36.2 (methylene chain), 52.4, 52.7 (methoxyl groups), 121.0, 128.6, 129.2, 129.3, 130.3, 138.8, 142.8, 159.6, 159.8, 166.7, 167.8 (aromatic rings and carbonyls); MS, *m/z* (rel intensity), 381 (M^+, 26), 380 (100). Found: C, 72.53; H, 7.15; N, 3.40%. Calcd for $C_{23}H_{27}NO_4$: C, 72.42; H, 7.13; N, 3.67%. **13c**: bp 130 °C (bath temp)/66 Pa; IR ($CHCl_3$), 1722 cm^{-1}; ^{1}H-NMR ($CDCl_3$) δ=0.20—2.10 (10H, m), 2.50—3.10 (3H, m), 3.53—3.93 (1H, m), 3.90 (3H, s), 3.97 (3H, s), 7.31—7.70 (3H, m), 7.84—8.07 (2H, m); ^{13}C-NMR ($CDCl_3$) δ=25.6, 25.9, 26.1, 29.1, 29.9, 30.9, 36.5 (methylene chain), 52.4, 52.7 (methoxyl groups), 120.3, 127.9, 128.7, 129.5, 130.8, 138.4, 143.2, 158.8, 159.5, 166.5, 167.9 (aromatic rings and carbonyls); MS *m/z*

(rel intensity), 367 (M^+, 27), 366 (100). Found: C, 71.87; H, 6.93; N, 3.70%. Calcd for $C_{22}H_{25}NO_4$: C, 71.91; H, 6.86; N, 3.81%. **13d**: bp 120 °C (bath temp)/66 Pa; IR ($CHCl_3$), 1721 cm^{-1}; ^{1}H-NMR ($CDCl_3$) δ=0.45—0.98 (4H, m), 1.00—1.75 (4H, m), 2.50—3.05 (3H, m), 3.30 (1H, dxt, J=12.0, 6.0 Hz), 3.87 (3H, s), 3.93 (3H, s), 7.38—7.60 (3H, m), 7.90—8.10 (2H, m); ^{13}C-NMR ($CDCl_3$) δ=24.8, 25.3, 31.5, 33.0, 33.8, 37.4 (methylene chain), 52.2, 52.8 (methoxyl groups), 127.6, 128.7, 130.1, 130.4, 136.3, 136.7, 142.5, 158.1, 164.4, 166.3, 168.2 (aromatic rings and carbonyls); MS, m/z (rel intensity), 353 (M^+, 76), 352 (100). Found: C, 71.37; H, 6.56; N, 3.96%. Calcd for $C_{21}H_{23}NO_4$: C, 71.34; H, 6.71; N, 3.94%. **13e**: bp 150 °C (bath temp)/93 Pa; IR ($CHCl_3$), 1721 cm^{-1}; ^{1}H-NMR ($CDCl_3$) δ=0.40—0.80 (4H, m), 1.05—1.80 (4H, m), 2.40—3.05 (3H, m), 3.32 (1H, dxt, J=12.1, 6.2 Hz), 3.91 (3H, s), 4.00 (3H, s), 7.40 (2H, d, J=8.5 Hz), 7.90 (2H, d, J=8.5 Hz); ^{13}C-NMR ($CDCl_3$) δ=25.5, 25.9, 31.5, 32.9, 33.7, 37.4, (methylene chain), 52.3, 52.9, (methoxy groups), 127.6, 128.4, 129.0, 131.5, 136.4, 142.6, 156.9, 164.2, 165.9, 167.7 (aromatic rings and carbonyls); MS, m/z (rel intensity), 389 (M^+, 25), 387 (M^+, 75), 386 (100); UV (EtOH, log ε) 252 (4.23), 287 (4.01), 345 (3.98) nm. Found: C, 64.69; H, 5.82; N, 3.88%. Calcd for $C_{21}H_{22}NO_4Cl$: C, 65.03; H, 5.72; N, 3.61%.

References

1) Preliminary report: see M. Nitta and T. Kobayashi, *Tetrahedron Lett.*, **25**, 959 (1984).

2) S. M. Rosenfeld and K. A. Choe, "Cyclophanes,Vol. 1," ed by P. M. Keehn and S. M. Rosenfeld, Academic Press, New York (1983).

3) a) N. L. Allinger, L. A. Freiberg, R. B. Hermann, and M. A. Miller, *J. Am. Chem. Soc.*, **85**, 1179 (1963); b) D. J. Cram, C. S. Montgomery, and G. R. Knox, *J. Am. Chem. Soc.*, **88**, 515 (1966); c) N. L. Allinger, T. J. Walter, and M. G. Newton, *J. Am. Chem. Soc.*, **96**, 4588 (1974); d) A. D. Wolf, V. V. Kane, R. H. Levin, and M. Jones, Jr., *J. Am. Chem. Soc.*, **95**, 1680 (1973); e) V. V. Kane, A. D. Wolf, and M. Jones, Jr., *J. Am. Chem. Soc.*, **96**, 2643 (1974); f) S. L. Kammula, L. D. Iroff, M. Jones, Jr., J. W. van Strate, W. H. de Wolf, and F. Biekelhaupt, *J. Am. Chem. Soc.*, **99**, 5815 (1977); g) J. Liebe, C. Wolff, and W. Tochtermann, *Tetrahedron Lett.*, **23**, 171 (1982); J. Liebe, W. Tochtermann, and J. Weiss, *Tetrahedron Lett.*, **24**, 2549 (1983); h) Y. Tobe, K. Kakiuchi, Y. Odaira, T. Hosaki, Y. Kai, and N. Kasai, *J. Am. Chem. Soc.*, **105**, 1376 (1983); Y. Tobe, K. Uda, K. Kakiuchi, and Y. Odaira, *Chem. Lett.*, **1983**, 1645.

4) H. Gerlach and E. Huber, *Helv. Chim. Acta*, **51**, 2027 (1968).

5) H. Reinshagen, G. Schulz, and A. Stutz, *Monatsh. Chem.*, **110**, 577 (1979).

6) T. Tachibana, M. Ando, and H. Kuzuhara, *Bull. Chem. Soc. Jpn.*, **56**, 3652 (1983).

7) T. Kobayashi and M. Nitta, *Chem. Lett.*, **1983**, 1233; T. Kobayashi and M. Nitta, *Bull. Chem. Soc. Jpn.*, **58**, 152 (1985).

8) M. E. Kuehne, S. J. Weaver, and P. Franz, *J. Org. Chem.*, **21**, 1582 (1964).

9) M. Nitta and T. Kobayashi, *J. Chem. Soc., Chem. Commun.*, **1982**, 877; M. Nitta and T. Kobayashi, *Tetrahedron Lett.*, **23**, 3925 (1982); M. Nitta and T. Kobayashi, *J. Chem. Soc., Perkin Trans. 1*, **1985**, 1401.

10) M. Nitta and T. Kobayashi, *Chem. Lett.*, **1983**, 51; M. Nitta and T. Kobayashi, *J. Chem. Soc., Perkin Trans. 1*, **1984**, 2103; M. Nitta, A. Yi, and T. Kobayashi, *Bull. Chem. Soc. Jpn.*, **58**, 991 (1985).

11) M. Nitta and T. Kobayashi, *Chem. Lett.*, **1983**, 1715; M. Nitta and T. Kobayashi, *Bull. Chem. Soc. Jpn.*, **57**, 1035 (1984); T. Kobayashi and M. Nitta, *Bull. Chem. Soc. Jpn.*, **58**, 1057 (1985); T. Kobayashi and M. Nitta, *Nippon Kagaku Kaishi*, **1985**, 451.

12) M. Nitta and T. Kobayashi, *Heterocycles*, **23**, 239 (1985).

13) T. Kaneda, T. Otsubo, H. Horita, and S. Misumi, *Bull. Chem. Soc. Jpn.*, **53**, 1015 (1980).

14) M. E. Kuehne, *J. Am. Chem. Soc.*, **81**, 5400 (1959).

15) M. H. Rosen and G. Bonet, *J. Org. Chem.*, **39**, 3805 (1974).

16) R. H. Wiley and B. J. Wakefield, *J. Org. Chem.*, **25**, 546 (1960).

Versatile Synthesis of Dialkyl Cyclopropylphosphonates *via* Reductive Phosphonation

Toshikazu HIRAO,* Masahiko HAGIHARA, and Toshio AGAWA
Department of Applied Chemistry, Faculty of Engineering, Osaka University, 2-1 Yamadaoka, Suita, Osaka 565
(Received June 10, 1985)

Reductive phosphonation of *gem*-dibromocyclopropanes was accomplished by the reaction with trialkyl phosphites, triethylamine, and water affording dialkyl cyclopropylphosphonates. This unique transformation proceeds by the virtue of trialkyl phosphites and dialkyl phosphonates.

The development of new routes for carbon–phosphorus bond formation is required for the synthetic utility of organophosphorus compounds. From this point of view, we have disclosed the palladium(0)-catalyzed phosphonation[1] as the necessary complement of carbon–phosphorus bond formation because the Arbuzov or Michaelis-Becker reaction is not generally applicable to the synthesis of alkenylphosphonates or arylphosphonates. Cyclopropylphosphonates are known as another class of less readily obtainable compounds due to the difficulty of nucleophilic displacement on a cyclopropane ring. In the course of our investigation[2,3] on reduction with dialkyl phosphonates (commercially named, dialkyl phosphites), we found a novel reductive phosphonation of *gem*-dibromocyclopropanes to give dialkyl cyclopropylphosphonates.[4] The present paper describes details of this methodology.

Results and Discussion

Treatment of the *gem*-dibromocyclopropanes **1** with triethyl phosphite in the presence of triethylamine and water at 90 °C gave mixtures of diethyl *cis*- and *trans*-cyclopropylphosphonates **2**. The

TABLE. PREPARATION OF THE DIALKYL CYCLOPROPYLPHOSPHONATES **2** AND **4**

Run	**1**				$P(OR^4)_3$ R^4, equiv.		Et_3N equiv.	H_2O equiv.	Reaction time/h[a]	Yield/%	
	R^1	R^2	R^3							**2** or **4**	**3**
1	n-C_6H_{13}	H	H	**1a**	Et	1.2	1.2	1.2	55	**2a** 16	27
2	**1a**					2	2	2	55	**2a** 28	32
3	**1a**					4	4	4	55	**2a** 32	48
4	**1a**					4	4	2	55	**2a** 51	17
5	**1a**					4	2	2	55	**2a** 70[b]	24
6	**1a**					4	4	0	55	**2a** 0	trace
7	H	$-(CH_2)_4-$		**1b**	Et	4	4	4	55	**2b** 25	63
8	**1b**					4	4	2	55	**2b** 46	18
9	**1b**					4	2	2	55	**2b** 54[c]	trace
10	**1b**					4	1	1	55	**2b** 52	trace
11	**1b**					4	2	—[d]	55	**2b** 3	trace
12	Ph	H	H	**1c**	Et	4	2	2	35	**2c** 50[e]	7
13	Me_3Si	H	H	**1d**	Et	4	2	2	25	**2d** 37	trace
14	Me_3SiCH_2	H	H	**1e**	Et	4	2	2	60	**2e** 39	trace
15	H	$-(CH_2)_6-$		**1f**	Et	4	2	2	55	**2f** 44	25
16	**1b**				*i*-Pr	4	2	2	45	**4b** 34	9
17	**1c**				*i*-Pr	4	2	2	25	**4c** 52	15
18	**1f**				*i*-Pr	4	2	2	45	**4f** 30	6
19	CN	Me	H	**1g**	Et	4	2	2	10	—	72
20	CO_2Me	Me	H	**1h**	Et	4	2	2	10	—	64
21	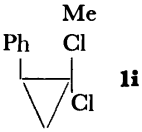 **1i**				Et	4	2	2	60	—[f]	—

a) Reaction temperature, 90 °C. b) *cis*:*trans*=1. c) *endo*:*exo*=1. d) EtOH (2 equiv.) was used instead of water. e) Diethyl *trans*-3-phenyl-2-propenylphosphonate (**5c**, 11%) and *trans*-3-ethoxy-1-phenyl-1-propene (**6c**, <1%) were produced as by-products. f) **1i** was recovered.

simultaneous reduction took place with phosphonation on a cyclopropane ring (reductive phosphonation). The *gem*-dibromocyclopropanes **1** were recovered almost quantitatively in the reaction without water, indicating that this method differentiates from the Arbuzov phosphonation. The molar ratio of reactants is a dominant factor for the successful results of this reductive phosphonation as shown in Table. The presence of a large quantity of water caused the preferential reduction of the *gem*-dibromocyclopropanes **1** into the corresponding monobromocyclopropanes **3** (runs 3 and 7). The formation of **3** is explained by the reduction of **1** with diethyl phosphonate and triethylamine as reported previously[2] because triethyl phosphite is considered to be hydrolyzed to diethyl phosphonate with water *in situ*. The increase in the amount of triethylamine lowered the yields of **2** (runs 4 and 8). Reductive phosphonation was efficiently performed in case **1**, triethyl phosphite, triethylamine, and water were used in the molar ratio of 1:4:2:2.

A variety of *gem*-dibromocyclopropanes were converted to **2** (Table). However, starting from *gem*-dibromocyclopropanes with an electron-withdrawing group such as ethoxycarbonyl or cyano group, reduction to the corresponding monobromocyclopropanes occurred exclusively (runs 19 and 20), maybe due to their susceptibility to reduction with diethyl phosphonate and triethylamine even at room temperature.[2] 1,1-Dichloro-2-phenylcyclopropane (**1i**) was not subjected to phosphonation under the conditions employed here (run 21). Use of triisopropyl phosphite yielded the corresponding diisopropyl cyclopropylphosphonate **4**. It should be noted that the formation of by-products (the cinnamylphosphonate and cinnamyl ether derivatives) was extremely depressed as compared to the reaction of **1c** with triethyl phosphite (runs 12 and 17).

The above-mentioned phosphonation seemed curious since diethyl phosphonate present *in situ* can reduce the *gem*-dibromocyclopropanes **1** to the monobromocyclopropanes **3** predominantly. One might consider that **3** intervenes as an intermediate capable of undergoing the Arbuzov phosphonation with triethyl phosphite. The independently prepared 1-bromo-2-phenylcyclopropane (**3c**), however, was not converted to the phosphonate **2c** on treatment with triethyl phosphite (4 equiv.) or with a mixture of triethyl phosphite (4 equiv.), triethylamine (2 equiv.), and water (2 equiv.) at 90 °C for 60 h. On the other hand, the reaction of 7,7-dibromonorcarane (**1b**) with triethyl phosphite, diethyl phosphonate, and triethylamine gave the corresponding cyclopropylphosphonate **2b**. This evidence implies that diethyl phosphonate plays an important role in the phosphonation reaction. Use of ethanol instead of water scarcely caused the present transformation because triethyl phosphite was not hydrolyzed to diethyl phosphonate in the absence of water (run 11).

As mentioned above, the cinnamyl derivatives were obtained as by-products (run 12), which are assumed to be resulted from the addition of diethyl phosphonate or ethanol to phenylallene. The allene formation is considered to be derived from 2-phenylcyclopropylidene intermediate. Ring cleavage occurred almost selectively in phosphonation of 1,1-dibromo-2,2-diphenylcyclopropane (**1j**), giving diethyl 3,3-diphenyl-2-propenylphosphonate (**5j**) and 3-ethoxy-1,1-diphenyl-1-propene (**6j**) together with a small amount of the cyclopropylphosphonate **2j**.

The reaction path to the cyclopropylphosphonate **2** might be postulated as depicted in the following scheme. The *gem*-dibromocyclopropane **1** undergoes debromination with the generated anion of diethyl phosphonate giving the carbanion **7**. Diethyl phosphonate is converted to diethyl phosphorobromidate and its degradation accompanies the deposition of $Et_3N \cdot HBr$.[2] Protonation of **7** with diethyl phosphonate or water gives the monobromocyclopropane **3**, which is consistent with reduction with diethyl phosphonate and triethylamine.[2] Elimination of Br^- from **7** results in the generation of the cyclopropylidene **8**. Prior to ring cleavage into the allene **9**, **8** is assumed to interact with triethyl phosphite to afford the ylide **10**. It is conceivable that the degradation of **10** completes the route to the cyclopropylphosphonate **2**.

Another possibility is proposed that **8** is subjected to α-addition of diethyl phosphonate, but excluded

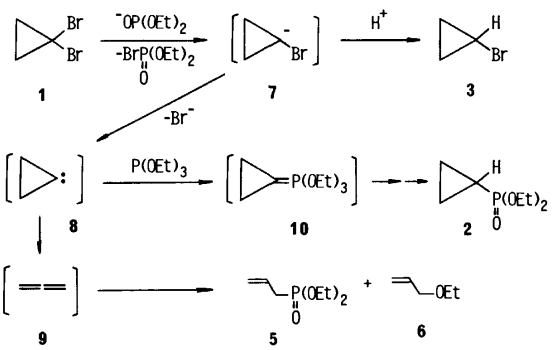

by the following observations. Treatment of **1c** with triethyl phosphite, diisopropyl phosphonate, and triethylamine gave the diethyl cyclopropylphosphonate **2c** exclusively. The formation of the diisopropyl cyclopropylphosphonate **4c** was not detected by GLC. The reverse combination of triisopropyl phosphite and diethyl phosphonate led to the exclusive formation of the diisopropyl cyclopropylphosphonate **4c**. These results support that the agent participating in carbon–phosphorus bond formation is trialkyl phosphite.

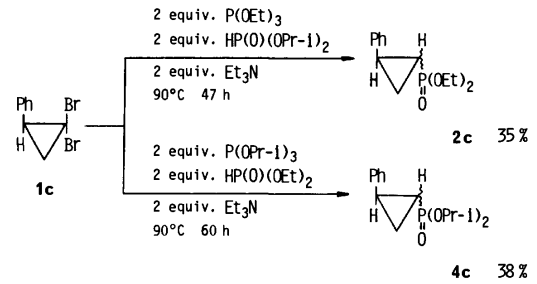

The α-proton of **2** is essentially derived from water, which was ascertained by the deuterium introduction (>90%) in the reaction of **1b** with deuterium oxide. In the case of **1c**, however, use of deuterium oxide changed the reaction course. Ring-opening phosphonation occurred predominantly producing diethyl 3-phenyl-2-propenyl-2-*d*-phosphonate.

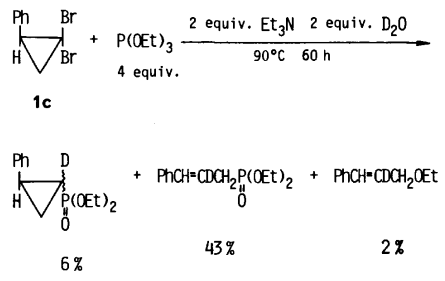

Preparation of cyclopropylphosphonates is not easily accessible because dialkyl diazomethylphosphonates commonly used for their synthesis[5] are potentially carcinogenic and explosive. The present method provides a facile synthesis of dialkyl cyclopropylphosphonates under the mild reaction conditions.

Experimental

IR spectra were taken on a JASCO IRA-1 spectrometer. NMR spectra were obtained on a JEOL JNM FX-90Q spectrometer with tetramethylsilane as an internal standard. Mass spectrometry was performed with Hitachi RMU-6E and JEOL JMS-DX 300 (high resolution) spectrometers.

Materials. *gem*-Dibromocyclopropanes were prepared according to the common method using a phase-transfer catalyst.[6] Trialkyl phosphites and dialkyl phosphonates were purified by distillation.

General Procedure for the Preparation of Dialkyl Cyclopropylphosphonates (2 or 4). To the *gem*-dibromocyclopropane **1** (5.0 mmol) were added trialkyl phosphite (20 mmol), triethylamine (10 mmol), and water (10 mmol) successively. The mixture was stirred at 90 °C for 25—60 h. During the reaction, the white precipitate ($Et_3N \cdot HBr$) separated. After the consumption of **1**, the salt was filtered off and washed with benzene (3×10 mL). The filtrate and washings were evaporated *in vacuo* and the residue was flash column chromatographed to give a mixture of dialkyl *cis*- and *trans*-cyclopropylphosphonates **2** or **4**. Further purification was done by distillation or rechromatography. These results are summarized in Table.

In the preparation of diethyl 2-phenylcyclopropylphosphonate (**2c**), diethyl *trans*-3-phenyl-2-propenylphosphonate (**5c**, 11%) and *trans*-3-ethoxy-1-phenyl-1-propene (**6c**, <1%) were obtained as by-products, which were purified by GLC (conditions: PEG 20 M column, 200 °C) after flash column chromatography.

2a: Bp 98—102 °C/0.07 mmHg† (Kugelrohr); IR (neat) 1240, 1020, 780 cm^{-1}; ^1H NMR ($CDCl_3$) δ=0.4—1.8 (m, 23H), 4.06 (quint, 4H, *J*=7.2 Hz). Found: C, 59.08; H, 10.73; P, 12.13; M^+, 262. Calcd for $C_{13}H_{27}O_3P$: C, 59.52; H, 10.37; P, 11.81; M^+, 262.

2b: Bp 118—120 °C/0.21 mmHg (Kugelrohr); IR (neat) 1240, 1020, 780 cm^{-1}; ^1H NMR ($CDCl_3$) *endo*: δ=0.72 (ddd, 1H, *J*=9.9, 8.5, 2.9 Hz, CHP), 1.0—2.2 (m, 16H), 4.10 (quint, 4H, *J*=7.1 Hz); *exo*: δ=0.55 (dt, 1H, *J*=5.6, 4.7 Hz, CHP), 1.0—2.2 (m, 16H), 4.07 (quint, 4H, *J*=7.1 Hz); ^{13}C NMR ($CDCl_3$) *endo*: δ=9.49, 14.75, 14.96, 15.88, 16.16, 18.11, 19.08, 19.35, 20.44, 60.37, 60.64; *exo*: δ=11.28, 15.83, 16.05, 16.26, 19.79, 20.44, 22.33, 22.50, 61.02, 61.29. Found: C, 57.13; H, 9.25; P, 13.10; M^+, 232. Calcd for $C_{11}H_{21}O_3P$: C, 56.88; H, 9.11; P, 13.34; M^+, 232.

2c: Oil; IR (neat) 1240, 1020, 780 cm^{-1}; ^1H NMR ($CDCl_3$) δ=1.10, 1.12 (t, 6H, *J*=7.1 Hz), 1.4—3.0 (m, 4H), 3.4—4.4 (m, 4H), 6.9—7.2 (m, 5H). Found: C, 61.18; H, 7.55; P, 12.02; M^+, 254. Calcd for $C_{13}H_{18}O_3P$: C, 61.41; H, 7.53; P, 12.18; M^+, 254.

2d: Oil; IR (neat) 1240, 1040, 780 cm^{-1}; ^1H NMR ($CDCl_3$) δ=0.00 (s, 9H), 0.2—0.8 (m, 3H), 1.37 (t, 6H, *J*=7.0 Hz), 4.10 (quint, 4H, *J*=7.0 Hz). High-resolution MS; Found: 235.0931. Calcd for $C_9H_{20}O_3PSi$ (M^+-CH_3): 235.0918.

2e: Oil; bp 98—100 °C/0.15 mmHg (Kugelrohr); IR

† 1 mmHg=133.322 Pa.

(neat) 1240, 1020, 790 cm^{-1}; ^1H NMR ($CDCl_3$) δ=0.22 (s, 9H), 0.4—1.2 (m, 6H), 1.32 (t, 6H, J=7.1 Hz), 4.10 (quint, 4H, J=7.1 Hz). Found: C, 49.65; H, 9.71; P, 11.49; M^+, 264. Calcd for $C_{11}H_{25}O_3PSi$: C, 49.97; H, 9.53; P, 11.72; M^+, 264.

2f: Oil; IR (neat) 1240, 1020, 780 cm^{-1}; ^1H NMR ($CDCl_3$) δ=0.7—2.2 (m, 15H), 1.33 (t, 6H, J=7.1 Hz), 4.06 (quint, 4H, J=7.1 Hz). High-resolution MS; Found: 260.1514. Calcd for $C_{13}H_{25}O_3P$ (M^+): 260.1540.

4b: Oil; IR (neat) 1250, 1010, 790, 770 cm^{-1}; ^1H NMR ($CDCl_3$) δ=0.4—2.2 (m, 23H), 4.4—4.9 (m, 2H). High-resolution MS; Found: 260.1522. Calcd for $C_{13}H_{25}O_3P$ (M^+): 260.1540.

4c: Oil; IR (neat) 1240, 1010, 770 cm^{-1}; ^1H NMR ($CDCl_3$) δ=1.0—1.5 (m, 15H), 2.1—2.7 (m, 1H), 4.1—4.9 (m, 2H), 7.1—7.5 (m, 5H). High-resolution MS; Found: 282.1389. Calcd for $C_{15}H_{23}O_3P$ (M^+): 282.1384.

4f: Oil; IR (neat) 1240, 1000, 780, 760 cm^{-1}; ^1H NMR ($CDCl_3$) δ=0.6—2.2 (m, 15H), 1.30 (d, 12H, J=6.7 Hz), 4.3—4.9 (m, 2H). High-resolution MS; Found: 288.1852. Calcd for $C_{15}H_{29}O_3P$ (M^+): 288.1852.

Phosphonation with Trialkyl Phosphite and Dialkyl Phosphonate. To the *gem*-dibromocyclopropane **1** (5.0 mmol) were added trialkyl phosphite (10 mmol), dialkyl phosphonate (10 mmol), and triethylamine (10 mmol). The mixture was stirred at 90 °C for 47—60 h. Workup was carried out as mentioned above to give **2** or **4**. Yields were shown in the equation or scheme. The selectivity was checked by GLC (conditions: PEG 20 M column, 200 °C).

Phosphonation in the Presence of D_2O. To the *gem*-dibromocyclopropane **1** (5.0 mmol) were added triethyl phosphite (20 mmol), triethylamine (10 mmol), and D_2O (10 mmol). The mixture was stirred at 90 °C for 60 h. Workup and isolation of products were done as mentioned above. Starting from **1b**, the corresponding α-deuteriocyclopropylphosphonate was obtained in 27% yield. Diethyl 2-phenylcyclopropyl-1-*d*-phosphonate (6%), diethyl 3-phenyl-2-propenyl-2-*d*-phosphonate (43%), and 3-ethoxy-1-phenyl-2-*d*-1-propene (2%) were obtained in the phosphonation reaction of **1c**. The olefinic geometry was not determined. In every case, the deuterium content was more than 90%.

This work was partially supported by the Grant-in-Aid for Developmental Scientific Research from the Ministry of Education, Science, and Culture.

References

1) T. Hirao, T. Masunaga, Y. Ohshiro, and T. Agawa, *Tetrahedron Lett.*, **21**, 3595 (1980); *Synthesis*, **1981**, 56; T. Hirao, T. Masunaga, N. Yamada, Y. Ohshiro, and T. Agawa, *Bull. Chem. Soc. Jpn.*, **55**, 999 (1982).

2) T. Hirao, T. Masunaga, Y. Ohshiro, and T. Agawa, *J. Org. Chem.*, **46**, 3745 (1981).

3) T. Hirao, S. Kohno, Y. Ohshiro, and T. Agawa, *Bull. Chem. Soc. Jpn.*, **56**, 1881 (1983); T. Hirao, T. Masunaga, K. -i. Hayashi, Y. Ohshiro, and T. Agawa, *Tetrahedron Lett.*, **24**, 399 (1983).

4) T. Hirao, M. Hagihara, Y. Ohshiro, and T. Agawa, *Synthesis*, **1984**, 60.

5) D. Seyferth, R. S. Marmor, and P. Hilbert, *J. Org. Chem.*, **36**, 1379 (1971); J. R. Reid and R. S. Marmor, *ibid.*, **43**, 999 (1978).

6) W. E. Keller, "Compendium of Phase-Transfer Reactions and Related Synthetic Methods," Fluka AG, 1979.

Aryliminodimagnesium Reagents. IX. The Reaction with Benzophenones. The Mechanism of Coordination and Electron Transfer Processes Distinct from That of Grignard Reaction

Masao Ōkubo
Department of Chemistry, Faculty of Science and Engineering, Saga University, Honjō-machi, Saga 840
(Received June 10, 1985)

In the reaction of aryliminodimagnesium reagents(ArN(MgBr)$_2$, Ar=C_6H_5, *p*-MeC_6H_4, and *p*-$MeOC_6H_4$) with some *p*-substituted benzophenones, the arylaminyl radicals(ArṄMgBr) derived from the reagents were detected by ESR in low concentrations and identified by computer simulation. From comparison of all the itemized facts characteristic of the reaction with those of Grignard reaction of the same substrates, the mechanisms of initial coordination and electron transfer of the two reactions were distinguished.

Aryliminodimagnesium reagents(ArN(MgBr)$_2$, aryl-IDMg) condense with diaryl ketones.[1,2] When the reagent has *o*-Me group, diarylmethanol is obtained as the sole abnormal product arising from ketyl radical *via* hydrogen abstraction from solvent.[2] In this paper, the identification of arylaminyl radical produced from IDMg reagent in the reaction with *p*-substituted benzophenones will be described first. On the basis of the fact that electron transfer is involved in both IDMg and Grignard[3] reactions with benzophenones, all the facts characteristic of each reaction will be itemized and compared. The distinctive mechanisms, consistent with the respective facts, for the initial processes of the two reactions will be proposed.

Results and Discussion

Identification of Arylaminyl Radicals. The ESR measurements were carried out at room temperature under the conditions similar to those of preparative reactions.[1,2] The benzophenones used are 4,4′-disubstituted ones, the substituents being Me_2N, MeO, Me, and Cl groups. The concentration of unsubstituted and *p*-substituted phenyl-IDMg reagents was 0.02 M[†] and the molar ratio of reagent to substrate was 2:1. The degassed and sealed solutions of reagent and substrate in tetrahydrofuran(THF) were mixed by breaking the seal.[3] The radical concentrations observed in this study were quite lower compared with those observed in the reactions with ArMgBr;[3] a high microwave power and a large modulation width(2.00 G, G=10^{-3} T) were supplied for obtaining the sufficient intensity of signals. The typical spectra obtained in the reactions of 4,4′-bis(dimethylamino)benzophenone with phenyl- and *p*-methoxyphenyl-IDMg are shown in Figs. 1a_1 and 1b_1, respectively. The spectra are incompletely resolved and slightly anisotropic, and the resolution was unimproved by dilution in the evacuated sample cell.

For the analysis of spectra 1a_1 and 1b_1, computor simulation with half width of 3.5 G was carried out by use of Lorentzian curve. The Mg-ketyl of the ketone was prepared by use of Mg-Hg amalgam; its ESR signal, observed under the same conditions of measurement, was simulated and overlapped with the simulated spectra of arylaminyl π-radicals,[4] $C_6H_5\dot{N}X$ and *p*-$MeOC_6H_4\dot{N}X$: The resultant spectra are shown

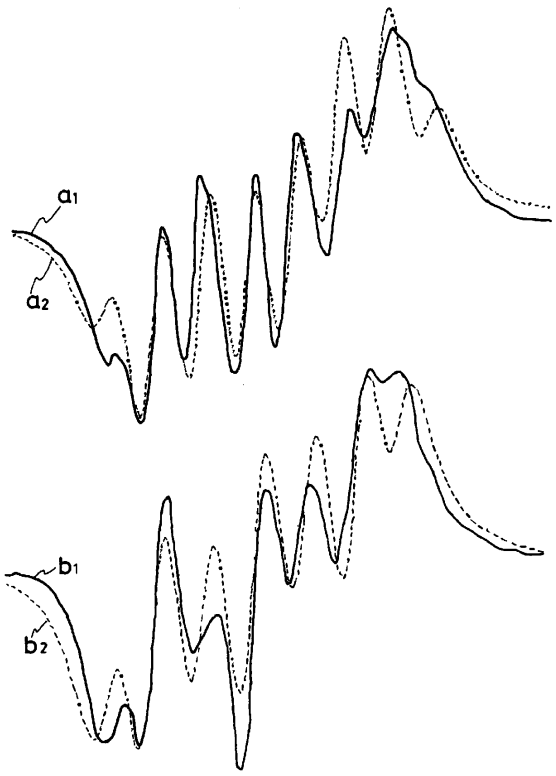

Fig. 1. ESR spectra of the mixtures of arylaminyl and ketyl radicals formed in the reaction of *p*,*p*′-$(Me_2N)_2$-benzophenone with IDMg reagents.
a_1: Observed in the reaction with C_6H_5-IDMg,
a_2: Simulated without 3.0 G shift of Mg-ketyl signal,
b_1: Observed in the reaction with *p*-$MeOC_6H_4$-IDMg,
b_2: Simulated without 3.0 G shift of Mg-ketyl signal.

† 1 M=1 mol dm^{-3}.

in Figs. $1a_2$ and $1b_2$, respectively. In both cases, the remarkable deviations are observed in two areas: The one at the left near to the center and the other near to the right end of each spectrum. The former deviation is ascribed to the slightly different *g*-factor of IDMg-ketyl from that of Mg-ketyl, since the best fits of $1a_2$ and $1b_2$ with $1a_1$ and $1b_1$, respectively, are obtained when the simulated signal of Mg-ketyl is shifted to the lower field by 3.0 G: The difference of *g*-factor originates from the presence of bromine atom combined to Mg atom of IDMg-ketyl. The latter deviation is ascribed to the decay of radicals during the course of scanning.

The spectrum observed in the reaction of the same ketone with *p*-methylphenyl-IDMg was simulated similarly. The values of splitting constans and *g*-factors given in Table 1 are reasonable as compared to those of various types of arylaminyl π-radicals($Ar\dot{N}X$: Ar=*t*-Bu, O-*t*-Bu, and H) reported previously.[5-7] The attempt to observe triplet state at 77 K was unsuccessful: The observed spectra are assignable to the mixtures of arylaminyl($Ar\dot{N}MgBr$) and ketyl ($Ar'_2\dot{C}OMgBr$) radicals interacting, if any, quite weakly with each other.

When the substituent on reagent is fixed, the shape of spectrum remains almost independent of the substituent on substrate, which, however, causes the gradual decrease in the signal strength according to the order: $Me_2N>MeO>Me>H>Cl$.[8] Since no diarylmethanol was detected, the observation implies that the electron-repelling substituent assists the substrate in rate-determining coordination of carbonyl oxygen to Mg atom of reagent and the resultant acceleration of electron transfer leads to the effective condensation(*vide infra*).[2,9]

Mechanistic Distinction between Grignard and IDMg Reactions. The electron transfer from reagent to substrate is involved in pathways for the formation of normal products in the reactions of benzophenone with both ArMgBr(***C***) and $ArN(MgBr)_2$(***N***): This is revealed not only by ESR measurement but also by use of *o*-Me-substituted reagents, which give rise to the increase in yields of abnormal products.[2,3] The coordination of carbonyl oxygen to Mg atom of reagent (or σ-complex formation, process I) due to the strong affinity of magnesium for oxygen, in addition to the subsequent electron transfer (process II), is also common to the two reactions. Accordingly, the itemized facts characteristic of the reactions observed in the previous and present studies (Table 2,

Table 1. Hyperfine splitting constants and *g*-factors of arylaminyl radicals derived from IDMg reagents in the reaction with 4,4'-bis(dimethylamino)benzophenone

Reagents	hfs/G (G=10^{-3} T)					*g*-factors
	a_N	$a_{p\text{-}H}$	$a_{o\text{-}H}$	$a_{m\text{-}H}$	a_{CH_3}	
$C_6H_5N(MgBr)_2$	9.80	5.75	5.20	0.73	—	2.0031
$p\text{-}CH_3C_6H_4N(MgBr)_2$	10.50	—	5.20	1.10	5.20	2.0031
$p\text{-}CH_3OC_6H_4N(MgBr)_2$	11.00	—	5.00	0.50	—	2.0031

Table 2. Itemized facts characteristic of the reactions of benzophenone with IDMg and Grignard reagents

	Items	$ArN(MgBr)_2$ (***N***)	ArMgBr (***C***)
[*a*]	Manner of Reaction	Condensation	Addition
[*b*]	Classification[i]	Type C	Type B
[*c*]	Favorable Substituents on Substrate	*p*-Me_2N, *p*-MeO	*p*-F, *p*-Cl
[*d*]	Abnormal Products		
	from Substrate	Diarylmethanol	TPE-diol[iv]
	from Reagent	Aniline	Biaryl
[*e*]	Character of Reagent		
	Oxidation Peak Potential[ii]	High	Low
	EDA	Weak	Strong
[*f*]	Radicals Observed at r.t.		
	from Substrate	Ketyl ○	Ketyl ◎
	from Reagent	Arylaminyl ○	Aryl ×
	Concentration	Low	High
[*g*]	Rate-determining Process[iii]	Coordination	Electron Transfer

i) Type A includes the reactions which are hardly controllable due to vigorous electron transfer.[9] ii) Ref. 11). iii) See text. iv) 1,1,2,2-Tetraphenylethan-1,2-diol.

[*a*—*g*]) are helpful in distinguishing the mechanisms from each other.

The fundamental fact for the distinction is that *one of the two initial processes is rate-determining*[g] and the subsequent ones for product formation are not. The rate-determining nature of process II in the reaction of ***C***[g] established by the thermochemical study of Holm[10] was confirmed by acceleration of ketyl formation by *p*-F- and *p*-Cl-substituents on benzophenone[*c*].[3,9] The rate-determining nature of process I in the reaction of ***N***[g] is suggested from the fact that *p*-Me_2N and *p*-MeO substituents on benzophenone favor the formation of products[*c*],[2,9] and is verified by the substituent effect on radical concentration. The rate-determining process moves between I and II depending on the electron-donating abilities(EDA) of reagents:[9] The weaker EDA of ***N*** than that of ***C***[*e*] is estimated by polarographic measurement of oxidation potentials.[11] On this basis, the mechanism of initial processes leading to the *monomeric* diarylmethanol in IDMg reaction is distinguished from that leading to the *dimeric* 1,1,2,2-tetraphenylethan-1,2-diol(TPE-diol) in Grignard reaction[*d*].

Since process II of the reaction of ***C*** is rate-determining, process I proceeds rapidly but incompletely. The "incomplete coordination" is substantiated by considering the two previous observations: The oligomeric aggregation of reagent molecules in the presence of oxygen-containing substances[12] and the presence of equilibrium between Grignard-ketyl and Mg–TPE–diolate[3,13] (Scheme 1a). The aggregation is best ascribed to the prior interaction of benzophenone molecules with ***C*** having strong EDA[*e*], and *the electron transfer from aggregated reagent molecules* give rise to production of Grignard-ketyls in the neighborhood of each other. This favors the formation of Mg–TPE–diolate[*d*], the equilibration with it being responsible for the ESR observation of long-lived Grignard-ketyl in moderately high concentration[*f*]. Aryl radicals, produced inside the reagent aggregate, are hardly observable by ESR[*f*] due to the favorable formation of biaryl[*d*] and also probably due to the delocalization of unpaired electrons in the aggregate.

In the reaction of ***N***, process II proceeds after the rate-determining σ-complex formation (process I) has been at least nearly completed[g]. The complex formation assists the substrate in lowering its HOMO and LUMO energy levels[8,14] and accepting electrons from ***N*** having weak EDA[*e*]. From the "complete σ-complex" surrounded by solvent molecules, both IDMg–ketyl and arylaminyl radicals are produced in monomeric states: They are thus short-lived and detectable in quite low concentration[*f*]. Most part of the two kinds of radicals recombine with each other leading to the formation of anil[1,2] (Scheme 1b), but a part of them abstracts hydrogen from solvent[*d*] especially when the radical recombination is retarded by *o*-Me substituent.[2]

The essential roles of processes I and II in the reactions of ***N*** and ***C***, respectively, are exemplified by the distinctive behaviors of the reagents towards sterically hindered 2,3,5,6-tetramethylbenzophenone. On the treatment with ***N***, neither ESR signal nor coloration of the mixture indicative of σ-complex formation is observed and the ketone is recovered unchanged. On the treatment with ***C***, in contrast, the ketyl accumulates gradually up to a very high concentration.[3] Whereas ***N*** having weak EDA is unable to transfer electrons *because the σ-complex formation is inhibited,* ***C*** having strong EDA transfers electrons *even though the coordination is incomplete.* The previous postulate on the possibility of produc-

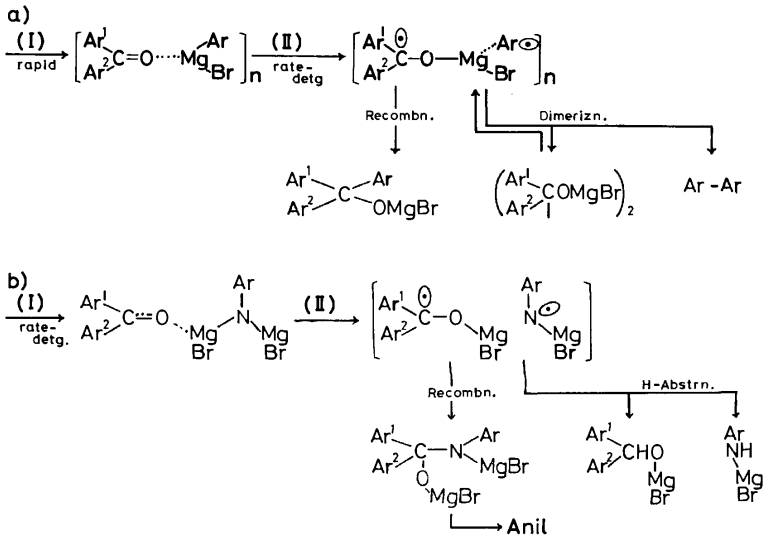

Scheme 1.

tion of "benzophenone anion radical" prior to the O–Mg bond formation in the reaction of ***C*** resembles the discussion given above. However, the aggregate formation, supposed in the earliest paper on Grignard-ketyls,[16] is verified to be essential in the reaction of ***C*** due to its strong EDA.

Experimental

Materials and Procedures. Benzophenone and aniline as well as their substituted derivatives were commercially available, and were purified by recrystallization or distillation if necessary. The preparation of stock solutions of reagents[1] and ESR measurements[3,16] were carried out according to the reported procedures.

The author wishes to express his gratitude to Professor Kazuhiko Ishizu, Ehime University, for helpful discussion. He also wishes to thank Dr. Noboru Takisawa and Mr. Toshiki Tsutsumi, Saga University, for computer simulation of ESR spectra.

References

1) M. Ōkubo and S. Ueda, *Bull. Chem. Soc. Jpn.*, **53**, 281 (1980).
2) M. Ōkubo, S. Hayashi, M. Matsunaga, and Y. Uematsu, *Bull. Chem. Soc, Jpn.*, **54**, 2337 (1981).
3) M. Ōkubo, *Bull. Chem. Soc. Jpn.*, **48**, 2057 (1975).
4) W. C. Danen and F. A. Neugebauer, *Angew. Chem., Int. Ed. Engl.*, **14**, 783 (1975).
5) S. F. Nelson, R. T. Randis, L. H. Kiehle, and T. H. Leung, *J. Am. Chem. Soc.*, **94**, 1610 (1972).
6) W. C. Danen, C. T. West, and T. T. Kensler, *J. Am. Chem. Soc.*, **95**, 5716 (1973).
7) R. Neta and R. W. Fessenden, *J. Chem. Phys.*, **78**, 523 (1974).
8) The unsuccessful detection of radical species in the previous study[9] is due to the use of benzophenone having no electron-repelling substituent.
9) M. Ōkubo, M. Yoshida, K. Horinouchi, H. Nishida, and Y. Fukuyama, *Bull. Chem. Soc. Jpn.*, **56**, 1196 (1983).
10) T. Holm and I. Crossland, *Acta Chem. Scand.*, B **28**, 809 (1974).
11) M. Ōkubo, T. Tsutsumi, A. Ichimura, and T. Kitagawa, *Bull. Chem. Soc. Jpn.*, **57**, 2679 (1984).
12) A. D. Vreugdenhil and C. Blomberg, *Recl. Trav. Chim. Pays-Bas*, **84**, 38 (1965); H. O. House, R. A. Latham, and G. M. Whitesides, *J. Org. Chem.*, **32**, 3481 (1967).
13) I. G. Lopp, J. D. Buhler, and E. C. Ashby, *J. Am. Chem. Soc.*, **97**, 4966 (1975).
14) S. Nagase and Y. Uchibori, *Tetrahedron Lett.*, **23**, 2585 (1982).
15) E. C. Ashby and A. B. Goel, *J. Am. Chem. Soc.*, **103**, 4983 (1982).
16) K. Maruyama, *Bull. Chem. Soc. Jpn.*, **37**, 897, 1013 (1964).

Isolation and Structures of Euphohelins, New Toxic Diterpenes from *Euphorbia Helioscopia* L.

Seiji KOSEMURA, Yoshikazu SHIZURI, and Shosuke YAMAMURA*
Department of Chemistry, Faculty of Science and Technology, Keio University, Hiyoshi, Kohoku-ku, Yokohama 223
(Received June 12, 1985)

Five new toxic diterpenes, euphohelins A, B, C, D, and E, have been isolated from the plant *Euphorbia helioscopia* L., and their stereostructures have also been elucidated on the basis of their spectral data coupled with some chemical evidence: euphornin, the known toxic diterpene, has been successfully converted into euphohelin A.

In connection with highly-oxygenated diterpenes which have antitumor activity or promote cancer development in tumor formation, we examined toxic substances of the plants *Euphorbiaceae* and could isolate euphoscopin A (**1**),[1,2] euphornin (**2**),[3] euphohelioscopin A (**3**),[2] euphohelionone (**4**),[4] and others from the plant *Euphorbia helioscopia* L. (Todai-Gusa in Japanese), as seen in Fig. 1. Further investigation of toxic compounds in the same plant resulted in the isolation of five new diterpenes, euphohelins A, B, C, D, and E (**5**, **6**, **7**, **8**, and **9**) in addition to the known diterpenes (**1**, **2**, and **3**) and others.[1-3]

Isolation of Euphohelins A, B, C, D, and E. Fresh leaves and roots of the plant *Euphorbia helioscopia* L. collected in Kanagawa Prefecture in the middle of June were immersed in methanol at room temperature, and then the methanol extract was concentrated and shaken with ethyl acetate. The ethyl acetate extract was partitioned between 90% aqueous methanol and "isooctane". The methanol extract was roughly separated by column chromatography [silica gel (Merck 7734)] using a gradient solution of hexane and ethyl acetate. The fraction eluted only with ethyl acetate was further separated by repeating preparative TLC (Kieselgen PF_{254}) using hexane–ethyl acetate

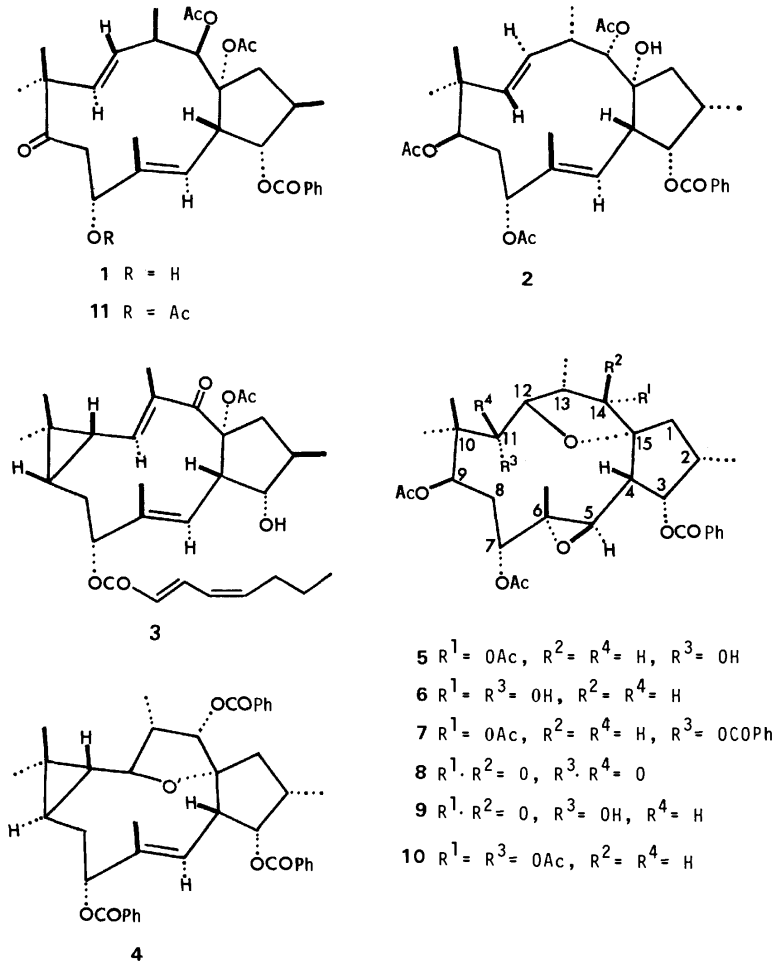

Fig. 1. Toxic diterpenes from *Euphorbia helioscopia* L.

Table 1. ^{1}H NMR Spectral data of euphohelins A (5), B (6), C (7), D (8), and E (9) and euphohelin a acetate (10) (δ from TMS)

Proton	5	6	7	8	9	10
C^1-H_2	1.91—2.23*	1.79—2.40*	1.93—2.63*	1.95—2.10*	1.93—1.98*	1.87—2.63*
C^2-H	2.10(m)	2.16—2.40*	1.93—2.63*	2.39—2.50*	2.36(m)	1.87—2.63*
C^3-H	5.63 (dd, J=6.5, 4.8 Hz)	5.63 (dd, J=5.6, 5.6 Hz)	5.66 (dd, J=6.3, 4.4 Hz)	5.74 (dd, J=6.0, 4.3 Hz)	5.74 (dd, J=6.1, 4.4 Hz)	5.65 (dd, J=6.6, 4.9 Hz)
C^4-H	2.33 (dd, J=9.9, 6.5 Hz)	2.16—2.40*	1.93—2.63*	2.39—2.50*	2.46 (dd, J=9.5, 6.1 Hz)	1.87—2.63*
C^5-H	3.66 (d, J=9.9 Hz)	3.66 (d, J=9.7 Hz)	3.70 (d, J=10 Hz)	3.73 (d, J=9.5 Hz)	3.68 (d, J=9.5 Hz)	3.66 (d, J=9.8 Hz)
C^7-H	5.06—5.10*	5.05 (dd, J=3.7, 3.4 Hz)	5.13—5.20*	5.02 (br. d, J= 5.9 Hz)	5.10 (dd, J=3.7, 3.4 Hz)	5.10 br. d, J= 5.4 Hz)
C^8-H_2	1.91—1.93*	1.79—1.94*	1.93—2.63*	1.95—2.10*	1.93—1.98*	1.87—2.62*
C^9-H	6.25 (dd, J=4, 4 Hz)	6.25 (dd, J=4.4, 3.9 Hz)	6.30 (br. d, J= 6.8 Hz)	6.59 (br. d, J= 7.8 Hz)	6.36 (dd, J=4.2, 3.9 Hz)	6.22 (br. d, J= 6.8 Hz)
C^{11}-H	3.30 (d, J=9.0 Hz)	3.22 (d, J=9.0 Hz)	5.13—5.20*		3.46 (d, J=8.8 Hz)	4.89 (d, J=9.5 Hz)
C^{12}-H	3.69*	3.65 (dd, J=9.0, 5.4 Hz)	4.05 (dd, J=9.3, 7.1 Hz)	4.67 (d, J=8.5 Hz)	3.95 (dd, J=8.8, 7.3 Hz)	3.87 (dd, J=9.5, 6.8 Hz)
C^{13}-H	2.51 (m)	2.16—2.40*	1.93—2.63*	2.77 (dq, J=8.5, 7.3 Hz)	2.35 (dq, J=7.3, 7.6 Hz)	1.87—2.63*
C^{14}-H	5.06—5.10*	4.06 (d, J=8.1 Hz)	5.13—5.20*			5.15 (d, J=7.3 Hz)
C^2-Me	1.07 (d, J=6.5 Hz)	1.18 (d, J=7.3 Hz)	0.88 (d, J=7.1 Hz)	1.10 (d, J=6.8 Hz)	1.05 (d, J=6.6 Hz)	0.97 (d, J=7.1 Hz)
C^6-Me	1.36 (s)	1.31 (s)	1.52 (s)	1.41 (s)	1.12 (s)	1.45 (s)
C^{10}-Me	0.93 (s)	0.92 (s)	0.81 (s)	0.97 (s)	0.96 (s)	0.77 (s)
C^{10}-Me′	0.93 (s)	0.92 (s)	1.12 (s)	1.11 (s)	1.01 (s)	1.00 (s)
C^{13}-Me	1.09 (d, J=7.2 Hz)	1.06 (d, J=6.6 Hz)	1.06 (d, J=5.6 Hz)	1.33 (d, J=7.3 Hz)	1.41 (d, J=7.6 Hz)	1.05 (d, J=5.9 Hz)
C^3-OCOPh	7.41—7.53 (3H, m) 8.20—8.25 (2H, m)	7.41—7.54 (3H, m) 8.20—8.25 (2H, m)	7.40—7.65 (3H, m) 8.19—8.24 (2H, m)	7.45—7.61 (3H, m) 8.23—8.33 (2H, m)	7.43—7.59 (3H, m) 8.26—8.31 (2H, m)	7.39—7.57 (3H, m) 8.18—8.24 (2H, m)
C^7-OAc	1.42 (s)	1.39 (s)	1.44 (s)	1.46 (s)	1.39 (s)	1.43 (s)
C^9-OAc	2.01 (s)	2.00 (s)	2.03 (s)	2.06 (s)	2.04 (s)	2.02 (s)
C^{11}-OAc						2.09 (s)
C^{14}-OAc	2.16 (s)		2.13 (s)			2.15 (s)
C^{11}-OCOPh			7.40—7.65 (3H, m) 8.02—8.06 (3H, m)			

* Overlapped with other signals.

(2:1) to afford euphohelins A, B, C, D, and E (**5**, **6**, **7**, **8**, and **9**) in 0.038, 0.0035, 0.021, 0.061, and 0.0042% yields, based on the weight of the methanol extract, respectively, in addition to the known diterpenes.[1-3] The structure of these newly isolated diterpenes, which are shown in Fig. 1, have been unambiguously determined on the basis of their spectral data coupled with some chemical evidence.

The Structure of Euphohelin A (5). Euphohelin A with a molecular formula $C_{33}H_{44}O_{11}$ has the IR absorption bands at 3500, 1730, 1600, and 1580 cm^{-1}, and its ^1H and ^{13}C NMR spectral data are described in Tables 1 and 2. As seen in Table 1, euphohelin A (**5**) has one benzoyloxyl group [δ 7.41—7.53 (3H), 8.20—8.25 (2H)], three acetoxyl groups [δ 1.42 (C^7-OAc), 2.01 (C^9-OAc), 2.16 (C^{14}-OAc)] and five methyls [δ 0.93 (6H, s), 1.07 (3H, d, J=6.5 Hz), 1.09 (3H, d, J=7.2 Hz), 1.36 (3H, s)]. As judged from Table 2, furthermore, euphohelin A is regarded as a tetracyclic diterpene, because it has no sp^2 carbon atom except for ten sp^2 carbon atoms included in one benzoyloxyl and three acetoxyl groups. In addition, one of the four rings must be a trisubstituted epoxide ring on the basis of a gated decoupling experiment at δ 56.0 together with selected decoupling ones: the doublet at δ 56.0 due to the C^5 carbon atom, which has a characteristically large $^1J_{C\text{-}H}$ (178.8 Hz), is coupled with the proton (C^5-H) (δ 3.66). As seen in Table 1 and Fig. 2, a detailed analysis of the ^1H NMR spectrum of euphohelin A (**5**) by homonuclear spin decoupling experiments indicated the presence of partial structures [A], [B], and [C] and three tertiary methyls. In addition, euphohelin A has one secondary hydroxyl group, which is accommodated in [C] on the basis of the following observation: on acetylation of euphohelin A (**5**) with acetic anhydride–pyridine giving rise to the corresponding acetate (**10**), the doublet at δ 3.30 in **5** was shifted to δ 4.89 in **10**. Another important information about euphohelin A will be obtained from its ^1H NMR spectrum, as follows. One of the methyl singlets due to the three acetoxyl groups in **5** is observed in higher magnetic field (δ 1.42) rather than the remaining ones (δ 2.01

Table 2. ^{13}C NMR Spectral data of euphohelins A and D (5 and 8) (δ from TMS)

Carbon	5	8
1	40.5 (t)	43.1 (t)
2	37.4 (d)	37.4 (t)
3	76.3 (d)	77.0 (d)
4	51.0 (d)	50.8 (d)
5	56.0 (d)	54.5 (d)
6	58.7 (s)	58.3 (s)
7	70.3 (d)	69.4 (d)
8	29.7 (t)	30.6 (t)
9	71.5 (d)	69.6 (d)
10	43.2 (s)	54.8 (s)
11	78.1 (d)	208.5 (s)
12	85.3 (d)	85.4 (d)
13	41.2 (d)	42.6 (d)
14	79.5 (d)	217.7 (s)
15	90.3 (s)	89.0 (s)
Me	13.8 (q)	13.4 (q)
	14.1 (q)	15.2 (q)
	17.1 (q)	15.8 (q)
	17.3 (q)	16.9 (q)
	17.9 (q)	22.4 (q)*
AcO	19.9 (q)	19.9 (q)
	20.7 (q)	21.1 (q)
	21.2 (q)	
	169.5 (s)	169.2 (s)
	169.6 (s)	169.3 (s)
	170.4 (s)	
PhCOO	128.4 (d)**	128.4 (d)**
	130.1 (s) (d)**	129.8 (s)
	132.8 (d)	130.3 (d)**
		132.9 (d)
	165.8 (s)	165.7 (s)

* This signal is assigned tentatively. ** Corresponding to two protons.

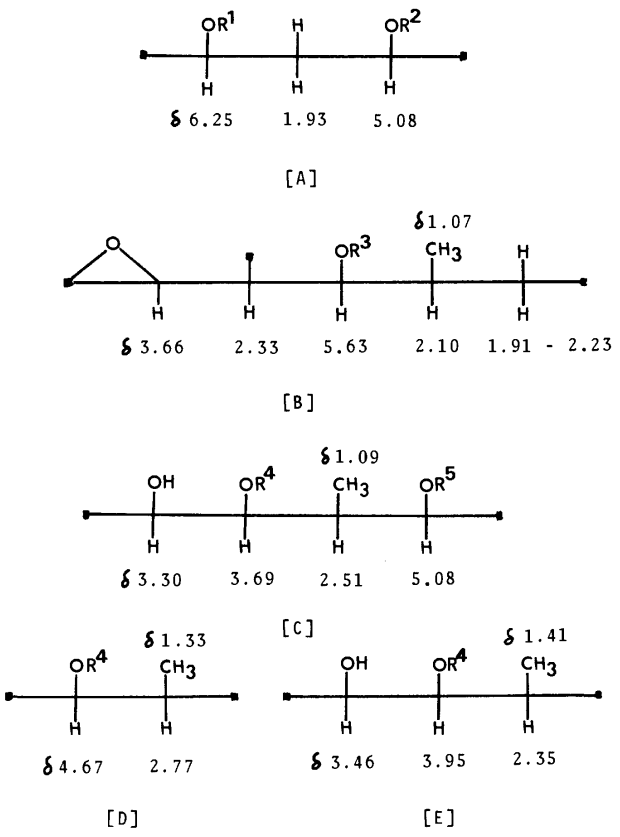

■ These are quaternary carbon atoms.

Fig. 2. Partial structures of euphohelins.

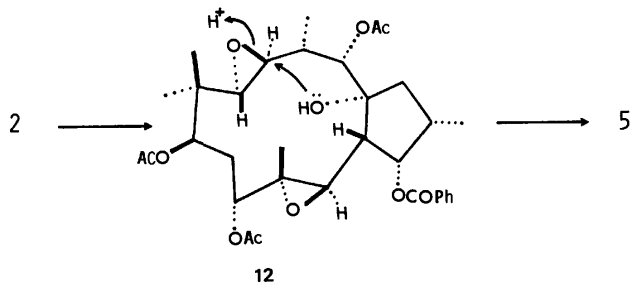

Fig. 3. Chemical conversion of euphornin (**2**) to euphohelin A (**5**).

and 2.16). This may be due to anisotropic effect of the benzoyloxyl group, as seen in the cases of euphornin (**2**)[3] and euphoscopin B (**11**).[1]

In the light of the above-mentioned results together with co-occurrence of euphoscopins A and B (**1** and **11**) and euphornin (**2**) and their ^{1}H NMR spectra, a tentative structure (**5**) is given to euphohelin A except for its stereochemistry (C^2-Me and C^{11}—C^{15}). Finally, the stereostructure of euphohelin A (**5**) was unambiguously determined in connection with euphornin (**2**), as follows.

Fortunately, euphornin (**2**), whose conformation strictly based on an X-ray crystallographic analysis, ^{1}H NMR spectrum, and molecular mechanics calculations,[3] was subjected to epoxidation using *m*-chloroperbenzoic acid in dichloromethane (room temp, 2 d) to give euphohelin A (**5**), 87% yield, through the corresponding diepoxide (**12**), as shown in Fig. 3., wherein one of the two epoxide rings was subsequently attacked by the hydroxyl group at C^{15}-position resulting in the formation of a tetrahydrofuran ring. Thus, the stereostructure of euphohelin A must be depicted as **5**, which is supported by its ^{1}H NMR spectrum: in consideration of the most plausible conformation, in which the acetoxyl group at C^7-position in **5** (δ 1.42) adopts the same situation as that in euphornin (**2**) and related diterpenes (δ 1.27—1.33), the two hydrogen atoms at C^{11}- and C^{12}-positions must be in a trans configuration having dihedral angle of 180° (J=9.0 Hz).

The Structure of Euphohelin B (6). Euphohelin B (**6**) with a molecular formula $C_{31}H_{42}O_{10}$ has the IR absorption bands at 3500, 1720, 1600, and 1580 cm^{-1}, and its ^{1}H NMR spectral data is also cited in Table 1. On a detailed comparison of the ^{1}H NMR spectra between euphohelins A and B, the NMR signal at δ 5.08 due to the proton (AcO-C^{14}-H) in **5** is not found in the latter, but instead a doublet is newly observed at δ 4.06, suggesting that euphohelin B (**6**) is a deacetyl derivative of euphohelin A (**5**) at C^{14}-position. Thus, euphohelin A was subjected to regioselective hydrolysis using one equivalent of KOH in methanol (room temp, 50 min) to afford euphohelin B (**6**) in 90% yield.

The Structure of Euphohelin C (7). Euphohelin C (**7**) has a molecular formula $C_{38}H_{46}O_{11}$ and its ^{1}H NMR spectrum indicates the presence of three acetoxyl and two benzoyloxyl groups. However, the IR spectrum of **7** has no absorption band assignable to a hydroxyl group. As seen in Table 1, the NMR signal at δ 3.30 (HO-C^{11}-H) in euphohelin A (**5**) is also not found in **7**, but instead the corresponding one is observed at δ 5.16, suggesting that euphohelin C has an additional benzoyloxyl group at C^{11}-position because the other corresponding signals are quite similar to one another. Thus, euphohelin A (**5**) was treated with benzoyl chloride in pyridine (room temp, overnight and then 60 °C, 1 h) to afford euphohelin C (**7**) in almost quantitative yield.

The Structure of Euphohelin D (8). The IR and ^{1}H NMR spectra of euphohelin D (**8**) having a molecular formula $C_{31}H_{38}O_{10}$ indicate the presence of one benzoyloxyl group and two acetoxyl groups (see Table 1), and any absorption band due to a hydroxyl group is not found in its IR spectrum. Furthermore, on the basis of detailed proton homonuclear spin decoupling and gated decoupling experiments, euphohelin D (**8**) has a trisubstituted epoxide ring (δ 54.5, $^1J_{C\text{-}H}$=178.8 Hz) and two partial structures [A] and [B], as seen in the case of euphohelin A (**5**). However, euphohelin D (**8**) with two carbonyl groups [δ 208.5 (s) and 217.7 (s)] possesses a partial structure [D] instead of [C] in **5** (see Fig. 2), suggesting that the two carbonyl groups are located at C^{11}- and C^{14}-positions. On Sarett oxidation at room temperature for 6 h, euphohelin B (**6**) was readily converted into euphohelin D (**8**) in 74% yield.

The Structure of Euphohelin E (9). On the basis of the IR and ^{1}H NMR spectra, euphohelin E (**9**) with a molecular formula $C_{31}H_{40}O_{10}$ has one secondary hydroxyl group [IR (film) 3500 cm^{-1}; δ 3.46 (1H, d, J=8.8 Hz)], two acetoxyl groups [δ 1.39 (3H, s) and 2.04 (3H, s)] and one benzoyloxyl group [δ 7.43—7.59 (3H, m) and 8.26—8.31 (2H, m)]. Further detailed proton homonuclear spin decoupling experiments of **9** indicate that it has a partial structure [E] instead of [C] in euphohelin A (**5**), in addition to the known moieties [A] and [B]. Thus, Sarett oxidation of euphohelin B (**6**) was carried out carefully at room temperature for 40 min to give rise to euphohelin E (**9**) in 65% yield, together with euphohelin D (**8**) in 18% yield.

Euphohelins, the highly-oxygenated diterpenes, belong to a small group of jatrophone-type ones,[5] and have been isolated only from the plant *Euphorbia helioscopia* L. collected in the middle of June and not found in April as well as early in May. Finally, from view points of their biogenesis and stereochemistry, it is quite interesting that euphohelins and the known macrocyclic diterpenes (**1**—**4**) co-occur in the same plant.

Experimental

All the melting points were uncorrected. ^1H and ^{13}C NMR spectra were taken on a JEOL JNM-FX 200 (199.5 MHz and 50.1 MHz) spectrometer, using $CDCl_3$ as solvent, unless otherwise stated. Chemical shifts are given in ppm from TMS as an internal standard. Coupling constants are given in Hz (s, singlet; d, doublet; t, triplet; q, quartet; m, multiplet). IR spectra were recorded on a JASCO Model A-202 spectrophotometer. Mass spectra were obtained on a Hitachi M-80 mass spectrometer operating with an ionization energy (70 eV). Optical rotations were taken on a JASCO DIP-360 polarimeter. Preparative and analytical TLC were carried out on Kieselgel 60 PF_{254} (E. Merck A.G. Germany), unless otherwise stated.

Isolation of Euphohelins. Fresh leaves and roots of the plant *Euphorbia helioscopia* L. (*ca.* 5 kg), which were collected at Atsugi in Kanagawa Prefecture in the middle of June, were hashed with a shears and immersed in MeOH (20 L) at room temperature for 2 months, and then filtered. The filtrate was concentrated under reduced pressure below 40 °C to leave a greenish brown oil (*ca.* 110 g) which was partitioned between water and AcOEt. The AcOEt layer was dried over large amounts to anhydrous Na_2SO_4 and then concentrated under reduced pressure to leave a greenish brown oil (28.5 g), which was further partitioned between 90% aq MeOH and isooctane (isooctane layer, *ca.* 8.1 g). The 90% aq MeOH layer was concentrated under reduced pressure to leave a greenish brown oil (*ca.* 20.1 g) which was dissolved in small amounts of MeOH and adsorbed on activated charcoal (*ca.* 30 g), and then eluted with MeOH (1.5 L) and $CHCl_3$ (2.0 L) quickly. The eluate was concentrated under reduced pressure to leave a greenish brown oil (19.5 g) which was roughly separated by column chromatography on silica gel (Merck 7734) (500 g) using a gradient solution of hexane and AcOEt [hexane–AcOEt (5:1) 0.5 L, hexane–AcOEt (3:1) 2 L, AcOEt 2 L] to afford six fractions (Fr. **1**, 400 mg; Fr. **2**, 2200 mg; Fr. **3**, 320 mg; Fr. **4**, 1140 mg; Fr. **5**, 500 mg; Fr. **6**, 420 mg) after removal of the nonpolar fraction containing hydrocarbons using hexane–AcOEt (5:1) (3.5 L). The first fraction was mainly comprised of a lot of hydrocarbons. Analytical TLC of the fraction **2**—**5** using hexane–AcOEt (2:1) showed the spots corresponding to euphoscopins A and B, euphornin, euphohelioscopins A and B, and the related known diterpenes.[1-3] Therefore, further separation of these fractions has not been carried out.

The most polar fraction **6**, which showed several new spots on analytical TLC plate [hexane–AcOEt (2:1)], was separated by preparative TLC using hexane–AcOEt (2:1) to afford euphohelin D (**8**) (97 mg), euphohelin C (**7**) (23 mg), euphohelin E (**9**) (4.6 mg), euphohelin A (**5**) (42 mg), and euphohelin B (**6**) (3.9 mg) in the order of increasing polarity: **8** as a colorless oil: $[\alpha]_D^{27}$ +46.9° (*c* 2.21, $CHCl_3$); IR (film) 1745, 1720, 1600, 1580, and 1245 cm^{-1}; Found: *m/z* 570.2469. Calcd for $C_{31}H_{38}O_{10}$: M, 570.2462. **7** as a colorless oil: $[\alpha]_D^{27}$ +44.6° (*c* 1.24, $CHCl_3$); IR (film) 1740, 1720, 1600, and 1240 cm^{-1}; Found: *m/z* 720.3144. Calcd for $C_{40}H_{48}O_{12}$: M, 720.3143. **9** as a colorless oil: $[\alpha]_D^{27}$ +24.9° (*c* 0.57, $CHCl_3$); IR (film) 3500, 1735, 1720, 1595, 1580, and 1250 cm^{-1}; Found: *m/z* 572.2632. Calcd for $C_{31}H_{40}O_{10}$: M, 572.2619. **5** as a colorless oil: $[\alpha]_D^{27}$ +31.8° (*c* 1.55, $CHCl_3$); IR (film) 3500, 1730, 1600, 1580, and 1240br. cm^{-1}; Found: *m/z* 616.2893. Calcd for $C_{33}H_{44}O_{11}$: M, 616.2880. **6** as a colorless oil: $[\alpha]_D^{27}$ +25.8° (*c* 0.76, $CHCl_3$); IR (film) 3500br., 1720, 1600, 1580, 1275, and 1250 cm^{-1}; Found: *m/z* 574.2752. Calcd for $C_{31}H_{42}O_{10}$: M, 574.2775.

Acetylation of Euphohelin A (5). Euphohelin A (5 mg) was dissolved in Ac_2O (0.3 mL) and pyridine (0.6 mL) at room temperature and allowed to stand at the same temperature overnight. After decomposition of excess Ac_2O with MeOH, the reaction mixture was partitioned between water and AcOEt. The AcOEt layer was dried over anhydrous Na_2SO_4 and then concentrated under reduced pressure to give an oil, which was purified by preparative TLC using hexane–AcOEt (2:1) to afford euphohelin A acetate (**10**) (5.1 mg) as a colorless oil: IR (film) 1740, 1720sh, 1600, 1580. and 1235 cm^{-1}; Found: *m/z* 658.3006. Calcd for $C_{35}H_{46}O_{12}$: M, 658.2987.

Reaction of Euphornin (2) with m-*Chloroperbenzoic Acid.* To a solution of euphornin (11.2 mg) in dry dichloromethane (1 mL) was added, with stirring, *m*-chloroperbenzoic acid (13.1 mg) at room temperature. The reaction mixture was further stirred at room temperature for 2 d, and then diluted with aqueous sodium hydrogensulfite and extracted with AcOEt. The AcOEt extract was dried over anhydrous Na_2SO_4 and concentrated under reduced pressure to leave an oil, which was purified by preparative TLC [hexane–AcOEt (1:1)] to afford euphohelin A (**5**) (10.3 mg) (TLC, IR and ^1H NMR spectra).

Regioselective Hydrolysis of Euphornin A (5). To a solution of euphohelin A (10.5 mg) in MeOH (2 mL) was added, with stirring, a solution of KOH (1 mg) in MeOH (0.1 mL) at room temperature. The reaction solution was further stirred at the same temperature for 50 min. After addition of one drop of AcOH, the reaction solution was partitioned between water and AcOEt. The AcOEt layer was dried over anhydrous Na_2SO_4 and then concentrated under reduced pressure to give a colorless oil which was purified by preparative TLC [hexane–acetone (1:1)] to afford euphohelin B (**6**) (8.8 mg) (TLC, IR, and ^1H NMR spectra).

Reaction of Euphohelin A (5) with Benzoyl Chloride. A solution of euphohelin A (3.1 mg) and benzoyl chloride (1 drop) in pyridine (1 mL) was stirred at room temperature for 24 h, and then at 60 °C for 1 h. After addition of MeOH, the reaction mixture was diluted with water and extracted with AcOEt. The AcOEt solution was dried over anhydrous Na_2SO_4 and concentrated under reduced pressure to leave an oil, which was purified by preparative TLC [hexane–AcOEt (1:1)] to give euphohelin C (**7**) (3.4 mg) (TLC, IR, and ^1H NMR spectra).

Sarett Oxidation of Euphohelin B (6). To a solution of euphohelin B (8.5 mg) in pyridine (0.4 mL) was added, with stirring, excess amounts of CrO_3–pyridine complex. The reaction mixture was further stirred at room temperature for 6 h. The reaction mixture was diluted with small amounts of $CHCl_3$ and chromatographed on silica gel (5 g). Elution with $CHCl_3$ afforded an oil, which was purified by preparative TLC [hexane–AcOEt (1:1)] to give rise to euphohelin D (**8**) as a colorless oil (6.2 mg) (TLC, IR, and ^1H NMR spectra).

Under essentially the same conditions as described above, euphohelin B (8.6 mg) in pyridine (0.6 mL) was also oxi-

dized with excess amounts of CrO_3-pyridine complex at room temperature. However, the oxidation reaction was stopped only in 40 min. According to the above-mentioned procedure, the reaction mixture was chromatographed on silica gel (5 g) and eluted with $CHCl_3$ to give an oil, which was subjected to preparative TLC [hexane–AcOEt (1:1)] to afford euphohelin D (**8**) (1.5 mg) and euphohelin E (**9**) (5.5 mg) [TLC, IR, and ^1H NMR spectra).

This research has been supported in part by grants from the Ministry of Education, Science and Culture as well as from the Foundation for the Promotion of Research on Medicinal Resources, to which grateful acknowledgment is made.

References

1) S. Yamamura, S. Kosemura, S. Ohba, M. Ito, and Y. Saito, *Tetrahedron Lett.*, **22**, 5315 (1981).

2) Y. Shizuri, S. Kosemura, J. Ohtsuka, Y. Terada, and S. Yamamura, *Tetrahedron Lett.*, **24**, 2577 (1983).

3) Y. Shizuri, S. Kosemura, J. Ohtsuka, Y. Terada, S. Yamamura, S. Ohba, M. Ito, and Y. Saito, *Tetrahedron Lett.*, **25**, 1155 (1984); S. Ohba, M. Ito, Y. Saito, Y. Shizuri, S. Kosemura, J. Ohtsuka, and S. Yamamura, *Acta Cryst.*, **C41**, 487 (1985).

4) Y. Shizuri, J. Ohtsuka, S. Kosemura, Y. Terada, and S. Yamamura, *Tetrahedron Lett.*, **25**, 5547 (1984).

5) S. M. Kupchan, C. W. Sigel,M. J. Maty, C. J. Gilmore, and R. F. Bryan, *J. Am. Chem. Soc.*, **98**, 2295 (1976).

The Pyrolyses of 1,1,4,4,-Tetraphenyl-1,4-butanediol and 1,1,4,4-Tetraphenyl-2-butene-1,4-diol Derivatives. Decomposition Reactions to Form Olefins *via* the Elimination of Two Mole Equivalents of the Hydroxydiphenylmethyl Radical

Katsuhiro SAITO,* Yoichi HORIE, Toshio MUKAI,† and Takashi TODA††
Department of Chemistry, Nagoya Institute of Technology, Gokiso-cho, Showa-ku, Nagoya 466
†*Department of Chemistry, Faculty of Science, Tohoku University, Aoba, Aramaki, Sendai 980*
††*Department of Industrial Chemistry, Faculty of Technology, Utsunomiya University, Ishii-cho 2753, Utsunomiya 321*
(Received June 18, 1985)

The pyrolysis of 1,1,2,4,4-pentaphenyl-1,4-butandiol, *trans*-1,2-bis(hydroxydiphenylmethyl)hexane, *trans*-1,2-bis(hydroxydiphenylmethyl)indan, and *cis-endo*- and *trans*-1,2-bis(hydroxydiphenylmethyl)bicyclo[2.2.1]-heptane gave styrene, cyclohexene, indene, and norbornene respectively, accompanied by benzophenone and benzhydrol. The pyrolysis of *trans*-1,2-bis(hydroxydiphenylmethyl)spiro[2.6]nona-4,6,8-triene afforded indene *via* rearrangement to form *trans*-1,2-bis(hydroxydiphenylmethyl)indan. The pyrolysis of *cis*-1,1,4,4-tetraphenyl-2-butene-1,4-diol afforded 2,2,5,5-tetraphenyl-2,5-dihydrofuran. On the other hand, *trans*-1,1,4,4-tetraphenyl-2-butene-1,4-diol afforded 1,2,4,4-tetraphenyl-3-buten-1-one. The mechanisms of these decomposition reactions are discussed.

Generally, vic-dicarboxylic acids (**1**) can be synthesized by Diels-Alder reactions readily and usually in good yields.[1] The introduction of double bonds to such vic-dicarboxylic acids by the elimination of the two carboxyl groups is a useful reaction for the synthesis of many organic compounds. Several types of such reactions have been developed and used as powerful synthetic methods.[2]

It is known that the pyrolysis of benzopinacol (**5**) gives benzophenone (**3**) and benzhydrol (**4**) *via* a disproportionation reaction of the initially formed hydroxydiphenylmethyl radical (**6**).[3] We investigated the application of this decomposition reaction to the preparation of the olefins from **1** in the expectation that 1,1,4,4-tetraphenyl-1,4-butanediol derivatives (**2**), which can be prepared by the Grignard reaction of **1**, would be pyrolyzed to form the olefins eliminating two mole equivalents of **6**, which in turn disproportionates to **3** and **4**. Various types of **2** were synthesized and pyrolyzed. The pyrolysis of several kinds of 1,1,4,4-tetraphenyl-2-butene-1,4-diol derivatives were also investigated. Here, we wish to report on these results.

Preparations of Glycols

The reaction of a cyclohexane derivative (**7**) with phenyllithium afforded the corresponding diketone (**8**) in a 53% yield; this diketone gave *trans*-1,2-bis(hydroxydiphenylmethyl)hexane (**9**) in a 52% yield in a reaction with phenyllithium. *trans*-1,2-Bis(hydroxydiphenylmethyl)indan (**11**) was prepared in a 62% yield by reaction of phenyllithium with indane derivative (**10**).[4] *cis-endo*- and *trans*-5,6-Bis(hydroxydiphenylmethyl)bicyclo[2.2.1]hept-2-ene (**13a** and **13b**) were synthesized in 71 and 87% yields respectively, by reactions of the corresponding diesters (**12a** and **12b**) with phenyllithium. *cis-endo*- and *trans*-1,2-Bis(hydroxydiphenylmethyl)bicyclo[2.2.1]heptane (**14a** and **14b**) were obtained almost quantitatively by catalytic hydrogenations of **13a** and **13b** respectively. *cis-endo*-8,9-Bis(hydroxydiphenylmethyl)tricyclo[3.2.2.$0^{2,4}$]non-2-ene (**17**) was synthesized in a overall yield of 77% from a corresponding diester (**15**) by reaction with phenyllithium *via* the dicarbonyl compound (**16**). *cis*- and *trans*-1,1,4,4-

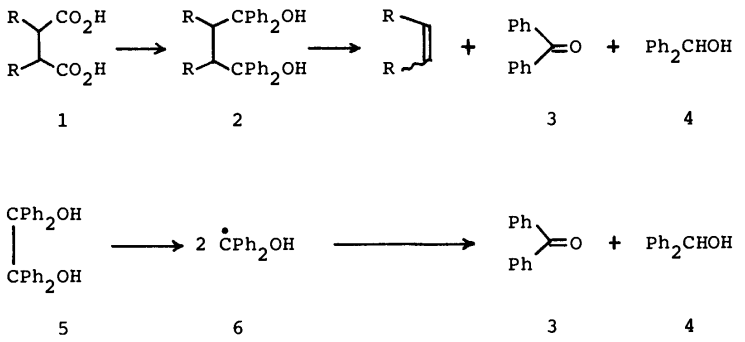

Fig. 1.

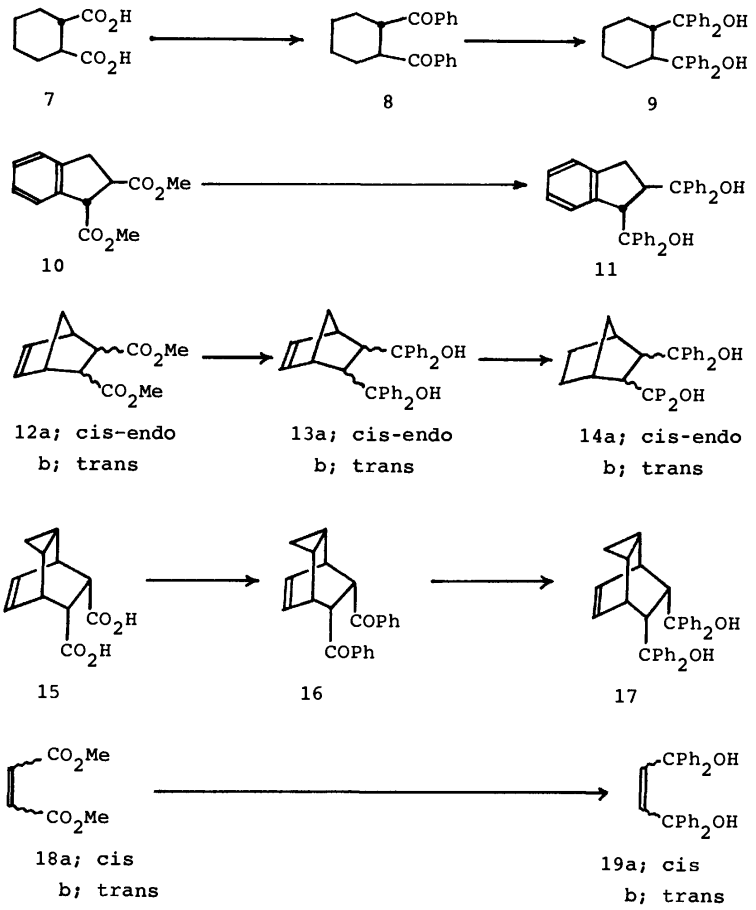

Fig. 2.

Tetraphenyl-2-butene-1,4-diol (**19a** and **19b**) were obtained in 25 and 31% yields respectively by reactions of the corresponding diesters (**18a** and **18b**) with phenyllithium.

1,1,2,4,4-Pentaphenyl-1,4-butandiol (**20**),[5] *trans*-1,2-bis(hydroxydiphenylmethyl)spiro[2.6]nona-4,6,8-triene (**30**),[6] and 1,2-bis(hydroxydiphenylmethyl)benzene (**35**)[7] were synthesized according to the literature.

Pyrolyses

Glycol **20** was pyrolyzed at 250 °C for 2 h to afford styrene (**21**, 40%), together with 1,1,3-triphenyl-1-propane (**22**, 11%), a cyclic ether (**23**, 46%), benzophenone (**3**, 60%), and benzhydrol (**4**, 10%). The pyrolysis of **9** under analogous conditions gave cyclohexene (**24**, 30%) accompanied by a cyclic ether (**25**, 35%), **3** (25%), and **4** (68%). The pyrolysis of **11** gave indene (**26**, 75%), **3** (99%), and **4** (60%). Pyrolysis of *cis-endo*-glycol **14a** afforded norbornene (**27**, 30%), along with a diphenylmethylene derivative (**28**, 37%), a cyclic ether (**29**, 9%), **3** (75%), and **4** (20%); on the other hand, the pyrolysis of *trans*-glycol **14b** gave **27** (27%), **28** (64%), **3** (95%), and **4** (15%). The cyclic ether **29** was not detected. The heating of **30** at 250 °C for 1 h afforded **26** (34%) and **11** (59%),[8] accompanied by **3** (44%) and **4** (26%).

The pyrolysis of *cis-endo*-glycol **13a** yielded cyclopentadiene (**31**, 55%), a cyclic ether **32** (68%), and **19a** (21%); on the other hand, *trans*-glycol **13b** afforded **31** (45%) and a diphenylmethylene derivative (**33**, 44%).[9] The pyrolysis of *cis-endo*-glycol **17** afforded tropylidene (**34**, 80%) and **32** (88%). The pyrolysis of *cis*-glyco **19a** afforded a cyclic ether **32** (53%) and **3** (58%), but *trans*-glycol **19b** gave **33** (45%). The pyrolysis of **35** was carried out at 350 °C in an autoclave, with *t*-butyl alcohol as the solvent, in order to trap benzyne, which was expected to be formed, but resulted in a quantitative formation of a cyclic ether **36**.[7]

Discussion

The mechanism of the formation of the olefins **21**, **24**, **26**, and **27** is considered to be as follows. A bond cleavage of the glycol **2** to form one mole equivalent of **6** gives a radical intermediate **37**, which affords the olefins by eliminating the other mole equivalent of **6**. On the other hand, the dehydration reaction of **2** forms **38**, which gives the diphenylmethylene deriva-

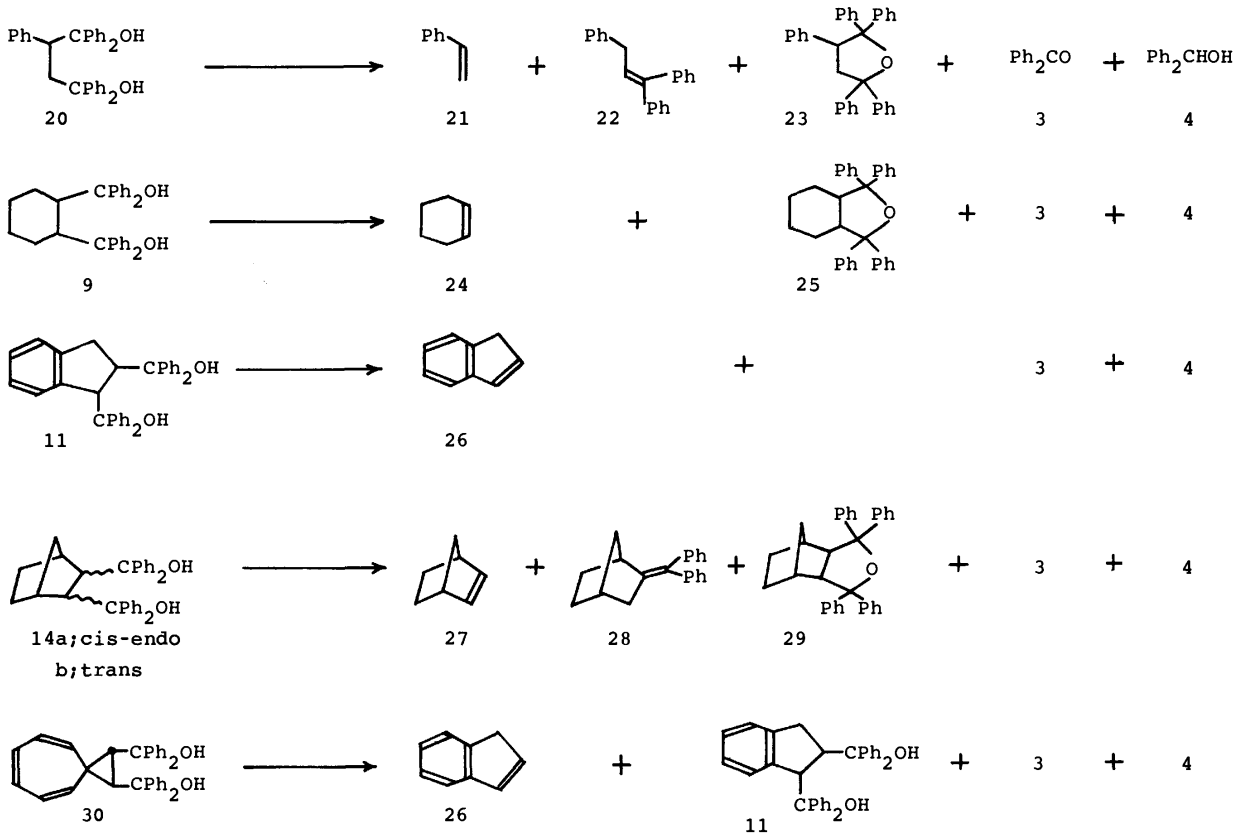

Fig. 3.

tive **39** by eliminating one mole equivalent of **6**.[10]

The formation mechanism of **33** can be considered to be as follows. An O–H bond fission of **19b**, followed by a 1,2-shift of the phenyl group, forms **40**, which gives **33** *via* a dehydration reaction.

The above-mentioned pyrolysis of the 1,2-bis(hydroxydiphenylmethyl) substituted hydrocarbons can be considered to be useful for the synthesis of olefinic compounds, because the desired olefins, styrene (**21**), cyclohexene (**24**), indene (**26**), and norbornene (**27**) are obtained. However, the other desired olefins, spiro[2.6]nonatetraene (**41**),[11] norbornadiene (**42**), and tricyclo[3.2.2.$0^{2,4}$]nonadiene (**43**) could not be obtained from the pyrolysis of **30**, **13**, and **17** respectively.

The spiro compound **30** is considered to have rearranged to **11** before the pyrolysis to afford **41** because of the high temperature.[8] The temperature needed by the pyrolysis seems also to be high enough to cause retro-Diels-Alder reactions in such compounds as **13** and **17**, which have double bonds at positions suitable for retro-Diels-Alder reactions. In order to cause the pyrolysis at lower temperature, pyrolyses of the glycols were also carried out in the presence of several kinds of radical initiators, however, no improvement was observed.

Experimental

All the melting and boiling points are uncorrected. The NMR spectra were measured with a Varian HA-100 or a Hitachi R-20B spectrometer with tetramethylsilane as the internal standard. The mass and IR spectra were recorded with Hitachi M-52 and DS-701G spectrometers respectively. Wako gel C-200 and Wako gel B-5F were used for column and thin-layer chromatography respectively.

All the pyrolysis reactions were carried out under a nitrogen stream without any solvent in a flask connected with three combined traps. The first trap was cooled with an ice-water bath while the second and last ones were cooled with a Dry Ice–acetone bath. Water formed by the dehydration reactions was swept away from the flask by a nitrogen stream and condensed in the first trap. The olefins formed were collected mainly in the second trap.

Preparations of Glycols

Preparation of **9**. A solution of **7** (6.88 g, 40 mmol) in anhydrous tetrahydrofuran (200 ml) was stirred with a solution of phenyllithium (320 mmol) in anhydrous ether (140 ml) at room temperature over a 1 h period. After further stirring at room temperature for 16 h, the reaction mixture was decomposed with water and extracted with ethyl acetate. The organic layer was washed with water and brine, and dried over anhydrous sodium sulfate. After

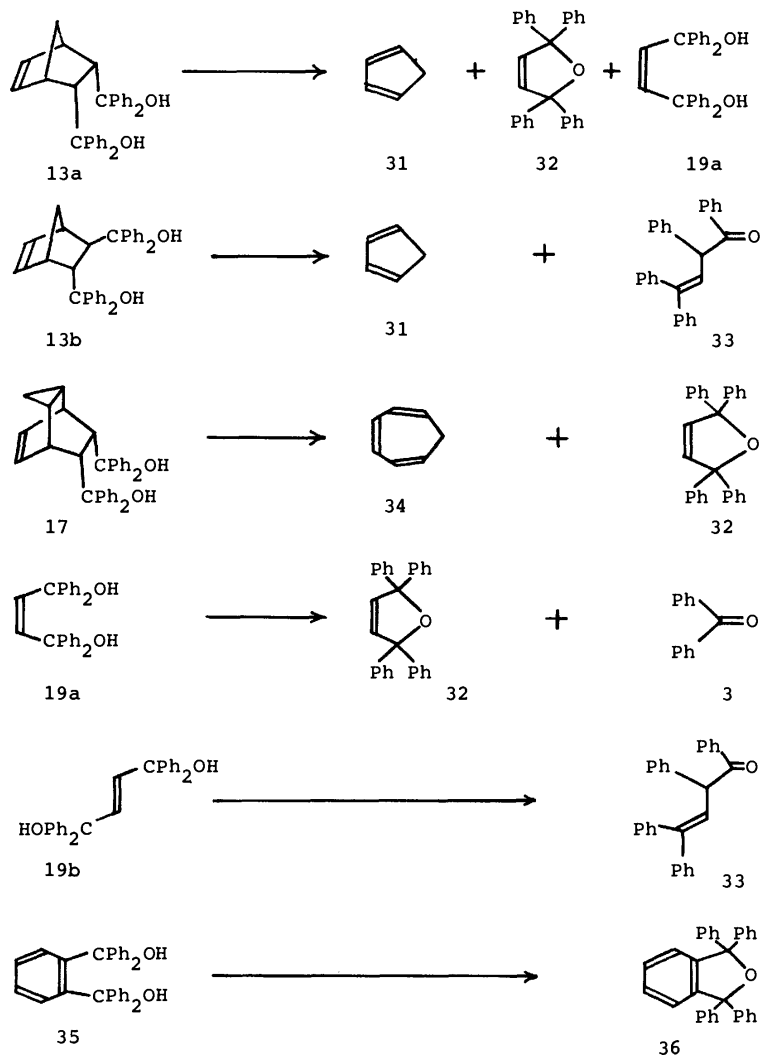
CPh2OH
CPh2OH
13a
31
Ph Ph
O
Ph Ph
32
CPh2OH
CPh2OH
19a
13b
33
17
34
19a
32
3
HOPh2C
19b
33
35
36

Fig. 4.

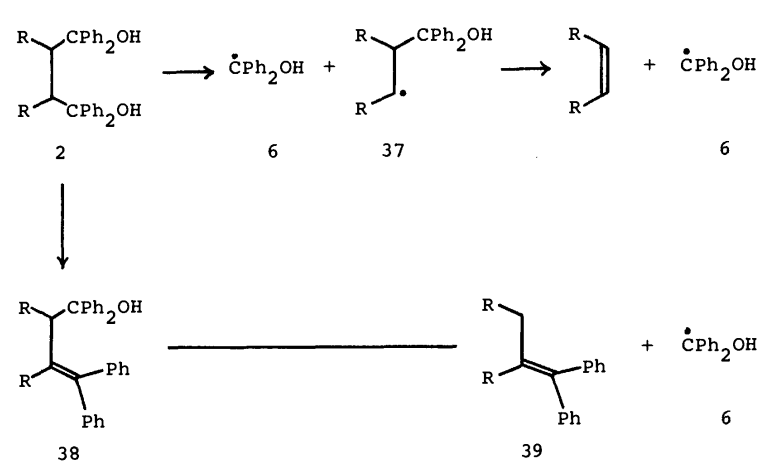
R
CPh2OH
2
6
37
6
38
39
Ph

Fig. 5.

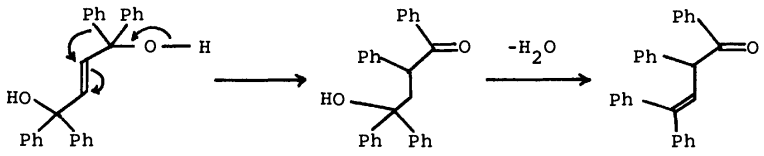

19b 40 33

Fig. 6.

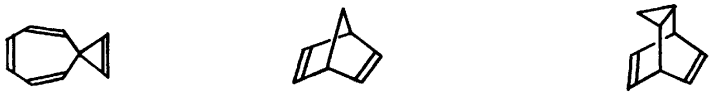

41 42 43

Fig. 7.

filtering, the solvent was removed on a rotary evaporator. The colorless residue was chromatographed on silica gel to give colorless crystals **8** (6.19 g, 53%) by the use of pet ether–benzene (3:7). Recrystallization from cyclohexane gave pure crystals of **8**.

8: Mp 115—116 °C. Found: C, 82.05; H, 6.86%. Calcd for $C_{20}H_{20}O_2$: C, 82.16; H, 6.89%. IR (KBr): 3100, 2950, 1670, 1600 cm^{-1}. ^1H NMR ($CDCl_3$) δ=1.43 (m, 8H), 3.82 (m, 2H), 7.0—7.5 (m, 10H). Mass *m/z* (rel intensity) 292 (M^+, 6.6), 105 (100), 77 (65).

A solution of **8** (7.70 g, 26 mmol) in anhydrous tetrahydrofuran (180 ml) was added to a solution of phenyllithium (204 mmol) in anhydrous ether (120 ml) at room temperature over a 1 h period and then further stirred for 20 h. The usual workup afforded a colorless tarry material, which was chromatographed on silica gel to give colorless crystals **9** (6.09 g, 52%) by the use of benzene–ether (9:1). Recrystallization from benzene gave pure crystals of **9**.

9: Mp 201—203 °C. Found: C, 84.57; H, 7.25%. Calcd for $C_{32}H_{32}O_2$: H, 85.67; H, 7.18%. IR (KBr): 3400, 3050, 1600 cm^{-1}. ^1H NMR ($CDCl_3$) δ=1.41 (m, 8H), 3.43 (m, 2H), 3.60 (bs, 2H), 7.1—7.5 (m, 20H). MS *m/z* (rel intensity) 430 (M^+, 25), 353 (100), 248 (71).

Preparation of ***11***. A solution of **10** (234 mg, 1 mmol) in anhydrous ether (10 ml) was added to a solution of phenyllithium (8 mmol) in anhydrous ether (10 ml) at room temperature, after which the mixture was stirred for 16 h. The usual workup gave a yellow oil, which was chromatographed on silica gel to give colorless crystals **11** (277 mg, 62%) by the use of benzene–ether (4:1). Recrystallization from ethyl acetate gave pure **11**.

11: Mp 189—190 °C. Found: C, 86.75; H, 6.23%. Calcd for $C_{35}H_{30}O_2$: C, 87.10; H, 6.27%. IR (KBr): 3570, 3070, 1600 cm^{-1}. ^1H NMR ($CDCl_3$) δ=2.05 (bs, 2H, OH), 2.65 (m, 1H), 2.95 (m, 1H), 3.46 (m, 1H), 4.42 (m, 1H), 6.28 (m, 1H), 6.75 (m, 1H), 6.93 (m, 1H), 7.0—7.4 (m, 21H). MS *m/z* (rel intensity) 446 (M^+), 282 (100), 191 (35), 183 (70), 167 (90).

Preparation of ***13a***. A solution of **12a** (420 mg, 2 mmol) in anhydrous ether (50 ml) was added to a solution of phenyllithium (16 mmol) in anhydrous ether (50 ml) at room temperature. After stirring at the boiling temperature for 4 h, the reaction mixture was treated as usual to give colorless crystals **13a** (650 mg, 71%), which were recrystallized from ethyl acetate.

13a: Mp 262—263 °C. Found: C, 86.44; H, 6.59%. Calcd for $C_{33}H_{30}O_2$: C, 86.43; H, 6.59%. IR (KBr): 3470, 3360, 1600 cm^{-1}. ^1H NMR ($CDCl_3$) δ=1.32 (m, 2H), 2.58 (bs, 2H), 4.24 (bs, 2H), 6.49 (m, 2H), 6.8—7.6 (m, 20H). MS *m/z* (rel intensity) 440 (M^+−18, 51), 381 (36), 258 (82), 183 (100), 167 (58).

Preparation of ***13b***. The same procedure as above, but using **12b** (420 mg, 2 mmol) and phenyllithium (16 mmol), gave colorless crystals **13b** (795 mg, 87%), which were then recrystallized from ethyl acetate.

13b: Mp 179—180 °C. Found: C, 86.38; H, 6.68%. Calcd for $C_{33}H_{30}O_2$: C, 86.43; H, 6.59%. IR (KBr): 3470, 3360, 1600 cm^{-1}. ^1H NMR ($CDCl_3$) δ=0.20 (m, 1H), 0.78 (m, 1H), 2.75 (bs, 2H), 3.07 (m, 1H), 3.52 (m, 1H), 3.80 (m, 1H), 5.20 (m, 1H), 6.28 (m, 1H), 6.83 (m, 1H). MS *m/z* (rel intensity) 458 (M^+, 5), 440 (8), 258 (45), 183 (100), 167 (28).

Preparation of ***14a***. A solution of **13a** (1.50 g, 3.1 mmol) in benzene (150 ml) was hydrogenated over palladium charcoal (10%, 150 mg) to absorb the hydrogen (70 ml, 3.1 mmol). After the subsequent removal of the palladium charcoal by filtration, the solvent was evaporated on a rotary evaporator to give colorless crystals **14a** (1.5 g, *ca.* 100%), which were then recrystallized from ethyl acetate.

14a: Mp 269—270 °C. Found: C, 86.09; H, 6.72%. Calcd for $C_{33}H_{32}O_2$: C, 86.05; H, 7.00%. IR (KBr): 3550, 3250, 1598 cm^{-1}. ^1H NMR ($CDCl_3$) δ=0.8—1.6 (m, 6H), 2.11 (m, 2H), 2.54 (m, 2H), 3.47 (bs, 2H), 7.1—7.5 (m, 20H). MS *m/z* (rel intensity) 442 (M^+−18, 8), 365 (6), 260 (100), 183 (44).

Preparation of ***14b***. A solution of **13b** (3.00 g, 6.2 mmol) in benzene (250 ml) was hydrogenated with palladium charcoal (10%, 200 mg) to absorb the hydrogen (145 ml, 6.2 mmol). The usual work-up afforded colorless crystals **14b** (3.00 g, *ca.* 100%), which were then recrystallized from ethyl acetate.

14b: Mp 191—193 °C. Found: C, 85.81; H, 6.90%. Calcd for $C_{33}H_{32}O_2$: C, 86.05; H, 7.00%. IR (KBr): 3550, 3240, 1600 cm^{-1}. ^1H NMR ($CDCl_3$) δ=0.7—1.5 (m, 6H), 2.32 (m, 3H), 2.59 (m, 1H), 3.22 (bs, 2H), 6.8—7.5 (m, 20H). MS *m/z* (rel intensity) 442 (M^+−18, 10), 424 (22), 365 (36),

260 (100), 183 (61).

Preparation of 17. A solution of **15** (6.50 g, 30 mmol) in anhydrous tetrahydrofuran (100 ml) was added to a solution of phenyllithium (240 mmol) in anhydrous ether (70 ml) at room temperature, after which the mixture was stirred for 17 h. The usual workup gave colorless crystals **16** (8.86 g, 90%), which were then recrystallized from benzene.

16: Mp 164—165 °C. Found: C, 83.85; H, 6.14%; M^+, 328. Calcd for $C_{23}H_{20}O_2$: C, 84.12; H, 6.14%; M^+, 328.

A solution of **16** (4.00 g, 12 mmol) in anhydrous tetrahydrofuran (100 ml) was added to a solution of phenyllithium (60 mmol) in anhydrous ether (200 ml) at room temperature, after which the mixture was stirred for 20 h. The usual workup gave colorless crystals **17** (5.00 g, 86%), which were then recrystallized from ethyl acetate.

17: Mp 284—285 °C. Found: C, 87.00; H, 6.66%. Calcd for $C_{35}H_{32}O_2$: C, 86.74; H, 6.66%. IR (KBr): 3470, 3060, 1600 cm^{-1}. ^1H NMR ($CDCl_3$) δ=0.5—1.2 (m, 4H), 2.65 (m, 2H), 3.91 (bs, 2H), 5.18 (bs, 2H), 6.04 (m, 2H), 6.9—7.6 (m, 20H). MS *m/z* (rel intensity) 466 (M^+−18, 38), 375 (16), 284 (64), 183 (100), 167 (47).

Preparation of 19a. A solution of **18a** (2.88 g, 20 mmol) in anhydrous ether (150 ml) was added to a solution of phenyllithium (160 mmol) in anhydrous ether (100 ml) at room temperature, after which the mixture was stirred for 19 h. After the usual workup, the brown tarry material was chromatographed on silica gel to yield colorless crystals **19a** (1.96 g, 25%), which were then recrystallized from benzene.

19a: Mp 215—217 °C. Found: C, 85.70; H, 6.10%. Calcd for $C_{28}H_{24}O_2$: C, 85.68; H, 6.16%. IR (KBr): 3550, 3050, 1670 cm^{-1}. ^1H NMR ($CDCl_3$) δ=4.80 (s, 2H), 6.17 (s, 2H), 7.2 (m, 20H). MS *m/z* (rel intensity) 374 (M^+−18, 19), 270 (100), 192 (26).

Preparation of 19b. The same procedure as above, but using **18b** (2.88 g, 20 mmol) and phenyllithium (160 mmol), afforded colorless crystals **19b** (2.43 g, 31%), which were then recrystallized from cyclohexane.

19b: Mp 219—221 °C. Found: C, 85.98; H, 6.13%. Calcd for $C_{28}H_{24}O_2$: C, 85.68; H, 6.16%. IR (KBr): 3550, 3050, 1670 cm^{-1}. ^1H NMR ($CDCl_3$) δ=4.71 (s, 2H), 6.38 (s, 2H), 7.3 (m, 20H). MS *m/z* (rel intensity) 374 (M^+−18, 13), 270 (100), 192 (24).

Pyrolyses of Glycols

Pyrolysis of 20. Glycol **20** (940 mg, 2 mmol) was pyrolyzed at 250 °C for 2 h to give **21** (84 mg, 40%). The residual resinous material was chromatographed on alumina to give a colorless oil (120 mg) and colorless crystals **23** (410 mg, 46%) using pet ether, **3** (210 mg, 60%) using pet ether-benzene (4:1), and **4** (30 mg, 10%) using ether. The colorless oil was distilled under reduced pressure to give a colorless oil **22** (62 mg, 11%).

22: Bp 0.1 Torr (1 Torr=133.322 Pa), 130 °C (bath temperature). Found: C, 92.96; H, 6.98%. Calcd for $C_{21}H_{18}$: C, 93.29; H, 6.71%. IR (neat): 3070, 2920, 1600 cm^{-1}. ^1H NMR ($CDCl_3$) δ=3.46 (d, 2H, J=7 Hz), 6.38 (t, 1H, J=7 Hz), 7.3 (bs, 15H). MS *m/z* (rel intensity) 270 (M^+, 61), 193 (100), 167 (36).

Pyrolysis of 9. Glycol **9** (3.00 g, 6.6 mmol) was pyrolyzed at 250 °C for 1.5 h to give **24** (165 mg, 30%). The residue was chromatographed on silica gel to give colorless crystals **25** (1.05 g, 35%), using pet ether-benzene (7:3), **3** (306 mg, 25%) using pet ether-benzene (1:4), and **4** (820 mg, 68%) using ether. The crystals **25** were purified by recrystallization from ethyl acetate.

25: Mp 199—201 °C. Found: C, 89.49; H, 7.09%. Calcd for $C_{32}H_{30}O$: C, 89.26; H, 7.02%. IR (KBr) 3070, 2920, 1600 cm^{-1}. ^1H NMR ($CDCl_3$) δ=1.5 (m, 8H), 3.3 (m, 2H), 7.0—7.4 (m, 20H). MS *m/z* (rel intensity) 353 (M^+−C_6H_5, 10), 246 (100), 168 (32).

Pyrolysis of 11. Glycol **11** (482 mg, 1 mmol) was pyrolyzed at 290 °C for 3 h to yield 26 (87 mg, 75%). The residue was chromatographed on alumina to give **3** (180 mg, 99%) using pet ether-benzene (4:1) and **4** (110 mg, 60%) using ether.

Pyrolysis of 14a. Glycol **14a** (500 mg, 1.1 mmol) was pyrolyzed at 290 °C for 3 h to yield **27** (32 mg, 30%). The residue was chromatographed on alumina to give colorless crystals **28** (105 mg, 37%) using pet ether, colorless crystals **29** (45 mg, 9%) and **3** (153 mg, 75%) using pet ether-benzene (4:1), and **4** (33 mg, 20%) using ether. The crystals **28** and **29** were recrystallized from benzene and ethanol respectively.

28: Mp 68—69 °C. Found: C, 92.26; H, 7.83%. Calcd for $C_{20}H_{20}$: C, 92.26; H, 7.74%. IR (KBr): 3030, 2960, 1600 cm^{-1}. ^1H NMR ($CDCl_3$) δ=1.3—1.9 (m, 6H), 2.05 (m, 1H), 3.01 (bs, 1H), 7.3 (bs, 10H). MS *m/z* (rel intensity) 260 (M^+, 100), 231 (80), 205 (14), 191 (27), 167 (36).

29: Mp 279—280 °C. Found: C, 89.54; H, 7.00%. Calcd for $C_{33}H_{30}O$: C, 89.55; H, 6.83%. IR (KBr): 3060, 2950, 1600 cm^{-1}. ^1H NMR ($CDCl_3$) δ=0.8—1.7 (m, 6H), 2.44 (bs, 2H), 4.01 (bs, 2H), 6.9—7.4 (m, 20H). MS *m/z* (rel intensity) 442 (M^+, 6), 366 (31), 289 (100), 260 (12), 194 (10).

Pyrolysis of 14b. Glycol **14b** (500 mg, 1.1 mmol) was pyrolyzed at 290 °C for 3 h to yield **27** (29 mg, 27%). The same procedure as above gave **28** (183 mg, 64%), **3** (170 mg, 95%), and **4** (20 mg, 15%).

Pyrolysis of 30. Glycol **30** (1.00 g, 2.1 mmol) was pyrolyzed at 250 °C for 1 h to yield **26** (80 mg, 34%). The residue was chromatographed on alumina to give **3** (169 mg, 44%), using pet ether-benzene (4:1), colorless crystals of **11** (585 mg, 59%) using benzene-ether (4:1), and **4** (100 mg, 26%) using ether.

Pyrolysis of 13a. Glycol **13a** (500 mg, 1.1 mmol) was pyrolyzed at 270 °C for 2 h to give **31** (40 mg, 55%). The residue was chromatographed on alumina to give colorless crystals **32** (284 mg, 68%) using pet ether and **19a** (88 mg, 21%) using benzene-ether (1:1). The crystals **32** were recrystallized from ethyl acetate.

32: Mp 184—185 °C. Found: C, 89.85; H, 5.83%. Calcd for $C_{28}H_{22}O$: C, 89.80; H, 5.92%. IR (KBr): 3050, 1590 cm^{-1}. ^1H NMR ($CDCl_3$) δ=6.42 (s, 2H), 7.2 (bs, 20H). MS *m/z* (rel intensity) 374 (M^+, 46), 297 (100), 269 (82), 220 (59).

Pyrolysis of 13b. Glycol **13b** was pyrolyzed at 250 °C for 2 h to give **31** (65 mg, 45%). The residue was submitted to thin-layer chromatography on silica gel, using pet ether-benzene (1:1) as the developing solvent to give colorless crystals **33** (370 mg, 44%, R_f=0.45). The structure of **33** was determined by comparison of its physical properties with the literature.[9]

Pyrolysis of 17. Glycol **17** (500 mg, 1 mmol) was pyrolyzed at 290 °C for 3 h to give **34** (75 mg, 80%). The residue was chromatographed on alumina to give **32** (322 mg, 83%) using pet ether.

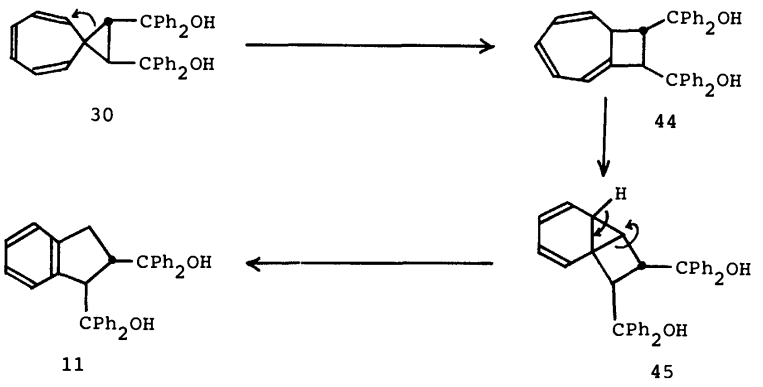

Fig. 8.

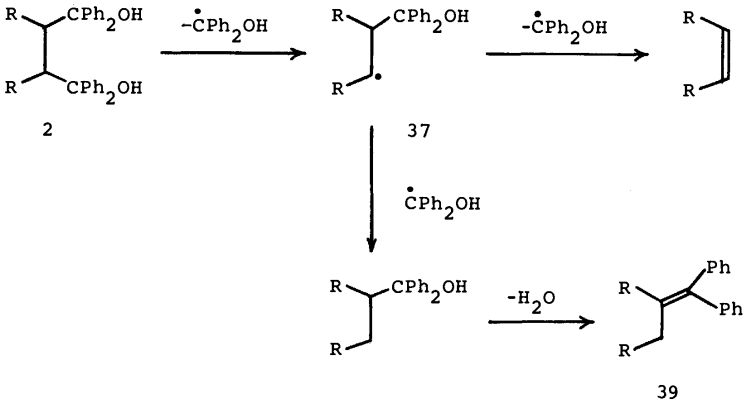

Fig. 9.

Pyrolysis of 19a. Glycol **19a** (1.00 g, 2.6 mmol) was pyrolyzed at 250 °C for 2 h. The residue was chromatographed on silica gel to yield colorless crystals **32** (506 mg, 53%) using pet ether and **3** (272 mg, 58%) using pet ether–benzene (4:1).

Pyrolysis of 19b. Glycol **19b** (1.00 g, 2.6 mmol) was pyrolyzed at 250 °C for 2 h. The residue was submitted to thin-layer chromatography on silica gel, using pet ether–benzene (1:1) as the developing solvent to give colorless crystals **33** (382 mg, 40%, R_f=0.45).

Pyrolysis of 35 A solution of **35** (1.00 g, 2.3 mmol) in *t*-butyl alcohol (40 ml) was heated at 330 °C for 5 h in an autoclave. The subsequent evaporation of the solvent gave colorless crystals **36** (950 mg, *ca.* 100%, mp 174—175 °C, lit,[7] 174—175 °C).

References

1) Wasserman, "Diels-Alder Reactions 2," Elsevier, New York (1965); R. B. Woodward and R. Hoffman, *Angew. Chem., Int. Ed. Engl.*, **8**, 781 (1969).

2) T. Toda, K. Saito, and T. Mukai, *Chem. Lett.*, **1973**, 1123; E. Grovenstein, Jr., D. V. Rao, and W. Taylor, *J. Am. Chem. Soc.*, **83**, 1705 (1961); C. M. Cimarudti and J. Wolinsky, *ibid.*, **90**, 113 (1968); P. Padrick, R. Klem, S. Superlock, J. J. Sins, E. E. van Tamelen, and T. Whitesides, *Tetrahedron Lett.*, **1968**, 5117; E. N. Cain, R. Vulkov, and S. Masamune, *J. Chem. Soc., Chem. Commun.*, **1969**, 98; B. M. Trost and F. Chen, *Tetrahedron Lett.*, **1971**, 2603; K. T. Mak, K. Srinivasachar, and N. C. Young, *J. Chem. Soc., Chem. Commun.*, **1979**, 1038.

3) D. C. Neckers and D. P. Colenbrander, *Tetrahedron Lett.*, **1968**, 5045.

4) T. Mukai, T. Nakazawa, and K. Isobe, *Tetrahedron Lett.*, **1968**, 565; K. Saito, T. Toda, and T. Mukai, *Bull. Chem. Soc. Jpn.*, **47**, 331 (1974).

5) R. E. Rutz, *J. Org. Chem.*, **27**, 2040 (1962).

6) T. Toda, K. Saito, and T. Mukai, *Tetrahedron Lett.*, **1972**, 1981; T. Toda, K. Saito, and T. Mukai, *Bull. Chem. Soc. Jpn.*, **52**, 151 (1979).

7) H. Hart, *J. Am. Chem. Soc.*, **85**, 1800 (1963); G. Wittig and M. Leo, *Chem. Ber.*, **64**, 2395 (1931).

8) The formation mechanism of the indane derivative (**11**) from the spiro compound (**30**) is considered to be as follows: a 1,7-shift of the carbon atom of the three-membered ring of **30** gives the bicyclo[5.2.0]nona-1,3,5-triene derivative (**44**), which then tautomerizes to the tricyclo[3.3.0.$0^{1,4}$]nonadiene (**45**). A cleavage of the three-membered ring of **45** followed by a hydrogen shift, affords **11**.[12]

9) R. E. Lutz, R. G. Bass, and D. W. Boykin, Jr., *J. Org. Chem.*, **29**, 3660 (1964).

10) A referee has suggested the possibility of a step-by-step decomposition as is shown in Fig. 9. We are indebted to the referee.

11) H. E. Simmons and T. Fukunaga, *J. Am. Chem. Soc.*, **91**, 6391 (1967); M. D. Gordon, T. Fukunaga, and H. E. Simmons, *ibid.*, **98**, 8401 (1976).

12) W. M. Jones and C. L. Ennis, *J. Am. Chem. Soc.*, **91**, 6391 (1969); K. Saito, T. Toda, and T. Mukai, *Bull. Chem. Soc. Jpn.*, **47**, 331 (1974).

 © 1985 The Chemical Society of Japan Bull. Chem. Soc. Jpn., 58, 3125—3130 (1985)

Formation and Reactions of 2-Substituted 4,4-Dimethyl-5(4*H*)-oxazolones.[1] The 5(4*H*)-Oxazolone as a Stable Intermediate in Peptide Bond Formation

Mitsuaki NARITA,* Kazunori ISHIKAWA,† Koji KUDO, and Takeshi ENDO†

Department of Industrial Chemistry, Faculty of Technology, Tokyo University of Agriculture and Technology, Koganei, Tokyo 184

†*Laboratory of Resource Utilization, Tokyo Institute of Technology, Nagatsuta, Midori-ku, Yokohama 227*

(Received May 24, 1985)

The reaction of Boc-Leu$_3$-Aib-OH with H-Leu$_3$-OBzl using DCC as a coupling reagent proceeded *via* the exclusive 2-substituted 4,4-dimethyl-5(4*H*)-oxazolone formation followed by a slow aminolysis. Similar treatment of Boc-Leu$_3$-Aib-OH with DCC in the presence of *p*-nitrophenol did not produce a *p*-nitrophenyl ester, but produced the 2-substituted 4,4-dimethyl-5(4*H*)-oxazolone (**1**) in a high yield within 20 min. The high potential for the oxazolone formation of Boc-Leu$_n$-Aib-OH (n=3 and 4) is apparently attributed to the conformational effect of C-terminal Aib residues, namely, the restriction of the backbone dihedral angles ϕ and ψ of Aib residues. Ring-opening reactions of oxazolones with hydroxy compounds were easily monitored by following the disappearance of the intense oxazolone peak at 1820 cm^{-1}. The oxazolone (**1**) reacted faster with HOSu than H-Leu$_3$-OBzl, followed by the slow aminolysis of the succinimide ester produced. In contrast, HOBt did not react with the oxazolones derived from Boc-Leu$_n$-Aib-OH (n=3 and 4), but strongly catalyzed the aminolysis of the oxazolones in dichloromethane to form peptide bonds in nearly quantitative yields. A little catalytic effect of acetic acid on the oxazolone aminolysis indicated that the oxazolone aminolysis in the presence of HOBt did not proceed through a simple acid catalytic pathway, but proceeded through a biphilic (electrophilic-nucleophilic) pathway.

The most common route to racemization during peptide bond formation involves a 5(4*H*)-oxazolone-mediated mechanism and, in many circumstances, a 5(4*H*)-oxazolone can be detected directly when an acylamino acid or peptide acid is converted to an activated derivative. Thus, the racemization and ring-opening reactions of 5(4*H*)-oxazolones with nucleophiles have been widely studied by many workers.[2] The role of 5(4*H*)-oxazolones in peptide synthesis has been reviewed by Kemp[3] and Benoiton[4] and, in their reviews, they considered the following issues: (a) the evidence for the intermediacy of 5(4*H*)-oxazolones in peptide coupling reactions, (b) the nature of the catalysis for the rate-determining ring closure, (c) the chemical behaviors of 5(4*H*)-oxazolones, and (d) the effect of substituents on the ease of 5(4*H*)-oxazolone formation. However, little attempt has been made concerning the possibility of using 5(4*H*)-oxazolones derived from peptides as coupling reagents because of lability of C$^\alpha$ hydrogen atoms.[2]

Recently we have demonstrated the usefulness of a novel strategy for solubility improvement in helical oligopeptides based on the restriction of the values of the backbone dihedral angles ϕ and ψ of Aib residues,[5] and the implication of the new findings for the study of artificial proteins containing Aib residues was discussed on the basis of the stabilizing efficacy of Aib residues on helical regions of proteins.[5–7] In the study of Aib-containing peptides,[5–7] we also found that the peptide containing an Aib residue at a C-terminal had high potential for the formation of 2-substituted 4,4-dimethyl-5(4*H*)-oxazolone and the oxazolone had low reactivity. Aib-containing peptides such as alamethicin, suzukacillin, and their peptide fragments have widely been studied mainly on their conformation.[8,9] But little information of the reactivity of an Aib residue is available.[8] Our attempts in this paper are directed towards elucidating the reactivity of a 2-substituted 4,4-dimethyl-5(4*H*)-oxazolone and exploring the possibility of using the 5(4*H*)-oxazolone as a coupling reagent, where the 5(4*H*)-oxazolone is free from racemization due to having a structure in which a labile C$^\alpha$ hydrogen atom of Ala is substituted with a methyl group.

Results

C-Terminal Aib residues are highly hindered[8] and the reaction of Boc-Leu$_3$-Aib-OH with H-Leu$_3$-OBzl using DCC as a coupling reagent proceeds *via* the exclusive 5(4*H*)-oxazolone formation followed by a slow aminolysis (Scheme 1). The characteristic IR absorption at 1820 cm^{-1} allows sensitive detection of the 5(4*H*)-oxazolone species. The IR spectrum of the reaction mixture in dichloromethane is shown in Fig. 1a. Similar treatment of Boc-Leu$_3$-Aib-OH with DCC in the presence of *p*-nitrophenol does not produce the *p*-nitrophenyl ester, but produces the oxazolone (**1**) in a high yield within 20 min (Scheme 1, Fig. 1b). The intense oxazolone peak at 1820 cm^{-1} indicates that the reaction is almost completed within 20 min, while the absence of the carbonyl band of *p*-nitrophenyl ester at about 1760 cm^{-1} indicates that the mixture does not contain the *p*-nitrophenyl ester (Fig. 1b). This is in remarkable contrast with the result that the same treatment of usual peptide acids produces exclusively corresponding *p*-nitrophenyl

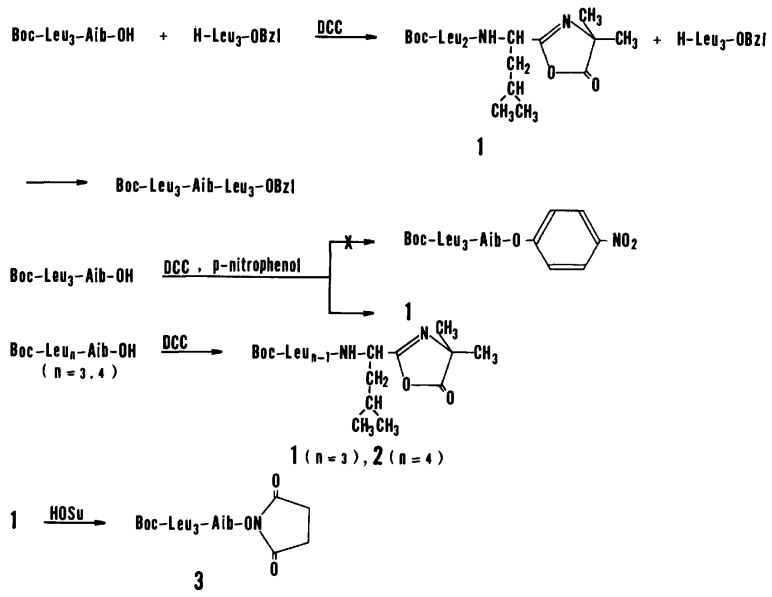

Scheme 1.

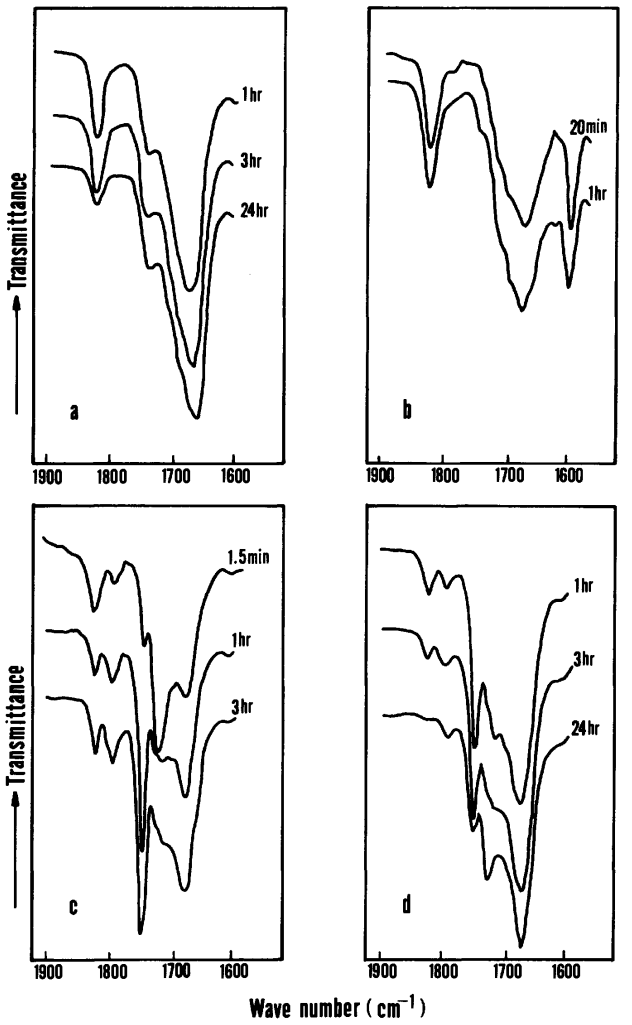

Fig. 1. Monitoring of the 5(4*H*)-oxazolone formation and the reaction of 5(4*H*)-oxazolone (**1**) with various nucleophiles by IR absorption spectra. The nucleophiles used are in the following: a, H–Leu_3–OBzl; b, *p*-nitrophenol; c, HOSu; d, HOSu, and H–Leu_3–OBzl.

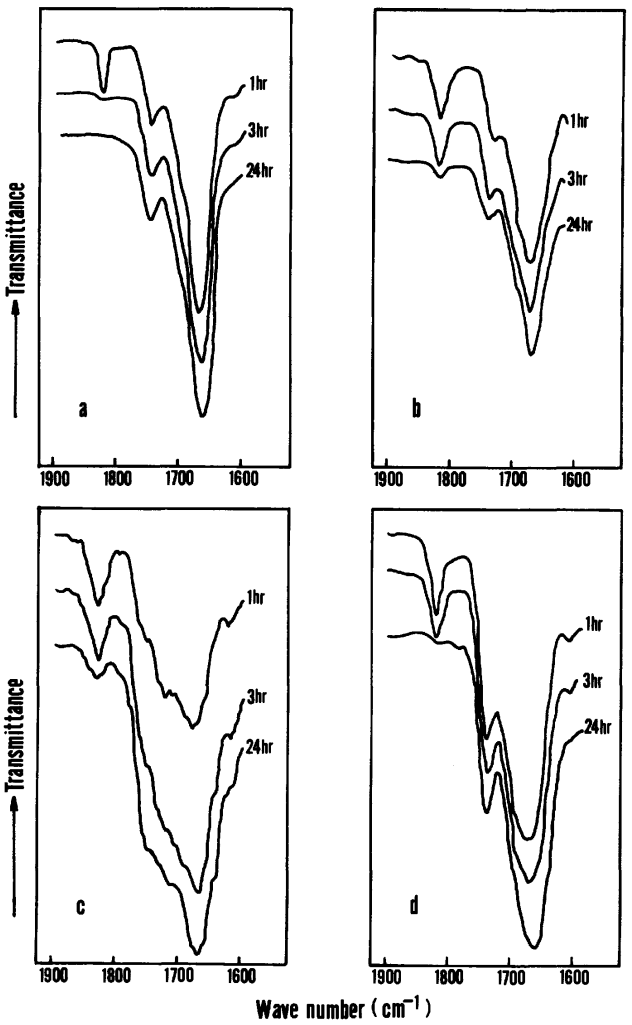

Fig. 2. Monitoring of the catalytic aminolysis of the oxazolone (**1**) with H–Leu_3–OBzl by IR absorption spectra. The catalysts used are in the following: a, HOBt; b, *p*-nitrophenol; c, acetic acid; d, imidazole.

esters of peptides. Treatment of Boc-Leu$_n$-Aib-OH (n=3 and 4) with DCC in the absence of nucleophiles begins to precipitate *N,N'*-dicyclohexylurea almost immediately and produces the corresponding 5(4*H*)-oxazolones in high yields (Scheme 1). Treatment of Boc-Leu$_3$-Aib-OH with acetic anhydride also produced the oxazolone (**1**). Ring-opening reactions of oxazolones with hydroxy compounds were easily monitored by following the disappearance of the intense oxazolone peak at 1820 cm^{-1}. The hydroxy compounds examined were in the following: *p*-nitrophenol, *o*-nitrophenol, pentachlorophenol, 2,4,6-trichlorophenol, 8-quinolinol, HOBt, and HOSu. For the hydroxy compounds, only HOSu reacted with the oxazolones at room temperature in dichloromethane to produce the succinimide ester (**3**) (Scheme 1, Fig. 1c). Even in the presence of amino component peptides such as H-Leu$_3$-OBzl and H-Leu$_n$-Aib-OBzl (n=3 and 4), the oxazolone (**1**) reacted faster with HOSu than the amino component peptides, followed by the slow aminolysis of the ester (**3**) (Fig. 1d). In contrast, HOBt does not react with the oxazolone under the same conditions, but strongly catalyzes the aminolysis of the oxazolone (**1**) in dichloromethane to form a peptide bond in a nearly quantitative yield. The catalytic effect of HOBt on the aminolysis were easily monitored by following the disappearance of the intense oxazolone peak at 1820 cm^{-1} (Fig. 2a). The reaction was also monitored by HPLC on a gel filtration column (Fig. 3). Other hydroxy compounds showed a little

Table 1. The coupling yields of the catalytic aminolysis of the oxazolones (**1**) and (**2**) with various amino component peptides in the presence of HOBt

Oxazolone	Product	Yield/%
1	Boc-Leu$_3$-Aib-Leu$_3$-OBzl	98
1	Boc-(Leu$_3$-Aib)$_2$-OBzl	97
1	Boc-(Leu$_3$-Aib)$_3$-OBzl	97
2	Boc-Leu$_4$-Aib-Leu$_4$-OBzl	95
2	Boc-(Leu$_4$-Aib)$_2$-OBzl	95
2	Boc-(Leu$_4$-Aib)$_3$-OBzl	93

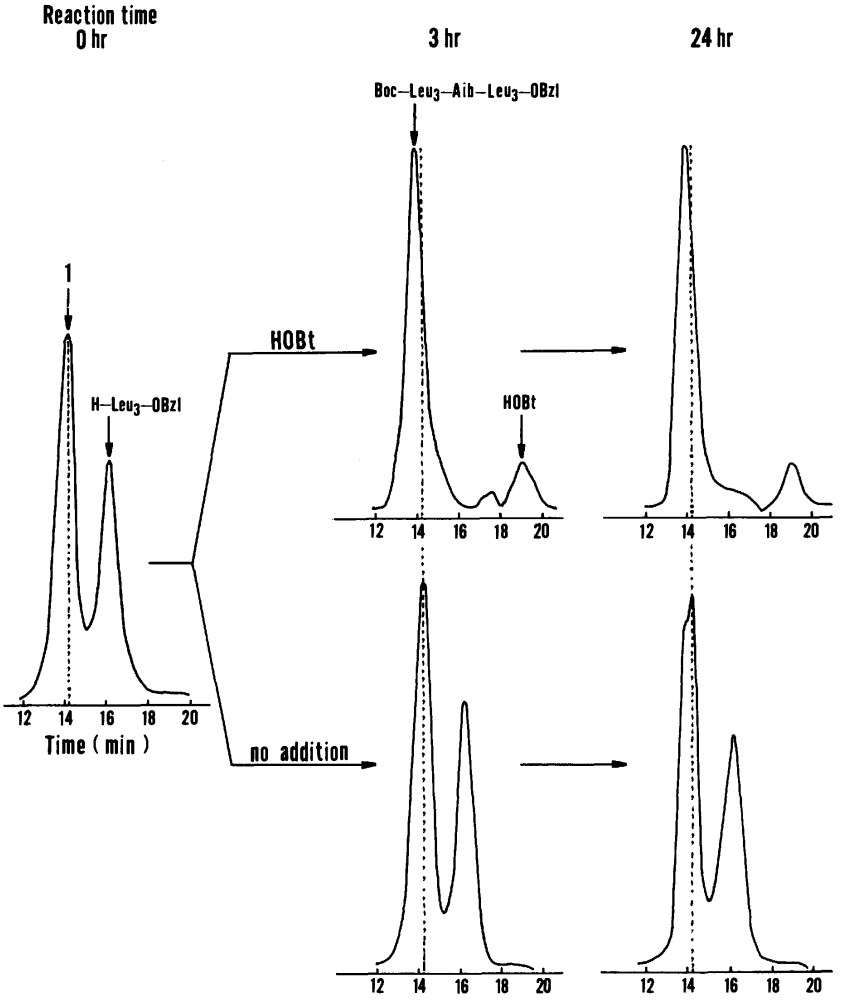

Fig. 3. Monitoring by HPLC of catalytic aminolysis of the oxazolone (**1**) with H-Leu$_3$-OBzl in the presence of HOBt.

catalytic effect on the aminolysis of the oxazolone (**1**) with H-Leu$_3$-OBzl (Fig. 2b). Acetic acid and imidazole also catalyze the aminolysis of the oxazolone (**1**) (Fig. 2c and 2d). The catalytic effect was in the following order: HOBt $\gg$ imidazole>acetic acid, *p*-nitrophenol, pentachlorophenol, *o*-nitrophenol, 2,4,6-trichlorophenol>8-quinolinol. The aminolysis of the oxazolones (**1**) and (**2**) with various amino component peptides is practically catalyzed by HOBt in dichloromethane to form peptide bonds in nearly quantitative yields. (Table 1).

Discussion

In the reaction of Boc-Leu$_n$-Aib-OH with DCC in the presence of nucleophiles except for HOSu, the exclusive formation of 5(4*H*)-oxazolones is very surprising. In a series of C-terminal-activated derivatives of peptides (the structure **4** in Scheme 2), the effect of substituents R_1 and R_2 on the ease of 5(4*H*)-oxazolone formation has been reported by Young.[10] If one assumes that 5(4*H*)-oxazolone formation occurs by a base-catalyzed path, then one expects the acidity of the amide at R_1 to be the major determinant, in accord with the simple acyl order, $CF_3CO>C_6H_5CO>CH_3CO$. The effect of R_2 on the ease of 5(4*H*)-oxazolone formation is difficult to rationalize due to the complexity of the situation. In the case of the reaction of Boc-Leu$_n$-Aib-OH with DCC, the ease of the 2-substituted 4,4-dimethyl-5(4*H*)-oxazolone formation is apparently attributed to the conformational effect of C-terminal Aib residues, namely, the extreme restriction of the backbone dihedral angles ϕ and ψ of Aib residues.[9a,9f,11] In term of activation entropy, the conformational restriction is clearly favorable for the intramolecular cyclization, the oxazolone formation. On the other hand, the low reactivity of the oxazolone with nucleophiles results from steric hindrance of both methyl groups on the oxazolone.

In the ring-opening reactions of (4S)-2-phenyl-4-benzyloxazolone with α nucleophiles (species containing two adjacent nucleophilic centers), biphilic (electrophilic-nucleophilic) pathways have been estimated.[12] HOSu has also been viewed as proceeding by a concerted mechanism involving nucleophilic-electrophilic attack of an anionic form (the transition state **5** in Scheme 2).[12] The high reactivity of HOSu with the oxazolone (**1**) derived from Boc-Leu$_3$-Aib-OH can be understood as involving a biphilic pathway through the transition state **5** (Scheme 2). No reaction of HOBt with the oxazolone (**1**) may be attributed to no contribution of the zwitterionic structures **6** and **7** (Scheme 2) due to weak basicity of the nitrogen atoms. No reaction of 8-quinolinol and *o*-nitrophenol with the oxazolone (**1**) may also be attributed to no contribution of the zwitterionic structures **8** and **9** (Scheme 2).

Catalytic effects of HOBt on the oxazolone aminolysis is quite significant. The pK_a value of HOBt (pK_a=4.00) is close to that of acetic acid (pK_a=4.05) and HOSu (pK_a=4.05). In the detailed studies on the acid catalysis of *p*-nitrophenyl ester aminolysis, Nakamizo proposed a bifunctional concerted mechanism that involves the 8-membered transition state **10** (Scheme 2).[13] A different transition state was also visualized by Muzalewski.[14] A little catalytic effect of acetic acid on the oxazolone aminolysis indicates that the oxazolone aminolysis in the presence of HOBt does not proceed through the

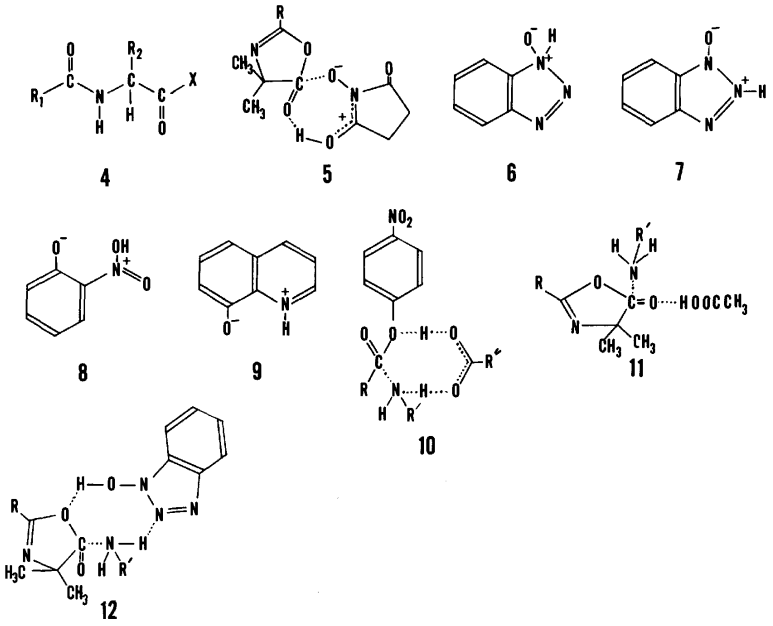

Scheme 2.

simple acid catalytic pathway (the transition state **11** in Scheme 2), but proceed through the biphilic pathway (the transition state **12** in Scheme 2).

Peptides having an α,α-disubstituted α-amino acid residue at C-terminal are expected to have high potential for the oxazolone formation due to the restriction of the backbone dihedral angles ϕ and ψ of the amino acid residue. The study for the reactivity of α,α-disubstituted α-amino acid residues will be in progress.

Experimental

General. The uncorrected capillary melting points will be reported. Analytical HPLC of the peptides was performed on a column packed with an acrylonitrile-divinylbenzene-styrene copolymer (7.5×500 mm) using a mini micro pump NSP-800-5DX (Nihon Seimitsu Kagaku) and a refractive index detector model RI-3H (Japan Analytical Industry). The operating conditions of HPLC were the following: Column with exclusion limit of 5000; solvent, DMF; flow rate, 1 ml/min; chart speed, 0.5 cm/min; temperature, room temperature. The IR spectra in the solid state were recorded for nujor mulls with a JASCO model DS-701G spectrometer. Those in solution were recorded employing 0.025 mm pathlength cells with potassium bromide windows. The concentration of the solution was kept near 4.0×10^{-2} M†.

Preparation of Oxazolones from Boc-Leu$_n$-Aib-OH (n=3 and 4) Using DCC as a Dehydration Reagent. Boc-Leu$_n$-Aib-OH (5 mmol) divided to five portions was added at 30 min intervals to an ice-chilled stirred solution of DCC (5 mmol) in 20 ml of dichloromethane. Precipitation of *N,N'*-dicyclohexylurea began almost immediately. After 1 h the solution was filtered and the dichloromethane was removed at room temperature under reduced pressure to give a solid material. The solid product was recrystallized from the appropriate solvents. The oxazolone (**1**), from ethyl acetate/hexane (1/5); yield, 80%; mp 161—163 °C.

Found: C, 60.91; H, 9.26; N, 10.63%. Calcd for $C_{27}H_{48}N_4O_6$ $0.5H_2O$: C, 60.76; H, 9.25; N, 10.50%.

The oxazolone (**2**), from tetrahydrofuran/hexane (1/3); yield, 83%; mp 205—207 °C.

Found: C, 62.05; H, 9.75; N, 11.09%. Calcd for $C_{33}H_{59}N_5O_7$ $0.5H_2O$: C, 61.98; H, 9.18; N, 10.62%.

Preparation of Oxazolones from Boc-Leu$_n$-Aib-OH (n=3 and 4) Using Acetic Anhydride as a Dehydration Reagent. A solution of a peptide (5 mmol) in acetic anhydride (20 ml) was heated at 110—120 °C for 15 min and then evaporated under reduced pressure. Last traces of acetic anhydride were removed by addition of toluene (10 ml) and evaporation, and the residual oxazolone recrystallized from the appropriate solvents. The yields of the oxazolones (**1**) and (**2**) were 95 and 78%, respectively.

IR Absorption Monitoring of the 5(4H)-Oxazolone Formation by the Reaction of Boc-Leu$_3$-Aib-OH with DCC in the Presence of Nucleophiles (H-Leu$_3$-OBzl, p-Nitrophenol, HOSu, and HOSu + H-Leu$_3$-OBzl). The formation of the 2-substituted 4,4-dimethyl-5(4*H*)-oxazolone (**1**) by the reaction of Boc-Leu$_3$-Aib-OH with DCC in the presence of nucleophiles were monitored by following the appearance of the intense oxazolone peak at 1820 cm^{-1}. The concentrations of Boc-Leu$_3$-Aib-OH, DCC, and nucleophiles were 4.0×10^{-1} M, respectively. The results were shown in Fig. 1.

Reactions of Oxazolones with Hydroxy Compounds. Ring-opening reactions of oxazolones with hydroxy compounds were carried out at room temperature in dichloromethane and monitored by following the disappearance of the intense oxazolone peak at 1820 cm^{-1}. The concentrations of the oxazolone and hydroxy compounds were 4.0×10^{-2} M, respectively, in the ring-opening studies.

Preparation of Boc-Leu$_3$-Aib-OH N-Hydroxysuccinimide Ester. To a solution of the oxazolone (**1**) from Boc-Leu$_3$-Aib-OH (1 mmol) in 10 ml of dichloromethane, *N*-hydroxysuccinimide (127 mg, 1.1 mmol) was added in one portion and the reaction was allowed to stir for 8 h at room temperature. The solvent was evaporated at room temperature under reduced pressure and 50 ml of water was added to dissolved unreacted *N*-hydroxysuccinimide. Crude product (530 mg, 73%), showing a single peak on HPLC, was obtained after filtration and washing with cold ether (to remove oxazolone). The product was recrystallized from ethyl acetate/hexane (1/2); yield, 87%; mp 133—137 °C.

Found: C, 56.16; H, 8.43; N, 10.40%. Calcd for $C_{31}H_{53}N_5O_9$ H_2O: C, 56.60; H, 8.43; N, 10.65%.

Peptide Bond Formation by the Reactions of the Oxazolone (1) with Amino Component Peptides. Ring-opening reactions of the oxazolone (**1**) with amino component peptides were carried out at room temperature in dichloromethane and monitored by following the disappearance of the intense oxazolone peak at 1820 cm^{-1}. The reactions were also monitored by HPLC on a gel filtration column. The concentrations of the oxazolone and amino component peptides were 4.0×10^{-2} M, respectively, in the ring-opening studies.

Catalytic Effects of Hydroxy Compounds on Peptide Bond Formation by the Reactions of the Oxazolone (1) with Amino Component Peptides. Accelerating effects of hydroxy compounds on the aminolysis of the oxazolone (**1**) were studied at room temperature in dichloromethane and monitored by following the disappearance of the intense oxazolone peak at 1820 cm^{-1}. The concentrations of the oxazolone, amino component peptide, and hydroxy compounds were 4.0×10^{-2} M, respectively, in the aminolysis. The reaction was also monitored by HPLC on a gel filtration column.

Preparation of Aib-containing Peptides Using the Oxazolones (1) and (2) as Coupling Reagents. A oxazolone (1.0 mmol) was added to a stirred mixture of an amino component peptide hydrochloride salt (1.0 mmol), *N*-methylmorpholine (1.0 mmol), and HOBt (1.0 mmol) in dichloromethane (20 ml). The reaction mixture was allowed to stir for 12 h at room temperature and then washed with water, 10% citric acid, and 5% sodium hydrogencarbonate, dried over sodium sulfate, and concentrated under reduced pressure. IR absorption spectra of crude products were free from the absorption band at 1820 cm^{-1} and in good agreement with those of authentic samples.[5,6]

† 1 M=1 mol dm^{-3}.

References

1) Part IV of "Peptides and Proteins Containing α,α-Disubstituted α-Amino Acid Residues," Part III, M. Narita, J.-Y. Chen, H. Sato, and Y. Kim, *Bull. Chem. Soc. Jpn.*, **58**, 2494 (1985). Abbreviations used are the following: Aib, α-aminoisobutyric acid residue; Leu, L-leucine residue; Boc, *t*-butoxycarbonyl; OBzl, benzyl ester; DCC, dicyclohexylcarbodiimide; HOBt, 1-hydroxy-1*H*-benzotriazole; HOSu, *N*-hydroxysuccinimide.

2) a) B. Iselin and R. Schwyzer, *Helv. Chim. Acta*, **43**, 1760 (1960); b) K. Lubke and E. Schroder, *Z. Naturforsch.*, **B16**, 765 (1961); c) D. Theodoropoulus and J. Gazopoulos, *J. Org. Chem.*, **27**, 2091 (1962); d) B. Liberek, *Tetrahedron Lett.*, **1963**, 925; e) M. W. Williams and G. T. Young, *J. Chem. Soc.*, **1964**, 3701; f) G. W. Anderson, F. M. Callahan, and J. E. Zimmerman, *Acta Chim. Acad. Sci. Hung.*, **44**, 51 (1965); g) M. Goodman and W. J. McGahren, *Tetrahedron*, **23**, 2017 (1967); h) M. Goodman and W. J. McGahren, *Tetrahedron*, **23**, 2031 (1967); i) B. Bator-Sawicka, *Rocz. Chem.*, **42**, 47 (1968); j) D. S. Kemp and J. Rebek, *J. Am. Chem. Soc.*, **92**, 5792 (1970); k) T. Wieland and A. Seelinger, *Chem. Ber.*, **104**, 3992 (1971); l) N. L. Benoiton and F. M. F. Chen, "Peptides, Structure and Biological Function," ed by E. Gross and J. Meienhofer, Pierce Chemical Co., Rockford, Illinois (1979) p. 261; m) J. Kovacs and Y. Hsieh, *J. Org. Chem.*, **47**, 4996 (1982); n) J. Kovacs, G. N. Jham, K. Y. Hui, E. M. Holleran, S. E. Kim, and T. Canavan, *Int. J. Peptide Protein Res.*, **24**, 161 (1984).

3) D. S. Kemp, "The Peptides," ed by E. Gross and J. Meienhofer, Academic Press, New York (1979), **Vol. 1**, p. 315.

4) N. L. Benoiton, "The Peptides," ed by E. Gross and J. Meienhofer, Academic Press, New York (1983), **Vol. 5**, p. 217.

5) M. Narita, M. Doi, H. Sugasawa, and K. Ishikawa, *Bull. Chem. Soc. Jpn.*, **58**, 1473 (1985).

6) M. Narita, K. Ishikawa, H. Sugasawa, and M. Doi, *Bull. Chem. Soc. Jpn.*, **58**, 1731 (1985).

7) M. Narita, J.-Y. Chen, H. Sato, and Y. Kim, *Bull. Chem. Soc. Jpn.*, **58**, 2494 (1985).

8) a) M. T. Leplawy, D. S. Jones, G. W. Kenner, and R. C. Sheppard, *Tetrahedron*, **11**, 39 (1960); b) D. S. Jones, G. W. Kenner, J. Preston, and R. C. Sheppard, *J. Chem. Soc.*, **1965**, 6227; c) G. Faust and H. Lange, *J. Prakt. Chem.*, **11**, 153 (1960).

9) a) A. W. Burgess and S. J. Leach, *Biopolymers*, **12**, 2599 (1973); b) A. W. Burgess and S. J. Leach, *Biopolymers*, **12**, 2691 (1973); c) R. Oekonomopulos and G. Jung, *Liebigs Ann. Chem.*, **1979**, 1151; d) R. Oekonomopulos and G. Jung, *Biopolymers*, **19**, 203 (1980); e) R. Nagaraj and P. Balaram, *Tetrahedron*, **37**, 1263 (1981); f) Y. Paterson, S. M. Rumsey, E. Benedetti, G. Némethy, and H. A. Scheraga, *J. Am. Chem. Soc.*, **103**, 2947 (1981); g) R. Nagaraj and P. Balaram, *Acc. Chem. Res.*, **14**, 356 (1981); h) R. O. Fox, Jr. and F. M. Richards, *Nature*, **300**, 325 (1982); i) C. P. Rao and P. Balaram, *Biopolymers*, **21**, 2461 (1982); j) T. S. Sudha, E. K. S. Vijayakumar, and P. Balaram, *Int. J. Peptide Protein Res.*, **22**, 464 (1983); k) E. K. S. Vijayakumar, and P. Balaram, *Tetrahedron*, **39**, 2725 (1983); l) R. R. Wilkening, E. S. Stevens, G. M. Bonora, and C. Toniolo, *J. Am. Chem. Soc.*, **105**, 2560 (1983); m) C. Toniolo, G. M. Bonora, A. Bavoso, E. Benedetti, B. D. Blasio, V. Pavone, and C. Pedone, *Biopolymers*, **22**, 205 (1983); n) A. K. Francis, M. Iqbal, P. Balaram, and M. Vijayan, *Biopolymers*, **22**, 1499 (1983); o) G. M. Bonora, C. Toniolo, B. D. Blasio, V. Pavone, C. Pedone, E. Benedetti, I. Lingham, and P. Hardy, *J. Am. Chem. Soc.*, **106**, 8152 (1984); p) G. M. Bonora, C. Mapelli, C. Toniolo, R. R. Wilkening, and E. S. Stevens, *Int. J. Biol. Macromol.*, **6**, 179 (1984).

10) G. T. Young, "Peptides, Proceedings of the Eighth European peptide Symposium," ed by L. Zervas, North-Holland Publ., Amsterdam (1967), p. 55.

11) a) G. R. Marshall, "Intra-Science Chemistry Report," ed by N. Kharasch, Gordon and Breach, New York (1971), p. 305.

12) M. Goodman and C. B. Glaser, *J. Org. Chem.*, **35**, 1954 (1970).

13) a) N. Nakamizo, *Bull. Chem. Soc. Jpn.*, **42**, 1071 (1969); b) N. Nakamizo, *Bull. Chem. Soc. Jpn.*, **42**, 1078 (1969).

14) F. Muzalewski, "Peptides 1971, Proceedings of the Eleventh European Peptide Symposium," ed by H. Nesvadba, North-Holland Publ., Amsterdam (1973), p. 39.

Photochemical Ring-expansion Reaction of 1,2-Benzisothiazolinones

Nobumasa KAMIGATA,* Satoshi HASHIMOTO, Michio KOBAYASHI, and Hiroshi NAKANISHI†

Department of Chemistry, Faculty of Science, Tokyo Metropolitan University, Fukazawa, Setagaya-ku, Tokyo 158

†*National Chemical Laboratory for Industry, Yatabe-Higashi 1-1, Tsukuba, Ibaraki 305*

(Received May 25, 1985)

The photochemical reaction of a series of 2-aryl-1,2-benzisothiazol-3(2*H*)-ones (**1**) under deaerated conditions was found to give dibenzo[*b*,*f*][1,4]thiazepin-11(10*H*)-ones (**2**). A mechanism through a biradical species is proposed for the photoreaction. When the photolysis of **1** was carried out in the presence of oxygen, 2-aryl-1,2-benzisothiazol-3(2*H*)-one 1-oxides (**11**) were formed together with compounds **2**.

In recent years much attention has been focused on the photochemistry of five-membered heterocyclic ring systems. These studies have dealt with the synthetic usefulness of the photochemistry of heterocyclic compounds as well as their reaction modes.[1-4] In earlier communications we reported that the photochemical reaction of 2-substituted 1,2-benzisothiazol-3(2*H*)-one 1,1-dioxides in benzene gave rise to *N*-substituted *o*-phenylbenzamides with the extrusion of sulfur dioxide,[5] whereas, the photolysis of 2-aryl-1,2-benzisothiazol-3(2*H*)-one, which corresponds to reduced derivatives of *N*-substituted 1,2-benzisothiazol-3(2*H*)-one 1,1-dioxides in benzene, gave dibenzothiazepinones.[6] We give here a full account for the photochemical behavior of a series of 2-aryl-1,2-benzisothiazol-3(2*H*)-ones (**1**).

Results and Discussion

When a deaerated solution of 2-(4-methoxyphenyl)-1,2-benzisothiazol-3(2*H*)-one (**1a**) in benzene was irradiated with 340-nm wavelength light, a single photoproduct was obtained. An assignment of this material as 7-methoxydibenzo[*b*,*f*][1,4]thiazepin-11-(10*H*)-one (**2a**) was made on the basis of its spectral data, especially its 400-MHz ^{1}H NMR spectrum.

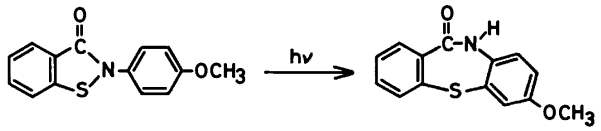

1a **2a**

Several related 2-aryl-1,2-benzisothiazol-3(2*H*)-ones (**1**) were also irradiated under similar conditions to give dibenzo[*b*,*f*][1,4]thiazepin-11(10*H*)-ones (**2**) as the only isolable photoproducts. The results are summarized in Table 1. A reaction mechanism which explains the phototransformation is outlined in Scheme 1. The photoexcited **1** undergoes homolytic cleavage of the weakest bond (S–N) in the molecule to give biradical (**3**). The initially-formed biradical attacks the ortho-position of the *N*-aryl group to give the cyclized product **5**. A subsequent 1,7-hydrogen shift of intermediate **5** leads to the final product. The last step of the sequence can proceed by either a thermal or photochemical hydrogen shift.

Recently, Rokach and Hammel reported that a small amount of a photo-ring expansion product was formed together with 3-phenylthiazol-2(3*H*)-one upon irradiation of 2-phenylisothiazol-3(2*H*)-one.[7] However, we could not detect the corresponding 3-aryl-2(3*H*)-benzothiazolone (**6**) in the reaction mixture.

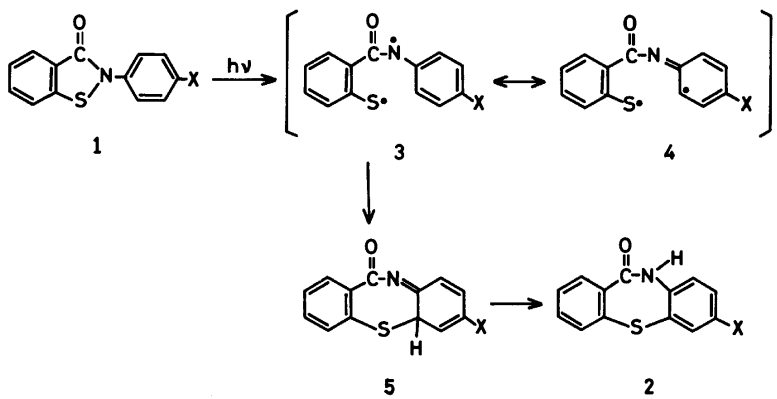

1 **3** **4** **5** **2**

Scheme 1.

According to the mechanism proposed,[7] a ring-contracted intermediate such as **7** would seem reasonable. The absence of compound **6** among the products suggests that this intermediate (*i.e.* **7**) is not formed in the photoreaction of **1**. The absence of **7**

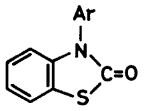

6

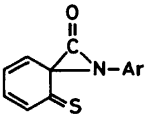

7

can be accounted for in terms of the high energy required to interrupt the aromaticity of the benzene ring. The photo-transposition reaction of the related 2-alkyl-1,2-benzisoxazol-3(2*H*)-one system to 3-alkyl-1,2-benzoxazol-2(3*H*)-one *via* the ring-contracted intermediate **8** was reported by Kinstle and co-workers.[8] Therefore, the absence of **7** can be also attributed to the instability of the C=S group (2pπ—3pπ) compared with the C=O group (2pπ—2pπ).

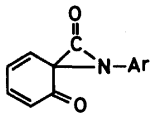

8

Recently, Kulyk and Neckers have reported the intermolecular photoaddition of the benzisothiazole system to alkenes and alkynes and demonstrated the synthetic usefulness of benzothiazepines.[9] Our present reaction is of interest from both mechanistic and synthetic points of view since medium-size seven-membered ring compounds are generally very difficult to prepare. Unfortunately, the yield of **2** is low as is shown in Table 1. This can be attributed to the fact that biradical **3** gives rise to polymeric compounds at a faster rate than an intramolecular reaction to give **2**. If this postulate is correct, the yield of **2** would be expected to improve with the use of a more viscous solvent. The irradiation of **1b** was carried out in *t*-butyl alcohol using a Tungsten filter. However, no difference in the yield of **2b** was observed. Then, **1b** was irradiated in *t*-butyl alcohol using a Pyrex, Corex or Vycor filter to determine whether the wavelength of light would affect the yield of **2**. A considerable improvement was observed with the latter two filters. When compound **1b** was irradiated through a Corex filter in either *t*-butyl alcohol, benzene or methanol, the yield of **2b** was low in the latter two solvents. The results are summarized in Table 2. These results imply that both the wavelength of the light and the solvent are important in the photoreaction of compound **1** to obtain the photoproduct **2** in a good yield. Since the yield of compound **2b** was improved upon irradiation through a Corex filter in *t*-butyl alcohol, several related compounds were irradiated under similar conditions (Table 3). We found that an improvement in the yield occurred only when the *N*-phenyl group of **1** possesses an electron-donating substituent.

We also studied the photoreaction of (*E*)-2-styryl-1,2-benzisothiazol-3(2*H*)-one (**9**) expecting the formation of a photoexpansion product (**10**). However,

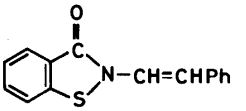

9

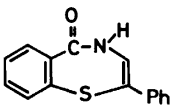

10

TABLE 1. PHOTOCHEMICAL REACTION OF **1** IN BENZENE[a]

X in **1**		Product	Yield/%[b]
1a	OCH_3	**2a**	13
1b	CH_3	**2b**	19
1c	H	**2c**	16
1d	Cl	**2d**	17
1e	CN	**2e**	11

a) The irradiation was carried out on a 2×10^{-3} M solution of **1** in benzene under degassed conditions using a 450 W medium-pressure mercury lamp (Hanovia) through a Tungsten glass filter (>340 nm). In case of **1e**, a Molybdenum glass filter (>320 nm) was employed. b) The yields are based on the starting material consumed.

TABLE 2. EFFECT OF WAVELENGTH AND VISCOSITY OF SOLVENT IN THE PHOTOLYSIS OF **1b**

Solvent	Rel. Viscosity η (m Poise)	Filter		Yield of **2b**/%
Benzene	6.5 (20 °C)	Tungsten	340 nm	19
t-BuOH	33.2 (30 °C)	Tungsten	340 nm	14
t-BuOH		Pyrex	300 nm	18
t-BuOH		Corex	280 nm	57
t-BuOH		Vycor	250 nm	54
t-BuOH	33.2 (30 °C)	Corex	280 nm	57
Benzene	6.5 (20 °C)	Corex	280 nm	13
MeOH	5.5 (20 °C)	Corex	280 nm	7

TABLE 3. PHOTOCHEMICAL REACTION OF **1** IN *t*-BUTYL ALCOHOL

X in **1**		Filter		Product	Yield/%
1a	OCH_3	Vycor	250 nm	**2a**	47
1b	CH_3	Corex	280 nm	**2b**	57
1c	H	Corex	280 nm	**2c**	31
1d	Cl	Vycor	250 nm	**2d**	13
1e	CN	Vycor	250 nm	**2e**	20

no photochemical transformation was observed upon irradiation for long periods of time (≈30 h) and all of the starting material **9** was recovered.

Irradiation of **1a** was also carried out in benzene using light of wavelength >340 nm in the presence of oxygen. Under these conditions, 2-(4-methoxyphenyl)-1,2-benzisothiazol-3(2*H*)-one 1-oxide (**11a**) was formed in 8% yield in addition to compound **2a**. The structure of **11a** was verified by a comparison with an authentic sample which was prepared by a treatment of **1a** with *N*-chlorosuccinimide, followed by a reaction with aqueous potassium hydrogencarbonate. Several related 2-aryl-1,2-benzisothiazol-3(2*H*)-ones **1** were also irradiated under similar conditions and were found to give the corresponding photo-oxidized product (**11**) together with compound **2**. The results are summarized in Table 4.

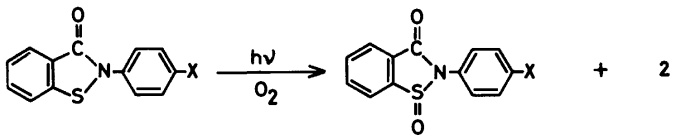

1 11

The mechanism of the photo-oxidation reaction is of considerable interest. We believe that compound **1** does not act as a sensitizer to form singlet oxygen since the triplet energy of **1** is estimated to be greater than 250 KJ per mol.[10] Therefore, the formation of singlet oxygen as the oxidant can be ruled out. Moreover, singlet oxygen is known not to oxidize diphenyl sulfide in benzene.[11] An alternate possibility involves the formation of an excited complex (**12**) resulting from the interaction of compound **1** and oxygen. Unfortunately, all attempts to detect such an intermediate by spectroscopic methods failed. Tezuka and co-workers have reported that a related complex, such as **13**, could indeed be detected spectroscopically in the photoreaction of diphenyl sulfide[12] with oxygen and they ruled out a mechanism which involves singlet oxygen as an intermediate.[13]

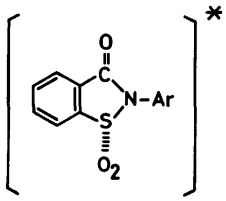

12

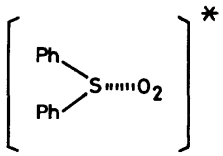

13

Table 4. Photochemical reaction of **1** in the presence of oxygen[a]

X in **1**		Solvent	Product	Yield[b]		
1a	OCH_3	Benzene	**12a**	8%	**2a**	12%
1a	OCH_3	Methanol	**12a**	9%	**2a**	11%
1b	CH_3	Benzene	**12b**	9%	**2b**	16%
1c	H	Benzene	**12c**	8%	**2c**	15%
1c	H	Methanol	**12c**	10%	**2c**	15%
1d	Cl	Benzene	**12d**	11%	**2d**	14%
1e	CN	Benzene	**12e**	17%	**2e**	29%

a) Irradiation with a medium-pressure 450 W mercury lamp (Hanovia) through a Tungsten filter (>340 nm) under bubbling oxygen. In case of **1e**, a Molybdenum filter (>320 nm) was used. b) Yields (isolated) are based on the starting materials consumed.

Experimental

Measurement. Melting points are uncorrected. The infrared absorption spectra were determined on a Hitachi Model 260—10 spectrophotometer using KBr disks. The electronic spectra were determined on a Hitachi Model 220A spectrophotometer. The NMR spectra were recorded at 60 and 400 MHz using a Hitachi R20B and a JEOL JNM-GX400 spectrometer, respectively, with Me_4Si as an internal standard. Mass spectra were determined with a JEOL JMS-DX300 mass spectrometer with a JEOL JMA 5000 mass-data system at an ionizing voltage of 20—70 eV. Elemental analyses were carried out using a Perkin Elmer 240 elemental analyzer.

Preparation of 2-Aryl-1,2-benzisothiazol-3(2H)-ones (1). An improved method of Reissert and Manns[14] was employed for the syntheses of **1**. A solution containing 2,2′-dithiobis[benzoyl chloride] (2.0 g, 5.0 mmol) in dry dichloromethane (100 cm^3) was added dropwise at the ambient temperature to a well stirred solution of substituted aniline (29 mmol) in dry dichloromethane (50 cm^3) over a period of 15 min. The resulting mixture was stirred at room temperature for 3 h; then, the solvent was evaporated under reduced pressure. The residue was stirred with 1 M† hydrochloric acid (100 cm^3) for 30 min at room temperature to remove any excess aniline. The solid product, *N,N′*-diaryl-2,2′-dithiobis[benzamide], was collected, washed with water, and dried in a desiccator. A solution of bromine (1.4 g, 8.7 mmol) in dichloromethane was added dropwise at ambient temperature to a well stirred suspension of the *N,N′*-diaryl-2,2′-dithiobis[benzamide] (5.8 mmol) in dichloromethane (150 cm^3) over a period of 3—5 min. Stirring was continued at room temperature overnight. Activated basic alumina (Wako Pure Chemical, 300 mesh, 20 g) was added to the reaction mixture and stirring was continued for an additional 3 h. Removal of the solvent left a pale-yellow residue which was chromatographed over an activated alumina column (300 mesh, 40 g) and eluted with chloroform to give pure **1**. The following compounds were prepared using the above procedure.

2-(4-Methoxyphenyl)-1,2-benzisothiazol-3(2H)-one (1a): Yield, 96%; mp 148—149 °C (lit[15], mp 147—149 °C); ^1H NMR (Me_2SO-d_6) 400 MHz, δ=3.819 (3H, s, OCH_3), 7.085 and 7.569 (2H and 2H, A_2B_2 quartet, J_{AB}=8.9 Hz, 3′- and 2′-H), 7.509 (1H, m, J_{5-4}=8 Hz, J_{5-6}=7.0 Hz, 5-H), 7.764 (1H, m, J_{6-5}=7 Hz, J_{6-7}=8 Hz, 6-H), 7.951 (1H, d, J_{7-6}=8 Hz, 7-H),

† 1 M=1 mol dm^{-3}.

and 8.042 (1H, d, J_{4-5}=8 Hz, 4-H); ^{13}C NMR (Me_2SO-d_6) 400 MHz, δ=163.23 (C=O), 129.58 and 140.10 (3a- and 7a-C), 126.00, 125.80, 132.27, and 121.68 (4-, 5-, 6-, and 7-C), 124.10 (1′-C), 126.60 (2′-C), 114.55 (3′-C), 158.18 (4′-C), and 55.41 (OCH_3).

*2-(4-Methylphenyl)-1,2-benzisothiazol-3(2H)-one (**1b**)*: Yield 96%; mp 136—137 °C (lit,[16] mp 135.5—136.5 °C); ^{1}H NMR (Me_2SO-d_6) 400 MHz, δ=2.360 (3H, s, CH_3), 7.333 and 7.570 (2H and 2H, A_2B_2 quartet, J_{AB}=8.9 Hz, 3′- and 2′-H), 7.509 (1H, m, J_{5-4}=8 Hz, J_{5-6}=7 Hz, 5-H), 7.760 (1H, m, J_{6-5}=7 Hz, J_{6-7}=8 Hz, 6-H), 7.951 (1H, d, J_{7-6}=8 Hz, 7-H), and 8.051 (1H, d, J_{4-5}=8 Hz, 4-H); ^{13}C NMR (Me_2SO-d_6) 400 MHz, δ=163.20 (C=O), 129.73 and 139.98 (3a- and 7a-C), 126.02, 125.85, 132.37, and 121.70 (4-, 5-, 6-, and 7-C), 134.55 (1′-C), 129.73 (2′-C), 124.37 (3′-C), 136.49 (4′-C), and 20.51 (CH_3).

*2-Phenyl-1,2-benzisothiazol-3(2H)-one (**1c**)*: Yield 91%; mp 141.5—142.5 °C (lit,[14] mp 143—144 °C); ^{1}H NMR ($CDCl_3$) δ=7.2—8.3 (9H, m); ^{13}C NMR (Me_2SO-d_6) δ=164.3 (C=O), 128.2 and 145.4 (3a- and 7a-C), 125.1, 126.6, 133.3, and 134.5 (4-, 5-, 6-, and 7-C), 133.9 (1′-C), 127.2 (2′-C), 129.6 (3′-C), and 128.8 (4′-C).

*2-(4-Chlorophenyl)-1,2-benzisothiazol-3(2H)-one (**1d**)*: Yield 87%; mp 128—129 °C (lit,[15] mp 129—130 °C); ^{1}H NMR ($CDCl_3$) 400 MHz, δ=7.504 and 7.743 (2H and 2H, A_2B_2 quartet, J_{AB}=8.9 Hz, 3′- and 2′-H), 7.52 and 7.74 (1H and 1H, m, J_{5-4}=8 Hz, J_{5-6}=7 Hz, and J_{6-7}=8 Hz, J_{6-5}=7 Hz, 5- and 6-H), 7.657 (1H, d, J_{7-6}=8 Hz, 7-H), and 8.170 (1H, d, J_{4-5}=8 Hz, 4-H); ^{13}C NMR ($CDCl_3$) 400 MHz, δ=164.03 (C=O), 129.41 and 139.66 (3a- and 7a-C), 127.22, 125.92, 132.50, and 120.09 (4-, 5-, 6-, and 7-C), 135.91 (1′-C), 125.48 (2′-C), 129.41 (3′-C), and 124.64 (4′-C).

*2-(4-Cyanophenyl)-1,2-benzisothiazol-3(2H)-one (**1e**)*: Yield 95%; mp 184.5—185.5 °C, IR (KBr) 2220 (m, C≡N) and 1652 cm^{-1} (s, amide C=O); ^{1}H NMR ($CDCl_3$) 60 MHz, δ=7.86 and 8.08 (2H and 2H, A_2B_2 quartet, J_{AB}=9 Hz) and 7.4—8.3 (4H, m); ^{13}C NMR ($CDCl_3$) 60 MHz, δ=164.1 (C=O), 124.5 and 131.9 (3a- and 7a-C), 127.4, 126.2, 133.2, and 120.1 (4-, 5-, 6-, and 7-C), 141.6 (1′-C), 123.2 (2′-C), 133.2 (3′-C), 118.2 (4′-C), and 109.5 (C≡N); UV (methanol) 203 (ε=3.5×10⁴), 239 (2.2×10⁴), 279 (1.7×10⁴), and 340 nm (7.8×10³); MS, *m/z* 252 (M^+). Anal. Calcd for $C_{14}H_8N_2OS$: C, 66.65; H, 3.20; N, 11.10. Found: C, 66.72; H, 3.09; N, 11.15.

*Photolysis of 2-Aryl-1,2-benzisothiazol-3(2H)-one (**1**) in a Degassed Solution.* A solution containing 0.44 mmol of 2-aryl-1,2-benzisothiazol-3(2*H*)-one (**1**) in 220 cm^3 of benzene or *t*-butyl alcohol was degassed by a freeze-thaw method and irradiated through a filter sleeve using a 450-W Hanovia medium-pressure mercury lamp for 2 h. The removal of the solvent under reduced pressure left a light-brown residue which was purified by silica-gel chromatography using dichloromethane-hexane as the eluent. Photoproduct **2** was isolated with recovered starting material **1**. The physical and spectral data, and analyses of the photoproducts **2** are as follows:

*7-Methoxydibenzo[b,f][1,4]thiazepin-11(10H)-one (**2a**).* Mp 234—235 °C; IR (KBr) 1655 (aromatic amide C=O) and 2900—3300 cm^{-1} (m, complex N-H); ^{1}H NMR (Me_2SO-d_6) 400 MHz, δ=3.734 (3H, s, OCH_3), 6.947 (1H, dd, J_{8-9}=8.8 Hz, J_{8-6}=2.9 Hz, 8-H), 7.114 (1H, d, J_{6-8}=2.9 Hz, 6-H), 7.152 (1H, d, J_{9-8}=8.8 Hz, 9-H), 7.44 and 7.48 (1H and 1H, m, 2- and 3-H), 7.525 (1H, d, J_{4-3}=7.3 Hz, 4-H), 7.678 (1H, d, J_{1-2}=7.3 Hz, 1-H), and 10.153 (1H, s, *N*-H); ^{13}C NMR (Me_2SO-d_6) 400 MHz, δ=168.07 (C=O), 131.30, 131.12, 131.69, and 128.81 (1-, 2-, 3-, and 4-C), 137.75 and 136.13 (4a- and 11a-C), 130.39, 156.34, and 132.74 (5a-, 7-, and 9a-C), 156.34, 115.78, and 124.21 (6-, 8-, and 9-C), and 55.48 (OCH_3); UV (methanol) 206 (ε=3.7×10³), 237 (1.5×10⁴), and 285 nm (5.4×10³); MS, *m/z* 257 (M^+). Anal. Calcd for $C_{14}H_{11}NO_2S$: C, 65.37; H, 4.31; N, 5.44. Found: C, 64.88; H, 4.36; N, 5.45.

*7-Methyldibenzo[b,f][1,4]thiazepin-11(10H)-one (**2b**).* Mp 274—275 °C; IR (KBr) 1660 (aromatic amide C=O) and 2900—3300 cm^{-1} (m, complex *N*-H); ^{1}H NMR (Me_2SO-d_6) 400 MHz, δ=2.240 (3H, s, CH_3), 7.119 (1H, d, J_{8-9}=8.1 Hz, 8-H), 7.158 (1H, d, J_{9-8}=8.1 Hz, 9-H), 7.377 (1H, broad s, 6-H), 7.43 and 7.47 (1H and 1H, m, J_{3-2}=J_{2-3}=7 Hz, J_{3-4}=J_{2-1}=7.3 Hz), 7.510 (1H, d, J_{4-3}=7.3 Hz, 4-H), and 7.671 (1H, s, *N*-H); ^{13}C NMR (Me_2SO-d_6) δ=168.20 (C=O), 131.17, 131.17, 131.71, and 128.70 (1-, 2-, 3-, and 4-C), 137.86 and 136.31 (4a- and 11a-C), 134.80, 134.80, and 137.26 (5a-, 7-, and 9a-C), 130.20, 122.93, and 132.53 (6-, 8-, and 9-C), and 19.86 (CH_3); UV (methanol) 208 (ε=4.2×10⁴) and 280 nm (4.2×10³); MS, *m/z* 241 (M^+). Anal. Calcd for $C_{14}H_{11}NOS$: C, 69.68; H, 4.59; N, 5.80. Found: C, 69.69; H, 4.65; N, 5.62.

*Dibenzo[b,f][1,4]thiazepin-11(10H)-one (**2c**).* Mp 264—265 °C; IR (KBr) 1645 (s, aromatic amide C=O) and 2900—3200 cm^{-1} (m, complex *N*-H); ^{1}H NMR (Me_2SO-d_6) δ=7.0—8.0 (m, aromatic-H); ^{13}C NMR (Me_2SO-d_6)δ=169.1 (C=O), 132.8, 132.1, 133.3, and 130.6 (1-, 2-, 3-, and 4-C), 140.6 and 137.1 (4a- and 11a-C), 133.3, 126.1, and 138.6 (5a-, 7-, and 9a-C), and 129.7, 132.1, and 123.9 (6-, 8-, and 9-C); UV (methanol) 206 (ε=4.1×10⁴), 240 (s), and 280 (s); MS, *m/z* 227 (M^+). Anal. Calcd for $C_{13}H_9NOS$: C, 68.70; H, 3.99; N, 6.16. Found: C, 68.65; H, 3.92; N, 6.10.

*7-Chlorodibenzo[b,f][1,4]thiazepin-11(10H)-one (**2d**).* Mp 300 °C<; IR (KBr) 1645 (s, aromatic amide C=O) and 2900—3300 cm^{-1} (m, complex *N*-H); ^{1}H NMR (Me_2SO-d_6) 400 MHz, δ=7.237 (1H, d, J_{8-9}=8.8 Hz, 9-H), 7.44 (1H, dd, J_{8-9}=8.8 Hz, J_{8-6}=2.3 Hz, 2-H), 7.49 (1H, dd, J_{2-3}=J_{2-1}=7.5 Hz, 2-H), 7.51 (1H, dd, J_{3-2}=J_{3-4}=7.5 Hz, 7-H), 7.54 (1H, d, J_{4-3}=7.5 Hz), 7.689 (1H, d, J_{1-2}=7.5 Hz, 1-H), and 10.774 (1H, s, *N*-H); ^{13}C NMR (Me_2SO-d_6) 400 MHz, δ=131.47, 131.26, 131.10, and 129.61 (1-, 2-, 3-, and 4-H), 138.89 and 135.40 (4a- and 11a-C), 139.01, 128.88, and 137.56 (5a-, 7-, and 9a-C), 131.47, 129.12, and 124.44 (6-, 8-, and 9-C), and 168.00 (C=O); UV (methanol) 208 (ε=4.0×10⁴), 245 (s), and 275 nm (s); MS, *m/z* 261 and 263 (M^+). Anal. Calcd for $C_{13}H_8NOSCl$: C, 59.66; H, 3.08; N, 5.35. Found: C, 59.58; H, 3.27; N, 5.40.

*7-Cyanodibenzo[b,f][1,4]thiazepin-11(10H)-one (**2e**).* Mp 292—293 °C; IR (KBr) 1660 (s, aromatic amide C=O), 2225 (m, C≡N), and 2900—3300 cm^{-1} (m, complex *N*-H); ^{1}H NMR (Me_2SO-d_6) δ=7.0—8.0 (7H, m, aromatic H) and 10.70 (1H, s, *N*-H); UV (methanol) 206 (3.6×10⁴), 220 (s), 258 (2.6×10⁴), and 280 nm (s); MS, *m/z* 252 (M^+). Anal. Calcd for $C_{14}H_8N_2OS$: C, 66.65; H, 3.20; N, 11.10. Found: C, 66.48; H, 3.05; N, 11.12.

*Preparation of (E)-2-Styryl-1,2-benzisothiazol-3(2H)-one (**9**).* To a mixture of 60 cm^3 of 25% aqueous ammonia and 60 cm^3 of THF was added 12.9 g of 2,2′-dithiobis[benzoyl chloride] in 150 cm^3 of THF at −15 °C over period of

30 min and the solution was stirred for additional 2 h. The solution was concentrated under reduced pressure. The remaining solid was washed with water, cold acetone, and then ether and dried in a desiccator to give 11.4 g of 2,2′-dithiobis[benzamide]: mp 239 °C (dec.); IR (KBr) 3400, 3200, 1640, and 1400 cm^{-1}. To a suspension of 3.8 g of the above compound in 15 cm^3 of carbon tetrachloride was added 2.5 g of bromine in 15 cm^3 of carbon tetrachloride over a period of 10 min. The mixture was stirred overnight, the solvent was evaporated under a reduced pressure and 3 g of sodium hydrogencarbonate in 50 cm^3 of water and 10 cm^3 of THF was added to the resulting residue and the mixture was stirred for 1 h. The solution was concentrated under reduced pressure to give 3.5 g of 1,2-benzisothiazol-3(2*H*)-one: mp 160—161 °C; IR (KBr) 3050, 2900, 2680, 1745, 1635, 1440, and 1325 cm^{-1}; ^1H NMR ($CDCl_3$) δ=7.2—8.2 (m); UV (methanol) 203 (ε=1.1×10⁴), 226 (1.6×10⁴), and 316 nm (4.4×10³).

A mixture containing 1.5 g of the above isothiazolone, 1.8 g of phenylacetaldehyde dimethyl acetal, and 10 mg of *p*-toluenesulfonyl chloride was heated at 100 °C for 20 h. The mixture was solidified on cooling to room temperature and the crude solid was purified by chromatography on a silica gel column using benzene as the eluent. The major fraction (2.1 g) obtained was identified as (*E*)-2-styryl-1,2-benzisothiazol-3(2*H*)-one (**9**) on the basis of the following data: mp 145—146 °C; IR (KBr) 1670, 1640, 1450, 1350, 1300, 1265, 1200, 935, and 740 cm^{-1}; ^1H NMR ($CDCl_3$) δ=6.31 (1H, d, J=14.0 Hz), 8.00 (1H, d, J=14.0 Hz) and 7.0—8.2 (9H, m); UV (methanol) 219 (ε=2.3×10⁴), 298 (1.4×10⁴), and 346 nm (1.6×10⁴). Anal. Calcd for $C_{15}H_{11}NOS$: C, 71.12; H, 4.38; N, 5.53. Found: C, 71.45; H, 4.28; N, 5.65.

Photolysis of (E)-2-Styryl-1,2-benzisothiazol-3(2H)-one (9). A solution containing 112 mg (0.44 mmol) of (*E*)-2-styryl-1,2-benzisothiazol-3(2*H*)-one (**9**) in 220 cm^3 of benzene or *t*-butyl alcohol was irradiated using a 450-W Hanovia medium-pressure mercury lamp through a Corex filter sleeve for 30 h. No photoconversion of the starting material was observed by HPLC or TLC. After removing the solvent under reduced pressure to give a solid, the ^1H NMR spectra was identical with that of the starting material **9**.

Photolysis of 2-Aryl-1,2-benzisothiazol-3(2H)-one (1) in the Presence of Oxygen. A solution containing 0.44 mmol of **1** in 220 cm^3 of benzene or methanol with bubbling of oxygen was irradiated through a filter sleeve using a 450-W Hanovia medium-pressure mercury lamp for 2 h. The removal of the solvent under reduced pressure left a light-brown residue which was purified by silica gel chromatography using dichloromethane–hexane as the eluent. Photo-oxidized product **11** was isolated with **2**.

Preparation of 2-Aryl-1,2-benzisothiazol-3(2H)-one 1-Oxide (11). To a solution containing 301 mg (2.25 mmol) of *N*-chlorosuccinimide in 40 cm^3 of dichloromethane was added 2.2 mmol of 2-aryl-1,2-benzisothiazol-3(2*H*)-one in 20 cm^3 of dichloromethane over a period 20 min at 0 °C. The mixture was then stirred for 1 h at room temperature. A solution containing 7 g of potassium hydrogencarbonate in 20 cm^3 of water was added to the reaction mixture and stirred for an additional 1 h. The organic layer was washed with water, dried over anhydrous magnesium sulfate, and concentrated under reduced pressure. The residual solid was purified by chromatography on silica gel using hexane–ethyl acetate as the eluent. 2-Aryl-1,2-benzisothiazol-3(2*H*)-one 1-oxides (**11a—e**) were obtained in 70—80% yield. The physical and spectral data are as follows:

2-(4-Methoxyphenyl)-1,2-benzisothiazol-3(2H)-one 1-Oxide (11a). Mp 147—148 °C; IR (KBr) 1715 (s, C=O), 1515 (s), 1260 (s, C-O-C, as), and 1100 cm^{-1} (s, S=O); ^1H NMR ($CDCl_3$) δ=3.84 (3H, s, OCH_3), 6.9—8.2 (4H, m), 7.02 and 7.41 (2H and 2H, A_2B_2 quartet, J_{AB}=8.9 Hz); ^{13}C NMR ($CDCl_3$) δ=164.7 (C=O), 128.2 and 145.6 (3a- and 7a-C), 125.1, 126.6, 133.2, and 134.4 (4-, 5-, 6-, and 7-C), 160.0 (1′-C), 129.2 (2′-C), 115.0 (3′-C), 126.1 (4′-C), and 55.5 (OCH_3); UV (methanol) 204 (ε=4.3×10⁴), 226 (1.8×10⁴), and 275 nm (5.8×10³); MS *m/z* 273 (M^+). Anal. Calcd for $C_{14}H_{11}NO_3S$: C, 61.53; H, 4.06; N, 5.13. Found: C, 61.06; H, 3.90; N, 5.03.

2-(4-Methylphenyl)-1,2-benzisothiazol-3(2H)-one 1-Oxide (11b). Mp 167.5—168.5 °C: IR (KBr) 1170 (s, C=O), 1315 (s), and 1100 cm^{-1} (s, S=O); ^1H NMR ($CDCl_3$) δ=2.28 (3H, s. CH_3), and 7.0—8.2 (8H, m); ^{13}C NMR ($CDCl_3$) δ=164.4 (C=O), 128.1 and 145.4 (3a- and 7a-C), 125.0, 126.5, 133.2, and 134.3 (4-, 5-, 6-, and 7-C), 131.0 (1′-C), 127.2 (2′-C), 130.2 (3′-C), 138.8 (4′-C), and 21.1 (CH_3); UV (methanol) 206 (ε=4.3×10⁴), 220 (s), 255 (s), and 275 nm (s); MS, *m/z* 257 (M^+). Anal. Calcd for $C_{14}H_{11}NO_2S$: C, 65.35; H, 4.31; N, 5.44. Found: C, 64.80; H, 4.08; N; 5.29.

2-Phenyl-1,2-benzisothiazol-3(2H)-one 1-Oxide (11c). Mp 136—137 °C; IR (KBr) 1685 (s, aromatic amide C=O) and 1100 (s, S=O); ^1H NMR ($CDCl_3$) δ=7.0—8.2 (m, aromatic-H); ^{13}C NMR ($CDCl_3$) δ=164.3 (C=O), 128.2 and 145.4 (3a- and 7a-C), 125.1, 126.6, 133.3, and 134.5 (4-, 5-, 6-, and 7-C), 133.9 (1′-C), 127.2 (2′-C), 129.6 (3′-C), and 128.8 (4′-C); UV (methanol) 204 (ε=4.29×10⁴) and 270 nm (s); MS, *m/z* 243 (M^+). Anal. Calcd for $C_{13}H_9NO_2S$: C, 64.18; H, 3.73; N, 5.76. Found: C, 63.85; H, 3.56; N, 5.85.

2-(4-Chlorophenyl)-1,2-benzisothiazol-3(2H)-one 1-Oxide (11d). Mp 139—140 °C; IR (KBr) 1720 (s, C=O), 1495 (s), 1310 (s), and 1195 cm^{-1} (s, S=O); ^1H NMR (acetone-d_6) 400 MHz, δ=7.595 and 7.616 (2H and 2H, A_2B_2 quartet J_{AB}=9.2 Hz, 2′- and 3′-H), 7.952 (1H, dt, J_{6-5}=J_{6-7}=8 Hz, J_{6-4}=1.2 Hz, 6-H), 8.024 (1H, dt, J_{5-4}=J_{5-6}=8 Hz, J_{5-7}=1.2 Hz, 5-H), 8.066 (1H, dd, J_{7-6}=8 Hz, J_{7-5}=1.2 Hz, 7-H), and 8.171 (1H, dd, J_{4-5}=8 Hz, J_{4-6}=1.2 Hz, 4-H); ^{13}C NMR (acetone-d_6) δ=164.4 (C=O), 128.1, 145.6 (3a- and 7a-C), 125.3, 126.9, 133.5, and 134.7 (4-, 5-, 6-, and 7-C), 132.7 (1′-C), 128.5 (2′-C), 129.9 (3′-C), and 134.7 (4′-C); UV (methanol) 205 (ε=4.4×10⁴), 225 (s), and 260 (s); MS, *m/z* 277 and 279 (M^+). Anal. Calcd for $C_{13}H_8NO_2SCl$: C, 56.22; H, 2.90; N, 5.04. Found: C, 56.14; H, 2.70; N, 5.07.

2-(4-Cyanophenyl)-1,2-benzisothiazol-3(2H)-one 1-Oxide (11e). Mp 146—147 °C; IR (KBr) 2240 (m, C≡N), 1720 (s, C=O), 1300 (s), and 1090 cm^{-1} (s, S=O); ^1H NMR ($CDCl_3$) δ=7.1—8.2 (m, aromatic-H); ^{13}C NMR ($CDCl_3$) δ=163.9 (C=O), 127.8 and 145.0 (3a- and 7a-C), 125.3, 126.9, 133.8, and 135.1 (4-, 5-, 6-, and 7-C), 138.8 (1′-C), 126.4 (2′-C), 133.4 (3′-C), 118.0 (4′-C), and 111.8 (C≡N); UV (methanol) 208 (ε=4.5×10⁴), 230 (s), 250 (s), and 280 nm (s); MS, *m/z* 268 (M^+). Anal. Calcd for $C_{14}H_8N_2O_2S$: C, 62.68; H, 3.01; N, 10.44. Found: C, 62.52; H, 2.97; N, 10.35.

References

1) P. Beak and W. Messer, *Org. Photochem.*, **2**, 117 (1969).
2) A. Lablache-Combier and M. A. Remy, *Bull. Soc. Chim, Fr.*, **35**, 679 (1971).
3) A. Lablache-Combier, "Photochemistry of Heterocyclic Compounds," ed by O. Buchardt, Wiley, New York (1976) p. 123.
4) A. Padwa, "Rearrangement in Ground and Excited State," ed by P. de Mayo, Academic Press, New York, Vol. 3, (1980) p. 501.
5) N. Kamigata, T. Saegusa, S. Fujie, and M. Kobayashi, *Chem. Lett.*, **1979**, 9.
6) N. Kamigata, S. Hashimoto, S. Fujie, and M. Kobayashi, *J. Chem. Soc., Chem. Commun.*, **1983**, 765.
7) J. Rokach and P. Hamel, *J. Chem. Soc., Chem. Commun.*, **1979**, 786.
8) L. J. Darlage, T. H. Kinstle, and C. L. McIntosh, *J. Org. Chem.*, **36**, 1088 (1971).
9) M. S. Kulyk and D. C. Neckers, *Tetrahedron Lett.*, **22**, 529, (1981); *J. Org. Chem.*, **47**, 4914 (1982).
10) S. L. Murov, "Handbook of Photochemistry," Marcel Dekker, Inc., New York (1973).
11) C. S. Foote and J. W. Peters, *J. Am. Chem. Soc.*, **93**, 3795 (1971); J. Goollnik, "Advanced Photochemistry," **6**, 1 (1968).
12) T. Tezuka, H. Miyazaki, and H. Suzuki, *Tetrahedron Lett.*, **1978**, 1959.
13) D. Sinnreich, H. Lind, and H. Batzen, *Tetrahedron Lett.*, **1976**, 3541.
14) A. Reissert and E. Manns, *Ber.*, **61**, 1308 (1928).
15) J. C. Grivas, *J. Org. Chem.*, **40**, 2031 (1975).
16) Y. Uchida and S. Kozuka, *J. Chem. Soc., Chem. Commun.*, **1981**, 510.

 © 1985 The Chemical Society of Japan Bull. Chem. Soc. Jpn., 58, 3137—3157 (1985)

Stereochemical Study on 1,3-Dipolar Cycloaddition Reactions of Heteroaromatic *N*-Ylides with Symmetrically Substituted cis and trans Olefins

Otohiko TSUGE,* Shuji KANEMASA, and Shigeori TAKENAKA
Research Institute of Industrial Science, and Department of Molecular Science and Technology, Interdisciplinary Graduate School of Engineering Sciences, Kyushu University, Kasugakoen, Kasuga 816
(Received July 8, 1985)

Stereochemistry of the cycloadditions of twenty-four heteroaromatic *N*-ylides with several symmetrically substituted cis and trans olefins has been investigated. Cyclic and acyclic cis olefins cycloadd to the anti form of the ylides in a highly *endo*-selective manner giving almost quantitative yields of stereospecific endo 3+2 cycloadducts. *N*-Ylides stabilized with a substituent of carbonyl type react with trans olefins to form mostly two stereoisomeric 3+2 cycloadducts to the anti form of the ylides. In most cases, they undergo the stereospecific interconversion through a retro cycloaddition process, the isomer ratios and the easiness of transformation depending upon the nature and size of substituents on the five-membered ring which has been built up in the cycloaddition step. On the other hand, *N*-ylides stabilized with a substituent of noncarbonyl type react with trans olefins to give stereospecific and stereoselective 3+2 cycloadducts as single isomers which are assigned as the cycloadducts to the syn form of the ylides.

1,3-Dipolar cycloaddition reaction is a process by which heterocyclic five-membered ring systems can be prepared. As exemplified below by the reaction between an azomethine ylide 1,3-dipole and an olefinic dipolarophile, this reaction involves several stereochemical and regiochemical aspects: the regioselectivity (the orientation between both an unsymmetrical 1,3-dipole and an olefin), the stereospecificity of a 1,3-dipole and an olefin (whether the stereochemistry of a 1,3-dipole and an olefin can be faithfully transmitted to the cycloadduct or not), and the stereoselectivity (the endo or exo approach between a 1,3-dipole and an olefin). Sixteen stereoisomers are possible for the cycloadduct of this reaction. Therefore, stereochemical and regiochemical control of this reaction is necessary for the wide applications of 1,3-dipolar cycloaddition reactions to organic synthesis as a useful process, especially the application to natural product synthesis.

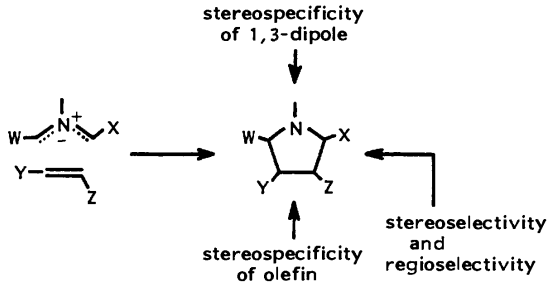

Among the above stereo- and regiochemical aspects, it has been well documented that 1,3-dipolar cycloadditions usually take place in a highly regioselective manner with the preservation of stereochemistry of olefins.[1-7] Some stereospecific cycloadditions have been also demonstrated by the use of highly reactive dipolarophiles and anti and syn, or trans and cis, azomethine ylides which can be selectively accessible by the thermal conrotatory ring opening of cis and trans aziridines, respectively.[8-15] In most cases, the selectivity between the endo and exo approaches is awfully poor.[8-12] Only when the azomethine ylide is substituted with an acyl group at the terminal carbon, stereoselective cycloadducts have been obtained.[13,14] However, the kind of approach (endo or exo) and the origin of stereoselectivity have not been solved since two geometrical isomers are possible for each isomer of the ylide and because it was hardly able to specify the species that was actually concerned in the cycloaddition.

Heteroaromatic *N*-ylides as reactive azomethine ylide 1,3-dipoles, readily available from nitrogen-containing aromatic heterocycles by the sequence of alkylation at the nitrogen and deprotonation, have been long applied to the cycloadditions with acetylenic dipolarophiles yielding fused heterocycles with a nitrogen at the point of fusion.[16-19] It is only quite recent that several reports on the stereochemical study of 1,3-dipolar cycloadditions of heteroaromatic *N*-ylides have started to appear, most of them being not inclusive but fragmentary.[20-28]

As shown below, the pyridinium methylide with a ylide-stabilizing substituent, as a representative of heteroaromatic *N*-ylides, contains both anti and syn azomethine ylide 1,3-dipolar structures. Unlike the open-chained systems derived from aziridines, there is no isomeric structure possible for both the anti and syn ylide. Accordingly, the simple structural analysis of cycloadducts formed in the reaction with an olefinic dipolarophile will give us answers to the following questions: 1) Which is more reactive, anti or syn ylide? 2) How is this cycloaddition stereospecific with respect to the ylide? 3) Is this reaction *endo*-selective or *exo*-selective?

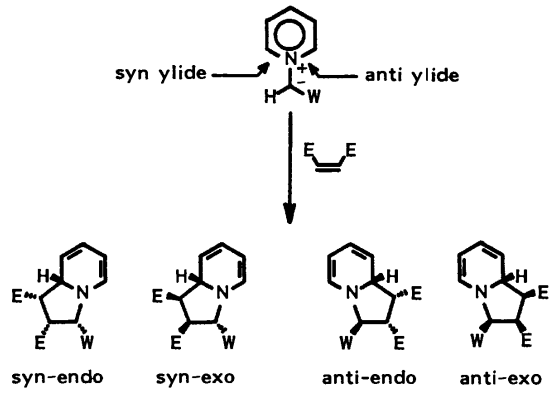

In the present paper, the 1,3-dipolar cycloaddition reactions of a variety of heteroaromatic *N*-ylides with symmetrically substituted cis and trans olefinic dipolarophiles were investigated, and it was attempted to figure out the stereochemical feature of 1,3-dipolar cycloaddition of heteroaromatic *N*-ylides on the basis of structural analysis of the cycloadducts.

Results and Discussion

In the present research were employed twenty-four heteroaromatic *N*-ylides involving six different heterocyclic ring systems (Scheme 1): Pyridinium methylides **1a—g** with several ylide-stabilizing substituents, pyridinium phenacylides **1h—n** substituted on the pyridine nucleus, isoquinolinium methylides **2a—d** also substituted at the ylide carbon, isoquinolinium 1-benzoylethylide **3**, quinolinium phenacylide **4**, pyridazinium phenacylide **5**, thiazolium methylides **6a** and **6b**, and benzothiazolium phenacylide **7**.

As these heteroaromatic *N*-ylides are all labile, they were generated *in situ* from the corresponding quaternary salts and triethylamine, and used without isolation for the cycloadditions to olefinic dipolarophiles.

Cycloadditions to Cyclic cis Olefins. The suspension of *N*-phenacylpyridinium bromide in dry chloroform containing an equivalent of *N*-methylmaleimide **8a** was treated with triethylamine at 0 °C. In a few minutes at room temperature, the suspension dissolved into a clean orange solution. After the reaction was completed (10 min), triethylamine hydrobromide was removed off by washing the reaction mixture with sufficient water. Dryness and evaporation of the chloroform under vacuum below room temperature gave a quantitative yield of the 1:1 adduct **9** as a single isomer (Scheme 2 and Table 2).

Other pyridinium methylides **1b—f** as well as **1a** readily reacted with several *N*-substituted maleimides **8a—d**, under similar conditions, to afford almost quantitative yields of the corresponding cycloadducts **10—18** as single isomers. Although the reaction of pyridinium *p*-nitrobenzylide **1g** with **8c** in chloroform was so sluggish that only 59% of the cycloadduct **19** was obtained after 24 h at room temperature with the recovery of *N*-(*p*-nitrobenzyl)pyridinium bromide (40%), the same reaction in dimethyl sulfoxide (12 h at room temperature) afforded a quantitative yield of **19** also as a single product.

A ^{1}H-NMR spectroscopic observation of the reaction of *N*-(2-furoylmethyl)pyridinium bromide with **8a** in the presence of triethylamine at 0 °C in deuteriochloroform showed that the cycloaddition was completed in a few minutes and that the only products formed in this solution were the cyclo-

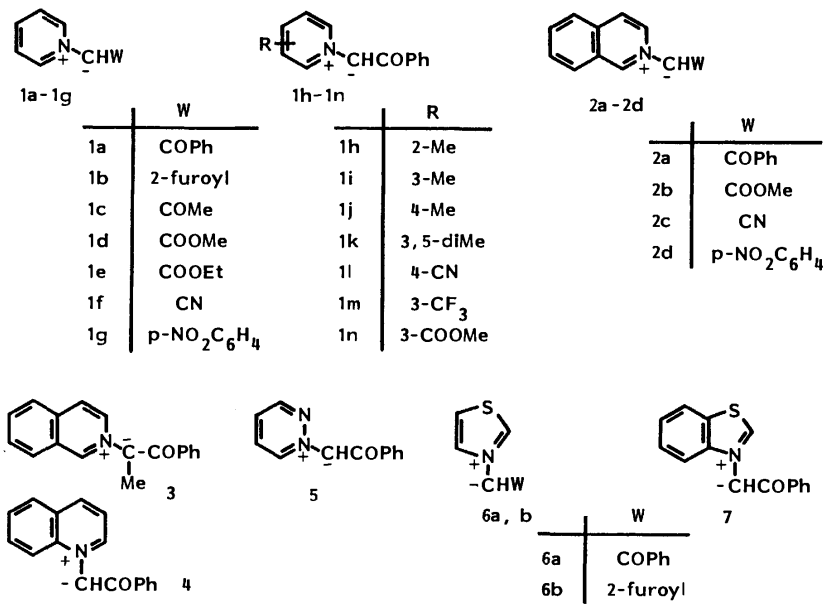

	W
1a	COPh
1b	2-furoyl
1c	COMe
1d	COOMe
1e	COOEt
1f	CN
1g	p-$NO_2C_6H_4$

	R
1h	2-Me
1i	3-Me
1j	4-Me
1k	3,5-diMe
1l	4-CN
1m	3-CF_3
1n	3-COOMe

	W
2a	COPh
2b	COOMe
2c	CN
2d	p-$NO_2C_6H_4$

	W
6a	COPh
6b	2-furoyl

Scheme 1.

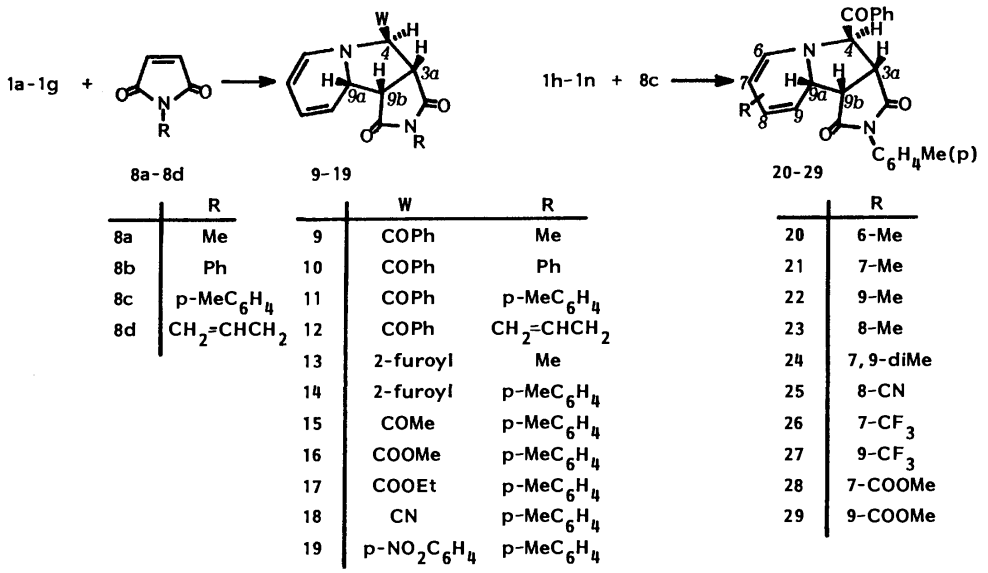

	R
8a	Me
8b	Ph
8c	p-MeC_6H_4
8d	CH_2=$CHCH_2$

	W	R
9	COPh	Me
10	COPh	Ph
11	COPh	p-MeC_6H_4
12	COPh	CH_2=$CHCH_2$
13	2-furoyl	Me
14	2-furoyl	p-MeC_6H_4
15	COMe	p-MeC_6H_4
16	COOMe	p-MeC_6H_4
17	COOEt	p-MeC_6H_4
18	CN	p-MeC_6H_4
19	p-$NO_2C_6H_4$	p-MeC_6H_4

	R
20	6-Me
21	7-Me
22	9-Me
23	8-Me
24	7, 9-diMe
25	8-CN
26	7-CF_3
27	9-CF_3
28	7-COOMe
29	9-COOMe

Scheme 2.

Table 1. Cycloadditions to cyclic cis olefins

Ylide	Olefin	Reaction conditions[a]			Product	Mp θ_m/°C	Yield/%[b]	
		Solvent[c]	Temp	Time/min				
1a	**8a**	CF	rt	10	**9**	150—153 (d)	100	
1a	**8b**	CF	rt	10	**10**	72—73	100	
1a	**8c**	DM	rt	10	**11**	59—62	100	
1a	**8d**	CF	rt	2 h	**12**	oil	100	
1b	**8a**	DM	rt	10	**13**	127—130 (d)	100	
1b	**8c**	CF	rt	10	**14**	145—146	100	
1c	**8c**	CF	rt	1 h	**15**	100—102	93	
1d	**8c**	CF	rt	10	**16**	133—136	100	
1e	**8c**	CF	rt	10	**17**	94—97	100	
1f	**8c**	CF	rt	20	**18**	oil	87	
1g	**8c**	DMSO	rt	12 h	**19**	146—147	100	
1h	**8c**	DM	rt	10	**20**	110—113	100	
1i	**8c**	DM	rt	10	**21** **22**	d) oil	100	(**21**:**22**=3:7)
1j	**8c**	DM	rt	10	**23**	70—75	98	
1k	**8c**	DM	rt	10	**24**	90—92 (d)	100	
1l	**8c**	DM	rt	10	**25**	124—127 (d)	100	
1m	**8c**	DM	rt	10	**26** **27**	80—85[e]	100	(**26**:**27**=1:2)
1n	**8c**	DM	rt	10	**28** **29**	92—96[e]	100	(**28**:**29**=5:3)
3	**8c**	CF	rt	10	**30**	176—178 (d)	100	
4	**8c**	CF	rt	10	**31**	218—220 (d)	100	
6a	**8c**	DM	rt	10	**32**	87—90	97	
6b	**8a**	DMSO	rt	10	**33**	178—179	100	
7	**8e**	CF	rt	3 h	**34**	195—196	97	
7	**35**	CF	rt	3 h	**36**	173—174	97	

a) All the ylides were generated *in situ* from the corresponding precursors and triethyamine. b) Isolated yields. The isomer ratios were determined by a ^{1}H-NMR spectroscopy. c) CF: chloroform; DM: dichloromethane; DMSO: dimethyl sulfoxide. d) Not separated. e) The melting points for the mixtures.

adduct **13** and triethylamine hydrobromide, no other product being formed. This indicates that **13** is the cycloadduct from a kinetically controlled reaction. The cycloadduct **13** was found too labile to be purified by crystallization. In deuteriochloroform **13** gradually decomposed even at room temperature and in 24 h at the same temperature it completely changed into a complex mixture of the secondary products. In deuteriobenzene the decomposition was suppressed, but when warmed at 50—60 °C the complete decomposition of **13** was observed in a few hours.

The other cycloadducts **9**—**19** showed comparable instability, their purification providing authentic samples for elemental analyses being unsuccessful. However, their structures were confirmed on the basis of the spectral data as well as the molecular weight measurement.

The ^{1}H-NMR spectra were most informative to determine the stereostructures of cycloadducts **9**—**19** (Table 2). Very small coupling constants between 4-H and 3a-H (0—0.8 Hz) confirm a trans relationship of these hydrogens. As the only possible manner of ring fusion at the 3a- and 9b-positions is cis geometry, 3a-H and 9b-H are cis each other. A structural inspection using molecular models shows that the coupling constants of 7.7—8.0 Hz are only possible for the cis configuration between 9b-H and 9a-H. Thus, all the cycloadducts **9**—**19** were assigned as the endo 3+2 cycloadducts to the anti ylides of **1a**—**g**. An additional evidence for the assigned structures is the extraordinarily big difference of chemical shifts between 7-H and 9-H. Since the difference of the corresponding hydrogens of 1-phenyl-1,2-dihydropyridine[29] is only 0.27 ppm (3-H: 5.21 ppm and 5-H: 4.94 ppm), this big differences which are more than 1.3 ppm must be because of the unusual low field shifts of 9-Hs. In the endo cycloadducts, these hydrogens are so closely located to a carbonyl of fused maleimide ring that they are suffering from its anisotropy showing unusual low chemical shifts.

When a substituent is introduced at the 2- or 3-position of pyridine nucleus of **1**, two unidentical ylide forms are possible. As each of them contains two 1,3-dipolar systems, anti and syn azomethine ylides, in the same molecule, there are four stereoisomers possible to form for the endo cycloadducts to a maleimide.

The reactions of pyridinium phenacylides **1h**—**n** bearing a variety of substituents on the pyridine ring with **8c** under similar conditions gave, in all cases, the endo 3+2 cycloadducts **20**—**29** to the corresponding anti ylides (Scheme 2, Table 1, and 2). When the 2-position of ylide is substituted by a methyl group, the cycloaddition occurred only at the 6-position of **1h** to give **20**, steric hindrance around the reaction sites being the major factor which determined the periselectivity of cycloaddition. In fact, the reaction of 2,6-dimethylpyridinium phenacylide with **8c** gave no cycloadduct under various reaction conditions. On the other hand, in the reactions of 3-substituted pyridinium ylides **1i**, **1m**, and **1n**, regioisomeric mixtures of endo 3+2 cycloadducts to the anti ylides, **21**+**22**, **26**+**27**, and **28**+**29** were obtained. On the basis of these results, it is easily indicated that two ylide forms of the 3-substituted pyridinium phenacylides actually exist and only the anti ylides of them preferentially participate in the cycloaddition to a cyclic dipolarophile. These regioisomers could not be separated each other because of their instability which will be discussed later.

Similar reactions of other heteroaromatic *N*-ylides

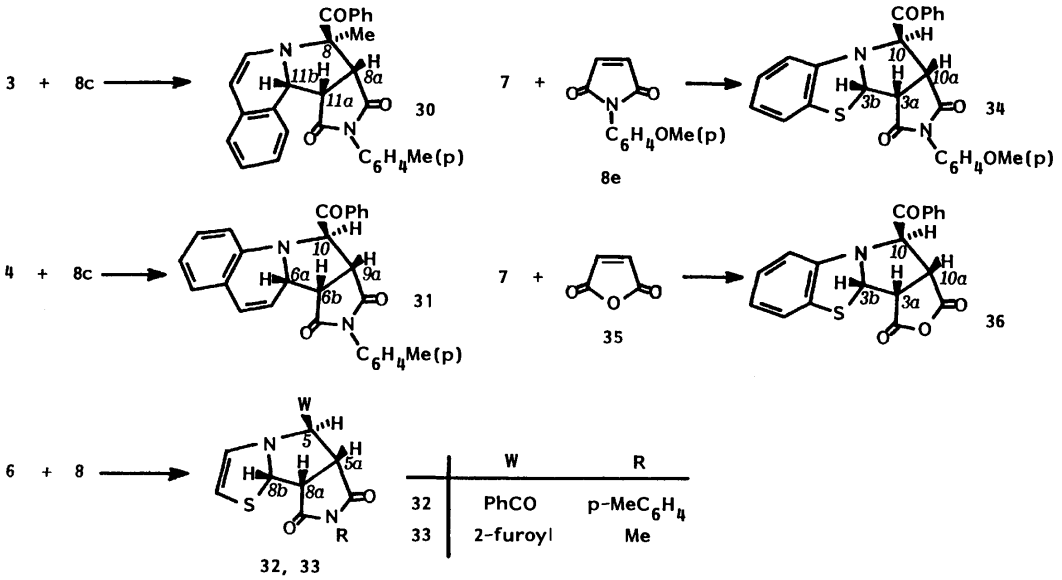

Scheme 3.

Table 2. Spectral data for the cycloadducts to cyclic cis olefins

	IR cm^{-1}	^{1}H-NMR spectra measured in $CDCl_3$ (δ, ppm and Hz)												MS *m/z*	
		4-H	3a-H	9b-H	9a-H	9-H	8-H	7-H	6-H	J_{4-3a}	J_{3a-9b}	J_{9b-9a}			
9	1780, 1697, 1680	5.36 d	3.69 dd	3.35 t	4.76 ddd	5.90 ddt	5.44 ddt	4.52 ddd	6.40 dt	0.6	7.7	7.7	2.93 (*N*-Me) s	308 (M^+)	a)
					5.8	10.0	5.8	8.0							
10	1776, 1720, 1705	5.48 d	3.96 dd	3.51 t	4.85 ddd	5.99 ddt	5.52 ddt	4.56 ddd	6.14 dt	0.8	8.0	8.0		370 (M^+)	
					5.9	9.9	4.3	7.4							
11	1780, 1710, 1690	5.48 d	3.93 dd	3.48 t	4.84 ddd	5.99 ddt	5.53 ddt	4.56 ddd	6.14 dd	0.6	8.0	8.0	2.34 (*p*-Me) s	384 (M^+)	
					5.9	9.8	4.2	7.8							
12	1775, 1710, 1690, 1600	5.37 d	3.64 dd	3.33 t	4.69 ddd	5.84 ddt	5.40 ddt	4.57 ddd	6.04 dt	0.7	7.8	7.8	4.01, 5.17, 5.61 (*N*-allyl) m m m	334 (M^+)	
					5.5	9.8	3.6	7.8							
13	1760, 1690, 1660	5.15 s	3.64 d	3.40 t	4.70 ddd	5.91 ddt	5.44 ddt	4.54 ddd	6.09 dt	0	7.9	7.9	2.92 (*N*-Me), 6.58, 7.38, 7.64 s dd dd dd (furoyl-H)	298 (M^+)	
					5.8	10.0	3.9	7.8							
14	1770, 1705, 1670	5.29 d	3.82 dd	3.53 t	4.82 ddd	5.98 ddt	5.51 ddt	4.62 ddd	6.16 dd	0.5	7.9	7.9	2.37 (*p*-Me), 6.58, 7.38, 7.64 s dd dd dd (furoyl-H)	374 (M^+)	a)
					5.9	10.0	4.0	7.5							
15	1780, 1720, 1710	4.51 s	3.91 d	3.33 t	4.79 ddd	5.8— 6.1m	5.48 ddt	4.31 ddd	5.8— 6.1m	0	7.9	7.9	2.28 (COMe), 2.32 (*p*-Me), s s		
					5.7	10.0	4.2	8.0							
16	1780, 1740, 1710	4.59 s	3.71 d	3.44 t	4.6— 4.9m	5.8— 6.1m	5.4— 5.6m	4.6— 4.8m	5.8— 6.1m	0	8.0	8.0	2.32 (*p*-Me), 3.74 (COOMe) s s	338 (M^+)	
					—	—	—	—							
17	1775, 1730, 1705	4.57 s	3.73 d	3.45 t	4.6— 4.9m	5.8— 6.2m	5.4— 5.6m	4.6— 4.9m	5.8— 6.2m	0	8.0	8.0	1.29, 4.18 (COOEt), 2.32 (*p*-Me) t q s	352 (M^+)	
					—	—	—	—							
18	1780, 1720, 1710	4.80 s	3.62 d	3.47 t	4.97 ddd	5.8— 6.2m	5.72 ddt	4.70 ddd	5.8— 6.2m	0	7.8	7.8	2.37 (*p*-Me) s		
					—	—	—	—							
19	1770, 1720, 1705	5.30 d	3.65 dd	3.38 t	4.83 ddd	5.99 ddt	5.60 ddt	4.63 ddd	6.10 dt	0.8	8.0	8.0	2.37 (*p*-Me) s	401 (M^+)	
					6.0	10.0	4.3	8.0							
20	1770, 1710, 1690	5.80 d	3.74 dd	3.41 t	4.83 ddd	5.37 ddd	5.89 ddd	4.71 dt	—	0.7	8.0	8.0	1.81 (6-Me), 2.37 (*p*-Me) s s	398 (M^+)	
					3.2	10.0	5.8	—							
21	1770, 1710[c]	5.42 s	3.91 br.d	3.44 t	4.38 dd	5.5—6.0 m		—	5.8— 6.0m	0	8.0	8.0	1.60 (7-Me), 2.37 (*p*-Me) s s	398[b] (M^+)	
22	1770, 1700	5.50 d	4.00 dd	3.59 t	4.18 d	—	5.77 d	4.88 dd	6.04 d	0.8	8.0	8.0	1.85 (9-Me), 2.37 (*p*-Me) s s	398 (M^+)	
					—	—	5.8	7.5							

Table 2. (Continued)

	IR cm^{-1}	^{1}H-NMR spectra measured in $CDCl_3$ (δ, ppm and Hz)											MS *m/z*	
		4-H	3a-H	9b-H	9a-H	9-H	8-H	7-H	6-H	J_{4-3a}	J_{3a-9b}	J_{9b-9a}		
23	1780, 1710	5.48 d	3.94 dd	3.44 t	4.27 ddd	5.25 m	—	4.76 dd	6.12 br.d	0.8	7.8	7.8	1.72 (8-Me), 2.37 (*p*-Me) s s	398 (M^+)
					4.5	—		—	7.4					
24	1780, 1700	5.47 s	3.98 d	3.55 t	4.07 d	—	5.68 br.s	—	5.80 br.s	0	8.0	8.0	1.60 (7-Me), 1.87 (9-Me), 2.36 (*p*-Me) s s s	412 (M^+)
						—	—	—	—					
25	2200, 1780, 1710	5.48 s	3.80 d	3.45 t	4.77 dd	6.10 dd	—	4.83 dd	6.22 d	0	8.0	8.0	2.37 (*p*-Me) s	409 (M^+)
					4.0	—		—	7.4					
26	1780, 1700, 1130—1180, 810[c]	5.51 s	3.73 dd	3.40 t	4.78 m	5.51 m	6.02 br.d	—	6.65 br.s	0.8	8.0	8.0	2.30 (*p*-Me) s	452[b] (M^+)
					—	10.0	—	—						
27		5.51 s	3.90 dd	3.45 t	4.39 dd	—	6.29 d	4.90 dd	6.49 d	0.8	8.0	8.0	2.30 (*p*-Me) s	
					—	—	7.3		6.5					
28	1780, 1710[c]	5.60 d	3.77 dd	3.65 t	4.87 m	4.90 m	5.40 dd	—	6.38 d	1.0	8.0	8.0	2.32 (*p*-Me), 3.63 (COOMe) s s	
					—	10.0	—	—						
29		5.52 d	3.97 dd	3.52 t	4.8— m	—	6.3— 6.5m	4.8— 5.0m	6.3— 6.5m	1.0	8.0	8.0	2.32 (*p*-Me), 3.72 (COOMe) s s	
					—	—	—	—						
		8-H	8a-H	11a-H	11b-H	5-H	6-H			J_{8-8a}	J_{8a-11a}	$J_{11a-11b}$		
30	1770, 1700, 1670	—	4.44 d	3.43 t	4.64 d	5.44 d	6.48 d			—	8.0	8.0	1.96 (8-Me), 2.18 (*p*-Me) s s	448 (M^+)
						8.0								
		10-H	9b-H	6b-H	6a-H	6-H	5-H			J_{10-9b}	J_{9b-6b}	J_{6b-6a}		
31	1780, 1700, 1680	5.80 d	3.78 dd	3.51 t	5.17 dt	6.43 dd	6.03 dd			1.0	8.0	8.0	2.35 (*p*-Me) s	434 (M^+)
					2.6	10.0								
		5-H	5a-H	8a-H	8b-H	2-H	3-H			J_{5-5a}	J_{5a-8a}	J_{8a-8b}		
32	1780, 1720, 1710	5.72 s	3.84 d	3.57 t	5.37 d	5.67 d	5.24 d			0	9.0	9.0	2.32 (*p*-Me) s	390 (M^+)
						4.5								
33	1770, 1705, 1680	5.48 s	3.63 d	3.51 t	5.34 d	5.89 d	5.19 d			0	8.0	8.0	2.90 (*N*-Me), 6.59, 7.41, 7.61 s dd dd dd (furoyl-H)	304 (M^+) a)
						4.3								
		10-H	10a-H	3a-H	3b-H					J_{10-10a}	J_{10a-3a}	J_{3a-3b}		
34	1780, 1700, 1680	6.05 d	4.03 dd	3.59 t	5.41 d					0.5	7.9	7.9	3.73 (*p*-MeO) s	456 (M^+) a, c)
36	1850, 1780, 1680	6.02 d	4.23 dd	3.73 t	5.33 d					1.0	8.6	8.6		351 (M^+) a, c)

a) ^{13}C-NMR spectrum is available in Experimental Section. b) Measured as a mixture with its stereoisomer. c) Satisfactory elemental analysis is available in Experimental Section.

3, **4**, **6**, and **7** with *N*-substituted maleimides **8** gave each single isomers of the 3+2 cycloadducts **30—34** in quantitative yields (Scheme 3 and Table 1). Their structures were assigned as the endo cycloadducts to the anti ylides on the basis of the spectral data shown in Table 2, especially of the close resemblance of coupling patterns of the methine hydrogens on the newly formed five-membered rings between **9—29** and **30—34**. The configuration at the 8-position of **30** was confirmed by the low field shift of 8-Me (1.96 ppm) owing to an anisotropy from the adjacent maleimide carbonyl, and by the comparison of chemical shifts of 8a-, 11a-, and 11b-H (4.44, 3.43, and 4.64 ppm, respectively) with those of the corresponding methine hydrogens in the endo 3+2 cycloadduct between the anti form of isoquinolinium *p*-nitrophenacylide and *N*-phenylmaleimide (8a-H: 4.11, 10a-H: 3.63, and 10b-H: 4.78 ppm).[30] The low field shift of 6-H of **31** is consistent with the assigned endo structure (6-H: 6.43 and 5-H: 6.03 ppm). A similar 3+2 cycloadduct **36** was obtained in the reaction of **7** with maleic anhydride **35**.

The heteroaromatic ring which has been incorporated from the heteroaromatic *N*-ylides into cycloadducts as a dihydro form tends to recover its aromaticity. This tendency induces the C–C bond cleavage into a betain intermediary and brings about further decomposition with the elimination of heteroaromatic ring.[31,32] Instability of these cycloadducts will be reduced if the remaining unsaturation on the incorporated heterocycles is consumed in another reaction.

With the aim of the formation of Diels-Alder cycloadducts, reactions of the 3+2 cycloadducts **9** and **13** with dimethyl acetylenedicarboxylate **37** were carried out. However, the 1:1 adducts **38** and **39** obtained were not the expected Diels-Alder cycloadducts but the Michael type adducts at the 7-position as shown in Scheme 4. Although **38** was found stable enough to be purified without serious decomposition, **39** was still unstable. So it was dehydrogenated with DDQ into the indolizine derivative **40**.

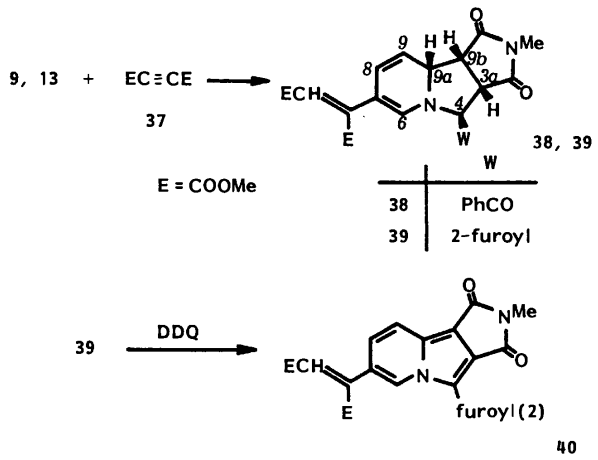

Scheme 4.

As described above, the cycloaddition reactions of heteroaromatic *N*-ylides to cyclic cis olefins proceed in a highly stereoselective manner giving quantitative yields of the endo 3+2 cycloadducts to the anti form of ylides. The reaction of a pyridinium methylide **1** carrying W as a ylide-stabilizing substituent with a maleimide is illustrated in Fig. 1 as an example. There is an attractive interaction working between the π conjugation on the pyridine nucleus and the additional unsaturations (carbonyls) of maleimide, only the endo approach of these reagents being preferred. The exclusive participation of the anti form of **1** may be partly because the endo approach toward the anti ylide **A** leads to a sterically less hindered transition state than that toward the syn ylide **B**. If the anti and syn forms of heteroaromatic *N*-ylides are energetically unidentical, unlike the pyridinium methylides such as **1a—g**, there should be some difference of stability between these two ylidic forms. It will be discussed later that the anti form of ylide is more stabilized than the syn form when the ylide is carrying a ylide-stabilizing substituent of carbonyl type.

Cycloaddition to Acyclic cis Olefins. In the reactions of the pyridinium phenacylide **1a** with such acyclic cis olefins as (*Z*)-1,2-dibenzoylethene **41b** and dimethyl maleate **41c**, the corresponding 3+2 cycloadducts could not be isolated because of their instability, only the pyridine-eliminated products being obtained.[32] However, maleonitrile **41a** produced a fairly stable cycloadduct **42** as a single stereoisomer in a quantitative yield as shown in Scheme 5 and Table 3.

It is clear that the cis geometry of the olefin **41a** has been retained in the cycloadduct **42**, for a similar stereospecific reaction of **1a** with fumaronitrile **55a**, the trans isomer of **41a**, provides two stereoisomeric 3+2 cycloadducts neither of which is identical with **42** as discussed later. The structure of **42** was independently assigned to be the endo 3+2 cycloadduct to the anti form of **1a** on the basis of the spectral data shown in Table 4, especially of a small

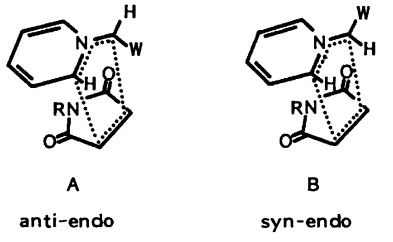

Fig. 1. Two endo approaches between **1** and a maleimide.

coupling constant between 2-H and 3-H (3.2 Hz).

Expecting the formation of stable 3+2 cycloadducts to acyclic cis olefins, several isoquinolinium methylides **2a—c** were allowed to react with **41a—d**, at room temperature in chloroform for less than an hour, to give only the endo cycloadducts **43—48** to the anti forms of **2** (Scheme 5 and Table 3). Similarly the thiazolium **6b** and benzothiazolium methylides **7** afforded the endo cycloadducts **50—52** in the stereoselective and stereospecific reactions with **41**.

The cycloadducts derived from the esteric dipolarophiles **41c** and **41d** are usually sensitive to dehydrogenation at one of the bonds newly formed in a cycloaddition step. In these cases, it is not easy to purify the crude cycloadducts since they undergo ready dehydrogenation during the purification by chromatography over silica gel or when warmed for a while in solution. Thus, the chromatographic treatment of **47** gave *trans*-2,3-dihydro-1,2,3-tris(methoxycarbonyl)pyrrolo[2,1-*a*]isoquinoline **53** in a fair yield. When isoquinolinium *p*-nitrobenzylide **2d** which was found not so highly reactive toward **41c** at room temperature in chloroform was allowed to react with **41c** under reflux in acetonitrile for 1 h, was obtained none of the cycloadduct **49** but the dehydrogenated product **54** as a single isomer.

All the spectral data for the stereoselective 3+2 cycloadducts **42—52** to the acyclic cis olefins **41** are

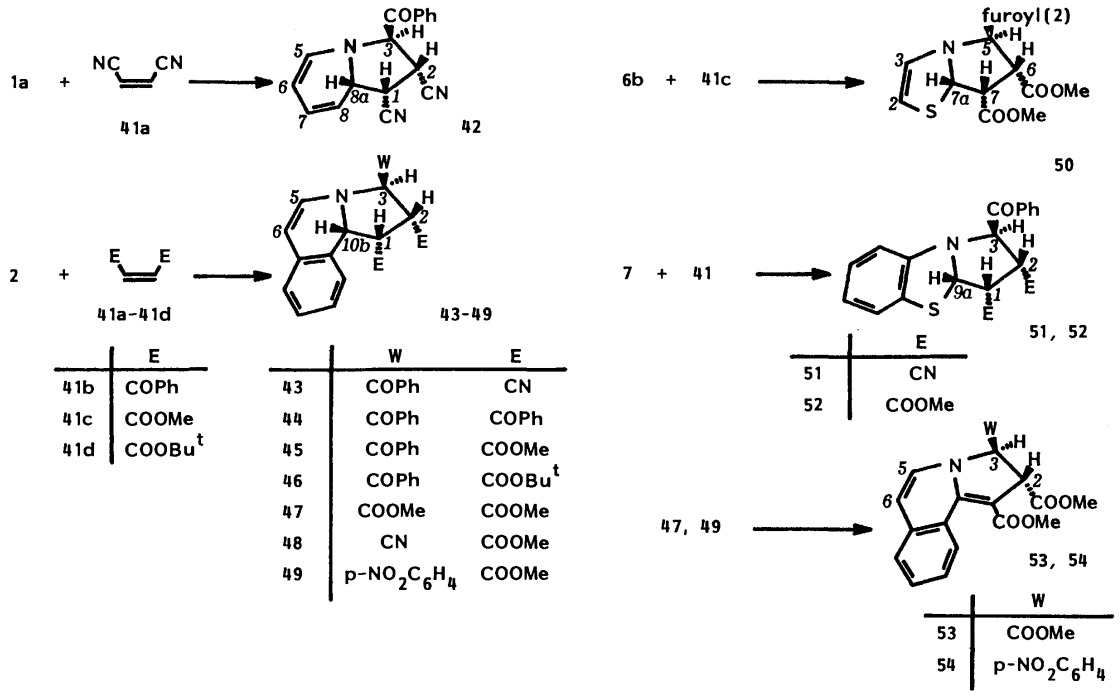

E	
41b	COPh
41c	COOMe
41d	$COOBu^t$

	W	E
43	COPh	CN
44	COPh	COPh
45	COPh	COOMe
46	COPh	$COOBu^t$
47	COOMe	COOMe
48	CN	COOMe
49	$p\text{-}NO_2C_6H_4$	COOMe

	E
51	CN
52	COOMe

	W
53	COOMe
54	$p\text{-}NO_2C_6H_4$

Scheme 5.

Table 3. Cycloadditions to acyclic cis olefins

Ylide	Olefin	Reaction conditions[a]			Product	Mp θ_m/°C	Yield/%[b]
		Solvent[c]	Temp	Time/min			
1a	**41a**	CF	rt	1 h	**42**	118—121 (d)	100
2a	**41a**	CF	rt	10	**43**	181—183 (d)	99
2a	**41b**	CF	rt	10	**44**	130—132 (d)	100
2a	**41c**	CF	rt	10	**45**	146—148	91
2a	**41d**	CF	rt	30	**46**	oil	100
2b	**41c**	CF	rt	10	**47**	147—149	93
2c	**41c**	CF	rt	10	**48**	oil	100
6b	**41c**	CF	rt	10	**50**	oil	92
7	**41a**	CF	rt	10	**51**	181—183 (d)	100
7	**41c**	CF	rt	20	**52**	119—122	100

a) All the ylides were generated *in situ* from the corresponding precursors and triethylamine. b) Isolated yields. c) CF: chloroform.

Table 4. Spectral data for the cycloadducts to acyclic cis olefins

	IR cm^{-1}	^{1}H-NMR spectra measured in $CDCl_3$ (δ, ppm and Hz)[a]												MS *m/z*	
		3-H	2-H	1-H	8a-H	8-H	7-H	6-H	5-H	J_{3-2}	J_{2-1}	J_{1-8a}			
42	2225, 1695	5.44 d	3.99 dd	3.59 dd	4.31 ddd	5.32 ddt	6.10 ddt	4.97 ddd	6.14 dt	3.2	8.8	6.0		275 (M^+)	
					4.3	10.0	6.0	7.2							
		3-H	2-H	1-H	10b-H			6-H	5-H	J_{3-2}	J_{2-1}	J_{1-10b}			
43	2240, 1680, 1625	5.77 d	4.23 dd	3.97 dd	4.68 d			5.48 d	6.50 d	3.2	9.0	6.8		325 (M^+)	b)
								7.5							
		6.08 d	4.28 m		4.63 d			5.42 d	6.69 d						
								7.5							
44	1700, 1690, 1680, 1640	5.42 d	5.16 dd	4.78 m				5.54 d	6.32 d	3.6	8.0	c)		483 (M^+)	b)
								7.5							
45	1730, 1690, 1630	5.70 d	3.98 dd	3.60 dd	5.24 d			5.02 d	6.08 d	6.4	7.4	5.3	3.31, 3.60 (COOMe) s s	391 (M^+)	d)
								8.0							
46	1730, 1670, 1620	5.63 d	3.83 t	3.49 dd	5.32 d			4.93 d	6.03 d	7.0	7.0	5.2	1.12, 1.39 ($COOBu^t$) s s		
								7.3							
47	1760—1720, 1620	4.71 d	3.50—3.85 m		5.34 d			5.04 d	6.12 d	7.0	b)	5.0	3.30, 3.68, 3.79 (COOMe) s s s	345 (M^+)	b, d)
								7.6							
48	1760—1720, 1630	5.00 d	3.50—3.85 m		5.40 d			5.19 d	6.07 d	7.8	b)	4.8	3.33, 3.75 (COOMe) s s	312 (M^+)	d)
								7.8							
		5-H	6-H	7-H	7a-H			2-H	3-H	J_{5-6}	J_{6-7}	J_{7-7a}			
50	1730, 1670, 1600	5.16 s	3.52 d	4.01 t	5.27 d			5.98 d	5.53 d	8.0	7.8	6.0	3.60, 3.71 (COOMe), 6.56, s s dd 7.32, 7.62 (furoyl-H) dd dd	e)	
								4.0							
		3-H	2-H	1-H	9a-H					J_{3-2}	J_{2-1}	J_{1-9a}			
51	2230, 1670	5.68 d	4.04 m	3.95 t	5.36 d					3.5	8.0	5.5		331 (M^+)	
52	1780, 1680	5.67 d	3.94 dd	3.65 t	5.88 d					7.3	7.3	5.5	3.53, 3.59 (COOMe)	397 (M^+)	

a) The only exception is **43** which was measured in acetonitrile-d_3 (the upper column) or in dimethyl-d_6 sulfoxide (the lower). b) Satisfactory elemental analysis is available in Experimental Section. c) No clear coupling was given because of the signal overlapping. d) Satisfactory high mass spectrum is available in Experimental Section. e) No parent ion peak was observed.

collected in Table 4. The assignment of signals in the ^{1}H-NMR spectra was based upon the decoupling of coupled signals by irradiation or deuterium labeling. The use of the monodeuterated derivative of **2a** in the reaction with **41c** succeeded in the introduction of a deuterium at the 3-position of **45**. The cycloadducts **45—48** are carrying two endo ester groups introduced from the esteric dipolarophiles **41c** and **41d**. The ones at the 1-position (3.30—3.33 ppm for COOMe and 1.12 ppm for COOBu^t) are more extensively shielded by the fused benzene ring than the others at the 2-position (3.65—3.75 ppm for COOMe and 1.39 ppm for COOBu^t), the assigned endo structures being confirmed.

As described above, the endo cycloadducts **9—36** to maleimides showed very small vicinal couplings (0—1.0 Hz) from a terminal methine hydrogen of ylidic origin. Although the cycloadducts **42—52** possess the same configuration to **9—36**, their coupling patterns are quite different. The corresponding vicinal couplings are varying in some wide range (3.2 to 8.0 Hz).

Figure 2 illustrates the conformations of pyrrolidine rings included as a part of the endo 3+2 cycloadducts to cyclic and acyclic cis olefins. A molecular model inspection indicates that the cycloadduct **C** to a maleimide is conformationally rigid. The cycloadduct **D** which carries such sterically small substituents as cyano moiety (E=CN) may take a conformation of close resemblance to **C**, since the gausch repulsion among substituents seems not critical. In these cases (cycloadducts **42**, **43**, and **51**), small coupling constants (3.2—3.5 Hz) were observed between 2-H and 3-H. When the substituents in **D** are bulky and therefore the gausch conformation becomes unstable, a rotation around C–C bonds takes place in a way to minimize the steric repulsion leading to **E**. The coupling constant between 2-H and 3-H becomes larger (6.4—8.0 Hz) and that between 1-H and 2-H slightly smaller (7.0—8.0 Hz) in the cycloadducts derived from the olefins **41b—d**.

The exclusive formation of endo cycloadducts to the anti forms of ylides in the reactions with acyclic cis olefins shows that the attractive interaction between the heteroaromatic plane of ylides and the additional unsaturations of olefins has overwhelmed the steric repulsion of all sorts. It is quite surprising that no any exo cycloadduct was formed in the reaction with **41d** which bears two bulky ester groups (COOBu^t).

The thermal stability for some of these cycloadducts will be discussed in the following section.

Cycloaddition to Acyclic trans Olefins. The reaction of **1a** with fumaronitrile **55a** in chloroform

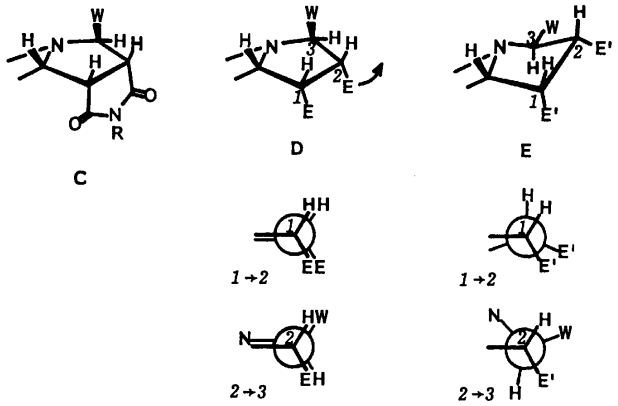

Fig. 2. Stable conformations for the newly formed five-membered rings.

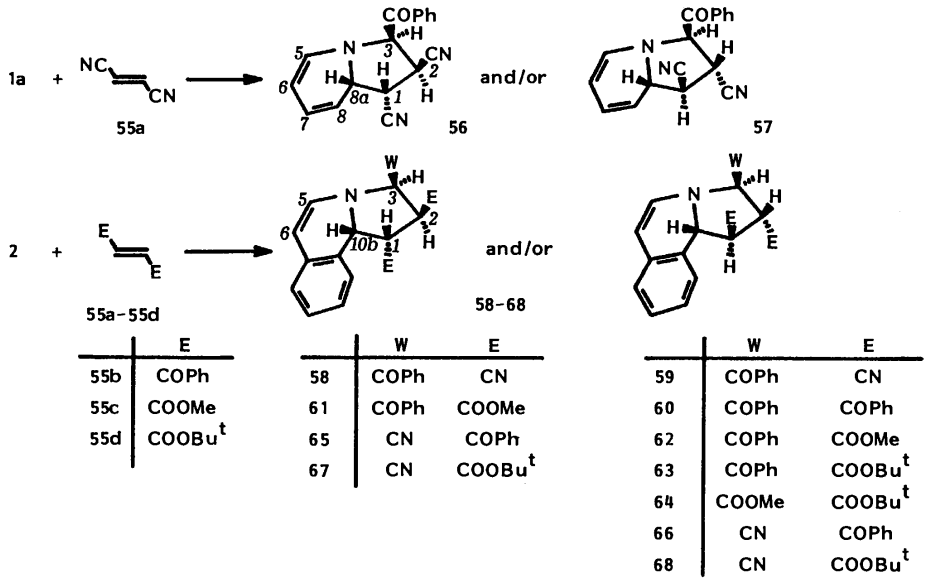

	E
55b	COPh
55c	COOMe
55d	COOBu^t

	W	E
58	COPh	CN
61	COPh	COOMe
65	CN	COPh
67	CN	COOBu^t

	W	E
59	COPh	CN
60	COPh	COPh
62	COPh	COOMe
63	COPh	COOBu^t
64	COOMe	COOBu^t
66	CN	COPh
68	CN	COOBu^t

Scheme 6.

at 0 °C for 5 min furnished a mixture of two stereoisomeric cycloadducts **56** and **57** (7:3), and for 1 h at the same temperature only **57**, both in quantitative yields (Scheme 6 and Table 5). On standing in solution (chloroform) at room temperature, **56** gradually changed into **57** and this clean isomerization was completed in 1 h, indicating that **56** and **57** are kinetically and thermodynamically controlled products, respectively. Although chromatographic separation of the kinetical cycloadduct **56** from the mixture with **57** was unsuccessful, the reaction of **1a** with **55a** in dimethyl sulfoxide under similar conditions precipitated almost pure **56** out of the solution.

Based upon the spectral data listed in Table 6, the structures of **56** and **57** were assigned to be the 1-endo-2-exo and 1-exo-2-endo cycloadducts to the anti form of **1a**, respectively. The isomer **57** shows a small coupling constant (2.8 Hz) between 2-H and 3-H which are in a trans relationship. This cycloaddition is highly stereospecific, so neither **56** nor **57** is identical with the cycloadduct **42** which was obtained as a single isomer from the cis olefin **41a** (Scheme 5). The stereospecific isomerization of **56** into **57** proceeds through a retro cycloaddition pathway as evidenced below. These facts were also helpful for the structural determination of **56** and **57**.

A similar reaction of isoquinolinium phenacylide **2a** with **55a** in dimethyl sulfoxide precipitated out the kinetically controlled cycloadduct **58** in a pure form together with **58**+**59** as a solution, and in chloroform the thermodynamically controlled 1-exo-2-endo isomer **59** was a major product in an equilibrium with **58** (Table 5). This equilibration can be achieved within a few minutes at room temperature in chloroform.

It was found that the isomerization of the 1-endo-2-exo cycloadducts into the 1-exo-2-endo cycloadducts was deeply related with thermal instability of these cycloadducts. They have a tendency of going back to the starting components, the heteroaromatic *N*-ylide and the dipolarophile, when heated or dissolved in solvent. This retro cycloaddition proceeds in a highly stereospecific fashion and is facilitated if both of the ylide and dipolarophile are carrying strongly electron-withdrawing substituents such as cyano and benzoyl moieties. Thus, the isomerization of **56** into **57** has taken place in the following way: The kinetic cycloadduct **56** is cleaved into **1a** and **55a** even at room temperature and then the dissociated species are

Table 5. Cycloadditions to acyclic trans olefins

Ylide	Olefin	Reaction conditions[a]			Product (yield/%)[b]		
		Solvent[c]	Temp	Time/min			
1a	**55a**	CF	0 °C	5	**56** (70)	**57** (30)	
		CF	0 °C	1 h		**57** (100)	
2a	**55a**	DMSO	rt	5	**58** (67)	**59** (33)	
		CF	rt	5	**58** (14)	**59** (86)	
		CF	rt	18 h	**58** (14)	**59** (86)	
2a	**55b**	CF or AN	rt	10		**60** (100)	
2a	**55c**	CF or AN	rt	10	**61** (50)	**62** (50)	
2a	**55d**	CF	rt	2 h		**63** (100)	
2c	**55d**	CF	rt	20		**64** (91)	
2d	**55b**	CF	rt	20	**65** (50)	**66** (50)	
		DMSO	rt	13 h	**65** (33)	**66** (67)	
		AN	rt	6 h	**65** (25)	**66** (75)	
2d	**55d**	CF or DMSO	rt	20	**67** (50)	**68** (13)	another isomer (37)[d]
5	**55c**	CF	rt	10		**69** (100)	
5	**55d**	CF	rt	5		**70** (99)	
6a	**55c**	CF	rt	10	**71** (50)	**72** (50)	
7	**55a**	CF	rt	10	**73** (68)	**74** (32)	
7	**55b**	DM	rt	10	**75** (45)	**76** (45)	
7	**55c**	CF	rt	3 h	**77** (82)		
7	**55d**	DM	rt	20		**78** (97)	
2d	**55b**	AN	rt	12 h			**79** (100)
2d	**55c**	AN	reflux	3			**80** (71)[e]
2d	**55d**	AN	rt	17 h			**81** (97)

a) All the ylides were generated *in situ* from the corresponding precursors and triethyamine. b) Isolated yields as single cycloadducts or mixtures of stereoisomeric cycloadducts. The isomer ratios were determined on the basis of the ^{1}H-NMR spectra of crude products. c) CF: chloroform; DMSO: dimethyl sulfoxide; AN: acetonitrile; DM: dichloromethane. d) Tentatively assigned as a cycloadduct to the syn form of **2d**. e) Containing 17% of the 1,10b-dehydrogenated derivative of **37**.

recombined into the thermodynamic isomer **57**, both processes being highly stereospecific.

When the 1-exo-2-endo cycloadduct **60**, the only product in the reaction of **2a** with (*E*)-1,2-dibenzoylethene **55b** at room temperature for 10 min, was warmed at 50—60 °C in dimethyl sulfoxide in the presence of *N*-methylmaleimide **8a**, the endo 3+2 cycloadduct of **8a** to the anti form of **2a** was formed in an excellent yield (Scheme 7). This result as an evidence for the retro cycloaddition process indicates that even the thermodynamically controlled cycloadducts may be readily dissociated into the starting ylide and olefin. An unusual isomerization of **44**, the cycloadduct of **2a** to (*Z*)-1,2-dibenzoylethene **41b**, occurred leading to **60** when warmed in dimethyl sulfoxide at 50—60 °C for 1 h. This reaction is also stereospecific, but with the complete inversion of stereochemistry of olefin part (from Z to E). As **41b** was found to isomerize into **55b** with comparable easiness under the reaction conditions, it can be concluded that this isomerization has been caused through the similar retro cycloaddition pathway and the additional olefin isomerization.

The cycloadducts carrying at least one esteric substituent, which were obtained in the reactions of **2b** or **55c** and **55d** as shown in Scheme 6 and Table 5, resist their dissociation into the starting ylides and olefins. Neither the incorporation of maleimide nor

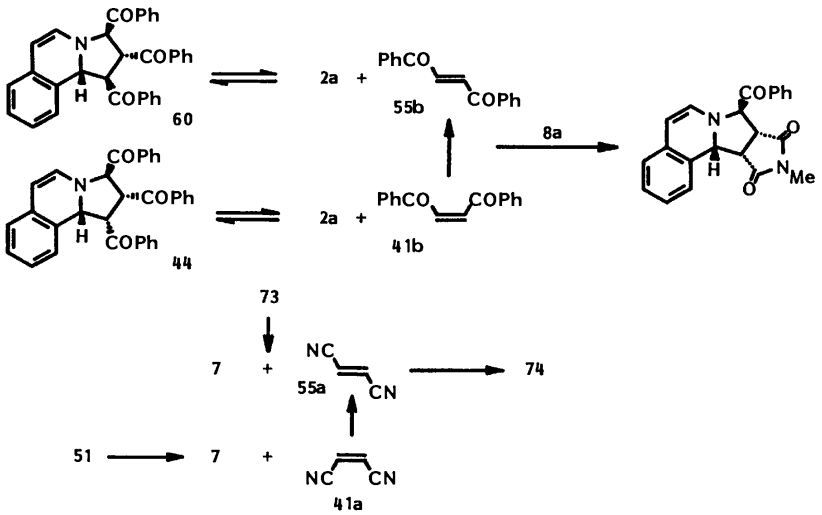

Scheme 7.

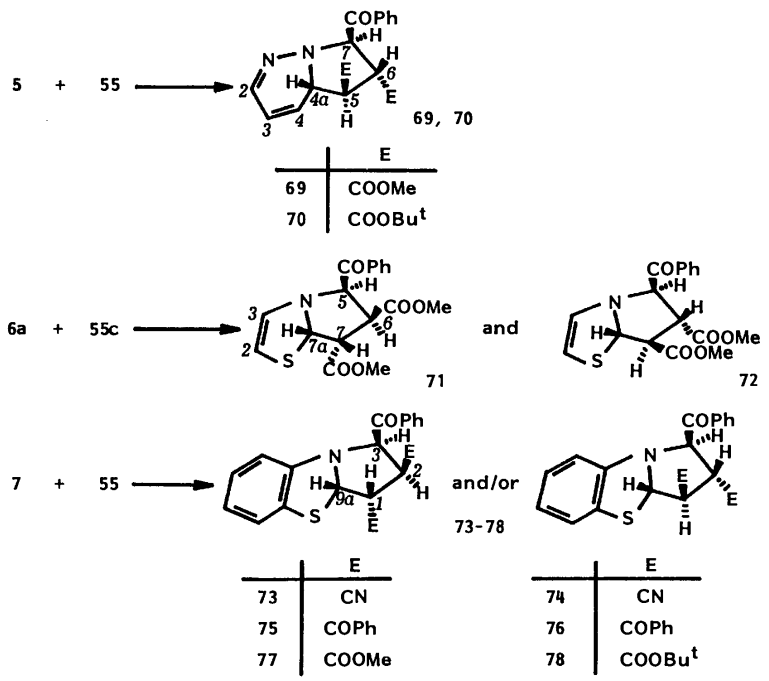

Scheme 8.

the change of isomer ratio was observed on their heating in the presence or absence of a maleimide. It was found, however, that the isomerization was catalyzed by palladium on charcoal. Thus, the mixture between **61** and **62** or among **67**, **68**, and their isomer[33] could isomerize into **62** or **68** in almost quantitative yield, respectively, when heated under reflux in benzene in the presence of palladium on charcoal.

Similar cycloadditions of other heteroaromatic *N*-ylides **5**, **6a**, and **7** with symmetrically substituted olefins **55** are shown in Scheme 8, the results in Table 5, and the spectral data of cycloadducts obtained in Table 6.

The first nine cycloadducts in Table 6 (compounds **55** to **77**) as kinetical products have the same stereochemistry as to the newly formed five-membered rings whose four consecutive methine hydrogens are in a cis-trans-cis relationship. The small trans coupling constants of **58**, **61**, **65**, and **67** (3.5—4.8 Hz) and the upfield shift of COOMe in **61** (3.14 ppm) and COOBu^t in **67** (1.08 ppm) at the 1-endo position are consistent with the proposed structures. On the other hand, the large trans couplings of **56**, **71**, **73**, **75**, and **77** will be because of the increase of dihedral angle by the rotation around the corresponding bonds. In the kinetic cycloadducts to **2**, for example **61**, such rotation is inhibited by the growing steric repulsion between the substituent at the 1-position and the extruding hydrogen at the 10-position.

The other fourteen cycloadducts (compounds **57** to **78**) as thermodynamic products have another stereochemistry on the five-membered rings whose four methine hydrogens are in a trans-trans-trans relationship that is thermodynamically more stable than the above cis-trans-cis succession. All the cycloadducts of this category show a similar coupling pattern. The trans couplings from the ylide hydrogen are generally small (2.8—5.8 ppm) and no strong shielding towards the substituents of olefins from the fused heterocyclic rings has been observed, the proposed structures being again confirmed.

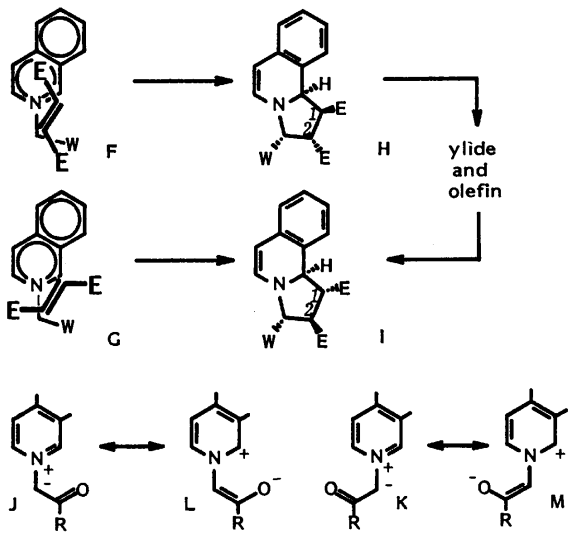

Fig. 3. Approaches of trans olefins to the anti form of heteroaromatic *N*-ylides.

As described above, the attractive interaction between the heteroaromatic ring of ylides and the substituents of olefins have determined the structures of cycloadducts in the 1,3-dipolar cycloadditions of heteroaromatic *N*-ylides to both cyclic and acyclic cis olefins. With trans olefins, the similar interaction also plays an important role as shown in Fig. 3 which illustrates the reaction of an isoquinolinium ylide as an example. One of the electron-withdrawing substituents E of trans olefin positively interacts with the heteroaromatic plane of the anti form of ylide, through the approach **F**, leading to the 1-endo-2-exo cycloadduct **H** as a kinetically controlled product. When both E and W are strongly electron-withdrawing, **H** is readily dissociated into the starting ylide and olefin, which are then recombined giving the thermodynamically more favored cycloadduct **I**, both in a highly stereospecific manner. Such dissociation of cycloadduct is inhibited under the conditions of cycloaddition reaction if it carries at least one esteric substituent. In this case, the formation of **H** and/or **I** is a result from the competition between the 1-endo-2-exo **F** and 1-exo-2-endo approach **G**, and hence from a cycloaddition path of kinetically controlled type. When E is small in size, the attractive interaction of E toward the ring in **F** is predominant, the cycloadduct **H** being the major product. However, when E is bulky, such interaction in **F** is reduced and instead the repulsion between the other E and W is increased. In the other approach **G**, an attractive interaction works between E and the edge of heteroaromatic plane, so that steric repulsion is not critical. This is the reason why the 1-exo-2-endo cycloadduct **I** was the only cycloadduct formed when both E and W are sterically crowded.

It is surprising that, in the approach **F**, the substituent W from the ylide has been sitting in such a direction as it causes some steric repulsion toward E. As shown by the exclusive participation of the anti form of ylide in the cycloadditions to cis olefins, there is no important attractive interaction working between E and W. Accordingly a reasonable explanation is that the anti ylide **J** is better stabilized than the syn ylide **K** so as to get a chance of participating to the cycloadditions. This stabilization may be caused by a proximate interaction of the both poles of 1,5-dipole **L** which arises from an extended conjugation of 1,3-dipole with the carbonyl. It is not confirmed so far, however, whether cyano moiety can act in the same manner or not.

Isoquinolinium *p*-nitrobenzylide **2d** might exist

Table 6. Spectral data for the cycloadducts to acyclic trans olefins

	IR cm^{-1}	^{1}H-NMR spectra measured in $CDCl_3$ (δ, ppm and Hz)[a]												MS *m/z*	
		3-H	2-H	1-H	8a-H	8-H	7-H	6-H	5-H	J_{3-2}	J_{2-1}	J_{1-8a}			
56	2250, 1690, 1640	5.41 d	3.16 dd	3.82 t	4.72 ddd	5.36 ddt	6.18 ddt	5.02 ddd	6.07 dt	6.8	7.8	7.8		275 (M^+)	b)
					4.0	9.5	5.8	7.5							
		3-H	2-H	1-H	10b-H			6-H	5-H	J_{3-2}	J_{2-1}	J_{1-10a}			
58	2240, 1690, 1630	6.00 d	4.25 dd	4.43 dd	5.06 d			5.37 d	6.44 d	7.5	4.8	6.4		325 (M^+)	b)
								7.9							
61	1740, 1730, 1670, 1620[c]	5.56 d	3.60—4.02 m		5.00 d			5.36 d	6.24 d	7.0	—	8.4	3.14, 3.58 (COOMe) s s	391 (M^+)[c]	
								7.4							
65	1680, 1660, 1590[c]	4.75 d	4.31 dd	4.80—4.95 m				5.37 d	—	7.8	3.5	—		404 (M^+)[c]	d)
								7.5							
67	2250, 2240, 1720, 1630[c]	4.31 d	3.35 dd	3.53 dd	4.90 d			5.34 d	6.19 d	7.0	4.0	7.4	1.08, 1.50 (COOBu^t) s s	396 (M^+)[c]	d)
								7.5							
		5-H	6-H	7-H	7a-H			2-H	3-H	J_{5-6}	J_{6-7}	J_{7-7a}			
71		5.37 d	3.67 dd	4.15 dd	5.64 d			5.90 d	5.34 d	7.0	10.2	9.0	3.51, 3.72 (COOMe) s s		
								4.2							
		3-H	2-H	1-H	9a-H					J_{3-2}	J_{2-1}	J_{1-9a}			
73	2240, 1680	5.70 d	3.42 dd	4.17 dd	5.58 d					7.0	9.2	7.5		331 (M^+)	e)
75	1680, 1650[c]	6.33 d	5.20 dd	4.96 dd	5.75 d					8.0	9.5	8.0		489 (M^+)[c]	d)
77	1780, 1680	5.50 d	3.77 dd	4.26 dd	5.89 d					7.4	9.8	7.9	3.42, 3.73 (COOMe) s s	397 (M^+)	e)

TABLE 6. (Continued)

	IR cm^{-1}	^{1}H-NMR spectra measured in $CDCl_3$ (δ, ppm and Hz)[a]												MS *m/z*	
		3-H	2-H	1-H	8a-H	8-H	7-H	6-H	5-H	J_{3-2}	J_{2-1}	J_{1-8a}			
57	2240, 1690 1630	5.37 d	3.98 dd	3.31 dd	3.95 ddd 4.8	5.56 ddt 9.5	6.12 ddt 6.0	5.08 ddd 7.3	6.23 dt	2.8	7.3	9.0		275 (M^+)	
		3-H	2-H	1-H	10b-H					J_{3-2}	J_{2-1}	J_{1-10b}			
59	2240, 1690, 1630	5.42 d	4.26 dd	3.38 dd	4.33 d			5.68 d 7.8	6.30 d	2.8	8.0	9.5		325 (M^+)	
		6.07 d	4.28 dd	3.79 dd	4.33 d			5.63 d 7.8	6.77 d	2.8	8.0	9.5			
60	1670, 1600	5.77 d	5.10 dd	4.92 dd	4.56 d			5.52 d 7.8	6.68 d	3.0	7.8	9.2		483 (M^+)	e)
		5.57 d	5.07 ddd	4.80 dd	4.63 dd			5.52 d 7.8	6.44 d	3.0	7.8	9.2			
62	1740, 1730, 1670, 1620[c]	5.43 d	4.08 dd	3.64 dd	4.67 d			5.46 d 7.6	6.23 d	3.7	8.0	9.5	3.68 (COOMe)	391 (M^+)[c]	
63	1720, 1690, 1620	5.41 d	3.75 dd	3.34 dd	4.67 d			5.44 d 7.4	6.17 d	4.0	8.8	9.5	1.41, 1.43 ($COOBu^t$) s s	475 (M^+)	b)
64	1720, 1670	4.57 d	3.58 dd	3.27 dd	4.76 d			5.37 d 7.7	6.05 d	4.0	8.8	9.5	1.44, 1.46 ($COOBu^t$) s s 3.78 (COOMe) s	429 (M^+)	
66	1680, 1660, 1590[c]	5.09 d	4.83 dd	4.46 dd	4.96 d			5.53 d 7.8	6.12 d	3.0	7.9	9.2		404 (M^+)[c]	d)
68	2240, 2250, 1720, 1630[c]	4.84 d	3.64 dd	3.25 dd	4.77 d			5.52 d 7.8	6.07 d	3.7	8.0	9.2	1.44, 1.49 ($COOBu^t$) s s	396 (M^+)[c]	d)

Table 6. (Continued)

	IR cm^{-1}	^{1}H-NMR spectra measured in $CDCl_3$ (δ, ppm and Hz)[a]										MS *m/z*	
		7-H	6-H	5-H	4a-H	4-H	3-H	2-H	J_{7-6}	J_{6-5}	J_{5-4a}		
69	1740, 1730, 1600	5.83 d	3.69 dd	3.80 dd	4.27 dd 5.0	5.65—6.03 m		6.64—6.80 m	3.2	7.5	9.0	3.59, 3.68 (COOMe) s s	342 (M$^+$) d)
70	2300, 1740, 1730	5.68 d	3.84 dd	3.50 dd	3.92 ddd 5.0	6.08 ddd 10.0	5.82 ddd	6.80 dd 3.5	4.0	8.0	10.4	1.44, 1.48 (COOBu^t) s s	426 (M$^+$) d)
		5-H	6-H	7-H	7a-H			2-H 3-H	J_{5-6}	J_{6-7}	J_{7-7a}		
72		5.50 d	3.93 dd	3.65 dd	5.15 d			5.96 d 5.28 d 4.2	4.3	7.8	7.8	3.73 (COOMe) s	
		3-H	2-H	1-H	9a-H				J_{3-2}	J_{2-1}	J_{1-9a}		
74	2240, 1680	5.73 d	4.16 dd	3.25 dd	4.95 d				3.8	8.4	8.4		331 (M$^+$) e)
76	1680, 1650[c]	5.77 d	5.02 dd	4.57 dd	5.42 d				4.5	8.1	8.0		489 (M$^+$)[c] d)
78	1720, 1700	5.44 d	3.68 dd	3.45 dd	5.56 d				5.8	8.5	7.5	1.28, 1.46 (COOBu^t) s s	481 (M$^+$) e)
		3-H	2-H	1-H	10b-H			6-H 5-H	J_{3-2}	J_{2-1}	J_{1-10a}		
79	1670, 1600, 1520, 1340	5.37 d	4.61 dd	4.80 t	5.10 d			5.49 d 5.22 d 7.4	5.0	8.0	8.0		496 (M$^+$) b)
80	1740	5.06 d	3.38 dd	f)	4.92 d			5.42 d 5.98 d 7.6	6.0	10.0	9.0	3.71, 3.97 (COOMe) s s	
81	1720, 1520, 1340, 1150	5.03 d	3.29 dd	3.52 dd	4.90 d			5.36 d 5.98 d 7.5	6.0	10.0	9.2	1.44, 1.47 (COOBu^t) s s	492 (M$^+$) b)

a) The following compounds were measured in other solvents: **58**, **59** (the upper column), **60** (the upper): in dimethyl-d_6 sulfoxide; **75**, **60** (the lower), **76**: in acetonitrile-d_3. b) Satisfactory high mass spectrum is available in Experimental Section. c) Measured as a mixture with its stereoisomer. d) Satisfactory elemental analysis for the mixture of two stereoisomers is available in Experimental Section. e) Satisfactory elemental analysis is available in Experimental Section. f) Overlapping with other signals.

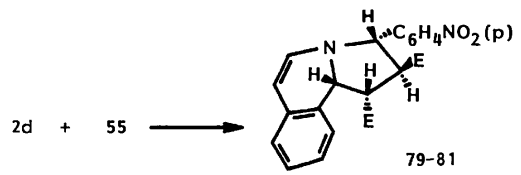

	E
79	COPh
80	COOMe
81	$COOBu^t$

Scheme 9.

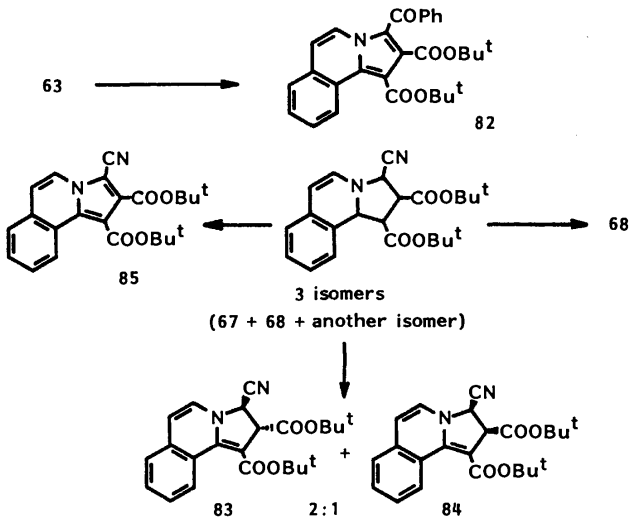

Scheme 10.

both as the anti and syn forms since no stabilization of anti ylide is expected in this case. Therefore, its cycloadditions to trans olefins will lead to the 1-endo-2-exo cycloadducts to the syn form, which are the most feasible products from the analysis of all possible attractive interactions and steric repulsions. As expected, the corresponding cycloadducts **79—81** were obtained as single stereoisomers (Scheme 9) and assigned as the 1-endo-2-exo cycloadducts to the syn form of **2d** on the basis of the spectral data shown in Table 6 and of the reaction mode of **2d** toward unsymmetrically substituted trans olefins.[34]

As shown in Scheme 10, some of the cycloadducts to trans olefinic esters undergo dehydrogenation reactions. The cycloadduct **63** was dehydrogenated into a pyrrolo[2,1-*a*]isoquinoline **82** when heated under reflux in benzene in the presence of 2,3-dichloro-5,6-dicyano-1,4-benzoquinone (DDQ). A mixture of three isomers formed from **2c** and **55d**, which was found to isomerize into the thermodynamically most stable cycloadduct **68** on heating in benzene in the presence of palladium on charcoal, was similarly dehydrogenated into the pyrrolo[2,1-*a*]isoquinoline **85** or the 2:1 mixture of stereoisomeric dihydropyrrolo[2,1-*a*]isoquinolines **83**+**84** when heated in ethanol or chromatographed over silica gel using benzene as an eluent, respectively.

Experimental

General. Melting points were determined on a Yanagimoto micro melting point apparatus and uncorrected. IR spectra were taken with a JASCO IRA-1 or a JASCO A-702 spectrometer. ^{1}H-NMR spectra were recorded on a Hitachi R-40 or a JEOL FX-100 instrument and ^{13}C-NMR spectra on a JEOL FX-100 spectrometer at 25.05 MHz. Chemical shifts are expressed in parts per million downfield from tetramethylsilane. Mass spectra were measured with a JEOL JMS-01SG-2 spectrometer at 70 eV of ionization energy. Elementary analyses were performed on a Hitachi 026 CHN analyzer. Thin-layer chromatography (TLC) was accompolished on 0.2 mm precoated plates of silica gel 60 F-254 (Merck) or of aluminum oxide 60 F-254 type-E (Merck). Visualization was with ultraviolet light (254 and 365 nm) and iodine. Wakogel C200 and C300 (Wako) and Silicagel 60 (Merck) were used for preparative column chromatography. Flash chromatography was carried out on an EYELA EF-10 apparatus using a column (20×180 mm) packed with Silicagel 60 (Merck, size: 0.04—0.063 mm). Solvents were evaporated with a Tokyo Rikakikai rotary evaporator type V.

Materials. The following olefins are commercially available and were used without further purification: *N*-methylmaleimide **8a**, maleic anhydride **35**, dimethyl maleate **41c**, fumalonitrile **55a**, and dimethyl fumarate **55c**. *N*-Substituted maleimides such as *N*-phenyl- **8b** (mp 89—90 °C), *N*-(*p*-methylphenyl)- **8c** (mp 152—153 °C), *N*-(2-propenyl)- **8d** (mp 52—53 °C), and *N*-(*p*-methoxyphenyl)-maleimide **8e** (mp 149—150 °C) were all prepared according to the reported method[35] which involves the aminolysis of **35** with the corresponding primary amines in ether at room temperature and the followed cyclization of the maleamic acids with acetic anhydride at 110—120 °C. *trans*-1,2-Dibenzoylethene **55b** was obtained by the Friedel-Crafts reaction of fumaroyl dichloride with benzene in the presence of aluminum chloride (**55b**: mp 108—110 °C).[36] Di-*t*-butyl fumarate **55d** was synthesized by the reaction of fumaroyl dichloride with 2 equivalents of *t*-butyl alcohol under reflux in ether for 2 h in the presence of *N*,*N*-dimethylaniline (**55d**: bp 113—115 °C/400 Pa; mp 59—60 °C; ^{1}H-NMR ($CDCl_3$) δ=1.50 (18H, s, $COOBu^t$) and 6.63 ppm (2H, s, =CH)). Maleonitrile **41** (bp 105—110 °C/2260 Pa) was prepared from the trans isomer **55a** according to the known method.[37] *cis*-1,2-Dibenzoylethene **41b** (mp 128—129 °C)[38] was given by a phothochemical isomerization from **55b**, and similarly di-*t*-butyl maleate **41d** from **55d** (**41d**: mp 64—65 °C; ^{1}H-NMR ($CDCl_3$) δ=1.50 (18H, s, $COOBu^t$) and 6.03 ppm (2H, s, =CH)).

Preparation of Quaternary Salts as the Precursors of Heteroaromatic N-*Ylides.* A mixture of heteroaromatic compound and slightly excess of alkylating reagent in dry ether was allowed to stir at room temperature for a few hours to a day precipitating the corresponding quaternary salt which was collected on a filter and washed with ether. The filtrate was again stirred at the same temperature

giving another portion of the precipitate of quaternary salt. The precursors of heteroaromatic *N*-ylides thus synthesized are as follows: *N*-phenacylpyridinium bromide:[39,40] mp 204—206 °C. *N*-(2-furoylmethyl)pyridinium bromide: mp 208—209 °C (IR (KBr) 1692 cm^{-1}; ^{1}H-NMR (DMSO-d_6) δ=6.38 (2H, s, CH_2), 6.87, 7.72, 8.20 (each 1H, dd, furoyl-H), 8.30 (2H), 8.72 (1H), and 9.07 ppm (2H, each dd, pyridyl-H); Found: C, 49.14; H, 3.84; N, 5.25%. Calcd for $C_{11}H_{10}O_2NBr$: C, 49.25; H, 3.73; N, 5.22%). *N*-acetonylpyridinium bromide:[39,40,41] hygroscopic solid (no melting point was measured). *N*-(methoxycarbonylmethyl)pyridinium chloride:[42] mp 170—173 °C. *N*-(ethoxycarbonylmethyl)pyridinium bromide:[40,43,44] mp 120—123 °C. *N*-(cyanomethyl)pyridinium bromide: mp 166—167 °C (Found: C, 42.07; H, 3.56; N, 14.26%. Calcd for $C_7H_7N_2Br$: C, 42.21; H, 3.52; N, 14.07%). *N*-(*p*-nitrobenzyl)pyridinium bromide:[44,45] mp 224—225 °C. *N*-phenacyl-2-methylpyridinium bromide:[46] mp 229—231 °C (dec). *N*-phenacyl-3-methylpyridinium bromide:[47] mp 185—187 °C. *N*-phenacyl-4-methylpyridinium bromide:[48] mp 274—276 °C (dec). *N*-phenacyl-3,5-dimethylpyridinium bromide: mp 200—203 °C (Found: C, 58.56; H, 5.33; N, 4.54%. Calcd for $C_{15}H_{16}ONBr$: C, 58.82; H, 5.23; N, 4.58%). *N*-phenacyl-4-cyanopyridinium bromide: mp 224—227 °C (dec) (Found: C, 55.22; H, 3.71; N, 9.42%. Calcd for $C_{14}H_{11}ON_2Br$: C, 55.43; H, 3.63; N, 9.24%). *N*-phenacyl-3-(trifluoromethyl)-pyridinium bromide: mp 197—198 °C (Found: C, 48.39; H, 3.25; N, 4.18%. Calcd for $C_{14}H_{11}ONF_3$: C, 48.55; H, 3.18; N, 4.05%). *N*-phenacyl-3-(methoxycarbonyl)pyridinium bromide:[49] mp 183—185 °C. *N*-phenacylisoquinolinium bromide:[39] mp 209—210 °C. *N*-(methoxycarbonylmethyl)-isoquinolinium bromide:[50] mp 159—160 °C (dec). *N*-(cyanomethyl)isoquinolinium bromide: mp 215—218 °C (dec) (Found: C, 52.64; H, 3.75; N, 11.39%. Calcd for $C_{11}H_9N_2Br$: C, 52.82; H, 3.63; N, 11.29%). *N*-(*p*-nitrobenzyl)isoquinolinium bromide:[39,40,51] mp 207—208 °C. *N*-(1-benzoylethyl)isoquinolinium bromide: mp 183—184 °C (Found: C, 63.30; H, 4.72; N, 4.07%. Calcd for $C_{18}H_{16}ONBr$: C, 63.16; H, 4.68; N, 4.09%). *N*-phenacylquinolinium bromide:[39,40] mp 173—175 °C (dec). *N*-phenacylpyridazinium bromide: mp 227—228 °C (dec) (Found: C, 51.42; H, 4.04; N, 10.04%. Calcd for $C_{12}H_{11}ON_2Br$: C, 51.61; H, 3.94; N, 10.04%). *N*-phenacylthiazolium bromide: mp 215—216 °C (Found: C, 46.39; H, 3.67; N, 5.20%. Calcd for $C_{11}H_{14}ONSBr$: C, 46.48; H, 3.52; N, 4.93%). *N*-(2-furoylmethyl)thiazolium bromide: mp 204—205 °C (IR (KBr) 1690 cm^{-1}; ^{1}H-NMR (DMSO-d_6) δ=6.37 (2H, s, CH_2), 6.88, 7.72, 8.20 (each 1H, dd, furyl-H), 8.44, 8.61, and 10.34 ppm (each 1H, dd, thiazolium-H); ^{13}C-NMR (DMSO-d_6) δ=59.36, 113.13, 120.41, 126.40, 138.14, 148.95, 161.68, 178.77, and 203.61 ppm; MS (rel intensity) *m/z* 190 (23), 95 (base peak), and 81 (8); Found: C, 39.43; H, 3.17; N, 5.04%. Calcd for $C_9H_8O_2NBr$: C, 39.43; H, 2.94; N, 5.11%). *N*-phenacylbenzothiazolium bromide:[53] mp 249—250 °C (dec).

General Procedure for the Cycloadditions to Cyclic cis Olefins. To the suspension of a quaternary salt was added an equivalent of cis olefin and then slowly a slight excess (1.1—1.2 equivalent) of triethylamine at 0 °C or room temperature. The resulting mixture was stirred at room temperature until all the salt dissolved into a clear solution. The solvent and time for each reaction are listed in Table 1. After the completion of reaction, the solution was poured into ice water and extracted with dichloromethane or chloroform. The extract was dried over $MgSO_4$ and evaporated under vacuum at or below room temperature. Mostly the residue solidified on the trituration with ether or petr. ether or their mixture. If the product is an oily material, the residue was subjected to an opperation for the complete elimination of reaction and extraction solvents under high vacuum at or below room temperature for at least a few hours. The yield as well as the melting point of each cycloadduct is given in Table 1. In most cases the purification of cycloadduct was unsuccessful affording no analytical samples of authentic purity because of their lability. Therefore the unpurified products were subjected to the spectral measurement whose results are listed in Table 2. Other data for the cycloadducts are given as follows: **9**: ^{13}C-NMR ($CDCl_3$) δ=25.41 (q, *N*-Me), 45.47, 51.30 (each d, 3a- and 9b-C), 59.24 (d, 9a-C), 70.59 (d, 4-C), 98.24 (d, 7-C), 114.13 (d, 9-C), 124.01, 128.95, 129.13, 129.30, 134.18 (each d), 134.07 (s), 176.07, 178.19 (each s, CON), and 194.19 ppm (COPh). **14**: ^{13}C-NMR ($CDCl_3$) δ=21.25 (*p*-Me), 44.56, 52.49 (3a- and 9b-C), 59.53 (9a-C), 71.86 (4-C), 97.69 (7-C), 112.78, 114.42, 119.71, 123.70, 125.99, 129.28, 129.81, 134.39, 147.54, 174.72 (CON), 176.89 (CON), and 177.71 ppm (furyl-CO). **26+27**: F-NMR ($CDCl_3$) δ=31.28 (7-CF_3) and 34.39 ppm (9-CF_3) with the ratio of 1:2. **33**: ^{13}C-NMR ($CDCl_3$) δ=24.78 (*N*-Me), 46.91, 51.25 (5a- and 8a-C), 67.52 (5-C), 70.98 (8b-C), 97.16, 112.72, 121.06, 132.92, 148.83, 149.42, 174.37 (CON), 176.80 (CON), and 183.06 ppm (furyl-CO). **34**: ^{13}C-NMR ($CDCl_3$) δ=47.60, 50.59 (each d, 3a- and 10a-C), 55.27 (q, OMe), 68.43 (d, 3b-C), 71.89 (d, 10-C), 173.30, 176.48 (each s, CON), and 194.02 ppm (s, COPh); Found: C, 68.54; H, 4.39; N, 6.15%. Calcd for $C_{26}H_{20}O_4N_2S$: C, 68.41; H, 4.42; N, 6.14%. **36**: ^{13}C-NMR ($CDCl_3$) δ=47.88, 51.09 (each d, 3a- and 10a-C), 69.32 (d, 3b-C), 71.93 (d, 10-C), 167.64, 172.08 (each d, CON), and 193.22 ppm (s, COPh); Found: C, 65.02; H, 3.68; N, 3.96%. Calcd for $C_{19}H_{13}O_4NS$: C, 64.96; H, 3.73; N, 3.99%.

Reaction of 9 with 37 Leading to 38. A mixture of each equivalents of the cycloadduct **9** and dimethyl acetylenedicarboxylate **37** in dichloromethane was refluxed for 10 min and the solvent was removed under vacuum. The residue was chromatographed over silica gel using hexane/ethyl acetate (3:1) to give 67% of **38**: pale yellow prisms; mp 200 °C; IR (KBr) 1780, 1720—1700, 1620, 1600, and 1580 cm^{-1}; ^{1}H-NMR (CD_3CN) δ=2.95, 3.47, 3.68 (each 3H, s, *N*-Me and COOMe), 3.54 (1H, dd, J_{9b-9a}=9.8 and J_{9b-3a}=7.4 Hz, 9b-H), 3.63 (1H, dd, J_{3a-9b}=7.4 and J_{3a-4}=0.5 Hz, 3a-H), 5.63 (1H, dd, J_{9a-9b}=9.8 and J_{9a-9}=8.0 Hz, 9a-H), 5.73 (1H, d, J_{4-3a}=0.5 Hz, 4-H), 5.79 (1H, ddd, J_{9-8}=9.8, J_{9-9a}=8.0, and J_{9-6}=1.0 Hz, 9-H), 6.57 (1H, dd, J_{8-9}=9.8 and J_{8-6}=3.4 Hz, 8-H), 6.84 (1H, dd, J_{6-8}=3.4 and J_{6-9}=1.0 Hz, 6-H), 7.36 (1H, br. s, HC=), 7.40—7.80, and 8.05—8.25 ppm (5H, m, COPh); ^{13}C-NMR ($CDCl_3$) δ=25.25 (q, *N*-Me), 51.31, 52.19 (each q, COO<u>Me</u>), 47.79 (d, 2×C, 3a- and 9b-C), 57.59 (d, 9a-C), 67.75 (d, 4-C), 102.04 (s, 7-C), 129.05 (d), 130.57 (d), 132.62 (d), 132.74 (s), 134.33 (d), 134.92 (d), 135.39 (d), 144.48 (d, CH=), 167.85 (s, 2×C, <u>C</u>OOMe), 174.60, 176.07 (each s, CON), and 194.92 ppm (s, <u>C</u>OPh); MS (rel intensity) *m/z* 450 (M^+, 22), 105 (base peak), and 77 (79).

Found: C, 63.85; H, 5.01; N, 6.34%. Calcd for $C_{24}H_{22}O_7N_2$: C, 63.99; H, 4.92; N, 6.22%.

Reaction of ***13*** *with* ***37*** *Leading to* ***39***. The similar procedure described above gave 70% of **39**: yellow solid; mp 117—118 °C; IR (KBr) 1770, 1720, and 1690 cm^{-1}; ^{1}H-NMR ($CDCl_3$) δ=3.07, 3.58, 3.72 (each 3H, s, *N*-Me and COOMe), 3.48 (1H, dd, J_{3a-9b}=8.7 and J_{3a-4}=2.0 Hz, 3a-H), 3.76 (1H, t, J_{9b-9a}=J_{9b-3a}=8.7 Hz, 9b-H), 5.22 (1H, d, J_{4-3a}=2.0 Hz, 4-H), 5.25—5.80 (2H, m, 9- and 9a-H), 6.60 (1H, dd, J_{8-9}=9.4 and J_{8-6}=3.5 Hz, 8-H), 6.63 (1H, dd, J=3.8 and 1.7 Hz, 4-H of furyl), 6.93 (1H, dd, J_{6-8}=3.5 and J_{6-9}=0.8 Hz, 6-H), 7.34 (1H, br. s, CH=), 7.50 (1H, dd, J=3.8 and 0.8 Hz, 5-H of furyl), and 7.72 ppm (1H, dd, J=1.7 and 0.8 Hz, 2-H of furyl); ^{1}H-NMR (CD_3CN) δ=2.96, 3.48, 3.67 (each 3H, s, *N*-Me and COOMe), 3.53 (1H, dd, J_{3a-9b}=8.5 and J_{3a-4}=2.4 Hz, 3a-H), 3.77 (1H, dd, J_{9b-9a}=9.5 and J_{9b-3a}=8.5 Hz, 9b-H), 5.36 (1H, d, J_{4-3a}=2.4 Hz, 4-H), 5.63 (1H, dd, J_{9a-9b}=9.5 and J_{9a-9}=8.5 Hz, 9a-H), 5.80 (1H, ddd, J_{9-8}=10.4, J_{9-9a}=8.5, and J_{9-6}=1.0 Hz, 9-H), 6.58 (1H, J_{8-9}=10.4 and J_{8-6}=3.4 Hz, 8-H), 6.69 (1H, dd, J=4.0 and 1.7 Hz, 4-H of furyl), 6.83 (1H, dd, J_{6-8}=3.4 and J_{6-9}=1.0 Hz, 6-H), 7.33 (1H, br. s, CH=), 7.64 (1H, dd, J=1.7 and 0.8 Hz, 5-H of furyl), and 7.83 ppm (1H, dd, J=4.0 and 0.8 Hz, 3-H of furyl); ^{13}C-NMR ($CDCl_3$) δ=25.19 (q, *N*-Me), 51.31, 52.13 (each q, COOMe), 47.79, 48.08 (each d, 3a- and 9b-C), 57.65 (d, 9a-C), 67.05 (d, 4-C), 102.56 (s, 7-C), 112.96 (d), 120.59 (d), 130.39 (d), 132.45 (s), 135.15 (d), 135.38 (d), 144.07 (d), 149.30 (s), 148.30 (d, CH=), 167.73 (s, 2×C, COOMe), 174.72, 175.83 (each s, CON), and 184.05 ppm (s, furyl-CO).

Purification of **39** in order to get the authentic sample failed due to its instability.

Dehydrogenation of ***39*** *into* ***40***. An equimolar mixture of **39** (347 mg, 0.79 mmol) and 2,3-dichloro-5,6-dicyano-1,4-benzoquinone (DDQ, 179 mg, 0.79 mmol) in 10 ml of dry benzene was heated under reflux for 21 h. The solvent was evaporated *in vacuo* and the residue was chromatographed over silica gel using ethyl acetate/hexane (1:1) giving 211 mg (61%) of **40**: pale yellow needles from ethyl acetate/hexane; mp 204 °C; IR (KBr) 1780, 1730, 1710, 1670, 1640, and 1270 cm^{-1}; ^{1}H-NMR ($CDCl_3$) δ=3.03, 3.72, 3.78 (each 3H, s, *N*-Me and COOMe), 6.54 (1H, dd, J_{7-8}=12.0 and J_{7-5}=3.3 Hz, 7-H), 6.62 (1H, dd, J=3.8 and 2.0 Hz, 4-H of furyl), 6.70 (1H, d, J_{8-7}=12.0 Hz, 8-H), 7.38 (1H, d, J_{5-7}=3.3 Hz, 5-H), 7.39 (1H, dd, J=3.8 and 0.9 Hz, 5-H of furyl), 7.67 (1H, dd, J=2.0 and 0.9 Hz, 3-H of furyl), and 7.98 ppm (1H, s, CH=); ^{13}C-NMR ($CDCl_3$) δ=24.35 (q, *N*-Me), 52.71 (q, 2×C, COOMe), 113.01 (d), 121.16 (d), 121.60 (d), 126.07 (s), 127.07 (s), 127.77 (s), 129.20 (s), 132.30 (s), 135.71 (d), 138.25 (d), 141.07 (d), 148.54 (d), 151.54 (s), 162.36, 163.07, 164.60, 164.78 (each s, CON and COOMe), and 170.48 ppm (s, furyl-CO); MS (rel intensity) *m/z* 436 (M^+, base peak), 320 (75), and 95 (76); Found: C, 60.55; H, 3.81; N, 6.56%. Calcd for $C_{22}H_{16}O_8N_2$: C, 60.55; H, 3.70; N, 6.42%.

General Procedure for the Cycloadditions to Acyclic cis Olefins. To the suspension of a quaternary salt in dry chloroform was added an equivalent of acyclic cis olefin and then slowly a slight excess (1.1—1.2 equivalent) of triethylamine at 0 °C. The cooling bath was removed and the reaction mixture was stirred at room temperature until all the suspension disappeared. After the reaction was complete, the mixture was poured into ice water and extracted with dichloromethane (twice). The combined extract was evaporated *in vacuo* below room temperature. The residue, in most cases, solidified on the trituration with ether, petr. ether, or their mixture. If the product is an oily material, the residue was evacuated below room temperature for a few hours. The yield and melting point of each cycloadduct is given in Table 3. The crude cycloadducts were all submitted for the ^{1}H-NMR spectral measurement from which the isomer formation was judged. Although some of the cycloadducts were successfully purified by crystallization below room temperature (down to −78 °C), the purification of the other failed because of their instability. The IR, ^{1}H-NMR, and mass spectra of each cycloadduct are listed in Table 4. Other data for the cycloadducts are given as follows: **43**: yellow needles from $CHCl_3$; Found: C, 77.28; H, 4.62; N, 12.85%. Calcd for $C_{21}H_{15}ON_3$: 77.52; H, 4.65; N, 12.92%. **44**: yellow grains from ether; Found: C, 81.90; H, 5.19; N, 3.15%. Calcd for $C_{33}H_{25}O_3N$: C, 81.96; H, 5.21; N, 2.90%. **45**: yellow prisms from ether; Found: *m/z* 391.1412. Calcd for $C_{23}H_{21}O_5N$: M, 391.1418. **47**: yellow needles from ether-petr. ether; Found: C, 62.33; H, 5.55; N, 4.09%. Calcd for $C_{18}H_{19}O_6N$: C, 62.60; H, 5.55; N, 4.06%; Found: *m/z* 345.1220. Calcd for $C_{18}H_{19}O_6N$: C, 345.1211. **48**: Found: *m/z* 312.1108. Calcd for $C_{17}H_{16}O_4N_2$: M, 312.1108. **51**: colorless plates from ethanol; Found: C, 68.71; H, 3.81; N, 12.51%. Calcd for $C_{19}H_{13}ON_3S$: C, 68.86; H, 3.95; N, 12.68%. **52**: pale yellow needles from benzene-hexane; Found: C, 63.47; H, 4.82; N, 3.53%. Calcd for $C_{21}H_{19}O_5NS$: C, 63.37; H, 4.79; N, 3.67%.

The crude cycloadduct **47** was dehydrogenated when chromatographed over silica gel using benzene as an eluent to give **53** in 36% yield: **53**: colorless needles from ether; mp 156 °C (lit.[54] mp 156—157 °C).

The reaction between each equivalent amounts of **2d** and **41c** in chloroform at room temperature for 10 h was carried out and the crude product which showed no clean formation of the cycloadduct **49** in its ^{1}H-NMR spectrum was subjected to a chromatography over silica gel using benzene as an eluent. The product **54** obtained in 40% yield was colored viscous oil whose purification by the repeated chromatography failed. **54**: IR (neat) 1760 cm^{-1}; ^{1}H-NMR ($CDCl_3$) δ=3.64, 3.78 (each 3H, s, COOMe), 3.97 (1H, d, J_{3-2}=4.7 Hz, 3-H), 5.38 (1H, d, J_{2-3}=4.7 Hz, 2-H), 6.23 (1H, d, J_{6-5}=6.9 Hz, 6-H), 6.57 (1H, d, J_{5-6}=6.9 Hz, 5-H), 7.20-8.30 (7H, m, ArH), and 9.89 ppm (1H, br. d, J_{10-9}=8.0 Hz, 10-H).

General Procedure for the Cycloadditions to Acyclic trans Olefins. To the suspension of a quaternary salt was added an equivalent of trans olefin and then slowly a slight excess (1.1—1.2 equivalent) of triethylamine at 0 °C. The resulting mixture was stirred at 0 °C or room temperature until all the salt dissapeared. The solvent and time for each reaction are listed in Table 5. After the completion of reaction, the mixture was poured into ice water and extracted with dichloromethane (twice). The extract was dried over $MgSO_4$ and evaporated under vacuum at or below room temperature. The crude product was submitted, after the complete elimination of the reaction and extraction solvents *in vacuo* below room temperature, for the ^{1}H-NMR measurement. The ^{1}H-NMR spectrum was inspected in order to know the isomer formation and

isomer ratio. The yield as well as the isomer ratio of each reaction is given in Table 5 and the IR, ^{1}H-NMR, and mass spectra in Table 6. Sometimes the crude cycloadducts solidified when triturated with ether, petr. ether, or their mixture. They were purified by crystallization below room temperature (down to −78 °C). However, in most cases not only the purification but the separation of isomers was unsuccessful because the cycloadducts were too labile against heating and chromatographic treatment. The unstable cycloadducts or the unseparable mixture of isomeric cycloadducts were assigned only on the basis of the spectral data. Other data and exceptional procedures for the cycloadducts are given as follows:

The reaction between **1a** and **55a**, 1 mmol each, in 10 ml of chloroform or dimethyl sulfoxide at 0 °C for 5 min precipitated almost pure **56**, whereas the same reaction in 50 ml of chloroform for 1 h gave a clean solution of **57**. **56**: pale yellow needles from chloroform; mp 120—121 °C (dec); Found: *m/z* 275.1034. Calcd for $C_{17}H_{13}ON_3$: M, 275.1058. **57**: yelow viscous oil.

The reaction between **2a** and **55a**, 1 mmol each, in 10 ml of dimethyl sulfoxide at room temperature for 5 min precipitated almost pure **58** which was collected on a filter and washed with ether, whereas the same reaction in 50 ml of chloroform gave a clean solution of **59** which was contaminated with a small amount of **58**. **58**: colorless prisms from acetonitrile; mp 179—182 °C (dec); Found: *m/z* 325.1210. Calcd for $C_{21}H_{15}ON_3$: M, 325.1214. **59**: yellow needles from chloroform–ether; mp 127 °C.

Other data are shown as follows: **60**: yellow needles from ether; mp 173 °C (dec); Found: C, 81.96; H, 5.21; N, 2.90%. Calcd for $C_{33}H_{25}O_3N$: C, 81.75; H, 5.15; N, 3.18%. **61+62**: viscous yellow oil. **63**: yellow prisms from ether; mp 84—86 °C (dec); Found: *m/z* 475.2373. Calcd for $C_{29}H_{33}O_5N$: M, 475.2357. **64**: viscous yellow oil. **65+66**: yellow solid from ether; mp 138—142 °C; Found: C, 80.18; H, 4.98; N, 6.92%. Calcd for $C_{27}H_{20}O_2N_2$: C, 79.90; H, 4.98; N, 6.92%. **67+68**+another isomer: yellow solid from ether; mp 67—70 °C; Found: C, 69.39; H, 7.06; N, 6.99%. Calcd for $C_{23}H_{28}O_4N_2$: C, 69.67; H, 7.12; N, 7.07%. **69**: colorless plates from ether; mp 130—132 °C (dec); Found: C, 62.98; H, 5.33; N, 8.29%. Calcd for $C_{18}H_{18}O_5N_2$: 63.15; H, 5.30; N, 8.18%. **70**: yellow viscous oil; Found: C, 67.36; H, 7.02; N, 6.50%. Calcd for $C_{24}H_{30}O_5N_2$: C, 67.58; H, 7.09; N, 6.59%. **71+72**: orange viscous oil. **73**: colorless needles from ethanol–hexane; mp 190—191 °C; Found: C, 69.05; H, 3.90; N, 12.44%. Calcd for $C_{19}H_{13}ON_3S$: C, 68.87; H, 3.96; N, 12.68%. **74**: colorless prisms from ethanol–hexane; mp 133—135 °C (dec); Found: C, 68.82; H, 4.09; N, 12.60%. Calcd for $C_{19}H_{13}ON_3S$: C, 68.87; H, 3.96; N, 12.68%. **75+76**: yellow prisms from ether; mp 64 °C; Found: C, 75.77; H, 5.00; N, 3.15%. Calcd for $C_{31}H_{23}O_3NS$: C, 76.07; H, 4.70; N, 2.86%. **77**: colorless needles from carbon tetrachloride; mp 104—105 °C (dec); Found: C, 63.14; H, 4.74; N, 3.50%. Calcd for $C_{21}H_{19}O_5NS$: C, 63.47; H, 4.82; N, 3.53%. **78**: pale yellow prisms from ether; mp 50 °C; Found: C, 67.66; H, 6.25; N, 3.26%. Calcd for $C_{27}H_{31}O_5NS$: C, 67.36; H, 6.44; N, 2.91%. **79**: pale yellow grains from ether; mp 93 °C; Found: *m/z* 496.1462. Calcd for $C_{32}H_{20}O_4N_2$: M, 496.1421. **80**: yellow solid; mp 80—82 °C. **81**: pale yellow grains from ether; mp 75—77 °C; Found: *m/z* 492.2258. Calcd for $C_{28}H_{32}O_6N_2$: M, 492.2258.

*Isomerization of **44** into **60** and of **41b** into **55b**.* The cycloadduct **44** was dissolved in dimethyl-d_6 sulfoxide in an NMR sample tube. The ^{1}H-NMR spectrum of the solution after 1 h at 50—60 °C showed the quantitative formation of **60**. Under the same conditions, **41b** was found to isomerize into **55b**.

*The Retro Cycloaddition of **60**.* The solution of each equivalent amounts of **60** and **8a** in dimethyl-d_6 sulfoxide was warmed at 50—60 °C for 24 h in an NMR tube. The quantitative formation of the endo cycloadduct of **8a** to the anti form of **2a** and the eliminated olefin **55b** was confirmed in the ^{1}H-NMR spectrum.

*Isomerization of **73** and **51** into **74** and of **41a** into **55a**.* The cycloadduct **73** or **51** was dissolved in acetonitrile-d_3 in an NMR tube. The ^{1}H-NMR spectrum of the solution after 24 h at room temperature showed the clean isomerization into **74**. Under the same conditions **41a** was found to isomerize completely into **55a**.

*Dehydrogenation of **63** Leading to **82**.* A mixture of each equivalent amounts of **63** and DDQ in benzene was heated under reflux for 23 h. The residue obtained by the removal of the benzene *in vacuo* was chromatographed over silica gel using benzene as an eluent giving 31% of **82**: pale yellow prisms from hexane; mp 153—154 °C; IR (KBr) 1720, 1710, and 1630 cm^{-1}; ^{1}H-NMR ($CDCl_3$) δ=1.05, 1.67 (each 9H, s, COOBu^t), 6.98 (1H, d, J=8.0 Hz, 6-H) 7.30—7.93 (8H, m, ArH), and 8.52 ppm (2H, m, 5- and 10-H); MS (rel intensity) *m/z* 471 (M^+, 34) and 359 (base peak).

Found: C, 73.68; H, 6.27; N, 2.99%. Calcd for $C_{29}H_{29}O_5N$: C, 73.86; H, 6.20; N, 2.97%.

*Isomerization of a Mixture of **67**, **68**, and Another Isomer into **68**.* The solution of 1.0 mmol of the mixture among **67**, **68**, and another isomer in 20 ml of dry benzene was heated under reflux in the presence of palladium on charcoal (10 mg) for 24 h. The benzene was evaporated *in vacuo* leaving the residue whose ^{1}H-NMR in $CDCl_3$ was identical with that of **68**.

*Dehydrogenation of a Mixture of **67**, **68**, and Another Isomer into the Dihydropyrrolo[2,1-a]isoquinolines **83+84** or the Pyrrolo[2,1-a]isoquinoline **85**.* The mixture of three isomers was heated under reflux in ethanol for 48 h and the residue after the evaporation of the ethanol *in vacuo* was chromatographed over silica gel using benzene as an eluent giving 40% of **85**: colorless needles from ether; mp 212 °C (dec); IR (KBr) 2220 and 1720 cm^{-1}; ^{1}H-NMR ($CDCl_3$) δ=1.63, 1.66 (each 9H, s, COOBu^t), 7.13 (1H, br. d, J=7.5 Hz, 6-H), 7.44—7.73 (3H, m, ArH), 8.39 (1H, m, 10-H), and 8.88 ppm (1H, d, J=7.5 Hz, 5-H); MS (rel intensity) *m/z* 347 (M^+, base peak).

Found: C, 70.68; H, 6.33; N, 6.87%. Calcd for $C_{23}H_{24}O_4N_2$: C, 70.39; H, 6.16; N, 7.14%.

The above mixture was subjected to a column chromatography over silica gel using benzene affording the eluent containing 2:1 mixture of **83** and **84** in 25% yield. Their separation by repeated chromatography failed. **83+84**: yellow oil; IR (neat) 2210, 1710, and 1680 cm^{-1}; ^{1}H-NMR $CDCl_3$) **83**: δ=1.48, 1.52 (each 9H, s, COOBu^t), 4.20 (1H, d, J_{2-3}=4.0 Hz, 2-H), 5.02 (1H, d, J_{3-2}=4.0 Hz, 3-H), 6.16 (1H, d, J_{6-5}=7.4 Hz, 6-H), and 6.70 ppm (1H, d, J_{5-6}=7.4 Hz, 5-H); **84**: δ=1.48, 1.51 (each 9H, s, COOBu^t), 4.10 (1H, d, J_{2-3}=11.8 Hz, 2-H), 5.13 (1H, d, J_{3-2}=11.8 Hz, 3-H), 6.13 (1H, d, J_{6-5}=7.4 Hz, 6-H), and 6.72 ppm (1H, d, J_{5-6}=7.4

Hz, 5-H).

References

1) R. Huisgen, *Angew. Chem.*, **75**, 604 and 742 (1963).
2) R. A. Firestone, *J. Org. Chem.*, **37**, 2181 (1972).
3) R. Huisgen, *J. Org. Chem.*, **41**, 403 (1976).
4) K. N. Houk, J. Sims, C. R. Watts, and L. J. Luskus, *J. Am. Chem. Soc.*, **95**, 7301 (1973).
5) D. S. C. Black, R. F. Crozier, and V. C. Davis, *Synthesis*, **1975**, 205.
6) C. G. Stuckwisch, *Synthesis*, **1973**, 469.
7) Y. Tamura, Y. Miki, and M. Ikeda, *J. Chem. Soc., Perkin Trans. 1*, **1976**, 1702.
8) P. Gilgen, H. Heimgartner, H. Schmid, and H.-J. Hansen, *Heterocycles*, **6**, 143 (1977).
9) A. Padwa and L. Gehrlein, *J. Am. Chem. Soc.*, **94**, 4932 (1972).
10) J. W. Lown and B. E. Landberg, *Can. J. Chem.*, **52**, 798 (1974).
11) A. Padwa and H. Ku, *J. Org. Chem.*, **44**, 255 (1979).
12) R. Huisgen, K. Matsumoto, and C. H. Ross, *Heterocycles*, **15**, 1131 (1981).
13) J. W. Lown and K. Matsumoto, *Can. J. Chem.*, *48*, 2215 (1970).
14) J. W. Lown and M. H. Akhtar, *Can. J. Chem.*, **50**, 2236 (1972).
15) P. B. Woller and N. H. Cromwell, *J. Org. Chem.*, **35**, 888 (1970).
16) K. Matsumoto, *Yuki Gosei Kagaku Kyokai Shi*, **32**, 731 (1974).
17) T. Uchida and K. Matsumoto, *Synthesis*, **1976**, 209.
18) G. Surpateanu, J. P. Catteau, P. Karafiloglou, and A. Lablache-Combier, *Tetrahedron*, **32**, 2647 (1976)
19) I. Zugrăvescu and M. Petrovanu, "N-Ylide Chemistry," McGraw-Hill Internatl. New York (1976).
20) O. Tsuge, S. Kanemasa, and S. Takenaka, *Heterocycles*, **20**, 1907 (1983).
21) G. A. Kraus and J. O. Nagy, *Tetrahedron Lett.*, **24**, 3427 (1983).
22) O. Tsuge, Y. Shimizu, H. Shimoharada, and S. Kanemasa, *Heterocycles*, **19**, 2259 (1982).
23) O. Tsuge, H. Shimoharada, and M. Noguchi, *Heterocycles*, **15**, 807 (1981).
24) M. Petrovanu, C. Luchian, G. Suprăteanu, and V. Bărboiu, *Rev. Roum. Chim.*, **24**, 733 and 1053 (1979).
25) M. Petrovanu, I. Drută, and M. V. Tri, *Rev. Roum. Chim.*, **23**, 781 (1978).
26) K. T. Potts, D. R. Choudhury, and T. R. Westby, *J. Org. Chem.*, **41**, 187 (1976).
27) B. E. Landberg and L. W. Lown, *J. Chem. Soc., Perkin Trans. 1*, **1975**, 1326.
28) G. Suprăteanu and A. Lablache-Combier, *Heterocycles*, **22**, 2079 (1984).
29) M. Saunders and E. H. Gold, *J. Org. Chem.*, **27**, 1439 (1962).
30) The reference compound is one of the first examples for the stereoselective cycloadducts of isoquinolinium ylides, while two methine hydrogens (8a-H and 11b-H) were incorrectly assigned. See Ref. 27.
31) O. Tsuge, S. Kanemasa, S. Kuraoka, and S. Takenaka, *Chem. Lett.*, **1984**, 281.
32) O. Tsuge, S. Kanemasa, S. Takenaka, and S. Kuraoka, *Chem. Lett.*, **1984**, 465.
33) This isomer was tentatively assigned as a cycloadduct to the syn form of **2d** by the careful reading of ^{1}H-NMR spectra for the mixture of three isomers (see Table 5).
34) The next paper in this series will describe the reaction of **2d** with acrylonitrile leading to the mixture of two endo cycloadducts to the anti and syn forms of **2d** (O. Tsuge, S. Kanemasa, and S. Takenaka, *Bull. Chem. Soc. Jpn.*, **58**, 3320 (1985).
35) M. P. Cava, A. A. Deana, K. Muth, and M. J. Mitchell, *Org. Syn.*, Coll. Vol., **5**, 944 (1973); C. S. Rondestredt Jr. and O. Vogl, *J. Am. Chem. Soc.*, **77**, 2313 (1955).
36) R. E. Lutz, *Org. Syn.*, Coll. Vol., **3**, 248 (1965).
37) G. E. Ficken, R. P. Linstead, E. Stephen, and M. Whalley, *J. Chem. Soc.*, **1958**, 3879.
38) L. Honer and E. Lingnau, *Ann. Chem.*, **591**, 21 (1955).
39) F. Kröhnke, *Chem. Ber.*, **68**, 1177 (1935).
40) C. A. Henrick, E. Ritchie, and W. C. Taylor, *Aust. J. Chem.*, **20**, 2441 (1967).
41) C. A. Henrick, E. Ritchie, and W. C. Taylor, *Aust. J. Chem.*, **20**, 2455 (1967).
42) C. Leonte and I. Zugrăvescu, *Tetrahedron Lett.*, **1972**, 2029.
43) F. Kröhnke, *Chem. Ber.*, **70**, 543 (1937).
44) C. A. Henrich, E. Ritchie, and W. C. Taylor, *Aus. J. Chem.*, **20**, 2467 (1967).
45) F. Kröhnke, *Chem. Ber.*, **72**, 83 (1939).
46) J. Fröhlich and F. Kröhnke, *Chem. Ber.*, **104**, 1631 (1971).
47) T. Sasaki, K. Kanematsu, and Y. Yukimoto, *J. Chem. Soc.*, **1970**, 481.
48) Y. Tamura, Y. Sumida, and M. Ikeda, *J. Chem. Soc., Perkin Trans. 1*, **1973**, 2901.
49) T. Sasaki, K. Kanematsu, Y. Yukimoto, and S. Ochiai, *J. Org. Chem.*, **36**, 813 (1970).
50) D. G. Farnum, R. J. Alamo, and J. M. Duston, *J. Org. Chem.*, **32**, 1130 (1967).
51) F. Kröhnke and H. Kübler, *Chem. Ber.*, **70**, 1117 (1937).
52) M. Petrovanu, A. Sauciuc, I. Gabe, and I. Zugrăvescu, *Rev. Roum. Chim.*, **14**, 1153 (1969).
53) F. Kröhnke and W. Friedrich, *Chem. Ber.*, **96**, 1195 (1963).
54) A. Kakei and S. Ito, *Bull. Chem. Soc. Jpn.*, **47**, 938 (1974).

The Crystal and Molecular Structure of Two Triple-layered Metaparacyclophanes

Yosuke KOIZUMI, Toshihiro TOYODA, Nobutami KASAI,†* and Soichi MISUMI*
The Institute of Scientific and Industrial Research, Osaka University, Mihogaoka, Ibaraki, Osaka 567
†*Department of Applied Chemistry, Faculty of Engineering, Osaka University, Yamadaoka, Suita, Osaka 565*
(Received July 18, 1985)

Molecular structures of triple-layered metaparacyclophanes containing two and one para-bridged, outside benzene rings([2.2]paracyclo(4,6)[2.2]metaparacyclophane (PMP) and [2.2]metacyclo(4,6)[2.2]metaparacyclophane (MMP), respectively) have been determined by means of X-ray diffraction. PMP: monoclinic, space group $P2_1/a$, a=15.989(1), b=9.932(1), c=5.991(1) Å, β=100.61(1)°, Z=2. MMP: monoclinic, space group $P2_1/c$, a=8.969(2), b=22.774(4), c=10.339(2) Å, β=119.32(1)°, Z=4. The structure of PMP was solved by the vector search method and that of MMP by the direct method. They are refined anisotropically by the least-squares procedure, final R values are 0.066 for PMP and 0.096 for MMP. Of the two possible conformers PMP has a centrosymmetric staircase structure(anti-form) whereas MMP takes a platform shape(syn-form).

Previously, a variety of triple-layered metaparacyclophanes has been synthesized by desulfurization of the corresponding dithiacyclophanes.[1] There have been discussed the assignment of their structures in detail and the conformational flipping of the meta-bridged benzene ring at the high temperature based on the NMR studies, and also the transannular electronic interactions between benzene rings.[2] In this paper, the crystal structure analysis of triple-layered metaparacyclophanes containing two and one para-bridged, outside benzene rings(PMP and MMP, respectively) is reported. A brief account of these metaparacyclophane structures has been given to prove the assigned structure in NMR studies.[2]

Experimental

Crystal Data. PMP. $C_{26}H_{26}$, M 338.5, monoclinic, space group $P2_1/a$(No. 14, absent reflections, $h0l$: $h=2n+1$, $0k0$: $k=2n+1$), a=15.989(1), b=9.932(1), c=5.991(1) Å, β=100.61(1)°, V=935.14(6) Å^3, D_m=1.20 g cm^{-3}, D_c=1.202 g cm^{-3} for Z=2. MMP. $C_{26}H_{26}$, M 338.5, monoclinic, space group $P2_1/c$(No. 14, absent reflections, $h0l$: $l=2n+1$, $0k0$: $k=2n+1$), a=8.969(2), b=22.774(4), c=10.339(2) Å, β=119.32(1)°, V=1841.2 Å^3, D_m=1.23 g cm^{-3}, D_c=1.221 g cm^{-3} for Z=4.

Both crystals were recrystallized from toluene. A colorless, platelet crystal of PMP with approximate dimensions of 0.3×0.4×0.4 mm and a colorless, hexagonal crystal of MMP with 0.4×0.2×0.4 mm were selected for the X-ray experiment. A Rigaku automated, four-circle diffractometer was used for the determination of unit-cell dimensions and the measurement of integrated intensities.

Intensity data were collected by the θ—2θ scan technique at a 2θ rate of 4° min^{-1}. The scan range for PMP was from $\{2\theta(\alpha_1)-1.0\}$° to $\{2\theta(\alpha_2)+1.0\}$° for Zr-filtered Mo $K\alpha$ radiation and that for MMP from $\{2\theta(\alpha_1)-0.8\}$° to $\{2\theta(\alpha_2)+0.8\}$° for graphite monochromatized Mo $K\alpha$ radiation (λ= 0.71069 Å). Backgrounds were counted for 10 s at both ends of a scan. Five standard reflections measured after every 50 reflections to monitor the stability and orientation of the crystals showed no significant decay throughout the data collection of both crystals. In total, 1864 non-zero reflections out of 2908 and 3152 out of 4499 were obtained for PMP and MMP, respectively($\sin\theta/\lambda<0.7$). Usual Lorentz and polarization corrections were made but absorption correction was ignored for both sets of data [μ(Mo)=0.72 cm^{-1} for PMP and MMP].

Structure Solution and Refinement

PMP. In order to obtain a clue to solve the structure, the benzene ring which is a main component of the molecule has been assumed as a rigid body, and the central benzene ring of the PMP molecule could be found by the vector search method(*XRICS*).[3] Successive Fourier synthesis phased by the six carbon atoms of the benzene ring could locate the remaining carbon atoms. The structure was refined anisotropically by the block-diagonal least-squares procedure(*HBLS* V).[4] The function minimized was $\sum w(\Delta F)^2$, where w=1. Hydrogen atoms were located on a difference Fourier map, which were included in the refinement with isotropic temperature factors. The R value converged to 0.066 for 1864 non-zero reflections. Final atomic parameters of carbon atoms are listed in Table 1a.††

MMP. The structure was solved by the direct method (*MULTAN*),[6] and refined by using the *HBLS* V program with anisotropic temperature factors and unit weight for all reflections. Hydrogen atoms were located on the calculated positions, which were confirmed on a difference Fourier map. They were refined isotropically. The final R value was 0.096 for 3152 non-zero reflections. Atomic parameters are given in Table 1b.††

Atomic scattering factors were taken from International Tables for X-Ray Crystallography.[7] Computations were done mainly on a NEAC 2200-500

†† Tables of anisotropic temperature factors, atomic parameters of hydrogen atoms, and observed and calculated structure factors are kept at the Chemical Society of Japan, Document No. 8550.

Table 1. Atomic parameters of carbon atoms in PMP and MMP with estimated standard deviations in parentheses

a. PMP Atom	x	y	z	B_{eq}/Å^2 [5]
C(1)	−0.2531(5)	0.2142(3)	0.0661(2)	3.6
C(2)	−0.1772(6)	0.3508(3)	0.0291(3)	4.3
C(3)	−0.1415(5)	0.3264(3)	−0.0608(2)	3.6
C(4)	−0.3244(5)	0.3092(3)	−0.1277(2)	3.9
C(5)	−0.3073(5)	0.2227(4)	−0.1946(2)	4.0
C(6)	−0.1051(5)	0.1528(3)	−0.1957(2)	3.6
C(7)	0.0893(5)	0.1961(3)	−0.1402(2)	3.6
C(8)	0.0718(5)	0.2825(3)	−0.0735(2)	3.5
C(9)	−0.1069(6)	0.0138(4)	−0.2343(2)	4.3
C(10)	−0.1901(5)	−0.0898(3)	−0.1723(2)	3.7
C(11)	−0.0939(5)	−0.0568(3)	−0.0798(2)	2.7
C(12)	−0.2143(4)	0.0328(3)	−0.0379(2)	2.6
C(13)	−0.1247(4)	0.0946(3)	0.0391(2)	2.7
b. MMP				
Atom	x	y	z	B_{eq}/Å^2
C(1)	1.0441(6)	0.1437(3)	0.5876(5)	3.8
C(2)	1.0340(6)	0.0749(3)	0.5856(5)	4.1
C(3)	0.9087(6)	0.0537(2)	0.6334(5)	3.7
C(4)	0.9589(7)	0.0451(3)	0.7828(6)	4.4
C(5)	0.8358(8)	0.0420(3)	0.8278(6)	5.0
C(6)	0.6648(7)	0.0523(3)	0.7285(6)	4.2
C(7)	0.6120(6)	0.0607(2)	0.5789(5)	3.5
C(8)	0.7342(6)	0.0566(2)	0.5334(5)	3.5
C(9)	0.4402(6)	0.0871(3)	0.4756(6)	4.0
C(10)	0.4503(6)	0.1554(2)	0.4780(5)	3.7
C(11)	0.5740(6)	0.1782(2)	0.4296(5)	3.0
C(12)	0.7485(6)	0.1727(2)	0.5292(5)	3.0
C(13)	0.8743(5)	0.1727(2)	0.4857(5)	3.1
C(14)	0.8269(5)	0.1941(2)	0.3438(5)	3.0
C(15)	0.6576(6)	0.2122(2)	0.2556(5)	3.1
C(16)	0.5270(5)	0.1991(2)	0.2870(5)	3.0
C(17)	0.3407(6)	0.2053(2)	0.1600(5)	3.7
C(18)	0.2697(6)	0.1503(3)	0.0555(5)	4.1
C(19)	0.4080(6)	0.1263(3)	0.0266(5)	3.9
C(20)	0.4631(7)	0.1586(3)	−0.0578(5)	4.2
C(21)	0.6329(7)	0.1550(3)	−0.0247(5)	4.4
C(22)	0.7491(6)	0.1206(3)	0.0928(5)	4.0
C(23)	0.6803(7)	0.0785(3)	0.1465(6)	4.2
C(24)	0.5123(7)	0.0814(3)	0.1141(5)	4.1
C(25)	0.9339(6)	0.1389(3)	0.1844(6)	4.5
C(26)	0.9443(6)	0.1950(3)	0.2748(6)	4.1

computer at the Computation Center, Osaka University and at the final stage an ACOS 850 computer at the Crystallographic Research Center, Institute for Protein Research, Osaka University was used.

Results and Discussion

Molecular Structure. PMP. The molecule has a centrosymmetric staircase structure, which is depicted in Fig. 1a(*ORTEP*).[8] Bond distances and bond angles are given in Fig. 2a.

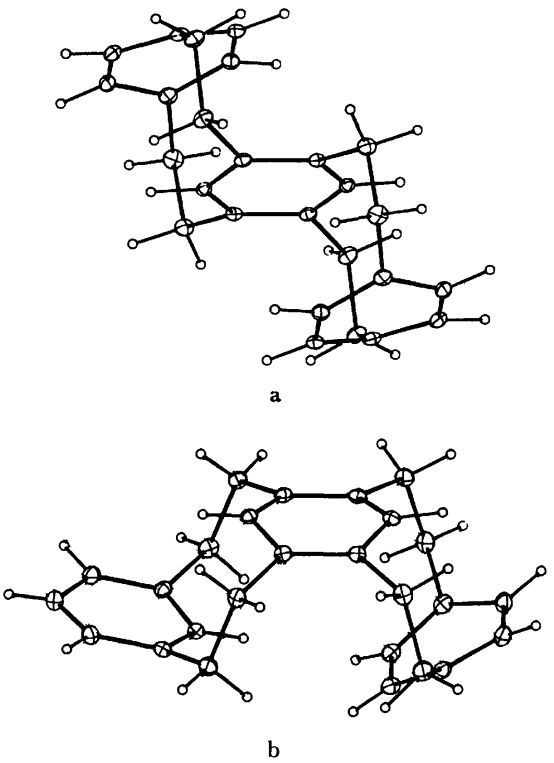

Fig. 1. A perspective view[8] of PMP (a) and MMP (b) molecules. Carbon atoms are represented by thermal ellipsoids with 10% probability level, hydrogen atoms as spheres with $B=1.0$ Å^2.

The outside para-bridged benzene ring is in a boat form as is found usually, the deformation angle p_1 at the C(3) atom(the dihedral angle between the plane defined by the C(4), C(5), C(7), and C(8) (Plane 1) and that by the C(3), C(4), and C(8) (Plane 2)) is 13.6° and that at the C(6), p_2 is 12.8°. The angle q_1 at the C(3) atom made by the C(2)–C(3) bond and the plane 2 is 15.4° and the corresponding angle q_2 at the C(6) is 15.2°, which are much larger than those in [2.2]paracyclophane.[9] The inner angles, C(4)–C(3)–C(8) and C(5)–C(6)–C(7) [117.4(3) and 117.5(3)°, respectively] in the benzene ring are smaller than 120°.

The center of the inside four-bridged benzene ring lies on a crystallographic center of symmetry, and this ring takes a chairform (Fig. 3a). The bending angle at the C(12) atom is 4.3°. The C(11)–C(12)–C(13) and C(11′)–C(12′)–C(13′) angles [both 123.9(3)°] are larger, and the other four angles [117.9(3) and 118.0(3)°] are smaller, than 120°.

In the ethylene bridges between the inside and outside benzene rings, the central C_{sp^3}–C_{sp^3} bonds are equal in length [1.579(4) and 1.572(4) Å]. Different from the corresponding angles in [2.2]paracyclophane and those of related compounds, the C(1)–C(2)–C(3) and C(6)–C(9)–C(10) angles[both 108.7(3)°] are smaller than the C(2)–C(1)–C(13) and C(9)–

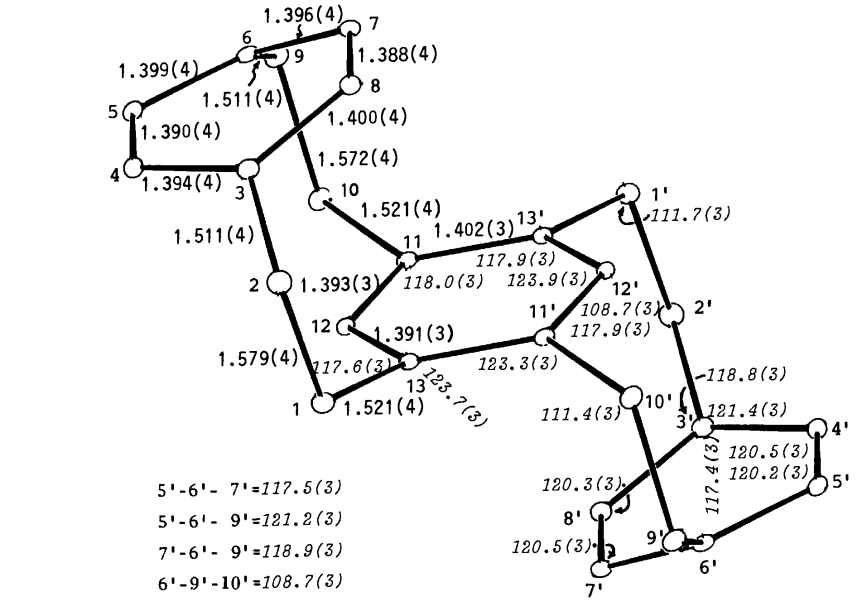

a

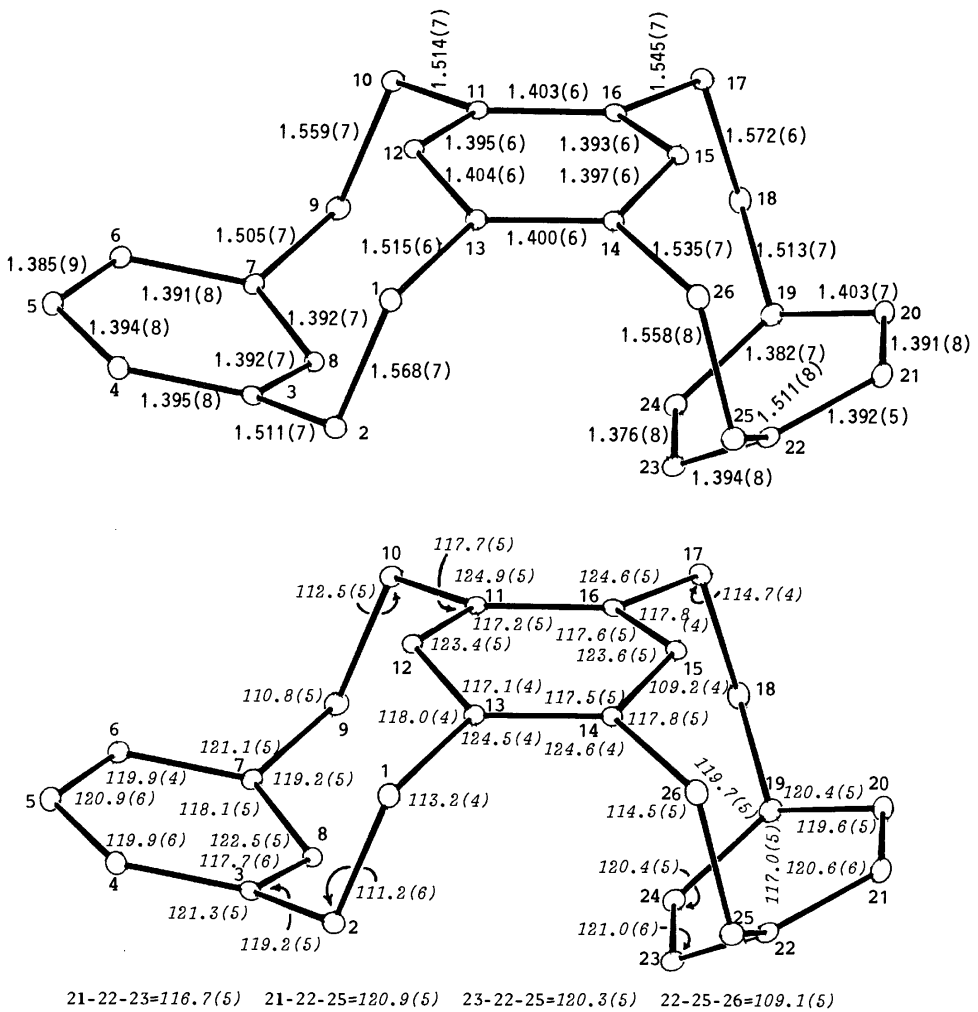

b

Fig. 2. Bond distances and bond angles in PMP (a) and MMP (b). Estimated standard deviations in parentheses.

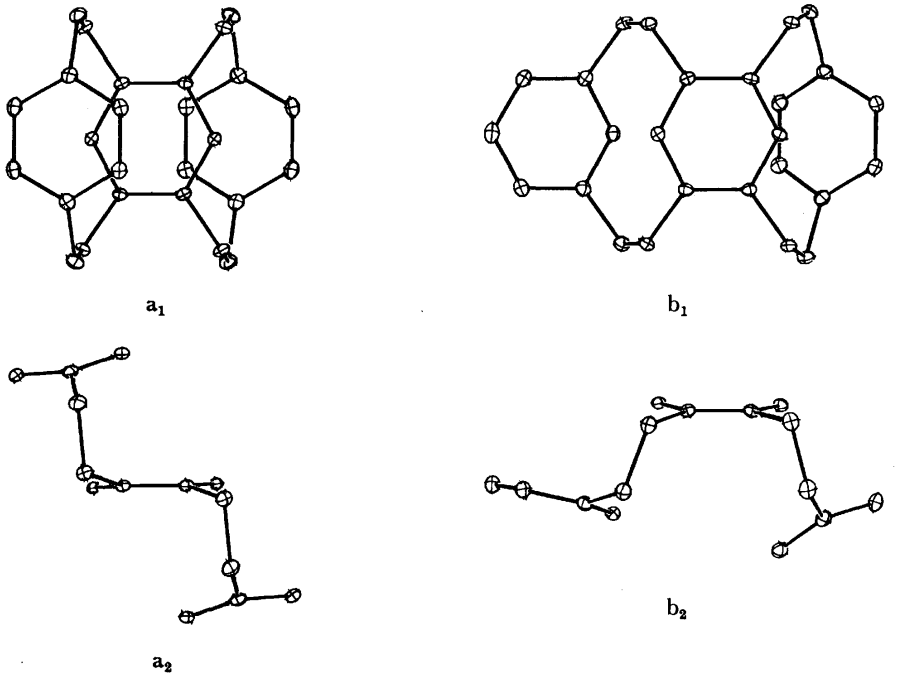

Fig. 3. Projections of molecules.
a_1: PMP molecule projected onto the plane defined by the C(11), C(13), C(11'), and C(13') atoms.
a_2: PMP molecule projected along the vector passing through the midpoints of the C(11)–C(13') and C(11')–C(13) bonds.
b_1: MMP molecule projected onto the plane defined by the C(11), C(13), C(14), and C(16) atoms.
b_2: MMP molecule projected along the vector passing through the midpoints of the C(13)–C(14) and C(11)–C(16) bonds.

C(10)–C(11) angles [111.7(3) and 111.4(3)°, respectively]. This fact is one of the features of [2.2]metaparacyclophane and the similar compounds.

The overlapping of three benzene rings is small: Between the outside and inside benzene rings the Plane 1 and the plane defined by the C(11), C(13), C(11'), and C(13') atoms makes an angle of 11.6°. Short nonbonded distances between atoms in the outside and inside benzene rings are given in Table 2, the closest distance, C(6)···C(11), is 2.780(4) Å.

MMP. A perspective view(*ORTEP*) of the molecule is drawn in Fig. 1b. The molecule has a platform shape(syn-form). Bond distances and bond angles are given in Fig. 2b. The projection of the molecule onto the least-squares plane of the C(11), C(13), C(14), and C(16) atoms and that along the vector passing through the midpoints of the C(13)–C(14) and C(11)–C(16) bonds are presented in Fig. 3b.

The outside meta-bridged benzene ring takes a boatform, the deformation angle p_1 at the C(5) atom is 4.9° and p_2 at the C(8) 9.2°. The C(4)–C(3)–C(8) [117.7(6)°] and C(6)–C(7)–C(8)[118.1(5)°] angles are smaller than 120°.

The central four-bridged benzene ring is also in a boatform, the deformation angle at the C(12) atom[14.8°] is larger than that at the C(15)[12.6°].

Table 2. Short nonbonded distances less than 3.6 Å between carbon atoms in benzene rings (l/Å) estimated standard deviations in parentheses

PMP		MMP	
C(5)···C(11)	3.442(4)	C(7)···C(11)	3.024(7)
C(6)···C(11)	2.780(4)	C(8)···C(11)	3.061(7)
C(7)···C(11)	2.974(4)	C(3)···C(12)	3.010(7)
C(8)···C(11)	3.510(4)	C(7)···C(12)	2.982(7)
C(3)···C(12)	2.981(4)	C(8)···C(12)	2.649(7)
C(4)···C(12)	3.111(4)	C(3)···C(13)	3.051(7)
C(5)···C(12)	3.103(4)	C(8)···C(13)	3.068(7)
C(6)···C(12)	2.970(4)	C(14)···C(21)	3.441(7)
C(7)···C(12)	3.117(4)	C(14)···C(22)	2.871(7)
C(8)···C(12)	3.126(4)	C(14)···C(23)	3.193(7)
C(3)···C(13)	2.793(4)	C(15)···C(19)	3.042(7)
C(4)···C(13)	3.451(4)	C(15)···C(20)	3.081(7)
C(7)···C(13)	3.497(4)	C(15)···C(21)	3.084(7)
C(8)···C(13)	2.982(4)	C(15)···C(22)	3.034(7)
		C(15)···C(23)	3.288(7)
		C(15)···C(24)	3.292(7)
		C(16)···C(19)	2.885(7)
		C(16)···C(20)	3.447(7)
		C(16)···C(24)	3.188(7)

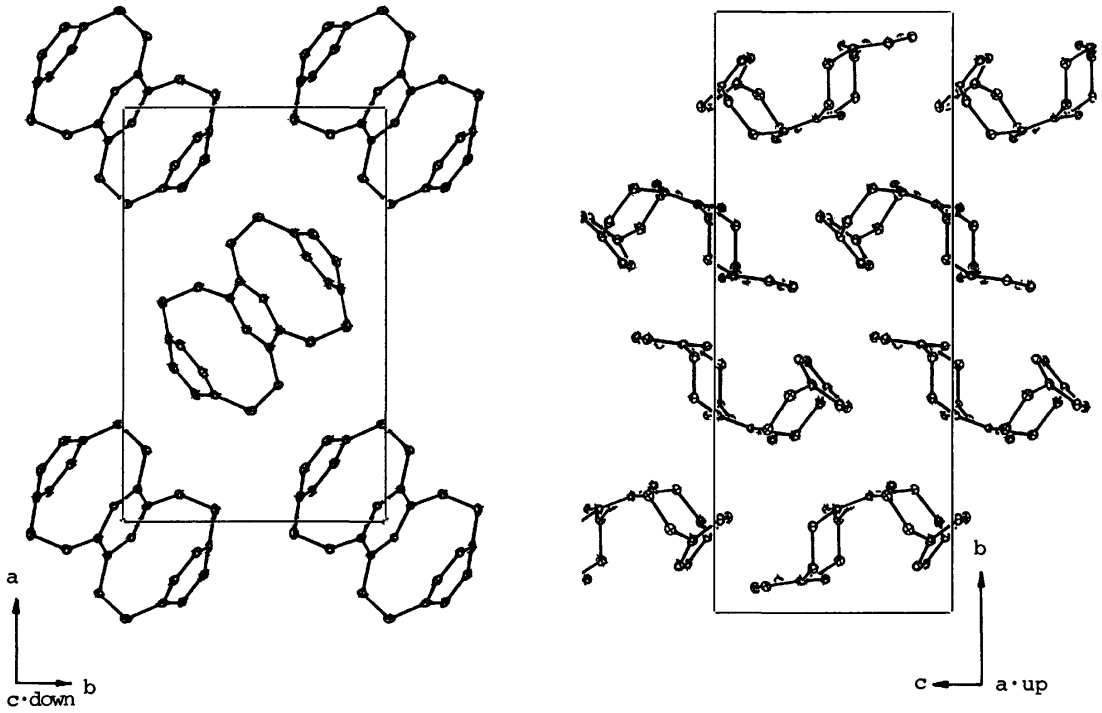

Fig. 4. Crystal structure[8] of PMP (a) and MMP (b) projected along an axis of the unit-cell. Carbon atoms are drawn as thermal ellipsoids with an arbitrary probability level.

The C(11)-C(12)-C(13) and C(14)-C(15)-C(16) angles are 123.4(5) and 123.6(5)°, respectively (Fig. 2b), which are larger than 120°. The other four inner angles [117.1(4) to 117.5(5)°] are smaller than 120°.

As a whole, the structure of the [2.2]metacyclophane moiety, consisting of the meta-bridged benzene and central benzene rings mentioned above and two ethylene bridges (Fig. 3b), is very similar to that of the two-third of the triple-layered metacyclophane-(*ud* isomer).[10,11] The closest intramolecular atomic contact is C(8)···C(12)[2.649(7) Å] (Table 2).

The third para-bridged benzene ring is also in a boatform. The deformation angles p_1 and q_1 at the C(19) atom are 13.9 and 14.9°, respectively, and those at the C(22) are p_2=14.8° and q_2=14.4°. These values of q's are larger than the corresponding angles in [2.2]paracyclophane.

Ethylene bridges in the [2.2]metaparacyclophane moiety, *i.e.* those between the central and third para-bridged benzene rings, have similar structure to those in the [2.2]metaparacyclophane moiety in PMP but slightly different structure from those in [2.2]paracyclophane moiety. The C(14)-C(26)[1.535(7) Å] and C(16)-C(17)[1.545(7) Å] bonds are longer, and the C(14)-C(26)-C(25)[114.5(5)°] and C(16)-C(17)-C(18) [114.7(4)°] angles are larger than the corresponding bond distances and bond angles in many [2.2]paracyclophanes, respectively. The torsion angles around the C(17)-C(18) and C(25)-C(26) bonds are equal[40.6 and 42.9°, respectively] but they are smaller than those around the C(1)-C(2)[59.8°] and C(9)-C(10) bonds[60.5°] in the [2.2]metacyclophane moiety of the present molecule.

The overlapping of the central and third para-bridged benzene rings are small. These two rings make an angle of 27.4°, which is much larger than the corresponding angle in the PMP molecule. Short nonbonded interatomic distances in the [2.2]metaparacyclophane moiety are C(14)···C(22) [2.871(7) Å] and C(16)···C(19)[2.885(7) Å].

Crystal Structure. The packing of PMP and MMP molecules in the crystal is shown in Fig. 4. In these two crystals molecules are packed rather loosely, and no short intermolecular contact less than 3.6 Å is found between non-hydrogen atoms.

The authors are grateful to Miss Nobuko Kanehisa who helped them at the final stage of the computation and for *ORTEP* drawing.

References

1) N. Kannen, T. Umemoto, T. Otsubo, and S. Misumi, *Tetrahedron Lett.*, **1973**, 4537; N. Kannen, T. Otsubo, Y. Sakata, and S. Misumi, *Bull. Chem. Soc. Jpn.*, **49**, 3307 (1976).

2) N. Kannen, T. Otsubo, Y. Sakata, and S. Misumi, *Bull. Chem. Soc. Jpn.*, **49**, 3203 (1976).

3) I. Tanaka, *XRICS*, "UNICS-Nagoya," Nagoya Univ., 1981, p. 37.

4) T. Ashida, *HBLS* V, The "Universal Crystallographic Computing System-Osaka," The Computing Center, Osaka

Univ., 1973, p. 55.
5) W. C. Hamilton, *Acta Crystallogr.*, **12**, 609 (1959).
6) G. Germain, P. Main, and M. M. Woolfson, *Acta Crystallogr., Sect. A*, **27**, 368 (1971).
7) International Tables for X-ray Crystallography, Vol. IV, Kynoch Press, Birmingham (1974), p. 71.
8) C. K. Johnson, *ORTEP* II, Report ORNL-5238, Oak Ridge National Laboratory, Tennessee (1976).
9) H. Hope, J. Bernstein, and K. N. Trueblood, *Acta Crystallogr., Sect. B*, **28**, 1733 (1972).

Activity and Selectivity Regulation of Synthesis Gas Reaction over Supported Ruthenium Catalysts

Kaoru FUJIMOTO,* Tatsuya NOBUSAWA, Takakazu FUKUSHIMA, and Hiro-o TOMINAGA
Department of Synthetic Chemistry, Faculty of Engineering, The University of Tokyo, Hongo, Bunkyo-ku, Tokyo 113
(Received February 15, 1985)

The catalytic activities of supported ruthenium for synthesis-gas conversion to hydrocarbons was found to be in the following order:

$$TiO_2 > Nb_2O_3 > ZrO_2 > SiO_2 > Ta_2O_5 > Al_2O_3 > V_2O_5 > Mo_3 > WO_3 > MnO_2 > ZnO$$

Turnover frequencies of the supported ruthenium increased with decrease in dispersion of the metal particles for every carrier material. Even the activities per unit weight of metals were higher for low-dispersion ruthenium on Al_2O_3, TiO_2, and ZrO_2. The chain-growth probability of a hydrocarbon product, which is characterized by the Schulz-Flory distribution, increased markedly with decrease in the metal dispersion irrespective of the carrier material. The catalytic activity of ruthenium particles with a dispersion level of 0.7 or higher reached a ceiling level at about 0.5 MPa, whereas that of low dispersed ruthenium increased almost linearly with an increase in reaction pressure (up to at least 2.0 MPa).

A supported ruthenium catalyst is one of the most active and promising catalysts for producing liquid hydrocarbons from synthesis gas.[1-3] Hydrocarbon products of Fischer-Tropsch (F-T) synthesis on supported ruthenium catalysts have been known to follow the Schluz-Flory distribution.[4,5] One of the most important targets regarding catalyst preparation for producing a liquid hydrocarbon by F-T synthesis is to control the probability of hydrocarbon chain growth. A maximization of the formation of C_5 to C_{20} hydrocarbons is especially important. Vannice *et al.*[3] and Kikuchi *et al.*[6] have reported that activities of supported ruthenium catalysts are markedly influenced by carrier materials and that, especially, Ru/TiO_2 is one of the most active and chain-growing catalysts. The activity and selectivity of a ruthenium catalyst are also influenced by the sizes of supported metals.[4-6] King has claimed that although the turnover frequency (TOF) of a synthesis-gas reaction increases with a decrease in the metal dispersion, no consistent relationship between the chain-growth probability of the product hydrocarbon and the dispersion exists.[7] Kellner and Bell have reported that the turnover frequency of a reaction on alumina-supported ruthenium catalysts under atmospheric conditions decreases moderately with an increasing dispersion (up to 0.7). The decrease is above 0.7, but neither the chain-growth probability nor the olefin-to-paraffin ratio is affected.[4]

The activity and selectivity of ruthenium catalysts should be determined under pressurized conditions using a synthesis gas of normal composition in order to determine the real performances of the F-T reaction, since they are very sensitive to these conditions.[1,2] In both of the studies mentioned above, the dispersions of supported ruthenium were controlled by regulating the ruthenium loading. This method is quite powerful for controlling metal dispersion; however, it has a disadvantages that the particle sizes are widely distributed.[8] Also, the range of the dispersion controlled by this method is not wide enough.

The present authors have developed a simple method for regulating the dispersion level of a supported ruthenium catalyst with constant loading and with the same source material and have shown that both activity and selectivity are influenced by either the carrier materials or the dispersion level of ruthenium.[5]

In the present work, the effects of carriers and the sizes of metal particles of supported ruthenium catalysts on the activity, selectivity, and other catalytic features (characterized by the CO conversion rate per weight of a catalyst, turn-over frequency, chain-growth probability, methane selectivity and pressure dependence) were studied under conditions normally utilized for F-T synthesis.

Experimental

Catalyst Preparation and Dispersion Measurements. All catalysts used in the present study contained 2 wt% of ruthenium. TiO_2 was obtained by the hydrolysis of titanium isopropoxide ($[(CH_3)_2CHO]_4Ti$), followed by calcining at 723 K for 3 h. This gave anatase type TiO_2. WO_3 and MoO_3 were prepared through the calcination (in air at 773 K for 7 h) of ammonium tungstate ($(NH_4)_2WO_4$) and ammonium molybdate ($(NH_4)_2\ MoO_4$), respectively. Alumina-magnesia(Al_2O_3-6MgO) was prepared by the calcination (in air at 723 K for 1 h) of a commercially available Al-Mg hydroxycabonate ($Mg_6Al_2(OH)_{16}CO_3$). Other metal oxides were used as received after calcining in air at 723 K for 1 h. SiO_2 (Aerosil-380) was obtained from Japan Aerosil Co. (380 m^2/g). A γ-Al_2O_3 (220 m^2/g) was prepared by hydrolyzing aluminium isopropoxide and calcining in air at 873 K for 3 h. Supported ruthenium catalysts were prepared by impregnating the carriers with $RuCl_3 \cdot 3H_2O$ from its aqueons solutions, drying at 353 K and then drying overnight at 393 K in an air oven. These catalysts were represented as H-(Highly-dispersed) catalysts.

Another group of catalysts represented as L-(Low-dispersed) catalysts were prepared by calcining H catalysts in air at 673 K for 3 h before reduction. The catalyst precursors were molded to granules (20—40 mesh) under pressure. The catalysts were activated in situ by reducing in flowing hydrogen at 453 K for 1 hr and then at 673 K for 2 h.

The chemisorption of CO was measured at room temperature using a flow-through cell connected to a glass vacuum system. A catalyst sample was first activated *in situ* as described above and then evacuated at 723 K for 3 h. The amount of desorped CO was determined as the difference between the first isotherm and the second isotherm which was measured following to evacuation for 30 min at room temperature after the first isotherm measurement. Metal dispersion was calculated assuming that one CO molecule was chemisorbed by one surface ruthenium atom.

Synthesis Gas Reaction and Product Analysis. Synthesis gas reactions were conducted in a flow-type fixed-bed reaction apparatus under pressurized conditions. A stainless-steel tube (inner diameter 8 mm, outer diameter 10 mm) was used as a reactor. The details of this apparatus has been described elswhere.[9] When highly active catalysts were used, they were diluted by α-Al_2O_3 (surface area<2 m^2/g) granules with the same size (20/40 mesh) in order to produce an even temperature profile over the catalyst bed (within 2K).

Activities and selectivities of the ruthenium catalysts were measured under the following reaction conditions: 503 K, 2.03 MPa, $H_2/CO=2$. The time factor (W/F) was adjusted to produce about 10% CO conversion.

Synthesis gas ($H_2/CO=2$) was introduced into the reactor after being purified by being passed through a series of silica-gel and activated charcoal columns. All products effluted from the catalyst bed were withdrawn in gaseous states from the high-pressure zone and were analyzed on-line by gas chromatographs. Hydrocarbons trapped in the catalyst bed during the reaction were extracted *in situ* with hot toluene for 1 h after a reaction was completed to be analyzed. CO, CH_4, and CO_2 were analyzed using an activated charcoal column. C_1–C_5 hydrocarbons were analyzed with a Porapak Q column, C_4–C_{20} hydrocarbons were analyzed with a Silicone SE-30/Chromosorb 101 column and C_{10}–C_{45} hydrocarbons were analyzed with a Dexil 300 GC column, respectively.

In all that follows, catalyst activity is defined by the equation:

Activity$=(CO_{in}-CO_{out})/W$ where CO_{in} and CO_{out} are the flow rates of carbon monoxide which enter and exit the reactor (moles/hour), respectively and W is the catalyst weight (gram).

Results and Discussion

Metal Dispersion. Table 1 shows the amount of CO chemisorption, metal dispersion, catalyst activities and turn-over frequencies. The dispersion level of supported ruthenium prepared without air calcination is distributed between 10 and 90%. Obviously, the dispersions of ruthenium on each of the four carriers (ZrO_2, SiO_2, Al_2O_3, TiO_2) were lowered due to air calcination prior to reduction.

Table 1. CO Chemisorption, dispersion and specific activity of supported ruthenium catalyst[a)]

Carrier	CO_{ch}[b)] μ-mol/g-cat	D_{Ru}[c)] %	N_{CO}[d)] $10^{-3}/s$	α[e)]
γ-Al_2O_3(H)	225	58.1	32	0.64
γ-Al_2O_3(L)	30.0	15.2	182	0.88
TiO_2(H)	174.3	88.7	42	0.62
TiO_2(L)	50.0	30.1	355	0.82
SiO_2(H)	51.4	26.4	143	0.66
SiO_2(L)	10.0	5.1	278	0.82
ZrO_2(H)	20.0	10.3	520	0.77
ZrO_2(L)	12.9	6.6	862	0.86
Nb_2O_5	44.7	22.6	390	0.73
Ta_2O_5	19.8	10.0	327	0.79
V_2O_5	144.9	73.2	37	0.65
MoO_3	124.9	63.1	30	0.66
WO_3	87.7	44.3	12	0.73
MnO_2	89.1	45.0	5.0	0.57
ZnO	40.9	20.7	11	0.66
$Al_2O_3 \cdot 6MgO$	110.5	55.8	2.8	0.56

a) 2 wt% Ru on carrier. b) CO chemisorption at room temperature. c) Dispersion of ruthenium. d) Turnover frequency. e) Chain growth probability.

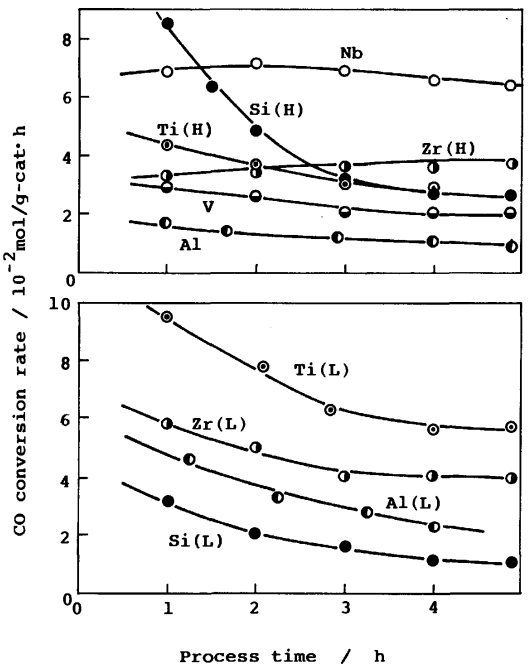

Fig. 1. Change in catalytic activity of supported ruthenium catalysts. Temperature: 503 K, Pressure: 2.03 MPa, H_2/CO: 2/1 mole ratio.

Since ruthenium chloride has been proven by our experiment to be converted to ruthenium oxide during air calcination, it can move easily on the carrier and aggregate into large particles as expected due to its high sublimation characteristics.

Characteristic Features of Synthesis-gas Reaction. As demonstrated in Fig. 1, the activities of most catalysts, expressed by CO conversion rates, decreased

with the processing time. Since deactivated catalysts restored their activities upon being treated with hydrogen at 673 K, the deactivation can be attributed to carbon deposition or an accumulation of wax on the catalysts. The activities and selectivities were expressed by average values which were measured between 4 and 5 h after starting.

The product hydrocarbon, eluted from the catalyst bed in a gaseous state, was characterized by the fact that hydrocabons higher than C_{15} are quite small, as demonstrated in Fig. 8. This was the same even with the L-catalysts whose chain-growth ability was high. It was caused by a trapping of high-boiling-point hydrocarbons in the catalyst bed.[5] A large amount of waxy hydrocarbon was extracted with hot toluene after the synthesis-gas reaction. By combining the extracted products with the gaseous products, the ratio of the amount of recovered hydrocarbons to the amount of consumed carbon monoxide (on carbon base) increased from 35 to 88% (for Ti-L-catalyst) and from 63 to 91% (Ti-H catalyst), respectively. The total hydrocarbon distributions, thus obtained, showed smooth profiles distributed from C_1 to C_{40}, or higher (Figs. 2 and 3). The distributions fit the Schulz-Flory equation very well as demonstrated by Figs. 4 and 5. It is clear from

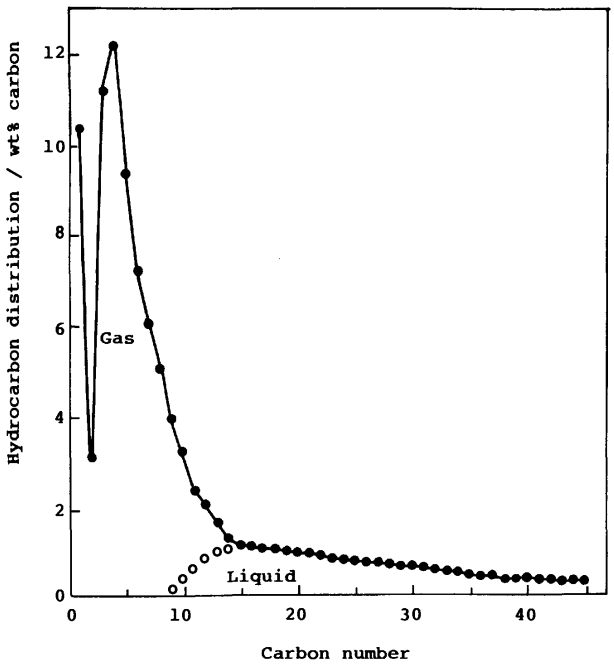

Fig. 2. Hydrocarbon distribution of the products on Ti-H catalyst. Temperature: 503 K, Pressure: 2.03 MPa, H_2/CO : 2/1 mol ratio.

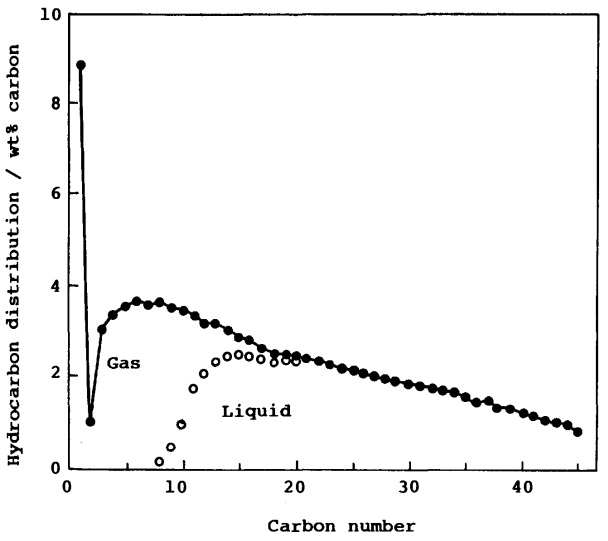

Fig. 3. Hydrocarbon distribution of the products on Ti-L catalyst. Temperature: 503 K, Pressure: 2.03 MPa, H_2/CO : 2/1 mole ratio.

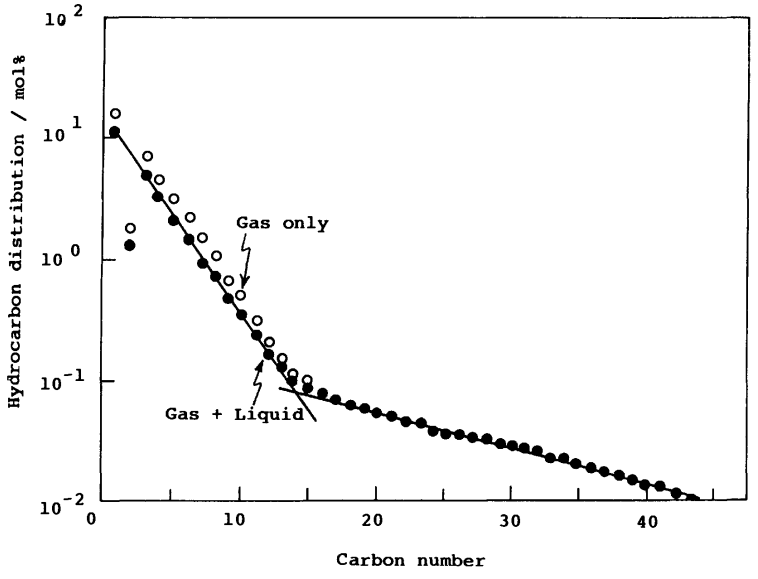

Fig. 4. Schluz-Flory plot of the product on Ti-H catalyst. Same product as shown in Fig. 2.

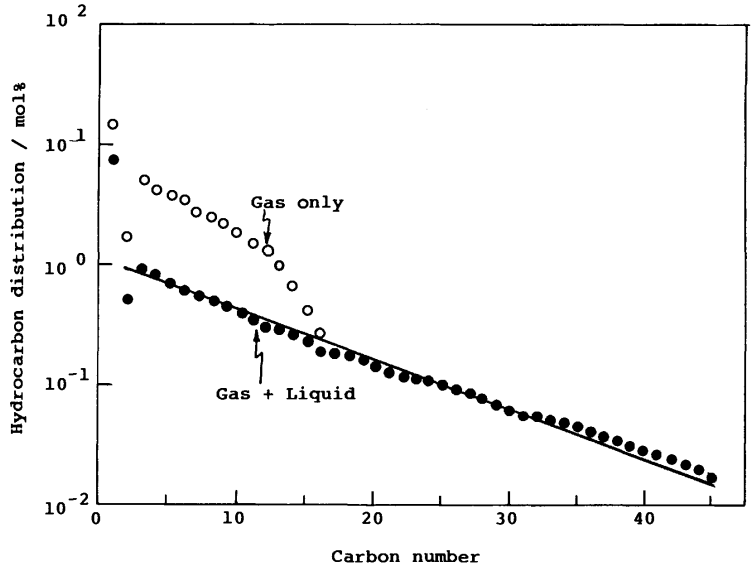

Fig. 5. Schluz-Flory plot of the product on Ti–L catalyst. Same product as shown in Fig. 3.

the data in Fig. 3 that the chain-growth probability (α value), which is determined from the distribution of gaseous hydrocarbons, agrees well with that obtained from the combined product. The α values of other catalysts were determined from the distribution of gaseous products. It is also worth while to note that the Schulz-Flory plot for a Ti–H catalyst can be expressed by two straight lines, whereas that of a Ti–L catalyst can be expressed by one straight line. This phenomenon will be discussed in the later chapter.

Controlling Factors of Catalyst Activity. The conversion levels, catalytic activities, methane selectivities, olefin content of products and chain-growth probabilities are shown in Tables 1 and 2. Although metal loadings are the same for all catalysts, metal dispersions are distributed from 5 to 89% and the activity per unit weight of catalysts are distrubued over a range of about 60 by factor. Figure 6 shows the relationship between ruthenium disperion and the turnover frequency (TOF). It is clear that the TOF is controlled not only by carrier materials, but also by the ruthenium dispersion. Catalysts can be classified into 3 groups: (1) Low dispersion-high TOF, (2) high dispersion-low TOF, and (3) low dispersion-low TOF. It is also demonstrated that a decrease in the dispersion by air calcination causes an increase in the TOF without exception. Similar facts have already been pointed out by King regarding methane synthesis.[7] or by Kikuchi *et al.*[6] for CO

Table 2. Performances of CO hydrogenation on supported ruthenium catalysts[a]

Carrier	W/F[b] g·cat·h/mol	CO conv. %	CH_4 select C·wt%	Olefine content C_2-C_{10}, mol%	Activity[c] molCO/g-cat·h
γ-Al_2O_3 (H)	4.9	4.8	12.0	45.9	0.97
γ-Al_2O_3 (L)	2.5	7.1	5.0	46.9	1.97
TiO_2 (H)	2.5	6.6	8.4	61.4	2.65
TiO_2 (L)	2.5	14.1	7.3	34.5	6.40
SiO_2 (H)	2.5	6.6	24.5	38.8	2.64
SiO_2 (L)	2.5	2.4	13.2	36.1	1.00
ZrO_2 (H)	2.5	9.3	18.7	24.8	3.74
ZrO_2 (L)	2.5	10.2	8.0	30.2	4.00
Nb_2O_5	2.5	16.7	12.9	24.1	6.27
Ta_2O_5	11.2	27.8	7.1	24.1	2.33
V_2O_5	2.5	5.2	10.1	65.3	1.94
MoO_3	11.0	16.0	13.4	5.4	1.35
WO_3	22.4	9.2	10.9	0.9	0.39
MnO_2	22.0	3.9	57.3	24.9	0.16
ZnO	21.5	3.6	5.1	43.4	0.16
Al_2O_3·6MgO	22.7	2.4	28.8	33.1	0.11

a) 2 wt% Ru on carrier. b) Contact time. c) Catalytic activity.

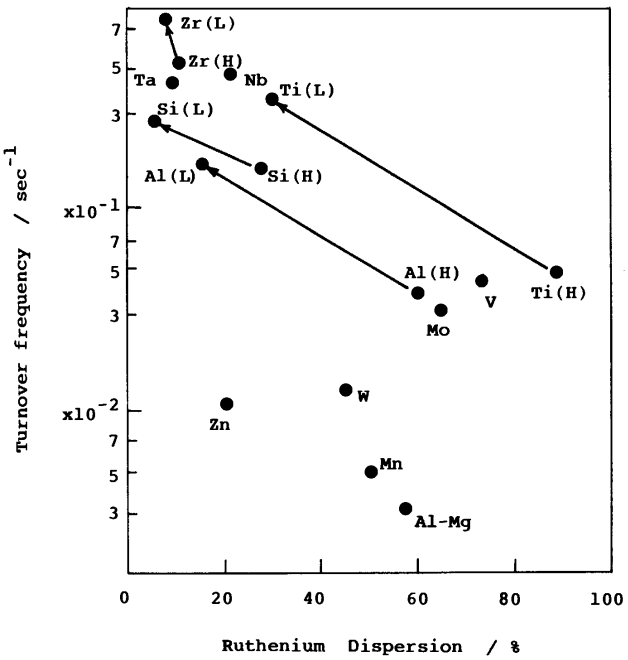

Fig. 6. Turnover frequency *vs.* ruthenium dispersion of supported ruthenium catalyst. Temperature: 503 K, Pressure : 2.03 MPa, H_2/CO : 2/1 mole ratio.

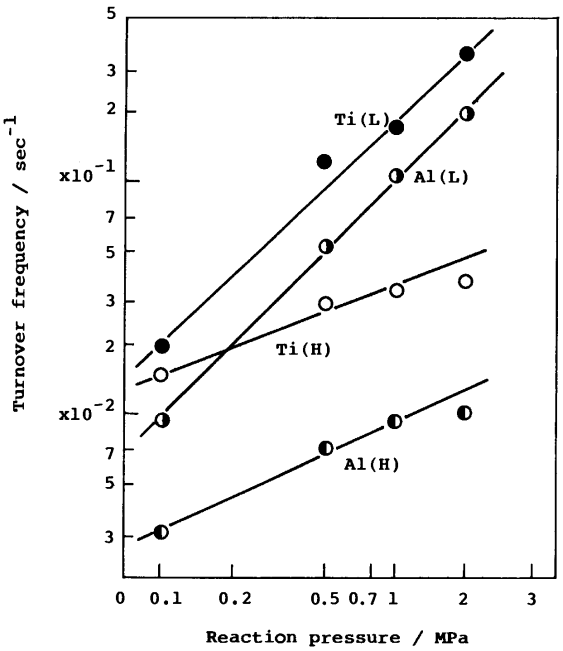

Fig. 7. Pressure dependency of the Ti–H, Ti–L, Al–H, and Al–L catalysts. Temperature: 503 K, H_2/CO: 2/1 mole ratio.

hydrogenation and by Kellner *et al.*[4] for the atomospheric Fischer-Tropsch synthesis. Not only the TOF but also activities per unit weight of ruthenium are higher for L-catalysts than for H-catalysts (Table 2). Thus, the fairly poor dispersion (less than 30%) of ruthenium is favored for the high activity of F-T synthesis. The reason for the high activity of the low-dispersed ruthenium has been discussed by Kellner *et al.*[4] however, the real reason has not been made clear yet. The L-catalyst exhibits, as will be shown in the later chapter, high activity under high reaction pressures.

On a similar dispersion basis, ruthenium showed a high activity when it was supported on Nb_2O_5, TiO_2, ZrO_2, SiO_2, or Ta_2O_5. ZnO, MnO_2, WO_3, and Al–Mg oxide showed poor abilities as carriers of ruthenium. Thus, it can be concluded that the selection of a carrier is also one of the essential factors in effecting catalytic activity. The effect of carrier materials on catalytic activity may be ascribed not only to the difference in metal dispersion, but also to some interaction between the carrier and the metal. In fact, by using carriers such as Nb_2O_5, TiO_2, Ta_2O_5, and V_2O_3, known to exhibit a SMSI effect,[10–12] highly active catalysts could be prepared.

Pressure Characteristics. It was also found that the degree of ruthenium dispersion affects the pressure characteristics of catalytic activity. It is very clear from Fig. 7 that the catalytic activity of a TiO_2-supported H-catalyst (Ti–H catalyst) increases markedly with an increase in pressure from 0.1 MPa to 0.51 MPa. However, above this the increase in the activity is quite small. The activity of a Ti–L catalyst increases almost linearly up to a pressure of 2.03 MPa. Thus, the activity of a H-catalyst is higher than that of a L-catalyst under atmospheric pressure, the reverse is true above 1.01 MPa. Not only the TiO_2 supported catalyst, but also the Ru/Al_2O_3 catalysts exhibit the same characteristics.

As can be seen in Fig. 7, the average reaction orders with respect to the total pressure at H_2/CO=2/1 were determined to be about 1 for both Ti–L and Al–L catalysts while those of Ti–H and Al–H catalysts are 0.4 and 0.6, respectively. It has been reported that the reaction order of the F-T reaction over Ru/Al_2O_3 catalysts are close to or higher than 1.0 with respect to hydrogen, whereas it is zero or negative with respect to carbon monoxide.[13,14] As the reaction order with respect to the total pressure is the sum of the orders with respect to the partial pressures of carbon monoxide and hydrogen, the low reaction order of an H-catalyst may due to a negative reaction order with respect to carbon monoxide. However, the details must be determined in further studies.

Controlling Factors of Product Selectivity.

a. Chain Growth. Figure 8 shows carbon number distributions of gaseous products under a standard condition with the above-mentioned 4 types of H- and L-catalysts. It is obvious that the distribution is less steep for L-catalysts than for H-catalysts, without exception. This indicates that the chain-growth probability is higher for L-catalysts. Figure 9 exhibits a clear inverse relationship between the dispersion and the growth probability, irrespec-

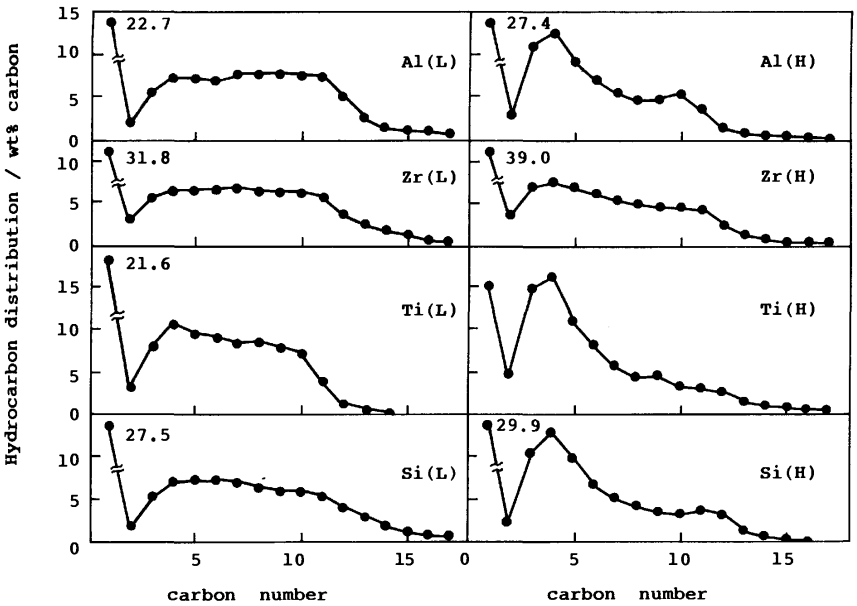

Fig. 8. Carbon number distribution of gaseous produts on L and H type ruthenium catalysts. Temperature: 503 K, Pressure: 2.03 MPa, H_2/CO : 2/1 mole ratio.

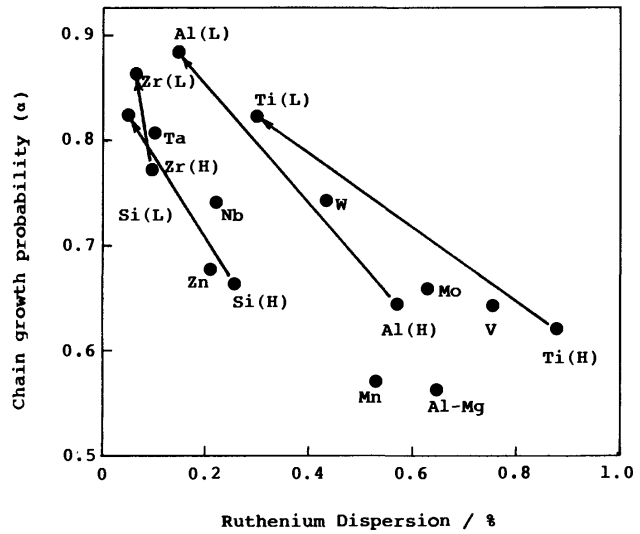

Fig. 9. Chain growth probability *vs.* ruthenium dispersion of supported ruthenium catalysts. Temperature: 503 K, Pressure: 2.03 MPa, H_2/CO : 2/1 mole ratio.

tive of carrier materials. It is also apparent that the calcination of the supported ruthenium chloride in air prior to hydrogen reduction caused the growth of ruthenium particles as well as the increase in the chain-growth probability. The results coincide well with that of Jacobs *et al.*[21], namely the values of α are mostly higher than 0.8 when the dispersion level is lower than 0.3. Thus, the regulating the dispersion level of ruthenium is one of the most effective methods for controlling the activity and the chain-growth ability of a catalyst.

Carrier material is also an important factor for regulating the α value. Ruthenium metals supported on TiO_2, Al_2O_3, or WO_3 exhibit high α values for a similar dispersion level. Among them, TiO_2 is an excellent carrier for a ruthenium catalyst with either CO conversion or carbon–carbon bond formation, as has already been shown.[16,17] However, supported ruthenium particles with the dispersion levels of 10% or lower exhibit high chain-growth probabilities irrespective of the carrier materials. This fact suggests that the carrier effect is reduced at low dispersion since there is a small contact area between ruthenium particle and the carrier surface.

b. Deviation from Schulz-Flory Distribution. Several examples have been reported where products on supported ruthenium catalysts do not follow the S-F distribution.[18–20] Jacobs *et al.* suggested that the unique distributions can be well simulated by assuming that the maximum carbon number of product hydrocarbon depends upon the sizes of metal particles.[21] In the present work, the S-F plots (Figs. 4 and 5) of products show that the distribution for an H-catalyst can be expressed by two straight lines, wheares that for an L-catalyst is well approximated by one straight line. The values of α obtained from the slopes of the plots are 0.87 for the Ti-L-catalyst, while 0.65 and 0.8 for the Ti-H-catalyst, respectively. The approximation using two staight lines had been also reported.[22]

The present authors explain the phenomenon as follows: It is common that a supported metal catalyst has a wide distribution regarding the size of metal particles when it is prepared by the impregnation method.[8] Thus, an H-catalyst should have particles with both "high" and "low" dispersions. The critical dispersion level of "high" and "low" is

Table 3. Isoparaffin formation[a)]

Catalyst	Ru/MoO_3	Ru/WO_3	Ru/TiO_2+WO_3[b)]	Ru/TiO_2+WO_3[b,c)]
Time Factor (W/F)	11.0	22.4	12.5	12.5
CO conversion/%	16.0	9.2	10.7	18.6[c)]
Hydrocarbon distribution/c-wt%				
C_1	24.8	12.4	16.1	18.1
C_2	6.6	3.3	5.3	4.3
C_3	10.8	5.6	10.2	9.0
C_4	11.8(0.4)[d)]	15.5(2.8)[d)]	15.5(>0.1)[d)]	15.8(0.2)[d)]
C_5	7.6(0.8)	15.4(50.4)	14.7(0.4)	13.2(1.0)
C_6	9.4(1.3)	13.8(8.2)	9.3(0.4)	10.6(1.7)
C_7	6.6(1.3)	12.2(10.0)	7.3(0.5)	8.4(2.0)
C_8	5.1(1.3)	9.9(8.0)	6.9(0.4)	6.8(3.0)
C_9	4.0(1.4)	5.7(8.5)	4.7(0.6)	5.6(3.7)
C_{10}^+	13.2	6.0	10.1	9.8

a) Temperature: 230 °C, Pressure: 21 bar, H_2/CO: 2/1. b) Ru/TiO_2: 20 wt%, WO_3: 80 wt%. c) 250 °C. d) Branched product/normal product.

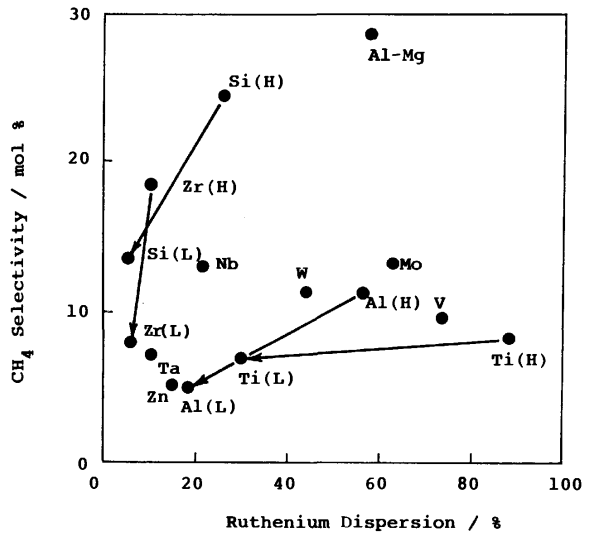

Fig. 10. Methane selectivity *vs.* ruthenium dispersion of supported ruthenium catalysts. Temperature: 503 K, Pressure : 2.03 MPa, H_2/CO : 2/1 mole ratio.

estimated to be about 30%, as described above. This classification is based on our finding that the chain-growth ability of a supported ruthenium catalyst is definitely divided at 30% of the dispersion.[23)] The products on the high- and low- dispersion particles supported on TiO_2 should have the α values of 0.65 and 0.87, respectively, under the conditions adopted. On the other hand, all metal particles on the Ti-L-catalyst should have a dispersion lower than 30%. Since smaller particles can easily aggregate to become large particles, due to sintering during air calcination,[8)] all products on these particles must have a chain-growth probability of 0.87.

c. Methane Selectivity. Points on plots of CH_4 selectivity *vs.* dispersion are scattered widely (Fig. 10). This suggests that the relationship between them is poor. However, for each set of the four carriers (TiO_2, Al_2O_3, ZrO_2, SiO_2) a decrease in the dispersion is necessarily accompanied by a decrease in the CH_4 selectivity. So long as the decrease in the dispersion brings about an increase in the chain-growth probabbility, as pointed out in the present paper, a decrease in the CH_4 selectivity can be expected due to the S-F equation. However, since the drastic decrease in the CH_4 selectivity (about 50%) for Ru/SiO_2 and the Ru/ZrO_2 catalysts is unable to be explained by the S-F theory, some unknown dispersion effect remains to be accounted for. Also, carrier materials, themselves, are the controlling factors of CH_4 selectivity. SiO_2, ZrO_2, Al-MgO_x, and Nb_2O_5 are favored for CH_4 formation whereas V_2O_5, TiO_2, Al_2O_3, and ZnO are effective for suppressing CH_4 formation. Thus, it is concluded a low-dispersion ruthenium catalyst supported on Al_2O_3 or TiO_2 is favored for selectively producing liquid hydrocarbons.

d. Isoparaffin Formation. It is interesting to note that with the MoO_3- and the WO_3- supported catalysts, methane selectivities are fairly low in spite of the low olefin contents in the products. Also, the high selectivities of isoparaffins are obtained, which are scarcely observed in products with other catalysts. These phenomena were especially marked in the case of the WO_3 carrier. As shown in Table 3, the ratio of branched paraffins to normal paraffins (i/n ratio) in hydrocarbons from C_4 to C_{10} is higher than 20 (in total). Isoparaffin formation was also observed (to some extent) when a mixed catalyst consisting of 2 wt% Ru/TiO_2 and WO_3 was subjected to a synthesis-gas reaction. The i/n ratio increased with an increased reaction temperature as demonstrated in Table 3. Isoparaffin formation could be attributed to the acidic character of MoO_3 and WO_3,[7)] which isomerize n-olefins produced on the ruthenium metal to isoolefins which are then hydrogenated to isoparaffins on the carriers or on the ruthenium.

Conclusion

It has been found that the specific activity of supported ruthenium for a synthesis-gas reaction is determined by both carrier materials and ruthenium dispersion, and the selectivity (carbon number distribution of product hydrocarbon) is essentially determined by the dispersion or particle-size distribution, but rather independent of the carrier.

Carrier materials affect both ruthenium dispersion and its catalytic activity. In more detail,

1) Carrier materials which are effective for giving small metal particles are V_2O_5, TiO_2, and Al_2O_3.

2) ZrO_2, SiO_2, TiO_2, and Nb_2O_3 promote the catalytic activity of ruthenium on them.

Effects of ruthenium dispersion on its catalysis are summarized as:

1) The specific activities of supported ruthenium catalysts increase markedly as the dispersion decreases, irrespective of the carrier materials.

2) Low-dispersion ruthenium exhibits a higher chain-growth probability, which is little affected by carrier materials.

3) The chain-growth probability is not uniform for a highly dispersed catalyst, which is suggested to be attributed to the wide distribution of particle sizes.

4) Catalytic activities of low-dispersion catalysts increase almost linearly up to a pressure at about 2.03 MPa. However, those of highly dispersed catalysts level off at around 1.01 MPa.

5) Isoparaffins are formed with high selectivities on MoO_3 and WO_3 supported catalysts. It is suggested that this is caused by their acid character.

References

1) F. S. Karn, J. F. Shultz, and R. B. Anderson, *Ind. Eng. Chem. Prod. Res. Dev.*, **4**, 265 (1965).

2) H. Shulz, "Chemierohstoffe aus Kohle" ed by J. Farbe, George Thieme Verlag, Stuttgart, (1977) pp. 334—355.

3) M. A. Vannice, *J. Catal.* **37**, 449 (1975).

4) C. S. Kellner and A. T. Bell, *J. Catal.* **71**, 288 (1981).

5) T. Fukushima, T. Nobusawa, K. Fujimoto, and H. Tominaga, *Nippon Kagaku Kaishi*, **1982**, 206.

6) E. Kikuchi, H. Nomura, M. Matsumoto, and Y. Morita, *App. Catal.*, **7**, 1 (1983).

7) D. L. King, *J. Catal*, **51**, 386 (1978).

8) J. R. Anderson, "Structure of Metallic Catalysts" Academic Press (1975).

9) K. Fujimoto, Y. Kudo, and H. Tominaga, *Nippon Kagaku, Kaishi*, **1982**, 207.

10) S. J. Tauster, S. C. Fung, and R. L. Garten, *J. Am. Chem. Soc.*, **100**, 170 (1978).

11) S. J. Tauster and S. C. Fung, *J. Catal*, **55**, 29 (1978).

12) K. Foger, *Catalysis, Science and Technology*, **6**, Springer Verlag (1984), p. 227.

13) M. A. Vannice, *Catal. Rev. -Sci. Eng*, **14**, 153 (1976).

14) R. B. Anderson, in "The Fischer-Tropsch Synthesis," Academic Press, (1984) p. 116.

15) K. Fujimoto, M. Kameyama, and T. Kunugi, *J. Catal*, **61**, 7 (1980).

16) M. A. Vannice and R. L. Garten, *J. Catal*, **56**, 236 (1979).

17) M. A. Vannice and R. L. Garten, *J. Catal*, **66**, 242 (1980).

18) J. R. Madon, *J. Catal*, **57**, 183 (1979).

19) Y. Okamura, Y. Iwasawa, K. Domen, and T. Onishi, 49th National Meeting of the Chemical Society of Japan, Tokyo, April 1984, Abstr., No. 1P05.

20) H. H. Nijs, P. A. Jacobs, and J. B. Uytterhoeven, *J. Chem. Soc., Chem. Commun.*, **1979**, 180.

21) H. H. Nijs and P. A. Jacobs, *J. Catal.*, **65**, 328 (1980).

22) C. N. Satterfield, G. A. Huff, and R. Summerhayes, *J. Catal.*, **80**, 486 (1983).

23) K. Fujimoto, M. Miyauchi, and H. Tominaga, 49th National Meeting, Japan Catalysis Society (1984).

 © 1985 The Chemical Society of Japan Bull. Chem. Soc. Jpn., 58, 3172—3175 (1985) [Vol. 58, No. 11

The Thermodynamic Behaviour of Nickel in a Molten LiF-KF-O^{2-} System

Yasuhiko ITO,* Hidetaka HAYASHI,† Yasuhiko ITOH,† and Shiro YOSHIZAWA†

Department of Nuclear Engineering, Faculty of Engineering, Kyoto University, Sakyo-ku, Kyoto 606

†*Department of Industrial Chemistry, Faculty of Engineering, Kyoto University, Sakyo-ku, Kyoto 606*

(Received May 20, 1985)

The thermodynamic behaviour of nickel in a molten LiF-KF-O^{2-} system was investigated by using $Pt(O_2)$/stabilized zirconia electrode as an oxide-ion-concentration indicator. The potentials of the $Pt(O_2)$/stabilized zirconia/LiF-KF-O^{2-} electrode and the Ni/NiO/LiF-KF-O^{2-} electrode at 550 °C were measured as :

$$E = 2.25 - \frac{RT}{2F} \ln X_{O^{2-}} \quad \text{(V. } vs. \text{ Li-K/Li}^+, \text{ K}^+\text{)}$$

and:

$$E = 1.42 - \frac{RT}{2F} \ln X_{O^{2-}} \quad \text{(V. } vs. \text{ Li-K/Li}^+, \text{ K}^+\text{)}$$

respectively. The solubility product of NiO in the melt was thus determined to be $K_{sp}=1.3\times10^{-6}$ at 550 °C. With these results, a potential-pO^{2-} diagram of the nickel in the system was presented.

Molten fluoride is a useful material for use in many energy processes, such as the Molten Salt Breeder Reactor and heat-storage systems.[1] To use this melt for such purposes, however, it is necessary to protect the metal container from the corrosion caused by any oxidizing agents as contaminated water and oxygen. The corrosion behaviour of metals in a fluoride melt is strongly dependent on the oxide film formed on the metal surface, the stability of which is influenced by the redox potential and the oxide-ion concentration in a melt system.

In this paper, an LiF-KF eutectic melt containing oxide ions has been selected as an example of a fluoride melt, and the oxide concentration and solubility product of NiO in this melt have been determined by the use of a stabilized zirconia electrode. Finally, a potential-pO^{2-} diagram of nickel has been constructed on the basis of a thermochemical analysis of this system. Recently it has been shown that a stabilized zirconia solid electrolyte can be used as an oxide-ion-concentration indicator in melt systems, especially molten chloride systems. Also, the solubility product of metal oxide,[2-4] and the chemical equilibrium associated with oxide ion[5] have been investigated by using this electrode. However, in molten fluoride systems, the solubility products of oxide were mainly determined by a chemical analysis method[6,7] that may derive higher solubility product values caused by colloidal metal oxide; this type of electrode has not been used as an oxide-ion indicator. By the use of a stabilized zirconia oxide indicator, not only a rigorous value of the solubility product, but also direct thermodynamic information about the oxide ion in the melt can be obtained.

Thermodynamic Description

By means of a constant-current electrolysis of a molten LiF-KF-O^{2-} system, the Li-K alloy is formed on the cathode; its composition is almost constant (Li:K=2:1) independent of the current densities.[8] That is, the single-electrode potential of the Li-K/Li^+, K^+ couple can be chosen as a common reference electrode in this system. In this paper, as will be described later, the potentials were measured with respect to a quasi-reference electrode, such as the Ni/NiO or Ni/NiF_2 electrode, but the data obtained were converted to the potential against the Li-K/Li^+, K^+ couple.

The emf of the electrochemical cell:

$$\text{Li-K/LiF-KF-O}^{2-}\text{/stabilized } ZrO_2/O_2(Pt) \qquad (1)$$

will obey the following Eq. 2 if the stabilized zirconia acts as an oxide-ion-concentration indicator:

$$E = E^\circ_{O_2/O^{2-}} - \frac{RT}{2F} \ln X_{O^{2-}} \qquad (2)$$

$X_{O^{2-}}$ represents the anionic mole fraction of the oxide ion in the melt. By the use of Eq. 2, the thermodynamic behaviour of nickel in this system can be described as below. To simplify the situation, only three chemical species are considered in this paper: Ni(s), the Ni(II) ion, and NiO(s). Among these three species, there exist the following three electrochemical or chemical equilibria:

$$\text{Ni(II)} + 2e^- = \text{Ni(s)} \qquad (3)$$

$$\text{NiO(s)} + 2e^- = \text{Ni(s)} + O^{2-} \qquad (4)$$

$$\text{NiO(s)} = \text{Ni(II)} + O^{2-} \qquad (5)$$

The equilibria involving the trivalent nickel ion, *e.g.* Ni(III) and Ni_2O_3(s), are not considered in this paper, since their existence has not been reported in the literature.[9]

The Nernst equation corresponding to the electrochemical equilibria 3 and 4 are expressed as Eqs. 6 and 7 respectively, while the equilibrium constant of Eq. 5 is expressed as Eq. 8 with the use of the solubility product of NiO, K_{sp}:

$$E_{Ni/Ni(II)} = E^\circ_{Ni/Ni(II)} + \frac{RT}{2F} \ln X_{Ni(II)} \quad (6)$$

$$E_{Ni/NiO} = E^\circ_{Ni/NiO} - \frac{RT}{2F} \ln X_{O^{2-}} \quad (7)$$

$$K_{sp} = X_{Ni(II)} \cdot X_{O^{2-}} \quad (8)$$

(when the melt is saturated with NiO(s))

When the melt is saturated with NiO, $E_{Ni/Ni(II)}$ is equal to $E_{Ni/NiO}$; hence, from Eqs. 6, 7, and 8, Eq. 9 can be derived:

$$E^\circ_{Ni/NiO} = E^\circ_{Ni/Ni(II)} + \frac{RT}{2F} \ln K_{sp} \quad (9)$$

For the drawing of the Potential-pO^{2-} diagram, the determination of the values of $E^\circ_{Ni/Ni(II)}$, $E^\circ_{Ni/NiO}$, and K_{sp} would seem to be necessary, but, as Eq. 9 is valid, it is sufficient to measure the values of K_{sp} and $E^\circ_{Ni/NiO}$. The K_{sp} value can be obtained from the emf response of the cell (1) to the amount of metal oxide (NiO in this case) added to the melt. That is, when the amount of NiO added to the melt is small, free oxide ions are produced corresponding to the amount of NiO added, and the potential shifts to the negative side according to the Nernst Eq. 2. However, once the melt is saturated with NiO, the added NiO does not dissociate any more and the emf remains constant. Hence, the intersection of the two lines gives the solubility of NiO, from which the solubility product, K_{sp} can be calculated by means of Eq. 10:

$$K_{sp} = [X^\circ_{NiO(added)}]^2 = [X^\circ_{Ni(II)(added)}][X^\circ_{O^{2-}(added)}] \quad (10)$$

where X°_{NiO} is the solubility of NiO.

Concerning the value of $E^\circ_{Ni/NiO}$, it can be calculated from the standard electrode potential, $E^\circ_{O_2/O^{2-}}$, of the reaction:

$$1/2\,O_2 + 2e^- = O^{2-} \quad (11)$$

and the difference ($E^\circ_{O_2/O^{2-}} - E^\circ_{Ni/NiO}$) which can be calculated from the standard free-energy change of the reaction:

$$NiO(s) = Ni(s) + 1/2O_2$$

Experimental Method and Apparatus

The experimental cell is shown in Fig. 1.

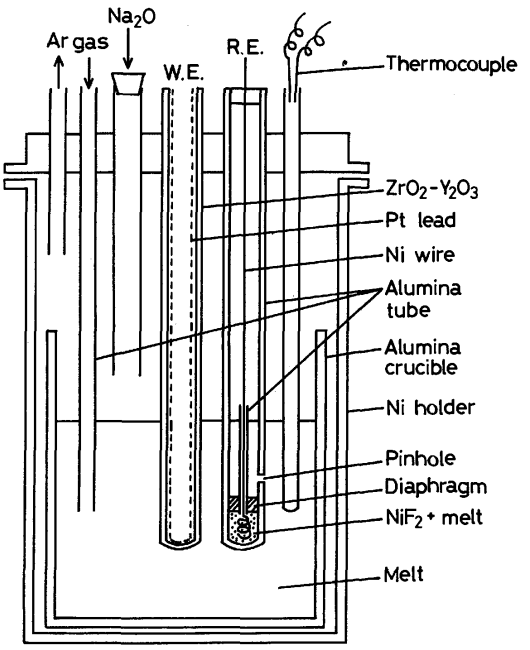

Fig. 1. Experimental cell.

Commercial LiF and KF (Reagent Grade, Wako Chemicals Co., Ltd.) were mixed, and the eutectic mixture was dried under a vacuum for a week at 200 °C, after which it was placed in a high-purity alumina crucible (Nippon Kagaku Togyo Co., Ltd., SSA-S) and melted under an argon (water content<10 ppm) atmosphere at 550 °C. By this procedure, the oxide-ion-concentration level could be reduced to the order of 10^{-4} mole fraction.[10] For an oxide ion indicating electrode, an yttria- or magnesia-stabilized zirconia tube (Nippon Kagaku Togyo Co., Ltd.) was used. The inside of the tube was coated with a platinum powder layer which acted as an air electrode. The measured emf was converted to the potential of the oxygen (Pt)/stabilized zirconia electrode, taking into account the partial pressure of oxygen in air. Several types of electrodes, for example, NiF_2/Ni and NiO/Ni electrodes, were used as quasi-reference electrodes, according to the experimental conditions. The potential of the quasi-reference electrode was calibrated *versus* the Li-K/Li^+, K^+ electrode potential before use. By means of a constant-current electrolysis between the graphite anode and the stainless-steel cathode, Li-K alloy of a finite composition (Li:K=2:1)[8] was deposited on the cathode. The cathode potential measured against the quasi-reference electrode was kept constant for several tens of minutes after the current interruption. From this constant potential value, the potential of the quasi-reference electrode against the Li-K/Li^+, K^+ electrode was determined. The oxide-ion concentration in the melt was controlled by adding the appropriate amount of dry Na_2O (Aldrich Co., Ltd.). For the solubility-product measurement of NiO(s), commercial NiO(s) (Wako

Chemicals Co., Ltd.) was added to the melt. The Ni/NiO electrode could be prepared by baking nickel wire for several tens of minutes in air at around 900 °C.

Results and Discussion

The relation between emf of the cell(1) and the oxide-ion concentration is shown in Fig. 2. A clear Nernst relation can be observed in the figure. From this straight line, obtained experimentally, the potential of the $Pt(O_2)$/stabilized zirconia/LiF-KF-O^{2-} electrode can be written as:

$$E = 2.25 - \frac{RT}{2F} \ln X_{O^{2-}} \text{ (V. vs. Li-K/Li}^+, \text{K}^+) \qquad (2')$$

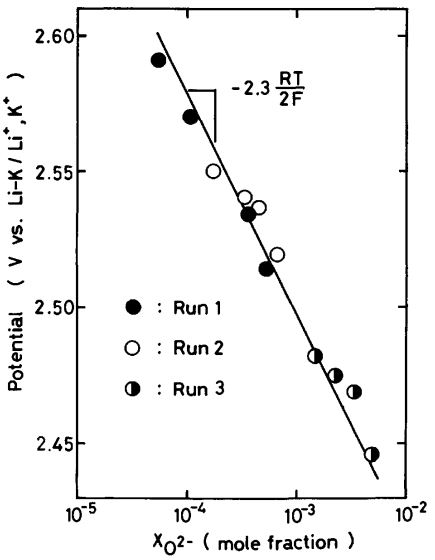

Fig. 2. Relation between emf of the cell: Li-K/LiF-KF-O^{2-}/stabilized zirconia/$Pt(O_2)$ and oxide-ion concentration.

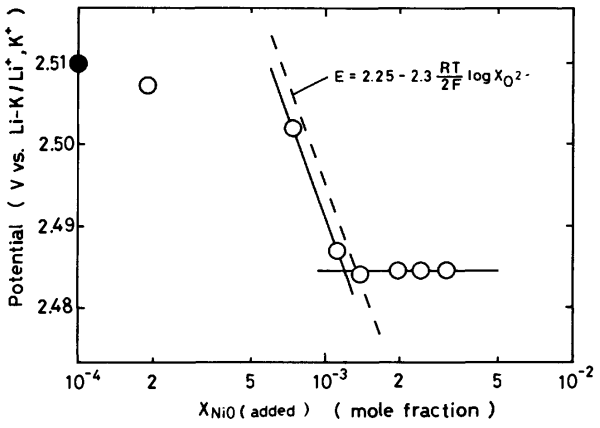

Fig. 3. Relation between $Pt(O_2)$/stabilized zirconia/LiF-KF-O^{2-} electrode potential and the added cmount of NiO (mole fraction).

Figure 3 shows the relation between the $Pt(O_2)$/stabilized zirconia/LiF-KF-O^{2-} electrode potential and the added NiO (expressed as a mole fraction). In the figure, the closed circle represents the potential before the addition of the NiO. This potential is determined by the concentration of the oxide ion contaminating the melt. In an early stage of the increase in the amount of NiO added, the potential response is not so quantitative because of the contaminating oxide ion, but when the amount of added NiO exceeds the contamination level, the potential shifts towards the negative side, obeying the Nernst equation. When the NiO in the melt is saturated, the potential remains constant at any amount of added NiO. From the intersection of the two lines, the K_{sp} values can be calculated by the use of Eq. 10.

In a practical calculation, however, the oxide-ion concentration, $X^\circ_{O^{2-}}$, due to the contamination before the experiment should also be taken into account. That is, the Ni(II)-ion concentration in the NiO-saturated melt is the difference between the measured oxide-ion concentrations, $X_{O^{2-}}$, and $X^\circ_{O^{2-}}$, thus, Eq. 10 is rewritten as:

$$K_{sp} = X_{Ni(II)} \cdot X_{O^{2-}} = [X_{O^{2-}} - X^\circ_{O^{2-}}] \cdot X_{O^{2-}} \qquad (10')$$

From Eq. 10′ and Fig. 3, and several other similar experimental results like Fig. 3 which are not given in this paper, the averaged K_{sp} value was determined to be 1.3×10^{-6} at 550 °C.

By the method described above, $E^\circ_{Ni/NiO}$ can be calculated from the standard free-energy change of reaction (12) and the $E^\circ_{O_2/O^{2-}}$ value of 2.25 V appearing in Eq. 2′ to be 1.42 V. That is, Eq. 7 is rewritten as:

$$E_{Ni/NiO} = 1.42 - \frac{RT}{2F} \ln X_{O^{2-}} \qquad (7')$$

The validity of Eq. 7′ was confirmed experimentally by using a cell similar to that in Fig. 1 and measuring the emf of the cell:

$$\text{Ni/NiO/LiF-KF-O}^{2-}\text{/stabilized zirconia/O}_2\text{(Pt)} \qquad (13)$$

The emf change of this cell with the time is shown in Fig. 4. About 2 h after the immersion of the Ni/NiO electrode in the melt, the emf remains almost constant at around 830 mV. This value exactly coincides with the value calculated from the difference between Eqs. 2′ and 7′.

From the data obtained above, the potential-pO^{2-} diagram of Ni-LiF-KF-O^{2-} system can be drawn as in Fig. 5.

After the experiment, the stabilized zirconia tube was examined carefully by visual observation; no mechanical damage nor chemical corrosion could be

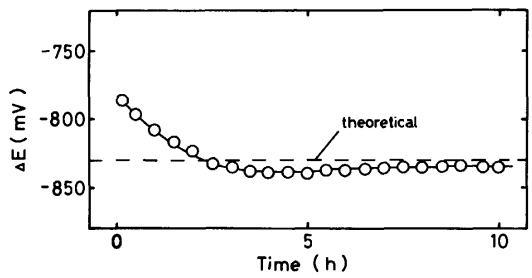

Fig. 4. Emf change of the cell: Ni/NiO/LiF–KF–O^{2-}/stabilized zirconia/Pt(O_2) with immersion time.

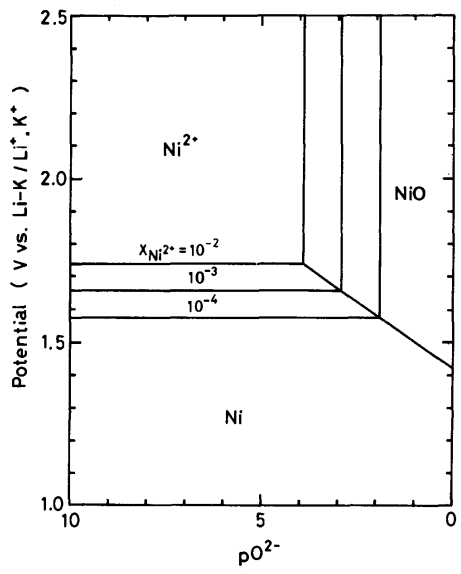

Fig. 5. Potential-pO^{2-} diagram of Ni–LiF–KF–O^{2-} system at 550 °C.

observed. During the whole experiment, reproducible measurements were possible. From these facts, it seems that stabilized zirconia can be used for an oxide-ion-concentration measurement in a fluoride melt at 550 °C.

Conclusion

The thermodynamic behaviour of nickel in a molten LiF–KF–O^{2-} system was investigated, and a potential-pO^{2-} diagram of the nickel in the system was presented, in which stabilized zirconia played an important role in measuring the oxide-ion concentration in the melt. The potential of the Pt(O_2)/stabilized zirconia/LiF–KF–O^{2-} electrode and the potential of the Ni/NiO/LiF–KF–O^{2-} electrode can be written as:

$$E = 2.25 - \frac{RT}{2F} \ln X_{O^{2-}} \quad \text{(V. } vs. \text{ Li-K/Li}^+, \text{ K}^+\text{: 550 °C)}$$

and:

$$E = 1.42 - \frac{RT}{2F} \ln X_{O^{2-}} \quad \text{(V. } vs. \text{ Li-K/Li}^+, \text{ K}^+\text{: 550 °C)}$$

respectively.

The solubility product of NiO in the melt was determined to be $K_{sp}=1.3\times10^{-6}$ at 550 °C.

Further refinement of the experimental technique might be necessary to get more rigorous and wider information. Especially, the improvement of the melt-purification technique and improvement of zirconia solid electrolyte might help us to get more reliable data. At least, though, this paper has shown that our method of using stabilized zirconia can offer useful information about the behaviour of metals in an oxide-ion-containing fluoride melt.

This work was supported by a Grant-in-Aid from the Ministry of Education, Science, and Culture.

References

1) "Molten Salt Technology," ed by D. G. Lovering Plenum Press (1982); "Advances in Molten Salt Chemistry," ed by C. E. Bamberger, Plenum Press (1975), Vol. 3.

2) R. Combes, M. N. Levelut, and B. Tremillon, *Electrochim. Acta*, **23**, 1291 (1978).

3) R. Combes, F. de Andrade, A. de Barros, and H. Ferreira, *Electrochim. Acta*, **25**, 371 (1980).

4) M. L. Deanhardt and K. H. Stern, *J. E. C. S.*, **128**, 2577 (1981).

5) K. H. Stern, *J. E. C. S.*, **127**, 2375 (1980).

6) C. E. Bamberger, R. G. Ross, and C. F. Baes, Jr, *J. Inorg. Nucl. Chem.*, **33**, 767 (1971).

7) C. E. Bamberger, R. G. Ross, and C. F. Baes, Jr., *J. Inorg. Nucl. Chem.*, **35**, 433 (1973).

8) K. Ema, Y. Ito, T. Takenaka, and J. Oishi, Abstract of the Spring Meeting of the Electrochemical Society of Japan (Yamanashi Pref., April, 1985).

9) J. A. Plambeck, "Encyclopedia of Electrochemistry of the Elements," Vol. X, Fused Salt Systems, ed by A. J. Bard, Marcel Dekker, New York (1976), Chap. 13, p. 349.

10) Y. Ito, T. Takenaka, K. Ema, and J. Oishi, *Denki Kagaku*, **51**, 864 (1983).

 © 1985 The Chemical Society of Japan Bull. Chem. Soc. Jpn., 58, 3176—3192 (1985) [Vol. 58, No. 11

Use of Propagators in the Hückel Model. VII. Thermochemical and Photochemical Rearrangement in Cycloheptatriene, Tropone, and Related Compounds

Masaaki YAMAMOTO, Kiyoshi NISHIKAWA, and Shigeyuki AONO*
Department of Chemistry, Faculty of Science, Kanazawa University, Marunouchi, Kanazawa 920
(Received March 4, 1985)

Hückel propagator theory has been applied to the analysis of photochemical and thermochemical rearrangement reactions, such as [1,3] sigmatropy, valence isomerization of norcaradiene, Cope rearrangement *et al.* In treatments employing the frontier orbital theory, the molecule is sometimes separated into two parts, and the orbital interaction between specified orbitals of two fragments is taken into account. In the propagator theory, the molecule is always considered as a whole, assuming a resonable transition state. In this transition state, the bond order between sites responsible for the reactions under consideration is estimated, and then the perturbing interaction between these sites is introduced. Then we can evaluate the extra energy to determine whether the reaction occures or not.

In the Hückel model the propagator is expressed in the M.O. basis set $\{|n>\}$ as[1)]

$$G(z) = \sum_n \frac{|n><n|}{z-\varepsilon_n}, \tag{1}$$

where ε_n and z are the energy eigenvalue and the complex variable, respectively. Using this propagator, we can easily obtain the bond order q_{rs} between sites r and s, and total energy as[1)]

$$q_{rs} = \frac{1}{2\pi i}\int_c G(r,s;z)\mathrm{d}z, \tag{2}$$

$$E = Tr\frac{1}{2\pi i}\int_c G(z)z\mathrm{d}z, \tag{3}$$

where integration is carried out along the Coulson contour which encloses poles of propagator corresponding to the occupied energy levels, and is assumed to include the spin summation.

In the previous papers, we have presented the perturbation theory[1)] to treat the chemical stability and reactivity,[2)] and the reactivity in the radiation field.[3)] Here we restrict ourselves to take into account the first order term with respect to the perturbation V. This is enough to the following analysis. The first order energy ΔE and that in the radiation field ΔE_f are given as follows:

$$\Delta E = \sum_{r,s} V_{rs}\frac{1}{2\pi i}\int_c G(s,r;z)\mathrm{d}z = \sum_{r,s} V_{rs}q_{sr}, \tag{4}$$

$$\Delta E_f = \frac{n|f_{\mathrm{HL}}|^2}{(\varepsilon_{\mathrm{LH}}-\omega)^2}\sum_{r,s} V_{rs}(q_{sr}^{\mathrm{L}}-q_{sr}^{\mathrm{H}}) \propto \sum_{r,s} V_{rs}(q_{sr}^{\mathrm{L}}-q_{sr}^{\mathrm{H}}). \tag{5}$$

The former is responsible for the thermochemical reaction, while the latter for the photochemical reaction. In the aboves, q_{rs} and q_{rs}^{P} are, respectively, the bond order and the partial bond order between r and s sites. f_{HL} is the interaction matrix element between electron and radiation field, and n and w are photon number and angular frequency. L and H represent LUMO and HOMO, respectively, and $\varepsilon_{\mathrm{LH}}=\varepsilon_{\mathrm{L}}-\varepsilon_{\mathrm{H}}$. In considering chemical reactivity for possible reaction pathes more over two, we can select, as a preferable reaction path. one with the lowest ΔE or ΔE_f. If the interaction is introduced only between r and s sites, Eqs. 4 and 5 simply become as

$$\Delta E \fallingdotseq 2Vq_{rs}, \tag{6}$$

$$\Delta E_f \propto Vq_{rs}^{\mathrm{LH}}, \tag{7}$$

where note that $V=V_{rs}=V_{sr}$, $q_{rs}=q_{sr}$, and $q_{rs}^{\mathrm{LH}}=q_{sr}^{\mathrm{LH}}$. The condition that $\Delta E<0$, which indicates the chemical bond being formed, holds for the following two cases:

$$q_{rs}<0,\ V>0 \quad \text{or} \quad q_{rs}>0,\ V<0. \tag{8}$$

The treatment of photochemical reaction is the same as that of thermochemical reaction except that we are using the partial bond order, and the condition that $\Delta E_f<0$ holds for the following two cases:

$$q_{rs}^{\mathrm{LH}}<0,\ V>0 \quad \text{or} \quad q_{rs}^{\mathrm{LH}}>0,\ V<0. \tag{9}$$

Accordingly, we have only to know the bond order or the partial bond order of molecule in question.

The sign of V_{rs} depends on phases of basis sets $|r>$ and $|s>$. Usually the direction of the basis set $\{|r>\}$ is determined so that the resonance integral β should be negative. In the case of π-electron system, and the sign of V_{rs} is negative when $|r>$ and $|s>$ have a facial symmetry, and positive when $|r>$ and $|s>$ have a point symmetry (see Fig. 1(a)).

However, V_{rs} generally has π- and σ-components. The former is perpendicular to the bond axes and the latter parallel. Interaction with the basis set of no direction, for example, the 1s orbital, has only the σ-component (see Fig. 1(b)). These considerations

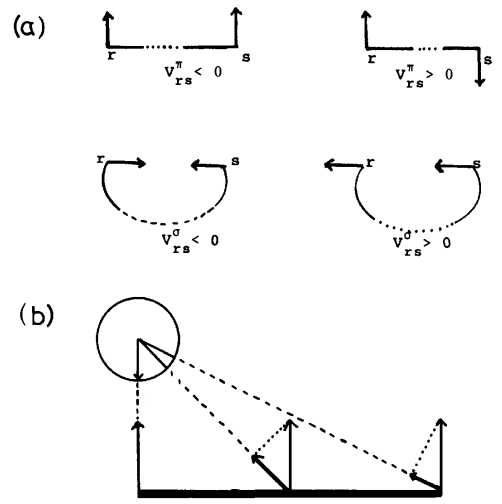

Fig. 1. Example of sign of V_{rs}.
(a) interactions between p orbitals, (b) interactions between s and p orbitals.

play a important role in the sigmatropic and ring closure reactions. For the ring closure reaction, there are two modes named conrotatory and disrotatory. If the π-orbitals are concerned with this, the relationship between the sign of V_{rs} and the mode are as follows ($V^{\sigma}_{rs}=V^{\sigma}_{sr}=V$):

$$V > 0 \text{ ; conrotatory,}$$
$$V < 0 \text{ ; disrotatory.} \qquad (10)$$

In treating reactivity, the frontier orbital theory and the Woodward-Hoffmann rule are sometimes used. These essence are the orbital interaction between specified orbitals and the conservation of orbital symmetry, respectively. They have made brilliant achievements[4,6] in explaining chemical reactions *e.g.* electrocyclic and sigmatropic reactions. However the former has a tendency of taking into account only for specified orbitals, and in the latter it is difficult to draw the correlation diagram for sigmatropic reaction which does not conserve the orbital symmetry. In the propagator method, the effect of all electrons are counted and we need not take care of the conservation of orbital symmetry at all.

Applications, Comparing with the Frontier Orbital Theory

In this section, We deal with the [1,3] sigmatropy, [1,5] prototropy, [1,3] prototropy, and ring closure reaction of *cis*-butadiene and compare the propagator method with the frontier orbital theory.[4]

Thermochemical [1,3] Sigmatropic Reaction.[6] A few thermal uncatalyzed [1,3] shifts are known. Berson and Nerson made a dramatic observation that

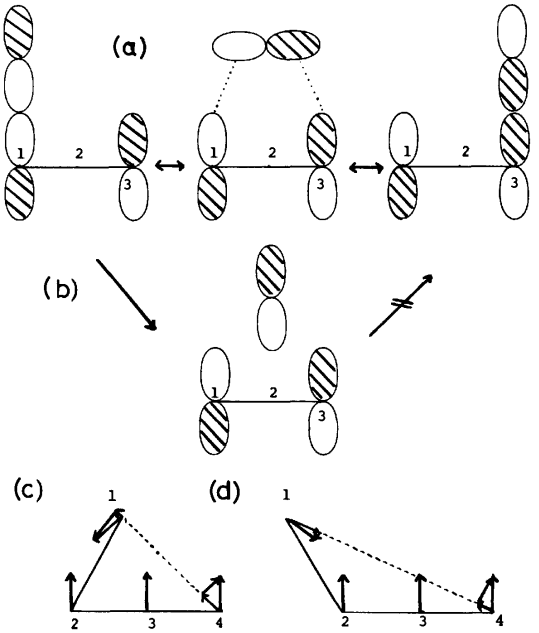

Fig. 2. (a), (b) The reaction path of the [1,3] sigmatropic reaction explained by the frontier orbital theory. (c), (d) The transition state in the [1,3] sigmatropic reaction in our treatment.

the system (a) undergoes a symmetry allowed suprafacial [1,3] shift with inversion at the migrating center, to give (b), at 307 °C.

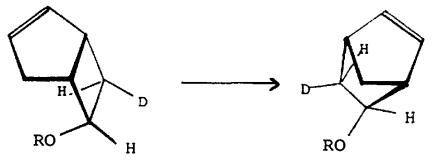

(a) (b)

In view of orbital interaction, this reaction is caused by the interaction between SOMO of the allyl radical and the $2p_z$ of carbon. Thus the frontier orbital theory predicts the reaction path shown in Fig. 2(a) rather than Fig. 2(b).

In our treatment of the [1,3] sigmatropy, this reaction is explained as follows: At first, considering the model for the transition state of the sigmatropic reaction as shown in Fig. 2(c), we calculate bond orders and determine signs of π and σ components of V_{rs} as

Site (r , s)	q_{rs}	V^{π}_{rs}	V^{σ}_{rs}	ΔE	reaction
1 , 2	0.8944	−	−	−	
1 , 3	0.0000	+	−		
1 , 4	−0.4472	+(−)	0	−(+)	YES(NO)

On the other hand, if we assume the transition state as shown in Fig. 2(d), the calculated results are shown in braces. In this case, it is impossible for the [1,3]-σ tropy to occur. So we conclude that the

transition state of the [1,3]-σ tropy is as shown in Fig. 2(c). In the above calculation, for simplicity, all resonance integrals are approximately equal to β and the coulomb integral is put 0.

Thermochemical [1,5]-Prototropy. Now, we deal with the [1,5] prototropy.[4] The treatment is the same as that of the [1,3]-σ tropy.

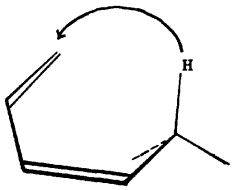

According to the frontier orbital theory, we consider the interaction between the H-1s orbital and SOMO of pentadienyl radical as shown in Fig. 3(a). In the present method, we assume the transition state as shown in Fig. 3(b) which is also schematically displayed in Fig. 3(c), and proceeds as same as in the case of the [1,3]-σ tropic reaction except for the sign of V_{rs}. In this case, the π-components of V_{1r} are 0 and the σ-component is negative. The result is shown as

Site(r , s)	q_{rs}	V_{rs}^{π}	V_{rs}^{σ}	ΔE	reaction
1 , 2	0.8711	0	−	−	YES
1 , 3	0.0000	0	−		
1 , 4	−0.3877	0	−	+	
1 , 5	0.0000	0	−		
1 , 6	0.3014	0	−	−	YES

When $q_{rs}V_{rs}$ is negative, the shorter R_{rs} is, the more the reaction will occur. Therefore, the hydrogen designated by 1 is most probably transfered to the site 6 ([1,5] sigmatropic reaction). It is noted that the most probable transition state of the [1,5] prototropic reaction is a cis type as shown in Fig. 3(c).

Photochemical [1,3]-Prototropy. The photochemical [1,3] prototropic reaction[6] as

$$CH_3\text{-}CH{=}CH_2 \rightleftharpoons CH_2{=}CH\text{-}CH_3$$

is easily understood by symmetry characters of orbitals. According to the frontier orbital theory, the reaction is explained by the interaction between LUMO of the allyl radical and the 1s of hydrogen as shown in Fig. 4(a).

While, in our theory this is explained as follows: At first, we assume the transition state shown in Fig. 4(b), and then evaluate the partial bond orders and signs of interaction matrix elements. The results are tabulated in the following:

Site(r , s)	q_{rs}^{LH}	V_{rs}^{π}	V_{rs}^{σ}	ΔE	reaction
1 , 2	−0.4472	0	−	+	
1 , 3	0.0000	0	−		
1 , 4	0.7236	0	−	−	YES

It is quite possible that the photochemical [1,3] prototropic reaction will occur.

Photochemical and Thermochemical Reactions of the Ring Closure of Butadiene. It is well known that in the case of photochemical reaction or thermochemical reaction, the mode of ring closure of butadiene[4] is disrotatory or conrotatory, respectively. According to the frontier orbital theory, the former is explained by the LUMO-LUMO interaction of two

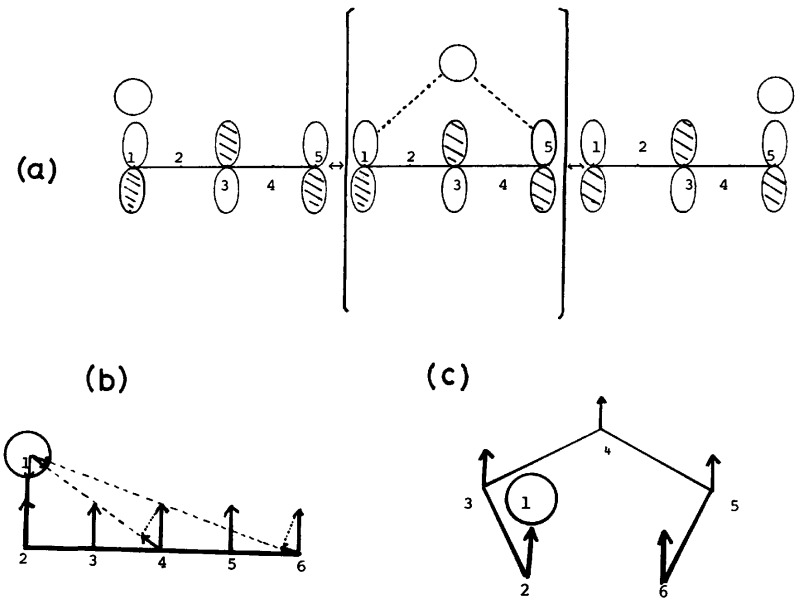

Fig. 3. (a) The reaction path in an example of [1,5] prototropic reaction explained by the frontier orbital theory. (b) The transition state in an example of the [1,5] prototropic reactionin our treatment. (c) The schematic representation of the transition state.

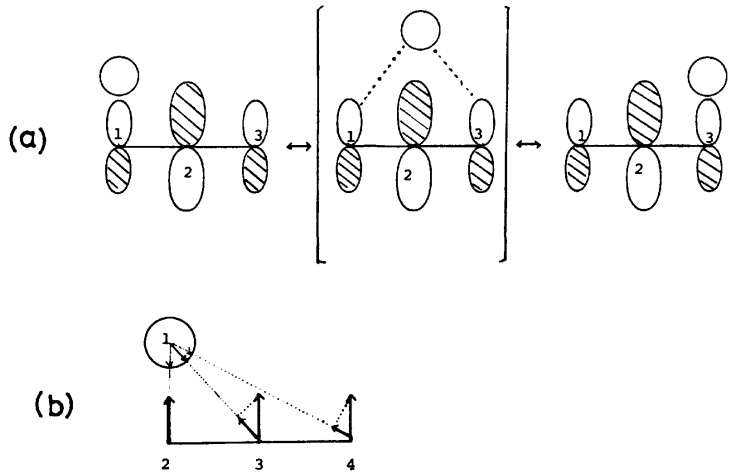

Fig. 4. (a) The reaction path of the photo-[1,3] prototropic reaction explained by the frontier orbital theory. (b) The transition state adopted in our treatment.

ethylene, and the latter by the HOMO-LUMO of two ethylene. (see Fig. 5(a), (b)). This consideration results that the modes of photochemical and thermochemical ring closure are disrotatory and conrotatory mode, respectively.

In view of the propagator method, the treatment is same as previous example, and it is natural to guess the transition state that all the carbons lie on the plane so that V_{14}^{π} and V_{14}^{σ} are negative (see Fig. 5(c)). In the case of photochemical reaction, since $q_{1,4}^{LH}$ is positive, this reaction occurs with the disrotatory mode. The result is shown as

Site (r , s)	q_{rs}^{LH}	V_{rs}^{π}	V_{rs}^{σ}	ΔE	reaction
1 , 2	−0.4472	−	0		
1 , 3	0.0000	−	0		
1 , 4	0.7236	−	−	−	YES

On the other hand, the thermochemical reaction of this is explained as follows: If the transition state is as same as that of photochemical reaction, this reaction will not occur, because $q_{14}<0$ and $V_{14}<0$. If we consider the transition state where the 2pπ orbitals at sites 1 and 4 twist considerably to the same direction as shown in Fig. 5(d), a positive V_{14}^{σ} shown in brace will produce a slight possibility of the conrotatoty ring closure. However, since V_{14}^{π} is still negative, we can assert this reaction hardly occurs.

Site (r , s)	q_{rs}	V_{rs}^{π}	V_{rs}^{σ}	ΔE	reaction
1 , 2	0.8944	−	0	−	
1 , 3	0.0000	−	0		
1 , 4	−0.4472	−	−(+)	+	NO

According to the Woodward-Hoffmann rule, the reactions are explained by the correlation diagrams.[6]

We have compared the propagator method with the frontier orbital theory or the Woodward-Hoffmann rule in these simple thermochemical and photochemical reactions, and get the same results. From now on, we are going to investigate the chemical reaction by the use of the propagator method and, if necessary, compare with the frontier orbital theory or the Woodward-Hoffmann rule.

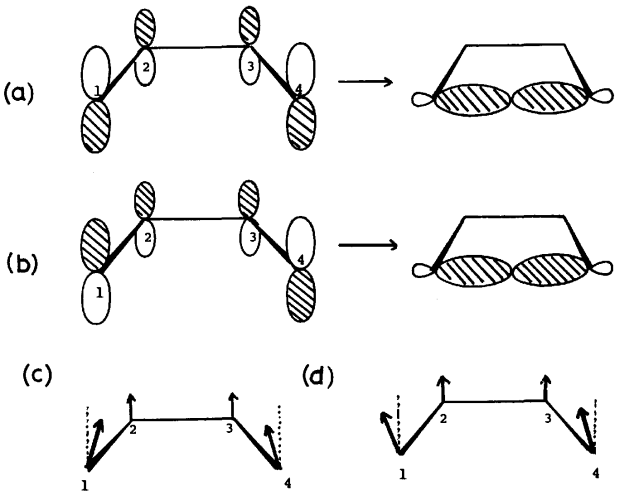

Fig. 5. (a), (b) The ring closure reaction of butadiene in photochemical and thermochemical reactions explained by the frontier orbital theory, respectively. (c), (d) The disrotatory and conrotatory modes of the transition state in the ring closure reacton of butadiene, respectively.

Thermochemical and Photochemical Reactions Cycloheptatriene and Norcaradiene Series

Cycloheptatriene and Norcaradiene.[5] Cycloheptatriene is the valence isomer of norcaradiene and this series undergo many queer rearrangements. We will try to predict these reaction pathes and sometimes compare with treatments with the frontier orbital

theory.

It is well known that cycloheptatriene and norcaradiene are with each other in thermal equilibrium.

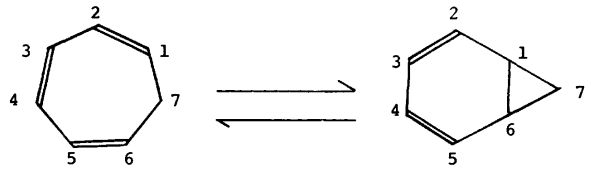

Cycloheptatriene Norcaradiene

It is natural to assume that in the transition state all the carbon atoms numbered from 1 to 7 lie on the molecular plane, but the interactions between sites 1 and 7 and between sites 6 and 7 are neglected because of σ-bond character (see Fig. 6(a)). Thus the treatment is nearly equal that for hexatriene. The result is shown as,

Site(r , s)	q_{rs}	V^{π}_{rs}	V^{σ}_{rs}	ΔE	reaction
1 , 4	−0.3877	−	0	+	
1 , 5	0.0000	−	0	+	
1 , 6	0.3014	−	0	−	YES

Therefore it is quite natural that a new bond is formed between sites 1 and 6. By the way, it is mentioned that the ring opening reaction is considerd as the reverse reaction of the ring closure, since all the elementary reactions are supposed to be reversible. According to the frontier orbital theory, this reaction is explained as the interaction of HOMO of heptatriene(see Fig. 6(b)), and the sites 1 and 6 will bind with the conrotatory mode.

Thermoisomerization of 2,5,7-Triphenylnorcaradiene.[5,8] In this section, we try to predict the mechanism of thermal isomerizations of 2,5,7-triphenylnorcaradiene. First we investigate the step(1)A.

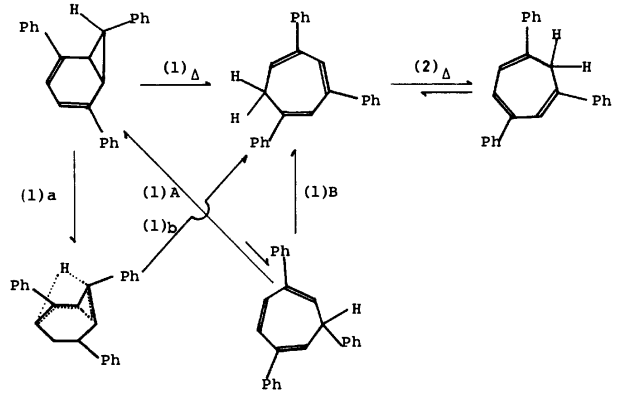

We begin with considering this reaction from the right side to the left side, assuming the transition state as shown in Fig. 7(a) for 2,5,7-triphenylcycloheptatriene. Namely this transition state is the same to that of hexatriene in the ring closure reaction except for three substituting phenyl radicals. The calculated parameters are given as

Site(r , s)	q_{rs}	V^{π}_{rs}	V^{σ}_{rs}	ΔE	reaction
1 , 4	−0.3681	−	0	+	
1 , 6	0.2716	−	−	−	YES
2 , 5	−0.0694	−	0	+	

Thus it is probable that between sites 1 and 6 a new σ-bond forms. If it is assumed that the reverse reaction proceeds along the same reaction path, the answer is given.

Next, we deal with the [1,5] prototropy in the step(1)B. It is natural to guess the transition state of 2,5,7-triphenylcycloheptatriene in this reaction is as shown in Fig. 7(b). That is to say, the carbon orbitals at site 7 rehybridizes from three sp^3 orbitals to two sp^2 and a $2p_z$, and then the carbon $2p_z$ binds not only with the H 1s, but also with π-orbitals of the substituting phenyl group and of the cycloheptatriene. Now we assume that for simplicity the resonance integral between H 1s and $2p_z$ at site 7 is nearly equal to β. The result is:

Site(r , s)	q_{rs}	V^{π}_{rs}	V^{σ}_{rs}	ΔE	reaction
1 , 8	−0.1489	0	−	+	
2 , 8	−0.2713	0	−	+	
3 , 8	0.1953	0	−	−	YES

Therefore, it is quite possible that H transfers from the carbon site 7 to the carbon site 3 or 4, and our prediction is agree with the experimental result.

In the next reaction(2), only the substituting positions of phenyl groups are different from the previous one. Thus the transition state shown in Fig. 7(c) yields the result:

Site(r , s)	q_{rs}	V^{π}_{rs}	V^{σ}_{rs}	ΔE	reaction
1 , 8	−0.1488	0	−	+	
2 , 8	−0.2799	0	−	+	
3 , 8	0.1863	0	−	−	YES
4 , 8	0.1786	0	−	−	YES
5 , 8	−0.2834	0	−	+	
6 , 8	−0.1353	0	−	+	

From these calculations the [1,5] prototropy (in our notation between 3 and 8, or 4 and 8) is quite probable.

According to the frontier orbital theory, the above two reactions are expressed as the orbital interaction between SOMO of cycloheptatrienyl radical and the H 1s (see Fig. 7(d)), but the position of H is not so clear. On the other hand, the position of H is almost fixed in our treatment, because we assume the transition state such that the H 1s binds with the carbon $2p_z$ at site 7.

Then, we try to predict the reaction path (1)a and (1)b. It is natural to assume the transition state as shown in Fig. 7(e). The mutual interaction energy

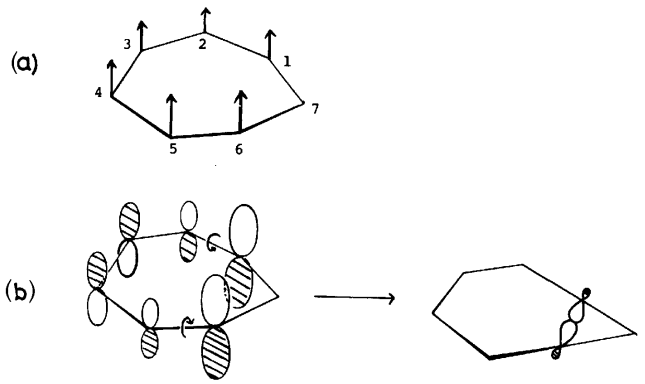

Fig. 6. (a) The transition state of cycloheptatriene in the ring closure reaction. (b) The reaction path from cycloheptatriene to norcaradiene explained by the Woodward-Hoffmann rule.

among three sp^3 hybridized orbitals are approximately, equal to β, because it is nearly equal to be $(\varepsilon_{2s}-\varepsilon_{2p})/4 \fallingdotseq -2\text{eV}$ (ε_{2s}, for example, the orbital energy of the carbon 2s), and the interactions between sites 1 and 7, between 6 and 8, and between 9 and 10 are approximately equal to 2β, because $\beta^{\sigma}_{rs} \fallingdotseq 2\beta^{\pi}_{rs}$. We have the result:

Site (r , s)	q_{rs}	V^{π}_{rs}	V^{σ}_{rs}	ΔE	reaction
1 , 10	−0.2326	0	−	+	
2 , 10	−0.0421	0	−	+	
3 , 10	0.0962	0	−	−	YES

Accordingly we may expect that the reaction will occur along this reaction path. But it seems considerably difficult to occur, because $q_{3,10}$ is not so

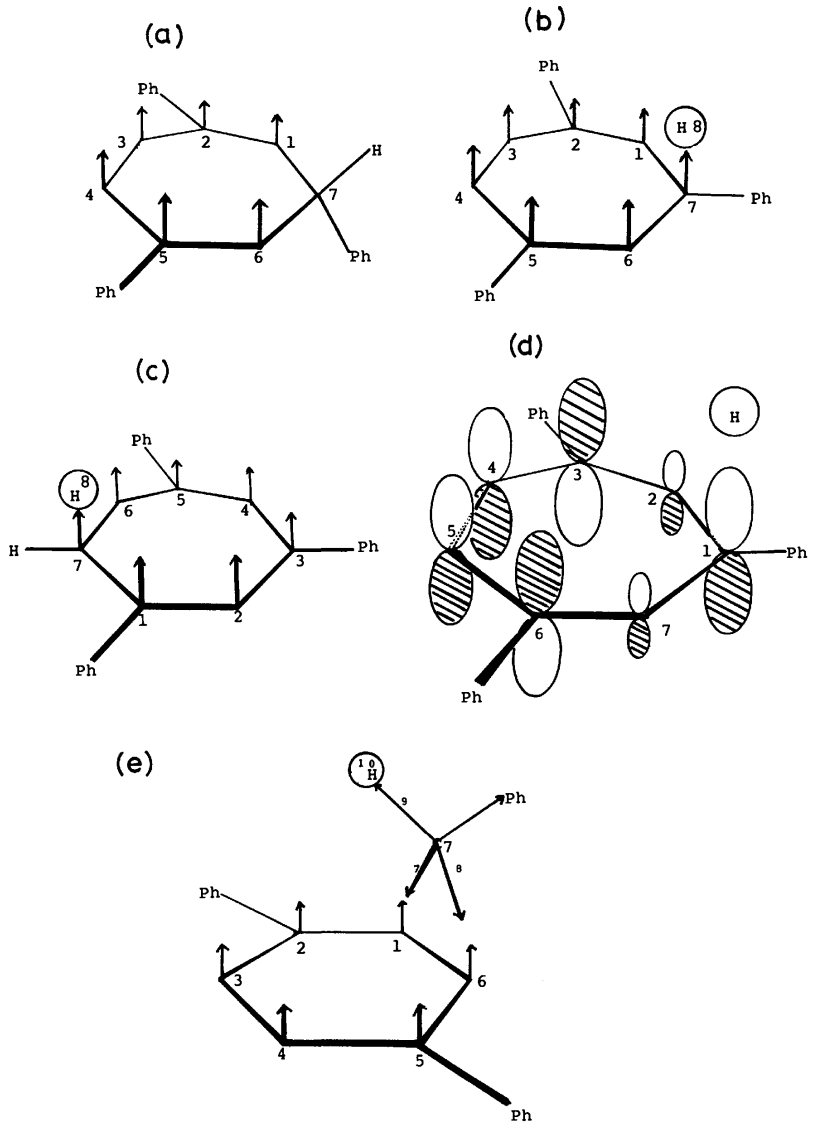

Fig. 7. (a), (b) The transition state of 2,5,7-triphenylcycloheptatriene in the ring closure reaction and the H-transfer, respectively. (c) The transition state of 1,3,5-triphenylcycloheptatriene in the H-transfer. (d) The reaction of 2,5,7-triphenylcycloheptatriene explained by the frontier orbital theory. (e) The transition state of 2,5,7-triphenylnorcaradiene in the H-transfer.

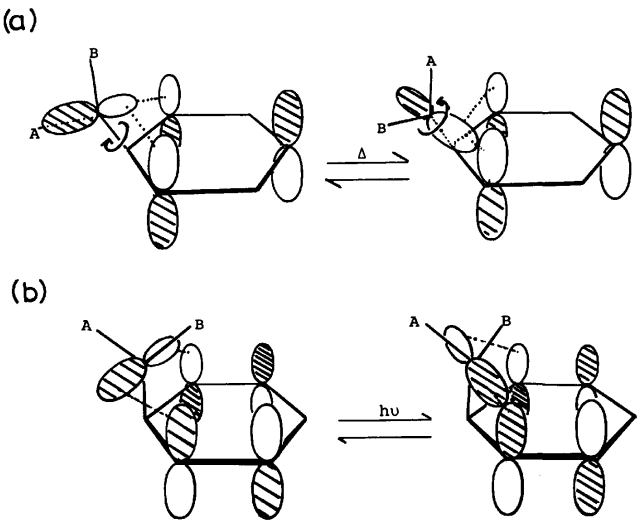

Fig. 8. (a) The reaction path and mode of the Berson-Willcott rearrangement explained by the frontier orbital theory. (b) The reaction path of photochemical isomerization of 2,5,7-triphenylnorcaradiene explained by the frontier orbital theory.

large.

Photoisomerization of 2,5,7-Triphenylcycloheptatriene. In this section we deal with the photochemical reaction of 2,5,7-triphenylcycloheptatriene.[5,9] It is shown as

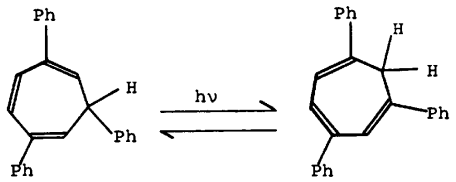

Then assuming the transition state shown in Fig. 7(b), we obtain the result:

Site (r , s)	q_{rs}^{LH}	V_{rs}^{π}	V_{rs}^{σ}	ΔE	reaction
1 , 8	0.2238	0	−	−	YES
2 , 8	0.1399	0	−	−	YES
3 , 8	−0.1745	0	−	+	

Therefore, the hydrogen will transfer from the carbon site 7 to the carbon site 1 or 2, the former being a little more probable. In this case, the former refers [1,7] prototropy and the latter gives the starting material. The same treatment for 1,4-diphenylcycloheptatriene gives the result that perfectly agrees with the experimental one.

BERSON-WILLCOTT Rearrangement

In this section, we deal with the thermoisomerization of methyl-substituted cycloheptatriene,[5] and compare the photoisomerization of triphenylnorcaradiene,[5] because these two reactions are similar in mechanism in spite of their difference in reaction characters.

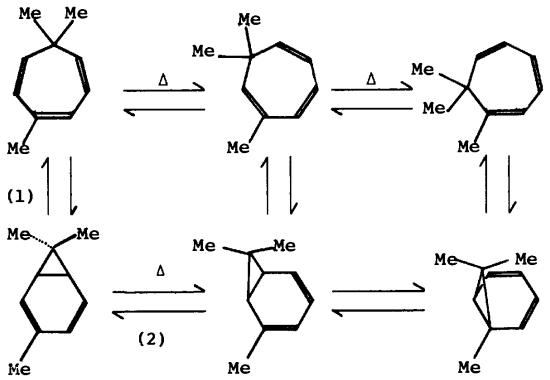

Berson and Willcott have observed a remarkable serise of the isomerization of methyl-substituted cycloheptatriene[10] as shown above. Woodward and Hoffmann expected that this [1,5] sigmatropic shift had to proceed with retention at the migrating carbon atom[6] as shown in Fig. 8(a). This condition implies that each group substituting the shifting carbon pivots 180° above the cyclohexatriene ring. However we have obtained a different result as will be mentioned below.

The structure of 3,7,7-trimethylcycloheptatriene is the same as that of cycloheptatriene except for the methyl groups at sites 3 and 7. If the carbons designated by 1~6 lying on the molecular plane have $2p_z$ orbitals, the interactions between these are negative, while the effect of two methyl groups at the site 7 are disregarded due to the σ-bond character. Assuming the transition state as shown in Fig. 9(a), we calculate bond orders and determine signs of π- and σ- components of interaction matrix elements:

Site (r , s)	$q_{rs}^{(1)}$	$q_{rs}^{(2)}$	$q_{rs}^{(3)}$	V_{rs}^{π}	V_{rs}^{σ}	ΔE	reaction
1 , 3	0.0661	0.0512	0.0856	−	0	−	
1 , 4	−0.3738	−0.3809	−0.3612	−	0	+	
1 , 5	−0.0231	−0.0168	−0.0307	−	0	+	
1 , 6	0.2913	0.2970	0.2814	−	0	−	YES

Therefore, it is quite possible that the sites 1 and 6 will bind with disrotatory mode (step(1)). This trend is also hold for cases(2; 2,7,7-trimethyl compound) and (3; 1,7,7-trimethyl compound). As is the case of

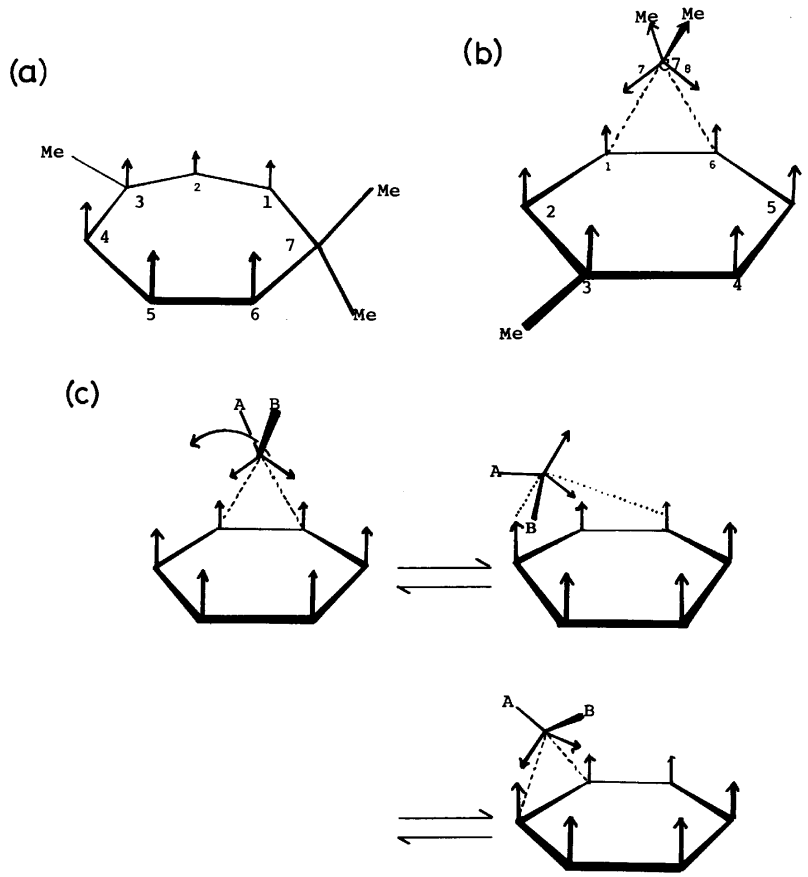

Fig. 9. (a) The transition state of 3,7,7-trimethylcycloheptatriene in the ring closure. (b) The transition state of 3,7,7-trimethylnorcaradiene in the sigmatropic reaction. (c) The reaction path of trimethylnorcaradiene series predicted in our treatment.

cycloheptatriene, we treat the ring opening reaction from norcaradiene to cyclohexatriene as a reverse reaction of the above.

Next we deal with the sigmatropic reaction of step(2). It is natural to guess the transition state shown in Fig. 9(b). Namely, the carbon which would transfer is in the sp^3 character, and the triangle formed by carbons numbered 1,6 and 7 is perpendicular to the molecular plane, and the six carbons lying on the molecular plane are conjugated like in benzene. The effect of two methyl groups is neglected. The interactions are put, $\beta_{17}=\beta_{68}\fallingdotseq\beta_{78}\fallingdotseq\beta$, for simplicity. Calculated bond orders and signs of V_{rs}^{π} and V_{rs}^{σ} are shown as

Site (r , s)	$q_{rs}^{(1)}$	$q_{rs}^{(2)}$	V_{rs}^{π}	V_{rs}^{σ}	ΔE	reaction
2 , 7	0.0119	0.0443	+	−		
3 , 7	0.1610	0.1713	+	−	+	
4 , 7	0.0673	−0.0204	+	+	+	
5 , 7	−0.3446	−0.3505	+	+	−	YES
6 , 7	−0.0638	0.0100	+	−		
1 , 8	0.0301	−0.0968	+	−		
2 , 8	−0.3541	−0.3386	+	+	−	YES
3 , 8	−0.0502	−0.0323	+	+		
4 , 8	0.1543	0.1612	+	−	+	
5 , 8	0.0237	0.0190	+	−		

It is quite possible that the sigmatropic reaction will occur without retention at the shifting center shown in Fig. 9(c). Our result is opposite to the prediction by Woodward and Hoffmann. However, the experimental proof has not yet given. The treatment of reactions for the 2-methyl compound is the same as the previous one, and the result is in the above table(2).

According to the frontier orbital theory, the transition state is assumed such that the three menbered ring of norcaradiene is cut at the carbon 7, and the sp^3 orbitals rehybridize to two sp^2 and a $2p_z$. The $2p_z$ and SOMO of cycloheptatrienyl radical interact with each other, so that this reaction occurs with retention at the resting center. Figure 9(c) might help to understand the difference of the reaction mode predicted by the propagator method and the frontier orbital theory.

Next we deal with the photochemical reaction which is similar to the Berson-Willcott rearrangement:[9]

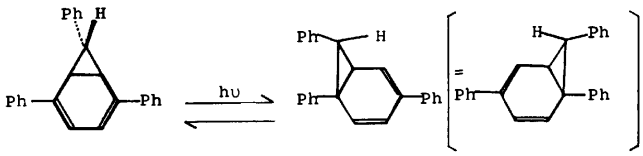

We begin with assuming the transition state of 2,5,7-triphenylnorcaradiene shown in Fig. 7(e) and evaluate the partial bond orders and signs of interaction matrix elements. The result is as follows:

Site (r , s)	q_{rs}^{LH}	V_{rs}^{π}	V_{rs}^{σ}	ΔE	reaction
2 , 7	0.1951	+	+	+	NO
4 , 7	−0.2534	+	−		
6 , 7	0.3373	−	−	−	

Thus we conclude that photoisomerization of 2,5,7-triphenylnorcaradiene which is similar to the Berson-Willcott rearrangement will not occur under the condition that the shifting carbon is in the sp^3-like state. This suggests that the present model of transition state is not adequate. Then we consider a new model that the shifting carbon is in sp^2 and $2p_z$ due to the effect of phenyl group substituting this carbon. It is noticed that there are interaction matrix elements among sp^3 orbitals, but between the sp^2 and $2p_z$ not. Under these considerations, we evaluate partial bond orders and signs of interaction matrix elements. The result is in the following:

Site (r , s)	q_{rs}^{LH}	V_{rs}^{π}	V_{rs}^{σ}	ΔE	reaction
2 , 7	−0.3642	+	+	−	YES
4 , 7	0.2813	+	−		

Conclusively, the phenyl group attached to the migrating carbon has a great influence on the photochemical [1,5] sigmatropy, and the shifting carbon may transfer without retention. This result is also explained by the frontier orbital theory, namely, by the interaction between the $2p_z$ of the shifting carbon and LUMO of cyclohexadienyl radical as shown in Fig. 8(b). We show the difference between the reaction mode predicted by the propagator method and that by the frontier orbital theory in Fig. 10.[6]

If in the molecule written as

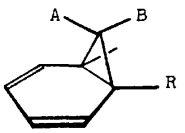

the similar reactions as mentioned in this section proceed with the retention at the migrating center, the slither mechanism is available not to loose the optical activity. However, if we employ the frontier orbital theory, the migrating center pivots in the thermal reaction resulting racemerization. On the other hand, in the optical reaction both treatments give the same results keeping the optical activity.

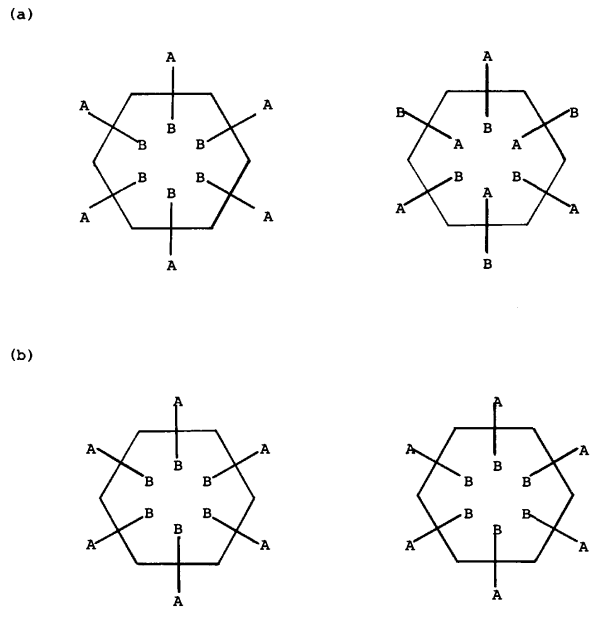

Fig. 10. The reaction modes of the Berson-Willcott rearrangement and photo-isomerization of 2,5,7-triphenylnorcaradiene predicted by the propagator method and the frontier orbital theory.
(a) Thermochemical reaction, (b) photochemical reaction.

Photochemical and Thermochemical Rearrangements of Tropone Ethylene Acetal

In this section, we deal with the photochemical and thermochemical rearrangement of tropone ethylene acetal.[5,11]

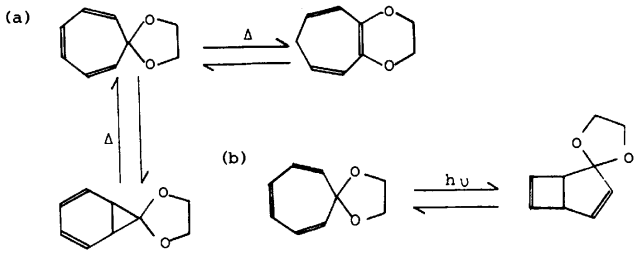

First we deal with the photoisomerization. It is natural to assume the transition state as shown in Fig. 11(a), where the effect of oxygen can be disregarded because of its σ-bond character. The calculated results are:

Site (r , s)	q_{rs}^{LH}	V_{rs}^{π}	V_{rs}^{σ}	ΔE	reaction
1 , 4	0.4356	−	0	−	YES
1 , 6	−0.5431	−	0	+	
2 , 5	−0.1076	−	0	+	

Therefore, this reaction will occur with disrotatory mode.

Next we consider the thermochemical reaction for two alternative pathes. A and B as shown in the following. We predict which path is suitable.

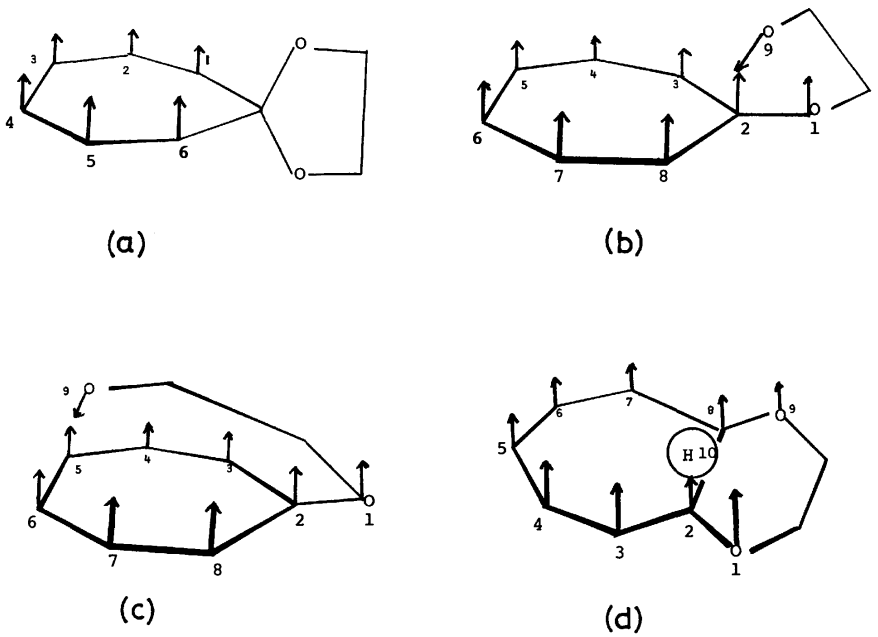

Fig. 11. (a), (b) The transition state of tropone ethylene acetal in the ring closure and O-transfer, respectively. (c), (d) The transition state of intermediate product of tropone ethylene acetal in the O-transfer and H-transfer, respectively.

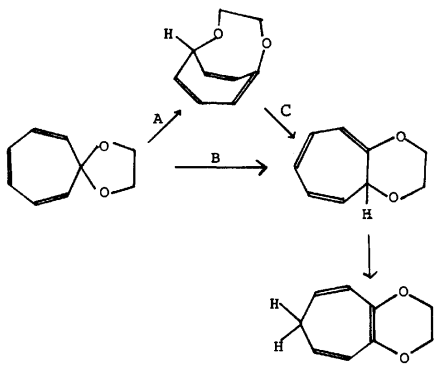

In the case of the first sigmatropy, we assume the transition state as shown in Fig. 11(b) and obtain the result as

Site (r , s)	q_{rs}	V^{π}_{rs}	V^{σ}_{rs}	ΔE	reaction
1 , 9	−0.1965	+ <	−	+	
2 , 9	0.7639	−	−	−	
3 , 9	−0.1498	+ <	−	+	NO
4 , 9	−0.1952	+ <	−	+	
5 , 9	0.1310	+ <	−	−	YES

Therefore it is quite possible that the [1,5] sigmatropy occurs. This implies the reaction path A to be preferable, and the "NO" for the 3,9 and 8,9 shifts mean the reaction path B is not acceptable. In order to predict the next step reaction, we assume the transition state as shown in Fig. 11(c) to get the results:

Site (r , s)	q_{rs}	V^{π}_{rs}	V^{σ}_{rs}	ΔE	reaction
1 , 9	−0.0438	+	−		
2 , 9	0.1217	−	−	−	YES
3 , 9	−0.2005	+ <	−	+	
4 , 9	−0.1563	+ <	−	+	
5 , 9	0.7960	+ <	−	−	
6 , 9	−0.2004	+ <	−	+	
7 , 9	−0.1976	+ <	−	+	
8 , 9	0.1749	+ <	−	−	YES

Therefore the reaction will occur on path C. In the above table, the latter "YES" refers to get the product and the former the reverse reaction. What reaction will follow the previous one? We assume the transition state as shown in Fig. 11(d) and calculate as follows:

Site (r , s)	q_{rs}	V^{π}_{rs}	V^{σ}_{rs}	ΔE	reaction
1 , 10	−0.1759	0	−	+	
3 , 10	−0.1766	0	−	+	
4 , 10	−0.2808	0	−	+	
5 , 10	0.2220	0	−	−	YES
6 , 10	0.1716	0	−	−	YES
7 , 10	−0.3133	0	−	+	
8 , 10	−0.1020	0	−	+	
9 , 10	0.0052	0	−	+	

It is expected that H will shift from the carbon site 2 to 5 or 6. Here we note that even for complicated reactions mentioned above the propagator method gives nice ways to predict the reaction path correctly.

Cope Rearrangement

Chair, Boat and Quasi-boat Model. The Cope rearrangement[7] is a kind of the [3,3] sigmatropic reaction as

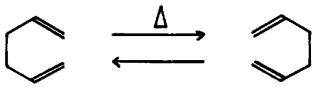

In view of the frontier orbital theory,[4] this reaction is explained as the interaction between two SOMO's of allyl radical. Therefore, the transition state of the Cope rearrangement, as is shown in Fig. 12(a)~(c) has three types named chair, boat and quasi-boat type referring to the relative positions of two allyl radicals.

Usually, the Cope rearrangement occurs through the transition state of chair type at low temperature, and the higher the temperature is, the more increasing the product through the boat type is. It is impossible for the simple frontier orbital theory to explain this experimental result, because SOMO of the allyl radical has no amplitude at site 2 so that there is no difference between chair and boat types. Fukui[4] explained this result by taking account of the interaction between LUMO and HOMO of the allyl radical.

In our treatment of the Cope rearrangement, we begin with assuming the transition state of 1,5-hexadiene as shown in Fig. 12(d) and (e), where at carbon sites 3 and 4 rehybridizations arise from three sp^3 to two sp^2 and a $2p_z$, so that sites 3 and 4 are coupled through $2p_z$'s. The resonance integral $\beta_{3,4}$ is approximated to be β for simplicity. Under these conditions calculations are carried out to give

Site (r , s)	q_{rs}	V^{π}_{rs}	V^{σ}_{rs}	ΔE	reaction
1 , 4	−0.3877	+	−	?	
1 , 6	0.3014	−	−	−	YES
2 , 5	−0.0867	+(−)	−	?(+)	(hinderance)

In the above, the results for the boat type are shown in braces. Because of the difference of V_{25}, the transition state of chair type is more stable than that of boat type.

The same treatment explains the following reaction

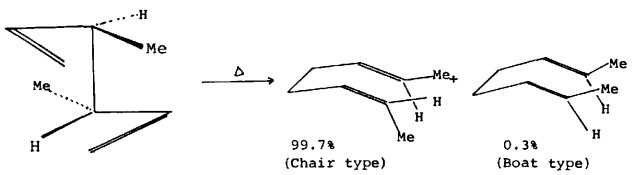

Thus we understand that the chair type is generally more stable than the boat type.

On the other hand for tropone, the experiment[13] suggests the quasi-boat rearrangement.

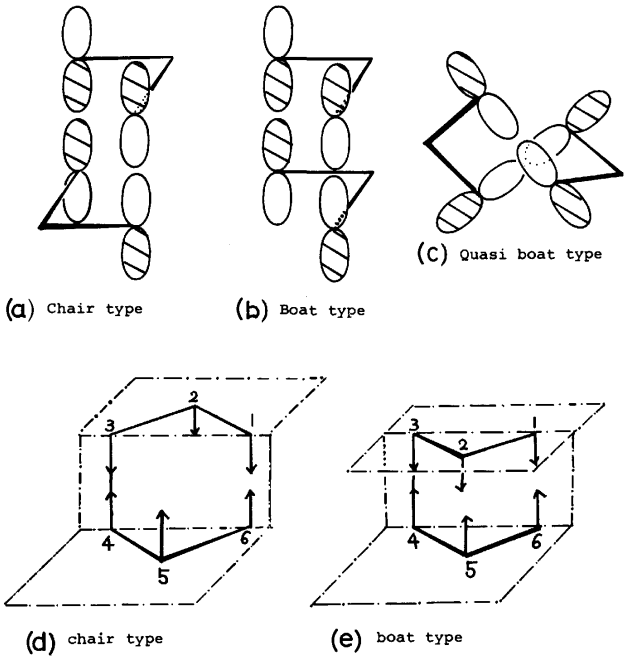

Fig. 12. (a), (b), (c) The possible transition states of the Cope rearrangement in the frontier orbital theory. (d), (e) The transition states of the Cope rearrangement in our treatmemt.

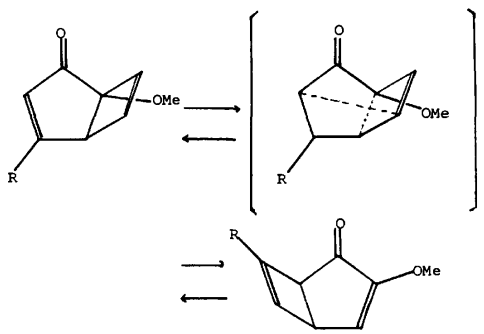

At sight, there be no interaction between two double bonds of molecular ends. If we make a model that carbons at sites 2, 4, 5, 7, and 8 are in sp^2-like state and the carbons at sites 3 and 6 are sp^3-like state, we can find that the σ-bond between sites 3 and 6 has a strain as shown in Fig. 13(a), and the resultant π-components are perpendicular to the left and right planes. So it is natural to imagine two double bond of molecular ends are conjugated with each other through the π-components at sites 3 and 6. As to the coupling parameteres, we put $\beta_{36} \fallingdotseq 2\beta$, $\beta_{23}=\beta_{34}=\beta_{56}=\beta_{67}=\alpha\beta$ ($\alpha>0$). We have tried two type parameters which are $\alpha=1.0$ and $\alpha=0.5$. The calculated results are shown as (a) and (b), respectively:

Site (r , s)	$q^{(a)}_{rs}$	$q^{(b)}_{rs}$	V^{π}_{rs}	V^{σ}_{rs}	ΔE	reaction
2 , 4	−0.0580	−0.0080	−	−	+	
2 , 5	−0.1245	−0.0182	−	−	+	
4 , 7	−0.1127	−0.0295	−	−	+	
4 , 8	−0.0285	0.0079	−	−	+(−)	
5 , 7	0.0496	−0.0026	−	−	−(+)	
5 , 8	0.1273	0.0313	−	−	−	YES

These two treatments give the qualitatively same results. Therefore, it is likely that a bond between sites 5 and 8 may be formed in the transition state in Fig. 13(a) and the reaction path should be such as shown above. Organic chemists[5,7] and R. Hoffmann[6] regard this reaction as a quasi-boat Cope rearrangement, as it is a [3,3] sigmatropic reaction. But this reaction is understood in a little different manner from the Cope rearrangement of 1,5-hexadiene series in the following sense:

(1) Due to π-components of the 3—6 bond, the double bonds at molecular ends do interact so that the resultant phase of bond order makes the reaction under consideration possible, together with the corresponding interaction matrix elements.

(2) It is also pointed out that in our treatment of the tight-binding approximation, the σ-character of the 3—6 interaction matrix element is fairly large to amount nearly 2β, and this effect is profoundly important in the present result.

Now, we turn to the experimental results. First we concern with the following reaction[14] which actually does not occur.

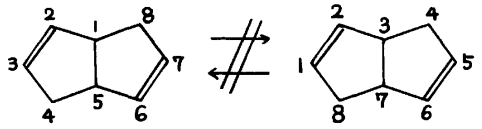

If this reaction would occur, it would be a pure Cope rearrangement through the transition state of the quasi-boat type. In view of our treatment, since the 1—5 σ bond is almost on plane, there is no π conjugation between two double bonds of molecular ends, namely these double double bonds are almost independent with each other. Therefore this molecule has no potential to make the rearrangement possible. Also a discussion has been given that, in the Dewar benzene series[15] having similar species of tropone series, the Cope rearrangement will occur through the quasi-boat type. If the reaction would occur, it would be shown schematically as

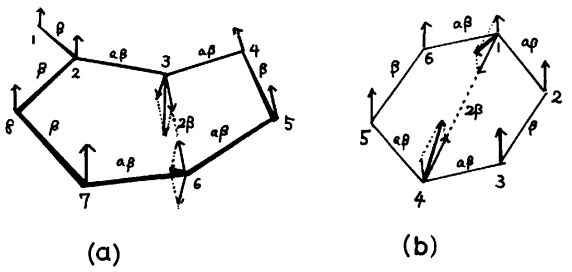

Fig. 13. (a) The transition state of the Cope rearrangement, through the quasi-boat. (b) The transition state of the Dewer benzene.

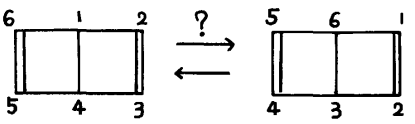

In view of our treatment, it does not occur. The reason is as follows: First, we assume the transition state of the Dewar benzene series as shown in Fig. 13(b), and calculate as useal. We can find there is no reaction mode in which ΔE is negative.

Site (r , s)	q_{rs}	V_{rs}^{π}	V_{rs}^{σ}	ΔE	reaction
2 , 5	−0.3333	−	0	+	NO
2 , 6	0.0000	−	0		

Untill now, we have considered the transition states of the Cope rearrangement: (1) chair type, (2) boat type, (3) quasi-boat type. However in literatures[5,7] we found four type states more than shown as

(4) allyl radical type (5) 1,4-biradical type

(6) ion-pair type (7) 1,4-dipole type

These concepts except (4) can be reinterpretended by our method in the following.

Cope Rearrangement Through the Allyl Radical. It was said that 1,5-hexadiene was cleaved to two allyl radicals, and each of them had a great concern with the Cope rearrangement at the beginning of reaction, but it was turned out to be uncorrect.[16] Doering[17] reported the next experimental result.

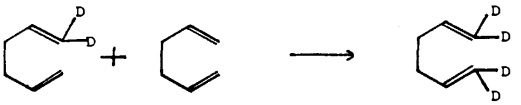

and then Wigfield[18] reported as,

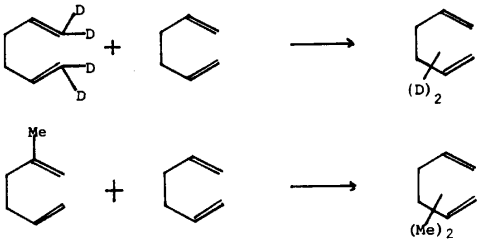

Observing these, it can be asserted that these reactions are of intermolecular character and do not concern with any intramolecular reaction (cleaving into two allyl radicals). We do not discuss these any longer.

Cope Rearrangement Through the 1,4-Biradical.
The reaction said to be a Cope rearrangement through the 1,4-biradical[19] is shown as

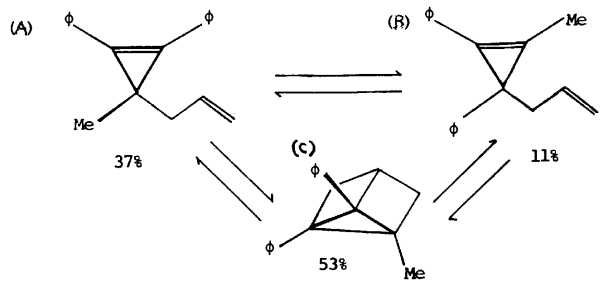

It is natural for our treatment to guess the transition state of (A) as shown in Fig. 14(a). Then we get calculated parameters as

Site (r , s)	q_{rs}	V^{π}_{rs}	V^{σ}_{rs}	ΔE	reaction
1 , 3	−0.0913	+	−		
1 , 6	0.1312	−	−	−	YES
2 , 5	−0.0913	+(−)	−	(+)	(hinderance)
2 , 6	0.1312	+	−		

In the above, the results for the boat type are in braces. Therefore, we find that the chair type is more stable than the boat type, because $q_{25}V_{25}$ is positive in the latter. In spite of the advantage of the chair type, why does the reaction which seems through the boat type occurs? If we choose the transition state of the intermediate product as shown in Fig. 14(b), the calculated parameters are:

Site (r , s)	q_{rs}	V^{π}_{rs}	V^{σ}_{rs}	ΔE	reaction
1 , 5	−0.0460	+	−		
2 , 5	−0.2833	+	0	−	YES
3 , 5	−0.0172	+	−	+	

Therefore, it is possible that this reaction will occur through the boat type.

In addition, we point out the [1,3] sigmatropy could occur, if groups or fragments inside the molecule could prevent sites 1 and 6 from approaching.

The reaction(B) presented at the beginning of this section is treated by the same method, considering effect of the different substituting group. The calculated parameters are:

Site (r , s)	q_{rs}	V^{π}_{rs}	V^{σ}_{rs}	ΔE	reaction
1 , 5	−0.0946	+	−		
1 , 6	0.2175	−	−	−	YES
2 , 5	−0.0932	+(−)	−	(+)	(hinderance)
2 , 6	0.1149	+	−		

In the above, the results for the boat type are shown in braces. Therefore, it is quite possible that this reaction from (B) to (C) will occur through the chair type. Then comparing the value of q_{16} between (A) and (B), we find that this is larger in (B) than in (A), implying that the transition state of (B) is perhaps preferable to that of (A). So the equilibrium probably tends to (A). Our prediction resultantly agrees with the experimental result.

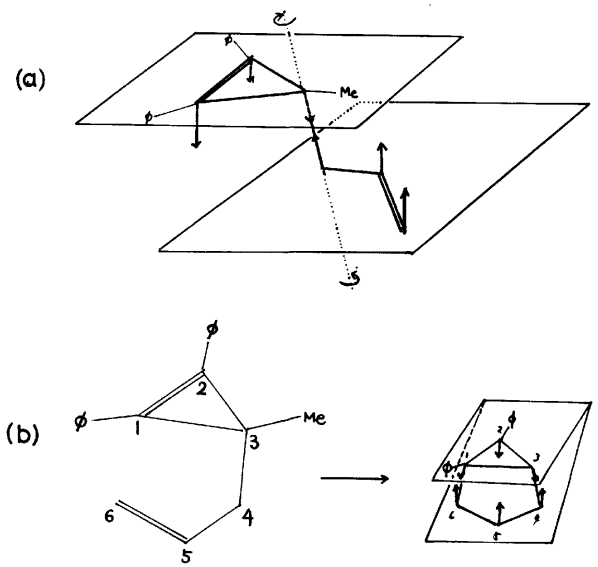

Fig. 14. The transition state of the Cope rearrangement, through the 1,4-biradical.

Cope Rearrangement Through the Ion Pair.
The ion pair or dipole models is rather a classical model. It is not acceptable from our viewpoint that the chemical reaction is genereated by quantum mechanical characters of electron, *i.e.* wavefunction or bond order. Employing our method, we can deal with reactions which have been explained by the ion pair model:[20]

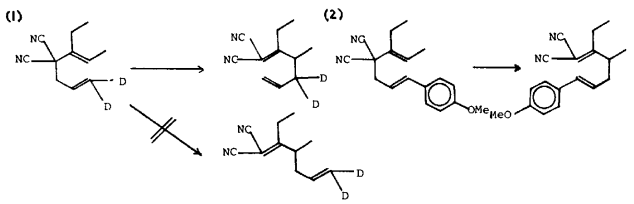

The difference between the above two reactions lies in environments, *i.e.*, sites 1 and 6 can easily approach with each other or not. We proceed under the following considerations:

(1) If sites 1 and 6 easily approach, the Cope rearrangenent will occur.

(2) If not, a possibility of the [1,3] sigmatropy increases.

Assuming the transition state for the first reaction as in Fig. 15(a), we calculate necessary parameters as

Site (r , s)	q_{rs}	V^{π}_{rs}	V^{σ}_{rs}	ΔE	reaction
1 , 5	−0.0946	+	−		
1 , 6	0.2175	−	−	−	YES
2 , 5	−0.0932	+	−		
2 , 6	0.1149	+	−		

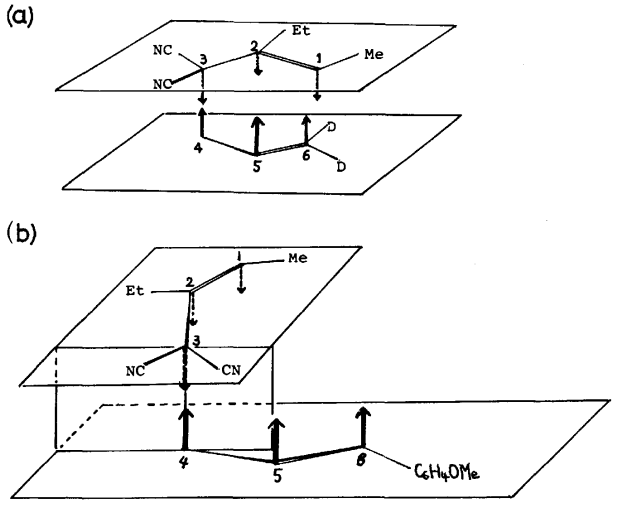

Fig. 15. The transition state of the Cope rearrangement (a) and the [1,3] sigmatropy (b), through the ion pair.

Thus, we can easily explain this reaction as a normal Cope rearrangement through the chair type corresponding to the case (1).

Next, we assume the transition state of the latter reaction as shown in Fig. 15(b), considering steric hinderance similar in the [1,3] sigmatropic reaction. Then we get the results:

Site (r , s)	q_{rs}	V^{π}_{rs}	V^{σ}_{rs}	ΔE	reaction
1 , 4	−0.2581	+	≒0	−	YES
1 , 6	0.1897	+	−		
2 , 5	−0.0620	+	−		
3 , 6	−0.2413	+	≒0	−	YES

The possibility of the 1—4 binding ([1,3] sigmatropy) is consistent with the experimental result. While the 3—6 binding is considered to be fairly difficult due to steric hinderance.

Cope Rearrangement Though the 1,4-Dipole Model. We deal with the reaction,

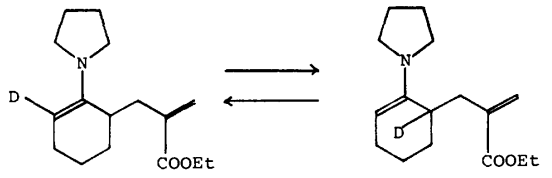

which has been explained to be a Cope rearrangement by the 1,4-dipole model.[21] In this case, either the Cope rearrangement and the [1,3] sigmatropy give the same product. As the steric effects scarcely hinder sites 1 and 6 approaching, we deal with this reaction as a Cope rearrangement. The chair type is sterically less hindered than the boat type is, as shown in Fig. 16. The required calculations are:

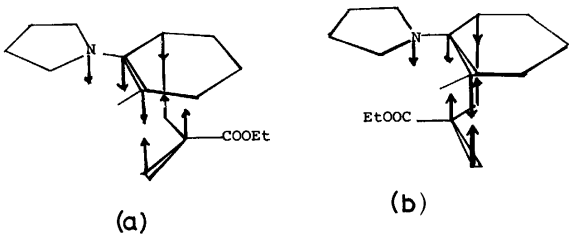

Fig. 16. The transition state of the Cope rearrangement, through the 1,4-dipole. (a) chair type, (b) boat type.

(Chair type)

Site (r , s)	q_{rs}	V^{π}_{rs}	V^{σ}_{rs}	ΔE	reaction
1 , 6	0.2070	−	−	−	YES
2 , 5	−0.0705	+	−		

It is noted here that there is little posibility of the [1,3] sigmatropic reaction because of a vanishingly small steric hinderance.

By the way, we examine why the 1,4-dipole model is not adequate. Assuming the structure,

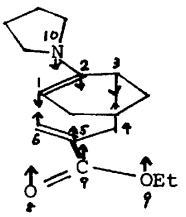

we can easily calculate the π-electron densities in the tight-binding approximation:

Site	r	q_r	Site	r	q_r
1	1.1347	$\delta-$	2	0.9526	$\delta+$
3	1.0202	$\delta-$	4	0.9823	$\delta+$
5	1.0290	$\delta-$	6	0.8256	$\delta+$
7	0.6489	$\delta+$	8	1.5926	$\delta-$
9	1.8964	$\delta+$	10	1.9172	$\delta+$

The net charge densitiy at site 7 is qualitatively positive ($\delta+$ in the above table), which is opposite to the transition state proposed in the reference.[7]

Claisen Rearrangement. The Cope rearrangement in which the double bond of the phenyl radical concerns with rearrangement is called the Claisen rearrangement. We present experimental examples below:[22,23]

(A)

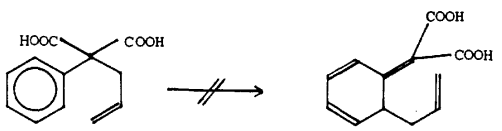

(B)

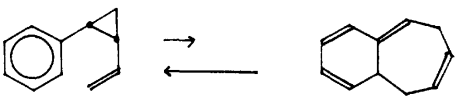

According to our treatment, we assume a transition state for the reactant of (A) as shown in Fig. 17(a), and evaluate bond orders and signs of interactions as

Site (r , s)	$q_{rs}^{(a)}$	$q_{rs}^{(b)}$	V_{rs}^{π}	V_{rs}^{σ}	ΔE	reaction
1 , 4	−0.2901	−0.2351	+	−		
1 , 6	0.1194	0.1706	+	−	−	YES
2 , 5	−0.0512	−0.1020	−	−	+	
3 , 6	−0.1597	−0.2103	+	−		

Then for the product (the right hand), assuming a transition state as in Fig. 17(b), we get bond orders and signs of interactions as in the above table(b).

In the aboves we find a considerbly larger values of q_{16} in the latter than in the former. It suggests the reverse reaction is easier to occur than the forward one does, and then the equilibrium tends strongly to the left. This consideration qualitatively explains the experimental result.

In order to predict the reaction(B), we assume transition states for reactant and product as in Fig. 17(c) and (d), respectively. Evaluated parameters are:

Site (r , s)	$q_{rs}^{(c)}$	$q_{rs}^{(d)}$	V_{rs}^{π}	V_{rs}^{σ}	ΔE	reaction
1 , 4	−0.3986	−0.3068	+	−		
1 , 6	0.1628	0.3805	+	−	−	YES
2 , 5	−0.0730	−0.0698	−	−	+	
3 , 6	−0.2195	−0.4503	+	−		

The value of q_{16} being considerably larger in the latter than in the former, the equilibrium seems to lean to the left side. It agrees with the experimental result, too.

Oxy-Cope Rearrangement. This and the related reactions have been classified by Berson[24] as the oxy-Cope rearrangement and the [1,3] sigmatropy systematically. First, we deal with the famous reaction

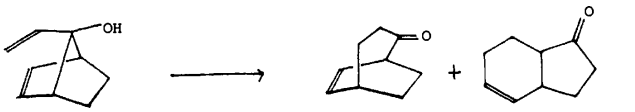

(1,3-σ tropy) (88%) (3,3-Cope) (7%)

Remembering the basic considerations previously given about the Cope rearrangement and the [1,3] sigmatropy, we assume the transition state as shown in Fig. 18(a). As to interaction matrix elements, $V_{16}^{\sigma}$is negative, V_{14}^{π}positive and V_{14}^{σ}vanishingly small. Due to the molecular shape, the distance between sites 1 and 6 is rather larger than that between sites 1 and 4. Under these considerations, calculations are carried

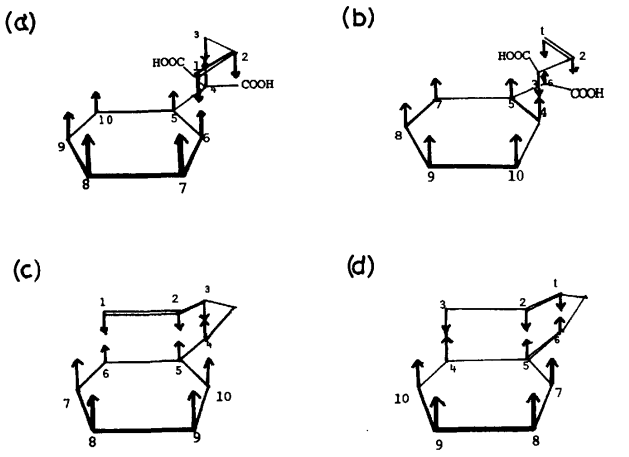

Fig. 17. The transition state of the Claisen rearrangement.

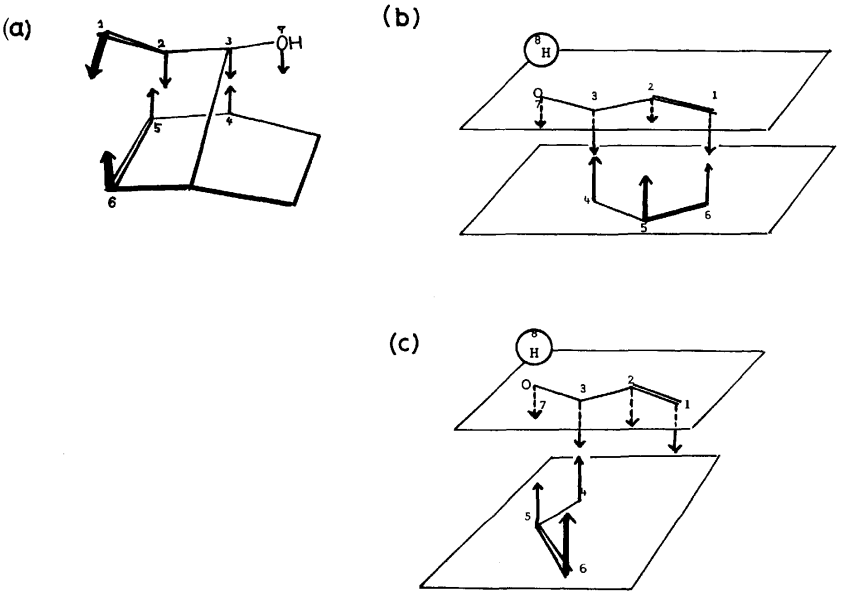

Fig. 18. The oxy-Cope rearrangement.

out as:

Site (r , s)	$q_{r,s}$	$V^{\pi}_{r,s}$	$V^{\sigma}_{r,s}$	ΔE	reaction
1 , 4	−0.3393	+	0	−	YES
1 , 6	0.2012	−	−	−	YES
2 , 5	−0.0748	−	−	+	
3 , 6	−0.3393	≒0	0	−	YES

Therefore, it is quite possible that the [1,3] sigmatropy occurs. In our notation, either the 1,4-transfer and the 1,6-transfer give products shown above, while the 3,6-transfer gives a queer material as

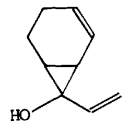

and it will be unstable.

Next, we deal with the competitive reactions, the Cope rearrangement *versus* prototropy shown as

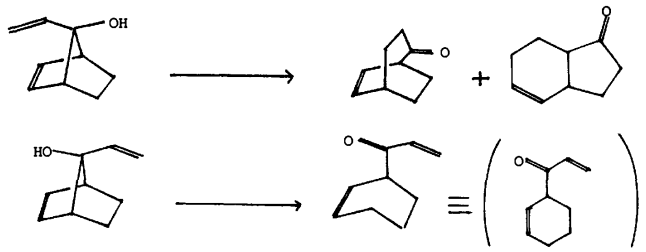

The transition state of this reaction is assumed as shown in Fig. 18(b), and the calculated parameters are:

Site (r , s)	$q_{r,s}$	$V^{\pi}_{r,s}$	$V^{\sigma}_{r,s}$	ΔE	reaction
1 , 6	0.2801	−(+)	0(−)	−(?)	YES
1 , 8	−0.2153	0	0		
2 , 8	−0.0674	0	+		
3 , 8	0.2278	0	+	+	
4 , 8	0.1661	0	−	−	YES
5 , 8	0.0169	0	−	+(−)	
6 , 8	−0.1227	0	−		

An other possile transition state is shown in Fig. 18(c). The results derived from this are the values in braces of the above table. These data suggest that only prototropy is possible.

The related reactions are reported by Thies[25] and by Mukai *et al.*[26] in other systems.

We expect that the Cope rearrangement will occur when the sites 1 and 6 can easily approach with each other, while the [1,3] sigmatropy takes place when sites 1 and 6 hardly approach due to some steric effect.

Concluding Remarks

From the preceding treatments, we can understand some advantages of our method:

(1) Our treatment is based on a reasonable assumption that the reaction will occur through a transition state in which the perturbing interaction makes energy lowering

(2) Considering the rearrangement reaction by use of the frontier orbital theory, we have to cut some bonds of molecule and take into account the interactions between the specified orbitals(*e.g.* HOMO, SOMO, or LUMO) of fragments. In our method, we need not such unnatural treatments but deal with the system always as a whole, taking into account the effect of all electrons in the molecule. We have only to assume the transition state of molecule in order to evaluate bond orders and interaction matrix elements.

(3) We need not to take care of the conservation of the orbital symmetry which is important in the Woodward-Hoffmann rule. Instead, the mutural phase of bond order at the place where the perturbing interaction takes place plays a important role, together with the sign of the interaction matrix element.

Conclusively we can say our treatment takes a step forward beyond the Woodward-Hoffmann rule or the frontier orbital theory.

References

1) S. Aono and K. Nishikawa, *Bull. Chem. Soc. Jpn.*, **53**, 3418 (1980); S. Aono, T. Ohmae, and K. Nishikawa, *Bull. Chem. Soc. Jpn.*, **54**, 1645 (1981); K. Nishikawa, M. Yamamoto, and S. Aono, *J. Chem. Phys.*, **78**, 5031 (1983).

2) T. Ohmae, K. Nishikawa, K. Deguch, and S. Aono, *Bull. Chem. Soc. Jpn.*, **54**, 2857 (1981).

3) T. Ohmae, K. Nishikawa, K. Deguch, and S. Aono, *Bull. Chem. Soc. Jpn.*, **54**, 3296 (1981).

4) K. Fukui, "Chemical Reactions and Electron Orbital," Maruzen (1976).

5) T. Mukai, Supplement of "Kagaku no Ryoiki," Vol. 93.

6) R. B. Woodward and R. Hoffmann, "The Conversation of Orbital Symmetry," Acadimic Press (1970).

7) T. Miyashi, A. Hazato, and T. Mukai, "Kagaku no Ryoiki," Vol. 33, No. 2, 62 (1979).

8) T. Mukai, H. Kubota, and T. Toda, *Tetrahedron Lett.*, **1967**, 3581.

9) T. Toda, M. Nitta, and T. Mukai, *Tetrahedron Lett.*, **1969**, 4401.

10) J. A. Berson, *Accounts Chem. Rev.*, **1**, 152 (1968).

11) T. Fukunaga, T. Mukai, Y. Akasaki, and R. Suzuki *Tetrahedron Lett.*, **1970**, (2975).

12) W. v. E. Doering and W. R. Roth, *Tetrahedron*, **18**, 67 (1962).

13) T. Miyashi, M. Nitta, and T. Mukai, *Tetrahedron Lett.*, **1967**, 3433.

14) J. E. Baldwin and M. S. Kaplan, *J. Am. Chem. Soc.*, **94**, 1794 (1972).

15) M. J. Goldstein and R. S. Leight, *J. Am. Chem. Soc.*, **99**, 8112 (1977).

16) R. P. Lutz, S. Bernal, R. O, Harries, and M. W. Mcnicholas, *J. Am. Chem. Soc.*, **93**, 3985 (1971).
17) W. v. E. Doering, V. G. Toscano, and G. H. Beasley, *Tetrahedron*, **27**, 5299 (1971).
18) D. C. Wigfield and K. Taymaz, *Tetrahedron Lett.*, **1975**, 3121.
19) A. Padwa and T. J. Blacklock, *J. Am. Chem. Soc.*, **100**, 1321 (1978).
20) A. C. Cope, E. G. Foster, and F. Daniels, *J. Am. Chem. Soc.*, **69**, 1893 (1947).
21) W. Ulrich and R. Gompper, *Angew. Chem., Int. Ed. Eng.*, **15**, 299 (1976).
22) E. N. Mavell and C. Lin, *J. Am. Chem. Soc.*, **100**, 877 (1978).
23) A. C. Cope, J. E. Meile, and D. W. H. Macdowell, *J. Am. Chem. Soc.*, **78**, 2551 (1956).
24) J. A. Berson and J. J. Gajewski, *J. Am. Chem. Soc.*, **86**, 5017, 5019 (1964).
25) R. W. Thies and E. P. Seitz, *J. Chem. Soc., Chem. Commun.*, **1976**, 864.
26) T. Mukai, A. Hazato, and T. Miyashi, *J. Am. Chem. Soc.*, **100**, 1008 (1978).

 © 1985 The Chemical Society of Japan Bull. Chem. Soc. Jpn., 58, 3193—3196 (1985)

Tungstic Acid-Tributyltin Chloride on a Charcoal Catalyst in the Epoxidation of Alkenes with Hydrogen Peroxide

Yasushi Itoi, Masami Inoue,* and Saburo Enomoto
Faculty of Pharmaceutical Sciences, Toyama Medical and Pharmaceutical University, 2630 Sugitani, Toyama 930-01
(Received May 10, 1985)

Several alkenes, such as cyclopentene, cyclohexene, 1-octene, 2-octene, 1-decene, styrene, and 1-methyl-1-cyclohexene, were epoxidized with aqueous (30%) hydrogen peroxide. *n*-Bu_3SuCl was a good co-catalyst of H_2WO_4 for the selective epoxidation. The conversion was improved by modifying charcoal as the carrier with such alkylating or alkylsilylating agents as *N,N*-dimethylformamide dibutyl acetal (DMFBA) or *N,O*-bis(trimethylsilyl)acetamide. Cyclopentene oxide, cyclohexene oxide, and 2-octene oxide were obtained from the corresponding olefins in the good yields of 74, 64, and 76% respectively by using DMFBA-modified charcoal as the support. The epoxidation was first-order with respect to both cyclohexene and H_2O_2. The apparent activation energy of the epoxidation of cyclohexene was 11.2 kcal/mol.

In the last decade much interest has been directed to the epoxidation of olefins for the synthesis of valuable key intermediates in the chemical industry. Also, attention has been paid to several kinds of hormones and mutagens involving an oxirane moiety in their structure. For the selective epoxidation of simple olefins, molybdenum complexes[1] are well known to catalyze under mild reaction conditions. Various complexes of Ti[2], Cr[3], and Pt[4] have also been used as catalysts for the epoxidation of allyl alcohols, alkenes, and terminal olefins respectively. However, among VIA-group metal oxides, tungstic acid (H_2WO_4) has not yet been found to catalyze the epoxidation of alkenes with *t*-butyl hydroperoxide. The use of H_2O_2 as an oxidizing agent has given diol exclusively.[5] Recently, however, it has been claimed that the addition of Me_3SnOH to tungstic acid catalyzes the epoxidation of cyclohexene with concentrated (70—90%) H_2O_2 to give cyclohexene oxide,[6] though the yields are not sufficiently high. Under the presence of phase-transfer agents, olefins have also been epoxidized with diluted aqueous H_2O_2 in the presence of Na_2WO_4-Na_3PO_4-H_3PO_4 at pH=9.[7] However, the use of a heterogenized tungstic acid catalyst in the epoxidation of olefins has not been proposed. Previously, authors have found that molybdenum oxide fixed on charcoal epoxidized olefins selectively with 30% H_2O_2 in the presence of *n*-Bu_3SnCl.[8] The yields were improved by using chemically modified charcoals as support.[9] When this catalyst system was applied to H_2WO_4, several alkenes, especially inner olefins, were epoxidized in good yields. In this report, the properties of tungsten catalysts will be studied in comparison with those of molybdenum catalysts.

Experimental

Materials. The cyclohexene, 30% aqueous hydrogen peroxide (Hayashi Pure Chemicals), *N,O*-bis(trimethylsilyl)acetamide, *N,N*-dimethylformamide dibutyl acetal, tungstic acid (Wako Pure Chemicals), organotin compounds (Kyodo Yakuhin), and charcoal (palm DC-5200) (Dia Catalysts & Chemicals) were purchased. The cyclohexene and other olefins were distilled before use.

Preparation of Catalyst. The H_2WO_4-charcoal catalyst was prepared by fixing H_2WO_4 on charcoal (65 mesh) by stirring it overnight with a H_2WO_4 solution dissolved with a small amount of 30% H_2O_2 in 2-propanol. The catalyst was then filtered off, washed with 2-propanol, and dried.

Pretreatment of Catalyst. Acid or Base Treatment of Charcoal. Charcoal powder (1 g) was dispersed in 25 mL of distilled water. The pH value of the charcoal-dispersed solution was adjusted at 2 to 12 by the addition of 0.1 M† HCl or 0.1 M NaOH. The solution, once heated, was left to stand at room temperature and the pH of the solution was readjusted. *Butylation or Trimethylsilylation of Charcoal.* Charcoal powder (1 g) was treated with *N,O*-bis(trimethylsilyl)acetamide or *N,N*-dimethylformamide dibutyl acetal in 20 mL of hexane by stirring at 50 °C. After 2 h, the charcoal was filtered off, washed with hexane, and dried.

Epoxidation Procedure. The tungstic acid–charcoal catalyst (0.4 g) was dispersed in 2-propanol (2 mL), and *n*-Bu_3SnCl (50 mg) was added. After the catalyst had stood at room temperature for 30 min, 2-propanol (4 mL), cyclohexene (1.5 g), and 30% hydrogen peroxide (1 to 2 mL) were added. The reaction was started at 50 °C±1° in an oil bath under magnetic stirring.

Analyses of Products. The reaction products were analyzed by means of gas-liquid chromatography (Shimadzu GC-8A), using OV-17 (3 mm i.d.×2 m in length) as the column-packing material and helium as the carrier gas (12.5 mL/min). The column temperature was programmed from 30° to 150 °C at a rate of 3°/min. The retention times were 1.4 min for cyclohexene, 6.0 min for cyclohexene oxide, 17.1 min for *trans*-1,2-cyclohexanediol monoisopropyl ether, and 17.6 min for *trans*-1,2-cyclohexanediol.

Results and Discussion

Epoxidation of Alkenes in the Presence of Tungsten Catalysts.

The oxidation of cyclohexene with aqueous (30%)

† 1 M=1 mol dm^{-3}.

Table 1. Oxidation of cyclohexene with 30% H_2O_2 in the presence of several tungstic catalysts

Catalyst	Conversion %	Yield/%		
		Epoxide[a]	Ether[b]	Diol[c]
H_2WO_4 (10 mg)	87.5	1.6	10.7	75.2
H_2WO_4-charcoal	34.8	5.5	6.6	22.7
H_2WO_4-*n*-Bu_3SnCl-charcoal	41.1	41.1	0	0
n-Bu_3SnCl-charcoal	0	0	0	0
Charcoal	0	0	0	0

Cyclohexene (1.6 M), H_2O_2 (1.6 M), 1.8% H_2WO_4-charcoal (0.4 g), *n*-Bu_3SnCl (1.58×10^{-2} M), and 2-propanol as the solvent were used. The reaction was carried out at 50 °C for 15 h. a) Cyclohexene oxide. b) *trans*-1,2-Cyclohexanediol monoisoporpyl ether. c) *trans*-1,2-Cyclohexanediol.

Table 2. Epoxidation of various olefins with 30% H_2O_2 on the H_2WO_4-*n*-Bu_3SnCl-charcoal catalyst

Olefin	Molar ratio of olefin to H_2O_2	Epoxide yield/%	By-product/%
Cyclopentene	1	74.4[a]	0
	2	81.0[b]	0
Cyclohexene	1	63.7[a]	0
	2	60.5[b]	0
1-Methyl-1-cyclohexene	2	53.7[b]	0
1-Octene	2	17.5[b]	0
2-Octene	1	76.3[a]	0
	2	56.0[b]	0
Styrene	2	30.3[b]	11.1[c]
1-Decene	2	16.5[b]	0

Olefin (1.6 M), H_2O_2 (0.8 or 1.6 M), 1.8%-H_2WO_4-charcoal (0.4 g), *n*-Bu_3SnCl (1.58×10^{-2} M), and 2-propanol as the solvent were used. Reaction was carried out at 50 °C for 15 h. a) Charcoal was pretreated with DMFBA. b) Charcoal was pretreated with BSA. c) Benzaldehyde.

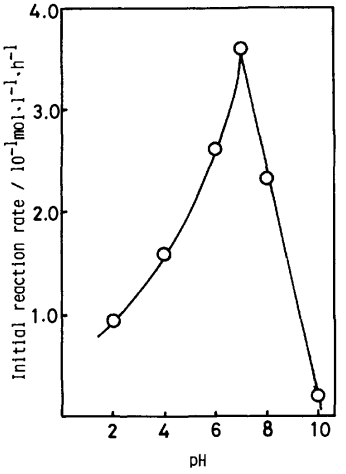

Fig. 1. Effect of pH of charcoal as support in the epoxidation of cyclohexene with 30% H_2O_2 on H_2WO_4-Bu_3SnCl-charcoal catalyst.
Cyclohexene 4.43 M, H_2O_2 8.02×10^{-1} M, 1.8%-H_2WO_4-charcoal 0.4 g, Bu_3SnCl 1.59×10^{-2} M, and solvent 2-propanol were used. Reaction was carried out at 50 °C.

H_2O_2 in the presence of H_2WO_4 catalysts was carried out in 2-propanol at 50 °C. The results are shown in Table 1. H_2WO_4 gave 1,2-cyclohexanediol, a hydrolysate of cyclohexene oxide, as the major product. Similar results were obtained in H_2WO_4-charcoal catalysts. However, the addition of *n*-Bu_3SnCl, as the best choice of the co-catalysts, prevented the hydrolysis and thus gave cyclohexene oxide selectively in a low yield (41%). The yield was not improved by changing the reaction conditions such as the solvent, the temperature, or the reaction time, since charcoal itself decomposed H_2O_2 considerably. By shaking the 2-propanol solution of H_2O_2 in the presence of a catalytic amount of charcoal (0.4g/5 mL) at 50 °C for 15 h, about three-tenths of the H_2O_2 was decomposed. We have observed that a chemically-modified charcoal supressed the decomposition of H_2O_2 to improve the yields of epoxides.[9] Therefore, charcoal was treated with DMFBA or BSA and several alkenes were epoxidized in the presence of H_2WO_4-*n*-Bu_3SnCl-charcoal catalysts. As is shown in Table 2, cyclic olefins of C_5–C_6 and inner olefins of 2-octene gave epoxides in 70—80% yields (based on H_2O_2), with a 1:2 ratio of olefins to H_2O_2. However, rather weak activity was observed in such terminal olefins as 1-octene and 1-decene. The order of yields closely resembled that obtained with the molybdenum oxide-*n*-Bu_3SnCl-charcoal (DMFBA) catalyst.[9]

Effect of the Pretreatment of Charcoal. In the oxidation of alkenes with aqueous H_2O_2, the pretreatment of charcoal drastically affected the conversion and the selectivity. Figure 1 shows the change in the conversions and selectivities when the epoxidation of cyclohexene was carried out in the presence of H_2WO_4 catalysts, using as supports charcoals which had been treated with solutions of various pH values. The oxidation rate for cyclohexene decreased according to the increase in the treated pH, though the selectivity was high. On the other hand, both the conversion and the selectivity

became poor on the acidic side. The best result was obtained by treating charcoal with a solution of pH 7. However, when equivalent amount of cyclohexene and H_2O_2 were used, the yield was as low as 40% by the decomposition of H_2O_2 on charcoal.

The suppression of the decomposition of H_2O_2 was examined by treating charcoal with various agents. The presence of such substituents as amino, carboxyl, and hydroxyl groups on the surface of charcoal is well known. We supposed that the decomposition of H_2O_2 was accelerated by those hydrophilic substituents on charcoal which concentrate H_2O_2 on the surface of charcoal. Therefore, the functional groups were blocked by alkylating or alkylsilylating agents, such as DMFBA, BSA, or diazomethane. Among those compounds, DMFBA is a good surface-modifier. The decomposition of H_2O_2 was suppressed by treating the charcoal with DMFBA; the decomposition rate of 50% in raw charcoal was decreased to 30% under heating for 15 h at 50 °C in a 2-propanol solution.

Effect of the Concentrations of Cyclohexene, H_2O_2 and H_2O on the Epoxidation. In the epoxidation of cyclohexene on H_2WO_4-*n*-Bu_3SnCl-charcoal catalysts, the concentrations of the olefins affected the rates. The initial rates of the oxidation of cyclohexene were first-order with respect to cyclohexene. Usually we used 4.43 M of cyclohexene in 2-propanol to keep a solution homogeneous by mixing in aqueous H_2O_2, cyclohexene, and 2-propanol. The reaction order with respect to the concentration of H_2O_2 was also unity. In the molybdenum oxide-*n*-Bu_3SnCl-charcoal catalyst, the initial rates of the oxidation of cyclohexene were zero-order for both cyclohexene and H_2O_2.[8] These results suggest that the affinity of cyclohexene or H_2O_2 to H_2WO_4 is weaker than that of the Mo catalyst. Though the presence of H_2O decreased the reaction rate in proportion to the amount added to the system, the selectivity to epoxide was excellent. Therefore, it was considered that a moderately hydrophobic surface was formed by the treatment of charcoal.

On the Arrhenius plot of the epoxidation of cyclohexene with H_2O_2 in the presence of the tungstic acid catalyst, an apparent activation energy of 11.2 kcal/mol (1 cal=4.184 J) was obtained. This value is smaller than those of molybdenum oxide-*n*-Bu_3SnCl-charcoal (13.5 kcal/mol),[8] or bis(dimethyldithiocarbamato)molybdenum(VI) oxide (19.0 kcal/mol).[10] Among the oxides of the VIA elements of the periodic table, Mo and W showed similar properties of giving epoxides selectively in the presence of alkyltin compounds. On the other hand, no epoxide was obtained with chromium(VI) oxide, not even in the presence of *n*-Bu_3SnCl, except for the use of $O_2Cr(NO_3)_2$ under mild reaction conditions (−78 °C).[3]

Effect of Organotin Compounds in the Selective Epoxidation. The effect of the co-catalyst of organotin compounds for H_2WO_4 was studied in the epoxidation of cyclohexene with aqueous (30%) H_2O_2. Different conversions and selectivities were obtained according to the kinds of substituents and alkyl groups of organotin chlorides, oxides, or acetates. Among these co-catalysts, *n*-Bu_3SnCl gave the highest yield (Table 3); the butyl group was more effective than the methyl or phenyl group. Furthermore, di or tributyltin compounds gave higher yields than monobutyltin compounds. These results

Table 3. Effects of various organotin compounds used as co-catalysts on the epoxidation of cyclohexene with 30% H_2O_2 on H_2WO_4-charcoal

Organotin compound	Conversion %	Yield/%		
		Epoxide[a]	Ether[b]	Diol[c]
Me_3SnCl	30.3	30.3	0	0
n-Bu_3SnCl	68.0	68.0	0	0
Ph_3SnCl	55.8	51.5	4.3	0
Me_3SnOH	30.4	30.4	0	0
$(n\text{-BuSnO})_2O$	42.8	35.6	7.2	0
n-Bu_2SnO	59.2	59.2	0	0
$(n\text{-}Bu_3Sn)_2O$	59.2	59.2	0	0
n-$Bu_2Sn(OCOCH_3)_2$	61.3	58.6	0	2.7
n-$BuSn(OCOCH_3)_3$	53.2	51.6	0	1.6
$Ph_3SnOCOCH_3$	58.0	52.5	5.5	0
$(Cyclohexyl)_3SnOH$	48.6	48.6	0	0
n-Bu_4Sn	64.6	38.5	26.0	0.1
Ph_4Sn	35.2	24.9	10.3	0

Cyclohexene (4.43 M), H_2O_2 (8.02×10^{-1} M), 1.8% H_2WO_4-charcoal (0.4 g), organotin compound (50 mg), and 2-propanol as the solvent were used. The reaction was carried out at 50 °C for 15 h. a) Cyclohexene oxide. b) *trans*-1,2-Cyclohexanediol monoisopropyl ether. c) *trans*-1,2-Cyclohexanediol.

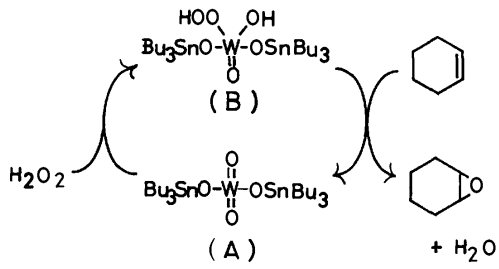

Chart 1.

suggest that the hydrophobic effect increases the yield of cyclohexene oxide. However, such tetraalkyltin as *n*-Bu_4Sn or Ph_4Sn gave lower selectivities for cyclohexene oxide. Therefore, the formation of tightly-bonded complexes between H_2WO_4 and such trialkyltin compounds of chloro, hydroxyl, oxy, or acetoxyl groups are considered to be an element for the selective epoxidation.

$$(HO)_2WO_2 + 2n\text{-}Bu_3SnCl \longrightarrow (n\text{-}Bu_3SnO)_2WO_2 + 2HCl$$

When cyclohexene and H_2O_2 were reacted in the presence of H_2WO_4 and *n*-Bu_3SnCl in 2-propanol at 50 °C for 15 h, white precipitates involving tungsten were obtained. These precipitates separated from the system and then catalyzed the selective epoxidation again. From these results, we considered the precipitates to be pre-active species with the (A) structure in Chart 1. The elemental analyses (C and H) of the precipitates were reasonable for (*n*-$Bu_3SnO)_2WO_2$. The treatment of Complex (A) with H_2O_2 gave an oxidized products. The IR spectra of this peroxy complex showed a remarkable decrease in the broad band at 800—900 cm^{-1}, probably because of the W=O bond observable in the IR spectra of H_2WO_4. Also, the absorption bands of Mo=O have been observed at 800—1000 cm^{-1}[11] in $(NH_4)_2[MoO_3F_2]$.

On the other hand, the band of the hydroxyl groups at 3400 cm^{-1} increased remarkably. Therefore, in our tungsten catalyst, a μ-peroxo-type[12] complex was suggested as an active species for the oxidation, as is shown in Chart 1 (B).

Then, the effect of the amount of *n*-Bu_3SnCl relative to that of H_2WO_4 in the epoxidation of cyclohexene was examined for the initial rate of the epoxidation. As is shown in Fig. 2, both the selectivity and the yield increased linearly with an increase in the amount of *n*-Bu_3SnCl and reached the saturation point at a molar ratio of 1:4 of H_2WO_4 to *n*-Bu_3SnCl. This fact supports a complex formation

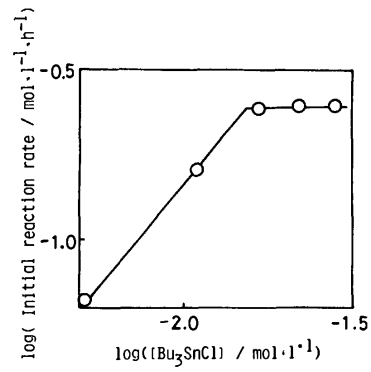

Fig. 2. Effect of the concentration of Bu_3SnCl as co-catalyst in the epoxidation of cyclohexene with 30% H_2O_2 on H_2WO_4–charcoal catalyst.
Cyclohexene 4.43 M, H_2O_2 8.02×10^{-1} M, 1.8%-H_2WO_4–charcoal 0.4 g, and solvent 2-propanol were used. Reaction was carried out at 50 °C.

between H_2WO_4 and *n*-Bu_3SnCl until the molar ratio of 1:4. Therefore, the organotin compounds bound on the acid groups of H_2WO_4 effectively prevent the hydrolysis of epoxides.

References

1) N. Indictor and W. F. Brill, *J. Org. Chem.*, **30**, 2074 (1965).
2) T. Katsuki and K. B. Sharpless, *J. Am. Chem. Soc.*, **102**, 5976 (1981).
3) N. Miyaura and J. K. Kochi, *J. Am. Chem. Soc.*, **105**, 2368 (1983); T. L. Siddall, N. Miyaura, J. C. Huffman, and J. K. Kochi, *J. Chem. Soc., Chem. Commun.*, **1983**, 1185.
4) G. Strukul and R. A. Michelin, *J. Chem. Soc., Chem. Commun.*, **1984**, 1538.
5) G. B. Payne and C. W. Smith, *J. Org. Chem.*, **22**, 1685 (1957).
6) Y. Watanabe, T. Nishizawa, and J. Kobayashi, U. S. Patent 3806467 (1974).
7) C. Venturello, E, Alneri, and M. Ricci, *J. Org. Chem.*, **48**, 3831 (1983).
8) Y. Itoi, M. Inoue, S. Enomoto, and Y. Watanabe, *Chem. Pharm. Bull.*, **32**, 41 (1984).
9) Y. Itoi, M. Inoue, and S. Enomoto, *Chem. Pharm. Bull.*, **33**, 3583 (1985).
10) T. Ikawa, M. Wakakura, T. Yamase, and S. Ozaki, *Sekiyu Gakkai Shi*, **18**, 492 (1975).
11) R. Mattes, K. Mennemenn, H. Rieskamp, and Heinz-J. Brockmeyer, Third International Conference on "The chemistry and uses of molybdenum," ed by H. F. Barry and P. C. H. Mitchell, Climax Molybdenum Development Co., Ltd., Michigan (1979), p. 28.
12) H. Mimoun, *J. Mol. Catal.*, **7**, 1 (1980).

Effects of Alkyl Chains of Thiacarbocyanine as the Sensitizer for the Photoreduction of Methylviologen in Micellar Phase

Masayuki NAKAGAKI, Hiroaki KOMATSU,* and Tetsurou HANDA†
Faculty of Pharmaceutical Sciences, Kyoto University, Yoshida-shimoadachi, Sakyo-ku, Kyoto 606
†*Gifu Pharmaceutical University, Mitahorahigashi, Gifu 502*
(Received May 23, 1985)

Photoinduced reduction of methylviologen (MV^{2+}) by ethylenediaminetetraacetate was investigated with 3,3′-dialkylthiacarbocyanines as a sensitizer in the micellar solution of a nonionic surfactant, heptaethylene glycol monododecyl ether. The alkyl chains of the dyes were found to have considerable effects on the reaction rate. The fluorescence yield of a dye having two long alkyl chains, 3,3′-dioctadecylthiacarbocyanine (C_{18-18}) in the micellar phase was larger than that of the dye having only one long alkyl chain, 3-methyl-3′-octadecylthiacarbocyanine (C_{1-18}). This result was discussed in terms of the large effective volume associated with the intramolecular twisting motion in the excited state of C_{18-18}. Also, from the fluorescence quenching experiments, it was found that MV^{2+} was of easier access to C_{18-18} than C_{1-18} in the micellar phase. Thus, the relatively higher stability of the excited state of C_{18-18} and the easier access of MV^{2+} to C_{18-18} were considered to be responsible for the faster reaction rate achieved by C_{18-18} than by C_{1-18} in the micellar solution.

Molecular organization plays important roles in complex biochemical processes. Components of metabolic pathways are compartmentalized in membranes which provide suitable microenvironments and which control the flow of reactants, transients and products. Micelles, monolayers and vesicles (liposomes) have been exploited as membrane mimetic agents.[1-6] Micelles have been extensively used to mimic membrane mediated processes in relatively simple systems.[6-8] To explain the enhancement of enzyme reactions in micelles, the involvements of hydrophobic interaction of the enzyme with the micelles, steric effects of the micelles and specific physical states of the substrates in the micelles have been suggested.[9-11]

For photoinduced reactions, micellar effects on the charge separation in exciplexes and on the prevention of the recombination of the photoproducts have been demonstrated.[12-14] On the other hand, the stability of the excited states of sensitizers and also the accessibility of substances to the sensitizers could be important factors in determining the efficiency of photoinduced reaction. The former would be closely correlated with the microenvironment around the sensitizer, that is, with the local effective polarity and viscosity in the vicinity of the sensitizers.[15] If an amphiphatic dye molecule having distinct hydrophobic and hydrophilic portions is used as a sensitizer, it can be expected that the sensitizer is provided with a different microenvironment in the micelle by changing the hydrophobic-hydrophilic balance, that is, by changing the numbers and/or length of the alkyl chains of the sensitizer. In this study, we investigate the photoinduced reduction of methylviologen by ethylenediaminetetraacetate, sensitized in aqueous solution by 3,3′-dialkylthiacarbocyanine incorporated in the nonionic micelle, heptaethylene glycol monododecyl ether. The effects of the alkyl chains of the sensitizers on the reaction are examined. The results obtained are discussed in relation to the stabilization of the excited state of the sensitizers in the micellar microenvironment and the accessibility of substrates from the aqueous phase to sensitizers in the micellar phase.

Experimental

3-Methyl-3′-octadecyl-2,2′-thiacarbocyanine (C_{1-18}) and 3,3′-dioctadecyl-2,2′-thiacarbocyanine (C_{18-18})(their structures are shown in Fig. 1) were purchased from the Japan Research Institute for Photosensitizing Dye Co., Ltd and used without further purification. Methylviologen (1,1′-dimethyl-4,4′-bipyridinium, MV^{2+}) dichloride (Sigma) and disodium ethylenediaminetetraacetate (EDTA) (Dojindo Laboratories) were used as received. The nonionic surfactant, heptaethylene glycol monododecyl ether (HED) was obtained from Nikko Chemicals Co., Ltd. The surface tension *versus* concentration curve for the aqueous HED solution gave no minimum around the critical micelle concentration (cmc), and the value of cmc agreed with the reported value,[16] 8×10^{-5} M.†† Sodium dodecyl sulfate (SDS) supplied from Nakarai Chemicals Co., Ltd was recrystallized twice from ethanol. Tris(hydroxymethyl)-aminomethane (Tris) of analytical grade was used as recieved. Water was doubly distilled from a quartz still and other solvents were distilled once.

For sample preparations, chloroform solutions of the cyanine dyes and HED were mixed and the solvent evaporated. The residue was dried overnight in a vacuum desiccator and then solubilized with 2×10^{-3} M MV^{2+} solution which was buffered with 2×10^{-3} M Tris and 2×10^{-3} M $EDTA^{3-}$ at pH 7.0, where EDTA (pK_a=2.0, 2.8, 6.1, 10.2)[17] is present as the trivalent anion. C_{1-18} and C_{18-18} are insoluble in water, and therefore, all of the dye is incorporated in the micellar phase. The sample solution was placed in a quartz cell (1×1×4 cm) fitted with a stopcock and was freed of oxygen by bubbling nitrogen gas and then degassed by aspiration at 2700 Pa (20 mmHg) prior to irradiation. The cell was immersed in a water bath (25.0 °C) with a quartz window.

Irradiations were carried out using a Kondo Sylvania

†† 1 M=1 mol dm^{-3}.

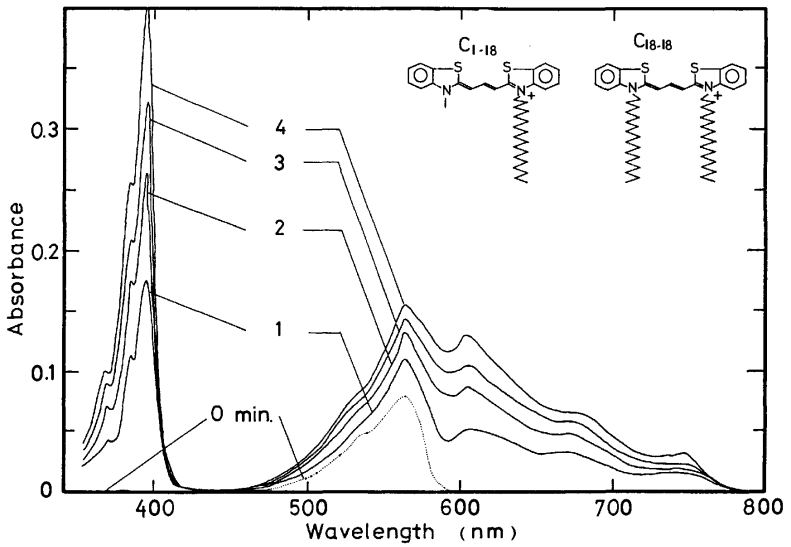

Fig. 1. Structures of sensitizers (C_{1-18} and C_{18-18}) and spectral changes of the solution due to the photoreduction of MV^{2+} using C_{18-18} as a sensitizer at 25.0 °C. 5×10^{-7} M of C_{18-18} is solubilized in 2×10^{-2} M HED micellar solution (2×10^{-3} M $EDTA^{3-}$, 2×10^{-3} M MV^{2+}, and 2×10^{-3} M Tris at pH 7.0). The solution is irradiated by a visible light ($\lambda>460$ nm) for 0, 1, 2, 3, and 4 min. The absorption band at 395 and 603 nm are contributed from MV^{+} formed by the reaction, and the band at 563 nm is attributed to C_{18-18} in the HED micellar phase.

1 kW tungsten halogen lamp. A Toshiba Y-46 cut-off filter was used to eliminate light of $\lambda<460$ nm. The distance from the irradiation source to the center of the cell containing sample solution was 10 cm. The sensitizer dyes had an absorption band around 560 nm in the micellar solution. On the other hand, reduced methylviologen (MV^{+}) formed by irradiation had an absorption maximum at about 603 nm. The latter band, however, resulted in faint reduction of the irradiation intensity (in this study, the reduction after 30 min's irradiation was at most 8% of the initial intensity).

The production of MV^{+} after intervals of irradiation was monitored by the absorption spectra on Shimadzu UV-180 spectrophotometer. The concentration of MV^{+} was calculated from the absorbance of the solution at 395 nm by taking $\varepsilon_{395nm}=3.8\times10^{4}$ M^{-1} cm.[18]

The measurement of the fluorescence yield was carried out for the dyes solubilized by HED in the buffer solution (2×10^{-3} M $EDTA^{3-}$ and 2×10^{-3} M Tris at pH 7.0) without MV^{2+}. The fluorescence spectra (excited at 530 nm) were observed with a Jasco FB-550 spectrofluorometer. The temperature was regulated at 25.0 °C by circulating water through the cuvette holders.

In order to determine the wavelength of the absorption maxima of the dyes in various solvents and micellar solutions, the first derivative absorption spectra were measured with a Hitachi-220 spectrophotometer.

The measurement of the viscosity of the various solvents has been described elsewhere.[19]

Results

Photoreduction of MV^{2+}. The deoxygenated solution containing a sensitizer dye in HED micellar phase and MV^{2+} in aqueous phase was irradiated with visible light. As a result, a blue color was developed in the presence of $EDTA^{3-}$. In Fig. 1, the changes of the absorption spectra are shown at varying irradiation times using C_{18-18} as a sensitizer. The development of absorption maxima at about 395 and 603 nm is charactaristic of the formation of MV^{+}.[20] Then, introduction of air into the cuvette resulted in the prompt reoxidation of MV^{+} to MV^{2+}

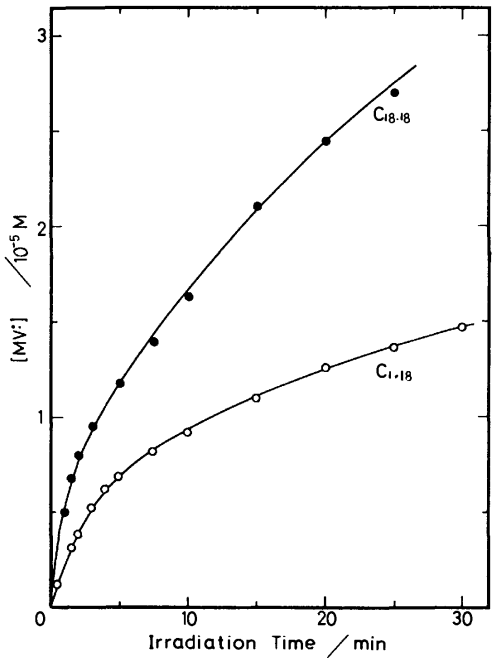

Fig. 2. Built-up of MV^{+} as a function of irradiation time.

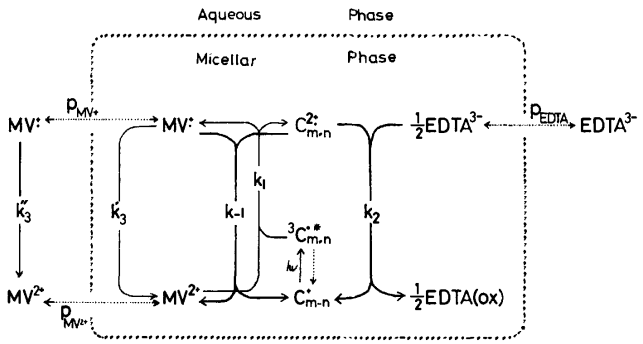

Fig. 3. The proposed mechanism of the photoreduction of MV^{2+} by $EDTA^{3-}$. C^{+}_{m-n} and $^3C^{+*}_{m+n}$ ($m=1$ or 18, $n=18$): sensitizer in the ground and the triplet exited state in the micellar phase, $C^{2+\cdot}_{m-n}$: sensitizer cation radical, EDTA(ox): the oxidized form of $EDTA^{3-}$, P_{MV2+}, P_{MV+}, and P_{EDTA}: the partition coefficient of MV^{2+}, MV^{+}, and $EDTA^{3-}$ from the aqueous to the micellar phase, and k_1, k_{-1}, k_2, and k_3: the rate constant of each reaction, respectively.

as manifested by decolorization.[20] The reduction of the concentration of the sensitizer dye after 30 min's irradiation was less than 5% of that before irradiation. Therefore, the contribution of the decrease of sensitizer to the formation rate of MV^{+} was not taken into account. In the dark or in the absence of $EDTA^{3-}$, no MV^{+} was produced.

In Fig. 2, the concentrations of MV^{+} formed are plotted against the irradiation time. The sensitizer dye having two long alkyl chains, C_{18-18}, exhibited faster formation of MV^{+} than C_{1-18} having only one long alkyl chain. In both cases, the formation rate of MV^{+} decreased with increase of the irradiation time. After removal of the light, the concentration of MV^{+} gradually decreased with increasing time owing to the reoxidation of MV^{+} to MV^{2+} by the small amount of dissolved oxygen in the solution. This reoxidation in the dark followed pseudo first-order kinetics, and the rate constant, k_3, had the same value in both sensitizers, being 5.4×10^{-5} s^{-1}. Such a reoxidation of MV^{+} to MV^{2+} may be considered to proceed not only after removal of the light but also during irradiation with light.

The proposed mechanism of the reaction is depicted in Fig. 3. Assuming that the concentration of the sensitizer cation radical ($C^{2+\cdot}_{m-n}$, $m=1$ or 18, $n=18$) is in the stationary state, and that mole of MV^{2+}, MV^{+}, and $EDTA^{3-}$ in the micellar phase is much smaller than the total mole in the micellar solution, the observed formation rate of MV^{+} can be written as

$$\frac{d[MV^+]_t}{dt} = \frac{k_1 k_2 [^3C^{+*}_{m-n}]_m [MV^{2+}]_m [EDTA^{3-}]_m^{1/2}}{k_{-1}(P_{MV+}[MV^+]_t) + k_2[EDTA^{3-}]_m^{1/2}} - k_3[MV^+]_t, \quad (1)$$

where $k_3=k_3'P_{MV+}+k_3''$. Here, $^3C^{+*}_{m-n}$ represents the sensitizer in the triplet excited state and P_{MV+} stands for the partition coefficient of MV^{+} from the aqueous to the micellar phases, $P_{MV+}=[MV^+]_m/[MV^+]_a$. The subscripts a, m, and t denote the concentration at the aqueous and the micellar phases and the total concentration in the micellar solution, respectively. For the case that $[MV^+]_t$ is small and $[MV^{2+}]_m$ is nearly equal to its initial value, $[MV^{2+}]_m^0$, and that $k_{-1}(P_{MV+}[MV^+]_t) \ll k_2[EDTA^{3-}]_m^{1/2}$, Eq. 1 reduces to

$$\frac{d[MV^+]_t}{dt} = k_1[^3C^{+*}_{m-n}]_m[MV^{2+}]_m^0, \quad (2)$$

which is the initial rate of formation of MV^{+} (V_{init}),

$$V_{Init} = k_1[^3C^{+*}_{m-n}]_m[MV^{2+}]_m^0. \quad (3)$$

Since $[MV^{2+}]_t \gg [MV^+]_t$ and $[MV^{2+}]_m$ in Eq. 1 is, in this experiment, nearly equal to $[MV^{2+}]_m^0$ which is constant, Eq. 1 becomes

$$\frac{d[MV^+]_t}{dt} = \frac{V_{Init}k_2[EDTA^{3-}]_m^{1/2}}{k_{-1}(P_{MV+}[MV^+]_t) + k_2[EDTA^{3-}]_m^{1/2}} - k_3[MV^+]_t, \quad (4)$$

which may be written as

$$\frac{1}{\frac{d[MV^+]_t}{dt} + k_3[MV^+]_t} = \frac{k_{-1}P_{MV+}}{V_{Init}k_2[EDTA^{3-}]_m^{1/2}}[MV^+]_t + \frac{1}{V_{Init}}. \quad (5)$$

Plots of $1/(d[MV^+]_t/dt+k_3[MV^+]_t)$ *versus* $[MV^+]_t$ according to Eq. 5 are shown in Fig. 4. Here, the observed values evaluated from Eqs. 6 and 7 were substituted for the values of $d[MV^+]_t/dt$ and $[MV^+]_t$, respectively.

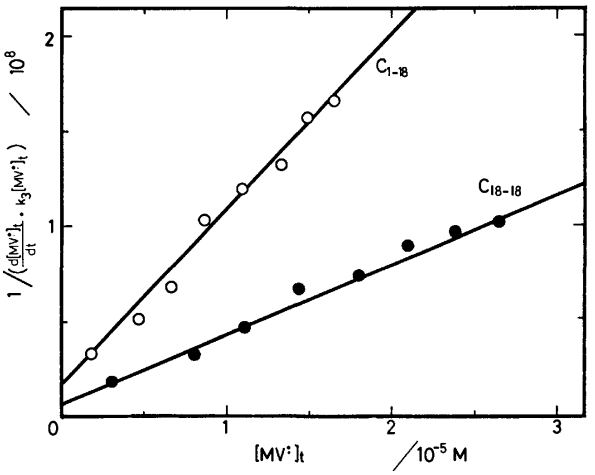

Fig. 4. Variation of $1/(d[MV^+]_t/dt+k_3[MV^+]_t)$ as a function of $[MV^+]_t$ according to Eq. 5.

$$\frac{d[MV^+]_t}{dt} = \frac{[MV^+]_{t(n+1)} - [MV^+]_{t(n)}}{t(n+1) - t(n)} \quad (6)$$

and

$$[MV^+]_t = \frac{[MV^+]_{t(n)} + [MV^+]_{t(n+1)}}{2} \quad (7)$$

where $[MV^+]_{t(n)}$ and $[MV^+]_{t(n+1)}$ are $[MV^+]_t$ at measuring time $t=t(n)$ and $t(n+1)$, respectively. These plots give straight lines and its intercept leads to values for V_{init} of 6.1×10^{-8} and 1.3×10^{-7} M·s^{-1} and $k_{-1}P_{MV+}/k_2[EDTA^{3-}]_m^{1/2}$ of 5.2×10^5 and 5.3×10^5 M^{-1} for C_{1-18} and C_{18-18}, respectively.

Absorption Maxima of Sensitizer Dyes in Various Solvents. In our previous studies,[19] it was found that C_{18-18} showed a marked dependence of its absorption maximum on the solvent polarity (solvatchroism). The solvatchroism for C_{1-18} was measured. C_{1-18} also showed considerably large shifts in its absorption maximum in various aliphatic alcohols as solvents. Figure 5 shows the relationship between the wave number at the absorption maximum ($\tilde{\nu}_{max}$) and the dielectric constant (D) of alcohols. In both dyes, the values of $\tilde{\nu}_{max}$ of sensitizer dyes increased linearly with increasing of D. The values of $\tilde{\nu}_{max}$ of sensitizer dyes in the HED micellar phase are shown by the arrows in Fig. 5. The D in the vicinity of dye molecules in the miceller phase, which is defined as the effective dielectric constant (D_{eff}) in this study, was estimated using the values of $\tilde{\nu}_{max}$ and D for alcohols. These procedures lead to values for D_{eff} of 18.5 and 20.0 for C_{1-18} and C_{18-18}, respectively. These results indicate that effective micropolarity in the vicinity of the chromophore of the dye in the micellar phase corresponds to that of 1-propanol or 1-butanol.

Fluorescence Quantum Yield of the Sensitizer Dyes. The fluorescence yields of the sensitizer dyes in the micellar phases and aliphatic alcohols were evaluated as the fluorescence intensities integrated over the spectra and divided by the absorbance at the excited wavelength (530 nm). Their results are presented in Fig. 6 as the value (ϕ_f^R) relative to that of 3,3'-diethyl-2,2'-thiacarbocyanine (C_{2-2}) in the aqueous phase (2×10^{-3} M EDTA-Tris buffered solution, pH 7.0) at 25.0 °C. Both C_{1-18} and C_{18-18} showed larger yields in the solvent of lower polarity, *e.g.* C_{1-18} had the yield of about 2.5 times larger in 1-octanol than in methanol. Furthermore, C_{18-18}, which has two long alkyl chains, has greater fluorescence yields than C_{1-18} in all solvents studied here. The fluorescence yields in the micellar phases are larger than that in the solvents where dyes are provided with the same dielectric constant in the micellar phases.

Fluorescence Quenching of Sensitizer Dyes in Micellar Phase by MV^{2+} in Aqueous Phase. Fluorescence quenchings of sensitizers solubilized in HED and HED-SDS mixed micellar phases by MV^{2+} as a quencher were measured. In the HED micellar solution, the quenching was slight, while in the mixed micellar solution, intense quenching was observed. If the Langmuir adsorption isotherm is applied to adsorption on the micellar surface of the quencher, MV^{2+}, the Stern-Volmer equation[21] can be written as

$$\frac{\phi_f^R}{\phi_f^{R(MV)}} = k_q\tau\frac{[MV^{2+}]_\infty P[MV^{2+}]}{1+P[MV^{2+}]}. \quad (8)$$

Here, $\phi_f^R/\phi_f^{R(MV)}$ is the ratio of relative fluorescence quantum yields with and without the quencher, k_q is the rate constant of quenching, τ is the lifetime of the excited state of the sensitizer, $[MV^{2+}]_\infty$ is the concentration of saturated adsorption of MV^{2+} on the micellar surface, and P is a constant giving the strength of adsorption of MV^{2+}. Equation 8 is rewritten as

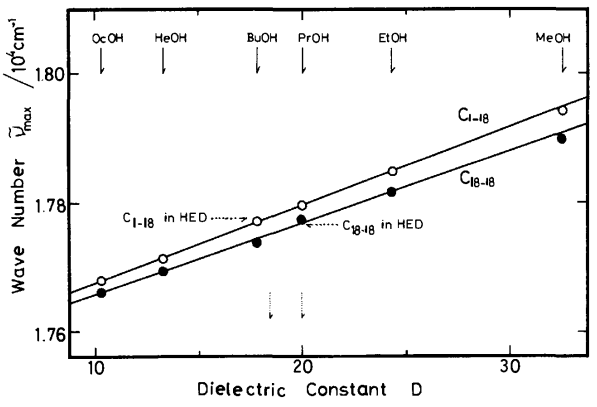

Fig. 5. Relationship of the wave number of absorption maxima ($\tilde{\nu}_{max}$) for C_{1-18} and C_{18-18} with dielectric constant D of solvent. MeOH: methanol, EtOH: ethanol, PrOH: 1-propanol, BuOH: 1-butanol, HeOH: 1-hexanol and OcOH: 1-octanol.

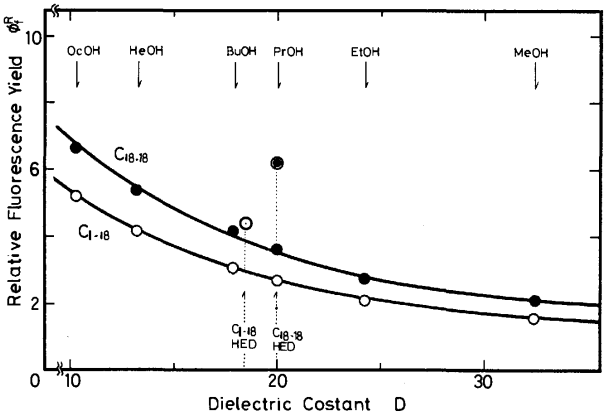

Fig. 6. Relationship of the relative fluorescence yield (ϕ_f^R) for C_{1-18} and C_{18-18} with dielectric constant D of solvent. ϕ_f^R is relative to the value for 3,3'-diethyl-2,2'-thiacarbocyanine (C_{2-2}) in the aqueous phase at 25.0 °C. (○) and (●): C_{1-18} and C_{18-18} in solvents, (⊙) and (◉): C_{1-18} and C_{18-18} in HED micellar phase.

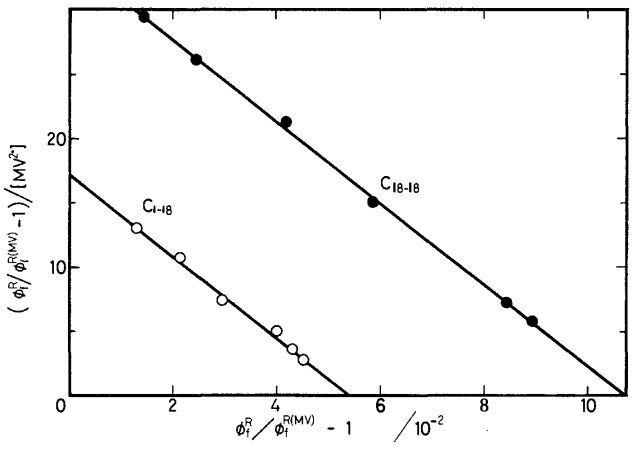

Fig. 7. Plots for fluorescence quenching of C_{1-18} and C_{18-18} in HED-SDS mixed micellar phase by MV^{2+} as a quencher, according to Eq. 9. The mole fraction of SDS in the mixed micelle is 0.1 (the total concentration of surfactants is 2×10^{-2} M). $\phi_f^R/\phi_f^{R(MV)}$ is the ratio of relative fluorescence yields without and with MV^{2+}

$$\left(\frac{\phi_f^R}{\phi_f^{R(MV)}}-1\right)\frac{1}{[MV^{2+}]} = P\left\{k_q\tau[MV^{2+}]_\infty-\left(\frac{\phi_f^R}{\phi_f^{R(MV)}}-1\right)\right\}. \quad (9)$$

In Fig. 7, the experimental values of $(\phi_f^R/\phi_f^{R(MV)}-1)/[MV^{2+}]$ for various amounts of MV^{2+} are plotted against the values of $(\phi_f^R/\phi_f^{R(MV)}-1)$ for the mole fraction of SDS in the mixed micelle of 0.1 (the total concentration of surfactants is 2×10^{-2} M). These plots yield straight lines, giving the same slope, P, in both dyes, with a value of P of 3.2×10^2. The intercept on the $(\phi_f^R/\phi_f^{R(MV)}-1)$ axis gives values for $k_q\tau[MV^{2+}]_\infty$ of 5.4×10^{-2} and 1.1×10^{-1} for C_{1-18} and C_{18-18}, respectively. These results indicate that C_{18-18} is more easily quenched by MV^{2+} than C_{1-18} in the micellar solution.

Discussion

Photoinduced reduction of MV^{2+} by EDTA was first observed with tris-(2,2′-bipyridine)ruthenium as a sensitizer by M. Calvin *et al.*[22] In our study, 3,3′-dialkylthiacarbocyanines in a nonionic micelle were adopted as a sensitizer. With increase of irradiation time, the concentration of MV^+ increased but the formation rate of MV^+ decreased. Equation 1, which represents the formation rate of MV^+, indicates that the decrease in the rate with irradiation time arises from the increase of $[MV^+]_t$. After removal of the light, the rate of disappearance of MV^+ due to reoxidation to MV^{2+} is equal to the second term, $k_3[MV^+]_t^2$ on the right-hand side of Eq. 1.

The initial rate of formation of MV^+, V_{init}, presented by Eq. 3 is proportional to the product of k_1 and $[^3C_{m-n}^{+*}]_m$, because $[MV^{2+}]_m$ is constant independent of a sensitizer. Therefore, the difference in V_{init} is estimated from the differences in k_1 and $[^3C_{m-n}^{+*}]_m$ for C_{1-18} and C_{18-18}.

Effects of Microenvironment on Fluorescence Yield. According to the proposed mechanism shown in Fig. 3, it is clear that the concentration of the sensitizer in the triplet excited state ($^3C_{m-n}^{+*}$) generated from the sensitizer in the singlet excited state ($^1C_{m-n}^{+*}$) plays an important role in the reaction. The relative yield of the intersystem crossing from the singlet excited state (ϕ_{isc}^R) is given by

$$\phi_{isc}^R = \alpha\frac{k_{isc}}{k_{rl}+k_f+k_{isc}}. \quad (10)$$

On the other hand, the relative fluorescence yield of the sensitizer (ϕ_f^R) is

$$\phi_f^R = \alpha'\frac{k_f}{k_{rl}+k_f+k_{isc}}, \quad (11)$$

and therefore, their ratio is

$$\frac{\phi_{isc}^R}{\phi_f^R} = \alpha''\frac{k_{isc}}{k_f}. \quad (12)$$

Here, k_{rl}, k_f, and k_{isc} are the rate constants for radiationless relaxation, radiative (fluorescence) relaxation and intersystem crossing of the excited state, $^1C_{m-n}^{+*}$, and α, α', and α'' are proportionality constants. Since k_f and k_{isc} are considered to be less dependent on the environmental properties,[23-25] the increase in ϕ_f^R is accompanied by the increase in ϕ_{isc}^R as shown in Eq. 12. Since $[^3C_{m-n}^{+*}]_m$ is proportional to ϕ_{isc}^R, $[^3C_{m-n}^{+*}]_m$ can be estimated using ϕ_f^R.

The increase in ϕ_f^R would result from the decrease of the rate constant of radiationless process, k_{rl}. It has been suggested that k_{rl} largely depends on the interaction of the excited dye molecule and the environment around it,[23] that is, the microenvironment in the vicinity of the dye molecule. The microenvironment would actually mean the local effective micropolarity and microviscosity around the dye molecule.

In order to evaluate the micropolarity, the wave number at the absorption maxima of dyes solubilized in the micellar phases were compared with their dependencies on solvent polarity. The reason for employing aliphatic alcohols to calibrate the micropolarity in the micellar phase have already been discussed in detail.[26-28] As seen from Fig. 5, the chromophores of C_{1-18} and C_{18-18} accommodated in the micellar phases are provided with a remarkably less polar environment in comparison with that in the aqueous phase, but they seem to be in a more polar environment than in a liquid hydrocarbon. These results indicate that the chromophores are

located in the surface region of the micelle. The chromophore having two long alkyl chains, C_{18-18}, seems to be located in a somewhat more polar environment than C_{1-18}.

As shown in Fig. 6, the fluorescence yields of both dyes are larger in the micellar phases than in the solvents where dyes are provided with the same dielectric constant in the micellar phases. The microenvironmental effects on the fluorescence yield of dyes would contain polarity and also viscosity factors. These are usually associated with each other in a complex way and can not be investigated separately.

Carbocyanine dyes have been known to exhibit intense twisting modes along the polymethine chain in the electronically excited state.[29-31] This is because in the excited state, the conjugated π electronic structure is broken; this allows twisting modes of the substituents at each end and a destruction of the initial planar structure. The ability of such an intramolecular twisting, which may be strongly affected from the viscosity in the vicinity of the dye molecule, is associated with the internal conversion process of the singlet excited state to the ground state and therefore, with the fluorescence yield.

The radiationless relaxation process of the excited state is divided as

$$k_{rl} = k_a + k_b. \tag{13}$$

Here, k_a is the rate constant of the usual internal conversion which is independent of the viscosity in the vicinity of the dye molecule but dependent on the polarity around the dye molecule. The quantity k_b is the rate constant for relaxation *via* a twisting mode which is influenced by the microscopic viscosity around the dye molecule. Using the Stokes equation, k_b is given as[32,33]

$$k_b = \beta\left(\frac{T}{\eta}\right). \tag{14}$$

Here, β is a function of the effective volume associated with the intramolecular twisting, η is the viscosity of the medium and T is absolute temperature. From Eqs. 11, 13, and 14, the following equation is derived[33]

$$\frac{1}{\phi_f^R} = \frac{1}{\phi_f^{0R}} + \left(\frac{A}{k_f}\right)\left(\frac{T}{\eta}\right). \tag{15}$$

Here, $A=\beta/\alpha'$ and ϕ_f^{0R} is the relative fluorescence yield when the relaxation via twisting mode is absent as $\phi_f^{0R}=\alpha' k_f/(k_a+k_{isc}+k_f)$. It is already known that the relation between the fluorescence yield of Auramine O and the viscosity of the mixed solvent is well described by Eq. 15.[32,38] Equation 15 was examined for C_{1-18} and C_{18-18} in aliphatic alcohols at 25 °C. In these cases, however, no simple correlation, as expected from Eq. 15, was obtained and this is explained by the effective polarity in these solvents. Eq. 15 was, therefore, examined for the viscosity change of a single solvent with change of temperature. Plots of the reciplocal of ϕ_f^R for C_{1-18} and C_{18-18} in ethanol, 1-propanol and 1-butanol *versus* T/η gave straight lines as expected from Eq. 15 (its figure[19] is not shown). The slope and the intercept of the lines allow k_f/A and ϕ_f^{0R} to be evaluated. Figure 8 shows plots of k_f/A and ϕ_f^{0R} as functions of D for C_{1-18} and C_{18-18}. It is seen from Fig. 8 that the greater the polarity of the solvent, the smaller is ϕ_f^{0R} and the larger is k_f/A. The k_f/A is the value which increases with increase of the effective volume associated with the twisting, because $A=\beta/\alpha'$. The larger value of k_f/A in a polar solvent is ascribed to the solvation of the dye molecule. In the same solvent, the value of k_f/A for C_{18-18} is about twice as large as that for C_{1-18}. This indicates that the twisting of the dye molecule affects the radiationless relaxation process of the electronic excited state remarkably and that long alkyl chains such as octadecyl groups have an important effect upon the twisting of the dye molecules and make a great contribution to the effective volume associated with

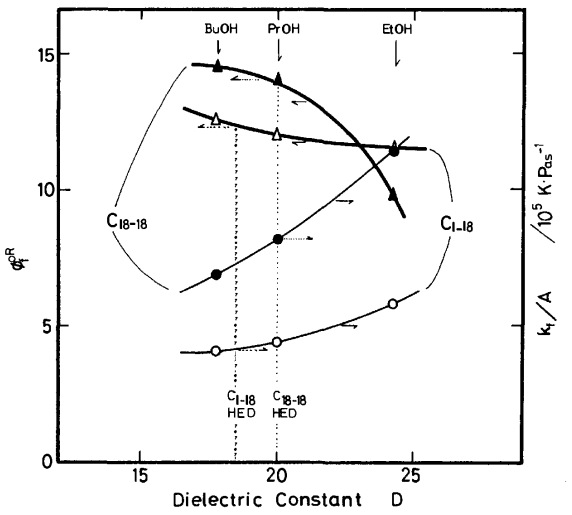

Fig. 8. ϕ_f^{0R} and k_f/A shown as functions of dielectric constant (D). ϕ_f^{0R}: the relative fluorescence yield when the relaxation via intrarotational mode is absent, k_f/A: the value increasing with increase of the effective volume associated with the twisting.

Table 1. Experimental results of C_{1-18} and C_{18-18} in micellar phase

Sensitizer Dye	ϕ_f^R	ϕ_f^{0R}	k_f/A / 10^5 K·Pa·s^{-1}	η_{eff} / 10^{-3} Pa·s
C_{1-18}	4.1	12.3	4.2	4.4
C_{18-18}	6.2	14.0	7.4	4.5

ϕ_f^R: Relative fluorescence yield, η_{eff}: effective microviscosity, ϕ_f^{0R} and k_f/A: see Eq. 15.

Table 2. Experimental values of C_{1-18} and C_{18-18} in micellar solution

Sensitizer dye	$\frac{V_{init}}{M \cdot s^{-1}}$	$\frac{\left(\frac{k_{-1}P_{MV^+}}{k_2[EDTA^{3-}]_m^{1/2}}\right)}{M^{-1}}$	$k_q \cdot \tau \cdot [MV^{2+}]_\infty$	k_q^R
C_{1-18}	6.1×10^{-8} (1)	5.2×10^{5}	5.4×10^{-2} (1)	1
C_{18-18}	1.3×10^{-7} (2.1)	5.3×10^{5}	1.1×10^{-1} (2.0)	1.3

V_{init}: The initial rate of formation of MV^+, τ: the life time of the excited state of sensitizer dye, k_q^R: the relative value of the rate constant of quenching.

the twisting.

If the polarity of the solvent is constant, Eq. 1 gives a straight line as mentioned before. Rearrangement of Eq. 15 leads to

$$\eta = \frac{T\phi_f^{0R}\phi_f^R}{(\phi_f^{0R}-\phi_f^R)\frac{k_f}{A}}. \quad (16)$$

When Eq. 16 is applied to micellar systems, the values in the solvent where dyes are provided with the same effective polarity in the micellar phase should be used. Therefore, the values of ϕ_f^{0R} and k_f/A of dye in alcohols of D, 18.5 for C_{1-18} and 20.0 for C_{18-18}, are assigned to those in the micellar phase (See Fig. 8). Substituting the value of ϕ_f^R in the micellar phase for ϕ_f^R in Eq. 16 yields values for the effective microviscosity in the micellar phase (η_{eff}). Table 1 shows the values of η_{eff} together with ϕ_f^R and k_f/A in the micellar phase. The η_{eff} has about the same value in both dyes, being 4.5×10^{-3}—4.6×10^{-3} Pas (4.5—4.6 cP).

As seen from Table 1, the difference in the values of ϕ_f^{0R} between both dyes is slight. Therefore, the large ϕ_f^R of C_{18-18} in the micellar phase compared with C_{1-18} can be ascribed to the relatively large effective volume ($1/A$) associated with the twisting. This indicates that the two long alkyl chains of C_{18-18} play an important role in the enhancement of the fluorescence yields. On the basis of an estimation of the fluorescence yield, it is suggested that the concentration of the sensitizer dye in the triplet excited state for C_{18-18} having two long alkyl chains is larger than that for C_{1-18} having only one long alkyl chain.

Access of MV^{2+} to Sensitizer Dye in Micellar Phase. As shown in Eq. 3, the initial rate of photoinduced reduction studied here is subject to the reaction between the sensitizer dye in the triplet state and MV^{2+} approching from aqueous to micellar phases. The D of dyes in the micelle indicated that the chromophore of C_{18-18} is located nearer to the micellar surface than that of C_{1-18}, and that C_{18-18} is more easily attacked by MV^{2+} at the miceller surface than C_{1-18}.

In order to obtain additional information about the accesibility of MV^{2+} to the excited sensitizer dye in the micellar phase, measurements of the quenching efficiency of fluorescence of the dye by MV^{2+} were carried out. From the experimental results, it was found that the value of P in Eq. 8 was the same for both dyes, indicating that the adsorption on the micellar surface of the quencher is not influenced by dyes in the micellar phase, and that the value of $k_q\tau[MV^{2+}]_\infty$ evaluated from experimental results was about 2.0 times larger for C_{18-18} than C_{1-18}. On the assumption that $(\tau)_{C(18-18)}/(\tau)_{C(1-18)} \approx (\phi_f^R)_{C(18-18)}/(\phi_f^R)_{C(1-18)}$, the following relation is obtained,

$$\frac{(k_q\tau[MV^{2+}]_\infty)_{C(18-18)}}{(k_q\tau[MV^{2+}]_\infty)_{C(1-18)}} = \frac{(k_q\tau)_{C(18-18)}}{(k_q\tau)_{C(1-18)}} \approx \frac{(k_q\phi_f^R)_{C(18-18)}}{(k_q\phi_f^R)_{C(1-18)}}, \quad (17)$$

because $[MV^{2+}]_\infty$ has the same value for both sensitizer dyes. Here, the parentheses show the terms for C_{1-18} and C_{18-18}, respectively. By using Eq. 17 and the values of ϕ_f^R and $k_q\tau[MV^{2+}]_\infty$ for C_{1-18} and C_{18-18}, the values of $(k_q)_{C(18-18)}/(k_q)_{C(1-18)}$ were evaluated. The results are presented in Table 2 as the value (k_q^R) relative to that of C_{1-18}. The value of k_q^R for C_{18-18} is 1.3 times larger than C_{1-18}. This difference in k_q^R may probably be ascribed to the difference in the location of the chromophores of these dyes in the micellar surface. Thus, it is also indicated from the data for the fluorescence quenching that C_{18-18} is more easily attacked by MV^{2+} than C_{1-18} at the micellar surface.

As shown in Table 2, the product of ϕ_f^R in the micellar phase and k_q^R, that is, $k_q\tau[MV^{2+}]_\infty$ is 2.0 times larger for C_{18-18} and agrees with the ratio of V_{init}, being 2.1. This indicates that the difference in V_{init} of C_{1-18} and C_{18-18} may be explained in terms of the difference in the fluorescence yield of the sensitizer dye in the micellar phase and in the accessibility of MV^{2+} to excited sensitizer dyes in the micellar phase.

References

1) M. Grätzel, "Micellization, Solubilization and Microemulsions," ed by K. L. Mittal, Plenum Press, New York (1977), p. 531.

2) M. Calvin, *Acct. Chem. Res.*, **10**, 369 (1978).

3) M. Mangel, *Biochim. Biophys. Acta*, **430**, 459 (1976).
4) Y. Toyoshima, M. Morino, H. Motoki, and M. Sukigara, *Nature*, **265**, 187 (1977).
5) W. Stillwell and H. Ti Tien, *Biochem. Biophys. Res. Commun.*, **81**, 212 (1978).
6) J. H. Fendler, "Membrane Mimetic Chemistry," Wiley, New York (1982).
7) J. H. Fendler and E. J. Fendler, "Catalysis in Micellar and Macromolecular Systems," Academic Press, New York (1975).
8) J. H. Fendler, *J. Phys. Chem.*, **84**, 1458 (1980).
9) S. G. Bhat and H. L. Brockman, *Biochemistry*, **21**, 1547 (1982).
10) P. S. De Arraujio, M. Y. Resseneu, J. M. H. Kremer, E. J. van Zolen, and G. H. de Hass, *Biochemistry*, **18**, 580 (1979).
11) M. Nakagaki and I. Yamamoto, *Yakugaku Zasshi*, **101**, 1099 (1981).
12) M. Grätzel, *Ber. Bunsenges. Phys. Chem.*, **84**, 981 (1980).
13) P. A. Brugger, P. P. Infelta, A. M. Braum, and M. Grätzel, *J. Phys. Chem.*, **84**, 2402 (1980).
14) Y. Yamaguchi, T. Miyashita, and M. Matsuda, *J. Phys. Chem.*, **85**, 1369 (1981).
15) T. Handa, H. Komatsu, and M. Nakagaki, *Progr. Colloid, Polymer Sci.*, **68**, 33 (1983).
16) H. Lange, *Proc. Inter. Cong. Surface Activity*, **3**, 279 (1960).
17) A. E. Martell and R. M. Smith, Eds., "Critical Stability Constants," Plenum Press, New York (1974), Vol. 1, P. 204.
18) M. S. Tunuli and J. H. Fendler, *J. Am. Chem. Soc.*, **103**, 2507 (1981).
19) T. Handa, H. Komatsu, K. Matsuzaki, and M. Nakagaki, *Nippon Kagaku Kaishi*, **1984**, 8.
20) E. M. Kosower and J. L. Cotter, *J. Am. Chem. Soc.*, **86**, 5524 (1964).
21) O. Stern and M. Volmer, *Physical. Z.*, **20**, 183 (1919).
22) W. E. Ford, J. F. Otvos, and M. Calvin, *Nature*, **274**, 505 (1978).
23) N. Mataga and T. Kubota, "Molecular Interactions and Electronic Spectra," Marcel Dekker, New York (1970), P. 139.
24) M. Gouterman, *J. Chem. Phys.*, **36**, 2846 (1961).
25) G. Robinson and R. Frosch, *J. Chem. Phys.*, **38**, 1187 (1964).
26) P. Mukerjee, C. Ramachandran, and R. Pyter, *J. Phys. Chem.*, **86**, 3189, 3198 (1982).
27) P. Mukerjee, J. R. Cardinal, *J. Phys. Chem.*, **82**, 1614 (1978) and 1620 (1978).
28) K. A. Zachariasse, N. Van Phuc, and B. Kozankiewicz, *J. Phys. Chem.*, **85**, 2676 (1981).
29) D. Dempster, T. Morrow, R. Rankin, and G. F. Thompson, *J. Chem. Soc., Faraday Trans. 2*, **68**, 1479 (1972).
30) R. H. Baker, M. Grätzel, and R. Steiger, *J. Am. Chem. Soc.* **102**, 847 (1980).
31) K. Onuki, K. Kurihara, Y. Toyoshima, and M. Sukigara, *Bull. Chem. Soc. Jpn.*, **53**, 1914 (1980).
32) G. Oster and Y. Nishijima, *J. Am. Chem. Soc.*, **78**, 1581 (1956).
33) Y. Nishijima, *Koubunshi*, **13**, 35 (1964).

Ultralow Interfacial Tension in the Vicinity of the Upper Critical Solution Temperature of the Mixture of Water and Isobutyric Acid

Makoto ARATONO* and Kinsi MOTOMURA
Department of Chemistry, Faculty of Science, Kyushu University, 33, Fukuoka 812
(Received May 24, 1985)

The ultralow interfacial tension of the binary liquid mixture of water and isobutyric acid has been measured as a function of temperature under atmospheric pressure in the vicinity of the upper critical solution temperature. It has been observed that the interfacial tension decreases monotonously as the temperature increases and is reduced to zero at the critical solution temperature. The results have been analyzed on the basis of the thermodynamics of interfaces. It has been found that the formation of interface is accompanied by increases in entropy and energy, which vanish at the critical solution temperature. This behavior has been considered in terms of the partial molar thermodynamic quantities of components. The brief discussion of the critical exponent has been also given for the present system.

The interfacial tension between two phases of a binary liquid mixture has been found to be reduced to zero as temperature approaches the critical solution temperature. In connection with the critical phenomena, therefore, it seems to be great interest to clarify the interfacial behavior in the vicinity of the critical solution temperature. However, the thermodynamic investigations of the interface are scarcely undertaken at temperatures near the critical solution temperature,[1-6] which is probably due to the difficulty of the precise measurement of ultralow interfacial tension. In our previous paper,[7] a new apparatus adopting a sessile drop technique was designed and the ultralow interfacial tension was measured accurately up to the value of 0.02 $\mu N\ m^{-1}$. Further it has been proved that the thermodynamic analysis of the interfacial tension measured as a function of thermodynamic variables is useful to shed light on the properties and structures of interfaces.[8-10] In the present paper, as a part of our thermodynamic studies of interfaces, the interfacial tension of the water–isobutyric acid mixture, of which the upper critical solution temperature is close to room temperature, was measured at temperatures near the upper critical solution temperature and analyzed on the basis of the thermodynamics of interfaces. The comment is also made on the critical exponent of this system.

Experimental

The purification of materials and the purity of isobutyric acid have been described previously.[7] The mutual solubility curve was drawn by using the phase separation temperature and phase mixing temperature determined visually according to the following procedure. The mixture of about 20 cm^3 was weighed and the sample tube was placed in a water bath having a volume of about 65 dm^3. The bath was thermostated by employing a mercury-toluene regulator; the temperature measured by a Beckmann thermometer was found to be constant within ±0.002 K. First, the temperature of the bath was set to a temperature about 0.1 K below or above the phase separation temperature expected. After the mixture was stirred by a magnetic rotor for about 10 min, the temperature was raised by about 0.01 K when the mixture was turbid and the temperature lowered when the mixture transparent. By repeating this procedure, the phase separation temperature and the phase mixing temperature were determined. Both temperatures were found to agree with each other within 0.01 K.

The sessile drop method was adopted to measure the interfacial tension between the two phases at temperatures near the upper critical solution temperature under atmospheric pressure. The apparatus and procedure of the measurement were described in detail in the previous paper.[7]

Results and Discussion

The phase separation and the phase mixing temperature were determined at about 70 different concentrations of the water–isobutyric acid mixture in the relatively narrow temperature range under atmospheric pressure. The mutual solubility curve is shown in Fig. 1 in the form of temperature T *vs.*

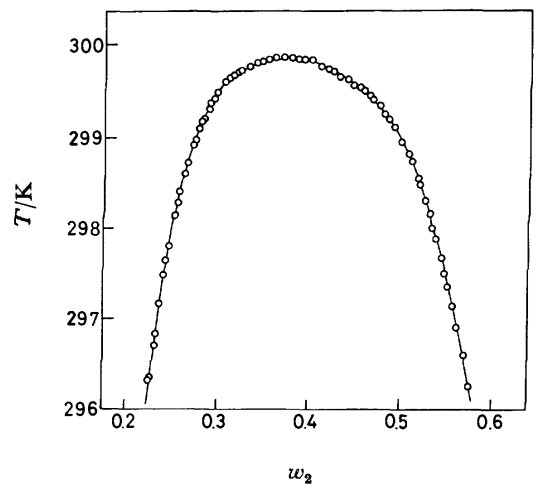

Fig. 1. Phase separation temperature *vs.* mass fraction curve under atmospheric pressure.

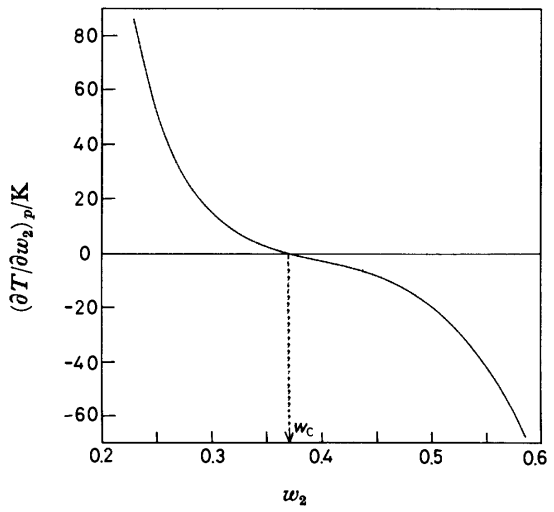

Fig. 2. $(\partial T/\partial w_2)_p$ *vs.* mass fraction curve under atmospheric pressure.

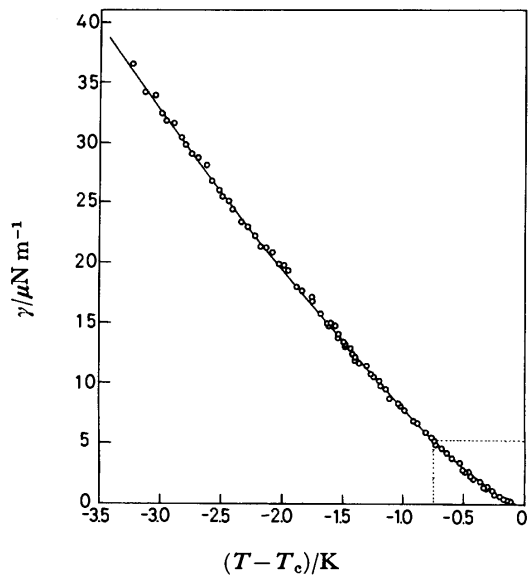

Fig. 3(a). Interfacial tension *vs.* temperature curve under atmospheric pressure.

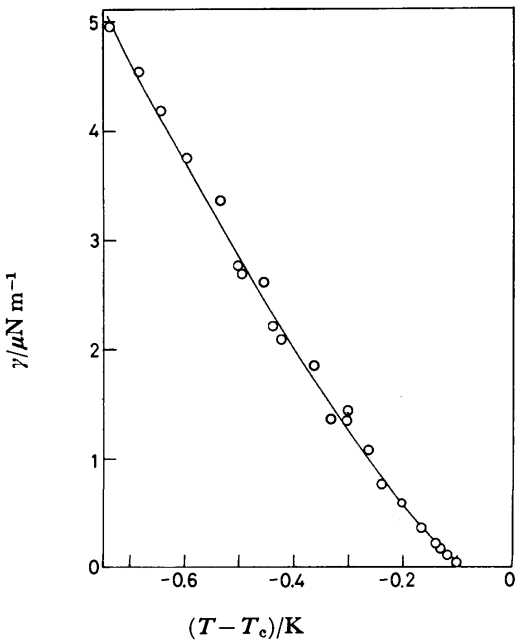

Fig. 3(b). Interfacial tension *vs.* temperature curve under atmospheric pressure.

mass fraction of isobutyric acid w_2 curve. The mass fraction at which the value of $\partial T/\partial w_2$ is zero was regarded as the critical composition w_c and the temperature corresponding to w_c as the upper critical solution temperature T_c. The $\partial T/\partial w_2$ *vs.* w_2 curve is shown in Fig. 2; the values of T_c and w_c were determined to be 299.88 K and 0.370, respectively.[11,12] At temperatures just below T_c, deep brown critical opalescence was observed. However, the determination of the phase separation and the phase mixing temperature was little affected by the opalescence.

The equilibrium interfacial tension γ was measured on critical mixtures at about 80 different temperatures in the vicinity of the critical solution temperature under atmospheric pressure. The γ *vs.* $T-T_c$ curve is drawn in Fig. 3(a) and the magnification of the curve very close to T_c is given in Fig. 3(b). It can be seen that the interfacial tension decreases monotonously from 35 to 0.02 μN m^{-1} with rising temperature in the narrow range of temperature. Further the γ value seems to approach zero at the critical solution temperature. This is the behavior expected for binary liquid mixtures having the upper critical solution temperature.[1-6] It is important to recognize that the slope of the curve is closely related to the entropy of interface formation.

By making use of Fig. 1, the interfacial tension shown in Fig. 3 can be plotted against the composition of the coexisting phases. The result is shown in Fig. 4 in the form of γ *vs.* w_2-w_c plot; the left and right parts of the curve correspond to the water-rich and acid-rich phases, respectively. It is seen that the interfacial tension decreases with decreasing the difference in composition between the conjugate phases and approaches zero at the critical composition. This is in harmony with the observation that an increase in mutual solubilities is responsible for a decrease in interfacial tension.[13,14] It is also seen that the curve is slightly unsymmetrical about the line parallel to the ordinate at the critical composition, which reflects the unsymmetry of the mutual solubility curve given in Fig. 1.

It has been well known that the temperature dependence of the interfacial tension in the vicinity of the critical solution temperature is described by the power law given by

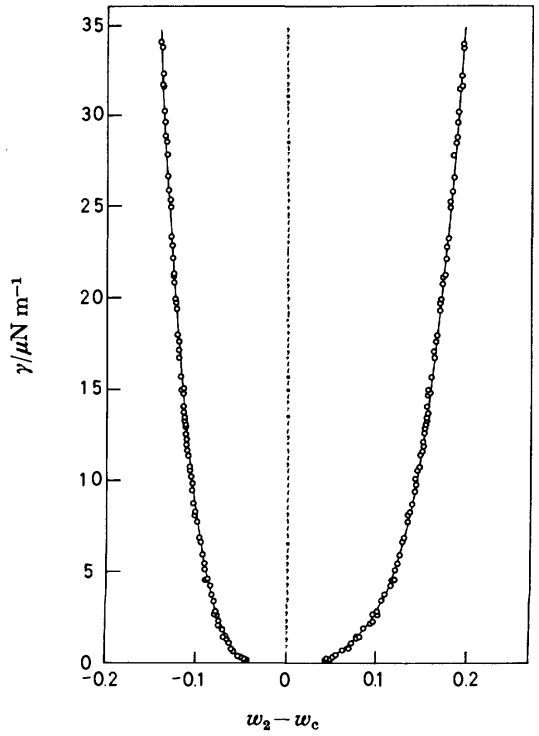

Fig. 4. Interfacial tension *vs.* mass fraction curve under atmospheric pressure.

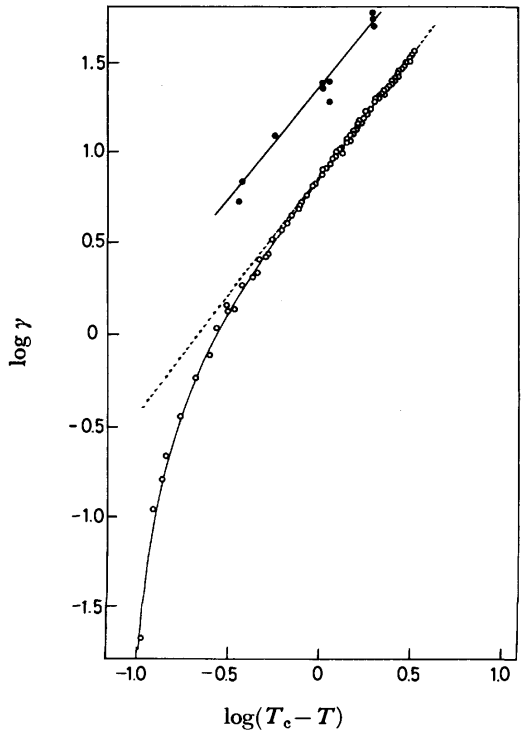

Fig. 5. log γ *vs.* log (T_c-T) curves under atmospheric pressure: (○) present study, (●) data from reference (6).

$$\gamma = k|T_c-T|^{\mu}, \tag{1}$$

where k is a proportionality constant and μ the critical exponent. Further, the temperature range where experimental results obey Eq. 1 has been discussed.[4] To examine the applicability of Eq. 1 to the present system, the value of log γ is plotted against log(T_c-T) in Fig. 5. It is seen that the curve follows the power law only in a limited temperature range and deviates from it at temperatures very close to T_c. The slope of the straight line was found to give $\mu=1.33$ in the range $0.003<(T_c-T)/T_c<0.01$. Also included in this figure for comparison are the results of Howland *et al.*;[6] they obtained $\mu=1.23\pm0.09$ by the unweighted least-squares analysis. It should be noted, however, the γ values of Howland *et al.* are higher than those of the present study and show considerable scatter. Furthermore, the lowest γ value measured is seen to be significantly high compared to that of the present study. Therefore, there seems to be some doubt as to whether Eq. 1 expresses the temperature dependence of the interfacial tension in the vicinity of T_c over a wide range of temperature.

To clarify the properties and structure of liquid/liquid interface, it is of great importance to examine the thermodynamic quantities of interface formation evaluated from experimental results by applying the thermodynamics of interfaces.[8-10] Immediately we notice that the temperature dependence of interfacial tension at constant pressure shown in Fig. 3 is closely related to the entropy of interface formation. The degree of freedom is two since the system under consideration is composed of two components and has two bulk phases separated by a plane interface. From the experimental point of view, therefore, it is convenient to choose temperature T and pressure p of the system as the independent variables. From Eqs. [8], [37], and [39] of Ref. (8), the interfacial tension is expressed in the differential form as

$$d\gamma = -\Delta s dT + \Delta v dp, \tag{2}$$

where Δs and Δv are the entropy and volume of interface formation, respectively. Thus we can estimate the value of Δs by applying Eq. 3 to the results given in Fig. 3:

$$\Delta s = -(\partial\gamma/\partial T)_p. \tag{3}$$

Figure 6 shows the change of the Δs value with temperature. It can be said that the interface formation of the binary mixture having upper critical solution temperature is accompanied by the increase in entropy. However, the value of Δs seems to decrease rapidly as the temperature approaches T_c and to be reduced to zero at T_c. Taking into account that the Δs values obtained for the systems of virtually immiscible oil and water are fairly larger than the above one and closely related to the mutual solubility between them,[10] it is also understandable

from Figs. 1 and 6 that the rapid decrease of the difference between the compositions of the two phases is responsible for the rapid decrease of the entropy of interface formation in the close vicinity of the critical solution temperature.

Now let us consider the contributions of components to the entropy of interface formation in some detail. According to the quasithermodynamics, the entropy of interface formation of two-component system can be expressed by use of the partial molar entropy changes of the components in the form[8]

$$\Delta s = \Gamma_1^I \Delta s_1 + \Gamma_2^I \Delta s_2, \tag{4}$$

where Γ_i^I is the number of moles of component i participating in the interface per unit area and Δs_i the partial molar entropy change of component i caused by the interface formation. In case that the two component are practically immiscible with each other, the two terms on the right side of Eq. 4 can be written as

$$\Gamma_i^I \Delta s_i = \Gamma_i^I (\bar{s}_i^I - s_i), \quad i=1, 2, \tag{5}$$

where $\bar{s}_i^I$ is the mean partial molar entropy in the interfacial region and s_i the partial molar entropy in the pure bulk phase. In the case of the present system where the two components are partly miscible with each other, on the other hand, $\Gamma_i^I \Delta s_i$ consists of two terms, *i.e.*, the one resulted from the transfer of component i from the component 1-rich phase α to the interfacial region and the other from the component 2-rich phase β; correspondingly, Γ_i^I is divided into the two parts $\Gamma_i^{I,\alpha}$ and $\Gamma_i^{I,\beta}$ which are attributable to the phases α and β, respectively. Therefore, it can be written as

$$\Gamma_i^I \Delta s_i = \Gamma_i^{I,\alpha}(\bar{s}_i^I - s_i^\alpha) + \Gamma_i^{I,\beta}(\bar{s}_i^I - s_i^\beta), \quad i=1, 2. \tag{6}$$

In the result, we have

$$\Delta s = [\Gamma_1^{I,\alpha}(\bar{s}_1^I - s_1^\alpha) + \Gamma_1^{I,\beta}(\bar{s}_1^I - s_1^\beta)] + [\Gamma_2^{I,\alpha}(\bar{s}_2^I - s_2^\alpha) + \Gamma_2^{I,\beta}(\bar{s}_2^I - s_2^\beta)]. \tag{7}$$

Comparing Eq. 7 with the positive value of Δs shown in Fig. 6, we may conclude, that the entropy of transfer of components from the two phases to the interfacial region, as a whole is positive. Accordingly, the contact of two different molecules which form a mixture with the upper critical solution temperature is said to be accompanied by an increase in entropy. Further, since the physical properties of the conjugate phases become identical as the temperature approaches the critical solution temperature, the partial molar entropies in the bulk phases and the interfacial region turn out to have the same values at T_c.

Now we can calculate the energy of interface formation Δu by applying the following equation to the above results;

$$\Delta u = \gamma + T\Delta s - p\Delta v. \tag{8}$$

The Δu *vs.* $T-T_c$ curve is shown in Fig. 7, where the value of $p\Delta v$ has been assumed to be negligibly small under atmospheric pressure when compared with the values of γ and $T\Delta s$ terms.[15-17] It is seen that the value of Δu is positive and reduced to zero at the critical solution temperature in a similar manner to that of Δs. The analog of Eq. 7 holds for Δu:

$$\Delta u = [\Gamma_1^{I,\alpha}(\bar{u}_1^I - u_1^\alpha) + \Gamma_1^{I,\beta}(\bar{u}_1^I - u_1^\beta)] + [\Gamma_2^{I,\alpha}(\bar{u}_2^I - u_2^\alpha) + \Gamma_2^{I,\beta}(\bar{u}_2^I - u_2^\beta)], \tag{9}$$

where $\bar{u}_i^I$ and u_i are the mean partial molar energy of component i in the interfacial region and the corresponding partial molar energy in the bulk phase, respectively. Therefore, we can say that the overall value of energy of transfer is positive and the differences among $\bar{u}_i^I$, u_i^α, and u_i^β disappear at the critical solution temperature. These facts lead us to the conclusion that the interface formation from the

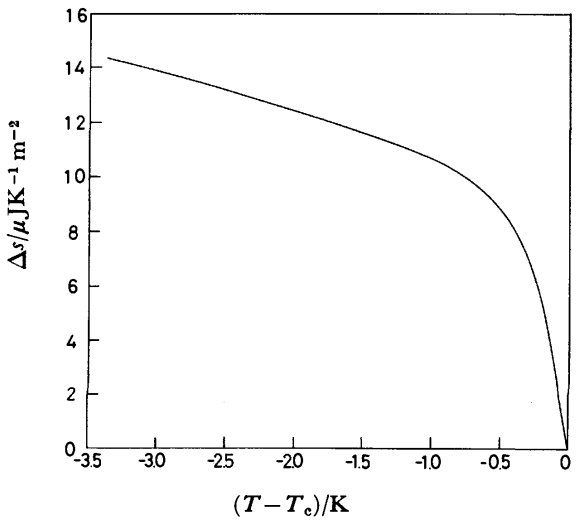

Fig. 6. Entropy of interface formation *vs.* temperature curve under atmospheric pressure.

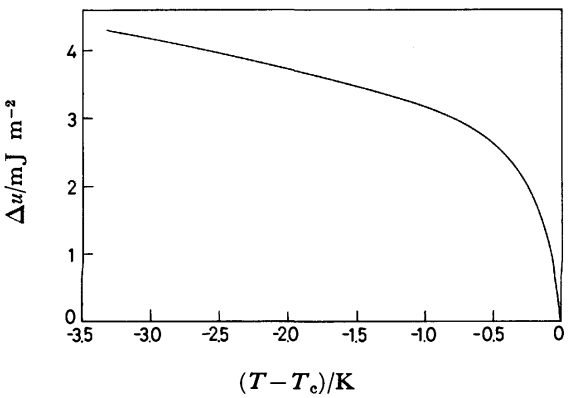

Fig. 7. Energy of interface formation *vs.* temperature curve under atmospheric pressure.

two conjugate phases of a binary system in the vicinity of the upper critical solution temperature is an unfavorable process from the viewpoint of energy, but favorable process from the viewpoint of entropy. Further information regarding the interfacial behavior of molecules will be provided by investigating a binary liquid mixture having the lower critical solution temperature.

The present work was supported by a Grant-in-Aid for Scientific Research No. 59470005 from the Ministry of Education, Science and Culture.

References

1) D. Atack and O. K. Rice, *Discuss. Faraday Soc.*, **15**, 210 (1953).
2) B. E. Sundquist and R. A. Oriani, *J. Chem. Phys.*, **36**, 2604 (1962).
3) C. Warren and W. W. Webb, *J. Chem. Phys.*, **50**, 3694 (1969).
4) A. W. Wims, J. V. Sengers, D. McIntyre, and J. S. Sherenshefsky, *J. Chem. Phys.*, **52**, 3042 (1970).
5) R. B. Heady and J. W. Cahn, *J. Chem. Phys.*, **58**, 896 (1973).
6) P. G. Howland, N. C. Wong, and C. M. Knobler, *J. Chem. Phys.*, **73**, 522 (1980).
7) M. Aratono and K. Motomura, *Bull. Chem. Soc. Jpn.*, **58**, 1853 (1985).
8) K. Motomura, *J. Colloid Interface Sci.*, **64**, 348 (1978).
9) K. Motomura, *Adv. Colloid Interface Sci.*, **12**, 1 (1980).
10) K. Motomura, H. Iyota, M. Aratono, M. Yamanaka, and R. Matuura, *J. Colloid Interface Sci.*, **93**, 264 (1983).
11) S. C. Greer, *Phys. Rev.*, **A14**, 1770 (1976).
12) T. S. Venkataraman and L. M. Narducci, *J. Phys.*, **C10**, 2849 (1977).
13) D. J. Donahue and F. E. Bartell, *J. Phys. Chem.*, **56**, 480 (1952).
14) T. Ikenaga, N. Matubayasi, M. Aratono, K. Motomura, and R. Matuura, *Bull. Chem. Soc. Jpn.*, **53**, 653 (1980).
15) K. Motomura, N. Matubayasi, M. Aratono, and R. Matuura, *J. Colloid Interface Sci.*, **64**, 356 (1978).
16) K. Motomura, M. Aratono, N. Matubayasi, and R. Matuura, *J. Colloid Interface Sci.*, **67**, 247 (1978).
17) M. Aratono, M. Yamanaka, N. Matubayasi, K. Motomura, and R. Matuura, *J. Colloid Interface Sci.*, **74**, 489 (1980).

 © 1985 The Chemical Society of Japan Bull. Chem. Soc. Jpn., 58, 3210—3214 (1985) [Vol. 58, No. 11

Effect of Inner-shell Excitations on the *W*-Value of Propane

Isao H. Suzuki* and Norio Saito
Electrotechnical Laboratory, Sakura-mura, Niihari-gun, Ibaraki 305
(Received June 5, 1985)

The dependence of the propane *W*-value on photon energy has been precisely measured near inner-shell excited states using monochromatized synchrotron radiation. The *W*-value showed an oscillatory variation in this energy region. A model has been proposed in which inner-shell excitation is assumed to give rise to a change in the energy of the electron ejected from the molecule having absorbed a photon. It has been found that the model can reproduce the oscillatory variation feature of the *W*-value. A post-collision interaction is suggested to take place just above the C-K edge of propane.

The *W*-value of ionizing radiation represents the mean energy expended by the radiation to produce an ion pair. A variety of studies were carried out regarding the *W*-values of gases (including propane) in a region higher than several keV.[1] However, a limited number of studies were performed for low energy radiation, although information on the *W*-values in this region is important for calculations regarding the radiation-transport phenomena.[2-7] Recently, Combecher reported on the electron *W*-value for propane in the energy region below 260 eV.[2] The *W*-value showed an increase with decreasing energy. This increase probably originated from the fact that the fraction of neutral excitations exceeded that of ionizations in electron-molecule collisions as the electron energy decreased. Srdoč measured the *W*-value of propane for photons from 90 eV to 280 eV using characteristic X-rays and filtered bremsstrahlung radiation.[3] The obtained data showed a slight increase with decreasing energy.

Samson and Haddad obtained the *W*-value of Xe for photons with energies from 12 eV to 90 eV.[4] Their results showed a distinct variation of the *W*-value over the energy region. This variation was ascribed to a change in the ejected electron energy which was caused by transitions to excited states of the Xe ion. Work on the *W*-value of methane for photons was performed in the ultra-soft X-ray region by the present authors.[5] An oscillatory variation near the C-K edge was found in the energy dependence of the *W*-value. Propane has the K-shell ionization energy of 290.6 eV.[8] Transitions of the K-electrons to unoccupied orbitals are supposed to take place slightly below the ionization threshold although there is no available data on the K-shell excitation spectrum.[9-11] These types of excitations and ionizations probably cause molecules to change into different types of states of the molecular ion. The *W*-value is expected to be affected by these ion states near the K-edge.

The present paper reports precise measurements of the *W*-value of propane for photons from 260 eV to 360 eV. The fine structure of the *W*-value found in this energy region is discussed in connection with the transitions of C-1s electrons.

Experimental and Analysis Method

Synchrotron radiation from the storage ring (electron energy: 400 MeV) at the Electrotechnical Laboratory was monochromatized by a plane grating monochromator.[12,13] The resolving power of the monochromator was about 150. The monochromatized photons entered a gas-flow proportional counter (Manson-04) with a thin film window. The window material was VYNS (thickness: 25 μg/cm²) or Al (1500 Å). Propane (purity: 99.99%) was introduced into the counter. The gas pressure was set to be 40 Torr for the Al window and 100 Torr for the VYNS window.

Signals from the counter were amplified and accumulated in a multichannel analyzer (MCA: Canberra-40). The resultant pulse height distributions of the signals were transferred to a micro-computer. Using this computer, the pulse height distributions were analyzed to obtain average pulse heights. The pulse height distribution can be approximately expressed by the following,[14,15]

$$f(z) = \frac{z^{x-1}\cdot\exp(-z/z_a)}{z_a^x\cdot\Gamma(x)}. \quad (1)$$

In the above equation, z indicates the number of electrons amplified by the electric field within the counter, z_a denotes the average gas amplification factor, x is the average number of the electrons initially generated by the radiation effect of a photon, and Γ is the gamma function. The distributions calculated using Eq. 1 were fitted to those obtained by observation.[14] This fitting procedure served to remove any interference due to contamination of the photon beam when the correct pulse height distributions were determined from the experimental data. The average pulse height distribution P is given by

$$P(E_p) = \int z\cdot f(z)\cdot dz = z_a\cdot x = \frac{z_a\cdot E_p}{W_p(E_p)}, \quad (2)$$

where E_p indicates the energy of a photon and W_p denotes the *W*-value.[3,5,14]

Using Eq. 2, relative *W*-values were obtained for photons with energies from 260 eV to 360 eV. Any nonlinearity of electric circuits (*e.g.*, preamp and MCA) was corrected for. Also, any change in P owing to a drift in the gas pressure was cancelled by performing several measurements at the same photon energy in the course of the experiment. There may be photoabsorption by propane in which only neutral fragments are produced but in which no ion pair are

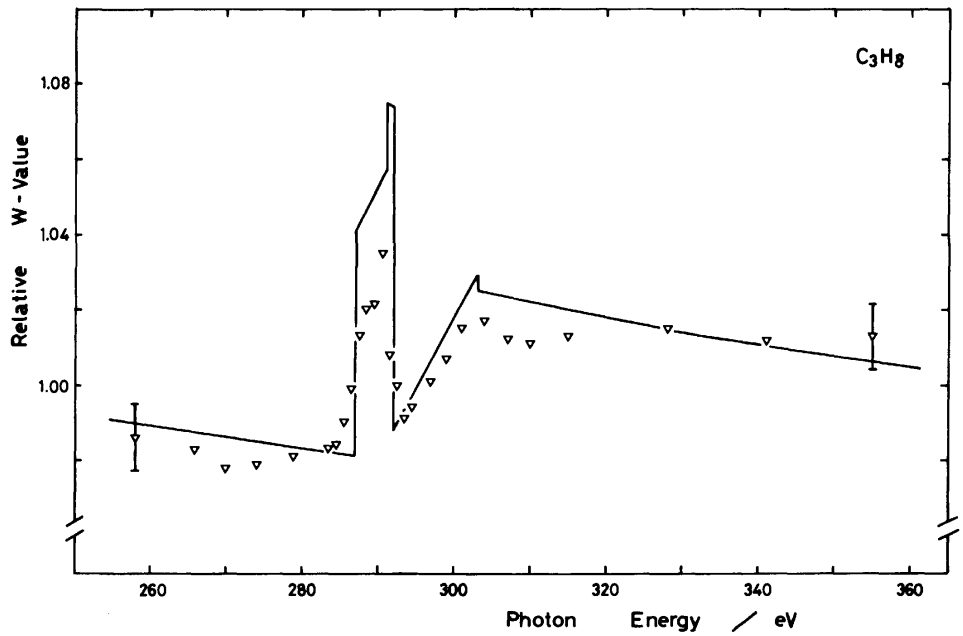

Fig. 1. Dependences of the propane W-value on the photon energy in the region from 260 eV to 360 eV. Open triangles indicate measured results. Solid curve denotes the calculated profile based on the present model. Bars indicate the error sizes of the measured data.

formed. This process should alter the W-value, although the present technique using a proportional counter can not count up these types of processes. At present, these processes are assumed to be negligible, by analogy of the results of ionization yield of methane by Backx and Van der Wiel.[16]

The photoabsorption spectrum was measured using a gas cell (length: 200 mm, inner diameter: 14 mm) with thin VYNS windows (for the entranee and exit of photon beams) and the proportional counter. The counter served to discriminate signals from the noise owing to a contamination of the photon beam, *e.g.*, higher order photons and stray photons with longer wavelengths.

Results and Discussion

The relative W-values derived from the measurements are shown with open triangles for photon energies from 260 eV to 360 eV in Fig. 1. The solid curve indicates a calculated profile based on the model described below. The measured W-value slightly decreases with increasing energy from 260 eV to 280 eV. The W-value shows a sharp rise at 286 eV, goes to a maximum at 291 eV and again decreases to a minimum at 294 eV. A linear dependence of the W-value data on the photon energy is seen from 294 eV to 304 eV. The W-value is essentially constant above 304 eV.

In order to clarify the origin of the variation in the W-value shown in Fig. 1, the present authors observed the photoabsorption spectrum of propane around the C-K edge (Fig. 2). Although the inner-shell excited states are not separated from one another (Fig. 2) owing to the low resolving power of

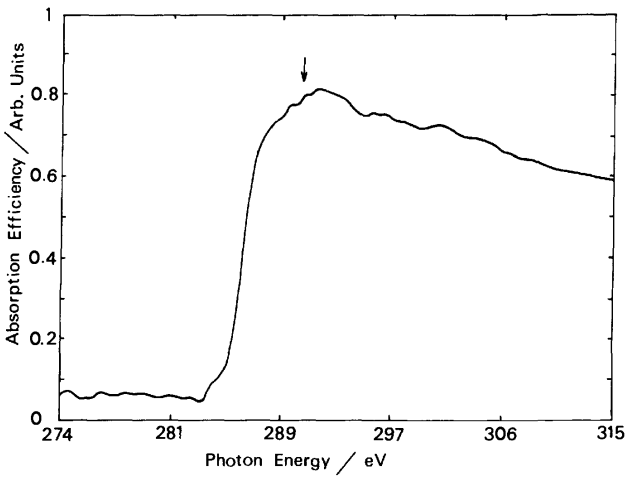

Fig. 2. Photoabsorption spectrum of propane in the region from 274 eV to 315 eV. Arrow indicates the threshold energy of the K-shell ionization (Ref. 8).

the present monochromator, the following items are possibly discernible in the figure. The absorption efficiency is low below 285 eV, becomes high at about 287 eV and has a maximum at around 291 eV. Above 291 eV, this efficiency gradually decreases with increasing photon energy. Judging from the inner-shell excitation spectra of methane and ethane,[9,10] the high efficiency at 287 eV can probably be ascribed to a transition of C-atomic orbitals, 1s→3s. In the cases of methane and ethane, the transition (1s→3s) is low in intensity. This type of transition is supposed to occur with a higher probability because of the poorer symmetry of propane relative to methane and

ethane. It is seen in Fig. 2 that this transition is followed by transitions to higher excited states (*e.g.*, 1s→3p) and to the ionized state.

As a result a comparison between the absorption spectrum and the energy dependence of the *W*-value for propane, a model is here proposed as follows.

i) Below 287 eV: Photons can only excite the valence electrons of propane, which occupy 10 molecular orbitals (composed of C-2s, C-2p, and H-1s orbitals) in the ground state. Ejected photoelectrons ionize ambient molecules and produce a number of ion pairs. On the other hand, the *W*-value of low energy electrons (W_e) can be approximately represented by the following expression.[1-4]

$$W_e(E) = \frac{E \cdot W}{E-U} \tag{3}$$

W denotes the *W*-value for radiation with a sufficiently high energy (24.0 eV),[1] U indicates the average energy of sub-ionization electrons, and *E* is the energy of an electron. Using Eq. 3, the photon *W*-value is given by

$$W_p(E_p) = \frac{E_p}{1+n_e} = \frac{E_p \cdot W}{E_p+W-E_v-U_2}, \tag{4}$$

where E_v is the average binding energy the valence electrons and n_e denotes the average number of ion pairs produced by the ejected photoelectrons. In the derivation of Eq. 4, the following relation was utilized.

$$n_e(E) = \frac{E}{W_e} = \frac{E_p-E_v-U_2}{W} \tag{5}$$

The term E_v is assumed to be 17.9 eV.[8] The average subionization energy, U_2, is assumed to be 25 eV from data regarding the *W*-value for low energy electrons.[2] Multiple ionizations of the valence electrons are at present assumed to be negligible because there is no available data for this type of process.

ii) Between 287 eV and 290.6 eV: Photons can excite the inner-shell electrons to the Rydberg orbitals and a hole can be formed in the inner-shell. (Unoccupied orbitals in the ground state are called Rydberg orbitals in the present study.) After this excitation, an Auger transition is supposed to occur since fluorescence yield is extremely low in a light element. Several types of Auger transitions have been reported in propane. The average energy of those Auger electrons has been estimated to be 248 eV from the work by Rye *et al.*[17] The average energy of the Auger electrons in the present case is supposed to be slightly different from 248 eV due to the existence of that electron in the Rydberg orbital. This average energy E_{RA} is assumed to be 255 eV, by analogy from a resonance-type Auger electron spectrum of CO.[18] The *W*-value is given by

$$W_p(E_p) = \frac{E_p}{1+n_e} = \frac{E_p \cdot W}{E_{RA}+W-U_2}. \tag{6}$$

In a comparison of Eq. 6 with Eq. 4, E_{RA} (255 eV) is lower than E_p-E_v (*e.g.*, 267.1 eV for the photon with energy of 285 eV). Thus, the *W*-value at 287 eV becomes higher than that at 285 eV. In the present model, it is assumed that the photoabsorption probability involving the valence electrons can be negligibly low above 287 eV on account of the spectrum shown in Fig. 2.

iii) Between 290.6 eV and 292 eV: The inner-shell electrons can be ejected from the molecule by the photons. The energy of this ejected photoelectron is very low. This electron is supposed to be retrapped through a post-collision interaction by that propane molecular ion when a second high-energy electron is ejected through an Auger transition, as seen in the case of CO.[19] The Auger electron obtains a somewhat higher energy owing to the existence of the slow photoelectron, compared to a normal Auger electron. The energy gain of the Auger electron is equal to the energy which the trapped electron loses. The average energy of the Auger electrons is here assumed to be (248 eV+E_p−288 eV).

iv) Between 292 eV and 302.6 eV: The inner-shell electrons can be ionized and can quickly escape from the molecular field. An Auger transition follows this photoelectron ejection. The photoelectron has an energy of E_p-E_k (E_k: the ionization energy of the inner-shell, 290.6 eV[8]), and the Auger electron has an average energy of 248 eV (E_A). The former electron can not ionize other ambient molecules because the electron energy is lower than the first ionization energy of the valence electron. (The vertical ionization energy 12.0 eV is considered here.[8])

v) Above 302.6 eV: The photoelectron ejected from the inner-shell has an energy higher than the first ionization energy of propane. This electron, as well as the Auger electron formed subsequently, can ionize other molecules. The *W*-value is expressed by

$$W_p(E_p) = \frac{E_p}{2+n_{e1}+n_{e2}} = \frac{E_p}{E_p+E_A+2W-E_k-U_1-U_2}, \tag{7}$$

where U_1 indicates the average energy of the sub-ionization electrons for the electron with kinetic energy between 12 eV and 60 eV. The U_1 value is assumed to be 11 eV on account of Combecher's study.[2]

The present model is summarized in Fig. 3. Initial and final configurations in the figure denote the configuration of the relevant electrons just after photoabsorption and that after the Auger transition if it happens, respectively. Based on the present model, the relative *W*-value has been calculated and drawn with the solid curve in Fig. 1. In this

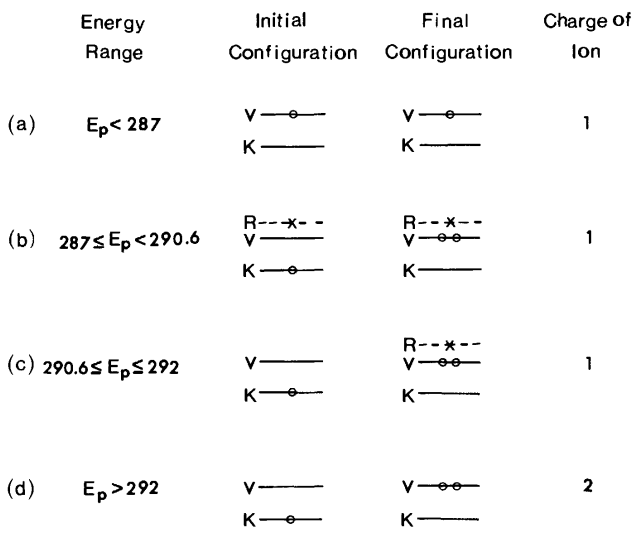

Fig. 3. Illustration of change in the electron configuration. Initial and final configurations indicate the electron configuration just after photoabsorption and that after the Auger transition if it happens, respectively. Charge of ion denotes the final charge state of the residual propane ion. E_p is the photon energy. V, K, and R mean the valence orbitals, the inner-shells and Rydberg orbitals, respectively. O and × represent a hole and an occupation by an electron, respectively.

calculation, the resolving power of the monochromator was not considered. The calculated curve reproduces the characteristics of the experimental results. Therefore, the present model is essentially correct.

There is a slight discrepancy between the experimental data and the calculated result around 290 eV. This discrepancy is probably caused by the low resolving power of the monochromator. However, the following can not be ruled out with respect to the reason for the discrepancy. Between 287 eV and 290.6 eV, the final configuration of the related electrons is not only one. One part of the final configuration may be the final configuration shown in Fig. 3(a); the configuration with one hole in the valence orbital, which is generated through the ejection of the electron promoted into the Rydberg orbital. From 290.6 eV to 292 eV, there is a possibility that some fractions of the slow photoelectrons are not retrapped by that molecular ion, although the energy of the electron may be lowered through a post-collision interaction. If this is the case, the final configuration is as shown in Fig. 3(d), with two holes in the valence orbitals. The two additional final states mentioned above should make the W-value lower than in a model neglecting these states. The calculated result derived from the above consideration is expected to be closer to the experimental data than that in Fig. 1.

If a post-collision interaction does not occur in the region from 290.6 eV to 292 eV, the minimum at 294 eV in the experimental results, shown in Fig. 1, should approach the threshold energy of the K-shell, 290.6 eV. The difference of about 3.5 eV can not be explained by the low resolving power of the monochromator. Thus, it is reasonably expected that the post-collision interaction takes place just above the C–K edge, as well as for CO and methane.[14,19] In methane, a minimum has appeared at 295 eV regarding the energy dependence of the W-value derived from measurements similar to those in the present work.[14] The inner-shell ionization energy of methane is 290.8 eV.[8] This type of post-collision interaction is limited to a narrower energy range in propane than in methane. This fact suggests the following. The more electrons exist in molecular orbitals, the more effectively the field of a doubly charged ion is shielded. This may result in there being no occurrence of a post-collision interaction of the photoelectron in propane at an electron energy lower than that in methane by about 1 eV.

The gap at 303 eV in the calculated curve originates from the adoption of the present values on U_1 and the vertical ionization energy. This gap could probably be removed if we could obtain a more reliable U_1 value and could utilize the adiabatic first ionization energy.

Summary

The energy dependence of the photon W-value for propane has been precisely determined in the region from 260 eV to 360 eV. An oscillatory structure has been found in the W-value near the C–K edge. This structure can essentially be explained by a plain model. In this model, transitions from the ground state to the inner-shell excited states and inner-shell ionization give rise to a change in the energy distribution of the ejected electrons. The Auger transitions are considered to represent the only processes for the re-occupation of the resultant hole in the inner-shell. This change in the energy distribution brings about the oscillatory structure regarding the W-value near the K-edge. The following, however, is necessary for a rigorous confirmation of the present model. The energy distribution of ejected electrons and the charge state of residual ions must be accurately determined as a function of photon energy. This type of information will be obtained soon since studies using synchrotron radiation are being vigorously advanced.

The authors wish to express their sincere thanks to the members of the accelerator group of the Electrotechnical Laboratory for providing synchrotron radiation.

References

1) H. O. Wyckoff, "Average Energy Required to Produce an Ion Pair," ICRU-Report, **31** (1979).
2) D. Combecher, *Radiat. Res.*, **84**, 189 (1980).
3) D. Srdoč, *Nucl. Instr. Meth.*, **108**, 327 (1973).
4) J. A. R. Samson and G. N. Haddad, *Radiat. Res.*, **66**, 1 (1976).
5) I. H. Suzuki and N. Saito, *Radiat. Phys. Chem.*, **26**, 305 (1985).
6) B. G. R. Smith and J. Booz, "Proceedings of Sixth Symposium on Microdosimetry, Commission of the European Communities," London (1978), p. 759.
7) D. Srdoč and B. Obelić, "Proceedings of Fifth Symposium on Microdosimetry," Commission of the European Communities, Luxembourg (1976), p. 1007.
8) J. J. Pireaux, S. Svensson, E. Basilier, P-Å. Malmqvist, U. Gelius, R. Caudano, and K. Siegbahn, *Phys. Rev. A*, **14**, 2133 (1976).
9) F. C. Brown, R. Z. Bachrach, and A. Bianconi, *Chem. Phys. Lett.*, **54**, 425 (1978).
10) A. P. Hitchcock and C. E. Brion, *J. Elect. Spectrosc.*, **10**, 317 (1977).
11) A. P. Hitchcock, *J. Elect. Spectrosc.*, **25**, 245 (1982).
12) T. Tomimasu, T. Noguchi, S. Sugiyama, T. Yamazaki, T. Mikado, and M. Chiwaki, *IEEE Trans. Nucl. Sci.*, NS-**30**, 3133 (1983).
13) N. Saito and I. H. Suzuki, Bull. Electrotechnical Laboratory, **49**, 689 (1985).
14) N. Saito and I. H. Suzuki, *Chem. Phys.* in press.
15) B. Breyer, *Nucl. Instr. Meth.*, **112**, 91 (1973).
16) C. Backx and M. J. Van der Wiel, *J. Phys. B.*, **8**, 3020 (1975).
17) R. R. Rye, D. R. Jennison, and J. E. Houston, *J. Chem. Phys.*, **73**, 4867 (1980).
18) L. Ungier and T. D. Thomas, *Phys. Rev. Lett.*, **53**, 435 (1984).
19) R. B. Key, Ph. E. Van der Leeuw and M. J. Van der Wiel, *J. Phys. B.*,**10**, 2521 (1977).

 © 1985 The Chemical Society of Japan Bull. Chem. Soc. Jpn., 58, 3215—3224 (1985)

A High-resolution ^{13}C NMR Study of Some Ethylene Oxide Oligomers, Cryptands and Crown Ethers Complexed with a Variety of Metal Ions in the Solid State. Conformational Change of Ligand Molecules as Viewed from the Conformation-dependent Displacements of ^{13}C Chemical Shifts

Ryoko TABETA and Hazime SAITÔ*
Biophysics Division, National Cancer Center Research Institute, Tsukiji 5-Chome, Chuo-ku, Tokyo 104
(Received July 11, 1985)

We recorded high-resolution solid-state ^{13}C NMR spectra of ethylene oxide oligomers, cryptands, and crown ethers complexed with metal ions, determined by cross polarization-magic angle spinning (CP-MAS) NMR method. It is found that peak-intensities of these complexes are significantly enhanced by the presence of metal ions which act toward conformational fixation of flexible ligand molecules. The ^{13}C chemical shifts of ethylene oxide oligomers complexed with $HgCl_2$ or $CdCl_2$ as open-chain analogues of crown ethers were successfully related with a pair of torsion angles of nearby single bonds. ^{13}C Chemical shifts of cyclic ionophores were displaced (up to 6 ppm) together with conformational changes of ligand molecules. In addition, the ^{13}C chemical shifts of the carbons neighbored with nitrogen atoms of cryptands [2.2.2] and [2.2.1] were well related with a pair of torsion angles of neaby bonds. Further, we found that several kinds of metal complexes with *cis-syn-cis* and *cis-anti-cis* isomers of dicyclohexano-18-crown-6 gave rise to substantially different spectral profiles, resulting in the occurrence of significant conformational changes of these ligand molecules as a result of complex formation.

It is well known that synthetic macrocyclic ionophores such as crown ethers and cryptands show a marked ability to form metal complexes with a variety of alkaline and alkaline earth metal ions[1–9] like naturally occurring ionophores such as valinomycin, nonactin, monensin, *etc.* These ionophores have gained much interest in relation to their models of naturally occurring antibiotics as carriers of cations through biological and model membranes, phase-transfer catalysis for salt solubility enhancement and anion activation in synthesis.[1–9] In many instances, these ligand molecules undergo marked conformational changes during ion-binding to achieve stability and ion-selectivity of complexes. Accordingly, it is very important to analyze these conformational changes of ligand molecules both in the solid

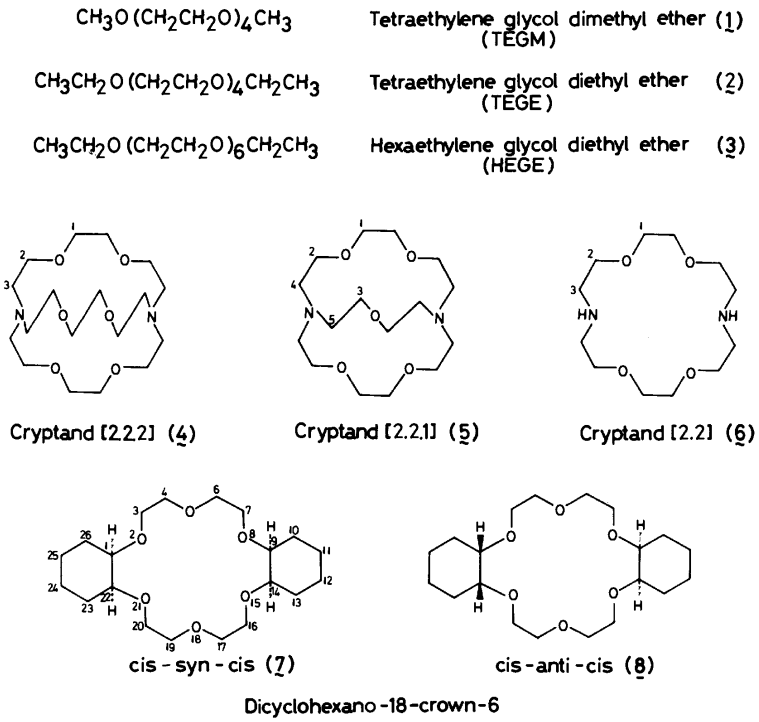

Fig. 1. Chemical structures of ethylene oxide oligomers, dicyclohexano-18-crown-6, and cryptands.

and solution, in order to gain insight of the manner of metal-ligand interaction in the complexes.

As a convenient complementary means to X-ray diffraction, we previously showed that the manner of such conformational changes in the ligand molecules in the solid state is conveniently examined when sizable amounts of displacements of the conformation-dependent ^{13}C chemical shifts, as determined by cross polarization-magic angle spinning (CP-MAS) technique, are seen for any carbons of backbones.[10-19] The major advantage of the present approach is to provide reference data to examine whether particular conformation observed in the solid state is retained in solution or not.

In order to gain insight how ^{13}C chemical shifts of these ligand molecules are varied with conformational changes associated with complexation, we recorded ^{13}C CP-MAS NMR spectra of ethylene oxide oligomers [tetraethylene glycol dimethyl ether (TEGM), tetraethylene glycol diethyl ether (TEGE), hexaethylene glycol diethyl ether (HEGE)], cryptands ([2.2.2], [2.2.1], and [2.2]), and *cis-syn-cis* and *cis-anti-cis* isomers of dicyclohexano-18-crown-6 (see Fig. 1 for chemical structure) complexed with a variety of metal ions. We studied ethylene oxide oligomers as open-chain analogues of cyclic ionophores, because conformations of the former resembles those of the latter and detailed X-ray diffraction data[20-23] are available for the former. We found that the ^{13}C chemical shifts were significantly varied among a variety of complexes, reflecting the conformational changes of ligand molecules. We also attempted to relate these displacements of shifts with a pair of torsion angles of the nearby single bonds. Finally, we compared ^{13}C chemical shifts between the solid and solution in order to evaluate whether or not the conformations achieved in the solid state are retained in solution.

Experimental

Materials. Tetraethylene glycol dimethyl ether (TEGM) and tetraethylene glycol diethyl ether (TEGE) were purchased from Tokyo Kasei Kogyo Co., Ltd., Tokyo and Aldrich Chemical Company, USA, respectively. Hexaethylene glycol diethyl ether (HEGE) was prepared by the reaction of hexaethylene glycol (Aldrich) and ethyl iodide over NaH dissolved in anhydrous dimethyl sulfoxide. $HgCl_2$ or $CdCl_2$ complexes were prepared by the procedure described by Iwamoto.[20-23]

Cryptands [2.2.2], [2.2.1], and [2.2] were purchased from Merck Chemical Company, West Germany. Colorless plate-shaped crystal of cryptand [2.2] with NaSCN was formed by dissolving these two chemicals in methanol-1-butanol solution. KSCN complex with cryptand [2.2] (colorless prism) was grown from benzene containing small amount of water.[24] $Pb(SCN)_2$ complex with cryptand [2.2](prism) was obtained by methanol-1-butanol solvent.[25] NaSCN and KSCN complexes with [2.2.1] were obtained from methanol-1-butanol solution.[26] $CaBr_2$,[27] $TlHCOO$,[28] NaSCN and KSCN complexes with cryptand [2.2.2] were obtained from methanol-ethyl acetate solvent, whereas $Ba(SCN)_2$ complex was obtained from methanol-1-butanol solvent.[29]

Cis-syn-cis and *cis-anti-cis* isomers of dicyclohexano-18-crown-6 (Aldrich Chemical Company, USA) were isolated by the procedure of Izatt *et al.*[30] utilizing OH_3ClO_4 and $Pb(ClO_4)_2$, respectively, as agents for complex formation. Plate-shaped. NaBr-complexes with both isomers were obtained from a solution of equimolecular quantity of individual *cis-syn-cis* or *cis-anti-cis* isomers and sodium bromide (5% excess) in ethanol-acetone which was allowed to evaporate in air.[31] In a similar manner, complexes with $La(NO_3)_3$,[32] KI_3,[33] $CsSCN$,[33] $Pb(ClO_4)_2$,[30] OH_3ClO_4,[30] KI,[34] NH_4SCN,[34] and $Ba(SCN)_2$[34] were prepared by the procedure published already.

^{13}C CP-MAS NMR Spectra. Single-contact ^{13}C CP-MAS NMR spectra were recorded on a Bruker CXP-300 spectrometer at 75.46 MHz, equipped with a CP-MAS NMR accessory. Samples were placed in an Andrew-Beams type rotor machined from perdeuterated poly(methylmethacrylate) and spun by compressed air. A contact time used was usually 800 μs, although several spectra were obtained by varying contact time from 500 μs to 5 ms. Repetition times were 2—4 s and spectral width and data points were 30 kHz and 8 K data points, respectively. Resolution-enhancement was made by a gaussian multiplication.[35] Spectra were accumulated more than 2000 times. Chemical shifts were calibrated through external benzene and converted to the values from tetramethylsilane (TMS).

High Resolution ^{13}C NMR. High resolution ^{13}C NMR spectra were recorded in deuterated chloroform and methanol on a Bruker CXP-300 spectrometer. Chemical shifts were calibrated with respect to external tetramethylsilane in a capillary.

Results

Figure 2 shows 75.46 MHz ^{13}C CP-MAS NMR spectra of ethylene oxide oligomers complexed with $HgCl_2$ or $CdCl_2$ in the solid state. The ^{13}C NMR signals of the terminal methoxyl or ethoxyl groups were readily assigned in view of the data of uncomplexed samples in chloroform solution (see Table 1). Several peaks were well resolved for the internal methylene carbons of polyether moiety and peak-positions and relative peak-intensities are summarized in Table 1. These ^{13}C NMR signals are also split into several peaks even in the uncomplexed molecules in solution state (Table 1). Such a splitting of peaks in the random-coil state is not necessarily caused by variations of local conformers among methylene groups but simply by substituent effects of the terminal methoxyl or ethoxyl groups. In particular, the peaks marked by **a** in the solid and solution states are assigned to the carbons which are neighbored with the terminal methoxyl or ethoxyl groups, in view of the relative peak-intensities and displacements of peaks (Table 1).

Table 1. ^{13}C Chemical shifts of oligomers of ethylene oxide complexed with $HgCl_2$ or $CdCl_2$ in the solid state[a] (ppm from TMS)

	Internal CH_2		Terminal	
	I[b]	II	CH_3	CH_2
TEGM-$HgCl_2$	72.1[c] (2), 71.2*(3), 69.2 (3)	—	58.9 (1) 58.2 (1)	
TEGM (soln)[d]	71.9[c] (2), 70.5*(4), 70.4 (2)	—	58.9 (2)	
TEGM-$CdCl_2$	71.9[c] (1), 70.5*(3), 69.5 (1), 68.2[c] (1)	67.1 (1) 67.9 (1)	60.5 (2)	
HEGE-$HgCl_2$	72.0[c] (2), 71.6 (2), 70.4*(6), 68.9 (2)	67.6 (1) 66.8 (1)	15.3 (2)	67[e] (2)
HEGE (soln)[d]	70.5*(10), 69.7[c] (2)		15.1 (2)	66.5 (2)
TEGE-$HgCl_2$	69.5*(8)		15.1 (2)	65.8 (2)
TEGE (soln)[d]	70.5*(6), 69.8[c] (2)		15.1 (2)	66.5 (2)

a) Numbers in parenthesis denote relative peak-intensities normalized to the total number of carbons. b) Peaks asterisked stand for the most intense signals. c) CH_2O group neighbored with the terminal CH_3 or CH_2CH_3 groups. d) In chloroform solution (uncomplexed). e) Superimposed on the internal CH_2 signals (peak II).

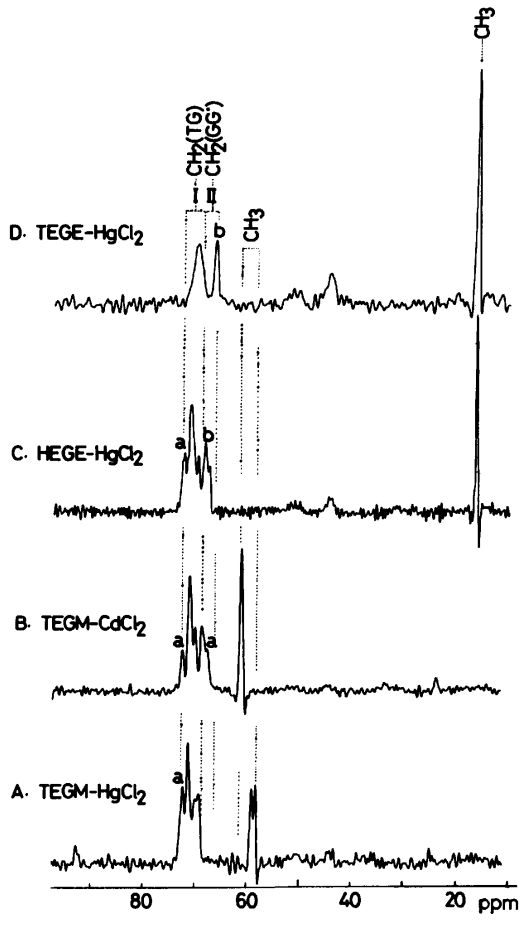

Fig. 2. 75.46 MHz ^{13}C CP-MAS NMR spectra of $HgCl_2$ or $CdCl_2$ complexes with ethylene oxide oligomers in the solid state. The peaks **a** and **b** stand for the peak of carbons neighbored with the terminal methoxyl (or ethoxyl) groups and methylene signal of the terminal ethoxyl groups, respectively.

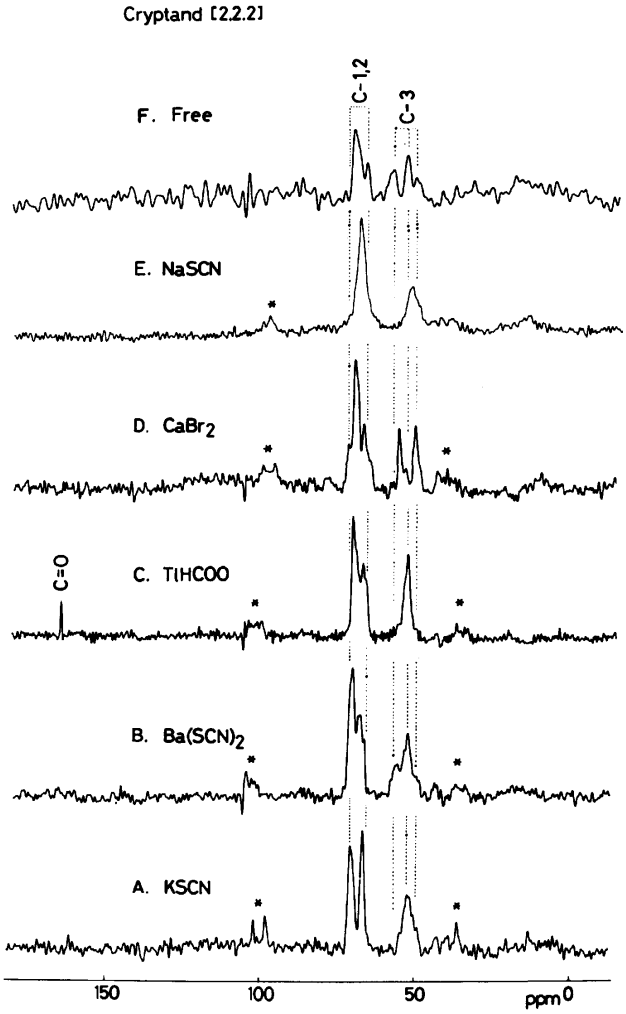

Fig. 3. 75.46 MHz ^{13}C CP-MAS NMR spectra of cryptand [2.2.2] complexed with a variety of metal ions in the solid state. The peaks asterisked are spinning side-bands of the central intense signals.

Figure 3 shows the ^{13}C CP-MAS NMR spectra of cryptand [2.2.2] complexed with a variety of metal ions. Interestingly, the peak-intensities of uncomplexed molecules are very weak as compared with those of the complexed molecules. The assignment of peaks was made on the basis of the solution NMR data. Spectral features are substantially different among complexes. Similarly, the splitting of the C-4,5 signals of cryptand [2.2.1] is quite different between the Na^+ and K^+ complexes, reflecting differences in the molecular conformations as revealed by X-ray diffraction[26] (Fig. 4). By contrast, very little change was observed among NaSCN, $Pb(SCN)_2$, and KSCN complexes with cryptand [2.2] (Table 2). The ^{13}C NMR spectra of uncomplexed [2.2] and [2.2.1] in the solid state turned out to be very difficult to observe, because molecular motion prevents from building up of ^{13}C NMR signals for the former and free molecule is in liquid state for the latter. These ^{13}C chemical shifts in the solid state are summarized in Table 2.

Figures 5 and 6 illustrate the ^{13}C CP-MAS NMR spectra of *cis-syn-cis* and *cis-anti-cis* isomers of dicyclohexano-18-crown-6, respectively, complexed with a variety of metal ions. Again, the peak-intensities of uncomplexed molecules are considerably suppressed as compared with those of the complexed molecules. It is expected that the ^{13}C NMR peaks of the C-1, C-9, C-14, and C-22 carbons of cyclohexane moiety in the solid state are split into a pair of doublet caused by the presence of the ether substituents at the axial (O_{ax}) and equatorial (O_{eq}) positions. The doublet peaks can be readily identified, because the center of the doublet should be very close to the ^{13}C NMR peaks observed in solution state (Table 3). The observation of the doublet peak was possible in solution state upon cooling (−75°)[36] and the magnitude of the separation of peaks (5—7 ppm) is similar to the data observed in the crystalline state (see Table 4). (Note that these doublet peaks are seen for the *cis-syn-cis* and *cis-anti-cis* isomers complexed with $La(NO_3)_3$ even at ambient

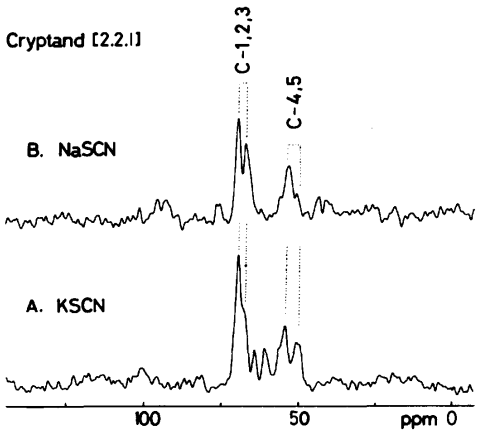

Fig. 4. 75.46 MHz ^{13}C CP-MAS NMR spectra of cryptand [2.2.1] complexed with KSCN (A) or NaSCN (B) in the solid state.

TABLE 2. ^{13}C CHEMICAL SHIFTS OF SOME CRYPTANDS COMPLEXED WITH A VARIETY OF METAL IONS IN THE SOLID AND SOLUTION (ppm FROM TMS, ±0.4 ppm FOR THE SOLID)

[2.2.2]	Free		$CaBr_2$		TlHCOO		$Ba(SCN)_2$		KSCN		NaSCN	
	Solid	Soln	Solid	Soln	Solid	Soln	Solid	Soln	Solid	Soln	Solid	Soln
C-1, C-2 a)	70.4 66.5	70.7 69.8	69.9(71.9) b) 67.3(65.1)	69.4 68.7	69.1 67.3	70.0 68.0	70.5 67.9	70.5 67.7	71.4 67.3	70.3 67.4	68.5	68.8 67.8
C-3	58.8 53.6 50.7	56.1	56.3 51.0	53.9	53.8	54.4	56.7 52.8	54.2	52.9	53.7	52.0	53.1

[2.2.1]	Free		KSCN		NaSCN	
	Solid	Soln	Solid	Soln	Solid	Soln
C-1, C-2, C-3 a)	—c)	70.5	69.6	69.1	69.8	68.8
	—	69.7	67.5	67.6	67.1	66.5
	—	69.9		69.5		67.0
C-4	—	56.5	56.2	57.7	56.4	52.8
C-5	—	56.3	54.4	53.6	53.8	53.6

[2.2]	Free		KSCN		NaSCN		$Pb(SCN)_2$	
	Solid	Soln	Solid	Soln	Solid	Soln	Solid	Soln
C-1, C-2 a)	—d)	70.4	70.2	70.6	68.5	69.2	70.6	70.3
	—	70.2		69.9		68.9	69.2	69.5
C-3	—	49.3	50.3	49.4	48.5	48.2	49.9	49.3

a) These peak cannot be distinguished in the solid state, although assigned separately in solution($CDCl_3$ or $CDCl_3$ containing a few drops of methanol): see Ref. 39. b) Shoulder peaks. c) Liquid state. d) Not detected.

temperature, see Table 3.) For NaBr complex with *cis-anti-cis* isomer,[31] the C-1 and C-14 carbons are ascribed to the O_{eq}, while the C-9 and C-22 are ascribed to the O_{ax} peak. The remaining ^{13}C NMR peaks resonating between 71 and 61 ppm are undoubtedly ascribed to the eight polyether carbons, C-3, 4, 6, 7, 16, 17, 19, 20.

Discussion

Peak-intensities. We found that the peak-intensities of the ^{13}C NMR spectra of uncomplexed cryptands and crown ethers in the solid state are generally weak or suppressed as compared with those of the complexed samples (Figures 3F, 5H, and 6H). In addition, no ^{13}C CP-MAS NMR data are available for uncomplexed cryptands [2.2.1] and [2.2] and ethylene oxide oligomers, because these samples except for cryptand [2.2] complex are in liquid state. The reason why the peak-intensities in the solid state are in many instances suppressed is undoubtedly caused by the presence of plausible molecular motion even in the solid state which might prevent from building up of the ^{13}C NMR signals through cross polarization.[37] In this connection, we were unable to observe ^{13}C CP-MAS NMR spectra of NaI complex with cryptand [2.2.2]. Further, the recording of the ^{13}C CP-MAS NMR spectra of 18-crown-6 complexed with a variety of metal ions was unsuccessful at room temperature because of the reason mentioned above (unpublished finding), although observation of the solid-state high-resolution ^{23}Na NMR signals of sodium complex by a single pulse experiment was not difficult.[38] Therefore, it is probable that the

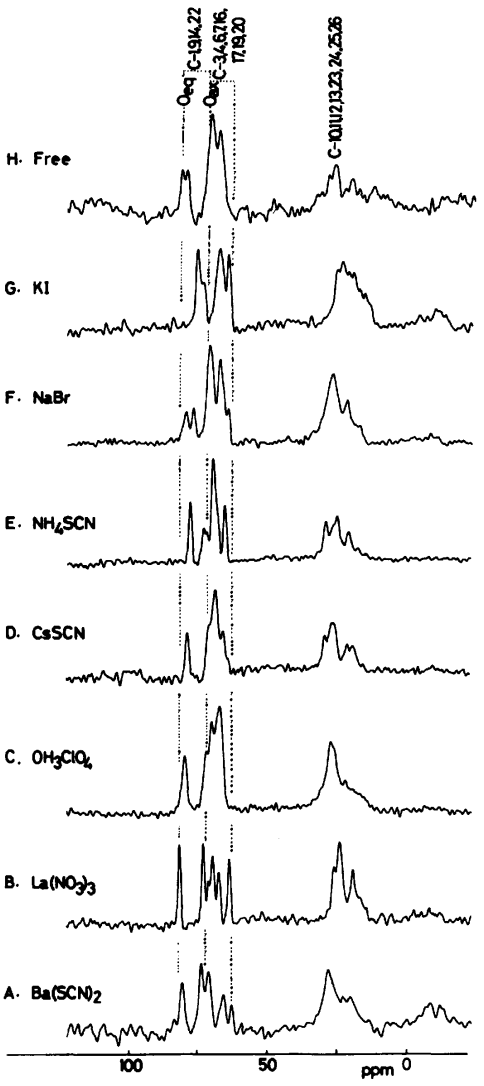

Fig. 5. 75.46 MHz ^{13}C CP-MAS NMR spectra of *cis-syn-cis* isomer of dicyclohexano-18-crown-6 complexed with a variety of metal ions in the solid state. Number of transients are 2000—5000.

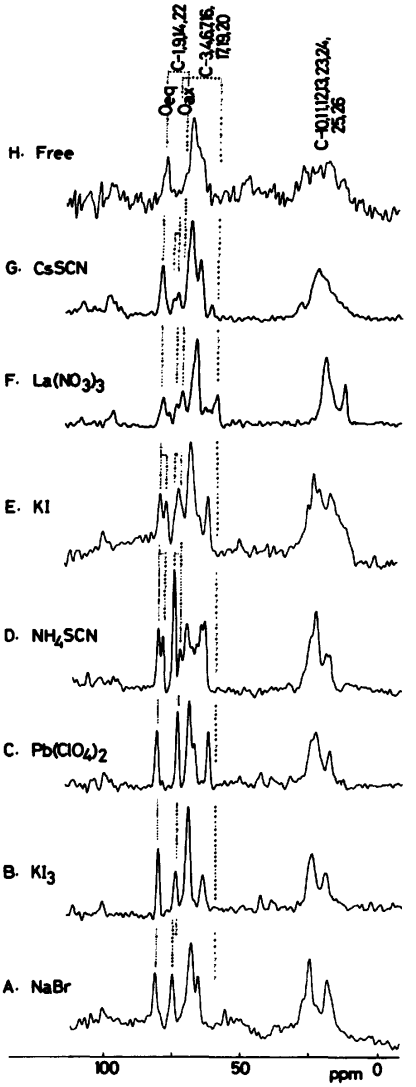

Fig. 6. 75.46 MHz ^{13}C CP-MAS NMR spectra of *cis-anti-cis* isomer of dicyclohexano-18-crown-6 complexed with a variety of metal ions in the solid state. Number of transients are 2000—5000.

TABLE 3. ^{13}C CHEMICAL SHIFTS OF *cis-anti-cis* AND *cis-syn-cis* ISOMERS OF DICYCLOHEXANO-18-CROWN-6 COMPLEXED WITH VARIOUS METAL IONS IN SOLUTION (ppm FROM TMS)[a]

Carbon No.	*cis-anti-cis*							
	Free / $CDCl_3$	KI / $CDCl_3$	CsSCN / $CDCl_3$	NaBr / CD_3OD	NH_4SCN / CD_3OD	$La(NO_3)_3$ / CD_3OD	$Pb(ClO_4)_2$ / DMSO-d_6	KI_3 / DMSO-d_6
1,9,14,22	77.4	78.3	77.8	78.6	79.0	81.7, 78.1	77.5	78.1
4,6,17,19	70.6	70.4	70.4	70.9	71.0	72.6, 71.3	70.7	70.8
3,7,16,20	67.9	66.3	66.9	67.0	67.0	68.5, 68.2	68.3	67.0
10,13,23,26	27.6	25.7	26.5	26.3	26.1	27.8, 25.9	28.2	26.4
11,12,24,25	22.0	21.4	21.7	21.9	21.8	22.3, 21.4	22.6	22.1
Carbon No.	*cis-syn-cis*							
	Free / $CDCl_3$	KI / CD_3OD	CsSCN / $CDCl_3$	NaBr / CD_3OD	NH_4SCN / CD_3OD	$La(NO_3)_3$ / CD_3OD	OH_3ClO_4 / CD_3OD	$Ba(SCN)_2$ / CD_3OD
1,9,14,22	77.5	78.2	77.5	78.2	78.1	81.3, 77.9	78.3	80.3
4,6,17,19	71.1	71.1	70.7	70.4	71.1	72.4, 70.9	71.2	70.8
3,7,16,20	68.0	67.3	67.4	66.9	67.5	68.5, 67.7	68.2	68.0
10,13,23,26	27.5	26.4	26.9	26.5	26.6	27.8, 25.6	27.3	26.3
11,12,24,25	22.0	22.0	21.7	21.9	22.0	22.3, 20.4	22.1	21.6

a) Assignment of peaks based on Ref. 36.

TABLE 4. ^{13}C CHEMICAL SHIFTS OF *cis-anti-cis* AND *cis·syn-cis* ISOMERS OF DICYCLOHEXANO-18-CROWN-6 COMPLEXED WITH VARIOUS METAL IONS IN THE SOLID STATE (±0.4 ppm; ppm FROM TMS)

Carbon No.	*cis-anti-cis*							
	Free	KI	CsSCN	NaBr	NH_4SCN	$La(NO_3)_3$	$Pb(ClO_4)_2$	KI_3
1,9,14,22	81.0 a)	81.7, 79.5 75.0, a)	81.1 77.0, 75.2	81.7 75.6	81.1, 79.5 75.4,[a] 73.2	80.7, 78.7 76.1, 73.6	81.9 74.4	81.1 74.6
4,6,17,19	71.1	70.8	71.0	68.7	75.4	69.0	70.3	70.4
3,7,16,20	68.1	64.5	67.5	66.3	73.2 70.8 68.9 67.1 65.9 64.5	65.7 61.1	68.3 63.1	65.1
10,13,23,26	b)	25.5	24.5	25.3	23.5	21.9	24.1	25.9
11,12,24,25		19.6	—	19.0	19.0	14.8	19.2	20.4
Carbon No.	*cis·syn·cis*							
	Free	KI	CsSCN	NaBr	NH_4SCN	$La(NO_3)_3$	OH_3ClO_4	$Ba(SCN)_2$
1,9,14,22	82.1 80.3	76.8 74.8	80.5 72.4	80.5, 77.6 71.6[c]	78.9 73.8, 72.8	82.7 74.0, 72.2	81.0 73.2	81.9 74.6
4,6,17,19	70.8	68.0	70.0	67.9	70.4	70.6	71.3	71.8
3,7,16,20	68.1	64.7	67.1	64.7	69.1	68.3 64.5	68.0	66.5 63.5
10,13,23,26	24.9	21.9	26.3	25.5	24.3(28.3)	25.5, 23.0	26.8	27.5
11,12,24,25	18.6	—	20.0	20.6	19.8	18.3	20.8	21.6

a) Overlapped with a signal of C-4,6,17,19,3,7,16,20. b) Obscured by line-broadening. c) Tentative assignment: another plausible assignment is one of C-4,6,17,19,3,7,16,20.

recording of the ^{13}C CP-MAS NMR spectra at lower temperature is very useful for the samples whose peak-intensities are suppressed at ambient temperature.

Ethylene Oxide Oligomers. Iwamoto[20-23] previously analyzed detailed molecular conformation of TEGM, HEGE, and TEGE complexed with $HgCl_2$ or $CdCl_2$ by X-ray diffraction method. The local conformations of these complexes are summarized in Fig. 7, as defined by sets of torsion angles. Our view is that the ^{13}C NMR signals of particular carbons are primarily influenced by the local conformations

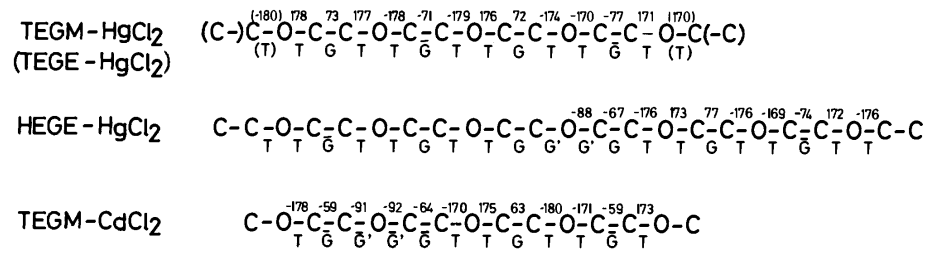

Fig. 7. Conformations of TEGM, TEGE, HEGE complexed with $HgCl_2$ or $CdCl_2$ in the solid state (Data taken from Refs. 20—23). The symbols T, G ($\bar{G}$), and G′ ($\bar{G}'$) stand for the *trans*, *gauche* (minus *gauche*), and torsion angle of about 90°, respectively.

defined by a pair of torsion angles of nearby single bonds. This view has been proven correct for a number of peptides, proteins, carbohydrates, and polysaccharides.[10—19] Accordingly, it is expected that the presence of the following two types of local TG and GG′ conformers in the complexes (Fig. 7) give rise to different types of signals:

$$-O-\overset{T}{\underset{}{C}}H_2-\overset{G}{\underset{}{C}}H_2-O \quad :TG \text{ conformer}$$

$$-O-\overset{G'}{\underset{}{C}}H_2-\overset{G}{\underset{}{C}}H_2-O \quad :GG' \text{ conformer}$$

where the symbols T and G stand for *trans* and *gauche* conformations, respectively, and G′ stands for the torsion angles of about 90°. It is expected from Figure 7 that the relative peak-intensity of the conformer TG with respect to that of the conformer GG′ is 8:0, 8:0, 10:2, and 6:2 for TEGM–$HgCl_2$, TEGE–$HgCl_2$, HEGE–$HgCl_2$ and TEGM–$CdCl_2$, respectively. Therefore, the peaks in regions I and II of the internal CH_2 group in Fig. 2 are ascribed to the TG and GG′ conformers, respectively, as substantiated from the relative peak-intensities of the individual peaks in Table 1 and the population of the TG and GG′ conformers in Fig. 7. Note that the peaks marked by **b** should be ascribed to the methylene carbons of the terminal ethoxyl groups in TEGE and HEGE, although they are within the region II of CH_2 (GG′). In particular, there exists no GG′ conformer in TEGE–$HgCl_2$ complex, as seen from Fig. 7. It is also mentioned that the TG and $T\bar{G}$ conformers gave the identical ^{13}C chemical shifts.

Torsion angles of the |T|, |G|, and |G′| rotamers are 174°±3°, 70°±3°, 90°±2°, respectively (Fig. 7) and the peaks of the TG and GG′ conformers should be observed as two separate single peaks. On the contrary, the TG signals are split into two or three signals as shown in Fig. 2, although the most intense with relative peak-intensity larger than 3 should be ascribed to the carbons at the central core of these oligomers which are not influenced by the presence of the terminal methoxyl or ethoxyl groups. Displacement of peaks from the most intense signals within the peaks of the TG conformers (region I) is less than 1.5 ppm and the positions of the TG conformers are well separated from those of the GG′ conformers which are resonated at higher field by 2 ppm. It is probable that direct effect of metal coordination over the carbon chemical shifts might have some contribution to the splittings of peaks. Such an effect, however, is not larger than 1.5 ppm, if it exists.

Cryptands. The individual assignment of peaks to the C-1 and C-2 in cryptands [2.2] and [2.2.2] and to the C-1, C-2, and C-3 in [2.2.1] in the solid state is difficult,[39] if one considers the maximum separation of the peaks is about 4 ppm which is in the range of the conformation-dependent ^{13}C chemical shifts of single carbon. However, we attempted to relate the ^{13}C chemical shifts of the C-4 plus C-5 and C-3 chemical shifts of cryptands [2.2.1] and [2.2.2], respectively, with the pairs of torsion angles, namely, rotation about N-C-4 and C-4-C-2, and N-C-5 and C-5-C-3 for cryptand [2.2.1] and rotation about N-C-3 and C-3-C-2 for cryptand [2.2.2]. It is now possible to plot the ^{13}C chemical shifts of the C-3 (for cryptand [2.2.2]), and C-4 plus C-5 (for cryptand [2.2,1]) against the torsion angles about N-C-4 and N-C-5 (cryptand [2.2.1]) and N-C-3 (cryptand [2.2.2]),[26—29,40] because the torsion angles C-4-C-2 and C-5-C-3

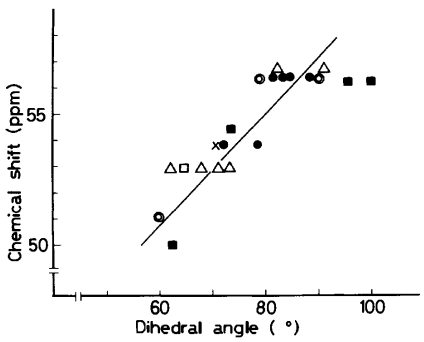

Fig. 8. A plot of C-3 (cryptand [2.2.2]), C-4 plus C-5 (cryptand [2.2.1]) ^{13}C chemical shifts of cryptands [2.2.2] and [2.2.1] against the N-C-3 ([2.2.2]) and N-C-4 and N-C-5 ([2.2.1]) torsion angles. □, K-[2.2.2]; △, Ba-[2.2.2]; ◎, Ca-[2.2.2]; ×, Tl-[2.2.2]; ●, Na-[2.2.1]; ■, K-[2.2.1].

(cryptand [2.2.1]) and C-3-C-2 (cryptand [2.2.2]) do not depart from the standard value (60°±10°) irrespective of the variety of complexes (Fig. 8).[41] Accordingly, it is found that the manner of peak-splittings in the C-3, C-4, and C-5 carbons of cryptands [2.2.2] and [2.2.1] can be well explained in terms of the variation of torsion angles characteristic of nearby local conformations.

Crown Ethers. Dalley *et al.*[42] showed by X-ray diffraction that in the both isomers the cavity surrounded by the six oxygen atoms is elliptical in shape with the two axial oxygen atoms O-21 and O-8 pointing out of the cavity. Consistent with this, the ^{13}C NMR spectra of free *cis-syn-cis* (Fig. 5H) and *cis-anti-cis* (Fig. 6H) are very similar (except for the doubling of the O_{eq} peak in the latter).[43] When NaBr or $Ba(SCN)_2$ salts[44] are complexed with *cis-anti-cis* or *cis-syn-cis* isomers, respectively, macrocyclic conformations are changed either to possess C_i symmetry[31] or to have C_2 symmetry.[44]

Interestingly, the ^{13}C chemical shifts of the O_{ax} and O_{eq} peaks of *cis-anti-cis* isomer are very similar among the eight kinds of complexes, suggesting the presence of similar conformation for cyclohexane moiety as observed for the NaBr complex. However, the conformations of the two cyclohexane moieties are not identical for the complexes with NH_4SCN, KI, $La(NO_3)_3$, and CsSCN, as manifested from the observation of the two pairs of doublets ascribable to the C-1, C-9, C-14, and C-22 carbons, probably reflecting the presence of some steric strain in the ligands. Conformation of two cyclohexane moieties becomes identical when KI_3 is coordinated to *cis-anti-cis* isomer in place of KI, although the ^{13}C NMR profile of polyether moiety remains unchanged. By contrast, the O_{eq} peaks are significantly displaced upfield for *cis-syn-cis* isomer complexed with KI, NaBr, and NH_4SCN (Fig. 5E-G). This finding is readily rationalized by the presence of strong ring strain in cyclohexane rings as a result of coordination at the polyether moiety.

The ^{13}C NMR peaks of the polyether carbons are in many instances split into two peaks, the intensity of which being 3:1 in spite of the presence of eight kinds of carbons. These doublet patterns are modified to yield three peaks (the intensity of which being 2:1:1) for *cis-syn-cis* isomer-$Ba(SCN)_2$ (Fig. 5A), four peaks for *cis-syn-cis* isomer-$La(NO_3)_3$ (Fig. 5B) or seven peaks for *cis-anti-cis* isomer-NH_4SCN complex (Fig, 6D). These observations are consistent with a possibility that local conformation of polyether moiety is C_2 or C_i symmetry, except for *cis-anti-cis* isomer-NH_4SCN complex whose arrangement of polyether moiety is highly distorted. It is interesting to note that the ^{13}C chemical shifts of the highest peak-intensity at 69-71 ppm in the solid state are not strongly varied among complexes with a variety of metal ions and are very close to those observed in solution state (70.8±0.4 ppm) (Table 3). Obviously, these peaks are straightforwardly ascribed to the carbons of the TG conformers in view of their chemical shifts as compared with those of ethylene oxide oligomers. This view is supported by X-ray diffraction study of *cis-anti-cis* isomer of NaBr complexes which is the only available detailed data of dicyclohexano-18-crown-6 complex: all of the torsion angles about the polyether moiety are within the typical TG conformer.[31]

Nevertheless, the upper peak of NaBr-*cis-anti-cis* isomer at 66.3 ppm should be ascribed to the TG conformer, although this position is rather high as compared with that of ethylene oxide oligomers. This may be caused by that the C-3, C-7, C-16, and C-20 peaks are not completely free from the substituent effect of cyclohexane rings. It is emphasized that the ^{13}C chemical shifts of peaks with lower peak-intensities vary with variety of metal ions, depending also on the conformation of the polyether moiety. In particular, the largest upfield displacement of peaks is 7.0 ppm for $La(NO_3)_3$-*cis-anti-cis* isomer. The observation of peaks at such a higher field region (>67 ppm) could be ascribed to the presence of the GG and TT conformers as seen for NaSCN-18-crown-6[45] or uncomplexed 18-crown-6.[46] Further study, however, is required to prove this view.

Conformation in Solution State. It is now possible to examine whether or not the conformations achieved in the solid state are also retained in solution by comparing the ^{13}C chemical shifts of solution with those of the solid state. This kind of information is closely related with stability of complexes in solution, because any conformational change of ligand molecules would lead to decomposition of complexes. It is worthwhile to note that metal complexes with cryptands are generally many orders of magnitude more stable than those with crown ethers.[8,9] In particular, the association constant of the potassium ion both in aqueous or methanol solutions decreases in the following order: [2.2.2]>[2.2.1]>*cis-syn-cis*>*cis-anti-cis*>[2.2]. In the case of the sodium ion, [2.2.1]>[2.2.2]. Consistent with this, [2.2.2] and [2.2.1] complexed with a variety of metal ions maintain their overall conformations achieved in the solid even in solution state, although conformational fluctuation about the N-C-3, N-C-4 or N-C-5 is evident as seen from the time-averaging process in the ^{13}C NMR signals, as judged from the similarity of the ^{13}C chemical shifts between the solid and solution. On the contrary, the presence of ring-puckering in two cyclohexane rings of the crown ethers as seen in solution state is responsible for reduction of stability and selectivity of complexes. Nevertheless, it appears that no drastic conforma-

tional change occurs between the solid and solution for [2.2] as inferred from Table 2, although association constant of this molecule is usually lower than crown ethers.[8,9] Obviously, consideration of steric requirement of ligand molecules in adapting to different metal ions is also very important to explain relative stability of complexes.

Concluding Remarks

We have showed that the ^{13}C NMR peaks of backbone carbons of ethylene oxide oligomers, crown ethers and cryptands exhibit substantial amounts of displacement of peaks (up to 6 ppm) upon complex formation with a variety of metal ions, as determined by cross polarization-magic angle spinning method. These changes of the ^{13}C chemical shifts are mainly ascribed to conformational changes induced by metal-binding as revealed by X-ray diffraction and can be utilized as intrinsic indicators of conformational changes. Analysis of ^{13}C NMR spectra in the solid state can be conveniently performed, when conformational features by X-ray diffraction studies are available. This approach is also suitable for comparative study of conformational changes of these ionophores induced by complexation with a variety of metal ions, even if detailed X-ray diffraction data are unavailable. Further, it is easily evaluated on the basis of the conformation-dependent ^{13}C chemical shifts whether or not the conformations of these ionophores achieved in the crystalline state is retained in solution state.

References

1) C. J. Pedersen, *Fed. Proc., Fed. Am. Soc. Exp. Biol.*, **27**, 1305 (1968).

2) J. J. Christensen, J. O. Hill, and R. M. Izatt, *Science*, **174**, 459 (1971).

3) C. J. Pedersen and H. K. Frensdorff, *Ang. Chem. Int. Ed. Eng.* **11**, 16 (1972).

4) J. M. Lehn, *Struct. Bonding*, **16**, 1 (1973).

5) M. R. Truter, *Struct. Bonding*, **16**, 71 (1973).

6) J. J. Christensen, D. J. Eatough, and R. M. Izatt, *Chem. Rev.*, **74**, 351 (1974).

7) B. C. Pressman, *Ann. Rev. Biochem.*, **45**, 501 (1976).

8) F. de Jong and D. N. Reinhoudt, *Adv. Phys. Org. Chem.*, **17**, 1 (1981).

9) B. Dietrich, "Inclusion Compound," Vol. 2, ed by J. C. Atwood, J. E. D. Davies and D. D. MacNicol, Academic Press, London (1984), Chap. 10.

10) H. Saitô, R. Tabeta, A. Shoji, T. Ozaki, I. Ando, and T. Asakura, "Magnetic Resonance in Biology and Medicine," ed by G. Govil, C. L. Kheterapal, and A. Saran, Tata McGraw-Hill, New Delhi (1985), pp. 195—215.

11) T. Taki, S. Yamashita, M. Satoh, A. Shibata, T. Yamashita, R. Tabeta, and H. Saitô, *Chem. Lett.*, **1981**, 1803.

12) H. Saitô, R. Tabeta, A. Shoji, T. Ozaki, and I. Ando, *Macromolecules*, **16**, 1050 (1983).

13) H. Saitô, R. Tabeta, T. Asakura, Y. Iwanaga, A. Shoji, T. Ozaki, and I. Ando, *Macromolecules*, **17**, 1405 (1984).

14) H. Saitô, R. Tabeta, A. Shoji, T. Ozaki, I. Ando, and T. Miyata, *Biopolymers*, **23**, 2279 (1984).

15) H. Saitô and R. Tabeta, *Chem. Lett.*, **1985**, 83.

16) H. Saitô, R. Tabeta, and T. Harada, *Chem. Lett.*, **1981**, 571.

17) H. Saitô and R. Tabeta, *Chem. Lett.*, **1981**, 713.

18) H. Saitô, R. Tabeta, and S. Hirano, "Chitin and Chitosan. Proceeding of the Second International Conference on Chitin and Chitosan," ed by S. Hirano and S. Tokura, The Japanese Society of Chitin and Chitosan (1982), pp. 71—76.

19) H. Orgura, K. Furuhata, H. Saitô, G. Izumi, M. Itoh, and Y. Shitori, *Chem. Lett.*, **1984**, 1003.

20) R. Iwamoto, *Bull. Chem. Soc. Jpn.*, **46**, 1114 (1973).

21) R. Iwamoto, *Bull. Chem. Soc. Jpn.*, **46**, 1118 (1973).

22) R. Iwamoto, *Bull. Chem. Soc. Jpn.*, **46**, 1123 (1973).

23) R. Iwamoto and H. Wakano, *J. Am. Chem. Soc.*, **98**, 3764 (1976).

24) D. Moras, B. Metz, M. Herceg, and R. Weiss, *Bull. Soc. Chim. France*, **1972**, 551.

25) B. Metz and R. Weiss, *Acta Cryst.*, **B29**, 1088 (1973).

26) F. Mathieu, B. Metz, D. Moras, and R. Weiss, *J. Am. Chem. Soc.*, **100**, 4412 (1978).

27) B. Metz, D. Moras, and R. Weiss, *Acta Cryst.*, **B29**, 1377 (1973).

28) D. Moras and R. Weiss, *Acta Cryst.*, **B29**, 1059 (1973).

29) B. Metz, D. Moras, and R. Weiss, *Acta Cryst.*, **B29**, 1382 (1973).

30) R. M. Izatt, B. L. Haymore, J. S. Bradshaw, J, J. Christensen, *Inorg. Chem.*, **14**, 3132 (1975).

31) D. E. Fenton, M. Mercer, M. R. Truter, *Biochem. Biophys. Res. Commun.*, **48**, 10 (1972); M. Mercer and M. R. Truter, *J. Chem. Soc., Dalton Trans*, **1973**, 2215.

32) M. E. Harman, F. A. Hart, M. B. Hursthouse, G. G. Moss, P. R. Raithby, *J. Chem. Soc., Chem. Commun.*, **1976**, 396.

33) C. J. Pedersen, *J. Am. Chem. Soc.*, **92**, 386 (1970).

34) C. J. Pedersen, *J. Am. Chem. Soc.*, **89**, 7017 (1967).

35) R. E. Ernst, *Adv. Magn. Reson.*, **2**, 1 (1966).

36) G. W. Buchanan, K. Bourque, J. W. Bovenkamp, A. Rodrique, and R. A. Bannard, *Tetrahedron Lett.*, **25**, 3963 (1984).

37) J. Schaeffer and E. O. Stejskal, "Topics in Carbon-13 NMR Spectroscopy," ed by G. C. Levy, Wiley-Interscience (1979) Vol. 3, pp. 283—324.

38) R. Tabeta and H. Saitô, Manuscript in preparation.

39) The ^{13}C NMR peaks of cryptand [2.2.1] in solution were already assigned individually (E. Schmidt, J.-M. Tremillon, J.-P. Kintzinger, and A. I. Popov, *J. Am. Chem. Soc.*, **105**, 7563 (1983).

40) D. Moras, B. Metz, and R. Weiss, *Acta Cryst.*, **B29**, 383 (1973).

41) In this treatment, we utilized X-ray diffraction data of the KI complex instead of the KSCN complex whose X-ray diffraction data are unavailable, although some of anions would alter the conformation of host molecules as seen in the case of KI and KI_3 complexes with *cis-anti-cis* isomer (Fig. 6E and 6B). It is probable, however, that the anion does not affect the conformation of host molecule as far as it is well separated from and not directly coordinated to the metal ion

as in the present situation (K^+-[2.2.2] complex).

42) N. K. Dalley, J. S. Smith, S. B. Larson, J. J. Christensen, and R. M. Izatt, *J. Chem. Soc., Chem. Commun.*, **1975**, 43.

43) As will be described in the next paragraph, doubling of the O_{eq} peak is ascribed to the presence of two kinds of cyclohexyl rings whose conformations are not identical.

44) N. K. Dalley, D. E. Smith, R. M. Izatt, and J. J. Christensen, *J. Chem. Soc., Chem. Commun.*, **1972**, 90.

45) M. Dobler, J. D. Dunitz, and P. Seiler, *Acta Cryst.*, **B30**, 2741 (1974).

46) J. D. Dunitz and P. Seiler, *Acta Cryst.*, **B30**, 2739 (1974).

 © 1985 The Chemical Society of Japan Bull. Chem. Soc. Jpn., 58, 3225—3228 (1985)

Studies of the Hydrous Niobium(V) Oxide Ion Exchanger. III. The Effect of Heat Treatment

Yasushi INOUE,* Hiromichi YAMAZAKI, and Yuzo MATSUDA
Department of Nuclear Engineering, Faculty of Engineering, Tohoku University, Aramaki, Sendai 980
(Received March 18, 1985)

The effects of heat treatments in air have been studied regarding the properties of a hydrous niobium(V) oxide ion exchanger in H^+ form. The exchanger lost 17 per cent of the initial ion-exchange capacity when it was heat-treated at 110 °C; thereafter the exchange capacity decreased progressively with temperature until 400 °C, at which point it retained about a half of the initial value. The exchanger began to crystallize into γ-phase at a temperature between 450 to 500 °C where the capacity disappeared. The γ-phase transformed to α-phase at a temperature above 800 °C. An examination of the uptake curves showed that less-acidic exchange sites were more resistant than more-acidic sites to heat treatment. The existence of three kinds of water in the exchanger (adherent, zeolitic, and bound) has been suggested on the basis of the ion-exchange capacity, the thermal-analysis curves, and water recovery brought about by humidifying.

Previous papers in this series described detailed studies regarding the synthesis, the acid-base properties, and the ion-exchange selectivity for various cations of a hydrous niobium(V) oxide ion exchanger.[1,2] The study on the effect of heat treatment regarding ion-exchange properties is also important, since most inorganic ion exchangers are expected to be superior to ion-exchange resins regarding thermal stability. As the hydrous niobium(V) oxide has an amorphous structure, this investigation may be helpful in considering the structure of the compounds by adding some strong circumstantial evidence: The relation between the ion-exchange capacity and the thermal behavior of water in the compound. As to the effect of thermal treatment, there have been many studies regarding the composition and the physical properties,[3-8] while there have been few reports on the ion-exchange properties.

The present paper describes the effect of heat treatment in air with regards to the composition and the ion-exchange properties of hydrous niobium(V) oxide. Furthermore, a classification of various water forms present in the exchanger is discussed, and the thermal stability of the material is compared with other hydrous oxides.

Experimental

Reagents and Apparatus. The hydrous niobium(V) oxide ion exchanger was prepared by pyrohydrolyzing a $NbCl_5$ solution, as has been previously described.[1,2] A thermal analysis was undertaken using a Shimadzu micro thermal analyzer, Model DT-20 B, connected to a thermal balance, Model TGC-20 H, for thermogravimetric analysis (TGA), and a high-temperature sample holder, Model MDH-20, for differential thermal analysis (DTA). The reference material for DTA was α-alumina. The measurement was performed in air at a heating rate of 10 °C min^{-1}.

X-Ray diffraction patterns were obtained by means of a Shimadzu X-ray diffraction unit, Model XD-3A, using Ni-filtered Cu $K\alpha$-radiation. The diffraction angle was calibrated using silicon powder.

Heat Treatment. About 8 g of the exchanger in H^+ form was heated in air to a constant weight at a constant temperature, which was controlled within an accuracy of 1% using an automatic temperature controller (Chino Workers, Ltd.). After cooling, the sample was immersed in water overnight, followed by the humidifying operation described previously.[1,2]

The other experimental procedures were the same as those described in the preceeding papers.

Results and Discussion

Effect of Heat Treatment on the Composition of Hydrous Niobium(V) Oxide. Figure 1 shows the relation between the water content immediately after the heat treatment (open mark) and that of the exchanger subjected to the humidifying operation

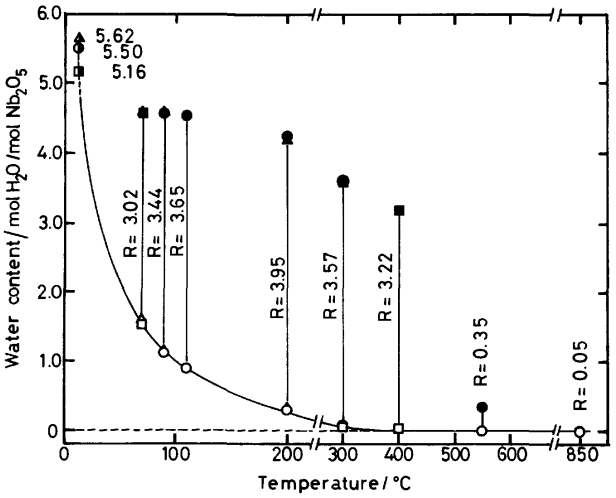

Fig. 1. Change in composition.
▲◑■: Sample R.T. Open marks: Immediately after heat treatment. Filled marks: Immersed in water, dried over saturated NaCl solution. R: Water recovery.

(filled mark). It should be noted that the water content was normalized to the number of moles of water per 1 mole of Nb_2O_5. In the case of the exchanger without heat treatment (designated as sample R.T.), there existed a fluctuation in the water content by an amount of 0.5 mol H_2O/mol Nb_2O_5. This fluctuation is insignificant in considering the effect of the heat treatment since the heat treatment, even at a temperature as low as 70 °C, led to the same composition irrespective of the original values. The amount of water contained in the exchanger immediately after the heat treatment at 70 °C was reduced to about 30% of the original value; then, it gradually decreased with temperature, and finally reached zero at 400 °C. This result is compatible with Lapitskii's observation that the water content of 6.93 mol H_2O/mol Nb_2O_5 at room temperature decreased to 1.79 mol H_2O/mol Nb_2O_5 at 110 °C and to almost zero at 400 °C, in spite of the difference in the experimental conditions.[4]

The following relation holds between the water content immediately after the heat treatment and that of the exchanger subjected to the humidifying operation. For the exchangers heated up to 400 °C, 3 to 4 mol of water per 1 mol of Nb_2O_5 were recovered, while for the samples heated over 550 °C, water was only slightly recovered by humidifying. Figure 2 shows the X-ray diffraction patterns of the samples subjected to the humidifying operation. The samples heated up to 400 °C, together with the sample R.T., have poor crystallinity. Over the range of 450—500 °C many peaks characteristic of γ-niobium(V) oxide, the low temperature phase of the compound reported by Brauer[3] and by Holtzberg *et al.*,[5] appeared and sharpened with increasing temperature, indicating an enhanced crystallization; the material crystallized completely in the γ-phase at a temperature between 600 to 650 °C. When the crystals were heated at a temperature above 800 °C, they were transformed to the α-phase. Therefore, the sudden decrease of water recovery at a temperature above 400 °C may be associated with the crystallization of the exchanger; this brings about a decrease in the space which can accommodate water molecules.

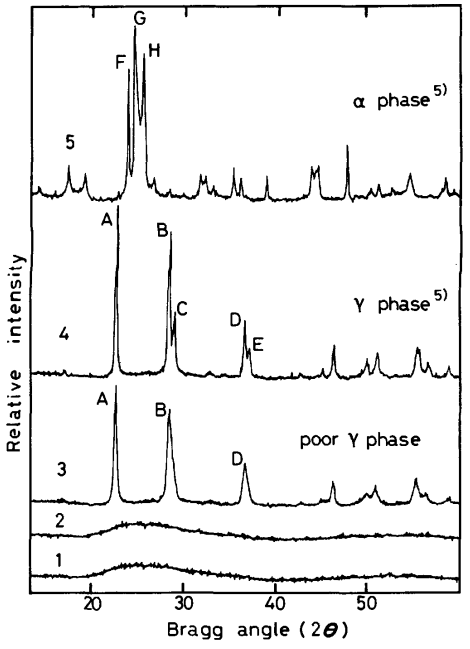

Fig. 2. X-Ray diffraction patterns.
Temperature of treatment; 1: R.T., 2: 400 °C, 3: 550 °C, 4: 650 °C, 5: 850 °C. Temperature range of transition; Poor γ-phase : 450—500 °C, γ-phase: 600—650 °C, α-phase: 800—850 °C.
Interplaner distance/nm; A: 0.393, B: 0.315, C: 0.309, D: 0.246, E: 0.243, F: 0.375, G: 0.364, H: 0.350.

Change in the Ion-exchange Capacity. In order to examine the effect of the heat treatment on the acid-base property of the exchanger, the uptake curves for Na^+ were measured as a function of the pH. The results are shown in Fig. 3. In the case of the exchangers heated up to 400 °C, the dissolution of a part of the exchanger in strong basic solutions limits the maximum cation-exchange capacity to the value at around pH 10.5. For the samples heated up to 110 °C, the decreases in the ion-exchange capacity were 0.06 and 0.13 mol Na^+/mol Nb_2O_5, respectively, at pH 7.6 (breaking point in the curve) and at pH 10; hence, nearly the same amount of exchange sites was destroyed in the pH ranges of either side of the breaking point. When the exchangers were heat-treated at 200 °C or higher, the capacity in a pH range lower than the breaking point decreased with

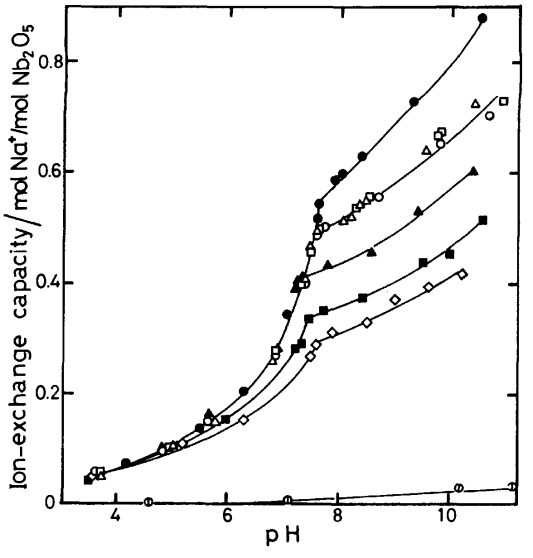

Fig. 3. Uptake curves for sodium ions.
Temperature of treatment; ●: R.T., △: 70 °C, □: 90 °C, ○: 110 °C, ▲: 200 °C, ■: 300 °C, ◇: 400 °C, ⓓ: 550 °C.

Table 1. Changes in ion-exchange capacity and water content

Temp of treatment °C	Difference in A[1] exchange capacity mol Na^+/mol Nb_2O_5	Difference in A/2[2] water content mol H_2O/mol Nb_2O_5	Difference in B[3] water content mol H_2O/mol Nb_2O_5	2B/A
70	0.14±0.01	0.07 ±0.01	0.60±0.04	9±2
200	0.24±0.01	0.12 ±0.01	1.27±0.04	11±1
300	0.34±0.01	0.17 ±0.01	1.58±0.04	9±1
400	0.39±0.01	0.19_5±0.01	1.93±0.04	9±1

1) Ion-exchange capacity at pH 10.0; difference between sample R.T. and sample thermally treated. 2) Difference in capacity was converted into that in water content. 3) Difference in water content between sample R.T. and heat-treated sample subjected to the humidifying operation.

the temperature, while in a pH range higher than that point, the curves were parallel to those for the samples heated at a temperature lower than 110 °C; the main part of the exchange sites, destroyed by the heat treatment at a temperature higher than 110 °C, was in the pH region lower than the breaking point. The exchange sites were completely destroyed at 550 °C. The sample heated at 850 °C exhibited no uptake of Na^+ throughout the pH region examined. From the above observations it is considered that the resistance to thermal decomposition is greater for less-acidic than for more-acidic ion-exchange sites.

Table 1 shows the relation between the decrease in ion-exchange capacity at pH 10 and that in the water content of the heat-treated samples subjected to the humidifying operation. Symbols A and B, respectively, are referred to the difference in the exchange capacity and in the water content between the sample R.T. and the heat-treated exchanger. As one mole of water should be liberated by a condensation of two moles of the OH groups which may act as ion-exchange sites, half of the difference in the ion-exchange capacity (A) is equivalent to a decrease of the water content due to the condensation of the exchange sites (A/2). As is shown in the right column in Table 1, the ratio of the loss of total water to the loss of water that originated from the exchange sites (OH groups), by heat treatment, 2B/A, did not change up to 400 °C. Hence, a constant amount of water molecules is considered to be fixed in the exchanger by OH groups through some kind of interaction such as a hydrogen bond (bound water); the irreversible condensation of the OH groups, which cannot be recovered by the humidifying operation, is accompanied by the irreversible release of water.

Thermal Analysis of the Samples. Figure 4 shows the TGA and DTA curves for the samples subjected to the humidifying operation. The TGA curves of the samples heat-treated up to 400 °C are similar to those of the sample R.T.; the sample lost weight abruptly up to around 100 °C and then,

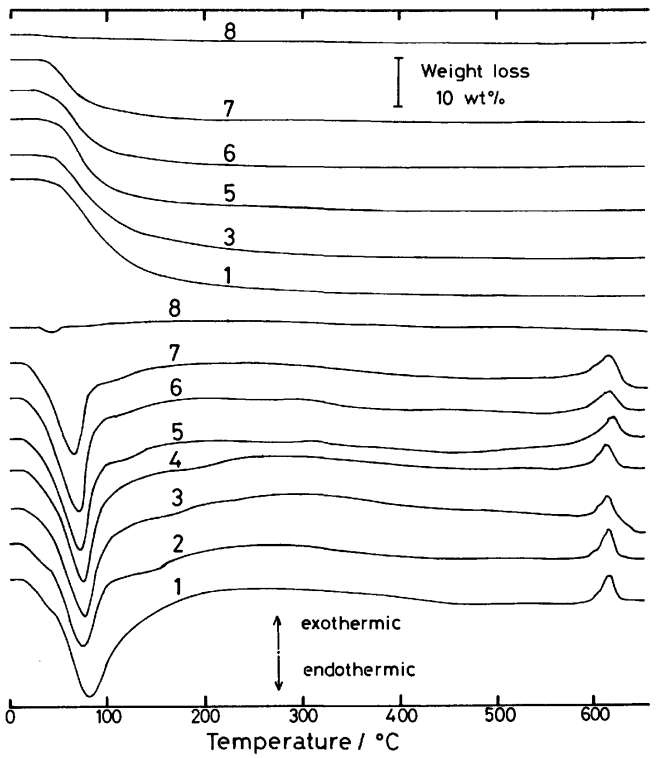

Fig. 4. TGA and DTA curves (Heat treatment, followed by humidiation).
Temperature of treatment; 1: R.T., 2: 70 °C, 3: 90 °C, 4: 110 °C, 5: 200 °C, 6: 300 °C, 7: 400 °C, 8: 550 °C.

gradually, up to about 600 °C, where the weight became constant. In contrast, the sample heated at 550 °C showed little weight loss up to 600 °C. In the DTA curves, large endothermic peaks appearing in the range lower than 200 °C sharpened as the temperature for heat treatment became higher. The position of the peak, observed at 70 to 80 °C for the samples heated below 400 °C, shifted to 45 °C and its area became very small when the sample was heated at 550 °C. Apparently, this observation is compatible with the changes in both the exchange capacity and

Table 2. Effect of heating time on the composition of sample

Heat treatment		Composition	
Temperature	Time	A	B
°C	h	mol H_2O/mol Nb_2O_5	
200	12	0.28±0.01	4.23±0.03
	72	0.26±0.01	4.15±0.03
400	12	0.02±0.01	3.22±0.03
	72	0.02±0.01	3.19±0.03

A: Immediately after heat treatment. B: Immersed into water, dried over sat. NaCl.

the degree of the recovery of water, with the temperature for heat treatment, if the peak is considered to correspond mainly to the release of water recoverable by humidifying, that is, a certain kind of zeolitic water. The shoulders observed at the high- and the low temperature sides, respectively, of the peak for the samples heat-treated at temperatures below 200 °C are attributable to the bound water liberated by the condensation of the hydroxyl groups and to the adherent water in the exchanger matrix. For the samples heat-treated below 400 °C, a small exothermic peak was observed at 605 °C; this peak can be assigned to crystallization. This temperature for crystallization is higher, by 100 °C, than that expected from the results in Fig. 2. This may be due to thermally non-equilibrium conditions in DTA measurements; incidentally, the exothermic peak shifted from 610 °C to 574 °C when the heating rate was decreased from 15 °C/min to 2 °C/min. Two exothermic peaks were observed at 375 °C and 545 °C by Sathyanarayana and Patel[6] and at 470 °C and 609 °C by Lapitskii.[4] In the present experiment, however, no exothermic peak was observed in the temperature region below 500 °C.

It is considered from above observations that the samples heated at temperatures up to 400 °C, keep the network structure essentially unchanged and, thereby, recover nearly a constant amount of the zeolitic water and some amount of the bound water, when humidified. When the exchanger is heat-treated at 550 °C or higher, the crystallization proceeds to an extreme and thereby almost all the water is not recovered by humidifying.

Effect of Heating Time. The thermal equilibrium is not always attained even when the exchanger is thermally treated until no weight loss is observed. To make clear this point, the effect of the heating time on the properties of the material was investigated at 200 °C and 400 °C. Table 2 shows that the composition of the exchangers (both immediately after the heat treatment and after the humidifying operation) is independent of the length of the heating period. There existed no difference in the uptake curves for Na^+, the thermal analysis curves, and the X-ray diffraction patterns between the samples heated for 12 h and those for 72 h. The materials, therefore, reach to thermal eqilibrium within 12 h.

Thermal Stability of the Exchanger. The thermal stability of hydrous niobium(V) oxide can be summarized as follows. The amount of water contained in the exchanger immediately after the heat treatment decreases with increasing temperature and becomes zero at 400 °C. The structure of the samples heated up to 400 °C, however, remains essentially unchanged, and the stabilized matrix can accomodate an approximately constant amount of a zeolitic water and some bound water when humidified. This brings about the recovery of a large part of the exchange sites; less acidic sites are more stable to thermal decomposition than more acidic sites. The ion-exchange capacity is halved when the exchanger is heat-treated at 400 °C. When the exchanger is heat-treated at temperatures above 500 °C, the crystallization of the matrix proceeds to an extreme and the structure changes completely. In this case, almost all the water is not recovered by the humidifying operation and, thereby, the sample has no ion-exchange capacity for Na^+ even in strong alkaline solution.

If the thermal stability of the exchangers is compared with hydrous titanium(IV) oxide[9] and hydrous tin(IV) oxide,[10] which have previously been investigated by the present authors, niobium(V) oxide is superior to these two hydrous oxides; hydrous titanium(IV) oxide, hydrous tin(IV) oxide, and niobium(V) oxide, respectively, keep 25, 29 and 57% of the original ion-exchange capacities for Na^+ when they are heat-treated at 300 °C.

References

1) Y. Inoue, H. Yamazaki, and Y. Kimura, *Bull. Chem. Soc. Jpn.*, **58**, 2481 (1985).
2) Y. Inoue, H. Yamazaki, K. Okada, and K. Morita, *Bull. Chem. Soc. Jpn.*, **58**, 2955 (1985).
3) G. Brauer, *Z. Anorg. Allg. Chem.*, **248**, 1 (1941).
4) A. V. Lapitskii, *Zh. Fiz. Khim.*, **26**, 56 (1952).
5) F. Holtzberg, A. Reisman, M. Berry, and M. Berkenblit, *J. Am. Chem. Soc.*, **79**, 2039 (1957).
6) D. N. Sathyanarayana and C. C. Patel, *Z. Anorg. Allg. Chem.*, **353**, 103 (1967).
7) V. A. Titova and I. G. Slatinskaya, *Russ. J. Inorg. Chem.*, **12**, 767 (1967).
8) V. V. Sakharov, N. E. Ivanova, S. S. Korovin, and M. A. Zakharov, *Russ. J. Inorg. Chem.*, **19**, 313 (1974).
9) Y. Inoue and M. Tsuji, *Bull. Chem. Soc. Jpn.*, **51**, 794 (1978).
10) Y. Inoue, H. Yamazaki, and H. Nakamizo, *Bull. Chem. Soc. Jpn.*, **58**, 1292 (1985).

Simultaneous Multielement Determination of Trace Metals in Seawater by Inductively Coupled Plasma Atomic Emission Spectrometry Using Chelating Resin Column Preconcentration

CHU Jia Cheng,† Tasuku AKAGI, and Hiroki HARAGUCHI*
Department of Chemistry, Faculty of Science, The University of Tokyo, 7-3-1, Hongo, Bunkyo-ku, Tokyo 113
(Received April 20, 1985)

Preconcentration of trace metals in seawater using a Chelex-100 resin column was investigated for simultaneous determination by inductively coupled plasma atomic emission spectrometry (ICP-AES). The optimum preconcentration conditions were examined in detail. With 100 ml of 1 M ammonium acetate buffer solution (1 M=1 mol dm^{-3}), the matrix elements in seawater could be removed sufficiently without loss of analytes. The concentration factor of 200 times could be achieved by dissolving the dried HNO_3 eluent of the column. The blanks of the method were negligibly small for most elements investigated. The detection limits were in the range of several ng/l to 100 ng/l for Al, Cd, Co, Cr, Cu, Fe, Mn, Mo, Ni, Pb, Ti, V, and Zn. The present technique was applied to the determination of trace metals in coastal and ocean seawater.

In recent years various methods for the determination of trace elements in seawater have been developed. Since the concentration levels of trace elements in seawater are very low, sensitive analytical techniques such as spectrophotometry,[1] atomic absorption spectrometry,[2-4] anodic stripping voltammetry,[5] isotope dilution mass spectrometry,[6] neutron activation analysis,[7] and X-ray fluorescence spectrometry[8] have been applied to seawater analysis.

Inductively coupled plasma atomic emission spectrometry (ICP-AES) which has the capability of simultaneous multielement detection has been often employed for determination of trace metals in seawater samples.[9-14] Adequate preconcentration techniques are, however, required prior to ICP-AES measurement because of insufficient sensitivity for the trace metal level in seawater and serious interferences caused by salts at high concentration. Therefore, preconcentration techniques such as solvent extraction,[9,10] coprecipitation,[11,12] and chelating exchange,[13,14] have been employed for seawater analysis with ICP-AES.

It has been shown that Chelex-100 chelating resin is an efficient exchanger of many trace metals and provides low analytical blank.[15] Further, as it is a strong chelator, it can remove metal ions from natural chelators existing in seawater.[15-17] Therefore, Chelex-100 resin may be useful for preconcentration of analytes prior to the ICP-AES measurement. Even so, it should be noted that Chelex-100 chelating resin often collects a part of Mg and Ca as well as trace metals in seawater.[18]

Berman *et al.* tried preconcentration of trace metals from seawater by Chelex-100 chelating resin followed by ICP-AES measurement.[13] They avoided the physical interference caused by salts using an ultrasonic nebulizer. Ammonium acetate buffer solution was known to remove the Mg and Ca cations from the resin,[19] but it also has the disadvantage to elute partly some of analytes such as Mn, Fe, and Cu.[20] Although an ICP-AES spectrometer equipped with a conventional cross flow nebulizer is widely prevailed, the preconcentration method using the Chelex-100 resin column and ICP-AES with a conventional cross flow nebulizer has not been reported. The Chelex-100 resin preconcentration procedure which allows minimum loss of analytes and efficient removal of matrix salts should be established in order to utilize ICP-AES effectively as a monitoring method of trace metals in seawater.

In this study, Chelex-100 resin column treatment is evaluated for preconcentration followed by ICP-AES measurement. Recoveries of trace metals and concentration of matrix elements in concentrated analysis solution are examined in detail for optimization of preconcentration conditions in ICP-AES analysis.

Experimental

Apparatus. An ICP instrument (Model Plasma Atomcomp Mk II from Jarrell-Ash Co., USA) was used with a conventional crossflow type nebulizer. The instrumental components and operating conditions for ICP-AES are summarized in Table 1. The emission lines used are shown in Table 2 along with the detection limit of each element. A pH meter (Model F-7, Horiba Seisakusho Ltd.) was used for the pH measurement. A class-100 clean booth (Model KCR-2D) was made by San-ei Seisakusho, and all column performance and preconcentration procedures were carried out in there.

Chemicals. All chemicals used were of analytical reagent grade or of better grade. The standard solutions for Al, Cd, Co, Cr^{3+}, Cu, Fe, Mg, Ni, Pb, Ti, and Zn were prepared from pure metals, and those for As, Cr^{6+}, Mo, V, Y, Na, K, and Ca from corresponding salts or oxides. HCl, HNO_3, acetic acid, and ammonium solution were of extra pure grade purchased from Wako Chemical Co., Ltd. HCl

† On leave from the Water Transportation Research Institute, Ministry of Communication, 12 Bei Huan Xi Road, Beijing.

TABLE 1. INSTRUMENTAL COMPONENTS AND OPERATING CONDITIONS

ICP spectrometer	Jarrell-Ash Plasma Atomcomp Mk II
RF frequency	27.12 MHz
RF Power	1.1 kW
Coolant gas	Argon 15 l/min
Auxiliary gas	Argon 0.5 l/min
Carrier gas	Argon 1.0 l/min
Observation height	17 mm above work coil
Nebulizer	Cross-flow type
Polychromator	Paschen-Runge type (75 cm focal length)
Grating	2400 grooves/mm
Reciprocal linear dispersion	0.54 nm/mm at 270 nm
Entrance slitwidth	25 μm
Exit slitwidth	50 μm

TABLE 2. ANALYTICAL WAVELENGTHS AND DETECTION LIMITS

Element	Wavelength[a]		Detection limit
	nm		μg/l
Al	I	308.2	10
As	I	193.6	40
Cd	I	228.8[b]	3
Co	II	228.6	4
Cr	II	205.5[b]	8
Cu	I	324.7	2
Fe	II	238.2	3
Mn	II	257.6	0.6
Mo	II	202.0	5
Ni	II	231.6[b]	10
Pb	II	220.3	20
Ti	II	334.9	1
V	II	292.4	8
Zn	I	213.8[b]	1

a) I and II indicate atomic and ionic lines, respectively. b) The 2nd order lines were used.

and HNO_3 used for resin purification and column conditioning were prepared by sub-boiling the acids of extra pure grade. Pure water for ordinary use was deionized/distilled water, and it was further purified by sub-boiling distillation when necessary. Ammonium acetate was prepared by mixing ammonium solution and acetic acid, and was purified by passing 2 times through the Chelex-100 column. Chelex-100 resin (200—400 mesh) was purchased from Bio Rad Laboratories, U.S.A. Before packing the resin in the column, the resin was kept for cleaning in 5 M HCl five times for 5 d, and then with pure water, 2 M HNO_3, and finally pure water. The HCl solution used for the resin cleaning was changed with new one everyday. The artificial seawater used for the recovery test was prepared after the prescription reported by Kester *et al.*[21] It contained 13 constituents whose concentrations

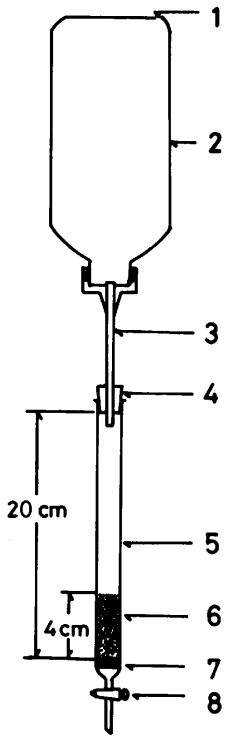

Fig. 1. Apparatus for preconcentration of trace elements in seawater.
1: Pin hole (0.5 mmφ), 2: Polyethylene bottle (1 l), 3: Polyethylene tube, 4: Silicone rubber stopper, 5: Glass column (14 mm I.D.), 6: Chelex-100 resin (200—400 mesh), 7: porous glass (pore size=35 μm), 8: Teflon stopcock.

are higher than 1 mg/l, and its salinity was adjusted at 35‰.

Column Preparation. The column system used is shown schematically in Fig. 1. The inner diameter of the column was 14 mm. A polyethylene bottle for the sample reservoir was connected with the column through the polyethylene tube. To avoid contamination the column system was designed as a closed one from the atmosphere, just being open to the air *via* a pin hole in the sample reservoir and a column outlet. Sample flow rate was controlled by the stopcock. All parts of the column were well precleaned with 1:1 HNO_3 and pure water. The Chelex-100 resin (dry weight 2.5 g) was packed in the column. The packed column was preconditioned with 10 ml of 2 M ammonium solution, 30 ml of sub-boiled pure water, and 20 ml of 1 M ammonium acetate buffer solution (pH 6) prior to each use. The length of the preconditioned resin in the column was about 40 mm.

Preconcentration Procedure. One liter of a seawater sample was filtered with Nuclepore filter (pore size 0.4 μm) and the pH of the solution was adjusted to pH 5.5—6 with 10 ml of 1 M ammonium acetate solution. The seawater sample was then taken into the sample reservoir and eluted at a flow rate of 2 ml/min through the preconditioned column. For removal of matrix salts the column was treated with 100 ml of 1 M ammonium acetate buffer (pH 6) and 50 ml of sub-boiled pure water after each seawater elution. Trace metals collected on the resin were then eluted with 25 ml of 2 M HNO_3 solution into a PTFE

beaker. The eluent in the beaker was heated to dryness on a hot plate, and then the residue was dissolved with 5 ml of 0.2 M HNO_3. Thus a 200-fold concentrated solution (hereafter called "analysis solution") was prepared for ICP-AES measurement. In case of the recovery test, the eluent was filled up to 50 ml with pure water.

Results and Discussion

pH Dependence of Calcium and Magnesium Concentrations in the Analysis Solution. In ICP-AES measurement, high concentrations of matrix elements in the analysis solution are sometimes prone to spectral and physical interferences.[22,23] Since parts of Ca and Mg in seawater were collected on the Chelex-100 resin,[18] the effects of Ca and Mg on the emission intensities of analytes were investigated by aspirating the test solutions which contained Ca and Mg at various concentrations. The emission intensities observed for the test solutions included both spectral and physical interferences. The emission intensities due to spectral interference were first corrected by using the correction coefficients for spectral interference,[11,12] which were estimated by introducing pure Ca or Mg solution (lower than 200 mg/l) into the ICP. Then physical interference was estimated. When the total concentration of the two elements was 1600 mg/l, the intensities were reduced by 10%. When their total concentration was smaller than 200 mg/l, the intensity changes due to the influences of nebulization process were negligibly small. Therefore, it was desirable that the total concentration of matrix elements was less than 200 mg/l.

The concentrations of Ca and Mg collected on 1 g resin are shown as a function of pH in Fig. 2. These values were obtained with artificial seawater which contained matrix elements at the same concentration levels as natural seawater, *i.e.*, 1350 mg of Mg/l and 400 mg of Ca/l. The concentrations of Ca and Mg on the resin increased at higher pH. The results agreed well with those reported previously.[24] When 2.5 g resin was used and the 200-times preconcentration was made even at pH 3, the concentrations of Mg and Ca in the final analysis solution were 2500 mg/l and 1200 mg/l, respectively. Matrix elements at such high concentration levels may seriously influence the analytical results in ICP-AES due to their spectral and physical interferences. Therefore, a proper procedure to remove matrix elements on the resin was necessary prior to elution of analyte elements.

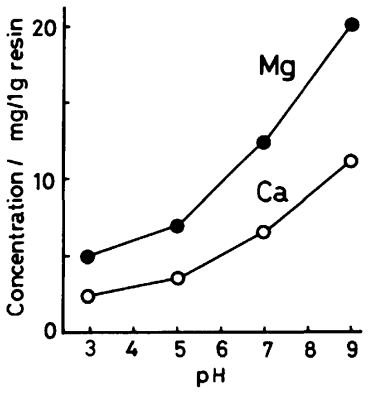

Fig. 2. pH Dependence of concentrations of Ca and Mg in 1 g resin after column preconcentration. The original concentrations of Ca and Mg were 400 mg/l and 1350 mg/l, respectively, which were the same as those in seawater.

Removal of Matrix Elements with Ammonium Acetate Buffer Solution. Kingston *et al.* reported that Mg and Ca retained on the resin could be removed by ammonium acetate solution.[19] However, excess amounts of ammonium acetate solution may cause loss of analytes.[20] In Table 3, the effect of ammonium acetate solution (pH 6) on removal of matrix elements are summarized. The values in the table are the concentrations in 50 ml of the eluent, when 1 l of artificial seawater was treated with the chelating resin column. As can be seen in Table 3, the concentrations of matrix elements were lowered remarkably when the volume of the buffer solution for washing was increased. In the analysis of natural seawater, the volume of the final analysis solution was 5 ml. Thus the concentration values should be multiplied by ten. Therefore, at least 100 ml of 1 M ammonium acetate buffer solution (pH 6) is required in treatment of natural seawater samples. Fortunately, the recoveries of all the elements were not affected by using the ammonium acetate buffer solution up to 100 ml. Thus 100 ml of the ammonium acetate solution was used for removal of matrix elements in natural seawater samples.

pH Dependence of Recoveries of Analytes. In Fig. 3, pH dependences of recoveries of Cu and Mn are shown. Since Cu has the largest stability constant and Mn has the smallest one with Chelex-100 resin, these two elements among fifteen elements were chosen as representative examples. In Fig. 3 the values indicated by black and white circles show the

Table 3. Concentrations (mg/l) of matrix elements in the 50 ml eluent after washing with various volumes of ammonium acetate buffer

Element	Volume of buffer[a] (ml)				
	0	50	100	200	300
Ca	337	18.6	3.1	0.9	0.6
Mg	500	11.1	4.5	2.0	1.2
Na	137	10.1	5.2	2.7	1.6
K	6	0.3	0.2	0.1	0.06

a) 1 M CH_3COOH/CH_3COONH_4 (pH 6) was used.

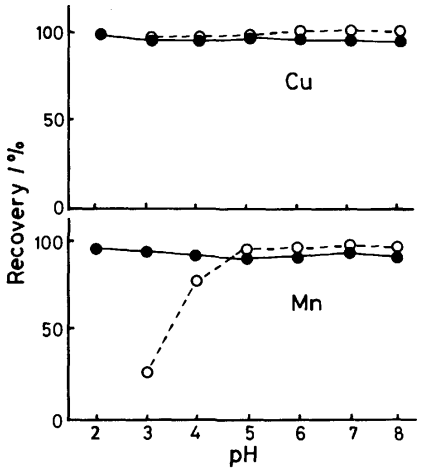

Fig. 3. pH Dependence of recoveries for Cu and Mn.
Black circles (●) indicate the values for pure water sample without washing with buffer solution.
White circles (○) indicate the values for artificial seawater after washing with 100 ml of 1 M ammonium acetate buffer solution.
The original concentrations of Cu and Mn were 100 μg/l.

experimental results for acidified water and artificial seawater used as the samples, respectively. Both solutions contained all the analytes at a concentration of 0.1 mg/l. In the case of artificial seawater the resin was treated with ammonium acetate buffer in order to remove the matrix elements. The pH dependences of recoveries for Al, Cd, Co, Fe, Mo, Ni, Pb, Ti, V, and Zn in acidified water was similar to those for Cu and Mn, *i.e.*, constant recoveries more than 90% in the pH range of 2—8. The pH dependences of the recoveries for As and Cr, however, were greatly different from those for the other elements, being less than 90% at any pH.

On the other hand, Mn in artificial seawater showed poor recovery at pH lower than 5 (see Fig. 3). The same deterioration in recovery from artificial seawater was also observed for Cd. Other elements such as Al, Co, Fe, Mo, Ni, Pb, Ti, V, and Zn showed constant recoveries similar to Cu (see Fig. 3). As mentioned previously, the concentrations of Ca and Mg in the analysis solution increased with pH, and so treatment with a large volume of ammonium acetate solution was needed for the removal of salts in the higher pH region. Thus pH 5.5—6 was chosen for preconcentration of the natural sample, which allowed efficient preconcentration of 12 elements including Mn and Cd on the chelating resin.

Recovery, Blank, and Detection Limits. The recovery and standard deviation obtained by the present method are summarized in Table 4. As can be seen in the table, the reproducibility in preconcentration is good for almost all elements except As and Cr. The poor reproducibilities of As and Cr may be caused by their poor recoveries in the column concentration, while other elements were quantitatively collected on the Chelex-100 resin with recoveries greater than 90%.

When natural seawater sample was analysed, the HNO_3 eluent from the column was heated to dryness. The recovery values including the drying process were examined by using artificial seawater which

TABLE 4. RECOVERIES OF METAL ELEMENTS ADDED TO SEAWATER OBTAINED BY CHELEX-100 PRECONCENTRATION AND ICP-AES METHOD

Element	Added	A[a] Recovery	A[a] C.v. (n=3)	B[b] Recovery
	μg	%	%	%
Al	100.2	97.6	4.0	92.7
As	100.7	7.3	6.8	—[c]
Cd	113.9	94.7	1.3	96.4
Co	100.5	95.9	2.1	95.0
Cr^{3+}	106.6	67.9	7.9	62.6
Cr^{6+}	103.5	32.7	—[d]	—[c]
Cu	102.9	100.2	0.7	97.1
Fe	99.0	98.1	2.7	93.0
Mn	101.4	98.7	2.2	96.8
Mo	92.8	90.5	—[d]	—[c]
Ni	102.5	96.5	1.3	97.1
Pb	96.8	92.6	0.8	97.9
Ti	100.0	96.8	1.3	92.4
V	100.1	95.4	1.8	—[c]
Zn	102.7	95.8	1.0	96.7

a) The 1 l seawater sample was concentrated to 50 ml without evaporation. b) The 1 l seawater sample was concentrated to 5 ml with evaporating the eluent to dryness. c) Not observed. d) Not estimated.

TABLE 5. BLANK AND ANALYTICAL DETECTION LIMITS

Element	Blank[a]	Analytical detection limit[a]
	μg/l	μg/l
Al	0.8	0.05
Cd	<0.02	0.02
Co	<0.02	0.02
Cr	<0.04	0.04
Cu	<0.01	0.01
Fe	0.08	0.02
Mn	0.004	0.003
Mo	0.02	0.02
Ni	<0.05	0.05
Pb	<0.1	0.1
Ti	<0.005	0.005
V	<0.04	0.04
Zn	0.08	0.005

a) Estimated for analysis solution with 200 fold concentration.

contained the analytes at the same levels as those in Table 4. The results are shown in the last column of Table 4. It can be seen that the recoveries of the analytes did not significantly deteriorate through drying.

Blank and detection limits in the present method were summarized in Table 5. The blank values were obtained by performing the same preconcentration procedure using 100 ml of sub-boiled pure water and were converted to the concentration corresponding to 1 l of an original sample. The analytical detection limits were calculated by dividing the detection limits (Table 2) for analytes by the concentration factor (200). As for Cd, Co, Cr, Cu, Ni, Pb, Ti, and V, the blank values were lower than the analytical detection limits. This may have resulted from the use of the well-closed column system, purification of chemicals, and a class-100 clean air system. The blank values for Al, Fe, and Zn were larger than the analytical detection limits. For these elements corrections of the blank values were carried out in the actual seawater analysis.

Application to Natural Seawaters. In Table 6 the analytical results for natural seawaters which were sampled on the cruises of the Tansei-Maru research vessel (the Ocean Research Institute, University of Tokyo) and the Toyoshio-Maru research vessel (Faculty of Applied Biological Science, Hiroshima University) are summarized. The analytical results for most elements except Mo in the ocean seawater sample were lower than those in the coastal seawater samples. The concentration levels in the ocean seawater were similar to those reported by Turekian *et al.*[25] The concentrations of Al, Fe, and Ti in the Seto Inland Sea water were much larger than those in the Tokyo Bay water.

The analytical results for several elements in seawater from the Tokyo Bay were compared with those obtained by the gallium coprecipitation method.[11] The concentrations of Al, Ni, Fe, Mn, and Zn obtained by the two analytical methods were consistent with each other. This indicates that the present method is accurate enough to apply to the multielement determination of trace metals in seawater.

TABLE 6. ANALYTICAL RESULTS FOR TRACE METALS IN NATURAL SEAWATERS[a]

Element	Concentration/μg/l			
	North Pacific Ocean	Inland Sea of Japan	Tokyo Bay[b]	
Al	2.6	93.9	11.0	(14.1)
Cd	<0.02	0.04	0.06	
Co	<0.02	0.15	0.30	
Cu	0.07	1.08	1.01	
Fe	0.28	67.1	9.46	(11.8)
Mn	0.04	5.73	5.69	(6.2)
Mo	10.6	9.32	9.38	
Ni	0.25	0.45	40.8	(41.0)
Pb	0.2	5.0	1.1	
Ti	0.01	2.48	0.23	(0.60)
V	2.98	3.32	3.26	
Zn	0.52	4.79	4.33	(5.3)

a) The seawater samples were stored after acidifying at pH 2 with HNO_3. b) The values in parenthesis were obtained by ICP-AES using gallium coprecipitation (Ref. 11).

Conclusion

The present Chelex-100 resin column method is convenient and effective for multielement preconcentration of trace metals in seawater. Ammonium acetate buffer solution reduced the concentration of remaining salts on the resin low enough so as to obtain a large concentration factor of 200 for the ICP-AES determination. Therefore, the present method can be successfully applied to determine trace metals such as Al, Cd, Co, Cu, Fe, Mn, Mo, Ni, Pb, Ti, V, Y, and Zn in coastal and open seawater. However, it does take about 9 h for one sample treatment by the column method, which may not be useful in routine analysis of seawater. A more efficient treatment system using the chelating resin, for example, a flow or batch preconcentration system is therefore required in such ICP-AES analysis.

The authors thank Prof. Keiichiro Fuwa in the University of Tokyo for his kind encouragement and valuable discussion. We also express our thanks to Prof. Hitoshi Sakai and his staff at the Ocean Research Institute in the University of Tokyo, and also to Prof. Hiroyuki Tsubota in the University of Hiroshima for their help in seawater sampling and valuable discussion. We are owed to Ms. J. E. Teague in preparation of the manuscript.

This research has been supported by the Grant-in-Aid for Scientific Research (No. 59470024) from the Ministry of Education, Science and Culture (1985).

References

1) K. Yoshimura, S. Nigo, and T. Tarutani, *Talanta*, **27**, 693 (1980).

2) L.-G. Danielsson, B. Magnusson, S. Westerlund, and K. Zhang, *Anal. Chim. Acta*, **144**, 183 (1982).

3) R. E. Sturgeon, S. S. Berman, A. Desaulniers, and D. S. Russell, *Talanta*, **27**, 85 (1980).

4) K. Fujiwara, S. Toda, and K. Fuwa, *Bull. Chem. Soc. Jpn.*, **54**, 3209 (1981).

5) C. Brihaye, G. Gillain, and G. Duyckaerts, *Anal. Chim. Acta*, **148**, 51 (1983).

6) A. P. Mykytiuk, D. S. Russell, and R. E. Sturgeon, *Anal. Chem.*, **52**, 1281 (1980).

7) K. Jørstad and B. Salbu, *Anal. Chem.*, **52**, 672 (1980).
8) F. Clanet, R. Deloncle, and G. Popoff, *Water Res.*, **15**, 591 (1981).
9) A. Miyazaki, A. Kimura, K. Bansho, and Y. Umezaki, *Anal. Chim. Acta*, **144**, 213 (1982).
10) C. W. McLeod, A. Otsuki, K. Okamoto, H. Haraguchi, and K. Fuwa, *Analyst (London)*, **106**, 419 (1981).
11) T. Akagi, K. Fuwa, and H. Haraguchi, *Anal. Chim. Acta*, in press.
12) T. Akagi, M. Matsui, Y. Nojiri, and H. Haraguchi, *Appl. Spectrosc.*, **39**, 662 (1985).
13) S. S. Berman, J. W. McLaren, and S. N. Willie, *Anal. Chem.*, **52**, 488 (1980).
14) H. Watanabe, K. Goto, S. Taguchi, J. W. McLaren, S. S. Berman, and D. S. Russell, *Anal. Chem.*, **53**, 738 (1981).
15) E. W. Davey and A. E. Soper, "Analytical Method in Oceanography," ed by T. R. P. Gibbs, Jr., Adv. Chem. Ser., American Chem. Soc., Washington, D. C. (1975), p. 147.
16) T. M. Florence and G. E. Batley, *Talanta*, **23**, 179 (1976).
17) T. M. Florence and G. E. Batley, *Talanta*, **24**, 151 (1977).
18) J. P. Riley and D. Taylor, *Anal. Chim. Acta*, **40**, 479 (1968).
19) H. M. Kingston, I. L. Barnes, T. J. Brady, T. C. Rains, and M. A. Champ, *Anal. Chem.*, **50**, 2064 (1978).
20) R. E. Sturgeon, S. S. Berman, J. A. H. Desaulniers, A. P. Mytytiuk, J. W. McLaren, and D. S. Russell, *Anal. Chem.*, **52**, 1585 (1980).
21) D. R. Kester, I. W. Duedall, D. N. Connors, and R. M. Pytkowicz, *Limnol. Oceanogr.*, **12**, 176 (1967).
22) S. Greenfield, H. McD.-McGeachin, and P. B. Smith, *Anal. Chim. Aca*, **84**, 67 (1976).
23) A. Sugimae, *Bunseki Kagaku*, **28**, 555 (1979).
24) K. Kawabuchi, M. Kanke, T. Muraoka, and M. Yamauchi, *Bunseki Kagaku*, **25**, 213 (1976).
25) M. S. Q.-Hunt and K. K. Turekian, *EOS*, **64**, 130 (1983).

X-Ray Diffraction, Raman, and NMR Studies on Tetrathiocyanato Complexes of Zinc(II), Cadmium(II), and Mercury(II) Ions in Aqueous Solution

Toshio YAMAGUCHI, Kiyoshi YAMAMOTO, and Hitoshi OHTAKI*
Department of Electronic Chemistry, Tokyo Institute of Technology, Nagatsuta, Midori-ku, Yokohama 227
(Received May 27, 1985)

X-Ray scattering, Raman, and ^{13}C- and ^{14}N-NMR measurements were performed on aqueous solutions containing tetrathiocyanato complex ions of Zn(II), Cd(II), and Hg(II). The radial distribution functions revealed that four thiocyanate ions tetrahedrally coordinated to Zn(II) and to Hg(II) ions through the N and S atoms, respectively, while Cd(II) ion was bound to two sulfur and two nitrogen atoms within the coordinated four SCN^- ions. The bond distances and bond angles are as follows: Zn-N 204 pm, Cd-N and Cd-S 225 and 265 pm, respectively, and Hg-S 254 pm, and Zn-N-C 145°, Cd-N-C and Cd-S-C 149° and 106°, respectively, and Hg-S-C 102°. The Raman bands of the C-S vibration within the tetrathiocyanato complexes of Zn(II), Cd(II), and Hg(II) ions in aqueous solutions appeared at 821 and 710 cm^{-1} for the Zn(II) and Hg(II) complexes, respectively, consistent with the values in the literature. The C-S stretching Raman bands of tetrathiocyanatocadmate(II) complex were resolved into two components at 779 and 732 cm^{-1}. The C-S frequency shifted toward the higher frequency side than that (747 cm^{-1}) of the free SCN^- ion in the case of the binding of SCN^- to metal ion *via* the N atom in the Zn(II) and Cd(II) cases, while the C-S bands influenced by the M-S bonding appeared on the lower frequency side in the Cd(II) and Hg(II) complexes. The ^{13}C chemical shifts of the tetrathiocyanato complexes in aqueous solutions showed the downfield and upfield shifts for Zn(II) and Hg(II), respectively, and the intermediate for Cd(II). The nitrogen-14 resonance in $[M(SCN)_4]^{2-}$ in aqueous solutions shifted upfield (−30.8 ppm) for Zn(II), downfield (30.3 ppm) for Hg(II), and in between for Cd(II) (−1.3 ppm). The trend of the ^{13}C- and ^{14}N-chemical shifts supported the different types of binding of ambient SCN^- ion deduced from the X-ray and Raman measurements.

Complex formation between thiocyanate ions and different metal ions has widely been investigated from interesting ambient nature of SCN^- ion, which can bind with metal ions through either the nitrogen or the sulfur atom depending on the central cation involved. Among these studies, thiocyanato complexes of the Group IIb metals are of particular interest,[1-21] since Hg(II) and Zn(II) ions behave as soft and hard acids, respectively, and Cd(II) ion has an intermediate character. From recent X-ray diffraction and Raman spectral studies[21] on the thiocyanate complexes of Zn(II), Cd(II), and Hg(II) ions in combination with the thermodynamic data[7] in dimethyl sulfoxide (DMSO), it has been established that thiocyanate ions coordinate to both Hg(II) and Cd(II) ions through the sulfur atom, but to Zn(II) ion through the nitrogen atom.

Formation of the thiocyanato complexes of Zn(II), Cd(II), and Hg(II) ions in aqueous solution has also been studied by thermodynamic,[1-5] Raman and infrared methods.[8-14] The results obtained from these studies are consistent with the conclusion that thiocyanate ions bind with Hg(II) ion through the sulfur atom, but to Zn(II) ion through the nitrogen atom, giving in both cases mononuclear species up to the tetra-complex. However, the coordination site of thiocyanato groups to Cd(II) ion in aqueous solution is still not conclusive.

Fronaeus and Larsson[9] interpreted two C-N absorption bands at 2098 and 2132 cm^{-1} in terms of the presence of mononuclear and bridged polymer species, respectively, in aqueous solutions having lower molar ratios of thiocyanate to cadmium ions. Taylor *et al.*[11] measured Raman spectra of the tetrathiocyanatocadmate(II) complex in aqueous solutions, suggesting that some SCN^- ions bound to Cd(II) through the N and some through the S atoms in the Cd(II) complex. In a recent Raman spectral measurement of thiocyanato complexes of Cd(II) ion in aqueous solutions, Antić-Jovanović *et al.*[14] assigned the band at 2132 cm^{-1} to the $[Cd(SCN)]^+$ complex, while the bands appearing at 2102 and 784 cm^{-1} were attributed to higher members of the stepwise $[Cd(NCS)_n]^{2-n}$ series. Their conclusion for the binding type of SCN^- to Cd(II) ions is consistent with that by Taylor *et al.*[11]

In crystal of $Cd(SCN)_2$,[18] a cadmium(II) ion is octahedrally surrounded by four sulfur and by two *trans*-nitrogen atoms with a slightly distorted geometry. In β-$Zn(NCS)_2$ crystal,[19] there are two crystallographically different Zn(II) ions, the one surrounded tetrahedrally by four N atoms and the other by four S atoms.

In the present study, we aimed at determining the structure of the tetrathiocyanato complex of Cd(II) ion in aqueous solution to clarify the type of binding of SCN^- ion by the X-ray diffraction, Raman, and NMR methods. The structure of tetrathiocyanato complexes of Zn(II) and Hg(II) ions in aqueous solution has also been determined for comparison.

Experimental

Preparation of Sample Solutions. If not otherwise

TABLE 1. THE COMPOSITION (mol/dm³), DENSITY d (g/cm³) AND STOICHIOMETRIC VOLUME V (10^6 pm³) PER SCN OF THE SAMPLE SOLUTIONS INVESTIGATED

	A	B	C	D
	Hg(II)	Cd(II)	Zn(II)	NH_4^+
M^{2+}	0.979	1.04	1.00	—
NH_4^+	5.02	5.04	5.03	7.12
SCN^-	6.98	7.12	7.03	7.12
H_2O	33.7	34.0	33.4	31.6
d	1.30	1.23	1.17	1.11
V	2.38	2.33	2.36	2.33

stated, all chemicals used were of analytical reagent grade purchased from Wako Pure Chemical Industries, Ltd.

Zinc(II) thiocyanate was prepared by reacting zinc(II) sulfate with a stoichiometric amount of barium(II) thiocyanate which had been recrystallized twice from water. Zinc(II) thiocyanate thus prepared was then recrystallized from water.

Cadmium(II) thiocyanate was prepared from cadmium(II) perchlorate and ammonium thiocyanate, the former reagent having been prepared by dissolving cadmium(II) oxide in an aqueous perchloric acid solution and then recrystallized twice from water. Cadmium(II) thiocyanate thus obtained was recrystallized twice from water.

Mercury(II) thiocyanate commercially available was recrystallized twice from water.

Ammonium thiocyanate purchased was used without further purification.

The sample solutions investigated were prepared by dissolving required amounts of zinc(II), cadmium(II), mercury(II), and ammonium thiocyanates in water so that the tetrathiocyanato species was predominantly formed according to thermodynamic data[1-5] in the literature which were assumed to be valid in relatively concentrated sample solutions. Density of the solutions was determined pycnometrically.

The composition of the solutions used for X-ray diffraction measurements is given in Table 1. The same samples were used for Raman and NMR studies.

X-Ray Data Collection. X-Ray scattering measurements were carried out at 23 °C with a JEOL θ-θ diffractometer by using Mo$K\alpha$ radiation (λ=71.07 pm). The scanning range of the scattering angle (2θ) was 2—140°, corresponding to the scattering vector $3\times10^{-3}< s/\mathrm{pm}^{-1}<0.16$ ($s=4\pi\sin\theta/\lambda$). Different slit combinations and step angles were used and a total amount of 80000 counts was collected at each angle. Details of the diffractometer and the method of measurements have been described elsewhere.[22,23]

Raman Measurements. Raman spectra of the sample solutions used in the X-ray measurements were recorded at room temperature on a JEOL JRS-SI spectrometer using the 514.5 nm line of NEC GLG3200 argon ion laser.

NMR Measurements. ^{13}C-NMR spectra of the sample solutions were obtained at room temperature in the pulsed Fourier transform mode at 25.00 MHz on a JEOL FX-100 spectrometer. ^{14}N-NMR spectra were measured at 7.14 MHz. Small amounts of deuterium oxide as the internal lock and DDS (sodium 2,2-dimethyl-2-silapentane-5-sulfonate) as the internal standard were added to the sample solutions.

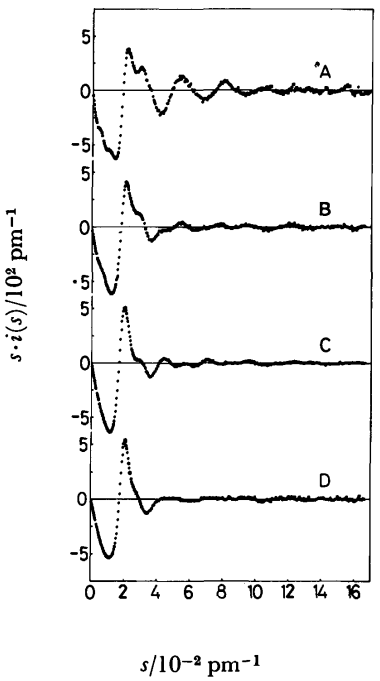

Fig. 1. Experimental structure functions $i(s)$ multiplied by s of aqueous solutions of mercury(II) thiocyanate (A), cadmium(II) thiocyanate (B), zinc(II) thiocyanate (C), and ammonium thiocyanate (D).

X-Ray Data Treatment. Experimental intensities were corrected for background, absorption, polarization, double scattering and Compton scattering and were scaled to absolute units in the usual manners described elsewhere.[22-26] The scattering factors of neutral atoms and the values for the Compton scattering and the anomalous dispersion effect were taken from the same sources previously described.[26]

The structure function $i(s)$ was obtained by

$$i(s) = I(s) - \Sigma x_j f_j^2(s), \quad (1)$$

where $I(s)$ is the scaled observed intensities, f_j the scattering factor of the jth atom corrected for anomalous dispersion and x_j the number of the jth atom in the stoichiometric volume containing one SCN^- ion. The structure functions of the sample solutions multiplied by s are shown in Fig. 1.

The radial distribution function was calculated by the Fourier transform of the $s\cdot i(s)$ values using the equation,

$$D(r) = 4\pi r^2\rho_0 + (2r/\pi)\int_{s_{min}}^{s_{max}} s\cdot i(s)M(s)\sin(rs)\mathrm{d}s. \quad (2)$$

Here, $M(s)$ is the modification function $[\Sigma x_j f_j(0)^2/\Sigma x_j f_j(s)^2]\exp(-0.01\ s^2)$, s_{min} and s_{max} denote, respectively, the lower and upper limits of the s values available in the experiments. The resulting $D(r)$ values are plotted in Fig. 2. All the calculations were performed by program KURVLR.[27]

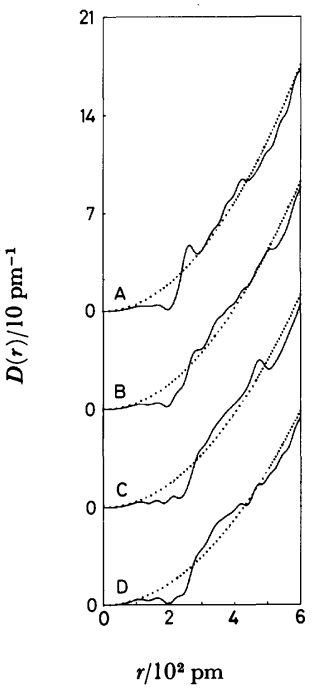

Fig. 2. Radial distribution functions $D(r)$ (solid lines) derived from the curves shown in Fig. 1. Dots show the values of $4\pi r^2\rho_0$.

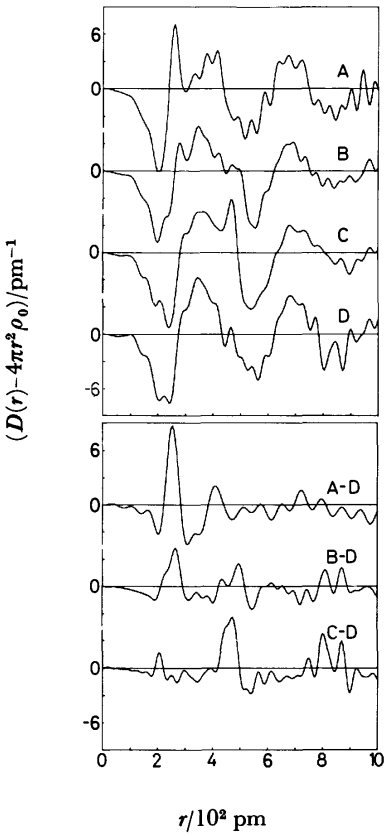

Fig. 3. Radial distribution functions of the form $D(r) - 4\pi r^2\rho_0$ derived from the curves in Fig. 1 (above). The figures below are the difference RDFs obtained by subtraction of curve (D) from curves (A), (B), and (C).

Results

X-Ray Radial Distribution Functions (RDFs). The total RDFs in the form of $D(r)-4\pi r^2\rho_0$ of Hg(II), Cd(II), Zn(II), and ammonium thiocyanate aqueous solutions of the stoichiometric volume per SCN ion are shown in Fig. 3 (upper figure). The peaks arising from the structure of SCN^- ion should appear at 120 pm (C-N), 165 pm (C-S), and 280 pm (S···N)[18-21] in all the RDFs. As is seen in Fig. 3 A through D, however, the large broad peak at 250—550 pm due to the hydration of SCN^- ion and the bulk water structure is dominant in the RDFs with distinct peaks at 255, 260, and 490 pm, respectively, in the RDFs of Hg(II), Cd(II), and Zn(II) thiocyanate solutions.

In order to extract the peaks originating from Hg(II), Cd(II), and Zn(II) thiocyanato complexes in the solutions, the RDF of NH_4SCN solution (Fig. 3 D) was subtracted from those of the metal thiocyanate solutions. Since an ammonium ion has a similar size as a water molecule and all the sample solutions contain an almost equal amount of SCN^- ions as well as the sum of $[NH_4^+]+[H_2O]$ (see Table 1), the bulk structure and the hydration structure of SCN^- ion may be similar in all the solutions at the first approximation. Thus, in the differences between the total RDFs A, B, or C and D (Fig. 3 lower figures, abbreviated as A-D, B-D, and C-D), the contribution of the bulk water and the SCN^- hydration structure is mostly eliminated and hence the peaks due to the metal thiocyanato complexes in the solutions are emphasized.

In the difference RDF of Hg(II) thiocyanate solution there are two peaks centered at 254 and 415 pm (Fig. 3 A-D). From the sum of the covalent radii of Hg and S (148 and 104 pm,[28] respectively) and the mean Hg-S bond length of 255 pm reported in a structure determination of $[Hg(SCN)_4][Cu(en)_2]$ crystal,[20] the first peak at 254 pm can be assigned to the Hg-S bonds within $[Hg(SCN)_4]^{2-}$. In the crystal structure of $[Hg(SCN)_4][Cu(en)_2]$, nonbonding Hg···N and interligand S···S interactions appear around 400 and 420 pm, respectively, and hence they are possibly responsible for the peak at 415 pm in the difference RDF of the Hg(II) thiocyanate solution.

In the case of Zn(II) thiocyanate solution, the difference RDF shows the distinct peaks at 204 and 462 pm. On the basis of the effective ionic radii of Zn and N atoms (60 and 146 pm[29], respectively) and the knowledge of the mean Zn-N (200 pm) and nonbonding Zn···S lengths (470 pm) within the $[Zn(NCS)_4]^{2-}$ moiety in β-$Zn(SCN)_2$ crystal,[19] the peaks around 204 and 462 pm are assignable to the Zn-N and Zn···S interactions within $[Zn(NCS)_4]^{2-}$, respectively.

The difference RDF of Cd(II) thiocyanate solution is more complex with peaks at 265, 435, and 490 pm with a shoulder at 225 pm. The values of 225 and 265 pm coincide well, respectively, with the sum of the effective ionic radii of Cd and N, and of Cd and S (Cd: 78 pm, N: 146 pm, S: 184 pm[29]). In the crystal structure of $Cd(SCN)_2$ having two Cd-N and four Cd-S bonds,[18] the Cd-N and Cd-S distances have been reported to be 224—225 and 271—280 pm, respectively. On the basis of these facts, it can be concluded that the peak at 265 pm with the shoulder at 225 pm consists of both Cd-S and Cd-N bonds within $[Cd(SCN)_4]^{2-}$ in the aqueous solution.

Model Calculations. A quantitative analysis of the X-ray scattering data was performed by comparing experimental values with theoretical ones calculated by a model both in the difference RDFs and in the difference structure functions.

A theoretical structure function of atom pair "i—j" was calculated by the Debye equation,

$$i(s)_{\text{calcd}} = n_{ij}f_i(s)f_j(s)\sin(sr_{ij})/(sr_{ij})\exp(-b_{ij}s^2), \quad (3)$$

where r_{ij}, b_{ij}, and n_{ij} represent the interatomic distance, the temperature factor and the number of interactions, respectively. The corresponding peak shape is obtained by the Fourier transform of the $s \cdot i(s)_{\text{calcd}}$ values using Eq. 2.

Firstly, the difference RDFs of Zn(II), Cd(II), and Hg(II) thiocyanate solutions were analyzed. In the difference RDF of the Hg(II) system (Fig. 3 A-D), the peak shape calculated for four Hg-S interactions was compared reasonably with the contour of the first peak at 254 pm, suggesting the tetrahedral coordination of four SCN^- ions to Hg(II). On the basis of the tetrahedral geometry of the $[Hg(SCN)_4]^{2-}$ complex, the interligand S···S interaction was estimated to be 415 pm, a corresponding peak appearing at 417 pm in the difference RDF. The nonbonding Hg···N interaction should also appear around 417 pm according to the crystal structure of $[Hg(SCN)_4]$-$[Cu(en)_2]$.[20] The distance of the Hg···C interactions within the $[Hg(SCN)_4]^{2-}$ complex in the solution was also estimated to be 330 pm from the crystal structure data.[20] The peak shapes calculated for these atom pairs are shown in Fig. 4. Subtraction of the sums of the peak shapes from the difference RDF gave the residue shown by dots in Fig. 4. Thus, the difference RDF of the Hg(II) thiocyanate solution was satisfactorily explained by the tetrahedral coordination model of four SCN^- ions to Hg(II) through the S atom.

A similar analysis applied to the difference RDF of the Zn(II) thiocyanate solution resulted in four Zn-N bonds from the area of the first peak at 204 pm. Four Zn···S interactions also explained satisfactorily the distinct peak at 460 pm. On the basis of the Zn-N and Zn···S distances with a linear SCN^- ion, the Zn···C interaction was expected to appear 310 pm, consistent well with the peak at 310 pm in the difference RDF (Fig. 5). The theoretical peak shapes due to the Zn-N, Zn···C, Zn···S, and interligand N···N interactions were calculated for the tetrahedral model of the $[Zn(NCS)_4]^{2-}$ complex and subtracted from the difference RDF. In the resulting residue shown by dots in Fig. 5, a small and broad peak still remains at 350—500 pm, which may be attributable to other interligand interactions such as N···C, N···S, C···S, and S···S. Small ripples left at 200—300 pm may be physically insignificant features judging from uncertainties in the difference RDF.

In the case of the Cd(II) thiocyanato complex, the first peak at 200—300 pm was analyzed by a trial-and-error method assuming various combinations of Cd-N and Cd-S interactions, and the most likely

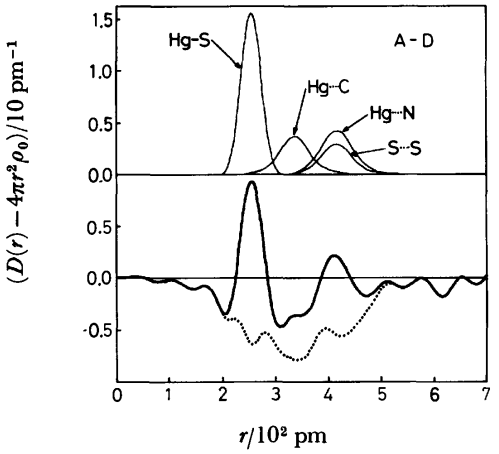

Fig. 4. Difference RDF of aqueous mercury(II) thiocyanate solution (solid line, below) obtained in Fig. 3A, and the residue (dots, below) obtained after subtraction of the peak shapes (solid line, above).

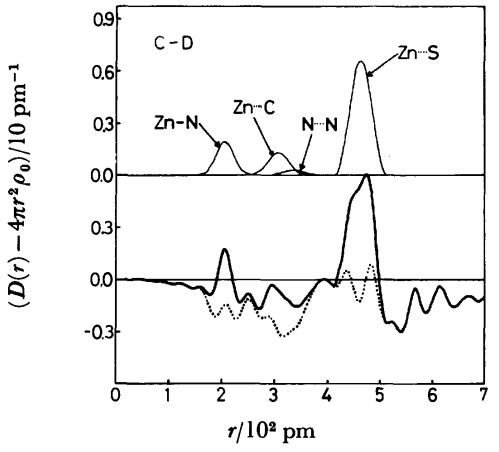

Fig. 5. Difference RDF of aqueous zinc(II) thiocyanate solution (solid line, below) obtained in Fig. 3C, and the residue (dots, below) obtained after subtraction of the peak shapes (solid line, above).

model attained was the one with two Cd–N and two Cd–S bonds per Cd(II). Nonbonding Cd···N and Cd···S interactions were assigned to the peaks at 440 and 490 pm, respectively, from the structural data of $Cd(SCN)_2$ crystal.[18] Cd···C and interligand N···N, S···S, and N···S distances were calculated from the tetrahedral geometry of the $[Cd(SCN)_4]^{2-}$ complex with the linear SCN^- ion coordinated and their peak shapes are shown in Fig. 6. Small peaks at 380—500 pm left after subtraction of the sum of the peak shapes from the difference RDF are probably related to other interligand interactions which were not taken into consideration. Since the X-ray scattering data can give the time- and space-averaged structure of a species, the present X-ray data for the Cd(II) thiocyanate solution could also be explained in terms of an equivalent mixture of $[Cd(SCN)_4]^{2-}$ having four Cd–S bonds and $[Cd(NCS)_4]^{2-}$ having four Cd–N bonds or a statistic mixture of $[Cd(NCS)_{4-n}(SCN)_n]^{2-}$ with the n value of 0 to 4. This problem will be discussed in more detail in a later section.

A direct comparison between experimental and theoretical difference structure functions was also performed by the least-squares method of minimizing the error square sum,

$$U = \sum_{s_{min}}^{s_{max}} s^2[\Delta i(s)_{obsd} - \Delta i(s)_{calcd}]^2. \quad (4)$$

Here, $\Delta i(s)_{obsd}$ denotes the difference structure functions experimentally obtained by subtraction of the total $i(s)$ values of NH_4SCN solution from those of metal thiocyanate solutions, s_{min} and s_{max} the lower and upper values of the s-range used in the calculations. Program NLPLSQ[30] was used for the calculations.

The model considered had the following characteristics.

(a) Four SCN^- ions coordinate to Zn(II) ion through the N atom, and to Hg(II) ion through the S atom. Cd(II) ion is bound with two SCN^- through the N atom, and the other two through the S atom.

(b) The interactions between atoms directly bonded to metal ion were taken into account by assuming the tetrahedral coordination of the atoms around the metal ion.

(c) The interactions between metal ion and the N or S atoms in SCN^- groups were defined by their interatomic distances, temperature factors, and number of interactions (=4), and the corresponding parameters r_{ij} and b_{ij} were allowed to vary independently with the coordination number fixed to the value of four. Parameters (r and b) due to the nonbonding M···C interactions were also allowed to vary in order to examine the deviation from the linearity of the SCN^- ions.

The final results of important parameters are summarized in Table 2. As shown in Fig. 7, the difference structure functions experimentally obtained are satisfactorily reproduced by the models, except for the data in the s-range less than 0.02 pm^{-1}, to which much longer interactions than those considered in the present models may contribute. On the basis of the M–N, M–C, and M–S distances within $[M(SCN)_4]^{2-}$, we see that the SCN^- ion within the complex has an almost linear structure.

Raman Spectra. Raman bands of the C–N and C–S stretching vibrations in the Zn(II), Cd(II), Hg(II), and ammonium thiocyanate solutions are shown by dots in Figs. 8 and 9, respectively.

A quantitative analysis of the Raman bands was performed by a nonlinear least-squares method by assuming the Lorentzian-Gaussian function expressed by

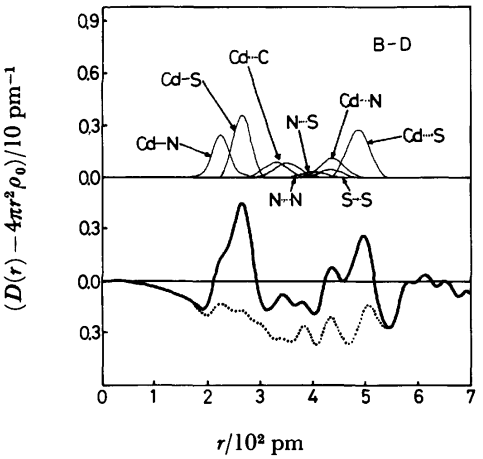

Fig. 6. Difference RDF of aqueous cadmium(II) thiocyanate solution (solid line, below) obtained in Fig. 3B, and the residue (dots, below) obtained after subtraction of the peak shapes (solid line, above).

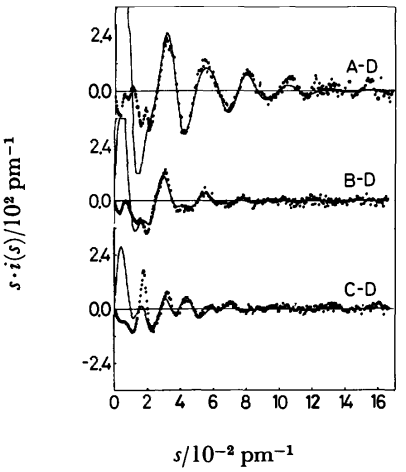

Fig. 7. Comparison between difference structure functions, $\Delta i(s)$, multiplied by s, and calculated values (solid lines) by the model with the parameter values given in Table 2. The symbols of the curves are the same as those used in Fig. 3.

TABLE 2. DISTANCES r (pm), TEMPERATURE FACTORS b (10^2 pm^2), NUMBER OF INTERACTIONS n AND THE BOND ANGLES (ϕ/°) USED IN THE MODEL CALCULATIONS DESCRIBED IN THE TEXT. THE ESTIMATED STANDARD DEVIATIONS ARE GIVEN IN PARENTHESES

		$[Hg(SCN)_4]^{2-}$	$[Cd(NCS)_2(SCN)_2]^{2-}$		$[Zn(NCS)_4]^{2-}$
M-N	r	415(4)	224.6(6)	435(2)	204.1(3)
	b	2.5[a]	0.25(8)	1.4(4)	0.30(5)
	n	4[a]	2[a]	2[a]	4[a]
M-C	r	335(4)	328(2)	349(3)	305[a]
	b	2.0[a]	1.5[a]	1.5[a]	1.0[a]
	n	4[a]	2[a]	2[a]	4[a]
M-S	r	253.5(5)	486.7(3)	264.9(3)	462(1)
	b	0.86(8)	1.8(2)	0.77(5)	1.5[a]
	n	4[a]	2[a]	2[a]	4[a]
N-N	r		367[b]		333[b]
	b		0.8[a]		1.0[a]
	n		1[a]		6[a]
S-S	r	414[b]	433[b]		414[b]
	b	2.5[a]	1.7[a]		2.5[a]
	n	6[a]	1[a]		6[a]
N-S	r		400[b]		
	b		1.5[a]		
	n		4[a]		
∠M-N-C			149(1)		145(1)
∠M-S-C		102(2)		106(1)	

a) Fixed. b) Assumed that ∠N-M-N= ∠N-M-S= ∠S-M-S=109.5°.

$$I(\nu) = I(\nu_0)[\exp\{-4\ln 2((\nu-\nu_0)/\sigma)^2\}\{1+(\nu-\nu_0)/\sigma\}^{-1}]^{1/2}, \quad (5)$$

where $I(\nu_0)$ denotes the peak height at the peak position ν_0, σ the half width. Parameters $I(\nu_0)$, ν_0, and σ were allowed to vary independently in the optimizing procedure.

Resolved peak components are shown by broken lines in Figs. 8 and 9, respectively, for the C-N and C-S bands. The sum of the components thus calculated is given by solid lines in the figures, which agrees well with the experimental values. The C-S and C-N frequencies thus determined are summarized in Table 3, together with those reported previously by other groups.[11,13,14]

As seen in Fig. 8, the C-N band at 2068 cm^{-1} observed in all the thiocyanate solutions is due to free SCN^- ion on the basis of the spectrum of the NH_4SCN solution. The higher C-N frequencies around 2100 cm^{-1} appearing in the metal thiocyanate solutions, the values of which agree well with those reported previously (Table 3),[11,14] are ascribed to SCN^- ions bound to a metal ion. As seen in Table 3, in the case of the bonding between SCN^- ion and a metal ion through the S atom, the C-N band appears at the higher frequency side than that of free SCN^- ion. The C-N frequency also increases when the

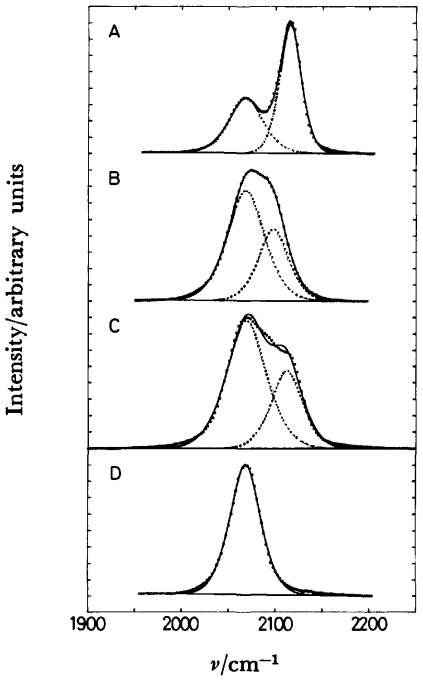

Fig. 8. Raman spectra of the C-N stretching bands of aqueous solutions of mercury(II) thiocyanate (A), cadmium(II) thiocyanate (B), zinc(II) thiocyanate (C), and ammonium thiocyanate (D). Dots represent the observed intensities and the solid line shows the sum of the components (broken lines) obtained by the least-squares fits.

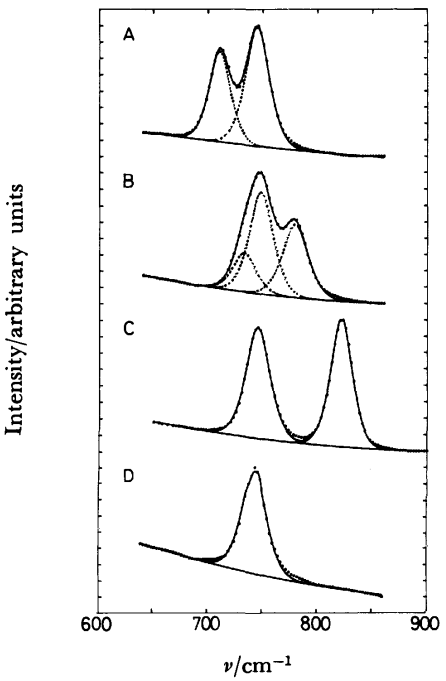

Fig. 9. Raman spectra of the C-S stretching bands of aqueous solutions of mercury(II) thiocyanate (A), cadmium(II) thiocyanate (B), zinc(II) thiocyanate (C), and ammonium thiocyanate (D). Dots represent the observed intensities and the solid line shows the sum of the components (broken lines) obtained by the least-squares fits.

Table 3. Raman frequencies of the C-S and C-N stretching bands of the tetrathiocyanato complexes of Hg(II), Cd(II), and Zn(II) ions in aqueous solutions

	Hg	Cd		Zn		
Binding atom	S	N	S	N	free SCN^- a)	Ref
C-S band	710	779	732	821	747	This work
	717	747		817	747	11)
				823	747	13)
		784			747	14)
C-N band	2117	2105		2114	2068	This work
	2114	2098		2110	2068	11)
		2102			2068	14)

a) Measured value in the present work.

nitrogen atom within SCN^- binds to a metal ion. Tramer[10] and Taylor *et al.*[11] have commented that the increasing C-N frequency on binding of SCN^- ion to a metal ion through the N atom is caused by the removal of repulsive interactions between the lone-pair electrons on the N atom. The shift of the C-N frequency thus is not applicable to specify the end atom of SCN^- bound to a metal ion.

On the other hand, the influence of complex formation between SCN^- and metal ions on the C-S frequency is more distinct (see Fig. 9 and Table 3). As seen in Fig. 9, the C-S frequency of SCN^- ions bound to a metal ion increases for the Zn(II) thiocyanate solution, but decreases for the Hg(II) system, relative to that of free SCN^- ion observed in the NH_4SCN solution. The C-S frequencies determined for the Zn(II) and Hg(II) thiocyanate solutions in the present analysis are in accordance with the previous values[11,13,14] and suggest that SCN^- ions are bound to Zn(II) ion through the N atom, and to Hg(II) ion through the S atom.

In the case of the Cd(II) thiocyanate solution, two C-S bands were observed at around 745 and 780 cm^{-1} (Fig. 9). These C-S frequencies have been reported in Refs. 11 and 14. However, a preliminary analysis of the C-S bands assuming two Lorentzian-Gaussian components failed, but the error square sum decreased significantly in the case of the calculation with three peaks and the whole contour of the C-S bands was satisfactorily reproduced. The final C-S frequencies obtained are given in Table 3 and the corresponding peaks are shown in Fig. 9. The lower and higher C-S frequencies (732 and 779 cm^{-1}) correspond well, respectively, to the presence of both N- and S-bindings to Cd(II) ion, which has been revealed by the X-ray diffraction study of the Cd(II) thiocyanate solution as described in a previous section.

NMR Spectra. The chemical shifts δ of ^{13}C- and ^{14}N-NMR spectra were measured as the internal standards DDS and NH_4^+ ion, respectively, in the Zn(II), Cd(II), Hg(II), and ammonium thiocyanate solutions and are summarized in Table 4. The differences between the chemical shifts for the metal thiocyanate solutions and that for the NH_4SCN solution are also given as $\Delta\delta(SCN^-)$ in Table 4.

Table 4. Chemical shifts (ppm) of Hg(II), Cd(II), Zn(II), and ammonium thiocyanate solutions

	^{13}C-NMR		^{14}N-NMR	
	δ(DSS)	$\Delta\delta(SCN^-)$	$\delta(NH_4^+)$	$\Delta\delta(SCN^-)$
$[Hg(SCN)_4]^{2-}$	130.1	−4.9	215.0	30.8
$[Cd(SCN)_4]^{2-}$	134.3	−0.7	182.9	−1.3
$[Zn(NCS)_4]^{2-}$	136.4	1.4	153.9	−30.3
NH_4SCN	135.0	0.0	184.2	0.0

The $\Delta\delta(SCN^-)$ of the nitrogen-14 resonance shifted downfield in the Zn(II) thiocyanate solution, but upfield in the Hg(II) thiocyanate solution. Howarth *et al.*[15] measured the ^{14}N-chemical shifts of many S- and N-bonding metal thiocyanato complexes in various solvents and have reported that the ^{14}N-resonance shifts downfield in the N-bonding complexes, but upfield in the S-bonding complexes, from that of the free thiocyanate ion. Thus, the present ^{14}N-chemical shifts of the Zn(II) and Hg(II) thiocyanate solutions suggest the coordination of SCN^- ions to Zn(II) ion *via* the N atom, and to Hg(II) ion *via* the S atom. In the Cd(II) thiocyanate solution, the $\Delta\delta(SCN^-)$ value is in between those for Zn(II) and Hg(II) cases. This can be interpreted in terms of the convolution of peaks of downfield and upfield shifts due, respectively, to both N- and S-bonding SCN^- ions for Cd(II) ion, together with the peak of free SCN^- ion.

The $\Delta\delta(SCN^-)$ values of the ^{13}C-resonance of Zn(II), Cd(II), and Hg(II) thiocyanate solutions have shown the downfield shift for Zn(II), the upfield for Hg(II), and the intermediate for Cd(II) (Table 4), the same trend but reverse order of the $\Delta\delta(SCN^-)$ values being found in the ^{14}N-chemical shifts. Thus, ^{13}C-chemical shifts of these solutions also indicate the different types of bonding of SCN^- ions to Zn(II), Cd(II), and Hg(II) ions in the thiocyanate solutions.

Discussion

The structural parameters of Zn(II), Cd(II), and Hg(II) thiocyanato complexes both in aqueous solution and in DMSO are compared in Table 5. The SCN^- ions are bound to Hg(II) through the S atom within the $[Hg(SCN)_4]^{2-}$ complex in both aqueous solution and in DMSO and the Hg-S bond length and the bond angle Hg-S-C are similar in the two solvents within experimental uncertainties.

The Zn-N distance within $[Zn(NCS)_4]^{2-}$ in H_2O is

TABLE 5. COMPARISON OF INTERATOMIC DISTANCES (pm) AND BOND ANGLES (ϕ/°) WITHIN THE TETRATHIOCYANATO COMPLEXES OF Hg(II), Cd(II), AND Zn(II) IONS IN H_2O AND IN DMSO

	Hg		Cd			Zn	
	H_2O	DMSO	H_2O		DMSO	H_2O	DMSO
Binding atom	S	S	N	S	S	N	N
r (M-N)	415	427	225	435	435[a]	204	193
r (M-C)	335	340	328	349	349[a]	305	308
r (M-S)	254	253	487	265	263[a]	462	473
∠M-N-C						145	180
∠M-S-C	102	108		106	106[a]		

a) The values determined for complex species in a DMSO solution of $\bar{n}=2.3$ in Ref. 21 where $\bar{n}$ denotes the average number of thiocyanato ions bound to the central metal ion.

somewhat longer than the corresponding distance in DMSO. In the analysis of the X-ray scattering data of a DMSO solution of Zn(II) thiocyanate,[21] the Zn-N distance within $[Zn(NCS)_4]^{2-}$ has not been directly determined because of a low Zn(II) concentration and fixed at the value (194 pm) found in β-$Zn(NCS)_2$ crystal, although the structure of the crystal has not been solved with a high precision (the R-value= 0.09[19]). The Zn-N distance obtained in the present study is in good agreement with the value estimated from the effective ionic radii (206 pm[29]). The Zn-N-C bond angle may also be affected from the errors of the same source.

Thus, a relatively hard acceptor Zn(II) ion prefers to bind with the nitrogen atom and a soft acceptor Hg(II) ion combines with the soft sulfur atom within an SCN^- ion in both aqueous and DMSO solutions.

The structural parameters of Cd(II) thiocyanate complex determined in DMSO were those of a mixture of $[Cd(SCN)_2]$ and $[Cd(SCN)_3]^-$ because the structure determination of cadmium(II) thiocyanato complexes in DMSO has been carried out in a solution of $\bar{n}=2.3$ ($\bar{n}$ is the average coordination number of SCN^- ion within the complexes). However, as far as Persson *et al.*[21] have examined, cadmium(II) ion combines with SCN^- ions through the S atoms in DMSO (see Table 5).

On the other hand, cadmium(II) ion binds with both nitrogen and sulfur atoms within SCN^- ions in the $[Cd(SCN)_4]^{2-}$ complex in water. This fact may be related to different donicities of H_2O and DMSO, the latter has a larger donor number than the former (H_2O: 18.0, DMSO: 29.8[31]). The larger electron donation from ligand solvent molecules toward the central metal ion may decrease the fractional charge of the metal ion and thus the metal ion becomes softer. Therefore the metal ion may prefer a soft ligand atom than a hard one in a solvent with a larger donicity. Water molecule having a larger acceptor number than DMSO (H_2O: 54.8, DMSO: 19.3[30]) may preferentially solvate to the sulfur atom than the nitrogen site and thus the N-end within SCN^- tends to bind to Cd(II) ion in H_2O, while the S-end may not be strongly solvated in DMSO. These two factors of different solvating properties of H_2O and DMSO may affect the bonding of SCN^- to Cd(II) ion. The Cd-S bond length and the bond angle Cd-S-C do not differ significantly in the two solutions.

The present X-ray scattering data of the Cd(II) thiocyanate solution have demonstrated the presence of two Cd-N and two Cd-S bonds per Cd(II) on the average within the tetrathiocyanatocadmate(II) ion in aqueous solution. By the X-ray diffraction experiment, however, the result is not distinguishable between the formation of the $[Cd(SCN)_2(NCS)_2]^{2-}$ complex and the statistic mixture of $[Cd(NCS)_{4-n}(SCN)_n]^{2-}$ with n=0—4. Thermodynamic quantities (ΔG°_n, ΔH°_n, and ΔS°_n for the stepwise formation of $[Cd(NCS)_n]^{(2-n)+}$ complexes) and Raman spectra of solutions containing the thiocyanato complexes with low $\bar{n}$ values in aqueous solution, details of which will be described elsewhere,[32] indicated that the first SCN^- ion coordinates to Cd(II) ion through the N atom and the second and third SCN^- ions combine with Cd(II) ion through the S and N atoms, respectively, and then, at the fourth step, the Cd-S bond forms. These results indicate that the X-ray diffraction data obtained for the tetrathiocyanatocadmate(II) solution should be interpreted in terms of the formation of the $[Cd(NCS)_2(SCN)_2]^{2-}$ with two Cd-N and two Cd-S bonds, but not the statistical mixture of $[Cd(NCS)_{4-n}(SCN)_n]^{2-}$ complexes.

The covalency of the metal-ligand bonds within thiocyanato complexes of Zn(II), Cd(II), and Hg(II) may be reflected on their bond lengths. The Zn-N distance (204 pm) is close to the value estimated from the effective ionic radii (206 pm) (*cf.* 201 pm for the sum of the covalent radii of the atoms[28]), while the Hg-S distance (254 pm) agrees well with the sum (252 pm) of covalent radii of the relevant atoms (*cf.* 280 pm for the sum of the ionic radii of Hg^{2+} and S^{2-}). Both Cd-N (225 pm) and Cd-S (265 pm) distances are close to those (224 and 264 pm, respectively) calculated using the effective ionic radii (*cf.* 218 and 252 pm, respectively, for the sum of the covalent radii of the atoms).

The authors thank Dr. Yoshiyuki Nakamura for ^{13}C-NMR measurements, and Dr. Masayoshi Harada for ^{14}N-NMR measurements. A part of the calculations was carried out by using M-200H computers at the Institute for Molecular Science. The present work has been financially supported, in

part, by a Grant-in-Aid for Scientific Research No. 57470054 of the Ministry of Education, Science and Culture.

References

1) P. Gerding, *Acta Chem. Scand.*, **20**, 2771 (1966).
2) P. Gerding, *Acta Chem. Scand.*, **22**, 1283 (1968).
3) S. Ahrland and L. Kullberg, *Acta Chem. Scand.*, **25**, 3692 (1971).
4) L. Ciavatta and M. Grimaldi, *Inorg. Chim. Acta*, **4**, 312 (1970).
5) Ts. Ruzhitski, V. V. Blokhin, and V. E. Mironov, *Russian J. Phys. Chem.*, **48**, 282 (1974).
6) S. Ahrland and N.-O. Björk, *Acta Chem. Scand., Ser. A*, **30**, 249 (1976).
7) S. Ahrland, I. Persson, and R. Portanova, *Acta Chem. Scand., Ser. A*, **35**, 49 (1981).
8) L. H. Jones, *J. Chem. Phys.*, **25**, 1069 (1956).
9) S. Fronaeus and R. Larsson, *Acta Chem. Scand.*, **16**, 1447 (1962).
10) A. Tramer, *J. Chem. Phys.*, **59**, 232 (1962).
11) K. A. Taylor, T. V. Lond II, and R. A. Plane, *J. Chem. Phys.*, **47**, 138 (1967).
12) R. E. Hester and K. Krishnan, *J. Chem. Phys.*, **48**, 1825 (1968).
13) D. P. Strommen and R. A. Plane, *J. Chem. Phys.*, **60**, 2643 (1974).
14) A. Antić-Jovanović, M. Jeremić, and D. A. Long, *J. Raman Spectrosc.*, **12**, 91 (1982).
15) O. W. Howarth, R. E. Richards, and L. M. Venanzi, *J. Chem. Soc.*, **1964**, 3335.
16) L. N. Mazalov, A. A. Voityuk, and G. K. Parygina, *Russ. J. Struct. Chem.*, **23**, 364 (1982).
17) A. L. Beauchamp and D. Goutier, *Can. J. Chem.*, **50**, 977 (1972).
18) M. Cannas, G. Carta, A. Cristini, and G. Marongiu, *J. Chem. Soc., Dalton Trans.*, **1976**, 300.
19) L. A. Aslanov, V. M. Zonov, and K. Kynev, *Sov. Phys. Crystallogr.*, **21**, 693 (1976).
20) H. Scouloudi, *Acta Crystallogr.*, **6**, 61 (1953).
21) I. Persson, Å. Iverfeldt, and S. Ahrland, *Acta Chem. Scand., Ser. A*, **35**, 295 (1981).
22) H. Ohtaki, M. Maeda, and S. Itoh, *Bull. Chem. Soc. Jpn.*, **47**, 2217 (1974).
23) H. Ohtaki, T. Yamaguchi, and M. Maeda, *Bull. Chem. Soc. Jpn.*, **49**, 701 (1976).
24) M. E. Milberg, *J. Appl. Phys.*, **29**, 64 (1958).
25) B. E. Warren and R. L. Mozzi, *Acta Crystallogr.*, **21**, 459 (1966).
26) T. Yamaguchi, G. Johansson, B. Holmberg, M. Maeda, and H. Ohtaki, *Acta Chem. Scand., Ser. A*, **38**, 437 (1984).
27) G. Johansson and M. Sandström, *Chem. Scr.*, **4**, 195 (1973).
28) L. Pauling, "The Nature of Chemical Bond," 3rd ed., Cornell University Press, Ithaca, N. Y. (1960).
29) R. D. Shannon, *Acta Crystallogr., Sect. A*, **32**, 751 (1976).
30) T. Yamaguchi, Doctor Thesis, Tokyo Institute of Technology, March (1978).
31) V. Gutmann, "Donor-Acceptor Approach to Molecular Interactions," Plenum Press, New York (1978).
32) S. Ishiguro, K. Yamamoto, and H. Ohtaki, to be published.

Ion-exclusion Chromatography of Weak Acids Using a Carbonic Acid Solution as Eluent

Hisaaki ITOH* and Yoshio SHINBORI
Faculty of Pharmaceutical Sciences, Josai University, Sakado, Saitama 350-02
(Received June 5, 1985)

Ion-exclusion chromatographic separation of organic acids using a carbonic acid solution as eluent is presented. This permits conductivity detection of ionic species without a suppressor as a post-column reactor. It was found that the proposed method was applicable to the separation of organic acids having pK_a over *ca* 3.5. This technique was applied to the determination of acetic acid in pharmaceuticals without tedious sample preparation.

In recent years, ion-exclusion technique, first reported by Wheaton and Bauman[1] for the separation of nonionic from ionic materials, has become of wider interest because of its ability to separate strong acids as a class from weak acids and also from each other.

Tanaka *et al.*[2] have indicated that ion-exclusion chromatography (IEC) using a hydrogen-type cation-exchange resin and flow-coulometric detection could be used for the separation of many weak acids from each other and for their determination. They[3] also have recently described the ion-exclusion behavior of a large number of strong and weak acids using water as eluent. Furthermore, Turkelson and Richards[4] have reported the use of IEC to separate most of the Krebs cycle acids, demonstrating that ion-exclusion can also separate weak acids from each other by the use of dilute hydrochloric acid solution as eluent.

Ion chromatography exclusion (ICE) technique, one of the modes of ion chromatography,[5] has also been successfully applied to the separation and analysis of many organic acids in various samples having complex matrices, *i.e.* brine,[6] foods,[7] and biologicals.[8] In this technique, using a dilute hydrochloric acid solution as eluent and conductivity detection, the separator column is connected with a so-called halide suppressor, which permits a sensitive detection of the ionic species in a sample solution with the reduction of the background conductivity. Although it has been proven that the ICE technique was a useful one for the analysis of organic acids, unfortunately, it has some disadvantages because of the use of the halide suppressor. In the suppression reaction procedure, the formation of silver chloride precipitation in the suppressor column causes an increase of back pressure in the system. Consequently, the retention time of the analyte will change and the detector response of the analyte will be diminished. Thus, the identification of unknown species will be somewhat difficult and the analytical precision in the quantification of the species will be poor, even though these problems may be improved by replacement with a different suppressor and/or by cutting off the consumed part of the suppressor.

In the previous communication,[9] we have briefly reported a new ion-exclusion technique using a carbonic acid solution as eluent and conductivity detection without a suppressor as a post column reactor. The present paper describes the elution behavior of several organic acids and the application to the acetate analysis to some pharmaceuticals.

Experimental

Materials. All reagents used were of reagent grade. All standard solutions, except for the solution of lithium lactate, valeric and hexanoic acid, were prepared by dissolving the acid and/or the corresponding sodium salt in distilled and deionized water (DI water). Valeric and hexanoic acid standard solutions were prepared by dissolving the acid in aliquots of 1 mol dm^{-3} NaOH solution and diluting with DI water. In addition, acetic acid standard solution for calibration was prepared by dissolving the potassium salt in DI water. The salt was dried in an electric drier oven at 110 °C for 24 h. Klinisalz® B Ringer's solution (Eisai) and Celtol® Intramuscular 1Gm (Takeda) were obtained from commercial sources. The aqueous solution of Celtol® injections was prepared by dissolving 0.5325 g of it (500 mg as Potency) in 5.0 cm^3 of the distilled water for injection and held in water bath at 25 °C.

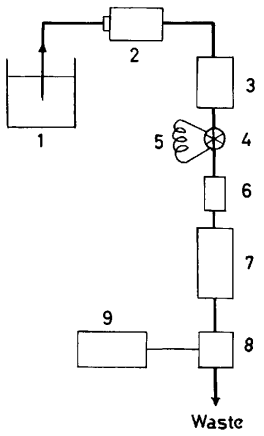

Fig. 1. Flow diagram of IEC system.
1: Eluent reservoir, 2: Pump, 3: Dionex Anion Suppressor (P/N 30828), 4: Injection valve, 5: Sample loop, 6: Dionex Anion Suppressor (P/N 38029), 7: Dionex ICE Separator (9 mm i.d. × 250 mm, P/N 30888), 8: Conductivity detector, 9: Recorder.

Chromatographic System. The Dionex Model 10 Ion Chromatograph equipped with conductivity detector was modified. The flow diagram of the modified system is shown in Fig. 1. Two Dionex anion suppressors[10] were used: One (9 mm i.d.×100 mm) between the pump and the injection valve and another (6 mm i.d.×60 mm) between the injection valve and the ICE Separator.[11] There are two reasons for introducing a suppressor before the ICE Separator. First, this column plays a role of a so-called guard column for the ICE Separator. Second, it neutralizes the sample solution and converts the sample ions into the corresponding acid forms. Thus, the system can be continually operated for 20 to 30 h depending upon the sample matrix and the flow rate without column regeneration. In addition, with a view to faster analysis, both the separator valve and the suppressor valve were bypassed by connecting the top of the suppressor column directly to the injection valve and the bottom of the ICE Separator directly to the conductivity cell inlet using a short length of tubings (0.5 mm i.d). The eluent reservoir contains a sodium carbonate solution and/or a standard sodium hydrogencarbonate/sodium carbonate solution which is commonly used for the anion analysis in ion chromatography. This solution is converted into a definite concentration of carbonic acid solution by passing it through the suppressor column. The injection volume was 50 mm^3. The strip chart recorder was operated at 1 mV full scale range and a chart speed of 30 cm h^{-1}. A 0.5 mol dm^{-3} sulfuric acid solution was used for column regeneration at flow rate of 1.0 cm^3 min^{-1}.

Results and Discussion

Elution Behavior of Organic Acids. In the previous paper,[9] it was shown that the presence of carbonic acid in the eluent dramatically improves the separation of organic acids such as formic, acetic, propionic, and butyric. Figure 2 typically shows the variation of the chromatographic capacity factor (k') of four organic acids with the concentration of carbonic acid in the eluent. The increase of each k' value was observed with the increase of the concentration of carbonic acid, that is, the decrease of pH of the eluent (pH 5.0 to 4.3). This is a characteristic effect of the pH of the eluent in ion-exclusion chromatographic separation.[4,12]

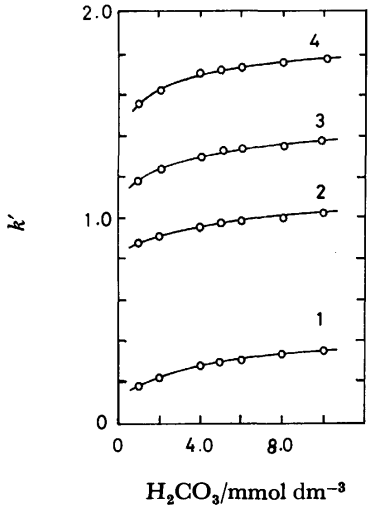

Fig. 2. Variation of the chromatographic capacity factor (k') with the concentration of carbonic acid solution.
Notations: 1 Formic acid, 2 acetic acid, 3 propionic acid, 4 butyric acid.

The factors which affect the separation characteristics in IEC are pK_a, structure and concentration of solute, temperature, eluent pH, nature of the resin, such as degree of cross linkage, and eluent flow rate *etc.*[1,6] Among these factors, generally, the pK_a of the solute can be used to predict its elution behavior. Because of a Donnan membrane effect, at a given eluent pH, the distribution of the solute between the occluded liquid inside the resin pores and the interstitial liquid of the resin particles depends upon its pK_a. The lower the pK_a, the smaller the distribution, that is, the lower the pK_a, the faster the elution. Indeed, Tanaka *et al.* have shown that this general rule holds for a large number of inorganic acids and also for some organic acids such as formic and acetic.[3]

Table 1 lists k' values of mono- and dicarboxylic acids and some substituted derivatives of these acids obtained by using carbonic acid solution (5.0 mmol dm^{-3}) as eluent together with their pK_a values. These k' data show that the general rule mentioned above holds only for acids of low molecular weight such as formic, acetic, succinic and glutaric *etc.*

Table 1. Chromatographic k' data

Acids	pK_a[a]	k'
Oxalic	1.19 (4.28)[b]	0
Pyruvic	2.49	0
Malonic	2.85 (5.69)	0
(*S*,*S*)-Tartaric	3.03 (4.36)	0
L-Malic	3.4 (5.1)	0.08
Formic	3.752	0.28
Lactic	3.862	0.28
Succinic	4.20 (5.64)	0.40
Glutaric	4.343 (5.42)	0.64
Adipic	4.430 (5.41)	0.97
Acetic	4.756	1.02
4-Oxovaleric	4.59	1.15
Propionic	4.874	1.33
Pimelic	4.509 (5.4)	1.64
Butyric	4.820	1.75
Valeric	4.86	2.85
Suberic	4.5 (4.7)	3.1
Hexanoic	4.88	5.0

a) Landolt-Börnstein, "Zahlenwerte und Funktionen," II B., 7 Teil, Springer (1960). b) Parenthesis: pK_2 value.

However, as the solutes become more aliphatic in nature, that is, with increase of the hydrophobic moiety, Van der Waals forces and/or the hydrophobic interactions between the hydrophobic moiety of the solute and the hydrocarbon portion of the resin become more dominant. Thus, the elution sequences differ from that predicted from the pK_a of solutes only. The k' values obtained show a tendency to increase with that of the hydrophobic moiety, that is, the molecular weight of solute regardless of its pK_a. In addition, hydroxy and keto carboxylic acids show smaller k' values than those of the corresponding normal acids because the introduction of such a hydrophilic group makes the acid stronger and increases the hydrophilicity of the solute.

In summary, although the definite correlation between k' value and pK_a of the solute was not observed from the results shown in Table 1, it can be seen that this technique is applicable for the separation of organic acids having pK_a over *ca* 3.5.

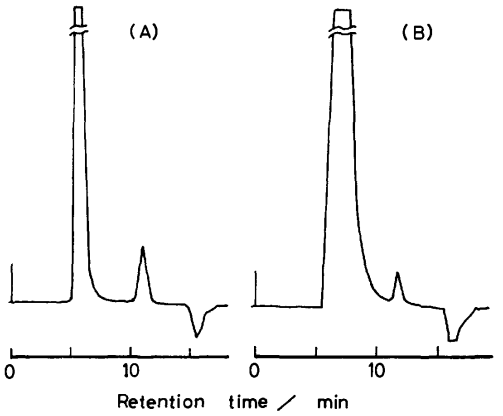

Fig. 3. Chromatograms of acetic acid in (A) Klinisalz® B Ringer's solution (×50 dilution) and (B) CEC injections solution (×200 dilution).
Chromatographic conditions. (A) Eluent: 5.0 mmol dm^{-3} carbonic acid solution, flow rate: 0.85 cm^3 min^{-1}, detector setting: 10 μS. (B) Eluent: 8.0 mmol dm^{-3} carbonic acid solution, flow rate: 0.75 cm^3 min^{-1}, detector setting: 3 μS.

Table 2. Replicate determination of acetic acid in pharmaceuticals. Peak heights[a)]

Klinisalz® B Ringer's solution (×50 dilution)	CEC injection solution (×200 dilution) A[b)]	B[c)]
25.5	9.8	33.7
26.0	10.0	33.4
25.8	10.4	33.5
25.7	9.6	33.0
26.0	10.2	33.2
Average 25.8	10.0	33.4
σ[d)] 0.2_0	0.2_9	0.2_4
R.S.D./%[e)] 0.8	2.9	0.7

a) Unit: mm. b) Sampling at 20 min after dissolution. c) Sampling at 6.0 hours after dissolution. d) Standard deviation. e) Relative standard deviation.

Application to the Determination of Acetic Acid in Pharmaceuticals. In order to evaluate the applicability of the present system, the determination of acetic acid in pharmaceutical samples, Klinisalz® B Ringer's solution and Celtol® injections, was undertaken. Klinisalz® B Ringer's solution contains NaCl, KCl, CH_3COONa, KH_2PO_4, $MgCl_2$, and xylitol as components. Celtol® injections contains cephacetrile sodium (CEC), which is one of the 3-(acetoxymethyl)-cephalosporins, and it is known that it partially decomposes to liberate acetic acid in aqueous solution and that the resulting desacetyl derivative has only a low potency. Thus, from the standpoint of quality control for both pharmaceuticals, it is required to analyze the acetic acid content.

The calibration curves constructed by using the peak height of standard acetate solution were linear over the range of 0.1—10 μg cm^{-3} and 0.5—30 μg cm^{-3} (as CH_3COO^-) at 3 μS and 10 μS, respectively. A relative standard deviation of 1.3% was obtained for five replicate injections of 1.0 μg cm^{-3} level at 10 μS. In addition, the detection limit established using 50 mm^3 standard injection was 40 ng cm^{-3}.

Both samples were directly injected without sample preparation except for diluting with DI water. The CEC solution was held in a cooling bath at 10 °C after dilution since CEC was stable in aqueous solution at low temperature.[13)]

The analytical results based on peak height measurements and chromatograms are shown in Table 2 and Fig. 3, respectively. For Klinisalz® B Ringer's solution, 11.81 μg cm^{-3} and 11.85±0.08 μg cm^{-3} are values calculated from the appended component table as taken and obtained from five replicate determinations, respectively. These data show that the method we describe is simple, precise and sensitive, which is applicable for routine analysis of the acetate of these pharmaceutical samples.

References

1) R. M. Wheaton and W. C. Bauman, *Ind. Eng. Chem.*, **45**, 228 (1953).
2) K. Tanaka, T. Ishihara, and H. Sunahara, *Bunseki Kagaku*, **24**, 235 (1975).
3) K. Tanaka, T. Ishizuka, and H. Sunahara, *J. Chromatogr.*, **174**, 153 (1979).
4) V. T. Turkelson and M. Richards, *Anal. Chem.*, **50**, 1420 (1978).
5) H. Small, T. Stevens, and W. C. Bauman, *Anal. Chem.*, **47**, 1801 (1975).
6) W. Rich, F. Smith, Jr., L. McNeil, and T. Sidebottom, "Ion Chromatographic Analysis of Environmental Pollutants," ed by J. D. Mulik, E. Sawicki, Ann Arbor Science,

Michigan (1979), Vol. 2, Chap. 2, pp. 17—29.

7) Dionex Application Note 19, "Analysis of Strong and Weak Acids in Coffee Extract," April (1979).

8) W. R. Rich, E. Johnson, L. Lois, B. E. Stafford, P. M. Kabara, and L. J. Marton, "Liquid Chromatography in Clinical Analysis," ed by L. J. Marton, P. M. Kabara, The Humana Press, New Jersey (1981), Chap. 17, pp. 393—407.

9) H. Itoh and Y. Shinbori, *Chem. Lett.*, **1982**, 2001.

10) Column packed with 20—40 μ Dionex DC-X8 resin, a microporous strong acid cation exchanger, which consists of a stylene/divinyl benzene copolymer containing sulphonic acid groups.

11) 9 mm i.d.×200 mm column packed with 9±0.5 μ DC-X8 resin.

12) R. M. Wheaton and W. C. Bauman, *Ann. N.Y. Acad. Sci.*, **57**, 159 (1953).

13) H. Itoh, Y. Shinbori, and N. Tamura, *Bunseki Kagaku*, **32**, 571 (1983).

 © 1985 The Chemical Society of Japan Bull. Chem. Soc. Jpn., 58, 3248—3251 (1985) [Vol. 58, No. 11

Thermal Reactions of the Nickel(II) Complexes Containing 1-Phenyl-1,2-ethanediamine in the Solid Phase

Yoshinori IHARA
Laboratory of Chemistry, Faculty of Education, Kanazawa University, Kanazawa 920
(Received June 20, 1985)

Nickel(II) complexes $[Ni(phenen)_2](ClO_4)_2$ and $[Ni(H_2O)_2(phenen)_2]X_2$ (phenen=1-phenyl-1,2-ethanediamine, X=Cl, Br, or NO_3) were prepared, and their thermal behavior was investigated in the solid phase. The nitrate showed a thermochromism consisting of two steps, violet→yellow→violet, which corresponds to a structural change from an octahedral diaqua complex to a square planar anhydride, and then to the octahedral dinitrato complex, respectively. Both the chloride and bromide were converted into the octahedral dianiono complexes by thermal deaquation-anation, retaining their octahedral configuration. However, no change was observed in the perchlorate, which is invariably square planar.

When two molecules of a *N*- and/or *C*-substituted ethylenediamine are coordinated to a nickel(II) ion, the resulting bis(diamine) complex is generally either square planar ($[Ni(diamine)_2]X_2$) or octahedral ($[NiX_2(diamine)_2]$ or $[NiA_2(diamine)_2]X_2$: X=a univalent anion, A=a solvent molecule). Two main factors for deciding whether X or A are coordinated or not can be distinguished: (i) the coordinating ability of these ligands, and (ii) the steric hindrance resulting from *N*- or *C*-substituents of the diamine.

Tsuchiya *et al.* have studied the relative stabilities of these two structures, and the ease of their interconversions, using many complexes containing different types of diamines, on the basis of their thermal reactions in the solid phase.[1-3] Recently, the author found more interesting examples of such a thermal transformation, including some octahedral→square planar→octahedral changes which are peculiarly thermochromic (violet→yellow→violet or blue), in the nickel(II) complexes with butanediamines[4] or 1,2-diphenyl-1,2-ethanediamines[5] in the solid phase. Such transformations were found to occur most easily in the case of the complex chloride or nitrate of *dl*-form diamines.

In a continuation of these studies, thermal reactions of the nickel(II) complexes of 1-phenyl-1,2-ethanediamine (phenen) were studied. The obtained results are reported in this paper. It is interesting to note that it was just these complexes, and those of 1,2-diphenyl-1,2-ethanediamines, that Lifschitz *et al.* studied and discussed in their historical paper on the structure of the nickel(II) complexes.[6]

Experimental

Preparation. Methyl 2-amino-2-phenylacetate[7] was converted into 2-amino-2-phenylacetamide by the method of Arpesella.[8] 1-Phenyl-1,2-ethanediamine was obtained by reducing the amide with $LiAlH_4$ according to the procedure described by Yano *et al.*[9]

The complexes were prepared following the method of Lifschitz *et al.*[6] with slight modifications.

(i) Complex chloride, nitrate, and perchlorate: To an aqueous solution of nickel(II) chloride or nitrate, an ethanolic solution of phenen was added in the molar ratio of 1:2. The violet crystals which separate out on standing were recrystallized from boiling water. The same procedure with nickel(II) perchlorate gave orange crystals of the complex perchlorate.

(ii) Complex bromide: When nickel(II) bromide was used in the method (i), a mixture of violet blue and violet crystals was almost always obtained irrespective of the organic solvent used (methanol or ethanol) and its concentration. The mixture was dissolved in boiling water, and the resulting solution was cooled rapidly on ice to yield pure violet crystals.

Measurements. Simultaneous TG and DSC measurements were carried out with a Rigaku Denki standard TG-DSC apparatus under a constant flow of nitrogen (20 ml/min). The heating rates and amounts of samples used are given in the figures.

The electronic spectra in the solid phase were measured by the diffuse reflectance method on a JASCO UVIDEC-410 spectrophotometer. The effective magnetic moments were evaluated from the susceptibilities measured by Gouy's method at room temperature.

Results and Discussion

Structures of the Original Complexes. The reflectance spectra of the chloride and perchlorate are shown in Fig. 1. The bromide and nitrate revealed

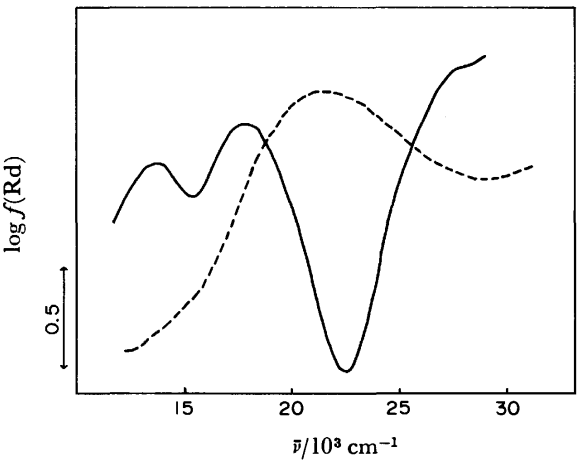

Fig. 1. Electronic spectra of $[Ni(H_2O)_2(phenen)_2]Cl_2$ (——) and $[Ni(phenen)_2](ClO_4)_2$ (----).

Table 1. Data on the elemental analyses, electronic spectra and magnetic moments of the original complexes

Complexes	Color	Analytical data[a]			Absorption maxima			μ_{eff}
		H (%)	C (%)	N (%)	$\bar{\nu}/10^3$ cm^{-1}			B.M.
$[Ni(H_2O)_2(phenen)_2]Cl_2$	Violet	6.24 (6.44)	43.52 (43.87)	12.72 (12.79)	13.5	17.9	28.1 sh	3.26
$[Ni(H_2O)_2(phenen)_2]Br_2$	Violet	5.40 (5.36)	36.44 (36.47)	10.57 (10.63)	13.5	18.2	29.4	3.17
$[Ni(H_2O)_2(phenen)_2](NO_3)_2$	Violet	5.75 (5.66)	39.13 (39.46)	17.11 (17.35)	13.5	17.9	27.5 sh	3.28
$[Ni(phenen)_2](ClO_4)_2$	Orange	4.56 (4.53)	36.26 (36.69)	10.57 (10.24)		22.3		Diamag.

a) Calculated values are in parentheses.

similar spectral patterns to that of the chloride. The spectral data of all the complexes are summarized in Table 1, together with their magnetic moments and analytical data. It is well understood from Fig. 1 and Table 1 that the violet complexes have an octahedral geometry and the orange perchlorate has a square planar one, leading to the formulas of the complexes given in Table 1.

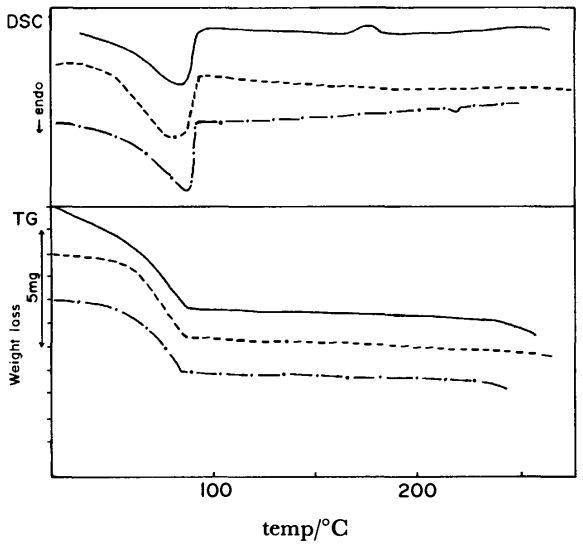

Fig. 2. TG–DSC patterns of $[Ni(H_2O)_2(phenen)_2]X_2$, where X=Cl (——), Br (----), and NO_3 (—·—). Heating rate: 1.25 °C min^{-1} for all complexes. Amount of sample used: 28.5 mg (chloride), 25.5 mg (bromide), and 20.1 mg (nitrate).

Thermal Analyses. The results of simultaneous TG–DSC measurements of the complexes are shown in Fig. 2. The results of the perchlorate are not shown, because it did scarcely show any change on TG and DSC curves before its decomposition. The weight losses observed below 100 °C correspond to the liberation of two moles of the coordinated water in the respective complexes (obsd. 8.07%, calcd. 8.23% for chloride; 6.86%, 6.84% for bromide; 7.46%, 7.34% for nitrate, respectively). The colors of the chloride and bromide were changed to violet blue and that of nitrate to yellow, after the dehydration.

On the DSC curves, a small exothermic peak is observed at 175 °C in the case of the chloride and an endothermic one at 215 °C in the case of the nitrate, after the peak caused by the dehydration. It is likely that these changes are not so drastic to bring about a distinct structural transformation, because no appreciable change was observed in the reflectance spectra of the complexes before and after the peak temperature.

On the other hand, the nitrate is strongly thermochromic, changing from yellow to violet at about 130 °C, after the color change by dehydration (violet→yellow) is over. This change indicates that, upon heating the yellow anhydrous complex a square planar-octahedral transformation takes place. But, the DSC curve remains nearly linear in this range irrespective of the obvious color change. Thus,

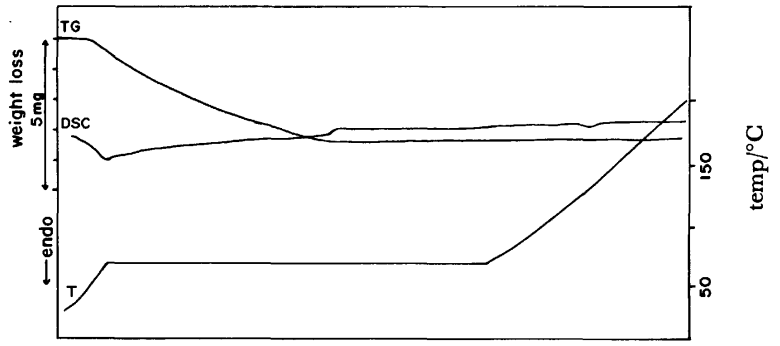

Fig. 3. TG–DSC pattern of $[Ni(H_2O)_2(phenen)_2](NO_3)_2$. Heating rate: 2.5 °C min^{-1} until 70 °C. After the dehydration was completed at 70 °C, heating was continued at the same rate. The sensitibity of DSC was the same as that of Fig. 2.

a more detailed measurement regarding this thermal reaction was tried, with the result is shown in Fig. 3. Avoiding an overlap with the dehydration peak, a measurement was performed by using an isothermal technique at 70 °C, under the conditions given in the caption of the figure.

The new small peak observed at about 130 °C revealed the existence of an endothermic reaction, which seems to correspond to the color change (yellow→violet). The peak is, however, too weak for estimating the amount of heat absorbed in the reaction.

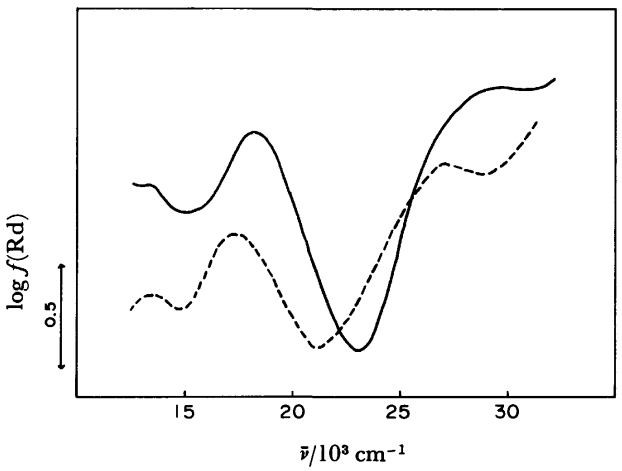

Fig. 4. Electronic spectra of $[Ni(H_2O)_2(phenen)_2]Br_2$ before heating (——) and after heating (----).

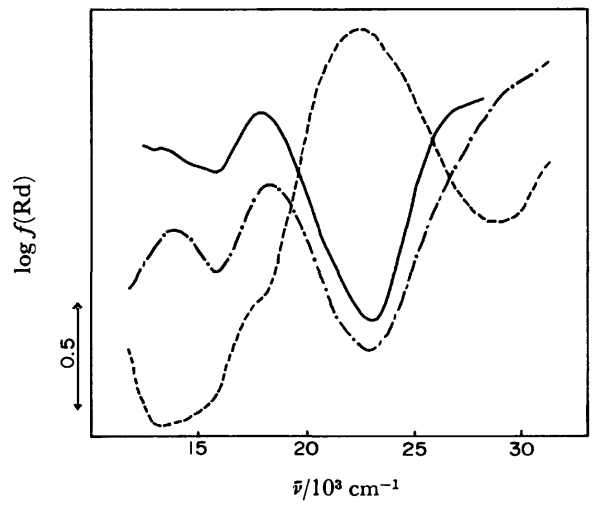

Fig. 5. Electronic spectra of $[Ni(H_2O)_2(phenen)_2](NO_3)_2$ before heating (——) and after heating at 70 °C (----) and at 150 °C (—·—).

Structures of the Complexes Obtained by Heating. The products of the thermal reactions were obtained by isothermal heating at the temperatures of the respective DSC peaks using an electric furnace in static air.

The reflectance spectra of the complex bromide and nitrate before and after heating are compared in Figs. 4 and 5, respectively. As shown in Fig. 4, the spectrum of the anhydrous complex bromide obtained upon heating is almost identical with that of the mother complex, except for a slight shift of the maximum peaks to longer wavelengths. The shifts can be attributed to an exchange of the coordinated species, *i.e.*, that of water molecules by bromide ions. A similar spectral change is also observed in the case of the chloride (Table 2). Consequently, both the chloride and bromide are found to undergo thermal deaquation-anation (Eq. 1; see below).

On the other hand, the spectrum of the yellow product of the nitrate is very similar to that of the complex perchlorate, but is completely different from those of the two violet species (Fig. 5). The violet product obtained by heating at 150 °C shows a spectral pattern nearly identical with that of the original octahedral dihydrate, while the pattern of the yellow product is that of a square planar nickel(II) complex, which have a broad and strong absorption band in the blue part of the spectrum. The data of the magnetic moments in Table 2 support these discussions.

The thermochemical changes observed can thus be represented by the following equations (as to the notations Oh, Oh′, and Sp, see below):

$$\underset{\text{Oh}}{[Ni(H_2O)_2(phenen)_2]X_2} \xrightarrow[\Delta]{-2H_2O} \underset{\text{Oh}'}{[NiX_2(phenen)_2]} \quad (X=Cl \text{ or } Br), \tag{1}$$

$$\underset{\text{Oh}}{[Ni(H_2O)_2(phenen)_2](NO_3)_2} \xrightarrow[\Delta]{-2H_2O} \underset{\text{Sp}}{[Ni(phenen)_2](NO_3)_2} \xrightarrow{\Delta} \underset{\text{Oh}'}{[Ni(NO_3)_2(phenen)_2]}. \tag{2}$$

TABLE 2. DATA ON THE ELEMENTAL ANALYSES, ELECTRONIC SPECTRA AND MAGNETIC MOMENTS OF THE COMPLEXES OBTAINED BY HEATING

Complexes	Color	Analytical data[a]			Absorption maxima $\bar{\nu}/10^3$ cm^{-1}			μ_{eff}
		H (%)	C (%)	N (%)				B.M.
$[NiCl_2(phenen)_2]0.75H_2O$[b]	Bluish violet	5.99 (6.19)	46.11 (46.25)	13.41 (13.48)	13.5	17.6	27.8 sh	3.23
$[NiBr_2(phenen)_2]$	Violet blue	4.82 (4.93)	39.67 (39.15)	11.50 (11.41)	13.5	17.4	27.2	3.13
$[Ni(phenen)_2](NO_3)_2$	Yellow					21.7		Diamag.
$[Ni(NO_3)_2(phenen)_2]0.75H_2O$[b]	Violet	5.16 (5.48)	41.28 (41.01)	17.53 (17.93)	13.7	18.3	27.0<	3.27

a) Calculated values are in parentheses. b) Very hygroscopic.

Table 3. Classification of thermal reactions of nickel(II) complexes containing *C*-substituted ethylenediamines

	Cl	Br	I	NO_3	ClO_4
pn[10]	Oh→Oh′	Oh→Oh′		Oh→Oh′	Oh→Sp
phenen	Oh→Oh′	Oh→Oh′		Oh→Sp→Oh′	Sp
i-bn[4]	Sp→Oh′	Sp	Sp	Sp	Sp
m-bn[4]	Sp	Sp	Sp	Sp→Oh′	Sp
dl-bn[4]	Oh→Sp→Oh′	Oh→Sp→Oh′		Oh→Sp	Oh→Sp
m-stien[5]	Sp	Sp	Sp	Sp	Sp
dl-stien[5]	Oh→Sp→Oh′	Oh→Sp→Oh′	Sp	Oh→Sp→Oh′	Sp

Abbreviations pn, phenen, *i*-bn, *m*-bn, *dl*-bn, *m*-stien, and *dl*-stien are 1,2-propanediamine, 1-phenyl-1,2-ethanediamine, 2-methyl-1,2-propanediamine, *meso*- and *dl*-2,3-butanediamine, and *meso*- and *dl*-1,2-diphenyl-1,2-ethanediamine, respectively. Oh and Sp denote an octahedral and a square planar structure. As to Oh→Oh′, Oh→Sp, Oh→Sp→Oh′, and Sp→Oh′, see text.

Only in the case of the nitrate, a square planar structure is observed as a stable product of the thermal reaction. The reason for the peculiarity of the nitrate showing such a transformation had been discussed in the preceding paper.[4,5]

Effects of Structures of Diamines upon Thermal Reactions. Table 3 summarizes the results of the thermal reactions of phenen complexes and those of the nickel(II) complexes with other *C*-substituted ethylenediamines already studied.

When the original species are octahedral, *i.e.* the diaqua bis(diamine)nickel(II) complexes, they are denoted by Oh in this Table. They contain monosubstituted, or *m*- or *dl*-disubstituted ethylenediamines, as shown below the table. When heated, they change in one of the three ways, *i.e.*: (i) simple deaquation leading to a square planar (Sp) species: Oh→Sp; (ii) single-step deaquation-anation leading to an octahedral dianiono species (Oh′): Oh→Oh′ (*cf.* Eq. 1); and (iii) two-step deaquation-anation: Oh→Sp→Oh′ (*cf.* Eq. 2). On the other hand, when the original species are square planar, they may remain unchanged upon heating, or may be converted into the octahedral dianiono species (simple anation, Sp→Oh′).

It can be seen that the phenen complexes easily undergo deaquation-anation either in one step or in two, producing dianiono complexes, retaining (or restoring) their octahedral configuration. An important reason for this easy anation can be found in the structure of the planar complex, $[Ni(phenen)_2]^{2+}$. It is clear that there is enough space above and below it to permit the anation of counter ions since the bulky phenyl groups can occupy the equatorial positions on the plane containing two diamines. On the other hand, in the complexes with *i*-bn, *m*-bn, or *m*-stien, at least two of their substituents are forced to occupy the axial positions. Such a conformation generates a large steric hindrance, preventing the approach of the other ligands and stabilizing the Sp structure.

The data in Table 3 (especially the comparison of phenen with bn and stien) lead, finally, to an impression that, for the square planar-to-octahedral transformation to occur, the steric hindrance of the ligands should be intermediate; it can be neither too large, nor too small. Diamines satisfying the following two conditions seemingly favor the transformation: (i) The substituent groups in the diamine protruding on the equatorial plane should be so bulky that they can influence the strength of axial coordination to some extent. (ii) The substituent groups protruding toward the axial directions are unnecessary for the reaction; if they exist, they should be as small as possible (*e.g.* methyl).

References

1) R. Tsuchiya, S. Joba, A. Uehara, and E. Kyuno, *Bull. Chem. Soc. Jpn.*, **46**, 1454 (1973).

2) H. Nishimoto, T. Yoshikuni, A. Uehara, E. Kyuno, and R. Tsuchiya, *Bull. Chem. Soc. Jpn.*, **51**, 1068 (1978).

3) Y. Ihara, E. Izumi, A. Uehara, R. Tsuchiya, S. Nakagawa, and E. Kyuno, *Bull. Chem. Soc. Jpn.*, **55**, 1028 (1982).

4) Y. Ihara, T. Kamishima, and R. Tsuchiya, *Thermochim. Acta*, **67**, 23 (1983).

5) Y. Ihara and R. Tsuchiya, *Bull. Chem. Soc. Jpn.*, **57**, 2829 (1984).

6) L. Lifschitz, J. G. Bos, and K. M. Dijkema, *Z. Anorg. Allg. Chem.*, **242**, 97 (1939).

7) E. L. Smith, D. H. Speckman, and J. Polglase, *J. Biol. Chem.*, **199**, 801 (1952).

8) L. Arpesella, A. La Manna, and M. Grassi, *Gazz. Chim. Ital.*, **85**, 1354 (1955).

9) S. Yano, M. Saburi, S. Yoshikawa, and J. Fujita, *Bull. Chem. Soc. Jpn.*, **49**, 101 (1976).

10) Y. Ihara and N. Nakamura, unpublished results.

 © 1985 The Chemical Society of Japan Bull. Chem. Soc. Jpn., 58, 3252—3258 (1985) [Vol. 58, No. 11

Use of Alternating Current Impedance Method in Diagnosing Electrode Kinetics of $[Fe(CN)_6]^{4-/3-}$ Complex Confined to Protonated Poly(4-vinylpyridine) Film on Graphite Surfaces

Takeo OHSAKA, Toru USHIROGOUCHI, and Noboru OYAMA*

Department of Applied Chemistry for Resources, Tokyo University of Agriculture and Technology, Koganei, Tokyo 184

(Received June 26, 1985)

A "heterogeneous" electron-transfer process of $[Fe(CN)_6]^{4-/3-}$ redox couple, which was confined electrostatically to the protonated poly(4-vinylpyridine) (PVP) film, at basal-plane pyrolytic graphite (BPG) electrode/PVP film interfaces and a "homogeneous" charge-transport process within the PVP film were examined by alternating current (ac) impedance method. The obtained impedance loci were found to correspond to those expected for the electrochemical impedance expressed by "Randles's equivalent circuit." The relevant kinetic parameters (*i.e.*, the standard rate constant, k° and the cathodic transfer coefficient, α) of the electrode reaction, the apparent diffusion coefficients, D_{app}, for the "homogeneous" charge-transport within the film, the double-layer capacity, C_{dl} and the solution resistance, R_{soln} were determined at various concentrations of $[Fe(CN)]^{3-}$ in PVP coatings. The obtained D_{app}, k°, and α values were compared with those recently obtained by normal pulse voltammetry. In addition, an equivalent circuit model is given for the impedance obtained for the redox reaction on a BPG electrode coated with a protonated PVP confining $[Fe(CN)_6]^{4-/3-}$ couple.

Recently, there has been much attention focused on the physical, electrochemical, photoelectrochemical, and other kinds of behavior of "polymer-coated electrode."[1] A key question concerning the behavior involves the kinetics of two distinct charge (ion or electron)-transfer processes: One is the "homogeneous" charge-transfer process within polymer coatings and another is the "heterogeneous" electron-transfer process between electrode and redox species (or sites) confined to polymeric domains. In a series of recent papers,[2-9] we have reported the kinetic study of these both charge-transfer processes for various polymer-coated electrode systems by means of a normal pulse voltammetry (NPV). They involve the $[Mo(CN)_8]^{4-/3-}$, $[Fe(CN)_6]^{4-/3-}$, $[W(CN)_8]^{4-/3-}$, and $[IrCl_6]^{3-/2-}$-protonated poly(4-vinylpyridine) (PVP) systems,[2-5] the $[Fe(CN)_5]^{3-/2-}$–PVP system,[4] the $[Fe(CN)_6]^{4-/3-}$–poly(*N*,*N*-dimethylaniline) system,[8] the $MV^{2+/+}$-Nafion® system (MV^{2+}: *N*,*N*′-dimethyl-4,4′-bipyridinium)[6] the poly(xylylviologen)-poly(*p*-styrenesulfonate) (PSS) system,[6] and the poly(methylviologen) (PMV), PMV–Nafion and PMV–PSS systems.[6,7,9] Some interesting results were obtained: (i) the values of the standard rate constant (k°) of the heterogeneous electron-transfer process and the apparent diffusion coefficient (D_{app}) for the diffusion-like charge-transport process within the polymer films are smaller than those for the corresponding solution-phase redox species, (ii) the k° and D_{app} depend on the concentration (c_p) of the redox species (or site) confined to the polymer, (iii) the k° and D_{app} change with the polymers confining the redox species (or site) and/or the supporting electrolytes, (iv) the transfer coefficient (α) of the heterogeneous electron-transfer process changes with c_p in some cases, and (v) there are linear relationships between $\log k^\circ$ and $\log D_{app}$. These results, which have not been completely explained yet, are of specific interest to this work.

In the present study, in order to obtain further information about the above-mentioned points, we examine the kinetics of the heterogeneous electron-transfer process of the $[Fe(CN)_6]^{4-/3-}$ couple confined to the protonated PVP coating on a pyrolytic graphite electrode as well as the homogeneous charge-transport process within the coating by means of ac impedance method, which has been recently increasingly gaining interest for characterization of the polymer films deposited on electrode surfaces (*e.g.*, glow-discharge polymer films prepared on Pt electrode from 4-vinylpyridine,[10] electropolymerized polypyrrole film,[11-13] polyacetylene film[14]). The data obtained are compared with those previously obtained by NPV. In addition, an equivalent circuit model for the impedance obtained with the redox reaction on a BPG electrode which is coated with a protonated PVP confining $[Fe(CN)_6]^{4-/3-}$ couple is represented.

Experimental

Materials. The basal-plane pyrolytic graphite (BPG) (Union Carbide Co.) disk electrodes (area: 0.17 cm^2) were prepared and mounted into glass tube with heat-shrinkable polyolefin tube as previously described.[15] Poly(4-vinylpyridine) (PVP) (Borden Inc., Philadelphia, Pa) was recrystallized from methanol–diethyl ether. Its average molecular weight was 7.4×10^5. Potassium hexacyanoferrate(III), $K_3[Fe(CN)_6]$, was of reagent grade (Merck). Aqueous solutions were prepared from doubly distilled water. The supporting electrolyte solution was 0.2 M (1 M=1 mol dm^{-3}) CF_3COONa (Aldrich) adjusted to pH 1.5 with CF_3COOH. Other chemicals were reagent grade and were used as received.

Apparatus and Procedures. The electrochemical measurement was made with a conventional potentiostatic device with three electrodes. The working electrodes were BPG disk electrodes coated with PVP films to which

$[Fe(CN)_6]^{3-}$ ions were confined electrostatically at various concentrations.[2-8, 15] The counter electrode was a spiral platinum wire with a surface area of *ca.* 20 cm^2. The reference electrode was a sodium chloride saturated calomel electrode (SSCE). All potentials were measured and are reported with respect to SSCE. The working electrode was potentiostated at a given dc potential and then a sinusoidal perturbation signal with an amplitude (ΔE) of 5.0 mV was superimposed onto the dc potential.

The ac impedance measurements were performed with a Frequency Response Analyzer (Solartron Model 1250) and a Potentiostat/Galvanostat 2000 (Toho Technical Research, Tokyo) equipped with GPIB interface. Measurements were carried out in the potentiostatic mode. The impedance diagrams were plotted in the frequency range from 1 Hz to 65 kHz at 10 points per frequency decade. The impedance data were transferred to the laboratory's minicomputer (NEC, PC-9801E) where calculation and tabulation were performed, and then graphically presented on a plotter (Hewlett Packard 7470A) in the form of complex impedance plane plots of Z'' *vs.* Z' and/or in the form of complex admittance plane plots of Y''/ω *vs.* Y'/ω, where Z and Y are the complex impedance and the complex admittance, respectively and superscripts $'$ and $''$ on Z and Y denote in-phase and quadrature (*i.e.*, 90° out-of-phase) components, and ω is the angular frequency. The tabulated data were stored on a computer disk file ready for further analysis.

Coatings of PVP were prepared by micropipetting 1 to 10 μl aliquots of a methanolic stock solution of PVP (0.5%) onto freshly cleaved BPG electrodes and allowing the solvent to evaporate.[2-5, 15, 16] Electrostatic binding of $[Fe(CN)_6]^{3-}$ ions to the protonated PVP coatings resulted from exposure of the coated electrodes to 0.2—10 mM solutions of $K_3[Fe(CN)_6]$ in a 0.2 M CF_3COONa solution (pH 1.5) for periods of 1 to 30 min depending on the desired quantity of incorporated $[Fe(CN)_6]^{3-}$. The quantities (coverage values) of $[Fe(CN)_6]^{3-}$ incorporated into the protonated PVP coatings were determined by transferring the electrodes into solutions containing only supporting electrolyte (0.2 M CF_3COONa-CF_3COOH (pH 1.5)) and integrating the current-time curves obtained when the potential was stepped to a value well beyond the voltammetric peak potential and held there until the rate of charge accumulation decreased to background levels. The coverage value was obtained in units of mol cm^{-2} and then the molar concentration (in units of mol cm^{-3}) was calculated by using the thickness of the PVP film estimated by assuming that the density of the wet PVP is 0.65 g cm^{-3}.[16]

Nitrogen gas was passed through the solutions to remove the dissolved oxygen before the measurements and over the solutions during the measurements. Experiments were conducted at 25 °C.

Results and Discussion

Impedance Measurements of the $[Fe(CN)_6]^{4-/3-}$-protonated PVP System. Figure 1 shows the typical cyclic voltammogram for the $[Fe(CN)_6]^{4-/3-}$ couple confined to the protonated PVP coating on a BPG electrode in a 0.2 M CF_3COONa solution (pH 1.5). The wave shape is similar to that for the solution-phase $[Fe(CN)_6]^{4-/3-}$ couple at a bare electrode, that is, the wave is diffusion-like, with broad peaks and a diffusion tail. The peak height and wave shape of the cyclic voltammogram remained substantially unchanged after 30 min when the electrode potential was scanned between −0.2 and 0.8 V *vs.* SSCE at 100 mV s^{-1}. The survival of the electrostatically bound $[Fe(CN)_6]^{4-/3-}$ couple for such long periods allowed us to carry out ac impedance measurements of this system.

In Fig. 2 are shown typical Cole-Cole plots (*i.e.*, plots of the quadrature component of the ac impedance *vs.* its real component) for the redox reaction of the $[Fe(CN)_6]^{4-/3-}$ couple confined to the protonated PVP film on BPG electrodes. The data in Fig. 2 show the complex plane impedance plots for the redox reaction of the $[Fe(CN)_6]^{4-/3-}$ couple at each formal redox potential. The formal redox potential for the $[Fe(CN)_6]^{4-/3-}$ confined to the protonated PVP film, which was estimated as the average of the anodic and cathodic peak potentials of the cyclic voltammograms (such as those shown in Fig. 1) for the redox reaction of the $[Fe(CN)_6]^{4-/3-}$ couple confined to the protonated PVP film, changed with the $[Fe(CN)_6]^{3-}$ concentration. Both of these curves were obtained at each formal redox potential, curve A taken at 0.275 V *vs.* SSCE and curve B at 0.265 V *vs.* SSCE. It can be seen that the impedance loci of these curves correspond to those expected for the electrochemical impedance represented by the well-known "Randles's equivalent circuit" (shown in Fig. 3).[17] The double-layer capacity C_{dl}, in parallel with the electron-transfer resistance R_{et}, gives rise to the circular part of the diagram (line I in Fig. 2). A straight line of unity slope (line II) corresponds to

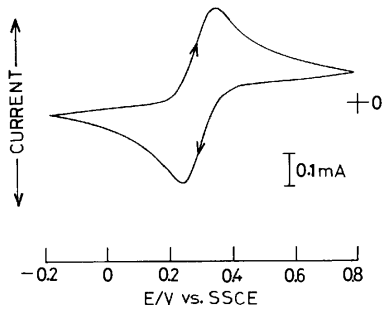

Fig. 1. A typical cyclic voltammogram for the oxidation-reduction of the $[Fe(CN)_6]^{4-/3-}$ redox couple confined to the protonated PVP film on a BPG electrode in a 0.2 M CF_3COONa solution (pH 1.5). Surface concentration of pyridine as PVP, Γ_{PVP}: 4.6×10^{-7} mol cm^{-2}. The concentration of $[Fe(CN)_6]^{3-}$ confined to protonated PVP film (thickness: 7.1×10^{-5} cm): 5.5×10^{-4} mol cm^{-3}. Scan rate: 100 mVs^{-1}.

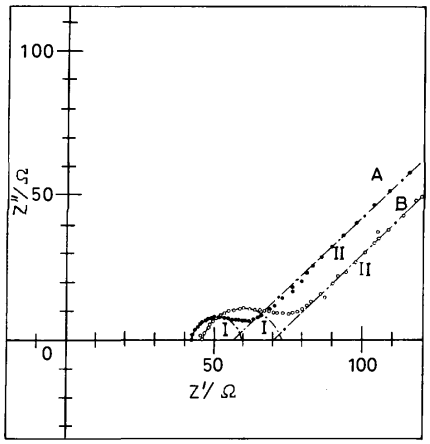

Fig. 2. Typical Cole-Cole plots for the redox reaction of the $[Fe(CN)_6]^{4-/3-}$ couple confined to the protonated PVP film on BPG electrodes in a 0.2 M CF_3COONa solution (pH 1.5). In both cases (A and B), the thicknesses of the PVP films were 8.7×10^{-5} cm and the surface concentration (Γ_{PVP}) of the pyridine site of PVP was 5.6×10^{-7} mol cm^{-2}. The concentrations (c_p) of $[Fe(CN)_6]^{3-}$ in PVP films were (A) 1.1×10^{-3} and (B) 4.1×10^{-4} mol cm^{-3}. The molar ratios of incorporated $[Fe(CN)_6]^{3-}$ to protonated pyridine site of PVP ($\Gamma_{[Fe(CN)_6]^{3-}}/\Gamma_{PVP}$) were (A) 0.17 and (B) 0.069. The dc potentails were set at (A) 0.275 and (B) 0.265 V *vs.* SSCE which were formal redox potentials in cases A and B. The amplitude of an imposed ac voltage was 5.0 mV.

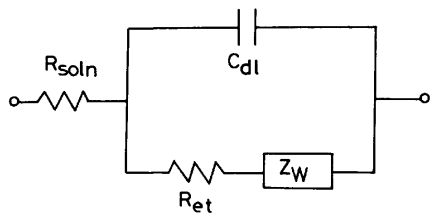

Fig. 3. Randles's equivalent circuit.
R_{soln} denotes solution resistance, R_{et} electron-transfer resistance, C_{dl} double-layer capacity, and Z_w Warburg diffusional impedance.

the Warburg diffusional impedance Z_w which arises as a consequence of diffusional polarization resulting from an imposed ac voltage.[18] Strictly speaking, the impedance plots shown in Fig. 2 are not perfectly semicircles. The center of the semicircle lies slightly below the real axis. This problem will be in detail discussed in the next section. As a first approximation, the impedance loci obtained may be expressed by the Randles's equivalent circuit. Thus, the kinetic parameters concerning the heterogeneous electron-transfer process and homogeneous charge-transport process (*i.e.*, the standard rate constant k° and the transfer coefficient α of heterogeneous electron-transfer and the apparent diffusion coefficient D_{app} for the charge-transport within polymer coatings) are estimated on the basis of the conventional analysis[18,19] of the complex impedance plane plots such as those shown in Fig. 2. According to the Randles's equivalent circuit shown in Fig. 3, the diameter of the semicircle equals the heterogeneous electron-transfer resistance R_{et}, while the double-layer capacity C_{dl} can be calculated from the angular frequency ω_{max} which corresponds to the maximum of the semicircle by using the relation $\omega_{max}R_{et}C_{dl}=1$ with $\omega=2\pi f$. From the R_{et} obtained, the k° can be calculated. The solution resistance R_{soln} is obtained from the high-frequency intercept with the real axis. Further, the diffusion coefficient can be obtained from the intercept of the line II with the real axis by knowing R_{soln} and C_{dl} and assuming that the diffusion coefficients for $[Fe(CN)_6]^{4-}$ and $[Fe(CN)_6]^{3-}$ are the same. It is apparent from curves A and B that the R_{soln} and R_{et} vary with the concentration of $[Fe(CN)_6]^{3-}$ in the PVP coatings. The values of R_{soln}, D_{app}, k°, and C_{dl} were estimated by the above-mentioned procedures and the data obtained are summarized below. The values of α were estimated from the analysis of the phase angle ϕ as mentioned below. By the similar analysis of ϕ, the k° values were also obtained.

The phase angle ϕ for the simple electrode process, $Ox+ne\rightleftarrows Red$, which is of great interest as a source of kinetic information about the heterogeneous electron-transfer reaction, can be expressed as follows:[18,19]

$$\cot\phi = 1 + \frac{(2D_{Ox}^{1-\alpha}D_{Red}^{\alpha}\omega)^{1/2}}{k^\circ}\cdot\left[\frac{1}{e^{(1-\alpha)\xi}(1+e^{-\xi})}\right] \quad (1)$$

with

$$\xi = \frac{nF}{RT}(E_{dc}-E_{1/2}), \quad (2)$$

where D_{Ox} and D_{Red} are the diffusion coefficients of Ox and Red, respectively, α is the cathodic transfer coefficient, E_{dc} is the applied dc potential, $E_{1/2}$ is the reversible half-wave potential of the Ox/Red couple, n is the number of electrons involved in the heterogeneous electron-transfer reaction, F is the Faraday constant, R is the gas constant, and T is the absolute temperature. The bracketed factor indicates that cot ϕ depends on the dc potential. That is, at large negative value of ξ, cot ϕ is close to 1 (*i.e.*, when $\xi\rightarrow-\infty$, cot $\phi\rightarrow1$). As ξ increases, cot ϕ increases and passes the maximum point. With further increase in ξ, cot ϕ decreases and at large positive value of ξ cot ϕ approaches to 1 (*i.e.*, when $\xi\rightarrow+\infty$, cot $\phi\rightarrow1$). The dc potential at which cot ϕ is a maximum is given by

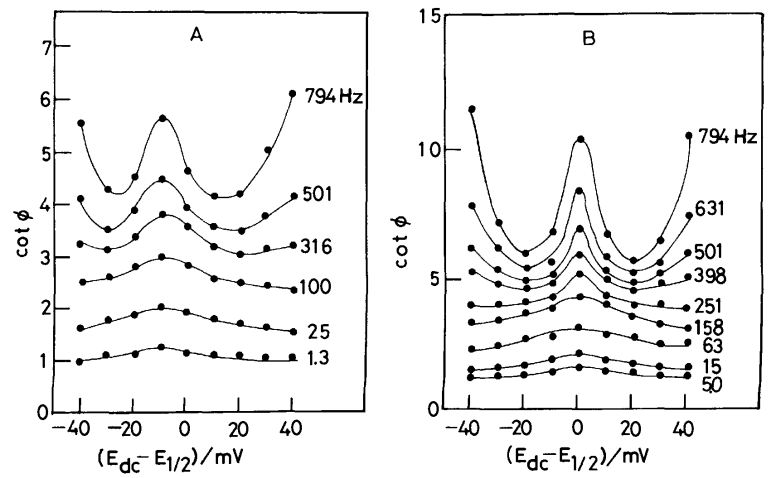

Fig. 4. Dependence of cot ϕ on E_{dc}.
The plots A and B correspond to cases A and B, respectively, shown in Fig. 2. The experimental conditions are the same as in Fig. 2. The numbers on respective plots indicate angular frequencies.

$$E_{dc} = E_{1/2} + \frac{RT}{nF} \ln \frac{\alpha}{1-\alpha}. \quad (3)$$

Thus, this maximum point is independent of nearly all experimental variables, for example, the amplitude of the applied ac voltage ΔE, the electrode area A and the angular frequency ω. The difference between $E_{1/2}$ and the potential of maximum cot ϕ provides transfer coefficient α. A typical example of such behavior is shown in Fig. 4. Note that the potential of maximum cot ϕ is independent of frequency, as predicted above. In the case of Fig. 4B (corresponding to curve B (c_p: 4.1×10^{-4} mol cm^{-3}) in Fig. 2), the maximum point is at $E_{dc}-E_{1/2}=0$ and thus α is 0.5. Similarly, in the case of Fig. 4A which corresponds to curve A (c_p: 1.1×10^{-3} mol cm^{-3}) in Fig. 2, the α value is estimated as 0.41. The dependence of α on c_p has been previously observed for the same redox system[4] as that examined here and for the other redox polymer-coated electrode systems.[2,3,5-9] The previous studies were conducted by NPV. The present data of α were in fair agreement with those obtained by NPV.

Further, it is also apparent from Fig. 4 that at higher frequencies, cot ϕ tends to increase as the value of $E_{dc}-E_{1/2}$ becomes larger. The reason for this behavior is not clear, but this may be probably due to the variation of C_{dl} in the dc potential region examined (see Fig. 7).

As can be seen from Eq. 1, plots of cot ϕ *vs.* $\omega^{1/2}$ yield k°, once α is known from the potential of maximum cot ϕ and the diffusion coefficients are known from the intercept of line II with the real axis or other measurements. Especially, at $E_{dc}=E_{1/2}$, $\xi=0$, and thus Eq. 1 can be reduced to Eq. 4

Typical examples of $[\cot\phi]_{E_{1/2}}$ *vs.* $\omega^{1/2}$ plots are shown in Fig. 5. As expected from Eq. 4, the straight

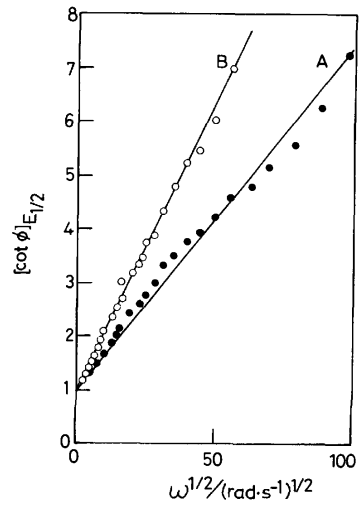

Fig. 5. Plots of $[\cot\phi]_{E_{1/2}}$ *vs.* $\omega^{1/2}$.
The plots A and B correspond to cases A and B, respectively, shown in Fig. 2. The experimental conditions and the symbols are the same as in Fig. 2. [cot $\phi]_{E_{1/2}}$ indicates cot ϕ at $E=E_{1/2}$.

$$[\cot\phi]_{E_{1/2}} = 1 + \left(\frac{D_{Ox}^{1-\alpha} D_{Red}^{\alpha}}{2}\right)^{1/2} \cdot \frac{\omega^{1/2}}{k^\circ}. \quad (4)$$

lines with the intercept of 1 on the ordinate can be obtained. The different slopes of these straight lines are ascribable to the different k°'s and/or D_{app}'s.

The data obtained for k° and D_{app} at the different concentrations of $[Fe(CN)_6]^{3-}$ in PVP coating are summarized in Fig. 6, where the data obtained by NPV are also shown for comparison. It can be seen from this figure that the k° values obtained from the R_{et} values by ac impedance method are almost equal to those obtained by NPV, while the D_{app} values are by about 1 to 2 orders of magnitude smaller than those obtained by NPV. The observed differences

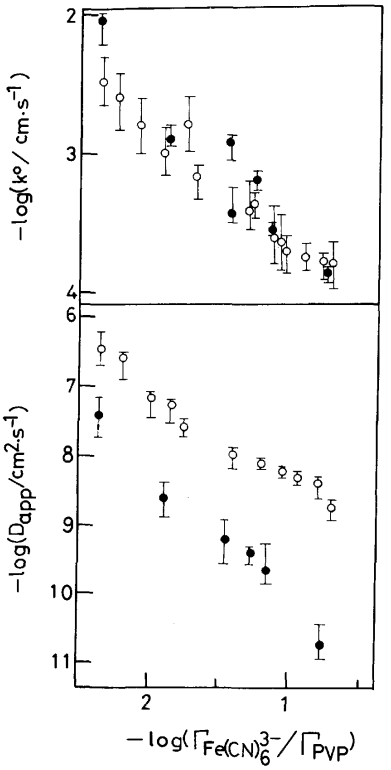

Fig. 6. Plots of the logarithms of D_{app} and k° *vs.* the logarithm of the molar ratio of incorporated $[Fe(CN)_6]^{3-}$ to the protonated pyridine site of PVP, $\Gamma_{[Fe(CN)_6]^{3-}}/\Gamma_{PVP}$. The thicknesses of the PVP films were 8.7×10^{-5} cm. Γ_{PVP}: 5.6×10^{-7} mol cm^{-2}. Supporting electrolyte: 0.2 M CF_3COONa–CF_3COOH (pH 1.5). The closed and open circles indicate the data obtained by ac impedance method and normal pulse voltammetry, respectively.

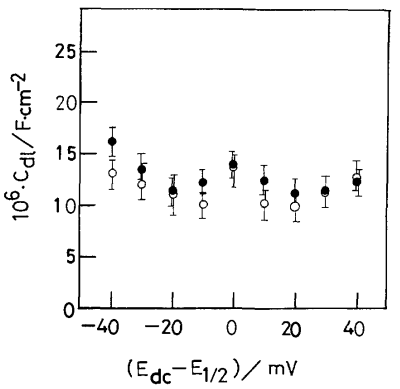

Fig. 7. Dependence of C_{dl} on $(E_{dc}-E_{1/2})$. c_p: (●) 1.1×10^{-3} and (○) 4.1×10^{-4} mol cm^{-3}. Other experimental conditions are the same as in Fig. 6.

between the D_{app} values obtained by the two methods seem not to be due to only the errors in the D_{app} estimation by ac impedance method, although the determination of D_{app} by ac impedance method is less accurate than the k° estimation. At the present stage,

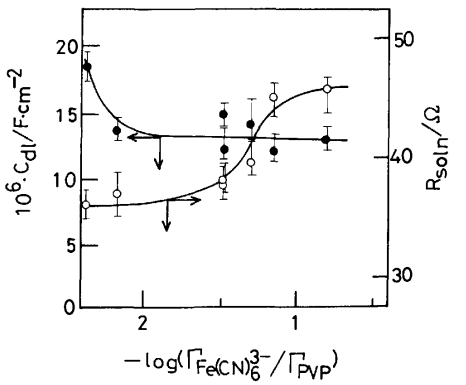

Fig. 8. Dependences of C_{dl} and R_{soln} on $-\log(\Gamma_{[Fe(CN)_6]^{3-}}/\Gamma_{PVP})$. The experimental conditions are the same as in Fig. 6. The values of C_{dl} and R_{soln} were obtained from the complex impedance loci such as those shown in Fig. 2 which were measured at the respective formal redox potentials, depending on $\Gamma_{[Fe(CN)_6]^{3-}}/\Gamma_{PVP}$.

we have no reasonable explanation for such differences in D_{app}'s, but this may be considered to be ascribed to the different time windows of these two methods in the D_{app} estimation, *i.e.*, the time window of ac impedance method is *ca.* one order of magnitude shorter than that of NPV. It is also apparent that the k° and D_{app} depend on the concentration (c_p) of $[Fe(CN)_6]^{3-}$ in polymer coatings, irrespective of the methods used. Such concentration dependences of k° and D_{app} may be understood by the same idea as that used previously:[2-6] As c_p increases, the extent of electrostatic cross-linking of PVP polymer by electrostatic force between multiply-charged anion (*i.e.*, $[Fe(CN)_6]^{3-}$) and positively charged protonated pyridine sites of PVP becomes higher and as a result the physical motion of $[Fe(CN)_6]^{3-}$ and/or supporting electrolytic ions through the film becomes more difficult.

Figure 7 shows the dependence of the double-layer capacity C_{dl} on the dc potential E_{dc}. It is obvious that C_{dl} depends on E_{dc} in the examined range of the potential. Such dependence of C_{dl} on E_{dc} seems to be almost the same irrespective of c_p. The values of C_{dl} are almost the same as those obtained with a bare BPG electrode in the same supporting electrolytic solution as that used here. Figure 8 shows the dependence of C_{dl} and the solution resistance (R_{soln}) upon c_p. The C_{dl} tends to decrease with an increase in c_p, while the R_{soln} increases with increasing c_p.

Equivalent Circuit Model for the Redox Reaction of $[Fe(CN)_6]^{4-/3-}$ Couple Confined to the Protonated PVP Coatings on BPG Electrodes. In the previous section, the impedance loci for the redox reaction of $[Fe(CN)_6]^{4-/3-}$ couple confined to the PVP coating on BPG electrodes were analyzed by assuming that the equivalent circuit for this redox reaction system can be expressed by the Randles's equivalent circuit (Fig.

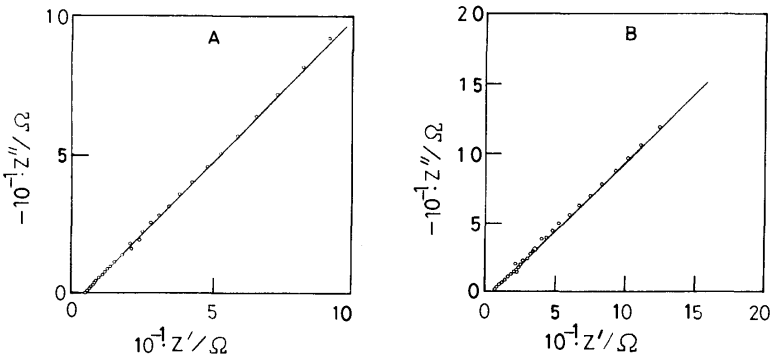

Fig. 9. The complex impedance plane plots finally obtained according to the procedure of De Levie *et al.*
The plots A and B correspond to cases A and B, respectively, shown in Fig. 2.

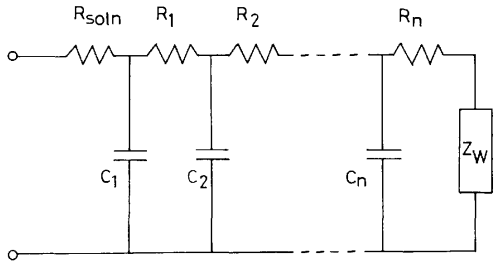

Fig. 10. The transmission line equivalent circuit obtained for the redox reaction of the $[Fe(CN)_6]^{4-/3-}$ couple confined to the protonated PVP film on BPG electrodes.
For the case A in Fig. 2, $R_{soln}=42\,\Omega$, $R_1=10\,\Omega$, $R_2=3\,\Omega$, $R_3=2\,\Omega$, $R_4=3\,\Omega$, $C_1=1.25\,\mu F$, $C_2=2\,\mu F$, $C_3=3\,\mu F$, and $C_4=6\,\mu F$, and for the case B in Fig. 2, $R_{soln}=45\,\Omega$, $R_1=14\,\Omega$, $R_2=7\,\Omega$, $R_3=5\,\Omega$, $C_1=1\,\mu F$, $C_2=1.7\,\mu F$, and $C_3=6\,\mu F$.

3). To elucidate equivalent circuit model expressing more exactly the actual redox reaction, the following procedure, originally suggested by De Levie *et al.*[20,21] for the analysis of ac impedance data, was used. The complex impedance representation such as that shown in Fig. 2 is first made and the frequency-independent resistance component R (in this case, solution resistance R_{soln}) can be obtained as an intercept on the abscissa by extrapolation of the impedance locus to infinite frequency. After subtraction of R_{soln}, the remaining impedance is transformed into an admittance, devided by ω, and the frequency-independent capacitance component C was determined as an intercept on the ordinate (*i.e.*, Y''/ω axis) by extrapolating the admittance locus to infinite frequency. A series of such procedures are repeated until the 45° straight line representing the Warburg impedance in the complex impedance plane can be obtained. The finally obtained complex plane impedance plots are shown in Fig. 9, and the equivalent circuit so obtained is shown in Fig. 10. The obtained equivalent circuit is well known as the so-called "transmission line equivalent circuit (TL equivalent circuit)."[22] The TL equivalent circuit of this type has been previously presented for the impedance for a porous electrode.[22-24] The similar equivalent circuit has been presented for electrodes where homogeneous or heterogeneous chemical processes are coupled to the heterogeneous electron-transfer step and also where adsorption of reactants or products or both occurs.[22] The obtainment of TL equivalent circuit can be considered to be due to a result of an "impedance dispersion."[25-28] This phenomenon, which is explained by the distribution of the time constants of the electrode processes, has been believed to be caused by (i) the influence of the microscopic roughness of the electrode surface, (ii) the selective adsorption phenomena, (iii) the non-uniform distribution of the current density on the surface, and so on. The same idea seems to be applicable to the present system. In order to obtain further information concerning this point, the kinetic study of electrode processes by ac impedance method is now extended to other polymer-coated electrode systems.

This work was partially supported by Grant-in-Aid for Scientific Research No. 59219008, for N. Oyama, from the Ministry of Education, Science, and Culture, Japan and the Nissan Science Foundation.

References

1) For example, R. W. Murray, "Electroanalytical Chemistry," ed by A. J. Bard, Marcel Dekker, New York (1984), Vol. 13, p. 191 and references therein.

2) N. Oyama, K. Sato, S. Yamaguchi, and H. Matsuda, *Denki Kagaku oyobi Kogyo Butsuri Kagaku*, **51**, 91 (1983).

3) K. Sato, S. Yamaguchi, H. Matsuda, T. Ohsaka, and N. Oyama, *Bull. Chem. Soc. Jpn.*, **56**, 2004 (1983).

4) N. Oyama, T. Ohsaka, M. Kaneko, K. Sato, and H. Matsuda, *J. Am. Chem. Soc.*, **105**, 6003 (1983).

5) N. Oyama, T. Ohsaka, and T. Ushirogouchi, *J. Phys. Chem.*, **88**, 5274 (1984).

6) T. Ohsaka, H. Yamamoto, M. Kaneko, A. Yamada, M. Nakamura, S. Nakamura, and N. Oyama, *Bull. Chem. Soc. Jpn.*, **57**, 1844 (1984).
7) T. Ohsaka, K. Sato, H. Matsuda, and N. Oyama, *J. Electrochem. Soc.*, in press (1985).
8) N. Oyama, T. Ohsaka, and T. Shimizu, *Anal. Chem.*, **57**, 1526 (1985).
9) N. Oyama, T. Ohsaka, H. Yamamoto, and M. Kaneko, *J. Phys. Chem.*, submitted.
10) K. Doblhofer, *Electrochim. Acta*, **25**, 871 (1980).
11) P. Burgmayer and R. W. Murray, *J. Am. Chem. Soc.*, **104**, 6139 (1982).
12) P. Burgmayer and R. W. Murray, *J. Phys. Chem.*, **88**, 2512 (1984).
13) R. A. Bull, F-R. F. Fan, and A. J. Bard, *J. Electrochem. Soc.*, **129**, 1009 (1982).
14) T. Osaka and T. Kitai, *Bull. Chem. Soc. Jpn.*, **57**, 759 (1984).
15) N. Oyama and F. C. Anson, *J. Am. Chem. Soc.*, **101**, 3450 (1979).
16) N. Oyama, S. Yamaguchi, Y. Nishiki, K. Tokuda, H. Matsuda, and F. C. Anson, *J. Electroanal. Chem.*, **139**, 371 (1982).
17) J. E. B. Randles, *Discuss. Faraday Soc.*, **1**, 11 (1947).
18) M. Sluyters-Rehbach and J. H. Sluyters, "Electroanalytical Chemistry," Vol. 4 (A. J. Bard, ed.), Marcel Dekker, New York (1970), p. 1.
19) A. J. Bard and L. R. Faulkner, "Electrochemical Methods, Fundamentals and Applications," Wiley, New York (1980), p. 316.
20) R. De Levie, J. W. Thomas, and K. M. Abbey, *J. Electroanal. Chem.*, **62**, 111 (1975).
21) R. De Levie and D. Vukadin, *J. Electroanal. Chem.*, **62**, 95 (1975).
22) E. Yeager and J. Kuta, "Physical Chemistry, An Advanced Treatise," ed by H. Eyring, Academic Press, New York, London (1970), Vol. 9A, p. 345.
23) L. E. A. Berlouis and G. J. Hills, *J. Electroanal. Chem.*, **180**, 401 (1984) and references therein.
24) R. De Levie, "Advances in Electrochemistry and Electrochemical Engineering," ed by P. Delehay and W. Tobias, Interscience, New York (1967), Vol. 6, p. 329.
25) V. Rammelt, G. Reinhard, and K. Rammelt, *J. Electroanal. Chem.*, **180**, 327 (1984) and references therein.
26) W. Scheider, *J. Phys. Chem.*, **79**, 127 (1975).
27) D. I. Leikis, E. S. Sevast'yanov, and L. L. Knots, *Russian J. Phys. Chem.*, **38**, 997 (1964).
28) R. J. Brodd, *J. Research, NBS*, **65A**, 275 (1961).

 © 1985 The Chemical Society of Japan Bull. Chem. Soc. Jpn., 58, 3259—3263 (1985)

A Study of the Inter-elemental Effect in the Carbon-furnace Atomic-absorption Spectrometry of Selenium and Mercury in Biological Samples by the Palladium-addition Method

Liu Ping, Wei Lei, Kazuko Matsumoto,†,* and Keiichiro Fuwa
Department of Chemistry, Faculty of Science, The University of Tokyo, Hongo, Bunkyo-ku, Tokyo 113
†*Department of Chemistry, School of Science and Technology, Waseda University, Okubo, Shinjuku-ku, Tokyo 160*
(Received July 13, 1985)

In the electrically-heated carbon-furnace atomic-absorption spectrometry of selenium and mercury, inter-elemental interference is present between the two elements. Mercury has no effect on selenium sensitivity in a simple inorganic selenium solution. When, however, the solution contains organic materials such as 0.5% albumin, the selenium sensitivity is decreased. The presence of mercury in addition to the organic material further decreases the sensitivity to about a half of that of a solution containing only selenium and albumin. The addition of 0.94 mmol dm^{-3} palladium ion completely removes the negative interferences due to organic materials and mercury. On the other hand, in mercury determination the presence of organic materials also decreases the mercury sensitivity. The addition of palladium, in contrast to selenium determination, enhances the mercury sensitivity about 50 times, independent of whether or not the solution contains organic materials.

It is known that some dolphins accumulate mercury and selenium in their livers at concentrations as high as 1.27 mmol dm^{-3}.[1,2] The chemical forms and the roles of these elements in livers are, however, still unknown. The concentration of the elements range from as low as 0.01 mmol dm^{-3} to more than 1.27 mmol dm^{-3}. As for the concentrations of these elements, it has been reported that the mercury concentration increases with the increase in the selenium concentration. However, there is no definite conclusion as to the cause of the accumulation of the two elements. This accumulation phenomenon is especially interesting from the viewpoints of the biochemical role of selenium in mammals, the toxicological effect of mercury, and the biochemical relation between the two elements.[3,4] Although the importance of selenium as an essential trace element is widely recognized today, no intensive study seems to have been carried out concerning the chemical forms and functions of these elements in dolphin livers. This is probably a result of the lack of a highly sensitive analytical method for these elements. Recently, the present authors have reported that the addition of palladium greatly enhances the sensitivities of both selenium and mercury, while removing interference due to organic materials in electrically-heated carbon-furnace atomic-absorption spectrometry.[5,6] In the present paper, inter-elemental interference between the two elements and the effects of organic materials on the sensitivities of the two elements in the palladium-addition method were studied. Although interference due to organic materials was investigated in previous studies[5,6] for both elements when they exist independently, it was found in the present study that the interference is completely different when the two elements co-exist in a solution. The correct estimation of such interference is indispensable to an accurate analysis of such samples as dolphin livers.

As for the palladium-addition method for selenium determination, Taga *et al.*[7] and S. X.-Quan *et al.*[8] have reported that palladium slightly enhances the sensitivity. However, our results show that the effect is remarkable and by far larger than has been reported previously. Moreover, there has been no report concerning the inter-elemental interference between selenium and mercury.

Experimental

Equipment and Measurement Conditions. A Shimadzu AA-640-13 atomic-absorption spectrometer equipped with a Shimadzu GFA-4 graphite-furnace atomizer was used. A selenium wavelength of 196.0 nm and a mercury wavelength of 253.7 nm were used. The measurement conditions were as follows; Se: dry 150 °C, 40 s, ramp mode; ash 500 °C, 60 s, ramp mode; atomize 2100 °C, 6 s, step mode; Hg: dry 150 °C, 40 s, ramp mode; ash 400 °C, 60 s, ramp mode; atomize 2000 °C, 6 s, step mode.

Reagents and Samples. Standard solutions of mercury ($HgCl_2$), selenium (Na_2SeO_3), and palladium ($PdCl_2$) were prepared by diluting a commercial 1000 mg dm^{-3} solution obtained from the Wako Co. Bovine albumin and methionine and selenomethionine from the Sigma Co. were used.

An extract solution of dolphin livers was prepared by extracting a homogenate of the livers with a 0.2 M ammonium acetate buffer (pH 7). The solution was then submitted to ultrafiltration with a YM-2 filter, Amicon Co.; the filtrate (M. W. less than 1000) was used for analysis. When comparing selenium results for undecomposed and acid-decomposed extract solutions, the filtrate was decomposed by adding HNO_3, H_2O_2, and $HClO_4$.

Procedure. A palladium solution of 9.4 mmol dm^{-3} was added to a sample solution before measurement so that the solution contained palladium at 0.94 mmol dm^{-3}.

Thirty mm^3 of the solution was then injected into a carbon furnace with an Eppendorf micropipette.

Results and Discussion

Effect of Palladium Addition for Sensitivity Enhancements of Selenium and Mercury in Biological Samples. The effect of palladium addition on selenium sensitivity was investigated; the results are shown in Fig. 1(A). Palladium neither enhances nor decreases the sensitivity for selenium when selenium exists in a solution as inorganic selenite. When selenium is added to an extract solution of dolphin livers, however, the selenium sensitivity is reduced to less than a twentieth; this negative interference is due to organic materials in the solution. However, the sensitivity is completely recovered to that of a simple inorganic selenium solution when 0.94 mmol dm^{-3} of palladium is added to the extract solution. The effect is remarkable, and it should be noted that the intercept of the calibration curve for the Pd-added extract solution corresponds to the selenium originally contained in the solution. In other words, selenium in such biological samples can be determined by the standard addition method with the aid of palladium addition.

On the other hand, in the mercury determination shown in Fig. 1 (B), palladium addition enhances the sensitivity about 50 times, even in a simple inorganic solution. Mercury sensitivity in an extract solution is so much decreased that no signal is observed. However, with the addition of palladium, mercury sensitivity is recovered to about a half of that of a simple inorganic mercury solution with palladium added.

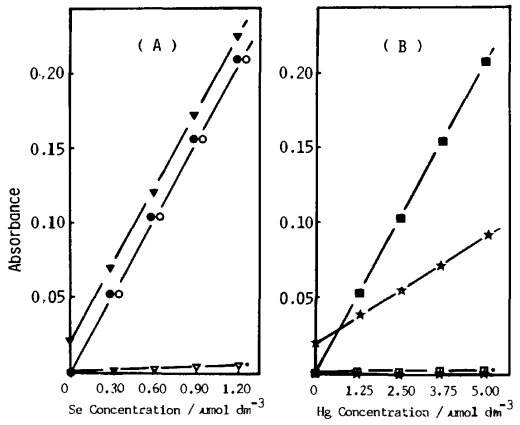

Fig. 1. Effect of palladium addition on selenium and mercury sensitivities.
(A) ○: An aqueous solution, ●: ○+Pd 0.94 mmol dm^{-3}, ▽: an extract solution of dolphin's livers, ▼: ▽+Pd 0.94 mmol dm^{-3}, (B) □: An aqueous solution, ■: □+Pd 0.94 mmol dm^{-3}, ☆: an extract solution of dolphin's livers, ★: ☆+Pd 0.94 mmol dm^{-3}.

Effect of Organic Materials on the Palladium-enhancement Effect. In order to study the effect of organic materials in the palladium-addition method, albumin was added to a selenium (1.27 μmol dm^{-3}) or mercury (9.97 μmol dm^{-3}) solution at various concentrations and the sensitivities were compared. Figure 2 clearly exhibits the effect. The existence of organic material, even at concentrations of less than 1%, drastically decreases the sensitivities of both selenium and mercury. The addition of palladium, however, completely restores the sensitivity to that of a solution without organic materials, even when albumin is present at concentrations of up to 2.0% during selenium determination. On the other hand, mercury sensitivity is increased by palladium addition at any albumin concentration, as is shown in Fig. 2.

Effect of Mercury in the Palladium-addition Method of Selenium. For the accurate determinations of mercury and selenium in extract solutions of dolphin's livers, inter-elemental effects between the two elements must be studied, especially with regard to the present palladium-addition method. The effect of palladium addition in the selenium analysis of a solution containing mercury is shown in Fig. 3. As Fig. 3 shows, the existence of mercury or the addition of palladium has no effect on the selenium sensitivity in a simple inorganic selenium solution. However, when the solution contains albumin (0.5%), the selenium sensitivity is decreased to about one-fifth of that of a simple inorganic selenium solution. The addition of palladium to a solution containing both selenium and organic materials restores the selenium sensitivity to that of a simple inorganic solution. Figure 3 also shows that the presence of mercury in addition to albumin further decreases the selenium sensitivity to about a half of that of a selenium solution containing only albumin.

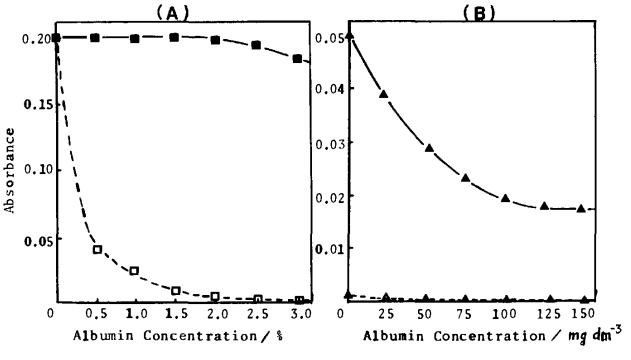

Fig. 2. Interference due to albumin in selenium and mercury determinations and effect of palladium addition for removal of the interference and enhancement of the sensitivity.
(A) Se 1.27 μmol dm^{-3}, □: without Pd, ■: with Pd (0.94 mmol dm^{-3}), (B) Hg 9.97 μmol dm^{-3}, △: without Pd, ▲: with Pd (0.94 mmol dm^{-3}).

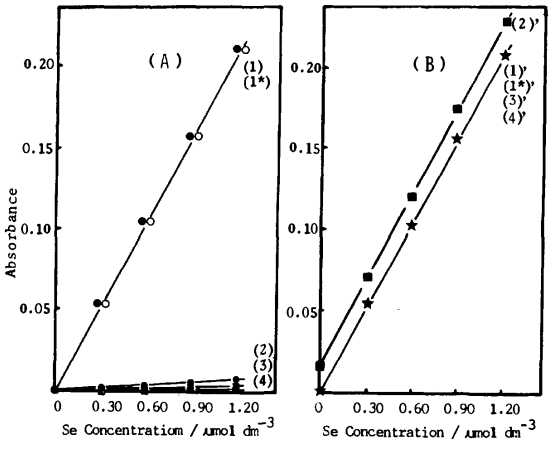

Fig. 3. Interferences of mercury and albumin on selenium determination and removal of the interferences by palladium addition.
(1): An aqueous selenium solution, (1*): (1)+Hg 1.25 μmol dm^{-3}, (2): an extract solution of dolphin's livers, (3): (1)+albumin 0.5%, (4): (3)+Hg 1.25 μmol dm^{-3}, (1)': (1)+Pd 0.94 mmol dm^{-3}, (1*)': (1*)+Pd 0.94 mmol dm^{-3}, (2)': (2)+Pd 0.94 mmol dm^{-3}, (3)': (3)+Pd 0.94 mmol dm^{-3}, (4)': (4)+Pd 0.94 mmol dm^{-3}.

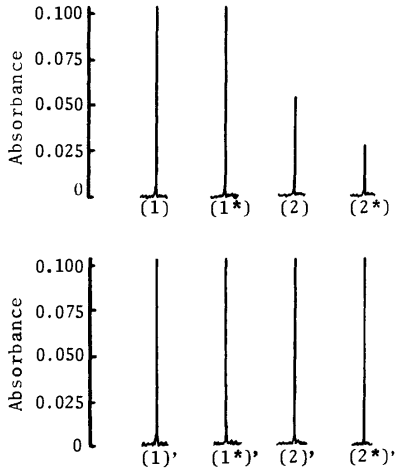

Fig. 4. Selenium sensitivity dependence on the chemical form and effect of palladium addition.
(1): Selenite (Se 0.63 μmol dm^{-3}), (1*): (1)+Hg 0.63 μmol dm^{-3}, (2): selenomethionine (Se 0.64 μmol dm^{-3}), (2*): (2)+Hg 0.63 μmol dm^{-3}, (1)': (1)+Pd 0.94 mmol dm^{-3}, (1*)': (1*)+Pd 0.94 mmol dm^{-3}, (2)': (2)+Pd 0.94 mmol dm^{-3}, (2*)': (2*)+Pd 0.94 mmol dm^{-3}.

The addition of palladium to such a solution completely restores the sensitivity. All the severe negative interferences due to organic materials and/or mercury can be completely removed by palladium addition, as is shown in (B) of Fig. 3.

In order to examine whether or not the selenium sensitivity is dependent on the chemical form, the sensitivities of selenite and selenomethionine solutions were compared. The effects of palladium addition were also compared for the two solutions; the results are shown in Fig. 4. It should be noted that the selenium sensitivity of selenomethionine is less than a half of that of a selenite solution. The presence of 0.63 μmol dm^{-3} of mercury does not affect the selenium sensitivity in a selenite solution. However, the sensitivity is decreased to nearly a half when selenium exists as selenomethionine. Considering the results of Figs. 3 and 4 together, it can be inferred that mercury decreases the selenium sensitivity only in organic-matrix solutions. "Organic matrix" means that either the solution contains organic substances in addition to inorganic selenium or selenium is contained as organic selenium molecules. The addition of palladium completely restores the sensitivity in any organic-matrix solution with or without mercury.

Effect of Selenium in the Palladium-addition Method of Mercury. It was found that selenium additionally enhances mercury sensitivity when added together with palladium. Figure 5 shows the dependence of the mercury sensitivity on the selenium concentration in a solution to which

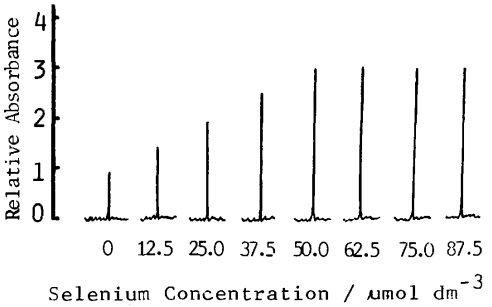

Fig. 5. Enhancement effect of selenium in palladium addition method of mercury. The solution contains Hg 0.05 mmol dm^{-3} and Pd 0.94 mmol dm^{-3}.

0.94 mmol dm^{-3} of palladium has already been added. The mercury sensitivity is linearly increased with an increase in the selenium concentration until it reaches 50 μmol dm^{-3}. At selenium concentrations higher than 50 μmol dm^{-3}, however, no more sensitivity enhancement is observed. It should be noted that 50 μmol dm^{-3} of selenium corresponds to a 1:1 molar ratio of Se and Hg; this suggests that the sensitivity enhancement may result from a 1:1 complex formation between Se and Hg, a complex which is retained in a carbon furnace up to higher temperatures than when only mercury is present. A similar enhancement effect for mercury by sulphur addition has been reported by Ediger.[9] The effect is believed to be due to the formation of mercury sulphide.

Effect of Palladium Addition for Mercury Determination in Solutions of Various Matrices. The effects

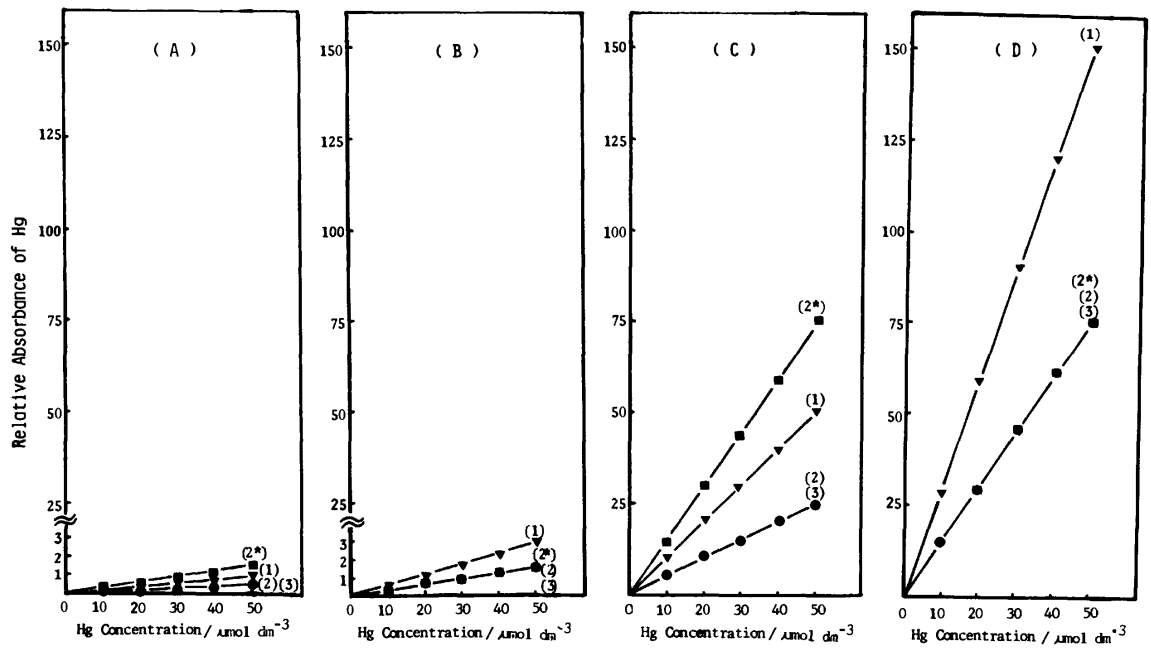

Fig. 6. Calibration curves for mercury in the presence or absence of selenium, organic materials and palladium. A (1): An aqueous solution of mercury (0.05 mmol dm^{-3}), (2): (1)+methionine 0.067 mmol dm^{-3}, (2*): (1)+selenomethionine 0.051 mmol dm^{-3}, (3): (1)+albumin 60 mg dm^{-3}. B (1): A(1)+selenite (Se 0.064 mmol dm^{-3}), (2): A(2)+selenite (Se 0.064 mmol dm^{-3}), (2*): same as A(2*), (3): A(3)+selenite (Se 0.064 mmol dm^{-3}). C (1): A(1)+Pd 0.94 mmol dm^{-3}, (2): A(2)+Pd 0.94 mmol dm^{-3}, (2*): A(2*)+Pd 0.94 mmol dm^{-3}, (3): A(3)+Pd 0.94 mmol dm^{-3}. D (1): A(1)+Se 0.064 mmol dm^{-3}+Pd 0.94 mmol dm^{-3}, (2): A(2)+Se 0.064 mmol dm^{-3}+Pd 0.94 mmol dm^{-3}, (2*): A(2*)+Pd 0.94 mmol dm^{-3}, (3): A(3)+Se 0.064 mmol dm^{-3}+Pd 0.94 mmol dm^{-3}.

Table 1. Comparison of selenium determinations for undecomposed and acid-decomposed extract solutions of dolphin livers (mmol dm^{-3})

Sample[a)]	Undecomposed solution	Acid-decomposed solution
1	26.8	24.1
2	14.1	17.1
3	16.4	15.2
4	9.5	10.3

a) One g of liver was extracted with a 10 cm^3 solution. The Extract solutions were as follows: 1, 1 mol dm^{-3} phosphate buffer (pH 7); 2, 1 mol dm^{-3}, phosphate buffer (pH 7) +1% SDS; 3, 1% NaCl; 4, 1 mol dm^{-3} phosphate buffer (pH 7) +2% Triton.

of selenium compounds, organic materials, and palladium on the mercury sensitivity are summarized in Fig. 6. Figure 6 (A) shows that the mercury sensitivity is reduced to almost a half of that of a simple mercury solution when methionine or albumin is present. On the contrary, the presence of selenomethionine increases the sensitivity about 1.5 times. When inorganic selenium is added to the solution of (A) in Fig. 6, the sensitivity is increased about 3 times. The fact that the sensitivities of (2) and (3) in Fig. 6 (B) are almost equal to that of (2*) suggests that the enhancement effect of selenium is independent of its chemical form. Although selenium enhances the mercury sensitivity in organic-matrix solutions, it cannot completely remove the negative interference due to organic materials, as is shown in Fig. 6 (B). Figure 6 (C) shows the effect of palladium. The addition of palladium enhances the mercury sensitivity about 50 times. This enhancement ratio is independent of whether the solution contains organic materials or selenium. The addition of both selenium and palladium enhances the mercury sensitivity about 150 times. This enhancement ratio is equal to the sum of the enhancement ratios of the two elements. Table 1 compares the selenium determinations obtained for undecomposed and acid-decomposed extract solutions of dolphin livers. All the measurements were done by means of the palladium-addition method; the results show that the present palladium-addition method makes possible the direct determination of selenium in an undecomposed solution containing organic materials.

The inter-elemental effects of selenium and mercury may be summarized as follows. Mercury decreases the selenium sensitivity, whereas selenium enhances the mercury sensitivity. The presence of organic materials decreases the sensitivities for both elements. The addition of palladium to a selenium solution

with an organic matrix completely removes the negative interferences caused by organic materials and mercury, whereas the addition of palladium enhances the mercury sensitivity in solutions with both inorganic and organic matrices.

References

1) J. H. Koeman, W. H. M. Peeters, C. H. M. Koudstaal-Hol, P. S. Tjioe, and J. J. M. Goeji, *Nature*, **245**, 385 (1973).

2) P. A. Pearce, J. M. Grucht, and J. A. Keith, Pesticide Section, Canadian Wildlife Service, Manuscript Reports, No. 24 (1973).

3) J. J. Rotruck, A. L. Pope, H. E. Ganther, A. B. Swanson, D. G. Hafeman, and W. G. Hoekstra, *Science*, **179**, 588 (1973).

4) W. G. Hoekstra, D. G. Hafeman, S. H. Oh, R. A. Sunde, and H. E. Ganther, *Fed. Proc.*, **32**, 885 (1973).

5) L. Ping, K. Matsumoto, and K. Fuwa, *Anal. Chim. Acta*, **171**, 279 (1985).

6) L. Ping, W. Lei, K. Matsumoto, and K. Fuwa, *Anal. Sci.*, **1**, 257 (1985).

7) Y. Taga, T. Yonemoto, A. Iwase, and K. Nakagawa, *Bunseki Kagaku*, **29**, 248 (1980).

8) S. X.-Quan and N. Z.-Ming, *Acta Chim. Sinica*, **39**, 575 (1981).

9) R. D. Ediger, *At. Abs. News*, **14**, 127 (1975).

A Synthesis of a Versatile Intermediate Leading to Thienamycin Analogs[1)]

Hiroshi MARUYAMA,*,† Masao SHIOZAKI, and Tetsuo HIRAOKA
Process Development Laboratories† and Chemical Research Laboratories, Sankyo Co., Ltd., Hiromachi, Shinagawa-ku, Tokyo 140
(Received May 8, 1985)

L-Threonine was converted to a versatile azetidinone derivative stereospecifically in 3 steps. This azetidinone was further transformed to (3*S*,4*R*)-3-[(*R*)-1-hydroxyethyl]-1-(4-methoxybenzyl)-4-[(phenylthio)-carbonylmethyl]-2-azetidinone (*S*-Phenyl thioester), a key intermediate for the synthesis of thienamycin and it's biologically active analogs. Since the thiol part of this *S*-phenyl thioester can be exchanged easily with other complex or useful thiols under mild conditions, important *S*-thioester precursors for the production of carbapenem analogs were obtained in high yield.

After the discovery of thienamycin,[2)] various analogs of 1-carbapenem antibiotics have been found and attracted many organic chemists to synthesize these compounds, as a result of which several synthetic methods have been reported.[3)] Recently the cyclization reaction for the formation of the carbapenem nucleus has been disclosed utilizing the trialkoxyphosphoranylidene-substituted *S*-thioester reaction,[4)] which is one of a number of versatile methods for the synthesis of carbapenem analogs. Thus the *S*-thioester of 4-carboxymethyl-2-azetidinone became an important intermediate in this route.

We have reported stereocontrolled syntheses of chiral and racemic intermediates (2-azetidinones) for thienamycin from D-*allo*-threonine,[5b)] *trans*-crotonic acid and L-threonine.[5)] This report describes the stereoselective synthesis of a precursor for thienamycin analogs (*S*-thioesters) from L-threonine by a stereocontrolled method.

(2*S*,3*R*)-2-Bromo-3-hydroxybutyric acid (**1**) was derived in high yield from L-threonine according to a known method.[6)] The butyric acid **1** was condensed with *N*-(4-methoxybenzyl)glycine *t*-butyl ester (**2**) to give the amide **3**. The amine **2** was synthesized from *t*-butyl bromoacetate and 4-methoxybenzylamine. The compound **3** was purified by silica-gel chromatography and then converted in good yield to the *cis*-epoxy amide **4** by treating with 1.05 equiv of lithium hexamethyldisilazide in tetrahydrofuran (THF). Without isolation, this epoxy amide **4** was cyclized

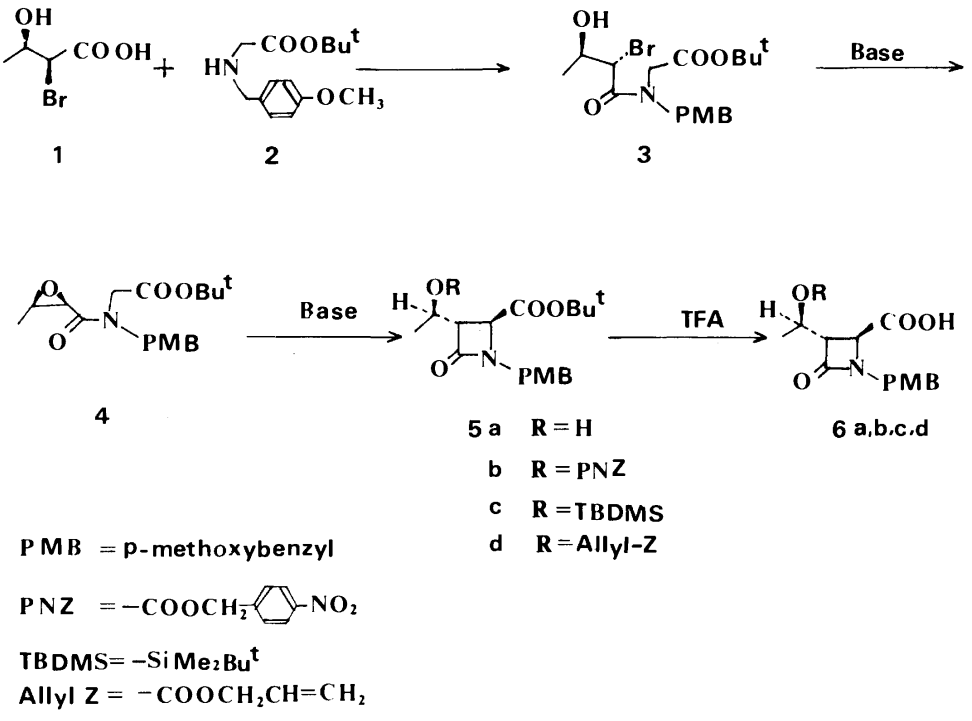

Scheme 1.

with lithium hexamethyldisilazide (1.05 equiv) in THF to give *t*-Butyl (2*S*,3*S*)-3-[(*R*)-1-hydroxyethyl]-1-(4-methoxybenzyl)-4-oxo-2-azetidinecarboxylate (**5a**) in 63.9% yield from the amide **3**. If necessary, this epoxy amide can be isolated as a stable intermediate.

As mentioned in the previous paper,[5b] when cyclization reaction was carried out at −78 °C, the reaction products contained cis-isomer as a minor product. But when the same reaction was run at 20—23 °C only one product of *trans*-**5a** was obtained without containing the cis-isomer, suggesting a kinetic control is operating. Thus in the compound **5a** the stereochemistry at the 3 and 4 position of the β-lactam and the side chain is exactly correct for thienamycin. These exact configurations were only attained through the epoxide **4** by the double inversion at the compound **3**. The hydroxyl function of **5a** was protected by appropriate groups such as *p*-nitrobenzyloxycarbonyl, *t*-butyldimethylsilyl, and allyloxycarbonyl group. The de-esterification of **5a**, **b**, **d** was carried out by treating with trifluoroacetic acid (TFA) at 0 °C, to give the corresponding free acid **6a**, **b**, **d** in quantitative yield. However the *t*-butyldimethylsilyl group of **5c** was not stable to TFA due to partial desilylation, so **5c** was de-esterified with sodium hydroxide (1.0 equiv) in ethanol. These

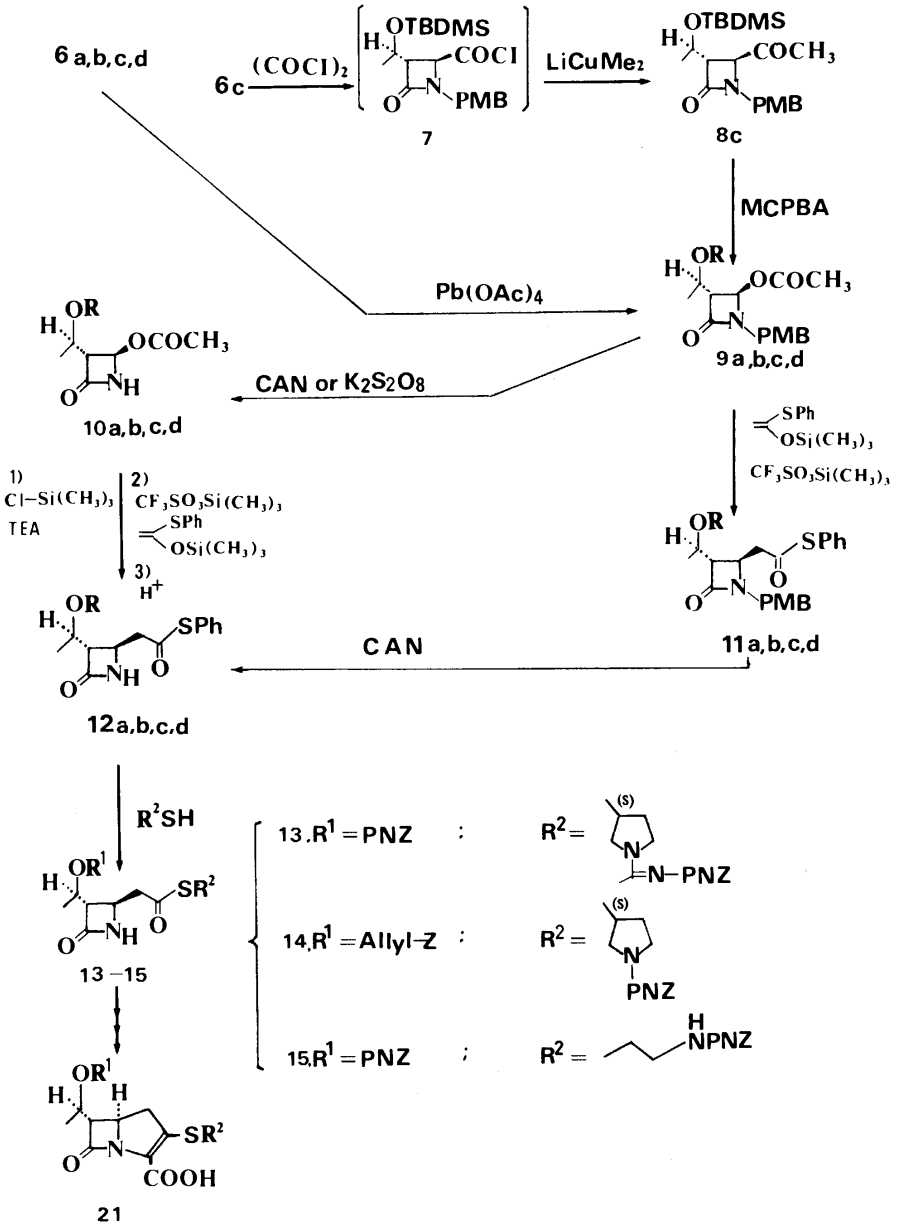

Scheme 2.

carboxylic acids were converted to 4-acetoxy-2-azetidinone derivatives by two methods: (i) The Baeyer-Villiger method[7] after conversion of the carboxylic acid to the acetyl group and (ii) the lead tetraacetate method.[8]

The carboxylic acid **6c** was converted with oxalyl di-chloride to the acid chloride **7** which was transformed into 4-acetyl derivative **8c** by reaction with lithium dimethylcuprate (I). By the Baeyer-Villiger reaction of **8c** with *m*-chloroperbenzoic acid (MCPBA), 4-acetoxy-2-azetidinone **9c** was obtained quantitatively. In this reaction the 3,4-*trans*-2-azetidinone derivative **9c** was formed selectively with retention of configuration as reported by Mislow and Brenner.[9] When this Baeyer-Villiger reaction was carried out starting from *N*-(2,4-dimethoxybenzyl) derivative **17**, no desired product **18** was obtained due to oxidation of the 2,4-dimethoxybenzene moiety. The same compound **9c** was also produced by treatment of **6c** with lead tetraacetate in *N,N*-dimethylformamide (DMF)–acetic acid.[10] Similarly, the carboxylic acids **6a**, **6b**, and **6d** gave the acetoxy derivatives **9a**, **9b**, and **9d**, respectively, by the same reaction in good yields. When starting from **6a**, a trace amount of the 3,4-cis isomer of **9a** was isolated. Removal of the *N*-protecting group of **9b,c,d** was achieved by treatment with cerium (IV) ammonium nitrate (CAN) or potassium peroxodisulfate ($K_2S_2O_8$) in good yield to afford **10b,c,d** respectively, which were identified by comparison with authentic samples. The same deprotection reaction by electrolysis seemed to be possible but tried without success (Pt or graphite as electrodes). The acetate **10b**, **c**, **d** were converted to the *S*-thioesters **12b**, **c**, **d** in quantitative yield by reaction with 1-phenylthio-1-trimethylsiloxyethylene in dichloromethane in the presence of trimethylsilyl trifluoromethanesulfonate as catalyst after trimethylsilylation of the N-atom.[11] The compound **9b—d** were also transformed to the 4-[(phenylthio)carbonylmethyl]-2-azetidinone derivatives **11b—d** in high yields by the same procedure. The *p*-methoxybenzyl group of **11b—d** was also removed with CAN in the same way to give the deprotected *S*-thioesters **12b—d**, respectively.

Generally *S*-thioesters such as **15** were synthesized by the condensation of thiol (**20**) and carboxylic acid (**19**) which was obtained, for example by reaction of the 4-acetoxy derivative **10b** with 1,1-bis(trimethylsiloxy)ethylene in the presence of a catalytic amount of trimethylsilyl trifluoromethanesulfonate. However, the yield of this condensation was unsatisfactory due to interaction of the triflate with the nitrogen part of the thiol **20**. Thus *S*-thioester exchange of **12** was tried and found to proceed under mild conditions to furnish many kind of useful *S*-thioesters, which were difficult to synthesize by the usual condensation reaction of an acid and thiol using dicyclohexylcarbodiimide. For example, in the case of the thiol **20** the reaction with **12b** proceeded smoothly in dichloromethane at room temperature in the presence of triethylamine to give the *S*-thioester **13**. This exchange reaction may be controlled by the acidity and nucleophilicity of the thiols, which is closely connected with the equilibrium constant. The compound **13** was already transformed to the carbapenem **21** by the cyclization using trialkyl phosphite.[4]

Thus we succeeded in finding a very simple method for the synthesis of the useful *S*-thioester derivatives. It seems that by this method several problems for the total synthesis of the trienamycin analogs were resolved. This *S*-thioester exchange method is useful and versatile together with an application of the previously reported cyclization by a new Wittig reaction.[4]

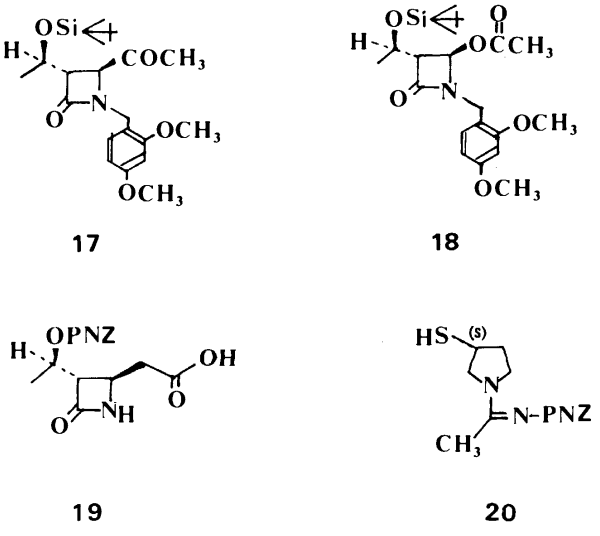

Scheme 3.

Experimental

All melting points were uncorrected. Optical rotation were obtained using a Perkin-Elmer 241 Polarimeter. ^{1}H NMR spectra were determined at 60 MHz with a Varian T-60 spectrometer using tetramethylsilane as internal standard. The IR absorption spectra were determined on a Jasco IR A-2 spectrophotometer. Preparative TLC was performed on silica-gel plate (Merk 60 PF254). Elemental analyses were performed by the Analytical Center of the Analytical and Metabolic Research Laboratories, Sankyo Company, Limited.

(2S,3R)-N-(4-Methoxybenzyl)-N-(t-butoxycarbonylmethyl)-2-bromo-3-hydroxybutyramide (3). To a stirred solution of (2*S*,3*R*)-2-bromo-3-hydroxybutyric acid **1** (50.96 g, 0.278 mol) were added amine **2** (70.14 g, 0.278 mol) in THF (1L), and *N,N'*-dicyclohexylcarbodiimide (57.3 g, 0.278 mol) at 20—30 °C with stirring. After 30 min, the precipitated urea

was filtered off and washed with a small amount of THF. The combined filtrate was evaporated, and chromatographed on silica-gel (900 g) with cyclohexane-EtOAc (2:1) to give amide **3** (81.9 g, 71.5%) as an oil; IR (Liquid) 1750, 1660 cm^{-1}; ^1H NMR ($CDCl_3$) δ=1.25 (3H, d, J=6.5 Hz), 1.40 (9H, s), 3.75 (3H, s), 3.90 (1H, d, J=3.5 Hz), 3.90—4.30 (1H, m), 4.20 and 4.75 (2H, ABq, J=12.5 Hz), 4.30 and 4.65 (2H, ABq, J=25.0 Hz), 6.70—7.30 (4H, m). MS m/z 336 (−79, Br).

*t-Butyl (2S,3S)-3-[(R)-1-Hydroxyethyl]-1-(4-methoxybenzyl)-4-oxo-2-azetidinecarboxylate (**5a**).* To a stirred solution of amide **3** (51.7 g, 0.124 mol) in THF (200 mL) was added lithium hexamethyldisilazide [$LiN(SiMe_3)_2$] solution [prepared by addition of n-BuLi solution (81.5 mL of 1.6 M[†] hexane solution, 0.13 mol) into a solution of hexamethyldisilazane (27 mL, 0.128 mol) in THF (75 mL) under nitrogen over a period of 15 min at 2—3 °C]. After 5 min the temperature was elevated to 20—23 °C and the same amount of [$LiN(SiMe_3)_2$] solution was further added to this solution at 20—23 °C and stirring was continued for 30 min. The reaction mixture was quenched with 10% HCl and evaporated to give an oily residue which was dissolved in ethyl acetate (EtOAc). This solution was washed with 5% $NaHCO_3$ and brine, dried ($MgSO_4$) and evaporated to give a crude oil which was chromatographed on silica-gel (1.5 Kg). Elution with cyclohexane-EtOAc (1:1) gave **5a** (26.6 g, 63.9%) as crystals; mp 75—76 °C; IR (KBr) 1760 cm^{-1}; ^1H NMR ($CDCl_3$) δ=1.25 (3H, d, J=6.5 Hz), 1.40 (9H, s), 2.50 (1H, d, J=4.0 Hz), 3.15 (1H, dd, J=3.0, 4.5 Hz), 3.75 (3H, s), 3.90 (1H, d, J=3.0 Hz), 4.00—4.40 (1H, m), 4.05 and 4.75 (2H, ABq, J=14.5 Hz), 6.80 (2H, d), 7.10 (2H, d). Found: C, 64.7; H, 7.47; N, 4.18%. Calcd for $C_{18}H_{25}NO_5$: C, 64.5; H, 7.51; N, 4.18%.

*t-Butyl (2S,3S)-3-[(R)-1-(t-Butyldimethylsiloxy)ethyl]-1-(4-methoxybenzyl)-4-oxo-2-azetidinecarboxylate (**5c**).* A mixture of **5a** (1.15 g, 3.43 mmol), t-butyldimethylsilyl chloride (1.48 g, 6.86 mmol) and 4-dimethylaminopyridine (837 mg, 6.86 mmol) in DMF (5 mL) was stirred for 16 h at room temperature. The reaction mixture was diluted with EtOAc, washed with dil HCl, water, 5% $NaHCO_3$, saturated NaCl, and dried ($MgSO_4$). After evaporation, the oily residue was chromatographed on silica-gel. Elution with cyclohexane-EtOAc (1:1) gave a crude **5c** (2.08 g) as an oil which was employed for the next reaction without further purification.

*t-Butyl (2S,3S)-1-(4-Methoxybenzyl)-3-[(R)-1-(p-nitrobenzyloxycarbonyloxy)ethyl]-4-oxo-2-azetidinecarboxylate (**5b**)* and *t-Butyl (2S,3S)-3-[(R)-1-(allyloxycarbonyloxy)ethyl]-1-(4-methoxybenzyl)-4-oxo-2-azetidinecarboxylate (**5d**).* 2-Azetidinone **5a** was converted to **5b** and **5d** by the similar reaction as in the case of **5c**.

Physical data **5b**: mp 75—76 °C; IR (KBr) 1770, 1760 cm^{-1}; ^1H NMR ($CDCl_3$) δ=1.35 (3H, d, J=6.5 Hz), 1.43 (9H, s), 3.40 (1H, dd, J=3.0, 7.0 Hz), 3.70 (3H, s), 3.85 (1H, d, J=3.0 Hz), 4.00 and 4.75 (2H, ABq, J=14.5 Hz), 4.90—5.31 (1H, m), 5.2 (2H, s), 6.50 (2H, d), 7.10 (2H, d), 7.81 (2H, d), 8.15 (2H, d). Found: C, 60.5; H, 5.82; N, 5.48%. Calcd for $C_{26}H_{30}N_2O_9$: C, 60.7; H, 5.88; N, 5.45%. **5d**: IR (Liquid) 1760 cm^{-1}; ^1H NMR ($CDCl_3$) δ=1.35 (3H, d, J=6.5 Hz), 1.40 (9H, s), 3.25 (1H, dd, J=3.0, 4.5 Hz), 3.75 (3H, s), 3.85 (1H, d, J=3.0 Hz), 4.00 and 4.75 (2H, ABq, J=14.5 Hz), 4.56 (2H, d, J=6.0 Hz), 4.92—5.20 (1H, m), 5.11—5.50 (2H, m), 5.70—6.10 (1H, m), 6.80 (2H, d), 7.15 (2H, d). MS m/z 419 (M^+).

*(2S,3S)-1-(4-Methoxybenzyl)-3-[(R)-1-(p-nitrobenzyloxycarbonyloxy)ethyl]-4-oxo-2-azetidinecarboxylic Acid (**6b**) and (2S,3S)-3-[(R)-1-(Allyloxycarbonyloxy)ethyl]-1-(4-methoxybenzyl)-4-oxo-2-azetidinecarboxylic Acid (**6d**).* 2-Azetidinone **6b** and **6d** were obtained from **5b** and **5d** with TFA as an oil in 99.2, 79.2% yield, respectively. Physical data: **6b**; IR (Liquid) 1760 cm^{-1}; ^1H NMR ($CDCl_3$) δ=1.25 (3H, d, J=6.5 Hz), 3.25 (1H, dd, J=3.0, 4.5 Hz), 3.75 (3H, s), 4.10 and 4.70 (2H, ABq, J=16 Hz), 4.11 (1H, d, J=3.0 Hz), 4.90—5.20 (1H, m), 5.10 (2H, s), 6.75 (2H, d), 7.10 (2H, d), 7.35 (2H, d), 8.15 (2H, d). MS m/z 456 (M^+). **6d**: ^1H NMR ($CDCl_3$) δ=1.40 (3H, d, J=6.5 Hz), 3.45 (1H, dd, J=3.0, 5.0 Hz), 3.79 (3H, s), 4.02 (1H, d, J=3.0 Hz), 4.00 and 4.85 (2H, ABq, J=14.0 Hz), 4.60 (2H, d, J=5.5 Hz), 5.00—5.31 (1H, m), 5.10—5.61 (2H, m), 5.70—6.20 (1H, m), 6.80 (2H, d), 7.15 (2H, d). MS m/z 363 (M^+).

*(2S,3S)-3-[(R)-1-(t-Butyldimethylsiloxy)ethyl]-1-(4-methoxybenzyl)-4-oxo-2-azetidinecarboxylic Acid (**6c**).* To a stirred solution of crude **5c** (230 mg) in EtOH (1.3 mL), was added 1 M NaOH (0.9 mL) and stirring continued at 60—70 °C for 2 h. The reaction mixture was diluted with water (10 mL) and acidified to pH 2 with dil HCl. The mixture was extracted with EtOAc and washed with water, saturated NaCl and dried ($MgSO_4$). After evaporation **6c** was obtained as crystals (201 mg, 100%): mp 107—109 °C; IR (KBr) 1758, 1720 cm^{-1}; ^1H NMR ($CDCl_3$) δ=0.30 (6H, s), 0.72 (9H, s), 1.10 (3H, d, J=6.0 Hz), 3.71 (3H, s), 3.72 (1H, t, J=2.5 Hz), 4.05 (1H, d, J=2.5 Hz), 4.07 and 4.70 (2H, ABq, J=15.0 Hz), 4.20 (1H, m), 6.81 (2H, d), 7.20 (2H, d), 7.91 (1H, s). Found: C, 60.8; H, 7.99; N, 3.51%. Calcd for $C_{20}H_{31}O_5NSi$: C, 61.1; H, 7.89; N, 3.56%.

*(2S,3S)-3-[(R)-1-(t-Butyldimethylsiloxy)ethyl]-1-(4-methoxybenzyl)-4-oxo-2-azetidinecarbonyl Chloride (**7**).* To a solution of **6c** (197 mg, 0.5 mmol) in THF (2 mL) and DMF (1 mL) was added oxalyl dichloride (0.5 mL) at 0 °C, and kept at 0 °C overnight. After evaporation, the resulted oily residue was used in the next reaction without purification.

*(3S,4S)-4-Acetyl-3-[(R)-1-(t-butyldimethylsiloxy)ethyl]-1-(4-methoxybenzyl)-2-azetidinone (**8c**).* To a stirred suspension of CuI (477 mg, 2.5 mmol) in ether (5 mL) was added a solution of MeLi (1.6 M solution in ether, 3.5 mmol) at 0 °C under nitrogen. After 5 min stirring at 0 °C, the solution was cooled to −78 °C, and a solution of acid chloride **7** (0.5 mmol) in ether (2 mL) and THF (0.5 mL) was added. After 15 min stirring at −78 °C, the reaction mixture was quenched with MeOH (1 mL), diluted with EtOAc, washed with water, saturated NaCl and dried ($MgSO_4$). After evaporation, the oily residue was chromatographed on silica gel. Elution with cyclohexane-EtOAc (3:1) gave **8c** (141 mg, 72% yield). Physical data of **8c**: IR (Liquid) 1758, 1710 cm^{-1}; ^1H NMR ($CDCl_3$) δ=0.04 (3H, s), 0.06 (3H, s), 0.85 (9H, s), 1.33 (3H, d, J=6.0 Hz), 2.00 (3H, s), 2.99 (1H, dd, J=2.5, 4.5 Hz), 3.74 (3H, s), 3.98 (1H, d, J=2.5 Hz), 4.11 and 4.59 (2H, ABq, J=14.0 Hz), 4.18 (1H, m, 6.83 (2H, d), 7.13 (2H, d). MS m/z 337 (M^+ −t-Bu).

*(3S,4S)-4-Acetoxy-3-[(R)-1-(t-butyldimethylsiloxy)ethyl]-1-(4-methoxybenzyl)-2-azetidinone (**9c**).* To a stirred solution

[†] 1 M=1 mol dm^{-3}.

of **8c** (412 mg, 1.05 mmol) in chloroform (5 mL) was added *m*-chloroperbenzoic acid (340 mg, 1.58 mmol) and the resulting solution was kept at room temperature overnight. The reaction mixture was diluted with EtOAc, washed with 5% $NaHCO_3$ (three times), saturated NaCl and dried ($MgSO_4$). After evaporation the oily residue was chromatographed on silica gel. Elution with cyclohexane–EtOAc (1:1) gave **9c** (369 mg, 86%) yield. Physical data **9c**: ^1H NMR ($CDCl_3$) δ=0.30 (3H, s), 0.80 (3H, s), 0.85 (9H, s), 1.20 (3H, d, J=6.0 Hz), 1.85 (3H, s), 3.08 (1H, dd, J=0.5, 3.0 Hz), 3.76 (3H, s), 3.90—4.20 (1H, m), 4.25 (2H, Bs), 6.01 (1H, d, J=0.5 Hz), 6.75 (2H, d), 7.15 (2H, d).

(2S,3S)-3-[(R)-1-Hydroxyethyl]-1-(4-methoxybenzyl)-4-oxo-2-azetidinecarboxylic Acid (6a). Azetidinone **5a** (20.0 g, 0.06 mol) was dissolved in trifluoroacetic acid (TFA, 50 mL) at 0 °C and stirred at the same temperature for 3 h. After evaporation of TFA, the residue was dissolved in benzene (100 mL) and evaporated again to remove the remaining TFA. The oily residue was dissolved in EtOAc (200 mL), which was washed with water, saturated $NaHCO_3$, saturated NaCl and dried ($MgSO_4$), and evaporated to give **6a** as crystals in quantitative yield; mp 100—102 °C; IR (KBr) 1740 cm^{-1}; ^1H NMR ($CDCl_3$) δ=1.30 (3H, d, J=6.5 Hz), 3.30 (1H, dd, J=3.5, 4.0 Hz), 3.75 (3H, s), 4.05 (1H, d, J=3.5 Hz), 4.00—4.40 (1H, m), 4.05 and 4.08 (2H, ABq, J=16.0 Hz), 6.45 (1H, Bs), 6.80 (2H, d), 7.15 (2H, d). Found: C, 60.2; H, 6.16; N, 4.93%. Calcd for $C_{14}H_{17}NO_5$: C, 60.2; H, 6.14; N, 5.02%.

(3S,4R)-4-Acetoxy-3-[(R)-1-hydroxyethyl]-1-(4-methoxybenzyl)-2-azetidinone (9a). To a solution of **6a** (2.80 g, 10 mmol) in DMF–AcOH (5:1, 10 mL) was added $Pb(OAc)_4$ (4.43 g, 10 mmol) with stirring under nitrogen. The mixture was stirred at 50—55 °C for 15 min, then the mixture was diluted with EtOAc (300 mL), washed with water (twice), 5% $NaHCO_3$, saturated NaCl and dried ($MgSO_4$). After evaporation of the solvent, the oily residue was chromatographed on silica gel (50 g). Elution with cyclohexane–EtOAc (1:2) gave **9a** (1.63 g, 51.3%) as crystals; mp 84—85 °C; IR (KBr) 1755 cm^{-1}; ^1H NMR ($CDCl_3$) δ=1.30 (3H, d, J=6.5 Hz), 2.5 (1H, dd, J=1.0, 4.0 Hz), 2.00 (3H, s), 3.10 (1H, Bd, J=7.0 Hz), 3.90—4.30 (1H, m), 3.80 (3H, s), 4.10 and 4.50 (2H, ABq, J=15.0 Hz), 5.75 (1H, d, J=1.0 Hz), 6.80 (2H, d), 7.15 (2H, d). Found: C, 61.32; H, 6.43; N, 4.81%. Calcd for $C_{15}H_{19}NO_5$: C, 61.4; H, 6.53; N, 4.78%.

By the lead tetraacetate method **6b** and **6d** were converted to corresponding **9b** and **9d** in 71.9 and 63% yield, respectively, as in the case of **9a**.

Physical data **9b**: IR (Liquid) 1770 cm^{-1}; ^1H NMR ($CDCl_3$) δ=1.43 (3H, d, J=6.5 Hz), 1.95 (3H, s), 3.35 (1H, dd, J=1.0, 6.5 Hz), 3.75 (3H, s), 4.10 and 4.50 (2H, ABq, J=14.5 Hz), 4.90—5.20 (1H, m), 5.23 (2H, s), 5.98 (1H, d, J=1.0 Hz), 6.78 (2H, d), 7.20 (2H, d), 7.52 (2H, d), 8.23 (2H, d). Found: C, 58.4; H, 5.31; N, 5.75%. Calcd for $C_{23}H_{24}N_2O_9$: C, 58.4; H, 5.08; N, 5.93%. MS m/z 472 (M^+). **9d**: IR (Liquid) 1765 cm^{-1}; ^1H NMR ($CDCl_3$) δ=1.40 (3H, d, J=6.5 Hz), 1.92 (3H, s), 3.28 (1H, dd, J=1.0, 6.5 Hz), 3.75 (3H, s), 4.10 and 4.50 (2H, ABq, J=15.0 Hz), 4.80—5.20 (1H, m), 4.40—4.70 (2H, m), 5.10—5.50 (2H, m), 5.70—6.20 (1H, m), 5.90 (1H, d, J=1.0 Hz), 6.75 (2H, d), 7.16 (2H, d). Found: C, 59.8; H, 6.03; N, 3.67%. Calcd for $C_{19}H_{23}NO_7$: C, 60.4; H, 6.14; N, 3.71%. MS m/z 377 (M^+).

(3S,4R)-4-Acetoxy-3-[(R)-1-(t-butyldimethylsiloxy)ethyl]-2-azetidinone (10c). To a solution of **9c** (408 mg, 1.0 mmol) in acetonitrile water (1:1, 32 mL) were added K_2HPO_4 (1.50 g) and $K_2S_2O_8$ (3.0 g). The mixture was stirred at 75 °C for 1 h under nitrogen, and concentrated *in vacuo* to half volume, and extracted with EtOAc. The extracts were washed with saturated $NaHCO_3$, saturated NaCl, dried ($MgSO_4$) and concentrated to an oily residue which was purified by preparative TLC plate on silica gel (20×20×0.2 cm). Development with cyclohexane–EtOAc (2:1) gave **10c** (115 mg, 41%) as crystals; mp 101—102 °C; IR (Nujol) 3200, 1785, 1745 cm^{-1}; ^1H NMR ($CDCl_3$) δ=0.07 (6H, s), 0.85 (9H, s), 1.24 (3H, d, J=6.5 Hz), 2.12 (3H, s), 3.20 (1H, dd, J=1.0, 3.0 Hz), 4.24 (1H, dq, J=3.0, 6.5 Hz), 5.89 (1H, d, J=1.0 Hz), 6.85 (1H, Bs); MS m/z 577 (M^+), 230, 188, 144; $[\alpha]_D^{24}$ +47.2 (c=1.0, $CHCl_3$).

(3S,4R)-4-Acetoxy-3-[(R)-1-(p-nitrobenzyloxycarbonyloxy)ethyl]-2-azetidinone (10b). To a stirred solution of **9b** (410 mg, 0.89 mmol) in acetone (3 mL) was added cerium(IV) ammonium nitrate (CAN) (910 mg, 1.75 mmol) at room temperature and stirring was continued for 1 h. The reaction mixture was diluted with EtOAc (30 mL) which was washed with water, saturated $NaHCO_3$, saturated NaCl and dried ($MgSO_4$). After evaporation an oily residue was purified by preparative TLC (20×20×0.2 cm) on silica gel with cyclohexane–EtOAc (1:1) to give deprotected **10b** (150 mg, 49% yield) as an oil; IR (Liquid) 3250, 1770 cm^{-1}; ^1H NMR ($CDCl_3$) δ=1.45 (3H, d, J=6.5 Hz), 2.10 (3H, s), 3.35 (1H, dd, J=2.5, 6.5 Hz), 4.90—5.51 (1H, m), 5.24 (2H, s), 5.81 (1H, d, J=2.5 Hz), 7.23 (1H, Bs), 7.50 (2H, d), 8.16 (2H, d).

(3S,4R)-4-Acetoxy-3-[(R)-1-(p-nitrobenzyloxycarbonyloxy)ethyl]-1-(4-methoxybenzyl)-2-azetidinone (9b). To a solution of **9a** (2.93 g, 10 mmol) in dichloromethane (20 mL) were added *p*-nitrobenzyloxycarbonyl chloride (6.45 g, 30 mmol) and 4-dimethylaminopyridine (3.66 g, 30 mmol) under ice cooling. After stirring for 1 h the reaction mixture was diluted with EtOAc and washed with dil HCl, water, saturated $NaHCO_3$, saturated NaCl and dried ($MgSO_4$). The solution was evaporated to afford an oily residue which was chromatographed on silica gel (50 g). Elution with cyclohexane–EtOAc (1:1) gave **9b** (300 mg, 74%) as an oil. The physical data was identical with that of an authentic sample obtained by the lead tetraacetate method.

(3S,4R)-4-Acetoxy-3-[(R)-1-(t-butyldimethylsiloxy)ethyl]-1-(4-methoxybenzyl)-2-azetidinone (9c) and *(3S,4R)-4-Acetoxy-3-[(R)-1-(allyloxycarbonyloxy)ethyl]-1-(4-methoxybenzyl)-2-azetidinone (9d).* Compound **9a** was converted to **9c** and **9d** by the similar reaction as in the case of **9b**, with *t*-butyldimethylsilyl chloride and imidazole, and allyloxycarbonyl chloride and 4-dimethylaminopyridine. The physical data were identical with that of authentic samples obtained in another route.

(3S,4R)-1-(4-Methoxybenzyl)-4-[(phenylthiocarbonyl)methyl]-3-[(R)-1-(p-nitrobenzyloxycarbonyloxy)ethyl]-2-azetidinone (11b). To a stirred solution of azetidinone **9b** (1.18 g, 2.5 mmol) in dichloromethane (10 mL) were added 1-phenylthio-1-trimethylsilyloxyethylene (2.74 g, 10 mmol) and trimethylsilyl trifluoromethanesulfonate (1.11 g, 1.25 mmol) at room temperature. The reaction mixture was kept at room temperature overnight, and diluted with EtOAc (100 mL),

washed with water, 5% $NaHCO_3$, saturated NaCl, and dried ($MgSO_4$). After evaporation, an oily residue was chromatographed on silica-gel (60 g). Elution with cyclohexane–EtOAc (1:1) gave **11b** (1.34 g, 94.9%); IR (Liquid) 1765 cm^{-1}; ^1H NMR ($CDCl_3$) δ=1.35 (3H, d, 6.5 Hz), 2.70—2.90 (2H, m), 3.15 (1H, dd, J=3.0, 7.0 Hz), 3.75 (3H, s), 3.80—4.10 (2H, m), 4.10 and 4.50 (2H, ABq, J=14.5 Hz), 4.90—5.30 (1H, m), 5.15 (2H, s), 6.75 (2H, d), 7.15 (2H, d), 7.35 (5H, s), 7.50 (2H, d), 8.15 (2H, d); MS m/z 564 (M^+).

(3S,4R)-3-[(R)-1-(t-Butyldimethylsiloxy)ethyl-1-(4-methoxybenzyl)-4-[(phenylthiocarbonyl)methyl]-2-azetidinone (11c) and (3S,4R)-3-[(R)-1-(Allyloxycarbonyloxy)ethyl]-1-(4-methoxybenzyl)-4-[(phenylthiocarbonyl)methyl]-2-azetidinone (11d). 2-Azetidinone **9c** and **9d** gave **11c** and **11d** respectively by the same reaction as in the case of **11b**.

Physical data **11c**: ^1H NMR ($CDCl_3$) δ=0.03 (6H, s), 0.83 (9H, s), 1.14 (3H, d, J=6.0 Hz), 2.76 (2H, d, J=6.0 Hz), 2.88 (1H, dd, J=2.0, 4.5 Hz), 3.75 (3H, s), 3.97 (1H, dt, J=2.0, 6.0 Hz), 4.16 (1H, dq, J=2.0, 6.0 Hz), 4.26 (2H, s), 6.77 (2H, d), 7.13 (2H, d), 7.35 (5H, Bs). **11d**: IR (Liquid) 1760 cm^{-1}; ^1H NMR ($CDCl_3$) δ=1.40 (3H, d, J=6.5 Hz), 2.84 (2H, d, J=5.5 Hz), 3.10 (1H, dd, J=2.0, 7.0 Hz), 3.76 (3H, s), 3.80—4.60 (1H, m), 4.10 and 4.50 (2H, ABq, J=14.0 Hz), 4.50—4.60 (2H, m), 4.80—5.20 (1H, m), 5.10—5.40 (2H, m), 5.60—6.10 (1H, m), 6.80 (2H, d), 7.12 (2H, d), 7.30—7.50 (5H, m). MS m/z 496 (M^+).

(3S,4R)-3-[(R)-1-(p-Nitrobenzyloxycarbonyloxy)ethyl]-4-[(phenylthiocarbonyl)methyl]-2-azetidinone (12b). To a stirred solution of cerium (IV) ammonium nitrate (3.0 g, 5.47 mmol) in water (2 mL) was added a solution of **11b** (203 mg, 0.36 mmol) in acetone (10 mL) and stirred for 2 h. The reaction mixture was diluted with EtOAc (200 mL), washed with water, 5% $NaHCO_3$, saturated NaCl and dried ($MgSO_4$). After evaporation an oily residue was chromatographed on silica-gel. Elution with cyclohexane–EtOAc (2:1) gave **12b** (111 mg, 69.5%) as an oil; IR (Liquid) 1770 cm^{-1}; ^1H NMR ($CDCl_3$) δ=1.44 (3H, d, J=6.5 Hz), 2.90—3.20 (3H, m), 3.86—4.10 (1H, m), 4.90—5.30 (1H, m), 5.15 (2H, s), 6.40 (1H, Bs), 7.45 (5H, s), 7.50 (2H, d), 8.15 (2H, d); MS m/z 444 (M^+).

(3S,4R)-3-[(R)-1-(t-Butyldimethylsiloxy)ethyl]-4-[(phenylthiocarbonyl)methyl]-2-azetidinone (12c) and *(3S,4R)-3-[(R)-1-Allyloxycarbonyloxy)ethyl]-4-[(phenylthiocarbonyl)methyl]-2-azetidinone (12d).* 2-Azetidinones **11c**, **11d** were converted to the corresponding **12c** and **12d** by the same reaction as in the case of **11b**.

Physical data **12c**: mp 95—96 °C; IR (Nujol) 1765, 1725 cm^{-1}; ^1H NMR ($CDCl_3$) δ=0.08 (6H, s), 0.87 (9H, s), 1.19 (3H, d, J=6.0 Hz), 2.55—3.25 (3H, m), 3.70—4.33 (2H, m), 6.20 (1H, Bs), 7.35 (5H, s); $[\alpha]_D^{24}$ +41.7 °C (C=1.64, $CHCl_3$). **12d**: IR (Liquid) 1770 cm^{-1}; ^1H NMR ($CDCl_3$) δ=1.40 (3H, d, J=6.5 Hz), 2.80—3.20 (3H, m), 3.80—4.20 (1H, m), 4.42—4.71 (2H, m), 4.80—5.20 (1H, m), 5.10—5.40 (2H, m), 5.60—6.10 (1H, m), 6.20 (1H, Bs), 7.32 (5H, s). Found: C, 5.81; H, 5.49; N, 3.89; S, 9.35%. Calcd for $C_{17}H_{19}NO_5S$: C, 58.4; H, 5.47; N, 4.00; S, 9.15%.

(3S,4R)-4-[(S)-[[1-[N-(p-Nitrobenzyloxycarbonyl)acetimidoyl]-3-pyrrolidinylthio]carbonylmethyl]]-3-[(R)-1-(p-nitrobenzyloxycarbonyloxy)ethyl]-2-azetidinone (13). To a stirred solution of 2-azetidinone **12b** (115 mg, 0.26 mmol) in dichloromethane (5 mL) were added 3-pyrrolidinethiol **20** (125 mg, 0.89 mmol) in dichloromethane (5 mL) and triethylamine (26 mg, 0.26 mmol) with stirring at room temperature and the resulting solution was kept at room temperature overnight. After evaporation, the oily residue was chromatographed on silica-gel. Elution with EtOAc gave **13** (168 mg, 98%) as an oil; IR (Liquid) 1770 cm^{-1}; ^1H NMR ($CDCl_3$) δ=1.22 (3H, d, J=6.0 Hz), 2.30 (3H, s), 1.60—2.60 (2H, m), 2.90 (2H, d, J=6.5 Hz), 3.04 (1H, Bd, J=7.0 Hz), 3.20—4.20 (6H, m), 4.90—5.20 (1H, m), 5.18 (2H, s), 5.13 (2H, s), 6.70 (1H, Bs), 7.25 (4H, d), 8.10—8.30 (4H, m).

(3S,4R)-3-[(R)-1-(Allyloxycarbonyloxy)ethyl]-4-[(S)-[[1-(p-nitrobenzyloxycarbonyl)-3-pyrrolidinylthio]carbonylmethyl]]-2-azetidinone (14). *S*-Phenyl thioester **12d** was converted to the corresponding exchanged *S*-thioester **14** by the same reaction as in the case of **13**; IR (Liquid) 1770 cm^{-1}; ^1H NMR ($CDCl_3$) δ=1.40 (3H, d, J=6.5 Hz), 1.60—2.70 (2H, m), 2.70—3.00 (3H, m), 3.20—4.21 (6H, m), 4.60 (2H, d, J=7.0 Hz), 4.80—5.21 (1H, m), 5.20—5.50 (2H, m), 5.20 (2H, s), 5.62—6.21 (1H, m), 6.40 (1H, Bs), 7.48 (2H, d), 8.15 (2H, d).

(3S,4R)-4-[[2-(p-Nitrobenzyloxycarbonylamino)ethylthio]carbonylmethyl]-3-[(R)-1-(p-nitrobenzyloxycarbonyloxy)ethyl]-2-azetidinone (15). To a stirred solution of 2-azetidinone **12b** (444 mg, 10 mmol) in dichloromethane (10 mL) were added 2-(*p*-nitrobenzyloxycarbonylamino)ethanethiol (512 mg, 20 mmol) and triethylamine (202 mg, 20 mmol) at room temperature and the solution was kept at the same temperature for 5 h. The mixture was diluted with EtOAc (50 mL) and washed with water, saturated $NaHCO_3$, saturated NaCl and dried ($MgSO_4$). After evaporation the oily residue was purified by column chromatography on silica-gel. Elution with cyclohexane–EtOAc gave **15** (431 mg, 73%) as an oil; IR (Liquid) 3260, 1760, 1740 cm^{-1}; ^1H NMR ($CDCl_3$) δ=1.42 (3H, d, J=6.5 Hz), 2.60—3.20 (4H, m), 3.20—3.50 (2H, m), 3.90—4.25 (2H, m), 4.80—5.30 (1H, m), 5.18 (2H, s), 5.26 (2H, s), 5.65 (1H, m), 6.90 (1H, Bs), 7.35—8.50 (8H, m).

References

1) A recent describing work similar to that at the beginning of this paper but with a slightly different nitrogen-protecting group has been disclosed in *Tetrahedron*, **40**, 1795 (1984).

2) J. S. Kahan, F. M. Kahan, R. Goegelman, S. A. Currie, M. Jackson, E. O. Stapley, T. W. Miller, A. K. Miller, D. Hendlin, S. Mochales, S. Hernandez, H. B. Woodruff, and J. Birnbaum, *J. Antibiot.*, **32**, 1 (1979); G. Albers-Schonberg, B. H. Arison, O. D. Hensens, J. Hirshfield, K. Hoogsteen, E. A. Kaczka, R. E. Rhodes, J. S. Kahan, F. M. Kahan, R. W. Ratcliffe, E. Walton, L. J. Ruswinkle, R. B. Morin, and B. G. Christensen, *J. Am. Chem. Soc.*, **100**, 6491 (1978).

3) a) For a recent review, see: T. Kametani, K. Fukumoto, and M. Ihara, *Heterocycles*, **17**, 463 (1982); b) L. D. Cama, K. J. Wildonger, R. Guthikonda, R. W. Ratcliffe, and B. J. Christensen, *Tetrahedron*, **39**, 2531 (1983).

4) A. Yoshida, Y. Tajima, N. Takeda, and S. Oida, *Tetrahedron Lett.*, **25**, 2793 (1984).

5) a) M. Shiozaki, N. Ishida, H. Maruyama, and T. Hiraoka, *Heterocycles*, **20**, 279 (1983); b) M. Shiozaki, N. Ishida, T. Hiraoka, and H. Maruyama, *Chem. Lett.*, **1983**,

169; c) M. Shiozaki, N. Ishida, T. Hiraoka, and H. Maruyama, *Tetrahedron*, **40**, 1795 (1984); d) M. Shiozaki, N. Ishida, H. Maruyama, and T. Hiraoka, *Tetrahedron*, **39**, 2399 (1983).

6) Y. Shimohigashi, M. Waki, and N. Izumiya, *Bull. Chem. Soc. Jpn.*, **52**, 949 (1979).

7) a) H. Gilman, R. G. Jones, and L. A. Woods, *J. Org. Chem.*, **17**, 1630 (1952); b) G. H. Posmen and C. E. Whitten, *Tetrahedron Lett.*, **11**, 4647 (1970).

8) a) P. J. Reider and E. J. J. Grabowski, *Tetrahedron Lett.*, **23**, 2293 (1982); b) Org. Reaction, 1972, 19, 279.

9) K. Mislow and J. Brenner, *J. Am. Chem. Soc.*, **75**, 2319 (1953).

10) a) T. Fukuyama, R. K. Frank, and C. F. Jewell, Jr., *J. Am. Chem. Soc.*, **102**, 2122 (1979); b) D. R. Kronenthal, C. Y. Han, and M. K. Taylor, *J. Org. Chem.*, **47**, 2765 (1982).

11) A. G. M. Barrett and P. Quayle, *J. Chem. Soc., Chem. Commun.*, **1981**, 1076.

 © 1985 The Chemical Society of Japan Bull. Chem. Soc. Jpn., 58, 3271—3276 (1985)

Catalytic Epoxidation of Olefins with *t*-Butyl Hydroperoxide in the Presence of Polymer-supported Vanadium(V) and Molybdenum(VI) Complexes

Toshiro YOKOYAMA, Masato NISHIZAWA, Tetsuo KIMURA, and Toshishige M. SUZUKI*
Government Industrial Research Institute, Tohoku, 4-2-1 Nigatake, Sendai 983
(Received May 13, 1985)

Oxovanadium(V) and oxomolybdenum(VI) ions have been incorporated into cross-linked polystyrene resins functionalized with iminodiacetic acid or diethylenetriamine derivatives. The polymer complexes have been used as catalysts in the epoxidation of olefins with *t*-butyl hydroperoxide. Vanadium(V) complexes promote epoxidation of allylic alcohols in a highly regioselective manner, *e.g.*, 2,3-epoxide has been preferentially obtained in 98% selectivity from (*E*)-geraniol at 80 °C. The catalytic activity of the vanadium(V) complexes is generally higher than that of the molybdenum(VI) complexes in the epoxidation of allylic alcohols whereas an opposed trend holds for the epoxidation of cyclohexene. Life time of catalysts have been examined by repeated use of the complexes in the epoxidation of (*E*)-geraniol at 80 °C in benzene. Approximately 15—25% of vanadium has been leaked out of the polymer beads on five time recycles leading to the decrease in the yield of 2,3-epoxide from initial value of 98% to 95—93%. Neither appreciable loss of metal nor reduction of catalytic activity has been observed in the molybdenum complex systems over five runs.

It is widely known that complexes of oxometal ions such as vanadium, molybdenum, and tungsten catalyze the epoxidation of olefins with alkyl hydroperoxides.[1-7] Recently anchoring of catalytically active transition metal complexes onto a polymer matrix received considerable attention[8,9] due to their potential advantages in practical synthesis, *i.e.*, i) the catalyst is easily separated from the reaction solution by filtration or centrifugation, ii) the recovered catalyst can be used repeatedly.

Several studies have been carried out on the catalytic epoxidation of olefins by polymer-anchored metal complexes.[10-13] However the functional groups so far used as metal-ion-binding unit were mostly monodentate and bidentate ligands, which often suffer from the disadvantage of the metal ion leaking from the polymer support. Accordingly a more stable metal-polymer linkage is required to avoid such leaking of metal ion into the reaction solution.

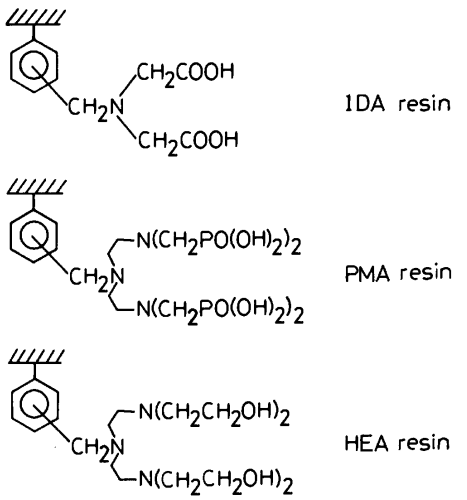

Fig. 1. Polymer chelating resins containing multidentate functional group.

Recently we have reported that the cross-linked polystyrene resins with a functional group having bis(phosphonomethyl)amino (PMA) and bis(2-hydroxyethyl)amino (HEA) moieties (Fig. 1) readily form metal complexes with oxovanadium(V) and oxomolybdenum(VI) ions in aqueous solution.[14] These polymer complexes were found to catalyze the epoxidation of (*E*)-geraniol with *t*-butyl hydroperoxide (*t*-BuOOH) without significant loss of the metal ion.[15] This is the full detailed description of the work including the preparation of the polymer complex catalysts, and the epoxidation of allylic alcohols and cyclohexene.

Experimental

Materials. Microreticular (Gel) and macroreticular (MR) types of polystyrene resins containing iminodiacetic acid (IDA) moieties are commercial products, *i.e.*, Dowex A-1 (Gel type, 25—50 mesh) and Lewatit-OC-1048 (MR-type, 25—50 mesh). The polymer matrices used for the preparation of PMA and HEA resins were Gel-type styrene-2%-divinylbenzene copolymer (from Kodac Co, 200—400 mesh) and MR-type styrene-10%-divinylbenzene copolymer (from Mitsubishi Chemical Co., 60—100 mesh). The surface area and mean pore radius of the MR-type resin were 7.3 $m^2 g^{-1}$ and 720 Å, respectively.

Preparation of the Chelating Resins. Both Gel- and MR-types of polystyrene beads were chloromethylated,[16] and then functionalized with diethylenetriamine (dien) to give a dien-resin in which diethylenetriamine is linked to the polymer uniquely through the secondary amino nitrogen.[17] The dien-resin was used as the starting material for the preparation of the PMA and HEA resins.

PMA Resin: To a refluxed mixture of dien-resin (Gel-type, 15 g), phosphorous acid (33 g) and 6 M HCl (80 cm^3, M=mol dm^{-3}) was added dropwise 37% of aqueous

formaldehyde solution (64 cm^3) in the course of 2 h. The reaction mixture was kept at refluxing temperature for an additional 3 h. The resin was filtered, washed with water, ethanol and then diethyl ether, and dried *in vacuo* at 50 °C. Yield: 25.3 g.

HEA Resin: The Gel-type of dien-resin (11 g) was stirred with aqueous ethylene oxide (9.6 g in 100 cm^3) for 3 h under ice cooling. After standing overnight at room temperature, the resin was filtered, washed throughly with water, ethanol and diethyl ether, and then dried *in vacuo* at 50 °C. Yield: 19.5 g.

Functionalization of the MR-type polystyrene resin was performed under similar conditions to those for the Gel-type of PMA and HEA resins.

Preparation of Polymer Complexes: Polymer complexes were generally prepared by the following procedures: One gram of dry resin was shaken with 10 mM of aqueous $NaVO_3$ or K_2MoO_4 solution (1000 cm^3) at pH about 4 for 24 h. The concentration of the remaining metal ion in the solution was analyzed by atomic absorption spectrometry to determine the amount of metal adsorbed on the resin. The polymer beads were filtered, washed throughly with distilled water, ethanol, diethyl ether, and then dried *in vacuo* at 50 °C.

Epoxidation of Olefins: A typical procedure for the epoxidation of allylic alcohols is as follows: In a 50 cm^3 round-bottomed flask equipped with a reflux condenser was placed a polymer complex containing 0.2—0.3 mmol of metal, 30 cm^3 of benzene, (*E*)-geraniol (4.0 g, 26 mmol) and 70% of aqueous *t*-BuOOH (4.0 g, 31 mmol). The reaction mixture was heated at 80 °C with stirring. The reaction was monitored by TLC. After the reaction was completed, the polymer beads were filtered off, and the filtrate acetylated by the published method[3] prior to the product analysis. The reaction conversion of allylic alcohol and the distribution of the products were analyzed on a GLC (2% OV-17 on Uniport HP, 80—100 mesh: 16 ft×1/8 in.) using methyl stearate as an internal standard. The geometry of the epoxide isomers was confirmed by ^1H NMR spectroscopy. Epoxidation of cyclohexene was carried out under conditions similar to those for the epoxidation of the allylic alcohols. The reaction solution was analyzed on a GLC (15% PEG-20M on Uniport S, 60—80 mesh, 16 ft×1/8 in.) using toluene as an internal standard.

Lifetime of the Catalysts: The polymer complexes were recovered by filtration at the end of the epoxidation of (*E*)-geraniol. After washing with benzene, the complexes were used in successive runs under identical conditions. The conversion and the selectivity were determined after each run as described above. In order to determine the amount of metal ion which leaked into the reaction solution, the polymer catalyst was removed by filtration. The filtrate was evaporated and extracted twice with 0.5 M HCl. The metal ion in the extract was determined by atomic absorption.

Catalytic Decomposition of t-BuOOH: Decomposition of *t*-BuOOH was monitored by iodometry in the absence of a substrate. To a mixture of the polymer complex (100 mg) and benzene (30 cm^3) was added 70% of aqueous *t*-BuOOH (4.0 g) and the whole heated at 80 °C with stirring. Small portions of the sample (1 cm^3) were withdrawn at appropriate intervals and titrated iodometrically according to the published method.[18]

Measurements: ^1H NMR spectra were measured with a JEOL FX-100 spectrometer in chloroform-*d* with TMS as an internal standard. The metal ion concentration was determined with a Shimadzu atomic absorption/flame photometer Model AA-610S. GLC-analysis was performed on a Varian Model 3700 gas-chromatograph equipped with an electron digital integrator Varian Model CDS-111.

Results

Polymer Catalysts. Analytical data and the amounts of the functional group contained in one gram of dry resin are shown in Table 1. The ligand contents of Gel- and MR-type resins (PMA and HEA) do not differ much from each other, indicating that the functionalization proceeds to a similar extent, irrespective of the type of polymer support. However the physical form of the Gel-type resin is affected by the solvent while the MR-type resin has only minor shrinking and swelling properties. Metal ions were incorporated into the polymer ligands by treating the

Table 1. Analytical data of polymer chelating resins and the maximum adsorption capacity for V(V) and Mo(VI)

Chelating Resin	Analytical Data	Ligand Capacity[a]	Ads. Capacity/(mmol/g-resin)[b]	
	N(%)	mmol/g-resin	V	Mo
Gel-IDA	6.27	4.46	1.7	1.1
MR-IDA	3.64	2.60	1.4	2.0
Gel-PMA	6.53	1.55	3.2	3.3
MR-PMA	5.54	1.32	3.3	4.0
Gel-HEA	7.32	1.74	3.1	3.2
MR-HEA	7.43	1.77	4.0	4.0

a) Calculated from the actual nitrogen content: Ligand capacity (mmol/g-resin) is estimated by $\frac{\%N}{14n}$, where %N=nitrogen in product, and n=number of nitrogen atoms in the ligand.[29] b) The amount of metal adsorbed on one gram of dry resin.

resins with aqueous Mo(VI) or V(V) solution at pH *ca.* 4.0, conditions under which the amounts of metal adsorbed are maximal. The maximum adsorption capacities of the present resins for Mo(VI) and V(V) are also given in Table 1. The amounts of metal adsorbed on one gram of PMA and HEA resins always exceed the ligand contents while those on IDA resins do not.

Epoxidation of Allylic Alcohols. The results of epoxidation of allylic alcohols are summarized in Table 2. (*E*)-Geraniol was epoxidized preferentially at the olefinic site close to the hydroxyl group regardless of the metal ion, the functional group or the type of polymer matrix. The following general features were observed in the present reactions: i) The conversion of (*E*)-geraniol and the selectivity toward the formation of 2,3-epoxide by vanadium catalysts are generally higher than those by the molybdenum complex systems. ii) Apparently complexes with the MR-type polymer matrix undergo epoxidation at a much faster rate than the corresponding complexes of the Gel-type polymer. iii) The catalytic activities are almost independent of the type of functional group. iv) The epoxidation rate is retarded by addition of an excess amount of *t*-butyl alcohol (*t*-BuOH). Vanadium complexes epoxidize (*E*)-geraniol almost quantitatively and the selectivity is remarkably high (≈98%). The reaction conversion and the selectivity are comparable to those observed with homogeneous $VO(acac)_2$ (acac=acetylacetonato) when MR–vanadium complexes were employed. The epoxidation of 2-cyclohexen-1-ol and linalool was carried out in a similar manner to that of (*E*)-geraniol in the presence of vanadium complexes of MR-type resin. The reaction of these secondary and tertiary alcohols required much longer reaction times and resulted in lower conversion.

The time-course plots of the epoxidation of (*E*)-geraniol by vanadium catalysts are illustrated in Fig. 2. The reaction at 80 °C is facile in the initial stage and in most of the cases 80% conversion was attained within 30 min. Although it takes longer reaction time, the epoxidation proceeds under moderate temperature (20 °C) by use of MR-vanadium catalysts. The vanadium complexes of IDA and PMA resins accomplished 80—90% conversion in 8 h whereas HEA resin required much longer induction periods.

Epoxidation of Cyclohexene. Epoxidation of cyclohexene with *t*-BuOOH (cyclohexene/*t*-BuOOH= 1) was carried out using vanadium(V) and molybdenum(VI) complexes of MR-type resins. Table 3 shows the conversion of cyclohexene and the selectivity toward the formation of cyclohexene oxide after a 24 h reaction period. In contrast to allylic alcohols, the epoxidation of a simple olefin catalyzed

Table 2. Catalytic epoxidation of allylic alcohols with polymer-supported metal complexes[a]

Substrate	Catalyst		Time/h	Conversion/%[b]	Selectivity/%[c]
	Resin	Metal			
(*E*)-Geraniol	Gel-IDA	V	24	100	98
		Mo	24	87	90
	MR-IDA	V	1	100	98
		Mo	24	96	82
	Gel-PMA	V	4	100	98
		Mo	24	89	81
	MR-PMA	V	1	100	98
		Mo	24	94	78
	Gel-HEA	V	4	100	98
		Mo	24	93	80
	MR-HEA	V	1.5	100	98
		Mo	24	98	71
		$VO(acac)_2$	0.5	100	98
2-Cyclo-hexen-1-ol	MR-IDA	V	6	89	87
	MR-PMA	V	24	53	88
	MR-HEA	V	24	100	90
Linalool	MR-IDA	V	24	70	53
	MR-PMA	V	24	48	53
	MR-HEA	V	24	70	55

a) Reaction was carried out at 80 °C. b) Conversion of allylic alcohol. c) Percentage of β,γ-epoxy alcohol in the products.

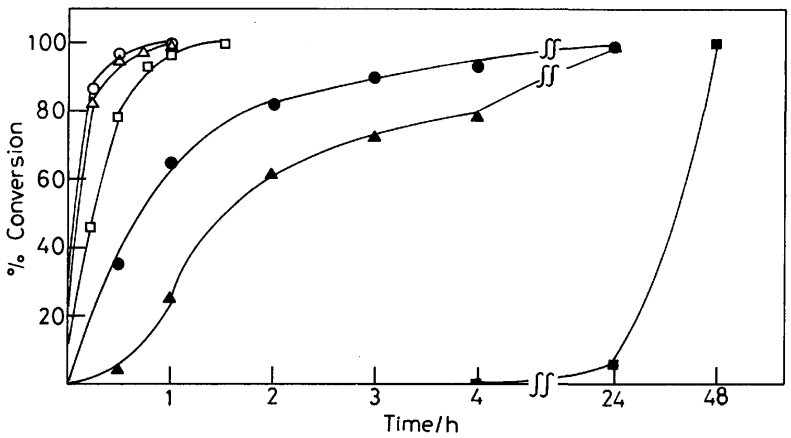

Fig. 2. Time-conversion profile of (*E*)-geraniol by polymer-anchored vanadium(V) complexes —○—: MR-IDA resin at 80 °C, —●—: MR-IDA resin at 20 °C, —△—: MR-PMA resin at 80 °C, —▲—: MR-PMA resin at 20 °C, —□—: MR-HEA resin at 80 °C, —■—: MR-HEA resin at 20 °C.

TABLE 3. EPOXIDATION OF CYCLOHEXENE WITH POLYMER-SUPPORTED METAL CATALYST[a]

Catalyst		Conversion/%[b]	Selectivity/%[c]
Resin	Metal		
MR-IDA	V	59	6
	Mo	77	59
MR-PMA	V	29	5
	Mo	88	55
MR-HEA	V	76	4
	Mo	86	54

a) Epoxidation was carried out at 80 °C for 24 h. b) Conversion of cyclohexene. c) Percentage of cyclohexene oxide in the products.

TABLE 4. METAL-CATALYZED DECOMPOSITION OF *t*-BuOOH (in benzene at 80 °C)

Catalyst		$t_{1/2}$(min)
Resin	Metal	
MR-IDA	V	210
	Mo	≫15,000
MR-PMA	V	90
	Mo	≫15,000
MR-HEA	V	90
	Mo	≫15,000

by molybdenum gave a higher conversion and better selectivity than the reaction by vanadium complexes. The vanadium catalyzed reactions generally gave several by-products involving polymerized compounds.

Lifetime of Catalysts. The lifetimes of the catalysts (MR-resins) were examined by their repeated use in the epoxidation of (*E*)-geraniol. The amount of metal ion leaked into the solution was determined for each run. Approximately 75% of the vanadium remained on MR-IDA and MR-HEA resins while more than 85% of the metal was still retained on the MR-PMA resin after five runs. The yield of 2,3-epoxide decreased only slightly, *i.e.*, the initial value of 98% decreased to 95—93% after fivefold recycling. In most cases notable change in selectivity has not been observed. Leakage of the metal ion does not take place in the absence of substrate and *t*-BuOOH. Neither appreciable loss of metal nor reduction of catalytic activity was observed in the molybdenum complex systems after five runs.

Catalytic Decomposition of t-BuOOH. The rates of consumption of *t*-BuOOH by the polymer complexes in the absence of substrate have been monitored by iodometry. Half-lives ($t_{1/2}$) of the reactions are given in Table 4. Obviously vanadium complexes remarkably facilitate the decomposition of *t*-BuOOH while those by molybdenum complexes are very slow.

Discussion

The major advantage of polymer-anchored catalysts over their homogeneous counterparts is the ease of recovering and recycling of the catalysts. So far bidentate ligands such as ethylenediamine,[10] acetylacetonato,[10,12] and dithiocarbamato[13] have been used as the polymer-metal (M=V(IV), Mo(V)) binding unit and the catalytic epoxidation of olefins has been carried out using the polymer complexes. However significant leakage of metal ion from the polymers inevitably took place during epoxidation, leading to a rapid lowering of the catalytic activity upon repeated use. Our catalyst systems, by contrast, are relatively long-lived. The catalytic activities after five

runs are essentially the same as those of the first run irrespective of the catalysts used. The polymer–metal bond in these complexes appears to be very durable toward the dissociation of the metal ion under the given catalytic conditions. It has been pointed out that the rate of dissociation of a chelated complex decreases significantly as the dentate number of the ligand increases.[19] This trend was exemplified by the studies on acid hydrolysis of a number of Mo(V) complexes.[20,21] The enhanced stability of the present complexes may be attributed to the increasing dentate number of the immobilized ligands.

Iminodiacetic acid (IDA) which is the functional group of the IDA resin acts as a tridentate ligand and is known to form 1:1 (ligand:metal) complexes with Mo(VI) and V(V).[22–24] The facial tridentate coordination of IDA group to the trioxomolybdenum(VI) was proposed on the basis of the ^{1}H-NMR study of the IDA–Mo(VI) complex[23] and confirmed in the solid state for a 2:1 complex $Na_4(MoO_3)_2(edta)\cdot 8H_2O$ (H_4edta=ethylenediaminetetraacetic acid).[25] The PMA and HEA resins formally contain two sets of tridentate ligands, bis(phosphonomethyl)amino and bis(2-hydroxyethyl)amino moieties, respectively. The maximum amount of metal ion adsorbed on PMA and HEA resins is much higher than the estimated amount of ligand contained in one gram of dry resin. It seems that each of the tridentate ligand having one nitrogen and two oxygens as the donating atoms forms 1:1 complexes with Mo(VI) and V(V) in a similar fashion to those for IDA and EDTA complexes. The coordination of the hydroxyl arms onto Mo(VI) has been demonstrated by ^{13}C-NMR study of the Mo(VI) complex with *N,N,N',N'*-tetrakis(2-hydroxyethyl)ethylenediamine.[14] The remaining coordination sites in the octahedral complexes are generally occupied with oxo ligands (or water) which can be replaced by the substrate or oxidizing agent in the epoxidation reaction. The higher durability of the PMA–V(V) complex toward metal dissociation suggests stronger coordination of the phosphonomethyl groups than that of the acetate or hydroxyl group.

As has been claimed earlier in the homogeneous catalyst systems[2,26] the high regioselectivity in the epoxidation of allylic alcohols can be interpreted by a mechanism in which coordination of the hydroxyl group of the substrate and *t*-BuOOH to the metal ion at neighbouring position is involved as the key intermediate. The fixed geometry of the allylic alcohols by the formation of such ternary complex results in preferential transfer of oxygen to an olefinic site close to the hydroxyl group. This may be supported by the observation that the rate of epoxidation is retarded in the presence of a large amount of *t*-BuOH which can compete with the substrate for coordination to the active center. With allylic alcohols vanadium complexes always gave a faster rate and better selectivity than the molybdenum complexes. A similar trend has been observed in the homogeneous catalyst system and has been attributed to the stronger coordination of hydroxyl group to vanadium.[2] In practice, the retardation by *t*-BuOH is more serious with vanadium complexes than with molybdenum complexes under similar reaction conditions.

Catalysts anchored on an MR-type resin always showed kinetic properties superior to those supported on a Gel-type resin. The MR-type resin has actual pores forming numerous channels which allow facile diffusion of the substrate into the polymer matrix.[27,28] On the other hand, the tight polymer network of the Gel-type resin may interfere with a smooth transfer of substrate to the active center.

Both vanadium and molybdenum complexes catalyze the decomposition of *t*-BuOOH to give peroxyl radicals.[4,6] Therefore the epoxidation of olefins catalyzed by these metal complexes involves competing with the metal-catalyzed decomposition of *t*-BuOOH. The vanadium-catalyzed decomposition of *t*-BuOOH is remarkably facile in the absence of a substrate, while in the presence of allylic alcohols, the epoxidation proceeds preferentially. An intramolecular oxygen transfer from peroxovanadium(V) complex to allylic alcohol seems to take place at a much faster rate than the decomposition of the peroxide when the olefins is fixed to metal through a functional group. On the contrary, the epoxidation of cyclohexene gave an extremely poor yield of epoxides indicating that the decomposition reaction takes place prior to the efficient oxygen transfer to the substrate. For the nonfunctionalized olefin the opportunity to form the stable ternary complex might be limited. Radicals produced by the homolytic decomposition of peroxide must be responsible for the formation of many kinds of by-products. Reactions involving such peroxyl radicals would be less remarkable in the molybdenum-catalyzed epoxidation since the rate of decomposition of *t*-BuOOH is significantly slow.

References

1) E. S. Gould, R. R. Hiatt, and K. C. Irwin, *J. Am. Chem. Soc.*, **90**, 4573 (1968).

2) M. N. Sheng and J. G. Zajacek, *J. Org. Chem.*, **35**, 1839 (1970).

3) K. B. Sharpless and R. C. Michaelson, *J. Am. Chem. Soc.*, **95**, 6136 (1973).

4) R. A. Sheldon and J. A. van Doorn, *J. Catal.*, **31**, 427 (1973).

5) A. O. Cheng and K. B. Sharpless, *J. Org. Chem.*, **42**, 1587 (1977).

6) R. A. Sheldon, *J. Mol. Catal.*, **7**, 107 (1980).

7) H. Mimoun, L. Saussine, E. Daire, M. Postel, J.

Fischer, and R. Weiss, *J. Am. Chem. Soc.*, **105**, 3101 (1983).
8) A. Akelah and D. C. Sherrington, *Chem. Rev.*, **81**, 557 (1981).
9) F. Ciardelli, G. Braca, C. Carlini, G. Sbrana, and G. Valentini, *J. Mol. Catal.*, **14**, 1 (1982).
10) G. L. Linden and M. F. Farona, *J. Catal.*, **48**, 284 (1977).
11) G. L. Linden and M. F. Farona, *Inorg. Chem.*, **16**, 3170 (1977).
12) S. Bhaduri, A. Ghosh, and H. Khwaja, *J. Chem. Soc., Dalton Trans.*, **1981**, 447.
13) S. Bhaduri and H. Khwaja, *J. Chem. Soc., Dalton Trans.*, **1983**, 415.
14) M. Nishizawa, T. Yokoyama, T. Kimura, and T. M. Suzuki, *Chem. Lett.*, **1983**, 1413; M. Nishizawa, T. Yokoyama, T. Kimura, and T. M. Suzuki, *Bull. Chem. Soc. Jpn.*, **57**, 2859 (1984).
15) T. Yokoyama, M. Nishizawa, T. Kimura, and T. M. Suzuki, *Chem. Lett.*, **1983**, 1703.
16) K. W. Pepper, H. M. Paisley, and M. A. Young, *J. Chem. Soc.*, **1953**, 4097.
17) T. M. Suzuki and T. Yokoyama, *Polyhedron*, **2**, 127 (1983); T. M. Suzuki and T. Yokoyama, *Polyhedron*, **3**, 939 (1984).
18) M. A. P. Dankleff, R, Curci, J. O. Edwards, and H. Y. Pynns, *J. Am. Chem. Soc.*, **90**, 3209 (1968).
19) K. Saito and Y. Sasaki, *Adv. Inorg. Bioinorg. Mechanisms*, **1**, 179 (1982).
20) Y. Sasaki and A. G. Sykes, *J. Chem. Soc., Dalton Trans.*, **1974**, 1468.
21) Y. Sasaki and A. G. Sykes, *J. Less-Common Met.*, **36**, 125 (1974).
22) R. J. Kula, *Anal. Chem.*, **39**, 1171 (1967).
23) M. A. Freeman, F. A. Schultz, and C. N. Reilley, *Inorg. Chem.*, **21**, 567 (1982).
24) S. Funahashi, K. Haraguchi, and M. Tanaka, *Inorg. Chem.*, **16**, 1349 (1977).
25) J. J. Park, M. D. Glick, and J. L. Hoard, *J. Am. Chem. Soc.*, **91**, 301 (1969).
26) K. B. Sharpless and T. R. Verhoeven, *Aldrichimica Acta*, **12**, 63 (1979).
27) R. B. Wesley and B. C. Gates, *J. Catal.*, **34**, 288 (1974).
28) S. L. Regen, D. Bolikal, and C. Barcelon, *J. Org. Chem.*, **46**, 2511 (1981).
29) L. R. Melby, *J. Am. Chem. Soc.*, **97**, 4044 (1975).

 © 1985 The Chemical Society of Japan Bull. Chem. Soc. Jpn., 58, 3277—3281 (1985)

A Kinetic Study on the Reaction of (Arylthio)trimethylgermane with Benzoyl Chloride Giving *S*-Aryl Thiobenzoate and Chlorotrimethylgermane

Seizi KOZUKA,* Shoji TAMURA, Tetsuya YAMAZAKI, Shigeru YAMAGUCHI, and Waichiro TAGAKI

Department of Applied Chemistry, Faculty, of Engineering, Osaka City University, Sugimoto 3-Chome, Sumiyoshi, Osaka 558

(Received June 1, 1985)

A kinetic study has been conducted on the reactions of (substituted arylthio)trimethylgermanes with aroyl chlorides giving *S*-aryl thioaroates and chlorotrimethylgermane. The rates of the reactions were distinctly accelerated in polar solvents. Both of the effects due to the substituents of the arylthio and the aroyl moieties gave positive ρ values especially in a polar solvent. A mechanism involving initial 5-coordination, ionic cleavage of the Ge–S bond giving arenethiolate ion, and followed by rate-determining addition of the thiolate to the carbonyl carbon, was suggested for the reaction.

Previously, we have reported kinetic and stereochemical studies on the reactions of methylthio- and (substituted arylthio)trimethylstannanes with haloalkanes.[1] Nucleophilic attacks of the sulfur atom on the haloalkanes have been suggested for the reactions based on the negative ρ value together with other kinetic and stereochemical results.

$$Me_3Sn\text{-}SR + R'\text{-}X \longrightarrow [Me_3Sn\text{-}S^+RR'\,X^-] \longrightarrow R\text{-}S\text{-}R' + Me_3Sn\text{-}X$$

R = substituted aryl ($\rho = -1.4$), Me
R′ = Me, Et, $C_6H_5CH_2$, 1-Me-heptyl (inversion)
X = I, Br, Cl.

Scheme 1.

On the other hand, quite different kinetic aspects were observed for the analogous reactions of arylthiosilanes. Namely, the reactions of (substituted arylthio)trimethylsilanes with a haloalkane were found to give the products in a similar way but with quite different kinetic results.[2] Phenacyl bromide was chosen as the haloalkane for the kinetic study because of the low reactivity of the arylthiosilanes towards common haloalkanes. A large positive ρ value (+2.2) was observed. The result was well recognized in terms of initial 5-coordination of the silicon atom and followed by the rate-determining Si–S bond cleavage (Scheme 2).

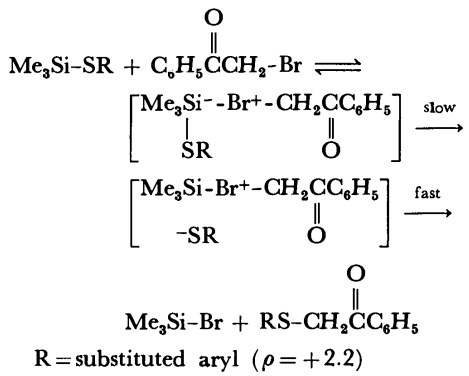

R = substituted aryl ($\rho = +2.2$)

Scheme 2.

A comparable difference was also observed between the analogous reactions of the arylthiostannanes and the arylthiosilanes with aroyl chlorides. The reactions of the (arylthio)trimethylstannanes with aroyl chlorides were found to give *S*-aryl thioaroates. The kinetic study on the reactions revealed opposite substituent effects due to the arylthio ($\rho_X = -1.6$) and the aroyl ($\rho_Y = +1.1$) moieties. Hereafter, the substituents on the arylthio and the aroyl groups are abbreviated as X and Y, respectively. Accordingly, the reaction was considered to involve a nucleophilic addition of the sulfur atom to the carbonyl carbon (Scheme 3).[3]

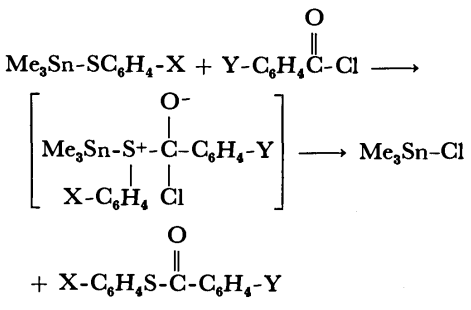

$\rho_X = -1.6$, $\rho_Y = +1.1$

Scheme 3.

Contrary to these results, the reactions of the (arylthio)trimethylsilanes with aroyl chlorides were found to give the same thioaroates but with quite different kinetic aspects. A large positive ρ value due to X ($\rho_X = +2.50$) was observed while that of Y was small negative ($\rho_Y = -0.87$). These results suggested initial 5-coordination followed by rate-determining formation of arenethiolate ion for the reaction (Scheme 4).[4]

A kinetic study on the reactions of the arylthiogermane analogs would be of interest since quite different kinetic aspects were observed for the reactions of the arylthiosilanes and the arylthio-

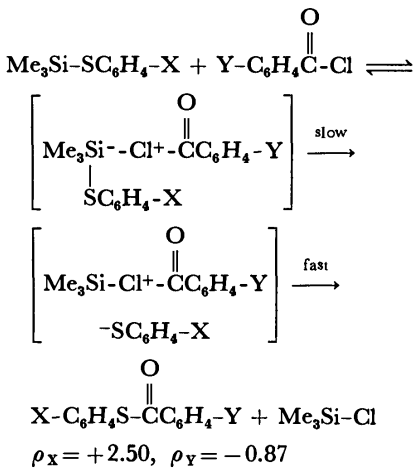

Scheme 4.

stannanes as far described. Substituted aroyl chlorides were chosen as the reactants because the reactions of these reagents have well been studied kinetically.[3,4]

Results and Discussion

The reaction of trimethyl(phenylthio)germane with benzoyl chloride was found to give chlorotrimethylgermane and *S*-phenyl thiobenzoate. No other product was found in the reaction solution by ^{1}H NMR analysis. The chlorogermane and the thiobenzoate were isolated and characterized.

The rate of the reaction of the phenylthiogermane with a small excess of benzoyl chloride was measured by monitoring the decrease in the ^{1}H NMR trimethyl signal of the starting phenylthiogermane (δ=0.47) and the increase in that of the chlorogermane

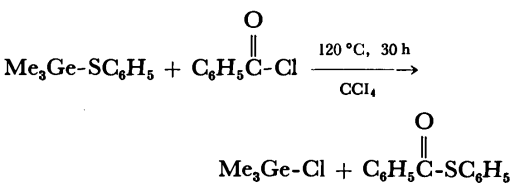

Scheme 5.

(δ=0.72). The reaction was found to obey a second order rate equation. The kinetic experiments were performed in various solvents at different temperatures. The results are given in Table 1 together with the activation parameters and the observed solvent effects. The possible reactions of the arylthiogermanes with the solvents were examined in control experiments. Small amounts of the solvolysis products were found on prolonged heating of the arylthiogermanes in some solvents. The rates (pseudo-first-order: k_1), however, were found much smaller and negligible comparing with those of the reactions with aroyl chlorides.

The activation parameters appeared in similar magnitudes with those of the analogous reactions which proceed by ionic processes.[1-3] Distinct solvent effects were observed as shown in Table 1. The results also suggest an ionic process for the reaction.

The effect of the substituents of the arylthio group (ρ_X) was examined to clarify the reaction mechanism. The results are shown in Table 2.

Clearly positive ρ_X values were observed for both the reactions carried out in carbon tetrachloride and in benzonitrile as the solvents. The positive ρ_X values would suggest 5-coordination of the germanium atom as was suggested for the reactions of the

TABLE 1. ACTIVATION PARAMETERS AND SOLVENT EFFECT ON THE RATE OF THE REACTION OF $Me_4GeSC_6H_5$ [0.131 mol dm^{-3}] WITH C_6H_5COCl [0.159 mol dm^{-3}] IN VARIOUS SOLVENTS

Solvent(ε)[a]	Temp	$k_2\times10^4$	$\Delta H^{\ddagger}_{400}$	$\Delta S^{\ddagger}_{400}$	k_{rel}[b]
	°C	dm^3 mol^{-1}	kJ mol^{-1}	J K^{-1} mol	
			(γ)		
CCl_4 (2.23)	110	1.85±0.31	37.0	−223	1.00
CCl_4	120	2.56±0.98	(0.999)		
CCl_4	130	3.45±0.28			
CH_2Br_2 (6.70)	110	5.78±0.33	45.6	−185	2.1
CH_2Br_2	120	8.76±0.09	(0.998)		
CH_2Br_2	130	19.8 ±0.20			
CH_2Cl_2 (8.90)	100	6.50±0.48	37.5	−208	4.9
CH_2Cl_2	110	9.18±0.87	(0.999)		
CH_2Cl_2	120	12.6 ±1.1			
C_6H_5CN (25.2)	40	7.83±0.42	63.0	−106	280
C_6H_5CN	50	15.2 ±1.1	(0.998)		
C_6H_5CN	60	34.6 ±3.0			
C_6H_5CN	70	62.9 ±3.9			

a) Dielectric constant. b) At 100 °C.

arylthiosilanes.[2,4,5] The enhanced ρ_X value observed in benzonitrile solution also suggests the rate-determining cleavage of the Ge–S linkage giving arenethiolate ion since the value is comparable with that of the dissociation of arenethiols.[6] The present reaction, thus once, appeared to be similar in the mechanism to that of the reactions of the arylthiosilanes with phenacyl bromide[2] and with aroyl chlorides[4] which involve initial 5-coordinations followed by rate-determining formations of arenethiolate ions. The effect of the substituent Y, (ρ_Y), however, strongly suggests that the rate-determining step of the present reaction is quite different from those of the reactions of the arylthiosilanes.[2,4]

As shown in Table 3, the effects of Y observed for the reactions in carbon tetrachloride were obscure, or rather U-shape plot was observed. On the other hand, the observed ρ_Y value is clearly positive for the reactions in benzonitrile as the solvent. The positive ρ_Y value strongly suggests an alternative mechanism for the reaction since a similar mechanism to that of the reactions of the arylthiosilanes demands a negative ρ_Y value (Scheme 4).[4]

The most appropriate mechanism for the reaction based on the kinetic results can be depicted as follows (Scheme 6).

The positive ρ_Y value observed in benzonitrile can be rationalized in terms of a rate-determining addition of the thiolate ion to carbonyl carbon giving the intermediate III. The positive ρ_X value would be originated from the both steps, the initial 5-coordination giving the intermediate I and the ionic fission of the Ge–S bond giving the ion pair II. Energetically disfavored equilibrium giving I and II might well account for the observed positive ρ_X values since favorable formations of I and II would disappear the effect of X or bring small negative ρ_X values.

It is uncertain, why the effects of Y in carbon tetrachloride gave a U-shaped Hammett plot. The electron-donating substituents Y may stabilize both the intermediates I and II. The stabilizations may slightly accelerate the reactions. Another process to rationalize the abnormal effects of Y is a charge-separated 4-center transition state which has been suggested for the reactions of the (aryloxy)trimethylstannanes with methanesulfonyl chloride.[7] The 4-center process may be favorable for the ionic reactions forced to proceed in nonpolar solvents. However, the observed solvent effects ($k_{C_6H_5CN}/k_{CCl_4}$= 280) are too large in comparison with that of the 4-center reaction which showed small and abnormal solvent effects.[8] Different mechanisms in individual solvents are not plausible in view of a clear isokinetic relationship in all the solvents examined as shown in Fig. 1.

The mechanism of the reactions of (substituted arylthio)trimethylgermanes with the aroyl chlorides has thus been found to be similar to that of the analogous reactions of the arylthiosilanes at the initial step and the following heterolysis of the metal-sulfur bond, but differ in the rate-determining step. The reactions of the arylthiosilanes involve rate-

Table 2. Rate constants for the reaction of $Me_3GeSC_6H_4$-X [0.131 mol dm^{-3}] with C_6H_5COCl [0.159 mol dm^{-3}]

X	Solvent	Temp °C	$k_2\times10^4$ dm^3 mol^{-1} s^{-1}	Remarks
m-Br	CCl_4	130	13.3 ±1.2	$\rho_{X(\sigma)}$=+1.46
m-Cl	CCl_4	130	9.46±0.73	γ=0.977
p-Cl	CCl_4	130	4.59±0.51	
H	CCl_4	130	3.45±0.21	
p-Me	CCl_4	130	1.37±0.01	
p-OMe	CCl_4	130	1.26±0.06	
m-Cl	C_6H_5CN	50	64.3 ±4.2	$\rho_{X(\sigma)}$=+2.32
p-Cl	C_6H_5CN	50	59.6 ±5.5	γ=0.982
H	C_6H_5CN	50	15.2 ±1.1	
p-Me	C_6H_5CN	50	5.27±0.32	
p-OMe	C_6H_5CN	50	2.43±0.67	

Table 3. Rate constants for the reaction of $Me_3GeSC_6H_5$ [0.131 mol dm^{-3}] with Y-C_6H_4COCl [0.159 mol dm^{-3}]

X	Solvent	Temp °C	$k_2\times10^4$ dm^3 mol^{-1} s^{-1}	Remarks
p-NO_2	CCl_4	130	26.8 ± 3.3	
m-Cl	CCl_4	130	7.03± 0.43	No linear
p-Br	CCl_4	130	4.75± 0.36	correlation
p-Cl	CCl_4	130	4.52± 0.33	in CCl_4.
H	CCl_4	130	3.45± 0.21	
p-Me	CCl_4	130	5.95± 0.54	
p-OMe	CCl_4	130	7.00± 0.27	
p-NO_2	C_6H_5CN	50	294 ±83	
m-Cl	C_6H_5CN	50	70.1 ± 1.1	$\rho_{Y(\sigma)}$=+1.90
p-Br	C_6H_5CN	50	38.3 ± 2.3	γ=0.990
p-Cl	C_6H_5CN	50	38.5 ± 0.8	
H	C_6H_5CN	50	15.2 ± 1.1	
p-Me	C_6H_5CN	50	6.05± 0.30	
p-OMe	C_6H_5CN	50	2.59± 0.32	

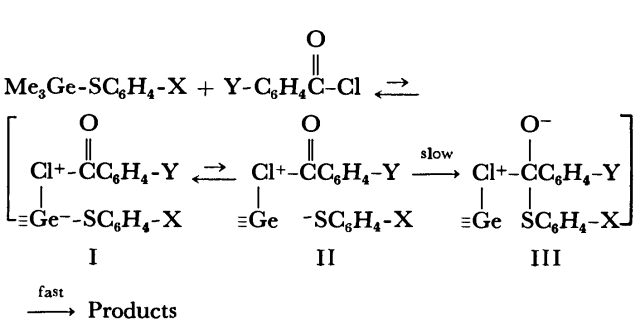

Scheme 6.

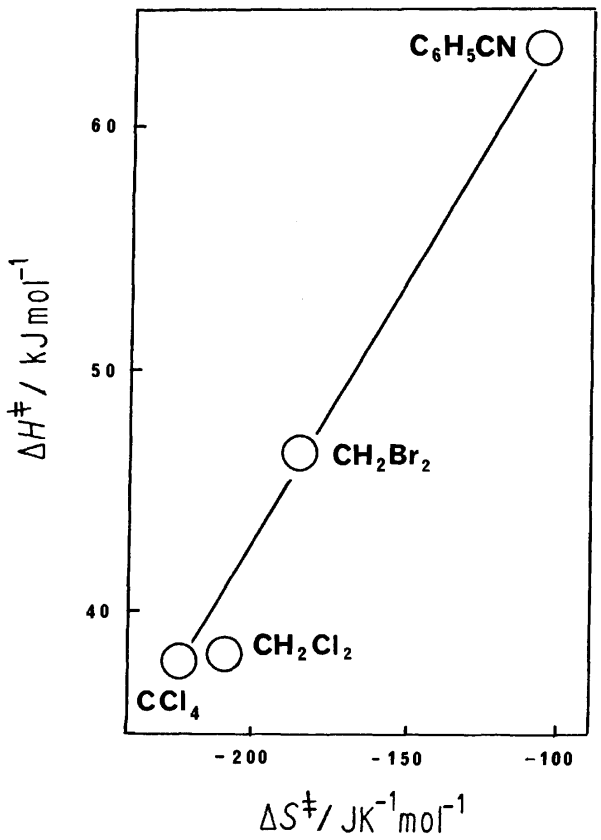

Fig. 1. Plot of $\Delta H^{\ddagger}$ *vs.* $\Delta S^{\ddagger}$ in various solvents.

determining heterolyses of the metal-sulfur bonds while the heterolysis is the second equilibrium step in the present reaction as shown in Scheme 6. The mechanism presently suggested is also different from that of the analogous reactions of the arylthiostannanes.[3] Thus, the reactions of the arylthiosilanes, -germanes, and -stannanes with aroyl chlorides have been found to proceed by individually different mechanisms.

Experimental

Materials. Solvents were dried and distilled. Substituted aroyl chlorides were purified by distillation or recrystallization before use.

Preparation of Tetramethylgermane. The germane was prepared by modified procedure of the literature.[9] In a 3-necked flask equipped with a stirrer, a refluxing condenser, and dropping funnel, 20 g of magnesium was placed and dry nitrogen gas was passed for 30 min. Dibutyl ether (300 cm^3) was added. Methyl iodide (114 g) diluted with dibutyl ether (*ca.* 70 cm^3) was added dropwise with cooling (ice bath) and stirring. After the addition, the Grignard solution was allowed to stand for 30 min with stirring. Tetrachlorogermane (25 g) dissolved in dibutyl ether (*ca.* 20 cm^3) was added dropwise with cooling (ice-salt bath, −15 °C) and vigorous stirring. The solution was gently heated up to 70 °C after the addition. Water was carefully added dropwise with cooling (ice bath) to consume the remaining Grignard reagent. The resulting mixture was distilled and low-boiling fraction containing tetramethylgermane, water, and dibutyl ether was collected (bp 42—89 °C). Water was separated from the distillate and the organic layer was dried (Na_2SO_4). Centrifugation of the reaction mixture to separate the precipitated magnesium salt and water, and followed by rough distillation was also effective to obtain crude tetramethylgermane. Fractional distillation gave tetramethylgermane, 4.92 g, bp 42—43 °C, ^{1}H NMR δ=0.15.

Preparation of Bromotrimethylgermane. Bromine (5.94 g) was added to tetramethylgermane (4.92 g) containing catalytic amount of aluminium trichloride (*ca.* 30 mg) with stirring. The mixture was allowed to stand overnight with stirring. Excess bromine was decolorized by addition of small amount of mercury. Bromotrimethylgermane was obtained by distillation, bp 113—114 °C, 5.94 g (81%), ^{1}H NMR δ=0.85.

Trimethyl(phenylthio)germane. The phenylthiogermane was prepared as follows: To chloroform (50 ml) solution of bromotrimethylgermane (1.0 g) and triethylamine (0.77 g), benzenethiol (0.56 g) was added and the mixture was refluxed for 2 h. The solvent was evaporated and hexane (30 ml) was added to precipitate the amine salt. Trimethyl(phenylthio)germane was obtained by distillation after evaporation of hexane, bp 62 °C/1 mmHg (133.332 Pa.), ^{1}H NMR δ=0.47. Other (arylthio)trimethylgermanes were prepared similarly. Substituents, bp at 1 mmHg, and ^{1}H NMR signals other than aryl protons are as follows: *p*-Methoxy-, 85 °C, δ=0.48 and 3.83; *p*-Methyl-, 83 °C, δ=0.47 and 2.37; *p*-Chloro-, 76 °C, δ=0.44; *m*-Chloro-, 87 °C, δ=0.42; *m*-Bromo-, 106 °C, δ=0.42.

Product Analysis. Trimethyl(phenylthio)germane (1.00 g, 5.1×10^{-3} mol) was heated with an equimolar amount of benzoyl chloride (0.71 g) in carbon tetrachloride (10 cm^3) in a sealed tube at 120 °C for 30 h. ^{1}H NMR Analysis of the solution showed signals only due to chlorotrimethylgermane and *S*-phenyl thiobenzoate. Chlorotrimethylgermane was isolated by distillation (bp 108—110 °C, 68%). *S*-Phenyl thiobenzoate was obtained from the residue and purified by recrystallization, mp 55 °C (from chloroform-hexane, 70%, lit,[10] 56 °C).

Kinetics. (Arylthio)trimethylgermanes (6.55×10^{-4} mol) and aroyl chlorides (7.55×10^{-4} mol) were dissolved in the solvent using 5 ml volumetric flask. The solutions were devided into 10 portions and sealed in glass tubes of *ca.* 0.7 cm^3 volume. The tubes were heated in a constant temperature bath (±0.1 °C) and samples were taken at appropriate time intervals and cooled (ice bath). Each sample of the solution was subjected to NMR analysis. Conversion at the time was measured by the relative intensities of the starting trimethyl (δ=0.42—0.48) and that of the product (chlorotrimethylgermane: δ=0.72) which were determined by 8 to 10 repeated scannings. The rate constant k was obtained by least squares calculation of second order rate equation.

The Reactions of the Arylthiogermanes with the Solvents Used for the Kinetics. Carbon tetrachloride solution of (*m*-chlolophenylthio)trimethylgermane (0.13 mol dm^{-3}) was heated at 130 °C for 22 h. The reaction conditions correspond to more than 80% completion of the reaction of the germane with the least reactive *p*-methoxybenzoyl chloride. The amount of chlorotrimethylgermane (δ=0.72)

was measured by ^{1}H NMR analysis. Pseudo-first-order rate constant (k_1) was estimated from the conversion. Similarly, other arylthiogermanes were heated in carbon tetrachloride or in dibromomethane and the amounts of the chlorogermane (in CCl_4) and the bromogermane (in CH_2Br_2) were measured. The arylthiogermanes, solvent, and k_1 at 130 °C were as follows: $Me_3GeSC_6H_4Cl$-*m*, CCl_4, 7×10^{-7} s^{-1}; $Me_3GeSC_6H_4OMe$-*p*, CCl_4, 1×10^{-6} s^{-1}; $Me_3GeSC_6H_5$, CH_2Br_2, 3×10^{-5} s^{-1}. No reaction was found with benzonitrile under the kinetic conditions (50 °C, 24 h). The solvolyses rates were thus found much smaller than those of the reactions with aroyl chlorides and can be neglected for the kinetic studies with aroyl chlorides.

References

1) S. Kozuka and S. Ohya, *Bull. Chem. Soc. Jpn.*, **51**, 2651 (1978).

2) S. Kozuka, T. Higashino, and T. Kitamura, *Bull. Chem. Soc. Jpn.*, **54**, 1420 (1981).

3) S. Kozuka and I. Naribayashi, *Bull. Chem. Soc. Jpn.*, **52**, 3638 (1979).

4) S. Kozuka and I. Naribayashi, *Memoirs of the Fac. of Engin. Osaka City University*, **22**, 115 (1981).

5) S. Kozuka and T. Kitamura, *Bull. Chem. Soc. Jpn.*, **52**, 3384 (1979).

6) F. G. Bordwell and H. M. Anderson, *J. Am. Chem. Soc.*, **75**, 6019 (1953).

7) S. Kozuka, S. Yamaguchi, and W. Tagaki, *Bull. Chem. Soc. Jpn.*, **56**, 573 (1983).

8) Abnormal solvent effect was observed for the reaction of trimethyl(phenoxy)stannane with methanesulfonyl chloride: k_{rel} in CCl_4, CH_2Br_2, CH_2Cl_2, C_6H_5CN, and CH_3CN were 1.00, 0.38, 0.32, 2.0, and 10, respectively.[7]

9) D. F. von de Vondil, *J. Organomet. Chem.*, **3**, 400 (1965).

10) "Beilstein Organishe Chemie" **9**, p 421.

 © 1985 The Chemical Society of Japan Bull. Chem. Soc. Jpn., 58, 3282—3290 (1985) [Vol. 58, No. 11

cis-Oxypalladation Complexes Derived from (1*R*,5*R*)-2(10),3-Pinadiene and Their Utilization in Pd(II)-catalyzed Enantioselective Cyclization of 2-(*trans*-2-Butenyl)phenols

Takahiro Hosokawa,* Yasushi Imada, and Shun-Ichi Murahashi*
Department of Chemistry, Faculty of Engineering Science, Osaka University, Machikaneyama, Toyonaka, Osaka 560
(Received June 19, 1985)

(1*R*,5*R*)-2(10),3-Pinadiene, when treated with either Na_2PdCl_4 in MeOH or $Pd(OAc)_2$ in AcOH and NaCl, gives di-μ-chloro-bis[(3,2,10-η-*cis*-4-methoxy or acetoxypinene)palladium(II)] (**4a**) or (**4b**), respectively. These complexes represent the firstly isolated *cis*-oxypalladation adduct. The ligand exchange of **4b** with AgOAc affords di-μ-acetato-bis[(3,2,10-η-*cis*-4-acetoxypinene)palladium(II)] (**5b**) which serves as the catalyst for the asymmetric cyclization of 2-(*trans*-2-butenyl)phenols leading to 2-vinyl-2,3-dihydrobenzofurans (**13**). Although the enantioselectivities induced in this asymmetric cyclization are not high (1—29% ee), noteworthy is that the *cis*-complex **5b** affords (*R*)-(−)-enantiomer of **13** while the parent di-μ-acetato-bis[(3,2,10-η-pinene)palladium(II)] give the (*S*)-isomer. As an application of the present asymmetric cyclization, attempts to synthesize (*S*)-(+)-tremetone have been made.

During the course of our study on the asymmetric cyclization of 2-allylphenols using (η^3-pinene)palladium(II) catalyst,[1,2] our interest has been extended to prepare η^3-allylpalladium(II) complexes bearing functionalized pinanyl ligands. For this purpose, (1*R*,5*R*)-2(10), 3-pinadiene (**1**) (verbenene) has been chosen as a precursor of the pinanyl ligand, since the reactions of 1,3-dienes with Pd(II) compounds in the presence of nucleophiles gives functionalized η^3-allylpalladium(II) complexes.[3] This type of reactions with oxygen nucleophiles such as alcohol[4] has been known to proceed by *trans*-addition; however, η^3-allylpalladium(II) complexes **4** obtained from **1** were the products derived from *cis*-addition. Although the stereochemistry of oxypalladation of alkenes has been extensively studied,[5] there has been no unambiguous examples of *cis*-oxypalladation complexes.[6] Described herein are the preparation and structural elucidation of the *cis*-oxypalladium complexes **4a**—**c**,[7] and their utilization as the catalyst for the asymmetric cyclization of 2-(*trans*-2-butenyl)-phenols.

Results and Discussion

Preparation of Di-μ-chloro-bis[3,2,10-η-cis-4-methoxy or Acetoxypinene)palladium(II)] (4). The synthesis of pinadiene **1** has been previously performed by bromination of α- or β-pinene with NBS followed by dehydrobromination.[8] Although this procedure seems to be a reasonable manipulation, the diene **1** was synthesized by utilizing palladium-catalyzed elimination of allylic acetates to dienes.[9] Thus, when a mixture of allylic acetates **2** and **3** (**2**/**3**=2/1), prepared from (−)-β-pinene and $Pb(OAc)_4$,[10] was treated with $Pd(OAc)_2$ (5 mol%) in the presence of PPh_3 (0.5 equiv), diene **1** was obtained in 72% yield {$[\alpha]_D$ +106° (CCl_4)}. The overall yield of **1** (32%) from β-pinene in this procedure is comparable to that in the previous method.[8]

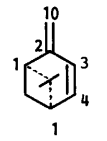

1

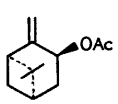

2

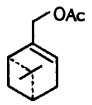

3

When the diene **1** thus obtained was allowed to react with an equimolar amount of Na_2PdCl_4 in MeOH, the *cis*-complex **4a** was formed as a single product in 66% isolated yield. The reaction of **1** with $Pd(OAc)_2$ in AcOH followed by addition of NaCl gave the complex **4b** (71%). The use of $Pd(OAc)_2$ in MeOH under otherwise the same conditions afforded two complexes **4a** (12%) and **4b** (14%). Also, the reaction of **1** with $Pd(OCOCF_3)(OOBu^t)$ in acetone and subsequent addition of NaCl gave the complex **4c** (85%).

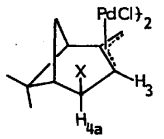

4a; X=OMe
4b; X=OAc
4c; X=OBu^t

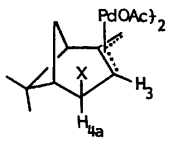

5a; X=OMe
5b; X=OAc
5c; X=H

The chloride ligand of complexes **4a** and **4b** is readily exchanged to acetate upon treatment with an equimolar amount of AgOAc. The complexes **5a** and **5b** thus obtained serve as the catalyst for the asymmetric cyclization of 2-(*trans*-2-butenyl)phenols (**12**). The results will be compared to those obtained by using the parent complex **5c** (X=H) (*vide infra*).

Structural Characterization. The structural elucidation of **4a**—**c** was undertaken by comparing the spectral data of **4a** and **4b** with those of the corresponding *trans*-isomers **7a** and **7b**. The authentic complexes **7a** and **7b** were prepared as

follows. The β-pinenes **6a** and **6b** bearing the substituent (X=OMe or OAc) at the C(4),*endo*-position were prepared from (−)-α-pinene by the reported method.[11,12] The reaction of **6a** with an equimolar amount of $Pd(OAc)_2$ in MeOH followed by addition of NaCl gave a 58% yield of complex **7a** (Eq. 1). Likewise, the *trans*-complex **7b** was obtained from **6b** in 52% yield. The reaction of β-pinene (**6c**) with $PdCl_2$ has been shown to proceed by the *exo*-attack of palladium at sterically less-hindered site of C(2)=C(10) olefin to give the complex **7c**.[13] The β-pinenes **6a** and **6b** react similarly with Pd(II) to afford the *trans*-complexes **7a** and **7b** as depicted in Eq. 1.

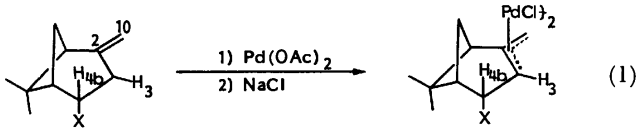

(1)

6a; X=OMe
6b; X=OAc
6c; X=H

7a; X=OMe
7b; X=OAc
7c; X=H

Comparison of the ^1H NMR spectral data shown in Table 1 unambiguously indicates the configurational difference between **4a** and **7a** or **4b** and **7b** (Entries 1, 2, 5, and 6), respectively. The following data in Table 1 support that the palladium is situated at the *exo*-position of all these complexes. Thus, the difference in chemical shifts between *gem*-dimethyl groups ($\Delta\delta$Me-8,9) of the *exo*-α-pinenes **4a**, **4b**, **8**, and **9** (group i) fall into the region of 0.36—0.48, whereas those of the *endo*-isomers **7a**, **7b**, **10**, and **11** (group ii) are in 0.26—0.36. Although these values tend to be lowered upon complexation, no significant difference was observed between the value of η^3-allyl complex and the corresponding α-pinene (*e.g.*, **4a** and **8**). If palladium in these complexes occupies the site opposite to that depicted, the relative chemical shift must differ greatly owing to the proximity of palladium to one of the Me group.[14] These considerations allow us to assign the *cis*-configuration of **4a** and **4b**.

The ^1H NMR spectrum of *trans*-complex **7a**

Table 1. ^1H NMR chemical shifts[a] of π-allyl complexes and α-pinene derivatives

Entry	Compd		H-10	H-3	H-4	J_{34}	J_{45}	Me-8	Me-9	$\Delta\delta$Me-8,9
	group (i)									
1	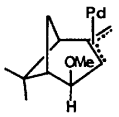	**4a**	3.03 3.73	3.99	3.52	4.5	2.5	0.99	1.39	0.40
2	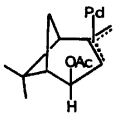	**4b**	3.08 3.69	4.15	4.88	5.0	2.6	1.04	1.40	0.36
3	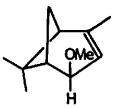	**8**	—	5.30	3.67	NA[b]	NA	0.85	1.33	0.48
4	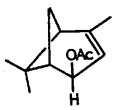	**9**	—	5.32	5.32	NA	NA	0.92	1.36	0.44
	group (ii)									
5	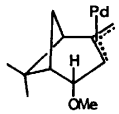	**7a**	3.08 3.75	3.96	3.65	0	2.4	1.11	1.38	0.27
6	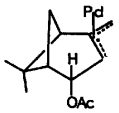	**7b**	3.09 3.77	3.89	5.07	0	2.4	1.13	1.39	0.26
7	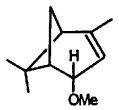	**10**	—	5.33	3.88	NA	NA	0.94	1.31	0.37
8	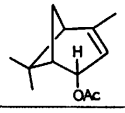	**11**	—	5.33	5.33	NA	NA	0.99	1.35	0.36

a) ^1H NMR spectra of complexes were obtained on a JEOL FX-100 ($CDCl_3$), and those of α-pinenes on a JEOL MH-100 (CCl_4) spectrometer. b) Not ascertainable.

showed no coupling between H-3 and H-4b (Table 1, Entry 5), while the coupling constant of 4.5 Hz was observed between H-3 and H-4a in the *cis*-complex **4a** (Entry 1). Similar observation was also made between the complexes **7b** and **4b**. The dihedral angle between H-3 and H-4b protons estimated by using a stereochemical model is roughly 80—90°, while that between H-3 and H-4a is around 30—40° because of the structural distortion of the pinanyl ligand. These angles, when applied to the Karplus equation, are in good agreement with the observed coupling constants. This also supports the configurational assignment of the complexes.

The present oxypalladation proceeds *via* π-coordination of Pd(II) to the C(3)=C(4) olefin (Scheme 1). The coordination is probably "slipped" away from the symmetrical position because of the steric factors. This allows the C(4) carbon to be more positive.[15] The *cis*-, *exo*-attack of nucleophiles on this carbon could be favorable,[16] similarly to the *cis*-oxymercuration of strained olefins such as norbornenes.[17]

*Asymmetric Cyclization of 2-(*trans*-2-Butenyl)phenols.* The results of the asymmetric cyclization of 2-(*trans*-2-butenyl)phenols (**12**) using the *cis*-complex **5b** (X=OAc) as the catalyst are shown in Table 2,

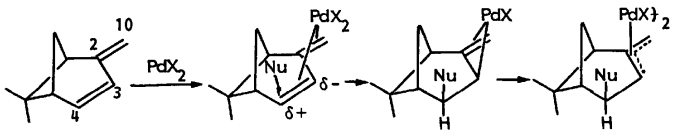

Scheme 1.

together with those obtained by using the parent complex **5c** (Eq. 2). Although the induced enantioselectivities (% ee) of product **13** are not much high in either case, the following two points are of noteworthy. 1) The acetoxy complex **5b** leads to the predominant formation of (*R*)-enantiomer of **13**, opposite to that with the complex **5c**. 2) The electron-withdrawing substituent (Y) of phenoxyl group provides a relatively higher enantiomer excess in either case, as has been observed previously,[2] and the enantioselectivity is not much affected by the steric factor of substituent Y.

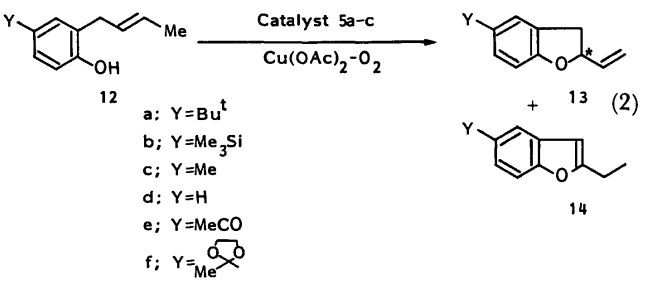

The mechanistic implication of these results may deserve comments. The internal chelation of the *cis*-OAc group in **5b** to palladium(II) blocks the front side corner of the pinanyl ligands. Accordingly, the bulky phenoxyl substituent of olefin **12** prefers to be far apart from the OAc group in the stage where the substrate approaches palladium. The π-complexation A shown in Scheme 2 is thus attained at the expence of steric interference between the Me substituent of

Table 2. Pd(II)-catalyzed asymmetric cyclization of 2-(*trans*-2-butenyl)phenols **12**[a]

Entry	Substrate, Y	Catalyst	Time[b] h	Cyclized product: Yield[c] %	Product ratio **13/14**	$[\alpha]_D$ of **13**[d] deg, (*c*, CCl_4)	Conf	ee[e] %
1	**12a**, 4-Bu^t	**5b** (X=OAc)	13	74	78/22	−6.34, (9.84)	*R*	25
2		**5c** (X=H)	4.8	78	82/18	+3.73, (10.8)	*S*	15
3	**12b**, 4-Me_3Si	**5b**	31	78	78/22	−5.04, (16.3)	*R*	17
4		**5c**	29	65	81/19	+4.40, (17.9)	*S*	15
5	**12c**, 4-Me	**5b**	12	51	78/22	−4.29, (9.46)	*R*	13
6		**5c**	11	76	83/17	+6.84, (3.86)	*S*	21[f]
7	**12d**, 4-H	**5b**	13	61	80/20	−4.58, (6.62)	*R*	18
8		**5c**	4.5	77	83/17	+4.53, (5.19)	*S*	18[g]
9	**12e**, 4-MeCO	**5b**	23	48	96/4	−0.79, (5.33)	*R*	~1
10		**5c**	11	74	96/4	+0.89, (2.71)	*S*	1[f]
11	**12f**, 4-	**5b**	23	79	80/20	−9.40, (4.31)	*R*	29
12	**12a**, 4-Bu^t	**5a** (X=OMe)	16	72	79/21	+0.24, (12.5)	*S*	1
13	**12d**, 4-H	**5a**	13	66	85/15	+0.92, (6.88)	*S*	4

a) The reaction conditions are shown in the text. b) Reaction time required for >98% completion. c) Isolated yield by Kugelrohr distillation. d) Measured at 25—29 °C. e) Determination of % ee for **13a**, **13b**, and **13f** is described in Experimental Section, and for others, see Ref. 2. f) Data from Ref. 2. g) Data from Ref. 1.

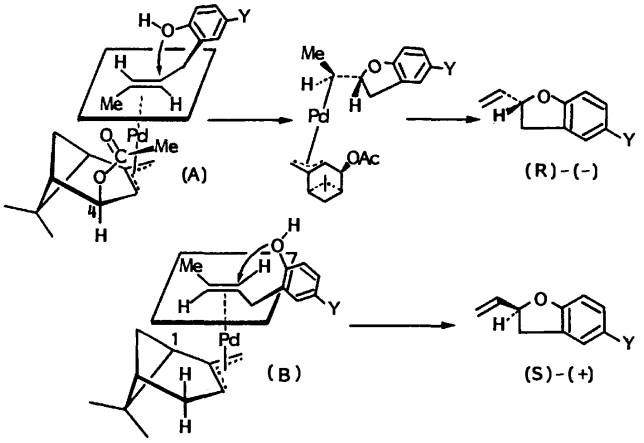

Scheme 2.

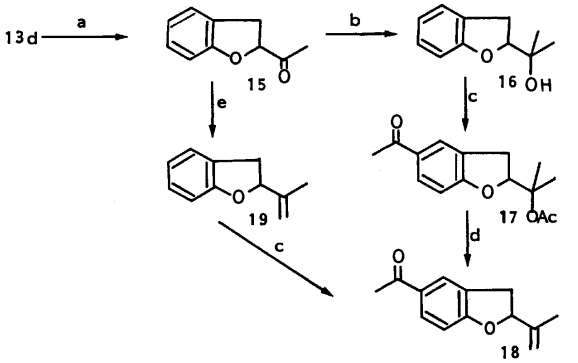

a, $Bu^tOOH/Pd(OCOCF_3)(OOBu^t)$; b, MeMgBr; c, $Ac_2O/SnCl_4$; d, 330 °C; e, $Ph_3P=CH_2$

Scheme 3.

olefin and the blocking OAc group. In the parent complex **5c**, the least steric hindrance is achieved if the Me group is situated in the "pocket" existing over the C(1) bridgehead hydrogen[2] (B in Scheme 2). *trans*-Oxypalladation from these arrangements followed by Pd–H elimination results in the formation of (*R*)- or (*S*)-enantiomer of **13**, respectively, as shown in Scheme 2.[18] The observed substituent (Y) effect common to both of the complexes suggests that the OAc group of pinanyl ligand does not alter the reaction pathways themselves.

In the case of complex **5a** (X=OMe), the two types of π-complexation (A and B) will be involved because the front-side corner must be less effectively blocked by the OMe group. In fact, the use of complex **5a** gives rise to poor enantioselectivity (1—4% ee) in the cyclization of **12a** and **12d** (Table 2, Entries 12 and 13).

As an application of the present asymmetric cyclization, the synthesis of optically active tremetone (**18**) was attempted. The oxidation of (+)-**13d** {$[\alpha]_D$ +4.11°, 16% ee} with Bu^tOOH in the presence of $Pd(OCOCF_3)(OOBu^t)$ as the catalyst gave (−)-2-acetyl-2,3-dihydrobenzofuran (**15**) {48%, $[\alpha]_D$ −9.30°} which was transformed into (*S*)-(+)-tremetone (**18**) by the following sequences (Scheme 3). Conversion of (−)-**15** into tertiary alcohol **16** with MeMgBr followed by acetylation ($SnCl_4$, Ac_2O) afforded 1-(5-acetyl-2,3-dihydro-2-benzofuranyl)-1-methylethyl acetate (**17**) (82%). Pyrolysis of the acetate **17** (330 °C, 1.5 min) gave (*S*)-(+)-tremetone (**18**) {$[\alpha]_D$ +10.4°, 17% ee[19,20]} in 76% yield. Alternatively, the Wittig reaction of (+)-**15** ($Ph_3P=CH_2$, 40 °C, 19 h, 33%) followed by acetylation ($SnCl_4$, Ac_2O, 89%) led to the formation of (*S*)-(+)-**18** {$[\alpha]_D$ +10.5°, 17% ee}.

The asymmetric cyclization of acetal **12f** (Y= 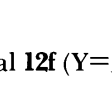) using *cis*-complex **5b** gave (*R*)-(−)-**13f** in 29% ee. Thus, the natural (*R*)-(−)-tremetone (**18**), one of biologically active components in the white snakeroot and others, which induces "tremble" in cattle and "milksickness" in higher animals and humans,[19,20] can be derived from either (*R*)-acetals **13f** or (*R*)-(−)-**13d** (Y=H).

Experimental

Optical rotation were measured with JASCO DIP-4 polarimeter with 1 dm-long cell at room temperature. ^1H NMR spectra were recorded on JMN-MH-60 (JEOL) and JMN FX-100 (JEOL) spectrometers. GLC analysis was performed on a JEOL Model JGC-20KFP flame ionization chromatograph using a 1 m×4 mm, 10% PEG 20 M on 80—100 mesh Celite column under the conditions of injection temperature (200 °C) and column temperature (100—230 °C). Preparative GLC was carried out on a JEOL Model JGC-20KT thermal conductive chromatograph using a 2 m×4 mm or 1 m×4 mm, 10% PEG 20 M on Celite column. Preparative thin-layer chromatography plates were made of silica gel 60 PF254 (Merck).

Palladium(II) acetate $[Pd(OAc)_2]$,[21] sodium tetrachloropalladate(II) (Na_2PdCl_4),[22] and (*t*-butyldioxy) (trifluoroacetato)palladium(II) $[Pd(OCOCF_3)(OOBu^t)]$[23] were prepared as the reported method. *t*-Butyl hydroperoxide (80%) is commercially avairable [Maruwaka Chemical Ind., Ltd. (Osaka)].

Preparation of (1R,5R)-2(10),3-Pinadiene (Verbenene) (1): A mixture of 2(10)-pinen-3-yl acetate (**2**) and 2-pinen-10-yl acetate (**3**) (**2**/**3**=2/1) (12.0 g, 61.8 mmol) prepared from (−)-β-pinene {$[\alpha]_D$ −20°, Tokyo Kasei} and $Pb(OAc)_4$,[10] was added to a stirred solution of $Pd(OAc)_2$ (0.690 g, 3.08 mmol) and PPh_3 (8.10 g, 30.8 mmol) in dry dioxane (72 mL) under argon. After the mixture was refluxed for 24 h, pentane (200 mL) was added to the reaction mixture. The resulting precipitate was removed by filtration, and the filtrate was washed with water (50 mL×2), 5% aqueous $NaHCO_3$ solution (50 mL), and brine (50 mL), and dried over Na_2SO_4. Evaporation followed by distillation gave pinadiene **1** (6.00 g, 72%): bp 60—65 °C (20 mmHg) (1 mmHg=133.322 Pa); $[\alpha]_D^{22}$ +106° (*c* 0.47, CCl_4); IR (neat) 3050, 2945, 1632, 1582, 1370, and 878 (C=CH_2) cm^{-1};

^{1}H NMR (100 MHz, CCl_4) δ=0.87 (3H, s, *gem*-Me), 1.36 (3H, s, *gem*-Me), 1.46 (1H, d, J=8.0 Hz), 2.25—2.65 (3H, m), 4.66 (2H, s, H-10), 6.02 (1H, d, J=8.0 Hz, H-3), and 6.32 (1H, dd, J=8.0 and 6.5 Hz, H-4).

Found: C, 89.17; H, 10.66%. Calcd for $C_{10}H_{14}$: C, 89.49; H, 10.51%. This compound has been reported to be prepared by dehydrobromination of 10-bromo-2-pinene with γ-collidine in 46—64% yields.[8]

Reaction of Pinadiene 1 with Na_2PdCl_4 in MeOH: Into a 0.1 M (1 M=1 mol dm^{-3}) solution of Na_2PdCl_4 in MeOH (10.0 mL, 1.00 mmol) was added pinadiene **1** (0.134 g, 1.00 mmol), and the solution was stirred for 1 h at room temperature. After removal of the solvent, the residue was extracted with CH_2Cl_2 (20 mL), and the extract was washed with brine (10 mL) and dried over Na_2SO_4. Evaporation followed by Al_2O_3 column chromatography (eluent CH_2Cl_2) afforded di-μ-chloro-bis[(3,2,10-η-*cis*-4-methoxypinene)palladium(II)] (**4a**) (0.204 g, 66%): mp 145—158 °C (decomp); IR (Nujol) 1356, 1250, 1104 (C-O), 982, and 788 cm^{-1}; The ^{1}H NMR spectral data of this compound **4a** are listed in Table 1, together with those of **4b**, **7a**, **7b**, **8**, **9**, **10**, and **11** described below.

Found: C, 43.69; H, 5.62; Cl, 11.32%. Calcd for $C_{11}H_{17}ClOPd$: C, 43.02; H, 5.58; Cl, 11.54%.

Reaction of Pinadiene 1 with $Pd(OAc)_2$ in AcOH: Into a suspended solution of $Pd(OAc)_2$ (0.449 g, 2.00 mmol) in AcOH (10 mL) was added pinadiene **1** (0.268 g, 2.00 mmol). After the solution was stirred for 1 h at room temperature, NaCl (0.350 g, 6.00 mmol) was added into the solution, and stirring was further continued for 30 min. The reaction mixture was extracted with CH_2Cl_2 (50 mL), washed with 5% aqueous $NaHCO_3$ solution (20 mL×2), and brine (20 mL) and dried over Na_2SO_4. Evaporation followed by Al_2O_3 column chromatography (eluent CH_2Cl_2) to give di-μ-chloro-bis[(3,2,10-η-*cis*-4-acetoxypinene)palladium(II)] (**4b**) (0.476 g, 71%): mp 117 °C; $[\alpha]_D^{22}$ −237° (*c* 0.22, MeOH); IR (Nujol) 1737 (C=O), 1241 (C-O), 1030, and 781 cm^{-1}.

Found: C, 43.36; H, 5.26; Cl, 10.72%. Calcd for $C_{12}H_{17}ClO_2Pd$: C, 43.01; H, 5.11; Cl, 10.58%.

Reaction of Pinadiene 1 with $Pd(OAc)_2$ in MeOH: The reaction of pinadiene **1** (0.460 g, 3.43 mmol) with $Pd(OAc)_2$ (0.770 g, 3.43 mmol) in MeOH (15 mL) was carried out according to the procedure described above. After usual workup, the crude oil was purified by preparative TLC [SiO_2, benzene-acetone (9:1)] to give **4a** (0.130 g, 12%, R_f 0.49) and **4b** (0.163 g, 14%, R_f 0.57).

Preparation of Di-μ-chloro-bis[(3,2,10-η-cis-4-t-butoxypinene)palladium(II)] (4c): The reaction of pinadiene **1** (0.067 g, 0.50 mmol) with $Pd(OCOCF_3)(OOBu^t)$ (0.154 g, 0.50 mmol) in acetone (2.5 mL) was carried out according to the procedure described above. After usual workup, Al_2O_3 column chromatography (eluent CH_2Cl_2) afforded complex **4c** (0.149 g, 85%): ^{1}H NMR (60 MHz, $CDCl_3$) δ=1.03 (3H, s, *gem*-Me), 1.25 (9H, s, Bu^t), 1.41 (3H, s, *gem*-Me), 2.00—2.75 (4H, m), 3.13 (1H, br), 3.75 (1H, br), 3.85—3.95 (1H, m), and 4.16—4.25 (1H, m).

Found: C, 48.29; H, 6.47%. Calcd for $C_{14}H_{23}ClOPd$: C, 48.15; H, 6.64%.

Ligand Exchange of Complex 4a and 4b with AgOAc: The reaction of chloride complex **4a** and **4b** with AgOAc in $CHCl_3$ was carried out according to the procedure described previously.[1]

Di-μ-acetato-bis[(3,2,10-η-cis-4-methoxypinene)palladium(II)] (5a): Yield 64%; IR (KBr) 1570, 1412, 1342, 1096, 976, 920, and 780 cm^{-1}; ^{1}H NMR (60 MHz, $CDCl_3$) δ=1.00 (3H, s, *gem*-Me), 1.41 (3H, s, *gem*-Me), 1.87—2.73 (4H, m), 2.01 (3H, s, OAc), 2.83 (1H, s, *syn*-H-10), 3.30 (3H, s, OMe), 3.47 (1H, dd, J=5 and 2 Hz, H-4), 3.66 (1H, s, *anti*-H-10), and 3.98 (1H, d, J=5 Hz, H-3).

Found: C, 47.17; H, 6.19%. Calcd for $C_{13}H_{20}O_3Pd$: C, 47.22; H, 6.10%.

Di-μ-acetato-bis[(3,2,10-η-cis-4-acetoxypinene)palladium(II)] (5b): Yield 84%; $[\alpha]_D^{27}$ −75° (*c* 0.25, MeOH); IR (KBr) 1730, 1570, 1416, 1240, and 1024 cm^{-1}; ^{1}H NMR (60 MHz, $CDCl_3$) δ=1.05 (3H, s, *gem*-Me), 1.43 (3H, s, *gem*-Me), 1.80—2.03 (1H, m), 1.96 (6H, s, OAc), 2.23—2.80 (3H, m), 3.35 (1H, s, *syn*-H-10), 3.52 (1H, d, J=2 Hz, *anti*-H-10), 3.85 (1H, d, J=5 Hz, H-3), and 4.72 (1H, dd, J=5 and 3 Hz, H-4).

Found: C, 47.29; H, 5.78%. Calcd for $C_{14}H_{20}O_4Pd$: C, 46.88; H, 5.62%.

Preparation of (1S,4S,5S)-2(10)-Pinen-4-yl Methyl Ether (6a): According to the sequence of G. Ohloff *et. al.*,[12] (−)-(1S,4S,5S)-2(10)-pinen-4-ol (**20**) was firstly prepared starting from (−)-α-pinene {$[\alpha]_D$ −29° (neat), Tokyo Kasei}. In this procedure, isomerization of (1S,5S)-2-pinen-4-one (verbenone) to (1S,5S)-2(10)-pinen-4-one was performed by Herrmann's method.[24] The alcohol **20** obtained in this way was transformed into the methyl ether **6a** by the following procedure.

Sodium hydride (0.068 g, 2.83 mmol) was added to a solution of alcohol **20** (0.400 g, 2.63 mmol) and MeI (0.436 g, 3.07 mmol) in dry DME (1.5 mL) over a period of 10 min with stirring at room temperature. After stirring for 10 min, a further quantity of MeI (0.100 g, 0.705 mmol) was added, and stirring was continued for additional 2 h. The DME and excess MeI were then removed by distillation at atmospheric pressure. To the remaining mixture was added ether (5 mL), and the resulting NaI was filtered off and washed with additional ether (10 mL). Evaporation of ether followed by distillation gave 2(10)-pinen-4-yl methyl ether (**6a**) (0.357 g, 82%): bp 90—95 °C (35 mmHg); IR (neat) 2935 (C-H), 1648, 1468, 1372, 1092, 874, and 846 cm^{-1}; ^{1}H NMR (60 MHz, CCl_4) δ=0.93 (3H, s, *gem*-Me), 1.25 (3H, s, *gem*-Me), 1.63—1.75 (1H, m), 2.18—2.93 (5H, m), 3.28 (3H, s, OMe), 3.63—3.98 (1H, m, H-4), and 4.63 (2H, d, J=2 Hz, H-10).

Preparation of (1S,4S,5S)-2(10)-Pinen-4-yl Acetate (6b): The alcohol **20** (0.584 g, 3.84 mmol) was acetylated by using Ac_2O (0.431 g, 4.22 mmol) in the presence of pyridine (0.455 g, 5.76 mmol). Usual workup followed by distillation gave 2(10)-pinen-4-yl acetate (**6b**) (0.653 g, 88%): bp 70—75 °C (2 mmHg); IR (neat) 2940 (C-H), 1738 (C=O), 1648, 1472, 1372, 1242, 1042, 1024, 880, and 852 cm^{-1}; ^{1}H NMR (60 MHz, CCl_4) δ=0.93 (3H, s, *gem*-Me), 1.30 (3H, s, *gem*-Me), 1.73—2.60 (6H, m), 1.96 (3H, s, OAc), 4.66 (2H, t, J=2 Hz, H-10), and 5.05—5.50 (1H, m, H-4).

Preparation of Di-μ-chloro-bis[(3,2,10-η-trans-4-methoxypinene)palladium(II)] (7a): Into a suspended solution of $Pd(OAc)_2$ (0.225 g, 1.00 mmol) in anhydrous MeOH (5 mL) was added methyl ether **6a** (0.166 g, 1.00 mmol). After the mixture was stirred for 30 min, NaCl (0.174 g, 3.00 mmol) was added to the solution, and stirring was continued for further 30 min. The solvent was then removed under reduced pressure, and the residue was extracted with

CH_2Cl_2 (50 mL×2), washed with brine (20 mL×2), and dried over Na_2SO_4. After evaporation of the solvent, the residual yellow oil was chromatographed on Al_2O_3 (15 g). Elution with $CHCl_3$ (100 mL) gave oily material which was purified by preparative TLC [benzene–EtOAc (4:1)] to give complex **7a** (0.179 g, 58%): R_f 0.75; mp 147—151 °C (decomp); IR ($CHCl_3$) 1470, 1252, 1086, 948, and 822 cm^{-1}.

Found: C, 43.02; H, 5.58; Cl, 11.54%. Calcd for $C_{11}H_{17}ClOPd$: C, 43.39; H, 5.69; Cl, 11.03%.

Preparation of Di-μ-chloro-bis[(3,2,10-η-trans-4-acetoxypinene)palladium(II)] (7b): The reaction of acetate **6b** (0.194 g, 1.00 mmol) and $Pd(OAc)_2$ (0.225 g, 1.00 mmol) was carried out according to the procedure described above. Chromatographic purification of the resulting oil followed by preparative TLC [benzene–EtOAc (4:1)] gave complex **7b** (0.174 g, 51%): R_f 0.70; mp 145 °C (decomp); $[\alpha]_D$ −94° (*c* 0.19, MeOH); IR ($CHCl_3$) 1740 (C=O), 1045, 1023, and 980 cm^{-1}.

Found: C, 43.65; H, 5.21; Cl, 10.32%. Calcd for $C_{12}H_{17}ClO_2Pd$: C, 43.00; H, 5.11; Cl, 10.58%.

(1S,4R,5S)-2-Pinen-4-yl Acetate (9): The pinene **9** bearing OAc group at the C(4),*exo*-position was prepared by the reaction of α-pinene with $Pb(OAc)_4$ followed by isomerization in AcOH[11] in 47% yield from α-pinene; bp 96—98 °C (8 mmHg); IR (neat) 2930, 1730 (C=O), 1372, 1240 (C–O), 1018, 970, and 773 cm^{-1}.

(1S,4R,5S)-2-Pinen-4-yl Methyl Ether (8): The pinene **8** bearing OMe group at the C(4),*exo*-position was synthesized by the hydrolysis of the acetate **9** followed by treatment with MeI in 61% yield from **9**; bp 83—85 °C (23 mmHg); IR (neat) 2920, 2815, 1468, 1445, 1192, 1138, 1086, and 959 cm^{-1}.

(1S,4S,5S)-2-Pinen-4-yl Methyl Ether (10): The pinene **10** bearing OMe group at the C(4),*endo*-position was prepared by treatment of (1*S*,4*S*,5*S*)-2-pinen-4-ol (**21**) with MeI in 84% yield. The alcohol **21** was obtained by MnO_2 oxidation of (1*S*,4*R*,5*S*)-2-pinen-4-ol followed by $LiAlH_4$ reduction;[12] bp 80—83 °C (20 mmHg); IR (neat) 2930, 2810, 1446, 1368, 1354, 1190, 1088, and 952 cm^{-1}.

(1S,4S,5S)-2-Pinen-4-yl Acetate (11): The esterification of alcohol **21** with Ac_2O gave the pinene **11** bearing OAc group at the C(4),*endo*-position in 89% yield: bp 90—95 °C (8 mmHg); IR (neat) 2940, 1740 (C=O), 1662, 1450, 1375, 1242, 1022, 976, and 810 cm^{-1}.

Found: C, 74.15; H, 9.40%. Calcd for $C_{12}H_{18}O_2$: C, 74.19; H, 9.34%.

*Preparation of 4-Substituted 2-(*trans*-2-Butenyl)phenols 12*: 4-*t*-Butyl-2-(*trans*-2-butenyl)phenol (**12a**) was prepared by *C*-alkylation of *p*-*t*-butylphenol with *trans*-1-chloro-2-butene (Tokyo Kasei). 4-Trimethylsilyl-2-(*trans*-2-butenyl)-phenol (**12b**) was synthesized by the silylation of 4-bromo-2-(*trans*-2-butenyl)phenol prepared by *O*-alkylation of *p*-bromophenol with 3-chloro-2-butene followed by the Claisen rearrangemet (200 °C, *N*,*N*-diethylaniline). The silylation procedure is as follows. Into a solution of 4-bromo-2-(*trans*-2-butenyl)phenol (3.40 g, 15.0 mmol) in dry THF (20 mL) was dropwise added Bu^nLi (1.6 M in hexane, 31 mL, 50 mmol) at −78 °C, and then chlorotrimethylsilane (5.7 mL, 45 mmol) was added to the solution at −78 °C. The mixture was warmed up to room temperature, stirred overnight, quenched with 2 M HCl (30 mL), and extracted with ether. Usual workup followed by distillation gave **12b** (2.56 g, 78%); bp 95—102 °C (1 mmHg); IR (neat) 3460 (OH) and 960 (C=C) cm^{-1}; ^1H NMR (60 MHz, CCl_4) δ=0.00 (9H, s, $SiMe_3$), 1.35—1.55 (3H, m, Me), 2.90—3.23 (2H, m, CH_2), 5.10 (1H, br s, OH), and 5.18—5.50 (2H, m, CH=CH). The acetal **12f** was synthesized as follows. A mixture of 4-acetyl-2-(*trans*-2-butenyl)phenol (**12e**) (1.14 g, 6.0 mmol), ethylene glycol (18.6 g, 300 mmol), and fumaric acid (0.06 g, 0.5 mmol) in dry benzene (20 mL) was refluxed with stirring. The water formed during the reaction was removed azeotropically (Dean-Stark trap) for 72 h. After the mixture was cooled to room temperature, benzene (200 mL) and K_2CO_3 was added until drying agent was coagulated. The solid was filtered off by suction. The filtrate was washed with 5% aqueous $NaHCO_3$ solution (20 mL) and brine (20 mL), and dried over Na_2SO_4. Evaporation of the solvent and addition of pentane induced crystallization to give ethylene acetal **12f** (1.07 g, 76%): IR (Nujol) 3370, 2930, 1611 (C=C), 1504, 1377, 1275, 1204, 1097, 1036, 971, 860, and 820 cm^{-1}; ^1H NMR (60 MHz, $CDCl_3$) δ=1.65 (3H, s, Me), 1.68—1.78 (3H, m, Me), 3.38 (2H, br s), 3.75—4.10 (4H, m, OCH_2CH_2O), 4.20—5.10 (1H, m, OH), 5.60—5.78 (2H, m, CH=CH), 6.81 (1H, d, *J*=9 Hz, ArH), and 7.20—7.40 (2H, m, ArH). Preparation of other phenols **12c—e** was described previously.[1,2]

Asymmetric Cyclization of 12: The cyclization of **12** (2.5 mmol) was performed by using di-μ-acetato-bis[(3,2,10-η-pinene)palladium(II) **5a—c** (0.125 mmol as a dimer) and $Cu(OAc)_2$ (0.0454 g, 0.25 mmol) in anhydrous MeOH (5 mL) under an atmosphere of O_2 (1 atm) at 35 °C according to the general procedure described previously.[1,2] The cyclized products **13** and **14** were isolated by Kugelrohr distillation and purified by either preparative GLC (20% PEG 20 M, 2 m) or TLC. The spectral and analytical data of newly obtained products are listed below.

2-Vinyl-5-t-butyl-2,3-dihydrobenzofuran (13a): Kugelrohr distillation, bp 120—129 °C (6 mmHg); IR (neat) 2970, 1500, 1240, 930, and 810 cm^{-1}; ^1H NMR (60 MHz, CCl_4) δ=1.15 (9H, s, Bu^t), 2.69 (1H, dd, *J*=15 and 8 Hz, H-3), 3.13 (1H, dd, *J*=15 and 9 Hz, H-3), 4.75—5.35 (3H, m, H-2 and CH_2=C), 5.57—6.12 (1H, m, CH=C), 6.35 (1H, d, *J*=9 Hz, ArH), and 6.78—7.02 (2H, m, ArH).

Found: C, 83.16; H, 8.87%. Calcd for $C_{14}H_{18}O$: C, 83.12; H, 8.97%.

5-t-Butyl-2-ethylbenzofuran (14a): Kugelrohr distillation, bp 135 °C (6 mmHg); IR (neat) 2970, 1480, 1370, 1270, and 800 cm^{-1}; ^1H NMR (60 MHz, CCl_4) δ=1.32 (9H, s, Bu^t), 1.35 (3H, t, *J*=8 Hz, Me), 2.73 (2H, q, *J*=8 Hz, CH_2), 6.20 (1H, br s, H-3), and 7.12—7.41 (3H, m, ArH).

Found: C, 83.03; H, 8.84%. Calcd for $C_{14}H_{18}O$: C, 83.12; H, 8.97%.

5-Trimethylsilyl-2-vinyl-2,3-dihydrobenzofuran (13b): TLC [SiO_2, hexane–$CHCl_3$ (4:1)], R_f 0.51; IR (neat) 2950, 1600, 1480, 1250, 1240, and 815 cm^{-1}; ^1H NMR (60 MHz, CCl_4) δ=0.00 (9H, s, $SiMe_3$), 2.88 (1H, dd, *J*=18 and 8 Hz, H-3), 3.40 (1H, dd, *J*=18 and 10 Hz, H-3), 5.05—5.83 (3H, m, H-2 and CH_2=C), 7.11 (1H, d, *J*=9 Hz, ArH), and 7.37—8.07 (2H, m, ArH).

5-Trimethylsilyl-2-ethylbenzofuran (14b): TLC (the same conditions as above), R_f 0.64; IR (neat) 2950, 1598, 1250, and 820 cm^{-1}; ^1H NMR (60 MHz, CCl_4) δ=0.00 (9H, s, $SiMe_3$), 1.15 (3H, t, *J*=8 Hz, Me), 2.80 (2H, q, *J*=8Hz, CH_2), 6.60 (1H, br s, CH=C), and 7.68—8.10 (3H, m, ArH).

5-Acetyl-2-vinyl-2,3-dihydrobenzofuran Ethylene Acetal (13f): TLC [SiO_2, hexane–EtOAc (5:1)], R_f 0.70; bp 122—124 °C (1 mmHg); $[\alpha]_D$ −9.40° (*c* 4.31, CCl_4); ^1H NMR (60 MHz, CCl_4) δ=1.48 (3H, s, Me), 2.83 (1H, dd, *J*=13 and 7 Hz, H-3), 3.28 (1H, dd, *J*=13 and 8 Hz, H-3), 3.53—3.91 (4H, m, OCH_2CH_2O), 4.78—5.39 (3H, m, H-2 and CH_2=), 5.92 (1H, ddd, *J*=15, 9, and 5 Hz, -CH=), 6.50 (1H, d, *J*=9 Hz, ArH), and 6.91—7.16 (2H, m, ArH).

Found: C, 72.39; H, 6.88%. Calcd for $C_{14}H_{16}O_3$: C, 72.40; H, 6.94%.

5-Acetyl-2-ethylbenzofuran Ethylene Acetal (14f): TLC (the same conditions as above), R_f 0.80; ^1H NMR (60 MHz, CCl_4) δ=1.31 (3H, t, *J*=8 Hz, Me), 1.61 (3H, s, Me), 2.78 (2H, q, *J*=8 Hz, CH_2), 3.64—4.05 (4H, m, OCH_2CH_2O), 6.30 (1H, s, H-3), and 7.23—7.34 (3H, m, ArH).

Determination of Enantiomer Excess of 13a (Y=Bu^t): The % ee determination of **13a** (Y=Bu^t) was attempted by using Eu(tfc)$_3$ through the NMR spectrum of methyl ester derived from $KMnO_4$ oxidation of **13a** followed by esterification.[2] However, during the workup process of $KMnO_4$ oxidation performed in MeCN–glyme solution, unreproducible results were obtained for this compound, because of the difference in solubility of the resulting enantiomeric potassium 5-*t*-butyl-2,3-dihydrobenzofuran-2-carboxylate into aqueous NaOH solution.[25] Hence, the enantiomer excess of **13a** was determined through the NMR spectrum of 2-(5-*t*-butyl-2,3-dihydro-2-benzofuranyl)-2-propanol (**22**) prepared by the same manner as that of **16** (see Scheme 3).

a) Transformation of 13a (Y=Bu^t) into Tertiary Alcohol 22: A solution of 2-vinyl-5-*t*-butyl-2,3-dihydrobenzofuran (**13a**) {0.270 g, 1.3 mmol, $[\alpha]_D^{21}$ −4.54° (*c* 8.58, CCl_4)}, $Pd(OCOCF_3)(OOBu^t)$ (0.040 g, 0.13 mmol), and Bu^{t}OOH (0.30 mL, 1.3 mmol) in benzene (6 mL) was stirred at 50 °C for 65 h. Evaporation of the solvent followed by addition of pentane afforded brown precipitate which was removed by filtration. Concentration of the filtrate followed by Kugelrohr distillation gave a 60:40 mixture (0.155 g) of 2-acetyl-5-*t*-butyl-2,3-dihydrobenzofuran (**23**) and unreacted **13a**. The compound **23** purified by preparative TLC [SiO_2, hexane–EtOAc (7:3)] showed the following characteristics: R_f 0.40; IR (neat) 2952, 2860, 1812, 1756, 1720, 1494, 1362, 1239, 1216, 1160, 1064, 962, and 829 cm^{-1}; ^1H NMR (60 MHz, $CDCl_3$) δ=1.29 (9H, s, Bu^t), 2.23 (3H, s, COMe), 3.29 (1H, d, *J*=8 Hz, H-3), 3.31 (1H, d, *J*=10 Hz, H-3), 4.95 (1H, dd, *J*=10 and 8 Hz, H-2), and 6.63—7.30 (3H, m, ArH). The acetylbenzofuran **23** (0.090 g, 0.41 mmol) was treated with MeMgBr (0.50 mmol) in dry ether (4 mL) at 0 °C. Usual workup followed by preparative TLC [SiO_2, benzene–EtOAc (4:1)] gave tertiary alcohol **22** (0.040 g, 42%): R_f 0.45; ^1H NMR (60 MHz, $CDCl_3$) δ=1.23 (3H, s, Me), 1.34 (3H, s, Me), 1.31 (9H, s, Bu^t), 2.03 (1H, br, OH), 3.18 (2H, d, *J*=9 Hz, H-3), 4.67 (1H, t, *J*=9 Hz, H-2), and 6.73—7.49 (3H, m, ArH).

b) Determination of Enantiomer Excess of 13a through tert-Alcohol 22: The ^1H NMR spectra ($CDCl_3$) of tertiary alcohol **22** (0.013 g) obtained above showed a triplet signal due to the C(2) proton at δ=4.67 (*J*=9 Hz). The proton was separated clearly into two sets of triplets (*J*=9 Hz) by addition of Eu(tfc)$_3$ (0.004 g). The relative peak areas of the three sets of splitting signals led to 18% ee for this compound. Thus, the maximum rotation of **13a** is estimated to be 25.4° (CCl_4). Using **13a** with different $[\alpha]_D$ values, the experiment was repeated three times, and the results were shown to be reproducible.

Application of this procedure to **13c** (Y=Me) led to the % ee in good agreement with that obtained by the previous method.[2]

Determination of Enantiomer Excess of 13b (Y=SiMe$_3$): Optically active **13b** (0.209 g, 0.96 mmol) of $[\alpha]_D^{23}$ −5.04° (*c* 16.3, CCl_4) was dissolved in CCl_4 (3 mL), into which was added trifluoroacetic acid (5 mL) at room temperature. After stirring for 24 h, the mixture was diluted with ether, poured into saturated $NaHCO_3$ solution (20 mL), and extracted with ether. Preparative TLC [SiO_2, hexane–EtOAc (4:1), R_f 0.80] followed by Kugelrohr distillation [bp 80—82 °C (1 mmHg)] gave **13d** (Y=H) (0.023 g, 17%), the $[\alpha]_D$ of which was −4.32° (*c* 1.16, CCl_4). This value corresponds to 17% ee based on the previously reported maximum rotation.[1] The maximum rotation of **13b** is thus estimated to be −30.3° (CCl_4).

Determination of Enantiomer Excess of 13f: Into a solution of **13f** {0.182 g, 0.78 mmol, $[\alpha]_D$ −9.40°} in ether (20 mL) was added 2 M HCl solution (20 mL). After the mixture was stirred at room temperature overnight, the ether layer was washed with water and brine, and dried over Na_2SO_4. Evaporation followed by preparative TLC [SiO_2, hexane–EtOAc (4:1), R_f 0.45] gave 4-acetyl-2-vinyl-2,3-dihydrobenzofuran (**13e**) (0.085 g, 58%), the $[\alpha]_D$ of which was −25.0° (CCl_4). This value corresponds to 29% ee.[2]

Preparation of 2-Acetyl-2,3-dihydrobenzofuran (15): A solution of 2-vinyl-2,3-dihydrobenzofuran **13d** {1.00 g, 6.84 mmol, $[\alpha]_D^{23}$ +4.11° (*c* 5.55, CCl_4)}, $Pd(OCOCF_3)(OOBu^t)$ (0.210 g, 0.68 mmol), and Bu^{t}OOH (1.76 mL, 14.7 mmol) in benzene (30 mL) was stirred at 50 °C for 16 h. The mixture was extracted with CH_2Cl_2, washed with a 10% aqueous Na_2SO_3 and brine, and dried over Na_2SO_4. Evaporation of the solvent gave oily material, which was dissolved into a small amount of ether. Addition of pentane to this solution afforded brown precipitate which was removed by filtration. Evaporation followed by Kugelrohr distillation gave 2-acetyl-2,3-dihydrobenzofuran **15** (0.532 g, 48%). Analytically-pure **15** was obtained by preparative GLC; bp 100—110 °C (2 mmHg); $[\alpha]_D^{24}$ −9.30° (*c* 1.52, CCl_4); IR (neat) 1720 (C=O) cm^{-1}; ^1H NMR (60 MHz, CCl_4) δ=2.27 (3H, s, COMe), 3.37 (2H, br d, *J*=9 Hz, H-3), 4.93 (1H, t, *J*=9 Hz, H-2), and 6.53—7.26 (4H, m, ArH).

Found: C, 73.58; H, 6.18%; M^+, 162. Calcd for $C_{10}H_{10}O_2$: C, 74.05; H, 6.22%; M, 162.

Preparation of 2-(2,3-Dihydro-2-benzofuranyl)-2-propanol (16): Into a solution of MeMgBr (11.6 mmol) in ether (30 mL) was slowly added a solution of **15** (0.754 g, 4.6 mmol) in ether (10 mL). The mixture was stirred for 1 h at room temperature and then acidified by 2 M HCl. Extraction with ether followed by Kugelrohr distillation gave tertiary alcohol **16** (0.580 g, 70%) which was purified by preparative GLC: bp 78—80 °C (0.1 mmHg); $[\alpha]_D^{24}$ +5.87° (*c* 1.02, EtOH); IR (neat) 3400 (OH) cm^{-1}; ^1H MNR (60 MHz, $CDCl_3$) δ=1.12 (3H, s, Me), 1.25 (3H, s, Me), 3.05 (2H, br d, *J*=9 Hz, H-3), 3.17—3.83 (1H, m, OH), 4.51 (1H, dd, *J*=10 and 9 Hz, H-2), and 6.60—7.25 (4H, m, ArH).

Preparation of 1-(5-Acetyl-2,3-dihydro-2-benzofuranyl)-1-methylethyl Acetate (17): A mixture of tertiary alcohol **16** (0.514 g, 2.88 mmol) and Ac_2O (0.894 g, 8.76 mmol) in

benzene (20 mL) was stirred at 0 °C while a solution of $SnCl_4$ (2.25 g, 8.64 mmol) in benzene (10 mL) was added dropwise over a period of 20 min. After stirring for further 30 min, the solution was poured into ice-water, extracted with ether until neutral, and dried over Na_2SO_4. Evaporation of the solvent gave acetate **17** (0.623 g, 82%) as solid which was recrystallized from pentane; mp 95.5—97.0 °C; IR (Nujol) 1730, 1664, 1610, 1270, 1250, 966, and 820 cm^{-1}; ^1H NMR (60 MHz, CCl_4) δ=1.48 (3H, s, Me), 1.55 (3H, s, Me), 1.94 (3H, s, OAc), 2.51 (3H, s, COMe), 3.17 (2H, d, J=9 Hz, H-3), 5.02 (1H, t, J=9 Hz, H-2), 6.73 (1H, d, J=9 Hz, ArH), and 7.57—7.92 (2H, m, ArH).

Found: 68.58; H, 6.83%. Calcd for $C_{15}H_{18}O_4$: C, 68.69; H, 6.92%.

Preparation of Tremetone (18): The acetate **17** (0.117 g, 0.45 mmol) was pyrolyzed at 330 °C for 1.5 min according to the procedure of Bonner *et al.*[20] The crude tremetone (**18**) formed in 76% yield (0.091 g, 75% pure) was purified by preparative GLC: $[\alpha]_D^{21}$ +10.4° (*c* 0.87, EtOH); IR (neat) 1678, 1608, and 1264 cm^{-1}; ^1H NMR (60 MHz, $CDCl_3$) δ=1.73 (3H, s, Me), 2.40 (3H, s, COMe), 2.95 (1H, dd, J=16 and 9 Hz, H-3), 3.35 (1H, dd, J=16 and 9 Hz, H-3), 4.85 (1H, br s, $=CH_2$), 5.03 (1H, br s, $=CH_2$), 5.15 (1H, t, J=9 Hz, H-2), 6.68 (1H, d, J=9 Hz, ArH), and 7.57—7.83 (2H, m, ArH). The spectral data agrees well with that reported previously.[26] The $[\alpha]_D$ value of +10.4° corresponding to 17% ee based on the reported maximum rotation.[19]

Found C, 76.80; H, 7.07%. Calcd for $C_{13}H_{14}O$: C, 77.20; H, 6.98%.

Tremetone (18) Prepared via *Wittig Reaction*: Into a solution of Bu^nLi (1.6 M in hexane, 2.10 mL, 3.36 mmol) in ether (8 mL) was added $[Ph_3PMe]^+Br^-$ (1.32 g, 3.70 mmol) by portions, and the mixture was stirred for 4 h at room temperature under argon. Into this mixture was added dropwise a solution of 2-acetyl-2,3-dihydrobenzofuran (**15**) {0.600 g, 3.70 mmol, $[\alpha]_D$ −9.30°} in ether (2 mL). The whole mixture was then heated at 40 °C for 19 h under argon, and the resulting solid was removed by filtration. The ether layer was washed with water until neutral, and dried over $CaCl_2$. Evaporation followed by Kugelrohr distillation gave 2-isopropenyl-2,3-dihydrobenzofuran (**19**) (0.180 g, 33%): bp 105—120 °C (2 mmHg); ^1H NMR (60 MHz, $CDCl_3$) δ=1.74 (3H, d, J=1 Hz, Me), 2.96 (1H, dd, J=16 and 9 Hz, H-3), 3.34 (1H, dd, J=16 and 9 Hz, H-3), 4.83—5.33 (3H, m, $C=CH_2$ and H-2), and 6.67—7.42 (4H, m, ArH). The dihydrobenzofuran **19** (0.174 g, 1.17 mmol) was converted into tremetone (**18**) (0.223 g, 94% pure) in 89% yield by the procedure using Ac_2O (0.364 g, 3.57 mmol) and $SnCl_4$ (0.917 g, 3.52 mmol) in benzene (15 mL). Preparative TLC (SiO_2, $CHCl_3$, R_f 0.27) followed by Kugelrohr distillation [bp 170 °C (2 mmHg)], gave pure **18** of $[\alpha]_D^{24}$ +10.5° (*c* 2.64, EtOH) in 17% ee.[19]

We wish to thank Mr. Satoru Yamamoto for the experimental assistance, and Mr. Yoshio Terawaki for measureing ^1H NMR spectra.

References

1) T. Hosokawa, T. Uno, S. Inui, and S.-I. Murahashi, *J. Am. Chem. Soc.*, **103**, 2318 (1981).

2) T. Hosokawa, C. Okuda, and S.-I. Murahashi, *J. Org. Chem.*, **50**, 1282 (1985).

3) The reaction of 1,3-diene with Pd(II) compounds in the presence of various nucleophiles, see: a) For oxygen nucleophiles: S. D. Robinson and B. L. Shaw, *J. Chem. Soc.*, **1963**, 4806; S. D. Robinson and B. L. Shaw, *ibid.*, **1964**, 5002; J. M. Rowe and D. A. White, *J. Chem. Soc., A*, **1967**, 1451; K. Dunne and F. J. McQuillin, *J. Chem. Soc., C*, **1970**, 2196; M. Takahashi, H. Suzuki, Y. Moro-oka, and T. Ikawa, *Chem. Lett.*, **1979**, 53; J.-E. Bäckvall, S. E. Byström, and R. E. Nordberg, *J. Org. Chem.*, **49**, 4619 (1984); b) For chloride nucleophiles: B. L. Shaw, *Chem. Ind.*, **1962**, 1190; J. Lukas, P. W. N. M. Van Leeuwen, H. C. Volger, and P. Kramer, *J. Chem. Soc., Chem. Commun.*, **1970**, 799; J. Lukas, P. W. N. M. Van Leeuwen, H. C. Volger, and A. P. Kouwenhoven, *J. Organomet. Chem.*, **47**, 153 (1973); c) For amine nucleophiles: B. Åkermark, J.-E. Bäckvall, A. Löwenborg, and K. Zetterberg, *J. Organomet. Chem.*, **166**, C33 (1979); d) For sulfur nucleophiles: M. Julia, M. Nel, and L. Saussine, *J. Organomet. Chem.*, **181**, C17 (1979); Y. Tamaru, Y. Yamada, M. Kagotani, H. Ochiai, E. Nakajo, R. Suzuki, and Z. Yoshida, *J. Org. Chem.*, **48**, 4669 (1983).

4) J.-E. Bäckvall, R. E. Nordberg, E. E. Björkman, and C. Moberg, *J. Chem. Soc., Chem. Commun.*, **1980**, 943.

5) J.-E. Bäckvall, B. Åkermark, and S. O. Ljunggren, *J. Am. Chem. Soc.*, **101**, 2411 (1979); O. S. Andell and J.-E. Bäckvall, *J. Organomet. Chem.*, **244**, 401 (1983), and references cited therein; D. E. James, L. F. Hines, and J. K. Stille, *J. Am. Chem. Soc.*, **98**, 1806 (1976); J. K. Stille and R. Divakaruni, *J. Organomet. Chem.*, **169**, 239 (1979).

6) Although a *cis*-oxypalladium adduct of cyclooctadiene has been reported, [M. Akbarzadeh and C. B. Anderson, *J. Organomet. Chem.*, **197**, C5 (1980)], this complex is the product of *trans*-oxypalladation of *cis*-, *trans*-1,5-cyclooctadiene.

7) This work has been reported as a preliminary communication; T. Hosokawa, Y. Imada, and S.-I. Murahashi, *Tetrahedron Lett.*, **1982**, 3373.

8) G. Zweifel and C. C. Whitney, *J. Org. Chem.*, **31**, 4178 (1966).

9) J. Tsuji, T. Yamakawa, M. Kaito, and T. Mandai, *Tetrahedron Lett.*, **1978**, 2075; B. M. Trost, T. R. Verhoeven, and J. M. Fortunak, *ibid.*, **1979**, 2301; R. O. Hutchins, K. Learn, and R. P. Fulton, *ibid.*, **1980**, 27.

10) L. E. Gruenewald and D. C. Johnson, *J. Org. Chem.*, **30**, 1673 (1965).

11) J. J. Hurst and G. H. Whitham, *J. Chem. Soc.*, **1960**, 2864; G. H. Whitham, *ibid.*, **1961**, 2232.

12) G. Ohloff and W. Giersch, *Helv. Chim. Acta*, **60**, 1496 (1977).

13) B. M. Trost, P. E. Strege, L. Weber, T. J. Fullerton, and T. J. Dietsche, *J. Am. Chem. Soc.*, **100**, 3407 (1978).

14) A. D. Buckingham and W. Urland, *Mol. Phys.*, **26**, 1571 (1973); T. Hosokawa, T. Ohta, and S.-I. Murahashi, *J. Organomet. Chem.*, **228**, C55 (1982).

15) L. L. Wright, R. M. Wing, and M. F. Rettig, *J. Am. Chem. Soc.*, **104**, 610 (1982); See also: O. Eisenstein and R. Hoffmann, *ibid.*, **102**, 6148 (1980); O. Eisenstein and R. Hoffmann, *ibid.*, **103**, 4308 (1981).

16) The *cis*-complexes **4a** and **4b** do not isomerize to the *trans*-complexes **7a** and **7b** under the reaction conditions.

17) R. D. Bach and R. F. Richter, *Tetrahedron Lett.*, **1971**, 3915; T. G. Traylor, *Acc. Chem. Res.*, **2**, 152 (1969); R. D.

Bach and R. F. Richter, *J. Am. Chem. Soc.*, **94**, 4747 (1972); W. Kitching, *Organomet. Chem. Rev.*, **3**, 61 (1968).

18) A recent review for this type of reactions, see: L. S. Hegedus, *Tetrahedron*, **40**, 2415 (1984).

19) D. M. Bowen, J. I. DeGraw, Jr., V. R. Shah, and W. A. Bonner, *J. Med. Chem.*, **6**, 315 (1963).

20) W. A. Bonner, N. I. Burke, W. E. Fleck, R. K. Hill, J. A. Joule, B. Sjöberg, and J. H. Zalkow, *Tetrahedron*, **20**, 1419 (1964).

21) T. A. Stephenson, S. M. Morehouse, A. R. Powell, J. P. Heffer, and G. Wilkinson, *J. Chem. Soc.*, **1965**, 3632.

22) P. Hass, "Handbuch der Präparativen Anorganischen Chemie," ed by G. Brauer, Ferdinand Enke Verlag, Stuttgart (1954), p. 1185.

23) H. Mimoun, R. Charpentier, A. Mitschler, J. Fischer, and R. Weiss, *J. Am. Chem. Soc.*, **102**, 1047 (1980).

24) J. L. Herrmann, G. R. Kieczykowski, and R. H. Schlessinger, *Tetrahedron Lett.*, **1973**, 2433.

25) In a preliminary report (T. Hosokawa, C. Okuda, S. Inui, and S.-I. Murahashi, 27th Symposium on Organometallic Chemistry, Tokyo, Nov. 1980, Abstr., No. B209), the % ee of **13a** was mistakenly determined to be 62% owing to this reason.

26) F. Bohlmann and U. Bühmann, *Chem. Ber.*, **105**, 863 (1972); and also see, M. Hirotani, J. O'Reilly, and D. M. X. Donnelly, *Tetrahedron Lett.*, **1977**, 651.

 © 1985 The Chemical Society of Japan Bull. Chem. Soc. Jpn., 58, 3291—3297 (1985)

3,3′-(Phenylphosphinylidene)bis[2(3*H*)-benzoxazolone] and 3,3′-(Phenylphosphinylidene)bis[2(3*H*)-benzothiazolone]. New Activating Agents

Mitsuru UEDA,* Amane MOCHIZUKI, Ichirō HIRATSUKA, and Hideaki OIKAWA
Department of Polymer Chemistry, Faculty of Engineering, Yamagata University, Yonezawa, Yamagata 992
(Received June 24, 1985)

New activating agents, 3,3′-(phenylphosphinylidene)bis[2(3*H*)-benzoxazolone] (**4**) and 3,3′-(phenylphosphinylidene)bis[2(3*H*)-benzothiazolone] (**5**), were readily prepared by the reaction of phenylphosphonic dichloride (**3**) with 2(3*H*)-benzoxazolone (**1**) and 2(3*H*)-benzothiazolone (**2**) respectively in the presence of triethylamine at room temperature. The new activating agents **4** and **5** were found to be useful for the preparation of amides, esters, and dipeptides under mild conditions. Furthermore, the direct polycondensation of isophthalic acid with aromatic diamines using the activating agent **4** in the presence of pyridine proceeded fast at room temperature to produce polyamides with inherent viscosities up to 0.80 dL/g.

As a part of our continuing research program on the synthesis of amides, esters and polyamides under mild conditions, our group has been studying the synthesis of new activating agents. In particular, our previous studies have resulted in a series of good leaving groups for use in the synthesis of active esters and amides.[1] Based on those studies, we showed that 3-substituted 1,2-benzisothiazole 1,1-dioxides,[2] active carbonate,[3] carbonamide,[4] and 1,2-benzisoxazol-3-yl diphenyl phosphate[5] species are new reactive activating agents for the synthesis of amides, esters and polyamides.

In the previous papers,[6,7] we showed that *N*-acyl derivatives of 2(3*H*)-benzoxazolone (**1**) or 2(3*H*)-benzothiazolone (**2**) are reactive acylating agents for the synthesis of amides and polyamides. This finding prompted us to develop further new activating agents. Recently, diphenyl 2,3-dihydro-2-oxo-3-oxazolylphosphonate has been shown to serve as a carbonyl activating agent to permit a direct preparation of versatile intermediate, 3-acyl-2(3*H*)-oxazolone or a one-step formation of amides from carboxylic acids.[8]

We now report that amides, esters, dipeptides and polyamides can be easily obtained from carboxylic acids and nucleophiles by the direct procedure using the new activating agents, 3,3′-(phenylphosphinylidene)bis[2(3*H*)-benzoxazolone] (**4**) and 3,3′-(phenylphosphinylidene)bis[2(3*H*)-benzothiazolone] (**5**).

Results and Discussion

Synthesis of Activating Agents 4 and 5. The new activating agent **4** was readily prepared by reacting **1** with phenylphosphonic dichloride (**3**) in the presence of triethylamine (TEA) in benzene at room temperature. Similarly, the reagent **5** was prepared by the reaction of **2** with **3** in acetonitrile (Scheme 1).

Recrystallization of these compounds from benzene gave white crystals. The structures of **4** and **5** were characterized by elemental analyses, MS, and IR spectroscopies. The IR spectrum of **4** showed carbonyl absorptions at 1780 and 1800 cm^{-1}, and P=O bond absorption at 1300 cm^{-1} On the other hand, the IR spectrum of **5** had carbonyl absorptions at 1690 and 1720 cm^{-1}, and the P=O bond absorption at 1240 cm^{-1}

Synthesis of Amides (8) and Esters (9). In order to clarify the reactivity of the activating agent **4**, we first studied the synthesis of benzanilide (**8a**) from benzoic acid (**6a**) and aniline (**7a**) in the presence of the reagent **4** by the direct procedure. This procedure consists of adding the reagent **4** to a solution of **6a** and **7a** in *N*-methyl-2-pyrrolidone (NMP) that contains a tertiary base to form benzoate ion. TEA as a tertiary base was used. The condensation proceeded rapidly at room temperature and gave **8a** in 90% yield, together with a small amount of 3-benzoyl-2(3*H*)-benzoxazolone (**10**). The most probable reaction pathway is as follows (Scheme 2).

The activating agent **4** first reacts with benzoate ion to form the mixed carboxylic-phosphoric anhydride (**11**), highly activated acylating agent. The activated intermediate **11** is less stable and its enhanced reactivity causes it to react rapidly with available nucleophiles, that is **7a** (Path A) and **1** (Path B) liberated in the first step. These reactions yield **8a** and **10**, respectively. To prevent the nucleophilic attack on the activated intermediate **11**

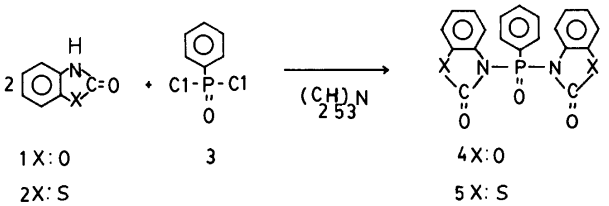

Scheme 1.

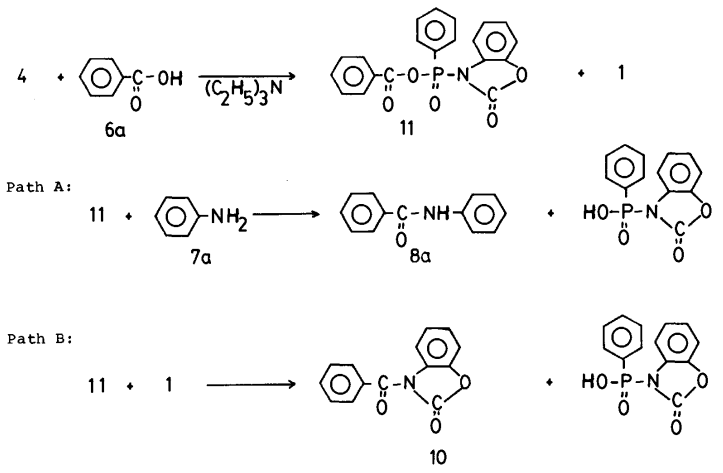

Scheme 2.

TABLE 1. YIELDS OF BENZANILIDE UNDER VARIOUS CONDITIONS[a)]

Ratio of 4/benzoic acid	Reaction time/h	Yield %
0.5	12	48
0.75	12	63
1.0	12	86
1.1	12	90
1.2	12	91
1.3	12	88
1.5	12	80
1.2	0.5	61
1.2	1.0	86
1.2	2.0	91
1.2	8.0	92
1.2	12	92

a) Reaction was carried out with 1 mmol of each monomer in the presence of TEA in NMP (2 ml) at room temperature.

by leaving group anion, pyridine (pK_a=4), less basic base than TEA (pK_a=11), was used because the acidity of **1** is about 8. Use of base TEA fully converts **1** to its anion. As would be expected, the formation of **10** was suppressed and the desired product **8a** was obtained in 98% yield.

Table 1 lists the effect of amount of the activating agent **4** and reaction time in the presence of TEA on the synthesis of **8a**. The best yield was obtained where 1.1—1.2 molar equivalent of **4** relative to **6a** was employed, and the reaction was completed in 2 h at room temperature.

On the bases of these results, the condensation of carboxylic acids (**6**) with amines (**7**) or phenols (**12**) was carried out using the activating agent **4** in the presence of TEA or pyridine in NMP (Scheme 3).

The reactions proceeded smoothly to give the corresponding amides (**8**) and esters (**9**) in good yields. Esterification required a 2 molar equivalent

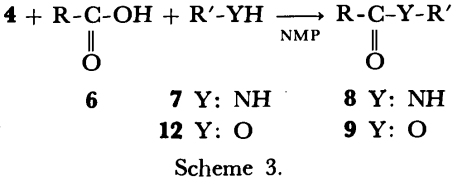

Scheme 3.

of base relative to **6**. Pyridine as a base was more favorable than TEA in the synthesis of amides, but was not effective for the synthesis of esters due to the formation of active amide **10** in fairly large quantities.

Amines reacted more rapidly with the activated intermediate **11** than did phenols. With this different reactivity, next the selective *N*-acylation and *N,O*-diacylation of *p*-aminophenol (**13**) were performed either in the presence of equivalent of **4** and **6a** or 2 molar equivalent of these to **13**, respectively. The corresponding amide, 4′-hydroxybenzanilide (**14**) or amide ester, 4′-(benzoyloxy)benzanilide (**15**) was obtained in good yield (Scheme 4). (Table 2).

Similarly, the conversions of carboxylic acids **6** into amides **8** using the new activating agent **5** were carried out by the direct procedure at room temperature in the presence of TEA. In this case, pyridine did not work well, and the reagent **5** was almost recovered unchanged from the reaction solution. Synthesis of amides using the reagent **4** accompanied the formation of **10** in the presence of TEA. However, when the reagent **5** was used, the formation of 3-benzoyl-2(3*H*)-benzothiazolone was not observed. The reactions of **6** with **7** in the presence of the reagent **5** proceeded smoothly to give the corresponding amides **8** in good yields. Subsequently, selective *N*-benzoylation of **13** and glucosamine hydrochloride (**16**) were performed in the presence of TEA at room temperature to give desired amides **14** and (**17**) having free hydroxyl groups in excellent yields (Scheme 5).

Table 2. Preparation of amides **8** and esters **9** using activating agent **4**[a)]

Carboxylic acid R-COOH, **6**	Amine or Phenol	Reaction condition		Product	Yield
		Base	Time/h		%
C_6H_5-	Aniline	TEA[b)]	2	*N*-Phenylbenzamide	90
C_6H_5-	Aniline	Py[c)]	2	*N*-Phenylbenzamide	98
C_6H_5-	Benzylamine	TEA	2	*N*-Benzylbenzamide	85
C_6H_5-	Benzylamine	Py	2	*N*-Benzylbenzamide	97
C_5H_{11}-	Aniline	TEA	2	*N*-Phenylhexanamide	83
C_5H_{11}-	Aniline	Py	2	*N*-Phenylhexanamide	82
C_5H_{11}-	Benzylamine	TEA	2	*N*-Benzylhexanamide	97
C_5H_{11}-	Benzylamine	Py	2	*N*-Benzylhexanamide	73
C_6H_5-CH=CH-	Aniline	Py	2	*N*-Phenylcinnamamide	87
C_6H_5-CH=CH-	Benzylamine	TEA	2	*N*-Benzylcinnamamide	95
C_6H_5-CH=CH-	Benzylamine	Py	2	*N*-Benzylcinnamamide	92
C_6H_5-	Phenol	TEA	3	Phenyl benzoate	82
C_6H_5-	*p*-Nitrophenol	TEA	3	*p*-Nitrophenyl benzoate	81
C_6H_5-	*p*-Nitrobenzyl alcohol	TEA	3	*p*-Nitrobenzyl benzoate	71
C_6H_5-	*p*-Aminophenol	TEA	2	4′-Hydroxybenzanilide	84
C_6H_5-	1/2 *p*-Aminophenol	TEA	4	4′-Benzoyloxybenzanilide	70

a) Reaction was carried out with 1 mmol of each reactants in NMP (2 ml). b) TEA: Triethylamine. c) Py: Pyridine.

Table 3. Preparation of amides **8**, **14**, and **17** using activating agent **5**[a)]

Carboxylic acid **6**	Amine **7**	Product	Yield
			%
C_6H_5-	C_6H_5-	*N*-Phenylbenzamide	94
C_6H_5-	C_6H_5-CH_2-	*N*-Benzylbenzamide	82
C_6H_5-	Cyclo-C_6H_{11}-	*N*-Cyclohexylbenzamide	91
n-C_5H_{11}-	C_6H_5-	*N*-Phenylhexanamide	92
n-C_5H_{11}-	C_6H_5-CH_2-	*N*-Benzylhexanamide	83
C_6H_5-CH=CH-	C_6H_5-	*N*-Phenylcinnamamide	93
C_6H_5-CH=CH-	C_6H_5-CH_2-	*N*-Benzylcinnamamide	96
C_6H_5-CH=CH-	Cyclo-C_6H_{11}-	*N*-Cyclohexylcinnamamide	97
o-NO_2-C_6H_4-	C_6H_5-CH_2-	*N*-Benzyl-*o*-nitrobenzamide	87
o-CH_3-C_6H_4-	C_6H_5-CH_2-	*N*-Benzyl-*o*-methylbenzamide	85
$(CH_3)_3$-C-	C_6H_5-	*N*-Phenyl-2,2-dimethylpropanamide	62
2,4,6-$(CH_3)_3C_6H_2$-	C_6H_5-CH_2-	*N*-Benzyl-2,4,6-trimethylbenzamide	91
C_6H_5-CO-$(CH_2)_2$-	C_6H_5-	*N*-Phenyl-3-benzoylpropanamide	93
C_6H_5-CO-$(CH_2)_2$-	C_6H_5-	*N*-Benzyl-3-benzoylpropanamide	98
C_6H_5-	*p*-HO-C_6H_4-	4′-Hydroxybenzanilide	80
C_6H_5-[b)]	D-Glucosamine	*N*-Benzoyl-D-glucosamine	90

a) Reaction was carried out with 1 mmol of the reactants in NMP(2 ml). b) Solvent: Sulfolane, Reaction time: 24 h.

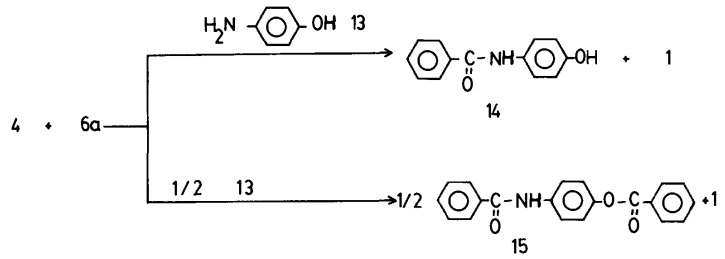

Scheme 4.

These results are summarized in Table 3.

Synthesis of Dipeptides (18). Peptide synthesis is essentially concerned with the formation of the amide bond. Therefore, the present reaction was applied to the preparation of dipeptides **18** (Scheme 6).

The *N*-protected α-amino acid (**19**), the α-amino acid ester hydrochloride (**20**), and the activating agent **4** or **5** were mixed in dichloromethane in the presence of 2 molar equivalent of TEA for 2 h at room temperature. The *N*-protected dipeptide **18** was isolated in the ordinary manner. The optical purity of the dipeptides was estimated by comparison of the specific rotation with the reported value. The *N*-protected dipeptide esters were obtained in the excellent yields with little racemization. These results are summarized in Tables 4 and 5.

Synthesis of Polyamides (21). In order to further demonstrate the preparative utility of our method, it was applied to the synthesis of aromatic polyamides **21**. Recent intensive investigations in the field of the synthesis of polyamides under mild conditions have resulted in the development of new methods including direct polycondensation by phosphorylation reactions and active esters. The direct polycondensation of dicarboxylic acid (**22**) with aromatic diamines (**23**) was carried out using the activating agent **4** in the presence of pyridine in polar aprotic solvents at room temperature (Scheme 7).

The effect of amount of the reagent **4** on the polycondensation of isophthalic acid (**22**) and 4,4′-oxydianiline (**23a**) is shown in Fig. 1. The inherent viscosity of the polymer reached its highest value with 30 mol% excess of the reagent **4** based on each

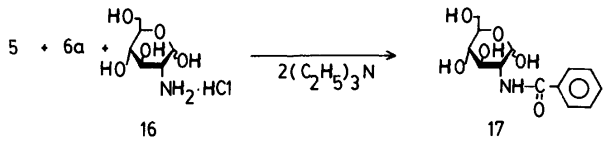

Scheme 5.

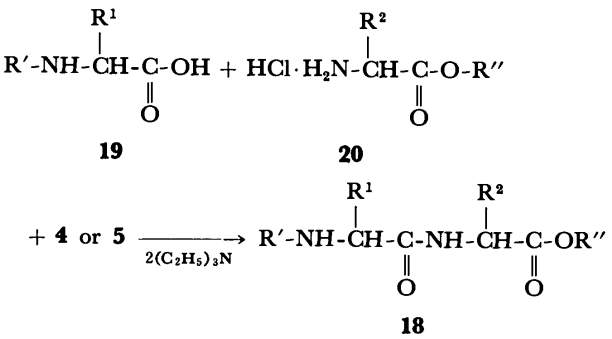

Scheme 6.

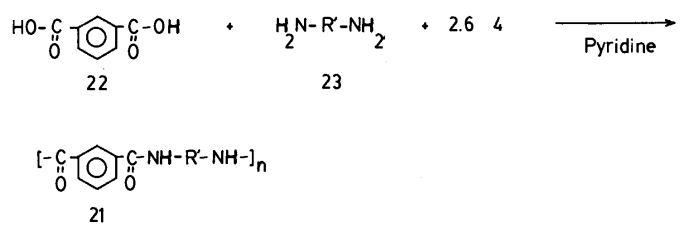

Scheme 7.

Table 4. Preparation of dipeptide esters **18** using activating agent **4**[a)]

N-Protected α-amino acid	α-Amino acid ester	Product	Yield %	Mp[θ_m/°C] found (reported)	[α]$_D$/°C(temp, *c*, solv.) (reported)
Z-Phe-OH	H-Leu-OMe	Z-Phe-Leu-OMe	93	110—111 (110—111)	−24.7(25°, 1.42, MeOH) −24.7(20°, 3.1, MeOH)[12)]
Z-Phe-OH	H-Gly-OEt	Z-Phe-Gly-OEt	97	110—111 (109—110)	−16.1(25°, 1.55, EtOH) −15.9(24°, 2.0, EtOH)[13)]
Z-Val-OH	H-Gly-OEt	Z-Val-Gly-OEt	90	168—169 (170—171)	−31.9(25°, 1.57, Dioxane) −31.6(20°, 1.28, Dioxane)[2)]
Z-Val-OH	H-Val-OEt	Z-Val-Val-OEt	94	115—116 (116—119)	−24.8(25°, 1.52, MeOH) −24.3(25°, 0.73, MeOH)[15)]
Z-Ala-OH	H-Gly-OEt	Z-Ala-Gly-OEt	96	99—100 (99—110)	−21.9(25°, 1.60, EtOH) −22.3(—, 3.65, EtOH)[14)]
Boc-Phe-OH	H-Val-OMe	Boc-Phe-Val-OMe	92	119—120 (115—117)	−10.6(25°, 1.56, DMF) −10.9(—, 2.01, DMF)[16)]
Boc-Phe-OH	H-Gly-OEt	Boc-Phe-Gly-OEt	95	87—88 (89—90)	−8.5(25°, 1.63, Dioxane) −8.1(—, 2.0, Dioxane)[17)]

a) Reaction was carried out with 1 mmol of each reactants in dichloromethane (2 ml) at room temperature.

Table 5. Preparation of dipeptides esters **18** using activating agent **5**[a]

N-Protected α-amino acid	α-Amino acid ester	Product	Yield %	Mp[θ_m/°C] found (reported)	[α]$_D$/°C(temp, *c*, solv.) (reported)
Z-Ala-OH	H-Gly-OEt	Z-Ala-Gly-OEt	76	99—100	−20.9(25°, 1.91 EtOH)
				(99—100)	−22.3(— , 3.65 EtOH)[14]
Z-Ala-OH	H-Val-OMe	Z-Ala-Val-OMe	98	84—85	−40.0(25°, 1.0 MeOH)
				(84)	−38.3(20°, 1.0 MeOH)[12]
Z-Val-OH	H-Gly-OEt	Z-Val-Gly-OEt	99	171—172	−31.3(25°, 1.28 Dioxane)
				(170—171)	−31.6(20°, 1.28 Dioxane)[2]
Z-Phe-OH	H-Gly-OEt	Z-Phe-Gly-OEt	93	109—110	−15.0(25°, 2.0 EtOH)
				(109—110)	−15.9(24°, 2.0 EtOH)[13]
Boc-Phe-OH	H-Gly-OEt	Boc-Phe-Gly-OEt	95	89—90	−8.75(25°, 2.0 Dioxane)
				(89—90)	−8.1 (— , 2.0 Dioxane)[17]
Z-Phe-OH	H-Leu-OMe	Z-Phe-Leu-OMe	92	111—113	−24.2(25°, 3.1 MeOH)
				(110—111)	−24.7(20°, 3.1 MeOH)[12]
Boc-Phe-OH	H-Val-OMe	Boc-Phe-Val-OMe	97	123—124	−10.0(25°, 2.01 DMF)
				(115—117)	−10.9(— , 2.01 DMF)[16]
Boc-Leu-OH	H-Leu-OMe	Boc-Leu-Leu-OMe	88	142—143	−48.6(25°, 0.36 MeOH)
				(139—140)	−49.1(— , 0.36 MeOH)[14]
Z-Tyr-OH	H-Gly-OEt	Z-Tyr-Gly-OEt	88	169—171	−24.0(25°, 5.0 DME)
				(168—169)	−23.6(20°, 5.0 DMF)[18]
Z-Val-OH	H-Val-OMe	Z-Val-Val-OMe	97	117—120	−24.0(25°, 1.75 MeOH)
				(116—119)	−24.3(25°, 0.73 MeOH)[15]

a) Reaction was carried out with 1 mmol of the reactants in dichloromethane (2 ml).

Table 6. Synthesis of polyamides **21** by direct polycondensation of isophthalic acid with diamines **23** using activaing agents **4**[a]

Diamine -⟨○⟩-R-⟨○⟩-	Solvent ml	Polymer ηinh(dl/g)[b]
-O-	NMP 2	0.55
-O-	NMP 1	0.80
-O-	HMPA 1	0.42
-CH_2-	NMP 2	0.51
-CH_2-	NMP 1	0.55
-CH_2-	HMPA 2	0.34
-CH_2-	HMPA 1	0.42
-CH_2-	DMAc 1	0.50

a) Polymerization was carried out with 1 mmol of each monomer using the activating agent **4** (2.6 mmol) in the solvent at room temperature. b) Measured at a concentration of 0.5 g/dl in concentrated sulfuric acid at 30 °C.

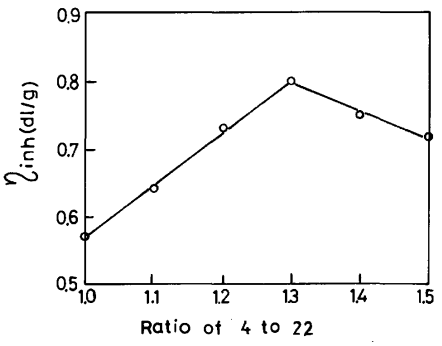

Fig. 1. Effect of amount of activating agent **4** on polycondensation.

monomer. Figure 2 shows the course of the polymerization in terms of inherent viscosity of the resulting polymer. Polycondensation took place rapidly and was almost completed within 2 h at room temperature. Table 6 shows the results of polycondensations of **22** with **23** in the presence of the reagent **4**. High-molecular-weight polyamides could be formed quite readily in polar aprotic solvents in which the polymers remained dissolved.

The polymers obtained were identified as polyamides by comparing their IR spectra with those of the authentic polyamides.

In summary, our studies indicate that the new activating agents **4** and **5** are very useful for the synthesis of amides, esters, dipeptides, and polyamides. These reagents are crystalline solids having excellent hydrolytic stability. Furthermore, 2(3*H*)-benzoxazolone **1** and 2(3*H*)-benzothiazolone **2**, leaving groups, are readily removed from the reaction products by washing the reaction mixture with 5% aqueous sodium carbonate.

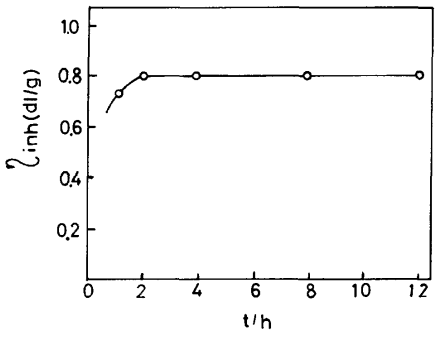

Fig. 2. Polycondensation of isophthalic acid **22** with 4,4′-oxydianiline **23a** using activating agent **4** in NMP at room temperature.

Experimental

Melting points were uncorrected. Infrared spectra were obtained using potassium bromide pellets with a JASCO IRA-1 spectrophotometer. 4,4′-Oxydianiline(**23a**) and 4,4′-methylenedianiline (**23b**) were recrystallized from tetrahydrofuran and benzene, respectively. *N*-Methyl-2-pyrrolidone (NMP), hexamethylphosphoric triamide (HMPA), and *N*,*N*-dimethylacetamide (DMAc) were purified by vacuum distillation and stored over 4 Å Molecular Sieves. *N*-Protected α-amino acids and α-amino acid ester hydrochlorides were prepared by usual procedures. The other reagents were used without further purification.

2(3H)-Benzoxazolone (1). This compound was prepared by the modified method reported by Böshagen.[9] To a ice-cold suspension of salicylohydroxamic acid (21 g, 0.14 mol) in tetrahydrofuran (45 ml), thionyl chloride (11 ml) was added dropwise over 30 min. Then excess thionyl chloride and the solvent were removed *in vacuo* to give a white paste, which was dissolved in toluene (300 ml). This solution was heated slowly to 80 °C and stirred at this temperature for 1 h, then at 120 °C for 2 h. The solvent was removed *in vacuo* to yield a white solid, which was dissolved in methanol. This solution was poured into water (500 ml). The product was collected by filtration, washed with water, and dried to give 13.5 g (73%). Recrystallization from water produced white needles. Mp 138—139 °C(lit,[9] 138 °C).

3,3′-(Phenylphosphinylidene)bis[2(3H)-benzoxazolone] (4). A solution of **1** (6.8 g, 0.05 mol) and TEA (7 ml, 0.05 mol) in dry benzene (40 ml) was cooled in an ice-water bath. To this solution was added dropwise with stirring a solution of **3** (4.9 g, 0.025 mol) in benzene (20 ml) under nitrogen. The addition was completed in 20 min, and stirring was continued at room temperature for an additional 1 h. The precipitate was separated by filtration and dried. To remove TEA·hydrochloride, the product was poured into water (100 ml). The precipitate was collected by filtration and dried *in vacuo*. Purification by recrystallization from benzene gave white needles; yield 6.3 g (64%). Mp 136 °C(by DTA); IR (KBr), 1800, 1780 (C=O), and 1300 cm^{-1} (P=O); MS, *m/z*, 392.3 (M^+). Found: C, 61.2; H, 3.5; N, 6.9%. Calcd for $C_{20}H_{13}N_2O_5P$: C, 61.23; H, 3.34; N, 7.14%.

3,3′-(Phenylphosphinylidene)bis[2(3H)-benzothiazolone] (5). 2(3*H*)-Benzothiazolone **2** was synthesized according to the method of Hunter[10] in 88% yield by the acid hydrolysis of 2-chlorobenzothiazole, which was prepared readily from 2-benzothiazolethiol and sulfuryl chloride;[11] mp 136—137 °C(lit,[10] 138 °C). A solution of **2** (5.53 g, 30 mmol) and TEA (8.4 ml, 60 mmol) in acetonitrile (12 ml) was cooled in an ice-water bath. To this solution was added dropwise with stirring a solution of **3** (2.98 g, 15 mmol) in acetonitrile (12 ml). The addition was completed in 5 min, and stirring was continued at room temperature for an additional 30 min. The solution was poured into water (100 ml). A precipitate formed and it was collected by filtration, washed with water, and dried *in vacuo*; yield 5.40 g (85%). Recrystallization from benzene produced white needles, mp 193 °C. IR(KBr), 1690, 1720 cm^{-1} (C=O), and 1240 cm^{-1} (P=O); MS, *m/z*, 424.4 (M^+). Found: C, 56.4; H, 3.2; N, 6.8%. Calcd for $C_{20}H_{13}N_2O_3PS_2$: C, 56.60; H, 3.08; N, 6.60%.

Amides (8). General Procedure: The activating agent **4** or **5** (1.1 mmol) was added to a solution of carboxylic acid **6** (1.0 mmol), amine **7** (1.1 mmol) and base (1.0 mmol) in NMP (2 ml). The solution was stirred at room temperature for 2 h, and then was poured into 5% aqueous sodium carbonate (50 ml). The precipitate was collected and dried. When TEA as a base was used, a small amount of **10** was formed (when **4** was used). But, it was removed by stirring in 5% aqueous sodium carbonate for 10 h.

Ester (9). General Procedure: A mixture of **4** (1.1 mmol), benzoic acid **6a** (1.0 mmol), phenol **12** (1.1 mmol) and TEA (2.2 mmol) was stirred at room temperature for 3 h. The reaction mixture was worked up as described above.

Protected Dipeptide Ester (18). General Procedure: To a solution of the *N*-protected α-amino acid **19** (1 mmol), the α-amino acid ester hydrochloride **20** (1 mmol) and TEA (2.0 mmol) in dichloromethane (2 ml), the reagent **4** or **5** (1.1 mmol) was added under nitrogen. The solution was stirred for 2 h at room temperature. After removal of the solvent *in vacuo*, the residue was dissolved in ethyl acetate and the organic solution was washed successively with 1 mol dm^{-3} hydrochloric acid, 5% aqueous sodium carbonate and saturated brine, and then dried with anhydrous sodium sulfate. After evaporation of ethyl acetate, the dipeptide was purified by recrystallization.

The crude products obtained (amides, esters, and dipeptide esters) were virtually pure (IR, ^{1}H-NMR spectra).

Polyamide (21). General Procedure: To a solution of isophthalic acid **22** (1.0 mmol), diamine **23** (1.0 mmol) and pyridine (2.2 mmol) in solvent was added the activating agent **4** (2.6 mmol). The mixture was stirred at room temperature for 2 h. The resulting viscous solution was diluted with solvent, and poured into methanol (200 ml). The polymer that precipitated was filtered, and was refluxed in methanol for 2 h. The fibrous polymer was collected and dried *in vacuo* at 100 °C. The yield was essentially quantitative. The inherent viscosity was measured at a concentration of 0.5 g/dl in concentrated sulfuric acid at 30 °C.

We are indebted to Mr. Sadao Kato for the performance of the elemental analyses.

References

1) Y. Imai and M. Ueda, *Yuki Gosei Kagaku Kyokai Shi*, **39**, 312 (1981).
2) M. Ueda, N. Kawaharasaki, and Y. Imai, *Synthesis*, **1982**, 933.
3) M. Ueda, H. Oikawa, and T. Teshirogi, *Synthesis*, **1983**, 908.
4) M. Ueda, H. Oikawa, N. Kawaharasaki, and Y. Imai, *Bull. Chem. Soc. Jpn.*, **56**, 2485 (1983). M. Ueda, N. Kawaharasaki, and Y. Imai, *Bull. Chem. Soc. Jpn.*, **57**, 85 (1984)
5) M. Ueda and H. Oikawa, *J. Org. Chem.* **50**, 760 (1985).
6) M. Ueda, T. Harada, H. Hirata, and Y. Imai, *Kobunshi Ronbunshu*, **38**, 787 (1981).
7) M. Ueda, A. Sato, and Y. Imai, *J. Polym. Sci. Polym. Chem. Ed.*, **15**, 2731 (1977).
8) T. Kunieda, Y. Abe, and M. Hirobe, *Chem. Lett.*, **1981**, 1427.
9) H. Böshagen, *Chem. Ber.*, **100**, 954 (1967).
10) R. F. Hunter, *J. Chem. Soc.*, **1930**, 135.
11) N. S. Moon, U.S. Patent 2469697 (1949). C.A. **43**, 6670c (1949).
12) S. Yamada and Y. Takeuchi, *Tetrahedron Lett.*, **1971**, 3595.
13) R. W. Young, K. H. Wood, R. J. Joyce, and G. W. Anderson, *J. Am. Chem. Soc.*, **78**, 2126 (1956).
14) H. Kinoshita, K. Inamoto, O. Miyano, and H. Kotake, *Bull. Chem. Soc. Jpn.*, **52**, 2619 (1979).
15) J. E. Shields, S. T. McDowell, J. Pavlos, and G. R. Gray, *J Am. Chem. Soc.*, **90**, 3549 (1968).
16) K. Inomata, H. Kinoshita, H. Fukuda, O. Miyano, Y. Yamashino and H. Kotake, *Chem. Lett.*, **1979**, 1265.
17) H. Ogura and K. Takeda, *Nippon Kagaku Kaishi*, **1981**, 836.
18) Y. Watanabe, N, Morita, K. Kamekawa, and T. Mukaiyama, *Chem. Lett.*, **1981**, 65.

Synthetic Studies of Pyridomycin. IV.[1] Syntheses of Some Twelve-membered Ring Compounds Designed for Construction of Intact Ring System with Exocyclic (*Z*)-*s*-Butylidene Side Chain in Pyridomycin

Mitsuhiro KINOSHITA* and Yasuharu MORI
Department of Applied Chemistry, Fuculty of Science and Technology, Keio University, Hiyoshi, Kohoku-ku, Yokohama 223
(Received July 1, 1985)

(2*R*,5*R*,6*S*,9*S*,10*S*,11*R*)-10-Hydroxy-2-[(1′*S*)-1′-hydroxy-1′-methylpropyl]-5,11-dimethyl-9-(3-pyridylmethyl)-6-(benzyloxycarbonylamino)-8-aza-1,4-dioxacyclododecane-3,7,12-trione and its 1′-*O*-methyl derivative, and (2*S*,1′*R*)-diastereomer of the latter have been enantiospecifically synthesized from sugar and L-threonine derivatives. The attempts to convert them into a pyridomycin precursor with the 2-(*Z*)-*s*-butylidene side chain were unsuccessful.

Pyridomycin(**1**) is an antimycobacterial antibiotic[2] produced by *Streptomyces pyridomyceticus*.[3] The most striking characteristic in its structure[4] is a novel heterocyclododecane system with unique exocyclic *s*-butylidene and 3-pyridylmethyl side chains. In the studies directed towerd the total synthesis of pyridomycin, it was first considered[1] that the cyclic compound **14** could serve as a synthetic precursor of **2** which was an intermediate of **1**, if the regiospecific dehydration[5] from **14** proceeded through an *anti*-elimination mechanism to generate the corresponding exocyclic (*Z*)-*s*-butylidene side chain in **2**. The synthetic segments, **3**[6] and **4** (or **5**),[1] utilizable to construct **14** together with L-threonine derivatives have already been enantiospecifically synthesized from D-glucose in our laboratories. Recently, an open chain model compound **8** prepared from **4** was treated with thionyl chloride in pyridine at −30 °C for 1 h to yield, in a 40% yield, a mixture[7] consisting of 16% methyl (*Z*)-2-benzyloxy-3-methyl-2-pentenoate **9** and each 42% of its regioisomers, **10** and **11** (Eq. 1). This fact indicated that the dehydration of **8** procceded through a concerted *anti*-elimination

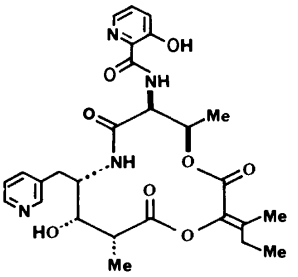

1

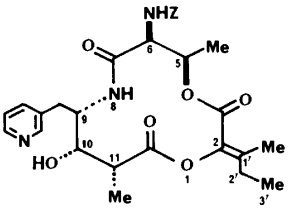

2
Z=COOCH$_2$Ph

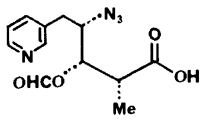

3

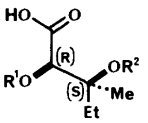

4: R^1, R^2 = H
5: R^1, R^2 =
6: R^1 = MOM, R^2 = Me

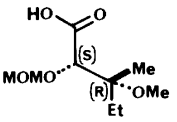

7

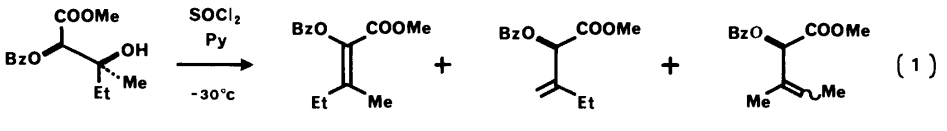

8 **9** **10** **11** (1)

Bz = PhCO

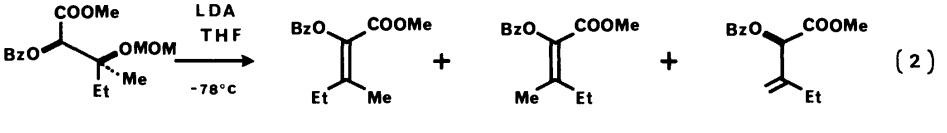

12 **9** **13** **10** (2)

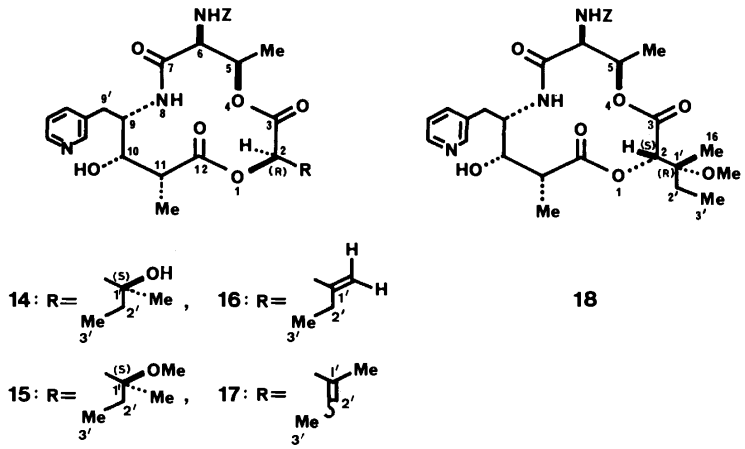

mechanism[5] to yield exclusively the *Z*-isomer **9**. In order to improve the regioselectivity in the formation of **9**, the treatment of **12** derived from **8** with 1.2 equivalents of lithium diisopropylamide (LDA) in THF at −78 °C for 30 min gave a 1:1:1 mixture[7] of **9**, **13**, and **10** in a 40% yield (Eq. 2). This reaction appeared to proceed by an ElcB like mechanism where competitive abstractions of the H-2 proton and the 3-methyl proton are followed by expulsion of the 3-methoxymethoxyl group. These observations suggested that the 12-membered cyclic substrates, **14** and **15** (or **18**) would be a key intermediate for the total synthesis of pyridomycin **1**. Herein we describe the enantiospecific syntheses of **14**, **15**, and its diastereomer **18**, along with the attempts made to convert them into **2** by β-elimination.

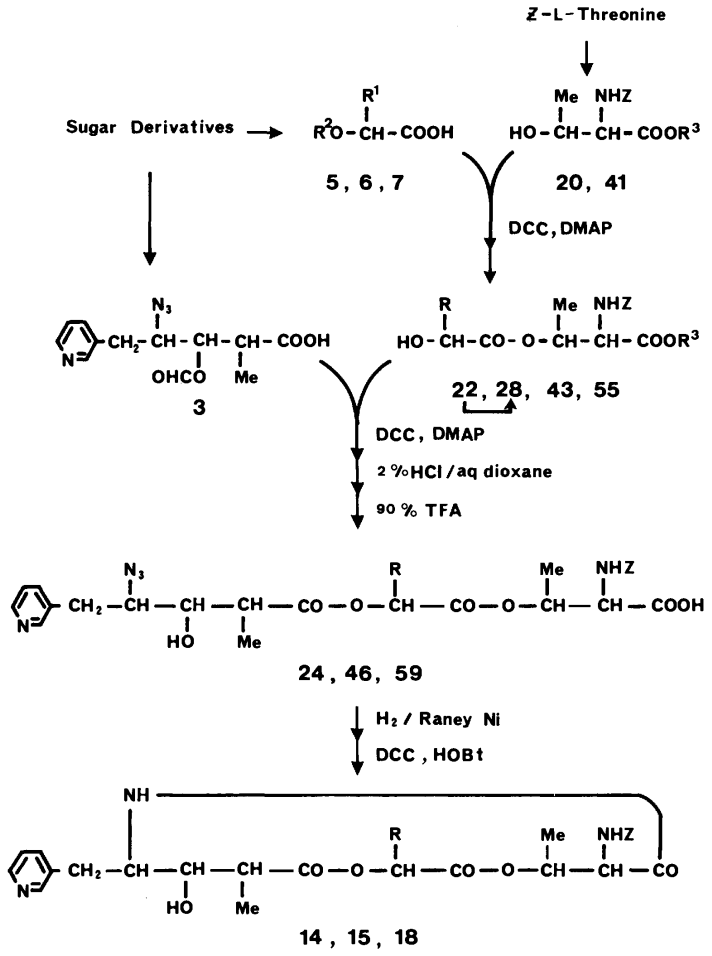

Scheme 1.

The synthetic routes are summarized in Scheme 1 accompanied by Charts 1, 2, and 3. *O-t*-Butyl-*N*-benzyloxycarbonyl-L-threonine[8] was converted, in a 92% yield, into the 2,2,2-trichloroethyl ester **19** by treatment with 2,2,2-trichloroethanol, dicyclohexylcarbodiimide (DCC), and 4-dimethylaminopyridine (DMAP)[9] in ethyl acetate. De-*O-t*-butylation of **19** with trifluoroacetic acid (TFA) afforded a 95% yield of **20**, which was condensed with **5**[1] in the presence of DCC and DMAP to give **21** in an 85% yield. Deisopropylidenation of **21** with 80% TFA followed by condensation of the resulting **22** with **3**[5] in the presence of DCC and DMAP afforded a 73% yield of **23**. One-step conversion of **23** into the seco amino acid **26** of the lactam **14** by treatment with Zn-dust in acetic acid was unsuccessful because of formation of many complex products. Treatment of **23** with Zn-dust in 1 M† aqueous ammonium acetate gave the azido acid **24** (53% yield) and the 5-membered lactam **25** (17.6% yield). De-*O*-formylation of **23** with 2% hydrogen chloride in 50% aqueous dioxane followed by treatment with Zn-dust in 1 M† aqueous ammonium acetate afforded a crude product, whose TLC showed the presence of **26** and **25**, indicating the absence of **24**. However, only the lactam **25** was isolated on the preparative TLC [silica-gel(Merck 5715), 3:1:1 *n*-BuOH–AcOH–H_2O] of the crude product.

On the other hand, treatment of **22** with Zn-dust in acetic acid provided a 98% yield of **27**, which was converted into the benzhydryl ester **28** in an 89% yield by treatment with diphenyldiazomethane in ethyl acetate. Coupling reaction of **28** and **3** with DCC and DMAP proceeded smoothly to afford **29** in an 86% yield. De-*O*-formylation of **29** with 2% hydrogen chloride in 50% aqueous dioxane followed by treatment with 90% TFA gave **24** in an 84% yield. The azido acid **24** was selectively hydrogenolized with Raney Ni in methanol to provide the seco amino acid **26** in good yield. Cyclization of **26** was performed according to the modified Okawa's method in 10^{-3} M DMF solution with DCC (20 equiv) and 1-hydroxybenzotriazole (HOBt, 5 equiv)[10] at 5 °C for 60 h to afford the intramolecular cyclization product **14** in a 37% yield. The cyclization of **26** which was carried out with Woodward's reagent *K* according to the procedure described in the previous paper,[11] gave a 1.5% yield of **14**.

Another route to **14** from **27** was also investigated. Treatment of **27** with *t*-butyl carbazate and DCC in ethyl acetate afforded the *N*-Boc-hydrazide **30** in an 82% yield. Condensation of **30** and **3** with DCC and DMAP gave a 91% yield of product **31**. De-*O*-formylation of **31** by treatment with 2 equivalents of hydrazine hydrate in ethanol afforded a 63% yield of **32**. Hydrogenolysis of **32** with Raney Ni in 50% acetic acid followed by exposure of the resulting amino acid *N*-Boc-hydrazide to 90% TFA gave the crude seco amino acid hydrazide trifluoroacetate, which was then cyclized by the azide method using HOBt as a catalyst according to the procedure described by Veber *et al.*[12] to yield a 2.9% yield of **14**. The structure of **14** thus obtained was confirmed by 250 MHz ^{1}H-NMR and MS.

Dehydration of **14** with thionyl chloride in pyridine was carried out in the same way as in the case of the model compound **8** to give a 79% yield of dehydration product (EIMS, *m/z* 553 (M^+)) after silica-gel column chromatography. The 250 MHz ^{1}H-NMR spectrum of this product revealed that it consisted mostly of a *ca.* 1:1 mixture of the undesired regioisomers, **16** and **17** (a mixture of geometrical isomers), being contaminated by a trace amount of **2** (see Expl.). Moreover, all attempts to separate these isomers on TLC were unsuccessful. Furthermore, though attempts to isomerize the mixture of **16** and

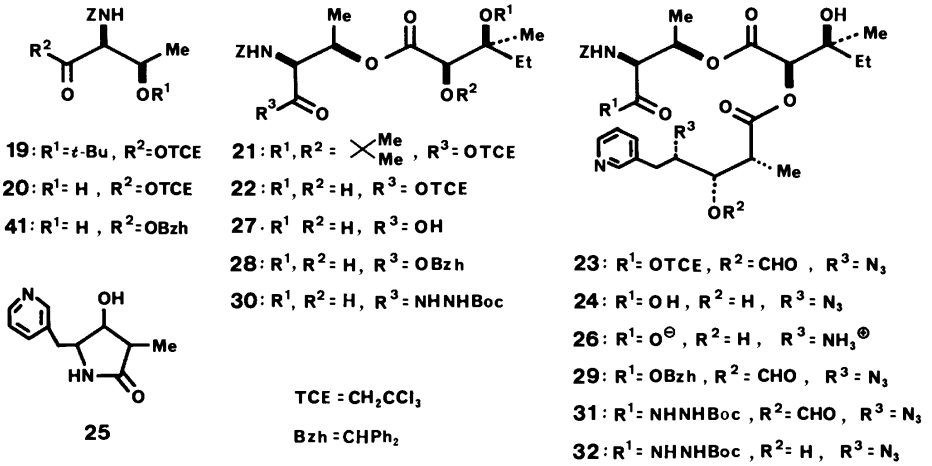

Chart 1.

† 1 M=1 mol dm^{-3}.

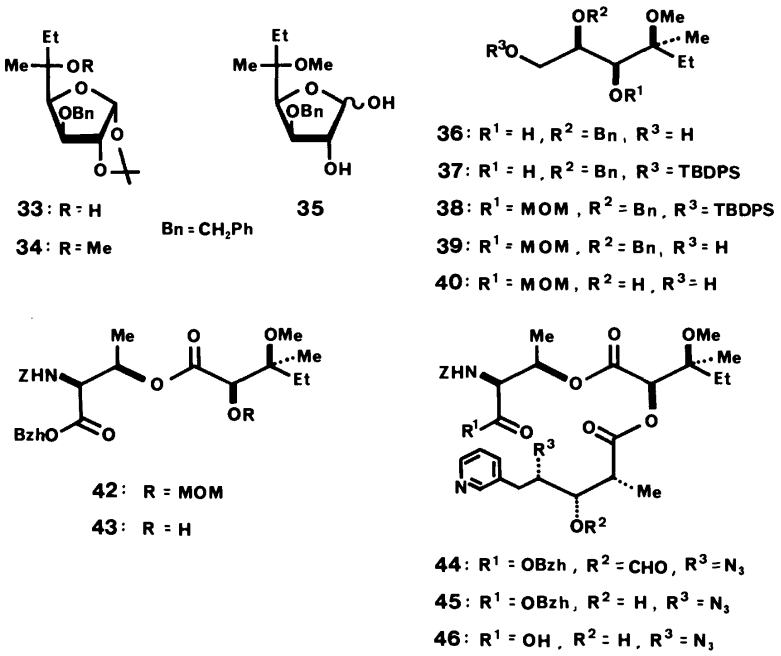

Chart 2.

17 to **2** were made under the following conditions; (a) triethylamine, DMF, 11—15 °C, 20 h, (b) LDA, THF, −75 °C, 1 h, (c) [RhCl(Ph$_3$P)$_3$],[13] ethanol, 100 °C, 3 h, (d) DBU, dioxane, 35 °C, 1.5 h, no appreciable change in the constitutional ratio of the starting olefins could be observed, with the exception of the condition (d) in which **16** was completely isomerized to **17**.

The second key intermediate **15** was next synthesized. The starting material **6** was derived from **33** which was previously prepared from D-glucose.[6] *O*-Methylation of **33** with sodium hydride and methyl iodide in DMF afforded a 77% yield of **34**, which was deisopropylidenated with boiling 50% aqueous acetic acid to give the lactol **35** in a 65% yield. Periodate oxidation of **35** followed by lithium aluminium hydride reduction afforded the diol **36** in a 67% yield. Selective *t*-butyldiphenylsilylation of **36** followed by methoxymethylation of the resulting silyl derivative **37** yielded **38**, which was then desilylated with tetrabutylammonium fluoride in THF to afford **39** in a 42% yield from **36**. Hydrogenolysis of **39** on Pd-black, followed by periodate oxidation of the resulting diol **40** gave the crude aldehyde, which was immediately oxidized with pyridine dichromate (PDC) in DMF to provide the carboxylic acid **6** in a 74% overall yield from **39**. *N*-Benzyloxycarbonyl-L-threonine was treated with diphenyldiazomethane to afford the benzhydryl ester **41** in an 80% yield. Condensation of **6** and **41** with DCC and DMAP followed by the sequential treatments of the resulting linear ester **42** with 90% TFA and with diphenyldiazomethane gave **43** in a 42% overall yield from **6**. Condensation of **43** and **3** with DCC and DMAP followed by the sequential treatments of the resulting linear ester **44** with 2% hydrogen chloride in 50% aqueous dioxane and with 90% TFA gave the azido acid **46** in a 57% overall yield from **43**. Selective hydrogenolysis of the azide group of **46** with Raney Ni in methanol followed by cyclization of the resulting seco amino acid with DCC (20 equiv) and HOBt (5 equiv) in 10^{-3} M DMF solution afforded the intramolecular cyclization product **15** in a 15% yield after sillica-gel column chromatography. The structure of **15** was also confirmed by ^{1}H-NMR and MS.

The elimination reaction of **15** was carried out with 2.2 equivalents of LDA in THF at −78 °C for 1 h. However, from the resulting light yellow solution, only the starting **15** was recovered in *ca.* 70% yield after silica-gel chromatography. This result showed that there occurred no base-promoted elimination from **15** through an ElcB like mechanism in contrast to the case of the acyclic model substrate **12**. This might be explained as follows. The ^{1}H-NMR spectrum of **15** revealed that **15** had a preferred rigid conformation. Unfortunately, because of this conformation, the base catalized enolization of the C-3 carbonyl group of **15** may be hardly stereoelectronically[14,15] or stereochemically assisted. In this respect, we were interested in the base-promoted elimination from the third cyclic substrate **18** which was the (2*S*, 1′*R*)-diastereomer of **15** and therefore might exist in a conformation different from **15**.

The preparation of **18** was started from **7**, the

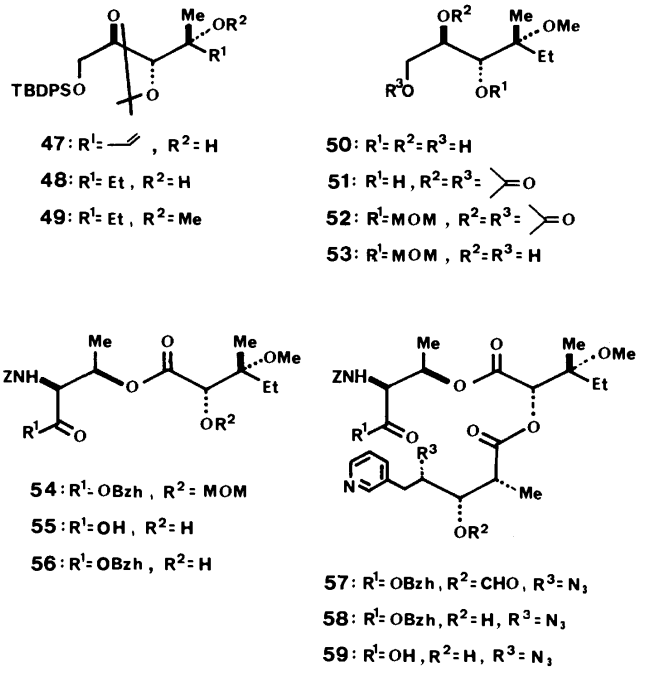

Chart 3.

enantiomer of **6**, in the same manner as that described in the preparation of **15**. The vinyl compound **47**[16] whose stereochemistry had been well confirmed, was hydrogenated on Pd–carbon to yield **48** in a 99% yield. *O*-Methylation of **48** with sodium hydride and methyl iodide in DMF afforded **49** in a 76% yield. The successive treatments with tetrabutylammonium fluoride and with 80% TFA gave **50** in a 67% yield. Reaction of **50** with *N,N'*-carbonyldiimidazole in benzene afforded the cyclic carbonate **51** as a sole product in a 61% yield. The *O*-methoxymethylated product **52** derived from **51** was decarbonated with sodium hydroxide in methanol to afford the crude diol **53**, which was subjected to the two-stage oxidation with sodium periodate in aqueous acetone and with PDC in DMF to provide **7** in a 51% overall yield from **52**. Condensation of **7** and **41** afforded an 85% yield of **54**, which was transformed, in a 65% yield, into the hydroxy benzhydryl ester **56** *via* **55** by the procedure described in the preparation of the diastereomer **43**. Condensation of **56** and **3** gave the linear ester **57** in a 72% yield, which was converted into the azido acid **59** *via* **58** in an 80% yield. Hydrogenolysis of **59** followed by cyclization with DCC and HOBt to afford **18** in a 15% yield after silica-gel column chromatography. The structure of **18** was confirmed by ^{1}H-NMR and MS. The elimination reaction of **18** was carried out in the same condition as in the case of **15** and no elimination reaction occurred. The starting **18** was recovered from the reaction mixture in *ca.* 60% yield.

Experimental

The melting points were determined on a micro hot-stage Yanaco MP-S3 and are uncorrected. The optical rotations were measured with a Carl Zeiss photoelectric polarimeter and a JASCO DIP-360 photoelectric polarimeter in chloroform unless stated otherwise. The ^{1}H-NMR spectra were recorded with either a Varian EM-390 or a Bruker WM 250 spectrometer in $CDCl_3$ using TMS as the internal standard. The IR spectra, EIMS, and SIMS were measured with a Hitachi Perkin-Elmer 225 spectrophotometer, a Hitach RMU-6M mass spectrometer, and Hitachi M-80 mass spectrometer, respectively. The TLC was carried out on Merck TLC plates (60F-254, 0.25 mm). The column chromatography was performed on silica-gel, Wakogel C-200. In general, the evaporation and concentration were carried out under reduced pressure below 30 °C unless otherwise noted.

N-Benzyloxycarbonyl-O-t-butyl-L-threonine 2,2,2-Trichloroethyl Ester (19). DCC (1.56 g, 7.573 mmol) was added at a time to an ice-cooled solution of *N*-benzyloxycarbonyl-*O*-*t*-butyl-L-threonine (2.23 g, 7.212 mmol), 2,2,2-trichloroethanol (0.696 ml, 7.212 mmol), and DMAP (59 mg, 0.48 mmol) in dry ethyl acetate (36 ml) and the mixture was stirred at 0 °C for 1.5 h. After the *N,N'*-dicyclohexylurea (DCU) had been filtered off, a small amount of acetic acid was added to the filtrate and the mixture (pH 3—4) was stirred under ice-cooling until unchanged DCC was destroyed. The DCU formed was filtered and the filtrate was evaporated to a white solid (3.41 g), which was chromatographed on silica-gel (200 g) with 12:2:1 benzene–hexane–ethyl acetate to afford **19** (2.91 g, 92%) as colorless needles. Recrystallization from pentane gave a pure sample: Mp 89—90 °C; $[\alpha]_D^{19}$ −5° (*c* 1.00); ^{1}H-NMR (90 MHz) δ=1.15 (9H, s), 1.28 (3H, d, J=6.5 Hz), 4.62 and 4.82 (2H, each d), 5.17 (2H, s), and 7.39 (5H, s).

Found: C, 48.76; H, 5.50; N, 3.01; Cl, 23.86%. Calcd for $C_{18}H_{24}NO_5Cl_3$: C, 49.05; H, 5.49; N, 3.18; Cl, 24.13%.

N-Benzyloxycarbonyl-L-threonine 2,2,2-Trichloroethyl Ester (20). A solution of **19** (1.89 g) in TFA (6.0 ml) was kept at room temperature for 5 min and then evaporated. The residue was repeatedly co-evaporated with ether and then dried over NaOH pellets under reduced pressure to give a crystalline solid (1.66 g), which was recrystallized from ether–pentane to afford **20** (1.56 g, 95%) as colorless needles: Mp 90—91 °C; $[\alpha]_D^{23}$ −21° (*c* 0.79); ^{1}H-NMR (90 MHz) δ=1.31 (3H, d, J=6.4 Hz); 4.77 and 4.88 (2H, each d), 5.17 (2H, s), and 7.40 (5H, s).

Found: C, 43.43; H, 4.13; N, 3.60; Cl, 27.58%. Calcd for $C_{14}H_{16}NO_5Cl_3$: C, 43.71; H, 4.19; N, 3.64; Cl, 27.58%.

N-Benzyloxycarbonyl-O-[(2R,3S)-2,3-dihydroxy-2,3-O-isopropylidene-3-methylpentanoyl]-L-threonine 2,2,2-Trichloroethyl Ester (21). To an ice-cooled solution of **5** (445 mg, 2.36 mmol), **20** (909 mg, 2.363 mmol), and DMAP (29 mg, 0.236 mmol) in dry ethyl acetate (8.4 ml) was added DCC (488 mg, 2.385 mmol) at a time and the mixture was stirred at 0 °C for 2 h. The DCU resulted was filtered off and the filtrate was evaporated to a pale yellow solid (1.43 g), which was chromatographed on silica-gel (100 g) with 10:1 benzene–ethyl acetate to afford **21** (1.12 g, 85%) as colorless needles. Recrystallization from ethyl acetate–

pentane gave a pure sample: Mp 108—109 °C; $[\alpha]_D^{23}$ +16° (*c* 0.55); IR (CCl_4) 3390 and 1720 cm^{-1}; ^{1}H-NMR (90 MHz) δ=0.99 (3H, t, *J*=6.5, 8.0 Hz), 1.12 (3H, s), 1.39 and 1.56 (each 3H, each s), 1.45 (3H, d, *J*=6.5 Hz), 1.5—2.0 (2H, m), 4.33 (1H, s), 4.67 (1H, dd, *J*=4.0, 11.0 Hz), 4.75 and 4.81 (2H, each *d*), 5.21 (2H, s), 5.53 (1H, dq), 5.3—5.7 (1H, br), and 7.43 (5H, s).

Found: C, 50.03; H, 5.55; N, 2.45; Cl, 19.37%. Calcd for $C_{23}H_{30}NO_8Cl_3$: C, 49.78; H, 5.45; N, 2.52; Cl, 19.17%.

N-*Benzyloxycarbonyl*-O-*[(2*R,*3*S)-*2,3-dihydroxy-3-methylpentanoyl]*-L-*threonine 2,2,2-Trichloroethyl Ester (22).* A solution of **21** (856 mg) in 80% aqueous TFA (10 ml) was allowed to stand at room temperature for 1 h and then evaporated. The residue (792 mg) was chromatographed on silica-gel (30 g) with 3:1 benzene–ethyl acetate to afford **22** (743 mg, 94%) as colorless needles: Mp 76—77 °C, $[\alpha]_D^{21}$ −41° (*c* 0.97); IR (CCl_4) 3440 and 1725 cm^{-1}; ^{1}H-NMR (90 MHz) δ=0.91 (3H, t, *J*=6.9, 7.9 Hz), 1.17 (3H, s), 1.42 (3H, d, *J*=6.5 Hz), 1.3—1.8 (2H, m), 2.78 (2H, br-s), 3.97 (1H, s), 4.5—4.8 (1H, m), 4.76 (2H, s), 5.18 (2H, s), 5.52 (1H, dq, *J*=3.5 Hz), 5.3—4.9 (1H, br), and 7.39 (5H, s).

Found: C, 46.82; H, 5.14; N, 2.52; Cl, 20.32%. Calcd for $C_{20}H_{26}NO_8Cl_3$: C, 46.66; H, 5.09; N, 2.72; Cl, 20.66%.

N-*Benzyloxycarbonyl*-O-*[(2*R,*3*S)-*2-((2*R,*3*S,*4*S)-*4-azido-3-formyloxy-2-methyl-5-(3-pyridyl)pentanoyloxy)-3-hydroxy-3-methylpentanoyl]*-L-*threonine 2,2,2-Trichloroethyl Ester (23).* To an ice-cooled solution of **22** (213 mg, 0.414 mmol), **3** (115 mg, 0.414 mmol), and DMAP (5.1 mg, 0.041 mmol) in dry ethyl acetate (2.9 ml) was added DCC (89.7 mg, 0.435 mmol) and the mixture was stirred at 0 °C for about 24 h. After the DCU had been filtered off, a small amount of acetic acid was added to the filtrate and the mixture was stirred at room temperature for 1 h. The DCU was removed by filtration and the filtrate was evaporated to a yellow syrup (447 mg), which was chromatographed on silica-gel (30 g) with 2:1 benzene–ethyl acetate to afford **23** (235 mg, 73%) as colorless syrup: $[\alpha]_D^{26}$ −8° (*c* 1.0); IR (CCl_4) 3440, 2110, and 1735 cm^{-1}; ^{1}H-NMR (90 MHz) δ=0.93 (3H, t, *J*=7.5 Hz), 1.23 (3H, s), 1.28 (3H, d, *J*=4.0 Hz), 1.40 (3H, d, *J*=9.0 Hz), 1.5—1.7 (2H, m), 2.5—3.3 (3H, m), 3.5—3.8 (1H, m), 4.0—4.3 (1H, br), 4.5—4.7 (1H, m), 4.76 (3H, s), 5.16 (2H, s), 5.2—6.0 (3H, m), 7.06 (5H, s), 7.2—7.4 (1H, m), 7.5—7.7 (2H, m), 8.20 (1H, s), and 8.4—8.6 (2H, m).

Found: C, 49.77; H, 5.06; N, 8.81%. Calcd for $C_{32}H_{38}N_5O_{11}Cl_3$: C, 49.59; H, 4.94; N, 9.04%.

N-*Benzyloxycarbonyl*-O-*[(2*R,*3*S)-*2-((2*R,*3*S,*4*S)-*4-azido-3-hydroxy-2-methyl-5-(3-pyridyl)pentanoyloxy)-3-hydroxy-3-methylpentanoyl]*-L-*threonine (24).* *(a) Preparation from 23.* To a stirred solution of **23** (25.5 mg, 0.033 mmol) in dry THF (0.25 ml) was added an aqueous 1 M ammonium acetate solution (0.022 ml) and then Zn-dust (21.5 mg, 3.3 mmol) at room temperature. After being stirred for 20 h at room temperature, the reaction mixture was filtered through a Celite and the filter cake was washed with chloroform. The filtrate and washings were evaporated and the residue was chromatographed on silica-gel (5 g) with 80:15:1 chloroform–methanol–acetic acid to give **24** (10.8 mg, 53%) and **25** (1.2 mg, 18%), whose R_f-values in the same solvent system were 0.37 and 0.13, respectively. **24**: Colorless syrup; IR ($CHCl_3$) 2100 cm^{-1}; ^{1}H-NMR (250 MHz) δ=0.88 (3H, t, *J*=8.0 Hz), 1.03 (3H, d, *J*=6.0 Hz), 1.24 (3H, s), 1.26 (3H, d, *J*=7.5 Hz), 1.53 (1H, dq, *J*=8.0 Hz), 1.66 (1H, dq), 2.9—3.2 (3H, m), 3.35 (1H, m), 3.68 (1H, d-like), 4.32 (1H, d, *J*=7.0 Hz), 4.73 (1H, s), 5.14 (2H, s), 5.4—5.8 (3H, m), 6.08 (1H, d, 10.0 Hz), 7.14—7.21 (1H, m), 7.2—7.4 (5H, m), 7.56—7.64 (1H, m), 8.47 (1H, m), and 8.56 (1H, d-like); SIMS, *m/z* 616 (M^+ +1). **25**: Colorless crystal, IR (KBr) 3300, 3180, 1700, and 1660 cm^{-1}; ^{1}H-NMR (250 MHz) δ=1.12 (3H, d, *J*=8.0 Hz), 2.54 (1H, dq, *J*=5.0 Hz), 2.91 (1H, dd, *J*=15.0, 8.0 Hz), 3.08 (1H, dd, *J*=10.0 Hz), 3.88 (1H, m), 4.07 (1H, m), 4.70 (1H, m), 7.85 (1H, d, *J*=8.0 Hz), 8.41 (1H, d, *J*=4.0 Hz), and 8.52 (1H, s).

(b) Preparation from 29. A solution of **29** (246 mg) in 25 ml of 2% HCl [in 50% (v/v) aqueous dioxane] was kept at 20 °C for 8 h and was concentrated to a syrup (250 mg), which was dissolved in 90% TFA (2.5 ml). The solution was kept at 20 °C for 0.5 h and then evaporated. The residue was co-evaporated with ether repeatedly to remove TFA and the final residue was chromatographed on silica-gel (20 g) with 90:10:1 chloroform–methanol–acetic acid to afford **24** (169 mg, 84% yield from **28**). This product was proved to be identical with the sample of **24** obtained in (a) by TLC and ^{1}H-NMR.

N-*Benzyloxycarbonyl*-O-*[(2*R,*3*S)-*2,3-dihydroxy-3-methylpentanoyl]*-L-*threonine (27).* To a solution of **22** (494 mg, 0.96 mmol) in acetic acid (5 ml) was added Zn-dust (2.2 g, 33.6 mmol) portionwise over a period of 1 h. After being stirred at 20 °C for 4 h, the reaction mixture was filtered through a Celite and the filter cake was washed with chloroform. The filtrate and washings were evaporated to a syrup (450 mg), which was chromatographed on silica-gel (25 g) with 80:5:1 chloroform–methanol–acetic acid to give **27** as a colorless glass (365 mg, 98%): ^{1}H-NMR (90 MHz, $CDCl_3$+D_2O) δ=0.88 (3H, t, *J*=7.5 Hz), 1.13 (3H, s), 1.33 (3H, d, *J*=6.0 Hz), 1.4—1.7 (2H, m) 3.90 (1H, s), 4.3—4.6 (1H, m), 5.08 (2H, s), 5.3—5.6 (1H, m), and 7.38 (5H, s).

N-*Benzyloxycarbonyl*-O-*[(2*R,*3*S)-*2,3-dihydroxy-3-methylpentanoyl]*-L-*threonine Benzhydryl Ester (28).* A mixture of benzophenone hydrazone (214 mg, 1.09 mmol), HgO (yellow) (239 mg, 1.10 mmol) and petroleum ether (0.3 ml) were stirred at room temperature for 5 h. The reaction mixture was filtered and the filtrate was evaporated to give a red-purple colored syrup of diphenyldiazomethane, which was dissolved in ethyl acetate (1.6 ml). To a solution of **27** (167 mg, 0.53 mmol) in ethyl acetate (1.6 ml) was added dropwise the above prepared solution of diphenyldiazomethane. After violent foaming had been settled, the reaction mixture was stirred at room temperature for 2 h, and then the excess diphenyldiazomethane was decomposed by addition of concd HCl under ice-cooling. The resulting mixture was washed with cold saturated aqueous $NaHCO_3$ and NaCl solutions, dried, and evaporated to a yellow syrup (359 mg), which was chromatographed on silica-gel (15 g) with 5:1 toluene–ethyl acetate to afford **28** (250 mg, 89%) as a syrup: $[\alpha]_D^{19}$ −4°, $[\alpha]_{365}^{19}$ −8° (*c* 1.81); ^{1}H-NMR (90 MHz) δ=0.83 (3H, t, *J*=6.0 Hz), 0.95 (3H, s), 1.33 (3H, d, *J*=6.0 Hz), 1.0—1.5 (2H, m), 1.6—2.0 (1H, br), 2.9—3.2 (1H, br), 3.81 (1H, br-d, *J*=10 Hz), 4.5—4.8 (1H, m), 5.13 (2H, s), 5.4—5.9 (2H, m), 6.80 (1H, s), and 7.2—7.6 (15H, m).

Found: C, 67.57; H, 6.46; N, 2.45%. Calcd for $C_{31}H_{35}NO_8$: C, 67.75; H, 6.41; N, 2.55%.

N-*Benzyloxycarbonyl*-O-*[(2*R,*3*S)-*2-((2*R,*3*S,*4*S)-*4-azido-3-formyloxy-2-methyl-5-(3-pyridyl)pentanoyloxy)-3-hydroxy-3-

methylpentanoyl]-L-threonine Benzhydryl Ester (29). To a solution of **28** (952 mg, 1.79 mmol), **3** (497 mg, 1.79 mmol), and DMAP (20 mg, 0.16 mmol) in dry ethyl acetate (15 ml) was added DCC (442 mg, 3.14 mmol) at a time and the mixture was stirred at room temperature for 48 h. The formed DCU was filtered off and the filtrate was concentrated and chromatographed on silica-gel (100 g) with 1:1 toluene–ethyl acetate to give **29** (1.23 g, 86%) as a glassy solid: ^{1}H-NMR (90 MHz) δ=0.85 (3H, t, J=7.5 Hz), 1.06 (3H, s), 1.20 (3H, d, J=9.0 Hz), 1.36 (3H, d, J=6.0 Hz), 1.2—1.5 (2H, m), 2.6—3.3 (3H, m), 3.5—3.8 (1H, m), 4.0—4.3 (1H, br), 4.5—4.8 (1H, m), 4.70 (1H, s), 5.3—5.8 (3H, m), 6.86 (1H, s), 7.1—7.4 (15H, m), 7.5—7.7 (1H, m), 8.16 (1H, s, CHO), and 8.4—8.6 (2H, m).

N-Benzyloxycarbonyl-O-[(2R,3S)-2,3-dihydroxy-3-methylpentanoyl]-L-threonine t-Butoxycarbonylhydrazide (30). To a solution of **27** (253 mg, 0.66 mmol) and Boc-NHNH$_2$ (105 mg, 0.79 mmol) in dry ethyl acetate (2.6 ml) was added DCC (143 mg, 0.69 mmol) and the mixture was stirred at room temperature for 2 h. The formed DCU was filtered off and the filtrate was concentrated and chromatographed on silica-gel (50 g) with 1:1 chloroform–ethyl acetate to give a glassy solid, which was again chromatographed on silica-gel (50 g) with 5:1 toluene-acetone to afford pure sample of **30** (286 mg, 82%) as a colorless glassy solid: $[\alpha]_D^{20}$ +50° (c 1.00); IR ($CHCl_3$) 3425, 3340, 1765, 1720, and 1685 cm^{-1}; ^{1}H-NMR (250 MHz) δ=0.86 (3H, t, J=7.0 Hz), 1.16 (3H, s), 1.24 (3H, d, J=6.0 Hz), 1.44 (9H, s), 1.40—1.60 (2H, m), 4.06 (1H, d, J=4.0 Hz), 4.50 (1H, dd, J=3.0, 10 Hz), 4.91 (1H, br-s), 5.10 (2H, s), 5.30—5.45 (2H, m), 6.45 (1H, d, J=2.0 Hz), 6.84 (1H, d, J=10 Hz), 7.36 (5H, s), and 8.80 (1H, d, J=2.0 Hz).

Found: C, 55.49, H, 7.10; N, 8.54%. Calcd for $C_{23}H_{35}N_3O_9$: C, 55.52; H, 7.09; N, 8.45%.

N-Benzyloxycarbonyl-O-[(2R,3S)-2-((2R,3S,4S)-4-azido-3-formyloxy-2-methyl-5-(3-pyridyl)pentanoyloxy)-3-hydroxy-3-methylpentanoyl]-L-threonine t-Butoxycarbonylhydrazide (31). To an ice-cooled solution of **30** (72.9 mg, 0.146 mmol), **3** (40.7 mg, 0.146 mmol), and DMAP (1.8 mg, 0.015 mmol) in dry ethyl acetate (0.8 ml) was added DCC (31.8 mg, 0.154 mmol) and the mixture was stirred at room temperature for 5 h. The DCU formed was filtered off and the filtrate was concentrated and chromatographed on silica-gel (10 g) with 1:3 chloroform–ethyl acetate to give **31** (100 mg, 91%) as a glassy solid: IR ($CHCl_3$) 2100 cm^{-1}; $[\alpha]_D^{17}$ 0°, $[\alpha]_{436}^{17}$ −39°, $[\alpha]_{365}^{17}$ −71° (c 0.84); ^{1}H-NMR (250 MHz) δ=0.93 (3H, t, J=7.0 Hz), 1.28 (3H, s), 1.29 (3H, d, J=8.0 Hz), 1.33 (3H, d, J=7.0 Hz), 1.5—1.65 (2H, m), 2.84 (1H, dd, J=11.0, 15 Hz), 3.04 (1H, dd, J=6.0 Hz), 3.16 (1H, dq, J=7.0 Hz), 3.65 (1H, br), 3.83 (1H, ddd, J=4.0 Hz), 4.48 (1H, d, J=10 Hz), 4.78 (1H, s), 5.12 (2H, ABq), 5.39 (1H, dd), 5.48 (1H, dq), 5.86 (1H, d, J=10 Hz), 7.2—7.35 (1H, m), 7.35 (5H, s), 7.63 (1H, d, J=10 Hz), 8.22 (1H, s), 8.53 (1H, d, J=4.0 Hz), 8.60 (1H, d, 2.0 Hz), and 8.74 (1H, br).

Found: C, 55.65; H, 6.35; N, 12.80%. Calcd for $C_{35}H_{47}N_7O_{12}$: C, 55.47; H, 6.25; N, 12.94%.

N-Benzyloxycarbonyl-O-[(2R,3S)-2-((2R,3S,4S)-4-azido-3-hydroxy-2-methyl-5-(3-pyridyl)pentanoyloxy)-3-hydroxy-3-methylpentanoyl]-L-threonine t-Butoxycarbonylhydrazide (32). A mixture of **31** (208 mg, 0.274 mmol), hydrazine hydrate (0.027 ml, 0.56 mmol), and ethanol (2 ml) was stirred at room temperature for 5 h. The reaction mixture was then concentrated and chromatographed on silica-gel (20 g) with 20:1 chloroform–methanol to afford a syrup of **32**. This syrup was again chromatographed on silica-gel (15 g) with 1:3 chloroform–ethyl acetate to give a pure sample of **32** (125 mg, 62.5%): IR ($CHCl_3$) 2100 cm^{-1}; $[\alpha]_D^{17}$ +9° (c 1.66).

Found: C, 56.18; H, 6.62; N, 13.17%. Calcd for $C_{34}H_{47}N_7O_{11}$: C, 55.96; H, 6.49; N, 13.44%.

(2R,5R,6S,9S,10S,11R)-10-Hydroxy-2-[(1'S)-1'-hydroxy-1'-methylpropyl]-5,11-dimethyl-9-(3-pyridylmethyl)-6-(benzyloxycarbonylamino)-8-aza-1,4-dioxacyclododecane-3,7,12-trione (14).

(a) *By HOBt-DCC Method:*[11] A solution of **24** (336 mg, 0.546 mmol) in methanol (30 ml) was stirred with a catalytic amount of Raney Ni (Nikko R-100) for 1 h under bubbling with hydrogen gas. The reaction mixture was filtered through a Celite and the catalyst was washed with a 1:1 methanol–dioxane. The combined filtrate and washings were evaporated to a glassy solid of crude **26**, To a solution of this residue in dry DMF (540 ml) was added HOBt (370 mg, 2.73 mmol) and then DCC (2.27 g, 11 mmol) portionwise at 0 °C with stirring. The mixture was kept at 5 °C for 60 h, after which time acetic acid (2 ml) was added to the mixture to decompose the unchanged DCC. The resulting mixture was then evaporated and the residue was taken with chloroform. The DCU undissolved was filtered and washed with chloroform twice. The combined filtrate and washings were washed with saturated aqueous $NaHCO_3$ and NaCl solutions successively, dried, and evaporated. The residue was chromatographed on silica-gel (20 g) with 15:1 chloroform–methanol to afford **14** (118 mg, 37%) as an amorphous powder: $[\alpha]_D^{18}$ −21° (c 0.96); EIMS, m/z 571 (M$^+$); ^{1}H-NMR (250 MHz) δ=0.93 (3H, t, J=7.5 Hz), 1.25 (3H, s), 1.31 (3H, d, J=6.5 Hz), 1.42 (3H, d, J=7.5 Hz), 1.52 and 1.65 (each 1H, each dq, J_{gem}=7.5 Hz), 2.55 (1H, q, J=0, 7.5 Hz), 2.6—2.8 (2H, m), 3.59 (1H, br-s), 4.03 (1H, q-like), 4.25—4.45 (2H, m), 4.96 (1H, s, H-2), 5.14 (2H, s), 5.34 (1H, dq, J=6.5, 7.0 Hz), 5.49 (1H, d, J=9 Hz), 6.26 (1H, d, J=9 Hz), 7.17 (1H, dd, J=5.0, 8.0 Hz), 7.37 (5H, s), 7.61 (1H, ddd, J=1.5, 1.8, 8.0 Hz), 8.46 (1H, dd, J=1.5, 5.0 Hz), and 8.54 (1H, d, J=1.8 Hz).

Found: C, 60.22; H, 6.69; N, 7,13%. Calcd for $C_{29}H_{37}N_3O_9$: C, 60.93; H, 6.52; N, 7.35%.

(b) *By Azide Method Using HOBt:*[12] A solution of **32** (87 mg, 0.119 mmol) in 50% aqueous acetic acid (8.7 ml) was stirred with Raney Ni for 3 h under bubbling with hydrogen gas. The mixture was filtered through a Celite and the filter cake was washed with methanol. The combined filtrate and washings were concentrated to a green syrup (250 mg), which was dissolved in 90% aqueous TFA (3 ml). The resulting solution was kept at room temperature for 1 h and then evaporated. The residue was co-evaporated with ether repeatedly to afford amorphous powder. A solution of this powder (250 mg) in dry DMF (3 ml) was acidified by addition of 6.53 M HCl in THF (0.109 ml, 0.715 mmol) at −25 °C. Isopentyl nitrite (0.020 ml, 0.145 mmol) was added and the solution stirred at −25 °C for 2 h. The resulting solution of the acyl azide was added to 100 ml of cold (−40 °C) DMF containing HOBt (81.1 mg, 0.6 mmol). The solution was neutralized by addition of triethylamine (0.150 ml, 1.062 mmol) and stored at −30 °C for 18 h and −5 °C for 24 h. The solvent was evaporated and the residue was partitioned between ethyl acetate (10 ml) and water (10 ml). The aqueous layer

separated was extracted with ethyl acetate (10 ml×5). The combined organic layers were washed with saturated aqueous $NaHCO_3$ and NaCl solutions, dried, and evaporated. The residue was chromatographed on silica-gel (20 g) with 10:1 chloroform–methanol to afford a syrup (3.5 mg). It was preparatively thin-layer chromatographed on PLC plate (Merck 5715) with 10:1 chloroform–methanol to give a pure sample of **14** (2 mg, 2.9%).

Dehydration Product (16+17) from 14. To a cold (−30 °C) solution of **14** (9 mg, 0.016 mmol) in dry pyridine (0.2 ml) was added freshly distilled $SOCl_2$ (0.012 ml, 0.16 mmol) under stirring. After being stirred at −20—−30 °C for 45 min, cold water was added and the mixture was extracted with chloroform (5×1 ml). The combined extracts were washed with saturated aqueous NaCl, dried, and evaporated to give a brown syrup (10 mg). It was chromatographed on silica-gel (2 g) with 30:1 chloroform–methanol to afford a colorless syrup of dehydration product (7 mg, 79%): EIMS, *m/z* 553 (M^+); ^{1}H-NMR (250 MHz) δ=1.08 (t, 3×H-3′ (**16**, **2**)), 1.31 (d, 5-Me, J=7.0 Hz), 1.38 (d, 11-Me (**16**, **17**), J=7.0 Hz), 1.39(d, H-5 (**2**), J=7.0 Hz), 1.50 (d, 11-Me (**2**), J=7.5 Hz), 1.63 (s, 1′-Me (**17**)), 1.67 (d, 3×H-3′ (**17**), J=7.0 Hz), 1.9—2.2 (2H, m, H-2′ (**16**, **2**)), 2.28 (*ca.* 0.5H, s, 1′-Me (**2**)), 2.50 (1H, dq, H-11, $J_{10,11}$=1.0 Hz), 2.60 (0.2H, dq, H-11 (**2**)), 2.90—3.05 (2H, m, 2×H-9′), 3.50—3.60 (1H, m, H-10), 4.02 (1H, q-like, H-9, $J\fallingdotseq$8 Hz), 4.29 (1H, t-like, H-6, $J\fallingdotseq$7 Hz), 4.35—4.50 (1H, br, OH), 5.14 (2H, s, $OC\underline{H}_2Ph$), 5.18 and 5.38 (each 0.5H, each s, H-2 (**16**, **17**)), 5.26 and 5.32 (each *ca.* 0.5H, each s, $\underline{H}_2C$=(**16**)), 5.38 (1H, dq, H-5, $J_{5,6}$=7.0 Hz), 5.40—5.50 (1H, br, 6-NH), 5.77 (*ca.* 0.5H, m, H-2′ (**17**)), 6.04 (1H, br-d, H—N(8), J=8 Hz), 7.18 (1H, dd, J=8.0, 4.5 Hz), 7.38 (5H, s, Ph), 7.62 (1H, ddd, J=2.0, 2.0 Hz), 8.46 (1H, dd), and 8.54 (1H, d).

Isomerization of Dehydration Products with DBU (16→17). A sample of the dehydration product (**16**+**17**) (7.9 mg) was dissolved in DBU (0.006 ml) and dry dioxane (0.01 ml), and then dioxane was removed by evaporation under reduced pressure. The residue was stored at 35 °C for 1.5 h. The reaction mixture was neutralized with aqueous 0.5 M HCl and then extracted thoroughly with chloroform. The combined extracts were washed with saturated aqueous NaCl, dried, and evaporated to give a yellow syrup, which was chromatographed on silica-gel (2 g) with 15:1 chloroform–methanol to afford a colorless syrup (2.7 mg) of **17** whose R_f-value was identical with the starting dehydration product: ^{1}H-NMR (250 MHz) δ=1.30 (3H, d, 5-Me, J=7.0 Hz), 1.39 (3H, 11-Me, J=7.5 Hz), 1.63 (3H, s, 1′-Me), 1.67 and 1.68 (each 1.5H, each d, 3×H-3′, J=7.0 Hz), 2.50 (1H, dq, H-11, $J_{10,11}$=1.0 Hz), 2.90—3.05 (2H, m, 2×H-9′), 3.50—3.60 (1H, m, H-10), 4.02 (1H, q-like, H-9, $J\fallingdotseq$8 Hz), 4.29 (1H, t-like, H-6, $J\fallingdotseq$7 Hz), 4.35—4.50 (1H, br, OH), 5.15 (2H, s, $OC\underline{H}_2Ph$), 5.18 and 5.38 (each 0.5H, each s, H-2), 5.38 (1H, dq, H-5, $J_{5,6}$=7.0 Hz), 5.40—5.50 (1H, br, 6-NH), 5.77 (1H, m, H-2′), 6.04 (1H, br-d, H-N(8), $J\fallingdotseq$8 Hz), 7.18 (1H, dd, J=8.0, 4.5 Hz), 7.38 (5H, s, Ph), 7.62 (1H, ddd, J=2.0, 2.0 Hz), 8.46 (1H, dd), and 8.54 (1H, d).

3-O-Benzyl-6-deoxy-5-C-ethyl-1,2-O-isopropylidene-5-O-methyl-α-D-glucofuranose (34). To a solution of **33** (5.37 g, 0.017 mol) in dry DMF (26 ml) was added 55% NaH (2.27 g, 0.052 mol) under ice-cooling. After the mixture had been stirred at room temperature for 0.5 h, methyl iodide (2.12 ml, 0.034 mol) was added to the mixture and stirring was continued for 1 h. The resulting mixture was poured into cold water and extracted with ethyl acetate. The extract was dried and evaporated to a brown syrup (8 g), which was chromatographed on silica-gel (200 g) with 5:1 toluene–ethyl acetate to afford **34** (4.38 g, 77%): A colorless syrup, $[\alpha]_D^{31}$ −68° (*c* 1.44); ^{1}H-NMR (90 MHz) δ=0.86 (3H, t, J=6.0 Hz), 1.30 (3H, s), 1.35 and 1.51 (each 3H, each s), 3.30 (3H, s), 3.90 and 4.15 (each 1H, each d, J=0, 3.0 Hz), 4.55 (1H, d, J=4.5 Hz), and 5.96 (1H, d).

Found: C, 67.55; H, 8.30%. Calcd for $C_{19}H_{28}O_5$: C, 67.83; H, 8.39%.

3-O-Benzyl-6-deoxy-5-C-ethyl-5-O-methyl-D-glucofuranose (35). A mixture of **34** (4.3 g) and 50% aqueous acetic acid (40 ml) was boiled under reflux for 5 h, and evaporated to a brown syrup, which was chromatographed on silica-gel (200 g) with 1:2 toluene-ethyl acetate to afford **35** (2.45 g, 65%).

Found: C, 64.73; H, 8.10%. Calcd for $C_{16}H_{24}O_5$: C, 64.84; H, 8.16%.

2-O-Benzyl-5-deoxy-4-C-ethyl-4-O-methyl-D-arabinitol (36). To a solution of **35** (2.35 g) in acetone (60 ml) was added a solution of sodium periodate (3.4 g) in water (40 ml). After the mixture had been stirred at room temperature for 3 h, a solution of the periodate (1.7 g) in water (20 ml) was added to the reaction mixture. The mixture was stirred in a dark place at room temperature for 1 h and filtered. Acetone was removed from the filtrate by concentration and the aqueous residue was extracted with chloroform. The extract was washed with saturated aqueous NaCl, dried, and evaporated. The residual syrup (1.74 g) was dissolved in dry THF (34 ml) and cooled in an ice-bath. Powdered $LiAlH_4$ (0.6 g, 155 mmol) was added slowly to the stirred solution and then stirred at room temperature for 2 h. Wet ether was added to the ice-cold reaction mixture to decompose the excess $LiAlH_4$. The mixture was filtered and the filter cake was washed with chloroform. The filtrate and washings were combined and evaporated to a yellow syrup (2 g), which was chromatographed on silica-gel (50 g) with 2:1 benzene–ethyl acetate to give **36** (1.4 g, 67%): a colorless syrup, $[\alpha]_D^{34}$ −25° (*c*, 1.00); ^{1}H-NMR (90 MHz) δ=0.88 (3H, t, J=7.5 Hz), 1.23 (3H, s), and 3.25 (3H, s).

Found: C, 67.06; H, 8.74%. Calcd for $C_{15}H_{24}O_4$: C, 67.13; H, 9.02%.

2-O-Benzyl-5-deoxy-4-C-ethyl-3-O-methoxymethyl-4-O-methyl-D-arabinitol (39). To a solution of **36** (1.43 g, 8.1 mmol) in dry DMF (14 ml) was added imidazole (817 mg, 12 mmol) and *t*-butyldiphenylsilyl chloride (TBDPSCl) (3.12 ml, 12 mmol), and the mixture was stirred at room temperature for 2 h. The resulting mixture was poured into cold water, and extracted with ethyl acetate. The extract was washed with a saturated aqueous NaCl solution, dried, and evaporated to a syrup, which was chromatographed on silica-gel (100 g) with 10:1 toluene–ethyl acetate to give a practically pure sample of **37** (a yellow syrup, 4.0 g, 97%). To an ice-cooled solution of this sample of **37** (4.0 g) in dry DMF (40 ml) was added methoxymethyl chloride (0.9 ml, 11.9 mmol) and diisopropylamine (2 ml, 11.5 mmol), and then the mixture was stirred at 60 °C for 2 h. The reaction mixture was poured into a cold water and extracted with ethyl acetate. The extract was washed with a saturated aqueous NaCl

solution, dried and evaporated to a crude syrup of **38** (4.0 g). To a solution of this syrup (4.0 g) in dry THF (20 ml) was added tetrabutylammonium, fluoride (1 M THF solution, 10 ml) dropwise under ice-cooling. After being stand at 0 °C for 2 h, the mixture was poured into an icewater and extracted with chloroform. The extract was washed with a saturated NaCl solution, dried, and evaporated to a syrup (4 g), which was chromatographed on silica-gel with 1:1 toluene–ethyl acetate to afford **39** (1.03 g, 42% from **36**): A colorless syrup; $[\alpha]_D^{33}$ −15° (*c* 1.00); ^{1}H-NMR (90 MHz) δ=0.87 (3H, t, *J*=7.2 Hz), 1.29 (3H, s), 1.57 (2H, q), 3.22 and 3.46 (each 3H, each s), 4.62 and 4.79 (each 2H, each s), and 7.38 (5H, s).

Found: C, 65.58; H, 8.87%. Calcd for $C_{17}H_{28}O_5$: C, 65.36; H, 9.03%.

(2R,3S)-(+)-3-Methoxy-2-(methoxymetoxy)-3-methylpentanoic Acid (6). A solution of **39** (740 mg) in methanol (7 ml) was stirred with Pd-black for 1 h under bubbling with hydrogen gas. The filtered solution was evaporated to a colorless syrup of **40** (700 mg), which was dissolved in acetone (7 ml) and to the solution a solution of sodium periodate (1.5 g, 7 mmol) in water (15 ml) was added dropwise under ice-cooling. After being stirred in a dark place at room temperature for 4 h, the reaction mixture was filtered, and acetone was removed by concentration. The resulting aqueous residue was extracted with chloroform. The extract was washed with saturated aqueous NaCl, dried, and evaporated to give 4-deoxy-3-*C*-ethyl-2-*O*-(methoxymethyl)-3-*O*-methyl-D-erythrose (colorless liquid, 780 mg). The crude aldehyde was dissolved in DME (1.8 ml) and to the solution PDC (5.4 g) was added. After being stirred at room temperature for 2 d, the mixture was filtered through silica-gel (10 g) with ether to remove the chromate. The filtrate was then evaporated to a syrup, which was chromatographed on silica-gel (30 g) with 80:5:1 chloroform–methanol–acetic acid to afford **6** (a colorless syrup, 480 mg, 74%): $bp_{0.1}$ 130 °C (bath temp); IR ($CHCl_3$) 1723 cm^{-1}; $[\alpha]_D^{29}$ +64° (*c* 1.09); ^{1}H-NMR (90 MHz) δ=0.92 (3H, t, *J*=7.5 Hz), 1.30 (3H, s), 1.73 (2H, q), 3.35 and 3.44 (each 3H, each s), 4.11 (1H, s) 4.60 and 4.85 (2H, m), and 7.79 (1H, br-s, COOH).

Found: C, 52.70; H, 8.69%. Calcd for $C_9H_{18}O_5$: C, 52.41; H, 8.80%.

N-Benzyloxycarbonyl-L-threonine Benzhydryl Ester (41). To a solution of *N*-benzyloxycarbonyl-L-threonine (500 mg, 1.97 mmol) in ethyl acetate (5 ml) was added dropwise a solution of diphenyldiazomethane in petroleum ether prepared from benzophenone hydrazone (580 mg, 2.95 mmol) and HgO (yellow) (640 mg, 2.95 mmol) in petroleum ether (0.3 ml) at room temperature for 5 h. After violent foaming had been settled, the reaction mixture was stirred at room temperature for 2 h and then excess diphenyldiazomethane was decomposed by addition of concd HCl. Water was added to the reaction mixture and extracted with ethyl acetate four times. The combined extracts were evaporated to a yellow syrup, which was chromatographed on silica-gel with 3:1 toluene–ethyl acetate to afford a pale yellow crystalline solid (662 mg, 80%). Recrystallization from hexane–ethyl acetate gave a pure sample of **41**: Colorless needles, mp 94—95 °C; $[\alpha]_D^{29}$ −19° (*c* 1,03); ^{1}H-NMR (90 MHz) δ=1.20 (3H, d, *J*=6.0 Hz), 1.8—2.1 (1H, br-s), 4.2—4.5 (2H, m), 5.10 (2H, s), 5.61 (1H, br-d, *J*=10 Hz), 6.90 (1H, s), and 7.36 (15H, s).

Found: C, 70.90; H, 6.07; N, 3.40%. Calcd for $C_{25}H_{25}NO_5$: C, 71.58; H, 6.01; N, 3.34%.

N-Benzyloxycarbonyl-O-[(2R,3S)-2-(methoxymethoxy)-3-methoxy-3-methylpentanoyl]-L-threonine Benzhydryl Ester (42). By the procedure described in the preparation of **21**, the mixture of **41** (712 mg, 1.7 mmol), **6** (350 mg, 1.69 mmol), ethyl acetate (8 ml), DMAP (20 mg, 0.16 mmol), and DCC (520 mg, 2.55 mmol) afforded **42** (650 mg, 65%) after silica-gel chromatography with 5:1 benzene–ethyl acetate: A colorless syrup, ^{1}H-NMR (90 MHz) δ=0.83 (3H, t, *J*=7.5 Hz), 1.12 (3H, s), 1.32 (3H, d, *J*=6.6 Hz), 1.53 (2H, q,), 3.18 and 3.28 (each 3H, each s), 4.00 (1H, s), 4.3—4.65 (1H, m), 4.39 and 4.48 (each 1H, ABq, J_{gem}=7.5 Hz), 5.13 (2H, s), 5.3—5.8 (2H, m), 6.86 (1H, s), and 7.10—7.50 (15H, m).

N-Benzyloxycarbonyl-O-[(2R,3S)-2-hydroxy-3-methoxy-3-methylpentanoyl]-L-threonine Benzhydryl Ester (43). A solution of **42** (650 mg) in 90% aqueous TFA (6 ml) was kept at room temperature for 1 h. Evaporation of the reaction mixture followed by co-evaporation with ether yielded a brown syrup (750 mg), which was chromatographed on silica-gel (30 g) with 80:5:1 chloroform–methanol–acetic acid to afford a colorless syrup (370 mg, 89%) of the hydroxy acid. By the same procedure as described in the preparation of **41**, the syrup (113 mg) was treated with diphenyldiazomethane to give a crude syrup (300 mg) of **43**, which was chromatographed on silica-gel (10 g) with 5:1 benzene–ethyl acetate to afford a pure sample of **43** (115 mg, 72%): A colorless syrup; $[\alpha]_D^{30}$ −2°, $[\alpha]_{365}^{30}$ −5° (*c* 2.24); ^{1}H-NMR (90 MHz) δ=0.86 (3H, t, *J*=7.5 Hz), 1.00 (3H, s), 1.31 (3H, d, *J*=7.5 Hz), 1.50 (2H, q), 2,83 (1H, br-s), 3.03 (3H, s), 3.96 (1H, s), 4.60 (1H, dd, *J*=3.0, 9.0 Hz), 5.10 (2H, s), 5.53 (1H, dq), 5.73 (1H, br-s), 6.86 (1H, s), and 7.07—7.47 (15H, m).

Found: C, 68.28; H, 6.62; N, 2.70%. Calcd for $C_{32}H_{37}NO_8$: C, 68.19; H, 6.62; N, 2.49%.

N-Benzyloxycarbonyl-O-[(2R,3S)-2-((2R,3S,4S)-4-azido-3-hydroxy-2-methyl-5-(3-pyridyl)pentanoyloxy)-3-methoxy-3-methylpentanoyl]-L-threonine (46). By the procedure described in the preparation of **29**, a mixture of **43** (117 mg, 0.207 mmol), ethyl acetate (2 ml), DMAP (2.5 mg, 0.02 mmol), and DCC (105 mg, 0.5 mmol) afforded **44** (105 mg, 63%) after purification through silica-gel (20 g) column with 3:1 toluene–ethyl acetate. A solution of **44** (105 mg) in 22 ml of a 2% HCl (in 50% (v/v) aqueous dioxane) was stirred at 35 °C for 10 h, and then evaporated to afford a syrup of **45**, which was dissolved in a 90% TFA (1 ml) and kept at room temperature for 30 min. The reaction mixture was evaporated and co-evaporated with ether. The final residue was chromatographed on silica-gel (10 g) with 80:5:1 chloroform–methanol–acetic acid to give **46** (70 mg, 57% from **43**) as a colorless glassy solid.

(2R,5R,6S,9S,10S,11R)-10-Hydroxy-2-[(1'S)-1'-methoxy-1'-methylpropyl]-5,11-dimethyl-9-(3-pyridylmethyl)-6-(benzyloxycarbonylamino)-8-aza-1,4-dioxacyclododecane-3,7,12-trione (15). By the procedure described in the preparation (a) of **14**, the azido acid **46** (110 mg) afforded a crude syrup of **15** which was purified through silica-gel column chromatography with 30:1 chloroform–methanol to provide a pure sample of **15** (16 mg, 15%) as a colorless glass: $[\alpha]_D^{27}$ −17° (*c* 0.53); ^{1}H-NMR (250 MHz) δ=0.85 (3H, t, *J*=6.2 Hz), 1.29 (3H, s), 1.30 (3H, d, *J*=7.5 Hz), 1.41 (3H, d, *J*=6.3 Hz), 1.71 (2H, q,

J=6.2 Hz), 2.59 (1H, q, J=6.3 Hz), 2.86—3.05 (2H, m), 3.21 (1H, s), 3.58 (1H, s-like), 3.93—4.10 (1H, m), 4.1—4.5 (2H, m), 5.00 (1H, s, H-2), 5.15 (2H, s), 5.40 (1H, dq, J=5.4, 7.5 Hz), 5.3—5.5 (1H, br), 6.25 (1H, br-d), 7.17 (1H, dd, J=5.0, 8.0 Hz), 7.38 (5H, s), 7.61 (1H, ddd, J=1.5, 1.8, 8.0 Hz), 8.46 (1H, dd, J=1.5, 5.0 Hz), and 8.53 (1H, d, J=1.8 Hz).

Found: m/z 585.2692. Calcd for $C_{30}H_{39}N_3O_9$: M, 585.2684.

5-O-(t-Butyldiphenylsilyl)-1-deoxy-2-C-ethyl-3,4-O-isopropylidene-D-ribitol (48). A solution of **47**[16] (3.0 g, 6.8 mmol) in methanol (30 ml) was stirred with 5% Pd-carbon (*ca.* 0.5 g) for 0.5 h under bubbling with hydrogen gas. The filtered solution was evaporated to a syrup of **48** (3.0 g, 99%). An analytical sample was obtained by silica-gel column chromatography with 10:1 toluene-ethyl acetate; colorless syrup, $[\alpha]_D^{31}$ +28° (c 1.09).

Found: C, 70.65; H, 8.40%. Calcd for $C_{26}H_{37}O_4Si$: C, 70.55; H, 8.64%.

5-O-(t-Butyldiphenylsilyl)-1-deoxy-2-C-ethyl-3,4-O-isopropylidene-2-O-methyl-D-ribitol (49). By the procedure described in the *O*-methylation of **33**, the sample of **48** (2.85 g) was *O*-methylated to afford a crude syrup of **49** (5 g), which was chromatographed on silica-gel (100 g) with 20:1 toluene-ethyl acetate to give a pure sample of **49** (2.24 g, 76%); a colorless syrup, $[\alpha]_D^{30}$ +35° (c 1.16); ^{1}H-NMR δ=0.86 (3H, t, J=7.5 Hz), 1.08 (9H, s), 1.12 (3H, s), 1.33 and 1.38 (each 3H, each s), 1.5—1.8 (2H, m), 3.15 (3H, s), and 3.5—3.8 (2H, m).

Found: C, 71.29; H, 8.62%. Calcd for $C_{27}H_{40}O_4Si$: C, 71.02; H, 8.82%.

1-Deoxy-2-C-ethyl-2-O-methyl-D-ribitol (50). To a cold solution of **49** (2.24 g) in dry THF (12 ml) was added (n-Bu)$_4$NF (7.75 ml of 1 M THF solution) dropwise. After being stirred at 5 °C for 3 h, the mixture was poured into a cold water and extracted with ethyl acetate. The extract was washed with saturated aqueous NaCl, dried, and evaporated to afford a syrup, which was dissolved in an 80% aqueous TFA (25 ml). After being kept at room temperature for 1 h, the mixture was evaporated. The residue (2.5 g) was chromatographed on silica-gel (100 g) with 15:1 chloroform–methanol to give a pure sample of **50** (5.8 g, 67%); a colorless syrup, $[\alpha]_D^{31}$ +9° (c 1.00); ^{1}H-NMR (90 MHz) δ=0.91 (3H, t, J=6.0 Hz), 1.21 (3H, s), 1.73 (2H, q), 2.7—3.1 (3H, br), and 3.23 (3H, s).

Found: C, 53.81; H, 9.90%. Calcd for $C_8H_{18}O_4$: C, 53.91; H, 10.18%.

1-Deoxy-2-C-ethyl-2-O-methyl-D-ribitol 4,5-carbonate (51). A solution of **50** (65 mg, 0.37 mmol) and *N,N'*-carbonyldiimidazole (72 mg, 0.444 mmol) in dry benzene (1.3 ml) was stirred at room temperature for 2 h, and the reaction mixture was then poured into a cold water and extracted with ethyl acetate. The extract was washed with saturated aqueous NaCl, dried, and evaporated. The residual syrup (80 mg) was chromatographed with 3:1 benzene–ethyl acetate to afford **17** (46 mg, 61%) as colorless crystals; mp 77—79 °C (hexane–ethyl acetate); $[\alpha]_D^{33}$ +17° (c 1.00); ^{1}H-NMR (90 MHz) δ=0.93 (3H, t, J=7.0 Hz), 1.18 (3H, s), 1.6—1.85 (2H, m), 2.9—3.1 (1H, br-s), 3.25 (3H, s), 3.88 (1H, d, J=4.5 Hz), and 4.4—5.0 (3H, m).

Found: C, 52.85; H, 7.75%. Calcd for $C_9H_{16}O_5$: C, 52.93; H, 7.90%.

1-Deoxy-2-C-ethyl-3-O-methoxymethyl-2-O-methyl-D-ribitol 4,5-carbonate (52). By the procedure described in the *O*-methoxymethylation of **47**, the sample of **51** (251 mg) was *O*-methyoxymethylated to afford a crude syrup of **52** (251 mg), which was chromatographed on silica-gel (25 g) with 5:1 benzene–ethyl acetate to give a pure sample of **52** (252 mg, 93%); a colorless syrup, $[\alpha]_D^{33}$ +30° (c 1.00); IR ($CHCl_3$) 1803 cm^{-1}: ^{1}H-NMR (90 MHz) δ=0.91 (3H, t, J=7.5 Hz), 1.20 (3H, s), 1.5—1.7 (2H, m), 3.23 and 3.43 (each 3H, each s), 3.91 (1H, d, J=1.0 Hz), and 4.3—5.1 (5H, m).

Found: C, 53.28; H, 7.97%. Calcd for $C_{11}H_{20}O_6$: C, 53.21; H, 8.12%.

(2S,3R)-(−)-3-Methoxy-2-(methoxymethoxy)3-methylpentanoic Acid (7). To a solution of **52** (251 mg, 1.08 mmol) in methanol (3 ml) was added an aqueous 1 M NaOH solution (2.2 ml). After being stirred at room temperature for 20 min, the reaction mixture was neutralized with CG-50 resin (H^+ type) to pH 6—8 under ice-cooling, and filtered. The filtrate and methanolic washings were combined and evaporated to give a crude syrup of **53**. The two-stage oxidation of the crude **53** was carried out by the same procedure described in the preparation of **6** from **40** to afford the enantiomeric **7** (114 mg, 51% yield from **52**). This sample of **7** was purified by bulb to bulb distillation; colorless syrup, $bp_{0.1}$ 130 °C (bath temp.); IR ($CHCl_3$) 1723 cm^{-1}; $[\alpha]_D^{28}$ −61° (c 0.96); the ^{1}H-NMR (90 MHz) and IR spectra were identical with those of **6**.

Found: C, 52.52; H, 8.61%. Calcd for $C_9H_{18}O_5$: C, 52.41; H, 8.80%.

N-Benzyloxycarbonyl-O-[(2S,3R)-2-(methoxymethoxy)-3-methoxy-3-methylpentanoyl]-L-threonine Benzhydryl Ester (54). The title compound **54** was prepared from **7** and **41** by the procedure described in the preparation of **42**. **54**: A colorless syrup, ^{1}H-NMR (90 MHz) δ=0.81 (3H, t, J=7.5 Hz), 1.13 (3H, s), 1.36 (3H, d, J=6.6 Hz), 1.2—1.5 (2H, m), 3.18 (3H, s), 3.31 (3H, s), 4.00 (1H, s), 4.36 and 4.53 (each 1H, ABq, J=7.5 Hz), 4.63 (1H, dd, J=2.5, 12 Hz), 5.15 (2H, s), 5.61 (1H, dq), 5.78 (1H, br-d), 6.90 (1H, s), and 7.13—7.58 (15H, m).

N-Benzyloxycarbonyl-O-[(2S,3R)-2-hydroxy-3-methoxy-3-methylpentanoyl]-L-threonine (55). **55**: Colorless needles, mp 120—121 °C; $[\alpha]_D^{28}$ +39° (c 1.25); ^{1}H-NMR (90 MHz) δ=0.83 (3H, t, J=7.5 Hz), 1.10 (3H, s), 1.30 (3H, d, J=6.0 Hz), 1.60 (2H, q), 3.15 (3H, s), 3.88 (1H, br), 4.08 (1H, s), 4.56 (2H, dd, J=1.0, 10 Hz), 5.08 (2H, s), 5.53 (1H, dq), 5.5—6.2 (2H, br), and 7.40 (5H, s).

N-Benzyloxycarbonyl-O-[(2S,3R)-2-hydroxy-3-methoxy-3-methylpentanoyl]-L-threonine Benzhydryl Ester (56). **56**: A colorless syrup, $[\alpha]_D^{30}$ +3°, $[\alpha]_{365}^{30}$ +16° (c 1.49); ^{1}H-NMR (90 MHz) δ=0.81 (3H, t, 7.5 Hz), 1.00 (3H, s), 1.33 (3H, d, J=6.6 Hz), 1.26—1.70 (2H, m), 2.8—3.0 (1H, m), 3.16 (3H, s), 3.73 (1H, s), 4.50—4.76 (1H, m), 5.15 (2H, s), 5.4—5.8 (2H, m), 6.83 (1H, s), and 7.13—7.58 (15H, m).

Found: C, 68.17; H, 6.61; N, 2.48%. Calcd for $C_{32}H_{37}NO_8$: C, 68.19; H, 6.62; N, 2.49%.

N-Benzyloxycarbonyl-O-[(2S,3R)-2-((2R,3S,4S)-4-azido-3-formyloxy-2-methyl-5-(3-pyridyl)pentanoyloxy)-3-methoxy-3-methylpentanoyl]-L-threonine Benzhydryl Ester (57). The compound **57** was prepard from **3** (118 mg) and **56** (232 mg) by the same procedure as described in the preparation of **44**. A practically pure sample of **57** (281 mg, 72%) was obtained

by silica-gel (25 g) column chromatography of the crude product with 1:1 toluene–ethyl acetate.

N-Benzyloxycarbonyl-O-[(2S,3R)-2-((2R,3S,4S)-4-azido-3-hydroxy-2-methyl-5-(3-pyridyl)pentanoyloxy)-3-methyoxy-3-methylpentanoyl]-L-threonine Benzhydryl Ester (58). A practically pure sample of **57** (281 mg) was dissolved in a 2% HCl solution in 50% aqueous dioxane (5 ml). After being stirred at 35 °C for 7 h, the reaction mixture was evaporated to a syrup of **58** which was used for the next preparation without further purification. A pure sample of **58** was obtained by silica-gel column chromatography with 40:1 chloroform–methanol; a colorless syrup, $[\alpha]_D^{31}$ +8°, $[\alpha]_{365}^{31}$ +17° (*c* 0.90).

Found: C, 64.91; H, 6.35; N, 8.75%. Calcd for $C_{43}H_{49}N_5O_{10}$: C, 64.90; H, 6.20; N, 8.80%.

(2S,5R,6S,9S,10S,11R)-10-Hydroxy-2-[(1'R)-1'-methoxy-1'-methylpropyl]-5,11-dimethyl-9-(3-pyridylmethyl)-6-(benzyloxycarbonylamino)-8-aza-1,4-dioxacyclododecane-3,7,12-trione (18). By the procedure described in the preparation of **15**, the title compound **18** was obtained in a 12% yield from **58** *via* the azido acid **59** as a colorless syrup: $[\alpha]_D^{29}$ −48° (*c* 0.89); ^{1}H-NMR (250 MHz) δ=0.88 (3H, t, *J*=8.3 Hz), 1.17 (3H, d, *J*=5.0 Hz), 1.33 (3H, d, *J*=8.0 Hz), 1.43 (3H, s), 1.65—1.90 (2H, m), 2.44 (2H, dq, *J*=1.5, 8.0 Hz), 2.9—3.2 (2H, m), 3.26 (3H, s), 3.60 (1H, br), 4.00—4.13 (1H, m), 4.0—4.5 (1H, br), 4.45 (1H, dd, *J*=5.0 Hz), 4.71 (1H, s, H-2), 5.00 (1H, dq), 5.13 (2H, s), 5.86 (1H, br-d), 6.76 (1H, br-d), 7.25 (1H, dd, *J*=5.0, 8.0 Hz), 7.36 (5H, s), 7.69 (1H, ddd, *J*=1.5, 1.8, 8.0 Hz), 8.51 (1H, dd, *J*=1.5, 5.0 Hz), and 8.59 (1H, d, *J*=1.8 Hz).

Found: *m/z* 585.2678. Calcd for $C_{30}H_{39}N_3O_9$: M, 585.2683.

We are grateful to Prof. Sumio Umezawa, Institute of Bioorganic Chemistry, and Prof. Hamao Umezawa, Institute of Microbial Chemistry, for the generous support of our program. We also thank Mr. Masaki Awamura and Mr. Noriyoshi Igami for their early contributions to this project, Mr. Saburo Nakada for elemental analyses, and Miss Yukiko Suzuki for 250 MHz ^{1}H-NMR analyses.

References

1) Part III: M. Kinoshita, H. Hamazaki, and M. Awamura, *Bull, Chem. Soc. Jpn.*, **51**, 3595 (1978).
2) K. Maeda, H. Kosaka, Y. Okami, and H. Umezawa, *J. Antibiot.*, **6A**, 140 (1953).
3) Y. Okami, K. Maeda, and H. Umezawa, *J. Antibiot.*, **7A**, 55 (1954).
4) G. Koyama, Y. Iitaka, K. Maeda, and H. Umezawa, *Tetrahedron Lett.*, **1967**, 3587.
5) An analogous example has been reported: A. Rosenthal and K. Shudo, *J. Org. Chem.*, **37**, 4391 (1972).
6) M. Kinoshita and S. Mariyama, *Bull. Chem. Soc. Jpn.*, **48**, 208 (1975).
7) The constituents of the mixture could not be separated each other by all the chromatographic techniques tried. The isomeric ratios were estimated by ^{1}H-NMR spectroscopy.
8) E. Wünsch and J. Jentsch, *Chem. Ber.*, **97**, 2490 (1964).
9) A. Hassner and V. Alexanian, *Tetrahedron Lett.*, **1978**, 4475.
10) K. Nakajima, T. Tanaka, M. Neya, and K. Okawa, *Bull. Chem. Soc. Jpn.*, **55**, 3237 (1982).
11) M. Kinoshita and M. Awamura, *Bull. Chem. Soc Jpn.*, **51**, 869 (1978).
12) R. T. Nutt, D. F. Veber, and R. Saperstein, *J, Am. Chem. Soc.*, **102**, 6539 (1980).
13) E. J. Corey and J. W. Suggs, *J. Org. Chem.*, **38**, 3224 (1973).
14) D. N. Kirk and M. P. Hartshorn, "Steroid Reaction Mechanism," Elsevier, New York (1968), p. 158.
15) K. Fukui, "Kagaku-hanno to Denshi no Kidō," Maruzen, Tokyo (1976), p. 59.
16) M. Arai, K. Tomooka, M. Nakata, and M. Kinoshita, Abstr-II, p. 1368, 49th National Meeting of Chemical Society of Japan, Tokyo, April 1984.

Stereoselective Oxylactonization. Preparation of 2-Deoxy-DL-ribono-1,4-lactone Derivatives from 3-Silyloxy-4-alkenamides

Yuh-ichiro ICHIKAWA, Tetsuo MIWA, and Koichi NARASAKA*
Department of Chemistry, Faculty of Science, The University of Tokyo, Hongo, Bunkyo-ku, Tokyo 113
(Received July 6, 1985)

The oxylactonization of 3-silyloxy-4-alkenamides proceeds stereoselectively by treatment with *m*-chloroperbenzoic acid to give the corresponding 2-deoxy-DL-ribono-1,4-lactone derivatives.

Halolactonization reaction of acyclic alkenoic acids or their derivatives has been used to functionalize double bonds in a stereoselective manner,[1] and widely applied to the synthesis of natural products.[2] It was expected that the development of oxylactonization in which alkenoic acid derivatives are converted to the corresponding hydroxy lactones in a one-pot manner would provide an effective method for the preparation of polyhydroxy compounds. Hence, the oxylactonization of 4-alkenoic acid derivatives was undertaken using *m*-chloroperbenzoic acid (MCPBA) as an oxidant.

When 4-pentenoic acid (**1a**) and the corresponding 3-phenylpropyl ester **1b** were treated with MCPBA at room temperature, the generation of the epoxides was observed. The successive lactonization to 5-hydroxy-4-pentanolide (**2**), however, proceeded very slowly.[3] On the other hand, the reaction of *N,N*-dimethyl-4-pentenamide (**1c**) with MCPBA was found to afford 5-hydroxy-4-pentanolide (**2**), however, even at room temperature.[4]

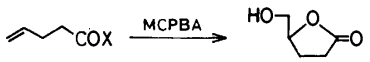

1a X=OH
b X=O(CH$_2$)$_3$Ph
c X=NMe$_2$

2

As an alkenamide is susceptible to the oxylactonization with MCPBA, we next investigated the stereochemical course of the oxylactonization of 3-hydroxy-4-pentenamide **3a**. The treatment of *N,N*-diisopropyl-3-hydroxy-4-pentenamide (**3a**) with a 4-molar amount of MCPBA in benzene at room temperature generated 3,4-*trans*(*erythro*)-3,5-dihydroxy-4-pentanolide (**4a**) predominantly along with the 3,4-*cis*(*threo*)-isomer **5a** (**4a**:**5a**=2.6:1).

Particularly interesting was that the oxylactonization of **3a** with MCPBA shows the opposite stereoselectivity to the halolactonization of 3-hydroxy-(or silyloxy)-4-alkenoic acids, which are generally converted to the 3,4-cis-substituted butanolides.[1c] Therefore, the stereoselectivity of this oxylactonization was examined in detail by introducing various protecting groups to the 3-hydroxyl group of the amide **3a**. When acyl groups such as acetyl, benzoyl, pivaloyl, and ethoxycarbonyl groups were employed for the protection of the 3-hydroxyl group, the yields of oxylactones **4** and **5** were very low because of the elimination of acyloxyl groups occurred under the reaction conditions. The reaction of the benzyl (Bn) ether **3b** and the methoxymethyl (MOM) ether **3c** with MCPBA proceeded smoothly, however, the stereoselectivity toward the *trans*(*erythro*)-lactone **4** was not improved (**4**:**5**=*ca.* 2:1).

The high selectivity was observed when the *t*-butyldimethylsilyl (TBS) ether **3d** was employed. The reaction of **3d** with MCPBA in benzene afforded the trans-substituted isomer **4d** in favorable selectivity. The structure of **4d** was confirmed by the transformation to 2-deoxy-DL-ribono-1,4-lactone[5] by removal of the TBS group with aqueous acetic acid in tetrahydrofuran at 80 °C.

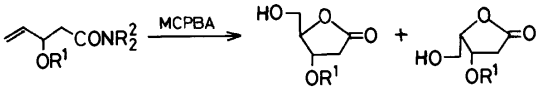

3 4 5

Table 1. Oxylactonization of the 3-hydroxy-4-pentenamide derivatives **3**

	R^1	R^2	Yield/%	(**4** : **5**)
3a	H	*i*-Pr	88	(2.6 : 1)
3b	Bn	Me	70	(2.1 : 1)
3c	MOM	Me	54	(1.9 : 1)
3d	TBS	*i*-Pr	90	(4.3 : 1)

Furthermore, (*E*) and (*Z*)-isomers of 3-silyloxy-4-hexenamide (**6a** and **6b**) were prepared and submitted to the reaction with MCPBA. In the oxylactonization of the (*Z*)-amide **6a**, the both stereoisomers **7a** and **8a** were formed in comparable amounts. On the other hand, it was noted that the 3,4-*trans*-substituted lactone **7b** was generated in good selectivity (**7b**:**8b**=3.9:1) from the (*E*)-hexenamide **6b**.

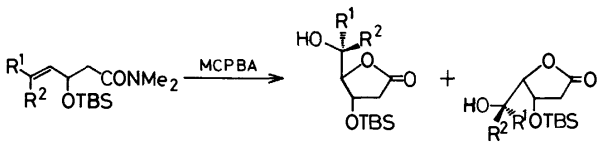

6 7 8

Table 2. Oxylactonization of the 3-silyloxy-4-hexenamides **6**

	R^1	R^2	Yield/%	(**7** : **8**)
6a	H	Me	63	(1.1 : 1)
6b	Me	H	79	(3.9 : 1)

From these results, the following speculation might be suggested for the *trans* stereoselection in the present oxylactonization. The lactonization is considered to proceed *via* unstable epoxy amides **10**, which are successively converted to hydroxy lactones by the intramolecular attack of the amide oxygen. The stereoselectivity is consequently directed in the epoxidation step. The epoxidation maybe proceeds through "the inside alkoxy transition state **9**"[6] in which MCPBA forms a hydrogen bond with the amide group[7] to result in the predominant formation of the *threo*-epoxide **10a**. The remarkable decrease of the selectivity in the case of the (*Z*)-amide **6a** is well explained by the steric interaction between the (*Z*)-methyl group and the TBS group in the preferred transition state **9**.

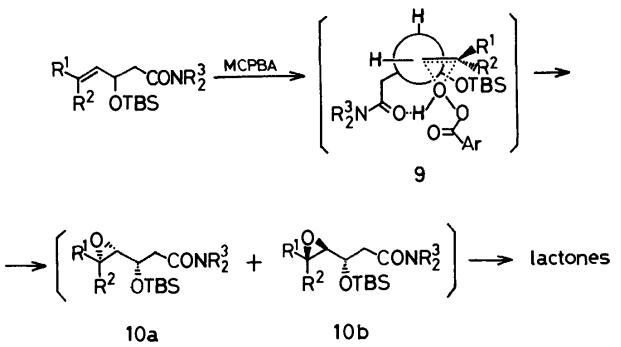

9

10a 10b

In conclusion, the oxylactonization of 3-silyloxy-4-alkenamides was found to proceed by the simple treatment with MCPBA to yield 2-deoxy-DL-ribono-1,4-lactone derivatives in good stereoselectivity. In contrast to *cis*-selective halolactonization, the present oxylactonization provides a useful method for the preparation of polyoxygenated 3,4-*trans*-substituted butyrolactones.

Experimental

All the melting and boiling points are uncorrected. The IR spectra were determined on a Hitachi Model 260-30 spectrometer. The ^{1}H NMR spectra were recorded with Hitachi R-24B and Varian EM-390 spectrometers in $CDCl_3$ with tetramethylsilane as an internal standard. Benzene was distilled and dried over sodium wire. Tetrahydrofuran (THF) was freshly distilled from sodium benzophenone ketyl. *N,N*-Dimethylformamide (DMF) was distilled from CaH_2 and stored over Molecular Sieve. Purification of products was performed by column chromatography on silica gel (Wakogel C-200 or Merck, Art. 9385 Kieselgel 60, 230—400 mesh).

Preparation of N,N-*Diisopropyl-3-hydroxyl-4-pentenamide (3a).* To a solution of lithium diisopropylamide (55 mmol) in THF (100 mL) was added a solution of *N,N*-diisopropylacetamide (7.16 g, 50 mmol) in THF (10 mL) at −78 °C, and the mixture was stirred for 1 h at −78 °C.[8] A THF (5 mL) solution of acrylaldehyde (3.36 g, 60 mmol) was added and then stirred for 15 min at −78 °C. To the mixture was added sat. aqueous NH_4Cl and the organic layer was extracted with dichloromethane. The separated organic layer was dried over Na_2SO_4 and was condensed under reduced pressure. Purification by column chromatography (hexane:ethyl acetate=3:1, v/v) and distillation gave the amide **3a** (8.21 g, 82%): Bp 101—102 °C/0.8 mmHg (1 mmHg=133.322 Pa). IR (neat) 3420, 1625 cm^{-1}. ^{1}H NMR δ=1.22 (6H, d, J=6.8 Hz), 1.38 (6H, d, J=6.8 Hz), 2.33 (1H, dd, J=8.3, 16.0 Hz), 2.55 (1H, dd, J=3.3, 12.0 Hz), 3.22—4.17 (2H, m), 4.32—4.70 (2H, m), 5.00—5.42 (2H, m), 5.88 (1H, ddd, J=5.4, 10.0, 17.0 Hz).

By the same procedure, the corresponding *N,N*-dimethyl amide (**3**, R^1=H, R^2=Me) was prepared in 82% yield: Bp 84—88 °C/0.35 mmHg. IR (neat) 3400, 1615 cm^{-1}. ^{1}H NMR δ=2.37 (1H, dd, J=7.8, 16.2 Hz), 2.59 (1H, dd, J=4.0, 16.2 Hz), 2.98 (3H, s), 3.03 (3H, s), 4.25—4.70 (2H, m), 5.02—5.43 (2H, m), 5.90 (1H, ddd, J=5.5, 10.0, 16.5 Hz).

Preparation of N,N-*Diisopropyl-3-t-butyldimethylsilyloxy-4-pentenamide (3d).* A mixture of **3a** (1.99 g, 10 mmol), triethylamine (1.52 g, 15 mmol), *t*-butyldimethylsilyl chloride (1.81 g, 12 mmol) and a catalytic amount of 4-dimethylaminopyridine in DMF (30 mL) was stirred for 3 h at room temperature.[9] Then pH 7 phosphate buffer (100 mL) was added, and the mixture was extracted with ether. The ether extract was washed with water and sat. aqueous NaCl and dried over Na_2SO_4. The ether solution was concentrated and the residue was purified by column chromatography on silica gel (hexane:ethyl acetate=10:1, v/v) and distillation to give the silylated amide **3d** (3.02 g, 96%): Bp 122 °C/0.4 mmHg. IR (neat) 1640 cm^{-1}. ^{1}H NMR δ=0.07 (6H, s), 0.88 (9H, s), 1.19 (6H, d, J=6.5 Hz), 1.34 (6H, d, J=6.5 Hz), 2.32 (1H, dd, J=6.0, 14.5 Hz), 2.62 (1H, dd, J=6.8, 14.5 Hz), 3.37—4.20 (2H, m), 4.73 (1H, br, q, J=6.5 Hz), 4.91—5.34 (2H, m), 5.90 (1H, ddd, J=5.5, 10.0, 16.5 Hz). Found: C, 64.59; H, 11.52; N, 4.52%. Calcd for $C_{17}H_{35}NO_2Si$: C, 65.12; H, 11.25; N, 4.47%.

Preparation of (Z)-N,N-*Dimethyl-3-t-butyldimethylsilyloxy-4-hexenamide (6a).* The reaction of lithiated *N,N*-dimethylacetamide with 2-butynal according to the procedure described above yielded *N,N*-dimethyl-3-hydroxy-4-hexynamide in 85% yield: Bp 125—126 °C/0.7 mmHg. The acetylenic amide was hydrogenated over 5% Pd/$BaSO_4$-quinoline catalyst[10] in methanol under usual pressure, and the hydroxyl group was silylated to give **6a** in 86% overall yield: Bp 120 °C (bath temp)/0.1 mmHg. IR (neat) 1650 cm^{-1}. ^{1}H NMR δ=0.02 (6H, s), 0.81 (9H, s), 1.60 (3H, d, J=5.5 Hz), 2.15 (1H, dd, J=4.8, 14.0 Hz), 2.63 (1H, dd, J=8.0, 14.0 Hz), 2.86 (3H, s), 2.98 (3H, s), 4.76—5.04 (1H, m), 5.10—5.55 (1H, m). Found: C, 61.77; H, 11.07; N, 5.20%. Calcd for $C_{14}H_{29}NO_2Si$: C, 61.93; H, 10.77; N, 5.16%.

Preparation of (E)-N,N-*Dimethyl-3-t-butyldimethylsilyloxy-4-hexenamide (6b).* As mentioned above, (*E*)-*N,N*-dimethyl-3-hydroxy-4-hexenamide was prepared by the reaction of lithiated *N,N*-dimethylacetamide with crotonaldehyde in 86% yield: Bp 99—100 °C/0.5 mmHg. The hydroxy amide was then silylated to give **6b** in 82% yield:

Bp 125—130 °C (bath temp)/0.3 mmHg. IR (neat) 1650 cm^{-1}. ^1H NMR δ=0.02 (6H, s), 0.87 (9H, s), 1.64 (3H, d, J=5.0 Hz), 2.22 (1H, dd, J=5.0, 13.5 Hz), 2.63 (1H, dd, J=8.0, 13.5 Hz), 2.88 (3H, s), 2.98 (3H, s), 4.33—4.73 (1H, m), 5.13—5.82 (2H, m). Found: C, 61.61; H, 11.00; N, 5.01%. Calcd for $C_{14}H_{29}NO_2Si$: C, 61.93; H, 10.77; N, 5.16%.

Oxylactonization of ***3d***. A benzene (2 mL) solution of the amide **3d** (152 mg, 0.48 mmol) was added to a suspension of MCPBA (70% pure, 478 mg, 1.94 mmol) in benzene (2 mL), and the mixture was stirred at 20—30 °C overnight. A mixture of sat. aqueous Na_2SO_3 and 10% aqueous K_2CO_3 was added and the mixture was extracted with ether. The ether extract was washed successively with 10% aqueous K_2CO_3 and sat. aqueous NaCl. After being dried over Na_2SO_4, the ether solution was condensed *in vacuo*. The residue was purified by column chromatography (hexane:ethyl acetate=3:1—1:1, v/v) to give the less polar **4d** (87.6 mg, 73%) and the more polar **5d** (20.7 mg, 17%).

*3-O-t-Butyldimethylsilyl-2-deoxy-*DL*-erythro-pentono-1,4-lactone (**4d**)*: Mp 54—55 °C (hexane). IR (CH_2Cl_2) 3620, 1785 cm^{-1}. ^1H NMR δ=0.09 (6H, s), 0.78 (9H, s), 2.28 (1H, dd, J=4.0, 16.5 Hz), 2.57 (1H, br s), 2.78 (1H, dd, J=6.5, 16.5 Hz), 3.53—3.82 (2H, m), 4.07—4.56 (2H, m). Found: C, 53.46; H, 9.23%. Calcd for $C_{11}H_{22}O_4Si$: C, 53.62; H, 9.00%. Hydrolysis of **4d** (49 mg, 0.20 mmol) in THF (0.5 mL), H_2O (0.5 mL), and acetic acid (1.5 mL) at 80 °C gave 2-deoxy-DL-ribono-1,4-lactone.[5]

*3-O-t-Butyldimethylsilyl-2-deoxy-*DL*-threo-pentono-1,4-lactone (**5d**)*: Mp 99—100 °C (cyclohexane). IR (CH_2Cl_2) 3620, 1785 cm^{-1}. ^1H NMR δ=0.09 (6H, s), 0.89 (9H, s), 2.37 (1H, br s), 2.40 (1H, dd, J=3.0, 17.5 Hz), 2.74 (1H, dd, J=5.7, 17.5 Hz), 3.58—4.07 (2H, m), 4.34—4.70 (2H, m). Found: C, 53.37; H, 8.93%. Calcd for $C_{11}H_{22}O_4Si$: C, 53.62; H, 9.00%.

The Oxylactonization of ***6a*** *and* ***6b*** *was Carried out by the Same Procedure.* *3-O-t-Butydimethylsilyl-2,6-dideoxy-*DL*-lyxo-hexono-1,4-lactone (**7a**)*: Bp 180—185 °C (bath temp)/2.5 mmHg. IR (CH_2Cl_2) 3480, 1775 cm^{-1}. ^1H NMR δ=0.09 (6H, s), 0.77 (9H, s), 1.19 (3H, d, J=6.0 Hz), 2.22 (1H, dd, J=4.0, 17.5 Hz), 2.37 (1H, br s), 2.78 (1H, dd, J=7.0, 17.5 Hz), 3.43—4.13 (2H, m), 4.22—4.60 (1H, m). Found: C, 55.26; H, 9.56%. Calcd for $C_{12}H_{24}O_4Si$: C, 55.34; H, 9.29%.

*3-O-t-Butyldimethylsilyl-2,6-dideoxy-*DL*-xylo-hexono-1,4-lactone (**8a**).* Mp 82—83.5 °C (cyclohexane). IR (CH_2Cl_2) 3580, 1785 cm^{-1}. ^1H NMR δ=0.12 (6H, s), 0.89 (9H, s), 1.25 (3H, d, J=6.2 Hz), 2.47 (1H, dd, J=3.3, 17.5 Hz), 2.65 (1H, br s), 2.77 (1H, dd, J=6.2, 17.5 Hz), 3.97—4.32 (2H, m), 4.42—4.69 (1H, m). Found: C, 55.24; H, 9.53%. Calcd for $C_{12}H_{24}O_4Si$: C, 55.34; H, 9.29%.

*3-O-t-Butyldimethylsilyl-2,6-dideoxy-*DL*-ribo-hexono-1,4-lactone (**7b**)*: Bp 150—160 °C (bath temp)/2 mmHg. IR (CH_2Cl_2) 3610, 1780 cm^{-1}. ^1H NMR δ=0.10 (6H, s), 0.76 (9H, s), 1.10 (3H, d, J=6.0 Hz), 2.18 (1H, dd, J=3.0, 17.5 Hz), 2.77 (1H, dd, J=6.5, 17.5 Hz), 2.80 (1H, br s), 3.57—4.13 (2H, m), 4.30—4.58 (1H, m). Found: C, 55.04; H, 9.51%. Calcd for $C_{12}H_{24}O_4Si$: C, 55.34; H, 9.29%.

*3-O-t-Butyldimethylsilyl-2,6-dideoxy-*DL*-arabino-hexono-1,4-lactone (**8b**)*: Mp 88.5—90.5 °C (cyclohexane). IR (CH_2Cl_2) 3610, 1780 cm^{-1}. ^1H NMR δ=0.13 (6H, s), 0.93 (9H, s), 1.35 (3H, d, J=6.0 Hz), 2.23 (1H, br d, J=4.5 Hz), 2.45 (1H, dd, J=3.0, 17.5 Hz), 2.75 (1H, dd, J=5.7, 17.5 Hz), 3.93—4.19 (2H, m), 4.57—4.80 (1H, m). Found: C, 55.04; H, 9.23%. Calcd for $C_{12}H_{24}O_4Si$: C, 55.34; H, 9.29%.

The authors are grateful to Professor Teruaki Mukaiyama for valuable discussion during this work.

References

1) a) P. A. Bartlett, "Olefin Cyclization Processes That Form Carbon-Heteroatom Bonds," in "Asymmetric Synthesis," ed by J. D. Morrison, Academic press, Inc., Orland (1984), Vol. 3, Chap. 6, pp. 417—425; b) P. A. Bartlett and J. Myerson, *J. Am. Chem. Soc.*, **100**, 3950 (1978); c) A. R. Chamberlin, M. Dezube, P. Dussault, and M. C. McMills, *ibid.*, **105**, 5819 (1983); d) Y. Tamaru, M. Mizutani, Y. Furukawa, S. Kawamura, Z. Yoshida, K. Yanagi, and M. Minobe, *ibid.*, **106**, 1079 (1984).

2) P. A. Bartlett, D. J. Tanzella, and J. F. Barstow, *Tetrahedron Lett.*, **23**, 619 (1982); N. J. Barnes, A. H. Davidson, L. R. Hughes, G. Procter, and V. Rajcoomar, *ibid.*, **22**, 1751 (1981); D. R. Williams, B. A. Barner, K. Nishitani, and J. G. Phillips, *J. Am. Chem. Soc.*, **104**, 4708 (1982).

3) By the treatment of **1a** with $HCOOH-H_2O_2$ at the elevated temperature, the lactone **2** was obtained in good yield: M. T. Dangyan and S. V. Arakelyan, *Nauch. Trudy Erevan. Gosudarst. Univ., Ser., Khim. Nauk*, **44**, 35 (1959); *Chem. Abstr.*, **53**, 21648i (1959).

4) During our investigation, it was reported that similar oxylactonization of an alkenamide proceeds by the acid catalyzed epoxidation ($CH_3COOH-H_2O_2$): M. Majewski and V. Snieckus, *J. Org. Chem.*, **49**, 2682 (1984).

5) The ^1H NMR and IR spectra are identical with those of the authentic sample: M. Murakami and T. Mukaiyama, *Chem. Lett.*, **1982**, 241.

6) K. N. Houk, S. R. Moses, Y.-D. Wu, N. G. Rondan, V. Jäger, R. Schohe, and F. R. Fronczek, *J. Am. Chem. Soc.*, **106**, 3880 (1984).

7) In the epoxidation of an olefinic amide, the interaction of the carbamoyl group with an peroxy acid by hydrogen bonding is probable from the following result. When ethyl 3-*t*-butyldimethylsilyloxy-4-pentenate was treated with MCPBA, almost equal amounts of both *threo* and *erythro* epoxides were obtained (*threo:erythro*=1.3:1). Furthermore, the formation of intermolecular hydrogen bonding between peroxy acids and amides has been reported: J. Škerjanc, A. Regent, and B. Plesničar, *J. Chem. Soc., Chem. Commun.*, **1980**, 1007.

8) D. Seebach and H. F. Leitz, *Angew. Chem., Int. Ed. Engl.*, **10**, 501 (1971).

9) S. K. Chaudhary and O. Hernandez, *Tetrahedron Lett.*, **1979**, 99.

10) D. J. Cram and N. L. Allinger, *J. Am. Chem. Soc.*, **78**, 2518 (1956).

 © 1985 The Chemical Society of Japan Bull. Chem. Soc. Jpn., 58, 3312—3319 (1985) [Vol. 58, No. 11

Diene-transmissive Diels-Alder Reaction Using 2-Ethoxy-3-methylene-1,4-pentadiene and 2-(2-Bromo-1-ethoxyethyl)-1,3-butadiene

Shuji KANEMASA, Hirohiko SAKOH, Eiji WADA, and Otohiko TSUGE*

Research Institute of Industrial Science, and Department of Molecular Science and Technology, Interdisciplinary Graduate School of Engineering Sciences, Kyushu University, Kasugakoen, Kasuga 816

(Received June 19, 1985)

A new cross-conjugated triene, 2-ethoxy-3-methylene-1,4-pentadiene, and a triene equivalent, 2-(2-bromo-1-ethoxyethyl)-1,3-butadiene, have been synthesized and their diene-transmissive Diels-Alder cycloadditions are investigated. The initial Diels-Alder reaction selectively occurs not across the diene part substituted with the alkoxyl moiety but the monosubstituted diene. Some cross types of diene-transmissive Diels-Alder reaction are demonstrated using the triene equivalent and two different dienophiles.

Recently, polyconjugated molecules of cross type called dendralene have received increasing attention in synthetic and theoretical field of chemistry.[1] Of special interest in organic synthesis is cross-conjugated triene because its reiterative Diels-Alder cycloadditions offer a useful process leading to substituted hydrocarbons of fused [6.6] ring systems.[2] We have reported a simple synthesis of bis(silyloxy) cross-conjugated trienes as functionalized dendralenes[3] and their multiple Diels-Alder reaction process termed diene-transmissive Diels-Alder reaction.[3,4] Stepwise sequence of this reaction using cross-conjugated triene equivalents is useful as a process for the cross type of reiterative Diels-Alder cycloaddition.[5]

The diene-transmissive Diels-Alder reaction starts with the first Diels-Alder cycloaddition across one of the two diene units of cross-conjugated triene and the second reaction is followed across the diene part which has been constructed in the first cycloaddition step. An attractive extension of this process is cross type of reaction in which two different dienophiles are used separatedly in each step.

We have planned to synthesize 2-ethoxy-3-methylene-1,4-pentadiene **1** from its precursor 2-(2-bromo-1-ethoxyethyl)-1,3-butadiene **2** with an aim of establishing a finely controlled diene-transmissive Diels-Alder reaction system of cross type.

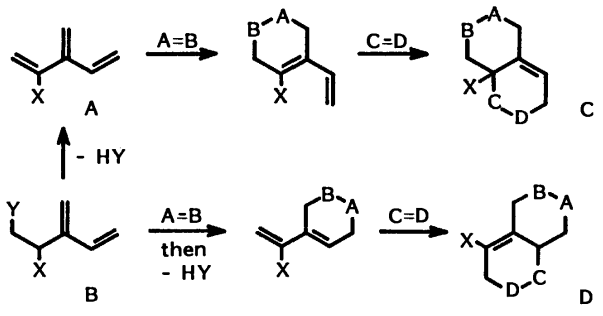

Scheme 1.

Scheme 1 shows a possible reaction mode of a cross-conjugated triene **A** with a diene-activating group X and its precursor **B**. As the diene-activating group X not only activates the diene as its carrier but also directs the regiochemistry of cycloaddition, it would be possible that the initial Diels-Alder reaction occurs across the diene part substituted with X under a regioselective control. The second cycloaddition with another dienophile, which is presumed also regioselective, gives a cross bis-cycloadduct **C**. On the other hand, the stepwise sequence of double cycloaddition of the precursor **B** using the same combination of dienophiles will lead to another bis-cycloadduct **D** which corresponds to an isomer of **C**.

Results and Discussion

The cross-conjugated triene **1** was synthesized in two steps starting from (1-methylene-2-propenyl)-magnesium chloride which is readily available from chloroprene. The cross-coupling reaction of (1-methylene-2-propenyl)magnesium chloride with 1-ethoxy-1,2-dibromoethane at 0 °C gave, after chromatography over silica gel and then distillation under vacuum, pure 2-(2-bromo-1-ethoxyethyl)-1,3-butadiene **2** in only 14% yield (Scheme 2). Although **2** was obtained in a better yield (40%, purity 68% (GLC)) in the same reaction using a catalyst Li_2CuCl_4[6] under milder conditions (−40 to −50 °C), the separation of **2** from one of the side products ended in failure.[7]

The dehydrobromination of **2** is a trouble-making

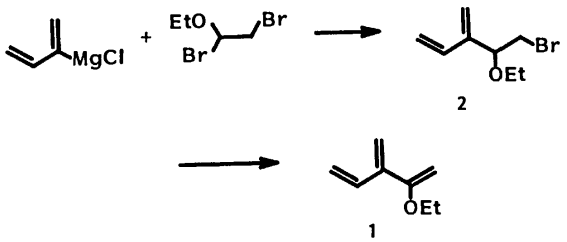

Scheme 2.

process. In order to avoid the polymerization of **1** as a labile product, **1** was separated from the reaction mixture by a vacuum distillation as soon as it was formed by the reaction of **2** with 1,8-diazabicyclo-[5.4.0]undec-7-ene (DBU) at 100—110 °C. Consequently, the cross-conjugated triene **1** isolated in 82% yield was contaminated with the unreacted **2** (18% (GLC)). As repeated distillation was found helpless, the triene of this purity (82%) was used for the following reactions.

A smooth cycloaddition took place between the triene **1** and *N*-methylmaleimide **3** under mild conditions (at room temperature for 24 h) to give 66% yield of a bis-cycloadduct **4** as the only isolated product, indicating that the initial Diels-Alder reaction was highly chemoselective. To our surprise, however, **4** was assigned as the bis-cycloadduct derived from the mono-cycloadduct **E** as shown in Scheme 3. Consequently the initial Diels-Alder reaction has favored the mono-substituted diene part which we assumed less reactive (See Scheme 1). As the stereostructure of **4** could not be determined only on the basis of the spectral data, the electronically and sterically most favorable approach in the second cycloaddition stage was taken into account.[8]

A similar reaction of **1** with dimethyl acetylenedicarboxylate **5** also produced the unexpected bis-cycloadduct **6** in 63% yield, which was readily dehydrogenated into tetramethyl 4-ethoxynaphthalene-1,2,6,7-tetracarboxylate **7** (81%) by the action of chloranil.

These unexpected diene reactivity is explained from a conformational point of view as shown in Fig. 1. There are two diene parts involved in the triene **1**, the monosubstituted "a" diene and the disubstituted "b" diene. The diene "b" can hardly occupy a planar s-cis conformation because of the steric hindrance between the two adjacent substituents (OEt and vinyl), while no such serious hindrance exists in the monosubstituted diene "a". Accordingly the initial Diels-Alder cycloaddition has occurred selectively across the diene "a".

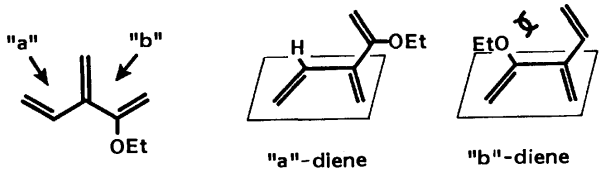

Fig. 1. s-cis Conformation for each diene part contained in the cross-conjugated triene **1**.

The use of two different dienophiles at each step of the above reaction, a cross type of cycloaddition, looks quite hard. Even though it is possible, a cross cycloadduct from this process can be obtained more easily by the stepwise sequence of double cycloaddition using the triene equivalent **2**. With this reason and because of the thermal instability of **1**, the stepwise cycloadditions of **2** were investigated.

The Diels-Alder cycloadditions of diene **2** with a variety of dienophiles **3**, **5**, **8**—**10** proceeded smoothly giving almost quantitative yields of cycloadducts **11**—**15** (Scheme 4). The results and reaction conditions are listed in Table 1. In the reactions with **3**, **8**, and **9**, each two diastereoisomeric cycloadducts were formed, but their ratios being slightly different (**11**, **12**: 1/2 and **14**: 1/1). The ratio of two regioisomeric cycloadducts of **15** was found to be 68/32 (para/meta) based on the GLC analysis, and about the same to that observed in the reaction of isoprene with **10** at 120 °C (para/meta=7/3).[9]

The diene functionality was revealed by dehydrobromination of the cycloadducts obtained above. Although **11** as an example resisted the dehydrobromination either when heated in benzene with triethylamine or refluxed in toluene with pyridine, successful dehydrobromination occurred by use of DBU. Thus, **12**, **14**, and **15** were converted into the corresponding dienes **16**, **18**, and **20**, respectively (Scheme 5 and Table 1). As these dienes are subject to the ready hydrolysis leading to enones, some of them were lost during the purification by column chromatography over silica gel.

The enones **17**, **19**, and **21** correspond to the Diels-Alder adducts of 2-acetyl-1,3-butadiene which can not be isolated because of its too easy dimerization.[10]

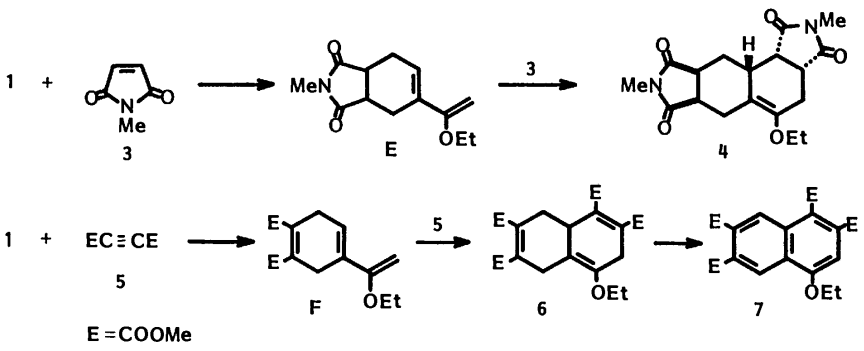

Scheme 3.

Accordingly, the diene **2** is a useful synthetic equivalent of 2-acetyl-1,3-butadiene.[11] An attempt of the second Diels-Alder reaction of the above dienes will be described later.

Dehydrobromination of the acetylene cycloadduct **13** with DBU gave no expected diene **F**, but instead the 4-(1-ethoxyethyl)- **22** and 4-vinylphthalate **23** in 95% of combined yield. The ready formation of **22**, presumably through a hydrogen migration of **F**, may have been driven by the aromatization on the six-membered ring. An attempt to trap the diene **F** with methyl propiolate **26** ended in failure, the same result being obtained.

The second Diels-Alder reactions were carried out using acetylenic dienophiles **5** and **26** (Scheme 6 and Table 1). The reaction of **16** with **5** gave a stereoselective cross bis-cycloadduct **24** along with its dehydrogenated derivative **25** in 78% of combined

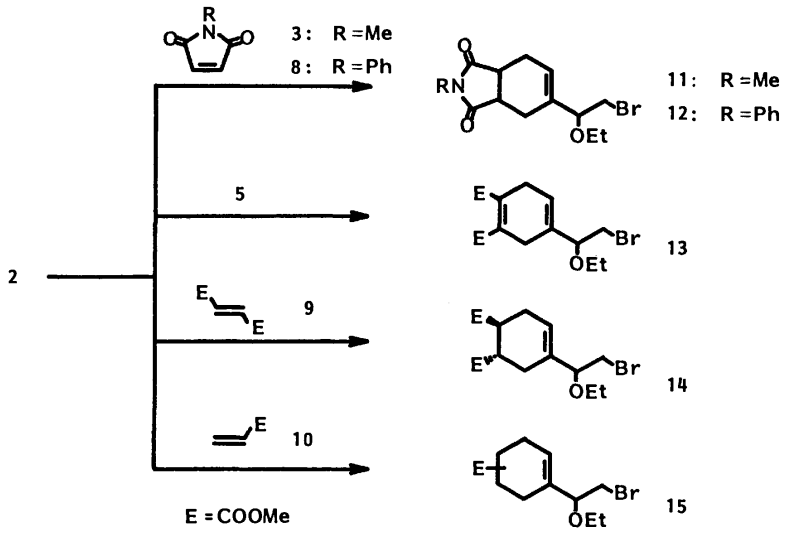

Scheme 4.

TABLE 1. STEPWISE SEQUENCE OF DIENE-TRANSMISSIVE DIELS-ALDER REACTIONS OF A CROSS-CONJUGATED TRIENE EQUIVALENT **2**

First cycloaddition		Reaction conditions			Product (yield/%)[a]
Diene	Dienophile	Solvent	Temperature	Time/h	
2	**3**	benzene	reflux	6	**11** (96)
2	**8**	benzene	reflux	6	**12** (98)
2	**5**	benzene	reflux	20	**13** (97)
2	**9**	benzene	reflux	24	**14** (96)
2	**10**	benzene	reflux	40	**15** (80)[b]
Diene formation		Reaction conditions			Product (yield/%)[a]
Bromide	DBU/Bromide	Solvent	Temperature	Time/h	
12	1.3	toluene	reflux	8	**16** (76), **17** (4)
14	1.5	toluene	reflux	20	**18** (59), **29** (20)
15	1.5	toluene	reflux	20	**20** (40), **21** (41)[c]
13	1.9	benzene	reflux	3	**22** (67), **23** (27)
Second cycloaddition		Reaction conditions			Product (yield/%)[a]
Diene	Dienophile	Solvent	Temp./°C	Time/h	
16	**5**	toluene	reflux	20	**24** (62), **25** (17)
16	**26**	toluene	110[d]	68	**27** (49)
18	**5**	toluene	reflux	6+15[e]	**29** (66)
20	**5**	toluene	reflux	6+15[e]	**30** (67)[c]

a) All isolated yields. b) Mixture of regioisomers (para : meta=68 : 32 (GLC)). c) Mixture of regioisomers (para : meta=2 : 1 (^{1}H-NMR)). d) Performed in a sealed tube. e) The latter is the reaction time after chloranil is added.

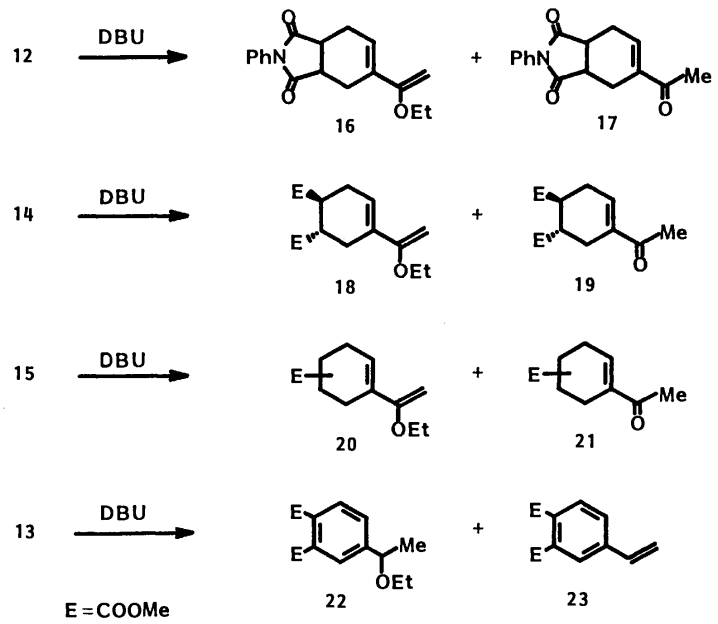

Scheme 5.

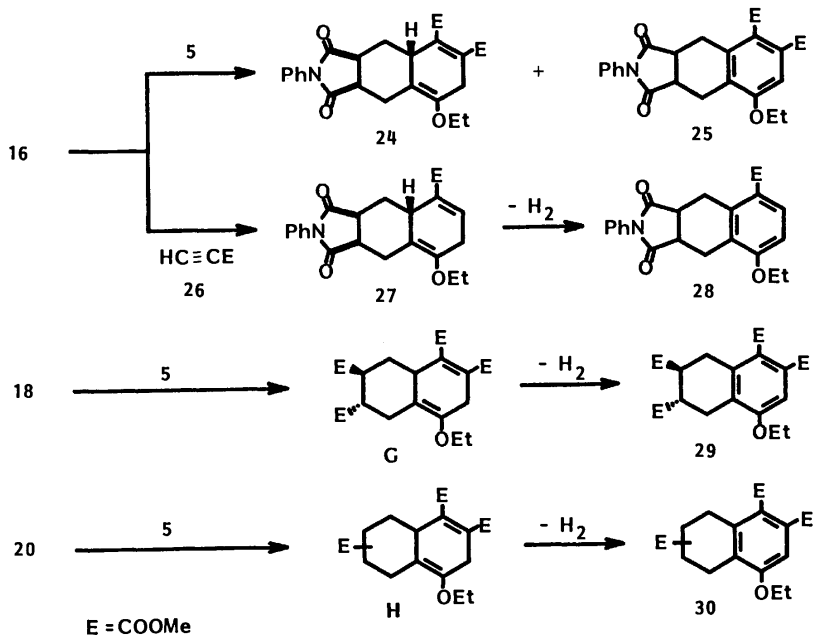

Scheme 6.

yield. As anticipated, an unsymmetrical acetylene **26** cycloadded to **16** under high regioselection, the stereo- and regioselective cross bis-cycloadduct **27** being isolated as the single product. The structures of **24** and **27** were hardly determined only on the basis of the spectral data, therefore based on the steric consideration in the approaches. These cycloadducts **24** and **27** were easily dehydrogenated with chloranil into the aromatic derivatives **25** and **28**, respectively, in high yields. A one-pot procedure for the second cycloaddition and dehydrogenation could be performed between **18** and **5** (similarly **20** and **5**) under the conditions shown in Table 1. This procedure gave the tetrahydronaphthalene derivatives **29** and **30** in good yields.

The both procedures of the diene formation by dehydrobromination and the second cycloaddition could be achieved in the same flask. First, the maleimide cycloadduct **11** or **12** was allowed to react with DBU under reflux in toluene and the excess or unreacted DBU was completely consumed by the action with methyl iodide (Scheme 7). Then, the diene **E** or **16** formed in solution was subjected to the second cycloaddition with **8** or **3**. Thus, a

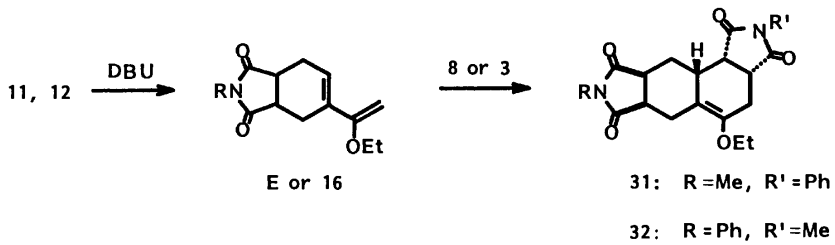

Scheme 7.

stereoselective cross bis-cycloadduct **31** (56%) or **32** (65%) was isolated through a column chromatography of the crude mixture.

Experimental

General and Materials. Melting points were measured on a Yanagimoto micro melting point apparatus and uncorrected. IR spectra were recorded on a JASCO A-702 and JEOL JIR-100 FT-IR spectrometers. ^{1}H-NMR spectra were taken at either 90 MHz (Hitachi R-40) or 100 MHz (JEOL FX-100), and ^{13}C-NMR at 25.05 MHz (JEOL FX-100). ^{1}H- and ^{13}C-NMR chemical shifts are recorded in δ values (ppm) relative to internal Me_4Si. Mass spectra were measured with a JEOL JMS-01SG-2 spectrometer at 75 eV of ionization energy. Elementary analyses were performed on a Hitachi 026 CHN micro analyzer. Analytical gas-liquid chromatography (GLC) was accomplished on a Yanaco G-2800 gas chromatograph equipped with a flame ionization detector (column: SE-30, 3.5×300 mm). Wakogel C300 and Florisil (100—200 mesh) were used for preparative column chromatography. Thin-layer chromatography (TLC) was accomplished on 0.2 mm precoated plates of silica gel 60 F-254 (Merck) and of aluminum oxide 60 F-254 type-E (Merck). Visualization was with ultraviolet light (254 and 365 nm) and iodine. Micro vacuum distillation was carried out with a Sibata GTO-250R Kugelrohr distilling apparatus. Solvents were evaporated with a Tokyo Rikakikai rotary evaporator type V.

Tetrahydrofuran (THF), benzene, and toluene were distilled over sodium wire immediately prior to their use. 1-Ethoxy-1,2-dibromoethane was prepared by the bromination of ethyl vinyl ether.[12] Methyl propiolate **26** was obtained by the esterification of commercial propiolic acid in the presence of *p*-toluenesulfonic acid.[13] Li_2CuCl_4 was prepared by mixing LiCl and $CuCl_2$ in 2:1 ratio.

2-(2-Bromo-1-ethoxyethyl)-1,3-butadiene **2** *and 2-Ethoxy-3-methylene-1,4-pentadiene* **1**. To a 0.1 M solution of (1-methylene-2-propenyl)magnesium chloride (20 ml, 20 mmol) was added dropwise a solution of 1-ethoxy-1,2-dibromoethane (2.7 ml, 20 mmol) in dry THF (20 ml) at 0 °C. The mixture was stirred at 0 °C for 6 h under nitrogen and then treated with water. Products were extracted in ether, the ether washed with 5% sodium hydrogencarbonate solution and with brine, dried over $MgSO_4$, and finally evaporated *in vacuo*. The residue was chromatographed over silica gel. An elution with hexane–benzene (2:1) gave 1.66 g (40%, purity 52% by GLC) of **2** which was purified by a vacuum distillation on Kugelrohr to afford pure **2** (0.58 g, 14%).

This compound **2** was also available by the following procedure: To a mixture of 1-ethoxy-1,2-dibromoethane (1.4 ml, 10 mmol) and Li_2CuCl_4 (220 mg, 1 mmol) in dry THF (10 ml) was added slowly a 0.1 M solution of (1-methylene-2-propenyl)magnesium chloride in THF (12 ml, 12 mmol) at −40 to −50 °C. The mixture was stirred at the same temperature for 4 h and treated with water. The same work up described above and a vacuum distillation gave 0.81 g of **2** (40%, purity 68% by GLC).

2: Colorless liquid; bp 80 °C (267 Pa) (bulb-to-bulb); IR (neat) 1580, 1120, and 1100 cm^{-1}; ^{1}H-NMR ($CDCl_3$) δ=1.20 (3H, t, $C\underline{H}_3CH_2$), 3.22—3.66 (4H, m, CH_2Br and $C\underline{H}_2Me$), 4.21 (1H, dd, J=4.3 and 7.8 Hz, $C\underline{H}OEt$), 5.10 (1H, d, J_{4-3}=11.0 Hz, one of 4-H), 5.26, 5.28 (each 1H, s, 1-H), 5.35 (1H, d, J_{4-3}=18.0 Hz, the other of 4-H), 6.32 (1H, dd, J_{3-4}=11.0 and 18.0 Hz, 3-H); ^{13}C-NMR ($CDCl_3$) δ=15.21 (q, Me), 35.21 (t), 64.82 (t), 79.79 (d, $\underline{C}HOEt$), 114.66, 117.24 (each t, 1- and 4-C), 135.56 (d, 3-C), and 143.66 (s, 2-C); MS *m/z* 206 and 204 (M^+).

Found: *m/z* 204.0125. Calcd for $C_8H_{13}OBr$: M, 204.0150.

A mixture of **2** (266 mg, 1.3 mmol) and DBU (395 mg, 2.6 mmol) was heated in a micro distilling flask at 100—110 °C under a reduced pressure (2666 Pa) while being distilled. The distillate collected in 30 min was purified by distillation on Kugelrohr to give **1** (132 mg, 82%, purity 82% by GLC).

1: Colorless liquid; GC/FT-IR (gas) 1585 and 980 cm^{-1}; ^{1}H-NMR ($CDCl_3$) δ=1.33, 3.78 (5H, $OC\underline{H}_2C\underline{H}_3$), 4.14, 4.26 (each 1H, d, J_{gem}=2.0 Hz, 1-H), 5.14 (1H, dd, J_{5-4}=10.5 and J_{gem}=2.0 Hz, one of 5-H), 5.22, 5.43 (each 1H, d, J_{gem}=2.0 Hz, 3-CH_2=), 5.43 (1H, dd, J_{5-4}=17.5 and J_{gem}=2.0 Hz, the other of 5-H), and 6.40 (1H, dd, J_{4-5}=17.5 and 10.5 Hz, 4-H); ^{13}C-NMR ($CDCl_3$) δ=14.47 (q, Me), 62.96 (t), 84.74 (t, 1-C), 114.47, 116.42 (each t, 5-C and 3-CH_2=), 135.56 (d, 4-C), 143.31 (s, 3-C), and 159.35 (s, 2-C); GC-MS *m/z* 124 (M^+).

Found: *m/z* 124.0872. Calcd for $C_8H_{12}O$: M, 124.0888.

Reaction of **1** *with* **3** *Leading to* **4**. A mixture of **1** (108 mg, purity 84%, 0.73 mmol) and **3** (193 mg, 1.74 mmol) in dry benzene (3 ml) was stirred at room temperature for 2 h. The residue which was obtained by evaporation of the solvent was chromatographed over silica gel using hexane–ethyl acetate (1:3) as an eluent to give 167 mg (66%) of **4**: Colorless solid; mp 113—116 °C; IR (KBr) 1770 and 1700 cm^{-1} (CO); ^{1}H-NMR ($CDCl_3$) δ=1.12 (3H, t, $CH_2C\underline{H}_3$), 1.84—3.32 (11H, m, 3×CH_2 and 5×CH), 2.88, 2.92 (each 3H, s, NMe), and 3.63 (2H, q, $C\underline{H}_2Me$); ^{13}C-NMR ($CDCl_3$) δ=15.01 (q, Me), 21.00, 23.54 (each t), 24.85 (d),

† 1 M=1 mol dm^{-3}.

25.68 (t), 32.75, 39.03, 40.15, 43.22 (each d), 64.76 (t), 113.25, 147.80 (each s), 177.47, 179.03, 179.77, and 180.11 (each s, CON); MS *m/z* 346 (M^+).

Found: *m/z* 346.1562. Calcd for $C_{18}H_{22}O_5N_2$: M, 346.1527.

Reaction of 1 with 5 Leading to 6 and Its Dehydrogenation into 7. A solution of **1** (103 mg, purity 82%, 0.68 mmol) and **5** (236 mg, 1.7 mmol) in dry benzene (2 ml) was refluxed for 6 h. The solvent was removed off *in vacuo* and the residue was chromatographed over silica gel. An elution with hexane-ethyl acetate (1:1) gave 176 mg (63%) of **6**: Colorless viscous liquid; IR (neat) 1725 cm^{-1} (CO); ^{1}H-NMR ($CDCl_3$) δ=1.26 (3H, t, $CH_2C\underline{H}_3$) 2.00—2.40 (1H, m), 2.60—3.98 (8H, m), 3.73, 3.86, and 3.90 (12H, s, COOMe); ^{13}C-NMR ($CDCl_3$) δ=15.40 (q, Me), 26.80, 27.24, 32.89 (each t), 36.60 (d), 52.29, 52.39 (each q, each 2×C, COO<u>Me</u>), 63.89 (t), 109.16, 129.28, 133.23, 134.98, 137.03, 142.58 (each s), 166.71, 167.77 (each s, <u>C</u>OOMe), and 168.07 (s, 2×C, <u>C</u>OOMe); MS *m/z* 408 (M^+).

Found: *m/z* 408.1373. Calcd for $C_{20}H_{24}O_9$: M, 408.1419.

A mixture of **6** (276 mg, 0.68 mmol) and chloranil (665 mg, 2.7 mmol) in toluene (6 ml) was refluxed for 72 h. Evaporation of the solvent and the chromatography over silica gel (hexane-ethyl acetate 1:1) gave 222 mg (81%) of **7**: Colorless prisms from hexane-ethyl acetate; mp 157—158 °C; IR (KBr) 1720 cm^{-1} (CO) ^{1}H-NMR ($CDCl_3$) δ=1.56, 4.26 ($OC\underline{H}_2C\underline{H}_3$), 3.92 (9H, s, COOMe), 4.01 (3H, s, COOMe), 7.28 (1H, s, 3-H), 8.14 (1H, s, 5-H), and 8.64 (1H, s, 8-H); ^{13}C-NMR ($CDCl_3$) δ=14.53 (q, Me), 52.95 (q, 4×C, COO<u>Me</u>), 64.89 (t), 105.83, 124.89 (each d), 126.60, 127.19 (each s), 127.83 (d), 129.66, 129.89, 131.01, 156.25 (each s), 166.37, 168.72 (each s, <u>C</u>OOMe), and 167.83 (s, 2×C, <u>C</u>OOMe); MS *m/z* 404 (M^+).

Found: C, 59.25; H, 4.97%. Calcd for $C_{20}H_{20}O_9$: C, 59.41; H, 4.99%.

Cycloadditions of 2 to Dienophiles 3, 5, and 8—10. General procedure is as follows: A mixture of **2** and dienophiles (1.2—2 equivalents) in dry benzene (2—3 ml per 1 mmol of **2**) was refluxed for the time shown in Table 1. The solvent was evaporated *in vacuo* and the residue was chromatographed over silica gel. The yields of cycloadducts are given in Table 1.

11: The reaction between **2** (308 mg, purity 85%, 1.28 mmol) and **3** (167 mg, 1.50 mmol) was followed by the chromatography with hexane-ethyl acetate (1:1) to give 389 mg (96%) of **11** in 2:1 ratio of diastereomers whose separation failed: Colorless viscous liquid; IR (neat) 1775 and 1710 cm^{-1} (CO); ^{1}H-NMR ($CDCl_3$) δ=1.12 (3H, t, $CH_2C\underline{H}_3$), 1.90—3.48 (10H, m), 2.88 (3H, s, NMe), 3.78 (1H, t, J=6.0 Hz, C<u>H</u>OEt), and 5.86 (1H, m, 6-H); ^{13}C-NMR ($CDCl_3$) the major: δ=14.91 (q, Me), 22.54, 23.66 (each t), 24.89 (q, NMe), 32.11 (t), 38.92, 39.22 (each d), 64.23 (t), 81.96 (d, <u>C</u>HOEt), 126.46 (d, 6-C), 136.68 (s, 5-C), and 179.42 (s, 2×C, CON); the minor: δ=14.68 (q, Me), 23.48 (t), 24.66 (q, NMe), 32.76 (t), 81.08 (d, <u>C</u>HOEt), 125.81 (d, 6-C), and 179.12 (s, CON); MS *m/z* 222 (M^+-CH_2Br).

Found: C, 49.36; H, 5.73; N, 4.43%. Calcd for $C_{13}H_{18}O_3NBr$: C, 49.38; H, 5.74; N, 4.43%.

12: The reaction between **2** (512 mg, purity 74%, 1.85 mmol) and **8** (539 mg, 3.11 mmol) and the followed chromatography using hexane-ethyl acetate (2:1) gave 685 mg (98%) of **12** as a mixture of two diastereomers in a ratio of 2:1, which could not be separated: Colorless viscous liquid; IR (neat) 1780 and 1720 cm^{-1} (CO); ^{1}H-NMR ($CDCl_3$) δ=1.07, 1.17 (3H, each t, $CH_2C\underline{H}_3$), 2.00—2.96 (4H, m), 3.08—3.52 (6H, m), 3.85 (1H, t, J=6.5 Hz, C<u>H</u>OEt), 5.98 (1H, m, 6-H), and 7.08—7.60 (5H, m, Ph); ^{13}C-NMR ($CDCl_3$) the major: δ=15.15 (q, Me), 23.20, 24.02, 33.04 (each t), 39.03, 39.42 (each d), 64.71 (t), 82.21 (d, <u>C</u>HOEt), 125.97 (d, 6-C), 126.16, 128.35, 128.89 (each d), 131.96 (s), 137.32 (s, 5-C), 178.60, and 178.74 (each s, CON); the minor: δ=14.86 (q, Me), 22.95, 23.88 (each t), 81.62 (d, <u>C</u>HOEt), 137.17 (s, 5-C), and 178.35 (s, CON); MS *m/z* 379 and 377 (M^+).

Found: C, 57.06; H, 5.27; N, 3.89%. Calcd for $C_{18}H_{20}O_3NBr$: C, 57.16; H, 5.33; N, 3.70%.

13: The reaction of **2** (557 mg, purity 68%, 1.85 mmol) with **5** (493 mg, 3.47 mmol) was followed by the chromatography using hexane-ethyl acetate (4:1) to afford **13** (619 mg, 97%): Colorless viscous liquid; IR (neat) 1725 cm^{-1} (CO); ^{1}H-NMR ($CDCl_3$) δ=1.20 (3H, t, $CH_2C\underline{H}_3$), 2.80—3.60 (8H, m), 3.76 (6H, s, COOMe), 3.91 (1H, t, J=6.5 Hz, C<u>H</u>OEt), and 5.76 (1H, m, 5-H); ^{13}C-NMR ($CDCl_3$) δ=15.15 (q, Me), 25.78, 28.26, 32.84 (each t), 52.24 (q, 2×C, COO<u>Me</u>), 64.66 (t), 82.55 (d, <u>C</u>HOEt), 122.17 (d, 5-C), 131.28, 131.86, 132.55 (each s), 167.92, and 168.12 (each s, <u>C</u>OOMe); MS *m/z* 315 (M^+-OMe).

Found: C, 48.19; H, 5.42%. Calcd for $C_{14}H_{19}O_5Br$: C, 48.43; H, 5.52%.

14: The reaction between **2** (327 mg, purity 74%, 1.18 mmol) and **9** (286 mg, 1.98 mmol) were followed by the chromatography with hexane-ethyl acetate (4:1) to give **14** (395 mg, 96%) as a 1:1 mixture of diastereomers: Colorless liquid; IR (neat) 1740 cm^{-1} (CO); ^{1}H-NMR ($CDCl_3$) δ=1.20 (3H, t, $CH_2C\underline{H}_3$), 1.90—2.50, 2.70—3.00 (6H, m), 3.69 (6H, s, COOMe), 3.84 (1H, t, J=6.5 Hz, C<u>H</u>OEt), and 5.74 (1H, m, 2-H); ^{13}C-NMR ($CDCl_3$) δ=15.21 (q, Me), 25.42, 25.77, 27.30, 27.65, 32.94, 33.41 (each t), 40.92, 41.21 (each d), 51.96 (q, 2×C, COO<u>Me</u>), 64.46, 64.58 (each t), 82.84 (d, <u>C</u>HOEt), 124.52, 124.99 (each d, 2-C), 133.39, 133.63 (each s, 1-C), 174.72, and 174.84 (each s, <u>C</u>OOMe); MS *m/z* 319 and 317 (M^+-OMe).

Found: C, 48.01; H, 6.07%. Calcd for $C_{14}H_{21}O_5Br$: C, 48.25; H, 6.06%.

15: The reaction of **2** (284 mg, 1.4 mmol) with **10** (0.25 ml, 2.8 mmol) and the followed chromatography with hexane-ethyl acetate (9:1) gave 322 mg (80%) of **15** as a mixture of two regioisomers in a ratio of 68:32 (GLC) whose separation was unsuccessful: Colorless liquid; IR (neat) 1735 cm^{-1} (CO); ^{1}H-NMR ($CDCl_3$) δ=1.19, 1.20 (3H, each t, $CH_2C\underline{H}_3$), 1.48—2.76 (7H, m), 3.20—3.60 (4H, m), 3.67 (3H, s, COOMe), 3.82 (1H, t, J=6.5 Hz, C<u>H</u>OEt), and 5.73 (1H, m, 2-H); ^{13}C-NMR ($CDCl_3$) including four sets of signals: δ=14.91 (q, Me), 21.78, 22.25, 23.66, 24.07, 24.60, 24.78, 25.36, 27.01, 27.12, 33.17, 33.64 (each t), 38.51, 38.63, 38.98 (each d), 51.31 (q, COO<u>Me</u>), 63.88, 64.05 (each t), 83.02 (d, <u>C</u>HOEt), 124.58, 125.23, 126.05, 126.35 (each d), 133.16, 133.45, 134.50, 134.68 (each s), 175.19, and 175.36 (each s, <u>C</u>OOMe); MS *m/z* 261 and 259 (M^+-OMe).

Found: C, 49.27; H, 6.56%. Calcd for $C_{12}H_{19}O_3Br$: C, 49.50; H, 6.58%.

Dehydrobromination of 12 Leading to 16 and 17. A solution of **12** (413 mg, 1.09 mmol) and DBU (216 mg, 1.42 mmol) in dry toluene (5 ml) was refluxed for 8 h. The

mixture was chromatographed over Florisil with hexane–ethyl acetate (2:1) giving 248 mg (76%) of **16**. Further elution with hexane–ethyl acetate (1:2) afforded **17** (11 mg, 4%).

16: Colorless solid; mp 66—69 °C; IR (KBr) 1780 and 1710 cm^{-1} (CO); ^{1}H-NMR (C_6D_6) δ=1.13, 3.42 (OCH_2CH_3), 1.66—2.08 (2H, m), 2.40—2.80 (3H, m), 2.92 (1H, dd, J_{gem}=15.0 and J_{vic}=2.5 Hz), 3.97, 4.37 (each 1H, d, J_{gem}=2.5 Hz, $=CH_2$), 6.38 (1H, m, 6-H), and 6.90—7.36 (5H, m, Ph); MS *m/z* 297 (M^+).

Found: C, 72.66; H, 6.49; N, 4.88%. Calcd for $C_{18}H_{19}O_3N$: C, 72.71; H, 6.44; N, 4.71%.

17: Colorless leaflets from dichloromethane–hexane; mp 114—115 °C; IR (KBr) 1770, 1700, and 1665 cm^{-1} (CO); ^{1}H-NMR ($CDCl_3$) δ=2.30 (3H, s, MeCO), 2.32—3.40 (6H, m), 7.02 (1H, ddd, *J*=2.0, 4.0, and 6.5 Hz, 6-H), and 7.10—7.74 (5H, m, Ph); MS *m/z* 269 (M^+).

Found: C, 71.26; H, 5.66; N, 5.38%. Calcd for $C_{16}H_{15}O_3N$: C, 71.36; H, 5.61; N, 5.20%.

*Dehydrobromination of **14** Leading to **18** and **19**.* A mixture of **14** (253 mg, 0.72 mmol) and DBU (165 mg, 1.08 mmol) in dry toluene (3 ml) was refluxed for 20 h and the solvent was removed *in vacuo*. The residue was chromatographed over Florisil with hexane–ethyl acetate (9:1) to give 115 mg (59%) of **18** as unstable material. Further elution with hexane–ethyl acetate (1:1) afforded 34 mg (20%) of **19**.

18: Colorless liquid; ^{1}H-NMR (C_6D_6) δ=1.13, 3.52 (OCH_2CH_3), 2.10—3.02 (6H, m), 3.38, 3.40 (each 3H, s, COOMe), 3.92, 4.10 (each 1H, d, J_{gem}=2.5 Hz, $=CH_2$), and 6.07 (1H, m, 2-H); ^{13}C-NMR (C_6D_6) δ= 14.57 (q, Me), 28.17, 28.36 (each t), 41.32, 41.96 (each d), 51.51 (q, 2×C, COOMe), 62.81 (t), 122.41 (d, 2-C), 130.84 (s, 1-C), 159.59 (s), and 174.70 (s, 2×C, COOMe).

19: Colorless liquid; IR (neat) 1740 and 1670 cm^{-1} (CO); ^{1}H-NMR ($CDCl_3$) δ=2.29 (3H, s, MeCO), 2.10—3.00 (6H, m), 3.67, 3.68 (each 3H, s, COOMe), and 6.84 (1H, m, 2-H); MS *m/z* 240 (M^+) and 43.

Found: C, 59.97; H, 6.76%. Calcd for $C_{12}H_{16}O_5$: C, 59.99; H, 6.71%.

*Dehydrobromination of **15** Leading to **20** and **21**.* A solution of **15** (228 mg, 0.78 mmol) and DBU (179 mg, 1.18 mmol) in dry toluene (3 ml) was refluxed for 20 h. The residue obtained by the evaporation of solvent was chromatographed over Florisil with hexane–ethyl acetate (9:1) gave 66 mg (40%) of unstable diene **20**. Further elution with hexane–ethyl acetate (2:1) afforded **21** (59 mg, 40%).

20: Colorless liquid as a mixture of two regioisomers (2:1); ^{1}H-NMR (C_6D_6) δ=1.10, 3.50 (OCH_2CH_3), 1.40—2.60 (7H, m), 3.30, 3.34 (3H, each s, COOMe), 3.94 (1H, d, J_{gem}=2.0 Hz, $=CH_2$), 4.17, 4.23 (1H, each d, J_{gem}=2.0 Hz, $=CH_2$), and 6.43 (1H, m, 2-H).

21: Colorless liquid as a 2:1 mixture of regioisomers; IR (neat) 1735 and 1685 cm^{-1} (CO); ^{1}H-NMR ($CDCl_3$) δ=1.50—2.68 (7H, m), 2.28 (3H, s, MeCO), 3.68, and 3.69 (3H, each s, COOMe); MS *m/z* 182 (M^+).

Found: *m/z* 182.0994. Calcd for $C_{10}H_{14}O_3$: M, 182.0942.

*Dehydrobromination of **13** Leading to **22** and **23**.* A mixture of **13** (236 mg, 0.68 mmol) and DBU (193 mg, 1.27 mmol) in dry toluene (4 ml) was refluxed for 3 h and the solvent was evaporated *in vacuo*. The residue was chromatographed over silica gel using hexane–ethyl acetate (3:1) to give **23** (41 mg, 27%) and then **22** (122 mg, 67%).

22: Colorless viscous liquid; IR (neat) 1725 cm^{-1} (CO); ^{1}H-NMR ($CDCl_3$) δ=1.19, 3.36 (OCH_2CH_3), 1.42 (3H, d, *J*=6.5 Hz, Me), 3.87, 3.89 (each 3H, s, COOMe), 4.46 (1H, q, *J*=6.5 Hz, CH(Me)OEt), 7.48 (1H, dd, *J*=1.5 and 8.0 Hz, 5-H), 7.63 (1H, d, *J*=1.5 Hz, 3-H), and 7.72 (1H, d, *J*=8.0 Hz, 6-H); ^{13}C-NMR ($CDCl_3$) δ=15.03, 23.66 (each q, Me), 52.19 (q, 2×C, COOMe), 63.99 (t), 76.62 (d, CH(Me)OEt), 126.11, 128.16, 128.98 (each d), 130.22, 132.22 (each s), 148.01 (s, 4-C), 167.32, and 167.79 (each s, COOMe); MS *m/z* 266 (M^+) and 251 (M^+—Me, base peak).

Found: C, 63.08; H, 6.69%. Calcd for $C_{14}H_{18}O_5$: C, 63.15; H, 6.81%.

23: Colorless liquid; IR (neat) 1725 cm^{-1}; ^{1}H-NMR ($CDCl_3$) δ=3.88, 3.89 (each 3H, s, COOMe), 5.39 (1H, dd, J_{gem}=0.5 and J_{vic}=11.0 Hz, one of $=CH_2$), 5.84 (1H, dd, J_{gem}=0.5 and J_{vic}=17.5 Hz, the other of $=CH_2$), 6.71 (1H, dd, *J*=11.0 and 17.5 Hz, CH=), 7.49 (1H, dd, *J*=2.0 and 8.0 Hz, 5-H), 7.66 (1H, d, *J*=2.0 Hz, 3-H), and 7.70 (1H, d, *J*=8.0 Hz, 6-H); MS *m/z* 220 (M^+) and 189 (M^+—OMe, base peak).

*Cycloaddition of **16** to **5** Leading to **24** and **25**.* A mixture of **16** (248 mg, 0.83 mmol) and **5** (237 mg, 1.67 mmol) in toluene (4 ml) was refluxed for 20 h and the solvent was evaporated *in vacuo*. The residue was chromatographed over silica gel with hexane–ethyl acetate (1:1) gave 227 mg (62%) of **24** and then 63 mg (17%) of **25**. A mixture of **24** (68 mg, 0.15 mmol) and chloranil (42 mg, 0.17 mmol) in toluene (3 ml) was refluxed for 36 h. Column chromatography of the crude mixture over silica gel (hexane–ethyl acetate (1:1)) afforded 53 mg (78%) of **25**.

24: Colorless solid; mp 85—87 °C; IR (KBr) 1775 and 1720 cm^{-1} (CO); ^{1}H-NMR ($CDCl_3$) δ=1.25 (3H, t, CH_2CH_3), 1.40—2.10 (2H, m), 2.50—3.92 (9H, m), 3.73, 3.79 (each 3H, s, COOMe), and 7.10—7.56 (5H, m, Ph); ^{13}C-NMR ($CDCl_3$) δ=15.30 (q, Me), 25.78, 27.34, 29.04 (each t), 37.33, 40.20, 40.30 (each d), 52.34 (q, 2×C, COOMe), 64.03 (t), 110.81 (s), 126.16 (d, 2×C), 128.35 (d), 129.04 (d, 2×C), 129.13, 131.86, 137.86, 143.12 (each s), 166.60, 167.77 (each s, COOMe), 177.04, and 177.91 (each s, CON); MS *m/z* 439 (M^+).

Found: C, 65.47; H, 5.80; N, 3.56%. Calcd for $C_{24}H_{25}O_7N$: C, 65.59; H, 5.73; N, 3.19%.

25: Colorless prisms from ethanol; mp 159—160 °C; IR (KBr) 1775 and 1720 cm^{-1} (CO); ^{1}H-NMR ($CDCl_3$) δ=1.42, 4.05 (OCH_2CH_3), 2.60—3.80 (6H, m), 3.84, 3.90 (each 3H, s, COOMe), 6.90—7.08, and 7.14—7.48 (each 3H, m, Ph and Ar); MS *m/z* 437 (M^+).

Found: C, 65.71; H, 5.37; N, 3.23%. Calcd for $C_{24}H_{23}O_7N$: C, 65.90; H, 5.30; N, 3.20%.

*Cycloaddition of **16** to **26** Leading to **27** and Dehydrogenation of **27** into **28**.* A solution of **16** (180 mg, 0.61 mmol) and **26** (255 mg, 3.03mmol) in dry toluene (6 ml) was heated in a sealed glass tube at 110 °C for 68 h. The solvent was evaporated *in vacuo* and the residue was chromatographed over silica gel using hexane–ethyl acetate (1:1) to give 113 mg (49%) of **27**. This product **27** (43 mg, 0.11 mmol) and chloranil (42 mg, 0.17 mmol) were refluxed in toluene (2 ml) for 48 h and the crude mixture was chromatographed, after evaporation of the solvent, over silica gel with hexane–ethyl acetate (1:1) to afford 33 mg (77%) of **28**.

27: Colorless prisms from ether; mp 140—141 °C; IR (KBr) 1775 and 1710 cm^{-1} (CO); ^{1}H-NMR ($CDCl_3$) δ=1.24

(3H, t, $CH_2C\underline{H}_3$), 1.20—1.60 (1H, m), 1.70—2.04 (1H, m), 2.72—3.90 (9H, m), 3.72 (3H, s, COOMe), 6.87 (1H, t, J=3.0 Hz, =CH), and 7.16—7.56 (5H, m, Ph); ^{13}C-NMR ($CDCl_3$) δ=15.15 (q, Me), 26.42, 27.01, 30.41 (each t), 35.05, 40.28, 40.57 (each d), 51.49 (q, COO<u>Me</u>), 63.58 (t), 112.72 (s), 125.99 (d, 2×C), 128.05 (d), 128.75 (d, 2×C), 130.63, 131.86 (each s), 135.21 (d), 142.72 (s), 166.09 (s, <u>C</u>OOMe), 177.07, and 178.07 (each s, CON); MS m/z 381 (M^+).

Found: C, 69.28; H, 6.08; N, 3.67%. Calcd for $C_{22}H_{23}O_5N$: C, 69.12; H, 6.04; N, 3.62%.

28: Colorless prisms from ethanol; mp 200—202 °C; IR (KBr) 1775 and 1705 cm^{-1} (CO); ^{1}H-NMR ($CDCl_3$) δ=1.42, 4.05 ($OC\underline{H}_2C\underline{H}_3$), 2.60—3.74 (6H, m), 3.84 (3H, s, COOMe), 6.74 (1H, d, J=9.0 Hz, 6-H), 6.84—7.00 (2H, m), 7.24—7.50 (3H, m), and 7.80 (1H, d, J=9.0 Hz, 7-H); MS m/z 379 (M^+).

Found: C, 69.44; H, 5.67; N, 3.66%. Calcd for $C_{22}H_{21}O_5N$: C, 69.65; H, 5.58; N, 3.69%.

*Cycloaddition of **18** to **5** and Subsequent Dehydrogenation Leading to **29**.* A solution of **18** (97 mg, 0.36 mmol) and **5** (77 mg, 0.54 mmol) in dry toluene (2 ml) was refluxed for 6 h. Chloranil (133 mg, 0.54 mmol) was added and the resulting mixture was further refluxed for 15 h. Column chromatography of the crude product over silica gel with hexane–ethyl acetate (2:1) gave 97 mg (66%) of **29**: Colorless needles from ethanol; mp 128—129 °C; IR (KBr) 1725 cm^{-1} (CO); ^{1}H-NMR ($CDCl_3$) δ=1.43, 4.08 ($OC\underline{H}_2C\underline{H}_3$), 2.40—3.40 (6H, m), 3.70, 3.72, 3.84, 3.87 (each 3H, s, COOMe), and 7.22 (1H, s, 3-H); MS m/z 408 (M^+).

Found: C, 59.03; H, 6.00%. Calcd for $C_{20}H_{24}O_9$: C, 58.82; H, 5.92%.

*Cycloaddition of **20** to **5** and Subsequent Dehydrogenation Leading to **30**.* A mixture of **20** (43 mg, 0.2 mmol) and **5** (44 mg, 0.31 mmol) in toluene (1.5 ml) was first refluxed for 6 h and further 15 h after chloranil (75 mg, 0.31 mmol) was added. The crude product was chromatographed over silica gel with hexane–ethyl acetate (3:1) to give **30** (48 mg, 67%) as a 2:1 mixture of regioisomers: Colorless solid; mp 117—123 °C; IR (KBr) 1725 cm^{-1} (CO); ^{1}H-NMR ($CDCl_3$) δ=1.43, 4.07 ($OC\underline{H}_2C\underline{H}_3$), 1.60—3.20 (7H, m), 3.69, 3.72, 3.84, 3.88, 3.89 (9H, each s, COOMe for the major and minor regioisomers), and 7.21 (1H, s, 3-H); MS m/z 350 (M^+).

Found: C, 61.77; H, 6.41. Calcd for $C_{18}H_{22}O_7$: C, 61.71; H, 6.33%.

*Cycloaddition of **11** to **8** Leading to **31**.* A mixture of **11** (167 mg, 0.53 mmol) and DBU (88 mg, 0.58 mmol) in dry toluene (4 ml) was refluxed for 6 h and then cooled to room temperature. After iodomethane (a few drops) and **8** (205 mg, 1.18 mmol) were added, the mixture was stirred at room temperature for 12 h. The crude product was chromatographed over silica gel with hexane–ethyl acetate (1:1) to afford **11** (34 mg, 20% recovered) and then **31** (121 mg, 56%): Colorless solid; mp 188—191 °C; IR (KBr) 1770 and 1700 cm^{-1} (CO); ^{1}H-NMR ($CDCl_3$) δ=1.16, 3.66 ($OC\underline{H}_2C\underline{H}_3$), 1.90—3.40 (11H, m), 2.93 (3H, s, NMe), and 7.00—7.56 (5H, m, Ph); MS m/z 408 (M^+).

Found: C, 67.46; H, 5.96; N, 6.86%. Calcd for $C_{23}H_{24}O_5N_2$: C, 67.63; H, 5.92; N, 6.86%.

*Cycloaddition of **12** to **3** Leading to **32**.* A mixture of **12** (160 mg, 0.42 mmol) and DBU (71 mg, 0.47 mmol) in toluene (4 ml) was refluxed for 6 h and cooled to room temperature. After iodomethane (a few drops) and **3** (94 mg, 0.85 mmol) were added, the mixture was stirred at room temperature for 24 h. The crude product was chromatographed over silica gel. An elution with hexane–ethyl acetate (2:1) gave **12** (18 mg, 11% recovered) and with hexane–ethyl acetate (1:2) **32** (112 mg, 65%): Colorless needles from ethanol; mp 105—107 °C; IR (KBr) 1770 and 1700 cm^{-1} (CO); ^{1}H-NMR ($CDCl_3$) δ=1.16, 3.64 ($OC\underline{H}_2C\underline{H}_3$), 2.00—3.40 (11H, m), 2.91 (3H, s. NMe), and 7.04—7.56 (5H, m, Ph); MS m/z 408 (M^+).

Found: m/z 408.1696. Calcd for $C_{23}H_{24}O_5N_2$: M, 408.1684.

We are grateful to Toyo Soda Manufactural Company for a generous sample of chloroprene.

References

1) H. Hopf, *Angew. Chem., Int. Ed. Engl.*, **23**, 948 (1984).
2) A. T. Blomquist and J. A. Verdol, *J. Am. Chem. Soc.*, **77**, 81 (1955); W. J. Bailey and J. Economy, *ibid.*, **77**, 1133 (1955); W. J. Bailey, C. H. Cunov, and L. Nicholas, *ibid.*, **77**, 2787 (1955).
3) O. Tsuge, E. Wada, and S. Kanemasa, *Chem. Lett.*, **1983**, 239; O. Tsuge, S. Kanemasa, H. Sakoh, and E. Wada, *ibid.*, **1984**, 273.
4) O. Tsuge, S. Kanemasa, H. Sakoh, and E. Wada, *Chem. Lett.*, **1984**, 277; O. Tsuge, E. Wada, S. Kanemasa, and H. Sakoh, *Bull. Chem. Soc. Jpn.*, **57**, 3221 (1984); O. Tsuge, S. Kanemasa, H. Sakoh, and E. Wada, *ibid.*, **57**, 3234 (1984).
5) O. Tsuge, E. Wada, S. Kanemasa, and H. Sakoh, *Chem. Lett.*, **1984**, 469 and 709.
6) S. Nunomoto, Y. Kawakami, and Y. Yamashita, *J. Org. Chem.*, **48**, 1912 (1983).
7) The unseparable side product was assigned as 4-ethoxy-3,6-dimethylene-1,7-octadiene on the basis of the ^{1}H-NMR spectrum of crude mixture.
8) Such high stereoselection has been observed in the previous cases (Ref. 4).
9) T. Inukai and T. Kojima, *J. Org. Chem.*, **31**, 1121 (1966).
10) M. F. Newmann, D. Martina, and F. Brion, *Angew. Chem., Int. Ed. Engl.*, **20**, 864 (1981).
11) A natural product synthesis using a 2-acetyl-1,3-butadiene equivalent has been reported: A. V. R. Rao, G. Venkatswamy, S. M. Javeed, V. H. Deshpande, and B. R. Rao, *J. Org. Chem.*, **48**, 1552 (1983).
12) O. Grummitt, E. P. Budewitz, and C. C. Chudd, *Org. Synth.*, Coll. Vol., **4**, 749 (1963).
13) E. H. Ingold, *J. Chem. Soc.*, **128**, 1199 (1925).

 © 1985 The Chemical Society of Japan Bull. Chem. Soc. Jpn., 58, 3320—3336 (1985) [Vol. 58, No. 11

Stereochemical Study on 1,3-Dipolar Cycloaddition Reactions of Heteroaromatic *N*-Ylides with Unsymmetrically Substituted Olefinic Dipolarophiles

Otohiko Tsuge,* Shuji Kanemasa, and Shigeori Takenaka
Research Institute of Industrial Science, and Department of Molecular Science and Technology, Interdisciplinary Graduate School of Engineering Sciences, Kyushu University, Kasugakoen, Kasuga 816
(Received July 8, 1985)

Regioselectivity and stereoselectivity of the cycloadditions of heteroaromatic *N*-ylides with unsymmetrically-substituted olefins such as methyl-substituted cis olefins, an acrylate, the related olefins, trans nitro olefins, and other trans olefins have been investigated. These cycloadditions are highly regioselective, while the stereoselectivity depends upon both the electronic and steric nature of substituents of the ylide and olefin. The 1-endo-2-exo cycloadducts of the anti form of ylides which have been formed as kinetically controlled products undergo the isomerization into either the 1-endo-2-exo cycloadducts of the syn ylides through a retro cycloaddition process or the 1-exo-2-endo cycloadducts of the syn ylides *via* betaine intermediates.

The preceding paper has dealt with the stereochemical study on the 1,3-dipolar cycloaddition reactions of heteroaromatic *N*-ylides to symmetrically substituted cis and trans olefins,[1] and some important stereochemical features in such cycloadditions have been figured out:

1) The anti form of ylides exclusively participates in the cycloadditions if the ylides are stabilized by a substituent of carbonyl type.

2) The reactions with cis olefins are highly stereoselective, the endo approach of olefins to the anti ylides being the only favored pathway.

3) If the cycloadducts formed are substituted by strongly electron-withdrawing groups, they suffer from the ready stereospecific dissociation into the starting ylides and olefins which then recombine in a stereospecific manner giving the thermodynamically more favored isomers.

4) After all, the stereochemical course of cycloadditions of heteroaromatic *N*-ylides depends upon the electronic nature and steric size of substituents on the olefins and ylides. The attractive secondary orbital interaction working between the olefin substituents and the heteroaromatic plane leads to the kinetically favored cycloadducts, and the steric repulsion working among the olefin substituents and the ylide ring and substituent favors the formation of thermodynamically controlled cycloadducts. The stereochemistry of the reactions is revealed as a result from the counter-balance of the above two interactions.

In the present paper, the cycloaddition reactions of heteroaromatic *N*-ylides to unsymmetrically substituted cis and trans olefins are investigated with the aim of knowing the generality and limitation of our rules which were outlined in the preceding paper and abstracted above. In the reactions with unsymmetrical olefins, of special interest are the regioselectivity, the stereoselectivity of ylide substituent (or the periselectivity), the stereoselectivity of olefin substituents (the endo and exo selectivity), and the thermodynamical stability of cycloadducts. For wide applications of the 1,3-dipolar cycloadditions to organic synthesis, it is necessary to discriminate among the factors which control the stereochemistry of cycloaddition and to understand which certain factor predominates over the other.

So far examples for the cycloadditions of heteroaromatic *N*-ylides to unsymmetrically substituted olefinic dipolarophiles are quite limited. In the most reported cases, the cycloadducts could not be isolated because of their instability[2] or, if isolated, their stereostructures remained unsolved.[3,4] It is only in recent year that the regio- and stereoselective cycloadducts of triazolium or dihydroisoquinolinium methylides to acrylic olefins have been reported to be the endo cycloadducts to the anti form of the ylides.[5,6] Some other unsymmetrical olefins have been employed in the cycloadditions to dihydroisoquinolinium methylides giving the regio- and stereoselective cycloadducts with a cis-trans-cis geometry as to the newly formed five-membered rings.

Results and Discussion

Thirteen heteroaromatic *N*-ylides **1**—**5** including five different types of heterocyclic systems were employed in the present work as shown in Scheme 1: Several pyridinium methylides **1a**—**e**, isoquinolinium methylides **2a**—**e**, pyridazinium **3**, thiazolium **4**, and benzothiazolium phenacylides **5**. These ylides are labile, so they were all generated *in situ* from the corresponding quaternary bromides and triethylamine in the presence of an olefinic dipolarophile.

After the cycloaddition was completed, triethylamine hydrobromide quantitatively formed was removed off by washing the reaction mixture with water. The crude mixture was submitted, in every case, to the ^{1}H-NMR measurement to get informations on the regio- and stereoselectivity of the

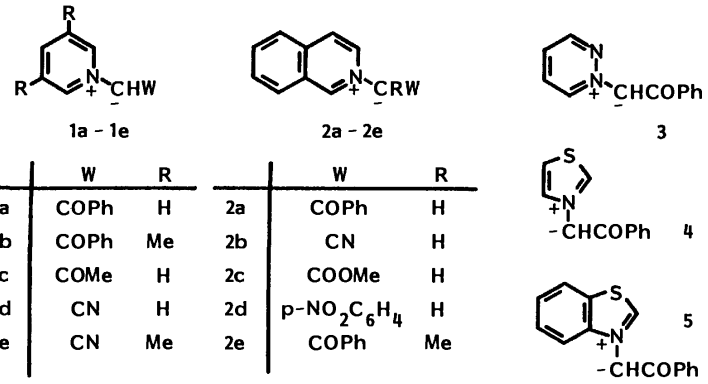

	W	R
1a	COPh	H
1b	COPh	Me
1c	COMe	H
1d	CN	H
1e	CN	Me

	W	R
2a	COPh	H
2b	CN	H
2c	COOMe	H
2d	p-$NO_2C_6H_4$	H
2e	COPh	Me

Scheme 1.

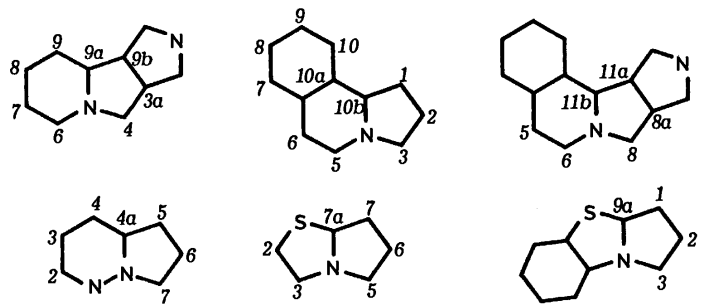

Fig. 1. Numberings for the cycloadducts formed in the reaction of heteroaromatic *N*-ylides to unsymmetrically substituted olefins.

cycloaddition, and then subjected to the isolation and purification procedure of products. Figure 1 shows the numberings for the ring systems of cycloadducts formed from the cycloadditions.

Cycloadditions to Methyl-substituted cis Olefins. We have recently found that such cis olefins as maleimides and maleates undergo the stereospecific and stereoselective cycloadditions to heteroaromatic *N*-ylides providing the endo 3+2 cycloadducts to the anti form of ylides.[1] When a methyl substituent is introduced at the olefin part of cis olefins, one of two possible endo approaches between the ylide and the methyl-substituted cis olefin may be disfavored because of the steric repulsion between the methyl moiety and a ylide-stabilizing substituent. Therefore, it is easily expected that the regioselectivity of cycloadditions to methyl-substituted cis olefins should be excellent in favor for the formation of cycloadducts with the methyl and ylide-stabilizing substituents in a 1,3-relationship.

The reaction of pyridinium phenacylide **1a** with *N*-(*p*-tolyl)citraconimide **6** in chloroform at room temperature produced a single isomer of the 3+2 cycloadduct **7** in a quantitative yield as shown in Scheme 2 and Table 1. Similarly 3,5-dimethylpyridinium phenacylide **1b** and pyridinium acetonylide **1c** gave almost quantitative yields of stereospecific, regio-, and stereoselective cycloadducts **8** and **9**, respectively, both as single isomers.

Although these cycloadducts **7**—**9** are all too unstable to be purified by recrystallization or column chromatography as is usual with the cycloadducts of heteroaromatic *N*-ylides to maleimides,[1] their structures were successfully determined as the 9b-methyl derivatives of the endo 3+2 cycloadducts of **6** to the anti form of **1** on the basis of the spectral data shown in Table 2. With the cycloadduct **7** as an example, the small coupling constant of 0.8 Hz between 3a-H and 4-H as well as the low field shift of 9-H compared with 7-H (5.49 and 4.82 ppm, respectively) is consistent with the endo cycloadduct to the anti ylide. It is clear that the methyl substituent is sitting at the 9b-position on the basis of the splitting patterns of methine hydrogens on the newly formed five-membered ring.

On the other hand, the reactions of pyridinium methylides **1d** and **1e** with a cyano moiety as a sterically small ylide-stabilizing substituent furnished each two regioisomeric cycloadducts **10**+**12** and **11**+**13**, respectively, whose separation was unsuccessful. The major products **12** and **13** were assigned as the 3a-methyl-substituted cycloadducts and the minor ones **10** and **11** the 9b-methyl derivatives by the careful reading of the ^{1}H-NMR spectral data. Such reversal of regioselectivity which should be deeply related with the steric size of the cyano moiety will be discussed later. The cycloadditions of isoquinolinium phenacylide **2a** to **6** and of **2a** to dimethyl citraconate

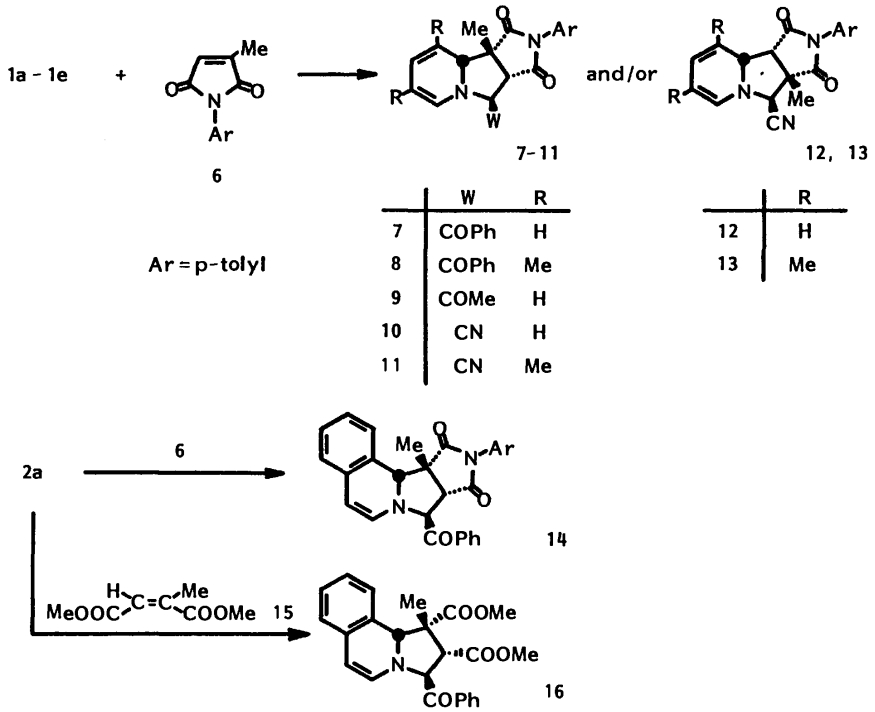

Scheme 2.

Table 1. Cycloadditions to citraconimide **6** and citraconate **15**

Ylide	Olefin	Reaction conditions[a]		Product[b]	Mp θ_m/°C	Yield/%[c]
		Temperature	Time h			
1a	**6**	rt	11	**7**	105—107	100
1b	**6**	rt	2	**8**	145—147	100
1c	**6**	rt	13	**9**	82—85	94
1d	**6**	rt	38	**10**+**12**	d)	100 **10** : **12**=1 : 2
1e	**6**	rt	19	**11**+**13**	d)	100 **11** : **13**=1 : 3
2a	**6**	rt	10 min	**14**	98—99	100
2a	**15**	reflux	20 min	**16**	oil	100

a) Solvent: chloroform. b) All yellow to pale yellow solid. c) All isolated yields. The isomer ratio was determined by the ^{1}H-NMR spectrum. d) Melting point was not taken.

15 took place, quite readily under milder conditions than the others, giving quantitative yields of regio- and stereoselective cycloadducts **14** and **15**, respectively.

The regioselectivity in the cycloadditions with such methyl-substituted cis olefins as **6** and **15** can be satisfactorily explained by the steric repulsion during the approach of the both reagents (Fig. 2). As has been demonstrated in the preceding work,[1] the cycloadditions of heteroaromatic *N*-ylides to a variety of cis olefins proceed through the endo approach to the anti form of ylides due to both the high stabilization of anti ylide and the minimization of steric repulsion from the ylide-stabilizing substituent. The same mode of approach may be applied to the present cases. Simple combination of the polarized structures of **1** and **6** leads to the approach **A** in

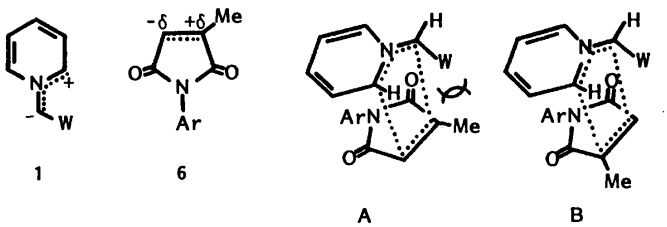

Fig. 2. Two regioisomeric endo approaches between **1** and **6**.

which some steric repulsion exists between the ylide-stabilizing substituent W and the methyl moiety. When W is small in size such as cyano group, the approach **A** is more favored providing **12** and **13** as major products. When the steric repulsion of W to the methyl is critical, the approach **A** becomes

Table 2. Spectral data for the cycloadducts to citraconic imide **6** and ester **15**

	IR (cm^{-1})	^{1}H-NMR Spectra measured in deuteriochloroform (δ, ppm, and Hz)											M$^+$ (m/z)
		4-H	3a-H	9b-H	9a-H	9-H	8-H	7-H	6-H	J_{4-3a}	J_{9b-9a}		
7	1780, 1700, 1680, 1640	5.44 d	3.68 d	Me	4.17 dd	5.49 ddt	5.95 ddt	4.82 ddd	6.13 dt	0.8	—	1.53^s(9b-Me), 2.37^s(p-Me)	a)
						4.0	10.0	6.0	7.5				
8		5.20 s	3.61 s	Me	3.77 s	Me —	5.64 br. s	Me —	5.82 br. s	0	—	1.60^s(7-Me), 1.66^s(9b-Me), 1.89^s(9-Me), 2.37^s(p-Me)	a)
9	1780, 1720, 1710	4.50 s	3.58 s	Me	3.94 dd	5.44 ddt	4.93 ddt	4.76 ddd	5.02 dt	0	—	1.40^s(9b-Me), 2.28^s(p-Me)	a)
						4.0	10.0	6.0	7.5				
10	2250, 1720, 1710[c]	b)	3.24 s	Me	4.45 dd	b)	b)	b)	b)	0	—	1.61^s(9b-Me), 2.37^s(p-Me)	
12		4.78 s	Me	3.10 d	b)	b)	b)	b)	b)	—	8.0	1.69^s(3a-Me), 2.37^s(p-Me)	
11	2250, 1770, 1720, 1680[c]	4.88 s	3.25 s	Me	4.25 s	Me —	5.47 br. s	Me —	5.70 br. s	0	—	1.55^s(7-Me), 1.61^s(9b-Me), 1.98^s(9-Me), 2.32^s(p-Me)	
13		4.80 s	Me	3.97 d	4.64 d	Me —	5.47 br. s	Me —	5.70 br. s	—	8.0	1.55^s(7-Me), 1.71^s(3a-Me), 1.93^s(9-Me), 2.32^s(p-Me)	
		8-H	8a-H	11a-H	11b-H			5-H	6-H	J_{8-8a}	$J_{11a-11b}$		
14	1770, 1700	5.48 d	3.80 d	Me	4.35 s			5.43 d	6.13 d	1.0	—	1.65^s(11a-Me), 2.30^s(p-Me)	448
									7.7				
		3-H	2-H	1-H	10b-H			6-H	5-H	J_{3-2}	J_{1-10b}		
16	1740—1720, 1620, 1600	5.65 d	3.68 d	Me	4.57 s			5.05 d	6.11 d	6.5	—	1.67^s(1-Me), 3.35^s, 3.64^s (1- and 2-COOMe)	405
									7.8				

a) No parent ion peak was observed. b) Could not be assigned because of the signal overlapping. c) Measured as mixtures of regioisomers.

disfavored and instead the other approach **B** is the only allowed pathway.

Cycloadditions to Acrylic and Related Olefins. The cycloadditions of **2a** with acrylonitrile **17a** and methyl acrylate **17b** as monosubstituted olefinic dipolarophiles were found to occur readily, at room temperature for 10 min, furnishing quantitaive yields of regioselective and stereochemically pure 3+2 cycloadducts **18** and **19**, respectively (Scheme 3 and Table 3). On the other hand, the isoquinolinium ylide **2d** having *p*-nitrophenyl moiety as a ylide-stabilizing substituent showed very poor stereoselectivity in the reaction with **17a**, a mixture of two stereoisomers **20** and **21** being obtained in 100% yield. They were tentatively assigned as the endo 3+2 cycloadducts to the anti and syn forms of the ylide **2d** on the ground of the mechanistic discussion described later. Unfortunately the similar reaction of **2d** with **17b** gave no 3+2 cycloadduct but the only obtained product **22** was the dehydrogenated cycloadduct, 1-methoxycarbonyl-3-(*p*-nitrophenyl)-2,3-dihydropyrrolo[2,1-*a*]isoquinoline.

Although quite sluggish, the cycloaddition of benzothiazolium *N*-pnenacylide **5** to **17a** gave 74% of the regio- and stereoselective cycloadduct **23** as a single product.

The structures of these cycloadducts were confirmed mainly on the basis of the ^{1}H-NMR spectral data listed in Table 4. The cycloadduct **19** which was obtained from **2a** and **17b** offers the most clear ^{1}H-NMR spectrum supporting the proposed stereostructure as shown in Fig. 3.

The ester methyl at the 1-position, appeared at 3.28 ppm, should be sitting in the midst of shielding zone of the fused benzene ring, and hence the relationship between 1-H and 10b-H is cis. The 1-H couples with one (Ha) of two adjacent methylene hydrogens with a small coupling constant of 2.3 Hz and the other (Hb) with a medium coupling of 8.0 Hz, indicating that Ha and Hb are trans and cis to 1-H, respectively. The molecular model for **19** with a confirmed stereochemistry at the 10b-, 1-, and 2-

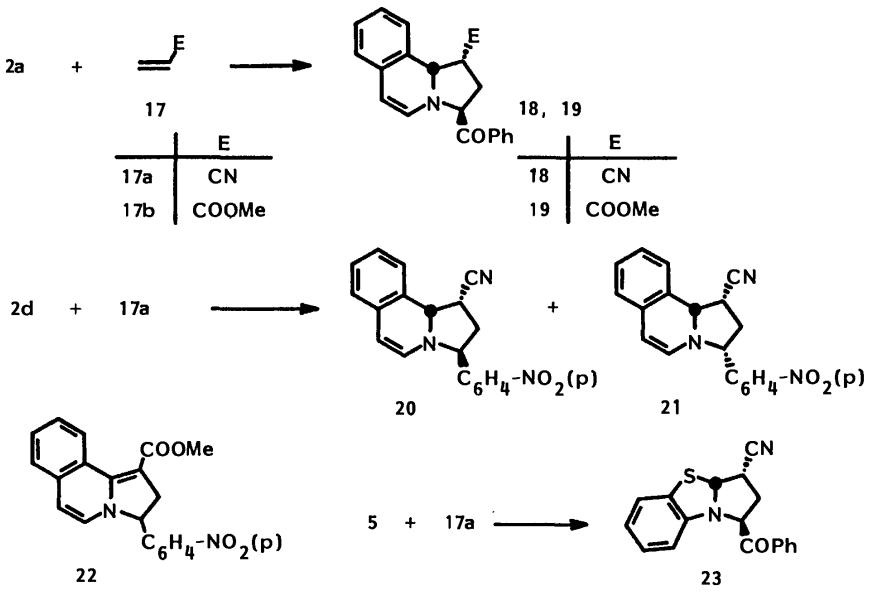

Scheme 3.

Table 3. Cycloaddition to acrylic **17** and related olefins **24**, **26**

Ylide	Olefin	Reaction conditions		Time/h	Product	Mp θ_m/°C	Yield/%[b]
		Solvent[a]	Temperature				
2a	**17a**	CF	rt	10 min	**18**	156—157	100
2a	**17b**	CF	rt	10 min	**19**	105—108	100
2d	**17a**	AN	rt	20 min	**20**+**21**[c]	oil	100
2d	**17b**	CF+AN[d]	rt	2	**22**	oil	60
5	**17a**	CF	rt	3	**23**	129—130	74
2d	**24**	AN	rt	2	**25**	oil	100
2a	**26**	CF	rt	10 min	**27**	73—76	100

a) CF: chloroform; AN: acetonitrile. b) All isolated yields. c) The isomer ratio could not be determined. d) chloroform: acetonitrile=25 : 1.

TABLE 4. SPECTRAL DATA FOR THE CYCLOADDUCTS TO ACRYLIC **17** AND RELATED OLEFINS **24, 26**

	IR (cm^{-1})	^{1}H-NMR Spectra (δ, ppm, and Hz)[a]								M$^+$(m/z)
		3-H	2-Ha[b]	2-Hb[c]	1-H	10b-H	6-H	5-H		
18	2240, 1670	5.39^{ddd}	2.78^{ddd}	2.27^{ddd}	3.62^{dddd}	4.96^{d}	5.40^{d}	6.37^{d}		300
		9.0	13.8	13.8	8.0	5.2	7.5	7.5		
		6.0	9.0	8.0	5.2					
		0.5	2.2	6.0	2.2					
					0.5					
19	1720, 1700, 1620, 1600	5.37^{dd}	2.52^{ddd}	2.03^{ddd}	3.37^{ddd}	5.11^{d}	5.04^{d}	6.16^{d}	3.28^{s}(COOMe)	333
		9.0	13.0	13.0	8.0	6.1	7.4	7.4		
		6.5	9.0	8.0	6.1					
			2.3	6.5	2.3					
22	1650, 1630, 1600, 1520	5.43^{dd}	3.57^{dd}	2.80^{dd}	—	—	6.16^{d}	6.64^{d}	3.59^{s}(COOMe), 9.81$^{br.\,d}$(10-H)	331
		12.0	15.3	15.3			7.5	7.5		
		6.5	12.0	6.5						
		3-H	2-Ha[b]	2-Hb[c]	1-H	9a-H				
23	2240, 1690	5.17^{ddd}	2.67^{ddd}	2.42^{ddd}	3.58^{ddt}	5.67^{d}				306
		7.8	13.0	13.0	7.0	5.6				
		6.0	7.8	7.0	5.6					
		0.8	5.6	6.0	5.6					
					0.8					
		3-H	2-Ha[b]	2-Hb[c]	1-H	10b-H	6-H	5-H		
25	1720, 1660, 1630, 1600	4.97^{dd}	3.22^{dd}	2.01^{dd}	—	5.56^{s}	5.16^{d}	5.95^{d}	0.82^{t}, 1.21^{t}, 3.80^{m}, 4.18^{m}(COOEt)	436
		8.7	13.0	13.0		—	7.6	7.6		
		6.5	8.7	6.5						
27	2250, 2200, 1680, 1630	5.37^{d}	—	4.43^{d}	—	5.57^{s}	5.44^{d}	6.56^{d}		401
		6.4		6.4		—	8.0	8.0		

a) **18, 19, 22, 27** were measured in CD_3CN and **23, 25** in $CDCl_3$. b) A hydrogen cis to 3-H. c) A hydrogen trans to 3-H.

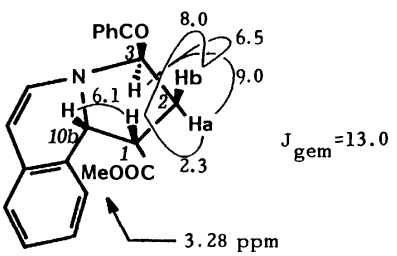

Fig. 3. Stereostructure and ^{1}H-NMR spectral data of **19**.

positions and with an undetermined configuration at the 3-position was built up and the coupling constants between 2-Hs and 3-H were estimated. As the result, the structure of **19** was determined as the endo 3+2 cycloadduct to the anti form of **2a**, whose formation was mostly predictable from our rule founded in the preceding paper.[1]

Contrary to the poor stereoselectivity of the cycloaddition between **2d** and **17a** mentioned above, a similar reaction of **2d** with diethyl 2-methylenemalonate **24** which carries two electron-withdrawing substituents at the same carbon was highly selective giving the single 3+2 cycloadduct **25** in a quantitative yield (Scheme 4 and Table 3).

The purification of **25** ended in failure because of its instability, but the ^{1}H-NMR spectrum as well as mass spectrum (Table 4) confirms the tetrahydropyrrolo[2,1-*a*]isoquinoline structure of **25**. The only ambiguousness is the configuration at the point of fusion (10b-H), which was tentatively assigned as shown in Scheme 4 (10b-H is trans to 3-H) on the basis of the mechanistic consideration discussed using Fig. 4 in the following section.

The stereo- and regioselective cycloadduct **27** was similarly obtained in the cycloaddition of **2a** to 2-benzylidenemalononitrile **26**.

The stereochemical features revealed in the cycloadditions to acrylic and related olefins are summarized in Fig. 4. It is quite understandable that the reactions of **2a** and **5** with acrylic olefins **17** have proceeded in a highly regio- and stereoselective fashion through the endo approach **C** (W=COPh, the case of isoquinolinium ylide) of **17** to the anti form of the ylides, because it is now known from our previous work[1] that the ylide **2a** as well as **5**, each of carbonyl-stabilized type, is more stabilized in the anti form than the syn form. On the other hand, the nonstereoselective cycloaddition of **2d** was also predictable. The ylide **2d** carrying a ylide-stabilizing substituent of noncarbonyl type has a similar stability in the anti and syn forms and hence the both endo approaches **C** and **D** (W=*p*-$NO_2C_6H_4$) seem

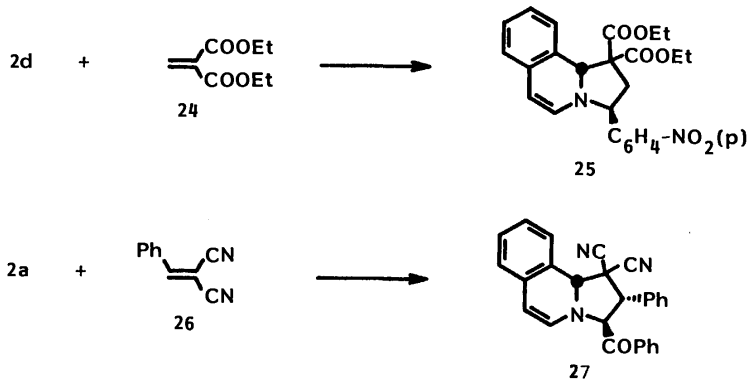

Scheme 4.

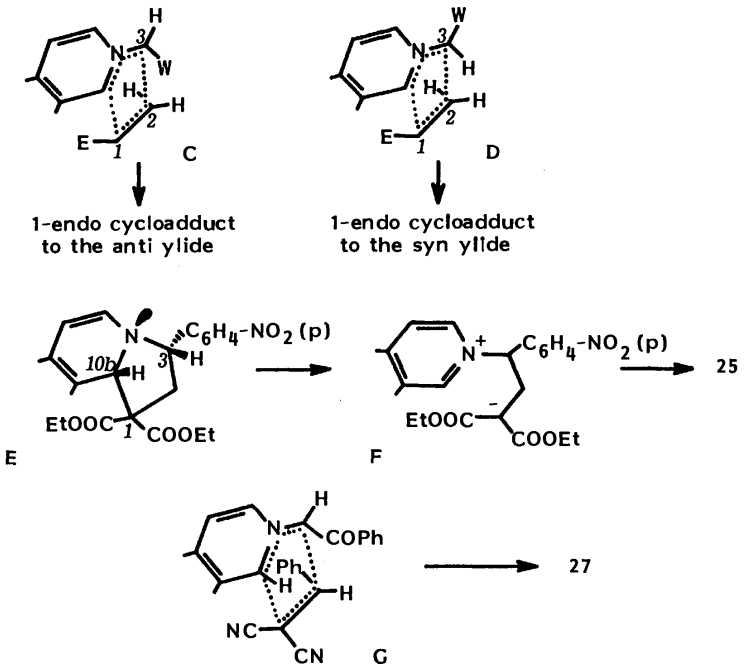

Fig. 4. Stereochemistry in the cycloadditions of **2** to acrylic **17** and related olefins **24, 26.**

likely to compete with the comparable easiness.

Surprising is the formation of single cycloadduct **25** in the reaction of **2d** with the 2-methylenemalonate **24.** We anticipated a kinetically nonstereoselective cycloaddition in this case because all the situation looked about the same to the cycloaddition to **17a.** This can be explained as follows: In this reaction also two isomeric cycloadducts **25** and **E** should have been formed through the energetically almost equal two endo approaches. As the both cycloadducts carry two electron-withdrawing ester groups at the 1-position, the 1—10b bond is readily cleaved into the stable betaine intermediate **F.** The recyclization of **F** must occur in a direction of producing the thermodynamically more stable cycloadduct **25** of the two. Such bond cleavage forming a betaine intermediate has been observed in the hydroalkylidenation reaction using pyridinium methylides[7] and will be discussed later.

In the cycloaddition between **2a** and 2-benzylidenemalononitrile **26** are possible two endo approaches to the anti form of **2a.** However, the reaction has trod the approach **G** leading to **27.** This high selectivity may be the result from either of the attractive interaction between the phenyl plane of **26** and the heteroaromatic plane of **2a** or the steric repulsion between the phenyl group and the benzoyl moiety of the anti form of **2a** as shown in Fig. 4.[8]

Cycloadditions to Nitro Olefins. The reactions of isoquinolinum ylides **2** with β-nitrostyrenes **28** proceeded at room temperature affording quantitative yields of 1 : 1 adducts in all cases (Scheme 5). The ^{1}H-NMR measurement of crude products showed that the product was, more or less in each case, composed of two stereoisomers of 3+2 cycloadduct and that the isomer ratio was dependent upon the solvent used for the ^{1}H-NMR measurement and also the time after the ^{1}H-NMR sample was prepared.

Although one isomer of the two or the both could be often separated in an almost pure form through crystallization or precipitation, it was unsuccessful to tell which of the two was the initial cycloadduct (kinetical product) because of the poor solubility and too rapid equilibration of the cycloadducts.

After all, it was concluded that the cycloadducts to **28** were under an equilibrium control (or thermodynamical control) and the energy barrier for the equilibrium was quite small. Their structures were assigned on the basis of the ^{1}H-NMR spectra, the chemical conversions, the molecular model inspection, and the proposed mechanism for the isomerization, all of which will be discussed soon later: **29**—**34**: the 1-endo-2-exo cycloadducts of the anti form of the ylides **2** as kinetically controlled products; **29′**—**34′**: the 1-exo-2-endo cycloadducts of the syn form of **2** as thermodynamically controlled products (Scheme 5).

Table 5 summarizes all the results obtained in the reactions of **2a**—**c** with several β-nitrostyrenes **28a**—**d**. The melting points are given only for the cycloadducts isolated in a pure form through crystallization or precipitation. The structural assignment for the cycloadducts formed from **2a**+**28a** and **2a**+**28d** was impossible because the only solvent in which they are satisfactorily soluble is DMSO, and in this solvent the equilibration between **29** and **29′** (also **32** and **32′**) is finished in a short time.

As shown in Scheme 5, the cycloadducts **31**+**31′** underwent the retro cycloaddition, in DMSO at room temperature, going back to the nitrostyrene **28c** and the ylide **2a** which was quantitatively captured with *N*-methylmaleimide **35** as the maleimide cycloadduct **36**. However, it is not likely that this retro reaction is deeply related with the isomerization between **31** and **31′** since the retro reaction is too slow compared with the isomerization (50 and 100% of **36** were formed after 4 and 48 h, respectively, at room temperature in

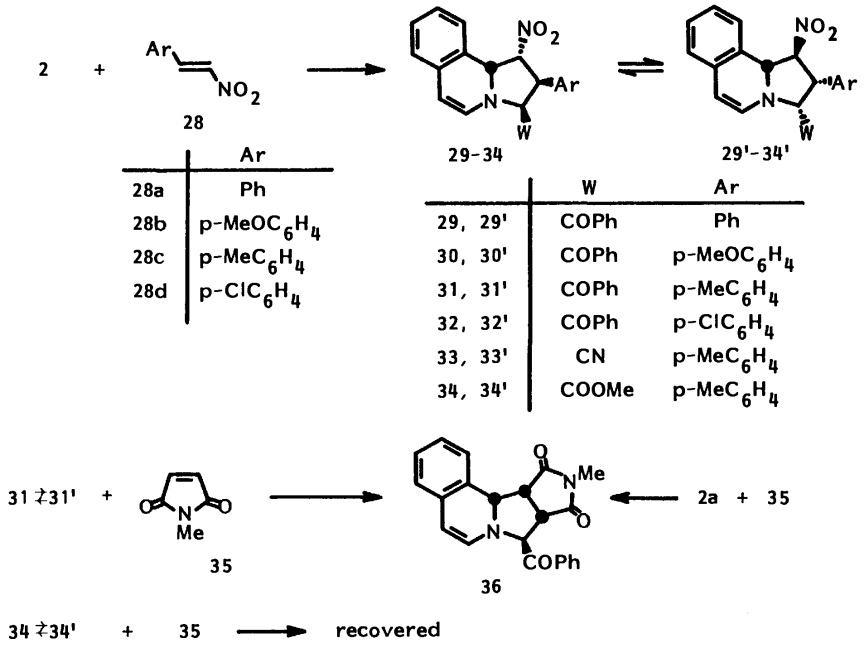

Scheme 5.

Table 5. Cycloadditions to β-nitrostyrenes **28**

Ylide	Olefin	Conditions[a]		Product[b]	Yield/%[c]	Mp(θ_m/°C) and solvent for crystallization[d]			Isomer ratio in DMSO-d_6[e]
		Temperature	Time/h						
2a	**28a**	rt	5 min	**29**⇄**29′**	100	**29** or **29′**	($CHCl_3$)	129—130	1 : 1
2a	**28b**	rt	5 min	**30**⇄**30′**	100	**30**	($CHCl_3$)	130—131 (d)	
2a	**28c**	rt	2	**31**⇄**31′**	100	**31**	(Me_2CO)	155—157 (d)	1 : 1
						31′	($CHCl_3$)	146—148 (d)	
2a	**28d**	rt	12	**32**⇄**32′**	100	**32** or **32′**	($CHCl_3$)	149—150	1 : 1
2b	**28c**	rt	1	**33**⇄**33′**	100	**33**	($CHCl_3$)	144—146	
2c	**28c**	rt	30 min	**34**⇄**34′**	100	**34′**	(EtOEt)	152—154	1 : 1

a) Carried out in chloroform. b) All yellow solid. c) Isolated yields. d) One isomer was less soluble than the other, being separated in a pure form. e) Very rapid equilibration was observed in DMSO. The ratio was based on the ^{1}H-NMR spectrum.

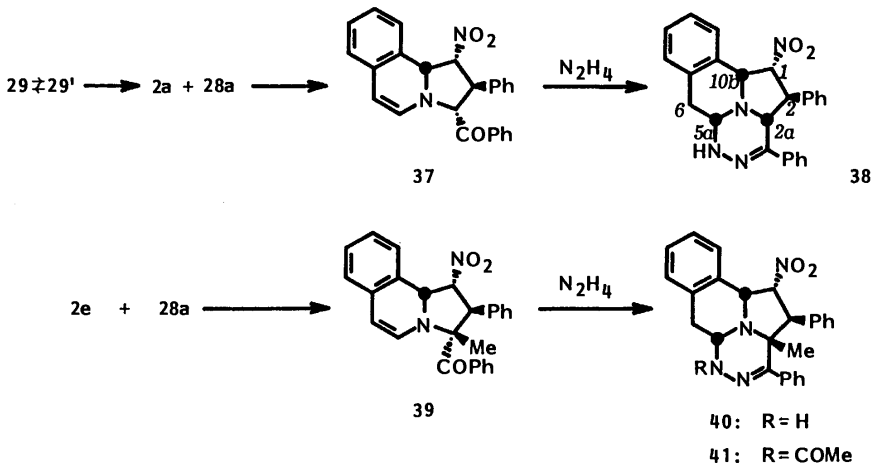

Scheme 6.

DMSO while the equilibration is completed in less than a few minutes under the same conditions). In fact, in spite of the ready isomerization between **34** and **34'**, the cycloadducts from the ylide **2c** bearing an ester substituent, at room temperature in DMSO, they never undergo the retro reaction with **35** even under harder conditions. As a conclusion, this rapid equilibration takes place *via* a betaine intermediate formed by the 1—10b bond cleavage of the cycloadduct. This will be discussed in detail in the following section.

The rapid equilibration is partly attributable to the high stability of the intermediary betaine compound (**J** in Fig. 6). If the 5—6 double bond of cycloadducts is reduced, such bond cleavage may be suppressed. In order to consume the 5—6 double bond and also to make the conformation of the pyrrolidine ring rigid, the equilibrating mixture of **29** and **29'** was allowed to react with hydrazine hydrate under reflux in ethanol producing a single isomer of the expected diazacyclazine derivative **38** (Scheme 6).

The structure of **38** was determined on the basis of the ^{1}H-NMR spectrum (Fig. 5) and the molecular model inspection: The 2-H is trans both to the 2a-H and 1-H (J_{2-2a}=3.5 and J_{2-1}=6.0 Hz) and the 1-H is cis to the 10b-H (from the molecular model analysis and J_{1-10b}=9.5 Hz). To our surprise, this coupling pattern around the pyrrolidine ring was found completely different from those of **29** (J_{3-2}=8.5, J_{2-1}=4.0, and J_{1-10b} could be about 7 Hz) and **29'** (J_{3-2}=J_{2-1}=J_{1-10b}=8.0 Hz), showing that **38** was derived from an isomeric cycloadduct **37** which was formed by the isomerization of **29** or **29'** under the reaction conditions. The coupling pattern of **31** with a medium-small-medium coupling was once observed in the 1-endo-2-exo cycloadducts of symmetrical trans olefins to the anti form of **2** as the kinetical products.[1]

Now, it is clear that **29** is the 1-endo-2-exo cycloadduct to the anti form of **2** as a kinetically

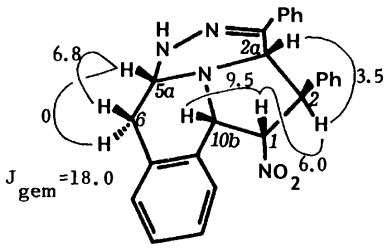

Fig. 5. Stereostructure and ^{1}H-NMR spectral data of **38**.

controlled product, **29'** is the 1-exo-2-endo cycloadduct to the syn form of **2** as a thermodynamically controlled product formed through the isomerization of **29** *via* a betaine intermediate, and that **38** was derived from another thermodynamical cycloadduct **37**, the 1-endo-2-exo 3+2 cycloadduct to the syn form of **2a**. This second thermodynamic cycloadduct **37** may have been formed, under forced conditions, through the retro cycloaddition of **29** (Scheme 6).

The similar reaction of isoquinolinium 1-benzoylethylide **2e** with **28a** and the subsequent cyclization with hydrazine gave **40** also as a single isomer in 21% of total yield. The structural inspection using the ^{1}H-NMR spectra of **40** and its *N*-acetylated derivative **41** confirmed the 1-endo-2-exo skeleton of the noniso-lated cycloadduct **39** as shown in Scheme 6.

The IR and ^{1}H-NMR spectra of the cycloadducts **29**—**34** and **29'**—**34'** are listed in Table 6. These spectra are consistent with the proposed structures for each isomers. The both ester methyls at the 3-position of **34** and **34'** are strongly shielded by the fused benzene ring and/or the adjacent phenyl ring.

The stereochemical variety in the cycloadditions of isoquinolinium ylides **2** to nitrostyrenes **28** is summarized in Fig. 6 with an exemplified reaction of **2a** with **28a**. This cycloaddition proceeds through the 1-endo-2-exo approach **H** of **28a** to the anti form of **2a**, just like the cycloadditions of heteroaromatic

Table 6. Spectral data for the cycloadducts to nitro olefins **28**

	IR (cm^{-1})	^{1}H-NMR Spectra (δ, ppm and Hz)						
		Solvent[a]	3-H	2-H	1-H	10b-H	6-H	5-H	Others
29	1670, 1630, 1540	D	6.27^d	4.43^{dd}	5.90^m	5.90^m	5.23^d	6.52^d	
				8.5	4.0	b)		7.0	
29'		D	5.90^m	4.75^t	5.90^m	5.12^d	5.60^d	6.43^d	
				8.0	8.0	8.0		7.2	
30	1670, 1620, 1540, 1510, 1250	A	6.15^d	4.55^{dd}	5.88^{dd}	6.03^d	5.28^d	6.50^d	3.67^s (*p*-MeO)
				8.5	4.4	6.6		7.4	
30'		A	5.84^d	4.73^t	5.88^{dd}	5.20^d	5.63^d	6.43^d	3.63^s (*p*-MeO)
				8.0	8.0	7.3		7.5	
31	1670, 1630, 1540, 1450, 1370, 1220	D	6.22^d	4.48^{dd}	5.84^{dd}	5.92^m	5.22^d	6.53^d	2.12^s (*p*-Me)
				8.5	4.0	7.0		7.5	
31'		A	5.83^d	4.73^t	5.90^{dd}	5.20^d	5.63^d	6.43^d	2.12^s (*p*-Me)
				8.8	8.8	7.9		7.7	
		D	5.23	4.70	5.90	5.12	5.59	6.43	
32	1670, 1630, 1540	D	6.26^d	4.59^{dd}	5.90^m	5.90^m	5.23^d	6.55^d	
				8.5	4.0	b)		7.3	
32'		D	5.90^m	4.79^{dd}	5.90^m	5.12^d	5.63^d	6.45^d	
				8.0	7.5	7.5		7.3	
33	2250; 1630, 1550, 1450, 1370	A	5.61^d	4.47^{dd}	6.02^{dd}	5.83^d	5.40^d	6.43^d	2.33^s (*p*-Me)
				8.2	5.5	7.2		7.8	
33'		CF	4.73^d	4.32^t	5.62^{dd}	5.18^d	5.77^d	6.35^d	2.32^s (*p*-Me)
				8.0	8.0	7.5		7.6	
		A	5.20	4.68	6.00	5.23	5.82	6.52	
34	1740, 1610, 1550, 1360	D	5.05^d	4.34^{dd}	5.92^m	5.92^m	5.13^d	6.34^d	2.27^s (*p*-Me), 3.17^s (COOMe)
				9.0	3.6	b)		7.7	
34'		A	4.63^d	4.68^t	5.98^t	5.22^d	5.62^d	6.38^d	2.29^s (*p*-Me), 3.23^s (COOMe)
				8.0	8.0	8.0		7.5	

a) D: DMSO-d_6; A: acetone-d_6; CF: $CDCl_3$. b) No coupling constant was given.

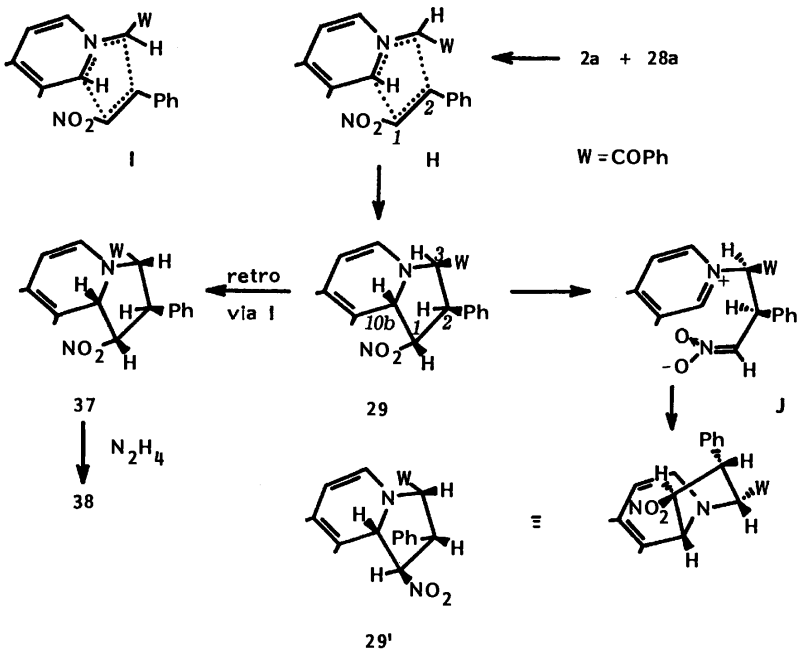

Fig. 6. Stereochemical course of the cycloaddition of **2a** to **28a**.

N-ylides to symmetrical trans olefins,[1] giving **29** as a kinetically controlled cycloadduct. This product **29** undergoes a rapid bond cleavage at the 1—10b bond leading to a betaine intermediate **J**. This easy betaine formation must have been induced by the anion stabilization with the nitro group and also by the cation stabilization in the isoquinolinium ring. The recyclization at the other side of the isoquinoline ring gives **29′** as a thermodynamically controlled cycloadduct. As the thermodynamical stability between **29** and **29′** looks about the same and the energy barrier between **29** and **J** and between **J** and **29′** might be small, they come into a rapid equilibration with the comparable isomer ratio. On the other hand, the kinetical cycloadduct **29** can undergo a slow retro cycloaddition providing **2a** and **28a** which recombine through the 1-endo-2-exo approach **I** to the syn form of **2a** giving the second thermodynamic cycloadduct **37**. Similar isomerization of the kinetical cycloadduct into two isomeric cycloadducts through a betaine intermediate or a retro cycloaddition path will be again discussed in the following section.

When the cycloadducts **29**—**32** and **29′**—**32′** were treated with bases, they were found to aromatize into the corresponding pyrrolo[2,1-*a*]isoquinoline derivatives **42**—**45** with the elimination of the nitro moiety (Scheme 7 and Table 7). Although the yields were not so high, such nitrous acid elimination is important as a method of synthesizing the indolizine derivatives carrying no electron-withdrawing substituent at the 1-position. It was also found that triphenylphosphine was even more effective, but the reaction mechanism is not clear so far.

The aromatization into the indolizines **46**—**47** carrying a nitro group at the 1-position was achieved by the usual dehydrogenation using DDQ (Scheme 7 and Table 7).

Cycloadditions to Unsymmetrical trans Olefins. Isoquinolinum methylides **2**, which belong to the most reactive heteroaromatic *N*-ylide, were found to react with unsymmetrically substituted trans olefins such as (*E*)-1-(*p*-methylbenzoyl)-2-phenylethene **48a**, cinnamaldehyde **48b**, crotonaldehyde **48c**, and (*E*)-1-benzoylpropene **48d** at room temperature, but rather slowly compared with the cycloadditions to other dipolarophiles previously employed. As the reactions under heating generally lead to the contamination of cycloadduct by some secondary products formed through the isomerization, dehydrogenation, or decomposition of the initially formed cycloadduct

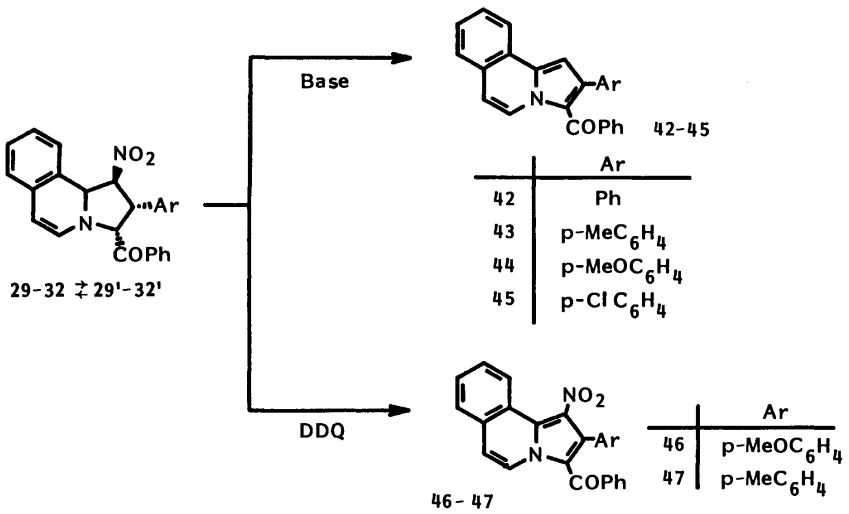

Scheme 7.

Table 7. Conversion of the cycloadducts of β-nitrostyrenes into benzo[*g*]indolizines

Cycloadduct	Base or oxidant	Reaction conditions		Time/h	Product[b]	Mp θ_m/°C	Yield/%[c]
		Solvent[a]	Temperature				
29⇄**29′**	PPh_3	AN	reflux	24	**42**	219—222	28
30⇄**30′**	NEt_3	CF	rt	21	**43**	191—193	58
31⇄**31′**	DBU	BZ	rt	22	**44**	203—205	28
	PPh_3	BZ	reflux	8			46
32⇄**32′**	PPh_3	AN	reflux	44	**45**	178—180	37
30⇄**30′**	DDQ	BZ	reflux	24	**46**	198—201	76
31⇄**31′**	DDQ	BZ	reflux	12	**47**	227—230	72

a) AN: acetonitrile; CF: chloroform; BZ: benzene. b) All yellow prisms. c) Isolated yields.

and since such cycloadducts are usually not so stable enough to be separated or purified safely, only limited numbers of dipolarophiles were used. No clear result was given in the reactions with such unreactive olefins as crotonates, cinnamates, (*E*)-4-phenyl-3-propen-2-one, and (*E*)-3-penten-2-one which required harder reaction conditions and therefore resulted in the complex mixture of products. The results are summarized in Scheme 8 and Table 8.

Three different types of 3+2 cycloadducts were isolated in the reactions with **48**, depending upon the nature of substituents of the ylide **2** and olefin **48** and also upon the reaction conditions. The reaction of **2a** with **48a** in acetonitrile precipitated a labile cycloadduct **49** in a pure form. This cycloadduct **49** was found to readily isomerize into **50** in DMSO even at room temperature. When the same reaction was carried out in chloroform, no precipitate appeared and only **50** was obtained in a quantitative yield. These facts indicate that **49** and **50** are the kinetic and thermodynamic cycloadducts, respectively. The third type of cycloadducts are **53**—**58** which were formed from either the alkyl-substituted vinyl ketone **48d**, the ylides **2b** and **2c** carrying a cyano or ester ylide-stabilizing substituent, or the other types of ylides **3** and **4**.

Each type of these cycloadducts showed a characteristic coupling pattern among the methine hydrogens on the newly formed five-membered ring as shown in Table 9. The product **49** showed similar couplings to the kinetically controlled cycloadduct between **2** and symmetrical trans olefins,[1] being assigned to be the 1-endo-2-exo cycloadduct to the anti form of **2a** as a kinetical product. Its isomer **50** exhibited a coupling pattern similar to both **38** (hence **37**) and the thermodynamically controlled cycloadduct of **2** to symmetrical trans olefins (1-exo-2-endo cycloadduct to the anti ylide). Based on this fact and also its chemical conversion into a diazacyclazine derivative which will be described

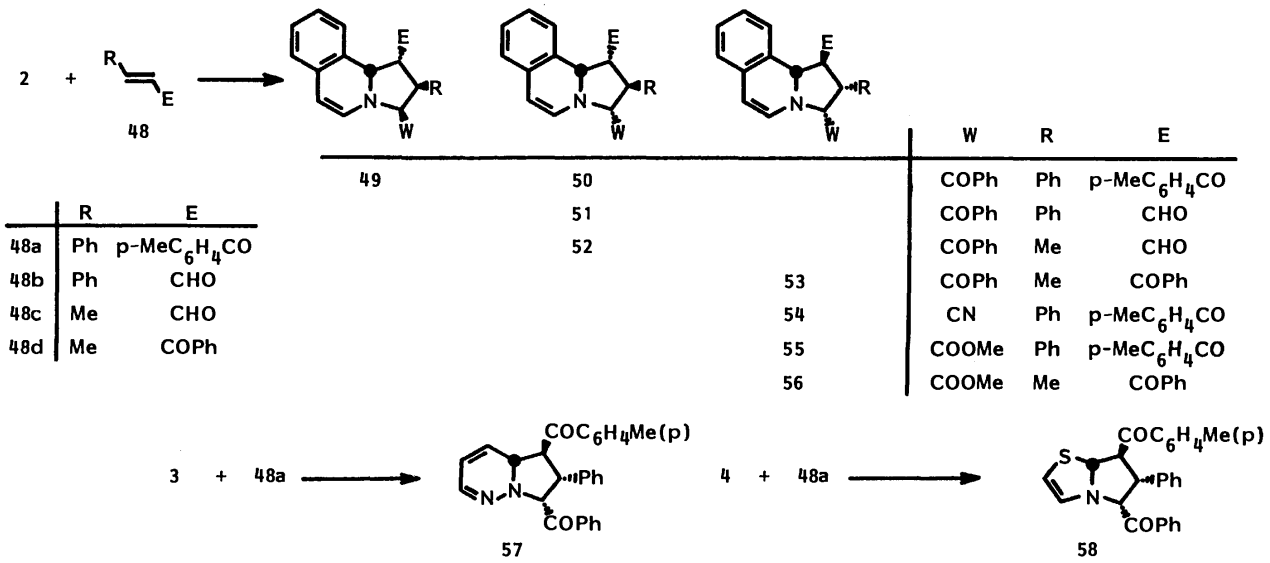

Scheme 8.

TABLE 8. CYCLOADDITIONS TO UNSYMMETRICAL TRANS OLEFINS **48**

Ylide	Olefin	Reaction conditions			Product (yield/%)[b]				
		Solvent[a]	Temperature	Time/h					
2a	**48a**	AN	rt	4	**49** (46)	**50** (54)			
		CF	rt	1.5		**50** (100)			
2a	**48b**	DM	rt	30 min		**51** (100)			
2a	**48c**	CF	rt	30 min		**52** (80)			c)
2a	**48d**	CF	rt	30 min			**53** (86)		c)
2b	**48a**	CF	rt	1			**54** (100)		
2c	**48a**	CF	rt	3			**55** (100)		
2c	**48d**	CF	rt	20 min			**56** (70)		c)
3	**48a**	CF	rt	14			**57** (100)		
4	**48a**	CF	rt	14			**58** (100)		

a) AN: acetonitrile; CF: chloroform; DM: dichloromethane. b) All isolated yields. c) An additional cycloadduct was formed but its stereostructure could not be determined.

Table 9. Spectral data for the cycloadducts to unsymmetrical trans olefins **48**

	IR (cm^{-1})	^{1}H-NMR Spectra measured in deuteriochloroform (δ, ppm, and Hz)										M^+ (m/z)
		3-H	2-H	1-H	10b-H	6-H	5-H	J_{3-2}	J_{2-1}	J_{1-10b}		
49	1680, 1660, 1635, 1605	6.00^d	4.16^{dd}	4.96^{dd}	5.16^d	5.16^d	5.83^d 7.4	8.0	5.5	7.6	2.33^s (p-Me)	496
50	1690, 1670, 1600	5.07^d	3.83^{dd}	4.62^{dd}	5.28^d	5.52^d	6.30^d 7.5	5.0	9.0	10.0	2.23^s (p-Me)	496
51	1660, 1620, 1595	5.02^d	3.93^{dd}	3.68^{ddd}	5.06^d	5.47^d	6.20^d 7.3	4.3	8.0	9.1	9.70^d (CHO)	379
52[a]	1720, 1690	4.69^d	2.68^{ddq}	3.06^{ddd}	5.07^d	5.40^d	6.16^d 7.5	4.5	7.6	8.9	1.28^d (2-Me), 9.73^d (CHO)	317
53[b]	1690, 1680, 1610, 1600	5.22^d	3.02^{ddq}	4.36^t	5.24^d	5.48^d	6.21^d 7.3	8.5	8.5	8.5	0.88^d (2-Me)	393
54	2220, 1678, 1605	4.60^d	3.87^t	4.71^{dd}	5.13^d	5.69^d	6.43^d 7.9	8.1	8.1	8.9	2.33^s (p-Me)	390
55	1740, 1660, 1620, 1600	4.40^d	3.87^{dd}	4.72^{dd}	5.20^d	5.60^d	6.39^d 7.4	9.0	8.1	8.7	2.33^s (p-Me), 3.20^s (COOMe)	423
56[c]	1740, 1670, 1620	4.23^d	2.92^{ddq}	4.40^{dd}	5.25^d	5.42^d	6.20^d 7.5	8.5	10.0	9.0	0.98^d (2-Me), 3.67^s (COOMe)	347
		7-H	6-H	5-H	4a-, 4-, 3-H		2-H	J_{7-6}	J_{6-5}	J_{5-4a}		
57	1690—1660, 1580	5.93^d	4.50^{dd}	4.93^t	5.10—5.94^m		6.72^m	7.9	9.0	9.0	2.37^s (p-Me)	d)
		5-H	6-H	7-H	7a-H	2-H	3-H	J_{5-6}	J_{6-7}	J_{7-7a}		
58	1680, 1670 1600	5.29^d	4.56^{dd}	4.93^{dd}	6.52^d	5.47^d	5.87^d 4.5	7.5	8.2	7.8	2.37^s (p-Me)	425

a) Contaminated by 20% of an isomer which shows 0.92^d (2-Me). b) Contaminated by 14% of an isomer which shows 1.03^d (2-Me). c) Contaminated by 30% of an isomer which shows 1.37^d (2-Me) and 3.77^s (COOMe). d) No parent ion peak was observed.

later, **50** was determined to be the 1-endo-2-exo cycloadduct to the syn form of **2a** as a thermodynamically controlled product, and the same to the others **51—52**.

The coupling pattern of the third type of cycloadducts **53—58** is close to the 1-exo-2-endo cycloadducts **29′—34′** of nitro olefins to the syn form of **2** (see Scheme 5 and Table 6). Thus, they were assigned to be the 1-exo-2-endo cycloadducts to the syn form of **2** as the cycloadducts isomerized through betaine intermediates.

To confirm the structures of the above cycloadducts, rather stable two cycloadducts **50** and **53** were subjected to the cyclization using hydrazine hydrate. As shown in Scheme 9, two types of diazacyclazine derivatives **59** and **60** were obtained. It is clear that the stereochemistry has not changed, in both cases, before and after the cyclization, because the starting materials **50** and **53** showed very similar couplings to those of the products **59** and **60**, respectively. Not only the coupling pattern but also the mode of cyclization supports the proposed

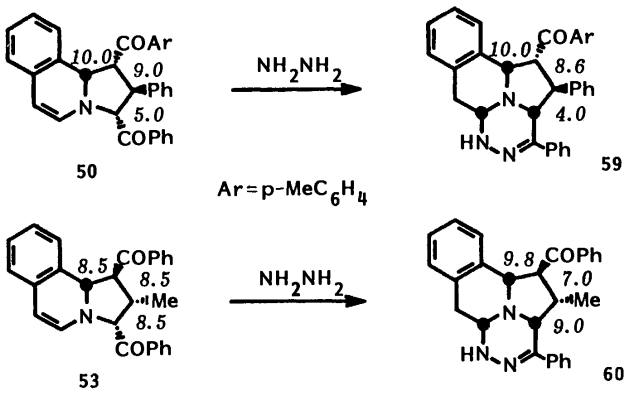

Scheme 9.

structures of **50** and **53**, and hence of **50—52** and **53—58**. Molecular model inspection shows that such hydrazine cyclization is possible only when the 3-benzoyl moiety is endo, and both **50** and **53** were assigned as the cycloadducts of syn ylide.

The stereochemical features observed in the cycloadditions of the ylides **2—4** with unsymmetrically substituted trans olefins **48** are symmarized in Fig. 7 with the cycloaddition example using **2**. In this case also, the kinetically favored approach is the 1-endo-2-exo approach **K** to the anti form of **2** forming the kinetical product **N**. The cycloadduct **49** is an example belonging to this kind. When W is strongly ylide-stabilizing and also the both olefin substituents R and COR′ are highly activating the olefin, the kinetical cycloadduct **N** suffers from a ready retro cycloaddition giving back to the ylide **2** and olefin **48**. They again undego a cycloaddition, but through a different approach **L**, the 1-endo-2-exo approach to the syn form of **2**, producing the thermodynamic cycloadduct **O**. The cycloadducts **50—52** are the examples. When the retro cycloaddition path is forbidden (W is cyano or ester, or the olefin substituents are not highly activating), the kinetical cycloadduct **N** takes another isomerization pathway. As have been observed for the nitrostyrene cycloadducts, the isomerization through a betaine intermediate **M** occurs leading to the 1-exo-2-endo cycloadduct **P** to the syn form of **2**. The cycloadducts **53—56** are the cases.

Experimental

Materials. *N*-Phenacyl-3,5-dimethylpyridinium bromide (mp 200—203 °C, Found: C, 58.56; H, 5.33; N, 4.54%. Calcd for $C_{15}H_{16}ONBr$: C, 58.82; H, 5.23; N, 4.58%) and *N*-cyanomethyl-3,5-dimethylpyridinium bromide (mp 143—145 °C, Found: C, 47.36; H, 4.84; N, 12.15%. Calcd for $C_9H_{11}N_2Br$: C, 47.58; H, 4.85; N, 12.33%) were prepared by

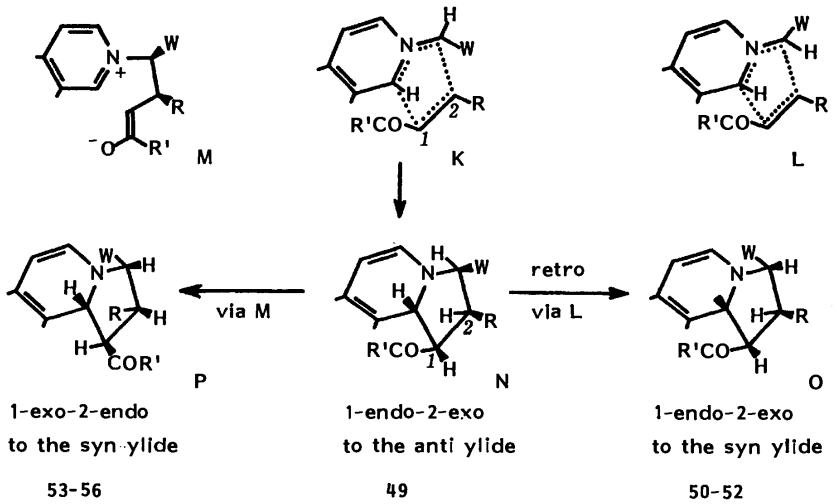

Fig. 7. Stereochemical course of the cycloaddition between **2** and **48**.

the reactions of 3,5-dimethylpyridine with α-bromoacetophenone and α-bromoacetonitrile, respectively. *N*-(*p*-Tolyl)citraconimide **6** was obtained by the reaction between citraconic anhydride and *p*-methylaniline followed by the treatment with acetic anhydride in the presence of sodium acetate.[9] Diethyl methylenemalonate **24** and benzylidenemalononitrile **26** were synthesized by the condensation of diethyl malonate with paraformaldehyde[10] and of malononitrile with benzaldehyde,[11] respectively. β-Nitrostyrenes **28a—d** were all prepared from the condensations between nitromethane and *p*-substituted benzaldehydes:[12] **28a**: Pale yellow prisms ($CHCl_3$), mp 58 °C; **28b**: Yellow prisms (EtOH), mp 81—82 °C; **28c**: Yellow needles ($CHCl_3$), mp 92—94 °C; **28d**: Pale yellow prisms ($CHCl_3$). (*E*)-1-(*p*-Methylbenzoyl)-2-phenylethene **48a** and (*E*)-1-benzoylpropene **48d** were obtained by the condensations between *p*-methylacetophenone and benzaldehyde[13] and between triphenylphosphonium phenacylide and acetaldehyde,[14] respectively. Other olefinic dipolarophiles **15—17**, **35**, and **48b—c** were all commercially available.

General Procedure for the Cycloadditions of 1a—e and 2a to Methyl-substituted Olefins 6 and 15. To the equivalent suspension of a ylide precursor and an olefin in dry chloroform (30 ml for the 1 mmol-scaled reaction), was slowly added an equivalent amount of triethylamine at room temperature. The mixture was allowed to stir at room temperature (one exception: The reaction between **2a** with **15** was carried out under reflux in chloroform) until all the precursor salts dissolved into a clear solution. After the completion of cycloaddition, the mixture was poured into ice water and extracted with chloroform twice (20 ml×2). The combined extracts were dried over $MgSO_4$ and evaporated *in vacuo* below room temperature. The crude oily material was weighed and subjected to the ^{1}H-NMR measurement. Often it solidified when triturated with petr. ether and/or ether. The reaction conditions, the melting points and yields of products are listed in Table 1. In every case the purification of cycloadduct was unsuccessful because of their lability. Therefore, the solidified products, or oily product itself, were submitted for the spectral measurement. Table 2 shows all the spectral data of cycloadducts **7—14** and **16**.

General Procedure for the Cycloadditions of 2 and 5 to Acrylic 17 and Related Olefins 24 and 26. The cycloadditions were performed by the similar procedures described above under the reaction conditions listed in Table 3. The melting points and yields of products are shown in Table 3 and the spectral data in Table 4. Other data are given as follows: **18**: Yellow prisms ($CHCl_3$–ether); ^{1}H-NMR ($CDCl_3$) δ=2.20—2.70 (2H, m, 2-H), 3.30—3.60 (1H, m, 1-H), 4.96 (1H, d, J_{10b-1}=5.2 Hz, 10b-H), 5.23 (1H, dd, J_{3-2}=9.0 and 6.0 Hz, 3-H), 5.37 (1H, d, J_{6-5}=7.5 Hz, 6-H), 6.16 (1H, d, J_{5-6}=7.5 Hz, 5-H), 6.90—7.70, and 7.80—8.10 ppm (9H, each m, ArH); Found: C, 80.06; H, 5.16; N, 9.04%. Calcd for $C_{20}H_{16}ON_2$: C, 79.98; H, 5.37; N, 9.33%. **19**: Yellow prisms (ether); Found: C, 75.42; H, 5.73; N, 4.28%. Calcd for $C_{21}H_{19}O_3N$: C, 75.65; H, 5.74; N, 4.20%. **20+21**: ^{13}C-NMR ($CDCl_3$) the major: δ=37.40 (t, 2-C), 38.57 (d, 1-C), 63.28, and 64.65 (each d, 3- and 10b-C); the minor: δ=35.20 (t, 2-C), 36.33 (d, 1-C), 63.57, and 65.92 ppm (each d, 3- and 10b-C). The intensity ratio was 2/1. **23**: colorless needles (EtOH); ^{13}C-NMR ($CDCl_3$) δ=33.3 (t, 2-C), 36.7 (d, 1-C), 68.0, 72.4 (each d, 3- and 9a-C), and 196.9 ppm (s, PhCO); Found: C, 70.44; H, 4.45; N, 9.07%. Calcd for $C_{18}H_{14}ON_2S$: C, 70.56; H, 4.61; N, 9.14%.

General Procedure for the Cycloadditions of 2 to Nitro Olefins 28. These cycloadditions were carried out using each equivalent amount of **2** and **28** according to the procedure mentioned above under the reaction conditions shown in Table 5. The results and the spectral data of cycloadducts are summarized in Table 5 and 6, respectively. The methods for separation of the isomeric cycloadducts and other data are given as follows:

29+29′: Either of **29** or **29′** was precipitated when the reaction mixture was condensed *in vacuo*. **29** or **29′**: Yellow needles ($CHCl_3$); MS *m/z* (rel intensity, %) 347 (M^+−49, 4), 105 (76), and 77 (base peak); Found: C, 75.85; H, 5.11; N, 7.16%. Calcd for $C_{25}H_{20}O_3N_2$: C, 75.74; H, 5.09; N, 7.07%.

30+30′: **30** was separated as precipitate during the cycloaddition in $CHCl_3$ and the evaporation of the filtrate gave a mixture of **30** and **30′**. **30**: Yellow needles ($CHCl_3$); MS *m/z* (rel intensity, %) 377 (M^+−49, 10), 348 (6), 228 (42), 105 (66), and 77 (base peak); Found: C, 72.75; H, 5.16; N, 6.79%. Calcd for $C_{26}H_{22}O_4N_2$: C, 73.22; H, 5.20; N, 6.57%. **30+30′**: Yellow solid; Found: C, 73.27; H, 5.10; N, 6.49%. Calcd for $C_{26}H_{22}O_4N_2$: C, 73.22; H, 5.10; N, 6.49%.

31+31′: **31′** was precipitated when the reaction mixture was condensed *in vacuo* at room temperature, and **31** was obtained as precipitate from the solution of **31′** in acetone. **31**: Yellow prisms (Me_2CO). **31′**: Yellow needles ($CHCl_3$); MS *m/z* (rel intensity, %) 377 (M^+−23, 17) and 361 (base peak); Found: C, 75.36; H, 5.28; N, 6.85%. Calcd for $C_{26}H_{22}O_3N_2$: C, 76.08; H, 5.40; N, 6.83%.

32+32′: Either of **32** or **32′** was isolated when the reaction mixture was evaporated *in vacuo* and the residue was triturated with ether. **32** or **32′**: Yellow needles ($CHCl_3$); MS *m/z* (rel intensity, %) 431 (M^+, 1) and 278 (base peak); Found: C, 69.78; H, 4.37; N, 6.18%. Calcd for $C_{25}H_{19}O_3N_2Cl$: C, 69.52, H, 4.40; N, 6.49%.

33+33′: **33′** was obtained as yellow viscous oil when the reaction solvent was removed *in vacuo*, and the solution of **33′** in $CHCl_3$ precipitated **33** after a long period of time at room temperature. **33**: Yellow needles ($CHCl_3$); MS *m/z* 315 (M^+−16), 290, and 282 (M^+−49, base peak); Found: C, 72.61; H, 5.22; N, 12.41%. Calcd for $C_{20}H_{17}O_2N_3$: C, 72.49; H, 5.17; N, 12.68%.

34+34′: **34′** was obtained when the oily crude product was treated with ether and isomerized in $CHCl_3$ at room temperature into a mixture of **34** and **34′**. **34′**: Yellow prisms (ether); MS *m/z* (rel intensity, %) 364 (M^+, 26), 317 (M^+−47, 72), and 258 (base peak); Found: C, 68.91; H, 5.63; N, 7.90%. Calcd for $C_{21}H_{20}O_4N_2$: C, 69.21; H, 5.53; N, 7.60%.

Retro Cycloadditions of 31+31′ and 34+34′ in the Presence of N-Methylmaleimide 35. A mixture of **31** and **31′** (1:1) in DMSO-d_6 was placed in an NMR sample tube and an equivalent amount of **35** was added. The resulting mixture was observed by ^{1}H-NMR spectroscopy. After 4 h at room temperature, each 50% of **31+31′** and **35** was consumed and the endo cycloadduct **36** was formed. And after 48 h at the same temperature, none of **31**, **31′**, and **35** was in the solution and the only compounds contained were **36** and **28c**. The similar procedure using a mixture of **34**, **34′**, and **35** in DMSO-d_6 showed no formation of the

cycloadduct between **28c** and **35**.

Reaction of 29+29′ with Hydrazine Hydrate Leading to 38. To a mixture of **29** and **29′** (396 mg, 1 mmol) in EtOH (20 ml), was added hydrazine hydrate (4 ml) and the resulting mixture was heated under reflux for 6 h. The residue, obtained by evaporation of the solvent *in vacuo*, was treated with ice water (20 ml) and then extracted with ether (20 ml×2). The ether was dried over $MgSO_4$ and evaporated *in vacuo*. The residue was chromatographed over silica gel (C-300) with chloroform giving 127 mg of **38** (31%): Colorless prisms (ether-petr. ether); mp 188 °C; IR (KBr) 3350, 1540, and 1360 cm^{-1}; ^{1}H-NMR ($CDCl_3$) δ=2.65 (1H, d, J_{gem}=18.0 Hz, 6-*endo*-H), 3.25 (1H, dd, J_{gem}=18.0 and J_{6-5a}=6.8 Hz, 6-*exo*-H), 3.53 (1H, dd, J_{2-1}=6.0 and J_{2-2a}=3.5 Hz, 2-H), 4.68 (1H, d, J_{5a-6}=6.8 Hz, 5a-H), 4.79 (1H, br.d, J_{2a-2}=3.5 Hz, 2a-H), 4.98 (1H, d, J_{10b-1}=9.5 Hz, 10b-H), 5.03 (1H, dd, J_{1-10b}=9.5 and J_{1-2}=6.0 Hz, 1-H), 5.96 (1H, br.s, NH, D_2O exchangable), and 6.90—7.50 ppm (14H, m, ArH); ^{13}C-NMR ($CDCl_3$) δ=31.77 (t, 6-C), 55.21, 58.67, 63.74, 64.42 (each d, 2-, 2a-, 5a-, and 10b-C), 95.27 (d, 1-C), 123.29, 125.67, 126.31, 127.53, 128.01, 128.31, 128.45, 128.89, 129.18, 131.91 (s), 134.20 (s), 135.76 (s), 141.12 (s), and 145.46 ppm (s, 3-C); MS *m/z* (rel intensity, %) 410 (M^+, 12), 364 (70), and 244 (base peak).

Found: C, 73.29; H, 5.36; N, 13.39%. Calcd for $C_{25}H_{22}O_2N_4$: C, 73.15; H, 5.40; N, 13.65%.

Cycloaddition between 2e and 28a Followed by Hydrazine Cyclization Leading to 40. A mixture of *N*-(1-benzoylethyl)isoquinolinium bromide (684 mg, 2 mmol) and **28a** (298 mg, 2 mmol) in dry chloroform (30 ml) was refluxed for 30 min in the presence of NEt_3 (0.28 ml, 2 mmol). The solvent was evaporated *in vacuo*, the residue treated with water (30 ml), extracted with ether (20 ml×2), the ether dried over $MgSO_4$, and then evaporated *in vacuo*. The residue was dissolved in EtOH (30 ml). After hydrazine hydrate (4 ml) was added, the mixture was heated under reflux for 22 h. The ethanol was evaporated *in vacuo*, the residue treated with water (10 ml), extracted with ether (20 ml×2), the ether dried over $MgSO_4$, and evaporated *in vacuo*. The residue was chromatographed over silica gel using chloroform as an eluent to give **40** (264 mg, 31%): Colorless solid; mp 109 °C; IR (KBr) 1550 cm^{-1}; ^{1}H-NMR ($CDCl_3$) δ=1.34 (3H, s, Me), 2.73 (1H, d, J_{gem}=18.0 Hz, 6-*endo*-H), 3.30 (1H, dd, J_{gem}=18.0 and J_{6-5a}=6.0 Hz, 6-*exo*-H), 3.92 (1H, d, J_{2-1}=6.8 Hz, 2-H), 4.78 (1H, d, J_{10b-1}=9.5 Hz, 10b-H), 4.90 (1H, d, J_{5a-6}=6.0 Hz, 5a-H), 5.27 (1H, dd, J_{1-10b}=9.5 and J_{1-2}=6.8 Hz, 1-H), 6.04 (1H, br.s, NH, D_2O exchangable), and 6.80—7.28 ppm (14H, m, ArH); MS *m/z* (rel intensity, %) 424 (M^+, 2), 275 (60), and 258 (base peak).

This product **40** was acetylated with acetic anhydride in the presence of a catalytic amount of pyridine at room temperature for 2 d to afford 43% of **41**: Colorless prisms (ether-hexane); mp 161 °C; IR (KBr) 1690 cm^{-1}; ^{1}H-NMR ($CDCl_3$) δ=1.33 (3H, s, Me), 2.37 (3H, s, COMe), 3.70 (1H, dd, J_{gem}=18.5 and J_{6-5a}=6.0 Hz, 6-*exo*-H), 3.90 (1H, dd, J_{gem}=18.5 and J_{6-5a}=3.7 Hz, 6-*endo*-H), 4.23 (1H, d, J_{2-1}=4.5 Hz, 2-H), 4.58 (1H, d, J_{10b-1}=8.0 Hz, 10b-H), 5.24 (1H, dd, J_{1-10b}=8.0 and J_{1-2}=4.5 Hz, 1-H), 5.47 (1H, dd, J_{5a-6}=6.0 and 3.7 Hz, 5a-H), and 6.90—7.70 ppm (14H, m, ArH); MS *m/z* (rel intensity, %) 466 (M^+, 1) and 258 (base peak).

Found: C, 72.27; H, 5.77; N, 12.14%. Calcd for $C_{28}H_{26}O_3N$: C, 72.08; H, 5.62; N, 12.01%.

General Procedure for the Aromatization of 29—32 and 29′—32′ Leading to 42—47. To the solution of **29—32** and **29′—32′** (1 mmol in 10 ml of solvent), was added an equivalent amount of PPh_3, NEt_3, DBU, or DDQ. The resulting mixture was allowed to react until all the cycloadduct was consumed (checked on TLC). The base, oxidant, solvent, temperature, and time are listed in Table 7. After the reaction was completed, the solvent was evaporated *in vacuo*. The residue was chromatographed over silica gel using benzene as an eluent to give the aromatized cycloadduct. The melting points and yields of products are summarized in Table 7. Other date are given as follows:

42: Yellow prisms (ether); IR (KBr) 1600 cm^{-1}; ^{1}H-NMR ($CDCl_3$) δ=6.82—7.78 (14H, m, ArH), 8.00—8.23 (1H, m, ArH), and 9.23 ppm (1H, d, J=8.0 Hz, 10-H); MS *m/z* (rel intensity, %) 347 (M^+, 8) and 380 (base peak).

Found: C, 86.24; H, 4.97; N, 4.35%. Calcd for $C_{25}H_{17}ON$: C, 86.43; H, 4.93; N, 4.03%.

43: Yellow prisms (ether); IR (KBr) 1610 and 1590 cm^{-1}; ^{1}H-NMR ($CDCl_3$) δ=2.20 (3H, s, *p*-Me), 6.70—7.20 (8H, m, ArH), 7.30—7.80 (5H, m, ArH), 8.00—8.20 (1H, m, ArH), and 9.25 ppm (1H, d, J=7.5 Hz, 10-H); MS *m/z* 361 (M^+).

Found: C, 85.87; H, 5.23; N 3.89%. Calcd for $C_{26}H_{19}ON$: C, 86.40; H, 5.30; N, 3.88%.

44: Yellow prisms (benzene-hexane); IR (KBr) 1600, 1520, and 1360 cm^{-1}; ^{1}H-NMR ($CDCl_3$) δ=3.64 (3H, s, OMe), 6.54 (2H, br.d, J=9.0 Hz, ArH), 6.80—7.15, 7.50—7.70 (12H, each m, ArH), 8.10 (1H, m, ArH), and 9.23 ppm (1H, d, J=8.0 Hz, 10-H); MS *m/z* (rel intensity, %) 377 (M^+, base peak), 348 (12), 300 (17), 188 (10), 105 (3), and 77 (7).

Found: C, 82.74; H, 5.07; N, 3.71%. Calcd for $C_{26}H_{19}O_2N$: C, 82.83; H, 5.04; N, 3.81%.

45: Orange prisms (ether); IR (KBr) 1610, 1590, 1450, and 1400 cm^{-1}; MS *m/z* (rel intensity, %) 383, 381 (M^+, 13, 40), 241 (94), and 78 (base peak).

Found: C, 78.34; H, 4.27; N, 3.83%. Calcd for $C_{25}H_{16}ONCl$: C, 78.64; H, 4.19; N, 3.67%.

46: Yellow prisms (ether); IR (KBr) 1730, 1620, and 1510 cm^{-1}; ^{1}H-NMR ($CDCl_3$) δ=3.66 (3H, s, OMe), 6.57 (2H, br.d, J=9.0 Hz, ArH), 6.90—7.30, 7.30—7.80 (11H, each m, ArH), 8.25—8.50 (1H, m, ArH), and 8.96 ppm (1H, d, J=7.8 Hz, 10-H); MS *m/z* (rel intensity, %) 422 (M^+, 24), 105 (68), and 77 (base peak).

47: Yellow prisms (ether); IR (KBr) 1600, 1570, and 1520 cm^{-1}; ^{1}H-NMR ($CDCl_3$) δ=2.31 (3H, s, *p*-Me), 6.87—7.89 (13H, m, ArH), 8.37—8.62 (1H, m, ArH), and 9.06 ppm (1H, d, J=8.0 Hz, 10-H); MS *m/z* (rel intensity, %) 406 (M^+, 56).

Found: C, 77.11; H, 4.63; N, 6.73%. Calcd for $C_{26}H_{18}O_3N_2$: C, 76.83; H, 4.46; N, 6.87%.

General Procedure for the Cycloadditions of 2—4 to Unsymmetrical trans Olefins 48. To the mixture of 1 mmol each of the ylide precursor and **48** in 30 ml of solvent, was added an equivalent amount of NEt_3. The resulting mixture was stirred at room temperature until all the suspension dissapeared. The reaction solvent and time are listed in Table 8. After the completion of cycloaddition, the mixture was poured into ice water and extracted twice (each 20 ml) with dichloromethane. The combined extracts were dried over $MgSO_4$ and evaporated

in vacuo giving crude cycloadduct. As the cycloadducts **49**—**58** are all too labile to be purified through a chromatography or from crystallization, they were subjected to the spectral measurement. The yields and spectral data of cycloadducts are shown in Table 8 and 9, respectively. Other data are given as follows:

49: Yellow needles (CH_3CN); mp 165—167 °C; **50**: Yellow solid; mp 94—96 °C; Found: C, 84.26; H, 5.83; N, 2.84%. Calcd for $C_{33}H_{27}O_2N$: C, 84.40; H, 5.80; N, 2.98%. **51**: Yellow needles (ether); mp 182—185 °C (dec). **52**: Yellow solid; mp 102—104 °C. **53**: Orange solid; mp 61—65 °C. **54**: Orange solid; mp 105—107 °C. **55**: Yellow solid; mp 79—82 °C. **56**: Orange solid; mp 64—70 °C.

*Hydrazine Cyclization of **50** Leading to **59**.* A mixture of **50** (928 mg, 2 mmol) and hydrazine hydrate (4 ml) in EtOH (50 ml) was refluxed for 14 h and the solvent was evaporated *in vacuo*. The residue was treated with ice water, extracted with ether (20 ml×2), the ether dried over $MgSO_4$, and evaporated *in vacuo*. The residue was chromatographed over silica gel (Merck C-200) with ethyl acetate–hexane (1:4) to give **59** (347 mg, 36%): Colorless prisms (Me_2CO); mp 132—133 °C; IR (KBr) 3350, 1700, 1660, and 1600 cm^{-1}; ^1H-NMR ($CDCl_3$) δ=2.28 (3H, s, *p*-Me), 2.77 (1H, br.d, J_{gem}=18.0 Hz, 6-*endo*-H), 3.11 (1H, dd, J_{2-1}=8.6 and J_{2-2a}=4.0 Hz, 2-H), 3.43 (1H, br.dd, J_{gem}=18.0 and J_{6-5a}=6.7 Hz, 6-*exo*-H), 4.09 (1H, dd, J_{1-10a}=10.0 and J_{1-2}=8.6 Hz, 1-H), 4.87 (1H, br.d, J_{5a-6}=6.7 Hz, 5a-H), 4.88 (1H, d, J_{2a-2}=4.0 Hz, 2a-H), 5.04 (1H, d, J_{10b-1}=10.0 Hz, 10b-H), 5.76 (1H, br.s, NH, D_2O exchangable), 6.56 (1H, br.d, J=8.0 Hz, ArH), and 6.64—7.46 ppm (17H, m, ArH); MS *m/z* (rel intensity, %) 483 (M^+, 7), 482 (9), and 244 (base peak).

Found: C, 79.50; H, 6.55; N, 7.92%. Calcd for $C_{33}H_{29}ON_3$: C, 79.82; H, 6.51; N, 7.76%.

*Hydrazine Cyclization of **53** Leading to **60**.* A mixture of **53** (786 mg, 2 mmol) and hydrazine hydrate (4 ml) in EtOH (50 ml) was refluxed for 14 h and the solvent was evaporated *in vacuo*. The residue was treated with ice water, extracted with ether (20 ml×2), the ether dried over $MgSO_4$, and evaporated *in vacuo*. The residue was chromatographed over silica gel with hexane–ethyl acetate (3:1) to give **60** (222 mg, 27%): Colorless needles (EtOH); mp 250—253 °C; IR (KBr) 3200 and 1660 cm^{-1}; ^1H-NMR ($CDCl_3$) δ=1.02 (3H, d, J=7.1 Hz, 2-Me), 2.60—3.08 (3H, m, 6-CH_2 and 2-H), 3.90 (1H, dd, J_{1-10b}=9.8 and J_{1-2}=7.0 Hz, 1-H), 4.38 (1H, br.t, J_{5a-6}=7.0 Hz, 5a-H), 4.65 (1H, d, J_{2a-2}=9.0 Hz, 2a-H), 5.17 (1H, d, J_{10b-1}=9.8 Hz, 10b-H), 6.08 (1H, br.s, NH, D_2O exchangable), and 6.60—7.92 ppm (14H, m, ArH); MS *m/z* (rel intensity, %) 407 (M^+, 24) and 130 (base peak).

Found: C, 79.37; H, 6.08; N, 10.38%. Calcd for $C_{27}H_{25}ON_3$: C, 79.58; H, 6.18; N, 10.31%.

References

1) O. Tsuge, S. Kanemasa, and S. Takenaka, *Bull. Chem. Soc. Jpn.*, **58**, 3137 (1985).

2) A. Kakei and S. Ito, *Bull. Chem. Soc. Jpn.*, **47**, 938 (1974).

3) J. Fröhlich and F. Kröhnke, *Chem. Ber.*, **104**, 1621 (1971).

4) J. Curtze, R. Dach, K. H. Duchardt, and F. Kröhnke, *Chem. Ber.*, **112**, 2197 (1979).

5) M. Petrovanu, C. Luchian, S. Supráteanu, and V. Bărboiu, *Rev. Roum. Chim.*, **24**, 1053 (1979).

6) Z. Bende, L. Töke, L. Weber, G. Tóth, F. Janke, and G. Csonka, *Tetrahedron*, **40**, 369 (1984).

7) O. Tsuge, S. Kanemasa, S. Kuraoka, and S. Takenaka, *Chem. Lett.*, **1984**, 281; O. Tsuge, S. Kanemasa, S. Takenaka, and S. Kuraoka, *ibid.*, **1984**, 465.

8) It is not clear so far whether an aryl group either at the 1- or 2-position can interact attractively with the hetero-aromatic plane of ylide or can not.

9) T. Oishi, *Polym. J.*, **12**, 799 (1980).

10) G. B. Bachman and H. A. Tanner, *J. Org. Chem.*, **4**, 493 (1939).

11) A. F. Odell and C. W. Hines, *J. Am. Chem. Soc.*, **35**, 82 (1913).

12) D. E. Worrall, C. S. Marvel, and W. H. Lycan, *Org. Synth.*, Coll. Vol. **1**, 413 (1941).

13) C. Weygand and H. Baumgärtel, *Ann. Chem.*, **469**, 253 (1929).

14) R. C. Fuson, R. Christ, and G. M. Whitman, *J. Am. Chem. Soc.*, **58**, 2450 (1936).

Total Synthesis of (−)-Deoxocassine and Its Diastereomers

Kazuo KURIHARA, Takashi SUGIMOTO, Yutaka SAITOH, Yukinobu IGARASHI, Hiroshi HIROTA, Yoshihiko MORIYAMA,† Takahiko TSUYUKI,* Takeyoshi TAKAHASHI,* and Qui KHUONG-HUU††

Department of Chemistry, Faculty of Science, The University of Tokyo, Hongo, Bunkyo-ku, Tokyo 113

††*Institut de Chimie des Substances Naturelles, Centre National de la Recherche Scientifique, 91190-Gif-sur-Yvette, France*

(Received July 12, 1985)

(−)-Deoxocassine [(2*R*,3*R*,6*S*)-6-dodecyl-2-methyl-3-piperidinol] and its diastereomers with 2*R*-configuration were synthesized starting from D-alanine by a route involving the intramolecular aminomercuration of an ε,ζ-unsaturated amine.

A number of piperidine alkaloids were isolated from plants of *Prosopis*,[1a] *Cassia*,[1b,c] *Azima*,[1d] and *Bathiorhamnus*[1c] species and from venoms of fire ants, *Solenopsis* species[1f] and their structures were elucidated. In these alkaloids, three substituents generally exist on the piperidine ring; a methyl or hydroxymethyl group at C-2, a hydroxyl or acyloxyl group at C-3, and a long alkyl side chain at C-6. Frequently there occur congeners from the same plant, and stereochemical investigation on the substituents between the congeners reveals that the same or homologous substituents on the same carbon atoms of the piperidine rings often possess the opposite configurations each other. For example, Christofidis *et al.*[1b] obtained three piperidine alkaloids, (+)-spectaline (**1**), (+)-iso-6-cassine (**2**), and (−)-cassine (**3**) from leaves of *Cassia spectablis* DC (Leguminosae). The absolute configurations of 2-methyl, 3-hydroxyl, and 6-alkyl side chain in these compounds were found to be (2*S*,3*S*,6*R*), (2*R*,3*R*,6*R*), and (2*R*,3*R*,6*S*) for **1**, **2**, and **3**, respectively.

Many synthetic investigations of the piperidine alkaloids have been reported.[2] Recently we reported a total synthesis of (−)-deoxoprosopinine and (−)-deoxoprosophylline[3] using an intramolecular aminomercuration.[4] From an interest in the occurrence of diastereomeric compounds such as **2** and **3** from the same origin, a total synthesis of (−)-deoxocassine (**4**)[5] and its diastereomers was planned. Although (−)-deoxocassine (**4**) is corresponding to a deoxo derivative of (−)-cassine (**3**), the compound (**4**) was also registered as desoxoprosafrinine and desoxoprosafrinone in Ratle's dissertation.[5] The original piperidine alkaloids, (−)-prosafrinine (**5**) and (−)-prosafrine (**6**) were isolated from *Prosopis africana* (GUILL and PERR.) TAUB.[1a] This paper describes a total synthesis of (−)-deoxocassine (**4**) and two diastereomers (**7** and **8**) with 2*R*-configuration starting from D-alanine by a route utilizing the intramolecular aminomercuration.[4]

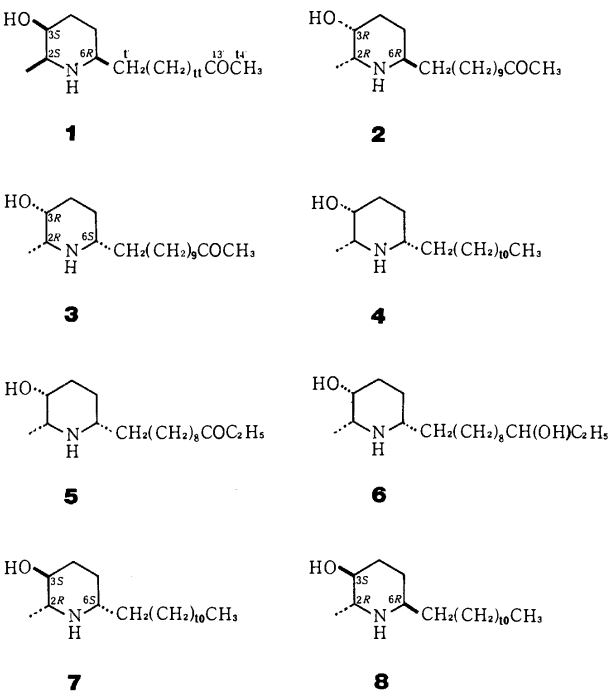

1 **2** **3** **4** **5** **6** **7** **8**

N-Phthaloylation[6] and the Rosenmund reduction[7] of D-alanine afforded (2*R*)-2-phthalimidopropanal (**9**), the aldehydic proton of which appeared as a sharp singlet at δ 9.68 in the ^{1}H NMR spectrum. The aldehyde (**9**) was treated with diallylzinc[8] in tetrahydrofuran (THF) at −30 to −10 °C to afford diastereomeric alcohols (**10** and **11**) in 51 and 10% yields, respectively. The major alcohol (**10**) showed double quartet signals due to $C_{(2)}$-H at δ 4.37 ($J_{2,3}$=4 Hz), while the corresponding signal of the minor alcohol (**11**) appeared at δ 4.42 as a quintet (J=7 Hz). The stereostructure of the major alcohol (**10**) was inferred to be an *erythro* isomer [(2*R*,3*S*)-2-phthalimido-5-hexen-3-ol] and the minor one (**11**) (2*R*,3*R*)-*threo* isomer by the Cram's rule, and these assignments were further confirmed by Horeau's method.[9] The *erythro* and *threo* isomers (**10** and **11**) were treated with racemic 2-phenylbutyric anhydride

† Present address: Institute of Chemistry, Kyoto Prefectural University of Medicine, Taishogun, Kita-ku, Kyoto 603.

and the reaction mixtures were worked up as usual, respectively. The 2-phenylbutyric acid obtained from the reaction with **10** showed $[\alpha]_D$ −0.015° (*c* 0.2, optical yield 10%) and the 2-phenylbutyric acid from **11** $[\alpha]_D$ +0.031° (*c* 0.2, optical yield 21%) showing that the asymmetric centers (C-3) of the secondary alcohols (**10** and **11**) possess *S* and *R* configurations, respectively.

Since the minor alcohol (**11**) with (3*R*)-configuration should be required for a preparation of (−)-deoxocassine (**4**), a direct conversion of the configuration at C-3 of the major alcohol (**10**) was attempted first using an adoptation of Mitsunobu's method.[10] However, treatment of **10** with an acid such as benzoic acid or formic acid in the presence of triphenylphosphine and diethyl azodicarboxylate did not afford any desired ester. When the reaction was conducted in the presence of *N*,*N*-dimethylformamide dineopentylacetal[10c,11] and bis(diethylamino)chlorophosphine,[10d,12] only a complex mixture was produced, respectively.

On oxidation with pyridinium chlorochromate, the main alcohol (**10**) gave a ketone (**12**) in 88% yield, which was subjected to reduction with zinc borohydride to afford two alcohols (**10** and **11**) in 25 and 53% yields, respectively. The main reduction product was completely identical, including the optical purity, with the alcohol (**11**) obtained as the minor product by the reaction of aldehyde (**9**) with diallylzinc.

The (2*R*,3*R*)-alcohol (**11**) was treated with methoxymethyl chloride in triethylamine and acetonitrile to afford (2*R*,3*R*)-*N*,*N*-phthaloyl-3-methoxymethoxy-5-hexen-2-amine (**13**) quantitatively. The methoxymethyl derivative (**13**) was subjected to hydroboration to give (4*R*,5*R*)-4-methoxymethoxy-5-phthalimido-1-hexanol (**14**) in 83% yield, which was oxidized with pyridinium chlorochromate. (4*R*,5*R*)-4-Methoxymethoxy-5-phthalimidohexanal (**15**), susceptible to air-oxidation, was obtained in 85% yield. The Wittig reagent which was generated from dodecyltriphenylphosphonium bromide (prepared by Chasin's procedure[13]) and butyllithium in hexane, was quickly treated with the aldehyde (**15**) in THF at −78 °C. The usual work-up gave (2*R*,3*R*)-3-methoxymethoxy-2-phthalimido-6-octadecene (**16**) in 60% yield. The olefin (**16**) is inferred to mainly consist of a (*Z*)-isomer, because no band due to *trans*-olefin was observed in the IR spectrum. This conclusion was confirmed by the separate synthetic route (*vide infra*).

The *N*-phthaloyl group of **16** was removed by treatment with an excess of hydrazine monohydrate to give (2*R*,3*R*,6*Z*)-3-methoxymethoxy-6-octadecen-2-amine (**17**), which, without purification, was subjected to the aminomercuration with mercury(II) acetate in methanol and successively to the demercuration with sodium borohydride. Since the reaction product was shown to be a complex mixture of several reaction products, the chromatographic separation was attempted, but the desired piperidine derivatives (**18** and/or **19**) could not be isolated. Then separation of the mixture was attempted after *N*-protection. However, neither *N*-*t*-butoxycarbonyl,[14] *N*-trityl, nor *N*-methoxycarbonyl derivative[15] could be prepared, while *N*-tosyl and *N*-acetyl derivatives could not be successfully deprotected. Then the mixture was treated with benzyloxycarbonyl chloride[16] and the reaction mixture was separated by silica-gel column chromatography to afford the sole product. The *N*-protected product was obtained only in a 15% isolation yield from **16** through three steps. The poor yield may be due to the facts that both dephthaloylation and aminomercuration yielded complex reaction mixtures. Any other diasteromeric isomer could not be isolated from the reaction mixture. The reaction product showed the molecular ion peak at *m/z* 461 and prominent fragment peaks at *m/z* 292 and *m/z* 91, indicating that the reaction product is one of the diastereoisomers of *N*-benzyloxycarbonylpiperidines (**20** and **21**).

The *N*-benzyloxycarbonylpiperidine was subjected to hydrogenolysis in the presence of 5% palladium on carbon to give the *N*-deprotected product (**18**) in 36% yield, which was successively treated with 1 M (1 M=1 mol dm^{-3}) hydrochloric acid in methanol at reflux temperature for 2 h. The reaction product, after alkalification, was extracted with ether and purified by column chromatography on alumina to give one diastereomer of (2*R*,3*R*)-6-dodecyl-2-methyl-3-piperidinols as white crystals, mp 47.5—48.5 °C, $[\alpha]_D^{18}$ −12.3°, in 44% yield. The physical and spectral data being identical with those of deoxocassine, and also desoxoprosafrinine and desoxoprosafrinone described in the Ratle's dissertation[5] (Table 1), the compound obtained by this preparation was determined to be (−)-deoxocassine (**4**) with a (2*R*,3*R*,6*S*)-configuration.

Stereochemistries of the synthetic (−)-deoxocassine (**4**) were further confirmed by ^{13}C and ^1H NMR and IR spectral measurements. The absolute configurations of (+)-spectaline (**1**) and (+)-iso-6-cassine (**2**) are (2*S*,3*S*,6*R*) and (2*R*,3*R*,6*R*), respectively and ^{13}C NMR shift values of C-2, C-3, C-6, and C-1′ are reported as shown in Table 2. The shift values observed in the synthetic (−)-deoxocassine (**4**) are nearly the same as those of the all-*cis*-substituted piperidine derivative, (+)-spectaline (**1**), indicating that two compounds possess the same relative configurations. Since the synthetic **4** possesses the (2*R*,3*R*) configuration, the stereochemistry of **4** was established to be (2*R*,3*R*,6*S*).

In ^1H NMR spectrum of the synthetic **4**, a methine proton at C-3 resonated at δ 3.56 as a multiplet signal, whose half-width was 4.8 Hz and a methine proton at C-2 was observed at δ 2.76 as double quartet

Table 1. Comparison of physical and spectral data of **4** with those of literature[5]

	4	Deoxoprosafrinone	Deoxoprosafrinine	Deoxocassine
mp (θ_m/°C)	47.5—48.5	50.5	50	50.5
$[\alpha]_D$	−12.3°	−8°	−12°	−11°
^{1}H NMR (δ)				
terminal-CH_3	0.88	0.88	0.88	0.88
$CH_{(2)}$-CH_3	1.11 (d, J=6.4 Hz)	1.11 (d, J=6.5 Hz)	1.11 (d, J=6.5 Hz)	1.08 (d, J=6.5 Hz)
-$(CH_2)_{11}$-	1.26	1.24	1.24	1.25
$C_{(3)}$-H	3.56	3.55	3.55	3.53
MS m/z (%)	283 (0.4) 114 (100) 96 (5)	283 (1) 114 (47) 96 (2.2)	284 (2) 114 (59) 96 (3)	

Table 2. ^{13}C NMR Spectra and $W_{1/2}$ and $J_{2,3}$ values of ^{1}H NMR spectra of **4**, **1**[1b], and **2**[1b]

	Synthetic-**4**	**1**	**2**
^{13}C NMR spectra (δ)			
C-3	68.02	67.6	68.9
C-2	57.27	57.0	50.4
C-6	55.85	55.7	49.5
C-1′	36.97	37.1	34.0
^{1}H NMR spectra (δ)			
$C_{(2)}$-H	2.76 (dq, $J_{2,3}$=1.4 Hz)	2.90 (br m, $J_{2,3}$=1.5 Hz)	3.06 (oct, $J_{2,3}$=3 Hz)
$C_{(3)}$-H	3.56 (m, $W_{1/2}$=4.8 Hz)	3.55 (br s, $W_{1/2}$=6 Hz)	3.66 (quint, J=6.5, 3.2, and 3 Hz)

signals with $J_{2,3}$=1.4 Hz, indicating that the $C_{(3)}$-H and $C_{(2)}$-H are in β-(equatorial) and β-(axial) orientations, respectively. These values are similar to those observed in (+)-spectaline (**1**), but apparently different from those of (+)-iso-6-cassine (**2**)[1b] (see Table 2).

In 2,6-dialkyl-3-piperidinols with all *cis*-configurations, two possible conformers (**A** and **B**) would exist in equilibrium and **A** is expected to be much more preferable, because of a formation of an intramolecular hydrogen bonding between the axial-OH and a lone pair of the nitrogen atom[17] and also a conformation with two alkyl side chain at C-2 and C-6 in equatorial orientations (Fig. 1). In a dilute solution of the synthetic **4** in carbon tetrachloride, the hydrogen-bonded OH absorption (E_b) was observed at 3523 cm^{-1} in the IR spectrum, while the free OH absorption (E_f) at 3629 cm^{-1} and their intensity ratio (E_b/E_f) was 14. These findings observed in ^{13}C and ^{1}H NMR and IR spectral measurements lead to the conclusion that the synthetic **4** is formulated as (2*R*,3*R*,6*S*)-6-dodecyl-2-methyl-3-piperidinol, identical with the natural (−)-deoxocassine.

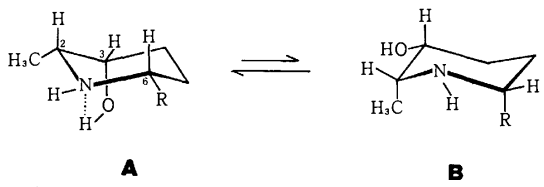

Fig. 1.

The *erythro*-alcohol (**10**) was treated with methoxymethyl chloride to afford a methoxymethyl derivative (**22**) in 98% yield, which was converted into (4*S*,5*R*)-4-methoxymethoxy-5-phthalimidohexanal (**24**) in 71% yield from **22** through **23**. The Wittig reaction gave (2*R*,3*S*)-3-methoxymethoxy-2-phthalimido-6-octadecene (**25**) in 62% yield, which was shown to contain a small amount of (*E*)-isomer; a very weak band at 964 cm^{-1} due to *trans*-olefin was observed together

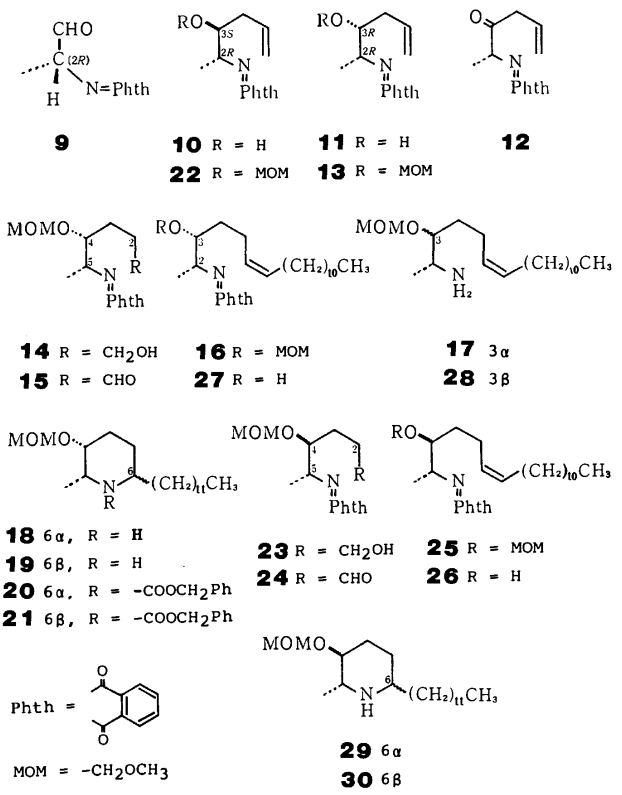

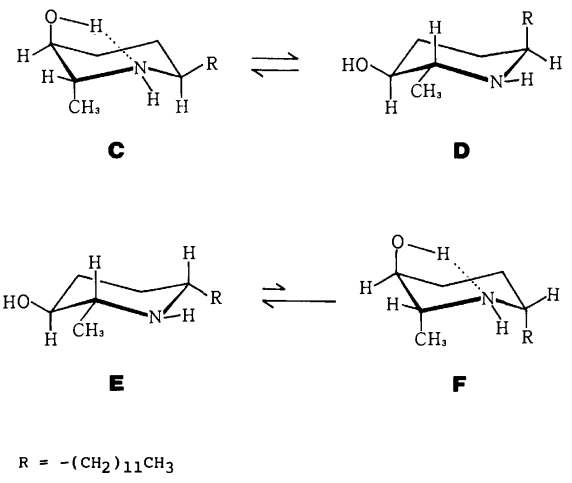

Fig. 2.

with an absorption at 765 cm^{-1} with medium intensity in the IR spectrum.

The olefin (**25**) was also prepared by the Grignard reaction. The *N*-phthaloyl aldehyde (**9**) was treated with a Grignard reagent prepared from (*Z*)-3-pentadecenyl bromide[3] and magnesium to give a diastereomeric mixture (3:1) of (2*R*,6*Z*)-2-phthalimido-6-octadecen-3-ols (**26** and **27**). Since the Grignard reagent reacted with also the phthaloyl group to yield a complex mixture, the isolation yield of the mixture of **26** and **27** was 23%. The configurations at C-3 were determined by the ^1H NMR spectral measurement. The major alcohol (**26**) showed double quartet signals ($J_{2,3}$=4 Hz) due to $C_{(2)}$-H at δ 4.35, while the minor alcohol (**27**) afforded a quintet signal (J=6.5 Hz) due to $C_{(2)}$-H at δ 4.43. These shift values and coupling constants are almost the same as those of the (3*S*)-alcohol (**10**) and (3*R*)-alcohol (**11**), respectively (*vide supra*). Methoxymethylation of the (2*R*,3*S*,6*Z*)-isomer (**26**) gave a methoxymethyl derivative in 54% yield, which was completely identical with **25**. Although this synthetic route containing the Grignard reaction consisted of only 2 steps, the overall yield was less than 10%. On the contrary, the route through the Wittig reaction comprised 5 steps and gave **25** in 12% overall yield. Both routes gave **25** in nearly the same yields, but the latter was much preferable to the former in respect of separation procedure of the reaction products.

On hydrazinolysis, the phthaloyl derivative (**25**) yielded (2*R*,3*S*,6*Z*)-3-methoxymethoxy-6-octadecen-2-amine (**28**) in 82% yield. The ε,ζ-unsaturated amine (**28**) was subjected to the aminomercuration and demercuration as before and separation by column chromatography on alumina gave two piperidine derivatives (**29** and **30**) in 17 and 43% yields, respectively. The piperidine derivatives (**29** and **30**) were heated under reflux in 4 M acetic acid overnight to give 6-dodecyl-2-methyl-3-piperidinols (**7**) and (**8**), respectively.

The stereochemistry of C-6 in **7** and **8** was determined by examining intensities of the IR absorption bands due to the intramolecular OH····N bonded (E_b) and free OH forms (E_f) in the dilute solution of **7** and **8** in carbon tetrachloride.[17] The piperidine derivative (**8**) obtained from the major product (**30**) exhibits free OH band at 3631 and 3626 cm^{-1} and hydrogen-bonded OH bands at 3531 cm^{-1} with approximately equal intensities (E_b/E_f=1), while the minor one (**7**) shows only free OH band at 3631 cm^{-1}. In 2α-methyl-3β-piperidinols with 6β-alkyl side chain, the conformation-determining effects of the *trans*-placed methyl and the alkyl side chain likely canceled out and two conformers (**C** and **D**) with the "OH-axial" and "OH-equatorial" conformations could exist in equilibrium. This is the case of **8**. On the other hand, the piperidine derivative (**7**) would exist exclucively in a triequatorial conformation (**E**) and, therefore, the IR spectrum of **7** measured in the dilute solution would exhibit no hydrogen-bonded OH band (Fig. 2). Thus the structures of two diastereomers **7** and **8** were determined to be (2*R*,3*S*,6*S*)- and (2*R*,3*S*,6*R*)-6-dodecyl-2-methyl-3-piperidinols, respectively.

Experimental

General Procedures. Melting points were measured on a Mel-temp capillary melting-point apparatus (Laboratory Devices) and uncorrected. IR spectra were measured

with a Hitachi 260-30, a Hitachi EPI-G2, a JEOL JIR-103 (FT), or a JEOL JIR-100 (FT) spectrometer. ^{1}H NMR spectra were taken with a Hitachi R-20B (60 MHz), a Hitachi R-24B (60 MHz), a Varian EM-390 (90 MHz), a JEOL FX-90Q (90 MHz), a JEOL JNM-PS100 (100 MHz), or a JEOL GX-270 (270 MHz) spectrometer and ^{13}C NMR spectra with a JEOL FX-90Q (22.5 MHz) or a JEOL GX-270 (67.8 MHz) spectrometer in $CDCl_3$ solution containing TMS as an internal standard. High and low resolution mass spectra were taken on a JEOL JMS-D300 mass spectrometer at 70 eV. Measurements of optical rotations were carried out with a JASCO DIP-181 polarimeter. Thin-layer chromatography (TLC) was carried out on Kieselgel GF_{254} (E. Merck) and Alumina B-10F (Wako) in 0.25mm-thickness for analytical use and 0.5 mm-thickness for preparative use. Wakogel C-200 (Wako), Aluminium Oxide W-200 neutral (ICN Pharmaceuticals), and Florisil 100-200 mesh (Wako) were used for column chromatography.

(2R)-2-Phthalimidopropanal (9). *N*-Phthaloyl-D-alanine (mp 144.5—145.0 °C, $[\alpha]_D^{22}$ +22.4°; 15 g) was dissolved in benzene (40 ml) and thionyl chloride (15 ml) was added. The mixture was refluxed for 1 h and then an excess of thionyl chloride was removed *in vacuo* completely, and the residue was allowed to stand overnight under reduced pressure.

A mixture of the acid chloride and 10% palladium on carbon (4 g) in benzene (150 ml) was refluxed with stirring, while hydrogen was bubbled continuously. The reaction was monitored by titration of evolved hydrogen chloride with alkali. After the usual work-up, crystallization from benzene gave (2*R*)-2-phthalimidopropanal (**9**; 10.4 g) as white crystals, mp 109.0—110.5 °C; $[\alpha]_D^{22}$ −32.5° (*c* 1.04, EtOH); ^{1}H NMR δ=1.62 (3H, d, *J*=7 Hz, C*H*$_3$-CH-(N=phth)-), 4.75 (1H, q, *J*=7 Hz; CH_3-C*H*(N=phth)-), 7.83 (4H, m; aromatic H's), and 9.68 (1H, s; -CHO); IR (KBr) 1768, 1730, 1710, 1385, 1032, 872, and 721 cm^{-1}; MS (EI) *m/z* (%) 174 (100); CI-MS (methane) *m/z* (%) 204 ([M+1]$^+$; 100) and 174 (14); Found: C, 64.90; H, 4.33; N, 6.99%. Calcd for $C_{11}H_9NO_3$: C, 65.02; H, 4.46; N, 6.89%.

(2R,3S)- and (2R,3R)-2-Phthalimido-5-hexen-3-ols (10 and 11). Allyl bromide (12.1 g) was added dropwise to THF (35 ml) containing zinc turnings (6.54 g) at room temperature under a nitrogen atmosphere, and then the mixture was heated at 50 °C for 1 h. After cooling, a small amount of unchanged zinc (0.84 g) was filtered off to give a yellow solution (50 ml; 1.74 mmol/ml) of diallylzinc, concentration of which was estimated from the amount of consumed zinc.

The solution (47 ml; 81.8 mmol) of diallylzinc was added dropwise to a solution of the aldehyde (**9**; 11 g, 54.5 mmol) in THF (120 ml) at −40 °C under a nitrogen atmosphere. After stirring for 1 h at −30 to −10 °C, THF-water (1:1, 30 ml) and 1 M hydrochloric acid (20 ml) were added, and the reaction product was extracted with ether (400 ml). The extract was washed with a saturated sodium hydrogencarbonate solution (30 ml) and a saturated sodium chloride solution (40 ml), dried over magnesium sulfate, and evaporated under reduced pressure to give a residue. The residue was chromatographed on a column of silica gel (250 g) using hexane–ethyl acetate (7:1) as eluent to give alcohol (**10**; 6.8 g) and alcohol (**11**; 1.34 g). **10**: mp 84.0—84.5 °C (from hexane-ethyl acetate); $[\alpha]_D^{28}$ −7.7° (*c* 0.31, EtOH); ^{1}H NMR δ=1.48 (3H, d, *J*=7 Hz; C*H*$_3$-CH-(N=phth)-), 2.29 (2H, t-like, *J*=6 Hz; -C*H*$_2$-CH=CH$_2$), 3.50 (1H, d, *J*=3 Hz; -OH), 4.07 (1H, m; -C*H*(OH)-), 4.37 (1H, dq, *J*=4 and 7 Hz; CH_3-C*H*(N=phth)-), 5.13 (2H, m, -CH=C*H*$_2$), 5.89 (1H, ddt, *J*=18, 9, and 6 Hz; -C*H*=CH$_2$), and 7.78 (4H, m; aromatic H's); IR (KBr) 3450, 1705, 1390, 1020, and 722 cm^{-1}; MS (EI) *m/z* (%) 227 (2), 204 (29), and 174 (56); CI-MS (methane) *m/z* (%) 246 ([M+1]$^+$; 100), 228 (91), 204 (30), and 174 (34); Found: C, 68.70; H, 6.23; N, 5.65%. Calcd for $C_{14}H_{15}NO_3$: C, 68.55; H, 6.16; N, 5.71%. **11**: mp 107.5—108.5 °C (from hexane-ethyl acetate); $[\alpha]_D^{30}$ −35.1° (*c* 0.30, EtOH); ^{1}H NMR δ=1.49 (3H, d, *J*=7 Hz; C*H*$_3$-CH(N=phth)-), 2.23 (2H, t-like, *J*=7 Hz; -C*H*$_2$-CH=CH$_2$), 3.17 (1H, d, *J*=8.5 Hz; -OH), 4.02 (1H, q, *J*=7 Hz; -C*H*(OH)-), 4.42 (1H, quint, *J*=7 Hz; CH_3-C*H*(N=phth)-), 5.05 (1H, d, *J*=18 Hz; $^{H}\!>\!C\!=\!C\!<^{H}_{H}$), 5.07 (1H, d, *J*=9 Hz, $^{H}\!>\!C\!=\!C\!<^{H}_{H}$), 5.90 (1H, ddt, *J*=18, 9, and 7 Hz; -C*H*=CH$_2$), and 7.80 (4H, m; aromatic H's); IR (KBr) 3510, 3260, 2940, 2920, 1690, 1640, 1560, 1395, 1392, 1168, 1022, and 722 cm^{-1}; MS (EI) *m/z* (%) 227 (9), 204 (82), and 174 (75); CI-MS (methane) *m/z* (%) 246 ([M+1]$^+$; 100), 228 (59), 204 (25), and 174 (16): Found: C, 68.82; H, 6.13; N, 5.97%. Calcd for $C_{14}H_{15}NO_3$: C, 68.55; H, 6.16 N, 5.71%.

(2R)-2-Phthalimido-5-hexen-3-one (12). A solution of (2*R*,3*S*)-2-phthalimido-5-hexen-3-ol (**10**; 10.1 g) in dichloromethane (60 ml) was added to a suspension of pyridinium chlorochromate (26.3 g) in dichloromethane (120 ml) and the mixture was stirred for 17 h at room temperature. The reaction mixture was decanted to afford a supernatant liquid and a black residue. The supernatant liquid was passed through a column of Florisil (45 g). The black residue was dissolved in a saturated sodium hydrogencarbonate solution and extracted with ether. The ethereal extract was washed with brine, dried over magnesium sulfate, and combined with the eluate from the Florisil column. The combined solution was evaporated and purified by column chromatography on silica gel (180 g). Elution with a mixture of hexane-acetone (4:1) afforded (2*R*)-2-phthalimido-5-hexen-3-one (**12**; 8.8 g) in 88% yield, mp 56.0—57.0 °C; $[\alpha]_D^{18}$ +23.0° (*c* 2.6 EtOH); ^{1}H NMR δ=1.67 (3H, d, *J*=7 Hz; C*H*$_3$-CH(N=phth)-), 3.27 (2H, d, *J*=7 Hz; -C*H*$_2$-CH=CH$_2$), 4.85 (1H, q, *J*=7 Hz; CH_3-C*H*(N=phth)-), 5.07 (1H, d, *J*=18 Hz; $^{H}\!>\!C\!=\!C\!<^{H}_{H}$), 5.11 (1H, d, *J*=9 Hz; $^{H}\!>\!C\!=\!C\!<^{H}_{H}$), 5.90 (1H, ddt, *J*=18, 9, and 7 Hz: -C*H*=CH$_2$), and 7.80 (4H, m; aromatic H's); IR (KBr) 1780, 1720, 1395, 1020, and 720 cm^{-1}; MS (EI) *m/z* (%) 243 (M$^+$; 3), 202 (42), and 174 (100); Found: C, 69.02; H, 5.12; N, 5.84%; MW 243.0881. Calcd for $C_{14}H_{13}NO_3$: C, 69.12; H, 5.39; N, 5.76%; M, 243.0894.

Reduction of Ketone (12) with Zinc Borohydride. Anhydrous zinc chloride (4.0 g) was added in ether (50 ml) and the mixture was refluxed for 1 h in a nitrogen atmosphere to yield an ethereal solution of zinc chloride, which was added dropwise to a suspension of sodium borohydride (2.7 g) in ether (150 ml). The mixture was stirred for 2 d at room temperature and decanted to afford a zinc borohydride solution (200 ml).

To an ice-cooled solution of (2*R*)-2-phthalimido-5-

hexen-3-one (**12**; 9.05 g) in ether (400 ml) the zinc borohydride solution (64 ml) above prepared was added in a nitrogen atmosphere and stirring was continued for 5 h at 0 °C. After addition of a solution (200 ml) of ammonium chloride, the organic layer was separated and evaporated to give a residue, which was chromatographed on silica gel. Elution with a mixture of hexane–ethyl acetate (5:1) afforded alcohol (**10**; 2.26 g) and alcohol (**11**; 4.87 g) in 25 and 53% yields, respectively. **10**: Mp 80.5—81.5 °C; $[\alpha]_D^{21}$ −10.4° (*c* 0.70, EtOH). **11**: Mp 107.5—108.5 °C; $[\alpha]_D^{22}$ −36.0° (*c* 3.0, EtOH).

*(2*R*,3*R*)-*N*,*N*-Phthaloyl-3-methoxymethoxy-5-hexen-2-amine (13).* Methoxymethyl chloride (12.7 g) was added to a mixture of alcohol (**11**; 4.86 g) and triethylamine (16.2 g) in acetonitrile (40 ml). The mixture was refluxed for 2.5 h in a flask equipped with a calcium chloride tube. After cooling to room temperature, water (30 ml) and a saturated solution (50 ml) of sodium hydrogencarbonate were added and the reaction product was extracted with ether. Evaporation and separation by column chromatography on silica gel (150 g) eluted with hexane–ethyl acetate (6:1) afforded (2*R*,3*R*)-*N*,*N*-phthaloyl-3-methoxymethoxy-5-hexen-2-amine (**13**; 5.71 g) quantitatively as a colorless oil, $[\alpha]_D^{23}$ −119° (*c* 0.36, $CHCl_3$); ^{1}H NMR δ=1.49 (3H, d, *J*=7 Hz; CH_3–CH(N=phth)–), 2.51 (2H, m; –CH_2–CH=CH_2), 3.00 (3H, s; CH_3O–), 4.28 (2H, m; –CH(N=phth)–CH(OMOM)–), 4.50 (2H, s; –OCH_2O–), *ca.* 5.16 (2H, m, –CH=CH_2), 6.00 (1H, ddt, *J*=17, 9, and 7 Hz; –CH=CH_2), and 7.80 (4H, m; aromatic H's); IR (neat) 2940, 1770, 1710, 1385, 1145, 1090, 1038, 920, 881, and 722 cm^{-1}; MS *m/z* (%) 248 (15) and 174 (100); CI-MS (methane) *m/z* (%) 290 ($[M+1]^+$; 13), 259 (18), 258 (100), 228 (13), and 174 (5); Found: C, 66.21; H, 6.81; N, 4.73%. Calcd for $C_{16}H_{19}NO_4$: C, 66.42; H, 6.62; N, 4.84%.

*(4*R*,5*R*)-4-Methoxymethoxy-5-phthalimido-1-hexanol (14).* A diborane solution (6 ml, *ca.* 12 mmol) in THF was added to a solution of the MOM-olefin (**13**; 922 mg) in THF (15 ml) in a nitrogen atmosphere at 0 °C and the reaction mixture was stirred at room temperature for 2 h. After an excess of diborane was destroyed by addition of water (1 ml), 2 M sodium hydroxide solution (4.5 ml) and 30% hydrogen peroxide (7 ml) were added at 0 °C, and the mixture was stirred at 50 °C for 1.5 h followed by extraction with ether (40 ml). The usual work-up afforded an oily residue, which was subjected to separation by column chromatography on silica gel (15 g). Elution with hexane-ethyl acetate (1:1) gave (4*R*,5*R*)-4-methoxymethoxy-5-phthalimido-1-hexanol (**14**; 815 mg) as an oil in 83% yield, $[\alpha]_D^{22}$ −58.9° (*c* 0.48, $CHCl_3$) ^{1}H NMR δ=1.49 (3H, d, *J*=6.5 Hz; CH_3–CH(N=phth)–), 1.77 (2H, m; –CH_2–CH_2OH), 2.65 (1H, m; –OH), 3.00 (3H, s; CH_3O–), 3.71 (2H, m; –CH_2–OH), 4.32 (2H, m; –CH(N=phth)–CH(OMOM)–), 4.53 (2H, s; –OCH_2O–), and 7.80 (4H, m; aromatic H's).

*(4*R*,5*R*)-4-Methoxymethoxy-5-phthalimidohexanal (15).* The MOM-alcohol (**14**; 603 mg) in dichloromethane (4 ml) was added to a suspension of pyridinium chlorochromate (1.5 g) in dichloromethane (7 ml) at room temperature. After stirring for 2.5 h, the reaction mixture was decanted to afford a supernatant liquid and a dark-brown residue. The supernatant liquid was diluted with ether, passed through a column of Florisil (6 g), and eluted with ether. The dark-brown residue was dissolved in a sodium hydrogencarbonate solution and extracted with ether. The ethereal extract was combined with the eluate from the Florisil column and chromatographed on a short column of silica gel. Elution with hexane–ethyl acetate gave MOM–aldehyde (**15**; 508 mg) in 85% yield, ^{1}H NMR δ=1.48 (3H, d, *J*=6.5 Hz CH_3–CH(N=phth)–), 1.90 (2H, m; –CH_2–CH_2–CHO), 2.64 (2H, td, *J*=9 and 1.5 Hz; –CH_2–CHO), 3.00 (3H, s; CH_3O–), 4.26 (2H, m; –CH(N=phth)–CH(OMOM)–), 4.46 (2H, s; –OCH_2O–), 7.89 (4H, m; aromatic H's), and 9.86 (1H, t, *J*=1.5 Hz; –CHO); IR (neat) 2935, 1770, 1710, 1381, 1140, 1030, 920, 881, and 721 cm^{-1}; MS (EI) *m/z* (%) 244 (5) and 174 (100); CI-MS (methane) *m/z* (%) 306 ($[M+1]^+$; 3), 275 (4), 274 (22), 260 (2), 245 (16), 244 (100), and 174 (4).

*(2*R*,3*R*,6*Z*)-3-Methoxymethoxy-2-phthalimido-6-octadecene (16).* Butyllithium (6.5 ml; 11.3 mmol) in hexane was added dropwise to a solution of dodecyltriphenylphosphonium bromide (7.5 g; 14.6 mmol) in dry THF at 0 °C under a nitrogen atmosphere. The red solution was stirred for 20 min at room temperature and 40 min at 40 °C, and then cooled to −78 °C. To the solution was added a solution of the MOM-aldehyde (**15**; 3.45 g) in THF (60 ml), and the mixture was stirred for 20 min at −78 °C and 20 min at 0 °C, and then allowed to stand overnight at room temperature. Ether (200 ml) and water (150 ml) were added and the ethereal layer was separated. The aqueous layer was extracted with ether and the extract was combined with the ethereal layer. The usual work-up gave an oily mixture, which was subjected to separation by column chromatography on silica gel (70 g). Elution was performed with hexane-ethyl acetate (6:1) to afford (2*R*,3*R*,6*Z*)-3-methoxymethoxy-2-phthalimido-6-octadecene (**16**; 3.12 g) as an oil, $[\alpha]_D^{21}$ −49.2° (*c* 0.62, $CHCl_3$); ^{1}H NMR δ=0.87 (3H, t-like, *J*=6 Hz; terminal CH_3), 1.27 (20H, br s; methylenes), 1.48 (3H, d, *J*=6.5 Hz; CH_3–CH(N=phth)–), 2.05 (4H, m –CH_2–CH=CH–CH_2–), 2.97 (3H, s; CH_3O–), 4.30 (2H, m; –CH(N=phth)–CH(OMOM)–), 4.51 (2H, s; –OCH_2O–), 5.39 (2H, t, *J*=5 Hz; –CH=CH–), and 7.77 (4H, m; aromatic H's); IR (neat) 2925, 1773, 1712, 1382, 1148, 1038, 922, 884, and 721 cm^{-1}; MS (EI) *m/z* (%) 457 (M^+; 0.1), 426 (1), 425 (3), and 174 (100); CI-MS (methane) *m/z* (%) 458 ($[M+1]^+$; 13), 427 (30), 426 (100), 397 (2), 396 (6), and 174 (4); Found: C, 73.53; H, 9.33; N, 3.03%. Calcd for $C_{28}H_{43}NO_4$: C, 73.48; H, 9.47; N, 3.06%.

*(2*R*,3*R*,6*Z*)-3-Methoxymethoxy-6-octadecen-2-amine (17).* 100% Hydrazine hydrate (0.2 ml) was added to a solution of phthalimido-olefin (**16**; 425 mg) in ethanol (4 ml) at room temperature and the mixture was stirred for 1 h. To the reaction mixture, ether (200 ml) and 2 M sodium hydroxide (10 ml) were added and the ethereal layer was separated. The aqueous layer was extracted with ether repeatedly and the extracts were combined with the ethereal layer. The usual work-up afforded crude ε,ζ-unsaturated amine (**17**; 512 mg) as a pale yellow oil, which was used for next synthetic step without any purification. **17** (crude): ^{1}H NMR δ=0.87 (3H, t-like, *J*=6 Hz; terminal CH_3); 1.07 (3H, d, *J*=7 Hz $C_{(2)}$–CH_3), 1.31 (22H, br s; methylenes), 1.4—2.2 (4H, m; –CH_2–CH=CH–CH_2–), 2.47 (2H, m; –NH_2), 3.37 (3H, s; CH_3O–), 4.65 (2H, s; –OCH_2O–), and 5.33 (2H, t-like, *J*=6 Hz; –CH=CH–); MS (EI) *m/z* (%) 327 (M^+; 3), 296 (4), 282 (6), 266 (3), and 44 (100); Found: *m/z* 327.3119. Calcd for $C_{20}H_{41}NO_2$: M, 327.3139.

*Crude (2*R*,3*R*,6*S*)-3-O-Methoxymethyldeoxocassine (18).*

Mercury(II) acetate (618 mg) was added to a solution of the ε,ζ-unsaturated amine (**17**; 512 mg) in methanol (4 ml) at room temperature, and the mixture was stirred for 2 d. To the reaction mixture, was added a solution of sodium borohydride (60 mg) in 2 M sodium hydroxide solution (6 ml). The reaction mixture was filtered and the filtrate was extracted with ether. The ethereal layer was worked up as usual to give crude (2*R*,3*R*,6*S*)-3-*O*-methoxymethyldeoxocassine (**18**; 249 mg) as a yellow oil.

*(2*R*,3*R*,6*S*)-N-Benzyloxycarbonyl-3-O-methoxymethyldeoxocassine (20).* Benzyloxycarbonyl chloride (180 mg) was added to an ice-cooled solution of the crude MOM-deoxocassine (**18**; 106 mg) and potassium carbonate (113 mg) in acetone (4 ml). The reaction mixture was stirred at 0 °C for 1.5 h and then for 1 d at room temperature, and filtered. The precipitates were washed with ether and the washings and the filtrate were combined. The usual work-up yielded an oily residue, which was subjected to separation by column chromatography on silica gel (7 g) eluted with hexane–ether (4:1) to afford a benzyloxycarbonyl derivative (**20**; 27.5 mg) as an oil, $[\alpha]_D^{17}$ −2.0° (*c* 1.8, EtOH); ^{1}H NMR δ=0.87 (3H, t-like, *J*=6 Hz; terminal CH_3), 1.28 (25H, br s; $C_{(2)}$–CH_3 and methylenes), 1.4—2.3 (4H, m; $-CH_2-CH_2-$), 3.38 (3H, s; CH_3O–), 3.4—5.3 (3H, m; $C_{(2)}$–H, $C_{(3)}$–H, and $C_{(6)}$–H), 4.63 (2H, s; $-OCH_2O-$), 5.12 (2H, s; $-CH_2-C_6H_5$), and 7.33 (5H, m; aromatic H's); IR (neat) 2925, 2850, 1700, 1300, and 1150 cm^{-1}; MS (EI) *m/z* 461 (M^+; 1), 429 (1), 292 (42), and 91 (100); Found: *m/z* 461.3544. Calcd for $C_{28}H_{47}NO_4$: M, 461.3504.

*Pure (2*R*,3*R*,6*S*)-3-O-Methoxymethyldeoxocassine (18).* The benzyloxycarbonyl derivative (**20**; 59 mg) in ethanol (5 ml) was subjected to hydrogenolysis in the presence of 5% palladium on carbon (146 mg) for 1 d. The usual work-up and separation by column chromatography on alumina (2 g) eluted with hexane–ether (1:1) affoded pure (2*R*,3*R*,6*S*)-3-*O*-methoxymethyldeoxocassine (**18**; 15 mg) as an oil, $[\alpha]_D^{16}$ −20° (*c* 0.57, $CHCl_3$); ^{1}H NMR δ=0.87 (3H, t-like, *J*=6 Hz; terminal CH_3), 1.14 (3H, d, *J*=7 Hz; $C_{(2)}$–CH_3), 1.27 (22H, br s; methylenes), 1.4—1.8 (4H, m; $-CH_2-CH_2-$), 1.8—3.7 (3H, m; $C_{(2)}$–H, $C_{(3)}$–H, and $C_{(6)}$–H), 3.37 (3H, s; CH_3O–), and 4.65 (2H, *AB*q, *J*=7 Hz; $-OCH_2O-$); MS (EI) *m/z* (%) 327 (M^+; 3), 312 (2), 296 (4), 282 (10), 266 (6), and 158 (100); Found: *m/z* 327.3098. Calcd for $C_{20}H_{41}NO_2$: M, 327.3145.

(−)-Deoxocassine (4). A solution of the methoxymethyl derivative (**20**; 13 mg) in 1 M hydrochloric acid–methanol was heated under reflux for 2 h. After cooling, 2 M sodium hydroxide solution (1.5 ml) was added and the reaction product was extracted with ether and worked up as usual to give a residue, which was subjected to column chromatographic separation on alumina (1 g). Elution with ether–methanol (9:1) gave (−)-deoxocassine (**4**; 5 mg) as white crystals, mp 47.5—48.5 °C (from methanol); $[\alpha]_D^{18}$ −12.3° (*c* 0.19; $CHCl_3$); ^{1}H NMR δ=0.88 (3H, t-like, *J*=6.0 Hz; terminal CH_3), 1.11 (3H, d, *J*=6.4 Hz $C_{(2)}$-CH_3), 1.26 (22H, br s; methylenes), 1.3—1.4 (2H, m; $C_{(5)}$–H_2), 1.4—1.5 (2H, m; $C_{(4)}$–H_2), 1.8—2.0 (1H, m; –NH), 2.4—2.7 (2H, m; $C_{(6)}$–H and –OH), 2.76 (1H, qd, *J*=6.5 and 1.4 Hz; $C_{(2)}$–H), and 3.56 (1H, m, $W_{1/2}$ 4.8 Hz; $C_{(3)}$–H); ^{13}C NMR δ=14.12, 18.66, 22.69, 25.83, 26.10, 29.35, 29.61, 29.66, 29.80, 31.92, 32.05, 36.97, 55.85, 57.27, and 68.02; MS (EI) *m/z* (%) 283 (M^+; 0.4), 282 (0.2), 268 (0.3), 114 (100), and 96 (5); Found: *m/z* 283.2875. Calcd for $C_{18}H_{37}NO$: M, 283.2875.

*(2*R*,3*S*,6*S*)- and (2*R*,3*S*,6*R*)-Deoxocassines (7 and 8).* (3*S*)-Diastereomers (**7** and **8**) of (−)-deoxocassine (**4**) were prepared from (2*R*,3*S*)-2-phthalimido-5-hexen-3-ol (**10**) according to the same procedures as described for preparation of **4**. (2*R*,3*S*)-*N*,*N*-phthaloyl-3-methoxymethoxy-5-hexen-2-amine (**22**): An oil, $[\alpha]_D^{19}$ +30.2° (*c* 0.26, $CHCl_3$); ^{1}H NMR δ=1.54 (3H, d, *J*=6.5 Hz; CH_3–CH(N=phth)–), 2.33 (2H, m; $-CH_2-CH=CH_2$), 3.40 (3H, s; CH_3O–), 4.40 (2H, m; $-CH$(N=phth)–CH(OMOM)–), 4.73 (2H, s; $-OCH_2O-$), 5.04 (2H, m; CH_2=CH–), 5.86 (1H, ddt, *J*=17, 9, and 7 Hz; $-CH=CH_2$), and 7.79 (4H, m; aromatic H's); IR (neat) 2925, 1772, 1710, 1385, 1142, 1095, 1035, 915, 876, and 715 cm^{-1}: MS (EI) *m/z* (%) 248 (52), 228 (20), and 174 (100); CI-MS (methane) *m/z* (%) 290 ($[M+1]^+$; 6), 259 (16), 258 (100), 228 (18), and 174 (13); Found: C, 66.49; H, 6.76; N, 5.06%. Calcd for $C_{16}H_{19}NO_4$: C, 66.42; H, 6.62; N, 4.84%. (4*S*,5*R*)-4-Methoxymethoxy-5-phthalimido-1-hexanol (**23**): An oil $[\alpha]_D^{19}$ −15.3° (*c* 0.30, $CHCl_3$); ^{1}H NMR δ=1.51 (3H, d, *J*=6.5 Hz; CH_3–CH(N=phth)–), 1.65 (2H, m; $-CH_2-CH_2OH$), 1.83 (1H, m; –OH), 3.41 (3H, s; CH_3O–), 3.58 (2H, m; $-CH_2-OH$), 4.40 (2H, m; $-CH$(N=phth)–CH(OMOM)–), 4.72 (2H, s; $-OCH_2O-$), and 7.76 (4H, m; aromatic H's); IR (neat) 3400, 2945, 1772, 1710, 1390, 1142, 1038, and 725 cm^{-1}; MS (EI) *m/z* (%) 174 (100); CI-MS (methane) *m/z* (%) 308 ($[M+1]^+$; 1), 277 (12), 276 (72), 247 (16), 246 (100), and 174 (11); Found: C, 62.28; H, 7.18; N, 4.64%. Calcd for $C_{16}H_{21}NO_5$: C, 62.52; H, 6.88; N, 4.56%. (4*S*,5*R*)-4-Methoxymethoxy-5-phthalimidohexanal (**24**): An oil; ^{1}H NMR δ=1.56 (3H, d, *J*=6.5 Hz; CH_3–CH(N=phth)–), 1.90 (2H, m; $-CH_2-CH_2-CHO$), 2.60 (2H, td, *J*=8.5 and 1.5 Hz; $-CH_2-CHO$), 3.43 (3H, s; CH_3O–), 4.35 (2H, m; $-CH$(N=phth)–CH(OMOM)–), 4.74 (2H, s; $-OCH_2O-$), 7.82 (4H, m; aromatic H's), and 9.78 (1H, t, *J*=1.5 Hz; –CHO); IR (neat) 2950, 1775, 1710, 1385, 1140, 1035, 920, 881, and 723 cm^{-1}; MS (EI) *m/z* (%) 274 (20), 244 (2), and 174 (100); CI-MS (methane) *m/z* (%) 306 ($[M+1]^+$; 6), 275 (9), 274 (57), 260 (5), 245 (17), 244 (100), and 174 (6). (2*R*,3*S*,6*Z*)-3-Methoxymethoxy-2-phthalimido-6-octadecene (**25**): An oil; $[\alpha]_D^{24}$ −14.9° (*c* 0.54, $CHCl_3$); ^{1}H NMR δ=0.88 (3H, t-like, *J*=6 Hz; terminal CH_3), 1.25 (20H, br s; methylenes), 1.54 (3H, d, *J*=6.5 Hz; CH_3–CH(N=phth)–), 1.96 (4H, m; $-CH_2-CH=CH-CH_2$), 3.42 (3H, s; CH_3O–), 4.32 (2H, m; $-CH$(N=phth)–CH(OMOM)–), 4.75 (2H, s; $-OCH_2O-$), 5.29 (2H, t, *J*=5 Hz; –CH=CH–), and 7.78 (4H, m; aromatic H's); IR (neat) 2925, 1775, 1710, 1382, 1142, 1040, 922, 882, and 723 cm^{-1}; MS (EI) *m/z* (%) 426 (3), 248 (9), and 174 (100); CI-MS (methane) *m/z* (%) 458 ($[M+1]^+$; 2), 427 (31), 426 (100), 397 (4), 396 (14), 276 (15), 248 (3), and 174 (21); Found: C, 73.39; H, 9.28; N, 3.00%. Calcd for $C_{28}H_{43}NO_4$: C, 73.48; H, 9.47; N, 3.06%. (2*R*,3*S*,6*Z*)-3-Methoxymethoxy-6-octadecen-2-amine (**28**): A pale yellow oil; MS (EI) *m/z* (%) 327 (M^+; 13), 312 (1), 296 (9), 282 (14), 266 (5), and 44 (100); Found: *m/z* 327.3145. Calcd for $C_{20}H_{41}NO_2$: M, 327.3139. (2*R*,3*S*,6*S*)- and (2*R*,3*S*,6*R*)-3-Methoxymethyldeoxocassines (**29** and **30**): To a solution of the ε,ζ-unsaturated amine (**28**; 558 mg) in methanol (20 ml) was added mercury(II) acetate (816 mg) at room temperature, and the mixture was stirred for 2 d. To the reaction mixture was added dropwise a solution of sodium borohydride (145 mg) in 2 M sodium hydroxide solution (15 ml). The usual work-up afforded a crude product, which was subjected to separation by preparative TLC (Wako Alumina B-10F, 20×20 cm, 20 plates, developed

with hexane–ether (1:1)). A band (R_f 0.80) was separated and eluted with ethyl acetate to afford **29** (95 mg) as an oil, and a band (R_f 0.63) afforded **30** (240 mg) as an oil. **29**: $[\alpha]_D^{24}$ +26.4° (*c* 0.33, $CHCl_3$); ^1H NMR δ=0.87 (3H, t-like, *J*=6 Hz; terminal CH_3), 1.15 (3H, d, *J*=6.5 Hz; $C_{(2)}$-CH_3), 1.27 (22H, br s; methylenes), 1.66 (3H, m), 2.15 (1H, m), 2.52 (2H, m), 3.03 (1H, m), 3.34 (3H, s; CH_3O-), and 4.63 (2H, *AB*q, *J*=6.5 Hz; -OCH_2O-), MS (EI) *m/z* (%) 327 (M^+; 1), 326 (2), 312 (3), 282 (23), 266 (16), and 158 (100); Found: *m/z* 327.3115. Calcd for $C_{20}H_{41}NO_2$: M, 327.3139. **30**: $[\alpha]_D^{24}$ +13.6° (*c* 0.12, $CHCl_3$); ^1H NMR δ=0.92 (3H, t-like, *J*=6 Hz; terminal CH_3), 1.19 (3H, d, *J*=7 Hz; $C_{(2)}$-CH_3), 1.30 (22H, br s; methylenes), 1.70 (4H, m), 2.72—3.55 (3H, m), 3.44 (3H, s; CH_3O-), and 4.77 (2H, *AB*q, *J*=10 Hz; -OCH_2O-); MS (EI) *m/z* (%) 327 (M^+; 1), 326 (1), 312 (20), 296 (3), 282 (20), 266 (10), and 158 (100); Found: *m/z* 327.3124. Calcd for $C_{20}H_{41}NO_2$: M, 327.3139. (2*R*,3*S*,6*S*)-Deoxocassine (**7**): A mixture of (2*R*,3*S*,6*S*)-3-methoxymethyldeoxocassine (**29**; 33.5 mg) and 4 M acetic acid (3 ml) was heated under reflux overnight. After neutralization with alkali, extraction with ether and the usual work-up afforded a crude product, which was purified by preparative TLC (Wako Alumina B-10F, 20×20 cm, developed with ether–methanol (20:1)). A band (R_f 0.30) was eluted with ethyl acetate–methanol (1:1) to afford (2*R*,3*S*,6*S*)-deoxocassine (**7**; 21 mg) as a pale yellow solid, $[\alpha]_D^{24}$ +13.1° (*c* 0.16, $CHCl_3$); ^1H NMR δ=0.87 (3H, t-like, *J*=6 Hz; terminal CH_3), 1.18 (3H, d, *J*=7 Hz; $C_{(2)}$-CH_3), 1.27 (22H, br s; methylenes), 1.43—2.25 (6H, m; -CH_2-CH_2-, -$\dot{N}H$, and -OH), 2.49 (2H, m), and 3.12 (1H, m); MS (EI) *m/z* 283 (M^+; 12), 282 (7), 268 (7), 265 (2), 250 (2), 114 (100), and 96 (29); Found: *m/z* 283.2875. Calcd for $C_{18}H_{37}NO$: M, 283.2877. (2*R*,3*S*,6*R*)-Deoxocassine (**8**): (2*R*,3*S*,6*R*)-3-*O*-Methoxymethyldeoxocassine (**30**; 34.7 mg) was deprotected as before to afford **8** (16.6 mg) as an amorphous solid, $[\alpha]_D^{24}$ −3.1° (*c* 0.15, $CHCl_3$); ^1H NMR δ=0.85 (3H, t-like, *J*=6 Hz; terminal CH_3), 1.13 (3H, d, *J*=7 Hz; $C_{(2)}$-CH_3), 1.25 (22H, br s; methylenes), 1.40—2.20 (6H, m; -CH_2-CH_2-, -$\dot{N}H$, and -OH), 2.87 (2H, m), and 3.35 (1H, m); MS (EI) *m/z* (%) 283 (M^+; 1), 282 (2), 268 (4), 265 (4), 250 (10), 114 (100), and 96 (39); Found: *m/z* 283.2873. Calcd for $C_{18}H_{37}NO$: M, 283.2877.

(2R,3S,6Z)-3-Methoxymethoxy-2-phthalimido-6-octadecene (25) (by Grignard reaction). A Grignard reagent[3] (0.68 mmol), prepared from (*Z*)-3-pentadecenyl bromide and magnesium, was added to a solution of *N*-phthaloyl aldehyde (**9**; 100 mg) in THF (1.5 ml) at −45 °C under a nitrogen atmosphere, and the reaction mixture was stirred at −30 °C for 6 h. The usual treatment gave a crude oil (320 mg), which was chromatographed on silica gel (6 g). Fractions containing diastereomeric alcohols (**26** and **27**), eluted with benzene–ether (19:1), were combined and further purified by preparative TLC (silica gel in 1 mm thickness, developed with benzene–ether (7:2) twice) to give a mixture (48 mg) of **26** and **27**. The separation of **26** and **27** was achieved by preparative TLC (silica gel in 0.3 mm thickness, developed with hexane–ethyl acetate (3:1) three times) to afford (2*R*,3*S*,6*Z*)- and (2*R*,3*R*,6*Z*)-2-phthalimido-6-octadecen-3-ols (**26** and **27**; in a ratio of *ca.* 3:1). **26**: mp 34.0—34.5 °C; $[\alpha]_D^{30}$ +9° (*c* 0.23, $CHCl_3$); ^1H NMR δ=0.87 (3H, t-like; terminal CH_3), 1.27 (18H, br s; methylenes), 1.43 (3H, d, *J*=7 Hz; CH_3-CH(N=phth)-), 1.50 (2H, m; -O-$\dot{C}H$-CH_2-), 2.10 (4H, m; -CH_2-CH=CH-CH_2-), 3.70 (1H, d, *J*=3 Hz; -OH), 4.00 (1H, m; -$\dot{C}H$-OH), 4.35 (1H, qd, *J*=7 and 4 Hz CH_3-CH(N=phth)-), 5.37 (2H, m; -CH=CH-), and 7.80 (4H, m; aromatic H's); IR (neat) 3400, 3300, 2920, 1775, 1710, 1390, 1020, 880, and 720 cm^{-1}; Found: C, 75.40; H, 9.80; N, 3.21%. Calcd for $C_{26}H_{39}NO_3$: C, 75.50; H, 9.51; N, 3.39%. **27**: mp 34.5—35.0 °C; $[\alpha]_D^{19}$ −9° (*c* 0.23, $CHCl_3$); ^1H NMR δ=0.89 (3H, t-like; terminal CH_3), 1.27 (18H, br s; methylenes), 1.40 (2H, m; -O-$\dot{C}H$-CH_2-), 1.46 (3H, d, *J*=6.5 Hz; CH_3-CH(N=phth)-), 2.10 (4H, m; -CH_2-CH=CH-CH_2-), 3.24 (1H, d, *J*=9 Hz; -OH), 3.92 (1H, m; -$\dot{C}H$-OH), 4.43 (1H, quint, *J*=6.5 Hz; CH_3-CH(N=phth)-), 6.37 (2H, m; -CH=CH-), and 7.80 (4H, m; aromatic H's); IR (neat) 3450, 2920, 1775, 1710, 1040, 880, and 720 cm^{-1}. Found: C, 76.64; H, 10.08; N, 3.19%. Calcd for $C_{26}H_{39}NO_3$: C, 75.50; H, 9.51; N, 3.39%.

The (2*R*,3*S*)-alcohol (**26**; 10 mg) was methoxymethylated with methoxymethyl chloride (82 mg) in acetonitrile (1 ml) containing triethylamine (91 mg) by the same procedure as before. A methoxymethyl derivative (**25**; 6 mg) was obtained as an oil, whose spectral data were completely identical with those of the specimen (**25**) obtained by the Wittig reaction.

The authors wish to express their thanks to Professor Takaharu Ohnishi, Tokyo Institute of Technology, for FT-IR measurement, Dr. Hajime Nagano, Ochanomizu University, for NMR measurement at 270 MHz, and Miss Toshiko Seki and Mrs. Kimiyo Saeki, The University of Tokyo, for micro analyses.

References

1) a) Q. Khuong-Huu, G. Rattle, X. Monseur, and R. Goutarel, *Bull. Soc. Chim. Berg.*, **81**, 425, 443 (1972); b) I. Christofidis, A. Welter, and J. Jadot, *Tetrahedron*, **33**, 977 (1977); c) D. Lythgoe and M. J. Vernengo, *Tetrahedron Lett.*, **1967**, 1133; d) G. J. H. Rall, T. M. Smalberger, and H. L. de Waal, *Tetrahedron Lett.*, **1967**, 3465; e) J. Bruneton and A. Cavé, *Tetrahedron Lett.*, **1975**, 739; f) J. G. MacConnell and M. S. Blum, *Tetrahedron*, **26**, 1129 (1971).

2) E. Brown and A. Bourgouin, *Chem. Lett.*, **1974**, 109; *Tetrahedron*, **31**, 1047 (1975); E. Brown and R. Dhal, *J. Chem. Soc., Perkin Trans. 1*, **1976**, 2190; E. Brown and R. Bonté, *Tetrahedron Lett.*, **1975**, 2881; *Bull. Soc. Chim. Fr.*, **1981**, II, 281; E. Brown, R. Dhal, and J. Lavoue, *Tetrahedron Lett.*, **1971**, 1055; E. Brown and R. Dhal, *Bull. Soc. Chim. Fr.*, **1972**, 4292; E. Brown, R. Dhal, and J. Lavoue, *C. R. Acad. Sci., Ser. C*, **272**, 958 (1971); E. Brown, R. Dhal, and P. F. Casals, *Tetrahedron*, **28**, 5607 (1972); S. Hanessian and R. Frenette, *Tetrahedron Lett.*, **1979**, 3391; M. Natsume and M. Ogawa, *Heterocycles*, **14**, 169, 615 (1980); G. Fodor, J.-P. Fumeaux, and V. Sankaran, *Synthesis*, **1972**, 464; A. J. G. Baxter and A. B. Holmes, *J. Chem. Soc., Perkin Trans., 1*, **1977**, 2343; A. B. Holmes, J. Thompson, A. Baxter, and J. Dixon, *J. Chem. Soc., Chem. Commun.*, **1985**, 37; M. Natsume and M. Ogawa, *Heterocycles*, **16**, 973 (1981); R. K. Hill and T. Yuri, *Tetrahedron*, **33**, 1569 (1977); A. Astier and M. M. Plat, *Tetrahedron Lett.*, **1978**, 2051; Y. Matsumura, K. Maruoka, and H. Yamamoto, *Tetrahedron Lett.*, **23**, 1929 (1982); K.

Maruoka, T. Miyazaki, M. Ando, Y. Matsumura, S. Sakane, K. Hattori, and H. Yamamoto, *J. Am. Chem. Soc.*, **105**, 2831 (1983); M. Bonin, J. R. Romero, D. S. Grierson, and H.-P. Husson, *Tetrahedron Lett.*, **23**, 3369 (1982); W. Carruthers, M. J. Williams, and M. T. Cox, *J. Chem. Soc., Chem. Commun.*, **1984**, 1235; T. Wakabayashi, K. Watanabe, Y. Kato, and M. Saito, *Chem. Lett.*, **1977**, 223.

3) Y. Saitoh, Y. Moriyama, T. Takahashi, and Q. Khuong-Huu, *Tetrahedron Lett.*, **21**, 75 (1980); Y. Saitoh, Y. Moriyama, H. Hirota, T. Takahashi, and Q. Khuong-Huu, *Bull. Chem. Soc. Jpn.*, **54**, 488 (1981).

4) J. J. Périé, J. P. Laval, J. Roussel, and A. Lattes, *Tetrahedron*, **28**, 675 (1972); Y. Moriyama, D. Doan-Hoynh, C. Monneret, and Q. Khuong-Huu, *Tetrahedron Lett.*, **1977**, 825.

5) G. Rattle, Thesis of Doctor of Science, The University of Paris, Orsay (1970).

6) G. H. L. Nefkens, G. I. Tesser, and R. J. F. Nivard, *Recl. Trav. Chim. Pays-Bas*, **79**, 688 (1960).

7) W. O. Foyé and W. E. Lange, *J. Am. Pharm. Assoc. Sci. Ed.*, **45**, 742 (1956).

8) M. Gaudemar, *Bull. Soc. Chim. Fr.*, **1962**, 974.

9) A. Horeau, *Tetrahedron Lett.*, **1961**, 506.

10) O. Mitsunobu and M. Yamada, *Bull. Chem. Soc. Jpn.*, **40**, 2380 (1967); A. K. Bose, B. Lal, W. A. Hoffman III, M. S. Manhas, *Tetrahedron Lett.*, **1973**, 1619; M. Asaoka, N. Yanagida, and H. Takei, *ibid.*, **21**, 4611 (1980); O. Mitsunobu and M. Eguchi, *Bull. Chem. Soc. Jpn.*, **44**, 3427 (1971).

11) H. Vorbrüggen and K. Krolikiewicz, *Angew. Chem., Int. Ed. Engl.*, **16**, 876 (1977).

12) P. G. Chantrell, C. A. Pearce, C. R. Toyer, and R. Twaits, *J. Appl. Chem.*, **14**, 563 (1964).

13) E. G. Perkins and D. G. Chasin, *Chem. Phys. Lipids*, **6**, 8 (1971).

14) M. Itoh, D. Hagiwara, and T. Kamiya, *Tetrahedron Lett.*, **1975**, 4393.

15) E. J. Corey, M. G. Bock, A. P. Kozikowski, A. V. Rama Rao, D. Floyd, and B. Lipshutz, *Tetrahedron Lett.*, **1978**, 1051.

16) *cf.* D. Ben-Ishai and A. Berger, *J. Org. Chem.*, **17**, 1564 (1952); M. Bergmann and L. Zervas, *Chem. Ber.*, **65**, 1192 (1932).

17) *e.g.*, H. S. Aaron and C. P. Ferguson, *Tetrahedron*, **30**, 803 (1974); M. Tichý and J. Sicher, *Tetrahedron Lett.*, **1962**, 511.

Reactivities of Stable Rotamers. XVI. Tributylstannane Reduction and Electron-impact Mass Spectra of Rotamers of 1,2,3,4-Tetrachloro-9-(2-chloro-1,1-dimethylethyl)triptycene and 1,2,3,4-Tetrachloro-9-(2-chloro-1-chloromethyl-1-methylethyl)triptycene[1)]

Katsumi YONEMOTO, Fumihiko KAKIZAKI, Gaku YAMAMOTO, Nobuo NAKAMURA, and Michinori ŌKI*

Department of Chemistry, Faculty of Science, The University of Tokyo, Bunkyo-ku, Tokyo 113

(Received July 26, 1985)

1,2,3,4-Tetrachloro-9-(2-chloro-1-chloromethyl-1-methylethyl)triptycene (**1**) and 1,2,3,4-tetrachloro-9-(2-chloro-1,1-dimethylethyl)triptycene (**2**) were reduced with tributylstannane in the presence of azobisisobutyronitrile in benzene. **1** was reduced to **2** which was further converted to a 9-*t*-butyltriptycene under the conditions. The chloromethyl group *sc* to the *peri*-chloro substituent was found to be *ca.* 7 times more reactive than the *ap* in *sc*-**1**. *sc*-**2** was consumed 1.7 times more rapidly than *ap*-**2**. The results are attributed to the participation of the *peri*-chloro substituent in the chlorine abstraction. Electron impact mass spectra of these compounds reveal that they give different intensities at a number of peaks. The difference is again attributed to the chloro participation in stabilizing the cation formed.

In one of the previous papers of this series, we pointed out that a radical reaction, chlorination of the methyl groups of the *t*-butyl group in 9-*t*-butyl-1,2,3,4-tetrachlorotriptycene (**3**), can be accelerated by the participation of the 1-chloro substituent.[2)] Since there are varieties of radical reactions known, the transition states of which should vary from the product-like to substrate-like, the degree of enhancement by the participation of the chloro substituent must be different from reaction to reaction. Alternatively, the degree of the chloro participation could tell the earliness or the lateness of the transition state of a reaction, if a common radical intermediate is to be formed by a variety of reactions.

The rotational barriers in 1,2,3,4-tetrachloro-9-(2-chloro-1-chloromethyl-1-methylethyl)triptycene (**1**) and 1,2,3,4-tetrachloro-9-(2-chloro-1,1-dimethylethyl)-triptycene (**2**) are known to be high enough so that any mixing of rotational isomers can be neglected during the course of reactions.[2)] The barrier to rotation of the radicals produced in the reaction may be assumed to be high as well from the results in the radical halogenations.[2)] To support this assumption, we may cite a fact that 9-*t*-alkyltriptycenes which possess the 9-substituent of a *t*-butyl type, one of the methyls of which is replaced by an sp^2 group, show high barriers as well.[3)] Therefore, any contamination by the contribution of other rotamer(s) during the

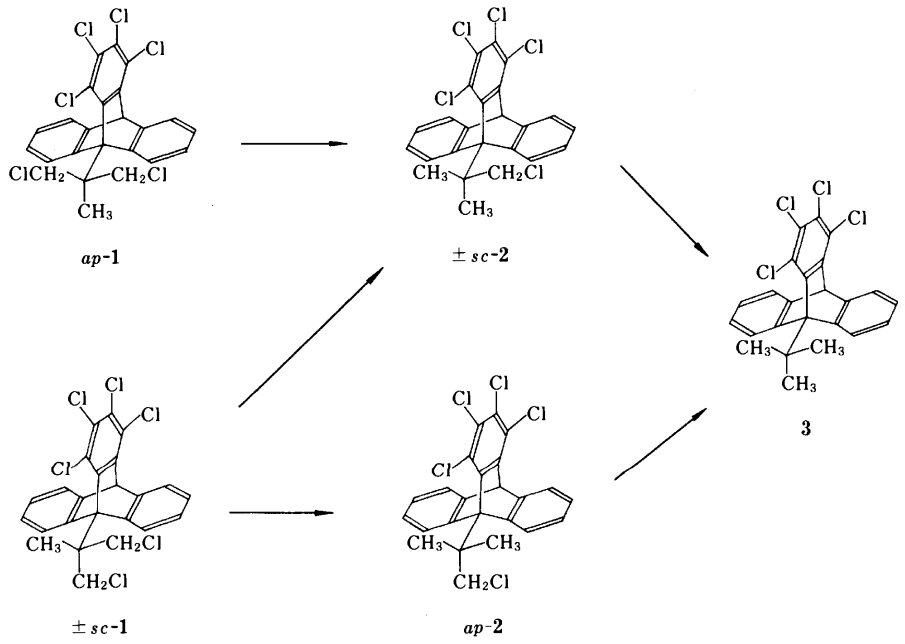

Scheme 1.

reaction may be neglected in this system, if the reaction is run in the vicinity of 100 °C for a week or so.

At an outset of investigations of other radical reactions, we chose reduction of rotamers of **1** and **2** with tributylstannane. The tributylstannane reduction of organic halides, which can be initiated by azobisisobutyronitrile, is known to proceed with radical intermediates: the rate-determining step is the abstraction of a halogen from the organic halides by tributylstannyl radicals.[4]

Compound **1** was prepared according to the method described before and separated into rotational isomers, *ap*-**1** and ±*sc*-**1**, by chromatography.[2] Although separation of *ap*-**2** and ±*sc*-**2** from the mixture of the two was reported to be tedious, as is shown in Scheme 1, if the tributylstannane reduction is successful for *ap*-**1**, it should give mixtures of ±*sc*-**2** and 9-*t*-butyl-1,2,3,4-tetrachlorotriptycene (**3**) in addition to the unreacted starting material, if any, of which separation by chromatography is not too difficult. Indeed, by this method, we could obtain sufficient quantity of ±*sc*-**2** for chracterization and some reactions.

The reaction of the halogen compounds with tributylstannane was generally carried out in benzene solutions, unless otherwise stated. The competitive reactions and determination of the relative rates of reactions were carried out as follows. Nearly equimolar mixtures of *ap*-**2** and ±*sc*-**2** or *ap*-**1** and ±sc-**1** were dissolved in benzene together with a reference compound, either 4-methoxytoluene or 1-methoxy-3,5-dimethylbenzene. Azobisisobutyronitrile was added to the mixture and then tributylstannane (equimolar with the mixture of the substrate) under a nitrogen atmosphere, and the mixture was heated at three temperatures. The decrease in the substrate was monitored by ^{1}H NMR spectroscopy and/or high pressure liquid chromatography (HPLC).

Although we wished to be quantitative, the reactions of **1** were not clean by any means: we found a number of peaks, though small, in HPLC charts in addition to the starting materials and the desired products, **2** and **3**. Especially the peak due to **3** was often in the midst of many small peaks which prevented us from obtaining reliable data of **2**. The yields of compound **2** (±*sc* and *ap*) from compound **1** were *ca.* 50% based on the consumed substrates. These results may be attributed to the strain of the molecules, which could make the aromatic chlorine substituents susceptible to the attack of the tributylstannyl radicals, and force us to be semiquantitative in discussion. The results of the reductions of *ap*-**1** and ±*sc*-**1** are compiled in Tables 1 and 2.

Though the reaction is not clean, we may take the ratio *ap*-**2**/*sc*-**2** in the reaction of ±*sc*-**1** as indicating the reactivity of the *sc* and the *ap*-chloromethyl groups in ±*sc*-**1**. Examination of the data in Table 1 reveals that the chloromethyl group *sc* to the *peri*-substituent is about 7 times more reactive than the *ap* group. By reducing the conversion ratio of ±*sc*-**1**, we should be able to expect that the consumption of ±*sc*-**2** is negligible. Yet the ratio *ap*-**2**/*sc*-**2** is almost constant. Thus the reactivity of the *sc*-chloromethyl group is indeed higher than that of the *ap*. This should be attributed to the participation of the *peri*-chloro substituent (**4**), which stabilizes the transition state of the reaction. This type of participation of a chlorine atom in stabilizing radicals has been reported.[5]

Table 1. Competitive reduction of the *sc* and *ap* chloromethyl groups in ±*sc*-**1**

Temperature/ °C	Conversion/ %	*ap*-**2**/ *sc*-**2**	Reaction time/ h
80	53	6.7	3
69	21	5.8	3
69	13	8	1.5
69	7	6	0.5

Table 2. Results of competitive reactions of ±*sc*-**1** and *ap*-**1** with tributylstannane after 3 h

Temperature/°C	Conversion/%		Product ratio
	±*sc*-**1**	*ap*-**1**	(*sc*-**2**/*ap*-**2**)
100	57	63	2.8
80	57	63	2.4
69	28	31	2.3

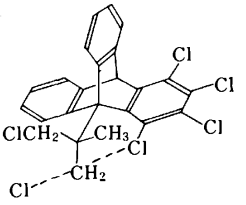

4

It is also noted that the relative reactivity of the *sc* chloromethyl group to that of the *ap* found in ±*sc*-**1** is much larger than that (1.6) in the radical chlorination of **3** with sulfuryl chloride.[2] The results will mean that the bond lengthening (C–Cl and C–H, respectively) in the transition states in these reactions are different to a considerable extent.

The data for the competitive reduction of *ap*-**1** and ±*sc*-**1**, shown in Table 2, indicate that the *ap*-form is a little more reactive than the *sc* and the product ratio (*ap*-**2**/*sc*-**2**) is larger than 2. If the two chloromethyl groups in *ap*-**1** had the same reactivity with the *sc*-chloromethyl group in ±*sc*-**1**, the followings could be

expected. Since there are two *sc*-chloromethyl groups in *ap*-**1**, the overall rates of reduction of either one of the groups are twice of that of the *sc*-chloromethyl group in ±*sc*-**1**. That means that ±*sc*-**2** is produced from *ap*-**1** with a factor of *ca.* 14 relative to the reduction of the *ap*-chloromethyl group in ±*sc*-**1**. Since the relative rate of formation of ±*sc*-**2** from ±*sc*-**1** is small, the formation of *sc*-**2** *via* this route may be neglected. Then the formation ratio (*ap*-**2**/*sc*-**2**) in the competitive reaction should be 2, if the reactivities of the *sc*-chloromethyl groups in *ap*-**1** and ±*sc*-**1** were the same. The observed ratios are significantly larger than 2 to indicate that the chloromethyl group in *ap*-**1** is more reactive than that in ±*sc*-**1** which is *sc* to the 1-chloro substituent for some reasons. The enhanced rates of decreasing in *ap*-**1** relative to those in *sc*-**1** may be also taken as supporting evidence for the above conclusion.

In the ground state, there are two Cl···CH_2Cl interactions[6] in *ap*-**1**, whereas there is only one such interaction in ±*sc*-**1**. This will necessarily make the Cl···CH_2Cl interactions in *ap*-**1** weaker than that in ±*sc*-**1**. The results then may show that this less stabilization in the ground state in *ap*-**1** is important. It may also be pointed out that three C–Cl dipoles are parallel in *ap*-**1** in close proximity (**5**) but one of them is more distant in ±*sc*-**1**: this should result in higher ground state energy of *ap*-**1** than that in ±*sc*-**1**. In addition, probably the steric congestion in *ap*-**1** is more effectively relieved than that in ±*sc*-**1** by the formation of transition state, because the congestedness in this molecule is expected to be greater than that in ±*sc*-**1**. Diagnosis of contributions of these factors awaits further investigations.

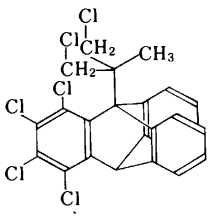

5

The reduction of ±*sc*-**2** and *ap*-**2** were not clean as well. The competitive reactions of ±*sc*-**2** and *ap*-**2** indicated that the *sc*-form was consumed 1.5, 1.6, and 2.0 times faster than *ap*-**2** at 100, 80, and 61 °C, respectively, after 3 h heating. We cannot postulate directly from the results that ±*sc*-**2** is more vulnerable to the attack of the tributylstannyl radicals than *ap*-**2** because of the complex nature of the reaction, but nonetheless it is tempting to consider so from the results with ±*sc*-**1** and *ap*-**1**. The interesting point here is that the difference in reactivities between the *sc*-chloromethyl group and the *ap* in **2** seems to be diminished considerably from the values observed in ±*sc*-**1**. We do not have good explanations for this finding but it could be postulated that the stabilization due to the Cl···CH_2Cl interaction, the congestedness, Coulombic interactions, and the enhanced electronegativity of the chloromethyl group in *ap*-**1** relative to that in ±*sc*-**2** are responsible.

Having had two rotamers of compound **2** in hand, we can now compare some properties of the rotamers of **2**, which cannot be examined as a mixture. As one of such examples we have taken the electron-impact mass spectra of the rotamers. Although there are ample reports which describe different fragment patterns of diastereomeric isomers,[7] those of rotational isomers are limited.[8] Therefore, it will be worthwhile to acquire mass spectral data of rotational isomers of **2** as well as **1**, because the mass spectra are usually obtained as a mixture of possible rotamers of a compound. We also expected that, from the results of ionization reactions of these isomers that showed significant stabilization of the *sc*-carbocation by the participation of the 1-chloro substituent in **2**,[9] the fragment species **6** should be more abundant than the fragment **7** in which no special stabilization is expected.

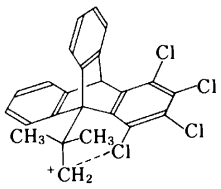

6

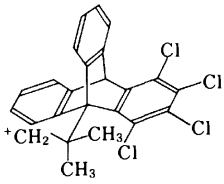

7

Sets of typical results are shown in Table 3. Since vaporization of the samples took place at 180—210 °C, we can assume that internal rotation is negligibly slow during the measurement. The intesities of the peaks varied from one measurement to another but the trends in intensities discussed below were reproducible. As expected, we observed a number of peaks in the mass spectra of which relative intensities were different from a rotamer to another. We will discuss the peaks corresponding to species which bear ^{35}Cl atoms only for the sake of simplicity and the absence of ambiguity in the discussion.

Base peaks in both ±*sc*-**2** and *ap*-**2** were mostly at *m/z* 356 which correspond to the loss of the 9-substituent and a chlorine atom with the gain of two hydrogen atoms. The loss is reasonable since removal of the 9-substituent and/or the chlorine atom at the 1-position relieves the strong steric strain. The features noticed in comparison of the two spectra due to ±*sc*-**2** and *ap*-**2** are that the relatively large molecular ion peak for the *ap*, the relatively large peak corresponding to $[M-35]^+$ for the *sc*, and

Table 3. Typical sets of mass spectral data of compounds **1** and **2**[a)]

Assignment	Compound **1**			Compound **2**		
	m/z	±*sc*	*ap*	*m/z*	±*sc*	*ap*
M^+	514	8.5	10.0	480	14.5	20.0
$[M-Cl]^+$	479	10.5	10.0	445	20.5	8.0
$[M-HCl]^+$	478	4.5	10.5	444	38.0	2.5
$[M-(Cl+HCl)]^+$	443	12.7	38.0			
$[M-2HCl]^+$	442	7.0	27.0			

a) Relative intensities to the base peaks which were at *m/z* 356 in all the cases shown here.

the relatively large peak corresponding to $[M-36]^+$ in the *sc*. The first two features both speak for the stabilization of $[M-35]^+$ species in the *sc* form which can be assigned to structure **6**. A part of the reasons for the less abundance of the M^+ peak for the ±*sc*-isomer must be attributed to the more intense peaks corresponding to $[M-35]^+$ and $[M-36]^+$. Since it is known that, if once the cationic species **6** is formed, it undergoes reactions, cyclization and olefin-formation,[9] this peak may be assigned to the cationic species formed after these reactions. Therefore, the abundance of $[M-36]^+$ peak in the mass spectra of the ±*sc*-form is also evidence for the stabilization of **6**.

In Table 3, are also included the electron impact mass spectra of ±*sc*-**1** and *ap*-**1**. Here again the base peaks were generally *m/z* 356. The features of the mass spectra of *ap*-**2** and ±*sc*-**2** are reproduced here again. Since both rotamers of **1** bear at least one *sc*-chloromethyl group to the *peri*-chloro, it may be fair to compare the results which correspond to the loss of the second chlorine atom. Although we could not observe a $[M-2Cl]^+$ peak, the peaks corresponding to $[M-(Cl+HCl)]^+$ and $[M-2HCl]^+$ are more abundant in the *ap* form than in the *sc*.[10] The anchimeric assistance in the fragmentation in mass spectra is again important.

Experimental

Substrates were prepared as reported previously,[2] except for ±*sc*-1,2,3,4-tetrachloro-9-(2-chloro-1,1-dimethylethyl)-triptycene (**2**), of which method of preparation is given below. The products were identified by comparison of their ^1H NMR spectra and retention times in HPLC.

Competitive Reactions. A nearly equimolar amount (*ca.* 5 mg or *ca.* 0.01 mmol) each of *ap* and ±*sc* isomers of **1** was weighed and dissolved in 1.3 mL of benzene. A small amount of azobisisobutyronitrile was added to the solution together with 60 µL of 1-methoxy-3,5-dimethylbenzene or 4-methoxytoluene. After purging of the air by nitrogen, 5.4 µL (0.02 mmol) of tributylstannane was added and the solution was sealed in a tube. The tube was heated at 100, 80, or 69 °C for 3 h by immersing the tube into a boiling bath of water, benzene, or hexane. Averages of 3 runs are given in Table 1. Competitive reactions between *ap*-**2** and ±*sc*-**2** were carried out similarly. A small amount of products which were derived by reduction of the aromatic chlorine atom(s) was detected but these were neglected in analyses.

Analysis of the Unreacted Materials and Products. Analysis was carried out with the use of a Waters HPLC apparatus equipped with a UV detecter at 254 nm, a microporasil column being used. Typical retention times for these compounds were as follows, when the flow rate of hexane was 1.5 mL min^{-1}: **3** 8.4 min, *ap*-**2** 11.5 min, ±*sc*-**2** 11.9 min, *ap*-**1** 14.7 min, ±*sc*-**1** 21.3 min. Intensities were measured by the weight method except for compound **2**, for which special care was taken because of the overlap of the corresponding peaks in HPLC. A calibration curve was drawn by comparing the intensities of the peaks due to the substrates and the products in HPLC with those of ^1H NMR spectra in the former case. The peak heights were used in the case of **2** and a calibration curve was drawn as well.

Mass Spectrometry. The electron-impact mass spectra were recorded on a JEOL-JMS-D300 mass spectrometer with 70 eV electrons. The temperature required for obtaining high enough vapor pressure for the measurement ranged from 180 to 210 °C. The intensities of peaks of interest changed from a measurement to another. Those data given in Table 3 are sets of typical values of which trends were reproducible.

±sc-*1,2,3,4-Tetrachloro-9-(2-chloro-1,1-dimethylethyl)-triptycene (2).* A solution of 110 mg (0.22 mmol) of *ap*-**1** in 12 mL of toluene was heated with 59 µL (0.22 mmol) of tributylstannane and a small amount of azobisisobutyronitrile under reflux for 6 h. The solvent was evaporated and the residue was chromatographed on a silica-gel plate with hexane-dichloromethane as an eluent. The desired product was obtained as crystals, mp 185.0—186.0 °C, in 16% yield. Found: C, 59.38; H, 3.71; Cl, 37.34%. Calcd for $C_{24}H_{17}Cl_5$: C, 59.72; H, 3.55; Cl, 36.73%. ^1H NMR ($CDCl_3$), δ=2.13 (3H, s), 2.32 (3H, s), 4.87 and 4.95 (2H, ABq, J=11.6 Hz), 6.06 (1H s), 6.9—7.2 (4H, m), 7.3—7.5 (2H, m), 7.8—8.0 (2H, m).

Although it was possible to increase the amount of ±*sc*-**2** in this reaction by increasing the reducing reagent, products derived by the reduction of aromatic chlorine atom(s) increase in its amount as well. Thus the above procedure is the optimum so far we have achieved. *ap*-**1** could be recovered in *ca.* 80% yield on an average.

This work was supported by a Grant-in-Aid for Scientific Research of the Ministry of Education,

Science and Culture, to which our thanks are due.

References

1) For Part XV, see K. Yonemoto, Y. Nakai, G. Yamamoto, and M. Ōki, *Chem. Lett.*, **1985**, 1739.

2) T. Morinaga, S. Seki, H. Kikuchi, G. Yamamoto, and M. Ōki, *J. Am. Chem. Soc.*, **102**, 1173 (1980); S. Seki, T. Morinaga, H. Kikuchi, T. Mitsuhashi, G. Yamamoto, and M. Ōki, *Bull. Chem. Soc. Jpn.*, **54**, 1465 (1981).

3) G. Yamamoto, A. Tanaka, and M. Ōki, *Bull. Chem. Soc. Jpn.*, **57**, 891 (1984).

4) H. G. Kuivila, *Acc. Chem. Res.*, **1**, 299 (1968).

5) C. R. Everly, F. Schweinsberg, and J. G. Traynham, *J. Am. Chem. Soc.*, **100**, 1200 (1978).

6) G. Izumi, G. Yamamoto, and M. Ōki, *Bull. Chem. Soc. Jpn.*, **54**, 3064 (1981).

7) M. M. Green, *Top. Stereochem.*, **9**, 35 (1976). For recent papers, see for example: A. Weisz, A. Mandelbaum, J. Shabanowitz, and D. F. Hunt, *Org. Mass. Spectrom.*, **19**, 238 (1984); V. Hanus, F. Turecek, A. Farag, and M. Tichy, *ibid.*, **19**, 459 (1984); I. Marksammer and A. Mandelbaum, *Tetrahedron*, **41**, 775 (1985).

8) H. Iwamura, *Tetrahedron Lett.*, **1973**, 232.

9) H. Kikuchi, S. Seki, G. Yamamoto, T. Mitsuhashi, N. Nakamura, and M. Ōki, *Bull. Chem. Soc. Jpn.*, **55**, 1514 (1982).

10) In one measurement, the peak at m/z 444 appeared as a very strong one. This peak involves contributions of the fragment $[M-2^{35}Cl]^+$ from $C_{24}H_{17}{}^{35}Cl_5$ and that $[M-2H^{35}Cl]^+$ from $C_{24}H_{17}{}^{35}Cl_4{}^{37}Cl$. However, this peak is omitted from the discussion for the following reasons. Firstly, the cause for the stabilization of $[M-2Cl]^+$ is difficult to find and, secondly, division of the contributions by the two kinds of fragments is not tried in this work.

 © 1985 The Chemical Society of Japan Bull. Chem. Soc. Jpn., 58, 3351—3355 (1985)

Kinetic Studies of Fast Equilibrium by Means of High-performance Liquid Chromatography. XII.[1] Rate Constants and Energy Barriers of Intramolecular Carbonyl-Nitrogen Bond Rotation of *o*-Substituted Acetanilides

Masataka Moriyasu,* Kazuko Kawanishi, Atsushi Kato, Yohei Hashimoto, Makiko Sugiura, and Torei Sai

Kobe Women's College of Pharmacy, Motoyamakita-machi Higashinada-ku, Kobe 658

(Received April 24, 1985)

A novel high-performance liquid chromatographic(HPLC) method has been proposed to determine the rate constants and activation energies of the interconversion between two labile species existing in equilibrium in solution. The rotational energy barriers to intramolecular bond rotation about the carbonyl-nitrogen bonds of several *o*-substituted acetanilides have been determined by this method. These energy barriers have been found to increase when bulkier groups are attached at the *o*-position on the benzene ring. These have also been determined by a dynamic nuclear magnetic resonance spectroscopic(DNMR) method, which gives good agreement with the HPLC results.

In our previous reports,[2,3] dynamic equilibria between two rotamers (*E*- and *Z*-form) of several anilides including formanilide and acetanilide derivatives have been investigated by means of high-performance liquid chromatography(HPLC). HPLC

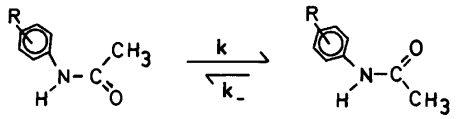

E-form Z-form

of several anilides at low temperatures have led to the successful separation of two labile rotamers. We have called the HPLC method dynamic high-performance liquid chromatography(DHPLC) in imitation of dynamic NMR. When the interconversion is relatively slow even at room temperature, either of the equilibrated species can be enriched by HPLC. In this case the rate constants and energy barriers to the interconversion can be easily determined.[4] On the other hand, when the interconversion is faster, as is the case for formanilide[2] and metal dithiocarbamates,[5] this treatment failed at room temperature, but was found possible under cooled conditions. This treatment was found to be inapplicable to acetanilides as the interconversion between the two rotamers of acetanilides are much faster than in the case of formanilide. Thus, when each of the portions collected were rechromatographed, howsoever carefully and quickly the experiments were carried out, almost equilibrated chromatograms were always obtained even at low temperatures. The difficulty has forced us to devise another method to determine the rate constants and energy barriers to the bond rotation. In this report, an approximate HPLC method is proposed to determine the energy barriers from the change in the HPLC chromatograms. We have determined the rate constants and energy barriers of intramolecular bond rotation of several *o*-substituted acetanilides. We have also determined the energy barriers by DNMR and compared both results. The attempt to determine the energy barriers in other acetanilides such as *m*- or *p*-substituted ones by means of HPLC was unsuccessful because the content of the *E*-form is low for these acetanilides.

Experimental

2-Methylacetanilide, 2-ethylacetanilide, 2-isopropylacetanilide, and 2,4-dimethylacetanilide were prepared by usual procedures from the corresponding aromatic amines and acetic anhydride.[6] The samples were twice recrystallized from hexane-acetone. The HPLC apparatus for use in low-temperature measurements was described in our previous communications.[3,5] The column effluent was passed through a narrow stainless steel tube (0.5 mm in internal diameter and 10—20 m in length) which was thermostated at 50—100 °C in an air bath prior to detection by means of a UV detector.[3] This treatment, however, was found not always to be necessary in this case because the ratios of the two rotamers were found to be unchanged in the presence and absence of heating. This suggests that either the absorption coefficients of the two rotamers are almost the same or the re-equilibrium is attained promptly before the column effluent reaches the cell of the UV detector even in the absence of the heating. The NMR instrument (Varian XL-200) was also similar to the one described previously.[3] In order to determine the energy barriers to bond rotation, the DNMR method was applied as follows: Total line shape analysis was carried out according to the DNMR3-IT$_2$[7] program after modifying the input and output modes partially. The calculation was made on an NEC ACOS series 77 system 1000 type computer at the Computation Center of Osaka University.

Theoretical

When the system composed of dynamic equilibria in solution is chromatographed, the separation and the interconversion will compete and complicated chromatograms may be obtained. This phenomenon

is sometimes observed in TLC,[8] GC,[9,10] and HPLC[11] included in our previous study.[2,5] In our series of measurements, we demonstrated the use of the HPLC method to investigate fast equilibria in solution. Two equilibrated species ($X \underset{k_-}{\overset{k}{\rightleftharpoons}} Y$) exist in solution, interconversion between two labile isomers being an example. The interconversion is assumed not to be rapid as compared with the separation speed by HPLC. Thus, when HPLC is carried out at low temperature, the two labile rotamers will be separated completely and interconversion between two isomers will not occur during chromatography (Fig. 1(a)). When the column temperature is slightly raised, interconversion between two labile species will occur to some extent. In this case, as shown in Fig. 1(b), the base line separation of the two species is no longer attained. When the interconversion X→Y (or Y→X) partially occurs during chromatography, the formed species Y (or X) will be eliminated from X (or Y) promptly, provided that the intrinsic retention time of X and Y differ markedly from one another. Thus, the peak area of X ($=S_X$) indicates the residual amount of X at a definite time t. The value t is approximated from the retention time of X ($=t_r$) as follows: When a sample composed of X and Y is introduced to HPLC from an injector, it reaches the column head after the lapse of a slight interval, t_1, and the separation process then begins with the slight interconversion between the two rotamers being attained during chromatography. After the lapse of time, t, X reaches the column end and the separation stops. It will still take some more time, t_2, before X reaches the cell of the detector. Assuming that the peak shape is symmetrical and that the separation is attained promptly near the column head, the following equation will apply: $t_r=t_1+t_2+t$. The residual amount of X at a time t is proportional to the product S_X in Fig. 1(b) and the flow rate v. When the flow rate is decreased with the column temperature being kept constant, a larger part of X should transform into Y during the chromatographic process. Thus, from the plot $S_X v$ *vs.* t, the rate constant of the bond rotation can be calculated. It is noteworthy here that in this method the transformed species is promptly eliminated from the peak and thus the effect of the reverse reaction can be approximately neglected, which differs from other kinetic methods. When the rate constants are measured at a variety of column temperatures, the rotational energy barrier can be calculated from the Arrhenius' plot.

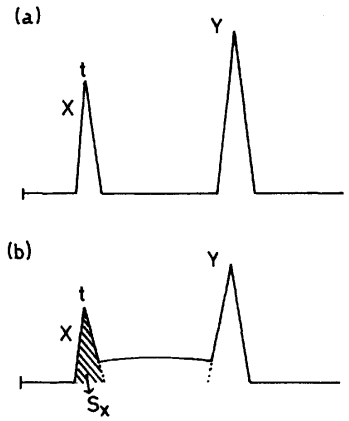

Fig. 1. Possible chromatogram patterns with partial interconversion during chromatography.

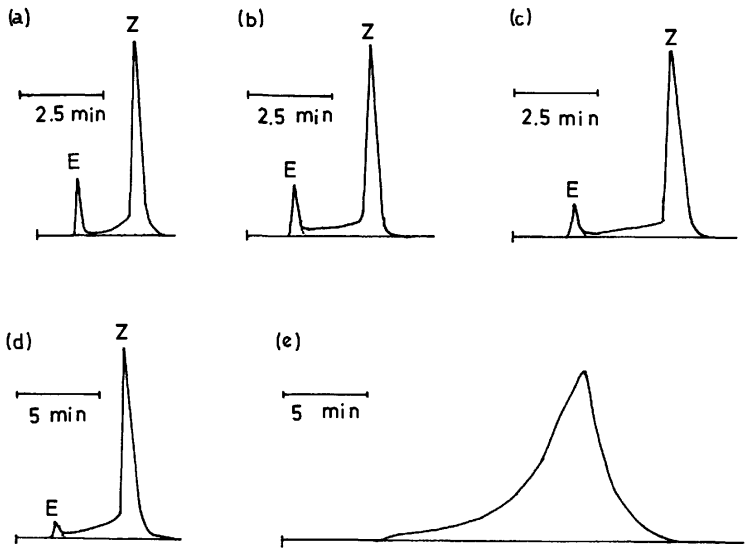

Fig. 2. HPLC chromatograms of 2-methylacetanilide at −35 °C under different flow rates. Flow rate: (a): 3.2 $cm^3 min^{-1}$, (b): 2.5 $cm^3 min^{-1}$, (c): 1.9 $cm^3 min^{-1}$, (d): 1.1 $cm^3 min^{-1}$, (e): 0.4 $cm^3 min^{-1}$. For other HPLC conditions, see text.

Results and Discussion

HPLC of 2-Methylacetanilide. As shown in the theoretical section, it is necessary to determine the void volume from the injector to the column head and from the column end to the cell of the UV detector. This was determined to be 0.25 cm^3 for the present HPLC apparatus by connecting a voidless 2-way union instead of the column and then injecting a sample to be detected. Thus, t_1+t_2 was calculated by dividing the dead volume by each flow rate.

Then, 2-methylacetanilide was chromatographed at low temperatures. The two rotamers of 2-methylacetanilide were separated under the HPLC conditions described previously;[3] solvent system: hexane:1-propanol:acetic acid=100:10:3; column: Polygosil 60—5 (4.6 mm×15 cm); flow rate: 2.0 cm^3 min^{-1}; detection: UV 254 nm. Under these conditions and the column temperature at −50 °C, base line separation of the two rotamers was achieved, and the equilibrium constants prior to HPLC could be determined. On the other hand, when the column temperature was higher than −20 °C, the two peaks coalesced, and consequently only one broad peak appeared on the chromatograms. Between these two extremes, two peaks, the larger one corresponding to the *E*-rotamer and the smaller one to *Z*-rotamer, appeared on the chromatograms with slight interconversion being attained during chromatography.[3] Then, the column temperature was adjusted from −40 to −25 °C, at various flow rates (0.3—4.0 cm^3 min^{-1}). The change of chromatograms at −35 °C is depicted in Fig. 2. With increasing flow rate, the interconversion is suppressed. The product of the peak area and the flow rate $S_X v$ is plotted against the residence time t and the results is shown in Fig. 3. From the slope of these linear lines, the rate constant k corresponding to the conversion from *E*-to *Z*-form at each temperature was determined. The results were 5.2×10^{-3}, 1.0×10^{-2}, 2.0×10^{-2}, and 3.7×10^{-2} s^{-1} at −40, −35, −30, and −25 °C, respectively. In Fig. 3, it is noteworthy that when the same amount of the sample was injected the extraporated values of $S_X v$ at $t=0$ were similar at different temperatures. This can reasonably be attributed to the fact that the initial content of the *E*-form before chromatography is similar for each sample.

With similar procedures, the reverse rate constant k from *Z*- to *E*-form at each temperature was deter-

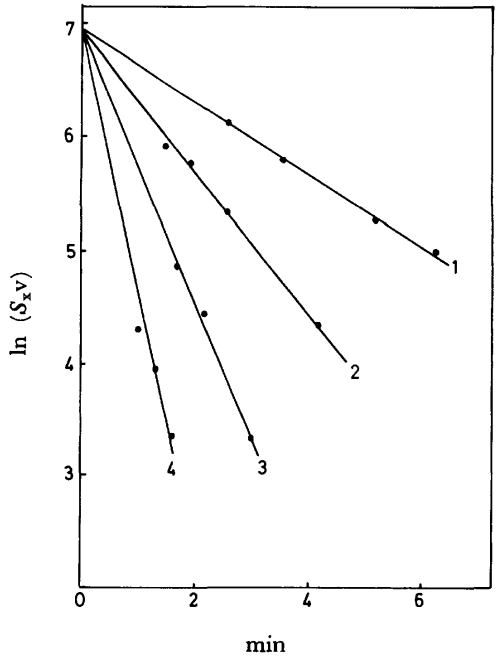

Fig. 3. Plots of residual amount of *E*-form of 2-methylacetanilide *vs.* residence time.
1: −40 °C, 2: −35 °C, 3: −30 °C, 4: −25 °C.

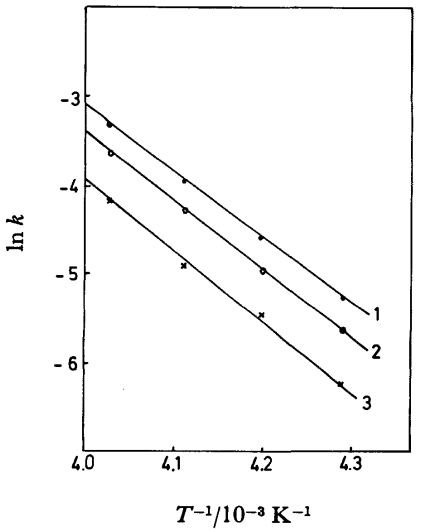

Fig. 4. Arrhenius' plot of *o*-substituted acetanilides by HPLC.
1: 2-Methylacetanilide, 2: 2-Ethylacetanilide, 3: 2-Isopropylacetanilide.

Table 1. Rate constants k and k_- of *o*-substituted acetanilides

	$k(s^{-1})$	$k_-(s^{-1})$	$K_{calcd}=k/k_-$	K_{obsd}		
				−50 °C	0° C	25 °C
2-Methylacetanilide	5.2×10^{-3}	6.1×10^{-4}	8.4	4.5	4.4	4.4
2-Ethylacetanilide	2.6×10^{-3}	3.8×10^{-4}	6.8	3.4	3.4	3.2
2-Isopropylacetanilide	2.0×10^{-3}	2.5×10^{-4}	7.8	2.6	2.5	2.6

Table 2. Energy barriers of bond rotation of *o*-substituted acetanilides

	E_a (kJmol^{-1})			
	HPLC[a] (−20——40 °C)		NMR[b] (10—50 °C)	
	$E \rightarrow Z$	$Z \rightarrow E$	$E \rightarrow Z$	$Z \rightarrow E$
2-Methylacetanilide	62.4	59.0	74.5	76.4
2-Ethylacetanilide	65.7	65.8	76.9	78.8
2-Isopropylacetanilide	68.2	66.5	84.0	82.0
2,4-Dimethylacetanilide	61.6	—	—	—

a) In eluent (hexane : 1-propanol : acetic acid = 100 : 10 : 3). b) In $CDCl_3$.

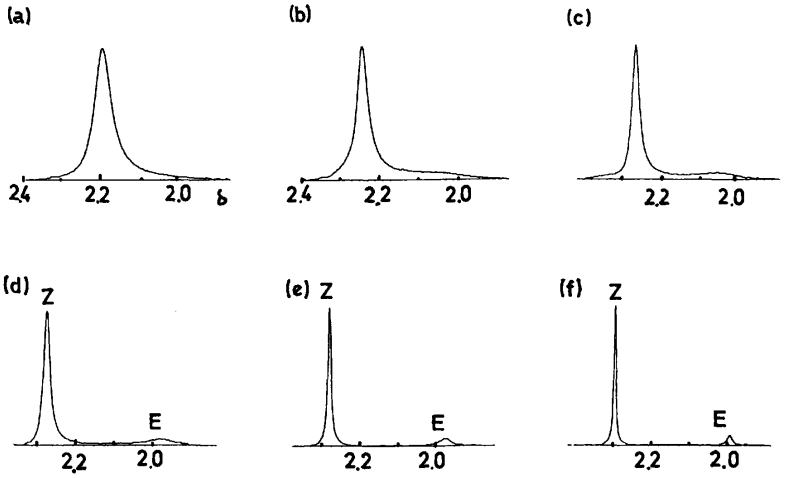

Fig. 5. ^{1}H-NMR spectra of 2-ethylacetanilide in $CDCl_3$ at different temperatures.
(a): 50 °C, $k = 6.7 \times 10^1$ s^{-1}, (b): 40 °C, $k = 2.7 \times 10^1$ s^{-1}, (c): 35 °C, $k = 1.6 \times 10^1$ s^{-1}, (d): 30 °C, $k = 9.8 \times 10^0$ s^{-1}, (e): 20 °C, $k = 3.4 \times 10^0$ s^{-1}, (f): 10 °C.

mined to be 6.1×10^{-4}, 1.0×10^{-3}, 1.6×10^{-3}, and 3.2×10^{-3} s^{-1} at −40, −35, −30, and −25 °C, respectively. Thus, the equilibrium constant K (=[*Z*-form]/[*E*-form]) should be from 8 to 12 over this temperature range. The equilibrium constant K can be directly determined by means of HPLC by dissolving 2-methylacetanilide in an HPLC eluent and then letting it stand for enough time to attain equilibrium between the two rotamers, followed by HPLC analysis at −50 °C.[3] The equilibrium constant at 25, 0, and −50 °C was thus determined and was found to be almost the same(K=4.5). Both results agree relatively well.

HPLC of Other o-Substituted Acetanilides. Using the procedure described above, the rate constants for the bond rotation were determined for other *o*-substituted acetanilides at low temperatures(−40 to −25 °C). The rate constants k and k_- at −40 °C are summarized in Table 1. These results suggest that when bulkier groups are attached at the *o*-position of the phenyl ring, intramolecular bond rotation becomes slow.

Energy Barriers to the Bond Rotation. Figure 4 indicates Arrhenius' plots (k *vs.* $1/T$) for *o*-substituted acetanilides. From the slope of these linear lines, the energy barriers to the bond rotation from the *E*- to the *Z*-form were calculated; they were found to increase slightly when bulkier groups were substituted. Using similar procedures, the energy

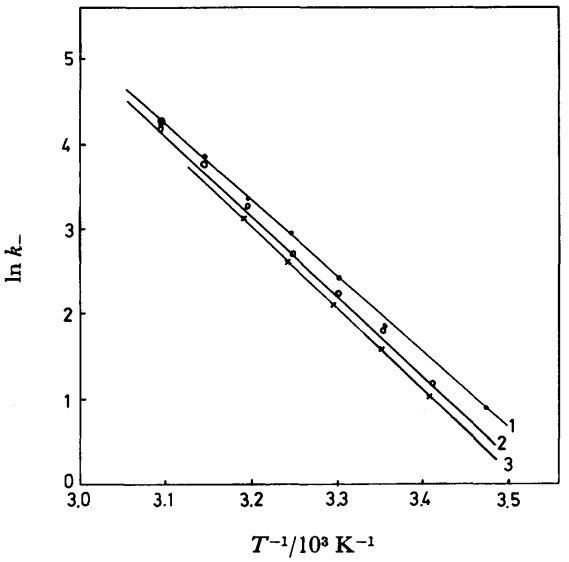

Fig. 6. Arrhenius' plot of *o*-substituted acetanilides by ^{1}H-NMR.
1: 2-Methylacetanilide, 2: 2-Ethylacetanilide, 3: 2-Isopropylacetanilide.

barriers of the reverse reaction (from *Z*- to *E*-form) were determined. These results are summarized in Table 2. The energy barriers of the bond rotation of forward and backward reactions were found to be closely similar.

DNMR Measurements. Previous NMR study have also demonstrated the presence of both *E*- and *Z*-forms for *o*-substituted acetanilides[12] but evaluation of the energy barriers by the DNMR method was not carried out as the percentages of the *E*-form are low, and consequently, total line shape analysis was difficult using relatively low field NMR instruments with low sensitivity. Figure 5 indicates 200 MHz ^{1}H-NMR spectra of 2-ethylacetanilide for the acetyl protons from 10 to 50 °C. Two sharp signals (δ=2.28 and 1.98 for *Z*- and *E*-form, respectively) at 10 °C are broadened with the rise of temperature and at 50 °C the two peaks coalesce. It is interesting to note that the change in the NMR spectra (Fig. 5) resembles that of the HPLC chromatograms (Fig. 2). The rate constants for the bond rotation at each temperature were determined by total line shape analysis (Fig. 5). The energy barrier corresponding to the conversion from the *Z*- to the *E*-form was calculated to be 78.8 kJ mol^{-1} from the Arrhenius' plots (Fig. 6). Similar experiments were carried out for 2-methylacetanilide and 2-isopropylacetanilide. The rate constants k_- at −30 °C were determined to be 1.1×10^1, 9.8×10^0, and 9.4×10^0 s^{-1}, for 2-methylacetanilide, 2-ethylacetanilide, and 2-isopropylacetanilide, respectively. The energy barriers were also calculated and the results are shown in Table. 1. In both NMR and HPLC the energy barriers are found to increase when bulkier substituents are introduced at the *o*-position. The energy barriers obtained by HPLC are somewhat smaller than those by NMR, which may be interpreted at least partially in terms of the difference in the polarity of the solvents and the temperature range. If these conditions are taken into consideration, both results agree fairly well. The energy barriers obtained by the present HPLC method are not always accurate because it may sometimes occur that the bond rotation is catalytically accelerated or suppressed on the surface of the adsorbent silica-gel. The authors, however, consider that the HPLC method will be a useful method for approximately estimating the energy barriers of fast equilibria.

The authors wish to express their gratitude to Dr. Usha Shome, National Botanical Research Institute, Lucknow, India, who kindly corrected the English of this paper.

References

1) Part XI. M. Moriyasu, A. Kato, and Y. Hashimoto, *J. Chem. Soc., Perkin Trans. 2*, in press.

2) M. Moriyasu, K. Kawanishi, A. Kato, and Y. Hashimoto, *Bull. Chem. Soc. Jpn.*, **57**, 1766 (1984).

3) M. Moriyasu, K. Kawanishi, A. Kato, and Y. Hashimoto, *Bull. Chem. Soc. Jpn.*, **58**, 2581 (1985).

4) a) H. Koller, R. Rimbock, and A. Mannschreck., *J. Chromatogr.*, **282**, 89 (1983); b) H. Scherubl, O. Fritzche, and A. Mannshreck., *Chem. Ber.*, **117**, 336 (1984).

5) M. Moriyasu, Y. Hashimoto, and M. Endo., *Bull. Chem. Soc. Jpn.*, **56**, 1972 (1983).

6) L. F. Fieser and K. L. Williamson, "Organic Experiments," 4th ed, ed by D. C. Heath and Company, Toronto (1979), p. 159.

7) DNMR3-IT$_2$ (J. Musso, G. Torrl, and M. Azzaro, J. Mag. Reson., to be published, QCPE 356) is an iterative version of the program DNMR3 for the calculation of complex exchange-broadened NMR spectra (D. A. Kleier and G. Binsch, J. Mag. Reson., 3, 2 (1970) 146, QCPE 165). Parameters are fitted using the Marquardt's algorithm (D. W. Marquardt, *J. Soc. Ind. App. Math.*, **11**, (1963) 431, QCPE).

8) R. A. Keller and J. C. Giddings., *J. Chromatogr.*, **3**, 205 (1960).

9) V. Schurig and W. Burkle, *J. Am. Chem. Soc.*, **104**, 7573 (1982).

10) W. Burkle, H. Karfunkel, and V. Scurig, *J. Chromatogr.*, **288**, 1 (1984).

11) C. Horvath and S. R. Lipsky, *Anal. Chem.*, **41**, 1227 (1969).

12) H. Kessler and A. Rieker, *Liebigs Ann. Chem.*, **708**, 57 (1967).

 © 1985 The Chemical Society of Japan Bull. Chem. Soc. Jpn., 58, 3356—3359 (1985)

Improved Synthesis and Crystal Structure of 7*H*-Dibenz[*a*,*kl*]anthracen-7-one

Shoji Fujisawa, Isao Oonishi,* Junji Aoki, Yuji Ohashi,†,†† and Yoshio Sasada†

Department of Chemistry, Faculty of Science, Toho University, Funabashi, Chiba 274
†*Laboratory of Chemistry for Natural Products, Tokyo Institute of Technology, Nagatsuta, Midori-ku, Yokohama 227*

(Received June 5, 1985)

An improved synthetic method gives pure 7*H*-dibenz[*a*,*kl*]anthracen-7-one, $C_{21}H_{12}O$, in a higher yield than those reported so far. The crystal structure has been determined by X-ray analysis. The space group is $Pn2_1a$, with unit cell dimensions of a=23.325(5), b=14.149(3), c=3.986(1) Å, and Z=4. The structure was solved by the direct method and refined by the block-diagonal least-squares method to an R value of 0.044. The molecule is greatly distorted from the planar conformation because of an intramolecular steric repulsion between the hydrogen atoms.

Bradley *et al.* reported[1] that the condensation of benz[*a*]anthracene-7,12-dione (**1**) with glycerol and concentrated sulfuric acid gave two products; 7*H*-benzo[*hi*]chrysen-7-one (8,9-BzBT, **2**) and 13*H*-dibenz-[*a*,*de*]anthracen-13-one (5,6-BzBT, **3**). In this case, the cyclization in the 11 and 12 positions of **1** should occur to produce 7*H*-dibenz[*a*,*kl*]anthracen-7-one (10,11-BzBT, **4**), although they did not mention it. Clar *et al.* reported[2] that 10,11-BzBT was prepared by decarboxylating its 13-carboxylic acid, which had itself been produced by the partial cyclization of 1,1′-binaphthyl-8,8′-dicarboxylic acid. However, this method requires many steps and gives only a poor yield. We reexamined the method reported by Bradley *et al.* and obtained 10,11-BzBT in a satisfactory yield.

Previously, we determined the crystal structures of 8,9-BzBT[3] and 5,6-BzBT.[4] These compounds are distorted from the planar conformation because of a steric repulsion between O and H, which are indicated by *. In 10,11-BzBT, the distortion from the planar structure is expected to be caused by the repulsion between the hydrogen atoms with *. The present paper deals with the crystal structure of **4** in comparison of the distortion modes with those of 8,9-BzBT and 5,6-BzBT.

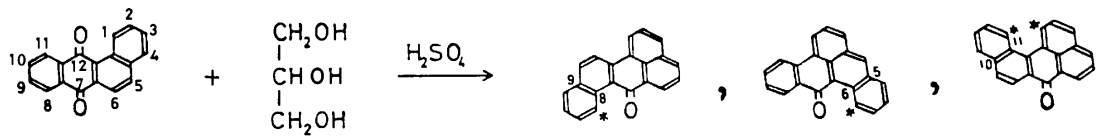

1 2 3 4

Experimental

Synthesis of o-(1-Naphthoyl)benzoic Acid. A mixture containing naphthalene (25.0 g) and finely powdered anhydrous aluminum chloride (50.0 g) was dissolved in 120 ml of 1,1,2,2-tetrachloroethane, into which phthalic anhydride (25.0 g) was added with stirring, the temperature being kept below 10 °C for 2 h. Then the mixture was kept at 20 °C for 8 h. The contents were poured into water (300 ml) containing a small amount of hydrochloric acid, and the whole was steam-distilled. The cold residue was extracted with a small amount of 4% aqueous sodium hydroxide, and then concentrated hydrochloric acid was added until the solution was made acidic. After the solution had stood overnight, the precipitated *o*-(1-naphthoyl)benzoic acid was collected and washed with water. Recrystallization from glacial acetic acid gave the *o*-(1-naphthoyl)benzoic acid as white plates; mp 175—176 °C (uncorrected). Yield, 42.7 g.

Synthesis of Benz[a]anthracene-7,12-dione. *o*-(1-Naphthoyl)benzoic acid (21.0 g) was mixed with concentrated sulfuric acid (210 ml), and the mixture was heated to 65 °C for 4 h. After cooling, the contents were poured into water (1 l). The precipitate was collected and washed thoroughly with water. The crude product (7.2 g) was then boiled for 2 h with glacial acetic acid. Yield, 6.0 g; green yellow needles; mp 167—168 °C.

Glycerol Condensation of Benz[a]anthracene-7,12-dione. To a mixture of benz[*a*]anthracene-7,12-dione (5.0 g), aniline (5.0 g), and 80% sulfuric acid (140 g), glycerol (14.0 g) was added, drop by drop, at 50 °C. The mixture was then heated at 100 °C for 8 h. After cooling, the contents were poured into a large amount of water, collected, and washed with hot water. The crude product (3.2 g), a brown mass with a mp of 123—153 °C, was extracted with acetone (50 ml). The extraction was carried

†† Present address: Department of Chemistry, Faculty of Science, Ochanomizu University, Otsuka, Bunkyo-ku, Tokyo 112.

out by means of hot filtration. The filtrate, on evaporation to dryness, gave a dark brown mass (1.4 g). A chlorobenzene solution of this product was passed through a column of silica-gel (300 mesh) and eluted with chlorobenzene. The products was developed into three bands. The red band was separated and concentrated, giving red needles. Yield 0.2 g; mp 197—198 °C. The intense yellow band, overlapping with a pale yellow band, was eluted with chlorobenzene and concentrated to give a yellow mass (1.1 g); mp 162—168 °C. This product was dissolved in a large amount of ethanol, and the solution was put into a column of alumina. The absorbed layer was developed into two bands; the lower layer, an intense yellow band, was separated and concentrated to give intense yellow needles. Yield, 0.3 g; mp 183—184 °C. The upper layer, a pale yellow band, gave pale yellow needles. Yield 0.7 g; mp 188—189 °C. The red needles (mp 197—8 °C) and the intense yellow needles (mp 183—4 °C) were proved to be 5,6-BzBT[4] and 8,9-BzBT[3], respectively. Thus, the pale yellow needles (mp 188—9 °C) were assumed to be 10,11-BzBT.

X-Ray Data Collection of 10,11-BzBT. The crystals (mp 188—9 °C) were grown from an ethanol solution. Crystals; $C_{21}H_{12}O$, M.W. 280.3, orthorhombic, a=23.325(5), b=14.149(3), c=3.986(1) Å, and U=1315.4(5) Å^3, D_X=1.415 g cm^{-3}; Z=4; space group, Pn2$_1$a; μ(Mo $K\alpha$)=0.90 cm^{-1}. The intensity data were collected on a Rigaku automated four-circle diffractometer, using the $\omega/2\theta$ scan technique with a scanning rate of 4° (2θ) min^{-1}. The crystal size was 0.5×0.3×0.1 mm. A total of 1220 independent reflections were measured (up to 2θ=55°) using graphite monochromated Mo $K\alpha$ radiation, of which 656 reflections with $|F_o|>3\sigma$ ($|F_o|$) were used for the analysis. Correction was made for the Lorentz and polarization factors, but not for absorption.

Structure Determination

The systematic absences of $0kl$ ($k+l=2n+1$) and $hk0$ ($h=2n+1$) indicated the space group to be Pnma or Pn2$_1$a. The packing consideration suggested a non-centrosymmetric arrangement, and the structure was successfully refined on the basis of the space group Pn2$_1$a. The structure was determined by the direct method, with the MULTAN78 program[5], and was refined by the block-diagonal least-squares method. The coordinates of the hydrogen atoms were derived from an idealized geometry and refined with the isotropic temperature factor. The final R became 0.044. No peaks higher than 0.3 eÅ^{-3} were found on the final difference map. The atomic-scattering factors were taken from Ref. 6. The final atomic parameters, with their standard deviations, are listed in Table 1. Lists of the observed and calculated structure factors, the anisotropic thermal parameters for the non-H atoms, and the positional parameters for the H atoms are deposited as Document No. 8547 at the office of the Chemical Society of Japan.

Table 1. Final atomic coordinates, with their estimated standard deviations, multiplied by 10^4 and 10 for B_{eq}

Atom	x	y	z	B_{eq}/Å^2 a)
C (1)	1086(2)	5879(4)	4212(17)	37(2)
C (2)	1481(3)	5202(4)	5337(18)	43(2)
C (3)	1963(3)	5473(4)	7027(18)	41(2)
C (4)	2590(2)	6736(5)	9007(18)	45(2)
C (5)	2726(3)	7682(5)	9267(18)	44(2)
C (6)	2353(2)	8362(4)	7914(17)	37(2)
C (7)	1482(2)	8788(4)	4724(18)	37(2)
C (8)	601(3)	9190(4)	1755(16)	39(2)
C (9)	67(3)	8970(4)	609(18)	40(2)
C (10)	−178(3)	8071(4)	1283(16)	36(2)
C (11)	155(2)	7373(4)	2888(15)	33(2)
C (12)	749(2)	7556(4)	3670(15)	30(1)
C (13)	1152(2)	6840(4)	4789(15)	31(1)
C (14)	1682(2)	7119(4)	6283(15)	31(1)
C (15)	2077(2)	6446(4)	7445(15)	34(2)
C (16)	1848(2)	8090(4)	6382(15)	32(1)
C (17)	933(2)	8486(4)	3349(15)	34(2)
C (18)	−749(3)	7866(5)	332(16)	43(2)
C (19)	−999(2)	7024(5)	1102(17)	43(2)
C (20)	−698(3)	6376(4)	3043(17)	42(2)
C (21)	−134(2)	6531(4)	3911(15)	36(2)
O	1641(2)	9613(3)	4482(14)	53(1)

a) The equivalent isotropic temperature factors were computed using the following expression: $B_{eq}=1/3\sum_{ij}a_ia_ja_i^*a_j^*$.

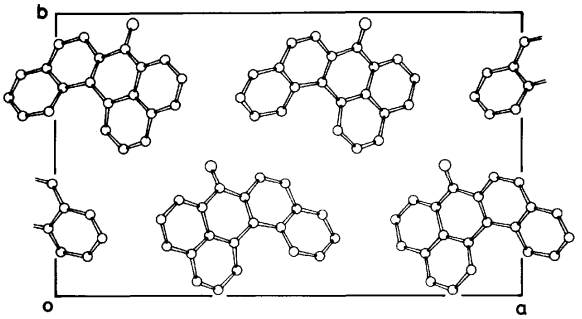

Fig. 1. Projection of the crystal structure along the c axis.

Results and Discussion

The present study has established the structure of **4**. This method is convenient for preparing not only 5,6-BzBT and 8,9-BzBT, but also 10,11-BzBT, since it gives pure 10,11-BzBT more easily and in a higher yield than the method described in Ref. 2.

Figure 1 illustrates the crystal structure of 10,11-BzBT viewed along the c axis. Molecules are stacked face-to-face along the c axis. The overlapping mode

is shown in Fig. 2. The stacking disorder found in the crystals of 8,9-BzBT and 5,6-BzBT is not observed here. There are two dimer pairs of molecules with different populations in the crystals of 8,9-BzBT and 5,6-BzBT. The mean interplanar distance is 3.582 Å, which is larger than that of 3.47 Å between the molecules with larger populations in 8,9-BzBT and 5,6-BzBT. There are no unusually short contacts between the molecules.

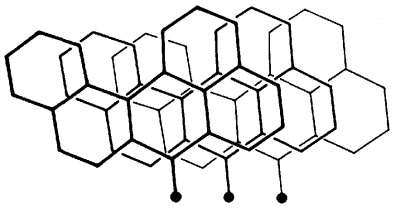

Fig. 2. Overlapping mode.

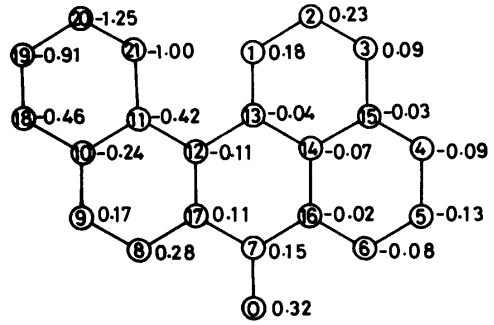

Fig. 3. Deviations of the atoms (l/Å) from the mean molecular plane.

The deviations of the atoms from the mean molecular plane are shown in Fig. 3. The bond distances and angles are listed in Tables 2 and 3 respectively. The molecules are greatly distorted from a planar conformation because of the steric repulsion, which is known as 1,7 interaction. The repulsion is released mainly by the enlargement of the C(1)–C(13)–C(12), C(11)–C(12)–C(13), and C(12)–C(11)–C(21) angles and the distortion from the planar conformation. The degree of the distortion was defined as the twisting angle around the pseudo bond of C(11)···C(13).[7] The angle of C(1)–C(13)···C(11)–C(21) is 33.4°. The corresponding angles (O–C···C–C) in 8,9-BzBT and 5,6-BzBT are 8.2° (Molecule A) and 6.3° (Molecule B) in the former, and 6.0° in the latter. These values are considerably smaller than that of

Table 2. Bond lengths (l/Å), with their estimated standard deviations

C (1) - C (2)	1.403 (10)	C (9) - C (10)	1.420 (10)
C (1) - C (13)	1.387 (9)	C (10) - C (11)	1.409 (9)
C (2) - C (3)	1.366 (10)	C (10) - C (18)	1.415 (9)
C (3) - C (15)	1.412 (9)	C (11) - C (12)	1.445 (8)
C (4) - C (5)	1.379 (10)	C (11) - C (21)	1.428 (9)
C (4) - C (15)	1.411 (9)	C (12) - C (13)	1.453 (9)
C (5) - C (6)	1.406 (10)	C (12) - C (17)	1.389 (8)
C (6) - C (16)	1.383 (9)	C (13) - C (14)	1.427 (9)
C (7) - C (16)	1.463 (9)	C (14) - C (15)	1.404 (9)
C (7) - C (17)	1.456 (9)	C (14) - C (16)	1.427 (9)
C (7) - O	1.228 (9)	C (18) - C (19)	1.362 (9)
C (8) - C (9)	1.363 (10)	C (19) - C (20)	1.390 (9)
C (8) - C (17)	1.414 (9)	C (20) - C (21)	1.377 (9)

Table 3. Bond angles (ϕ/°) with their estimated standard deviations

C (2) - C (1) - C (13)	122.8 (7)	C (1) - C (13) - C (12)	124.0 (6)
C (1) - C (2) - C (3)	120.5 (7)	C (1) - C (13) - C (14)	116.0 (6)
C (2) - C (3) - C (15)	119.1 (7)	C (12) - C (13) - C (14)	119.7 (6)
C (5) - C (4) - C (15)	120.7 (7)	C (13) - C (14) - C (15)	121.2 (6)
C (4) - C (5) - C (16)	119.6 (7)	C (13) - C (14) - C (16)	120.8 (6)
C (5) - C (6) - C (16)	120.5 (7)	C (15) - C (14) - C (16)	117.8 (6)
C (16) - C (7) - C (17)	118.9 (6)	C (3) - C (15) - C (4)	119.7 (6)
C (16) - C (7) - O	120.1 (7)	C (3) - C (15) - C (14)	120.0 (6)
C (17) - C (7) - O	121.0 (7)	C (4) - C (15) - C (14)	120.3 (6)
C (9) - C (8) - C (17)	119.4 (6)	C (6) - C (16) - C (7)	120.6 (6)
C (8) - C (9) - C (10)	120.6 (6)	C (6) - C (16) - C (14)	120.7 (6)
C (9) - C (10) - C (11)	119.5 (6)	C (7) - C (16) - C (14)	118.7 (6)
C (9) - C (10) - C (18)	120.7 (6)	C (7) - C (17) - C (8)	116.3 (6)
C (11) - C (10) - C (18)	119.8 (6)	C (7) - C (17) - C (12)	121.0 (6)
C (10) - C (11) - C (12)	120.1 (6)	C (8) - C (17) - C (12)	122.6 (6)
C (10) - C (11) - C (21)	117.1 (6)	C (10) - C (18) - C (19)	121.5 (7)
C (12) - C (11) - C (21)	122.7 (6)	C (18) - C (19) - C (20)	119.0 (7)
C (11) - C (12) - C (13)	124.3 (6)	C (19) - C (20) - C (21)	121.2 (7)
C (11) - C (12) - C (17)	116.5 (6)	C (11) - C (21) - C (20)	120.7 (6)
C (13) - C (12) - C (17)	119.2 (6)		

Table 4. Comparison of steric hindrance

Molecule	ϕ/°	d(C···C)/Å
1	41.0	2.971
	41.5	2.944
2[a] A	39	3.01
B	30	2.87
3[a] A	30.1	2.94
B	37.6	2.96
4	31.4	3.03
5	33.4	2.993

1): Tetrabenzo[*a,cd,j,lm*]perylene,[8] 2): Diphenanthro-[5,4,3-*abcd*: 5′,4′,3′-*jklm*]perylene,[9] 3): Anthra[2,1,9,8-*hijkl*]benzo[*de*]naphtho[2,1,8,7-*stuv*]pentacene,[7] 4): Benzo[*c*]phenanthrene,[10] 5): This molecule.
a) A and B indicate the crystallographically independent molecules.

10,11-BzBT. On the other hand, similar distortion modes are observed in several related molecules, whose twisting angles are listed in Table 4 together with the C···C distances. The 1,7 interaction appears to play an important role in the distortion of such overcrowded molecules.

References

1) W. Bradley and F. K. Sutcliffe, *J. Chem. Soc.*, **1952**, 1247.
2) E. Clar and W. Willicks, *Liebigs Ann.*, **601**, 193 (1956).
3) S. Fujisawa, S. Sato, and Y. Saito, *Acta Crystallogr., Sect. B*, **37**, 2194 (1981).
4) I. Oonishi, S. Fujisawa, J. Aoki, Y. Ohashi, and Y. Sasada, *Bull. Chem. Soc. Jpn.*, **57**, 3048 (1984).
5) P. Main, L. Lessinger, M. M. Woolfson, G. Germain, and J. P. Declercq (1978), MULTAN78. A System of Computer Programs for Automatic Solution of Crystal Structure from X-ray Diffraction Data, Univ. of York, England, and Lauvain, Belgium.
6) "International Tables for X-ray Crystallography," Vol. IV, Birmingham, Kynoch Press (1974).
7) S. Fujisawa, I. Oonishi, J. Aoki, Y. Ohashi, and Y. Sasada, *Bull. Chem. Soc. Jpn.*, **55**, 3424 (1982).
8) Y. Kohno, M. Konno, Y. Saito, and H. Inokuchi, *Acta Crystallogr., Sect B*, **31**, 2076 (1975).
9) I. Oonishi, S. Fujisawa, J. Aoki, and T. Danno, *Bull. Chem. Soc. Jpn.*, **51**, 2256 (1978).
10) F. L. Hirshfeld, S. Sandler, and G. M. J. Schmidt, *J. Chem. Soc.*, **1962**, 2108.

Optical Absorption and Conductimetric Studies on Ionic Dissociation of Metallotetraphenylporphyrins in Ethanol Solutions

Mikio HOSHINO,* Shunzo KATAYAMA, and Kiyoko YAMAMOTO
The Institute of Physical and Chemical Research, Wako, Saitama 351-01
(Received June 17, 1985)

Optical absorption spectra of chloro[tetraphenylporphyrinato(2-)]metals, $M^{III}Cl(tpp)$ (M=Mn, Fe, Co, and In), and diacetato[tetraphenylporphyrinato(2-)]tin(IV), $Sn^{IV}(CH_3COO)_2(tpp)$, in ethanol and benzene solutions were measured. A marked difference in the absorption spectra between the ethanol and benzene solutions was observed for $Mn^{III}Cl(tpp)$, $Fe^{III}Cl(tpp)$, and $Co^{III}Cl(tpp)$, while a small difference for $In^{III}Cl(tpp)$ and $Sn^{IV}(CH_3COO)_2(tpp)$. The electric conductivity measurements demonstrated that $M^{III}Cl(tpp)$ (M=Mn, Fe, Co, and In) undergoes ionic dissociation in ethanol, whereas $Sn^{IV}(CH_3COO)_2(tpp)$ does not. Solvent effects on the optical absorption spectra observed for ethanol and benzene solutions of the metallotetraphenylporphyrins are discussed on the basis of (1) the ionic dissociation revealed from the conductivity measurements and (2) charge-transfer (from porphyrin ligand to the central metal) character of the electronic absorption bands.

Synthetic metalloporphyrins have received much attention because of their importance as a model compound of natural metalloporphyrins that dominate electron-transport phenomena occurring in life.[1,2] Furthermore, the chemical and physical properties of these porphyrins strikingly depend on the nature of the central metal. For these reasons, studies of synthetic metalloporphyrins have been carried out by many researchers in diversed fields.[3-6]

Recently, the study of solar energy conversion and storage has been increasingly important subject of photochemistry.[7-9] Since metalloporphyrins efficiently absorb visible light from the sun, the photochemistry of them has been subjected to numerous studies, in particular, on electron transfer reactions between the excited states of porphyrins and electron-acceptor molecules.[10-16]

Despite of the importance of metalloporphyrins as mentioned above, conductivity measurements of them in solutions have not yet been carried out. The conductivity measurements have been proved of great use for the study of the ionic dissociation of solute molecules in solutions.

In the present study we have measured optical absorption spectra and conductivity of metalloporphyrins in ethanol and benzene solutions. The metalloporphyrins used are chloro[tetraphenylporphyrinato(2-)]metals, $M^{III}Cl(tpp)$ (M=Mn, Fe, Co, and In), and diacetato[tetraphenylporphyrinato(2-)]-tin(IV). The optical absorption spectra of the former three porphyrins in ethanol solutions were found to differ markedly from those in benzene solutions. On the other hand, the spectra of the latter two porphyrins showed slight difference between the ethanol and benzene solutions. We consider that this result is interpreted in terms of either (1) ligation of an ethanol molecule in the vacant axial position of metalloporphyrins or (2) ionic dissociation of metalloporphyrins. The conductivity measurements give a clear solution for this problem. On the basis of the optical absorption spectroscopic and conductivity measurements, the dissolved states of these metalloporphyrins are discussed in detail.

Experimental

Chloro[tetraphenylporphyrinato(2-)]metals, $M^{III}Cl(tpp)$ (M=Mn, Fe, Co, and In), and diacetate[tetraphenylporphyrinato(2-)]tin(IV) (these are abbreviated, respectively, as $Mn^{III}Cl(tpp)$, $Fe^{III}Cl(tpp)$, $Co^{III}Cl(tpp)$, $In^{III}Cl(tpp)$, and $Sn^{IV}(CH_3COO)_2(tpp)$ hereafter), were synthesized and purified according to the literature.[17-20] Reagent grade ethanol and benzene were fractionally distilled after being dried over molecular sieves to remove traces of water: conductivity of dry ethanol was obtained to be 2×10^{-8} S cm^{-1} and that of dry benzene, 1.0×10^{-9} S cm^{-1} at 25 °C.

Optical absorption spectra were recorded on a Hitachi 330 spectrophotometer.

The electric conductivity of solutions was measured at 1000 Hz by the conductance-linear-bridge method as described in the previous paper.[21] The resistance readings of the linear-bridge were calibrated by substitution method with a precision decade resistance box (Dekastat RS-624 from Electro Scientific Industries: the accuracy is ±0.005%). A conductivity cell which is specially designed for solutions of low conductivity was used throughout this study. The cell constant was determined to be 0.1348 cm^{-1} with the use of standard potassium chloride solutions. The experimental error of the conductivity measurements was less than 0.1%. All the measurements were carried out at 25.00±0.01 °C by using a water bath equipped with a thermostat.

The thermodynamic ion-association constants, K_A, for the reactions

$$Cl^- + [M^{III}(tpp)]^+ \rightleftarrows M^{III}Cl(tpp)$$
(M: Mn, Fe, Co, and In)

and

$$[Sn^{IV}(CH_3COO)(tpp)]^+ + CH_3COO^- \rightleftarrows Sn^{IV}(CH_3COO)_2(tpp) \quad (1)$$

can be calculated from the conductivity data on the basis of the Fuoss-Hsia conductance theory.[22-24] The revised

Fuoss-Hsia equation for the molar conductivity, Λ, of an associated symmetrical electrolyte is given by

$$\Lambda = \Lambda^{\infty} - S\cdot c^{1/2}\cdot\gamma^{1/2} + E\cdot c\cdot\gamma\log(c\cdot\gamma) + J_1\cdot c\cdot\gamma - J_2^{3/2}(c\cdot\gamma)^{3/2} - K_A\cdot c\cdot\gamma\cdot f_{\pm}^2\cdot\Lambda \quad (2)$$

with

$$K_A = (1-\gamma)/c\cdot\gamma^2\cdot f_{\pm}^2 \quad (3)$$

where Λ^{∞} is the limiting molar conductivity; c, the molar concentration; γ, the degree of dissociation; S, the Onsager limiting slope; $f_{\pm}$, the mean ionic activity coefficient, and E, J_1, and J_2 are the theoretical coefficients, respectively. The coefficients, J_1 and J_2, are formulated as a function of the mean distance (a) of closest approach of positive and negative ions. These coefficients were used for the evaluation of a.

The mean activity coefficient $f_{\pm}$, was estimated by means of Debye-Hückel equation:

$$\log f_{\pm} = -A|z_+z_-|\sqrt{I}/(1+B\cdot a\cdot\sqrt{I}) \quad (4)$$

where z_+ and z_- are the charge numbers of the positive and negative ions, respectively, I is the ionic strength, and A and B are the theoretical coefficients. The values of permitivity and viscosity of ethanol used in the present calculation were taken from literature.[25] A set of Λ^{∞}, K_A, and a values was obtained in such a way that the theoretical equation gives the best fit to the conductivity data obtained experimentally. All the calculations were performed on a FACOM computer using a FORTRAN program (JCCOND) which was kindly supplied from Professor J. C. Justice in Université de Paris.

Results and Discussion

Optical Absorption Spectra. Figure 1 shows the optical absorption spectra of $Mn^{III}Cl(tpp)$ in benzene and ethanol solutions at room temperature. The spectrum observed in ethanol is found to differ considerably from that in benzene. When the solvent is changed from benzene to ethanol, the absorption bands located around 1.3 and 2.7×10^4 cm^{-1} are red-shifted and those around 1.7 and 2.1×10^4 cm^{-1}, to the contrary, are blue-shifted. The solvent effects on the optical absorption spectra are closely related to the nature of each electronic band.

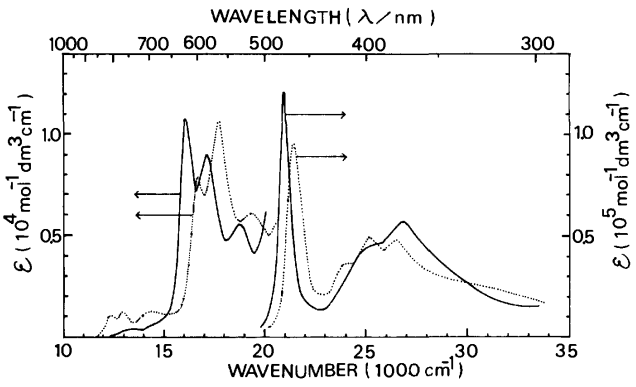

Fig. 1. Optical absorption spectra of $Mn^{III}Cl(tpp)$ in benzene (——) and in ethanol (----) solution.

The theoretical calculation has been carried out in order to elucidate the significant difference in the optical absorption spectra between manganese(III) porphyrin and usual metalloporphyrin such as zinc(II) porphyrin.[26-27] For manganese(III) porphyrin, d levels of the central manganese atom are very close to the porphyrin π levels, resulting in strong mixing of the d and π levels. As a consequence of the strong mixing, porphyrin has a number of charge-transfer bands in the UV-visible region of the absorption spectrum.[28] On the other hand, d levels of zinc(II) porphyrin are too low to make a strong mixing with the porphyrin π levels.

The location of the electronic bands having charge-transfer character in the spectra of manganese porphyrin is known to vary depending on the nature of the axial ligands as well as the negative ion in the axial position.[27] Boucher[28] has studied the absorption spectra of manganese(III) protoporphyrin IX dimethyl ester complexes in coordinating and non-coordinating solvents. The spectra observed in benzene solutions are characteristically different for each of the halide ion complexes of the manganese(III) porphyrin. However, the spectra observed in methanol solutions are independent of the axial halide ions. These results are well interpreted in terms of the ionic dissociation of the manganese(III) porphyrin in methanol solutions:[28]

$$[Mn^{III}X\ \text{porphyrin}]\ (X\text{: halogen atom}) \longrightarrow X^- + [Mn^{III}\ \text{porphyrin}]^+$$

No ionic dissociation is observed for the benzene solutions.

The above discussion is also acceptable for the interpretation of the absorption spectra of $Mn^{III}Cl(tpp)$: $Mn^{III}Cl(tpp)$ undergoes ionic dissociation in ethanol, while it does not in benzene. The previous studies on one-electron reduction induced by γ-rays at 77 K have strongly suggested that $Mn^{III}Cl(tpp)$ in ethanol dissociated into Cl^- and $[Mn^{III}(tpp)]^+$.[29] Furthermore, the conductivity measurements, as will be described later, confirmed the ionic dissociation of $Mn^{III}Cl(tpp)$ in ethanol solutions.

Figure 2 shows the optical absorption spectra of $Fe^{III}Cl(tpp)$ in benzene and ethanol solutions. The spectrum observed in ethanol differs markedly from that in benzene. In comparison with the spectrum measured in benzene, four major features are recognized for the spectrum in ethanol: (1) The 1.5×10^4 cm^{-1} band loses its intensity without shift, (2) The 1.95×10^4 cm^{-1} band is red-shifted, (3) The 2.4×10^4 cm^{-1} band is slightly blue-shifted, and (4) The 2.7×10^4 cm^{-1} band is largely blue-shifted.

The situation of the metal d levels and porphyrin π levels in iron(III) porphyrins is very similar to that in manganese(III) porphyrins.[27] Thus, we can expect

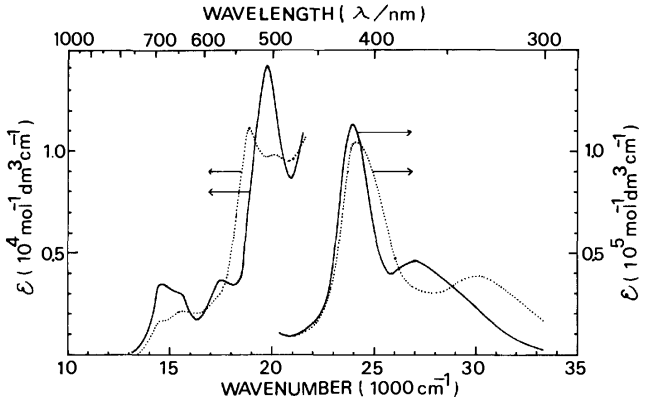

Fig. 2. Optical absorption spectra of $Fe^{III}Cl(tpp)$ in benzene (——) and in ethanol (----) solution.

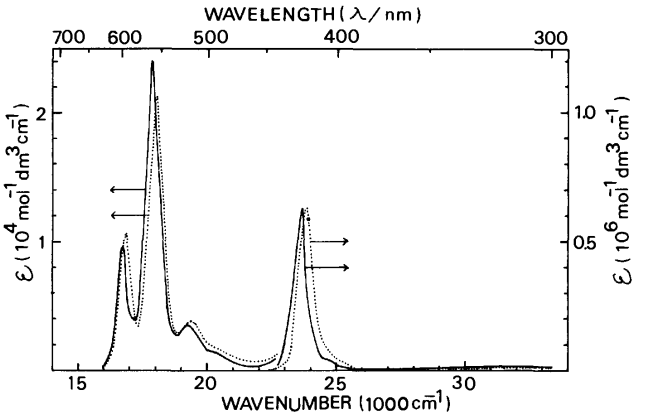

Fig. 3. Optical absorption spectra of $In^{III}Cl(tpp)$ in benzene (——) and in ethanol (----) solution.

that the electronic bands of $Fe^{III}Cl(tpp)$ have a charge-transfer character as in the case of $Mn^{III}Cl(tpp)$.[27] In fact, the theoretical calculation involving the configuration interaction between the porphyrin π states and the charge-transfer (from porphyrin to iron(III)) states gives a consistent interpretation for the optical absorption spectra of $Fe^{III}Cl(tpp)$.[30] Since the charge-transfer character of the electronic bands depends on the d levels of the central metal and the porphyrin π levels, the absorption spectrum of $Fe^{III}Cl(tpp)$ is regarded to vary by the coordinating nature of the solvents. Therefore, the absorption spectrum of $Fe^{III}Cl(tpp)$ as well as $Mn^{III}Cl(tpp)$ observed in non-coordinating solvent, benzene, is considered to differ from that in coordinating solvent, ethanol.

A significant change in the absorption spectra of $Fe^{III}Cl(tpp)$ between ethanol and benzene solutions suggests that ionic dissociation of $Fe^{III}Cl(tpp)$ occurs in ethanol solutions.

The absorption spectra of $Co^{III}Cl(tpp)$ in benzene and ethanol solutions exhibit two distinct features: (1) the Soret (*ca.* 2.3×10^4 cm^{-1}) and Q (*ca.* 1.8×10^4 cm^{-1}) bands in an ethanol solution become narrower than those in a benzene solution and (2) although the peak maximum of the Soret band observed for an ethanol solution is remarkably red-shifted by *ca.* 1.1×10^4 cm^{-1}, the Q band is slightly blued-shifted by *ca.* 0.2×10^4 cm^{-1} in comparison with each band observed for a benzene solution.

The absorption spectrum in the ethanol solution is in good agreement with that observed for the six-coordinated $Co^{III}(tpp)$.[31] Therefore, the species in the ethanol solution is presumed to be $Co^{III}Cl(tpp)(C_2H_5OH)$ or $[Co^{III}(tpp)(C_2H_5OH)_2]^+$ in which ethanol molecule(s) are located in the axial position(s). The spectrum observed for the benzene solution is ascribed to the five-coordinated species, $Co^{III}Cl(tpp)$.[32]

It is suggested that cobalt porphyrins have a number of charge-transfer transitions as in the case of nickel porphyrins.[27] A significant difference in the spectra between ethanol and benzene solutions is interpreted by assuming that the absorption bands, in particular the Soret band, have a charge-transfer character.

As to the ionic dissociation of $Co^{III}Cl(tpp)$, paper electrophoresis study has revealed that $Co^{III}Cl(tpp)$ in ethanol is dissociated as[32]

$$Co^{III}Cl(tpp) + 2C_2H_5OH \longrightarrow Cl^- + [Co^{III}(tpp)(C_2H_5OH)_2]^+$$

Here, C_2H_5OH molecules in $[Co^{III}(tpp)(C_2H_5OH)_2]^+$ are assumed to be located in the axial positions. The ionic dissociation of $Co^{III}Cl(tpp)$ in ethanol was also suggested on the basis of the optical and ESR studies of one-electron reduced species of $Co^{III}Cl(tpp)$ produced by γ-radiolysis of the ethanol solution at 77 K.[29]

Figure 3 shows the optical absorption spectra of $In^{III}Cl(tpp)$ in benzene and ethanol solutions. The spectra differ remarkably from those of $Mn^{III}Cl(tpp)$, $Fe^{III}Cl(tpp)$, and $Co^{III}Cl(tpp)$ but are very similar to those of usual metallotetraphenylporphyrins such as tetraphenylporphyrinato(2-)zinc(II). This fact suggests that the absorption bands scarcely have a charge-transfer character. In fact, only small difference in the spectra between ethanol and benzene solutions is observed. Both the Q and Soret bands are found to be slightly blue-shifted on going from benzene to ethanol solutions as shown in Fig. 3. This result may be interpreted in terms of general solvent effects on the optical absorption bands.

There have been no reports on the ionic dissociation of $In^{III}Cl(tpp)$ in ethanol solutions. However, we assumed the dissociation of $In^{III}Cl(tpp)$ in ethanol solutions in order to elucidate the electron-transfer reaction from the photoexcited triplet state of $In^{III}Cl(tpp)$ to methylviologen.[16] The electiric conductivity measurements, as will be shown later, confirmed the ionic dissociation:

$$In^{III}Cl(tpp) + 2C_2H_5OH \longrightarrow Cl^- + [In^{III}(tpp)(C_2H_5OH)_2]^+$$

Table 1. Molar conductivities Λ of $Mn^{III}Cl(tpp)$, $Fe^{III}Cl(tpp)$, $Co^{III}Cl(tpp)$, $In^{III}Cl(tpp)$, and $Sn^{IV}(CH_3COO)_2(tpp)$ in ethanol solutions at 25 °C

$Mn^{III}Cl(tpp)$		$Fe^{III}Cl(tpp)$		$Co^{III}Cl(tpp)$		$In^{III}Cl(tpp)$		$Sn^{IV}(CH_3COO)_2(tpp)$	
10^4c	Λ	10^4c	Λ	10^4c	Λ	10^4c	Λ	10^4c	Λ
mol dm^{-3}	S cm^2 mol^{-1}	mol dm^{-3}	S cm^2 mol^{-1}	mol dm^{-3}	S cm^2 mol^{-1}	mol dm^{-3}	S cm^2 mol^{-1}	mol dm^{-3}	S cm^2 mol^{-1}
1.995	30.91	0.80	28.81	1.601	29.76	0.5472	29.39	4.097	3.10
2.993	30.55	1.00	28.64	2.002	29.52	0.7290	29.13	8.193	3.02
4.989	29.97	1.20	28.50	3.203	28.93	0.9113	28.89	10.241	3.00
6.984	29.52	1.60	28.23	4.984	28.21	1.0935	28.69	16.386	2.98
9.977	28.96	2.00	28.00	8.007	27.26	1.4580	28.30	20.483	2.80
14.058	28.35			10.008	26.71	1.8230	27.96		
20.082	27.64			20.017	24.64				

Table 2. Limiting molar conductivities Λ^∞, ion-association constants K_A, and ion-size parameter a, of $Mn^{III}Cl(tpp)$, $Fe^{III}Cl(tpp)$, $Co^{III}Cl(tpp)$, and $In^{III}Cl(tpp)$ in ethanol solutions at 25 °C

	Λ^∞	K_A	$^aJ_2$
	S cm^2 mol^{-1}	dm^3 mol^{-1}	nm
$Mn^{III}Cl(tpp)$	32.75±0.02	18±2	1.24±0.4
$Fe^{III}Cl(tpp)$	30.10±0.01	94±1	1.14±0.1
$Co^{III}Cl(tpp)$	31.64±0.01	82±2	1.42±0.2
$In^{III}Cl(tpp)$	30.71±0.01	282±4	1.14±0.1

where C_2H_5OH molecules in $[In^{III}(tpp)(C_2H_5OH)_2]^+$ are assumed to occupy the axial positions.

The optical absorption spectra of $Sn^{IV}(CH_3COO)_2$-(tpp) in benzene and ethanol solutions are very similar to those of $In^{III}Cl(tpp)$. The peak maxima observed for a benzene solution are located at 1.66×10^4, 1.78×10^4, and 1.93×10^4 cm^{-1} in the Q band region and at 2.34×10^4 cm^{-1} in the Soret band region. When the solution is changed from benzene to ethanol, the Q band peaks are slightly blue-shifted by *ca.* 0.1×10^4 cm^{-1} and the Soret band peak, by *ca.* 0.3×10^4 cm^{-1}. No significant differences in the spectra between the two solutions are observed, indicating that the charge-transfer character in the optical absorption is very weak. The small blue shift of the Q and Soret band observed in ethanol solutions is regarded as being due to the general solvent effects similar to the case of $In^{III}Cl(tpp)$.

Electric Conductivity Measurements. The molar conductivities, Λ, for $Mn^{III}Cl(tpp)$, $Fe^{III}Cl(tpp)$, $Co^{III}Cl(tpp)$, $In^{III}Cl(tpp)$, and $Sn^{IV}(CH_3COO)_2(tpp)$ in ethanol solutions at 25 °C are summarized in Table 1. The Λ values of the former four porphyrins are obtained to be 24—31 S cm^2 mol^{-1} in their concentration range 5×10^{-5}—2×10^{-3} mol dm^{-3}. However, the Λ value of $Sn^{IV}(CH_3COO)_2(tpp)$ is extremely small in comparison with those of the former four porphyrins. Taking account of the limiting molar conductivity of acetate ion in ethanol (λ^∞=17.9 S cm^2 mol^{-1}),[33] we conclude that $Sn^{IV}(CH_3COO)_2(tpp)$ is hardly dissociated in ethanol solutions.

In Table 2 are listed the values of Λ^∞, K_A, and a determined for $Mn^{III}Cl(tpp)$, $Fe^{III}Cl(tpp)$, $Co^{III}Cl$-(tpp), and $In^{III}Cl(tpp)$ in ethanol solutions at 25 °C. The values of Λ^∞ are calculated to be 30—33 S cm^2 mol^{-1}. Since λ^∞_- of Cl^- in ethanol is reported to be 24.3 S cm^2 mol^{-1},[34] the limiting molar conductivities of $[M^{III}(tpp)]^+$ ions (λ^∞_+) are determined to be 8.45, 5.80, 7.34, and 6.41 S cm^2 mol^{-1} for M=Mn, Fe, Co, and In, respectively. The fact that $[M^{III}(tpp)]^+$ gives the λ^∞_+ values smaller than the λ^∞_- value of Cl^- is ascribed to the ion size in solutions: $[M^{III}(tpp)]^+$ has a larger size than Cl^-.

The K_A values obtained for the four metallotetraphenylporphyrins are found to decrease in the sequence $In^{III}Cl(tpp) \gg Fe^{III}Cl(tpp) \cong Co^{III}Cl(tpp) > Mn^{III}Cl(tpp)$. By using K_A values, we can calculate the degree of ionic dissociation, γ, from the equation 3. When $c=10^{-4}$ mol dm^{-3}, the values of γ are obtained to be 0.998, 0.992, 0.993, and 0.970 for $Mn^{III}Cl(tpp)$, $Fe^{III}Cl(tpp)$, $Co^{III}Cl(tpp)$, and $In^{III}Cl$-(tpp) in ethanol solutions, respectively. Since the absorption spectroscopic measurements in the present study were carried out in the concentration range 10^{-5}—10^{-4} mol dm^{-3}, the major species (>90%) in the ethanol solutions of $M^{III}Cl(tpp)$ (M=Mn, Fe, Co, and In) are ascribed to $[M^{III}(tpp)]^+$ produced by the ionic dissociation of $M^{III}Cl(tpp)$. Presumably, $[M^{III}(tpp)]^+$ in ethanol solution has two axial ethanol molecules to be formulated as $[M^{III}(tpp)(C_2H_5OH)_2]^+$.

The mean distance (a_{J_2}) of the closest approach of $[M^{III}(tpp)]^+$ and Cl^- is calculated from J_2 to be 1.1—1.4 nm. These values of the distance are found to be in good agreement with those estimated from the Stokes' law.[38] In comparison with the distance-(0.22—0.24 nm) between the central metal and Cl atom in $M^{III}Cl(tpp)$,[18,35-37] the distance of the closest approach in ethanol solution is very large. It is likely that the solvent sphere around Cl^- and the axial ethanol molecules in $[M^{III}(tpp)(C_2H_5OH)_2]^+$ afford the large value of the distance of the closest approach.

Conclusion

The optical absorption spectra of $M^{III}Cl(tpp)$ (M=Mn, Fe, and Co) in ethanol solutions markedly differ from those in benzene solutions, whereas the spectra of $In^{III}Cl(tpp)$ and $Sn^{IV}(CH_3COO)_2(tpp)$ in ethanol solutions are rather similar to those in benzene solutions. The electric conductivity measurements carried out for the ethanol solutions revealed that $M^{III}Cl(tpp)$ (M=Mn, Fe, Co, and In) undergo ionic dissociation, while $Sn^{IV}(CH_3COO)_2$-(tpp) does not. A marked difference in the absorption spectra between the ethanol and benzene solutions of $M^{III}Cl(tpp)$ (M=Mn, Fe, and Co) is concluded to be caused not only from the ionic dissociation but also from the charge-transfer character of the absorption bands. This conclusion is further supported by the facts that (1) $In^{III}Cl(tpp)$ undergoes ionic dissociation in ethanol without giving rise to substantial difference in the absorption spectra between ethanol and benzene solutions and (2) the absorption spectra of $In^{III}Cl(tpp)$ in ethanol and benzene solutions are very similar to those of $Sn^{IV}(CH_3COO)_2(tpp)$ which is demonstrated to be nondissociative in an ethanol solution.

We thank Professor Reita Tamamushi of Fukushima University for critical reading of the manuscript.

References

1) D. Ostefeld and M. Tsutsui, *Accounts Chem. Res.*, **7**, 52 (1974).
2) D. Dolphin and R. H. Felton, *Accounts Chem. Res.*, **7**, 26 (1974).
3) W. C. Lin, "The Porphyrins," ed by D. Dolphin, Academic Press, New York (1978), Vol. IV, Chap. 7.
4) J. Fajer and M. S. Davis, "The Porphyrins," ed by D. Dolphin, Academic Press, New York (1978), Vol. IV, Chap. 4.
5) A. Wolberg and J. Mansassen, *J. Am. Chem. Soc.*, **92**, 2982 (1970).
6) M. Gouterman, R. A. Mathies, and B. E. Smith, *J. Chem. Phys.*, **52**, 3795 (1979).
7) A. B. P. Lever, B. S. Ramaswamy, and S. Licoccia, *J. Photochem.*, **19**, 173 (1982).
8) J. R. Bolton, "Solar Power and Fuels," Academic Press, New York (1977).
9) G. Sprintschnik, H. W. Sprintshnik, P. P. Kirsh, and D. G. Whitten, *J. Am. Chem. Soc.*, **99**, 4974 (1979).
10) J. Kiwi, and M. Gratzel, *J. Am. Chem. Soc.*, **101**, 7214 (1979).
11) I. Okura, and N. K. Thuan, *J. Chem. Soc., Faraday Trans. 1*, **76**, 2209 (1980).
12) T. Matsuo, K. Ito, and K. Takama, *Chem. Lett.*, **1980**, 1009.
13) D. Holten, M. W. Windsor, W. W. Parson, and M. Gouterman, *Photochem. Photobiol.*, **28**, 951 (1978).
14) T. L. Netzel, M. A. Bergkamp, and C. K. Chang, *J. Photochem.*, **17**, 451 (1981).
15) M. Migita, T. Okada, N. Mataga, S. Nishitani, N. Kurata, Y. Sakata, and S. Misumi, *Chem. Phys. Lett.*, **84**, 263 (1981).
16) M. Hoshino, H. Seki, and H. Shizuka, *J. Phys. Chem.*, **89**, 470 (1985).
17) G. D. Dorough, J. R. Miller, and F. M. Huennekens, *J. Am. Chem. Soc.*, **73**, 4315 (1951).
18) T. Sakurai, K. Yamamoto, H. Naito, and N. Nakamoto, *Bull. Chem. Soc. Jpn.*, **49**, 3042 (1976).
19) A. D. Alder, F. R. Long, F. Kampas, and J. Kim, *J. Inorg. Nucl. Chem.*, **32**, 2443 (1970).
20) M. Bhatti, W. Bhatti, and E. Mast *Nucl. Chem. Lett.*, **8**, 133 (1972).
21) S. Katayama, *Bull. Chem. Soc. Jpn.*, **46**, 106 (1973).
22) R. M. Fuoss and K. L. Hsia, *Proc. Natl. Acad. Sci. U. S.*, **57**, 1550 (1966).
23) K. L. Hsia and R. M. Fuoss, *J. Am. Chem. Soc.*, **90**, 3055 (1968).
24) R. Fernandez-Prini, *Trans. Faraday Soc.*, **65**, 3311 (1969).
25) G. J. Janz and R. P. T. Tomkins, "Nonaqueous Electrolyte Handbook," Academic Press, New York and London (1972), Vol. I, p. 94.
26) a) M. Zerner and M. Gouterman, *Theoret. Chim. Acta*, **4**, 44 (1966); b) M. Zerner, M. Gouterman, and H. Kobayashi, *Theoret. Chim. Acta*, **6**, 363 (1966); c) M. Gouterman, L. K. Hanson, G. E. Khalil, W. L. Leenstra, and J. W. Buchler, *J. Chem. Phys.*, **62**, 2343 (1975).
27) L. J. Boucher, *Coord. Chem. Rev.*, **7**, 289 (1972).
28) L. J. Boucher, *J. Am. Chem. Soc.*, **90**, 6640 (1968).
29) M. Hoshino, S. Konishi, and M. Imamura, *Bull. Chem. Soc. Jpn.*, **57**, 1713 (1984).
30) H. Kobayashi, T. Higuchi, Y. Kaizu, H. Osada, and M. Aoki, *Bull, Chem. Soc. Jpn.*, **48**, 3137 (1975).
31) K. Yamamoto and S. Tonomura, *Sci. Papers Inst. Phys. Chem. Res.*, **58**, 122 (1964).
32) K. Yamamoto, *Sci. Papers Inst. Phys. Chem. Res.*, **71**, 111 (1977).
33) "Landolt-Börnstein Tablellen," Springer-Verlag, II Band, 7 Teil, Electrische Eigenschaften II (1960), p. 622.
34) D. Dobos, "Electrochemical Data," Elsevier Sci. Pub. Co.: Amsterdam-Oxford-New York (1975).
35) A. Tulinsky and B. M. L. Chen, *J. Am. Chem. Soc.*, **99**, 3647 (1977).
36) R. G. Ball, K. M. Lee, A. G. Marshall, and J. Trotter, *Inorg. Chem.*, **19**, 1463 (1980).
37) J. L. Hoard, G. H. Cohen, and M. D. Glick, *J. Am. Chem. Soc.*, **89**, 1992 (1967).
38) R. A. Robinson and R. H. Stokes, "Electrolyte Solutions," Butterworths: London (1959), p. 43.

Magnetic-field Effect on the Thermal Decomposition of Dilauroyl Peroxide

Yoshifumi TANIMOTO,* Masato NISHINO, and Michiya ITOH
Faculty of Pharmaceutical Sciences, Kanazawa University, Takara-machi, Kanazawa 920
(Received April 24, 1985)

Synopsis. In the thermal decomposition of dilauroyl peroxide in octane, the yield of docosane increases by 3—6% in the presence of magnetic fields (0.15—1 T). The results are interpreted in terms of a radical-pair model.

Magnetic-field effects on photochemical reactions have been extensively and successfully studied in the last decade.[1,5] On the other hand, there have been few reports on the thermal reactions, since the first observation of the effect on the reaction of pentafluorophenylmethyl chloride with C_4H_9Li in hexane.[2] Recently, though, Imoto and Nomoto[3] studied the magnetic-field effect on the radical polymerization of methyl methacrylate initiated with poly(2-hydroxyethyl methacrylate). In the present paper, we have studied the magnetic-field effect on the thermal decomposition of dilauroyl peroxide in octane. In the presence of magnetic fields (0.15—1 T), the yield of docosane, a cage product, increases by 3—6%. The results are interpreted in terms of a radical-pair model.

Experimental

The octane solution (0.2 ml) of dilauroyl peroxide (0.05 mol dm^{-3}) in a NMR tube was placed in a home-made heat bath at the center of an electromagnet (JASCO, MCD-1BS). The temperature of the bath was kept at 97 °C by circurating ethylene glycol from a thermostat.

The decrease in dilauroyl peroxide was monitored by means of iodometric titration. Its half-lifetime was about 20 min. The reaction time was set at 90 min in order to decompose 96% of the peroxide.

The yields of the three products, docosane, undecane, and 1-undecene, were determined by means of vapor-phase chromatography VPC, using hexadecane as the external standard. Since undecane and 1-undecene showed the same retention time under our VPC conditions, the sum of the yields was measured.

Results and Discussion

In the thermal decomposition of dilauroyl peroxide, the yields of docosane, undecane, and 1-undecene have been reported to be 56, 36, and 9% in octane, and 58, 16, and 4% in *o*-dichlorobenzene, respectively.[4] Since *o*-dichlorobenzene is a radical scavenger, these facts imply that docosane is a cage product, while the larger amounts of undecane and 1-undecene are mainly formed *via* free-radical reactions. Figure 1 shows the magnetic-field dependence of the product yields in the decomposition of dilauroyl peroxide. The yield of docosane increases by 3—6% in the presence of magnetic fields. On the other hand, the yield of the undecane/1-undecene mixture is almost magnetic-field-independent, though the data points are rather scattered. This scattering is because the

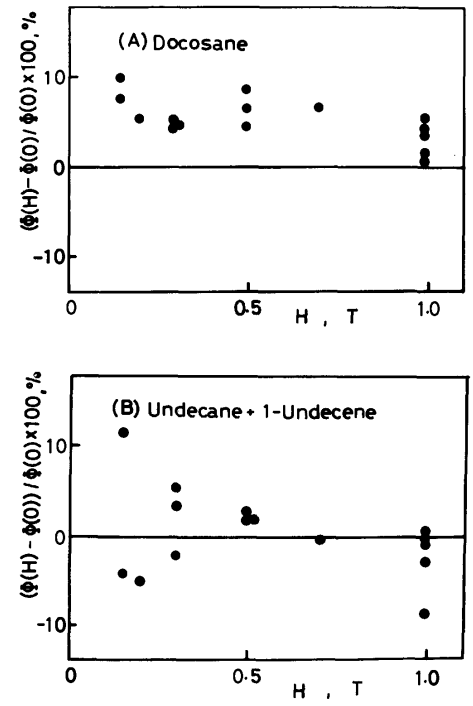

Fig. 1. Magnetic field dependence of the relative yields of (A) docosane and (B) the undecane/1-undecene mixture. Here, $\Phi(0)$ and $\Phi(H)$ represent the yields in the absence and presence of a magnetic field H, respectively.

TABLE 1. MAGETIC-FIELD EFFECT ON THE RELATIVE PRODUCT YIELDS (%) FOR THE THERMAL DECOMPOSITION OF DILAUROYL PEROXIDE AT 1 T

	Isopropyl iodide (mol dm^{-3})	
	0	1.5
Docosane	3.0±2.0	2.9±1.3
Undecane/ 1-undecene	−2.7±2.9	−0.7±3.5
No. of runs	5	11

VPC peak of the mixture appears just after the intense peak of the solvent under our VPC conditions.

To check the influence of a radical scavenger, isopropyl iodide is added into the solution. The VPC peak of the mixture remarkably decreases in intensity, while that of docosane is insensitive to the scavenger. This also implies that docosane and undecane/1-undecene are mostly a cage product and free-radical products respectively. The magnetic-field effects on the product yields in the absence and in the presence of the scavenger are shown in Table 1. The

lack of any significant change in the magnetic-field effect by the scavenger supports the assignment of products presented above.

A proposed mechanism for the present thermal decomposition of dilauroyl peroxide is as follows:

$$C_{11}H_{23}COO_2COC_{11}H_{23} \xrightarrow{\Delta} {}^1(C_{11}H_{23}COO\cdot \cdot OCOC_{11}H_{23}) \quad (1)$$

$${}^1(C_{11}H_{23}COO\cdot \cdot OCOC_{11}H_{23}) \longrightarrow {}^1(C_{11}H_{23}\cdot \cdot C_{11}H_{23}) + 2CO_2 \quad (2)$$

$${}^1(C_{11}H_{23}\cdot \cdot C_{11}H_{23}) \longrightarrow C_{22}H_{46} \quad (3)$$

$${}^1(C_{11}H_{23}\cdot \cdot C_{11}H_{23}) \longrightarrow {}^3(C_{11}H_{23}\cdot \cdot C_{11}H_{23}) \quad (4)$$

$${}^{1,3}(C_{11}H_{23}\cdot \cdot C_{11}H_{23}) \longrightarrow 2C_{11}H_{23}\cdot \quad (5)$$

$$2C_{11}H_{23}\cdot \longrightarrow C_{11}H_{24} + CH_2{=}CH(CH_2)_8CH_3 \quad (6)$$

The initial step in the reaction is the homolysis of the oxygen–oxygen bond to generate a singlet radical pair of the lauroyloxyl radicals, (1). The decarboxylation of the lauroyloxyl radical, (2), is probably a very rapid process, since no appreciable amount of undecyl laurate, the product to be expected from the reaction of the radical, is detected.[4] The decarboxylation of lauroyloxyl radicals generates a singlet pair of the undecyl radicals. From the singlet radical pair, there are three processes; *i.e.*, a recombination into docosane, a cage product (3), an intersystem crossing to the triplet radical pair (4), and a diffusive separation into free radicals (5). The singlet-triplet intersystem crossing of the undecyl radical pair occurs *via* electron-nuclear hyperfine interaction. The rate is reduced in the presence of an external magnetic field because of the Zeeman splitting of the triplet sublevels (hfc mechanism). Therefore, this reduction in the intersystem-crossing rate leads to an increase in the yield of docosane, the cage product, in magnetic fields. Although an external magnetic field is also expected to decrease the yield of the free-radical products, the undecane/1-undecene mixture, this decrease is not so clear as that of the cage product because of the experimental error.

In the singlet-sensitized photolysis of dibenzoyl peroxide,[5] phenyl benzoate is detected as a cage product, and its magnetic-field effect (an 8% decrease at 4.3 T) is interpreted in terms of the Δg mechanism, in which the singlet-triplet intersystem crossing of the benzoyloxyl-phenyl radical pair is enhanced because of the difference in the g values of the component radicals. In the present reaction, the yield of docosane increases in the presence of relatively weak magnetic fields (0.15—1 T). Therefore, the magnetic-field effect observed here is mostly attributable to that on the undecyl radical pair by the hfc mechanism. The difference between dibenzoyl peroxide and dilauroyl peroxide reactions might be attributable to that in the decarboxylation rate of the intermediate radicals.

References

1) For example, see: Y. Tanimoto, H. Udagawa, Y. Katsuda, and M. Itoh, *J. Phys. Chem.*, **87**, 3976 (1983), and the references therein.

2) R. Z. Sagdeev, Yu. N. Molin, K. M. Salikhov, T. V. Leshina, M. A. Kamkha, and S. M. Shein, *Org. Magn. Resonance*, **5**, 603 (1973).

3) M. Imoto and K. Nomoto, *Makromol. Chem. Rapid Commun.*, **2**, 703 (1981).

4) R. A. Cooper, R. G. Lawler, and H. R. Ward, *J, Am. Chem. Soc.*, **94**, 545 (1972).

5) Y. Tanimoto, H. Hayashi, S. Nagakura, H. Sakuragi, and K. Tokumaru, *Chem. Phys. Lett.*, **41**, 267 (1976).

Viscosity *B* Coefficients for Polymethylenebis(trimethylammonium) Dibromides in Aqueous Solutions

Kunio TAMAKI* and Akifumi FUJIWARA
Department of Chemistry, Yokohama City University, Kanazawa-ku, Yokohama 236
(Received May 16, 1985)

Synopsis. The viscosity *B* coefficients of the Jones-Dole equation for *N,N'*-polymethylenebis(trimethylammonium) dibromides $[(CH_3)_3N(CH_2)_nN(CH_3)_3]Br_2$ (n=3—8, 10, and 12) and for comparison for alkyltrimethylammonium bromides $C_nH_{2n+1}N(CH_3)_3Br$ (n=2—6) in aqueous solutions at 25 and 35 ° have been determined, and the effect of structural changes in the solvent water upon the dissolution of both series of electrolytes is discussed.

In a previous paper,[1] the balance of ionic hydration and hydrophobic hydration in aqueous solutions of *N,N'*-polymethylenebis(trimethylammonium) dibromides ($[(CH_3)_3N(CH_2)_nN(CH_3)_3]Br_2$, which will be abbreviated as, MeC_nMe) were discussed on the basis of the changes in the heat capacity upon dissolution in water. In this paper, an experimental study of the viscosity *B* coefficients for a series of MeC_nMe and, for comparison, for a series of alkyltrimethylammonium bromides ($C_nH_{2n+1}N(CH_3)_3Br$, which will be abbreviated as C_nMe) in aqueous solutions will be reported.

Experimental

MeC_nMe except for MeC_7Me and C_nMe were the same samples as those described in a previous paper.[1] MeC_7Me was prepared by the reaction of 1,7-dibromoheptane with an excess of trimethylamine in ethanol, and was purified several times by recrytallization from ethanol. Water was triply distilled.

The viscosities were measured at 25 and 35 °C with an automatic viscometer of the Shibayama Scientific Co., Ltd. The densities were measured using a vibrating-tube densimeter, twin-type SS-D-200 of the Shibayama Scientific Co., Ltd. The detailed procedure was described in a previous paper.[2] The electrical conductivities were measured with a Yokogawa audio-frequency bridge using a frequency of 1000 Hz.

Results and Discussion

The Viscosity B *Coefficients of Electrolytes.* The viscosity of an aqueous solution of an electrolyte, η, can be represented by the Jones-Dole equation:

$$\eta=\eta_0(1+Ac^{1/2}+Bc) \quad (1)$$

where η_0 is the viscosity of water, c is the molar concentration, A is a constant related to the ion-ion interaction, and B is the viscosity *B* coefficient. The constant A was interpreted theoretically by Falkenhagen and Vernon,[3] and can be calculated using the data of the limiting equivalent conductivities of the salt, cation, and anion. Equation 1 may be converted to,

$$\eta/\eta_0-1-Ac^{1/2}=Bc \quad (2)$$

When the left-hand side of Eq. 1, using the calculated values of A, is plotted against c, the viscosity *B* coefficient is obtained as the slope of a linear line. Figures 1 and 2 show the results of plotting Eq. 2 for MeC_nMe and C_nMe respectively. The values of A and B for both series of compounds are summarized in Table 1. The *B* values for C_2Me, C_4Me, and C_6Me are in reasonable agreement with the values reported by Tanaka *et al.*[4] The *B* values for both series of compounds increase approximately linearly with the number of carbon atoms in the polymethylene or alkyl group, n.

The temperature dependence of the *B* values is a factor of the solute-solvent interaction; the *B* values increase with the temperature for a solvent-structure-breaking salt, and decrease with temperature for a solvent-structure-making solute.[5] For the MeC_nMe series, it may be seen in Table 1 that the *B* values for MeC_3Me and MeC_4Me increase as the temperature is

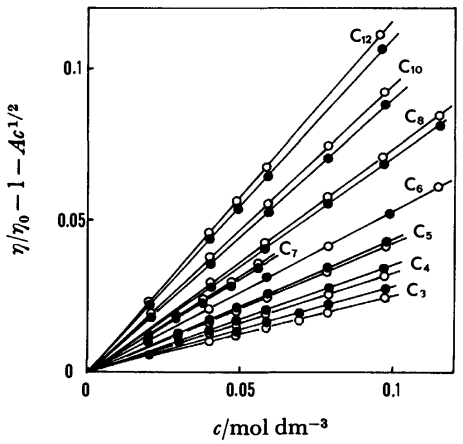

Fig. 1. Plots of $\eta/\eta_0-1-Ac^{1/2}$ against c for MeC_nMe. ○, 25 °C; ●, 35 °C.

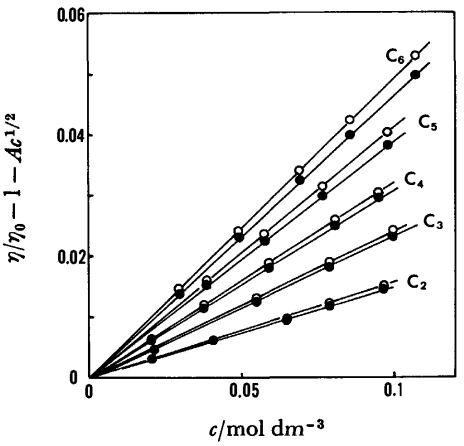

Fig. 2. Plots of $\eta/\eta_0-1-Ac^{1/2}$ against c for C_nMe. ○, 25 °C; ●, 35 °C.

Table 1. The values of A, B, and B_{ion}

n	A		B		B_{ion}	
	$dm^{3/2}\ mol^{-1/2}$		$dm^3\ mol^{-1}$		$dm^3\ mol^{-1}$	
T/°C	25	35	25	35	25	35
			$[(CH_3)_3N(CH_2)_nN(CH_3)_3]Br_2$			
3	0.0143	0.0147	0.260	0.284	0.340	0.336
4	0.0146	0.0151	0.330	0.353	0.410	0.405
5	0.0150	0.0154	0.426	0.440	0.506	0.492
6	0.0154	0.0159	0.536	0.537	0.616	0.589
7	0.0158	0.0163	0.643	0.635	0.723	0.687
8	0.0162	0.0167	0.733	0.708	0.813	0.760
10	0.0167	0.0172	0.945	0.909	1.024	0.961
12	0.0170	0.0176	1.165	1.115	1.245	1.167
			$C_nH_{2n+1}N(CH_3)_3Br$			
1			0.076[a]	0.087[a]	0.116	0.113
2	0.0065	0.0067	0.151	0.148	0.191	0.174
			0.16[b]			
3	0.0068	0.0070	0.239	0.229	0.279	0.255
4	0.0071	0.0073	0.326	0.310	0.366	0.336
			0.31[b]			
5	0.0073	0.0075	0.414	0.388	0.454	0.414
6	0.0075	0.0077	0.494	0.461	0.534	0.487
			0.45[b]			

a) Ref. 6; b) Ref. 4.

raised from 25 to 35 °C, and these salts may therefore be considered to behave as structure-breaking salts in the water phase. The B values of MeC_6Me are insensitive to the temperature. With MeC_7Me and higher homologs, the B values decrease with an increase in the temperature, therefore these salts exhibit a water-structure-making-effect. It was noted in previous work[1] on the change of heat capacity upon dissolution that MeC_6Me exhibited a slight tendency to behave as a structure-making solute. The classification of the behavior of a salt in water is somewhat dependent on the experimental method adopted.

With the C_nMe series, viscometric studies of tetramethylammonium bromide $(CH_3)_4NBr$, abbreviated as C_1Me in this paper, have been reported by several investigators, and the results by Out and Los[6] are included in Table 1. The B values for C_1Me increase with the temperature; this salt may be considered to act as a structure-breaking salt. The B values of C_2Me are insensitive to the temperature, and it seems to be a borderline salt. The B values for C_3Me and the higher homologs decrease with the temperature, and they are to be classified as hydrophobic structure-makers.

Figure 3 shows the changes in the viscosity B coefficients which occur as the temperature is raised from 25 to 35 °C, ΔB, as a function of n for MeC_nMe and C_nMe. If we take one-half the values of ΔB for

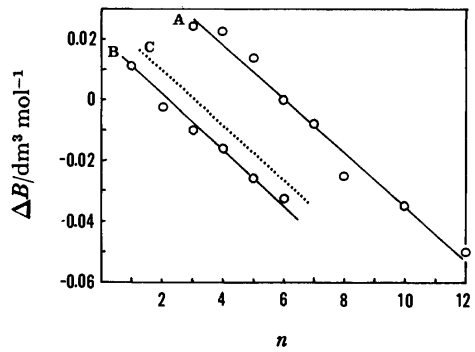

Fig. 3. Plots of ΔB aganist n. A, MeC_nMe; B, C_nMe; C, $-(CH_2)_nN(CH_3)_3Br$.

MeC_nMe, the values of ΔB for a series of $-(CH_2)_nN\cdot(CH_3)_3Br$ can be estimated. The ΔB *vs.* n relation thus obtained is plotted as a dotted line in Fig. 3. It is found that, for the same number of n, the values of ΔB for $-(CH_2)_nN(CH_3)_3Br$ are higher than those of ΔB for C_nMe. This fact indicates that the hydrophobic character of the polymethylene chain in MeC_nMe is considerably diminished as compared with that of the alkyl chain in C_nMe with the same number of n.

The Viscosity B Coefficients of Ions. The B values of electrolytes are determined by adding the individual contributions of the ions. Out and Los[6] reported the ionic B values of the Br^- ion as a function of temperature according to the convention of Gurney[7] that the ionic B values for K^+ and Cl^- ions are equal. The ionic B values of Br^- ion[6] are -0.040 and $-0.026\ dm^3\ mol^{-1}$ at 25 and 35 °C, respectively. The B values of organic ions obtained are included in Table 1. With the MeC_nMe^{2+} series, the ionic B values of MeC_3Me^{2+} and MeC_4Me^{2+} ions vary little with temperature. The ionic B values of MeC_5Me^{2+} and the higher homologous ions decrease with the temperature, so they are classified as structure-making ions. With the C_nMe series, the ionic B values of C_1Me^+ are practically constant between 25 and 35 °C. The B values of C_2Me^+ and the higher homologous ions decrease with the temperature, so they are classified as structure-making ions.

References

1) K. Tamaki and R. Furuya, *Bull. Chem. Soc. Jpn.*, **57**, 3325 (1984).

2) K. Tamaki, Y. Ōhara, M. Inabe, T. Mori, and F. Numata, *Bull. Chem. Soc. Jpn.*, **56**, 1930 (1983).

3) H. Falkenhagen and E. L. Vernon, *Z. Physik.*, **33**, 140 (1932).

4) M. Tanaka, S. Kaneshina, W. Nishimoto, and H. Takabatake, *Bull. Chem. Soc. Jpn.*, **46**, 364 (1973).

5) R. L. Kay, T. Vituccio, C. Zawoyski, and D. F. Evans, *J. Phys. Chem.*, **70**, 2336 (1966).

6) D. J. P. Out and J. M. Los, *J. Solution Chem.*, **9**, 19 (1980).

7) R. W. Gurney, "Ionic Processes in Solution," McGraw-Hill, New York (1953) p. 159.

Formation of α-Methylstyrene Dimer Radical Cations *via* Molecular Aggregates Studied by Pulse Radiolysis

Yukio YAMAMOTO,* Yukio CHIKAI, and Koichiro HAYASHI
The Institute of Scientific and Industrial Research, Osaka University, 8-1 Mihogaoka, Ibaraki, Osaka 567
(Received May 30, 1985)

Synopsis. Pulse radiolysis of α-methylstyrene was carried out in 1,2-dichloroethane, and the effect of additives on the formation of the dimer radical cations was investigated. In the presence of excess amounts of hexenes and biphenyl, the dimer radical cations are suggested to be formed *via* molecular aggregates by charge-transfer reactions.

The initiation processes of the radiation-induced cationic polymerization of styrene derivatives have been studied by pulse radiolysis methods.[1-4] Monomer and dimer radical cations and propagating cations have been detected as transient species responsible for the cationic polymerization. The monomer radical cations are quite short-lived, and the mechanistic details have been obtained by the pulse radiolysis at low temperature, −165 °C, in a mixture of isopentane and butyl chloride.[3] The following reaction scheme has been proposed for styrene and α-methylstyrene (MS):

$$\text{S(solvent)} \rightsquigarrow S^+ + e \quad (1)$$

$$S^+ + \text{M(monomer)} \longrightarrow S + M^+ \quad (2)$$

$$S^+ + M_2 \longrightarrow S + (M_2)^+ \quad (3)$$

$$S^+ + M_2 \longrightarrow S + M\text{-}M^+ \quad (4)$$

$$M^+ + M \rightleftharpoons (M_2)^+ \quad (5)$$

$$M^+ + M \longrightarrow M\text{-}M^+ \quad (6)$$

$$(M_2)^+ \longrightarrow M\text{-}M^+ \quad (7)$$

$$M\text{-}M^+ + M \longrightarrow \cdot M\text{-}M\text{-}M^+ \quad (8)$$

where $M\text{-}M^+$ and $(M_2)^+$ are the bonded and associated dimer radical cations, respectively. The formation of the dimer radical cations *via* molecular aggregates, M_2, has been proposed to account for their rapid formation during pulse irradiation.[2,3] The existence of the molecular aggregates, however, has been ruled out by another research group.[4] In the present study, the pulse radiolysis of MS was carried out in 1,2-dichloroethane at room temperature (*ca.* 22 °C) by using 8 ns electron pulses. The effect of additives on the formation of the dimer radical cations was examined in order to investigate the contribution of such neutral molecular aggregates.

Experimental

MS and 1,2-dichloroethane (Wako Chemicals) were successively washed three times with an aqueous solution of NaOH and with distilled water and then distilled over CaH_2. The middle fractions were stored under vacuum over CaH_2. Cyclohexene and 1-hexene (Wako Chemicals) were distilled over CaH_2 and stored under vacuum. Zone-refined biphenyl (BP) (Tokyo Kasei) was used without further purification. Bu_4NPF_6 (Bu, butyl) was prepared from Bu_4NBr and KPF_6 and twice recrystallized from a water-methanol mixture. The samples for the pulse radiolysis were prepared in a high vacuum operation and sealed into Suprasil cells of 10-mm optical path length. The pulse radiolysis techniques employed in this laboratory have been described elsewhere.[5]

Results and Discussion

The transient absorption spectra of MS in 1,2-dichloroethane are shown in Fig. 1. According to the literature,[3] the absorption band at 470 nm is assigned to the bonded dimer radical cations, although the possibility of a contribution of another type of dimer radical cations, associated ones, to the absorption still remains.[2] In this paper, the dimer radical cations having the 470-nm band are tentatively represented by $M\text{-}M^+$, and their formation processes are discussed.

At the higher concentration, 0.1 mol dm^{-3} (Fig. 1 (A)), the formation of $M\text{-}M^+$ seems to be almost completed within the pulse duration, 8 ns, and the 470-nm band decreases as a function of time. The absorption bands at 350 and 690 nm assigned to the monomer radical cations, M^+, are negligible even at the end of the pulse. The absorption below 400 nm with a relatively slow decay rate is attributed to

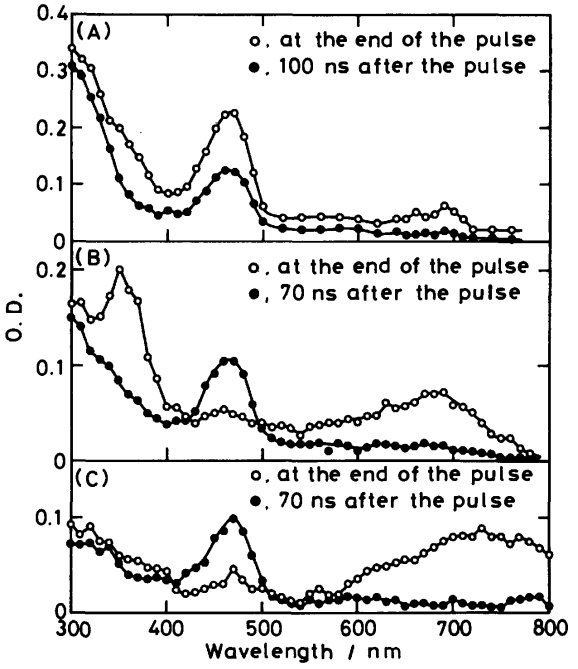

Fig. 1. Transient absorption spectra of MS solutions: (A) [MS]=0.1 mol dm^{-3}; (B) [MS]=0.01 mol dm^{-3}; and (C) [MS]=0.01 mol dm^{-3} in the presence of 0.5 mol dm^{-3} cyclohexene.

radical species such as benzyl-type radicals. The formation of the associated dimer radical cations having absorption bands at 620 and 1600 nm seems to be less important at room temperature than at −165 °C.[3]

At the low MS concentration, 0.01 mol dm^{-3} (Fig. 1 (B)), a rapid decay of the absorption due to M^+ can be seen, and the 470-nm band increases after the pulse. The absorption of M-M^+ attained a maximum at 70 ns. The effect of Bu_4NPF_6 was examined in order to establish the formation of M-M^+ from M^+. As has been reported,[6,7] the addition of Bu_4NPF_6 results in the stabilization of radical cations toward neutralization through ion-pair formation. When 5×10^{-3} mol dm^{-3} Bu_4NPF_6 was added to the 0.01 mol dm^{-3} MS solution, the formation of M-M^+ was enhanced, and the decay of M^+ became slightly slower. Therefore, the enhancement of the M-M^+ formation is attributable to the stabilization of M^+ toward neutralization with Cl^-, the product of dissociative electron capture by the solvent. That is to say, the growth of the 470-nm band is a result of the reaction of M^+ taking place in competition with the neutralization.

In the 0.01 mol dm^{-3} MS solution containing 0.5 mol dm^{-3} cyclohexene (Fig. 1 (C)), the 470-nm band increases after the pulse similarly to that in the solution not containing cyclohexene. However, no absorption peak is observed at 350 nm. The result can be explained by assuming that M-M^+ is formed *via* the MS molecular aggregates by the charge-transfer reaction probably from the cyclohexene dimer radical cations.[8] A similar result was obtained for the 0.01 mol dm^{-3} MS solution containing 0.5 mol dm^{-3} 1-hexene.

When 0.1 mol dm^{-3} BP was added to the 0.01 mol dm^{-3} MS solution, the transient absorption spectrum obtained at the end of the pulse was similar to that of the BP solution not containing MS. The absorption bands at 370 and 680 nm are assigned to BP^+, although the former band includes the absorption by the triplet excited state of BP. As the absorption of BP^+ decayed, the 470-nm band appeared, whereas no absorption peak due to M^+ was observed at any stage after the pulse. It was demonstrated that the decay of BP^+ is accelerated in the presence of added MS resulting in the direct formation of M-M^+. The result may be explained by the occurrence of the charge-transfer from BP^+ to the MS molecular aggregates.

From the results presented above, it seems likely that the MS molecular aggregates exist and contribute to the formation of M-M^+. Clearly further investigation is required to reveal the nature of the molecular aggregates.

References

1) H. Yoshida, M. Noda, and M. Irie, *Polymer J.*, **2**, 359 (1971).

2) K. Hayashi, M. Irie, D. Lindenau, and W. Schnabel, *Eur. Polym. J.*, **13**, 925 (1977).

3) S. Egusa, Y. Tabata, S. Arai, A. Kira, and M. Imamura, *J. Polym. Sci., Polym. Chem. Ed.*, **16**, 729 (1978).

4) O. Brede, J. Bös, W. Helmstreit, and R. Mehnert, *Radiat. Phys. Chem.*, **19**, 1 (1982).

5) Y. Yamamoto, S. Nishida, K. Yabe, K. Hayashi, S. Takeda, and K. Tsumori, *J. Phys. Chem.*, **88**, 2368 (1984).

6) S. Mah, Y. Yamamoto, and K. Hayashi, *J. Phys. Chem.*, **87**, 297 (1983).

7) S. Mah, Y. Yamamoto, and K. Hayashi, *Radiat. Phys. Chem.*, **23**, 137 (1984).

8) B. Badger and B. Brocklehurst, *Trans. Faraday Soc.*, **65**, 2576 (1969).

Olefin Hydrogenation over ZSM-5 Type Zeolite Catalysts Modified with Alkaline Earth Metals

Tsuneji SANO,* Kiyomi OKABE, Hiroshi SHOJI,† Kenji SAITO,†
Yoshiro YASUMOTO, Hiroyuki HAGIWARA, and Haruo TAKAYA
Catalysis Division, National Chemical Laboratory for Industry, Yatabe, Ibaraki 305
(Received May 30, 1985)

Synopsis. Olefin hydrogenation was carried out over ZSM-5 type zeolite catalysts modified with various alkaline earth metals. It was found that the catalytic activity of H-ZSM-5 for the olefin hydrogenation decreases upon such a modification.

Several papers have claimed that alumina, silica-alumina gels, and crystalline aluminosilicates (mordenite) are effective for the hydrogenation of ethylenic double bonds.[1-5] Recently, our previous communications have dealt with the conversion of the synthesis gas to hydrocarbons in a two-stage system consisting of a methanol synthesis reactor, followed by a hydrocarbon-forming reactor containing H-ZSM-5 zeolite. It has also been shown that the H-ZSM-5 zeolite catalyst is active for olefin hydrogenation.[6,7]

In this paper, it will be shown that the activity of the H- ZSM-5 zeolite catalyst in the olefin hydrogenation decreases when it is modified with alkaline earth metals.

Experimental

The H-ZSM-5 catalysts modified with alkaline earth metals were synthesized hydrothermally from ZSM-5 zeolite in the presence of alkaline earth metal acetates. Crystallization was carried out in a 300 ml stainless steel autoclave at 150—160 °C for 15—24 h. The precipitate was filtered off, washed thoroughly with distilled water, and calcined at 500 °C for 15 h in order to remove an organic base. It was then protonated in a hydrochloric acid solution of 1 M (1 M=1 mol dm^{-3}) and calcined in air at 500 °C for 6 h. Some analytical data are given in Table 1. The synthetic alkaline earth metal-modified ZSM-5 catalyst had a well defined ZSM-5 type structure, as demonstrated by the X-ray powder diffraction pattern.

The silicalite and silica gel used were prepared as follows. The silicalite was synthesized from tetraethoxysilane in the method described above. The silica gel was obtained by the hydrolysis of tetraethoxysilane. The precipitate was filtered off, dried at 100 °C, and then calcined at 500 °C for 10 h.

TABLE 1. PREPARATION OF VARIOUS ALKALINE EARTH METAL-MODIFIED H-ZSM-5 TYPE ZEOLITE CATALYSTS

Catalyst	Atomic ratios[a]		BET surface area ($m^2 g^{-1}$)
	Si/Al	Alkaline earth metal/Al	
1. H-ZSM-5	120		342
2. Mg-H-ZSM-5	94	1.30	336
3. Ca-H-ZSM-5	117	1.63	341
4. Sr-H-ZSM-5	93	1.29	301
5. Ba-H-ZSM-5	90	1.35	301
6. Silicalite[b]	—		345

a) Determined by X-ray fluoresence spectrometry.
b) Prepared from tetraethoxysilane.

† Present address: Maruzen Petrochemical Co., Ltd., Hatchobori, chuo-ku, Tokyo 104.

Hydrogenation was carried out at 400 °C and at a space velocity (SV) of 5000 h^{-1} under 40 kg cm^{-2}, using a high-pressure fixed-bed system. The reaction gas was composed of 2.5 mol% C_2H_4 (or C_3H_6), 50 mol% H_2, and 47.5 mol% Ar. The catalyst was packed into a quartz tube reactor, which was set in the pressure vessel. The effluent gas was led directly to sampling valves of a Yanaco AG-1000TFH auto gas chromatograph for analysis. The ethylene (or propylene)-based yields of the products were calculated by using argon as the internal standard.

The temperature programmed desorption (TPD) spectra of NH_3 over various catalysts were measured using a conventional TPD apparatus. The measurement was done from 100 °C to 600 °C with a heating rate of 5 °C min^{-1} and with nitrogen as the carrier gas (flow rate, 100 ml min^{-1}). The catalyst charged was 0.30 g.

Results and Discussion

Figure 1 shows some typical results for the hydrogenation of ethylene or propylene over various alkaline earth metal-modified ZSM-5 catalysts. The shaded parts in Fig. 1 indicate C_2 to C_5 olefins. Products both lower and higher in molecular weight were formed through a variety of reactions, such as polymerization, isomerization, cracking, and hydrogenation. The yields of light olefins and higher-carbon-number hydrocarbons (C_6^+) increased in the following order: H-ZSM-5≈Mg-H-ZSM-5<Ca-H-ZSM-5<Sr-H-ZSM-5<Ba-H-ZSM-5. In the case of the C_2H_4 (or C_3H_6)-H_2 system over these catalysts, hardly no aromatic hydrocarbons(BTX) were obtained as compared with those obtained in the C_2H_4 (or C_3H_6)-He system over the H-ZSM-5 catalyst (self-hydrogenation). In addition, the hydrogenation of these olefins was carried out over silicalite and silica gel of a very high purity. However, these olefins were hardly hydrogenated at all over these catalysts.

The TPD spectra of H-ZSM-5 zeolite exhibited two peaks, whose temperatures at the peak maximum were about 170 and 450 °C. By the addition of alkaline earth metals, the amount of desorbed NH_3 above 350 °C, which corresponded to that of the second peak, of various catalysts decreased in the following order: H-ZSM-5>Ca-H-ZSM-5>Mg-H-ZSM-5>Sr-H-ZSM-5>Ba-H-ZSM-5. In Fig. 2 are plotted the molar ratios of the C_2 to C_5 paraffins (C_2^-—C_5^-) to the C_2 to C_5 olefins ($C_2^=$—$C_5^=$) over these catalysts (given in Fig. 1) against the normalized amount of desorbed NH_3 [based on that of H-ZSM-5]. Except for Mg-H-ZSM-5, the (C_2^-—C_5^-)/($C_2^=$—$C_5^=$) molar ratio decreased as the amount of

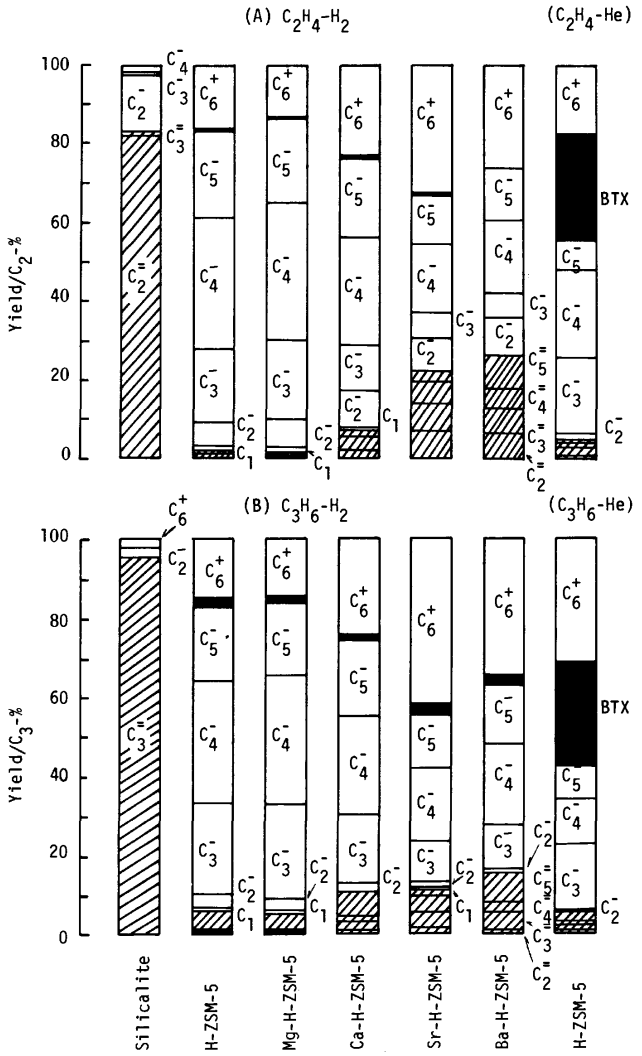

Fig. 1. Olefin hydrogenation over ZSM-5 type zeolite catalysts modified with various alkaline earth metals. Reaction conditions: $P=40$ kg cm^{-2}, $T=400$ °C, SV $=5000$ h^{-1}
Shaded parts indicate C_2 to C_5 olefins.

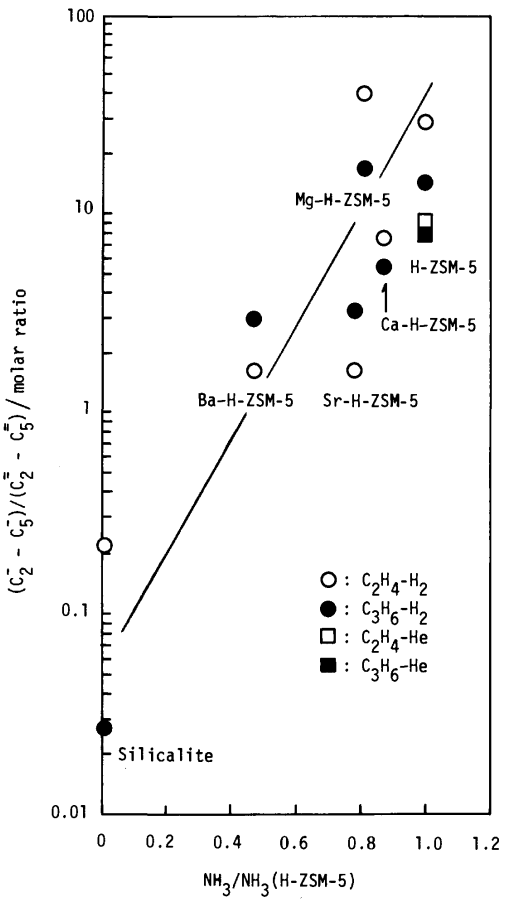

Fig. 2. Relation between the $(C_2^-—C_5^-)/(C_2^=—C_5^=)$ molar ratio and the amount of desorbed NH_3 of various catalysts. $(C_2^-—C_5^-)$:C_2 to C_5 paraffins, $(C_2^=—C_5^=)$: C_2 to C_5 olefins.

desorbed NH_3 decreased, namely, the basicity of alkaline earth metal increased. The temperature at the peak maximum of the second peak of the Mg-H-ZSM-5 catalyst hardly differed from that of H-ZSM-5.

Moreover, the impurities presented in the H-ZSM-5 zeolite were carefully analyzed by means of X-ray fluoresence spectrometry and inductively coupled argon plasma emission spectrometry. Only a trace amount of Fe (0.0065 wt%) was detected. The other metals were far below the detection limit of the inductively coupled argon plasma emission spectroscope (Shimadzu ICPS-50).

From these results, it can be concluded that the olefins are hydrogenated on the acidic sites of the H-ZSM-5 zeolite catalyst and that this hydrogenation activity decreases upon modification with alkaline earth metals.

The increase in the C_6^+ yield over the catalyst modified with alkaline earth metals may be attributed to the occurrence of the other reactions, such as polymerization, isomerization, and cracking, which take place in preference to the hydrogenation.

The limited data of the present work can not serve to clarify the detailed mechanism of this alternation of the acid property in zeolites.

This work is a part of the "C_1 Chemistry Project," a National Research and Development Program of the Agency of Industrial Science and Technology, Ministry of International Trade and Industry (M.I.T.I.), Japan.

References

1) G. Paravano, E. F. Hammel, and H. S. Taylor, *J. Am. Chem. Soc.*, **70**, 2269 (1948).
2) V. C. F. Holm and R. W. Blue, *Ind. Eng. Chem.*, **43**, 501 (1951); **44**, 107 (1952).
3) S. G. Hindin and S. W. Weller, *J. Phys. Chem.*, **60**, 1501 (1956).
4) P. J. Lucchesi, J. L. Carter, and D. J. C. Yates, *J. Phys. Chem.*, **66**, 1451 (1962).
5) Kh. M. Minachev, V. I. Garanin, V. V. Kharlamov, and T. A. Isakaya, *Kinetika i Kataliz*, **13**, 1101 (1972).
6) T. Sano, H. Hagiwara, K. Okabe, H. Takaya, H. Okado, and K. Saito, *Sekiyu Gakkaishi*, in press.
7) H. Hagiwara, T. Sano, H. Okado, K. Saito, K. Okabe, and H. Takaya, *Sekiyu Gakkaishi*, submitted for publication.

Preparation of (L-Cysteinato)(L- or D-histidinato)chromium(III) Complex

Yoshio ODAKA, Yuichi HASEGAWA, and Masatoshi WATABE*
General Education Department, Kogakuin University, Hachioji, Tokyo 192
(Received March 29, 1985)

Synopsis. Mixed-ligand chromium(III) complexes of the form [Cr(L-cys)(L-or D-his)] (L-cys=L-cysteinate and L-his=L-histidinate anions) were prepared. Isolated isomers of each complex were assigned structures on the basis of their high-speed liquid chromatograms and the distribution of the isomers.

Recently we have reported the preparation and stereochemistry of L- or D-aspartato(L-histidinato)-chromium(III) and bis(aspartato)chromate(III) complexes.[1] Hoggard prepared two of three isomers of the bis(L-histidinato)chromium(III) complex,[2] and Meester *et al.* prepared only one of three isomers of the bis(L-cysteinato)chromate(III) complex, the structure of which was determined as a trans sulfur isomer by X-ray crystallography.[3] Here, we report the preparation, chromatography, and absorption spectra of the chromium(III) complexes containing D- or L-his and L-cys.

Experimental

Preparations of [Cr(L-cys)(L- or D-his)] L-histidine (0.01 mol) and L-cysteine(0.01 mol) were dissolved in 80 cm^3 of water heated on a steam bath. The solution was added to an aqueous solution (60 cm^3) containing $Cr(NO_3)_3 \cdot 9H_2O$ (0.01 mol 4.00 g). After the mixture was heated for 10 min on the steam bath, the pH of the solution was adjusted to 7 with a 1-mol dm^{-3} NaOH solution. The solution was heated for 30 min, evaporated to 30—40 cm^3 and then loaded onto a column (50×500 mm) of QAE Sephadex A-25 anion resin in a chloride form. The column was kept at about 0 °C by circulating ethylene glycol-water. Three bands descended, the first was cations and the second and the third were neutral species corresponding to two isomers of the desired complex which were called A1 and A2, respecively. These two eluates were frozen as quickly as possible and evaporated at 0 °C. Two isomers of [Cr(L-cys)(D-his)] were obtaind by a similar method using D-histidine instead of L-histidine and were called B1 and B2 in the order of the elution in chromatography. As the two isomers in each D- and L-his complex easily isomerize to each other, they should be dissolved in ice-water. Anal. Calcd for $CrC_9H_{13}N_4O_4S \cdot H_2O$: C, 31.52; H, 4.40; N, 16.33%. Found (A1): C,31.01 H,3.95; N, 15.99%. Found (B1): C,31.32; H, 4.21; N, 16.15%. Calcd for $CrC_9H_{13}N_4O_4S \cdot 2H_2O$: C, 29.94; H, 4.74; N, 15.52%. Found (A2): C, 29.44; H, 4.94; N, 14.93%. Found (B2): C, 29.84; H, 5.12; N, 15.21%.

Measurements. The electronic absorption spectra were measured with a JASCO 505 spectrophotometer. The complexes were dissolved in water at 0 °C. The cell was treated with ethyleneglycol to prevent it from becoming wet with dew. The chromium content was determined with an atomic absorption photometer(Nippon Jarrel-Ash AA-845). Chromatographic separation was carried out with a JASCO-LCP-350. A 300×4 mm column containing a QAE Sephadex A-25 anion resin in a chloride form was used. The complexes were eluted with water at a flow rate of 0.1 cm^3 min^{-1} at a pressure of 40 kg cm^{-2}.

Results and Discussion

Figure 1 shows the six possible isomers of [Cr(L-cys)(L- or D-his)]. These isomers are denoted as L- or D-series with respect to the his ligand used and called L(or D)-*trans*(NNi), L(or D)-*trans*(NN), and L(or D)-*trans*(NO), where the left side N in parenthesis indicates that the nitrogen of cysteine and the following Ni, N, and O stand for the imidazole nitrogen, the nitrogen, and the oxygen atoms of coordinated histidine. Figure 2 shows high-speed liquid chromatograms of A1 and A2 together with that for [Cr(L-asp)(L-his)][1a](isomers CL1 and CL2) since the tridentate cysteinate coordinates with N,O,S atoms and the aspartate with N,O,O atoms so that the geometry and spectral behavior are expected to be similar in both complexes. The "a" in Fig. 2 represents a marker. Since all isomers of [Cr(L-cys)(L- or D-his)] isomerize in water at room temperature, the chromatograms in Fig. 2 show two peaks. Peak b corresponds to isomer A1 and peak c to isomer A2. These were determined by observing the time dependence of the peak heights. The same situation occurs in the chromatogram of [Cr(L-cys)(D-his)]. The peak of A1 appears a little later than that of CL1 and A2 elutes a little faster than CL3 of [Cr(L-asp)-(L-his)].

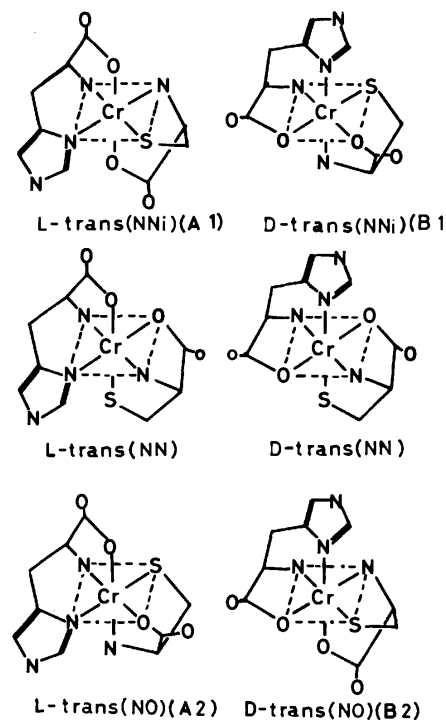

Fig. 1. The six possible isomers of [Cr(L-cys)(L- or D-his)], The isomers obtained are shown in parenthesis.

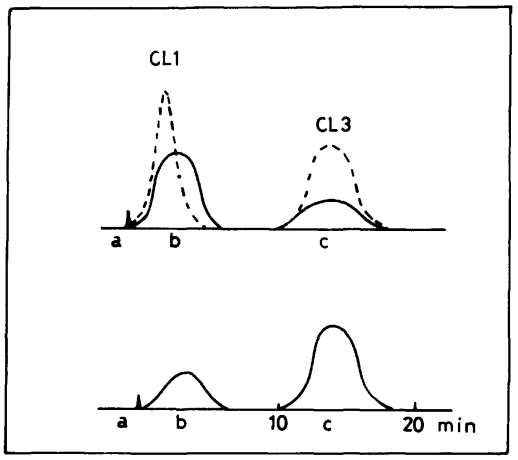

Fig. 2. High-speed liquid chromatograms indicating a mixture of [Cr(L-cys)(L- or D-his)] together with that of [Cr(L-asp)(L-his)]. Upper; from Al, lower; from A2. CL1 (*trans* (NNi)), CL2 (*trans* (NN)), and CL3 (*trans* (NO)) are the prepared isomers of [Cr (L-asp) (L-his)] in the order of elution.

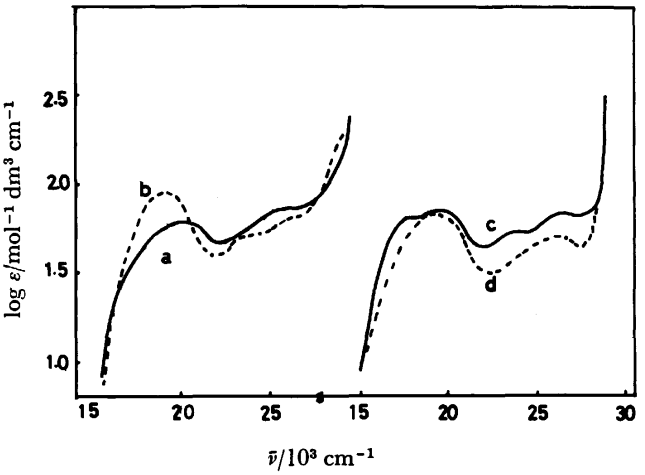

Fig. 3. Visible absorption spectra of [Cr(L-cys)(L- or D-his)]: Left a: Al and b: A2; right c: Bl and d: B2.

Though there are small differences in the peak positions, isomer Al can be assigned as L-*trans*(NNi) or L-*trans*(NN) and isomer A2 as L-*trans*(NO) by taking into consideration that the value of the dipole moment of the [Cr(L-cys)(L-his)] complex may be similar to that of [Cr(L- or D-asp)(L-his)]. In the same way, isomer Bl can be assigned as D-*trans*(NNi) or D-*trans*(NN) and isomer B2 as D-*trans*(NO). Figure 3 shows the visible absorption spectra of [Cr(L-cys)(L-or D-his)]. There are some peaks in the visible absorption spectra of [Cr(L-cys)(L-or D-his)] in both the first and second absorption band regions. Thioether complexes did not show any charge-transfer absorption[4] in the first and second absorption band regions. We tried to change the thiolate complex to a thioether complex by adding dimethyl sulfate. However, it was uncertain whether they were due to a d-d transition or a sulfite charge transfer since the thiolate complex could not be changed quantitatively to a thioether complex by adding dimethyl sulfate. Some infomation was, nevertheless, obtained; the band widths of isomers A2 and B2 in the first absorption band region were narrower than those of isomers Al and Bl, which indicates that A2 and B2 have a *trans*(NO) configuration (facial geometry when CrN_3O_3 type).

It is necessary to assign the first eluted isomers (Al and Bl). We have prepared mixed-ligand type, $[Co(N)_3(O)_3]$ and $[Cr(N)_3(O)_3]$, complexes containing two different tridentate ligands, such as [Co(L- or D-asp)(L-his)] and [Cr(L- or D-asp)(L-his)]. In all cases, the yields of the *trans*(NN) isomers were the lowest of all the possible isomers. In general, yields of isomers are dependent on the steric repulsion between ligands and on the electronic effect, such as the trans effect of a sulfur atom in chromium(III) complexes. We tentatively assigned Al as L-*trans*(NNi), A2 L-*trans*(NO), Bl D-*trans*(NNi) and B2 D-*trans*(NO). Though the isomerization of the complexes in solution could not be studied, it is interesting to note that the isomers of [Cr(L-cys)(L-or D-his)] isomerize in water at temperatures greater than 5 °C, when we consider the role of chromium(III) complexes containing cysteine in biological reactions.[6,7]

References

1) a) M. Watabe, H. Yano, Y. Odaka, and, H. Kobayashi, *Inorg. Chem.*, **20**, 3623 (1981); b) M. Sato, M. Kosaka, and M. Watabe, *Bull. Chem. Soc. Jpn.*, **58**, 874 (1985).
2) P. E. Hoggard, *Inorg. Chem.*, **20**, 415 (1981).
3) P. D. Meester, D. J. Hodgson, H. S. Freeman, and, C. J. Moore, *Inorg. Chem.*, **16**, 1494 (1976).
4) K. Okamoto, K. Wakayama, H. Einaga, S. Yamada, and J. Hidaka, *Bull. Chem. Soc. Jpn.*, **56**, 165 (1983).
5) M. Watabe, H. Yano, and, S. Yoshikawa, *Bull. Chem. Soc. Jpn.*, **52**, 61 (1979).
6) W. Y. Mertz, *Fed. Proc.*, **33**, 659 (1974).
7) W. Y. Mertz, E. W. Toepfer, E. E. Roginski, and M. M. Polansky, *Fed. Proc.*, **33**, 2275 (1974).

The Electrochemical Cleavage of Carbon-Halogen Bonds of Haloferrocenes

Tetsuo SAJI* and Naoyuki ITO
Department of Chemical Engineering, Tokyo Institute of Technology, Ohokayama, Meguro-ku, Tokyo 152
(Received June 8, 1985)

Synopsis. The cyclic voltammetric studies for haloferrocenes, FcX (X=Cl, Br, and I), in etylene glycol dimethyl ether at −45 °C have been reported. The cyclic voltammogram and the absorption spectrum of the solution after the exhaustive controlled-potential reduction for the reduction step of haloferrocene show a quantitative formation of ferrocene and a cleavage of the carbon-halogen bond of haloferrocene.

A vast amount of information regarding the organic chemistry of ferrocene (FcH) has been reported since its discovery.[1] The chemistry of ferrocene is similar to that of aromatic hydrocarbons. For example, ferrocene very readily undergoes Fridel-Craft acylation, alkylation, metalation by butyllithium.

It is known that FcH and its derivatives can be oxidized to ferrocenium cation (FcH^+) electrochemically as well as chemically.[2] On the other hand, Mugnier *et al.* and we ourselves have reported that ferrocene can be reduced quasireversibly in etylene glycol dimethyl ether (DMeE) at −45 °C, and that a stable ferrocene anion (FcH^-) exists for a few minutes.[3,4] Only a few cases of the electrochemical reduction of ferrocene dirivatives have been reported.[5] Such electron-rich anions are interesting in their reactivity.[6] The present note will deal with voltammetric and controlled-potential electrolytic studies of haloferrocenes undertaken in order to examine the mechanism of the reduction process.

Experimental

Iodoferrocene (FcI) was prepared by the reaction of (chloromercurio) ferrocene with iodine.[6] Chloroferrocene (FcCl) and bromoferrocene (FcBr) were prepared by the halogen-exchange reaction of FcI with copper(I) salts.[7] These complexes were purified by sublimation and identified on the basis of their melting points and elemental analyses on C, H, N, and halogen. The preparation of the test solutions and the procedures for the electrochemical measurements has been described previously.[4] Chloroferrocene: mp 56—56.5 °C (lit,[7] 56—56.5 °C). Found: C, 53.85; H, 4.04; N, 0.00, Cl, 16.78%. Calcd for $C_{10}H_9ClFe$: C, 54.47; H, 4.11; N, 0.00; Cl, 16.08%. Bromoferrocene: mp 30.5—31 °C (lit,[9] 30—31 °C). Found: C, 44.84; H, 3.32; N, 0.00; Br, 31.78%. Calcd for $C_{10}H_9BrFe$: C, 45.33; H, 3.42; N, 0.00; Br, 30.16%. Iodoferrocene: mp 48—49 °C (lit,[10] 49—49.5 °C). Found: C, 38.40; H, 2.84; N, 0.00; I, 41.23. Calcd for $C_{10}H_9IFe$:C, 38.50; H, 2.91; N, 0.00; I, 40.68%.

Results and Discussion

Figure 1 shows a cyclic voltammogram for 0.6 mM (mmol dm^{-3}) of FcCl in 0.2 M tetrabutylammonium perchlorate (TBAP) in DMeE, recorded at −45 °C with a scan rate of 0.2 V s^{-1}. It exhibits one reversible one-electron step at +0.04 V *vs.* Ag/$AgNO_3$(sat.), and two reduction steps at −3.35 V (reduction peak potential, E_{pc}) and −3.56 V, where potentials are indicated in terms of the potential at the midpoint between the cathodic peak potential (E_{pc}) and the anodic one (E_{pa}), $(E_{pa}+E_{pc})/2$, except for the case of the first reduction step. The reversal current peak of the step at −3.35 V can not be observed, even with a scan rate of 2 V s^{-1}. The step at −3.56 V was quasireversible. After the cathodic sweep was reversed at a potential less than the first reduction step, a small reversible one-electron oxidation step appeared at −0.13 V (Fig. 1-b). The half-wave potentials and the reversibilities of the second reduction and small oxidation steps were the same as those for the reduction and oxidation steps of FcH under the same conditions (Table 1). At room temperature, the first reduction step was observed at −3.28 V (E_{pc}), but the second reduction step was masked by the ultimate current rise. Similar voltammograms were obtained for FcBr and FcI. Table 1 lists the voltammetric results of these compounds. The first reduction peak potentials become more positive in the order of substituents, I>Br>Cl. This order agrees with that of the reactivities of haloferrocenes for photosubstitution.[11]

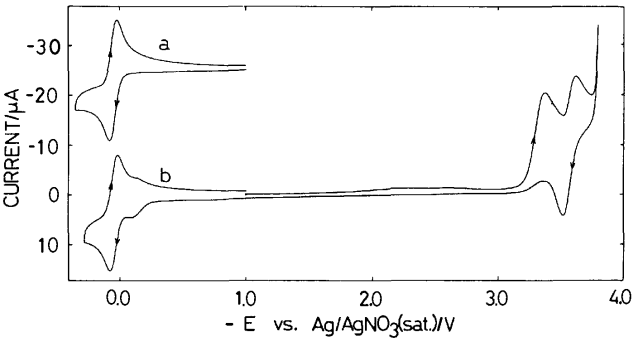

Fig. 1. Cyclic voltammogram of 0.6 mM chloroferrocene in 0.2 M TBAP-DMeE at −45 °C. Scan rate 0.2 V s^{-1}.

TABLE 1. THE VOLTAMMETRIC DATA OF CHLORO-, BROMO-, AND IODO- FERROCENES IN 0.2 M TBAP-DMeE AT −45 °C. SCAN RATE: 0.2 V s^{-1}

Compound	$E_{1/2}^{ox}$ a,b	$E_{1/2}^{ox}$ a,c	E_p^{red} a,d	$E_{1/2}^{red}$ a,e
Chloroferrocene	+0.04	−0.13	−3.35	−3.56
Bromoferrocene	+0.03	−0.13	−3.29	−3.57
Iodoferrocene	+0.01	−0.13	−3.23	−3.57
Ferrocene		−0.13		−3.58

a) *Vs.* Ag/$AgNO_3$(sat.) in V. b) Half-wave potential of the oxidation step in V. c) Half-wave potential of the small oxidation step after cathodic sweep in V. d) Peak potential of the first reduction step in V. e) Half-wave potential of the second reduction step in V.

An exhaustive controlled potential reduction of 2.0 mM FcCl in 0.5 M TBAP-DMeE with a Pt electrode held at −3.4 V at room temperature was undertaken in order to study the product for the reduction of FcCl. The solution of the reduced product was yellow. A cyclic voltammogram of this solution agreed with that of ferrocene under the same conditions. The peak current of this oxidation step showed that FcCl is quantitatively converted into ferrocene. The absorption spectrum of this solution also agreed with that of ferrocene.

Consequently, the electrochemical reduction of haloferrocene (FcX) may be said to result in the cleavage of the carbon-halogen bond and may proceed through the following process in the same manner as aromatic hydrocarbons:[12]

$$\mathrm{FcX} \overset{+e}{\rightleftharpoons} \mathrm{FcX^-}$$
$$\longrightarrow \mathrm{Fc\cdot} + \mathrm{X^-}$$
$$\mathrm{Fc\cdot} \overset{+e}{\longrightarrow} \mathrm{Fc^-}$$
$$\overset{+H^+}{\longrightarrow} \mathrm{FcH}$$

Such a quantitative formation of the ferrocenyl radical can be used in the preparation of ferrocene derivatives in place of the photolytic method.[11,13]

References

1) See, for example: "Gmeline Handbuch der Anorganishen Chemie," Bd. 14, Teil A, Ferrocene 1—7, Springer, Berlin (1974—1980).

2) M. D. Morris and G. L. Kok, "Encyclopedia of Electrochemistry of the Elements," XIII, ed by A. J. Bard, Marcel Dekker, New York (1979), Chap. XIII-1.

3) Y. Mugnier, C. Moise, J. Tirouflet, and F. Laviron, *J. Organomet. Chem.*, **186**, C49 (1980).

4) N. Ito, T. Saji and S. Aoyagui, *J. Organomet. Chem.*, **247**, 301 (1983).

5) See, for example, N. e. Murr and A. Chaloyyard, *J. Organomet. Chem.*, **193**, C60 (1980); C. Elschenbroichh and M. Cais, *ibid.*, **18**, 135 (1969). A. M. Hartley and R. E. Visco, *Anal. Chem.*, **35**, 1871 (1963).

6) J. R. Hamon, D. Astruc, and P. Michaud, *J. Amer. Chem. Soc.*, **103**, 758 (1981).

7) H. Shechter and J. F. Helling, *J. Org. Chem.*, **26**, 1034 (1961).

8) M. Sato, T. Ito, I. Motoyama, K. Watanabe, and K. Hata, *Bull. Chem. Soc. Jpn.*, **42**, 1976 (1969).

9) R. W. Fish and M. Rosenblum, *J. Org. Chem.*, **30**, 1253 (1965).

10) M. D. Rausch, *J. Org. Chem.*, **26**, 1802 (1961).

11) K. Shibata, Y. Saito, M. Matsui, and Y. Takase, *Bull. Chem. Soc. Jpn.*, **57**, 3349 (1984).

12) L. G. Feoktistov, "Reduction of Halogenated Organic Compounds," in Organic Electrochemistry," ed by M. M. Baizer and H. Lund, Marcel Dekker, New York (1983), Chap. 7.

13) T. Sato, S. Shimada, and K. Hata, *Bull. Chem. Soc. Jpn.*, **42**, 2731 (1969).

Substituent Effect on Stereoselectivity for Cobalt(III), Chromium(III), and Manganese(III) Complexes of Ring-substituted 1-*l*-Menthyloxy-3-benzoylacetones[1)]

Michio NAKAMURA, Hisashi ŌKAWA,* and Sigeo KIDA
Department of Chemistry, Faculty of Science, Kyushu University 33, Hakozaki, Higashi-ku, Fukuoka 812
(Received June 14, 1985)

Synopsis. Stereoselectivities of tris(1-*l*-menthyloxy-3-benzoylacetonato)M(III) ([M(*l*-moba)$_3$] (M=Co^{III}, Cr^{III}, Mn^{III})) and its homologs [M(*l*-moba-Br)$_3$] and [M(*l*-moba-Me)$_3$] (possessing bromo and methyl substituents at the 4-position of the aromatic ring, respectively) were examined by CD spectra. The stereoselectivity increased in the order [Co(*l*-moba-Br)$_3$]<[Co(*l*-moba)$_3$]<[Co(*l*-moba-Me)$_3$], and this trend was explained in terms of the electronic effect of the substituents on the interligand CH/π-interaction.

In the previous paper we showed that tris(1-*l*-menthyloxy-3-benzoylacetonato)M(III) complexes, [M(*l*-moba)$_3$] (M=Co^{III}, Cr^{III}, Mn^{III}), were obtained predominantly in one isomer, *cis-Δ*, probably because of the intramolecular, interligand CH/π-interactions operating between the phenyl and the *l*-menthyl groups (Fig. 1, R=H).[2)] The interligand CH/π-interaction was supported by the enhanced selectivities in tris{1-*l*-menthyloxy-3-(2-naphthoyl)acetonato}M(III) complexes[3)], [M(*l*-mona)$_3$], compared with those in [M(*l*-moba)$_3$] because the π-system of the naphthyl group which is larger than the phenyl group give rise to a more efficient interaction with the *l*-menthyl group.

In order to obtain further evidences for the CH/π-interaction, we prepared in this study H(*l*-moba) homologs with bromo and methyl substituents at the 4-position of the aromatic ring (abbreviated as H(*l*-moba-Br) and H(*l*-moba-Me), respectively), and the stereoselectivities of their cobalt(III), chromium(III), and manganese(III) complexes were examined in comparison with those of [M(*l*-moba)$_3$].

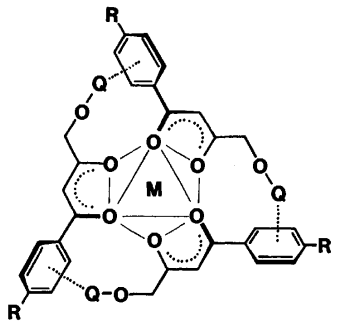

Fig. 1. Schematical representation of interligand CH/π-interaction supposed for [M(*l*-moba-R)$_3$] (Q=*l*-menthyl)

TABLE 1. ELEMENTAL ANALYSES OF THE COMPLEXES

Complex	Found(%)		Calcd(%)	
	C	H	C	H
Co(*l*-moba-Br)$_3$·H$_2$O	57.63	6.37	57.20	6.40
Cr(*l*-moba-Br)$_3$·3H$_2$O	55.79	6.50	55.91	6.51
Co(*l*-moba-Me)$_3$	72.28	8.50	72.25	8.37
Cr(*l*-moba-Me)$_3$	72.60	8.51	72.73	8.45
Mn(*l*-moba-Me)$_3$	71.37	8.38	71.29	8.45

Experimental

H(*l*-moba-Br) and H(*l*-moba-Me) were synthesized in a way similar to that for H(*l*-moba), using *p*-bromoacetophenone and *p*-methylacetophenone instead of acetophenone, respectively.[2)]

The metal complexes, [M(*l*-moba-Br)$_3$] and [M(*l*-moba-Me)$_3$] (M=Co^{III}, Cr^{III}, Mn^{III}), were prepared in the same way as that of [M(*l*-moba)$_3$].[2)] The elemental analyses for the complexes are given in Table 1.

The electronic and circular dichroism (CD) spectra were measured in carbon tetrachloride on a Shimadzu Multipurpose Spectrophotometer Model MPS-5000 and a JASCO J-500C Spectropolarimeter, respectively.

Results and Discussion

The spectral data are listed in Table 2. The electronic spectra of the cobalt complexes closely resemble those of previously reported tris(1,3-diketonato)cobalt(III) complexes.[2-5)] In Fig. 2 the spectrum of [Co(*l*-moba-Me)$_3$] is shown with the CD spectrum as an example. [Co(*l*-moba-Me)$_3$] exhibits intense circular dichroism in the d-d band region, a positive CD at 15.2×10^3 cm^{-1}($\Delta\varepsilon$=+2.27) and a negative CD at 17.3×10^3 cm^{-1}($\Delta\varepsilon$=−10.00), demonstrating that the chirality is configurational in

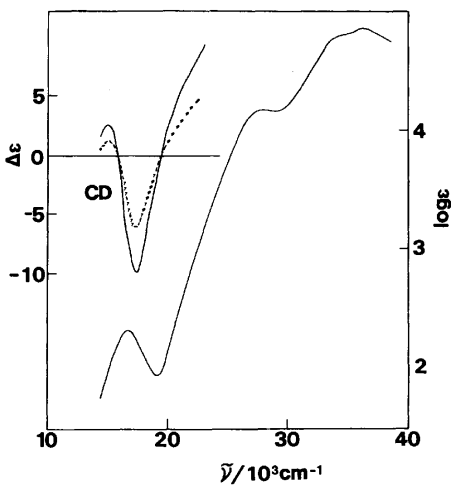

Fig. 2. Electronic and CD spectra of [Co(*l*-moba-Me)$_3$] (——) and [Co(*l*-moba)$_3$] (----) in carbon tetrachloride.

Table 2. Electronic and CD spectral data in carbon tetrachloride

	CD[a] $\Delta\varepsilon$/dm^3 mol^{-1} cm^{-1} ($\tilde{\nu}$/10^3 cm^{-1})		Absorption $\tilde{\nu}$/10^3 cm^{-1} (log ε)
[Co(*l*-moba-Br)$_3$]	+0.32(15.1)	− 1.73(17.3)	16.6(2.24), 27.4(sh), 35.1(sh), 36.8(4.80)
[Co(*l*-moba-Me)$_3$]	+2.36(15.2)	−10.00(17.3)	16.6(2.28), 27.5(4.16), 35.4(sh), 36.8(4.82)
[Cr(*l*-moba-Br)$_3$]	+0.17(15.9)	− 0.74(18.3)	17.1(2.03), 21.7(4.41), 32.0(4.42) 37.3(4.57)
[Cr(*l*-moba-Me)$_3$]	+0.79(16.2)	− 3.90(18.4)	17.6(2.02), 27.5(4.46), 32.3 (sh) 34.7(sh), 37.0(4.51)
[Mn(*l*-moba-Me)$_3$]	+0.15(18.2)	− 0.33(21.9)	8.0(2.18), 16.7(sh), 22.2(sh), 26.3(sh), 32.3(4.63), 38.5(4.42)

a) CD spectral data for [M(*l*-moba)$_3$]: +1.6(15.2) −6.1(17.4) for [Co(*l*-moba)$_3$], +0.56(15.9) −1.60(18.5) for [Cr-(*l*-moba)$_3$], and +0.10(18.0) −0.24(22.0) for [Mn(*l*-moba)$_3$].

origin. The CD pattern is the same as that of [Co(*l*-moba)$_3$], but the intensity is much higher than that of [Co(*l*-moba)$_3$] as seen in Fig. 2. In comparison with the CD spectra of *Λ*-[Co(acac)$_3$][5] and [Co(*l*-moba)$_3$],[2] the preferred configuration of [Co(*l*-moba-Me)$_3$] was shown to be of *cis*-*Δ*. Similarly, the circular dichroism of [Co(*l*-moba-Br)$_3$] exhibited the same pattern as that of [Co(*l*-moba)$_3$][2] and [Co(*l*-mona)$_3$][3] in the d-d band region. However, its CD intensity was weaker than that of [Co(*l*-moba)$_3$] (See Table 2).

The electronic spectra of [Cr(*l*-moba-Br)$_3$] and [Cr(*l*-moba-Me)$_3$] resemble those of tris(1,3-diketonato)chromium(III) complexes previously reported.[2,6,7] Their CD spectral pattern in the visible region indicated the predominant formation of the *cis*-*Δ* isomer.[2]

The manganese complex [Mn(*l*-moba-Me)$_3$] also showed fairly intense CD at 18.2×10^3 and 21.9×10^3 cm^{-1}. It is presumed that the *cis*-*Δ* isomer also predominates in this case by analogy with the case of the cobalt(III) and chromium(III) complexes.

Thus, all the complexes showed a stereoselectivity which led to the formation of the *cis*-*Δ* isomer. From Table 2, it is seen that the CD intensity induced at the d-d band region increases generally in the order, [M(*l*-moba-Br)$_3$]<[M(*l*-moba)$_3$]<[M(*l*-moba-Me)$_3$], for each metal ion, suggesting the stereoselectivity enhanced in this order provided that the CD intensity of the *cis*-*Δ* isomer is not significantly affected by the substituents on the ring. The trend can be reasonably explained in terms of the electronic effect of the substituents on the ring. That is, the π-electron density of the ring should increase in the order 4-BrC$_6$H$_4$<C$_6$H$_5$<4-CH$_3$C$_6$H$_5$, and thence the interligand CH/π-interaction (Fig. 1) becomes more effective in this order.

The authors are grateful to Mr. Y. Hisaeda for measuring CD spectra.

References

1) Noncovalent Interactions in Metal Complexes. Part X. Part IX: S. Maeda, M. Nakamura, M. Mikuriya, T. Shinmyozu, H. Ōkawa, and S. Kida, *Mem. Fac. Soc., Kyushu Univ., Ser. C*, **15**, 63 (1985).

2) H. ŌKawa, K. Ueda, and S. Kida, *Inorg. Chem.*, **21**, 1594 (1982).

3) M. Nakamura, H. Ōkawa, and S. Kida, *Inorg. Chim. Acta*, **96**, 111 (1984).

4) A. Y. Girgis and R. C. Fay, *J. Am. Chem. Soc.*, **92**, 7061 (1970).

5) R. B. Von Deele and R. C. Fay, *J. Am. Chem. Soc.*, **93**, 4936 (1971).

6) T. S. Piper and R. L. Carlin, *J. Am. Chem. Soc.*, **36**, 3330 (1962).

7) J. P. Fackler, Jr., T. S. Davis, and I. D. Chawla, *Inorg. Chem.*, **4**, 130 (1965).

The Reaction of Dimethyl *N*-Benzoylcarbonimidodithioates with Amines

Naoaki FUKADA,* Masahiro HAYASHI, and Yukari SUZUKI
Department of Chemistry, Faculty of Science, Chiba University, Yayoicho, Chiba 260
(Received May 16, 1985)

Synopsis. 1-Substituted 3-benzoyl-2-methylisothioureas and 1,3-disubstituted 2-benzoylguanidines were synthesized from dimethyl *N*-benzoylcarbonimidodithioates and amines. From ethylenediamine and 2-aminoethanol, imidazolidine and oxazolidine derivatives were obtained respectively.

In recent years, α-oxoketene dithioacetals have been widely used for the preparation of heterocycles and intermediates in organic synthesis. However, relatively few studies have been reported on the reactions of the corresponding aza-analog *N*-acylcarbonimidodithioic acid dithioesters. In our continuing study of the reactions of amides with carbon disulfide,[1,2] we have previously reported the general synthesis of dimethyl *N*-aroylcarbonimidodithioates from aromatic amide, carbon disulfide, and sodium hydride.[3] The dithioesters reacted with hydrazine hydrate to give 3-aryl-5-methylthio-1*H*-1,2,4-triazoles in good yields.[3] Augustin *et al.* reported the syntheses of dimethyl *N*-cinnamoyl- and *N*-aroylcarbonimidodithioates, and their reactions with nucleophilic compounds.[4–7] Recently Potts *et al.* used diethyl *N*-benzoylcarbonimidodithioates and the potassium enolates of methyl ketones to prepare *N*-acyl-β-enamino ketones.[8]

In this note, we wish to report the reactions of dimethyl *N*-benzoylcarbonimidodithioates **1** obtained from 2-methyl- and 4-nitrobenzamides with several amines. When equimolar mixtures of **1** and amines

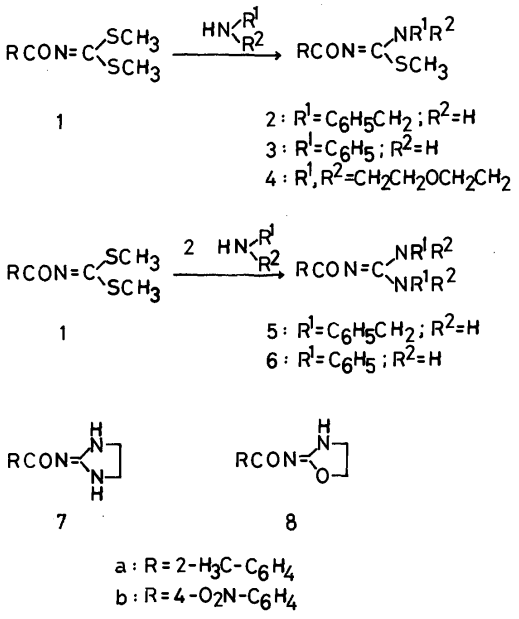

(benzylamine, aniline, and morpholine) were heated in ethanol, 1-substituted 3-benzoyl-2-methylisothioureas **2**—**4** were obtained in good yields. Two moles of the amines (benzylamine and aniline) gave 1,3-disubstituted 2-benzoylguanidines **5** and **6**. For the latter reactions it was necessary to heat in boiling xylene. Although early reports[9,10] described the preparation of compounds of these types (**2**—**6**), the method reported here is more convenient. From ethylenediamine and 2-aminoethanol, the cyclized compounds, 2-(benzoylimino)imidazolidines **7** and 2-(benzoylimino)oxazolidine **8** respectively, were obtained.

These results are similar to those of the reaction of α-oxoketene dithioacetals with amines[11] and offer new possibilities in preparing heterocycles.

Experimental

*1-Substituted 3-Benzoyl-2-methylisothioureas (**2**—**4**).*
General Procedure. A mixture of dimethyl *N*-benzoylcarbonimidodithioate (**1**, 0.002 mol),[3] amine (benzylamine, aniline, or morpholine; 0.0022 mol), and ethanol (30—40 ml) was refluxed for 1—3 h. The solvent was then removed, and the residual solid was recrystallized.

*1-Benzyl-2-methyl-3-(2-methylbenzoyl)isothiourea (**2a**)*: Recrystallized from ethanol; IR (KBr) 3160 m (NH) and 1590 *vs.* cm^{-1} (C=O); UV (EtOH) λ_{max} 244sh (log ε 4.13), 249 (4.15), 255 (4.15), 262sh (4.22), and 282 nm (4.47); ^{1}H NMR (CCl_4) δ=2.55 (s, 3H, CH_3), 2.58 (s, 3H, CH_3), 4.55 (d, 2H, CH_2), 7.2—8.5 (m, 9H, C_6H_4 and C_6H_5), and 11.77 (br s, 1H, NH); MS *m/z* 298 (M^+).

*1-Benzyl-3-(4-nitrobenzoyl)-2-methylisothiourea (**2b**)*: Recrystallized from ethanol; IR (KBr) 3250 w (NH) and 1580 *vs.* cm^{-1} (C=O); MS *m/z* 329 (M^+).

*2-Methyl-3-(2-methylbenzoyl)-1-phenylisothiourea (**3a**)*: Recrystallized from hexane–ethanol; IR (KBr) 1605 *vs.* cm^{-1} (C=O); MS *m/z* 284 (M^+).

*2-Methyl-3-(4-nitrobenzoyl)-1-phenylisothiourea (**3b**)*: Recrystallized from ethanol; IR (KBr) 1615 m cm^{-1} (C=O); MS *m/z* 315 (M^+).

*4-[2-Methylbenzoylimino(methylthio)methyl]morpholine (**4a**)*: Recrystallized from ethanol; IR (KBr) 1604 s cm^{-1} (C=O); UV (EtOH) λ_{max} 240 (log ε 4.27) and 281 nm (4.23); MS *m/z* 278 (M^+).

*4-[Methylthio(4-nitrobenzoylimino)methyl]morpholine (**4b**)*: Recrystallized from ethanol; IR (KBr) 1630 s cm^{-1} (C=O); MS *m/z* 309 (M^+).

*1,3-Disubstituted 2-Benzoylguanidines (**5** and **6**).*
General Procedure. A mixture of **1** (0.002 mol), amine (benzylamine or aniline; 0.0044 mol), and xylene (30—40 ml) was refluxed for 5 h. In the case of **6a**, ethanol was used as the solvent. The solvent was removed, and the residual solid was recrystallized.

*1,3-Dibenzyl-2-(2-methylbenzoyl)guanidine (**5a**)*: Recrystallized from ethanol; IR (KBr) 3295 *vs.* (NH) and 1615 *vs.* cm^{-1} (C=O); MS *m/z* 357 (M^+).

*1,3-Dibenzyl-2-(4-nitrobenzoyl)guanidine (**5b**)*: Recrystallized from hexane–ethanol; IR (KBr) 3398 s (NH) and 1612 s cm^{-1} (C=O); MS *m/z* 388 (M^+).

*1,3-Diphenyl-2-(2-methylbenzoyl)guanidine (**6a**)*: Recrystallized from ethanol; IR (KBr) 3380 m, 3250 s (NH), and 1680 *vs.* cm^{-1} (C=O); UV (EtOH) λ_{max} 234sh (log ε 4.33) and 278 nm (4.42); MS *m/z* 329 (M^+).

Table 1. Yields and analytical data

Compound	Yield %	Mp θ_m/°C	Molecular formula	Found (Calcd) (%) C	H	N	S
2a	97	71—72	$C_{17}H_{18}N_2OS$	68.40 (68.43)	6.14 (6.08)	9.50 (9.39)	10.44 (10.75)
2b	83	120—121	$C_{16}H_{15}N_3O_3S$	58.48 (58.35)	4.68 (4.59)	12.73 (12.76)	9.80 (9.73)
3a	66	71—72	$C_{16}H_{16}N_2OS$	67.43 (67.58)	5.73 (5.67)	9.59 (9.85)	11.12 (11.28)
3b	85	153—154[a]	$C_{15}H_{13}N_3O_3S$	57.25 (57.13)	4.18 (4.16)	13.37 (13.33)	10.25 (10.17)
4a	87	91—92	$C_{14}H_{18}N_2O_2S$	60.66 (60.41)	6.52 (6.52)	10.10 (10.06)	11.26 (11.52)
4b	55	152—154	$C_{13}H_{15}N_3O_4S$	50.46 (50.48)	4.90 (4.89)	13.56 (13.58)	10.05 (10.37)
5a	78	146—147	$C_{23}H_{23}N_3O$	77.13 (77.28)	6.50 (6.49)	11.70 (11.76)	
5b	77	154—156	$C_{22}H_{20}N_4O_3$	67.73 (68.03)	5.29 (5.19)	14.26 (14.42)	
6a	57	134—135	$C_{21}H_{19}N_3O$	76.49 (76.57)	5.87 (5.81)	12.76 (12.76)	
6b	84	145—147	$C_{20}H_{16}N_4O_3$	66.52 (66.66)	4.56 (4.48)	15.46 (15.55)	
7a	96	162—163	$C_{11}H_{13}N_3O$	65.05 (65.01)	6.43 (6.45)	20.90 (20.68)	
7b	94	252—253[b]	$C_{10}H_{10}N_4O_3$	51.31 (51.28)	4.49 (4.30)	23.93 (23.92)	
8b	63	236—238	$C_{10}H_9N_3O_4$	51.05 (51.07)	3.90 (3.86)	17.93 (17.87)	

a) Lit,[7] mp 148—150 °C. b) Decomp.

*1,3-Diphenyl-2-(4-nitrobenzoyl)guanidine (**6b**)*: Recrystallized from ethanol; IR (KBr) 3375 m (NH) and 1600 s cm^{-1} (C=O); MS *m/z* 360 (M^+).

*Imidazolidines **7** and Oxazolidine **8*** were prepared from ethylene diamine and 2-aminoethanol respectively as has been described for the preparation of **2—4**.

*2-(2-Methylbenzoylimino)imidazolidine (**7a**)*: Recrystallized from ethanol; IR (KBr) 3340 s (NH) and 1600 *vs.* cm^{-1} (C=O); UV (EtOH) λ_{max} 244 nm (log ε 4.48); MS *m/z* 203 (M^+).

*2-(4-Nitrobenzoylimino)imidazolidine (**7b**)*: Recrystallized from *N,N*-dimethylformamide-ethanol; IR (KBr) 3310 s (NH) and 1620 *vs.* cm^{-1} (C=O); MS *m/z* 234 (M^+).

*2-(4-Nitrobenzoylimino)oxazolidine (**8b**)*: Recrystallized from *N,N*-dimethylformamide; IR (KBr) 3290 s (NH) and 1620 *vs.* cm^{-1} (C=O); MS *m/z* 235 (M^+).

The authors wish to thank Dr. Tatsuo Takeshima for his helpful suggestions and warm encouragement.

References

1) T. Takeshima, M. Ikeda, M. Yokoyama, N. Fukada, and M. Muraoka, *J. Chem. Soc., Perkin Trans. 1*, **1979**, 692.
2) T. Takeshima, N. Fukada, E. Ohki, and M. Muraoka, *J. Chem. Res. (S)*, **1979**, 212.
3) M. Sato, N. Fukada, M. Kurauchi, and T. Takeshima, *Synthesis*, **1981**, 554.
4) M. Augustin, M. Richter, and S. Salas, *J. Prakt. Chem.*, **322**, 55 (1980).
5) M. Richter, C. Herrmann, and M. Augustin, *J. Prakt. Chem.*, **322**, 434 (1980).
6) M. Richter, K. Strauss, H.-D. Schädler, and M. Augustin, *J. Prakt. Chem.*, **324**, 625 (1982).
7) M. Richter, K. Strauss, and M. Augustin, *Z. Chem.*, **22**, 103 (1982).
8) K. T. Potts, A. J. Ruffini, and G. R. Titus, *J. Org. Chem.*, **48**, 625 (1983).
9) H. L. Wheeler and H. F. Merriam, *J. Am. Chem. Soc.*, **23**, 283 (1901).
10) T. B. Johnson and L. H. Chernoff, *J. Am. Chem. Soc.*, **34**, 164 (1912).
11) For example, G. Kobayashi, S. Furukawa, and Y. Matsuda, *Yakugaku Zasshi*, **86**, 1152 (1966); M. Augustin, Ch. Groth, H. Kristen, K. Peseke, and Ch. Wiechmann, *J. Prakt. Chem.*, **321**, 205 (1979); A. Kumar, V. Aggarwal, H. Ila, and H. Junjappa, *Synthesis*, **1980**, 748.

Reactions of Trimethylsilylmethyl Azide with Aromatic Acid Derivatives Catalyzed by Fluoride Ion

Kozaburo NISHIYAMA,* Hiroyuki MIKUNI, and Mari HARADA
Department of Chemistry, Tokyo Metropolitan University, 2-1-1, Fukasawa, Setagaya-ku, Tokyo 158
(Received May 28, 1985)

Synopsis. The treatment of an aromatic acid halide with trimethylsilylmethyl azide (TMSMA) in the presence of potassium fluoride and crown ether gave triazine, methanediamine, and benzamide derivatives, while the reaction of acid anhydride with TMSMA gave tertiary amine together with methanediamine and benzamide under similar conditions.

We are currently interested in the reactivities and the synthetic utilities of azide compounds containing silicon atoms.[1] Trimethylsilylmethyl azide (TMSMA) has various reaction sites and a synthetic applicability as a synthon for the amination of aromatic halides,[1b] 1,3-dipolar cycloaddition,[2] or heterocumulenes.[3] In this paper, we describe unexpected reactions involving TMSMA with acid derivatives to give triazine, methanediamine, tertiary amine, and benzamide derivatives.

Results and Discussion

A mixture of benzoyl chloride and TMSMA in the presence of potassium fluoride and a catalytic amount of 18-crown-6 in benzene was heated to reflux for 50 h. Surprisingly, the extract with dichloromethane gave 30% of 1,3,5-tribenzoylhexahydro-1,3,5-triazine (**1a**) and 34% of *N,N'*-dibenzoylmethanediamine (**2a**) together with 16% of benzamide.

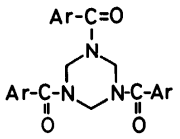

1

$ArCONHCH_2NHCOAr$

2

a, $Ar=C_6H_5$
b, $Ar=p\text{-}NO_2C_6H_4$
c, $Ar=p\text{-}MeC_6H_4$

Without either potassium fluoride or crown ether, no products were formed. Other aroyl chlorides were treated in a similar manner and the results are listed in the Table. With *p*-nitrobenzoyl chloride, both triazine **1b** and methanediamine **2b** along with *p*-nitrobenzamide were isolated, though the product distribution was different from that of benzoyl chloride itself. When *p*-methylbenzoyl chloride was employed, only triazine **1c** was obtained in a much higher yield (73%) as the sole product. As for the formation of these compounds, it has been reported that benzonitrile, 1,3,5-trioxane, and a catalytic amount of concd sulfuric acid gave either triazine **1a**[4] or methanediamine **2a**,[5] depending on the conditions.

As a reaction pathway, we assumed that the

TABLE. REACTION OF TMSMA WITH AROYL CHLORIDES AND BENZOIC ANHYDRIDE[a]

Substrate	KF	Yield/%[b]			$ArCONH_2$
		1	**2**	**3**	
C_6H_5COCl	1 equiv	30	34		16
$p\text{-}NO_2C_6H_4COCl$	1 equiv	9	38		7
$p\text{-}MeC_6H_4COCl$	1 equiv	73			
$(C_6H_5CO)_2O$	1 equiv	0	28	3	4
	3 equiv	0	10	22	4

a) Reaction conditions were cited in experimental section. b) Based on used acid derivatives.

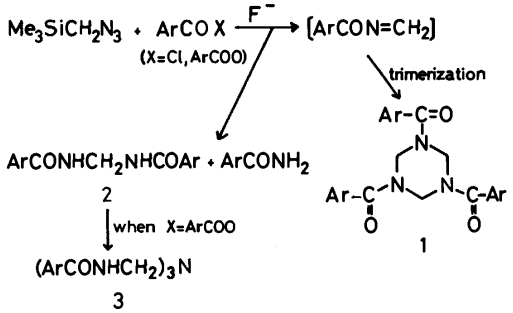

Scheme

desilylation of TMSMA induced by fluoride ions gave $K^+[CH_2N_3]^-$, followed by an evolution of nitrogen to form $K^+[CH_2{=}N]^-$ at the temperature, which afforded *N*-benzoylmethanimine ($ArCON{=}CH_2$) *via* a nuclereophilic attack on acid chloride. The triazine derivative **1** would be obtained by a trimerization of the species. Such a trimerization of methanimine has been reported;[6] 1,3,5-tris(benzylsulfonyl)hexahydro-1,3,5-triazine was transformed from phenylmethanesulfonamide and 1,3,5-trioxane *via* *N*-(benzylsufonyl)methanimine ($PhCH_2SO_2N{=}CH_2$), in which 3,4-dihydro-1*H*-2,3-benzothiazine 2,2-dioxide was also obtained as a thermodynamically controled product. In our case, however, the intramolecular cyclization product, 1-isoindolinone, was not detected even when the reaction time was prolonged.

When benzoic anhydride was employed, 28% of methanediamine **2a**, 3% of tris(benzoylaminomethyl)-amine (**3a**), and 4% of benzamide, along with the

$(RCONHCH_2)_3N$ **3**, a, R=Ph; b, R=Me

starting material, were obtained. With a three-fold excess of potassium fluoride to benzoic anhydride, the yield of **2a** was decreased to 10%, while that of amine **3a** was increased to 22%. Ethyl benzoate and acetic anhydride gave neither **1**, **2**, nor **3**.

From reported investigations[4,5,6] and these results, the reaction pathway to **1** and **2** might be competitive (as shown in the Scheme) and the formation of **3** would be rationalized by a nucleophilic attack of benzoyloxy anions towards **2**. However, it was not easy to confirm the reaction course.

Experimental

Melting points are uncorrected. ^{1}H NMR spectra were determined with a Hitachi R-600 or a JEOL PS-100 spectrometer using tetramethylsilane as an internal standard. IR spectra were taken on a Hitachi 260-10 infrared spectrometer and mass spectra were measured with a JEOL DX-300 spectrometer. Aroyl chlorides, potassium fluoride, and 18-crown-6 were commercial products and were purified when necessary. Trimethylsilylmethyl azide was prepared from trimethylsilylmethyl chloride and sodium azide according to a reported method.[1d]

Reaction of Aroyl Chloride with TMSMA. A mixture of benzoyl chloride (1.40 g, 10 mmol), TMSMA (1.94 g, 15 mmol), KF (0.58 g, 10 mmol), and 18-crown-6 (26 mg, 0.1 mmol) in benzene (10 cm^3) was heated to reflux for 50 h with stirring. To the reaction mixture was added a 10% sodium carbonate solution (30 cm^3). Stirring was continued for 24 h. The reaction mixture was extracted with dichlromethane. After drying over magnesium sulfate and evaporating the solvent *in vacuo*, the residual solid was chromatographed on alumina. Rapid elution with benzene/chloroform gave 405 mg (30%) of 1,3,5-tribenzoylhexahydro-1,3,5-triazine (**1a**), recrystallized from ethanol, colorless prisms, mp 216—218 °C (lit,[4] 220—222 °C), mass spectrum *m/z* 399 (M^+), and 435 mg (34%) of *N,N'*-dibenzoylmethanediamine (**2a**), recrystallized from methanol, colorless needles, mp 215—216 °C (lit,[5] 216—218 °C), *m/z* 254 (M^+). Further elution with methanol afforded 197 mg (16%) of benzamide. ^{1}H NMR spectra of **1a** and **2a**: **1a** ($CDCl_3$) δ=5.41 (6H, s) and 7.48 (15H, m); **2a** (DMSO-d_6) δ=5.08 (2H, t, J=6 Hz), 7.5—8.1 (10H, m) and 9.15 (2H, t, J=6 Hz).

Other aroyl chlorides were similarly treated unless otherwise mentioned. With *p*-nitrobenzoyl chloride (1.85 g, 10 mmol), the reaction time was prolonged to 120 h. To the reaction mixture was added chloroform and water. A precipitated solid was filtered and then washed with hot acetonitrile, giving 160 mg of a colorless solid, which was found to be 1,3,5-tris(*p*-nitrobenzoyl)hexahydro-1,3,5-triazine (**1b**, 9%), mp >260 °C, ν_{max} 1650 and 1530 cm^{-1}. The ^{1}H NMR spectrum in DMSO-d_6 showed at δ=5.38 (6H, s) and 7.76, 8.26 (12H, AA'BB'q, J=8 Hz). Found: C, 53.46; H, 3.33; N, 15.60%. Calcd for $C_{24}H_{18}N_6O_9$: C, 53.93; H, 3.39; N, 15.73%. Column chromatography on alumina of the combined filtrate gave 650 mg (38%) of *N,N'*-bis(*p*-nitrobenzoyl)methanediamine (**2b**), recrystallized from acetonitrile, colorless needles, mp 245—246 °C, *m/z* 344 (M^+), ^{1}H NMR (DMSO-d_6) δ=5.08 (2H, t, J=6 Hz), 8.35, 8.54 (12H, AA'BB'q, J=9 Hz), and 9.65 (2H, t, J=6 Hz), ν_{max} 3290, 1630, and 1510 cm^{-1}. Found: C, 51.97; H, 3.42; N, 16.27%. Calcd for $C_{15}H_{12}N_4O_6$: C, 52.33; H, 3.51; N, 16.27%. *p*-Nitrobenzamide along with unidentified products was also obtained.

When *p*-methylbenzoyl chloride (1.55 g, 10 mmol) was employed, 1,3,5-tris(*p*-methylbenzoyl)hexahydro-1,3,5-triazine (**1c**) was obtained in 73% (1.07 g) yield. The compound was recrystallized from ethanol to give colorless needles, mp 211—212 °C, *m/z* 441 (M^+). The IR spectrum showed at 1660 and 1640 cm^{-1} and the ^{1}H NMR spectrum in $CDCl_3$ showed signals at δ=2.40 (9H, s), 5.40 (6H, s), and 7.28 (12H, m). Found: C, 73.23; H, 6.07; N, 9.48%. Calcd for $C_{27}H_{27}N_3O_3$: C, 73.45; H, 6.17; N, 9.52%.

Reaction of Acid Anhydride with TMSMA. The reaction of benzoic anhydride (2.26 g, 10 mmol) with TMSMA (1.94 g, 15 mmol) was carried out as metioned above. Extraction with CH_2Cl_2 and column chromatography eluted by benzene/chloroform gave 350 mg (28%) of **2a** and 41 mg (3%) of tris(benzoylaminomethyl)amine (**3a**), recrystallized from ethanol, colorless plates, mp 188—189 °C, *m/z* 416 (M^+), ν_{max} 3320 and 1645 cm^{-1}. ^{1}H NMR ($CDCl_3$) δ=4.73 (6H, d, J=7 Hz), 7.0—7.7 (15H, m), and 8.10 (3H, t, J=7 Hz). Found: C, 69.05; H, 5.71; N, 13.28%. Calcd for $C_{24}H_{24}N_4O_3$: C, 69.21; H, 5.80; N, 13.45%. Benzamide (48 mg, 4%) was also obtained by elution with methanol on alumina. With 3 equiv of KF, yields of **2a**, **3a**, and benzamide were 127 mg (10%), 305 mg (22%), and 48 mg (4%), respectively.

References

1) a) K. Nishiyama and H. Karigomi, *Chem. Lett.*, **1982**, 1477; b) K. Nishiyama and N. Tanaka, *J. Chem. Soc., Chem. Commun.*, **1983**, 1322; c) K. Nishiyama and A. Watanabe, *Chem. Lett.*, **1984**, 455; d) idem, *ibid.*, **1984**, 773; e) K. Nishiyama, *Yuki Gosei Kagaku Kyokai Shi*, **43**, 176 (1985); f) K. Nishiyama and I. Miyata, *Bull. Chem. Soc. Jpn.*, **58**, 2419 (1985).

2) O. Tsuge, S. Kanemasa, and K. Matsuda, *Chem. Lett.*, **1983**, 1311.

3) O. Tsuge, S. Kanemasa, and K. Matsuda, *J. Org. Chem.*, **49**, 2688 (1984).

4) M. A. Gradsten and M. W. Polloch, *J. Am. Chem. Soc.*, **70**, 3079 (1948); W. D. Emmons, H. A. Rodewicz, W. N. Cannon, and R. M. Ross, *ibid.*, **74**, 5524 (1952).

5) E. E. Magat, B. F. Faris, J. E. Reith, and L. F. Salisbury, *J. Am. Chem. Soc.*, **73**, 1028 (1951).

6) O. O. Orazi and R. A. Corral, *J. Chem. Soc., Chem. Commun.*, **1976**, 470.

Palladium-catalyzed Displacement of Aryl Halide by Tin Analogue of Reformatsky Reagent

Masanori KOSUGI, Yoshikazu NEGISHI, Masayuki KAMEYAMA, and Toshihiko MIGITA*
Department of Chemistry, Faculty of Technology, Gunma University, Kiryu, Gunma 376
(Received May 28, 1985)

Synopsis. Reaction of ethyl α-(tributylstannyl)acetate with aryl bromides in the presence of zinc bromide or chloride and a catalytic amount of dichlorobis(tri-*o*-tolylphosphine)palladium was found to give ethyl arylacetates in good yields except with the aryl bromide having *p*-acetyl or *p*-nitro group.

Transition metal-catalyzed displacement of aryl halides by an enolate-like reagent giving a carbon–carbon bond is of recent interest.[1,2] We have reported the aromatic displacement by enolate-like tin reagents (α-stannyl ketone and/or stannyl enol ether) catalyzed by dichlorobis(tri-*o*-tolylphosphine)-palladium.[3] The nickel or palladium-catalyzed arylation[4] and alkenylation[5] of Reformatsky reagent have also been reported, but these reactions seem to have disadvantage in the low catalytic efficiencies and the limitation in a functional group exsisting in the aryl halide.

In this note, we report the displacement of aryl halides by organotin analogue of Reformatsky reagent in the presence of palladium complex.

$$n\text{-}Bu_3SnCH_2CO_2Et + ArX \xrightarrow{[Pd]} ArCH_2CO_2Et + n\text{-}Bu_3SnX$$

The reaction gave aryl acetate in moderate yields together with 1-arylbutane and biaryl which were formed through butyl transfer from the tin compound and homocoupling of the aryl bromides, respectively. Results are shown in Table 1. Similarly to the reaction of tin enolate, dichlorobis(tri-*o*-tolylphosphine)palladium was the best catalyst among the palladium complexes examined here. However, in contrast with the reaction of tin enolate,[3] proper solvents were polar aprotic ones, such as hexamethylphosphoric triamide (HMPA), *N*-methyl-2-pyrolidone (NMP), *N*,*N*-dimethylformamide (DMF), or dimethyl sulfoxide (DMSO). We chose DMF as a solvent, with which a relatively short reaction time was required.

As can be seen in Table 1, however, the yield was not particularly good, and sometimes was not reproducible. This is probably due to instability of α-stannyl acetate as well as α-stannyl ketone or stannyl enol ether under the reaction conditions. After many trials to overcome the difficulty, the addition of an equimolar amount of zinc bromide or chloride to the reaction system was found to enhance the yield of the product to almost quantitative, as shown in Table 2.

As Table 2 shows, zinc bromide or chloride was an especially effective additive, while other Lewis acids seem to deactivate the catalyst. Based on these results, the best reaction conditions were found to be as follows; a mixture of ethyl α-stannylacetate (1.3 mmol), bromobenzene (1.0 mmol), zinc bromide (1.3 mmol), $PdCl_2[P(o\text{-tolyl})_3]_2$ (0.01 mmol), and DMF (2 cm^3) was heated under argon at 80 °C for 5 h. Usual workup gave ethyl phenylacetate in 71% isolated yield. Table 3 shows the results with various aryl bromides.

The yield was greatly improved compared with

Table 1. Reaction of $Bu_3SnCH_2CO_2Et$ with PhBr in the presence of various palladium complexes[a]

Catalyst[b]	Solvent	Temp/°C	Time/h	Yield/%[c]		
				$PhCH_2CO_2Et$	PhBu	PhPh
None	HMPA	80	20	0		
A	HMPA	80	20	25	4	trace
B	HMPA	80	20	trace	4	8
C	HMPA	80	20	36	10	12
D	HMPA	80	20	59	21	8
D	HMPA	80	5	49		
D	DMSO	100	20	42		
D	NMP	80	5	65		
D	NMP	100	5	52		
D	DMF	80	5	67		
D	DMF	100	5	54		
D	PhH	80	20	25		
D	THF	80	20	34		

a) $Bu_3SnCH_2CO_2Et$ (1.1 mmol), PhBr (1.0 mmol), Catalyst (0.01 mmol), Solvent (0.5 cm^3). b) A; $Pd(PPh_3)_4$, B; $PdCl_2(PhCN)_2$, C; $PdCl_2(PPh_3)_2$, D; $PdCl_2[P(o\text{-tolyl})_3]_2$. c) GLC yield based on bromobenzene.

Table 2. Effect of additives

$$Bu_3SnCH_2CO_2Et + PhBr \xrightarrow[\text{in DMF } 80\,^\circ C,\ 5h.]{[Pd]^{a)}} PhCH_2CO_2Et + Bu_3SnBr$$

1.3 mmol, 1.0 mmol

Additive (1.3 mmol)	Yield of $PhCH_2CO_2Et$/%[b]
None	67
$ZnBr_2$	100
$ZnCl_2$	100
ZnF_2	53
$TiCl_4$	0
$SnCl_4$	0
$BF_3 \cdot OEt_2$	0

a) $PdCl_2[P(o\text{-tolyl})_3]_2$ (0.01 mmol). b) GLC yield based on bromobenzene.

Table 3. Reaction of $Bu_3SnCH_2CO_2Et$ with ArX

ArX	Isolated yield of $ArCH_2CO_2Et$/%
PhCl	0
PhBr	71
PhI	31*
p-MeC_6H_4Br	93
m-MeC_6H_4Br	60
o-MeC_6H_4Br	71
p-ClC_6H_4Br	89
o-ClC_6H_4Br	66
p-$MeOC_6H_4Br$	47
o-$MeOC_6H_4Br$	82
p-$MeCOC_6H_4Br$	22* mp 61 °C (lit,[4] 62—68 °C)
p-NCC_6H_4Br	67 mp 90 °C (lit,[4] 88 °C)
p-$O_2NC_6H_4Br$	34 mp 62 °C (lit,[4] 64 °C)

* GLC yield based on the halide.

that with Reformatsky reagent. In our case, the best substrate was bromide, and iodide which was a better substrate in Reformatsky reaction gave poor results, and chloride did not react at all. The reaction with aryl bromides having *p*-acetyl or *p*-nito group gave the product in low yields. These tendencies were also observed in other cross-coupling reactions, where the palladium catalyst having tri-*o*-tolylphosphine as a ligand was used.[3,6,7]

The mechanistic role of zinc salts which enhance the yields of the reaction products is not yet clear. The metal exchange between zinc salts and organotin producing Reformatsky reagent seems unlikely, considering the above difference in behaviors of iodobenzene and bromobenzene.

Experimental

IR spectra were recorded on Jasco A-100 spectrophotometer. ^1H NMR spectra were recorded on a Varian EM-360 instrument. GLC analyses were carried out with Ohkura 802 instrument, using columns (1.5 m) packed with 10% Silicone SF-96 and SE-30 on Celite 545.

Materials. Ethyl α-(tributylstannyl)acetate was prepared by the reaction of tributyltin ethoxide with ketene.[8] bp 117—119 °C/0.2 mmHg. (lit,[8] 150—152 °C/1.6 mmHg (1 mmHg=133.322 Pa)). Aryl bromides and palladium catalyst have already reported.[3]

Reaction Procedure. Zinc bromide (1.3 mmol) was placed in 10 cm^3 flask, and heated at 140 °C for 1 h under reduced pressure. Then, a mixture of ethyl α-(tributylstannyl)acetate (1.3 mmol), aryl bromide (1.0 mmol), $PdCl_2[P(o\text{-tolyl})_3]_2$ (0.01 mmol), and DMF (2 cm^3) was added into the flask, and heated under argon at 80 °C for 5 h. The reaction mixture was washed with water to remove the solvent, extracted with ether, and dried with anhydrous sodium sulfate. After column chromatography on silica gel, the product was isolated by distillation or crystallization.

Products. All the products were known and their structures were identified with IR and ^1H NMR spectra. Ethyl phenylacetate,[9,10a] ethyl *p*-methylphenylacetate,[10b] ethyl *m*-methylphenylacetate,[10c] ethyl *o*-methylphenylacetate,[10d] ethyl *p*-chlorophenylacetate,[10e] ethyl *o*-chlorophenylacetate,[10f] ethyl *p*-methoxyphenylacetate,[4,10g] ethyl *o*-methoxyphenylacetate,[10h] ethyl *p*-acetylphenylacetate,[4] ethyl *p*-cyanophenylacetate,[4] and ethyl *p*-nitrophenylacetate.[4]

The gift of tributyltin oxide by Kohriyama Kasei Co. is gratefully acknowledged.

References

1) M. F. Semmelhack, B. P. Chong, R. D. Stauffer, T. D. Rogerson, A. Chong, and R. D. Jones, *J. Am. Chem. Soc.*, **97**, 2507 (1975).

2) M. W. Rathke and A. A. Millard, *J. Am. Chem. Soc.*, **99**, 4833 (1977).

3) M. Kosugi, I. Hagiwara, T. Sumiya, and T. Migita, *Bull. Chem. Soc. Jpn.*, **57**, 242 (1984); I. Kuwajima and H. Urabe, *J. Am. Chem. Soc.*, **104**, 6831 (1982).

4) J. F. Fauvarque and A. Jutand, *J. Organomet. Chem.*, **177**, 273 (1979).

5) J. F. Fauvarque and A. Jutand, *J. Organomet. Chem.*, **209**, 109 (1981).

6) M. Kosugi, M. Kameyama, and T. Migita, *Chem. Lett.*, **1983**, 927.

7) M. Kosugi, M. Ishiguro, Y. Negishi, H. Sano, and T. Migita, *Chem. Lett.*, **1984**, 1511.

8) I. F. Lutsenko and S. V. Ponomarev, *Zh. Obsch. Khim.*, **31**, 2025 (1961); *Chem. Abst.*, **55**, 27024d (1961).

9) C. J. Pouchert, "The Aldrich Library of Infrared Spectra", 2nd ed., (1975).

10) J. G. Grasselli and W. M. Richey, "Atlas of Spectra Data and physical Constants for Organic Compounds." 2nd Ed., CRC Press. Inc. (1975). a; a583, b; a618, c; a617, d; a616, e; a354, f; a352, g; a524, h; a521.

Peterson Olefination of (α-Methoxybenzyl)silane with Aldehydes and Ketones Leading to Vinyl Ethers

Shuji KANEMASA, Junji TANAKA, Hideki NAGAHAMA, and Otohiko TSUGE*

Reserach Institute of Industrial Science, and Department of Molecular Science and Technology, Interdisciplinary Graduate School of Engineering Sciences, Kyushu University, Kasugakoen, Kasuga 816

(Received June 6, 1985)

Synopsis. (α-Methoxybenzyl)trimethylsilane is deprotonated with butyllithium and then allowed to react with a variety of carbonyl compounds giving vinyl ethers which are convertible into methyl ketones under mild conditions.

Although a variety of α-hetero-substituted organosilanes have been utilized in organic synthesis as an attracting member of isolable α-hetero organometallics, only limited applications of α-hydroxy or α-alkoxy alkylsilanes are known.[1] The present paper describes the vinyl ether synthesis using (α-methoxybenzyl)trimethylsilane **1** which is readily available through the 1,2-anionic rearrangement of silyl moiety of benzyl silyl ether.[2]

When the silane **1** was treated with a mixture of butyllithium and *N,N,N′,N′*-tetramethyl-1,2-ethanediamine (TMEDA) in dry THF at 0 °C, the solution immediately began to color and became deep red in 5 min. In this solution, the silyl-stabilized carbanion **2** was found to form in an excellent yield. Benzaldehyde **3a** was added and the mixture was allowed to stir at 0 °C and then at room temperature until all the silane **1** was consumed (checked on TLC). From the above procedure, 83% yield of **4a** was given as 7:2 mixture of E and Z isomers.

As shown in Scheme 1 and Table 1, the silyl-stabilized carbanion **2** was allowed to react with several carbonyl compounds. The reactions with aromatic aldehydes **3b—f**, heteroaromatic aldehydes **3g—h**, an α,β-unsaturated aldehyde **3i**, aliphatic aldehydes **3j—k**, and ketones **5a—d** gave the corresponding vinyl ethers in good yields as mixtures of E and Z isomers. Their structures were determined on the basis of the spectral data and elementary analyses.

Some of the vinyl ethers thus obtained were readily hydrolyzed under mild conditions. When the vinyl ethers **4** were heated in methanol in the presence of a catalytic amount of hydrochloric acid the correspond-

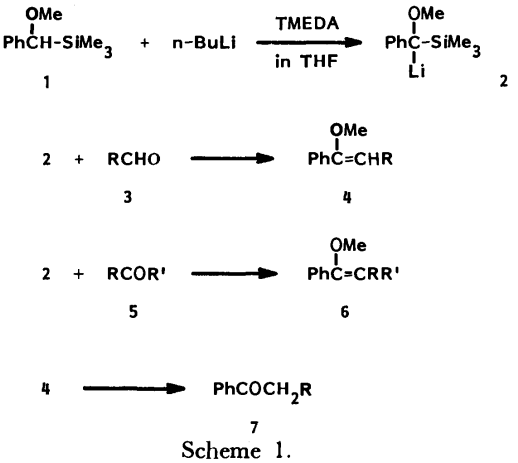

Scheme 1.

TABLE 1. PETERSON OLEFINATION OF (α-METHOXYBENZYL)TRIMETHYLSILANE **1**

Carbonyl compound	Reaction time/h[a]	Product		Yield[b] %	E/Z[c]	OMe[d] E	OMe[d] Z	=CH-[d] E	=CH-[d] Z	others[d]	C=C	M+ m/z
			R									
3a	5.5	**4a**	Ph	83	7/2	3.74	3.57	5.77	5.65		1630	210
3b	20	**4b**	*o*-MeC_6H_4	78	7/2	3.77	3.52	5.75	6.16	2.25E 2.32Z (*p*-Me)	1625	224
3c	19.5	**4c**	*m*-MeC_6H_4	83	7/2	3.72	3.57	5.76	6.05	2.16E 2.34Z (*m*-Me)	1630	224
3d	6.5	**4d**	*p*-MeC_6H_4	71	7/2	3.72	3.58	5.76	6.07	2.22E 2.32Z (*p*-Me)	1630	224
3e	20	**4e**	*o*-ClC_6H_4	68	1/1	3.76	3.51	5.85	6.39		1630	244, 246
3f	19.5	**4f**	*m*-ClC_6H_4	92	7/2	3.76	3.59	5.70	5.93		1630	244, 246
3g	15.5	**4g**	2-Furyl	65	3/1	3.71	3.62	5.69	6.20		1630	200
3h	16	**4h**	2-Thienyl	62	6/1	3.73	3.65	5.98	6.48		1630	216
3i	18	**4i**	PhCH=CH (t)	76	3/1	3.64	3.57	5.65[d]	6.06[d]		1625	236
3j	20	**4j**	*n*-Pr	70	1/1	3.60	3.50	4.71[t]	5.29[t]		1660	176
3k	20	**4k**	*i*-Pr	77	1/1	3.55	3.48	4.52[d]	5.12[d]		1650	176
3l	20.5	**4l**	*t*-Bu	76	3/2	3.52	3.39	4.79	5.04	0.92E 1.19Z (*t*-Bu)	1650	190
			R R′									
5a	6	**6a**	Ph Ph	70	—	3.36		—			1610	286
5b	5.5	**6b**	Ph Me	94	2/1	3.34	3.18	—		1.92E 2.14Z (Me)	1630	224
5c	6	**6c**	Et Et	79	—	3.18		—			1650	190
5d	13	**6d**	$(CH_2)_4$	60	—	3.39		—			1660	188

a) All the reactions were performed by using each 1.5 equivalent amounts of butyllithium, carbonyl compounds, and TMEDA in dry THF under nitrogen. In the beginning the reaction mixture was stirred at 0 °C for 1 h and then at room temperature for the time shown in Table. b) All isolated yields as mixtures of E and Z isomers. c) Determined by ^{1}H-NMR spectra. d) Measured in deuteriochloroform. All the signals appear as singlets otherwise cited. d: doublet; t: triplet.

Table 2. Hydrolysis of the vinyl ethers

Vinyl ether	Conditions[a]	Product	R	Yield/%[b]
4a	reflux in MeOH 3 h	**7a**	Ph	86
4f	reflux in MeOH 6 h	**7b**	*m*-ClC_6H_4	91
4i	reflux in MeOH 5 h	**7c**	PhCH=CH (t)	86[c]
	rt in HCOOH 5 h	**7c**		35
4l	reflux in MeOH 3 h	**7d**	*t*-Bu	78

a) The reaction in MeOH was carried out in the presence of a catalytic amount of HCl. b) All isolated yields. c) Containing 42% of 3-methoxy-1,4-diphenyl-1-butanone.

ing methyl ketones **7a—d** were given as shown in Scheme 1 and Table 2. A part of **7c** underwent the double bond migration into a conjugated ketone and the subsequent methanol addition gave 3-methoxy-1,4-diphenyl-1-butanone (42%).

Experimental

General Procedure for the Reaction of 1 with Carbonyl Compounds 3 and 5. To the solution of TMEDA (2.3 ml, 1.5 mmol) in dry THF (distilled over lithium aluminum hydride immediately before use, 2 ml) was added at 0 °C under nitrogen butyllithium (15% content in hexane, 0.94 ml, 1.5 mmol). After 5 min, the silane **1** (0.194 g, 1.5 mmol in 0.5 ml of THF) was added slowly by the use of a syringe, the color of solution turning deep red. After an additional 5 min at the same temperature, carbonyl compounds **3** or **5** (1.5 mmol for **3a—f, 3i, 5a—d**, and 2.0 mmol for **3g—h, 3j—l** in 1 ml of THF) were added dropwise. The resulting mixture was stirred at 0 °C under nitrogen for 1 h and then at room temperature for the time shown in Table 1. Aqueous ammonium chloride solution (**3—5** ml) was added and the mixture was extracted with ether (20 ml×2). The ether extracts were combined and washed with saturated sodium chloride three times, and finally dried over anhydrous magnesium sulfate. The residue obtained by evaporation of the ether *in vacuo* was chromatographed over silica gel using hexane-benzene (5:1) as an eluent giving viscous oil of vinyl ethers **4** and **6**. The yields, E/Z ratios, ^{1}H-NMR, IR, and mass spectral data are listed in Table 1. As the separation of the E and Z isomers by repeated column chromatography were unsuccessful, purified E/Z mixtures were submitted to elementary analyses.

Other data for the vinyl ethers **4** and **6** are as follows: **4a**: colorless oil (E/Z=7/2), Found: C, 85.49; H, 6.64%. Calcd for $C_{15}H_{14}O$: C, 85.68; H, 6.71%. **4b**: colorless oil (E/Z=7/2), Found: C, 85.83; H, 7.13%. Calcd for $C_{16}H_{16}O$: C, 85.68; H, 7.19%. **4c**: colorless oil (E/Z=7/2), Found: C, 85.62; H, 7.27%. Calcd for $C_{16}H_{16}O$: C, 85.68; H, 7.19%. **4d**: pale yellow oil (E/Z=7/2), Found: C, 85.55; H, 7.10%. Calcd for $C_{16}H_{16}O$: C, 85.68; H, 7.19%. **4e**: colorless oil (E/Z=1/1), Found: C, 73.75; H, 5.55%. Calcd for $C_{15}H_{13}OCl$: C, 73.62; H, 5.35%. **4f**: colorless oil (E/Z=7/2), Found: C, 73.82; H, 5.55%. Calcd for $C_{15}H_{13}OCl$: C, 73.62; H, 5.35%. **4g**: pale yellow oil (E/Z=3/1), ^{1}H-NMR ($CDCl_3$) δ=5.53, 6.72 (1H, 3:1, d, J=3.0 Hz, 3-H of furyl), 6.15, 6.43 ppm (1H, 3:1, m, 4-H of furyl), Found: *m/z* 200.0840. Calcd for $C_{13}H_{12}O_2$: M, 200.0837. **4h**: pale yellow oil (E/Z=6/1), Found: C, 72.06; H, 5.57%. Calcd for $C_{13}H_{12}OS$: C, 72.19; H, 5.59%. **4i**: pale yellow oil (E/Z=3/1), ^{1}H-NMR ($CDCl_3$) δ=5.65 (3/4H, d, J=9.0 Hz, C<u>H</u>=C(OMe)Ph of E isomer), 6.06 (1/4H, d, J=9.5 Hz, C<u>H</u>=C(OMe)Ph of Z isomer), 6.37 (3/4H, d, J=17.0 Hz, PhC<u>H</u>=CHCH= of E isomer), 6.50 (1/4H, d, J=17.5 Hz, PhC<u>H</u>=CHCH= of Z isomer), and 6.84 ppm (3/4H, dd, J=9.0 and 17.0 Hz, PhCH=C<u>H</u>CH= of E isomer). **4j**: colorless oil (E/Z=1/1), ^{1}H-NMR ($CDCl_3$) δ=0.89, 0.98 (each 3/2H, t, CH_3), 1.28—1.70 (2H, m, $CH_2C\underline{H}_2CH_3$), 2.07, 2.26 (each 2/2H, q, =CHC<u>H</u>$_2$-), 4.71 (1/2H, t, J=7.5 Hz, =C<u>H</u>CH_2 of E isomer), and 5.29 ppm (1/2H, t, J=8.0 Hz, =C<u>H</u>CH_2 of Z isomer), Found: *m/z* 176.1200. Calcd for $C_{12}H_{16}O$: M, 176.1207. **4k**: colorless oil (E/Z=1/1), ^{1}H-NMR ($CDCl_3$) δ=0.97, 1.06 (each 3/2H, d, $\underline{Me}_2CH$), 2.26 (1/2H, m, $Me_2C\underline{H}$ of E isomer), 3.20 (1/2H, m, $Me_2C\underline{H}$ of Z isomer), 4.52 (1/2H, d, J=9.5 Hz, =CH- of E isomer), and 5.12 ppm (1/2H, d, J=9.5 Hz, of Z isomer), Found: *m/z* 176.1202. Calcd for $C_{12}H_{16}O$: M, 176.1202. **4l**: the E and Z isomers were separated through the column chromatography over silica gel using hexane-benzene (5:1). *E*-**4l**: colorless oil, Found: *m/z* 190.1307. Calcd for $C_{13}H_{18}O$: M, 190.1357; *Z*-**4l**: colorless oil, Found: *m/z* 190.1352. Calcd for $C_{13}H_{18}O$: M, 190.1357. **6a**: colorless prisms from benzene-hexane, mp 110—111 °C, Found: C, 88.08; H, 6.34%. Calcd for $C_{12}H_{18}O$: C, 87.92; H, 6.31%. **6b**: colorless oil (E/Z=2/1), Found: C, 85.51; H, 7.11%. Calcd for $C_{16}H_{16}O$: C, 85.68; H, 7.19%. **6c**: colorless oil, ^{1}H-NMR ($CDCl_3$) δ=0.92, 1.03 (each 3H, t, $C\underline{H}_3CH_2$), 1.93, 2.23 (each 2H, q, $CH_3C\underline{H}_2$), and 7.18 ppm (5H, br.s, ArH), Found: *m/z* 190.1295. Calcd for $C_{13}H_{18}O$: M, 190.1357. **6d**: colorless oil, ^{1}H-NMR ($CDCl_3$) δ=1.55—1.90 and 2.20—2.70 ppm (each 4H, m, CH_2), Found: *m/z* 188.0830. Calcd for $C_{13}H_{16}O$: M, 188.1119.

General Procedure for the Hydrolysis of 4. The vinyl ether **4** was heated under reflux in methanol containing a catalytic amount of hydrochloric acid until **4** was completely consumed (checked on TLC). The methanol was evaporated *in vacuo*, the residue was treated with water, extracted with ether (twice), the ether was washed with aqueous sodium hydrogencarbonate, and dried over magnesium sulfate. The residue obtained by the removal of the ether *in vacuo* was chromatographed over silica gel using hexane-benzene (2:1) as an eluent. The reaction conditions and yields are listed in Table 2. All the methyl ketones **7** are known compounds, therefore their structures were confirmed by the comparison of melting points and/or spectral data with those of authentic samples. **7b**: colorless prisms; mp 43 °C;[3] IR (neat) 1690 cm^{-1}; ^{1}H-NMR ($CDCl_3$) δ=4.13 (2H, s, CH_2) and 6.98—7.55 ppm (9H, m, ArH); MS *m/z* 230, 232 (M^+) and 105 (base peak). **7c**: colorless prisms (benzene-hexane), mp 88—89 °C,[4] IR (KBr) 1660 cm^{-1}, ^{1}H-NMR ($CDCl_3$) δ=3.79 (2H, m, CH_2), 6.35 (2H, m, C<u>H</u>=C<u>H</u>), and 7.00—8.00 ppm (10H, m, ArH), MS *m/z* 222 (M^+) and 105 (base peak). **7d**: colorless oil,[5] IR (neat) 1660 cm^{-1}; ^{1}H-NMR ($CDCl_3$) δ=1.03 (9H, s, *t*-Bu), 2.79 (2H, s, CH_2), and 7.20—7.88 ppm (5H, m, ArH), MS *m/z* 176 (M^+) and 77 (base peak).

References

1) P. Magnus and G. Roy, *J. Chem. Soc., Chem. Commun.*, **1979**, 822; P. Magnus and G. Roy, *Organometallics*, **1**, 553 (1982); A. Murai, A. Abiko, N. Nishida, and T. Masamune, *Tetrahedron Lett.*, **25**, 4951 (1984); O. Tsuge, S. Kanemasa, H. Nagahama, and J. Tanaka *Chem. Lett.*, **1984**, 1803: S. Kanemasa, J. Tanaka, H. Nagahama, and O. Tsuge, *ibid.*, **1985**, 1223.

2) A. Wright and R. West, *J. Am. Chem. Soc.*, **96**, 3214 (1974).

3) A. Fischer, B. A. Grigor, J. Packer, and J. Vaughan, *J. Am. Chem. Soc.*, **83**, 4208 (1961).

4) H. Wieland and H. Stenzl, *Chem. Ber.*, **40**, 4803 (1907).

5) B. S. Kupin and A. A. Petrov, *Zh. Obshch. Khim.*, **31**, 2958 (1961).

Synthetic Studies on the Validamycins. XII. Synthesis of Optically Active Valienamine and Validatol

Seiichiro OGAWA,* Yasushi SHIBATA, Taisuke NOSE, and Tetsuo SUAMI
Department of Applied Chemistry, Faculty of Science and Technology, Keio University, Hiyoshi, Yokohama 223
(Received June 6, 1985)

Synopsis. (+)-Valienamine and (+)-validatol have been totally synthesized as the peracetyl derivatives starting from a common synthetic intermediate, (1*S*)-(1,3/2)-4-methylene-5-cyclohexene-1,2,3-triol.

Valienamine (**1a**) is an unsaturated branched-chain aminocyclitol found in the structural unit of the antibiotic validamycins[1] and several pseudo-oligosaccharidic α-glucosidase inhibitors.[2] Later, **1a** itself was shown to be an α-glucosidase inhibitor.[3] Hydrogenolysis of validamycin A produced validatol (**2a**), resulting from a reductive elimination of the imino group of the aminocyclitol part.[4]

We have reported the synthesis of the racemic forms of **1a**[5–7] and **2a**,[8] and Paulsen and Heiker have first synthesized the optically active **1a** starting from quebrachitol (L-2-*O*-methyl-*chiro*-inositol).[9]

We now describe a facile synthesis of the penta-*N*,*O*-acetyl derivative (**1b**) of **1a** from the optically active diene intermediate (**4**), following the route previously used for preparation of its racemate.[6,7] In addition, a new synthesis of the tetra-*O*-acetyl derivative (**2b**) of **2a** is reported.

Dehydrobromination of (1*R*)-(−)-1,2,3-tri-*O*-acetyl-(1,3/2,4,6)-4-bromo-6-bromomethyl-1,2,3-cyclohexanetriol (**3**)[10] with 1,8-diazabicyclo[5.4.0]undec-7-ene (DBU) in toluene afforded exclusively the diene (**4**), which was, without purification, treated with equimolar amount of *m*-chloroperbenzoic acid (MCPBA) in dichloromethane to oxidize the exomethylene group. A mixture of the products was fractionated by a silica-gel column to give the spiro oxiranes **5** (27%) and **6** (12%). Their structures were confirmed by comparison of the ^{1}H NMR spectra with those of the respective racemates.[6,7] Chlorination of **5** with concd hydrochloric acid in tetrahydrofuran (THF) followed by acetylation gave the chloride (**7**) in 92% yield. Treatment of **7** with sodium azide in *N*,*N*-dimethylformamide (DMF) at 60 °C gave selectively the azide (**8**) in a quantitative yield. Reduction of **8** with hydrogen sulfide followed by the conventional acetylation gave **1b**, mp 92.5—95 °C, $[\alpha]_D$ +20° ($CHCl_3$), in 94% yield. The ^{1}H NMR spectrum was superposable on that of an authentic sample.[1,5]

On the other hand, a new synthesis of **2b** was attempted by reduction of **7**. Direct hydrogenolysis of **7** in the presence of Raney nickel and a basic resin gave a complex mixture of products. Therefore, dechlorination was first carried out by treatment of **7** with lithium aluminum hydride (LAH) in THF, and then the product was hydrogenated in the presence of Raney nickel and successively acetylated to give **2b**, $[\alpha]_D$ −16° ($CHCl_3$), in 19% yield, together with tri-*O*-acetyldeoxyvalidatol[4,8] (**9**) (17%). Formation of **9** suggested that the initial dechlorination involved an attack of a hydride ion at C-6 giving an allyl alcohol (**10**). Hydrogenation of **4** with platinum oxide gave only **9** in 56% yield.

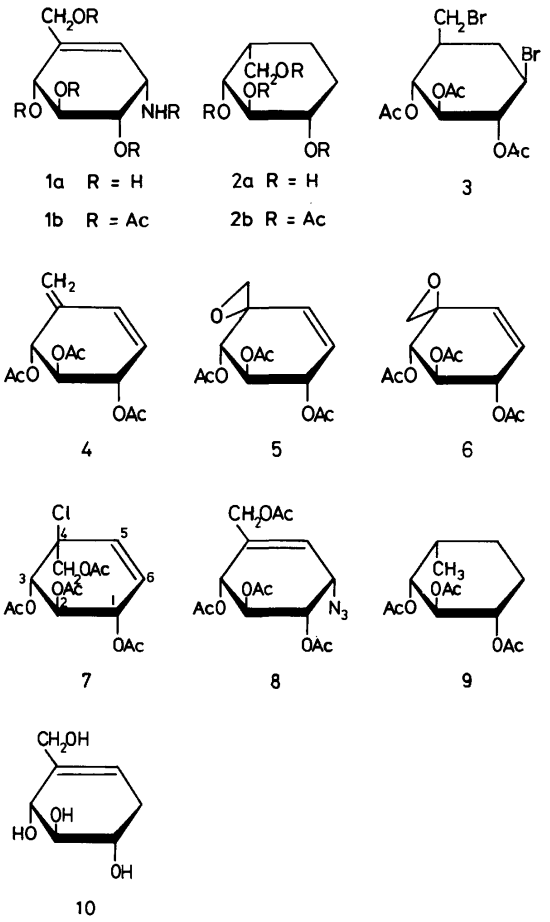

Experimental

Melting points were determined on a Büchi 510 capillary melting-point apparatus and are uncorrected. Optical rotations were measured on a Jasco DIP-4 polarimeter. The ^{1}H NMR spectra were recorded on a Varian EM-390 (90 MHz) spectrometer for solutions of chloroform-*d*. The silica gel used for column chromatography was Wakogel C-300 (Wako Co., Osaka). The structures of the optically active compounds synthesized were confirmed by comparison of the ^{1}H NMR spectra with those of the corresponding racemic modifications.

(2R)-(+)-2,3,4-Tri-O-acetyl-1,7-anhydro-(1,2,4/3)- (5) and (1,3/2,4)-1-C-Hydroxymethyl-5-cyclohexene-1,2,3,4-tetrol (6). Treatment of (1*R*)-(−)-1,2,3-tri-*O*-acetyl-(1,3/2,4,6)-4-bromo-6-bromomethyl-1,2,3-cyclohexanetriol[9] (**3**) (1.0 g, 2.3 mmol) with DBU in toluene similarly as described in the preparation of the racemate[8] gave a diene (**4**) (574 mg), which was, without isolation, subjected to an oxidation

with MCPBA in dichloromethane.[6,7] A crystalline mixture of the products (540 mg) was fractionated by a silica-gel column (18 g) with 1:10 2-butanone–toluene as an eluant to give 82 mg (12%) of **6** as plates (from ethanol): mp 114—115 °C; $[\alpha]_D^{24}$ +147° (*c* 1.03, $CHCl_3$). The second fraction gave 179 mg (27%) of **5** as plates (from ethanol): mp 102—103 °C; $[\alpha]_D^{22}$ +65° (*c* 1.0, $CHCl_3$).

Found for **5**: C, 54.78; H, 5.46%, and for **6**: C, 54.64; H, 5.73%. Calcd for $C_{13}H_{16}O_7$: C, 54.93; H, 5.67%.

(2S)-(+)-1,2,3-Tri-O-acetyl-(1,3/2,4)-4-C-acetoxymethyl-4-chloro-5-cyclohexene-1,2,3-triol (7). Treatment of **5** (119 mg, 0.42 mmol) with concd hydrochloric acid (0.044 ml) in THF (4.8 ml) similarly as described in the preparation of the racemate.[6,7] The product was crystallized from ethanol to give 141 mg (92%) of **7** as thin needles: mp 103.5—105 °C; $[\alpha]_D^{18}$ +60° (*c* 1.02, $CHCl_3$).

Found: C, 49.71; H, 5.48%. Calcd for $C_{15}H_{19}ClO_8$: C, 49.66; H, 5.28%.

(1S)-1,2,3-Tri-O-acetyl-(1,3,6/2)-4-acetoxymethyl-6-azido-4-cyclohexene-1,2,3-triol (8). The chloride (**7**) (67 mg, 0.18 mmol) was treated with sodium azide in DMF similarly as described in the preparation of the racemate[6,7] to give 68 mg (99%) of **8** as a syrup: $[\alpha]_D^{20}$ +40° (*c* 1.0, $CHCl_3$).

Found: C, 48.79: H, 5.25; N, 11.44%. Calcd for $C_{15}H_{19}N_3O_8$: C, 48.78; H, 5.19; N, 11.38%.

(1S)-1,2,3-Tri-O-acetyl-(1,3,6/2)-6-acetamido-4-acetoxymethyl-4-cyclohexene-1,2,3-triol [penta-N,O-acetyl-(+)-valienamine] (1b). The azide (**8**) (90 mg, 0.24 mmol) was reduced with hydrogen sulfide and then acetylated similarly as described in the preparation of the racemate[6,7] to give 88 mg (94%) of **1b** as needles (from ethanol–toluene): mp 92.5—95 °C; $[\alpha]_D^{21}$ +20° (*c* 1.04, $CHCl_3$) [lit.[1] mp 95 °C, $[\alpha]_D^{23}$ +30.2° ($CHCl_3$)].

Found: C, 53.27; H, 6.01; N, 3.42%. Calcd for $C_{17}H_{23}NO_9$: C, 52.98; H, 6.02; N, 3.63%.

(3R)-1,2,3-Tri-O-acetyl-(1,3,4/2)-4-acetoxymethyl-1,2,3-cyclohexanetriol [tetra-O-acetyl-(−)-validatol] (2b) and (3R)-1,2,3-Tri-O-acetyl-(1,3,4/2)-4-methyl-1,2,3-cyclohexanetriol [tri-O-acetyl-(−)-deoxyvalidatol] (9). A mixture of **7** (66 mg, 0.18 mmol), lithium aluminum hydride (42 mg), and THF (7.5 ml) was refluxed for 9 h. To a cooled mixture was added water (1.5 ml), and an insoluble material was removed by filtration and the filtrate was concentrated. The residue was treated with acetic anhydride (0.6 ml) and pyridine (0.6 ml) at room temperature overnight. The product was then hydrogenated in ethyl acetate (10 ml) in the presence of Raney nickel T-4[11] (0.5 ml) at room temperature overnight (initial hydrogen pressure of 3.4 kg cm^{-2}). The products were separated by a silica-gel column with 1:8 2-butanone-toluene to give first 8.7 mg (17%) of **9** as a syrup: $[\alpha]_D^{23}$ −7.9° (*c* 0.37, $CHCl_3$).

Found: C, 57.38; H, 7.13%. Calcd for $C_{13}H_{20}O_6$: C, 57.34; H, 7.40%.

The second fraction gave 12 mg (19%) of **2b** as a syrup: $[\alpha]_D^{25}$ −16° (*c* 0.52, $CHCl_3$).

Found: C, 54.84; H, 6.79%. Calcd for $C_{15}H_{22}O_8$: C, 54.54; H, 6.71%.

Catalytic Hydrogenation of 4. The crude **4** (139 mg) was hydrogenated in ethyl acetate (10 ml) in the presence of platinum oxide (10 mg) at room temperature overnight (initial hydrogen presure of 3.4 kg cm^{-2}). The product was purified by a silica-gel column with 1:10 2-butanone-toluene to give 91 mg (56%) of **9** as a syrup: $[\alpha]_D^{21}$ −8.6° (*c* 1.0, $CHCl_3$).

The authors wish to thank Mr. Saburo Nakada for his elemental analyses.

References

1) Y. Kameda and S. Horii, *J. Chem. Soc., Chem. Commun.*, **1972**, 746.
2) E. Truscheint, W. Frommer, B. Junge, L. Müller, D. D. Schmidt, and W. Wingender, *Angew. Chem.*, **93**, 738 (1981).
3) Y. Kameda, N. Asano, M. Yoshikawa, and K. Matsui, *J. Antibiot.*, **33**, 1575 (1980).
4) S. Horii, T. Iwasa, E. Mizuta, and Y. Kameda, *J. Antibiot.*, **24**, 59 (1971).
5) S. Ogawa, T. Toyokuni, and T. Suami, *Chem. Lett.*, **1980**, 713.
6) S. Ogawa, T. Toyokuni, Y. Iwasawa, Y. Abe, and T. Suami, *Chem. Lett.*, **1982**, 279.
7) T. Toyokuni, S. Ogawa, and T. Suami, *Bull. Chem. Soc. Jpn.*, **56**, 1161 (1983).
8) S. Ogawa, T. Toyokuni, M. Omata, N. Chida, and T. Suami, *Bull. Chem. Soc. Jpn.*, **53**, 455 (1980).
9) H. Paulsen and F. R. Heiker, *Angew. Chem., Int. Ed. Engl.*, **19**, 904 (1980); *Liebigs Ann. Chem.*, **1981**, 2180.
10) S. Ogawa, Y. Iwasawa, T. Nose, T. Suami, S. Ohba, M. Ito, and Y. Saito, *J. Chem. Soc., Perkin Trans. I*, **1985**, 903.
11) S. Nishimura, *Bull. Chem. Soc. Jpn.*, **32**, 61 (1959).

UV Photoelectron Spectra of Peralkylated Catenates of Group 4B Elements (Silicon, Germanium, and Tin)

Kunio MOCHIDA,* S. D. WORLEY,*,† and J. K. KOCHI*,††

Department of Chemistry, Faculty of Sciences, Gakushuin University, 1-5-1 Mejiro, Tokyo 171

†*Department of Chemistry, Auburn University, Alabama 36849, U.S.A*

††*Department of Chemistry, University of Houston, University Park, Houston, TX 77004, U.S.A*

(Received June 7, 1985)

Synopsis. The low-energy photoelectron spectra (PES) of twelve peralkylated catenates of group 4B elements (silicon, germanium, and tin) were recorded. The trends in the energies and the nature of the metal-metal and metal-carbon bonds are discussed.

In connection with predicting rates of the reactions and the products for processes involving electron transfer, UV photoelectron spectra (PES) of the organometals, particularly of group 4B metals, have received considerable attention.[1] These PES studies have mainly focussed on the metal-carbon,[2-8] metal-hydrogen,[9-15] and metal-halogen bonds[16-24] of the group 4B metals. However, there are a few reports on PES of the metal-metal bonds of the group 4B metals.[25-29] Compounds which contain metal-metal bonds have attracted increasing interest in comparison with those of carbon-carbon double bonds.[30,31] The carbon-carbon double bonds have, of course, already been very extensively studied by PES.[32] Here we present the PES of twelve peralkylated catenates of group 4B elements, $R_3M\text{-}M'R_3$ (R=Me, Et; M, M'=Si, Ge, Sn) to explain trends in the energies and the nature of metal-metal and metal-carbon bonds.

Results and Discussion

Although the PES of permethylated and perethylated catenates of group 4B elements (silicon, germanium, and tin) are slightly different from the spectrum of carbon analogue, 2,2,4-trimethylpentane,[28] these spectra show similar patterns, each exhibiting three bands of increasing intensity. The vertical ionization potentials corresponding to the highest three occupied orbitals are summarized in Table 1, together with the designated symmetry and the principal contributions to MO's.[28] The highest occupied molecular orbital (HOMO), which is of principal concern to us, is associated with ionization from M-M' σ bonding orbital (a_1), while the next two bands correspond to M-C and/or M'-C bonding orbitals (e).

Table 1. Ionization potentials (eV) of group 4B dimetals

Compound	M-M' (a_1)	C-M (e)	C-M' (e)
$Me_3SiSiMe_3$	8.68	10.23, 10.67	
$Me_3SiGeMe_3$	8.62	9.91	10.50
$Me_3GeGeMe_3$	8.60	9.87, 10.40	
$Me_3SiSnMe_3$	8.39	9.71	10.41
$Me_3GeSnMe_3$	8.36	9.65	10.09
$Me_3SnSnMe_3$	8.20	9.26, 9.62	
$Et_3SiSiEt_3$	8.39	9.40, 9.78	
$Et_3SiGeEt_3$[a]	8.24	b)	9.75
$Et_3GeGeEt_3$	8.33	9.14, 9.53	
$Et_3SiSnEt_3$	8.10	8.90	9.70
$Et_3GeSnEt_3$	8.05	8.79	9.29
$Et_3SnSnEt_3$	7.82	8.49, 8.87	

a) The PES resolution was rather poor due to the complexity of the compounds under study. b) This band was not resolved from leading edge of the 9.75 eV band.

The bands corresponding to M-M' σ bonding orbital ionization of a series of kindred catenates of group 4B elements will appear at lower ionization potentials than the bands corresponding to the interaction of this 4B atom with the methyl or ethyl group, since each group 4B atom studied has an ionization potential much lower than carbon. The first ionization potentials of a series of kindred catenates of group 4B elements shown in Table 1 are essentially the same as those of the parent metal (C, 11.26; Si, 8.15; Ge, 7.88; Sn, 7.34 eV),[33] indicating that electrons ionized are localized relatively at the M-M' bonds. The first ionization potential of a series of peralkylated catenates of group 4B elements decreases generally in order: Si-Si>Si-Ge>Ge-Ge>Si-Sn>Sn-Sn in accord with the M-M' ionic bond dissociation energy. The internal consistency of the data is illustrated in Fig. 1 by a comparison of the ionization potentials of the permethylated derivatives with the perethylated analogues.

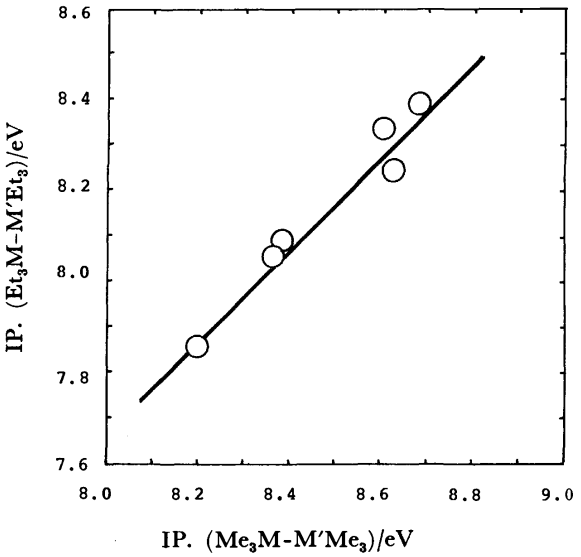

Fig. 1. First ionization potential of $Me_3M\text{-}M'Me_3$ *vs.* the first ionization potential of $Et_3M\text{-}M'Et_3$ (M, M' =Si, Ge, Sn).

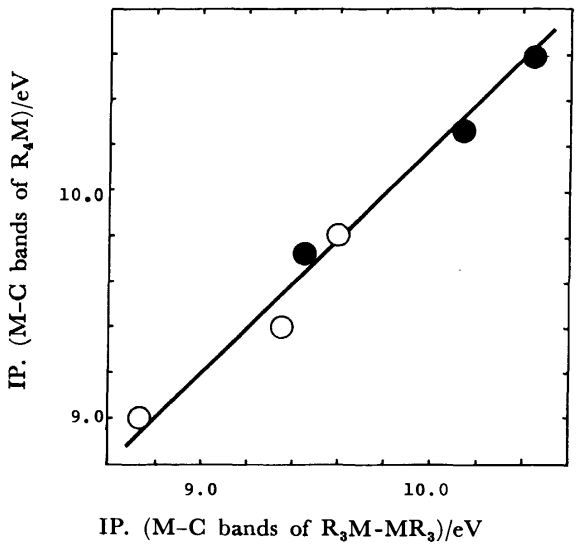

Fig. 2. The mean value of two bands of M-C bonding orbitals of R_3M–MR_3 *vs.* the first ionization potential of R_4M (M=Si, Ge, Sn); ●; permethylated derivatives, ○; perethylated derivatives.

Furthermore, the average of the next two bands corresponding to M-C bonding orbitals of kindred catenates of group 4B elements is close in energy and linearly related to the M-C σ bonding orbital (the HOMO) of R_4M (Si, 10.57, 9.8; Ge, 10.23, 9.4; Sn, 9.70, 9.0 eV for R=Me, Et).[2,15] The correlation of the average of bands corresponding to M-C bonding orbitals of kindred catenates of group 4B elements with M-C σ bonding orbitals (the HOMO) of R_4M is illustrated in Fig. 2. Figure 2 shows that interaction between the M-M bond and the M-C bond is weak.[25]

The ionization potentials of peralkylated catenates of group 4B elements in this study should provide interesting criteria for evaluating electron transfer processes involving catenates of group 4B elements.

Experimental

Peralkylated catenates of group 4B elements (silicon, germanium, and tin) and the photoelectron spectrometer used in these studies have been described previously.[34]

References

1) For example; J. K. Kochi, "Organometallic Mechanism and Catalysis," Academic Press, New York (1978), Part 3.
2) S. Evans, J. C. Green, P. J. Joachim, A. F. Orchard, D. W. Turner, and J. P. Maier, *J. Chem. Soc., Faraday Trans. 2*, **1972**, 905.
3) S. Cradock, E. A. V. Ebsworth, W. J. Savage, and R. A. Whiteford, *J. Chem. Soc., Faraday Trans. 2*, **68**, 934 (1972).
4) A. E. Jonas, G. K. Schweitzer, F. A. Grimm, and T. A. Carlson, *J. Electron Spectros.*, **1**, 29 (1972).
5) R. Boschi, M. F. Lappert, J. B. Pedley, W. Schmidt, and B. T. Wilkins, *J. Organomet. Chem.*, **50**, 69 (1973).
6) A. Schweig, U. Weidner, and G. Manual, *J. Organomet. Chem.*, **54**, 145 (1973).
7) A. Hosomi and T. G. Traylor, *J. Am. Chem. Soc.*, **97**, 3682 (1975).
8) C. L. Wong, K. Mochida, A. Gin, M. A. Weiner, and J. K. Kochi, *J. Org. Chem.*, **44**, 3979 (1979).
9) A. W. Potts and W. C. Price, *Proc. Roy. Soc., Ser. A*, **326**, 165 (1971).
10) W. B. Perry and W. L. Jolly, *Chem. Phys. Lett.*, **17**, 611 (1972).
11) S. Cradock and R. A. Whiteford, *J. Chem. Soc., Faraday Trans. 2*, **1972**, 281.
12) S. Cradock and R. A. Whiteford, *J. Chem. Soc., Faraday Trans. 2*, **1972**, 934.
13) L. Szepes, G. Náray-Szabó, F. P. Colonna, and G. Distefano, *J. Organomet. Chem.*, **117**, 141 (1976).
14) G. Distefano, S. Pignataro, L. Szepes, and J. Borossay, *J. Organomet. Chem.*, **104**, 173 (1976).
15) G. Beltram, T. P. Fehler, K. Mochida, and J. K. Kochi, *J. Electron Spectros.*, **18**, 153 (1980).
16) D. C. Frost, F. G. Herring, A. Katrib, R. A. N. McLean, J. E. Drake, and N. P. C. Westwood, *Can. J. Chem.*, **49**, 4033 (1971).
17) M. B. Hall, M. F. Guest, I. H. Hillier, D. R. Lloyd, A. F. Orchard, and A. W. Potts, *J. Electron Spectros.*, **1**, 497 (1973).
18) D. R. Lloyd and J. R. Robert, *J. Electron Spectros.*, **7**, 325 (1975).
19) C. Glidewell, *Inorg. Chim. Acta.*, **13**, L11 (1975).
20) A. Flamini, E. Semprini, F. Stefani, S. Sorriso, and G. Cardaci, *J. Chem. Soc., Dalton Trans*, **1976**, 731.
21) G. C. Stocco and A. F. Orchard, *Chim. Ind. (Milan)*, **59**, 122 (1977).
22) J. E. Drake, B. M. Glavincevski, and K. Gorzelska, *Can. J. Chem.*, **57**, 2278 (1979).
23) J. E. Drake, B. M. Glavincevski, and K. Gorzelska, *J. Electron Spectros.*, **17**, 73 (1979).
24) J. E. Drake, B. M. Glavincevski, and K. Gorzelska, *J. Electron Spectros.*, **16**, 331 (1979).
25) H. Bock and W. Ensslin, *Angew. Chem.*, **83**, 435 (1971).
26) C. G. Pitt, M. Bursey, and P. F. Rogerso, *J. Am. Chem. Soc.*, **92**, 519 (1970).
27) H. Bock, W. Ensslin, F. Feher, and R. Freund, *J. Am. Chem. Soc.*, **98**, 668 (1976).
28) L. Szepes, T. Korányi, G. Náray-Szabó, A. Modelli, and G. Distefano, *J. Organomet. Chem.*, **217**, 35 (1981).
29) H. Sakurai, M. Ichinose, M. Kira, and T. G. Traylor, *Chem. Lett.*, **1984**, 1383.
30) H. Sakurai, *Kagaku No Ryoiki*, **29**, 36 (1975).
31) R. West, "Comprehensive Organometallic Chemistry," ed by G. Wilkinson, F. G. A. Stone, and E. W. Abel, Pergamon Press (1982), Vol. 2, p. 365.
32) For example; D. W. Turner, C. Baker, A. D. Baker, and C. R. Brunde, "Molecular Photoelectron Spectroscopy," John Wiley & Sons, New York (1970).
33) C. E. Moore, National Bureau of Standards Circular 467, Vol. 3, U. S. Government Printing Office, Washington, D. C. (1958).
34) K. Mochida, A. Itani, M. Yokoyama, T. Tsuchiya, S. D. Worley, and J. K. Kochi, *Bull. Chem. Soc. Jpn*, **58**, 2149 (1985).

Cycloreversion Reaction of Cage Compounds Initiated by Aminium Cation Radical Salts[1)]

Eietsu HASEGAWA and Toshio MUKAI*
Department of Chemistry, Faculty of Science, Tohoku University, Sendai 980
(Received June 18, 1985)

Synopsis. Treating cage compounds **1** with triarylaminium cation radical salts, **3** and **4**, resulted in the effective conversion of **1** to dienes **2**. The cation radical isomerization induced by electron-transfer from **1** to aminium salt was suggested by the effect of substituent of **1** as well as by the effect of addition of electron donors as quenchers.

Since it was suggested that certain aminium cation radicals play a role of useful one-electron oxidation reagents, [2)] much attention has centered on the cation radical reactions initiated by the aminium cation radical salts.[3)] For instance, Bauld recently reported noticeable aspects of the cation radical pericyclic reactions induced by tris(*p*-bromophenyl)aminium cation radical salt.[4)] On the other hand, Gassman claimed that the aminium salt-catalyzed Diels-Alder reaction proceeds not only by the simple cation radical mechanism but involves the protic acid generation mechanism.[5)] This controversy has prompted us to examine the catalytic character of aminium cation radical salts. For this purpose, we chose cage compounds **1** as reaction substrates, because the cation radicals of **1** cleanly isomerize to those of dienes **2** without any side reactions, and because the electron-donating ability of **1** can be controlled by changing the substituent on the phenyl group.[6)]

Upon stirring a dichloromethane solution of bisphenylated cage compound **1a** and tris(*p*-bromophenyl)aminium hexachloroantimonate **3**[2)] for 1 min at room temperature, quantitative conversion of **1a** to the corresponding diene **2a** was observed, whereas a similar treatment with tris(*p*-methylphenyl)aminium hexachloroantimonate **4**[3i)] gave a lower conversion (22%). This finding can be rationalized in terms of the electron-donating property of neutral amines, **5** and **6**. Since the oxidation potential of **5** ($E_{1/2}^{ox}$=1.05 V)[7,8)] is higher than that of **6** ($E_{1/2}^{ox}$=0.75 V),[7,8)] the electron-transfer from **1a** to aminium cation radical salt **3** is certainly more favorable than that to **4**. The involvement of electron-transfer was furthermore confirmed by the substituent effect of **1** on the reaction with **4** (Table 1). The reactivity of **1a** was lower than those of **1b** and **1c** (see No. 1,2, and 4 in Table 1), while no isomerization was observed for **1d** under similar reaction conditions (No. 6). More facile transformation was observed for **1b** than for **1c** (No. 3 and 5). A correlation of the reactivities with the electron-donating abilities of cage compounds **1** (**1b**>**1c**>**1a**>**1d**) suggests that the reaction efficiency depends on an electron-transfer process from **1** to aminium salt in the first step of the reaction.

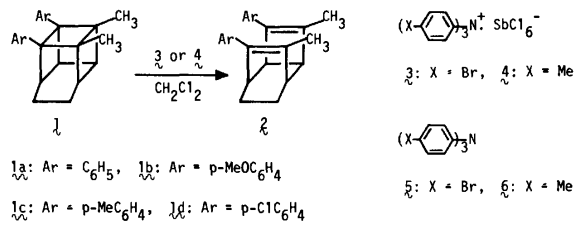

Scheme 1.

Quenching by electron donors is a useful technique for exploring electron-transfer reactions. Substituted benzenes such as 1,4-dimethoxybenzene ($E_{1/2}^{ox}$=1.34 V),[7,9)] 1,3,5-trimethoxybenzene ($E_{1/2}^{ox}$=1.49 V),[7,9)] and toluene ($E_{1/2}^{ox}$=1,98 V),[7,9)] which have oxidation potentials similar to or higher than **1a**, apparently did not quench the reaction of **1a** with **3**. However, 1,2,4,5-tetramethoxybenzene (TMB) effectively quenched the isomerization of **1a** to **2a** (conversion of **1a**=31%). When **3** was added to a dichloromethane solution of **1a** and TMB, the deep blue color of the solution immediately turned to yellow. On the other hand, **2a** was obtained in a similar yield (26%) when **1a** was added to a yellow solution of TMB and **3**. Since electron-transfer from TMB ($E_{1/2}^{ox}$=0.81 V)[7,9)] to **3** is more favorable than that from **1a**, the concentration of TMB cation radical must be even higher than that of the cation radical of **1a** at the initial reaction step. Therefore, **2a** would be mainely formed by an interaction of **1a** with initially formed TMB cation radical. The proposed reaction mechanism is summarized in Scheme 2.

TABLE 1. CYCLOREVERSION REACTION OF CAGE COMPOUNDS **1** BY tris(*p*-METHYLPHENYL)AMINIUM HEXACHLOROANTIMONATE **4**[a)]

No.	Cage(Ar)	$E_{1/2}^{ox}$ / V *vs.* SCE	10⁴×[**4**] / mol dm⁻³	Reac. time / min	Conversion[b)] / %
1	**1a**(C_6H_5)	1.41	2.80	1.0	22
2	**1b**(p-$MeOC_6H_4$)	1.09	2.80	1.0	100
3	**1b**	1.09	0.56	0.5	100
4	**1c**(p-MeC_6H_4)	1.28	2.80	1.0	100
5	**1c**	1.28	0.56	0.5	55
6	**1d**(p-ClC_6H_4)	1.49	2.80	1.0	0

a) [**1**]=2.37—2.42×10⁻² mol dm⁻³ in dichloromethane. b) Determined by ¹H NMR.

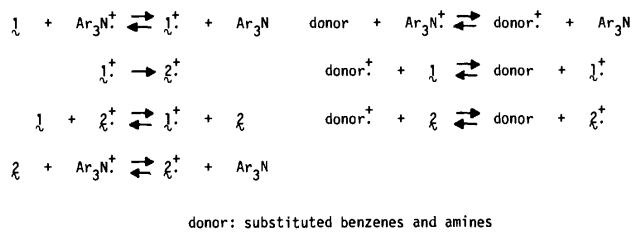

Scheme 2.

The aminium salt-catalyzed cycloreversion reaction of **1a** was relatively sensitive to addition of amine derivatives. For instance, addition of alkylamines such as 1,4-diazabicyclo[2.2.2]octane ($E_{1/2}^{ox}$=0.68 V),[7,9] triethylamine ($E_{1/2}^{ox}\simeq$1.0 V),[10] or diethylamine ($E_{1/2}^{ox}\simeq$1.3 V)[10] completely quenched the trans formation of **1a** to **2a**. By contrast, triphenylamine ($E_{1/2}^{ox}$=0.92 V)[7,8] did not quench the cycloreversion reaction of **1a**. These observations are consistent with the fact that alkylamine cation radicals are less stable than arylamine cation radicals.[11] In fact, although the deep blue color of **3** immediately disappeared upon adding the alkylamines to a dichloromethane solution of **3**, triphenylamine did not affect the color of the reaction solution. Therefore, triphenylamine cation radical possessing a relatively long lifetime would interact with **1a**,[3a] resulting in the formation of **2a** *via* cation radicals of **1a** and **2a**. Interestingly the reaction was quenched by pyridine (conversion of **1a**=21%), even though the electron-donating ability of pyridine ($E_{1/2}^{ox}\simeq$2.1 V)[10] is lower than that of toluene which did not quench the reaction. Since **3** was rapidly decolorlized by pyridine in the presence of **1a** but not in its absence, it appears that a direct interaction between **3** and pyridine is not important. A possible interpretation might be provided by assuming that pyridine interacts with the cation radicals of **1a** and **2a**, which are formed by reversible electron-transfer with **3**, to promote the conversion of amine cation radical to neutral amine.

On the other hand, although a protic acid-catalyzed the isomerization of **1a** to **2a**, the reaction efficiency was even lower than that of aminium salt initiated reaction ([**1a**]=2.11×10^{-2} mol dm^{-3}, [HBF_4]$\simeq$ 4×10^{-2} mol dm^{-3}, stirred for 15 min in mixed solvent: CH_2Cl_2/CH_3CN=3/1, conversion of **1a**=17%).

All these findings suggest that the electron-transfer of cage compounds **1** to the aminium cation radical salt initiates the cation-radical isomerization of **1** to dienes **2** which proceeds *via* a cation-radical chain mechanism.[6,12]

Experimental

Measurements and Materials. ^{1}H NMR (60 MHz) were measured on a Varian EM-360A Spectrometer, where CCl_4 containing TMS as an internal standard was used as a solvent. Cage compounds **1** were synthesized according to the literature.[13] Aminium salts were prepared by the reported method.[2,3i]

Aminium Salt-catalyzed Reaction of Cage Compounds 1. The following is a general procedure. To a dichloromethane solution of cage compound **1** (3 ml), aminium salt dissolved in dichloromethane (1 ml) was added ([**1**]=2.32—2.45×10^{-2} mol dm^{-3}, [aminium salt]= 2.80×10^{-4} mol dm^{-3}). After stirring at room temperature, the reaction was quenched by addition of CH_3ONa (28% in methanol: commercial grade). To the reaction solution, 4 ml of dichloromethane and 10 ml of water were added, and then the organic layer was washed with water. Solvent was evaporated after drying (Na_2SO_4). The conversion of **1** was measured by ^{1}H NMR.

The experiments for the effects of additives were carried out under the same conditions as above ([additive]= 2.26—2.47×10^{-2} mol dm^{-3}).

References

1) Organic Thermal Reactions 63. Part 62: T. Miyashi, Y. Nishizawa, Y. Fujii, K. Yamakawa, M. Kamata, S. Akao, and T. Mukai, submitted to *J. Am. Chem. Soc.*

2) F. A. Bell, A. Ledwith, and D. C. Sherrington, *J. Chem. Soc., (C)*, **1969**, 2719.

3) a) A. Ledwith, *Acc. Chem. Res.*, **5**, 133 (1972); b) P. Beresford, M. C. Lambert, and A. Ledwith, *J. Chem. Soc., (C)*, **1970**, 2508; c) R. W. Hoffman, and W. Burth, *J. Chem. Soc., Chem. Commun.*, **1983**, 345; d) W. Schmidt and E. Steckhan, *Angew. Chem., Int. Ed. Engl.*, **17**, 673 (1978); **18**, 801 (1979); e) F. Ciminale and L. Lopez, *Tetrahedron Lett.*, **26**, 789 (1985); f) C. Jones, *J. Org. Chem.*, **46**, 3370 (1981); g) I. Ahmad, D. Bethell, and V. D. Parker, *J. Chem. Soc., Perkin Trans. 2*, **1984**, 1572; h) C. B. Little and G. B. Schuster, *J. Am. Chem. Soc.*, **106**, 7167 (1984); i) D. H. R. Barton, R. K. Haynes, G. Leclerc, P. D. Magnus, and I. D. Menzies, *J. Chem. Soc., Perkin Trans. 1*, **1975**, 2055; j) S. F. Nelsen and R. Akaba, *J. Am. Chem. Soc.*, **103**, 2096 (1981).

4) a) D. J. Bellville, D. D. Wirth, and N. L. Bauld, *J. Am. Chem. Soc.*, **103**, 718 (1981); b) D. J. Bellville and N. L. Bauld, *ibid.*, **104**, 2665 (1982); c) R. A. Pabon, D. J. Bellville, and N. L. Bauld, *ibid.*, **105**, 5158 (1983); d) N. L. Bauld and R. A. Pabon, *ibid.*, **105**, 633 (1983); e) R. A. Pabon, D. J. Bellville, and N. L. Bauld, *ibid.*, **106**, 2730 (1984).

5) P. G. Gassman and D. A. Singleton, *J. Am. Chem. Soc.*, **106**, 6085 (1984); **106**, 7993 (1984).

6) a) K. Okada, K. Hisamitsu, and T. Mukai, *J. Chem. Soc., Chem. Commun.*, **1980**, 941; b) T. Mukai, K. Sato, and Y. Yamashita, *J. Am. Chem. Soc.*, **103**, 670 (1981); c) K. Okada, K. Hisamitsu, and T. Mukai, *Tetrahedron Lett.*, **22**, 1251 (1981); d) K. Okada, K. Hisamitsu, T. Miyashi, and T. Mukai, *J. Chem. Soc., Chem. Commun.*, **1982**, 974; e) Y. Takahashi, K. Sato, T. Miyashi, and T. Mukai, *Chem. Lett.*, **1984**, 1553.

7) All potentials given in the text are referenced to the SCE electrode.

8) R. F. Nelson and R. N. Adams, *J. Am. Chem. Soc.*, **90**, 3925 (1968).

9) C. K. Mann and K. K. Barns, "Electrochemical Reactions in Nonaqueous Systems," Marcel Dekker, New York, 1970.

10) The reported data of $E_{1/2}^{ox}$(V *vs.* Ag/Ag$^+$)[9] were corrected to the SCE electrode by using the equation: $E_{1/2}^{ox}$(V *vs.* SCE)$\simeq E_{1/2}^{ox}$(V *vs.* Ag/Ag$^+$)+0.3.[9]

11) a) Y. L. Chow, W. C. Danen, S. F. Nelsen, and D. H. Rosenblatt, *Chem. Rev.*, **78**, 243 (1978); b) R. I. Walter, *J. Am. Chem. Soc.*, **77**, 5999 (1955); c) L. Hagopian, G. Köhler, and R. I. Walter, *J. Phys. Chem.*, **71**, 2290 (1967).

12) Gassman suggested that the protic acid could originate from loss of protons from cation-radical intermedites in certain cases of Diels-Alder reactions initiated by aminium salt.[5] Although the effect of amines may remind us of the protic acid generation, it would be unnecessary to adopt the acid-catalyzed mechanism in our case since the proton generation from the cation radicals of **1** or **2**[14] would be impossible.

13) T. Mukai and Y. Yamashita, *Tetrahedron Lett.*, **1978**, 357.

14) H. D. Roth, M. L. M. Schilling, T. Miyashi, and T. Mukai, *Tetrahedron Lett.*, **24**, 5815 (1983).

Synthesis of Alkyl Dihydrogenphosphate by the Reaction of Alcohols and Silyl Polyphosphate

Yoshiki OKAMOTO

The Institute of Scientific and Industrial Research, Osaka University, 8-1, Mihogaoka, Ibaraki, Osaka 567

(Received June 27, 1985)

Synopsis. Alkyl dihydrogenphosphates were readily prepared by phosphorylation of alcohols with trimethylsilyl polyphosphate or polyphosphorylated silica-gel.

Various methods have been reported for phosphorylation of alcohols.[1] However, there are a few methods which are well suited to preparation of alkyl dihydrogenphosphate (**1**) for industrial use.[2] The cheapest and convenient method is the phosphorylation with powdery diphosphorus pentaoxide (Eq. 1),

$$3ROH + 1/2P_4O_{10} \longrightarrow \underset{\mathbf{1}}{(RO)P(O)(OH)_2} + \underset{\mathbf{2}}{(RO)_2P(O)OH} \quad (1)$$

which has been widely used for industrial production of surfactants of **1**.[3] But, this reaction was always accompanied by the formation of considerable amounts (16—20%) of dialkyl hydrogenphosphate (**2**). Furthermore, vigorous stirring and careful control of the temperature are required, because the reaction is heterogeneous and much exothermic.

In this report, a new selective synthetic method of **1** by phosphorylation of alcohols with trimethylsilyl polyphosphate (**3**) is described. Trimethylsily polyphosphate (**3**) is readily prepared by refluxing the benzene solution of diphosphorus pentaoxide and hexamethyldisiloxane.[4,5] Alcohol reacts smoothly with **3** to give alkyl trimethylsilyl hydrogenphosphate (**4**), which is easily hydrolyzed with water into **1** (Eq. 2). For the purpose of synthesis of **1**, the trimethylsilyl polyphosphate (**3**),

$$n\mathrm{ROH} + \underset{\mathbf{3}}{\left[\begin{array}{c}O\\ \|\\ -O-P-O-\\ |\\ OSiMe_3\end{array}\right]_n} \longrightarrow \underset{\mathbf{4}}{n\mathrm{RO}-\overset{O}{\overset{\|}{P}}-OH} \xrightarrow{H_2O} \underset{\mathbf{1}}{n\mathrm{RO}-\overset{O}{\overset{\|}{P}}-OH} + n/2Me_3SiOSiMe_3 \quad (2)$$
$$\quad\quad\quad

Table 2. Preparation of several alkyl dihydrogenphosphates (**1a—h**) by the reaction of trimethylsilyl polyphosphate (**3**)[a]

Compd. No.	ROH	Yield %	Mp θ_m/°C	Lit, Mp(θ_m/°C)
1a	$CH_3(CH_2)_6CH_2OH$	76	129—130[b]	129—130[6]
1b	$CH_3(CH_2)_8CH_2OH$	73	45—47	45—46[7]
1c	$CH_3(CH_2)_{10}CH_2OH$	72	54—56[d]	—
1d	$CH_3(CH_2)_{12}CH_2OH$	75	67—69	66—68[2]
1e	$CH_3(CH_2)_{14}CH_2OH$	76	75—77	74—75[8]
1f	$C_6H_5CH_2OH$	61	152—154[c]	150—153[6]
1g	Borneol	65	195—197[b]	194—196[6]
1h	Cholesterol	82	185—187	186—188[9]

a) With trimethylsilyl polyphosphate(**3**) prepared from P_4O_{10} 7.1 g (25 mmol) and $Me_3SiOSiMe_3$ 16.2 g (100 mmol), alcohol (100 mmol) was phosphorylated in benzene (100 mmol) at the refluxing temperature for 2 h. b) Monoanilinium salts. c) Dianilinium salt. d) Elemental analysis, Found: C, 54.40; H, 10.42; P, 11.33%. Calcd for $C_{12}H_{27}O_4P$: C, 54.12; H, 10.22; P, 11.63%.

Table 3. Results of phosphorylation of 1-decanol with polyphosphorylated silica-gel (**5**)[a]

Polyphosphorylated silica-gel (**5**) Reagent ratio (weight ratio) P_4O_{10}/Silica-gel	Yields of phosphates/%	
	$C_{12}H_{21}OP(O)(OH)_2$(**1b**)	$(C_{12}H_{21}O)_2P(O)OH$(**2b**)
1/8	52	2
1/5	58	4.5
1/2	64	9
Without silica-gel	69	18

a) With polyphosphorylated silica-gel (**5**) prepared from P_2O_{10} 7.1 g (25 mmol) and prescribed amounts of silica-gel, 1-decanol 15.8 g (100 mmol) was phosphorylated in benzene (100 ml) at the refluxing temperature for 4 h.

combined alkaline extacts were acidified with 60 ml of 10% hydrochloric acid solution, and again extacted three times with 100 ml of ether. The ethereal solution was dried (Na_2SO_4), and evaporation of the ether gave 17.0 g of colorless crystalline product (76% yield) in an almost pure state. However, the product **1a**, **f**, and **g**, which did not crystalize, were characterized as anilinium salts. The **1/2** ratios of these products were determined by elemental analysis or alkalimetry.[10]

Typical Procedure 2: Reaction With Polyphosphorylated Silica-gel (5). The mixture of dry silica-gel (20 g, Kieselgel 60, 70—230 mesh, Merck for chromatography, calcinated at 900 °C for 4 h), diphosphorus pentaoxide (7.1 g, 25 mmol), and 100 ml of benzene was stirred at refluxing temperature for 3 h. 1-Decanol (15.8 g, 100 mmol) was added to the mixture and it was stirred at the same temperature for 4 h. After the reaction, the solvent was removed off, and 100 ml of water was added into the residue to hydrolyze the silyl phosphate. The mixture was filtered, and the silica-gel was washed twice with 100 ml of ether. The combined ether solutions were extracted three times with 20 ml of 5% sodium hydroxide solution. The combined alkaline extracts were acidified with 60 ml of 1 mol dm^3 hydrochloric acid solution, and again extracted three times with 100 ml of ether. The ethereal solution was dried and evaporation of the ether gave a mixture of decyl dihydrogenphosphate (**1b**) and didecyl hydrogenphosphate (**2b**) in 58% and 4.5% yields, respectively.

References

1) K. Sasse, "Organische Phosphorverbindungen Teil 2," in "Methoden der Organischen Chemie, Band XII/2" ed by E. Müller, Georg Thieme Verlag, Stuttgart (1967) p. 145; B. Gallenkamp, W. Hofe, B.-W. Kruger, F. Maurer, and T. Pfister, "Organische Phosphorverbindungen II," in "Methoden der Organischen Chemie," ed by M. Regitz, Georg Thieme Verlag, Stuttgart (1982), p. 485; E. Cherbuliez, "Organic Phosphorus Compounds Vol 6, Chap 15, Organic Derivatives of Phosphoric Acid," ed by G. M. Kosolapoff and L. Maier, Wiley Interscience, New York (1973), p. 211; L. A. Slotin, *Synthesis*, **1977**, 737.

2) A. K. Nelson and A. D. Toy, *Inorg. Chem.*, **2**, 775 (1963); G. Imokawa, H. Tsutsumi, and T. Kurosaki, *J. Am. Oil Chemists' Soc.*, **55**, 389 (1978).

3) E. Cherbuliez and H. Weniger, *Helv. Chim. Acta*, **28**, 1584 (1945); **29**, 2006 (1946).

4) T. Imamoto, H. Yokoyama, and M. Yokoyama, *Tetrahedron Lett.*, **22**, 183 (1981).

5) The composition of **3** was recently disclosed on the base of ^{31}P NMR measurement; K. Yamamoto and H. Watanabe, *Chem. Lett.*, **1982**, 1225.

6) T. Obata and T. Mukaiyama, *J. Org. Chem.*, **32**, 1063 (1967).

7) A. K. Nelson and A. D. F. Toy, U. S. patent, 3, 146, 255 (1964).

8) H. N. Christensen, *J. Biol. Chem.* **132**, 399 (1940).

9) F. Ramirez, J. F. Marecek, and S. S. Yemul, *J. Org. Chem.*, **48**, 1417 (1983).

10) K. Onoda and K. Hamada, *Yukagaku*, **7**, 426 (1967).

Chemistry of *N*-Nitrososulfonamides. Substitution Reaction by the Acetyl Group

Masaaki IWATA* and Hiroyoshi KUZUHARA
Riken (The Institute of Physical and Chemical Research), Wako, Saitama 351-01
(Received April 1, 1985)

Synopsis. The *N*-nitroso group on *N*-nitrososulfonamides was substituted for the acetyl group in chloroform to give *N*-acetylsulfonamides in moderate yields.

We started the present research in order to understand fundamental chemical properties of sulfonamides. From attempts to survey the reactivity of the sulfonamide group, we found a new substitution reaction of the *N*-nitroso derivatives for an acetyl group without a base.

Nitrosation of sulfonamide was performed in quantitative yield by use of a modified procedure using a sodium nitrite-acetic anhydride-acetic acid mixture.[1-3] Thus, α,ω-bis(*N*-nitrososulfonamide)s, **2a—c**, were prepared from the corresponding sulfonamides **1a—c**. The nitroso group could be removed by either light, protic solvents, radical initiator such as AIBN, or L-ascorbic acid to regenerate the corresponding sulfonamides.

It was predicted that acid anhydride and *N*-nitrososulfonamide can be disposed to take a six-membered cyclic transition state advantageous for the lowered activation energy upon a substitution reaction through an intermediate (**5**). When a suspended mixture of **2a**, acetic anhydride, and chloroform was refluxed, **3a** (diacetyl sulfonamide) and **4a** (monoacetyl sulfonamide) were obtained in 54 and 13% yields, respectively. In the same way, **2b** and **2c** gave the corresponding diacetyl sulfonamides, **3b** and **3c**, in 38 and 29% yields, respectively. Usual acetylation of **1a** employing acetic anhydride and pyridine afforded neither mono- nor diacetyl sulfonamide. In addition, more drastic acetylation using acetyl chloride unsatisfactorily gave **3c** and **4c**. These results indicate that the acetyl substitution reaction of *N*-nitrososulfonamides effectively proceeds through such a transition state **5** as predicted.

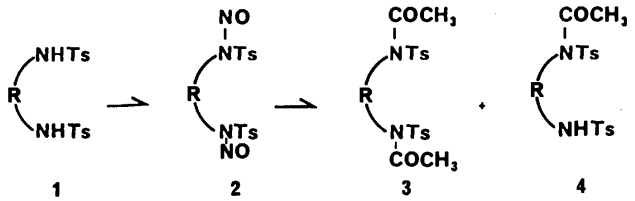

1 2 3 4

a R = $-CH_2-C_6H_4-CH_2-$

b R = $-(CH_2)_6-$

c R = $-(CH_2)_2-$

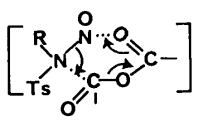

5

IR and ^{1}H-NMR spectral data suggested the stronger electrophilic nature of the acetyl group on *N*-acetylsulfonamides than those in usual acetates and acetamides. When a mixture of **3a** and anhydrous potassium carbonate in a mixed solvent of methanol-water was refluxed,[4] **1a** was obtained in quantitative yield.

The net cycle of introduction-removal of the *N*-acetyl group regarding sulfonamides will become a possible route to utilize the *N*-acetyl group as a protecting group for a variety of synthetic purpose.

Experimental

^{1}H-NMR spectra were recorded on a JEOL JNM GX-400 (400 MHz) spectrometer with Me_4Si as the internal standard in $CDCl_3$; chemical shifts (δ) and coupling constants (J) are in parts per million and Herz, respectively. Infrared spectra (IR) was obtained on a Shimadzu IR-27G spectrophotometer. Electronic absorption spectra (UV) were recorded on a Hitachi 124 spectrophotometer. Mass spectra (MS; rel. intensity) were recorded with a Hitachi RMU-6MG spectrometer by using an ionizing potential at 20 eV. Merck silica-gel 60 (Art. 7734, 0.063—0.20) was used for column chromatography and Merck precoated silica-gel 60 F_{254} plates (Art. 5715, 20×20) were used for thin-layer chromatography (TLC). The solvent system employed for column chromatography and TLC was benzene-ethyl acetate (10:1 v/v) and R_f values are referred to this solvent system, unless otherwise noted. α,ω-Disulfonamides (**1**) were prepared by the previously described method.[5] Elemental analyses were performed at Riken. The uncorrected melting points were measured with a micro melting-point apparatus (Yanagimoto Seisakusho).

N-Nitrosation of Sulfonamides. Optimal *N*-nitrosation was achieved by the following modified method of that described by de Boer *et al.*[2b] To a suspended mixture of sulfonamide (**1**) (1 g), acetic anhydride (10 ml), and acetic acid (2 ml), was added sodium nitrite (2 mol eq to **1**) portion by portion at *ca.* 10 °C, while rapidly stirred. After stirring for 30 min at room temperature, water (30 ml) was added to quench the reaction. The mixture was stirred for 30 min at *ca.* 10 °C. Crystalline α,ω-bis(*N*-nitrososulfonamide)s (**2**) were collected by filtration and washed well with water. This pale-yellow crystalline solid was pure enough.

2a: (90% yield) mp 131—133 °C. Calcd for $C_{22}H_{22}N_4S_2O_6$: C, 52.58; H, 4.41; N, 11.15; S, 12.76%. Found: C, 52.36; H, 4.40; N, 10.91; S, 12.72%. IR (KBr) 1510(N=O), and 1380 and 1170(SO_2) cm^{-1}. R_f 0.75.

2b: (99% yield) mp 86—88 °C. Calcd for $C_{20}H_{26}N_4S_2O_6$: C, 49.78; H, 5.43; N, 11.61; S, 13.29%. Found: C, 50.26; H,

5.49; N, 10.77; S, 13.33%. IR (KBr) 1510(N=O), and 1375 and 1169(SO_2) cm^{-1}. R_f 0.75.

2c: (99% yield) mp 120 °C (decomp). Calcd for $C_{16}H_{18}N_4S_2O_6$: C, 45.06; H, 4.25; N, 13.14; S, 15.04%. Found: C, 45.34; H, 4.26; N, 12.96; S, 14.88%. IR (KBr) 1516(N=O), and 1384, 1188, 1174, and 1155(SO_2) cm^{-1}. R_f 0.75.

Reaction of N-Nitrososulfonamides with Acetic Anhydride in Chloroform. When a suspended mixture of *N*-nitrososulfonamide (**2**) (1 g), acetic anhydride (1 ml) and chloroform (20 ml) was refluxed, the suspension disappeared in 10 min. The reaction was monitored by tlc till no more change was observed (15—30 h). After cooling, the reaction mixture was evaporated and the residue was chromatographed on a silica-gel column. Thus **2a** gave *N,N'*-diacetyl-*N,N'*-ditosyl-α,α'-*p*-xylenediamine (**3a**) in 54% yield and *N*-acetyl-*N,N'*-ditosyl-α,α'-*p*-xylenediamine (**4a**) in 13% yield.

Recrystallization of **3a** from diethyl ether gave colorless crystals; mp 178—180 °C. Calcd for $C_{26}H_{28}N_2S_2O_6$: C, 59.07; H, 5.34; N, 5.30; S, 12.13%. Found: C, 59.06; H, 5.36; N, 5.10; S, 12.10%. IR (KBr) 1700(C=O), and 1350 and 1160(SO_2) cm^{-1}. ^{1}H-NMR; 2.31 ($COCH_3$), 2.43 (CH_3), and 5.07 (CH_2). MS; *m/z* 444 (0.4%), 374 (100%), and 332 (38%).

Recrystallization of **4a** from diethyl ether gave colorless crystals; mp 142—143 °C. Calcd for $C_{24}H_{26}N_2S_2O_5$: C, 59.24; H, 5.39; N, 5.76; S, 13.18%. Found: C, 59.27; H, 5.45; N, 5.58; S, 12.96%. IR (KBr) 3280(NH), 1700(C=O), and 1358, 1318, 1163, and 1148(SO_2) cm^{-1}. ^{1}H-NMR; 2.28 ($COCH_3$), 2.44 and 2.45 (CH_3), 4.11 (J=6.11, CH_2), 4.62 (J=6.11, NH), and 5.02 (CH_2). MS; *m/z* 445 (0.9%), 332 (87%), 290 (100%).

N,N'-Diacetyl-*N,N'*-ditosyl-1,6-hexanediamine (**3b**) was obtained from **2b** in 29% yield (R_f 0.5, benzene-ethyl acetate 4:1 v/v), accompanied by two other unidentified products at R_f 0.8 and 0.66. Recrystallization of **3b** from acetone-diethyl ether gave colorless crystals; mp 155—157 °C. Calcd for $C_{24}H_{32}N_2S_2O_6$: C, 56.67; H, 6.34; N, 5.51; S, 12.61%. Found: C, 56.70; H, 6.36; N, 5.33; S, 12.50%. IR (KBr) 1700(C=O), and 1360 and 1158(SO_2) cm^{-1}. ^{1}H-NMR; 1.37 (CH_2), 1.71 (CH_2), 2.32 ($COCH_3$), 2.45 (CH_3), 3.76 (J=7.56, NCH_2). MS; *m/z* 337 (100%), 296 (30%), and 254 (42%).

N,N'-Diacetyl-*N,N'*-ditosyl-1,2-ethanediamine (**3c**) was obtained from **2c** in 38% yield (R_f 0.58, benzene-ethyl acetate 4:1 v/v), accompanied by an unidentified product at R_f 0.77. Recrystallization of **3c** from benzene gave colorless fine needles; mp 215—216 °C. Calcd for $C_{20}H_{24}N_2S_2O_6$: C, 53.08; H, 5.35; N, 6.19; S, 14.17%. Found: C, 53.02; H, 5.33; N, 6.16; S, 14.02%. IR (KBr) 1700(C=O), and 1340 and 1170(SO_2) cm^{-1}. ^{1}H-NMR; 2.43 ($COCH_3$), 2.45 (CH_3), and 4.01 (NCH_2). MS; *m/z* 240 (27%), 226 (4.2%), and 184 (100%).

Reaction of Sulfonamide (1c) with Acetyl Chloride. To a suspended mixture of 0.5 g of **1c** in 20 ml of chloroform, 1 ml of acetyl chloride was added all at once. To the mixture, 1 ml of triethylamine was added at 0—5 °C. After 15 min, the reaction was found to be almost completed on TLC. After evaporation of solvents, the residue was chromatographed on a silica-gel column eluted with chloroform-acetone (93:7 v/v), to give 49 mg (8% yield) of **3c** and 152 mg (27%) of *N*-acetyl-*N,N'*-ditosyl-1,2-ethanediamine (**4c**). The rest was the unchanged starting **1c**. **4c** was obtained as colorless viscous liquid (spontaneous cryst.). Calcd for $C_{18}H_{22}N_2S_2O_5$: C, 52.66; H, 5.40; N, 6.83; S, 15.62%. Found: C, 52.59; H, 5.39; N, 6.74; S, 15.43%. IR (KBr) 3250(NH), 1700(C=O), and 1360, 1328, and 1158(SO_2) cm^{-1}. ^{1}H-NMR; 2.31 ($COCH_3$), 2.44 and 2.46 (CH_3), 3.24 (J=6.10, NCH_2), 3.88 (J=6.10, NCH_2), 4.95 (J=6.10, NH). MS; *m/z* 255 (18%), 213 (3.2%), 197 (19%), and 184 (100%).

Spontaneous Decomposition of N-Nitrososulfonamide (2a) in Ethanol. When an ethanolic solution of **2a** (0.315 mg/20 ml) was allowed to stand on a bench top, the reaction induced by ambient room light was monitored by repetitive measurements of the UV spectra (every day in the range 210—350 nm). The original shoulder band at 250 nm revealed hypochromism and a band at 290 nm, hyperchromism, having an isosbestic point at 271 nm. After 47 d, the decomposition of **2a** became less significant. The eventual UV spectrum was superimposable to that of **1a**.

Removal of the N-Nitroso Group in N-Nitrososulfonamide (2c) with L-Ascorbic Acid. When a mixture of 0.43 g (1 mmol) of **2c** and 0.178 g (1 mmol) of L-ascorbic acid in 20 ml of ethanol was heated at *ca.* 70 °C overnight, **1c** was the only isolable product in quantitative yield. At the lowered temperature, the reactioin was markedly retarded.

Removal of N-Acetyl Group in N-Acetylsulfonamide (3a) with Potassium Carbonate. When a mixture of 90 mg of **3a** and 0.188 g (8 mmol eq) of anhydrous potassium carbonate in a mixed solvent of methanol-water (20 ml:1 ml) was refluxed for 1 h, **1a** was obtained in quantitative yield (76 mg) after silica-gel chromatography eluted with chloroform–methanol (17:3 v/v).

We are grateful to Dr. Haruo Homma and his staff at Riken for performing elemental analyses and Dr. Jun Uzawa and Mrs. Tamiko Chijimatsu at Riken for recording ^{1}H-NMR spectra.

References

1) a) B. C. Challis and J. A. Challis, "The Chemistry of Amides," ed by Zabicky, J. Interscience Publishers, London, 1970; pp. 780. b) B. C. Challis and S. A. Kryptpoulos, *J. Chem. Soc., Chem. Commun.*, **1976**, 877.

2) a) E. H. White, *J. Am. Chem. Soc.*, **77**, 6008 (1955). b) T. J. de Boer and H. J. Backer, *Org. Synth.* Coll. Vol. IV, 225 (1963). c) C. G. Overberger and J.-P. Anselme, *J. Org. Chem.*, **28**, 592 (1963).

3) K. Yoshida and K. Yano, *Bull. Chem. Soc. Jpn.*, **55**, 2200 (1982).

4) J. E. Nordlander, M. J. Payne, M. A. Balk, J. L. Gress, F. D. Harris, J. S. Lane, R. F. Lewe, S. E. Marshall, D. Nagy, and D. J. Rachin, *J. Org. Chem.*, **49**, 133 (1984).

5) M. Iwata and H. Kuzuhara, *Bull. Chem. Soc. Jpn.*, **55**, 2153 (1982).

Stereoselective Synthesis of (*E*)-Alkylidenesuccinates by Palladium-catalyzed Carbonylation

Keiji YAMAMOTO,* Ryoji DEGUCHI, and Jiro TSUJI
Department of Chemical Engineering, Tokyo Institute of Technology, Meguro-ku, Tokyo 152
(Received May 30, 1985)

Synopsis. (*E*)-Alkylidenesuccinates have been prepared stereoselectively starting with acrylates by a three-step procedure involving a palladium-catalyzed carbonylation of allylic carbonates.

The well-known Stobbe condensation of aldehydes with an ester of succinic acid is rather limited to the use of aromatic aldehydes, because in the case of aliphatic ones possible isomerization of the produced alkylidenesuccinic acids often yields positional as well as geometrical isomers.[1]

We report here that (*E*)-alkylidenesuccinic acid esters can readily be prepared by a three-step procedure which consists of a base-catalyzed addition of acrylates to aliphatic aldehydes,[2] carbonate formation of the resulting allylic alcohols, and facile palladium-catalyzed carbonylation of the allylic carbonates reported recently by one of us.[3] Scheme 1 shows the procedure.

Although the addition of acrylates to common aldehydes was found to take place slowly but in moderate yields, the yield in carbonate formation was rather inconsistent with recovery of the starting allylic alcohols (40—85% yield).

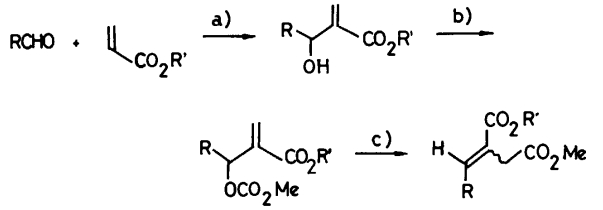

a) 1,4-Diazabicyclo[2.2.2]octane (DABCO) (20 mol%). b) $ClCO_2Me$/pyridine/benzene. c) $Pd(OAc)_2+2PPh_3$ (2 mol%)/CO (20 kg/cm²).

Scheme 1.

The decarboxylation-carbonylation was carried out by using allyl methyl carbonates thus obtained in the presence of a catalytic amount (2 mol%) of a palladium(0)-phosphine complex generated *in situ* under carbon monoxide pressure at 50 °C.[3]

It should be mentioned that the palladium-catalyzed carbonylation is very characteristic of allylic carbonates, other allylic derivatives, such as halides or acetates, being hardly applicable to the catalytic process.

In Table 1 are summarized the results of the preparation of alkylidenesuccinates (**2**).

Three points may be worth commenting: 1) CO pressure affects significantly both the yield of **2** and the selectivity for *E*/*Z* isomers (Table 1, entries 1—3). 2) Satisfactorily high *E*-selectivity (entries 3—5) must be a direct consequence of the carbonylation from *anti*-η^3-allylpalladium intermediate which contains an alkoxycarbonyl group at 2-position. 3) While an isopropyl ester in **1b** has no effect in favor of forming (*E*)-**2b**, an isopropyl substituent of R in **1c** enhances *E*-selectivity of **2c**.

In addition to these results, it was found that the carbonylation of the corresponding cyano analogue of **1**, which was obtained similarly starting with acrylonitrile, afforded mainly (*Z*)-alkylidenesuccinic acid mononitrile (**3**) (*E*/*Z*=1/6), reflecting *syn*-η^3-allylpalladium intermediate to be carbonylated preferably. It follows, therefore, that effect of an alkoxycarbonyl group at 2-position of *anti*-1,2-disubstituted η^3-allylpalladium is steric rather than electronic.

TABLE 1. PREPARATION OF (*E*)-ALKYLIDENESUCCINATES (**2**)

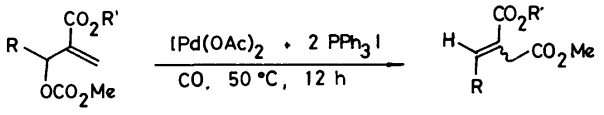

1a—c **2a—c**

Entry	Substrate, **1** R	R′		CO kg/cm²	Yield %	**2**	*E* : *Z*[a]	By-product[b] %
1	*i*-Bu	Me		10	27		7 : 1[c]	60
2	*i*-Bu	Me	**1a**	15	79	**2a**	8 : 1	10
3	*i*-Bu	Me		25	82		11 : 1	5
4	*i*-Bu	*i*-Pr	**1b**	20	70	**2b**	10 : 1	—
5	*i*-Pr	Me	**1c**	20	67	**2c**	14 : 1	—

a) Determined by GLC analysis. b) Allylic methyl ether (*E*/*Z*=5/1). c) Isolated by preparative GLC.

Experimental

Preparation of 3-(Methoxycarbonyloxy)-2-methylenealkanoate (1). A typical procedure is as follows: A mixture of isovaleraldehyde (40 mmol), methyl acrylate (40 mmol), and DABCO (8 mmol) was stirred at room temperature for several days.[2] Remaining acrylate was removed *in vacuo*, the residue was taken up in dichloromethane, washed with 1M HCl(1 M=1 mol dm^{-3}), and dried ($MgSO_4$). The concentrated material was distilled under reduced pressure to give methyl 3-hydroxy-5-methyl-2-methylenehexanoate, bp 48—50 °C/2 Torr (52% yield) (1 Torr=133.322 Pa). The latter (10 mmol) was treated with methyl chloroformate (30 mmol) and pyridine (30 mmol) in dry benzene (50 mL) in a usual manner giving methyl 3-(methoxycarbonyloxy)-5-methyl-2-methylenehexanoate (**1a**), bp 62—64 °C/2 Torr (85%).

Similarly, from isopropyl 3-hydroxy-5-methyl-2-methylenehexanoate (bp 65—67 °C/3 Torr, 62%), isopropyl 3-(methyoxycarbonyloxy)-5-methyl-2-methylenehexanoate (**1b**) was obtained and purified by column chromatography (70% yield with 43% recovery of the starting alcohol). From methyl 3-hydroxy-4-methyl 2-methylenepentanoate (bp 78—80 °C/4 Torr, 51%), methyl 3-(methoxycarbonyloxy)-4-methyl-2-methylenepentanoate (**1c**) was prepared and purified similarly as above (40% yield with 26% recovery of the starting material).

Proton NMR data of **1a—c** are given below: ^{1}H NMR (90 MHz, $CDCl_3$, TMS) **1a**: δ=0.93 (d, J=5.9 Hz, 3H), 0.96 (d, J=5.7 Hz, 3H), 1.54—1.68 (m, 3H), 3.78 (s, 3H), 3.79 (s, 3H), 5.47—5.61 (m, 1H), 5.84 (br s, 1H), and 6.30 ppm (br s, 1H). **1b**: 0.94 (d, J=6.4 Hz, 3H), 0.95 (d, J=6.2 Hz, 3H), 1.29 (d, J=6.4 Hz, 6H), 1.35—1.58 (m, 2H), 1.60—2.04 (m, 1H), 3.77 (s, 3H), 5.10 (sept, J=6.3 Hz, 1H), 5.45 (br t, J=7.2 Hz, 1H), 5.77 (t, J=1.2 Hz, 1H), and 6.18 (d, J=0.7 Hz, 1H). **1c**: 0.92 (d, J=6.6 Hz, 3H), 0.96 (d, J=6.8 Hz, 3H), 1.82—2.26 (m, 1H), 3.78 (s, 3H), 3.79 (s, 3H), 5.34 (dd, J=0.9 and 5.5 Hz, 1H), 5.80 (t, J=1.0 Hz, 1H), and 6.37 (d, J=0.9 Hz, 1H).

General Procedure for the Palladium-catalyzed Carbonylation. In a 50 mL micro-autoclave with glass lining were placed under a nitrogen atmosphere an allylic carbonate (**1**) (5 mmol), $Pd(OAc)_2$ (2 mol%) and PPh_3 (4 mol%). Carbon monoxide was introduced (20 kg/cm^2) and the mixture was heated at 50 °C overnight with stirring. The red-brown solution was filtered through a short Florisil column to remove the catalyst, the latter being rinsed with little ether. The filtrate was condensed *in vacuo*, and the residue was purified by distillation under reduced pressure (Kugelrohr) to give the corresponding alkylidenesuccinate (**2**). (*Z*)-Isomer as a minor component was isolated by preparative GLC and identified by ^{1}H and/or ^{13}C NMR. Yields and the ratios of *E*- and *Z*-isomers of **2** are summarized in Table 1, and spectral and analytical data of **2a—c** and **3** are given below:

Dimethyl (E)-(3-Methylbutylidene)succinate (2a): ^{1}H NMR 0.94 (d, J=6.4 Hz, 6H), 1.32—1.92 (m, 1H), 2.09 (dd, J=6.4 and 7.5 Hz, 2H), 3.36 (s, 2H), 3.68 (s, 3H), 3.75 (s, 3H), and 7.00 (t, J=7.5 Hz, 1H). ^{13}C NMR (22.5 MHz) δ=22.4 (MeX2), 28.2, 32.2, 38.0, 51.9 (OMeX2), 125.9, 144.9, 167.4, and 171.2 ppm. IR (neat) 1263, 1715, and 1745 cm^{-1}. Anal. Calcd for $C_{11}H_{18}O_4$: C, 61.82; H, 8.47%. Found: C, 61.82; H, 8.37%. (*Z*)-**2a**: ^{1}H NMR 0.92 (d, J=6.2 Hz, 6H), 1.20—1.90 (m, 1H), 2.47 (dd, J=6.8 and 7.5 Hz, 2H), 3.28 (s, 2H), 3.68 (s, 3H), 3.74 (s, 3H), and 6.09 (t, J=7.5 Hz, 1H).

1-Isopropyl 4-Methyl (E)-2-(3-Methylbutylidene)succinate (2b): ^{1}H NMR 0.94 (d, J=6.4 Hz, 6H), 1.26 (d, J=6.4 Hz, 6H), 1.60—2.00 (m, 1H), 2.08 (t, J=7.3 Hz, 2H), 3.34 (s, 2H), 3.67 (s, 3H), 5.06 (sept, J=6.3 Hz, 1H), and 7.04 (t, J=7.6 Hz, 1H). ^{13}C NMR 21.8 (MeX2), 22.5 (MeX2), 28.3 32.4, 37.9, 51.9, 68.1, 126.6, 144.1, 166.4, and 171.4. IR (neat) 1260, 1710, snf 1740 cm^{-1}. Anal. Calcd for $C_{13}H_{22}O_4$: C, 64.44; H, 9.15%. Found: C, 64.18; H, 9.07%. (*Z*)-**2b**: ^{1}H NMR 0.93 (d, J=6.6 Hz, 6H), 1.25 (d, J=6.4 Hz, 6H), 1.44—1.85 (m, 1H), 2.47 (t, J=7.2 Hz, 2H), 3.26 (s, 2H), 3.67 (s, 3H), 5.07 (sept, J=6.3 Hz, 1H), and 6.05 (t, J=7.5 Hz 1H). ^{13}C NMR 21.8 (MeX2), 22.4 (MeX2), 28.8, 38.4, 40.4, 51.8, 67.8, 126.0, 145.9, 166.8, and 172.0.

Dimethyl (E)-(2-Methylpropylidene)succinate (2c): ^{1}H NMR 1.04 (d, J=6.6 Hz, 6H), 2.24—2.95 (m, 1H), 3.36 (s, 2H), 3.68 (s, 3H), 3.74 (s, 3H), and 6.77 (d, J=10.1 Hz, 1H). ^{13}C NMR 21.9 (MeX2), 28.5, 32.2, 52.0 (OMeX2), 123.2, 152.1, 167.6, and 171.3. IR (neat) 1265, 1710, and 1740 cm^{-1}. Anal. Calcd for $C_{10}H_{16}O_4$: C, 59.98; H, 8.05%. Found: C, 60.33; H, 8.07%. (*Z*)-**2c**: ^{1}H NMR 1.02 (d, J=6.6 Hz, 6H), 3.12—3.48 centered at 3.37 (decoupled) (m, 1H), 3.24 (s, 2H), 3.68 (s, 3H), 3.74 (s, 3H), and 5.84 (d, J=9.9 Hz, 1H).

Methyl (Z)-3-Cyano-6-methyl-3-heptenoate (3): ^{1}H NMR 0.96 (d, J=6.4 Hz, 6H), 1.56—2.12 (m, 1H), 2.32 (dd, J=7.0 and 7.3 Hz, 2H), 3.24 (s, 2H), 3.75 (s, 3H), and 6.33 (t, J=7.7 Hz, 1H). ^{13}C NMR 22.2 (MeX2), 28.2, 39.0, 40.6, 52.4, 108.0, 116.9, 151.1, and 169.5. IR (neat) 1260, 1740, and 2200 cm^{-1}. Anal. Calcd for $C_{10}H_{15}NO_2$: C, 66.27; H, 8.34;, N, 7.73%. Found: C, 66.16; H, 8.40; N, 7.58%. (*E*)-**3**: ^{1}H NMR 0.93 (d, J=6.4 Hz, 6H), 1.56—1.96 (m, 1H), 2.10 (dd, J=6.6 and 7.3 Hz, 2H), 3.26 (s, 2H), 3.75 (s, 3H), and 6.58 (t, J=7.6 Hz, 1H). ^{13}C NMR 22.2 (MeX2), 28.1, 34.1, 37.7, 52.4, 107.8, 116.7, 150.8, and 168.9.

References

1) W. S. Johnson and G. H. Daub, *Organic Reactions*, Vol. 6, pp 1—73 (1951).

2) A. B. Baylis and N. E. Hilman, Ger. Pat. 2155113; *Chem. Abstr.*, **77**, 34174q (1972); S. E. Drewes and N. D. Emslie, *J. Chem. Soc., Perkin Trans. 1.* **1982**, 2079; also, H. M. R. Hoffmann and J. Rabe, *Angew. Chem. Intern. Edn.*, **22**, 795 (1983).

3) J. Tsuji, K. Sato, and H. Okumoto, *J. Org. Chem.*, **49**, 134 (1984).

Convenient Synthesis of β-Truxinic Acid *via* Photodimerization of *p*-Nitrophenyl Cinnamate in the Crystalline State

Tadatomi NISHIKUBO,* Eiji TAKAHASHI, Takatoshi MIYAJI, and Takashi IIZAWA
Department of Applied Chemistry, Faculty of Engineering, Kanagawa University, Rokkakubashi, Kanagawa-ku, Yokohama 221
(Received June 13, 1985)

Synopsis. β-Truxinic acid was synthesized in extremely high yield *via* a topochemical photodimerization of *p*-nitrophenyl cinnamate crystals, followed by the hydrolysis of the obtained dimer.

Since topochemical photodimerizations of cinnamic acid derivatives have been investigated extensively by Schmidt and his co-workers,[1] the photodimerizations of cinnamic acids and other olefinic compounds in the crystalline state, which is very interesting as crystal engineering, have been reported. The stable α-form of (*E*)-cinnamic acid gives α-truxillic acid selectively whereas the metastable β-form of (*E*)-cinnamic acid yields pure β-truxinic acid at low temperature. However, the metastable form of (*E*)-cinnamic acid is transformed to the stable form at temperatures higher than 50 °C in the crystalline state. Recently, although many substituted α-truxillic acids or β-truxinic acids were prepared[2-5] by the topochemical photodimerizations of the corresponding forms of substituted (*E*)-cinnamic acids, the unsubstituted β-truxinic acid has not been obtaind by topochemical photodimerization on a preparative scale so far due to the above transformation.

This article reports on the successful photodimerization of *p*-nitrophenyl cinnamate (NPC) in a crystalline state at various temperatures to give β-truxinic acid in high yield per reaction. As shown in Fig. 1, the rate of photochemical reaction of NPC embeded in KBr pellet was much faster than those of cinnamic acid (CA) and phenyl cinnamate (PC). This means that NPC has a high photochemical reactivity in the crystalline state.

Therefore, the photochemical reaction of NPC has been carried out under various conditions. The results are summarized in Table 1. The yield of bis(*p*-nitrophenyl) β-truxinate (BNPT) was not affected by the reaction temperature, the solvent and air. However, the yield was dependent on the irradiation time. The yield of BNPT was also affected by the amounts of NPC suspended in hexane, because a small amount of the suspended NPC was soluble in hexane. (*E*)-NPC in a hexane solution changed to the (*Z*)-isomer (confirmed by HPLC) upon irradiation by UV light.

According to the intensity of the X-ray diffraction patterns, the crystallinity of NPC decreased extremely along with the progress of the reaction. Then, new weak peaks, which seem to be peaks of the dimer crystal, appeared. However, the diffraction pattern of as-prepared BNPT was quite different from that of the recrystallized BNPT. This is good evidence that the reaction of NPC proceeded topochemically.

Recently, we have found[6] that the pendant 4-nitrophenoxide moiety acts as an excellent photosensitizer for a pendant cinnamic ester in a polymer film and a diluted solution of the polymer. From these results, it seems that 4-nitrophenoxide on NPC

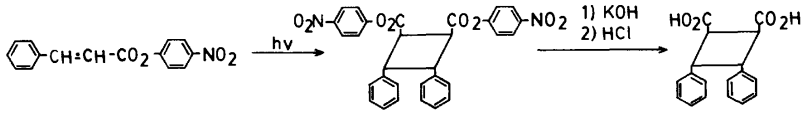

(NPC) (BNPT)

Table 1. Photochemical reaction of NPC in the crystalline state

Run No.	Cinnamic ester/g/l	Dispersant	Irradiation conditions		Yield
			Temp/°C	Time/h	%
1	NPC (4.0)	Hexane	30	3	67.3
2	NPC (12.0)	Hexane	30	3	80.2
3	NPC (20.0)	Hexane	30	3	88.9
4	NPC (40.0)	Hexane	30	3	84.4
5	NPC (40.0)	Hexane	30	3	85.2[a]
6	NPC (40.0)	Hexane	−10	3	89.9
7	NPC (40.0)	Hexane	50	3	90.7
8	NPC (40.0)	Hexane	30	6	99.2
9	NPC (80.0)	Hexane	30	10	91.1
10	NPC (40.0)	Water	10	3	89.4

a) The reaction was carried out in N_2.

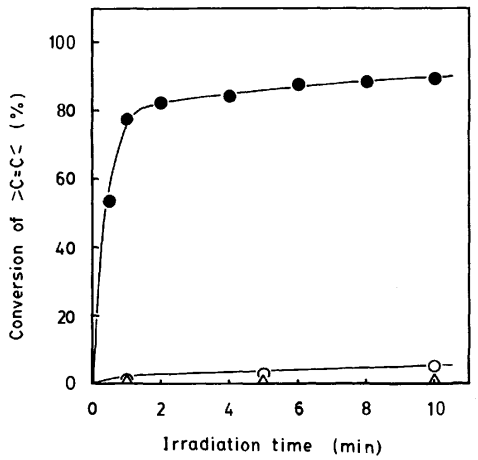

Fig. 1. The rates of disappearance of C=C group in cinnamic acid and its esters.
(△): CA, (○): PC, (●): NPC.

also acted as a photosensitizer in the crystalline state.

The BNPT obtained by a photodimerization reaction in a crystalline state was successfully hydrolyzed in high yield to give β-truxinic acid using excess potassium hydroxide in methanol.

From these results, we reveal here that NPC is an excellent starting compound for obtaining an unsubstituted β-truxinic acid by crystal engineering.

Experimental

NPC (mp 144—145 °C)[7] was prepared through a reaction of cinnamoyl chloride with 4-nitrophenol. Then it was recrystallized twice from methanol.

Measurement of the Rate of Photochemical Reaction of NPC in KBr Pellet. NPC (10^{-6} mol) with KBr (0.089 g) was ground and molded into pellet form. The pellet fastened to a plate was irradiated using 250-W high-pressure mercury lamp (Ushio Electric Co., USH-250D) at a distance of 30 cm. The rate of the disappearance of the absorption peak due to a C=C group at 1640 cm^{-1} was measured by IR spectrometry (JASCO model A-202).

Synthesis of BNPT by Photodimerization of NPC in the Crystalline State. NPC crystals (1.6—80 g) were dispersed in hexane (400 ml) in a Pyrex flask. The flask was then irradiated with a 100-W high-pressure mercury lamp (Ushio Electric Co., UM-102) at various temperatures. Then the progress of the reaction was monitored by measuring the decrease of NPC and the increase of BNPT by HPLC [JASCO model; Twincl, detecter; uvidec-100-III, column (4.6 mm×250 mm) packed with a silicagel-ODS-10, elutant; water-acetonitrile (ratio; 4/6)] and/or from UV spectrum of NPC (absroption maximum; 271 nm in THF) by the spectrometry (Shimazu model; UV-240). The final product was filtered off, washed with hot methanol, and recrystallized twice from 2-butanone. Mp 192—193 °C. IR (KBr) 1750 (C=O), 1520 and 1350 ($-NO_2$), 1150 cm^{-1} (C-O-C). NMR ($CDCl_3$) δ=4.6 (s, 2H, C-CH-C), and 7.1—8.5 (m, 9H, aromatic protons). Found: C, 66.51; H, 4.10; N, 5.10%. Calcd for $C_{30}H_{22}N_2O_8$: C, 66.91; H, 4.12; N, 5.20%.

Synthesis of β-truxinic acid by Hydrolysis of BNPT. BNPT (53.8 g; 0.1 mol) and potassium hydroxide (28.1 g; 0.5 mol) were dissolved in methanol (250 ml). Then, the solution was refluxed for 5 h. The reaction mixture was poured into water (750 ml) the PH of the solution was adjusted to 3 with concd HCl solution. The precipitated β-truxinic acid was filtered off, washed with water, and dried. Yield: 28.6 g (96.7%). The crude β-truxinic acid was recrystallized twice from acetic acid. Mp 209—210 °C (Lit,[8] 209—210 °C).

The authors thank professor M. Hasegawa of the University of Tokyo for his helpful advice.

References

1) a) G. M. J. Schmidt, *Pure Appl. Chem.*, **27**, 647 (1971); b) G. M. J. Schmidt *et al.* "Solid State Photochemistry," Verlag Chemie, New York (1976).

2) M. D. Cohen, G. M. J. Schmidt, and F. I. Sonntag, *J. Chem. Soc.*, **1964**, 2000.

3) a) F. Nakanishi, H. Nakanishi, M. Tsuchiya, and M. Hasegawa, *Bull. Chem. Soc. Jpn.*, **49**, 3096 (1976); b) F. Nakanishi, M. Ishii, and H. Nakanishi, *Bull. Chem. Soc. Jpn.*, **57**, 3335 (1984).

4) J. P. Glusker D. E. Zacharias, and H. L. Carrell, *J. Chem. Soc., Perkin Trans. 2*, **1975**, 68.

5) a) J. A. R. P. Sarma and G. R. Desiraju, *J. Chem. Soc., Chem. Commun.*, **1984**, 145; b) G. R. Desiraju, R. Kamala, B. H. Kumari, and J. A. R. P. Sarma, *J. Chem. Soc. Perkin Trans. 2*, **1984**, 181.

6) T. Iizawa, T. Nishikubo, E. Takahashi, and M. Hasegawa, *Makromol. Chem.*, **184**, 2297 (1983).

7) M. L. Bender, G. R. Schonbaum, and B. Zerner, *J. Am. Chem. Soc.*, **84**, 2540 (1962).

8) H. Stobbe, *Ber.*, **55**, 2225 (1922).

The 1-Octanol/Water Partition Coefficient of Mercury

Shoichi OKOUCHI* and Sokichi SASAKI
Chemical Laboratory, College of Engineering, Hosei University, Koganei, Tokyo 184
(Received February 8, 1985)

Synopsis. The 1-octanol/water partition coefficient of metallic mercury was measured as a useful parameter for predicting the environmental behavior or fate of mercury. The partition coefficient obtained was 4.15±0.20 at 298 K; it slightly decreased from 4.80 to 3.80 as the temperature rose from 278 to 308 K. The partition coefficient of metallic mercury is very low in comparison with those of such nonpolar organic compounds as benzene and tetrachloromethane. Therefore, it was found that metallic mercury has a tendency to be further concentrated in the atmosphere.

It is well known that mercury has been released to the environment[1] by the combustion of fossil fuels. It has been increasingly important to predict how contaminants will behave upon their release to the environment in order to assess the potential hazards of contaminants. Several models[2,3] have been developed which predict environmental behavior or fate from accessible physico-chemical properties, such as vapor pressure, aqueous solubilities, Henry's constant, the soil-sorption constant, and the bioconcentration factor. The soil-sorption constant based on the organic carbon content[4,5] and, in particular, the bioconcentration factor[6,7] are complicated to measure experimentally, therefore, they have been correlated to the 1-octanol/water partition coefficient,[16] which is relatively measurable. The partition coefficient is, then, very useful parameter in predicting the environmental behavior of a contaminant.

In this work, the partition coefficient of metallic mercury is experimentally determined; no information on this has previously been reported.

Experimental

All the chemicals used were of an analytical-reagent grade. The metallic mercury was further purified in the usual manner.[8] The 1-octanol/water was distilled twice to remove trace amounts of impurities, which tended to produce emulsions.[9] Doubly distilled water was used throughout this work.

By shaking an octanol solution containing a few drops of the purified metallic mercury and 0.001 mol dm^{-3} of hydrazine used as a reducing agent to prevent the mercury oxidation,[8] the mercury was dissolved into the 1-octanol (approximately 0.8 mg-mercury/cm^3). A 2-cm^3 aliquot of the 1-octanol solution and 20 cm^3 of the distilled water were then shaken for 24 h at a constant temperature in a closed 25-cm^3 centrifuge tube. After equilibrium and then centrifugation, the two phases were separated and analyzed by means of the cold-vapor atomic-absorption method.[10] The mercury concentrations in the two phases were constant after 24 h of shaking and thereafter remained constant over a period of several days. The 1-octanol/water partition coefficient was determined in the temperature range from 278 to 308 K.

Results and Discussion

Figure 1 shows the effect of the temperature on the 1-octanol/water partition coefficient, K_{OW}. The partition coefficient was 4.15±0.20 at 298 K, but it slightly decreased from 4.80 to 3.80 as the temperature rose from 278 to 308 K. The K_{OW} value of metallic mercury thus obtained is very low in comparison with those of nonpolar organic compounds, for example, 1.34×10^2 [11] for benzene and 4.37×10^2 [11] for tetrachloromethane, and with that of 1.66×10^6 [16]for PCB (aroclor 1242).

Table 1 shows the soil-sorption constant, based on the organic carbon content, K_{OC}, and the bioconcentration factor, K_B, of metallic mercury and organic compounds calculated using the correlation equations of Karickhoff *et al.*[6] and Veith *et al.*[5] from the partition coefficient. The sorption by a soild phase, such as soil, a suspended solid, and sediment, and the

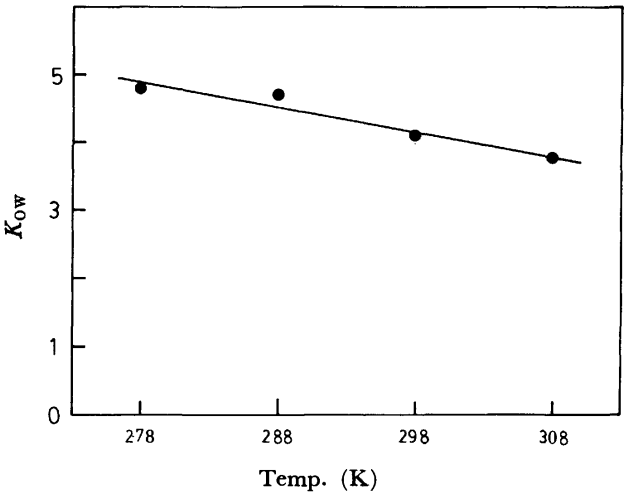

Fig. 1. Effect of temperature on the 1-octanol/water partition coefficient of metallic mercury, K_{OW}.

TABLE 1. THE VALUES OF K_{OW}, K_{OC}, K_B, AND $K_V^{(i)}/K_V^{(O_2)}$.

Contaminant	K_{ow}	K_{OC}[6]	K_B[5]	$K_V^{(i)}/K_V^{(O_2)}$
Mercury	4.15	2.6	6.7×10^{-1}	0.94[12]
Benzene	1.34×10^2 [11]	8.3×10^1	1.3×10^1	0.56[13]
Tetrachloromethane	4.37×10^2 [11]	3.0×10^2	$3.5\times10_1$	0.62[14]
PCB (aroclor 1242)	1.66×10^6 [16]	1.0×10^6	3.9×10^4	0.22[15]

uptake by the aquatic-biota phase for mercury are much less than those for nonpolar organic compounds such as benzene and tetrachloromethane, and for PCB (aroclor 1242). In addition, Okouchi *et al.*[12] has reported that the volatilization rate of metallic mercury from water to the atmosphere is more rapid than those of benzene,[13] tetrachloromethane,[14] and PCB (aroclor 1242)[15] by factors of about 1.7, 1.5, and 4.3 respectively, judging from the volatility coefficient ($K_v^{(i)}/K_v^{(O_2)}$) as is shown in Table 1. The volatility coefficient represents the comparative volatilization rate of a volatile contaminant $K_v^{(i)}$ with oxygen $K_v^{(O_2)}$.

Therefore, from the 1-octanol/water partition coefficient of mercury measured in this work, it was found that metallic mercury has a tendency to be further concentrated in the atmosphere because of very low sorption by the particulate soild phase and uptake by the aquatic-biota phase.

References

1) R. W. Klusman and C. P. Matoske, *Environ. Sci. Technol.*, **17**, 2511 (1983).
2) "Modeling the Fate of Chemicals in Aquatic Environment," ed by K. L. Dickson, A. W. Maki, and J. Carins, Jr., Ann Arbor Science, Ann Arbor Michigan (1982).
3) ACS Symposium Series 225, "Fate of Chemicals in the Environment," ed by R. L. Swann and A. Eschenroeder, American Chemical Society, Washington, D.C. (1983).
4) W. B. Neely, D. R. Branson, and G. Eblau, *Environ. Sci. Technol.*, **8**, 1113 (1974).
5) G. D. Veith, D. L. DeFoe and B. V. Bergstedt, *J. Fish. Res. Board Can.*, **36**, 1040 (1979).
6) S. W. Karickhoff, D. S. Brown, and T. A. Scott, *Water Res.*, **13**, 241 (1979).
7) G. G. Briggs, Proc. 7th British Insecticide and Fungicide Conf., 83 (1973).
8) D. N. Glew and D. A. Hames, *Can. J. Chem.*, **49**, 3114 (1971).
9) C. T. Chiou, V. H. Freed, D. W. Schmedding, and R. L. Kohnert, *Environ. Sci. Technol.*, **11**, 475 (1977).
10) S. Okouchi and S. Sasaki, *Bull. Chem. Soc. Jpn.*, **54**, 2513 (1981).
11) D. Mackay, A. Bobra, and W. Y. Shiu, *Chemosphere*, **9**, 701 (1980).
12) S. Okouchi, S. Sasaki, and Y. Harano, *Bull. Chem. Soc. Jpn.*, **57**, 338 (1984).
13) J. H. Smith, D. C. Bomberger, Jr., and D. L. Haynes, *Environ. Sci. Technol.*, **14**, 1332 (1980).
14) P. V. Roberts and P. G. Dandliker, *ibid.*, **17**, 484 (1983).
15) D. F. Paris, W. C. Steen, and G. L. Baughman, *Chemosphere*, **4**, 319 (1978).
16) A. Leo, C. Hansch, and D. Elkins, *Chem. Reviews*, **71**, 525 (1971).

Temperature Dependence of Walden Product of 18-Crown-6-K^+ Complex in Water

Yasuyuki TAKEDA* and Osamu ARIMA
Department of Chemistry, Faculty of Science, Chiba University, Yayoi-chō, Chiba 260
(Received March 19, 1985)

Synopsis. Limiting ionic molar conductivities of the 18-crown-6-K^+ complex in water were determined at 15 and 35 °C. Walden product values of the complex at 15, 25, and 35 °C are nearly identical within experimental errors of conductance measurements. Solvation properties of the complex in water were discussed in detail.

From a viewpoint of solution chemistry, it is interesting to study solvation properties of crown ether-alkali metal ion complexes as well as medium effects on stabilities of the complexes. It has been carried out by various methods and the information on solute-solvent interactions regarding the crown ether complexes has been reported. For example, density and speed-of-sound measurements suggested that hydration number of K^+ in 18-crown-6 (18C6) is zero.[1] The data for entropies of transfer from water to methanol of the 18C6-K^+ complex indicate that the complex in water undergoes hydrophobic hydration.[2] It was concluded from the results of viscosity measurements that the dragging resistance of the 18C6-K^+ complex is nearly the same as that of the free 18C6 in water.[3] It was reported from conductance study that the 18C6-K^+ complex acts as a structure breaker in water.[4,5] In a series of our conductance studies,[4-7] limiting ionic molar conductivity at 25 °C of the 18C6-K^+ complex in a given solvent was compared with that of $(n\text{-}C_4H_9)_4N^+$ since they have almost the same size, and Walden products of the complex at 25 °C in various solvents were discussed.

In this work, in order to obtain more detailed information about solvation behavior of the 18C6-K^+ complex in water, limiting ionic molar conductivities of the complex in water were determined at 15 and 35 °C, and temperature dependence of Walden products for the complex was investigated.

Experimental

18-Crown-6 and extremely pure potassium chloride were obtained from Nisso Co., Ltd. and Merck Japan Ltd., respectively. The 18C6 was recrystallized three times from acetonitrile and, prior to use, dried at 70 °C in a vacuum oven. The potassium chloride was used without further purification. Conductivity of water was less than $2\times10^{-7}\ \Omega^{-1}\ cm^{-1}$. Conductance measurements were made on a Fuso conductivity apparatus, model 362 A, in a water bath thermostated at 10, 15, 20, 25, 35, 45±0.01 °C. Two cells were used with cell constants of 0.059707 and 0.093938 cm^{-1}.

The experimental procedures to obtain formation constants and limiting ionic molar conductivities of the 18C6-K^+ complex were described in the previous paper.[7] For each conductance measurement system, total concentrations of KCl and 18C6 were kept below 5×10^{-3} and 3×10^{-2} mol dm^{-3}, respectively.

Table 1. $\log K_{ML^+}$ values of the 18C6-K^+ complex and Λ° values of the 18C6 complex with potassium chloride in water at various temperatures

Temp/°C	$\log(K_{ML^+}/mol^{-1}\ dm^3)$	$\Lambda^\circ/\Omega^{-1}\ cm^2\ mol^{-1}$
10	2.288±0.008	—
15	2.253±0.012	81.2±0.5
20	2.135±0.011	—
25	2.034±0.004	101.7±0.3[4]
35	1.940±0.004	124.2±0.5
45	1.790±0.020	—

Results and Discussion

Formation constant (K_{ML^+}) and limiting ionic molar conductivity (λ°) of the 18C6-K^+ complex were obtained in the same manner described in the previous study.[7] M^+ and L designate an alkali metal ion and a crown ether, respectively. It is assumed that the association between a cation and an anion is negligible and that 18C6 forms a 1:1 complex with K^+. Corrections for viscosity changes due to solute were neglected. The $\log K_{ML^+}$ values of the 18C6-K^+ complex and the limiting molar conductivity (Λ°) values of the 18C6 complex with potassium chloride in water at various temperatures are listed in Table 1.

The $\log K_{ML^+}$ value at 25 °C determined in this study is in good agreement with those by Izatt *et al.*[8] (2.03±0.10, by calorimetric titration) and Stover[9] (2.029±0.028, by isotachophoresis); however, it is slightly lower than those by Frensdorff[10] (2.06±0.04, using cation-selective electrode by potentiometry) and Høiland *et al.*[1] (2.0476±0.0015, using cation-exchange membrane by potentiometry). The $\log K_{ML^+}$ *vs.* T^{-1} plots in Fig. 1 show a linear relationship. Enthalpy change (ΔH) and entropy change (ΔS) were calculated from these data by using equations, $\Delta G = -RT\ln K_{ML^+}$ and $\Delta G = \Delta H - T\Delta S$, ΔG being free energy change. The ΔH and ΔS values are

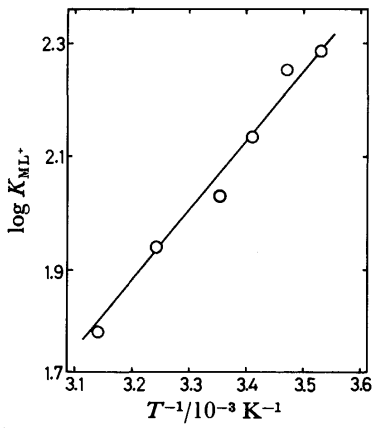

Fig. 1. $\log K_{ML^+}$ *vs.* T^{-1} plots for the 18C6-K^+ complex in water.

TABLE 2. $\lambda^\circ/\Omega^{-1}\,cm^2\,mol^{-1}$ AND WALDEN PRODUCTS IN WATER AT VARIOUS TEMPERATURES

Temp/°C	η_o/cP* [12]	18C6-K^+		$(n\text{-}C_4H_9)_4N^+$		Cl^-
		λ°	$\lambda^\circ\eta_o$	λ° [13]	$\lambda^\circ\eta_o$	λ°
10	1.306	—	—	12.56	0.1640	—
15	1.138	19.8	0.22_5	—	—	61.4_1 [12]
25	0.8903	25.3 [4]	0.22_5	19.31	0.1719	76.39 [13]
35	0.7194	32.0	0.23_0	—	—	92.2_1 [12]
45	0.5963	—	—	30.40	0.1813	—

* η_o denotes viscosity of water, 1 P=0.1 Pa s.

-25.01 kJ mol^{-1} and -44.34 J K^{-1} mol^{-1}, respectively; they agree well with those by Izatt *et al.*[8] ($\Delta H=-25.9$ kJ mol^{-1}, $\Delta S=-47.6$ J K^{-1} mol^{-1}). Values of log K_{ML^+} at 25 °C (2.140 ± 0.022), ΔH (-23.43 ± 0.83 kJ mol^{-1}), and ΔS (-37.60 ± 3.22 J K^{-1} mol^{-1}) determined by Michaux and Reisse[11] (log K_{ML^+}: using electrode by potentiometric titration, ΔH and ΔS: by calorimetric measurement) are relatively larger than those by us.

Thus, conductometry is a very accurate and reliable method for obtaining formation constants and thermodynamic parameters of crown ether-metal ion complexes.

As can be seen from Table 2, λ° values at 15 and 35 °C of the 18C6-K^+ complex are nearly equal to and larger than those at 25 and 45 °C of $(n\text{-}C_4H_9)_4N^+$, respectively; both mobilities of the 18C6-K^+ complex and $(n\text{-}C_4H_9)_4N^+$ gradually increase with an increase in temperature. This indicates that the 18C6-K^+ complex is more mobile than $(n\text{-}C_4H_9)_4N^+$ in water as reported previously.[4] The explanation for the results was offered in the preceding paper.[4] Walden product values of the 18C6-K^+ complex in water at 15, 25, and 35 °C are nearly identical within experimental errors of conductance measurements (Table 2). This may reflect the effects caused by the following two factors. (1) There exist possible interactions between the central potassium ion and water molecules on two axial sides of the 18C6 plane, and between ether oxygen atoms of the 18C6 and water molecules *via* hydrogen bonding. The interactions may be weakened with an increase in temperature. Thus, the 18C6-K^+ complex is more mobile than expected at a higher temperature. This would cause a positive temperature coefficient of Walden product of the 18C6-K^+ complex in water. (2) The 18C6-K^+ complex acts as a structure breaker in an aqueous solution.[4,5] Since hydrogen-bonded structure of water gradually disappears at a higher temperature, the 18C6-K^+ complex is less mobile than expected. This would cause a negative temperature coefficient of Walden product. These two factors compensate each other, resulting in no temperature dependence of Walden product of the 18C6-K^+ complex.

Values of $\lambda^\circ(K^+)/\lambda^\circ$(18C6-$K^+$) for CH_3OH, CH_3CN, DMF, DMSO, propylene carbonate, and water are 1.31, 1.41, 1.24, 1.46, 1.34, and 2.90, respectively. These were calculated from the data in Ref. 4. If the radii of moving entities of K^+ and 18C6-K^+ complex in the nonaqueous solvents (*i.e.*, effective radii) are considered to be 2.9 and 4.9 Å, respectively, the $\lambda^\circ(K^+)/\lambda^\circ$(18C6-$K^+$) value is about 1.6 ($\lambda^\circ=0.819/\eta_o r$, r being radius). The former was evaluated from Stokes' radii of K^+ in the nonaqueous solvents, and the latter is the crystal ionic radius itself evaluated from the crystal ionic radius of K^+ and the 18C6 volume. Experimental $\lambda^\circ(K^+)/\lambda^\circ$(18C6-$K^+$) values of the nonaqueous solvents are very much closer to the calculated value (1.6) compared to that of water (2.90). This indicates that the 18C6-K^+ complex is not so much strongly solvated in the nonaqueous solvents as K^+. From the fact that there is no large difference in Walden products of the 18C6-K^+ complex among these solvents (including water)[4] and that the Walden product value of K^+ for water is very much larger than those for the other solvents,[4] the considerably high $\lambda^\circ(K^+)/\lambda^\circ$(18C6-$K^+$) value of water is attributed completely to the role of K^+ as a structure breaker in water. This is supported by the data that the $\lambda^\circ(K^+)/\lambda^\circ$(18C6-$K^+$) value of water decreases with an increase in temperature ($\lambda^\circ(K^+)$ [12]$=59.6_6$ at 15 °C and 88.2_1 at 35 °C). From the fact that the 18C6-K^+ complex in water shows no temperature dependence of Walden product, whereas Walden product of K^+ in water decreases with an increase in temperature, the negative temperature coefficient of the $\lambda^\circ(K^+)/\lambda^\circ$(18C6-$K^+$) value for water may be caused entirely by the decrease of iceberg structure in water at a higher temperature.

References

1) H. Høiland, J. A. Ringseth, and T. S. Brun, *J. Solution Chem.*, **8**, 779 (1979).
2) M. H. Abraham and H. C. Ling, *Tetrahedron Lett.*, **23**, 469 (1982).
3) F. Kawaizumi, I. Yajima, H. Nomura, and Y. Miyahara, *Bull. Chem. Soc. Jpn.*, **57**, 2565 (1984).
4) Y. Takeda, *Bull. Chem. Soc. Jpn.*, **56**, 866 (1983).
5) Y. Takeda, *Bull. Chem. Soc. Jpn.*, **58**, 1259 (1985).
6) Y. Takeda, *Bull. Chem. Soc. Jpn.*, **54**, 3133 (1981).
7) Y. Takeda, H. Yano, M. Ishibashi, and H. Isozumi, *Bull. Chem. Soc. Jpn.*, **53**, 72 (1980).
8) R. M. Izatt, R. E. Terry, B. L. Haymore, L. D. Hansen, N. K. Dalley, A. G. Avondet, and J. J. Christensen, *J. Am. Chem. Soc.*, **98**, 7620 (1976).
9) F. S. Stover, *J. Chromatogr.*, **298**, 203 (1984).
10) H. K. Frensdorff, *J. Am. Chem. Soc.*, **93**, 600 (1971).
11) G. Michaux and J. Reisse, *J. Am. Chem. Soc.*, **104**, 6895 (1982).
12) R. A. Robinson and R. H. Stokes, "Electrolyte Solutions," Butterworths, London (1959).
13) R. L. Kay and D. F. Evans, *J. Phys. Chem.*, **70**, 2325 (1966).

A Molecular Mechanical Calculation along the Intrinsic Reaction Coordinate

Seikichi Cho
Department of Chemistry, Faculty of Education, Gunma University, 4-2 Aramakicho, Maebashi, Gunma 371
(Received June 14, 1985)

Synopsis. A normal coordinate analysis was applied to nonequilibrium states composed of atoms. A normal coordinate, Q_k, can be the intrinsic reaction coordinate if, and only if, all the first-order differentials have vanished except the k-th one. The HNC-to-HCN isomerization reaction was treated with the *ab initio* STO-3G potential surface: we thus observed several interesting features.

Molecular mechanical calculations usually utilize empirical expressions of the potential energy, which approximate near the equilibrium state of atoms in the system. The adiabatic potential energy surface can now be calculated at the *ab initio* SCF or a more elaborate level over a wide range of nonequilibrium states. The extension of the molecular mechanical calculation to nonequilibrium states or to the "reaction coordinates" is desirable. This paper concerns this extension by means of *ab initio* STO-3G SCF calculations with standard parameters.[1]

The relative kinetic energy[2] of an N atomic system can be calculated from the total kinetic energy minus the translational energy of, and the rotational energy around, the center of gravity:

$$T = T^{\mathrm{tot}} - T^{\mathrm{trans}} - T^{\mathrm{rot}} = \frac{1}{2}\sum_{i,j=1}^{3N} T_{ij}\dot{q}_i\dot{q}_j, \tag{1}$$

and the potential energy is approximated by the Taylor expansion to the second order:

$$V = V_0 + \sum_{i=1}^{3N} d_i q_i + \frac{1}{2}\sum_{i,j=1}^{3N} F_{ij}q_iq_j, \tag{2}$$

$$d_i = \frac{\partial V}{\partial q_i}, \qquad F_{ij} = \frac{\partial^2 V}{\partial q_i \partial q_j}.$$

As is well-known, Eqs. 1 and 2 can be transformed simply, by the introduction of a normal coordinate,[3] Q, to:

$$T = \frac{1}{2}\sum_{i=1}^{f} \dot{Q}_i^2, \tag{3}$$

$$V = V_0 + \sum_{i=1}^{f} g_i q_i + \frac{1}{2}\sum_{i=1}^{f} \lambda_i Q_i^2, \tag{4}$$

so that the Lagrange equations of motion are given by:

$$\frac{d^2Q}{dt^2} + g_i + \lambda_i Q_i = 0, \quad i = 1,2,\cdots\cdots,f. \tag{5}$$

The ordinary solution of Eq. 5 involves the simple harmonic motion around the center, $-g_i/\lambda_i$, and ν_i, the frequency:

$$Q_i = A\sin(2\pi\nu_i t+\alpha) - g_i/\lambda_i, \ \nu_i = \frac{1}{2\pi}\sqrt{\lambda_i}, \tag{6}$$

where A and α are determined from the initial conditions. The simple harmonic motion is generally thought to be a very fast motion of the nuclei. However, if we assume an infinitely slow motion[4] of the nuclei as the initial condition, the solutions are quite different from Eq. 6:

$$\frac{Q_i}{(g_i+\lambda_i Q_i)} = -\tau^2 = const.,$$

or:

$$Q_i = \frac{-\tau^2 g_i}{(1+\tau^2\lambda_i)}. \tag{7}$$

Thus, the normal coordinates are the solutions of the infinitely slow motion, *i.e.*, the "trajectories." If, and only if, all the gradients, g_i's, except one, say g_k, are zero, the nonvanishing trajectory is given by Q_k. This is the necessary and sufficient condition of the so-called "intrinsic reaction coordinate," previously defined by Fukui.[5]

The present normal coordinate analysis was applied to the HNC-to-HCN isomerization reaction using the *ab initio* STO-3G potential surface. The intrinsic reaction coordinate of this system was previously determined by Ishida *et al.*[6] by means of the gradient method: it was also treated by Cerjan and Miller[7] by making explicit use of the second-order derivatives of the potential energy surface. The equilibrium state of HNC has three vibrational modes, a NH-stretching vibration (4224 cm^{-1}), a CH-stretching vibration (2410 cm^{-1}), and a doubly-degenerate HNC bending vibration (758 cm^{-1}). All the reaction coordinates are, of course, zero. If the curvature of the potential energy surface is small enough for nuclei to reach far from the equilibrium position at a small excess vibrational energy, a chemical reaction will take place. Therefore, the initial step was taken along the lowest frequency vibration, the HNC bending. The step size was 0.2 Å. Departing from the equilibrium state, none of the gradients vanish, and no unique reaction coordinate is found. The distance to the bottom of a valley of the potential energy surface is found to be:

$$d_i = -g_i/\lambda_i, \tag{8}$$

d_3, corresponding to ν_3, being the largest in absolute value. Moving towards the bottom of valleys along ν_1 and ν_2, g_1 and g_2 become zero and the nonvanishing reaction coordinate remains Q_3.

The second step is to "walk uphill" along the reaction coordinate Q_3, taking care of the sign of the gradient. The process was repeated until the saddle point was reached, where the gradient along the reaction coordinate was zero. Then the reaction coordinate turned to "walk downhill" to the point of the HCN equilibrium. The whole process is

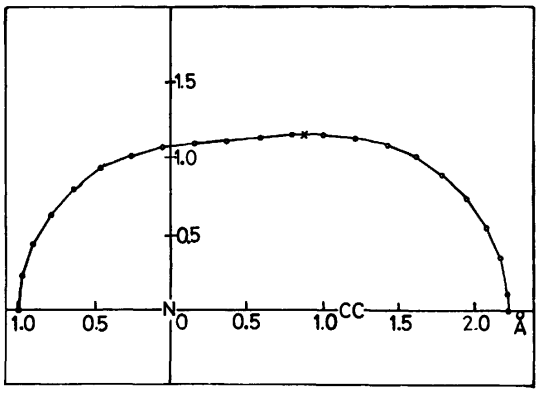

Fig. 1. The intrinsic reaction coordinate of H atom in the HNC-HCN isomerization reaction. The points denoted by —○— were calculated at the *ab initio* STO-3G potential surface and the solid lines connected these points. The symbol —⨯— is the saddle point. The N atom, denoted by N, is fixed at the origin and the C atom, denoted by C, moves slightly on the abscissa.

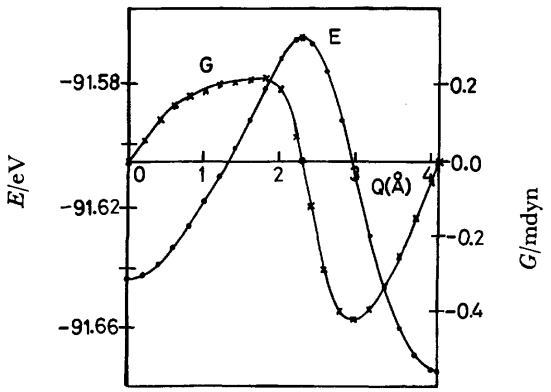

Fig. 2. The potential energy and the gradient curve along the intrinsic reaction coordinate of HNC-HCN reaction. The points denoted by —●— and —⨯— were calculated on the STO-3G potential surface. The point where the gradient is vanishing corresponds to the saddle point.

demonstrated graphically in Figs. 1 and 2, which completely reproduce those given by Ishida *et al.*[6]

More interesting features are seen in the variations of vibrational frequencies with the progress of the chemical reaction (Fig. 3). The frequency along the reaction coordinate is imaginary over a rather wide range. (The scattering of points is probably due to

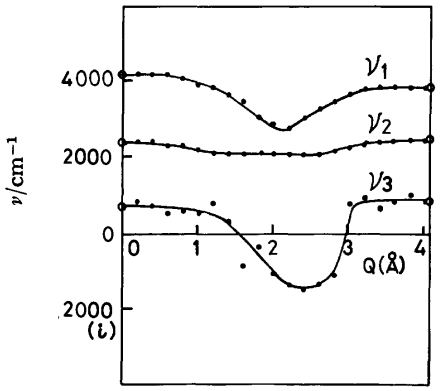

Fig. 3. The variation of the vibrational frequencies along the intrinsic reaction coordinate of HNC-HCN reaction. ν_1 corresponds to the NH or the CH stretching, ν_2 to the CN stretching, and ν_3 to the HNC bending vibrations. The points were calculated on the STO-3G potential surface.

errors in the numerical differentiation, as revealed by the lowest eigenvalue.) The CN stretching frequency is fairly constant throughout the whole process, while the NH stretching vibration transforms to the CH stretching vibration in the region of the transition state. These facts seem reasonable from the standpoint of chemistry.

The whole calculation, including the numerical differentiation to the second order, was carried out on the HITAC M-240H computer located at Gunma University. A more efficient program[8] and a more faster computer may facilitate the molecular mechanical analysis of chemical reactions.

References

1) W. J. Hehre, R. F. Stewart, and J. A. Pople, *J. Chem. Phys.*, **51**, 2651 (1969).

2) S. Cho, *Sci. Rep. Fac. Educ., Gunma Univ.*, **32**, 7 (1983) (Japanese).

3) E. B. Wilson, Jr., *J. Chem. Phys.*, **7**, 1047 (1939); **9**, 76 (1941).

4) K. Fukui, S. Kato, and H. Fujimoto, *J. Amer. Chem. Soc.*, **97**, 1 (1975).

5) K. Fukui, *J. Phys. Chem.*, **74**, 4161 (1970).

6) K. Ishida, K. Morokuma, and A. Komornicki, *J. Chem. Phys.*, **66**, 2153 (1977).

7) C. J. Cerjan and W. H. Miller, *J. Chem. Phys.*, **75**, 2800 (1981).

8) J. A. Pople, R. Krishnan, H. B. Schlegel, and J. S. Binkley, *Int. J. Quantum Chem. Symp.*, **13**, 225 (1979).

^{15}N NMR Spectra of Cobalt(III) Complexes Containing $^{15}NO_2^-$

Yoshio ODAKA, Akira YAMASAKI, and Masatoshi WATABE*
General Education Department, Kogakuin University, Hachioji, Tokyo 192
(Received April 25, 1985)

Synopsis. The nitrogen-15 nuclear magnetic resonance spectra of the cobalt(III) complexes containing $^{15}NO_2^-$ were first measured; the coordination chemical shifts, $\Delta\delta$ ($=\delta_{complex}-\delta_{free}$), were found to be from 135.0 to 161.5 ppm. The relationship between $\Delta\delta$ and the geometrical configuration was discussed in terms of the paramagnetic anisotropy of the cobalt(III) ion.

The nuclear magnetic resonance spectroscopy of nitrogen in coordination compounds is an area of considerable potential interest. Only a few ^{15}N chemical shift data of the cobalt(III) complexes have, however, been reported.[1-4] In our previous paper,[5] we reported the ^{15}N-NMR data for the bis (L-aspartato)cobaltate(III) and discussed the main factor which affects the ^{15}N chemical shift by using the magnetic anisotropy[6,7] of the central cobalt ion. This method could explain the trend of the ^{15}N chemical shifts of $[Co(L\text{-}asp)_2]^-$ to a certain extent. However, it is necessary to collect a great many ^{15}N chemical-shift information concerning metal complexes. Herein we report on the ^{15}N NMR spectroscopy of the cobalt(III) complexes containing the $^{15}NO_2^-$ ion.

Experimental

Cis-$[Co(^{15}NO_2)_2(en)_2]Cl$[8] is prepared from $[Co(CO_3)(en)_2]$-Cl, and *trans*-$[Co(^{15}NO_2)_2(en)_2]Cl$,[9] from $Co(NO_3)_2\cdot 6H_2O$. These cis and trans complexes are too insoluble in water for the ^{15}N NMR spectra to be measured. In order to change the counter anion, a solution of these complexes was placed in a Sephadex C-25 cation-exchange column (Cl^- form). After the column had then been swept with water, the adsorbed material was eluted with 1 mol dm^{-3} sodium aspartate. The eluate was concentrated with a rotary evaporator at about 5 °C. The resulting complexes, $[Co(NO_2)_2(en)_2]$ aspNa, were very soluble in water. *Cis*-$[CoCl(^{15}NO_2)(en)_2]Cl$[10] and *trans*-$[CoCl(^{15}NO_2)(en)_2]NO_3$[11] were prepared from *trans*-$[Co(^{15}NO_2)_2(en)_2]NO_3$. These two complexes are soluble enough in water for the ^{15}N NMR spectra to be measured. The ^{15}N NMR spectra were measured in the Fourier transform mode with a Varian FT-80A spectrometer. The chemical shifts at 8.104 MHz were determined by the use of a 2-kHz range and a 16-K memory and were measured with respect to external ^{15}N ammonium chloride or ^{15}N sodium nitrite in D_2O. About 200 mg of material was dissolved in 1.5 cm^3 of H_2O in a 10-mm tube, and the spectra were accumulated 50000-70000 times at 37 °C.

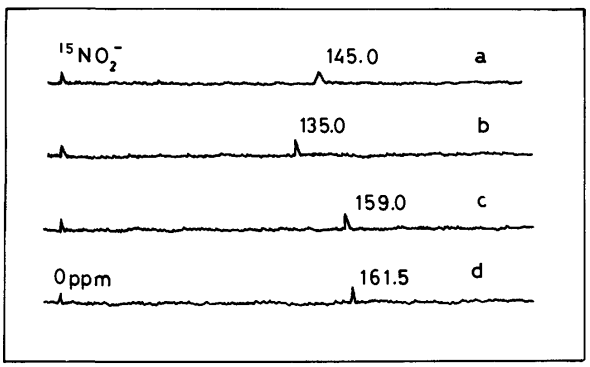

Fig. 1. ^{15}N NMR spectra in H_2O; a; *cis*-$[Co(NO_2)_2(en)_2]^+$, b; *trans*-$[Co(NO_2)_2(en)_2]^+$, c; *cis*-$[CoClNO_2(en)_2]^+$, d; *trans*-$[CoClNO_2(en)_2]^+$.

Results and Discussion

Figure 1 shows the ^{15}N NMR spectra of *trans*- and *cis*-$[Co(^{15}NO_2)_2(en)_2]$aspNa (asp=aspartate), *trans*-$[CoCl(^{15}NO_2)(en)_2]Cl$, and *cis*-$[CoCl(^{15}NO_2)(en)_2]NO_3$. The chemical shifts of the nitrogen-15 of the NO_2^- type coordinating to the cobalt(III) ion, were first obtained. The sharp singlet peaks on the left side of all the spectra are the peaks of the ^{15}N-enriched sodium nitrite. The chemical shifts are interpreted by means of Ramsey equations[12] as

$$\delta = \delta_p + \delta_d + \delta_i, \quad (1)$$

where the δ_p term is the paramagnetic component, the δ_d term is the diamagnetic term, and the δ_i term is the anisotropy term, which arises from the effects of neighboring atoms. Since the metal ion was the same in all cases, the paramagnetic and the diamagnetic contribution should be fairly constant, as was suggested by Bose and Abott[3]. Nakashima *et al.*[4] stated that the chemical shift, δ_i, induced by the paramagnetic anisotropy of cobalt(III) ion is of minor importance to the ^{15}N chemical shifts; this is in contrast with the finding that they are of dominant importance to the ^1H chemical shift. However, we reported in our previous paper that the

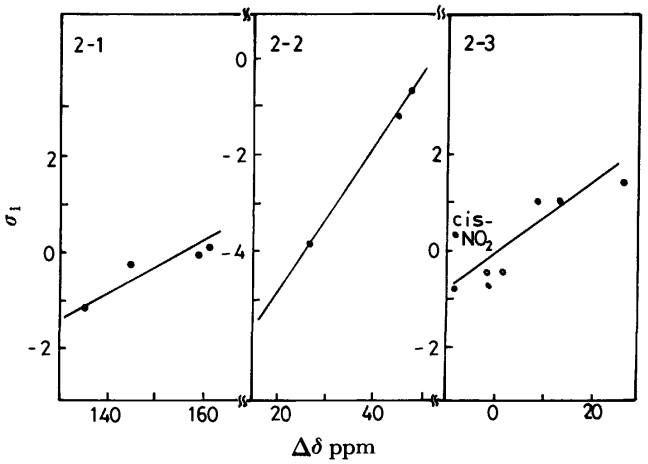

Fig. 2. The correlation between $\Delta\delta$obsd and σ_1, NO_2^- complex (from NO_2^-)(Fig. 2-1), ^{15}N-aspartate complex (from ^{15}N-asp)(Fig. 2-2), and the $^{15}NH_3$ complex (from $[Co(^{15}NH_3)_6]^{3+}$(Fig. 2-3), In Fig. 2-3, ○: Denotes the cis complex, ●: The trans complex.

calculated anisotropy shift could be correlated with the observed ^{15}N chemical shift if the former values are multiplied about 10 or 20 times. We tried again to calculate the δ_i term by using the method demonstrated by Yoneda.[7] For the complexes dealt with here, we postulate the following values $\delta(^1H) \propto \delta(^{15}N)$; $\langle r^{-3} \rangle = 5.77$ a.u, which is the value for $[Co(NH_3)_6]^{3+}$; the distance between nitrogen-15 and metal is 1.95 Å (=3.68 a.u.); $\delta(NO_2) = -4073$ ppm; $\delta(Cl) = -5910$ ppm, and $\delta(en/2) = -4603$ ppm. If the coordinated NO_2^- is placed in the Z axis, then $\theta = 0$, $\varphi = 0$, and the chemical shifts ($[Co(NH_3)_6]^{3+}$ is taken as a standard) can easily be evaluated to be as follows; −1.13 for *trans*-$[Co(NO_2)_2(en)_2]^+$, −0.28 for *cis*-$[Co(NO_2)_2(en)_2]^+$, 0.08 for *trans*-$[CoClNO_2(en)_2]^+$, and −0.21 for *cis*-$[CoClNO_2(en)_2]^+$. The correlation between the calculated and the experimental values is shown in Fig. 2-1. The slope is 0.040, and the standard deviation, R, is 0.925. This value is smaller than those for $[Co(L\text{-asp})_2]^-$ (0.154) and R(0.996)(Fig. 2-2). In Fig. 2-3, the correlation between the calculated chemical shift and the ^{15}N chemical shift of $[CoX(NH_3)_5]^{n+}$ is shown. The slope for the trans complex is 0.068, and R, 0.929. These good standard deviations of the three series confirm that paramagnetic anisotropy is one of the factors influencing the ^{15}N chemical shift of the cobalt(III) complexes. The ^{15}N chemical shift of the cis NH_3 of $[CoNO_2(NH_3)_5]^{2+}$ is not in line with those of the other $[CoX(NH_3)_5]^{n+}$-type complexes. We considered that hydrogen bonding exists in *cis*-$[CoNO_2(NH_3)_5]^{2+}$ between the NH_3 hydrogen and NO_2^- and that this hydrogen-bonding ^1H atom may influence the magnetic field around the ^{15}N atom. Fung *et al.*[13] reported that the chemical shifts of ^{15}N directly bound to cobalt are hardly affected at all by the solvents. This implies intramolecular hydrogen bonding. The difference in the slopes among the three series is natural because the atoms around the cobalt are different. Though, in every series, the experimental values are ten times those calculated, the calculated chemical shifts are useful in predicting which complex among similar complexes shows the chemical shift at a higher magnetic field.

References

1) S. W. Lehman and B. M. Fung, *Inorg. Chem.*, **11**, 214 (1972).
2) R. Hagen, J. P. Warren, D. H. Hunter, and J. D. Robert, *J. Am. Chem. Soc.*, **95**, 5712 (1973).
3) K. S. Bose and E. H. Abott, *Inorg. Chem.*, **16**, 3190 (1977).
4) Y. Nakashima, M. Muto, J. Takagi, and K. Kawano, *Chem. Lett.*, **1975**, 1075.
5) M. Watabe, M. Takahashi, and A. Yamasaki, *Inorg. Chem.*, **22**, 2650 (1983).
6) R. Freeman, G. R. Murray, and R. E. Richards, *Proc. Soc. London., Ser. A*, **242**, 455 (1957).
7) H. Yoneda, Y. Nakashima, *Bull. Chem. Soc. Jpn.*, **47**, 669 (1974).
8) *Inorg. Synth.*, Vol. XIV, p. 72.
9) *Inorg. Synth.*, Vol. IV, p. 176.
10) A. Werner, *Ann.*, **386**, 248 (1912).
11) A. Werner, *Ann.*, **386**, 251 (1912).
12) N. F. Ramsey, *Phys. Rev.*, **91**, 903 (1953).
13) B. M. Fung, S. C. Wei, T. H. Martin, and I. Yuan. Wei, *Inorg. Chem.*, **12**, 1203 (1973).

Behavior of Polyacrylamide-Acyclic Poly(oxyethylene)-coated Ion-selective Electrodes in Nonaqueous Solvents

Toshio NAKAMURA,* Kazuyuki OGIWARA, Kosuke IZUTSU, and G. A. RECHNITZ†
Department of Chemistry, Faculty of Science, Shinshu University, Asahi, Matsumoto 390
†*Department of Chemistry, University of Delaware, Newark, Delaware 19716, U.S.A.*
(Received June 1, 1985)

Synopsis. Ion-selective electrodes constructed with polyacrylamide(PAA) coupled to acyclic poly(oxyethylene) neutral carriers, tetraethylene glycol monododecyl ether (POE4) or hexaethylene glycol monododecyl ether (POE6), were reported. Nernstian responses were obtained to magnesium and barium ions in AN with the PAA-POE4 membrane and to copper(II) and silver(I) ions in DMSO with the PAA-POE6 membrane.

Ion-selective electrodes have been shown to be useful for analytical and physicochemical studies in nonaqueous and mixed solvents[1] and their applications are steadily increasing. Ion-selective electrodes applicable in nonaqueous solutions, however, have mainly been limited to those with glass- or crystalline- sensing elements because of possible damage to or dissolution of the electrode components by organic solvents. Development of other types of ion-selective electrodes for use in nonaqueous solutions is desirable.

Recently we showed that a gelatine membrane electrode coated on a copper disk was durable in dimethyl sulfoxide(DMSO) and could respond in a Nernstian way to the activities of the magnesium and calcium ions in DMSO.[2] We also showed that a platinum disk electrode coated with polyacrylamide (PAA) polymer coupled to macrocyclic polyether neutral carrier (dibenzo-18-crown-6) could serve as a barium ion sensor durable for at least twenty days in acetonitrile(AN).[3] In the present report, we will report the behavior of electrodes which have been prepared by coating a platinum disk with a membrane of PAA coupled to acyclic poly(oxyethylene) neutral carriers. As the acyclic poly(oxyethylene), tetraethylene glycol monododecyl ether (POE4) and hexaethylene glycol monododecyl ether (POE6) were used. The PAA-POE4 electrode showed a Nernstian response to the activities of the magnesium and barium ions in AN and the PAA-POE6 electrode showed a Nernstian response to those of the copper(II) and silver(I) ions in DMSO.

Experimental

Apparatus. Potentiometric measurements were carried out at 25 °C with a Beckman Φ71 digital pH/mV meter and a Yokogawa Denki type 3056 strip chart recorder. Construction of the indicator electrode is similar to that reported before.[3] The silver/silver ion reference electrode and the salt bridge were as shown below in Cell I.

Reagents. The POE4 and POE6 were obtained from Tokyo Kasei Kogyo Co. Ltd. All other chemicals were the same as those used in the previous reports.[2,3]

Preparation of PAA-POE4 and PAA-POE6 Conjugates. The acyclic neutral carriers, POE4 and POE6, were conjugated at the carboxyl group of the carboxyl-modified polyacrylamide by esterification in benzene under the coexistence of *p*-toluenesulfonic acid as a catalysis.[4] The products were washed with tetrahydrofuran and dried under high vacuum.

Construction and Preparation of the Indicator Electrode. The indicator electrodes were constructed using either PAA-POE4 or PAA-POE6. Small amounts of the respective materials were dissolved in 5 μl of water and spread on the end surface of a 3 mm platinum disk. After flushing with nitrogen gas to volatile water, it was placed in a desiccator with silica gel for a few hours. The electrode was then conditioned in 0.01 M Et_4NClO_4–AN (1 M=1 mol dm^{-3}) or 0.01 M Et_4NClO_4–DMSO for 1 d. The electrodes should be stored in the same solution for repeated use.

Measurements of the Electrode Potential. The response of the electrodes was tested in the following cell,

$$\mathrm{Ag}\,|\,0.005\ \mathrm{M}\ \mathrm{AgNO_3} + 0.01\ \mathrm{M}\ \mathrm{Et_4NClO_4(D)}\,\|$$
$$0.05\ \mathrm{M}\ \mathrm{Et_4NClO_4(D)}\,\|\,C\ \mathrm{M(ClO_4)}_x + 0.01\ \mathrm{M}$$
$$\mathrm{Et_4NClO_4(D)}\,|\,\mathrm{Polymer\ Membrane}\,|\,\mathrm{Pt}\cdots\ \mathrm{Cell\ I}$$

where D denotes AN or DMSO. $M(ClO_4)_x$ is the perchlorate of the cation to be tested (sodium, potassium, silver(I), magnesium, barium, copper(II) or zinc(II) ion). All the solutions were freshly prepared daily. The concentration, C in mol dm^{-3}, of the metal perchlorate was usually increased by the standard addition method to obtain calibration curves. Steady state potentials were read to ±0.1 mV. The electrode potentials were not significantly affected by a change in stirring rate.

Results and Discussion

The membrane electrodes, PAA-POE4 and PAA-POE6, constructed in this experiment were durable in AN and DMSO for at least about a week. The responses of these electrodes to the magnesium, barium, copper(II), and silver(I) ions in AN or DMSO are summarized in Table 1. Some typical calibration curves are also shown in Fig. 1. The activity of the metal ion, $a_{M^{n+}}$, was calculated by using the Debye-Hückel equation as previously described.[2] The results in Table 1 have not been corrected for the change of the liquid junction potential between the sample solution and the salt bridge of Cell I, but its effect seems to be small. In AN, the PAA-POE4 membrane electrode could respond in a Nernstian way to the activities of the magnesium and barium ions between the concentration ranges 5.0×10^{-7} M—5.0×10^{-3} M and 6.8×10^{-6} M—1.5×10^{-3} M, respectively. In DMSO, the PAA-POE6 electrode could respond in a Nernstian way to the activities of copper(II) and silver(I) ions between the concentration ranges 1.5×10^{-5} M—1.6×10^{-3} M and 6.2×10^{-5} M—1.1×10^{-2} M, respectively. The response of the PAA-POE4 electrode to the activity of the silver(I)

Table 1. The responses of the polymer membrane electrodes to some metal ions in nonaqueous solvents at 25 °C[a)]

Ion	$2r_c$,Å	Solvent	Slope (mV/$pa_{M^{n+}}$)	Range of the linear response ($pa_{M^{n+}}$)
PAA-POE4				
Mg^{2+}	1.30	AN	29.2±1.1 (5)	6.7—3.0
Ba^{2+}	2.70	AN	26.8±2.1 (4)	5.7—3.4
Ag^{+}	2.52	DMSO	48.5±2.1 (3)	4.3—2.3
PAA-POE6				
Cu^{2+}	1.44	DMSO	30.4±1.5 (10)	5.2—3.2
Ag^{+}	2.52	DMSO	61.3±1.5 (3)	4.3—2.1

a) The figures in parentheses denote the number of experiments. r_c : crystallographic ionic radius.

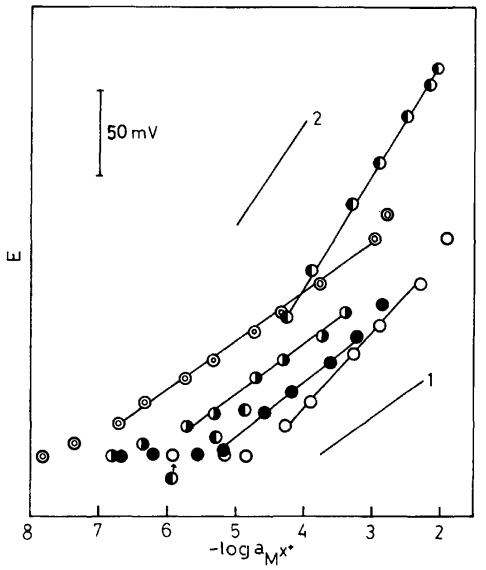

Fig. 1. Calibration curves in nonaqueous solvents at 25 °C. Lines 1 and 2, theoretical slope for divalent cations (29.6 mV/$pa_{M^{2+}}$) and for univalent cations (59.2 mV/$pa_{M^{+}}$), respectively. ◎, Mg^{2+} in AN with PAA-POE4; ◑, Ba^{2+} in AN with PAA-POE4; ○, Ag^{+} in DMSO with PAA-POE4; ◐, Ag^{+} in DMSO with PAA-POE6; ●, Cu^{2+} in DMSO with PAA-POE6.

ion in DMSO was sub-Nernstian between the concentration of 6.2×10^{-5} M and 6.5×10^{-3} M. In all cases, the steady state potential was reached within ten minutes after each increase of the ionic concentration. Both electrodes of PAA-POE4 and PAA-POE6, however, showed poor responses to sodium and potassium ions in AN. These electrodes also showed poor responses to sodium, potassium, and zinc(II) ions in DMSO. The approximate selectivity coefficient obtained for the magnesium ion *vs.* barium ion, $\log k_{Mg^{2+},Ba^{2+}}$, was 1.2 by the mixed solution method in AN in the case of PAA-POE4 electrode.

Yanagida *et al.*[5)] showed a specific interaction of the magnesium ion with POE4 in acetone and suggested that the so called "hole-size rule" in the complexation of metal ions with crown ethers could be applicable to complexation with such acyclic polyethers as POE4 and POE6. If we consider that the magnesium ion in AN reacts with POE4 to form a stable complex, the response of the PAA-POE4 electrode to a wide concentration range of the magnesium ion in AN may be reasonable. But the electrode could also respond, though in a narrower concentration range, to the barium ion with a larger ionic size. The fact that the response to the silver(I) ion in DMSO was Nernstian with the PAA-POE6 electrode but was sub-Nernstian with the PAA-POE4 electrode may also be related to the hole sizes of POE4 and POE6. It seems reasonable to assume that complexation of the metal ions with POE4 or POE6 is essential for the electrode response. For correlation between the electrode response and the hole size concept, however, more detailed data will need to be obtained. In connection with this, solvents may play important roles on the electrode behavior through their solvation to the metal ions and also to the electrode materials. The extremely slow and poor response behavior of the electrode constructed of polyacrylamide polymer alone in AN has been reported before.[3)] The present experiment confirms that the presence of the neutral carrier, POE4 or POE6, in the membrane serves to stabilize the electrode potential and to improve the reproducibility and dynamic response behavior. Further experiments concerning the response behavior of these electrodes in other aprotic organic solvents and the application of these electrodes to obtain information about the solvent effect on the cations used in this experiment are now under investigation in this laboratory.

References

1) For review, E. Pungor, K. Tóth, P. G. Klatsmányi, and K. Izutsu, *Pure Appl. Chem.*, **55**, 2029 (1983).

2) T. Nakamura, S. Morozumi, and K. Izutsu, *Chem. Lett.*, **1982**, 1317.

3) T. Nakamura and G. A. Rechnitz, *Anal. Chem.*, **57**, 393 (1985).

4) C. F. H. Allen and F. W. Spangler, "Organic Syntheses Collective," ed.-in-chief E. C. Horning, Wiley, New York (1955), Vol. 3, p. 203.

5) S. Yanagida, K. Takahashi, and M. Okahara, *Bull. Chem. Soc. Jpn.*, **51**, 3111 (1978).

Induced Circular Dichroism of Bis(tropolonato)copper(II) with Optically Active Amines

Tasuku MURAKAMI
Faculty of Education, Iwate University, Ueda, Morioka 020
(Received June 18, 1985)

Synopsis. Bis(tropolonato)copper(II) forms adducts with chiral aromatic amines and exhibits circular dichroism(CD) induced for d-d and intra-ligand transitions. The applicability of the dispersion-induced CD theory to this complex system is discussed.

In a previous paper, we reported the CD spectra of some copper(II) β-diketonates in optically active bases such as (+)-1-phenylethylamine.[1] The chiral base coordinates at the axial position of the complexes to form mono base-adducts, gives a dissymmetric influence to the parent achiral complexes, and induces optical activities to their electronic transitions.

Dispersion-induced circular dichroism(DICD) treatment has been developed by Schipper for the interaction between achiral and chiral species with no specific orientation; for example, an achiral solute/chiral solvent system.[2,3] He applied this theory to the above system of copper(II) β-diketonates with optically active amines and his results supported most of our discussion.[2]

However, the examined achiral complex/chiral amine couples were so limited that the observations and theoretical applications could not be generalized. Thus, we have studied more systems including a tropolonate complex and (+)-1-(1-naphthyl)ethyl- and (+)-1-(2-naphthyl)ethylamine.

Experimental

Bis(tropolonato)copper(II), $Cu(trop)_2$, was prepared according to the literature.[4] (+)-1-(1-Naphthyl)ethylamine was commercially available and distilled before use. $[\alpha]_D^{20}=+58.2°$ (c=2, methanol). 1-(2-Naphthyl)ethylamine was prepared from 2′-acetonaphthone according to literature[5] and resolved by the use of (+)-tartric acid. For its (+)-antipode, $[\alpha]_D^{20}=+19.6°$ (c=3.5, methanol). Chloroform of spectro-grade was used as solvent without further purification.

TABLE 1. THE VALUES OF $\Delta\varepsilon$ AND STABILITY CONSTANT(K_b) FOR THE 1:1 BASE-ADDUCTS OF $Cu(trop)_2$ IN CHLOROFORM

(+)-Amine	K_b, M^{-1} (25 °C)	$\Delta\varepsilon$, $cm^{-1}M^{-1}$ ($\tilde{\nu}/10^3\,cm^{-1}$)
1-Phenylethylamine	2.3	+0.009(12.7), −0.002(16.7) −0.32(25.6), +0.55(30.0)
1-(1-Naphthyl)-ethylamine	3.1	+0.027(12.4) −1.01(24.8), +0.64(30.4)
1-(2-Naphthyl)-ethylamine	2.6	−0.65(25.6), +0.66(29.8)

Upon the addition of bases, the visible absorption band shifts to a longer wavelength with a much-increased intensity (Fig. 1). From this spectral change, the formation of mono base-adducts is obvious.[6] The formation constant (K_b) of the adducts was determined by the ordinary spectrophotometric method.[7] The values of K_b are listed in Table 1.

The spectra of the chiral amine-adducts were obtained for the chloroform solutions containing 5×10^{-3} M of complex and 1—1.5 M of amines(1 M=1 mol dm^{-3}). Under this condition, approximately 70% of the parent complex transforms to the adduct, in spite of the low K_b values. The values of $\Delta\varepsilon$ summarized in Table 1 are based on the adduct concentration, whereas the vertical scales of Fig. 1 refer to 1 mol of the copper ion. Since tropolone seems to undergo no corbonyl reactions,[4] the chelated tropolonate appeared stable even in the presence of primary amines.

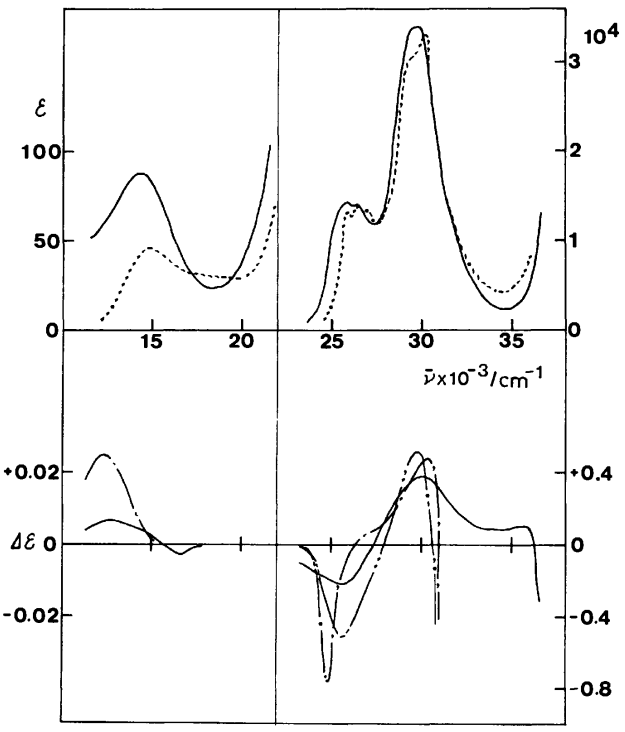

Fig. 1. Absorption and CD spectra of $Cu(trop)_2$ with the addition of (+)-amines in chloroform; the concentration of complex is about 5×10^{-3} M and the numbers in parentheses represent mole ratios in amine/complex. ----, no amine added; ——, (+)-1-phenylethylamine (200); — — —, (+)-1-(1-naphthyl)ethylamine (190); — — — —, (+)-1-(2-naphthyl)ethylamine (240).

Results and Discussion

Figure 1 shows the absorption and CD spectra of $Cu(trop)_2$ in chloroform containing (+)-amines. The main CD band in the visible region appears at the lower wavenumber side of the broad d-d absorption band. This is the same result as those for the β-diketonate complexes as previously reported.[1] Therefore, this CD band originates from the two low-energy transitions, $d_{z^2} \rightarrow d_{x^2-y^2}$ and $d_{xy} \rightarrow d_{x^2-y^2}$. As suggested by Schipper,[2] only the latter, which is *z*-polarized magnetic dipole-allowed in a parent molecular symmetry D_{4h}, mainly contributes the optical activity.

Two intense absorption bands are observed at around 26000 and 30000 cm^{-1} as shown in Fig. 1, and at a higher wavenumber another more intense band is expected to appear.[4] Free tropolone also exhibits three bands, each located at a slightly higher wavenumber compared with the corresponding three bands of $Cu(trop)_2$.[4,8,9] Such a red shift of the intra-ligand band due to the complex formation has been also observed for other ligands, acetylacetone, salicyl-aldehyde, and so on.[10,11] Thus, from the positions and intensities, the two bands at 26000 and 30000 cm^{-1} are supposedly associated with the intra-ligand transitions, although their more detailed nature is not clear so far.

Upon the addition of amine, the tropolone bands shift slightly to lower wavenumbers. Any of three (+)-amines used induces similar optical activities; a negative band at 26000 and a positive one at 30000 cm^{-1}. These (+)-amines show an intrinsic negative CD band at the lowest energy transition which corresponds to the L_b band of phenyl or naphthyl ring.[12,13] On the basis of these findings, the induced CD of this region is discussed as follows.

(1) Schipper has suggested that DICD bands for the electric dipole-allowed transitions of achiral species have the same sign as that of the intrinsic CD of the inducing transition of chiral species.[2] However, the induced optical activity observed possesses different signs as mentioned above. This discrepancy between the DICD theory and the observation would be caused by the assumption that the achiral and chiral species have no orientational correlation. In the amine-adducts, the amine molecule acts as ligand rather than as mere solvent and coordinates to the copper ion. Therefore, the chiral amine and the achiral tropolonate will have a fairly fixed orientation, although the aromatic chromophore of the amine will rotate, to some extent, around the tetragonal axis in the solution. The two tropolone transitions in question possess different polarizations along the tropolone plane,[9] which may be responsible for their opposite-signed CD bands.

(2) The exciton coupling between the transitions of the tropolonate rings cannot constitute the inducing mechanism, since only one CD component appears under the lobe of each absorption band, as previously mentioned.[1]

(3) The inherent CD intensity associated with the L_b band of (+)-1-(1-naphthyl)ethylamine is much different from that of (+)-1-(2-naphthyl)ethylamine; the value of $\Delta\varepsilon$ at 320 nm is -0.03 for the former and -0.27 for the latter in chloroform.[14] This comes from the polarization of the L_b transition which is along the long axis of the naphthalene plane. In spite of such a different electric inducing power,[2] these two (+)-amines induce comparable optical activities for each of the two tropolonate transitions. This also suggests that the orientation between the chromophores of the chiral amine and the achiral tropolonate ring is significant as mentioned above.

The author thanks Prof. Masahiro Hatano for his permission of use of Jasco J-500c spectropolarimeter.

References

1) T. Murakami and M. Hatano, *Inorg. Chem.*, **14**, 999 (1975).
2) P. E. Schipper, *J. Am. Chem. Soc.*, **98**, 7938 (1976).
3) P. E. Schipper and A. Rodger, *J. Am. Chem. Soc.*, **107**, 3459 (1985).
4) J. W. Cook, A. R. Gibb, R. A. Raphael, and A. R. Somerville, *J. Chem. Soc.*, **1951**, 503.
5) A. W. Ingersoll, "Organic Syntheses," Wiley, New York (1943), Coll. Vol. 2, p. 503.
6) L. L. Funck and T. R. Ortolano, *Inorg. Chem.*, **7**, 567 (1968).
7) K. Ueda, *Bull. Chem. Soc. Jpn.*, **51**, 805 (1978).
8) M. Tsuboi, *Bull. Chem. Soc. Jpn.*, **25**, 369 (1952).
9) H. Hosoya, J. Tanaka, and S. Nagakura, *Tetrahedron*, **18**, 859 (1956).
10) S. Yamada and R. Tsuchida, *Bull. Chem. Soc. Jpn.*, **29**, 694 (1956).
11) K. Sone, *J. Am. Chem. Soc.*, **75**, 5207 (1953).
12) J. R. Platt, *J. Chem. Phys.*, **17**, 484 (1949).
13) H. E. Smith and T. C. Willis, *J. Am. Chem. Soc.*, **93**, 2282 (1971).
14) T. Murakami, unpublished data.

Chlorination of Poly(vinyltoluene) by Electrolysis in an Organic/Water Suspension System

Yoshiharu MATSUDA, Masayuki MORITA,* Hiroshi YAMAMOTO, Hiroyuki WATANABE,† Tooru SEITA,† and Akira AKIMOTO†

Department of Industrial Chemistry, Faculty of Engineering, Yamaguchi University, Tokiwa-dai 2557, Ube 755

†*Research Laboratory, Toyo Soda Manufacturing Co., Ltd., Tonda 4560, Shin-nanyo 746*

(Received April 20, 1985)

Synopsis. Chlorinated poly(vinyltoluene) was synthesized by controlled-current electrolysis of poly(vinyltoluene) in a suspension system consisting of aqueous and organic solutions. A high Cl-content polymer, in which Cl was introduced to the methyl group and the main chain, was obtained without changes in the molecular-weight distribution of the polymer.

Chlorinated poly(vinyltoluene) (C-PVT) and its derivatives are promising materials as sensitive nega-type microresists which cross-link under electron beam or X-ray irradiation.[1-3] Among them, poly[(chloromethyl)styrene] (CMS) has been synthesized by the chloromethylation of polystyrene (PS)[4] (Scheme 1). This method, however, involves a rather

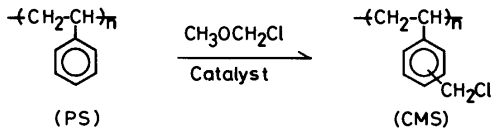

Scheme 1.

complicated procedure and tends to change the molecular-weight (MW) distribution of the product polymer.[3] On the other hand, a direct chlorination of poly(vinyltoluene) (PVT) by Cl_2 gas or thionyl chloride with some catalysts also yields C-PVT.[5] However, with this method it is difficult to control the Cl content and the substitution position in the polymer. We have found a simple process for introducing Cl to the methyl group as well as to the main chain of PVT which involves electrolysis.

There has been much work concerning the electro-halogenation of aromatic compounds with low molecular weights,[6] but little is known about the electro-halogenation of macromolecular compounds.[7] The principal reason for this is the difficulty in choosing a homogeneous electrolyte system. In this work, we have employed a suspended system consisting of an organic solution and an aqueous electrolytic solution.

Experimental

The starting PVT was prepared at Toyo Soda Manufacturing Co. Two kinds of polymers were used; one was a mixture of *m*- and *p*-isomers ($\overline{Mn}\simeq40000$: PVT-I), and the other consisted of *p*-isomer only ($\overline{Mn}\simeq170000$: PVT-II). The polydispersivity ($\overline{Mw}/\overline{Mn}$) was about 1.1 for both polymers. An electrolytic synthesis was conducted in a suspension system consisting of aqueous and organic solutions. The aqueous phase contained an acid, HCl, which acted as both a supporting electrolyte and a Cl source. The organic solvent was dichloromethane (CH_2Cl_2), chloroform ($CHCl_3$), or benzene (C_6H_6), which dissolved the substrate PVT. The electrolytic cell was a normal beaker-type, one-compartment cell (volume: $\simeq$50 cm^3). The anode was a platinum wire (surface area: 3.5 cm^2), and the cathode was a platinum sheet (surface area: 6.5 cm^2). Controlled-current electrolysis was carried out with vigorous stirring of the solution using a magnetic stirrer while water-cooling the cell (16°—20 °C). The electric charge was normally 2.41×10^5 C (2.5 F) per mol of monomer. Such a charge ideally enables 1.25 atoms of Cl per monomer unit to be introduced to PVT.

The product polymer, separated from the organic phase, was purified by reprecipitation. No attempt was made to exclude light during the electrolysis, but the isolated products were stored under an Ar atmosphere while shielding the container from light. The Cl content in the product was determined by an elemental analysis, and the MW distribution of the polymer was estimated by gel permiation chromatography (GPC). The chlorinated position in the product polymer was determined by ^{1}H NMR spectroscopy (solvent: $CDCl_3$, standard reference: TMS).

Results and Discussion

Table 1 shows the results of the electro-chlorination of PVT in organic/water suspension systems. An estimation of the MW distribution of the products was based on the shape of the GPC curves, and is qualitatively described in the last column of Table 1 (symbols A, B, and C). The values of $\overline{Mw}/\overline{Mn}$ were determined from the calibration curve of the standard PS, and were $\simeq$1.1 for the products labeled "A", $\simeq$1.3 for "B", and $\simeq$2.1 (or above) for "C". As shown in the table, PVT-I was highly chlorinated, and the MW distribution was little changed by the chlorination. It was assumed that the electro-chlorination of PVT proceeds with a two-electron transfer, like the anodic halogenation of usual organic substances.[6,8] Thus, a Cl content of 1.14 in the product (Run 2) is equivalent to a 91% current efficiency. During the chlorination of PVT-II, the MW distribution of the product tended to spread, though Cl was introduced into PVT with 0.9 atoms or more per monomer unit (Runs 3—5). The product labeled "C" in the table was not satisfactory as a microresist.[3] A change in the MW distribution was not observed upon decreasing the PVT-II concentration (Runs 6 and 7), but the Cl content in the product was also lowered ($<$0.1).

The effective chlorination of PVT-II without any change in the MW distribution became feasible upon

Table 1. Electro-chlorination of poly(vinyltoluene) in organic/water suspension systems

Run[a]	Organic Solvent[b]	W[c] wt%	Current[d] A	Cell voltage[e] V	Electric charge F[f] (unit-VT mol)$^{-1}$	Cl content in the product atom (unit-VT)$^{-1}$	MW distribution of the product[g]
1	CH_2Cl_2	3	0.5	4	2.5	1.08	A
2	CH_2Cl_2	5	0.5	4	2.5	1.14	A
3	CH_2Cl_2	5	0.3	3	2.5	0.98	C
4	CH_2Cl_2	5	0.5	3	2.5	0.93	C
5	CH_2Cl_2	5	0.7	5	0.5	0.22	C
6	CH_2Cl_2	1	0.5	4	2.5	<0.1	B
7	CH_2Cl_2	1	0.1	2	2.5	<0.1	B
8	$CHCl_3$	1	0.1	2	2.5	0.29	A
9	C_6H_6	1	0.1	2	2.5	0.47	A
10	C_6H_6	3	0.1	2	2.5	0.89	A
11	C_6H_6	3.3	0.5	3	2.5	0.86	A
12	C_6H_6	1	0.2	2	10.0	1.38	B

a) Runs 1 and 2: PVT-I($\overline{Mn}\simeq40000$), Runs 3—12: PVT-II($\overline{Mn}\simeq170000$), b) Organic phase/aqueous phase (12 mol dm^{-3} HCl)=1:1 by volume, c) W is PVT concentration in organic phase, d) Surface area of the anode (Pt): 3.5 cm^2, e) Voltage at the beginning of the electrolysis, f) F denotes 96485 C (2.5 F=2.41×10^5 C), g) Represented qualitatively; A denotes $\overline{Mw}/\overline{Mn}\simeq1.1$, B≃1.3, C≳2.1, ($\overline{Mw}/\overline{Mn}$ of the original PVT≃1.1).

choosing an appropriate solvent for the organic phase. Regarding electrolysis in a $CHCl_3/H_2O$ suspension (Run 8), the MW distribution was little spread, but the Cl content was relatively low. The use of C_6H_6 as a solvent brought about an improvement in the Cl content without broadning of the MW distribution (Runs 9—11). The Cl content increased upon increasing the PVT concentration, but the influence of the current density on the Cl content was rather small. An increase in the electric charge lead to a high Cl content in the product (Run 12). In this case, however, the current efficiency fell to 30% or less, and the MW distribution of the polymer tended to spread. This is probably due to the electrochemical reduction of the product C-PVT at the counter electrode (cathode), where a subtraction of the Cl from the C-PVT and/or a reductive cross-linking of the polymer might occur.

The differences in the results regarding electro-chlorination between PVT-I and PVT-II are probably responsible for the differences in the mean molecular weight and/or the isomer ratio of the starting PVT. On the other hand, solvent properties, such as the donor- and acceptor numbers[9], apparently affected the results of the PVT-II chlorination. It is supposed that the molecular Cl_2 formed by a side reaction is more polarized in CH_2Cl_2 than in C_6H_6. The activated Cl_2 in CH_2Cl_2 would promote the polymer chains to cross-link with each other.

The ^{1}H NMR spectra of the product polymer suggested that chlorination occurred at the methyl group of toluene as well as at the α- and β-positions of the chain (Scheme 2). A variation in the

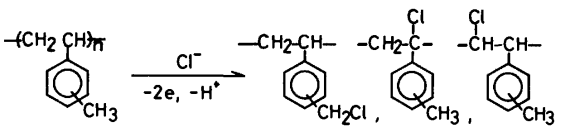

Scheme 2.

experimental conditions (such as the PVT concentration and the current density) did not seem to affect the chlorinated positions. In the electro-halogenation of low molecular-weight aromatics such as alkylbenzenes[6,10] and alkoxybenzenes,[11–13] nuclear-substituted compounds have been main products. During the present electro-chlorination of PVT, however, nuclear substitution was not detected. The differences in the substitution position might originate from the difference in the solvent that was used. That is, homogeneous organic solutions containing polar solvents were used in previous work for the chlorination of alkyl- or alkoxybenzenes.[6,10–13] However, a suspension of C_6H_6 (or CH_2Cl_2)/H_2O was employed in the present work. These solvent effects, which relate to the details of the reaction mechanism, are now under investigation.

References

1) J. Kosar, "Light-Sensitive System," John Wiley, New York (1965), p. 141.
2) H. Y. Ku and L. C. Scala, *J. Electrochem. Soc.*, **116**, 980 (1969).
3) S. Imamura, *J. Electrochem. Soc.*, **126**, 1628 (1979).
4) G. O. Jones, *Ind. Eng. Chem.*, **44**, 2686 (1952).
5) P. H. Jessie, M. C. Dewilde, and G. Smet, *J. Polymer Sci.*, **16**, 429 (1955).
6) *e.g.* M. Mastragostino, G. Casalbore, and S. Valcher, *J. Electroanal. Chem. Interfacial Electrochem.*, **56**, 117 (1974).
7) S. P. Prokopchuk, USSR Patent 740796 (1980); *Chem. Abstr.*, **93**, 115270a (1980).
8) D. K. Kyriacou, "Basics of Electroorganic Synthesis," John Wiley, New York (1981), p. 56.
9) V. Gutmann, *Electrochim. Acta*, **21**, 661 (1976).
10) Y. Matsuda, A. Terashima, and K. Nakagawa, *Denki Kagaku*, **51**, 790 (1983).
11) T. Matsue, M. Fujihira, and T. Osa, *J. Electrochem. Soc.*, **126**, 500 (1979).
12) Y. Matsuda and H. Hayashi, *Chem. Lett.*, **1981**, 661.
13) Y. Matsuda, A. Terashima, N. Sakota, and K. Nakagawa, *Denki Kagaku*, **49**, 669 (1981).

 © 1985 The Chemical Society of Japan Bull. Chem. Soc. Jpn., 58, 3415—3422 (1985)

Comparison of the Excited-state Dipole Moments and Polarizabilities Estimated from Solvent Spectral Shifts with Those from Electrooptical Measurements

Takehiro ABE* and Idowu IWEIBO†
College of General Education, Tohoku University, Kawauchi, Sendai 980
(Received June 3, 1985)

On the assumption that the average energy for all transitions from a low-lying excited state to all other states was approximately the same as that for all transitions from the ground state to all excited states, Abe's improved expression for the solvent spectral frequency shift (*Bull. Chem. Soc. Jpn.*, **54**, 327 (1981)) was applied to spectral data for some neutral organic molecules in solution in order to estimate their excited-state dipole moments and polarizabilities. The changes in the dipole moments and/or polarizabilities of these molecules upon excitation were compared with those obtained from electrooptical measurements. Both methods give results that are consistent.

Many theories[1-11] have hitherto been proposed regarding solvent spectral frequency shifts of organic molecules. On the basis of some of these, dipole moments and polarizabilities have been estimated for the excited states of organic molecules. Such detailed information, which essentially leads to knowledge regarding excited-state structures of organic molecules, may help in the understanding of the photophysics and photochemistry of such molecules. Alternatively, changes in the dipole moments and/or polarizabilities upon excitation have been obtained for many organic molecules in the vapor phase, in solution, or in a crystalline host from electrooptical measurements. In particular, the magnitudes of the changes in the dipole moments of some substituted benzenes, directly determined by a technique involving the optical Stark effect[12] in the gas phase, seem to be very reliable. On the basis of a few assumptions, the values of the excited-state dipole moments and/or polarizabilities of molecules in solution or in a crystalline host have been obtained using electric-field perturbation techniques. Recently, Morales,[13] Prabhumirashi *et al.*,[14,15] and Koutek[16] have tried to compare their results, which were obtained from solvent spectral shifts, with those obtained from electrooptical measurements. Their comparisons appear, however, to be insufficient as will be shown below.

Until now, there has been no detailed and systematic study comparing the excited-state dipole moments and/or polarizabilities estimated from the solvent spectral shifts with those determined from electrooptical measurements. Such comparisons are necessary, in part, to justify the theoretical expressions for the solvent spectral frequency shifts and, in part, to confirm the reliability of the electrooptical measurements or to reveal any inadequacies leading to discrepancies in both methods of measurement and in their variants. Electrooptical measurements are, in general, difficult. In particular, the most reliable technique regarding the optical Stark effect in the gas phase is confined to vaporizable substances, while measurements of solvent spectral shifts are easy and widely applied. It is, therefore, desirable to find a solvent spectral shift theory that gives excited-state dipole moment and polarizability values that are comparable to those of electrooptical measurements. This paper applies Abe's generalized equation,[4] which includes all interaction modes, to data for a representative group of compounds. There is, generally, reasonable agreement between the results of the present type analysis and those for electrooptical measurements. This shows that the use of a multiple linear regression analysis to compute the excited-state dipole moment and polarizability without introducing solvent macroscopic parameters, such as the relative permittivity and the refractive index, is certainly an advantage.

Theory

According to Abe's improved theory,[4] the wave number (σ_{i0}) of a transition from the ground state to the ith-excited state of a neutral solute molecule in solution is given by:

$$\sigma_{i0} = \sigma_{i0}^{\circ} + A \times \frac{(d^s/M_r^s)^{2/3}(p_{00}^s)^2}{(r_A+r_s)^4} + B \times \frac{(d^s/M_r^s)^{2/3}\alpha_{00}^s}{(r_A+r_s)^4}, \quad (1)$$

where

$$r_A = (3M_r^A/4\pi L d^A)^{1/3}, \quad (2)$$

$$r_S = (3M_r^s/4\pi L d^s)^{1/3}, \quad (3)$$

$$A = \frac{\pi}{hc}\left(\frac{4\pi L}{3}\right)^{2/3} \times \left[\frac{2\{(p_{00}^A)^2 - p_{00}^A p_{ii}^A \cos\theta\}}{3(4\pi\varepsilon_0)^2 kT} + \frac{(\alpha_{00}^A - \alpha_{ii}^A)}{4\pi\varepsilon_0}\right], \quad (4)$$

and

$$B = \frac{\pi}{hc}\left(\frac{4\pi L}{3}\right)^{2/3} \frac{1}{4\pi\varepsilon_0} \times \left[\{(p_{00}^A)^2 - (p_{ii}^A)^2\} + \frac{3}{2} \times \left(\frac{\Delta E_0^A \alpha_{00}^A}{1+\Delta E_0^A/\Delta E_0^s} - \frac{\Delta E_i^A \alpha_{ii}^A}{1+\Delta E_i^A/\Delta E_0^s}\right)\right]. \quad (5)$$

†Present address: Department of Chemistry, University of Ibadan, Ibadan, Nigeria.

The corresponding transition energy (in cm^{-1}) of the molecule in a vapor state is denoted by σ_{i0}°. For example, the superscripts/subscripts (A and s) denote the solute and solvent molecules, respectively. The symbol c is the speed of light in vacuum, h the Planck constant, L the Avogadro constant, ε_0 the permittivity of a vacuum, M_r the relative molecular mass, and d the density. Moreover, p_{00} and α_{00} denote the electric dipole moment and the electric isotropic polarizability, respectively, for the ground state. The corresponding values for the ith-excited state are p_{ii} and α_{ii}. The angle between $\boldsymbol{p}_{00}^{A}$ and $\boldsymbol{p}_{ii}^{A}$ is denoted by θ. In addition, ΔE_0 and ΔE_i denote the average transition energies for all transitions from the ground state and the ith-excited state, respectively, to all other excited states. The average transition energy (ΔE_0) is usually replaced by the ionization potential (I_0) of the ground state. Similarly ΔE_i is replaced by the ionization potential of the excited state as given by $\Delta E_i^{A}=I_0^{A}-hc\sigma_{i0}^{\circ}$.[4,17] However, Amos and Burrows[1a,18] stated that the average transition energies in Abe's previous expression[17] should be approximately the same for transitions from a ground state and an excited one. In applying Eq. 1, therefore, we have adopted this assumption of Amos and Burrows:

$$\Delta E_i^{A} = \Delta E_0^{A} = I_0^{A}. \tag{6}$$

As is described in a previous paper,[4] Eq. 1 has been derived on the assumption that a spherical solute molecule exhibits no effective hydrogen bonds or complexes with spherical solvent molecules.

Explicitly, we can rewrite Eq. 1 with the use of Eq. 6 as

$$C \times (p_{00}^{A}\cos\theta)p_{ii}^{A} + D \times (p_{ii}^{A})^2 + E \times \alpha_{ii}^{A} = \sigma_{i0}^{\circ} - \sigma_{i0} + F, \tag{7}$$

where

$$G = \frac{(d^s/M_r^s)^{2/3}}{(r_A+r_s)^4} \times \frac{\pi}{hc}\left(\frac{4\pi L}{3}\right)^{2/3}, \tag{8}$$

$$C = G \times \frac{2(p_{00}^{s})^2}{3(4\pi\varepsilon_0)^2kT}, \tag{9}$$

$$D = G \times \frac{\alpha_{00}^{s}}{4\pi\varepsilon_0}, \tag{10}$$

$$E = G \times \left\{\frac{(p_{00}^{s})^2}{4\pi\varepsilon_0} + \frac{3}{2} \times \frac{I_0^{s}I_0^{A}\alpha_{00}^{s}}{I_0^{s}+I_0^{A}}\right\}, \tag{11}$$

and

$$F = G \times \left[\frac{2(p_{00}^{s})^2(p_{00}^{A})^2}{3(4\pi\varepsilon_0)^2kT} + \frac{1}{4\pi\varepsilon_0} \times \{(p_{00}^{s})^2\alpha_{00}^{A} + \alpha_{00}^{s}(p_{00}^{A})^2\} + \frac{3}{2} \times \frac{I_0^{s}I_0^{A}\alpha_{00}^{s}\alpha_{00}^{A}}{I_0^{s}+I_0^{A}}\right]. \tag{12}$$

Unfortunately, except for nonpolar solute molecules, we can not obtain directly reliable values for p_{ii}^{A} and α_{ii}^{A} by means of a least-squares analysis of data regarding solvent spectral shifts by means of Eq. 7. This is because a cubic equation with respect to p_{ii}^{A} must be solved in the case of polar solute molecules. Solving the equation is not practicable. We, therefore, proceed to obtain values of p_{ii}^{A} and α_{ii}^{A} by the following method for a polar solute molecule.

Calculation 1. At first we assumed $(p_{00}^{A}\cos\theta)p_{ii}^{A}(1)=\{(p_{ii}^{A}(1)\}^2$ in Eq. 7 and obtained the first approximate values of $p_{ii}^{A}(1)$ and $\alpha_{ii}^{A}(1)$ by the least-squares method. Next, we wrote the second approximate values as $p_{ii}^{A}(2)=p_{ii}^{A}(1)+\Delta(p)$ and $\alpha_{ii}^{A}(2)=\alpha_{ii}^{A}(1)+\Delta(\alpha)$ in Eq. 7. On the assumption that $2p_{ii}^{A}(1) \gg \Delta(p)$, values of $\Delta(\alpha)$ and $\Delta(p)$ were then obtained by the least-squares method as well as those of $p_{ii}^{A}(2)$ and $\alpha_{ii}^{A}(2)$. The same calculation was repeated until both values for $\Delta(p)$ and $\Delta(\alpha)$ became smaller than 10^{-4} of a unit of measurement of the electric dipole moment or the polarizability.

On the other hand, we adopted the following (Calculations 2 and 3) for a nonpolar solute molecule having no dipole moments in either the ground or the excited states.

Calculation 2. When the value of σ_{i0}° was known, we obtained a value for α_{ii}^{A} by averaging the values of α_{ii}^{A} for all solvents by means of Eq. 7.

Calculation 3. When the σ_{i0}° value was unknown, at first we arbitrarily assumed the first appropriate approximate value of $\sigma_{i0}^{\circ}(1)$ for σ_{i0}° in Eq. 7 and obtained a first approximate value of $\alpha_{ii}^{A}(1)$ by the least-squares method. The second approximate values for σ_{i0}° and α_{ii}^{A} were then given as $\sigma_{i0}^{\circ}(2)=\sigma_{i0}^{\circ}(1)+\Delta(\sigma)$ and $\alpha_{ii}^{A}(2)=\alpha_{ii}^{A}(1)+\Delta(\alpha)$ and the final values for σ_{i0}° and α_{ii}^{A} were obtained by repeating the iterative procedure adopted in Calculation 1.

In applying Eq. 7, we always assumed the temperature to be 20 °C and, unless it is otherwise stated, that all the electric dipole moments and ionization potentials for molecules in the vapor phase were taken from Refs. 19 and 20. Values for α_{00} were calculated from sums of bond refractions. Moreover, we excluded data for solvents lacking information regarding their dipole moments and ionization potentials and of solvents which are capable of forming hydrogen bonds and complexes with solutes. We used the spectral data reported by the same authors for solutes.

Results and Discussion

Benzene, Naphthalene, and Anthracene. The solvent effects on the position of the ^1L_b transition of benzene were investigated by Macovei.[21] We have assumed Macovei's value of 39539 cm^{-1} for σ_{i0}° and have chosen data for 13 solvents (out of his reported total of 27 solvents) by excluding hydrogen bonding solvents. This is because benzene is low in the scale regarding hydrogen-bond acceptor strength determined by Kamlet and Taft.[22] Similarly, we chose data for only 10 and 9 solvents for the ^1L_b and ^1L_a transitions, respectively, in naphthalene from the data of Weigang and Wild.[23,24] For calculations regarding anthracene, data for 25 solvents were taken from the report of Nicol *et al.*[25] The values of α_{ii}^{A} (estimated by Calculation 2) are listed in Table 1, where $\Delta\alpha=\alpha_{ii}^{A}-\alpha_{00}^{A}$.

Except for the expression for the dipole–dipole interaction term between the solute and solvent molecules in Eq. 1, the latter is essentially the same as Abe's previous expression.[17] Accordingly, the application of Eq. 7 to a nonpolar solute gives the same correlation between the experimental frequencies and

TABLE 1. THE $\Delta\alpha$ VALUES FOR NONPOLAR SOLUTE MOLECULES

Molecule	Method	α_{00}^{A}	r_A	α_{ii}^{A}	$\Delta\alpha$
		10^{-24} cm^3	nm	10^{-24} cm^3	10^{-24} cm^3
Benzene					
^1L_b	Calcd 2	10.38	0.328	13.96	3.58
	Obsd	—	—	—	1.2±0.6[a,b]
Naphthalene					
^1L_b	Calcd 2	17.04	0.354	22.13	5.09
	Obsd	—	—	—	1.9±0.3[a]
^1L_a	Calcd 2	17.04	0.354	28.36	11.32
	Obsd	—	—	—	9.8±1.6[a]
Anthracene					
^1L_a	Calcd 2	23.69	0.384	42.89	19.2
	Obsd	—	—	—	16.7±2.3[a,c]
Lycopene					
	Calcd 3	72.06	0.7[d]	312.1	240.0
	Obsd	—	—	—	246±22[e]

a) Ref. 26. b) This experimental value was reduced under the assumption that no change in polarizability occurred in the direction perpendicular to the molecular plane. c) Ref. 27. d) Ref. 29. e) Ref. 28.

the frequencies calculated by Eq. 7 as was found using Abe's previous expression. The latter correlation was discussed in detail by Nicol *et al.*[25]

The observed $\Delta\alpha$ values for the aromatic hydrocarbon molecules in Table 1 are those measured by Mathies and Albrecht[26] for molecules dissolved in a rigid solution of 3-methylpentane at 77 K and by Liptay *et al.*[27] for anthracene in cyclohexane at 25 °C by means of electric field techniques.

Table 1 shows that the large $\Delta\alpha$ values estimated using Eq. 7 for the ^1L_a transitions of naphthalene and anthracene roughly approach those determined by electrooptical measurements. The difference was a maximum of 16%, and the small $\Delta\alpha$ values estimated using Eq. 7 for the ^1L_b transitions of benzene and naphthalene were higher by a factor of *ca.* 3 than those of the electrooptical measurements. The significantly large differences in the $\Delta\alpha$ values for the ^1L_b transitions obtained by using the two different methods may be due to a number of causes: (1) The present theoretical model for the solvent shift assumes spherical shapes for the solute and solvent molecules. The estimation of r_A using Eq. 2 may, therefore, be inappropriate for plane hydrocarbon molecules whose shapes considerably deviate from the spherical model. This is why we consider it inappropriate to extend the application of Eq. 7 to largely plane polynuclear hydrocarbons such as tetracene and perylene, although the $\Delta\alpha$ values for these molecules have been obtained from electrooptical measurements.[27] An arbitrary choice of smaller r_A values for benzene and naphthalene in our calculations minimized the differences in the $\Delta\alpha$ values obtained from both methods. (2) It has been reported that some excited-state polarizabilities vary with solvents to some extent.[27,28] The $\Delta\alpha$ values of Mathies and Albrecht are those for the hydrocarbons in 3-methylpentane at 77 K, while the $\Delta\alpha$ values in our present estimation correspond to those for the hydrocarbons in a vapor phase at 20 °C. Moreover, the electrooptical measurements of Mathies and Albrecht contain a few assumptions. Accordingly, some difference in the $\Delta\alpha$ values obtained by both methods may be unavoidable. (3) The differences may also result, in part, from the present assumption regarding Eq. 6.

In Table 1, the application of Eq. 7 gives $\Delta\alpha$ values which are larger than those determined by Mathies and Albrecht by less than 3×10^{-24} cm^3. This means that the excited-state polarizabilities estimated using Eq. 7 may be larger than those of Mathies and Albrecht by less than 3×10^{-24} cm^3. Compared to the polarizability values, the difference of *ca.* 3×10^{-24} cm^3 is small. Thus, we may conclude that our present application of Eq. 7 gives a reasonable estimation of the excited-state polarizabilities for the aromatic hydrocarbon molecules and that the estimation is better with a larger $\Delta\alpha$ value.

Lycopene. The r_A value of lycopene was taken to be 0.7 nm, the value that Myers and Birge[29] estimated for β-carotene from crystallographic data, as both lycopene and β-carotene have the same molecular formula ($C_{40}H_{56}$) and are similar in shape. The ionization potential of the ground state of a lycopene molecule having 11 conjugated double bonds was extrapolated to be 7.48 eV (1 eV=1.602×10^{-19} J) from the linear relationship[30] between the observed ionization potentials and the Hückel HOMO energy levels for ethylene, *s-trans*-1,3-butadiene and hexatriene. We used the reported spectral data[31] for the first transition in lycopene. The σ_{i0}° value of 23050 cm^{-1} and the $\Delta\alpha$ value in Table 1 were estimated according to Calculation 3. Obviously, the $\Delta\alpha$ value so estimated from solvent frequency shifts closely agrees with that obtained from the electric field-induced spectral change of lycopene in 3-methylpentane at 25 °C by Seibold *et al.*[28] (Table 1).

Chlorobenzene. Macovei[32] has investigated in detail the effects of a solvent on the 0-0 vibrational component[33] of the 37052-cm^{-1} π-π^* band of chloro-

Table 2. The dipole moments and polarizabilities of the first excited states of chlorobenzene and fluorobenzene

	Chlorobenzene	Fluorobenzene
P^A_{00}/D	1.782	1.66
$\alpha^A_{00}/10^{-24}$ cm^3	12.30	10.29
cos θ	1	1
P^A_{ii}/D	1.47	1.42
$\alpha^A_{ii}/10^{-24}$ cm^3	16.11	13.48
Δp/D	−0.31	−0.24
$\lvert\Delta p\rvert_{obsd}$/D	0.24±0.08[a]	0.30±0.07[b]
$\Delta\alpha/10^{-24}$ cm^3	3.81	3.20

a) Ref. 12e. b) Ref. 12d.

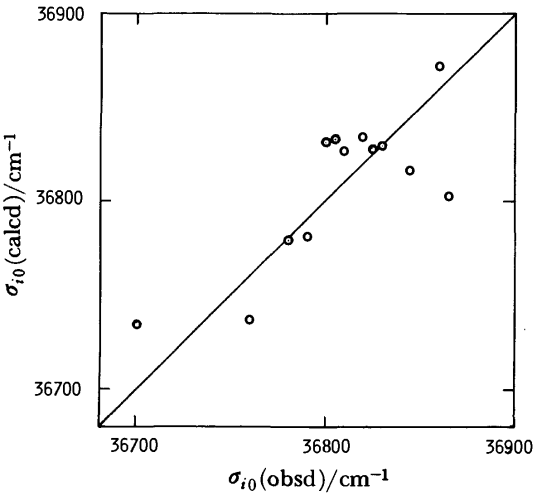

Fig. 1. A plot of the experimental frequency of the 0-0 band of the first transition of chlorobenzene *vs.* the frequency calculated.

benzene in the vapor phase. We chose data for 13 solvents from his spectral data involving 27 solvents. The data for carbon tetrachloride as a solvent were excluded since this molecule forms weak donor-acceptor complexes with benzene and substituted benzenes.[34] The values of p^A_{ii} and α^A_{ii} estimated by means of Calculation 1 are shown in Table 2. Even if a value of −1.0 was used for cosθ, we still obtained the same excited-state values recorded in Table 2, where $\Delta p=|p^A_{ii}|-|p^A_{00}|$. By using the p^A_{ii} and α^A_{ii} values so estimated, one can calculate the frequencies according to Eq. 1. We show in Fig. 1 the correlation between the experimental frequencies (σ_{i0} (obsd)) and the calculated ones (σ_{i0} (calcd)) for the ^1L_b band of chlorobenzene, as a representative example for the polar solutes. On the whole, the correlation is good.

The observed $|\Delta p|$ values (Table 2) determined by Lombardi *et al.*[12] by means of the optical Stark effect in the vapor phase are very reliable. As Lombardi[12a,c] clearly described, however, the sign of Δp cannot be determined using their experimental method. In the case of chlorobenzene, therefore, the two possible values of 2.03 and 1.55 D (1 D=3.333×10^{-30} Cm) are consistent with each measured splitting.[12e] By comparing the changes in rotational constants upon excitation, Wu and Lombardi[12e] expected the larger value for p^A_{ii}=2.03 D to be correct one. Their choice of 2.03 D, however, is not consistent with the theoretical results predicted by Kimura and Nagakura[35] by means of an MO calculation. Their theoretical results showed that the electron density on the chlorine atom in the first excited state of chlorobenzene should be slightly less than that of the chlorine atom in the ground state. This means that the value of p^A_{ii} is slightly less than that of p^A_{00}, since the substituent is the negative end of the dipole in both the ground and the excited states. Accordingly, the smaller value of p^A_{ii}=1.55 D should be the preferred experimental value of Wu and Lombardi. Our estimation of p^A_{ii}=1.47 D closely agrees with their reliable experimental value. By applying McRae's equation[36] to the solvent spectral frequency data for chlorobenzene, Macovei[32] also obtained a good result of p^A_{ii}=1.526 D. Thus, the comparable results on chlorobenzene, as determined by the electrooptical measurement and our present analysis, show that upon the assumption of Eq. 6, Eq. 1 can be applied for estimating the excited-state dipole moment of a polar solute molecule.

Fluorobenzene. There is a limited amount of data regarding polar solvents which do not form hydrogen bonds with fluorobenzene. Unfortunately, no desirable data regarding solvent effects for the 0-0 band (37829 cm^{-1})[37] of the first $\pi\cdot\pi^*$ transition in fluorobenzene in a vapor state are available. We were, therefore, restricted to using the undesirable data of Bowden and Braude[38] who reported that fluorobenzene in both cyclohexane and ethanol showed the 0-0 band to be at the same position (37590 cm^{-1}).

We wrote an equation for each solvent (cyclohexane or ethanol) according to Eq. 7. By solving the two equations simultaneously, we first obtained the two possible p^A_{ii} values, 1.42 and 242.70 D. For probabilistic reasons, however, the smaller value (1.42 D) was adopted as p^A_{ii} and the α^A_{ii} value was obtained as shown in Table 2. Huang and Lombardi[12d] determined the two possible excited-state dipole moments to be 1.37 and 1.96 D. They selected the larger value of 1.96 D as they did for chlorobenzene. According to Kimura and Nagakura,[35] the theoretical results regarding fluorobenzene are similar to those for chlorobenzene. If, by the same reasoning as we adopted in the case of chlorobenzene, we select their smaller value of 1.37 D as the experimental excited-state dipole moment of fluorobenzene, the p^A_{ii} value of 1.42 D estimated by the present method agrees well with the experimental value of 1.37 D.

Aniline. We chose the solvent spectral data of Mataga[39] for the first absorption band (35490 cm^{-1})[37] of aniline in vapor: 34800 (cyclohexane), 34700 (1,2-dichloroethane) and 34600 cm^{-1} (acetonitrile). In the present case, the angle θ between $\boldsymbol{p}^A_{00}$ and $\boldsymbol{p}^A_{ii}$ was

Table 3. Changes in the dipole moment and polarizability on excitation in aniline[a)]

cos θ	P_{ii}^{A}/D	Δp/D	$\Delta\alpha/10^{-24}$ cm^3
1.0	1.35	−0.13	9.56
0.8	1.69	0.21	9.46
0.5845	2.33	0.85	9.22
0.4	3.48	2.00	8.60
0.2	8.19	6.71	3.50
0.0	8.43	6.95	37.42
−0.2	−8.07	6.59	3.98
−0.4	−3.48	2.00	8.61
−0.5845	−2.33	0.85	9.22
−0.8	−1.69	0.21	9.46
−1.0	−1.35	−0.13	9.56

a) r_A=0.331 nm, P_{00}^{A}=1.48 D, and α_{00}^{A}=11.73×10^{-24} cm^3.

unknown. Consequently, we calculated the excited-state values for the possible values of cosθ according to Calculation 1 and give examples of the results in Table 3. By varying r_A in steps over a range from 0.2 to 0.4 nm, we found that Δp varies little with our choice for r_A. However, Δα depends on r_A considerably. According to Lombardi's experimental result of $|\Delta p|_{obsd}$= 0.85±0.15 D,[12a)] the value for p_{ii}^{A} should be either 0.63 or 2.33 D. In Table 3, the larger value (2.33 D) was reproducible by the present method to give cosθ=±0.5845. The angle of p_{ii}^{A} when the value of the moment is 2.33 D and cosθ=0.5845 is the same as when the p_{ii}^{A} moment is −2.33 D and cosθ=−0.5845=cos(180°− 54.23°). However, the direction of the former moment is different from that of the latter moment, as are shown in Fig. 2. Table 3 shows that the application of Eq. 7 gives no excited-state dipole moment smaller than 1.35 D in absolute value. Accordingly, the smaller (0.63 D) of the two possible experimental values proposed by Lombardi may be discarded on the basis of disagreement with the results of the solvent spectral-shift method. Lombardi[12a)] also explained his preference for the larger value of the excited-state dipole moment. Thus, the angle between $\boldsymbol{p}_{00}^{A}$ and $\boldsymbol{p}_{ii}^{A}$ is expected to be 54.23°. There is, therefore, two possible directions for the excited-state dipole moment as are shown by p_{ii}^{A}=±2.33 D in Fig. 2. The frequencies calculated using estimated values of p_{ii}^{A} and α_{ii}^{A} for cosθ=±0.5845 were 34820 (obsd, 34800), 34680 (obsd, 34700) and 34600 cm^{-1} (obsd, 34600 cm^{-1}) for the solvents of cyclohexane, 1,2-dichloroethane, and acetonitrile, respectively.

The ground-state dipole moment of aniline was calculated by Hehre *et al.*[40)] to be 1.44 D by means of *ab initio* MO theory. Their calculated components for the dipole moment and the direction of the ground-state dipole moment (p_{00}^{A}) are shown in Fig. 2. All the MO calculations of Baba,[41)] Mataga,[39)] and Hirota and Nagakura[42)] show a decrease in the π-electron density at the nitrogen atom in the excited state of aniline. This decrease only increases the magnitude of the excited-state dipole moment component parallel to the plane containing both the benzene ring and the nitrogen atom in the same direction as that of the corresponding ground-state dipole moment component. Accordingly, the positive and negative terminals of the dipole moment component in question will not change sign upon excitation. In Fig. 2, only the positive moment (p_{ii}^{A}=2.33 D) of the two possible moments of ±2.33 D for p_{ii}^{A} does clearly not change the sign of the dipole moment component. Thus, the direction of the excited-state dipole moment may be predicted as shown by p_{ii}^{A}=2.33 D in Fig. 2.

The p_{ii}^{A} value for aniline has been estimated by Mataga (2—2.5 D),[39)] Murrell (5 D),[43)] Iweibo *et al.* (a value nearly equal to p_{00}^{A}),[44)] Suppan (5.2 D),[5)] and Prabhumirashi *et al.* (2.12 D)[14,15)] from solvent shifts of absorption and/or fluorescence spectra. Mataga and Murrell used an equation for solvent shifts of absorption and fluorescence spectra.[45,46)] Suppan used a similar equation. Iweibo *et al.* and Prabhumirashi *et al.* used an approximation (Eq. 46 of Ref. 1a) of McRae's general expression.[36)] Since such an ap-

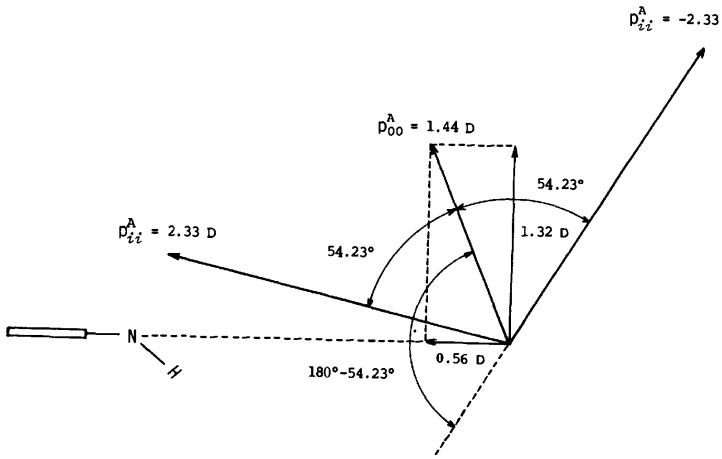

Fig. 2. The predicted directions of the ground- and excited-state dipole moments of aniline. The direction of the arrow denotes a moment from a positive charge to a negative one.

Table 4. The excited-state dipole moment and polarizability of retinal

	Present work[a]	Ponder and Mathies[b]	
		solid matrix[c]	gas phase
$\alpha^{A}_{ii}/10^{-24}\,cm^3$	102.26		
$\Delta\alpha/10^{-24}\,cm^3$	66.37	180±20	60[e]
$\Delta\alpha^{d}_{x}/10^{-24}\,cm^3$		600±100	200±20
P^{A}_{ii}/D	7.82	19.8±0.7	7±1

a) $\alpha^{A}_{00}=35.89\times10^{-24}\,cm^3$ and $\cos\theta=1$. b) Ref. 48. c) In poly(methyl methacrylate) films. d) A change in a long-axis polarizability on excitation. e) We so estimated this value that the ratios of $\Delta\alpha_x/\Delta\alpha$ became the same for both the solid matrix and the gas phase.

proximation obviously neglects the dispersion effect, the excited-state dipole moments estimated from such measurements will, for less polarized molecules, show sufficient departure from those of the electrooptical measurements. The fortuitously good estimate of Prabhumirashi *et al.* seems to be due to their choice of a rather small value of 0.146 nm for r_A. Except for Suppan, all of the above authors assumed collinear ground- and excited-state dipole moments. In view of the molecular structure[47] and the *ab initio* calculation[40] of the ground-state dipole moment for aniline, it seems difficult to assume such collinear dipole moments.

Retinal. Recently, Ponder and Mathies[48] have obtained the excited-state dipole moment and polarizability of *all-trans*-retinal from measurements of electric-field-induced changes in its optical absorption spectrum. We attempt to estimate the values of p^{A}_{ii} and α^{A}_{ii} for retinal by applying Eq. 7 to the available spectral data of Corsetti *et al.*[49] We chose 9 data points including those of 5 polar solvents from a total of 16 data points. From an extrapolation of a good linear relationship between absorption maxima (in cm^{-1}) of retinal in various nonpolar solvents and refractive indices of the solvents, we estimated the σ°_{i0} value of retinal to be 29210 cm^{-1}. The ionization potential of the retinal was estimated to be 8.31 eV as in the case of lycopene where parameters of the coulomb and resonance integrals for an oxygen atom were those referred to in Ref. 30. We used values of 4.55 D for p^{A}_{00} and 0.458 nm for r_A. These values were obtained by Myers and Birge[50] upon assuming a spherical model. Following Ponder and Mathies,[48] we assumed that both p^{A}_{00} and p^{A}_{ii} were parallel. Listed in Table 4 are the values of p^{A}_{ii} and $\Delta\alpha$ estimated by means of Calculation 1, in addition to the experimental results of Ponder and Mathies. The former values which were estimated by the present analysis agree well with the latter ones which were obtained from electrooptical measurements in a gas phase.

Azulene. The excited-state dipole moments and/or polarizabilities of azulene were obained from electrooptical measurements[51–55] as listed in Table 5. Hochstrasser and Noe,[51] Barker *et al*,[52] and Clark and Small[55] applied the Stark spectroscopy of mixed molecular crystals to the absorption systems of azulene. Mathies and Albrecht[52] adopted electric field broadening experiments for the absorption spectrum of azulene in 3-methylpentane at 77 K. Using reaction fields, Baumann[54] analyzed data obtained from electrooptical absorption and dielectric measurements for azulene in cyclohexane at 298 K.

We estimated the first and second excited-state dipole moments and polarizabilities of azulene by applying Calculation 1 to the available spectral data[23,24] as shown in Table 5. We chose 11 data points including 6 for nonpolar solvents and 5 for polar ones. For r_A we used the value of 0.308 nm, whose cube was already estimated by Baumann[54] for the spherical model of the azulene molecule. In the case of azulene, $\cos\theta$ obviously takes a value of either 1 or −1. Setting $\cos\theta=1$, yielded negative excited-state dipole moments. We, therefore, assumed that $\cos\theta=-1$.

As shown in Table 5, the present analysis gives the first and second excited-state dipole moments that are opposite in direction to that of the ground state. This result agrees with that obtained from the electrooptical measurements. The present analysis gives a far smaller decrease in the polarizability of the first excitation than do the measurements of Baumann. The first excited-state dipole moment estimated in the present analysis agrees roughly with those obtained from the electrooptical measurements. However, the present analysis shows that the magnitude of the second excited-state dipole moment is larger than that of the first excited state; electrooptical measurements show a reverse situation. The above differences between the present solvent shift method and the electrooptical

Table 5. The excited-state dipole moments[a] and polarizabilities of azulene

	Present work[b]	Baumann[c]	Clark and Small[d]	Mathies and Albrecht[e]	Hochstrasser, Noe *et al.*[f]
The first excited state					
P^{A}_{ii}/D	−0.817	−0.564	−0.26	—	−0.42
$\alpha^{A}_{ii}/10^{-24}\,cm^3$	15.80	11.44	—	—	—
The second excited state					
P^{A}_{ii}/D	−2.124	−0.348	−0.17	−0.44	−0.31
$\alpha^{A}_{ii}/10^{-24}cm^3$	22.00	—	—	—	—

a) The signs of P^{A}_{ii} were determined relative to P^{A}_{00}. b) $r_A=0.308$ nm, $P^{A}_{00}=0.795$ D, $\alpha^{A}_{00}=16.664\times10^{-24}\,cm^3$, and $\cos\theta=-1$. c) Ref. 54: $\alpha^{A}_{00}=15.52\times10^{-24}\,cm^3$. d) Ref. 55. e) Ref. 53. f) Refs. 51 and 52.

TABLE 6. THE EXCITED-STATE DIPOLE MOMENT AND POLARIZABILITY OF *p*-NITROANILINE

cos θ	Present work[a]		Electrooptical measurements
	P_{ii}^{A}	α_{ii}^{A}	P_{ii}^{A}
	D	10^{-24} cm^3	D
1.0	9.21	62.39	14[b], 15.5±2.8[c]
0.9	10.32	60.40	
0.8	11.75	57.51	
0.7	13.68	53.05	
0.6	16.41	45.59	
0.5	20.59	31.57	

a) P_{00}^{A}=6.29 D, α_{00}^{A}=13.983×10^{-24} cm^3 and r_A=0.336 nm. b) Ref. 56. c) Ref. 57.

measurements may be ascribed to the same reasons preferred for the aromatic hydrocarbons above. More reliable excited-state dipole moments for azulene must wait for determinations regarding the optical Stark effect in the gas phase.

p-Nitroaniline. From the electrooptical absorption measurements, Czekalla and Wick[56] and Liptay *et al.*[57] obtained the p_{ii}^{A} values listed in Table 6. In order to make a comparison with their values, we applied Eq. 7 to the solvent spectral shift data of Kamlet and Taft[22] for the observed 34210 cm^{-1} absorption maximum[58] of *p*-nitroaniline in a vapor phase. We chose 7 data points relative to their 9 non-hydrogen-bonding solvents. The value of 6.29 D[59] was used for p_{00}^{A}. The direction of the ground-state dipole moment may obviously not lie in the plane of the benzene ring of *p*-nitroaniline for the same reason as described in the case of aniline. In using Calculation 1, therefore, we changed the value of cosθ to be within the range of 0.5—1.0. The results of the calculation are shown in Table 6.

The electrooptical measurements made by both Czekalla and Wick[56] and Liptay *et al.*[57] assumed that the ground- and excited-state dipole moments were parallel to each other. With this assumption, the results of their measurements can be compared with our present calculation only when cosθ=1. Their values are considerably higher than that estimated by the present analysis. Czekalla and Wick completely neglected the effects of the ground- and excited-state polarizabilities of *p*-nitroaniline, while Liptay *et al.* neglected only the contribution of its excited-state polarizability. The large difference in the p_{ii}^{A} value using the two methods seems to be mainly due to their neglect of the contributions due to these polarizabilities. Thus, at the present stage, we have no reliable value for an electrooptically determined excited-state dipole moment in the case of *p*-nitroaniline.

The p_{ii}^{A} value has been estimated by Abe (10.26 D),[60] Suppan (16.3 D),[61] Millefiori *et al.* (10.13—10.50 D),[58,62] and Koutek (15.5 D)[16] from solvent spectral-shift theories. Koutek has applied the local reaction fields of Block and Walker[63] and Wertheim[64] to the already presented equations based on McRae's theory.[36] The expressions used by Suppan and Millefiori *et al.* lack any consideration of the polarizabilities and are based on the assumption that the ground- and excited-state dipole moments were parallel to each other. Koutek's treatments are also insufficient regarding these points. Thus, much weight cannot be credited to results from such computations.

References

1) Almost all references concerning the solvent effects on the frequency shifts of electronic spectra up to 1975, are cited in the following reviews: a) A. T. Amos and B. L. Burrows, *Adv. Quant. Chem.*, **7**, 289 (1973); b) M. F. Nicol, *Appl. Spectrosc. Rev.*, **8**, 183 (1974); c) C. N. R. Rao, S. Singh, and V. P. Senthilnathan, *Chem. Soc. Rev.*, **5**, 297 (1976).

2) A. E. Lutskii, A. V. Shepel, and M. R. Kreslavskii, *Opt. Spektrosk.*, **40**, 150 (1976).

3) K. Hirano, *Nippon Kagaku Kaishi*, **1978**, 481.

4) T. Abe, *Bull. Chem. Soc. Jpn.*, **54**, 327 (1981).

5) P. Suppan, *Chem. Phys. Lett.*, **94**, 272 (1983).

6) A. Botrel, F. Corre, and A. le Beuze, *Chem. Phys.*, **74**, 383 (1983).

7) R. G. E. Morales, *Spectrosc. Lett.*, **16**, 899 (1983).

8) K. S. Schweizer and D. Chandler, *J. Chem. Phys.*, **78**, 4118 (1983).

9) A. Raudino, F. Zuccarello, and G. Buemi, *J. Chem. Soc., Faraday Trans. 2*, **79**, 1759 (1983).

10) R. Constanciel and R. Contreras, *Theor. Chim. Acta*, **65**, 1 (1984).

11) R. Bonaccorsi, R. Cimiraglia, and J. Tomasi, *J. Mol. Struct.*, **107**, 197 (1984).

12) a) J. R. Lombardi, *J. Chem. Phys.*, **50**, 3780 (1969); b) K. -T. Huang and J. R. Lombardi, *J. Chem. Phys.*, **51**, 1228 (1969); c) J. R. Lombardi, *J. Am. Chem. Soc.*, **92**, 1831 (1970); d) K. -T. Huang and J. R. Lombardi, *J. Chem. Phys.*, **52**, 5613 (1970); e) C. Y. Wu and J. R. Lombardi, *J. Chem. Phys.*, **55**, 1997 (1971).

13) R. G. E. Morales, *J. Phys. Chem.*, **86**, 2550 (1982).

14) L. S. Prabhumirashi, *Spectrochim. Acta*, **39A**, 91 (1983).

15) a) L. S. Prabhumirashi, D. K. N. Kutty, and A. S. Bhide, *Spectrochim. Acta*, **39A**, 663 (1983); b) L. S. Prabhumirashi and R. S. Satpute, *Spectrochim. Acta*, **40A**, 953 (1984).

16) B. Koutek, *Collect. Czech. Chem. Commun.*, **43**, 1680 (1984).

17) T. Abe, *Bull. Chem. Soc. Jpn.*, **38**, 1314 (1965).

18) A. T. Amos and B. L. Burrows, *Theor. Chim. Acta*, **29**, 139 (1973).

19) "Kagaku Binran," ed by the Chemical Society of Japan, Maruzen Publishing Co., Tokyo (1975), Kisohen (Fundamental Part), II, pp. 1275, 1279, 1404.

20) "CRC Handbook of Chemistry and Physics, 61st Edition (1980—1981)," ed by R. C. Weast and M. J. Astle, CRC Press, p. E-64.

21) V. Macovei, *Rev. Roum. Chim.*, **20**, 1413 (1975).

22) M. J. Kamlet and R. W. Taft, *J. Am. Chem. Soc.*, **98**, 377 (1976).

23) O. E. Weigang, Jr., *J. Chem. Phys.*, **33**, 892 (1960).

24) O. E. Weigang, Jr. and D. D. Wild, *J. Chem. Phys.*, **37**, 1180 (1962).
25) M. Nicol, J. Swain, Y. -Y. Shum, R. Merin, and R. H. H. Chen, *J. Chem. Phys.*, **48**, 3587 (1968).
26) R. Mathies and A. C. Albrecht, *J. Chem. Phys.*, **60**, 2500 (1974).
27) W. Liptay, G. Walz, W. Baumann, H. -J. Schlosser, H. Deckers, and N. Detzer, *Z. Naturforsch.*, **26a**, 2020 (1971).
28) K. Seibold, H. Navangul, and H. Labhart, *Chem. Phys. Lett.*, **3**, 275 (1969).
29) A. B. Myers and R. R. Birge, *J. Chem. Phys.*, **73**, 5314 (1980).
30) A. Streitwieser, Jr., "Molecular Orbital Theory for Organic Chemists," John Wiley and Sons, New York (1961), pp. 135, 192.
31) F. Feichtmayr, E. Heilbronner, A. Nürrenbach, H. Pommer, and J. Schlag, *Tetrahedron*, **25**, 5383 (1969).
32) V. Macovei, *Rev. Roum. Chim.*, **21**, 193 (1976).
33) H. Sponer and S. H. Wollam, *J. Chem. Phys.*, **9**, 816 (1941).
34) C. N. R. Rao, S. N. Bhat, and P. C. Dwivedi, *Appl. Spectrosc. Rev.*, **5**, 1 (1972).
35) K. Kimura and S. Nagakura, *Mol. Phys.*, **9**, 117 (1965).
36) E. G. McRae, *J. Phys. Chem.*, **61**, 562 (1957).
37) W. W. Robertson and F. A. Matsen, *J. Am. Chem. Soc.*, **72**, 5252 (1950).
38) K. Bowden and E. A. Braude, *J. Chem. Soc.*, **1952**, 1068.
39) N. Mataga, *Bull. Chem. Soc. Jpn.*, **36**, 1607 (1963).
40) W. J. Hehre, L. Radom, and J. A. Pople, *J. Am. Chem. Soc.*, **94**, 1496 (1972).
41) H. Baba, *Bull. Chem. Soc. Jpn.*, **34**, 76 (1961).
42) F. Hirota and S. Nagakura, *Bull. Chem. Soc. Jpn.*, **43**, 1010 (1970).
43) J. N. Murrell, *Tetrahedron*, **19**, Suppl. 2, 277 (1963).
44) I. Iweibo, R. A. Oderinde, and J. A. Faniran, *Spectrochim. Acta*, **38A**, 1 (1982).
45) N. Mataga, Y. Kaifu, and M. Koizumi, *Bull. Chem. Soc. Jpn.*, **28**, 690 (1955); **29**, 465 (1956).
46) a) E. Lippert, *Z. Naturforsch.*, **10a**, 541 (1955); b) E. Lippert, *Z. Elektrochem.*, **61**, 962 (1957).
47) D. G. Lister and J. K. Tyler, *J. Chem. Soc., Chem. Commun.*, **1966**, 152.
48) M. Ponder and R. Mathies, *J. Phys. Chem.*, **87**, 5090 (1983).
49) J. P. Corsetti and B. E. Kohler, *J. Chem. Phys.*, **67**, 5237 (1977).
50) A. B. Myers and R. R. Birge, *J. Am. Chem. Soc.*, **103**, 1881 (1981).
51) R. M. Hochstrasser and L. J. Noe, *J. Chem. Phys.*, **50**, 1684 (1969).
52) J. W. Barker, L. J. Noe, and A. P. Marchetti, *J. Chem. Phys.*, **59**, 1304 (1973).
53) R. Mathies and A. C. Albrecht, *J. Chem. Phys.*, **60**, 1420 (1974).
54) W. Baumann, *Chem. Phys.*, **20**, 17 (1977).
55) R. Clark and G. J. Small, *J. Chem. Phys.*, **66**, 1779 (1977).
56) J. Czekalla and G. Wick, *Z. Elektrochem.*, **65**, 727 (1961).
57) W. Liptay, W. Eberlein, H. Weidenberg, and O. Elflein, *Ber. Bunsengeselshaft Phys. Chem.*, **71**, 548 (1967).
58) S. Millefiori, F. Zuccarello, and G. Buemi, *J. Chem. Soc., Perkin Trans. 2*, **1978**, 849.
59) A. L. McClellan, "Table of Experimental Dipole Moments," Freeman, San Francisco (1963).
60) T. Abe, *Bull. Chem. Soc. Jpn.*, **41**, 1260 (1968).
61) a) M. B. Ledger and P. Suppan, *Spectrochim. Acta*, **23A**, 641 (1967); b) P. Suppan, *J. Chem. Soc. (A)*, **1968**, 3125.
62) S. Millefiori, G. Favini, A. Millefiori, and D. Grasso, *Spectrochim. Acta*, **33A**, 21 (1977).
63) M. Block and S. M. Walker, *Chem. Phys. Lett.*, **19**, 363 (1973).
64) M. S. Wertheim, *Mol. Phys.*, **25**, 211 (1973).

Photochemical Magnetic Field Effects of 4-Methyl-2-quinolinecarbonitrile

Norisuke HATA* and Naoya NISHIDA
Department of Chemistry, College of Science and Engineering, Aoyama Gakuin University, Chitosedai, Setagaya-ku, Tokyo 157
(Received July 10, 1985)

The irradiation of 4-methyl-2-quinolinecarbonitrile **1** in ethanol or cyclohexane resulted in the formation of 2-(1-hydroxyethyl)-4-methylquinoline **2** or 2-cyclohexyl-4-methylquinoline **3** in the yield of *ca.* 48 or 65%. The effects of an external magnetic field upon the photosubstitution reaction were investigated in either the absence or presence of 1,3-pentadiene (triplet quencher). In the case of the photosubstitution reaction (**1**→**2**) in ethanol, the chemical yield of **2** increased quadratically with an increase in the field strength (magnetic field effect due to Δg mechanism) and it also showed a minimum at approximately 1.1T (magnetic field effect due to HFI-J mechanism). The addition of 1,3-pentadiene caused a complete disappearance of the Δg magnetic field effect. Thus, the formation of **2** at a zero field was concluded to occur from the S_1-state *via* the singlet hydrogen-bonded radical pair. In the case of the photosubstitution reaction (**1**→**3**) in cyclohexane, the chemical yield of **3** decreased steeply upon the application of a magnetic field of 40mT (magnetic field effect due to HFI mechanism) and a further increase in the field strength resulted in a quadratic increase in the yield (magnetic field effect due to Δg mechanism). Neither an HFI nor a Δg magnetic field effect was observed in the presence of 1,3-pentadiene. The reaction was thus concluded to proceed from the S_1 and T_1 states *via* the singlet and triplet radical pairs. Reaction mechanisms deduced from the external magnetic field effects were consistent with the results of Stern-Volmer analyses.

Photochemical reactions proceeding *via* a radical-pair intermediate in solution can generally be expected to show an external magnetic field effect which arises from an electronic Zeeman interaction (Δg mechanism), electron-nuclear hyperfine interaction (HFI mechanism), or hyperfine-interaction mechanism including an electron-exchange interaction (HFI-J mechanism) in a radical-pair intermediate (*cf.* Appendix).[1] The magnetic field effect due to the HFI-J mechanism is considered to be particularly interesting and important from the viewpoint of mechanistic photochemistry, becuase it is expected when hydrogen- or electron-transfer between a photoexcited molecule and the hydrogen-bonded species occurs to form an appropriate hydrogen-bonded radical pair or radical ion-pair intermediate in a solvent cage.[2] In 1976 this type of magnetic field effect was found for the first time by one (N.H.) of the authors in the case of the photochemical isomerization of isoquinoline *N*-oxide in ethanol.[2] In order to find a second example of the magnetic field effect due to the HFI-J mechanism, in the present investigation, the photoinduced substitution reaction of 4-methyl-2-quinolinecarbonitrile in ethanol and in cyclohexane were studied in both the absence and presence of a magnetic field.[3]

Experimental

Materials. The 4-methyl-2-quinolinecarbonitrile **1** used as a sample was prepared from 4-methylquinoline *N*-oxide according to a method (Reissert reaction) given in the literature;[4] it was then purified by recrystallization from methanol several times; mp 97—98°C. 1,3-Pentadiene used as a triplet quencher was a Chemical-pure product of Tokyo Kasei Kogyo Co., which was further purified by distillation; bp 42—43.5°C. The ethanol and cyclohexane used as the photoreaction medium were Reagent-grade products of Wako Pure Chemical Industries; the former was used without further purification, while the latter was purified by silica-gel chromatography.

Isolation and Identification of Photoproducts. 4-Methyl-2-quinolinecarbonitrile **1** (50 mg) dissolved in 50-cm³ of ethanol (or cyclohexane) in a Pyrex vessel was irradiated with a 100 W high-pressure immersion mercury lamp (Riko Kagaku Sangyo Co.) for 5 h (or 8 h) in an atmosphere of nitrogen at room temperature. After the removal of the solvent under reduced pressure, unreacted **1** and product **2** (or **3**) were separated by means of silica-gel TLC (Merck TLC silica-gel plate $60F_{254}$; layer thickness, 2 mm; the eluent, hexane–diethyl ether (1:2) for the separation of **1** and **2**, and hexane–ethyl acetate (5:1) for the separation of **1** and **3**). The product **2** was 2-(1-hydroxyethyl)-4-methylquinoline, which has been identified previously;[5] mp 82—82.5°C; the yield, *ca.* 48%. The product **3** was a colorless liquid; bp 121°C/2 mm, mp (the picrate) 182°C; the yield, *ca.* 65%. It was identified as 2-cyclohexyl-4-methylquinoline by the following analytical data. NMR($CDCl_3$) δ(ppm): 8.2—7.3 (m, 5H, aromatic), 2.70 (s, 3H, $-CH_3$), 2.2—1.1 (m, 11H, $-C_6H_{11}$). MS: 225(M^+). Found (the picrate): C, 58.46; H, 4.86; N, 12.05%. Calcd for $C_{22}H_{22}N_4O_7$ (the picrate): C, 58.15; H, 4.85; N, 12.33%.

Stern-Volmer Experiments. A determination of the quantum yields (the disappearance of **1** and the formation of **2** or **3**) was performed in a quartz cell (4.5-cm in diameter and 1-cm in length) containing the ethanolic solution (or cyclohexane solution) of **1** (1.62×10^{-3} mol dm^{-3}) and 1,3-pentadiene (0—10.0×10^{-3} mol dm^{-3}) under a nitrogen atmosphere at room temperature. The light source employed was a Ushio Super-high-pressure Mercury Lamp (USH-500D) equipped, for the 313-nm irradiation, with a filter combination of a nickel sulfate solution with Toshiba filters UV-29 and UV-D33S. The light intensity was determined by means of a potassium tris-(oxalato)ferrate (III) actinometer. The amounts of unreacted **1** and product **2** (or **3**) were determined by means of a silica-gel chromatographic separation, using the same eluent as that described before, combined with a spectrophotometric determination.

Magnetic Perturbation Experiments. A 50-cm³ of ethanolic solution (or cyclohexane solution) containing 4-

TABLE 1. SPECTRAL DATA OF SOME AZAAROMATIC NITRILES[6-8]

Nitriles		Solvents[a]	Absorption[b] λ_{max}/nm (ε_{max})	Fluorescence λ_{max}/nm	Phosphorescence[b] λ_{max}/nm
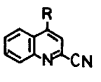	R=H	MCH	330 (2800)	Non	482
		EtOH	331 (2650)	372.5	484
	$R=CH_3$	MCH	330.5 (2600)	Non	483
		EtOH	331 (2300)	365	486
	R=H	MCH	331 (5600)	339 (Very weak)	Non
		EtOH	332 (5600)	365	Non
	$R=CH_3$	MCH	340 (6200)	350 (Very weak)	Non
		EtOH	341 (6100)	370	Non

a) MCH: Methylcyclohexane, EtOH: Ethanol. b) The value of the first maximum.

methyl-2-quinolinecarbonitrile **1** (35 mg) and 1,3-pentadiene (0 or 3.0×10^{-1} mol dm^{-3}) in a quartz vessel (44×45×25 mm) was placed in an electromagnet (EEO-1815) supplied by the Maezumi Electric Company and subsequently, irradiated with two 500 W Super-high-pressure Mercury Lamps (USH-500D) equipped with a Toshiba filter UV-31 for 40 min at room temperature while nitrogen was bubbled. The unreacted **1** and product **2** (or **3**) were separated by means of silca-gel TLC in the same manner as that described before and the amounts were determined spectrophotometrically.

Spectroscopic Measurements. UV absorption spectra were taken with a Shimadzu recording spectrophotometer, UV-220. Fluorescence and phosphorescence spectra were determined with a Hitachi recording fluorescence spectrophotometer, MPF-2A. Reagent-grade ethanol (Wako Pure Chemical Industries) and Spectro-grade methylcyclohexane (Dotite Spectrosol) were used as the solvent. NMR spectra were taken in $CDCl_3$ with a Hitachi-Perkin Elmer NMR spectrometer R-20 at 60 MHz, using TMS as the internal standard. Mass spectra were measured with a Hitachi mass spectrometer, RMU-6M.

Results and Discussion

Photochemical Reactions and the Stern-Volmer Analyses. It has been already reported in previous papers[5] that the irradiation of 2-quinolinecarbonitriles in alcoholic solvents generally results in the replacement of the cyano group at the 2-position of a quinoline nucleus by hydroxyalkyl group. As has been described in the Experimental section, when 4-methyl-2-quinolinecarbonitrile **1** in ethanol was irradiated in an atmosphere of nitrogen, 2-(1-hydroxyethyl)-4-methylquinoline **2** was obtained in a *ca.* 48% yield (Eq. 1). In the case of a cyclohexane solution, there also occurred a similar photosubstitution reaction to give rise to 2-cyclohexyl-4-methylquinoline **3** in a yield of *ca.* 65% (Eq. 2).

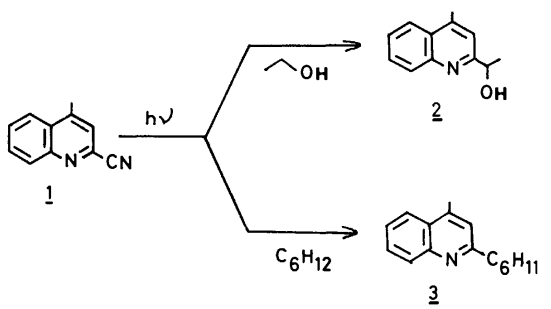

(1)

(2)

In order to characterize the excited states responsible for the photosubstitution reaction of 4-methyl-2-quinolinecarbonitrile **1** in ethanol or cyclohexane, the effects of 1,3-pentadiene upon the quantum yield (Φ_{-1}) of the disappearance of **1** and that (Φ_2 or Φ_3) of the formation of **2** or **3** were examined. The excitation energy of the lowest triplet state of 4-methyl-2-quinolinecarbonitrile was estimated, from the first maximum of the phosphorescence spectrum (Table 1), to be *ca.* 247 kJ mol^{-1}; hence 1,3-pentadiene was used as a triplet quencher for the photochemical reaction of **1**.

Figure 1 shows a plot of $\Phi^{\circ}_{-1}/\Phi_{-1}$ or Φ°_{2}/Φ_2 against the concentration of 1,3-pentadiene ([C_5H_8]) for the photosubstitution reaction (**1**→**2**) in ethanol (Stern-Volmer plot), where the quantum yield (Φ°_{-1}) of the disappearance of **1** and that (Φ°_{2}) of the formation of **2** at [C_5H_8]=0 were 0.0825 and 0.0461, respectively. As can be seen from Fig. 1, Φ_2 was independent of the concentration of 1,3-pentadiene, whereas Φ_{-1} decreased with an increase in the concentration of 1,3-pentadiene until it became constant above a concentration of 7.0×10^{-3} mol dm^{-3} 1,3-pentadiene. The results clearly indicate that the photosubstitution reaction (**1**→**2**) proceeds from the S_1 state and that some complicating reactions occur from the T_1 state.

Figure 2 shows Stern-Volmer plots for a photosubstitution reaction (**1**→**3**) in cyclohexane, where the quantum yield (Φ°_{-1}) of the disappearance of **1** and that (Φ°_{3}) of the formation of **3** at [C_5H_8]=0 were 0.0374 and 0.0271, respectively. Both quantum yields, Φ_{-1} and Φ_3, decreased with an increase in the concentration of 1,3-pentadiene until no further quenching occurred above a concentration of 1.7×10^{-3} mol dm^{-3} 1,3-pentadiene. This means that, unlike the case of the photosubstitution reaction **1**→**2**, both S_1 and T_1 states are responsible for the photosubstitution reaction **1**→**3**.

The chemical yield, Y_S or Y_T, of the S_1- or T_1-born product **3** was estimated from the Stern-Volmer plot (curve (a) in Fig. 2) in the following manner. The chemical yield (Y) of **3** at [C_5H_8]=0 is given by the sum of Y_S and Y_T (Eq. 3). The chemical yield (Y_S) of the S_1-born product **3** is given by Eq. 4, where $(\Phi^{\circ}_{3}/\Phi_3)_0$ and $(\Phi^{\circ}_{3}/\Phi_3)_s$ represent, respectively, Φ°_{3}/Φ_3 at [C_5H_8]=0 and [C_5H_8]>1.7×10^{-3} mol dm^{-3}. Y_S and Y_T were thus

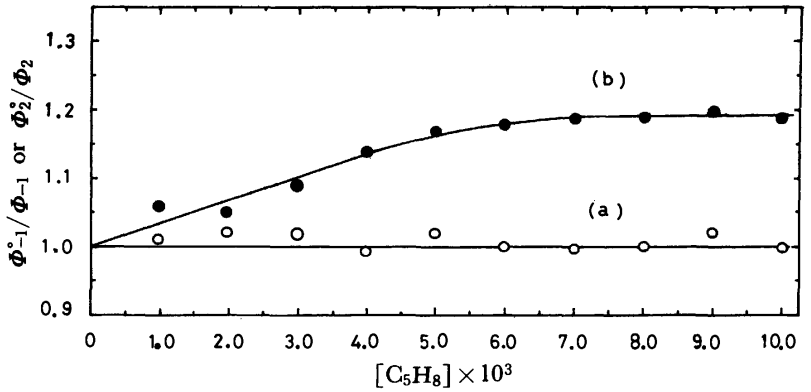

Fig. 1. Triplet quenching of the photosubstitution reaction (**1**→**2**) in ethanol. [**1**]=1.62×10^{-3} mol dm^{-3}.
(a) —○—: $\Phi^{\circ}_{2}/\Phi_{2}$, (b) —●—: $\Phi^{\circ}_{-1}/\Phi_{-1}$.

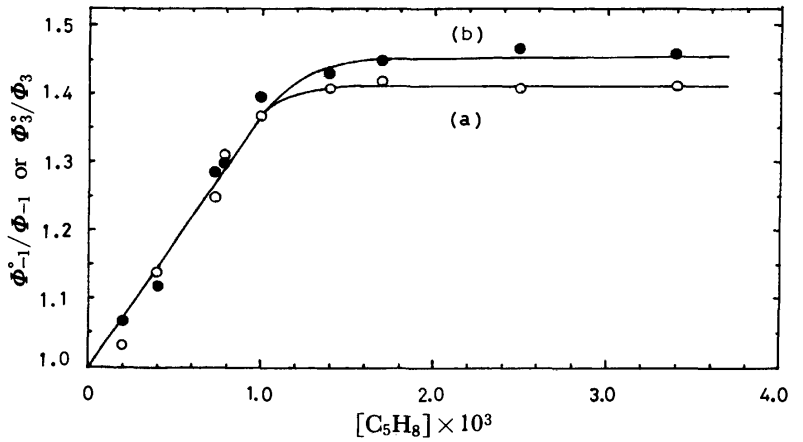

Fig. 2. Triplet quenching of the photosubstitution reaction (**1**→**3**) in cyclohexane. [**1**]=1.62×10^{-3} mol dm^{-3}.
(a) —○—: $\Phi^{\circ}_{3}/\Phi_{3}$, (b)—●—: $\Phi^{\circ}_{-1}/\Phi_{-1}$

$$Y = Y_s + Y_T \quad (3)$$

$$Y_s = Y(\Phi^{\circ}_{3}/\Phi_{3})_0/(\Phi^{\circ}_{3}/\Phi_{3})_s \quad (4)$$

evaluated by substituting $(\Phi^{\circ}_{3}/\Phi_{3})_s$=1.41 and Y=65% into Eqs. 3 and 4 to be 46 and 19% respectively.

Magnetic Field Effects. In the case where the photochemical reactions in solution proceed *via* a radical-pair intermediate (as is shown in Scheme 1), the chemical yield of the cage product or escape product shows a magnetic field dependence provided that the rate of the intersystem crossing of a radical pair is influenced by an external magnetic field.[1] As will be briefly described in Appendix, such a field dependence of chemical yield has been currently classified into six patterns (Figs. 5 and 6), depending on whether the product is a cage- or escape-product and an S_1- or T_1-born product and also whether the magnetic perturbation is due to Δg, HFI, or HFI-J mechanism. Consequently, an examination of the field dependence of chemical yield is supposed to furnish quite significant information regarding photochemical reaction mechanism.[6]

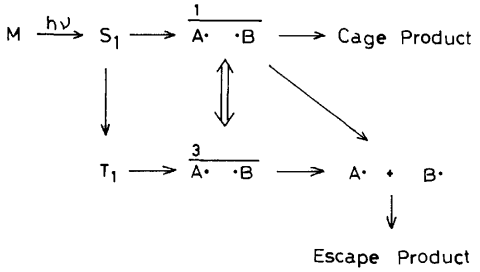

Scheme 1.

As mentioned before, the Stern-Volmer plots (Fig. 1) of the photoinduced substitution reaction (**1**→**2**) in ethanol revealed the S_1 state to be responsible for this reaction. Previously,[7,8] it had also been demonstrated from the solvent dependence of the absortpion and fluorescence spectra of 2-quinolinecarbonitriles (*cf.* Table 1) that a hydrogen-bonding interaction between the ring nitrogen and an ethanol does exist in the S_1 state, although there is no appreciable interaction in the S_0 state.[9] Furthermore, the photoreaction has been reasonably assumed to proceed *via* the S_1 state through hydrogen abstraction by the ring nitrogen from the

hydrogen-bonded ethanol.[7] Hence, as is shown in Scheme 2, it seems quite reasonable to assume that the S_1-born singlet hydrogen-bonded radical pair **2a** is formed as a transient intermediate of this reaction. If this assumption is valid, the magnetic field effect due to the HFI-J mechanism (curve (3) in Fig. 5) may be expected for the photosubstitution reaction **1**→**2**, just as the case of the photoisomerization of isoquinoline *N*-oxide in ethanol;[2] it is because the radical centers in the radical pair **2a** are in close proximity as a result of hydrogen-bonding interaction between the two radicals (consequently, the electron-exchange interaction is much greater than the electron-nuclear hyperfine energy). On the other hand, the photosubstitution reaction (**1**→**3**) in cyclohexane was demonstrated from Stern-Volmer plots (Fig. 2) to occur from both the S_1 and T_1 states. Therefore, as is shown in Scheme 3, if the reaction proceeds *via* the S_1-born singlet and T_1-born triplet radical pairs, **3a** and **3a'**, as the reactive intermediate, then it may be subject to a magnetic field effect due to Δg or HFI mechanism (curve (1) or (2) in Fig. 5 and curve (1') or (2') in Fig. 6), because either the radical pair **3a** or **3a'** is not a hydrogen-bonding pair of radicals in close proximity and therefore the electron-exchange interaction is disregarded. For these reasons, the effects of an external magnetic field on the photoinduced substitution reactions of 4-methyl-2-quinolinecarbonitrile **1** in ethanol and in cyclohexane were investigated in either the absence or presence of 1,3-pentadiene (triplet quencher).

First we will describe the magnetic field effect upon the photosubstitution reaction (**1**→**2**) in ethanol. Figure 3 shows the results when the chemical yield of **2** is plotted as a function of the field strength in the absence and presence of 1,3-pentadiene, where the conversion remained almost constant (20—22%). In the absence of 1,3-pentadiene, as is shown by curve (a) in Fig. 3, the chemical yield of **2** was *ca.* 48% at the zero field, but it increased quadratically with an increase in the field strength to be *ca.*58% at about 1.5 T (the

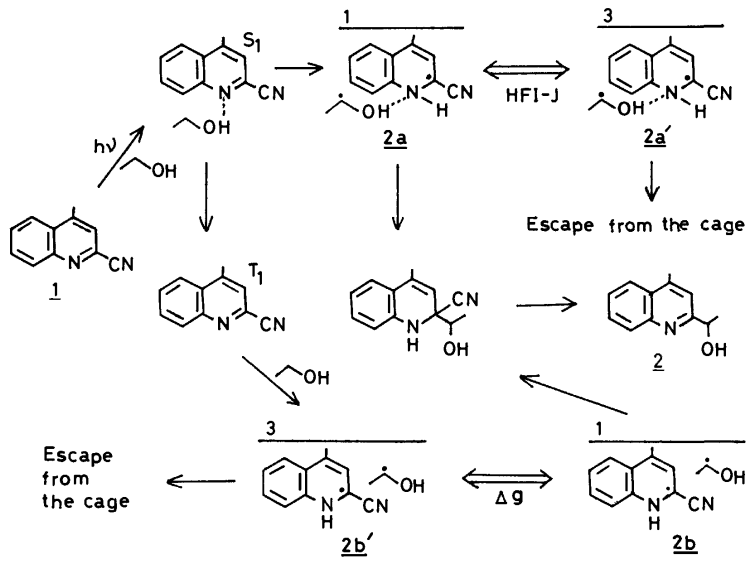

Scheme 2.

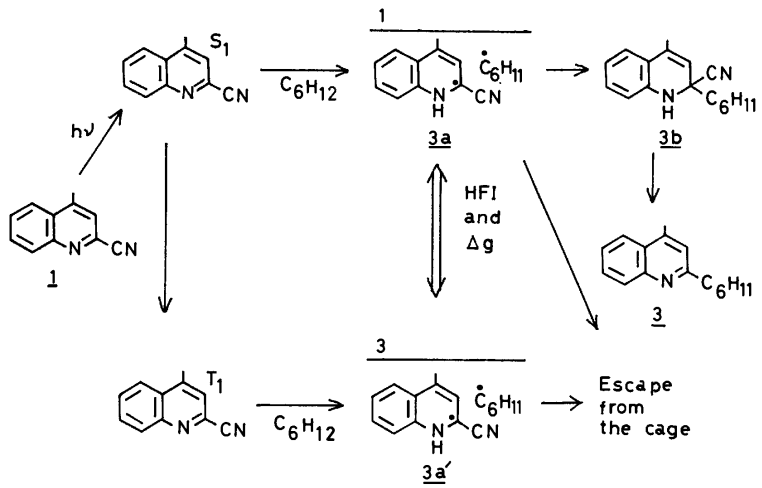

Scheme 3.

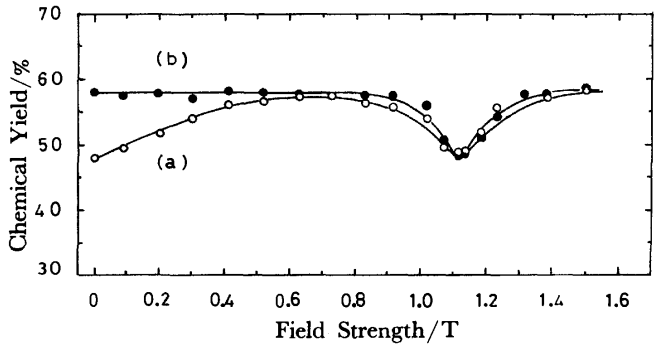

Fig. 3. External magnetic field effect upon the photosubstitution reaction (**1**→**2**) in ethanol. Chemical yield of **2** *vs.* magnetic field strength. [**1**]= 4.01×10^{-3} mol dm^{-3}.
(a) —○—: $[C_5H_8]=0$, (b) —●—: $[C_5H_8]=3.0\times10^{-1}$ mol dm^{-3}.

magnetic field effect due to Δg mechanism); this is the same pattern as for the field dependence of the chemical yield of the S_1-born escape product or the T_1-born cage product (curve (1′) in Fig. 6). The chemical yield of **2** also showed a minimum (*ca.* 49%) at approximately 1.1 T (the magnetic field effect due to HFI-J mechanism); this is the same pattern as for the field dependence of the chemical yield of the S_1-born cage product or the T_1-born escape product (curve (3) in Fig. 5). The Δg magnetic field effect, as is shown by curve (b) in Fig. 3, disappeared completely upon the addition of 1,3-pentadiene, although the magnetic field effect due to the HFI-J mechanism was still observed. Thus, the chemical yield of **2** was *ca.* 58% at a magnetic field below 0.8 T, but it decreased steeply with an increase in the field strength to become *ca.* 48% at about 1.1 T. A further increase in the magnetic field resulted in a steep increase in the chemical yield until it became approximately constant (*ca.* 58%). The results explicitly indicate that the Δg or the HFI-J magnetic field effect observed in a photochemical reaction can be assigned to the field dependence of the chemical yield of the T_1- or S_1-born cage product.

Such an examination of the magnetic field effects leads to the conclusion that a photosubstitution reaction of 4-methyl-2-quinolinecarbonitrile **1** in ethanol (Eq. 1) proceeds according to the mechanism shown in Scheme 2. Thus, the photoexcitation of **1** into the S_1 state results in the formation of a hydrogen bond between the ring nitrogen and an ethanol. This is followed by hydrogen abstraction by the ring nitrogen from the hydrogen-bonded ethanol, which gives rise to the singlet hydrogen-bonded radical pair **2a** that is responsible for the formation of **2** (S_1-born cage product). The S_1-born singlet hydrogen-bonded radical pair **2a** undergoes a magnetic perturbation due to the HFI-J mechanism. As a result, the chemical yield of the S_1-born cage product **2** comes to show a minimum at approximately 1.1 T. In addition, an observation of the magnetic field effect due to the Δg mechanism (which disappears upon the addition of 1,3-pentadiene) indicates, unambiguously, that in the T_1 state there also occurs hydrogen abstraction by the ring nitrogen from an ethanol to yield the triplet radical pair **2b′**. The T_1-born triplet radical pair **2b′**, because of its triplet character, undergoes a diffusive separation into the solvent bulk to cause some complicating radical reactions. It should also be noted that a magnetic field effect due to the HFI mechanism, ascribed to the T_1-born triplet radical pair **2b′** (curve (2′) in Fig. 6), was not observed in this reaction system. This implies that, unless a magnetic field is applied to this system, the triplet radical pair **2b′** does not undergo an intersystem crossing to the singlet radical pair **2b** responsible for the formation of **2** (T_1-born cage product). This agrees well with the conclusion from Stern-Volmer analyses (Fig. 1) that the photosubstitution reaction **1**→**2** proceeds from the S_1 state, while some complicating reactions occur from the T_1 state.

As a general rule (*cf.* Appendix), a magnetic field effect due to the Δg or the HFI mechanism should be expected when the two components of a field-sensitive radical pair in a solvent cage is sufficiently far apart that the electron-exchange interaction can be neglected. On the other hand, a magnetic field effect due to the HFI-J mechanism should be expected when the two component radicals are in close proximity as a result of a hydrogen-bonding interaction (the electron-exchange interaction can not be disregarded). Thus, it may be considered that the S_1-born singlet radical pair **2a** which undergoes a magnetic perturbation due to HFI-J mechanism is a hydrogen-bonding pair, whereas the T_1-born triplet radical pair **2b′** which is subject to a magnetic perturbation due to the Δg mechanism is a nonhydrogen-bonding pair. This in turn leads to the conclusion that hydrogen-bonding interaction between the ring nitrogen and an ethanol does exist in the S_1 state, but that it is negligibly small in the T_1 state. This agrees well with the previously obtained conclusion from solvent-effect studies on the fluorescence and phosphorescence spectra of 2-quinolinecarbonitriles (*cf.* Table 1).[9]

Next, we describe the effect of an external magnetic field on a photosubstitution reaction (**1**→**3**) in cyclohexane. Figure 4 shows the results when the chemical yield of **3** is plotted against the field strength in either the absence or presence of 1,3-pentadiene. In either case the conversion was almost independent of the field strength (19—21%). In the absence of 1,3-pentadiene, as can be seen from curve (a) in Fig. 4, the chemical yield of **3** was *ca.* 65% at a zero field. However, it steeply decreased upon the application of a magnetic field of 40 mT to be *ca.* 54% (the magnetic field effect due to HFI mechanism). This is the same pattern as that for the field dependence of the chemical yield of the S_1-born escape product or the T_1-born cage product (curve (2′) in Fig. 6). A further increase in the field strength resulted in a quadratic increase in the chemical yield (the

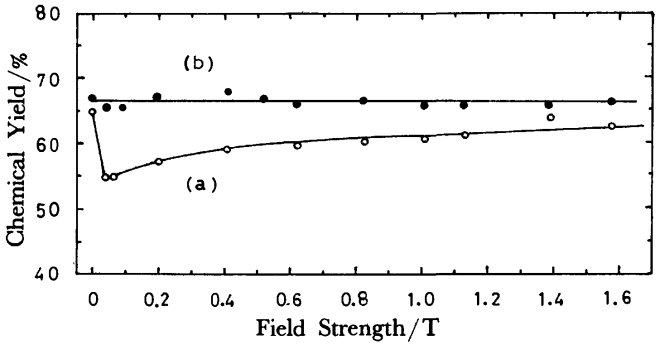

Fig. 4. External magnetic field effect upon the photosubstitution reaction (**1**→**3**) in cyclohexane. Chemical yield of **3** *vs.* magnetic field strength. [**1**]=4.01 ×10^{-3} mol dm^{-3}.
(a) —○—: [C_5H_8]=0, (b) —●—: [C_5H_8]=3.0×10^{-3} mol dm^{-3}.

magnetic field effect due to Δg mechanism). This is the same pattern as the field dependence of chemical yield of the S_1-born escape product or the T_1-born cage product (curve (1′) in Fig. 6). The addition of 1,3-pentadiene, however, caused a complete disappearance of these magnetic field effects; as a result, the chemical yield of **3** became independent of the field strength to show *ca.* 67%. This means that both the HFI and Δg magnetic field effects observed in this reaction can be assigned to the field dependence of chemical yield of the T_1-born cage product. Also, the fact that the product **3** was obtained in a high yield (*ca.* 67%), even in the presence of 1,3-pentadiene, suggests strongly that the photosubstitution reaction proceeds from the S_1 state as well as the T_1 state. This is consistent with a conclusion from Stern-Volmer analyses (Fig. 2).

The external magnetic field effects described above lead to the conclusion that the photosubstitution reaction of 4-methyl-2-quinolinecarbonitrile **1** in cyclohexane (Eq. 2) proceeds according to the mechanism shown in Scheme 3. Thus, the photochemical reaction is initiated by a hydrogen abstraction from cyclohexane by the ring nitrogen, which occurs from both the S_1 and T_1 states, to yield the S_1-born singlet radical pair **3a** and T_1-born triplet radical pair **3a′** as transient intermediates. The S_1-born singlet radical pair **3a** undergoes mostly efficient cage recombination to generate the product **3** (S_1-born cage product). On the other hand, the T_1-born triplet radical pair **3a′** undergoes partly hyperfine-induced intersystem crossing to the singlet radical pair **3a** responsible for the formation of **3** (T_1-born cage product) and partly diffusive separation into the solvent bulk.

As can be seen from Fig. 4, a magnetic field effect which could be ascribed to the S_1-born singlet radical pair **3a** was not observed at all, although the formation of the product **3** undoubtedly occurs from the S_1 state, probably, *via* the intermediate **3a**. This may be interpreted as follows. As is shown in Scheme 3, the S_1-born singlet radical pair **3a** undergoes mainly the following two processes; one of them is a cage recombination (**3a**→**3b**) or diffusive separation of the component radicals, while the other is a magneto-sensitive intersystem crossing (**3a**→**3a′**) which occurs with a rate of the order of 10^7—10^8 s^{-1} *via* electron-nuclear hyperfine interaction. Therefore, if the cage recombination takes place in competition with the intersystem crossing, the singlet radical pair **3a** is supposed to be subject to a magnetic perturbation due to the Δg or HFI mechanism. However, the fact that such a magnetic field effect as shown in curve (1) or (2) in Fig. 5 is not observed at all implies that the cage recombination is much faster than an intersystem crossing. A similar interpretation has been made regarding the photochemical magnetic field effect of 1-isoquinolinecarbonitriles in ethanol.[6]

The chemical yield, Y_S or Y_T, of the S_1-born or T_1-born cage product **3** was estimated from data regarding the magnetic field effects in the absence of 1,3-pentadiene (curve (a) in Fig. 4) in the following way. The chemical yield ($Y°$) of **3** at a zero field is equal to the sum of Y_S and Y_T (Eq. 5). The chemical yield (Y^H) of **3** at a magnetic field of 40 mT is given by Eq. 6, where the chemical yield of the T_1-born cage product **3** at a magnetic field of 40 mT is assumed to be $(1/3)Y_T$ because the number of effective working channels for the hyperfine-induced intersystem crossing of a radical pair reduces by the application of a magnetic field from three ($T_{0,\pm}$↔S) to one (T_0↔S). Thus, Y_S and Y_T were evaluated by substituting $Y°$=65% and Y^H=54% into

$$Y° = Y_S + Y_T \quad (5)$$

$$Y^H = Y_S + (1/3)Y_T \quad (6)$$

Eqs. 5 and 6 to be 48.5 and 16.5% respectively. These values approximately agree with those (Y_S=46% and Y_T=19%) obtained by Stern-Volmer analyses (Fig. 2).

Conclusion

The second example of a magnetic field effect due to the HFI-J mechanism (ascribed to the S_1-born singlet radical pair) was found for the case of a photoinduced substitution reaction of 4-methyl-2-quinolinecarbonitrile in ethanol (Eq. 1). This reaction also showed the magnetic field effect due to the Δg mechanism which can be ascribed to the T_1-born triplet radical pair. In the case of a photosubstitution reaction in cyclohexane (Eq. 2), the formation of a T_1-born triplet radical pair intermediate was concluded by the observation of magnetic field effects due to the HFI and Δg mechanisms. However, a magnetic field effect which could be ascribed to an S_1-born singlet radical pair was not observed. From the experimental results, the photosubstitution reaction of 4-methyl-2-quinolinecarbonitrile in ethanol or cyclohexane was unambiguously deter-

mined to proceed according to the mechanism shown in Scheme 2 or 3. This is consistent with the results of Stern-Volmer analyses. The present studies explicitly demonstrate that magnetic-perturbation experiments are quite useful for the mechanistic elucidation of photochemical reactions in solutions.

Appendix

Magnetic Field Dependence of the Chemical Yield of Photoproduct. Scheme 1 shows the case of a compound M in a solution absorbing light and, thus, being excited into S_1 and T_1 states. It thus forms singlet and triplet radical-pair intermediates. The S_1-born singlet radical pair, because of its singlet character, mostly undergoes recombination or disproportionation within a solvent cage to give rise to the S_1-born cage product. On the other hand, the T_1-born triplet radical pair, because of its triplet character, undergoes a diffusive separation into a solvent bulk to give the T_1-born escape product. Also, the intersystem crossing of the radical-pair intermediates results in the formation of the S_1-born escape product or T_1-born cage product. If such an intersystem crossing is subject to a magnetic perturbation, the chemical yield of the cage- or escape-product comes to show a magnetic-field dependence (external magnetic field effect upon photochmical reactions in solution).[1]

If the exchange interaction between the unpaired electrons in a radical pair is neglected, the singlet (S) and triplet ($T_{0,\pm}$) levels being degenerate, the rate of the intersystem crossing may be affected by an external magnetic field in the following ways. (1) Electronic Zeeman interaction (Δg mechanism); the external magnetic field causes the intersystem crossing ($S \leftrightarrow T_0$) of a radical pair by virtue of the different g-values of the component radicals. (2) Electron-nuclear hyperfine interaction (HFI mechanism); the external magnetic field causes the number of effective working channels for the hyperfine-induced intersystem crossing of a radical pair to reduce from three ($S \leftrightarrow T_{0,\pm}$) to one ($S \leftrightarrow T_0$).

On the other hand, when the unpaired electrons in a radical pair is in close proximity as a result of a hydrogen-bonding interaction between the two component radicals, the electron-exchange interaction may be greater than the electron-nuclear hyperfine energy; the singlet (S) and triplet ($T_{0,\pm}$) levels of the pair are nondegenerate, having an energy gap of $2|J|$, where J denotes the electron-exchange integral. In this case, the intersystem crossing $S \leftrightarrow T_+$ or $S \leftrightarrow T_-$ may be induced by an electron-nuclear hyperfine interaction mechanism at the magnetic field in which the S level is in resonance with the T_+ or T_- level (HFI-J mechanism).

Figure 5 shows the field dependence of chemical yield of the S_1-born cage product (CP-S_1) or the T_1-born escape product (EP-T_1). In Fig. 6 the field dependence of chemical yield of the S_1-born escape product (EP-S_1) or T_1-born cage product (CP-T_1) is also shown. In the case of a magnetic field effect due to the Δg mechanism, the chemical yields of CP-S_1 and EP-T_1 (or EP-S_1 and CP-T_1) decrease (or increase) quadratically with an increase in the field strength (curve (1) in Fig.5 or curve (1′) in Fig. 6). In the case of a magnetic field effect due to the HFI mechanism, the chemical yields of CP-S_1 and EP-T_1 (or EP-S_1 and CP-T_1) increase (or decrease) steeply at a very low field (curve (2) in Fig. 5 or curve (2′) in Fig. 6). Also, in the case of a magnetic field effect due to the HFI-J mechanism, the chemical yields of CP-S_1 and EP-T_1 (or EP-S_1 and CP-T_1) show a minimum (or a maximum) at a particualr magnetic field (curve (3) in Fig.5 or curve (3′) in Fig. 6).

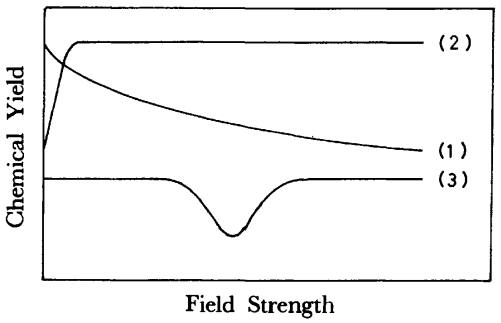

Fig. 5. Magnetic field dependence of the chemical yield of S_1-born cage product (CP-S_1) and T_1-born escape product (EP-T_1).
(1): Δg mechanism, (2): HFI mechanism, (3): HFI-J mechanism.

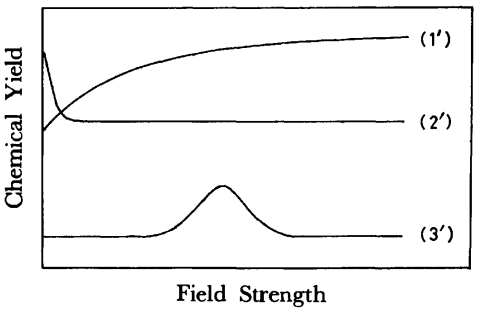

Fig. 6. Magnetic field dependence of the chemical yield of S_1-born escape product (EP-S_1) and T_1-born cage product (CP-T_1).
(1′): Δg mechanism, (2′): HFI mechanism, (3′): HFI-J mechanism.

References

1) See, for example, "Spin Polarization and Magnetic Effects in Radical Reactions," ed by Yu. N. Molin, Elsevier, Amsterdam (1984), Chap. 5.

2) N. Hata, *Bull. Chem. Soc. Jpn.*, **58**, 1088 (1985); Preliminary reports, N. Hata, *Chem.Lett.*, **1976**, 547; **1978**, 1359.

3) Preliminary reports, N. Hata, and M. Hokawa, *Chem.Lett.*, **1981**, 507; N. Hata and N. Nishida, *Chem. Lett.*, **1983**, 1043.

4) H. Menze, *Ber.*, **69**, 1566 (1936).

5) N. Hata, I. Ono, and S. Ogawa, *Bull. Chem. Soc. Jpn.*, **44**, 2286 (1971); N. Hata, I. Ono, S. Matono, and H. Hirose, *Bull. Chem. Soc. Jpn.*, **46**, 942 (1973).

6) N. Hata, *Nippon Kagaku Kaishi*, **1984**, 1759. It has been reported that examination of the magnetic-field and heavy-atom effects on the photosubstitution reaction of 1-isoquinolinecarbonitrile or photochemical substitution and decyanation reactions of 3-methyl-1-isoquinolinecarbonitrile in ethanol were quite useful for the mechanistic elucidation of the reactions. From the experimental results, the photosubstitution reaction was revealed to proceed *via* the S_1 and/or T_1 states through hydrogen abstraction by the ring

nitrogen from ethanol, whereas the photodecyanation reaction was concluded to occur from the S_1 state through hydrogen abstraction by the ring nitrogen from the methyl group at the 3-position of an isoquinoline nucleus.

7) N. Hata and T. Saito, *Bull. Chem. Soc. Jpn.*, **47**, 942 (1974).

8) N. Hata and R. Ohtsuka, *Chem.Lett.*, **1975**, 1107.

9) In previous papers,[6-8] hydrogen-bonding interaction of the ring nitrogen of some azaaromatic nitriles in the S_0, S_1, or T_1 state with an ethanol has been discussed on the basis of the solvent effect of absorption and emission spectra (*cf.* Table 1). The absorption spectrum, both the spectral shape and maximum wavelength (the extinction coefficient), was essentially unchanged in either methylcyclohexane (MCH) or ethanol (EtOH). This means that there is no appreciable hydrogen-bonding interaction between the ring nitrogen and an ethanol in the S_0 state. On the other hand, the fluorescence spectrum showed a remarkable dependence on the solvent. The non-fluorescence (or very weak fluorescence) in MCH was interpreted in terms of a mixing of the S_1 (π,π^*) state with a closely lying ^1n, π^* state through the vibronic coupling, and the fluorescence activation in ethanol was attributable to a great decrease in such a vibronic mixing owing to the formation of hydrogen bond between the ring nitrogen and an ethanol in the S_1 state. The phosphorescence spectrum, which was observed only in the case of 2-quinolinecarbonitriles, was not affected significantly by changing the solvent from MCH to EtOH, indicating that hydrogen-bonding interaction of the ring nitrogen with an ethanol is negligibly small in the T_1 state as well as in the S_0 state.

Reaction of Malonaldehyde with Nucleic Acid. II. Formation of Fluorescent Pyrimido[1,2-*a*]purin-10(3*H*)-one Mononucleotide

Hiroshi SETO,* Tomoyuki TAKESUE,† and Tadashi IKEMURA†
Tokyo Metropolitan Research Laboratory of Public Health, Sinjuku-ku, Tokyo 160
†*College of Science and Technology, Nihon University, Chiyoda-ku, Tokyo 101*
(Received April 10, 1985)

The reaction of malonaldehyde under acidic conditions (pH 4.5) with guanosine 5′-monophosphate resulted in the formation of fluorescent 3-(β-D-ribofuranosyl)pyrimido[1,2-*a*]purin-10(3*H*)-one 5′-phosphate (**3a**). This adduct was also isolated from malonaldehyde-reacted RNA. The amount of **3a** in the modified RNA was estimated to be 0.4 per cent by weight. The fluorescence spectrum of **3a** (E_x max. 360 nm, E_m max. 500 nm) was similar to that of guanine- and guanosine-malonaldehyde adducts which have the same type base structure. On the other hand, another type of fluorophore (E_x max. 390 nm, E_m max. 460 nm) was also formed in the reaction of malonaldehyde with a nucleic acid polymer. Thus, at least two different types of fluorophores are present in malonaldehyde-reacted nucleic acid.

Malonaldehyde (1), an end product of lipid peroxidation and a side product of prostagrandin and thromboxane biosynthesis in animal tissues,[1] is mutagenic[2–4] and carcinogenic.[4–6] These toxicological data suggest chemical interactions between 1 and various biological macromolecules. Therefore, the presence of 1 in foods[7] and in living organs[8,9] in which the lipid fraction has undergone oxidation may be of physiolosical significance. Malonaldehyde is reactive toward DNA to form fluorescent products which are accounted for by cross-linking of DNA between amino groups of the bases of DNA.[10] Recently, Nair *et al.*[11] reported novel adducts from the modification of adenine and cytosine by 1. As previously reported,[12] the adducts formed by the reaction of 1 with guanosines are fluorescent pyrimido[1,2-*a*]-purin-10(3*H*)-one nucleosides. Malonaldehyde also reacts with DNA or RNA (presumably with guanine base), as we previously reported.[12] However, a difference was apparent between the fluorescence spectra of the modified DNA and that of the modified guanosines. An investigation regarding the reactions of 1 with guanosine 5′-monophosphate (5′-GMP) and polyguanylic acid (poly[G]) is of interest in connection with an elucidation of the effect of the phosphate group on the fluorescence (FL) spectrum.

The present paper describes the isolation and characterization of 5′-GMP-malonaldehyde and guanine-malonaldehyde adducts and the formation of a pyrimido[1,2-*a*]purine-10(3*H*)-one base by the reaction of 1 with RNA. We also describe the formation of another fluorophore which is resistant to enzymic digestion.

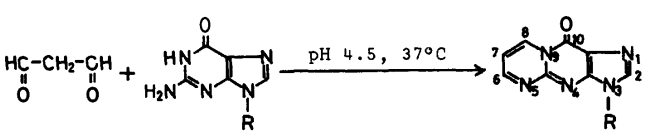

1 **2a**: R = Ra **3a**: R = Ra
2b: R = H **3b**: R = H

Ra = β-D-ribofuranosyl 5′-monophosphate

Scheme 1.

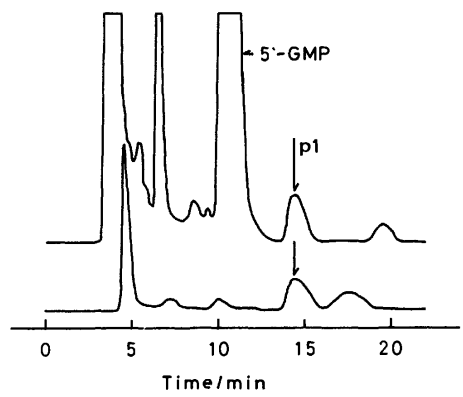

Fig. 1. HPLC chromatograms of 5′-GMP-malonaldehyde reaction mixture. Column: Partisil 10 SAX (4.6φ×250 mm). Upper: UV 254 nm, range 16, 10 μl inj, Lower: FL 365-460 nm, 50 μl inj.

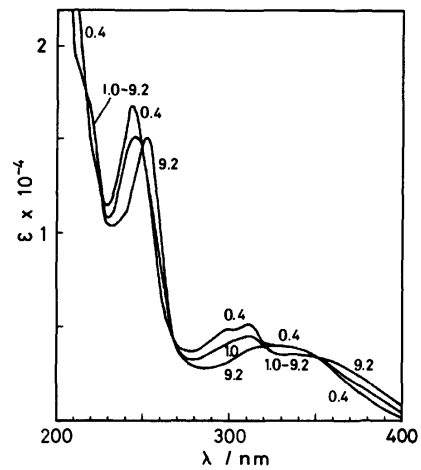

Fig. 2. UV absorption spectra of **3a** at various pH values.

Results and Discussion

5′-GMP-malonaldehyde Adduct. Figure 1 shows an HPLC chromatogram of a reaction mixture of 5′-GMP (**2a**) with 1. The fluorescence peak pl (estimated yield, 2.2%) appeared after the reaction. The

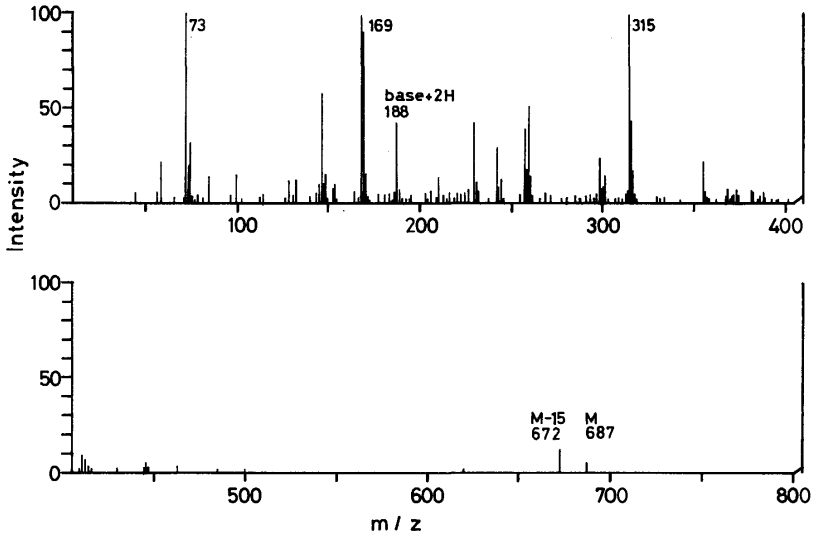

Fig. 3. EI mass spectrum of the TMS derivative of **3a**.

product, a labile light-brown solid (purity 99% as determined by HPLC analysis), was deduced to be 3-(β-D-ribofuranosyl)pyrimido[1,2-*a*]purin-10(3*H*)-one 5′-phosphate (**3a**) from the following chemical and spectroscopic evidence.

TBA (2-thiobarbituric acid)[13] and Molish tests[14] were positive. No carbonyl group (ketone or aldehyde) was detected in the 2,4-dinitrophenylhydrazine test.[14] The pH profile of the UV absorption of compound **3a** is shown in Fig. 2. The pK_a value was calculated spectrophotometrically as 1.23.

The EI mass spectrum of trimethylsilylated **3a** (TMS-**3a**) showed M^+ at *m/z* 687 and an $(M-15)^+$ peak at *m/z* 672 (intensity ratio: *m/z* 687/ *m/z* 672=0.35)(Fig. 3). An important peak of the base was observed at *m/z* 188 $(base+2H)^+$. In the mass spectra of nucleotide-TMS, the base ion is usually accompanied by ions b+H and b+2H.[15] The ions of characteristically high abundance in the spectrum are *m/z* 315 ($HOP(OTMS)_3$) and *m/z* 169 ($C_8H_{13}O_2Si$) from ribotide. The molecular weight of TMS-**3a** was confirmed by the CI mass spectrum, which showed an MH at *m/z* 688. The molecular formula of **3a**, $C_{13}H_{14}N_5O_8P$, was established by high-resolution mass spectrometry (found: *m/z* 687.2186. Calcd for $C_{13}H_{10}N_5O_8P(TMS)_4$: M, 687.2161).

The IR (KBr) spectrum showed absorption bands at 3280 (O–H) and 1725 (C=O) cm^{-1}. The UV spectrum of **3a** was similar to that of pyrimido[1,2-*a*]purin-10(3*H*)-one nucleosides.[12]

A part of the proton NMR spectrum of **3a** is shown in Fig. 4. The characteristic double doublet peaks are typical AMX-type signals due to the -CH=CH-CH= group. The ^{13}C-NMR spectrum showed the existence of 3 carbons (δ 112.3, 142.5, and 163.4 (each d)) in addition to those of **2a** (Fig. 5).

Guanine-malonaldehyde Adduct. The adduct was deduced to be pyrimido[1,2-*a*]purin-10(3*H*)-one (**3b**) from spectroscopic evidence (UV, IR, NMR, and MS).

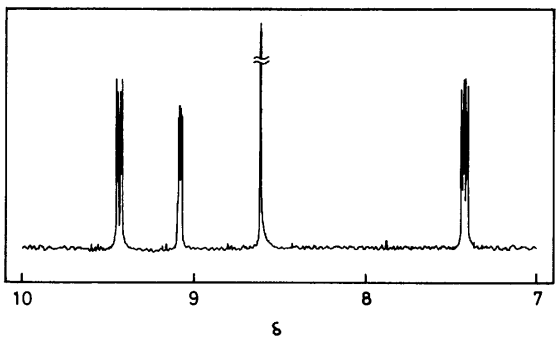

Fig. 4. ^1H-NMR spectrum of **3a**.

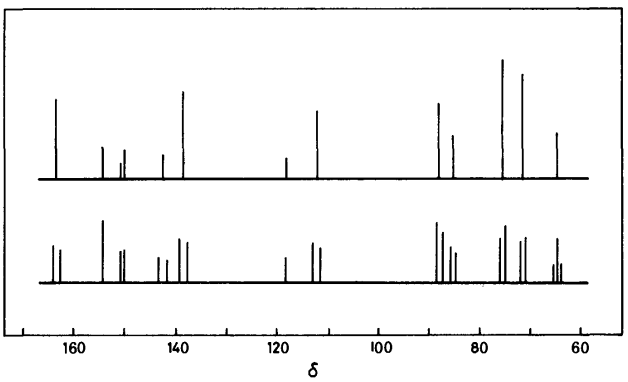

Fig. 5. ^{13}C-NMR spectra of **3a**. Upper: Complete decoupling, Lower: Off-resonance decoupling.

Figure 6 shows an HPLC chromatogram of the extract containing **3b** (peak p2) from the precipitate. The fluorescent product, a yellow amorphous solid, was obtained in 8.4% yield after purification (purity 97% as determined by HPLC analysis). Compound **3b** showed chemical properties similar to those of **3a** in TBA[13] and the 2,4-dinitrophenylhydrazine tests.[14] The UV absorption of **3b** at various pH values is illustrated in Fig. 7. The pK_a value was calculated to be 1.89.

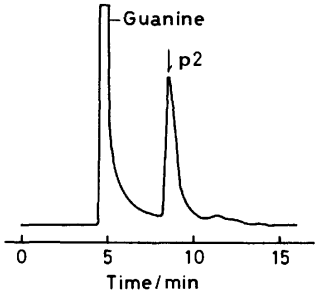

Fig. 6. HPLC chromatogram of the hot water extract from guanine-malonaldehyde reaction mixture. Column: Partisil 10 SCX (4.6φ×250 mm), UV 254 nm, range 16, 10 μl inj.

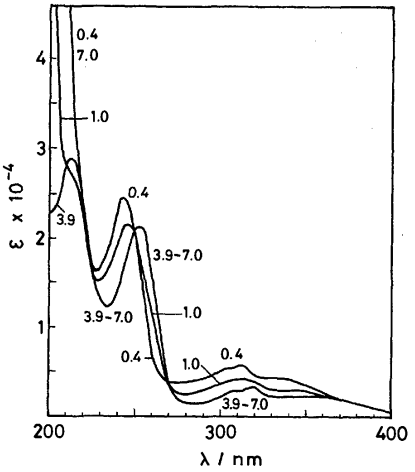

Fig. 7. UV absorption spectra of **3b** at various pH values.

Comparison with the Fluorescence Spectra The Fluorescence(FL) spectra of nucleic acid- and the analog-malonaldehyde adducts are summarized in Fig. 8. The FL spectra of **3a** and **3b** coincided with those of pyrimido[1,2-*a*]purin-10(3*H*)-one nucleosides. It seems that the effect of the phosphate moiety on the FL spectrum is negligible. However, the FL spectra (named Type I) of polymer-malonaldehyde adducts can be distinguished from those (named Type II) of the monomeric compounds which contain a pyrimido[1,2-*a*]purin 10(3*H*)-one base. The spectral difference between the two groups can presumably be attributed to their different structures.

*Isolation of **3a** from the Modified RNA.* Figure 9 shows an HPLC chromatogram of digested RNA which had been modified by 1. The product in peak p3 was separated and characterized. Peak p3 gave UV and FL spectra essentially identical with those of **3a**. The absorbance ratio (A 319 nm/ A 251 nm) of the compound (0.24) was in fair agreement with that of **3a** (0.22), and the retention time of p3 on HPLC coincided with that of **3a**. TMS-treated p3 gave an EI mass spectrum similar to that of **3a**. The molecular ion M^+ at *m/z* 687, $(M-15)^+$ at *m/z* 672 and $(base+2H)^+$ at *m/z* 188 were observed. The product at p3 was therefore identified as compound **3a**.

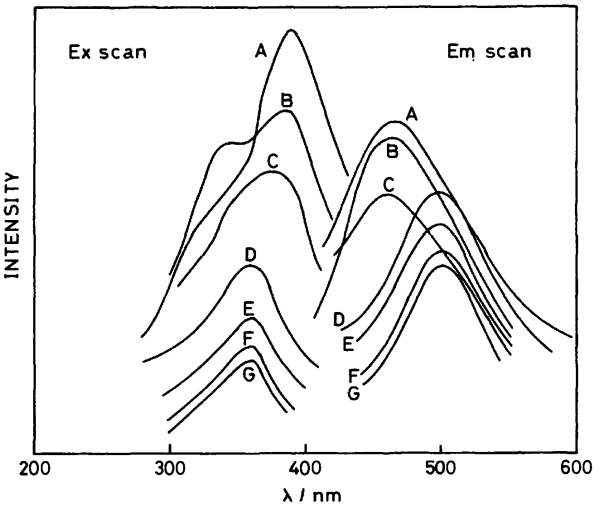

Fig. 8. Fluorescence spectra of malonaldehyde-reacted nucleic acid and analogs. Solvent: water. Substrate (E_x max./nm, E_m max./nm) A: DNA (390,460), B: RNA (390, 460), C: poly[G] (380, 460), D: 5′-GMP (358, 500), E: guanine (363, 500), F: guanosine (360, 500), G: 2′-deoxyguanosine (360, 500). Fluorescence emission spectra were measured by holding fluorescence excitation at 365 nm. Fluorescence excitation spectra were measured by holding fluorescence emission at 460 nm. Concentration of the solution was not normalized.

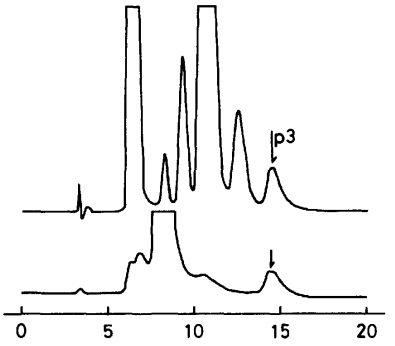

Fig. 9. HPLC chromatograms of the digested RNA solution. The sample for injection was cleaned-up on a DEAE Sephadex column. Column: Partisil 10 SAX (4.6φ×250 mm). Upper: UV 254 nm, range 8, 10 μl inj., Lower: FL 365—460 nm, 50 μl inj.

The amount of **3a** formed in RNA (20 mg) modified by 1 was estimated to be 85 μg (210 nmol, 0.4 wt%) by an HPLC determination. The total amount of 1 incorporated into the RNA was at least 420 nmol as determined by the TBA method.[13] Thus, the modified RNA contains significant amounts of 1 incorporated by some other types of reaction. When the digested RNA solution was applied to a DEAE Sephadex column, a yellow fluorescent band, which contained the major fluorophore, was observed on top of the column bed. This fluorescent substance become strongly bound to the gel.

Tappel *et al.* suggested that the reaction of 1 with DNA produces interstrand crosslinking (N=CH-CH=CH-N)[10] and determined the crosslinks by a fluorescence measurement.[13] However, our result shows that at least two types of FL products (corresponding to Type I and Type II) are formed in the reaction of 1 with nucleic acid. It is necessary to elucidate the structure and properties of Type-I fluorophore.

Experimental

Apparatus. Melting points are uncorrected. IR, UV, and FL spectra were recorded on Hitachi EPI-G3, Shimadzu UV 240, and Shimadzu RF-500 spectrophotometers, respectively. NMR spectra were obtained on a JEOL FX-270 spectrometer with 1,4-dioxane as an internal standard in D_2O at room temperature. Mass spectra were recorded on a JEOL D-300 mass spectrometer. TLC analyses were carried out with Wako polyamide FM plates (5×10 cm). Analytical HPLC was carried out with a Shimadzu LC-2 equipped with UV (254 and 330 nm) and FL (E_x 365 nm, E_m 460 nm) detectors, on a Partisil 10 SAX (4.6ϕ×250 mm) column (the mobile phase was 0.05 M KH_2PO_4 (1M=1 mol dm^{-3}) pH 3.5) and a Partisil 10 SCX (4.6ϕ×250 mm) column (the mobile phase was 0.05 M $NH_4H_2PO_4$). The inlet of the FL detector was connected to the outlet of the UV detector.

Determination of Malonaldehyde Incorporated into Nucleic Acid Polymers. A 0.5 ml aliquot of the solution to be analyzed was taken, and 2 ml of 0.6% 2-thiobarbituric acid and 0.5 ml of glacial acetic acid were then added. The mixture was kept in boiling water for 30 min, and the absorbance was measured at 532 nm.

Reaction of Malonaldehyde with 5'-GMP. 5'-GMP·2Na (**2a**) was purchased from Yamasa Shoyu Co. Ltd., Tokyo. Malonaldehyde (1) was prepared by the hydrolysis of 1,1,3,3-tetraethoxypropane (4.4 g, 0.02 mol) with 0.1 M HCl (200 ml). The mixture was stirred at 40 °C for 40 min, then adjusted to pH 4.5. A solution of 1 (0.02 mol), **2a** (4.1 g, 0.01 mol) and KH_2PO_4 (27.2 g, 0.2 mol) in two liters of water was kept at 37 °C for 7 d, then concentrated to about 400 ml at 40 °C. Acetonitrile was then added, and the whole was kept overnight in a refrigerator (4 °C). The precipitate was collected by filtration, washed with acetonitrile and redissolved in a small amount of water. It was then subjected to DEAE Sephadex A-25 chromatography (5ϕ×70 cm, 0.01 M KH_2PO_4, pH 3.5). The fluorescent fractions were collected, concentrated, and purified by Partisil 10 SAX chromatography (8ϕ×250 mm, 0.1 M KH_2PO_4, pH 3.5). The fraction containing **3a** was applied to a Unisil C-18 column (8ϕ×250 mm, water) for desalting. The product solution was evaporated to dryness *in vacuo*.

Reaction of Malonaldehyde with Guanine. A solution of 1,1,3,3-tetraethoxypropane (5.5 g, 25 mmol) in 25 ml of 1 M HCl was kept at 40 °C for 40 min. Subsequently, guanine (0.75 g, 5 mmol, Yamasa Shoyu Co. Ltd.) and 25 ml of 1 M HCl were added. The mixture was stirred at 40 °C for 1 h. The precipitate was collected by centrifugation (2500 min^{-1}, 10 min), washed with ethyl alcohol, and then centrifuged again. The guanine-malonaldehyde adduct was extracted from the precipitate with hot water (60 °C). The extract was cleaned on a polyamide column (5ϕ×30 cm, water). The fluorescent fractions were collected and concentrated to remove sedimenting guanine. The solution was purified by Partisil 10 SCX chromatography (8ϕ×250 mm, 0.1 M $NH_4H_2PO_4$). Finally, the eluate containing guanine-malonaldehyde adduct (**3b**) was evaporated *in vacuo*.

Reaction of Malonaldehyde with DNA, RNA, or Poly [G]. Calf thymus DNA, baker's yeast RNA, and poly [G] were purchased from Sigma Chemical Co., St. Louis, MO. A mixture containing 10 mg of nucleic acid and 136 mg of KH_2PO_4 (1 mmol) in 10 ml of 1 (0.01 M) solution was maintained at 37 °C for 10 d. The solution was dialyzed against distilled water for 5 d, then evaporated *in vacuo* to give a modified nucleic acid.

Isolation of 5'-GMP-malonaldehyde Adduct (3a) from the Modified RNA. The malonaldehyde-reacted RNA (20 mg) was hydrolyzed in 10 ml of buffer solution (1 mM KH_2PO_4, 0.1 mM $ZnCl_2$, pH 5.3) with 1 mg of Nuclease P_1 from *Penicillium citrinum* (Yamasa Shoyu Co. Ltd.) at 37 °C for 2 d. The digested RNA solution was cleaned on a DEAE Sephadex A-25 column (10ϕ×150 mm, 0.01 M KH_2PO_4, pH 3.5). The eluate was concentrated to 2 ml, then chromatographed on a Partisil 10 SAX column (4.6ϕ× 250 mm, 0.05 M KH_2PO_4, pH 3.5). The fractions of 5'-GMP-malonaldehyde adduct (**3a**) were collected, desalted and evaporated *in vacuo*.

3a: Mp>200 °C (dec); R_f=0.67 polyamide/H_2O, R_f=0.34 DEAE ppc/0.03 M KH_2PO_4, pH 3.5); pK_a 1.23; UV (H_2O) 214(ε 22000), 251(ε 15000), 318(ε 3000), and 350 nm (ε 2900); ^{1}H NMR (D_2O) δ=4.09 (2H, br., m, C_5'-H), 4.39(1H, br., m, C4'-H), 4.54(1H, br., dd, C_3'-H), 4.82(1H, br., dd, C_2'-H), 6.22(1H, d, J=5.5 Hz, C_1'-H), 7.39(1H, dd, J=3.8 and 7.1 Hz, C_7-H), 8.63(1H, s, C_2-H), 9.06(1H, dd, J=2.0 and 3.8 Hz, C_6-H), and 9.37(1H, dd, J=2.0 and 7.0 Hz, C_8-H); ^{13}C NMR (D_2O) δ=64.8(t), 71.5(d), 75.5(d), 85.4(d), 88.1(d), 112.3(d), 118.4(s), 138.4(d), 142.5(d), 150.1(s), 150.7(s), 154.3(s), and 163.4(d).

3b: Mp>270 °C (dec); R_f=0.62 polyamide/H_2O, R_f= 0.58 CM ppc/0.025M $NH_4H_2PO_4$); pK_a 1.89; UV (H_2O) 215(ε 21000), 251(ε 17000), 305(ε 3000), 316(ε 3500), and 350 nm (ε 3000); IR (KBr) 1720 cm^{-1} (C=O); MS EI(70 ev) m/z 187 (M^+), Found: m/z 187.0493. Calcd for $C_8H_5N_5O$: M, 187.0493, CI(isobutane) m/z 188 (QM^+); ^{1}H NMR(D_2O) δ=7.33(1H, dd, J=2.0 and 7.3 Hz, C_7-H), 8.33(1H. s, C_2-H), 8.97(1H, dd, J=2.0 and 4.0 Hz, C_6-H), and 9.21(1H, dd, J=2.0 and 7.1 Hz, C_8-H).

References

1) W. A. Pryor, "Free Radicals in Biology," Academic Press, New York (1976) Vol. 1 and 2.

2) F. H. Mukai and B. D. Goldstein, *Science*, **191**, 868 (1976).

3) A. K. Basu and L. J. Marnett, *Carcinogenesis*, **4**, 331 (1983).

4) P. E. Hartman, *Environ. Mutagen*, **5**, 603 (1983).

5) R. J. Shamberger, T. L. Andreone, and C. E. Willis, *J. Natl. Cancer Inst.*, **53**, 1771 (1974).

6) R. P. Bird, H. H. Draper, and V. E. O. Valli, *J. Toxicol. Environ. Health*, **10**, 897 (1982).

7) E. A. Jacobson, H. L. Newmark, R. P. Bird, and W. R. Bruce, *Nutr, Rep. Int.* **28**, 509 (1983).

8) D. H. Boehme, R. Kosecki, S. Carson, F. Stern, and N. Marks, *Brain Res.*, **136**, 11 (1977).

9) K. Nakashima, T. Ando, K. Nakamura, and S.

Akiyama, *Chem. Pharm. Bull.*, **31**, 2523 (1983).
10) U. Reiss, A. L. Tappel, and K. S. Chio, *Biochem. Biophys. Res. Commun.*, **48**, 921 (1972).
11) V. Nair, G. A. Turner, and R. J. Offerman, *J. Am. Chem. Soc.* **106**, 3370 (1984).
12) H. Seto, T. Okuda, T. Takesue, and T. Ikemura, *Bull. Chem. Soc. Jpn.*, **56**, 1799 (1983).
13) F. W. Summerfield and A. L. Tappel, *Anal. Biochem.*, 111, 77, (1981).
14) D. J. Pasto and C. R. Johnson, "Organic Structure Determination," Prentice-Hall Inc., Eaglewood Cliffs, New Jersey (1969), Chap. 3.
15) A. M. Lawson, R. N. Stillwell, M. M. Tacker, K. Tsuboyama, and J. A. McCloskey, *J. Am. Chem. Soc.*, **93**, 1014 (1971).

Cation-binding Properties of Ionophorous Cyclic Octapeptide in Acetonitrile Solution

Toshimi SHIMIZU,* Yoshio TANAKA, and Keishiro TSUDA
Research Institute for Polymers and Textiles, Yatabe-Higashi 1-1-4, Tsukuba, Ibaraki 305
(Received June 7, 1985)

Complex formation of synthetic cyclic octapeptide, cyclo[Gly-L-Lys(Z)-Sar-L-Pro]$_2$, with alkali and alkaline earth metal ion was investigated by CD and NMR spectroscopy. Titration curves obtained from CD data revealed three kinds of CGLSP2(P)/cation(C) complexes. P_2C ("peptide sandwich"), PC ("1 : 1"), and PC_2 ("cation sandwich") complexes occurred in the complexation between CGLSP2 and Ba^{2+}. In the presence of Li^+, Mg^{2+}, or Ca^{2+}, the existence of PC and PC_2 was assumed. K^+ and Na^+ form only a PC species with CGLSP2. By analyzing the titration curves, 1 : 1 complex-formation constants (K_1) were evaluated. The K_1 values decrease in the order $Ba^{2+}>Ca^{2+}>Mg^{2+}>Li^+\gg Na^+$, K^+. ^{1}H- and ^{13}C-NMR data showed that CGLSP2 in acetonitrile exists in at least five different conformational states in a free state. A predominant conformer had a C_2-symmetric structure containing two cis Lys-Sar peptide bonds. After the addition of equimolar amounts of $Ba(ClO_4)_2$, these conformations converged into a single C_2-symmetric one with all-trans peptide bonds. This corresponds to a PC species. On further addition of the salt, CGLSP2 changed the conformation into an asymmetric structure with one cis Lys-Sar peptide bond. This corresponds to a PC_2 species.

Ionophores form stable and lipophilic complexes with Na^+, K^+, and Ca^{2+} *etc.*, and are able to transport them across artificial and biological membranes. Some cyclic oligopeptides have an interesting feature to bind a specific alkali and alkaline earth metal ion.[1-4] In the light of this characteristic, cation extraction,[5] cation transport through a liquid membrane,[6,7] and liquid membrane electrode[8] have been examined by using cyclic peptides. We also reported behavior of cyclic octapeptide, cyclo[Gly-L-Lys(Z)-Sar-L-Pro]$_2$ (CGLSP2) as an ionophorous agent.[9] CGLSP2 could transport or extract Ba^{2+} and Ca^{2+} preferably over Mg^{2+}, K^+, Rb^+, and Na^+. Among physiological cations, Ca^{2+}/Mg^{2+} selectivity in the cation extraction reached 1.5×10^2. Thus, CGLSP2 can compete in this high discrimination ability with naturally occurring antibiotics.[10]

Valinomycin is a macrocyclic dodecadepsipeptide, displaying an exceptionally high selectivity for K^+ over Na^+. The feature can be interpreted in terms of a limited structure of the cyclic backbone in the complexed state.[11] On the other hand, a variety of conformations have been detected for the uncomplexed form in solution.[12] They are found to be highly dependent on solvent polarity. In this way, the cation-binding specificity of valinomycin is based on a conformational rearrangement accompanying complex formation. In particular, CGLSP2 contains four N-substituted peptide bonds (Lys–Sar and Sar–Pro bonds) which are able to take cis as well as trans geometry.[13,14] Therefore, a number of conformations are allowed by random distribution of the cis and trans peptide bonds.

From this point of view, we have studied a cation binding of CGLSP2 with alkali and alkaline earth metal ions in an acetonitrile solution by CD and NMR spectroscopy. Acetonitrile was chosen as a suitable aprotic medium. Its resolution of cation complexes is better than that of protic solvents such as water or methanol. Since CD spectra are very sensitive to peptide conformation upon complexation, they serve to follow a change of complexed species. In addition, it takes the advantage that complex-formation constants can be determined for a certain binding species.[15,16] On the other hand, NMR spectra give information about the structure of that species. Since cis-trans isomerism is slow on the NMR time scale, the conformations can be detected individually by NMR. This paper focused on resolutions and identifications of several complexed species.

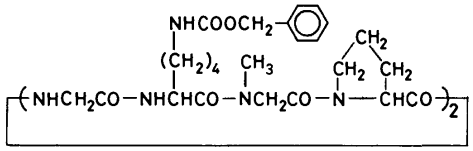

cyclo[Gly-L-Lys(Z)-Sar-L-Pro]$_2$ (CGLSP2)

Experimental

The preparation and physical characteristic of the cyclic octapeptide, cyclo[Gly-L-Lys(Z)-Sar-L-Pro]$_2$ (CGLSP2) are reported in our preceding paper.[9]

^{1}H-NMR spectra were obtained at 360 MHz on a NICOLET NT-360 spectrometer with a NIC 1180 Computer Data System, operating in the Fourier transform mode with quadrature detection. ^{13}C-NMR spectra were recorded on a Varian CFT-20 spectrometer at 20 MHz, in the Fourier transform mode with proton-noise decoupling. All the chemical shifts are given in parts per million (ppm) relative to the internal tetramethylsilane.

Circular dichroism spectra were recorded on a JASCO J-40A automatic recording spectropolarimeter equipped with a J-DPY data processor at 20 °C. Measurements were carried out using a quartz cell with 0.1-cm path length over 250 nm to 200 nm. Data are represented as molar ellipticities. Unless otherwise noted, spectrophotometric-grade acetonitrile was used as the solvent.

Alkali metal cations used for binding studies were Li^+ (1.20

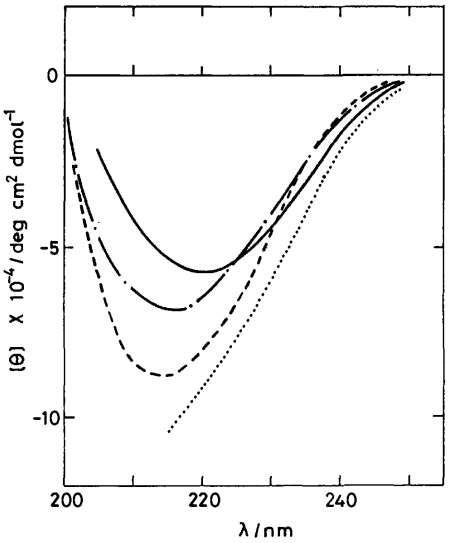

Fig. 1. CD spectra of CGLSP2 in various solvents. Acetonitrile (——), methanol (— — —), 2,2,2-trifluoroethanol (– – – – –), and 1,4-dioxane (·····). Peptide concentration; 6.23×10^{-4} mol dm^{-3}.

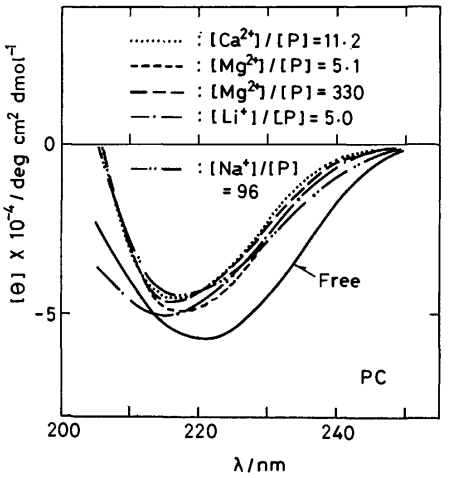

Fig. 2. CD spectra of CGLSP2 in acetonitrile in the presence of lithium, sodium, magnesium, and calcium perchlorate. Molar ratios of a salt to CGLSP2 are shown in the figure. Peptide concentration; 2.47×10^{-4} mol dm^{-3}.

Å), Na^+ (1.90 Å), and K^+ (2.66 Å), and alkaline earth metal cations Mg^{2+} (1.30 Å), Ca^{2+} (1.98Å), and Ba^{2+} (2.70 Å). The value in parentheses indicates each ionic diameter. The cations were dissociated from the corresponding perchlorates. In the case of K^+, acetonitrile/water (95/5, by volume) mixture was used to dissolve the salt. Both CD and NMR measurements were performed after the complexation equilibrium was completely established on addition of each salt.

Results and Discussion

CD Spectra of Cyclic Octapeptide in a Free and a Complexed State. CD spectra of CGLSP2 in various solvents (acetonitrile, methanol, 2,2,2-trifluoroethanol, and 1,4-dioxane) are shown in Fig. 1. Dielectric constant of each solvent is 37.5, 32.7, 26.7, and 2.2, respectively. A large negative Cotton effect appeared at 214—221 nm, which is mainly attributed to an $n\rightarrow\pi^*$ transition of the amide bond. The extremum is shifted to longer wavelength when dielectric constant of the solvent increased. At the same time ellipticity of the negative band decreased. There seems to be no remarkable differences in conformation in these solvents.

When cations smaller than 2.00 Å (Li^+, Na^+, Mg^{2+}, and Ca^{2+}) were added stepwise to a solution of CGLSP2 in acetonitrile, a small spectral change was observed, as shown in Fig. 2. There was a slight decrease of the negative ellipticity. The extremum was shifted 216—218 nm from 221 nm for the free peptide. These spectra are designated type I.

In the presence of cations larger than 2.00 Å [Ba^{2+} (small amounts) and K^+ (large amounts)], the 221-nm negative band decreased in intensity and the extremum was shifted to longer wavelength. In addition,

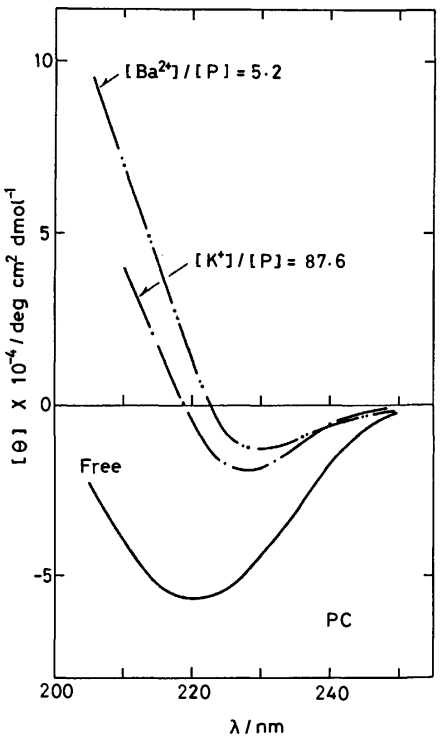

Fig. 3. CD spectra of CGLSP2 in acetonitrile in the presence of potassium and barium perchlorate. Unless otherwise noted, the conditions are the same as those described in Fig. 2.

appearance of a strong positive band around 200—210 nm could be observed (Fig. 3). These are referred to type II. Besides these two types of spectra, a group of spectra designated as type III were found. They were characterized by a small negative ellipticity at 235—250 nm and a relatively sharp negative band at 210—220 nm (Fig. 4). These spectra appeared in the presence of large amounts of Ba^{2+}, Ca^{2+}, and Li^+. The above

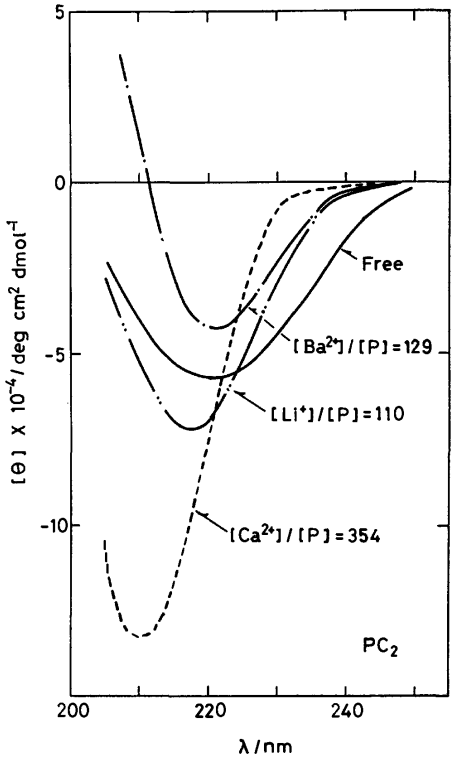

Fig. 4. CD spectra of CGLSP2 in acetonitrile in the presence of lithium, calcium, and barium perchlorate. Unless otherwise noted, the conditions are the same as those described in Fig. 2.

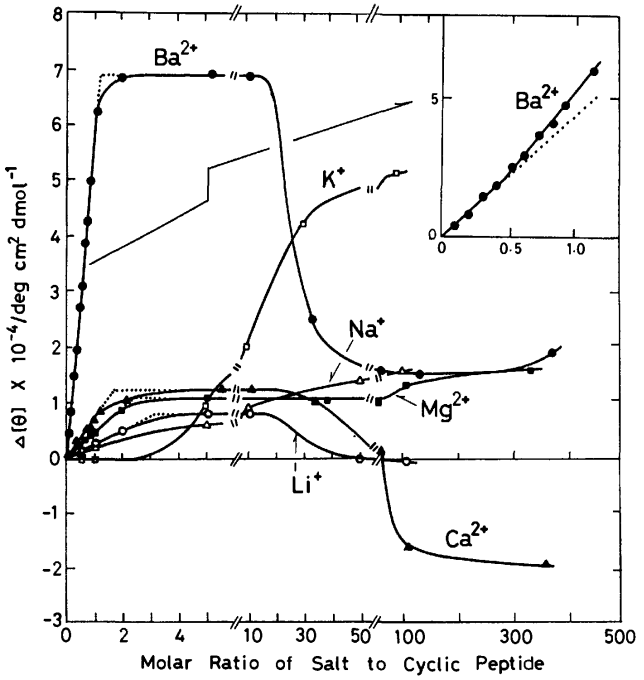

Fig. 5. Titration curves of CGLSP2 for various metal perchlorates in acetonitrile. $\Delta[\theta]$ indicates the difference between the molar ellipticity of a complexed peptide and that of a free peptide.

results suggest that several complexed species exist with different stoichiometries. Moreover, they vary with peptide/cation sets. To clarify these features, we obtained titration curves for each cation from CD spectra.

Titration Curves. Titration curves were depicted, in which the changes in molar ellipticities at a certain wavelength were plotted against the molar ratio of metal salt to cyclic peptide. Titration curves generated from several wavelength (210—230 nm) showed no remarkable differences. Figure 5 indicates the titration curves at 220 nm for Li^+, Na^+, K^+, Mg^{2+}, Ca^{2+}, and Ba^{2+}. Three representative curves were depicted according to cations. The first is a titration curve for Ba^{2+}. After adding less than half equivalent of Ba^{2+}, the increase of the ellipticity was linear with the amount of the salt. As the molar ratio further increased (0.5—1.1 equiv), the straight line became another one with a slightly larger slope than that at the early part of titration. After the addition of more than two equivalents of Ba^{2+}, two plateaus that correspond to type II and type III were observed. This finding suggests that CGLSP2 forms at least three types of complexes with Ba^{2+}. At the peptide concentration over the range of 10^{-5}—10^{-3} mol dm^{-3} we have studied, the first species of the complexation may be expressed as P_2C, where P is the cyclic peptide and C is a metal cation. The second and the third step can be interpreted in terms of the formation of a 1:1 PC species and a 1:2 PC_2 species, respectively. The above feature of binding is similar to those found for other cyclic peptides.[16-18]

In the case of Li^+-, Mg^{2+}-, and Ca^{2+}-titration curves, a clear folding could not be observed around the molar ratio of 0.5. Only one plateau is observed within the addition of less than 400 equiv of the cation. It would be associated with the formation of a 1:1 complex. At the late part of titration, the decrease of ellipticity for Li^+ and Ca^{2+}, or the increase of ellipticity for Mg^{2+} indicates an appearance of PC_2 species in place of PC.

K^+- and Na^+-titration curves showed a gradual increase of the ellipticity when the molar ratio increased. The last part of titration with K^+ corresponds to type II which is similar to the case of the first plateau in Ba^{2+} titration (Fig. 3). CD spectrum of CGLSP2 in the presence of 96 equiv of Na^+ resembles closely to that of a 1:1 complex between CGLSP2 and Ca^{2+} (Fig. 2). The above results support that a single complexation step in K^+- and Na^+-titration curve is associated with the formation of a 1:1 complex.

Complex-formation Constants. The data obtained from CD spectra and CD-titration curves revealed the following. (1) P_2C ("peptide sandwich"), PC ("1:1"), and PC_2 ("cation sandwich") complexes occur in the complexation between CGLSP2 and Ba^{2+}. (2) In the Li^+, Mg^{2+}, and Ca^{2+} systems, the existence of PC and PC_2 is assumed. (3) K^+ and Na^+ form only a PC species with CGLSP2. Of course, one can not exclude an existence of alternate complexed species in the presence of larger amount of cations than that we have

Table 1. Complex-formation constants (K_1) of CGLSP2 with various metal perchlorates in acetonitrile at 20°C

Cation	Charge density$\times10^{-10}$/s A m^{-3}	K_1/mol^{-1} dm^3
Li^+	12.1	$(2.4\pm0.2)\times10^3$
Na^+	4.46	Very low
K^+	1.62	Very low
Mg^{2+}	26.8	$(5.6\pm0.9)\times10^3$
Ca^{2+}	7.90	$(7.6\pm1.9)\times10^3$
Ba^{2+}	3.17	$(2.7\pm0.7)\times10^4$

studied. From the region of a 1:1 complex formation in the titration curves, complex-formation constants (K_1) were determined so as to satisfy a normalized α-ϕ curves calculated by Prestegard and Chan.[19] The obtained values are given in Table 1. The affinity of Ba^{2+} for CGLSP2 in acetonitrile ($K_1\approx2.7\times10^4$ mol^{-1} dm^3) is *ca.* 10-fold smaller than that of K^+ for valinomycin ($K_1\approx3\times10^5$ mol^{-1} dm^3 in CH_3CN).[20] In addition, CGLSP2 binds Ca^{2+} favorably ($K_1\approx7.6\times10^3$ mol^{-1} dm^3). This affinity is *ca.* 10-fold smaller than that of a naturally occurring cyclic decapeptide, antamanide which forms a very stable complex with Ca^{2+} ($K_1=1\times10^5$ mol^{-1} dm^3 in CH_3CN).[21] The K_1 sequences were $Ba^{2+}>Ca^{2+}>Mg^{2+}>Li^+\gg Na^+$, K^+. It can be clearly seen that doubly charged cations are bound preferentially over monovalent cations. Between cations having similar ionic diameter (Ba^{2+} and K^+), the ratio of the binding constants, $K_1(Ba^{2+}):K_1(K^+)$, is approximate 10^4. Similar trend could be seen between Ca^{2+} and Na^+ [$K_1(Ca^{2+}):K_1(Na^+)\approx10^3$]. The binding of both Na^+ and K^+ is much lower than that of the other cations, even the smaller cations, Li^+ or Mg^{2+}. As observed with the complex formation between cyclo-(L-Val-Gly-Gly-L-Pro)$_3$ and Li^+, or Mg^{2+},[16] high charge density of the cations may serve to form a stable 1:1 complex.

Rate of Complex Formation. Kinetics of a 1:1 complex formation between CGLSP2 and $Ba(ClO_4)_2$ was investigated in acetonitrile by CD spectroscopy. The complexing reaction was started by combining solutions of the salt (1.14 equiv) and the cyclic peptide. Immediately after mixing, the ellipticity at 220 nm was measured at 1-min intervals. Under these conditions, formation of a 1:1 complex is clearly demonstrated by the titration curves shown in Fig. 5. Consequently, equilibrium was already reached even after 1 min. This result indicates that the rate of complex formation between CGLSP2 and Ba^{2+} is fairly rapid. Formation and dissociation of the complex can be expressed by the following scheme;

$$P + C \underset{k_d}{\overset{k_f}{\rightleftharpoons}} PC$$

where k_f and k_d is rate constants of the complex formation and dissociation, respectively. Assuming the half-life of free cyclic peptide (P) is 1 min, we can

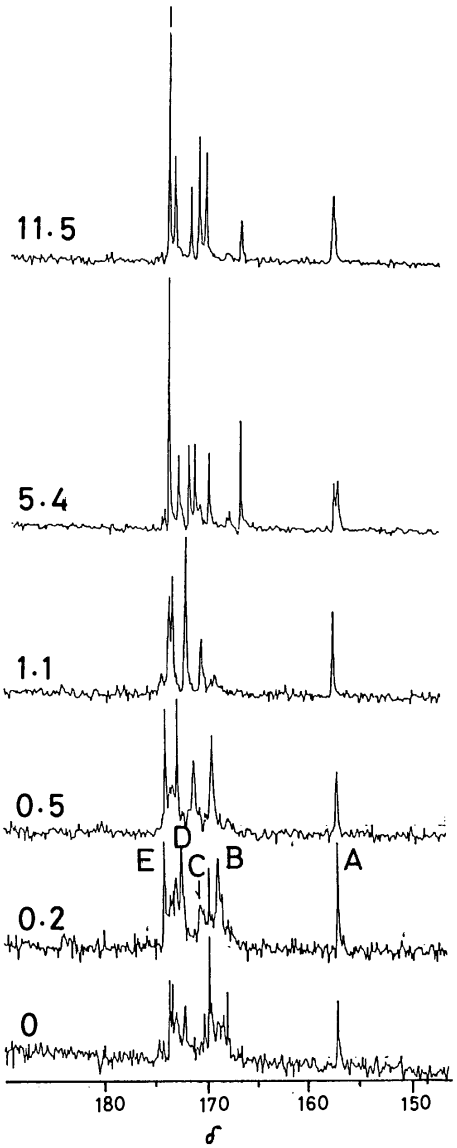

Fig. 6. ^{13}C-NMR spectra of C=O region of CGLSP2 in acetonitrile-d_3 when barium perchlorate was added. Numbers represent the molar ratio of salt to peptide. Peptide concentration; 54.2 g dm^{-3}. Temperature; 25°C.

evaluate the rate constant (k_f) roughly in the same manner as described by Kimura and Imanishi.[4] The k_f value obtained was larger than 66 (mol^{-1} dm^3 s^{-1}) at 20°C. This value appears to be lower than that reported for valinomycin/K^+ complex (3.5×10^7 mol^{-1} dm^3 s^{-1} in methanol).[22] However, it is at least 300-fold larger than that reported for complex formation between cyclo[L-Lys(Z)-L-Pro]$_4$ and Ba^{2+} [0.2 mol^{-1} dm^3 s^{-1} in ethanol/ water (95/5, v/v) mixture].[4]

NMR Investigation. Titration of CGLSP2 with $Ba(ClO_4)_2$ was investigated in acetonitrile-d_3 by NMR spectroscopy (^{1}H and ^{13}C). The number of both C=O carbon resonances and N-CH_3 proton resonances serves to clarify the symmetry of the ring. In addition, the chemical shifts of Pro C^β and C^γ carbon are indica-

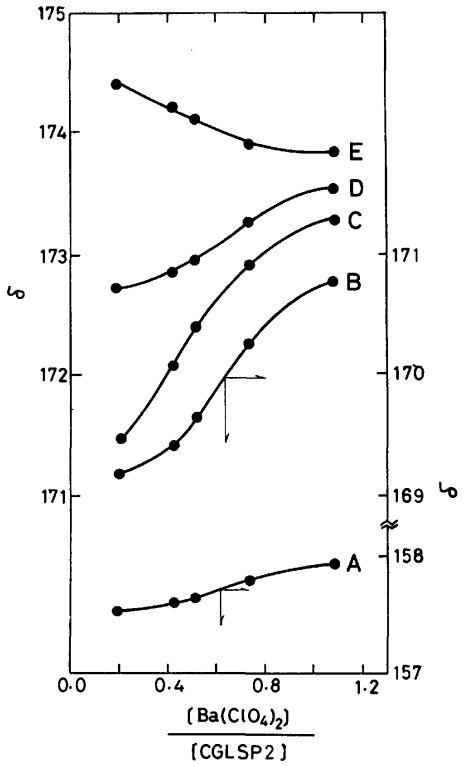

Fig. 7. Shift of carbonyl resonances of CGLSP2 in acetonitrile-d_3 when barium perchlorate was added.

tive of a cis-trans isomerism around Sar–Pro peptide bonds.[13,23] The chemical shifts of Sar N–CH_3 protons reflect a cis-trans isomerism around Lys–Sar peptide bonds.[23,24] In Fig. 6, spectral change of carbonyl resonance region in ^{13}C-NMR is presented. A large number of resonances appeared in the absence of barium salt. When the salt was added stepwise to the solution (<1.1 equiv of Ba^{2+}), five signals became pronounced with increasing in concentration of the salt. This finding indicates that CGLSP2 converged into a single C_2-symmetric conformation from multiple conformations in a free state by the complex formation with Ba^{2+}. That species in a complexed state corresponds to PC that is responsible for type I spectrum in CD. Figure 7 indicates the shift of the five carbonyl carbon resonances caused by the addition of $Ba(ClO_4)_2$. A downfield shift was observed for the signals A, B, C, and D except the signal E. This downfield shift is considered to be caused by ion-dipole interactions between Ba^{2+} and carbonyl groups.[4,17,25] Accordingly, differences in their chemical shifts ($\Delta\delta$) between the cases containing 0.2 and 1.1 equiv of Ba^{2+} were determined. The difference ($\Delta\delta$) of the signals B and C is at least two times larger than that of the other signals A, D, and E. Assignment of the signals were carried out by comparison with the signals of a precursory linear peptides and related compounds,[9] and on the basis of literature information.[26] The Pro C=O, Lys(Z) C=O, Gly or Sar C=O, and Lys(Z) NHCOO carbon resonances must be located in this order from the lowfield. Thus,

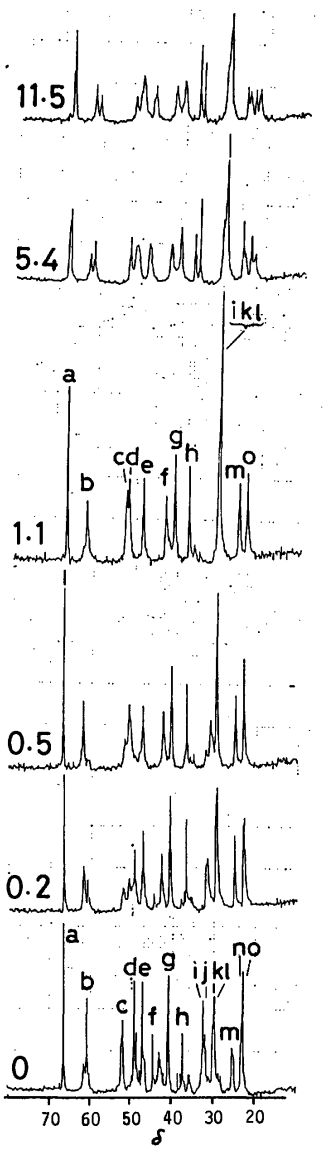

Fig. 8. ^{13}C-NMR spectra of upfield regions of CGLSP2 in acetonitrile-d_3 when barium perchlorate was added. Numbers represent the molar ratio of salt to peptide. Tentative resonance assignments were indicated; (a) $\underline{C}H_2$–C_6H_5, (b) Pro C^{α}, (c) Pro C^{δ}, (d) Lys C^{α}, (e) Sar C^{α}, (f) Gly C^{α}, (g) Lys C^{ε}, (h) Sar N–CH_3, (i) Lys C^{δ}, (j) Pro C^{β}(cis), (k) Pro C^{β}(trans), (l) Lys C^{β}, (m) Pro C^{γ}(trans), (n) Pro C^{γ}(cis), and (o) Lys C^{γ}.

the signals B and C can be attributed to Gly C=O and Sar C=O carbon. Therefore, four carbonyl oxygens of Gly and Sar residues are considered to participate to bind Ba^{2+} cooperatively in the C_2-symmetric conformer. At this time, the side-chain carbonyl groups of Lys residue do not involve in complexation, since the signal A can be assigned to carbonyl carbon of benzyloxycarbonyl group of Lys.

Further addition of more than 1.1 equiv of the salt produced another pattern of signals which was ascribable to a new complexed species. As judged from the number and peak area of resonances in the pres-

ence of 5.4 equiv of the salt, the new species possesses an asymmetric conformation. This conformer corresponds to PC_2 that is responsible for type III spectrum in CD.

Upfield regions of the ^{13}C-NMR spectra of CGLSP2 are given in Fig. 8. Remarkable spectral changes were observed in Pro C^{β} and C^{γ} resonance regions (δ 20—35). As the molar ratio of salt to peptide increases, the Pro C^{β} and Pro C^{γ} carbon signals (j and n) involving in a cis Sar-Pro peptide bond in free peptide diminished and alternatively signals (k and m) arising from the trans peptide bond became predominant. In the presence of 1.1 equiv of the salt, only one signal attributed to the trans Sar-Pro peptide bond appeared at δ 30.31 for Pro C^{β} carbon and δ 25.31 for Pro C^{γ} carbon.[13,24] Even when the salt was further added, the resonances of Pro C^{β} and Pro C^{γ} carbon remained within the region associated with trans Sar-Pro bond.

Similarly, ^1H-NMR spectra were investigated while $Ba(ClO_4)_2$ was added stepwise to CGLSP2 in acetonitrile-d_3. They also suggested a conformational convergence into the single C_2-symmetric conformation. In Fig. 9 , spectral change of N-CH_3 resonance region is shown. In the absence of the salt, a strong signal appears at δ 2.87, in addition to a single resonance at δ 2.92 and three pairs of six signals at δ 2.83, 2.90, 2.96, 2.98, 3.17, and 3.20. Therefore, free CGLSP2 exists in at least five different conformational states (two C_2-symmetric conformers and three asymmetric ones) in acetonitrile. As previously reported,[9] conformational distribution of these conformers is similar to that in chloroform. Moreover, a predominant C_2-symmetric conformer includes two cis Lys-Sar peptide bonds that are the same in chloroform. The temperature dependences of predominant NH proton resonances (not shown) were found to be $\approx$0 ppm deg^{-1} for Lys NH protons and $\approx 7\times10^{-3}$ ppm deg^{-1} for Gly NH protons in acetonitrile-d_3. This result suggests that Lys NH protons of the predominant conformer are shielded from the solvent. ^{13}C-NMR measurement showed that Pro C=O carbon resonance (the signal E) is shifted to upfield upon complexation (Fig. 7). Together with these results, Lys NH protons could be intramolecularly hydrogen-bonded to Pro C=O oxygens in (some) conformers of the free peptide. Consequently, the upfield shift of Pro C=O carbon resonance may be attributed to the destruction of hydrogen bonds in the complex formation.[6]

With increasing in Ba^{2+} concentration (<1.0 equiv of Ba^{2+}), a strong N-CH_3 signal (○) at δ 2.87 disappeared gradually. At the same time, a new N-CH_3 signal (▲) appeared at δ 3.10 upon the addition of 0.25 equiv of Ba^{2+}, and its intensity increased. In the presence of 0.5—1.0 equiv of Ba^{2+}, one major signal was observed at δ 3.09. Further addition of the salt (>1.0 equiv of Ba^{2+}) produced a new pair of signals (●) at δ 3.03 and 2.84. In the presence of more than 5.6 equiv of Ba^{2+}, only this

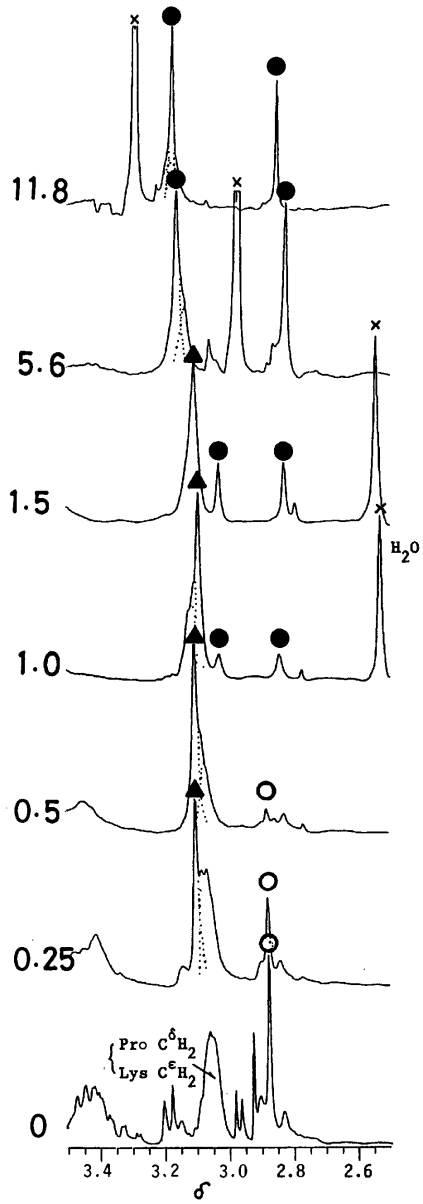

Fig. 9. ^1H-NMR spectra of N-CH_3 region of CGLSP2 in acetonitrile-d_3 when barium perchlorate was added. Numbers represent the molar ratio of salt to peptide. Peptide concentration; 32.0 g dm^{-3}. Temperature; 20°C.

$$C_2(ctttcttt) \rightleftharpoons C_2' \rightleftharpoons A' \rightleftharpoons A'' \rightleftharpoons A'''$$

c: cis, t: trans

$$C_2(tttttttt)\cdot M^{2+} \qquad [PC]$$

$$M^{2+}{:}A(ctttttttt)\cdot M^{2+} \qquad [PC_2]$$

Fig. 10. Scheme for the complexation of CGLSP2 with $Ba(ClO_4)_2$ or $Ca(ClO_4)_2$, which was deduced from ^1H- and ^{13}C-NMR spectroscopy. C_2 and C_2' represent distinct C_2-symmetric conformers. A, A', A'', and A''' represent asymmetric conformers. M^{2+} means Ba^{2+} or Ca^{2+}. Peptide-bond sequences in parentheses are given for the linkage of Lys(Z)-Sar-Pro-Gly-Lys(Z)-Sar-Pro-Gly-Lys(Z) on the ring.

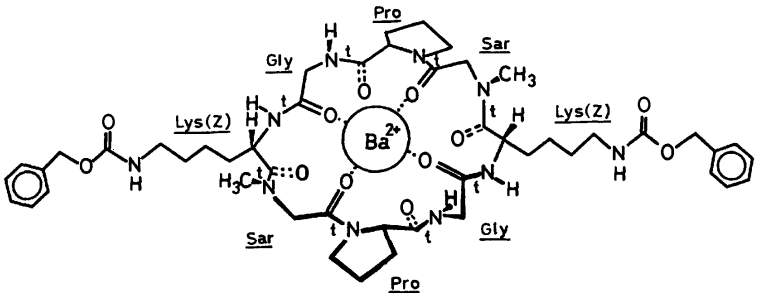

Fig. 11. Schematic representation of a proposed conformation of the 1:1 complex between CGLSP2 and barium cation.

pair of signals exist. These features are consistent with those observed in ^{13}C-NMR measurement, which demonstrates the existence of two complexation steps. However, in ^{1}H- and ^{13}C-NMR spectra, we could not resolve and identify the P_2C species that was detected in a CD spectrum. It has been reported that a resonance for N–CH_3 protons involved in a trans peptide bond occurs in a lower field region than that involved in a cis peptide bond.[24,27] Thus, the N–CH_3 signal marked with (▲) could be associated with trans Lys–Sar peptide bond. In a similar way, the lowfield signal of the two marked with (●) is ascribed to N–CH_3 protons associated with the trans Lys–Sar bond, and the highfield signal is ascribed to those of the cis Lys–Sar bond.

By the combination of the above ^{1}H- and ^{13}C-NMR data, the cis-trans arrangements of peptide bonds in CGLSP2 can be deduced for each complexed species in Ba^{2+} binding. A PC (1:1) complex has an all-trans peptide bonds. In contrast to this, a P_2C (2:1) complex contains one cis Lys–Sar peptide bond. Both conformations are absent in a free state. Moreover, it is of interest that the structure of CGLSP2/Ba^{2+} (1:1) complex in acetonitrile is different from that of CGLSP2/Ca^{2+} (1:1) complex in chloroform/acetonitrile (5/3, v/v) mixture.[9] In order to obtain further details, we measured ^{13}C- and ^{1}H-NMR spectra of the 1:1 Ca^{2+} complex with CGLSP2 in acetonitrile. As a result, the chemical shifts of Sar N–CH_3, Pro C^{β}, and Pro C^{γ} resonances are indicative of the occurrence of all-trans peptide bond arrangement. This fact indicates that the structural difference between Ca^{2+}- and Ba^{2+} -complex is not affected by the nature of cation but by that of solvent. From the above, the following scheme may be proposed for the Ba^{2+} binding and the Ca^{2+} binding by CGLSP2 in acetonitrile. It is shown in Fig. 10.

Inspection of a CPK molecular model having all-trans peptide bonds revealed that four coplanar carbonyl groups form a cavity for binding a cation. The barium or calcium ion may be bound favorably by the carbonyl groups of the two Sar and two Gly residues. This is supported by the chemical shift change of each carbonyl resonances upon complexation (Fig. 7). Figure 11 indicates a proposed conformation of 1:1 complex between CGLSP2 and Ba^{2+}, in which the divalent charge of the cations enhances the stability of 1:1 complex more effectively than the fitness of the cation size to cavity. Actually, CGLSP2 had poor affinity for K^{+} that is suitable for the cavity size.

Cyclo(L-Pro–Sar)$_4$ showed a conformational multiplicity that is based on cis/trans isomerism of all N-substituted peptide bonds.[14,28,29] In this respect, CGLSP2 has a localized distribution of N-substituted peptide bonds,[9] when compared with other cyclic octapeptides.[7,29] Therefore, this approach might provide CGLSP2 with a relatively limited structure of the cyclic backbone similarly to that of valinomycin. However, the ratio of the complex-formation constants, $K_1(Ca^{2+}):K_1(Mg^{2+})$, was very low ($\approx$1.4) in acetonitrile (Table 1). We have reported that the Ca^{2+} transport and extraction by CGLSP2 is much higher than Mg^{2+}.[9] Particularly, the ratio of the extraction equilibrium constants, $K_{ex}(Ca^{2+}):K_{ex}(Mg^{2+})$, was about 150. This high Ca^{2+}/Mg^{2+} selectivity disagrees with that of complex formation. It can be interpreted in terms of three constituent equilibria of the extraction process;[30] (1) distribution of CGLSP2 between the two phases, (2) complex formation of CGLSP2 with the metal cation in the aqueous phase, and (3) ion-pair extraction of CGLSP2/metal cation/picrate-anion species. The Ca^{2+}/Mg^{2+} selectivity of CGLSP2 has no relation with equilibrium (1). Therefore, the Ca^{2+} -selective transport and extraction by CGLSP2 may be closely related to the equilibria (2) and/or (3). With regard to the equilibrium (2), it could be owing to the high Ca^{2+}/Mg^{2+} selectivity of complex formation in the aqueous solution. This could not be confirmed experimentally because CGLSP2 was insoluble in water. With regard to the equilibrium (3), it could be attributed to the fairly poor solubility of the CGLSP2/Mg^{2+}/picrate-anion species into the chloroform phase in comparison with the corresponding Ca^{2+}-complexed ion pair.

References

1) L. V. Sumskaya, T. A. Balashova, I. I. Mikhaleva, T. S. Chumburidze, E. I. Melnik, V. T. Ivanov, and Yu. A. Ovchinnikov, *Bioorg. Khim.*, **3**, 5 (1977).
2) E. R. Blout, *Biopolymers*, **20**, 1901 (1981).
3) D. W. Hughes and C. M. Deber, *Biopolymers*, **21**, 169

(1982).
4) S. Kimura and Y. Imanishi, *Biopolymers*, **22**, 2383 (1983).
5) C. M. Deber, P. D. Adawadkar, and J. Tom-Kun, *Biochem. Biophys. Res. Commun.*, **81**, 1357 (1978).
6) C. M. Deber and P. D. Adawadkar, *Biopolymers*, **18**, 2375 (1979).
7) S. Kimura and Y. Imanishi, *Biopolymers*, **23**, 563 (1984).
8) F. Behm, D. Ammann, W. Simon, K. Brunfeldt, and J. Halstrøm, *Helv. Chim. Acta*, **68**, 110 (1985).
9) T. Shimizu and Y. Tanaka, *Int. J. Peptide Protein Res.* (to be published).
10) D. R. Pfeiffer, P. W. Reed, and H. A. Lardy, *Biochemistry*, **13**, 4007 (1974).
11) K. Neupert-Laves and M. Dobber, *Helv. Chim. Acta*, **58**, 432 (1975).
12) Yu. A. Ovchinnikov, V. T. Ivanov, and A. M. Shkrob, "Membrane-Active Complexones," Elsevier, Amsterdam (1974).
13) D. E. Dorman and F. A. Bovey, *J. Org. Chem.*, **38**, 2379 (1973).
14) T. Shimizu, Y. Tanaka, and K. Tsuda, *Int. J. Peptide Protein Res.*, **22**, 194 (1983).
15) M. M. Shemyakin, Yu. A. Ovchinnikov, V. T. Ivanov, V. K. Antonov, E. I. Vinogradova, A. M. Shkrob, G. G. Malenkov, A. V. Estratov, I. A. Laine, E. I. Melnik, and I. D. Ryabova, *J. Membr. Biol.*, **1**, 402 (1969).
16) D. Baron, L. G. Pease, and E. R. Blout, *J. Am. Chem. Soc.*, **99**, 8299 (1977).
17) C. H. Niu, V. Madison, L. G. Pease, and E. R. Blout, *Biopolymers*, **17**, 2747 (1978).
18) T. Shimizu, Y. Tanaka, and K. Tsuda, *Bull. Chem. Soc. Jpn.*, **55**, 3817 (1982).
19) J. H. Prestegard and S. I. Chan, *Biochemistry*, **8**, 3921 (1969).
20) M. C. Rose and R. W. Henkens, *Biochim. Biophys. Acta*, **372**, 426 (1974).
21) Th. Wieland, H. Faulstich, W. Burgermeister, W. Otting, W. Mohle, M. M. Shemyakin, Yu. A. Ovchinnikov, V. T. Ivanov, and G. G. Malenkov, *FEBS Lett.*, **9**, 89 (1970).
22) Th. Funk, F. Eggers, and E. Grell, *Chimia*, **26**, 637 (1972).
23) T. Shimizu, Y. Tanaka, and K. Tsuda, *Biopolymers*, **22**, 617 (1983).
24) F. A. Bovey, J. J. Ryan, and F. P. Hood, *Macromolecules*, **1**, 305 (1968).
25) M. Ohnishi, M. C. Fedarko, J. D. Baldeschwieler, and L. F. Johnson, *Biochem. Biophys. Res. Commun.*, **46**, 312 (1972).
26) K. Wüthrich, "NMR in Biological Research: Peptides and Protein," North-Holland Publishing Company, Amsterdam (1976), p. 157.
27) M. Sisido, Y. Imanishi, and T. Higashimura, *Biopolymers*, **11**, 399 (1972).
28) T. Shimizu, K. Ueno, Y. Tanaka, and K. Tsuda, *Int. J. Peptide Protein Res.*, **22**, 231 (1983).
29) T. Shimizu and S. Fujishige, *Biopolymers*, **19**, 2247 (1980).
30) F. Vögtle and E. Weber, "Host Guest Complex Chemistry III," Springer-Verlag, Berlin (1984) p. 1.

Preparation of Pyrido- and Azepino-fused Cycl[3.2.2]azines[1)]

Michihiko NOGUCHI,* Noriyuki TANIGAWA, and Shoji KAJIGAESHI
Department of Industrial Chemistry, Faculty of Engineering, Yamaguchi University, Tokiwadai, Ube 755
(Received June 17, 1985)

Pyrido- and azepino-fused cycl[3.2.2]azines were obtained by the reaction of the corresponding pyrido- and azepino[*hi*]indolizines with electron-deficient acetylenes in the presence of appropriate oxidants. The reaction pathway of their preparation was proposed to be a sequence of Michael addition of indolizine to acetylene, 10π-electrocyclic reaction of Michael adduct, and dehydrogenation by means of the chemical conversions of the isolated intermediates.

Much attention has been paid for the synthesis of the heterocyclic compounds with new ring systems because of their chemical and physicochemical as well as biological interests.

Recently, we reported the interesting physical properties of 4*H*-benzo[*hi*]pyrrolo[2,1,5-*cd*]indolizin-4-ones[2)] and cyclohepta[*hi*]pyrrolo[2,1,5-*cd*]indolizines,[3)] which were prepared by the oxidation of 5,6-dihydro-4*H*-benzo- and 4,5,6,7-tetrahydrocyclohepta[*hi*]pyrrolo [2,1,5-*cd*]indolizines,[4)] respectively. In the continuation of our studies on [*ef*]fused cycl[3.2.2]azine systems, our attention was focused on the synthesis of pyrido- and azepino-fused cycl[3.2.2]azines as aza-analogs of the above two systems.

We wish to report here the synthesis of 2,3-dihydro-1*H*-pyrido- and 1,2,3,4-tetrahydro[3,4,5-*hi*]pyrrolo[2, 1,5-*cd*]indolizines from the corresponding [*hi*]fused indolizines. A mechanistic aspect for the cyclazine synthesis was also described.

Results and Discussion

5-Cyano-2-ethoxycarbonyl-2,3-dihydro-1*H*-pyrido- (**2a**) and 6-cyano-2-ethoxycarbonyl-1,2,3,4-tetrahydroazepino [3,4,5-*hi*]pyrrolo[2,1,5-*cd*]indolizine (**2b**) were prepared by the intramolecular 1,3-dipolar addition of pyridinium-1-dicyanomethylides **1** according to the procedure developed by us.[5)] It was proved that the cyano group at 5 or 6-position of **2** hindered the reaction with acetylenes, so **2a** and **2b** were converted to 2,3-dihydro-1*H*-pyrido- (**3a**) and 1,2,3,4-tetrahydroazepino[3,4,5-*hi*]pyrrolo[2,1,5-*cd*]indolizine (**3b**), respectively, with alkaline hydrolysis followed by decarboxylation. In order to protect the amine moiety, **3a** was again converted to carbamate **4a**, which was allowed to react with dimethyl acetylenedicarboxylate (DMAD) in toluene under reflux for 20 h in the presence of palladium-charcoal (Pd/C) to give 2-ethoxycarbonyl-2,3-dihydro-5,6-bis(methoxycarbonyl)-1*H*-pyrido[3,4,5-*hi*]pyrrolo [2,1,5-*cd*]indolizine (**5a**) in 59% yield. The azepinopyrroloindolizine **5b** was also obtained from **4b** and DMAD in 68% yield.

The reactions of **4a** and **4b** with dibenzoylacetylene (DBZA) were carried out in tetrahydrofuran (THF) at 0°C in the presence of 2,3-dichloro-5,6-dicyano-1,4-benzoquinone (DDQ) to afford the expected pyrido- and azepinopyrroloindolizines, **6a** and **6b**, in 57 and 49% yields, respectively (Scheme 1).

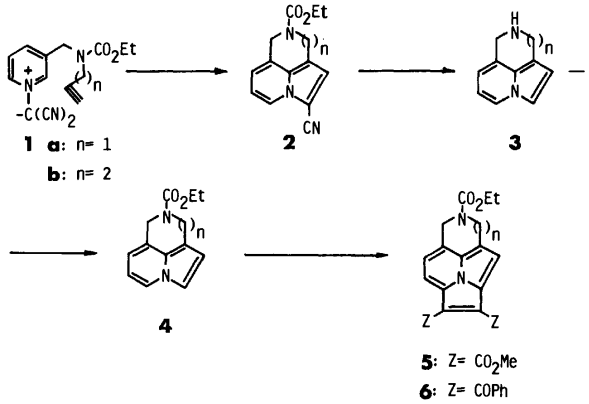

Scheme 1.

The analytical data and spectroscopic properties of **5** and **6** were consistent with the proposed structures. Especially, in ^{1}H NMR spectrum of **6a** or **6b**, one pair of the signals assignable to ethyl, methylene, and olefin protons were observed. The spectra of **6a** in deuteriochloroform at elevated temperatures revealed that the signals corresponding to two isomers were coalesced at *ca.* 50°C and sharpened again with an increase of the temperature. From these findings, we concluded that **6** in the solution was consisted of two conformational isomers concerning to the azepine ring.

In recent investigations of the mechanism on the cyclazine synthesis from indolizine, the isolation of intermediary products under the conditions without dehydrogenating reagents and their chemical conversions revealed considerably reliable reaction profiles.[6,7)] A proposed mechanism[7)] for the reaction with electron-deficient acetylene is as follows: Indolizine **A** attacks nucleophilically on acetylene to give the zwitterionic intermediate **B**, which leads to Michael adduct **C** and [8+2] cycloadduct **D**. The cycloadduct **D** is converted to more stable isomer(s) by the migration of hydrogen atom and finally dehydrogenated to the cyclazine.

In the synthesis of the benzo- and cyclohepta-fused cyclazines,[4)] some, at least more than two, intermediary products leading to cyclazines were also detected by ^{1}H NMR spectra and thin-layer chromatographies (TLC) of the reaction mixtures and, however, had not been identified owing to their thermodynamically

liablities. The 6-vinylindolizine derivative **7b**, the initially-formed product, was isolated in 62% yield as a pure form at the first time in the reaction of **4b** with DBZA in THF at 0°C without DDQ. The structural elucidation of **7b** was accomplished on the basis of its spectral data and elemental analysis. Particularly, its ^{1}H NMR spectrum showed a broad doublet at δ 8.46 assignable to the proton at 8-position. The similar reaction of **4a** with DBZA gave the 5-vinylindolizine **7a**, whose structure was confirmed by its ^{1}H NMR spectral data compared with those of **7b**.

While the treatment of **7b** with an equimolar DDQ in THF at 0°C gave the cyclazine **6b** in 84% yield, the similar treatment in dioxane under reflux afforded 6-(1,2-dibenzoylvinyl)-2-ethoxycarbonyl-1,2-dihydroazepino[3,4,5-*hi*]indolizine (**8b**) in 73% yield, which was formed by the oxidation of cyclic methylene moiety of **7b**. On the other hand, the reaction of **4b** with DMAD in dioxane without Pd/C gave a (1:4) mixture of **5b** and an intermediate **9b** similar to **7b**. The mixture was treated with an equimolar DDQ under reflux to give a mixture of **5b**, **9b**, and 2-ethoxycarbonyl-1,2-dihydroazepino[3,4,5-*hi*]pyrrolo[2,1,5-*cd*]indolizine (**10b**), then, with two equimolar DDQ to give **10b** in 66% yield as a sole product (Scheme 2).

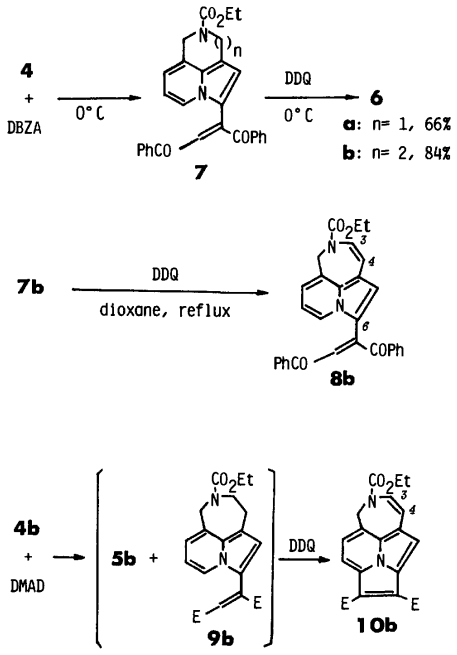

Scheme 2.

These results implied the possibility of the conversion of Michael adduct **C** to cyclazine system in the above-mentioned pathway or, circumstantially, of the interconversion between these two systems, which had been overlooked by preceding investigators.

In the actual synthesis of **6b** from **4b** and DBZA in the presence of DDQ, the examination by TLC revealed that the 6-vinylindolizine **7b** was converted to another intermediate, which was oxidized to the cyclazine **6b** finally.

From these results, we believe that the cyclazine synthsis from [*hi*]fused indolizines and acetylenes proceeds in a stepwise manner than in a concerted one.[8] Also, we suggest that vinylindolizines such as **7** or **9**, the Michael type adducts, would undergo 10π-electrocyclic reaction to give 1,2,3,4,7,7a-hexahydroazepino- or 2,3,6,6a-tetrahydro-1*H*-pyrido[3,4,5-*hi*]pyrrolo[2,1,5-*cd*]indolizines, which are converted to more stable isomer(s) and oxidized to the cyclazines (Scheme 3).

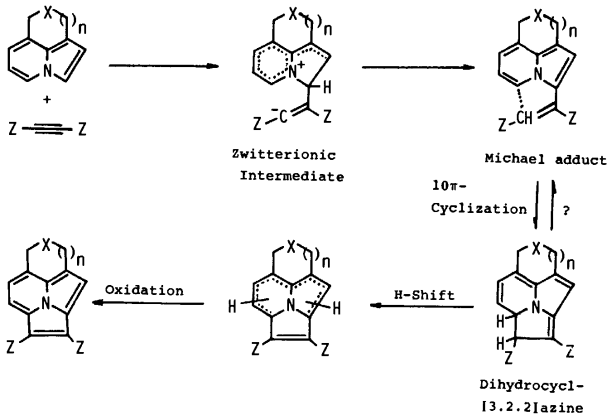

Scheme 3.

Experimental

All melting points are uncorrected. The IR spectra were measured on a JASCO IRA-1 spectrometer as potassium bromide pellets. ^{1}H NMR spectra were obtained on a JEOL JMN-MH-100 spectrometer with tetramethylsilane as an internal standard. Mass spectra were determined with a JEOL JMS-D mass spectrometer equipped with a direct inlet and at an ionization energy of 75 eV. Elemental analyses were performed on a Hitachi 026 CHN analyzer. The TLC was accomplished on 0.2 mm precoated plates of silica gel 60 F-254 (Merck) or on 0.2 mm precoated plates of aluminium oxide 60 F-254 type E (Merck). Visualization was made with ultraviolet light (254 and 365 nm). For the preparative column chromatography, Wakogel C-300 was used.

Preparations of Cyanoindolizines **2**: The pyridinium-1-dicyanomethylides **1** were prepared from the corresponding 3-(aminomethyl)pyridines and tetracyanooxirane and converted to cyanoindolizines **2** by the heating in toluene similarly to the reported method.[5]

*3-[N-(Ethoxycarbonyl)propargylaminomethyl]pyridinium-1-dicyanomethylide (**1a**)*: Yield 58%; yellow prisms; mp 81—84°C.

Found: C, 64.05; H, 5.16; N, 19.56%. Calcd for $C_{15}H_{14}N_4O_2$: C, 63.82; H, 5.00; N, 19.85%; M, 282.

*3-[N-(Ethoxycarbonyl)-3-butynylaminomethyl]pyridinium-1-dicyanomethylide (**1b**)*: Yield 55%; yellow prisms; mp 119—120°C.

Found: C, 65.09; H, 5.48; N, 18.96%. Calcd for $C_{16}H_{16}N_4O_2$: C, 64.85; H, 5.44; N, 18.91; M, 296.

*5-Cyano-2-ethoxycarbonyl-2,3-dihydro-1H-pyrido[3,4,5-hi]-indolizine (**2a**)*: Yield 75%; colorless needles; mp 104—105°C; IR (KBr) 2200 (CN) and 1700 cm^{-1} (CO); ^{1}H NMR ($CDCl_3$) δ=1.30 (3H, t, $-CH_3$, J=7 Hz), 4.20 (2H, q, $-CH_2-$, J=7 Hz),

4.8 (4H, m, 1 and 3-H), 6.7—6.9(2H, m, 8 and 9-H), 7.09 (1H, s, 4-H), and 8.06 (1H, br d, 7-H, J=6 Hz).

Found: C, 65.96; H, 5.12; N, 16.23%. Calcd for $C_{14}H_{13}N_3O_2$: C, 65.87; H, 5.13; N, 16.46%; M, 255.

*6-Cyano-2-ethoxycarbonyl-1,2,3,4-tetrahydroazepino[3,4,5-hi]indolizine (**2b**)*: Yield 87%; colorless prisms; mp 126—127 °C; IR (KBr) 2200 (CN) and 1960 cm^{-1} (CO); ^{1}H NMR ($CDCl_3$) δ=1.2—1.4 (3H total, m, $-CH_3$), 3.1—3.2 (2H, m, 4-H), 3.8 (2H, t, 3-H, J=6 Hz), 4.0—4.2 (2H, m, $-CH_2-$), 4.74 (2H, br s, 1-H), 6.7 (2H, m, 9 and 10-H), and 8.04 (1H, br d, 8-H, J=6 Hz).

Found: C, 67.05; H, 5.65; N, 15.34%. Calcd for $C_{15}H_{15}N_3O_2$: C, 66.90; H, 5.61; N, 15.61%; M, 269.

*Conversion of Cyanoindolizines **2** to Indolizines **3** (Typical Procedure)*: **2a** (3.9 mmol) was refluxed in 15% ethanolic potassium hydroxide (100 ml) for 10 h and ethanol was removed to give a residue. The residue was made acidic with concd hydrochloric acid (150 ml) and refluxed for 3 h. The solution was concentrated *in vacuo* and made basic with sodium hydroxide and extracted with ether (50 ml×5). The ethereal layer was collected, dried, and evaporated to give the indolizine **3a** (0.56 g, 91%).

*2,3-Dihydro-1H-pyrido[3,4,5-hi]indolizine (**3a**)*: Colorless prisms; mp 97—99 °C; IR (KBr) 3200 cm^{-1} (NH); ^{1}H NMR ($CDCl_3$) δ=2.3 (1H, s, NH), 3.96, 4.12 (2H each, 2s, 1 and 3-H), 6.15 (1H, d, 9-H, J=6 Hz), 6.34 (1H, t, 8-H, J=6 Hz), 6.50 (1H, d, 4-H, J=2 Hz), 7.12 (1H, d, 5-H, J=2 Hz), and 7.62 (1H, d, J=6 Hz); MS m/z 158(M^+).

Found: C, 75.93; H, 6.42; N, 17.57%. Calcd for $C_{10}H_{10}N_2$: C, 75.92; H, 6.37; N, 17.71%; M, 158.

*1,2,3,4-Tetrahydroazepino[3,4,5-hi]indolizine (**3b**)*: Yield 98%; colorless needles; mp 87—89 °C; IR (KBr) 3260 cm^{-1} (NH); ^{1}H NMR($CDCl_3$) δ=2.0 (1H, s, NH), 3.0—3.2 (4H, m, 3 and 4-H), 4.06 (2H, s, 1-H), 6.3 (2H, m, 9 and 10-H), 6.52 (1H, d, 5-H, J=2 Hz), 7.18 (1H, d, 6-H, J=2 Hz), and 7.62 (1H, dd, 8-H, J=5 and 3 Hz); MS m/z 172 (M^+).

Found: C, 76.54; H, 7.18; N, 16.24%. Calcd for $C_{11}H_{12}N_2$: C, 76.71; H, 7.02; N, 16.27%; M, 172.

Reaction of [hi]Fused Indolizines with DMAD (Typical Procedure): To a solution of **3a** (4.65 mmol) and triethylamine (6 mmol) in THF (20 ml), ethyl chloroformate (5 mmol) was added and the mixture was allowed to stand at room temperature overnight. After being filtrated the precipitates, the filtrate was concentrated to give a residue, which was treated with a short column chromatography (silica gel-chloroform) to afford **4a** quantitatively. Without further purification, **4a** was reacted with DMAD (5 mmol) in toluene (30 ml) under reflux in the presence of 0.5 g of 5% Pd/C overnight and the reaction mixture was worked up usually to give the cyclazine **5a**.

*2-Ethoxycarbonyl-2,3-dihydro-1H-pyrido[3,4,5-hi]indolizine (**4a**)*: Pale yellow oil; ^{1}H NMR ($CDCl_3$) δ=1.20 (3H, t, $-CH_3$, J=7 Hz), 4.12 (2H, q, $-CH_2-$, J=7 Hz), 4.62, 4.72 (2H each, 2s, 1 and 3-H), 6.1—6.3 (2H, m, 8 and 9-H), 6.46 (1H, d, 4-H, J=2 Hz), 7.03 (1H, d, 5-H, J=2 Hz), and 7.46 (1H, br d, 7-H, J=6 Hz).

*2-Ethoxycarbonyl-2,3-dihydro-5,6-bis(methoxycarbonyl)-1H-pyrido[3,4,5-hi]pyrrolo[2,1,5-cd]indolizine (**5a**)*: Yellow prisms; mp 95—96 °C; IR (KBr) 1725 and 1675 cm^{-1} (CO); ^{1}H NMR ($CDCl_3$) δ=1.34 (3H, t, $-CH_3$, J=7 Hz), 4.01, 4.05 (3H each, 2s, $-CH_3$), 4.23 (2H, q, $-CH_2-$, J=7 Hz), 5.2—5.3 (4H, br, 1 and 3-H), 7.36 (1H, br s, 4-H), 7.68 (1H, d, 8-H, J=8 Hz), and 8.35 (1H, d, J=8 Hz); MS m/z 370 (M^+).

Found: C, 61.65; H, 4.98; N, 7.89%. Calcd for $C_{19}H_{18}N_2O_6$: C, 61.61; H, 4.90; N, 7.56%; M, 370.

*2-Ethoxycarbonyl-1,2,3,4-tetrahydroazepino[3,4,5-hi]indolizine (**4b**)*: Pale yellow oil; ^{1}H NMR ($CDCl_3$) δ=1.1—1.3 (3H total, m, $-CH_3$), 3.1—3.3 (2H total, m, 4-H), 3.7—3.9 (2H total, m, 3-H), 4.0—4.2 (2H total, m, $-CH_2-$), 4.64, 4.68 (2H total, 2s, 1-H), 6.4 (2H, m, 9 and 10-H), 6.58 (1H, br s, 5-H), 7.24 (1H, br s, 6-H), and 7.70 (1H, br d, 8-H, J=6 Hz).

*2-Ethoxycarbonyl-1,2,3,4-tetrahydro-6,7-bis(methoxycarbonyl)-azepino[3,4,5-hi]pyrrolo[2,1,5-cd]indolizine (**5b**)*: Yellow prisms; mp 133—135 °C; IR (KBr) 1730, 1690, and 1665 cm^{-1} (CO); ^{1}H NMR ($CDCl_3$) δ=1.2—1.3 (3H total, m, $-CH_3$), 3.4—3.5 (2H total, m, 4-H), 3.94 (2H total, m, $-CH_2-$), 5.15, 5.20 (2H total, 2s, 1-H), 7.4 (1H, br s, 5-H), 7,60, 7.63 (1H total, 2d, 9-H, J=8 Hz each), 8.30, and 8.32 (1H total, 2d, 8-H, J=8 Hz each); MS m/z 384 (M^+).

Found: C, 62.51; H, 5.23; N, 7.31%. Calcd for $C_{20}H_{20}N_2O_6$: C, 62.49; H, 5.24; N, 7.29%; M, 384.

Reaction of [hi]Fused Indolizines with DBZA (Typical Procedure): To a cooled at 0 °C and stirred solution of **4a** (1 mmol) in THF (10 ml), DBZA (1 mmol) in THF (5 ml) was added dropwise for 10 min. After the consumption of the starting materials being confirmed by TLC, DDQ (1.1 mmol) in THF (5 ml) was added to the mixture, which was allowed to stir for additional 10 min at the same temperature. The resultant hydroquinone was filtered off and the filtrate was evaporated to dryness. Chromatography on silica gel with chloroform as an eluent gave **6a** (264 mg, 57%).

*5,6-Dibenzoyl-2-ethoxycarbonyl-2,3-dihydro-1H-pyrido[3,4,5-hi]pyrrolo[2,1,5-cd]indolizine (**6a**)*: Yellow prisms; mp 69—71 °C; IR (KBr) 1690 and 1655 cm^{-1}(CO); ^{1}H NMR ($CDCl_3$) δ=1.35 (3H, t, $-CH_3$, J=7 Hz), 4.30 (2H, q, $-CH_2-$, J=7 Hz), 5.3(4H, br, 1 and 3-H), 7.3—7.6 (7H, m, 8-H and phenyl protons), 7.6—7.9 (5H, m, 4-H and phenyl protons), and 8.14 (1H, d, 7-H, J=8 Hz); MS m/z 462 (M^+).

Found: C, 75.49; H, 5.10; N, 5.87%. Calcd for $C_{29}H_{22}N_2O_4$: C, 75.31; H, 4.80; N, 6.06%; M, 462.

*6,7-Dibenzoyl-2-ethoxycarbonyl-1,2,3,4-tetrahydroazepino[3,4,5-hi]pyrrolo[2,1,5-cd]indolizine (**6b**)*: Yellow prisms; mp 147—150 °C; IR (KBr) 1700 and 1650 cm^{-1} (CO); ^{1}H NMR ($CDCl_3$) δ=1.2—1.4 (3H total, m, $-CH_3$), 3.4—3.5 (2H total, m, 4-H), 3.95 (2H, br t, 3-H, J=7 Hz), 4.1—4.3 (2H total, m, $-CH_2-$), 5.22, 5.27 (2H total, 2s, 1-H), 7.2—7.5 (7H, m, 5-H and phenyl protons), 8.15, and 8.19 (1H total, 2d, 8-H, J=8 Hz each); MS m/z 476 (M^+).

Found: C, 75.50; H, 5.10; N, 5.67%. Calcd for $C_{30}H_{24}N_2O_4$: C, 75.61; N, 5.08; N, 5.88%; M, 476.

*Identification of Primarily-formed Intermediates in the Reaction of [hi]Fused Indolizines **4** with DBZA or DMAD (Typical Procedure)*: DBZA (1 mmol) in THF (5 ml) was added to a solution of **4b** (1 mmol) in THF (10 ml) for 10 min at 0 °C under nitrogen atmosphere. The reaction mixture was stirred for additional 10 min at the same conditions, evaporated to dryness, and a reddish crystalline **7b** (296 mg, 62%) was obtained from ether.

*6-(1,2-Dibenzoylvinyl)-2-ethoxycarbonyl-1,2,3,4-tetrahydroazepino[3,4,5-hi]indolizine (**7b**)*: Red prisms, mp 170—171 °C; IR (KBr) 1690 and 1650 cm^{-1} (CO);^{1}H NMR ($CDCl_3$) δ=1.99 (3H, t, $-CH_3$, J=7 Hz), 2.9—3.1 (2H, m, 4-H), 3.72 (2H, br t, 3-H, J=6 Hz), 4.07 (2H, q, $-CH_2-$, J=7 Hz), 4.6—4.8 (2H, br s, 1-H), 6.6—6.8 (3H, m, 5, 9, and 10-H), 7.3—7.6 (7H, m, vinyl and phenyl protons), 7.8—8.0 (4H, m, phenyl protons), and 8.46 (1H, br d, 8-H, J=6 Hz); MS m/z 478 (M^+).

Found: C, 75.13; H, 5.60; N, 6.02%. Calcd for $C_{30}H_{26}N_2O_4$: C, 75.29; H, 5.48; N, 5.85%; M, 478.

The reaction of **4a** with DBZA gave a reddish amorphous **7a** (62%), whose structure was confirmed by ^{1}H NMR spectral data without satisfactory analytical data.

*5-(1,2-Dibenzoylvinyl)-2-ethoxycarbonyl-2,3-dihydro-1H-pyrido[3,4,5-hi]indolizine (**7a**)*: ^{1}H NMR ($CDCl_3$) δ=1.90 (3H, t, $-CH_3$, J=7 Hz), 4.32 (2H, q, $-CH_2-$, J=7 Hz), 4.70, 4.75 (2H each, 2s, 1 and 3-H), 6.6—6.8 (3H, m, 4, 8, and 9-H), 7.2—7.6 (7H, m, vinyl and phenyl protons), 7.7—8.0 (4H, m, phenyl protons), and 8.33 (1H, br d, 7-H, J=6 Hz).

The formation of 6-vinylindolizine **9b** from **4b** and DMAD was elucidated by the ^{1}H NMR spectrum of the reaction mixture in octadeuteriodioxane. It showed three singlets at δ 3.78 and 3.92 (methyl protons), 6.04 (vinyl proton), and a doublet at δ 8.00 (8-H, J=6 Hz) besides the other protons overlapped with those of **5b**.

*Reactions of 6-Vinylindolizines **7** with DDQ (Typical Procedure)*: A mixture of **7b** (0.21 mmol) and DDQ (0.22 mmol) in THF (5 ml) was stirred at 0 °C for 30 min and evaporated *in vacuo* to give a residue. The residue was treated with a short column chromatography (silica gel-chloroform) to give **6b** (84 mg, 84%).

A mixture of **7b** (0.42 mmol) and DDQ (0.44 mmol) in dioxane (10 ml) was refluxed for 10 min. After the usual working-up, 145 mg(73%) of **8b** was obtained.

*6-(1,2-Dibenzoylvinyl)-2-ethoxycarbonyl-1,2-dihydroazepino[3,4,5-hi]indolizine (**8b**)*: Red prisms; mp 132—134 °C; IR (KBr) 1690 and 1655 cm^{-1} (CO); ^{1}H NMR ($CDCl_3$) δ=1.26 (3H, t, $-CH_3$, J=7 Hz), 4.18 (2H, q, $-CH_2-$, J=7 Hz), 4.61 (2H, br s, 1-H), 5.90 (1H, d, 4-H, J=8 Hz), 6.60 (1H, d, 3-H, J=8 Hz), 6.7—6.8 (3H, m, 5, 9, and 10-H), 7.3—7.6 (7H, m, vinyl and phenyl protons), 7.8—8.0 (4H, m, phenyl protons), and 8.51 (1H, dd, 8-H, J=6 and 4 Hz); MS m/z 476 (M^+).

Found: C, 75.52; H, 5.14; N, 5.82%. Calcd for $C_{30}H_{24}N_2O_4$: C, 75.61; H, 5.08; N, 5.88%; M, 476.

*Reactions of 6-Vinylindolizine **9b** with DDQ (Typical Procedure)*: DDQ (3.5 mmol) was added to a (1:4) mixture of **5b** and **9b**, from indolizine **4b** (1.64 mmol) and DMAD (1.76 mmol), in dioxane (20 ml) and the reaction mixture was refluxed for 30 h. The resultant hydroquinone was removed by filtration and the filtrate was worked up usually to give **10b** (412 mg, 66%).

*2-Ethoxycarbonyl-6,7-bis(methoxycarbonyl)-1,2-dihydroazepino[3,4,5-hi]pyrrolo[2,1,5-cd]indolizine (**10b**)*: Orange prisms; mp 118—120 °C, IR (KBr) 1720 and 1700 cm^{-1} (CO); ^{1}H NMR ($CDCl_3$) δ=1.28 (3H, t, $-CH_3$, J=7 Hz), 4.04, 4.07 (3H each, 2s, $-CH_3$), 4.24 (2H, q, $-CH_2-$, J=7 Hz), 5.21 (2H, s, 1-H), 6.43 (1H, d, 4-H, J=8 Hz), 6.84 (1H, br d, 3-H, J=8 Hz), 7.42 (1H, s, 5-H), 7.70 (1H, d, 9-H, J=8 Hz), and 8.34 (1H, d, 8-H, J=8 Hz); MS m/z 476 (M^+).

Found: C, 75.50; H, 5.10; N. 5.67%. Calcd for $C_{30}H_{24}N_2O_4$: C, 75.61; H, 5.08; N, 5.88%; M, 476.

This work was partly supported by Grant-in-Aid for Scientific Research (No. 59750691) from the Ministry of Education, Science and Calture to M. N.

References

1) Studies on Nitrogen-bridged Heterocycles. V. Part IV in this series: M. Noguchi, N. Tanigawa, H. Okumura, and S. Kajigaeshi, submitted to *Heterocycles*.

2) M. Noguchi, N. Tanigawa, T. Yamamoto, and S. Kajigaeshi, *Chem. Lett.*, **1985**, 873.

3) M. Noguchi, N. Tanigawa, H. Okumura, and S. Kajigaeshi, submitted to *Heterocycles*.

4) M. Noguchi, N. Tanigawa, and S. Kajigaeshi, *J. Heterocycl. Chem.*, **22**, 1049 (1985).

5) M. Noguchi, H. Kan, and S. Kajigaeshi, *Chem. Pharm. Bull.*, **31**, 3342 (1983).

6) S. Ikeda, S. Kajigaeshi, and S. Kanemasa, *Chem. Lett.*, **1976**, 367.

7) Y. Yamashita, D. Suzuki, and M. Masumura, *Heterocycles*, **22**, 705 (1984).

8) A. Galbraith, T. Small, R. A. Barnes, and V. Boekelheide, *J. Am. Chem. Soc.*, **83**, 453 (1961).

The Decomposition of *t*-Butyl Heptafluoroperoxybutyrate in Aromatic and Aliphatic Solvents

Hideo SAWADA, Hidehiko HAGII, Kazuyoshi AOSHIMA,
Masato YOSHIDA,† and Michio KOBAYASHI*,†

Chemicals and Explosives Research Laboratory, Nippon Oil & Fats Co., Ltd., Taketoyo, Chita-gun, Aichi 470-23
†*Department of Chemistry, Faculty of Science, Tokyo Metropolitan University, Fukazawa, Setagaya-ku, Tokyo 158*
(Received June 26, 1985)

Kinetical studies and products analyses of the thermal decomposition of *t*-butyl heptafluoroperoxybutyrate (TBH) in benzene, octane, nitrobenzene, pyridine, and methoxybenzene have been carried out. In benzene and octane, the decomposition appears to be entirely a radical process. In nitrobenzene and pyridine, the reactions are found to give ionic decomposition products exclusively. On the other hand, the decomposition of TBH in methoxybenzene is characteristic of mixed ionic and radical cleavages.

Although the mechanisms for the thermolysis of a series of peroxy esters have been extensively investigated,[1] studies on fluorinated peroxy esters are very limited. Fluorinated peroxy esters are expected to show a different decomposition behavior from corresponding aliphatic peroxy esters due to the strong electron-withdrawing properties of fluoroalkyl groups. Strong electron-withdrawing groups in peroxide weaken the O–O bond and lower the energy level of an antibonding (σ^*) O–O bond.[2] Bartlett and Traylor reported that the *t*-butyl peroxy esters derived from a strong organic acid might well undergo an ionic cleavage with a Criegee rearrangement.[3] Recently, we also reported that *t*-butyl heptafluoroperoxybutyrate (TBH) decomposes in methanol to give methyl heptafluorobutyrate and *t*-butyl hydroperoxide in good yields according to the following transesterification.[4]

$$C_3F_7CO_2OC(CH_3)_3 \xrightarrow[CH_3OH]{} C_3F_7CO_2CH_3 + (CH_3)_3COOH$$

However, we found that the thermal decomposition of TBH suffered extreme solvent effects. In this paper, we wish to report on studies regarding the reaction mechanism for the thermal decomposition of TBH in benzene, octane, nitrobenzene, pyridine, and methoxybenzene.

Results and Discussion

The thermal decomposition of TBH in benzene was monitored by iodometry at various temperatures from 60.0 to 80.0 °C; the rate of decomposition deviated upwards remarkably from a first-order rate plot after about 30% of the reaction. However, the rate of decomposition of TBH was found to follow very well a first-order equation when pyridine was added in order to suppress the autocatalyzed decomposition by produced heptafluorobutyric acid. The anomalous behavior regarding the thermal decomposition of highly acid-sensitive peroxy esters is well-known and in order to prevent autocatalysis, pyridine has usually been used.[5,6] The decomposition of 0.02 M†† TBH in benzene was carried out at 75.0 °C in the presence of various (0.005—0.025 M) amounts of pyridine. It was found that as the amount of pyridine was increased, the decomposition rates of TBH decreased and the apparent rate constants leveled off at about 0.015 M pyridine as shown in Fig. 1. Products attributable to a reaction between TBH and pyridine were not obtained except for pyridinium heptafluorobutyrate. In the

††1 M=1 mol dm^{-3}.

TABLE 1. RATE CONSTANTS AND ACTIVATION PARAMETERS FOR THE THERMAL DECOMPOSITION OF TBH IN BENZENE

Temp/°C	Initial Conc. M[a]	k_d(s^{-1})×10^5	ΔH^*/kJ mol^{-1}	ΔS^*/JK^{-1} mol^{-1}
65.0	0.02[b]	1.56±0.01		
70.0		3.09±0.02	112.6	−4.2
75.0		5.27±0.04		
80.0		9.08±0.10		
60.0	0.10[c]	0.95±0.02		
65.0		1.61±0.02		
70.0		2.70±0.03	108.8	−15.5
75.0		5.23±0.07		
80.0		9.18±0.10		
60.0	0.10[d]	0.96±0.03		
65.0		1.93±0.06	118.4	13.4
70.0		3.57±0.08		
75.0		6.35±0.07		

a) M=mol dm^{-3}. b) 0.02 M pyridine was added. c) 0.10 M pyridine was added. d) 0.10 M 2,6-lutidine was added.

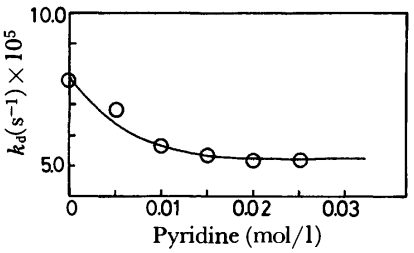

Fig. 1. Effect of added pyridine on the apparent rate constants for the thermal decomposition of 0.02 mol/l TBH in benzene at 75.0 °C.

Table 2. Products from the thermal decomposition of 0.10 M TBH and 0.10 M pyridine in benzene at 80 °C for 11 h and in octane at 100 °C for 10 h

Benzene Product	mol/mol	Octane Product	mol/mol
$(CH_3)_2C=CH_2$	Trace	$(CH_3)_2C=CH_2$	0.01
$(CH_3)_2CO$	0.02 (0.20)[a]	C_3F_7H	—[b]
$C_3F_7CO_2C(CH_3)_3$	0.02	$(CH_3)_2CO$	Trace
$PhCH_3$	0.03	$C_3F_7CO_2CH_3$	0.30
$C_6H_3(CH_3)_3$	0.01	$C_3F_7CO_2C(CH_3)_3$	0.03
Ph-Ph	0.01	$CH_3COCH=C(CH_3)_2$	Trace
$C_3F_7CO_2H$	0.63[c]	$C_3F_7CO_2H$	0.02
$CH_3COCH=C(CH_3)_2$	0.01		
$(CH_3)_3COC(CH_3)_3$	0.04		

a) 1.0 M pyridine was used. b) Heptafluoropropane could be detected by GC–MS, however, the exact yield could not be determined. c) Isolated yield of pyridinium heptafluorobutyrate recrystallized from toluene.

absence of pyridine, the decomposition of TBH gave a considerable amount of 2-methoxy-1-propene (**1**: $CH_3OC(CH_3)=CH_2$, 0.15 mol/mol peroxide) in addition to the products listed in Table 2. The production of propene shows the acid-catalyzed decomposition of TBH.

$$C_3F_7\overset{\overset{O}{\|}}{C}OOC(CH_3)_3 \xrightarrow{H^+} C_3F_7\overset{\overset{+O-H}{\|}}{C}OOC(CH_3)_3 \longrightarrow$$

$$C_3F_7CO_2H + CH_3O-\overset{\overset{CH_3}{|}}{\overset{+}{C}}-CH_3 \xrightarrow{-H^+} CH_3O-\overset{\overset{CH_3}{|}}{C}=CH_2$$

(**1**)

The rates of decomposition of TBH in benzene in the presence of an equimolar amount of 2,6-lutidine, which is known to play the role of a proton acceptor and not a nucleophile, gave similar values as those for TBH, using pyridine as a suppresser. These results indicate that pyridine or lutidine played the role of the suppresser of the heptafluorobutyric acid-catalyzed decomposition.

The rate constants and activation parameters for the thermal decomposition of TBH in several solvents are summarized in Table 3. The decomposition was extremely solvent-dependent as shown in Table 3, while the thermal decomposition of nonfluorinated peroxy esters, for example, *t*-butyl peroxyacetate in aliphatic and aromatic solvents showed a weak solvent dependence.[7]

As shown in Tables 1 and 3, the activation parameters for the thermal decomposition of TBH in benzene and octane have similar values as those for the homolytic decomposition of non-fluorinated peroxy esters; *t*-butyl peroxybenzoate in chlorobenzene, ΔH^*=140.2 KJ mol^{-1}, ΔS^*=32.6 JK^{-1} mol^{-1};[5] *t*-butyl phenylperoxyacetate in chlorobenzene, ΔH^*=116.7 kJmol^{-1}, ΔS^*=8.4 JK^{-1} mol^{-1}.[8] The products obtained from the thermal decomposition of TBH in benzene and in octane are shown in Table 2. The decomposition of TBH in benzene gave no ionic Criegee rearrangement products such as 2-methoxy-1-propene, but heptafluorobutyric acid, toluene, biphenyl, *t*-butyl heptafluorobutyrate, acetone, and condensation products of acetone such as mesityl oxide and 1,3,5-trimethylbenzene. The production of toluene, biphenyl, *t*-butyl heptafluorobutyrate, acetone, and acetone derivatives indicates that TBH decomposes homolytically in benzene. The generation of the radical species was also confirmed by ESR studies. In studies on the decomposition of TBH using nitrosodurene as a spin-trapping reagent, the ESR signal of some nitroxide radicals were observed: one signal was assigned to the adduct of methyl radical to nitrosodurene from the following h.f.s.c.; a_N=14.0 G, $a_{\beta\text{-H}}$=12.2 G, g=2.0068, (lit, a_N=13.70 G, $a_{\beta\text{-H}}$=12.17 G, g=2.0060).[9] Formation

Table 3. Rate constants and activation parameters for the thermal decomposition of 0.10 M TBH & 0.10 M pyridine in various solvents

Solvent	Temp/°C	$k_d(s^{-1})\times10^5$	ΔH^*/kJ mol^{-1}	ΔS^*/JK^{-1} mol^{-1}
Octane	85.0	0.51±0.01		
	90.0	0.95±0.01	136.8	34.7
	95.0	1.75±0.04		
	100.0	3.41±0.06		
$PhNO_2$	40.0	3.26±0.04		
	45.0	6.36±0.03	85.8	−56.9
	50.0	9.31±0.23		
Pyridine	30.0	2.74±0.03		
	40.0	7.66±0.11	75.3	−82.8
	50.0	18.68±0.18		
$PhOCH_3$	55.0	5.01±0.05		
	60.2	8.56±0.11	95.4	−37.2
	65.0	13.78±0.22		
	70.0	24.44±0.45		

of this nitroxide is explained by the decomposition of a cage-escaped *t*-butoxyl radical to acetone and methyl radical.

$$\cdot OC(CH_3)_3 \longrightarrow \cdot CH_3 + (CH_3)_2CO$$

$$\cdot CH_3 + ArNO \longrightarrow ArNO\cdot \quad (CH_3 \text{ on } \cdot)$$

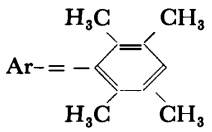

No adduct radical due to $C_3F_7\cdot$ and nitrosodurene was observed.[10]

In the decomposition of TBH in octane, the heptafluoropropane (**2**), and methyl heptafluorobutyrate (**3**) were produced, and their production can be attributed to homolytic cleavages of TBH. Thus, the decomposition of TBH in octane may also be proceeded by a homolytic cleavage, according to Scheme 1. The homolysis of TBH in octane was further confirmed by ESR studies using nitrosodurene as a spin-trapping reagent. When TBH was decomposed in the presence of nitrosodurene, ESR signals of more than three nitroxide radicals were observed; the main signal was a triplet of doublet with coupling to nitrogen and hydrogen. This signal is probably due to the adduct radical of the secondary alkyl radicals to nitrosodurene. Also, the adduct radical of $C_3F_7\cdot$ to nitrosodurene could not be observed in this case. The radicals generated by the homolysis of TBH did not attack nitrosodurene but abstracted a hydrogen atom from solvent octane to give a mixture of secondary alkyl radicals ($C_8H_{17}\cdot$) which could be trapped by nitrosodurene. In order to confirm this, an ESR study of TBH in cyclohexane was also carried out. In this case, the spin adduct of the produced single radical (cyclohexyl radical) to nitrosodurene was observed; a_N=13.4 G, a_H=6.7 G, g=2.0059, (lit, a_N=13.57 G, a_H=6.93 G, g=2.0060).[9]

$$C_3F_7C(=O)\text{-}OOC(CH_3)_3 \longrightarrow \overline{C_3F_7C(=O)\text{-}O\cdot \quad \cdot OC(CH_3)_3} \longrightarrow$$

$$(CH_3)_2CO + C_3F_7C(=O)\text{-}O\cdot + \cdot CH_3 \longrightarrow C_3F_7CO_2CH_3 \quad (\mathbf{3})$$

Fate of the cage-escaped radical:

$$C_3F_7\cdot + RH(\text{solvent}) \longrightarrow C_3F_7H + R\cdot \quad (\mathbf{2})$$

$$\cdot OC(CH_3)_3 \longrightarrow \cdot CH_3 + (CH_3)_2CO$$

$$\cdot CH_3 + RH \longrightarrow CH_4 + R\cdot$$

Scheme 1.

As mentioned before, it was considered that TBH decomposes homolytically in octane and in benzene. However, the activation parameters for the thermal decomposition of TBH in benzene have smaller values compared with those in octane, and heptafluorobutyric acid was obtained in much higher (63%) yield than that in octane. These results suggest that the induced decomposition of TBH by the cyclohexadienyl radicals, which were formed by the attack of radicals to benzene, may occur, in part, in benzene.

On the other hand, the activation parameters for the thermal decomposition of TBH in nitrobenzene and pyridine have similar values as those for the ionic decomposition of other *t*-butyl peroxy esters accompanied by a Criegee rearrangement; for instance, *t*-butyl peroxytosylate in methanol, $\Delta H^{\ddagger}$=90.0 kJmol^{-1}, $\Delta S^{\ddagger}$=3.8 JK^{-1}mol^{-1}.[3] It was also found that TBH decomposed in nitrobenzene and pyridine to give one molar equivalent of heptafluorobutyric acid and several Criegee rearrangement products such as 2-methoxy-1-propene (**1**), 2,2-dimethoxypropene (**4**), and 1-methoxy-1-methylethyl heptafluorobutyrate (**5**) as shown in Table 4. 2,2-Dimethoxypropane is probably produced by the reaction of a 1-methoxy-1-methylethylium ion with water (giving acetone and methanol) followed by a reaction involving the evolved methanol with another 1-methoxy-1-methylethylium ion. These results indicate that the decomposition of TBH in nitrobenzene and pyridine is principally an ionic decomposition accompanied by a Criegee rearrangement, according to the following scheme. However, nonfluorinated *t*-butyl peroxy esters are reported to decompose homolytically even in a polar solvent such as nitrobenzene.[11]

$$C_3F_7C(=O)\text{-}OOC(CH_3)_3 \xrightarrow{\text{ionic cleavage}}$$

$$[C_3F_7C(=O)\text{-}O^- \ {}^+O\text{-}C(CH_3)_2\text{-}CH_3] \xrightarrow{\text{Criegee rearrangement}}$$

$$[C_3F_7C(=O)\text{-}O^- \ {}^+C(OCH_3)(CH_3)\text{-}CH_3] \rightarrow C_3F_7C(=O)\text{-}O\text{-}C(OCH_3)(CH_3)\text{-}CH_3 \quad (\mathbf{5})$$

$$[C_3F_7C(=O)\text{-}O^- \ {}^+C(OCH_3)(CH_3)\text{-}CH_3] \rightarrow CH_3\text{-}C(OCH_3)=CH_2 + C_3F_7CO_2H \quad (\mathbf{1})$$

Scheme 2.

In the decomposition of TBH in pyridine, 2-*t*-butoxy-2-methoxypropane (**6**) was obtained in 21% yield. The formation of this product may be explained by a nucleophilic attack of the N-lone pair of pyridine on a peroxidic α-oxygen of peroxy ester to give *t*-butoxide ion which reacted with 1-methoxy-1-methylethylium ion. It was reported that a reaction of *t*-butyl perbenzoate with dimethyl sulfide occurred at the peroxidic α-oxygen of the benzoyloxyl group to form a dimethylbenzoyloxysulfonium ion, not at the *t*-butoxyl

Table 4. Products from the thermal decomposition of 0.10 M TBA in nitrobenzene[a] at 70 °C for 7 h, in pyridine at 50 °C for 12 h and in methoxybenzene[a] at 70 °C for 7 h

Product	$PhNO_2$ mol/mol	C_5H_5N mol/mol	$PhOCH_3$ mol/mol
$(CH_3O)C(CH_3)=CH_2$	0.19	0.46	0.14
$(CH_3)_2C(OCH_3)_2$	0.06	—	0.02
$C_3F_7CO_2C(CH_3)_3$	0.02	—	0.28
$C_3F_7CO_2C(CH_3)_2(OCH_3)$	0.05	—	0.02
$C_3F_7CO_2H$	0.90	0.97(0.91)[b]	0.59
$CH_3CO_2CH_3$	—	0.03	—
$(CH_3)_2CO$	—	—	0.07
$CH_3OC_6H_4CH_3$	—	—	0.10
$(CH_3)_2(CH_3O)COC(CH_3)_3$	—	0.21	—
$C_5H_5N\rightarrow O$	—	0.07	—

a) 0.1 M pyridine was added to suppress the acid-catalyzed decomposition. b) Isolated yield of pyridinium heptafluorobutyrate.

oxygen to form dimethyl-*t*-butoxysulfonium ion.[12] The peroxidic α-oxygen of a heptafluorobutyryloxyl group should be more electropositive than the *t*-butoxyl oxygen. α-Oxygen in a peroxy ester O–O bond is estimated to be more electropositive than α-oxygen according to a MO calculation.[13] Therefore, a nucleophilic attack of pyridine on the heptafluorobutyryloxyl peroxidic oxygen rather than on the *t*-butoxyl oxygen is expected to be favored.

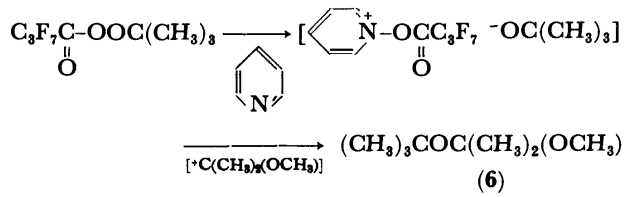

(6)

In a thermal decomposition of TBH in methoxybenzene, the values of the activation enthalpy and entropy for the thermal decomposition of TBH were $\Delta H^{\ddagger}=95.4\,kJmol^{-1}$, $\Delta S^{\ddagger}=-37.2\ JK^{-1}mol^{-1}$. These values are larger than those for a thermal decomposition of TBH in nitrobenzene. Ionic Criegee type rearrangement products such as 2-methoxy-1-propene (**1**), 2,2-dimethoxypropane (**4**), and 1-methoxy-1-methylethyl heptafluorobutyrate (**5**) were obtained as the decomposition products in methoxybenzene. Furthermore, acetone (**7**), *t*-butyl heptafluorobutyrate (**8**), and methoxymethylbenzene (**9**), which would result from a homolytic cleavage, were also obtained as shown in Table 4. From these results, it may be concluded that the thermal decomposition of TBH in methoxybenzene is characteristic of mixed ionic and radical cleavages.

Thus, the decomposition of TBH was affected by the polarity of the solvents; the rate of decomposition increased with the dielectric constant of a solvent (ε). In a nonpolar solvent such as octane (ε=1.90) and benzene (ε=2.27), the decomposition proceeds homolytically and the ionic decomposition becomes dominant in a polar solvent such as nitrobenzene (ε=34.6), and pyridine (ε=12.3). In methoxybenzene (ε=4.30), the decomposition is characteristic of mixed ionic and radical cleavages. Although the dielectric constant of nitrobenzene is larger than that of pyridine, the decomposition in pyridine is faster than that in nitrobenzene. This may be due to a nucleophilic attack of pyridine to the O–O bond of TBH.

Experimental

The ^{1}H-NMR spectra were taken with a JEOL JNM-MH-100 spectrometer. The mass spectra were measured with a JEOL JMS-D300 spectrometer. ESR signals were taken with a JES-PE-3X spectrometer. GLC analyses were performed on a Shimadzu GC-4APTF gas chromatograph. IR spectra were recorded on a JASCO A-3 spectrophotometer. Benzene, octane, nitrobenzene, pyridine, and methoxybenzene were purified according to conventional methods. Heptafluorobutyryl chloride was prepared by a reaction of heptafluorobutyric acid and phosphorus pentachloride. The pure acid chloride had a bp of 39—40 °C/760 mmHg (1 mmHg=133.322 Pa), (38—39 °C/740 mmHg[14]) and $\nu_{C=O}$ 1795 cm^{-1}. *t*-Butyl hydroperoxide (commercial grade of Nippon Oil & Fats Co.) was distilled prior to use, bp 32—35 °C/15 mmHg.

Preparation of t-Butyl Heptafluoroperoxybutyrate (TBH). Heptafluorobutyryl chloride (77 g, 0.33 mol) was added to *t*-butyl hydroperoxide (35 g, 0.39 mol) in pentane (55 g) at −2 °C and the mixture was cooled to −10 °C. Dry pyridine (31 g, 0.39 mol) was added dropwise with stirring over a period of 20 min while the temperature was maintained below 0 °C. The reaction mixture was then kept at −5 °C—−10 °C for an additional 40 min. The resulting mixture containing a white precipitate was poured into 100 mL of cold aqueous 10% hydrochloric acid and was thoroughly stirred. The pentane layer was separated, washed twice with 100 mL of cold aqueous 5% sodium hydroxide, and finally with 100 mL of cold water. After being dried over anhydrous magnesium sulfate, the solution was concentrated to give 42 g of a crude colorless peroxy ester. This was carefully distilled to give a pure colorless peroxy ester, bp 39.5—40.0 °C/17 mmHg. The infrared spectra exhibited the characteristic peroxy ester carbonyl band at 1815 cm^{-1}. ^{1}H-NMR ($CF_2ClCFCl_2$) δ=1.36 (9H, s). MS *m/z* 286 (M^+), 271, 197, 169, 150, 119, 100, 73, 69, 58, 57 (base), 55, 45, 43, 42, 39, 31, 29, 27, and 15; Anal. Calcd for $C_8H_9O_3F_7$: C, 33.58; H, 3.17%. Found: C, 32.50; H, 2.99%.

Kinetic Measurement. A solution of TBH in a degassed sealed tubes were immersed in a constant-temperature bath. Each sample tube was taken out after appropriate time intervals and immersed in a Dry Ice–acetone bath to quench the reaction; the amount of the residual TBH was estimated by iodometric titration.

Decomposition Products of TBH. The products of the decomposition of TBH were identified by GC–MS and by their retention times of GLC compared with those of authentic samples. The yield of heptafluorobutyric acid was determined by titration after hydrolysis of the reactants. Yields of the other products were determined by GLC using internal standards.

The authors wish to express their thanks to Mr. Shigehiko Yamaguchi at the Tsukuba Central Research Laboratory of Nippon Oil & Fats Co., Ltd. for GC–MS spectrometric measurement.

References

1) G. Bouillon, C. Lick, and K. Schank, "The Chemistry of Peroxides," ed by S. Patai, Wiely-Interscience, New York (1983), Chap. 10.

2) O. Kikuchi, *Yuki Gosei Kagaku Kyokai Shi*, **37**, 678 (1979).

3) P. D. Bartlett and T. G. Traylor, *J. Am. Chem. Soc.*, **83**, 856 (1961).

4) H. Sawada, H. Hagii, K. Aoshima, and T. Arai, *Bull. Chem. Soc. Jpn.*, **57**, 1161 (1984).

5) P. D. Bartlett and R. R. Hiatt, *J. Am. Chem. Soc.*, **80**, 1398 (1958).

6) P. D. Bartlett and D. M. Simons, *J. Am. Chem. Soc.*, **82**, 1753 (1960).

7) T. Koenig, J. Huntington, and R. Cruthoff, *J. Am. Chem. Soc.*, **92**, 5413 (1970).

8) P. D. Bartlett and C. Rüchardt, *J. Am. Chem. Soc.*, **82**, 1398 (1960).

9) S. Terabe, K. Kuruma, and R. Konaka, *J. Chem. Soc., Perkin Trans. 2*, **1973**, 1252.

10) In the photolysis of C_3F_7I in the presence of nitrosodurene, the adduct radical of $C_3F_7\cdot$ to nitrosodurene was observed: a_N=10.8 G, a_F=16.3 G, g=2.0066.

11) M. Trachtman and J. G. Miller, *J. Am. Chem. Soc.*, **84**, 4828 (1962).

12) W. A. Pryor and W. H. Hendrickson, Jr., *J. Am. Chem. Soc.*, **97**, 1580 (1975); **105**, 7114 (1983).

13) T. Yonezawa, H. Kato, and O. Yamamoto, *Bull. Chem. Soc. Jpn.*, **40**, 307 (1967).

14) W. T. Miller, Jr., E. Bergman, and A. H. Fainberg, *J. Am. Chem. Soc.*, **79**, 4159 (1957).

Total Syntheses of (±)-Aerothionin, (±)-Homoaerothionin, and (±)-Aerophobin-1

Shigeru NISHIYAMA and Shosuke YAMAMURA*
Department of Chemistry, Faculty of Science and Technology, Keio University, Hiyoshi, Kohoku-ku, Yokohama 223
(Received July 17, 1985)

(±)-Aerothionin, (±)-homoaerothionin, and (±)-aerophobin-1 have been successfully synthesized using phenolic oxidation of the methyl pyruvate oxime derivative with thallium(III) trifluoroacetate as a key step. The stereostructure of aerophobin-2 has been also established by comparison of the ^{1}H NMR spectrum with those of related compounds.

Recently, enlarged synthetic attention has been focused on marine natural products having physiological activities.[1] Among them, several sponges have served attractive bromine-containing metabolites derived from tyrosine, which in biosynthetic pathway seem to involve phenolic oxidation affording dimerization, cyclization and so on.

As a part of our approach directed toward total syntheses of these natural products using thallium(III) salt-induced phenolic oxidation as a key step,[2] we have already accomplished total synthesis of bastadins isolated from the sponge *Ianthella basta*.[3] Along this line, our attention turned to aerothionin (**1**),[4] homoaerothionin (**2**),[4] aerophobin-1 (**3**),[5] and -2 (**4**)[5] which are also metabolites of such sponges as *Aplysia fistularis, Verongia thiona* and *V. aerophoba*. Especially, the absolute stereostructure of **1** was established by an X-ray crystallographic analysis coupled with circular dichroism,[6] and its synthetic effort was also made by Thomson *et al.*,[7] wherein sodium borohydride reduction of tetradehydroaerothionin did not yield natural *trans, trans*-aerothionin, but *cis, cis*-aerothionin.

Configurations of the hydroxyl group at C^6-position in aerophobin-1 (**3**) and its congener (**4**) possessing 2-aminohomoistamine moiety instead of histamine in **3** remained unsettled. From a biogenetic point of view, however, they should have the same stereostructures as that of **1**. Accordingly, it was expected that the spiroisoxazoline derivative (**14a**) would be a potent intermediate for syntheses of aerothionin (**1**), homoaerothionin (**2**) and aerophobin-1 (**3**), respectively, and the ketone (**11**) conceivable as a precursor of **14a** might be obtained by the two-electron oxidation process (*i.e.* **9**→**11**) involving attack of a hydroxyimino group to a carbonium ion generated on phenolic oxidation. We describe herein total syntheses of **1**, **2**, and **3** as well as determination of aerophobin-2 (**4**).

When a readily accessible azulactone (**5**)[4] was submitted to alkaline hydrolysis followed by oximation and benzylation, the tribenzyl derivative (**6**) was obtained in 31% yield, together with the enamine (**7**) in 14% yield, from which on treatment with the same reaction sequence **6** was further obtained. The structure of **6** could be confirmed by its successful conversion to a known alkaline degradation product of **1**,[4] *N,N'*-bis[3-(3,5-dibromo-2-hydroxy-4-methoxyphenyl)-2-hydroxyiminopropionyl]-1,4-butanediamine (**8**) by treatment with 1,4-butanediamine followed by hydrgenolysis. Furthermore, transesterification of **6** in methanol containing K_2CO_3 afforded the corresponding methyl ester, which on hydrogenolysis led to the desired dihydroxy derivative (**9**) in moderate yield.

The methyl ester (**9**) so far obtained was oxidized with thallium(III) trifluoroacetate (TTFA) in trifluoroacetic acid (room temp, 4 h) to afford **10**, **11** and **12** as isolable products in 21, 27, and 3% yields, respectively. The aspect of the TTFA oxidation is compatible, except for the dimer (**12**), with the results reported by Forrester *et al.*,[8] in which they examined several oxidation reactions of phenols [A] using MTA, $Pb(OAc)_4$, Ag_2O, Br_2, and TBCO as oxidant to afford [B] and [C].

As seen in the case of *cis,cis*-aerothionin formation,[7] on treatment of **11** with $NaBH_4$, the undesired **13a** was also obtained in high yield together with trace amount of **14a**. However, evaluation of several reaction conditions provided an improvement to pro-

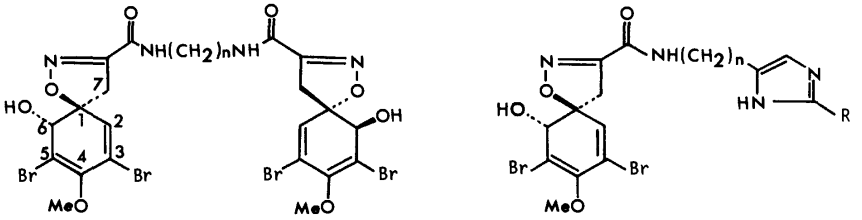

1 n = 4
2 n = 5
3 n = 2, R = H
4 n = 3, R = NH_2

Fig. 1. Some novel spiroisoxazolines from marine sponges.

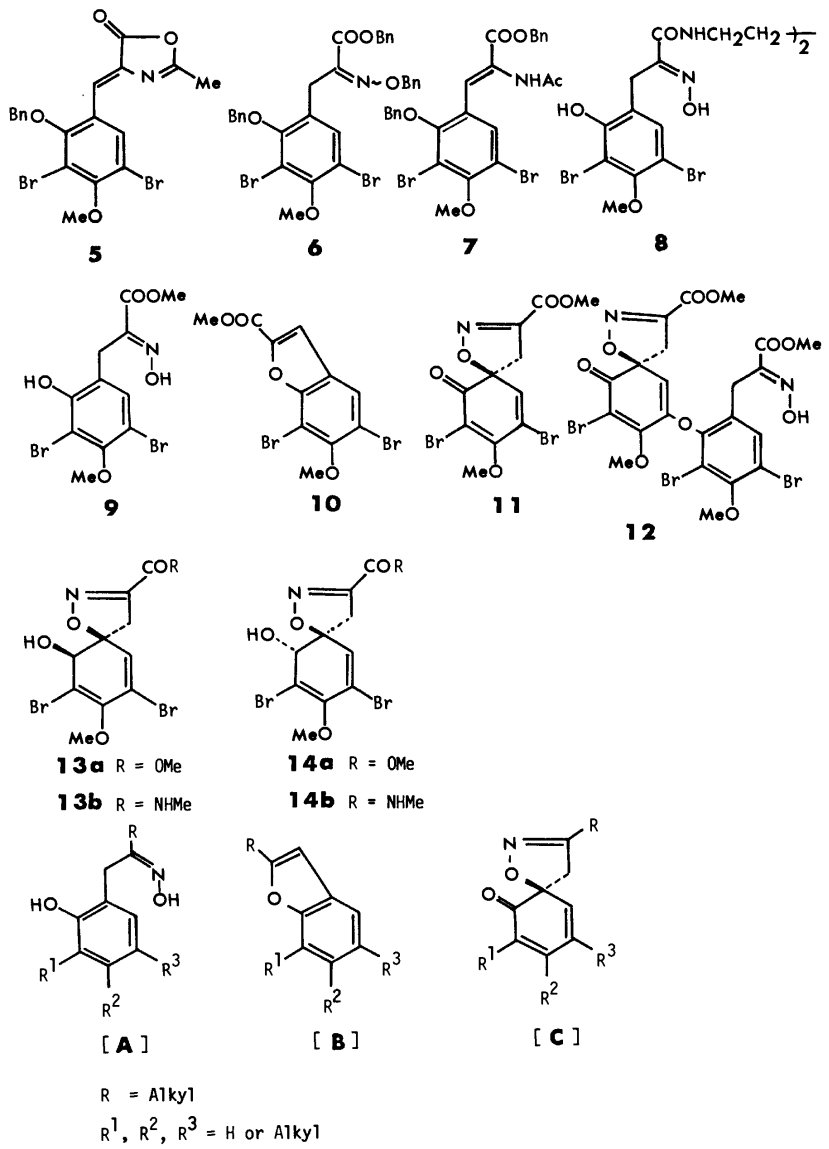

Fig. 2.

duce **14a** in preparative scale. Namely, reduction of **11** was carried out with excess $Zn(BH_4)_2$ in ether (room temp, 7 min) to afford a 1.3:1 mixture of **13a** and **14a**, in 70% yield, which were easily separable on preparative TLC. The stereostructures of **13a** and **14a** could be established on the basis of exhaustive comparison of both ^1H NMR spectra with those of **1** and *cis,cis*-aerothionin which has a cis vicinal relationship between a hydroxyl group and an oxygen atom in the spiroisoxazoline unit, as seen in Table 1.

Finally, amidation of **14a** with 1,4-butanediamine, 1,5-pentanediamine and histamine (room temp, overnight) successfully afforded aerothionin (**1**), homoaerothionin (**2**) and aerophobin-1 (**3**), in 18, 4.4 and 82% yields, respectively. Interestingly, on the other hand, the ester (**13a**), which has the trans relationship between the hydrogen atom attached to the carbon atom bearing the hydroxyl group and the oxygen atom in a spiroisoxazoline ring, was quite unstable to amines. The amides (**1**), (**2**), and (**3**) thus obtained were indistinguishable with authentic samples under the full range of spectral (IR, ^1H NMR, and mass) and chromatographical (TLC and HPLC) means. However, in the cases of **1** and **2**, a possibility that each product consists of a mixture of the natural product and its concomitant diastereomer, could not be ruled out. Unfortunately, up to date we have no reliable solution for it.

The stereostructure of aerophobin-2 could be established as depicted in **4** on the basis of exhaustive comparison of the ^1H NMR spectrum with those of **13b** and **14b**: particularly, the resonances of δ 4.14 and 6.35 ascribed to C^6-H and C^2-H are rather agreeable with those of δ 4.08 and 6.40 in **14b** than those of δ 4.40 and 6.55 in **13b**. Furthermore, while *cis,cis*-aerothionin, **13a** and **13b** have the broad signals attributable to the two geminal protons at C^7-position in their ^1H NMR spectra, the NMR signals due to the corresponding

Table 1. ^{1}H NMR Chemical shifts (δ) of aerothionin (1), *cis,cis*-aerothionin,[7] aerophobin-1 (3), aerophobin-2 (4)[5] and related compounds[a]

Proton	1[b]	*cis,cis*-Aerothionin[b]	3[c]	4[c]	13a[b]	14a[b]	13b[c]	14b[c]
C^2-H	6.53	6.60	6.40	6.35	6.58	6.52	6.55	6.40
C^6-H	4.18 (7.5)	4.52 (7.5)	4.08	4.14	4.53 (7.5)	4.22 (7.5)	4.40	4.08
C^6-OH	5.40 (7.5)	4.97 (7.5)			4.98 (7.5)	5.38 (7.5)		
C^7-H	3.15 (18)	3.2—3.5	3.03 (18)	3.20 (17.5)	3.42	3.17 (18)	3.3—3.4	3.05 (18)
	3.85 (18)		3.77 (18)	3.85 (17.5)		3.85 (18)		3.78 (18)
OMe	3.77	3.73	3.73	3.79	3.68[d]	3.73[d]	3.75	3.73
NMe							2.85	2.83
$-CH_2-$	1.62	1.62	2.83 (7.5)	2.01 (7)				
				2.67 (7)				
Imidazole			6.90	6.47				
			7.67					
$OCNCH_2-$	3.2—3.5	3.2—3.5	3.52 (7.5)	3.43 (7)				
NH	7.60	7.55						
COOMe					3.70[d]	3.83[d]		

a) Coupling constants (in Hz) are given in parentheses. b) Acetone-d_6 as solvent. c) Methanol-d_4 as solvent. d) May be reversed.

protons in **1**, **2**, **3**, **14a**, and **14b** are observed as two doublets because of an interaction of the hydroxyl group with one of the geminal protons. Accordingly, it is reasonable that aerophobin-2 (**4**) exhibiting two doublets at δ 3.20 and 3.85 should possess the same structure unit as those of the latter compounds.

Experimental

All the melting points were obtained on a Mitamura Riken melting point apparatus and uncorrected. IR spectra were recorded on a JASCO Model A-202 spectrophotometer. ^{1}H NMR spectra were obtained on a Varian EM-390 NMR spectrometer (90 MHz) using tetramethylsilane as an internal standard. High resolution mass spectra were obtained on a Hitachi M-80 GC-MS spectrometer operating with an ionization energy (70 eV). Preparative and analytical TLC were carried out on silica-gel plates (Kieselgel 60 F_{254}, E. Merck A.G. Germany) using UV light and/or 5% molybdophosphoric acid in ethanol for detection, unless otherwise stated. HPLC were performed on a JASCO Trirotar-II apparatus using a 4.6×250 mm Develosil 60-3 column with hexane–AcOEt (v/v 1:1) at 1 ml/min flow rate.

Benzyl 2-Benzyloxyimino-3-(2-benzyloxy-3,5-dibromo-4-methoxyphenyl)propionate (6). The azulactone (**5**)[4] (8.22 g) was hydrolyzed at 100 °C for 9 h with KOH (11 g) in dioxane (50 ml)–H_2O (50 ml). After addition of hydroxylamine hydrochloride (3.7 g), the reaction mixture was allowed to stand at room temperature overnight, and then acidified with 2M HCl(1M=1 mol dm^{-3}) and extracted with AcOEt. The AcOEt layer was washed with brine, dried over anhydrous Na_2SO_4, and then evaporated. The residue was treated with benzyl chloride (6 ml) and K_2CO_3 (6 g) in DMF (50 ml) at room temperature overnight. The mixture was partitioned between AcOEt and H_2O, and then the AcOEt layer was washed with brine, dried over anhydrous Na_2SO_4, and then evaporated under reduced pressure to leave a crude syrup, which was submitted to silica-gel column chromatography (250 g) using benzene as eluant to give **6** (3.42 g) and **7** (1.4 g). **6**: mp 83—85 °C from hexane–AcOEt; IR (film) 1720, 1600, and 1580 cm^{-1}: ^{1}H NMR ($CDCl_3$) δ=3.85(3H, s), 3.88(2H, s), 4.88(2H, s), 5.12(2H, s), 5.22(2H, s), and 7.2—7.5(16H, complex); Found: *m/z* 651.0244. Calcd for $C_{31}H_{27}NO_5{}^{79}Br_2$: M, 651.0254. **7**: mp 159—160 °C from hexane–AcOEt; IR (film) 3250, 1730, 1660, 1575, and 1520 cm^{-1}; ^{1}H NMR ($CDCl_3$) δ=1.93(3H, s), 3.90(3H, s), 4.90(2H, s), 5.25(2H, s), 7.2—7.5(10H, complex), and 7.55 (1H, s); Found: *m/z* 586.9952. Calcd for $C_{26}H_{23}NO_5{}^{79}Br_2$: M, 586.9943.

Methyl 2-Hydroxyimino-3-(3,5-dibromo-2-hydroxy-4-methoxyphenyl)propionate (9). A mixture of the tribenzyl derivative (2.16 g) and K_2CO_3 (0.91 g, 2 equiv mol) in dioxane (10 ml)–MeOH (10 ml) was stirred at room temperature for 40 min. The mixture was partitioned between AcOEt and H_2O, and the organic layer was washed with 2M HCl and then dried over anhydrous Na_2SO_4. After evaporation of the solvent, the residue was hydrogenated at room temperature overnight in the presence of catalytic Pd–C (10%) in dioxane (20 ml)–AcOH (20 ml) to afford the methyl ester (**9**) (0.97 g): mp 148—149 °C from hexane–AcOEt; IR (film) 3300, 1730, 1700 sh., 1650, 1590, and 1550 cm^{-1}; ^{1}H NMR ($CDCl_3$) δ=3.85 (3H, s), 3.88(3H, s), 3.92(2H, s), and 7.42(1H, s); Found: *m/z* 396.8984. Calcd for $C_{11}H_{11}NO_5{}^{79}Br^{81}Br$: M, 396.9005.

N,N'-Bis[3-(3,5-dibromo-2-hydroxy-4-methoxyphenyl)-2-hydroxyiminopropionyl]-1,4-butanediamine (8). A mixture of **6** (2.76 g, 4 mmol) and 1,4-butanediamine (0.16 ml, 1.6 mmol) was kept at room temperature for 6 d, and then heated at 60 °C for 6 h. The resulted syrup was passed through a silica-gel column (20 g) using hexane–AcOEt (2:1) as eluant to afford the desired amide (1.63 g): mp 108—110 °C from hexane–AcOEt. A 857 mg portion of the product was submitted to hydrogenolysis in the presence of catalytic Pd–C (10%) in dioxane (40 ml)–AcOH (40 ml) at room temperature for 3 d to yield **8** (564 mg): mp 189—190 °C from ether–acetone [lit,[4] mp 188.5—189.5 °C].

TTFA Oxidation of 9. To a solution of TTFA (1.33 g, 2.4 mmol) in TFA (30 ml) was added the ester (**9**) (0.43 g, 1.1 mmol) in TFA (10 ml). The mixture was stirred at room temperature for 4 h, and then partitioned between $CHCl_3$ and H_2O. The organic layer was dried over anhydrous Na_2SO_4 and evaporated under reduced pressure to give a brownish residue, which was further separated by preparative TLC using hexane–AcOEt (2:1) to afford **10** (81 mg), **11** (114 mg), and **12** (12 mg), respectively. The physical data of these products are as follows: **10**: mp 141.5—143 °C from hexane–AcOEt; IR (film) 1720 sh., 1600, 1575, and 1550 cm^{-1};

^{1}H NMR (acetone-d_6) δ=3.97(6H, s), 7.70(1H, s), and 8.07(1H, s); Found: m/z 363.8763. Calcd for $C_{11}H_8O_4{}^{79}Br^{81}Br$: M, 363.8768. **11** as a colorless oil: IR (film) 1710, 1670, 1585, and 1530 cm^{-1}; ^{1}H NMR ($CDCl_3$) δ=3.27(1H, d, J=18Hz), 3.65(1H, d, J=18Hz), 3.93(3H, s), 4.20(3H, s), and 6.78(1H, s); Found: m/z 394.8809. Calcd for $C_{11}H_9NO_5{}^{79}Br^{81}Br$: M, 394.8826. **12** as a colorless oil: IR (film) 3300, 1725, 1680, 1650 sh., 1595, and 1555 cm^{-1}: ^{1}H NMR ($CDCl_3$) δ=3.10(1H, d, J=18Hz), 3.57(1H, d, J=18Hz), 3.80(3H, s), 3.83(3H, s), 3.90(3H, s), 3.8—3.9(2H, overlapped with MeO signals), 4.32(3H, s), 4.92(1H, s), and 7.50(1H, s); Found: m/z 712. Calcd for $C_{22}H_{19}N_2O_{10}{}^{79}Br^{81}Br$: M, 712. The molecular ion peak at m/z 712 has not been detected by high resolution mass spectrum, but observed in quite low intensity on measurement of its normal mass spectrum.

Reduction of 11 with Zinc Borohydride. The dienone (**11**) (103 mg) in CH_2Cl_2 (3 ml) was treated, at room temperature for 7 min, with excess $Zn(BH_4)_2$ in ether (2 ml), and then the mixture was quenched as usual to give a crude product, which was separated by preparative TLC using hexane–AcOEt (5:1) to afford **13a** (41 mg) and **14a** (30 mg). Their physical data are as follows: **13a** as a syrup: IR (film) 3470, 1730, 1620, 1595, and 1575 cm^{-1}; Found: m/z 394.8987. Calcd for $C_{11}H_{11}NO_5{}^{79}Br_2$: M, 394.9002. **14a** as a syrup: IR (film) 3450, 1725, 1630, 1590, and 1580 cm^{-1}; Found: m/z 396.8979. Calcd for $C_{11}H_{11}NO_5{}^{79}Br^{81}Br$: M 396.8983.

Synthesis of Aerothionin (1). A mixture of **14a** (19 mg, 0.05 mmol) and 1,4-butanediamine (2 µl, 0.02 mmol) was allowed to stand at room temperature overnight. Direct separation of the mixture by preparative TLC [benzene–acetone (5:1)] afforded aerothionin (**1**) (3 mg, 18% yield based on 1,4-butanediamine) and unreacted **14a** (7.2 mg). The IR and ^{1}H NMR spectra of the synthetic compound (**1**) were completely identical with those of an authentic sample, and the both aspects in HPLC (retention time, 7 min) were indistinguishable.

Synthesis of Homoaerothionin (2). The ester (**14a**) (8 mg, 0.02 mmol) was treated with 1,5-pentanediamine (1 µl, 0.009 mmol) according to essentially the same procedure as described above to yield homoaerothionin (**2**) (0.3 mg, 4.4%) and unreacted **14a** (7.5 mg). The IR, ^{1}H NMR, and HPLC (retention time, 6.5 min) of the product were identical with those of an authentic sample.

Synthesis of Aerophobin-1 (3). A mixture of **14a** (4.5 mg, 0.01 mmol) and histamine (12.5 mg, 0.1 mmol) in MeOH (0.1 ml)–dioxane (0.1 ml) was kept at room temperature overnight, and then directly purified by preparative TLC using $CHCl_3$–MeOH (3:1) to afford aerophobin-1 (**3**) (4.4 mg, 82%) (IR and ^{1}H NMR spectra).[5] Further acetylation of the synthetic compound (**3**) was carried out using Ac_2O–pyridine (1:1) as usual to afford the corresponding *O*-acetyl derivative, whose spectral data were superimposable with those of an authentic sample.

Syntheses of 13b and 14b. A mixture of **6** (1.06 g) and methylamine (40% aq solution, 1.5 ml) in THF (10 ml) was kept at room temperature for 13 h. The resulted mixture was acidified with 2M HCl, and then partitioned between AcOEt and H_2O. The organic layer was washed with aq $NaHCO_3$ and dried over anhydrous Na_2SO_4. After removal of the solvent under reduced pressure, the crystalline residue was recrystallized from hexane–AcOEt to give the corresponding amide (0.6 g, 65%): mp 112—113 °C. In the next step, a 544 mg portion of the amide was hydrogenated at room temperature for 8 h in dioxane (15 ml)–AcOH (15 ml) in the presence of catalytic Pd–C (10%) to afford the hydroxy derivative (272 mg, 73%): mp 143—145 °C from hexane–AcOEt. According to essentially the same procedure as described in **9** the hydroxy amide (450 mg, 1.1 mmol) was oxidized with TTFA (1.26 g, 2.3 mmol) in TFA to give the spiroisoxazoline derivative [41 mg, 9.2% (mp (dec)<170 °C)] as well as the benzofuran (14 mg, 3.4%) and the dimer (98 mg, 24%).

To a solution of the spiroisoxazoline derivative (16 mg) in CH_2Cl_2 was added excess $Zn(BH_4)_2$. After stirring at room temperature for 1.5 h, the reaction mixture was quenched by usual manner. The crude product was separated by preparative TLC using hexane–AcOEt (1:1) to give **13b** (4.6 mg, 29%) and **14b** (4.2 mg, 27%), the physical data of which were shown below: **13b**: mp 182—185 °C (dec.) from hexane–AcOEt; IR (film) 3350, 1640, 1600, 1565, and 1545 cm^{-1}; Found: m/z 393.9172. Calcd for $C_{11}H_{12}N_2O_4{}^{79}Br_2$: M, 393.9164. **14b** as a syrup: IR (film) 3360, 1660, 1630 sh., 1595, 1580, and 1550 cm^{-1}; Found: m/z 395.9141. Calcd for $C_{11}H_{12}N_2O_4{}^{79}Br^{81}Br$: M, 395.9142.

The authors wish to thank Prof. Forrester (University of Aberdeen) for providing them with authentic samples of aerothionin, homoaerothionin and *cis-cis* aerothionin, and also Dr. G. Sodano (Instituto per la Chimica di Molecole di Intersse Biologico del C.N.R.) for providing them with the ^{1}H NMR spectra of aerophobin-1 and its acetate in addition to an authentic sample of the latter. This research has been supported in part by grants from the Takeda Science Foundation as well as from the Kawakami Memorial Foundation, to which grateful acknowledgment is made.

References

1) For a preliminary report of a part of this work see: S. Nishiyama and S. Yamamura, *Tetrahedron Lett.*, **24**, 3351 (1983).

2) D. J. Faulkner, "*Antibiotics from Marine Organisms*" in "*Topics in Antibiotic Chemistry*" ed by P. G. Sammes, Ellis Horwood LTD., Chichester (1978), Vol. 2, p. 9.

3) S. Nishiyama and S. Yamamura, *Tetrahedron Lett.*, **23**, 1281 (1982); S. Nishiyama, T. Suzuki, and S. Yamamura, *ibid.*, **23**, 3699 (1982); S. Nishiyama, T. Suzuki, and S. Yamamura, *Chem. Lett.*, **1982**, 1851.

4) E. Fattorusso, L. Minale, G. Sodano, K. Moody, and R. H. Thomson, *Chem. Commun.*, **1970**, 752; K. Moody, R. H. Thomson, E. Fattorusso, L. Minale, and G. Sodano, *J. Chem. Soc. Perkin I*, **1972**, 18.

5) G. Cimino, S. De Rosa, S. De Stefano, R. Self, and G. Sodano, *Tetrahedron Lett.*, **24**, 3029 (1983).

6) J. A. McMillan, I. C. Paul, Y. M. Goo, and K. L. Rinehart, Jr., *Tetrahedron Lett.*, **22**, 39 (1981).

7) A. R. Forrester, R. H. Thomson, and S. -On Woo, *Justus Liebigs Ann. Chem.*, **1978**, 66.

8) A. R. Forrester, R. H. Thomson, and S. -On Woo, *J. Chem. Soc. Perkin I*, **1975**, 2340.

Synthetic Studies of Rifamycins. VIII.[1] An Improved Practical Synthesis of the Ansa-chain Compounds for the Rifamycin W Synthesis

Masaya NAKATA, Kazunobu TOSHIMA, Toshiyuki KAI, and Mitsuhiro KINOSHITA*
Department of Applied Chemistry, Faculty of Science and Technology, Keio University, Hiyoshi, Kohoku-ku, Yokohama 223
(Received July 10, 1985)

The improved practical synthesis of 6,8,10-tri-*O*-acetyl-3-*C*-(acetoxymethyl)-3,5,7,9,11-pentadeoxy-1,2-*O*-isopropylidene-5,7,9,11-tetra-*C*-methyl-L-*erythro*-D-*altro*-β-L-*talo*-dodecodialdofuranose-(1,4) 12-(diethyl acetal) (**3**), a useful synthetic segment for the rifamycin W ansa-chain, is described. The key intermediate, 3-*O*-benzyl-2,4,7-trideoxy-5,6-*O*-isopropylidene-2,4-di-*C*-methyl-*aldehydo*-D-*glycero*-D-*allo*-heptose (**22**), was synthesized in a 29.4% yield from methyl 4,6-*O*-benzylidene-3-deoxy-3-*C*-methyl-α-D-altropyranoside (**8**) in 15 steps. The coupling of **22** with the lithium reagent prepared from butyllithium and 3-*C*-(benzyloxymethyl)-3,5,6-trideoxy-5-iodo-1,2-*O*-isopropylidene-α-D-ribo-5-hexenofuranose afforded only the "Cram" product **24** in a 61% yield. The homogeneous hydrogenation of **24** with [$RhCl(Ph_3P)_3$] gave 8-*O*-benzyl-3-*C*-(benzyloxymethyl)-3,5,7,9,12-pentadeoxy-1,2:5,6-di-*O*-isopropylidene-5,7,9-tri-*C*-methyl-D-*erythro*-D-*altro*-L-*talo*-dodecofuranose-(1,4) (**25**) and its C-5 epimer in 95 and 3.8% yields respectively. 6,8-Di-*O*-benzyl-3-*C*-(benzyloxymethyl)-3,5,7,9-tetradeoxy-1,2-*O*-isopropylidene-5,7,9-tri-*C*-methyl-D-*altro*-β-L-*talo*-decodialdofuranose-(1,4), derived from **25** in a 91% yield, was subjected to coupling with 3,3-diethoxy-2-lithio-1-propene to afford about 1.7:1 excess of the "Cram" product (**30**, 59% yield). The conversion of **30** into **3** was accomplished by the sequence of reactions involving homogeneous hydrogenation, debenzylation, and acetylation in a 75% yield. The 24-step synthesis of **3** from **8** was achieved in a 7% overall yield.

For the purpose of synthesizing practically the optically active natural macrolides such as rifamycins and erythronolides which contain a long chain consisting of many consecutive chiral carbon atoms, it is indispensable to realize the highly diastereoselective connections between the selected chiral carbon chain segments which can be effectively synthesized from appropriate chiral compounds, but on the other hand each resulting coupling product must naturally be transformed into each target compound as effectively as possible. In the studies directed toward the total synthesis of rifamycin W (**1**), the selected ansa-chain compound **2**[2] corresponding to the C-17 – C-29 portion of **1** was first synthesized from the sugar derivative **8** in our laboratories. In this synthesis, the precursor **3** of **2** was prepared in good yield from **5** by the sequence of reactions involving the highly diastereoselective coupling of **4** and **5** followed by the stereospesific homogeneous hydrogenation of the major "Cram" product and two successive transformations. However, the 7-steps synthesis of **5** from **7**, involving the coupling of **6** with **7** followed by the stereospecific homogeneous hydrogenation of the desilylated compound of the major "Cram" product and four successive transformations, was not satisfactory because of the low overall yield caused by the requirement of many steps of transformation not directly neccessary for the connection of carbon chains in the synthetic route. Moreover, the long way (18 steps) to **7** from **8** was also undesirable for the large scale preparation of **7**. In our recent synthetic studies of **3** directed at the total synthesis of rifamycin W, it was found that a modified synthetic route which was shorter by five steps than the old route effected a 2-fold improvement in the overall

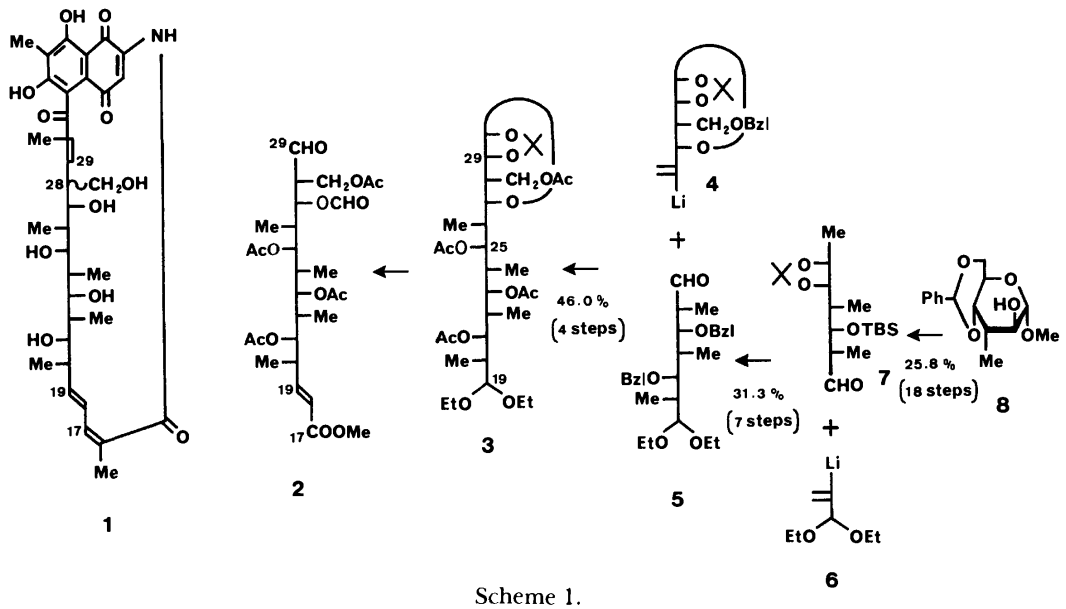

Scheme 1.

yield of **3** from the starting material **8** with no sacrifice in the stereoselectivities of the peculiar carbon chain connections which we have termed a "two stage coupling," and were effectively used in the old route. In this paper, we wish to report the improved practical synthesis of **3**, the most important key intermediate for the rifamycin W ansa-chain synthesis.

The starting material, methyl 4,6-*O*-benzylidene-3-deoxy-3-*C*-methyl-α-D-altropyranoside (**8**)[3,4] was *O*-benzylated and the resulting **9** was treated with 75% dichloroacetic acid (DCA) to afford the crystalline derivative **10**. The selective 6-*O*-mesylation of **10** followed by reduction with lithium aluminium hydride gave **11**. The acetolysis of **11** followed by the hydrolysis yielded **12** in a 71% overall yield from **8**.

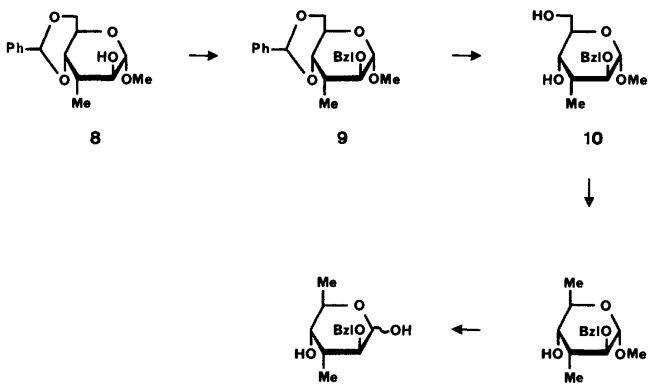

Scheme 2.

The Grignard reaction of **12** with 10 equimolar amounts of methylmagnesium iodide in ether gave **13** in an 86% yield as a sole product. The (2S)-configuration of **13** was confirmed by conversion to the known 1,4-lactone **14**[5] by the sequence of reactions involving periodate-oxidation, debenzylation, and bromine-oxidation. The isopropylidenation of **13** with 2,2-dimethoxypropane (DMP) in acetone containing a catalytic amounts of concd sulfuric acid gave the 5,6-isopropylidene derivative **15** without the

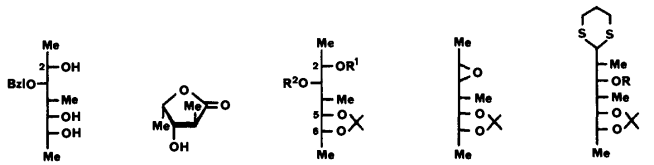

Scheme 3.

formation of the undesired 2,5-isopropylidene derivative.[2] Subsequent acetylation of **15** gave the crystalline derivative **16** in an 89% yield from **13**. The hydrogenolysis of **16** was reproducibly carried out with an atmospheric pressure of hydrogen and a freshly prepared palladium black in a 9:1 mixture of ethyl acetate–methanol. The resulting debenzylated product was immediately mesylated to afford **17** in a 95% yield. The mesylate **17** was then treated with sodium methoxide in chloroform to afford the epoxide **18** in an 81% yield after distillation. The nucleophilic addition of 2-lithio-1,3-dithiane to the *cis*-epoxide **18** gave regiospecifically only the desired C-6-adduct **19** in a 93% yield. The structure of **19** could be determined by the coupling feature (double doublet) of the acetoxymethine proton in the ^{1}H-NMR spectrum of its acetate **20**. The reason for this high regioselectivity in ring-opening of the *cis*-epoxide has been reasonably explained in the preceding paper.[2]

The benzylation of **19** provided, in a 91% yield, the benzyl ether **21**, whose dithioacetal group was cleaved with a 1:1 mixture of mercury(II) chloride and red mercury(II) oxide to generate the aldehyde **22** in a 65% yield together with the 27% yield of the deisopropylidenation heptopyranose **23**. The latter could

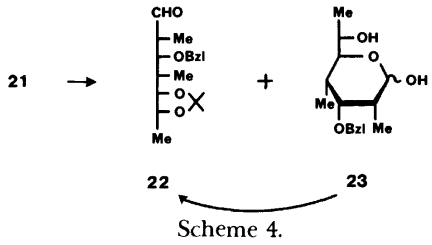

Scheme 4.

be converted to the former, in a 67% yield, by a sequence of reactions involving sodium borohydride reduction, isopropylidenation, and Swern oxidation, therefore the yield of **22** from **21** amounted to an 83% (or to a 29.4% overall yield from**8**).

With the aldehyde **22** corresponding to the central portion of the rifamycin W ansa-chain now in hand, the next stage was elaboration of it to the key intermediate **3** using our "two stage coupling." The coupling of **22** with the lithium reagent **4**, prepared from the corresponding iodide[2] (3 equiv) and butyllithium (2.8 equiv) in ether at −95—−90 °C, was carried out in ether at −95—−90 °C to afford a sole coupling product **24** in a 61% yield based on **22**. The homogeneous hydrogenation of **24** with 0.25 equimolar amounts of chlorotris(triphenylphosphine)rhodium(I) in benzene under an atmospheric pressure of hydrogen gave the hydrogenated products **25** and **26** in 95 and 3.8% yields respectively. We could confidently predict the structures of **24**, **25**, and **26** as depicted in Scheme 5 by the fact that in the old synthetic route (Scheme 1)[2] the "two stage coupling" of **4** and **5** gave predominantly the precursor of **3**. This prediction was confirmed in the later stage of this ansa-chain synthesis.

The benzylation of **25** followed by the selective deisopropylidenation of the resulting benzyl ether **27** afforded **28**, which was subjected to the periodate-oxidation to give the aldehyde **29** in a 91% yield from

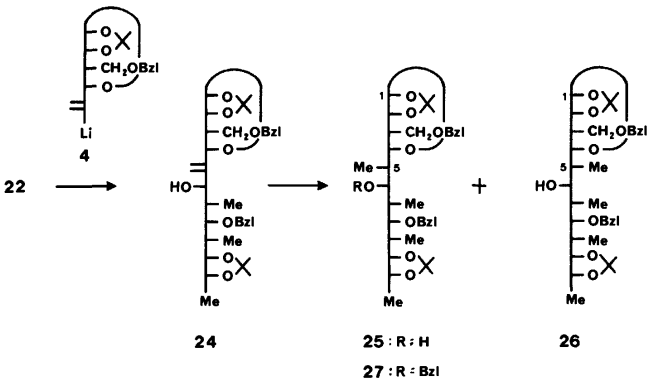

Scheme 5.

25. The coupling of **29** with the lithium reagent **6**, prepared from 3 equiv of 2-bromo-3,3-diethoxy-1-propene[2,6] and 2.5 equiv of butyllithium in THF at −110—−108°C, was performed in THF at −110—−108°C to afford, after column-chromatographic separation, **30** and **31** in 59 and 35% yields respectively based on **29**. The homogeneous hydrogenation of the

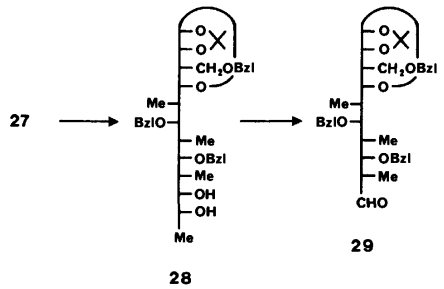

Scheme 6.

major product **30** with 0.25 equimolar amounts of rhodium catalyst gave **32** and its C-11 epimer **33** in 83 and 3.6% yields respectively. The major product **32** was debenzylated with lithium in liquid ammonia to afford **34**, which was acetylated with acetic anhydride and 4-dimethylaminopyridine (DMAP) in ethyl acetate to give the target key intermediate **3** in a 90% yield from **32**. The ^{1}H-NMR spectrum, R_f-value on TLC, and mp of **3** were identical with those of the authentic sample.[2] This result established the structures of **30—33**, together with those of the first "two stage coupling" products **24—26**. The overall yield of **3** from **8** (24 steps) thus amounted to a 7%, whereas the 29 steps overall yield of **3** from **8** in the old route was 3.5%.

Having achieved improved practical synthesis of **3**, we now undertake the total synthesis of rifamycin W.

Experimental

Melting points were determined on a micro hot-stage Yanaco MP-S3 and were uncorrected. The specific rotations were measured with a Carl Zeiss or JASCO DIP-360 photoelectric polarimeter in chloroform unless stated otherwise. IR spectra were recorded on a Hitachi Perkin-

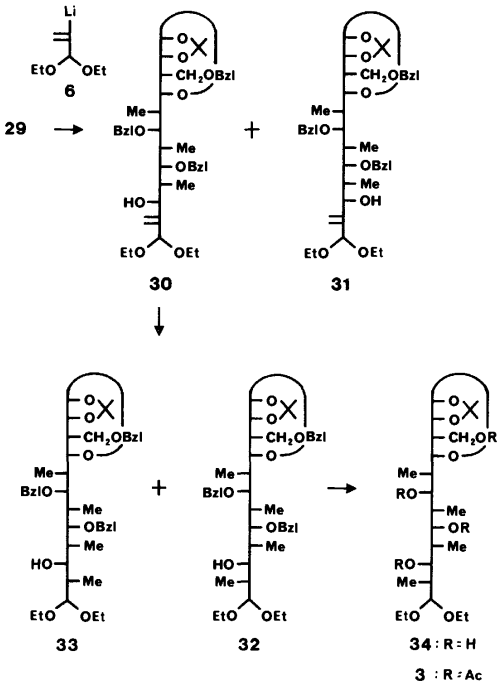

Scheme 7.

Elmer 225 spectrometer and ^{1}H-NMR spectra on either a Varian EM-390 or a Bruker WM 250 spectrometer in $CDCl_3$ using TMS as internal standard. Mass spectra were recorded on Hitachi M-80 mass spectrometer. Silica-gel TLC and column chromatography were performed on Merck TLC 60F-254 and Wakogel C-200, respectively. In general, evaporation of solvents was carried out under reduced pressure below 35°C.

Methyl 2-O-Benzyl-4,6-O-benzylidene-3-deoxy-3-C-methyl-α-D-altropyranoside (9). To an ice-cold stirred solution of **8** (31.1 g, 111 mmol) in dry DMF (218 ml), sodium hydride (5.30 g, 221 mmol) was added portionwise. The mixture was stirred at room temperature for 1 h and then ice-cooled. Benzyl bromide (26.4 ml, 221 mmol) was added dropwise and the resulting mixture was stirred at room temperature for 2 h. The reaction mixture was poured into ice water (600 ml) and the resulting mixture was extracted with ethyl acetate (300 ml×3). The extracts were washed with a saturated aqueous NaCl solution, dried, and evaporated. The residue was chromatographed on silica gel (1.5 kg) with 40:1 benzene–ethyl acetate to afford **9** (40.1 g, 98%) as a colorless syrup: R_f=0.72 (5:1 benzene–ethyl acetate); $[\alpha]_D^{27}$ −24° (*c* 2.10); ^{1}H-NMR δ=1.17 (3H, d, 3-Me, J=7.0 Hz), 2.30—2.70 (1H, m, H-3), 3.33 (3H, s, OMe), 3.60—4.30 (5H, m, H-2, 4, 5,6, and 6′), 4.54 (2H, s, $OC\underline{H}_2Ph$), 4.62 (1H, s, H-1), 5.55 (1H, s, $C\underline{H}Ph$), and 7.38 (10H, s, 2×Ph).

Found: C, 71.38; H, 7.05%. Calcd for $C_{22}H_{26}O_5$: C, 71.33; H, 7.07%.

Methyl 2-O-Benzyl-3-deoxy-3-C-methyl-α-D-altropyranoside (10). To an ice-cold sample of **9** (35.0 g, 94.5 mmol) was added ice-cold 75% aqueous dichloroacetic acid (350 ml). After being stirred at 0°C for 0.5 h, the reaction mixture was poured into a cold saturated aqueous $NaHCO_3$ solution (3 l). The mixture was extracted with chloroform (1 l×3) and the extracts were washed with a saturated aqueous NaCl solution (1 l), dried, and evaporated. The crystalline residue was washed with cold hexane to remove benzalde-

hyde and a practically pure sample of **10** (22.1 g, 83%) was obtained: mp 68.0—69.0 °C (colorless plates from acetone); R_f=0.09 (3:1 benzene–ethyl acetate); $[\alpha]_D^{23}$ +42° (*c* 1.38); ^{1}H-NMR δ=1.09 (3H, d, 3-Me, J=7.0 Hz), 1.20—2.40 (3H, m, H-3 and 2×OH), 3.33 (3H, s, OMe), 3.45—4.30 (5H, m, H-2, 4, 5, 6, and 6′), 4.51 (2H, s, OC$\underline{H}_2$Ph), 4.61 (1H, s, H-1), and 7.35 (5H, s, Ph).

Found: C, 63.76; H, 7.99%. Calcd for $C_{15}H_{22}O_5$: C, 63.81; H, 7.85%.

Méthyl 2-O-Benzyl-3,6-dideoxy-3-C-methyl-α-D-altropyranoside (11). To an ice-cold solution of **10** (48.6 g, 172 mmol) in dry pyridine (486 ml) was added mesyl chloride (14.6 ml, 189 mmol) over a period of 5 min. After being stirred at 0 °C for 1 h, the reaction mixture was poured into cold water (450 ml) and the resulting mixture was extracted with ethyl acetate (400 ml×3). The extracts were evaporated and the residue was resolved in ethyl acetate (250 ml). The solution was washed successively with saturated aqueous $KHSO_4$ (100 ml), $NaHCO_3$ (100 ml), and NaCl (100 ml) solutions, dried, and evaporated. To an ice-cold stirred solution of this crude syrup (62.0 g) of the 6-mesylate in dry ether (930 ml), $LiAlH_4$ (14.4 g, 379 mmol) was added portionwise over a period of 10 min. After being stirred at room temperature for 2 h, $Na_2SO_4 \cdot 10H_2O$ (122 g, 379 mmol) was added to the reaction mixture, and the resulting insoluble matter was filtered and the filter cake was washed thoroughly with chloroform. The combined filtrate and washings were evaporated and the residue was chromatographed on silica gel (1.5 kg) with 3:1 benzene–ethyl acetate to afford **11** (41.9 g, 91%) as a colorless syrup: R_f=0.42 (2:1 benzene–ethyl acetate); $[\alpha]_D^{30}$ +15° (*c* 1.37); ^{1}H-NMR δ=1.10 (3H, d, 3-Me, J=7.5 Hz), 1.27 (3H, d, 5-Me, $J_{5,6}$=6.3 Hz), 1.91 (1H, d, OH, J=7.5 Hz), 1.90—2.30 (1H, m, H-3), 3.31 (1H, dd, H-2, $J_{1,2}$=3.0 Hz, $J_{2,3}$=6.5 Hz), 3.40 (3H, s, OMe), 3.59 (1H, dd after addition of D_2O, H-4, $J_{3,4}$=3.8 Hz, $J_{4,5}$=6.3 Hz), 3.89 (1H, dq, H-5, $J_{4,5}$=6.3 Hz), 4.55 and 4.67 (each 1H, ABq, OC$\underline{H}_2$Ph, J_{gem}=12.0 Hz), 4.58 (1H, d, H-1, $J_{1,2}$=3.0 Hz), and 7.34 (5H, s, Ph).

Found: C, 67.65; H, 8.22%. Calcd for $C_{15}H_{22}O_4$: C, 67.64; H, 8.33%.

2-O-Benzyl-3,6-dideoxy-3-C-methyl-D-altropyranose (12). To an ice-cold stirred solution of **11** (10.0 g, 37.5 mmol) in acetic anhydride (300 ml), concd H_2SO_4 (0.30 ml) was added. After being stirred at 0 °C for 10 min, the reaction mixture was poured into a cold saturated aqueous $NaHCO_3$ solution (250 ml) and the resulting mixture was extracted with ethyl acetate (200 ml×1+100 ml×1). The extracts were washed with a saturated aqueous NaCl solution (150 ml), dried, and evaporated to give a yellow syrup (11.4 g). To a solution of this syrup in methanol (113 ml) was added dropwise 1 M† aqueous NaOH solution (113 ml) and the mixture was kept at room temperature for 3.5 h. The reaction mixture was then neutralized (pH 7) with CO_2 gas and evaporated. The residue was triturated with acetone and the insoluble matter was removed by filtration and the filter cake was washed with acetone. The combined filtrate and washings were evaporated and the residue was chromatographed on silica gel (260 g) with 1:2 toluene–ethyl acetate to afford **12** (9.06 g, 96%) as a colorless syrup: R_f=0.41 (1:2 toluene–ethyl acetate); $[\alpha]_D^{18}$ −29° (*c* 1.19, MeOH, after 2d); ^{1}H-NMR δ=1.10—1.30 (6H, m, 2×Me), 2.15—2.55 (1H, m, H-3), 2.60 (0.6H, d, α-OH, J=3.0 Hz), 3.19 (0.4H, br, β-OH-4), 3.44 (0.6H, d. α-OH, J=3.0 Hz), 3.55—4.20 (3H, m, H-2, 4, and 5), 4.04 (0.4H, d, β-OH-1, J=6.0 Hz), 4.55 and 4.65 (ABq, OC$\underline{H}_2$Ph, J_{gem}=12.0 Hz), 4.56 (s, OC$\underline{H}_2$Ph), 5.22 (0.4H, dd, β-H-1, $J_{1,2}$=4.5 Hz), 5.41 (0.6H, d, α-H-1, $J_{1,2}$=0 Hz), and 7.34 and 7.37 (each s, Ph).

Found: C, 66.92; H, 8.01%. Calcd for $C_{14}H_{20}O_4$; C, 66.64; H, 7.99%.

3-O-Benzyl-1,4,7-trideoxy-4-C-methyl-D-glycero-D-glucoheptitol (13). A solution of **12** (8.70 g, 34.5 mmol) in dry ether (25 ml) was added dropwise to an ice-cold stirred ether solution of methylmagnesium iodide [prepared from magnesium turnings (8.39 g, 345 mmol) and methyl iodide (21.5 ml, 345 mmol) in dry ether (84 ml)]. After being stirred at 35 °C for 20 h, a saturated aqueous NH_4Cl solution was carefully added to the ice-cold reaction mixture. The organic layer was separated and the aqueous layer was extracted with chloroform (300 ml×3). The combined organic layers were dried and evaporated to a syrup (9.52 g), which was chromatographed on silica gel (463 g) with 1:5 toluene–ethyl acetate to afford **13** (8.00 g, 86%) as a colorless syrup and unchanged **12** (0.72 g, 8.3%). **13**: R_f=0.33 (1:5 toluene–ethyl acetate); $[\alpha]_D^{17}$ +3°, $[\alpha]_{365}^{17}$ +18° (*c* 3.81); ^{1}H-NMR δ=0.90 (3H, d, Me, J=7.5 Hz), 1.14 (3H, d, Me, J=6.0 Hz), 1.21 (3H, d, Me, J=6.0 Hz), 1.70—2.00 (1H, m, H-4), 2.10—2.40, 2.40—2.70, and 2.90—3.15 (each 1H, each br, 3×OH), 3.55—4.15 (4H, m, H-2, 3, 5, and 6), 4.70 and 4.79 (each 1H, ABq, OC$\underline{H}_2$Ph, J_{gem}=12.0 Hz), and 7.40 (5H, s, Ph).

Found: C, 66.87; H, 8.93%. Calcd for $C_{15}H_{24}O_4$: C, 67.13; H, 9.02%.

(2S,3S,4S)-3-Hydroxy-2-methyl-4-pentanolide (14). A solution of $NaIO_4$ (82 mg, 0.38 mmol) in water (0.8 ml) was added to a solution of **13** (68.6 mg, 0.256 mmol) in acetone (0.69 ml) under ice-cooling. After being stirred for 20 min, the mixture was diluted with water and extracted with ether. The extracts were washed with a saturated aqueous NaCl solution, dried, and evaporated. The residual syrup (49.4 mg) was hydrogenolyzed in *t*-BuOH (0.98 ml) with palladium black at 28 °C for 40 min under bubbling with H_2 gas. The filtered solution was evaporated to a colorless syrup (29.2 mg), which was then oxidized with bromide (0.0148 ml, 0.287 mmol) in 50% aqueous dioxane (0.29 ml) at room temperature for 7.5 h. The reaction mixture was extracted with ethyl acetate, and the extracts were washed with saturated aqueous $Na_2S_2O_3$ and NaCl solutions, dried, and evaporated. The residue was chromatographed on silica gel (2 g) with 1:5 toluene–ethyl acetate to give **14** (13.8 mg, 46% from **13**) as a colorless oil. The ^{1}H-NMR spectrum of **14** was identical with that of the authentic sample.[5]

3-O-Benzyl-1,4,7-trideoxy-5,6-O-isopropylidene-4-C-methyl-D-glycero-D-gluco-heptitol (15). To an ice-cold stirred solution of **13** (8.00 g, 29.8 mmol) and DMP (7.30 ml, 59.6 mmol) in dry acetone (160 ml) was added dropwise concd H_2SO_4 (0.008 ml). After being stirred at 0 °C for 0.5 h, the reaction mixture was neutralized with solid Na_2CO_3. The insoluble matter was filtered and washed with acetone. The combined filtrate and washings were evaporated to afford a crude sample of **15** (8.30 g, 90%) as colorless needles. This sample was pure enough for the next step without further purification. An analytical sample was obtained after silica-gel column chromatography with 20:1 chloroform–acetone: mp 53—54 °C; R_f=0.88 (1:5 toluene–ethyl acetate); $[\alpha]_D^{15}$ +28° (*c* 0.79); ^{1}H-NMR δ=0.86 (3H, d, Me, J=6.6 Hz), 1.11 (3H, d,

†1 M=1 mol dm^{-3}.

Me, J=6.0 Hz), 1.16 (3H, d, Me, J=6.0 Hz), 1.30 and 1.45 (each 3H, each s, CMe_2), 1.60—2.00 (1H, m, H-4), 2.47 (1H, d, OH, J=3.0 Hz), 3.61 (1H, dd, H-3, $J_{3,4}$=2.0 Hz, $J_{2,3}$=7.5 Hz), 3.77 (1H, ddd, H-2, $J_{1,2}$=6.0 Hz), 4.06 (1H, dd, H-5, $J_{5,6}$=6.0 Hz, $J_{4,5}$=10.5 Hz), 4.25 (1H, dq, H-6, $J_{6,7}$=6.0 Hz), 4.71 and 4.79 (each 1H, ABq, $OC\underline{H}_2Ph$, J_{gem}=11.7 Hz), and 7.37 (5H, s, Ph).

Found: C, 70.06; H, 9.02%. Calcd for $C_{18}H_{28}O_4$: C, 70.10; H, 9.15%.

2-O-*Acetyl-3*-O-*benzyl-1,4,7-trideoxy-5,6*-O-*isopropylidene-4*-C-*methyl*-D-glycero-D-gluco-*heptitol* (**16**). To a solution of the crude sample of **15** (8.30 g, 26.9 mmol) in ethyl acetate (83 ml) were added acetic anhydride (3.81 ml, 40.4 mmol) and DMAP (3.45 g, 28.2 mmol). After being stirred at room temperature for 0.5 h, the reaction mixture was diluted with ethyl acetate (83 ml) and washed with water (50 ml) and a saturated aqueous NaCl solution (50 ml), dried, and evaporated. The residue was chromatographed on silica gel (283 g) with 5:1 toluene-ethyl acetate to afford **16** (9.30 g, 89% from **13**) as colorless crystals: mp 78—78.5 °C (plates from acetone-hexane); R_f=0.78 (2:1 toluene-ethyl acetate); $[\alpha]_D^{17}$ +3°, $[\alpha]_{365}^{17}$ +14° (c 5.72); IR (KBr) 1728 cm^{-1}; ^{1}H-NMR δ=0.87 (3H, d, Me, J=7.2 Hz), 1.11 (3H, d, Me, J=6.0 Hz), 1.20 (3H, d, Me, J=6.0 Hz), 1.27 and 1.45 (each 3H, each s, CMe_2), 1.70—2.00 (1H, m, H-4), 1.92 (3H, s, OAc), 3.85 (1H, dd, H-3, $J_{3,4}$=1.5 Hz, $J_{2,3}$=9.0 Hz), 4.05—4.45 (2H, m, H-5 and 6), 4.73 (2H, s, $OC\underline{H}_2Ph$), 5.12 (1H, dq, H-2, $J_{1,2}$=6.0 Hz), and 7.30 (5H, s, Ph).

Found: C, 68.48; H, 8.47%. Calcd for $C_{20}H_{30}O_5$: C, 68.54; H, 8.63%.

2-O-*Acetyl-1,4,7-trideoxy-5,6*-O-*isopropylidene-3*-O-*mesyl-4*-C-*methyl*-D-glycero-D-gluco-*heptitol* (**17**). A mixture of **16** (998 mg, 2.85 mmol), palladium black (freshly prepared from 1 g of palladium(II) chloride), ethyl acetate (9 ml), and methanol (1 ml) was vigorously stirred at 25 °C for 3.5 h under bubbling with H_2 gas, and the suspension was filtered. The filtrate was evaporated to a colorless syrup (741 mg, 100%), which was mesylated with mesyl chloride (0.661 ml, 8.54 mmol) in dry pyridine (7.4 ml) at room temperature for 2 h. The reaction mixture was poured into cold water (7.4 ml) and the resulting mixture was extracted with ethyl acetate (10 ml×3). The extracts were washed successively with saturated aqueous $KHSO_4$ (6 ml×5), $NaHCO_3$ (6 ml), and NaCl (6 ml) solutions, dried, and evaporated. The residue was chromatographed on silica gel (50 g) with 3:1 toluene-ethyl acetate to afford **17** (918 mg, 95%) as colorless crystals: mp 88—90 °C (needles from hexane); R_f=0.51 (3:2 toluene-ethyl acetate); $[\alpha]_D^{16}$ 0°, $[\alpha]_{365}^{16}$ −32° (c 1.48); IR (KBr) 1738 cm^{-1}; ^{1}H-NMR δ=0.93 (3H, d, Me, J=7.2 Hz), 1.14 (3H, d, Me, J=6.0 Hz), 1.27 (3H, d, Me, J=6.0 Hz), 1.33 and 1.44 (each 3H, each s, CMe_2), 1.75—2.10 (1H, m, H-4), 2.09 (3H, s, OAc), 3.04 (3H, s, OMs), 3.94 (1H, dd, H-5, $J_{5,6}$=6.0 Hz, $J_{4,5}$=10.5 Hz), 4.26 (1H, dq, H-6, $J_{6,7}$=6.0 Hz), and 5.00—5.40 (2H, m, H-2 and 3).

Found: C, 49.95; H, 7.48; S, 9.27%. Calcd for $C_{14}H_{26}O_7S$: C, 49.69; H, 7.74; S, 9.47%.

2,3-Anhydro-1,4,7-trideoxy-5,6-O-*isopropylidene-4*-C-*methyl*-D-glycero-D-allo-*heptitol* (**18**). To an ice-cold stirred solution of **17** (4.36 g, 12.9 mmol) in chloroform (43.6 ml) was added 3.23 M sodium methoxide in methanol (5.68 ml). After being stirred at 0 °C for 0.5 h, the reaction mixture was neutralized with CO_2 gas and poured into cold water (50 ml). The mixture was extracted with dichloromethane (30 ml×3) and the extracts were washed with a saturated aqueous NaCl solution (50 ml), dried, and evaporated. The residue was chromatographed on silica gel (75 g) with 3:1 benzene-ethyl acetate to afford oily **18** (2.32 g, 90%), which was subjected to bulb-to-bulb distillation to give a pure sample of **18** (2.09 g, 81%) as a colorless oil: bp 100—106 °C (bath temp)/8.5 Torr; R_f=0.42 (3:1 toluene-ethyl acetate); $[\alpha]_D^{15}$ +49° (c 0.77); ^{1}H-NMR δ=0.94 (3H, d, Me, J=6.0 Hz), 1.19 (3H, d, Me, J=6.0 Hz), 1.31 (3H, d, Me, J=6.0 Hz), 1.37 and 1.50 (each 3H, each s, CMe_2), 1.50—1.90 (1H, m, H-4), 2.83 (1H, dd, H-3, $J_{3,4}$=9.0 Hz, $J_{2,3}$=4.5 Hz), 3.00 (1H, dq, H-2, $J_{1,2}$=6.0 Hz), 3.98 (1H, dq, H-5, $J_{5,6}$=6.0 Hz, $J_{4,5}$=9.0 Hz), and 4.28 (1H, dq, H-6, $J_{6,7}$=6.0 Hz).

Found: C, 65.91; H, 9.87%. Calcd for $C_{11}H_{20}O_3$: C, 65.97; H, 10.07%.

2,4,7-Trideoxy-5,6-O-*isopropylidene-2,4-di*-C-*methyl*-D-glycero-D-allo-*heptose Trimethylene Dithioacetal* (**19**). To a cold (−40 °C) stirred solution of 1,3-dithiane 97% (4.26 g, 34.4 mmol) in dry THF (42.6 ml), 1.28 M butyllithium in hexane (26.9 ml, 34.4 mmol) was added dropwise under argon. After being stirred at −20 °C for 2 h, the mixture was recooled to −40 °C and a solution of **18** (1.38 g, 6.89 mmol) in dry THF (2.8 ml) was added dropwise to this stirred solution. After standing at 2 °C for 2 d, the reaction mixture was poured into cold water (70 ml) and the resulting mixture was extracted with chloroform (50 ml×3). The extracts were washed with water (50 ml) and a saturated aqueous NaCl solution (50 ml), dried, and evaporated. The residue was chromatographed on silica gel (200 g) with 2.5:1 hexane-ethyl acetate to afford **19** (2.05 g, 93%) as a colorless syrup: R_f=0.30 (2.5:1 hexane-ethyl acetate); $[\alpha]_D^{30}$ +16° (c 1.50); ^{1}H-NMR δ=0.91 (3H, d, Me, J=6.3 Hz), 1.12 (3H, d, Me, J=6.0 Hz), 1.14 (3H, d, Me, J=7.0 Hz), 1.30 and 1.41 (each 3H, each s, CMe_2), 1.70—2.50 (4H, m, H-2,4, and $SCH_2C\underline{H}_2CH_2S$), 2.70—3.20 (5H, m, OH and $SC\underline{H}_2CH_2C\underline{H}_2S$), 3.58 (1H, dd after addition of D_2O, J=4.5 and 7.5 Hz), 4.02 (1H, dd, H-5, $J_{4,5}$=10.0 Hz, $J_{5,6}$=6.0 Hz), 4.22 (1H, dq, H-6, $J_{6,7}$=6.0 Hz), and 4.57 (1H, d, H-1, $J_{1,2}$=3.0 Hz).

Found: m/z 320.1471. Calcd for $C_{15}H_{28}O_3S_2$: M, 320.1477.

Acetyl Derivative **20**. R_f=0.53 (3:1 hexane-ethyl acetate); $[\alpha]_D^{18}$ 0°, $[\alpha]_{365}^{18}$ 0° (c 0.33); IR (KBr) 1749 cm^{-1}; ^{1}H-NMR δ=5.11 (1H, dd, H-3, J=3.0 and 9.0 Hz).

Found: C, 56.24; H, 8.15; S, 17.44%. Calcd for $C_{17}H_{30}O_4S_2$: C, 56.32; H, 8.34; S, 17.69%.

3-O-*Benzyl-2,4,7-trideoxy-5,6*-O-*isopropylidene-2,4-di*-C-*methyl*-D-glycero-D-allo-*heptose Trimethylene Dithioacetal* (**21**). By the procedure described in the preparation of **9**, a sample of **19** (305 mg, 0.952 mmol) afforded, after silica-gel (19.5 g) column chromatography with 50:1 toluene-ethyl acetate, **21** (357 mg, 91%) as a pale yellow syrup. An analytical sample was obtained after silica-gel column chromatography with 50:1 toluene-ethyl acetate: R_f=0.70 (5:1 toluene-ethyl acetate); $[\alpha]_D^{15}$ −20° (c 1.02); ^{1}H-NMR δ=0.96, 1.09, and 1.12 (each 3H, each s, 3×Me, J=7.2, 6.0, and 7.5 Hz), 1.30 and 1.43 (each 3H, each s, CMe_2), 1.55—3.00 (8H, m, H-2, 4, and $SCH_2CH_2CH_2S$), 3.70 (1H, dd, H-3, J=2.1 and 10.2 Hz), 4.00—4.30 (2H, m, H-5 and 6), 4.60 (1H, d, H-1, $J_{1,2}$=2.7 Hz), 4.74 (2H, s, $OC\underline{H}_2Ph$), and 7.20—7.45 (5H, m, Ph).

Found: C, 64.19; H, 8.18; S, 15.26%. Calcd for $C_{22}H_{34}O_3S_2$: C, 64.35; H, 8.35; S, 15.62%.

3-O-*Benzyl-2,4-7-trideoxy-5,6*-O-*isopropylidene-2,4-di*-C-*methyl-aldehydo*-D-glycero-D-allo-*heptose* (**22**) *and Deisopropylidenation Heptopyranose* **23**. To a mixture of **21** (233 mg, 0.567 mmol) and mercury(II) oxide (540 mg, 2.49 mmol) in

aqueous 80% acetone (16.3 ml) was added mercury(II) chloride (677 mg, 2.49 mmol) at room temperature with efficient stirring. The mixture was stirred at 60 °C for 10 min, cooled, and filtered with a Celite. The filter cake was washed with acetone, and then the filtrate and washings were combined. After the subsequent removal of the acetone by concentration, the aqueous residue was extracted with chloroform (10 ml×3) and the extracts were washed with an aqueous 10% KI solution (8 ml×2) and a saturated aqueous NaCl solution (8 ml), dried, and evaporated. The residue was chromatographed on silica gel (9.1 g) with 20:1 toluene–ethyl acetate to afford **22** (118 mg, 65%) as a colorless syrup: R_f= 0.48 (20:1 toluene–ethyl acetate); ^{1}H-NMR δ=0.91, 1.11, and 1.14 (each 3H, each d, 3×Me, J=6.6, 6.0, and 7.0 Hz), 1.28 and 1.42 (each 3H, each s, CMe_2), 2.00—2.40 (1H, m, H-4), 2.60—3.00 (1H, m, H-2), 3.90—4.20 (2H, m, H-3 and 5), 4.23 (1H, dq, H-6, $J_{5,6}$=$J_{6,7}$=6.0 Hz), 4.53 and 4.63 (each 1H, ABq, $OC\underline{H}_2Ph$, J=12.0 Hz), 7.34 (5H, s, Ph), and 9.83 (1H, d, H-1, $J_{1,2}$=3.0 Hz). The elution of the silica-gel column with ethyl acetate gave **23** (42.6 mg, 27%) as a colorless syrup: R_f=0.37 and 0.46 (10:1 chloroform–methanol); ^{1}H-NMR δ=0.90—1.30 (9H, m, 3×Me), 1.40—2.00 (2H, m, H-2 and 4), 2.40—2.80 and 3.30—3.60 (each 1H, each br, 2×OH), 3.50—4.20 (3H, m, H-3, 5, and 6), 4.64 (2H, s, $OC\underline{H}_2Ph$), 4.80—5.20 (1H, m, H-1), and 7.36 (5H, s, Ph).

*Transformation of **23** into **22**.* To a solution of **23** (50 mg, 0.18 mmol) in 95% ethanol (0.5 ml) was added $NaBH_4$ (13.5 mg, 0.357 mmol) and the mixture was stirred at room temperature for 24 h. The reaction mixture was neutralized with CO_2 gas and then evaporated. The residue was taken up with chroloform and an insoluble matter was filtered off. The filter cake was washed with chroloform and the combined filtrate and washings were evaporated. The residue (50.4 mg, 100%) was dissolved in dry DMF (0.5 ml) and to this were added DMP (0.044 ml, 0.36 mmol) and *dl*-10-camphorsulfonic acid (4.1 mg, 0.018 mmol). The mixture was stirred at room temperature for 3 h and poured into a cold solution of 0.1 M aqueous NaOH. The mixture was extracted with ethyl acetate and the extracts were washed with a saturated aqueous NaCl solution, dried, and evaporated. The residue was chromatographed on silica gel (3 g) with 3:1 toluene–ethyl acetate to afford an alcohol. DMSO (0.0271 ml) was added to a solution of oxalyl dichloride (0.0164 ml, 0.191 mmol) in dry dichloromethane (0.83 ml) cooled to −60 °C. After being stirred at −60 °C for 15 min, a solution of the above alcohol (41 mg) in dry dichloromethane (0.32 ml) was added to the mixture and the new mixture was stirred at −60 °C for 15 min. After being added triethylamine (0.0881 ml, 0.636 mmol), the mixture was stirred at −25 °C for 15 min. Ether (2 ml) and water (2 ml) were added and the two layers were separated. The aqueous layer was extracted with ether and the combined organic layers were washed with a saturated aqueous NaCl solution, dried, and evaporated. The residue was chromatographed on silica gel (2 g) with 20:1 toluene–ethyl acetate to afford a syrup (37 mg, 67% from **23**). The ^{1}H-NMR spectrum and TLC of this sample were identical of them of **22**.

*8-O-Benzyl-3-C-(benzyloxymethyl)-3,5,7,9,12-pentadeoxy-1,2:10,11-di-O-isopropylidene-7,9-di-C-methyl-5-methylene-*D-glycero-D-allo-L-talo-*dodecofuranose-(1,4) (**24**).* To a cooled (−90—−95 °C) solution of 3-*C*-(benzyloxymethyl)-3,5,6-trideoxy-5-iodo-1,2-*O*-isopropylidene-α-D-ribo-5-hexenofuranose[2] (0.451 g, 1.08 mmol) in dry ether (10 ml) was added 1.48 M butyllithium in hexane (0.68 ml, 1.01 mmol) over a period of 5 min under argon. After being stirred at the same temperature for 0.5 h, a solution of **22** (0.116 g, 0.361 mmol) in dry ether (0.23 ml) was added to the mixture over a period of 2 min, and stirring was continued at the same temperature for 20 min. To the reaction mixture was added a saturated aqueous NH_4Cl solution, and the separated aqueous layer was extracted with ether. The organic layers were combined, washed with a saturated aqueous NaCl solution, dried, and evaporated. The residual yellow syrup (0.553 g) was chromatographed on silica gel (83 g) with 5:1 toluene–ethyl acetate to afford **24** (0.170 g) contaminated with a small amount of impurity. This was again chromatographed on silica gel (17 g) with 2.5:1 hexane–ethyl acetate to afford a pure sample of **24** (0.134 g, 61%) as a colorless syrup: R_f=0.19 (5:1 toluene–ethyl acetate); $[\alpha]_D^{18}$ +36° (*c* 0.69); ^{1}H-NMR δ= 0.91, 0.97, and 1.11 (each 3H, each d, 3×CMe, J=6.5, 7.5, and 6.0 Hz), 1.28, 1.32, 1.41, and 1.47 (each 3H, each s, 2×CMe_2), 2.00—2.55 (3H, m, H-3, 7, and 9), 2.88 (1H, br s, OH), 3.40—4.90 (12H, m, H-2,4,6,8,10,11, $C\underline{H}_2OBzl$, and 2×$OC\underline{H}_2Ph$), 5.30 and 5.37 (each 1H, each br s, C=CH_2), 5.81 (1H, d, H-1, $J_{1,2}$=3.3 Hz), 7.33 and 7.36 (each 5H, each s, 2×Ph).

Found: C, 70.81; H, 8.15%. Calcd for $C_{36}H_{50}O_8$: C, 70.79; H, 8.25%.

*8-O-Benzyl-3-C-(benzyloxymethyl)-3,5,7,9,12-pentadeoxy-1,2:10,11-di-O-isopropylidene-5,7,9-tri-C-methyl-*D-erythro-D-altro-L-talo-*dodecofuranose-(1,4) (**25**) and* D-allo *Epimer (**26**).* A solution of **24** (0.123 g, 0.201 mmol) and chlorotris(triphenylphosphine)rhodium(I) (0.0465 g, 0.0502 mmol) in benzene (6.1 ml) was stirred under an atmospheric pressure of hydrogen at room temperature for 4.5 h. The reaction mixture was then evaporated and the residue was passed through Florisil (100—200 mesh, 2.5 g) with ether and again evaporated. The residue was chromatographed on silica gel (16 g) with 4:1 toluene–ethyl acetate to afford **25** (0.117 g, 95%) and **26** (0.0047 g, 3.8%) as colorless syrups: **25**, R_f=0.29 (4:1 hexane–acetone); $[\alpha]_D^{26}$ +38° (*c* 0.75); ^{1}H-NMR (250 MHz) δ=0.78 (3H, d, 5-Me, J=6.5 Hz), 0.97 (3H, d, 9-Me, J=6.8 Hz), 0.99 (3H, d, 7-Me, J=6.8 Hz), 1.14 (3H, d, 3×H-12, J=6.5 Hz), 1.28, 1.32, 1.43, and 1.49 (each 3H, each s, 2×CMe_2), 1.70—1.80 (1H, m, H-5), 2.00—2.15 (1H, m, H-7), 2.15—2.30 (2H, m, H-3 and 9), 3.26 (1H, d, OH, J=2.3 Hz), 3.46 (1H, dd, one of $C\underline{H}_2$OBzl, J=5.3 Hz, J_{gem}=9.8 Hz), 3.71 (1H, dd, H-8, $J_{7,8}$=3.8 Hz, $J_{8,9}$=5.0 Hz), 3.79 (1H, dd, one of $C\underline{H}_2OBzl$, J=7.8 Hz, J_{gem}=9.8 Hz), 3.94 (1H, dd, H-10, $J_{9,10}$=10.5 Hz, $J_{10,11}$=5.0 Hz), 3.99 (1H, d, H-6, $J_{5,6}$=9.0 Hz, $J_{6,7}$=0 Hz), 4.22 (1H, dq, H-11), 4.37 (1H, dd, H-4, $J_{3,4}$=11.3 Hz, $J_{4,5}$=1.3 Hz), 4.46 and 4.67 (each 1H, ABq, $OC\underline{H}_2Ph$, J=12.0 Hz), 4.52 (2H, s, $OC\underline{H}_2Ph$), 4.70 (dd, H-2, $J_{1,2}$=$J_{2,3}$=3.5 Hz), 5.76 (1H, d, H-1), and 7.20—7.40 (10 H, m, 2×Ph).

Found: C, 70.05; H, 8.42%. Calcd for $C_{36}H_{52}O_8$: C, 70.56; H, 8.55%.

26, R_f=0.20 (4:1 hexane–acetone); ^{1}H-NMR (250 MHz) δ=0.94 and 1.00 (each 3H, each d, 7- and 9-Me, J=7.3 and 7.5 Hz), 1.08 (3H, d, 5-Me, J=7.3 Hz), 1.12 (3H, d, 3×H-12, J=6.5 Hz), 1.28, 1.32, 1.42, and 1.47 (each 3H, each s, 2×CMe_2), 1.90—2.05 (1H, m, H-5), 2.05—2.30 (3H, m, H-3, 7, and 9), 2.55 (1H, d, OH, J=3.8 Hz), 3.51 (1H, dd, one of $C\underline{H}_2$ OBzl, J=5.3 Hz, J_{gem}=10.0 Hz), 3.62 (1H, dd, H-8, J=3.5 and 6.5 Hz), 3.68 (1H, dd, one of $C\underline{H}_2OBzl$, J=10.0 Hz, J_{gem}=10.0 Hz), 3.84 (1H, dd, H-4, $J_{3,4}$=10.0 Hz, $J_{4,5}$=3.8 Hz), 3.94 (1H, ddd, H-6, $J_{5,6}$=6.3 Hz, $J_{6,7}$=2.5 Hz), 4.03 (1H, dd, H-10, $J_{9,10}$=10.0 Hz, $J_{10,11}$=5.0 Hz), 4.17 (1H, dq, H-11), 4.39 (2H,

s, OCH$_2$Ph), 4.56 and 4.67 (each 1H, ABq, OCH$_2$Ph, J=11.3 Hz), 4.66 (1H, dd, H-2, $J_{1,2}$=$J_{2,3}$=4.0 Hz), 5.68 (1H, d, H-1), and 7.20—7.40 (10H, m, 2×Ph).

*6,8-Di-O-Benzyl-3-C-(benzyloxymethyl)-3,5,7,9,12-pentadeoxy-1,2:10,11-di-O-isopropylidene-5,7,9-tri-C-methyl-*D-erythro-D-altro-L-talo-*dodecofuranose-(1,4) (27).* By the procedure described in the preparation of **9**, a sample of **25** (1.05 g, 1.71 mmol) afforded, after silica-gel column chromatography with 15:1 toluene–ethyl acetate, **27** (1.16 g, 97%) as a colorless syrup: R_f=0.26 (15:1 toluene–ethyl acetate); $[\alpha]_D^{30}$ −10° (*c* 1.86); ^{1}H-NMR δ=0.85, 0.93, 0.98, and 1.07 (each 3H, each d, 4×CMe, J=7.5, 7.5, 7.0, and 6.0 Hz), 1.29, 1.33, and 1.45 (3H, 6H, and 3H, each s, 2×CMe$_2$), 1.70—2.40 (4H, m, H-3, 5, 7, and 9), 3.30—4.40 [7H, m, H-4, 6, 8, 10, 11, and CH$_2$OBzl, including dd of 3.42 (1H, J=6.0 and 9.0 Hz)], 4.51 (4H, s, 2×OCH$_2$Ph), 4.50 and 4.77 (each 1H, ABq, OCH$_2$Ph, J_{gem}=12.0 Hz), 4.69 (1H, dd, H-2, $J_{1,2}$=$J_{2,3}$=3.9 Hz), 5.80 (1H, d, H-1), and 7.31 (15H, s, 3×Ph).

*6,8-Di-O-Benzyl-3-C-(benzyloxymethyl)-3,5,7,9,12-pentadeoxy-1,2-O-isopropylidene-5,7,9-tri-C-methyl-*D-erythro-D-altro-L-talo-*dodecofuranose-(1,4) (28).* A solution of **27** (1.21 g, 1.72 mmol) in 75 (v/v)% aqueous acetic acid (24 ml) was stirred at 50°C for 1.5 h, then evaporated. The residue was chromatographed on silica gel (36 g) with 2:1 toluene–ethyl acetate to afford **28** (1.11 g, 97%) as a colorless syrup: R_f=0.31 (2:1 toluene–ethyl acetate); $[\alpha]_D^{30}$ −27° (*c* 1.50); ^{1}H-NMR δ=0.85, 0.97, 1.04, and 1.16 (each 3H, each d, 4×CMe, J=7.5, 7.5, 6.0, and 6.0 Hz), 1.27 (6H, s, CMe$_2$), 1.60—2.35 (4H, m, H-3, 5, 7, and 9), 3.35—4.90 (10H, m, H-2, 4, 6, 8, 10, 11, CH$_2$ OBzl, and OCH$_2$Ph), 4.53 and 4.58 (each 2H, each s, 2×OCH$_2$ Ph), 5.78 (1H, d, H-1, $J_{1,2}$=3.0 Hz), 7.30 (10H, s, 2×Ph), and 7.33 (5H, s, Ph).

Found: C, 72.20; H, 7.92%. Calcd for $C_{40}H_{54}O_8$: C, 72.48; H, 8.21%.

*6,8-Di-O-Benzyl-3-C-(benzyloxymethyl)-3,5,7,9-tetradeoxy-1,2-O-isopropylidene-5,7,9-tri-C-methyl-*D-altro-β-L-talo-*decodialdofuranose-(1,4) (29).* To an ice-cold solution of **28** (0.933 g, 1.41 mmol) in acetone (9.3 ml) was slowly added a solution of $NaIO_4$ (0.904 g, 4.23 mmol) in water (9.0 ml). After being stirred at room temperature for 5 h, the mixture was diluted with water (9.0 ml) and saturated with NaCl. The mixture was extracted with ethyl acetate (15 ml×3) and the extracts were washed with a saturated aqueous NaCl solution, dried, and evaporated. The residue was chromatographed on silica gel (15 g) with 10:1 toluene–ethyl acetate to afford **29** (0.840 g, 97%) as a colorless syrup: R_f=0.51 (5:1 toluene–ethyl acetate); ^{1}H-NMR δ=0.80, 0.83, and 1.15 (each 3H, each d, 3×CMe, J=7.5, 7.2, and 6.3 Hz), 1.25 and 1.26 (each 3H, each s, CMe$_2$), 1.70—2.45 (3H, m, H-3, 5, and 7), 2.70—2.95 (1H, m, H-9), 3.35—4.35 [5H, m, H-4, 6, 8, and CH$_2$OBzl, including dd of 3.46 (1H, J=6.6 and 9.6 Hz) and d of 4.28 (1H, J=0 and 10.2 Hz)], 4.46 and 4.50 (each 1H, two center peaks of ABq, OCH$_2$Ph), 4.53 (2H, s, OCH$_2$Ph), 4.55 and 4.85 (each 1H, ABq, OCH$_2$Ph, J=12.0 Hz), 4.69 (1H, dd, H-2, $J_{1,2}$= $J_{2,3}$=3.3 Hz), 5.82 (1H, d, H-1), 7.35 (15H, s, 3×Ph), and 9.83 (1H, s, CHO).

*6,8-Di-O-benzyl-3-C-(benzyloxymethyl)-3,5,7,9,11-pentadeoxy-1,2-O-isopropylidene-5,7,9-tri-C-methyl-11-methylene-*L-glycero-D-altro-β-L-talo-*dodecodialdofuranose-(1,4) 12-(Diethyl Acetal) (30) and* D-glycero-D-altro-β-L-talo *Epimer (31).* To a solution of 2-bromo-3,3-diethoxy-1-propene (846 mg, 4.05 mmol) in dry THF (5.7 ml) cooled at −108—−110°C was added 1.40 M butyllithium in hexane (2.41 ml, 3.37 mmol) under argon. After being stirred at the same temperature for 15 min, a solution of **29** (832 mg, 1.35 mmol) in dry THF (2.5 ml) was added to the mixture and stirring was continued at the same temperature for 0.5 h. The reaction was quenched by adding a saturated aqueous NH_4Cl solution (5 ml) and the mixture was then extracted with ether (10 ml×3) at room temperature. The organic layer were washed with a saturated aqueous NaCl solution, dried, and evaporated. The residue was chromatographed on silica gel (150 g) with 9:1 toluene–ethyl acetate to afford **30** (592 mg, 58.8%) and **31** (351 mg, 34.8%) as colorless syrups: **30**, R_f=0.32 (9:1 toluene–ethyl acetate); ^{1}H-NMR δ=0.87, 0.99, and 1.02 (each 3H, each s, 3×CMe, J=6.6, 7.5, and 7.5 Hz), 1.15—1.30 (12H, m, 2×OCH$_2$Me and CMe$_2$), 1.80—2.40 (4H, m, H-3, 5, 7, and 9), 3.30—4.40 (10H, m, H-4, 6, 8, 10, 2×OCH$_2$Me, and CH$_2$ OBzl), 4.50—5.00 (8H, m, H-2, 12, and 3×OCH$_2$Ph), 5.30—5.50 (2H, m, C=CH$_2$), 5.80 (1H, d, H-1, $J_{1,2}$=4.5 Hz), and 7.32 (15H, s, 3×Ph).

31, R_f=0.23 (9:1 toluene–ethyl acetate); ^{1}H-NMR δ=0.84, 0.92, and 1.04 (each 3H, each s, 3×CMe, J=6.6, 7.0, and 7.0 Hz), 1.10—1.30 (12H, m, 2×OCH$_2$Me and CMe$_2$), 1.75—2.40 (4H, m, H-3, 5, 7, and 9), 3.30—4.40 (10H, m, H-4, 6, 8, 10, 2×OCH$_2$Me, and CH$_2$OBzl), 4.50—5.00 (8H, m, H-2, 12, and 3×OCH$_2$Ph), 5.35—5.50 (2H, m, C=CH$_2$), 5.80 (1H, d, H-1, $J_{1,2}$=4.5 Hz), and 7.30 and 7.34 (10H and 5H, each s, 3×Ph).

*6,8-Di-O-benzyl-3-C-(benzyloxymethyl)-3,5,7,9,11-pentadeoxy-1,2-O-isopropylidene-5,7,9,11-tetra-C-methyl-*L-erythro-D-altro-β-L-talo-*dodecodialdofuranose-(1,4) 12-(Diethyl Acetal) (32) and* D-threo-D-altro-β-L-talo *Epimer (33).* A solution of **30** (256 mg, 0.343 mmol) and chlorotris(triphenylphosphine)-rhodium(I) (79.4 mg, 0.0858 mmol) in benzene (13 ml) was stirred under an atmospheric pressure of hydrogen at room temperature for 1 d. The reaction mixture was then evaporated and the residue was passed through Florisil (100—200 mesh, 20 g) with ether and again evaporated. The residue was chromatographed on silica gel (45 g) with 4:1 hexane–acetone to afford **32** (212 mg, 82.7%), **32**+**33** (21.7 mg, 8.4%), and **33** (9.3 mg, 3.6%) as colorless syrups: **32**, R_f=0.28 (4:1 hexane–acetone); $[\alpha]_D^{29}$ −35° (*c* 0.97); ^{1}H-NMR δ=0.82, 0.85, 0.92, and 1.05 (each 3H, each d, 4×CMe, J=7.5 Hz), 1.20 (6H, t, 2×OCH$_2$Me, J=7.5 Hz), 1.27 (6H, s, CMe$_2$), 1.60—2.40 (5H, m, H-3, 5, 7, 9, and 11), 3.35—4.40 (10H, m, H-4, 6, 8, 10, 2×OCH$_2$Me, and CH$_2$OBzl), 4.50—5.00 (8H, m, H-2, 12, and 3×OCH$_2$Ph), 5.80 (1H, d, H-1, $J_{1,2}$=4.2 Hz), and 7.30 and 7.33 (10H and 5H, each s, 3×Ph).

Found: C, 72.20; H, 8.43%. Calcd for $C_{45}H_{64}O_9$: C, 72.16; H, 8.61%.

33, R_f=0.19 (4:1 hexane–acetone); ^{1}H-NMR δ=0.80—1.30 (24H, m, 8×CMe), 1.70—2.40 (5H, m, H-3, 5, 7, 9, and 11), 3.25—4.40 (10H, m, H-4, 6, 8, 10, 2×OCH$_2$Me, and CH$_2$-OBzl), 4.45—4.90 (8H, m, H-2, 12, and 3×OCH$_2$Ph), 5.82 (1H, d, H-1, $J_{1,2}$=3.6 Hz), and 7.32 and 7.37 (10H and 5H, each s, 3×Ph).

*6,8,10-Tri-O-acetyl-3-C-(acetoxymethyl)-3,5,7,9,11-pentadeoxy-1,2-O-isopropylidene-5,7,9,11-tetra-C-methyl-*L-erythro-D-altro-β-L-talo-*dodecodialdofuranose-(1,4) 12-(Diethyl Acetal) (3).* To a solution of **32** (362 mg, 0.484 mmol) in dry ether (7.25 ml) was added liquid ammonia (36 ml), and then lithium (270 mg, 39 mmol) was added under cooling (−78°C). After the mixture was stirred at the same temperature for 4 h, the excess lithium was destroyed by adding of solid NH_4Cl. The mixture was then diluted with ether and allowed to concentrate spontaneously. The residue was taken with ether

and the solution was washed with a saturated aqueous NaCl solution, dried, and evaporated. The residual colorless syrup (231 mg, 100%) of **34** was dissolved in ethyl acetate (2.3 ml) and to this were added acetic anhydride (0.365 ml, 3.86 mmol) and DMAP (354 mg, 2.90 mmol). After being stirred at room temperature for 4 h, the reaction mixture was diluted with ethyl acetate (5 ml) and washed with a saturated aqueous NaCl solution (3 ml), dried, and evaporated. The residue was chromatographed on silica gel (30 g) with 3:2 toluene–ethyl acetate to afford **3** (280 mg, 90%) as colorless needles. The ^{1}H-NMR spectrum, R_f-value on TLC, and mp of this sample were identical with those of the authentic sample.[2]

We are grateful to Prof. Sumio Umezawa, Institute of Bioorganic Chemistry, and Prof. Hamao Umezawa, Institute of Microbial Chemistry, for the generous support of our program. The authors wish to thank Mr. Saburo Nakada for carrying out the microanalyses, and Mr. Seiichi Sato for his early contribution to this project. Supports by the Ministry of Education, Science and Culture (Grant-in-Aid for special research) and the Asahi Glass Foundation for Contribution to Industrial Technology are deeply acknowledged.

References

1) Part VII: M. Nakata, S. Wada, K. Tatsuta, and M. Kinoshita, *Bull. Chem. Soc. Jpn.*, **58**, 1801 (1985).

2) M. Nakata, H. Enari, and M. Kinoshita, *Bull. Chem. Soc. Jpn.*, **55**, 3283 (1982).

3) M. Nakata, Y. Ikeyama, H. Takao, and M. Kinoshita, *Bull. Chem. Soc. Jpn.*, **53**, 3252 (1980).

4) T. D. Inch and G. J. Lewis, *Carbohydr. Res.*, **15**, 1 (1970).

5) M. Nakata, H. Takao, Y. Ikeyama, T. Sakai, K. Tatsuta, and M. Kinoshita, *Bull. Chem. Soc. Jpn.*, **54**, 1749 (1981).

6) J. Ficini and J. -C. Depezy, *Tetrahedron Lett.*, **1969**, 4797; A. B. Smith, III, P. A. Levenberg, P. J. Jerris, R. M. Scarborough, Jr., and P. M. Wovkulich, *J. Am. Chem. Soc.*, **103**, 1501 (1981).

Brillouin Scattering of Supercooled Liquids. II. Diisobutyl Phthalate

Shinobu KODA, Ryuki HASHITANI, and Hiroyasu NOMURA*
Department of Chemical Engineering, School of Engineering, Nagoya University, Chikusa-ku, Nagoya 464
(Received April 3, 1985)

The Brillouin scattering spectra of diisobutyl phthalate were measured over a wide range of temperatures. The sound velocity dispersion was observed in the GHz region in a temperature range between 240 and 340 K. We concluded that the sound dispersion of the sample was attributed to the structural relaxation of a supercooled liquid. The relaxation curve of the longitudinal modulus was obtained by a superposition method and could be analyzed using a generalized B.E.L. model with a parameter of $K=0.3$—0.5. The viscoelastic relaxation in the GHz region was found to have a narrower distribution of relaxation times than in the MHz region.

It is well known that molecules in a liquid state are in an ordered structure at local and very short separations. However, at the greater separations, this ordered structure becomes indistinct. Therefore, when a mechanical force is suddenly applied to liquids, they at first respond elastically, just as if they were solid bodies, but relax as viscoelastic bodies. In order to better understand local structures of liquids and solutions regarding molecular interaction forces, it is very important to know the relaxation mechanism of liquids and solutions under such external forces as mechanical and electrical. However, it has been roughly estimated that the structural relaxation times of ordinary liquids are of an order of 10^{-13} s. Because of their low viscosities, we can not measure the relaxation times directly by means of relaxation spectroscopy. In order to study the dynamic properties of liquids, supercooled liquids are suitable materials, since such liquids have a large viscosity coefficient and their characteristic relaxation times are so long that they fall within measurable frequency ranges. Our final goal is to determine the dynamic properties of liquids and solutions. Supercooled materials will present useful information.

Most investigations regarding the dynamic properties of supercooled liquids were carried out in the megahertz regions and relaxation curves were obtained by superimposing data at different temperatures on the basis of a reduced procedure. The Brillouin scattering method is also a very useful technique for studying the viscoelastic properties of liquids. It provides information about the dynamic properties of liquids in the GHz range. Scattering is due to local thermal density fluctuations in the liquid phase.

In our previous paper,[1] the sound velocities of tri-*o*-tolyl phosphate in the GHz region were measured using the Brillouin scattering method with wide scattering angles and temperature ranges. The relaxation curves of the obtained longitudinal modulus were expressed by the B. E. L. model. However, the K parameter, which involves a distribution of the relaxation times, was somewhat different from those obtained in the MHz region.

In this paper, we report on the experimental results of Brillouin scattering in diisobutyl phthalate for a wide range of temperatures. The molecular dimension and symmetry of diisobutyl phthalate are quite different from those of tri-*o*-tolyl phosphate which was previously investigated. Viscoelastic relaxation, obtained from sound dispersion curves in the GHz region, are discussed on the basis of a generalized B. E. L. equation for bulk and shear moduli and is compared with the results from the MHz region.[2] The temperature dependence of the K parameter in the generalized B. E. L. equation is also discussed.

Experimental

Diisobutyl phthalate, guaranteed grade, was obtained from Nakarai Chemicals Co., Ltd. The sample was distilled under reduced pressure at 4 mmHg†, and poured into a scattering cell by filtration using a millipore filter with a pore size of 1.0 μm.

The Rayleigh-Brillouin spectra were obtained with a pressure-scanning Fabry-Perot interferometer, using a He-Ne laser (NEC., GLG 5800, output 50 mW). Detailed descriptions of the apparatus and experimental procedures are given in previous papers.[1,3] Measurements were performed over a temperature range between 197 and 348 K for various scattering angles (30 to 150°). The accuracy of the sound velocity was within ±1.0%.

Velocities at 5 MHz were measured using an ultrasonic interferometer over a temperature range between 273 and 333 K. Ultrasonic absorption coefficients were also measured at a frequency of 5 MHz by the usual pulse method. The refractive indexes of the samples were measured using an Abbe refractometer between 258 and 318 K. Values at the lower and higher temperatures were estimated by extrapolating the temperature dependences of the velocity and the refractive index.

Results

Figure 1 shows the typical Rayleigh-Brillouin spectra of diisobutyl phthalate at a constant scattering angle, $\theta=90°$, as a function of temperature. The sound velocity, V, can be calculated from the values of the Brillouin frequency shift, $\Delta\omega$, and the scattering angle, θ, by the following relation;

$$V=\left(\frac{\Delta\omega}{\omega_0}\right)\frac{c}{2n\sin(\theta/2)}, \quad (1)$$

† 1 mmHg=133.322 Pa.

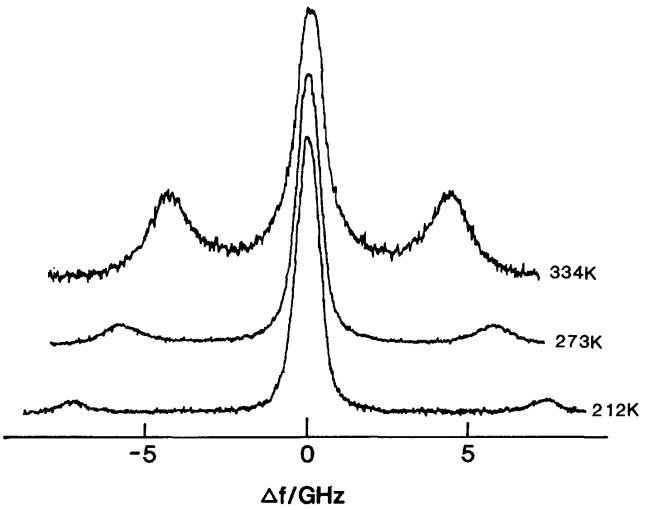

Fig. 1. Representative Brillouin spectra. (θ=90°).

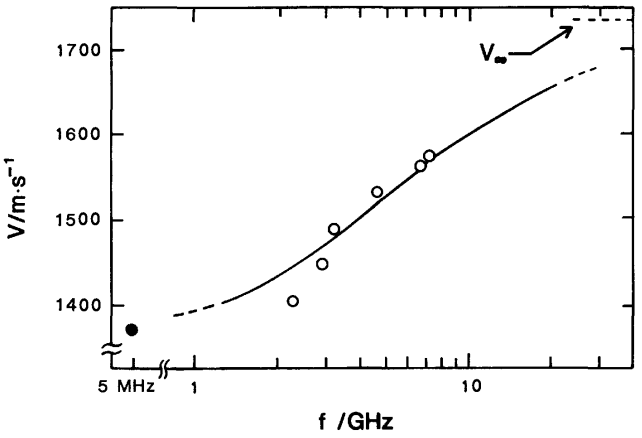

Fig. 2. Frequency dependence of the sound velocity at 298 K.
(○); Brillouin scattering method, (●) ; ultrasonic data (5 MHz).

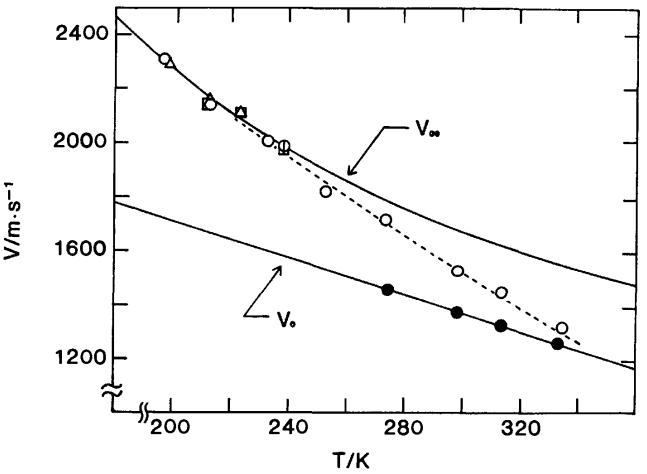

Fig. 3. Temperature dependence of the sound velocity.
(○); θ=90°, (□); θ=130°, (⊕); θ=140°, (△); θ=145°, (⊞); θ=150°, (●); ultrasonic data (5 MHz).

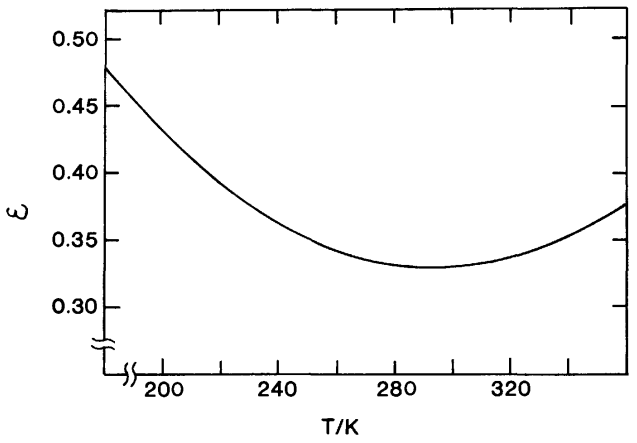

Fig. 4. Temperature dependence of the relaxation strength, ε.

where ω_0 is the frequency of the incident light, c the velocity of light, and n the refractive index of the sample.

Figure 2 shows a plot of the sound velocities against the frequencies at 298 K. The sound velocity dispersion was observed in the GHz region. The temperature dependence of the sound velocities, which were obtained at various scattering angles, is shown in Fig. 3. As can be seen, a clear sound velocity dispersion was obtained in the mid temperature range. In the low temperature region, below 238 K, although velocities were measured for various scattering angles, these velocities were independent of the scattering angles, that is, were independent of the frequencies. These velocities can be considered as those at the high frequency limit for various temperatures. The temperature dependence of the velocities at the high frequency limit, V_∞, can be represented by the following equation by analogy with the temperature dependence of the shear modulus.[2)]

$$V_\infty = \frac{a}{T(\mathrm{K})} + b. \quad (2)$$

The numerical values of a and b are 3.59×10^5 m s^{-1}·K and 479 m s^{-1}, respectively. Those were determined by a curve fitting method, using data from the lower temperature regions. For the low frequency limit of the sound velocity, V_0, values measured by an ultrasonic interferometer operating at 5 MHz were employed. The temperature dependence of V_0 can be expressed as V_0=−3.43 T(K)+2400.[2)]

Discussion

Generally, the origin of sound velocity dispersion in the GHz region is mainly ascribed to the following two relaxation processes. One is vibrational relaxation, which is due to an energy transfer from vibrational modes of a molecule to translational motion. The other is a viscoelastic relaxation, that is, structural relaxation.

The temperature dependence of the relaxation

strength, $\varepsilon=(V_\infty^2-V_0^2)/V_\infty^2$, is shown in Fig. 4. As can be seen, ε decreases with increasing temperature. If the velocity dispersion were due to vibrational relaxation, ε would increase with increasing temperature.[4] It might be, therefore, concluded that the observed sound velocity dispersion is not mainly due to vibrational relaxation, but to the viscoelastic relaxation. This is also true for tri-*o*-tolyl phosphate in the GHz region. This conclusion can be supported by taking into consideration the fact that observed value of $\varepsilon=0.331$ (at 298 K) is one order of magnitude larger than $\varepsilon=0.0315$ (at 298 K) estimated using the Planck-Einstein relation with frequencies of the vibrational modes.

At this stage, shear modulus data in the GHz region are not available by any method. Thus, longitudinal data cannot be divided into that related to the bulk and shear modulus, respectively, through the relation $M^*=K^*+4/3\,G^*$ (where K^* and G^* refer to the bulk and shear modulus respectively, and the superscript* refers to the complex modulus). Therefore, our data analysis was constrained to only longitudinal data, that is, M' (hereafter the real and imaginary parts of the complex are distinguished by ′ and ″, respectively).

The storage modulus, which is the real part of the complex longitudinal modulus M^*, can be estimated by $M'=\rho V^2$, where ρ is the density. According to a data analysis which was proposed by Lamb's school, a reduced plot of $(M'-M_0)/(M_\infty-M_0)$ against $\omega\eta_s/G_\infty$ was carried out and is shown in Fig. 5, where ω is the angular frequency ($\omega=2\pi f$). η_s/G_∞ ($=\tau_s$) corresponds to the relaxation time of the Maxwell element for a single relaxation, where η_s is the shear viscosity and G_∞ is the complex shear modulus at the high frequency limit. The temperature dependences of the viscosity and the density of the sample investigated here can be found in the literature.[5] The values of G_∞ at each temperature that were used were determined at an ultrasonic frequency at low temperatures.[5] As can be seen in Fig. 5, a master curve has been found in spite of the wide temperature and frequency ranges within the experimental error.

Assuming the generalized B. E. L. equation for K^* and G^*,[2] respectively, the expression for M^* is given as

$$\frac{M^*-M_0}{M_\infty-M_0}=C\left[1+\frac{1}{i\zeta\omega\tau_s}+2K\left(\frac{1}{i\zeta\omega\tau_s}\right)^{1/2}\right]^{-1}+(1-C)\left[1+\frac{1}{i\omega\tau_s}+2K\left(\frac{1}{i\omega\tau_s}\right)^{1/2}\right]^{-1}$$

$$C=\frac{K_\infty-K_0}{M_\infty-M_0}=1-\frac{4}{3}\frac{G_\infty}{M_\infty-M_0}$$

$$\zeta=\frac{\tau_v}{\tau_s}=\frac{\eta_v}{\eta_s}\frac{G_\infty}{M_\infty-M_0}=\frac{3}{4}\frac{\eta_v}{\eta_s}(1-C), \quad (3)$$

where K is an adjustable parameter for the broadness of the relaxation region. The K parameter is assumed to be the same for both shear and bulk relaxation processes.[2]

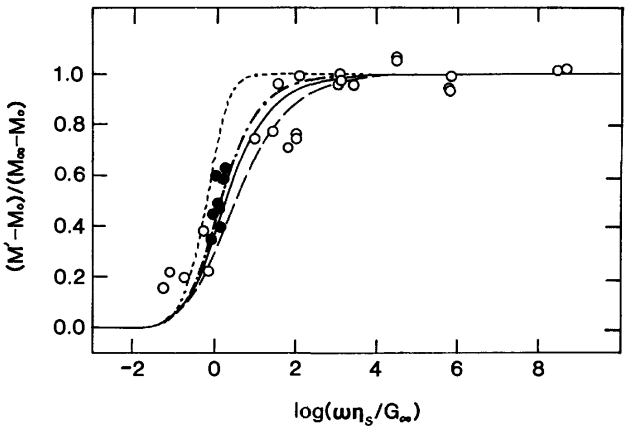

Fig. 5. Values of the normarized longitudinal modulus, $(M'-M_0)/(M_\infty-M_0)$ plotted as a function of $\log(\omega\eta_s/G_\infty)$.
(------); K=0, (—·—·-); K=0.3, (——); K=0.5, (— — —); K=1.0.
(●): Data at 25℃.

The value of C was estimated from data regarding the temperature dependence of the relaxation strength (Fig. 4) and G_∞'s which are also found in the literature.[5] C has a constant value of 0.35 in the low temperature range (from 197 to 300 K) but at higher temperatures, C increases slightly (C=0.40 at 320 K). The values of ζ can be estimated from data regarding η_v/η_s, which can be determined by measurements of the ultrasonic absorption coefficient at the low frequency limit, using the following equation.[2]

$$\lim_{\omega\to 0}\frac{\alpha}{\omega^2}=\frac{1}{2\rho v_0^3}(\eta_v+4/3\,\eta_s). \quad (4)$$

The obtained value of η_v/η_s is 2.64.

Calculated curves of $(M'-M_0)/(M_\infty-M_0)$ are drawn in Fig. 5 for K=0, 0.3, 0.5, and 1.0, by lines using Eq. 3 with the observed values of C and ζ. The curve with K=0 corresponds to that of the Maxwell model for a single relaxation. The curve with K=1.0 corresponds to the original B. E. L. equation and is in good agreement with those obtained in the MHz region for many supercooled liquids (as reported by Barlow *et al.*).[6-11] As can be seen in Fig. 5, the curve for K=1.0 is considerably broader than that obtained experimentally. The curve for K=0.3 and/or 0.5 reproduces the experimental values within experimental error. In the higher temperature region, that is, in the low frequency region, a deviation from the B. E. L. model was appeared. This deviation may be due to the rotational molecular motion of molecules in the liquid.

Previously,[1] we suggest that the relaxation curves of the longitudinal modulus for tri-*o*-tolyl phosphate in the GHz region could be reproduced by the B. E. L. model with a parameter of K=0.5. Therefore, both results for tri-*o*-tolyl phosphate and diisobutyl phthalate indicate the same tendency; that is, the longitudinal modulus obtained from the measure-

ments in the GHz region at various temperatures can be apparently composed with a master curve using the B. E. L. method, like that for the MHz region. However, the K parameter obtained from data in the GHz region was somewhat different from that in the MHz region. If the superposition procedure were to hold completely, the values of K which were obtained from data in the GHz and MHz regions should coincide with each other.

The solid circles in Fig. 5 represent the data obtained at a constant temperature of 298 K as a function of the frequency. According to the superposition procedure, these data for the GHz region at log $(\omega\eta_s/G_\infty)\simeq 0$ correspond to that around a frequency of 50 MHz at about 250 K. The data in the MHz region should correspond to the spectrum for $K=1.0$. On the other hand, as shown in Fig. 5, the data in the GHz region at 298 K do not coincide with the spectrum for $K=1.0$ and the data in the GHz region give a narrower relaxation spectrum than the spectrum for $K=1.0$. This fact clearly suggests that the distribution of the relaxation times at 298 K is different from that at 250 K.

At this stage, we would like to limit ourselves to pointing out that the distribution of the relaxation times of the longitudinal modulus of supercooled liquids may depend on the temperature. In order to confirm this fact more clearly, measurements over a frequency range between 300 and 700 MHz are needed. Work along this line is in progress and will be reported elsewhere.

References

1) S. Koda, H. Nomura, M. Nakamura, and Y. Miyahara, *Bull. Chem. Soc. Jpn.*, **58**, 1484 (1985).
2) G. Harrison, "The Dynamic Properties of Supercooled Liquids," Academic Press, London, (1976).
3) H. Nomura, H. Shimizu, Y. Tanaka, S. Koda, T. Okunishi, S. Kato, and Y. Miyahara, *Bull. Chem. Soc. Jpn.*, **55**, 3899 (1982).
4) For example, K. Takagi, and K. Negishi, *J. Appl. Phys.*, **16**, 1319 (1977).
5) A. J. Barlow, A. Erginsav, and J. Lamb, *Proc. Roy. Soc.*, **A 298**, 481 (1967).
6) J. Lamb, *Proc. Inst. Mech. Eng., Part 3*, **182**, 293 (1967).
7) A. J. Barlow, J. Lamb, A. J. Matheson, P. R. K. L. Padmini, and J. Richter, *Proc. Roy. Soc.*, **A298**, 467 (1967).
8) A. J. Barlow, A. Erginsav, and J. Lamb, *Proc. Roy. Soc.*, **A309**, 473 (1969).
9) A. J. Barlow and Erginsav, *Proc. Roy. Soc.*, **A327**, 175 (1972).
10) A. J. Barlow and R. P. Singth, *J. Chem. Soc., Faraday Trans. 2*, **68**, 1404 (1972).
11) A. J. Barlow, J. Lamb, and N.Ş. Taşköprülü, *J. Acoust. Soc. Am.*, **46**, 569 (1969).

Kinetic Study of the Thermal Decomposition of Isocyanic Acid in Shock Waves

Okitsugu KAJIMOTO,† Osamu KONDO, Kazuo OKADA, Jiro FUJIKANE, and Takayuki FUENO*
Department of Chemistry, Faculty of Engineering Science, Osaka University, Toyonaka, Osaka 560
(Received May 25, 1985)

Thermal decomposition of isocyanic acid HNCO diluted to less than 2.0 mol% in argon was studied behind incident shock waves over the temperature range 2100—2500 K. The decomposition course was followed by monitoring the light absorption of HNCO and NH($^3\Sigma^-$) at 206 and 336 nm, respectively. It is confirmed that the primary step of the decomposition is a bimolecular process HNCO+Ar→NH($^3\Sigma^-$)+CO+Ar, ΔH°_0=337 kJ mol^{-1}, with the low-pressure limit rate constants $k=10^{17.23\pm0.36}\exp[-(402\pm17)\text{ kJ mol}^{-1}/RT]$ cm^3 mol^{-1} s^{-1}. The siglet-to-triplet crossing point is estimated on the basis of the RRKM low-pressure-limit rate constant calculations. The overall decomposition mechanism is suggested and its validity is confirmed by computer simulation of the time-concentration profiles of NH($^3\Sigma^-$) at varying temperature.

Decomposition of isocyanic acid (HNCO) as a possible source of the imino radical (NH) has already been investigated by several groups of workers. Holland *et al.*[1] first photolyzed HNCO to observe a strong absorption by NH. Wooley and Back[2] found that the primary process of the HNCO photolysis at 206.2 nm involves the following two branches with nearly equal probabilities:

$$\text{HNCO} + h\nu \longrightarrow \begin{cases} \text{NH} + \text{CO} \\ \text{H} + \text{NCO} \end{cases}$$

Pyrolysis of HNCO was also studied by Back and Childs[3] at the temperature range 550—770 °C. Unfortunately, however, the overall decomposition process was so complex because of the secondary reactions as well as the surface effects that the kinetic features of even the primary step remained to be disclosed.

In the present investigation, isocyanic acid diluted in argon has been decomposed in incident shock waves over the temperature range 2100—2500 K. Time-resolved measurements of the light absorptions of both reactant and product radicals at elevated temperatures greatly facilitated kinetic studies of the decomposition. Of the following three conceivable initial steps of decomposition:

		ΔH°_0(kJ mol^{-1})[5,6]	
HNCO + Ar	→ NH($^1\Delta$) + CO + Ar	488	(1a)
	→ NH($^3\Sigma^-$) + CO + Ar	337	(1b)
	→ H + NCO + Ar	474	(1c)

the spin-forbidden reaction 1b has been concluded to be the most dominant, just as in the case of the hydrazoic acid (HN_3) decomposition studied previously.[4] The overall decomposition mechanism was inferred on this basis, and its validity was confirmed from the computer tracing of the time histories of the NH($^3\Sigma^-$) concentrations at varying temperature.

Experimental

(A) Materials. Isocyanic acid was synthesized by heating a mixture of potassium cyanate and stearic acid for 8 h on an oil bath at 95 °C. All the volatile substances were collected in a trap maintained at −196 °C. Impurities that remained were carbon dioxide and water, which were removed by successive trap-to-trap distillations at −60 °C and −20 °C. Purity of the resulting isocyanic acid was checked by the mass,[9] IR,[10] and UV[11] spectrometries.

Sample gases of various concentrations (0.1—2.0 mol%) were prepared by diluting isocyanic acid with high purity (99.999%) argon. They were allowed to stand in 10-l Pyrex bulbs for at least 10 h before use. No trace of polymerization of HNCO was perceived in these diluted gas samples.

(B) Kinetic Measurements. A stainless-steel shock tube of 10.4 cm diameter was used. The driver and driven sections were 2.0 and 3.0 m in length, respectively. A 25-l dump tank was attached to the end wall of the driven section in order to prevent the driven gas from being heated further by reflected shock waves. An involatile substance was found to be formed near the end of the driven section unless such a tank was used. The two sections were separated by a Mylar diaphragm of 0.10, 0.18, or 0.25 mm thickness. The bursting pressures of these Mylar sheets were *ca.* 4, 7, and 10 atm,[12] respectively. The driven section was evacuated to less than 2×10^{-5} Torr[12] before charging it with a gas sample. A diaphragm of selected thickness was used in combination with a driver gas, H_2 or He, of given driven pressures, so that the net pressure of the reaction zone could vary from 500 to 1500 Torr. The temperature, pressure, and density of shocked gas were calculated from the measured shock velocity by assuming an ideal shock behavior. Both the boundary layer effects and the effects of reaction heat were estimated to be unimportant under our experimental conditions.

The light absorption at 206.2±2.8 nm was utilized to follow the concentration of HNCO. A home-made microwave-operated I_2 lamp, together with a Bausch-Lomb MC-20 grating monochromator, was used to isolate the 206.2 nm atomic line. The NH($A^3\Pi$–$X^3\Sigma^-$) absorption was also followed at the wavelength 335.96±0.14 nm.[13] A 400-W Ushio high-pressure mercury lamp and a Rikotsusho MC-50 grating monochromator were used for this purpose. The wavelength scale of the monochromator was calibrated by using an NH lamp[14] which was microwave-operated on a flowing mixture of 1 Torr of ammonia and 4 Torr of argon.

The light which passed an appropriate optical path was collected on an EMI-9634Q photomultiplier. Its time-dependent output signal was amplified with a Keithley 102B amplifier and stored in a Kawasaki Electronica TM-1450

†Present address: Faculty of General Education, The University of Tokyo, Meguro-ku, Tokyo 153.

transient memory. The stored signal was displayed on an oscilloscope for photographing or on a pen recorder.

Results

(A) Kinetics of the HNCO Decay. In all experiments, the HNCO absorption increased abruptly upon the arrival of incident shock wave, and then decreased gradually with elapsing time. At the shock wave temperatures above 2500 K, the effects of unidentified emission were found to be inevitable. Below 2200 K, on the other hand, the absorption often showed an irregular increase, especially when the pressure of the reaction zone exceeded 1000 Torr. Observations of the HNCO decay were thus limited to the temperature range between 2200 and 2500 K.

At temperatures between 2200 and 2500 K, the observed HNCO decay signals were smooth enough and well reproducible. It is believed that the initial decays of HNCO observed in this temperature region are entirely due to its decomposition effected by the shock heating. This point was corroborated from the observations of the concurrent increase in concentration of the NH radicals as the primary decomposition product, as will be demonstrated shortly below.

The absorption coefficient of HNCO at each experimental temperature was evaluated from the absorbance extrapolated to time zero and the calculated initial post-shock concentration of HNCO. The absorption coefficients thus obtained were essentially constant at $(1.37\pm0.20)\times10^5$ $cm^2 mol^{-1}$ over the temperature range studied.

By use of the average absorption coefficient $\varepsilon = 1.37\times10^5$ $cm^2 mol^{-1}$, the absorbance-time records were converted into concentration-time curves. First-order plots of the HNCO concentration against the particle time t were satisfactorily linear during the initial 100 μs. The first-order rate constants k_{1st} obtained from such plots for several typical runs are listed in Table 1, together with the relevant shock parameters.

Plots of log k_{1st} against $1/T$ gave three separate straight lines which were parallel-shifted upward as the total pressure P_2 was increased stepwise (500, 900, and 1300 Torr). The second-order rate constants k_{2nd} were obtained by dividing k_{1st} by the post-shock argon concentration. The values of k_{2nd} obtained for typical runs are given in the final column of Table 1.

The Arrhenius plots of k_{2nd} were found to give a single straight line. Figure 1 shows such plots for a total of 22 runs. Evidently, the HNCO decay is in the low-pressure region under our experimental conditions. The least-squares treatment of all the data given in Fig. 1 resulted in the following Arrhenius expression:

$$k_{2nd} = 10^{17.23\pm0.36} \exp[-(402\pm17)\text{kJ mol}^{-1}/RT] \quad \text{cm}^3\,\text{mol}^{-1}\,\text{s}^{-1}. \quad (1)$$

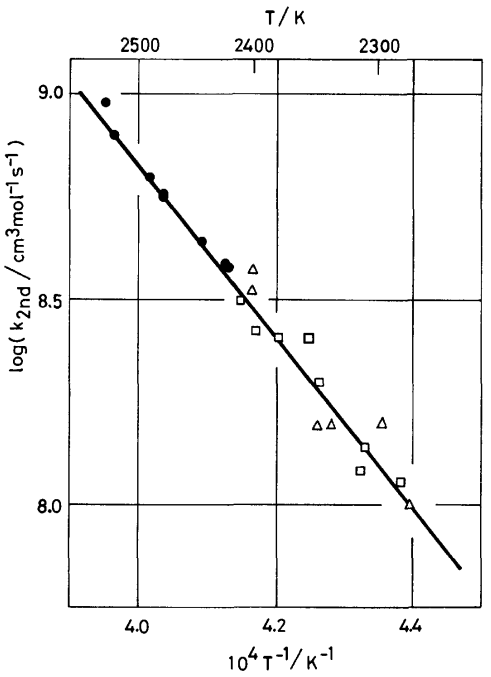

Fig. 1. Arrhenius plots of the second-order rate constants (k_{2nd}) for the decay of HNCO. The approximate Total pressures and the concentrations of HNCO in Ar were as follows: ●, 500 Torr, 2.0 mol%; □, 900 Torr, 0.5 mol%; △, 1350 Torr, 0.5 mol%.

Table 1. Rate data for the shock wave decomposition of HNCO

m	P_2	ρ_{21}	T_2	[Ar]	$[HNCO]_0$	k_{1st}	k_{2nd}
mol%	Toor		K	10^{-6} mol/cm^3	10^{-8} mol/cm^3	10^3 s^{-1}	10^8 cm^3 mol^{-1}s^{-1}
2.00	494	3.57	2523	3.07	6.27	2.41	7.86
2.00	511	3.56	2489	3.23	6.59	2.00	6.20
2.00	520	3.56	2478	3.30	6.73	1.95	5.61
2.00	528	3.55	2421	3.43	7.00	1.30	3.77
0.500	880	3.54	2411	5.82	2.93	1.83	3.14
0.500	892	3.53	2346	6.07	3.05	1.20	1.98
0.500	933	3.52	2282	6.52	3.28	0.735	1.13
0.500	1316	3.54	2401	8.75	4.50	3.20	3.66
0.500	1378	3.53	2337	9.41	4.73	1.48	1.57
0.500	1346	3.51	2275	9.44	4.74	0.965	1.02

TABLE 2. DATA FOR THE OBSERVATION OF THE $NH(^3\Sigma^-)$ ABSORPTION

m	P_2	ρ_{21}	T_2	[Ar]	$[HNCO]_0$	k_{1b}
mol%	Toor		K	10^{-6} mol/cm^3	10^{-8} mol/cm^3	10^8 cm^3 mol^{-1} s^{-1}
0.491	573	3.505	2230	4.12	2.02	0.532
0.498	555	3.471	2081	4.28	2.13	0.105
0.201	528	3.554	2526	3.35	0.674	8.78
0.201	516	3.536	2425	3.41	0.684	3.56
0.200	532	3.526	2281	3.94	0.788	0.902
0.200	996	3.495	2209	7.23	1.45	0.465
0.200	1052	3.469	2108	8.01	1.60	0.169
0.100	1375	3.546	2479	8.90	0.890	4.11
0.100	1469	3.503	2240	10.5	1.05	0.689
0.100	1523	3.490	2206	11.1	1.11	0.369

(B) Rate Constants for the $NH(^3\Sigma^-)$ Formation. Observation of the $NH(^3\Sigma^-)$ absorption at 336 nm was feasible at reaction temperatures down to 2100 K. At any temperature between 2100 and 2500 K, the absorption started up sharply upon the arrival of the incident shock. It increased monotonously until it reached a maximum, beyond which it decreased gradually. As the reaction temperature was raised, the absorption increased more abruptly, thus reaching its maximum in a shorter time interval and then decreasing faster. The maximum absorption became larger correspondingly. These qualitative features of absorption suffice to indicate an initial production of $NH(^3\Sigma^-)$ by the shock heating, followed by its decay due to subsequent reactions with coexistent species.[15]

The rates of the $NH(^3\Sigma^-)$ formation were evaluated from the initial slope of the absorption-time profile, assuming the average absorption coefficient $\varepsilon=1.0\times10^7$ cm^{2}mol^{-1} for $NH(^3\Sigma^-)$.[4] The resulting rates were divided by the concentration product of Ar and HNCO, to obtain the second-order rate constant k_{1b}. The values of k_{1b} thus obtained for some representative runs are given in Table 2, together with the shock parameters.

Figure 2 shows the Arrhenius plots of k_{1b} obtained for a total of 31 runs. Irrespective of the total pressure ranging from 500 to 1500 Torr, all the experimental points are seen to be fitted by a single straight line. The results indicate that the unimolecular decomposition of HNCO into $NH(^3\Sigma^-)$+CO is in the low-pressure limit. The least-squares treatment of the data gave the following Arrhenius expression:

$$k_{1b} = 10^{17.38\pm0.29}\exp[-(412\pm13)\text{kJ mol}^{-1}/RT]\ \text{cm}^3\,\text{mol}^{-1}\,\text{s}^{-1}. \quad (2)$$

Shown with a dotted line in Fig. 2 is the k_{2nd}, Eq. 1. The essential agreement between these two lines can be taken as a strong indication that HNCO decomposes mostly into $NH(^3\Sigma^-)$+CO.

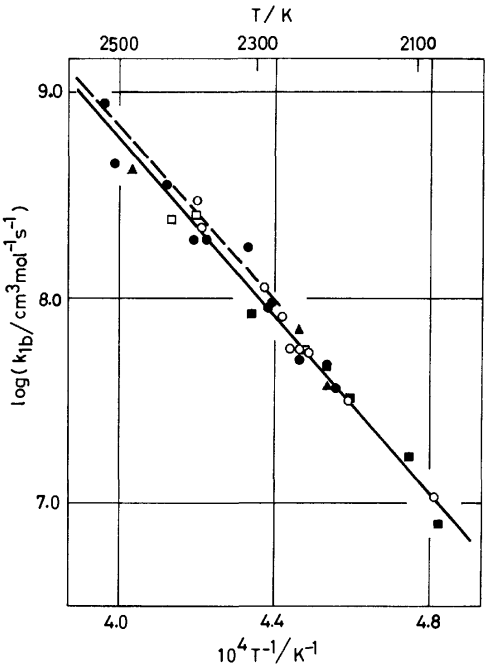

Fig. 2. Arrhenius plots of the second-order rate constants (k_{1b}) for HNCO+Ar→$NH(^3\Sigma^-)$+CO+Ar determined from the initial slope of the $NH(^3\Sigma^-)$ absorption. The approximate total pressures and the concentrations of HNCO in Ar were as follows: ○, 550 Torr, 0.5 mol%; ●, 550 Torr, 0.2 mol%; ■, 1000 Torr, 0.2 mol%; □, 1000 Torr, 0.1 mol%; △, 1500 Torr, 0.1 mol%. The rate constant of HNCO disappearance, k_{2nd}, is also shown with a dotted line.

Discussion

(A) Primary Decomposition Step. The close agreement between k_{2nd} and k_{1b} strongly suggests that HNCO is decomposed into $NH(^3\Sigma^-)$ and CO. The decomposition step is evidently bimolecular in type at least under our experimental conditions. The low-pressure limit behavior in the ordinary pressure regime has also been reported for other four-atomic molecules such as HN_3,[4] NH_3,[16] C_2N_2,[17,18] H_2O_2,[19] and SO_3,[20] diluted in inert gas.

The activation energy of k_{2nd}, E_a=402 kJ mol^{-1}, is noticeably greater than the heat of reaction ΔH°_0=337 kJ mol^{-1} for the triplet path 1b but is clearly smaller than the heat of reaction ΔH°_0=488 kJ mol^{-1} for the singlet path 1a. Similar situations have been noted in the thermal decompositions of HN_3[4] and N_2O,[21]

where the observed activation energies are in between the heats of reaction for the lowest triplet path and the higher singlet path.

In order to estimate the threshold energy for reaction 1b, we have undertaken RRKM calculations of the low-pressure limit rate constants:

$$k^{\mathrm{RRKM}} = (\lambda Z/Q_{\mathrm{v}})\exp(-E_0/RT)\int_0^{\infty} N(\varepsilon+E_0)\exp(-\varepsilon/RT)\mathrm{d}\varepsilon. \quad (3)$$

The various symbols appearing in Eq. 3 have their usual meanings.[22]

In calculating k^{RRKM}, we adopted the Whitten-Rabinovitch approximation[23] to $N(\varepsilon+E_0)$. The collision diameter between HNCO and Ar was assumed to be 0.39 nm. The six vibrational normal-mode frequencies of HNCO were all taken from the literature:[8] 3535, 2274, 1327, 808.0, 672.5, and 563.5 cm^{-1}.

We first calculated the k^{RRKM} as the functions of E_0 and T. Then we searched for a value of E_0 such that the observed temperature dependence of $k_{2\mathrm{nd}}$ (Eq. 1) was best reproduced. For the sake of simplicity, we neglected possible minor temperature dependence of the collisional efficiency λ. The best fit was achieved when we chose E_0=439 kJ mol^{-1}. The resulting RRKM rate constant was

$$k^{\mathrm{RRKM}} = \lambda 10^{17.76}\exp(-402\mathrm{kJ\ mol^{-1}}/RT)\ \mathrm{cm^3\ mol^{-1}s^{-1}}. \quad (4)$$

Comparison of Eq. 4 with Eq. 1 leads to the collisional efficiency λ=0.30. The λ value thus obtained does not seem to be unreasonable in view of the fact that the decompositions of most four-atomic molecules take on λ of the order of 0.1.[24] In addition, the critical energy E_0=439 kJ mol^{-1} of our choice suggests that the singlet and triplet potential energy curves cross each other at 102 kJ mol^{-1} *above* the zero point energy level of $NH(^3\Sigma^-)$+CO. The situation is very similar to the case of HN_3.[4] The schematic potential energy diagrams for both cases are compared in Fig. 3.[25]

The critical energy E_0 for reaction 1b is smaller than the heats of reaction for paths 1a and 1c by 49 and 35 kJ mol^{-1}, respectively. Because reaction 1b of our major concern is found to be in the low-pressure limit region, the contributions of 1a and 1c to the decomposition are likely to be negligible under the experimental conditions adopted in this work.[26]

(B) Overall Decomposition Mechanism. On the basis of the previously reported results on the photolysis of HNCO[27,28] as well as the mechanism proposed for the pyrolysis of HN_3,[4] we here assume the overall mechanism of the HNCO thermal decomposition to be such as follows:

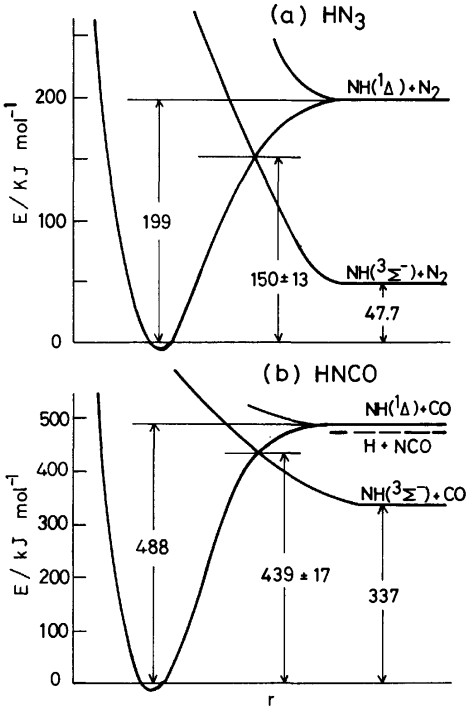

Fig. 3. Schematic potential energy curves of HN_3 (a) and HNCO(b).

		ΔH°_0(kJ mol^{-1})[5,6]
$HNCO+Ar$	$\xrightarrow{1b}$ $NH(^3\Sigma^-)+CO+Ar$	337
$NH(^3\Sigma^-)+HNCO$	$\xrightarrow{2}$ NH_2+NCO	99
$H+HNCO$	$\xrightarrow{3}$ NH_2+CO	−38
NH_2+HNCO	$\xrightarrow{4}$ NH_3+NCO	26
$2NH(^3\Sigma^-)$	$\xrightarrow{5}$ N_2+2H	−272
$2NH_2(+Ar)$	$\xrightarrow{6}$ $H_2NNH_2(+Ar)$	−277
$H+NH_2+Ar$	$\xrightarrow{7}$ NH_3+Ar	−448
$2H+Ar$	$\xrightarrow{8}$ H_2+Ar	−432
$NH(^3\Sigma^-)+NH_2(+Ar)$	$\xrightarrow{9}$ $HNNH_2(+Ar)$	−361
$H+HNNH_2$	$\xrightarrow{10}$ $2NH_2$	−34
$2NCO$	$\xrightarrow{11}$ N_2+2CO	−546

In order to examine the validity of this mechanism, the simultaneous kinetic equations for the various species involved were solved numerically (GEAR method) on a computer. Specifically, we aimed at comparing the calculated time-concentration profiles of $NH(^3\Sigma^-)$ with the observed ones at varying temperature. The rate constants used for computations are summarized in Table 3. Most of these data were either taken directly from the literature[29-31] or estimated judiciously by the procedures analogous to those delineated previously for the case of HN_3.[4]

The time-concentration profiles of $NH(^3\Sigma^-)$ were

TABLE 3. RATE CONSTANTS USED FOR COMPUTER SIMULATION OF THE HNCO DECOMPOSITION

Reaction	Rate constant ($cm^3\,mol^{-1}\,s^{-1}$)	Reference
1b	$k_{1b}=10^{17.23}\exp(-402\,kJ\,mol^{-1}/RT)$	This work
2	$k_2=10^{11.5}\exp(-106\,kJ\,mol^{-1}/RT)$	a)
3	$k_3=10^{11}$	a)
4	$k_4=10^{11.5}\exp(-50\,kJ\,mol^{-1}/RT)$	a)
5	$k_5=2.0\times10^{13}$	b)
6	$k_6=1.5\times10^{13}$	29)
7	$k_7=2.2\times10^{15}$ [Ar]	30)
8	$k_8=6.5\times10^{17}\,T^{-1}$ [Ar]	31)
9	$k_9=1.5\times10^{13}$	a)
10	$k_{10}=10^{11}$	a)
11	$k_{11}=10^{12}$	a)

a) Estimated, b) Adjusted.

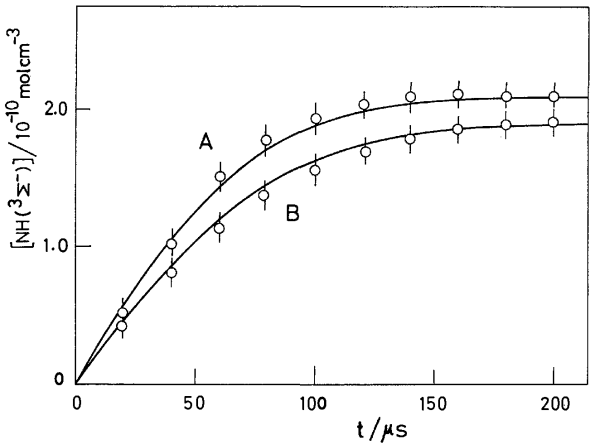

Fig. 4. Comparisons of the computed NH($^3\Sigma^-$) concentration profiles (——) with the observed (O): (A)NHCO=0.20 mol%, T_2=2281 K, P_2=532 Torr; (B) HNCO=0.20 mol%, T_2=2108 K, P_2=1052 Torr. The vertical lines indicate the range of uncertainty due to the low S/N ratio.

found to be governed by the rates of the initial process 1b and the NH "recombination" reaction 5. The rate constants for reactions 6—8, 10, and 11 had virtually no effects on the calculated profiles. In practice, we adopted k_{2nd} (Eq. 1) rather than k_{1b} (Eq. 2) as the rate constant for reaction 1b since there may well exist some uncertainty in the absorption coefficient of NH($^3\Sigma^-$). The rate constant of reaction 5 was most influential in the determination of the position as well as the height of the peak of the calculated profiles. We thus adjusted the value of k_5 so as to best reproduce the observed profiles of NH($^3\Sigma^-$) at various temperatures studied. The best fit was obtained when k_5 was taken to be constant at 2×10^{13} $cm^3\,mol^{-1}\,s^{-1}$ within the temperature range studied. This value agrees well with 2.5×10^{13} $cm^3\,mol^{-1}\,s^{-1}$ adopted previously.[4]

Figure 4 shows examples of the calculated time histories of the NH($^3\Sigma^-$) concentration. Circles shown in Fig. 4 are the concentrations calculated from the observed absorption profiles of NH($^3\Sigma^-$) by using $\varepsilon=1.0\times10^7$ $cm^2\,mol^{-1}$ as the absorption coefficient of NH($^3\Sigma^-$). Agreements between the calculated curves and the observed are satisfactory. The results lend strong support not only to the overall decomposition mechanism assumed but also to the various assumptions invoked as well as the experimental techniques adopted in the present work.

In conclusion, the primary process of the shock-wave decomposition of HNCO in argon at the total pressure range 550—1500 Torr is a bimolecular reaction, giving rise exclusively to NH($^3\Sigma^-$). The activation energy E_a=402 kJ mol^{-1} for this "triplet" process is evidently higher than its heat of reaction $\Delta H°_0$=337 kJ mol^{-1}, indicating that the singlet-triplet potential-energy curve crossing occurs at a level above the dissociation limit. The kinetic behavior is found to conform to the RRKM theory in the low-pressure limit.

This work was supported in part by the Grant-in-Aid for Scientific Research No. 59030074 from the Ministry of Education.

References

1) R. Holland, R. N. Dixon, D. A. Ramsay, and D. W. G. Style, *Nature*, **182**, 336 (1958).

2) W. D. Wooley and R. A. Back, *Can. J. Chem.*, **46**, 295 (1968).

3) R. A. Back and J. Childs, *Can. J. Chem.*, **46**, 1023 (1968).

4) O. Kajimoto, T. Yamamoto, and T. Fueno, *J. Phys. Chem.*, **83**, 429 (1979).

5) The heats of reaction, $\Delta H°_0$, given in this paper are all based primarily on the relevant heat-of-formation data taken from S. W. Benson, "Thermochemical Kinetics," 2nd ed., John Wiley, New York (1976).

6) Piper[7] reviewed the thermochemical data on the heat of formation for the NH radical critically, concluding that the value given in JANAF Table,[8] 377 kJ mol^{-1} for $\Delta H°_{f0}$, must be lowered to 352 kJ mol^{-1}. In the present paper, all the thermochemical values pertaining to the NH radical have been based on this new value.

7) L. G. Piper, *J. Chem. Phys.*, **70**, 3417 (1979).

8) D. R. Stull and H. Prophet, "JANAF Thermochemical Tables," 2nd ed, Nationsl Bureau of Standards, Washington, D. C. (1971).

9) J. Y. P. Mui and R. A. Back, *Can. J. Chem.*, **41**, 826 (1963).

10) G. Herzberg and C. Reid, *Disc. Faraday Soc.*, **9**, 92

(1950).

11) R. N. Dixon and G. H. Kirby, *Trans. Faraday Soc.*, **64**, 2002 (1968).

12) 1 atm=101325 Pa and 1 Torr=(1/760) atm.

13) J. M. Lentz, *J. Quant. Spectrosc. Radiant Transfer*, **13**, 297 (1973).

14) I. Hansen, K. Höninghaus, C. Zetzsch, and F. Stuhl, *Chem. Phys. Lett.*, **42**, 370 (1976).

15) These features alone can by no means rule out the possibility that HNCO is first decomposed to give rise to $NH(^1\Delta)$, which is then rapidly quenched to $NH(^3\Sigma^-)$ on collisions with the reactant HNCO. In our previous investigation of the HN_3 decomposition,[4] we considered such a process beside the process giving $NH(^3\Sigma^-)$ directly. However, the conclusion was that the triplet path was evidently preponderant over the singlet path under the experimental conditions adopted there. Whether or not the triplet path is the major step of the initial decomposition in the present HNCO case also, is to be judged cautiously from the magnitudes as well as the temperature dependences of the rate constants observed for both the HNCO decay and the $NH(^3\Sigma^-)$ production.

16) K. W. Michael and H. Gg. Wagner, Proceeding of the 10th Internat. Symp. Combust., **1964**, 353 (1965).

17) W. Tsang, S. H. Bauer, and M. Cowperthwait, *J. Chem. Phys.*, **36**, 1768 (1962).

18) T. Fueno, K. Tabayashi, and O. Kajimoto, *J. Phys. Chem.*, **77**, 575 (1973).

19) H. Kijewski and J. Troe, Int. *J. Chem. Kinet.*, **3**, 223 (1971).

20) D. C. Astholz, K. Glänzer, and J. Troe, *J. Chem. Phys.*, **70**, 2409 (1979).

21) J. Troe and H. Gg. Wagner, in "Physical Chemistry of Fast Reactions," ed by B. P. Levitt, Plenum Press, London (1973), Vol. 1, p. 1.

22) P. J. Robinson and K. A. Holbrook, "Unimolecular Reactions," Willey-Interscience, London (1972).

23) G. Z. Whitten and B. S. Rabinovitch, *J. Chem. Phys.*, **38**, 2466 (1963).

24) The formal spin "forbiddenness" of the present triplet reaction should not be taken literally as such. Even though the spin is certainly not conserved during the decomposition, the reaction is in reality a unimolecular process in its low-pressure limit, where the thermal activation step is rate-controlling. The activation step itself would not necessarily involve the spin conversion.

25) The thermochemical values used in our previous study of HN_3 decomposition[4] have been recalculated according to Piper's heat of formation for NH,[6] and the values thus modified are given in Fig. 3(a).

26) The RRKM rate constants calculated for reactions 1a and 1c are indeed an order of magnitude smaller than the observed rate constants (1) and (2).

27) R. A. Back, *J. Chem. Phys.*, **40**, 3493 (1964).

28) N. J. Friswell and R. A. Back, *Can. J. Chem.*, **46**, 527 (1968).

29) P. V. Khe, J. C. Soulignac, and R. Lesclaux, *J. Phys. Chem.*, **81**, 210 (1977).

30) S. Gordon, W. Mulac, and P. Nangia, *J. Phys. Chem.*, **75**, 2087 (1971).

31) D. L. Baulch, D. D. Drysdale, D. G. Horne, and A. C. Lloyd, "Evaluated Kinetic Data for High Temperature Reactions," Butterworths, London (1972) Vol. 1.

Photoionization Study of the Sulfur Monoxide Radical Produced by Pyrolysis of Ethylene Sulfoxide

Eisuke NISHITANI, Kenichi FUKUDA, and Ikuzo TANAKA*
Department of Chemistry, Tokyo Institute of Technology Ohokayama, Meguro-ku, Tokyo 152
(Received June 10, 1985)

Sulfur monoxide (SO) radical has been produced in the gas phase by pyrolysis of ethylene sulfoxide (C_2H_4=SO) at 510 °C. The vacuum ultraviolet photoionization efficiency curve between 915 and 1220 Å has been obtained for the first time. Several thermodynamic data about C_2H_4=SO have also been obtained from direct photoionization. The values of the bond energies of $D_0(C_2H_4$=SO) and $D_0(C_2H_4$=SO^+) are 4640±30 and 5160±30 cm^{-1} respectively. Ionization potentials (IP) of the SO($X^3\Sigma^-$) radical and C_2H_4=SO, and the appearance potential (AP) of SO^+ fragment ion from C_2H_4=SO are 10.28±0.01, 9.49±0.02, and 10.13±0.01 eV. In the system of C_2H_4=SO, the AP is lower than the IP and this phenomenon has only been found in this system.

The sulfur monoxide (SO) radical has been studied as an important intermediate in reactions involving oxygen atoms and molecules containing sulfur. It has also been found in interstellar space by radio telescopes.[1] In addition, the SO radical is a very interesting radical from the point of electronic structure because of the isoelectronic species of diatomic sulfur (S_2) and molecular oxygen (O_2). In contrast to the large amount of spectroscopic data obtained for O_2, SO, and S_2 in several low-lying electronic states,[2] our current knowledge concerning the SO radical in the vacuum ultraviolet region is very limited. Though autoionization in radicals has been rarely observed in this region so far, it is expected that the autoionization peaks might appear in the SO radical because of the similarity to O_2.

Since the far ultraviolet absorption spectrum of O_2 was observed by Price and Collins in 1935,[3] absorption spectra, the photoionization efficiency curves and photoelectron spectra of O_2 have been intensively studied. A high resolution (FWHM 0.07 Å) photoionization study of O_2 has been carried out by Dehmer and Chupka.[4] For the S_2 radical, the relative photoionization efficiency curve has been observed by Berkowitz *et al.*[5] in the gas phase by thermal vaporization of HgS. They found that an autoionization structure emerged, but the peak shapes were not clear enough to allow spectroscopic studies.

Compared to the study of these species, at the present stage, very few works have been carried out on the SO radical in the vacuum ultraviolet region. Donovan *et al.*[6] have obtained the absorption spectrum of the SO radical and studied the Rydberg series (The $D^3\Pi$ and $E^3\Pi$ states) converging to the $X^2\Pi$ state of SO^+. The photoelectron spectrum of the SO radical produced by discharge of CS_2 and O_2 was also observed by Jonathan *et al.* in 1974.[7]

The present work reports the first mass spectrometric analysis of the relative photoionization efficiency curve of the SO radical produced by pyrolysis of ethylene sulfoxide (C_2H_4=SO). The synthesis of C_2H_4=SO[8] and production of the SO radical by its pyrolysis has been reported.[9] Also the $a^1\Delta$ state of the SO radical produced by pyrolysis of C_2H_4=SO was analyzed from the microwave spectrum by Saito in 1970.[10]

The pyrolysis and photoionization in the present system are described below:

$$C_2H_4{=}SO \xrightarrow{\Delta} C_2H_4(X^1A_{1g}) + SO(a^1\Delta)$$

$$SO(a^1\Delta) + M \longrightarrow SO(X^3\textstyle\sum^-) + M$$

$$SO(X^3\textstyle\sum^-) + h\nu \longrightarrow SO^+(X^2\Pi) + e \quad \text{(IP)} \quad (1)$$

$$C_2H_4{=}SO + h\nu \longrightarrow C_2H_4{=}SO^+ + e \quad \text{(IP)} \quad (2)$$

$$C_2H_4{=}SO + h\nu \longrightarrow C_2H_4(X^1A_{1g}) + SO^+(X^2\Pi) + e \quad \text{(AP)} \quad (3)$$

From the threshold energies for above processes, the bond energies of $D_0(C_2H_4$=SO) and $D_0(C_2H_4$=SO^+) were determined. The IP of the SO radical in process (1) obtained from mass spectrometric photoionization is in excellent agreement with the results of photoelectron studies[7] and photofragmentation studies of sulfur dioxide.[11] The IP of C_2H_4=SO in process (2) and the AP of SO^+ from C_2H_4=SO in process (3) were obtained. Thus, these threshold energies indicate that the AP of SO^+ from C_2H_4=SO should be lower than the IP of the SO radical. This unique phenomenon was first observed in the system of C_2H_4=SO.

On the other hand, in process (1) the relative photoionization efficiency curve of the SO radical was obtained by scanning the excitation wavelength. Rather strong autoionization peaks were observed on this curve. But these peaks could not be assigned due to the lack of strong vibrational progressions such as are found for O_2^+.

Experimental

The experimental arrangement is shown in Fig. 1. The apparatus consisted of a hydrogen discharge light source operated at 0.4 A dc with about 700 V across the tube, a 50 cm Seya-Namioka type vacuum monochromator with a resolution of 2.3 Å (FWHM) which dispersed and refocused the monochromatic light into the ionization chamber, a set of

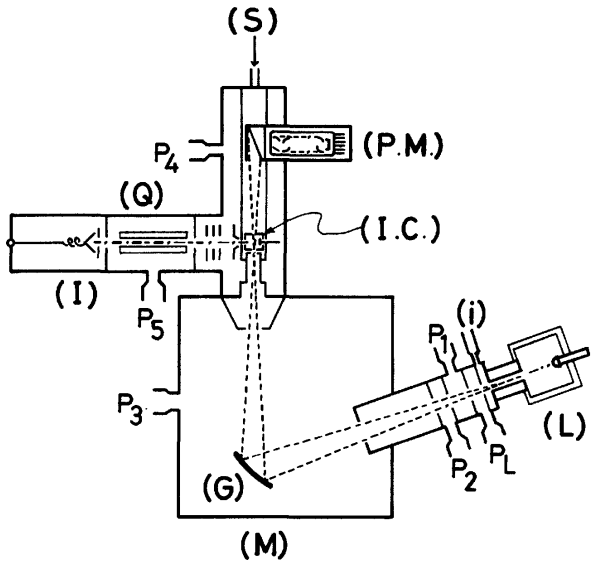

Fig. 1. Schematic diagram of the experimental apparatus. L; light source, i; gas inlet, G; grating, M; monochromator, I.C.; ionization chamber, Q; quadrupole mass filter, P.M.; photon monitor, I; ion multiplier, S; sample gas inlet, P_L, P_1—P_5; differential pumping system.

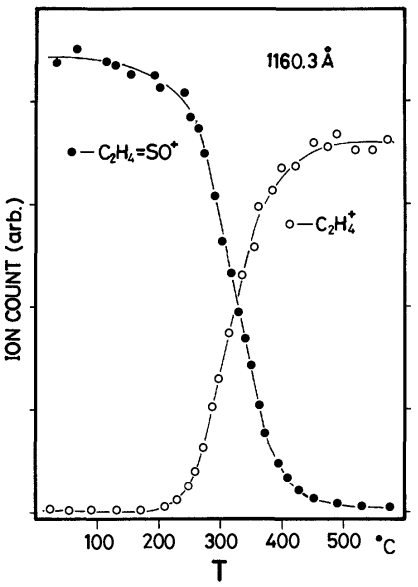

Fig. 2. Temperature variation of the ion counts of C_2H_4=SO and C_2H_4.
● denotes the ion counts of C_2H_4=SO, O denotes the ion counts of C_2H_4 produced by pyrolysis from C_2H_4=SO.

ion extraction and focusing lenses, and a quadrupole mass spectrometer (NEVA NAG-520) for ion detection.

Ion counts were measured by an electronmultiplier (Murata EMS-6081B), and photon counts were measured by the scintillation counter of a photomultiplier (HTV R-268) coated with sodium salicylate. After each signal had been amplified and identified by a fast pre-amplifier (ORTEC 9301) and an amplifier-discriminator (ORTEC 9302), it was integrated by the counter (ORTEC 9315). The accumulation of signals and control of the experimental apparatus were regulated by a microcomputer (NEC PC-9801). The relative photoionization efficiency was derived by the normalization method, dividing the ion counts by the photon counts.

In order to obtain radicals by pyrolysis, a tape-heater wrapped around a 10 mm diameter quartz tube was used at about 20 cm upstream from the ionization chamber. The temperature was varied in the region between room temperature and 580 °C. The total pressure was measured by a capacitance manometer (MKS-Baratoron). The sample pressure was typically about 0.6 m Torr in the ionization chamber.

In order to investigate the temperature dependence of pyrolysis of C_2H_4=SO, ion counts for several species were measured in the range, room temperature to 580 °C. The sample was irradiated by light at 1160.3 Å, whose energy is higher than either of the IPs of the parent molecule or ethylene produced by pyrolysis, but it was lower than the AP of the fragment ethylene ion from the parent molecules. The SO^+ radical ion could not be used for monitoring the pyrolysis because its IP is higher than the AP of the SO^+ fragment ion from the parent molecules. The temperature dependence of ion counts produced by irradiation at 1160.3 Å is shown in Fig. 2. At 300 °C, the ion counts of C_2H_4=SO^+ were reduced to one-half of those at room temperature. With a further rise in the temperature, they were rarely observed. On the other hand, ion counts of ethylene increased up to 500 °C, and above 500 °C they remained stationary. Thus, the temperature of the pyrolysis was maintained at 510 °C throughout this experiment.

Results and Discussion

The relative photoionization efficiency curve of SO^+ from the SO radical for the wavelength region 915—1220 Å, is shown in Fig. 3, where the hydrogen discharge lamp was used as a source at a wavelength resolution (FWHM) of 2.3 Å. In the present experiment, the accuracy of the wavelength was determined to be within about 0.5 Å from H Lyman-α and H Lyman-β in the light source. For excited $O_2(a^1\Delta_g)$, Jonathan *et al.*[13] examined the photoelectron spectrum of the ($^2\Delta_g \leftarrow {}^1\Delta_g$ and $^2\Phi_u \leftarrow {}^1\Delta_g$) ionization transition using phase-sensitive detection. These transitions from the $a^1\Delta$ state could not be being observed in the present photoionization efficiency curve, the reason that the excited $SO(a^1\Delta)$ may have almost completely been deactivated. The photoionization efficiency rises sharply at 1206.3±0.5 Å (=10.28±0.01 eV), and above this threshold there is a gradual increase in ionization cross section. Somewhat strong peaks, assigned to autoionization structures, have been detected between 1010 and 920 Å from which the autoionization structures have been determined. But along the SO^+ photoionization curve there are no very strong vibrational progressions like O_2^+ between 1005 Å (the threshold of IP) and 850 Å.[4] Therefore, spectroscopic studies could not be done as successfully of the autoionization peaks in SO^+ as those of the broad ones S_2^+.[5]

Furthermore, to obtain various thermodynamic data

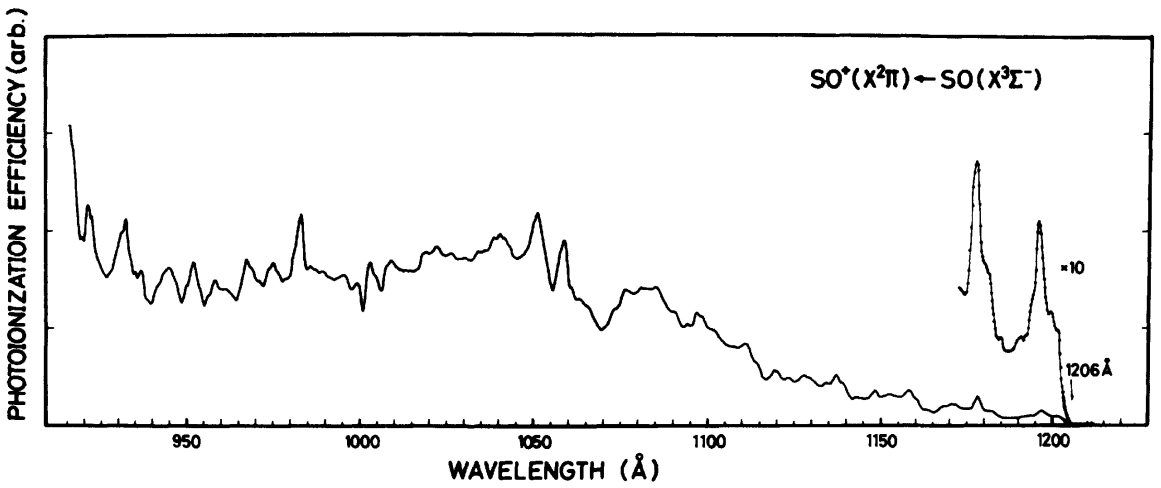

Fig. 3. Photoionization efficiency curve for SO^+ from the SO radical taken between 1220 and 915 Å at a wavelength resolution (FWHM) of 2.3 Å at 510°C.

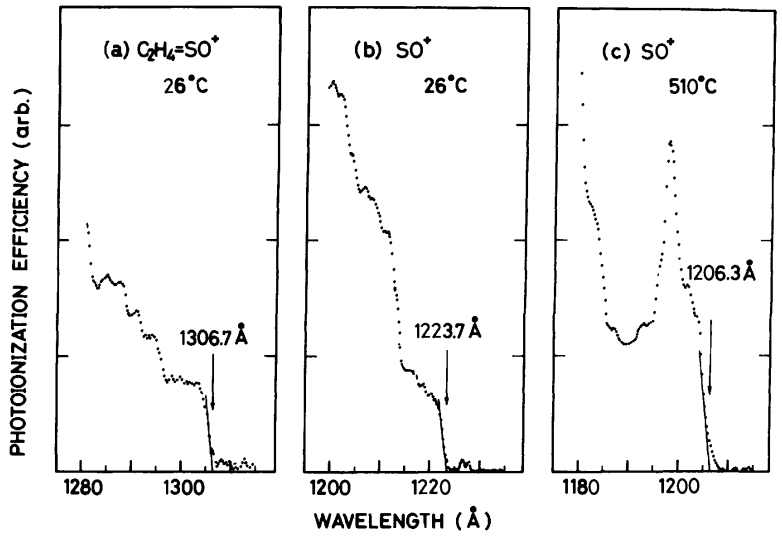

Fig. 4. The relative photoionization cross sections in the neighborhood of the threshold energies.
(a) The ion counts of C_2H_4=SO^+ at the room temperature, (b) The ion counts of SO^+ fragment ion from C_2H_4=SO at room temperature, (c) The ion counts of the SO radical at 510°C.

Table 1. Summary of photoionization data for the system of ethylene sulfoxide

Ion	Threshold eV[a)]	Process	Temperature °C
SO^+	10.28±0.01	$SO(X^3\Sigma^-)+h\nu\rightarrow SO^+(X^2\Pi)+e$	510
SO^+	10.13±0.01	C_2H_4=SO+$h\nu\rightarrow C_2H_4(X^1A_{1g})+SO^+(X^2\Pi)+e$	26
C_2H_4=SO^+	9.49±0.02	C_2H_4=SO+$h\nu\rightarrow C_2H_4$=SO^++e	26

a) Estimated uncertainties.

relating to C_2H_4=SO, the threshold energies were measured. Figure 4 shows the relative photoionization cross section of (a) C_2H_4=SO at room temperature, (b) SO^+ fragment ion from C_2H_4=SO at room temperature, (c) SO^+ ionized directly from the SO radical at 510°C. $C_2H_4^+$ fragment ions at room temperature were not observed. These threshold energies are summarized in Table 1.

The IP of SO in the present work is in excellent agreement with the value of 10.29±0.02 eV obtained from photoelectron spectra by Jonathan *et al.*[7] and that of 10.21 eV obtained from the photofragmentation method by Dibeler and Liston.[11] Though, it was assumed that SO^+ ions might appear from $SO(a^1\Delta)$

produced by pyrolysis of C_2H_4=SO in the region longer than 1206.3 Å (=10.28 eV) by means of an allowed $SO^+(X^2\Pi)\leftarrow SO(a^1\Delta)$ ionization transition, in fact, SO^+ ions were not observed in this region as can be seen in Fig. 4(c). This results from the fact that the excited $SO(a^1\Delta)$ was almost completely deactivated to the ground state before it reached to the ionization chamber.

The AP of SO^+ fragment ion from C_2H_4=SO and the IP of C_2H_4=SO were determined. It is worth noting that the IP of the SO radical is about 0.15 eV higher than the AP of SO^+ from C_2H_4=SO. In the pyrolysis of C_2H_4=SO described in process (1), C_2H_4=SO must correlate to $SO(a^1\Delta)$ from spin conservation, thus decomposition to $C_2H_4+SO(a^1\Delta)$ is an endothermic reaction. The values of ΔH_f in the following reactions are derived by using the transition energy of $SO(a^1\Delta\leftarrow X^3\Sigma^-)$ from chemiluminescence studies of Barnes *et al.*[12]

$$C_2H_4{=}SO \begin{cases} \rightarrow C_2H_4+SO(a^1\Delta) \\ \qquad\qquad \Delta H_f = 13.3\pm0.1 \text{ kcal/mol}^\dagger \\ \rightarrow C_2H_4+SO(X^3\Sigma^-) \\ \qquad\qquad \Delta H_f = -3.5\pm0.1 \text{ kcal/mol} \end{cases}$$

The transitions to $SO^+(X^2\Pi)$ from both $SO(a^1\Delta)$ and $SO(X^3\Sigma^-)$ are allowed. It seems that the exothermicity of the reaction in pyrolysis contributes to the ionization of SO from parent molecule. Therefore, it stands to reason that the AP of SO^+ from C_2H_4=SO is lower than the IP of the SO radical. From these results and the IP of C_2H_4=SO, the following bond energies of $D_0(C_2H_4{=}SO)$ and $D_0(C_2H_4{=}SO^+)$ were obtained;

$$D_0(C_2H_4{=}SO) = 4640\pm30 \text{ cm}^{-1}$$

$$D_0(C_2H_4{=}SO^+) = 5160\pm30 \text{ cm}^{-1}$$

Furthermore, from a consideration of the temperature dependence of C_2H_4=SO, the activation energy in the system of C_2H_4=SO has been estimated.

This reaction is regarded as a first-order irreversible unimolecular decomposition reaction of the plug type, and, so, the following equation in logarithmic form is obtained;

$$\ln(C_0/C) = (k/v)l, \tag{4}$$

where C_0 and C are sample concentrations of the entrance and exit regions of the pyrolysis tube, respectively, and k is the rate constant, v is the flow rate, and l is the length of the pyrolysis tube. From the expressions for the rate constant, k expressed in terms of the frequency factor A, and the activation energy E, we obtain the following equation;

$$\ln(\ln(C_0/C)) = -E/RT + \ln Al/v. \tag{5}$$

†1 cal_{th}=4.184 J.

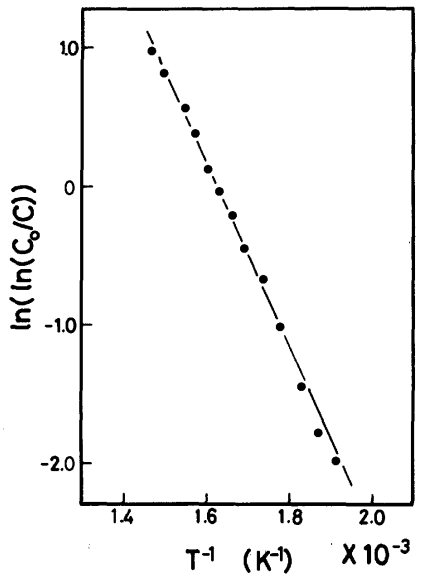

Fig. 5. Arrhenius plot of $\ln(\ln(C_0/C))$ versus T^{-1} obtained from the ion counts of C_2H_4=SO^+ in Fig. 2.

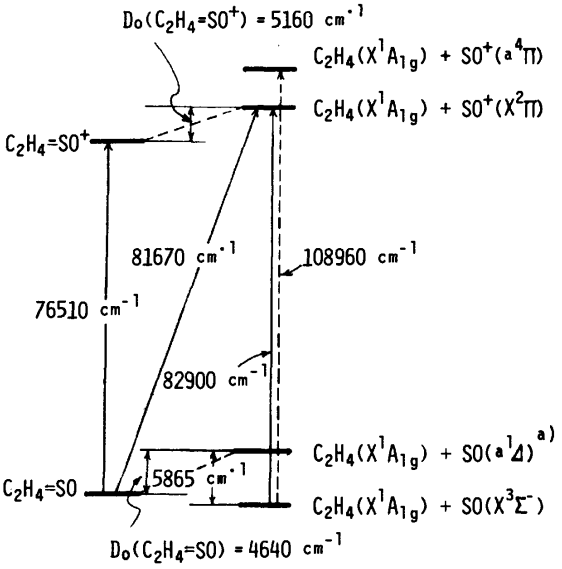

Fig. 6. The energy diagram of C_2H_4=SO and SO.
a) The energy difference between $a^1\Delta$ and $X^3\Sigma^-$ from Ref. 12.

Then the plot of $\ln(\ln(C_0/C))$ versus T^{-1} will yield the activation energy E from slope of the curve.

The plot of $\ln(\ln(C_0/C))$ versus T^{-1} which was obtained from the ion counts of C_2H_4=SO^+ in Fig. 2 is shown in Fig. 5. The activation energy was estimated to be 13.6 kcal/mol and was in excellent agreement with the value of $D_0(C_2H_4{=}SO)$ obtained from the above discussion.

The energy diagram of C_2H_4=SO and SO is summarized in Fig. 6.

Although the electronic state of C_2H_4=SO has not yet been studied, it is presumed that the electron in the highest occupied molecular orbital is an antibonding electron because the bond energy of the neutral state is

less than that of the ionic state.

The authors would like to thank Dr. S. Saito of Institute for Molecular Science for preparing ethylene sulfoxide.

References

1) C. A. Gottlieb and J. A. Ball, *Astrophys. J.*, **184**, L59 (1973): **187**, L47 (1974).

2) a) W. C. Swope, Y. P. Lee, and H. F. Schafer III, *J. Comput. Phys.*, **26**, 243 (1978); *J. Chem. Phys.*, **70**, 947 (1979); **71**, 3761 (1979); b) G. Theodorakopoulos, S. D. Peyerimhoff, and R. J. Bunker, *Chem. Phys. Lett.*, **81**, 413 (1981).

3) W. C. Price and G. Collins, *Phys. Rev.*, **48**, 714 (1935).

4) P. M. Dehmer and W. A. Chupka, *J. Chem. Phys.*, **62**, 4525 (1975).

5) J. Berkowitz and C. Lifshiz, *J. Chem. Phys.*, **48**, 4346 (1968).

6) a) R. J. Donovan, D. Husan, and P. T. Jackson, *Trans. Faraday Soc.*, **65**, 2930 (1969); b) R. J. Donovan and D. J. Little, *Spectrosc. Lett.*, **4**, 213 (1971).

7) a) N. Jonathan, D. J. Smith, and K. J. Ross, *Chem. Phys. Lett.*, **9**, 217 (1971); b) J. M. Dyke, L. Golob, N. Jonathan, A. Morris, M. Okuda, and D. J. Smith, *J. Chem. Soc., Faraday Trans. 2*, **70**, 1818 (1974).

8) K. Kondo and A. Negishi, *Tetrahedron*, **27**, 4821 (1971).

9) S. Saito, *Bull. Chem. Soc. Jpn.*, **42**, 667 (1969).

10) S. Saito, *J. Chem. Phys.*, **53**, 2544 (1970).

11) V. H. Dibeler and S. K. Liston, *J. Chem. Phys.*, **49**, 482 (1968).

12) I. Barnes, K. H. Becker, and E. H. Fink, *Chem. Phys. Lett.*, **67**, 310 (1979).

13) N. Jonathan, A. Morris, M. Okuda, K. J. Ross, and D. J. Smith, *J. Chem. Soc., Faraday Trans. 2*, **70**, 1810 (1974).

 © 1985 The Chemical Society of Japan Bull. Chem. Soc. Jpn., 58, 3480—3485 (1985) [Vol. 58, No. 12

Internal Energy Distributions of NH($A^3\Pi$). An Application of Phase Space Theory to the Electron-impact Dissociation

Ikuo Tokue* and Yoshio Ito
Department of Chemistry, Faculty of Science, Niigata University, Niigata 950-21
(Received June 27, 1985)

Internal energy distributions of NH(A) produced by electron impact on NH_3, HN_3, and HNCO are compared with those predicted by use of the phase space theory based on the method of Light and Pechukas. The values predicted under conservation of energy and total angular momentum are found to be inconsistent with the experimental results. The observed values are well simulated *via* the introduction of a nonstatistical bias by representing the selective coupling between the reaction coordinate and the rotational modes of the products. The dynamics for formation of NH(A) is discussed.

The decomposition of polyatomic molecules is a typical example of unimolecular reactions. Unimolecular processes only proceed at an appreciable rate when the reacting molecule posseses an internal energy greater than a certain threshold value corresponding to the activation energy. These active molecules arise in the process of chemical reaction as a result of inelastic molecular collisions, or on electron, or photon, impact. The basic idea of the statistical theory of unimolecular reactions[1] is that an active molecule is considered as a closed system whose states are distributed with equal probability over hypersurfaces of constant total energy.

The transition state theory[2] of chemical reactions identifies the transition complex having activation energy along the reaction coordinate. In the reactions such as bond dissociations, however, there is little or no potential-energy barrier along the reaction coordinates. Light and Pechukas[3] treated atom-molecule reactions which proceed without activation energy under the requirement that the reaction complex can dissociate over the orbital angular momentum barrier in the final state. Their method was successfully applied to the photodissociation $NH_3 \rightarrow NH(c^1\Pi)+H_2$.[4] Mies[5] pointed out that their space theory is a special microcanonical version of the transition state theory for the "loose complex," where the activated complex is the rotational barrier in the asymptotic channel. Horie and Kasuga[6] proposed another statistical model including the law of angular momentum conservation and discussed the decomposition $H_2O \rightarrow H+OH(A^2\Sigma^+)$ through electron or photon impact.

We previously reported formation and internal energy distributions of NH($A^3\Pi$) by electron impact on NH_3,[7] HN_3,[8] and HNCO.[9] The basic idea of Light and Pechukas[3] can be applied to these electron-impact dissociations. In the present paper, the observed distributions of NH(A) from NH_3, HN_3, and HNCO are compared with those predicted by a statistical calculation based on the method of Light and Pechukas.[3] In order to give an account of the observed values, we have introduced a nonstatistical bias by representing the selective coupling between the reaction coordinate and the rotational mode of the products. On comparison between the observed distributions and the predicted by the statistical calculations, the dynamics for formation of NH(A) is discussed.

Method of Calculation

Outline of Calculation. The main requirements imposed on the system[1] are that the reaction proceeds *via* an intermediate complex with a long lifetime and that the coupling between different degrees of freedom must ensure a sufficiently intensive energy exchange between them. This statistical theory assumes that the size of the phase volume accesible to the active and activated molecules is limited only by the condition that the energy is constant. Furthermore, conservation of the total angular momentum of the system imposes an additional restriction on the size of the phase volume of the active and activated molecules. This restriction is especially important for "loose" activated molecules. Moreover, the conservation of angular momentum is important when the active molecule arises as a result of excitation by electron impact. This is connected with the fact that, due to electron impact, a large amount of electronic-vibrational excitation energy is usually transferred to the molecule, but the rotational angular momentum of the molecule is very little changed.

To evaluate the energy distribution, we introduce the available energy (E_{av}) defined by the difference between the vertical and the adiabatic energy required for decomposition. The probability of decomposition of the parent molecule to a given state is the same to all the states to be accessible under conservation of energy and total angular momentum. Thus, for this system, the validity of the microcanonical distribution is assumed. Accordingly, after decomposition, E_{av} is allowed to be distributed among all the degrees of freedom in the products. The initial angular momentum $\boldsymbol{J}$ (momentums are written throughout in units of $\hbar$) possessed by the parent molecule as molecular rotation must be equal to the sum of those of the molecular rotations of the fragments and the orbital angular momentum between them.

Theoretical Energy Distributions of the NH(A) Product.

We treat here a direct dissociation into final fragments such as Reactions 1 and 2, and do not consider an indirect process such as Reaction 3, where one of the products are quasibound in an intermediate state.

$$NH_3 \longrightarrow NH(A)+H_2(X), \quad (1)$$

$$NH_3 \longrightarrow NH(A)+H(ls)+H(ls), \quad (2)$$

$$NH_3 \longrightarrow NH_2^*+H(ls), \quad (3a)$$

$$NH_2^* \longrightarrow NH(A)+H(ls), \quad (3b)$$

$$HN_3 \longrightarrow NH(A)+N_2(X), \quad (4)$$

$$HNCO \longrightarrow NH(A)+CO(X). \quad (5)$$

The calculation of the internal energy distributions was carried out on the basis of the following methods: Method 1 is a simple statistical calculation under the requirement of conservation of energy. Method 2 is the statistical calculation based on the method of Light and Pechukas.[3] In Method 3, a nonstatistical bias is introduced into the population distribution.

In the case of a reaction such as M→NH+B, where B is a diatomic molecule, $\boldsymbol{J}_N$, $\boldsymbol{J}_B$, $\boldsymbol{J}$, $\boldsymbol{l}$, $\boldsymbol{k}$, their space-fixed z components, v_N, and v_B can be used to specify the quantum states of all the products. The v_N and v_B are the vibrational quantum numbers of NH and B, respectively. The $\boldsymbol{J}_N$ and $\boldsymbol{J}_B$ are the rotational angular momenta of NH and B, respectively, $\boldsymbol{l}$ is the orbital angular momentum among the fragments, $\boldsymbol{k}$ is an intermediate angular momentum associated with a vector sum $\boldsymbol{J}_N+\boldsymbol{J}_B$, and $\boldsymbol{J}$ corresponds to the total angular momentum $\boldsymbol{J}=\boldsymbol{k}+\boldsymbol{l}$. The angular momenta are restricted by energy conservation and by the triangle inequalities:[10] namely, the corresponding quantum numbers k and J can have the values $|J_N-J_B|\leq k\leq J_N+J_B$ and $|k-l|\leq J\leq k+l$.

On the assumption of a Boltzmann temperature of 298 K for the ground state of parent molecules, the distribution of J, $P(J)$, was evaluated by use of the rotational constants.[11] The total number of the J state among various product states with E_{av} is given by

$$N(J,E_{av})=\sum_{v_N}\sum_{v_B}\sum_{J_N}\sum_{J_B}\sum_{l=0}^{l_{max}} 1, \quad (6)$$

under conservation of total energy that $E_{av}=E_{tr}+E_{rot}+E_{vib}$, where E_{tr} denotes the translational energy, and E_{rot} and E_{vib} are the rotational and the vibrational energies of all the fragments,[12] respectively. Light and Pechukas[3] derived the quantum number of the maximum orbital angular momentum, l_{max}, from the interaction potential between the products. However, no information is found about the interaction potential among the fragments from parent molecules. In this study, the interaction constant (spherically averaged sum of dipole-induced dipole and dispersion contributions) denoted by C are estimated on the basis of the method of Hirschfelder *et al.*[13] by use of data on the polarizabilities, dipole moments, ionization potentials for H[14] and diatomic fragments.[12,13] Dipole moment and polarizabiliy of NH(A) are assumed to be 3.34×10^{-30} Cm (1 D) and 1×10^{-30} m^3, respectively. The interaction constants thus obtained are listed in Table 1. In preliminary analysis, the internal energy distributions evaluated are found to be rather insensitive to l_{max}.

The probability of dissociation into each accessible final state having J is $P(J)/N(J,E_{av})$. Thus, the rotational distribution in the v_N level of NH(A) can be reperesented with collection of all the states having J_N and v_N as follows:

$$P(J_N,v_N,E_{av})=\sum_{v_B}\sum_{J_B}\sum_{l}\sum_{J}P(J)/N(J,E_{av}), \quad (7)$$

under the conservation of energy and the restriction based on the two triangle inequalities on angular momenta. In Reaction 2, we must exclude summation over v_B and J_B from Eqs. 6 and 7. Equation 7 is summed to give the vibrational distribution of NH(A),

$$P(v_N,E_{av})=\sum_{J_N}P(J_N,v_N,E_{av}). \quad (8)$$

In calculation of the rotational distribution of NH(A) by Method 1, Eq. 7 is replaced by

$$P(J_N,v_N,E_{av})=\sum_{v_B}\sum_{J_B} 1, \quad (9)$$

where the sum includes, of course, the accessible states under conservation of energy.

In electron-impact dissociation at energies over the onset for formation of NH(A), an available energy (E_{av}) converting into the translational and internal energies of products cannot be given very clearly because collisions with electrons are essentially an energy-loss process. Thus, E_{av} was treated as an adjustable parameter.

Following a series of diagnostic calculation for Reactions 1, 2, 4, and 5, a nonstatistical bias is introduced into the rotational distribution (Method 3) with the view of agreement with the observed values: namely, Eq. 7 is multiplied by a factor of $\exp(-\beta|E_{av}-E_{rot}|)$, where β is a parameter representing the strength of coupling between the reaction coordinate and the rotation of the fragments. This factor realizes the resonance feature in energy transfer of the available energy into the rotation of the fragments. Thus, in Method 3, the validity of the microcanonical distribution no longer holds good. The parameter β represents insufficientness in energy exchange among various degrees of freedom at the energy partitioning process.[15] When β decreases to zero, Method 3 apparently results in Method 2.

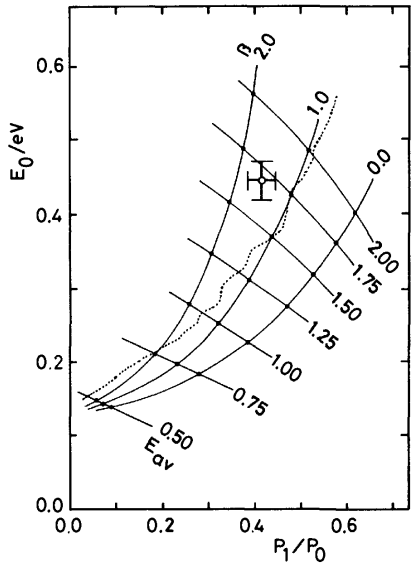

Fig. 1. Rotational energy (E_0) *versus* vibrational population ratio (P_1/P_0) predicted for Reaction 1: the open circle with error bars shows the observed values at electron energy of 17 eV. The dotted line shows the results by Method 1. The solid line with β=0 shows those by Method 2 and the others with β=1.0 and 2.0 show those by Method 3.

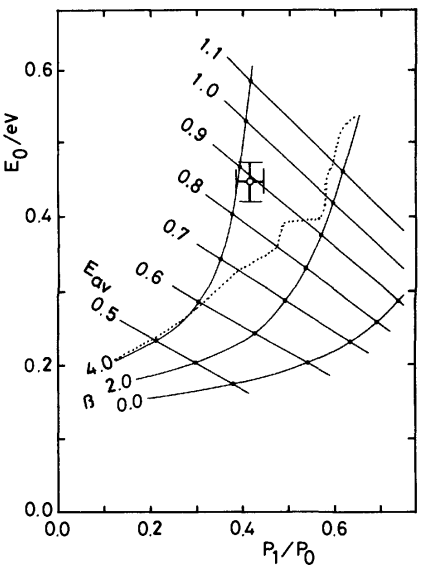

Fig. 2. The same as Fig. 1 but for Reaction 2.

Results and Discussion

Vibrational Population Ratio versus *Rotational Energy of NH(A).* In the analysis of the emission intensities of the NH(A-X) spectrum, we used the relative vibrational population ($P_v/P_{v=0}$) and the rotational temperature (T_v) of the v=0 and 1 levels of the NH(A) state. Although the rotational distribution evaluated by use of the statistical methods can be approximated by a Boltzmann temperature, the population decreases more rapidly with increasing J_N and

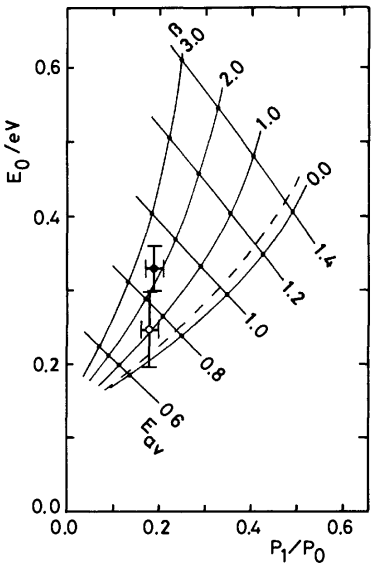

Fig. 3. The same as Fig. 1 but for Reaction 4. The open and the closed circles with error bars show the results at electron energies of 7 and 10 eV, respectively.

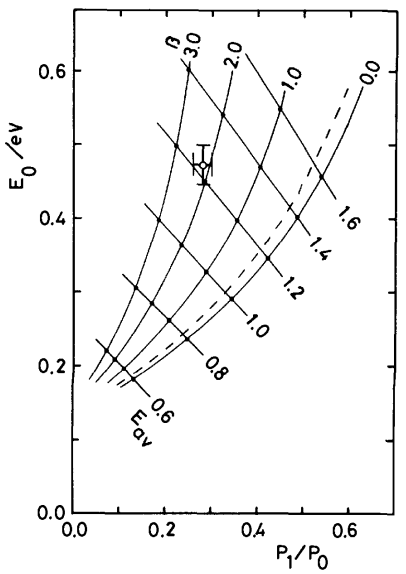

Fig. 4. The same as Fig. 1 but for Reaction 5.

disappears suddenly. Henthforce, the observed rotational distributions were compared with those predicted in the form of E_v being the rotational energy concerning with the v level.

In Figs. 1—4, E_0 is plotted *versus* P_1/P_0 comparing the observed values with the predicted by three methods. The observed results from NH_3 and HN_3 are nearly consistent with the predicted by Method 1 for Reactions 1 and 4, respectively, but are inconsistent with those by Method 2. On the contrary, the results predicted for Reactions 2 and 5 by both Methods 1 and 2 cannot explain the observed values from NH_3 and HNCO, respectively. These imply that the agreement between the observed and the predicted for

TABLE 1. THE P_1/P_0 AND E_0 OBSERVED AND PREDICTED WITH THE BEST FIT E_{av} AND β

Molecules Reactions	Methods	P_1/P_0	E_0 eV	E_{av}[a] eV	β[a] eV^{-1}	C 10^{-78} J m^6
NH_3	Obsd[b]	0.415±0.02	0.447±0.03			
1	1	0.460	0.403	1.40	—	
1	3	0.415	0.447	1.685	1.515	1.83
2	1	0.490	0.392	0.75	—	
2	3	0.414	0.446	0.893	3.686	1.23[c]
HN_3	Obsd[d]	0.18±0.01	0.245±0.05			
4	1	0.214	0.233	0.8	—	
4	3	0.182	0.248	0.75	1.01	2.74
HNCO	Obsd	0.28±0.02	0.48±0.04			
5	1	0.44	0.387	1.4	—	
5	3	0.280	0.471	1.23	2.06	2.92

a) The best fit values used for simulation. b) Observed at electron energy of 17 eV. c) Sum of one H–H and two NH–H attractive contributions. d) Observed at electron energy of 7 eV.

Reactions 1 and 4 by Method 1 is specious because Method 2 is more accurate than Method 1. Accordingly, in order to explain the observed results, we have introduced a nonstatistical bias and have adjusted not only E_{av} but the coupling parameter β. Table 1 lists the predicted E_0 and P_1/P_0 by use of best fit E_{av} and β comparing with the observed.

Recently, Kajimoto[15] has treated the rotational distributions of NH($c^1\Pi$) through photolysis of NH_3 by use of a nonstatistical bias representing the coupling between the bending motion of NH_3 precursor and the rotation of NH(c). On the assumption of vibrational energy of 21 kJ/mol (0.22 eV) for bending motion of NH_3, the observed distributions has been well simulated by use of β=0.024 mol/kJ (2.3 eV^{-1}). On the contrary, the best-fit E_{av} and β for formation of NH(A) through electron impact on NH_3, HN_3, and HNCO are 0.8—1.7 eV and 1.0—3.7 eV^{-1}, respectively. This implies that many vibrational motions of precursor are strongly coupled with the rotation of NH(A).

Formation of NH(A) from NH_3. In electron-impact dissociation of NH_3, NH(A) is produced *via* two different channels.[7] One corresponds to Reaction 1 *via* a triplet precursor with the onset energy of 8.0 eV and the other corresponds to Reaction 2 with the onset energy of 12.3 eV. Reactions 1 and 2 similarly contribute to the formation of NH(A) at the lowest impact energy of 17 eV, to which the population analysis could be applied, while Reaction 2 is main contributors of the formation of NH(A) above 17 eV. The rotational distributions of the v=0 and 1 levels of NH(A) are found to vary only moderately from 17 up to 92 eV. This indicates that the rotational distribution of NH(A) produced *via* Reaction 1 is nearly equal to those *via* Reaction 2.

The observed values are shown in Fig. 5 comparing with the results predicted for Reactions 1 and 2. The distributions predicted for Reaction 1 is in fairly good agreement with the observed, while those for Reaction 2 is inconsistent with the observed. The results for Reaction 1 by Method 3, however, rather overestimate

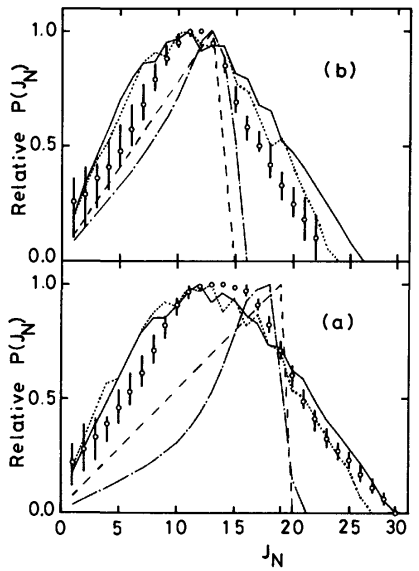

Fig. 5. The relative rotational distributions of NH(A) from NH_3 for (a) the v=0 level and (b) the v=1 level: ------, Method 1 for Reaction 1; ——, Method 3 for Reaction 1; ———, Method 1 for Reaction 2; —·—·—, Method 3 for Reaction 3. The open circles with error bars show the observed values.

the distributions of the v=1 level above J_N=15. This is due to the application of single coupling constant β to the distributions of both the v=0 and 1 levels. The difference between the observed distributions and the predicted for Reaction 2 seems to originate in the application of the method of Light and Pechukas.[3]

In unimolecular reactions into an atom(s)+diatomic product such as Reaction 2, the predicted distribution is extremely nonthermal and strongly depends on E_{av}. In case of electron-impact excitation, the electron energy for impinging electron is not so monoenergetic, contrary to photon excitation. On the basis of the Franck-Condon principle, the distribution of E_{av} may be determined by reflecting the position probability function associated with the normal vibrations of the ground state of parent molecule onto the potential

energy surface of the precursor state. Accordingly, E_{av} is expected to have a rather broad distribution. In such a case, it is necessary to take the weighted mean of the population distributions obtained for a wide range of values of E_{av}. On the assumption of a Gaussian distribution for E_{av}, Horie and Kasuga[6] reproduced the rotational distribution of OH(A) produced by electron impact on H_2O. When both the ground and the precursor states of NH_3 are well informed, we expect to give an account of the observed rotational distribution of NH(A) for Reaction 2 by Method 3 using a suitable distribution of E_{av}. On the contrary, in unimolecular reactions into two diatomic products such as Reactions 1, 4, and 5, the predicted distribution is nearly thermal and only moderately depends on E_{av}. In this case, even if we do not consider the distribution of E_{av}, we can reproduce the observed distribution by use of the best fit E_{av} and β. The value of E_{av} thus obtained means rather an averaged value. Incidentally, for Reaction 3b, calculation of the internal energy distributions of NH(A) by Method 2 by use of a variety of Boltzmann temperatures for NH_2* failed in agreement with the observed.

Runau *et al.*[16] reported in their *ab initio* study that the SCF potential curve calculated for Reaction 1 correlates with the $^3A_2''$ state (point group D_{3h}), which corresponds to excitation out of the $3a_1$ (C_{3v}) MO into the $4a_1$ (Rydberg 3s+H 1s) orbital. This $^3A_2''$ precursor (the lowest triplet state) belongs to the Rydberg state having a planar geometry since one of the lone pair electrons is mainly excited into the atomic orbital of the N atom. Thus, the excitation from the non-planar ground state into the planar triplet precursor causes the strong excitation of the umbrella inversion of NH_3. The rotational distributions of the departing fragments are selectively enhanced during subsequent bond-dissociation process. This gives rise to the breakdown of the assumption of the microcanonical distribution.

Formation of NH(A) from HN_3 and HNCO. The molecular structures of the ground state of HN_3[17] and HNCO[18] are trans bent in equilibrium (point group C_s). On the basis of CNDO/S study, we reported[8,9] that the precursor forming NH(A) from HN_3 and HNCO is presumably the $2^3A''$ state corresponding to excitation out of the 9a′ MO into the 3a″ MO. This result for HN_3 is supported by *ab initio* study.[19]

The observed rotational distributions of the $v=0$ level of NH(A) from HN_3 depend on the impact energy, while those from HNCO is independent of the impact energy. In HN_3, the values near the onset are compared with those predicted since the foregoing energy dependence is due to two different channels for formation of NH(A).

In the previous report for HNCO,[9] T_0 and P_1/P_0 are compared with those predicted by a simple statistical calculation based on the information theory.[20] This method assumes complete randomization of the available energy among all degrees of freedom in the products under the requirement of conservation of energy. The results predicted by use of E_{av}=0.7 eV show that the internal energy of NH(A) is selectively enhanced in the dissociation of the precursor state of HNCO. The present results show that the rotational distributions of NH(A) from HN_3 and HNCO are selectively enhanced much more than predicted by Method 2. Thus, the assumption of the microcanonical distribution cannot apply to Reactions 4 and 5. It can be concluded that the molecular structure of the $2^3A''$ precursor state of HN_3 and HNCO in equilibrium is fairly different from each ground state. For HN_3, Moore and Rosengren[21] found that the HN-NN stretch is strongly mixed with the H-N-N bend on the ground state. This suggests that the HN-NN stretching motion enhances the angular momentum of the separating NH+N_2 products when HN_3 dissociates.

Conclusion

On comparison of the observed and predicted internal energy distributions of NH(A), the assumption of the microcanonical distribution is found to be inapplicable to formation of NH(A) from NH_3, HN_3, and HNCO. The good agreement with the observed results is obtained by introduction of a coupling parameter, which represents the resonance feature in energy transfer process of the available energy. This result leads to selective excitation of the rotation of the fragments during bond-dissociation process.

Even if the phase space theory cannot be applied to the dissociation of such a small molecule, the internal energy distribution predicted can be used to estimate the mean available energy in electron-impact dissociation. Furthermore, this method including a nonstatistical bias can be used as a convenient criterion for prediction of whether the available energy is completely randomized among all the degrees of freedom in the products or a specific mode is enhanced.

References

1) See, for example, W. Frost, "Theory of Unimolecular Reactions," Academic Press, New York (1973), and E. E. Nikitin, "Theory of Elementary Atomic and Molecular Processes in Gases," translated by M. J. Kearsley, Clarendon Press, Oxford (1974).

2) H. Eyring, D. Walter, and D. Kimball, "Quantum Chemistry," Wiley, New York (1944).

3) J. C. Light, *J. Chem. Phys.*, **40**, 3221 (1964); P. Pechukas and J. C. Light, *J. Chem. Phys.*, **42**, 3281 (1965); P. Pechukas, J. C. Light, and C. Rankin, *J. Chem. Phys.*, **44**, 794 (1966).

4) N. Washida, G. Inoue, M. Suzuki, and O. Kajimoto, *Chem. Phys. Lett.*, **114**, 274 (1985).

5) F. H. Mies, *J. Chem. Phys.*, **51**, 798 (1969).

6) T. Horie and T. Kasuga, *J. Chem. Phys.*, **40**, 1683 (1964).

7) I. Tokue and M. Iwai, *Chem. Phys.*, **52**, 47 (1980).

8) I. Tokue and Y. Ito, *Chem. Phys.*, **79**, 383 (1983).
9) I. Tokue and Y. Ito, *Chem. Phys.*, **89**, 51 (1984).
10) D. W. Wardlaw and R. A. Marcus, *Chem. Phys. Lett.*, **110**, 230 (1984).
11) G. Herzberg, "Electronic Spectra and Electronic Structure of Polyatomic Molecules," Van Nostrand, Princeton (1966).
12) K. P. Huber and G. Herzberg, "Constants of Diatomic Molecules," Van Nostrand-Reinhold, New York (1979).
13) J. O. Hirschfelder, C. F. Curtiss, and R. B. Bird, "Molecular Theory of Gases and Liquid," Wiley, New York (1963).
14) T. M. Miller and B. Bederson, *Adv. At. Mol. Phys.*, **13**, 1 (1977).
15) O. Kajimoto, "Laser Chemistry," ed by S. Tsuchiya, Japan Scientific Society's press, Tokyo (1984), Chap. 3, pp. 61—72.
16) R. Runau, S. D. Peyerimhoff, and R. J. Buenker, *J. Mol. Spectrosc.*, **68**, 253 (1977).
17) M. Winnewisser and R. L. Cook, *J. Chem. Phys.*, **41**, 999 (1964).
18) L. Fusina and I. M. Mills, *J. Mol. Spectrosc.*, **86**, 488 (1981).
19) T. Fueno, private communications.
20) R. B. Bernstein and R. D. Levine, "Advances in Atomic and Molecular Physics," ed by D. R. Bates, Academic Press, New York (1975), p. 215.
21) C. B. Moore and Kj. Rosengren, *J. Chem. Phys.*, **44**, 4108 (1966).

Preparation, Crystal Structure, and Stereochemical Properties of {*N,N'*-Ethylenebis(1,1,1-trifluoro-4-imino-2-pentanonato)} (L-methioninato)cobalt(III)

Ken-ichi OKAMOTO,* Katsuhiro MATSUTANI, and Yuki FUJII†
Department of Chemistry, University of Tsukuba, Sakura, Ibaraki 305
†*Department of Chemistry, Ibaraki University, Mito, Ibaraki 310*
(Received July 9, 1985)

The $(-)_{435}$ isomer of the {*N,N'*-ethylenebis(1,1,1-trifluoro-4-imino-2-pentanonato)}(L-methioninato)cobalt(III) complex, $(-)_{435}$-[Co(tfac$_2$en)(L-met)], was preferentially crystallized from an equilibrium mixture of the $(-)_{435}$ and $(+)_{435}$ isomers in methanol. The crystal structure of the $(-)_{435}$ isomer was determined by X-ray diffraction. The $(-)_{435}$ isomer is of a Λ-cis-β_2 type in which the quadridentate tfac$_2$en takes a nonplanar configuration, and the L-methioninate is bound to the cobalt atom by nitrogen and oxygen atoms as a bidentate ligand. The electronic absorption, CD, and ^{1}H NMR spectral behaviors of both $(-)_{435}$ and $(+)_{435}$ isomers are discussed in relation to their geometrical and absolute configurations.

Mixed cobalt(III) complexes with quadridentate Schiff base and bidentate ligands (such as amino carboxylates and β-diketonates) have been investigated regarding their kinetic and thermodynamic stereoselectivities.[1-6] Some of these have been determined by X-ray crystal structure analyses.[7-10] Concerning these cobalt(III) complexes, it has been known that a quadridentate Schiff base, which usually contains salicylideneaminate moieties, selectively takes a nonplanar cis-β configuration[11a] by coordination.[1-10] Further, complexes with amino carboxylate as a bidentate ligand preferentially take a mer(N)[11b] configuration.[1-5] In order to elucidate the source of a regioselective effect due to the quadridentate Schiff base, we employed in this work *N,N'*-ethylenebis(1,1,1-trifluoro-4-imino-2-pentanonate), tfac$_2$en, which has flexible β-imino ketone moieties instead of salicylideneaminate ones. Also, its cobalt(III) complex with L-methioninate was prepared.

The present paper deals with the crystal structure of $(-)_{435}$-[Co(tfac$_2$en)(L-met)], which was preferentially crystallized from an equilibrium mixture of the $(-)_{435}$ and $(+)_{435}$ isomers in methanol. The absorption and CD spectra of the $(-)_{435}$ and $(+)_{435}$ isomers are discussed in comparison with those of corresponding cobalt(III) complexes with a quadridentate Schiff base, together with their stereochemical properties.

Experimental

1) Preparation of [Co(tfac$_2$en)(L-met)]. A warm solution (*ca.* 40 °C) containing 0.57 g of L-methionine in 15 cm^3 of water was added to a hot solution (*ca.* 40 °C) containing 1.5 g of [Co(tfac$_2$en)] (prepared by a procedure similar to that described in the literature[16,17]) in 80 cm^3 of methanol. The solution was vigorously stirred in the open for about 4 h at room temperature. The color of the solution changed from orange-brown to green. After filtration, the green filtrate was concentrated to about 10 cm^3 and appeared as a green crude product. The product (collected by filtration) was dissolved in a small amount of methanol and then slowly recrystallized by evaporating the solvent at room temperature to form the $(-)_{435}$ isomer as massive crystals in about 80% yield. A piece of crystal, thus obtained, was used for an X-ray diffraction study. Found: C, 37.84; H, 4.08; N, 7.83%. Calcd for [Co(tfac$_2$en)(L-met)]=$CoC_{17}H_{22}N_3O_4SF_6$: C, 38.00; H, 4.13; N, 7.82%. $[M]^{25}_{435}=-52900°$ / mol dm^{-3} m (mixed solvent of *N,N*-dimethylformamide (DMF)–$CHCl_3$ (1:4 in volume); concentration, 1.0×10^{-3} mol dm^{-3}).

When the green crude product or the pure $(-)_{435}$ isomer obtained above was recrystallized from a methanol–water (4:1) mixture, the complex consisted of two kinds of crystalline forms, a large amount of massive crystals ($(-)_{435}$ isomer) and a small amount of needle-shaped crystals ($(+)_{435}$ isomer). The needle-shaped crystals could be sorted by hand. Yield; about 15%. Found: C, 38.04; H, 4.13; N, 8.08%. Calcd for [Co(tfac$_2$en)(L-met)]: C, 38.00; H. 4.13; N, 7.82%. $[M]^{25}_{435}=+50100°$ / mol dm^{-3} m (mixed solvent of DMF–$CHCl_3$ (1:4); concentration, 1.0×10^{-3} mol dm^{-3}).

2) General Data. The electronic absorption spectra were recorded with JASCO UVIDEC-1 and UVIDEC-610 spectrophotometers and the CD spectra with a JASCO J-20 spectropolarimeter. All measurements were carried out at room temperature. Rotations at 435 nm were measured with a JASCO DIP-140 polarimeter at 25 °C. The ^{1}H NMR spectra were recorded with a Hitachi R-20 spectrometer at 35 °C, using tetramethylsilane (TMS) as an internal reference. X-Ray analysis calculations were carried out on a FACOM M-380 computer at the Uviversity of Tsukuba.

3) X-Ray Characterization. Unit cell parameters and intensity data for the single crystal (*ca.* $0.1\times0.12\times0.5$ mm^3) were measured on a Rigaku-denki four-circle diffractometer (AFC-5) with graphite-monochromatized Mo$K\alpha$ radiation. The unit-cell parameters were determined by a least-squares refinement based on 44 reflections. Systematic absences led to an assignment of the space group $P2_12_12_1$. The crystal data are summarized in Table 1.

Intensity data were collected by a ω—2θ scan technique up to $2\theta=60°$ with a scan rate of 3 °/min. The intensity data were converted to F_o data in the usual manner. Absorption corrections were not applied. A total of 2059 independent reflections with $F_o>3\sigma(|F_o|)$ were considered as 'observed' and used for the structure analysis.

4) Determination of the Crystal Structure. The position of the cobalt atom was obtained from a three-dimentional Patterson function. Difference Fourier maps, based on the cobalt position, revealed all the non-hydrogen atoms. The

TABLE 1. CRYSTAL DATA

Compound	$CoC_{17}H_{22}N_3O_4SF_6$
Formula weight	537.37
Crystal system	Orthorhombic
Space group	$P2_12_12_1$
a/Å	12.623(2)
b/Å	19.404(5)
c/Å	9.153(2)
Cell volume/Å^3	2241.9(8)
Z	4
D_x/g cm^{-3}	1.592
D_m/g cm^{-3}	1.59
μ(Mo $K\alpha$)/cm^{-1}	9.70

TABLE 2. POSITIONAL AND THERMAL PARAMETERS

Atom	X	Y	Z	B_{eq}/Å^3
Co	0.15075(13)	0.11730(8)	0.06267(16)	3.56
S1	0.4793(4)	0.1738(3)	−0.2118(5)	6.76
N1	0.2568(8)	0.1000(5)	−0.0905(9)	3.62
N2	0.0585(8)	0.1268(6)	0.2267(11)	4.61
N3	0.2359(9)	0.1838(6)	0.1675(11)	4.10
O1	0.2078(8)	0.0409(5)	0.1543(9)	4.73
O2	0.3156(8)	−0.0484(5)	0.1230(10)	5.32
O3	0.0615(8)	0.0550(5)	−0.0394(10)	5.00
O4	0.0894(7)	0.1891(4)	−0.0504(10)	4.40
C1	0.2844(11)	0.0059(6)	0.0859(12)	3.83
C2	0.3291(10)	0.0456(6)	−0.0468(12)	3.87
C3	0.4382(13)	0.0715(10)	−0.0038(16)	6.65
C4	0.5118(15)	0.0918(11)	−0.1280(21)	8.65
C5	0.4266(20)	0.1441(13)	−0.3869(21)	11.79
C6	−0.0364(13)	0.0487(9)	−0.0018(17)	5.47
C7	−0.0984(17)	0.0087(9)	−0.1179(23)	7.04
C8	−0.0887(12)	0.0689(8)	0.1185(17)	5.47
C9	−0.0381(13)	0.1039(7)	0.2356(15)	5.39
C10	−0.1014(13)	0.1176(10)	0.3783(16)	6.88
C11	0.1118(12)	0.1622(7)	0.3544(13)	4.64
C12	0.2293(12)	0.1616(8)	0.3244(15)	5.16
C13	0.2649(11)	0.2414(8)	0.1205(16)	4.75
C14	0.3192(15)	0.2938(9)	0.2181(25)	8.48
C15	0.2387(12)	0.2646(7)	−0.0229(17)	5.08
C16	0.1499(13)	0.2387(6)	−0.0906(13)	4.66
C17	0.1170(15)	0.2707(9)	−0.2360(20)	6.81
F1	−0.1954(11)	0.0000(13)	−0.0899(22)	21.33
F2	−0.0966(12)	0.0408(8)	−0.2481(15)	12.56
F3	−0.0586(15)	−0.0496(7)	−0.1501(17)	14.60
F4	0.1055(17)	0.2259(7)	−0.3354(11)	14.11
F5	0.0217(10)	0.2993(7)	−0.2238(13)	10.70
F6	0.1748(10)	0.3186(8)	−0.2830(18)	14.92

$B_{eq}=8\pi^2\,(U_{12}+U_{22}+U_{33})/3$.

structure was refined by a full-matrix least-squares refinement of the positional and anisotropic thermal parameters of all the non-hydrogen atoms (program RFINE by L. W. Finger was used). The neutral atomic scattering factors for all the non-hydrogen atoms were taken from the literature.[18] The final R and R_w values converged to 0.086 and 0.098, respectively. The absolute configuration was determined on the basis of the known configuration of L-methioninate.[19] The final atomic parameters are given in Table 2. A list of structure factors (Table A), anisotropic thermal parameters of non-hydrogen atoms (Table B), and the projected figure of the crystal structure (Fig. A) are kept at the Chemical Society of Japan as Document No. 8551.

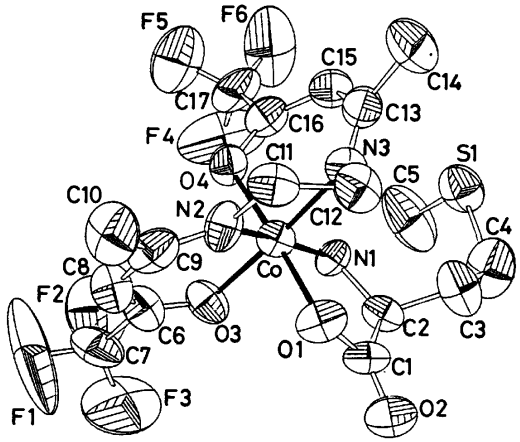

Fig. 1. A perspective drawing of (−)$_{435}$-Λ-cis-β_2-[Co(tfac$_2$en) (L-met)] with the numbering scheme of atoms.

Results and Discussion

Description of the Structure. A perspective drawing of (−)$_{435}$-[Co(tfac$_2$en)(L-met)] is given in Fig. 1, together with a numbering scheme. The bond lengths and angles (with their standard deviations) for the (−)$_{435}$ isomer are listed in Table 3. The L-methioninate ligand coordinates to a cobalt atom with nitrogen and oxygen atoms serving as a bidentate ligand. The tfac$_2$en Schiff base, which coordinates as a quadridentate ligand, takes the cis-β_2 configuration by coordination.[11] Namely, the cobalt atom is surrounded by a meridional N_3O_3 structure and the nitrogen atom in the L-met (N1) is located on the trans position of the nitrogen atom (N2) of the tfac(1) moiety (tfac; 1,1,1-trifluoro-4-imino-2-pentanonate). The absolute configuration of (−)$_{435}$-[Co(tfac$_2$en)(L-met)] was determined to be Λ on the basis of the known absolute configuration, $S(C)$, of the asymmetric carbon atom of the L-methioninate.[19] Thus, the structure of the (−)$_{435}$ isomer is denoted as the Λ-cis-β_2 type (Fig. 1). This has a similar structure to those of [Co(α-Me-sal$_2$en)(L-isoleu)][9] and [Co(α-Me-sal$_2$en)(N-Bz-L-ala)][10] (α-Me-sal$_2$en; N,N'-ethylenebis(*o*-hydroxy-α-methylbenzylideneaminate, L-isoleu; L-isoleucine, and N-Bz-L-ala; N-benzyl-L-alanine). These results coincide with the fact that the cis-α structure of the cobalt(III) Schiff base complexes is unstable and such a complex has not been found yet.[1-5,9,10]

The bond lengths and angles of (−)$_{435}$-[Co(tfac$_2$en)(L-met)] are similar to those of cobalt(III) complexes with amino carboxylate and quadridentate Schiff bases such as salen and α-Me-sal$_2$en (Table 3).[9,10] The Co–O and Co–N bond lengths of the tfac$_2$en ligand are somewhat longer than those of [Co(α-Me-sal$_2$en)(L-isoleu)][9] and [Co(α-Me-sal$_2$en)(N-Bz-L-ala)],[10] while the distances of the L-methioninate, Co–O1 1.849(9) Å and Co–N1 1.968(9) Å, are significantly shorter than those of the N-Bz-L-ala and L-isoleu in the α-Me-sal$_2$en complexes.[9,10] On the contrary, the chelate angles for the L-met,

Table 3. Intermolecular distances and bond angles (with e.s.d.'s)

(a) Bond distances (l/Å)			
Co-N1	1.968(9)	Co-N2	1.909(10)
Co-N3	1.933(11)	Co-O1	1.849(9)
Co-O3	1.898(9)	Co-O4	1.900(9)
S1-C4	1.814(22)	S1-C5	1.829(21)
N1-C2	1.451(15)	N2-C9	1.300(19)
N2-C11	1.513(17)	N3-C12	1.501(17)
N3-C13	1.253(18)	O1-C1	1.337(15)
O2-C1	1.175(15)	O3-C6	1.289(19)
O4-C16	1.282(16)	C1-C2	1.546(16)
C2-C3	1.517(21)	C3-C4	1.520(25)
C6-C7	1.532(26)	C6-C8	1.342(22)
C8-C9	1.421(21)	C9-C10	1.554(21)
C11-C12	1.509(22)	C13-C14	1.517(25)
C13-C15	1.427(21)	C15-C16	1.377(21)
C16-C17	1.526(22)	C7-F1	1.263(26)
C7-F2	1.345(25)	C7-F3	1.273(23)
C17-F4	1.265(21)	C17-F5	1.329(23)
C17-F6	1.259(23)		
(b) Bond angles (ϕ/°)			
N1-Co-N2	172.7(4)	N1-Co-N3	95.1(4)
N1-Co-O1	85.5(4)	N1-Co-O3	86.8(4)
N1-Co-O4	90.8(4)	N2-Co-N3	83.4(5)
N2-Co-O1	87.6(4)	N2-Co-O3	95.0(4)
N2-Co-O4	96.3(4)	N3-Co-O1	95.3(4)
N3-Co-O3	177.2(5)	N3-Co-O4	90.4(4)
O1-Co-O3	86.8(4)	O1-Co-O4	173.4(4)
O3-Co-O4	87.5(4)	C4-S1-C5	100.2(10)
Co-N1-C2	110.9(7)	Co-N2-C9	126.0(9)
Co-N2-C11	112.3(8)	C9-N2-C11	121.6(11)
Co-N3-C12	104.7(8)	Co-N3-C13	126.0(10)
C12-N3-C13	126.8(12)	Co-O1-C1	118.5(7)
Co-O3-C6	119.9(9)	Co-O4-C16	117.7(9)
O1-C1-O2	124.3(11)	O1-C1-C2	112.3(10)
O2-C1-C2	123.4(11)	N1-C2-C1	110.4(10)
N1-C2-C3	113.6(11)	C1-C2-C3	107.0(10)
C2-C3-C4	116.5(13)	S1-C4-C3	113.9(13)
O3-C6-C7	110.6(14)	O3-C6-C8	131.6(15)
C7-C6-C8	117.8(15)	C6-C8-C9	122.5(14)
N2-C9-C8	122.5(13)	N2-C9-C10	118.4(13)
C8-C9-C10	119.0(14)	N2-C11-C12	107.0(10)
N3-C12-C11	103.1(11)	N3-C13-C14	121.9(14)
N3-C13-C15	122.0(13)	C14-C13-C15	115.7(14)
C13-C15-C16	119.2(13)	O4-C16-C15	129.0(12)
O4-C16-C17	113.2(13)	C15-C16-C17	117.7(13)
C6-C7-F1	115.0(19)	C6-C7-F2	111.8(15)
C6-C7-F3	114.2(18)	F1-C7-F2	105.0(19)
F1-C7-F3	108.2(19)	F2-C7-F3	101.5(17)
C16-C17-F4	112.2(14)	C16-C17-F5	110.0(15)
C16-C17-F6	116.2(16)	F4-C17-F5	104.1(17)
F4-C17-F6	109.2(17)	F5-C17-F6	104.1(15)

Table 4. Displacements of atoms from the least-squares plane (d/Å) and dihedral angles between the planes

Least-square planes:

plane(1); $0.4109X-0.7637Y+0.4979Z+0.6449=0$

Co −0.0258 N1 0.0833 N2 0.1031 N3 −0.0913 O3 −0.0310

plane(2); $-0.7088X+0.0866Y+0.7001Z+0.7608=0$

Co 0.0110 N3 0.0326 O1 −0.0410 O3 0.0504 O4 −0.0442

plane(3); $-0.6434X-0.6255Y-0.4423Z+2.8790=0$

Co −0.0222 N1 −0.0544 N2 −0.0507 O1 0.0711 O4 0.0609

tfac(1); $0.2575X-0.8507Y+0.4582Z+0.9085=0$

N2 −0.0431 O3 0.0349 C6 −0.0220 C8 −0.0201 C9 0.0574

tfac(2); $0.5818X-0.6342Y-0.5092Z+1.4335=0$

N3 0.1242 O4 −0.0017 C13 −0.1535 C15 0.0365 C16 0.0198

met; $-0.6759X-0.5172Y-0.5251Z+2.8872=0$

N1 0.1280 O1 −0.0383 O2 0.0895 C1 −0.0110 C2 −0.1528

Dihedral angles between the planes:

plane(1)-tfac(1)	10.4°	plane(2)-plane(3)	84.7°
plane(1)-plane(2)	89.5°	plane(2)-tfac(1)	86.3°
plane(1)-plane(3)	89.6°	plane(2)-met	86.2°
plane(1)-tfac(2)	62.0°	plane(3)-met	8.1°
plane(1)-met	81.7°	plane(3)-tfac(1)	80.6°
plane(2)-tfac(2)	34.5°	plane(3)-tfac(2)	75.7°

N1-Co-O1 85.5(4)°, and for the tfac$_2$en, N2-Co-N3 83.4(5)° and N3-Co-O4 90.4(4)°, are approximately in agreement with those of the cobalt(III) complexes with α-Me-sal$_2$en and amino carboxylate.[9,10]

The angles among the planes of the three equatorial planes, plane(1)-plane(3), of the octahedron around the cobalt atom and the planes passing through tfac(1), tfac(2), and the L-met moieties are summarized in Table 4. These dihedral angles are affected by the highly strained conformational state about the coordinated ethylene ring, N2-C11-C12-N3, and the coordination geometry around the azomethine nitrogens, N2 and N3, as in the case of the cobalt(III) complexes with a quadridentate Schiff base.[7-10] In the present complex, however, the dihedral angle between plane(1) and tfac(1) is 10.4° and is smaller than the corresponding angles of [Co(salen)(acac)] (17.9°)[7] and [Co(α-Me-sal$_2$en)(*N*-Bz-L-ala)](29.3°).[10] This seems to reflect the difference in the rigidity between the 1,1,1-trifluoro-4-imino-2-pentanonate and salicylideneaminate moieties.

Absorption and CD Spectra. The electronic absorption and CD spectra of $(-)_{435}$-Λ-cis-β_2-and $(+)_{435}$-[Co(tfac$_2$en)(L-met)] are shown in Fig. 2 and their data are summarized in Table 5. The absorption spectral behaviors of the $(-)_{435}$-Λ-cis-β_2 and $(+)_{435}$ isomers closely resemble each other, showing identical peaks at 17.24, 29.76, and 38.17×10^3 cm^{-1}. The $(-)_{435}$-Λ-cis-β_2 isomer exhibits four CD bands in the region of 14—35×10^3 cm^{-1}, corresponding to absorption peaks and shoulders as shown in Fig. 2. The $(+)_{435}$ isomer exhibits CD patterns that are almost enantiomeric relative to that of the $(-)_{435}$-Λ-cis-β_2 one. These facts indicate that the $(+)_{435}$ isomer can safely be assigned a Δ-cis-β_2 structure.

The configurational CD curve (Λ) and the vicinal CD curve (L) due to a coordinated L-met of the $(-)_{435}$-Λ-cis-β_2 isomer are shown in Fig. 2. These were calculated using the following equations:

$$(\text{L}) = 1/2 \times \{\Delta\varepsilon(-) + \Delta\varepsilon(+)\}$$

$$(\Lambda) = 1/2 \times \{\Delta\varepsilon(-) - \Delta\varepsilon(+)\}$$

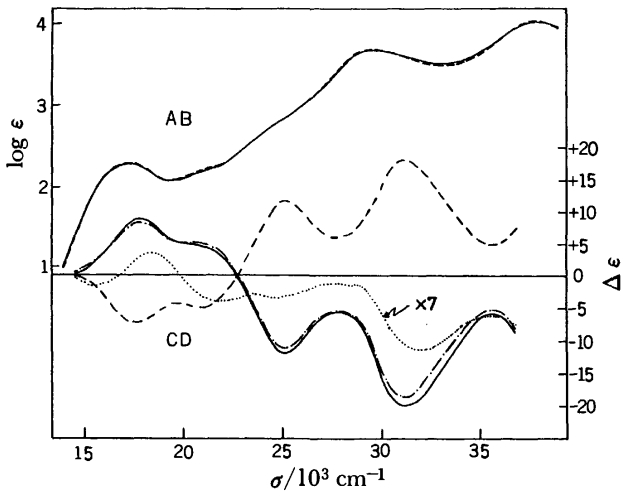

Fig. 2. Absorption and CD spectra of *cis*-β_2-[Co(tfac$_2$en)(L-met)] in DMF-$CHCl_3$ (1:4) mixture: $(-)_{435}$-*Λ-cis*-β_2 (——) and $(+)_{435}$-*Δ-cis*-β_2 (------). Two calculated CD curves of the vicinal (·····) and configurational (—·—·—·—) effects are also shown.

TABLE 5. ABSORPTION AND CD SPECTRAL DATA OF [Co(tfac$_2$en)(L-met)][a]

Isomer	Absorption maxima $\sigma/10^3$ cm^{-1} (log ε/mol^{-1} dm^3 cm^{-1})	CD extrema $\sigma/10^3$ cm^{-1} ($\Delta\varepsilon$/mol^{-1} dm^3 cm^{-1})
$(-)_{435}$-Λ-cis-β_2	17.24 (2.31)	17.54 (+8.43)
	21.28 (2.21 sh[b])	20.83 (+4.15)
	24.50 (2.75 sh)	24.69 (−12.25)
	29.76 (3.69)	30.86 (−20.54)
	38.17 (4.08)	
$(+)_{435}$-Δ-cis-β_2	17.24 (2.33)	17.24 (−7.68)
	21.28 (2.23 sh)	20.83 (−5.26)
	24.50 (2.75 sh)	24.69 (+11.28)
	29.76 (3.71)	30.67 (+17.62)
	38.17 (4.10)	

a) Solvent; DMF-$CHCl_3$ (1:4) mixture. b) sh; shoulder.

where $\Delta\varepsilon(-)$ and $\Delta\varepsilon(+)$ denote the CD curves of the $(-)_{435}$ and $(+)_{435}$ isomers, respectively. The calculated configurational curve (Λ) shows almost the same pattern as the $(-)_{435}$-Λ-cis-β_2 isomer over the whole region and the positive CD sign in the first d-d absorption band region (Fig. 2). A similar configurational CD behavior has also been observed for the Λ-cis-β_2 isomers of cobalt(III) complexes with a sal$_2$en-type Schiff base and amino carboxylate.[5] The vicinal CD contribution (L) in the first d-d absorption band region is quite similar to those of sal$_2$en and α-Me-sal$_2$en cobalt(III) complexes with L-amino carboxylates chelated by their nitrogen and oxygen atoms (Fig. 2).[5] This fact coincides with the results of the present X-ray crystal analysis: (1) the coordinated atoms of L-met in [Co(tfac$_2$en)(L-met)] are nitrogen and oxygen and (2) the conformation of the N-O chelate ring of the coordinated L-met is quite similar to those of the L-amino carboxylates in α-Me-sal$_2$en complexes.[9,10]

It is interesting to note that the CD intensities in the d-d absorption band regions of Λ- or Δ-cis-β_2-[Co(tfac$_2$en)(L-met)](Fig. 2 and Table 5) are stronger than those of optically active cobalt(III) complexes with the linear quadridentate ligands such as ethylenediamine-*N,N'*-diacetate (edda) and its derivatives.[20] The absorption shoulder at 24.50×10^3 cm^{-1} and the CD band at 24.69×10^3 cm^{-1} seem to correspond to the second d-d absorption band due to their position and the absorption intensity (log ε=2.75). Also, the CD intensity is quite strong compared with that of cobalt(III) complexes with an edda-type ligand.[20] This intense CD band in the second d-d absorption band region seems to arise from a coordination of the alcoholic oxygen atoms of the Schiff base ligand to the cobalt(III) ion.[21] Such an increase of CD intensity has also been observed in the case of sal$_2$en-type complexes.[1,2,4,5]

The Λ- or Δ-cis-β_2 isomer of [Co(tfac$_2$en)(L-met)] exhibit an absorption band at 29.76×10^3 cm^{-1} and the CD band at *ca.* 30×10^3 cm^{-1} (Fig. 2). It has been known that the sal$_2$en-type complexes of Cu(II), Ni(II), Co(II), Co(III), and so on exhibit broad absorption bands and CD bands at *ca.* 30×10^3 cm^{-1} due to ligand π-π* transitions. This is mostly associated with an azomethine chromophore.[12-15] This suggests that the absorption and CD bands at *ca.* 30×10^3 cm^{-1} are assignable to the ligand π-π* transition due to azomethine moieties in the tfac$_2$en ligand. In the simple sal$_2$en-type complexes of Cu(II), Ni(II), Co(II), and Co(III), π-π* transitions split into two CD components with different signs due to the exciton interaction.[12-15] However, *Λ-* or *Δ-cis*-β_2-[Co(tfac$_2$en)(L-met)] exhibits only one CD band for this transition region and no exciton couplet was observed (Fig. 2). A similar trend was also observed for cis-β_2 type cobalt(III) complexes with a sal$_2$en-type Schiff base and bidentate ligands.[1-5] These facts suggest that the two azomethine moieties in *Λ-* or *Δ-cis*-β_2-[Co(tfac$_2$en)(L-met)] form a negligible dihedral angle which gives rise to non-zero components regarding the exciton interaction between them.

Properties. The $(-)_{435}$-Λ- and $(+)_{435}$-Δ-cis-β_2 isomers of [Co(tfac$_2$en)(L-met)] showed no mutarotation in *N,N*-dimethylformamide, dimethyl sulfoxide, and chloroform. However, they did exhibit mutarotation in methanol and showed the same optical rotation under equilibrium conditions (Fig. 3). The absorption spectral change during mutarotation was very small for each of the $(-)_{435}$-Λ- and $(+)_{435}$-Δ-cis-β_2 isomers and plots of ln $\alpha_\infty-\alpha_t$ *vs.* time for each mutarotation gave a straight line with the same slope ($k_{obsd}=9.50\times10^{-5}$ s^{-1}) up to at least 90% completion,[22] where α_t and α_∞ denote the optical rotation at 435 nm at time t and at equilibrium, respectively. Accordingly, it is obvious that the two isomers of *cis*-β_2-[Co(tfac$_2$en)(L-met)] isomerize in methanol to give a mixture of both isomers under equilibrium conditions. As shown in Fig. 4, the ^{1}H NMR spectra of the $(-)_{435}$

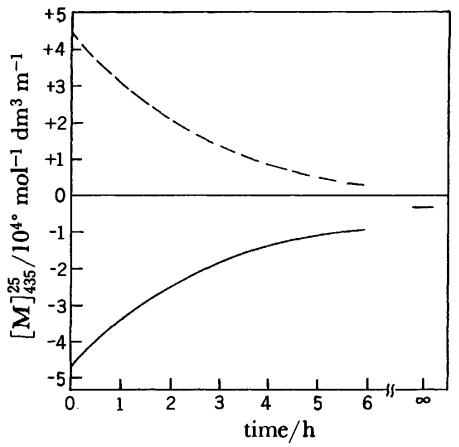

Fig. 3. Mutarotation of *cis*-β_2-[Co(tfac$_2$en)(L-met)] in CH_3OH at 25 °C: $(-)_{435}$-*Λ-cis*-β_2 (——) and $(+)_{435}$-Δ-*cis*-β_2 (------).

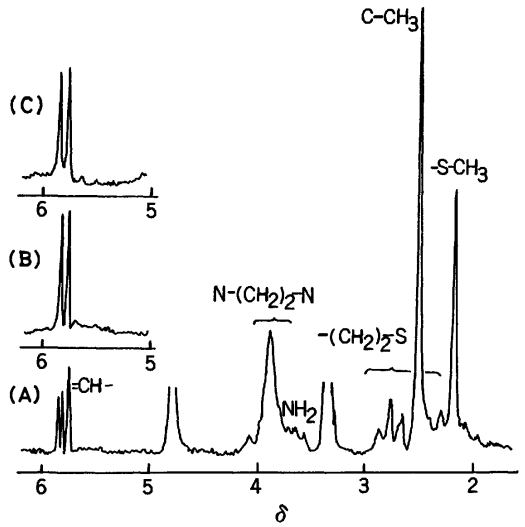

Fig. 4. ^{1}H NMR spectrum of *cis*-β_2-[Co(tfac$_2$en)(L-met)] in CD_3OD under equilibrium condition (A), and the C=CH signals of the $(-)_{435}$ (B) and $(+)_{435}$ (C) isomers soon after dissolution.

and $(+)_{435}$ isomers closely resemble each other except for the C=CH signal, supporting a similar geometrical structure to each other. From the intensity of the ^{1}H NMR signal for C=CH, the isomeric ratio in the equilibrium mixture, Λ-cis-β_2: Δ-cis-β_2, was estimated to be about 1:1. This ratio differs significantly from those in *cis*-β_2-[Co(sal$_2$en)(L-met)] (1.5:1) and *cis*-β_2-[Co(α-Me-sal$_2$en)(L-met)](2:1). This difference of diastereomeric stereoselectivity may be partly due to the flexibility of the β-imino ketone moieties as compared with those of salicylideneaminate. The $(-)_{435}$-Λ-cis-β_2 isomer was crystallized in high yield (*ca.* 80% for the total complex) from the solution, regardless of a 1:1 formation of the $(-)_{435}$-Λ- and $(+)_{435}$-Δ-cis-β_2 isomers under equilibrium conditions. Since the complex was labile in isomerization, the preferential crystallization of the $(-)_{435}$-Λ-cis-β_2 isomer could be safely ascribed to a thermodynamic origin. That is, a second-order asymmetric transformation from the Δ-cis-β_2 isomer to the Λ-cis-β_2 isomer due to the lower solubility of the latter. This kind of preferential crystallization is quite rare in cobalt(III) complexes.

In the case of [Co(tfac$_2$en)(L-met)], a cis-β_2 isomer was formed in the 100% regioselectivity as observed for the sal$_2$en-type Schiff base complexes.[1-5,9,10] Therefore, the regioselective behavior seems to be common in mixed cobalt(III) complexes with various kinds of quadridentate Schiff bases and amino carboxylate. It is fairly difficult, however, to explain the stereochemical reason for the high regioselectivity toward the cis-β_2 structure, *mer*(N_3O_3), as the corresponding cis-β_1 isomer, *fac*(N_3O_3), has not been found yet. It is probable that an electrostatic repulsion among three negatively charged oxygen atoms is much weaker in the *mer*(N_3O_3) configuration than in the *fac*(N_3O_3) configuration. Thus, the cis-β_2 isomer is thermodynamically more stable than the cis-β_1 isomer.[10]

References

1) Y. Fujii, T. Isago, M. Sano, N. Yanagibashi, S. Hirasawa, and S. Takahashi, *Bull. Chem. Soc. Jpn.*, **49**, 3509 (1976).

2) Y. Fujii, M. Sano, and Y. Nakano, *Bull. Chem. Soc. Jpn.*, **50**, 2609 (1977).

3) Y. Fujii, K. Shiono, K. Ezuka, and T. Isago, *Bull. Chem. Soc. Jpn.*, **53**, 3537 (1980).

4) Y. Fujii, M. Matsufuru, A. Saito, and S. Tsuchiya, *Bull. Chem. Soc. Jpn.*, **54**, 2029 (1981).

5) Y. Fujii, Y. Kuwano, S. Takahashi, K. Shimizu, and K. Hiroi, *Bull. Chem. Soc. Jpn.*, **55**, 2598 (1982).

6) M. Nakamura, H. Okawa, T. Inazu, and S. Kida, *Bull. Chem. Soc. Jpn.*, **55**, 2400 (1982).

7) N. A. Bailey, B. M. Higson, and E. D. Mckenzie, *J. Chem. Soc., Dalton Trans.*, **1972**, 503.

8) M. Calligaris, G. Manzini, G. Nardin, and L. Randaccio, *J. Chem. Soc., Dalton Trans.*, **1972**, 543.

9) Y. Kushi, R. Tamura, M. Kuramoto, T. Yoshizawa, H. Yoneda, and Y. Fujii, *J. Chem. Soc., Chem. Commun.*, **1978**, 266.

10) Y. Kushi, T. Tada, Y. Fujii, and H. Yoneda, *Bull. Chem. Soc. Jpn.*, **55**, 1834 (1982).

11) a) The cis-α and cis-β denote the trans(O) and cis(O) configurations of the coordinated quadridentate Schiff base ligand, respectively, when the remaining two coordination sites occupy the cis position. b) β_1 and β_2 refer to the two configurational isomers, *fac(N)* and mer(N), for the $[Co(N)_3(O)_3]$-type complex, as shown in Ref. 1—5, 8, and 9.

12) B. Bosnich, *J. Am. Chem. Soc.*, **90**, 627 (1968).

13) R. S. Downing and F. L. Urbach, *J. Am. Chem. Soc.*, **92**, 5861 (1970).

14) R. L. Farmer and F. L. Urbach, *Inorg. Chem.*, **9**, 2562 (1970).

15) A. Pasini, M. Gullotti, and R. Ugo, *J. Chem. Soc., Dalton Trans.*, **1977**, 346.

16) P. J. McCarthy, R. J. Hovey, K. Ueno, and A. E. Martell, *J. Am. Chem. Soc.*, **77**, 5820 (1955).

17) Y. Fujii, M. Ito, and K. Akiyama, *Bull. Chem. Soc.*

Jpn., **54**, 2527 (1981).
18) "International Tables for X-Ray Crystallography," Kynoch Press, Birmingham (1974), Vol. IV.
19) J. P. Greenstein and M. Winitz, "Chemistry of the Amino Acids," Wiley, New York (1961), Vol. 3, Chap. 33.
20) M. Okabayashi, K. Okamoto, H. Einaga, and J. Hidaka, *Bull. Chem. Soc. Jpn.*, **56**, 157 (1983).
21) K. Ogino, K. Uchida, T. Nishida, J. Fujita, and K. Saito, *Chem. Lett.*, **1973**, 679; Y. Nishida, "Optical Rotatory Dispersion and Circular Dichroism," in "Chelate Chemistry," ed by K. Ueno, Nankodo, Tokyo (1976), Vol. 2, Chap. 7.
22) Y. Fujii, T. Kobayashi, M. Matsufuru, and S. Takahashi, *Bull. Chem. Soc. Jpn.*, **56**, 3608 (1983).

Preparation and Stereochemistry of Cobalt(III) Complexes Containing (3*S*,8*S*)-3,8-Dimethyl-1,1,10,10-tetraphenyl-4,7-diaza-1,10-diphosphadecane or (4*S*,9*S*)-2,4,9,11-Tetramethyl-5,8-diaza-2,11-diphosphadodecane (*SS*-Me$_2$-mm-PNNP). Molecular Structure of (+)$_{589}$-*Λ*-*cis*-*β*-[Co(acac)(*SS*-Me$_2$-mm-PNNP)](ClO$_4$)$_2$·H$_2$O (acac=C$_5$H$_7$O$_2^-$)

Masamichi Atoh, Kazuo Kashiwabara, and Junnosuke Fujita*
Department of Chemistry, Faculty of Science, Nagoya University, Chikusa-ku, Nagoya 464
(Received July 16, 1985)

Two new optically active quadridentate phosphine ligands, (3*S*,8*S*)-3,8-dimethyl-1,1,10,10-tetraphenyl-4,7-diaza-1,10-diphosphadecane(*SS*-Me$_2$-pp-PNNP) and (4*S*,9*S*)-2,4,9,11-tetramethyl-5,8-diaza-2,11-diphosphadodecane-(*SS*-Me$_2$-mm-PNNP) and their cobalt(III) complexes, *trans*-[CoCl$_2$(*SS*-Me$_2$-pp- or *SS*-Me$_2$-mm-PNNP)]$^+$, *Λ*-*cis*-*β*-[Co(acac)(*SS*-Me$_2$-pp-PNNP)]$^{2+}$ (acac=2,4-pentanedionate ion), *Λ*-*cis*-*β*-[Co(CO$_3$)(*SS*-Me$_2$-pp-PNNP)]$^+$, and *Δ*- and *Λ*-*cis*-*β*-[Co(acac)(*SS*-Me$_2$-mm-PNNP)]$^{2+}$ were prepared and characterized. The molecular structure and the absolute configuration of (+)$_{589}$-*Λ*-*cis*-*β*-[Co(acac)(*SS*-Me$_2$-mm-PNNP)](ClO$_4$)$_2$·H$_2$O were determined by X-ray analysis. Crystal data; monoclinic, C2, *a*=28.274(4)Å, *b*=9.266(1)Å, *c*=11.0901(9)Å, *β*=92.97(1)°, *V*=2901.6(5)Å^3, and *Z*=4. Three five-membered chelate rings in the complex form distorted gauche (*δλλ*) conformations, and the methyl group on carbon of the apically linked chelate ring takes an axial disposition. Stereochemistry of all the complexes was discussed on the basis of the NMR, absorption and CD spectra.

In a previous paper,[1] cobalt(III) complexes containing 1,1,10,10-tetraphenyl-4,7-diaza-1,10-diphosphadecane (pp-PNNP) or 2,11-dimethyl-5,8-diaza-2,11-diphosphadodecane (mm-PNNP) were prepared, and the absorption spectra and stereochemistry were compared with those of the corresponding (2-aminoethyl)-diphenylphosphine (edpp) complexes. All of these quadridentate phosphine complexes formed stereoselectively a particular geometrical isomer. Introduction of asymmetric carbon atoms into a chelate ligand often brings about remarkable stereoselectivity in the formation of a particular optical isomer.[2] In this paper, we have prepared two optically active quadridentate phosphine ligands, (3*S*,8*S*)-3,8-dimethyl-1,1,10,10-tetraphenyl-4,7-diaza-1,10-diphosphadecane (*SS*-Me$_2$-pp-PNNP) and (4*S*,9*S*)-2,4,9,11-tetramethyl-5,8-diaza-2,11-diphosphadodecane (*SS*-Me$_2$-mm-PNNP), and their cobalt(III) complexes. The structure and absolute configuration of (+)$_{589}$-[Co(acac)(*SS*-Me$_2$-mm-PNNP)](ClO$_4$)$_2$·H$_2$O (acac=2,4-pentanedionate ion) have been determined by the X-ray diffraction method. Stereochemistry of other complexes was discussed by comparing the NMR, absorption, and circular dichroism spectra with those of the structurally known (+)$_{589}$-complex.

Experimental

Phosphine ligands, *SS*-Me$_2$-pp- and *SS*-*Me*$_2$-mm-PNNP, were prepared and handled under an atmosphere of nitrogen until they formed cobalt(III) complexes. All solvents used for preparing the ligands and complexes are deoxygenated by bubbling nitrogen for 20 min immediately before use. ^{1}H NMR, absorption and circular dichroism spectra were recorded on a Jeol JNM GX-400 spectrometer, a Hitachi 323 spectrophotometer and a Jasco J-40CS spectropolarimeter, respectively.

Preparation of Ligands. The optically active quadridentate phosphine ligands were prepared according to the synthetic route given in Scheme 1.

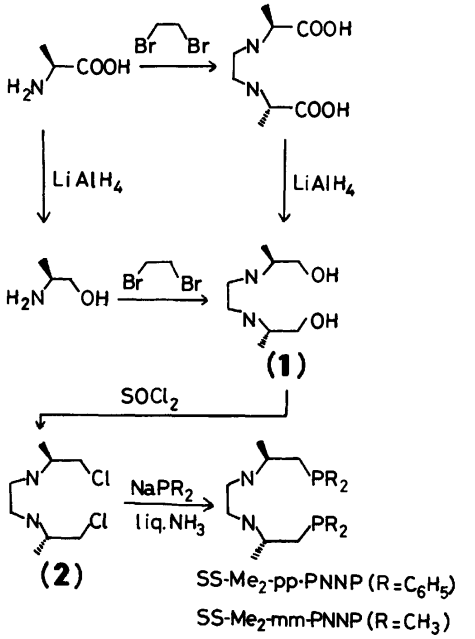

Scheme 1.

(2*S*,7*S*)-2,7-Dimethyl-3,6-diaza-1,8-octanediol (**1**) was prepared from (*S*)-alaninol (2-amino-1-propanol)[3] by a modified method of Holdiness *et al.*[4] (method **a**), or from (2*S*,7*S*)-2,7-dimethyl-3,6-diaza-octanedionic acid (EDDP)[5] (method **b**). Method **a**: To (*S*)-alaninol (63.8 g, 0.85 mol) in a 1 dm^3 three-necked round bottom flask was added dropwise 1,2-dibromoethane (25.3 g, 0.125 mol) over 1 h at 100 °C with stirring. Stirring was continued for 4 h at 100 °C, and then the solution was cooled to 0 °C and mixed with KOH (19.6 g, 0.35 mol) in ethanol (200 cm^3). After 1 h KBr precipitated was filtered, and the filtrate was evaporated under reduced pressure to remove ethanol, yielding an oily liquid. The liquid was distilled at *ca.* 130 Pa, giving unreacted (*S*)-alaninol at *ca.* 50 °C and the desired **1** at *ca.* 160 °C. Yield: 15.1 g, mp 99 °C, [*α*]$_D$=+28 °(H$_2$O, 25 °C). Elemental analysis

was performed on the hydrochloride salt of **1** (*vide infra*). Method **b**: To $LiAlH_4$ (15 g) in THF (400 cm^3) at 0 °C was added EDDP (14.8 g, 72.5 mmol) in small portions with stirring. The mixture foamed violently. The resulting solution was stirred at 0 °C for 30 min and then refluxed for 10 h. After cooling an aqueous solution (*ca.* 100 cm^3) saturated with KNa[*d*-tartrate]·$4H_2O$ was added dropwise to the solution. A white precipitate was filtered and washed twice with ethanol (50 cm^3×2). The filtrate and washings were combined, and the solvent was evaporated under reduced pressure. An oily liquid obtained was vacuum-distilled under the same conditions as in Method **a** to yield **1**. Yield: 6.05 g.

(2*S*,7*S*)-2,7-Dimethyl-1,8-dichloro-3,6-diazaoctane dihydrochloride (**2**) was prepared from **1**. HCl gas was bubbled under cooling into a chloroform solution (150 cm^3) of **1** (6.0 g, 34 mmol) in a 1 dm^3 three-necked round bottom flask, yielding white crystals (Found: C, 38.39; H, 8.93; N, 11.04%. Calcd for $C_8H_{22}N_2Cl_2O_2$=**1**·2HCl: C, 38.56; H, 8.93; N, 11.24%.). To the mixture was added $SOCl_2$ (12.5 g, 0.121 mol) dropwise over 15 min under cooling. The resulting solution was refluxed for 4 h in a water bath (60 °C), and then cooled in an ice bath. White crystals formed were filtered and recrystallized from hot isopropyl alcohol (200 cm^3). Yield: 4.5 g. Found: C, 33.72; H, 7.04; N, 9.84%. Calcd for $C_8H_{20}N_2Cl_4$(**2**): C, 33.59; H, 7.05; N, 9.79%.

(3S,8S)-3,8-Dimethyl-1,1,10,10-tetraphenyl-4,7-diaza-1,10-diphosphadecane (SS-Me$_2$*-pp-PNNP).* To liquid ammonia (250 cm^3) containing metallic sodium (1.33 g, 57.8 mmol) in a 500 cm^3 three-necked round bottom flask was added dropwise diphenylphosphine[6] (11.0 g, 59.1 mmol) over 5 min with stirring at −78 °C. After stirring for 1 h, the color of the solution changed from deep blue to orange. To the orange solution was added compound **2** (4.15 g, 14.5 mmol) in small portions with stirring. Stirring was continued for 1 h, giving a colorless solution. After liquid ammonia had been evaporated, water (100 cm^3) and then diethyl ether (80 cm^3) were added to the residue with stirring. The ethereal layer was separated from the aqueous layer and dried over $MgSO_4$ (*ca.* 3 g) overnight. A viscous liquid was obtained by removing the solvent and unreacted diphenylphosphine under vacuum. The product (*ca.* 6.0 g) was used for preparing cobalt(III) complexes without further purification.

(4S,9S)-2,4,9,11-Tetramethyl-5,8-diaza-2,11-diphosphadodecane (SS-Me$_2$*-mm-PNNP).* To liquid ammonia (100 cm^3) containing metallic sodium (0.6 g, 26 mmol) in a 300 cm^3 three-necked round bottom flask was added dropwise tetramethyldiphosphine[7] (1.5 g, 12.3 mmol) with stirring at −78 °C. After stirring for 1 h, compound **2** (1.8 g, 6.3 mmol) was added to the resulting orange solution in small portions with stirring. After 1 h liquid ammonia was evaporated, and then water (50 cm^3) and diethyl ether (50 cm^3) were added successively to the residue with stirring. The ethereal layer was separated from the aqueous layer, dried over $MgSO_4$ (*ca.* 2 g) overnight, and then distilled under reduced pressure to remove the solvent and unreacted dimethylphosphine. The colorless oily product thus obtained (*ca.* 1.3 g) was used for preparing cobalt(III) complexes without further purification.

Preparation of Complexes. trans-*[CoCl*$_2$*(SS-Me*$_2$*-pp-PNNP)]ClO*$_4$·*0.5H*$_2$*O*: To a methanol solution (50 cm^3) of $Co(ClO_4)_2·6H_2O$ (1.30 g, 3.55 mmol) was added *SS*-Me_2-pp-PNNP (1.75 g, 3.99 mmol) with stirring. An orange solution was obtained. Methanol was removed under reduced pressure, and the residue was dissolved in dichloromethane (250 cm^3). Chlorine gas was bubbled into the dichloromethane solution for 10 min, and then nitrogen gas for 20 min to remove excess Cl_2. To the resulting green solution was added methanol (20 cm^3), and the solution was evaporated to a small volume under reduced pressure, yielding a green precipitate (the solution should not be evaporated to dryness since perchlorates of complexes are potentially explosive in a solid state). The precipitate was dissolved in hot methanol (150 cm^3). Solid $NaClO_4·H_2O$ (22 g) was dissolved in the solution, which was stored in a refrigerator overnight. Green crystals yielded were filtered, washed with water and then diethyl ether, and air-dried. Yield: 627 mg. Additional crystals (234 mg) were obtained by concentrating the filtrate. Total yield: 34%. Found: C, 51.24; H, 5.00; N, 3.67%. Calcd for $C_{32}H_{39}N_2Cl_3CoO_{4.5}P_2$: C, 51.18; H, 5.23; N, 3.73%. The complex is soluble in methanol, dichloromethane, chloroform and acetone, but not in water, diethyl ether and benzene.

trans-*[CoCl*$_2$*(SS-Me*$_2$*-mm-PNNP)]ClO*$_4$·*0.5H*$_2$*O*. To *cis*-$[CoCl_2(en)_2]Cl$[8] (en=ethylenediamine) (2.5 g, 8.76 mmol) in a mixture of water (10 cm^3) and methanol (40 cm^3) was added *SS*-Me_2-mm-PNNP (0.871 g, 3.30 mmol) with stirring. After 1 h the solution was mixed with concd HCl(10 cm^3) and stirred for 4 h, the temperature of the solution being gradually raised from room temperature to 45 °C. The solution was cooled, filtered to remove $[Co(en)_3]Cl_3$ precipitated, and the filtrate was evaporated to dryness. Methanol (100 cm^3) was added to the residure, and the solution was filtered to remove insoluble $[Co(en)_3]Cl_3$. The filtrate was diluted with water (500 cm^3), and the solution was applied on a column (ϕ 8 cm×5 cm) of SP-Sephadex C-25 (Na^+ form). By elution with 0.05 mol dm^{-3} HCl, a blue eluate was collected, and evaporated to dryness under reduced pressure. The blue complex was extracted from the residue with ethanol, and the extract was evaporated again to dryness under reduced pressure. The residue was mixed with $LiClO_4·3H_2O$ (2 g) in water (15 cm^3), and the solution was stored in a refrigerator overnight, yielding blue crystals, which were filtered, washed with water and air-dried. Yield: 267 mg. Found: C, 28.73; H, 6.57; N, 5.06%. Calcd for $C_{12}H_{31}N_2Cl_3CoO_{4.5}P_2$: C, 28.68; H, 6.02; N, 5.57%. The complex is soluble in water, methanol and acetone, but not in dichloromethane, chloroform, diethyl ether and benzene.

Λ-cis*β*-*[Co(acac)(SS-Me*$_2$*-pp-PNNP)](ClO*$_4$*)*$_2$·*H*$_2$*O*. A methanol solution (75 cm^3) containing *trans*-$[CoCl_2(SS$-Me_2-pp-PNNP)]ClO_4·0.5H_2O$ (200 mg, 0.266 mmol) and Li(acac) (30 mg, 0.28 mmol) was stirred at room temperature for 7 h. The resulting orange-red solution was diluted with water (700 cm^3), and the solution was applied on a column (ϕ 3.5 cm×100 cm) of SP-Sephadex C-25. By elution with 0.2 mol dm^{-3} NaBr, a very small red band, a large red one, and a brown one were eluted successively. The eluate of the second red band was collected and concentrated to a small volume under reduced pressure. The red complex was extracted with chloroform, and the extract was evaporated to dryness. The residue was dissolved in water (10 cm^3), and the solution was mixed with $NaClO_4·H_2O$ (0.2 g) in water (1 cm^3). Red crystals formed were filtered, washed with a very small amount of water and then diethyl ether, and air-dried. Yield: *ca.* 50 mg. Found: C, 50.29; H, 5.19; N, 3.28%. Calcd for $C_{37}H_{47}N_2Cl_2CoO_{11}P_2$: C, 50.07; H, 5.34; N, 3.16%. The complex is soluble in water, methanol, dichloromethane and acetone, but not in diethyl ether and benzene.

(−)$_{589}$-Δ-cisβ-[Co(acac)(SS-Me$_2$-mm-PNNP)](ClO$_4$)$_2$·0.5NaClO$_4$·H$_2$O and (+)$_{589}$-Λ-cisβ-[Co(acac)(SS-Me$_2$-mm-PNNP)](ClO$_4$)$_2$·H$_2$O. A mixture of [Co(acac)$_3$][9] (380 mg, 1.08 mmol), *SS*-Me$_2$-mm-PNNP (200 mg, 0.320 mmol) and active charcoal (*ca.* 50 mg) in methanol (100 cm^3) was stirred at room temperature for 10 h, and filtered. The filtrate was diluted with water (1 dm^3) and applied on a column (φ3.5 cm×10 cm) of SP-Sephadex C-25. After complexes with the +1 charge contained in the adsorbed product had been eluted with 0.05 mol dm^{-3} NaCl, those with the +2 charge were eluted with 0.2 mol dm^{-3} NaCl. The orange eluate obtained was diluted with water (3 dm^3) and applied on a column (φ 3 cm×30 cm) of SE-Toyopearl.[10] Yellow-orange and orange bands (F-1 and F-2) were eluted successively with 0.3 mol dm^{-3} NaCl. Each eluate of F-1 and F-2 was mixed with excess NaClO$_4$·H$_2$O (*ca.* 2 g), and concentrated to a small volume under reduced pressure, yielding orange crystals which were filtered, washed with cold water, and air-dried. Yield (F-1): 10 mg. Found: C, 29.43; H, 5.72; N, 3.99%. Calcd for $C_{17}H_{39}N_2Cl_{2.5}CoNa_{0.5}O_{13}P_2$: C, 29.15; H, 5.61; N, 4.00%. Yield (F-2): 80 mg. Found: C, 32.04; H, 5.96; N, 4.52%. Calcd for $C_{17}H_{39}N_2CoCl_2O_{11}P_2$: C, 31.94; H, 6.15; N, 4.38%. Both complexes are soluble in water, methanol and acetone, but not in chloroform, dichloromethane, diethyl ether and benzene. Complexes F-1 and F-2 were assigned as the *Δ-cisβ* and *Λ-cisβ* isomers, respectively (*vide post*).

Λ-cisβ-[Co(CO$_3$)(SS-Me$_2$-pp-PNNP)]ClO$_4$·1.5(NaClO$_4$)·H$_2$O. To a methanol solution (100 cm^3) of *trans*-[CoCl$_2$(*SS*-Me$_2$-pp-PNNP)]ClO$_4$·0.5H$_2$O (300 mg, 0.40 mmol) were added (NH$_4$)$_2$CO$_3$ (100 mg, 1.04 mmol) and active charcoal (50 mg). The mixture was stirred for 2 h at room temperature and filtered. The filtrate was diluted with water (2 dm^3), and the solution applied on a column (φ 3.5 cm×90 cm) of SP-Sephadex C-25. The adsorbed product was eluted with 0.05 mol dm^{-3} NaCl, and the eluate of the first main red band was concentrated to a small volume under reduced pressure. The concentrate was mixed with chloroform to extract the red complex into the chloroform layer. The chloroform was evaporated under reduced pressure, and the residue was dissolved in water (25 cm^3). The solution was mixed with NaClO$_4$·H$_2$O (3.0 g) in water (5 cm^3), and stored in a refrigerator overnight, yielding a pink precipitate, which was filtered, washed with a small amount of water, and air-dried. Yield: 205 mg. Found: C, 42.74; H, 4.12; N, 2.85%. Calcd for $C_{33}H_{40}N_2CoCl_{2.5}Na_{1.5}O_{14}P_2$: C, 42.50; H, 4.32; N, 3.00%. The complex is soluble in water, methanol, acetone, dichloromethane and chloroform, but not in diethyl ether and benzene.

Optical Resolution of cisβ-[Co(acac)(pp-PNNP)](ClO$_4$)$_2$·H$_2$O. The complex was prepared by the method reported[1] and resolved by the follwing method. An aqueous solution of *cisβ*-[Co(acac)(pp-PNNP)](ClO$_4$)$_2$·H$_2$O (*ca.* 100 mg) was applied on a column (φ 3.5 cm×100 cm) of SP-Sephadex C-25. On elution with 0.1 mol dm^{-3} Na$_2$[Sb$_2$(*d*-tartrate)$_2$], two bands appeared. The eluate of the fast-moving band was collected, diluted ten times with water, and the solution was applied on a column (φ 3.5 cm×5 cm) of SP-Sephadex C-25. The adsorbed complex was eluted with 0.2 mol dm^{-3} NaCl. On addition of excess NaClO$_4$·H$_2$O the eluate gave crystalline (+)$_{589}$-*cisβ*-[Co(acac)(pp-PNNP)](ClO$_4$)$_2$·NaCl. From the slow-moving band the antipode was obtained. Found: C, 46.93; H, 4.74; N, 2.99%. Calcd for $C_{35}H_{41}N_2Cl_3CoNaO_{10}P_2$: C, 46.71; H, 4.51; N, 3.11%.

X-Ray Analysis. Single crystals of (+)$_{589}$-[Co(acac)(*SS*-Me$_2$-mm-PNNP)](ClO$_4$)$_2$·H$_2$O were obtained by recrystallizing the complex from methanol-water (3:2). Crystal data are as follows; Formula: $C_{17}H_{39}N_2Cl_2CoO_{11}P_2$, FW=639.3, Crystal system: monoclinic, Space group: C2, a=28.274(4) Å, b=9.266(1) Å, c=11.0901(9) Å, β=92.97(1)°, V=2901.6(5) Å^3, D_m=1.45 g cm^{-3}, D_x=1.46 g cm^{-3}, Z=4, μ(Mo $K\alpha$)=0.962 mm^{-1}. A specimen with dimensions 0.30×0.40×0.76 mm^3 was used for the X-ray work. Diffraction data were collected on a Rigaku AFC-5 four-circle diffractometer with graphite monochromatized Mo $K\alpha$ radiation at 298 K. Within the range $2\theta<60°$, 3229 independent reflections ($|F_o| \geqq 3\sigma(|F_o|)$) were obtained. In order to determine the absolute configuration, intensity data for Bijvoet pair reflections were also collected up to $2\theta=40°$. The intensity data were corrected for Lorentz-polarization effects, and for absorption. The calculations of the structure analysis were performed on a HITAC M-200H computer at the Computer Center of the Institute for Molecular Science with the Universal Crystallographic Computation Program System UNICS III[11]. The coordinate of the cobalt atom was deduced from a three dimensional Patterson function, and those of other atoms except hydrogens were determined by successive Fourier syntheses. The positions of all the hydrogen atoms were identified in subsequent difference-Fourier maps. The structure was refined by the block-diagonal least-squares method with anisotropic thermal parameters for non-hydrogen atoms and isotropic for hydrogens. The weighting scheme $\sigma_w=[\sigma_{count}^2+(0.015|F_o|)^2]^{-1}$ was employed. At the final stage, refinements were carried out on two enantiomeric models, *Δ* and *Λ*, using 4503 intensities including the Bijvoet pair reflections. The R and R_w values were reduced to 0.053 and 0.078, respectively for the *Λ*-configuration, whereas the values were 0.062 and 0.086 for the *Δ*-configuration, respectively. Thus application of the R-factor ratio test[12] showed that the *Δ*-model can be rejected at the 99.5% confidence level. This result confirms that two asymmetric carbon atoms in the *SS*-Me$_2$-mm-PNNP ligand have the *S*-configuration. Table 1 lists the atomic parameters for non-hydrogen atoms. Complete lists of observed and calculated structure factors, hydrogen atomic parameters, and thermal parameters for non-hydrogen atoms are preserved by the Chemical Society of Japan (Document No. 8552).

Results and Discussion

The optically active quadridentate phosphine ligands, *SS*-Me$_2$-pp- and *SS*-Me$_2$-mm-PNNP were prepared from (*S*)-alanine according to the same route as that for achiral pp- and mm-PNNP ligands.[1] The cobalt(III) complexes with these chiral ligands were also prepared by methods similar to those for the corresponding achiral PNNP complexes.[1] Chemical properties such as stability or solubility in various solvents of the new complexes are similar to those of the corresponding PNNP complexes.

The absorption spectra of [CoCl$_2$(*SS*-Me$_2$-pp- or *SS*-Me$_2$-mm-PNNP)]$^+$ shown in Fig. 1 are very similar to those of *trans*-[CoCl$_2$(pp- or mm-PNNP)]$^+$,[1] respectively, indicating the trans (Cl,Cl) isomer. The spectral data are listed in Table 2. On the other hand,

Table 1. Positional parameters for non-hydrogen atoms

Atom	x	y	z	B_{eqv}/Å^2
Co	1332(1)	0	2582(1)	2.9
P(1)	1104(1)	−1920(2)	1512(1)	3.8
P(2)	1435(1)	1407(2)	1031(1)	4.1
N(1)	1315(2)	−1368(6)	4026(4)	3.7
N(2)	2013(1)	−383(5)	2623(4)	3.4
C(1)	520(2)	−1822(11)	734(6)	6.0
C(2)	1478(2)	−2647(8)	398(6)	5.2
C(3)	1336(3)	3318(8)	1351(6)	6.4
C(4)	1134(3)	1146(11)	−457(6)	7.1
C(5)	1065(2)	−3312(8)	2639(6)	5.1
C(6)	996(2)	−2671(8)	3893(6)	4.7
C(7)	494(2)	−2301(10)	4108(6)	5.7
C(8)	1812(2)	−1818(8)	4352(5)	4.4
C(9)	2163(2)	−755(8)	3908(5)	4.3
C(10)	2297(2)	836(8)	2126(5)	4.5
C(11)	2824(3)	512(11)	2050(7)	6.9
C(12)	2075(2)	1180(8)	896(6)	5.2
C(13)	1436(3)	3368(9)	5141(7)	6.0
C(14)	1197(2)	2343(7)	4220(5)	4.0
C(15)	713(2)	2338(8)	4024(6)	5.0
C(16)	474(2)	1461(8)	3195(5)	4.6
C(17)	−59(2)	1565(11)	2965(7)	6.6
O(1)	1489(1)	1548(5)	3698(3)	3.9
O(2)	669(1)	457(5)	2546(3)	4.0
Cl(1)	2617(1)	5348(2)	2641(1)	4.9
Cl(2)	4377(1)	660(3)	2311(2)	6.8
O(3)	2325(3)	4829(11)	3329(6)	11.1
O(4)	2482(4)	6668(9)	1936(7)	13.1
O(5)	2779(5)	4384(9)	1723(9)	18.2
O(6)	3022(3)	5662(18)	3153(10)	19.6
O(7)	4350(4)	2146(11)	2165(8)	13.4
O(8)	4482(3)	199(11)	3488(6)	12.1
O(9)	4081(4)	−221(14)	1657(10)	17.2
O(10)	4817(5)	416(15)	1877(11)	18.3
O(w)	1078(2)	9458(9)	6528(6)	8.9

The x, y, and z values are multiplied by 10^4. The thermal parameters are given by the equivalent temperature foctors.

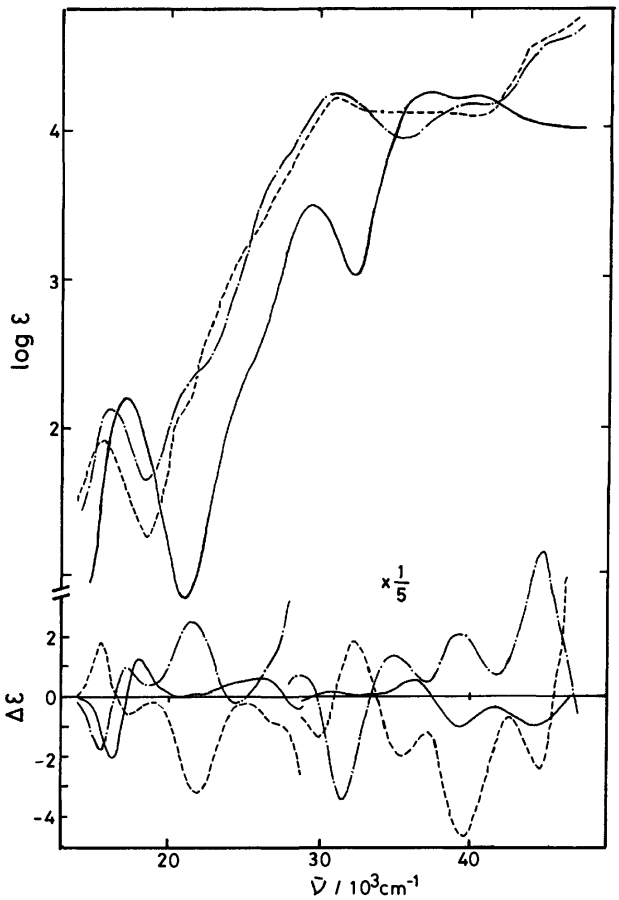

Fig. 1. Absorption and CD spectra of *trans*-[$CoCl_2$-(*SS*-Me_2-mm-PNNP)]$^+$ (——), *trans*-[$CoCl_2$(*SS*-Me_2-pp-PNNP)]$^+$ (-·—·-), and *trans*(Cl,Cl),*cis*(P,P)-[$CoCl_2$(*S*-pdpp)$_2$]$^+$ (------).

Table 2. Absorption (AB) and CD spectral data in the visible to near ultraviolet region (Solvent: CH_3OH, at 298K)

Complex	AB ($\tilde{\nu}$/10^{3}cm^{-1} (logε))	CD ($\tilde{\nu}$/10^{3}cm^{-1} ($\Delta\varepsilon$))
(+)$_{589}$-*trans*-[$CoCl_2$(*SS*-Me_2-pp-PNNP]$^+$	16.15(2.12), 21.5(2.3)[a], 26.5(3.6)[a], 31.05(4.15)[a], 39.5(4.15)[a], 45.0(4.58)[a]	15.75(+1.00), 17.25(+1.00), 21.75(+2.56) 24.50(−0.25), 28.90(+3.63), 31.50(−17.3) 35.00(+6.81), 39.50(+10.5), 45.00(+20.4)
(+)$_{589}$-*trans*-[$CoCl_2$(*SS*-Me_2-mm-PNNP)]$^+$	16.95(2.20), 24.5(2.2)[a], 29.40(3.48), 37.10(4.24), 40.2(4.21)[a]	16.50(+2.08), 18.25(+1.24), 26.50(+0.55), 28.8(−0.41), 30.75(+0.64), 36.50(+2.61) 39.50(−5.19), 44.50(−5.30)
(+)$_{589}$-*Λ*-*cisβ*-[Co(acac)(*SS*-Me_2-pp-PNNP)]$^{2+}$	19.20(2.90), 28.0(3.9)[a], 32.0(4.36)	18.7(+7.25), 21.0(−1.52), 25.0(−7.0)[a], 28.0(−29.6), 31.3(+38.2), 35.5(−5.03), 39.5(−10.3), 44.0(+14.7)
(+)$_{589}$-*Λ*-*cisβ*-[Co(CO_3)(*SS*-Me_2-pp-PNNP)]$^+$	19.50(2.41), 24.5(2.49)[a], 31.75(4.10), 38.00(3.88), 44.5(4.5)[a]	18.40(+2.02), 20.75(−1.78), 24.75(+0.40), 31.25(−6.02), 34.0(+1.45), 37.5(+2.15)[a], 40.10(−2.80)
(+)$_{589}$-*Λ*-*cisβ*-[Co(acac)(*SS*-Me_2-mm-PNNP)]$^{2+}$	20.0(2.67)[a], 22.7(2.73), 29.7(3.45)[a], 39.5(4.39)	20.00(+6.11), 23.25(−1.19), 25.75(2.2)[a], 29.70(−11.9), 34.0(+0.9), 36.9(−14.2), 40.7(−8.24), 45.3(−0.70)
(−)$_{589}$-*Λ*-*cisβ*-[Co(acac)(*SS*-Me_2-mm-PNNP)]$^{2+}$	21.8(2.72), 29.8(3.44)[a], 39.0(4.39)	20.0(−4.92), 23.0(+0.90), 29.8(+10.8), 34.3(−0.98), 36.5(+8.79), 40.5(−15.1), 44.5(+3.26)

a) Shoulder.

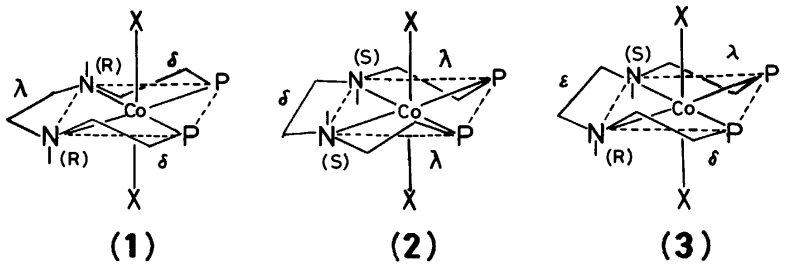

Fig. 2. Three possible diastereomers of *trans*-[$CoCl_2$(*SS*-Me_2-pp-PNNP)]$^+$.

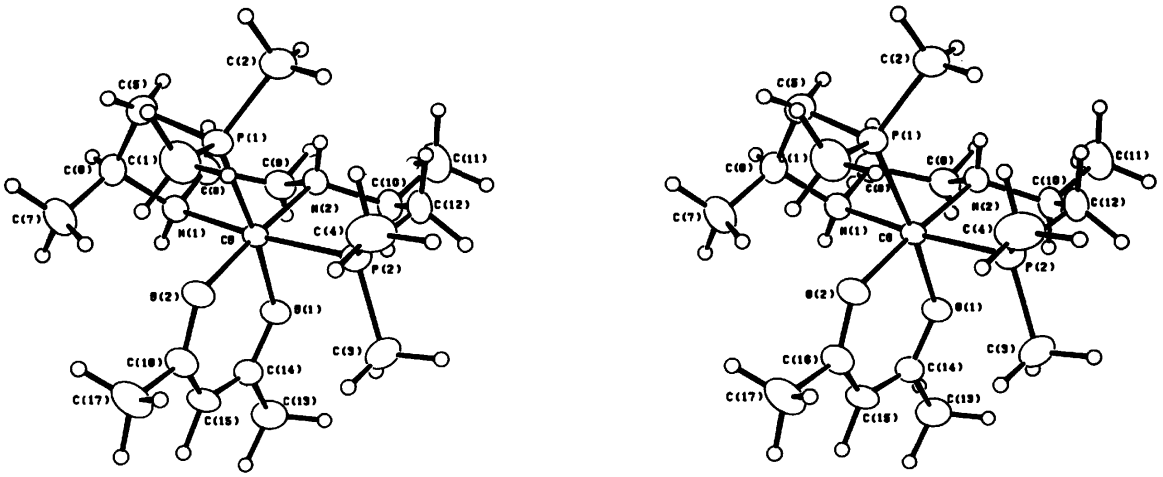

Fig. 3. ORTEP stereoview of $(+)_{589}$-*Λ*-*cisβ*-[Co(acac)(*SS*-Me_2-mm-PNNP)]$^{2+}$.

the CD spectrum of [$CoCl_2$(*SS*-Me_2-pp-PNNP)]$^+$ is nearly enantiomeric to that of *trans*(Cl,Cl),*cis*(P,P)-[$CoCl_2$(*S*-pdpp)$_2$]$^+$ (*S*-pdpp=(*S*)-$NH_2CH(CH_3)CH_2P(C_6H_5)_2$)[13] over the whole region as shown in Fig. 1, although the structures of the two complexes are similar, and all the chiral carbon atoms are the same *S* configuration. For the *SS*-Me_2-pp-PNNP complex, there are two more chiral sources, the chiral nitrogen atoms and the chiral conformation of the N–N chelate ring. In a previous paper,[13] we reported that the vicinal effect of the chiral nitrogen atom in the *trans*(Cl,Cl),*cis*(P,P)-[$CoCl_2$(N–P)$_2$]$^+$-type complex is very small, since the CD spectra of *S*-pdpp and *S*-prdpp (*S*(C),*S*(N)-$CH_2CH_2CH_2NHCHCH_2P(C_6H_5)_2$) complexes of this type are very similar. The latter complex has a chiral nitrogen donor atom of the *S*-configuration. Thus the effect of chiral conformation of the N–N chelate ring may be responsible for the big difference in CD spectra between the *SS*-Me_2-pp-PNNP and the *S*-pdpp complexes. The *trans*-[$CoCl_2$(*SS*-Me_2-pp-PNNP)]$^+$ complex has three possible diastereomers as shown in Fig. 2. The methyl groups of the *δ* and *λ* N–P chelate conformations have equatorial and axial dispositions, respectively, to the chelate ring. Since the complex shows only one kind of methyl signal in the ^{1}H NMR spectrum (-CH_3: 1.83 ppm), isomer **3** in Fig. 2 which has an equatorial and an axial methyl group can be excluded. Isomer **2** will be the least stable among the three isomers because of two axially disposed methyl groups. Thus the complex can be assigned as isomer **1**, where both methyl groups take an equatorial disposition, and the N–P and N–N chelate rings have the *δ* and *λ* conformations, respectively. In this isomer both nitrogen donor atoms become necessarily the *R* configuration. A structurally related tetraammine complex, $(-)_{589}$-*trans*-[$Co(NO_2)_2$(*SS*-3,8-Me_2-trien)]ClO_4 (*S,S*-3,8-Me_2-trien=(*SS*)-$NH_2CH_2CH(CH_3)NHCH_2CH_2NHCH(CH_3)CH_2NH_2$) forms three chelate rings of *δ*, *λ*, and *δ* conformations, and has two equatorial methyl groups and two *R*-nitrogen donor atoms.[14] The *trans*(Cl,Cl),*cis*(P,P)-[$CoCl_2$(*S*-pdpp)$_2$]$^+$ complex has no N–N chelate ring, and the N–P chelate rings will be stabilized in the *δ* conformation with an equatorial methyl group.[13] Thus the enantiomeric CD pattern of the *SS*-Me_2-pp-PNNP complex to that of the *S*-pdpp complex may be attributable to the extremely strong vicinal effect of the *λ*-(N–N) chelate ring compared with that of *δ*-(N–P) chelate one. Five-membered N–P chelate rings in cobalt(III) complexes often form a distorted gauche (nearly envelope) conformation,[15] and the vicinal effect of such a chelate ring would be smaller than that of a chelate ring with the typical gauche conformation.

The CD spectrum of the *SS*-Me_2-mm-PNNP complex resembles that of the *SS*-Me_2-pp-PNNP complex in the Ia absorption band region (14000—19000 cm^{-1}),

indicating similar chiral skeletal structures for both complexes. In the higher energy region, however, the CD spectra are quite different from each other. These differences may be attributable to the difference in substitutent on the phosphorus atom, methyl and phenyl groups.

For the [Co(O–O)(*SS*-Me_2-pp- or *SS*-Me_2-mm-PNNP)]$^{n+}$-type complexes (O–O=acac, CO_3^{2-}), two geometrical isomers cisα and cisβ are possible, and each geometrical isomer can form diastereomers arising from the chiral carbon and nitrogen atoms. The structure of $(+)_{589}$-[Co(acac)(*SS*-Me_2-mm-PNNP)]$(ClO_4)_2\cdot H_2O$, which was formed in much larger amounts than the other $(-)_{589}$-isomer, was determined by X-ray analysis. Figure 3 shows a stereoview of the complex cation with the numbering scheme of the atoms. The selected bond distances and angles are listed in Table 3. The complex ion has the *Λ*-cisβ configuration. The three chelate rings form distorted gauche ($\delta\lambda\lambda$) or envelope conformations as shown in Fig. 4. One methyl group (C(7)) at C(6) lies in an axial disposition to the chelate ring, while the other methyl group (C(11)) is in an equatorial disposition to the chelate ring. Such an axial methyl group has been found in *Λ*-cisβ-[Co(CO_3)(*SS*-3,8-Me_2-trien)]ClO_4.[16,17]

The Co–P distances (2.208(2), 2.196(2) Å) are slightly shorter than those found in [Co(edmp)$_2$(dmpe)]$Br_3\cdot 2H_2O$ (Co–edmp=2.294(3), 2.245(4); Co–dmpe=2.273(4), 2.295(3) Å),[18] $(+)_{589}$-*Λ*-[Co(en)$_2$(dmpe)]$Br_3\cdot 1.5H_2O$ (2.264(3), 2.248(3) Å),[19] and $(+)_{589}$-*Λ*-*fac*-[Co(edmp)$_3$]$Br_3\cdot 3H_2O$ (2.231(5), 2.239(4), 2.242(5) Å,[20] where edmp and dmpe denote $NH_2CH_2CH_2P(CH_3)_2$ and $(CH_3)_2PCH_2CH_2P(CH_3)_2$, respectively. The bond distances of Co–N(1) and Co–O(1) (trans to the P atom) are longer by 0.057 and 0.043 Å, respectively, than those of Co–N(2) and Co–O(2) (cis to the P atom), indicating trans influence of the P donor atom.[15] The average Co–N distance (2.015 Å) is fairly longer than that of the corresponding central two Co–N bonds in $(+)_{589}$-*Λ*-cisβ-[Co(CO_3)(*SS*-3,8-Me_2-trien)]ClO_4 (1.949 Å),[17] whereas the N–Co–N angles of these phosphine and trien complexes are similar (85.2(2) and 86.7(2)°, respectively). The chelate angles of P(1)–Co–N(1) (84.7(1)°) and P(2)–Co–N(2) (86.6(1)°) are nearly the same as those (84—86°) found in the edpp ($NH_2CH_2CH_2P(C_6H_5)_2$)[13,15] and edmp[18,20] complexes of cobalt(III).

The geometrical structure of the other isomer $(-)_{589}$-[Co(acac)(*SS*-Me_2-mm-PNNP)]$^{2+}$ can be assigned as the cisβ form, since it shows two kinds of –CH_3(acac) signals at 2.50 and 2.68 ppm in the ^{1}H NMR spectrum. Figure 5 compares the absorption and CD spectra with those of $(+)_{589}$-*Λ*-cisβ-[Co(acac)(*SS*-Me_2-mm-PNNP)]$^{2+}$. The CD spectrum of the $(-)_{589}$-isomer is nearly enantiomeric to that of the $(+)_{589}$-*Λ*-cisβ-isomer over the whole region. Thus the $(-)_{589}$-isomer is assigned as the *Λ*-cisβ-isomer. This isomer has further two possible

Table 3. Selected bond lengths(l/Å) and bond angles(ϕ/°) for $(+)_{589}$-*Λ*-cisβ-[Co(acac)(*SS*-Me_2-mm-PNNP)]$(ClO_4)_2\cdot H_2O$.

Co	–P(1)	2.208(2)	N(2)	–C(9)		1.505(7)
Co	–P(2)	2.196(2)	N(2)	–C(10)		1.506(8)
Co	–N(1)	2.043(5)	C(5)	–C(6)		1.535(10)
Co	–N(2)	1.986(4)	C(6)	–C(7)		1.491(9)
Co	–O(1)	1.936(4)	C(8)	–C(9)		1.500(9)
Co	–O(2)	1.893(4)	C(10)	–C(11)		1.529(9)
P(1)	–C(1)	1.825(6)	C(10)	–C(12)		1.505(9)
P(1)	–C(2)	1.798(7)	C(13)	–C(14)		1.527(10)
P(1)	–C(5)	1.803(7)	C(14)	–C(15)		1.375(9)
P(2)	–C(3)	1.830(8)	C(15)	–C(16)		1.378(9)
P(2)	–C(4)	1.833(8)	C(16)	–C(17)		1.518(9)
P(2)	–C(12)	1.837(7)	C(14)	–O(1)		1.269(7)
N(1)	–C(6)	1.509(8)	C(16)	–O(2)		1.314(8)
N(1)	–C(8)	1.493(8)				
P(1)	–Co –P(2)	96.0(1)	C(4)	–P(2)	–C(12)	109.0(4)
P(1)	–Co –N(1)	84.7(1)	Co	–N(1)	–C(6)	116.7(3)
P(1)	–Co –N(2)	96.6(1)	Co	–N(1)	–C(8)	108.4(4)
P(2)	–Co –N(1)	172.1(1)	C(6)	–N(1)	–C(8)	110.5(5)
P(2)	–Co –N(2)	86.6(1)	Co	–N(2)	–C(9)	106.9(3)
P(1)	–Co –O(1)	172.7(1)	Co	–N(2)	–C(10)	113.5(3)
P(1)	–Co –O(2)	85.7(1)	C(9)	–N(2)	–C(10)	112.9(4)
P(2)	–Co –O(1)	91.2(1)	P(1)	–C(5)	–C(6)	111.5(5)
P(2)	–Co –O(2)	91.8(1)	N(1)	–C(6)	–C(5)	107.1(5)
N(1)	–Co –O(1)	88.3(2)	N(1)	–C(6)	–C(7)	111.6(6)
N(1)	–Co –O(2)	96.1(2)	C(5)	–C(6)	–C(7)	113.7(5)
N(2)	–Co –O(1)	84.9(2)	N(1)	–C(8)	–C(9)	111.6(5)
N(2)	–Co –O(2)	177.4(2)	N(2)	–C(9)	–C(8)	107.6(4)
N(1)	–Co –N(2)	85.5(2)	N(2)	–C(10)	–C(11)	114.3(6)
O(1)	–Co –O(2)	93.0(2)	N(2)	–C(10)	–C(12)	106.7(5)
Co	–P(1) –C(1)	115.8(3)	C(11)	–C(10)	–C(12)	110.6(6)
Co	–P(1) –C(2)	120.9(2)	P(2)	–C(12)	–C(10)	108.4(4)
Co	–P(1) –C(5)	103.3(2)	C(13)	–C(14)	–C(15)	120.7(6)
C(1)	–P(1) –C(2)	104.0(3)	C(13)	–C(14)	–O(1)	113.0(5)
C(1)	–P(1) –C(5)	106.1(4)	C(15)	–C(14)	–O(1)	126.3(6)
C(2)	–P(1) –C(5)	105.5(3)	C(14)	–C(15)	–C(16)	123.8(6)
Co	–P(2) –C(3)	113.1(2)	C(15)	–C(16)	–C(17)	121.5(6)
Co	–P(2) –C(4)	123.2(3)	C(15)	–C(16)	–O(2)	125.3(6)
Co	–P(2) –C(12)	100.3(2)	C(17)	–C(16)	–O(2)	113.2(6)
C(3)	–P(2) –C(4)	103.5(4)	Co	–O(1)	–C(14)	125.4(4)
C(3)	–P(2) –C(12)	106.7(4)	Co	–O(2)	–C(16)	125.7(4)

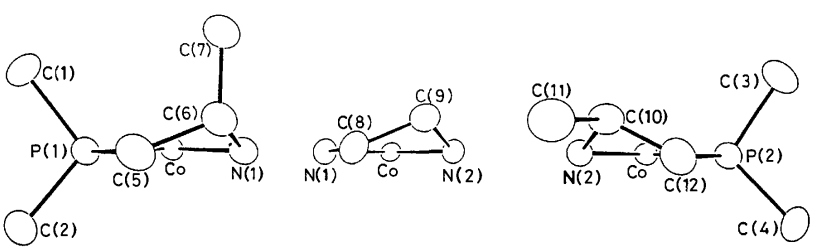

Fig. 4. Three chelate rings of $(+)_{589}$-*Λ*-cisβ-[Co(acac)(*SS*-Me_2-mm-PNNP)]$^{2+}$.

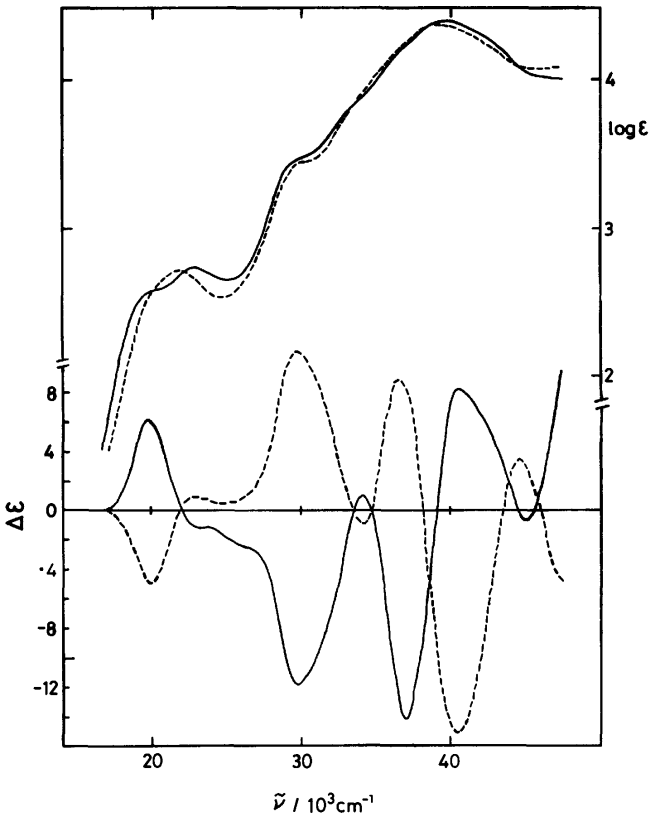

Fig. 5. Absorption and CD spectra of $(+)_{589}$-Λ-*cis*β-[Co(acac)(*SS*-Me$_2$-mm-PNNP)]$^{2+}$ (——) and $(-)_{589}$-Λ-*cis*β-[Co(acac)(*SS*-Me$_2$-mm-PNNP)]$^{2+}$ (------).

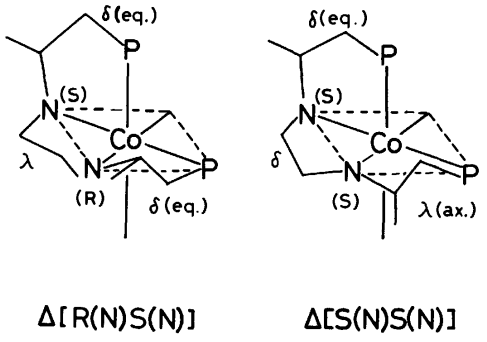

Fig. 6. Two possible diastereomers of Λ-*cis*β-[Co(acac)(*SS*-Me$_2$-mm-PNNP)]$^{2+}$.

diastereomers arising from the absolute configuration of the nitrogen donor atom as shown in Fig. 6. In the Λ[*R*(N)*S*(N)]-isomer, both methyl groups on carbon take an equatorial disposition, while in the Λ[*S*(N)*S*(N)]-isomer, the methyl group on carbon of the meridional-(PNN) coordination moiety (in-plane) becomes axial. No *cis*β complex having such an axial "in-plane" methyl group has been reported probably because of large intra- and interligand steric interactions with this methyl group. Thus the $(-)_{589}$-isomer can be assigned as the Λ[*R*(N)*S*(N)]-*cis*β-isomer shown in Fig. 6. This isomer was obtained by reaction of [Co(acac)$_3$] with the ligand in methanol in poor yield, the formation ratio of it to the other $(+)_{589}$-Λ-*cis*β-isomer being *ca.* 1/8. The

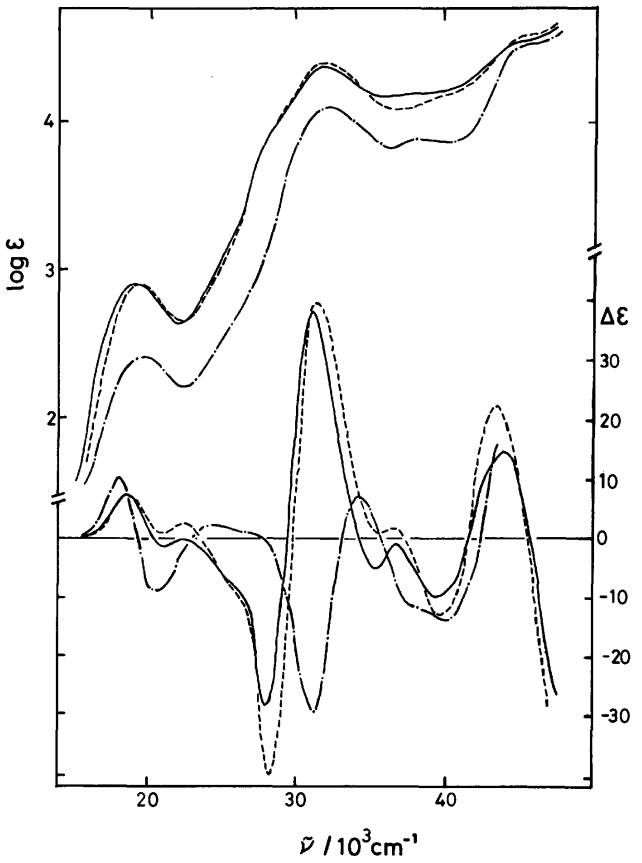

Fig. 7. Absorption and CD spectra of $(+)_{589}$-Λ-*cis*β-[Co(acac)(*SS*-Me$_2$-pp-PNNP)]$^{2+}$ (——), $(+)_{589}$-Λ-*cis*β-[Co(acac)(pp-PNNP)]$^{2+}$ (------) and $(+)_{589}$-Λ-*cis*β-[Co(CO$_3$)(*SS*-Me$_2$-pp-PNNP)]$^+$ (-·—·-).

reaction of *trans*-[CoCl$_2$(*SS*-Me$_2$-mm-PNNP)]$^+$ with Li(acac) in methanol afforded only the Λ-*cis*β-isomer, no other isomer being formed. In either experiment no *cis*α-isomer was yielded. These experimental results indicate that [Co(acac)(*SS*-Me$_2$-mm-PNNP)]$^{2+}$ is the most stable in the Λ[*R*(N)*R*(N)]-*cis*β structure, although this structure has an axially disposed methyl group on carbon of the apically linked N–P chelate ring. The reason for such selectivity is not clear at present. Saburi *et al.*[16] reported that structurally related [Co(CO$_3$)(*SS*-3,8-Me$_2$-trien)]$^+$ is more stable in the Λ-*cis*β form than in other forms. Complexes of such a (3*S*,8*S*)-dimethyl-substituted quadridentate ligand seem to be stabilized in the Λ-*cis*β form, irrespective of the kind of terminal donor atoms.

Both [Co(acac)(*SS*-Me$_2$-pp-PNNP)]$^{2+}$ and [Co(CO$_3$)(*SS*-Me$_2$-pp-PNNP)]$^+$ yielded only the $(+)_{589}$-isomer by reactions of *trans*-[CoCl$_2$(*SS*-Me$_2$-pp-PNNP)]$^+$ with Li(acac) and $(NH_4)_2CO_3$, respectively. For the acac complex, the reaction of [Co(acac)$_3$] with the ligand also formed only the same isomer. The ^{1}H NMR spectra of these acac and carbonato complexes clearly indicate that both of them are the *cis*β isomer. Figure 7 shows absorption and CD spectra of these complexes together with those of $(+)_{589}$-*cis*β-[Co(acac)(pp-PNNP)]$^{2+}$.

The CD spectral patterns of both *SS*-Me_2-pp-PNNP complexes resemble that of $(+)_{589}$-*Λ-cisβ*-[Co(acac)(*SS*-Me_2-mm-PNNP)]$^{2+}$ in the first absorption band region, a positive and a negative CD band from the low energy side. Thus the complexes can be assigned as the *Λ-cisβ*-isomer. All the nitrogen donor atoms in these isomers will have the same *R* configuration as those in *Λ-cisβ*-[Co(acac)(*SS*-Me_2-mm-PNNP)]$^{2+}$, since the *R*(N)*S*(N) isomer has two methyl groups in an axial disposition, and the *S*(N)*S*(N) isomer can not form the *Λ* configuration. As stated above, the *SS*-Me_2-pp-PNNP complexes formed only the *Λ-cisβ*-isomer. Neither the *cisα*- nor the *Δ-cisβ*-isomer which corresponds to the minor product ($(-)_{589}$-isomer) of [Co(acac)(*SS*-Me_2-mm-PNNP)]$^{2+}$ was detected.

The *cisβ*-[Co(acac)(pp-PNNP)]$^{2+}$ complex, which was only isomer obtained from *trans*-[$CoCl_2$(pp-PNNP)]$^+$ and Li(acac) in methanol,[1] shows an absorption spectrum nearly the same as that of the corresponding *SS*-Me_2-pp-PNNP complex. The CD spectrum of the resolved $(+)_{589}$-isomer is also very similar to that of the *SS*-Me_2-pp-PNNP complex which was assigned to the *Λ* configuration. Thus $(+)_{589}$-*cisβ*-[Co(acac)(pp-PNNP)]$^{2+}$ is assigned as the *Λ*-isomer,[21] and the two nitrogen donor atoms will have the same *R* configuration as those in the *SS*-Me_2-pp-PNNP complex. The presence of two chiral carbon atoms in the *SS*-Me_2-pp-PNNP complex seems to little affect both absorption and CD spectra.

The authors wish to thank the Ministry of Education for Scientific Research Grant-in-Aid No. 58470032 and 60470046, and the Institute for Molecular Science for the use of a diffractometer and a HITAC M-200H computer.

References

1) M. Atoh, K. Kashiwabara, and J. Fujita, *Bull. Chem. Soc. Jpn.*, **58**, 2793 (1985).

2) M. Saburi and S. Yoshikawa. *Kagaku Sosestu*, **1976**, No. 13, p. 109.

3) O. Vogl and M. Pöhm, *Monatsh. Chem.*, **83**, 541 (1952).

4) M. R. Holdiness, Z. H. Islaili, and J. B. Justice, *J. Chromatogr.*, **224**, 415 (1981).

5) a) F. C. Bersworth, British Patent, 723, 316 (1955); b) L. N. Schoenberg, D. W. Cooke, and C. F. Liu, *Inorg. Chem.*, **7**, 2386 (1966).

6) L. Horner, P. Beck, and H. Hoffmann, *Chem. Ber.*, **92**, 2092 (1959).

7) H. Neibergall and B. Langefeld, *Chem. Ber.*, **95**, 64 (1962).

8) *Inorg. Synth.*, **2**, 223 (1946).

9) *Inorg. Synth.*, **5**, 188 (1957).

10) M. Fujita, Y. Yoshikawa, and H. Yamatera, *Chem. Lett.*, **1982**, 432.

11) T. Sakurai and K. Kobayashi, *Rikagaku Kenkyusho Hokoku*, **55**, 69 (1978).

12) W. C. Hamilton, *Acta Crystallogr.*, **18**, 502 (1965).

13) I. Kinoshita, Y. Yokota, K. Matsumoto, S. Ooi, K. Kashiwabara, and J. Fujita, *Bull. Chem. Soc. Jpn.*, **56**, 1067 (1983).

14) M. Ito, F. Marumo, and Y. Saito, *Acta Crystallogr.*, **B28**, 463 (1972).

15) M. Atoh, K. Kashiwabara, H. Ito, T. Ito, and J. Fujita, *Bull. Chem. Soc. Jpn.*, **57**, 3139 (1984), and references cited therein.

16) M. Saburi, T. Sato, and S. Yoshikawa, *Bull. Chem. Soc. Jpn.*, **49**, 2100 (1976).

17) K. Toriumi and Y. Saito, *Acta Crystallogr.*, **B31**, 1247 (1975).

18) T. Ohishi, S. Ohba, K. Kashiwabara, Y. Saito, and J. Fujita, *Bull. Chem. Soc. Jpn.*, **57**, 877 (1984).

19) S. Ohba, Y. Saito, T. Ohishi, K. Kashiwabara, and J. Fujita, *Acta Crystallogr.*, **C39**, 49 (1983).

20) I. Kinoshita, K. Kashiwabara, J. Fujita, K. Matsumoto, and S. Ooi, *Bull. Chem. Soc. Jpn.*, **54**, 2683 (1981).

21) In a previous paper (Ref. 22)), we incorrectly assigned the absolute configuration of $(+)_{589}$-*cisβ*-[Co(acac)(*SS*-Me_2-pp-PNNP)]$^{2+}$, $(+)_{589}$-*trans*(P,N)- and $(+)_{589}$-*trans*(P,P)-[Co(acac)(edpp)$_2$]$^{2+}$, and $(+)_{589}$-*trans*(P,N)-[Co(O–O)(edpp)$_2$]$^+$ (O–O=CO_3^{2-}, $C_2O_4^{2-}$ and $CH_2(CO_2)^{2-}$) to *Δ*. All of these isomers should be assigned to *Λ*.

22) M. Atoh, I. Kinoshita, K. Kashiwabara, and J. Fujita, *Bull. Chem. Soc. Jpn.*, **55**, 3179 (1982).

Na^+/H^+ Ion-exchange Process on Layered Hydrous Titanium Dioxide

Takayoshi SASAKI,* Mamoru WATANABE, Yū KOMATSU, and Yoshinori FUJIKI
National Institute for Research in Inorganic Materials, 1-1 Namiki, Sakura-mura, Niihari-gun, Ibaraki 305
(Received July 3, 1985)

The Na^+/H^+ ion-exchange on layered hydrous titanium dioxide, $H_2Ti_4O_9 \cdot 1.2—1.3H_2O$, has been studied from chemical and structural aspects. The ion-exchange reaction proceeded stepwise through two stages [0—50%, 50—72% conversion]. In stage I a discontinuous change in interlayer distance took place and the 1/2-exchanged phase with a widened interlayer distance appeared. The exchange in stage II proceeded *via* a solid solution and resulted in the 3/4-exchanged phase. The variation in unit cell dimensions indicates that these partially exchanged phases were formed by swelling the spacing of adjacent $[Ti_4O_9^{2-}]_n$ sheets. The structural and the thermoanalytical data can be interpreted on the basis of the structural model in which sodium ions and water molecules are arranged in a double row in the interlayer region.

Layered hydrous titanium dioxide, $H_2Ti_4O_9 \cdot 1.2—1.3H_2O$, has recently been prepared from potassium tetratitanate ($K_2Ti_4O_9$) by extracting interlayered potassium ions.[1-3] This material is attractive since it is one of the first hydrous metal oxides with a layer structure which act as inorganic ion exchangers. The material has a layer structure which consists of the host macroanion, $[Ti_4O_9^{2-}]_n$ sheets, and exchangeable protons (see Fig. 1).[4] Two types of exchangeable protons exist in the interlayer region; one oxonium ion and one hydroxylated proton per chemical formula. The unit cell has two equivalent interlayer spaces which are shifted by $b/2$ along the b axis. Each space contains two oxonium ions and two hydroxylated protons. This means that the material has four independent exchange sites. The authors have studied the K^+/H^+ ion-exchange process and obtained the satisfactory interpretation on the reaction mechanism which is consistent with the structural model described above:[4] Potassium ions replace the four exchange sites one by one. It is interesting and important to examine the exchange behavior of another ion to investigate whether the analogous explanation can be applied or not.

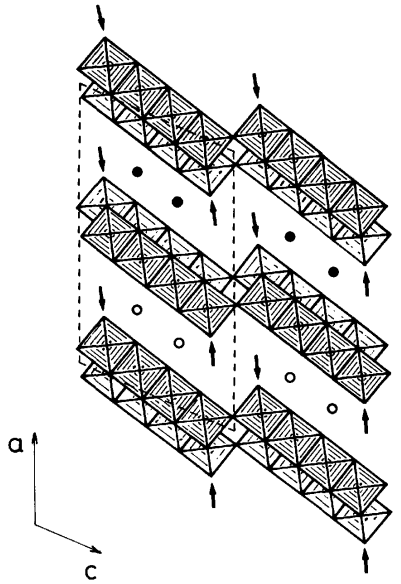

Fig. 1. Idealized representation of the crystal structure of layered hydrous titanium dioxide projected along (010). Arrows and circles show the possible positions of hydroxyl bonds and hydronium ions, respectively.

The ion-exchanged phases of layered hydrous titanium dioxide can be regarded as hydrated phases of alkali metal tetratitanate. Since these hydrated phases are chemically active, they are promising as catalyst carriers and starting or intermediate materials for further syntheses. There have been several reports on the hydrated phases which are obtained by hydrolyzing potassium tetratitanate.[1-3,5,6] This field is, however, in a state of confusion because the studies were not done systematically and they do not agree with each other. Moreover, no study has yet appeared on the hydrated phases of sodium tetratitanate. Thus it is significant to characterize the Na^+-exchanged phases from the viewpoint of clarifying the system of the hydrated phases of alkali metal tetratitanate.

This paper describes the Na^+/H^+ ion-exchange behavior on layered hydrous titanium dioxide and characterization of the Na^+-exchanged phases. The ion-exchange mechanism is discussed from chemical and structural aspects.

Experimental

Reagents. The titanium dioxide used was of 99.98% purity. All the other chemicals were of reagent grade. Distilled, deionized water was used throughout the experiments.

Preparation of Layered Hydrous Titanium Dioxide. Potassium tetratitanate ($K_2Ti_4O_9$) was grown in a fibrous form by slowly cooling a mixture of K_2O–$3TiO_2$ in a K_2MoO_4 flux melt from 1150 °C to 950 °C.[7] Layered hydrous titanium dioxide was obtained by extracting interlayered potassium ions from potassium tetratitanate:

$$K_2Ti_4O_9(s) + 2H^+(aq) + 1.2—1.3H_2O(aq) \longrightarrow H_2Ti_4O_9 \cdot 1.2—1.3H_2O(s) + 2K^+(aq)$$

The potassium ion extraction was performed by a column technique; about 15 g of potassium tetratitanate in a column (2.5 cm i.d.) was treated with a 1 mol dm^{-3} HCl solution until

the potassium ion concentration in the effluent decreased to be negligible. The resulting product was washed with water and was dried over a saturated NaCl solution (relative humidity: 70%) to a constant weight. The material used in this experiment had a composition of $H_2Ti_4O_9 \cdot 1.2H_2O$ (theoretical ion-exchange capacity: 5.57 mequiv g^{-1}) because the weight loss at 800 °C was 10.9%.

Titration Experiment. The titration experiment was carried out batchwise by shaking a weighed amount of the material with a 0.1 mol dm^{-3} (NaCl+NaOH) solution at 25±0.5 °C. The solution to solid ratio was 0.1 dm^3 g^{-1} and the ratio of NaCl/NaOH varied from 0.1 M/0.0 M to 0.0 M/0.1 M (1 M=1 mol dm^{-3}). After shaking for 4 d, an aliquat of the supernatant solution was pipetted and its sodium ion content as well as pH value was measured. The sodium ion uptake was calculated from the difference between initial and equilibrium concentrations of the solution. The solid was filtered off, washed with water and then dried over a saturated NaCl solution to a constant weight. The solid was characterized by chemical analysis, thermal analysis and powder X-ray diffractometry.

Apparatus. A TOA HM-20E digital pH meter was used to measure pH values of the solution. Sodium ion contents in the solution were determined by a Hitachi 180-80 atomic absorption spectrophotometer. X-Ray powder diffraction patterns were recorded by using a Philips PW-1130 type diffractometer with Ni-filtered Cu $K\alpha$ radiation (λ=1.5405 Å). Silicon or titanium dioxide (rutile) was used as an internal standard. The lattice constants were refined by the least-squares method.[8] The DTA-TG measurement was performed by using a Rigaku Denki M 8075 thermal analyzer at a heating rate of 10 °C min^{-1}.

Results and Discussion

Ion-exchange Process. Figure 2 shows the sodium ion titration curve. After an initial rising portion, the pH value increased rather gradually up to approximately 40% conversion. A pH jump was observed at 40—50% conversion and then the curve had a mild slope region again. At the uptake of 4.0 mequiv g^{-1}, the pH value increased steeply, indicating that the apparent capacity was approximately 3/4 of the theoretical limit.

Figure 3 shows the X-ray powder diffraction patterns of the ion-exchanged solids at various loading levels which were obtained in the titration experiment. The X-ray patterns changed continuously up to the loading level of 0.5 mequiv g^{-1}. This means that layered hydrous titanium dioxide (designated as phase HH) can accommodate sodium ions by forming a solid solution in this region. This region corresponded to the initial rising portion of the titration curve. Beyond this loading level, two immiscible solid phases were present; one was the resulting phase of the solid solution and the other was the exchanged phase with a widened interlayer distance of 11.2 Å. The latter phase increased as the exchange proceeded, and was observed alone near 50% conversion. This phase was verified as the 1/2-exchanged phase since the chemical composition was determined to be $Na_{0.98}H_{1.02}Ti_4O_9 \cdot 3.3H_2O$

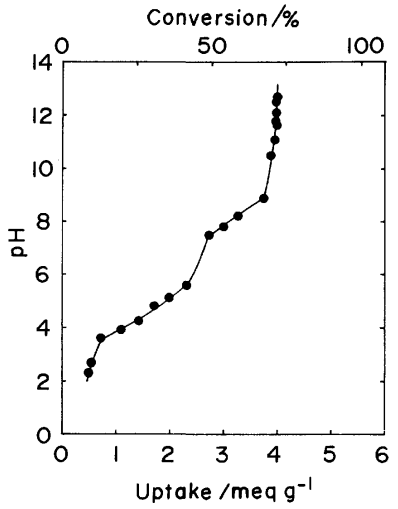

Fig. 2. Sodium ion titration curve. Exchanger: 0.2 g, Titrant: 20 cm^3 of 0.1 mol dm^{-3} (NaCl+NaOH) solution.

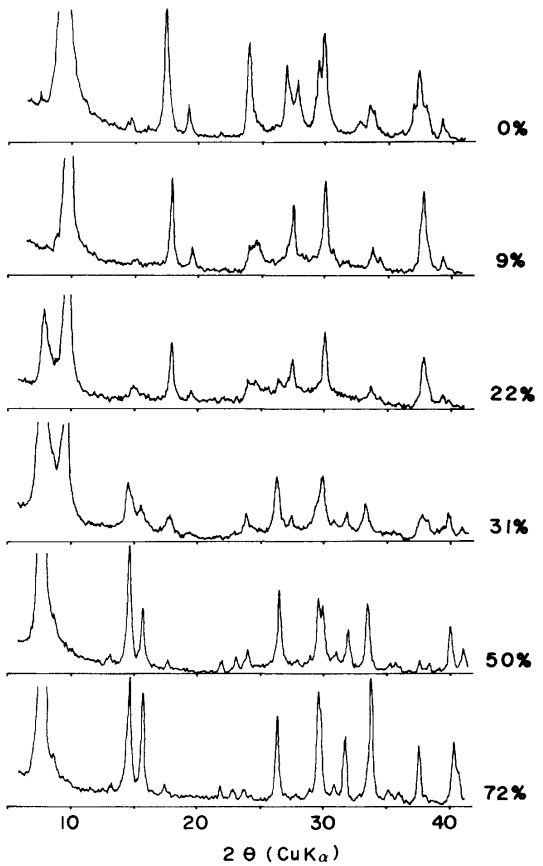

Fig. 3. X-Ray powder diffraction patterns of the sodium ion-exchanged solids at various loading levels. Numerals represent the percent uptake of sodium ion.

(termed phase Na1). Further exchange took place without an appreciable change in interlayer distance and water content. This indicates that sodium ions were taken into phase Na1 *via* a solid solution. The 3/4-exchanged phase (phase Na2) was formed at a result of this solid solution.

From the above results, the Na^+/H^+ ion-exchange process can be divided into two stages; stage I [0—50% conversion] and stage II [50—72%]. The ion-exchange reaction in each stage can be formulated as follows: stage I:

$$H_2Ti_4O_9 \cdot 1.2H_2O(s) + Na^+(aq) + 2.1H_2O(aq) \quad [9.1\ Å] \longrightarrow NaHTi_4O_9 \cdot 3.3H_2O(s) + H^+(aq) \quad [11.2\ Å]$$

stage II:

$$NaHTi_4O_9 \cdot 3.3H_2O(s) + 0.4Na^+(aq) \quad [11.2\ Å] \longrightarrow Na_{1.4}H_{0.6}Ti_4O_9 \cdot 3.3H_2O(s) + 0.4H^+(aq) \quad [11.2\ Å]$$

where numerals in brackets give the interlayer distance (d_{200}), and the subscripts "s" and "aq" represent solid and aqueous phases, respectively.

Figure 4 gives the approximate ratios of the above mentioned phases as a function of sodium ion uptake, which were estimated from the relative intensities of the (200) reflection.

Interpretation of the Ion-exchange Process. Analogously to the K^+/H^+ exchange process,[4] the Na^+/H^+ exchange proceeded in a stepwise fashion *via* several partially exchanged phases with different interlayer distances. Table 1 summarizes the salt forms of the solid phases that appeared in both processes. The two processes tended to be divided at $n/4$ of the theoretical ion-exchange capacity (n=1,2,3,4). This phenomenon is consistent with the structural model of phase HH in which four independent exchange sites exist. The Na^+/H^+ exchange process can be interpretted as follows: Two of the four sites are replaced simultaneously to form the 1/2-exchanged phase (stage I). The third site is occupied in stage II, which results in the 3/4-exchanged phase.

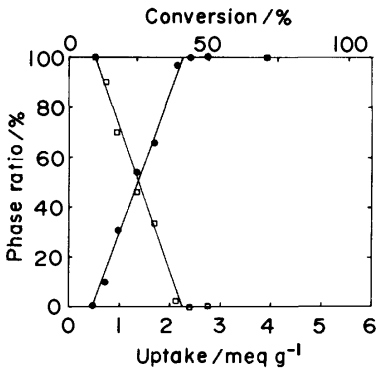

Fig. 4. Approximate ratios of the sodium ion-exchanged phases as a function of uptake.
□: Phase HH, ●: phase Na1, ■: phase Na2.

On the other hand, there are several differences between the Na^+/H^+ and K^+/H^+ exchange processes.

i) A complete exchange was not achieved for the Na^+/H^+ exchange.

ii) A 1/4-exchanged phase as well as a fully-exchanged one did not appear in the Na^+/H^+ exchange process.

iii) Phases Na1 and Na2 have larger interlayer distances than the corresponding K^+-exchanged phases.

Item i) may be due to the higher hydration energy of sodium ion than potassium ion:[9] A cation must give up a part or all of hydrated water when it enters into a host lattice. Therefore, a cation with a higher hydration energy is more difficult to be ion-exchanged.

Fact ii) may be explained by the idea that the ion-exchange behavior is rather dependent on the relative stability of the solid phases formed than the acidities of exchangeable protons.

Item iii) will be discussed in the next section.

Characterization of the Ion-exchanged Phases. The X-ray powder patterns of phases Na1 and Na2 could be indexed as a *C* base-centered monoclinic lattice. The X-ray data of phase Na1 is given in Table 2. The refined lattice constants are listed in Table 3 together with the values for phase HH.

Phase Na1 has the largely expanded *a* axis while the other three parameters were almost equal to those of phase HH. This means that phase Na1 was formed by swelling the interlayer spacing while the host framework of $[Ti_4O_9^{2-}]_n$ was remained unchanged.

Phase Na1 contains 1 mol of sodium ion and ≈3 mol of water per formula weight in the interlayer region. In contrast sodium tetratitanate ($Na_2Ti_4O_9$) accommodates 2 mol of interlayered sodium ion per formula weight. This means that phase Na1 accom-

Table. 1. Comparison of the Na^+/H^+ and K^+/H^+ ion-exchange processes

Conversion	Na^+/H^+ exchange		K^+/H^+ exchange[a]	
	Salt form	d_{200}/Å	Salt form	d_{200}/Å
0	$\overline{HH}\cdot 1.2H_2O$	9.1	$\overline{HH}\cdot 1.2H_2O$	9.1
1/4	—	—	$\overline{K_{0.5}H_{1.5}}\cdot 0.6H_2O$	8.6
1/2	$\overline{NaH}\cdot 3.3H_2O$	11.2	$\overline{KH}\cdot 0.5H_2O$	9.0
≈3/4	$\overline{Na_{1.4}H_{0.6}}\cdot 3.3H_2O$	11.2	$\overline{K_{1.4}H_{0.6}}\cdot 1.2H_2O$	9.8
1	—	—	$\overline{KK}\cdot 2.2H_2O$	10.9

a) Data taken from Ref. 4). b) d_{200}: Interlayer distance. c) $\overline{M_xH_{2-x}}\cdot nH_2O$ is the abbreviated form of $M_xH_{2-x}Ti_4O_9\cdot nH_2O$.

TABLE 2. X-RAY POWDER DIFFRACTION PATTERN FOR PHASE NaI

h k l	d_{calc}/Å	d_{obsd}/Å	Intensity
2 0 0	11.24	11.18	vs
2 0 $\bar{1}$	10.06	10.04	w
2 0 1	6.72	6.74	vw
4 0 $\bar{1}$	6.03	6.05	s
4 0 0	5.62	5.62	m
4 0 $\bar{2}$	5.03	5.03	vw
6 0 $\bar{1}$	4.05	4.05	vw
6 0 $\bar{2}$	3.868	3.866	vw
4 0 $\bar{3}$	3.842	3.842	vw
6 0 0	3.747	3.746	vw
1 1 0	3.711	3.713	w
3 1 0	3.363	3.362	s
4 0 2	3.360		
8 0 $\bar{2}$	3.016	3.014	s
8 0 $\bar{1}$	3.012		
5 1 $\bar{1}$	2.977	2.979	m
5 1 0	2.886	2.888	vw
8 0 0	2.810	2.807	m
4 0 3	2.660	2.662	s
1 1 3	2.542	2.541	vw
8 0 1	2.506	2.505	vw
10 0 $\bar{1}$	2.388	2.389	w
6 0 $\bar{5}$	2.346	2.346	vw
6 0 3	2.240	2.240	m
8 0 $\bar{5}$	2.201	2.201	w
10 0 1	2.056	2.055	vw
10 0 $\bar{5}$	2.012	2.012	m
12 0 $\bar{1}$	1.976	1.976	w
8 0 $\bar{6}$	1.921	1.920	m
0 2 0	1.881	1.881	m
12 0 0	1.873	1.873	vw
2 2 0	1.856	1.854	w
1 1 5	1.856		
0 2 1	1.855		

TABLE 3. LATTICE CONSTANTS OF THE SODIUM ION-EXCHANGED PHASES

phase	a/Å	b/Å	c/Å	β/°
HH[a]	19.968(4)	3.746(1)	12.025(2)	114.01(1)
NaI	24.337(5)	3.763(1)	12.078(3)	112.52(2)
Na2	24.378(4)	3.781(1)	12.054(3)	113.10(1)

a) Data taken from Ref. 4). b) Numerals in parentheses give the estimated standard deviations in the last digit.

modates a double number of interlayered species compared with the case of sodium tetratitanate. Phase NaI has a larger interlayer distance than sodium tetratitanate (d_{200}=8.38 Å)[10] by 2.8 Å, which is equal to the diameter of a water molecule. We can propose the structural model to explain the above facts: Interlayered sodium ions and water molecules are arranged in a double row which lies on the levels at y=0 and 1/2, as shown in Fig. 5. Although there may be other possible structural models for phase NaI, the model in Fig. 5 is appropriate to explain the ion-exchange behavior and thermoanalytical data described later. For example, this model gives a good explanation for the fact iii). (The corresponding K^+-

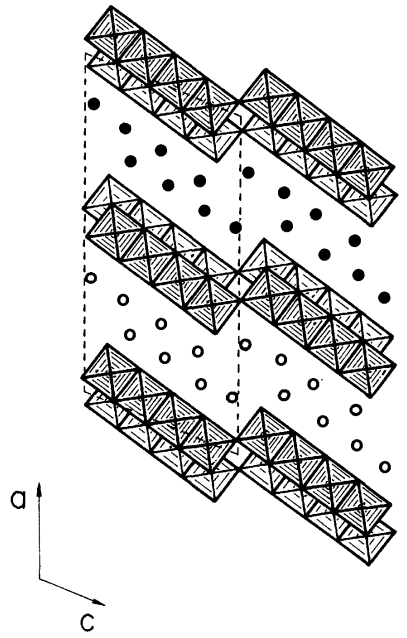

Fig. 5. Idealized structural model for phase NaI. (Projection along (010)).
●: y=1/2, ○: y=0.
Each circle is occupied at 25 and 75% by sodium ion and water molecule, respectively.

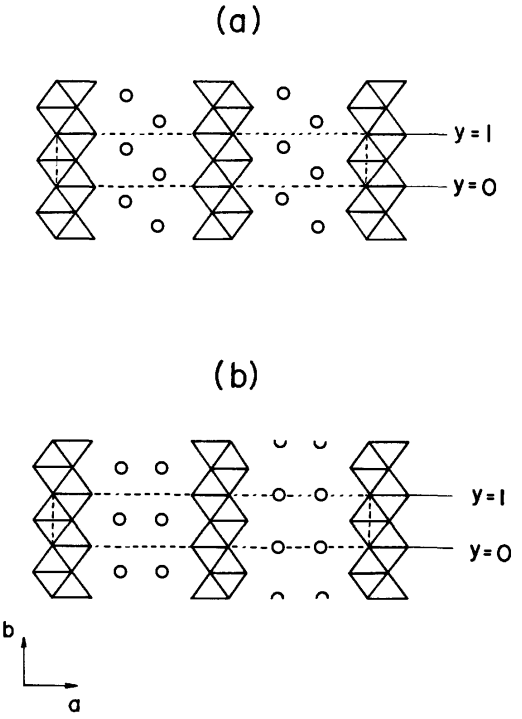

Fig. 6. Models for the arrangement of interlayered species. (Projection along (001)).
(a) Fully K^+-exchanged phase, (b) Phase NaI.
In the fully K^+-exchanged phase each circle is occupied evenly by potassium ion and water molecule, and in phase NaI at 25 and 75% by sodium ion and water molecule, respectively.

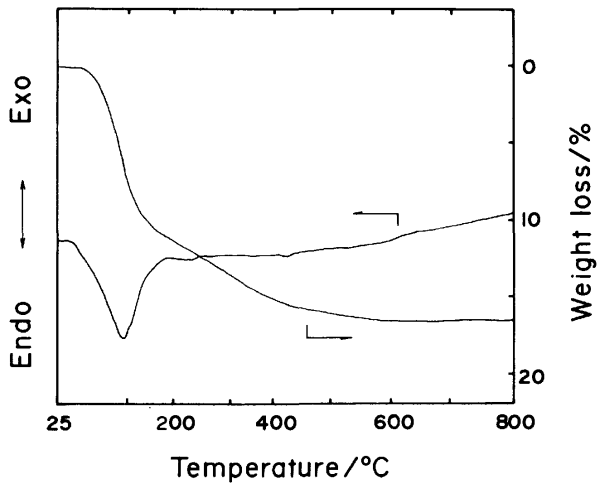

Fig. 7. DTA-TG curve of phase Na1. Heating rate: 10°C min^{-1}.

exchanged phase has a single row arrangement.)[4]

The similar double row arrangement of interlayered species has been reported for the fully K^+-exchanged phase.[4] The double row is tilted with respect to the (010) plane in this case: Potassium ions and water molecules occupy the sites which are shifted above and below the levels at $y=0$ and 1/2 (see Fig. 6). This tilt is considered to be due to the accommodation of relatively large interlayered species; potassium ions (ionic radius: 1.51 Å) and water molecules (1.40 Å).[11] On the contrary, phase Na1 can accommodate the interlayered species at the same y level since sodium ion is much smaller in size (1.16 Å)[11] than potassium ion.

The dehydration of phase Na1 took place apparently in two steps as shown in Fig. 7. The weight losses in each step were 10.0 and 6.5% and corresponded to the loss of 2.3 mol of hydrated water up to 100°C and then 1.5 mol in the temperature range of 100—600°C. When phase Na1 was heated at 100°C, the interlayer spacing decreased to 8.4 Å. The resulting material easily rehydrated to restore the original state by being exposed to moisture in the air. Being heat-treated up to 600°C, the material was decomposed into sodium hexatitanate ($Na_2Ti_6O_{13}$) and anatase (TiO_2).

In summary, the dehydration process can be written in the following scheme:

$$\begin{array}{lll} & NaHTi_4O_9\cdot 3.3H_2O & [11.2\ \text{Å}] \\ \text{step I} & 100°C \downarrow \quad \uparrow \text{in the air} & \\ & NaHTi_4O_9\cdot H_2O & [8.4\ \text{Å}] \\ \text{step II} & 100\text{—}600°C \downarrow & \\ & 1/2Na_2Ti_6O_{13}+TiO_2 & \end{array}$$

The process can be understood on the basis of the structural model described above (see Fig. 8). In step I the double row arrangement of interlayered species is destroyed by evaporating 8 water molecules per unit cell (2 mol/formula weight). The resulting phase has a single row arrangement of sodium ions and water molecules. This inference is consistent with the shrinkage of interlayer distance, 2.8 Å, which is in good agreement with the size of a water molecule. The weight loss in step II corresponds to the removal of remaining interlayered water molecules and the condensation of the host framework. The layer structure cannot be maintained by such a dehydration.

The water content and interlayer distance of phase Na2 were almost equal to those of phase Na1. This fact implies that phase Na1 has some space in the interlayer region which can accommodate additional sodium ions.

The authors would like to express their gratitude to

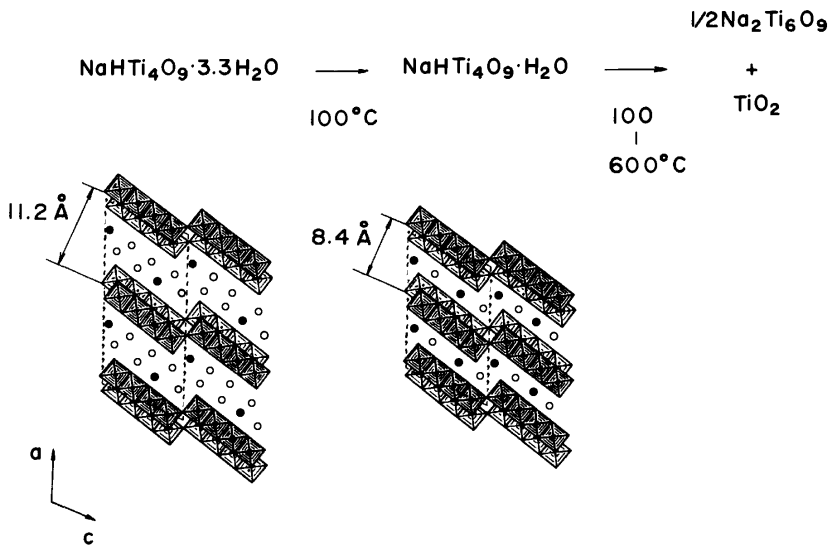

Fig. 8. Schematic explanation of the dehydration process of phase Na1. The closed circles and open ones denote sodium ions and water molecules, respectively. The configurations of the interlayered species are tentative.

Dr. Takefumi Mitsuhashi, National Institute for Research in Inorganic Materials, for his valuable discussion on the thermal analysis.

References

1) R. Marchand, L. Brohan, and M. Tournoux, *Mat. Res. Bull.*, **15**, 1129 (1980).
2) N. Ohta and Y. Fujiki, *Yogyo Kyokai Shi*, **88**, 1 (1980).
3) H. Izawa, S. Kikkawa, and M. Koizumi, *J. Phys. Chem.*, **86**, 5023 (1982).
4) T. Sasaki, M. Watanabe, Y. Komatsu, and Y. Fujiki, *Inorg. Chem.*, **24**, 2265 (1985).
5) Y. Fujiki, F. Izumi, T. Ohsaka, and M. Watanabe, *Yogyo Kyokai Shi*, **85**, 475 (1977).
6) T. Shimizu, H. Yanagida, M. Hori, K. Hashimoto, and Y. Nishikawa, *Yogyo Kyokai Shi*, **87**, 565 (1979).
7) Y. Fujiki and N. Ohta, *Yogyo Kyokai Shi*, **88**, 111 (1980).
8) D. E. Appleman and H. T. Evans, *NTIS Document*, No. PB-216188 (1973).
9) H. F. Halliwell and S. C. Nyburg, *Trans. Faraday Soc.*, **59**, 1126 (1963).
10) M. Dion, Y. Piffard, and M. Tournoux, *J. Inorg. Nucl. Chem.*, **40**, 917 (1978).
11) R. D. Shannon and C. T. Prewitt, *Acta Crystallogr., Sect. B*, **25**, 925 (1973).

Structural Studies of Thiocyanato and Isothiocyanato Cobalt(III) Complexes Ligating Diamine-*N,N'*-polycarboxylates

Yoshikiyo KATO, Hiroaki ISAGO,† Hiroshi OGINO,*,† Koshiro TORIUMI,†† and Tasuku ITO††
Department of Chemistry, Faculty of General Education, Yamagata University, Yamagata 990
†*Department of Chemistry, Faculty of Science, Tohoku University, Sendai 980*
††*Department of Applied Molecular Science, Institute for Molecular Science, Okazaki 444*
(Received July 3, 1985)

Crystal and molecular structures of NH_4[Co(NCS)(hedtra)]·H_2O and K[Co(SCN)(edtra)]·1.5H_2O have been determined by single-crystal X-ray analyses, where $hedtra^{3-}$ and $edtra^{3-}$ denote *N*-(2-hydroxyethyl)ethylenediamine-*N,N',N'*-triacetate and ethylenediamine-*N,N,N'*-triacetate ions, respectively. Crystal data are as follows: For the former species, triclinic, space group P1, a=7.477(2)Å, b=9.135(2)Å, c=6.899(1)Å; α=84.37(2)°, β=107.31(2)°, γ=108.35(2)°, V=427.0(2)Å^3, Z=1; for the latter species, monoclinic, space group $P2_1/a$, a=15.288(2)Å, b=7.059(1)Å, c=14.373(2)Å, β=107.55(1)°, V=1479.0(4)Å^3, Z=4. It has been proved unequivocally that the former species contains N-bonded SCN^- ligand and the latter species, the S-bonded ligand. Coordination geometry around the cobalt atom in each species deviates considerably from the regular octahedron, so that a very open space is created around the Co-NCS or Co-SCN moiety. This structural feature may be associated with the facile formation of the novel S-bonded species.

Quite recently, a pair of linkage isomers, $[Co(NCS)L]^{n-}$ and $[Co(SCN)L]^{n-}$, were prepared, where L denotes ethylenediamine-*N,N,N',N'*-tetraacetate ion ($edta^{4-}$) and *N*-(2-hydroxyethyl)ethylenediamine-*N,N',N'*-triacetate ion ($hedtra^{3-}$); *n* is 2 for $edta^{4-}$ and 1 for $hedtra^{3-}$.[1] When [Co(hedtra)(H_2O)] is allowed to react with SCN^-, comparable amounts of both $[Co(SCN)(hedtra)]^-$ and $[Co(NCS)(hedtra)]^-$ are formed simultaneously in an early stage of the reaction. Then, the thiocyanato (S-bonded) isomer changes to the isothiocyanato (N-bonded) isomer, because the N-bonded isomer is thermodynamically more stable than the S-bonded isomer. Therefore, the novel S-bonded isomer can be obtained in a good yield by controlling the reaction time.

Although the simultaneous formation of both $[Co(SCN)(NH_3)_5]^{2+}$ and $[Co(NCS)(NH_3)_5]^{2+}$ was also observed by the direct reaction of $[Co(NH_3)_5(H_2O)]^{3+}$ with SCN^-, the yield of the S-bonded isomer was much lower than that of the N-bonded isomer.[1] In the reaction of $[Co(CN)_5(H_2O)]^{2-}$ with SCN^-, the initial product has been found to be the N-bonded isomer $[Co(CN)_5(NCS)]^{3-}$.[2] Therefore, in the systems of $[Co(NH_3)_5(H_2O)]^{3+}$ and $[Co(CN)_5(H_2O)]^{2-}$, the N-bonded isomers are formed more easily than the S-bonded isomers. In order to elucidate the reason why $[Co(SCN)(hedtra)]^-$ is formed in a good yield, X-ray structural studies were undertaken for single crystals of K[Co(SCN)(edtra)]·1.5H_2O and NH_4[Co(NCS)(hedtra)]·H_2O, where $edta^{3-}$ denotes ethylenediamine-*N,N,N'*-triacetate ion.

Experimental

Materials. Ammonium salt of the complex, NH_4[Co(NCS)(hedtra)]·H_2O, was prepared from the corresponding potassium salt K[Co(NCS)(hedtra)]·2.5H_2O[1] by use of ion-exchange resin (QAE Sephadex). Slow evaporation of an aqueous solution saturated with the ammonium salt gave reddish violet needle crystals of NH_4[Co(NCS)(hedtra)]·H_2O. Found: C, 30.74; H, 4.90; N, 13.10%. Calcd for NH_4[Co(NCS)(hedtra)]·H_2O: C, 30.85; H, 4.94; N, 13.08%.

Potassium salt of the complex, K[Co(SCN)(edtra)]·1.5H_2O, was prepared by a method similar to NH_4[Co(SCN)(hedtra)]·0.3H_2O.[1] Found: C, 26.09; H, 3.41; N, 10.29%. Calcd for K[Co(SCN)(edtra)]·1.5H_2O: C, 26.74; H, 3.71; N, 10.14%. Blue plate crystals of K[Co(SCN)(edtra)]·1.5H_2O were obtained by dropwise addition of 0.3 ml of methanol to an aqueous solution of the complex (10 mg of complex in 6 ml of water) and by leaving the solution in a refrigerator for two weeks.

X-Ray Analyses. Diffraction data were obtained on a Rigaku automated four circle diffractometer AFC-5 with graphite monochromatized Mo$K\alpha$ radiation (λ=0.71073 Å). Intensity data were corrected for the Lorentz-polarization effects and for absorption. The lattice parameters were obtained from the least-squares fit of 50 (for NH_4[Co(NCS)(hedtra)]·H_2O) and 35 (for K[Co(SCN)(edtra)]·1.5H_2O) 2θ values with $25° < 2\theta < 30°$.

The structures of both complexes were solved by standard heavy-atom techniques and refined by block-diagonal least square methods. The weight (w) was taken as $w=[\sigma_c^2+(0.015|F_o|)^2]^{-1}$. The scattering factors for non-hydrogen atoms were taken from the literatures.[3] For hydrogen, the values given by Stewart *et al.* were used.[4] All the hydrogen atoms were located by difference syntheses and included in the refinement with isotropic temperature factors. Absolute configuration of the NH_4[Co(NCS)(hedtra)]·H_2O was determined by using anomalous scattering technique. Least-squares calculation including the anomalous scattering corrections for non-hydrogen atoms gave R and R_w values of 0.023 and 0.029. The enantiomeric structure was refined under identical conditions to give R and R_w values of 0.032 and 0.045, respectively. The crystal specimen of NH_4[Co(NCS)(hedtra)]·H_2O used in the X-ray work has the absolute configuration illustrated in Fig. 1 ($\Lambda(R,R)\Delta(R,G)$ form, *vide infra*). When the *R*-factor ratio test[5] was applied to the R_w values, the alternative model was rejected at the less than 0.005 significant level. Crystallographic data and the final R indices are summarized in Table 1. The final fractional atomic coordinates and equivalent isotropic thermal parameters for non-hydrogen atoms of NH_4[Co-

TABLE 1. CRYSTALLOGRAPHIC PARAMETERS

	$NH_4[Co(NCS)(hedtra)]\cdot H_2O$	$K[Co(SCN)(edtra)]\cdot 1.5H_2O$
Formula	$CoSC_{11}H_{19}N_4O_7\cdot H_2O$	$KCoSC_9H_{11}N_3O_6\cdot 1.5H_2O$
Crystal system	Triclinic	Monoclinic
Space group	P1	$P2_1/a$
a/Å	7.477(2)	15.288(2)
b/Å	9.135(2)	7.059(1)
c/Å	6.899(1)	14.373(2)
α/deg	84.37(2)	—
β/deg	107.31(2)	107.55(1)
γ/deg	108.35(2)	—
V/Å^3	427.0(2)	1479.0(4)
Z	1	4
d_c/g cm^{-3}	1.67	1.86
d_m/g cm^{-3}	1.67	1.83
Crystal size/mm	0.56×0.16×0.14	0.4×0.4×0.3
Scan range/degree	1.3+0.5 tanθ	1.2+0.5 tanθ
Scan mode	θ—2θ	θ—2θ
$2\theta_{max}$/deg	55	55
μ/mm^{-1}	1.21	1.65
Unique reflections	2322	3822
Observed reflections[a)]	2039	3086
R	0.023	0.029
R_w	0.029	0.038

a) $|F_o|>3\sigma(|F_o|)$.

TABLE 2. FRACTIONAL COORDINATES (×10^4) AND EQUIVALENT ISOTROPIC THERMAL PARAMETERS (Å^2) FOR NON-HYDROGEN ATOMS OF $NH_4[Co(NCS)(hedtra)]\cdot H_2O$

Atom	x	y	z	B_{eq}
Co	5000(1)	5000(1)	5000(1)	1.5
S	1808(1)	8695(1)	4216(2)	3.8
O(1)	4606(3)	3815(2)	7375(3)	2.2
O(2)	4779(3)	1591(3)	8917(4)	2.7
O(3)	7155(3)	6511(2)	6588(3)	2.1
O(4)	10197(3)	6896(3)	8566(4)	3.4
O(5)	2865(3)	3439(2)	3443(3)	2.1
O(6)	797(4)	2945(3)	366(4)	3.6
O(7)	7349(3)	9904(2)	494(4)	2.9
N(1)	6805(3)	3839(2)	5106(4)	1.7
N(2)	5399(3)	5916(2)	2378(4)	1.5
N(NCS)	3314(4)	6206(3)	5039(4)	2.3
C(1)	6829(4)	3746(3)	2957(4)	2.0
C(2)	6959(4)	5332(3)	2037(4)	1.9
C(3)	5978(5)	2308(3)	5996(5)	2.2
C(4)	5067(4)	2557(3)	7585(5)	2.0
C(5)	8769(4)	4671(3)	6439(5)	2.1
C(6)	8739(4)	6140(3)	7282(5)	2.0
C(7)	3465(4)	5286(3)	843(5)	2.0
C(8)	2250(4)	3768(3)	1536(5)	2.1
C(9)	6061(4)	7644(3)	2296(5)	2.1
C(10)	6310(5)	8302(4)	258(5)	2.9
C(NCS)	2708(4)	7250(3)	4710(5)	2.2
N(a)	589(4)	10070(3)	8557(5)	3.1
O(w)	9560(4)	1333(3)	−5447(4)	3.3

TABLE 3. FRACTIONAL COORDINATES (×10^4) AND EQUIVALENT ISOTROPIC THERMAL PARAMETERS (Å^2) FOR NON-HYDROGEN ATOMS OF $K[Co(SCN)(edtra)]\cdot 1.5H_2O$

Atom	x	y	z	B_{eq}
K	1672(1)	−3076(1)	9593(1)	4.5
Co	184(1)	288(1)	6888(1)	1.7
S	1519(1)	−798(1)	6663(1)	2.9
O(1)	163(1)	−1596(3)	7840(1)	2.7
O(2)	−325(1)	−1947(4)	9139(2)	4.6
O(3)	−447(1)	−1295(2)	5832(1)	2.3
O(4)	−1812(1)	−2607(3)	5143(2)	3.5
O(5)	810(1)	1950(3)	7903(1)	2.5
O(6)	1734(2)	4448(3)	8178(2)	4.7
N(1)	−1007(1)	988(3)	7021(1)	2.1
N(2)	105(1)	2467(3)	6033(1)	2.2
N(SCN)	2827(2)	−294(6)	8501(2)	6.5
C(1)	−1164(2)	3006(4)	6710(2)	2.7
C(2)	−856(2)	3207(4)	5805(2)	2.8
C(3)	−929(2)	635(4)	8062(2)	2.8
C(4)	−333(2)	−1109(4)	8383(2)	2.9
C(5)	−1706(2)	−305(4)	6376(2)	2.6
C(6)	−1315(2)	−1505(4)	5729(2)	2.3
C(7)	822(2)	3844(4)	6547(2)	3.0
C(8)	1162(2)	3438(4)	7629(2)	2.9
C(SCN)	2279(2)	−505(5)	7759(2)	3.6
O(w1)	1560(1)	790(3)	9863(1)	4.1
O(w2)	−52(5)	−4433(9)	10598(5)	9.0

(NCS)(hedtra)]·H_2O and K[Co(SCN)(edtra)]·1.5H_2O are given in Tables 2 and 3.

All calculations were carried out on the HITAC M-200H computer at the Computer Center of the Institute for Molecular Science using the Universal Crystallographic Computation Program System UNICS III.[6] The lists of structure factors and anisotropic thermal parameters are deposited at the Office of the Chemical Society of Japan (Document No. 8553).

Results and Discussion

Description of the Molecular Structures of [Co(NCS)(hedtra)]$^-$ and [Co(SCN)(edtra)]$^-$. Figures 1 and 2 show, respectively, stereoscopic views of the complex anions, [Co(NCS)(hedtra)]$^-$ and [Co(SCN)(edtra)]$^-$.

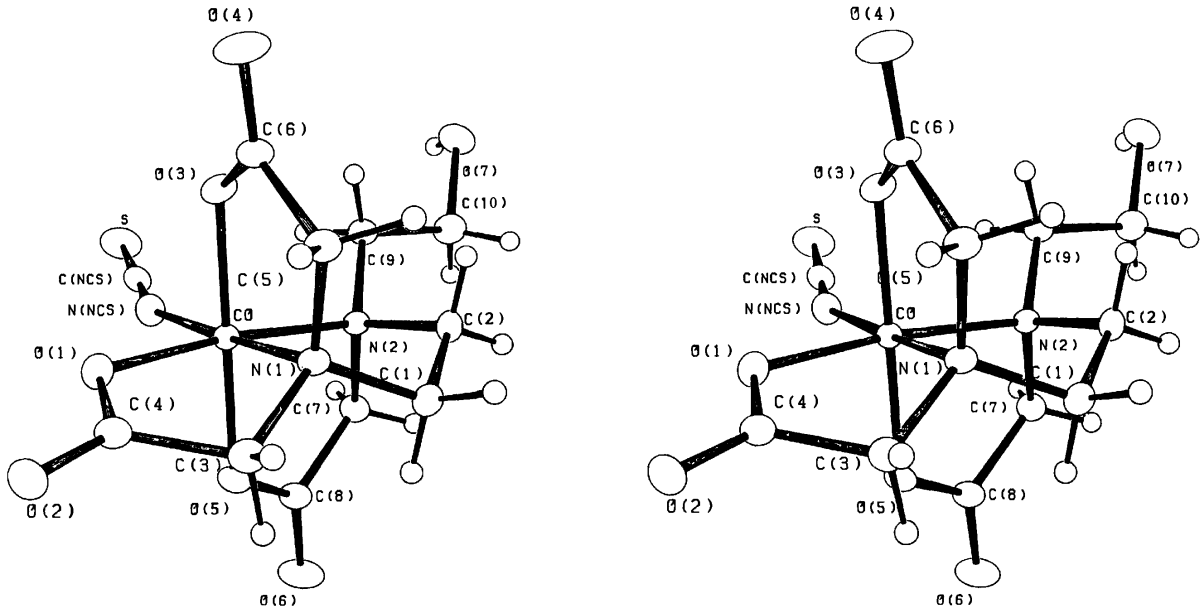

Fig. 1. Stereoscopic view of $[Co(NCS)(hedtra)]^-$.

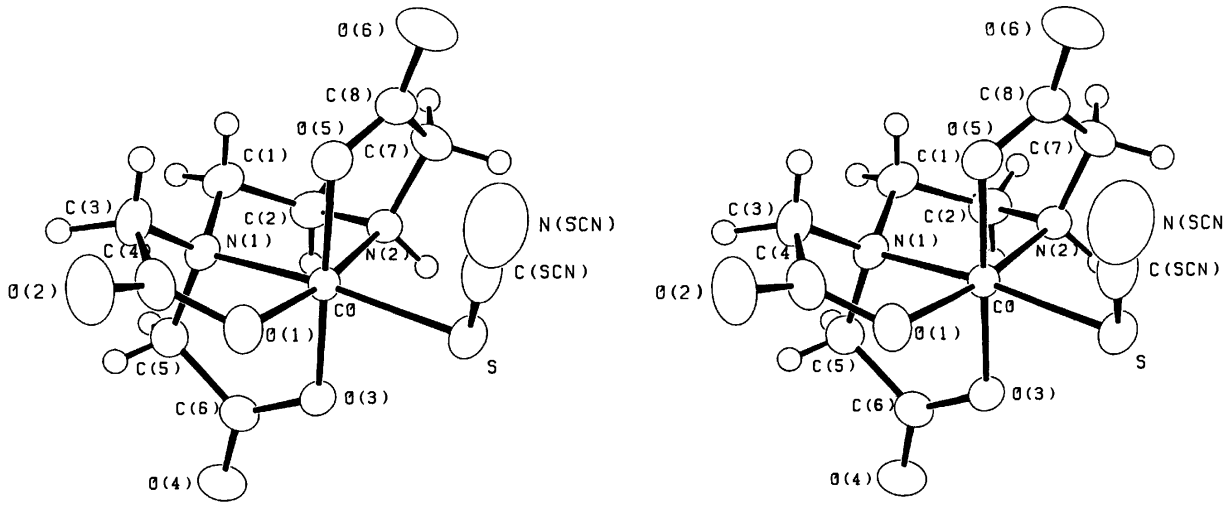

Fig. 2. Stereoscopic view of $[Co(SCN)(edtra)]^-$.

The relevant bond lengths and bond angles based on the atomic numbering scheme in these figures are listed in Tables 4—7. The present structural determinations prove unequivocally that $[Co(NCS)(hedtra)]^-$ contains isothiocyanato ligand and $[Co(SCN)(edtra)]^-$, thiocyanato ligand. The diamine-*N*,*N*′-polycarboxylate ions, $hedtra^{3-}$ and $edtra^{3-}$, act as pentadentate ligands. In each complex, isothiocyanato or thiocyanato ligand exists in the plane containing cobalt atom and two amino nitrogen atoms. Wiekliem and Hoard have pointed out for $[Co(edta)]^-$ that the strain in the complex can be expressed by the deviation from planarity of acetate (N–C–C–O–Co) rings.[7] The out-of-plane acetate rings (*R* rings) of the complexes studied here are less strained than the in-plane acetate rings (*G* rings), because the deviation from the planality of the *R* rings is smaller than that of the *G* rings. Similar trends have been observed for other related complexes, $[Co(Hedta)(H_2O)]$[8] and $[Co(NO_2)(edtra)]^-$.[9] The strains existing in the complexes are also disclosed in the Co–O bond lengths: The Co–O bond lengths of the *G* rings are longer than those of the *R* rings.

The bond angle of Co–N(NCS)–C(NCS) in $[Co(NCS)(hedtra)]^-$ is 157.1(3)°. This value deviates significantly from the values commonly found for various N-bonded complexes. The reported values lie in the range of 163.5—177.6°.[10–14] The deviation may come from a packing effect, because any specific group which can interact with the Co–NCS group is absent. The value of the bond angle of Co–S(SCN)–C(SCN) in $[Co(SCN)(edtra)]^-$ (102.9(1)°) is within the range of

Table 4. Bond lengths (l/Å) for NH_4[Co(NCS)-(hedtra)]·H_2O

Co-O1	1.918(2)	Co-O3	1.883(2)
Co-O5	1.893(2)	Co-N1	1.944(3)
Co-N2	1.982(2)	Co-N(NCS)	1.924(3)
S-C(NCS)	1.626(4)	O1-C4	1.284(4)
O2-C4	1.228(4)	O3-C6	1.277(4)
O4-C6	1.233(3)	O5-C8	1.296(4)
O6-C8	1.216(3)	O7-C10	1.424(4)
N1-C1	1.498(4)	N1-C3	1.492(3)
N1-C5	1.487(3)	N2-C2	1.510(4)
N2-C7	1.493(3)	N2-C9	1.499(3)
N(NCS)-C(NCS)	1.156(4)	C1-C2	1.510(4)
C3-C4	1.519(5)	C5-C6	1.522(5)
C7-C8	1.519(4)	C9-C10	1.513(5)

Table 5. Bond angles (degree) for NH_4[Co(NCS)-(hedtra)]·H_2O

O1-Co-O3	91.3(1)	O1-Co-O5	87.7(1)
O1-Co-N1	83.8(1)	O1-Co-N2	171.0(1)
O1-Co-N(NCS)	94.8(1)	O3-Co-O5	178.4(1)
O3-Co-N1	87.4(1)	O3-Co-N2	94.4(1)
O3-Co-N(NCS)	89.6(1)	O5-Co-N1	91.2(1)
O5-Co-N2	86.5(1)	O5-Co-N(NCS)	91.7(1)
N1-Co-N2	89.4(1)	N1-Co-N(NCS)	176.7(1)
N2-Co-N(NCS)	92.3(1)	Co-O1-C4	114.8(2)
Co-O3-C6	115.5(2)	Co-O5-C8	115.2(2)
Co-N1-C1	105.9(2)	Co-N1-C3	105.5(2)
Co-N1-C5	108.5(2)	C1-N1-C3	113.4(2)
C1-N1-C5	112.2(2)	C3-N1-C5	110.9(2)
Co-N2-C2	105.4(2)	Co-N2-C7	105.0(2)
Co-N2-C9	115.5(2)	C2-N2-C7	111.5(2)
C2-N2-C9	108.8(2)	C7-N2-C9	110.6(2)
Co-N(NCS)-C(NCS)	157.1(3)	N1-C1-C2	106.8(2)
N2-C2-C1	110.5(2)	N1-C3-C4	108.2(3)
O1-C4-O2	124.4(3)	O1-C4-C3	114.7(3)
O2-C4-C3	121.0(3)	N1-C5-C6	111.3(3)
O3-C6-O4	123.8(3)	O3-C6-C5	113.4(2)
O4-C6-C5	119.9(3)	N2-C7-C8	111.9(2)
O5-C8-O6	123.3(3)	O5-C8-C7	115.2(2)
O6-C8-C7	121.5(3)	N2-C9-C10	114.0(3)
O7-C10-C9	108.5(3)	S-C(NCS)-N(NCS)	178.7(2)

those reported for various S-bonded complexes (90—109°).[12,15]

The C-N (SCN) bond length of [Co(NCS)(hedtra)]$^-$ (1.156(4) Å) is essentially identical with those of [Co(SCN)(edtra)]$^-$ (1.150(5) Å), other cobalt(III) complexes containing thiocyanate ion such as [Co(SCN)$(NH_3)_5]^{2+}$ (1.14(4) Å)[15] and [$(CN)_5$Co(SCN)Co$(NH_3)_5$] (1.145(7) Å)[12] and uncoordinated thiocyanate ion (1.158(5) Å and 1.149(7) Å).[16] Therefore, the C-N bond lengths of thiocyanate ion are hardly influenced by the bonding mode of thiocyanate ion. The C-S bond lengths, however, are influenced by the bonding mode: 1.664(3) Å for [Co(SCN)(edtra)]$^-$, 1.627(4) Å for [Co(NCS)(hedtra)]$^-$, 1.645(5) Å for [$(CN)_5$Co(SCN)Co$(NH_3)_5$],[12] and 1.644(4) and 1.646(5) Å for free thiocyanate ion.[16] The C-S bond lengths change in the following order: Co-NCS<SCN$^-$≃Co-SCN-Co<Co-SCN.

Table 6. Bond lengths (l/Å) for K[Co(SCN)-(edtra)]·1.5H_2O

Co-O1	1.915(2)	Co-O3	1.897(2)
Co-O5	1.892(2)	Co-N1	1.952(2)
Co-N2	1.949(2)	Co-S	2.292(1)
S-C(SCN)	1.664(3)	O1-C4	1.288(4)
O2-C4	1.233(4)	O3-C6	1.299(3)
O4-C6	1.227(3)	O5-C8	1.295(3)
O6-C8	1.216(4)	N1-C1	1.490(4)
N1-C3	1.486(4)	N1-C5	1.495(3)
N2-C2	1.500(3)	N2-C7	1.485(4)
N(SCN)-C(SCN)	1.150(5)	C1-C2	1.518(4)
C3-C4	1.519(4)	C5-C6	1.508(4)
C7-C8	1.511(4)		

Table 7. Bond angles (degree) for K[Co(SCN)-(edtra)]·1.5H_2O

O1-Co-O3	92.8(1)	O1-Co-O5	89.6(1)
O1-Co-N1	83.6(1)	O1-Co-N2	170.7(1)
O1-Co-S	94.4(1)	O3-Co-O5	177.6(1)
O3-Co-N1	87.9(1)	O3-Co-N2	92.4(1)
O3-Co-S	87.1(1)	O5-Co-N1	92.1(1)
O5-Co-N2	85.3(1)	O5-Co-S	92.9(1)
N1-Co-N2	88.8(1)	N1-Co-S	174.5(1)
N2-Co-S	93.7(1)	Co-O1-C4	112.8(2)
Co-O3-C6	114.5(2)	Co-O5-C8	115.4(2)
Co-N1-C1	106.5(2)	Co-N1-C3	105.2(2)
Co-N1-C5	107.3(2)	C1-N1-C3	114.8(2)
C1-N1-C5	112.2(2)	C3-N1-C5	110.3(2)
Co-N2-C2	106.4(2)	Co-N2-C7	107.9(2)
C2-N2-C7	114.1(2)	Co-S-C(SCN)	102.9(1)
N1-C1-C2	106.5(2)	N2-C2-C1	108.5(2)
N1-C3-C4	107.5(2)	O1-C4-O2	123.7(3)
O1-C4-C3	116.2(3)	O2-C4-C3	120.1(3)
N1-C5-C6	112.5(2)	O3-C6-O4	123.4(2)
O3-C6-C5	116.5(2)	O4-C6-C5	120.0(2)
N2-C7-C8	111.2(2)	O5-C8-O6	124.2(3)
O5-C8-O7	115.0(3)	O6-C8-C7	121.5(3)
S-C(SCN)-N(SCN)	178.7(2)		

Infrared spectroscopy has been used for the determination of the bonding mode of thiocyanate ion.[17] The C-S stretching frequencies change in the order M-SCN<SCN$^-$<M-NCS and provide a good diagnostic test for the bonding mode.[18] The order is consistent with the change in the bond lengths shown above. Although it has been stated that the C-N stretching frequencies are generally higher for M-SCN than for M-NCS, the reverse is also sometimes true.[19] This comes from the fact that the C-N bond length is almost constant regardless of the bonding mode.

Description of the Crystal Structures of NH_4[Co(NCS)-(hedtra)]·H_2O and K[Co(SCN)(edtra)]·1.5H_2O. The stereoscopic view of the crystal structure for NH_4[Co(NCS)(hedtra)]·H_2O is given in Fig. 3. The crystals of the compound belong to the space group P1 with one molecule in a unit cell as shown in Table 1. This necessitates the occurrence of a spontaneous resolution. This was confirmed by the measurement of the CD spectrum of the solution which was prepared by dissolving a single crystal in water. The absolute

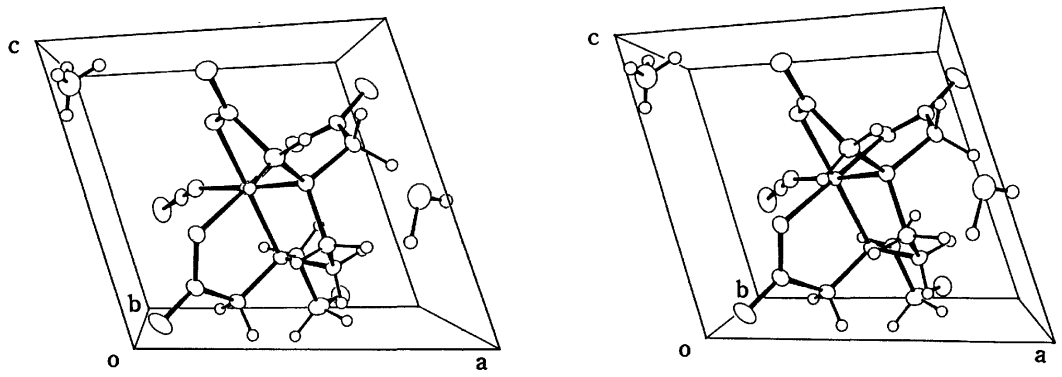

Fig. 3. Stereoscopic view of $NH_4[Co(NCS)(hedtra)]\cdot H_2O$.

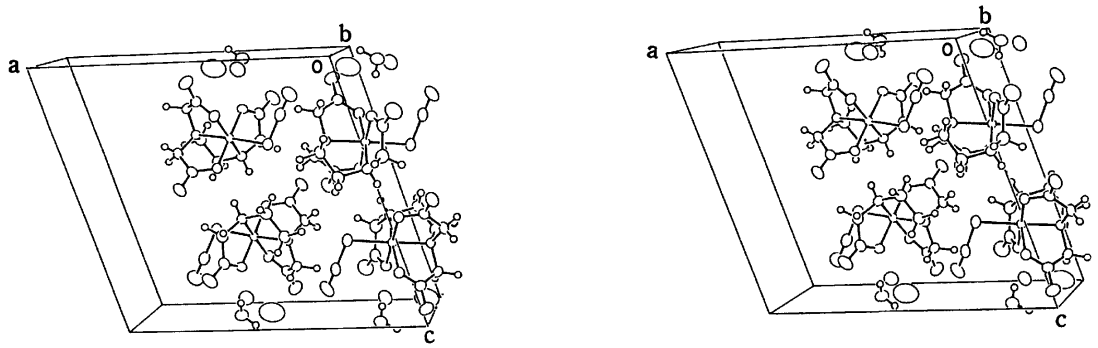

Fig. 4. Stereoscopic view of $K[Co(SCN)(edtra)]\cdot 1.5H_2O$.

configuration of the complex in the crystal used for X-ray analysis was $\Lambda(R,R)\Delta(R,G)$, showing that two R rings take Λ configuration and that one R ring (N2–C7–C8–O5–Co) and G ring take Δ configuration.

The stereoscopic view of the crystal structure for $K[Co(SCN)(edtra)]\cdot 1.5H_2O$ is given in Fig. 4. A unit cell of the complex is composed of four molecules which are two pairs of enantiomers, thus forming a racemic crystal.

Steric Circumstances around Cobalt(III) Centers in Thiocyanato and Isothiocyanato Cobalt(III) Complexes. The complexes, $[Co(NCS)(hedtra)]^-$ and $[Co(SCN)(edtra)]^-$, are so distorted that large open spaces are created around the coordination sites of N-bonded and S-bonded thiocyanate ions. This is evidenced by the fact that an angle of O(1)–Co–N(2) at the same side as NCS^- (or SCN^-) is opened to 189.0(1)° in $[Co(NCS)(hedtra)]^-$ and to 189.3(1)° in $[Co(SCN)(edtra)]^-$. We have attempted to evaluate the magnitude of the open spaces of these and the related complexes: The R_v value defined in Eq. 1 was calculated.

$$R_v = \sum_{cis} V_{do} / \sum_{cis} V_{ro} \qquad (1)$$

For a thiocyanato or an isothiocyanato complex, let us consider the plane which is perpendicular to the Co–SCN (or NCS) bond axis and involves the center of the cobalt atom (Fig. 5). The plane will hereafter be

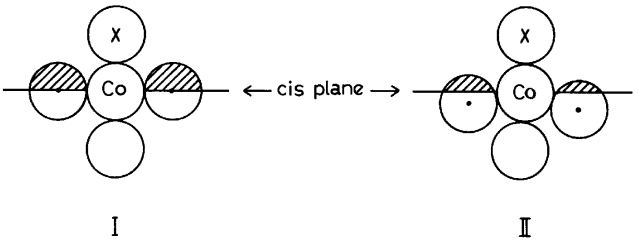

Fig. 5. Schematic expression of V_{do} (shaded part) of thiocyanato or isothiocyanato complex ($[CoXA_5]$). X denotes sulfur or nitrogen atom in thiocyanate. When $[CoXA_5]$ is a regular octahedron in geometry, V_{do} corresponds to V_{ro}. I: Regular octahedral $[CoXA_5]$. II: Distorted octahedral $[CoXA_5]$.

referred to as the cis plane. If the geometry of the complex is a regular octahedron, the centers of four donor atoms in cis position (A_1, A_2, A_3, and A_4) must be involved in the cis plane. In an actual complex, however, the four donor atoms deviate more or less from the cis plane. The space occupied by a cis donor atom is divided into two parts by the cis plane. The quantity given in Eq. 1, V_{do}, denotes the volume of the part of the side containing the thiocyanato ligand. Hence the term $\sum_{cis} V_{do}$ denotes the sum of the V_{do} values of the four atoms in the cis plane. The V_{ro} value is defined as the V_{do} value obtained when the geometry of the complex is assumed to be a regular octahedron. According to the definition, $\sum_{cis} V_{ro}$ can be expressed as follows:

TABLE 8. THE V_{do} AND R_v VALUES OF THE THIOCYANATO AND ISOTHIOCYANATO COMPLEXES AND RELATED COMPLEXES

Complex	Co-X bond	V_{do}/Å^3	R_v	Ref
$[Co(NCS)(hedtra)]^-$	Co-N(NCS)	1.84	0.73	This work
$[Co(SCN)(edtra)]^-$	Co-S	2.14	0.85	This work
$[Co(Hedta)(H_2O)]$	Co-O(H_2O)	2.22	0.88	8
$[Co(NO_2)(edtra)]^-$	Co-N(NO_2)	2.12	0.84	9
$[Co(SCN)(NH_3)_5]^{2+}$	Co-S	2.91	1.01	15
$[Co(NH_3)_5(NCS)$- in dimer[a]	Co-N(NCS)	3.00	1.04	12
$[Co(CN)_5(SCN)$- in dimer[a]	Co-S	3.83	1.00	12

a) Dimer means $[(NH_3)_5Co(NCS)Co(CN)_5]$.

$$\sum_{cis} V_{ro} = \frac{1}{2}(\text{the sum of the volume occupied by the donor atoms } A_1, A_2, A_3, \text{ and } A_4) \quad (2)$$

Therefore, if the complex in question takes the geometry of a regular octahedron, the R_v value must be unity. When there is a large open space around the coordination site of the thiocyanato ligand, the R_v value becomes smaller than unity. In the calculation of the R_v values, all donor atoms are assumed to be spherical and have covalent radii (C, 0.77; N, 0.70; O, 0.66).[20] The R_v and V_{do} values thus obtained are summarized in Table 8. For the $[Co(NO_2)(edtra)]^-$ and $[Co(Hedta)(H_2O)]$ complexes, the Co-NO_2 and Co-OH_2 bonds are regarded as Co-SCN (or NCS) bond.

There is a remarkable difference between the R_v values of the complexes containing diamine-*N*,*N*′-polycarboxylate and the other complexes: The former complexes show smaller R_v values (<0.9) than the latter complexes (≈1). This means that the pentaammine and pentacyano complexes are almost regular octahedral in geometry, while the complexes containing diamine-*N*,*N*′-polycarboxylates are considerably distorted octahedral molecules so that very open spaces are created around the Co-X bond (X=SCN^-, NCS^-, H_2O, or NO_2^-). Therefore, the sixth coordination sites of the pentaammine and pentacyano complexes which accommodate thiocyanato ligand are more crowded than those of the diamine-*N*,*N*′-polycarboxylato complexes.

Steric Factor Controlling the Formation of the Thiocyanato and Isothiocyanato Linkage Isomers. The reactions of $[Co(NH_3)_5(H_2O)]^{3+}$ and $[Co(CN)_5(H_2O)]^{2-}$ with SCN^- lead to the almost exclusive formation of N-bonded isomers.[1,2] In the system of $[CoL(H_2O)]^{n-}$ containing diamine-*N*,*N*′-polycarboxylate ion, however, spontaneous formation of both N-bonded and S-bonded isomers was observed. This may be due to the difference in the steric circumstances around the coordination sites which accommodate thiocyanate ions.

The substitution reactions of $[Co(NH_3)_5(H_2O)]^{3+}$, $[Co(CN)_5(H_2O)]^{2-}$, and $[CoL(H_2O)]^{n-}$ will proceed through *D* or I_d mechanism to produce five coordinate intermediate, because substitution reactions of most cobalt(III) complexes have been believed to proceed through the mechanism.[21] The vacant coordination site of the intermediate yielded from $[CoL(H_2O)]^{n-}$ would be much less crowded than those from $[Co(NH_3)_5(H_2O)]^{3+}$ and $[Co(CN)_5(H_2O)]^{2-}$.

The size of a sulfur atom is larger than that of a nitrogen atom. The Co-SCN bond in S-bonded isomers is bent (<CoSC=≈100°), while the Co-NCS bond is approximately linear. Therefore, the coordination of the sulfur end in thiocyanate ion requires a larger open space around the coordination site than that of the nitrogen end. The smaller open space in $[Co(NH_3)_5]^{3+}$ and $[Co(CN)_5]^{2-}$ intermediates cannot accept the sulfur end favorably, but the larger open space in $[CoL]^{n-}$ intermediate can accept not only the nitrogen end but also the bulky sulfur end.

References

1) H. Ogino and H. Isago, *Chem. Lett.*, **1984**, 561.
2) I. Stolz, W. K. Wilmarth, and A. Haim, *Inorg. Chem.*, **7**, 1250 (1968).
3) "International Tables for X-ray Crystallography"; Kynoch Press: Birmingham, England, 1974; Vol. IV.
4) R. F. Stewart, E. R. Davidson, and W. T. Simpson, *J. Chem. Phys.*, **42**, 3175 (1965).
5) W. C. Hamilton, *Acta Crystallogr.*, **18**, 502 (1965).
6) T. Sakurai and K. Kobayashi, *Rikagaku Kenkyusho Hokoku*, **55**, 69 (1979).
7) H. A. Wiekliem and J. L. Hoard, *J. Am. Chem. Soc.*, **81**, 549 (1959).
8) H. Okazaki, K. Tomioka, and H. Yoneda, *Inorg. Chim. Acta*, **74**, 169 (1983).
9) J. D. Bell and G. L. Blackmer, *Inorg. Chem.*, **12**, 836 (1973).
10) G. R. Clark and G. J. Palenik, *Inorg. Chem.*, **9**, 2754 (1970).
11) G. J. Palenik, M. Mathew, W. L. Steffen, and G. Baren, *J. Am. Chem. Soc.*, **97**, 1059 (1975).
12) F. R. Fronczek and W. P. Schaefer, *Inorg. Chem.*, **14**, 2066 (1975).
13) A. J. Carty, P. C. Chieh, N. C. Taylor, and Y. S. Wong, *J. Chem. Soc., Dalton Trans.*, **1976**, 572.
14) J. H. Nelson, J. J. MacDougall, N. W. Alcock, and F. Mathew, *Inorg. Chem.*, **21**, 1200 (1982).
15) M. R. Snow and R. F. Boomsa, *Acta Crystallogr., Sect., B*, **28**, 1908 (1972).
16) J. J. MacDougall, J. H. Nelson, W. C. Fultz, J. L. Burmeister, E. M. Holt, N. W. Alcock, *Inorg. Chim. Acta*, **63**, 75 (1982).

17) R. A. Bailey, S. L. Kozak, T. W. Michelsen, and W. N. Mills, *Coord. Chem. Rev.*, **6**, 407 (1971).
18) A. Turco and C. Pecile, *Nature*, **191**, 66 (1961).
19) D. A. Buckingham, I. I. Creaser, and A. M. Sargeson, *Inorg. Chem.*, **9**, 655 (1970).
20) L. Pauling, "The Nature of the Chemical Bond," 3rd ed., Cornell University Press (1960).
21) C. H. Langford and H. B. Gray, "Ligand Substitution Processes," W. A. Benjamin, Inc., New York (1965).

The Synthesis and Thermal Behavior of Barium Bis(hydrogenphosphoramidate) and Barium Phosphoramidate

Shoji SATO and Makoto WATANABE*
Department of Industrial Chemistry, Chubu University, Matsumoto-cho, Kasugai, Aichi 487
(Received July 9, 1985)

Barium bis(hydrogenphosphoramidate) monohydrate and barium phosphoramidate monohydrate were made by mixing a solution of potassium hydrogenphosphoramidate and a solution of barium chloride at pH 6.1—6.4 and 10.0—10.5 respectively. Both products were stable at room temperature. Barium bis(hydrogenphosphoramidate) monohydrate was decomposed by water to produce the orthophosphate. This was condensed to make polyphosphates above 100 °C and finally formed barium metaphosphate above 500 °C. The thermal products of the hydrogenphosphoramidate did not produce any phosphate with imino groups. Barium phosphoramidate produced ortho-, di-, imidodi-, and triphosphates when it was heated above 200 °C. These thermal products were converted to dibarium diphosphate in air above 500 °C.

Among many phosphorus–nitrogen compounds, phosphazenes are probably the best-known and the most intensively investigated compounds. Some of them are already used as industrial materials and products. There are a series of phosphorus–nitrogen compounds which have amino groups on a P atom. These compounds can be used as a new type of chemical fertilizer with a P–N covalent bond and as flameproof materials because they produce polyphosphates having imino and amino groups when they are heated. They can also be used as starting materials for the preparation of many organic and inorganic phosphorus compounds.

In our previous papers,[1-4] the synthesis and the thermal behavior of magnesium and calcium phosphoramidates and hydrogenphosphoramidates were reported. Both the hydrogenphosphoramidates were unstable even at room temperature and decomposed to polyphosphates, while the phosphoramidates were stable at room temperature. These phosphoramidates and hydrogenphosphoramidates were decomposed to polyphosphates above room temperature in air. This paper will describe the synthesis and the thermal behavior of barium bis(hydrogenphosphoramidate) and phosphoramidate.

Experimental

Preparation of Barium Bis(hydrogenphosphoramidate). Potassium hydrogenphosphoramidate was made by the method described in a previous paper;[5] 0.08 mol of the phosphoramidate was dissolved in 85 cm^3 of water. The aqueous solution of barium chloride, which was made by dissolving 0.04 mol of barium chloride dihydrate in 40 cm^3 of water, was added to the phosphoramidate solution below 5 °C to prevent the hydrolysis of the phosphoramidate. The pH of the solution was 6.1—6.4 during the treatment. A white precipitate was filtered off and washed with cold water, ethanol, and then acetone. The product was dried at 50 °C for 1 d under reduced pressure.

Preparation of Barium Phosphoramidate. Potassium hydrogenphosphoramidate(0.04 mol) was dissolved in 400 cm^3 of water. Barium chloride dihydrate (0.04 mol) was dissolved in 120 cm^3 of water. The solution was poured into the phosphoramidate solution and the resulting solution was stirred for 5—10 min. During the treatment, the temperature of the phosphoramidate solution was kept below 5 °C to prevent the hydrolysis of the phosphoramidate; the pH of the solution was kept at 10.0—10.5 with aqueous ammonia. The white precipitate thus obtained was removed by filtration. Acetone was added to the mother liquor and the white product was filtered off, washed with 50-V% aqueous ethanol, ethanol, and then acetone. The product was dried at 25 °C for 1 d under reduced pressure.

Chemical Analysis. Phosphorus in a sample was determined colorimetrically by dissolving about 0.2 g of the sample in 100 cm^3 of a 6%-EDTA (disodium dihydrogen ethylenediaminetetraacetate dihydrate) aqueous solution. Barium and nitrogen in a sample were estimated by the gravimetric technique and the Kjeldahl method respectively.

Paper Chromatography and Colorimetry of Phosphates. The thermal products of barium hydrogenphosphoramidate were dissolved in a 6%-EDTA aqueous solution and those of barium phosphoramidate were dissolved in the EDTA solution of pH 9—10 controlled with aqueous ammonia. The one-demensional paper-chromatographic separation and the colorimetric determination of the phsophate species in the EDTA solutions were made by the method described in our previous paper.[1]

X-Ray Diffractometry. An X-ray diffraction diagram of a powder sample was taken with nickel-filtered Cu $K\alpha$ radiation using a Toshiba X-ray diffractometer, ADG-102.

IR Spectrophotometry. An IR spectrum of a sample was recorded on a JASCO IR spectrophotometer, A-3, using the KBr disc method.

^{31}P NMR Measurement. The nuclear magnetic resonance data were taken with a JNM-GX270 spectrograph on the aqueous solutions of the thermal products located by paper chromatography. As is customary, the NMR chemical shifts are reported relative to external 85%-orthophosphoric acid with positive shifts being downfield.

DTA and TG. A sample was heated at a rate of 5 °C min^{-1} in air by means of a Cho Balance TRDA$_1$-H apparatus.

Results and Discussion

Barium Bis(hydrogenphosphoramidate). The yield of the product was about 10.2 g. Found: P, 18.4; N, 7.9; Ba, 38.5%. Calcd for $Ba(HPO_3NH_2)_2 \cdot H_2O$: P, 17.8; N, 8.1; Ba, 39.5%. In this manner, the product was

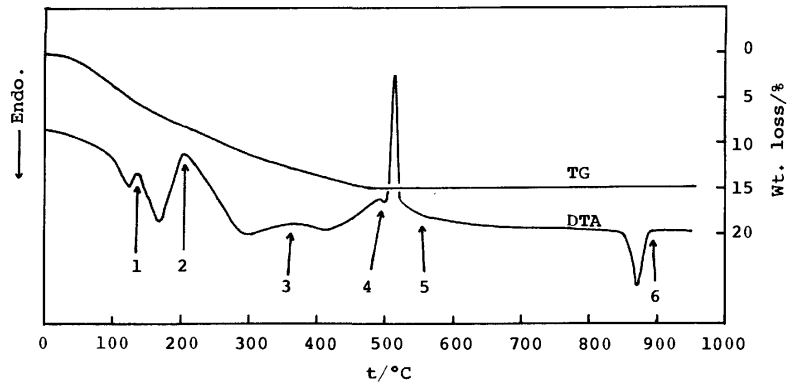

Fig. 1. DTA and TG curves of $Ba(HPO_3NH_2)_2 \cdot H_2O$ in air.

TABLE 1. WEIGHT LOSS AND COMPOSITION OF THE THERMAL PRODUCTS OF $Ba(HPO_3NH_2)_2 \cdot H_2O$

Sample	Total N/%	N/% as NH_4^+	Wt. loss /%	X-Ray dif.	Ortho & Amido	Di & Imidodi	Tri	Higher
Amido[a]	7.9	—	—	—	100	—	—	—
1	5.8	2.2	4.1	Am[b]	47.3	24.7	12.9	15.1
2	2.4	2.2	7.7	Am	10.3	15.8	16.4	57.5
3	0.6	—	11.7	Am	—	—	—	—
4	0	0	13.9	Am	—	—	—	—
5	0	0	15.0	$Ba(PO_3)_2$ JCPDS card 20-141	—	—	—	—
6	0	0	15.1	Am	—	—	—	—

a) $Ba(HPO_3NH_2)_2 \cdot H_2O$. b) Amorphous.

found to be barium bis(hydrogenphosphoramidate) monohydrate. The X-ray diffraction diagram of the product was the same as that of $Ba_{1/2}HPO_3NH_2 \cdot H_2O$ (JCPDS card, No. 18—170), but the careful measurement of the heating weight loss of the product, as will be shown later, also supported the above conclusion. Magnesium and calcium bis(hydrogenphosphoramidate) slowly decomposed to polyphosphates at room temperature,[1,2] while the product obtained in this work was very stable and did not decompose at room temperature. To study the thermal behavior of the product, DTA and TG curves of the product were taken with the result shown in Fig. 1. The samples as numbered on Fig. 1 were removed from a furnace, cooled in a silica-gel desiccator, and subjected to further analysis. The results are shown in Table 1, and Figs. 2 and 3. The hydrogenphosphoramidate showed two endothermic peaks accompanying weight loss below 200°C. The following dehydration reaction may be written for the endothermic process:

$$Ba(HPO_3NH_2)_2 \cdot H_2O \longrightarrow Ba(HPO_3NH_2)_2 + H_2O. \quad (1)$$

As Table 1 shows, the thermal product 1 exhibited less N content than that of $Ba(HPO_3NH_2)_2$ and contained ammonium ions. The N content of the product 2 was less than that of the product 1. Almost all the nitrogen of the product 2 was present as ammonium ions. The IR spectra of the thermal products 1 and 2 showed peaks

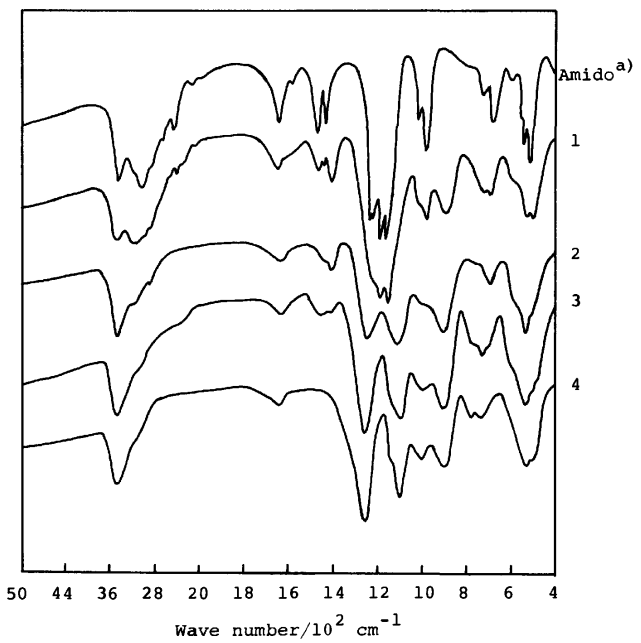

Fig. 2. IR spectra of the thermal products of $Ba(HPO_3NH_2)_2 \cdot H_2O$.
a): $Ba(HPO_3NH_2)_2 \cdot H_2O$.

of NH_4^+ at 1400 cm^{-1}, P-O-P and/or P-N(H)-P at 900 cm^{-1}, and $(PO_2)^-$ at 1220—1250 cm^{-1}. The paper-chromatographic analysis of the thermal products 1 and 2 agreed well with these results. Since the thermal

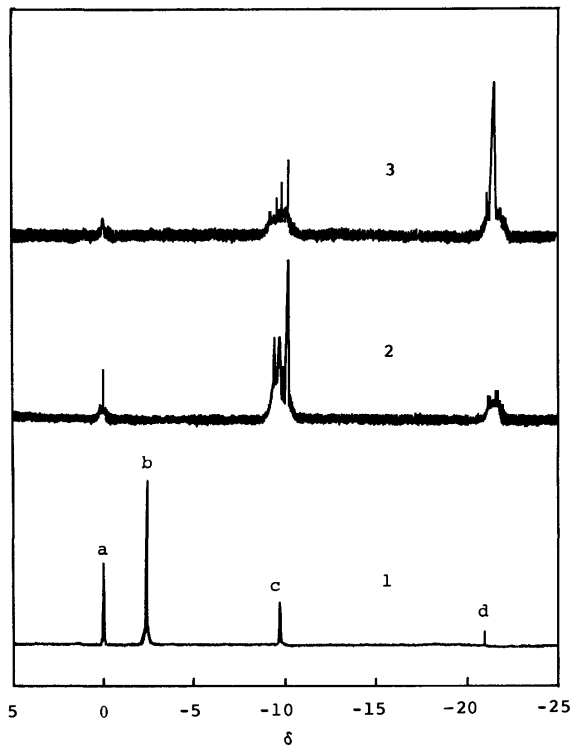

Fig. .3 ^{31}P NMR spectra of the thermal products of $Ba(HPO_3NH_2)_2 \cdot H_2O$ in air.
a: Orthophosphate, b: phosphoramidate, c: end-PO_4 group, d: middle-PO_4 group.

products other than 1 and 2 contained insoluble material and the separation of the phosphate species was poor, the paper-chromatographic analysis of the products was not possible. The above results do not indicate clearly that P-NH_2 linkages thermally decompose to form P-N(H)-P linkages with the elimination of ammonia as follows:

$$-\overset{|}{\underset{|}{P}}-NH_2 + NH_2-\overset{|}{\underset{|}{P}}- \longrightarrow -\overset{|}{\underset{|}{P}}-N(H)-\overset{|}{\underset{|}{P}}- + NH_3. \quad (2)$$

Accordingly, a ^{31}P NMR study of the thermal products was made. The ^{31}P NMR spectrum of the thermal product 1 showed peaks due to orthophosphate (0 ppm), phosphoramidate (−2.4 ppm), an end-PO_4 group (−9.8 ppm), and a middle-PO_4 group (−20.9 ppm). The thermal product 2 showed the NMR peaks of orthophosphate, an end-PO_4 group, and a middle-PO_4 group. Accordingly, these thermal products did not contain any substance with P-N(H)-P linkages. The hydrogenphosphoramidate did not form thermal products with imino groups. According to the above results, one can write the following reactions for the thermal decomposition of the hydrogenphosphoramidate to orthophosphate and condensation of the orthophosphate to polyphosphates:

$$Ba_{1/2}HPO_3NH_2 + H_2O \longrightarrow Ba_{1/2}NH_4HPO_4, \quad (3)$$

$$2Ba_{1/2}NH_4HPO_4 \begin{cases} \nearrow Ba(HO_3POPO_3H) + 2NH_3 + H_2O, & (4) \\ \searrow Ba(HO_3POPO_3NH_4) + NH_3 + H_2O, & (5) \end{cases}$$

$$Ba(HO_3POPO_3H) + Ba_{1/2}NH_4HPO_4 \longrightarrow Ba_{3/2}[HO_3POP(O_2)OPO_3H] + NH_3 + H_2O. \quad (6)$$

The thermal product 3 contained only a small amount of nitrogen and the product 4 contained no nitrogen. The IR spectra of these products were similar to that of polyphosphate with a meta composition. The ^{31}P NMR spectrum of the product 3 showed a small orthophosphate peak and peaks of end- and middle-PO_4 groups. Therefore, the successive broad endothermic peaks were found to be caused by the condensation of ortho- and polyphosphates to polyphosphate with a meta composition. The thermal products 1-3 showed weak unknown X-ray diffraction peaks and the product 4 was amorphous by X-ray diffractor. The product 5 showed X-ray diffraction peaks of barium metaphosphate(JCPDS card, No. 20—141). The large exothermic peak at about 510 °C is responsible for the conversion of amorphous barium metaphosphate into the crystalline form. The measured weight losses of the products 5 and 6 were close to the calculated one according to the following reaction:

$$Ba(HPO_3NH_2)_2 \cdot H_2O \longrightarrow Ba(PO_3)_2 + 2NH_3 + H_2O. \quad (7)$$

The last endothermic peak at about 870 °C was found to be caused by the melting of the barium metaphos-

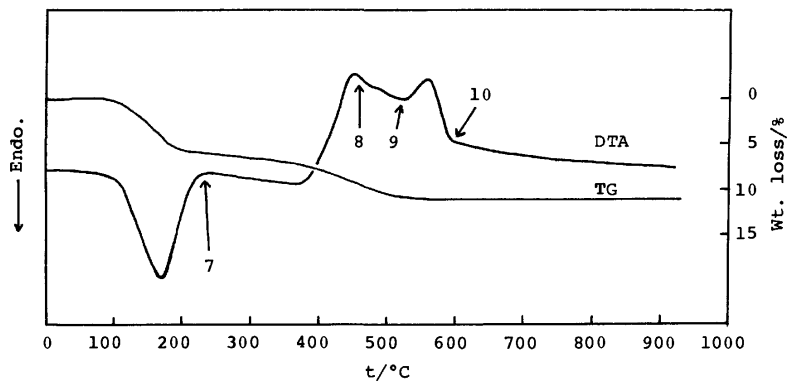

Fig. 4. DTA and TG curves of $BaPO_3NH_2 \cdot H_2O$ in air.

Table 2. Weight loss and composition of the thermal products of $BaPO_3NH_2 \cdot H_2O$

Sample	Total N/%	N/% as NH_4^+	Wt. loss /%	X-Ray dif.	Ortho & Amido	Di & Imidodi	Tri
Amido[a]	5.4	—	—	—	100	—	—
7	5.2	1.8	6.6	Un[b]	78.1	21.9	0
8	4.0	1.8	7.9	Un	56.2	37.3	6.5
9	0.5	0.3	10.1	Am[c]	11.4	77.2	11.4
10	0	0	10.8	$Ba_2P_2O_7$ JCPDS card 9-45	2.3	97.7	0

a) $BaPO_3NH_2 \cdot H_2O$. b) Unknown pattern. c) Amorphous.

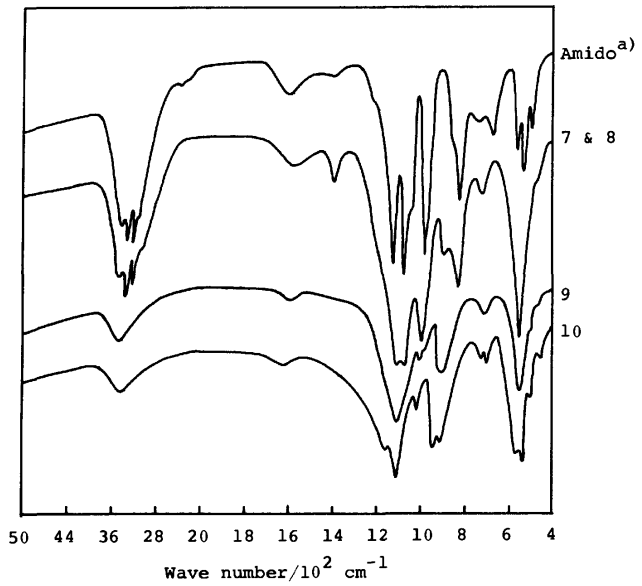

Fig. 5. IR spectra of the thermal products of $BaPO_3NH_2 \cdot H_2O$.
a): $BaPO_3NH_2 \cdot H_2O$.

phate.

Barium Phosphoramidate. The yield of the product was about 8.5 g. Found: P, 12.3; N, 5.4; Ba, 54.7%. Calcd for $BaPO_3NH_2 \cdot H_2O$: P, 12.4; N, 5.6; Ba, 54.2%. Accordingly, the product is barium phosphoramidate monohydrate. As will be described in the later part of this section, the study of the heating weight loss of the product supported this conclusion. The phosphoramidate was stable and did not decompose at room temperature. To study the thermal behavior of the product, DTA and TG curves of the product were taken with the result in Fig. 4. The chemical analysis data, the IR spectra, and the ^{31}P NMR spectra of the thermal products are shown in Table 2, and Figs. 5 and 6 respectively. The first large endothermic reaction accompanied by rapid weight loss seemed to be caused mainly by removal of the bound water because the measured weight loss was close to the calculated one according to the reaction:

$$BaPO_3NH_2 \cdot H_2O \longrightarrow BaPO_3NH_2 + H_2O. \quad (8)$$

As Table 2 shows, the nitrogen content of the thermal

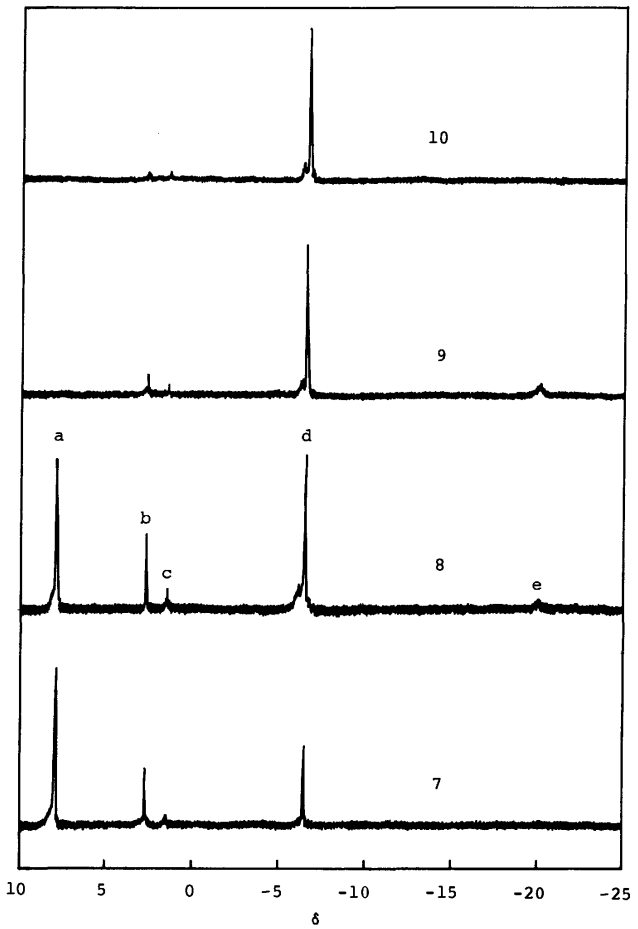

Fig. 6. ^{31}P NMR spectra of the thermal products of $BaPO_3NH_2 \cdot H_2O$ in air.
a: Phosphoramidate, b: orthophosphate, c: imidodiphosphate,[6] d: end-PO_4 group, e: middle-PO_4 group.

product 7 was less than that of $BaPO_3NH_2$. The product contained ammonium ions and ortho-, and diphosphate and/or imidodiphosphate other than the phosphoramidate. The IR spectrum of the product 7 exhibited absorptions of NH_4^+ at 1400 cm^{-1} and P–O–P and/or P–N(H)–P linkages at 900 and 720 cm^{-1}. These results indicate that barium phosphoramidate monohydrate reacts at this stage according to the following processes other than reaction 8:

$$BaPO_3NH_2 + H_2O \longrightarrow BaNH_4PO_4, \quad (9)$$

$$BaNH_4PO_4 \longrightarrow BaHPO_4 + NH_3, \quad (10)$$

$$2BaHPO_4 \longrightarrow BaO_3POPO_3Ba + H_2O, \quad (11)$$

$$2BaPO_3NH_2 \longrightarrow BaO_3PN(H)PO_3Ba + NH_3. \quad (12)$$

As Fig. 6 shows, the product 7 contained phosphoramidate, orthophosphate, imidodiphosphate, and diphosphate. (Barium phosphoramidate, tribarium bis(phosphate), and dibarium diphosphate showed ^{31}P NMR peaks at about 7.8—8.0, 2.8, and −5.6—−6.3 ppm respectively in a 6%-EDTA solution of pH 9—10 controlled with aqueous ammonia). So all the above reactions 9—12 take place at this stage. The intensity of the imidodiphosphate peak was weak and the rate of the Reaction 12 seemed to be much slower than those of the other reactions. According to Table 2, successive slow weight loss was due to the elimination of ammonia. Since the NMR spectrum of the product 8 exhibited peaks with stronger intensity than that of the product 7 at the same δ, the above reactions 9—12 may take place rapidly over the temperature range of 400—500 °C. The total energy of the reactions was considered to be exothermal. As Table 2 and Fig. 6 show, the thermal products 8 and 9 contained triphosphate. It is not probable that orthophosphate with Ba/P ratio of 1.0 would form triphosphate over this low temperature range. The problem can be solved by taking into account the following reorganization or disproportionation reaction in this system:

$$2BaNH_4PO_4 \longrightarrow Ba_{3/2}PO_4 + Ba_{1/2}(NH_4)_2PO_4. \quad (13)$$

The chemical species, $Ba_{1/2}(NH_4)_2PO_4$, can form triphosphate according to the reaction as follows:

$$Ba_{1/2}(NH_4)_2PO_4 + 2BaNH_4PO_4 \longrightarrow Ba_{5/2}[O_3POP(O_2)OPO_3] + 4NH_3 + 2H_2O. \quad (14)$$

The product 10 contained small amounts of ortho- and imidodiphosphates other than diphosphate and did not contain higher polyphosphates, so the reorganization or the decomposition of the triphosphate to diphosphate may occur according to the reaction:

$$Ba_{5/2}[O_3POP(O_2)OPO_3] + Ba_{3/2}PO_4 \longrightarrow 2Ba_2(O_3POPO_3). \quad (15)$$

The NMR data also showed that imidodiphosphate gradually converted to diphosphate. The reaction written below can be responsible for the conversion:

$$BaO_3PN(H)PO_3Ba + H_2O \longrightarrow BaO_3POPO_3Ba + NH_3. \quad (16)$$

We thank Dr. S. Motojima and Dr. H. Ishihara, Department of Industrial Chemistry, Gifu University, for providing the ^{31}P NMR spectral data of many samples.

References

1) M. Watanabe, T. Inagaki, and S. Sato, *Bull. Chem. Soc. Jpn.*, **56**, 458 (1983).
2) M. Watanabe, T. Inagaki, Y. Morii, and S. Sato, *Setsuko To Setsukai*, No. 184, p. 111 (1983).
3) M. Watanabe, Y. Morii, and S. Sato, *Bull. Chem. Soc. Jpn.*, **57**, 2087 (1984).
4) M. Watanabe, Y. Morii, and S. Sato, *Bull. Chem. Soc. Jpn.*, **57**, 2914 (1984).
5) "Shin Zitsuken Kagaku Koza," ed by the Chemical Society of Japan, Maruzen, Tokyo (1976), Vol. 8-[I], p. 354.
6) M. M. Crutchfield, C. H. Dungan, J. H. Letcher, V. Mark, and J. R. Van Wazer, "Topics in Phosphorus Chemistry," Interscience Publishers, New York (1967), Vol. 5, p. 227.

 © 1985 The Chemical Society of Japan Bull. Chem. Soc. Jpn., 58, 3518—3523 (1985) [Vol. 58, No. 12

Studies on Mixed Chelates. XIV. Influences of Solvent Polarity, and of Substituent Groups in β-Diketonate Ligands, on the Electronic Spectra of 5-Coordinated Mixed Copper(II) Chelates in Organic Solutions[1)]

Yutaka FUKUDA,* Mayumi YASUHIRA, and Kozo SONE
Department of Chemistry, Faculty of Science, Ochanomizu University, Otsuka, Bunkyo-ku, Tokyo 112
(Received July 22, 1985)

Several chelates of copper(II), Cu(tmen)(dike)X, were newly obtained where tmen=*N,N,N′,N′*-tetramethylethylenediamine, dike= a β-diketonate ion, and X^-= a halide or pseudohalide anion. These complexes exist as 5-coordinated species, with axially coordinated X^-, in nonpolar solvents. In more polar solvents, they are ionized according to the solvent polarity, and form the following equilibrium mixtures:

$$[Cu(tmen)(dike)X] \rightleftharpoons [Cu(tmen)(dike)]^+ + X^-$$

5-coordinated 4-coordinated (solvated, tetragonal)

This equilibrium is controlled by (a) the strengths of acceptor and donor properties of the solvent, which can be expressed by its polarity factor (Pf), *i.e.*, a linear combination of the donor number and acceptor number of the solvent, and (b) the changes of the ligand field strength of dike caused by the electron-withdrawing and -releasing properties of its α-substituent groups.

In the previous papers,[1-3)] we reported the properties of mixed Cu(II) chelates of the general formula Cu(diam)(dike)X in solid state and in various solvents.*[1)]

All these chelates are easily soluble in various organic solvents, and characteristic solvatochromism (color change caused by the nature of the solvent) is observed in their solutions. Moreover, in the same solvent, the spectral and conductivity behaviors of the chelates with different anions show drastic changes according to the coordination power of the anion (anion effect).

When X^-=ClO_4^-, or NO_3^-, *e.g.* with [Cu(tmen)(acac)]ClO_4, the solvatochromism observed is mainly due to the solute-solvent interaction between the chelate cation and the solvent molecules. On the other hand, when X^-= a halide or pseudohalide anion, *e.g.* with [Cu(tmen)(acac)Cl], the chelate exists as 5-coordinated green species in solid crystals and in nonpolar solvents. Here the solvatochromism observed in polar solvents is due to the competition of X^- and solvent molecules for the axial site(s) of the chelate cation, which leads to complicated solute-solute-solvent interactions.

In these former studies, a large number of chelates with various diamines and β-diketonates were prepared and studied, with ClO_4^- or NO_3^- as X^-, but only the chelates with tmen and acac were reported so far with a halide or pseudohalide anion as X^-.[4)] In continuation of these studies, therefore, we have prepared the latter type of chelates with tmen and various β-diketonates such as tfac, hfac and dipm. The effects of α-substituents in them, the anion (X^-), and solvent polarity on the formation of the 5-coordinated complexes in their solutions will be discussed in this paper.

Experimental

Materials. The ligands used (tmen and dike) and metal salts were "Guaranteed Grade" or "Extra Pure," and the solvents used for physical measurements were "Dotite Spectrosol" of Dojindo Laboratories, or "Guaranteed Grade" of Wako Pure Chemical Industry Co. Ltd. They were used without further purification.

Preparation of New Chelates. 1) Cu(tmen)(dike)X(dike =dipm, tfac, or hfac, X^-=Cl^- or Br^-): These complexes could be obtained by concentrating methanol solutions of the mixtures of CuX_2($CuCl_2 \cdot 2H_2O$ or $CuBr_2$), tmen, and dike of which molar ratio was 1:1:1. The hfac-Cl-chelate was rather difficult to prepare, because the deep green crystals of the mixed chelate [Cu(tmen)(hfac)Cl] contained small amounts of its disproportionation products, *i.e.*, blue plates of [$Cu(tmen)Cl_2$] and light green crystals of [$Cu(tmen)(hfac)_2$]. The compositions of these by-products were ascertained by elemental analyses. To remove them, the crude deep green products were recrystallized from $CHCl_3$ or DCE, and washed with cold DCE and ether. Among these complexes, the tfac- and hfac-chelates are all green and stable in atmospheric moisture but the dipm-chelates absorb water to form the monohydrates, showing the color change from green to bluish-violet(Cu(tmen)(dipm)X·H_2O, see Table 1).

2) Cu(tmen)(dike)X(dike=dipm or tfac, X^-=NCS^-; dike=tfac, X^-=I^-). These compounds could be obtained by the anion exchange of [Cu(tmen)(dike)]NO_3 with NaX in acetone, which is very similar to the method described before.[3)] As the iodide complexes were very difficult to crystallize, we could obtain only one of them, Cu(tmen)(tfac)I. The green crystals obtained were recrystallized from DCE.

*[1)] Abbreviations used in this article are as follows: diam= *N*-alkylated ethylenediamine, tmen=*N,N,N′,N′*-tetramethylethylenediamine, dike= a β-diketonate ligand ($R_1COCHCOR_2^-$), acac=acetylacetonate (R_1=R_2=CH_3), hfac=hexafluoroacetylacetonate (R_1=R_2=CF_3), tfac=trifluoroacetylacetonate (R_1=CH_3, R_2=CF_3), dipm=dipivaloylmethanate (R_1=R_2=$C(CH_3)_3$); DCE=1,2-dichloroethane, NM=nitromethane, DMF=*N,N*-Dimethylformamide, DMSO=dimethyl sulfoxide.

TABLE 1. ANALYTIAL DATA, COLOR, AND MAGNETIC MOMENTS OF THE COMPLEXES OBTAINED[a)]

Complex	C(%)	H(%)	N(%)	Color	μ_{eff}/BM
Cu(tmen)(tfac)Cl	35.76(35.87)	5.60(5.47)	7.61(7.61)	light green	1.87
Cu(tmen)(tfac)Br	31.90(32.01)	5.00(4.88)	6.77(6.79)	deep green	1.85
Cu(tmen)(tfac)I	28.39(28.74)	4.33(4.39)	6.09(6.09)	deep green	1.81
Cu(tmen)(tfac)NCS	36.57(36.87)	5.24(5.16)	10.79(10.75)	green	1.86
Cu(tmen)(dipm)Cl·H_2O	48.86(49.02)	8.81(8.95)	6.86(6.73)	bluish violet	1.84
Cu(tmen)(dipm)Br·H_2O	43.73(44.30)	6.01(6.08)	8.05(8.09)	bluish violet	1.80
Cu(tmen)(dipm)NCS	51.26(51.34)	8.38(8.38)	9.99(9.98)	bluish green	1.90
Cu(tmen)(hfac)Cl	31.25(31.29)	4.13(4.06)	6.79(6.63)	green	1.88
Cu(tmen)(hfac)Br	28.36(28.31)	3.69(3.67)	6.00(6.00)	green	1.87

a) Calculated values are shown in parentheses.

Elemental analyses of the prepared chelates were performed at the Laboratory of Organic Microanalysis of the Institute of Physical and Chemical Research.

Physical Measurements. The electronic spectra of the complex solutions (5×10^{-3} mol dm^{-3}) in visible region were measured with a Hitachi 340 Recording Spectrophotometer at room temperature (20—25 °C) in 10 mm quartz cells. Infrared spectra (400—5000 cm^{-1}) were measured as Nujol mulls with a JASCO IR-A3 Grating Spectrophotometer. Magnetic susceptibility measurements were performed with a Shimadzu Torsion Magnetometer MB-100 at room temperature. Electric conductivities of the solutions (1×10^{-3} mol dm^{-3}) were measured with a Conductivity Outfit Model AOC-10 (Denki-Kagaku-Keiki Co. Ltd.) at 25±0.2 °C. TG-DTA measurements were performed with a Differential Thermal Analyser TGD-3000 M (Sinku-Riko) under static air with the heating rate of 3 °C/min.

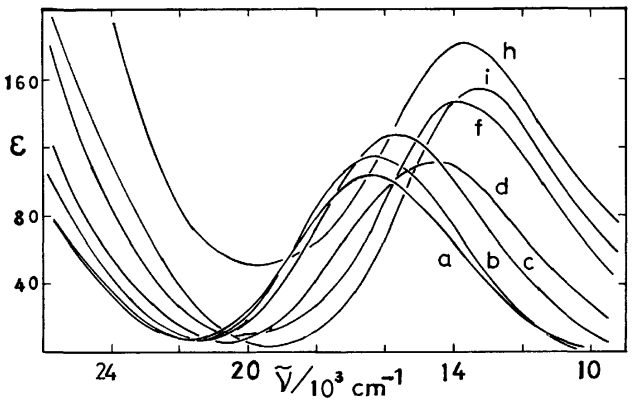

Fig. 1. Absorption spectra of [Cu(tmen)(tfac)Cl] in various solvents. The alphabetic notations a to i, on each curve are those for the solvents, and are the same as those in Table 2.

Results and Discussion

Properties of the Solid Complexes. In Table 1, the analytical data, magnetic moments at room temperature and colors of the mixed chelates obtained in this study are summarized. All of the analytical data agree fairly well with the proposed formulas. The dipm-halide complexes are monohydrates. When they were dried under reduced pressure, their colors turned from bluish violet to green. The loss of one H_2O in this process was confirmed by TG-DTA method. The magnetic moments of all these chelates were normal, showing that they are mononuclear Cu(II) chelates. Solid reflectance spectra of these chelates were very similar to those in nonpolar solvents (see Table 2). The bands of $\tilde{\nu}_{C\equiv N}$ of NCS^- in the IR spectra of the thiocyanate chelates with dipm, acac, and tfac appeared at 2070—2075 cm^{-1}, and those of $\tilde{\nu}_{C\text{-}S}$ of these three chelates at 770—780 cm^{-1}, indicating that the NCS^- ions in them are N-bonded monodentate.[5)] All these results, and comparison with the previous data,[3,4)] support that the green solid chelates with the general formula [Cu(tmen)(dike)X] (X^-: halide or pseudohalide ion; dike: dipm, acac, tfac, or hfac) are all 5-coordinated. Their structure, therefore, is quite different from the planar one expected for the nitrates or perchlorates, [Cu(tmen)(dike)]X ($X^-=NO_3^-$ or ClO_4^-).

Electronic Spectra of the Chelates in Various Solvents. The characteristic properties of the chelates obtained are (1) their high solubility in various solvents, and (2) the drastic change in the color of the solution observed in going from one solvent to another, that is, strong solvatochromism of their solutions. In Fig. 1, the spectral changes of [Cu(tmen)(tfac)Cl] in various solvents are shown as an example of this solvatochromism. There are, in addition, (3) notable anion effect and (4) substituent effect of dike on the colors (or absorption spectra) of such solutions. All the spectral data ($\tilde{\nu}_{max}$ and ε_{max} values of the d-d band) obtained are summarized in Table 2, including the previous data on Cu(tmen)(acac)X. A plot of $\tilde{\nu}_{max}$ values of the tfac-chelates is given in Fig. 2, which indicates the effects (2) and (3) more clearly.

At first, comparing the spectral and conductivity data (Table 3) of the chelates reported before, it can be seen that ClO_4^- acts only as a counter ion of the chelate cation, and does not interact in any solvent with the latter. Consequently, the structure of [Cu(tmen)(tfac)]-ClO_4 in solution depends only on the donor properties of the solvent used (Gutmann's donor number=DN), as was reported previously in similar systems.[4)] In other words, there exist only solute-solvent interactions in these systems: the spectral changes observed in such a

TABLE 2. THE $\tilde{\nu}_{max}$ (IN 10^3 cm^{-1}) AND ε_{max} (IN PARENTHESES) VALUES OF THE COMPLEXES IN VARIOUS SOLVENTS[a)]

Cu(tmen)(tfac)X	H_2O (=a)	MeOH (=b)	EtOH (=c)	DMSO (=d)	DMF (=e)	NM (=f)	CH_3CN (=g)	DCE (=h)	Aectone (=i)
X=Cl	16.46(103)	16.33(114)	15.69(128)	14.60(111)	13.94(137)	13.89(147)	13.79(148)	13.75(181)	13.33(158)
X=Br	16.50(84)	16.39(92)	15.94(103)	15.57(87)	14.93(82)	14.39(113)	14.50(107)	13.89(147)	13.70(182)
X=I	16.46(111)	16.46(115)	16.20(128)	15.69(105)	15.94(97)	16.20(93)	16.46(109)	13.99(183)	14.34(146)
X=NCS	16.39(103)	16.00(116)	15.15(129)	15.57(111)	15.21(110)	14.71(131)	14.87(128)	14.39(156)	14.24(116)
Cu(tmen)(dipm)X									
X=Cl·H_2O	—	17.02(117)	16.81(124)	16.30(126)	15.38(102)	15.33(104)	15.15(114)	14.29(167)	13.99(171)
X=Br·H_2O	—	17.02(126)	16.88(134)	16.39(126)	16.46(110)	17.39(96)	16.81(115)	14.66(177)	14.55(168)
X=NCS	—	16.95(131)	16.53(135)	16.39(132)	16.46(117)	16.00(106)	16.20(121)	14.93(156)	15.04(151)
Cu(tmen)(hfac)X									
X=Cl	—	15.21(105)	14.29(132)	14.18(129)	14.18(121)	13.89(132)	13.89(132)	13.61(142)	13.79(133)
X=Br	—	15.27(106)	14.34(147)	14.08(141)	13.99(153)	13.99(173)	13.94(179)	13.75(200)	13.89(195)
Cu(tmen)(acac)X									
X=Cl	16.89(101)	16.89(123)	16.67(133)	16.00(121)	14.71(114)	14.53(128)	14.53(132)	14.03(169)	13.83(153)
X=Br	16.89(101)	16.84(108)	16.72(130)	16.21(129)	16.21(112)	15.82(103)	16.08(112)	14.45(173)	14.39(154)
X=I	16.89(97)	16.92(106)	16.75(111)	16.26(113)	16.50(100)	18.48(96)	17.27(100)	15.15(135)	16.47(94)
X=NCS	16.86(99)	16.84(121)	16.29(123)	16.21(125)	16.21(111)	15.48(118)	15.67(115)	14.71(153)	14.79(138)

a) The notation of the respective solvent in parentheses is used in this article (see Figs. 1, 2 and 5).

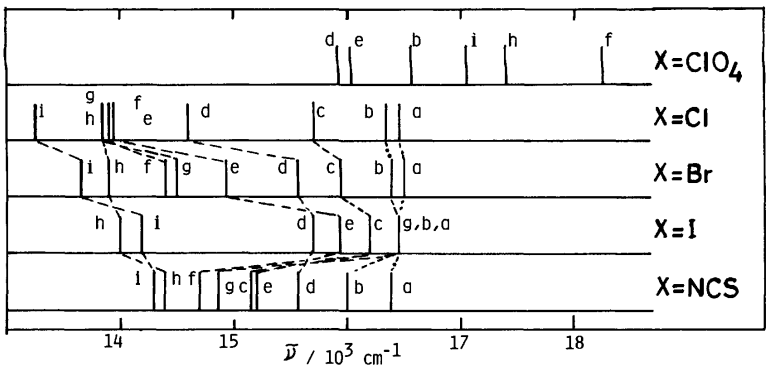

Fig. 2. The $\tilde{\nu}_{max}$ values of the complexes Cu(tmen)(tfac)X in various organic solvents. As to the notations a to i, *cf.* Fig. 1. The data for X=ClO_4 were taken from Ref. 2.

system will be called "Type A Solvatochromism." The characteristics of this solvatochromism are summarized schematically below, taking [Cu(tmen)(tfac)]ClO_4 as an example.

$[Cu(tmen)(tfac)]^+ \longrightarrow [Cu(tmen)(tfac)(Solv)_2]^+$

Structure: More planar $\longrightarrow$ Tetragonal

$\longrightarrow$ More octahedral

$\tilde{\nu}_{max}$ of the solution: Higher $\longrightarrow$ Lower

Solvent Polarity (DN): Small $\longrightarrow$ Large

Color of the Complex: Violet $\longrightarrow$ Blue

(Type A Solvatochromism)

The behaviors of halide- and NCS-chelates in various solvents are now very different. Here the anion in the complex can be coordinated to the chelate cation as well as the solvent molecules, so that the competition of these two types of ligands for the axial site(s) of the chelate cation takes place. These situations are so-called "solute-solute-solvent interaction," and are schematically shown in Fig. 3.

In a polar solvent, the negative center of the 5-coordinated complex, *i.e.*, the X^- anion, attracts the positive ends of the solvent molecules (hydrogen bond will be formed when the solvent is amphiprotic). The

TABLE 3. ELECTRIC CONDUCTIVITY DATA OF Cu(tmen)(dike)X IN VARIOUS SOLVENTS[a,b)]

Complex	CH_3CN	NM	DCE
Cu(tmen)(dipm)Cl·H_2O	67.2(45)	38.5(45)	0.7(4)
Cu(tmen)(acac)Cl	46.2(33)	43.7(51)	0.6(3)
Cu(tmen)(tfac)Cl	15.5(11)	7.8(9)	0.3(2)
Cu(tmen)(hfac)Cl	6.2(4)	2.0(2)	0.3(2)
Cu(tmen)(dipm)Br·H_2O	106.3(76)	60.1(71)	1.5(8)
Cu(tmen)(acac)Br	—	70.5(83)	1.2(6)
Cu(tmen)(tfac)Br	49.2(35)	17.5(21)	0.3(2)
Cu(tmen)(hfac)Br	17.2(12)	6.6(8)	0.6(3)
Cu(tmen)(tfac)I	120.9(86)	54.8(65)	4.3(22)
Cu(tmen)(dipm)NCS	99.0(71)	44.9(53)	1.3(7)
Cu(tmen)(acac)NCS	—	56.6(65)	1.1(6)
Cu(tmen)(tfac)NCS	43.7(31)	13.8(16)	0.3(2)

a) Standard values for a 1:1 electrolyte are 140, 85, and 20 in CH_3CN, NM, and DCE, respectively.[10] b) The values in parentheses are the degree of the dissociation (%) of the anion based on the standard values given in a).

Cu–X bond is weakened by this interaction, and finally dissociates off the X^- anion. In the previous paper,[4] we emphasized this effect, and stated that the main driving force to dissociate the anion X^- from such a complex is the anion solvation power of the solvent used, which is expressed as the acceptor number (AN),[6,7] the E_T value,[8] or the Z value.[9]

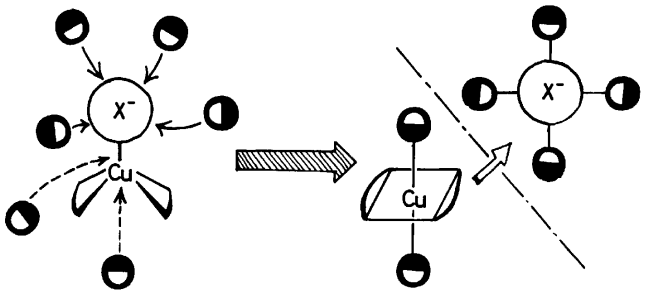

Fig. 3. Schematic representation of the dissociation process of the 5-coordinated complex in a polar organic solvent. The solvent molecules are shown here by half-shadowed balls; their white and dark halves, respectively, correspond to the positive and negative ends of the molecules.

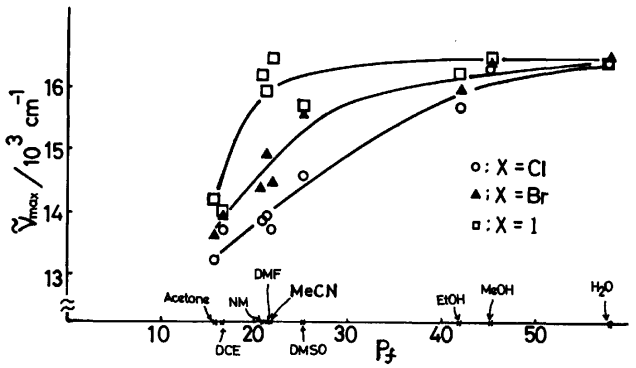

Fig. 4. The correlation between the $\tilde{\nu}_{max}$ values of the complexes Cu(tmen)(tfac)X in various solvents and the solvent parameter P_f.

A look at Fig. 3 suggests, however, that there is another cooperative factor, *i.e.*, the coordination power of the solvent to the metal ion which corresponds to the donor number (DN) of the solvent. In fact, although there is a general correlation between the $\tilde{\nu}_{max}$ of the solutions of these types of chelates and AN of their solvents,*2) there are certain deviations which indicate that, when two solvents have similar AN values, the one with the larger DN favors the change shown in Fig. 3.

Taking this into account, we have newly introduced a new polarity parameter of the solvent, polarity factor (P_f), which is a linear combination of AN and DN. Figure 4 shows the relation between the $\tilde{\nu}_{max}$ of the tfac-halide-chelates and P_f values of the solvents which, in this paticular case, were taken to be equal to

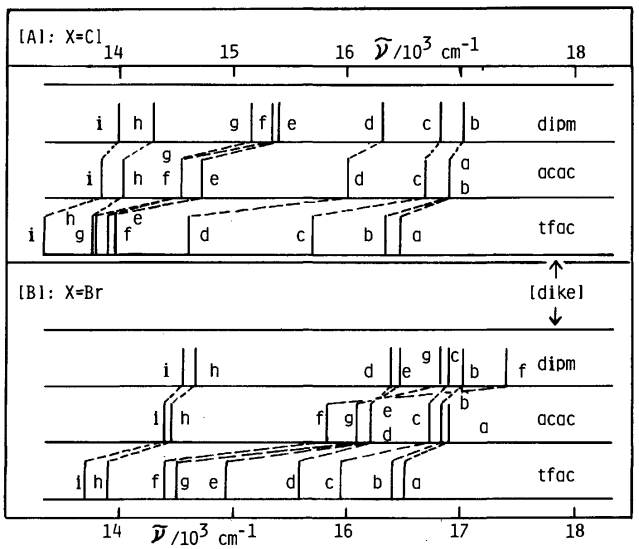

Fig. 5. The $\tilde{\nu}_{max}$ values of the complexes Cu(tmen)(dike)X in various solvents, [A]=[Cu(tmen)(dike)Cl] and [B]=[Cu(tmen)(dike)Br]. As to the notations a to i, *cf.* Fig. 1.

(AN+0.2DN). The fact that the change in Fig. 3 is favored with the increase of this P_f, and in the order of $I^->Br^->Cl^-$, is clearly seen from these curves. Similar curves can also be obtained for the Cl- or Br-acac-chelates, although the points for the I-acac-complex tend to scatter.[1)]

Previous results showed that, in general, increasing strength of the Cu^{2+}–X^- bond brings about the stabilization of 5-coordinate species which, in its turn, is reflected on the decrease of its $\tilde{\nu}_{max}$. Comparing the $\tilde{\nu}_{max}$ values in solvents of very low P_f (DCE or acetone) where the 5-coordinate species predominate, it can be seen that they change in the order of $Cl^-<Br^-<I^-$, indicating that the stabilities of the 5-coordinated species are in the opposite order. The conductivity data (see below) also show that the Cl-complex is more stable than the Br-complex, and the I-complex is the most unstable, as the 5-coordinate species in the same solvent. Thus it is evident that the stability order of the 5-coordinate complexes, [Cu(tmen)(dike)X], in solution is $Cl^->Br^->I^-$. Comparison with the data of the NCS-complex shows that it comes between Cl^- and Br^-, or sometimes near Cl^- or Br^- in this series, although its exact position seems to depend markedly on the solvent used.

Figure 5 shows the $\tilde{\nu}_{max}$ diagram of the Cl- and Br-complexes with different kinds of dike in various solvents, including the data of the corresponding acac-complexes reported previously. The $\tilde{\nu}_{max}$ of a chelate containing Cl^- or Br^- changes, in general, in the order of MeOH>EtOH>DMSO>DMF>NM>CH_3CN>DCE≃ acetone in various solvents (*i.e.*, nearly in the order of P_f), with some ambiguity at hfac-chelates. And, in the same solvent, for example in MeOH, EtOH, or DMSO, it changes as dipm>acac>tfac>hfac, with

*2) This correlation of $\tilde{\nu}_{max}$ with AN (and that with Pf) can be understood with the view that the $\tilde{\nu}_{max}$ of a solution is determined by the position of the equilibrium (1) in it (see later). In fact, the absorption band observed is a superposition of the band of [Cu(tmen)(dike)X] and that of [Cu(tmen)-(dike)(Solv)$_2$]$^+$, and the latter is susceptible to type A solvatochromism, changing somewhat from one solvent to another. Nevertheless, examination of the data indicates, in most cases, that the above view can be taken as a reasonable approximation.

the change of the α-substituent groups in dike. This is the same as the order of the ligand field strengths of the dike ligands, although the degree of the shift of the $\tilde{\nu}_{max}$ from one another is different in each solvent; *e.g.*, in MeOH and EtOH the shifts of the $\tilde{\nu}_{max}$ of the hfac-chelate from that of the dipm-chelate are rather large, but that in DCE is very small.*3) The conductivity data (see below), on the other hand, reveal that the degree of dissociation of the dipm-chelate (for example, Cu(tmen)(dipm)Cl: 45 % in CH_3CN) is, in most cases, larger than those of the corresponding chelates of acac, tfac, or hfac, which decreases in this order (33, 11, and 3%, respectively, in CH_3CN). All these data mean that, as the equatorial ligand field of the chelate is weakened by the α-substituents, the coordination of the axial ligand X^- is strengthened, and the equilibrium leading to the tetragonal, solvated [Cu(tmen)(dike)] cation (see below) is thus shifted to the left hand side.

The characteristics of the spectral changes in the present systems, which will be called "Type B Solvatochromism," can thus be summarized as follows:

$$[Cu(tmen)(dike)X] + n(Solv) \rightleftharpoons [Cu(tmen)(dike)(Solv)_2]^+ + X^-(Solvated) \quad (1)$$

Structure: 5-Coordinated $\rightleftharpoons$ Tetragonal

$\tilde{\nu}_{max}$ of the solution : Lower ⟶ Higher

Solvent Polarity (Pf) : Small ⟶ Large

Anion Effect(X^-): Cl^- ⟶ (NCS^-) ⟶ Br^- ⟶ I^-

Substituent Effect(dike): hfac ⟶ tfac ⟶ acac ⟶ dipm

Color of Solution: Green ⟶ Bluish violet

(Type B Solvatochromism)

The anion effect and substituent effect may be called, respectively, the "Axial Ligand Field Variation Effect" and "Equatorial Ligand Field Variation Effect" on the Type B solvatochromism. Owing to the latter effect, the tetragonal structure is stabilized especially in the case of the dipm chelates. This may be reflected in the easy formation of monohydrates of these chelates, Cu(tmen)(dipm)X·H_2O (see experimental).

Electric Conductivities of the Chelates. Electric conductivity data (molar conductance) of the chelates in three solvents(CH_3CN, NM, and DCE) are summarized in Table 3. These and similar results obtained in other solvents in Table 2 can be explained as follows, supporting the conclusions of the spectral observations.

1) In alcohols and H_2O, almost all of the complexes dissociate strongly into $[Cu(tmen)(dike)(Solv)_2]^+$ and X^-, except the hfac-Cl-complex which decomposes into [Cu(tmem)(hfac)$_2$] and [Cu(tmen)Cl_2] in water (see next section). This is quite natural because the solvents have large DN and AN, so that their P_f are high, and the equilibrium (1) is shifted strongly to the right hand side.

2) In a solvent with a lower P_f, such as CH_3CN or NM, there is a smaller ionization of the complexes, *i.e.*, the equilibrium (1) is shifted to the right to a limited extent.

3) In the case of 2), there is a characteristic anion effect on the equilibrium. For example, the equilibrium of [Cu(tmen)(tfac)X] is shifted to the left hand side in the order of $Cl^- > NCS^- > Br^- > I^-$ in most solvents, as pointed out in last section.

4) In the case of 2), there is also a notable substituent effect on the equilibrium, as stated in the last section. The stability of the 5-coordinate species is found to increase as follows:

$$\text{dipm} < \text{acac} < \text{tfac} < \text{hfac},$$

although an apparent reversal of dipm and acac is observed at times (*cf.* the data in NM).

5) In a solvent with very low P_f such as DCE or acetone, most of the chelates studied here exist as the stable 5-coordinate green species. In this case, notable anion effects and substituent effect cannot be observed.

Ligand Rearrangement Reaction of Cu(tmen)(hfac)Cl. As mentioned above, the tfac- or hfac-chelates containing electron-withdrawing CF_3 groups have a weak equatorial ligand field and favor axial coordination of the anion X^-. In the extreme case of the hfac-Cl-chelate, these effects make the 5-coordinate species unstable, so that a ligand rearrengment reaction (or disproportionation) occurs in water:

$$2[Cu(tmen)(hfac)Cl] \rightleftharpoons [Cu(tmen)(hfac)_2] + [Cu(tmen)Cl_2].$$

The identity of each of the two disproportionation products was checked by their elementary analyses and spectral properties reported in the literature.[11] A very similar disproportionation was formerly observed with analogous Ni(II) chelates,[12] where the reaction could occur also in solid state and with other dike, *e.g.*, acac:

$$2[Ni(tmen)(acac)X(OH_2)] \xrightarrow{\Delta}$$

greenish blue

$$[Ni(tmen)(acac)_2] + [Ni(tmen)X_2]$$

green violet

The non-charged stable chelate, [Ni(tmen)(acac)$_2$], formed by this thermal reaction was very volatile, so it was easy to separate the two disproportionation products from each other.[12]

In the copper system, at present, we could not observe such a thermal reaction. Any drastic weight loss, or release or absorption of heat, could not be observed by TG-DTA technique, until a complicated decomposition begins to take place. This difference

*3) In the case of the bromide-dipm complex, the $\tilde{\nu}_{max}$ of most complexes tend to flock together, showing type A solvatochromism to some extent, and only those in DCE and acetone are left apart from them. This is similar to the result observed with the iodide-tfac complex (*cf.* Fig. 2), and indicates that the stronger ligand field of dipm hinders the coordination of Br^- quite remarkably, while the weaker tfac can do so only toward I^-.

between the Cu(II)- and the Ni(II)-chelates may be explained by the crystal field stabilization energies and the complex-forming powers of these metal ions (Irving-William's rule) and the Jahn-Teller effect in the copper(II) system. More precise work along this line is now in progress.

The present work was partially supported by a Grant-in-Aid for Scientific Research (No. 59430009) from the Ministry of Education, Science and Culture.

References

1) Part XIII: Y. Fukuda, H. Kimura, and K. Sone, *Bull. Chem. Soc. Jpn.*, **55**, 3738 (1982).

2) For $X^-=ClO_4^-$ and NO_3^-: a) Y. Fukuda and K. Sone, *Bull. Chem. Soc. Jpn.*, **45**, 465 (1972); b) Y. Fukuda, A. Shimura, M. Mukaida, E. Fujita, and K. Sone, *J. Inorg. Nucl. Chem.*, **36**, 1265 (1974); c) Y. Fukuda, Y. Miura, and K. Sone, *Bull. Chem. Soc. Jpn.*, **50**, 142 (1977).

3) For X^-=pseudohalide ions: a) Y. Fukuda, N. Sato, N. Hoshino, and K. Sone, *Bull. Chem. Soc. Jpn.*, **54**, 428 (1981) (*cf.* Footnote of Ref. 1). For X^-= a halide ion: b) see Ref. 1.

4) K. Sone and Y. Fukuda, "Ions and Molecules in Solutions," ed by N. Tanaka *et al.*, Elsevier, Amsterdam (1983), pp. 251—266.

5) K. Nakamoto, "Infrared and Raman Spectra of Inorganic and Coordination Compounds," 3rd ed, John Wiley & Sons, New York (1978).

6) V. Gutmann, "The Donor-Acceptor Approach to Molecular Interactions," Plenum Press, New York (1978); and also "Coordination Chemistry in Non-Aqueous Solutions," Springer-Verlag, Vienna (1968).

7) U. Mayer, "Ions and Molecules in Solutions," ed by N. Tanaka *et al*,, Elsevier, Amsterdam (1983), pp. 219—236.

8) C. Reichardt, *Angew. Chem. Int. Ed. Engl.*, **4**, 29 (1965).

9) E. M. Kosower, *J. Am. Chem. Soc.*, **80**, 3253 (1958); "An Introduction to Physical Organic Chemistry," John Wiley & Sons, New York, (1968).

10) W. J. Geary, *Coord. Chem. Rev.*, **7**, 81 (1971).

11) I. Bertini and F. Mani, *Inorg. Chem.*, **6**, 2032 (1967).

12) N. Hoshino, Y. Fukuda, and K. Sone, *Chem. Lett.*, **1979**, 437.

Solvent Effect on Adsorption of TCNQ onto Metal Oxides

Kunio Esumi,* Kazuaki Miyata, and Kenjiro Meguro
Department of Applied Chemistry, Institute of Colloid and Interface Science, Science University of Tokyo, Kagurazaka, Shinjuku-ku, Tokyo 162
(Received April 22, 1985)

7,7,8,8-Tetracyanoquinodimethan (TCNQ) was adsorbed on the surfaces of alumina and titania from three basic solvents. The amount of TCNQ adsorbed decreased with an increase in the acid-base interaction between TCNQ and the basic solvent for both metal oxides. The TCNQ anion radicals were formed as a result of electron transfer from the metal oxide surfaces to adsorbed TCNQ. Further, the concentration of TCNQ anion radicals formed on the oxides after the TCNQ adsorption decreased also with an increase in the acid-base interaction between TCNQ and the basic solvent.

It is well known[1,2] that, when strong electron acceptors or donors are adsorbed on metal oxides, the corresponding radicals are formed as a result of electron transfer. By measuring the concentrations of the radicals formed, the electron-donor-acceptor properties of metal oxides have been evaluated.[3–5] Furthermore, Esumi *et al.*[6,7] attempted to determine the distribution of Lewis sites with different strengths of metal oxides; they found that the distribution of Lewis sites with different strengths on alumina was much wider than that on titania.

Recently, the acid-base theory has been applied to colloidal systems. Fowkes *et al.*[8] studied the interactions between polymers and inorganic solids by using the Drago correlation[9] of the heats of acid-base interaction and reported that strong polymer adsorption is observed only from solvents more neutral than the adsorbate polymer or the adsorbent surface sites. Thus, the acid-base interaction is a very important factor at interfaces.

In this work, electron-donor-acceptor interactions on metal oxides were examined by means of 7,7,8,8-tetracyanoquinodimethan(TCNQ) adsorption from various solvents.

Experimental

Materials. Two kinds of metal oxides, alumina and titania, were used. These metal oxides were prepared as follows: excess aqueous methanol (water: methanol,4:1 in weight) was vigorously added into a butanolic solution of each alkoxide. Stirring was continued for 5 h at about 90 °C. The precipitate was then separated by centrifuging, washed with methanol, finely ground, and then evacuated at 100 °C. The dried products were calcined for 2 h at 500 °C.

The TCNQ was obtained from Wako Chemicals and purified by repeated recrystallization. The solvents used in this study were dried by the use of molecular sieves.

Procedure. The metal oxide was placed in a L-type test tube, and a solution of TCNQ in an organic solvent was then poured in. After the tube had subsequently been shaken for 2 h at 25 °C, the dispersion thus obtained was used for the zeta potential measurement. The metal oxide was collected by centrifuging and dried at room temperature *in vacuo*. The dried sample was then used for the ESR measurement.

The ESR spectra were measured by means of a Japan Electrons Optics Laboratory ESR spectrometer (JES-FE3X) operating with an X-band microwave 100 kHz field modulation. The radical concentrations were estimated by comparing the area under the absorption curves for the sample and for standard solutions of 2,2-diphenyl-1-picrylhydrazyl in benzene.

The zeta potential of metal oxide after the adsorption was measured by means of an electrophoresis apparatus (Laser Zee 500, Pen Kem).

The amount of TCNQ adsorbed was determined from the difference in concentrations before and after the adsorption. The absorbance of TCNQ was measured by means of an UV spectrophotometer (Hitachi 220A). The maximum absorption wavelengths of the absorption band of TCNQ in the three basic solvents were 393 nm in acetonitrile, 395 nm in ethyl acetate, and 403 nm in 1,4-dioxane.

The specific surface areas of the samples were determined with a Sorptograph, Model ADS-1B (Shimadzu Seisakusho Co., Ltd.).

Results and Discussion

The amount of TCNQ in solutions adsorbed on the surfaces of alumina and titania was determined using three basic solvents: acetonitrile, a very weak base; ethyl acetate, a weak base, and 1,4-dioxane, a moderately weak base. The adsorption isotherms of TCNQ from these basic solvents are given in Fig. 1; it is apparent that their isotherms may be classified as the Langmuir type for both metal oxides. From the Langmuir plots of these isotherms, the saturated amounts of TCNQ were obtained; their values are listed in Table 1. It may be seen that the amount of TCNQ adsorbed decreases very appreciably with an increase in the basicity of the solvent for both metal oxides. To interpret this result in terms of the acid-base theory, the Drago equation[9] was employed:

$$-\Delta H^{ab} = C_A C_B + E_A E_B$$

where E and C are the Drago constants for the acidic compound(A) and the basic compound(B). Drago determined many E and C values for organic solvents from measurements of the heat of acid-base interaction made by his group and by others using calorimetric and spectroscopic methods.[9,10] These studies demonstrated that the Drago equation usually predicted ΔH^{ab} values within 3%. A very useful approach for relating the

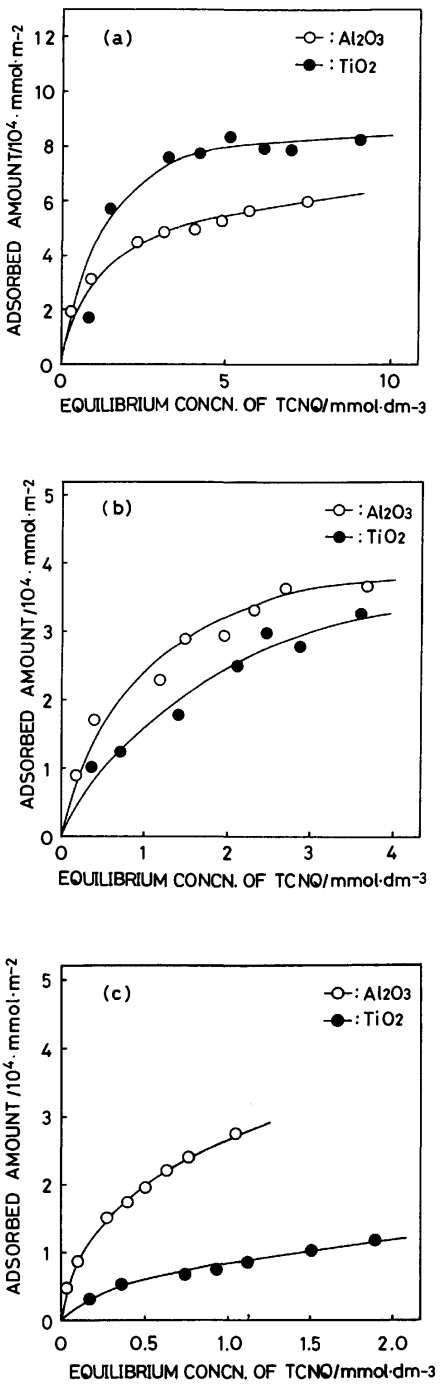

Fig. 1. Adsorption isotherms for TCNQ adsorbing from basic solvents onto metal oxides: (a) Acetonitrile, (b) Ethyl acetate, (c) 1,4-Dioxane.

Table 1. Data of TCNQ adsorption

Sample	Color of oxide surfaces		
	Acetonitrile	Ethyl acetate	1,4-Dioxane
Alumina	Blue green	Yellowish green	Yellowish white
Titania	Violet	Pale violet	—
	Amount adsorbed ($\times 10^4$ mmol/m^2)		
Alumina	6.2	4.4	2.9
Titania	7.7	5.7	1.7

Table 2. Acid-base parameters

Solvent	C_B	E_B	$-\Delta H^{ab}$ with TCNE[a] (kcal/mol)
Acetonitrile	1.34	0.889	3.51
Ethyl acetate	1.74	0.975	4.27
1,4-Dioxane	2.38	1.09	5.23

a) TCNE (C_A=1.51, E_A=1.68). (1 cal$_b$=4.184 J).

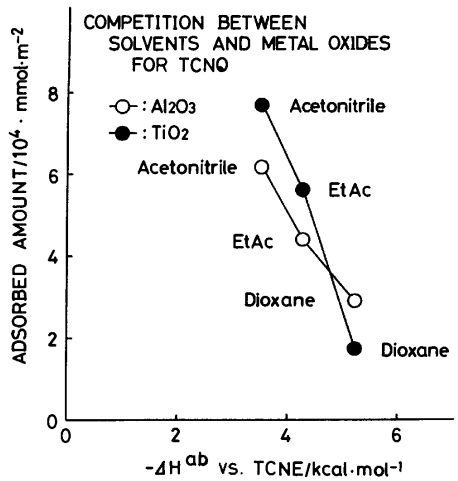

Fig. 2. Saturated amount of TCNQ adsorbing onto metal oxides *vs.* acid-base interaction enthalpy.

interfacial interactions quantitatively has been the Drago equation of enthalpy changes in acid-base complexation. When the Drago equation is applied to this work, the basic compounds correspond to the solvents, such as acetonitrile, ethyl acetate, and 1,4-dioxane, and the acidic compound, to TCNQ. The E and C values for three basic solvents are available,[9] but not for TCNQ. Therefore, in this study, the E and C values[9] of tetracyanoethylene(TCNE), which is similar to TCNQ, are employed insteads of these of TCNQ. These acid-base parameters are listed in Table 2.

Figure 2 shows the amount of TCNQ saturated on alumina and titania as a function of ΔH^{ab}; the amount of TCNQ saturated decreases with an increase in the acid-base interaction (ΔH^{ab}) between the basic solvent and TCNQ.

When TCNQ was adsorbed from the solutions on alumina and titania, the surfaces of the metal oxides developed a remarkable coloration. The color was dependent on the kind of solvent; the results are shown in Table 1. It has previously been reported[4,5] that the adsorption of electron acceptors on metal oxides produces a surface coloration and gives unresolved ESR spectra. The samples colored by the TCNQ adsorption gave unresolved ESR spectra with a g-value of 2.003. These spectra have been identified[4,5] as being those of TCNQ anion radicals.

The above results support the idea that the TCNQ anion radicals are formed as a result of electron transfer from the metal oxide surface to the TCNQ adsorbed.

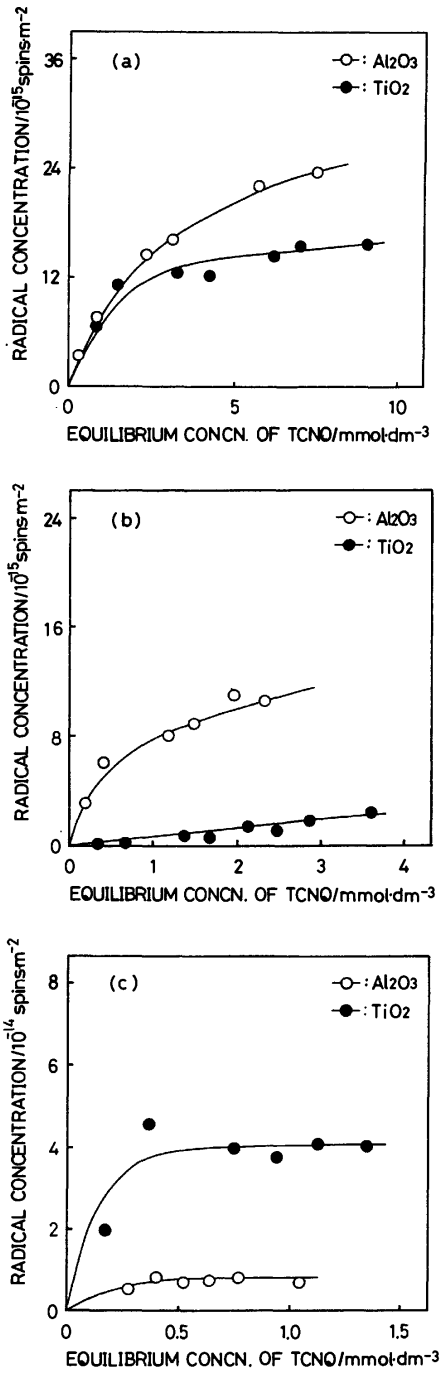

Fig. 3. TCNQ radical concentration onto metal oxides *vs.* equilibrium concentration of TCNQ into basic solvent:
(a) Acetonitrile, (b) Ethyl acetate; (c) 1,4-Dioxane.

The TCNQ-radical concentrations formed on the surface of metal oxides are plotted against the equilibrium concentration of TCNQ in Fig. 3. The TCNQ-radical concentration decreased with an increase in the basicity of the basic solvents. Furthermore, in order to compare the TCNQ-radical concentration on the surface of metal oxide as a function of ΔH^{ab}, the TCNQ-radical concentration corresponding to the half-value of the saturated amount of TCNQ was obtained; the results are illustrated in Fig. 4. The TCNQ-radical concentrations of alumina decreased gradually in the weak acid-base interaction and steeply in the moderate acid-base interaction. On the other hand, in the case of titania, they decreased steeply in the weak acid-base interaction and gradually in the moderate acid-base interaction. The TCNQ-radical concentrations on alumina were larger than those on titania for two of the three basic solvents, but not 1,4-dioxane, indicating that the concentration of electron-donor sites having relatively weak strengths on alumina is larger than that on titania. Furthermore, in the case of 1,4-dioxane, the TCNQ-radical concentration on titania was larger than that on alumina. This result suggests that the concentration of electron-donor sites having relatively strong strengths on titania is larger than that on alumina. These results agreed fairly well with similar measurements previously reported by us.[6]

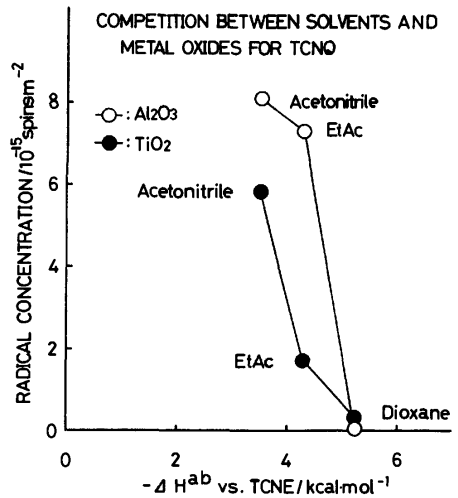

Fig. 4. TCNQ radical concentration corresponding to half-value of saturated amount of TCNQ onto metal oxides *vs.* acid-base interaction enthalpy.

The zeta potentials of metal oxides before and after TCNQ adsorption were also measured. The zeta potential of alumina and titania in the basic solvent alone decreased with an increase in the basicity of the solvents. In this case, the acid sites of alumina and titania interacted with the basic solvent. After the TCNQ adsorption, the zeta potentials of alumina and titania decreased with an increase in the concentration of TCNQ for the three basic solvents. Further, the magnitude of the decrease in the zeta potential of both metal oxides was dependent on the acid-base interaction between TCNQ and the basic solvent; the order of magnitude of the decrease was acetonitrile>ethyl acetate>1,4-dioxane. Labib *et al.*[11] measured the zeta-potential for several solids in a series of organic liquids chosen to cover a wide range of electron-donor properties; they reported that, for most of the solids, the zeta potential changes its sign for

some value of the liquid donicity because of the acid-base interaction between solids and organic liquids.

The electron-donor sites of metal oxides for the electron transfer are considered as follows: two possible electron-donor sources exist on the alumina surface. One of these has electrons trapped at intrinsic defects, while the other has hydroxide ions. Free electrons derived from the intrinsic defects on the surface of the alumina would normally be expected to participate in the electron-transfer adsorption. However, since it has been reported[1] that the electron-donor defect site on the surface of alumina was created at an activation temperature above 500 °C, it may be suggested that the electron-donor defect site does not play an important role in this study. The other site is the surface hydroxide ions which have been confirmed to exist on the surface of alumina. The ionization potentials of the hydroxide ions are comparatively small[12] (≈2.6 eV in the gas phase). It seems likely that the surface hydroxide ions on alumina as an electron-donor site can be attributed to the electron-transfer adsorption. Indeed, Fomin *et al.*[13] have reported that electron transfer from the hydroxide ion can occur in certain solvent systems, provided a suitable acceptor molecule is present. The electron-donor sites of titania have been associated with surface hydroxide ions and Ti^{3+} ions.[14] The latter site has been reported[14] to be formed at high temperatures *in vacuo*. In the present study, the hydroxide ions on the titania surface have been found to operate mainly as an electron-donor site.

The authors are indebted to Mr. Shizuo Sugimoto for obtaining the ESR spectra.

References

1) B. D. Flockhart, J. A. N. Scott, and R. C. Pink, *Trans. Faraday Soc.*, **62**, 730 (1966).
2) B. D. Flockhart, I. R. Leith, and R. C. Pink, *Trans. Faraday Soc.*, **66**, 469 (1970).
3) A. J. Tench and R. L. Nelson, *Trans. Faraday Soc.*, **63**, 2254 (1967).
4) H. Hosaka, T. Fujiwara, and K. Meguro, *Bull. Chem. Soc. Jpn.*, **44**, 2616 (1971).
5) K. Meguro and K. Esumi, *J. Colloid Interface Sci.*, **59**, 93 (1977).
6) K. Esumi and K. Meguro, *J. Colloid Interface Sci.*, **66**, 192 (1978).
7) K. Esumi and K. Meguro, *J. Japan Soc. Colour Mater.* **58**, 9 (1985).
8) F. M. Fowkes, "Physico-chemical Aspects of Polymer Surfaces," Vol. 2, Plenum Press (1983), p. 583.
9) R. S. Drago, L. B. Parr, and C. S. Chamberlain, *J. Am. Chem. Soc.*, **99**, 3203 (1977).
10) R. S. Drago, G. C. Vogel, and T. E. Needham, *J. Am. Chem. Soc.*, **93**, 6014 (1971).
11) M. E. Labib and R. Williams, *J. Colloid Interface Sci.*, **97**, 356 (1984).
12) V. M. Vedeneev *et.al.*, "Cleavage Energies of Chemical Bonds. Ionization Potentials and Electron Affinity," Handbook Izd. AN USSR (1960).
13) G. V. Fomin, L. A. Blyumenfel'd, and V. I. Sukhorukov, *Proc. Acad. Sci. U. S. S. R.*, **157**, 819 (1964).
14) M. Che, C. Naccache, and B. Imelik, *J. Catal.*, **24**, 328 (1972).

CO_2 Laser-induced Decomposition of 1,1,2-Trichloroethane

Hiroo OGURA
The Institute of Space and Astronautical Science, Komaba, Meguro-ku, Tokyo 153
(Received June 15, 1985)

$CH_2ClCHCl_2$ was photolyzed with a focusing geometry using the P(24) line of the 10.6 μm CO_2 band (940.6 cm^{-1}). The final products of neat photolysis were *cis*- and *trans*-CHCl=CHCl, $CH_2=CCl_2$, $CH_2=CHCl$, CH≡CCl, CH≡CH, and C_4H_2. The relative yield of $CH_2=CCl_2$ in particular was strongly dependent on $CH_2ClCHCl_2$ pressure and sensitive to the addition of H atom containing molecules. A series of diagnostic experiments shows that the dichloroethene isomers are formed by three different processes, *i.e.*, infrared multiphoton decomposition, collision-induced decomposition, and radical chain reaction. Infrared mulitiphoton decomposition and collision-induced decomposition give rise to *cis*- and *trans*-CHCl=CHCl predominantly, while the radical chain reaction generates the dichloroethene isomers in comparable amounts at high reactant pressures, the most probable initiation step being the C-Cl bond-scission reaction of the parent molecule. Formation mechanisms for other minor products are also discussed.

Infrared multiphoton decomposition (IRMPD) of halogenated ethanes has been extensively studied.[1-12] In these studies it has been shown that molecular elimination of hydrogen halide is the predominant dissociation channel. Among the partially chlorofluorinated ethanes, CH_2XCHXY (X,Y=Cl,F) is unique in that it undergoes molecular elimination of HX (X=Cl,F) giving more than one haloethene. This was confirmed in chemical activation studies,[13,14] in a shock tube study,[15] and in flow tube studies[16,17] on $CH_2ClCHCl_2$ and CH_2FCHF_2, which decompose to three isomeric dichloro- and difluoroethenes, respectively.

In a previous study[9] we showed that $CH_2ClCHFCl$ is also decomposed upon an infrared multiphoton excitation (IRMPE) to $CH_2=CFCl$, *trans*- and *cis*-CHF=CHCl in the primary step and that the branching ratio of $CH_2=CFCl$ is remarkably increased with respect to those of *trans*- and *cis*-CHF=CHCl as the reactant pressure is increased up to 3 Torr (1 Torr=133.322 Pa). These results suggest a mechanistic change in the formation of $CH_2=CFCl$ at higher reactant pressures. We have extended the study on CH_2XCHXY to $CH_2ClCHCl_2$ and CH_2FCHF_2[18] and report in this paper the results of $CH_2ClCHCl_2$. A series of diagnostic experiments such as product yield dependence on reactant and buffer gas pressure was carried out and the results were interpreted on the basis of the simple extended threshold model presented by Hackett *et al.*[4]

Experimental

The experimental apparatus and analytical procedure used are essentially the same as those in a previous study and have been fully described.[9] Only a brief description will be given here. The pulse beam from a Lumonics 103-2 TEA CO_2 laser with N_2 added was passed through an aperture (14 mm in diameter) and focused in an irradiation cell (46-mm diameter, 22-cm long, NaCl windows) by means of Ge lens (12.7-cm focal length). The principal line used in these experiments was the P(24) line of the 10.6 μm band at 940.6 cm^{-1}. The output pulse was attenuated by CaF_2 flats and the incident pulse energy was measured with a calibrated pyroelectric detector, the repetition rate being 1 Hz for all runs. MKS Baratron transducers were used for the pressure measurements.

All photolysis products were identified by comparative GC retention times with known samples, in particular, with the IRMPD products of $CH_2ClCHFCl$.[9] For quantitative determination of the photolysis products, temperature programmed gas chromatographic analyses were carried out using Porapak N column (flame ionization detector). The reactant (Tokyo Kasei Co. Ltd.) was purified by gas chromatography using octane/Porasil C (Durapak) column, and then further distilled under vacuum at low temperature.

Results

Upon the photolysis at 940.6 cm^{-1}, which falls within a band of $CH_2ClCHCl_2$ corresponding to a CH_2 wagging vibration,[19] several products were observed by gas chromatography. The final products detected were

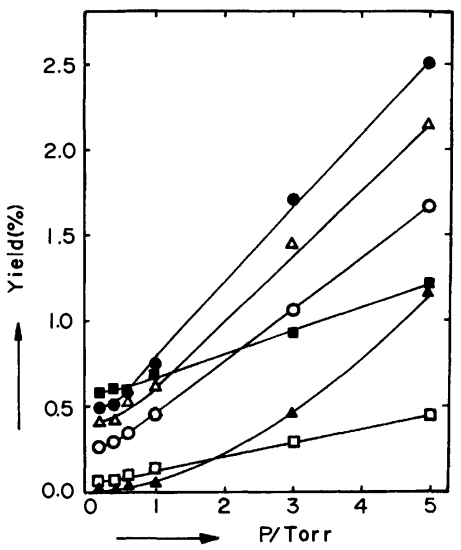

Fig. 1. Product yields as a function of reactant pressure. (Conditions: pulse energy E_0=0.136 J/pulse, pulse number n=500, excitation line ν=940.6 cm^{-1}). ●: *cis*-CHCl=CHCl, ○: *trans*-CHCl=CHCl, ▲: $CH_2=CCl_2$, △: CH≡CCl(×10), □: $CH_2=CHCl$(×10), ■: CH≡CH(×100).

Table 1. Pressure dependence of relative yields[a)]

P/Torr	0.20	0.40	0.60	1.0	3.0	5.0
CH≡CH	1.16	1.14	0.95	0.87	0.54	0.48
CH≡CCl	8.38	8.17	9.01	8.24	8.46	8.56
CH_2=CHCl	0.93	1.08	1.38	1.66	1.68	1.78
CH_2=CCl_2	3.32	3.04	4.44	7.27	27.2	46.7
trans-CHCl=CHCl	53.8	53.5	57.0	60.1	62.6	66.6
cis-CHCl=CHCl	100	100	100	100	100	100
	(0.495)	(0.524)	(0.587)	(0.742)	(1.71)	(2.52)

a) Relative yields at E_0=0.136 J/pulse and 500 shots. The yield of *cis*-CHCl=CHCl in % conversion per 500 shots (in parenthesis) is taken as 100.

CH_2=CCl_2, *trans*- and *cis*-CHCl=CHCl, CH_2=CHCl, CH≡CCl, CH≡CH, and C_4H_2. C_4H_2, which was formed in trace amounts at high substrate pressures and high laser fluences, was identified by comparing the rentention time with that of the C_4H_2 prepared from C_6H_6: C_6H_6 of about 30 Torr was irradiated by the CO_2 laser at 1043.1 cm^{-1}, C_4H_2 being trapped from the effluent of the gas chromatograph and identified by mass spectrometry. CHCl=CCl_2, CH_2ClCH_2Cl, and $CHCl_2CHCl_2$ were sought by using octane/Porasil C column at 110 °C, but were found in trace amounts or not found at all, no quantitative determination of CHCl=CCl_2 being made.

A series of diagnostic experiments was performed to establish the unimolecular dissociation and subsequent reaction mechanism of $CH_2ClCHCl_2$ subjected to the intense CO_2 laser irradiation. In each diagnostic experiment the relevant photolysis parameter was varied, the other parameters being kept constant or same.

Dependence on Reactant Pressure. Product yields as a function of $CH_2ClCHCl_2$ pressure were investigated at the pulse energy of 0.136 J/pulse, product yields and relative yields being shown in Fig. 1 and Table 1, respectively. Figure 1 shows that all product yields increase as the substrate pressure is increased, in particular, the increase in the yield of CH_2=CCl_2 with higher reactant pressure is most significant: The yield of CH_2=CCl_2 at 5.0 Torr is more than 70 times greater than that at 0.2 Torr, while those of *trans*- and *cis*-CHCl=CHCl are increased by a factor of 5—6 of their yields at 0.2 Torr. From the viewpoint of relative yields, the yield of *cis*-CHCl=CHCl being arbitrarily taken as 100, those for *trans*-CHCl=CHCl, CH_2=CCl_2, and CH_2=CHCl show an increase with higher reactant pressure, in particular, that of CH_2=CCl_2 increases much more rapidly than that of *trans*-CHCl≡CHCl, while that of CH=CH shows an opposite trend. In the case of CH≡CCl there appears to be no discernible pressure dependence. Major products are *cis*- and *trans*-CHCl=CHCl at lower pressures, CH_2=CCl_2 being less important than CH≡CCl, whereas CH_2=CCl_2 becomes major product at higher pressures together with *cis*- and *trans*-CHCl=CHCl.

Dependence on Pulse Number. The effects of pulse number on product yields were examined at 0.2 and 5.0 Torr reactant pressure and pulse energy of 0.202 J/pulse. All product yields, even those for minor products, are proportional to pulse number n up to 500, which affirms that all the products are formed upon each pulse irradiation, *viz.*, within the time interval between pulses.

Table 2. Pulse energy dependence of relative yields[a)]

E_0/(J/pulse)	0.311	0.202	0.136	0.0916
CH≡CH	4.46	2.58	1.16	0.35
CH≡CCl	12.4	9.94	8.38	5.49
CH_2≡CHCl	1.41	1.04	0.93	0.23
C_4H_2	1.22	0.61	b)	b)
CH_2=CCl_2	5.00	4.19	3.32	2.49
trans-CHCl=CHCl	50.0	49.2	53.8	60.5
cis-CHCl=CHCl	100	100	100	100
$d\times10^5$/(pulse)$^{-1}$	8.24	3.97	1.68	0.754

a) Relative yields at 0.20 Torr $CH_2ClCHCl_2$ pressure as compared to the yield of *cis*-CHCl=CHCl. b) Yield is too small to be quantitatively determined.

Dependence on Pulse Energy. Product yields as a function of pulse energy were investigated at 0.2 Torr substrate pressure. All yield, as mentioned above, is propertional to pulse number, indicating pseudo-first order decay of the parent molecule over a fairly wide range of conversion. The dissociation rate constant(d) could be defined by $d=-(1/n)\ln(1-X)$, where X is the dissociated fraction of $CH_2ClCHCl_2$ after irradiation of n pulses. Log d is correlated linearly with log E_0 in the pulse energy (E_0) range of 0.311—0.0916 J/pulse with a slope of 1.98. The slope value obtained is somewhat larger than the standard 3/2 power dependence of d on E_0 for a "tightly" focused geometry. It has been recognized that at relatively low pulse energy and local fluence below the critical fluence, the power dependence of d is higher than the standard value, and approaches 1.5 as E_0 increases.[20] At higher fluences where the 3/2 power law holds, main contribution of the irradiated volume to the dissociation yield comes from the reaction zone where the laser fluence exceeds the critical fluence for $CH_2ClCHCl_2$ decomposition and all molecules contained dissociate with unit probability. Since the observed power dependence of d

Table 3. Effects of additives on product relative yields[a)]

Gas	Neat	N_2	NO	CF_4	H_2	CH_4	C_2H_6
CH≡CH	0.48	0.32	0.34	0.13	2.36	9.61	b)
CH≡CCl	8.56	6.32	6.66	4.89	5.06	5.79	3.73
CH_2=CHCl	1.78	1.98	2.21	1.82	21.2	4.10	6.25
CH_2=CCl_2	46.7	44.7	40.4	41.1	17.6	5.39	4.31
trans-CHCl=CHCl	66.6	66.5	70.2	68.5	69.0	73.0	71.7
cis-CHCl=CHCl	100	100	100	100	100	100	100
	(2.52)	(1.48)	(1.31)	(0.906)	(0.863)	(0.610)	(0.549)

a) Relative yields at E_0=0.136 J/pulse as compared to the yield of *cis*-CHCl=CHCl in % conversion per 500 shots (in parenthesis). Reactant pressure is 5.0 Torr, those of additives being 5.0 Torr. b)The GC peak was masked by an impurity contained in the C_2H_6.

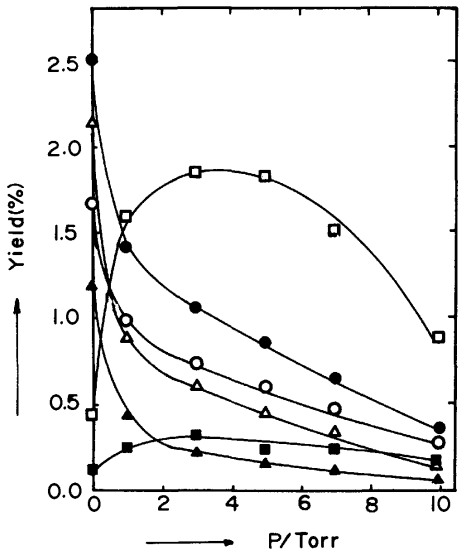

Fig. 2. Product yields as a function of H_2 pressure. (Reactant pressure=5.0 Torr, E_0=0.136 J/pulse, n=500, =940.6 cm^{-1}).
●: *cis*-CHCl=CHCl, ○: *trans*-CHCl=CHCl, ▲: CH_2=CCl_2, △: CH≡CCl(×10), □: CH_2=CHCl(×10), ■: CH≡CH(×10).

is not so far from 1.5, the relative yields with respect to the yield of *cis*-CHCl=CHCl, as predicted from the simple extended threshold model, change slightly with increasing E_0, at most 10 for that of *trans*-CHCl=CHCl (Table 2). However, the increase in the relative yields of minor products and the decrease in that of *trans*-CHCl=CHCl with increasing pulse energy are worthy of note to discuss the photolysis mechanism.

Effects of Additives on Product Yields. The product yields as a function of several additive pressure up to 5—10 Torr were examined at 5.0 reactant pressure and 0.136 J/pulse laser energy. Upon the addition of N_2, NO, and CF_4, all the product yields decrease monotonically as the pressure is increased. The yield-pressure behaviors for these molecules are similar to one another, the relative yields being little affected by the presence of these additives and by increasing the additive pressure. On the other hand, by the addition of H_2, CH_4, and C_2H_6 , the yield of CH_2=CCl_2 together with its relative yield is decreased more rapidly and significantly than those of *cis*- and *trans*-CHCl=CHCl. The yield of CH_2=CHCl increased markedly upon the addition of H_2 and C_2H_6 at lower additive pressures and then decreases slowly with higher additive gas pressure. The yield-pressure behaviors for H_2 and C_2H_6 are similar to each other, the increase in the yield of CH_2=CHCl being more significant upon the addition of H_2. While the relative yield of CH_2=CHCl is increased by the addition of CH_4 as in the case of H_2 and C_2H_6 addition, its yield is decreased slightly by the presence of CH_4. At the same time the yield of CH≡CH is increased to small extent at lower H_2 pressures and then decreased slowly with increasing H_2 pressure. Similarly, at lower CH_4 pressures it is increased by a factor of 2 greater than that by the same amount of H_2 addition. The relative yields at the additive gas pressure of 5.0 Torr are summarized in Table 3. The yield-pressure plot in the presence of H_2 is shown in Fig. 2, the relative yields being summarized in Table 4.

Discussion

Primary Photolysis. The final product dis-

Table 4. Dependence of relative yields[a)] on H_2 pressure

P/Torr	1.0	3.0	5.0	7.0	10.0
CH≡CH	1.70	2.88	2.36	3.66	2.91
CH≡CCl	6.39	5.68	5.06	5.10	3.65
CH_2=CHCl	11.2	17.3	21.2	23.1	24.1
CH_2=CCl_2	31.2	20.4	17.6	16.4	12.6
trans-CHCl=CHCl	70.1	70.3	69.0	71.2	71.3
cis-CHCl=CHCl	100	100	100	100	100
	(1.41)	(1.07)	(0.863)	(0.653)	(0.364)

a) Relative yields at E_0=0.136 J/pulse as compared to the yield of *cis*-CHCl=CHCl in % conversion per 500 shots(in parenthesis). Reactant pressure was 5.0 Torr for these runs.

tribution obtained in the neat photolysis of $CH_2ClCHCl_2$ in the pressure range up to 5 Torr (Table 1) suggests that $CH_2=CCl_2$, *trans*- and *cis*-CHCl=CHCl are important products, *trans*- and *cis*-CHCl=CHCl being the major products over the whole pressure range examined and $CH_2=CCl_2$ formation being significant only at higher pressures. As can be seen from Table 1, all the products as well as their relative yields are relatively constant at reactant pressures below 0.4 Torr. At these pressures the effects of collisions would not be important, since all product yields increase linearly with the substrate pressure. The principal mode of dissociation at lower pressures would be the direct elimination of HCl upon the infrared multiphoton absorption. Molecular elimination of HCl is in line with the IRMPD studies on related systems[7-9] and with a chemical activation study on this system:[13]

$$CH_2ClCHCl_2 + nh\nu \longrightarrow CH_2=CCl_2 + HCl, \quad (1)$$

$$\longrightarrow trans\text{-}CHCl=CHCl + HCl, \quad (2)$$

$$\longrightarrow cis\text{-}CHCl=CHCl + HCl. \quad (3)$$

By analogy with the chemically activated $CH_2ClCHCl_2$, the reactant molecule upon the IRMPE would eliminate HCl *via* three-center reaction together with more common four-center reaction mentioned above:

$$CH_2ClCHCl_2 + nh\nu \longrightarrow CH_2ClCCl: + HCl, \quad (4)$$

$$CH_2ClCCl: \longrightarrow trans\text{-}CHCl=CHCl, \quad (5)$$

$$\longrightarrow cis\text{-}CHCl=CHCl. \quad (6)$$

There is now sufficient evidence for the vibrational excitation of HCl eliminated by the IRMPD of halogenated ethanes. It has been shown that the *trans*- and *cis*- CHCl=CHCl produced from the chemically activated $CH_2ClCHCl_2$, in particular those formed *via* three-center reaction, have enough internal energy to undergo isomerization. The threshold energies for $CH_2=CCl_2$, CHCl=CHCl *via* four-center reaction, and CHCl=CHCl *via* three-center reaction have been estimated to be 57.1, 58.8, and 60.0 kcal/mol(1 cal_{th}= 4.184 J), respectively. Formation of *cis*-form is favored channel in both four- and three-center eliminations, *cis*-form being thermodynamically more stable than *trans*-form by 0.650 kcal/mol.[21] Activation energy for the isomerization of *cis*-CHCl=CHCl is reported to be 56.9 kcal/mol.[22] In the case of CHCl=CHCl isomers it is not possible to distinguish between three- and four-center eliminations, $CH_2=CCl_2$ being attributed to four-center reaction. The contribution of three-center elimination is estimated to be 25% for chemically activated $CH_2ClCHCl_2$.[13] Similarly, three-center elimination would not predominate over four-center reaction in the IRMPD of $CH_2ClCHCl_2$. The relative yield of $CH_2=CCl_2$ at reactant pressures below 0.4 Torr is about 50 times smaller than that of *trans*- plus *cis*-CHCl=CHCl, which can be partly ascribed to the 7 times smaller statistical weight of $CH_2ClCHCl_2$ activated complexes leading to $CH_2=CCl_2$.[13] Dai *et al.* also observed the very small relative yield of $CH_2=CCl_2$ with respect to those of *trans*- and *cis*-CHCl=CHCl in their SiF_4 sensitized IR laser pyrolysis of $CH_2ClCHCl_2$, and suggested that the activation energy of $CH_2=CCl_2$ formation should be higher than those of *trans*- and *cis*-CHCl=CHCl by more than 5 kcal/mol, the activation energies for *cis*- and *trans*-CHCl=CHCl obtained being 58.5 and 59.5 kcal/mol, respectively.[23] This higher activation energy for $CH_2=CCl_2$ is not consistent with the lower threshold estimated from the chemical activation study, a good agreement being seen between the laser pyrolysis and chemical activation results for the activation energies of 1,2-dichloroethene production.

According to the simple extended threshold model for multiple dissociation channels,[4] the reaction zone with a "tightly" focused laser beam is divided by individual critical fluence and all molecules contained in the volume defined by the threshold fluence contours decompose *via* individual channel with unit probability. At low pressures the relative yields from various channels are the ratios of the individual reaction volume. This model would be applicable approximately to our system, although a slight deviation of d at 0.2 Torr from the standard 3/2 power law is observed in the present experiments. The very small relative yield of $CH_2=CCl_2$ indicates that the critical fluence for $CH_2=CCl_2$ formation locate spacially inside those of *trans*- and *cis*-CHCl=CHCl channels in the photolysis cell: In terms of threshold energy $CH_2=CCl_2$ formation channel has higher threshold energy than those of CHCl=CHCl channels.

The activation energy for the C–Cl bond rupture was estimated to be 64 kcal/mol from the laser pyrolysis results.[23] This energy threshold is very close to those for the HCl elimination channels and the C–Cl bond fission would take place in the primary photolysis:

$$CH_2ClCHCl_2 + nh\nu \longrightarrow CH_2ClCHCl\cdot + Cl \quad (7)$$

Since the threshold energy of C–C bond scission is about 85 kcal/mol,[13] the C–C bond rupture channel might contribute to IRMPD to very minor extent. Actually no CH_3Cl, CH_2Cl_2, CH_2ClCH_2Cl, and $CHCl_2$-$CHCl_2$ were found in the product analysis.

Secondary Photolysis. The formation of the minor products by one step from the parent molecule is unlikely from the viewpoint of threshold energy and from mechanistic considerations. Nagai and Katayama reported that the major product of TEA CO_2 laser-induced reaction of *trans*-CHCl=CHCl is the *cis*-form, minor products being CH≡CH and CH≡CCl with a ratio of 1:3.[24] $CH_2=CCl_2$ was also reported to dissociate

to CH≡CCl upon an intense CO_2 laser irradiation.[25] The IR laser photolysis of *trans*-CHCl=CHCl and CH_2=CCl_2 in their ground vibrational states using the same excitation line as that for $CH_2ClCHCl_2$ did not give any appreciable amounts of the dissociation products. It is now recognized that polyatomic products formed in the primary photolysis are in their vibrationally excited states where they can absorb the laser photons efficiently and suffer from secondary photolysis.[9,10]

In the IRMPD of the dichloroethenes HCl elimination and C–Cl bond scission need 60—70 and 80—90 kcal/mol, respectively, isomerization channel being the lowest in *trans*- and *cis*-CHCl=CHCl:

$$cis(trans)\text{-}CHCl{=}CHCl^{\dagger} + mh\nu \longrightarrow trans(cis)\text{-}CHCl{=}CHCl \quad (8)$$

$$\longrightarrow CH{\equiv}CCl + HCl, \quad (9)$$

$$\longrightarrow CHCl{=}CH\cdot + Cl, \quad (10)$$

where CHCl=CHCl† denotes the CHCl=CHCl molecule excited to its quasicontinuum region or very close to it by the primary photolysis. As shown in Table 2, the relative yields of CH≡CCl and CH≡CH are increased with an increase in the laser energy, while that of *trans*-CHCl=CHCl with respect to *cis*-CHCl=CHCl is decreased with higher pulse energy. This strongly suggests that CH≡CCl is derived from *trans*- and *cis*-CHCl=CHCl predominantly. The relative yield of CH_2=CCl_2, however, shows a similar behavior to those of minor products, indicating that its dissociation is not so significant in the secondary photolysis as those of CHCl=CHCl isomers.

Similarly, the radicals primarily formed by the C–Cl bond scission would be decomposed by the secondary photolysis:

$$\cdot CHClCH_2Cl^{\dagger} + mh\nu \longrightarrow CH_2{=}CHCl + Cl \quad (11)$$

CH≡CH might be formed by the sequential elimination of Cl atom from CHCl=CHCl in a similar manner to CH_2=CHCl.[26] Under the present conditions, however, it seems more likely that CH≡CH is derived by the H-atom abstraction reaction of CH≡C· radical, since C_4H_2 is observed at higher laser energies. Thus CH≡CCl rather than CHCl=CH· radical would be further dissociated:

$$CH{\equiv}CCl^{\dagger} + m'h\nu \longrightarrow CH{\equiv}C\cdot + Cl, \quad (12)$$

$$CH{\equiv}C\cdot + CH_2ClCHCl_2 \longrightarrow CH{\equiv}CH + CH_2ClCCl_2\cdot, \quad (13)$$

$$2CH{\equiv}C\cdot \xrightarrow{M} C_4H_2\cdot \quad (14)$$

Effects of Pressure on Mechanism. The increase in the product yields in % conversion (Table 1) indicates that the collisional effects outside the reaction zone become significant at higher pressures, since the volume of reaction zone in which the fluence exceeds the lowest critical value and the fluence distribution are unaltered with increasing the reactant pressure at a given pulse energy, the absorption along the laser beam being neglected. As the substtrate pressure is increased, collisional energy transfer between the reactant molecules excited by the laser outside the reaction zone can drive them to higher energy levels than those excited upon the laser irradiation:

$$2CH_2ClCHCl_2^{\dagger} \longrightarrow CH_2ClCHCl_2^{*} + CH_2ClCHCl_2, \quad (15)$$

where $CH_2ClCHCl_2^{\dagger}$ and $CH_2ClCHCl_2$* stand for the $CH_2ClCHCl_2$ molecules excited below and above the dissociation threshold, respectively. The difference of critical energies between the HCl elimination and the C–Cl bond rupture is so small that the $CH_2ClCHCl_2$* molecule excited above the critical energy by the energy-pooling process would exit *via* both channels.

Since the yields of secondary products as well as those of primary products are increased with higher reactant pressure, other process of collisional energy transfer at higher pressures must be operative. At higher pressures many collisions are avialable to establish higher energy distribution of the reactant molecule, Reaction 15 being merely a simplified form of this process. Collisional energy transfer from energized parent molecule to other species occurs with a time scale comparable to the pulse duration.[23] This is the basis of IR laser pyrolysis experiment, except that IR sensitizers are in general much stronger absorbers of the laser photons and have higher energy threshold for their decomposition than $CH_2ClCHCl_2$. Thus the products formed by the collision-induced decomposition would be further dissociated as a result of intermolecular energy transfer:

$$CHCl{=}CHCl + CH_2ClCHCl_2^{\dagger} \longrightarrow CHCl{=}CHCl^{*} + CH_2ClCHCl_2, \quad (16)$$

$$CH{\equiv}CCl + CH_2ClCHCl_2^{\dagger} \longrightarrow CH{\equiv}CCl^{*} + CH_2ClCHCl_2, \quad (17)$$

$$\cdot CHClCH_2Cl + CH_2ClCHCl_2^{\dagger} \longrightarrow \cdot CHClCH_2Cl^{*} + CH_2ClCHCl_2. \quad (18)$$

Collisionally excited $CH_2ClCHCl_2$*, CHCl=CHCl*, ·$CHClCH_2Cl$*, and CH≡CCl* above the dissociation thresholds undergo decomposition analogous to Reactions 1—12.

In the presence of additives, the energy-pooling process 15 is suppressed by collisional deactivation of $CH_2ClCHCl_2^{\dagger}$ with the additive gases, and, as a reslut, the dissociation yields decrease monotonically. As mentioned earlier (Table 3), all the products yields at 5.0 Torr reactant pressure are decreased and their relative yields are little affected by the addition of N_2,

NO, and CF_4. These observations indicate that $CH_2ClCHCl_2$ is free from rotational bottlenecking due to its high density of rotational-vibrational states and these molecules are serving to quench the highly vibrationally excited parent molecules. The efficiency of collisional deactivation appears to be dependent on the molecular size of quenchers, since Table 3 shows that CF_4 quenches more efficiently than N_2 and NO. On the other hand, H_2, CH_4, and C_2H_6 decrease the yields of primary products more significantly and influence the relative yields remarkably, in particulr, those of $CH_2=CCl_2$, $CH_2=CHCl$, and $CH\equiv CH$. Therefore, other interaction than collisional quenching must be sought in the case of H_2, CH_4, and C_2H_6 addition.

$CH_2ClCHCl_2$ is found to react primarily by radical chain propagation in thermal reactor, molecular elimination of HCl being operative at the same time.[16,17] Radical chain reactions give the same dichloroethene isomers as those by unimolecular HCl elimination:

$$Cl + CH_2ClCHCl_2 \longrightarrow CH_2ClCCl_2\cdot + HCl, \quad (19)$$

$$\longrightarrow \cdot CHClCHCl_2 + HCl, \quad (20)$$

$$CH_2ClCCl_2\cdot \longrightarrow CH_2=CCl_2 + Cl, \quad (21)$$

$$\cdot CHClCHCl_2 \longrightarrow cis\text{-}CHCl=CHCl + Cl, \quad (22)$$

$$\longrightarrow trans\text{-}CHCl=CHCl + Cl, \quad (23)$$

The radical chain terminates by[17]

$$Cl + CH_2ClCCl_2\cdot \longrightarrow CHCl=CCl_2 + HCl,$$

$$Cl + \cdot CHClCHCl_2 \longrightarrow CHCl=CCl_2 + HCl.$$

In the presence of H_2, CH_4, and C_2H_6, Cl atom can abstract H atom from these molecules and inhibit the radical chain, depending on their rates of H-atom abstraction reactions:

$$Cl + RH \longrightarrow HCl + R\cdot, \ R=H, CH_3, \text{ and } C_2H_5 \quad (24)$$

The yield of $CH_2=CCl_2$ and those of *trans*- and *cis*-CHCl=CHCl formed by the radical chain reactions would be comparable, since the rate constants for Reactions 19 and 20 were found to be similar to each other.[27] The significant decrease in the relative yield of $CH_2=CCl_2$ upon the addition of the H atom containing molecules could be ascribed to Reaction 24, which inhibits the radical chain. The decrease also provides an evidence that the relative yield of $CH_2=CCl_2$ derived from the radical chain reaction is much greater than those by IRMPD and collision-induced decomposition (Table 3). The rate constant of Reaction 24 becomes greater in the order of H_2, CH_4, and C_2H_6.[28] In the case of H_2 the rate constant of Reaction 24 is about 25 times smaller than that of Reaction 19 plus 20 at 300 K. As shown in Table 4, the relative yield of $CH_2=CCl_2$ is appreciably decreased by the addition of only 1.0 Torr H_2, which implies that Reaction 24 is competitive with Reactions 19 and 20 at this pressure. Its rate constant becomes comparable to those of Reactions 19 and 20 at higher temperature, since its activation energy is greater than those of Reactions 19 and 20. Therefore, as a result of the collisional energy transfer the system is effectively at higher temperatures. The relative yield of $CH_2=CCl_2$ in the presence of H_2 up to 10 Torr is greater than those upon the addition of 5.0 Torr CH_4 and C_2H_6, indicating that inhibition of the radical chain by H_2 is imcomplete over the pressure range examined.

Table 5. Dependence of relative yields[a] on C_2H_6 pressure

P/Torr	1.0	2.0	3.0	5.0
$CH\equiv CCl$	7.89	6.20	4.82	3.73
$CH_2=CHCl$	5.82	6.44	6.09	6.25
$CH_2=CCl_2$	5.38	4.63	4.41	4.31
trans-CHCl=CHCl	75.4	74.1	73.1	71.7
cis-CHCl=CHCl	100 (1.26)	100 (0.897)	100 (0.798)	100 (0.549)

a) Relative yields at 5.0 Torr reactant pressure and E_0=0.136 J/pulse as compared to the yield of *cis*-HCl=CHCl in % conversion per 500 shots(in parenthesis). C_2H_2 was not measured by the same reason as in Table 3.

As the rate of the reaction of Cl atom with C_2H_6 is much faster than that with $CH_2ClCHCl_2$, C_2H_6 would inhibit the radical chain completely. The relative yields of the dichloroethene isomers change very slightly with increasing C_2H_6 pressure (Table 5), showing the radical chain is completely stopped by the addition of C_2H_6. The slight decrease in the relative yields would result from the decrease in the effective temperature with higher C_2H_6 pressure. In a tightly focused geometry and at a given pulse energy, as mentioned earlier, the volume of reaction zone where the fluence exceeds the lowest critical value and IRMPD takes place would remain rather constant with increasing reactant pressure. Thus the increase in the product yields (in % conversion) with increasing pressure could be attributed to the contribution from the collision-induced decomposition outside the reaction zone. With reference to Tables 1 and 5, at 5.0 Torr $CH_2ClCHCl_2$ with 1.0 Torr C_2H_6 added, where the radical chain reactions are negligible, the yield of *cis*-CHCl=CHCl is seen to be about 2.5 times greater than that *via* the neat IRMPD at 0.2 Torr. Since at 0.2 Torr $CH_2ClCHCl_2$ pressure collisional effects can be considered to be very small, the relative yields of the dichloroethene isomers obtained in the presence of 1.0 Torr C_2H_6 would reflect the product distribution in the collision-induced decomposition to a considerable extent. The relative yield of $CH_2=CCl_2$ observed at 1.0 Torr C_2H_6 and pulse energy of 0.136 J/pulse is roughly similar to that in the neat photolysis at 0.2 Torr reactant pressure. This may suggest that the energy

distribution of the dissociating $CH_2ClCHCl_2$ molecules by IRMPE is not so different from that excited by energy-pooling process. A considerably higher *trans/cis* ratio in the collision-induced decomposition than that in the neat IRMPD at the low reactant pressure, may result from the more significant thermarization of the *trans/cis* ratio due to higher substrate pressure in the former.

Upon the addition of H_2 (Fig. 2), the yields of CH_2=CHCl and CH≡CH are increased markedly. It is tempting to ascribe their formation to the H-atom abstractions of CHCl=CH· and CH≡C· radicals, which are generated by the C–Cl bond rupture of CHCl=CHCl and CH≡CCl, respectively. Table 4 shows that the relative yield of CH_2=CHCl upon the addition of H_2 is greater than that of CH≡CCl. However, it is unlikely that the branching ratio of C–Cl bond-scission channel with higher energy threshold is greater than that of lower HCl elimination channel. In addition, the yield-pressure behavior of CH_2=CHCl in presence of C_2H_6 is similar to that of H_2 addition, while upon the addition of CH_4 its yield is decreased slightly. Therefore, H atom generated by Reaction 24 and that emitted by the decomposition of C_2H_5· radical would be participated in the formation of CH_2=CHCl in the presence of H_2 and C_2H_6· CH_3· radical requires much higher energy than C_2H_5· radical:

$$C_2H_5\cdot \xrightarrow{(M)} C_2H_4 + H, \qquad (25)$$

$$H + CHCl{=}CHCl \longrightarrow \cdot CHClCH_2Cl^* \longrightarrow CH_2{=}CHCl + H. \qquad (26)$$

In a similar manner, the following reaction is possible:

$$H + CH{\equiv}CCl \longrightarrow CH{\equiv}CH + Cl$$

In contrast to CH_2=CHCl, the yield of CH≡CH upon the addition of CH_4 is greater than that upon the addition of H_2, indicating that H-atom arstraction is more important for the fromation of CH≡CH and, as a result, that the C–Cl bond scission of CH≡CCl is an important source of Cl atom. The relative yield of CH≡CH in the neat photolysis becomes smaller than that of CH_2=CHCl with increasing reactant pressure. Most probable initiation reaction of the radical chain would be the C–Cl bond rupture of $CH_2ClCHCl_2$.

References

1) K. Nagai and M. Katayama, *Bull. Chem. Soc. Jpn.*, **51**, 1269 (1978).
2) Y. Makide, S. Kato, T. Tominaga, and K. Takeuchi, *Appl. Phys. B*, **28**, 341 (1982).
3) A. V. Baklanov, Yu. N. Molin, and A. K. Petrov, *Chem. Phys. Lett.*, **68**, 329 (1979).
4) P. A. Hackett, C. Wills, M. Drouin, and E. Weinberg, *J. Phys. Chem.*, **84**, 1873 (1980).
5) P. J. Papagiannakopolous, K. Kosnik, and S. W. Benson, *Int. J. Chem. Kinet.*, **14**, 327 (1982).
6) T. H. Richardson and D. W. Setser, *J. Phys. Chem.*, **81**, 2310 (1977).
7) Y. Ishikawa and S. Arai, *Chem. Phys. Lett.*, **103**, 68 (1983).
8) Y. Ishikawa and S. Arai, *Bull. Chem. Soc. Jpn.*, **57**, 691 (1983).
9) H. Ogura and T. Yano, *Bull. Chem. Soc. Jpn.*, **58**, 1239 (1985).
10) T. Yano, S. Ozaki, H. Ogura, and E. Tschuikow-Roux, *J. Phys. Chem.*, **89**, 1108 (1985).
11) S. Kato, Y. Makide, K. Takeuchi, and T. Tominaga, *J. Phys. Chem.*, **88**, 3977 (1984).
12) C. R. Quick, Jr. and C. Wittig, *J. Chem. Phys.*, **72**, 1694 (1980).
13) K. C. Kim and D. W. Setser, *J. Phys. Chem.*, **78**, 2166 (1974); *ibid.*, **76**, 283 (1972).
14) B. E. Holmes, D. W. Setser, and G. O. Prichard, *Int. J. Chem. Kinet.*, **8**, 215 (1976); D. W. Follner and G. O. Prichard, *Int. J. Chem. Kinet.*, **6**, 573 (1974); G. O. Prichard and J. T. Bryant, *J. Phys. Chem.*, **72**, 1603 (1968).
15) M. V. C. Sekhar and E. Tschuikow-Roux, *J. Phys. Chem.*, **78**, 472 (1974).
16) D. H. R. Barton, *J. Chem. Soc.*, **1949**, 148.
17) T. Teramoto, M. Kitabatake, and T. Onouchi, *Kogyo Kagaku Zasshi*, **68**, 460 (1964).
18) H. Ogura, *Bull. Chem. Soc. Jpn.*, submitted 1985.
19) R. H. Harrison and K. A. Kobe, *J. Chem. Phys.*, **26**, 1411 (1957).
20) K. Takeuchi, I. Inoue, R. Nakane, Y. Makide, S. Kato, and T. Tominaga, *J. Chem. Phys.*, **76**, 398 (1982).
21) N. C. Craig, L. P. Pipper, and V. L. Wheeler, *J. Phys. Chem.*, **75**, 1453 (1971).
22) P. M. Jeffers, *J. Phys. Chem.*, **78**, 1469 (1974).
23) H. Dai, E. Specht, M. Berman, and C. B. Moore, *J. Chem. Phys.*, **77**, 4494 (1982).
24) K. Nagai and M. Katayama, *Chem. Phys. Lett.*, **5**, 329 (1977).
25) C. Reisler, F. M. Lussier, C. C. Jensen, and J. I. Steinfeld, *J. Am. Chem. Soc.*, **101**, 350 (1979).
26) K. Nagai and M. Katayama, *Chem. Lett.*, **1979**, 969.
27) C. Cillien, P. Goldfinger, G. Huybrechts, and G. Martens, *Trans. Faraday Soc.*, **63**, 1631 (1967).
28) P. H. Wine and D. H. Semmes, *J. Phys. Chem.*, **87**, 3572 (1983); D. D. Davis, W. Braun, and A. M. Bass, *Int. J. Chem. Kinet.*, **2**, 101 (1970).

Photolytic Generation and the Subsequent Dimerization of 4-Alkyl-1-methylpyridinyl Radicals in Solution as Studied by Steady-state and Kinetic ESR Spectroscopy

Kimio Akiyama, Toru Ishii, Shozo Tero-Kubota,† and Yusaku Ikegami*
Chemical Research Institute of Non-Aqueous Solutions, Tohoku University, Katahira 2-1-1, Sendai 980
†*Institute for Molecular Science, Myodaiji, Okazaki 444*
(Received July 18, 1985)

1-Methylpyridinyl and 4-alkyl-1-methylpyridinyl (alkyl=methyl, ethyl, isopropyl, and *t*-butyl) radicals were generated photolytically from their dimers in solution. Hyperfine splitting constants for these radicals were assigned and the temperature dependence was discussed. Absolute dimerization rates of these radicals in the range of −50—−100 °C were determined by analyzing the ESR signal decay during the dark period. A nearly constant activation energy of dimerization was observed for five radicals, while the frequency factor decreased with the bulkiness of 4-substituent, which are discussed in terms of the steric hindrance for the dimerization.

Electron spin resonance (ESR) spectra of the neutral pyridinyl radicals prepared by one-electron reduction of the corresponding pyridinium salts have been successfully analyzed.[1] However, the isolable radicals in solution are restricted to those having electron-withdrawing and delocalizing group at 2- or 4-position of the pyridine ring. In our recent studies,[2] it was established that some pyridinyl radicals are equilibrated with the dimers and the interconversion between the radical and the dimer is completely reversible for an intermittent photolysis or a temperature change. A kinetic ESR method was applied to such equilibrium systems and elucidated the dimerization mechanism showing a two-step decay of the ESR signal due to the radical generated photolytically. Further, the time-resolved ESR studies revealed that the precursor of the radical generated upon light irradiation was singlet radical pair for the reason that the A/E polarized transient ESR spectra were observed in solution.[3,4]

Based upon these results, we attempted the generation of simple 4-alkyl-substituted pyridinyl radicals which might be produced by photoirradiation of the corresponding dimers. In spite of the radical formation from the singlet radical pair, the pair has relatively long lifetime enough to cause ST_0-mixing and to escape from the primary cage. The ESR spectra

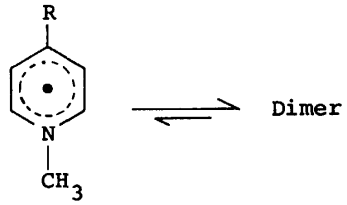

1 R=H
2 R=CH_3
3 R=CH_2CH_3
4 R=$CH(CH_3)_2$
5 R=$C(CH_3)_3$

of five pyridinyl radicals, **1**—**5**, were then observed during the continuous irradiation and analyzed to obtain the hyperfine splitting (hfs) constants. The kinetic ESR study was also carried out to determine the activation parameters of the second-order dimerization.

Experimental

Vacuum line technique was standard in the preparation and purification of the radicals and solvents. Each pyridinyl radical was prepared from the corresponding pyridinium iodide by the reduction with 3% sodium-amalgam in degassed acetonitrile at about −30 °C and extracted with a nonpolar solvent such as methylcyclohexane. All pyridinium iodides were obtained by treating the pyridines with methyl iodide without solvent, and recrystallized from ethanol. Solvents for the measurements were transferred by the trap-to-trap method using a vacuum system. Steady-state ESR measurements were carried out with a Varian E-109E EPR spectrometer. A high pressure Hg-lamp (Ushio 500 W) as a light source was equipped with a UV-31 glass filter to prevent undesirable decomposition of radicals. Spectral simulation and McLachlan calculation were performed by using a Sharp MZ-80C microcomputer. Kinetic ESR technique was described previously.[2]

Results and Discussion

Hfs Constants of 4-Alkyl-1-methylpyridinyl Radicals. The 4-alkyl-1-methylpyridinyl radicals dimerize in solution at room temperature forming covalently-bonded dimers, which show a broad absorption band in the near UV region. As the radical-dimer equilibrium is in favor of the dimer side, no ESR signal was observed at room temperature for all radicals examined. Either photolysis or rise in temperature of a dimer solution led to exhibit the ESR spectrum. The interconversion between the radical and the dimer was completely reversible at temperatures below 80 °C. Figure 1a shows the ESR spectrum observed during a continuous irradiation to the dimer of 1-methylpyridinyl radical (**1**) in 2-methyltetrahydrofuran (MTHF) at −40 °C. Hyperfine structure of the spectrum was reasonably analyzed on the computer simulation (Fig. 1b). The hfs constants were assigned tentatively according to the types of splitting and by comparing them with the spin density calculations by the McLachlan procedure. The constants and assignments are given in Table 1 together with those of the other alkyl-substituted pyridinyl radicals. As seen in Table 1, changes in the constants with the substitution of 4-alkyl group are negligibly small compared with the substitution of electron-withdrawing or delocalizing groups.[5] Relatively large

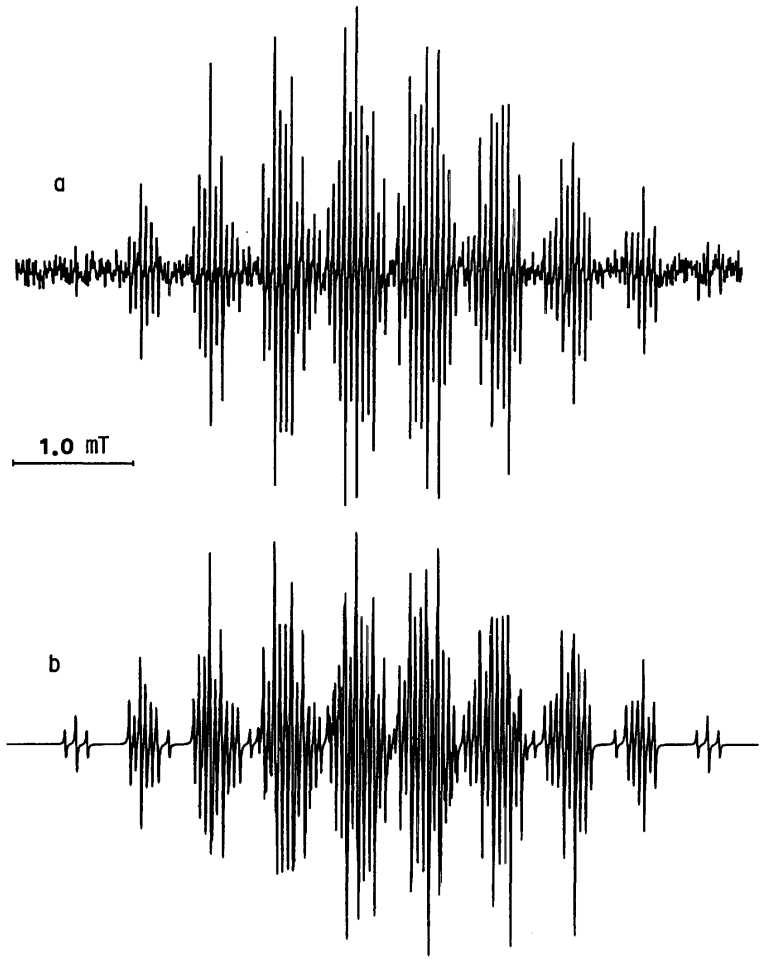

Fig. 1. ESR spectrum of the 1-methylpyridinyl radical generated by light irradiation of the dimer solution in MTHF at −40 °C. (a) Measured and (b) simulated.

Table 1. Hyperfine splitting constants (a in mT) for the 4-alkyl-1-methylpyridinyl radicals in MTHF at −40 °C

Position	R at 4-position				
	H	CH_3[a)]	CH_2CH_3	$CH(CH_3)_2$	$C(CH_3)_3$
1	0.678	0.639	0.647	0.663	0.665
2, 6	0.577	0.584	0.586	0.584	0.585
3, 5	0.092	0.113	0.108	0.107	0.106
N	0.535	0.491	0.495	0.494	0.494
4	1.118				
R (β-H)		1.168	0.871	0.566	
R (γ-H)			b)	0.018	0.022

a) Measured in toluene. b) Unresolved.

hfs constants were observed at 4-, 2-, and 6-positions, where would apt to couple in the dimerization.

The hfs constants of β-protons of 4-alkyl groups, ring nitrogen, and N-methyl protons showed dependence on temperature, while the other constants were almost independent. Temperature dependence of the hfs constants of pyridinyl radicals having polarizable groups has been discussed in terms of polarity change of the solvent and the restricted rotation of substituents.[5,6] On the other hand, the temperature dependent hfs constants of 1-hydropyridinyls have been analyzed using the model of localized out-of-plane vibration of the protons.[7] For the present radicals, the comparatively large dependence was found with temperature coefficients of 5.4×10^{-4} and 8.3×10^{-4} mT/°C for the β-protons in **3** and **4**, respectively. These values can be interpreted by the existence of restricted rotation of the alkyl groups. This is supported by the small hfs constants, 0.871 mT for **3** and 0.566 mT for **4**, compared with 1.168 mT for **2** in which the methyl group rotates freely in temperature range examined (−80—+40 °C). After the usual manner to interprete the internal rotation of alkyl groups by ESR spectroscopy, we found that the conformation of the alkyl groups is similar to those of 1-alkyl-4-methoxycarbonylpyridinyl radicals reported previously.[6]

The hfs constant of the N-methyl protons reflects the spin density on the bonded nitrogen atom and the conformational change around this atom. The nitrogen spin density also correlates with the spin densities on the adjacent atoms with the Karplus-

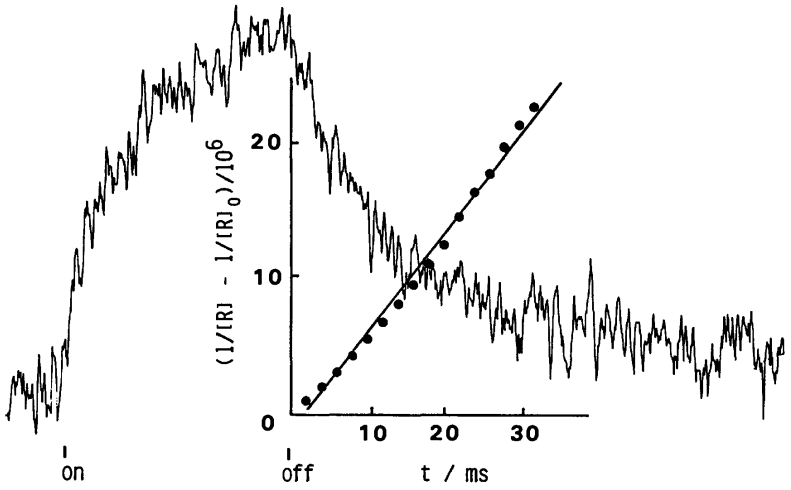

Fig. 2. Growth and decay curve of the 1-methylpyridinyl radical in MTHF solution at −76°C. Insert is the second-order plot.

TABLE 2. KINETIC PARAMETERS FOR THE DIMERIZATIONS OF THE 4-ALKYL-1-METHYLPYRIDINYL RADICALS IN MTHF

No.	R at 4-position	k_{exp}[a)] / mol^{-1}dm^{3}s^{-1}	log A / mol^{-1}dm^{3}s^{-1}	E_a / kJ mol^{-1}
1	H	5.4×10^7	10.2	8.79
2	CH_3	4.3×10^7	10.0	8.37
3	CH_2CH_3	3.0×10^7	9.8	8.79
4	$CH(CH_3)_2$	1.4×10^7	9.5	8.75
5	$C(CH_3)_3$	1.3×10^7	9.4	8.37

a) Observed value at −80°C.

Fraenkel relation.[8] In the present radicals, since the spin densities at 2- and 6-positions were independent of temperature, the latter contribution to the change of the nitrogen spin density with temperature can be ignored, though the overlapping between the $p\pi$-orbital of the nitrogen and the 1s orbital of the bonded methyl protons may vary with the structural change. It is rather indicative of the presence of the out-of-plane vibration of the *N*-methyl group that the temperature coefficients for a^N and $a^H_{N\text{-}CH_3}$ showed the opposite signs each other. With a lowering of temperature, $a^H_{N\text{-}CH_3}$ would decrease and a_N increases, because the out-of-plane vibrational amplitude decreases. Sander and Dohrmann[7] reported the temperature dependent hfs constants of protons and nitrogen for 1-hydropyridinyl radicals and estimated the frequencies of the out-of-plane vibrations of the protons. Das and Fraenkel[9] suggested that the out-of-plane vibration of the N-H proton probably contributes to the temperature dependent hfs constants of the dihydropyrazine cation radical. In our case, the observed temperature coefficient of 1.3×10^{-4} mT/°C for nitrogen is small for the conformational change with temperature, compared with those of 1-hydropyridinyl radicals. This may be due to the low vibrational frequency and the small displacement of N-CH_3 group from the π-plane.

Kinetic Treatment of the Dimerization. The dimers of the 4-alkyl-substituted pyridinyl radicals have a dihydropyridine type structure and show each a broad absorption band in the near UV region. Light irradiation to this band causes a homocentric C-C bond cleavage, resulting the appearance of ESR signal of the monomeric radical. After the pulse irradiation, the radical dimerizes and then the signal decays in the intermittent dark period. Figure 2 shows a growth and decay of the ESR signal measured during the photolysis of the dimer of 1-methylpyridinyl in MTHF at −76°C. The signal was accumulated 2000 transient times. Although the signal-to-noise ratio is rather poor, the decay curve could be analyzed in terms of a second-order kinetics. The straight line inserted in Fig. 2 represents a least squares fit to the points according to the equation:

$$1/[R] = k_{exp}t + 1/[R]_0 \quad (1)$$

where $[R]_0$ is the concentration of the radical at time t=0 after an onset of the dark period. This equation is best explained by the C-C bond formation of two radicals. The dimerization rate constants (k_{exp}) were estimated by obtaining values from three independent measurements at −80°C. The constants are listed in Table 2.

The rates were also measured in the temperature range −50—−100°C. Figure 3 presents the Arrhenius plots for the dimerization of **1**—**5**. The activation

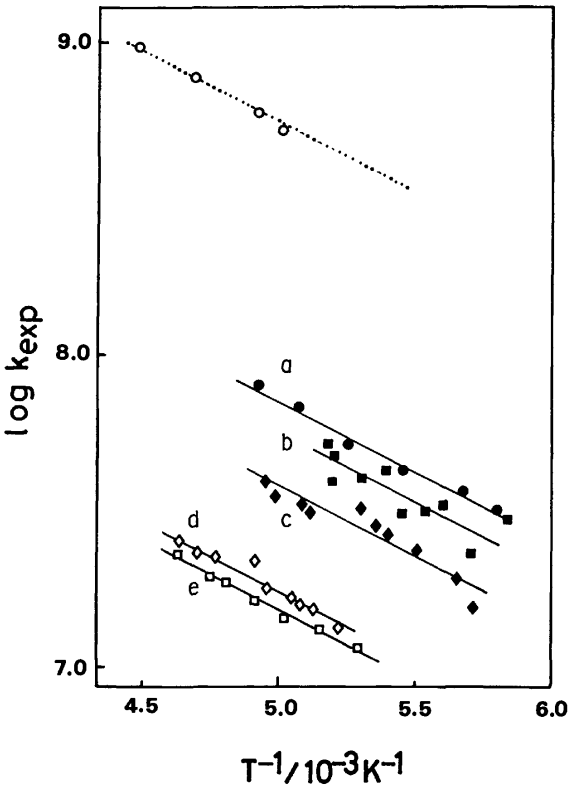

Fig. 3. Dimerization rate constants *vs.* $1/T$ for a: **1**, b: **2**, c: **3**, d: **4**, and e: **5**. A dotted line represents the diffusion-controlled rate constants (see text).

energies (E_a) and frequency factors (A) were each estimated by the least squares method from the plots, as summarized in Table 2. Because of the low yield of **2** from the dimer, the integrated signal intensities of ESR showed a poor reproducibility, leading to a significant deviation of the plot. The rates observed for **5** were slightly larger than those reported reviously.[4] This is caused by that, in the previous study, the concentration ($\approx 10^{-4}$ mol dm^{-3}) of the standard 2,2-diphenyl-1-picrylhydrazyl (DPPH) solution used to evaluate the initial concentration of radical was far different from the radical concentration ($\approx 10^{-6}$ mol dm^{-3}) produced by light irradiation.[10] In the present work, a standard DPPH solution of *ca.* 10^{-6} mol dm^{-3} was used.

A dotted line in Fig. 3 represents the diffusion-controlled second-order rate constants estimated by use of the Smoluchowsky-Stoles-Einstein relation:[11]

$$k_{diff} = 8RT/3 \times 10^3 \eta(T) \quad (2)$$

where $\eta(T)$ denotes the temperature-dependent viscosity of solvent MTHF.[12] From the slope of the line, we obtain the activation energy of 8.98 kJ mol^{-1} for a diffusion in MTHF and the frequency factor of log A=11.1 mol^{-1} dm^{-3} s^{-1}. It is implied from Eq. 2 that the diffusion-controlled rate constants for a bimolecular reaction are independent of the size of the reactants. This may be true to the radicals in which the electron is completely delocalized so that the reaction is equally probable at any direction, but it would be unadaptable to saturated or σ-type radicals, in which the unpaired electron is localized and the reaction therefore occurs at a particular site on the radical.

The radical **5** forms only the 2,2′-dimer composed of its diastereoisomers.[4] On the other hand, **1** forms the 4,4′-dimer at the temperature range 30—−70 °C.[11] Since the highest spin density is located at 4-position, as discussed on the basis of the steady-state ESR experiments, this position would be the most active site for dimerization. However, when a sterically large group such as *t*-butyl is substituted at this position, the dimerization occurs at the position having next higher spin density, *i.e.* 2- or 6-position, forming 2,2′-dimer. In spite of the delocalized unpaired electron, the coupling reaction of pyridinyls proceeds in a site-selective manner like σ-type radical. Even if the above factor shifts the diffusion rates for the present radicals from that expressed by Eq. 2, the observed rates are two or three orders of magnitude smaller than that of diffusion encounter. The slow rate is ascribed to the small frequency factor. The activation energies in Table 2 agree well with that of diffusion in the MTHF solution within experimental error limit. Although the frequency factors are small compared with that of diffusion, the values of 10^{9-10} mol^{-1} dm^3 s^{-1} are larger than those in the dimerizations of spin-delocalized π-radicals such as triphenylmethyl and triphenylimidazolyl.[14,15] The values for the present radicals are rather comparable to those of spin-localized alkyl radicals.[16]

Although the activation energy is nearly constant for the dimerizations of **1**—**5**, the rate constant and the frequency factor are significantly affected by the size of 4-substituent. Since the bulky substituent prevents the bond formation at 4-position, the dimerization occurs at 2-position. Thus, with a decrease in the probability of 4,4′-dimer formation, the frequency factor and the rate decreased. In order to extend further discussion, the thermodynamic parameters of the monomer-dimer equilibria for **1**—**5** should be obtained. Determination of the parameters, however, has been unsuccessful, because the radical concentrations could not be determined by reason of that each equilibrium inclines overwhelmingly toward the dimer side even at 70 °C.

References

1) For recent review, see E. M. Kosower, "Topics in Current Chemistry," ed by F. L. Boschke, Springer, Berlin Heiderberg (1983), Vol. 112, pp. 117—162.

2) K. Akiyama, S. Kubota, and Y. Ikegami, *Chem. Lett.*, **1981**, 469; S. Tero-Kubota, Y. Sano, and Y. Ikegami, *J. Am. Chem. Soc.*, **104**, 3711 (1982); K. Akiyama, S. Tero-Kubota, and Y. Ikegami, *ibid.*, **105**, 3601 (1983).

3) K. Akiyama, S. Tero-Kubota, T. Ikenoue, and Y. Ikegami, *Chem. Lett.*, **1984**, 903; K. Akiyama, S. Tero-Kubota, Y. Ikegami, and T. Ikenoue, *J. Am. Chem. Soc.*, **106**, 8322 (1984).

4) K. Akiyama, S. Tero-Kubota, Y. Ikegami, and T.

Ikenoue, *J. Phys. Chem.*, **89**, 339 (1985).
5) S. Kubota and Y. Ikegami, *J. Phys. Chem.*, **82**, 2739 (1978).
6) K. Akiyama, S. Kubota, and Y. Ikegami, *J. Phys. Chem.*, **85**, 120 (1981).
7) U. Sander and J. K. Dohrmann, *Ber. Bunsenges. Phys. Chem.*, **83**, 1258 (1979); **84**, 270 (1980).
8) M. Karplus and G. K. Fraenkel, *J. Chem. Phys.*, **35**, 1312 (1961).
9) M. R. Das and G. K. Fraenkel, *J. Chem. Phys.*, **42**, 792 (1865).
10) R. S. Alger, "Electron Paramagnetic Resonance: Techniques and Applications," John Wiley & Sons, New York (1968).
11) A. M. North, *Quart. Rev., Chem. Soc.*, **20**, 421 (1966); E. McLaughlin, *Trans. Faraday Soc.*, **55**, 28 (1959).
12) D. Nicholls, C. Sutphen, and M. Szwarc, *J. Phys. Chem.*, **72**, 1021 (1968).
13) The dimer is characterized with the following data: ^{1}H-NMR (CD_3COCD_3) δ=2.72 (6H, s), 2.83 (2H, m), 4.24 (4H, dd), 5.78 (4H, d).
14) F. S. D'yachikovskii, N. N. Bubnov, and A. E. Shilov, *Dokl. Akad. Nauk SSSR*, **122**, 629 (1958).
15) K. Maeda and T. Hayashi, *Bull. Chem. Soc. Jpn.*, **43**, 429 (1970).
16) D. Griller and P. R. Marriott, *Int. J. Chem. Kinet.*, **11**, 1163 (1979); R. W. Fessenden, *J. Phys. Chem.*, **68**, 1508 (1964).

Preparation of Polyoxa- and Dioxapolythia[*n*](1,1′)-ruthenocenophanes and Their Metal Complexes

Yoichi HABATA, Sadatoshi AKABORI,* and Masaru SATO†
Department of Chemistry, Faculty of Science, Toho University, Funabashi, Chiba 274
†*Chemical Analysis Center, Saitama University, Urawa, Saitama 338*
(Received July 25, 1985)

Polyoxa- and dioxapolythia[*n*]ruthenocenophanes were prepared by the reaction of 1,1′-diacetoxyruthenocene with α-(2-bromoethyl)-ω-bromopoly(oxyethylene) in the presence of alkali metal hydroxides and by the reaction of 1,1′-bis(2-chloroethoxy)ruthenocene with dithiolate in the presence of sodium hydroxide, respectively. The extraction ability of their compounds was excellent for mercury(II) and thallium(I) ions. The ruthenocenophanes with oxygen atoms attached to the ruthenocene nucleus showed excellent extraction ability for a silver(I) ion, although the corresponding ferrocenophane analogs decomposed in similar reaction conditions. The ruthenocenophanes formed 1 : 1 complexes with mercury(II) and silver(I) ions. ^{1}H-NMR, electronic, and IR spectral data of their complexes showed the presence of direct electronic interaction between the mercury-(II) or silver(I) ion and the ruthenium atom of ruthenocenophanes.

For the purpose of syntheses of crown compounds possessing specific properties, several research groups to date have reported on the syntheses and complexing ability of crown ether typed compounds containing a ferrocene nucleus in their macrocyclic skeleton.[1-5] Morrison *et al.* reported on the Ru–Hg and the Fe–Hg interaction in the mercury adducts of ruthenocene and ferrocene.[6] However, Biernat *et al.* suggested that the interaction between the iron atom of the ferrocene nucleus and the complexed rubidium ion was not present from their electronic spectral data.[1b] Our X-ray analysis elucidated no interaction between the iron atom of 1,4,7,10,13-pentaoxa[13](1,1′)ferrocenophane and the complexed sodium cation in the solid state.[5b] The above results suggest that the soft mercury(II) and silver(I) ions which were incorporated by the crown site of the ferroceno-crown ethers might cause the strong interaction with the iron atom of the ferrocene nucleus. Although the compound **2** with sulfur atoms at the 1,*n*-position of the ferrocenophane was not decomposed by treating with silver(I) and mercury(II) ions, the compound **1** with oxygen atoms at the 1,*n*-position of the ferrocene nucleus, decomposed by their metal ions.

1 : X=Y=O
2 : X=S, Y=O or S
3 : X=S, Y=O
4 : X=Y=S

a : n=1, b : n=2, c : n=3, d : n=4

The enhanced stability of the silver complexes of **2** may be attributed to the pπ-dπ interaction of sulfur and iron atoms of the ferrocene nucleus of **2**.[2d] It is well-known[7] that ruthenocene is more stable for oxidation compared with ferrocene as seen by the reduction potential of both metallocene. Therefore, in this paper, we wish to report on the synthesis of polyoxa- and dioxapolythia[*n*]-(1,1′)ruthenocenophanes and their complexing ability with transition metal ions, along with alkali and alkaline earth metal ions.[8]

Results and Discussion

Syntheses of Polyoxa[n](1,1′)- (10) and Oxathia[n]-(1,1′)ruthenocenophanes (11). In order to obtain the starting material of **10**, 1,1′-diacetoxyruthenocene **6** was prepared according to the method of the synthesis of 1,1′-diacetoxyferrocene.[5b] 1,1′-Dilithioruthenocene which was prepared by the reaction of ruthenocene with butyllithium in the presence of *N,N,N′,N′*-tetramethylethylenediamine (TMEDA), was reacted with 1,2-dibromo-1,1,2,2-tetrafluoroethane to give 1,1′-dibromoruthenocene **5** in 53% yield. Compound **5** was reacted with copper(II) acetate to give **6** in 53% yield. After **6** had been hydrolyzed by alkali metal hydroxide, α-(2-bromoethyl)-ω-bromopoly(oxyethylene) (**9**) was immediately added to the hydrolyzate. The stirring was

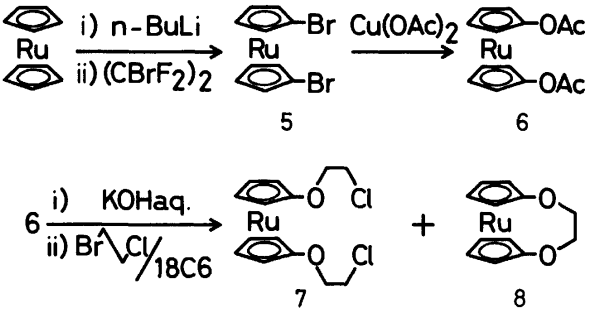

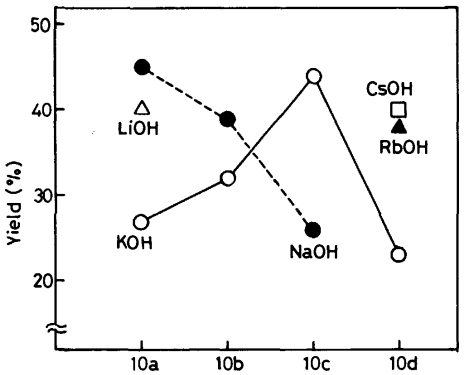

Fig. 1. The relationship between yields and alkali metal hydroxids on the syntheses of **10a—d**.

continued for 5 h at reflux temperature under nitrogen. The reaction mixture was treated by the usual method and subsequently separated by Silica-gel TLC to give 10. In the above reactions several kinds of alkali metal hydroxide were used for hydrolysis. As shown in Fig. 1, the use of sodium and potassium hydroxides resulted maximum yield of **10a** and **10c**, respectively. In the synthesis of **10d**, the use of cesium hydroxide was most favorable. This result is correlated to the cavity size of metallocenophanes.[9,10] Compound **7**, the starting material for dioxapolythia[n](1,1′)ruthenocenophanes, was synthesized by the reaction of **6** with 1-bromo-2-chloroethane in the presence of a catalytic amount of 18-crown-6. To prepare **11a**, a mixture of **7** and sodium sulfide in *N*,*N*-dimethylformamide (DMF) was stirred at reflux temperature for 9 h. The reaction mixture was treated by the usual method and separated by silica-gel TLC to give **11a** in 11% yield. The compound **7** was reacted with disodium 1,2-ethanedithiolate in ethanolic tetrahydrofuran (THF) to give **11b** and **11c** in 25 and 5% yields, respectively. The possible mechanism of the formation of **11c** in the above reaction may be the same as that for ferrocene analogues.[5f] Similarly, **7** was reacted with disodium 2,2′-thiobis(ethanethiolate) in ethanolic THF to give only **11c** in 63% yield.

The ^{1}H-NMR and ^{13}C-NMR spectra of **10**—**11** are summarized in Table 1. The structures of the new compounds were determined on the basis of ^{1}H-NMR, ^{13}C-NMR, mass spectra and elemental analyses. For example, the molecular formula of **10c** was deduced to be $C_{18}H_{24}O_5Ru$ by the elemental analysis and mass spectroscopy (M^+ 422). As the ^{1}H-NMR spectrum of **10c** showed α- and β-protons of the ruthenocene nucleus appeared as two triplets (J=1.8 Hz) at δ 4.63 and 4.24, respectively and the methylene protons appeared as a multiplet of the A_2B_2 type at δ 3.89—3.49 and a singlet at δ 3.58. In the completely decoupled ^{13}C-NMR spectrum of **10c**, bridge-head, α-, and β-carbons of the ruthenocene nucleus appeared at δ 128.3, 60.2, and 64.8 ppm, respectively. Furthermore, eight methylene carbons appeared as four signals at δ 71.2, 70.4, 69.8, and 69.1 ppm. The structures of the new other compounds were also determined by a similar method described above.

The Extraction Ability. The measurement of extraction ability was carried out by the method

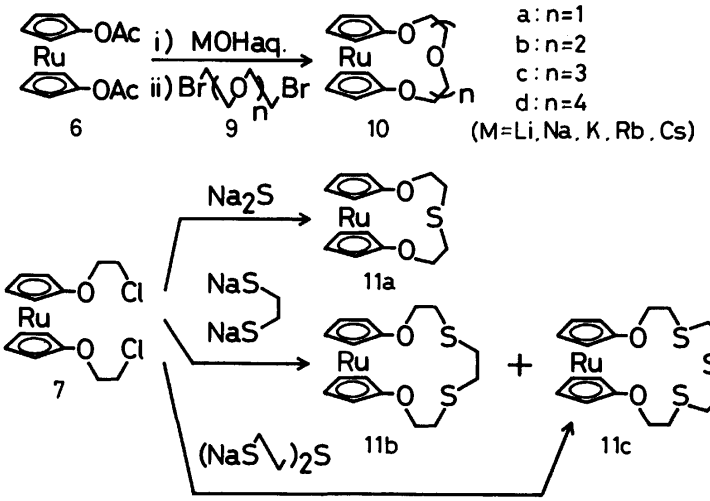

Table 1. ^{1}H- and ^{13}C-NMR spectral data of **10** and **11**

Compd	^{1}H-NMR Spectra (chemical shift/ppm)[a]	^{13}C-NMR Spectra (chemical shift/ppm)[b]
10a	4.68 (J=1.8Hz, 4H), 4.21 (J=1.8Hz, 4H), 4.04—3.63 (m, 8H)	126.7 (Cb), 59.7 (Cα), 64.3 (Cβ), 71.7, 67.7 (CH_2)
10b	4.65 (t, J=1.8Hz, 4H), 4.23 (t, J=1.8Hz, 4H), 3.95—3.52 (m, 8H), 3.60 (s, 4H)	128.4 (Cb), 60.2 (Cα), 64.6 (Cβ), 71.1, 71.0, 69.1 (CH_2)
10c	4.63 (t, J=1.8Hz, 4H), 4.25 (t, J=1.8Hz, 4H), 3.87—3.56 (m, 8H), 3.58 (s, 8H)	128.3 (Cb), 60.2 (Cα), 64.8 (Cβ), 71.2, 70.4, 69.8, 69.1 (CH_2)
10d	4.62 (t, J=1.8Hz), 4.25 (t, J=1.8Hz, 4H), 3.89—3.49 (m, 8H), 3.58 (s, 12H)	128.2 (Cb), 60.1 (Cα), 64.9 (Cβ), 71.0, 70.3, 70.0, 69.9, 69.1 (CH_2)
11a	4.91 (t, J=1.8Hz, 4H), 4.44 (t, J=1.8Hz, 4H), 4.22 (t, J=6.2Hz, 4H), 3.06 (t, J=6.2Hz, 4H)	126.8(Cb), 60.2 (Cα), 64.5 (Cβ), 72.4, 30.8 (CH_2)
11b	4.64 (t, J=1.8Hz, 4H), 4.29 (t, J=1.8Hz, 4H), 3.95 (t, J=6.2Hz, 4H), 2.90 (s, 4H), 2.82 (t, J=6.2Hz, 4H)	128.4 (Cb), 60.5 (Cα), 65.0 (Cβ), 73.7, 33.3, 31.3 (CH_2)
11c	4.72 (t, J=1.8Hz, 4H), 4.31 (t, J=1.8Hz, 4H), 3.88 (t, J=6.2Hz, 4H), 2.86 (s, 8H), 2.81 (t, J=6.2Hz, 4H)	128.1 (Cb), 60.2 (Cα), 65.2 (Cβ), 72.5, 33.7, 32.5, 31.6 (CH_2)

a) Compounds **10** and **11** were measured in CD_3CN and DMSO-d_6, respectively. b) Compounds **10** and **11** were measured in $CDCl_3$.

Table 2. Percentage of metal picrates extracted from the aqueous to organic phase[a,b]

Compd	3b	3c	3d	4a	4b	4c	10a	10b	10c	10d	11a	11b	11c
Ag^+	99	99	99	96	98	100	13	11	60	53	53	94	82
Hg^{2+}	95	95	99	12	20	20	12	80	85	20	20	22	34
Tl^+	2	33	87	0	1	2	2	37	37	0	0	0	0

a) Solvent: Water and dichloromethane (1:1). Concentration of ruthenocenocrown ether: 7×10^{-4} M. (1 M=1 mol dm^{-3}) Concentration of picric acid: 7×10^{-5} M. Concentration of metal nitrates: 0.1 M. b) Mercurydichloride was used in place of nitrate.

Table 3. Electronic and IR spectral data of compounds **10**—**15**

Compd	Electronic spectral data [nm (ε)][a]	Infrared spectral data (cm^{-1})[b]
10c	321(300)	3080, 3060, 1475, 440, 385
12c	287(2500, sh)	3070, 1475, 435, 385
10d	321(300)	3100, 3080, 1480, 430, 384
12d	287(2500, sh)	3090, 1480, 430, 385
14d	269(7400, sh), 299(7700), 357(750, sh), 459(310)	3100, 3030, 1510, 450, 460, 470, 380
11b	309(310)	3080, 1480, 434, 370
13b	330(2100), 429(200)	3080, 1475, 435, 375
15b	318(370)	3085, 1484, 439, 390
11c	315(310)	3080, 1480, 435, 380
13c	307(5500)	3090, 1494, 446, 375
15c	313(380)	3090, 1484, 437, 383

a) in CH_3CN. b) CsI disk.

described in a previous paper.[5f] Their results are summarized in Table 2. The extraction ability of their compounds toward alkali and alkaline earth metal ions was very low and/or negligible in value and this tendency was the same for the ferrocene analogues.[5b,f] However, the extraction ability of **10** and **11** toward silver(I), mercury(II), and thallium(I) ions was excellent and showed ionic selectivity. Although ferrocenophanes bearing oxygen atoms at the 1,1′-positions were decomposed by the attack of silver(I) ion, **10** and **11** showed excellent extraction ability without decomposition. This result is explicable by means of the higher stability of ruthenocene nucleus than that of the ferrocene nucleus for oxidation by silver(I) nitrate, because the oxidation potential of ruthenocene (0.693 eV) is higher than that of ferrocene (0.307 eV).[7] The compounds **10c** and **11b** showed the highest extraction ability toward silver(I) ion due to the fitness of the diameter of the guest ion on the hole size of the host molecule. Furthermore, the extraction ability of the ruthenocenophanes containing soft sulfur atoms for silver(I) ions as shown in **3**, **4**, and **11** was higher than that of polyoxa[*n*]ruthenocenophanes **10** containing no sulfur atoms. This result is in accord with the HSAB rule.[11] However, the extraction ability of the ruthenocenophanes containing sulfur atoms except **3** toward mercury(II) and thallium(I) ions was lower than that of **10**. These results show that the extraction ability also depends on the hetero-atom (Y); *i.e.* compounds **3** and **10** (Y=O) showed the good extraction ability toward mercury(II) and thallium(I) ions, while compounds **4** and **11** (Y=S) showed low or negligible extraction ability. Consequently, in the ruthenoceno crown ethers, the selectivity toward a metal cation can be controlled not only by the kind and number of heteroatoms and cavity size, but also the position of the heteroatoms.

*Isolation of Silver(I) and Mercury(II) Complexes of **10** and **11**.* A solution of ruthenoceno-crown ethers (**10** and **11**) in ether was reacted with an equimolar of silver(I) nitrate or mercury(II) chloride in acetonitrile solution to give 1:1 complexes in good yield. The melting or decomposition points of their silver and mercury complexes were higher than those of the metal free ligands, respectively.

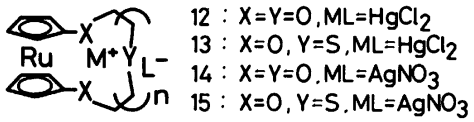

12 : X=Y=O, ML=$HgCl_2$
13 : X=O, Y=S, ML=$HgCl_2$
14 : X=Y=O, ML=$AgNO_3$
15 : X=O, Y=S, ML=$AgNO_3$

a: n=1, b: n=2, c: n=3, d: n=4

*Electronic, Infrared, and ^{1}H-NMR Spectral Change of Compounds **10** and **11** to Their Mercury(II) and Silver(I) Complexes.* The electronic and infrared spectral data of the title compounds are summarized in Table 3. In the electronic spectra of mercury(II) complexes (**12** and **13**), the wavelength of maximum absorption showed a blue shift about 8—34 nm and their molecular coefficient increased when compared with those of the free ligands (**10** and **11**). Only the **12b** showed red shift about 11 nm, but ε increased to the same extent as the other mercury(II) complexes. Derisovich *et al.*[12] described the electronic spectra of ruthenocene–$HgCl_2$ adduct as showing an intense band at 280 nm, which is absence in ruthenocene itself. This fact suggests that mercury(II) complexes (**12** and **13**) have the interaction between the ruthenium atom of ruthenoceno-crown

Table 4. ^{1}H-NMR spectral data of compounds **12**—**15**

Compd	(chemical shift/ppm)[a] Cp-ring protons		Methylene protons			
	Hα	Hβ	-OCH$_2$		-SCH$_2$	
12c	4.87(t, *J*=1.8Hz, 4H), (+0.22)	4.53(t, *J*=1.8Hz, 4H), (+0.28)	3.57(s, 8H), (+0.02)	3.91—3.57(m, 8H) (+0.03)		
12d	4.85(t, *J*=1.8Hz, 4H), (+0.19)	4.51(t, *J*=1.8Hz, 4H), (+0.26)	3.56(s, 8H), (+0.01)	3.90—3.55(m, 8H) (0.05—+0.01)		
13b	4.83(t, *J*=1.8Hz, 4H), (+0.15)	4.43(t, *J*=1.8Hz, 4H), (+0.15)	3.88(t, *J*=6.2Hz, 4H), (+0.01)		2.82(s, 8H), (0.00)	2.81(t, *J*=6.2Hz, 4H) (−0.01)
13c	4.87(t, *J*=1.8Hz, 4H), (+0.19)	4.54(t, *J*=1.8Hz, 4H), (+0.26)	3.85(t, *J*=6.2Hz, 4H), (+0.04)		2.82(s, 8H), (0.00)	2.81(t, *J*=6.2Hz, 4H) (+0.02)
14d	6.06(t, *J*=2.5Hz, 4H), (+1.43)	5.72(t, *J*=2.5Hz, 4H), (+1.47)	4.55(t, *J*=4.0Hz, 4H), (+0.85)	3.80(t, *J*=4.0Hz, 4H), (−0.08)	3.50(s, 4H), (−0.08)	3.55—3.45(m, 8H) (+0.01—−0.08)
15b	4.75(t, *J*=1.8Hz, 4H), (+0.07)	4.28(t, *J*=1.8Hz, 4H), (+0.00)	3.88(t, *J*=6.2Hz, 4H), (+0.01)		2.96(s, 4H), (+0.14)	2.96(t, *J*=6.2Hz, 4H) (+0.14)
15c	4.75(t, *J*=1.8Hz, 4H), (+0.07)	4.43(t, *J*=1.8Hz, 4H), (+0.02)	3.89(t, *J*=6.2Hz, 4H), (+0.07)		3.02(s, 8H), (+0.22)	3.06(t, *J*=6.2Hz, 4H) (+0.25)

a) Compound **14** was measured in CD_3CN. Compounds **12**, **13**, and **15** were measured in DMSO-d_6. A downfield shift is denoted as a positive value. Shift changes are presented in parentheses.

ethers and mercury(II) chloride. The maximum absorption of **13**, containing sulfur atoms, was in a longer wavelength range than that of **12** containing no sulfur atom. This result may be explained by a difference in the coordination ability between the sulfur and oxygen atoms toward the mercury(II) ion.[11] That is, the sulfur atoms of **11** are so strongly coordinated to the mercury(II) ion that the interaction between Ru and Hg(II) is weakend.

On comparison of the IR spectra of mercury(II) complexes with their free ligands, slight differences were observed at the C–H and C–C streching bands and Cp–Ru–Cp ring tilting band of the ruthenocene nucleus. Morrison *et al.*[6] reported that the antisymmetric C–C streching band at 1400 cm^{-1} region of the mercury(II) adduct of ruthenocene was split into two absorption bands because of ring tilting derived from the $HgCl_2$ interaction. However, the absorption band at 1400 cm^{-1} of the mercury(II) complexes (**12** and **13**) did not show the spliting in the IR spectra. Therefore, the bridging between the two Cp rings by the crown moiety of the ruthenocenophanes may be inhibit the tilting of the Cp rings. As the ^{1}H-NMR spectral changes showed the β-protons of the ruthenocene nucleus of all mercury complexes (**12** and **13**) were more shifted downfield than the α-protons, whereas the ethylene protons were only little downfield shifted by 0.01—0.05 ppm. From their spectral data of the mercury complexes (as shown in Table 4), two types of complexing form are anticipated as follows: (i) the mercury ion incorporated into the crown cavity has an interaction with the ruthenium atom of the ruthenocene nucleus. (ii) the mercury(II) ion is coordinated to the ruthenium atom from the opposite site of the macrocyclic ring. On the other hand, **14d** showed characteristic spectral data in contrast to other silver complexes. For example, in the electronic spectra of **14d**, new and very intense absorption appeared at 299 (ε 7700), 357 (sh), and 459 nm (310), whereas **15** showed merely a little increase of ε (+60—+70) and a slight shifting of the d-d transition band of the ruthenocene nucleus. As early as 1952, Wilkinson reported[13] that the electronic spectra of the ruthenicinium cation which was prepared from ruthenocene and perchloric acid employing controlled potential anodes showed characteristic bands at 320 (ε *ca.* 10000), 400(sh), and 450 nm (sh). This tendency was very similar to that of **14d**. In the complex **14d** the silver(I) cation is incorporated into the cavity of macrocyclic polyether and coordinated weakly toward the six oxygen atoms although the complexed silver(I) cation in the complex **15** is coordinated more strongly toward the sulfur atoms. Therefore, the distance between the silver(I) cation and the ruthenium atom in the complex **14d** is shorter than that in the complex **15**. So, it is suggested that the electron transfer from the ruthenium atom to the complexed silver(I) ion in **14d** leads to the change of the ruthenocene nucleus to the ruthenicinium cation form. A similar phenomenon was also observed in the mercury complex **13b** and **13c**. Some remarkable differences were also observed in the IR spectrum of **14d**. Apparently, the C–H stretching band at the 3080 cm^{-1} region shifted to low frequency by about 50 cm^{-1} and the Cp–Ru–Cp ring tilting band at 430 cm^{-1} was split into three bands at 450, 460, and 470 cm^{-1}. Complexes **15b** and **15a** showed no characteristic change in the IR spectrum as **14d** did. Furtheremore, the ^{1}H-NMR spectrum of **14d** changed dramatically as shown in Fig. 2. The α- and β-protons of the Cp rings were shifted downfield by 1.43 and 1.47 ppm, respectively. The methylene protons near the ruthenocene nucleus were more shifted downfield (0.85—0.10 ppm) than other methylene protons. However, in **15c** carrying sulfur atoms as donor atoms, only the methylene protons attached to sulfur atoms were shifted (+0.22 ppm), and the Cp ring protons and the methylene protons attached to oxygen atoms were shifted slightly. This result suggests that the silver(I) ion of **14d** is coordinated with the crown site near the ruthenocene nucleus and then interacts with the ruthenium atom, while **15b** and **15c** has no interaction between ruthenium atom of ruthenocene and the incapsulated silver(I) ion.

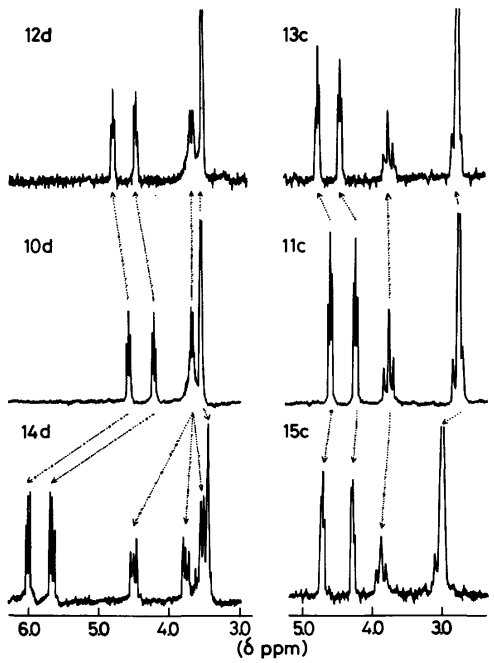

Fig. 2. ^{1}H-NMR Spectra of **10d**, **11c**, **12d**, **13c**, **14d**, and **15c**.

Experimental

The melting points are uncorrected. The mass spectra were taken on a Hitachi M 80 mass spectrometer. The ^{1}H-NMR (90 MHz) and the ^{13}C-NMR (22.5 MHz) were obtained on a JEOL-FX-90Q spectrometer, with TMS as an internal standard. The electronic spectra were obtained on a Hitachi Model 330 spectrometer. The IR spectra were measured on a JASCO DS-701G Diffraction Grating Infrared Spectrometer.

Materials. The silica-gel used for thin-layer chromatography was Wako gel B-5F. Ruthenocene,[13] 1,5-dibromo-3-oxapentane (**9a**),[14] and 1,8-dibromo-3,6-dioxaoctane (**9b**)[15] were prepared according to the procedure described in the literature. Compounds **9c** and **9d** were prepared by the same manner as described for **9a**.

1,1'-Dibromoruthenocene (5). To a solution of butyllithium in hexane (100 cm^3, 144 mmol) and TMEDA (30 cm^3, 199 mmol) in hexane (15 cm^3) was added ruthenocene in hexane (300 cm^3) under nitrogen. After mixture had been stirred for 5 h at room temperature, 1,2-dibromo-1,1,2,2-tetrafluoroethane (26.8 cm^3, 103 mmol) was added dropwise for 1 h at −60 °C. The stirring was continued overnight at −60 °C. After the solution had been warmed to room temperature, water (15 cm^3) was added to the reaction mixture. The aqueous solution was extracted with three 300 cm^3 portions of hexane. The hexane extracts were combined, washed with water, and concentrated *in vacuo*. The yellow solid was sublimed at 130 °C/0.3 mmHg. The pure product was obtained as pale yellow needles by recrystallization from hexane in 53% yield. Mp 117—118 °C, ^{1}H-NMR ($CDCl_3$) δ= 4.51 (t, J=1.8 Hz, 4H), 4.86 (t, J=1.8 Hz, 4H). Found: C, 30.87; H, 2.22%. Calcd for $C_{10}H_8Br_2Ru$: C, 30.87; H, 2.08%. MS (60 eV): m/z 389 (M^+).

1,1'-Diacetoxyruthenocene (6). Compound **5** (16.7 g, 83 mmol) and copper(II) acetate (92 g, 460 mmol) in 50% aqueous ethanol (600 cm^3) were refluxed for 1.5 h under nitrogen. After the mixture had been cooled to room temperature, the resulting solid was removed by filtration. The solid was washed with ether (20 cm^3) three times. The ethereal layer combined was dried over anhydrous magnesium sulfate and the ether was removed *in vacuo*. The residue was chromatographed on silica-gel (benzene–ethyl acetate as eluent). The pure product was obtained as pale yellow needles by recrystallization from hexane in 53% yield. Mp 74.5—75 °C. ^{1}H-NMR ($CDCl_3$) δ=4.94 (t, J=1.8 Hz, 4H), 4.42 (t, J=1.8 Hz, 4H), 2.12 (s, 6H). Found: C, 48.69; H, 4.07%. Calcd for $C_{14}H_{14}O_4Ru$: C, 48.41; H, 4.06%. MS (60 eV): m/z 348 (M^+).

Polyoxa[n](1,1')ruthenocenophanes (10a—d). As a typical example, preparation of 1,4,7,10,13-pentaoxa[13](1,1')ruthenocenophane (**10c**) is described here. After a mixture of **6** (452 mg, 1.30 mmol) and potassium hydroxide (423 mg, 7.55 mmol) in water (15 cm^3) was stirred for 30 min under nitrogen, 1,11-dibromo-3,6,9-trioxaundecane (**9c**) (510 mg, 1.59 mmol) in 60% aqueous ethanol (60 cm^3) was added to the mixture at once. The stirring was continued for 5 h. The reaction mixture was cooled and extracted with three 30 cm^3 portions of ether. The ethereal extract was washed with water (30 cm^3), and was evaporated. The resulting solid was chromatographed on silca-gel TLC (hexane–acetone as eluent). The main fraction was extracted with acetone and the solution was evaporated *in vacuo*. Recrystallization of the resulting solid from hexane (10 cm^3) gave **10c** as pale yellow crystals in 44% yield. Mp 94.5—95 °C. Found: C, 51.42; H, 5.54%. Calcd for $C_{18}H_{24}O_5Ru$: C, 51.29; H, 5.75%. MS (60 eV): m/z 422 (M^+).

1,4,7-Trioxa[7](1,1')ruthenocenophane (10a). Mp 97.5—98 °C. Found: C, 50.26; H, 4.80%. Calcd for $C_{14}H_{16}O_3Ru$: C, 50.44; H, 4.85%. MS (60 eV): m/z 334 (M^+).

1,4,7,10-Tetraoxa[10](1,1')ruthenocenophane (10b). Mp 70—70.5 °C. Found: C, 50.71; H, 5.40%. Calcd for $C_{16}H_{20}O_4Ru$: C, 50.89; H, 5.35%. MS (60 eV): m/z 378 (M^+).

1,4,7,10,13,16-Hexaoxa[16](1,1')ruthenocenophane (10d). Mp 29—30 °C. Found: C, 51.37; H, 5.80%. Calcd for $C_{20}H_{28}O_6Ru$: C, 51.59; H, 6.07%. MS (60 eV): m/z 465 (M^+).

1,1'-Bis(2-chloroethoxy)(1,1')ruthenocene (7). After **6** (2.164 g, 6.21 mmol) had been reacted with sodium hydroxide (1.558 g, 38.9 mmol) in water (10 cm^3) for 30 min in the presence of 18-crown-6 (438 mg, 1.83 mmol) under nitrogen, 1-bromo-2-chloroethane (28.4 g, 198 mmol) was added to the mixture at once. The stirring was continued for 5 h at a reflux temperature. The reaction mixture was cooled, and extracted with three 300 cm^3 portions of ether. The extracts were combined, washed with water, and concentrated *in vacuo*. The residual solid was chromatographed on silica gel (benzene as eluent). The first fraction was extracted with acetone and the solution was evaporated *in vacuo*. Recrystallization of the residue from hexane gave **8** as white needles in 1% yield, mp 120—121.0 °C. ^{1}H-NMR ($CDCl_3$) δ=4.84 (t, J=1.8 Hz, 4H), 4.31 (t, J=1.8 Hz, 4H), 4.00 (s, 4H). MS (60 eV): m/z 289 (M^+). Found: C, 49.53; H, 4.14%. Calcd for $C_{12}H_{12}O_2Ru$: C, 49.81; H, 4.18%. The second fraction was extracted with acetone and the product was recrystallized from hexane to gave **7** as a white amorphous solid in 40% yield, mp 78.5—79.0 °C. MS (60 eV): m/z 388 (M^+). Found: C, 43.16; H, 4.14%. Calcd for $C_{14}H_{16}O_2Cl_2Ru$: C, 43.30%; H, 4.16%.

1,7-Dioxa-4-thia[7](1,1')ruthenocenophane (11a). To sodium sulfide nonahydrate (328 mg, 1.37 mmol) in reflux-

ing DMF (30 cm³) was added **7** (251 mg, 0.65 mmol) in DMF (30 cm³). After the mixture had been cooled to room temperature, water (60 cm³) was added and the resulting mixture was extracted with three 30 cm³ portions of chloroform. The extracts were combined and concentrated *in vacuo*. The residue was chromatographed on silica-gel TLC (benzene as eluent). The main fraction was extracted with acetone and the solvent was removed. Recrystallization of the crude product from hexane gave **11a** as white needles in 17% yield, mp 117—117.5 °C. Found: C, 48.14; H, 4.68%. Calcd for $C_{14}H_{16}O_2SRu$: C, 48.12; H, 4.62%. MS (60 eV): *m/z* 350 (M^+).

1,10-Dioxa-4,7-dithia[10](1,1')ruthenocenophane (11b). A solution of **7** (282 mg, 0.73 mmol) in THF (50 cm³) and a mixture of 1,2-ethanedithiol (300 mg, 3.19 mmol) and sodium hydroxide (230 mg, 5.95 mmol) in ethanol (50 cm³) were added dropwise to ethanolic THF (ethanol:THF=1:1) (240 cm³) over a 2.5 h under reflux. The refluxing was continued for 14 h with stirring and then the reaction mixture was cooled and concentrated *in vacuo*. The residual oil was separated by alumina column chromatography (benzene as eluent) and then TLC (silica gel, benzene as eluent). The first fraction in TLC was extracted with acetone and recrystallized from hexane to give **11b** as white needles in 25% yield, mp 116.5—117.0 °C. MS (60 eV): *m/z* 409 (M^+). Found: C, 46.94; H, 4.86%. Calcd for $C_{16}H_{20}O_2S_2Ru$: C, 46.92; H, 4.93%. The second fraction in TLC was extracted with acetone and recrystallized from hexane to give **11c** as white needles in 5% yield, mp 113—113.5 °C. MS (60 eV): *m/z* 469 (M^+). Found: C, 46.03; H, 5.05%. Calcd for $C_{18}H_{24}O_2S_3Ru$: C, 46.03; H, 5.15%.

1,13-Dioxa-4,7,10-trithia[13](1,1')ruthenocenophane (11c). A solution of **7** (314 mg, 0.91 mmol) in THF (50 cm³) and a solution of bis(2-mercaptoethyl) sulfide (640 mg, 4.16 mmol) and sodium hydroxide (330 mg, 8.25 mmol) in ethanol (50 cm³) were added dropwise to refluxing ethanolic THF (ethanol:THF=1:1) (300 cm³) at the same rate for 2.5 h. The stirring was continued for 14 h at a refluxing temperature. The reaction mixture was cooled and concentrated *in vacuo*. The residual oil was chromatographed on alumina column (benzene as eluent). The main fraction was combined and concentrated. Recrystallization of the crude product from hexane gave **11c** as white needles in 63% yield. The pure **11c** obtained by this reaction was identified by comparison with the melting point, R_f value of TLC and the special data of the authentic sample.

Method of Solvent Extraction. Extraction ability of ruthenoceno-crown ethers toward alkali, alkaline earth, and some non-transition and transition metal ions was examined by the extraction method described in the previous paper.[5f] All metals used were metal nitrates, except for mercury(II) chloride.

Mercury(II) Chloride Complexes (12 and 13). A solution of ruthenoceno-crown ether (**10** or **11**, 0.06 mmol) in ether (5 cm³) was added to a solution (15 cm³) containing mercury(II) chloride (0.06 mmol) in ether (15 cm³). As the ethereal solution was concentrated to 10 cm³ *in vacuo*, a yellow solid was precipitated. Recrystallization of the solid from acetonitrile (2 cm³) gave pure mercury complexes in 80—90% yiled as yellow needles.

12a: Mp 210 °C (decomp). Found: C, 27.77; H, 2.65%. Calcd for $C_{14}H_{16}O_3Ru\ HgCl_2$: C, 27.80; H, 2.67%.

12b: Mp 200 °C (decomp). Found: C, 29.59; H, 3.08%. Calcd for $C_{16}H_{20}O_4Ru\ HgCl_2$: C, 29.61; H, 3.11%.

12c: Mp 160 °C. Found: C, 31.23; H, 3.44%. Calcd for $C_{18}H_{24}O_5Ru\ HgCl_2$: C, 31.20; H, 3.40%.

12d: Mp 150 °C (decomp). Found: C, 32.29; H, 3.67%. Calcd for $C_{20}H_{28}O_6Ru\ HgCl_2$: C, 32.58; H, 3.84%.

13b: Mp 184—185.5 °C. Found: C, 28.11; H, 2.91%. Calcd for $C_{16}H_{20}O_2S_2Ru\ HgCl_2$: C, 28.22; H, 2.97%.

13c: Mp 166—167 °C. Found: C, 28.97; H, 3.27%. Calcd for $C_{18}H_{24}O_2S_3Ru\ HgCl_2$: C, 29.17; H, 3.27%.

Silver(I) Nitrate Complex (14d). A solution of **10d** (129 mg, 0.28 mmol) in acetonitrile (2 cm³) was added to a solution of silver(I) nitrate (55 mg, 0.32 mmol) in acetonitrile (2 cm³) at one time. After 1.5 h, the resulting precipitate was filtered and then a small amount of ether was added dropwise to the filtrate to give orange crystals in 19% yield. Mp 113—115 °C. Found: C, 40.54; H, 4.64; N, 6.71%. Calcd for $C_{25.5}H_{35.5}N_{3.5}RuAg$: C, 40.67; H, 4.86; N, 6.64%.

Silver(I) Nitrate Complexes (15). A solution of ruthenoceno-crown ether (0.06 mmol) in acetonitrile (2 cm³) was added to silver(I) nitrate (0.06 mmol) in acetonitrile (2 cm³). The resulting crystals were collected by filtration and washed with small portions of acetonitrile to give **15** in 76% yield as white needles.

15b: Mp 170 °C (decomp). Found: C, 33.02; H, 3.48; N, 2.50%. Calcd for $C_{16}H_{20}NO_5S_2RuAg$: C, 33.16; H, 3.49; N, 2.42%.

15c: Mp 167—169 °C (decomp). Found: C, 33.64 ; H, 3.66; N, 2.13%. Calcd for $C_{18}H_{24}NO_5S_3RuAg$: C, 33.80; H, 3.79; N, 2.19%.

We wish to thank the Nukada Scholarship of Toho University for financial support.

References

1) a) G. Oepen and F. Vogtle, *Liebigs Ann. Chem.*, **1979**, 1094; b) J. F. Biernat and T. Wilczewski, *Tetrahedron*, **36**, 2521 (1980); c) A. Ratajczk and B. Czeh, *Polish J. Chem.*, **54**, 57 (1980); d) B. Czech and A. Ratajczk, *ibid.*, **54**, 767 (1980).

2) a) M. Sato, M. Kubo, S. Ebine, and S. Akabori, *Tetrahedron Lett.*, **1982**, 185; b) M. Sato, H. Watanabe, S. Ebine, and S. Akabori, *Chem. Lett.*, **1982**, 1753; c) M. Sato, M. Kubo, S. Ebine, and S. Akabori, *Bull. Chem. Soc. Jpn.*, **57**, 421 (1984); d) M. Sato, S. Tanaka, S. Ebine, K. Morinaga, and S. Akabori, *Bull. Chem. Soc. Jpn.*, **57**, 1929 (1984).

3) B. Czech, A. Czech, S. I. Kang, and R. A. Bartish, *Chem. Lett.*, **1984**, 37.

4) T. Izumi, T. Tezuka, S. Yusa, and A. Kasahara, *Bull. Chem. Soc. Jpn.*, **57**, 2435 (1984).

5) a) S. Akabori, H. Fukuda, Y. Habata, M. Sato, and S. Ebine, *Chem. Lett.*, **1982**, 1393; b) S. Akabori, Y. Habata, Y. Sakamoto, M. Sato, and S. Ebine, *Bull. Chem. Soc. Jpn.*, **56**, 537 (1983); c) S. Akabori, Y. Habata, and M. Sato, *ibid.*, **58**, 783 (1985); d) S. Akabori, Y. Habata, and M. Sato, *ibid.*, **57**, 68 (1984); e) S. Akabori, Y. Habata, M. Sato, and S. Ebine, *ibid.*, **56**, 1459 (1983); f) S. Akabori, S. Shibahara, Y. Habata, and M. Sato, *ibid.*, **57**, 63 (1984).

6) W. H. Morrison, Jr. and D. N. Hendrickson, *Inorg. Chem.*, **11**, 2921 (1972).

7) T. Kuwan, D. E. Bublitz, and G. Hoh, *J. Am. Chem. Soc.*, **82**, 5811 (1960).

8) A preliminary report: S. Akabori, Y. Habata, and M. Sato, *Chem. Lett.*, **1985**, 1063.

9) R. N. Green, *Tetrahedron Lett.*, **1972**, 1973.

10) L. Pauling, "The Nature of the Chemical Bond," Cornell University Press, Itaka, New York (1960), Chap. 13.
11) T. -L. Ho, "Hard and Soft Acids and Bases Principle in Organic Chemistry," Academic Press, New York and London (1977), p. 167.
12) L. I. Denisovich, N. Zakurin, A. A. Bezrukova, and S. P. Gubin, *J. Organomet. Chem.*, **81**, 207 (1974).
13) G. Wilkinson, *J. Am. Chem. Soc.*, **74**, 6146 (1952).
14) P. Pertici, G. Vitulli, M. Paci, and L. Porri, *J. Chem., Soc., Dalton Trans.*, **1980**, 1961.
15) Von A. Luttringhaus, F. Cramer, H. Prinzbach, and F. M. Henglein, *Liebigs Ann. Chem.*, **1958**, 185.

exo-Selective Peripheral Cycloaddition Reactions of Pyrido[2,1-*a*]isoindole

Shoji KAJIGAESHI,* Seiji MORI, Shizuo FUJISAKI, and Shuji KANEMASA†,*
Department of Industrial Chemistry, Faculty of Engineering, Yamaguchi University, Tokiwadai, Ube 755
†*Research Institute of Industrial Science, Kyushu University, Kasugakoen, Kasuga 816*
(Received August 2, 1985)

Pyrido[2,1-*a*]isoindole cycloadds to olefinic dipolarophiles in a highly *exo*-selective fashion giving the kinetically controlled cycloadducts which gradually isomerize into the Michael adducts. With acetylenic dipolarophiles, the hydrogen-migrated cycloadducts are the only products. The mechanism of cycloadditions is discussed.

Some time ago the first example of stereochemical study on the peripheral cycloaddition reactions of indolizines to olefins was reported.[1] These cycloadditions are stereospecific and highly *exo*-selective. Nevertheless the stepwise mechanism through zwitterionic intermediates was proposed since Michael type adducts were formed in some cases.

Thereafter a great number of cycloadditions of a variety of heteroaromatic *N*-ylides[2] and peripheral azomethine ylides[3–5] have been investigated, and these ylides were found to react with olefinic dipolarophiles in an exclusively *endo*-selective fashion. The high selectivity might be due to the positive interaction between the heteroaromatic plane and the unsaturated substituents of dipolarophiles.

We came to wonder why the indolizine cycloaddition showed such an exceptional *exo*-selectivety. Is it due to the stepwise reaction pathway?. If so, how? More informations on the stereoselectivity of the analogous cycloadditions are needed.

In the present paper, the cycloadditions of pyrido[2,1-*a*]isoindole with olefinic dipolarophiles were investigated and it was found that these reactions proceeded not *via* the zwitterionic intermediates but through synchronous cyclization pathway. The *exo*-selection might be a result from the $8\pi+2\pi$ concerted cycloaddition.

Results and Discussion

Pyrido[2,1-*a*]isoindole **4** is a known compound which was synthesized by the photoreaction between 2-bromopyridine and benzyl bromide.[6] Our approach to **4** starts with the reduction of ethyl 2-(2-pyridyl) benzoate **1** into 2-(2-pyridyl)benzyl alcohol **2** with lithium aluminum hydride, bromination of **2** into 6*H*-pyrido[2,1-*a*]isoindolium bromide **3** with hydrobromic acid, and the final step of dehydrobromination of **3** with aqueous sodium carbonate (Scheme 1).

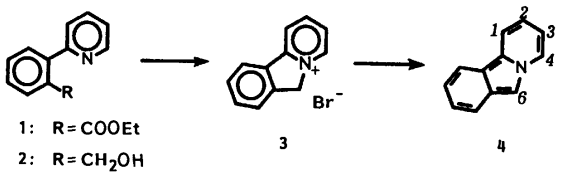

Scheme 1.

An advantage of this preparation is that the starting ester **1** is readily available in large quantities through the reaction of pyridine with 2-lithiotoluene and the subsequent several steps can be all performed in large scales. Furthermore, the salt **3** as the precursor of air-sensitive **4** can be safely stored without any serious decomposition.

Rapid cycloadditions were found to occur when **4** was allowed to react with electron-deficient olefins at 0 °C, but the cycloadducts formed were too labile to be isolated. They gradually changed into the corresponding Michael adducts. Accordingly, the structural analyses of the cycloadducts were based only on the ^{1}H-NMR spectra.

Equivalent amounts of **4** and dimethyl maleate **5**

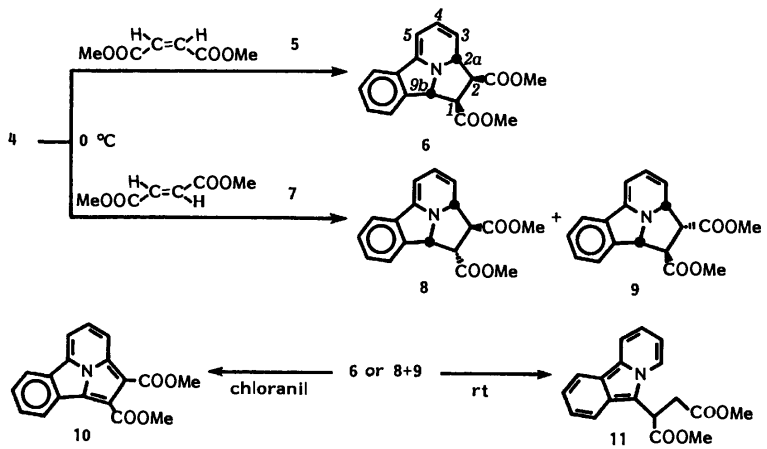

Scheme 2.

TABLE 1. ^{1}H-NMR SPECTRA OF THE OLEFIN CYCLOADDUCTS **6**, **8**, **9**, **14**, **15**

	Chemical shifts in δ and coupling constants in Hz																			
	9b-H		1-H		2-H		2a-H		3-H		4-H		5-H							
6	5.06^d	5.3	2.57^{dd}	10.5	3.12^{dd}	10.0	4.57^{dd}	5.5	5.85^{dd}	9.6	6.25^{dd}	5.8	5.58^d						3.70^s (2-COOMe), 3.80^s (1-COOMe)	
8	5.23^d	10.0	b)		b)		4.20^{dd}	5.6	5.85^{dd}	9.6	6.36^{dd}	6.0	5.70^d						3.35^s (1-COOMe), 3.72^s (2-COOMe)	
9	4.92^d	7.0	2.90^{dd}	5.6	b)		4.89^{dd}	5.5	5.65^{dd}	10.0	6.34^{dd}	6.0	5.49^d						3.57^s (2-COOMe), 3.79^s (1-COOMe)	
14	4.79^{dd}	5.0	1.52^{ddd}	10.0	2.63^q	10.0	4.14^{dd}	5.2	5.66^{dd}	9.2	6.16^{dd}	6.0	5.45^d							
		10.0	2.10^{dt}	10.0																
			13.5 (gem)																	
15	4.86^{dd}	4.8	1.44^{ddd}	10.2	2.86^{ddd}	9.2	4.14^{dd}	5.2	5.63^{dd}	9.4	6.16^{dd}	5.8	5.48^d						3.66^s (2-COOMe)	
		9.5	2.49^{dt}	9.5																
			13.5 (gem)																	

a) All the spectra were taken in $CDCl_3$ at 0°C. b) Overlapping with other signals. c) No clear coupling was given.

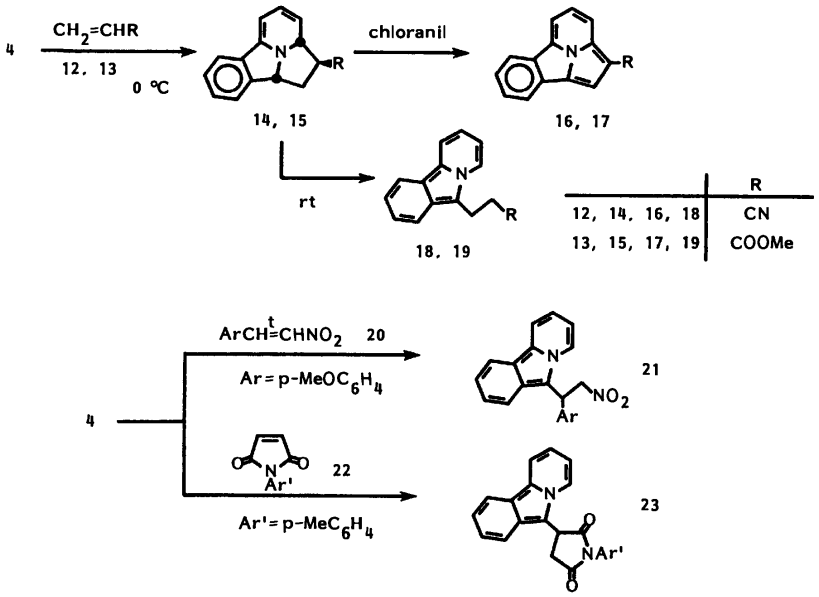

Scheme 3.

were dissolved in $CDCl_3$ at 0°C in an NMR sample tube and immediately subjected to the ^{1}H-NMR measurement. Only observed were the signals for the *exo*-selective and *cis*-specific cycloadduct **6**, indicating the quantitative formation of **6** (Scheme 2). On the other hand, the reaction of **4** with dimethyl fumarate **7** at 0°C formed the 7:3 mixture of two isomeric cycloadducts **8** and **9**. On standing at room temperature, these cycloadducts **6**, **8**, and **9** gradually isomerized into the same compound **11** which was isolated by the evaporation of the solvent and identified as the Michael adduct shown in Scheme 2.

The structural assignment of **6**, **8**, and **9** was based on the coupling constants among the methine hydrogens on the newly formed five-membered rings and the chemical shifts of ester methyls (Table 1). The stereochemistry of the starting olefins **5** and **7** must be retained in the cycloadducts and a molecular model inspection indicates that the only configuration for the points of fusion is cis (the methine hydrogens at the 2a- and 9b-positions are cis to each other). The 1—9b couplings of **6** and **9** are small to medium and the ester methyls at the 1-position of **8** and the 2-position of **9** are shielded. These informations are enough to determine the stereostructures of cycloadducts: **6**: 1-*exo*-2-*exo*-; **8**: 1-*endo*-2-*exo*-; **9**: 1-*exo*-2-*endo*-cycloadducts.

The cyclic structures of **6**, **8**, and **9** were confirmed by their dehydrogenation with chloranil at 0°C into dimethyl indolizino[3,4,5-*ab*]isoindole-1,2-dicarboxylate **10** which was no longer labile.

The regioselective and stereoselective cycloadducts **14** and **15** were formed also as unstable products in similar reactions of **4** with acrylonitrile **12** and methyl acrylate **13** (Scheme 3). They again isomerized into the

Table 2. Michael adducts **11**, **18**, **19**, **21**, **23** and indolizino[3,4,5-*ab*]isoindoles **10**, **16**, **17**

	Yield/%[a]	Mp(θ_m/°C)	IR/cm^{-1}	^{1}H-NMR in $CDCl_3$ (δ, ppm)	M$^+$(m/z)[b]
11	96[c] 93[d]	108—109	1730 (CO)	2.80 (1H, dd, J=17.5 and 6.0 Hz, one of CH_2), 3.60 (1H, dd, J=17.5 and 8.8 Hz, the other of CH_2), 3.58, 3.60 (each 3H, s, COOMe), 5.00 (1H, dd, J=6.0 and 8.8 Hz, CH)	311
18	82	136—137	2240 (CN)	2.61, 3.57 (each 2H, t, J=7.4 Hz, CH_2)	220
19	83	78—80	1735 (CO)	2.74, 3.62 (each 2H, t, J=7.6 Hz, CH_2), 3.66 (3H, s, COOMe)	253
21	83	140—143		3.58 (3H, s, *p*-OMe), 5.06 (1H, dd, J=16.0 and 8.0 Hz, one of CH_2), 5.18 (1H, dd, J=16.0 and 7.3 Hz, the other of CH_2), 5.50 (1H, dd, J=7.3 and 8.0 Hz, CH)	346
23	99	229—230	1770 (CO) 1710 (CO)	2.31 (3H, s, *p*-Me), 2.92 (1H, dd, J=19.0 and 5.4 Hz, one of CH_2), 3.24 1H, dd, J=19.0 and 9.5 Hz, the other of CH_2), 4.80 (1H, dd, J=5.4 and 9.5 Hz, CH)	
10	94[c] 92[d]	184—185	1730 (CO) 1700 (CO)	4.18, 4.30 (each 3H, s, COOMe)	307
16	74	162—163	2210 (CN)	7.60 (1H, s, 1-H)	216
17	60	119—120	1690 (CO)	4.12 (3H, s, COOMe), 8.20 (1H, s, 1-H)	249

a) Isolated yield. b) All as base peaks. c) From the maleate **5**. d) From the fumarate **7**.

Table 3. Hydrogen-migrated cycloadducts **27—29** to acetylenic dipolarophiles **24—26**

Acetylene	Conditions	Product Mp(θ_m/°C)	Yield %	Spectral data[a]
24	0.5 h at rt in C_6H_6	**27** (146—147)	71	IR (cm^{-1}): 1710 and 1700 (CO) ^{1}H-NMR: δ=2.31 (1H, dddd, J=16.5, 15.0, 3.0, and 2.0 Hz, one of 3-H), 2.88 (1H, dt, J=16.5, and 6.3 Hz, the other of 3-H), 3.84, 3.92 (each 3H, s, COOMe), 4.80 (1H, dd, J=15.0 and 6.3 Hz, 2a-H), 5.97 (1H, ddd, J=10.0, 6.3, and 2.0 Hz, 4-H), 6.88 (1H, dd, J=10.0 and 3.0 Hz, 5-H) MS (m/z): 309 (M$^+$)
25	3 h at 45°C in $CHCl_3$	**28** (129—130)	60	IR (cm^{-1}): 1690 (CO) ^{1}H-NMR: δ=2.25 (1H, ddt, J=16.5, 3.0, and 2.5 Hz, one of 3-H), 2.50 (3H, s, 1-Me), 2.75 (1H, dt, J=16.5 and 6.4 Hz the other of 3-H), 3.80 (3H, s, COOMe), 4.71 (1H, dd, J=16.5 and 6.4 Hz, 2a-H), 5.83 (1H, ddd, J=9.6, 6.4, and 2.5 Hz, 4-H), 6.97 (1H, dd, J=9.6 and 3.0 Hz, 5-H) MS (m/z): 265 (M$^+$)
26	1 h at rt in $CHCl_3$	**29** (83—85)	68	IR (cm^{-1}): 1700 (CO) ^{1}H-NMR: δ=2.30 (1H, dddd, J=17.2, 16.0, 3.2, and 2.5 Hz, one of 3-H), 2.80 (1H, dt, J=17.2 and 6.3 Hz, the other of 3-H), 3.84 (3H, s, COOMe), 4.79 (1H, dd, J=16.0 and 6.3 Hz, 2a-H), 5.90 (1H, ddd, J=9.8, 6.3, and 2.5 Hz, 4-H), 6.66 (1H, s, 1-H), 7.02 (1H, dd, J=9.8 and 3.2 Hz, 5-H) MS (m/z): 251 (M$^+$)

a) IR and ^{1}H-NMR spectra were measured as KBr disks and in $CDCl_3$, respectively.

Michael adducts **18** and **19** at room temperature and were dehydrogenated into the aromatized heterocycles **16** and **17** on treatment with chloranil at 0°C.

On the other hand, the reactions of **4** with (*E*)-1-(*p*-methoxyphenyl)-2-nitroethene **20** and *N*-(*p*-methylphenyl)maleimide **22** at 0°C provided no trace of the corresponding cycloadducts, only the Michael adducts **21** and **23** being observed in the reaction mixtures. By the evaporation of the reaction solvent, they were isolated as the sole products.

The spectral data of the Michael adducts **11**, **18**, **19**, **21**, and **23** as well as the indolizino[3,4,5-*ab*]isoindoles **10**, **16**, and **17** are summarized in Table 2. All the indolizino[3,4,5-*ab*]isoindoles show intense fluorescence in solution.

With acetylenic dipolarophiles such as dimethyl acetylenedicarboxylate **24**, methyl 2-butynoate **25**, and methyl propynoate **26** readily reacted **4** at room temperature giving the stable 1:1 adducts **27—29** all as yellow fluorescent materials (Scheme 4).

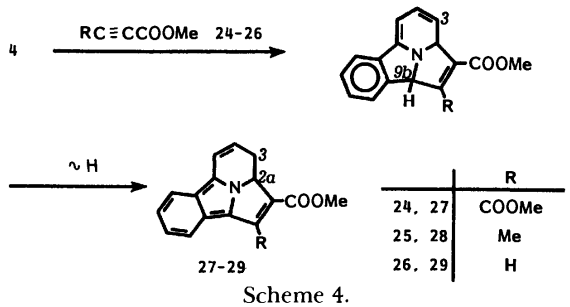

Scheme 4.

These regioselective products **27—29** were assigned as the hydrogen-migrated cycloadducts, from the 9b- to the 3-position, on the basis of the ^{1}H-NMR spectra shown in Table 3.

In the previous paper on the *exo*-selective cycloadditions of indolizines to olefinic dipolarophiles,[1] we proposed the stepwise mechanism *via* a zwitterionic intermediate **B**. This mechanism was based upon the formation of either the cycloadduct **D** or the Michael adduct **E** depending on the nature of dipolarophile and upon no interconversion between **D** and **E**. However, we would have to amend the reaction path because we now know that the Michael adduct **H** is the secondary product formed from the cycloadduct **G** (Scheme 5). The revised pathway is **A**→**C**→**D** or **A**→**C**→**E**.

In the cases of indolizines, two isomerization paths from **C**, the hydrogen migration from the 2a- to the 5-position leading to **D** and the bond cleavage into **B** (and hence **E**), presumably happened to compete. Once **D** and **E** are formed, there should be little chance of their interconversion. In the present cases, the similar hydrogen migration of **G** is suppressed by the influence of the additional fused benzo moiety, the cycloadduct **G** getting a chance of bond cleavage into **H**.

The acetylene cycloadduct **I** lies in a quite different situation. To accomplish the maximum extension of conjugation, the methine hydrogen at the 9b-position migrates long way to the 3-position giving **J** which was the isolated product. Since this migration may quickly occur, no Michael adduct **K** was obtained.

According to our study on the stereoselectivity of the cycloadditions of azomethine ylides involved as a part of heterocycles, all tested cases have shown the exclusive endo selectivity in the reactions with olefinic dipolarophiles[2-5] (Scheme 6); pyridinium, quinolinium, isoquinolinium, thiazolium, benzothiazolium methylides, anhydro-3*H*-pyrido[1,2,3-*de*]quinoxalinium hydroxide, thiazolo[4,3-*a*]isoindole, and imidazo[1,2-*c*]-thiazole.

Indolizine and pyrido[2,1-*a*]isoindole can be also regarded as the peripheral azomethine ylide 1,3-dipoles as illustrated with the charge-separated form **M** in Scheme 6. If the azomethine ylides participated in the $4\pi+2\pi$ cycloadditions, no satisfactory explanation for the high *exo*-selection would be available. We so far believe that the cycloadditions of indolizine and pyrido[2,1-*a*]isoindole to olefins belong to an $8\pi+2\pi$ synchronous cycloaddition.

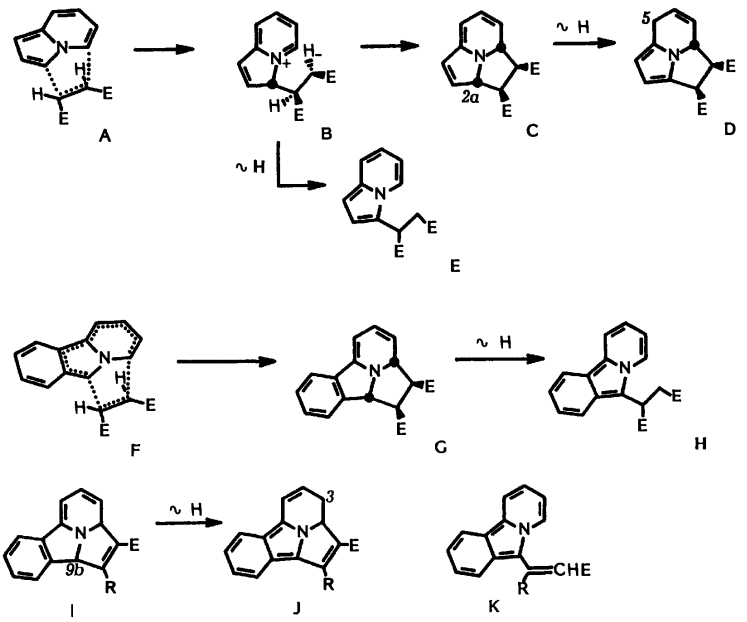

Scheme 5.

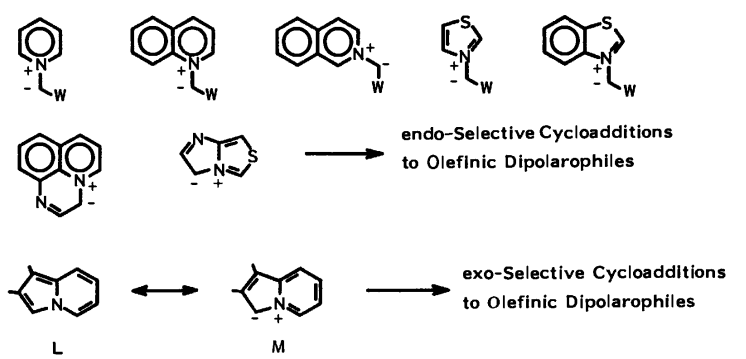

Scheme 6.

Experimental

Melting and boiling points are all uncorrected. Spectral characterization was carried out with the following instruments: IR: JASCO IRA-1 spectrometer; ^{1}H-NMR: JEOL JNM-MH 100 spectrometer using tetramethylsilane as an internal standard; MS: JEOL JMS-100 mass spectrometer using a direct insertion probe at 70 eV of ionization energy. Elementary analyses were obtained on Shimadzu CHN-1A micro analyzer. Melting points were taken in capillaries on Mitamura Riken melting point measurement apparatus. Solvents were evaporated *in vacuo* using a rotary evaporator.

2-(2-Pyridyl)benzyl Alcohol **2**. To a suspension of lithium aluminum hydride (2.66 g, 0.07 mol) in dry ether (250 ml), was added slowly ethyl 2-(2-pyridyl)benzoate **1**[7] (10.59 g, 0.047 mol) in ether (200 ml) in 10 min. The mixture was stirred at room temperature for 1 h and poured into ice water. The ether separated was dried over $MgSO_4$, evaporated *in vacuo*, and the residual oil was distilled under vacuum to give **2** (8.13 g, 94%) as colorless liquid: Bp 159—164 °C/266 Pa; IR (Nujol) 3280 cm^{-1} (OH); ^{1}H-NMR ($CDCl_3$) δ= 4.46 (2H, s, CH_2), 6.10 (1H, br. s, OH), 7.14—7.86, and 8.52 (8H, m, ArH); MS *m/z* 185(M^+, base peak). Found: C, 77.7; H, 6.1; N, 7.4%. Calcd for $C_{12}H_{11}NO$: C, 77.8; H, 6.0; N, 7.6%.

6H-Pyrido[2,1-a]isoindolium Bromide **3**. A mixture of **2** (0.65 g, 3.5 mmol) and concd hydrobromic acid (48% content, d=1.48, 0.4 ml, 3.5 mmol) was warmed at 90 °C for 1.5 h. All the voratile materials were removed by evaporation *in vacuo* and the residue was treated with methanol to give **3** (0.77 g, 89%) which was purified by crystallization from ethanol: Colorless plates; mp 203—205 °C (lit,[6] mp 207.5—209.5 °C); ^{1}H-NMR (CF_3COOH) δ=5.53 (2H, s, CH_2), 7.30—8.32, and 8.70 (8H, m, ArH).

Pyrido[2,1-a]isoindole **4**. To a saturated aqueous solution of **3**, was added saturated aqueous solution of sodium carbonate at room temperature to give yellow precipitate of **4** in a quntitative yield: Yellow needles from ethanol; mp 221—223 °C (lit,[6] 225 °C).

General Procedure for the Cycloadditions of 4 to Olefins. Freshly prepared **4** (84 mg, 0.5 mmol) was added to a solution of olefins (0.5 mmol) in 1 ml of $CDCl_3$ at 0 °C. This mixture was transferred into an NMR sample tube and subjected to the ^{1}H-NMR measurement at 0 °C. In about 5 min, all the starting materials disappeared and instead very clean spectrum of the cycloadduct was observed. All the operations of integration, expansion, and decoupling were carried out at 0 °C. The ^{1}H-NMR spectra of **6**, **8**, **9**, **14**, and **15** are listed in Table 1.

General Procedure for the Michael Adduct Formation. The Michael adduct was obtained according to either of the following two procedures: 1) The solution of cycloadduct prepared above was allowed to stand at room temperature for 1 d and the solvent was evaporated *in vacuo* to give the Michael adduct. 2) An equivalent mixture of **3** (0.75 g, 3.0 mmol) and olefin in methanol (5 ml) was treated with triethylamine (5 mmol). The mixture was stirred at room temperature for 1 h and the solvent was evaporated *in vacuo*. The residue was triturated with cold 2-propanol or chromatographed over silica gel with chloroform to give the Michael adduct. The spectral data as well as melting points are summarized in Table 2. Other data are given below:

11: Yellow needles from methanol, Found: C, 69.6; H, 5.5; N, 4.3%. Calcd for $C_{18}H_{17}NO_4$: C, 69.4; H, 5.5; N, 4.5%.

18: Yellow needles from methanol. Found: C, 81.7; H, 5.6; N, 12.4%. Calcd for $C_{15}H_{12}N_2$: C, 81.8; H, 5.5; N, 12.7%.

21: Yellow prisms from methanol. Found: C, 72.7; H, 5.1; N, 8.2%. Calcd for $C_{21}H_{18}N_2O_3$: C, 72.8; H, 5.2; N, 8.1%.

23: Pale yellow prisms from acetone-methanol. Found: C, 77.5; H, 5.1; N, 8.2%. Calcd for $C_{23}H_{18}N_2O_2$: C, 77.9; H, 5.1; N, 7.9%.

General Procedure for the Indolizino[3,4,5-ab]isoindole Formation. A mixture of freshly prepared **4** (0.17 g, 1.0 mmol) and 1.2 equiv of olefin in dichloromethane (5 ml) was stirred at 0 °C for 15 min and chloranil (0.5 g, 2.0 mmol) was introduced. The resulting mixture was stirred at 0 °C for 1 h. The precipitate was removed by filteration and washed with boiling chloroform (15 ml×2). The combined filtrates were evaporated *in vacuo* and the residue was chromatographed over silica gel using chloroform as the eluent. The intensely fluorescent fraction gave the indolizino[3,4,5-*ab*]isoindoles, whose spectral data and melting points are given in Table 2. Other data are as follows:

10: Yellow plates from acetone. Found: C, 70.6; H, 4.3; N, 4.5%. Calcd for $C_{18}H_{13}NO_4$: C, 70.4; H, 4.3; N, 4.6%.

16: Yellow needles from methanol. Found: C, 83.3; H, 3.9; N; 13.0%. Calcd for $C_{15}H_8N_2$: C, 83.3; H, 3.7; N, 13.0%.

17: Yellow needles from petr. ether. Found: C, 77.0; H, 4.3; N, 5.8%. Calcd for $C_{16}H_{11}NO_2$: C, 77.1; H, 4.4; N, 5.6%.

General Procedure for the Cycloadditions of 4 to Acetylenes. An equimolar mixture of freshly prepared **4** and acetylene was allowed to react under the conditions shown in Table 3. After the solvent was evaporated *in vacuo*, the residue was chromatographed over silica gel with chloroform. The data of the product are listed in Table 3. Other data are as follows:

27: Yellow prisms from acetone. Found: C, 70.2; H, 4.8; N, 4.2%. Calcd for $C_{18}H_{15}NO_4$: C, 69.9; H, 4.9; N, 4.5%.

28: Yellow needles from petr. ether. Found: C, 77.1; H, 5.7; N, 5.5%. Calcd for $C_{17}H_{15}NO_2$: C, 77.0; H, 5.7; N, 5.3%.

References

1) S. Ikeda, S. Kajigaeshi, and S. Kanemasa, *Chem. Lett.*, **1976**, 367.

2) O. Tsuge, S. Kanemasa, and S. Takenaka, *Bull. Chem. Soc. Jpn.*, **58**, 3137 and 3320 (1985).

3) S. Kanemasa, S. Kobira, and S. Kajigaeshi, *Chem. Lett.*, **1980**, 951.

4) S. Kanemasa, S. Ikeda, H. Shimoharada, and S. Kajigaeshi, *Chem. Lett.*, **1982**, 1533.

5) O. Tsuge, S. Kanemasa, and T. Hamamoto, *Chem. Lett.*, **1982**, 1491.

6) A. Fozard and C. K. Bradsher, *J. Org. Chem.*, **32**, 2966 (1967).

7) C. K. Bradsher and C. F. Voigt, *J. Org. Chem.*, **36**, 1603 (1971).

Extraction-spectrophotometric Study of the System Technetium-Chromotropic Acid-Long Chain Quaternary Ammonium Salt

Feliçiá Grases,* Juan Gabriel March, Félix Mata,† and Alberto Peñafiel†
Department of Analytical Chemistry, Faculty of Sciences, University of Palma de Mallorca, 07071-Palma de Mallorca, Spain
†*Nuclear Medicine Section, Residencia Sanitaria "Virgen de Lluch," Palma de Mallorca, Spain*
(Received July 30, 1984)

A simple and highly selective extraction-spectrophotometric determination of technetium is described. The ion-associate formed between the technetium-chromotropic acid (CA) anion and trioctylmethylammonium (TOMA) is extracted with toluene in acidic media. The absorption maximum of the extracted species occurs at 630 nm, the molar absorptivity being 3.1×10^3 dm^3 mol^{-1} cm^{-1}. The composition of the ion-associate is estimated to be $[Tc(CA)_2(TOMA)_3]$.

Radiochemical methods are the most widely used procedures so far for technetium determination. These methods, however, require extensive chemical separation and purification to remove interferences and this can be difficult and laborious. The recent increase in technetium production has aroused interest in the development of methods of analysis that could be used to supplement the radiochemical ones. Methods described so far for technetium determination by means of nonradiochemical processes are however very scarce.[1] On the other hand, the recent production of appreciable quantities of technetium has allowed initiation of the study of its chemical behavior,[2] that has been restricted for a long time due to available quantities of this element being very small. In this aspect it can be pointed out that, although some complexes of the element were isolated for its different states of oxidation and even in some cases its structure was determined, knowledge of the behavior of this element in solution is still unknown in many aspects.

The present paper is concerned with the spectrophotometric determination of traces of technetium by extracting its complex with chromotropic acid in the presence of Adogen 464. The absorbance of the organic phase is very stable and is thus suitable for routine work. This system seems worthwhile because of the simplicity and high selectivity of the procedure.

Experimental

Reagents and Apparatus. Stock solution of chromotropic acid (CA) (supplied by Panreac) included a 7.5 g dm^{-3} aqueous solution of the compound ($C_{10}H_8O_8S_2\cdot 2H_2O$). Trioctylmethylammonium chloride (TOMA), better known as Adogen 464 (supplied by Serva) included a 2.5 g dm^{-3} solution in toluene.

Technetium-99 in solution form, as ammonium pertechnetate, was obtained from Amersham/Searle Co., Arlington Heights, Ill. A technetium solution of 119 ppm was prepared by dilution of the primary standard with water.

A Perkin-Elmer 552 spectrophotometer with 1.0-cm cells was used.

Extraction Procedure. To a series of 100 cm^3 separatory funnels, add 5 cm^3 of chromotropic acid (7.5 g dm^{-3}), 2 cm^3 of 18% L-ascorbic acid, 2.5 cm^3 of concentrated HCl (11.8 mol dm^{-3}), and the volume of technetium solution necessary for the final concentration to be between 0.5—6 ppm, and dilute to 25 ml with water. Mix well, and warm in a steam bath for 10 min. Add 5 ml of Adogen 464 (2.5 g dm^{-3}) and shake on a mechanical shaking apparatus for 30 min. Allow to stand for adequate time to separate the layers and discard the aqueous layer. Measure the absorbance of the organic layer at 630 nm using toluene as a reference.

Results and Discussion

Absorption Spectra. Maximum absorption of the

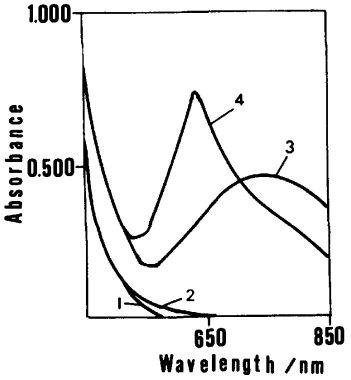

Fig. 1. Absorption spectra for Tc-CA complex. [CA]=4.4×10^{-3} mol dm^{-3}, [Ascorbic acid]=0.1 mol dm^{-3}, [Tc]=23.8 ppm, $[TOMA]_{org}=6\times10^{-3}$ mol dm^{-3}. 1: Reagent blank in aqueous solution, 2: Reagent blank in toluene phase, 3: Complex Tc-CA in aqueous solution, 4: Ion pair Tc-CA-TOMA in toluene phase. The extraction was carried out using 5 cm^3 of aqueous phase and 5 cm^3 of toluene phase.

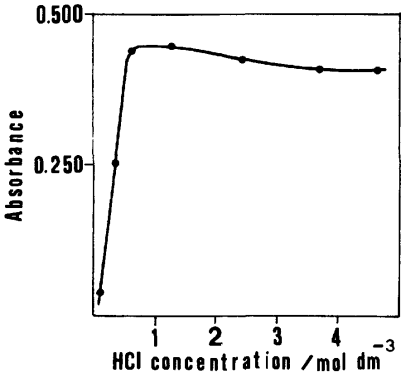

Fig. 2. Absorbance at 740 nm *versus* HCl concentration. [CA]=4.4×10^{-3} mol dm^{-3}, [Ascorbic acid]=0.1 mol dm^{-3}, [Tc]=23 ppm.

TABLE 1. CHARACTERISTICS OF THE PHOTOMETRIC METHODS FOR TECHNETIUM DETERMINATION

Reagent	λ_{max}/nm	ε/dm^3 mol^{-1} cm^{-1}	Main interferences	Ref.
1,5-Diphenylcarbazide	520	48600	Fe(III), Cr(VI), Ce(IV)	4
Thiocyanate	510	47500	U(VI), Fe(III), Mo(VI)	5
Mercaptoacetic acid	655	1800	Mo(VI), Cr(VI), Ru(VII), U(VI), Fe(III)	6
3,4-Toluenedithiol	450	15000	Mo(VI), Cr(VI), Ru(VII)	7
Thiocyanate	585	16500	Fe(III), Mo(VI)	8
Thiocyanate	510	50000	Fe(III), Mo(VI)	8

Tc-CA complex in aqueous media occurs at 740 nm ($\varepsilon=2.0\times10^3$ dm^3 mol^{-1}cm^{-1}), as can be seen in Fig. 1. The absorption spectrum (Fig. 1) of the extracted ternary system shows important changes of absorptivity and the maximum position ($\lambda_{max}=630$ nm, $\varepsilon=3.1\times10^3$ dm^3 mol^{-1}cm^{-1}) as a result of the ion-associate formation and extraction (the band shift involved is about 110 nm).

Effect of the Variables. The effect of pH on the formation of the Tc-CA complex was investigated. It was deduced from this study that complex formation is detected only when the assay takes place in acid medium as can be seen in Fig. 2. Maximal absorbance corresponds to hydrochloric acid interval concentrations of 0.6—1.4 mol dm^{-3}. At higher concentration, the absorbance decreases slightly, probably as a consequence of complex destruction. At lower hydrochloric acid concentrations, the absorbance decreases markedly. Formation of the Tc-CA complex only in strong acid medium can be explained admitting that the reduction process of Tc(VII) is more favored in this medium and not as a consequence of instability of complex species formed at lower hydrochloric acid concentrations. Thus, it has been proved that once having obtained the colored species in 1.2 mol dm^{-3} hydrochloric acid, they are not destroyed until pH=5 when basifying.

Ascorbic acid is used to reduce Tc(VII), the most stable species of the element in aqueous solution, to Tc(V), the probable oxidation state required for the CA color development. Other reductants produced either no color, or not as much color as ascorbic acid. Thus, tin(II) chloride seems. to be too strong and in the presence of a little excess of this reductant, absorbance decreases notably. The color does not develop in the absence of this special reductant because the CA is unable to act as a reductant by itself. The color appearance is not instantaneous and is favored by means of calefaction. It has been proved that for maximum color development, 10 min calefaction in a steam bath is necessary. A final concentration of 0.5% ascorbic acid is sufficient for maximum color development.

The effects of changing the CA and TOMA concentrations on the absorbance of the ternary complex were examined. The absorbance was found to increase rapidly on addition of CA up to a technetium:CA mole ratio of 1:12, when higher than this value it was practically independent of reagent concentration. For TOMA, this ratio was 1:8. It should be remembered that a very large excess of surfactant can retard the rate at which the phases separate and remain clear.[3] The stability of the ternary complex was studied. The absorbance of the extracted phase was stable at least for 24 h.

Nature of the Ion-associate. To determine the composition of the formed species, the Yoe-Jones method was used. Thus, stoichiometries of 1:2 (Tc:CA) and 1:2:3 (Tc:CA:TOMA) were found, suggesting that the extracted species is an ion-associate with formula $Tc(CA)_2(TOMA)_3$. This is in good agreement with the hypothesis that suggests the V oxidation state for technetium.

Characteristics of the Analytical Method. When the recommended procedure was used, Beer's law was followed in the range 0.5—6 μg Tc cm^{-3}. The molar absorptivity and precision of the method were established by carrying out ten parallel experiments. The molar absorptivity thus obtained is 3.1×10^3 dm^3 mol^{-1} cm^{-1}, which corresponds to a Sandell sensitivity of 31.9 ng Tc cm^{-2} for A=0.001. The relative standard deviation was 1.3% (95% confidence).

The selectivity of the method was tested by application of the recommended procedure in the presence of several foreign ions. A 100-fold amount of each of Ca, Sr, Ba, Mg, Ag, Ni, Co(II), Zn, Mn(II), Pb, Al, Cr(III), Fe(III), Mo(VI), W(VI), U(VI), Re(VII), V(V), NO_3^-, and SO_4^{2-} did not interfere. Only Cu(II) causes some serious interference. Thus, the presence of Cu(II) in large amounts prevents complex formation. Only 0.5 ppm of Cu(II) is tolerated. It is important to point out that U(VI), Re(VII), W(VI), and Mo(VI) which frequently accompany technetium and cause important disturbances in most of nonradiochemical procedures for technetium determination, do not cause any interference. This selectivity compares favorably with those obtained for other technetium complexes used spectrophotometrically (Table 1).

Finantial support by the CAICYT (Grand No. 2060-83) is gratefully acknowledged.

References

1) J. H. Kaye and N. E. Ballou, *Anal. Chem.*, **50**, 2076 (1978).

2) E. Deutsch and K. Libson, *Comments Inorg. Chem.*, **3**, 83 (1984).

3) D. Nonova and S. Pavlova, *Anal. Chim. Acta*, **123**, 289 (1981).

4) F. J. Miller and H. E. Zittel, *Anal. Chem.*, **35**, 299 (1963).
5) C. E. Crouthamel, *Anal. Chem.*, **29**, 1756 (1957).
6) F. J. Miller and P. F. Thomason, *Anal. Chem.*, **32**, 1429 (1960).
7) F. J. Miller and P. F. Thomason, *Anal. Chem.*, **33**, 404 (1961).
8) O. H. Howard and C. W. Weber, *Anal. Chem.*, **34**, 530 (1962).

Electrodeposition of Catalytically Active Cobalt Powder from Aqueous Sulfate Electrolytes

A. M. Abd El-Halim*,† and Reda Mohamed Khalil
Department of Chemistry, Faculty of Science, King Abdulaziz University, Jeddah, Saudi Arabia
(Received July 23, 1984)

The electrodeposition of cobalt powder was investigated from aqueous sulfate solutions containing 0.0125—0.0500 $CoSO_4 \cdot 7H_2O$ (I), 0.23—1.00 $(NH_4)_2SO_4$ (II), 0.1 H_3BO_3 and 0.07 mol dm^{-3} $Na_2SO_4 \cdot 10H_2O$. The effects of the bath composition, the pH, the deposition current density and the duration of electrolysis on the cathodic polarization and the efficiency of cobalt electrodeposition, as well as on the morphology and the catalytic activity (towards the decomposition of 0.4% H_2O_2 solution) of the as-deposited cobalt powders were discussed. X-Ray diffraction studies proved that cobalt powders were very pure and deposited in the hexagonal close-packed structure with the orientations (100), (002), and (101). Cobalt powder deposited with an efficiency of 32% and had a catalytic activity approaching 100% could be obtained from the above-mentioned bath formula containing 0.05 mol dm^{-3} (I) and 0.46 mol dm^{-3}(II). The optimum operation conditions to achieve these characteristics were: pH 4.78, $j=10\,A\,dm^{-2}$ and $t=15$ min.

Little use has been made of pure cobalt deposits and this seems to be due to commercial and technical reasons.[1] However, cobalt powder is important in metalloceramics industry[2] and in manufacture of alloys characterized by a desired protective, decorative, and magnetic properties.[3,4]

The electrochemistry of cobalt is not well established, the number of contributions on the subject is low, and the data on this process is incomplete.[2] However, the electrodeposition of cobalt powder was investigated from sulfate[5] and tetrafluoroborate[6] aqueous solutions. On the other hand, the deposition of cobalt powder is favored by nonaqueous media and has been investigated in a two-layer bath.[7] The electrolyte was an aqueous solution of $CoCl_2 \cdot 6H_2O$ and the organic medium was 0.5% solution of oleic acid in toluene. The process was further developed to yield cobalt powder proper for use in the production of magnets.[8]

The present study was undertaken to investigate the electrodeposition of cobalt powder in dilute aqueous sulfate solutions. The process may be suitable for recovery of Co^{2+} ions from industrial effluents in form of fine grained powder of beneficial use as a catalyst.

Experimental

The baths used for electrodeposition of cobalt were prepared in distilled water using AnalaR grade chemicals (BDH). The symbol, composition, pH, and specific conductance of each of these baths are given in Table 1. The experimental arrangement for electrodeposition consisted of a Perspex cell with a copper cathode positioned midway between two plane parallel platinum anodes; all electrodes were of the same geometrical area. The anodes were surrounded by asbestose diaphragms to preclude oxidation of Co^{2+} ions and errors in the measured potentials caused by the oxygen evolved at the anodes.

The cathodic polarization curves were measured relative to the saturated calomel electrode (SCE) by means of a Wenking potentioscan model POS 73 and recorded automatically with a Philips x-y recorder model PM 8132. The cathodic efficiencies (f%) were determined by the use of a standard copper coulometer. The morphology of the as-formed cobalt powders was examined with a scanning electron microscope (JEOL model JSM 35). X-Ray diffraction studies were carried out by a Philips X-ray diffractometer PW 1390 with a nickel filter and copper radiation. The percentage decomposition (D%) of 0.4% H_2O_2 solution (at 40 °C) on the surface of the electrodeposited powders was considered as a measure for their catalytic activity. Therefore, a definite volume (50 ml) of the H_2O_2 solution was passed (single-pass) over a fixed bed (0.15 g) of the test powder with a constant flow-through rate (150 ml h^{-1}) by the aid of a MICROPERPEX peristaltic pump (LKB Bromma model 2132). D% was calculated by measuring the exact concentrations of H_2O_2 spectrophotometrically before and after its passage over the powder.

The electrodeposition experiments were carried out (in a selected bath) at various pH values; current densities, j (A dm^{-2}) and durations, t (min) using stationary electrodes. The pH of the bath was adjusted by additions of concentrated H_2SO_4 (98%) or NaOH solutions. One variable was changed

Table 1. Composition, pH and specific conductance (C) of cobalt deposition baths

Bath Co.	Contents in the bath/mol dm^{-3}				pH	C/ohm^{-1} cm^{-1}
	$CoSO_4 \cdot 7H_2O$	$(NH_4)_2SO_4$	H_3BO_3	$NaSO_4 \cdot 10H_2O$		
1	0.0125	1.00	0.1	0.07	5.43	0.129
2	0.0250	1.00	0.1	0.07	4.94	0.130
3	0.0500	1.00	0.1	0.07	4.72	0.135
4	0.0500	0.46	0.1	0.07	4.78	0.066
5	0.0500	0.23	0.1	0.07	4.85	0.044

†Permanent address: Department of Chemistry, Faculty of Science, Ain Shams University, Abbassia, Cairo, Egypt.

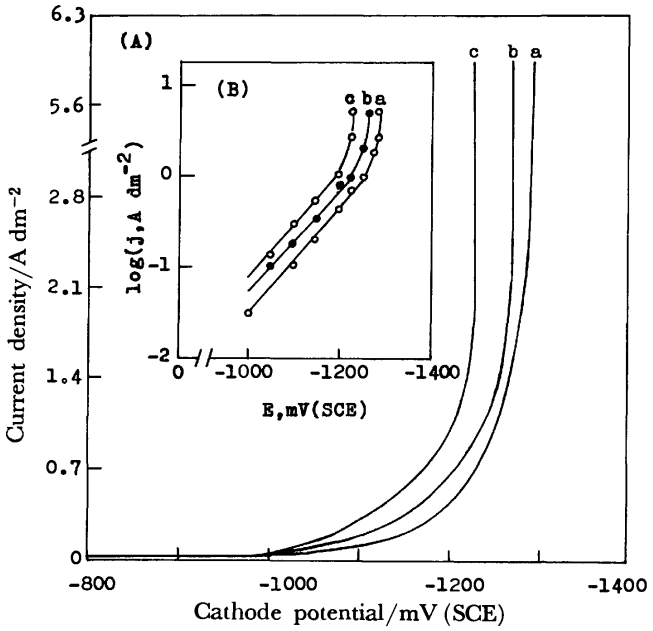

Fig. 1. (A) Polarization curves and (B) Tafel lines for cobalt electrodeposition from Baths: Co. 1 (Curve a), Co. 2 (Curve b), and Co. 3 (Curve c).

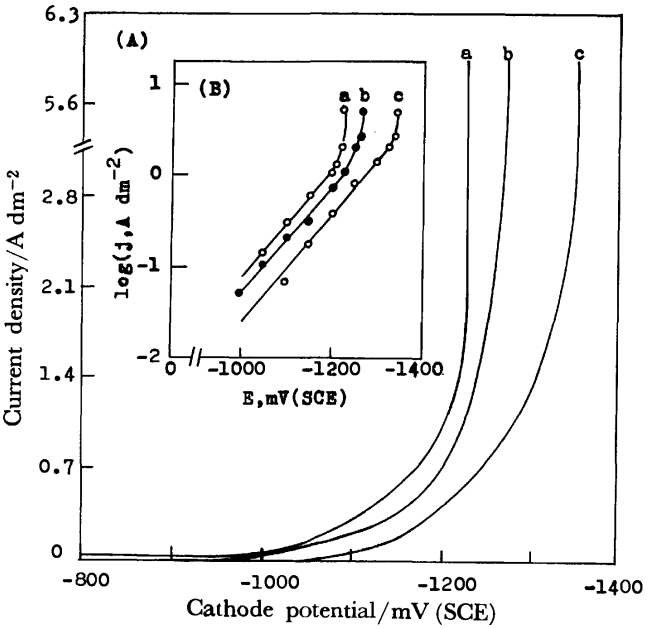

Fig. 2. (A) Polarization curves and (B) Tafel lines for cobalt electrodeposition from Baths Co. 3 (Curve a), Co. 4 (Curve b), and Co. 5 (Curve c).

while the other two were held constant. Unless otherwise stated, all types of measurements were carried out at 25 °C.

Results and Discussion

Polarization Curves. The cathodic polarization curves for cobalt electrodeposition from Baths Co. 1—3 are shown in Fig. 1(A). The curves are characterized by an initial rapid potential-shift to the more negative values followed by a gradual increase with rise of current density and then the potential remains almost constant. This indicates that the electrodeposition of cobalt is attended by a high activation polarization.[9] This can be seen more clearly in Fig. 1(B) which shows that the Tafel relation holds good within the current density range 0—1 A dm^{-2}. Furthermore, the Tafel lines and the polarization curves shift to less negative potentials with increase in the concentration of Co^{2+} ion in the bath. This could be attributed to the corresponding decrease in the activation and the concentration polarizations.[10] However, regardless of the concentration of Co^{2+} ion in the bath, codeposition and vigorous evolution of hydrogen could be easily seen.

Decreasing the concentration of $(NH_4)_2SO_4$ in Baths Co. 3—5 which was expected to decrease the cathodic polarization *via* decreasing the stability constants of the Co^{2+}-ammonium complex ions,[11] is in practice found to has the opposite effect, *viz.* increasing the polarization (Figs. 2(A) and (B)). In addition, a corresponding decrease in the specific conductance of these baths is observed (Table 1).

As can be seen in Fig. 3(A), the cathodic polarization increases with increase in the pH of Bath Co. 4 over the range 2.1—9.6. This feature could be ascribed to the corresponding increase in the hydrogen overvoltage[12]

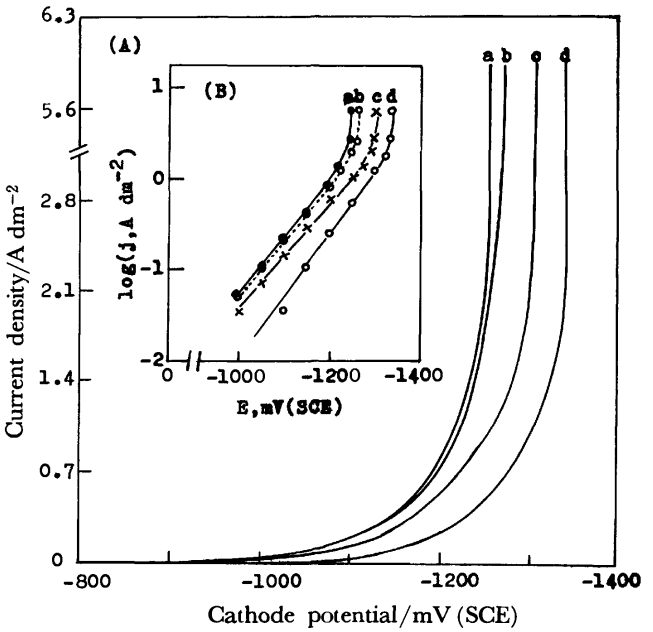

Fig. 3. (A) Polarization curves and (B) Tafel lines for cobalt electrodeposition from Bath Co. 4 at pH 2.1 (Curve a), pH 4.78 (Curve b), pH 7.7 (Curve c), and pH 9.6 (Curve d).

and the observed increase in the activation polarization of the cobalt deposition reaction (see Fig. 3(B)). In addition, at a low pH the rate of hydrogen evolution is so high that most of the gas formed escapes as bubbles. Increase in pH produces a state at which bubble formation is not fast enough for the gas to escape and consequently hydrogen adsorption occurs giving rise to an increase in the cathode potential.[6]

Current Efficiency. The percentage current efficiency (f%) of cobalt deposition increases with increase in the concentration of Co^{2+} ion in Baths Co. 1—3

Table 2. Effect of the bath composition on the efficiency and the catalytic activity of cobalt deposits

Property	Bath Co.				
	1	2	3	4	5
f %[a]	10.65	20.04	30.49	32.22	34.79
D %[b]	82.45	89.55	94.97	97.62	95.86

a) j=6.6 A dm^{-2}, t=10 min. b) j=10 A dm^{-2}, t=30 min.

Table 3. Effect of pH in bath Co. 4 on the efficiency and the catalytic activity of cobalt deposits

Property	pH			
	2.1	4.78	7.7	9.6
f %[a]	31.33	32.22	29.70	21.56
D %[b]	94.50	97.62	95.35	96.20

(a) and (b) are the same as in Table 2.

(Table 2). This effect could be due to the corresponding decrease of the concentration and the activation polarizations of cobalt deposition (Figs. 1(A) and (B)) and the simultaneous inhibition of discharge of H^+ ions. However, a general increase in the efficiency with concentration of the depositable metal ion in the bath was reported in previous studies.[10,13]

As the concentration of ammonium sulfate decreases in Baths Co. 3—5, there is a regular trend of increase in the efficiency of cobalt deposition (Table 2). This could be attributed to the expected decrease in the stability constant of Co^{2+}-ammonium complex ions[11] and the consequent increase in the concentration of the free Co^{2+} ions in the cathode layer. A similar increase in the efficiency with decrease in the concentration of the complexing agent has been observed during the electrodeposition of other metal powders.[13]

Bath Co. 4 is distinguished by a comparatively high current efficiency and the produced powder is characterized by the highest catalytic activity. Therefore, this bath was selected to explore the effect of the variables pH, j, and t on the electrodeposition of cobalt powder.

The data of Table 3 show that the efficiency from the as-prepared Bath Co. 4, of pH 4.78, decreases slightly with lowering of the pH to 2.1. This could be due to the competition between Co^{2+} ions and H^+ ions for discharge. This result is in good agreement with that obtained for the electrodeposition of cobalt from an acidic chloride bath.[14] On the other hand, the efficiency decreases considerably with rise of the pH over the range 4.78—9.60. This could be explained by the observed increase in the cathodic polarization with pH (Fig. 3).

The efficiency of cobalt deposition from Bath Co. 4 decreases gradually with increase in the current density (Table 4). This feature may be ascribed to the depletion of Co^{2+} ions in the cathode layer, arising from the increased rate of deposition, and the preferential discharge of hydrogen at high current densities. Similar results have been observed in several acidic plating electrolytes.[15,16]

Table 4. Effect of current density on the efficiency and the catalytic activity of cobalt deposits from bath Co. 4

Property	j/A dm^{-2}			
	2.0	6.6	10.0	13.2
f %[a]	43.65	32.22	30.35	28.26
D %[b]	98.15	97.90	97.62	94.32

a) pH=4.78, t=10 min. b) pH=4.78, t=30 min.

Table 5. Effect of deposition time on the efficiency and the catalytic activity of cobalt deposits from bath Co. 4

Property	t/min			
	10	15	20	30
f %[a]	32.22	32.18	28.41	11.04
D %[b]	100.00	99.00	98.10	97.62

a) pH=4.78, j=6.6 A dm^{-2}. b) pH=4.78, j=10 A dm^{-2}.

A regular trend of decrease in efficiency with increase in deposition time is represented in Table 5. Actually, this is an unfavourable feature and could be avoided by using soluble cobalt anodes or replenishing the Co^{2+} ions in the bath.

Surface Morphology. The powder obtained from Bath Co. 1 consists of fine crystals which have a characteristic fern-like shape (Fig. 4(A)). On increasing the concentration of Co^{2+} ions in Baths Co. 2 and 3, there is a growth habit modification towards the formation of coarser leaf-like dendritic deposit (Fig. (4B)). This change could be due to the decrease in the concentration and the activation polarizations (Figs. 1(A) and (B)) and the increase in diffusion of Co^{2+} ions which enable preferential growth on certain crystallographic planes and directions.[17]

The inclusion of lower concentrations of ammonium sulfate in Baths Co. 4 and 5 results in the formation of dispersed nodular deposit and better coverage of the cathode surface (Fig. 4(C)). This result is in agreement with the observed increase in the cathodic polarization (Fig. 2) and the correspondingly expected increase in the nucleation sites.[10]

On lowering the pH of Bath Co.4 from 4.78 to 2.10, there is no remarkable change in the growth morphology of the deposit other than refinement of the crystal size. In contrast, increase in pH of Bath Co. 4 over the range 4.78—9.60 leads to passivation of the cathode and formation of isolated dendritic clusters (Fig. 4(D)). This could be due to the polarization increasing effect with pH (Fig. 3) resulting from the increase in adsorption of hydrogen onto the cathode surface[6] and the consequent inhibition of Co^{2+} ions deposition.

The effects of the deposition current density (1.3—13.2 A dm^{-2}) and duration of electrolysis (3—30 min) on the morphology of cobalt powder from Bath Co. 4 (pH=4.78) were also examined. At a low current density (j=1.3 A dm^{-2}) small dihedral grains randomly oriented at the cathode are obtained (Fig. 5(A)). A regular trend of increasing grain size and transformation to

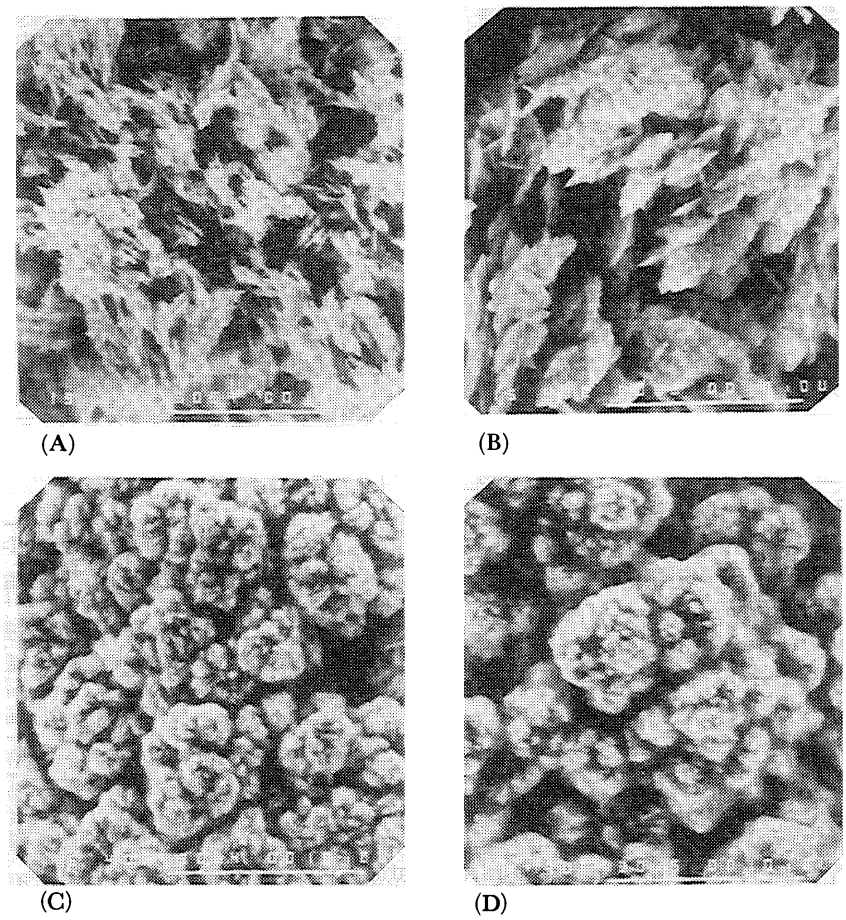

Fig. 4. Electron micrographs of cobalt powders from Baths Co. 1 (A), Co. 3 (B), Co. 4 at pH 4.78 (C), and Co. 4 at pH 7.7 (D); j=6.6 A dm^{-2}, t=10 min and magnification (×4000).

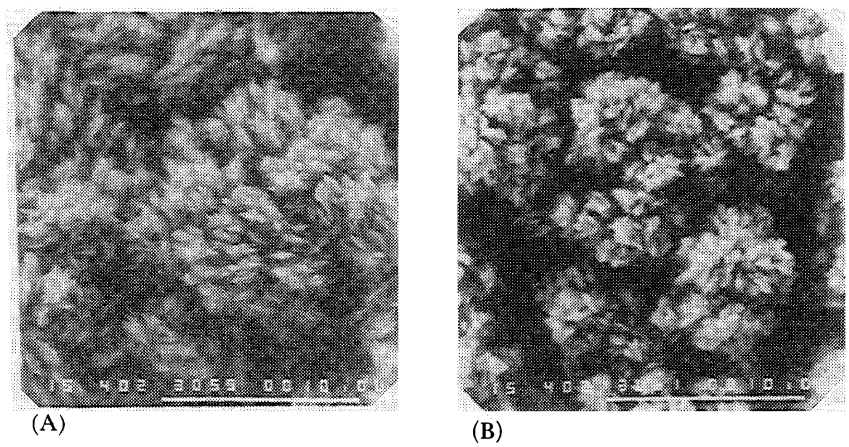

Fig. 5. Electromicrographs of cobalt powders from Bath Co. 4 at j=1.3 A dm^{-2} and t=10 min (A) and at j=6.6 A dm^{-2} and t=3 min (B); pH=4.78 and magnifications (×4000).

nodular dendrites is observed with increase in current density, as can be seen in Fig. 4(C). This feature could be attributed to the increase in the rate of discharge of Co^{2+} ions with current density; whereas, the cathodic polarization remains constant (Fig. 2(A)). Such conditions favour enlargement of the crystal size without considerably affecting the nucleation density.[15,18]

For short deposition times (t=3 min), isolated clusters of fine crystals are formed (Fig. 5(B)). On increasing the deposition time, there is a corresponding increase in the grain size of the cobalt deposit and better coverage of the cathode as shown in Fig. 4(C). These results could be ascribed to the fact that bigger grains are more stable thermodynamically, and if the system has enough time it will reach its most stable state.[19] This phenomenon would result from redissolution and recrystallization of the deposits, through the formation of local cells between them.[18] However, similar results and ex-

Table 6. X-Ray diffraction patterns of cobalt deposit from bath Co. 4

Line	2θ	d/Å	I/I_o	hkl	Observed parameters		Standard parameters	
					a/Å	c/Å	a/Å	c/Å
1	41.60	2.1690	20	100	2.505	4.065	2.507	4.070
2	44.50	2.0342	60	002				
3	47.50	1.9120	100	101				

planations were reported for the electrodeposition of cadmium.[15]

X-Ray Diffractometry. X-Ray structural studies were carried out on the electrodeposited cobalt powders from the under test baths at a current density of 10 A dm^{-2} and duration for 30 min. Table 6 shows as for example the data for the deposit formed in Bath Co. 4. Regardless of the composition or the pH of the examined baths, the obtained data reveal that cobalt powders are deposited in the hexagonal close-packed structure and exhibit the orientations (100), (002), and (101). Moreover, the powders are deposited in a very pure form as could be find out from the good agreement between the values of the calculated and the standard lattice parameters.

Catalytic Activity. In general the catalytic activity (D%) of the electrodeposited cobalt powder, towards the decomposition of 0.4% H_2O_2 solution, is relatively high (82—100%) and this seems to be a specific property. However, the catalytic activity increases with increase of Co^{2+} ions concentration in Baths Co. 1—3 and decrease of ammonium sulfate concentration in Baths Co. 3—5 (Table 2). These effects may be due to the corresponding morphological transformations (Figs. 4A—C) which would result in an increased surface area of the deposit and accordingly increase its catalytic activity.[20]

The effects of the variables, pH, current density, and deposition time on the catalytic activity of cobalt powders formed in Bath Co. 4 were also examined. A negligible change in the catalytic activity is observed with altering the pH over the range 2.1—9.6 (Table 3). This may be referred to the slight effect of pH on the surface morphology of the deposit (Figs. 4(C) and (D)).

The catalytic activity of the deposited powder at the lowest current density (2.0 A dm^{-2}) and the shortest deposition time (10 min) is almost 100%. However, the catalytic activity decreases gradually with increasing current density (Table 4) and increasing deposition time (Table 5). These results may be due to the corresponding enlargement of the cobalt grain size and formation of clusters rather than disperse deposit as mentioned above in the discussion of the surface morphology. However, it seems probable that the catalytic activity of the cobalt powder is, in general, a morphological-sensitive property.

Conclusions

The electrodeposition of cobalt powder from sulfate electrolytes can be controlled by the bath composition, the pH, the current density, and the duration. The obtained data show that the effects of these variables on the cathodic polarization influence to a great extent the surface morphology of the electrodeposited cobalt powder. In addition, the catalytic activity seems to be a morphological-sensitive property. Accordingly, the optimum bath is found to contain 0.05 $CoSO_4 \cdot 7H_2O$, 0.46 $(NH_4)_2SO_4$, 0.1 H_3BO_3, and 0.07 mol dm^{-3} $Na_2SO_4 \cdot 10H_2O$. This bath yields the best depoit, characterized by a catalytic activity of 99%, with an efficiency of 32% at the most suitable operating conditions: pH=4.78, j=10 A dm^{-1} and t=15 min.

References

1) F. A. Lowenheim, "Modern Electrolating," Wiley, New York (1974), p. 141.
2) A. Calusaru, "Electrodeposition of Metal Powders," Elsevier, Amsterdam (1979), p. 387.
3) J. Spiro and F. Wohlgemuth, U.S. Patent 2519585 (1950).
4) F. R. Morral, *Plating*, **59**, 131 (1972).
5) P. C. Baldwin, U.S. Patent 3672968 (1972).
6) Y. M. F. Marikar and K. I. Vasu, *Chemical Era*, **6**, 5 (1970).
7) Yu, I. Khimchenko, E. P. Zhelibo, and V. V. Myalkovsky, *Sov. Powder, Metall. Met. Ceram.*, **14**, 266 (1975).
8) T. N. Amelichkina and E. P. Zhelibo, *Sov. Powder, Metall. Met. Ceram.*, **15**, 337 (1976).
9) T. Yannakopoulos and A. Brenner, *J. Electrochem. Soc.*, **103**, 521 (1958).
10) A. M. Abd El-Halim, *J. Appl. Electrochem.*, **14**, 587 (1984).
11) L. G. Sillén and A. M. Martell, "Stability Constants of Metal-Ion Complexes," Chemical Society, London (1971), p. 84.
12) S. S. Abd El Rehim, *Acta Chim. Acad. Sci. Hung.*, **82**, 535 (1974).
13) A. M. Abd El-Halim and R. M. Khalil, *Surf. Technol.*, **23**, 215 (1984).
14) J. Scoyer and R. Winand, *Surf. Technol.*, **5**, 169 (1977).
15) A. M. Abd El-Halim and M. I. Sobahi, *Surf. Technol.*, **19**, 45 (1983).
16) C. K. Mital, *J. Electrochem. Soc. India*, **22**, 251 (1973).
17) R. Walker and A. Sandford, *Chem. Ind. (London)*, **1979**, 642.
18) S. Itoh, N. Yamazoe, and T. Seiyama, *Surf. Technol.*, **5**, 27 (1977).
19) J. Cl. Puippe and N. Ibl, *Plat. Surf. Finish.*, **1980**, 68.
20) K. Appelt, Z. Dominiczak, A. Nowacki, and M. Paszhiewicz, *Electrochim. Acta*, **10**, 617 (1965).

 © 1985 The Chemical Society of Japan Bull. Chem. Soc. Jpn., 58, 3560—3562 (1985) [Vol. 58, No. 12

Spectrophotometric Determination of Rhodium(III) and Iridium(III) with 3-Hydroxy-2-methyl-1,4-naphthoquinone 4-Oxime

Kamini SHRAVAH and S. K. SINDHWANI*
Department of Chemistry, University of Delhi, Delhi-7, India
(Received August 15, 1984)

Rhodium(III) and iridium(III) form 1:3 and 1:2 (metal:ligand) complex, respectively with 3-hydroxy-2-methyl-1,4-naphthoquinone 4-oxime (HMNQM). The complexes are soluble in 20% ethanol. The reagent has been used for the spectrophotometric determination of Rh(III) and Ir(III). The optimum ranges of concentration for the determination of Rh(III) and Ir(III) are 0.27—5.24 and 1.51—15.85 over the pH range 5.0—7.5 and 5.3—8.0, respectively. The Sandell sensitivities for the determination of Rh(III) and Ir(III) are 0.0042 and 0.015 $\mu g\,cm^{-2}$, respectively. The determinations have also been carried out in the presence of foreign ions.

When ethanolic solution of 3-hydroxy-2-methyl-1,4-naphthoquinone 4-oxime was added to Rh(III) or Ir(III) solution, a yellow or orange brown colored complex was formed. The present study was undertaken to investigate the possibility of the use of HMNQM as a reagent for spectrophotometric determination of rhodium or iridium. Optimum conditions for the determination of rhodium(III) or iridium(III) alone or in presence of diverse ions have also been investigated.

Experimental

Reagents and Apparatus. Preparation of 3-hydroxy-2-methyl-1,4-naphthoquinone 4-oxime (HMNQM) has been reported earlier.[1] The 1×10^{-2} M (1 M=1 mol dm^{-3}) solution of HMNQM was prepared in ethanol (95%).

Buffer solutions were prepared by mixing 0.2 M sodium acetate and 0.2 M acetic acid in the required proportions. For higher pH, sodium hydroxide was added.

Rhodium(III) Solution. A standard solution of rhodium(III) was prepared by dissolving rhodium trichloride (Johnson Matthey) in double distilled water containing 1 M hydrochloric acid. The solution was standardized gravimetrically by precipitating rhodium as the sulfide, followed by ignition to the oxide and then reduction to the metal in an atmosphere of hydrogen and cooling in carbon dioxide. Subsequent dilutions were made by diluting the stock solution, maintaining acidity at 1 M.

Iridium(III) Solution. A standard solution of iridium was prepared by dissolving iridium(III) chloride (Johnson Matthey) in double distilled water containing 1 M hydrochloric acid. The iridium solution was standardized gravimetrically by precipitating iridium as the hydrated oxide, followed by careful ignition in air and then reduction to the metal in presence of hydrogen gas and cooling in an atmosphere of carbon dioxide. Subsequent dilutions were made by diluting the stock solution and keeping the acidity at 1 M.

Reagent grade chemicals were used in the study of interferences. Double distilled water was used throughout the work.

A Unicam SP 600 spectrophotometer was used for measuring absorbance and an ECIL expanded scale pH meter PH821A was used for pH measurements.

Absorption Spectra and Effect of pH. Both rhodium and iridium complexes show the maximum absorption at 470 and 480 nm respectively (Fig. 1). Subsequent studies have been carried out at this wavelength. A plot of absorbance *vs.* pH shows that the absorbances remain constant in the pH range 5.0—7.5 and 5.3—8.0 for Rh(III) and Ir(III), respectively. Further studies have been carried out at pH 6.0 and 6.5 for rhodium and iridium, respectively.

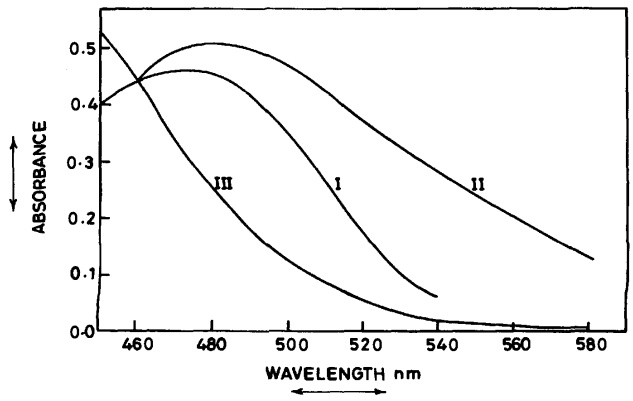

Fig. 1. Absorption spectra of I rhodium(III) complex *vs.* reagent, rhodium 2×10^{-5} M; II iridium(III) complex *vs.* reagent, iridium 4×10^{-5} M; III reagent *vs.* water, HMNQM 2×10^{-4} M.

Rate of Color Development and Stability of the Complexes. The rate of reaction between metal and HMNQM is slow at room temperature. The color intensity was found to increase when the solutions containing a fixed amount of Rh(III) or Ir(III) and excess of reagent were heated on a water bath for various intervals of time and absorbances were measured at 470 or 480 nm for Rh or Ir, respectively. Results of this study show that complete complex formation takes place on heating the contents for about 50 min and 3 h for rhodium and iridium, respectively.

The Rh-HMNQM and Ir-HMNQM complexes were found to be quite stable and absorbances were found to remain constant up to 48 and 24 h, respectively.

Effect of Ethanol Concentration. The precipitated complexes were found to be soluble in ethanol. It has been found that 20% (v/v) ethanol is sufficient to dissolve the precipitate completely. Subsequent studies for rhodium and iridium have been carried out in 20% ethanol medium.

Effect of Reagent Concentration. A plot of absorbance *vs.* moles of ligand shows that at least eight and five times molar excess of the reagent is required for maximum complex formation for rhodium and iridium, respectively (Fig. 2). In further studies ten times molar excess of the reagent was used for both metal.

Adherence to Beer's law, Optimum Range and Sensitivity. Beer's law is obeyed up to 5.97 and 17.68 ppm (1 ppm=1 $\mu g\,cm^{-1}$) while the optimum concentration ranges for accurate determination, as determined from Ringbom plot

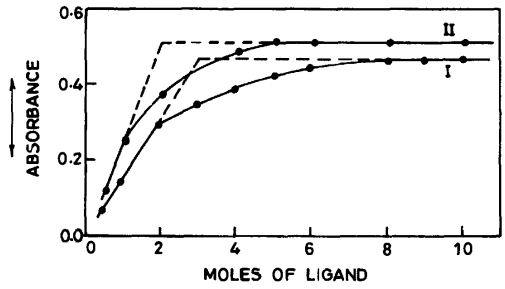

Fig. 2. Effect of reagent concentration, I: Rh(III)-complex Rh=2×10^{-5}M, II: Ir(III)-complex Ir=4×10^{-5}M.

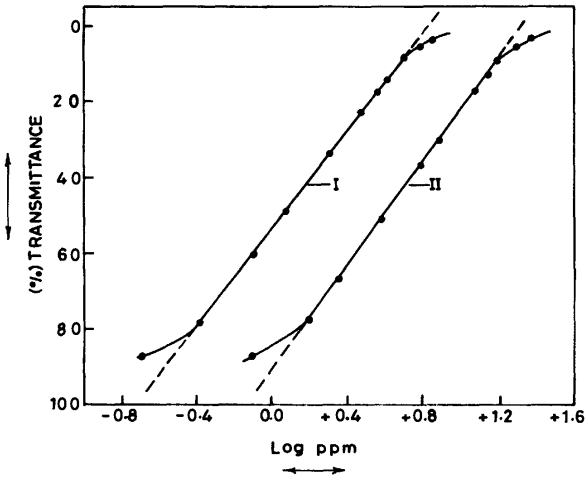

Fig. 3. Ringbom plot for I Rh(III)-HMNQM complex; II Ir(III)-HMNQM complex.

(Fig. 3), are 0.27—5.24 and 1.51—15.85 ppm for rhodium and iridium respectively. The sensitivity in terms of Sandell's definition, is 0.0044 μg Rh/cm^2 and 0.015 μg Ir/cm^2 for log I_o/I=0.001 with molar absorptivity 2.32×10^4 and 1.27×10^4 l mol^{-1} cm^{-1}, respectively.

Recommended Procedure. To a suitable aliquot containing 6.7—131.0 μg of Rh(III) or 37.7—396.2 μg of Ir(III) is added ten times molar excess of reagent. The pH is adjusted between 5.0—7.5 for rhodium and 5.3—8.0 for iridium with acetate buffer and dilute solution of sodium hydroxide. The contents are heated on a boiling water bath for 1 and 3 h, respectively for rhodium and iridium, cooled to room temperature (30±5 °C). The total volume is raised to 25 cm^3 with double distilled water, keeping 20% ethanol concentration. The absorbance of the solution is measured at 470 nm for rhodium and 480 nm for iridium against reagent blank prepared under similar conditions. Knowing the absorbance, the amount of rhodium or iridium is deduced from the calibration graph.

Molar Composition of the Complexes. The composition of the complexes were determined by Job's method of continuous variations[2,3] (Fig. 4) and mole ratio method[4] (Fig. 2). Both of these methods show that the stoichiometric ratio of metal to HMNQM in the complex is 1:3 (Rh:HNMQM) and 1:2 (Ir:HMNQM).

Absorbance Deviations. Measured under experimental conditions, absorbance of six solutions, each containing 2.06 ppm of rhodium, gave mean absorbance of 0.465 with average relative deviation of ±0.32% and maximum relative

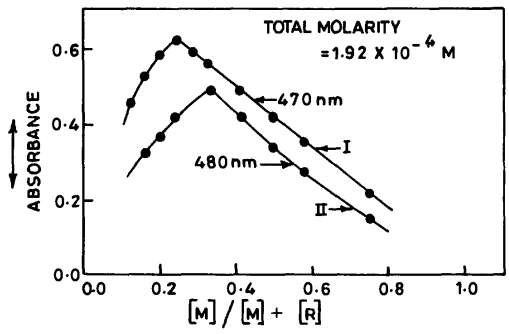

Fig. 4. Composition by Job's method, I: Rh(III)-complex, II: Ir(III)-complex.

deviation of ±0.64% with standard deviation of 0.002. Seven solutions each containing 7.68 ppm of iridium gave an average absorbance of 0.51 with standard deviation of 0.0026. The average relative deviation was found to be ±0.39% and average maximum deviation was ±0.78%.

Effect of Diverse Ions. The effect of diverse ions was studied in the determination of rhodium and iridium following the recommended procedure. The amounts (in ppm) of ions which do not cause any interference with 2.06 ppm of rhodium are given below in parentheses. Masking agents, wherever used, have been mentioned against each:

Chloride (700), bromide (300), iodide or nitrate or sulfate (200), fluoride (600), nitrite or phosphate (150), sulfite or oxalate or EDTA (100), tartrate (50), thiocyanate (80), Ca(II) (100), Ba(II) or Hg(II) (80), Mg(II) or Zn(II) or Cd(II) or Pb(II) (40), Al(III) (20), Mn(II) (30), Fe(II) or Co(II) or Ni(II) or Cu(II) (10, EDTA), Sn(II) (40, F^-), As(III) (50), Ag^I(I) (20, Cl^-), Sb(III) (25), Pd(II) (2, I^-), Os(VIII) (2, SCN^-), V(IV) or Th(IV) (20, F^-), U(VI) (10, PO_4^{3-}). Thiourea, thiosulfate, citrate, Ru(III), Ir(III), and Pt(IV) interfere and attempts to mask the cations were unsuccessful.

For 7.68 ppm of iridium(III), the limits of tolerance are; chloride (100), bromide or nitrate (300), iodide or fluoride (400), nitrite (50), citrate (70), tartrate or oxalate or thiocyanate (100), phosphate, sulfite (150), EDTA (80), sulfate (200), Ca(II) (80), Ba(II) or Cd(II) or Cr(III) (70), Mg(II) or Zn(II) (50), Al(III) (10), Hg(II) or Mn(II) (100), Fe(II) or Co(II) or Ni(II) or Cu(II) (15, EDTA), Sn(II) (20, F^-), As(III) (20), Ag^I(I) (40, Cl^-), Pd(II) (10, I^-), Os(VIII) (4, SCN^-), V(IV) (10, F^-), U(VI) (70, PO_4^{3-}). However, interference due to thiosulfate, thiourea and Ru(III), Rh(III), and Pt(IV) could not be avoided.

Discussion

Quite a few satisfactory reagents are known for the spectrophotometric determination of rhodium. Several methods for the spectrophotometric determination of Rh have been reviewed by Beamish.[5] Tin bromide[5] is a sensitive reagent for rhodium, though the method is not selective and stability of the complex is also low (3 h). The HMNQM method is more sensitive than *N,N'*-bis(3-dimethylaminopropyl)dithiooxamide,[5] *o*-mercaptobenzamide[6] and oximidobenzotetronic acid or α-isonitrosobenzotetronic acid.[7] Most of the associated metals interfere in the case of these reagents.

†Removed by centrifugation.

Table 1. Sensitivities of reagents for Rh and Ir

Reagent	Sensitivity μg Rh/cm²	Reagent	Sensitivity μg Ir/cm²
Tin(II) bromide	0.0035/427 nm	Leucocrystal Violet	0.004/590 nm
N,N-Dimethyl-*p*-nitrosoaniline	0.0015/510 nm	*o*-Dianisidine[a]	0.016/530 nm
Oximidobenzotetronic acid or α-isonitrosobenzotetronic acid	0.07/475 nm	*N,N*-Dimethyl-*p*-nitrosoaniline	0.010/530 nm
N,N'-bis(3-dimethylaminopropyl) dithiooxamide	0.012/420 nm	Oximidobenzotetronic acid or α-isonitrosobenzotetronic acid	0.020/480 nm
o-Mercaptobenzamide	0.014/377 nm	Cerium(IV) sulfate sulfuric acid	0.12/510 nm
Acenaphthenequinone monoxime	0.0036/390 nm	Acenaphthenequinone monoxime	0.021/385 nm
3-Hydroxy-2-methyl-1,4-naphthoquinone 4-oxime (Present method)	0.0044/470 nm	3-Hydroxy-2-methyl-1,4-naphthoquinone 4-oxime (Present method)	0.015/480 nm

a) 3,3'-Dimethoxybiphenyl-4,4'-diamine.

In *N,N*-dimethyl-*p*-nitrosoaniline[5] full color development takes place within 10 min of heating, but after 20 min absorbance begins to decrease and also the volume of the buffer solution used has a pronounced effect on the absorbance of the complex. In acenaphthenequinone monoxime[8] EDTA, NTA, SCN^-, $S_2O_3^{2-}$, Ir, Pt, Cu, Fe, and cerium(IV) cause serious interference. Recently 1-phenyl-3-(2-pyridyl)thiourea[9] has been successfully used for the determination of rhodium. The disadvantage is that the absorption maximum lies in UV region.

For the determination of iridium with Leucocrystal Violet,[10] Rh and Fe(III) interfere seriously. This method depends upon a specific composition of the dissolved iridium salt and aged iridium solutions give green solutions of lower absorbance than those which are freshly prepared. Tin bromide method[11,12] is not selective. This method is sensitive to certain variation in the procedure such as time of contact, temperature, quantity of reagent, and hydrobromic acid. In *o*-dianisidine[13] method, there is interference from associated metals and from oxidants and sulfuric acid solution cannot be used. The absorbance is sensitive to the amount of reagent and to the acidity of the medium. In *N,N*-dimethyl-*p*-nitrosoaniline[14] method, the composition of the complex is not known and the method offers no specificity among platinum metals and there is interference from nonvolatile acids. The method is sensitive to changes in the conditions. In acenaphthenequinone monoxime[15] method, most of the platinum metals interfere and prior separation of iridium is necessary and sensitivity is also low.

The present method, using 3-hydroxy-2-methyl-1,4-naphthoquinone 4-oxime involves simple technique. The method is quite sensitive and the complexes are stable for a long time. Other factors such as effect of buffer, pH, heating time, amount of reagent do not have any effect on the absorbance. Most of the associated metals do not interfere. The sensitivity is comparable (Table 1) with other methods known for the purpose.

One of the authors (K. S.) thanks the Council of Scientific and Industrial Research, New Delhi, for financial assistance.

References

1) Miss Kamini, F. Kamil, and S. K. Sindhwani, *J. Indian Chem. Soc.*, **60**, 388 (1983).
2) P. Job, *Ann. Chim.*, **9**, 113 (1928).
3) H. Irving and T. B. Pierce, *J. Chem. Soc.*, **1959**, 2565.
4) J. H. Yoe and A. L. Jones, *Ind. Eng. Chem. Anal. Ed.*, **16**, 111 (1944).
5) F. E. Beamish, "Analytical Chemistry of Noble Metals," Pergamon, London (1966), p. 409.
6) K. Sur and S. C. Shome, *Anal. Chim. Acta*, **48**, 145 (1969).
7) G. S. Manku, A. N. Bhat, and B. D. Jain, *Talanta*, **14**, 1229 (1967).
8) S. K. Sindhwani and R. P. Singh, *Microchem. J.*, **18**, 686 (1973).
9) Yu. I. Usatenko, N. R. Meshcheryakova, and V. P. Pedan, *Zh. Anal. Khim.*, **34**, 1211 (1979).
10) G. H. Ayres and W. T. Bolleter, *Anal. Chem.*, **29**, 72 (1957).
11) S. S. Berman and W. A. E. McBryde, *Analyst*, **81**, 566 (1956).
12) A. D. Westland and F. E. Beamish, *Mikrochim. Acta*, **1956**, 1974.
13) S. S. Berman, F. E. Beamish, and W. A. E. McBryde, *Anal. Chim. Acta*, **15**, 363 (1956).
14) A. D. Westland and F. E. Beamish, *Anal. Chem.*, **27**, 1776 (1955).
15) S. K. Sindhwani and R. P. Singh, *Z. Anal. Chem.*, **268**, 31 (1974).

 © 1985 The Chemical Society of Japan Bull. Chem. Soc. Jpn., 58, 3563—3565 (1985)

X-Ray Fluorescence Study of Manganese Compounds at Stoichiometric Compositions

M. Ghodsi,* P. H. Duvigneaud, and G. Glade
Service de Chimie Industrielle et Chimie des Solides, Université Libre de Bruxelles, Belgium
(Received August 17, 1984)

Manganese oxides and other inorganic compounds were studied by electron induced X-ray fluorescence. Mn $L\alpha$ energy shifts were measured with respect to pure manganese $L\alpha$ maximum. Those shifts were shown to be a smooth function of manganese partial charge if the latter is calculated from Sanderson's electronegativity scale. The results are in good agreement with Yokokawa's previous work on oxides.

Increasing interest in X-ray analysis methods in such field as industry and research is duly justified by numerous advantages they offer. For example, X-ray fluorescence allows the study of amorphous substances and detection limits of heavy elements can be reduced to a very low level (*ca.* 100 ppm) by use of an ultrathin counter window (polypropylene 1 μm). The cold cathod tube (windowless tube) appears as a very efficient tool for the electronic excitation of K bands of light elements (boron included) and of L bands of heavier elements ($Z>20$). On the other hand, electronic excitation permits the surface analysis of samples in connection with the low penetration depth of the rays.[1]

Furthermore, this method gives access to the stoichiometric composition of samples owing to the energy shift of the characteristic bands (the so-called chemical shift) and can be successfully applied to the study of transition metal oxides[2] the importance of which is well known. Particulary, Mn $L\alpha$ energy shifts (corresponding to the transition L_{III} $M_{IV,\ V}$) can be linked with partial charge of manganese in its compounds.

Experimental

The spectrometer is an "INEL-Alpha 2020" model allowing the study of light elements owing to the use of an electron tube ("Elent 20"). This device, working under a primary vacuum, has been described elsewhere.[3] Table 1 gives the conditions of use of the spectrometer for the Mn $L\alpha$ measurements.

Materials. Each of the synthesized systems has been duly characterized by X-ray diffraction analysis. Results are summarized in Table 2. Manganosite[4] is prepared by a careful decarbonation of precipitated $MnCO_3$. Precipitation is obtained under pure N_2 atmosphere by the reaction

$$Mn(NO_3)_2 + (NH_4)_2CO_3 \longrightarrow MnCO_3 + 2NH_4^+ + 2NO_3^-. \quad (1)$$

After Reaction 1 has been completed, $MnCO_3$ is washed and decomposed at 500 °C in presence of N_2 96%–H_2 4%. Operation is complete after 48 h. Manganese(II) oxide (Riedel-De Haen-high grade purity) has also been investigated. X-Ray diffraction analysis gives a composition of 90% manganosite and 10% MnO_2 (pyrolusite). Dimanganese trioxide has been synthesized by modifying a method initially proposed by Krull.[5] $Mn(OH)_2$ is precipitated from manganese(II) acetate according to the reaction

Table 1. Experimental conditions for the study of Mn $L\alpha$

Excitation source	Electron tube
Voltage	3kV
Intensity	800μA
Analyzing crystal	RbAP(2d=26.12Å)
Detection	Flow proportional counter (90% Argon–10% methane)

Table 2. X-Ray diffraction analysis of the samples

Chemical species	Name	Lattice
MnO synth.	Manganosite	Cubic
MnO (RDH)	MnO 90% manganosite MnO_2 10% pyrolusite	
$Mn(OH)_2$	Pyrochroite	Hexagonal
Mn_2O_3	Partridgeite	Orthorhombic
Mn_3O_4	Hausmannite	Tetragonal
MnO_2	Pyrolusite	Tetragonal

$$Mn(CH_3COO)_2 + 2OH^- \longrightarrow Mn(OH)_2 + 2CH_3COO^-. \quad (2)$$

Initial reactives concentration is chosen as high as possible in order to obtain very small particles[6] and hence to improve the oxidation kinetics. The oxidation step has been performed for 6 h under pure oxygen. The system consists of Partridgeite, as shown by X-ray analysis. Mn_3O_4 is prepared by a prolonged heating of MnO_2 in presence of air (1050 °C) and characterized as Hausmannite.[7] $Mn(OH)_2$ is precipitated in an oxygen-free dilute aqueous ammonia, starting from $MnCl_2$. The hydroxide is vacuum dehydrated in presence of P_2O_5 for 48 h. Electrolytic manganese (99.99%) is polished up to complete disappearance of superficial oxide. Evolution of the surface state is measured by the intensity of the O $K\alpha$ peak. Other samples ($MnSO_4$, $MnCl_2$) though of high purity grade, have been recrystallized. In order to avoid granulometry effects,[8] a mixture of oxides (MnO 50%–MnO_2 50% and MnO 80%–MnO_2 20%) has been prepared from sieved powders (size less than 30 μm).

Energy Shifts. One of the most interesting characteristics of low energy X-ray emission bands is the change occurring in spectra when the valence state of the element under study is modified.[9,10] Since emitted soft X-rays are connected with transitions finding their origin in external levels of an atom, corresponding photon energy must be sensitive to the oxidation state of the element. Hence, significant changes in energy position of the intensity maxima can occur. Furthermore, new transitions unobserved in pure elements, can

TABLE 3. Mn L_α ENERGY SHIFTS IN MANGANESE COMPOUNDS

Compound	E/eV	ΔE Mn L_α/eV
Mn	634.7	—
MnO	635.4	+0.7
MnO(RDH)	635.4	+0.7
$Mn(OH)_2$	635.7	+1.0
Mn_3O_4	635.6	+0.9
Mn_2O_3	636.0	+1.3
MnO_2	636.1	+1.4
MnO 50%-MnO_2 50%	636.0	+1.3
MnO_2 20%-MnO 80%	635.7	+1.0
$MnCl_2$	636.0	+1.3
$MnSO_4$	636.3	+1.6

appear in their compounds.[11] If ΔE represent the energy shift of the element band maximum in a compound compared with that of the pure element, one generally finds:

$$\Delta E(K\alpha) < \Delta E(K\beta) < \Delta E(L). \quad (3)$$

If the element's oxidation state increases. As a rule, the higher the formal positive change, the more energetic the electronic transition. In the opposite case (element negatively charged), ΔE will be negative. This is only in case of light elements compounds (sulfides[12] oxides[13]) that K shifts can easily be observed. For heavier elements, only the L energy shifts can provide the required information.

Results and Discussion

Mn $L\alpha$ maxima positions (transitions between L_{III} and $M_{IV,V}$ levels) have been measured. Each point of the curve intensity *versus* angle is provided by a hundred seconds counting time, angular increment being equal to 0.01°.[2] ΔE (eV) is obtained by comparison with pure manganese $L\alpha$. Table 3 shows the observed energy shifts. All ΔE's correspond to an energy increase of the transition and appear to be directly linked with the manganese oxidation state. It is worthwhile to remark that MnO (Riedel-De Haen) behaves in the same way as pure manganosite despite the high MnO_2 concentration revealed by X-ray diffraction. This can be explained by the relatively low excitation depth. As shown by Feldman,[14] the penetration depth of the electrons in the sample is given by:

$$R(\text{Å}) = \frac{250<A>}{\rho<Z>^{n/2}} E^{n/2} \quad (4)$$

where n=1.2 (1−0.29 log<Z>), <A> is the mean atomic weight and ρ the specific mass gr/cm³) of the sample. <Z> is the mean atomic number and E (keV) is the electrons kinetic energy. Accordingly, excitation depth is *ca.* 800 Å in case of MnO. It seems obvious to assume that the particle nucleus consists of undetected MnO_2 as a result of uncompleted particle reduction. It can be pointed out that the mixture (MnO 50%-MnO_2 50%) exhibits the same overall chemical shift as Mn_2O_3.

Figure 1 represents the observed energy shift as a function of manganese partial charge calculated from Sanderson electronegativities scale[15] which appears to give a better correlation with experimental evidence than Pauling's scale.[16,17] As a matter of fact, one observes a smooth variation of ΔE as a function of q_{Mn}. Those results are in good agreement with those of Yokokawa *et al.*[18] on Si $K\alpha$ and Al $K\alpha$ chemical shifts in oxide glasses.

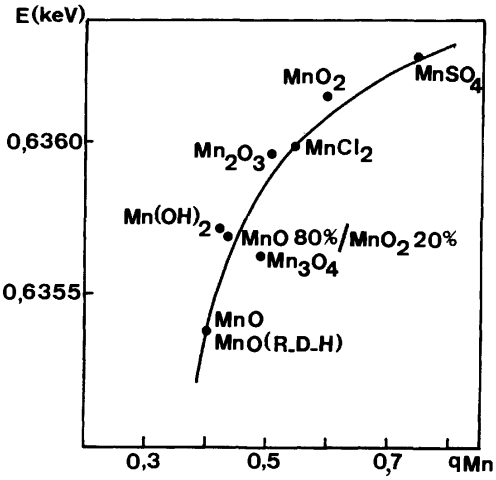

Fig. 1. MnL_α Energy shifts *versus* manganese partial charge in its compouds.
As an example, the solid line is a fifth order polynomial approximation (correlation coefficient: 0.94).

Conclusions

Soft X-ray fluorescence is an useful tool in the study of transition metal compounds. Particularly, L energy shifts give a rapid estimate of the mean stoichiometry of a compound or mixtures of compounds. Furthermore, the use of the electrons tube gives access, in contrast with Auger spectroscopy, to a relatively important analysis depth (*ca.* 1000 Å); accordingly, the contribution of possible superficial impurities is highly reduced. Finally, in view of the industrial importance of manganese and transition compounds, study of the L energy shifts provides a useful method for the rapid determination of mineral ores and metallurgy products.

The authors are indebted to the "Fonds National de la Recherche Scientifique" (FNRS-Belgium) for part of the financial support for the investigation.

References

1) A. Roche, M. Charbonnier, F. Gaillard, M. Romand, and R. Bador, *Appl. Surf. Sci.*, **9**, 227 (1981).
2) T. Birchall, J. A. Connor, and I. A. Hillier, *J. Chem. Soc., Dalton Trans.*, **1976**, 270.
3) R. Bador, M. Romand, M. Charbonnier, and A. Roche, *Adv. X-ray Anal.* **24**, 351 (1981).
4) J. Millar, *J. Am. Chem. Soc.*, **50**, 1875 (1928).
5) R. Krull, *Z. Anorg. Allg. Chem.*, **208**, 134 (1932).
6) A. E. Nielsen, "Kinetics of Precipitation," Pergamon Press (1964).
7) T. Shomate, *J. Am. Chem. Soc.*, **65**, 785 (1943).
8) B. Holynska and A. Markowicz, *X-ray Spectrom.*, **11**,

117 (1982).
9) "Electron Spectroscopy," ed by D. A. Shirley, North Holland (1971).
10) "Electronic Structure and Properties of Solids," ed by W. A. Harrison-Freeman and Co. (1980).
11) D. W. Fischer, *Adv. X-Ray Anal.*, **13**, 159 (1970).
12) T. Maekawa, N. Kikuchi, N. Fukuda, and T. Yokokawa, *Bull. Chem. Soc. Jpn*, **51**, 777 (1978).
13) N. Kikuchi, T. Maekawa, and T. Yokokawa, *Bull. Chem. Soc. Jpn.*, **52**, 1260 (1979).
14) C. F. Feldman, *Phys. Rev.* **117**, 455 (1960).
15) R. T. Sanderson, "Chemical Bonds and Bond Energy," Academic Press (1976).
16) L. Pauling, "The Nature of the Chemical Bond" Cornell Univ. Press, Ithaca, New York (1960).
17) W. Gordy and J. O. Thomas, *J. Chem. Phys.* **24**, 439 (1956).
18) T. Maekawa and T. Yokokawa, *Spectrochim. Acta*, **37B**, 713 (1982).

Photoredox Chemistry of Chloro and Bromo Complexes of Copper(II) in Methanolic Medium

Pazhayirayyathu Geeverghese DAVID* and Paulo Augusto Correa DA SILVA
Departamento de Química, Universidade de Brasília, Brasília, Brazil
(Received August 20, 1984)

Investigation of the photoreduction of copper(II) to copper(I) in methanolic solutions of copper(II) chloride and copper(II) bromide indicates the halide-to-copper(II) charge-transfer (CT) responsible for the photoreduction. Quantum yields for the formation of copper(I) as a function of irradiating wavelength and copper(II) halide concentration show that $[Cu(CH_3OH)_5Cl]^+$ and $[Cu(CH_3OH)_4Cl_2]$ have identical photoreaction efficiency, while $[Cu(CH_3OH)_4Br_2]$ is more photoreactive than $[Cu(CH_3OH)_5Br]^+$. In the copper(II) chloride system the chloride-to-copper(II) CT band centered around 272 nm appears to be responsible for the photoreaction, while the bromide-to-copper(II) CT band centered around 245 nm effects the photoreaction in copper(II) bromide system.

Qualitative aspects of the photochemistry of copper(II) salts in organic solvents have been investigated[1] since 1804. We have reported recently the quantitative aspects of the photoredox chemistry of copper(II) perchlorate in methanolic medium;[2] the primary photoprocess is the homolytic cleavage of copper(II)–methanol bond caused by the broad methanol-to-copper(II) charge-transfer absorption with λ_{max} at 235±2 nm. Kochi[3] employed copper(II) chloride in the chlorination of organic compounds. The primary photoprocess was proposed to be the redox reaction of chloro complexes of copper(II), forming copper(I) and Cl atoms. The present work deals with the quantitative aspects of the photoredox chemistry of chloro and bromo complexes of copper(II) in methanolic medium.

Experimental

Copper(II) perchlorate (Alfa Inorganics) was purified by recrystallization from hot water and dried under vacuum. Copper(II) chloride, copper(II) bromide, lithium chloride, and lithium bromide were reagent grade chemicals (BDH) and were dried under vacuum before use. Methanol and methyl methacrylate were purified by published procedures.[4]

Gross irradiations, from which no quantum yield data were desired, were carried out in a Rayonet photochemical reactor fitted with RPR 3500 Å lamps. Photochemical irradiations, from which quantum yields were to be determined, were performed with a Hanovia 901C-1 150 W xenon lamp dispersed through a Bausch and Lomb 33-86-40 monochromator. Intensity reductions were accomplished by Baird-Atomic neutral density filters. Samples were irradiated in a 1-cm rectangular cell (volume 4.5 cm^3) fitted with ground joint and teflon stopper. The cell was thermostated at 25±0.1 °C by circulating water through the cell holder from a constant-temperature water bath. All methanolic copper(II) solutions were deaerated by bubbling oxygen-free dry nitrogen. Manipulations of methanol and methanolic solutions were carried out in a dry box in an oxygen-free dry-nitrogen atmosphere.

Source intensities were measured by potassium trioxalatoferrate(III) actinometry.[5] Copper(I) was determined spectrophotometrically as the $[Cu(dmp)_2]^+$ complex (dmp=2,9-dimethyl-1,10-phenanthroline) which has a characteristic absorption maximum at 450 nm (ε=7530 $dm^3\ mol^{-1}\ cm^{-1}$ in methanol). A large excess of dmp was always employed. Absorption due to $[Cu(dmp)_2]^{2+}$ at 450 nm (ε=150 $dm^3\ mol^{-1}\ cm^{-1}$ in methanol) was taken into consideration in computing the concentration of copper(I). Formaldehyde formed during the photolysis was determined by the published procedure.[2] Techniques utilized in chemical scavenging experiments with methyl methacrylate have been described.[6]

Results and Discussion

Irradiation of methanolic solutions of copper(II) chloride and copper(II) bromide at 350 nm resulted in the formation of copper(I) and formaldehyde as the products, the concentration of formaldehyde being always half of that of copper(I). At this wavelength the predominant light absorbing species are the halo complexes of copper(II). The results obtained are shown in Table 1. These results are identical to those reported earlier by us for the photolysis of methanolic solution of copper(II) perchlorate[2] in which the photoactive species is $[Cu(CH_3OH)_6]^{2+}$. However, the photopolymer obtained in the radical scavenging experiments using methyl methacrylate yielded positive tests for both the hydroxyl and halogen end

TABLE 1. STOICHIOMETRIC RELATION BETWEEN COPPER(I) AND FORMALDEHYDE IN THE PHOTOLYSIS OF COPPER(II) HALIDES IN METHANOL MEDIUM

$[CuX_2]$	$[Cu^+]$	$[CH_2O]$	$\frac{[Cu^+]}{[CH_2O]}$
1.0×10^{-2}*	8.04×10^{-4}	4.03×10^{-4}	1.99
1.0×10^{-2}	7.60×10^{-3}	3.80×10^{-3}	2.00
7.0×10^{-3}*	5.22×10^{-4}	2.60×10^{-4}	2.01
7.0×10^{-3}	4.15×10^{-4}	2.10×10^{-4}	1.98
4.0×10^{-3}*	3.31×10^{-4}	1.66×10^{-4}	1.99
4.0×10^{-3}	2.55×10^{-4}	1.28×10^{-4}	1.99
1.0×10^{-3}*	1.00×10^{-4}	5.00×10^{-5}	2.00
1.0×10^{-3}	8.60×10^{-5}	4.28×10^{-5}	2.01
1.0×10^{-4}*	8.95×10^{-6}	4.50×10^{-6}	1.99
1.0×10^{-4}	9.50×10^{-6}	4.80×10^{-6}	1.98

All the concentrations are in mol dm^{-3}. Wavelength of irradiation 350 nm. Time of irradiation was adjusted to maintain the photolysis between 5—10% of the initial copper(II) concentration. Copper(II) halide concentrations before the photolysis are indicated. Asterisks indicate copper(II) chloride solutions and the others copper(II) bromide.

groups for the chloride and bromide salts.[7] As the concentration of methyl methacrylate was increased (at constant initial concentration of 0.001 mol dm^{-3} for the copper(II) halides) the concentration of OH end group decreased, while the concentration of halogen end group increased. At [methyl methacrylate]> 0.1 mol dm^{-3}, the concentration of halogen end groups was large and unaffected by further increases in the concentration of methyl methacrylate, while the concentration of OH end group was virtually zero. These results indicate that the halogen atoms are produced in the primary photoreaction and the $\cdot CH_2OH$ radicals[8] are formed as product of secondary reactions of halogen atoms with methanol. If $\cdot CH_2OH$ were a primary product, with X$\cdot$ being formed *via* scavenging of $\cdot CH_2OH$ by X^-, the opposite result would be expected. The observation suggests instead that methyl methacrylate and methanol are competitive scavengers of halogen atoms. Hence, we suggest the homolytic cleavage of Cu(II)-X producing Cu(I) and X$\cdot$ as the primary photoprocess. The halogen atom may reoxidize copper(I) to copper(II) or may be scavenged by CH_3OH yielding $\cdot CH_2OH$ and HX. It has been reported that the principal reaction of the radical $\cdot CH_2OH$ is reduction of copper(II) leading to copper(I) and formaldehyde.[2] This is in agreement with the present result $[Cu^+]/[CH_2O]=2.0$ (Table 1). The following Eqs. may summarize the above observations.

$$CuX^+(\text{or } CuX_2) \xrightarrow{h\nu} [Cu^+\cdot X] \quad (\text{or } [CuX\cdot X]) \quad (1)$$

$$[Cu^+\cdot X](\text{or } [CuX\cdot X]) \longrightarrow Cu^+ + \cdot X \quad (\text{or } Cu^+ + X^- + \cdot X) \quad (2)$$

$$\cdot X + CH_3OH \longrightarrow \cdot CH_2OH + HX \quad (3)$$

$$\cdot CH_2OH + Cu^{2+} \longrightarrow Cu^+ + HCHO + H^+ \quad (4)$$

Quantum yields for the formation of copper(I) in the photoreduction of copper(II) chloride as a function of initial copper(II) chloride concentration are presented in Table 2. For [copper(II) chloride]<0.002 mol dm^{-3} the light absorption was incomplete (pathlength 1.0 cm) and was taken into account in calculating the quantum yields. Manahan and Iwamoto have shown that in methanol $[Cu(CH_3OH)_5Cl]^+$ and $[Cu(CH_3OH)_4Cl_2]$ are the predominant species.[9] The absorption spectra of these species in methanol are not known. However, the work of Baaz *et al.* has proved that in acetonitrile medium the mono- and dichlorocopper(II) complexes have nearly identical absorption spectra with absorption maximum at 310 nm.[10] We repeated the work of Baaz *et al.* in methanol medium using $Cu(ClO_4)_2$ and LiCl. Addition of LiCl to methanolic solution of $Cu(ClO_4)_2$ (5.0×10^{-4} mol dm^{-3}) gave rise to an absorption with maximum at 272 nm. This absorption centered around 272 nm increased until the ratio $[Cu(ClO_4)_2]/[LiCl]=1.0$. Further increase in LiCl concentration produced a slow and steady decrease in the absorption. This agrees with the findings of Baaz *et al.* that the mono- and dichlorocopper(II) complexes have nearly identical absorption spectra. Also the present results indicate that the molar absorptivity of the dichlorocopper(II) complex is less than that of the monochloro complex. The spectra of copper(II) chloride obtained as a function of concentration corroborate the above observations. An increase in ε for the band centered around 272 nm is observed upto a copper(II) chloride concentration 3.0×10^{-4} mol dm^{-3}. Further increase in concentration showed a decrease in these ε values. This indicates that $[Cu(CH_3OH)_6]^{2+}$ and $[Cu(CH_3OH)_5Cl]^+$ are at equilibrium at concentrations of copper(II) chloride $\leq3.0\times10^{-4}$ mol dm^{-3}, while $[Cu(CH_3OH)_5Cl]^+$ and $[Cu(CH_3OH)_4Cl_2]$ are at equilibrium for higher concentrations of copper(II) chloride. The constancy of the quantum yields for the concentration range $1.0\times10^{-4}-2.0\times10^{-3}$ mol dm^{-3} (Table 2) indicates that the monochloro and the dichlorocopper(II) complexes have nearly identical photoreduction efficiency. This behavior is different from that observed for the photoreduction of copper(II) bromide (see below). The decrease in quantum yields for concentrations higher than 2.0×10^{-3} mol dm^{-3} (Table 2) is probably a consequence of depth effect,[2] or reoxidation of copper(I) by Cl_2^- radicals. Increase in the concentration of copper(II) chloride increases the concentration of free Cl^- which may compete with methanol in scavenging Cl atoms. The Cl_2^- species may reoxidize copper(I) with consequent reduction in quantum yield, or may be scavenged by methanol producing $\cdot CH_2OH$ and HCl. However, the final products and the ratio $[Cu^+]/[CH_2O]$ will be unaffected by these reactions. Quantum yield for the formation of copper(I) as a function of irradiating wavelength (Fig. 1) indicate that a charge-transfer band centered around 272 nm is, in fact, responsible for the photoreduction of copper(II) in methanolic solution of copper(II) chloride.

Table 2. Quantum yield for the formation of copper(I) in methanolic solutions of copper(II) chloride

$[CuCl_2]$ / mol dm^{-3}	Φ[a]	$[CuCl_2]$ / mol dm^{-3}	Φ[a]
6.0×10^{-5}	0.077	3.0×10^{-3}	0.060
1.0×10^{-4}	0.079	4.0×10^{-3}	0.041
2.5×10^{-4}	0.077	6.0×10^{-3}	0.030
5.0×10^{-4}	0.080	8.0×10^{-3}	0.025
1.0×10^{-3}	0.078	1.0×10^{-2}	0.022
2.0×10^{-3}	0.079	1.5×10^{-2}	0.020

a) All$\pm$0.001; irradiating wavelength 300 nm; incident intensity $6.67\pm0.01\times10^{14}$ q s^{-1}.

Photoredox chemistry of copper(II) bromide does not parallel that of copper(II) chloride. Quantum yields as a function of initial concentration of copper(II) bromide (Table 3) show that higher concentrations are more effective. The quantum yield values in the concentration range 5.0×10^{-5} to 5.0×10^{-4} mol dm^{-3} are similar to those reported for the photoreduction of copper(II) perchlorate in methanol.[2] A substantial

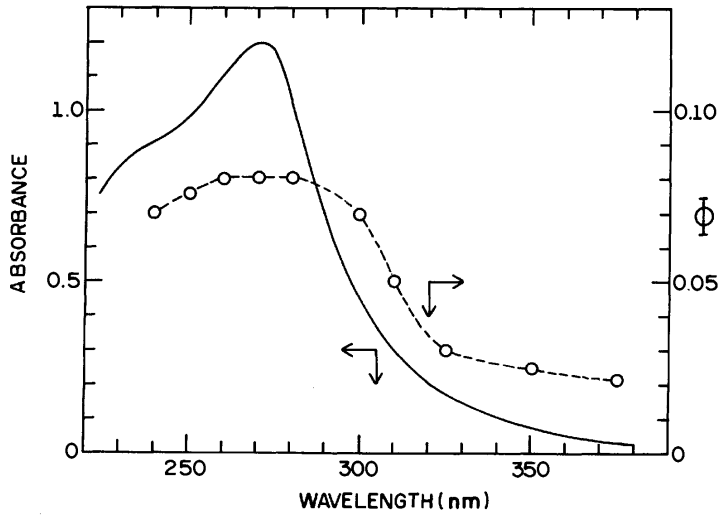

Fig. 1. Electronic absorption spectrum of 5.0×10^{-4} mol dm^{-3} copper(II) chloride in methanol (continuous line), and the variation of quantum yield for the formation of copper(I) as a function of irradiating wavelength (broken line). Initial copper(II) chloride concentration employed for the irradiations was 5.0×10^{-4} mol dm^{-3}.

Table 3. Quantum yield for the formation of copper(I) in methanolic solutions of copper(II) bromide

$[CuBr_2]$ / mol dm^{-3}	Φ[a]	$[CuBr_2]$ / mol dm^{-3}	Φ[b]
5.0×10^{-5}	0.110	1.0×10^{-2}	0.40
1.0×10^{-4}	0.087	2.0×10^{-2}	0.60
2.0×10^{-4}	0.055	3.0×10^{-2}	0.85
5.0×10^{-4}	0.028	4.0×10^{-2}	1.10
8.0×10^{-4}	0.024	5.0×10^{-2}	1.40
1.0×10^{-3}	0.035	6.0×10^{-2}	1.35
2.0×10^{-3}	0.052	8.0×10^{-2}	1.30
4.0×10^{-3}	0.105	1.0×10^{-1}	1.15
8.0×10^{-3}	0.150		

a) All±0.001. b) All±0.01; irradiating wavelength 250 nm; incident intensity $2.32\pm0.01\times10^{14}$ q s^{-1}.

increase in the quantum yields occurs for [copper(II) bromide]>8.0×10^{-4} mol dm^{-3}. We have reported recently[11] that only $[Cu(CH_3OH)_6]^{2+}$, $[Cu(CH_3OH)_5Br]^+$, and $[Cu(CH_3OH)_4Br_2]$ are important in methanolic medium at low concentrations of copper(II) (3.0×10^{-4} mol dm^{-3}) and [LiBr] up to 0.1 mol dm^{-3}. In methanol the monobromo and dibromo complexes of copper(II) have distinctly different spectra and, hence, their formation can be identified.[11] Spectral identification of the monobromo- and dibromocopper(II) complexes in methanolic solutions of copper(II) bromide was carried out in the concentration range 5.0×10^{-5}—8.0×10^{-3} mol dm^{-3}. A graph of molar absorptivity *vs.* wavelength showed an increase in molar absorptivity for $\lambda>235$ nm and a decrease for $\lambda<235$ nm with an isosbestic point at 235 nm in the concentration range 5.0×10^{-5}—5.0×10^{-4} mol dm^{-3}. In agreement with our earlier work[11] this result shows an equilibrium involving $[Cu(CH_3OH)_6]^{2+}$ and $[Cu(CH_3OH)_5Br]^+$. For concentrations higher than 5.0×10^{-4} mol dm^{-3} a general increase in molar absorptivity was observed for all wavelengths in the range 400—220 nm, the increases being larger for $\lambda<290$ nm. These results indicate the increasing formation of $[Cu(CH_3OH)_4Br_2]$ at the expense of the other two species when the [copper(II) bromide]>5.0×10^{-4} mol dm^{-3}. The increase in quantum yields for [copper(II) bromide]>8.0×10^{-4} mol dm^{-3} shows that $[Cu(CH_3OH)_4Br_2]$ is more photoactive than the other two species. Also a quantum yield which exceeds unity indicates that the deactivation reactions are less efficient in the photolysis of $[Cu(CH_3OH)_4Br_2]$ in comparison to that of $[Cu(CH_3OH)_5Br]^+$. The principal deactivation processes may be represented by the reverse of Eq. 1 (primary cage recombination) and the reoxidation of copper(I) by ·X (secondary recombination) represented by Eq. 5.

$$Cu^+ + \cdot X \xrightarrow{X^-} CuX^+(\text{or } CuX_2) \qquad (5)$$

Since for every copper(I) ion formed photochemically (Eq. 1) another copper(I) is formed thermally (Eq. 4), a quantum yield of 2.0 is attainable if Eqs. 1—4 represent entirely the photoreaction and the ensuing thermal reactions. However, the fact that this value is not attained experimentally indicates the importance of deactivation processes.

The nearly identical quantum yield values for the photoreduction of copper(II) perchlorate and copper(II) bromide in the concentration range 5.0×10^{-5}—5.0×10^{-4} mol dm^{-3} (compare this work with the results of Ref. 2) may indicate either that $[Cu(CH_3OH)_6]^{2+}$ and $[Cu(CH_3OH)_5Br]^+$ have nearly identical photoreduction efficiency or $[Cu(CH_3OH)_5Br]^+$ is photochemically inactive. The former seems more plausible. Since $[Cu(CH_3OH)_5Br]^+$, which is in equilibrium with $[Cu(CH_3OH)_6]^{2+}$ at this concentration range, is respon-

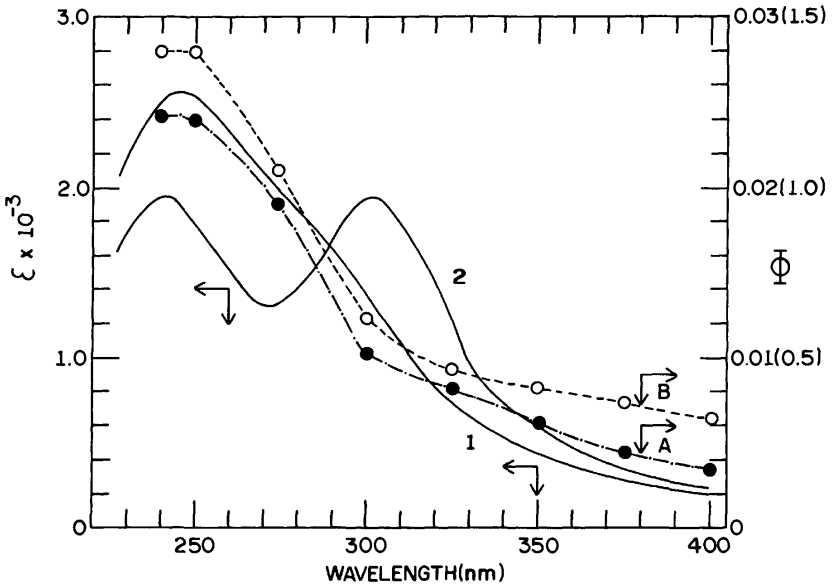

Fig. 2 Electronic absorption, spectra of $[Cu(CH_3OH)_5Br]^+$ and $[Cu(CH_3OH)_4Br_2]$ (1 and 2, respectively) in methanol, and variation of quantum yields as a function of irradiating wavelength (A and B). Curve A is for an initial concentration of copper(II) bromide 8.0×10^{-4} mol dm^{-3} and curve B for 5.0×10^{-2} mol dm^{-3}. The numbers in parentheses (right ordinate scale) are for curve B.

sible for the absorption of a significant part of the incident light its photoinertness could signify a reduction in quantum yield in comparison to that of copper(II) perchlorate solution in which the only light absorbing species is $[Cu(CH_3OH)_6]^{2+}$. Hence, the nearly identical quantum yields in the two solutions signify, quite probably, that the two species, $[Cu(CH_3OH)_6]^{2+}$ and $[Cu(CH_3OH)_5Br]^+$, have nearly identical photoreduction efficiency. The decrease in quantum yield for copper(II) bromide concentrations higher than 5.0×10^{-2} mol dm^{-3} is similar to that observed for copper(II) chloride solutions and, hence, could be the consequence of depth-effect,[2] or reoxidation of copper(I) by Br_2^- radicals.[2,12] Quantum yields as a function of irradiating wavelength (Fig. 2) shows that charge-transfer transitions occurring at wavelengths below 300 nm is in fact responsible for the photoreduction. This points to $[Cu(CH_3OH)_4Br_2]$ as the photoactive species which has the CT band centered around 245 nm.

A plausible explanation for the difference in the photoreactivities of $[Cu(CH_3OH)_5Br]^+$ and $[Cu(CH_3OH)_4Br_2]$ is that the Cu–Br distances are different in the two species. Barnes and Day[13] have showed that an increase in the internuclear distance increases the energy of the charge-transfer transition. Hence, the high energy charge-transfer transition in the dibromo complex (Fig. 2) may signify a longer Cu–Br bond in this compound in comparison to that of the monobromo complex.[14] This could mean a larger distance between Cu(I) and ·Br in the excited state of the dibromo complex and, hence, could render their separation more efficient (and cage-recombination less probable) leading to an increase in the product quantum yield.

References

1) V. Balzani and V. Carassiti, "Photochemistry of Coordination Compounds," Academic Press, London (1970), p. 272.

2) P. A. C. da Silva and P. G. David. *Bull. Chem. Soc. Jpn.*, **55**, 2673 (1982).

3) J. K. Kochi, *J. Am. Chem. Soc.*, **84**, 2121 (1962).

4) P. G. David and E. L. Wehry, *Mol. Photochem.*, **5**, 21 (1973).

5) J. G. Calvert and J. N. Pitts, Jr., "Photochemistry," Wiley, New York (1966).

6) F. David and P. G. David, *J. Phys. Chem.*, **80**, 579 (1976).

7) Radical scavenging experiments yielded positive tests for the formation of $\cdot CH_2OH$ radicals in the photolysis of methanolic solutions of copper(II) perchlorate (Ref. 2).

8) The radical $\cdot CH_2OH$ is responsible for the positive OH end-group test in the photopolymers. The analysis does not distinguish between incorporation of CH_2OH or OH as end group in the photopolymer.

9) S. E. Manahan and R. T. Iwamoto, *J. Electroanal. Chem.*, **13**, 411 (1967).

10) M. Baaz, V. Gutmann, G. Hampel, and J. R. Masaguer, *Monatsh. Chem.*, **93**, 1416 (1962).

11) P. G. David, *Polyhedron*, **4**, 437 (1985).

12) Br_2^- radicals are formed by the scavenging of Br atoms by bromide ions.

13) J. C. Barnes and P. Day, *J. Chem. Soc.*, **1964**, 3886.

14) The bromide-to-copper(II) CT transition is centered around 300 nm in the monobromo complex; the band centered around 240 nm could be methanol-to-copper(II) CT band. The absorption centered around 245 nm in the dibromo complex represents, quite probably, two CT bands (bromide-to-copper and methanol-to-copper) superimposed one over the other.

New Amino-protective Reagents for *t*-Butoxycarbonylation and Benzyloxycarbonylation of Amines and Amino Acids

Sunggak Kim,* Jae In Lee, and Kyu Yang Yi
Department of Chemistry, Korea Advanced Institute of Science and Technology, Seoul 131, Korea
(Received September 11, 1984)

New amino-protective reagents for *t*-butoxycarbonylation and benzyloxycarbonylation of amines and amino acids have been developed. *t*-Butyl 2-pyridyl carbonate and *t*-butyl *S*-(2-pyridyl) thiocarbonate react cleanly with various amines and amino acids to afford *N*-Boc amines and *N*-Boc amino acids in high yields. Benzyl 2-pyridyl carbonate and *O*-benzyl *S*-(2-pyridyl) thiocarbonate are also found to be very effective in the benzyloxycarbonylation of amino acids.

The *t*-butoxycarbonyl (Boc) group is one of the most important amino-protective groups along with benzyloxycarbonyl (Cbz) group in peptide synthesis because the *t*-butoxycarbonyl group is cleanly cleaved by cold trifluoroacetic acid, hot formic acid, or hydrochloric acid and *N*-Boc amino acids are resistant to racemization during peptide synthesis.[1] Since *t*-butyl chloroformate is only fairly stable below 10 °C,[2] considerable efforts have been devoted to the development of a variety of useful and reliable reagents for the preparation of *N*-Boc amino acids during last 30 years.[3] In view of the great importance of the *t*-butoxycarbonyl group in peptide synthesis, a great need still exists for an efficient and stable reagent for the *t*-butoxycarbonylation of amines and amino acids.

Since it has been found that *S*-(2-pyridyl) thioates and 2-pyridyl esters are very useful active esters as acylating agents in the synthesis of peptides,[4] ketones,[5] and carboxylic esters,[6] we have been interested in the utilization of 2-pyridyl ester moieties for the *t*-butoxycarbonylation and the benzyloxycarbonylation of amino acids. Recently, we have communicated that *t*-butyl 2-pyridyl carbonate (BPC) is very effective in the *t*-butoxycarbonylation of amino acids.[7] The present paper describes a full detail of (i) the preparation of BPC, *O*-*t*-butyl *S*-(2-pyridyl) thiocarbonate (BPT), benzyl 2-pyridyl carbonate (BZBC), and *O*-benzyl *S*-(2-pyridyl) thiocarbonate (BZPT) and (ii) their use for the *t*-butoxycarbonylation and the benzyloxycarbonylation of amines and amino acids.

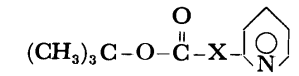

BPC: X = O
BPT: X = S

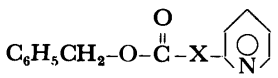

BZPC: X = O
BZPT: X = S

Results and Discussion

t-Butyl 2-Pyridyl Carbonate (BPC). BPC was originally prepared by the reaction of 2-pyridyl chloroformate, generated from an excess amount of phosgene and 2-pyridinol in the presence of pyridine, with equimolar amounts of *t*-butyl alcohol and pyridine in dichloromethane at room temperature and obtained in 65—70% yield along with a small amount of di-2-pyridyl carbonate (Eq. 1). In order to avoid the formation of di-2-pyridyl carbonate, we attempted to isolate 2-pyridyl chloroformate but it decomposed rapidly during usual workup, yielding 2-pyridinol as a major product. Thus, di-2-pyridyl carbonate was removed by filtration through a short column of silica gel with dichloromethane as an eluant. Recently, we have found that BPC can be prepared by the reaction of di-2-pyridyl carbonate[8] with an equimolar amount of *t*-butyl alcohol in the presence of 0.1 equiv of 4-dimethylaminopyridine[9] in dichloromethane at room temperature for 24 h in 80% yield. Di-2-pyridyl carbonate was conveniently prepared in 90% yield by treatment of phosgene with 2 equiv of 2-pyridinol in the presence of 2 equiv of triethylamine in dichloromethane (Eq. 2).

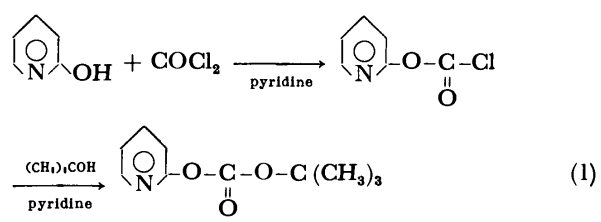

(1)

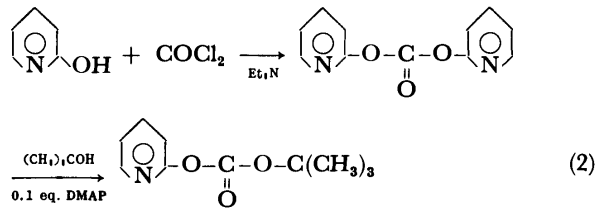

(2)

O-t-Butyl S-(2-Pyridyl) Thiocarbonate (BPT). The preparation of BPT was turned out to be very difficult. First, we adopted a similar scheme utilized in the preparation of BPC. (2-Pyridylthio)carbonyl chloride was prepared by a known procedure.[10] Unexpectedly, reaction of (2-pyridylthio)carbonyl chloride with equimolar amounts of *t*-butyl alcohol and triethylamine did not give the desired product. Instead *S*,*S*-di(2-pyridyl) dithiocarbonate was isolated in an essentially quantitative yield. Furthermore, the reaction of (2-pyridylthio)carbonyl chloride with equimolar amounts of *t*-butyl alcohol and pyridine did not occur to an observable extent, though the similar type of a reagent, *O*-*t*-butyl *S*-(4,6-dimethyl-2-pyrimidinyl) thiocarbonate, has been prepared in a high yield by use of pyridine as a base in a similar manner.[11]

Recently, we have found that *S*-(2-pyridyl) thioates are rapidly and cleanly esterified with alcohols in the presence of copper(II) bromide in acetonitrile.[6c] Thus, reaction of *S,S*-di(2-pyridyl) dithiocarbonate, which was prepared in 91% yield by the reaction of phosgene with 2 equiv of 2-pyridinethiol in the presence of 2 equiv of triethylamine in dichloromethane, with *t*-butyl alcohol in the presence of 1 equiv of copper(II) bromide in acetonitrile at room temperature was attempted. However, a desired product was not obtained. Furthermore, on the basis of a previous result obtained with BPC, we attempted the reaction of *S,S*-di(2-pyridyl) dithiocarbonate with equimolar amounts of *t*-butyl alcohol and 4-dimethylaminopyridine. However, the reaction did not proceed to an observable extent in dichloromethane, tetrahydrofuran, or *N,N*-dimethylformamide (DMF) at room temperature for 5 h.

Finally, we were able to prepare BPT by treatment of *S,S*-di(2-pyridyl) dithiocarbonate with 0.5 equiv of copper(II) *t*-butoxide in tetrahydrofuran at room temperature for 2 h (Eq. 3). BPT was obtained in 79%

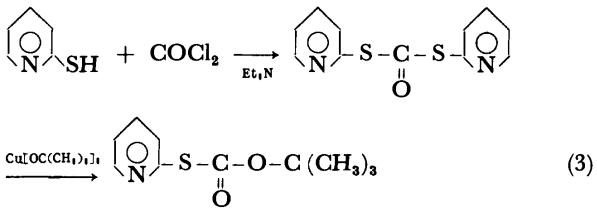

(3)

yield as a relatively stable oily compound. Attempts to crystallize the product were failed.

Benzyl 2-Pyridyl Carbonate (BZPC) and O-Benzyl S-(2-Pyridyl) Thiocarbonate (BZPT). BZPC was easily prepared in 80% yield as an oil by the reaction of benzyl chloroformate with equimolar amounts of 2-pyridinol and triethylamine in dichloromethane (Eq. 4). Similarly, BZPT was prepared in a high yield from equimolar amounts of benzyl chloroformate and 2-pyridinethiol in the presence of triethylamine in dichloromethane and obtained as an oil (Eq. 4).

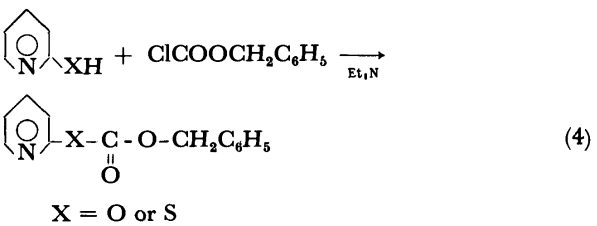

(4)

X = O or S

t-*Butoxycarbonylation of Amines and Amino Acids.* First, reaction of BPC with a variety of structurally different amines was examined. Simple amines such as propylamine, benzylamine, and piperidine were rapidly and quantitatively converted into the corresponding *t*-butyl carbamates in dichloromethane at room temperature within 2 h. However, the *t*-butoxycarbonylation of sterically hindered secondary amines such as diisopropylamine and 2,6-dimethylpiperidine, and relatively unreactive amines like aniline did not occur in dichloromethane to an observable extent, even after forcing conditions such as prolonged stirring at elevated temperatures. Thus, proper conditions to effect the *t*-butoxycarbonylation of sterically hindered amines were studied. Among the solvents employed, acetonitrile and DMF gave the best results in terms of the rapidity and the yield of the reaction and are generally recommended, though DMF is considered to be slightly better than acetonitrile. Reaction of diisopropylamine with BPC in DMF at 80 °C for 48 h afforded *N*-(*t*-butoxycarbonyl)diisopropylamine in 83% yield, whereas the reaction in acetonitrile at 80 °C required 60 h for completion of the reaction. Similarly, aniline was converted into *N*-(*t*-butoxycarbonyl)-aniline in high yields in DMF or acetonitrile at 80 °C. The *t*-butoxycarbonylation of imidazole and benzimidazole with BPC in DMF or acetonitrile did not occur under forcing conditions. The results obtained with several amines are summarized in Table 1.

In order to find out optimum conditions for the *t*-butoxycarbonylation of amino acids with BPC, we briefly examined the effects of bases, solvents, and reaction time by use of L-phenylalanine as a model compound. With aqueous DMF as the solvent, the effect of four bases was briefly examined at room temperature and it was found that the yield of Boc–Phe was the highest using 1.5 equiv of triethylamine (96% isolated yield): Sodium hydrogencarbonate (75%), sodium carbonate (72%), and sodium hydroxide (70%), though the reason for these results are unclear. However, the *t*-butoxycarbonylation proceeded much more rapidly with sodium hydroxide (1 h for complection of the reaction): sodium carbonate (5 h), sodium hydrogencarbonae (16 h), and triethylamine (12 h). Although aqueous DMF and aqueous dioxane were found to be equally effective in the *t*-butoxycarbonylation of amino acids, the reaction occurred more rapidly in aqueous DMF than in aqueous dioxane. For example, the reaction of L-phenylalanine with equimolar amounts of BPC in the presence of 1.5 equiv of triethylamine in aqueous DMF at room temperature afforded *N*-Boc–Phe in 96% yield in 12 h, whereas the reaction in aqueous dioxane required 16 h. The pronounced difference in the reaction rate was observed in L-leucine. The reaction in aqueous DMF required 4 h for completion of the reaction, whereas the reaction in aqueous dioxane required 16 h.

On the basis of these results obtained, the standard conditions employed for the *t*-butoxycarbonylation of amino acids with BPC involved the use of 1.5 equiv of triethylamine and aqueous DMF at room temperature. As shown in Table 2, the *t*-butoxycarbonylation of various amino acids used in this study was normally complete within 12 h at room temperature and the corresponding *N*-Boc amino acids were isolated in high yields. The identities of

Table 1. Preparation of *N*-Boc amines[a]

Amine	Solvent	Temp/°C	Time/h	Isolated Yield/%[b]
$CH_3CH_2CH_2NH_2$	CH_2Cl_2	r.t	0.25	97
$C_6H_5CH_2NH_2$	CH_2Cl_2	r.t	2	95
$(CH_3CH_2)_2NH$	CH_2Cl_2	r.t	1.5	94
	CH_2Cl_2	r.t	0.25	95
$CH_3CH_2C(CH_3)_2NH_2$	CH_2Cl_2	r.t	36	92
$C_6H_5NH_2$	CH_3CN	80	60	92
	DMF	80	48	92
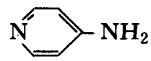	DMF	80	12	80
$(CH_3)_2CHNHCH(CH_3)_2$	CH_3CN	80	60	86
	DMF	80	48	83
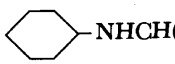	DMF	80	30	86
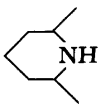	DMF	80	36	81

a) The reaction was carried out on an 1—3 mmol scale of amine with 1.0 equiv of the reagent. b) Yields were based on the amine.

Table 2. Preparation of *N*-Boc amino acids in aqueous DMF[a]

Amino acid	*t*-Butyl 2-pyridyl carbonate (BPC) Time/h	Yield/%	Mp/θ_m/°C	$[\alpha]_D$/°	*O*-*t*-Butyl *S*-(2-pyridyl) thiocarbonate (BPT) Time/h	Yield/%	Mp/θ_m/°C	$[\alpha]_D$/°
Ala	8	90	145—147[b]	−23.8 (0.9, AcOH)	16	84	76—77	−23.6 (1.5, AcOH)
Cys[b]	10	85	173—176	−57.1 (1.3, AcOH)	12	84	173—175	−55.2 (1.0, AcOH
Cys-Cys	8	87	140—142	−112.0 (0.7, AcOH)	20	83	141—143	−109.7 (1.4, AcOH)
Leu	4	94	70—74[c]	−23.1 (1.1, AcOH)	12	95	70—74[c]	−25.5 (1.1, AcOH)
Met[b]	7	96	137—139	+17.5 (1.4, MeOH)	8	90	136—139	+17.7 (1.7, MeOH)
Phe[b]	12	96	221—224	+28.0 (1.3, MeOH)	16	89	221—224	+27.8 (2.2, MeOH)
Pro	6	98	133—135	−60.7 (0.9, AcOH)	4	95	134—135	−61.0 (0.7, AcOH)
Ser[b]	7	93	139—141	+13.1 (1.2, DMF)	10	85	139—141	+12.9 (0.4, DMF)
Thr[b]	8	98	152—155	+10.2 (1.7, MeOH)	12	92	152—154	+9.8 (2.7, MeOH)
Try	4	98	137—138	−21.5 (1.0, AcOH)	8	89	136—138	−20.9 (0.8, AcOH)
Tyr[b]	6	88	212—215	+3.8 (1.1, AcOH)	16	92	206—208	+3.4 (3.2, AcOH)
Val	9	92	141—143[b]	−5.9 (1.1, AcOH)	12	80	77—78	−5.1 (1.5, AcOH)

a) Mp and $[\alpha]_D$ values of the known compounds were within the limit of error in comparison with the reported data and $[\alpha]_D$ values were measured at room temperature (15—25 °C). See Refs. 3, 11, and 12 for the reported data. b) Dicyclohexylammonium salt. c) Monohydrate.

N-Boc amino acids were confirmed by comparison of mp, NMR, and IR data and $[\alpha]_D$ values with reported data.[12] Furthermore, it is noteworthy that a by-product, water-soluble 2-pyridinol, can be easily removed from the reaction mixture by simple aqueous workup.

The *t*-butoxycarbonylation using BPT was performed on several amino acids under the similar conditions employed in the *t*-butoxycarbonylation of amino acids using BPC. In general, the reaction occurred smoothly but somewhat slowly in aqueous DMF at room temperature, when compared with reaction using BPC. Some experimental results are summarized in Table 2. It is noteworthy that 2-pyridinethiol, generated from the reaction, can be easily removed from the reaction mixture by washing with aqueous $CuSO_4$ solution. However, di-2-pyridyl disulfide was sometimes formed to some extent due to oxidation of 2-pyridinethiol during the reaction and it was removed by column chromatographic separation in such cases. In comparison with BPC, BPT has several disadvantages over BPC with respects to the difficulty of its preparation, an oily nature of BPT, and workup procedures.

Benzyloxycarbonylation of Amino Acids. Although benzyl chloroformate has been widely used for the preparation of *N*-Cbz amino acids, it is thermally unstable and decomposes to yield carbon dioxide and benzyl chloride when it is stored at room temperature over a long period of time. In view of

Table 3. Preparation of *N*-Cbz amino acids in aqueous DMF[a]

Amino acid	Benzyl 2-pyridyl carbonate (BZPC) Time/h	Yield/%	Mp/θ_m/°C	$[\alpha]_D$/°	*O*-Benzyl *S*-(2-Pyridyl) Thiocarbonate (BZPT) Time/h	Yield/%	Mp/θ_m/°C	$[\alpha]_D$/°
Ala	0.3	85	83—85	−14.1 (1.5, AcOH)	0.5	87	84—85	−13.9 (1.5, AcOH)
Cys-Cys	1	95	68—69	−81.2 (1.3, AcOH)	1	90	68—69	−81.2 (1.3, AcOH)
Ile	0.5	86	42—43	+5.5 (1.2, EtOH)	0.5	87	42—44	+5.6 (1.9, EtOH)
Met	0.5	82	67—68	−21.1 (2.5, MeOH)	0.5	85	65—67	−19.8 (1.8, MeOH)
Phe	0.5	90	86—88	+5.4 (0.4, AcOH)	0.5	92	86—88	+5.4 (0.4, AcOH)
Pro	0.3	88	75—76	−58.3 (0.2, AcOH)	1	85	75—76	−59.0 (0.2, AcOH)
Ser	0.3	90	110—111	+5.0 (2.3, AcOH)	0.3	95	110—111	+5.0 (2.3, AcOH)
Thr[b]	0.5	86	185—187	−2.8 (1.7, AcOH)	0.5	78	183—186	−2.7 (1.7, AcOH)
Try	0.3	97	Oil	+2.1 (2.4, AcOH)	0.3	94	Oil	+2.1 (2.4, AcOH)

a) Mp and $[\alpha]_D$ values of the known compounds were within the limit of error in comparison with the reported data and $[\alpha]_D$ values were measured at room temperature (15—25 °C). See Refs. 3c and 13 for the reported data. b) Dicyclohexylammonium salt.

encouraging results obtained with BPC, we turned our attention to BZPC and BZPT for the introduction of benzyloxycarbonyl group in amino acids under mild conditions. Thus, the reaction of BZPC and BZPT with several amino acids was briefly examined under similar conditions employed for the *t*-butoxycarbonylation of amino acids with BPC and the results are summarized in Table 3.[13]

It was found that the benzyloxycarbonylation with BZPC and BZPT proceeded much faster than the *t*-butoxycarbonylation with BPC. The reaction was normally complete within 0.5 h in aqueous DMF at room temperature and the corresponding *N*-Cbz amino acids were isolated in excellent yields.

Experimental

NMR spectra were recorded with a Varian T-60A spectrometer, and chemical shifts are expressed as δ units relative to tetramethylsilane. Infrared spectra were recorded on a Perkin-Elmer 267 and the frequences are given in reciprocal centimeters. Melting points were determined on an Electrothermal melting point apparatus and are uncorrected. Reported boiling points are those observed during distillation with a Kugelrohr apparatus and uncorrected. Optical rotations were measured with an automatic polarimeter AUTOPOL III. Elemental analysis were performed by Korea Research Institute of Chemical Technology and Lucky Central Research Institute.

Commercially available amines and amino acids were used without further purification and all amino acids used in this study were L-configuration.

Since the reactions performed are all similar in many respects, typical reactions will be described as specific examples.

Di-2-pyridyl Carbonate. To a diluted solution of phosgene (2.5 M† in toluene, 2 ml, 5.0 mmol) with dichloromethane (8 ml) at 0 °C was added a solution of 2-pyridinol (950 mg, 10 mmol) and triethylamine (1.214 g, 10.2 mmol) in dichloromethane (20 ml). The reaction mixture was stirred at 0 °C for 1 h, washed with cold 5% $NaHCO_3$ (20 ml), cold saturated NaCl (20 ml), dried over $MgSO_4$ and filtered. The filtrate was concentrated to dryness to give di-2-pyridyl carbonate (972 mg) in 90% yield. Di-2-pyridyl carbonate could be recrystallized from dichloromethane–petrolem ether (811 mg, 75%). Mp 84—86 °C. NMR($CDCl_3$) δ=7.10—7.46 (m, 4H), 7.64—8.00 (m, 2H), 8.36—8.52 (m, 2H); IR(KBr) 1770 cm^{-1}. Found: C, 61.03; H, 3.45; N, 13.15%. Calcd for $C_{11}H_8O_3N_2$: C, 61.11; H, 3.73; N, 12.96%.

t-Butyl 2-Pyridyl Carbonate (BPC). *A*: The procedure using 2-pyridyl chloroformate is as follows. To a diluted solution of phosgene (2.5 M in toluene, 20 ml, 50 mmol) with dichloromethane (20 ml) at −10—0 °C was slowly added a solution of 2-pyridinol (951 mg, 10 mmol) and pyridine (870 mg, 11 mmol) in dichloromethane (40 ml). After being stirred at −10—0 °C for 15 min, excess phosgene and solvents were evaporated under reduced pressure and then the residue was dissolved with dichloromethane (30 ml). A solution of *t*-butyl alcohol (815 mg, 11 mmol) and pyridine (830 mg, 10.5 mmol) in dichloromethane (20 ml) was added to the flask at room temperature. The reaction mixture was stirred at room temperature for 5 h and diluted with dichloromethane (30 ml). The resulting solution was washed with saturated $NaHCO_3$ (30 ml) and brine (30 ml), dried over $MgSO_4$, and evaporated to dryness under reduced pressure. The crude product was purified by filtration through a short column of silica gel using dichloromethane as an eluant to afford *t*-butyl 2-pyridyl carbonate (1.37 g, 70%). The product could be recrystallized from hexane. Mp 48—49 °C. NMR($CDCl_3$) δ=1.60 (s, 9H), 7.00—7.39 (m, 2H), 7.62—7.97 (m, 1H), 8.30—8.50 (m, 1H); IR(KBr) 1755 cm^{-1}. Found: C, 62.13; H, 6.86; N, 6.98%. Calcd for $C_{10}H_{13}O_3N$: C, 61.53; H, 6.71; N, 7.17%.

B: The procedure using di-2-pyridyl carbonate is as follows. To a stirred solution of di-2-pyridyl carbonate (1.08 g, 5.0 mmol) in dichloromethane (15 ml) at room temperature were added *t*-butyl alcohol (370 mg, 5.0 mmol) and 4-dimethylaminopyridine (61 mg, 0.5 mmol) and stirring was continued at room temperature for 24 h. The reaction mixture was diluted with dichloromethane (30 ml), washed with saturated NH_4Cl (30 ml) and brine (20 ml), dried over $MgSO_4$, and concentrated to dryness. The crude product was purified by filtration through a short column of silica gel using dichloromethane as an eluant to afford *t*-butyl 2-pyridyl carbonate (780 mg, 80%).

S,S-Di(2-pyridyl) Dithiocarbonate. To a solution of 2-pyridinethiol (1.112 g, 10 mmol) and triethylamine (1.02 g, 10 mmol) in dichloromethane (40 ml) at 0 °C was slowly added a solution of phosgene (2.5 M in toluene, 2 ml, 5 mmol). After being stirred at 0 °C for 1 h, the reaction mixture was washed with saturated $NaHCO_3$ (30 ml) and brine (30 ml), dried over $MgSO_4$, and evaporated to

† 1 M=1 mol dm^{-3}.

dryness to afford the desired product (1.13 g) in 91% yield as an oil. The crude product was pure enough using for further reactions. NMR($CDCl_3$) δ=6.66—6.97 (m, 2H), 7.10—7.33 (m, 4H), 8.03—8.30 (m, 2H); IR(film) 1715 cm^{-1}. Found: C, 53.31; H, 3.13; N, 11.42%. Calcd for $C_{11}H_8ON_2S_2$: C, 53.21; H, 3.25; N, 11.28%.

O-t-Butyl S-(2-Pyridyl) Thiocarbonate (BPT). To a solution of *t*-butyl alcohol (371 mg, 5 mmol) in tetrahydrofuran (7 ml) at 0°C under nitrogen was added butyllithium (1.6 M in hexane, 3.2 ml, 5 mmol). After being stirred at 0°C for 10 min, the solution was added to the suspended solution of copper(II) bromide (560 mg, 2.5 mmol) in tetrahydrofuran (4 ml) and the resulting mixture was stirred at room temperature for 0.5 h. To a solution of *S,S*-di(2-pyridyl) dithiocarbonate (1.24 g, 5 mmol) in tetrahydrofuran (4 ml) at 0°C was added a solution of copper(II) *t*-butoxide and the resulting solution was allowed to warm to room temperature with stirring for 2 h. After the reaction mixture was evaporated to dryness, the residue was dissolved in dichloromethane (40 ml). The dichloromethane solution was washed with saturated NH_4Cl (30 ml) and brine (30 ml), dried over $MgSO_4$, and concentrated. The residue was subjected to silica-gel column chromatography with hexane-ethyl acetate (2:1) as an eluent to affors *O-t*-butyl *S*-(2-pyridyl) thiocarbonate (834 mg) in 79% yield as an oil. NMR ($CDCl_3$) δ=1.66 (s, 9H), 7.13—7.40 (m, 1H), 7.64—7.81 (m, 2H), 8.47—8.64 (m, 1H); IR(film) 1730 cm^{-1}. Found: C, 56.29; H, 6.43; N, 6.53%. Calcd for $C_{10}H_{13}O_2NS$: C, 56.85; 6.20; N, 6.63%.

Benzyl 2-Pyridyl Carbonate (BZPC). To a solution of benzyl chloroformate (1.71 g, 10 mmol) in dichloromethane (10 ml) at 0°C was added a solution of 2-pyridinol (1.00 g, 10.5 mmol) and triethylamine (1.06 g, 10.5 mmol) in dichloromethane (20 ml). After being stirred at room temperature for 1 h, the reaction mixture was diluted with dichloromethane (30 ml) and washed with saturated NH_4Cl (20 ml) and brine (20 ml). The dichloromethane solution was dried over $MgSO_4$ and evaporated to give benzyl 2-pyridyl carbonate (2.20 g, 96%). The crude product was purified by filtration through a short column of silica gel with ethyl acetate-hexane (1:3) as an eluant to give benzyl 2-pyridyl carbonate (1.83 g) in 80% yield as an oil. NMR($CDCl_3$) δ=5.32 (s, 2H), 7.00—7.39 (m, 2H), 7.41 (b.s, 5H), 7.61—7.96 (m, 1H), 8.30—8.50 (m, 1H); IR(film) 1750 cm^{-1}. Found: C, 68.40; H, 4.89; N, 5.69%. Calcd for $C_{13}H_{11}O_3N$: C, 68.12; H, 4.84; N, 6.11%.

O-Benzyl S-(2-Pyridyl) Thiocarbonate (BZPT). To a solution of benzyl chloroformate (1.71 g, 10 mmol) in dichloromethane (10 ml) at 0°C was added a solution of 2-pyridinethiol (1.17 g, 10.5 mmol) and triethylamine (1.06 g, 10.5 mmol) in dichloromethane (20 ml). After being stirred at room temperature for 1 h, the reaction mixture was diluted with dichloromethane (30 ml) and washed with saturated NH_4Cl (20 ml) and brine (20 ml). The dichloromethane solution was dried over $MgSO_4$ and evaporated to dryness. The residue was purified by filtration through a short column of silica gel with ethyl acetate-hexane (1:3) as an eluant to afford *O*-benzyl *S*-(2-pyridyl) thiocarbonate (2.06 g) in 84% yield as an oil. NMR($CDCl_3$) δ=5.29 (s, 2H), 7.09—7.32 (m, 1H), 7.34 (b.s, 5H), 7.57—7.82 (m, 2H), 8.42—8.63 (m, 1H); IR(film) 1720 cm^{-1}. Found: C, 63.93; H, 4.38; N, 6.04%. Calcd for $C_{13}H_{11}O_2NS$: C, 63.66; H, 4.52; N, 5.71%.

Preparation of N-Boc-Benzylamine. To a stirred solution of benzylamine (215 mg, 2.0 mmol) in dichloromethane (6 ml) at room temperature was added BPC (391 mg, 2.0 mmol). The reaction mixture was stirred at room temperature for 2 h, diluted with dichloromethane (30 ml), and washed with saturated $NaHCO_3$ (20 ml). The dichloromethane solution was dried over $MgSO_4$ and evaporated to dryness. The residue was recrystallized from dichloromethane-petroleum ether to give *N*-Boc-benzylamine (390 mg) in 95% yield. Mp 53—54°C (lit,[3a] 53—54°C); NMR($CDCl_3$) δ=1.50 (s, 9H), 4.30 (d, 2H, *J*=6 Hz), 4.64—5.31 (m, 1H), 7.28 (b.s, 5H); IR (KBr) 1680 cm^{-1}.

Preparation of N-Boc-2,6-Dimethylpiperidine. To a stirred solution of 2,6-dimethylpiperidine (115 mg, 1.0 mmol) in DMF (4 ml) at room temperature was added BPC (200 mg, 1.0 mmol). The reaction mixture was stirred at 80°C for 36 h, diluted with diethyl ether (30 ml), and washed with saturated $NaHCO_3$ (20 ml) and water (20 ml). The aqueous layer was extracted with diethyl ether (30 ml×2). The combined ether extracts were dried over $MgSO_4$ and evaporated to dryness. The curde product was distilled to give *N*-Boc-2,6-dimethylpiperidine (173 mg, 81%): Bp 102—108°C/38.5 mm Hg[†]); NMR ($CDCl_3$) δ=1.25 (d, 2H, *J*=7 Hz), 1.54 (s, 9H), 1.38—2.00 (m, 6H), 4.04—4.63 (m, 2H); IR(film) 1690 cm^{-1}. Found: C, 67.35; H, 10.62; N, 6.40%. Calcd for $C_{12}H_{12}O_2N$: C, 67.57; H, 10.87; N, 6.57%.

Preparation of N-Boc-Proline. *(A) BPC Method:* To a solution of L-proline (230 mg, 2.0 mmol) in DMF-water (2:1, 12 ml) was added triethylamine (303 mg, 3.0 mmol). After the reaction mixture was stirred at room temperature for 10 min, BPC (392 mg, 2.0 mmol) was added and the resulting mixture was stirred at room temperature for 6 h. The reaction mixture was adjusted to pH 3.5 by addition of 0.025 M oxalic acid and extracted with dichloromethane (30 ml×3). The dichloromethane solution was washed with water (20 ml) and brine (20 ml), dried over $MgSO_4$, and evaported to dryness *in vacuo* to give *N*-Boc-proline (424 mg, 98%) as a syrup, which can be crystallized from ethyl acetate-petroleum ether. Mp 133—135°C (lit,[3c] 136—137°C); $[\alpha]]_D$ −60.7° (0.9, AcOH, 20°C) [lit,[3c] $[\alpha]_D$ −60.57° (0.974, AcOH, 25°C)].

(B) BZPC Method: To a solution of L-proline (232 mg, 2.0 mmol) and triethylamine (303 mg, 3.0 mmol) in DMF-water (1:1, 8 ml) was added a solution of BZPC (423 mg, 2.0 mmol) in DMF (2 ml). The reaction mixture was stirred at room temperature for 4 h, acidified with 0.025 M oxalic acid (pH 3.5), and extracted with ethyl acetate (30 ml×3). The extracts were washed with saturated $CuSO_4$ (20 ml×2) and brine (30 ml), dried over $MgSO_4$, and evaporated to dryness *in vacuo*. The residue was crystallized from ethyl acetate-petroleum ether to give *N*-Boc-proline (408 mg, 95%). Mp 134—135°C; $[\alpha]_D$ −61.0° (0.7, AcOH, 18°C).

Preparation of N-Cbz-Phenylalanine. To a solution of L-phenylalanine (330 mg, 2.0 mmol) and triethylamine (301 mg, 3.0 mmol) in DMF-water (1:1, 8 ml) was added a solution of BZPT (492 mg, 2.0 mmol) in DMF (2 ml). The reaction mixture was stirred at room temperature for 0.5 h, acidified with 0.025 M oxalic acid (pH 3.5) and extracted with ethyl acetate (30 ml×3). The combined extracts were washed with saturated $CuSO_4$ (20 ml×2) and brine (20 ml), dried over $MgSO_4$, and evaporated to dryness. The crude product was crystallized from dichloromethane-petroleum ether to give *N*-Cbz-phenylalanine (534 mg, 89%). Mp 86—88°C (lit,[3c] 86—87°C); $[\alpha]_D$ +5.4° (0.4, AcOH, 20°C) [lit, [3c] $[\alpha]_D$ +5.54° (0.361, AcOH, 18°C)]. In the case of using BZPC, the com-

[†]1 mmHg=133.322 Pa.

bined extracts were washed with water and brine. Otherwise, the experimental procedure is almost same as described above.

Spectral Data of N-*Boc Amines.* *N*-Boc-propylamine: Bp 65—70 °C/38 mmHg; NMR ($CDCl_3$) δ=1.00 (t, 3H, J=6 Hz), 1.56 (s, 9H), 1.25—1.94 (m, 2H), 3.06 (q, 2H, J=6 Hz), 4.50—5.07 (m, 1H); IR (film) 1700 cm^{-1}. *N*-Boc-diethylamine: Bp 74—76 °C/38 mmHg; NMR ($CDCl_3$) δ=1.25 (t, 6H, J=7 Hz), 1.57 (s, 9H), 3.26 (q, 4H, J=7 Hz); IR (film) 1690 cm^{-1}. *N*-Boc-piperidine: Bp 92—95 °C/38 mmHg; NMR ($CDCl_3$) δ=1.50 (s, 9H), 1.40—1.76 (m, 6H), 3.12—3.58 (m, 4H); IR (film) 1685 cm^{-1}. *N*-Boc-di-*s*-butylamine: Bp 92—95 °C/38 mmHg; NMR ($CDCl_3$) δ=0.85 (t, 3H, J=7 Hz), 1.28 (s, 6H), 1.50 (s, 9H), 1.53 (q, 2H, J=7 Hz), 4.19—4.63 (m, 1H); IR (film) 1705 cm^{-1}. *N*-Boc-aniline: Mp 133—135 °C (lit,[14] 135.5—138 °C); NMR ($CDCl_3$) δ=1.60 (s, 9H), 6.49—7.40 (m, 6H); IR (KBr) 1685 cm^{-1}. *N*-Boc-4-aminopyridine: Mp 139—142 °C; NMR ($CDCl_3$) δ=1.56 (s, 9H), 7.25—7.50 (m, 2H), 8.06—8.80 (m, 3H); IR (KBr) 1715 cm^{-1}. Found: C, 61.88; H, 7.47; N, 14.15%. Calcd for $C_{10}H_{14}O_2N_2$: C, 61.84; H, 7.27; N, 14.42%. *N*-Boc-diisopropylamine: Bp 70—75 °C/26 mmHg; NMR ($CDCl_3$) δ=1.20 (d, 12H, J=7 Hz), 1.51 (s, 9H), 3.40—4.10 (m, 2H); IR(film) 1685 cm^{-1}. *N*-Boc-*N*-isopropylcyclohexylamine: Bp 95—100 °C/48 mmHg; NMR ($CDCl_3$) δ=1.22 (d, 6H, J=6 Hz), 1.54 (s, 9H), 1.60—2.14 (m, 10H), 3.33—4.02 (m, 2H); IR (film) 1680 cm^{-1}. Found: C, 69.65; H, 11.87; N, 5.60%. Calcd for $C_{14}H_{27}O_2N$: C, 69.67; H, 11.27; N, 5.80%.

References

1) E. Gross and J. Meienhofer, "The Peptides, Analysis, Synthesis, Biology," Academic Press, New York (1981), Vol. 3.; T. W. Greene, "Protective Groups in Organic Synthesis," Wiley, New York (1981) and references cited therein.

2) A. R. Choppine and J. W. Rogers, *J. Am. Chem. Soc.*, **70**, 2967 (1948).

3) For recently developed reagents, see: a) T. Kunieda, T. Higuchi, Y. Abe, and M. Hirobe, *Tetrahedron Lett.*, **21**, 3065 (1980); b) J. W. Scott and D. Parker, *Org. Prep. Proced. Int.*, **12**, 242 (1980); c) Y. Kita, J. Haruta, H. Yasuda, K. Fukunaga, Y. Shirouchi, and Y. Tamura, *J. Org. Chem.*, **47**, 2697 (1982); d) R. B. Harris and I. B. Wilson, *Tetrahedron Lett.*, **23**, 231 (1983); e) S. Kim and H. Chang, *J. Chem. Soc., Chem. Commun.*, **1983**, 1357.

4) W. Broadbent, J. S. Morley, and B. E. Stone, *J. Chem. Soc. C*, **1967**, 2632; T. Mukaiyama, R. Matsueda, and M. Suzuki, *Tetrahedron Lett.*, **1970**, 1901.

5) a) M. Araki, S. Sakata, H. Takei, and T. Mukaiyama, *Bull. Chem. Soc. Jpn.*, **47**, 1777 (1974); b) M. Onaka, T. Goto, and T. Mukaiyama, *Chem. Lett.*, **1979**, 1483; c) S. Kim and J. I. Lee, *J. Org. Chem.*, **48**, 2608 (1983).

6) a) E. J. Corey and K. C. Nicolaou, *J. Am. Chem. Soc.*, **96**, 5614 (1974); b) H. Gelach and A. Thalmann, *Helv. Chim. Acta*, **57**, 293 (1974); c) S. Kim and J. I. Lee, *J. Org. Chem.*, **49**, 1712 (1984).

7) S. Kim and J. I. Lee, *Chem. Lett.*, **1984**, 237.

8) S. Kim, J. I. Lee, and Y. K. Ko, *Tetrahedron Lett.*, in press.

9) For reviews, see: G. Höfle, W. Steglich, and H. Vorbrüggen, *Angew. Chem., Int. Ed. Engl.*, **17**, 569 (1978); E. F. V. Scriven, *Chem. Soc. Rev.*, **12**, 129 (1983).

10) E. J. Corey and D. A. Clark, *Tetrahedron Lett.*, **1979**, 2875.

11) T. Nagasawa, K. Kuroiwa, K. Narita, and Y. Isowa, *Bull. Chem. Soc. Jpn.*, **46**, 1269 (1973).

12) H. Otsuka and K. Inouye, *Bull. Chem. Soc. Jpn.*, **37**, 1465 (1964); K. Hoffmann, R. Schmiechen, R. D. Wells, Y. Wolmann, and N. Yanaihara, *J. Am. Chem. Soc.*, **87**, 611 (1965); E. Schnabel, *Justus Liebigs Ann. Chem.*, **702**, 188 (1967) and Refs. 3 and 11.

13) M. Bergmann and L. Zervas, *Ber.*, **65**, 1192 (1932); K. Hoffmann, A. Jöhl, A. E. Furlenmeier, and H. Kappeler, *J. Am. Chem. Soc.*, **79**, 1636 (1957); H. Schwarz, F. M. Burpus, and J. H. Page, *ibid.*, **79**, 5697 (1957) and Ref. 11.

14) L. A. Carpino, *J. Am. Chem. Soc.*, **82**, 2725 (1960).

Refractive Indices, Dielectric Constants, and Order Parameter of Four Alkyl/Alkoxyphenylcyclohexanecarboxylate Liquid Crystals in the Nematic Phase

Krishnakali KALI, Sushmita SEN, and Subir Kumar ROY*
Optics Department, Indian Association for the Cultivation of Science, Jadavpur, Calcutta-700032, India
(Received October 2, 1984)

The extraordinary and ordinary refractive indices, n_e and n_o, and the densities of four liquid crystals 4-pentylphenyl *trans*-4′-pentylcyclohexanecarboxylate, 4-ethoxyphenyl *trans*-4′-propylcyclohexanecarboxylate, 4-ethoxyphenyl *trans*-4′-butylcyclohexanecarboxylate, and 4-methoxyphenyl *trans*-4′-pentylcyclohexanecarboxylate have been reported at different temperatures. The effective polarizabilities α_e and α_o in the nematic phase have been calculated using 1) Neugebauer and 2) Vuks methods. The order parameter S calculated from the two methods were comparable. The dielectric constants $\varepsilon_\parallel$ and $\varepsilon_\perp$, parallel and perpendicular to the long axis of the molecules have been measured at 1 kHz at different temperatures. The order parameters for the liquid crystals were then evaluated from dielectric anisotropy $\Delta\varepsilon(=\varepsilon_\parallel-\varepsilon_\perp)$, polarizability anisotropy $\Delta\alpha(=\alpha_e-\alpha_o)$ and dipole moment μ, using Maier and Meier equation and were found only slightly less than those obtained from refractive indices method. It was concluded that Maier and Meier equation also could be used to evaluate the order parameter of liquid crystals of molecules having dipole moments 2 Debye or less.

The knowledge of dielectric constants $\varepsilon_\parallel$ and $\varepsilon_\perp$, parallel and perpendicular to the long molecular axis helps us to select a liquid crystal for a specific electrooptical display device. The values of dielectric anisotropy $\Delta\varepsilon(=\varepsilon_\parallel-\varepsilon_\perp)$ and polarizability anisotropy $\Delta\alpha(=\alpha_e-\alpha_o)$ where α_e and α_o are the effective polarizabilities of the nematic medium and the dipole moment μ may be useful for the evaluation of order parameter of liquid crystals using Maier and Meier equation.[1] de Jeu and Lathouwers[2,3] observed that in the case of liquid crystals with zero or small dipole moment, the average dielectric constant $\bar{\varepsilon}=1/3\,(\varepsilon_\parallel+2\varepsilon_\perp)$ practically coincides with the dielectric constant ε_{iso} in the isotropic phase. They pointed out that these results indicate that the Maier and Meier equation gives qualitatively the correct picture of dielectric properties of liquid crystals. But for the lack of information on molecular polarizabilities, dipole moments, and their angle with the long molecular axis, the model could not be tested for quantitative measurements. Recently Sen *et al.*[4] observed that in the case of liquid crystals of strongly polar molecules having dipole moments of 4—5 Debye,† the order parameter S obtained from Maier and Meier equation using dielectric anisotropy and polarizability anisotropy are much less than the values obtained from other methods. Sen *et al.*[4] pointed out that the short range antiferroelectric dipole correlation of permament dipole moment μ in strongly polar nematics as proposed by Madhusudana and Chandrasekhar[5] might cause a large decrease in $\varepsilon_\parallel$ thus decreasing the order parameter. The object of the present investigation is to evaluate the order parameter S of liquid crystals with dipole moments about 2 Debye from the measurements of refractive indices and densities, and to compare these S values with those obtained from dielectric anisotropy $\Delta\varepsilon$ and polarizability anisotropy $\Delta\alpha$, using the Maier and Meier equation.[1]

†1D=3.3×10^{-30}cm.

Experimental

The structural formulae and nematic-isotropic transition temperatures of four liquid crystals which were obtained from Merck are given below. The general formula for these compounds is

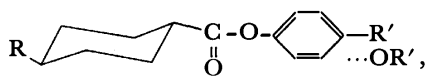

where R and R′=Alkyl and OR′=Alkoxy.

1) 4-Pentylphenyl *trans*-4′-pentylcyclohexanecarboxylate (D-55)

$$C \xrightarrow{37^\circ C} N \xrightarrow{47^\circ C} I$$

2) 4-Ethoxyphenyl *trans*-4′-propylcyclohexanecarboxylate (D-302)

$$C \xrightarrow{48^\circ C} N \xrightarrow{78^\circ C} I$$

3) 4-Ethoxyphenyl *trans*-4′-butylcyclohexanecarboxylate (D-402)

$$C \xrightarrow{37^\circ C} N \xrightarrow{75^\circ C} I$$

4) 4-Methoxyphenyl *trans*-4′-pentylcyclohexanecarboxylate (D-501)

$$C \xrightarrow{40^\circ C} N \xrightarrow{71^\circ C} I$$

The liquid crystals were used in the investigations without further purification.

Measurement of Refractive Indices. The refractive indices n_o and n_e for the ordinary and extraordinary refracted rays in the nematic phase and the refractive index n in the isotropic phase at different temperatures were measured by means of an Abbe refractometer. The glass prisms of the refractometer were first treated with an aqueous solution of 3% poly (vinyl alcohol) and dried. The prism was then rubbed with a lens paper along the length of prism several times. A little of the liquid crystal was dropped on the lower prism

and was spread with a spatula. These operations helped to align the liquid crystal along the length of the prism surface. The arrangement was complete when the upper prism was clamped in place.

Two positions of a nicol placed over the eyepiece allow distinct separation of bright and dark space corresponding to n_e and n_o (in the nematic $n_e > n_o$). The temperature was maintained constant within ±0.2°C by means of a thermostat.

The densities of the liquid crystal in the nematic and isotropic phases were determined by introducing a weighed sample of the liquid crystal into a capillary tube placed in a thermostat. The length of the column in the capillary was measured at different temperatures with a travelling microscope. The density was calculated after correcting for the expansion of the glass tube.

Measurements of Dielectric Constants $\varepsilon_{\parallel}$ and $\varepsilon_{\perp}$. The static dielectric constants were measured at a frequency of 1 kHz using a GR-1620 capacitance bridge reading to an accuracy of 0.01%. A parallel plate capacitor with stainless steel electrodes of 2 cm×1 cm separated by a 1 mm teflon spacer, served as the sample holder. The temperature of the sample was measured with a thermocouple mounted directly on one of the electrodes. A magnetic field 1.0 T was used to align the liquid crystal molecules parallel and perpendicular to the electrode surfaces. The temperature of the sample holder was maintained constant within ±0.2°C by means of a thermostat. The cell was calibrated with freshly distilled toluene and chlorobenzene and the values agree to 0.1% of the standard value.[6]

Results

Refractive Indices and Polarizabilities. The experimental values of refractive indices n_e, n_o, and n and the densities of the liquid crystals are given in Tables 1 (a, b, c, d) and Fig 1. The effective polarizabilities α_e and α_o in the nematic state were calculated using two methods. 1) Neugebauer's[7] method of anisotropic internal field given by

$$n_{e,c}^2 - 1 = 4\pi N\alpha_{e,c}/(1 - N\alpha_{e,c}\gamma_{e,o}), \quad (1)$$

where N is the number of molecules per 1 cm³ and $\gamma_{e,o}$ are internal field constants. The relevant equations for calculating the polarizabilities are

$$\frac{1}{\alpha_e} + \frac{2}{\alpha_o} = \frac{4\pi N}{3}\left[\frac{n_e^2+2}{n_e^2-1} + \frac{2(n_o^2+2)}{(n_o^2-1)}\right], \quad (2)$$

$$\alpha_e + 2\alpha_o = \alpha_{//} + 2\alpha_{\perp} = \frac{9}{4\pi N}\left(\frac{n^2-1}{n^2+2}\right). \quad (3)$$

Table 1a. Refractive indices, density and order parameter S for D-55

T/°C	n_o	n_e	ρ/g cm^{-3}	$\bar{\alpha}$/Å^3	Vuks' Method			Neugebauer's Method		
					α_o/Å^3	α_e/Å^3	S	α_o/Å^3	α_e/Å^3	S
36	1.4730	1.5304	0.9508	41.632	39.683	45.532	.70	39.995	44.908	.69
37	1.4724	1.5301	0.9501	41.623	39.664	45.550	.70	39.989	44.900	.69
39	1.4724	1.5272	0.9468	41.623	39.757	45.357	.67	40.058	44.753	.66
41	1.4720	1.5250	0.9486	41.629	39.818	45.241	.65	40.090	44.708	.65
43	1.4722	1.5217	0.9449	41.643	39.867	45.020	.61	40.206	44.518	.60
45	1.4736	1.5163	0.9431	41.652	40.190	44.571	.52	40.413	44.132	.52
47	1.4870		0.9416							
48.5	1.4862		0.9389							
51.5	1.4848		0.9357							
					$\alpha_{\perp}$= 38.869 (Å)^3	$\alpha_{\parallel}$= 47.2717 (Å)^3		$\alpha_{\perp}$= 39.310 (Å)^3	$\alpha_{\parallel}$= 46.398 (Å)^3	

Table 1b. Refractive indices, density and order parameter S for D-302

T/°C	n_o	n_e	ρ/g cm^{-3}	$\bar{\alpha}$/Å^3	Vuks' Method			Neugebauer's Method		
					α_o/Å^3	α_e/Å^3	S	α_o/Å^3	α_e/Å^3	S
51	1.4705	1.5448	1.0118	33.1706	31.1645	37.1733	.75	31.4817	36.5486	.75
54.5	1.4700	1.5417	1.0093	33.1730	31.2352	37.0442	.72	31.5438	36.4314	.72
57	1.4693	1.5401	1.0074	33.1790	31.2605	37.0092	.71	31.5646	36.4078	.71
60	1.4684	1.5384	1.0048	33.1960	31.2950	36.9931	.71	31.5954	36.3972	.71
63	1.4680	1.5356	1.0024	33.2063	31.3670	36.8800	.69	31.6581	36.3028	.69
66	1.4677	1.5327	1.0000	33.2183	31.4441	36.7570	.66	31.7181	36.2188	.66
69	1.4677	1.5289	0.9974	33.2293	31.5552	36.5697	.62	31.8137	36.0606	.63
72	1.4674	1.5263	0.9947	33.2550	31.6408	36.4781	.60	31.8919	35.9812	.61
75	1.4677	1.5222	0.9921	33.2713	31.7757	36.2608	.56	32.0104	35.7932	.56
77	1.4680	1.5198	0.9900	33.2956	31.8844	36.1550	.53	32.1633	35.5604	.50
78	1.4698	1.5146	0.9888	33.3126	32.0789	35.7753	.46	32.2666	35.4048	.46
79	1.4845		0.9849							
80	1.4842		0.9841							
84.5	1.4824		0.9804							
88	1.4810		0.9776							
					$\alpha_{\perp}$= 30.7379 (Å)^3	$\alpha_{\parallel}$= 38.7851 (Å)^3		$\alpha_{\perp}$= 31.1611 (Å)^3	$\alpha_{\parallel}$= 37.9387 (Å)^3	

TABLE 1c. REFRACTIVE INDICES, DENSITY AND ORDER PARAMETER S FOR D-402

T/°C	n_o	n_e	ρ/g cm^{-3}	$\bar{\alpha}$/Å^3	Vuks' Method			Neugebauer's Method		
					α_o/Å^3	α_e/Å^3	S	α_o/Å^3	α_e/Å^3	S
40	1.4730	1.5508	1.0106	35.0349	32.8309	39.4324	.73	33.1803	38.7443	.73
44	1.4723	1.5469	1.0072	35.0449	32.9238	39.2740	.70	33.2561	38.6227	.70
45.5	1.4712	1.5473	1.0063	35.0406	32.8772	39.3628	.72	33.2233	38.6752	.71
52	1.4703	1.5408	1.0012	35.0499	33.0334	39.0702	.67	33.3455	38.4589	.67
55.5	1.4695	1.5380	0.9986	35.0513	33.0898	38.9691	.65	33.4004	38.3531	.65
59.5	1.4686	1.5345	0.9958	35.0389	33.1471	38.8183	.63	33.4507	38.2154	.62
64	1.4685	1.5288	0.9923	35.0433	33.3030	38.5099	.57	33.5646	38.0007	.58
67	1.4682	1.5256	0.9897	35.0539	33.3974	38.3626	.55	33.6578	37.8462	.55
69	1.4680	1.5234	0.9879	35.0629	33.4629	38.2637	.53	33.7192	37.7505	.53
71	1.4680	1.5207	0.9860	35.0756	33.5470	38.1216	.50	33.7745	37.6779	.51
73	1.4690	1.5164	0.9841	35.0939	33.7161	37.8363	.45	33.9132	37.4554	.46
74	1.4698	1.5137	0.9832	35.1016	33.5238	37.6430	.45	34.0195	37.2659	.42
75.5	1.4840		0.9815							
76.5	1.4835		0.9791							
78	1.4828		0.9778							
80	1.4820		0.9761							
					$\alpha_\perp$= 32.1041 (Å)^3	$\alpha_\parallel$= 41.1670 (Å)^3		$\alpha_\perp$= 32.5785 (Å)^3	$\alpha_\parallel$= 40.2182 (Å)^3	

TABLE 1d. REFRACTIVE INDICES, DENSITY AND ORDER PARAMETER S FOR D-501

T/°C	n_o	n_e	ρ/g cm^{-3}	$\bar{\alpha}$/Å^3	Vuks' Method			Neugebauer's Method		
					α_o/Å^3	α_e/Å^3	S	α_o/Å^3	α_e/Å^3	S
40	1.4772	1.5445	1.0164	34.870	32.975	38.646	.73	33.270	38.070	.73
50	1.4742	1.5389	1.0087	34.900	33.065	38.561	.71	33.355	37.990	.71
60.5	1.4725	1.5302	1.0068	34.720	33.084	37.993	.63	33.354	37.452	.63
65	1.4723	1.5256	0.9970	34.956	33.430	38.005	.59	33.665	37.540	.59
70	1.4732	1.5180	0.9924	34.996	33.710	37.570	.50	33.921	37.148	.49
72.5	1.4752	1.5112	0.9896	35.033	34.000	37.107	.40	34.186	36.728	.39
74.5	1.4865		0.9861							
75.5	1.4860		0.9854							
					$\alpha_\perp$= 32.533 (Å)^3	$\alpha_\parallel$= 40.283 (Å)^3		$\alpha_\perp$= 32.936 (Å)^3	$\alpha_\parallel$= 39.477 (Å)^3	

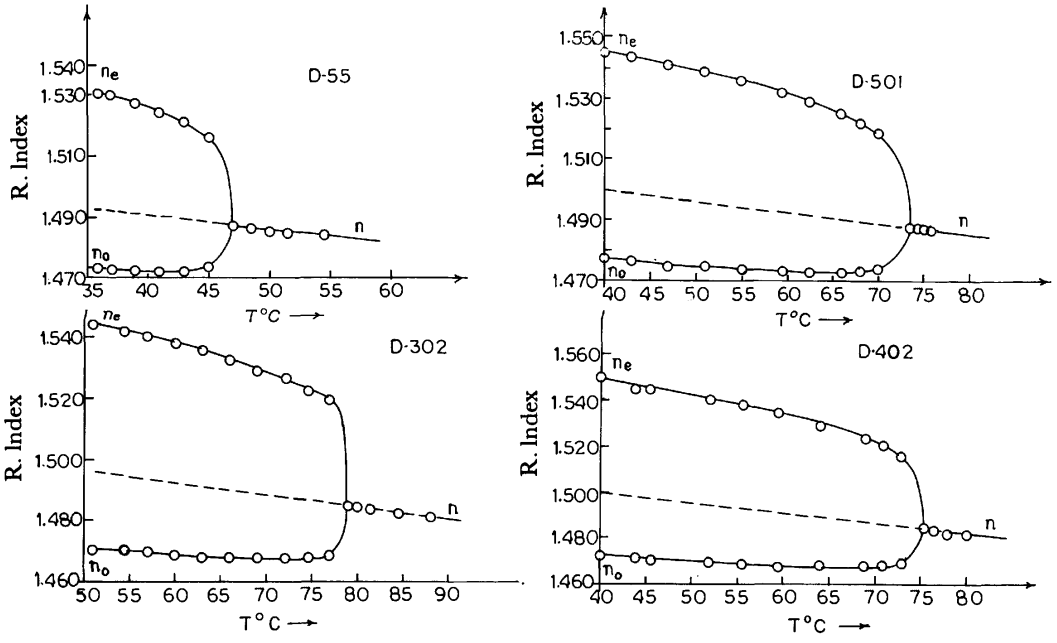

Fig. 1. Refractive index anisotropy plots for D-55, D-501, D-302, and D-402.

2) Vuks'method[8] of isotropic internal field given by

$$\frac{n_{e,o}^2-1}{\overline{n^2}+2}=\frac{4\pi N\alpha_{e,o}}{3}, \quad (4)$$

where $\overline{n^2}=1/3\ (n_e^2+2n_o^2)$.

The values of effective polarizabilities α_e and α_o obtained from the two methods are included in Tables 1 (a, b, c, d). Since the principal polarizabilities $\alpha_\parallel$ and $\alpha_\perp$, parallel and perpendicular to the long axis of the molecules in the crystalline state, were not available, the method of Haller *et al.*[9] was adopted. Graphs were plotted with $\log \alpha_e/\alpha_o$ *vs.* $\log (T_c-T)$ where T_c is the nematic-isotropic transition temperature. These plots are straight lines at lower temperatures and intersect the $\log \alpha_e/\alpha_o$ axis at 0 K assumed to correspond to $\log \alpha_\parallel/\alpha_\perp$ in the crystalline state. From Eq. 3 the values of $\alpha_\parallel$ and $\alpha_\perp$ are obtained. The order parameter S was then calculated from the relation $S=\alpha_e-\alpha_o/\alpha_\parallel-\alpha_\perp$.

Dielectric Constants $\varepsilon_\parallel$ and $\varepsilon_\perp$ and the Order Parameter. The experimental values of dielectric constants $\varepsilon_\parallel$ and $\varepsilon_\perp$ of the liquid crystals in nematic state and that in the isotropic phase ε_{iso} are given in Table 2. The dielectric anisotropy is shown in Fig. 2. The order parameter was calculated using the Maier and Meier equation,[1]

$$\Delta\varepsilon=4\pi NhF\left[\Delta\alpha-\frac{F\mu^2}{2kT}(1-3\cos^2\beta)\right]S, \quad (5)$$

where N is the number of molecules per 1 cm^3, $h=3\overline{\varepsilon}/(2\overline{\varepsilon}+1)$, the cavity field factor, $F=1/(1-\overline{\alpha}f)$, the reaction field factor, and $f=4\pi N(2\overline{\varepsilon}-2)/3(2\overline{\varepsilon}+1)$, μ the dipole moment of the molecule, $\Delta\alpha$=polarizability anisotropy $=\alpha_e-\alpha_o$, and $\Delta\varepsilon=\varepsilon_\parallel-\varepsilon_\perp$ dielectric anisotropy.

The dipole moments μ of the liquid crystal molecules were determined in dilute solutions in benzene and included in Table 2. The angle between the resultant moment and the long axis of the molecules of the liquid crystals (β) was calculated from the alkoxyl

Table 2. Values of dielectric permittivities $\varepsilon_\parallel$, $\varepsilon_\perp$, and ε_{iso}

D-55			D-302			D-402			D-501		
T/°C	$\varepsilon_\parallel$	$\varepsilon_\perp$	T/°C	$\varepsilon_\parallel$	$\varepsilon_\perp$	T/°C	$\varepsilon_\parallel$	$\varepsilon_\perp$	T/°C	$\varepsilon_\parallel$	$\varepsilon_\perp$
37.5	2.940	3.419	51	3.2816	4.5447	40	3.2720	4.4947	43	3.4125	4.4595
40	2.958	3.396	54.5	3.2798	4.5150	52	3.2355	4.3607	47	3.3583	4.4137
42	2.958	3.382	60	3.2952	4.4732	59.5	3.2483	4.2246	51	3.3685	4.2837
44	2.984	3.351	66	3.3024	4.4155	69	3.3229	4.0941	55	3.3182	4.2423
46	2.997	3.313	72	3.3369	4.2613	73	3.3572	4.0179	60.5	3.3372	4.1875
50 iso	3.226		77	3.3566	4.1899	77 iso	3.7435		65	3.3560	4.1244
52	3.217		80	3.4673	4.0482	80	3.7143		70	3.4083	3.9952
54	3.208		84.5 iso	3.8518		85	3.6798		74 iso	3.8101	
			88	3.8308		88	3.6548		76	3.7936	
			90	3.8208					78	3.7727	
									80	3.7563	
									85	3.7110	
μ=1.99 D, β=66°			μ=2.17 D, β=72°			μ=2.08 D, β=72°			μ=2.23 D, β=68°		

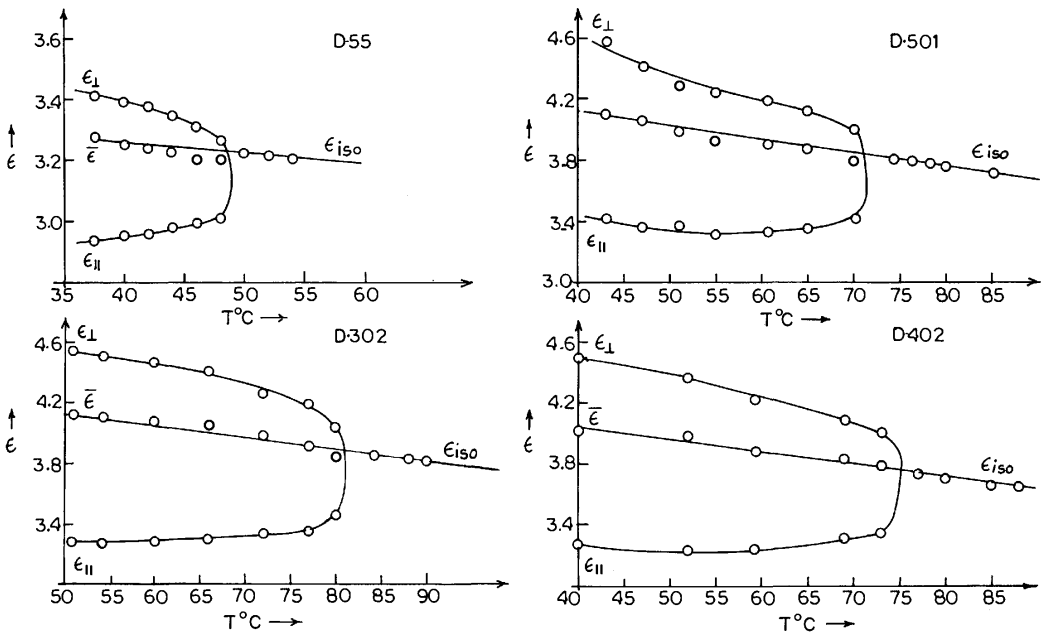

Fig. 2. Dielectric anisotropy plots for D-55, D-501, D-302, and D-402.

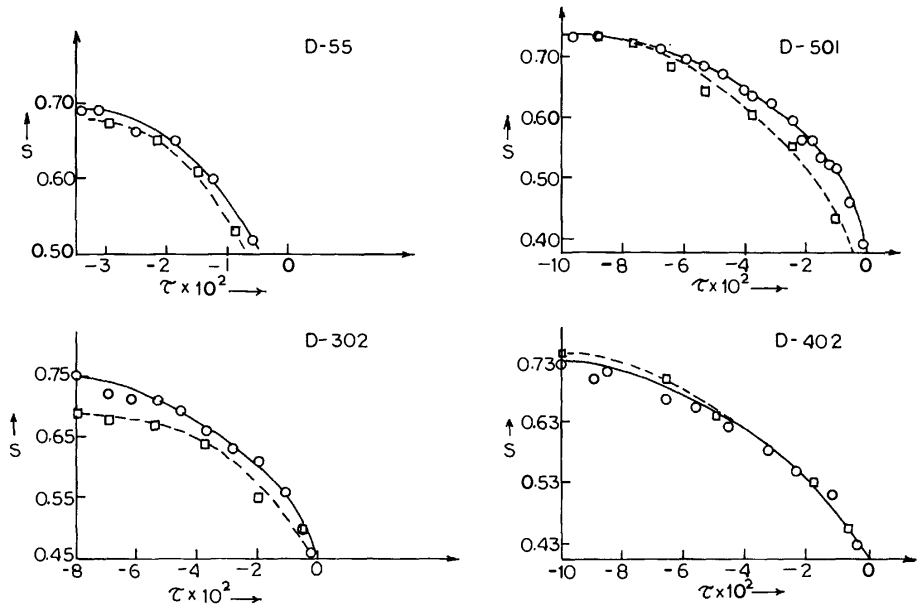

Fig. 3. Plots of order parameter S *vs.* $\tau=(T-T_{NI})/T_{NI}$.
By O—Neugebauer's method, and □—Maier and Meier's method.

group moment and ester group moment reported in the literature.[10] The angle β for the different samples is given in Table 2.

Discussion

It can be seen from Tables 1 (a, b, c, d) that the order parameters S for the liquid crystals under study, obtained from the refractive indices using 1) Neugebauer and 2) Vuks methods are comparable. The S value decreases with increase of temperature till it suddenly vanishes at the clearing temperature. The order parameters for these liquid crystals have not been reported so far.

From Fig. 2, it can be seen that the average dielectric constants $\bar{\varepsilon}=(\varepsilon_{\parallel}+2\varepsilon_{\perp})/3$ in the nematic phase practically coincide with the dielectric constants ε_{iso} in the isotropic phase. These results are similar to those reported by de Jeu[3] in the case of liquid crystals of very small or zero dipole moment but unlike to the case of liquid crystals having large dipole moment (μ=4—5 Debye) of which the average dielectric constant ε_{iso} in the isotropic phase reported by different workers.[11,12]

From Table 2, it can be seen that the values of the order parameter S, calculated from the values of the dielectric anisotropy $\Delta\varepsilon$, polarizability anisotropy $\Delta\alpha$ and dipole moment μ using the Maier and Meier equation for the alkoxyphenyl *trans*-4′-alkylcyclohexanecarboxylates, compare very well at all temperatures with those obtained from refractive index methods. Similarly for alkylphenyl *trans*-4′-alkylcyclohexanecarboxylates, the order parameters S from the Maier and Meier equation also agree well with those obtained from the refractive index methods, though the former values are only slightly less than the latter. The slight discrepancy may be due to the estimation of the angle β made by the resultant moment with the long axis of the molecule. So, it appears that for liquid crystals having dipole moment of about 2D, or so, the Maier and Meier equation with dielectric anisotropy $\Delta\varepsilon$, provides another method for the determination of the order parameter.

The inapplicability of the Maier and Meier theory[1] for dielectric constants in strongly polar nematics might be due to short range antiferroelectric dipole correlation of the permament dipole moment as proposed by Madhusudana and Chandrasekhar,[5] which might cause a large decrease in $\varepsilon_{\parallel}$ in strongly polar nematics (μ>4 D); Such a decrease in $\varepsilon_{\parallel}$ in less polar nematics ($\mu\approx$2D) might not affect the dielectric anisotropy and hence the order parameter very effectively.

Of course some more liquid crystals having moments of more or less 2D should be studied before drawing definite conclutions.

Our sincere thanks to Dr. S. B. Roy for his guidance.

References

1) W. Maier and G. Meier., *Z. Naturforsch.*, *A*, **16**, 262 (1961).

2) W. H de Jeu and Th. W. Lathouwers, *Z. Naturforsch.*, *A*, **29**, 905 (1974).

3) W. H. de Jeu and Th. W. Lathouwers, *Z. Naturforsch.*, *A*, **30**, 79 (1975).

4) S. Sen, P. Brahma, S. K. Roy, and S. B. Roy, *Acta Phys. Pol.*, *A*, **65**, 47 (1984).

5) N. V. Madhusudana and S. Chandrasekhar, Proc, International Conf. on Liquid Crystals, Bangalore (1973), p. 427.

6) C. D. Hodgman, R. C. Weast, R. S. Shanklend, and S. M. Selby, "Handbook of Chemistry and Physics," The Chemical Rubber Publishing Co., Cleveland, Ohio (1962)

pp. 2556—2557.
7) H. E. J. Neugebauer, *Can. J. Phys.*, **32**, 1 (1954).
8) M. F. Vuks, *Opt. Spektrosk*, **20**, 361 (1966).
9) I. Haller, H. A. Huggins, H. R. Lilienthal, and T. R. McGuire, *J. Phys. Chem.*, **77**, 950 (1973).
10) V. I. Minkin, O. A. Osipov, and Y. A. Zhadanov, "Dipole Moments in Organic Chemistry," Plenum Press, NY-London (1970), p. 91.
11) M. Schadt, *J. Chem. Phys.*, **56**, 1494 (1972).
12) B. R. Ratna and R. Sashidhar, *Pramana*, **6**, 278 (1976).

Studies on Double Malonates. II.† Potassium Rare Earth Malonates, $K_5Ln(C_3H_2O_4)_4$ (Ln=Gd–Ho or Y)

Mahadeo Anant NABAR* and Bharat Nilkanth JUKAR

Department of Chemistry, University of Bombay, Vidyanagari, Bombay-400 098, India

(Received May 4, 1984)

Double malonates of some of the rare earths with potassium having formula $K_5Ln(C_3H_2O_4)_4$ were synthesized. The lattice parameters of the compounds were determined by X-ray powder diffractometry. Infrared absorption spectroscopy was employed to throw some light on the nature of Ln–O bonding, while the thermoanalytical techniques were made use of in proposing the thermal decomposition mechanism of some of the double malonates.

Davitashvili and his coworkers have carried out a systematic study of the double oxalates of rare earth elements with alkali metals.[1–5] However, practically no attention has been paid to the corresponding double compounds of malonic acid — the next higher homologue of oxalic acid; the only report available in the literature being on the cerium(III) double malonates.[6] Thus, it was thought worthwhile to carry out systematic work on such type of double malonates, taking rare earths and different alkali or pseudo alkali metals.[7] The present paper, which is a part of this investigation, deals with the potassium double malonates, $K_5Ln(C_3H_2O_4)_4$, where Ln=Gd–Ho or Y.

Experimental

Synthesis. The normal rare earth malonates were precipitated by adding slowly about 14 cm^3 of aqueous potassium malonate solution (134 mg $(C_3H_2O_4)^{2-}$ cm^{-3}), to the aqueous *ca.* 0.011 M rare earth nitrate solution, with constant stirring. The precipitate obtained was filtered, washed free of nitrate ions and excess of potassium malonate, and dried over silica gel under vacuum till constant weight.

The normal rare earth malonates were dissolved in the aqueous potassium malonate solution in Ln^{3+}: $(C_3H_2O_4)^{2-}$ molar proportion of 1 : 5 since it was observed that for the molar proportions equal to 1 : 2, 1 : 3, and 1 : 4, a syrupy product was obtained on evaporation. The turbid mixture was warmed to get a clear solution, which gave the desired product when allowed to crystallize slowly over silica gel. The crystals formed were picked up from the mother liquor and were washed with 50 cm^3 of 90% methanol; dried over silica gel under vacuum and stored in a desiccator because of its hygroscopic nature. All the chemicals used were of reagent grade quality.

It is interesting to note here that although the normal rare earth malonates and potassium malonate were mixed in the Ln^{3+}: $(C_3H_2O_4)^{2-}$ mole ratio as 1 : 5, the synthesized compounds were in the mole ratio 1 : 4.

Chemical Analysis. The rare earth contents of the double malonates were determined complexometrically. The potassium percentage was determined flame photometrically.

The malonate contents were determined using ion-exchange technique. Since the compounds tend to hydrolyse on dissolving in water, known volume of dilute hydrochloric acid was used for dissolution. The sample solution was passed through a cation exchanger (Seralite SRC 120) in hydrogen form (washed free of excess acid used for regeneration) at a rate of 2—3 cm^3min^{-1}. As the malonate ion gets adsorped on the strongly acidic sulphonated resin,[8] the column was eluted with 100—150 cm^3 of hot deionised water (363—373 K), to facilitate the complete desorption of the anion. The rate of flow of the effluent was 6—7 cm^3min^{-1} while washing the column with hot water so as to keep the resin warm throughout. The eluate thus obtained contains the malonic acid (equivalent to the malonate ion in the compound) plus the hydrochloric acid used for dissolution. This eluate was titrated with standard sodium hydroxide solution. The hydrochloric acid used for the dissolution was determined by following the same procedure as used for the sample solution so as to compensate for procedural errors. The reading corresponding to malonic acid was obtained by subtracting the reading corresponding to hydrochloric acid from the total reading for the eluate. The analytical results are given in Table 1.

Table 1. Results of chemical analysis of $K_5Ln(C_3H_2O_4)_4$

Ln	K/%		Ln/%		$C_3H_2O_4$/%	
	Calcd	Found	Calcd	Found	Calcd	Found
Gd	25.70	25.93	20.67	20.78	53.63	53.40
Tb	25.65	25.73	20.84	20.90	53.51	53.71
Dy	25.61	25.45	21.13	21.23	53.26	53.45
Ho	25.45	25.71	21.46	21.35	53.09	53.00
Y	28.26	28.60	12.84	12.61	58.90	58.60

Instrumentation. Nickel filtered Cu $K\alpha$ radiation (mean λ=154.18 pm), operated on Philips X-ray diffractometer model No. PW 1009/30-NRD 1023, was used for the X-ray powder diffraction study. The relative intensities of the reflexions were calculated by taking that of the highest peak as 100.

The densities of the double malonates were determined by floatation method, using bromoform–hexane mixture as the working medium.

The densities of the double malonates were determined by malonates, were made in the frequency range 4000—400 cm^{-1} with a Perkin-Elmer model 377, by CsBr disc method; while the spectra of some of the intermediates obtained by isothermally heating the original compound, were scanned on Beckman IR-4250 spectrophotometer in the frequency range 4000—200 cm^{-1} using KBr pellet technique.

The TG and DTG curves of the gadolinium and holmium double malonates were scanned on a sophisticated Mettler Recording Vacuum Thermoanalyser (No. 84), in dry air, with a flow rate of 100 cm^3min^{-1}. A Pt/Pt–Rh thermocouple

† For Part I, See M. A. Nabar and B. N. Jukar, *Can. J. Chem.*, **62**, 348 (1984).

†† 1 M=1 mol dm^{-3}.

TABLE 2. CRYSTAL DATA FOR $K_5Ln(C_3H_2O_4)_4$

Ln	a/pm	b/pm	c/pm	β/deg	V/pm$^3\times10^6$	D_{calcd}/Mg m^{-3}	D_{obsd}/Mg m^{-3}
Gd	743±1	1367±2	991±1	93.10±0.16	1005	2.51	2.48
Tb	746±1	1366±3	989±1	13.79±0.17	1006	2.52	2.50
Dy	746±1	1367±2	987±1	93.46±0.10	1005	2.53	2.52
Ho	742±1	1363±2	985±1	93.20±0.10	996	2.56	2.54
Y	746±1	1365±2	988±1	93.28±0.13	1004	2.29	2.30

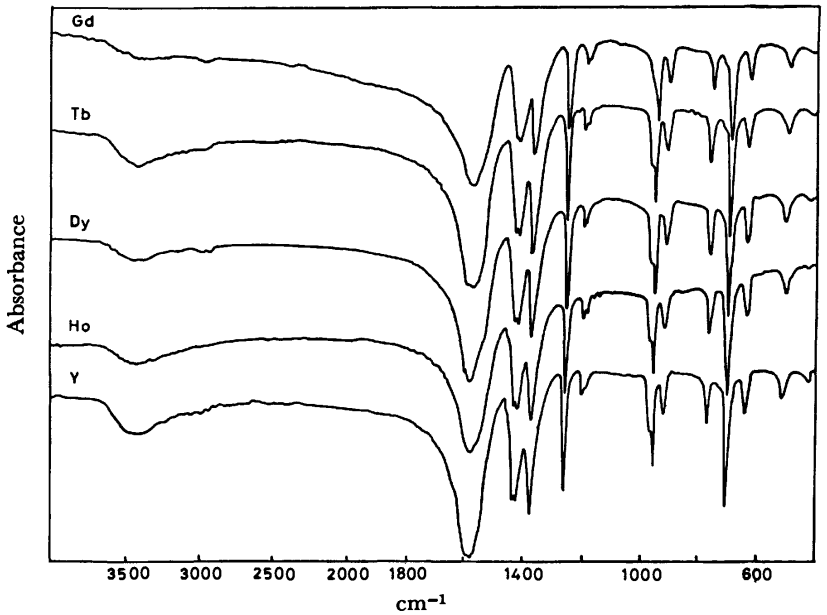

Fig. 1. Infrared absorption spectra of $K_5Ln(C_3H_2O_4)_4$.

was used for temperature detection. The samples were heated in an alumina crucible of volume 0.5 cm^3, at a rate of 10 K min^{-1}. The DTA curves were obtained with the help of an instrument fabricated in this laboratory.[7]

Results and Discussion

X-Ray Diffraction Study. The X-ray powder patterns for the present compounds show that the compounds are isomorphous. On analyzing with Ito's method,[9] the double malonates were found to possess a monoclinic symmetry, with two molecules per unit cell. The systematic absence of reflexes ($0k0 : k=2n+1$), suggests that the probable space group is $P2_1/m$ or $P2_1$. The lattice parameters were refined by least squares method. The unit cell dimensions and the other relevant data are given in Table 2. The decrease in unit cell volumes is not regular as is normally expected. The cell dimension "c" decreases from gadolinium to holmium linearly with decrease in ionic radii, but such regular decrease in "a" and "b" is not observed. The complete indexed data of dysprosium double malonate are given in Table 3, as a representative.

Infrared Spectroscopic Studies. The double malonates are isomorphous and hence expectedly their infrared spectra exhibit similar patterns (Fig. 1). The assignments for the various bands are based on the earlier reports.[6,10,11]

A very strong band at ≈1585 cm^{-1} and a strong one at ≈1380 cm^{-1} have quite easily been assigned to the

TABLE 3. X-RAY POWDER DIFFRACTION DATA FOR $K_5Dy(C_3H_2O_4)_4$

h k l	d_{calcd}/pm	d_{obsd}/pm	I/I_0
0 1 1	799	798	31
1 0 0	745	745	31
0 2 0	683	684	31
1 0 $\bar{1}$	612	614	31
0 0 2	493	492	35
1 2 1	441	441	27
1 1 $\bar{2}$	404	404	15
2 0 0	372	370	77
0 0 3	328	328	100
2 2 1	306	306	12
2 0 $\bar{2}$	306		
2 0 2	289	290	19
1 4 2	260	259	92
0 0 4	246	247	19
1 5 1	247		
3 1 0	244	244	12
2 1 3	236	235	15
1 1 $\bar{4}$	235		
3 1 2	214	214	15
2 5 1	213		
2 3 3	212	212	23
1 6 1	212		
1 5 $\bar{3}$	204	204	42
3 2 3	185.3	185.4	27
2 3 4	183.1	183.3	19

asymmetric and symmetric stretching vibrations of OCO group, respectively. It can be seen that these frequencies in case of the double malonates have shifted to higher and lower values, respectively, as against the corresponding frequencies in potassium malonate[10] (1563 and 1405 cm^{-1}), suggesting an increase in the covalent nature of Ln–O bond. A band with medium intensity at $\approx$780 cm^{-1} and the one with a strong intensity at $\approx$710 cm^{-1}, are probably due to OCO deformation vibrations.

The C–H stretching vibrations are observed as two very weak bands in the region 3000—2900 cm^{-1}. Strong bands at $\approx$1440 and $\approx$1260 cm^{-1} are attributed to CH_2 bending and wagging modes, respectively.

A weak broad absorption is observed in the OH stretching region, probably due to the moisture absorbed by these hygroscopic compounds.

Thermoanalytical Investigation. In order to get the insight of the thermal decomposition mechanism, the double malonates of gadolinium and holmium were subjected to the thermoanalytical investigation as representatives of the series. The corresponding thermal curves are reproduced in Figs. 2 and 3. The thermoanalytical data are given in Table 4.

The anhydrous nature of the double malonates is reflected in non observance of the dehydration stage on the thermal curves; and the decomposition of both the compounds commences at 543 K. The breaks corresponding to the formation of an intermediate of probable composition $K_{10}Ln_2O(CO_3)_3(OCOCHOCO)_4$ are observed on the TG curves at 613 and 623 K for gadolinium and holmium compounds, respectively. Formation of such a type of intermediate has also been reported in the thermal decomposition of lanthanum malonate pentahydrate.[12] It is apparent from the TG and DTG curves of both the double malonates that the decomposition of holmium compound to $K_{10}Ho_2O(CO_3)_3(OCOCHOCO)_4$ is a two stage process, the first one involving formation of $K_{10}Ho_2O(CO_3)_{1.5}(OCOCHOCO)_{5.5}$, whereas the corresponding two stages in case of gadolinium double malonate are probably overlapped. The non observance of the first stage on the TG and DTG curves of gadolinium compound can probably be due to the comparatively larger amount of the sample taken in this case (57.77 mg as against 25.9 mg of holmium double malonate). A very sharp exotherm observed at 578 K on the DTA curve of holmium double malonate can be attributed to the formation of the first stage intermediate, $K_{10}Ho_2O(CO_3)_{1.5}(OCOCHOCO)_{5.5}$. From the analogy with

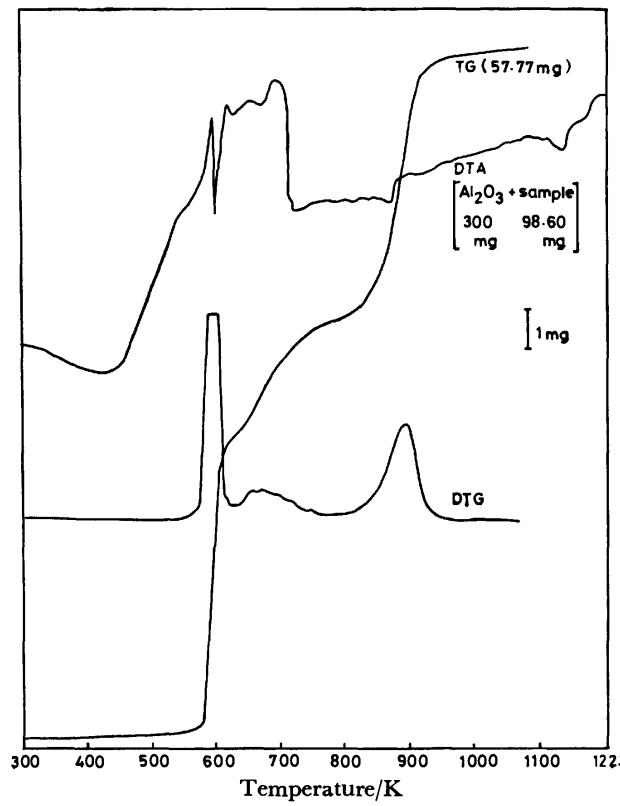

Fig. 2. Thermoanalytical curves of $K_5Gd(C_3H_2O_4)_4$.

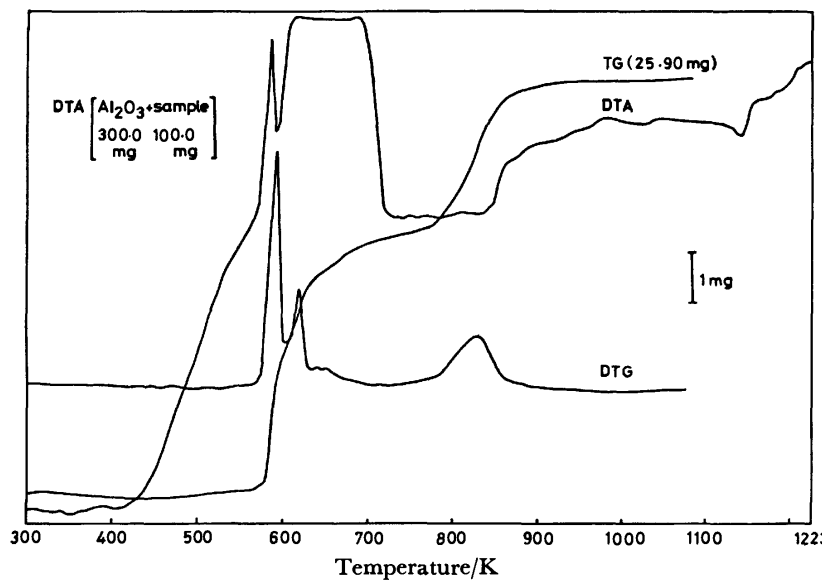

Fig. 3. Thermoanalytical curves of $K_5Ho(C_3H_2O_4)_4$.

TABLE 4. THERMOANALYTICAL RESULTS FOR $K_5Ln(C_3H_2O_4)_4$

DTA temp/K	TG temp range/K	DTG temp/K	% Loss		Interpretation
			Calcd	Obsd	
Ln=Gd					
					$2K_5Gd(C_3H_2O_4)_4$
588 (exo)					↓
608 (exo)	543— 613	588	14.20	13.31	$K_{10}Gd_2O(CO_3)_3(OCOCHOCO)_4$
648 (exo)					↓
693	613— 743	663	4.28	5.02	$K_{10}Gd_2O_2(CO_3)_{2.5}(OCOCHOCO)_{3.5}$
					↓
873 (endo)	743—1023	883	12.30	12.05	$5K_2CO_3+Gd_2O_3$
1153 (endo)	—	—	—	—	Melting of K_2CO_3
Ln=Ho					
					$2K_5Ho(C_3H_2O_4)_4$
					↓
578 (exo)	543— 593	593	10.05	9.92	$K_{10}Ho_2O(CO_3)_{1.5}(OCOCHOCO)_{5.5}$
					↓
598—683 (broad, exo)	593— 623	613	4.00	5.10	$K_{10}Ho_2O(CO_3)_3(OCOCHOCO)_4$
					↓
	623— 723	643	4.20	4.05	$K_{10}Ho_2O_2(CO_3)_{2.5}(OCOCHOCO)_{3.5}$
					↓
	723— 983	823	12.20	12.04	$5K_2CO_3+Ho_2O_3$
1158 (endo)	—	—	—	—	Melting of K_2CO_3

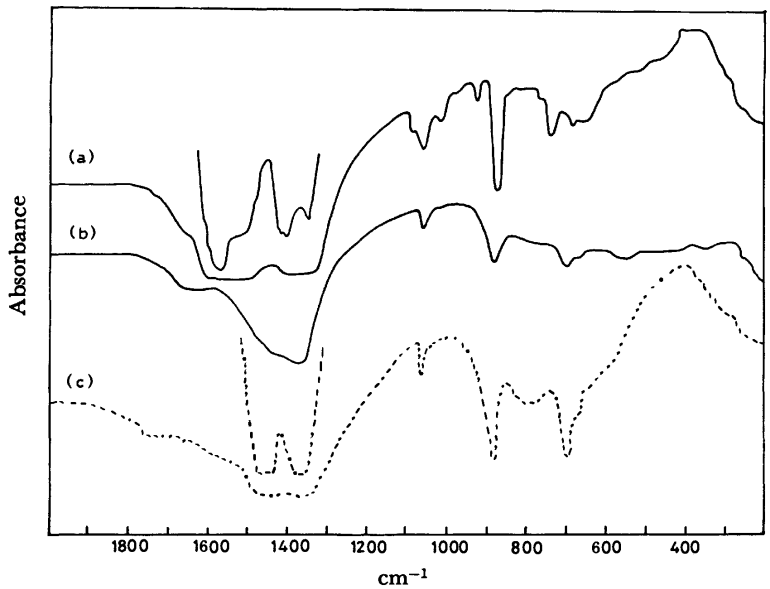

Fig. 4. Infrared absorption spectra of $K_5Ho(C_3H_2O_4)_4$ heated at a) 648 K, b) 723 K, and c) K_2CO_3.

the holmium compound, a similar sharp exotherm at 588 K in case of gadolinium compound can be accounted for the formation of a similar intermediate.

The intermediate $K_{10}Ln_2O(CO_3)_3(OCOCHOCO)_4$, decompose exothermically to give $K_{10}Ln_2O_2(CO_3)_{2.5}$-$(OCOCHOCO)_{3.5}$ in the temperature range 613—743 and 623—723 K, in case of gadolinium and holmium compounds, which in turn decompose to give mixture of respective rare earth oxide and potassium carbonate, at temperatures 1023 and 983 K, respectively. The endothermic effect observed at 873 K on the DTA curve of gadolinium compound is probably due to the final decomposition; however, the corresponding effect in case of holmium double malonate is not easily discernible. The endothermic activities observed at about 1153 K in case of both the compounds are probably due to the melting of potassium carbonate formed (mp of K_2CO_3 is 1174 K[13]).

The following mechanism can thus be proposed for the decomposition of the double malonates:

$$2K_5Ln(C_3H_2O_4)_4 \longrightarrow K_{10}Ln_2O(CO_3)_{1.5}(OCOCHOCO)_{5.5} \longrightarrow K_{10}Ln_2O(CO_3)_3(OCOCHOCO)_4 \longrightarrow K_{10}Ln_2O_2(CO_3)_{2.5}(OCOCHOCO)_{3.5} \longrightarrow 5K_2CO_3 + Ln_2O_3$$

The holmium double malonate heated isothermally at 550 K (21 % loss), on qualitative analysis indicated the presence of carbonate. The infrared spectra of the

intermediate (Fig. 4a) exhibits no bands ascribable to CH_2 wagging mode, indicating the absence of malonate group. A very weak band, however, is detected at $\approx 3000\ cm^{-1}$, suggesting the presence of CH group. These observations support the assumption that the (OCOCHOCO) group is present in the intermediate. The intermediate obtained was contaminated with free carbon which might have formed due to the disproportionation of liberated CO, as has been suggested earlier in the study of lanthanum oxalate.[14]

The spectrum of the final decomposition product exhibits the bands characteristic of potassium carbonate and holmium sesquioxide (Fig. 4b).

The authors are indebted to Mr. P. V. Adarkar for extending the spectral facility and to the Director, Tata Institute of Fundamental Research, Bombay, for the X-ray facility. We are also thankful to Mr. Chakraborty, Radiochemistry Division, B.A.R.C., for the facility of Mettler Thermo Analyser. One of the authors (B.N.J.) is grateful to the University of Bombay for financial assistance.

References

1) E. G. Davitashvili and M. E. Modebadze, *Soobshch. Akad. Nauk Gruz. SSR*, **39**, 305 (1965).
2) E. G. Davitashvili, M. E. Modebadze, and N. G. Sheliya, *Soobshch. Akad. Nauk Gruz. SSR*, **40**, 325 (1965).
3) E. G. Davitashvili, N. G. Sheliya, and M. E. Modebadze, *Zn. Neorg. Khim.*, **14**, 917 (1969).
4) E. G. Davitashvili, M. E. Modebadze, and N. G. Sheliya, *Zh. Neorg. Khim.*, **16**, 655 (1971).
5) Zh. Sh. Kublashvili and E. G. Davitashvili, *Zh. Neorg. Khim.*, **16**, 1526 (1971).
6) J. Mach, *Monatsh. Chem.*, **100**, 1839 (1969).
7) B. N. Jukar, Ph. D. Thesis, University of Bombay, 1982.
8) O. Samuelson, "Ion Exchange Separation in Analytical Chemistry," John Wiley and Sons, Inc., New York (1963), p. 176.
9) T. Ito, "X-ray Studies on Polymorphism," Maruzen Co. Ltd., Tokyo (1950), p. 187.
10) M. J. Schmelz, I. Nakagawa, S. Mizushima, and J. V. Quagliano, *J. Am. Chem. Soc.*, **81**, 287 (1959).
11) B. S. Azikov, S. E. Kharzeeva, Z. A. Grankina, and V. V. Serebrennikov, *Zh. Neorg. Khim.*, **13**, 1831 (1968).
12) K. Nagase, K. Muraishi, M. Kikuchi, and N. Tanaka, *Thermal Anal. (Proc. Int. Conf. Therm. Anal.)* 6th, **2**, 159 (1980).
13) "Handbook of Chemistry," 12th ed, ed by N. A. Lange, McGraw-Hill, New York, (1967), p. 493.
14) A. Glasner and M. Steinberg, *J. Inorg. Nucl. Chem.*, **16**, 279 (1961).

Effects of Solvents and pH on the Spectral Behavior of 2-(*p*-Aminophenyl)benzimidazole

Ashok Kumar MISHRA and Sneh Kumar DOGRA*

Department of Chemistry, Indian Institute of Technology, Kanpur-208016, U.P., India

(Received May 4, 1984)

The absorption and fluorescence spectra in different solvents and at various pH have indicated that monocation and dication of 2-(*p*-aminophenyl)benzimidazole ($PBNH_2$) are formed by protonating first the tertiary amine nitrogen atom and then the amino group, both in S_0 and S_1, whereas the monoanion in S_0 is obtained by deprotonating the imino group but in S_1, it is formed by deprotonating the amino group. Dianion at H_15 in S_1 is obtained by deprotonating the amino and then imino group.

The spectral shift, shape of the spectral band, Stokes' shift *etc.* depend upon the geometry of the molecule in the ground and excited states, the nature and the position of functional group in the molecule and nature of solvents.[1] In case of biphenyl,[2] S_1 state is relatively more planar than S_0 and large Stokes' shift has been attributed to this change in the geometry on excitation and broad absorption band involving overlapping of two transitions. The presence of groups, like alkyl, amino, vinyl, and phenyl, at the para position shift the long wavelength band towards red and make the molecule a little more planar.[3,4] The presence of these groups at the ortho position shift the spectra towards blue unless the biphenyl molecule along with the substituents form a rigid planar molecule. Similarly in case of 2-phenylnaphthalene,[5] the Stokes' shift of 1770 cm^{-1} is attributed both to the phenyl group rotation and solvent stabilization.

Recently our study on 2-phenylbenzimidazole (PBI)[6] has shown that the Stokes' shift is quite small ($\approx$324 cm^{-1}), indicating that this molecule is planar or nearly planar in S_0 and S_1 states. The presence of amino group in the ortho position of 2-phenyl-substituted benzimidazole leads to a rigid molecule, formed through the intramolecular hydrogen bonding, thus leading to two four-membered ring systems.[7a] The present study of 2-(*p*-aminophenyl)benzimidazole ($PBNH_2$) was carried out to study the above-mentioned effects and the changes observed in the absorption and fluorescence spectra in different solvents and at various pH. The equilibrium constants of various prototropic reactions are calculated both in S_0 and S_1 states.

Experimental

$PBNH_2$ was prepared by heating an equimolar mixture of *o*-phenylenediamine and *p*-aminobenzoic acid at 250 °C, as described in literature[8] and purified further by recrystallization from ethanol. The purity was checked by getting similar fluorescence maxima when excited with different excitation wavelengths. BDH spectrograde methanol, analytical grade sulfuric acid and sodium hydroxide were used as such. Analytical grade acetonitrile (E. Merck), cyclohexane, ether, dioxane, heptane (BDH), and ethanol were further purified by methods described in literature.[9] Triply distilled water was used for the preparation of aqueous solutions. A modified Hammett's acidity scale[10] (H_0) for H_2SO_4–H_2O mixture and Yagil's[11] basicity scale (H_-) for NaOH-H_2O mixture were used for the solutions below pH 1 and above pH 13 respectively.

Absorption spectra were recorded in a Cary 17-D spectrophotometer. Fluorescence spectral measurements were carried out on a recording spectrofluorometer, fabricated in our laboratory and details are described elsewhere.[12] The band width of excitation radiation is 8 mn and both the monochromators are calibrated, from time to time with low pressure mercury lamp. pH in the range 1—13 were measured on a Toshniwal pH meter, model CL-44A. The concentrations of the solutions were of the order of 10^{-5} to 10^{-4} M†. Quinine sulfate in 0.1 M H_2SO_4[13] was taken as the standard for measuring quantum yields, and wavelength used for excitation was 315 nm. The solutions for absorptiometric and fluorimetric titrations were prepared just before the measurements. In fluorimetric titrations, isosbestic wavelengths were used for excitation of different species. The values for dication–monocation, monocation–neutral and neutral–monoanion are 295, 320, and 315 nm respectively.

Results and Discussion

Effect of Solvents on Absorption and Fluorescence Spectra. The absorption and fluorescence spectra of $PBNH_2$ were observed in solvents of different polarity and of hydrogen bond formation tendency. The former is shown in Fig. 1 and the latter in Fig. 2. The absorption maxima, log ε_{max} (except in heptane where the saturated solution was used) are listed in Table 1, whereas the fluorescence maxima and fluorescence quantum yields are listed in Table 2. The two normal band systems of benzimidazole molecule (278, 272 nm, L_b; 243 nm, L_a) are kept intact except that both are red shifted (333, 318 nm, L_b; 277, 268, 258 nm, L_a) and the third band system, λ_{max} (abs) $\approx$207 nm is also observed. The L_b band system is similar to that of benzimidazole, but the structure is lost and is also red shifted as the polarity of the solvent increases except in water, where the broad band is red shifted with respect to heptane but blue shifted with respect to methanol and acetonitrile, the latter being a weakly hydrogen accepting solvent. The behavior of the 207 nm band system is similar to that of L_b one under the similar environments. Whereas the structure of L_a band system also undergoes the similar changes as the L_b one, the band maxima is regularly blue shifted.

The data of Table 2 indicate that the fluorescence spectrum of $PBNH_2$ is nicely structured in less polar solvents and can be explained by the vibrational frequency of $\approx$1450 cm^{-1} in S_0 state. The fluorescence

† 1 M = 1 mol dm^{-3}.

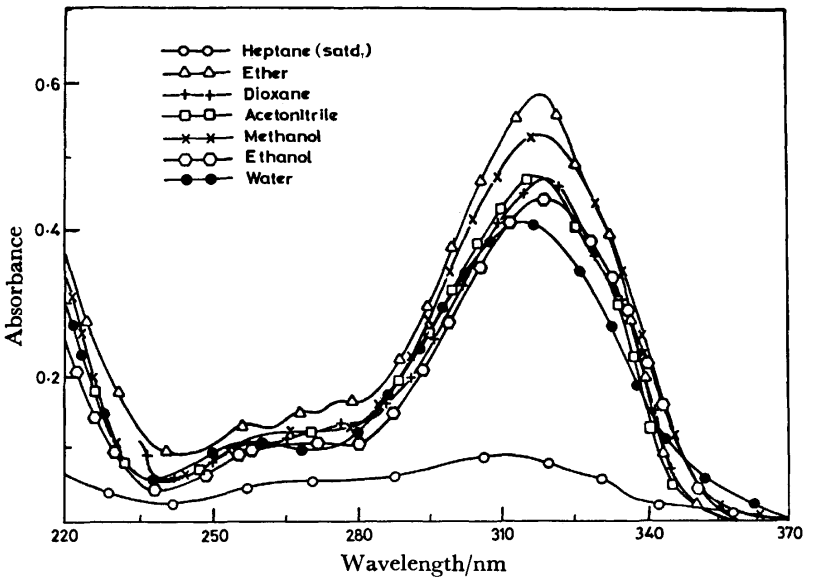

Fig. 1. Absorption spectra of $PBNH_2$ in various solvents at 298 K. (concn 2.5×10^{-5} M)

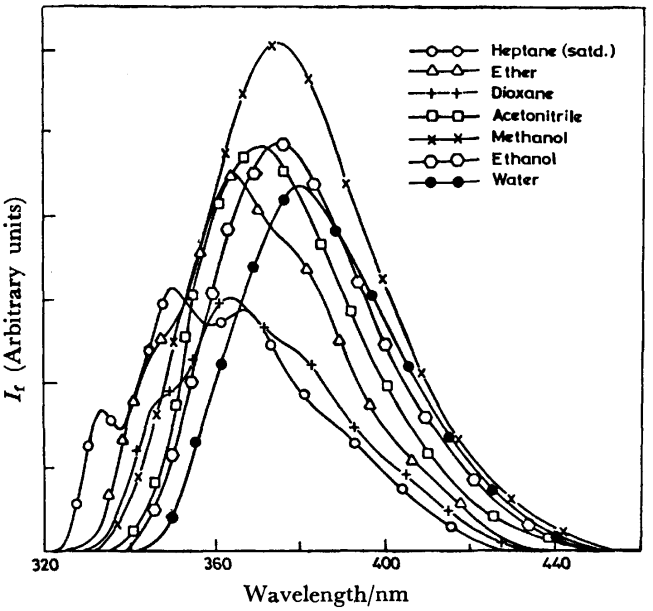

Fig. 2. Fluorescence spectra of $PBNH_2$ in various solvents at 298 K. (concn 2.5×10^{-5} M)

spectrum of $PBNH_2$ is similar to that of 2-phenylbenzimidazole (PB)[6] and the vibrational frequency in $PBNH_2$ is nearly equal to that observed in PB ($\approx$1500 cm^{-1}). The 0-0 band in the fluorescence spectrum of $PBNH_2$ in heptane can be assigned to the shortest wavelength band of 334 nm. Structure of the band is lost and the band is regularly red-shifted with the increase in the polarity and hydrogen bond formation tendency of solvents, but this effect was not as large as observed for 2-(*m*-aminophenyl)benzimidazole.[7b] The fluorescence quantum yield of $PBNH_2$ increases under the similar conditions in contrast to PB[6] (for this compound the quantum yield remains nearly constant *i.e.* 0.12+0.01 for these solvents), 2-(*m*-aminophenyl)benzimidazole ($MBNH_2$, in this case the quantum yield decreases from 0.146 to 0.08 for solvents ranging from heptane to water) and is even slightly larger than that of benzimidazole in ethanol[14] (0.7). Another fluorescence band is observed at long-wavelength (maximum at 500 nm) and its intensity is much smaller than that of short-wavelength fluorescence band, however the ratio (I_{382}/I_{500}) remains unchanged with the change in the concentration (10^{-5} to 10^{-3} M) of solute, change of solvent and pH of the solution.

It has been shown by Tway and Love[15] that the longwavelength transition in benzimidazole and 2-(4-thiazolyl)benzimidazole is of π-π^* character in non-aqueous polar solvents. Further, the absorption and fluorescence spectra of these compounds are affected by the nature of solvents although the effect is small. Similarly to other amino substituted benzimidazoles or indazoles, $PBNH_2$ also possesses two positions which can accept protons and two sites which can donate protons to the solvents. Thus the spectral shifts observed depend upon the preferential interactions of the solvents with the solute molecule. The high extinction coefficient, red shift in λ_{max} (abs) with increase in the polarity of solvents and high fluorescence yield, all confirm the π—π^* nature of the transition. The small blue shift noticed in water relative to methanol or acetonitrile tells that water is acting as better hydrogen donor solvent to the lone pair of the amino group rather hydrogen acceptor one.

Fluorescence results can also be explained exactly on the same lines. Stokes' shift [ν_{max}(abs)$-\nu_{max}$(fluo)], thought it is large, does not increase significantly with the increase in the polarity of solvents. This indicates that there is no significant change in dipole moment of $PBNH_2$ in S_1 state from that in S_0 and this could be due to the charge migration from carbocyclic ring to the heterocyclic ring, leaving some positive charge

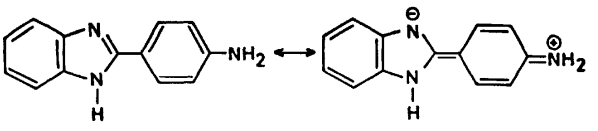

Table 1. Absorption maxima and $\log \varepsilon_{max}$ of $PBNH_2$ in various solvents and at different pH at 298 K

Solvent	λ_{max}(abs)/nm, ($\log \varepsilon_{max}$)					
Heptane	207		270		310	330[a]
Dioxane	—	258 (3.64)	268 (3.70)	277 (3.73)	318 (4.27)	333 (4.09)
Ether	210 (4.35)	257 (3.71)	268 (3.87)	276 (3.82)	316 (4.37)	331 (4.21)
Acetonitrile	211 (4.32)	257 (3.68)	267 (3.64)		316 (4.27)	
Methanol	210 (4.37)	≈260 (3.68)	(broad)		317 (4.32)	
Ethanol	210 (4.38)	260 (3.62)	(broad)		318 (4.27)	
Water (neutral)	207 (4.39)	255 (3.73)	(broad)		313 (4.30)	
10^{-3} M H_2SO_4 (monocation)		230	262		330	
1 M H_2SO_4 (dication)		240	245		295	
pH 12 (monoanion)			260		305 317	332

a) Weak shoulder.

Table 2. Fluorescence maxima and ϕ_f of $PBNH_2$ in various solvents and at different pH at 298 K

Solvent	λ_{max}(flu)/nm				ϕ_f
Heptane	334	350	368	384	0.485
Dioxane		348	363	380	0.453
Ether		348	363	380	0.775
Acetonitrile			370		0.822
Methanol			376		0.900
Ethanol			378		0.836
Water (neutral)			382		0.852
10^{-3} M H_2SO_4 (monocation)			394		0.06
H_0^{-3} H_2SO_4 (dication)			380		0.30
pH 12[a] (monoanion)		352	368	385	—
H_- 16 (dianion)			430		—

a) Fluorescence spectrum recorded at 77K.

on the carbocyclic ring, as shown below. The presence of long-wavelength fluorescence band could not be explained from this study and is still under investigation.

Effect of pH. The absorption (Fig. 3) and fluorescence spectra (Fig. 4) of $PBNH_2$ have been studied in the H_0/pH/H_- range of −9 to 16. The absorption and fluorescence maxima of various forms are reported in Tables 1 and 2 respectively. Starting with H_0 = −9, the absorption spectrum shows a long wavelength band at 295 nm. With decreasing hydrogen ion concentration, a red shifted band appears at pH 5 with λ_{max} (abs) at ≈330 nm; at pH ≈8 the absorption band appears at 310 nm; at pH 12 a structured absorption spectrum with λ_{max}(abs) at 317 nm is observed and no further change is noted in absorption spectrum after pH 13. Under the similar conditions upto pH 8, the fluorescence bands observed were at 380, 394, and 382 nm respectively and follows the same trend as observed in absorption. No extra fluorescence band is observed in the pH/H_- range of 8 to 14 besides that at 382 nm. This band is quenched at H_-=14. A new red shifted and broad fluorescence band (430 nm) starts appearing at H_-=−15 and its formation is not complete even at H_-=16, the highest basic concentration used.

Comparing the absorption and fluorescence spectra with the solvent study, 310 and 382 nm (pH 8), 340 and 394 nm (pH≈5), 295 and 380 nm (H_0≈−9) and 317 nm (pH≈12) bands could be assigned to the respective spectra of neutral, monocation, dication, and monoanion species respectively. Since the energy difference between the two observed band maxima corresponding to L_a and L_b of different species either remain nearly the same or increases with the change in hydrogen ion concentration, it can be concluded that no crossing of L_a and L_b occurs, *i.e.* the long-wavelength absorption and fluorescence bands for all of these species belong to the same electronic state (L_b).

The following trend in the absorption and fluorescence spectra is generally observed during protonation or deprotonation of heterocyclic molecules if π-π^* is the lowest energy transition: i) A blue shift in absorption and fluorescence spectra is observed on protonation of amino group and the spectra resembles with the parent molecule.[16] ii) A broad red shifted absorption and fluorescence band is noticed if the tertiary nitrogen atom is protonated[17] and iii) red shift is observed in the spectral behavior if imino or amino group is deprotonated.[18] Further, pK_a for the deprotonation of imino group in benzimidazoles is ≈12±2 whereas that for amino group is >14 and amino group becomes relatively much more acidic in S_1 state as compared to imino group.[16,19,20] The anion formed in the former case is generally fluorescent but that formed in the latter case is nonfluorescent,[19] with the exception of 2-naphtylamine,[21] iv) lastly, proton induced quenching of the fluorescence of neutral amines are generally observed at moderate hydrogen ion concentration before forming ammonium ion in S_1.[22]

With the above points in mind and the spectral behavior as shown in Figs. 3 and 4, it is clear that the monocation is formed by protonating the tertiary nitrogen atom and the dication by protonating both

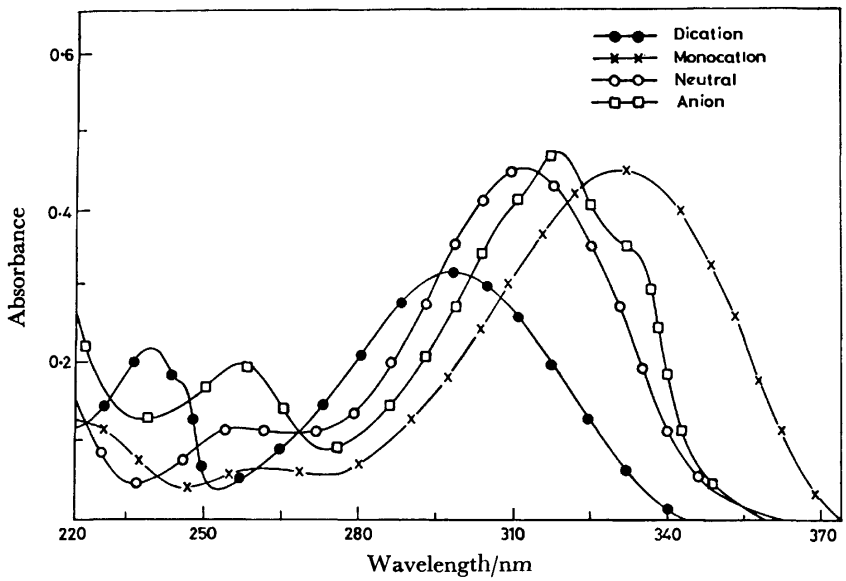

Fig. 3. Absorption spectra of various prototropic forms of $PBNH_2$ at 298 K. (concn 2.5×10^{-5} M)

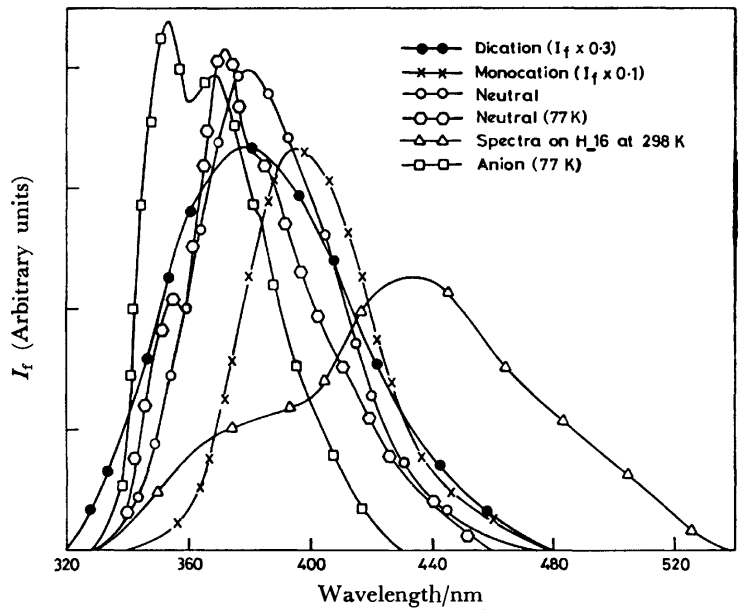

Fig. 4. Fluorescence spectra of various prototropic forms of $PBNH_2$ at 298 K and 77 K.

tertiary and primary amine nitrogen atoms, both in S_0 and S_1 states. This also agrees with the results that the pK_a value for benzimidazole molecule is nearly 5.3 and that for amino group is $\approx$4.0. Further, the λ_{max} (abs), 295 nm, of dication of $PBNH_2$ agrees nicely with the monocation of 2-phenylbenzimidazole.[6] The exact agreement may be accidental but it clearly tells that the effect of anilinium ion is similar to that of phenyl group. The ground state pK_a value for the deprotonation of imino group in benzimidazole is 13.2 and is decreased or increased further if an electron removing or electron donating group, respectively, is substituted in the parent molecule. Similar pK_a value for the deprotonation of aromatic amine is more than 14. The pK_a value of 13.0, observed for above kind of reaction in $PBNH_2$ clearly indicates that monoanion formed in S_0 state is from the deprotonation of the imino group. Further, as mentioned earlier, it has been noticed that increase in the acidity of amino group upon excitation to S_1 state is larger than that of imino group,[16,19,20] the imino anion formed by the deprotonation of amino group is nonfluorescent[19] with the exception of 2-naphthylamine,[21] whereas anion formed by the deprotonation of imino group is generally fluorescent.[18,26,27] With the above results and from our results it is clear that monoanion in S_1 state is formed by the deprotonation of amino group and not imino group as no new fluorescence spectrum was observed with the depletion of neutral $PBNH_2$ in the pH range 8—14. To substantiate this point further, the fluorescence spectrum of $PBNH_2$ at pH 12 is taken at 77 K and is shown in Fig. 4, with the data in Table 2. At

TABLE 3. GROUND AND EXCITED STATE EQUILIBRIUM CONSTANTS OF $PBNH_2$ AT 298 K

Equilibrium	pK_a	pK_a^*			
		F.C. (abs)[a]	F.C.[a] (flu)	F.C.[a] (ave)	(F.T.)[b]
Dication–monocation	1.40	−7.92	−0.42	−4.18	−1.6
		7.50			
Monocation–neutral	5.05	11.03	6.58	8.80	5.00
		4.45			
Neutral–anion	13.00[c]	—	—	—	12.18[d]

a) Förster cycle method. b) Fluorimetric titration. c) Deprotonation of pyrrolic group. d) Deprotonation of amino group.

such a low temperature and in frozen state, the geometry of the species and the nature of the environments in S_1 state corresponds to that of ground state *i.e.* the species present in S_1 is the monoanion formed by the deprotonation of imino group. Though the absorption spectra of the monoanion at 77 K is not observed but the nature of vibrational mode interacting with the electronic mode obtained from the absorption spectrum at 298 K seems to be the smae as observed from the fluorescence spectrum of monoanion of $PBNH_2$ at 77 K. This will give a support to our assignment of monoanion species in S_0 and S_1 states.

The 430 nm fluorescence band, observed at 298 K and at H_15 and 16, could be assigned to the formation of dianion. This species is formed by the deprotonation of imino nitrogen atom, and is consistent with the above-mentioned conclusions. The dianion could have also been obtained by the second deprotonation of amino group but this has been rejected on the ground that the fluorescence observed from the dianion, formed by the double deprotonation of amino group in case of 9-phenanthrylamine,[23] 1- and 2-naphthylamines[28] is blue shifted, both in comparison to neutral and monoanion species whereas this one is red shifted with respect to neutral one.

The values of pK_a for various equilibria calculated spectrophotometrically are listed in Table 3. The values of pK_a^* obtained by fluorimetric titration curves (Fig. 5) as well as by Förster cycle method,[25] wherever applicable, are also listed in Table 3. These values depict the general behavior of the benzimidazoles and prove the assignment of the various species as mentioned earlier. pK^* values for monocation–neutral and neutral–monoanion equilibria are nearly equal to that for benzimidazole molecule, indicating that the presence of electron-donating amino group at the proper position of the phenyl group does not allow the phenyl group to behave as electron-withdrawing group. The results of fluorimetric titration curves (Fig. 5) are also consistent with the earlier findings *i.e.* arylammonium ions are stronger acids in S_1 state, the value of dissociation constant obtained for monocation–neutral equilibrium agrees with that of ground state value (this behavior is common for the protonation of tertiary nitrogen atom[26,27] and the relative increase in the acidity of amino group upon excitation to S_1 state is more than that of imino group. The large difference between the pK_a^* values obtained by Förster cycle

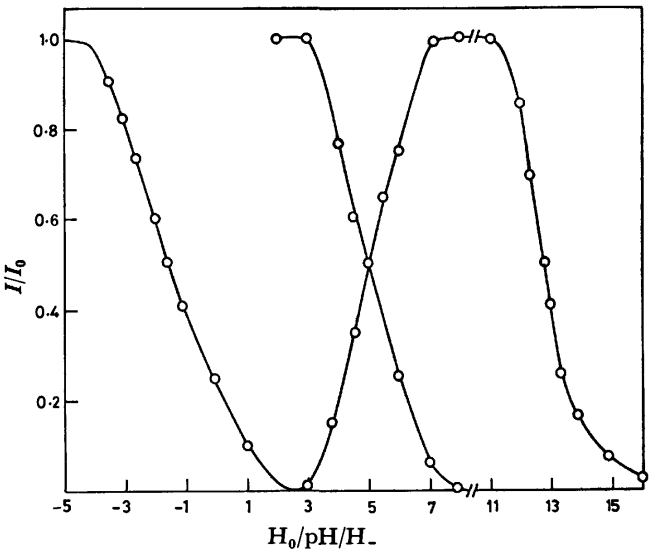

Fig. 5. Plot of relative fluorescence intesity(I/I_0) of different species as a function of H_0/pH/H_.
I/I_0 of dication in the range $H_0 = -9$ to pH=3; I/I_0 of monocation or neutral molecule in the pH range of 3 to 9; I/I_0 of neutral molecule in the pH range 11 to $H_- = 16$.

method, using absorption or fluorescence data, for the dication–monocation equilibrium (7.50 pK_a units) and monocation–neutral equilibrium (4.45 pK_a units) could be due to the unequal solvent relaxation or it may however, be due to use of band maxima in stead of 0-0 band.

References

1) T. C. Werner, "Modern Fluorescence Spectroscopy," ed by E. L. Wehry, Plenum Press, New York (1976), Vol. 2, p. 277.

2) B. Tinland, *J. Mol. Struct.*, **3**, 161 (1969); O. Gropen and H. Seip, *Chem. Phys. Lett.*, **11**, 445 (1971).

3) F. Momicchioli, M. Brumi, and I. Baraldi, *J. Phys. Chem.*, **76**, 3983 (1972).

4) J. B. Berlman, *J. Chem. Phys.*, **52**, 5616 (1970).

5) H. Holloway, R. Nauman, and J. Wharton, *J. Phys. Chem.*, **72**, 4468 (1968).

6) A. K. Mishra and S. K. Dogra, *Spectrochim. Acta, Part A*, **39**, 609 (1983).

7) a) A. K. Mishra and S. K. Dogra, *J. Photochem.*, in press; b) *Indian J. Phys.*, **58B**, 480 (1984).

8) D. W. Hein, R. J. Alheim, and J. J. Leavitt, *J. Am. Chem. Soc.*, **79**, 427 (1957).
9) J. A. Riddick and W. B. Bunger, "Organic Solvents," Wiley Interscience, New York (1970).
10) M. J. Jorgenson and D. R. Hartter, *J. Am. Chem. Soc.*, **85**, 878 (1963).
11) G. Yagil, *J. Phys. Chem.*, **71**, 1034 (1967).
12) M. Swaminathan and S. K. Dogra, *Indian J. Chem.*, **22A**, 853 (1983).
13) G. G. Guilbault, "Practical Fluorescence," Marcel Dekker, Inc., New York (1971), p. 13.
14) J. W. Longworth, R. O. Rahn, and R. G. Schulman, *J. Chem. Phys.*, **45**, 2030 (1966).
15) P. C. Tway and L. T. C. Love, *J. Phys. Chem.*, **86**, 5223 (1982).
16) A. K. Mishra and S. K. Dogra, *J. Photochem.*, **23**, 163 (1983) and references mentioned there.
17) A. K. Mishra, M. Swaminathan, and S. K. Dogra, *J. Photochem.*, **26**, 49 (1984) and references mentioned there.
18) M. Swaminathan and S. K. Dogra, *J. Photochem.*, **21**, 245 (1983) and references listed there.
19) A. K. Mishra and S. K. Dogra, *J. Chem. Soc., Perkin Trans. 2*, **1984**, 943.
20) M. Swaminathan and S. K. Dogra, *J. Am. Chem. Soc.*, **105**, 6263 (1983).
21) Th. Förster, *Z. Elektrochem.*, **54**, 577 (1950).
22) K. Tsutsumi and H. Shizuka, *Chem. Phys. Lett.*, **52**, 485 (1977); *Z. Phys. Chem.* (Frankfurt am Main), **111**, 129 (1978); H. Shizuka, K. Tsutsumi, H. Takauchi, and I. Tanaka, *Chem. Phys.*, **59**, 183 (1981); S. Tobita and H. Shizuka, *Chem. Phys. Lett.*, **75**, 140 (1980); K. Tsutsumi, S. Sekiguchi, and H. Shizuka, *J. Chem. Soc., Faraday Trans. 1*, **78**, 1087 (1982).
23) M. Swaminathan and S. K. Dogra, *Can. J. Chem.*, **61**, 1064 (1983).
24) P. J. Kovi, A. C. Capomacchia, and S. G. Schulman, *Anal. Chem.*, **44**, 1611 (1972).
25) Th. Förster, *Z. Elektrochem.*, **54**, 42, 531 (1950).
26) M. Swaminathan and S. K. Dogra, *Indian J. Chem.*, **22A**, 278 (1983).
27) M. Swaminathan and S. K. Dogra, *Indian J. Chem.*, **22A**, 408 (1983).
28) A. K. Mishra, M. Swaminathan, and S. K. Dogra, *J. Photochem.*, **28**, 89 (1985).

Kinetics and Mechanism of the Interaction of Iminodiacetate with *cis*-Tetraamminediaquacobalt(III) Ion in Acidic Media

Prabir BHATTACHARYA and Pradyot BANERJEE*

Department of Inorganic Chemistry, Indian Association for the Cultivation of Science, Jadavpur, Calcutta 700 032, India

(Received July 5, 1984)

Kinetics of the reaction of iminodiacetate ($Hida^-$) with *cis*-tetraamminediaquacobalt(III) have been studied spectrophotometrically at pH 3.0—4.15, $[\text{iminodiacetate}]_T = 0.03$—0.4 mol dm^{-3}, $I = 0.5$ mol dm^{-3} ($NaClO_4$), in the temperature range 30—50 °C. The reaction is governed by the rate law:

$$\text{rate} = \{k_{-1} + k_1[\text{iminodiacetate}]_T\}[\text{complex}],$$

where k_{-1} and k_1 denote the reverse aquation and anation rate constants respectively. At 40 °C the k_{-1} values increase with pH and show a limiting tendency at pH≈4. The pH-anation rate profile indicates no reaction at pH<1.5 and in the range 3.5—3.9, k_1 remains constant. The pH dependence on rate is expressed as $k_1 = k_A K_{AH}/([H^+] + K_{AH})$, where k_A is the anation rate arising from the aqua complex ion and $Hida^-$ species and K_{AH}, the dissociation constant for the iminodiacetic acid. The value of k_A at 40 °C = $(5 \pm 0.02) \times 10^{-5}$ mol^{-1} dm^3 s^{-1}. The activation parameters, ΔH^* and ΔS^* for the anation step are 170 ± 2 kJ mol^{-1} and 239 ± 3 JK^{-1}mol^{-1}. The reaction is believed to operate through the initial complexation at the carboxylate end followed by a fast intramolecular proton transfer with simultaneous ring closure to form a chelated product. The complexation probably takes place through a dissociative interchange (I_d) mechanism.

Mixed-ligand complex formation has several important biological implications because of the enhanced probability of bringing two different ligands together or of facilitating enzyme-substrate interaction through a bridging metal ion. Bulky ligands, especially those which form multimembered chelate rings, inhibit substitution reactions and usually tend to mask out the influence of bonding and charge on the substitution rates.[1] Unfortunately anation reactions involving such multidentate ligands and an inert metal centre are not explored much. Herein we report the kinetics of interaction of *cis*-tetraamminediaquacobalt(III) ion with iminodiacetate ($Hida^-$).

Experimental

Reagents. The *cis*-tetraamminediaquacobalt(III) perchlorate is prepared following literature method[2] and its purity is checked by spectral and elemental analyses.

The tetraammine(iminodiacetato)cobalt(III) perchlorate has been prepared for the first time by us using the following procedure.

0.44 g (0.15 mole) disodium iminodiacetate monohydrate is dissolved in miniumm volume of water. pH of the solution is adjusted with dilute $HClO_4$ (0.1 mol dm^{-3}) to ≈4.0 and the solution is heated on water bath. To this hot solution is added with stirring an aqueous hot solution of 0.86 g (0.125 mole) *cis*-$[Co(NH_3)_4(H_2O)_2](ClO_4)_3$. Total volume of the solution is kept at ≈15 cm^3. The mixture is heated on the water bath for about 30 min. Pink colored solid product separates out from the solution. It is then cooled. The solution is filtered, the solid is washed with a little cold water followed by cold ethanol and finally dried over fused $CaCl_2$. The purity of the complex is ascertained by elemental analyses: Calcd for $[Co(NH_3)_4(Hida)](ClO_4)_2$: Co, 12.87; C, 10.48; H, 3.93; N, 15.29%. Found: Co, 12.73; C, 10.25; H, 3.79; N, 15.32%. Molar conductance (Λ_M at 25° (in water)) = 240 cm^2 Ω^{-1} mol^{-1}.

Disodium iminodiacetate monohydrate (Fluka AG) is used as received. Recrystallized sodium perchlorate (E. Merck) is used for ionic strength adjustments. pH of the reacting solutions is maintained with dilute perchloric acid prepared from 70% $HClO_4$ (E. Merck).

In addition to the elemental analysis and conductance data, spectral measurements of the synthesized complex furnish further evidence regarding the mode of binding of the acid in the complex. It is well known that amino acids form chelated species with metal ions binding through carboxylato (O^-) and amino (N) groups. The position and intensities of the first and second bands of a freshly prepared solution (at pH=4.0, I=0.5 mol dm^{-3} ($NaClO_4$)) of the isolated complex (λ_{max}, 508 nm; $\varepsilon = 90 \pm 1$ dm^3 mol^{-1} cm^{-1} and λ_{max}, 354 nm; $\varepsilon = 60 \pm 1$ dm^{3}mol^{-1}cm^{-1}) corresponding to $^1A_{1g} \rightarrow {}^1T_{1g}$ and $^1A_{1g} \rightarrow {}^1T_{2g}$ transitions match very well with those of tetraammine(amino acidato)cobalt(III) species.[3] For a tridentate ligand like *N*-methyliminodiacetate ($mida^{2-}$), Bailey *et al.*[4] have isolated an intermediate $[Cr(mida)(Hmida)(H_2O)]$ during the anation studies of $[Cr(mida)(H_2O)_3]^+$ with $Hmida^-$. In this intermediate $Hmida^-$ is coordinated as a bidentate ligand through nitrogen and one CO_2^- group and one carboxyl group (protonated) remains uncoordinated. The mode of bonding of $Hida^-$ in our complex follows the same fashion resulting in a 1 : 2 electrolyte. IR spectrum in KBr discs shows a strong absorption at 1630 cm^{-1} assignable to $[\nu_{COOM} + \delta_{d(NH_3)}]$. Free carboxyl stretching frequency generally encountered at ≈1700 cm^{-1} is probably masked by the presence of this strong band and does not appear. The presence of a sharp band at 555 cm^{-1} strongly indicates the occurance of ν(M–N(amino acid)) bonding.[5]

Measurements. The kinetics of the reaction have been followed with a Pye-Unicam SP8-150 spectrophotometer equipped with a thermostated cell compartment. pH of all the solutions has been measured with a Beckman pH meter (4500). The kinetic spectra has been recorded with a Hitachi 330 spectrophotometer. The spectral change observed during the reaction of *cis*-$[Co(NH_3)_4(H_2O)_2]^{3+}$ with iminodiacetate at pH 3.0—4.15 leads to an increase in the absorption maxima at 354 ± 2 and 508 ± 1 nm, and the rates of the reaction were followed by product absorption at 508 nm. Kinetics of the reaction were measured under pseudo-first-order conditions having $[\text{complex}] = 2 \times 10^{-3}$ mol dm^{-3} and $[\text{iminodiacetate}]_T = 0.03$—0.4 mol dm^{-3} in the pH region 3.0—4.15 at temperatures 30—50 °C. Examination of the

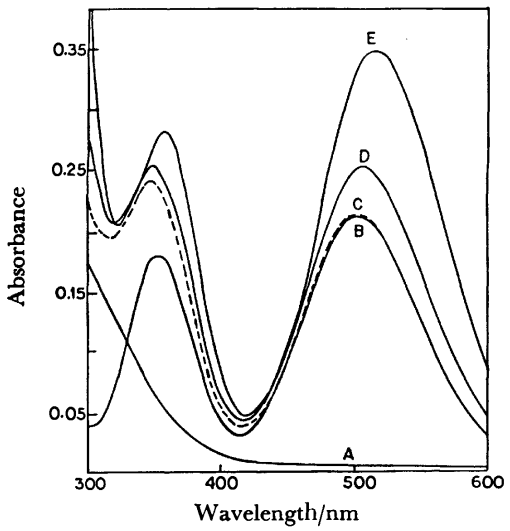

Fig. 1. Absorption spectra: (A) [iminodiacetate] = 0.4 mol dm^{-3}, pH = 4.00±0.01, I = 0.5 mol dm^{-3}; (B) [Co(NH$_3$)$_4$(H$_2$O)$_2^{3+}$] = 4×10^{-3} mol dm^{-3}, pH = 4.00±0.01; (C) [Co(NH$_3$)$_4$(H$_2$O)$_2^{3+}$] = 4×10^{-3} mol dm^{-3}, [iminodiacetate] = 0.4 mol dm^{-3}, pH = 4.00±0.01, I = 0.5 mol dm^{-3} and temperature ≈15 °C (spectrum recorded within 2 min. of mixing); (D)→(E) Change in absorbance with time during the reaction in solution (C) by gradually raising the temperature to 40 °C; curve (E) actually denotes the infinite time spectrum of the reacting solution.

absorbances at infinite time (A_∞) for reacting solutions indicates an equilibrium for the anation process.[6] The approach to equilibrium first-order rate constants (k_{app}) are evaluated from the plots of $\log(A_\infty - A_t)$ *vs.* time (t). These plots are good straight lines for more than three half-lives of the reaction, free from any kinetic complications.

Results and Discussion

A close perusal of the kinetic spectra (Fig. 1) shows that curve (C) departs largely in the range 300—400 nm, though the visible region logically shows no progress in the reaction. The origin of the departure in the region mentioned is due to the absorbance of excess iminodiacetate (curve A) and if we subtract it from that in curve(C), there is practically no difference. This result suggests that no complex of significant stability is formed by association of the diaquacobalt(III) species and iminodiacetate at the time of mixing. The curve(E) shows that the absorbance maximum value at 354 nm is also little higher (*ca.* 15%) than that of the corresponding value of the isolated product under the same conditions (*vide supra*). This also originates from the residual absorbance of iminodiacetate.

At a constant pH, the rate of reaction is shown to be linearly dependent on total iminodiacetate concentration, [iminodiacetate]$_T$. Plots of k_{app} *vs.* [iminodiacetate]$_T$ are straight lines having appreciable intercepts (Fig. 2). The intercept should correspond to the reverse aquation path which has earlier been predicted from the inconcurrence of A_∞ values. With [iminodiacetate]$_T$ present in > ten fold excess over the complex, the rate law (1) is found to apply.

$$\text{Rate} = \{k_{-1} + k_1[\text{iminodiacetate}]_T\}[\text{complex}], \quad (1)$$

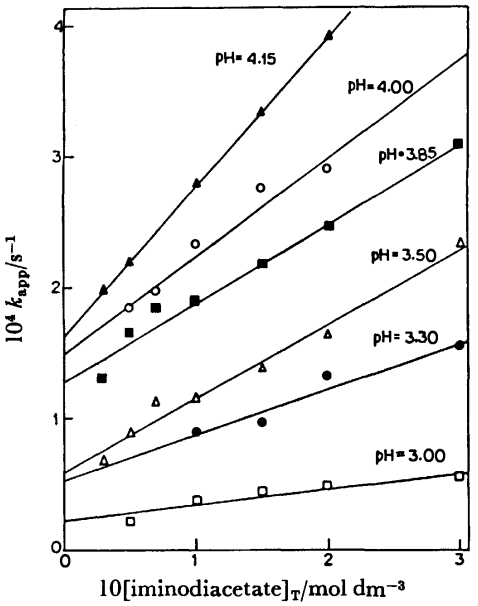

Fig. 2. Plots of k_{app} *vs.* [iminodiacetate]$_T$ at 40 °C, [complex] = 2×10^{-3} mol dm^{-3}, I = 0.5 mol dm^{-3} and pH = 3.0—4.15.

Table 1. Kinetic parameters obtained in the anation reaction of *cis*-[Co(NH$_3$)$_4$(H$_2$O)$_2$]$^{3+}$ with iminodiacetate

Temp/°C	pH	$10^4\,k_{-1}/s^{-1}$	$10^4\,k_1/mol^{-1}\,dm^3\,s^{-1}$
40	3.0	0.22±0.01	1.24±0.02
	3.3	0.53±0.02	3.47±0.02
	3.5	0.60±0.02	5.60±0.03
30	3.85	0.29±0.01[a]	0.79±0.01
35		0.56±0.01[a]	4.41±0.02
40		1.29±0.03[a]	5.97±0.03
50		3.81±0.04[a]	68.70±0.08
40	4.0	1.50±0.01	7.49±0.02
	4.15	1.62±0.02	11.46±0.06

a) Activation parameters obtained from the data corresponding to k_{-1} are ΔH^*_{-1} = 100±4 kJ mol^{-1}, ΔS^*_{-1} = −1±0.5 JK^{-1} mol^{-1}.

where k_{-1} denotes the rate constant for the aquation path and k_1, the second order anation rate constant. The least-squares values of k_{-1} and k_1 obtained at different pH and temperatures are shown in Table 1. The k_{-1} values increase with pH and show a limiting tendency at pH ≃4. The pH-anation rate profile (Fig. 3) clearly indicates three important generalisations; (i) in the high acid region where pH <1.5, there is no reaction, (ii) at pH >3.5, Hida$^-$ is the only species in solution, (iii) at pH >3.9, the reaction rate starts to increase. All three observations can be rationalized into the following derivations.

$$H_2ida \overset{K_{AH}}{\rightleftharpoons} Hida^- + H^+, \quad (2)$$

$$[Co(III)]_T + Hida^- \underset{k_{-1}}{\overset{k_A}{\rightleftharpoons}} \text{products}, \quad (3)$$

$$k_1 = \frac{k_A K_{AH}}{[H^+] + K_{AH}}. \quad (4)$$

The expression (4) is justified by the pH-anation rate

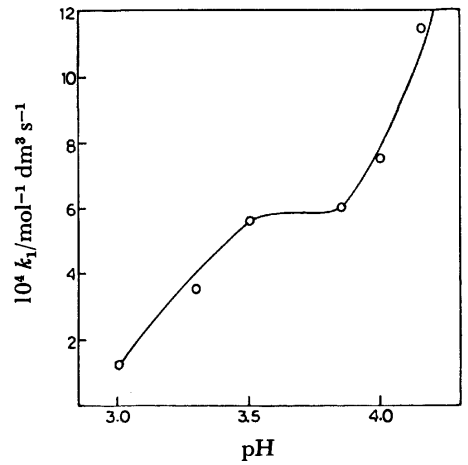

Fig. 3. pH-anation rate profile at 40 °C and I=0.5 mol dm^{-3}.

profile. At relatively high pH, $[H^+] \ll K_{AH}$ ($=3.55\times 10^{-3}$ mol dm^{-3} at 40 °C[7]), the rate becomes acid-independent since $k_1=k_A$. At very low pH when $[H^+] \gg K_{AH}$, $k_1=k_AK_{AH}[H^+]^{-1}$. Thus a plot of k_1 *vs.* $[H^+]^{-1}$ should produce strict linearity in the region of pH<2 having slope ($=k_AK_{AH}$) and $k_A=(5.0\pm0.2)\times 10^{-5}$ mol^{-1} dm^3 s^{-1} at 40 °C obtained by extrapolation of the data to $[H^+]^{-1}=0$, as we were unable to carry out experiments at pH <2 (the reaction rate becoming increasingly slow at lower pH). At pH >3.9 the increase in rate may be ascribed to the onset of protic equilibrium of the diaqua complex. The *cis*-labilisation phenomenon of coordinated-OH group is well documented in literature.[8-10]

The activation parameters obtained by analysing the kinetic data according to the Eyring equation are shown in Table 2. This also includes the comparable kinetic parameters for analogous systems. There is however not a large difference in the anation rates (k_1^x) of *cis*-$[Co(NH_3)_4(H_2O)_2]^{3+}$ with NCS$^-$, Hsal$^-$, Hphthal$^-$, and Hida$^-$. If it is assumed that the mechanism is a dissociative interchange (I_d) type (Eqs. 5 and 6), the rate constant k_1 is a measure of $K_{IP}k_i$.

$$[Co(NH_3)_4(H_2O)_2]^{3+} + \text{Hida}^- \overset{K_{IP}}{\rightleftharpoons} [Co(NH_3)_4(H_2O)_2{}^{3+}\text{Hida}^-], \quad (5)$$

$$[Co(NH_3)_4(H_2O)_2{}^{3+}\text{Hida}^-] \xrightarrow{k_i} [Co(NH_3)_4(\text{Hida})]^{2+} + 2H_2O. \quad (6)$$

The relative small difference in the values of k_1^x (x= NCS$^-$, Hsal$^-$, Hphthal$^-$, and Hida$^-$) is thus indicative of a dissociative activation since the value of $K_{IP}k_i$ are likely to remain fairly constant for similarly charged ligands. The activation parameters also support this mechanism. Assuming an I_d mechanism for any reaction, the activation parameters for the anation step imply more bond breaking than bond making in the transition state. If, however, the entering group is forming a bond in the transition state (associative in nature), stringent steric requirements have to be met and the entropy of activation would be relatively negative. The activation parameters obtained for the aquation step (Table 1) are in excellent agreement with those obtained for the aquation reaction of $[Co(NH_3)_4(NCS)(H_2O)]^{2+}$ ($\Delta H^*=102\pm7$ kJ mol^{-1}, $\Delta S^*=3\pm5$ JK^{-1} mol) and of $[Co(NH_3)_5Cl]^{2+}$ ($\Delta H^*=99.2$ kJ mol^{-1}, $\Delta S^*=-6.7$ JK^{-1}mol^{-1}).[12]

From a detailed analysis of kinetic data, Jordan[13] has suggested that the initial complexing of a metal

Table 2. Anation rate constants[a] and activation parameters

Nucleophile	$10^4 k_1^x$/mol^{-1} dm^3 s^{-1}	ΔH^*/kJ mol^{-1}	ΔS^*/JK^{-1} mol^{-1}	Ref.
NCS$^-$	2.44±0.07[b]	143±2	141±5	8
Hsal$^-$	7.5 ±0.01	138±3	135±4	9
Hphthal$^-$	14.1 ±0.02[c]	116±2	70±4	11
Hida$^-$	5.60±0.03	170±2	239±3	This work

a) All at temp 40 °C and ionic strength=0.5 mol dm^{-3}. b) Represents k_1 value at pH=2.0 where no contribution from aquahydroxocobalt(III) is present, since an unusual *cis*-labilisation for the hydroxo group even at pH> 2.4 has been encountered in this reaction. c) At pH 3.5 no contribution for phthal^{2-} is observed and the rate-law is fully described by an equation analogous to (1).

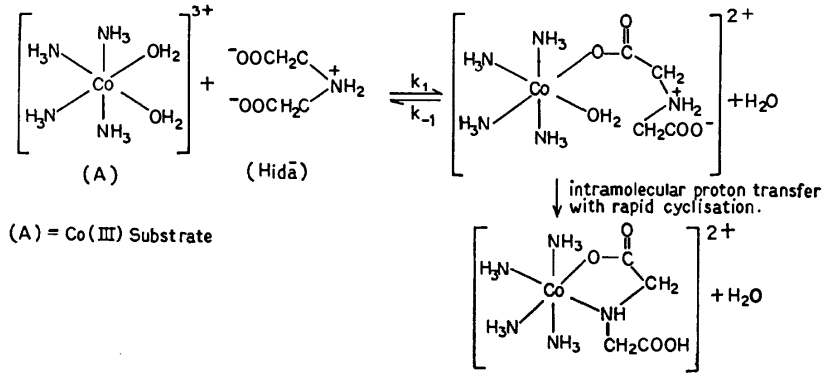

Scheme 1.

ion by a simple amino acid (⁻O–N) occurs at the carboxylato group and chelate ring closure is an important kinetic factor specially for those amino acids with $pK_1 > 8$ even in a less labile system like nickel(II). With an inert metal centre, it is generally believed[14] that the initial complexing is the rate determining step followed by a rapid cyclization to form the chelated species. All these considerations lead us to the postulation of a total reaction as in Scheme 1.

References

1) V. S. Sharma and D. L. Leussing, "Metal Ions in Biological Systems," ed by H. Siegel, Marcell Dekker, Inc., New York (1973), Vol. 2, p. 127.

2) J. Springborg and C. E. Schaffer, *Inorg. Synth.*, **18**, 83 (1978).

3) W. U. Malik, R. Bembi, and Sushila, *J. Inorg. Nucl. Chem.*, **39**, 345 (1977).

4) A. A. T. Bailey, S. Dutta-Chaudhuri, C. J. O'Connor, and A. L. Odell, *J. Chem. Soc., Dalton Trans.*, **1976**, 2103.

5) K. Nakamoto, "Infrared and Raman Spectra of Inorganic and Coordination Compounds," Wiley, New York (1977), p. 308.

6) The higher the incoming ligand concentration, the more complete the reaction becomes. At $[\text{iminodiacetate}]_T \gtrsim 0.15$ mol dm^{-3}, the A_∞ values become almost equal to the absorbance maximum of the isolated tetraammine(iminodiacetato)cobalt(III) product. The percentage of equilibrium reaction varies from *ca.* 85—95 in the range of $[\text{iminodiacetate}]_T$, 0.03—0.40 mol dm^{-3}.

7) This value has been obtained by extrapolation of the corresponding parameter at other temperatures (S. Chaberek Jr. and A. E. Martell, *J. Am. Chem. Soc.*, **74**, 5052 (1952)).

8) M. C. Ghosh and P. Banerjee, *J. Coord. Chem.*, **13**, 237 (1984).

9) M. C. Ghosh, P. Bhattacharya, and P. Banerjee, *Transition Met. Chem.*, **9**, 68 (1984).

10) S. Balt, *Recl. Trav. Chim. Pays-Bas*, **91**, 1026 (1972).

11) P. Bhattacharya and P. Banerjee, unpublished results.

12) A. W. Adamson and R. G. Wilkins, *J. Am. Chem. Soc.*, **76**, 3379 (1954).

13) R. H. Voss and R. B. Jordan, *J. Am. Chem. Soc.*, **98**, 2173 (1976).

14) R. G. Wilkins, "The Study of Kinetics and Mechanism of Reactions of Transition Metal Complexes," Allyn and Bacon, Boston (1974), p. 196.

Kinetics and Mechanism of Ce(IV) Oxidation of Free and Coordinated Glyoxylic Acid

Nirod Kumar MOHANTY* and Rabindra Kumar NANDA†

Post-graduate Department of Chemistry, Sambalpur University, Sambalpur, Orissa, India

†*Department of Chemistry, Utkal University, Bhubaneswar-4, Orissa, India*

(Received October 30, 1984)

The kinetics and mechanism of Ce(IV) oxidation of glyoxylic acid and pentaammineglyoxylatocobalt(III) perchlorate have been investigated in acidic sulfate media in the temperature range 35 to 50 °C and at ionic strength 0.95 M. The rate of decrease of [Ce(IV)] was found to be first order in [substrate] and [Ce(IV)]. The observed second order rate constant, k_{obsd}, for the disappearance of [Ce(IV)] is satisfactorily given by,

$$k_{obsd} = \frac{k_1 + k_2K_3[HSO_4^-]/[H^+]}{1 + K_3[HSO_4^-]/[H^+]} \quad \text{(for glyoxylato complex)}$$

and

$$k_{obsd} = \frac{k_1}{1 + K_3[HSO_4^-]/[H^+]} \quad \text{(for glyoxylic acid)}$$

Both $Ce(SO_4)_2$ and $[Ce(SO_4)_3]^{2-}$ appear to be the oxidant species for coordinated glyoxylate while for free glyoxylic acid $Ce(SO_4)_2$ seems to be the only oxidant species. The values of k_1 and k_2 and the associated activation parameters have been computed. A suitable mechanism has been suggested for the reaction.

The mechanism of Ce(IV) oxidation of carboxylic acids has been extensively investigated.[1,2] Literature survey indicates that Ce(IV) oxidation of carboxylates coordinated to inert metal ion centres has been very sparsely investigated.[3–10] Ce(IV) in $HClO_4$ and H_2SO_4 media exists as different species.[11,12] So far attempt has not been made to establish the mechanism and the nature of reactive cerium species for the oxidation of carboxylates coordinated to metal centers. In the present investigation Ce(IV) oxidation of pentaammineglyoxylatocobalt(III) ion and glyoxylic acid in H_2SO_4–$HClO_4$ media has been undertaken to explore the mechanism, to determine the nature of active cerium species and to establish the complex formation, if any, between the substrate and the oxidant. The products of oxidation have been characterised. For comparison, Ce(IV) oxidation of free glyoxylic acid has also been studied.

Experimental

Pentaammineglyoxylatocobalt(III) perchlorate was prepared by the method of Price and Taube[13] and the purity of the complex was checked by estimating cobalt as described in literature.[14] Cerium(IV) sulfate solution was prepared by dissolving cerium(IV) sulfate (A.R., B.D.H.) in calculated amount of standard sulfuric acid and was standardized against standard ammoniumiron(II) sulfate using *N*-phenylanthranilic acid as indicator.[15] Sodium hydrogensulfate solution of known concentration was prepared by partial neutralisation of standard sulfuric acid with calculated amount of standard sodium hydroxide solution. Glyoxylic acid (A.R., E. Merck) was used as such for oxidation studies. All other chemicals were of reagent grade. All the solutions were prepared from double distilled water, the second distillation being from alkaline $KMnO_4$ in an all-glass distillation set.

Kinetics

To follow the kinetics of the reaction, known amounts of sulfuric acid, perchloric acid, sodium hydrogensulfate and cerium(IV) solutions were transferred into a 50 ml reaction flask and allowed to equilibrate at the reaction temperature. In another flask solution of the substrate (to be oxidized) of known concentration was equilibrated at the same temperature. After thermal equilibrium was attained a known volume of the substrate was transferred to the reaction flask and the volume was made up to the mark with distilled water previously equilibrated at the same temperature. Aliquots of the reaction mixture were drawn out at known time intervals and the reaction was quenched in ice–cold water. The optical density of the quenched solutions was measured at preset wavelengths (410 and 430 nm for glyoxylato complex and 340 and 390 nm for glyoxylic acid). One cm matched quartz cells were used for all measurements, distilled water being taken as 100 precent transmission standard. The oxidations were carried out under second-order conditions.

Stoichiometry

Stoichiometry of the Ce(IV) oxidation of pentaammineglyoxylatocobalt(III) ion was determined as follows: Oxidation of this compound produced Co^{2+} as one of the products which was detected by the formation of the usual blue $[Co(SCN)_4]^{2-}$ species with NH_4-SCN solution. To determine the stoichiometry of the reaction, to a known amount of complex solution was added cerium(IV) sulfate in 4 to 5 fold excess in presence of excess sulfuric acid and allowed to react at 35 °C. Two aliquots of the reaction mixture were withdrawn. One aliquot was added to a calculated volume of ice–cold sulfuric acid to quench the reaction.[9,10] The solution was diluted to a known volume and the optical density of this solution was measured at the wavelength mentioned earlier at which the molar extinction coefficient of Ce(IV) had been determined previously in a separate experiment. From the knowledge of the extinction coefficient and the optical density of the reaction mixture at any time t, unreacted

[Ce(IV)] at that time was calculated. In the second aliquot (after quenching the reaction under ice-cold conditions) [Co(II)] was determined spectrophotometrically using the method of Kitson.[16] In this context it may be noted that the parent cobalt(III) complex was found not to absorb at these wavelengths under the experimental conditions. The stoichiometry for glyoxylato complex was found to be one. To determine the stoichiometry of oxidation of glyoxylic acid, 4—5 fold excess of a known amount of cerium(IV) sulfate was added to a known amount of glyoxylic acid at room temperature. Aliquots of the reaction mixture were withdrawn from time to time and cooled to ice-temperature and the optical density of the mixture was measured at the wavelength mentioned earlier. After about 24 h the absorbance of the reaction mixture was found to be unchanged indicating complete oxidation of glyoxylic acid. The stoichiometry calculated as the ratio of [Ce(IV)] consumed to the total [glyoxylic acid] was found to be 2.

Second Order Rate Expression

In the concentration range studied, preliminary experiments showed that Co(II) and Ce(III) did not absorb in the wavelength range 340—430 nm (at which all optical density measurements were made), the only absorbing species being the cobalt(III) substrate and Ce(IV). Let (i) D_0 and D_t be the optical densities of the reaction mixture at "zero" time and at time "t" respectively, (ii) "x" moles of substrate (henceforward will be known as "sub") react with "y" moles of Ce (IV) at time "t" (iii) E_1 and E_2 be the extinction coefficients of the substrate and Ce(IV) respectively, it is possible to derive the relationship

$$x = (D_0 - D_t)/(E_1 + SE_2) \quad (1)$$

Where "S" is the stoichiometry of the reaction given by

$$y = Sx \quad (2)$$

Thus from the knowledge of S, D_0, D_t, E_1, and E_2 it was possible to calculate x and y from Eqs. 1 and 2 respectively and the observed second order rate constant, "k_{obsd}" from the second order rate expression (3)

$$\ln\frac{([\mathrm{Sub}]_0 - x)}{([\mathrm{Ce(IV)}]_0 - y)} = \ln\frac{[\mathrm{Sub}]_0}{[\mathrm{Ce(IV)}]_0} + (b[\mathrm{Sub}]_0 - a[\mathrm{Ce(IV)}]_0)k_{obsd}\cdot t \quad (3)$$

for the stoichiometric reaction: a Sub + b Ce(IV) → products ($a=b=1$ for glyoxylato complex; $a=1$ and $b=2$ for glyoxylic acid) The experimental results were found to fit best to the above second order rate expression (Eq. 3). The k_{obsd} values were calculated from this expression using the method of least squares with the IBM 1130 computer of Utkal University. The k_{obsd} values and the least squares deviation are collected in Tables 1 and 2. The rate was found not to vary with ionic strength in the range 1 to 2 M†.

Product Analysis

Both glyoxylic acid and glyoxylato complex were found to produce formic acid on oxidation. Following the method of Sengupta and Aditya,[17] formic acid was separated by distillation from the reaction mixture. It was detected by the usual tests and estimated by titrating it with standard potassium permanganate

TABLE 1. EFFECTS ON $[HSO_4^-]/[H^+]$ ON THE OBSERVED SECOND ORDER RATE CONSTANT (k_{obsd}) FOR THE Ce(IV)-OXIDATION OF GLYOXYLATO COMPLEX

[Complex] = 2.0×10^{-3} M and [Ce(IV)] = 1.0×10^{-3} M

$[HSO_4^-]$ M	$[H^+]$ M	$[HSO_4^-]/[H^+]$	k_{obsd} $M^{-1}s^{-1}$	k_{calcd} $M^{-1}s^{-1}$	k_{obsd} $M^{-1}s^{-1}$	k_{calcd} $M^{-1}s^{-1}$	k_{obsd} $M^{-1}s^{-1}$	k_{calcd} $M^{-1}s^{-1}$
			35+0.1 °C		40+0.1 °C		45+0.1 °C	
0.95	0.95	1.0	0.44±0.05	0.47	0.88±0.04	0.83	1.38±0.02	1.35
0.95	0.80	1.19	0.45±0.03	0.43	0.87±0.06	0.74	1.28±0.08	1.19
0.95	0.65	1.46	0.39±0.02	0.38	0.69±0.04	0.65	1.02±0.06	1.09
0.95	0.55	1.72	0.38±0.03	0.35	0.59±0.03	0.59	0.91±0.04	0.93
0.95	0.50	1.90	0.37±0.03	0.34	0.54±0.03	0.56	0.84±0.03	0.88
0.85	0.95	0.90	0.62±0.03	0.50	0.96±0.05	0.89	1.75±0.08	1.46
0.75	0.95	0.79	0.64±0.05	0.54	1.03±0.07	0.97	1.65±0.10	1.60
0.60	0.95	0.63	0.69±0.05	0.62	1.13±0.06	1.14	1.81±0.10	1.90
0.50	0.95	0.53	0.70±0.04	0.70	1.26±0.06	1.30	1.84±0.15	2.19
0.45	0.95	0.47	0.64±0.01	0.75	—	—	2.17±0.12	2.37
0.32	0.95	0.34	0.81±0.02	0.94	1.65±0.09	1.82	2.55±0.22	3.10
0.24	0.95	0.25	1.10±0.04	1.15	2.04±0.09	2.27	3.54±0.21	3.89
0.20	0.95	0.21	1.22±0.05	1.31	2.29±0.11	2.59	—	—
0.15	0.95	0.16	1.57±0.05	1.60	2.86±0.15	3.19	—	—
0.135	0.95	0.14	1.65±0.05	1.71	3.49±0.01	3.44	—	—
0.125	0.95	0.13	1.93±0.05	1.80	3.37±0.19	3.62	—	—
0.095	0.95	0.10	2.11±0.12	2.13	4.53±0.24	4.32	—	—

k_{calcd} stands for the rate constant calculated from Eq. 11 using the best values of k_1 and k_2.

† 1 M = 1 mol dm^{-3}.

Table 2. Effect of $[HSO_4^-]/[H^+]$ on the observed second order rate constant (k_{obsd}) for the Ce(IV)-oxidation of glyoxylic acid

[Glyoxylic Acid] = 2.5×10^{-5} M and [Ce(IV)] = 1.0×10^{-4} M

$[HSO_4^-]$ / M	$[H^+]$ / M	$[HSO_4^-]/[H^+]$	k_{obsd} / $M^{-1}s^{-1}$	k_{calcd} / $M^{-1}s^{-1}$	k_{obsd} / $M^{-1}s^{-1}$	k_{calcd} / $M^{-1}s^{-1}$	k_{obsd} / $M^{-1}s^{-1}$	k_{calcd} / $M^{-1}s^{-1}$
			40±0.1 °C		45±0.1 °C		50±0.1 °C	
0.95	0.95	1.0	18.54±0.35	21.63	31.55±0.32	32.06	49.29±0.71	48.74
0.95	0.80	1.19	18.11±0.18	18.44	28.44±0.38	27.14	39.84±1.05	41.27
0.95	0.55	1.72	14.82±0.23	12.92	18.62±0.30	19.01	33.72±0.63	28.91
0.95	0.50	1.90	14.50±0.78	11.72	17.96±1.35	17.25	26.30±0.50	26.23
0.85	0.95	0.90	24.38±0.47	24.06	34.13±0.15	35.40	53.70±1.2	53.87
0.75	0.95	0.79	29.85±1.49	27.21	39.69±0.89	40.07	—	—
0.60	0.95	0.63	33.00±0.54	33.51	48.56±1.32	49.35	—	—

k_{calcd} stands for the rate calculated from Eq. 12 using the best value of k_1.

solution.[18] It was found that 1 mole of formic acid was produced per mole of the substrate, *i.e.*, glyoxylic acid and glyoxylato complex. The stoichiometry of the reactions can be represented as

$$CHOCOOH + 2\,Ce(IV) + H_2O = 2Ce(III) + HCOOH + 2H^+ + CO_2$$

$$[(NH_3)_5CoOCOCHO]^{2+} + Ce(IV) + H_2O + 4H^+ = Ce(III) + HCOOH + Co^{2+} + CO_2 + 5NH_4^+$$

Results and Discussion

In acidic sulfate media Ce(IV) exists mainly in form of three ionic species, namely, $[CeSO_4]^{2+}$, $Ce(SO_4)_2$, and $[Ce(SO_4)_3]^{2-}$ according to the following equilibria[12]:

$$Ce^{4+} + HSO_4^- \overset{K_2}{\rightleftharpoons} [CeSO_4]^{2+} + H^+ \quad (4)$$

$$[CeSO_4]^{2+} + HSO_4^- \overset{K_2}{\rightleftharpoons} Ce(SO_4)_2 + H^+ \quad (5)$$

$$Ce(SO_4)_2 + HSO_4^- \overset{K_3}{\rightleftharpoons} [Ce(SO_4)_3]^{2-} + H^+ \quad (6)$$

It is obvious from the above three equilibria that the proportions of Ce^{4+} and the three sulfatocerate species in solution are determined by the amounts of free HSO_4^- and H^+ ions. It is possible to express the concentrations of the various Ce(IV) species in terms of the total cerium(IV) ion concentration and the stability constants K_1, K_2, and K_3 as under:

$$[Ce^{4+}] = [Co(IV)]_T/K_1K_2R^2(1+RK_3) \quad (7)$$

$$[CeSO_4^{2+}] = [Ce(IV)]_T/K_2R(1+RK_3) \quad (8)$$

$$[Ce(SO_4)_2] = [Ce(IV)]_T/(1+RK_3) \quad (9)$$

$$[Ce(SO_4)_3^{2-}] = RK_3[Ce(IV)]_T/(1+RK_3) \quad (10)$$

where $R = [HSO_4^-]/[H^+]$

The values of K_1, K_2, and K_3 at 25 °C and ionic strength 2.0 M have been reported to be 3500, 200, and 20 respectively.[12] The ratio $[HSO_4^-]/[H^+](=R)$ maintained throughout the present investigation is in the range 0.1 to 2.0. Eq. 7 indicates that $[Ce^{4+}]$ is negligibly small compared to $[Ce(IV)]_T$ (for example, when $R=1$, $[Ce^{4+}]$ is one in 14×10^6 and was not considered to be one of the reactive species). To determine the active cerium species the concentrations of the various sulfatocerate species were varied by varying $[HSO^-]_4/[H^+]$ ratio. Such a variation resulted in a change in the rate of oxidation indicating that one or more of the sulfatocerate species acted as the oxidizing species. $[HSO_4^-]/[H^+]$ could be varied by adding different amounts of $NaHSO_4$, H_2SO_4, and $HClO_4$ to the reaction medium such that

$$[HSO_4^-] = [H_2SO_4] + [NaHSO_4]$$

and

$$[H^+] = [H_2SO_4] + [HClO_4],$$

the dissociation of HSO_4^- was assumed to be negligible under the present experimental conditions.

In Ce(IV)-oxidation of substrates, in aqueous H_2SO_4 media, usually the formation of precursor complex[17,20,21] between the substrate and sulfatocerate species has been visualized. The formation of such complexes has been established spectrophotometrically:[9,10] Two solutions, one containing Ce(IV) and the other containing the substrate, both having the same amount of HSO_4^- and H^+, on mixing had optical density less than the sum of the optical densities of the two individual solutions. This method could be applied to systems where the rate of oxidation was slow enough such that there was no change in optical density due to oixdation during the spectral measurements. Unfortunately, the oxidation of glyoxylic acid and glyoxylato complex were too fast to establish the precursor complex formation by the above method though we have been successful in establishing this fact in the case of pentaamminebis(oxalato)cobalt(III) ions.[22] Therefore, we presume the complex formation between Ce(IV) and the substrates (glyoxylic acid and glyoxylato complex).

To establish the nature of the active cerium species, one and more than one species at a time were considered and the corresponding rate expression was deduced. The experimental data fitted best to the rate expression 11 in case of glyoxylato complex and 12 in case of glyoxylic acid.

$$k_{obsd} = (k_1+k_2K_3R)/(1+K_3R) \quad (11)$$

and

$$k_{obsd} = k_1/(1+K_3R) \quad (12)$$

TABLE 3. RATE AND ACTIVATION PARAMETERS OF THE Ce(IV)-OXIDATION OF PENTAAMMINEGLYOXYLATOCOBALT(III) ION AND GLYOXYLIC ACID

Substrate	Pentaammineglyoxylatocobalt(III)			Glyoxylic acid		
Temp/°C	35±0.1	40±0.1	45±0.1	40±0.1	45±0.1	50±0.1
$k_1/M^{-1}\,s^{-1}$	6.01±0.07	12.45±0.05	21.75±0.7	457.5±3.0	673.5±3.0	1023±7.5
$k_2/M^{-1}\,s^{-1}$	0.19±0.01	0.24±0.01	0.33±0.03	—	—	—
ΔH^*(kcal/mol), k_1-path		25.4±0.6			15.5±0.2	
ΔH^*(kcal/mol), k_2-path		9.5±2.0			—	—
ΔS^*(e.u.), k_1-path		27.5±0.2			3.0±0.1	
ΔS^*(e.u.), k_2-path		−31.0±0.6			—	

The known values of k_{obsd}, K_3, and R were used as the inputs and the parameters k_1 and k_2 were calculated by the method already indicated.[14] Value of K_3 has been reported by Hardwick and Robertson[12] to be 20 at μ=2.0 M and temperature 25 °C while in the present investigation the reactions have been studied at μ=0.95 M and at temperature range 35—50 °C. To examine the change, if any, of K_3 with the change of ionic strength and temperature we have measured K_3 values, following the method of Hardwick and Robertson, in the temperature range 30—40 °C and ionic strength 1.0 to 2.0 M and found K_3 to be temperature and ionic strength independent in this range. Therefore, the value of K_3 reported by these authors[12] has been used for the iteration process. The best values of k_1 and k_2 have been presented in Table 3. The activation parameters for the k_1 and k_2 paths, calculated from transition state equation, have been collected in Table 3.

The form of the rate laws 11 and 12 indicates that for glyoxylato complex the oxidation proceeds *via* two kinetic paths (k_1 and k_2) while for glyoxylic acid *via* k_1 path only. Assuming that oxidation proceeds *via* precursor complex formation between the substrate and the oxidant, $Ce(SO_4)_2$ and $[Ce(SO_4)_3]^{2-}$ are the oxidant species for glyoxylato complex, and only $Ce(SO_4)_2$ is the oxidant for glyoxylic acid the following general reaction scheme may be written down:

$$\text{Substrate} + Ce(SO_4)_2 \overset{K_1'}{\rightleftharpoons} (\text{Complex})_1 \xrightarrow{k_1'} \text{Products}$$

$$\text{Substrate} + [Ce(SO_4)_3]^{2-} \overset{K_2'}{\rightleftharpoons} (\text{Complex})_2 \xrightarrow{k_2'} \text{Products}$$

The rate of Ce(IV) loss, $-d[Ce(IV)]_T/dt$, is given by

$$-\frac{1}{b}\left(\frac{d[Ce(IV)]_{Total}}{dt}\right) = [\text{Substrate}]_{Total}\{k_1[Ce(SO_4)_2] + k_2[Ce(SO_4)_3^{2-}]\}$$

(where $k_1=k_1'K_1'$ and $k_2=k_2'K_2'$)

Substituting for $[Ce(SO_4)_2]$ and $[Ce(SO_4)_3^{2-}]$ from Eqs. 9 and 10 respectively, it is possible to show that the observed second order rate constant k_{obsd} is given by the expression 11. In the absence of k_2 path Eq. 11 reduces to Eq. 12. Thus kinetic results support that when glyoxylic acid is coordinated to positively charged $(NH_3)_5Co(III)$ moiety, $[Ce(SO_4)_3]^{2-}$, in addition to $Ce(SO_4)_2$, acts as the oxidant species. This may be attributed to the fact that the substrate and the oxidant being oppositely charged, complex formation and subsequent electron transfer between them becomes favorable. The specific rate constants for the $Ce(SO_4)_2$-path are greater than those for the $[Ce(SO_4)_3]^{2-}$-path in case of the glyoxylato complex. This is again probably due to the greater complex forming ability of $Ce(SO_4)_2$ with the substrate compared to $[Ce(SO_4)_3]^{2-}$, *i.e.*, the precursor complex of $Ce(SO_4)_2$ is considered to be innersphere type. Higher reactivity of glyoxylic acid compared to glyoxylato complex in $Ce(SO_4)_2$-path is worth noting. This implies that when glyoxylate is coordinated to a positively charged center, electron transfer becomes difficult from electrostatic considerations. The lower reactivity of $[(NH_3)_5CoC_2O_4H]^{2+}$ towards Ce(IV), compared to oxalic acid, has been similarly accounted for by Saffir and Taube.[3] The present kinetic results further indicate that $[CeSO_4]^{2+}$ is not a reactive species for both the substrates which may be due to very low concentration of $[CeSO_4]^{2+}$ under the present experimental conditions (R=0.1 to 2.0). For example, when R=2, Eqs. 8, 9, and 10 indicate that percentages of $[CeSO_4]^{2+}$, $Ce(SO_4)_2$, and $Ce(SO_4)_3]^{2-}$ respectively are 0.002, 4.76, and 95.2. A possible mechanism consistent with our observations is delineated below:

1. Glyoxylic Acid

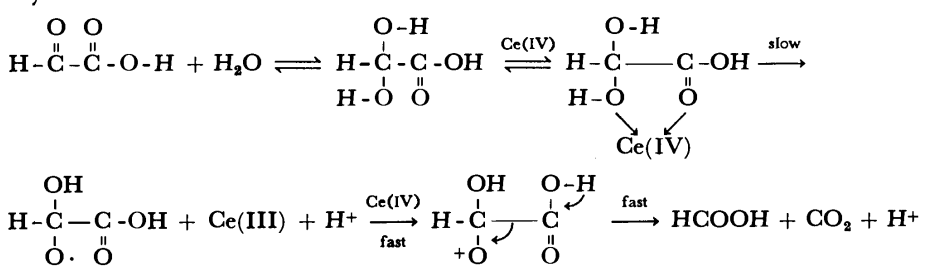

2. Glyoxylatopentaamminecobalt(III) Ion

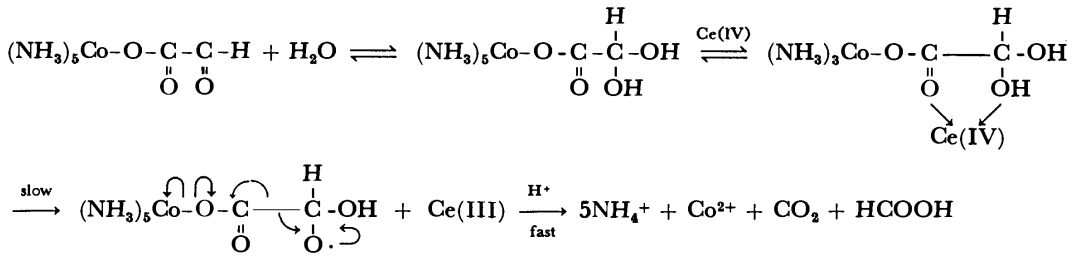

The mechanism presented above invokes that the formation of a radical is rate limiting. Formation of such radicals in the oxidation of carboxylic acids by Ce(IV) has long since been suggested.[3,19,23] The reaction can also proceed *via* the formation of the radical at other donor atoms. Further, the reaction products can also be explained by a concerted mechanism suggested by Gould and Srinivasan.[24] However, with the kinetic results at hand it is not possible to answer all these questions.

References

1) "Oxidation in Organic Chemistry," 1st ed, ed by K. B. Wiberg, Academic Press, New York and London (1965).
2) W. A. Waters, "Mechanisms of Oxidation of Organic Compounds," Methuen & Co. Ltd., London and John Wiley & Sons, Inc., New York (1965).
3) P. Saffir and H. Taube, *J. Am. Chem. Soc.*, **82**, 13 (1960).
4) R. T. M. Fraser and H. Taube, *J. Am. Chem. Soc.*, **82**, 4152 (1960).
5) J. P. Candlin and H. Halpern, *J. Am. Chem. Soc.*, **85**, 2518 (1963).
6) J. E. Teggins, M. T. Wang, and R. M. Milburn, *Advan. Chem. Ser.*, No. 37, 226 (1963).
7) R. Robson and H. Taube, *J. Am. Chem. Soc.*, **89**, 6487 (1967).
8) J. E. French and H. Taube, *J. Am. Chem. Soc.*, **91**, 6951 (1969).
9) M. W. Hsu, H. G. Kruszyna, and R. M. Milburn, *Inorg. Chem.*, **8**, 2201 (1969).
10) H. G. Kruszyna and R. M. Milburn, *Inorg. Chem.*, **10**, 1578 (1971).
11) T. J. Hardwick and E. Robertson, *Can. J. Chem.*, **29**, 818 (1951).
12) T. J. Hardwick and E. Robertson, *Can. J. Chem.*, **29**, 828 (1951).
13) H. J. Price and H. Taube, *J. Am. Chem. Soc.*, **89**, 269 (1967).
14) A. C. Dash and R. K. Nanda, *Inorg. Chem.*, **12**, 2024 (1973).
15) A. I. Vogel, "A Text Book of Quantitative Inorganic Analysis," 3rd ed., John Wiley and Sons, Inc., New York (1962), p. 319.
16) R. E. Kitson, *Anal. Chem.*, **22**, 664 (1950).
17) K. K. Sengupta and S. Aditya, *Z. Phys. Chem.* (Frankfurt am Main), **38**, 25 (1963).
18) Ref. 15, p. 301.
19) B. Krishna and K. C. Tiwari, *J. Chem. Soc.*, **1961**, 3097.
20) V. K. Grover and Y. K. Gupta, *Bull. Chem. Soc. Jpn.*, **43**, 2445 (1970).
21) K. K. Sengupta and S. Aditya, *J. Electrochem. Soc.*, **32**, 200 (1964).
22) N. K. Mohanty and R. K. Nanda, *Indian J. Chem.*, **21A**, 582 (1982).
23) P. Levesley and W. A. Waters, *J. Chem. Soc.*, **1955**, 217.
24) E. S. Gould and V. S. Srinivasan, *Inorg. Chem.*, **20**, 208 (1981).

Extraction Chromatographic Separation of Uranium (VI) with Amberlite LA-1 from Malonic Acid

Prakash NARAYANAN and S. M. KHOPKAR*

Department of Chemistry, Indian Institute of Technology, Bombay-400 076, India

(Received November 26, 1984)

Uranium(VI) was extracted between pH 2.5 to 6.0 from 0.01 mol dm^{-3} malonic acid on a column of silica gel with Amberlite LA-1 as the extractant. It was stripped from the column with 1—2 mol dm^{-3} of hydrochloric, sulfuric, and nitric acids. Uranium(VI) was separated from alkali, alkaline earths, manganese, iron, cobalt, nickel, zinc, yttrium, lanthanum, cerium in binary mixtures by exploiting the difference in the pH of formation of malonato complexes. Uranium was separated from zirconium, hafnium, thorium, scandium, and titanium by taking its advantage of stability of chloro or sulfato complexes. The method was tested for the standard reference rock samples.

Solvent extraction separations of uranium(VI) from mineral acid media using liquid anion exchanger has been studied, but such studies from the organic acid media are lacking. The separation of uranium by extraction chromatography using sulfate media was carried out with Alamine-336[1] or Amberlite LA-2.[2] The studies from nitrate media[3–5] made use of tridodecylamine or trioctylamine as extractants. However, maximum work has been carried out from chloride media,[6–9] where Teflon was used as the stationary support with normal trioctylamine as the stationary phase. Such methods permitted the separation of uranium from actinide elements. In continuation of our work[10] with dicarboxylic acids, such as malonic acid, as the complexing media, extraction chromatographic studies were extended for the separation of uranium (VI) on silica-gel column coated with Amberlite LA-1 as the stationary phase. This paper describes some novel methods for the separation of uranium(VI) from associated elements. The method was tested for the analysis of uranium(VI) from rock samples.

Experimental

Apparatus and Chemicals. The apparatus used was similar to one described earlier.[11] The stock solution of uranium(VI) was prepared by dissolving 1.055 g of uranyl (VI) nitrate (BDH, England) in 100 cm^3 of demineralized water containing 1% of nitric acid. The solution was standardized gravimetrically.[12] It was found to contain 4.9 mg cm^{-3} of uranium(VI). A solution containing 98 μg cm^{-3} was prepared by appropriate dilution. Silica gel (100—200 mesh) was made hydrophobic by procedure described earlier.[11] The column (10×0.7 cm) was packed with silica gel coated with Amberlite LA-1.

General Procedure. An aliquot of solution containing 98 μg of uranium(VI) was mixed with 5 cm^3 of 0.01 mol dm^{-3} malonic acid, and the pH of the solution was adjusted between 2.5—6.0 with 0.01 mol dm^{-3} malonic acid or sodium hydroxide. Then the solution was passed on the column when uranium(VI) was extracted in the stationary phase containing Amberlite LA-1. It was then stripped with various mineral acids and alkalies. Ten fractions each of 5 cm^3 were collected and uranium(VI) from each fraction was determined spectrophotometrically at 530 nm as its complex with 4-(2-pyridylazo)resorcinol (PAR).

Results and Discussion

The study of extraction of uranium(VI) as a function of pH was carried out in the pH range 1.0—8.0. The extraction commenced at pH 1.0 (45.2 %) and it was quantitative in the range 2.5 to 6.0. On further increase of the pH the extraction decreased. The optimum pH for the quantitative extraction of uranium (VI) was therefore 2.5 to 6.0 (Fig. 1).

The extraction of uranium(VI) was carried out by varying the concentration of malonic acid from 1×10^{-4} mol dm^{-3} to 5×10^{-1} mol dm^{-3}. The extraction was quantitative from 1×10^{-3} mol dm^{-3} to 2.5×10^{-1} mol dm^{-3}. At higher concentration of malonic acid there was a decrease in the extraction, probably due to the setting up of a competitive equilibrium between the anionic metal malonato complex and the simple malonate anion for Amberlite LA-1. All the extractions were carried out with 1×10^{-2} mol dm^{-3} malonic acid as it was adequate for complex formation (Fig. 2).

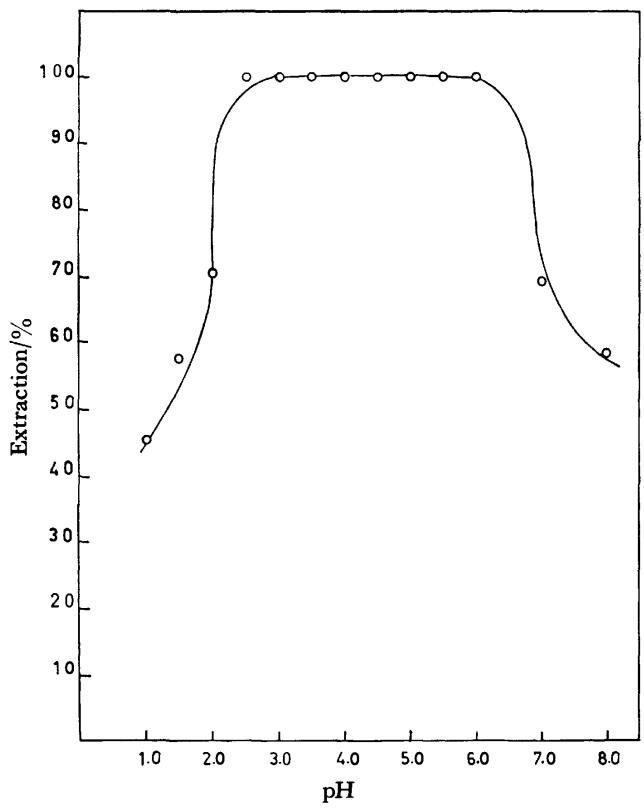

Fig. 1. Effect of pH on extraction of uranium(VI) from malonic acid.

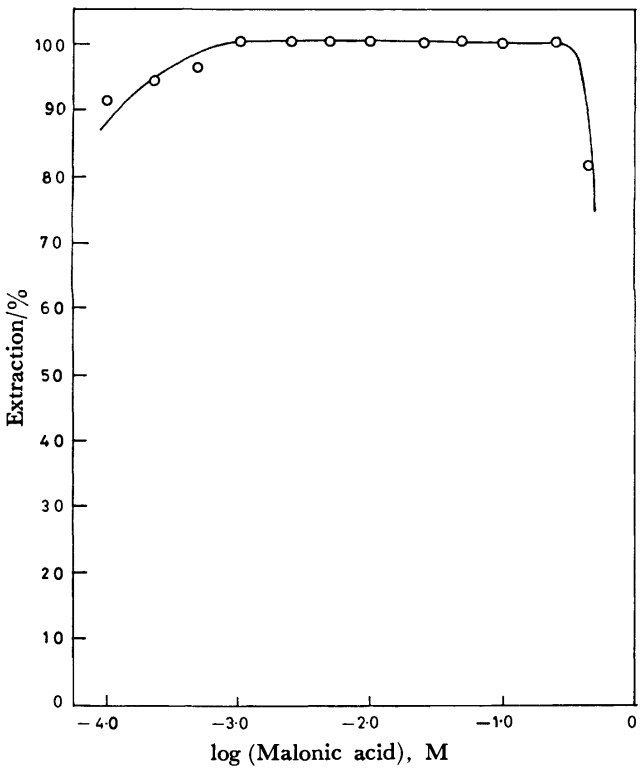

Fig. 2. Effect of malonic acid concentration. (1 M=1 mol dm^{-3}).

On the basis of batch extraction,[13] the probable mechanism of extraction involves the following transformations:

$$UO_2(NO_3)_2 + 2(\text{malonic acid}) \longrightarrow UO_2(\text{malonate})_2^{2-} + 2HNO_3 + 2H^+ \quad (1)$$

$$[(R_2NH_2)_2(\text{malonate})]_o + [UO_2(\text{malonate})_2]_w^{2-} \longrightarrow [(R_2NH_2)_2 \cdot UO_2(\text{malonate})_2]_o + (\text{malonate})_w^{2-} \quad (2)$$

where subscript o and w refer to organic and aqueous phase respectively.

The uranium(VI) was stripped after its extraction from the stationary phase with hydrochloric, sulfuric, and nitric acids and aqueous ammonia. The stripping was quantitative with 1.0 to 2.0 mol dm^{-3} for all acids, or with 0.5 to 1.0 mol dm^{-3} of aqueous ammonia. Since uranium(VI) formed anionic sulfato complex at lower concentration of sulfuric acid, hence could not strip uranium (*i.e.* <0.25 mol dm^{-3}). At high concentration of hydrochloric acid (>6.0 mol dm^{-3}), uranium(VI) formed negatively charged chloro complex, which in turn was reextracted in the extractant. These facts formed the basis for its separation from several metal ions (Fig. 3).

Separation of Uranium(VI) from Binary Mixtures. Uranium(VI) was separated from several elements in binary mixtures by utilizing the differences in their capacity to form anionic complexes. Thus, since alkali, alkaline earths, iron(II), yttrium, zinc, cadmium, lead, nickel, cobalt, aluminium, manganesee(II), lanthanum, and cerium(III) could not form anionic malonato complexes they were not extracted and hence were separated from uranium(VI). Uranium(VI) was then subsequently stripped from the column with 2 mol dm^{-3} nitric acid. Further, since uranium formed anionic sulfato complex at lower concentration of sulfuric acid, it was possible to separate it from scandium, titanium(IV), vanadium(V), iron(III), bismuth(III) as they could not form such complexes and were stripped out with 0.1 mol dm^{-3} sulfuric acid. Uranium which was retained in the form of anionic sulfato complex in the liquid anion exchanger and was subsequently stripped with 2 mol dm^{-3} nitric acid. Uranium(VI) also formed negatively charged chloro complex at 6 mol dm^{-3} hydrochloric acid but zirconium, hafnium, and thorium could not form such chloro complex and hence were stripped out first with 6 mol dm^{-3} hydrochloric acid and then uranium(VI) was stripped with 2 mol dm^{-3} nitric acid.

Separation of Uranium(VI) from Multicomponent Mixtures. The differences in acidity at which various metals formed mineral acid complexes or inability of few to form malonato complexes was exploited to develop new separations. A mixture of lead, bismuth, and uranium (VI) were passed on the column at pH 5.0, when malonato complexes of bismuth and uranium(VI) were extracted, while lead passed through the column as the uncomplexed species. Then bismuth was stripped with 0.1 mol dm^{-3} sulfuric acid and finally uranium (VI) was stripped with 2.0 mol dm^{-3} nitric acid.

The separation of yttrium, scandium and uranium (VI) was carried out by passing the mixture through the column, when yttrium passed through as it could not form extractable malonato complex, while scandium was stripped with 0.1 mol dm^{-3} sulfuric acid fol-

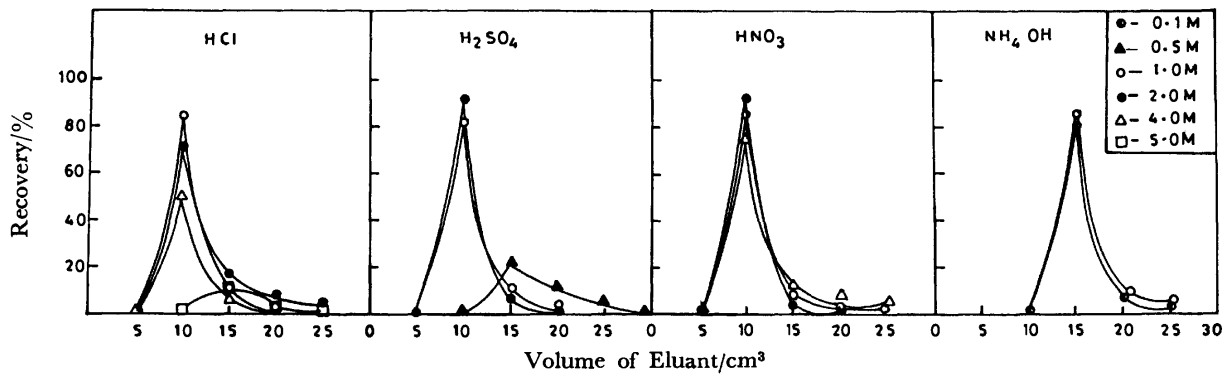

Fig. 3. Elution behavior of uranium(VI) in malonate media with various eluants.

lowed by stripping of uranium(VI) with 2 mol dm^{-3} nitric acid.

The separation of chromium(III), vanadium(V), and uranium(VI) was achieved by washing out chromium (III) with water followed by stripping of vanadium(V) with 0.1 mol dm^{-3} sulfuric acid and uranium(VI) finally with 2 mol dm^{-3} nitric acid.

The separation of uranium(VI) from aluminium, iron(III) or titanium(IV) was effected by passing the mixture through the column. Aluminium was washed with water as it did not form extractable malonato complex. Iron(III) or titanium(IV) was stripped with 0.1 mol dm^{-3} sulfuric acid and finally uranium (VI) was stripped from the column with 2 mol dm^{-3} nitric acid.

The separation of cerium(III), zirconium(IV) or hafnium(IV) was effected by washing cerium(III) with water, zirconium(IV) or hafnium(IV) was stripped latter with 6 mol dm^{-3} hydrochloric acid and finally uranium with 2 mol dm^{-3} nitric acid.

An interesting separation of uranium from lanthanum, thorium, and zirconium was achieved by passing the mixture through the column. When lanthanum was washed with water, thorium was stripped with 0.25 mol dm^{-3} sulfuric acid when zirconium and uranium (VI) were retained on the column as their sulfato complexes. Zirconium was stripped with 6 mol dm^{-3} hydrochloric acid when uranium(VI) was retained on the column as its chloro complex which was finally stripped with 2 mol dm^{-3} nitric acid (Table 1)(Fig. 4).

In all the separation it was interesting to note that uranium could be separated from other elements in the presence of various mineral acids. At 0.1 mol dm^{-3} sulfuric acid uranium(VI) forms anionic sulfato[14] complex, and thus it was possible to separate it from scandium, titanium, vanadium, iron(III), and bismuth. Similarly uranium(VI) forms chloro complex[15] with 6 mol dm^{-3} hydrochloric acid and gets reextracted where other elements like zirconium, hafnium, and thorium could be stripped with 6 mol dm^{-3} hydrochloric acid. Since uranium(VI) did not form nitrato complex at lower concentration of nitric acid, it was possible to strip uranium(VI) with 2 mol dm^{-3} nitric acid in all such cases.

Separation of Uranium(VI) from Rock Sample. About 0.5 g of the sample was heated with a mixture of hydrofluoric and nitric acid in a platinum crucible. It was then diluted to 100 cm^3 with 0.1 mol dm^{-3} nitric acid. To an aliquot of the solution 5 cm^3 of 0.01 mol dm^{-3} malonic acid was added and the pH was adjusted to 5.0. It was then passed through the

TABLE 1. SEPARATION OF URANIUM(VI) FROM MULTICOMPONENT MIXTURES

	Mixtures	Taken μg	Found μg	Recovery %	Eluant
1)	Pb	100	100	100.0	Water
	Bi(III)	100	98.6	98.6	0.1 M† H_2SO_4
	U(VI)	98	97	98.9	2.0 M HNO_3
2)	Y	100	100	100.0	Water
	Sc	100	100	100.0	0.1 M H_2SO_4
	U(VI)	98	98.2	100.2	2.0 M HNO_3
3)	Cr(III)	100	100	100.0	Water
	V(V)	100	99.3	99.3	0.1 M H_2SO_4
	U(VI)	98	98.2	100.2	2.0 M HNO_3
4)	Al	100	100	100.0	Water
	Fe(III)/Ti(IV)	96.5	95.4	98.8	0.1 M H_2SO_4
	U(VI)	98	97.2	99.1	2.0 M HNO_3
5)	Ce(III)	100	100	100.0	Water
	Zr(IV)/Hf(IV)	50	49	98.0	6 M HCl
	U(VI)	98	97.5	99.4	2.0 M HNO_3
6)	La	100	100	100.0	Water
	Th	100	101	101.0	0.25 M H_2SO_4
	Zr(IV)	50	49	98.0	6.0 M HCl
	U(VI)	98	96.3	98.2	2.0 M HNO_3

† 1 M = 1 mol dm^{-3}.

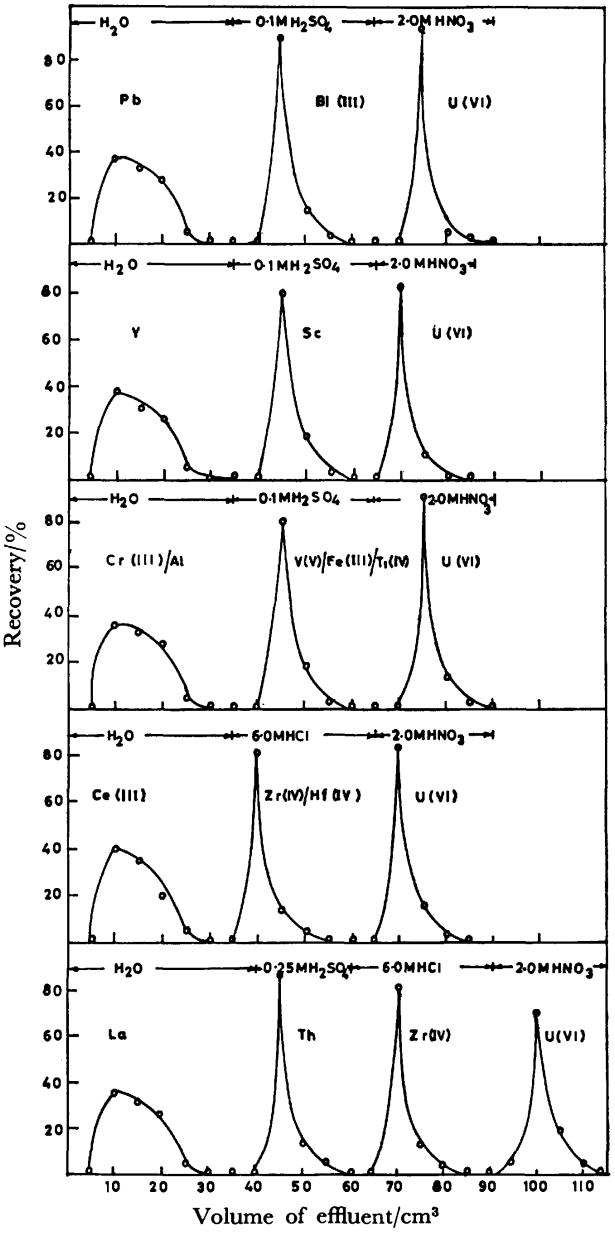

Fig. 4. Separation of uranium(VI) from multicomponent mixtures.

column when elements such as sodium, potassium, calcium, magnesium, manganese, pass through the column. The elements zirconium, thorium, and iron were coextracted with uranium. Thorium and iron (III) were stripped with 0.25 mol dm^{-3} sulfuric acid, while zirconium was stripped with 6 mol dm^{-3} hydrochloric acid under this circumstances uranium(VI) remained on the column either as sulfato complex or chloro complex. Finally uranium was stripped with 2 mol dm^{-3} nitric acid and was determined as usual. The results showed amount of uranium as a mixed oxide as 0.029% against 0.03% in the first sample and 0.079% against 0.08% in the second sample.

The separation of uranium(VI) from lead, bismuth, thorium, zirconium, and hafnium is of significance in the analysis of fission products. Also separation from aluminium, cadmium, iron, titanium, scandium, and cerium is of great importance. The proposed method is simple and rapid.

We are thankful to Council of Scientific and Industrial Research for sponsoring this project and awarding Senior Research Fellowship to one of us (PN).

References

1) S. M. Itani, Ph. D. Thesis, "Chromatographic Separation and Spectrophotometric Determination of Uranium," Iowa State University, Iowa, USA, IST-385, (1970).
2) T. Shimizu, *J. Chromatogr.*, **96**, 262 (1974).
3) D. Gourisse and A. Chesne, *Anal. Chim. Acta*, **45**, 321 (1969).
4) E. Cerrai and C. Testa, *J. Chromatogr.*, **6**, 443 (1961).
5) H. Beranova and M. Tejnecky, *Collect. Czech. Chem. Commun.*, **37**, 3579 (1972).
6) R. Krefeld, G. Rossi, and Z. Hainski, *Mikrochim. Acta*, **1965** 133.
7) J. Mikulski, K. A. Gavrilov, and V. Knobloch, *J. Chromatogr.*, **17**, 197 (1965).
8) J. Mikulski, *Nucleonika*, **11**, 57 (1966).
9) I. Stronski, *Radiochem. Radioanal. Lett.*, **1**, 191 (1969).
10) P. Narayanan and S. M. Khopkar, *J. Radioanal. Nucl. Chem.*, **84**, 33 (1984).
11) P. Narayanan and S. M. Khopkar, *Anal. Lett.*, **16**, 443 (1983).
12) A. I. Vogel, "Textbook of Quantitative Inorganic Analysis," 3rd ed, Longmans, London (1964), p. 540.
13) M. B. Dalvi and S. M. Khopkar, *Talanta*, **25**, 599 (1978).
14) S. M. Khopkar and A. K. De, *Anal. Chim. Acta*, **23**, 147 (1960).
15) K. A. Kraus and F. Nelson, *Proc. Intern. Conf. Peaceful Uses of Atomic Energy, Geneva*, **7**, 113 (1956).

 © 1985 The Chemical Society of Japan Bull. Chem. Soc. Jpn., 58, 3606—3612 (1985) [Vol. 58, No. 12

Thermal Studies of 1,2-Propanediamine Complexes of Zinc(II) and Cadmium(II) in the Solid Phase

Ashutosh GHOSH, Goutam DE, and Nirmalendu RAY CHAUDHURI*

Department of Inorganic Chemistry, Indian Association for the Cultivation of Science, Jadavpur, Calcutta-700 032, India

(Received January 28, 1985)

$[ML_3]X_2 \cdot nH_2O$, where M = Zn^{II} and Cd^{II}; L = 1,2-propanediamine; X = Cl^-, Br^-, $0.5SO_4^{2-}$, and $0.5SeO_4^{2-}$ and n = 1, 1.5, and 2, have been synthesized and their thermal investigations carried out. $ZnL_{1.5}Cl_2$, $CdL_{1.5}X_2$ (X = Cl^- and Br^-), and $CdLX_2$ (X = Cl^-, $0.5SO_4^{2-}$, and $0.5SeO_4^{2-}$) have been synthesized pyrolytically in solid state from their parent diamine complexes. These $ML_{1.5}X_2$ complexes are expected to exist as $[ML_3][MX_4]$. Only $[CdL_3][CdBr_4]$ species has been synthesized from solution. Syntheses of $ZnLCl_2$, $CdLCl_2$, and $CdLBr_2$ from solution have also been reported. IR spectra suggest that symmetry of the chelate ring in mono(diamine) complexes is lowered in comparison to the other complexes. $ML_{1.5}Cl_2$ show isomorphism with each other. Thermal stability sequence of $[ML_3]X_2$ (X = Br^-, $0.5SO_4^{2-}$ and $0.5SeO_4^{2-}$) is $SO_4^{2-} < SeO_4^{2-} \leqslant Br^-$. $[ZnL_3]X_2$ and $ZnLX_2$ appear thermally more stable than those of cadmium complexes. All these complexes are thermally less stable than those of 1,2-ethanediamine complexes reported by us earlier.

We carried out thermal investigations of a good number of diamine complexes, synthesized several novel diamine complexes pyrolytically in solid state from the parent diamine complexes[1-7] and noticed, several interesting observations relating to the structures of diamine complexes derived in solid state with respect to the parent diamine complexes. Recently, we reported the thermal behavior of 1,2-propanediamine complexes of nickel(II)[8] and observed some noticeable difference in the thermal behavior from those of 1,2-ethanediamine and 1,3-propanediamine complexes of nickel(II) due to the methyl substitution in the methylene group of the diamine.

The coordination chemistry of d^{10} metal(II) is interesting. They show a variety of coordination numbers and geometries. The chemistry of diamine complexes of d^{10} metal(II) halides are now well established. Although the chemistries of zinc and cadmium are very similar, it is found that the effect of size is to make Cd^{II} more likely than Zn^{II} to assume a coordination number six.[9] In this context thermal studies on 1,2-propanediamine complexes of MX_2 (M = Zn^{II} and Cd^{II}; X = Cl^-, Br^-, $0.5SO_4^{2-}$, and $0.5SeO_4^{2-}$) are relevent.

Experimental

Preparation of the Complexes. $[ZnL_3]Cl_2 \cdot 2H_2O$ (**1**), $[ZnL_3]Br_2 \cdot 1.5H_2O$ (**2**), $[CdL_3]Cl_2 \cdot 2H_2O$ (**5**), and $[CdL_3]Br_2 \cdot 2H_2O$ (**6**): 1,2-propanediamine (4 mmol) was added dropwise with vigorous stirring to MX_2 (M = Zn^{II} or Cd^{II}; X = Cl^- or Br^-) (1 mmol) dissolved in ethanol. The desired complexes were separated out and purified by washing with ethanol.

*$CdLCl_2$ (**5b**) and $CdLBr_2$ (**6b**).* These complexes were prepared by stoichiometric addition of the ligand to the metal salts adopting similar procedure as described above.

*$[ZnL_3]SO_4 \cdot H_2O$ (**3**), $[ZnL_3]SeO_4 \cdot 1.5H_2O$ (**4**), $[CdL_3]SO_4$ (**7**), and $[CdL_3]SeO_4 \cdot 1.5H_2O$ (**8**).* 1,2-Propanediamine (4 mmol) was added dropwise with vigorous stirring to MX_2 [M = Zn^{II} or Cd^{II}; X = $0.5SO_4^{2-}$ or $0.5SeO_4^{2-}$] (1 mmol) dissolved in minimum quantity of water. The derived com-

TABLE 1. ANALYTICAL DATA OF 1,2-PROPANEDIAMINE(L) COMPLEXES OF ZINC(II) AND CADMIUM(II)

Compound		Elemental analyses/%[a]		
		Metal	Nitrogen	Halogen/sulfur/selenium
$[ZnL_3]Cl_2 \cdot 2H_2O$	(**1**)	16.3(16.6)	20.9(21.3)	17.6(18.0)
$ZnL_{1.5}Cl_2$[b]	(**1a**)	26.1(26.4)	16.8(16.9)	28.6(28.7)
$[ZnL_3]Br_2 \cdot 1.5H_2O$	(**2**)	13.5(13.8)	17.7(17.7)	33.8(33.7)
$[ZnL_3]SO_4 \cdot H_2O$	(**3**)	16.3(16.3)	20.5(20.9)	7.6(7.9)
$[ZnL_3]SeO_4 \cdot 1.5H_2O$	(**4**)	14.4(14.3)	18.1(18.3)	16.8(17.2)
$[CdL_3]Cl_2 \cdot 2H_2O$	(**5**)	25.4(25.5)	19.1(19.0)	15.9(16.1)
$CdL_{1.5}Cl_2$[b]	(**5a**)	37.9(38.2)	14.1(14.3)	23.8(24.1)
$CdLCl_2$[b]	(**5b**)	43.8(43.7)	10.7(10.9)	27.6(27.6)
$[CdL_3]Br_2 \cdot 2H_2O$	(**6**)	21.2(21.2)	15.8(15.8)	29.8(30.1)
$CdL_{1.5}Br_2$[b]	(**6a**)	29.2(29.3)	10.7(10.9)	41.1(41.7)
$CdLBr_2$	(**6b**)	32.3(32.4)	8.0(8.1)	46.0(46.2)
$[CdL_3]SO_4$[c]	(**7**)	25.8(26.1)	19.2(19.5)	7.5(7.4)
$CdLSO_4$[b]	(**7b**)	39.5(39.8)	9.5(9.9)	11.1(11.3)
$[CdL_3]SeO_4 \cdot 1.5H_2O$	(**8**)	21.9(22.3)	16.5(16.6)	15.0(15.6)
$CdLSeO_4$[b]	(**8b**)	33.7(34.1)	8.2(8.5)	23.4(23.9)

a) Figures in parentheses are the required percentages. b) Synthesized in the solid state. c) Analyzed in anhydrous form.

plexes were separated out on evaporating the mixture on a constant temperature bath (50±2 °C). The zinc and cadmium complexes were purified by washing with ethanol and isopropanol, respectively.

$[CdL_3][CdBr_4]$ (6a). To the aqueous solution (2 ml) of 1 mmol, $[CdL_3]Br_2\cdot 1.5H_2O$, 1 mmol $[Et_4N]_2[CdBr_4]$ (dissolved in 10 ml acetonitrile) was added with stirring. To the resulting solution ether was added till the desired product was separated out. It was purified by washing with ether. All the complexes were dried in $CaCl_2$ desiccator.

$ZnL_{1.5}Cl_2$ (1a), $CdL_{1.5}Cl_2$ (5a), and $CdL_{1.5}Br_2$ (6a). These complexes were synthesized by keeping the complexes **1**, **5**, and **6** at 170, 145, and 165 °C, respectively, following the method reported earlier.[4,5,7] Similarly $CdLCl_2$ (**5b**), $CdLSO_4$ (**7b**), and $CdLSeO_4$ (**8b**) were prepared from complexes **5**, **7**, and **8** at 210, 235, and 235 °C, respectively. Thermal curves do not tally the temperatures at which thermolytic syntheses were carried out. The respective temperatures are very much optimum for isolation of the complexes in pure form.

Analytical data for the above complexes are presented in Table 1.

The apparatus employed for carrying out thermal analysis is same as reported earlier.[1-8] Tables 2a and 2b list the thermal data.

Results and Discussion

Diamine Complexes of Zinc Chloride. IR spectra (Table 3a) of $[ZnL_3]Cl_2\cdot 2H_2O$ (**1**) show that the diamines are chelated in it.[10] This tris species starts deaquation at 65 °C and transforms to $ZnL_{1.5}Cl_2$ (**1a**) at 175 °C showing three endothermic peaks in the DTA curve overlapping to each other (Fig. 1). Isolation of deaquated species is not feasible here like the

Table 2a. Thermal parameters of 1,2-propanediamine(L) complexes of zinc(II)

Decomposition reaction	Temperature range/°C	DTA peak temperature/°C
$[ZnL_3]Cl_2\cdot 2H_2O$ (**1**) → $ZnL_{1.5}Cl_2$ (**1a**)	65—175	105, 135, 165
$ZnL_{1.5}Cl_2$ → $ZnLCl_2$	185—270	205, 229, 247
$ZnLCl_2$ → $ZnCl_2$	270—410	365
$[ZnL_3]Br_2\cdot 1.5H_2O$ (**2**) → $[ZnL_3]Br_2\cdot H_2O$	55— 82	75
$[ZnL_3]Br_2\cdot H_2O$ → $[ZnL_3]Br_2$	82—125	115
$[ZnL_3]Br_2$ → ZnL_2Br_2	140—217	185, 205
ZnL_2Br_2 → $ZnLBr_2$	217—310	220
$ZnLBr_2$ → $ZnBr_2$	310—405	368, 375
$[ZnL_3]SO_4\cdot H_2O$ (**3**) → $[ZnL_3]SO_4$	45— 85	82
$[ZnL_3]SO_4$ → ZnL_2SO_4 (**3a**)	85—130	120
ZnL_2SO_4 → $ZnLSO_4$	185—270	260
$ZnLSO_4$ → $ZnSO_4$	270—390	305, 388, 358[a], 372
$[ZnL_3]SeO_4\cdot 1.5H_2O$ (**4**) → $[ZnL_3]SeO_4\cdot H_2O$	40— 75	70
$[ZnL_3]SeO_4\cdot H_2O$ → $[ZnL_3]SeO_4$	75—105	90
$[ZnL_3]SeO_4$ → ZnL_2SeO_4 (**4a**)	120—165	155
ZnL_2SeO_4 → $ZnSeO_4$	217—392	260, 280[a]

a) Denotes exothermic peaks, rest are endothermic.

Table 2b. Thermal parameters of 1,2-propanediamine(L) complexes of cadmium(II)

Decomposition reaction	Temperature range/°C	DTA peak temperature/°C
$[CdL_3]Cl_2\cdot 2H_2O$ (**5**) → $CdL_{1.5}Cl_2$ (**5a**)	75—150	115, 145
$CdL_{1.5}Cl_2$ → $CdLCl_2$ (**5b**)	165—210	205
$CdLCl_2$ → $CdCl_2$	245—355	265, 330[a], 332, 337
$[CdL_3]Br_2\cdot 2H_2O$ (**6**) → $[CdL_3]Br_2\cdot H_2O$	50— 80	70
$[CdL_3]Br_2\cdot H_2O$ → $[CdL_3]Br_2$	80—100	95
$[CdL_3]Br_2$ → $CdL_{1.5}Br_2$ (**6a**)	100—170	165
$CdL_{1.5}Br_2$ → $CdBr_2$	180—355	200, 230, 328, 330, 340
$[CdL_3]SO_4$ (**7**) → CdL_2SO_4 (**7a**)	82—123	118
CdL_2SO_4 → $CdLSO_4$ (**7b**)	180—239	232
$CdLSO_4$ → $CdL_{0.66}SO_4$	245—272	265
$CdL_{0.66}SO_4$ → $CdSO_4$	282—322	288, 318
$[CdL_3]SeO_4\cdot 1.5H_2O$ (**8**) → $[CdL_3]SeO_4\cdot H_2O$	50— 66	63
$[CdL_3]SeO_4\cdot H_2O$ → $[CdL_3]SeO_4$	66—100	88
$[CdL_3]SeO_4$ → CdL_2SeO_4 (**8a**)	100—135	125
CdL_2SeO_4 → $CdLSeO_4$ (**8b**)	190—240	231
$CdLSeO_4$ → $CdSeO_4$	255—305	288, 294[a]

a) Denotes exothermic, rest are endothermic.

Table 3a. IR spectral data (4000—600 cm^{-1}) of 1,2-propanediamine(L) complexes of zinc(II) and cadmium(II) in KBr

Compound	Assignments							
	$\nu(NH_2)$	$\nu(CH_2)$	$\delta(NH_2)$	$\delta(CH_2)$	$\rho_w(CH_2)$	$\tau(NH_2)+\rho_w(NH_2)+\tau(CH_2)$	Stretching vibration of skeleton $\nu(C-N)+\nu(C-C)$	$\rho_r(CH_2)$
$[ZnL_3]Cl_2\cdot 2H_2O$[a]	3315 s, 3280 s, 3235 s, 3160 m	2960 m, 2935 m, 2870 m	1590 ms, 1557 sh	1462 sh, 1455 m,	1388m, 1378 sh, 1370 m	1336 w, 1303 m, 1227 vw, 1192 m, 1149 m	1100 w, 1070 ms, 1027 sh, 1015 vs, 985 sh	932 m, 900 vw, 835 w, 630 mb
$ZnL_{1.5}Cl_2$	3315 s, 3260 ms, 3170 m	2960 m, 2930 m, 2875 w	1580 ms, 1560 sh	1455 w	1390 w 1370 w	1330 vw, 1305 w, 1265 vw, 1190 w, 1140 w	1100 w, 1065 m, 1028 sh, 1010 vs, 984 sh	930 m, 900 vw, 835 w, 625 mb
$[CdL_3]Cl_2\cdot 2H_2O$[a]	3315 s, 3275 s, 3235 s, 3160 m	2960 ms, 2930 m, 2975 m	1585 s, 1555 sh	1458 m	1390 m, 1370 m,	1347 vw, 1335 vw, 1302 w, 1265 vw, 1182 m, 1135 ms	1095 w, 1055 s, 1000 sbr	922 ms, 898 w, 821 w, 650 sh,
$CdL_{1.5}Cl_2$	3315 vs, 3255 s, 3160 w	2950 ms, 2920 m, 2870 m	1575 ms, 1555 sh	1455 w	1380 w, 1370 w	1325 vw, 1300 w, 1260 vw, 1180 w, 1120 w	1095 w, 1050 m, 990 vs	920 ms, 890 w, 820 w, 650 w
$CdLCl_2$	3322 s, 3300 vs, 3272 ms, 3245 s, 3150 w	2998 sh, 2960 m, 2940 m, 2919 sh, 2879 w	1582 s, 1560 w	1468 w, 1460 w, 1450 w	1392 m, 1378 w	1327 vw, 1305 w, 1260 vw, 1192 m, 1130 m	1100 w, 1055 m, 1038 ms, 1027 m, 1001 s	930 m, 899 vw, 828 w, 615 ms
$CdL_{1.5}Br_2$	3320 vs, 3255 s, 3155 w	2955 ms, 2920 m, 2870 m	1575 s, 1555 sh	1455 w	1390 w, 1375 w	1330 vw, 1305 w, 1260 vw, 1180 m, 1120 w	1090 w, 1050 m, 978 vs	922 ms, 890 w, 821 w, 655 vw
$CdLSO_4$	3322 s, 3300 vs, 3265 ms, 3240 s, 3140 w	2960 m, 2935 m, 2918 sh, 2875 m	1578 s, 1555 sh	1465 w, 1450 w, 1447 w, 1442 sh	1388 m, 1370 w	1320 vw, 1300 w, 1258 vw, 1185 sh b)	1041 ms, 1027 s, 1015 ms, 991 s, 978 m[c]	920 m, 890 w, 820 w, 610 vs, 605 sh
$CdLSeO_4$	3322 s, 3300 vs, 3265 ms, 3240 vs, 3140 w	2960 m, 2935 m, 2918 sh, 2875 m	1578 s, 1555 sh	1460 w, 1450 w, 1445 w, 1440 sh	[388 w, 1370 w	1320 vw, 1300 w, 1258 vw, 1183 m, 1132 m	(1118 m, 1041 ms, 1108 m)[d], 1026 s, 1099 m, 1015 ms, 1090 sh[d], 991 s	920 m, 602 ms, (898 vs, 875 vs, 833 m)[d], 820 vw

a) Bands due to H_2O vibration are omitted; spectra of the other tris complexes are similar. b) Spectra complicated, not distinguishable due to overlapping of sulfate and ligand bands. c) Bands due to SO_4^{2-} vibration. d) Bands due to SeO_4^{2-} vibration: vs=very strong, s=strong, ms=medium strong, m=medium, w=weak, vw=very weak, sh=shoulder.

TABLE 3b. FAR-INFRARED SPECTRAL DATA[a] (600—100 cm^{-1}) OF 1,2-PROPANEDIAMINE(L) COMPLEXES OF ZINC(II) AND CADMIUM(II) IN POLYTHENE DISC

Compound	Assignments		
	$\rho_r(NH_2)+\nu(M-N)+$chelate ring bend	$\nu_t(M-X)$	$\nu_b(M-X)$
$ZnL_{1.5}Cl_2$	528 s, 520 sh, 442 vs, 430 sh, 340 sh	279 vs br, 126 w	—
$CdL_{1.5}Cl_2$	580 s, 515 m, 435 s, 425 sh, 340 m	280 w, 260 vs, 245 vs	—
$CdLCl_2$	570 sh, 530 m, 461 m, 447 ms, 358 m	268 s	184 vs, 178 vs
$CdL_{1.5}Br_2$	595 s, 525 w, 505 w, 435 m, 422 m, 340 w	188 vs, 170 vs	—
$CdLSO_4$	565 sh, 518 m, 450 m, 422 ms, 345 w	—	—
$CdLSeO_4$	565 sh, 518 m, 449 m, 419 ms, 408 s[b], 345 w	—	—

a) Done in FT-IR spectrometer, Polytec FIR 30. vs=very strong, br=broad, s=strong, ms=medium strong, m=medium, w=weak, sh=shoulder. b) Band due to SeO_4^{2-} vibration.

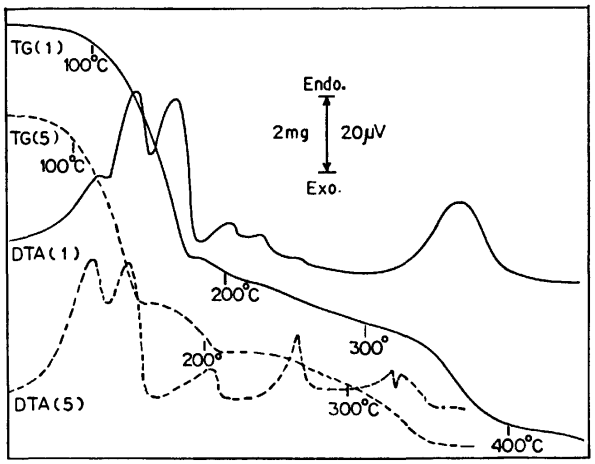

Fig. 1. Thermal curves of ——, $[ZnL_3]Cl_2\cdot 2H_2O$ (**1**) and - - -, $[CdL_3]Cl_2\cdot 2H_2O$ (**5**). Sample weights: **1**, 16.75 mg: **5**, 15.30 mg.

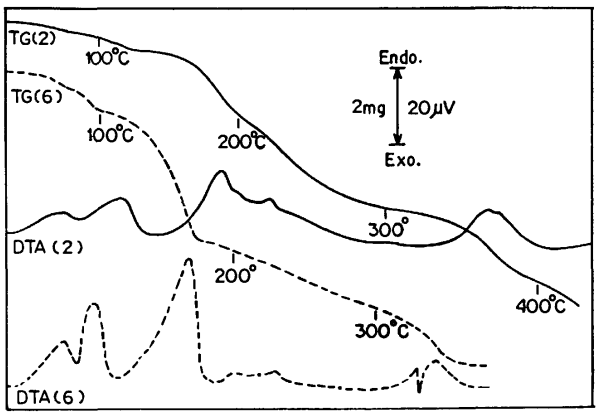

Fig. 2. Thermal curves of ——, $[ZnL_3]Br_2\cdot 1.5H_2O$ (**2**) and - - -, $[CdL_3]Br_2\cdot 2H_2O$ (**6**). Sample weights: **2**, 13.46 mg: **6**, 16.62 mg.

corresponding 1,2-ethanediamine complex.[4] The synthesis of $ZnL_{1.5}Cl_2$ in solid state appears very interesting as such type of zinc diamine complex species is not known in literature although we reported[7] the synthesis of $NiL_{1.5}Cl_2$ (L=1,4-butanediamine), where diamine behaves as chelating as well as bridging bidentate ligand. The complex **1a** may be presumed to exist in dimeric form. But dimerization of the complex **1a** becomes possible if one ligand (L) acts here as bridging bidentate. Interesting observation is that IR spectra of complex **1** and **1a** show practically no difference with respect to diamine bands (Table 3a). This observation does not support the bridging behavior of diamine in $ZnL_{1.5}Cl_2$.† So it may be thought that all the diamine present in complex **1a** are chelated which is possible if the species exists as $[ZnL_3][ZnCl_4]$. The far-infrared spectrum (Table 3b) of **1a** shows a very strong band at $\approx$279 cm^{-1} and a weak band at $\approx$126 cm^{-1} which supports the existence of $[ZnCl_4]^{2-}$ [13] anion in complex. We tried to prepare this species from the equimolecular mixture of $[ZnL_3]Cl_2\cdot 2H_2O$ and $[Et_4N]_2[ZnCl_4]$, but we always obtained $ZnLCl_2$. On the other hand, synthesis of $[Fe(bpy)_3][FeBr_4]$[14] from the pyrolysis of $[Fe(bpy)_3]Br_2$ in solid state does not rule out the above possibility. On further heating $ZnL_{1.5}Cl_2$ starts decomposition at 185 °C and transforms to $ZnCl_2$ through nonisolable intermediate $ZnLCl_2$ as supported from the TG curve (Fig. 1, Table 2a). Three broad overlapping endotherms in the DTA profile account the elimination of 0.5 molecule diamine per zinc atom from $ZnL_{1.5}Cl_2$. Endothermic peak appearing at 365 °C is due to the elimination of last molecule of diamine.

Diamine Complexes of Zinc Bromide. IR spectrum (Table 3a) of $[ZnL_3]Br_2\cdot 1.5H_2O$ (**2**) with respect to the diamine bands is similar to $[ZnL_3]Cl_2\cdot 2H_2O$ suggesting practically no difference in the nature of bonding between the two complex species. Complex **2** upon heating becomes anhydrous at 125 °C in two steps (Fig. 2, Table 2a). The anhydrous compound is isolable by temperature arrest technique. It decomposes at 140 °C and transforms to $ZnBr_2$ at 405 °C through the formation of unstable intermediates ZnL_2Br_2 and $ZnLBr_2$ as is evident from the TG curve. Three overlapping endotherms account for the elimination of two molecules of diamine per zinc atom. Last two overlapping endotherms account for the elimination of residual diamine (Fig. 2). None of the inter-

† It is well established fact that different IR active vibrations will be allowed for chelated and bridged diamine in the respective metal complexes.[10-12] If there is any real evidence for bridging as well as chelating behavior of diamine in complex (**1a**), then it should show some distinguishable difference in IR spectrum from that of (1).

mediate species is isolable in solid state by arresting temperature.

Diamine Complexes of Zinc Sulfate. $[ZnL_3]SO_4 \cdot H_2O$ (**3**) shows almost similar IR spectra with that of complex **1**. It becomes anhydrous at 85 °C showing an endothermic peak at 82 °C in DTA curve. On further heating the dehydrated complex starts to lose diamine and transforms to ZnL_2SO_4 (**3a**) at 130 °C (Fig. 3) showing an endothermic peak at 120 °C in DTA curve. We could not characterize the derived bis species owing to its extreme hygroscopic nature. So the prediction about the role of the SO_4^{2-} in the complex ZnL_2SO_4 is not possible here. But from our previous study[4] and the preference of tetracoordination of zinc(II) enables us to conclude that probably SO_4^{2-} is not coordinated here. On further heating the complex ZnL_2SO_4 decomposes in a complicated way. However, the TG curve indicates the decomposition taking place through the formation of an unstable intermediate $ZnLSO_4$.

Diamine Complexes of Zinc Selenate. IR spectra of $[ZnL_3]SeO_4 \cdot 1.5H_2O$ (**4**) show very close similarity with those of the complexes **1**, **2**, and **3**. It becomes anhydrous at 105 °C through the formation of monohydrate at 75 °C (Fig. 4). The anhydrous species starts decomposition at 120 °C and transforms to ZnL_2SeO_4 (**4a**) at 165 °C. Characterization of this bis species in solid state in anhydrous form is also not possible owing to the similar reason stated in the corresponding sulfate. The TG curve shows that it decomposes to $ZnSeO_4$ in single step. But the corresponding DTA curve shows an endotherm followed by an exotherm. The exothermic peak appearing at 280 °C might be due to the decomposition of ligand. This is very much likely as the residue obtained at 292 °C is $ZnSeO_4$+carbon.

Diamine Complexes of Cadmium Chloride. IR spectrum of $[CdL_3]Cl_2 \cdot 2H_2O$ (**5**) (Table 3a) is similar to its zinc analogue. It starts deaquation at 75 °C and transforms to an isolable intermediate, $CdL_{1.5}Cl_2$ (**5a**) at 150 °C like that of complex (**1**) (Fig. 1). Here also, the later compound gives identical IR spectrum with that of its parent tris complex. Far-infrared spectrum (Table 3b) of $CdL_{1.5}Cl_2$ shows bands at 280(w), 260(s), and 245 cm^{-1} (s). These bands suggest here also the presence of $[CdCl_4]^{2-}$ anion in it[13,14] like that of zinc complex. It is noticed that the derived $[CdL_3][CdCl_4]$ appears to be isomorphous with $[ZnL_3][ZnCl_4]$ as is evident from their similar X-ray diffraction patterns (Table 4). Here also for comparative study we tried to prepare $[CdL_3][CdCl_4]$ by mixing $[CdL_3]Cl_2$ and $[Et_4N]_2[CdCl_4]$ in 1 : 1 proportion but failed to prepare it in pure form owing to the presence of $CdLCl_2$ in appreciable amount which could not be separated by

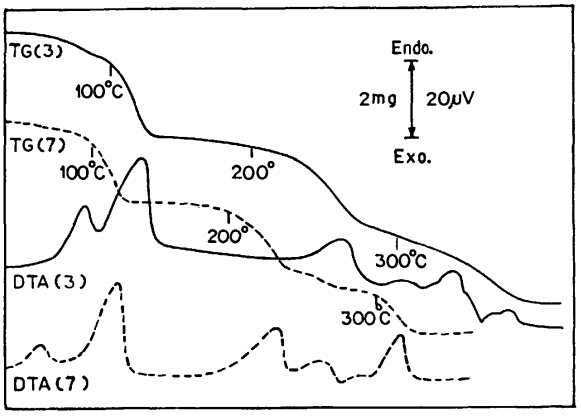

Fig. 3. Thermal curves of ——, $[ZnL_3]SO_4 \cdot H_2O$ (**3**) and - - -, $[CdL_3]SO_4$ (**7**). Sample weights: **3**, 12.21 mg: **7**, 10.96 mg.

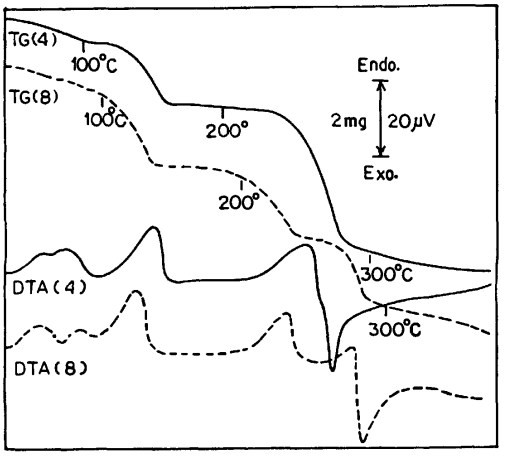

Fig. 4. Thermal curves of ——, $[ZnL_3]SeO_4 \cdot 1.5H_2O$ (**4**) and - - -, $[CdL_3]SeO_4 \cdot 1.5H_2O$ (**8**). Sample weights: **4**, 13.00 mg: **8**, 12.39 mg.

Table 4. The prominent lines in the X-ray powder photographs of the diamine complexes[a]

$ZnL_{1.5}Cl_2$ d, Å	$CdL_{1.5}Cl_2$ d, Å	$CdL_{1.5}Br_2$[b] d, Å
8.80 vs[a]	8.76 vs	7.44 w
5.70 s	6.78 s	6.42 s
5.29 s	5.44 w	5.81 w
4.84 m	4.90 m	5.16 vw
4.56 m	4.47 s	4.80 w
4.26 w	4.02 m	4.45 s
3.86 s	3.78 w	3.98 vw
3.53 w	3.62 vw	3.66 s
3.42 w	3.38 m	3.47 w
3.29 vw	3.23 vw	3.24 vw
2.93 vw	2.78 m	3.04 s
2.67 m	2.68 m	2.83 m
2.48 w	2.48 vw	2.68 vw
2.39 m	2.39 w	2.51 vw
2.18 w	2.26 w	2.38 w
2.06 w	2.13 vw	2.27 vw
2.00 vw	2.04 w	2.18 vw
1.93 vw	1.93 vw	2.10 s
1.88 m	1.80 w	1.99 w
1.77 vw	1.75 vw	1.90 w

vs=very strong, s=strong, m=medium, w=weak, vw=very weak. a) Intensities estimated visually. b) The X-ray powder photograph of $[CdL_3][CdBr_4]$ synthesized from solution is identical to it.

any means. The complex **5a** on further heating transforms to an isolable intermediate having composition $CdLCl_2$ (**5b**) unlike the corresponding zinc complex. IR spectra of this mono(diamine) species shows chelating bidentate character of the diamine whereas, $CdenCl_2$ synthesized by us earlier[5] possesses bridged en. $CdLCl_2$ synthesized from solution also shows similar physicochemical property with that of **5b**. Far-infrared spectral data of $CdLCl_2$ (**5b**) and $CdLBr_2$†† (**6b**) are presented in Table 3b. Compariosn of the spectrum shows the presence of ν_t(Cd–Cl) at 268 cm^{-1} and ν_b (Cd–Cl) at 178 and 184 cm^{-1} in $CdLCl_2$ and ν_t(Cd–Br) at 207 cm^{-1} and ν_b(Cd–Br) at 154 and 163 cm^{-1} in $CdLBr_2$. These data clearly indicate the presence of bridging and terminal coordination of the halogen in the mono(diamine) complex. Reported crystal structure of analogous compound $[Cd(dmpd)X_2]$[17] (dmpd =2,2-dimethyl-1,3-propanediamine) also corroborates our proposed bonding character of halogens and diamines to the metal ion. Again the splitting of the IR bands of the complex **5b** (Table 3a and b) in the region ≈3300, ≈1000, and 500 cm^{-1} which are due to ν_{NH_2}, ν_{CN}, and ν_{MN} indicate that the symmetry of the chelate ring is lowered in the complex. The decomposition of $CdLCl_2$ appears very complicated (Fig. 1). It initially melts showing an endothermic peak at 265 °C, then it decomposes and transforms to $CdCl_2$ at 355 °C. DTA curve shows overlapping endotherms as well as exotherm for the elimination of residual diamine from $CdLCl_2$.

Diamine Complexes of Cadmium Bromide. $[CdL_3]Br_2 \cdot 2H_2O$ (**6**) starts decomposition at 50 °C and becomes anhydrous at 100 °C through the formation of monohydrate at 80 °C (Fig. 2, Table 2b). The derived anhydrous compound immediately starts decomposition and transforms to an isolable intermediate $CdL_{1.5}Br_2$ (**6a**) at 170 °C. This on further heating transforms to $CdBr_2$ at 355 °C. The DTA curve shows initially two overlapping endotherms for the elimination of water, then a prominent endotherm for the elimination of 1.5 molecule of diamine. The elimination of residual diamine occurs showing two overlapping broad endotherms and then an endotherm followed by one exotherm and endotherm (Fig. 2). IR spectra of $CdL_{1.5}Br_2$, $[CdL_3]Br_2$, and $CdL_{1.5}Cl_2$ are very similar. The far-infrared spectral data of **6a** show bands at 170 and 188 cm^{-1} which are also found in $[Et_4N]_2[CdBr_4]$[15] supporting the presence of $[CdBr_4]^{2-}$ anion in **6a**. Again we prepared $[CdL_3][CdBr_4]$ from solution and observed similar thermal behavior, IR spectral data like $CdL_{1.5}Br_2$ (**6a**) isolated pyrolytically in solid state. X-ray powder patterns (Table 4) of two $CdL_{1.5}Br_2$ also appear same. The above observations suggest that the complex $CdL_{1.5}Br_2$ exists actually in $[CdL_3][CdBr_4]$ form.

Diamine Complexes of Cadmium Sulfate. $[CdL_3]SO_4$ (**7**) is hygroscopic in character. This complex starts decomposition at 82 °C and becomes CdL_2SO_4 (**7a**) at 123 °C (Fig. 3, Table 2b). Initial loss in TG curve and its corresponding endotherm in DTA curve (Fig. 3) is due to the elimination of water adsorbed while exposing the complex **7** in air. The derived bis species on further heating generates $CdSO_4$ at 322 °C through two intermediates, $CdLSO_4$ (**7b**) and $CdL_{0.66}SO_4$ at 239 and 272 °C, respectively. The mono(diamine) species is isolable in solid state. The corresponding DTA curve shows altogether six endothermic peaks. The first three endotherms are due to water elimination and the first and second molecules of diamine, respectively. Fourth endotherm is due to elimination of 0.33 mole of diamine. The last two overlapping endotherms (Fig. 3) are due to elimination of 0.66 mole of diamine. Although we could not separate $CdL_{0.66}SO_4$ in pure form, but formation of this type of complex is not unlikely as literature show examples of this type of complex.[18,19] CdL_2SO_4 is also hygroscopic in nature like the corresponding zinc salts. As Cd^{II} prefers O_h coordination and complex like $[Cd(tn)_2SO_4]$ (tn=1,3-propanediamine)[5] is known, SO_4^{2-} coordination is expected in this bis(diamine) species. IR spectrum of $CdLSO_4$ is almost identical to that of $CdLCl_2$ (Table 3a). The far-infrared spectra of these two complexes are also similar (Table 3b), though one could expect some M–O stretching vibration along with M–N stretching vibrations in the far-infrared region (500—200 cm^{-1}) owing to the coordination of SO_4^{2-} to the metal atom. So it is clear that M–O stretching force constants are much smaller than the M–N stretching force constants here.[20]

Diamine Complexes of Cadmium Selenate. $[CdL_3]SeO_4 \cdot 1.5H_2O$ (**8**) becomes anhydrous at 100 °C through the formation of monohydrate at 66 °C (Fig. 5). The derived anhydrous species immediately starts deamination and transforms to CdL_2SeO_4 (**8a**) at 135 °C. This on further heating decomposes at 190 °C and transforms to $CdSeO_4$ through the formation of an isolable intermediate, $CdLSeO_4$ (**8b**) at 240 °C. The corresponding DTA curve shows first an endotherm for the elimination of 0.5 mole of water, then an endotherm overlapping with another prominent endotherm for the elimination of residual water and one diamine molecule. The fourth endotherm accounts for the second molecule of diamine. The residual diamine elimination is associated with first an endotherm immediately followed by an exotherm. Appearance of exotherm might be due to the same reason as stated in the corresponding zinc complex. Here also, bis(diamine) species shows hygroscopic character. $CdLSeO_4$ appears to be isomorphous with $CdLSO_4$. It is interesting to note that $[ZnL_3]SeO_4$ does not yield any $ZnLSeO_4$ while pyrolysis. This type of anomaly occurs probably due to the size factor of the two metal ions.

It is noticed that the decomposition temperature of $[ML_3]X_2$ (M=zinc(II) and cadmium(II); X=Br^-, $0.5SO_4^{2-}$, and $0.5SeO_4^{2-}$) follows the sequence $SO_4^{2-} < SeO_4^{2-} \leqslant Br^-$. $[ZnL_3]X_2$ and $ZnLX_2$ appear thermally more stable than those of cadmium complexes (Tables 2a and b). Our earlier investigation shows that zinc and cadmium complexes of 1,2-ethanediamine are thermally more stable than the corresponding 1,2-propanediamine complexes. $[ML_3]SO_4$ [M=zinc(II) or cadmium(II)] complexes particularly show surprisingly less stability than the corresponding 1,2-ethanediamine

†† Synthesized from solution for characterizing ν_t and ν_b (M–X) band from far-infrared spectra.

complexes.

References

1) G. De, P. K. Biswas, and N. Ray Chaudhuri, *Bull. Chem. Soc. Jpn.*, **56**, 3145 (1983).
2) S. Mitra, G. De, and N. Ray Chaudhuri, *Thermochim. Acta*, **66**, 187 (1983).
3) S. Mitra, G. De, and N. Ray Chaudhuri, *Thermochim. Acta*, **71**, 107 (1983).
4) G. De and N. Ray Chaudhuri, *Thermochim. Acta*, **66**, 349 (1983).
5) G. De and N. Ray Chaudhuri, *Thermochim. Acta*, **77**, 1 (1984).
6) G. De, P. K. Biswas, and N. Ray Chaudhuri, *J. Chem. Soc., Dalton Trans.*, **1984**, 2591.
7) G. De and N. Ray Chaudhuri, *Bull. Chem. Soc. Jpn.*, **58**, 715 (1985).
8) A. Ghosh, G. De, and N. Ray Chaudhuri, *J. Therm. Anal.*, **32**, 447 (1985).
9) F. A. Cotton and W. Wilkinson, "Advanced Inorganic Chemistry," 4th ed, John Wiley and Sons, Inc., New York (1980), p. 590.
10) K. Krishnan and R. A. Plane, *Inorg. Chem.*, **5**, 852 (1966).
11) G. Newman and D. B. Powell, *J. Chem. Soc.*, **1961**, 477.
12) T. Iwamoto and D. F. Shriver, *Inorg. Chem.*, **10**, 2428 (1971).
13) J. S. Avery, C. D. Burbridge, and D. M. L. Goodgame, *Spectrochim. Acta*, **24A**, 1721 (1968).
14) S. K. Dhar and F. Basolo, *J. Inorg. Nucl. Chem.*, **25**, 37 (1963).
15) J. E. D. Davis, and D. A. Long, *J. Chem. Soc., A*, **1968**, 2054.
16) D. M. Adams, J. Chatt, J. M. Davidson, and, J. Gerratt, *J. Chem. Soc.*, **1963**, 2184.
17) F. Cariati, G. Ciani, L. Menabue, G. C. Pellacani, G. Rassu, and A. Sironi, *Inorg. Chem.*, **22**, 1897 (1983).
18) B. Banerjee, P. K. Biswas, and N. Ray Chaudhuri, *Thermochim. Acta*, **68**, 261 (1983); B. Banerjee and N. Ray Chaudhuri, *ibid.*, **71**, 93 (1983).
19) G. Bach, C. T. Mortimer, and E. G. Tyler, *J. Chem. Soc. A*, **1967**, 925; **1969**, 512.
20) T. J. Lane, J. A. Durkin, and R. J. Hooper, *Spectrochim. Acta*, **20**, 1013 (1964); I. Nakagawa, R. J. Hooper, J. L. Walter, and T. J. Lane, *ibid.*, **21**, 1 (1965).

Über die Reaktion von Harnstoff mit Ammoniumhydrogenamidophosphat unter dem Atmosphärendruck

Choichiro SHIMASAKI* und Mitsunari HARA
Fakultät für Ingenieurwissenschaften, Universität Toyama, Nakagawasonomachi, Takaoka, Toyama 933
(Eingangsdatum: 22. Juni 1985)

Die Reaktion von Harnstoff mit Ammoniumhydrogenamidophosphat ($NH_4HPO_3NH_2$) im Schmelzzustand unter dem Atmosphärendruck ergibt, daß die Bildung des Guanidinumions (GH^+) zusammen mit dem Phosphation bei *ca.* 160 °C die maximale Hitze, und nach 7 Stunden die maximale Ausbeute erreicht. Aus IR Spektren und ^{31}P NMR-Spektren von Reaktionsgemischen und der Entwicklungsbetrag des Ammoniakgases wurde keine Zwischenprodukte, wie Ammoniumureidophosphat, aufgestellt. Die frühere Hauptreaktion der Bildung von GH^+ ist das Deamidieren von $NH_4HPO_3NH_2$. Die gebildete GH^+ und das Phosphation bilden mit zunehmender Reaktionstemperatur jeweils die Ringverbindungen wie Triazinverbindungen und die Polmerisaten wie Pyro-, Tripoly-, und Metaphosphat. Das aus $NH_4HPO_3NH_2$ isolierende Ammoniak unterdrückt die Zersetzung von Harnstoff zu Cyansäure und befördert die Transition zu Cyanamid. Die Bildung von GH^+ ist von der Reaktion von Cyanamid mit NH_4^+ abhängig.

Außer Dicyandiamid als Rohstoff sind die meisten Herstellungsmethoden der Guanidiniumsalze bekannt. Als eine durchführbare Methode für die Industrieherstellung des Guanidiniumsalzes wurde an den Gebrauch des Harnstoffs als Rohstoff gedacht. Unter dem Atmosphärendruck wurden die Reaktionen von Harnstoff mit Ammoniumsalz unter dem Silikagel-Katalysator[1] und von Harnstoff mit Ammoniumamidosulfat,[2] Ammoniummetaphosphat,[3] oder Phosphorpentaoxyd[4] unter dem Nichtkatalysator festgestellt.

Bis jetzt ist die Reaktion von Harnstoff mit $NH_4HPO_3NH_2$ nicht sehr bekannt. Auf der anderen Seite wurden in bezug auf Ammoniumamidosulfat die Literaturen von Boivin und Lovecy,[5] und von Tanihara[6] erkannt. In der jetzigen Abhandlung wird der Mechanismus der Reaktion von Harnstoff mit $NH_4HPO_3NH_2$ untersucht und die Veränderung der physikochemischen Eigenschaften von Guanidiniumsalz diskutiert.

Durchführung der Experimente

Materialien. $NH_4HPO_3NH_2$ wurde nach der Methode[7] zusammengesetzt, die in der früheren Abhandlung beschrieben ist. Das Produkt wurde unter 3333 Pa bei Raumtemperatur für zwei Tage getrocknet und mit Daten von IR Spektren,[8] Röntgenbeugungsbildern,[9] und Elementaranalysen identifiziert.

Apparate und Verfahren. Eine bestimmte Quantität von Harnstoff und $NH_4HPO_3NH_2$ (Molenverhältnis=1.0, Gesamtsumme=3.0 g) wurde in einen Dreihalskolben mit einem Rührwerk hineingetan. Die Reaktion unter dem Atmosphärendruck wurde durchgeführt. Bevor das Reaktionsgemisch erwärmt wurde, wurde das System mit Stickstoffgas durchgefüllt. Die Erwärmung wurde mit dem Thermoregler des Ölbad durchgeführt. Während die Wärme konstant gehalten wurde, wurde die Temperature mit einer Aufheizgeschwindigkeit von 5 °C/min zur gewünschten Temperatur gebracht. Nach der vorgeschriebenen Reaktionszeit wurde das Reaktiongefäß vom Ölbad, während der Einleitung des Stickstoffgases, genommen und für eine Stunde liegengelassen wie es war. Das Reaktionsgemisch wurde anschließend im Vakuumexsikkator mittels P_2O_5 getrocknet. Auch die Abtrennung des entstehenden Ammoniakgases vom Reaktionsgemisch konnte durch dauerndes Durchleiten des trockenden Stickstoffgases ins Reaktionsgefäß erfolgen. Das Ammoniakgas wurde durch rasches Durchleiten des Gasgemisches durch eiskaltes 1 M H_2SO_4 (1 M=1 mol dm^{-3}) restlos absorbiert.

Der Ammoniakgehalt wurde mit Lösung der Schwefelsäure nach der Kjeldahl Methode bestimmt. Der Phosphorgehalt wurde mittels einer gravimetrischen Methode[10] analysiert und mittels Papierchromatographie[11] mit sauren und basischen Lösungsmitteln getrennt. Der Guanidiniumiongehalt wurde mittels der kalorimetrischen Analyse bestimmt. Die DTA, DSC, und TG Kurven wurden in der Luft mit einer Aufheizgeschwindigkeit von 5 °C/min mit einem Rigaku TG-DTA Thermoflex aufgenommen. Für DTA und DSC wurde α-Al_2O_3 als Bezugsmittel gebraucht. Die Röntgenbeugungsbilder wurden mit einem Shimadzu-Beugungsmesser (Cu $K\alpha$-Strahlung, Ni-gefiltert) erhalten. Die IR Spektren wurden mittels Präparation von KBr-Presslingen mit einem Beugungsgitter IR Spektrometer der JASCO aufgenommen. Die ^{31}P NMR Spektren wurden mit einem JEOL JNM-FX 90 QFT Spektrometer aufgenommen. Als Lösungsmittel wurde schweres Wasser verwendet.

Ergebnisse und Diskussionen

Thermische Reaktion. Die DSC und TG Kurven der Probe sind in Abb. 1 dargestellt. Die DSC Kurve ergibt komplizierte endotherme Spitzen zwischen 130 und 220 °C, unter denen die erste Spitze (zwischen 130 und 145 °C) aus dem eutektischen Punkt von $NH_4HPO_3NH_2$ und Harnstoff ist. Die folgenden Spitzen zwischen 160 und 220 °C werden komplizierter, da in diesem Temperaturgebiet die Schmelzreaktion zu entstehen beginnen. Im Temperaturgebiet über 220 °C werden die endotherme und exotherme Spitzen nicht beobachtet. In dieser Temperatur hat sich herausgestellt, daß die Reaktion zum Abschluß kommt. Die TG Kurve zeigt, daß der Prozeß der Gewichtsverluste von der Probe in der Nähe der Temperatur 130 °C anfängt und mit zunehmender Temperatur der Prozentsatz der Gewichtsverluste abnimmt.

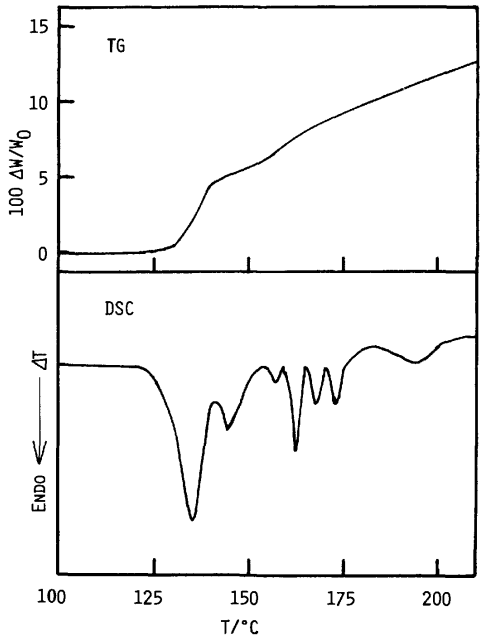

Abb. 1. DSC-TG-Kurven des äquimolekularen Gemisches von $NH_4HPO_3NH_2$-$(NH_2)_2CO$ in Luft.

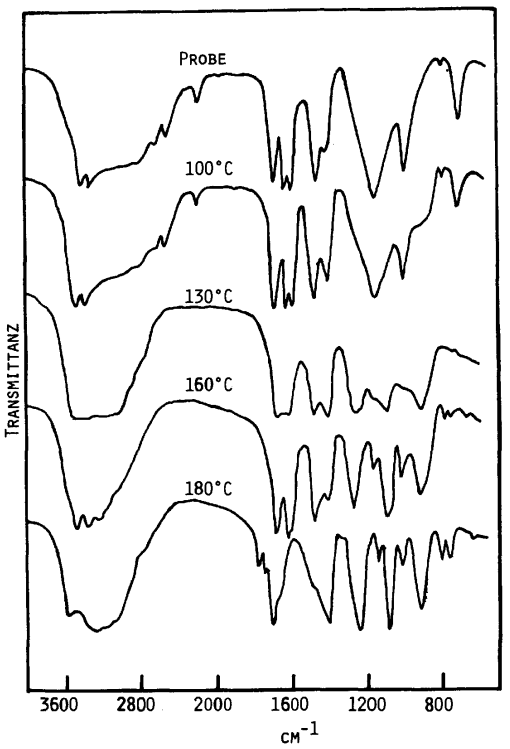

Abb. 2. IR-Spektren des äquimolekularen Gemisches von $NH_4HPO_3NH_2$-$(NH_2)_2CO$ in verschiedenen Temperaturen.

TABELLE 1. PAPIERCHROMATOGRAPHIE VON HEIZPRODUKTE

Reaktionstemperatur/°C	R_f wert (Farbe)			
Probe	0.078 (Helles blau)	0.396 (Rot)		
100	0.078 (Helles blau)	0.400 (Rot)		
110	0.076 (Helles blau)	0.400 (Rot)		
120	0.074 (Helles blau)	0.398 (Rot)		
130	0.078 (Helles blau)	0.402 (Rot)		
140	0.074 (Helles blau)	0.400 (Rot)		
150			0.105 (Rot)	0.345 (Rot)
160			0.104 (Rot)	0.346 (Rot)
170			0.108 (Rot)	0.341 (Rot)
180			0.101 (Rot)	0.345 (Rot)
190			0.101 (Rot)	0.340 (Rot)
200			0.102 (Rot)	0.347 (Rot)
$(NH_2)_2CO$		0.410 (Rot)		
$NH_4HPO_3NH_2$	0.077 (Helles blau)			
$(NH_2CNHNH_2)_2H_3PO_4H_2O$			0.103 (Rot)	0.342 (Rot)

IR Spektren. Abbildung 2 zeigt den Effekt der Heiztemperatur auf IR Spektren von der Probe. Die Absorption infolge eines Guanidiniumions zeigt sich bei 160°C, was mit den Ergebnissen der Papierchromatographie (Tabelle 1) übereinstimmt. Die Absorption infolge einer P-O-P Bindung sich zeigt und die Intensität der Absorption wird mit zunehmender Temperatur vergrößert, was mittels Papierchromatographie bei aller Reaktionsgemischen beobachtet wurde. Die Absorption eines Ammoniumions wird mit zunehmender Temperatur vergrößert, andererseits nehmen die entsprechenden Absorptionen von P-O-H und P-N-H Bindungen mit zunehmender Temperatur ab. Dies bedeutet, daß eine Amido Gruppe ein Ammoniumion umwandelt und als Ammoniakgas langsam in die Luft freigegeben wird.

Röntgenbeugungsbild. Abbildung 3 zeigt das Röntgenbeugungsbild des thermischen Zerfallprodukts von der Probe. Die Intensitäten der Beugungslinien von $NH_4HPO_3NH_2$ und Harnstoff nehmen mit zunehmender Temperatur ab. Die erstere geht bei 160°C und die letztere bei 170°C vollstandig verloren. Bei 120°C werden neue Spitzen erreicht, dann werden die Intensitäten vergrößert. Diese neuen Spitzen entspre-

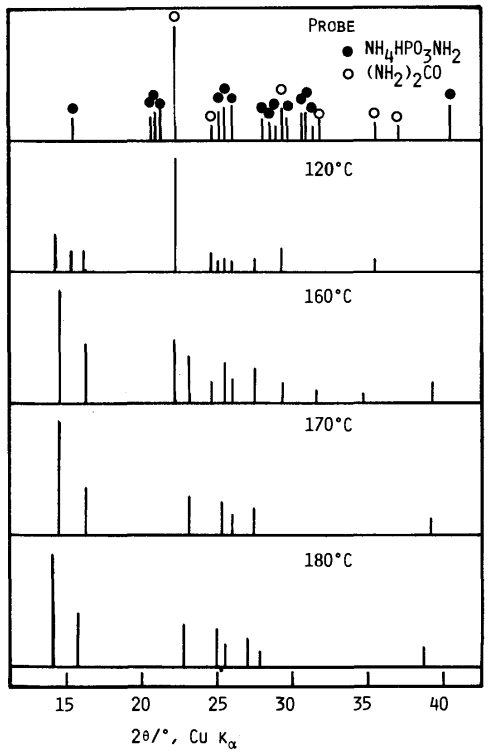

Abb. 3. Röntgenbeugungsbilder des äquimolekularen Gemisches von $NH_4HPO_4NH_2$-$(NH_2)_2CO$ in verschiedenen Temperaturen.

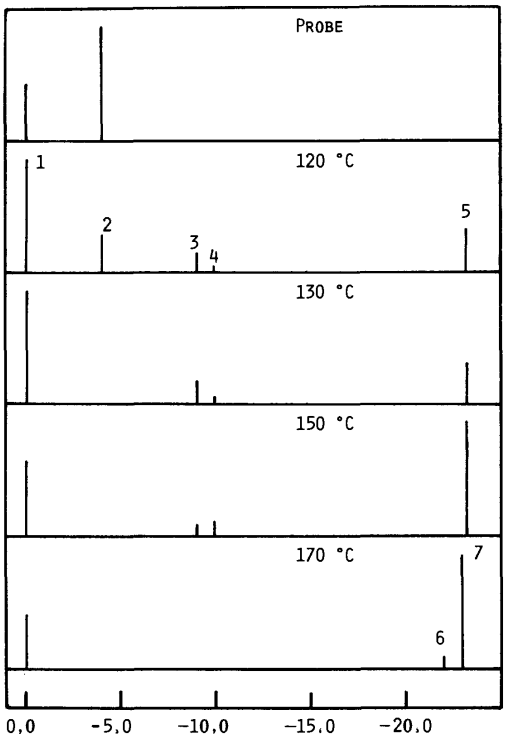

Abb. 4. ^{31}P NMR-Spektren des äquimolekularen Gemisches von $NH_4HPO_3NH_2$-$(NH_2)_2CO$ in verschiedenen Temperaturen.
1: Orthophosphat, 2: Amidophosphat, 3: Diphosphat, 4: Endgruppe des PO_4 von Triphosphat, 5: Mittegruppe des PO_4 von Triphosphat, 6: Endgruppe des PO_4 von Polyphosphat, 7: Mittegruppe des PO_4 von Polyphosphat.

chen Guanidiniumsalz. Die bei 130—150 °C gebildeten Heizprodukte sind hygroskopisch und adhäsiv, und noch dazu amorph. Die Resultate der Papierchromatographie deuten an, daß bei diesen Temperaturen $NH_4HPO_3NH_2$ festgestellt wird und als eutektisches Gemisch existiert. Aus den Resultaten der Röntgenbeugungsbilder und Papierchromatographie wurde die Existenz von Biuret nicht festgestellt. Aus diesem Grunde wird der Schluß gezogen, daß die Reaktion der Kondensationspolymerisation nicht aus Harnstoff entstehen, sondern aus der Bildungsreaktion des Guanidiniumsalzes.

^{31}P NMR-Spektren. Die ^{31}P NMR-Spektren in Abb. 4 zeigen, daß die Heizprodukte Orthophosphat, Diphosphat, und Triphosphat auch noch bei 120 °C $NH_4HPO_3NH_2$ enthalten. Bei allen Heizprodukten wird die Spitze der P-NH-P Bindung in den Spektren nicht festgestellt. Man kommt zu dem Schluß gezogen, daß Imidophosphat weder stabil noch aktiv ist. Der Bildungsprozeß von Ortho-, Di-, und Triphosphat wurde auf die gleiche Weise ausgeführt, die in der vorliegenden Abhandlung[12] erwähnt ist. Das Polyphosphat entstand nach

$$NH_4O\text{-}\underset{\underset{O}{\|}}{P}\text{-}OH \rightleftharpoons NH_4O\text{-}\overset{\overset{O}{\|}}{P}\text{-}O^- \longrightarrow$$

$$NH_4O\text{-}\overset{\overset{O}{\|}}{\overset{+}{P}}\text{-}\overset{-}{O} + NH_3 \longrightarrow \overset{ONH_4}{\overset{+}{P}}\text{-}O\text{-}\left[\begin{array}{c}ONH_4\\ P\text{-}O\\ \|\\ O\end{array}\right]_n\begin{array}{c}ONH_4\\ P\text{-}O^-\\ \|\\ O\end{array} \quad (1)$$

Reaktionsmechanismus von Harnstoff mit $NH_4HPO_3NH_2$. Watt und Post[13] gehen vermutlich über den Bildungsprozeß von Harnstoff zu Guanidiniumsalz, daß zuerst durch die Dehydrierung des Harnstoffes Cyanamid gebildet wird und bei der Reaktion mit Ammoniumsalz Guanidiniumsalz ergibt. Trotzdem in unserem Experiment konnte Cyanamid als Zwischenprodukt nicht nachgewiesen werden. Aus der thermodynamischen Betrachtung über die Reaktionstemperatur unter 300 °C ist es unmöglich, daß nach Dehydrierung und Ammoniakentzug aus Harnstoff Cyanamid und Cyansäure entstehen.[14] Aber man kann für möglich halten, daß Cyanamid sowohl gegen das System $NH_4HPO_3NH_2$-Harnstoff als auch gegen das System Ammoniumamidosulfat-Harnstoff[2] in der konjugierten Reaktion entsteht. Bei der thermischen Zersetzung von $NH_4HPO_3NH_2$ ist zuerst durch Ammoniakentzug die Bildung von Imidodiphosphat möglich:

$$2NH_4HPO_3NH_2 \rightleftharpoons NH(NH_4HPO_3)_2 + NH_3. \quad (2)$$

Es wird geschlossen, daß das Gebilde Imidodiphosphat ebenso leicht die Hydrolyse wie die Diammoniumimidobisulfat[15] beginnt. Der Effekt der Reaktionstemperatur und Reaktionszeit auf die Bildung von Guanidiniumsalz ist in Abb. 5 gezeigt. Bis 120 °C der

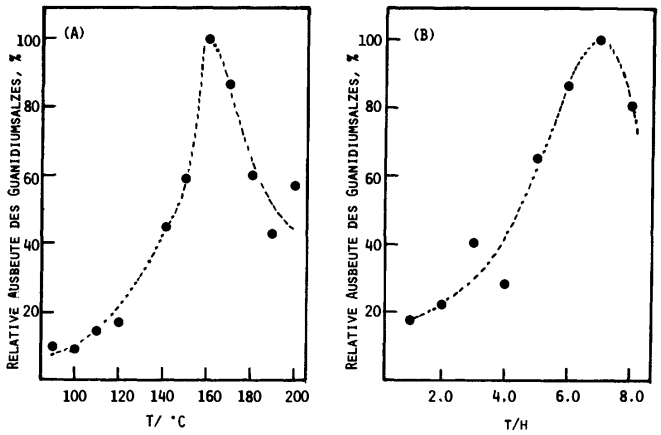

Abb. 5. Relative Ausbeute des Guanidiniumsalzes in Abhängigkeit von der Reaktionstemperatur (A) und dem Reaktionszeit (B).
(A) Reaktionszeit bei der Durchführung aller Experimente: 5 h.
(B) Reaktionstemperatur bei der Durchführung aller Experimente: 160°C.

Reaktionstemperatur wird die Bildung des Guanidiniumsalzes nicht festgestellt. Dieses Resultat stimmt mit den Resultaten von Röntgenbeugungsbilder und IR und ^{31}P NMR Spektren überein. Die Reaktion des Ammoniakentzuges bei 120°C stammt nicht aus dem Harnstoff, sondern $NH_4HPO_3NH_2$. Bei der Reaktionstemperatur über 130°C nimmt die Bildung des Guanidiniumsalzes bedeutend zu und bei 160°C erreicht die maximale Ausbeute des Guanidiniumsalzes. Zudem bei 170°C zeigt sich eine abnehmende Tendenz der Ausbeute des Guanidiniumsalzes. Aus den obigen Resultaten wird geschlossen, daß Ammoniakentzug besser ist als Dehydrierung aus Harnstoff und die Bildungsreaktion von Cyansäure vorwärtskommt. Außerdem wurde der Effekt der Reaktionszeit bei der Reaktionstemperatur 160°C untersucht. Es hat sich herausgestellt, daß in sieben Stunden die maximale Ausbeute von Guanidiniumsalz erreicht wird. Weitere Versuche haben gezeigt, daß die Entwickelungsmenge des Ammoniakgases bei einer Laufzeit der Reaktion bei 160°C bis zu sieben Stunden eine gleichmäßig steigende Kurve ergibt. Diese gefundene Ammoniakmenge entspricht gemäß Gl. 2 den berechneten Werten. In der Reaktionszeit über sieben Stunden fängt die Zersetzung des Guanidiniumsalzes an.

Der Bildungsmechanismus von Guanidiniumsalz braucht unbedingt die Dehydrierung aus Harnstoff nach

$$(NH_2)_2CO \rightleftharpoons NH_2CN + H_2O. \quad (3)$$

Die Hydrolysereaktion des Imidobiphosphates entsteht anschließend aus

$$NH(NH_4HPO_3)_2 + H_2O \longrightarrow NH_4HPO_3NH_2 + NH_4H_2PO_4. \quad (4)$$

Die Reaktion des gebildeten $NH_4H_2PO_4$ mit dem unreaktiven $NH_4HPO_3NH_2$ ergibt Imidobiphosphat und $(NH_4)_2HPO_4$ nach

$$2\,NH_4HPO_3NH_2 + NH_4H_2PO_4 \longrightarrow NH(HPO_3NH_2)_2 + (NH_4)_2HPO_4. \quad (5)$$

Diese Reaktion trägt zu der Bildung von NH_2CN mäß Gl. 3 bei, gleich wie Gl. 4. Schließlich hat es dazugeführt, daß die Reaktion von Cyanamid mit $NH_4H_2PO_4$ oder $(NH_4)_2HPO_4$ Guanidiniumphosphat gebildet wird:

$$NH_2CN + NH_4^+ \longrightarrow GH^+. \quad (6)$$

Dabei entstehen gleichzeitig als Nebenreaktion die gebildeten Phosphate wie $NH_4H_2PO_4$ und $(NH_4)_2HPO_4$ und aus dem unreaktiven Harnstoff wurden mit zunehmender Reaktionstemperatur die polymerisaten wie Pyro-, Tripoly-, und Metaphosphate und die Ringverbindungen wie Triazinverbindungen gebildet.

Literaturen

1) L. G. Boatright, U. S. Patent 2783276 (1957); N. Hamada, H. Sugahara, und T. Maebara, Japanisches Patent 45-28365 (1970).
2) J. S. Mackay, U. S. Patent 2464247 (1949); P. E. Gagnon, J. L. Boivin, und C. Haggart, *Can. J. Chem.*, **34**, 1662 (1956).
3) L. E. Craig und J. T. Minor, U. S. Patent 3009949 (1961).
4) J. S. Mackay, U. S. Patent 2469338 (1949).
5) J. L. Boivin und A. L. Lovecy, *Can. J. Chem.*, **33**, 1222 (1955).
6) K. Tanihara, *Nippon Kagaku Kaishi*, **1979**, 486; **1980**, 1094.
7) F. A. Cotton, "Inorganic Syntheses," Vol. XIII, p. 23 (1972).
8) D. E.C. Corbridge und E. J. Lowe, *J. Chem. Soc.*, **1954**, 493.
9) A. H. Herzog und M. L. Nielsen, *Anal. Chem.*, **30**, 1490 (1958).
10) "Bunseki Kagaku Binran," herausgegeben von der Japanischen Gesellschaft für Analytische Chemie, Maruzen, Tokyo (1971), pp. 204, 1492.
11) M. Takimoto und K. Koeda, *Kogyo Kagaku Zasshi*, **63**, 797 (1960).
12) C. Shimasaki, Y. Oono, F. Takai, M. Shoji, und M. Yoshizawa, *Nippon Kagaku Kaishi*, **1982**, 376; C. Shimasaki, S. Ookawa, und R. Isizaka, *Bull. Chem. Soc. Jpn.*, **58**, 592 (1985).
13) G. W. Watt und R. G. Post, *Ind. Eng. Chem.*, **45**, 846 (1953).
14) G. Ostrogovich und R. Bacaloglu, *Rev. Roum. Chim.*, **10**, 1125 (1965).
15) Y. Ito, *Kogyo Kagaku Zasshi*, **73**, 281 (1970).

Aromatic Stabilization of the Dewar-Chatt-Duncanson Bonding Model

Jun-ichi AIHARA
Department of Chemistry, Faculty of Science, Shizuoka University, Oya, Shizuoka 422
(Received July 30, 1985)

Synopsis. Metal–olefin complexes can be considered as aromatics if their conjugated systems are described well by the Dewar-Chatt-Duncanson bonding model.

Stable complexes between transition metal salts and olefins have long been known,[1] but not understood until comparatively recently.[2–5] Zeise's salt is a typical example of such complexes. Ethylene in this salt occupies the fourth coordination site of the square-planar platinate ion with the C–C axis perpendicular to the platinum-ligand plane.[6] In this note, the author would like to point out that many such metal–olefin complexes are essentially aromatic, being stabilized by cyclic conjugation.

The useful bonding model for the metal–olefin complexes was presented by Dewar[7] and by Chatt and Duncanson.[8] They proposed that the bonding consists of a two-way donor-acceptor mechanism: σ donation of the π-bonding electrons of the olefin to vacant orbitals on the metal and π back donation of metal valence electrons to the π^* orbital of the olefin. The extent of back bonding varies depending upon the substituents on ethylene and other ligands on the metal. This bonding model has been referred to as a Dewar-Chatt-Duncanson model. It is noteworthy that few qualitative pictures have served us as beautifully as the Dewar-Chatt-Duncason model.[3]

This bonding model is shown graphically in Fig. 1. The basis-set orbitals for the Hückel calculation are two valence orbitals of the metal (**1** and **2**) and two carbon $2p_z$ orbitals of ethylene (**3** and **4**). In many complexes, **1** is a metal d_{xz} orbital while **2** is a metal d_{z^2} orbital or one of the dp^2- or d^2p^2-hybrid orbitals.[2–8] These two metal orbitals are represented by unconnected vertices because they are orthogonal to each other.

Such a conjugated system is depicted in terms of five resonance integrals and four Coulomb integrals. Coulomb integral parameters for **1** and **2** are denoted by h_1 and h_2, respectively. Four of the resonance integrals have a negative sign and one has a positive sign, reflecting the phase change which results from the nodal characteristic and the position of the metal d_{xz} orbital relative to the carbon $2p_z$ orbitals. Resonance integral parameters between metal and carbon valence orbitals are denoted by $\pm k_a$ and k_b, where k_a and k_b are positive in sign. The resonance integral parameter for the ethylene π bond is equal to unity. The Hückel calculation then demonstrates that the four basis-set orbitals combine to form two bonding and two antibonding molecular orbitals. Four electrons fill the two bonding molecular orbitals.

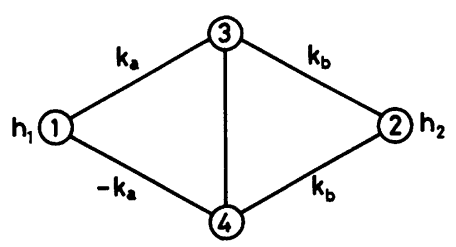

Fig. 1. Graphic representation of the Dewar-Chatt-Duncanson bondng model (k_a, k_b>0).

We then apply our graph theory of aromaticity[9] to this Dewar-Chatt-Duncanson bonding model. A characteristic polynomial for this conjugated system is obtainable by expansion of the Hückel secular determinant.[9] It is written as

$$P(X) = X^4 - (h_1+h_2)X^3 - (1+2k_a^2+2k_b^2-h_1h_2)X^2 + (h_1+h_2+2h_1k_b^2+2h_2k_a^2+2k_a^2-2k_b^2)X + (4k_a^2k_b^2-h_1h_2+2h_1k_b^2-2h_2k_a^2). \quad (1)$$

Zeros of this polynomial represent the energies of molecular orbitals for the conjugated system. The corresponding reference polynomial is derived graph-theoretically from the characteristic polynomial.[9] It is written as

$$R(X) = X^4 - (h_1+h_2)X^3 - (1+2k_a^2+2k_b^2-h_1h_2)X^2 + (h_1+h_2+2h_1k_b^2+2h_2k_a^2)X + (2k_a^2k_b^2-h_1h_2). \quad (2)$$

Zeros of this polynomial represent the energies of hypothetical molecular orbitals which the system would possess if it were totally deprived of aromaticity.[9] A conjugated system defined by this polynomial is named an olefinic reference structure.[9] Total energy for each system is given by summing energies of four electrons in the two bonding molecular orbitals.

The difference in total energy between a real conjugated system and its olefinic reference system is defined as resonance energy due to cyclic conjugation.[9] Resonance energy of the system in question is a function of h_1, h_2, k_a, and k_b. Here, h_1 must not be smaller than h_2 since **1** and **2** are electron-donating and accepting orbitals, respectively. For symplicity, h_2 is set equal to $-h_1$, and k_a equal to k_b. Here, h_1 takes a positive value. This way of choosing the parameter set satisfies the empirical fact that the metal-ethylene bond is essentially electroneutral, with donation and back-acceptance approximately balanced.[3,4] A couple of realistic values were chosen independently for h_1 and k_a. The resonance energy values thus determined for the metal–ethylene bonding system are listed in Table 1. It is worth noting that the resonance energy stays positive in sign for all parameter values. It varies in the range 0.173—0.775 β, where β is an absolute value of β. This value is comparable to the resonance energy of benzene, 0.273 β.

The nodal property of the metal d orbitals is known to aromatize the olefin–tricarbonyliron complexes.[10,11] It is now true for the present Dewar-Chatt-Duncanson

Table 1. Resonance energies of the Dewar-Chatt-Duncanson bonding model in units of β.

k_a	h_1		
	0.00	0.50	1.00
0.50	0.173	0.395	0.373
1.00	0.404	0.659	0.775

model. The presence of one phase change in the metal-olefin conjugated system makes it a Möbius system with four bonding electrons. Möbius systems are characterized by the $4n$ rule for aromaticity,[12] in contrast to the common $4n+2$ Hückel rule. The Möbius ring found along the periphery of the bonding network (Fig. 1) can, therefore, be considered to be aromatic in nature. This is the primary reason why an entire metal-ethylene conjugated system can be regarded as an aromatic species. Furthermore, it is quite likely that many other metal-olefin complexes are totally or partly stabilized by such a bonding pattern.

Bicyclo[1.1.0]butadiene has a similar bonding network, but has no phase change along the periphery. In fact, it has a large negative resonance energy of $-0.473\ \beta$. Thus, bicyclo[1.1.0]butadiene must differ in stability from the Dewar-Chatt-Duncanson bonding model. This suggests that any metal-olefin complexes whose conjugated system is analogous to bicyclo[1.1.0]-butadiene, if any, must be very unstable.

Now, several stabilizing mechanisms have been clarified for organometallic conjugated systems and polyhedral molecules. Multicenter bonds and/or a network of three-center bonds stabilize polyhedral cluster compounds.[13,14] Metallocenes and olefin-tricarbonyliron complexes are stabilized by the bonds formed between metal atoms and carbocyclic rings.[11,15] Formation of all these bonds is obviously associated with aromatization. The binding of olefins to transition metals has also occupied a central position in organometallic chemistry.[1-8] As has been seen above, the Dewar-Chatt-Duncanson model is stabilized by aromatization.

This work was supported by a Grant-in-Aid for Scientific Research (No. 60540283) from the Ministry of Education, Science and Culture.

References

1) F. A. Cotton and G. Willkinson, "Advanced Inorganic Chemistry: A Comprehensive Text," Fourth Ed., Wiley-Interscience, New York (1980); J. E. Huheey, "Inorganic Chemistry: Principles of Structure and Reactivity," Second Ed., Harper & Row, New York (1978).
2) K. S. Wheelock, J. H. Nelson, L. C. Cusachs, and H. B. Jonassen, *J. Am. Chem. Soc.*, **92**, 5110 (1970).
3) T. A. Albright, R. Hoffmann, J. C. Thibeault, and D. L. Thorn, *J. Am. Chem. Soc.*, **101**, 3801 (1979).
4) T. Ziegler and A. Rauk, *Inorg. Chem.*, **18**, 1558 (1979); P. J. Hay, *J. Am. Chem. Soc.*, **103**, 1390 (1981); K. Kitaura, S. Sakaki, and K. Morokuma, *Inorg. Chem.*, **20**, 2292 (1981); F. U. Axe and D. S. Marynick, *J. Am. Chem. Soc.*, **106**, 6230 (1984).
5) Many references in this area are cited in Ref. 3.
6) J. A. Wunderlich and D. P. Mellor, *Acta Cryst.*, **8**, 57 (1955).
7) M. J. S. Dewar, *Bull. Soc. Chim. Fr.*, **18**, C79 (1951).
8) J. Chatt and L. A. Duncanson, *J. Chem. Soc.*, **1953**, 2939.
9) J. Aihara, *J. Am. Chem. Soc.*, **98**, 2750, 6840 (1976); *Kagaku No Ryoiki*, **30**, 379 (1976); *Pure Appl. Chem.*, **54**, 1115 (1982); *Netsu Sokutei*, **12**, 61 (1985); I. Gutman, M. Milun, and N. Trinajstić, *J. Am. Chem. Soc.*, **99**, 1692 (1977).
10) D. M. P. Mingos, *J. Chem. Soc., Dalton Trans.*, **1977**, 20, 26, 31.
11) J. Aihara, *Bull. Chem. Soc. Jpn.*, **51**, 1541 (1978).
12) E. Heilbronner, *Tetrahedron Lett.*, **1964**, 1923.
13) J. Aihara, *J. Am. Chem. Soc.*, **100**, 3339 (1978).
14) J. Aihara, *Bull. Chem. Soc., Jpn.*, **52**, 2202 (1979).
15) J. Aihara, *Bull. Chem. Soc., Jpn.*, **58**, 266 (1985).

Potential Energies of Rotation of Double Bond in Ethylene Molecule and Ion

Hiroshi ICHIKAWA,* Yukiko EBISAWA, and Atsushi SHIGIHARA
Hoshi College of Pharmacy, Ebara, Shinagawa-ku, Tokyo 142
(Received July 6, 1985)

Synopsis. MP3/6-31G** calculations show that the potential barrier of a double-bond rotation in an ethylene ion is 137 kJ mol^{-1} (about half that of the molecular state) and that the orthogonally twisted ion has a C_{2v} symmetry. The geometries are discussed in relation to the total energies.

It is often said that geometrical isomers cannot be distinguished by a mass spectral observation.[1,2] This is dramatically emphasized by the fact that benzene and its linear isomer, 1,3-hexadien-5-yne, give the same mass spectra upon electron-impact ionization.[3] Unsuccessful trials for characterizing geometrical isomers have so far simply suggested that the double bond in an ionized organic molecule easily becomes twisted and changes its geometry. Using the ethylene system, we studied this problem in order to give an answer to the fundamental question regarding organic mass spectrometry. This subject has also drawn some conceptional interests regarding chemical bonding as an example of an isovalent hyperconjugation.[4]

The method for evaluating such rotational energy is straightforward: Simply obtain the energetic difference between the lowest- and highest-energy configurations of the ethylene ion. However, as care must be taken regarding the calculation for determining a twisted geometry, since in an ionic state, the D_2 or D_{2d} (at 90°) symmetry of a molecular state is possibly degraded to C_2 or C_{2v} (or even C_1 or Cs) due to a lack of one of the π electrons. There are some reports regarding Hartree-Fock[5] (HF) MO theoretical calculations for determining the rotational energy of ionized ethylene.[6–8] However, they deal with only the D_{2d} symmetry for a perpendicular structure. In addition, as is often said, a HF calculation regarding a reaction in which the number of bonds changes, is generally unreliable since the energy difference of the electron correlation between the systems becomes non-negligible. Therefore, previous results must be carefully checked. We have performed second- and third-order Møller-Plesset purterbation calculations[9] based on the HF or the UHF (unrestricted Hartree-Fock[10]) 6-31G**[11] (MP3/6-31G**) to obtain the most reliable rotational barrier values presently available.[12]

a. Geometries in an Ethylene Molecule. The various states of an ethylene molecule have been thoroughly studied through experiments[13] and theoretical calculations.[14,15] In order to check the reliability of the present method, we will compare the calculated values with experimental values and previous calculations. The geometries that are obtained by MP3/6-31G** are:

Ground state (D_{2h}):

R_{CC} = 1.333 (exptl 1.339,[13] CIPSI[16] 1.344,[14] CEPA[17] 1.336[15])

R_{CH} = 1.080 (exptl 1.086,[13] CEPA 1.074[15])

∠HCH = 116.6 (exptl 117.6,[13] CEPA 116.3[15])

Twisted triplet state (D_{2d}):

R_{CC} = 1.459 (CIPSI 1.463,[14] CEPA 1.459[15])

R_{CH} = 1.081 (CEPA 1.074[15])

∠HCH = 117.0 (CEPA 117.2[15])

The present method has been shown to be excellent for reproducing experimental values as well as previous calculations, especially regarding the CEPA results.

b. Rotational Barrier of a Ethylene Molecule and Its Ion. The rotational barrier of an ethylene molecule has been observed to be 273 kJ mol^{-1}.[13] The HF/6-31G** result gives a value that is too low (176 kJ mol^{-1}). However, the MP3/6-31G** result as well as previous CIPSI and CEPA calculations give very good experimental values (272, 263, and 280 kJ mol^{-1}, respectively). This shows the necessity for the inclusion of an electron correlation and also demonstrates the appropriateness of MP3/6-31G**.

Table 1 shows the geometries and the total energies of D_{2d} and C_{2v} ethylene ions where a C_1 atom carries an unpaired electron. Figure 1 shows plots of the total energy *vs.* the twist angle (θ). As expected, when θ is 90°, the C_{2v} structure is more stable than D_{2d}.

As can be seen in Figure 1, the rotational barrier in ionic state is found to be about half (137 kJ mol^{-1}) that of the neutral state. The PE of the twisted molecule has been reported to increase steeply as the twist angle (θ) increases.[14] However, that of the ion does not change until θ is 20°. This indicates that the double bond in an ionic state is very flexible regarding rotation in accordance with experience from organic mass spectrometry.

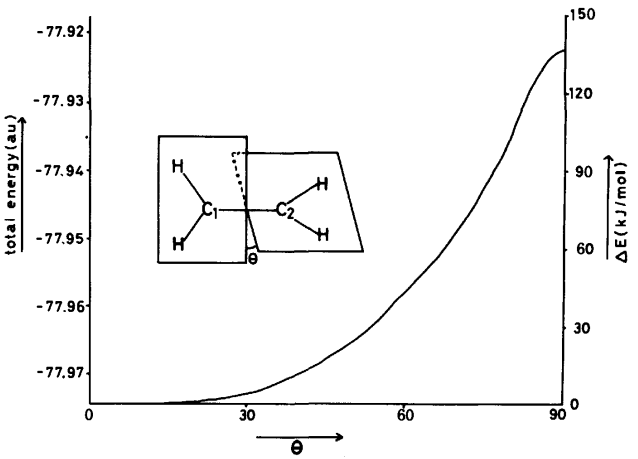

Fig. 1. Total energies *vs.* twist angle (θ) by MP3/6-31G**. All geometrical parameters except the fixed twist angle were optimized with respect to the total energy.

Table 1. Geometries and total energies of ethylene ion by MP3/6-31G**[a)]

	Planar: D_{2h} θ=0	Perpendicular: D_{2d} θ=90	Perpendicular: C_{2v} θ=90
$R(C_1-C_2)$	1.4167[b)]	1.4106	1.4118
$R(C_1-H)$	1.0824	1.0909	1.0891
$R(C_2-H)$			1.0927
HC_1H	118.8[c)]	117.6	119.7
HC_2H			116.0
Total energy	−77.974663[d)]	−77.922613	−77.922954

a) The geometry optimization was carried out by the Fletcher-Powell method.[22] b) In A. c) In degree. d) au (1 au=2625.5 kJ mol^{-1}).

c. Geometries of the Ethylene Ions. Mulliken and Roothaan proposed that the ethylene ion is an example of isovalent hyperconjugation and predicted a twist angle of 30° from a plane.[4] This is the result of a compromise between normal π bonding (planar structure) and hyperconjugative π bonding (perpendicular structure). This prediction was supported by ultraviolet studies regarding a series of Rydberg states of ethylene, which converge to the ethylene ion.[18] It has been reported that the non-plane structure can be produced by using the ab initio SCF MO CI method.[19] We have tried to reproduce this structure by optimizing all of the geometrical parameters. However, like all other reports regarding reasonably extensive SCF MO CI calculations,[20,21] a planar ion is found to be the most stable and to have a D_{2h} symmetry. It should be noted that the total energy that we have obtained is the lowest (−77.974663 au).

We have tried the Cs, C_{2v}, and D_{2d} structures for the perpendicular ion. The C_{2v} structure was found to be the most stable: The lowering of the order from a D_{2d} symmetry is caused by a configurational difference in which the unpaired electron occupies only one of the methylene groups. Interestingly, the C–C bondlength is maintained at almost the same independance regarding the twist angle (θ), even at 90°.

In summary, an MP3/6-31G** calculation shows that the potential barrier of a double-bond rotation in an ethylene ion is 137 kJ mol^{-1}, about half that of the molecular state. Also, an orthogonally twisted ion has a C_{2v} symmetry.

Refernces

1) F. W. McLafferty, "Interpretation of Mass Spectra," W. A. Benjamin, New York (1966), Chap. 6.

2) H. Budzikiewicz, C. Djerassi, and D. H. Williams, "Mass Spectrometry of Organic Compounds," Holden-Day, San Francisco (1967), Chap. 1.

3) R. S. Berry, J. Clardy, and M. E. Schafer, *J. Am. Chem. Soc.*, **86**, 2738 (1964); *Tetrahedron Lett.*, **1965**, 1003.

4) R. S. Mulliken and C. C. J. Roothaan, *Chem. Rev.*, **41**, 219 (1947).

5) G. G. Hall,*Proc. R. Soc. London, Ser. A*, **205**, 541 (1951); C. C. J. Roothaan, *Rev. Mod. Phys.* **23**, 69 (1951).

6) W. A. Latham, W. J. Hehre, and J. A. Pople, *J. Am. Chem. Soc.*, **93**, 808 (1971).

7) D. J. Bellville and N. L. Bauld, *J. Am. Chem. Soc.*,**104**, 294 (1982).

8) J. Kalcher and G. Olbrich, *J. Mol. Struct.*, **104**, 341 (1983).

9) C. Moller and M. S. Plesset, *Phys. Rev.*, **46**, 618 (1934).

10) J. A. Pople and R. K. Nesbet, *J. Chem. Soc.*, **1964**, 571.

11) P. C. Hariharan and J. A. Pople, *Theoret. Chim. Acta*, **28**, 213 (1973).

12) We have used GAUSSIAN 80H program (a Hitac version of GAUSSIAN 80 (QCPE No. 437, Indiana University, IN)) at the computer center of the University of Tokyo.

13) H. O. Kalinowski and H. Kessler, *Topics Stereochim.*, **7**, 295 (1973).

14) M. Said, D. Maynau, J. -P. Malrieu, and M. -A. Barcia Bach, *J. Am. Chem. Soc.*, **106**, 571 (1984).

15) H. J. Kohler and H. Lischka, *J. Am. Chem. Soc.*, **104**, 5884 (1982).

16) B. Huron, J. P. Malrieu, and P. Rancurel, *J. Chem. Phys.*, **58**, 5745 (1973).

17) W. Meyer, *J. Chem. Phys.*, **58**, 1017 (1973).

18) H. Koppel, W. Domcke, L. S. Cederbaum, and W. v. Niessen, *J. Chem. Phys.*, **69**, 4252 (1978).

19) R. J. Buenker, S. D. Peyerimhoff, and H. L. Hsu, *Chem. Phys. Lett.*, **11**, 65 (1971).

20) P. D. Foo and K. K. Innes, *J. Chem. Phys.*, **60**, 4582 (1974).

21) W. R. Rodwell, M. F. Guest, D. T. Clark, and D. Shuttlesworth, *Chem. Phys. Lett.*, **45**, 50 (1977).

22) R. Fletcher and M. J. D. Powell, *Compt. J.*, **6**, 163 (1963).

Synthesis and Characterization of a Chloro-bridged Binuclear Iron(III) Complex

Naohide MATSUMOTO,* Chikako YOSHIMURA, Yonezo MAEDA,†
Hisashi OKAWA,† and Akira OHYOSHI

Department of Synthetic Chemistry, Faculty of Engineering, Kumamoto University, Kurokami 2-39-1, Kumamoto 860
†Department of Chemistry, Faculty of Science, Kyushu University, Hakozaki, Higashi-ku, Fukuoka 812

(Received May 24, 1985)

Synopsis. A chloro-bridged binuclear iron(III) complex $[Fe_2ClL](BPh_4)$, where $[H_4L]$ and BPh_4^- denote *N,N,N′,N′*-tetrakis(3-salicylideneaminopropyl)ethylenediamine and tetraphenylborate, respectively, was prepared and characterized by elemental analysis, electrical conductivity, Mössbauer spectrum, and cryomagnetic data. The magnetic susceptibility data of the complex was analyzed by the Heisenberg model on the basis of a binuclear structure $\hat{H}=-2J\hat{S}_1\cdot\hat{S}_2$ ($S_1=S_2=5/2$), leading to an antiferromagnetic interaction parameter of $J=-3.9\,cm^{-1}$.

Chloro-bridged iron(III) complexes are rare, although a number of oxo-bridged iron(III) complexes are well known.[1] In this study, a chloro-bridged binuclear iron(III) complex $[Fe_2ClL](BPh_4)$ is reported, where $[H_4L]$ and BPh_4^- denote a decadentate binucleating ligand *N,N,N′,N′*-tetrakis(3-salicylideneaminopropyl) ethylenediamine and tetraphenylborate, respectively. The complex was characterized by elemental analysis, electrical conductivity, Mössbauer spectrum, and cryomagnetic data, and their physical properties were compared with those of the corresponding mononuclear complex chloro[*N,N*-bis(3-salicylideneaminopropyl) methylaminato] iron(III).

Experimental

Physical Measurements. Elemental analyses (C, H, N) were performed by Mr. Shinichi Miyazaki at the Technical Service Center of Kumamoto University, and an analysis of Cl was carried out by the Fajans method. Melting points were measured on a Yanagimoto micro melting point apparatus and were uncorrected. Electrical conductivity measurements were carried out on a Denki Kagaku AOC-10 type digital conductometer at *ca.* 10^{-3} mol dm^{-3} in methanol or *N,N*-dimethylformamide. The ^{1}H NMR spectrum was recorded on a JEOL MH 100 spectrometer, where the solvent used was chloroform-*d* and shift measurements were made relative to tetramethylsilane. Magnetic susceptibilities were obtained by the Faraday method in a temperature range between liquid nitrogen temperature and room temperature, according to the literature.[2] The susceptibility was corrected for the diamagnetism of the component atoms by the use of Pascal's constants. An effective magnetic moment was calculated using $\mu_{eff}=2.828\sqrt{\chi_A T}$, where χ_A is the magnetic susceptibility per iron atom. The Mössbauer spectroscopy was effected by using an instrument described elsewhere.[3] An isomer shift is reported with respect to the centroid of the spectrum of an iron foil enriched with ^{57}Fe at 295 K. This was also used as a standard material for a velocity calibration.

Syntheses. Binucleating Ligand [H4L]: N,N,N′,N′-Tetrakis(3-aminopropyl)ethylenediamine hexahydrobromide was prepared according to a method described in the literature.[4] A mixture of *N,N,N′,N′*-tetrakis(3-aminopropyl)ethylenediamine hexahydrobromide, salicylaldehyde, and triethylamine with a mole ratio of 1:4:6 in ethanol was stirred on a water bath. Yellow crystals precipitated and were collected and recrystallized from a mixture of chloroform and ethanol. Found: C, 71.58; H, 7.48; N, 11.93%. Calcd for $C_{22}H_{28}N_6O_4$: C, 71.56; H, 7.44; N, 11.92%. Mp 112 °C, ^{1}H NMR ($CDCl_3$) δ=1.7 [8H, m, $4CH_2$], 2.4 [12H, t, $6CH_2$], 3.5 [8H, t, $4CH_2$], 6.6—7.3 [16H, m, $4C_6H_4$], 8.2 [4H, s, 4CH=N].

[Fe2ClL](BPh4). The ligand $[H_4L]$ (10 mmol) and anhydrous iron(III) chloride (20 mmol) were mixed in 100 cm^3 of methanol. To the mixture was added triethylamine (40 mmol) and the resulting solution was warmed at 50 °C for 30 min and then filtered. To the filtrate was added a solution of sodium tetraphenylborate (20 mmol) in 30 cm^3 of methanol. This was warmed at 50 °C for 1 h to yield fine black crystals. These were collected, washed with methanol, and dried *in vacuo*. Found: C, 67.75; H, 6.06; N, 7.22; Cl, 3.24%. Calcd for $C_{66}H_{68}N_6BClO_4Fe_2$: C 67.91; H, 5.87; N, 7.20; Cl, 3.04%. Mp 255 °C (decomp), Λ_M 47.4 Scm^2 mol^{-1} (DMF).

Chloro[N,N-bis(3-salicylideneaminopropyl)methylaminato]-iron(III) [FeClL′]. The mononuclear chloro complex [FeClL′], used as a reference complex, was prepared according to a method described in the literature.[5] Found: C, 56.75; H, 5.80; N, 9.50%. Calcd for $C_{21}H_{25}N_3ClO_2Fe$: C, 56.97; H, 5.69; N, 9.49%. Mp 219 °C, Λ_M 0.0 Scm^2 mol^{-1}(MeOH).

Results and Discussion

The molar electrical conductance of the complex was 47.4 Scm^2 mol^{-1} in *N, N*-dimethylformamide,[6] indicating that the complex has a formula of $[Fe_2ClL]^+(BPh_4)^-$, although this value is slightly smaller than the expected value (65—90 Scm^2 mol^{-1}) of a 1:1 electrolyte in DMF.[7] The molar electrical conductance of the mononuclear complex shows that the complex is uncharged and has a formula of [FeCLL′].

The magnetic moment of the mononuclear complex [FeClL′] is independent of the temperature over the temperature range studied within the experimental error (*ca.* 5.9 BM), typical of a high spin (S=5/2) iron(III) complex. On the other hand, the magnetic moment of $[Fe_2ClL](BPh_4)$ gradually increased from 4.8 BM at 90 K to 5.6 BM at 300 K. Plots of χ_A and $1/\chi_A$ *vs.* temperature for [FeClL′] and $[Fe_2ClL](BPh_4)$ are shown in Fig. 1. The magnetism of the mononuclear chloro complex [FeClL′] obeys the Curie law, while that of the complex $[Fe_2ClL](BPh_4)$ obeys the Curie-Weiss law ($\chi_A=C/(T+\theta)$) with a Weiss constant of θ=50 K. This suggests antiferromagnetic interaction between iron (III) centers. The Mössbauer spectrum of $[Fe_2ClL](BPh_4)$ at 296 K showed a doublet with parameters of IS=0.380, QS=0.741, Γ=0.370 mms^{-1}, typical of a high-spin (S=5/2) center.

The magnetic susceptibilities of the complex $[Fe_2ClL](BPh_4)$ were analyzed by the Heisenberg model

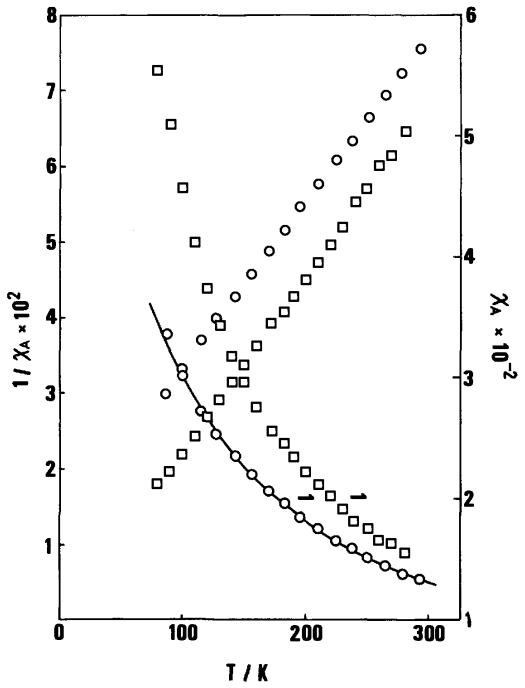

Fig. 1. Plots of χ_A and $1/\chi_A$ *vs.* temperature for [FeClL'] (□) and [Fe_2ClL](BPh_4) (○), where the solid line of χ_A *vs.* T plot for [Fe_2ClL](BPh_4) represents the theoretical curve of Eq. 1 with the parameters of $g=2.00$, $J=-3.9\,cm^{-1}$, and $p=0.015$.

on the basis of a binuclear structure. The magnetic susceptibility per iron atom of a binuclear structure ($S_1=S_2=5/2$) is given by Eq. 1,

$$\chi_A = \frac{Ng^2\beta^2}{kT}\frac{55+30x^{10}+14x^{18}+5x^{24}+x^{28}}{11+9x^{10}+7x^{18}+5x^{24}+3x^{28}+x^{30}}(1-p) + \frac{35Ng^2\beta^2}{12kT}p \quad (1)$$

where $x=\exp(-J/kT)$ and p is the amount of magnetically dilute ferric impurity which possibly coexists with the dimer. Other symbols have their usual meanings. An isotropic g value of 2.00 was assumed, and the best fit to the data gave $J=-3.9\,cm^{-1}$ and

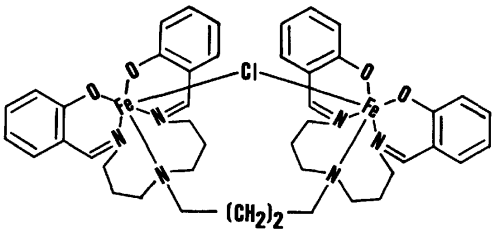

Fig. 2. A proposed structure for $[Fe_2ClL]^+$.

$p=0.015$. A theoretical χ_A *vs.* T curve using the above parameters is represented as a solid line in Fig. 1. On the basis of the electrical conductance and the magnetic property, it can be concluded that the complex [Fe_2ClL](BPh_4) assumes a binuclear structure with a chloro-bridge as shown in Fig. 2.

A number of oxo-bridged binuclear iron(III) complexes have been known and the antiferromagnetic interaction parameters vary from *ca.* $-10\,cm^{-1}$ to *ca.* $-100\,cm^{-1}$,[1] indicating that the antiferromagnetic interaction of the chloro-bridged complex is considerably smaller than those of the oxo-bridged complexes.

This work was in part supported by a Grant-in-Aid for Scientific Research No. 59740300 from the Ministry of Education, Science and Culture.

References

1) F. E. Mabbs, V. N. McLachlan, D. McFadden, and A. T. Mcphail, *J. Chem. Soc., Dalton Trans.*, **1973**, 2016, and references therein.

2) M. Mikuriya, H. Okawa, and S. Kida, *Bull. Chem. Soc. Jpn.*, **54**, 2943 (1981).

3) H. Ohshio, Y. Maeda, and Y. Takashima, *Inorg. Chem.*, **22**, 2684 (1983).

4) W. Gauss, P. Moser, and G. Schwarzenbach, *Helv. Chim. Acta*, **35**, 2360 (1952).

5) N. Matsumoto, S. Ohta, C. Yoshimura, A. Ohyoshi, S. Kohata, H. Okawa, and Y. Maeda, *J. Chem. Soc. Dalton Trans.*, in press.

6) The complex [Fe_2ClL](BPh_4) is sparingly soluble in methanol, dichloromethane, and acetonitrile but soluble in *N,N*-dimethylformamide and dimethylsulfoxide.

7) W. J. Geary, *Coord. Chem. Rev.*, **7**, 81 (1971).

Preparation and Characterization of (Iminodiacetato)cobalt(III) Complexes with L-Methioninate and *S*-Methyl-L-cysteinate

Hideki UMEHARA,* Takashi ISAGO, Ken-ichi OKAMOTO, and Jinsai HIDAKA
Department of Chemistry, University of Tsukuba, Sakura, Ibaraki 305
(Received June 21, 1985)

Synopsis. The (iminodiacetato)(L-methioninato or *S*-methyl-L-cysteinato)cobalt(III) complex was prepared and separated into three geometrical isomers by ion-exchange chromatography. The isomers were characterized from the electronic absorption, ^{1}H NMR and CD spectra.

The bis or mixed type cobalt(III) complexes with branched terdentate ligands such as D- or L-aspartate (D- or L-asp), L-methioninate (L-met), and *S*-methyl-L-cysteinate (L-smc), have been investigated in concerning with the spectrochemical and stereochemical properties.[1–5] Regarding the CD spectral analysis of the complexes, however, the branched terdentate ligand such as D- or L-asp was troublesome because of the CD contribution due to *R*(*C*) or *S*(*C*) of the ligand.[3] In this work, we extended the study to the spectrochemical property of the L-met and L-smc cobalt(III) complexes with iminodiacetate (ida) which is a typical linear terdentate ligand. Each complex prepared was chromatographically separated into three possible geometrical isomers and the isomers were characterized from the absorption and ^{1}H NMR spectra.

Experimental

Preparation of Complexes. *1) [Co(ida)(L-met)]*: To a solution containing 0.89 g of iminodiacetic acid and 1.0 g of L-methionine in 30 cm^3 of water (adjusted to pH 8 by NaOH solution) was added a solution containing 1.6 g of $CoCl_2 \cdot 6H_2O$ in 30 cm^3 of water, and then 2 g of PbO_2 and 0.5 g of activated charcoal. The mixture was mechanically stirred at 70 °C for 30 min, cooled to room temperature, and then filtered. The filtrate was passed through a Dowex 1-X8 column (4.5 cm×20 cm) and then a Dowex 50W-X8 one (4.5 cm×20 cm) in order to remove the charged compounds. The eluate concentrated to *ca.* 5 cm^3 was poured onto a Dowex 50W-X8 column (Na^+ form, 200—400 mesh, 3.0 cm×100 cm), and eluted with water. Three colored bands, dark violet (A1), purple (A2), and pink-violet (A3), were eluted in this order. A1, A2, and A3 eluates contained *trans*(N_iN)-, *trans*(N_iS)-, and *trans*(N_iO)-[Co(ida)(L-met)], respectively (A1:A2:A3=*ca.* 55:40:5).[6] A1 and A2 eluates were separately concentrated to dryness. A1 isomer was recrystallized from as little water as possible by adding ethanol. A2 isomer was recrystallized from a little water. A3 eluate was concentrated to a small volume with a rotary evaporator and then kept in a refrigerator overnight. The crystals obtained were filtered and washed with ethanol and ether. Found for A1: C, 28.78; H, 4.99; N, 7.36%. Calcd for [Co(ida)(L-met)]·$2H_2O$=$CoC_9H_{15}N_2O_6S \cdot 2H_2O$: C, 28.88; H, 5.12; N, 7.49%. Found for A2: C, 31.21; H, 4.65; N, 7.93%. Calcd for [Co(ida)(L-met)]·$0.5H_2O$: C, 31.13; H, 4.64; N, 8.07%. Found for A3: C, 30.51; H, 4.77; N, 7.92%. Calcd for [Co(ida)(L-met)]·H_2O: C, 30.34; H, 4.81; N, 7.86%.

2) [Co(ida)(L-smc)]. This noncharged complex was prepared and separated by the same procedure as described in *1)*, using *S*-methyl-L-cysteine (0.91 g) instead of L-methionine, except for adjusting the solution to pH 6. Three colored eluates, dark violet (B1), purple (B2), and pink-violet (B3), contained *trans*(N_iN)-, *trans*(N_iS)-, and *trans*(N_iO)-[Co(ida)(L-smc)], respectively. B2 and B3 isomers were obtained by a procedure similar to that used for A3 in *1)*. For B1 isomer being unstable, after the fractions containing only the *trans*(N_iN) isomer were concentrated, a large amount of ethanol was immediately added to it. Gray-violet powder was filtered and washed with ethanol and ether. Found for B1: C, 26.38; H, 4.86; N, 7.70%. Found for B3: C, 26.72; H, 4.71; N, 7.89%. Calcd for [Co(ida)(L-smc)]·$2H_2O$=$CoC_8H_{13}N_2O_6S \cdot 2H_2O$: C, 26.67; H, 4.76; N, 7.78%. Found for B2: C, 27.91; H, 4.55; N, 7.94%. Calcd for [Co(ida)(L-smc)]·H_2O: C, 28.08; H, 4.42; N, 8.19%.

Measurements. The electronic absorption spectra were recorded with JASCO UVIDEC-1 and -610 spectrophotometers and the CD spectra with a JASCO J-20 spectropolarimeter. The ^{1}H NMR spectra were recorded on a JEOL JNM-FX-100 NMR spectrometer in D_2O. Sodium 2,2-dimethyl-2-silapentane-5-sulfonate was used as an internal reference.

Results and Discussion

Three geometrical isomers were isolated for each of [Co(ida)(L-met)] and [Co(ida)(L-smc)] (Fig. 1), and their absorption and CD spectra are shown in Fig. 2. Their absorption spectral behaviors are quite similar to those of the corresponding isomers of [Co(D-or L-asp)(L-met or L-smc)] over the whole region.[2] Considering the splittings of the first d-d absorption bands estimated semiempirically,[2,7] it is assigned that A1 and B1 are *trans*(N_iN), A2 and B2 *trans*(N_iS), and A3 and B3 *trans*-(N_iO) (Fig. 1).[6]

The *S*-methyl proton signals of A1 (δ 1.89), B1 (δ 1.79 and 2.02 (*ca.* 4:1 in intensity)), A3 (δ 1.89), and B3 (δ 1.96) appear in the higher field than those of A2 (δ 2.30) and B2 (δ 2.33 and 2.40 (*ca.* 7:2)).[8] These suggest that the *S*-methyl group occupies the trans position to the nitrogen atom of ida for A2 and B2, and to its oxygen atom for A1, A3, B1, and B3, because the resonance lines due to the *S*-methyl group in the trans position to the oxygen atom can be expected to shift to higher field than that to the nitrogen one, as in the case of the cobalt(III) complexes with D- or L-aspartate, L-histidinate, and L-methioninate.[2,4] Therefore, the

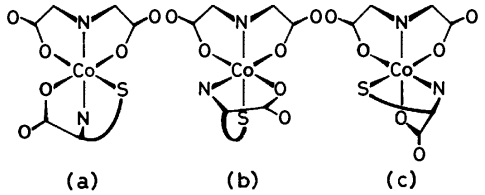

Fig. 1. Three possible isomers of [Co(ida)(L-met or L-smc)]; (a) *trans*(N_iN), (b) *trans*(N_iS), and (c) *trans*(N_iO). The N-S ring is a six-membered ring for L-met and a five-membered one for L-smc.

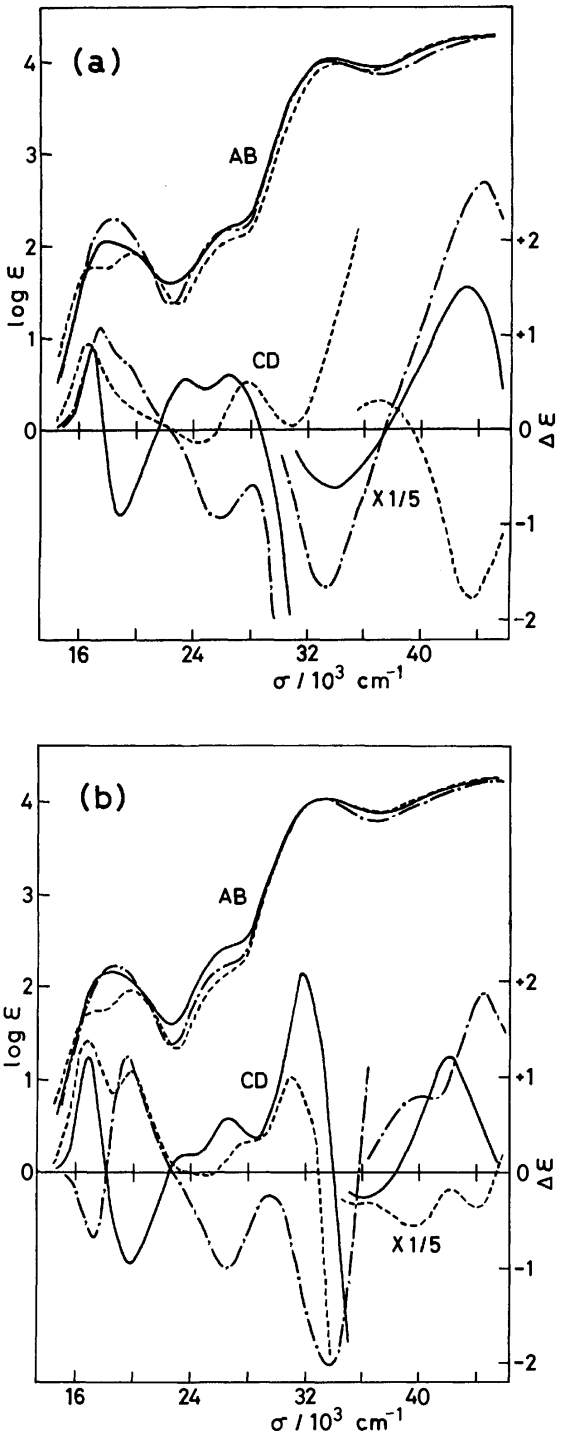

Fig. 2. Absorption and CD spectra of (a) [Co(ida)(L-met)] and (b) [Co(ida)(L-smc)]; *trans*(N_iN) (------), *trans*(N_iS) (——), and *trans*(N_iO) (—·—·—·—).

results from the ^{1}H NMR spectra of the three isomers for [Co(ida)(L-met or L-smc)] support the assignment on the basis of the absorption spectra.

Trans (N_iO)-[Co(ida)(L-met)] exhibits the CD spectrum almost enantiomeric to the *trans*(N_iS) isomer in the d-d absorption band region (Fig. 2(a)), reflecting that the two geometrical isomers have mutually quasi-enantiomeric configurations (Fig. 1). Here, it should be noted that, in the first d-d absorption band region, the enantiomeric CD spectral relation of the *trans*(N_iO) and *trans*(N_iS) isomers of [Co(ida)(L-met)] is opposite in sign to that of the corresponding isomers of [Co(D- or L-asp)(L-met)].[2] *Trans*(N_iO)- and *trans*(N_iS)-[Co(ida)(L-smc)] also exhibit enantiomeric CD patterns on the whole, but an interesting deviation is observed in the first d-d absorption band region (Fig. 2(b)). Namely, the CD band at *ca.* 17×10^3 cm^{-1} of the *trans*(N_iO) L-smc isomer exhibits the reversed sign of the corresponding CD band of the *trans*(N_iO) L-met one, though the CD pattern of the *trans*(N_iS) L-smc isomer coincides well with that of the *trans*(N_iS) L-met one (Fig. 2). This deviation is probably related to the difference of the configurations around the sulfur donor atoms or the flexibilities of the N-S rings in *trans*(N_iO)-[Co(ida)(L-met)] and -[Co(ida)(L-smc)].

References

1) J. Hidaka, S. Yamada, and Y. Shimura, *Chem. Lett.*, **1974**, 1487; K. Okamoto, K. Wakayama, H. Einaga, S. Yamada, and J. Hidaka, *Bull. Chem. Soc. Jpn.*, **56**, 165 (1983).

2) T. Isago, K. Igi, and J. Hidaka, *Bull. Chem. Soc. Jpn.*, **52**, 407 (1979).

3) S. Yamada, J. Hidaka, and B. E. Douglas, *Inorg. Chem.*, **10**, 2187 (1971); J. I. Legg and J. A. Neal, *Inorg. Chem.*, **12**, 1805 (1973); M. Watabe and S. Yoshikawa, *Bull. Chem. Soc. Jpn.*, **48**, 2185 (1975).

4) K. Okamoto, H. Maki, and J. Hidaka, *Bull. Chem. Soc. Jpn.*, **57**, 595 (1984).

5) M. Watabe, H. Yano, and S. Yoshikawa, *Bull. Chem. Soc. Jpn.*, **52**, 61 (1979).

6) N_i denotes an imino nitrogen atom in the coordinated ida.

7) M. Suzuki, O. Arisato, K. Okamoto, H. Einaga, and J. Hidaka, *Bull. Chem. Soc. Jpn.*, **57**, 2751 (1984).

8) The coordinated sulfur atom of each isomer is possible to take two absolute configurations, *R* and *S*.

A New Gas Sampler for Pyrolytic Sulfurization Gas Chromatography

Itsuro KAWAI* and Tadashi HARA†

Department of Environment and Safety Engineering, Fukui Institute of Technology, Gakuen-cho Fukui 910

†*Department of Chemical Engineering, Faculty of Engineering, Doshisha University, Karasuma Imadegawa, Kamigyo-ku, Kyoto 602*

(Received July 31, 1985)

Synopsis. A new gas sampler was designed and constructed by the use of a commercially available pyrolytic apparatus. This sampler made easier heating and crushing an ampoule, and introducing a liberated gas into a gas chromatograph than those by the conventional gas sampler.

One of the most important operations in the pyrolytic sulfurization gas chromatography[1-4] was to introduce a liberated gas into a gas chromatograph. Therefore, a new gas sampler was constructed by combining a crushing device as shown in Fig. 1 with a Shimadzu PYR-1A pyrolyzer. The sampler thus constructed has advantages in heating and crushing an ampoule and introducing the liberated gas into a gas chromatograph compared with the conventional gas sampler. The elemental analysis of polymer and carboxylic acid samples was tried by the pyrolytic sulfurization gas chromatography with the new gas sampler. The results obtained were almost satisfactory.

Experimental

Apparatus. The axial compression load method was adopted to crush an ampoule containing a sample. Figure 1 shows the crushing device of the new gas sampler. The crushing device was made of a stainless steel tube of 170 mm in length, 8 mm in outside diameter and 6 mm in inside diameter, and the device had a junction at about 45 mm from the one end. By the use of this junction, crushed pieces was able to remove easily, and the inner part of the crushing device was easily cleaned. An ampoule containing a sample was placed at position C, and crushed by pushing plunger D to the direction of the torsion. The gas sampler was heated by electric furnace F and the carrier gas was passed through A to B. The crushing device was combined with a Shimadzu PYR-1A pyrolyzer, and gas chromatograms were taken on a Shimadzu GC-4B gas chromatograph.

Reagents. Sulfur used as reagent was obtained by purifying[5] commercially available sulfur (chemical pure). Homopolymers, copolymers and terpolymers used as samples were commercially available products. Carboxylic acids and other organic compounds used as samples were of JIS special grade.

Procedure. The liberated gas was introduced into a gas chromatograph by either of the following two methods by operating a carrier gas stopcock of the pyrolytic apparatus: (a) An ampoule containing a sample was crushed while a carrier gas was passing through the crushing device. (b) An ampoule containing a sample was crushed while the carrier gas was stopped in the crushing device, and the liberated gas was introduced into the gas chromatograph with the carrier gas. In both cases, the introduced gas was analyzed under the following conditions: For polymer samples, a 2 m Silica-gel (60—80 mesh) column was used at the flow rate of 50 ml min^{-1} He carrier, and for carboxylic acid samples, a 0.25 m Chromosorb 104 (80—100 mesh) column connected with a 1.75 m Porapak Q (80—100 mesh) column in series was used at the flow rate of 30 ml min^{-1}. All the chromatograms were obtained at the programmed temperature of 20 °C min^{-1} over 80—180 °C.

Results and Discussion

Both ends of an ampoule containing a sample were conical and sharp. Figure 2 shows the crushing direction of an ampoule containing a sample. It was proved from the results of compression test (n=3) by means of a Toyo Baldwin UTM-5000-E universal testing machine of Fukui industrial laboratory that the axial compression load (A) (within 10 kg) necessary for crushing an ampoule containing a sample was smaller than the lateral compression load (B) (about 40 kg).

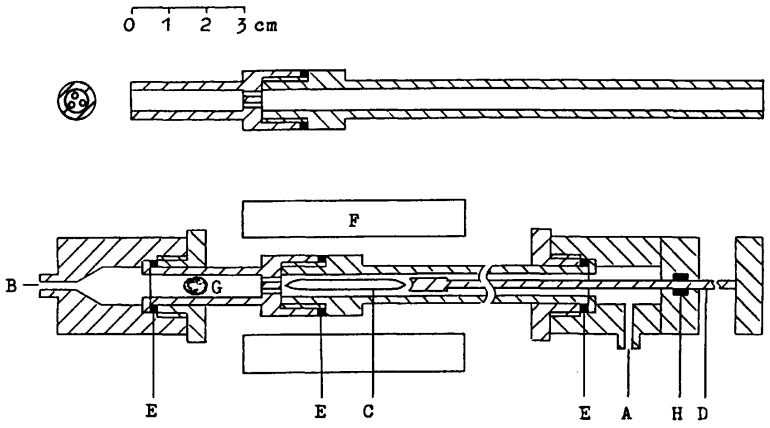

Fig. 1. Crushing device.
A: Carrier gas inlet, B: carrier gas outlet, C: ampoule containing a sample, D: plunger for crushing an ampoule, E: seals, F: electric furnace, G: filter, and H: silicone rubber gasket.

Table 1. Analytical results of polymers

Sample	C/wt%		H/wt%		O/wt%		N/wt%	
	CH Anal.[a]	PSGC	CH Anal.[a]	PSGC	CH Anal.[b]	PSGC	CH Anal.[a]	PSGC
Nylon	63.68	63.41	9.80	9.53	14.14	14.33	12.73	11.72
Polyethylene glycol	53.92	53.79	9.39	9.67	36.69	36.54		
Poly(vinyl alcohol)	52.86	52.56	8.92	9.13	38.22	38.31		
Methyl methacrylate-styrene copolymer	76.05	76.08	8.15	8.48	15.80	15.44		
Acrylonitrile-stylene copolymer	85.66	85.30	7.20	7.26			7.14	7.44
Methyl methacrylate-acrylonitrile-styrene copolymer	81.19	81.38	7.76	7.98	6.26	5.99	4.79	4.65
Acrylonitrile-butadiene-stylene copolymer	85.26	85.68	8.11	7.90			6.63	6.42

a) The sample compositions analyzed at the Elemental Analysis Center of the Pharmaceutical Department of Kyoto University. b) Obtained by subtracting the sum of the C, H, and N values from the total amount of a sample. Column: Silica gel 2 m×4ϕ SUS; Column temp: 80°C→180°C(20°C/min); Carrier gas: He 50 ml min^{-1}.

Table 2. Analytical results of carboxylic acids

Sample	C/wt%			H/wt%			O/wt%		
	Theor.	Found	Error	Theor.	Found	Error	Theor.	Found	Error
Heptadecanoic acid	75.50	75.35	0.15	12.67	12.94	0.27	11.83	11.71	0.21
Benzoic acid	68.86	68.68	0.16	5.00	5.05	0.05	26.16	26.27	0.11
Tartaric acid	32.01	32.06	0.05	4.03	4.02	0.01	63.96	63.92	0.04
Mandelic acid	63.15	63.36	0.21	5.30	5.38	0.08	31.55	31.26	0.29
Malic acid	35.83	35.92	0.09	4.51	4.55	0.04	59.66	59.53	0.13
p-Hydroxybenzoic acid	60.87	60.59	0.28	4.38	4.57	0.19	34.75	34.84	0.09
Gallic acid	44.69	45.01	0.32	4.29	4.21	0.08	51.02	50.78	0.24

Column: Chromosrb 104 0.25 m×4ϕ SUS and Porapak Q 1.75 m×4ϕ SUS; Column temp: 80°C→180°C(20°C/min); Carrier gas: He 30 ml min^{-1}.

Fig. 2. Crushing direction of an ampoule containing a sample.
A: Axial compression, and B: lateral compression.

Therefore, the crushing method by means of the axial compression load was adopted in the following experiment. This crushing method was easily carried out by pushing the plunger in the crushing device shown in Fig. 1. The gas in an ampoule is easily liberated because the ampoule is dashed to pieces. When the liberated gas was introduced into the gas chromatograph, both the methods, (a) and (b), mentioned above gave the same gas chromatogram. The (a) method was not always applicable on account of the imperfect crushing of an ampoule, while the (b) method was always possible after confirmation of the complete crushing of an ampoule. Tables 1 and 2 show the results of elemental analyses of polymers by the (a) method, and carboxylic acids by the (b) method, respectively. Both organic halogen and organometallic compounds were also analyzed and reasonable results were obtained. This new gas sampler has the following features: (1) Connecting the gas sampler with a pyrolyzer is easier than attaching the conventional gas sampler to a gas chromatograph directly. (2) Heating and crushing an ampoule are easier than those in the conventional gas sampler. (3) The load necessary for crushing an ampoule is less than that for the conventional gas sampler. (4) Analytical operation can be continuously performed by using a carrier gas stopcock of a pyrolytic apparatus.

Reference

1) T. Hara and S. Ito, *Bull. Chem. Soc. Jpn.*, **44**, 2427 (1971).
2) K. Tsuji, K. Fujinaga, and T. Hara, *Bull. Chem. Soc. Jpn.*, **50**, 2292 (1977).
3) T. Hara, K. Fujinaga, and K. Tsuji, *Bull. Chem. Soc. Jpn.*, **51**, 1110 (1978).
4) T. Hara, K. Fujinaga, and F. Okui, *Bull. Chem. Soc. Jpn.*, **53**, 951 (1980).
5) T. Hara, K. Fujinaga, K. Tsuji, and F. Okui, *Bull. Chem. Soc. Jpn.*, **51**, 3079 (1978).

The Reaction of 5-Cyano- and 5-Methoxycarbonyl-7-oxabicyclo[2.2.1]hept-2-enes with Chlorotrimethylsilane/Sodium Iodide Reagent

Takao KIBAYASHI, Yasutaka ISHII,* and Masaya OGAWA
Department of Applied Chemistry, Faculty of Engineering, Kansai University, Senriyama, Suita, Osaka 564
(Received June 26, 1985)

Synopsis. Reactions of 5-cyano- and 5-methoxycarbonyl-7-oxabicyclo[2.2.1]hept-2-enes with a chlorotrimethylsilane/sodium iodide reagent in acetonitrile gave 2-furanpropanenitrile and 5-methoxycarbonyl-1,3-cyclohexadiene in good yields, respectively.

In recent years, Olah[1-4] has developed an equivalent of iodotrimethylsilane generated *in situ* from chlorotrimethysilane and sodium iodide (Me_3SiCl/NaI). Treatments of appropriate oxygen-containing compounds such as ethers, esters and lactones with this reagent afford a silicon-oxygen bonded intermediate which then can be converted to another product through a subsequent step.

Previously, we reported the synthesis of 7-oxabicyclo-[2.2.1]hept-2-enes and their stereochemistries.[5] These compounds were allowed to react with Me_3SiCl/NaI to induce the rearrangement and deoxygenation of oxabicyclo[2.2.1]heptene ring. We describe here the rearrangement of 5-cyano-7-oxabicyclo[2.2.1]hept-2-ene (**1**) to 2-furanpropanenitrile (**3**) and the deoxgenation of 5-methoxycarbonyl-7-oxabicyclo[2.2.1]hept-2-ene (**2**) to 5-methoxycarbonyl-1,3-cyclohexadiene (**4**). (Eq. 1)

Results and Discussion

The Reaction of 1 with Me_3SiCl/NaI. An isomeric mixture of **1** (endo/exo≒1/1), derived from furan and acrylonitrile, was allowed to react with Me_3SiCl/NaI in acetonitrile at room temperature to give a rearranged product **3** in fairly good yield. (Table 1)

An approximately stoichiometric reaction of **1** with Me_3SiCl/NaI provided **3** in 91% yield. When $MeSiCl_3$ was employed instead of Me_3SiCl, **1** was rearranged slowly to **3** in 81% yield. However, the same reaction using three equiv of NaI to $MeSiCl_3$ took place rapidly giving **3** in good yield (94%). Conventionally, compound **3** has been prepared by a somewhat difficult method.[6-8] Thus, the present method seems to be favorable for preparing **3**. This rearrangement was expected to proceed catalytically, but a reaction with 0.1 equiv of Me_3SiCl/NaI merely afforded **3** at a yield of 12%. Lengthening the reaction time, however, led to an increase of **3** (46%).

The rearrangement of **1** to **3** may be illustrated by an attack by a cationic species, $[CH_3CN^+-SiMe_3]I^-$,[9] to a cyano group of **1**, followed by a cleavage of the C–C bond to form **3**. (Scheme 1)

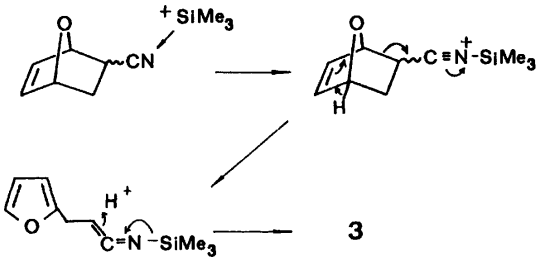

Scheme 1.

The Reaction of 2 with Me_3SiCl/NaI. A reaction of **2** with Me_3SiCl/NaI, followed by hydrolysis with water, gave deoxygenated products, **4** and **5**, as well as **6** in which the O–C bond was cleaved. However, their yields changed extremely due to the orientation of the methoxycarbonyl group of **2**. The isomeric **2** (endo/exo≒3/2), derived from furan and methylacrylate, was treated with 1.2 equiv of Me_3SiCl/NaI to form about 30% of **4** and benzoic acid **5** (3%). (Table 2) The yield of **4** increased to 43% when an excess amount of Me_3SiCl/NaI was used (Run 2).

TABLE 1. RING CLEAVAGE OF 5-CYANO-7-OXABICYCLO-[2.2.1]HEPT-2-ENE[a]

Run	**1**[b]:Me_3SiCl:NaI	Time	Yield[c] of **3**
	mmol	h	%
1	10: 12 : 12	3	91.3
2	10: 12[d]: 12	20	81.1
3	10: 10[d]: 30	3	93.6
4	10: 1 : 1	20	11.5
5	10: 1 : 1	70	46.0

a) Reactions were carried out in acetonitrile (10 ml) at room temperature. b) An isomeric mixture of *endo*-and *exo*-**1** (1:1) was used. c) Estimated by v.p.c. d) $MeSiCl_3$ was used instead of Me_3SiCl.

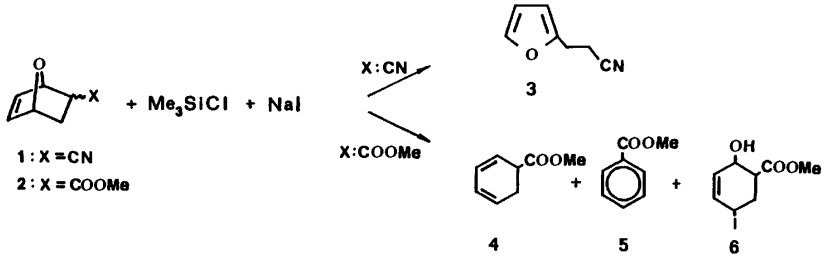

Equation 1.

Table 2. Ring cleavage of 5-methoxycarbonyl-7-oxabicyclo [2.2.1] hept-2-ene[a)]

Run	2 endo:exo	Time h	Yield/%[b)] 4	5	6
1	3:2	20	29.3	1.0	—
2[c)]	3:2	20	43.0	8.2	—
3[d)]	3:2	20	11.4	2.3	—
4	endo	20	42.8	11.6	27.2
5[e)]	endo	20	56.1	7.0	—
6[e)]	endo	48[f)]	67.3	13.4	—
7[e)]	endo	1[g)]	62.6	16.0	—
8[h)]	exo	20	9.2	4.0	—

a) **2** (10 mmol) was allowed to react with Me_3SiCl (12 mmol) and NaI (12 mmol) in acetonitrile (10 ml) at room temperature. b) Isolated yield c) Me_3SiCl (30 mmol) and NaI (30 mmol) were used. d) $MeSiCl_3$ was used instead of Me_3SiCl. e) Me_3SiCl (20 mmol) and NaI (20 mmol) were used. f) At 0 °C. g) At 40 °C. h) About 50% of *exo*-**2** was converted to furan and methyl acrylate.

Again, the $MeSiCl_3$/NaI reagent was milder than the Me_3SiCl/NaI one (Run 3). The reaction of *endo*-**2** with Me_3SiCl/NaI led to **4**(43%), **5**(12%), and **6**(27%). The yield of **4** increased to 67% upon using 2.0 equiv of Me_3SiCl/NaI at 0 °C for 48 h (Run 6). When the same reaction was carried out at 40 °C, the reaction was completed within 1 h to give **4** in 63% yield. **4** was prepared from 3,6-dihydrobenzoic acid by Boeckman,[10] but the procedure is somewhat difficult.

In contrast to the case of *endo*-**2**, *exo*-**2** reacted with Me_3SiCl/NaI under similar conditions yielding **4** in poor yield (9%), and most of *exo*-**2** was converted to furan and methyl acrylate, corresponding to retro-Diels-Alder products. Although the differences in the reactivity of *endo*- and *exo*-**2** with Me_3SiCl/NaI is still unclear, we believe that a cationic species, $[CH_3CN^+-SiMe_3]I^-$,[9] has difficulty in attacking the bridge-oxgen atom of *exo*-**2** in which a methoxycarbonyl group is oriented in the same direction as the bridge-oxygen atom.

Experimental

All of the starting materials were commercially available and were used without further purification except for the solvents. 7-Oxabicyclo[2.2.1]heptenes, **1** and **2**, were prepared according to procedures described in the literature.[5,11] IR spectra were taken with a JASCO-A202 spectrometer, and the ^1H- and ^{13}C-NMR spectra were recorded on a JEOL PMX-60 spectrometer and a Hitachi R-90H, respectively. GLC analyses were performed on a Yanaco-G1800 instrument.

General Method for Ring Cleavage of 7-Oxabicyclo[2.2.1]hept-2-enes. Reactions were normally conducted at a 10-mmol scale in a 25-ml flask fitted with a condenser under a nitrogen atmosphere. To a solution of chlorotrimethylsilane (12 mmol) and sodium iodide (12 mmol) in acetonitrile (10 ml) was added 7-oxabicyclo[2.2.1]hept-2-ene (10 mmol). The mixture was stirred for 20 h at room temperature and was then quenched by water. After washing with a solution of sodium thiosulfate, products were extracted with ether. The extract was washed again with water and dried over anhyd sodium sulfate. After evaporation of the ether, the products were isolated by chromatography on silica gel (hexane:ethyl acetate=10:1 eluent) and were identified by their spectral data.

2-Furanpropanenitrile (3): ^{13}C-NMR ($CDCl_3$) δ=151.4(s), 141.8(d), 118.7(s), 110.3(d), 106.6(d), 24.2(t), 16.5(t); ^1H NMR(CCl_4) δ=7.31 (d, 1H), 6.29 (t, 1H), 6.16 (d, 1H), 2.96 (t, 2H), 2.62 (t, 2H); IR (neat) 2950 cm^{-1}, 2250 cm^{-1}, 1420 cm^{-1}, 1110 cm^{-1}, 740 cm^{-1}; MS *m/z* 121.0 (M^+).

5-Methoxycarbonyl-1,3-cyclohexadiene (4): ^{13}C-NMR($CDCl_3$) δ= 174.2(s), 125.5(d), 125.0(d), 123.7(d), 123.1(d), 51.9(q), 39.1 (d), 24.8(t); ^1H-NMR(CCl_4) δ=5.76 (d, 4H), 3.36 (s, 3H), 3.21 (t, 1H), 2.40 (d, 2H); MS *m/z* 138.1 (M^+).

4-Iodo-6-methoxycarbonyl-2-cyclohexen-1-ol (6): ^{13}C-NMR ($CDCl_3$) δ= 174.1(s), 128.9(d), 126.1(d), 68.4(d), 52.1(q), 45.1(d), 38.8(d), 28.9(t); ^1H-NMR (CCl_4) δ=6.2—5.5 (m, 2H), 5.12 (s, 1H), 3.80 (s, 3H), 3.1—2.4 (m, 5H); IR (KBr) 3500 cm^{-1}, 1740 cm^{-1}, 1430 cm^{-1}, 1165 cm^{-1}; mp 75—76 °C; MS *m/z* 282.2 (M^+); Found: C, 34.10%, H, 3.81%. Calcd for $C_8H_{11}O_3I$: C, 34.05%, H, 3.82%.

References

1) G. A. Olah, S. C. Narang, B. G. B. Gupta, and R. Malhotra, *J. Org. Chem.*, **44**, 1247 (1979).

2) G. A. Olah, S. C. Narang, B. G. B. Gupta, and R. Malhotra, *Synthesis*, **1979**, 61.

3) G. A. Olah, M. Arvanaghi, and Y. D. Vankar, *J. Org. Chem.*, **45**, 3531 (1980).

4) G. A. Olah, A. Husain, B. P. Singh, and A. K. Mehrotra, *J. Org. Chem.*, **48**, 3667 (1983).

5) S. Iwase, S. Maeda, S. Hamanaka, and M. Ogawa, *Nippon Kagaku Kaishi*, **1975**, 1934.

6) F. Sorm, and J. Brondejs, *Collect, Czech. Chem. Commun.*, **12**, 444 (1947).

7) J. M. Patterson, *Org. Syn.* Coll. Vol. V, 585.

8) M. F. Obstain, J. F. Pegues, and L. A. Paquette, *J. Org. Chem.*, **45**, 167 (1980).

9) The cationic spacies, $[CH_3CN^+-SiMe_3]I^-$, was suggested by Olah[4] to generate *in situ* from Me_3SiCl and NaI in acetonitrile.

10) R. K. Boeckman, Jr., M. Ramaiak, and J. B. Medwid, *Tetrahedron Lett.*, **1977**, 4485.

11) Francis Brion, *Tetrahedron Lett.*, **23**, 5299 (1982).

A Straightforward Access to 5-Deoxy-D-arabinono-1,4-lactone, a Versatile Intermediate in the Lauraceae Lactones Syntheses

Sigeru Torii,* Tsutomu Inokuchi, and Yoshinori Masatsugu
Department of Industrial Chemistry, School of Engineering, Okayama University, Okayama 700
(Received July 8, 1985)

Synopsis. 5-Deoxy-D-arabinono-1,4-lactone (**2**) was synthesized by a RuO_4-catalyzed oxidative cleavage of 6-deoxyglucal diacetate (**5d**), derived from D-glucal triacetate (**3**), followed by alkaline hydrolysis and acidic work-up.

Chiral γ-lactones are versatile building blocks in natural product synthesis and their syntheses from readily available carbohydrates are currently an important area of research.[1] In connection with our programs dealing with the total synthesis of the lauraceae lactones, *i.e.*, (−)-litsenolide B_1 (**1a**) and B_2 (**1b**),[2] we sought a simple method for the preparation of optically active derivatives of β-hydroxy-γ-methyl-γ-lactone. Although 5-deoxy-L-arabino-γ-lactone [(2*R*,3*S*,4*S*)-2,3-dihydroxy-4-pentanolide] is easily accessible from L-rhamnose,[3,4] the preparation of its antipode, 5-deoxy-D-arabinono-1,4-lactone (**2**) whose chirality at the C(3) and C(4) carbons coincides with asymmetric carhons of **1**, is not explored to data due to the scant availability of 6-deoxy-D-mannose. More recently, on the other hand, derivation of (3*R*,4*R*)-pentan-4-olide from D-(+)-ribonic acid by the double

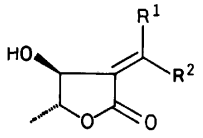

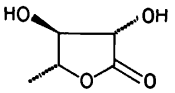

1a: R^1 = H, R^2 = $(CH_2)_9C{\equiv}CH$
1b: R^1 = $(CH_2)_9C{\equiv}CH$, R^2 = H

2

deoxygenation at the C(2) and C(5) positions and its utilization in the synthesis of (−)-litsenolide C_1 and C_2 has been reported.[2d] We describe here a facile synthesis of **2** from the commercially available D-glucal triacetate (**3**)[5] *via* the oxidative cleavage of carbon–carbon double bond of the corresponding 6-deoxyglucal diacetate (**5d**).

Deoxygenation at the C(6) position of **3** to **5d** is the initially requested task in the present synthesis. According to the procedure reported preliminarily by Fraser-Reid *et al.*,[6] we first attempted to transform **3** to the *p*-toluenesulfonate **5a** by selective sulfonylation of the primary hydroxyl group of D-glucal (**4**). After alkaline hydrolysis of **3** with aqueous potassium carbonate, the liberated triol **4** was treated successively with *p*-toluenesulfonyl chloride in pyridine at range 0—50 °C for extended period and then with excess acetic anhydride. Unfortunately, no intended tosylation was observed in this reaction and the starting **3** was recovered. However, the selective sulfonylation of **4** was successfully achieved by using more reactive methanesulfonyl chloride and the desired **5b** was obtained in 52% overall yield from **3** when the reaction was followed by acetylation with acetic anhydride after mesylation. Displacement of the mesylate **5b** with lithium iodide in 2-butanone heated at reflux produced the 6-iodo derivative **5c** which was in turn reduced to the key intermediate **5d** with tributyltin hydride in 91% yield (from **5b**).

In the preceding article[7] we described a ruthenium tetroxide-catalyzed oxidative cleavage of enolic olefins of cyclic structure, giving the corresponding carboxylic acids in good yields. Taking into the advantage of this procedure, the conversion of **5d** into the carboxylic acid **6** was attempted. Thus, the treatment of **5d** with ruthenium tetroxide, generated *in situ* from a catalytic amount of ruthenium dioxide and a stoichiometric amount of sodium periodate (3 equiv) in a biphase solution of carbon tetrachloride and water (1:1 v/v), provided the tri-*O*-acyl-D-arabinonic acid **6** in 78% yield. Finally, the hydrolysis of **6** with aqueous potassium carbonate followed by acidic work-up with 10% hydrogen chloride furnished the desired **2** in 89% yield.

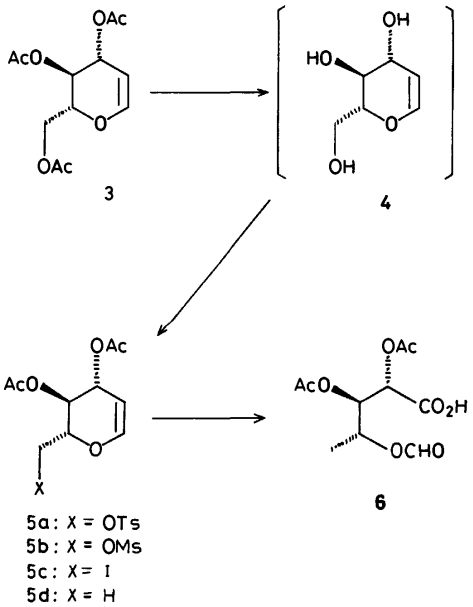

3 **4**

5a: X = OTs
5b: X = OMs
5c: X = I
5d: X = H

6

Experimental

Melting points are uncorrected and boiling points are indicated by an air-bath temperature without correction. IR spectra were recorded with a JASCO IRA-1 grating spectrometer. Unless otherwise noted, ^1H NMR spectra were determined with either a Hitachi R-24 (60 MHz) or a JEOL FX-100 (100 MHz). ^{13}C NMR spectra were recorded with a JEOL FX-100 (25.05 MHz) spectrometer. Optical rotations were taken on a JASCO DIP-140 digital polarimeter. Ele-

mental analyses were performed in our laboratory.

3,4-Di-O-acetyl-6-O-methylsulfonyl-1,5-anhydro-2-deoxy-D-arabino-hex-1-enitol (5b). To a solution of D-glucal triacetate (**3**, 1.0 g, 3.67 mmol) in EtOH (10 ml) was added 2M K_2CO_3 (5.5 ml) (1 M=1 mol dm^{-3}). After stirring for 19 h at room temperature, the mixture was filtered and the filtrate was concentrated *in vacuo*. The remaining solid was dried at 50—60 °C for 24 h at diminished pressure and then dissolved in pyridine (7 ml). To this solution was added methanesulfonyl chloride (0.43 ml, 5.56 mmol) at −20 °C and the resulting solution was stirred for 6.5 h at −20 °C and allowed to warm gradually to room temperature. After recooling to 0 °C, the mixture was treated with acetic anhydride (1.4 ml, 14.7 mmol) at 0 °C and stirred for 1 h at 0 °C and additional 17 h at room temperature. The mixture was poured into saturated $NaHCO_3$ and extracted several times with AcOEt. The extracts were washed with 5% $NaHCO_3$ and saturated NaCl, dried (Na_2SO_4), and concentrated. Purification of the crude products on column chromatography (SiO_2, hexane–AcOEt 5:1) gave 590 mg (52%) of **5b**: Mp 47—51 °C (from ether); $[\alpha]_D^{17}$ +15.0 °(*c* 1.6 in EtOH); IR (Nujol) 1730 (ester C=O), 1641 (C=C),1352, 1240, 1220, 1161, 1070, 1039, 963, 929 cm^{-1}; ^{1}H NMR (60 MHz, $CDCl_3$) δ=2.07, 2.11 (s, 6, CH_3CO), 3.09 (s, 3, CH_3SO_2), 4.20—4.60 (m, 1, CH-O), 4.42 (m, 2, CH_2OSO_2), 4.91 (d, d, *J*=6, 3 Hz, 1, O-C=CH), 5.13—5.50 (m, 2, CH-O), 6.51 (d, *J*=6 Hz, 1, O-CH=C). Found: C, 42.97; H, 5.35. Calcd for $C_{11}H_{16}O_8S$: C, 42.86; H, 5.23.

3,4-Di-O-acetyl-6-iodo-1,5-anhydro-2,6-dideoxy-D-arabino-hex-1-enitol (5c). A mixture of **5b** (667 mg, 2.17 mmol) and LiI (487 mg, 3.26 mmol) in 2-butanone (15 ml) was heated at reflux for 29 h. After cooling, the mixture was filtered and the filtrate was concentrated *in vacuo*. The residue was purified on column chromatography (SiO_2, hexane–AcOEt 5:1) to give 676 mg (92%) of **5c**: Bp 119—120 °C/2.5 Torr (1 Torr=133.3 Pa); $[\alpha]_D^{13}$ −3.43° (*c* 1.76 in EtOH); IR (neat) 3040, 3000, 1740, 1725 (ester C=O), 1640 (C=C), 1420, 1363, 1220, 1130, 1078, 1037, 945, 809, 745 cm^{-1}; ^{1}H NMR (60 MHz, $CDCl_3$) δ=2.06, 2.10 (s, 6, CH_3CO), 3.35 (d, *J*=1.5 Hz, 1, CH_2I), 3.44 (s, 1, CH_2I), 3.90—4.30 (m, 1, CH-O), 4.38 (m, 1, O-C=CH), 5.17—5.88 (m, 2, CH-O), 6.50 (d, *J*=6 Hz, 1, O-CH=C); ^{13}C NMR ($CDCl_3$) δ=2.0 (t), 20.8 (q), 21.0 (q), 66.6 (d), 69.7 (d), 74.8 (d), 98.8 (d), 145.3 (d), 169.3 (s), 170.1 (s). Found: C, 35.19; H, 3.73. Calcd for $C_{10}H_{13}IO_5$: C, 35.32; H, 3.86.

3,4-Di-O-acetyl-1,5-anhydro-2,6-dideoxy-D-arabino-hex-1-enitol (5d). A solution of **5c** (357 mg, 1.05 mmol) and *n*-Bu_3SnH (920 mg, 3.16 mmol) in toluene (7 ml) was stirred at room temperature for 4.5 d under nitrogen atmosphere. Evaporation of the solvent followed by column chromatography (SiO_2, hexane–AcOEt 15:1) of the residue gave 222 mg (99%) of **5d**: Bp 87—88 °C/2 Torr; $[\alpha]_D^{15}$ −47.7° (*c* 1.36 in EtOH); IR (neat) 3040, 1735 (ester C=O), 1644 (C=C), 1375, 1220, 1109, 1045, 1022, 910 cm^{-1}; ^{1}H NMR (100 MHz, $CDCl_3$) δ=1.31 (d, *J*=7 Hz, 3, CH_3), 2.04, 2.09 (s, 6, CH_3CO), 4.09 (d, q, *J*=7, 6.5 Hz, 1, CH-O), 4.75 (d, d, *J*=6.5, 3.3 Hz, 1, O-C=CH), 4.99 (d, d, *J*=8, 6 Hz, 1, CH-O), 5.32 (d, d, d, *J*=8, 3.3, 1.5 Hz, 1, CH-O), 6.40 (d, d, *J*=6.5, 1.5 Hz, O-CH=C); ^{13}C NMR ($CDCl_3$) δ=16.6 (q), 20.9 (q), 21.1 (q), 68.3 (d), 71.9 (d), 72.5 (d), 98.8 (d), 146.0 (d), 169.9 (s), 170.6 (s). Found: C, 56.23; H, 6.75. Calcd for $C_{10}H_{14}O_5$: C, 56.07; H, 6.59.

2,3-Di-O-acetyl-4-O-formyl-5-deoxy-D-arabinonic Acid (6). A solution of **5d** (71 mg, 0.33 mmol) in CCl_4 (5 ml) was mixed with a solution of $NaIO_4$ (211 mg, 0.99 mmol) in H_2O (5 ml) and to this mixture was added $RuO_2 \cdot 2H_2O$ (3 mg, 0.02 mmol). After vigorous stirring for 1 h at room temperature, the reaction was quenched with a small amount of 2-propanol. The CCl_4 layer was separated and the aqueous layer was acidified with aqueous 5% HCl and extracted several times with AcOEt. The combined extracts were filtered and the filtrate was dried (Na_2SO_4) and concentrated to give 67 mg (78%) of **6**: $[\alpha]_D^{16}$ +37° (*c* 0.75 in EtOH); IR($CHCl_3$) 3600—2400 (COOH), 1740, 1720 (C=O), 1365, 1205, 1160, 1120, 1040, 840, 930 cm^{-1}; ^{1}H NMR (60 MHz, $CDCl_3$) δ=1.30 (d, *J*=6 Hz, 3, CH_3), 2.11, 2.17 (s, 6, CH_3CO), 4.90—5.70 (m, 3, CH-O), 8.02 (s, 1, CHO), 8.50 (br, 1, COOH). Satisfactory elemental analysis for the methyl ester of **6**; Found: C, 47.70; H, 5.95. Calcd for $C_{11}H_{16}O_8$: C, 47.83; H, 5.84.

5-Deoxy-D-arabinono-1,4-lactone (2). To a solution of **6** (207 mg, 0.79 mmol) in MeOH (10 ml) was added 2 M K_2CO_3 (2 ml) at 3—5 °C. After stirring for 20 h at room temperature, the mixture was acidified to pH 2—3 with 10% HCl and concentrated *in vacuo*. The remaining solids were washed several times with hot AcOEt and the washings were filtered, dried (Na_2SO_4), and concentrated. The crude product was purified on column chromatography (SiO_2, hexane–AcOEt 2:1) to give 92.3 mg (89%) of **2**: Mp 124.5—125.5 °C (from methanol) (lit, data of L-enantiomer[3] 125 °C); $[\alpha]_D^{13}$ +37.3 °(*c* 1.01 in EtOH) (lit, data of L-enantiomer[3] −34—−39°); IR (KBr) 3400 (OH), 1758 (lactone C=O), 1390, 1363, 1330, 1230, 1195, 1144, 1095, 1055, 1019, 945, 870 cm^{-1}; ^{1}H NMR (400 MHz, CD_3OD)[8] δ=1.41 (d, *J*=6.3 Hz, 3, CH_3), 3.76 (d, d, *J*=8.8, 8.3 Hz, 1, CH-O), 4.15 (d, q, *J*=8.3, 6.3 Hz, 1, CH-O), 4.28 (d, *J*=8.8 Hz, 1, CH-O), 4.84 (s, OH); ^{13}C NMR (CD_3OD) δ=18.0 (q), 75.1 (d), 78.2 (d), 80.1 (d), 176.0 (s). Found: C, 45.32; H, 5.95. Calcd for $C_5H_8O_4$: C, 45.46; H, 6.10.

The authors are grateful to the Ministry of Education, Science, and Culture for a financial support by a Grant-in-Aid for Scientific Research (No. 60470089).

References

1) S. Hanessian, "Total Synthesis of Natural Products: The 'Chiron' Approach," Pergamon Press, Oxford (1983); T. D. Inch, *Tetrahedron*, **40**, 3161 (1984).

2) Isolation a) K. Takeda, K. Sakurai, and H. Ishii, *Tetrahedron*, **28**, 3757 (1972); b) M. Niwa, M. Iguchi, and S. Yamamura, *Chem. Lett.*, **1975**, 655; c) J. C. V. Martinez, M. Yoshida, and O. R. Gottlieb, *Tetrahedron Lett.*, **1979**, 1021: *Phytochemistry*, **20**, 459 (1981); Chiral Synthesis d) S. -Y. Chen and M. M. Joullié, *J. Org. Chem.*, **49**, 2168 (1984); Racemic synthesis e) R. H. Wollenberg, *Tetrahedron Lett.*, **21**, 3139 (1980); f) P. Barbier and C. Benezra, *ibid.*, **23**, 3513 (1982); g) K. Tanaka, M. Terauchi, and A. Kaji, *Bull. Chem. Soc. Jpn.*, **55**, 3935 (1982); h) A. S. Kende and B. H. Toder, *J. Org. Chem.*, **47**, 163 (1982).

3) P. Andrews, L. Hough, and J. K. N. Jones, *J. Am. Chem. Soc.*, **77**, 125 (1955). Synthesis of *dl*-**2**; J. Jary and K. Kefurt, *Collect. Czech. Chem. Commun.*, **27**, 2561 (1962).

4) T. Ohgi, S. M. Hecht, *J. Org. Chem.*, **46**, 1232 (1981).

5) Obtainable from Pfanstiehl Laboratories, Waukegan, IL 60085; W. Roth and W. Pigman, "Methods in Carbohydr. Chem., ed by R. L. Whistler, M. L. Wolfrom, and J. N. BeMiller, Academic Press, New York (1963), Vol. 2 pp. 405—408.

6) D. B. Tulshian and B. Fraser-Reid, *J. Am. Chem. Soc.*, **103**, 474 (1981).

7) S. Torii, T. Inokuchi, and K. Kondo, *J. Org. Chem.*, December issue (1985).

8) We are grateful to Otsuka Pharmaceutical Company for a kind measurement of 400 MHz NMR.

Optical Resolution of 3a,4,7,7a-Tetrahydro-4,7-methano-1*H*-indene Derivatives

Toshio Ito, Yoshio Okamoto,† and Takeshi Matsumoto*
Department of Chemistry, Faculty of Science, Hokkaido University, Sapporo, 060
†*Department of Chemistry, Faculty of Engineering Science, Osaka University, Toyonaka 560*
(Received July 10, 1985)

Synopsis. (1*RS*,3a*RS*,4*RS*,7*SR*,7a*SR*)-3a,4,7,7a-Tetrahydro-4,7-methano-1*H*-inden-1-ol was resolved kinetically and its C-1 epimer was resolved chromatographically. Absolute configurations of these resolved compounds were determined.

Optically active 3a,4,7,7a-tetrahydro-4,7-methano-1*H*-indene(dicyclopentadiene) and allied compounds seem useful chiral synthons for syntheses of optically active natural products,[1] because they contain at least four asymmetric centers and a variety of reactive sites. We report here optical resolution of (1*RS*,3a*RS*,4*RS*,7*SR*,7a*SR*)-3a,4,7,7a-tetrahydro-4,7-methano-1*H*-inden-1-ol-[(±)-**1**] and its C-1 epimer (±)-**2** (Fig. 1).[2]

Titanium(IV) tartrate-catalyzed asymmetric epoxidation developed by Sharpless *et al.*[3] was adopted for kinetic resolution of (±)-**1**. Allylic alcohol (±)-**1** (50 mmol) was treated with 0.6 mol eq of *t*-butyl hydroperoxide in the presence of diisopropyl tartrate and Ti(*i*-PrO)$_4$ as catalyst to afford epoxy compound (−)-**6** and starting material enriched in (+)-**1** in 38 and 34% isolated yields, respectively (Fig. 2). Specific rotation of the resolved **1** was +78°(*c* 1.00, $CHCl_3$). A portion of this sample was esterified with (*S*)-2-methoxy-2-trifluoromethylphenylacetyl chloride ((*S*)-MTPACl)[4] to yield (*S*)-MTPA ester **5**, which was found to be a mixture of diastereomers by the 400 MHz ^{1}H NMR spectrum. The diasteromeric excess was 68.2%. Optically pure (+)-**1** was readily obtained by recrystallization in 63% yield, from the 68.2% e. e. **1**.

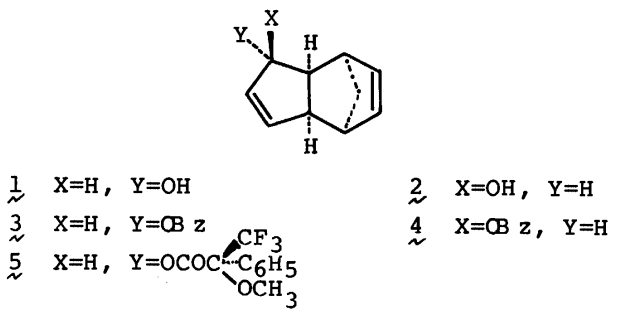

Fig. 1.

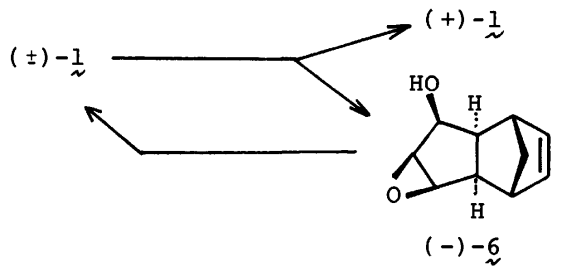

Fig. 2.

Next, the absolute configuration of the above optically active alcohol was determined by the allyl benzoate rule.[5] Alcohol (+)-**1** (68.2% e.e.) was converted to its benzoate **3**, whose CD spectrum exhibited a positive first Cotton effect peak at 222 nm. Therefore the absolute configuration of (+)-**1** was determined to be as shown in Fig. 3.

Produced epoxy alcohol (−)-**6** had low optical purity (39% e.e., by ^{1}H NMR of (*S*)-MTPA ester), and was not synthetically useful. Therefore (−)-**6** was reverted to **1**. Epoxy alcohol (−)-**6** was reduced with $TiCl_3$–$LiAlH_4$[6] to give (±)-**1** in 65% yield (Fig. 2).

The above kinetic resolution is practical for preparing a large quantity of optically active (+)-**1**. However, the method is operationally not so simple. On the other hand, the resolution by chromatography developed by one of us (Y. O.)[7] is simple. Although this method is at present not so practical for large scale preparation, resolution of dicyclopentadiene derivatives by means of the (+)-PTrMA-coated silicagel column[7] was next attempted. Dicyclopentadiene, (±)-**1** and (±)-**2**, and acetates of (±)-**1** and (±)-**2** were not resolved. Since it was reported that aryl groups strongly interacted with (+)-PTrMA,[7] (±)-**1** and (±)-**2** were

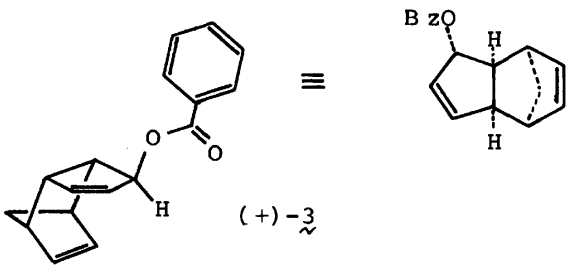

Fig. 3.

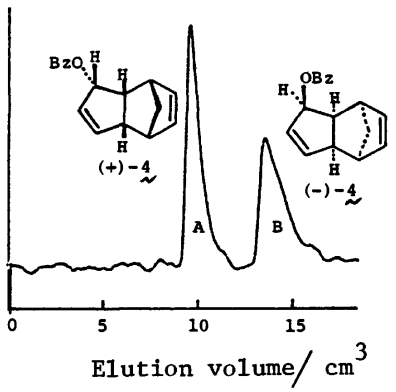

Fig. 4. Resolution of (±)-**4**(0.4 mg). (+)-PTrMA column, 25×0.46 (i.d.); eluent, MeOH; flow rate 0.76 cm^3 min^{-1}; temperature 25 °C.

benzoylated. While benzoate (±)-**3** was not separated (R_s=0.5), its C-1 epimer (±)-**4** was cleanly resolved (R_s=2.02, Fig. 4). The eluents A and B contained respectively enantiomers (+)-**4** and (−)-**4** with the absolute configuration shown in Fig. 4, which was proved as follows. Alcohol (+)-**1** (68.2% e.e.) with known configuration was converted to (−)-**2**,[2] which in turn was benzoylated and passed through the (+)-PTrMA column. The main peak coincided in retention volume with that of the eluent B (Fig. 4).

Experimental

Measurements. Melting points were uncorrected. IR spectra were measured with a JASCO model IR-S spectrophotometer. Unless otherwise noted, ^{1}H NMR spectra were recorded at 60 MHz (HITACHI R-20B). ^{1}H NMR spectra at 400 MHz were taken on a JEOL JNM FX-400. Low resolution mass spectra were obtained with a HITACHI model RMS-6U instrument. Optical rotations and CD spectra were measured by means of a JASCO model DIP-SL automatic polarimeter and a JASCO J-20 automatic recording spectropolarimeter respectively. The high-performance liquid chromatography was accomplished on a Waters associates model 6000A chromatograph equipped with a Waters associates R-401 RI detector.

Kinetic Resolution of (±)-1 and Absolute Configuration of (+)-1. A mixture of (±)-**1** (7.1 g, 50.0 mmol), diisopropyl (2*R*,3*R*)-tartrate (13.5 g, 57.7 mmol) and Ti(*i*-PrO)$_4$ (14.9 cm^3, 50.0 mmol) in dry CH_2Cl_2 (500 cm^3) was stirred at −20 °C. Anhydrous *t*-BuOOH (11.3 g, 30.0 mmol) in dry CH_2Cl_2 (about 24 w/w%) was then added, and the resulting mixture was maintained at −20 °C in a freezer. After 4 d, the cold reaction mixture was poured into a precooled (−20 °C) solution of 1000 cm^3 of acetone containing 14 cm^3 of water. The resulting mixture was stirred for 1 h at −20 °C and for 30 min at room temperature. After *ca.* 400 cm^3 of the acetone was evaporated, the residue was diluted with ether (400 cm^3) and filtered. The filtrate was concentrated and diluted again with 430 cm^3 of ether, and then 1 M NaOH soution (170 cm^3) (1 M=1 mol dm^{-3}) was added to the ether solution. The resulting homogeneous mixture was stirred for 1 h at 0 °C. After hydrolysis of the tartrate was complete, the ether layer was separated and the aqueous layer was extracted with ether (3×100 cm^3). The combined ether extracts were washed with water and NaCl solution. After drying (Na_2SO_4), the solvent was evaporated to give 5.8 g of an oily residue, which was chromatographed on silica gel (200 g) with 30% AcOEt in hexane. The elution gave 2.4 g (34%) of (+)-**1** and 3.0 g (38%) of (−)-**6**. (+)-**1**: $[\alpha]_D$=+78° (*c* 1.00, $CHCl_3$); mp 50—52 °C. (−)-**6**: $[\alpha]_D$=−32.6 (*c* 4.05, $CHCl_3$); mp 35—38 °C; IR($CHCl_3$) 3560, 1255 cm^{-1}; ^{1}H NMR ($CDCl_3$) δ=6.06 (2H, t, *J*=1.0 Hz), 3.78 (1H, t, *J*=1.5 Hz), 3.41 (1H, t, *J*=2 Hz), 3.27 (1H, d, *J*=2 Hz), 3.2—2.8 (2H, m), 1.49 and 1.30 (ABq, *J*=8 Hz); *m/z* 148 (M−H_2O). Found: C, 73.03; H, 7.39. Calcd for $C_{10}H_{12}O_2$: C, 73.14; H, 7.37%. E. e. was 68.2% for (+)-**1**; two kinds of peaks due to C-7a-H of (+)-**1** (*S*)-MTPA ester were observed at 2.70 (84%) and 2.60 (16%) in the 400 MHz ^{1}H NMR spectrum. For (−)-**6**, e. e. was 39%; two kinds of peaks due to C-6-H of (−)-**6** (*S*)-MTPA ester appeared at 4.85 (69.5%) and 4.82 (30.5%) in the 400 MHz ^{1}H NMR spectrum.

Recrystallization of (+)-**1** (68.2% e.e., 1.0 g) from petroleum ether three times afforded optically pure (+)-**1** (0.63 g, 63%) $[\alpha]_D$=+115.1 ° (*c* 1.00, $CHCl_3$); mp 69.5—72.0 °C. (*S*)-MTPA ester of (+)-**1**: $[\alpha]_D$=+138° (*c* 1.00, $CHCl_3$); IR (neat) 3120, 1750, 1625, 1460, 1225, 1170 cm^{-1}; ^{1}H NMR ($CDCl_3$, 400 MHz) δ=7.53 (2H, m), 7.39 (3H, m), 6.06 (1H, dd, *J*=6, 3 Hz), 5.91 (1H, dt, *J*=6, 2 Hz), 5.88 (1H, dd, *J*=6, 3.5 Hz), 5.57 (1H, dt, *J*=6, 2 Hz), 5.18 (1H, q, *J*=2 Hz), 3.56 (3H, q, *J*=1 Hz), 3.54 (1H, m), 3.42 (1H, br s, W_H=10 Hz), 2.84 (1H, br s, W_H=9 Hz), 2.70 (1H, qd, *J*=2, 8 Hz), 1.63 (1H, td, *J*=1.5, 8 Hz), 1.43 (1H, br d, *J*=8 Hz).

$TiCl_3$-$LiAlH_4$ Reduction of (−)-6. To an ice-cooled suspension of $TiCl_3$ (110 mg, 0.71 mmol) in dry THF (3.3 cm^3) was added $LiAlH_4$ (6.8 mg, 0.18 mmol). The resulting mixture was stirred for 20 min at 0 °C, and (−)-**6** (39% e.e., 39 mg, 0.23 mmol) in dry THF (0.5 cm^3) was added. Stirring was continued for 10 min. Celite, anhydrous Na_2SO_4 (each 500 mg), and saturated aq NH_4Cl solution (0.5 cm^3) were then added successively. The resulting mixture was filtered, and the solid material was washed with AcOEt (3×20 cm^3). The combined organic solution was washed with aq NaCl solution and dried (Na_2SO_4). The solvent was evaporated to give an oily residue, which was purified by preparative TLC to afford 22 mg (65%) of (±)-**1**.

References

1) For examples: coriolin; T. Ito, N. Tomiyoshi, K. Nakamura, S. Azuma, M. Izawa, F. Maruyama, M. Yanagiya, H. Shirahama, and T. Matsumoto, *Tetrahedron Lett.*, **23**, 1721 (1982); *Tetrahedron*, **40**, 241 (1984). PGF_2; D. Brewster, M. Myers, J. Ormerod, P. Otter, A. C. B. Smith, M. E. Spinner, and S. Turner, *J. Chem. Soc., Perkin Trans. 1*, **1973**, 2796. Vervenalol; T. Sakan and K. Abe, *Tetrahedron Lett.*, **1968**, 2471.

2) Woodward and Katz had prepared (±)-**1** and (±)-**2** and resolved (±)-**1** *via* 3β-acetoxy-Δ^5-etiocholenate, but the absolute configuration of these resolved compounds had not been determined; R. B. Woodward and T. J. Katz, *Tetrahedron*, **5**, 70 (1959).

3) V. S. Martin, S. S. Woodard, T. Katsuki, Y. Yamada, M. Ikeda, and K. B. Sharpless, *J. Am. Chem. Soc.*, **103**, 6237 (1981).

4) J. A. Dale, D. L. Dull, and H. S. Mosher, *J. Org. Chem.*, **34**, 2543 (1969).

5) N. Harada, J. Iwabuchi, Y. Yokota, H. Uda, and K. Nakanishi, *J. Am. Chem. Soc.*, **103**, 5590 (1981).

6) J. E. McMurry and M. P. Fleming. *J. Org. Chem.*, **40**. 2555 (1975).

7) Y. Okamoto, S. Honda, I. Okamoto, and H. Yuki, *J. Am. Chem. Soc.*, **103**, 6971 (1981).

Absolute Configurations of Novel Axially Dissymmetric 10,10′-Dihydroxy-9,9′-biphenanthryl and Its Related Compounds

Koji YAMAMOTO,* Hitoshi FUKUSHIMA, Hiroya YUMIOKA, and Masao NAKAZAKI
Department of Chemistry, Faculty of Engineering Science, Osaka University, Toyonaka, Osaka 560
(Received July 13, 1985)

Synopsis. Stereoselective oxidative coupling of 10-hydroxy-1,2,3,4-tetrahydrophenanthrene derived from methyl 3-methoxy-2-naphthoate gave (−)-(*S*)-10,10′-dihydroxy-1,1′,2,2′,3,3′,4,4′-octahydro-9,9′-biphenanthryl which was converted into (+)-(*S*)-10,10′-dimethoxy-9,9′-biphenanthryl assigning the *S* configuration to (−)-10,10′-dihydroxy-9,9′-biphenanthryl.

Recently, we found that the novel axially dissymmetric molecule, 10,10′-dihydroxy-9,9′-biphenanthryl (**14**), has been used for synthesis of chiral crown ether with high enantiomer selectivity toward primary amines[1] and enantioselective reduction of ketones.[2] Here we report the determination of the absolute configuration of chiral 10,10′-dihydroxy-9,9′-biphenanthryl (**14**) and its related compounds.

Lithium aluminium hydride reduction of methyl 2-methoxy-3-naphthoate (**1**)[3] furnised the alcohol (**2**) which was converted to the bromide (**3**) with phosphorus tribromide, then submitted to the malonic ester synthesis under usual reaction conditions to afford the ester (**4**) (32.5% yield from **1**). After the side chain of **4** was extended by routine method (*via* cyanide), the resulting acid (**8**) (94% yield from **4**) was cyclized with polyphosphoric acid to yield the expected cyclic ketone (**9**) in 89% yield. Wolff-Kishner reduction of **9** followed by hydrolysis with AcOH–H_2O–concd HCl (10:5:1) gave the naphthol derivative (**11**) (69.7% yield from **9**). Stereoselective oxidative coupling of **11** was carried out using optically active amine–copper(II) complex, which prepared *in situ* by treating (−)-(*S*)-1,2-diphenylethylamine[4] and $Cu(NO_3)_2 \cdot 3H_2O$ in methanol. The coupling product was purified by recrystallization from benzene to give an optically pure specimen of the binaphthol derivative (−)-(**12**) (79% yield,$[\alpha]_D^{21}$ −29.0° ($CHCl_3$).[5] Comparison of the CD spectra of (−)-**12** with that of authentic (−)-(*S*)-2,2′-dihydroxy-3,3′-dimethyl-1,1′-binaphthyl[7] let us to conclude that these two compounds have the same configuration. Methylation of (−)-(**13**) which was dehydrogenated with 2,3-dichloro-5,6-dicyano-1,4-benzoquinone to give (+)-(*S*)-10,10′-dimethoxy-9,9′-biphenanthryl (**15**) (45% yield from **12**, $[\alpha]_D^{23}$ +26° ($CHCl_3$)). This dextrorotatory compound (**15**) could also be derived from (−)-10,10′-dihydroxy-9,9′-biphenanthryl (**14**)[2] by methylation with methyl *p*-toluenesulfonate. These correlation enable us to assign *S* configurations to (−)-**14** and its related compounds.

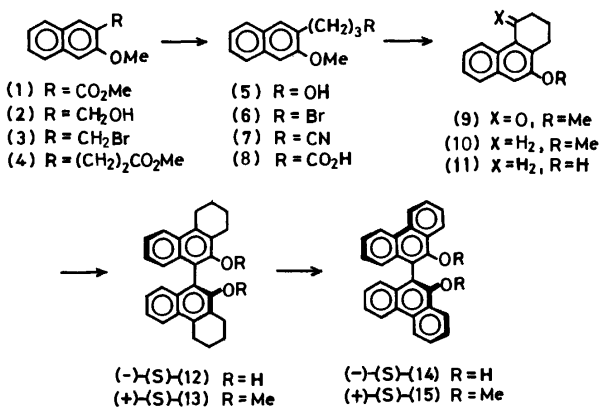

Experimental

Melting points are uncorrected. IR, NMR, UV, and CD spectra were recorded on a Hitachi 260-10, a JNM-MH-100, a Hitachi 220A, and a JASCO J-20 spectrometer, respectively.

3-Methoxy-2-naphthaleneethanol (2). A solution of **1** (23.6 g, 0.109 mol) in dry THF (150 ml) was added to a suspension of $LiAlH_4$ (2.5 g, 66 mmol) in dry THF (150 ml). The mixture was refluxed for 8 h with stirred and cooled in an ice-bath. To the chilled reaction mixture was added aq HCl, and extracted with ether. The ether extract was washed with water, dried ($MgSO_4$), concentrated, and recrystallized from benzene, giving 13.9 g (68% yield) of **2**: Mp 72—73 °C; IR (KBr) 3450 cm^{-1} (OH) (Found: C, 75.95; H, 5.79%).

2-Bromomethyl-3-methoxynaphthalene (3). To a stirred solution of **2** (11.9 g, 63.4 mmol) in dry ether (150 ml) was added dropwise a solution of phosphorus tribromide (8.6 g, 31.8 mmol) in dry ether (70 ml) at room temperature. The mixture was stirred for further 4 h, and quenched with water (90 ml). After a usual work-up, the crude product was recrystallized from hexane–benzene to give **3** (13 g, 81%), mp 150—151 °C (Found: C, 57.77; H, 4.50%).

Methyl 3-Methoxy-2-naphthalenepropionate (4). The alykylation of malonic ester with **3** (12.3 g, 48 mmol) was carried out according to literature[8] using sodiomalonate (prepared from sodium (1.84 g, 0.08 g-atom), ethyl malonate (21 g, 0.19 mol), and absolute ethanol (28 ml). The resulting diester was saponified by refluxing for 3 h with KOH (30 g) in 80% ethanol (280 ml). After a usual work-up, the resulting dicarboxylic acid (7 g) was decarboxylated by heating at 200 °C for 1 h. The routine esterification of the monocarboxylic acid with methanol and concd H_2SO_4 afforded **4** (6.7 g, 59%): Bp 160—162 °C (0.9 mmHg); IR (film) 1730 cm^{-1} (C=O) (Found: C, 74.01; H, 6.42%).

3-Methoxy-2-naphthalenepropanol (5). Hydride reduction of **4** was carried out followed by the same method as described of **2**, using **4** (6.7 g, 27.5 mmol) and $LiAlH_4$ (0.63 g, 16.5 mmol). The product was distilled to give **5** (5.5 g, 93%): Bp 168—169 °C (0.7 mmHg); IR (film) 3450 cm^{-1} (OH).

2-(3-Bromopropyl)-3-methoxynaphthalene (6). The alcohol (**5**) (5.2 g, 24 mmol) was converted into the bromide (**6**) following the same method as described for **3**. Recrystallization of the product from ethanol afforded **6** (4.1 g, 61%): mp 56—57 °C (Found: C, 60.22; H, 5.39%).

2-(3-Cyanopropyl)-3-methoxynaphthalene (7). A mixture of **6** (3.87 g, 13.9 mmol), KCN (2.55 g, 13.9 mmol), and 80% ethanol (30 ml) was refluxed for 6 h. After removal of the solvent, the reaction mixture was diluted with water and the product was extracted with ether. The etheral extract was dried ($MgSO_4$), concentrated, and recrystallized from methanol, giving 3.0 g (95%) of **7**: Mp 74—75 °C; IR (KBr)

2250 cm^{-1} (C≡N) (Found: C, 79.98; H, 6.78%).

3-Methoxy-2-naphthalenebutyric acid (8). A solution of **7** (2.7 g, 12.2 mmol), KOH (5.4 g, 96 mmol), and 70% ethanol (30 ml) was refluxed for 4 h, and the chilled reaction mixture was quenched with 2M HCl (200 ml) (1 M=1 mol dm^{-3}). The separated product was extracted with chloroform. The extract was dried ($MgSO_4$), concentrated, and recrystallized from methanol, giving 2.8 g (95%) of **8**: mp 93—94 °C (Found: C, 73.73; H, 6.66%).

10-Methoxy-1,2,3,4-tetrahydro-4-phenanthrenone (9). A solution of **8** (2.55 g, 10.6 mmol) and polyphosphoric acid (40 g) was stirred for 1 h at 60 °C. The hot mixture was poured onto ice-water and the product was extracted with ether. The ether solution was washed with water and dried ($MgSO_4$). After evaporation of the solvent, the residue was recrystallized from hexane to give **9** (2.13 g, 89%): Mp 83—84 °C; IR (KBr) 1660 cm^{-1} (C=O) (Found: C, 79.73; H, 6.30%).

10-Methoxy-1,2,3,4-tetrahydrophenanthrene (10). Wolff-Kishner reduction of **9** (0.9 g, 4 mmol) using KOH (0.9 g, 16 mmol), 100% hydrazine hydrate (0.8 g, 6 mmol), and diethylene glycol (20 ml) was carried out according to literature[9] to give **10** (0.64 g, 75%). Recrystallization from methanol furnished colorless needles: Mp 72—73 °C (Found: C, 84.84; H, 7.63%).

10-Hydroxy-1,2,3,4-tetrahydrophenanthrene (11). A solution of **10** (0.12 g, 0.57 mmol) in a mixture of 10:5:1 acetic acid, water, and concd HCl (16 ml) was refluxed for 15 h. The mixture poured onto ice-water and the product was extracted with ether. After a usual work-up, the crude product was recrystallized from hexane to give **11** (0.1 g, 93%): Mp 127—128 °C; IR (KBr) 3300 cm^{-1} (OH) (Found: C, 84.72; H, 7.15%).

(−)-10,10′-Dihydroxy-1,1′,2,2′,3,3′,4,4′-octahydro-9,9′-biphenanthryl (12). To a chilled solution (−5 °C) of (−)-(*S*)-diphenylethylamine ($[\alpha]_D^{23}$ −50.8° (EtOH), 99% optical purity[7]) (1.3 g, 6.6 mmol) and Cu $(NO_3)_2 \cdot 3H_2O$ (0.3 g, 1.24 mmol) in methanol (4 ml), was added a solution of **11** (0.12 g, 0.605 mmol) in methanol (1 ml). After stirring at −5 °C for 1 h under N_2, the mixture was quenched with 3% aq HCl (20 ml) and the product was extracted with ether. Work-up followed by recrystallization from benzene gave an optically pure (−)-**12**[5] (93 mg, 79%): Mp 216—218 °C; $[\alpha]_D^{21}$ −30.1° ($CHCl_3$); IR (KBr) 3520 cm^{-1} (OH); ^{1}H-NMR ($CDCl_3$) δ=1.76—2.18 (m, 8H), 2.88 (t, 4H), 3.22 (t, 4H), 5.09 (s, 2H), 7.00—7.46 (m, 6H), and 8.00 (d, 2H); UV (MeOH) 285 (log ε 4.13), 295 (4.13), 318 (3.83), and 333 nm (3.92); CD (MeOH) $[\theta] \times 10^{-3}$ (nm) +5.5 (272), −11.4 (296), −6.6 (307), −10.3 (318), −8.2 (324), −8.9 (328), and +2.0 (337); Found: C, 85.35; H, 6.70%. Calcd for $C_{28}H_{26}O_2$: C, 85.24; H, 6.64%.

(+)-10,10′-Dimethoxy-1,1′,2,2′,3,3′,4,4′-Octahydro-9,9′-biphenanthryl (13). To a boiling suspension of **12** (80 mg, 0.203 mmol), *t*-BuOK (50.2 mg, 0.447 mmol), and dry THF (4 ml) was added a solution of methyl *p*-toluenesulfonate (84 mg, 0.447 mmol) in dry THF (1 ml) under N_2. The reaction mixture was refluxed for further 5 h, cooled in an ice-bath, quenched with water, and extracted with ether. After a usual work-up, the product was recrystallized from benzene to give (+)-**13** (77 mg, 90%): Mp 170—171 °C; $[\alpha]_D^{19}$ +28.9° ($CHCl_3$); ^{1}H-NMR ($CDCl_3$) δ=1.71—2.19 (m, 8H), 2.63—3.37 (m, 8H), 3.27 (s, 6H), 7.05—7.35 (m, 6H), and 7.97 (d, 2H) (Found: C, 85.40; H, 7.23%).

(−)-10,10′-Dimethoxy-9,9′-biphenanthryl (15). a) Dehydrogenation of 13: A Solution of **13** (20.5 mg, 0.09 mmol) and 2,3-dichloro-5,6-dicyano-1,4-benzoquinone (20.5 mg, 0.09 mmol) in benzene (1 ml) was refluxed for 3 h. Evaporation of the solvent left a solid material which was recrystallized from benzene to give **15** (10 mg, 50%): Mp 251—253 °C; $[\alpha]_D^{23}$ +26.4° ($CHCl_3$); ^{1}H-NMR ($CDCl_3$) δ=3.46 (s, 6H), 7.20—7.82 (m, lOH), 8.22—8.36 (m, 2H), and 8.65—8.85 (m, 4H) (Found: C, 87.72; H, 5.67%).

b) Methylation of (−)-14: The same method as described for **13**, using (−)-**14** ($[\alpha]_D^{23}$ −71° ($CHCl_3$), 98% optical purity)[2] (0.1 g, 0.259 mmol), *t*-BuOK (60 mg, 0.52 mmol), methyl *p*-toluenesulfonate (0.1 g, 0.53 mmol) afforded **15** (70 mg, 65%): mp 251—253 °C; $[\alpha]_D^{23}$ +25.5° ($CHCl_3$).

References

1) K. Yamamoto, H. Fukushima, Y. Okamoto, K. Hatada, and M. Nakazaki, *J. Chem. Soc., Chem. Commun.*, **1984**, 1111.

2) K. Yamamoto, H. Fukushima, and M. Nakazaki, *J. Chem. Soc., Chem. Commun.*, **1984**, 1490.

3) R. Huisgen and H. Nakaten, *Justus Liebig Ann. Chem.*, **586**, 84 (1954).

4) M. Nakazaki, I. Mita, and N. Toshima, *Bull. Chem. Soc. Jpn.*, **36**, 161 (1963).

5) The optical purity of (−)-**12** was determined by h.p.l.c. analysis with a column packed with (+)-poly (triphenylmethyl methacrylate) (elution with methanol).[6]

6) Y. Okamoto, S. Honda, I. Okamoto, H. Yuki, S. Murata, R. Noyori, and H. Takaya, *J. Am. Chem. Soc.*, **103**, 6971 (1981).

7) R. C. Helgeson, J. M. Timko, P. Moreau, S. C. Peacock, J. M. Mayer, and D. J. Cram, *J. Am. Chem. Soc.*, **96**, 6762 (1974).

8) M. Nakazaki, K. Yamamoto, S. Isoe, and M. Kobayashi, *J. Org. Chem.*, **44**, 2160 (1979).

9) M. Nakazaki, K. Yamamoto, and M. Maeda, *J. Org. Chem.*, **45**, 3229 (1980).

Strong Embedding Effect of Decalin Walls on Cation Complexation in Crown Ethers

Kazuya KOBIRO,* Mitsuru TAKAHASHI, Shigeki TAKADA, Yoshinobu ODAIRA, and Yoshikane KAWASAKI
Department of Applied Fine Chemistry, Faculty of Engineering, Osaka University, Suita, Osaka 565
(Received July 15, 1985)

Synopsis. Cylindrical crown ether, tridecalino-18-crown-6, shows strong embedding effect toward coordinated thallium ion.

Increasing attention has been paied to the host molecules such as cryptands,[1] spherands,[2] and cavitands,[2] which have not only high complexing ability but also high complexing selectivity. In this context, we designed a new class of cylindrical crown ether with bicycloalkane walls.[3] In this cylindrical system, it is expected that the coordinated metal ion may be embedded strongly by bicycloalkane moieties spread out above and below the crown ether ring. In this paper, we wish to report on strong embedding effect of three decalin moieties of tridecalino-18-crown-6† (**1**).

Results and Discussion

In the present cylindrical system, the embedding effect of bicycloalkane moieties constructing cylinder wall on complexation of cations can be estimated by the differences in magnitude between total stability of complexes and coordination ability of ethereal oxygen atoms. From the above concept, we selected thallium(I) and dimethylthallium(III) ions as stability and coordination probes, respectively, because it is well-known that the ionic radius of thallium(I) ion (1.40 Å)[4] and that of dimethylthallium(III) ion (1.25 Å)[5] are very close to that of potassium (1.33 Å)[4] and that the larger spin-spin coupling constants between thallium nucleus and methyl protons reflect the stronger coordination ability of ligands surrounding cation.[6]

First, spin-spin coupling constants between thallium nuclei and methyl protons of dimethylthallium (III) ion complexes were measured to estimate coordination ability of oxygens. As shown in Table 1, the cylindrical crown ethers, **1**, didecalino-18-crown-6 (**2**), and dibicyclooctano-18-crown-6† (**3**) had larger coupling constants than that of 18-crown-6 (**4**). These strong coordinations of cylindrical crown ether oxygens are ascribed to the location of oxygen atoms at the entropically favorable positions before and after complexation.

Next, complexation constants, K_c, were measured to determine total complex stabilities in chloroform according to Kimura's method.[7b,8] As is indicated in Table 1, these crown ethers showed similar complexing behavior toward potassium and thallium(I) ions.[9] Interestingly, tridecalino-18-crown-6 (**1**) having similar coordination ability to **2** gave ten-fold larger stability than that of **2** in chloroform. From these results, it may be concluded that total stability of complexes is mainly influenced by the bicycloalkane moieties of cylindrical system and, in addition, three decalin walls exhibit efficient embedding effect toward coordinated thallium ion.

TABLE 1. THE VALUES OF COUPLING CONSTANTS, J(Tl-CH$_3$), OF COMPLEXES AND COMPLEXATION CONSTANTS, K_c

Crown ether	J(Tl-CH$_3$)/Hz[a]	log K_c	
	δ	K$^+$	Tl$^+$
None	400(1.23)		
1	435(1.24)[b]	10.07	9.36
2	434(1.15)	9.36	8.26
3	440(0.93)	9.37	8.28
4	430(0.89)		
5[c]	417(0.90)	7.46	6.22

a) In CD_3CN, 100 MHz spectra unless otherwise stated. b) In CD_3CN, 60 MHz spectrum. c) Dibenzo-18-crown-6.

TABLE 2. EXTRACTION CONDITIONS

Crown ether	Metal ion	Concentration/mol dm^{-3}	
		(CE)°	M°
1	K$^+$, Tl$^+$	1×10^{-4}	$1-5\times10^{-4}$
2, 3	K$^+$	1×10^{-4}	$0.2-1\times10^{-4}$
2, 3	Tl$^+$	1×10^{-4}	$1-5\times10^{-4}$
5[a]	K$^+$, Tl$^+$	1×10^{-4}	$1-5\times10^{-3}$

a) Dibenzo-18-crown-6.

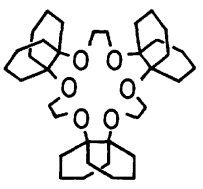

1

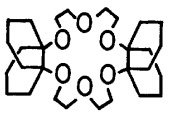

2

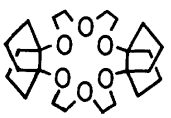

3

Experimental

^{1}H NMR specra were taken with JEOL JMN-PS-100 (100 MHz) and HITACHI R-600S (60 MHz) spectrometers in CD_3CN solutions with Me_4Si as an internal standard.

†Ortho fused cyclic compounds are tentatively named "decalino" and "bicyclooctano" for decahydronaphtho[4*a*,8*a*,] and octahydropentaleno[3*a*,6*a*], respectively.

Electronic spectra were measured on a HITACHI 356 spectrophotometer.

Tridecalino-18-crown-6 (1). **1** was prepared from 1,2:7,8-didecalino-3,6-dioxaoctane-1,8-diol and 4,5-decalino-3,6-dioxaoctane-1,8-diol ditosylate by the method similar to that described previously[3b] and recrystallized from 1,2-dimethoxyethane (29%): mp 197—198 °C; IR (KBr) 1100, 1090 cm^{-1}, ^1H NMR ($CDCl_3$) δ=1.00—2.48 (m, 48H), 3.20—4.08 (m, 12H); ^{13}C NMR ($CDCl_3$, 60 °C) δ=21.7 (t, 6C), 23.0 (t, 6C), 30.8 (t, 6C), 61.7 (t, 6C), 78.0 (s, 6C); MS *m/z* 588 (M^+). Found: C, 73.30; H, 10.34%. Calcd for $C_{36}H_{52}O_6$: C, 73.43; H, 10.27%.

Dibicyclooctano-18-crown-6 (3). **3** was prepared from *cis*-bicyclo[3.3.0]octane-1,5-diol as described previously[3a] and recrystallized from ether: mp 73—75 °C; IR (KBr) 1150, 1120, 1090 cm^{-1}; ^1H NMR ($CDCl_3$) δ=1.12—2.20 (m, 24H), 3.65 (br s, 16H); ^{13}C NMR ($CDCl_3$) δ=21.8 (t, 4C), 36.9 (t, 8C), 64.1 (t, 4C), 71.1 (t, 4C), 91.7 (s, 4C); MS *m/z* 424 (M^+). Found: C, 67.67; H, 9.56%. Calcd for $C_{24}H_{40}O_6$: C, 67.89; H, 9.50%.

Preparation of Crown Ether Complexes with Dimethylthallium(III) Perchlorates. Complexes were prepared by the method similar to that described previously[5] in an appropriate solvent (2-propanol, acetone, or acetonitrile-d_3) and purified by recrystallization from acetone/peteroleum ether or dichloromethane/hexane.

Metal Picrates. Potassium and thallium picrates were prepared according to the described methods.[7]

Extraction. The extraction procedures were similar to those described by Kimura.[7b,8] Equal volumes (10 ml) of chloroform solution of crown ether and aqueous metal picrate solution were placed in a stoppered flask and shaken for 40 min at 25±0.1 °C. After the phase separated, aliquots varying from 0.50 to 8.00 ml of organic phase (depending on its color intensity) were very carefully removed from organic phase and evaporated to dryness. Aliquots varying from 4.00 to 20.00 ml of acetonitrile were added to the residue. Then concentration of the metal complex with crown ethers were determined spectrophotometrically. In the case of thallium picrate, a mixture of equal volumes of chloroform and acetonitrile was employed as a solvent for spectrophotometry, because a considerable amount of uncomplexed crown ether which was insoluble in acetonitrile existed. The molar absorptivities of picrates were 1.50×10^4 mol dm^{-3} cm^{-1} for potassium and thallium(I) picrates at 374 nm.

Calculations. The extraction equilibirium constant, K_e, for 1:1 crown ether/metal ion complexes is defined by

$$M^+_{aq} + Pic^-_{aq} + CE_{org} \rightleftharpoons M(CE)Pic_{org}$$

$$K_e = \frac{[M(CE)Pic]_{org}}{[M^+]_{aq}[Pic^-]_{aq}[CE]_{org}} \quad (1)$$

where M^+, Pic^-, and CE are metal ion, picrate anion, and crown ether, respectively. The existence of uncomplexed crown ether and complexed crown ether in aqueous solution is negligible, because these cylindrical crown ethers have very lipophilic bicycloalkane moieties. Therefore, the following assumption can be made:

$$D = [M(CE)A]_{org}/[M^+]_{aq} \quad (2)$$

$$[M^+]_{aq} = [Pic^-]_{aq} = M^\circ - A \quad (3)$$

$$[CE]_{org} = (CE)^\circ - A, \quad (4)$$

where M° and $(CE)^\circ$ denote the initial alkali metal ion and initial crown ether concentration, respectively, and A the concentration of picrate transferred to the chloroform solution. Then Eq. 1 is rewritten as follows:

$$D = K_e(M^\circ - A)[(CE)^\circ - A]. \quad (5)$$

The K_e values were calculated directly by Eq. 5 and checked by the slope of the plots, log D *vs.* log $(M^\circ - A)[(CE)^\circ - A]$, being unity.

The distribution and complexing constants, K_d and K_c, respectively, are defined by

$$M^+_{aq} + Pic^-_{aq} \rightleftharpoons MPic_{org}$$

$$K_d = \frac{[MPic]_{org}}{[M^+]_{aq}[Pic^-]_{aq}} \quad (6)$$

$$MPic_{org} + CE_{org} \rightleftharpoons M(CE)Pic_{org}$$

$$K_c = \frac{[M(CE)Pic]_{org}}{[MPic]_{org}[CE]_{org}} \quad (7)$$

$$K_e = K_c/K_d. \quad (8)$$

The K_c values are estimated form Eq. 8. The reported K_d values (K^+ 2.67×10^{-3} and Tl^+ 4.68×10^{-2}) were quoted for K_c calcuration.[7b,8]

Extraction conditions were listed in Table 2.

References

1) F. Kotzyba-Hibert, J. M. Lehn, and P. Vierling, *Tetrahedron Lett.*, **1980**, 941.

2) D. J. Cram and J. M. Cram, "Designed Complex-Science and Application," in "Selectivity- a Goal for Synthetic Efficiency," ed by W. Bartmann and B. M. Trost, Verlag Chimie Weinheim (1984), pp. 43—64.

3) a) K. Kobiro, Y. Tanaka, K. Okubo, Y. Hiramatsu, K. Kakiuch, Y. Tobe, and Y. Odaira, *Chem. Lett.*, **1983**, 1507; b) K. Kobiro, K. Ohnishi, K. Kakiuchi, Y. Tobe, and Y. Odaira, *Bull. Chem. Soc. Jpn.*, **58**, 1333 (1985).

4) R. M. Izatt, D. J. Eatoug, and J. J. Christiansen, "Thermodynamics of Cation-Macrocylic Compound Interaction," in "Structure and Bonding," ed by J. D. Dunitz, P. H. Konstanz, C. K. Jorgensen, and D. R. Marburg, Springer-Verlag, Berlin (1973), Vol 16, pp. 161—189.

5) Y. Kawasaki and R. Kitano, *Chem. Lett.*, **1978**, 1425.

6) G. D. Shier and R. S. Drago, *J. Organomet. Chem.*, **5**, 330 (1966); Y. Kawasaki and M. Aritomi, *ibid.*, **104**, 39 (1976); P. J. Burke, R. W. Matthews, and D. G. Gillies, *ibid.*, **118**, 129 (1976).

7) a) M. A. Coplan and R. M. Fuoss, *J. Phys. Chem.*, **68**, 1177 (1964); b) T. Maeda, K. Kimura, and T. Shono, *Fresenius' Z. Anal. Chem.*, **298**, 363 (1979).

8) K. Kimura, T. Maeda, and T. Shono, *Talanta*, **26**, 945 (1979).

9) The similar tendency was observed for silver ion.

A HPLC Study of Adsorption of Organic Solutes on Cellulose Acetate

Yoshiaki Kiso
Laboratory of Sanitary Engineering, Faculty of Engineering, Toyohashi University of Technology, Tenpaku-cho, Toyohashi 440
(Received June 26, 1985)

Synopsis. The liquid chromatographic technique was useful for the measurement of adsorption of some nonionic organic solutes on cellulose acetate. It was recognized that there were linear correlations between logarithmic capacity factors measured by HPLC, log k', and logarithmic 1-octanol: water partition coefficients, log P.

In the reverse osmosis process, the adsorption of organic solutes on a cellulose acetate membrane is assumed to be important for the permeabilities of the solutes and the membrane fouling.[1-3] The interaction between cellulose acetate (CA) and some organic or inorganic solutes has been investigated with the high performance liquid chromatograhy (HPLC).[4,5] Y. Taketani *et al.*[4] estimated the distribution coefficients for solutes between the stationary phase around CA and the bulk phase, K_A'. The values of K_A' for some organic solutes were more than unity. These results rather suggested that the organic solutes were adsorbed on the CA surface. However, the factors affecting the adsorption of organic solutes on the CA surface were known little. The objects of this work are to confirm the usefulness of liquid chromatography for the measurement of adsorption characteristics and to examine the effects of molecular structures on adsorption.

Experimental

The HPLC column was prepared by packing cellulose acetate (acetyl content 39.8%, Kodak 4644, 200/325 mesh) into a stainless steal column (I. D.=4.6 mm, L=250 mm). The moving phase was water and a solvent velocity was 0.5 ml min^{-1}. The HPLC apparatus used was a Toyosoda HLC-803A connected with a RI detector. The solutes used for this study were listed in Table 1. The concentrations of organic solutes in sample solution were less than 1%. The capacity factor for each solute, k', was calculated by the following equation;

$$k' = (t_i - t_0)/t_0, \quad (1)$$

where t_i and t_0 are the retention times of solute i and D_2O, respectively.

Results and Discussion

The capacity factors of all alcohols and ketones in Table 1 were positive and these solutes seemed to be adsorbed on CA. It was also recognized that more hydrophobic solutes were adsorbed more. However, more hydrophobic compounds such as benzene, nitrobenzene or acetophenone did not elute and seemed to be adsorbed strongly on CA. These facts suggested that these HPLC conditions were useful for the measurement of relatively weak interaction between CA and organic solutes. From these results, it was attempted to correlate log k', with logarithmic 1-octanol: water partition coefficients,[6] log P, logarithmic activity coefficients at infinite dilution calculated by the UNIFAC method,[7] ln γ^∞, or the connectivity index,[8] $^1\chi^v$. These results were shown in Figs. 1, 2, and 3.

In the cases of ketones except acetyl acetone and aliphatic alcohols except 2-methyl-2-propanol, it was recognized that log k' was related linearly to log P as follows:

$$\text{1-alkanols; } \log k' = 0.675 \log P - 0.914 \quad (N = 9,\ r = 0.9961) \quad (2)$$

$$\text{2-alkanols; } \log k' = 0.699 \log P - 1.048 \quad (N = 5,\ r = 0.9986) \quad (3)$$

$$\text{ketones; } \log k' = 0.613 \log P - 0.451 \quad (N = 9,\ r = 0.9901) \quad (4)$$

Table 1. Organic solutes

No.	Solute	log P[a]	lnγ^∞[b]	$^1\chi^v$[c]	No.	Solute	log P[a]	lnγ^∞[b]	$^1\chi^v$[c]
1	Methanol	−0.77	—	0.447	16	2-Hexanol	1.76[d]	10.326	2.951
2	Ethanol	−0.31	1.637	1.023	17	2-Methyl-2-propanol	0.35	—	1.724
3	1-Propanol	0.25	3.397	1.523	18	2-Ethyl-2-propanol	0.89	—	2.284
4	1-Butanol	0.88	5.176	2.023					
5	1-Pentanol	1.56	6.954	2.523	20	Acetone	−0.24	2.984	1.204
6	1-Hexanol	2.03	8.735	3.023	21	2-Butanone	0.29	4.738	1.765
7	2-Methyl-1-propanol	0.65	5.173	1.879	22	2-Hexanone	1.38	8.224	2.765
8	2-Ethyl-1-propanol	1.42	6.954	2.379	23	3-Methyl-2-butanone	0.71[d]	6.481	2.148
9	2-Methyl-1-hexanol	2.44[d]	10.505	3.417	24	4-Methyl-2-pentanone	1.15[d]	8.221	2.621
10	Benzyl alcohol	1.10	5.374	2.841	25	3-Pentanone	0.83[d]	6.484	2.325
11	*dl*-1-Phenylethanol	1.36	7.605	3.195	26	Cyclopentanone	0.37	5.311	2.411
12	Cyclohexanol	1.23	9.077	3.117	27	Cyclohexanone	0.81	7.054	2.911
13	2-Propanol	0.05	4.866	1.413	28	4-Methylcyclohexanone	1.35[d]	8.790	3.305
14	2-Butanol	0.61	6.701	1.951	29	Acetophenone	1.58	7.189	2.865
15	2-Pentanol	1.29[d]	8.520	2.451	30	Acetyl acetone	0.34	1.886	1.911

a) 1-Octanol: water partition coefficient.[6] b) Logarithmic activity coefficient at infinit dilution calculated by the UNIFAC method.[7] c) Connectivity Index.[8] d) Calculated value.

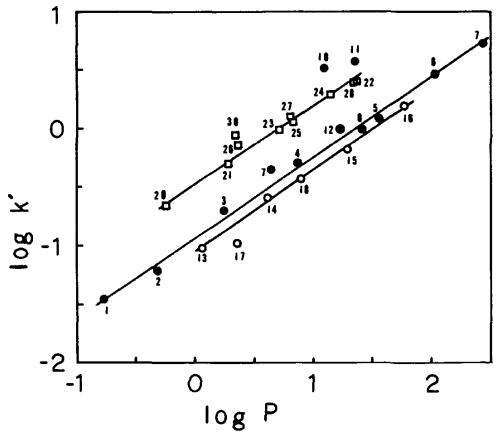

Fig. 1. The relationship between log P and log k' (numbers in figure mean the solute numbers).
●; 1-alkanol, ○; 2-alkanol, □; ketone.

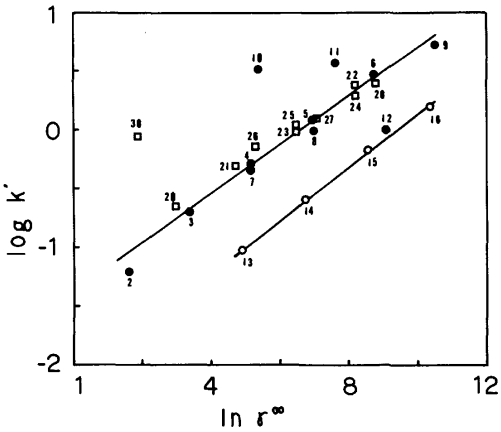

Fig. 2. The relationship between ln γ^{∞} and log k'.

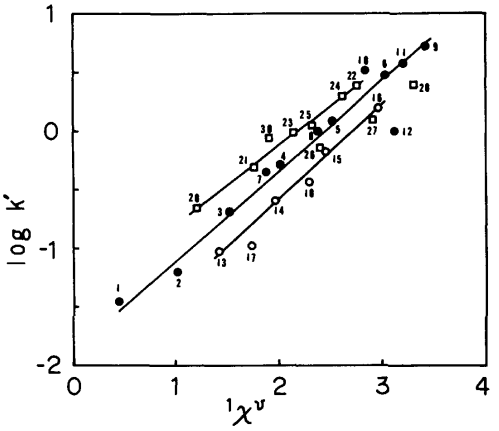

Fig. 3. The relationship between connectivity index $^1\chi^v$ and log k'.

These results indicated that the adsorption of organic solutes was controlled by the hydrophobicity of solutes and that the effect of hydrophobicity in these solutes was equivalent because the slopes in these equations were almost equal. These results showed that the functional group affected the adsorption, because the intercept of ketones was larger than that of alcohols and acetyl acetone was above the line of ketones in Fig. 1. It was assumed that the steric factors also influenced the adsorption from the following results; (a) the intercept of 2-alkanols was a little less than 1-alkanols, and (b) the log k' value of 2-methyl-2-propanol was less than the value estimated by Eq. 3.

Table 2. Solutes eluted earlier than D_2O

Solute	Retention time/min
D_2O	6.27
NaCl	5.57
Glucose	5.65
Lactose	5.57
Tween-20	5.51
PEG(#6000)	5.35
PVP(K-90))	4.35

The log k' values of benzyl alcohol and dl-1-phenylethanol were larger than those estimated by using Eq. 2. Acetophenone, nitrobenzene and benzene, whose log P values were 1.58, 1.85, and 2.15 respectively, did not elute under these conditions. These results suggested that the phenyl group was adsorbed more easily than the aliphatic group. Considering the results of aromatic compounds and ketones, it was assumed that unsaturated bonds in solutes also affected the adsorption on CA.

The relationship between log k' and ln γ^{∞} or $^1\chi^v$ was also linear as shown in Figs. 2 or 3, and these tendencies were similar to those in Fig. 1. From these results, it was assumed that the adsorption of organic solutes on CA was able to be correlated with some free energy parameters or some structure parameters.

The results for solutes whose retention time was less than that of D_2O are shown in Table 2. Glucose and lactose, the most hydrophilic solutes, were not adsorbed on CA. Polymer solutes (PEG and PVP) and Tween-20, which caused the membrane fouling,[3] were not adsorbed on CA and it seems that the retention time of these solutes decreased as molecular weight increased. Y. Taketani *et al.*[4] showed a similar tendency by using PEG. These facts seem to be caused by the size exclusion effect, because the large specific area of CA[4] suggested that there are many micro pores on the surface of cellulose acetate particles.

The author is greatly indebted to Dr. Toshio Sugita for HPLC available for this study.

References

1) T. Matsuura and S. Sourirajan, *J. Appl. Polym. Sci.*, **17**, 3683 (1973).
2) C. Kamiszawa and S. Ishizaka, *Bull. Chem. Soc. Jpn.*, **45**, 2967 (1972).
3) Y. Kiso, T. Kitao, M. Sugahara, and Y. Terashima, *Nippon Kagaku Kaishi*, **1981**, 1805.
4) Y. Taketani, T. Matsuura, and S. Sourirajan, *Separation Sci. Technol.*, **17**, 821 (1982).
5) H. Nomura, S. Yoshida, M. Senō, H. Takahashi, and T. Yamabe, *J. Appl. Polym. Sci.*, **22**, 2609 (1978).
6) C. Hansch and A. Leo, "Substituent Constants for Correlation Analysis in Chemistry and Biology," John Wiley & Sons, Inc., New York (1979).
7) A. Fredenslund, R. L. Jones, and J. M. Praunsnizt, *AIChE J.*, **21**, 1086 (1975).
8) L. B. Kier and L. H. Hall, "Molecular Connectivity in Chemistry and Drug Research," Academic Press (1976).

Reaction of Leucomalachite Green with Chloranil

Norio NISHIMURA* and Takushi MOTOYAMA
Department of Chemistry, School of Science, Okayama University, Tsushima, Okayama 700
(Received February 25, 1985)

Synopsis. The reaction of Leucomalachite Green with chloranil to produce Malachite Green cations has been carried out in acetonitrile. Prior to the formation of the cations, a 1:1 CT complex is formed between the reactants. The equilibrium and the rate constants were estimated.

In preceding papers,[1,2] the proton/deuteron transfer reactions of Leucocrystal Violet (LCV) with tetracyanoethylene (TCNE) and chloranil (CA) under high pressures and in various solvents have been reported. It was concluded that both reactions probably proceed *via* an outer CT complex followed by a pair of radical ions. However, the electronic spectra assigned to the complex were observed only at low temperatures. This made the accurate estimation of thermodynamic quantities impossible.

This paper is concerned with the reaction of Leucomalachite Green (LMG) with CA. When the acetonitrile solutions of LMG and CA were mixed, a broad absorption spectrum ($\lambda_{max}\approx670$ nm) appeared at room temperatures. The color becomes deep upon cooling. Similar phenomena were observed in various solvents and LMG–TCNE system, too. Therefore, this blue-colored substance can be assigned to the CT complex formed between LMG and CA. The equilibrium constant K_1 for the formation of the complex was estimated by means of the Lang plot and checked by the Benesi-Hildebrand (B-H) plot modified as follows:

$$\frac{[\mathrm{LMG}]_0[\mathrm{CA}]_0}{A([\mathrm{LMG}]_0+[\mathrm{CA}]_0-A/\varepsilon)}=\frac{1}{([\mathrm{LMG}]_0+[\mathrm{CA}]_0-A/\varepsilon)}\cdot\frac{1}{K\varepsilon}+\frac{1}{\varepsilon}, \quad (1)$$

where A is the absorbance at 720 nm (1 cm cell), and ε is the molar extinction coefficient at this wavelength. In this study, the concentration ranges were: $[\mathrm{LMG}]_0=(2.5—12.8)\times10^{-3}$ mol dm^{-3}, $[\mathrm{CA}]_0=(7.9—10.4)\times10^{-3}$ mol dm^{-3}. The Lang and the modified B-H plots were repeated until an assumed pair of ε and K values became self-consistent. The results are given in Table 1.

The rate of reactions was followed by monitoring the absorbance at 620 nm which is assigned to Malachite Green cations (MG^+). Within the time interval of the kinetic measurement, the absorbance at 720 nm has not changed appreciably. This made the simultaneous estimations of the equilibrium and the rate constants possible. Figure 1 shows the time dependence of the absorption spectrum. The broad line at the bottom (500—900 nm) is due to the CT complex[3] (denoted as LMG→CA hereafter). It was found that the rate of appearance of MG^+ at the initial stage (conversion<0.5%) follows the overall second-order kinetics:

Table 1. Equilibrium constants and thermodynamic parameters for the formation of the CT complex in the LMG–CA system

Temp	$10^{-3}K_1\varepsilon$	K_1
°C	dm^6 mol^{-2} cm^{-1}	dm^3 mol^{-1}
15	3.03±0.04	6.70±0.74
20	2.67±0.06	5.90±0.69
25	2.28±0.02	5.04±0.52
30	2.02±0.01	4.46±0.45
ε/dm^3 mol^{-1} cm^{-1}=452±43		
ΔH/kJ mol^{-1}=−20.1±0.4		
ΔS(298K)/J mol^{-1} K^{-1}=−51.6±2.9		

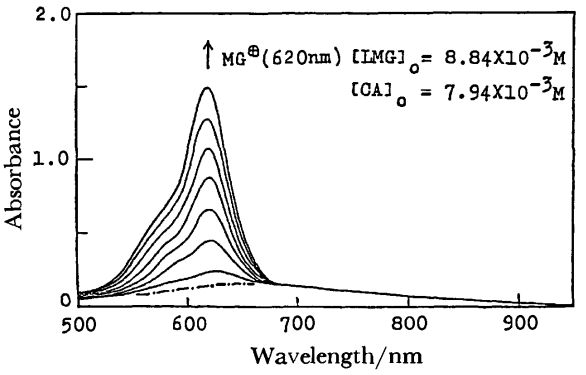

Fig. 1. Time dependence of the absorption spectrum for the reaction of LMG with CA in acetonitrile at 25 °C. Time intervals are 5 min.

$$\mathrm{d}[\mathrm{MG}^+]/\mathrm{d}t=k_{obsd}[\mathrm{LMG}]_0[\mathrm{CA}]_0 \quad (2)$$

If the proposed mechanism for the LCV–TCNE and LCV–CA systems[2] is valid for the LMG–CA system, too, the reaction route may be as follows:

$$\mathrm{LMG}+\mathrm{CA}\underset{\text{fast}}{\overset{K_1}{\rightleftharpoons}}\mathrm{LMG}\longrightarrow\mathrm{CA}\overset{K_2}{\underset{\text{fast}}{\rightleftharpoons}}$$

$$(\mathrm{LMG})^{+\cdot}(\mathrm{CA})^{-\cdot}\xrightarrow[\text{slow}]{k_1}\mathrm{MG}^+ + \cdots$$

From the above scheme, k_{obsd} can be expressed by

$$k_{obsd}=K_1K_2k_1=K_1k. \quad (3)$$

The kinetic data and the activation parameters are given in Table 2. Figure 2 shows the energy profile. The numerical value in parenthesis is the one assumed for the LCV–CA system.[2]

It is interesting to compare the above results with those for the LCV–CA system. There are two notable points. The equilibrium constant K_1 for the formation of the CT complex is considered considerably

TABLE 2. RATE CONSTANTS k_{obsd} AND k DEFINED BY Eq. 3 AND THE ACTIVATION PARAMETERS RELATED TO k

Temp	$10^4 k_{obsd}$	$10^5 k$
°C	$dm^3 mol^{-1} s^{-1}$	s^{-1}
15	0.396±0.033	0.59±0.11
20	0.654±0.005	1.11±0.15
25	1.02 ±0.02	2.02±0.25
30	1.54 ±0.03	3.45±0.48
$\Delta H^{\neq}$(300K)/kJ mol^{-1}=83.6±0.8		
$\Delta S^{\neq}$(300K)/J $mol^{-1} K^{-1}$=−54.7±3.0		

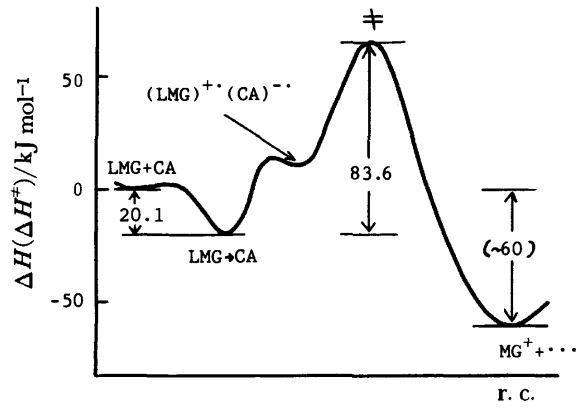

Fig. 2. Energy profile for the reaction of LMG with CA.

larger for the LMG–CA system than for the LCV–CA system, as judged from the spectral intensity observations. The second point is the k_{obsd}-value is about 10^3times smaller than that for the LCV–CA system (0.11 $dm^3 mol^{-1} s^{-1}$ at 25 °C). The $\Delta H^{\neq}$ and $\Delta S^{\neq}$ for the LCV–CA system in acetonitrile are 27.9 kJ mol^{-1} and −169 J $mol^{-1} K^{-1}$, respectively.[4] The above distinctive points are difficult to interpret in connection with the structural difference between LMG and LCV alone. We tentatively measured the ^{1}H NMR spectra and examined the chemical shift of the hydrogen being abstracted. The data are as follows: δ=2.18 in CCl_4, 2.58 in $CDCl_3$, and 3.74 in CD_3CN (s, 1H) for LMG. These values may be compared with the normal values δ=5.10—5.54 (s, 1H) for triphenylmethane, 4-diphenylmethyl-*N*,*N*-dimethylbenzenamine, and LCV, for which the solvent dependency on δ was small. The extraordinarily high-field shift and its very large solvent dependence for LMG alone in this series of compounds are very hard to interpret, and therefore require more fundamental investigations aside from this work. What we now can say is that if this high-field shift is due to the electronic effect (charge shift), it would give rise to the large K_1-value and hence the large activation energy compared with those for the LCV–CA system.

Experimental

Commercial LMG and CA were recrystallized twice from a benzene–ethanol mixture. Solvents were purified as usual manners. A Union 401 spectrophotometer was used for spectral measurements. The temperature was regulated within ±0.1 K. ^{1}H-NMR spectra were recorded on a Hitachi R-600 FT NMR spetrometer.

References

1) N. Nishimura and T. Motoyama, *Bull. Chem. Soc. Jpn.*, **57**, 1 (1984).

2) N. Nishimura and T. Motoyama, *Bull. Chem. Soc. Jpn.*, **58**, 1013 (1985).

3) There is a possibility of the existence of two kinds of CT complexes: CT_1(R′→CA, R′=phenyl) and CT_2(R→CA, R=*p*-dimethylaminophenyl). As far as the electronic spectrum was examined, no distinction was observed. If it is assumed that the equilibrium constant of CT_1 is similar to that for benzene-CA system (0.35 dm^3 mol at 25 °C[5]), K_1 in Table 1 may be regarded as the one for CT_2.

4) N. S. Isaacs, K. Javaid, and E. Rannale, *J. Chem.Soc. Perkin 2*, **1978**, 709 (data recalculated).

5) S. Fukuzumi and J. K. Kochi, *J. Org. Chem.*, **46**, 4116 (1981).

Laser Photolysis Study on the Duroquinone-photosensitized Isomerization of Stilbenes in Micellar Solution

Yoshifumi TANIMOTO,* Masanari TAKAYAMA, Sayaka SHIMA, and Michiya ITOH
Faculty of Pharmaceutical Sciences, Kanazawa University, Takara-machi, Kanazawa 920
(Received April 4, 1985)

Synopsis. Photoinduced electron-transfer reaction between the excited triplet duroquinone and *trans*- and *cis*-stilbenes generates *trans*-stilbene cation radical in SDS micellar solution, suggesting that the *cis-trans* isomerization of stilbene occurs *via* an electron-transfer mechanism.

Recently, an increasing interest has been paid to the photosensitized isomerization of stilbenes in electron-transfer reactions.[1-5] In the present paper, we have studied a photoinduced electron-transfer reaction between duroquinone and stilbenes in sodium dodecyl sulfate (SDS) micellar solution by nanosecond laser flash photolysis. It is shown that the electron-transfer from both *trans*- and *cis*-stilbenes to the excited triplet duroquinone generates only the *trans*-stilbene cation radical in the nanosecond timescale; the *cis-trans* photoisomerization of stilbene mostly occurs *via* an electron-transfer mechanism.

Experimental

Duroquinone (DQ) and *trans*-stilbene (TS) were purified by recrystallization. *cis*-Stilbene (CS) was purified by distillation; its purity was determined to be >95% by gas chromatography. Sodium dodecyl sulfate (for biological use, SDS) was used as supplied. Water was distilled and deionized.

The laser flash photolysis measurements were carried out in deaerated solutions at room temperature using a Molectron UV-12 N_2 laser (337 nm) as the exciting light source.[6]

Results and Discussion

Figure 1 shows transient absorption spectra of SDS micellar solutions containing DQ and stilbenes. In the absence of stilbenes, a weak triplet-triplet absorption of DQ appears in the 400—500 nm region.[7,11] In the presence of TS, a new intense band appears at ≈480 nm (the growth and decay rates are 1.1×10^6 and 1.5×10^4 s^{-1}, respectively), which is assigned to the TS cation radical (TS^+).[8] In contrast to this, no appreciable transient absorption due to TS^+ is observed in acetonitrile solution. In the aqueous micellar solution both DQ and TS are mostly solubilized in the micellar phase, since they are almost insoluble in water. This local high concentration of solute molecules in the micellar phase leads to a high efficiency of the electron transfer reaction in the micellar solution. From the plots of the growth rate *versus* the TS concentration shown in Fig. 2A, the apparent bimolecular electron-transfer rate constant was estimated to be 1.6×10^9 $mol^{-1}dm^3s^{-1}$ in the present micellar solution. The intercept in the figure deviates slightly from the origin. This is mostly due to the contamination of the T-T absorption intensity of DQ at the lower TS concentrations. Further, the absorption of the duroquinone anion radical (DQ^-), a counter radical, is expected to occur in the 400 nm region.[7] However, it is not observed clearly because of overlap with the absorption bands of the excited triplet duroquinone ($^3DQ^*$) and the TS^+ radical in this wavelength region. The TS^+ radical is mostly formed *via* the photoinduced electron-transfer reaction between $^3DQ^*$ and TS.

On the other hand, in a solution containing DQ and

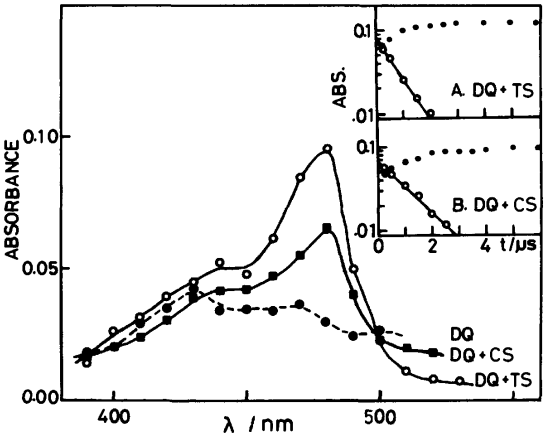

Fig. 1. Transient absorption spectra of 0.4 mol dm^{-3} SDS micellar solutions containing 6×10^{-4} mol dm^{-3} DQ (---●---), DQ and 4×10^{-4} mol dm^{-3} TS (—○—), and DQ and 3×10^{-4} mol dm^{-3} CS (—■—), at 1 μs delay after laser excitation. Inserts show typical time profiles of the absorption intensities at 480 nm for the solutions containing DQ and TS, (A), and DQ and CS, (B).

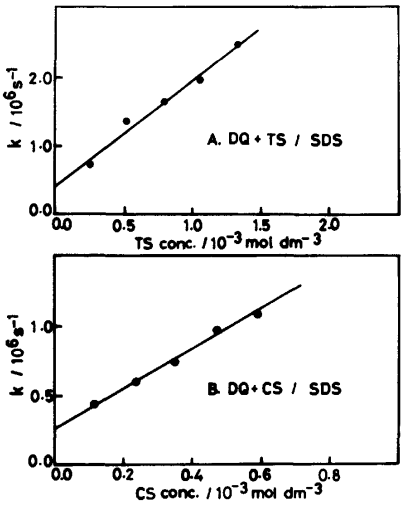

Fig. 2. Concentration dependence of the growth rate, k, of the 480 nm band for TS, (A) and CS, (B). The concentrations of SDS and DQ were 0.4 and 5×10^{-3} mol dm^{-3}, respectively.

CS, a band appears at ≈480 nm (the growth and decay rates are 0.7×10^6 and 1.5×10^4 s^{-1}, respectively) as shown in Fig. 1, though the absorption of CS^+ is reported to appear at 515 nm.[8] Since the band is similar to that of TS^+ in the figure, it is assigned to the TS^+ radical. In the photolysis of the micellar solution of DQ and CS, the $CS^+\rightarrow TS^+$ isomerization occurs rapidly, since no appreciable absorption due to CS^+ appears in the nanosecond timescale. The apparent bimolecular rate constant for CS was found to be 1.5×10^9 mol^{-1} dm^3 s^{-1} (see Fig. 2B). This is almost the same as that for TS.

The unusual $CS^+\rightarrow TS^+$ isomerization has been reported for the photobleaching of CS^+ in CCl_4 rigid glass at low temperature,[8] for the 9,10-dicyanoanthracene-sensitized oxidation of CS in acetonitrile,[2] and for the electron impact of CS.[9] The present result clearly demonstrates that the TS^+ radical is also produced by the electron transfer reaction between the excited triplet DQ and CS, whereas generation of TS^+ *via* a singlet-sensitized reaction is well known.[2]

Furthermore, the formation of CS was detected in a gas chromatograph of the photolysed solution of DQ and TS. The fact suggests that *trans-cis* isomerization of stilbene occurs *via* an electron-transfer mechanism, though triplet sensitized isomerization of stilbene *via* an energy transfer mechanism is well known.[10]

The photoreaction of DQ with TS may be interpreted in the following scheme:[1,3]

$$DQ \xrightarrow{h\nu} {}^1DQ^* \longrightarrow {}^3DQ^* \quad (1)$$

$${}^3DQ^* + TS \longrightarrow {}^3(DQ^{\cdot}TS^{+}) \quad (2)$$

$${}^3(DQ^{\cdot}TS^{+}) \rightleftharpoons {}^1(DQ^{\cdot}TS^{+}) \quad (3)$$

$${}^3(DQ^{\cdot}TS^{+}) \longrightarrow DQ + {}^3TS^* \quad (4)$$

$${}^3(DQ^{\cdot}TS^{+}) \longrightarrow DQ^{\cdot} + TS^{+} \quad (5)$$

$${}^1(DQ^{\cdot}TS^{+}) \longrightarrow DQ + TS \quad (6)$$

$${}^1(DQ^{\cdot}TS^{+}) \longrightarrow DQ^{\cdot} + TS^{+} \quad (7)$$

In the micellar solution of DQ and TS, the electron-transfer between $^3DQ^*$ and TS generates a triplet pair of DQ^- and TS^+, $^3(DQ^-\ TS^+)$. Here, we assume the radical ion pair as an intermediate by analogy with the electron-transfer reaction of DQ and diphenylamine in SDS micellar solution.[11] It is expected that there are three processes from the triplet pair; *i.e.*, intersystem crossing to the singlet pair, (3), back electron-transfer to generate the excited triplet TS, (4), and separation into free radicals, (5). *trans-cis* Isomerization may occur *via* the excited triplet TS as suggested by Leshina *et al.*[3]

On the other hand, in the micellar solution of DQ and CS, electron-transfer between $^3DQ^*$ and CS generates a triplet pair of DQ^- and CS^+, $^3(DQ^-\ CS^+)$, followed by a rapid isomerization:

$${}^3DQ^* + CS \longrightarrow {}^3(DQ^{\cdot}CS^{+}) \longrightarrow {}^3(DQ^{-}TS^{+}) \quad (8)$$

After the generation of $^3(DQ^-\ TS^+)$, the reaction processes are similar to those mentioned above. Furthermore, since the lifetime of TS^+ is relatively long (≈65 μs), an apparent *cis-trans* isomerization of TS^+ may also occur *via* an electron hole transfer from CS to TS^+ as an inter-micellar process, as proposed for the $[Ru(bpy)_3]^{2+}$ sensitized isomerization of stilbazole in SDS solution,[4] and for the singlet 9,10-dicyanoanthracene-sensitized isomerization of CS in acetonitrile:[5]

$$TS^{+} + CS \longrightarrow TS + CS^{+} \quad (9)$$

Furthermore, the observation of the magnetic field effect (1 T) on the transients was attempted in these micellar solutions. However no detectable effect was observed, suggesting that the triplet-singlet intersystem crossing of the radical ion pair is not the rate-determining step in the reaction. The magnetic field effects on the photosensitized isomerization of stilbene in organic solvents[3] and on the electron-transfer between the excited duroquinone and diphenylamine in SDS solution[11] are reported.

Finally, we believe that the present transient spectroscopic results indicate the importance of $CS^+\rightarrow TS^+$ isomerization in the triplet sensitized electron-transfer reaction of stilbenes in micellar solution.

References

1) H. D. Roth and M. L. M. Schilling, *J. Am. Chem. Soc.*, **101**, 1898 (1979); *ibid.*, **102**, 4303 (1980).
2) L. T. Spada and C. S. Foote, *J. Am. Chem. Soc.*, **102**, 391 (1980).
3) T. V. Leshina, K. M. Salikhov, R. Z. Sagdeev, S. G. Belyaeva, V. I. Maryasova, P. A. Purtov, and Yu. N. Molin, *Chem. Phys. Lett.*, **70**, 228 (1980); T. V. Leshina, S. C. Belyaeva, V. I. Maryasova, R. Z. Sagdeev, and Yu. N. Molin, *ibid,*, **75**, 438 (1980).
4) K. Takagi, K. Aoshima, Y. Sawaki, and H. Iwamura, *J. Am, Chem. Soc.*, **107**, 47 (1985).
5) F. D. Lewis, J. R. Petisce, J. D. Oxman, and M. J. Nepras, *J. Am. Chem. Soc.*, **107**, 203 (1985).
6) Y. Tanimoto, H. Udagawa, Y. Katsuda, and M. Itoh, *J. Phys. Chem.*, **87**, 3976 (1983).
7) E. Amouyal and R. Bensasson, *J. Chem. Soc., Faraday Trans, 1*, **72**, 1274 (1976).
8) T. Shida and W. H. Hamill, *J. Chem. Phys.*, **44**, 2375 (1966).
9) R. Gooden and J. I. Brauman, *J. Am. Chem. Soc.*, **104**, 1483 (1982).
10) M. Sumitani, K. Yoshihara, and S. Nagakura, *Bull. Chem. Soc. Jpn.*, **51**, 2503 (1978), and references therein.
11) Y. Tanimoto, K. Shimizu, H. Udagawa, and M. Itoh, *Chem. Lett.*, **1983**, 353.

Phase Diagrams in Binary Systems of Octafluoronaphthalene and Polynuclear Aromatic Compounds

Shigeyoshi MIYAGISHI,* Akira ISOMI, Mayumi IWATA, Tsuyoshi ASAKAWA, and Morie NISHIDA
Department of Industrial Chemistry, Faculty of Technology, Kanazawa University, Kanazawa 920
(Received July 13, 1985)

Synopsis. Solid-liquid phase diagrams were obtained for binary mixtures of octafluoronaphthalene with six polynuclear aromatic compounds, pyrene, phenanthrene, naphthalene, 1,5-naphthylenediamine, anthracene, and phenothiazine, and for mixtures of naphthalene and pyrene. The first four systems all formed well-defined 1:1 molecular complexes with congruent melting points.

In the course of our experiments on the photochemical reaction of octafluoronaphthalene (OFN) with pyrene, we observed that a solid was formed on mixing these two substances in methanol. The solid had a surprisingly high melting point compared with OFN and pyrene. Experimental evidence has indicated that hexafluorobenzene,[1-10] pentafluorobenzene,[4] pentafluorobenzonitrile,[9,11] and decafluorobiphenyl[5] form complexes with aromatic hydrocarbons. OFN has not been reported to produce complexes with the aromatic hydrocarbons except for benzene.[5] On the intermolecular force resulting in formation of such complex, opinions have differed.[5,6] Our attention is being paid to whether perfluoro-aromatic compounds always form molecular complexes with the aromatic hydrocarbons or not, and what kind of force acts between them. As the first step, the phase diagrams of binary mixtures of OFN and several polynuclear compounds were examined.

Experimental

OFN (guaranteed reagent, Tokyo Chemical Industry) was recrystallized from methanol and sublimed *in vacuo*. Pyrene (Katayama Chemicals) was of analytical grade, phenanthrene (Tokyo Chemical Industry) was zone-refined material, and anthracene (Wako Pure Chemical Industries) was a standard reagent. Naphthalene (Katayama Chemicals), 1,5-naphthylenediamine (Wako Pure Chemical Industries), and phenothiazine (Nakarai Chemicals), respectively, were reagent grade.

A mixture of a known composition of OFN and one of the other compounds was made up by weight and dissolved in diethyl ether. After the ether was evaporated at room temperature and atmospheric pressure, a part of the mixture (about 5 mg) was sealed in an aluminum vessel (15 mm^3). Calorimetric experiments were done on a differential scanning calorimeter (Daini-Seikosha DSC-560S).[12] The scanning rate was 5 $K\,min^{-1}$. Repeated heating produced lowering of the transition temperatures in the systems except for the naphthalene-pyrene system.

Results and Discussion

The phase diagrams for OFN+pyrene, OFN+phenanthrene, OFN+naphthalene, and OFN+1,5-naphthylenediamine, respectively, indicated clearly the formation of a 1:1 molecular complex between OFN and the other component (Figs. 1—4). The system

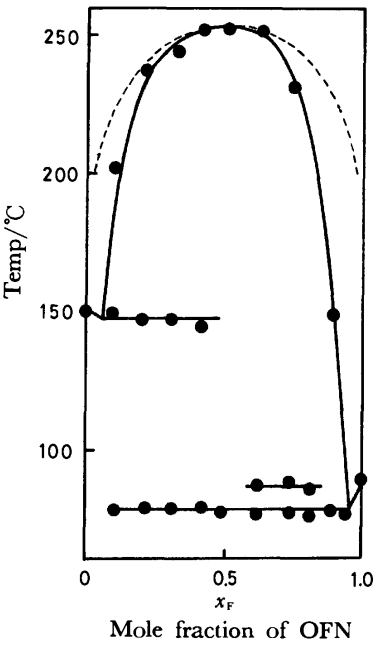

Fig. 1. Phase diagram of the OFN-pyrene system. The dotted curve is the calculated values from Eq. 2.

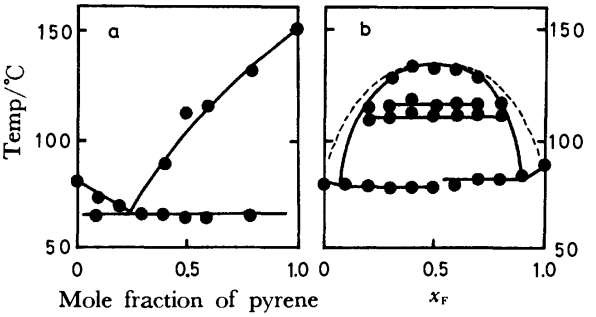

Fig. 2. Phase diagram of the naphthalene-pyrene system(a); the solid curves were calculated from Eq. 1, and that of the OFN-naphthalene system(b); the dotted curve was calculated from Eq. 2.

naphthalene+pyrene was studied in comparison with the system OFN+pyrene. It is seen from Fig. 2-a that naphtalene and pyrene form a simple eutectic. For such a binary mixture the thermodynamic equation relating the melting point of one component of the mixture to the composition of the solution is

$$\ln x = (\Delta H_1/R)(1/T_1 - 1/T), \quad (1)$$

where x is the mole fraction of the first component, and ΔH_1 and T_1 are the enthalpy of fusion and melting temperature of pure 1. The solid curve in Fig. 2-a

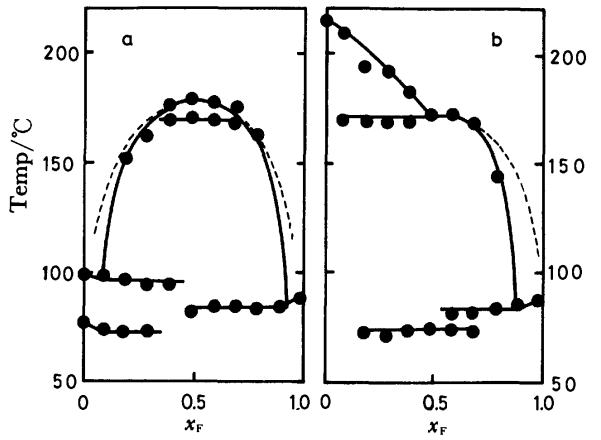

Fig. 3. Phase diagrams of the OFN-phenanthrene system(a) and the OFN-anthracene system(b). The dotted curves were calculated from Eq. 2.

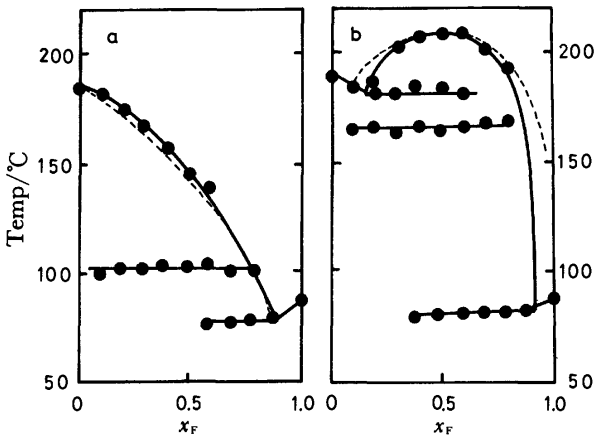

Fig. 4. Phase diagram of the OFN-phenothiazine system(a), the dotted curve was calculated from Eq. 1, and that of the OFN-1,5-naphthylenediamine system(b), the dotted curve was calculated from Eq. 2.

represents the melting temperatures calculated from Eq. 1 and is in good agreement with the experimental points. This evidence means that formation of the complex between OFN and pyrene results from the presence of fluorine atoms in OFN. Although in the system OFN+anthracene the compound molecule may be made from one OFN and one anthracene molecules, its melting temperature was lower than that of anthracene. The system OFN+phenothiazine did not give a congruent melting temperature.

The dotted curves in Figs. 1—4 represent the values calculated from Eqs. 1 or 2.[13]

$$-\ln x(1-x) + \ln 0.25 = \Delta H_c/R(1/T - 1/T_c), \quad (2)$$

here T_c is the melting temperature of the compound, and ΔH_c is its enthalpy of fusion. The equations assume ideal mixing in solution and for ΔH to be independent of temperature. The systems with congruent melting points exhibited negative deviation from Eq. 2, while the phase diagram for the system OFN+phenothiazine deviated positively from Eq. 1. The system OFN+phenothiazine seems to interact differently than the other systems. The other transition points, which were indicated in Figs. 1—4, were detected. Although some of these points may correspond to the phase transition of the molecular complexes, further investigation is required.

Thanks are given to Mrs. Kumiko Kawai for her assistance in drawing the figures.

References

1) C. R. Patrick and G. S. Prosser, *Nature*, **187**, 1201 (1960).
2) J. C. A. Boeyens and F. H. Herbstein, *J. Phys. Chem.*, **69**, 2153 (1965).
3) W. A. Duncan and F. L. Swinton, *Trans. Faraday Soc.*, **62**, 1082 (1966); W. A. Duncan, J. P. Sheridan, and F. L. Swinton, *Trans. Faraday Soc.*, **62**, 1090 (1966).
4) D. V. Fenby, I. A. Mclure, and R. L. Scott, *J. Phys. Chem.*, **70**, 602 (1966).
5) E. Mclaughlin and C. E. Messer. *J. Chem. Soc., (A)*, **1966**, 1106.
6) T. G. Beaumont and K. M. C. Davis, *J. Chem. Soc., (B)*, **1967**, 1131.
7) D. A. Armitage and K. W. Morcom, *Trans. Faraday Soc.*, **65**, 688 (1969).
8) D. A. Armitage, T. G. Beaumont, K. M. C. Davis, D. J. Hall, and K. W. Morcom, *Trans. Faraday Soc.*, **67**, 2548 (1971).
9) D. A. Armitage, J. M. T. Brindley, D. J. Hall, and K. W. Morcom, *J. Chem. Thermodynamics*, **7**, 97 (1975).
10) G. Griffith, P. R. Jackson, E. Kenyon-Blair, and K. W. Morcom, *J. Chem. Thermodynamics*, **15**, 1001 (1983).
11) D. J. Hall, K. W. Morcom, and J. M. T. Brindley, *J. Chem. Thermodynamics*, **6**, 1133 (1974).
12) The points in Figs. 1—4 are the temperatures at the intersection of the base line of a DSC curve with the tangent of the peaks. The tangent of a curve on a lower temperature side of the peak was used for the first peak, while for the subsequent peak the tangent on its higher temperature side was used.
13) I. Prigogine and R. Defay, "Thermodynamique Chimique," (1950), Japanese Ed., Misuzu Shobo (1966) p. 386.

A Common Factor Determining the Features of the Photocatalytic Hydrogenation and Isomerization of Alkenes over Ti-Si Oxides

Sukeya KODAMA,* Hiroaki NAKAYA, Masakazu ANPO, and Yutaka KUBOKAWA
Department of Applied Chemistry, University of Osaka Prefecture, Sakai, Osaka 591
(Received July 26, 1985)

Synopsis. On addition of SiO_2 to TiO_2 photocatalysts, it has been found that the yields of C_2H_6 and CH_4 in the photocatalytic hydrogenation of propylene as well as that of 1-butene in the photocatalytic isomerization of *cis*-2-butene decrease simultaneously. This gives some support for the mechanisms for both reactions where [Ti^{3+}–O^-] pairs are important.

It is well-known that in the photocatalytic reactions associated with the decomposition of water over Pt-loaded TiO_2 where charge separation takes place efficiently the reduction reactions by electrons and the oxidation reactions by holes proceed on different parts of the catalyst.[1] We have recently shown that a close association of photo-formed electrons and holes plays a significant role in some photocatalytic reactions.[2] For example, in the photocatalytic hydrogenation of propylene over TiO_2 the photo-formed trapped electron-hole pairs [Ti^{3+}–O^-] play a significant role in formation of the C=C bond fission products such as CH_4 and C_2H_6.[3] Furthermore, in the photocatalytic isomerization of 2-butene the [Ti^{3+}–O^-] pairs or Ti^{3+} (trapped electrons) are important to bring about the double bond shift in the isomerization.[4] According to such a reaction model, it would be expected that the decreases in the yields of CH_4 and C_2H_6 (hydrogenation) and 1-butene (isomerization) take place simultaneously, if removal of the trapped electrons (Ti^{3+}) is caused by in some way. Such features have been actually observed with the photocatalytic reactions over Ti–Si oxides.

Experimental

Propylene and *cis*-2-butene obtained from Takachiho Kagakukogyo Co. were purified by vacuum distillation. Ti–Si oxides with various compositions were prepared by coprecipitation of a mixed solution of $TiCl_4$ and $Si(OC_2H_5)_4$ with aqueous solution of ammonia, and by heating in air for three hours at 500 °C.[5] These catalysts were subjected to oxygen treatment for one hour at 500 °C followed by evacuation at the same temperature. *Cis*-2-butene of 4.0 kPa was introduced over the catalysts (500 mg) which had been spread on the quartz window, having a surface of *ca.* 20 cm^2. The photoisomerization was carried out by UV irradiation from a high pressure mercury lamp (Toshiba, SHL-100UV) without a filter for one hour at the ice-water temperature. The photocatalytic hydrogenation of propylene over water adsorbed catalysts was performed at room temperature in the same experimental conditions as above. Gas samples were analyzed by gas chromatography using silica gel and 2,4-dimethylsulfolane columns.

Results and Discussion

The hydrocarbon products in the photocatalytic hydrogenation of propylene by adsorbed water (reaction I) are CH_4, C_2H_6, and C_3H_8. As shown in Fig. 1, the formation rates of the products, especially those of CH_4 and C_2H_6 decrease drastically with increasing content of SiO_2 up to 60%. With the photocatalytic hydrogenations of alkenes and alkynes over TiO_2, it has recently been shown that the photo-formed [Ti^{3+}–O^-] pairs participate in formation of the products accompanied by fission of the C=C or C≡C bond.[3] It appears therefore that such a decrease in the yields of C_2H_6 and CH_4 may be explicable by the concept that the concentration of [Ti^{3+}–O^-] pairs decreases on the addition of SiO_2.

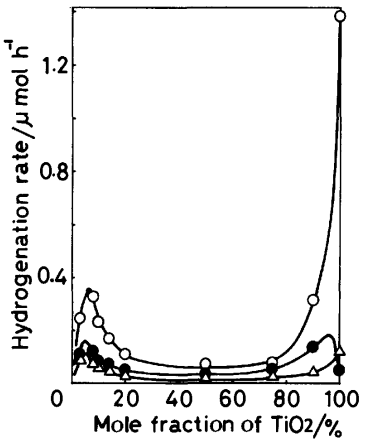

Fig. 1. Photocatalytic hydrogenation of propylene over binary Ti–Si oxides. ○: C_2H_6; ●: C_3H_8; △: CH_4.

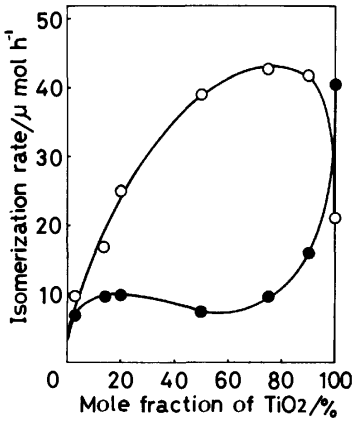

Fig. 2. Photocatalytic isomerization of *cis*-2-butene over binary Ti–Si oxides at 0 °C. ○: *trans*-2-butene; ●: 1-butene.

In the photocatalytic isomerization of *cis*-2-butene (reaction II) over Ti–Si oxides, both isomerizations to

trans-2-butene and 1-butene take place, though the isomerizations in the dark scarcely proceed at 0 °C. The rates of formation of *trans*-2-butene and 1-butene, as a function of the TiO_2 content, are shown in Fig. 2. The yield of 1-butene *i.e.* the selectivity toward 1-butene formation decreases in the range up to 60% TiO_2.

According to our recent work[4] in the photocatalytic isomerization of 2-butene the interaction of $[Ti^{3+}-O^-]$ pairs or O^- species with butene results in opening of its C=C bond, *i.e.* in formation of a radical, which participates in the photocatalytic isomerization. In the double bond shift isomerization, H atoms are removed from and added to the radical. Since H atoms are supplied from surface OH groups according to the process $OH^- \rightarrow O^{2-}+H^+$, the neutralization of protons is necessary. For this purpose the electrons trapped on Ti^{4+} ions (Ti^{3+}) are used. Accordingly, if the trapped electrons (Ti^{3+}) are removed, *i.e.* the O^- species are formed in place of the $[Ti^{3+}-O^-]$ pairs, the double bond shift isomerization would be unexpected to occur. The *cis-trans* isomerization will proceed, since it has been shown previously[4] that the interaction of the O^- species with alkene brings about the weakening of its C=C bond.[6] Replacement of the $[Ti^{3+}-O^-]$ pairs by the O^- species would result in simultaneous increase and decrease in the yields of *trans*-2-butene and 1-butene, respectively. Such feature was actually observed with the range above 90% of TiO_2. It was found that the selectivity of *trans*-2-butene formation in the photocatalytic isomerization of *cis*-2-butene is increased with Pt-loaded TiO_2 where removal of the trapped electrons (Ti^{3+}) is expected to occur. This suggests that the occurrence of the *cis-trans* isomerization is closely associated with such removal of the trapped electrons.

The considerations described above suggest that the decrease in the yields of CH_4 and C_2H_6 (reaction I) and 1-butene (reaction II) caused by the addition of SiO_2 is explicable by the same factor, *i.e.* the decrease in the concentration of $[Ti^{3+}-O^-]$ pairs brought about by removal of the trapped electrons(Ti^{3+}). Apart from the nature of such removal, which will be described later, it should be noted that such a simultaneous decrease in the yields of CH_4 and C_2H_6 and of 1-butene in both reactions would give some support for the mechanisms proposed for both reactions where the $[Ti^{3+}-O^-]$ pairs play a significant role.

In the range below 50% of TiO_2, the reversed behavior is observed, *i.e.* simultaneous increase in the yields of CH_4 and C_2H_6 and 1-butene takes place. Such feature might be explained in a similar manner, *i.e.* in the increase in the concentration of $[Ti^{3+}-O^-]$. In any events, those results will again give additional support for the proposed reaction model.

As for the removal of the trapped electrons (Ti^{3+}), the followings may be mentioned. It is well-known that trapping or recombination centers are formed by addition of a foreign material to a semiconductor. This would be the case for the present system, since formation of Lewis acid sites has been reported for Ti-Si oxides.[5] At present the depth of the traps is unknown, they appear deep enough to remove the trapped electrons (Ti^{3+}).

In the region of lower Ti contents, we have recently reported formation of a new active phase arising from a high dispersion of Ti ions.[7] In this state the radiationless transfer of photon energy absorbed by TiO_2 is suppressed because of a high coordination unsaturation. This would be expected to facilitate formation of the $[Ti^{3+}-O^-]$ pairs. Further work is necessary to clarify the nature of such phenomena.

References

1) *e. g.* B. Kraeutler and A. J. Bard, *J. Am. Chem. Soc.*, **100**, 5985 (1978).

2) M. Anpo, I. Tanahashi, and Y. Kubokawa, *J. Chem. Soc., Faraday Trans. 1*, **78**, 2121 (1982).

3) M. Anpo, N. Aikawa, S. Kodama, and Y. Kubokawa, *J. Phys. Chem.*, **88**, 2569 (1984); M. Anpo, N. Aikawa, and Y. Kubokawa, *ibid.*, **88**, 3998 (1984).

4) S. Kodama, M. Yabuta, and Y. Kubokawa, *Chem. Lett.*, **1982**, 1671; S. Kodama, M. Yabuta, M. Anpo, and Y. Kubokawa, *Bull. Chem. Soc. Jpn.*, **58**, 2307 (1985).

5) K. Shibata, T. Kiyoura, J. Kitagawa, T. Sumiyoshi, and K. Tanabe, *Bull. Chem. Soc. Jpn.*, **46**, 2985 (1973); M. Itoh, H. Hattori, and K. Tanabe, *J. Catal.*, **35**, 225 (1974).

6) The O^- species will trap an electron to form an O^{2-} ion at the end of their life. It seems that its life time is not necessarily the same as the time to complete the isomerization, being probably much longer. Further work is necessary to clarify this point.

7) M. Anpo, H. Nakaya, S. Kodama, Y. Kubokawa, K. Domen, and T. Onishi, *J. Phys. Chem.*, to be published.

The Microwave Spectrum of (Z)-(Acrylaldehyde Oxime)

Mariko TERASHIMA and Osamu OHASHI*

Department of Chemistry, Faculty of Science and Technology, Sophia University, Chiyoda-ku, Tokyo 102

(Received August 8, 1985)

Synopsis. The microwave spectrum of (*Z*)-(acrylaldehyde oxime) was observed in the frequency region from 10 to 40 GHz.

Several a-type R-branch transitions in the ground vibrational state were identified and the rotational constants in MHz were determined to be A=17430.7(35), B=3022.514(15), and C=2576.504(16). The conformation of (*Z*)-(acrylaldehyde oxime) has been plausibly deduced to be the s-trans Z-form from the rotational constants experimentally determined. The angle of C-C=N is discussed.

The gas chromatogram and proton magnetic resonance spectrum of acrylaldehyde oxime have suggested that this molecule has two geometrical isomers.[1] One of them is an E-form of which the microwave spectroscopic study has been reported.[2] The other one is a Z-form which has not been determined to be whether the s-trans Z-form or s-cis Z-form, or both (See Fig. 1). It is interesting to determine the molecular conformation of (*Z*)-(acrylaldehyde oxime) in gas phase. We have observed the microwave spectrum of (*Z*)-(acrylaldehyde oxime) and discussed its conformation and the angle of C-C=N.

Experimental

Acrylaldehyde oxime was prepared and purified by the method described elsewhere.[2] No attempt was made to separate the E- and Z-species; all measurements were made with the equilibrium mixture of the isomers at room temperature, using a flowing system in which the sample was put into a sample cell at the one end and pumped out from the other end during the measurement of the spectrum.

The spectrometer used has been described elsewhere.[2]

Results and Discussion

The first survey of the rotational spectrum was made in the frequency region of 26.5 to 40 GHz at the Stark field of 100 V/cm.

Bunches of relatively weak absorption lines that might be ascribed to the Z conformer were found with the frequency interval of about 5600 MHz, while groups of strong lines which had been assigned to the E-conformer were observed with the frequency interval of about 4600 MHz.

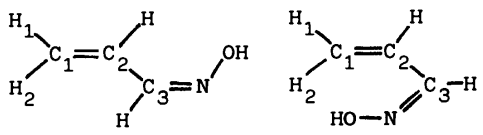

s-trans Z-form s-cis Z-form

Fig. 1. Two possible geometrical isomers and the numbering of carbon and hydrogen atoms of (*Z*)-(acrylaldehyde oxime).

In the first place, four transitions of J=5←4 and J=6←5 with K_{-1}=1 and six lines of J=5←4, 6←5, and 7←6 with K_{-1}=2 in the frequency region of 26.5 to 40 GHz were tentatively assigned and they led to the prelimenary rotational constants which were employed to predict the other transition lines. Then, forty a-type R-branch transition lines in the ground vibrational state were assigned in the frequency region of 10 to 40 GHz as listed in Table 1. The rotational and centrifugal distortion constants finally determined are shown in Table 2, together with the rotational

Table 1. Observed transition frequencies (MHz) of (*Z*)-(acrylaldehyde oxime)

Transition	Obsd	$\Delta\nu$[a]	Transition	Obsd	$\Delta\nu$[a]
2_{12}—1_{11}	10752.05	0.02	5_{14}—4_{13}	29063.63	0.02
2_{02}—1_{01}	11187.84	0.02	6_{16}—5_{15}	32177.93	−0.04
2_{11}—1_{10}	11644.15	0.12	6_{06}—5_{05}	33242.38	0.01
3_{13}—2_{12}	16121.73	0.02	6_{25}—5_{24}	33547.80	−0.06
3_{03}—2_{02}	16756.12	−0.11	6_{52}—5_{51}	33620.67	0.15
3_{22}—2_{21}	16797.18	0.08	6_{51}—5_{50}		0.15
3_{21}—2_{20}	16837.65	−0.20	6_{43}—5_{42}	33629.17	0.06
3_{12}—2_{11}	17459.57	0.01	6_{42}—5_{41}		0.00
4_{14}—3_{13}	21483.88	−0.09	6_{34}—5_{33}	33646.25	0.15
4_{04}—3_{03}	22294.24	−0.00	6_{33}—5_{32}	33654.08	−0.17
4_{23}—3_{22}	22388.23	0.11	6_{24}—5_{23}	33898.89	−0.01
4_{32}—3_{31}	22416.76	0.54	6_{15}—5_{14}	34845.88	0.06
4_{31}—3_{30}		−0.33	7_{17}—6_{16}	37506.39	0.07
4_{22}—3_{21}	22489.78	0.02	7_{07}—6_{06}	38637.93	0.07
4_{13}—3_{12}	23267.13	0.04	7_{26}—6_{25}	39113.17	−0.01
5_{15}—4_{14}	26836.62	−0.06	7_{62}—6_{61}	39223.26	−0.01
5_{05}—4_{04}	27792.39	−0.01	7_{61}—6_{60}		−0.01
5_{24}—4_{23}	27972.25	−0.02	7_{53}—6_{52}	39230.07	−0.05
5_{42}—4_{41}	28018.55	0.34	7_{52}—6_{51}		−0.05
5_{41}—4_{40}		0.33	7_{44}—6_{43}	39243.94	−0.01
5_{33}—4_{32}	28029.10	0.27	7_{43}—6_{42}		−0.22
5_{32}—4_{31}	28031.38	−0.41	7_{35}—6_{34}	39268.54	−0.02
5_{23}—4_{22}	28174.57	−0.02	7_{34}—6_{33}	39286.78	−0.06
			7_{25}—6_{24}	39667.21	−0.02

a) $\Delta\nu=\nu_{obsd}-\nu_{calcd}$.

Table 2. Observed and calculated rotational constants of (*Z*)-(acrylaldehyde oxime)

	Obsd	Calcd[a]	
		s-trans	*s-cis*
A/MHz	17430.7(35)	16309	9111
B/MHz	3022.514(15)	3232.61	6040.54
C/MHz	2576.504(16)	2697.87	3632.41
Δ_J/kHz	0.74(13)		
Δ_{JK}/kHz	−5.21(35)		
κ	−0.939948	−0.92143	−0.12099
ΔI[b]/amu·Å^2	−0.0493788		

Numbers in parentheses represent 2.5 times the standard deviation. a) Calculated from the molecular parameters in Table 3. b) $\Delta I=I_c-I_a-I_b$.

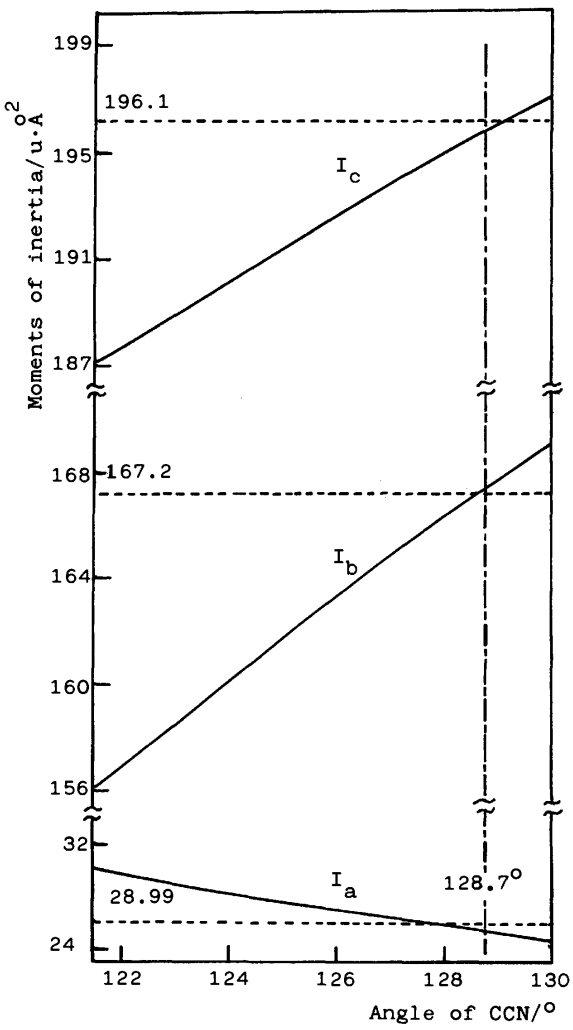

Fig. 2. The dependence of the moments of inertia, I_a, I_b, and I_c, on the angle of CCN. The solid lines indicate the calculated moments of inertia and the dotted lines show the observed ones.

constants calculated from the molecular models (See Fig. 1 and Table 3).

From the comparison of the experimental and calculated rotational constants shown in Table 2, it is conclued that the s-trans Z conformer is attributed to the spectrum analyzed in this work.

Table 3. Structural parameters assumed for (*Z*)-(acrylaldehyde oxime)

Bond length	l/Å	Bond angle	θ/°
C=C	1.345[a]	H_1-C=C	121.45[a]
C=C	1.470[a]	H_2-C=C	119.97[a]
C_1-H	1.086[a]	C_1=C_2-H	122.83[a]
C_2-H	1.084[a]	C=C-C	119.83[a]
C=N	1.276[b]	C-C=N	121.77[b]
N-O	1.408[b]	H-C=N	115.55[b]
O-H	0.956[b]	C=N-O	110.20[b]
C_3-H	1.086[b]	N-O-H	102.68[b]

The numbering of carbon and hydrogen atoms is given in Fig. 1. a) Ref. 3, Cherniak and Costain, *J. Chem. Phys.*, **45**, 104 (1966). b) Ref. 4, Levine, *J. Chem. Phys.*, **38**, 2326 (1963).

No spectrum of any other conformer has been detected. This suggests that the population or dipole moment, or both of the other conformer is too small to be detected.

Figure 2 shows how the moments of inertia, I_a, I_b, and I_c, depend on the angle of C-C=N keeping the other structural parameters constant. According to Fig. 2, the angle of C-C=N may be plausibly determined to be 128.7°. This unexpectedly large angle is thought to be due to the steric effect between the vinyl and hydroxyl groups. However, the moments of inertia, I_a, I_b, and I_c, may largely depend on the other structural parameters, particularly the bond length of C_2–C_3 and C=N, and the angle of C=C-C and C=N-O.

The more data than we have now are needed in order to come to the final conclusion about this angle.

References

1) S. Masuda, H. Kihara, and T. Ota, *Nippon Kagaku Kaishi*, **1974**, 608.

2) M. Niwase, K. Kubota, K. Yoshida, T. Sakaizumi, M. Onda, O. Ohashi, and I. Yamaguchi, *Bull. Chem. Soc. Jpn.*, **57**, 2408 (1984).

3) E. A. Cherniak and C. C. Costain, *J. Chem. Phys.*, **45**, 104 (1966).

4) I. N. Levine, *J. Chem. Phys.*, **38**, 2326 (1963).

Extractability of Copper(II) and Zinc(II) with Crown Ethers as Picrates

Yuko HASEGAWA,* Hiroaki TANABE, and Satoshi YOSHIDA
Department of Chemistry, Science University of Tokyo, Kagurazaka, Shinjuku-ku, Tokyo 162
(Received July 2, 1985)

Synopsis. The extraction of copper(II) and zinc(II) with picrate ion and 12-crown-4(1,4,7,10-tetraoxacyclododecane) or 15-crown-5(1,4,7,10,13-pentaoxacyclopentadecane) into benzene or chloroform has been measured. The extraction of copper(II) is better than that of zinc(II), in spite of the similar ionic size, although the difference is much smaller than that in the extraction of these metal ions with β-diketones.

The study of extractions of metal ions with crown ethers has been developed in relation to the agreement between the size of the metal ion and the cavity size of the crown ether.

Since both copper and zinc ions are stable in the divalent state and have about equal size, and their size is also close to the cavity size of 12-crown-4(12C4) or 15-crown-5(15C5), a similar extraction may be expected.

On the other hand, it has been reported that the extraction of copper(II) with a given β-diketone is much better than that of zinc(II).[1]

In the present paper, the extraction of copper and zinc ions with 12C4 and 15C5 from lithium picrate solution into benzene or chloroform has been measured, in order to compare the extractability of these metal ions as ion pairs to the extractability as the chelates.

Experimental

All the procedures were performed at 25±0.5 °C. The crown ethers were obtained from the Aldrich Chemical Co., USA and Merck Inc., West Germany. The lithium picrate solution was prepared by neutralizing picric acid solution with lithium hydroxide. All other reagents were employed without purification.

An aqueous solution containing metal(II) nitrate (2.5×10^{-2} M, 1 M=1 mol dm^{-3}) and lithium picrate and the same volume of benzene or chloroform containing a certain amount of 12C4 or 15C5 were placed in a stoppered glass tube and agitated mechanically for an hour. The two phases were then centrifuged and the metal(II) in the organic phase was back extracted with 0.1 M perchloric acid. The amount of the metal(II) was measured by an atomic absorption method. The metal(II) concentration in the aqueous phase was regarded as the total concentration added initially. The distribution ratio was defined by the following equation.

$$D = [M(II)]_{o,total}/[M(II)]_{a,total}$$

The distribution constants of 12C4 and 15C5 were determined as follows: the crown ethers were distributed between water and benzene or chloroform. The concentration of each crown ether distributed between both phases was measured spectrometrically using sodium chloride and lithium dipicrylamide. The detailed procedure was reported elsewhere.[2]

Results and Discussion

Figure 1 shows the dependence of the picrate ion concentration on the extraction of copper and zinc ion with 15C5 into benzene or chloroform. The slopes of the curves are +2, except in the higher picrate concentration region. When 12C4 was used, the distribution ratio also increased in proportion to the second order of the picrate ion concentration. Since the extraction was not good, a higher concentration of

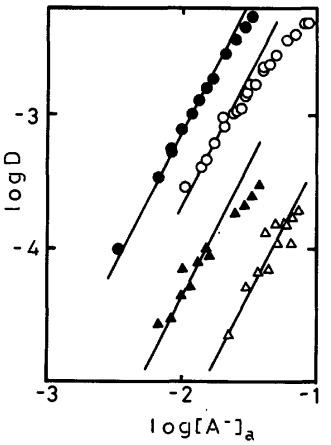

Fig. 1. Extraction of copper(II) (circles) and zinc(II) (triangles) into benzene (open symbols) or chloroform (closed symbols) containing 15C5 as a function of picrate ion concentration.

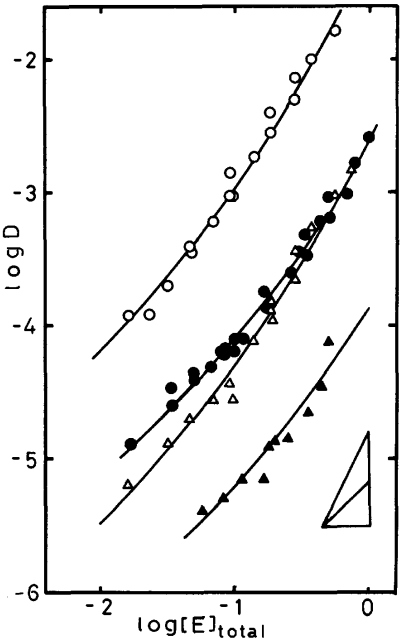

Fig. 2. Distribution ratio of copper(II) (circles) and zinc(II) (triangles) with 12C4 (closed symbols) or 15C5 (open symbols) at 2.5×10^{-2} M picrate concentration as a function of crown ether concentration in benzene.

Table 1. Summary of constants

Org. solvent	Ether[b]	log K_D	Cu(II)[a] log Kex_1	Cu(II)[a] log Kex_2	Zn(II)[a] log Kex_1	Zn(II)[a] log Kex_2
C_6H_6	12C4	−0.82	0.0_9	0.5_0	-1.0_5	-0.7_2
	15C5	−0.84	1.0_4	2.0_2	-0.2_6	0.6_4
$CHCl_3$	12C4	0.90	0.6_4	3.0_7	-0.1_5	1.8_0
	15C5[4]	0.88	2.0_9	4.4_4	1.0_1	3.2_8

a) Diameter (nm)[3]: 0.15 for 4 coordination, 0.18 for 6 coordination. b) cavity size (nm)[2]: 0.1—0.13 (12C4), 0.17—0.22 (15C5).

the metal ions should be employed for an accurate determination of the distribution ratio. Consequently, the nitrate concentration was as high as 0.05 M. However, the species extracted does not seem to include nitrate ions, because the value of the slope of +2 indicates that two picrate ions were present and there was no room for additional anions.

Figure 2 shows the dependence of the crown ether concentration on the extraction of these metal ions into benzene at a constant picrate concentration. The slope of the extraction curves seems to change from one to two. It suggests that the species extracted would have a 2:1 as well as a 1:1 stoichiometry of the crown ether to the metal ion.

From these results, the distribution ratio, D, can be represented as,

$$D = \frac{[MEA_2]_o + [ME_2A_2]_o}{[M^{2+}]_a} = Kex_1[A^-]_a^2[E]_a + Kex_2[A^-]_a^2[E]_a^2 \quad (1)$$

here, the subscripts "o" and "a" denote the organic and the aqueous phases, respectively, $Kex_n=[ME_nA_2]_o/[M^{2+}]_a[A^-]_a^2[E]_a^n$, and $[E]_a=[E]_{total}/(1+K_D)$ and $K_D(=[E]_o/[E]_a)$ is the distribution constant of the crown ethers. The extraction data were analyzed by a successive approximation method. The extraction constants obtained are listed in Table 1 together with the distribution constants of these crown ethers.

As seen in Table 1, the frame size of the crown ether does not seem to change the general features of the extraction of the crown ether itself. The increase of hydrocarbon segments in the frame may be more favorable to the extraction, because the segments give more hydrophobic character to the crown ether. At the same time, the increase in the hydrophobic tendency should be cancelled out by the increase in the hydrophilic tendency of the molecule, because in a series of the crown ethers such as 12C4, 15C5, and 18C6, an increase of one hydrocarbon segment, $-CH_2-CH_2-$ in the frame always causes an increase of one oxygen atom, and the oxygen atom should give hydrophilic tendency to the molecule through hydration.

On the other hand, the extraction of the metal ions with 15C5 is always better than that with 12C4 by a factor of about one order of magnitude as seen in Fig. 2. That is, the frame size seems to change the extraction of metal ions definitely. Although the reason is not clear, it may reflect that on the complexation of the metal ion with the crown ether, the oxygen atoms in the crown ether interact with metal ions, and hence the balance between the hydrophilic and hydrophobic tendency would be broken, or the stability of the complex with 12C4 would be different from that with 15C5.

The difference of organic solvents influences the extraction of the crown ethers themselves more remarkably than that of the ion pairs of the metal(II), as is seen in Table 1. This fact may also reflect that the oxygen atoms in the frame of the crown ethers may solvate more easily with chloroform, probably through a hydrogen bond, than with benzene.

Table 1 also shows that the extraction of copper ion with either 12C4 or 15C5 is better by a factor of one order than that of zinc ion, when the metal ions are extracted with the same crown ether into the same organic solvent. The extraction constant of bis(acetylacetonato) copper(II) (log $Kex=-3.47$) is larger than that of zinc chelate (log $Kex=-10.69$). The difference has been explained in terms of the different electronic structure, that is, since zinc ion forms stable octahedral chelates with the coordination number of six, the central zinc ion in the chelate may interact more with water molecules than the central copper(II) ion in the chelate.[1] On the other hand, it has been reported[4] that zinc(II) takes four coordination when the metal ion is extracted as ion pairs with trioctylphosphine oxide and perchlorate or halide ions. If the zinc ion also takes on a tetrahedral structure instead of an octahedral one on extraction with the crown ethers and picrate ions, the zinc ion in the ion pairs should not hydrate more than the ion in the chelates. Accordingly, the difference of the extraction of these metal ions would be smaller than that with β-diketones.

Without information on the thermodynamic properties such as the changes in the free energy, the enthalpy, and the entropy on the complexation or the extraction, it is impossible to discuss the extractability of these ion pairs in more detail.

The authors wish to express their gratitude to Messrs. T. Nakano, Y. Morimoto, and T. Miura for their experimental aid.

References

1) T. Sekine and N. Ihara, *Bull. Chem. Soc. Jpn.*, **44**, 2942 (1971).
2) Y. Hasegawa, T. Nakano, Y. Odori, and Y. Ishikawa, *Bull. Chem. Soc. Jpn.*, **57**, 8 (1984).
3) "Kagaku Binran," ed by Japan Chemical Society, Maruzen, Tokyo (1984).
4) H. Moriya and T. Sekine, *Bull. Chem. Soc. Jpn.*, **45**, 1626 (1972).

NMR Spectra of Substituted 2-(2-Nitrovinyl)thiophenes

Hajime SATONAKA* and Michio WATANABE†

Industrial Research Institute of Kanagawa Prefecture, 3173, Showa-machi, Kanazawa-ku, Yokohama 236

†*Permachem Asia Ltd., 2-14-5, Hiranuma, Nishi-ku, Yokohama 220*

(Received June 1, 1985)

Synopsis. ^{1}H and ^{13}CNMR spectra are reported for substituted 2-(2-nitrovinyl) thiophenes. The proton chemical shifts and coupling constants were correlated closely with those of methyl *trans*-3-(5-substituted 2-thienyl) acrylates. We have found that the additivity rule for ^{13}C chemical shifts of simple substituted thiophenes is applicable to the shifts of the ring carbons in substituted 2-(2-nitrovinyl) thiophenes.

The antibacterial property of 2-(2-nitrovinyl) thiophene has been well known.[1] Recently, we also reported some new antibacterial and fungicidal (nitrovinyl) thiophenes.[2]

We examined the substituent effect in ^{1}H and ^{13}C NMR spectra of a series of substituted 2-(2-nitrovinyl) thiophenes.

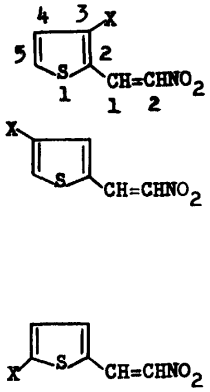

X=H	1
X=CH_3	2
X=Br	3
X=OCH_3	4
X=Cl	5
X=Br	6
X=I	7
X=OCH_3	8
X=CH_3	9
X=Cl	10
X=Br	11
X=I	12
X=CHO	13
X=$COCH_3$	14
X=COOH	15
X=$COOCH_3$	16
X=NO_2	17
X=CH=$CHNO_2$	18

^{1}H NMR spectra of substituted (2-nitrovinyl) thiophenes are very similar to those of methyl *trans*-3-(substituted 2-thienyl)acrylate.[3] Thus, assignment was made easily by comparing the spectra of two series of the compounds. The results are given in Table 1. The chemical shifts of protons in 5-substituted 2-(2-nitrovinyl)thiophenes (X=H, OCH_3, CH_3, Cl, Br, I, CHO, $COCH_3$, $COOCH_3$, and NO_2) against those of the corresponding protons in methyl *trans*-3-(5-substituted 2-thienyl)acrylates give good linear correlations [δH(3)[3] r 0.963, p 0.970, s 0.038; δH(4) r 0.992, p 0.963, s 0.062: δH(α)[4] r 0.726, p 0.726, s 0.121; and δH(β) r 0.959, p 1.05, s, 0.048], where r designates correlation coefficient, p slope, and s standard deviation.

^{13}CNMR chemical shifts (Table 2) were assigned as described below. C(β) substituted by NO_2 was unambiguously identified by its broad line width and lower intensity. The quaternary ring carbons were identified by lower intensity. C(2) and another carbon carrying the substituent were assigned on the basis of the substituent effect on substituted thiophenes.[5,6] The protonated carbons were assigned in comparison with the coupling constants between coarbons and protons. C(α) was easily identified by the smallest one bond coupling in the protonated carbons. C(3) and C(4) in 5-substituted 2-(2-nitrovinyl) thiophenes were assigned on the basis of the long-range couplings with H(α), because C(3) couples considerably with H(α), but C(4) does not.

Good linear correlations were obtained between the ^{13}C chemical shifts of the ring in substituted 2-(2-nitrovinyl) thiophenes and the corresponding chemical shifts in substituted thiophenes[6] [δC(2) r 0.988, p 0.909, s 0.793; δC(3) r 0.944, p 0.900, s 1.77; δC(4) r 0.997, p 1.01, s 1.15; and δC(5) r 0.998, p 0.945, s 1.30]. These results suggest that the additivity rule for ^{13}C chemical shifts of simple substituted thiophenes is

TABLE 1. ^{1}H NMR CHEMICAL SHIFTS AND COUPLING CONSTANTS OF SUBSTITUTED 2-(2-NITROVINYL)THIOPHENES

Compounds	Chemical shifts (δ)						Coupling constants/Hz								
	H(3)	H(4)	H(5)	H(α)	H(β)	Others	J_{34}	J_{35}	J_{45}	$J_{\alpha\beta}$	$J_{3\alpha}$	$J_{5\alpha}$	$J_{3\beta}$	$J_{5\beta}$	Others
1	7.76	7.25	7.85	8.26	7.77		3.7	1.2	5.1	13.5	0.5	0.6	0.4	0.4	
2	—	7.09	7.72	8.26	7.62	2.46(CH_3)	—	—	4.9	13.5	—	0.5	—	0.4	0.4(J_{CH_3-4}) 0.4(J_{CH_3-5})
3	—	7.30	7.93	8.15	7.88		—	—	5.4	13.5	—	0.6	—	0.4	
4	7.41	—	6.90	8.11	7.75	3.85(OCH_3)	—	1.8	—	13.4	0.5	0.5	0.4	0.4	
5	7.72	—	7.76	8.20	7.87		—	1.5	—	13.4	0.5	0.6	0.4	0.4	
6	7.75	—	7.87	8.22	7.86		—	1.5	—	13.5	0.5	0.6	0.5	0.4	
7	7.80	—	7.99	8.24	7.84		—	1.3	—	13.5	0.5	0.6	0.5	0.4	
8	7.50	6.47	—	8.15	7.49	4.04(OCH_3)	4.2	—	—	13.2	0.5	—	0.4	—	
9	7.56	6.95	—	8.18	7.62	2.56(CH_3)	3.7	—	—	13.2	0.5	—	0.4	—	0.5(J_{CH_3-3}) 0.9(J_{CH_3-4})
10	7.64	7.20	—	8.19	7.75		4.0	—	—	13.4	0.5	—	0.4	—	
11	7.59	7.32	—	8.21	7.77		4.0	—	—	13.4	0.5	—	0.4	—	
12	7.45	7.48	—	8.23	7.75		3.9	—	—	13.5	0.5	—	0.4	—	
13	7.89	8.04	—	8.31	7.99	10.04(CHO)	4.0	—	—	13.5	0.6	—	0.4	—	
14	7.81	7.91	—	8.26	7.93	2.60($COCH_3$)	4.0	—	—	13.5	0.6	—	0.4	—	
15	7.79	7.81	—	8.27	7.93	5.99(COOH)	4.0	—	—	13.6	0.6	—	0.4	—	
16	7.79	7.82	—	8.27	7.94	3.91($COOCH_3$)	4.0	—	—	13.6	0.6	—	0.4	—	
17	7.82	8.10	—	8.27	8.09		4.4	—	—	13.5	0.6	—	0.4	—	
18	7.84	7.84	—	8.28	7.88		—	—	—	13.5	0.6	—	0.4	—	

TABLE 2. ^{13}C NMR CHEMICAL SHIFTS OF SUBSTITUTED 2-(2-NITROVINYL)THIOPHENES

Compounds	Chemical shifts (δ)							
	C(2)	C(3)	C(4)	C(5)	C(α)	C(β)	Others	
1	134.7	135.6	129.7	132.9	132.7	136.4		
2	128.9	147.1	132.7	131.4	131.2	135.5	14.4(CH_3)	
3	129.7	120.3	132.9	133.0	130.2	137.8		
4	133.0	125.5	160.3	105.3	132.7	136.6	58.0(OCH_3)	
5	135.4	133.8	127.3	127.2	131.5	137.8		
6	136.1	136.3	111.9	129.9	131.3	137.8		
7	136.8	141.5	79.4	135.7	131.0	137.7		
8	121.1	137.8	107.3	173.3	134.4	133.0	61.3(OCH_3)	
9	132.8	137.0	128.6	148.8	133.1	135.3	15.7(CH_3)	
10	133.9	135.7	129.4	136.4	132.0	136.7		
11	136.7	136.4	133.1	119.4	131.7	136.9		
12	140.9	137.1	140.0	82.8	131.2	137.1		
13	142.2	135.4	137.8	148.1	131.8	139.6	181.4(CHO)	
14	141.2	135.5	134.2	149.1	131.9	139.0	26.8($COCH_3$)	191.0($COCH_3$)
15	140.3	135.0	134.9	139.6	131.9	138.7	162.4(COOH)	
16	140.5	134.9	134.9	138.6	131.8	138.9	52.9($COOCH_3$)	162.2($COOCH_3$)
17	140.9	133.5	130.4	155.1	131.1	140.4		
18	139.7	136.2	136.2	139.7	131.6	138.6		

TABLE 3. MELTING POINTS AND ANALYTICAL DATA OF NEW 2-(2-NITROVINYL)THIOPHENES

Compounds	Mp/θ_m/°C	Formula	Found (%)				Calcd (%)			
			C	H	N	S	C	H	N	S
4	118	$C_7H_7NO_3S$	45.30	3.82	7.70	17.40	45.40	3.81	7.56	17.31
5	118	$C_6H_4ClNO_2S$	38.18	2.09	7.26	16.98	38.01	2.13	7.39	16.91
7	106	$C_6H_4INO_2S$	25.50	1.49	5.07	11.52	25.64	1.43	4.98	11.41
8	129	$C_7H_7NO_3S$	45.33	3.85	7.43	17.43	45.40	3.81	7.56	17.31
12	138	$C_6H_4INO_2S$	25.73	1.52	4.85	11.59	25.64	1.43	4.98	11.41
14	154	$C_8H_7NO_3S$	48.79	3.51	7.02	16.32	48.72	3.58	7.10	16.26
15	199(dec)	$C_7H_5NO_4S$	42.05	2.63	7.00	16.17	42.21	2.53	7.03	16.10
16	173	$C_8H_7NO_4S$	45.28	3.20	6.51	15.18	45.07	3.31	6.57	15.04
18	197(dec)	$C_8H_6N_2O_4S$	42.57	2.76	12.49	14.02	42.48	2.67	12.38	14.17

applicable to the shifts of the ring carbons in substituted 2-(2-nitrovinyl)thiophenes.

Chemical shifts of the ring carbons are not always correlated closely with those of hydrogen atoms attached to them. In all the compounds stuidied, $\delta H(\alpha)$ appeared at considerably lower field than $\delta H(\beta)$. In contrast, $\delta C(\alpha)$ appeared at higher field than $\delta C(\beta)$, except for **8**. The substituent effect of methoxy group may be transmitted more strongly by the contribution of resonance structures to $\delta C(\beta)$ in **8**, as to $\delta H(\beta)$ in methyl *trans*-3-(5-methoxy 2-thienyl)acrylate.[3] In 4-substituted compounds, $\delta H(3)$ appeared at lower field than $\delta H(5)$, but $\delta C(3)$ at higher field than $\delta C(5)$. These facts can be a reason for the poor correlations between δH and δC. It is exceptional that plot of $\delta H(\beta)$ *vs.* $\delta C(\beta)$ gave a good correlation (r 0.985, p 11.9, s 0.315). Besides, $\delta C(\beta)$ of 5-substituted compounds (X=H, OCH_3, CH_3, Cl, Br, I, CHO, $COCH_3$, $COOCH_3$, and NO_2) against Hammett's σ_p value[7,8] gave a good correlation (r 0.900, p 6.43, s 8.90). The effect of the substituent on the 5-position may be transmitted more regularly to $\delta H(\beta)$ and $\delta C(\beta)$ than others as observed with methyl *trans*-3-(5-substituted 2-thienyl)acrylates.[3]

Experimental

^1H and ^{13}CNMR spectra were recorded on a JEOL FX-90Q spectrometer. ^1H(±0.01 ppm) and ^{13}C(±0.1 ppm) chemical shifts were measured from internal TMS reference in $(CD_3)_2CO$ solution at probe temperature. ^1H spectra were obtained, using 45° pulse flip angle and 900 or 1100 Hz spectra width and proton decoupled ^{13}C spectra, using 30° pulse flip angle and 4500 or 5000 Hz spectra width. Proton coupled ^{13}C spectra were obtained by the normal gate decoupling technique in $(CD_3)_2SO$ solution.

Thiophenes (**1**, **2**, **3**, **6**, **9**, **10**, **11**, **13**, and **17**) were prepared according to the reported methods.[1,9-10] Melting points and analytical data of new compounds are given in Table 3.

The authors wish to thank Professor Minoru Hirota of Yokohama National University for his kind suggestions and encouragement.

References

1) A. Vecchi and G. Melone, *J. Org. Chem.*, **22**, 1636 (1957).
2) H. Satonaka, *Jpn. Kokai Tokkyo Koho*, 59-84882 (1984); 60-81179 (1985).
3) H. Satonaka, *Bull. Chem. Soc. Jpn.*, **57**, 473 (1984).
4) The notations H(α), H(β), C(α), and C(β) are hereafter used for H(1), H(2), C(1), and C(2) of an olefinic side chain, respectively.
5) K. Takahashi, T. Sone, and K. Fujieda, *J. Phys., Chem.*, **74**, 2765 (1970).
6) S. Gronowitz, I. Johnson, and A. B. Hornfeldt, *Chem. Scr.*, **7**, 76 (1975).
7) H. H. Jaffe, *Chem. Revs.*, **53**, 191 (1953).
8) J. Hine, "Physical Organic Chemistry," 2nd ed. McGraw Hill, New York (1962), p. 87.
9) W. J. King and F. F. Nord, *J. Org. Chem.*, **14**, 405 (1949).
10) S. Gronowitz and E. Sandberg, *Ark. Kemi*, **32**, 217 (1970).
11) V. I. Rogovik and Ya. L. Gol'dfarb, *Izv. Akad. Nauk SSSR, Ser. Khim.*, **1963**, 2178.

A Kinetic Study of Thermal Rotational Isomerization of 5,10,15,20-Tetrakis(*o*-aminophenyl)porphyrin and 5,10,15,20-Tetrakis(*o*-pivaloylaminophenyl)porphyrin

Keiichiro HATANO,* Kazunori ANZAI, Akemi NISHINO, and Keiko FUJII
Department of Pharmaceutical Sciences, Nagoya City University, Mizuho-ku, Nagoya 467
(Received June 26, 1985)

Synopsis. Rates of thermal interconversion of atropisomers of 5,10,15,20-tetrakis(*o*-aminophenyl)porphyrin and 5,10,15,20-tetrakis(*o*-pivaloylaminophenyl)porphyrin have been determined.

It is well known that four atropisomers of *ortho*-substituted tetraarylporphyrins can be thermally or photochemically interconverted by rotation about a porphyrin-aryl bond.[1-4,6] In a previous paper,[4] we reported the isomerization reactions of tetrakis-(*o*-cyanophenyl)porphyrin (ToCNPP) atropisomers. Herein we report the isomerization rates of 5,10,15,20-tetrakis(*o*-aminophenyl)porphyrin ($ToNH_2PP$) and 5,10,15,20-tetrakis(*o*-pivaloylaminophenyl)porphyrin (ToPivPP) studied at various temperatures in order to compare the effects of the *ortho* substituents on the atropisomerization.

Experimental

$ToNH_2PP$ was synthesized by methods described in the literature.[1] Calcd for $C_{44}H_{34}N_8 \cdot H_2O$; C, 76.21; H, 5.20; N, 16.16. Found: C, 76.38; H, 4.68; N, 16.01%. The separation of $ToNH_2PP$ into the four atropisomers was carried out by column chromatography on silica gel eluted with 98:2 chloroform-methanol. The preparation and purification of the four atropisomers of ToPivPP was described previously.[5]

The isomerization reactions of $ToNH_2PP$ were conducted in toluene or 1,1,2-trichloroethane solutions heated at a temperature range of 65 to 95 °C. The quantity of each isomer at appropriate reaction times was evaluated spectrometrically on the chloroform extracts of the TLC spots, or measured directly by the integrated peak area recorded on a TLC scanner.

The isomerization reactions of ToPivPP were monitored by the NMR spectral changes recorded on a JEOL FX-100 spectrometer operating in FT mode. The NMR signals due to the methyl protons of the pivaloylamino substituent allow an unambiguous assignment to each of the four conformations as described.[5] The isomerization of ToPivPP was carried out by dipping an NMR tube containing a toluene-d_8 solution of the isomers into the heated oil bath.

Results and Discussion

Thermal rotation of one substituted phenyl ring about the phenyl–porphyrin bond lead to the stereochemical isomerization reactions among the atropisomers of $ToNH_2PP$ or ToPivPP as shown schematically in Fig. 1. The R_f values on TLC eluted with 95:5 chloroform–methanol are 0.26, 0.18, 0.07, and 0.03 for $\alpha\beta\alpha\beta$-, $\alpha\alpha\beta\beta$-, $\alpha\alpha\alpha\beta$-, and $\alpha\alpha\alpha\alpha$-isomer of $ToNH_2PP$, respectively.

On permitting a toluene solution of $ToNH_2PP$ isomers to stand for 2 d at 80 °C, the four isomers were present in 0.15, 0.27, 0.49, and 0.09 ratio for the $\alpha\beta\alpha\beta$-, $\alpha\alpha\beta\beta$-, $\alpha\alpha\alpha\beta$-, and $\alpha\alpha\alpha\alpha$-isomers, respectively. The ratio was close to the statistical 1:2:4:1 ratio expected in equilibrium for the case where there is no mutual interaction between the *ortho* substituents.[4] The free energy difference corresponding to the small deviation from the ideal ratio was evaluated to be at most 0.4 kJ mol^{-1}. This value is small enough to be ignored in the rate constant determination. Therefore the rate data could be processed by assuming the idealized statistical ratio at equilibrium. Under these conditions, each isomer is considered to possess four equivalent rotational bonds. Thus, a relationship in the rate constants is deduced as follows: $k_r=k_2=k_6=k_4/2=k_1/4=k_3/4=k_5/4$, where k_r is the rate constant for the rotation about one phenyl–porphyrin bond of any isomer. The observed rate constants entered in Fig. 1 are consistent with this relationship within the experimental errors. The values of k_r were determined from several independent experiments at 65, 75, 85, 93, and 95 °C.

The equilibrium mixture of ToPivPP atropisomers produced by heating a solution of $\alpha\alpha\alpha\alpha$-

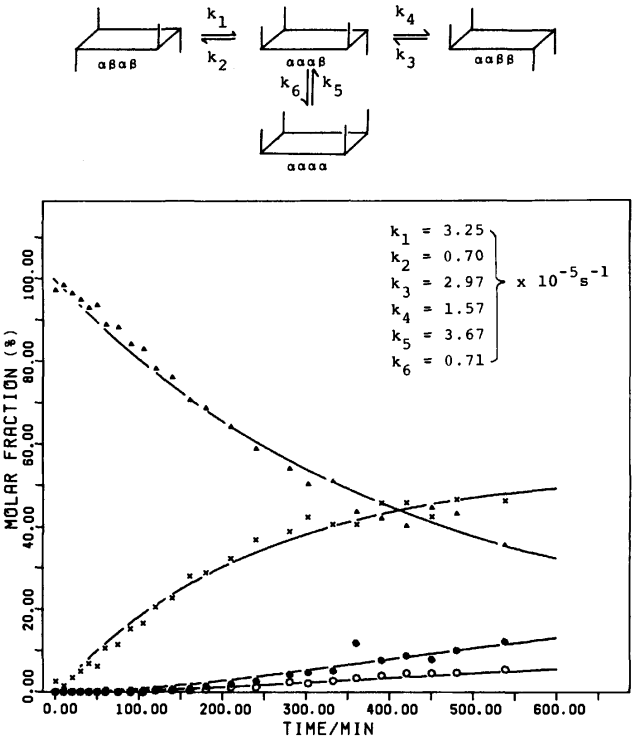

Fig. 1. Time course of isomerization starting from $\alpha\alpha\alpha\alpha$- isomer of $ToNH_2PP$ at 65 °C.
(○) $\alpha\beta\alpha\beta$; (●) $\alpha\alpha\beta\beta$; (×) $\alpha\alpha\alpha\beta$; (▲) $\alpha\alpha\alpha\alpha$. The solid lines are the best fit curves computed from the rate constants in the frame.

Table 1. Activation parameters for the rotation of the *ortho*-substituted phenyl ring about the porphyrin-phenyl bond in free base tetraaryl porphyrins

Substituent group	ΔG^*/kJ mol^{-1}					ΔH^*/kJ mol^{-1}	ΔS^*/J deg	Ref
	296 K	333 K	338 K	354 K	433 K	(333 K)		
Piv[a]		125.6				66.6	−177	This work
HA[b]				118.5[c]		54.4	−168[c,d]	(6)
NH_2	113.2[e]	115.6[e]	115.9	117.0[e]	122.3[e]	91.6	−72	This work
CN		103.0[c]				87.0	−60	(4)
OH	100							(2)
CH_3O					108			(3)

a) Pivaloylamino. b) Hexadecyloylamino. c) Derived from the rate constant for the isomerization of *αααα*- to *ααaβ*-isomer. d) 354 K. e) Extrapolated value.

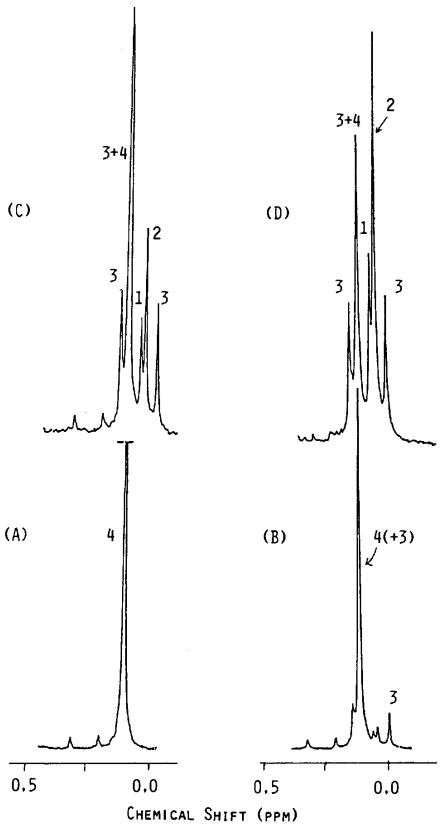

Fig. 2. NMR spectral changes during atropisomerization of ToPivPP at 90°C. Reaction time (A) 0 h (B) 30 h (C) 76 h (D) more than 720 h and the signal assignment 1.*αβαβ*; 2.*ααββ*; 3.*αααβ*; 4.*αααα* are shown.

isomer at 90°C for more than 30 d contained four isomers in a ratio of 0.14:0.28:0.47:0.11 for the respective *αβαβ*, *ααββ*, *αααβ*, and *αααα*-isomers. This ratio is surprisingly close to the statistical ratio.[6] Hence, the rate determination was carried out with the *αααα*-isomer by assuming the same relationship as in the $ToNH_2PP$ case. The outline of the NMR spectral changes during the atropisomerization reaction of ToPivPP and the signal assignment to each isomer are shown in Fig. 2. The rate constants for rotation about one axis were determined graphically. The k_r values for ToPivPP were obtained at 60, 90, and 103°C. The derived kinetic parameters are listed in Table 1.

The rotational barrier is brought about mainly by the steric hindrance of the *ortho* substituent on the phenyl ring. The bulk of the substituents is the most important factor to affect the height of the barrier. The evaluation of the barrier depending on the *ortho* substituents requires comparison of data at the same temperature. For this purpose, the extrapolation using the Arrhenius activation energy measured in a wide range of temperatures will be effective. The thermochemical activation parameters reported for some *ortho* substituents of tetraarylporphyrin free bases are summarized in Table 1 using the data of the NH_2 group as a common standard. The order of Piv>HA~NH_2>CN>CH_3O~OH with decreasing ΔG^* values was observed as the effect of substituents. The order is reasonable in view of the bulk of the *ortho* substituents, although the high barrier for the NH_2 group is remarkable. The actual friction for rotational isomerization generated by the two protons of NH_2 may be much more resistive than that expected by the simple comparison of the ionic radii.

Another remarkable feature of the kinetic parameters is the difference in the entropy of activation dependent on the substituents. All ΔS^* took negative values.[6] The order was Piv~THA>NH_2~CN with decreasing of the absolute values of ΔS^*. The order is also compatible with the bulk of the *ortho* substituents. This suggests that a bulky substituent at the *ortho* position makes a large contribution to the entropy term in the energy of activation for the rotational isomerization reaction.

References

1) J. P. Collman, R. R. Gagne, C. A. Reed, T. R. Halbert, G. Lang, and W. T. Robinson. *J. Am. Chem. Soc.*, **97**, 1427 (1975).

2) L. K. Gottwald and E. F. Ullman. *Tetrahedron Lett.*, **1969**, 3071.

3) J. W. Dirks, G. Underwood, J. C. Matheson, and D. Gust, *J. Org. Chem.*, **44**, 2551 (1979).

4) K. Hatano, K. Anzai, T. Kubo, and S. Tamai, *Bull. Chem. Soc. Jpn.*, **54**, 3518 (1981).

5) K. Anzai and K. Hatano, *Chem. Pharm. Bull.*, **32**, 1273 (1984).

6) R. A. Freitag, J. A. Mercer-Smith, and D. G. Whitten, *J. Am. Chem. Soc.*, **103**, 1226 (1981), communicated a nonstatistical distribution of ToPivPP atropisomers detected by spectrophotometric methods although the ratio was unreported. It seems that there is some disagreement in the spectral observations for ToPivPP between these authors and us.[5] Their rate data obtained at two temperatures for ToPivPP were not entered in Table 1.

Bromochlorination of Conjugated Dienes with Dichlorobromate(1-) Ion

Takeshi NEGORO* and Yoshitsugu IKEDA
Department of Chemistry, Faculty of Education, Wakayama University, Sakaedani, Wakayama 640
(Received July 22, 1985)

Synopsis. The reactions of some conjugated dienes with tetrabutylammonium dichlorobromate (1-) (**1**) were found to give the bromochloroalkenes in good yields, 1,2-addition predominating. Appreciable *anti*-Markownikoff adduct was obtained from 1,3-butadiene. An $AdEC_2$-type mechanism is suggested.

The ratio of 1,2- to 1,4-addition of bromine (and bromine chloride) to conjugated dienes has been shown to be markedly dependent on the brominating (and bromochlorinating) agents employed.[1,2] The predominance of 1,2-addition was observed for the reaction with a tribromide ion.[2,3] However, no studies have been carried out on the reaction with tetrabutylammonium dichlorobromate (1-) (**1**) as a bromochlorinating agent. We have reported that the additions of **1** to alkenes are strikingly different from that of molecular bromine chloride (BrCl).[4,5] In this paper, we will report the bromochlorination of some conjugated dienes with **1**.

Results and Discussion

The reaction of **1** with 1, 3-butadiene (**2a**), 2-methyl-1, 3-butadiene (**2b**), *cis*- and *trans*-1,3-pentadienes (**2c** and **2d**), and cyclopentadiene (**2e**) in dichloromethane gave the corresponding bromochloroalkenes in good yields (Table 1). In the cases of **2b** and **2e**, a small amount of 1, 4-dichloro adducts (**6**) was isolated.

TABLE 1. REACTIONS OF DIENES WITH **1**[a]

Dienes	1,2-Adduct[b]		1,4-Adduct[b]		Yield/%[c]
	3	**4**	**5**	**6**	
2a	99.0[d]		1.0		98
2b	78.6	11.0	9.2	1.2	98
2c	66.2	29.4	4.4		99
2d	87.1	5.1	7.8		99
2e	93.2		0.9	5.9[e]	93

a) Reactions were carried out with 30 mmol of **1**, 36 mmol of diene, and 100 ml of CH_2Cl_2 at −12°C. b) The products are identified as follows: from **2a**, 4-bromo-3-chloro-1-butene (**3a**), 3-bromo-4-chloro-1-butene (**3a′**), *trans*-1-bromo-4-chloro-2-butene (**5a**); from **2b**, 4-bromo-3-chloro-3-methyl-1-butene (**3b**), 4-bromo-3-chloro-2-methyl-1-butene (**4b**), 1-bromo-4-chloro-2-methyl-2-butene (**5b**),1,4-dichloro-2-methyl-2-butene (**6b**); from **2c** and **2d**, *cis*- and *trans*-5-bromo-4-chloro-2-pentenes (**3c** and **3d**), *threo*- and *erythro*-4-bromo-3-chloro-1-pentenes (**4c** and **4d**), *trans*-1-bromo-4-chloro-2-pentene (**5c**=**5d**); from **2e**, *trans*-4-bromo-3-chlorocyclopentene (**3e**), *cis*-3-bromo-5-chlorocyclopentene (**5e′**), *cis*- and *trans*-3,5-dichlorocyclopentenes (**6e′** and **6e**). Percentages are normalized to 100%. c) Based on **1**. Total bromochloralkene yields determined by GLC using 1,2-dibromobutane as an internal standard. d) **3a**:**3a′**=84:16. e) **6e**:**6e′**=35:65.

Furthermore, in all cases, the yield of 1, 4-bromochloro adducts (**5**) decreased by the prolonged reaction time, producing **6**. It was shown that **6** is also formed upon treatment of **5** with tetrabutylammonium chloride in CH_2Cl_2. Therefore, it probably arises by the halogen-exchange reaction of 5 with generating chloride ions in the reaction system. Control experiments showed that all the 1, 2-bromochloro adducts (**3** and **4**) are stable under the reaction conditions.

A common characteristic of the present reaction is the highly selective formation of the 1, 2-bromochloro adducts. Moreover, the addition to the 3, 4-bond in **2c**, **2d**, and **2e** gave completely *anti*-stereospecific products (**4c**, **4d**, and **3e**).

In the case of **2a**, the reaction gave a mixture of 4-bromo-3-chloro-1-butene (**3a**) and 3-bromo-4-chloro-1-butene (**3a′**) as the 1, 2-adducts.

$$\underset{\textbf{2a}}{CH_2{=}CHCH{=}CH_2} + \textbf{1} \longrightarrow \underset{\textbf{3a},\ 84\%}{CH_2BrCHClCH{=}CH_2} + \underset{\textbf{3a}',\ 16\%}{CH_2ClCHBrCH{=}CH_2}$$

Fig. 1.

When the reaction of **2a** with **1** was carried out in the presence of a free radical inhibitor, 2,6-di-*t*-butyl-4-methylphenol or oxygen, the product composition did not change within experimental errors. This result indicates that the lack of regiospecificity cannot be ascribed to a radical process.[6]

The reaction of **2a** with **1** was investigated in a variety of solvents. The reaction in chloroform, dichloromethane, 1,2-dichloroethane, acetic anhydride, and nitromethane gave nearly the same ratio of **3a** and **3a′** (84:16) within an experimental error (±1%). The amount of the 1,4-adduct (**5a**) was less than 2% in all the solvents employed. A similar solvent independency on the regiochemistry has been previously observed for the reaction of 1-phenylpropenes with **1**.[5]

In contrast to the present results, the high preference of 1,4-addition has been observed for the reaction of BrCl (and Br_2) with conjugated dienes.[1,2,7] Furthermore, dependence of the 1,2- *vs.* 1,4-addition of Br_2 to **2a** on solvent polarity has been reported.[7] We have also found that BrCl reacted with **2a** to give a mixture of **3a** and **5a** (**3a**:**5a**=27:73). None of the *anti*-Markownikoff adduct (**3a′**) was detected by ^{13}C-NMR analysis of the product mixture.

Thus, the addition to dienes appeared to be very different in reactions with **1** and with BrCl. Therefore, the present reaction cannot be explained on the basis of any accepted mechanism involving a bromonium ion intermediate for the addition of BrCl (and Br_2).[2,3] We would like to suggest another possible mechanism

which involves the attack of chloride ions on a three-center bound π complex-type intermediate (**7**) with little delocalization of the positive charge across the allylic system: a similar mechanism has been suggested for the addition of **1** to alkenes.[4,5]

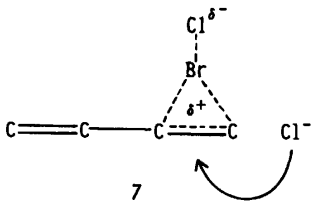

7

Experimental

The NMR and mass spectra were recorded on a JEOL JNM FX-60Q and JMS-D-300 mass spectrometer, respectively. The GLC analyses were performed on a Yanako G-180 Gas Chromatograph with a Silicone SE-30 (2.5%)-Chromosorb WAW DMCS (2 m) column at 50 °C with helium as a carrier gas (35 ml/min). All the organic starting materials were distilled before use.

*Reaction of **2a** with **1**.* Details of the reaction have been reported previousiy.[4] To a solution of **2a** (3.0 ml, 36 mmol) in CH_2Cl_2 (100 ml) was added **1** (11.8 g, 30 mmol) at −12 °C over 20 min with stirring. After the usual work-up, distillation afforded 3.83 g (75.3%) of a mixture of **3a** and **3a′**: Bp 46—48 °C/26 mmHg (1 mmHg=133.322 Pa); MS M$^+$ at *m/z*=168, 170, 172 (100:132:35); Found: *m/z* 167.9330. Calcd for C_4H_6BrCl: M, 167.9342. ^{13}C-NMR showed a 84:16 mixture of **3a** and **3a′**, respectively. ^{13}C-NMR ($CDCl_3$) (an asterisk indicates **3a′**) δ=35.0, 47.0*, 51.1*, 60.2, 119.7, 135.2, 135.5*. Although attempts to separate **3a** and **3a′** were unsuccessful, these assignments were supported for dibromo and dichloro analogs as follows: 3,4-dichloro-1-butene, ^{13}C-NMR ($CDCl_3$) δ=47.3, 60.1, 119.7, 134.8; 3,4-dibromo-1-butene, ^{13}C-NMR ($CDCl_3$) δ=34.5, 50.5, 119.8, 136.0. The structure of the minor 1,4-adduct (**5a**) was verified by comparison of the spectra of the sample prepared by the reaction of **2a** with BrCl.[2] **5a**, ^{1}H-NMR ($CDCl_3$) δ=3.90—4.10 (4H, m, CH_2Br and CH_2Cl), 5.90—6.01 (2H, m, CH=CH); ^{13}C-NMR ($CDCl_3$) δ=30.9, 43.5, 130.3 (2C).

*Reaction of **2b—e** with **1**.* The reactions were carried out similarly to those of **2a**. The relative amounts of the products were determined by the peak areas of GLC (Table 1). All the reaction products were identified by comparing GLC and NMR spectra with the authentic samples prepared by the reaction of BrCl with these dienes.[1,2] The ^{1}H-NMR spectra of the products correspond well with those reported in the literatures.[1,2]

*Reaction of **2a** with **1** Under Various Conditions.* When **2a** was treated with **1** in CH_2Cl_2 as described above, O_2 was bubbled during the reaction. ^{13}C-NMR analysis of the residue showed an 85:15 mixture of **3a** and **3a′**, respectively. The reaction was carried out with 12 mmol of **2a**, 10 mmol of **1**, and 3 mmol of 2,6-di-*t*-butyl-4-methylphenol in CH_2Cl_2 (50 ml). After the usual work-up, ^{13}C-NMR analysis of the residue showed an 86:14 mixture of **3a** and **3a′**, respectively.

To 12 mmol of **2a** in 50 ml of the solvent ($CHCl_3$, CH_2Cl_2, CH_2ClCH_2Cl, $(CH_3CO)_2O$, and CH_3NO_2) was added 10 mmol of **1** at −12 °C over 5 min with stirring. After the usual work-up, the residues were subjected to GLC and ^{13}C-NMR analyses. In all cases, GLC analysis showed over 98% of the 1, 2-adducts. ^{13}C-NMR analysis showed nearly the same ratio of **3a** and **3a′** (84:16) within an experimental error (±1%).

Halogen Exchange Reaction. To 5 mmol of **5a** in CH_2Cl_2 (25 ml) was added 10 mmol of tetrabutylammonium chloride and the mixture was allowed to stand for 24 h at 0 °C with stirring. After the usual work-up, GLC analysis showed the composition to be: **5a**, 5%; *trans*-1,4-dichloro-2-butene (**6a**), 95%. Similar treatment of **5b—e** and **5e′** with chloride ions gave over 95% of the corresponding 1,4-dichloro compounds.

References

1) V. L. Heasley, C. N. Griffith, and G. L. Heasley, *J. Org. Chem.*, **40**, 1358 (1975).
2) G. E. Heasley, J. M. Bundy, V. L. Heasley, S. Arnold, A. Gipe, D. McKee, R. Orr, S. L. Rodgers, and D. F. Shellhamer, *J. Org. Chem.*, **43**, 2793 (1978).
3) G. Bellucci, G. Berti, R. Bianchini, G. Ingrosso, and K. Yates, *J. Org. Chem.*, **46**, 2315 (1981).
4) T. Negoro and Y. Ikeda, *Bull. Chem. Soc. Jpn.*, **57**, 2111 (1984).
5) T. Negoro and Y. Ikeda, *Bull. Chem. Soc. Jpn.*, **57**, 2116 (1984).
6) V. L. Heasley, D. W. Spaite, D. F. Shellhamer, and G. E. Heasley, *J. Org. Chem.*, **44**, 2608 (1979).
7) V. L. Heasley, G. E. Heasley, R. A. Loghry, and M. R. McConnell, *J. Org. Chem.*, **37**, 2228 (1972).

Palladium-catalyzed Reaction of Stannyl Sulfide with Aryl Bromide. Preparation of Aryl Sulfide

Masanori KOSUGI,* Toshimi OGATA, Masahiro TERADA, Hiroshi SANO, and Toshihiko MIGITA*
Department of Chemistry, Faculty of Technology, Gunma University, Kiryu, Gunma 376
(Received August 5, 1985)

Synopsis. Tributylstannyl alkyl or aryl sulfide and bis(tributylstannyl) sulfide were found to be useful to prepare aryl sulfides in good yields under the usual conditions of the palladium-catalyzed reaction with aryl bromides.

Versatility of organotin reagents can be found in that organotin compounds having either carbon–tin bond[1] or heteroatom–tin bond can be utilized in palladium-catalyzed cross-coupling with organic halides. Thus, silylstannane,[2] distannane,[3] and aminostannane[4] transfer silyl, stannyl, and amino groups to aryl halides, respectively. However, palladium-catalyzed alkoxylation or acyloxylation of aryl halides by using the alkoxy or acyloxy tin compounds is not attained so far. In contrast, stannyl sulfide, an analogue of stannyl alkoxide, was found to undergo the cross-coupling with aryl bromides.[6]

In this note, we report the palladium-catalyzed reaction of stannyl sulfides with aryl bromides.

$$n\text{-Bu}_3\text{SnSR} + \text{ArBr} \xrightarrow{[\text{Pd}]} \text{ArSR} + n\text{-Bu}_3\text{SnBr}$$

Previously we reported that aryl phenyl or aryl alkyl sulfides were formed by the reaction of sodium benzenethiolate or alkanethiolate with aryl iodides or bromides, catalyzed by palladium.[5] The present method is an alternative one without any use of strong base and is applied to aryl bromides bearing wider variety of substituents. Results are summarized in Table 1.

The reaction took place with either butylthio or phenylthio tin compounds and gave the sulfides in good yields regardless of the nature of functional groups in substrates. With mesityl bromide, the yield was rather low probably due to steric hindrance. As the yield did not depend on the solvent polarity, we chose aromatic hydrocarbon for the convenience of its removal in workup processes.

The reaction of bis(tributylstannyl) sulfide was exemplified for the preparation of symmetrical sulfide as shown in Table 2, although the palladium-catalyzed reaction of aryl iodides or vinyl bromides with bis(triethylstannyl) sulfide has appeared in a recent review of Beletskaya[6] without any reference cited. The reaction was carried out under similar conditions to those shown in Table 1. The reaction gave the sulfide in moderate yields except with aryl bromides having ortho substituents. A similar situation was also observed in the reaction with vinyl bromides, showing that steric hindrance might be an important factor in these reactions. Trials for the preparation of unsymmetrical sulfides by using a mixture of two bromides were failed.

Experimental

IR spectra were recorded on a Jasko A-100 spectrophotometer. ^{1}H NMR spectra were recorded on a Varian EM-360 instrument. GLC analyses were carried out with an Ohkura 802 instrument, using columns (1.5 m) packed with 10% Silicone SF-96 and SE-30 on Celite 545.

Materials. Tributylstannyl butyl and phenyl sulfide were prepared by treating the corresponding thiols with tributyltin oxide in the presence of base (sodium ethoxide).[7] Bis(tributylstannyl) sulfide was prepared by the reaction of tributyltin oxide with thiourea.[7] Palladium complex and halide were already reported.[1b]

Reaction Procedures. A mixture of stannyl sulfide (1.3 mmol), halide (1.0 or 2.0 mmol), tetrakis(triphenylphosphine)palladium (1 mol%), and toluene or xylene (1 cm^3) was heated under argon at 120 °C for 20 h. After the reaction mixture was washed with aqueous potassium fluoride and filtered to remove tributyltin fluoride, the organic layer was extracted with ether and dried over magnesium sulfate. The product was distilled by Kugelrohr.

Products. Most of the products were known and their structures were identified by IR and ^{1}H NMR spectra.

Di-p-tolyl Sulfide: ^{1}H NMR (CCl_4) δ=2.29 (s, 6H) and 6.8—7.3 (m, 8H). Found: C, 78.05; H, 6.73%. Calcd for $C_{14}H_{14}S$: C, 78.46; H, 6.58%.

Bis(p-chlorophenyl) Sulfide: Found: C, 56.94; H, 3.19%. Calcd for $C_{12}H_8Cl_2S$: C, 56.49; H, 3.16%.

Bis(p-acetylphenyl) Sulfide: IR (CCl_4) 1270 and 1690 cm^{-1} (C=O). ^{1}H NMR (CCl_4) δ=2.50 (s, 6H) and 7.34 and 7.55 (ABq, J=9Hz, 8H). Found: C, 71.19; H, 5.23%. Calcd for $C_{14}H_{14}O_2S$: C, 71.09; H, 5.22%.

Bis(p-cyanophenyl) Sulfide: IR (CCl_4): 2230 cm^{-1} (CN). ^{1}H

TABLE 1. REACTION OF TRIBUTYLSTANNYL BUTYL OR PHENYL SULFIDE WITH ARYL BROMIDES

$$\text{Bu}^n_3\text{SnSR}^1 + \text{X-C}_6\text{H}_4\text{Br} \xrightarrow{[\text{Pd}]^{a)}} \text{X-C}_6\text{H}_4\text{SR}^1 + \text{Bu}^n_3\text{SnBr}$$

R^1	X	Yield of $ArSR^1$/%[b]	R^1	X	Yield of $ArSR^1$/%[b]
Bu^n	H	86	Ph	*p*-Cl	74
Ph	H	(83)	Ph	*o*-Cl	73
Ph	*p*-Me	(76)	Ph	*p*-MeCO	67
Ph	*o*-Me	(67)	Ph	*p*-CN	72
Ph	*p*-MeO	100	Ph	*p*-NO_2	52
Ph	*o*-MeO	66	Ph	2,4,6-Me_3	34

a) $Pd(PPh_3)_4$, b) GLC yields based on the bromide, in parentheses isolated yields.

TABLE 2. REACTION OF BIS(TRIBUTYLSTANNYL) SULFIDE WITH ARYL OR VINYL BROMIDES

$Bu^n_3SnSSnBu^n_3 + 2R\text{-}Br \xrightarrow{[Pd]^{a)}} R\text{-}S\text{-}R + 2Bu^n_3SnBr$

R-Br	Yield of RSR/%[b]	R-Br	Yield of RSR/%[b]
C_6H_5-	75	*p*-$MeCOC_6H_4$-	52
p-MeC_6H_4-	23	*p*-NCC_6H_4-	57
m-MeC_6H_4-	50	*p*-$O_2NC_6H_4$-	44
p-MeC_6H_4-	60	2,4,6-$Me_3C_6H_2$-	3[c]
p-$MeOC_6H_4$-	62	(E) PhCH=CH-	77
m-ClC_6H_4-	60	Me_2C=CH-	25
p-ClC_6H_4-	86	Me_2C=CMe-	0

a) $Pd(PPh_3)_4$, b) Isolated yields based on the bromide, c) GLC yield.

NMR (CCl_4) δ=7.32 and 7.55 (ABq, J=8Hz). Found: C, 71.56; H, 3.54; N, 11.72%. Calcd for $C_{14}H_8N_2S$: C, 71.16; H, 3.41; N, 11.86%.

Bis(p-*nitrophenyl*) *Sulfide*: IR (CCl_4) 1350 and 1515 cm^{-1} (NO_2). ^1H NMR (CCl_4) δ=7.63 and 8.07 (ABq, J=9Hz). Found: C, 52.32; H, 2.86; N. 10.19%. Calcd for $C_{12}H_8N_2O_4S$: C, 52.17; H, 2.92; N, 10.14%.

The gift of tributyltin oxide by Kohriyama Kasei Co. is gratefully acknowledged.

References

1) a) M. Kosugi, K. Sasazawa, Y. Shimizu, and T. Migita, *Chem. Lett.*, **1977**, 301; b) M. Kosugi, I. Hagiwara, T. Sumiya, and T. Migita, *Bull. Chem. Soc. Jpn.*, **57**, 242 (1984); c). J. W. Labadie, D. Tueting, and J. K. Stille, *J. Org. Chem.*, **48**, 4634 (1983).

2) H. Azizian, C. Eaborn, and A. Pidcock, *J. Organometal. Chem.*, **215**, 49 (1981).

3) M. Kosugi, T. Ohya, and T. Migita, *Bull. Chem. Soc. Jpn.*, **56**, 3855 (1983).

4) M. Kosugi, M. Kameyama, and T. Migita, *Chem. Lett.*, **1983**, 927.

5) T. Migita, T. Shimizu, Y. Asami, J. Shiobara, Y. Kato, and M. Kosugi, *Bull. Chem. Soc. Jpn.*, **53**, 1385 (1980).

6) I. P. Beletskaya, *J. Organometal. Chem.*, **250**, 551 (1983).

7) A. G. Davies and P. J. Smith, "Comprehensive Organometallic Chemistry," ed by Sir G. Wilkinson, Vol. 2, Pergamon Press (1982) p. 604.

Substituent Effects on Cation-extraction and Transport Properties of a Series of 4′-Substituted Benzo-15-Crown-5 Derivatives

Hiroshi TSUKUBE,* Kentaro TAKAGI, Tatsuo HIGASHIYAMA, Tadashi IWACHIDO, and Naomi HAYAMA
Department of Chemistry, College of Liberal Arts and Science, Okayama University, Okayama 700
(Received August 7, 1985)

Synopsis. The substituent effects on chemical functions of benzo-15-crown-5 derivatives were found to be considerably large and often comparable to the ring-size effects. For example, 4′-aminobenzo-15-crown-5 transported K^+ ion 14-times faster than 4′-nitrobenzo-15-crown-5, while 4′-nitrobenzo-18-crown-6 showed 12-times higher transport rate than 4′-nitrobenzo-15-crown-5.

Macrocyclic crown ethers form stable and selective complexes with alkali and alkaline earth cations, and show characteristic cation-transport and related functions.[1] Since their cation-binding properties are largely changed by chemical modifications of crown ether structures,[2] a variety of functional substituents have been introduced into crown ether skeletons. Here we examined the cation-extraction and transport properties of a series of 4′-substituted benzo-15-crown-5 derivatives, and found that the substituent effects on chemical functions of crown ethers were considerably large and often comparable to the crown ring-size effects. Although several types of benzo-crown ether derivatives have been prepared as cation-binders, carriers, and catalysts,[3] this is the first report concerning substituent effects on the cation-transport phenomena.[4] Therefore, the present study may offer the further possibilities in the designing new functional benzo-crown ethers and related polymers.

Results and Discussion

1. Substituent Effects on Cation-extraction Properties of Benzo-15-Crown-5 Derivatives. The cation-extraction properties of a series of benzo-15-crown-5 derivatives **1**, **3**, **4**, and **5** were examined by equilibrating a CH_2Cl_2 solution of a crown ether with an aqueous solution of metal perchlorate.

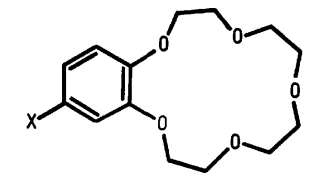

1: X=NH_2
2: X=t-C_4H_9
3: X=H
4: X=Br
5: X=NO_2

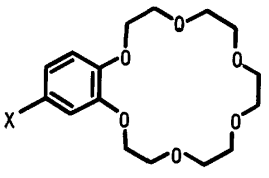

6: X=NO_2

Fig. 1. Examined benzo-crown ethers.

The examined benzo-15-crown-5 derivatives extracted Na^+ and K^+ ions much more effectively than Li^+ and Cs^+ ions under the employed conditions (Table 1). Their extraction properties were generally controlled by guest cation-crown ring size fitness, and also largely influenced by the natures of 4′-substituents attached to benzene ring. For example, crown **1** bearing electron-donating -NH_2 group showed higher extraction abilities for Na^+ and K^+ ions than crowns **4** and **5** bearing electron-withdrawing -Br and -NO_2 substituents. Smid *et al.* have measured the stability constants for some Na^+·benzo-15-crown-5 complexes in acetone and observed somewhat similar substituent effects: $K\times10^{-3}$ (M^{-1})=8.21 for **1**; 2.05 for **4**; 0.165 for **5**.[4a] As shown before,[4] substituent groups attached to benzene rings may change basicities of two aromatic ether oxygen atoms. (1 M=1 mol dm^{-3}).

4′-Nitrobenzo-18-crown-6 (**6**) extracted K^+ ion more effectively than 4′-nitrobenzo-15-crown-5 (**5**). Since K^+ ion fits ring size of 18-membered crown ether more tightly than that of 15-membered one, crown ring size effects seemed to be a dominant factor as reported frequently.[1] However, its extraction efficiency and selectivity for K^+ ion were lower than those of benzo-15-crown-5 derivatives **1** and **3**. These observations strongly suggest that the nature of substituent is a more important factor in determining extraction ability than ring size of parent crown ether.

2. Substituent Effects on Cation-transport Properties of Benzo-15-Crown-5 Derivatives. The transport experiments were performed in the CH_2Cl_2 liquid membrane,[5] in which crown ether solubilizes guest cation salt into the membrane and facilitates transport from source aqueous phase through CH_2Cl_2 membrane to receiving aqueous phase. The measured values of initial cation-transport rates are summarized in Table 2.

The transport rates of Na^+ and K^+ ions with benzo-

Table 1. Extraction properties of benzo-crown ethers

Crown	Extraction Percentage/%[a]			
	Li^+	Na^+	K^+	Cs^+
1	0	3.6	13.6	0.4
3	0.4	3.8	10.4	0
4	0	0.8	2.8	0
5	0.2	1.8	3.6	0
6	0	3.4	4.6	2.1

Conditions: Aqueous phase; Metal perchlorate, 0.02 mmol/H_2O, 2 ml. Organic phase; Crown, 0.15 mmol/CH_2Cl_2, 3 ml. a) [Metal salt extracted in CH_2Cl_2]/[Metal salt added initially]×100 was shown, which was calculated from the difference in the extraction percentages of crown-containing and blank (no crown) systems.

Table 2. Transport properties of benzo-crown ethers

Crown	Transport Rate ($\times 10^6$ mol/h)[a]			
	Li^+	Na^+	K^+	Cs^+
1	0.1	0.7	9.9	1.1
2	<0.1	0.6	9.1	1.2
3	<0.1	0.6	8.9	0.7
4	<0.1	0.2	2.3	0.3
5	<0.1	0.1	0.7	<0.1
6	<0.1	0.4	8.7	3.0

Conditions; Source aqueous phase; Metal perchlorate, 0.5 mmol/H_2O, 5 ml. Membrane phase; Crown, 0.05 mmol/CH_2Cl_2, 12 ml. Receiving aqueous phase; H_2O, 5 ml. a) The values indicated were calculated from the difference in the transport rates of carrier-containing and blank (no carrier) systems. Reproducibility was confirmed as ±15% or better.

15-crown-5 derivatives also showed a pronounced dependence on the natures of 4′-substituents attached to benzo-crown ring. The electron-withdrawing substituents such as -Br and -NO_2 groups largely decreased transport rates of Na^+ and K^+ ions, though electron-donating -NH_2 and -t-C_4H_9 groups offered fast transport rates. As a result, a 14-fold difference in the transport rates of K^+ ion was observed between benzo-15-crown-5 derivatives **1** and **5**. When 4′-nitrobenzo-18-crown-6 (**6**) was employed as a carrier, its transport rate of K^+ ion was 12-times higher than that of 4′-nitrobenzo-15-crown-5 (**5**), but lower than those of 4′-amino- and 4′-*t*-butylbenzo-15-crown-5 derivatives **1** and **2**. Since we confirmed that the leakages of the examined benzo-crown ethers **1**—**6** were almost negligible,[6] the present results demonstrate that transport profiles are easily modified by simple substitution of benzo-crown ether. In other words, the nature of substituent introduced into crown ether skeleton should be seriously considered in the modification and functionalization of benzo-crown ether type ligand system.

Experimental

1. Materials. 4′-Substituted benzo-crown ethers **1**, **4**, **5**, and **6** were prepared as decribed before,[4a] and showed satisfactory Mass, ^{1}H-NMR, and ir spectral data. Crowns **2** and **3** were purchased from Merck Japan and Parish Chemical, respectively. Other employed reagents were commercially available and used without further purifications.

2. Extraction Procedures. The extraction abilities of crown ethers were estimated on the basis of the partition of metal perchlorate between CH_2Cl_2 (3 ml) and aqueous solution (2 ml). After extraction experiments (3 h), the aqueous phase was separated and the concentrations of K^+, Na^+, and ClO_4^- ions were determined by means of ion-selective electrodes (Orion Model 931901, 971100, and 938100). The crown **2** was not examined here, because of its low solubility into the CH_2Cl_2.

3. Transport Procedures. The transport experiments were carried out at room temperatue in a U-tube glass cell (2.0 cm, i. d.) as reported before.[5] The crown in CH_2Cl_2 (12 ml) was placed in the base of the U-tube, and two aqueous phases (5 ml, each) were placed in the arms of the U-tube, floating on the CH_2Cl_2 membrane. The membrane phase was constantly stirred with a magnetic stirrer. The transported amounts of K^+, Na^+, and ClO_4^- ions were also determined by ion-selective electrode techniques.

References

1) a) D. J. Cram and J. M. Cram, *Acc. Chem. Res.*, **11**, 8 (1978); b) J. M. Lehn, *ibid.*, **11**, 49 (1978); c) R. M. Izatt and J. J. Christensen, "Synthetic Multidentate Macrocyclic Compounds," Academic Press, New York (1978).

2) a) G. W. Gokel and S. H. Korzeniowski, "Macrocyclic Polyether Syntheses," Springer-Verlag, Berlin (1982); b) F. Vögtle, "Host Guest Complex Chemistry" I, Springer-Verlag, Berlin (1982).

3) a) S. Shinkai, T. Ogawa, Y. Kusano, O. Manabe, K. Kikukawa, T. Goto, and T. Matsuda, *J. Am. Chem. Soc.*, **104**, 1960 (1982); b) A. Warshawsky and N. Kahana, *ibid.*, **104**, 2663 (1982); c) V. Thanbel and V. Krishnan, *ibid.*, **104**, 3643 (1982); d) M. Berthet and E. Sonveaux, *J. Chem. Soc., Chem. Commun.*, **1983**, 10; e) E. Weber, *Angew. Chem. Suppl.*, **1983**, 840.

4) a) Substituent effects on the complex stabilities of benzo-15-crown-5 derivatives have been reported: R. Ungaro, B. E. Haj, and J. Smid, *J. Am. Chem. Soc.*, **98**, 5198 (1976); b) Substituent effects on the extraction properties of dibenzo-18-crown-6 systems: K. H. Pannell, W. Yee, G. S. Lewandos, and D. C. Hambrick, *J. Am. Chem. Soc.*, **99**, 1457 (1977).

5) a) K. Maruyama, H. Tsukube, and T. Araki, *J. Am. Chem. Soc.*, **104**, 5197 (1982); b) H. Tsukube, *J. Chem. Soc., Perkin Trans. 1*, **1985**, 615.

6) After transport experiments, the employed benzo-crown ethers remained in the membrane phase quantitatively, excepting for crown **1** (≈91%).

Possible Interpretation of Inactivity of Novel Gramicidin S Analogs by CD Spectral Analysis of Tetrapeptide Derivatives Related to the Analogs[1)]

Kazuki SATO, Ukon NAGAI,* and Makoto TAMAKI†
Mitsubishi-Kasei Institute of Life Sciences, 11 Minamiooya, Machida, Tokyo 194
†*Department of Chemistry, Faculty of Science, Toho University, Miyama, Funabashi, Chiba 274*
(Received August 9, 1985)

Synopsis. CD spectral analysis of chromophoric derivatives of tetrapeptides related to the β-turn part of [D-Val$^{1,1'}$]- and [D-Val$^{1,1'}$, L-Phe$^{4,4'}$]-gramicidin S indicated that they had very low preference for β-turn formation. The results suggested that neither analog could take gramicidin S-like β-sheet conformation. It seems noteworthy that the side-chain bulkiness of the 4th amino acid of a tetrapeptide affects the stability of β-turn.

In the previous papers, we reported that the CD spectra of *N*-(2,4-dinitrophenyl) tetrapeptide *p*-nitroanilides reflected well the β-turn preference of the tetrapeptide sequences.[2-4)] β-Turn preferences of the tetrapeptides related to the β-turn part of gramicidin S (GS), *cyclo*(-L-Val$^{1,1'}$-L-Orn$^{2,2'}$-L-Leu$^{3,3'}$-D-Phe$^{4,4'}$-L-Pro$^{5,5'}$-)$_2$ (Fig. 1),[5)] had good correlation with antibiotic activities of the GS analogs having similar tetrapeptides sequences at their β-turn parts.[3)]

Recently, one of the authors (M. Tamaki) and his co-workers synthesized [D-Val$^{1,1'}$]- and [D-Val$^{1,1'}$, L-Phe$^{4,4'}$]-GS and found that both analogs were inactive against Gram-positive bacteria.[6)] In this paper, we attempted to explain the inactivity of the analogs by β-turn preference of their partial sequences. First, we synthesized Dnp-L-Ala-D-Ala-L-Pro-D-Ala-pNA (**2D**) and Dnp-L-Ala-L-Ala-L-Pro-D-Ala-pNA (**2L**) as models of the partial sequences of [D-Val$^{1,1'}$]- and [D-Val$^{1,1'}$, L-Phe$^{4,4'}$]-GS, respectively. Especially, **2D** was of interest due to the LDLD sequence which have never been examined yet.

Figure 2 shows the CD spectra of **2D** and **2L** together with those of Dnp-L-Leu-D-Ala-L-Pro-L-Val-pNA (**1D**)[2)] and Dnp-L-Leu-L-Ala-L-Pro-L-Val-pNA (**1L**)[2)], which are model peptides for [D-Ala$^{4,4'}$]-GS,[7,8)] and [L-Ala$^{4,4'}$]-GS,[8)] respectively. Compound **2D** sbowed strong Cotton effect above 250 nm typical for the exciton coupling between the two terminal chromophores, though it was a little weaker than that of GS-model peptide **1D**. So, β-turn preference of the sequence in **2D** seems to be high enough to allow the GS-analog containing the similar sequence to take GS-like conformation. On the other hand, **2L** did not show any particular CD patterns above 250 nm suggesting that **2L** took random conformation. The CD spectrum seems to be explained by the summation of CD of a Dnp-L-amino acid and a D-amino acid *p*-nitroanilide as in the case of **1L**. So, the inactivity of [D-Val$^{1,1'}$, L-Phe$^{4,4'}$]-GS seems to be due to the difficulty of taking GS-like β-sheet conformation as in the case of [L-Ala$^{4,4'}$]-GS.[8)]

Though CD spectra of **2D** suggested that [D-Val$^{1,1'}$]-GS had some possibility of taking GS-like β-sheet conformation, the analog was inactive and showed different CD spectra from that of GS.[6)] Based on the molecular model study, we considered that the bulky D-Val side chain might destabilize the β-turn conformation because of large steric hindrance with carbonyl oxygen of the L-Pro residue (cf. Fig. 1). So, we

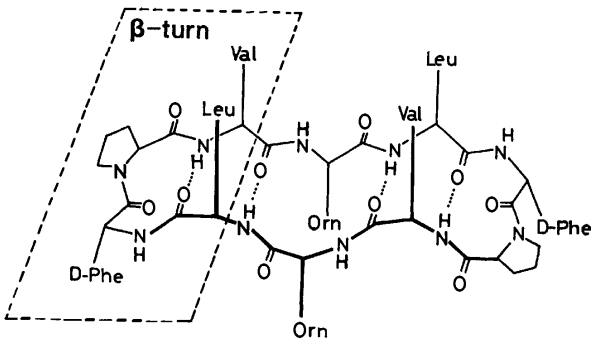

Fig. 1. β-Sheet conformation of gramicidin S.

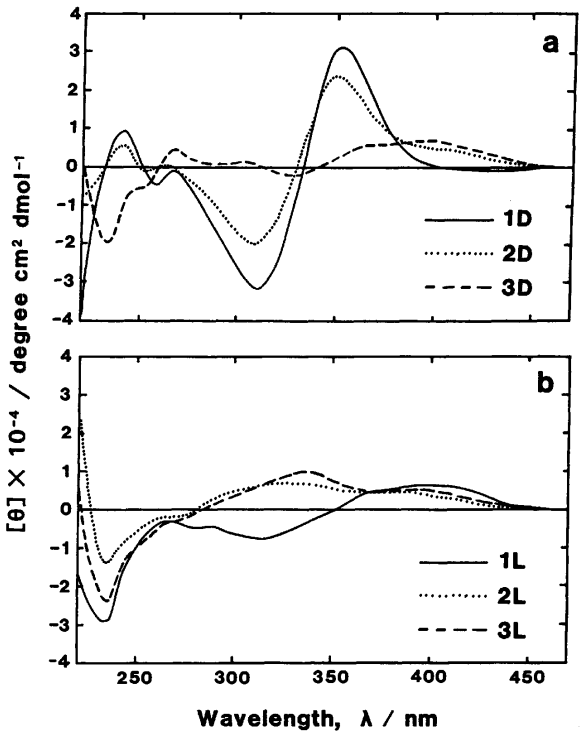

Fig. 2. CD spectra of (a) Dnp-X-D-Ala-L-Pro-Y-pNA and (b) Dnp-X-L-Ala-L-Pro-Y-pNA in MeOH. ——: X=L-Leu, Y=L-Val (**1D**, **1L**); ·····: X=L-Ala, Y=D-Ala (**2D**, **2L**); ------: X=L-Leu, Y=D-Val (**3D**, **3L**).

TABLE 1. YIELDS AND ANALYTICAL DATA OF SYNTHETIC PEPTIDES

Compound	Yield	Mp	$[\alpha]_D^{23}$ [a]	R_f^1	R_f^2	R_f^3	Found (%)			Calcd (%)		
	%	θ_m/°C	°				C	H	N	C	H	N
4L	72	192—193	41.8	0.67	0.32	0.79	55.68	6.61	14.33	55.34	6.54	14.67
5D	65	115—118	67.2	0.63	0.24	0.77	54.52	6.59	15.20	54.73	6.62	15.32
5L	68	118—120	24.4	0.63	0.24	0.80	54.24	6.64	15.09	54.29	6.65	15.19[b]
2D	81	146—148	117.2	0.62	0.18	0.76	50.18	4.86	18.01	50.08	5.01	17.97[c]
2L	97	274—276	47.6	0.70	0.17	0.79	50.39	4.91	17.53	50.08	5.01	17.97[c]
6D	72	226—229	140.1	0.67	0.29	0.81	56.86	6.87	13.84	57.02	6.98	13.85
6L	82	100—104	41.1	0.69	0.25	0.88	56.58	6.87	13.69	57.02	6.98	13.85
7D	57	112—116	53.7	0.77	0.25	0.79	57.33	7.33	13.15	57.40	7.55	13.39[c]
7L	76	117—120	14.0	0.77	0.25	0.88	57.12	7.30	12.99	57.40	7.55	13.39[c]
3D	71	120—124	84.8	0.75	0.27	0.79	53.46	5.76	16.01	53.33	5.79	16.05[d]
3L	79	125—127	63.2	0.75	0.29	0.83	53.38	5.73	15.79	53.33	5.79	16.05[d]

a) *c* 1, MeOH. b) $0.25H_2O$. c) $0.5H_2O$. d) $0.75H_2O$.

synthesized Dnp-L-Leu-D-Ala-L-Pro-D-Val-pNA (**3D**) and Dnp-L-Leu-L-Ala-L-Pro-D-Val-pNA (**3L**) as closer models to the original sequences of the GS analogs. Tetrapeptide **3D** as well as **3L** showed weak CD bands above 250 nm (Fig. 2). The result suggested that **3D** did not prefer to take β-turn conformation and therefore [D-Val$^{1,1'}$]-GS did not take GS-like β-sheet conformation.

Consequently, inactivity of both [D-Val$^{1,1'}$]- and [D-Val$^{1,1'}$, L-Phe$^{4,4'}$]-GS seems to be caused by the reluctance of their partial sequences to take β-turn conformation. However, the reason of reluctance seems to be different; partial sequence of the former has some potential to take β-turn conformation except for the steric hindrance of bulky D-Val side chain, whereas, that of the latter has not such potential at all.

Present study proves that CD spectra of the chromophoric derivatives of peptides are useful for interpreting the structure-activity relationships of GS analogs, and suggests that the bulkiness of the 4th-position amino acids as well as their configurations[9] has a significant effect on β-turn formation.

Experimental

All the melting points were uncorrected. Thin-layer chromatographies were carried out on Merck silica gel 60 F_{254} plates with the following solvent systems: R_f^1, $CHCl_3$–MeOH (5:1, v/v); R_f^2, $CHCl_3$–MeOH–AcOH (95:5:1, v/v); R_f^3, *n*-BuOH–AcOH–pyridine–H_2O (4:1:1:2, v/v). Optical rotations were measured on an Union automatic polarimeter PM-201. CD spectra were recorded on a JASCO J-40A spectropolarimeter at the concentration of 0.1 mM (1 M=1 mol dm^{-3}) at 23 °C. All the peptides were synthesized according to schemes shown in Fig. 3 by similar manners as reported previously,[3] and the results are summarized in Table 1.

We thank Professors Michiaki Takimoto of Toho University and Ichiro Muramatsu of Rikkyo University for helpful discussion, Miss Rika Kato of Mitsubishi-Kasei Institute of Life Sciences for her technical assistance, and the members of Analysis Center of Mitsubishi Chemical Industries Ltd. for elemental analysis.

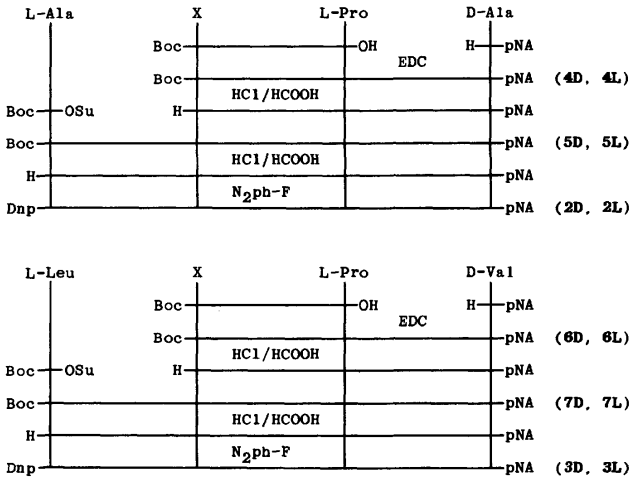

Fig. 3. Synthetic schemes of Dnp-tetrapeptide-pNA. Affix **D** or **L** means X=D-Ala or L-Ala, respectively.

References

1) Studies on β-turn of peptides. Part XI. For Part X, see M. Kawai, K. Sato, and U. Nagai, *Int. J. Peptide Protein Res.*, **24**, 607 (1984).
2) K. Sato, M. Kawai, and U. Nagai, *Biopolymers*, **20**, 1921 (1981).
3) K. Sato, M. Kawai, and U. Nagai, *Bull. Chem. Soc.Jpn.*, **56**, 1527 (1983).
4) K. Sato, U. Nagai, and T. Higashijima, *Bull. Chem. Soc. Jpn.*, **56**, 1657 (1983).
5) The abbreviations used in this paper are those recommended by IUPAC-IUB: *Eur. J. Biochem.*, **138**, 9 (1984). Additional abbreviations: EDC, 1-ethyl-3-(3-dimethylaminopropyl)carbodiimide: pNA, *p*-nitroanilide; GS, gramicidin S.
6) M. Tamaki, T. Okitsu, M. Araki, H. Sakamoto, M. Takimoto, and I. Muramatsu, *Bull. Chem. Soc. Jpn.*, **58**, 531 (1985).
7) S. Lee, R. Ohkawa, and N. Izumiya, *Bull. Chem. Soc. Jpn.*, **44**, 158 (1971).
8) M. Kawai and U. Nagai, *Biopolymers*, **17**, 2649 (1978).
9) K. Sato, R. Sugawara, and U. Nagai, *Int. J. Peptide Protein Res.*, **24**, 600 (1984).

Further Evidence for the Regioselectivity Rules in Nucleophilic Aromatic Photosubstitution

Kiyoshi MUTAI* and Ryoichi NAKAGAKI†

Department of Chemistry, College of Arts and Sciences, The University of Tokyo, Komaba, Meguro-ku, Tokyo 153

†*Institute for Molecular Science, Myodaiji, Okazaki 444*

(Received May 24, 1985)

Synopsis. In order to assess the validity of our regioselectivity rules for nucleophilic aromatic photosubstitution, 4-nitronaphthyl ethers were designed and their photochemical behavior was studied by applying frontier molecular orbital theory. The results provide supporting evidence for our rules.

In a previous paper[1] we proposed two rules to rationalize the regioselectivities observed in nucleophilic aromatic photosubstitutions; namely, (rule 1) photosubstitutions accompanying direct addition of a nucleophile to an excited aromatic substrate substituted with a strongly electron-withdrawing group (s) show HOMO-controlled regioselectivity, and (rule 2) those involving photoinduced electron transfer from a nucleophile to an aromatic substrate show LUMO-controlled regioselectivity, where, HOMO and LUMO, refer to those of the aromatic substrate in the ground state.

The objectives of the present paper are to extend the scope of application of these rules to naphthalene derivatives and, thus, to provide further evidence for the rules.

By analogy with the substituted benzenes previously reported to undergo photorearrangement,[2] naphthalene derivatives **1** and **2** are designed and submitted to photoreaction.

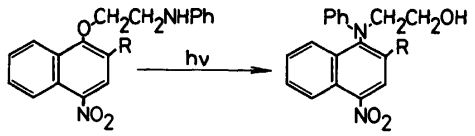

1, R = H
2, R = OMe

3, R = H
4, R = OMe

HOMO-controlled Photosubstitution. Since 1-methoxy-4-nitro- and 1,2-dimethoxy-4-nitronaphthalenes can be regarded as simplified models for the nitroaromatic moieties of **1** and **2**, respectively, nucleophilic photosubstitutions of these model compounds were examined.

In Fig. la, the frontier electron density (FED) maps of the HOMO and LUMO of 1-alkoxy-4-nitronaphthalene are depicted. The values were calculated by the CNDO/2 approximation, assuming that the alkoxyl group can be replaced with a hydroxyl without causing any significant change in the FED distribution pattern.[1] According to frontier molecular orbital theory, photosubstitutions are expected to occur at the carbons with high FED, *i.e.* C_1–OR, C_2 or C_4–NO_2. All the reactions so far reported (with cyanide, hydride as BH_4^-, and methoxide ions)[3] have been observed at the position with the highest FED, C_4. Although the FED map in the LUMO suggests that the C_4-substitutions may also be interpreted as LUMO-controlled, electron transfer pathway cannot be expected for these

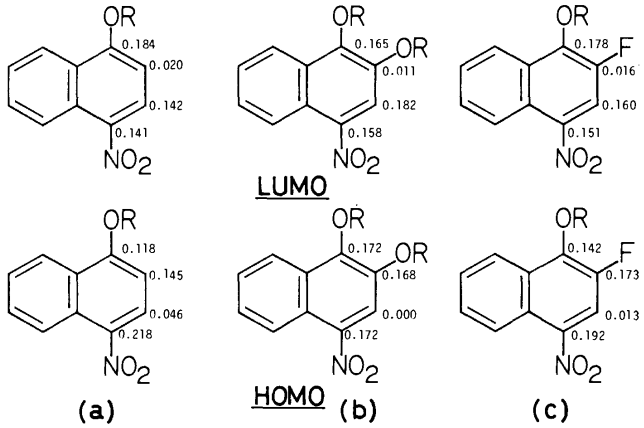

Fig. 1. Frontier electron density (FED) maps of the HOMO and LUMO of (a) 1-alkoxy-4-nitro-, (b) 1,2-dialkoxy-4-nitro-, and (c) 1-alkoxy-2-fluoro-4-nitronaphthalene.

nucleophiles, which have shown no tendency of electron release in the photosubstitutions of benzene derivatives.[1]

The photoreaction of 1,2-dimethoxy-4-nitronaphthalene has not been reported, but for the present purpose we could adopt 2-fluoro-1-methoxy-4-nitronaphthalene as a good substitute, because the FED maps of the HOMO's and LUMO's of these two models show a similar pattern (Fig. 1b and 1c). Nucleophilic photosubstitutions of 2-fluoro-1-methoxy-4-nitronaphthalene have been reported to occur[4] at C_1 with hydroxide ion, at C_2 with methoxide ion, and at C_4 with cyanide ion. A secondary reaction has been noted in the case of methoxide ion, replacing the nitro group at C_4 (an example of the photoreaction of the original model compound, 1,2-dimethoxy-4-nitronaphthalene). These three positions, C_1, C_2, and C_4, bear comparably large FED's (0.142, 0.173, and 0.192, respectively) and, therefore, the observed regioselectivity towards nucleophiles is consistent with rule 1.

LUMO-Controlled Photosubstitution. For the photoreactions accompanying electron transfer or the LUMO-controlled reactions, substitution in both **1** and **2** should occur at C_1 (intramolecular reaction at C_4 is sterically impossible) to afford rearranged products. On irradiating solutions of **1** and **2**, containing a catalytic amount of triethylamine, with a high-pressure Hg lamp, **3** and **4**, respectively, were isolated as reaction products in good yields (Eq. 1).[5] It is also noticeable that the photosubstitution observed for **2** occurred only at C_1 and not at C_2; because the C_2 carbon is bonded to a good leaving group and its FED of the HOMO is sufficiently large to accept a nucleophile, the substitution should occur, at least partly, at this position if the reaction takes

the HOMO-controlled pathway. This fact also underlines the importance of the LUMO in this photorearrangement. A marked contrast with the HOMO-controlled reactions strongly suggests that the rearrangements took place *via* electron transfer.

So far as we judge only by the structure of the product **3**, the observed regioselectivity of **1** is explicable either by rule 1 or rule 2, since its C_1 carbon has high FED's in both HOMO and LUMO. Rigorously speaking, it is difficult to rule out the HOMO-controlled mechanism. However, the LUMO-controlled pathway is more plausible, because even the nitroaromatic moiety with an additional electron-donating substituent, methoxyl group, in **2** is supposed to be able to accept an electron from the anilino moiety as discussed above and the counterpart in **1**, lacking in the methoxyl, is expected to have a larger electron affinity.

In order to obtain further supporting evidence for electron transfer process, we have tried to detect a transient species formed immediately after photoexcitation of **1** by means of nanosecond laser flash photolysis. However, it was found that the observation of transient spectra attributable to the charge-separated biradical consisting of the donor cation and acceptor anion was difficult due to strong fluorescence from the naphthalene moiety. Thus, no direct evidence for photoinduced electron transfer has been obtained.

Experimental

The details of the MO calculations have been described in a previous paper.[1] ^{1}H-NMR Spectra were recorded on a Varian EM-390 spectrometer. Melting points are uncorrected. Homogeneity of the compounds was established by HPLC on a JASCO FLC-A10 using methanol as an eluent.

1-(2-Bromoethoxy)-4-nitronaphthalene. To a mixture of 3.82 g (20 mmol) of 4-nitro-1-naphthol[6] and 9.30 g (50 mmol) of 1,2-dibromoethane in 15 ml of water containing 3 ml of dioxane was added a solution of 0.8 g (20 mmol) of sodium hydroxide in 10 ml of water under reflux with stirring during 1.5 h, and reflux was continued for 2 d. After cooling, the reaction mixture was poured into 30 ml of 5% aqueous sodium hydroxide solution and extracted with three 10-ml portions of dichloromethane. The extracts were collected and the solvent was removed by distillation. Chromatography on 80 g of active alumina eluting with benzene–dichloromethane mixture afforded 1.95 g (33%) of the bromide as yellow cyrstals: mp 77—78 °C; ^{1}H NMR ($CDCl_3$) δ= 3.76 (2H, t, J=5 Hz, CH_2Br), 4.46 (2H, t, J=5 Hz, OCH_2), 6.63 (1H, d, J=9 Hz, H-2), 7.3—7.8 (2H, m, H-6 and H-7), 8.0—8.35 (2H, m, H-5 and H-8), 8.63 (1H, d, J=9 Hz, H-3).

Found: C, 48.72; H, 3.26; N, 4.97%. Calcd for $C_{12}H_{10}NO_3Br$: C, 48.67; H, 3.40; N, 4.73%.

1-(2-Bromoethoxy)-2-methoxy-4-nitronaphthalene. This compound was prepared from 2-methoxy-4-nitro-1-naphthol[7] by a procedure similar to that described above for the bromide in a yield of 32%: mp 115—116 °C; ^{1}H NMR ($CDCl_3$) δ=3.71 (2H, t, J=6 Hz, CH_2Br), 4.02 (3H, s, OCH_3), 4.60 (2H, t, J=6 Hz, OCH_2), 7.4—7.7 (2H, m, H-6 and H-7), 8.17 (1H, s, H-3), 8.2—8.7 (2H, m, H-5 and H-8).

Found: C, 47.74; H, 3.71; N, 4.35%. Calcd for $C_{13}H_{12}NO_4Br$: C, 47.87; H, 3.71; N, 4.30%.

1-(2-Anilinoethoxy)-4-nitronaphthalene (1). This compound was prepared from aniline and the corresponding bromide by a reported procedure[2b] in a yield of 59%: mp 161—162 °C; ^{1}H NMR ($CDCl_3$–DMSO-d_6) δ=3.5—3.8 (2H, m, CH_2N), 4.37 (2H, t, J=6 Hz, OCH_2), 5.56 (1H, t, J=5 Hz, NH), 6.2—7.2 (6H, m, C_6H_5 and H-2), 7.2—7.8 (2H, m, H-6 and H-7), 8.25—8.4 (2H, m, H-3 and H-8), 8.54 (1H, dd, J=2 and 8 Hz, H-5).

Found: C, 69.88; H, 5.00; N, 9.08%. Calcd for $C_{18}H_{16}N_2O_3$: C, 70.12; H, 5.23; N, 9.08%.

1-(2-Anilinoethoxy)-2-methoxy-4-nitronaphthalene (2). This compound was prepared[2b] from aniline and the corresponding bromide in a yield of 88%: mp 110.5—112 °C; ^{1}H NMR ($CDCl_3$) δ=3.60 (2H, t, J=5 Hz, CH_2N), 3.97 (3H, s, OCH_3), *ca.* 4.3 (1H, br s, NH), 4.43 (2H, t, J=5 Hz, OCH_2), 6.6—7.3 (5H, m, C_6H_5), 7.4—7.6 (2H, m, H-6 and H-7), 8.17 (1H, s, H-3), 8.15—8.3 (1H, m, H-8), 8.5—8.7 (1H, m, H-6).

Found: C, 67.18; H, 5.33; N, 8.02%. Calcd for $C_{19}H_{18}N_2O_4$: C, 67.44; H, 5.36; N, 8.28%.

1-[N-(2-Hydroxyethyl)anilino]-4-nitronaphthalene (3). The amine **1** (370 mg, 1.2 mmol) dissolved in a mixture of methanol (800 ml), acetonitrile (150 ml), and triethylamine (10 ml) was irradiated with a 400 W high-pressure Hg lamp for 50 min. Usual workup and chromatography on 50 g of silica gel eluting with a 1:1 mixture of benzene and dichloromethane afforded **3** (293 mg, 79%) as brick-red crystals: mp 131—132 °C; ^{1}H NMR ($CDCl_3$) δ=1.70 (1H, t, J=5 Hz, OH), 3.7—4.2 (4H, m, NCH_2CH_2O), 6.7—7.25 (5H, m, C_6H_5), 7.50 (1H, d, J=9 Hz, H-2), 7.4—7.8 (2H, m, H-6 and H-7), 8.01 (1H, dd, J=*ca.* 1.5 and 9 Hz, H-8), 8.31 (1H, d, J=9 Hz, H-3), 8.65 (1H, dd, J=*ca.* 1.5 and 9 Hz, H-5).

Found: C, 70.07; H, 4.95; N, 8.81%. Calcd for $C_{18}H_{16}N_2O_3$: C, 70.12; H, 5.23; N, 9.08%.

1-[N-(2-Hydroxyethyl)anilino]-2-methoxy-4-nitronaphthalene (4). Irradiation of the amine **2** under similar conditions to those used for **3** and usual workup afforded **4** as brick-red crystals in a yield of 53%: mp 117—118 °C; ^{1}H NMR ($CDCl_3$) δ=*ca.* 2.63 (1H, br t, J=*ca.* 5 Hz, OH), 3.75 (4H, br m, NCH_2CH_2O), 3.93 (3H, s, OCH_3), 6.45—7.2 (5H, m, C_6H_5), 7.35—7.6 (2H, m, H-6 and H-7), 7.7—7.9 (1H, m, H-8), 8.11 (1H, s, H-3), 8.4—8.6 (1H, m, H-5).

Found: C, 67.69; H, 5.54; N, 8.12%. Calcd for $C_{19}H_{18}N_2O_4$: C, 67.44; H, 5.36; N, 8.28%.

We are grateful to Professor Koichi Ohno and Dr. Akinori Inoue, the University of Tokyo, for their advice and help in calculation. This work was supported by the Joint Studies Program (1984) of the Institute for Molecular Science.

References

1) K. Mutai, R. Nakagaki, and H. Tukada, *Bull. Chem. Soc., Jpn.*, **58**, 2066 (1985).

2) a) K. Mutai and K. Kobayashi, *Bull. Chem. Soc. Jpn.*, **54**, 462 (1981); b) K. Mutai, K. Yokoyama, S. Kanno, and K. Kobayashi, *ibid.*, **55**, 1112 (1982).

3) R. L. Letsinger and R. R. Hautala, *Tetrahedron Lett.*, **1969**, 4205; W. C. Petersen and R. L. Letsinger, *ibid.*, **1971**, 2197.

4) J. G. Lammers and J. Lugtenburg, *Tetrahedron Lett.*, **1973**, 177; J. G. Lammers, Thesis, University of Leiden, Leiden, The Netherland, 1974, cited as Ref. 47 in J. Cornelisse and E. Havinga, *Chem. Rev.*, **75**, 353 (1975).

5) For the solutions of *ca.* 10^{-4} mol dm^{-3}, the rearrangement occurred in more than 90% yields, as monitored by HPLC at 254, 300, and 350 nm. The yields described in Experimental are the results obtained in preparative scale, adopting higher concentrations and prolonged time of irradiation.

6) A. Fischer, M. A. Riddolls, and J. Vaughan, *J. Chem. Soc, (B)*, **1966**, 106.

7) W. Bradley and R. Robinson, *J. Chem. Soc.*, **1934**, 1484; H. Cassebaum, *Chem. Ber.*, **90**, 2876 (1957).

A Novel Synthesis of Dihydropyranoflavonols

Sudhakar Rao TAKKELLAPATI, Hari Har MATHUR, and Girish Kumar TRIVEDI*
Department of Chemistry, Indian Institute of Technology, Bombay-400 076, India
(Received August 9, 1984)

Synopsis. Condensation of 6-formyl-7-hydroxy-2,2-dimethylchroman with ω-nitrostyrene in the presence of triethylamine yields 3-nitro-8,8-dimethyl-2-phenyl-7,8-dihydro-2*H*,6*H*-benzo[1,2-*b*:5,4-*b'*]dipyran which on treatment with hydrogen peroxide gives 3-hydroxy-8,8-dimethyl-2-phenyl-7,8-dihydro-4*H*,6*H*-benzo[1,2-*b*:5,4-*b'*]dipyran-4-one.

The occurrence of dihydropyrano- and pyranoflavonols in nature is well known[1-5] and there are very few reports on the synthesis of the title compounds and their dehydrogenated products.[5-8] Till now most of the syntheses reported are mainly based on the well known Algar-Flynn-Oyamada reaction[6-8] wherein 6-acetyl-7-hydroxychromans have been used as the starting materials. Now here in we wish to report a new route for the synthesis of dihydropyranoflavonols, starting from 6-formyl-7-hydroxy-2,2-dimethylchroman (**1**) and ω-nitrostyrene (**2**—**4**). This method consists of the synthesis of 3-nitro-8,8-dimethyl-2-phenyl-7,8-dihydro-2*H*,6*H*-benzo[1,2-*b*:5,4-*b'*]dipyran and its conversion to 3-hydroxy-8,8-dimethyl-2-phenyl-7,8-dihydro-4*H*,6*H*-benzo[1,2-*b*:5,4-*b'*]dipyran-4-one *via* hydrogen peroxide treatment.

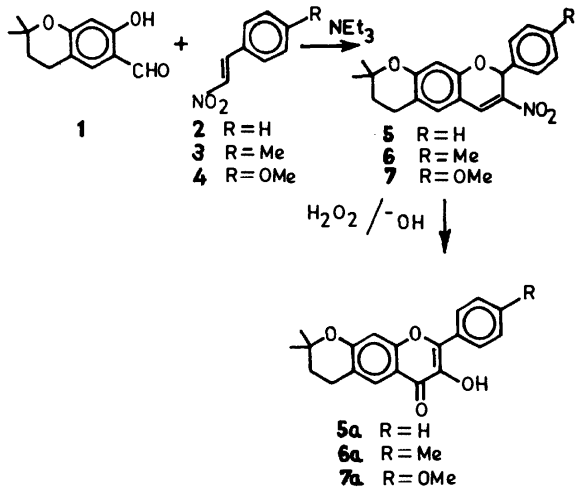

Experimental

Proton NMR spectra were obtained in $CDCl_3$ solution, unless otherwise stated, containing Me_4Si as reference using a Varian XL-100 spectrometer. Infrared spectra were recorded on a Perkin Elmer Model 618 instrument. UV spectra were recorded in $CHCl_3$ on a Varian Superscan-3 spectrometer. Mass spectra were determined on a MAT 112 S mass spectrometer. Melting points were taken in open capillaries and were not corrected.

*General Procedure for the Synthesis of 3-Nitro-8,8-dimethyl-2-phenyl-7,8-dihydro-2*H,6H*-benzo[1,2-*b*:5,4-*b'*]dipyran (**5**—**7**).* 4 mmol of 6-formyl-7-hydroxychroman (**1**) and 8 mmol of ω-nitrostyrene (**2**—**4**) were taken in a round bottom flask to which 5 ml of triethylamine was added and refluxed for 30 min on a water bath. Then the remaining triethylamine was evaporated off and the resulting solid mass was dissolved in dichloromethane and filtered. The solid residue after repeated washings with dichloromethane was discarded and the combined washings and filtrate on concentration and chromatography (pet. ether) yielded the trace amount of unreacted nitrostyrene, 6-formyl-7-hydroxychroman and 3-nitro-8,8-dimethyl-2-phenyl-7,8-dihydro-2*H*,6*H*-benzo[1,2-*b*:5,4-*b'*]dipyran consecutively. Crystallization was achieved from methanol. The yields of isolated compounds were varying from 30 to 35%.

*3-Nitro-8,8-dimethyl-2-phenyl-7,8-dihydro-2*H,6H*-benzo[1,2-*b*:5,4-*b'*]dipyran (**5**)*: Mp 210 °C; IR: 1320, 1560 (NO_2) cm^{-1}; NMR: δ=1.32 (3H, s), 1.34 (3H, s), 1.8 (2H, t, *J*=6 Hz), 2.72 (2H, t, *J*=7 Hz), 6.3 (1H, s), 6.34 (1H, s), 7.02 (1H, s), 7.36 (5H, s), 8.04 (1H, s); MS *m/z* (relative intensity) 55 (53), 63 (42), 69 (52), 77 (42), 115 (34), 139 (22), 178 (34), 235 (38), 291 (100), 337 (M^+, 50). Found: C, 71.10; H, 5.58; N, 4.13%. Calcd for $C_{20}H_{19}NO_4$: C, 71.22; H, 5.64; N, 4.15%.

*3-Nitro-8,8-dimethyl-2-(4-methylphenyl)-7,8-dihydro-2*H,6H*-benzo[1,2-*b*:5,4-*b'*]dipyran (**6**)*: Mp 146—148 °C; IR: 1320, 1560 (NO_2) cm^{-1}; NMR (DMSO-d_6): δ=1.23 (6H, s), 1.65 (2H, t, *J*=7 Hz), 2.2 (3H, s), 2.46 (2H, t, *J*=7 Hz), 6.13 (1H, s), 6.46 (1H, s), 7.16 (4H, s, br), 7.26 (1H, s), 8.26 (1H, s); MS *m/z* (relative intensity) 91 (9), 119 (7), 151 (11), 178 (12), 221 (8), 249 (39), 250 (25), 305 (100), 351 (M^+, 46). Found: C, 71.62; H, 5.88; N, 3.93%. Calcd for $C_{21}H_{21}NO_4$: C, 71.79; H, 5.98; N, 3.99%.

*3-Nitro-8,8-dimethyl-2-(4-methoxyphenyl)-7,8-dihydro-2*H,6H*-benzo[1,2-*b*:5,4-*b'*]dipyran (**7**)*: Mp 163—164 °C; IR: 1310, 1550 (NO_2) cm^{-1}; NMR: δ=1.32 (3H, s), 1.34 (3H, s), 1.79 (2H, t, *J*=7 Hz), 2.71 (2H, t, *J*=7 Hz), 3.78 (3H, s), 6.26 (1H, s), 6.48 (1H, s), 6.84 (2H, d, *J*=9 Hz), 7.02 (1H, s), 7.32 (2H, d, *J*=9 Hz), 8.02 (1H, s); MS *m/z* (relative intensity) 55 (21), 69 (25), 77 (19), 165 (22), 265 (39), 266 (20), 321 (100), 367 (M^+, 19). Found: C, 68.43; H, 5.63; N, 3.76%. Calcd for $C_{21}H_{21}NO_5$: C, 68.66; H, 5.72; N. 3.81%.

*General Procedure for the Conversion of 3-Nitro-8,8-dimethyl-2-phenyl-7,8-dihydro-2*H,6H*-benzo[1,2-*b*:5,4-*b'*]dipyran (**5**—**7**) to 3-Hydroxy-8,8-dimethyl-2-phenyl-7,8-dihydro-4*H,6H*-benzo[1,2-*b*:5,4-*b'*]dipyran-4-one (**5a**—**7a**)*: To a solution of 3-nitro-8,8-dimethyl-2-phenyl-7,8-dihydro-2*H*,6*H*-benzo[1,2-*b*:5,4-*b'*]-dipyran in methanol (20 ml) were added sodium hydroxide (2 M (1 M=1 mol dm^{-3}), 1 ml) and hydrogen peroxide (2 ml, 15%) while stirring at 35 °C. The stirring was continued for further 18 h. Removal of the solvent and crystallization from ethanol gave the crystalline dihydropyranoflavonol in 70—82% yield. The structures of all the compounds were confirmed by comparison with the literature data.

*3-Hydroxy-8,8-dimethyl-2-phenyl-7,8-dihydro-4*H,6H*-benzo-[1,2-*b*:5,4-*b'*]dipyran-4-one (**5a**)*: Mp 200—201 °C; lit,[6] mp 200—201 °C; IR: 1632 (C=O), 3300 (OH) cm^{-1}; NMR: δ=1.42 (6H, s, *gem*-dimethyl), 1.91 (2H, t, *J*=7 Hz, C_7-H), 2.95 (2H, t, *J*=7 Hz, C_6-H), 6.95 (1H, s, C_{10}-H), 7.42—7.64 (3H, m, phenyl), 8.0 (1H, s, C_5-H), 8.1—8.32 (2H, m, phenyl); MS *m/z* (relative intensity) 104 (49), 149 (22), 267 (89), 322 (M^+, 100); UV: λ_{max} (log ε): 263 (4.19), 333 (4.36), 363 (sh) (4.18) nm.

*3-Hydroxy-8,8-dimethyl-2-(4-methylphenyl)-7,8-dihydro-4*H,6H*-benzo[1,2-*b*:5,4-*b'*]dipyran-4-one (**6a**)*: Mp 188—190 °C IR: 1635 (C=O), 3250 (OH) cm^{-1}; NMR: δ=1.41 (6H, s, *gem*-dimethyl), 1.9 (2H, t, *J*=7 Hz, C_7-H), 2.42 (3H, s, methyl), 2.93 (2H, t, *J*=7 Hz, C_6-H), 6.92 (1H, s, C_{10}-H), 7.34 (2H, d, *J*=8 Hz, $C_{3'}$-H and $C_{5'}$-H), 9.98 (1H, s, C_5-H), 8.14 (2H, d, *J*=

8 Hz, $C_{2'}$–H and $C_{6'}$–H); MS *m/z* (relative intensity) 119 (24), 149 (15), 280 (58), 321 (8), 336 (M^+, 100); UV: λ_{max} (log ε) 260 (4.23), 332 (4.26), 351 (4.33), 367 (sh) (4.24) nm.

*3-Hydroxy-8,8-dimethyl-2-(4-methoxyphenyl)-7,8-dihydro-4*H, *6*H-*benzo[1,2*-b:*5,4*-b′*]dipyran-4-one* (**7a**): Mp 198—200 °C;lit,[8] mp 199—200 °C; IR: 1630 (C=O), 3300 (OH) cm^{-1}; NMR: δ= 1.42 (6H, s, *gem*-dimethyl); 1.92 (2H, t, *J*=7 Hz, C_7–H), 2.95 (2H, t, *J*=7 Hz, C_6–H), 3.91 (3H, s, methoxy), 6.92 (1H, s, C_{10}–H), 7.03 (2H, d, *J*=9 Hz, $C_{3'}$–H and $C_{5'}$–H), 7.97 (1H, s, C_5–H), 8.2 (2H, d, *J*=9 Hz, $C_{2'}$–H and $C_{6'}$–H); MS *m/z* (relative intensity) 135 (29), 149 (18), 296 (13), 298 (10), 337 (5), 352 (M^+, 100); UV: λ_{max} (log ε): 262 (4.2), 332 (4.35), 358 (4.38) nm.

References

1) J. F. Connet, F. Kozzek, and J. Pavre-Bonvin, *Phytochemistry*, **12**, 2773 (1973).
2) A. V. Rama Rao, M. Varadan, and K. Venkataraman, *Indian J. Chem.*, **7**, 101 (1969).
3) M. C. Do Nascimento, R. L. De Vasconcellos Dias, and W. B. Mors, *Phytochemistry*, **15**, 1553 (1976).
4) R. K. Gupta, M. Krishnamurthy, and E. A. Sherif, *Indian J. Chem.*, **19B**, 616 (1980).
5) S. K. Mukherjee, S. C. Sarkar, and T. R. Seshadri, *Tetrahedron*, **25**, 1063 (1969).
6) A. S. Sonde, Ph. D. Thesis, IIT Bombay, 1974.
7) S. B. Malik, P. Sharma, and T. R. Seshadri, *Indian J. Chem.*, **15B**, 493 (1977).
8) K. J. Rajendra Prasad, C. S. R. Iyer, and P. R. Iyer, *Indian J. Chem.*, **22B**, 693 (1983).
9) V. K. Ahluwalia, K. K. Arora, and R. S. Jolly, *Indian, J. Chem.*, **21B**, 629 (1982).

Atomic Absorption Spectrophotometric Determination of Cadmium

Mohamed A. KABIL* and Mohamed A. MOSTAFA
Department of Chemistry, Faculty of Science, Mansoura University, Mansoura, A.R. Egypt
(Received August 4, 1984)

Synopsis. In the determination of cadmium by atomic absorption spectrophotometry(AAS), the interfering effects of different species can be completely eliminated by adding excess cyanide. The mechanism by which the cyanide eliminates interference by influencing the atomization process is discussed. Also the AAS for the analysis of cadmium in complex form is elaborated. The aim of this investigation is to achieve a determinate characterization of compound formation. The way to reach this purpose is the utilization of the continuous titration technique.

The interfering effects on cadmium are rarely mentioned in the literature and what has been published are concerned with its determination.[1-3] In this work the effects of some inorganic and organic compounds have been examined and the feasibility of the compound formation is elaborated.

When solutions of cadmium complexes are examined, the absorption signals are mainly depend on the extent to which the ligands affect the atomization processes of Cd. In this respect, the work of Fujiwara[4] is important. He observed a significant difference in the absorbances in the lower part of the air–acetylene flame for the transition metal complexes. These differences were attributed to the type of complex present in solution.

Cyanide has already been successfully applied in AAS for some metals.[5-7] Since cyanide forms very stable complexes with most of transition metal ions,[8] elimination of the interfering effects by adding cyanide was examined.

Experimental

Atomic absorption spectrophotometer, Unicam SP '90 A series 2 fitted with a new HTA photomultiplier tube No. R 270 from EMI. Air was supplied through PU 9003 air compressor. Acetylene was obtained from cylinders after passing through concentrated sulfuric acid and glass wool for purification. A continuous titration device[9,10] was attached to the instrument and the results were computed using a CASIO FX-502 P type programmable pocket calculator. Absorbance values were recorded with a Philips PM 8251 single-pen recorder.

The instrumental parameters were: Lamp current, 4 mA; wavelength, 228.8 nm; slit width, 0.1 mm; observation height, 0.4 cm; air flow rate, 5 $dm^3 min^{-1}$, fuel flow rate, 1.0 $dm^3 min^{-1}$.

All solutions were prepared from B. D. H. Chemicals, Stock solutions of metals and organic compounds were prepared using twice distilled water; aliquots were suitably diluted to give the desired concentration used for the experiments. Stock solution of cadmium was prepared from $CdCl_2 \cdot H_2O$. The concentration of cadmium in the stock solution was 100 $\mu g cm^{-3}$.

The complexes, dibromobis(acetyltrimethylammonium-4-phenylthiosemicarbazide)cadmium(II) chloride [$Cd(H_2atpts)_2Br_2]Cl_2$, bis(1-anthraniloyl-4-phenylsemicarbazide) cadmium(II) [$Cd(Hapsc)_2$], bis(1-benzoyl-4-phenylthiosemicarbazide)cadmium(II) monohydrate [$Cd(Hbpts)_2] \cdot H_2O$, dibromo(acetylpyridinium-4-phenylthiosemicarbazide) cadmium(II) chloride [$Cd(H_2apts)Br_2]Cl$, acetato(1-acetyl-4-phenylthiosemicarbazide)cadmium(II) monohydrate [Cd(Hapts)(ac)]$\cdot H_2O$ and bis(1-anthraniloyl-4-phenylthiosemicarbazide)cadmium(II) [$Cd(Haptsc)_2$] were prepared as mentioned in the literature.[11,12] Other complexes; tris(1,2-propanediamine-$N,\overline{N}$)cadmium(II) dithionate [$Cd(pn)_3]S_2O_6$ and tris(1,2-ethanediamine-$N,\overline{N}$)cadmium (II) hydroxide [$Cd(en)_3](OH)_2$ were also prepared as mentioned earlier.[13] The 4.44×10^{-5} M (1 M=1 mol dm^{-3}) solutions of cadmium complexes were prepared by dissolving the appropriate weight of the solid complex in a few amount of *N,N*-dimethylformamide(DMF) and completed to the mark using twice distilled water.

Results and Discussion

Effect of potassium cyanide. Figure 1 shows the change in the absorption signal of cadmium as a function of [cyanide]/[Cd] molar ratio. There is a decrease in the signal with distinct break-point corresponding to [CN]/[Cd], 4:1 molar ratio, followed by a sharp enhancement to 130% of the recovery, giving a plateau.

The interpretation of the cyanide behaviour can be discussed on the basis of three main steps which may take place during its continuous increase in the flame, (i) Vaporization of the solid cyano complex particles followed by a decomposition giving Cd atoms which react instantaneously with the oxidizing species in the flame forming cadmium compound(s) essentially CdO, (ii) After the particular stoichiometric ratio is attained at 4:1 for CN:Cd, the excess of CN radical in the flame reacts with the cadmium compound(s) according to the following equation.

$$CdO + CN \longrightarrow Cd + N + CO$$

(iii) The continuous increase of the CN radical scavenging the excess oxidizing species, thus performing a reducing environment for increasing the Cd atom population. There is a balance between the CN

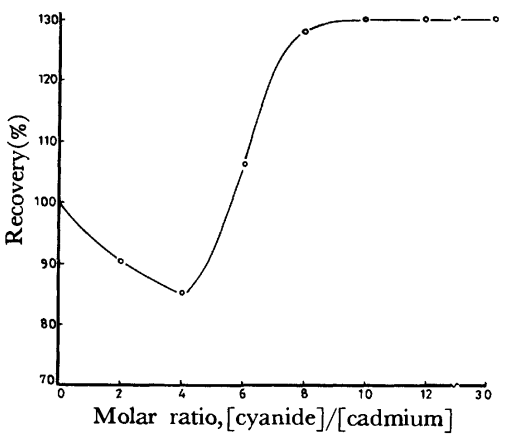

Fig. 1. Titration of 5 ppm Cd (4.44×10^{-5} mol dm^{-3}) with KCN.

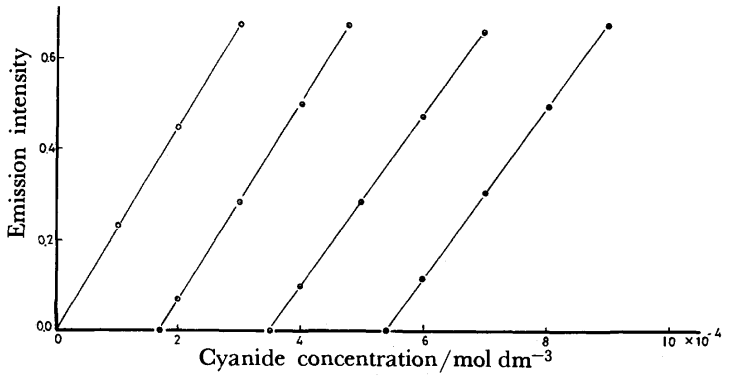

Fig. 2. Changes of cyanide band emission intensity as a function of cyanide concentration, (O) emission signal in absence of Cd, (⊙), (◒), and (●) in presence of 4.44×10^{-5}, 8.89×10^{-5}, and 1.33×10^{-4} mol dm^{-3} of Cd respectively.

radical and the excess oxidizing species in the flame at the plateau.

To assess both the formation of (4:1) molar ratio of CN:Cd and the presence of CN radical in the flame, we measured the emission intensity at 358 nm. Figure 2 curve (o) indicates the initial existence of CN radical in the flame at the starting of the titration process and in absence of the analyte (Cd). On conducting the titration in the presence of 4.44×10^{-5}, 8.89×10^{-5}, and 1.33×10^{-4} M of cadmium, the curves (⊙, ◒, and ●) of Fig. 2 are attained, respectively. These curves show, the emission intensity of CN radical, which disappears at the beginning of the titration and continued till the CN ion concentration reaches the stoichiometric ratio 4:1 for CN:Cd. Thence the emission intensity of CN radical increasing of CN ion.

Elimination of interferences. Different and diverse Cd(II) complexes are investigated. The relationship between the free Cd atom population and the height of measurement above the burner top is measured. The distribution curves in Fig. 3 clearly indicate the differences in the thermal stabilities of the tested complexes. Different times in the flame are required to achieve the same ratio of free atoms from various compounds. The general applicability of the cyanide addition to Cd(II) complexes is indicated by the data in Table 1.

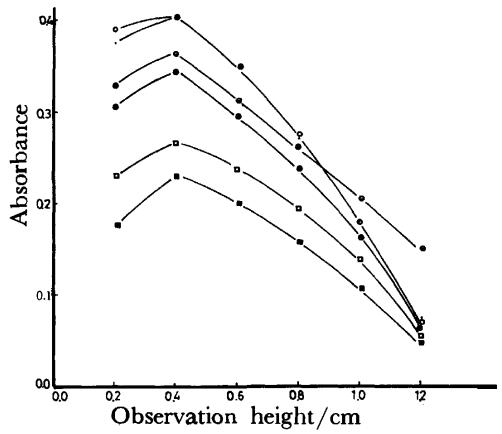

Fig. 3. Distribution of cadmium atoms as a function of observation height for different cadmium(II) complexes (5 ppm of Cd), (O)$[Cd(H_2atpts)_2Br_2]Cl_2$, (·) $CdCl_2$, (◒)$[Cd(Hapsc)_2]$, (●)$[Cd(Hbpts)_2]\cdot H_2O$, (□)$[Cd(pn)_3]S_2O_6$, and (■)$[Cd(en)_3](OH)_2$.

Table 1. Determination of Cd(II) complexes without and with masking by 0.05 M KCN (in all cases, the amount of complex taken corresponds to 5 μg cm^{-3} of Cd)

Cd(II) Complex	Cd Recovery/%	
	without masking	with masking
$[Cd(H_2atpts)_2Br_2]Cl_2$	100	100
$[Cd(Hapsc)_2]$	90	100
$[Cd(Hbpts)_2]\cdot H_2O$	86	98
$[Cd(H_2apts)Br_2]Cl$	100	100
$[Cd(Hapts)(ac)]\cdot H_2O$	108	98
$[Cd(Hptsc)_2]$	110	102
$[Cd(pn)_3]S_2O_6$	66	98
$[Cd(en)_3](OH)_2$	58	100

References

1) R. T. T. Rantala and D. H. Loring, *At. Spectrosc.*, **6**, 163 (1980).
2) W. M. Blakemova and S. M. Billedeau, *J. Assoc. Anal. Chem.*, **64**, 1284 (1981).
3) B. Magnusson and S. Westerlund, *Anal. Chim. Acta*, **131**, 63 (1981).
4) K. Fujiwara, H. Haraguchi, S. Toda, and K. Fuwa, *Bunseki Kagaku*, **25**, 255 (1976).
5) M. M. M. El-Defrawy, J. Posta, and M. T. Beck, *Anal. Chim. Acta*, **115**, 155 (1980).
6) M. M. M. El-Defrawy, J. Posta, and M. T. Beck, *Anal. Chim. Acta*, **102**, 185 (1978).
7) M. M. M. El-Defrawy, M. A. Mostafa, and A. M. Abdallah, Egyptian Chemical Society, XII Egyptian Chemical Conference, Cairo, 7—10 April, 1984.
8) A. G. Sharpe, "The Chemistry of Cyano Complexes of Transition Metals," Academic Press, London (1976).
9) R. W. Looyenga and C. O. Huber, *Anal. Chim. Acta*, **55**, 179 (1971).
10) J. Posta and J. Lakatos, *Magy. Kem. Folyoirat*, **86**, 284 (1980).
11) A. A. El-Asmy and M. M. Mostafa, *Polyhedron*, **2**, 591 (1983).
12) A.M. Shallaby, M. M. Mostafa, and A. A. El-Asmy, *Acta Chim. Hung.*, **114**, 9 (1983).
13) G. Marcu, M. Somay, and C. Varhelyi, *Stud. Univ. Babes-Bolyai, Ser. Chem.*, **23**, 3 (1978).

1,8-Diazabicyclo[5.4.0]undec-7-ene. An Effective and Selective Catalyst for the *t*-Butyldimethylsilylation of Alcohols

Sunggak KIM* and Heung CHANG
Department of Chemistry, Korea Advanced Institute of Science and Technology, Seoul 131, Korea
(Received October 11, 1984)

Synopsis. The use of 1,8-Diazabicyclo[5.4.0]undec-7-ene (DBU) as a catalyst has been found to be very effective and selective in the *t*-butyldimethylsilylation of primary and secondary alcohols.

In view of the great importance of the *t*-butyldimethylsilyl group in the protection of alcohols,[1] various synthetic methods have been reported in the literature after discovery by Corey.[2,3]

We have found that DBU is an effective and selective catalyst for the *t*-butyldimethylsilylation of alcohols (Eq. 1). Under the present reaction conditions, it is assumed that DBU forms a complex with *t*-butyldimethylchlorosilane (TBDCS) which subsequently reacts with alcohols to give *t*-butyldimethylsilyl ethers (Eq. 2). Furthermore, in view of large steric requirements of the complex, it is expected that high selectivity between primary alcohols and secondary alcohols can be achieved by use of DBU as a catalyst.

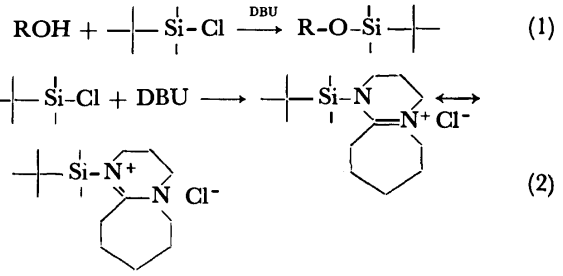

(1)

(2)

Table 1 includes several experimental results and shows the efficiency, the applicability, and the scope of this procedure. When primary alcohols such as phenethyl alcohol and nonyl alcohol were allowed to react with equimolar amounts of TBDCS and DBU in dichloromethane at room temperature, the reaction was complete within 20 min and the *t*-butyldimethylsilyl ethers were obtained in high yields. Application of 0.2 equiv of DBU in the presence of 1 equiv of triethylamine in dichloromethane at room temperature for 4 h resulted in clean silylation of alcohols. Furthermore, the silylation of alcohols using DBU proceeded smoothly in various solvents such as *N,N*-dimethylformamide, acetonitrile, and tetrahydrofuran. Similarly, secondary alcohols were cleanly silylated to the corresponding *t*-butyldimethylsilyl ethers in high yields at room temperature within 4 h. As we expected from large steric requirements of the complex as shown in Eq. 2, this procedure reaches a limit with tertiary alcohols. Thus, the *t*-butyldimethylsilylation of 2-phenyl-2-butanol did not occur to an observable extent, even after prolonged stirring.

TBDCS has been used in the selective protection of primary alcohols in the presence of secondary alcohols due in part to steric bulkiness of *t*-butyldimethylsilyl group.[4] It has been reported that the use of 4-dimethylaminopyridine (DMAP)[5] as a catalyst is very

TABLE 1. PREPARATION OF *t*-BUTYLDIMETHYLSILYL ETHERS AT ROOM TEMPERATURE[a]

No.	Alcohol	Amine[b]	Solvent	Time	Yield/%[c]	Bp θ_b/°C/Torr[d]
		A	CH_2Cl_2	20 min	98	80—82/0.5[3h]
		B	CH_2Cl_2	4 h	96	
1	$C_6H_5CH_2CH_2OH$	C	CH_2Cl_2	20 min	98	
		A	DMF	10 min	95	
		A	CH_3CN	20 min	96	
		A	THF	20 min	98	
2	$C_6H_5CH_2OH$	C	CH_2Cl_2	20 min	90	64—67/0.5[3g]
3	$C_6H_5CH{=}CHCH_2OH$	B	CH_2Cl_2	5 h	93	93—96/0.5[3c]
4	$CH_3(CH_2)_7CH_2OH$	A	CH_2Cl_2	20 min	90	106—110/1.7[3c]
5	$C_6H_5CH(OH)CH_3$	A	CH_2Cl_2	4 h	98	58—61/0.5
6	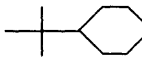	B	DMF	20 min	95	88—90/1.0[3b]
		C	CH_2Cl_2	1 h	89	
7	$C_6H_5C(CH_3)C_2H_5$ OH	A	DMF	24 h	0	
		A	CH_2Cl_2	24 h	0	
8	$CH_3(CH_2)_2CH(OH)CHCH_2OH$ C_2H_5	A	CH_2Cl_2	30 min	89 (99:1:0)	
		B	CH_2Cl_2	2 h	94 (99:1:0)	
9	$C_6H_5CH(OH)CH_2OH$	B	CH_2Cl_2	4 h	95 (97:1:2)	
10	$CH_3CHCH_2CH_2OH$ OH	A	CH_2Cl_2	20 min	92 (97:3:0)	
		B	CH_2Cl_2	1 h	93 (98:2:0)	

a) For selective silylation of selected diols, 1.0 equiv of TBDCS was used, Otherwise, 1.1 equiv of TBDCS was employed. b) A: 1.1 equiv DBU, B: 0.2 equiv DBU/1 equiv Et_3N, C: 1.1 equiv DBN. c) The numbers in parentheses indicate the ratio of the primary silyl ether, the secondary silyl ether, and the bissilyl ether, respectively. The product ratios were determined by GLC analysis. d) Spectral data of silyl ethers were in satisfactory agreement with reported or expected values. 1 Torr=133.322 Pa.

effective in the selective *t*-butyldimethylsilylation of primary alcohols in the presence of secondary alcohols, whereas the use of imidazole does not give satisfactory results.[3b] We have found that DBU can be utilized for the selective silylation of primary alcohols in the presence of secondary alcohols. For example, reaction of 2-ethyl-1,3-hexane-diol with 1 equiv of TBDCS and 1.1 equiv of DBU gave almost exclusively the primary silyl ether with a trace amount (<1%) of the secondary silyl ether, whereas it is known that the use of imidazole gives a mixture of all the possible isomers without high selectivity. Similar results were obtained with 1,3-butanediol and 1-phenyl-1,2-ethanediol. The selectivity achieved with DBU as a catalyst is superior to imidazole and is comparable to DMAP as a catalyst in the selective silylation of primary alcohols.[3b]

It is noteworthy that 1,5-diazabicyclo[4.3.0]non-5-ene (DBN) was also found to be effective in the *t*-butyldimethylsilylation of alcohols.

In conclusion, the present procedure offers the advantages of the ready availability of DBU, the rapidity of the reaction, the wide choice of solvents, and the high selectivity between primary alcohols and secondary alcohols.

Experimental

^{1}H-NMR spectra were recorded with a Varian T-60A spectrometer and infrared spectra were recorded on a Perkin-Elmer 267. GLC analysis was performed on a Varian 2800 gas chromatograph using FID detector. All analyses were carried out on 10 ft×0.125 in. 10% Carbowax 20 M. Reported boiling points are those observed during distillation with a Kugelrohr apparatus and are uncorrected.

Since the reaction were performed are all similar in many respects, typical reactions will be described as specific examples.

t-Butyldimethylsilylation of Cinnamyl Alcohol. To a solution of cinnamyl alcohol (270 mg, 2.0 mmol), DBU (60 mg, 0.4 mmol), and triethylamine (205 mg, 2.0 mmol) in dichloromethane (5 ml) at room temperature was added *t*-butyldimethylchlorosilane (335 mg, 2.2 mmol). The reaction mixture was stirred at room temperature for 5 h, diluted with dichloromethane (40 ml), and washed with cold 5% HCl solution (20 ml), saturated $NaHCO_3$ solution (20 ml), and brine (20 ml). The organic layer was dried over anhydrous $MgSO_4$ and evaporated to dryness. The residue was distilled *in vacuo* to give *t*-butyldimethylsilyl cinnamyl ether (465 mg, 93%). Bp 93—96 °C/0.5 Torr (lit,[3c] bp 90—92 °C/0.3 Torr). ^{1}H-NMR (CCl_4) δ=0.10 (s, 6H), 1.0 (s, 9H), 4.35 (d, 2H, J=6), 6.20—6.80 (m, 2H), 7.25 (s, 5H).

Selective t-Butyldimethylsilylation of 2-Ethyl-1,3-hexanediol. To a solution of 2-ethyl-1,3-hexanediol (290 mg, 2.0 mmol), DBU (58 mg, 0.4 mmol), and triethylamine (210 mg, 2.0 mmol) in dichloromethane (6 ml) at room temperature was added *t*-butyldimethylchlorosilane (298 mg, 2.0 mmol). The reaction mixture was stirred at room temperature for 2 h, diluted with dichloromethane (30 ml), and washed with cold 5% HCl solution (20 ml), saturated $NaHCO_3$ solution (20 ml), and brine (20 ml). The organic layer was dried over anhydrous $MgSO_4$ and evaporated to dryness to afford the primary silyl ether (486 mg) in 94% yield. The product was subjected to GLC analysis, which showed 99% of the primary silyl ether and <1% of the secondary silyl ether without any contamination of the bissilyl ether. For the characterization of the products, a mixture of all the possible isomers was prepared by the known procedure, while the primary silyl ether was also prepared by use of DMAP–Et_3N.[3b]

References

1) T. W. Greene, "Protective Groups in Organic Synthesis," Wiley, New York (1981).

2) E. J. Corey and A. J. Venkateswarlu, *J. Am. Chem. Soc.*, **94**, 6190 (1972).

3) a) T. J. Barton and C. R. Tulley, *J. Org. Chem.*, **43**, 3649 (1978); b) S. K. Chaudhary and O. Hernandez, *Tetrahedron Lett.*, **1979**, 99; c) G. A. Olah, B. G. B. Gupta, S. C. Narang, and R. Malhorta, *J. Org. Chem.*, **44**, 4272 (1979); d) T. Morita, Y. Okamoto, and H. Sakurai, *Tetrahedron Lett.*, **21**, 835 (1980); e) M. Lissel and J. Weiffen, *Synth. Commun.*, **11**, 545 (1981); f) E. J. Corey, H. Cho, C. Rucker, and D. H. Hua, *Tetrahedron Lett.*, **22**, 3455 (1981); g) Y. Kita, J. Haruta, J. Segawa, and Y. Tamura, *Synthesis*, **1981**, 451; h) L. Lombardo, *Tetrahedron Lett.*, **25**, 227 (1984); i) S. Kim and H. Chang, *Synth. Commun.*, **14**, 899 (1984).

4) K. K. Ogilvie and D. J. Iwacha, *Tetrahedron Lett.*, **1973**, 317; G. Just and S. Kim, *ibid.*, **1976**, 1063; K. K. Ogilvie, S. L. Beaucage, A. L. Schiffman, N. Y. Theriault, and K. L. Sadana, *Can. J. Chem.*, **56**, 2768 (1978).

5) For excellent reviews, see: G. Höfle, W. Steglich, and H. Vorbrüggen, *Angew. Chem. Int. Ed. Engl.*, **17**, 569 (1978); E. F. V. Scriven, *Chem. Soc. Rev.*, **12**, 129 (1983).

A Mechanistic Investigation of the Todd Reaction

Anne Kong and Robert Engel*
Queens College, The City University of New York, Flushing, NY 11367, U.S.A.
(Received November 14, 1984)

Synopsis. The Todd reaction, involving formation of a dialkyl phosphorochloridate by reaction of a dialkyl phosphonate with tetrachloromethane under basic conditions, has been determined to involve the intermediacy of the trichloromethanide anion.

The Todd reaction, a synthetically valuable method for the preparation of dialkyl phosphoramidates[1] and dialkyl phosphorochloridates,[2] was the subject of early kinetic investigations by Steinberg.[3] On the basis of the kinetic data, several possible mechanisms for the reaction were proposed, two of these involving the intermediacy of the trichloromethanide anion. We have now obtained direct evidence for the intermediacy of this species in the Todd reaction under carefully defined conditions, giving foundation for a detailed mechanism.

The chemistry of the trichloromethanide anion has become quite well known since the postulation of its intermediacy in the Todd reaction. Hine[4] first gained positive data for the dissociation of the trichloromethanide anion into chloride ion and dichlorocarbene during the hydrolysis of chloroform. It was later noted that dichlorocarbene so produced could add to olefins.[5] Should the Todd reaction proceed through a route involving the trichloromethanide anion, it would be anticipated that dichlorocarbene would be produced which is capable of being trapped.

The formation of dialkyl (or diaryl) phosphorochloridate in the Todd reaction occurs with near violent rapidity upon addition of small amounts of base (amine) to a mixture of dialkyl (or diaryl) phosphonate and tetrachloromethane as shown in Scheme 1.

$$(RO)_2POH + CCl_4 \xrightarrow{Et_3N} (RO)_2\overset{O}{\overset{\|}{P}}Cl + HCCl_3$$
$$R = CH_3,\ C_2H_5,\ C_6H_5$$

Scheme 1.

We have confirmed and extended several earlier observations[3] regarding this reaction: 1) In the absence of base, no reaction occurs, even with prolonged heating. 2) The reaction is not influenced by the presence of free radical initiators or inhibitors. 3) The only phosphorus-containing side products are those as reported by Steinberg,[3] the hypophosphate and pyrophosphate, resulting from further reaction of the initially generated dialkyl (diaryl) phosphorochloridate; under GLC analysis using either thermal conductivity or hydrogen flame detection capable of detecting products at amounts less than 0.1 % conversion, no formation of the dialkyl trichloromethylphosphonate could be observed. This material is easily formed in an Arbuzov-type reaction with a trialkyl phosphite as shown in Scheme 2. 4) The reaction may be accomplished in the presence or absence of solvent, which simply serves to moderate the reaction.

$$(RO)_3P + CCl_4 \xrightarrow{\Delta} (RO)_2\overset{O}{\overset{\|}{P}}CCl_3 + RCl$$

Scheme 2.

The general procedure for performing and analyzing reactions involved placement of the dialkyl (diaryl) phosphonate (0.1 mol) with the solvent (if any) and a weighed amount of a suitable inert standard (for quantitative GLC analysis) in a reaction flask equipped with a dropping funnel, reflux condenser, and magnetic stirrer. If amine were used as base, an equivalent amount (0.1 mol) was then added; if the sodium salt of the dialkyl phosphonate were used, sodium or sodium hydride was added with stirring until all had reacted. Tetrachloromethane was then added dropwise at ambient temperature, and stirring continued for 2 h.

An immediate analysis was made using GLC to determine quantitatively chloroform generated, and to note the presence of the phosphorochloridate using one of the following columns: (a) 5′×1/4″ 1.5 % OV-101 on Chrom GHP, (b) 5′×1/4″ 30 % SE-30 on Chromsorb W, or (c) 5′×1/4″ 20 % Apiezon L on Chromsorb W. As the phosphorochloridates underwent significant decomposition under the analytical conditions, the reaction mixture was then treated with an excess of abs ethanol and triethylamine for conversion of the phosphorochloridate to the phosphate. A further chromatographic analysis was then made to determine the yield of the phosphate, and by inference the phosphorochloridate (*minimal* yield). The phosphate was also isolated from the reaction mixture and its structure was confirmed by ^{1}H-NMR analysis (Varian EM-360).

In all attempts using a tertiary amine to initiate the reaction and cyclohexene as solvent or cosolvent, the reaction proceeded "normally" yielding only the products found in the absence of solvent. It had been anticipated that cyclohexene would serve to trap any dichlorocarbene which would result from trichloromethanide decomposition.

Attempts using a less than one equivalent amount of preformed anion of dialkyl phosphonate produced similar results (Scheme 3). When a small amount of anion was generated by addition of sodium hydride

$$(RO)_2POH + NaH \xrightarrow{\bigcirc} (RO)_2PONa$$
$$<0.1\ \text{equiv} \qquad \downarrow CCl_4$$
$$(RO)_2\overset{O}{\overset{\|}{P}}Cl + HCCl_3$$
$$R = CH_3,\ C_2H_5$$

Scheme 3.

Table 1.

Starting Materials			Product Yields		
R	Base	Solvent	$CHCl_3$/%	$(RO)_2P(O)Cl$/%	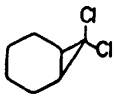 /%
CH_3	Et_3N[a]	Toluene	69.0	63.6	—
C_2H_5	Et_3N[a]	Toluene	63.9	61.0	—
C_6H_5	Et_3N[a]	Tolnene	57.9	48.2	—
CH_3	Et_3N[a]	Cyclohexene	70.6	67.3	0[e]
C_2H_5	Et_3N[b]	Cyclohexene	69.8	61.5	0[e]
C_6H_5	Et_3N[a]	Cyclohexene	60.3	51.8	0[e]
C_2H_5	Na[b]	Cyclohexene	53.1	42.1	0[e]
C_2H_5	NaH[c]	Cyclohexene	71.4	62.7	0[e]
CH_3	NaH[d]	THF	40.6	29.2	—
CH_3	NaH[d]	Cyclohexene	31.7	48.2	22.6

a) Equiv amounts of base, CCl_4, and dialkyl (diaryl) phosphonate. b) Preformed anion with 0.1 equiv Na; Yields based on 0.5 equiv CCl_4. c) Preformed anion with 0.015 equiv NaH; Yields based on CCl_4 as limiting reagent. d) Preformed anion with 1.0 equiv NaH. e) Below detectable limits.

and to this was added tetrachloromethane, rapid reaction ensued generating phosphorochloridate and chloroform with an average conversion of 60 % based on tetrachloromethane.

This result could be observed in the absence of solvent or in the presence of varying amounts of several solvent systems (tetrahydrofuran, toluene, cyclohexene). Again, with cyclohexene no trapping of dichlorocarbene could be noted using GLC techniques.

Finally the reaction was performed by the conversion of the entire amount of dialkyl phosphonate to the anion form using sodium hydride. To this system in cyclohexene was added an equivalent amount of tetrachloromethane. Analysis of the reaction mixture showed the formation of dialkyl phosphorochloridate along with 7,7-dichloronorcarane, the product of dichlorocarbene addition to cyclohexene, with an average 50 % conversion. Typical results are illustrated in Table 1.

The verification of the intermediacy of the trichloromethanide anion along with prior data regarding the phosphorus stereochemistry (retention) for this type of reaction[6,7] supports the overall mechanism as illustrated in Scheme 4. In the presence of any proton source the trichloromethanide anion accepts a proton with extreme rapidity precluding decomposition to dichlorocarbene. In the absence of any such proton source, the resultant trichloromethanide anion leads to products derived from dichlorocarbene.

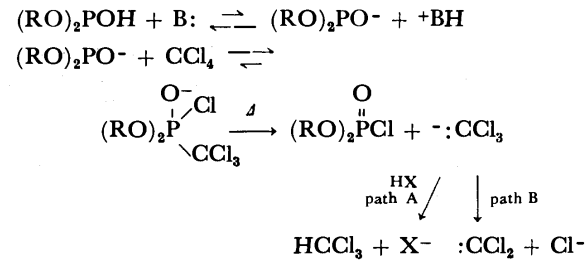

Scheme 4.

The authors wish to thank Dr. H. S. Aaron for helpful discussions, and the PSC-BHE Research Award Program for financial support.

References

1) F. R. Atherton, H. T. Openshaw, and A. R. Todd, *J. Chem. Soc.*, **1945**, 660.
2) F. R. Atherton and A. R. Todd, *J. Chem. Soc.*, **1947**, 674.
3) G. M. Steinberg, *J. Org. Chem.*, **15**, 673 (1950).
4) J. Hine, *J. Am. Chem. Soc.*, **72**, 2438 (1950).
5) W. v. E. Doering and A. K. Hoffmann, *J. Am. Chem. Soc.*, **76**, 6162 (1954).
6) L. P. Reiff and H. S. Aaron, *J. Am. Chem. Soc.*, **92**, 5275 (1970).
7) G. R. Van den Berg, D. H. J. M. Platenburg, and H. P. Benschop, *J. Chem. Soc., Chem. Commun.*, **1971**, 606.

Spectrophotometric Determination of Cobalt(II) with Thiocyanate. A Modification for Increasing Sensitivity and Selectivity

Ajai Kumar SINGH,* Dinesh KUMAR, and Mohan KATYAL
Department of Chemistry, Indian Institute of Technology, New Delhi 110 016, India
(Received December 18, 1984)

Synopsis. The ion association complex formed between $[Co(SCN)_4]^{2-}$ and 3,3'-(1,1'-biphenyl-4,4'-diyl)bis[2,5-diphenyl-2*H*-tetrazolium] dichloride, commercially known as neotetrazolium chloride, has been extracted into isobutyl methyl ketone and used for the photometric determination of 2.5—9.8 μg cm^{-3} cobalt at pH 3.5—5.0 (acetate buffer). Sandell's sensitivity of the method (0.02 μg cm^{-2}) is better than most of the other thiocyanate methods known so far. Interference of diverse ions has been studied. Using the higher tolerances of anions, many cations interfering in the other thiocyanate methods have been masked, thus making the present procedure more selective. The method has been applied to wire alloys.

Thiocyanate is among the most commonly used spectrophotometric reagents[1] of cobalt. The tetrathiocyanatocobaltate(II) as well as its ion associates with a variety of counter ions have been employed for the determination of the metal,[2,3] but the sensitivity exceeding 0.04 μg cm^{-2} (for 0.001 absorbance) has been rarely reported. In the course of studies on tetrazolium salts it has been observed that the ion pair formed between neotetrazolium chloride (NTC) and $[Co(SCN)_4]^{2-}$ is highly absorbing in isobutyl methyl ketone (MIBK) medium in comparision to other ion pairs of the anions investigated so far (Sandell's sensitivity 0.02 μg cm^{-2}). The detailed results of these investigations are reported in the present note.

The aqueous solution of $[Co(SCN)_4]^{2-}$ on mixing with NTC solution forms a greenish blue precipitate which is extractable into organic solvents. However the absorbance of this ion pair has been found maximum in MIBK. The tolerance of anions is more in this system than other Co–SCN systems and therefore can be utilized to create a more selective method for the determination of cobalt(II) with thiocyanate.

Experimental

Apparatus. Unicam SP 500 and 700 spectrophotometers were used for absorbance measurements and a Elico LI-10 pH meter for measuring pH.

Reagents. A stock solution 0.01 M (1 M = 1 mol dm^{-3}) of cobalt(II) was prepared by dissolving $CoSO_4 \cdot 7H_2O$ (BDH, A. R.) in doubly distilled water. It was standardized by titration with ethylenediaminetetraacetic acid (EDTA) before use. The solution of NTC, procured from Aldrich (U. S. A.), was prepared in 50% ethanol. Thiocyanate solution(10%) was prepared by dissolving the requisite amount in doubly distilled water. All other solutions of cations and anions were prepared by dissolving analytical grade chemicals in doubly distilled water.

Recommended Procedure. To a suitable aliquot containing 20 to 70 μg of cobalt add acetate buffer of pH 4.5, 10% ammonium thiocyanate and 0.4% NTC solution(4.0 cm^3 each). To this mixture add 2 cm^3 of water and 5 cm^3 (*N,N*-dimethylformamide) (DMF) to dissolve the precipitate. Extract the complex with 7 cm^3 MIBK and measure the absorbance of organic layer after centrifugation, at 620 nm against water blank. Deduce the metal content from calibration curve.

Results and Discussion

Spectral Behavior of the Complex and Effect of pH. The ion associate absorbs maximum at 620 nm. Absorbance remains maximum in the pH range 2.5 to 5.0. The variation in pH does not affect the absorbing characteristics of the complex. Reagent blank does not absorb at 620 nm. Acetate buffer is most suitable for pH adjustment .

Effect of Thiocyanate and NTC Concentration. For 1 cm^3 of 1 mM cobalt solution the maximum absorbance is attained in the presence of 3.7 cm^3 NTC solution (0.04 %). At least 3 cm^3 of 10 % thiocyanate solution should be added for full color development. The excess of either reagent does not affect the absorbance.

Effect of DMF and Stability of the Complex. At least 4.5 cm^3 of DMF should be added in the estimation of 1 cm^3 cobalt(II) to dissolve the precipitate. Excess up to 8 cm^3 does not have any effect but beyond this the extraction becomes erratic due to very slow irreproducible separation of the immiscible layers. The color does not fade even on keeping the solution for 12 h.

Characteristics of the Complex. Beer's law is obeyed up to 13 μg cm^{-3} at pH 4.5. The optimum concentration, evaluated by Ringbom method, is 2.5 to 9.8 μg cm^{-3}. The Sandell's sensitivity is 0.02 μg of cobalt cm^{-2}. The molar absorptivity is 3.0×10^3 l mol^{-1} cm^{-1}. The metal: NTC ratio, as found by Job's method of continuous variation, is 1 : 1. The species $(NTC)^{2+} \cdot [Co(SCN)_4]^{2-}$ are most probably responsible for the absorption. The standard deviation for the mean absorbance 0.345 has been found to be 0.003.

Effect of Diverse Ions. Synthetic solutions containing known amounts of diverse ions and cobalt(II) were prepared and the recommended procedure was followed for determination of the metal. An error of 2 % in the absorbance measurement was considered tolerable. In the determination of 8.4 μg cm^{-3} cobalt the anions tolerated (in μg cm^{-3} given in parentheses) are as follows: fluoride, chloride, iodide, nitrate(1000 each); phosphate (1250); oxalate(1280); nitrite (1200); bromide(625); thiosulfate (600); citrate, tartrate (480), and thiourea (150). The metal ions tolerated are: Ca(II), Sr(II), Ba(II), Ni(II), Cd(II), Mn(II), Al (III), Ti(IV) (250 μg cm^{-3} each); Zn(II) or Fe(II) (50 μg cm^{-3}); and Cu(II) (10). EDTA interferes seriously. All other metal ions which form colored complex with thiocyanate also interfere in this system. However, 100 μg cm^{-3} of iron can be masked with

Table 1. Determination of cobalt in alloys

Alloy	Cobalt/%		No. of detn.	Relative standard deviation
	Reported	Found		%
"K" Monel wire	0.51	0.50	6	3.8
Nilo "K" wire	17.4	17.6	6	2.0

fluoride. Tolerance of copper can be improved up to 60 μg cm^{-3} by using thiourea as masking agent. Similarly mixture of citrate and tartrate improves the tolerance of nickel up to 1000 μg cm^{-3}.

Determination of Cobalt in Alloys. To exhibit the advantages of higher sensitivity and selectivity of this method, the contents of cobalt in some wire alloys have been estimated using SCN and NTC as chromogenic reagent. The detailed procedure is given below.

Weighed samples of "K" Monel wire and Nilo "K" wire were dissolved in concentrated nitric acid. Excess acid was evaporated off and the residue was dissolved in doubly distilled water. By applying the recommended procedure the cobalt contents of the samples were determined. To mask copper, nickel, and iron present in these alloys requisite amounts of thiourea, citrate, tartrate, and fluoride were added. The results are reported in Table 1.

Comparision with Other Methods Based on Thiocyanate. The present method is better in sensitivity than most of the other methods based on thiocyanate. Sensitivities are compared in Table 2. The high molecular weight and conjugation of NTC^{2+} ion is responsible.

Table 2. Sensitivities of thiocyanate methods for the photometric determination of cobalt(II)

Method	Sensitivity (μg Co cm^{-2})	Reference
Thiocyanate (isopentyl alcohol)	0.055 (620 nm)	1, 4
Thiocyanate + tetraphenylarsonium ion (chloroform)	0.034 (620 nm)	1, 4
Thiocyanate + 1,1-diantipyrinylethane	0.075 (625 nm)	4
Thiocyanate + tributylammonium salt	0.045 (615 nm)	4
Thiocyanate + 2,3,5-triphenyltetrazolium salt	0.055 (625 nm)	1, 5
Thiocyanate + Neotetrazolium chloride	0.020 (620 nm)	Present method

References

1) E. B. Sandell, "Colorimetric Determination of Traces of Metals," 3rd ed, Interscience, New York (1965), p. 414.
2) F. D. Snell, "Photometric and Fluorimetric Methods of Analysis (Meatal)," Part 1, Wiley, New York (1978).
3) E. B. Sandell and H. Onishi, "Photometric Determination of Traces of Metals," Wiley, 4th ed, New York (1979), p. 536.
4) I. V. Pyatnitskii, "Analytical Chemistry of Cobalt," Israel Programme for Scientific Translations, Jerusalem (1966), p. 104
5) M. C. Mehra and D. LeBlenc, *Microchem. J.*, **24**, 435 (1979).

A CIDEP Study of the Addition of Trialkylsilyl Radicals to Substituted *p*-Benzoquinones

Marjory T. CRAW, Angelo ALBERTI,† M. Catherine DEPEW, and Jeffrey K. S. WAN*
Department of Chemistry, Queen's University, Kingston, Ontario, Canada K7L 3N6
(Received January 5, 1985)

Synopsis. Evidence has been obtained through the combined ESR and CIDEP techniques for the two distinct pathways in which trialkylsilyl radicals add to substituted *p*-benzoquinones *via* the carbonyl oxygen as well as the ring carbon–carbon double bonds. The results represent the first observation of CIDEP from organic radicals containing an organosilyl group in solution.

The reaction of organosilyl radicals with carbonyl compounds has received considerable attention in the past decade.[1-4] While it is generally accepted that the most *stable* adduct formed between a trialkylsilyl radical and 2,6-di-*t*-butyl-*p*-benzoquinone (DTBQ) at room temperature is the adduct to the carbonyl oxygen, recent experiments at low temperature with 3,6-dimethylthieno[3,2-*b*]thiophen-2,5-dione[5] indicate that the faster reaction is the addition of the trialkylsilyl radicals to the ring carbon–carbon double bond. Although CIDEP has been detected previously from trialkylsilyl radicals in solution, it is possible that in a fast reaction involving a primarily polarized organosilyl radical and a quinone the secondary racical adduct may retain and exhibit the initial polarization. In an ideal case, the magnitude of the secondary polarization is a direct measure of the relative efficiencies of the different reaction pathways. We wish to report here the first observation of CIDEP of the trialkylsilyl radical adducts to DTBQ formed by two distinct mechanisms.

When *t*-butylbenzene solutions of DTBQ and triethylsilane were photolyzed in the microwave cavity of an ESR spectrometer at −50 °C a first derivative spectrum (Fig. 1a) was observed which showed *a* triplet attributable to the oxygen adduct (**1**) (a_H=1.08 G (1G ≈10^{-4})) and *a* broad doublet due to the ring adduct (**2**) (a_H=7.03 G).

The polarization spectrum of the same system obtained in the CIDEP experiment is shown in Fig. 1b. The totally emissive character of the polarization spectrum is consistent with the photochemistry of the triplet DTBQ which must lead to the formation of two primary, emissive radicals, DTBQH* and $R_3\dot{S}i$*. In the present system with excess benzoquinone, the addition reactions of $R_3\dot{S}i$* to the ground state benzoquinone molecules are so rapid (faster or comparable to the spin lattice relaxation rate of $R_3\dot{S}i$*) that only the radical adducts (**1**) and (**2**) are observed in the cw spectrum. However, in the polarization spectrum, additional emissive lines due to the semiquinone radical DTBQH* are also apparent. In order to avoid the complication of the polarization spectrum due to the overlapping semiquinone radicals, triethylsilane was replaced with hexamethyldisilane as the reactant. In such a system the overall reaction can be represented by the following steps:

[1] ^{3}DTBQ* + $Me_3SiSiMe_3$ ⟶ DTBQ-$SiMe_3$* + $Me_3\dot{S}i$*,

[2] $Me_3\dot{S}i$* + DTBQ ⟶ (**1**) and (**2**).

The cw and the polarization spectra of the DTBQ/hexamethyldisilane system at 23 °C are shown in Fig. 1c and 1d, respectively. At room temperature, the predominant radical adduct was (**1**), while a weak polarized spectrum of the ring adduct (**2**) was observable in the CIDEP experiment.

The present results clearly establish that there are two distinct pathways for the addition of trialkylsilyl radicals to *p*-benzoquinones. The variation of temperature in the reaction system further confirms that the most thermally stable adduct is the oxygen adduct. At room temperature with DTBQ most of our previous

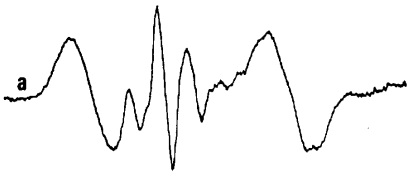

Fig. 1a. Cw ESR first derivative spectrum observed during the photolysis of DTBQ and triethylsilane in *t*-butylbenzene at −50 °C;

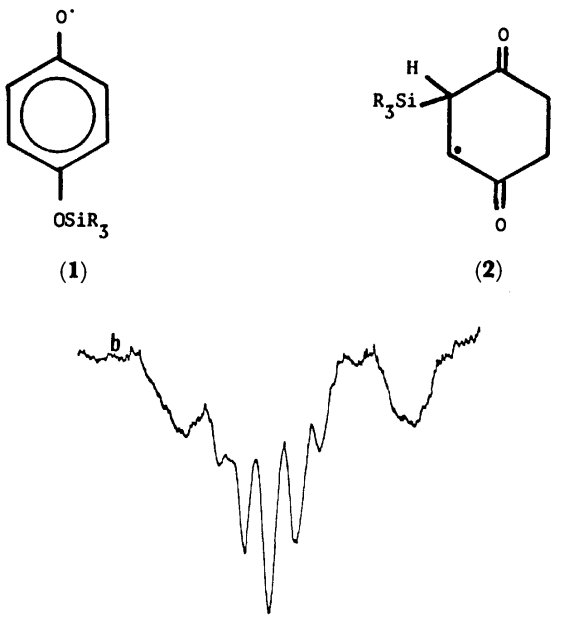

Fig. 1b. Polarization spectrum of the same system in 1a at −50 °C;

† On leave from Istituto dei Composti del Carbonio Contenenti Eteroatomi e loro Applicazioni, CNR, 40064 Ozzano Emillia, Italy.

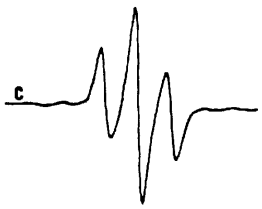

Fig. 1c. Cw ESR first derivative spectrum observed during the photolysis of DTBQ and hexamethyldisilane at 23 °C;

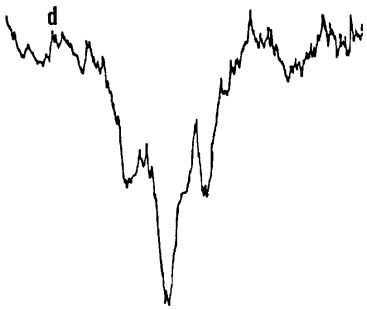

Fig. 1c. Polarization spectrum of the same system in 1c at 23 °C.

studies of the reactions of organometallic radicals, $\dot{M}R_3$, indicate the predominant formation of adducts of the type (**1**). In a more interesting study of the photochemical and thermal reactions of $Me_3Sn–\dot{M}n(CO)_5$, we have shown[6] that at room temperature the two primary radicals, $Me_3\dot{S}n$ and $\dot{M}n(CO)_5$ behaved very differently towards the addition mechanism to DTBQ: The $Me_3\dot{S}n$ radicals added to the carbonyl oxygen of DTBQ while the $\dot{M}n(CO)_5$ radicals attacked only at the carbon–carbon double bond of the ring. These results can be explained by the reversibility and endothermicity of the addition of stannyl radicals to ethylenic double bonds.[7]

Experimental

Cw ESR spectra were recorded on a Varian E-3 X-band spectrometer with 100 kHz field modulation. Irradiation in cw experiments was accomplished by using a 200 watt super pressure mercury lamp. For CIDEP experiments, a Molectron nitrogen laser (1 MW) was used as the excitation source and the ESR transients were directly detected without modulation using a Hewlett Packard wide band preamplifier and a Princeton Applied Research model 162 boxcar integrator and a Nicolet microcomputer controlled digital oscilloscope with a Hewlett Packard 7475A digital plotter.

Chemicals were supplied by Aldrich, the *p*-benzoquinone was sublimed and the tertiary butylbenzene distilled before use.

This research is supported by the operating grant and an International Scientific Collaboration award from the Natural Science and Engineering Research Council of Canada.

References

1) A. R. McIntosh and J. K. S. Wan, *Mol. Phys.*, **22**, 183 (1971); *Can. J. Chem.*, **49**, 817 (1971).

2) A. Alberti and A. Hudson, *J. Chem. Soc., Perkin Trans. 2*, **1978**, 1098; *J. Organomet. Chem.*, **164**, 219 (1979).

3) C. Chatgiliawglu, J. C. Scaiano, and K. U. Ingold, *J. Am. Chem. Soc.*, **103**, 3231 (1981); *ibid.*, **104**, 5119 (1982).

4) For a review, see K. A. M. Creber, K. S. Chen, and J. K. S. Wan, *Rev. Chem. Intermediates*, **5**, 37 (1984).

5) G. F. Pedulli and A. Alberti, private communication.

6) T. Foster, K. S. Chen, and J. K. S. Wan, *J. Organomet. Chem.*, **184**, 113 (1980).

7) R. A. Jackson, "Essays in Free Radical Chemistry," Chem. Soc. London (1970).